ICCTP 2009

Critical Issues in Transportation Systems Planning, Development, and Management

PROCEEDINGS OF THE NINTH INTERNATIONAL CONFERENCE ON CHINESE TRANSPORTATION PROFESSIONALS

August 5–9, 2009
Harbin, China

SPONSORED BY
North American Chinese Overseas Transportation Association (NACOTA)

Harbin Institute of Technology

Transportation and Development Institute (T&DI)
of the American Society of Civil Engineers

EDITED BY
Yinhai Wang, Ph.D.
Ping Yi, Ph.D.
Shi An, Ph.D.
Hua Wang, Ph.D.

Published by the American Society of Civil Engineers

ICCTP 2009

Critical Issues in Transportation Systems Planning, Development, and Management

PROCEEDINGS OF THE NINTH INTERNATIONAL CONFERENCE ON CHINESE TRANSPORTATION PROFESSIONALS

August 5–9, 2009
Harbin, China

SPONSORED BY
North American Chinese Overseas Transportation Association (NACOTA)

Harbin Institute of Technology

Transportation and Development Institute (T&DI)
of the American Society of Civil Engineers

EDITED BY
Yinhai Wang, Ph.D.
Ping Yi, Ph.D.
Shi An, Ph.D.
Hua Wang, Ph.D.

Published by the American Society of Civil Engineers

Copyright and Disclaimer

ISBN: 978-0-7844-1064-6

Any statements expressed in these materials are those of the individual authors and do not necessarily represent the views of ASCE, which takes no responsibility for any statement made herein. No reference made in this publication to any specific method, product, process or service constitutes or implies an endorsement, recommendation, or warranty thereof by ASCE. The materials are for general information only and do not represent a standard of ASCE, nor are they intended as a reference in purchase specifications, contracts, regulations, statutes, or any other legal document.

ASCE makes no representation or warranty of any kind, whether express or implied, concerning the accuracy, completeness, suitability, or utility of any information, apparatus, product, or process discussed in this publication, and assumes no liability therefore. This information should not be used without first securing competent advice with respect to its suitability for any general or specific application. Anyone utilizing this information assumes al liability arising from such use, including but not limited to infringement of any patent or patents.

Copyright © 2009 by the American Society of Civil Engineers.
All Rights Reserved.

ASCE and American Society of Civil Engineers—Registered in U.S. Patent and Trademark Office.

American Society of Civil Engineers
ASCE International Headquarters
1801 Alexander Bell Drive
Reston, VA 20191-4400 USA

Call Toll-Free in the U.S.: 1-800-548-2723 (ASCE)
Call from anywhere in the world: 1-703-295-6300
Internet: http://www.pubs.asce.org

This product was produced for the American Society of Civil Engineers by Omnipress.

Duplication of this product and its content in print or digital form for the purpose of sharing with others is prohibited without permission from the American Society of Civil Engineers.

Photocopies and reprints.

You can obtain instant permission to photocopy ASCE publications by using ASCE's online permission service (www.pubs.asce.org/authors/RightslinkWelcomePage.html). Requests for 100 copies or more should be submitted to the Reprints Department, Publications Division, ASCE, (address above); email: permissions@asce.org. A reprint order form can be found at www.pubs.asce.org/authors/reprints.html.

In no event will ASCE, Omnipress or its suppliers be liable for any consequential or incidental damages to your hardware or other software resulting from the installation and/or use of this product.

No part of the product navigation and "Help" files may be reproduced or used without writter permission from Omnipress.
© 2009 Omnipress - All rights reserved.

Preface

This is to continue the North American Chinese Overseas Transportation Association (NACOTA) tradition of organizing at least two major transportation conferences each year, one in Washington D.C. and the other in China. The 9th ICCTP in Harbin represents the NACOTA summer conference in 2009, which is jointly hosted with Harbin Institute of Technology with the sponsorship of the Transportation and Development Institute (T&DI) of American Society of Civil Engineers (ASCE). In the past five years, NACOTA has held its summer conferences in Wuhan, Dalian, Xi'an, Shanghai, and Chengdu, at a different city each year to generate grassroots impact and promote NACOTA.

Established in January 1996, NACOTA is a non-profit professional organization with its members working or studying in the transportation or related fields and who are interested in contributing to the transportation development in China. The main objectives of NACOTA include: promote transportation development in China by providing knowledge and expertise through its members; strengthen the links between transportation professionals and students in North America and other parts of the world and their counterparts in China; promote networking among Chinese overseas transportation professionals and students; and disseminate information on state-of-the-art transportation developments and major events in China to NACOTA members, partners, and friends.

Only since a couple of years ago have NACOTA started producing conference proceedings. As we continue to generate widespread interest in such events, we have gained a great deal of experience in organizing large conferences and producing high quality articles in the proceedings. This year, for example, a total of 948 papers were received from authors of eight countries and regions, including Mainland China, Taiwan, the United States, Canada, United Kingdom, Germany, Japan, and Korea. To ensure the quality of the ICCTP 2009 proceedings, rigorous technical evaluation and English editing efforts had been made. As a result, only about 50% of the submitted papers were accepted for publication in the ICCTP 2009 proceedings. Those selected papers cover all the twelve key theme areas of transportation as planned for the conference.

As NACOTA continues to grow we hope more people will join our organization as a member, a partner, or a friend. Only with your continued support and contributions can we carry on the NACOTA tradition to best benefit you and the society.

Acknowledgements

The editorial board of this proceedings and the executive committee of 9th International Conference for Chinese Transportation Professionals (ICCTP 2009) would like to thank all the authors who submitted their papers to this conference. Those papers selected for publication were revised multiple times and the authors were very cooperative and supportive during the process.

Harbin Institute of Technology (HIT) kindly hosted the ICCTP 2009 conference and offered numerous supports to ensure a successful conference. The hard work from HIT faculty, staff, and students definitely deserve kudos. The T&DI of ASCE not only sponsored the conference, but also helped recruiting volunteers for English-editing the papers. These volunteers' helps were essential for the quality of this proceedings and their timely efforts are highly appreciated. In particular, special gratitude goes to Dr. Louis F. Cohn and Ms. Eva Lerner-Lam for their advice and to Ms. Donna Dickert and Mr. Jonathan C. Esslinger for their hard work to publish the proceedings.

ICCTP 2009 is the 9th summer conference of NACOTA. We would like to thank the members of NACOTA, Board of Directors, and Advisory Committee for their advice and consistent support. In particular, we want to recognize the contribution and timely support of Dr. Fang (Clara) Fang who handled the financial duties throughout the entire process for NACOTA.

Lastly, we would like to thank all the conference organizers, staff, editors (including English editors), and ICCTP 2009 participants for their contributions and hope that everyone finds the proceedings both informative and enjoyable.

Table of Contents

Transportation Safety

Information Needs of Urban Transit Travelers—The Case of Wuhan, China 1
Zhengdong Huang, Xuejun Liu, and Jie Li

Study on the Rational Size of the Box Girder Used in Cable-Stayed Bridge Based on ANSYS 8
Xia-lin Yang, Xue-xian Sun, Ya-ping Wu, and Xiao-dong Mao

Research on the Crashworthiness of Two-Layer Thin-Walled Structures 15
Shourne Xiao, Qiyu Shan, Guangwu Yang, and Hanzhen Chen

Effects of Roadway Lighting Level on the Pedestrian Safety 21
Huaguo Zhou and Ping Hsu

Analysis of a New Combined Micropile Structure for Preventing Slope Slippage and Its Application in a Practical Project 30
S. G. Xiao, K. Cui, D. P. Zhou, and J. Feng

Experimental Research on the Mechanical Parameter of Fly Ash Soil 41
Han-bing Liu, Chang-yu Li, and Hai-bin Wei

The Bearing Character of Bridge Piles in Karst Areas 49
Hourong Kang, Xiedong Zhang, and Hong Li

The Analysis of Traffic Landscape from Users' Perspective: The Case of the Zhangjiang Tram 56
Na Li, Xiaohong Chen, and Wen Xiong

Traffic Incident Acoustic Recognition Based on Wavelet Decomposition and SVM 65
Xianglong Luo, Qisheng Wu, and Guohong Niu

Gray-Periodic Extensional Combinatorial Model for Road Traffic Accidents in Cold Regions 71
Shi An and Lilan Li

A Multi-Objective Decision Model of Traffic Rescue Service Site Location on Road 80
Gan Chai, Chengwei Fang, Jiaxiang Zhou, and Shui Wan

The Method of Road Safety Analysis Based on Two-Dimensional Speed Difference **87**
Xingwang Liu and Jingmei Wu

Risk Evaluation for Highway Transportation of "Toxic Gas" Hazardous Materials—Based on a Back Propogation (BP) Neural Network **93**
Kai-zheng Liu and Hao-zue Liu

Study on Different Residual and Weight Coefficient in Model Updating of Bridge Structure **100**
Jie Li, Min-shui Huang, and Hong-ping Zhu

Study on a Passageway Location Model on Underground Expressway **108**
Yucong Hu, Bingqiang Situ, Wenzhou Jin, and Qin Liu

Optimum Choice for the Construction Management Plan Based on Entropy Weight **115**
Yong-Fen Ruan, Jin-Ping Wang, Wang Dong, and Mou Jie

Lane Change Behavior Character and Its Influence to Traffic Safety on Urban Roads **122**
Y. Zhang, Q. Huang, M. Zhang, and X. Yu

Study on the Rules of Crash Distribution **129**
X. Zhong, X. Chen, and Z. Wei

Quick Maintenance for Tunnel Lining Voids with Polymer Grouting Technology **136**
Jianguo Xu, Fuming Wang, and Bo Wang

Safe Spacing Research Based on the Theory of Cellular Automation on Freeways in Foggy Weather **142**
Q. Shi, Z. Huang, and W. Liu

Simulation of Turning Stability Control for Two-Motor-Drive Electric Vehicles **150**
Shaobo Xie, Cheng Lin, Peng Liu, and Xiaowei Zhang

The Simulation Analysis of Passenger Evacuation in One Metro Station Based on Exodus **157**
Y. F. Ye, Q. F. Hu, and H. W. Huang

Research of Company Freight Traffic Generation Prediction Models in **164**

High-Tech Park
Ke Zheng and Yaping Zhang

Bending Vibration Suppression of High Speed Railway Passenger Car Body 171
Caihong Huang, Jing Zeng, and Ren Luo

Analysis of Deformation Characteristics of Collision Vehicles Using Close-Range Photogrammetry 177
Z-M. Tao and Y-L. Pei

Traffic Safety Evaluation of the 30 Provincial Capital in China Based on Principal Component Analysis 185
Sheqiang Ma, Chunfu Shao, Zhuanglin Ma, and Dong Liu

Study on Spatial Information Model and Database of Traffic Facilities Management Systems Based on ArcGIS 192
Y. Wang, S. Dong, H. Kui, T. Gao, H. Yu, H. Wang, and Y. Liu

Expressway Data De-Noised Approach Based on Wavelet Analysis 198
Zhenjun Wang, Jizhen Guan, Jianling Yu, and Jing Liu

Influence Analysis of Deep Discount Policy on Public Transit Ridership 204
Yan Han, Hongzhi Guan, and Xuejiao Fang

Design and Validation of Wireless Dynamic Testing System for Bridge Based on the 941B Type Vibration Sensor 211
Zhonglong Li, Lianzhen Zhang, Xiaodi Zhu, Hongjiang Gu, and Zitian Jiang

Application of Fractal Theory in Pavement Surface Texture Measurement 219
Yan Yuan, Anxing Lai, and Yun Que

Research on Application of Externally Prestressing for Simple-Continuous Bridge 226
Kejian Sheng, Rongda Li, and Zonglin Wang

Restraint Efficacy Analysis and Structure Optimization for the Design of Airplane Metal Chocks 234
Fuhai Li, Hongbin Gu, and Hongyu Yao

The Comparison of Three Getting Signal Control Delay Video Methods at Signalized Intersection 241
Huiling Zhang, Keping Li, Hongbo Qian, and Guimin Su

Enhancing Immersion through Adjusting Parameters of Vehicle Driving Simulator 247
Xiaobo Zhou, Shunying Zhu, Hong Wang, and Bing Liu

A Calculation Method for the Information Utility of Traffic Guide Signs 254
Li-Li Zhu, Jian-Jun Shi, and Xin-dong Chen

Safety Evaluation Methods of Road Traffic Based on Gray Cluster Theory 260
L. Wei and Z. Guan

Road Traffic Control Information and Traffic Resource Analysis System 268
Hui Zhang, Zhongzhen Yang, Yonglei Jiang, and Haigui Kang

Research on the Crashworthiness Optimization of Curved-Road Concrete Barriers 277
Zhengbao Lei, Lan Liu, Zuo Peng, and Shijing Hou

Highway Accidents Analysis with Panel Data Model 287
T. Xu, X. Sun, Y. He, and C. Xie

The Impacts of Differential Speed Limits on Speed 294
Shicui Liu, Xiaoduan Sun, Yulong He, and Shuzhan Hou

Study on the Influence of Coarse Aggregate on the Pavement Performance of Road Cement Concrete 300
Ai-qin Shen, Jian-ping Xiong, Jun-hui He, and Tai-jun Liu

Research on the Competitiveness of China's Ports 307
B. Liu and C. Liu

Equilibrium Model of Trip Modes in Road Traffic and Orientation of Charge Policy 317
Linlin Wu, Qifen Zha, and Jianyi Liu

Analysis of the Influence of Emergent Incident on Expressways by Simulation 323
M. Li, W. Jin, and S. Fang

Optimization of Regional Traffic Structure from the Perspective of Sustainable Development 330
Linlin Wu, Qifen Zha, and Jianyi Liu

Performance Evaluation of Waterproof Bond Layer Materials Based on 336

Grey Target Theory
Xin Yu

Probabilistic Pedestrian-Vehicle Conflict Micro-Model in Non-Signal Controlled Multi-Lane Segments **343**
S. Lu, S. Fang, and S. Zheng

Research on Simulation of Train Tracing Operation Based CBTC **351**
Z. Ma, X. Chai, and L. Chong

Research on Rapid Curing Technology of Lime-Flyash-Cement Stabilized Macadam **357**
Yuanzhao Chen, Zhenxia Li, and Xuancang Wang

Experimental Research on Shear Connectors' Stress of Composite Beam Bridge under Complex Stress Condition **365**
Shibo Zhang, Ronghui Wang, Junping Zhang, and Lingling Gong

A Retrograde Vehicle Detection Method Based on the Optical Flow Field **371**
You-ting Zhao, Xi-ying Li, and Zhen-bo Wang

Research on a Risk Analysis System of Vessel-Bridge Collision **378**
Tao Fu, Junjie Wang, and Junjian Zhang

Methods of Setting Maximum Speed Limits on Freeways **384**
Guozhu Cheng and Yulong Pei

Study on the Carrying Capability of Preplanned Regional Earthquake Evacuation Corridor Based on Macro-Simulation **390**
Yang Wang, Zhijie Li, Jing Cao, and Xiaokuan Yang

The Analysis of Traffic Flow State on Foggy Expressway Based on Fuzzy Clustering **398**
Jianjun Wang, Chenfeng Xie, Zhenwen Chang, and Jingjing Zhang

Research on the Impact of Drivers' Heart Rate on Longitudinal Slope of Freeway Tunnel **405**
Jianyou Zhao, Cao He, and Yanni Shi

A Study on Cable-Removing Scheme of the Cable-Stay System of the Zhijing River Bridge **413**
Jianjun Wei and Nianhe Chen

Design Theory for Speed Control by Using Constant Edge Rate **419**
Bing Liu, Shunying Zhu, Hong Wang, Jing Xia, and Qinmei Sun

Optimization of Dynamic Dispatching Decisions of Local Wagon-Flows in Terminals with IRTS **425**
Zuoan Hu and Yusong Yan

Laboratory Evaluation of the Warm Mix Asphalt Performance in Liaoning **433**
Yanhai Yang, Huaizhi Zhang, and Yaodong Wu

Model of High Speed Railway Wheel Ovalization **440**
Xueshan Zhang, Xinbiao Xiao, and Xuesong Jin

From Time Based Speed Series to Behavior Sequence: The Transformations and Applications of VTDR Data **449**
Zhenfeng He and Zhenzhi Huang

Road Safety in Sections under Mixed Flow Traffic Environment **456**
Sisi Liu, Xiaoduan Sun, and Yulong He

Analysis on Vehicle No-Sideslip Single Side Skid Equivalent Frictional Coefficient **463**
Yongheng Yue, Qiang Zhao, and Qingdong Xia

Discussion on Methods of Traffic Routes' Alignment Survey and Application of Principle of Least Squares **470**
Yubao Liang, Baoxi He, Shaotang Liu, and Qianli Ma

A Study on Speeding Driving Based on Expected Speed **480**
Chen Hu, Xiaoduan Sun, and Shicui Liu

Vehicle Tracking from Videos Based on Mean Shift Algorithm **486**
Chang-Zhen Xiong, Yi-Gui Pang, Zheng-Xi Li, Ya-Li Liu, and Ying-Hong Li

The Evaluation of Micro-Benefit on Highway Construction Investments **494**
Hong Chen, Yujia Tian, Dianliang Xiao, and Fengxia Wang

Noise Source Identification and Noise Reduction of a Double Crank Four Ring-Plate-Type Cycloid Reducer **501**
B. Yang, Y. Liu, and X. Zhang

Analysis Model for Operating Speed on Two-Lane Secondary Highway **507**

Dianliang Xiao and Yujia Tian

Study on the Method for Calculating Ship Squat in the Restricted Channel **515**

Zhong-Yi Zheng, Long-Hui Gang, and Hong-Xi Li

A Study on Driver's Dynamic Visual Characteristics **521**

Fei Song and Xiao-kuan Yang

Study of Hydrodynamic Pressure on the Cylindrical Pile-Cap Pier in Deep Water Subjected to Seismic Action **528**

Haopeng Liu, Bo Song, and Guoming Zhang

Influencing Factors Contributing to Rear-End Collisions on Highways: PCA Based Investigation and Findings **536**

H. Jun, H. Xu, Y. Pei, and H. Ji

Passenger Transport Demand Prediction for Newly-Built Regions **542**

Maomin Zhang and Yisheng Liu

The Method to Identify Black Spots of Long Highway Tunnel **549**

Zhuanglin Ma, Chunfu Shao, Shengrui Zhang, and Juan Zhang

Study on the Relationship of Traffic Flow Complexity and Traffic Conflict on Urban Road **555**

Zhihong Xu, Xuewu Chen, and Meikin Zhang

Control and Monitoring of Surface Subsidence for Shallow Tunnel under Existing Railway **562**

Xinzheng Wang and Liying Xing

Voids Classification Standard for Cement Concrete Pavement Slabs Based on Service Life **569**

Sheng Zeng and Jia Xu

Design of 3D Virtual Simulation and Evaluation System for Road Traffic Signs **575**

Haifeng Jiang, Zhiyong Zhang, Jian Chen, and Zhengpeng Fang

Using VISSIM to Calculate the Capacity of Urban Expressway Interchange **583**

X. Zang and W. Zhou

RGB Based Crowded Pedestrian Counting in Red Light Time **590**

G. Y. Zhang, Q. Zhao, Z. W. Luo, and H. Wei

Impact of Posted Speed Limits on Operating Speed in Urban Expressways **597**

H. Wang, X. Sun, B. Li, and Y. He

Nonparametric Analysis of Timely Distribution of Traffic Crash **605**

Yaping Zhang, Xiang Lan, Ke Zhang, Lihua Liu, and Xu Yao

Evaluation of Fire Risk at Highway Tunnels **611**

Jing Huang, Shao Yun Ren, and Wei Zhang

The Analysis of Rural Road Safety and Its Strategies **618**

Feng Sun

A Traffic Accident Reconstruction Study on Continuous Collision of Three Cars **624**

Qiang Yu, Lang Wei, and Tao Chen

Study on the Preventive Maintenance Time for Asphalt Pavement **630**

Ronghue Ying, Ting Wu, Lijuan Wang, and Zhaoguang Hou

Wavy Road Elevation Measurement Based on the Principle of Inertia **637**

Y. Han and H. Wang

Investigation of Relationship between Level of Service and Safety **643**

Xuesong Wang, Hangfei Lin, and Xiaohong Chen

Research and Application of Graphic-Attributes Integration Based on Web GIS in Aviation Accident Investigation **650**

Rui-shan Sun, Ding Yuan, and Zi-nan Xie

Study and Implementation on JPEG Image Enhancement System of Tire Mark **656**

Tao Chen and Lang Wei

Analysis of Characters and Causes of Road Traffic Accident Migration **662**

Chengwu Jiao, Manjuan Yang, and Yubo Hao

A Time-Varying Route Optimization Model for Urban Hazmat Transportation **669**

Yunpeng Wang, Wencai Sun, Shiwu Li, Weiyuan Sun, Jingjing Tian, Haiwei Wang, Hui Wang, Yi Chen, and Gang Cao

A Speed Limit Model of Vehicle for Urban Road Hazmat Transportation **676**
Yunpeng Wang, Wencai Sun, Shiwu Li, Gunan Li, Jingjing Tian, Hui Wang, and Wanji Chen

Risk Assessment of Road Operation Environment under Atrocious Weather Condition **683**
Yan Ma, Zhong-yin Guo, Hua Guo, and Yong-gang Xu

Study on Accident Reconstruction Model Based on Reverse-Reasoning Method **693**
Lili Zheng, Tongqiang Ding, Jianfeng Xi, Jian Sun, and Jiang Li

Evaluation Study of the Median Markings in Undivided Highway Tunnels **700**
Fengxiang Guo, Jian Xiong, Hongqi Liu, Huasen Wan, and Yaqin Qin

The Numerical Analysis of Sound and Vibration from a Tire by FEM and BEM **706**
Liang Chang, Wang-Xin Xiao, and Wei-Ping Xie

Technology Research on the Vehicle Collision Accident Self-Alarm System **712**
Zhe-Wen Tian, Jia-Qi Xu, Qian Feng, Shuai Lei, and Xiao-Ming Mei

Research on Pedestrian Safety under Rapid Development of Motorization **719**
Shuling Wang, Zhili Lui, Jifu Guo, and Yanyan Chen

Gradually Rolling Prediction of the Use-Level of Road Network Based on BP Neural Network **725**
Tao Zhang, Xiang-shen Hou, Xin-kai Li, Hai-min Jing, and Bing-qian Zheng

Identification of Hazardous Locations Based on Integrated Highway Safety State Analysis **733**
Yan Wang and Zhongyin Guo

Analysis of Crowd Behavior in Route Choice Based on Dynamic Programming **742**
Xiaobei Jiang, Hui Xiong, and Hongwei Guo

Vehicle Dynamics Model in Two-Dimension Collision Accident **751**
Yi Cao, Yu-long Pei, and Wen-sen Xiang

Vehicle Trajectory Model in Two-Dimension Collision Accidents **757**
Yu-long Pei, Yi Cao, and Jun Ai

Analysis of Runway Incursion in Civil Airport Based on Bayesian Network **763**
Yang Gao and Yang Li

Investigation of the Relationship between Red-Light-Running Frequencies and Intersection Features **769**
Yiyi Cai, Xuesong Wang, and Xiaohong Chen

Effect of Sunlight Glare on Drivers' Psychophysiological Characteristics **777**
Han Gao and Yulong Pei

Evaluation of Road Traffic Safety Based Improved Fuzzy-AHP Method **783**
Liwei Hu, Yulong Pei, Zhuo Qiu, and Ze Liu

Road Traffic Safety Micro-Evaluation Based on Bayes Theory **790**
Leilei Dai, Yulong Pei, and Shaohua Ping

Impact Analysis on Countdown Device on Transit Priority Signal Control **796**
Ke-ping Li, Yu-pu Dong, and Hong-bo Qian

Driving Simulation Study on Traffic Flow Characteristics on the Climbing Lane on a Two-Lane Rural Road **804**
Yaqin Qin, Jian Xiong, Hongqi Liu, Fengxiang Guo, and Huasen Wan

A Safety Protection Technology System on Highway Roadside in China **812**
Yang Li, Rongguo Ma, Yuxin Niu, and Longfei Wang

Study on Pedestrian Safety and Countermeasures in Crosswalks around Campus—Case Study at Ludong University in Yantai **819**
Jiuchun Gu, Chunyan Mu, Liangshen Wang, Kening Liu, and Jing Sun

Enhancing Airport Security and Place Marketing with Spider Web Networking **826**
Li-Yen Hsu

Dynamic Response of a Magnetically Levitated Vehicle in a Crosswind **832**
Jian-Jun Wu and Xiao-Hong Shi

Research on the Design of Inner Horizontal Surface of the Airport **841**

Rui-shan Sun, Li-xan Zhang, and Hong-yuan Zhao

Grey Relational Analysis Method of Main Reasons of Road Traffic Accidents **847**

Jianfeng Xi, Shuangwei Wang, Na Zhou, Yan Gao, and Zhenglin Ding

Study on Fuzzy Neural Network Model of Vehicle-Bicycle Conflicts at Grade Intersection Based on Failure Tree Analysis **854**

Ying-hui Liang and Xing-qiang Zhang

Research on the Prediction Model of Traffic Accidents Using the Least Square Support Vector Machine **861**

Wei-hua Zhang, Qian Sun, and Hao Sun

Study of Anti-Slide Pile Composed of Arch and Truss Structure Based on FEM **871**

Chenglin Han, Xiedong Zhang, and Liang Yin

Analysis of the Influences of Fatigue on Driver's Behavior Characteristics **878**

Y. Ma, Y. Pei, and Y. Wang

Dilemma Zone Modeling Using Yellow-Onset Vehicular Trajectory Data **886**

Heng Wei and Zhixia Li

Evaluating the Impacts of Ramp Configurations and Influential Factors on Freeway Exit Ramps **895**

Hongyun Chen and Jian John Lu

Uncertainty Analysis of Collision Velocity in Motor Vehicle Crash Using Evidential Reasoning Algorithm **906**

Ruiguang Shen, Jun Ai, and Yulong Pei

Choice of Reasonable Longitudinal Gradient at Alignments of Mountain Highways Based on Driver's Physiological Reactions **914**

Xian-Qiang Ren, Jian-Yi Liu, and Song Gao

Impacts of Road Sight Distance on Safe Driving Conditions **920**

Xian-Qiang Ren, Jian-Yi Liu, and Song Gao

A Study on Multifactorial Prediction Model for the Road Traffic Accidents **927**

Zhao-hui Liu

Case Studies for Shaking Table Tests on Seismic Soil-Pile Group-Bridge Structure Interaction in Liquefiable Ground 934
Liang Tang, Xianzhang Ling, Pengju Xu, Xia Gao, and Liquan Wu

CT Scan on Frozen Roadbed Soil under Dynamic Triaxial Test Condition of Beilu River Section, Qinghai-Tibet Railway of China 942
Lixia Wang, Xianzhang Ling, Feng Zhang, Yibin Pu, and Liquan Wu

Freeze-Thaw Stability of Slopes in Seasonally Frozen Regions of the Northeast China 951
Lina Wang, Xianzhang Ling, Feng Zhang, Xia Gao, and Liquan Wu

Stability and Reinforcement Methods of a High Slope at the Hang-Yong Natural Gas Pipeline in China 958
Liquan Wu, Feng Zhang, Xianzhang Ling, Huoming Yu, Tianhong Chen, and Wei Liu

Stability of Slope with the Weak Structural Plane Based on 2-D Nonlinear Finite Element Method 965
Feng Zhang, Liquan Wu, Xianzhang Ling, Zhanyuan Zhu, and Lina Wang

Vibration Characteristics of Permafrost Embankment Induced by Passing Trains in Qinghai-Tibet Railway in Winter 973
Zhanyuan Zhu, Xianzhang Ling, Lina Wang, Feng Zhang, Shijun Chen, and Liquan Wu

Reliability Analysis of Cable-Stayed Bridge under Reaction of Seldom Occurred Earthquake 980
Feng-chen Li, Li-na Zhang, Da-peng Wang, Ze-ping Yang, and Ou Yang

Transportation Planning and Operations

The Key Technology of "One Road One Line with Straight Driving" Public Transportation System 986
Zhiyong Guo, Wei Wang, and Xuewu Chen

Research on Urban Public Transit Dispatching System Based on Real-Time Prediction and Game Theory 993
Hui-ying Wen, Gong Cheng, and Peng-fei Li

Individual and Population Learning in Route Choice Behavior of Drivers: Experiment and Model 1001
Liang Pu, Hong-zhi Guan, Zi-xu Lu, Shan Huang, and Jia Fang

Research on a Generalized Cost Model for Optimization of Ningbo-Zhoushan Port's Collection and Distribution System 1014
W. Liu, H. Pan, and X. Pi

Assessing Performance of Public Transit Network Using Network-Based Accessibility Measures 1021
Fangqiang Lu and Xuewu Chen

Modeling Study of Coal Allocation and Distribution Plan Based on Graph Theory and Fuzzy Optimization Method 1027
Liang Xian, Hui Wang, and Jin Zhang

A Comprehensive Bus Line Evaluation Method Based on Fuzzy C-Means Clustering Algorithm 1034
Suping Chen, Xuewu Chen, and Min Yang

A Nonlinear Model for Decision-Making for Container Slot Chartering and Allocation under Liner Shipping Alliance 1041
Ji-hong Chen and Hong Zhen

Study on the Model of Hub Location under Earthquake Conditions 1048
Shi An, Lei Ye, and Candong Wang

Empirical Correlation Analysis of Parking Arrival and Departure Rates for Urban Parking Facilities 1056
Jun Chen, Huanhuan Chao, and Hua Bai

Transit Network Optimization Method Based on BRT Attracting Region: A Case Study of Changzhou 1063
Zimu Li, Xuewu Chen, and Xiaoqing Liu

Efficiency Evaluation of Urban Transit Terminals Based on the Cloud Model 1070
Shijun Yu, Yingshun Liu, and Yongneng Xu

Travel Mode Choice in Large Cities of China Based on Loss Aversion Theory 1077
Xuemei Zhou, Yan Meng, and Di Di

Topological Properties of Public Transport Networks: A Temporal Perspective 1084
Xiao-Yong Yan and Ming-Sheng Wang

Conventional Bus Stop Capacity in Peak **1090**
Haijian Bai, Wenquan Li, and Ruijuan Dong

Inhabitant Trip Behavior Similar to Quantum Transition **1097**
Rong-Han Yao and Dian-Hai Wang

Study and Simulation of Behavioral Decision-Making Model of Through Bicycles Passing Vehicles at Signalized Intersection **1104**
Xing-qiang Zhang, Shen Wang, and Ying-hui Liang

An Optimization Model for Bus Rapid Transit **1111**
Bo Yan, Yonglei Jiang, Bin Yu, and Zhongzhen Yang

A Model of Mixed Land Use and Trip Production by BP Neural Network **1117**
Yue Zhao, Chunfu Shao, and Zhihua Xiong

Assessment Methodology for Road Network Travel Time Reliability under Ice and Snowfall Conditions **1124**
Junqiang Leng, Yaping Zhang, and Yuquan Leng

Multi-Section Short-Term Traffic Flow Prediction Based on Multi-Dimensional Time Series **1131**
Gangliang Chen and Lin Cheng

Research on the Characteristics of Time Headway Distribution in Expressway Weaving Section of Type A **1137**
Changlong Xue, Jiaqi Xhao, and Yulong Pei

An Improved Ant Colony Algorithm for Placing-In and Taking-Out of Wagons in Branch-Shaped Sidings **1144**
Qianqian Guo, Shaoquan Ni, Chengbing Li, and Dingjun Chen

A Study on Vehicle Trip Distribution Forecasting Based on BP Neural Network **1150**
Xiang-hai Meng, Qing Liu, Ying-chun Du, and Jian Lu

Bus Service Frequency Multi-Objective Optimal under Snowy Day **1156**
Jian Wang, Xiaowei Hu, and Chunbin Hu

Capacity Model of Low Channeling Roundabout Based on Vehicle Arrival Characteristics **1162**
Ruijuan Dong, Weihua Zhang, and Haijian Bai

The Reasonable Distance of Unsignalized Crosswalks Based on Traffic Flow, Stability, and Efficiency **1168**
Shunying Zhu, Jing Xia, Hong Wang, and Bing Liu

Study on the Green Traffic Planning System of New Rural Communities **1175**
Chang-hong Li and Cong-hong Liu

Predicting Methods of Trip Modal-Split Based on Structural Model **1181**
Zhuping Zhou, Gang Ren, and Wei Wang

A Multi-Class Multi-Modal Combined Model for TDM Measures Evaluation in Large Scale Urban Transportation Network **1188**
Tianran Zhang, Dongyuan Yang, Chao Yang, and Yali Zhao

Nonlinear Analysis of Prestressed Steel Box Beams **1198**
Yanmin Jia

Algorithm of PFE and Its Application in Shenzhen Urban Transport Simulation System **1203**
Tao Lin and Xiaotian Cui

The Applied Research on Forecasting Cargo Volume of Northeast Economic Zone by Systemic Dynamics **1209**
Shuzhi Zhao, Tonghe Ni, and Yonggang Zhu

A Study on the Location Selection of Public Traffic Transfer Hub Based on Improved Particle Swarm Algorithm **1216**
Lifan Lin, Weihua Zhang, Jinxin Hu, and Qian Sun

Region Public Transportation Timetable Optimization Based on Node and Line's Wait Analysis **1223**
Wen-xia Sun, Ti Song, and Li-xia Ma

Study on the Method of "Inverse Four-Step" Regulatory Transportation Planning **1231**
Jin Wang, Xiaoguang Yang, and Xianyao Zhao

Robust Optimization Approach for Transportation Network Design under Demand Uncertainty **1237**
Yafeng Yin and Yingyan Lou

Analysis on Standards Used in Traffic Impact Study **1249**

Lei Lei, Jing Cao, and Xiaokuan Yang

Study on the Location Parking Index Based on Function Division of Parking Space **1258**

Lin-bo Li, Man Wang, and Bing Wu

Study on Traffic Impedance Based on Grey Theory **1266**

Qiu-ping Wang, Ye-fan Du, and Jin-pu Wu

The Attitude and Psychological Demand Related Determinants of Public Transport Use **1273**

Xia Wan, Jun Chen, and Wei Wang

A Study on the Matching of Urban Form and Traffic Pattern **1280**

Haifeng Li

Study on Road Network Reserved Capacity on Different Levels of Service and Stochastic Conditions **1286**

Zhengwei Liu and Lin Cheng

Expansion and Validation of Beijing Household Interview Survey Data **1293**

Kai Xian, Zhili Liu, Dexin Zhang, and Huabing Du

Modeling Logistics and Supply Chain with an Integrated Land Use Transport Model: PECAS **1300**

Ming Zhong, John Douglas Hunt, and John Edward Abraham

Research on the Bicycle Capacity of Signalized Intersection Based on Fluid Diffusion Characteristics **1306**

Lilan Li, Yaping Zhang, Xiang Lan, Ruimin Ye, and Yuping Wang

Analysis and Evaluation of Expressway Planning Schemes Based on Integrated Macro and Micro Simulation **1312**

Dui-dui Liang, Yun-tao Chang, Zhong-Ren Peng, and Ying Pang

Evaluation of Traffic Impact on Land Development Projects Based on Matter-Element Analysis **1319**

Ying Pang, Yun-tao Chang, Zhong-ren Peng, and Dui-dui Liang

Research on Model of Public Transportation Network Optimization Based on the Demand of Citizen Trips **1326**

Yongzheng Kang, Xueqin Niu, and Ruifen Liu

Urban Transport Network Capacity Considering Level of Service **1332**
Huapu Lu, Xinxin Yu, Haiwei Wang, Changzhi Bian, and Ziyin Deng

The Balance Lines of International Freight and Incidentals **1338**
Xian Liu

Traffic Management on an At-Grade Signalized Intersection Connecting to Urban Expressway Ramps **1343**
Kejun Long, Jianlong Zheng, Xiaoguang Yang, and Zhigang Zhou

Pedestrian Simulation Research of Subway Station in Special Events **1351**
Guanghua Zhao, Guanghou Zhang, Yanyan Chen, and Ping Wu

Association of Signal-Controlled Method at Roundabout and Capacity **1359**
Yu Bai, Kun Xue, and Tao Wang

Case Study on the Computing Model of the Driving-Into Rate of Service Area **1371**
Liying Mu, Hongjun Cui, and Hongqi Hui

Research on Dynamic Characteristics of Road Network in Snowy Conditions **1378**
Xiaoqiang Ren, Longhai Yang, Xiqiao Zhang, and Dongxu Fan

A Study on the Headway Distribution of the Xueyuan Roundabout **1385**
Ping Han and Dian-hai Wang

Study on Intersections with Median BRT Stations: Focused on Pedestrian Street-Crossing Characteristics **1392**
Ruhua Zhang, Xianyuan Zhu, and Li Lei

The Analysis of Transportation Demand Generation Mechanisms of the Urban Agglomerations in China **1400**
Zhi Dong, Bing Wu, and Linbo Li

Study on Residential Daily En-Route Travel Choice Behavior with Traffic Information: Application of RP/SP Joint Survey and Disaggregate Model **1406**
Yi Zhang, Meiping Yun, and Xiaoguang Yang

A Particle Swarm Optimization Algorithm for Bilevel Programming Models in Urban Traffic Equilibrium Network Design **1412**
Hui Hu

Study on Inter-regional Transportation Infrastructure Integration Planning in China 1419
Chaoyang Li and Yi Zhang

Repositioning of Empty Containers in the Transpacific Market: A Case Study 1425
Yu Zhang and Cristiano Facanha

Further Development of the German Highway Capacity Manual (HBS2011) 1439
Ning Wu

Operational Performance Evaluation of Different Exit Ramps on Florida's Freeways by Considering Number of Lane Change 1445
Jian John Lu, Linjun Lu, and Tangyi Guo

Strategic Transport Model of Beijing and Application to City Centre Transport Policies Evaluation 1453
Rui Zhang and Haiyan Wu

Emergency Response Systems and Technologies

Real-Time Monitoring System Architecture of Hazardous Goods Logistics Based on RFID 1459
Minai He

Public Transport Incident Prediction Method by Road Traffic Delays 1465
H. Z. Gao, Y. Han, L. L. Zang, C. Xu, and H. N. Wu

The Application of the Maximal Coverage and Partial Coverage Model in the Shelter Location Problem 1472
Xiao-Qiang Ren, Juan Chen, Gao Guo, and Wen-Ping Cai

A Framework of the Traffic Organization Simulation System for Freeway Emergency Response 1479
Shaowu Cheng, Xiaofei Ye, Shi An, and Tingting Yang

Application of Locating Technology in the Highway Emergency Response System 1484
Hantao Zhao, Yunpeng Wang, Shiwu Li, and Hongyan Mao

Accident Prevention and Inducement Strategy in Highway Tunnel 1490
Heng Ding, Xiao-yan Zheng, Wei-hua Zhang, and Zhong-jie Zhao

Locating Emergency Response Facilities for Hazardous Materials Transportation with Probabilistic Response Time 1498
Qingping Gao, Yu Luo, Qipeng Yan, and Yu Lin

Test and Analysis of Rail Break Emergency Treatment Device for Railway Switches 1504
Xiangguo Li, Mingsheng Wang, Yunqing Zhang, Chao Ma, and Musong Li

Capacity Reliability of Road Network under Adverse Weather Conditions Based on Fuzzy Theory 1510
Xi-qiao Zhang, Shi An, Yan-hong Tang, and Hong-fei Sheng

Real-Time Dispatching and Routing for Emergency Vehicles after Earthquake Disasters 1516
Wen-Ping Cai, Lei He, and Gao Guo

Establishment of Construction Safety Early-Warning System for Mountainous Freeways 1523
Kaifeng Wang, Xiedong Zhang, Xiaohuang Wang, Jianyi Yu, and Sheng Yi

A Study of Vehicle and Materials Depot Location Problems for Winter Road Maintenance 1530
W. P. Cai, G. Liu, and W. S. Cao

Analysis of City Transportation Networks' Travel Time Reliability during Adverse Weather 1536
Jian Wang, Guanglin Sun, and Xiaowei Hu

A Study of Transit Evacuation Route Planning Based on Time-Expanded Network 1543
D. L. Zhang, J. X. Cui, and G. Liu

Integrated Arterial Signal and Access Control Strategy under Non-Notice Emergency Evacuation: Modeling and Simulation-Based Analysis 1550
Heng Wei, Harikishan Perugu, Qingyi Ai, and Xiaokuan Yang

Impacts of the Modernization of Global Navigation Satellite Systems on Intelligent Transport Systems 1564
Xin Shi

Intelligent Transportation Systems

Car-Following Criteria at a Signalized Intersection in Beijing 1570

Q. Yu, J. Liu, and J. Rong

Study of Driver's EEG and Application in Intelligent Transportation Systems **1576**

Junqiang Peng and Pingdong Wu

Short-Term Forecasting of Uncertain Traffic States **1584**

Zhihua Xiong, Zhisheng Yao, and Chunfu Shao

Dynamic Model of Transit Signal Priority on Colored Time Petri Net **1590**

Ciyun Lin, Zhaosheng Yang, and Bowen Gong

Bus Location Display System Based on GPRS **1597**

Song Gao, Ling-yong Zhang, and Lei Zhong

Short-Term Traffic Flow Prediction Based on EMD and Artificial Neural Network **1605**

Xianglong Luo, Guohong Niu, and Qianjiao Wu

The Research of Signal Phase Sequences Based on the Conglomeration of Pedestrians and Bicycles **1611**

Jin-guang Liu, Quan Yu, Jian Rong, and Xiao-ming Liu

Effects of Lane Changing in Heterogeneous Traffic Flow **1618**

Fa Zhang and Qiao-xia Zhao

Detecting the Type of Multi-Fractality in Traffic Time Series **1624**

J. Yu, D. Liu, P. Shang, Z. Wang, and L. Guan

Link Average Speed of Traffic Flow Estimation Method Based on Floating Car **1631**

W. Zhu, A. Chang, G. Jiang, and W. Zhang

A "Reality Vision" Navigation Technique Based on Sequence Geo-Referenced Image Databases **1637**

Qingwu Hu, Shoujun Liu, and Kai Mao

Signal Timing and Coordination—An Art of Engineering **1648**

Z. Tian

Highway Traffic Parameters Estimation by Using Cell Dwell Time **1656**

H. Wang, Y. Han, and Z. Liang

Real-Time Optimization Model of Intelligent Public Transport **1662**

Network and Its Algorithm
S. Bao, Y. Han, and L. Wang

Frequency Optimization Model for a Public Traffic Scheduling System **1669**
C. Xu, F. Wu, Y. Han, H. Gao, Y. Zhang, and Z. Li

Mixed Traffic Micro-Simulation of Urban Branch Roads **1676**
B. Liu, X. Lv, W. Li, Q. Li, and X. Wang

Track Access Technology of Traffic Accident Vehicles Based on Video **1682**
B. Liu, X. Wang, W. Li, and X. Wang

Collision Avoidance among Multiple Ship Agents **1688**
M. Pan, F. Yan, L. Zhao, and M. Inaishi

Traffic Signal Control Optimization of Urban Arterials Based on a Method of Main Intersection Control Strategies **1695**
B. Liu, X. Yan, J. Wu, L. Li, and X. Wang

An Interval-Varying Floating Car Data Clustering Approach Based on Self-Organizing Maps **1701**
Q. Li, J. Cao, and Y. Yue

A Route-Based Model for Determining Interconnection of Isolated Traffic Signals **1707**
W. Ma, Y. Lin, and X. Yang

Optimal Setting of the VMS's Future Range Based on the Characteristics of Driving Speed **1713**
T. Wang and J. Chen

Urban Road Travel Speed Estimation Based on Low Sampling Floating Car Data **1719**
Y. Yue, H. X. Zou, and Q. Q. Li

Experimental Study on Sound Countermeasures against Driver Fatigue **1726**
R. Fang, X. Zhao, K. Mao, J. Ron, and X. Liu

The Evaluation of Level of Service for Expressway in Operating Stage **1734**
Hong-ping Li and Yu-long Pei

Vehicle Detection from Videos Containing Complex Background Based on Bayesian Statistical Modeling **1741**

Ying-hong Li, Ya-li Liu,Yi-gui Pang, and Yi-xin Yin

An Improved Ant Colony Algorithm for the Shortest Path Problem in Time-Dependent Networks **1748**

Hui Gao, Yongqiang Liu, Qing Chang, and Huagang Xiong

Intelligent Emergency Traffic Evacuation Spatial Decision Support System for Urban Disasters **1755**

Zhichong Zou and Yaowu Wang

Estimation of Original-Destination Matrices for Public Traffic Passenger Flow **1762**

Jian Zhang, Wenquan Li, and Jinhuan Zhao

New Methods for Research in Multi-Agent Traffic Signal Control **1769**

Qian-jiao Wu and Rong Lan

An AHP-Based Performance Evaluation Model of Transportation Control System: The Experience from West Liaohe Rd., Dalian **1776**

Jianmei Ding and Changhoug Wang

An Optimized Signal Control Method for a Freight Arterial Transport System **1783**

Changhong Wang and Jianmei Ding

A Reserve Capacity Model of Optimal Traffic Lane Allocating **1790**

Peng Zhang and Wen-quan Li

Side Road Traffic Considered in Transit Signal Priority Control **1797**

Jia Xu and Hangfei Lin

Short-Term Traffic Flow Prediction with ACD and Particle Filter **1804**

G. Y. Zhang, Q. Zhao, Z. W. Luo, and H. Wei

ALINEA-Based Urban Expressway On-Ramp Metering Strategy **1811**

Fei Zhang, Yuchuan Du, and Lijun Sun

An Active Parking Guidance Information System Based on Dynamic Agent Negotiation **1819**

Longfei Wang, Hong Chen, and Yang Li

Research on Vehicle Information Extraction from High-Resolution Satellite Images **1825**

Qi Sun, Yanping Liang, Qulin Tan, and Sulan Zhang

Map Matching Algorithm of a Center Terminal Based on the Road Network Topological Structure **1832**
Zhaosheng Yang and Zhijian Wang

An Improved A* Algorithm for the Intelligent Transportation System **1839**
Yan Li and Yang Gao

Study of the Parking Guidance Reliability of Urban Parking Variable Message Signs **1846**
Dongping Li, Kefei Yan, and Xiaotian Cui

Study on Signal Timing Methods of Optimizing Urban Transportation Network Efficiency **1855**
Xianmin Song, Dianhai Wang, and Ying Peng

The Prediction of Urban Bus Travel Time **1863**
Rui Li and Wenquan Li

A New Cellular Automaton Traffic Flow Model for an Off-Ramp Junction of a Chinese Urban Expressway **1870**
Yusheng Ci, Lina Wu, Yulong Pei, and Xianzhang Ling

A Manual Calibration Method for Simulation of a Freeway Weave Section **1877**
Jingguo Dai, Jian Sun, and Keping Li

Efficient Link Travel Time Estimation for Signalized Link by Small Size Probe Reports **1884**
Qiang Li, Tomio Miwa, and Taka Morikawa

Phase and Timing Optimization at Actuated-Coordinated Signal Control Intersection **1892**
Chengyuan Mao and Yulong Pei

Signal Intersection Optimal Control Model of Small Region Based on Traffic Equilibrium Theory **1898**
Wei Liu, Hai-xian Jiao, and Wei-yong Gong

A Novel Real-Time Road Shape Describing and Parameter Obtaining Method **1904**
Meng Wu, Yang Gao, and Peng He

Adaptive Control Method of Multi-Phase Intersection Based on Traffic **1910**

Status Identification
Wenchen Yang, Zhaocheng He, and Ningning Chen

A Collaborative Software Framework Design in Supporting GLITS I-75 Integrated Freeway and Arterial Operation Project 1920
Ken Yang

Investment and Finance for the Intelligent Transportation System in China 1927
Mingquan Wang, Yali Zhao, Dongyuan Yang, Xiaofa Shi, and Ying Hui

Advanced Traveler Information Impact on Truck Route Choice 1934
Xiao Qin, Junhee Han, and Bruce X. Wang

Identifying Alternative Routes with Integration of ITS into Traffic-Diversion Strategies 1946
Heng Wei, Yinhai Wang, Abi Mogharabi, and Qingyan (Ken) Yang

An EEG Predictor of Driving Fatigue 1958
Xiaoli Xie, Xiaoming Liu, Jiangbi Hu, Xintao Cao, and Weili Wang

Energy Saving and Alternative Energy

Calculation Method for Braking Torque of Self-Excited Retarder 1966
Xiaojun Yang, Ren He, and Haijun Shen

Fuzzy Control of AMT Clutch Engagement during the Vehicle Starting 1974
Wen-guang Liu and Ren He

Ration Effect of Rheological and Combustion Properties of Coal-Oil-Water Slurry 1983
Qiang Zhang, Ying Tian, and Da-feng Tian

Research on the 25kW FCPS's Temperature Controlling Simulation 1988
Xianjun Hou, Wengang Gui, Xue Jin, and Mu Pan

Study on Energy Consumption by Land Cargo Transportation 1996
Shunquan Huang, Siqin Yu, and Zhongmin Liu

Case Study: Analysis of CO_2 Emissions Caused by Customers Transportation in Shanghai and Shenzhen IKEA 2003
Yali Zhao and Dongyuan Yang

Effect of Electro-Mechanical Coupling on Dynamic Performance of 2009

Crankshaft of ISG HEV
J. Zhou, F. Sun, X. Hu, and X. Cheng

Forecast the Automobile Population Based on Scenario Analysis **2016**
Yuee Gao, Yanjiang Lou, and Chao Wang

The Research of Control Strategy of Permanent Magnet Synchronous Motor for Hybrid Electric Vehicles **2023**
Hong Xing Wu, Jian Fei Shi, Heng Ji, and Guo Ping Zhao

Automotive Exhaust Treatment and Environmental Protection

Monitoring Model for Three-Way Catalyst Converter Efficiency Based on Exotherm **2029**
Xiaohong Peng and Zhaowen Qiu

Study on Burner Type Diesel Particulate Filter System Using Compressed Air from Turbocharger **2035**
X. Li, X. Zi, F. Yan, G. Yao, and J. Suo

Runnoff Pollutants Control by Asphalt Permeable Pavement **2044**
Xiaoguang Xie, Yongpeng Xu, and Long Wang

Research on Numerical Simulation of Pollutant Dispersion at Expressway Toll Plazas Based on Multi-Influencing Factors **2051**
Z. Qi, J. He, X. Li, C. Zhao, and X. Bao

Several Questions of Highway Influence Assessment on Dongting Lake Ecosystem in China **2058**
Su Liu, Yaping Zhang, and Zhuokui Xu

Research on Urban Intersection Vehicle Emission Reduction Based on Microcosmic Simulation **2068**
Y. Wang, D. Guo, S. Li, C. Zheng, Wenjuan E, Y. Chen, and X. Lu

The Method of Determining Traffic Impact Range of Developing Project Based on Threshold Value **2075**
Chao Zhou, Xiaoning Wang, and Shuanglong Deng

Calculation Method on Traffic Noise Pollution of Interchange Based on Geometric Alignment **2082**
Xiaoning Wang, Jingjing Tong, and Ke Deng

The Study on Design Method of Vehicle Intake Silencer Based on Three-Dimension/One-Dimension Models Coupling **2088**
J. Li and Q. Guan

Study on Traffic Noise Characteristics of Large Grade Interchange **2095**
Dejun Wang, Xiaoning Wang, and Lianghao Luo

New Technology on Transportation Infrastructure (Pavement, Bridge)

Effect of Density Variation of Coarse Aggregate on Asphalt Mixture Properties **2101**
Zhe-sheng Ge and Ke Xu

Study of an Image-Based Gradation Measurement Techniques of the Asphalt Mixture **2106**
Z. Y. Sun, C. F. Wang, and A. M. Sha

Analysis of Thermal Stress Response in Asphalt Overlay **2114**
Wensheng Xu, Wei Tian, and Hui Luo

Effect by Different Factors on Ductility of Evaporated Residue of Modified Emulsion Asphalt **2122**
Zhipeng Fu, Zhanliang Liu, and Lin Jing

Analysis of Elastic Slab on Non-Uniform Support Foundation Using a Weighted-Residual Method **2128**
Zhu Luo and Zhi Fu

Plastic Behavior for Compaction Pile with Hole Expanded by Blasting or Tamping Techniques **2135**
Xiaowei Li, Junhai Zhao, Xueying Wei, Haibing Xiao, and Qing Ma

Bridge Damage Assessment by Dynamic Response in Time Domain **2144**
Jianqing Bu, Zhanyou Yan, and Xiangguo Li

Viscoelastic Mechanical Properties of Crumb Rubber Modified Asphalt Mixture **2153**
Lan Wang, Chun-qing Chang, and Yong-ming Xing

Viscoelastic Analysis of Asphalt Pavement Using a Regularized Interconversion Technique between Creep and Relaxation **2159**

Yaoting Zhu, Lu Sun, and Kesi You

Performance of Pavement Plate Reinforced with Modified Unsaturated Polyester Fiberglass Reinforced Plastic **2165**

Wei Xu, Guang-yuan Li, and Guo-ping Cen

Study on Permanent Deformation Characteristics of Asphalt Pavement Based on Discrete Element Method **2171**

J. Z. Pei and M. F. Chang

Mechanism of Rutting Formation in Long and Steep Climbing Sections of Asphalt Pavement **2179**

J. Z. Pei, Y. Chen, and M. F. Chang

Study on Safety Stability of Excavating Shallow Depth Neighborhood Tunnel in Traversing Construction **2188**

Yun-peng Li, Chang-ling Han, and Chuan-zhi Ai

New Concrete Improving Performance of Airfield Pavement **2195**

Guangyuan Li and Wei Xu

Constitutive Relationship of Asphalt Mixture for Finite Element Method **2201**

Shaopeng Wu, Hong Wang, and Yao Yao

Limit Value of Railway Bridge for Traffic Safety **2207**

Zhihui Zhou, Wenxiao Qin, Jun Zhang, and Qingyuan Zeng

Finite Element Analysis on Shear-Lag Effect in Curved Continuous Box Girder with Corrugated Steel Webs **2213**

Zhaotong Hu and Xi Chen

Nonlinear Analysis of Time-Dependent Effect for Reinforced Concrete Thin-Wall Box Girders Exposed to Fire **2219**

Gang Zhang, Shuan-hai He, and Ling-bo Wang

Construction Control of Cable-Stayed Bridges Based on ANN and GA Hybrid Algorithm **2225**

Zeying Yang, Haiming Yi, Jianbo Qu, Junjie Song, and Xuefu Li

Experimental Investigation of the First Precast Bi-Pre-Stressing Simple Girder Concrete Bridge **2230**

Minjuan Zhou and Nan Wang

Study on Long-Term Behavior and Ultimate Strength of CFST Columns **2239**

Xianyan Zhou, Guohui Cao, Ran He, and Xiangrong Liu

Observation and Theoretical Analysis of the Temperature Field on the Cross Section of Concrete Filled Steel Tubes Arch Bridge Rib **2249**

Hang Sun, Hongfei Sheng, Yan Li, and Jianglong Li

Influencing Factor Analyses of Section Types on Vehicle-Bridge Interaction of Concrete Box Girder with Corrugated Steel Webs **2256**

Baodong Liu, Pengfei Li, and Lingxiang Xue

Model Test Study of System Transformation for Jiangdong Bridge **2262**

Ruili Shen, Dongchun Qi, Maolin Tang, and Yong Yan

Experimental Study on Performance of the Bridge Deck Pavement of SF-PFSC **2271**

Wenling Tian, Xiaowei Wang, Shuling Gao, Mingjie Zhou, Xiaoyan Zhao, and Erlong Zhang

Study on Experiment of Concrete Mixed with II Degree Flyash under the Corrosion of Freeze Thawing **2278**

Lihua Lu, Sili Chen, Xiating Feng, and Haixia Sun

Experimental Research on the Shear Strength Deterioration between the Freezing and Thawing Surface of Melting Soil Slope in Seasonal Frozen Regions **2284**

Yong-chun Cheng, Qi Ge, and Yan He

Design and Construction of Overlay with Mechanical Joint Element on Used Concrete Pavement **2291**

Mingjie Zhou, Xioayan Zhao, Wenling Tian, Xiaowei Wang, and Xinwei Xu

Resilient Modulus of the Graded Aggregate Material under Long-Term Dynamic Repeat Load **2297**

Long Wang, Xiaoguang Xie, and Bin Xu

Prediction of the Soft Roadbed Deformation Based on a Creep Damage Model **2303**

Y. L. Wang and Y. Wang

Research on Relationship between Fine Aggregate Angularity and Asphalt Mixture's Anti-Shear Ability **2310**

Chang-jun Zhou, De-cheng Feng, Wen-xin Zuo, and Quan Lei

Application of High Performance Concrete Mixed with Steel Slag Powder in Concrete Pavements **2316**

Yunfeng Li, Fanying Kong, and Rongqiang Du

Mechanical Characteristics of Reinforced Gravity Oblique High U-Shaped Abutment **2323**

Li-hui Qin and Gui-wei Liu

Application of Thermal Stress Controlling in Construction of Large Bridge Cushion Cap **2330**

Wei Xu, Jianwen Zou, and Huixing Ren

Impact of Gradation Types on Freeze-Thaw Performance of Asphalt Mixtures in Seasonal Frozen Region **2336**

Decheng Feng, Junyan Yi, Lei Wang, and Dongsheng Wang

Study on Shear Properties for Adherence of New and Old Concrete and Its Practical Calculation **2343**

L. Li and Z. L. Wang

Research on Flame-Retardant Technique in Application of Asphalt Pavement in Highway Tunnel **2350**

Lun Ji, Yi-qiu Tan, Guang-yuan Qi, and Zheng-jin Chen

Fracture Mechanics Analysis of Cracking in Asphalt Pavement Widening **2359**

Jun-hui Zhang, Jian-long Zheng, and Bao-shan Huang

Sensitivity Analysis of the Dynamical Parameters on Road Materials **2366**

Hai-bin Wei, Han-bing Liu, He-feng Zhang, and Chang-yu Li

Dynamic Effects of Moving Vehicular Loads on Continuously Reinforced Concrete Pavements on Winkler Foundation **2373**

Shihua Liang, Xueqiang Yang, Tian Qi, and Ganbin Liu

Theoretical Analysis of Design Parameters on Semi-Rigid Asphalt Pavement with Flexible Base **2381**

Ruibo Ren, Hiwen Li, and Zheren Wang

Seismic Hybrid Simulation of a Multi-Span Bridge **2387**

Xin-jiang Cai and Shi-zhu Tian

Experimental Study on Behavior of Geotextile-Reinforced Soil **2393**
You-chang Hu, Hai Song, and Zheng-jun Zhao

Study on the Frost Resistance Test Method of Lime-Fly Ash Stabilized Material Base Course **2403**
Zhiguo Chen, Zheren Wang, Xiwei Wang, and Yufeng Zhao

Computer-Aided Error Detection of Horizontal and Vertical Alignment in Highway Construction **2412**
Su Liu, Yaping Zhang, and Lu Yu

An Estimate Method for Accuracy of Fitting Horizontal Alignment in Old-Highway Based on Fitting Normal Error **2418**
Su Liu, Yaping Zhang, and Yuqin Feng

Effects of Layer Interface Conditions on Fatigue Behavior of Asphalt Pavements with Semi-Rigid Bases **2426**
Yan-qing Zhao, Chang-hong Zhou, and Yi-qiu Tan

Damage Model Analysis of SBS Modified Asphalt Mixture **2436**
Ronghua Ying, Xiao Chen, Ting Wu, and Zhiyong Zhang

Flutter Derivatives Identification of Aeroelastic Model of Hangzhou Bay Bridge **2444**
F. Y. Xu, X. L. Hu, and A. R. Chen

A Discontinuous Numerical Method for Asphalt Mixture **2450**
Changhong Zhou, Yanqing Zhao, and Zheren Wang

A Safety Evaluation Method of Existing Flexible Suspension Bridge with Double Cable **2456**
Li-Xia Lin, Ya-Ping Wu, and Nan-Hong Ding

Relation of Stability Coefficient to Design Parameters for Curved Continuous Rigid Frame Bridges with Long-Span and High-Pier **2463**
Jun-li Wang and Shuan-hai He

A Study on Spatial Correlation and Power Spectrum of Natural Wind at Xihoumen Bridge **2469**
Ming Liu, Haili Liao, Mingshui Li, and Cunming Ma

Influence Factors Analysis of Buffeting Response of Self-Anchored Cable-Stayed Suspension Bridge **2475**

Haixin Huang, Ying Zhang, Bo Liu, and Fuyou Xu

Stiffness Reduction Factor of Reinforced Concrete Bridge Pier Considering Characters of Nonlinear **2482**

Pengfei Luo, Dongjian Shen, Haijie Mi, Xiangya Kong, and Jianxin Wang

A Fuzzy Neural Network Technique for Crack Assessment of RC Bridges **2491**

Zhijian Hu and Zhaofang Hu

Experimental Research on the Combined-Method of Vacuum Well-Point Dewatering and Preloading **2500**

Hai-xu Yang, Hai-biao Wang, Xi-bin Dong, and Jian-ming Yin

Experimental Research and Damage Model of Square Concrete-Filled Steel Tube Subjected to Cyclic Loading **2506**

Xi-kai Du, Tie-cheng Wang, Hongming He, and Kai Yi

Function Design of Cement Stabilized Crushed Stone Drainage Base **2512**

Lin Tian, Xiaoguang Xie, and Decheng Feng

Heat Reflection Coating Design and Performance **2519**

Decheng Feng and Xin Zhang

Research on Key Question of Joint of Large Span Pre-Stressed Box-Girder Concrete Continuous Rigid Frame Bridge with High Piers **2526**

Guanghui Wang, Chenglong Wei, and Xiaoyan Liu

Research on Structural Design of Interlocking Concrete Block Pavement for Rural Road **2535**

Songlin Ma, Xiangshen Hou, and Dayong Wu

The Analysis of Dowel and Tie Bars Effects on Curling Up in Concrete Pavement Slabs **2539**

Xinkai Li, Songlin Ma, and Xiangshen Hou

Experimental Analysis of Interface Bond Performance of UTW **2545**

Yuqiang Huang, Decheng Feng, Xinkai Li, and Deyou Feng

The Analysis of the Correlation between International Roughness Index and Body Ride Comfort **2554**

Xiangshen Hou, Xuerong Liang, Songlin Ma, and Hua Wang

The Application of Anti-Rutting Agent on Improving the High- **2562**

Temperature Stability of Asphalt Pavement
Ping Li, Hui-Shan Li, Han-Qing Liu, and Yu Qian

Shake Table Test on Seismic Response of Non-Free Liquefiable Site **2569**
X. Z. Ling, X. Gao, L. Tang, P. J. Xu, and L. Q. Wu

Rut-Resisting Capacity of the Whole Surface Course in Continuous Upgrade under Heavy Loading **2577**
Hongxin Guan, Qisen Zhang, Yang Xu, and Libo Zhou

Integration of Fortran with ANSYS in Transient Thermal Simulation **2583**
Tao Zhang and Yanlin Yu

Study on Asphalt Treated Permeable Base in Permafrost Regions **2589**
Xi-bin Dong, Hai-biao Wang, and Li-hui Li

Continuous Test for Construction Quality of Mixed Filling Roadbed **2595**
Caixia Wang, Guanghui Xu, Haibin Cai, and Dapeng Song

An Evaluation of the Effectiveness of Geo-Textile-Binder-Aggregate System for Surface Treatment of Distressed Asphalt Pavement **2602**
Yanping Sheng, Shuanfa Chen, and Linbing Wang

Laboratory Investigation of Reclaimed Asphalt Pavement Mixed with Pure Binder Using X-Ray CT Scanner **2611**
Cristian Druta, Linbing Wang, and Tulong Zhu

Influence of Curing Regime on the Ductility of Ultra-High Performance Fiber Reinforced Concrete (UHPFRC) **2621**
Songlin Yang and Bo Diao

NURBS Strands Modeling of Prestressed Concrete Bridges **2628**
Dawei Yang and Qiao Huang

Highway Maintenance and Management

Performance Model for Pavement Maintenance of Expressway in Northwest of China **2635**
Yan Zhang, Chen Zhao, and Wei-sheng Li

Pavement Crack Automatic Recognition Based on Wiener Filtering **2641**
J. Zhang, A. Sha, Z. Y. Sun, and H. G. Gao

Determine Old Asphalt Pavement Milling Thickness Based on **2648**

Pavement Surface Deflection Control
Chao-hui Wang and Xiao-zhao Wang

Stability and Reinforcement Analysis of a High and Steep Cataclastic Rock Slope **2657**
Zuyin Zou, Zhanyuan Zhu, Lianjin Tao, and You Mo

Research on the Mechanism for Preventing Reflective Cracks in Old Cement Concrete Pavement Reconstruction **2664**
Liang Wang, Jinhua Song, Sheng Feng, Zhiping Jia, and Yuchao Lian

Study on Prolonging Asphalt Pavement Fatigue Life Based on Vision Transverse Intervention **2670**
Xiaodong Pan, Peng Hu, Zhen Yang, and Cheng Chi

Reliability Analysis on Pavement Skid-Resistant Performance in Expressway Tunnel **2679**
Jian-guo Yang, Yong-li Xie, Xiao Zhang, and Wei Ma

Influence of Crack Size of Old Concrete Pavement Slab on Structure Stress of Asphalt Overlay **2686**
M. Zheng and S. Chen

Stability Analysis of Excavating Rock Slope Based on the Catastrophe Theory **2692**
Xiao-zhao Wang and Si-chang Wang

Reinforcement Learning Control for On-Ramp Metering Based on Traffic Simulation **2701**
Xingju Wang, Bohang Liu, Xueqin Niu, and Toshihiko Miyagi

A Fatigue Test on Fiber Reinforced Asphalt Mixtures **2708**
Yang Guo, Yinghua Zhao, and Naisheng Guo

Analysis Method for the Prestressed Concrete Bridges Based on Time-Dependent Theory **2715**
Hong-Lin Wu

An Analytical Method for Predicting the Service Life of Bridge Structures **2720**
Xiaoguang Wu, Jun Liu, and Yanwei Li

A Study of Cold In-Place Recycling Mixture Used as Binder Course in China **2730**

Jonathan Jia, Jinhai Yan, and Zhouhui Tao

Optimization of Vehicle Routing for Plowing and Snow Disposal **2738**
Dali Zhang

Expressway Pavement-Performance Indexes Prediction Based on Gray Model GM(1,1,λ) **2745**
Li-juan Zhang and Fu-you Xu

Experimental Tests and Finite Element Modeling of Shrinkage Behavior in Cement Stabilized Aggregate Base **2754**
Qiang Li, Fujian Ni, and Zaixin Li

Research on Automatic Identification Method of Pavement Sag Deformation **2761**
Jiaqiu Wang, Songlin Ma, and Li Jiang

The Experimental Study of Effects of Herbaceous Plant Protecting Slope in Cold Area **2767**
Hai-biao Wang, Bi-feng Jiang, Xi-bin Dong, and Hai-xu Yang

Effect of Inorganic Salts on Frost Resistance of Concrete **2773**
Yong Ge, Wencui Yang, Jie Yuan, and Baosheng Zhang

Effect of Lightweight Aggregate with Different Moisture of Autogenous Shrinkage and Stress under Partially Restrained Condition **2779**
Shuhui Dong, Baosheng Zhang, Yong Ge, and Jie Yuan

Dynamic Response of Saturated Asphalt Pavement Based on Three Dimensional Finite Element Simulation **2786**
Zejiao Dong, Liping Cao, and Xiaoliang Cheng

Permanent Deformation Characteristic of Asphalt Mixture Considering Pavement Temperature Distribution **2793**
Liping Cao, Zejiao Dong, and Lijun Sun

Basic Study on Fractal Characteristic of Pore Structure in Cement Mortar **2801**
Shanshan Jin, Jinxi Zhang, Shuang Li, and Meng Fan

Node-Importance-Degree-Based Logistics Node Analysis **2808**
Li Li and Guoquan Yao

Study on Evaluation Method of Expressway Roughness **2814**

Shuyun Wang, Jinxi Zhang, and Yaping Cui

Transportation Management, Economy, and Policy

Research on Cost Control in Logistics Enterprises **2821**
Lingxiang Jian and Dongbing Li

Simulation Study on a Freeway Climbing Lane **2827**
Xiaomeng Cai, Q. Li, and Z. Wang

Hybrid Genetic and Taboo Search Algorithm for Solving the Bus Timetable Problem **2834**
C. Ren, W. Lu, L. Zhao, C. Yin, and H. Wang

Analysis of the Competitive Strategy of the Core Enterprises in Virtual Intermodal Freight-Transportation Enterprise **2840**
Dapeng Liu, Xiamiao Li, Minghua Zeng, and Xiaodong Cao

Optimization of Transportation Enterprises Pricing Strategies **2846**
Bailing Wang and Hui Li

Coordinated Development between Transportation System and Socio-Economic System Research Based on SEM **2852**
Shengrong Lu, Huiyuan Jiang, and Yao Liu

Study on the Structure of Digitized Transport Networks and Evaluation of Some Logistics Policies **2858**
ZhongZhen Yang, Yonglei Jiang, and Lianjie Jin

Research on Optimization of Crew Scheduling of the Passenger Dedicated Line Based on a Genetic Ant Colony Algorithm **2866**
Z. Tian, S. Ni, T. Chen, and Q. Song

Analysis for Principal-Agent Relationship between Owner and Construction Agent of Agent-Construction Project **2873**
Wenyi Zhao, Xuancang Wang, and Ting Zhan

Research on Calculation of Important Parameters of Freeway Financial Post-Evaluation **2878**
Y. Wang, S. Zhu, H. Wang, W. Xin, and M. Li

Empirical Research on Applicable Principle for Toll Mode of Highway **2886**
Ying Zhang and Guang Yang

Research on Travel Behavior Changes under Vehicle-Use-Restriction Measures during the Olympic Games 2893
Chun Yan Li, Sheng Yang Sun, and Ji Fu Guo

Study on Congestion Pricing Model of Bus Lane Mixed Use by Carpool Vehicles 2900
Dawei Pan, Wei Deng, and Renjie Qian

Principle Analysis and State Evaluation on Coordinated Development among Transportation Modes 2906
Hai-bo Zou

Evaluating the Equity Impacts of Rural Road Investment Projects on Household Welfare Based on a Quantile Regression Approach: Evidence from Fujian Province 2913
Y. Tian, Y. Li, and X. Chen

Study on Using OD Traffic Flow to Identify the Special Boundary of the Expressway Influence Zone 2920
Li-Ying Situ, Shun-Ying Zhu, and Hong Wang

Transport Strategy for Sustainable Development of Jiao Dong Economic Region 2927
S. Wang, S. Zhang, and L. Ren

Research of Road Transportation Sustainable Development Based on Ecological Footprint Model 2935
Xiao-xia Wang, Lei Fang, Xiao-xia Wang, and Jian-feng Lu

A Study on Signal Timing Optimization of Individual Intersections Based on an Ant Colony Algorithm 2942
Ling-jie Li, Xiao-kuan Yang, and Zhi Xu

Study on the Optimization of Vessel Scheduling Design Based on Soft Time Windows under Voyage Charters 2951
Ming Sun, Feifei Fei, and Xuefeng Wang

Congestion Pricing Revenue Redistribution Strategy Based on Traffic Behavior 2957
Z. B. Zhao, Y. Tian, and Y. Chen

Investment and Financing Influence Analysis and Countermeasures for Highway Construction in the Period of China's 11th Five-Year Plan 2963

Ruoqi Zhang, Minglan Chen, Xiurong Cai, and Fang Liu

A Study on the Financing Mode of Assets Securitization in Port Project **2969**

Su Yu

Study on the Capacity of Right-Turn Movement under Pedestrians' Influence at Signalized Intersections **2976**

Wanchao Zhang, Xiaokuan Yang, and Zhi Xu

Ramp Metering Strategies in a Corridor Network **2983**

Qiong Tian, Haijun Huang, and Hai Yang

Efficiency Loss of the Multiclass, Multicriteria Stochastic User Equilibrium Traffic Assignment against Stochastic System Optimization **2990**

Xiaojun Yu, Haijun Huang, and Tianliang Liu

The Application of TUXEDO Middleware in a Network-Based Train Working Diagram Compilation System **2997**

Hongxia Lu, Shaoquan Ni, Jinshan Pan, and Bin Liu

Analyzing the Effects of the Growth of Maritime Industries on the Regional Economy with Dynamic Inverse Matrix **3004**

Yajun Li and Zhongzhen Yang

Optimization Theory of Regulation on Rural Transit Market Based on Rule of Transport Equality **3011**

Changan Zheng, Maosheng Li, and Qisen Zhang

Analyzing the Motivation of Queue-Jumping Driving-Action on Transportation Systems by Prospect Theory **3019**

Maosheng Li, Qinglong Zhong, and Dafei Chen

Modeling Passenger Choice Behavior in Chinese Multi-Airport Regions **3028**

Jiangtao Liu

Design and Realization of Decision-Making and Analysis Assistant System on National Integrated Transportation Information **3034**

J. Zhang, C. Shao, C. Zhang, and Z. Ma

Pricing Model for Expressway with Elastic Demand **3042**

Huapa Lu, Xinxin Yu, Haiwei Wang, and Changzhi Bian

Research on Conversion Coefficients between Bicycle, Electric **3049**

Bicycle, and Pedestrian on Urban Road Intersection
Ai-Zeng Li, Xin-Sheng Song, Wei Wang, and Wen-Quan Li

Simulation Analysis of Merging Area on Urban Expressway in Alternate Rules Based on Cellular Automata Model **3055**
Shun Fang, Xiaoning Zhang, and H. M. Zhang

A Study on the Bus Delay Model at Bus Stops **3062**
Zhi Xu, Vincent Kwami Akpakli, and Xiao-kuan Yang

A Google-Map Integrated Web-Based Stated Preference Survey for Modeling Personal Mobility **3072**
Kai Liu and Yasuo Asakura

Evaluation of Supervision Engineer's Control over Investment Based on AHP **3079**
T. Lu and Q. Li

Technical Efficiency of Container Terminals in China Using a Multi-Activity Data Envelopment Analysis Model **3086**
Ying Li and Lixin Miao

Expressway Operation Financial Benefit Evaluation under Uncertainty **3093**
Liye Zhang and Chang Li

Research on the Differences in Regional Economy and Transportation among the Three Regions in China **3099**
Kechao Sun, Qingnian Zhang, and Xinjie Zhang

Evaluation and Optimization of Public Transport Subsidies for Alternative Energy **3105**
Yuan Fang, Xiqun Chen, and Xinmiao Yang

Study on the Control Strategy of Gas Injection of Gas Engines **3112**
Song Gao, Yu-ming Li, and Ling-yong Ling

Logistics

Design of Intelligent Decision Module for Storage Location Assignment in AS/RS **3118**
Yanru Zhu, Guiliang Zhou, and Lina Mao

Optimization of Open Vehicle Route to Reduce Fuel Consumption Based on Genetic Algorithm **3124**

Yong Peng and Haiying Zhu

Research on Location of Railway Logistics Center **3131**

Xionghuan Jin, Haihong Xie, Bo Jiang, and Lan Xu

Study on Logistics Center Location Bi-Level Programming Model and Algorithm Based on Competition **3137**

Xiaojun Guan, Xifu Wang, Cuihua Wang, and Yana Yan

A Model and Heuristic Algorithm for Inventory Routing Problem in Emergency Logistics **3147**

Binglei Xie and Xiaoming Hu

Study on Multi-Dimensional Structure Model for Agricultural Products Logistics Organization in China **3154**

Xinsheng Yao, Guangyin Xu, Jianhua Qu, Jianguang Wei, and Shasha Fan

Mean-CVaR Model of Wholesale Price Contracts and Dual Purchase Contracts in the Supply Chain **3160**

Y. G. Mu, Q. Mai, Z. B. Zhao, and Y. J. Feng

Structure System Model of Modern Logistics **3167**

Lijun Chen and Xuewu Chen

Multi-Objective Interval Number Model of Intermodal Transport under Uncertain Environment **3174**

Longhai Yang, Xiaowei Hu, and Jian Wang

A Model on Risk Evaluation for Emergency Guarantee Mechanism of Food Logistics **3180**

Xiangrong Huang and Ruhe Xie

Logistics Distribution Information System Based on 3rd Generation Mobile Communication Technology **3187**

Zhongwei Wang, Hongbo Wang, and Yan Pang

Theory Study on Correlation Stability and Profit Allocation of Supply Chain **3197**

Hui Hu and Chuantao Wang

Optimal Dynamic Substitution Policy for Components in an Assemble-to-Order System **3204**

Yongqiang Liu, Qing Chang, Xiaohong Zhang, and Hui Gao

Coordination Policies of Supply Chain Where Deterioration Begins at a Random Time Point 3210
Yongqiang Liu, Qing Chang, Xiaohong Zhang, and Hui Gao

Grey Correlation Analysis on Logistics Energy Consumption 3216
Zhiyi Lei

Research on Taboo Simulated Annealing Combinatorial Optimization Algorithm of Location Routing Problem with Pickups and Deliveries 3222
Dawei Hu, Dengdian Xuan, Huigang Lin, and Xiaofen Guo

Electrical Appliance Reversion Logistics Network Planning 3229
Gang Zhao, Xi Nan, and Kecong Lu

A New Organizational Structure Pattern of Owners Based on Multi-Project 3236
Qiaoting Dong, Yingming Shen, Huijun Li, and Zhijun Chen

Dynamic Alliance of Road Logistics Enterprise Based on Ant Colony Algorithm 3243
Xiaobo Liao and Yamin Huo

Optimization of Emergency Material Dispatch Problem Based on Adaptive Genetic Algorithm 3249
Xuejun Feng, Qinying Zhang, and Wei Wang

An Algorithm for Vehicle Routing Problem with Soft Time Windows Using Tabu Search 3257
Lixin Zhang and Huimin Niu

Research on Dynamic Safety Stock Based on Short-Term Weather Forecasting 3263
Wei Liu, Shuzhi Zhao, Wei Wang, and Bo Peng

Study of Operational Characteristics of HAZMAT Vehicles Based on GPS Data 3269
Zhenguo Liu, Xiaofa Shi, and Ying Hui

Risk Evaluation Model for Construction of a Logistics Park Based on Principal Component Analysis 3276
Yuzhou Wang, Qing Huang, Bin Chen, and Dewu Liu

Vehicle Operations Technologies

Parameter Sensitivity Analysis of Accident Reconstruction Model Based on Orthogonal Design 3283
Tiefang Zou, Zhi Yu, Ming Cai, and Jike Liu

Study on the Key Technology of Captive Model's Numerical Test 3289
Xiao Wang, Bing Xiao, Bo Yang, and Aiguo Shi

Simulation and Analysis for Stick-Slip Vibration of Locomotive with Hollow-Shaft Drive System 3299
Jianxin Liu, Huaiyun Zhao, and Wanming Zhai

Fatigue Life Prediction of Rubber Nodes 3306
Huichao Wu, Pingbo Wu, and Qingqun Lan

Application Research of GPS Based on Google Earth Platform 3312
Zhen-Bo Wang, Rui-Xiang Chen, Niandong Jiang, Hui Zhang, and ZhiRen Sha

A Study of the Fuzzy PID Control Over the Hydraulic Semi-Active Suspension in Consideration of Automotive Engine and Passenger-Seat System 3318
Xiang Chen, Guo-fang Li, En-yong Wang, and Xin-jia Jiang

Study on Power Control of Electric Power Steering System 3327
Chunyan Mu, Jingnuo Yu, Wansheng Zhao, and Jianxia Liu

Rail and Transit Systems

Simulation of Wheel/Rail Noise of High Speed Train Running on the Slab Track 3333
Xinwen Yang and Caiyun Yan

Study of Influence of Subway Station Excavation on Existing Metro Deformation 3339
Yun-Peng Li and Zhi-Yin Wang

Influence of Longitudinal Connection Mode of Ballastless Slab Track on Vibration Characteristic of Train-Ballastless Slab Track-Subgrade System 3346
Qing-Yuan Xu and Zhi-Ping Zeng

Vehicle Semi-Active Suspension System Simulation with Variable Structure Control Method 3354
Zhongji Li and Huanyun Dai

Structural Noise of Longitudinal Stiffened Concrete Cylindrical Shell **3361**
Weiping Xie and Liangming Sun

Research on Greedy Train Rescheduling Algorithm **3368**
Z. He, H. Li, J. Miao, L. Meng, and B. Mao

Impact on Regularity of Track from Pile Underpinning of Light Railway Bridge **3378**
Xiangguo Li, Hailong Wang, Quan Zhou, Jianqing Bu, and Musong Li

Train-Carried Rail Signal Parameters Test System Based on Spectrum Correction Method and Virtual Instrumentation **3387**
Y. Guo, G. Cheng, and S. Sha

Study on Style Protection and Urban Traffic Planning of Harbin Jingyu Street **3393**
X. Yao, Y. Zhang, and Y. Liu

Study on the System Design and Optimal Models of Urban Rail Transit Traction Calculation System **3399**
Hongbo Liu, Hongxia Lu, Miaomiao Lu, and Jie Zhang

Characteristic Analysis of Urban Rail Transit Network Considering Demand and Operation: A Case on Shanghai **3406**
C. Yang and Y. Wang

Adaptability Assessment and Maintenance Technology Research of Existing Railway Line Speed Increases to 200 km/h **3413**
Ping Wang, Rong Chen, and Xiaoping Chen

Analysis on Mechanical Performances of High-Speed Railway Transition Curves **3420**
Xiangguo Li, Musong Li, Chao Ma, Jianqing Bu, and Liangliang Zhu

Research on Dynamic Measuring System and Model of Novel High Speed Railway Vehicle Bogie **3428**
X. Wang, J. Su, Y. Lin, and D. Zhou

Empirical Research on Urban Rail Transit Operation Performance Based on FCE–AHP **3435**
Xinlong Jiao

The Application of Functionally Gradient Material to Problems of **3443**

Wheel-Rail Contact

Jun Zhang, Liping Sun, Shengwu Wang, and Xuesong Jin

Analysis about Business Investing and Financing Models of Urban Rail Transit **3449**

Xiao Tian Cui and Hui Xie

Characteristics of Fundamental Data for Railway Maintenance and the Construction of Integrated Data Platform **3456**

Futian Wang, Mei Sun, and Jianglin Zhou

Track Structure Vibration Characteristic Analysis Based on FEM 3D Model **3463**

Linya Liu and Zhuqing Lu Lu

Measurement and Simulation Study on Ground Subsidence Induced by Shield Tunneling in Sandy Stratum **3469**

Haixia Sun, Wen Zhao, and Lihua Lu

Information Needs of Urban Transit Travelers – The Case of Wuhan, China

Zhengdong Huang[12] Xuejun Liu[3] Jie Li[3]

[1] School of Urban Design, Wuhan University. Donghu Nanlu 8, 430072 Wuhan, China; PH (+86 27) 68772147; FAX(+86 27) 68773062; email:zdhuang@whu.edu.cn
[2] Research Center for Digital City, Wuhan University
[3] School of Urban Design, Wuhan University, Donghu Nanlu 8, 430072 Wuhan, China

ABSTRACT:

While the structure and functions of transit information systems have been widely explored, there exist bottlenecks of information quality. Transit information providers need to understand the travelers' needs correctly. To find out the structure of transit information needs, a survey on transit travelers has been conducted in Wuhan, China. It is discovered that the transit travelers in Wuhan rely heavily on conventional means in making trip plans, and the potential of internet-based spatial transit information service has not yet been fully explored. The investigation reflects the current situation of intelligent transit passenger service, as well as the potentials of development in the future.

INTRODUCTION

One of the major components of an Advance Public Transportation System (APTS) is the Transit Traveler Information System (TTIS). An important objective of TTIS is to provide accurate and opportune information so as to attract more travelers. This is accomplished by incorporating routes, fares, schedules and other dynamic data, into one cohesive database for such applications as pre-trip planning and in-vehicle information provision (Casey and Labell, 2000). Transit information service involves a variety of strategies and methods, ranging from paper route maps to interactive trip planning.

The development of the Information and Communication Technologies (ICT) has facilitated dissemination of traveling information. Real-time bus location and web-based information delivery system have been deployed and tested (Maclean and Dailey, 2002). Transit information service requires efficient transit data model, which in most cases makes use of spatial data modeling technologies. The system may be constructed in a web-based GIS framework so that transit passengers may plan their trips interactively (Peng and Huang, 2000). From the last decade, many cities have been providing public transit information through internet and mobile service (Lu, 1999). Good data quality and reliable bus system operation are important factors for the success of TTIS.

While the structure and functions of transit information systems are widely explored, there exist bottlenecks of information quality. A TTIS should satisfy the information needs of transit travelers. However, there has been inadequate study on the type and structure of information for this purpose. Previous studies have identified varied usefulness of different types of information. Chorus *et al* (2007) have found out that there is basically a genuine need for time-related and cost-related information. For the more advanced types of information, travelers especially need those that make travelling 'easier', rather than that facilitate advanced searching possibilities. Another research declares that real-time information yields only very modest improvements in passenger service measures such as the origin-to-destination travel times and the variability of trip times (Hickman and Wilson, 1995).

To find out the type and structure of transit information needs, a survey on transit traveler has been conducted in Wuhan, China. The questionnaire for the survey concerns with evaluation of current transit system, means and contents of information acquisition, as well as expectation of types of information in the future. This paper introduces the survey structure and describes the outcomes and implications from the survey.

SURVEY DESIGN AND IMPLEMENTATION IN WUHAN, CHINA

Wuhan administration covers a total area of 8,494 square kilometers, with a total population of 8 million. The built-up area is 356 square kilometers, which served by a transit system of 216 bus routes and 1,800 stop platforms. The bus transit system has an average route length of 18.65 km, and a high overlapping rate of 5.0. These two indicators are much higher than those of the national standard. From the perspective of spatial distribution, bus stops are evenly deployed, which covers more areas than by the national standard (Huang, 2003).

The objectives of the survey are to clarify the structure and content of information needs in bus transit trips, and to evaluate the level of information service in existing operational system. The content of the field survey is comprised of four aspects. These are basic information of respondents, status of bus transit service, trip information needs, and bus transfer. The contents of these aspects are:

- The basic information section includes gender, age, monthly income, residence place, and transport vehicle ownership.
- Questions on the status of bus transit service concern with how the traveler evaluate Wuhan bus transit as a whole system, including easiness of information acquisition, service quality, walking distance at trip ends.
- The main section of the survey is the information needs in transit travel, aiming at acquiring the contents and degree of information needs. The questions concern with way and source of acquiring trip information, as well as expected information source and media.

- The section of transfer investigates the situation and problems encountered in bus transfer.

The questionnaire has totally 19 questions, printed on two sides of one sheet. In the summer of 2007, the field survey was conducted on sites around bus stops, squares and public activity centers. Among the 2,000 valid feedbacks, 52.8% are young respondents between the age of 20 to 30, and 54.7% are males.

FINDINGS FROM THE SURVEY

Transit environment in Wuhan

Bus transit system in Wuhan is the dominant mode of public transport. Other modes include several passenger ferry lines, as well as a nine-kilometer light rail that attracts few trips. Two big rivers and several large lakes shape the city into a unique spatial structure, which partly explain the high overlapping rate of bus lines. The survey investigates the current situation by inviting the respondents to evaluate the bus transit system. Three aspects are involved, i.e., the performance, time cost at trip ends, and easiness of information acquisition.

- Transit performance: Average transfer times and ticket price are appreciated by transit travelers, accounting for 36.4% and 38.5% respectively. However, punctuality and driving behavior are two big problems, which indicate a low system performance.
- Time cost at trip ends: 78.5% of the respondents walk to their boarding bus stops from their origins. With regard to the time cost in reaching the origin stop, 49.0% of the travelers are found to be “within 5 minutes”, and 31.6% fall between “5 to 10 minutes”. Similar trend has been found for walking time from last alighting stop to destination (**Figure 1**). These reflect the rational spatial distribution of bus stops in Wuhan.
- Easiness of information acquisition: Although more bus travelers regard “very easy” than those feeling “difficult”, the majority (75.3%) of respondents report “easy” for acquiring information.

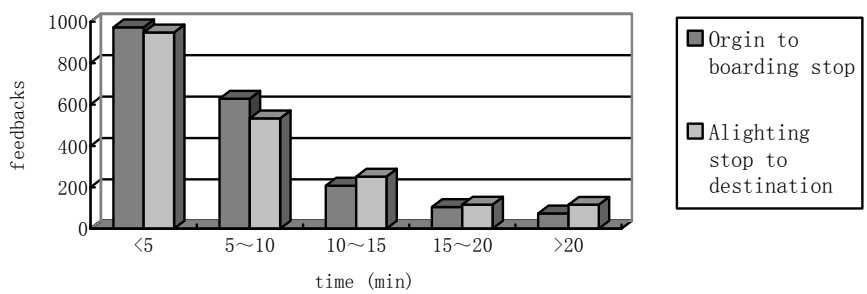

Figure 1. Time cost at both ends of transit trip.

STRUCTURE OF INFORMATION NEEDS

Bus travelers may need information on boarding stops, routes, transfers and schedule. It was envisaged that there is varied degree of demand on these factors. Four choices are provided for the expected information needs, including boarding stop, trip route, trip time and transfer stop. Respondents may make multiple choices in the form. Results reveal that exact information on boarding stop and trip route are slightly more attractive to travelers, with approximately 40% selection each. Choices of trip time and transfer stop are selected by 33% of the respondents each (**Figure 2**). The revealed choices have also indicated a slight gender difference. Although this is a question with multiple choices, we have identified limited forms with multiple selections. Among the 2,000 respondents, 431 people made two choices, 137 people made three choices, and 94 people selected all four choices.

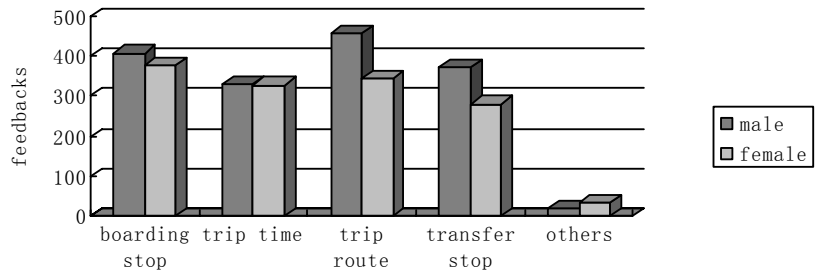

Figure 2. Expected bus transit information by gender.

For pre-trip planning, nearly half of the respondents (926 cases) would pursue least transfer times. This can be partly explained by the current route-based fare system, i.e., each route has a fixed fare regardless what distance the traveler takes, and the passenger needs to buy a ticket upon boarding. Bus travelers are also seeking least travel time and distance (770 cases), as well as shortest walking distance at both bus trip ends (663 cases). Other less selected choices include cheap fare and comfortableness.

MEANS OF INFORMATION ACQUISITION IN TRANSIT TRAVEL

The survey investigates revealed and expected information acquisition, as well as a comparison between two types of information delivery. Listed information sources in the survey include stop plate, paper map, friends, internet, telephone, and mobile SMS.

- Revealed information source: The most popular information source that travelers are utilizing reveals to be stop plates (1163 cases) and asking family member or colleagues or friends (817 cases). Travelers also frequently use transport maps (400 cases) and internet searching (394 cases). Telephone inquiry (150 cases) is less popular information source. It is also found out that female travelers have a

stronger inclination than the males in asking people for trip advice.

- Expected information source: The option of asking people is not included in this question, which makes it possible to emphasis the importance of the future information source. The stop plate remains to be the most popular information source (1114 cases). Internet searching (638 cases) is regarded as a very important means, while paper map (388 cases), mobile SMS (353 cases) and telephone inquiry (331 cases) are less popular in the expectation. These data indicate that bus travelers are expecting some improvements on the information and communication technology.
- Information media: Two options were given for the preference in internet searching, i.e., text-based and map based. Conforming to previous envision, most travelers would prefer internet maps (1299 cases). In fact, maps provide more spatial orientation for travelers, but a system providing maps is more expensive.

TRANSFER ISSUES

Convenience of transfer is an important indicator for transit performance. Issues related to transfer include the connection of transfer platforms, walking distance in transfer and transfer time.

- Connections between transfer platforms: Two major problems on transfer platforms are identified from the investigation. The first one is that a stop is composed of two or more platforms, and a transfer has to be carried out between them (853 cases). But there is no clear transfer guidance between the links. The other problem is a consequence from the multi-platform layout, i.e., travelers cannot find the correct platform at a stop (835 cases). Also, there are complains on long walking distance (632 cases).
- Walking distance in transfer: Many transfers are made by walking less than 50m with no crossing (745 cases), and by waiting at the same platform (513 cases). All other situations receive moderate number of feedbacks between 260 and 310 cases. This indicates the complex transfer situation in Wuhan.
- Transfer time: A majority of transfers are made within 10 minutes, with 652 cases of “less than 5 minutes” and 1036 cases of “5 to 10 minutes”. However, regarding “longest waiting time ever experienced”, 73.3% of the reporters claim that they have experienced waiting more than 15 minutes in a transfer.

DISCUSSION AND CONCLUSIONS

The survey outputs reflect the current situation of bus information needs in the city of Wuhan, China. Firstly, finding stop platforms in complicated spatial surroundings and long transfer distance are main problems. Secondly, transit travelers in Wuhan are trying to seek trips with least transfers, which conforms to early

findings from other cities in China (e.g. Yang et al., 2000). Thirdly, bus travelers are mostly using conventional methods to acquire trip information, including inquiring other people, reading on stop plates and browsing maps. The trip information is usually acquired during bus trips, with very little proportion of pre-trip planning. Fourthly, data from existing sources has low quality in terms of spatial location and transfer guidance. Finally, real time bus information provision is still far from implementation.

A complete bus trip consists of a series of activities, including finding and walking to the boarding stop, traveling on bus, possible transit transfer, and traveling from alighting stop to destination. The survey on structure and content of information needs helps to identify key factors in bus trips. Findings from the survey also justify a multi-layer representation of transit system, such as the multi-tier transit data model proposed by Huang et al (2007).

The survey may also provide information for predicting transit trip activities, such as choice of information source, preference among alternatives, and selection of transfer types. These activities are related to the travelers' socio-economic status.

ACKNOWLEDGEMENT

The research is funded by the Chinese National Natural Science Foundation (70671076) and the Chinese National High-tech R&D Program (863 Program: 2007AA11Z207).

REFERENCES

Casey, R. F., and Labell, L. N. (2000). "Advanced Public Transportation Systems: The State of the Art Update 2000." *FTA-MA-26-7007-00-1*, Volpe National Transportation Systems Center.

Chorus, C. G., Arentze, T. A., Timmermans, H. J. P., Molin, E. J. E., and Van Wee, B. (2007). "Travelers' Need for Information in Traffic and Transit: Results from a Web Survey." *Journal of Intelligent Transportation Systems*, 11(2), 57 - 67.

Hickman, M. D., and Wilson, N. H. M. (1995). "Passenger travel time and path choice implications of real-time transit information." *Transportation Research Part C: Emerging Technologies*, 3(4), 211-226.

Huang, Z. (2003). "Data Integration for Urban Transport Planning. PhD dissertation," PhD Dissertation, Utrecht University, The Netherlands.

Huang, Z., Yu, Z., and Wang, B. (2007). "A Multi-tier Data Model For Urban Public Transportation." *Geomatics and Information Science of Wuhan Univeristy*, 32(4), 22-25.

Lu, H. (1999). "The status quo and prospect of development and application of the intelligent public transport system in Japan." *Urban planning overseas*(1), 5-8.

Maclean, S., and Dailey, D. (2002). "Wireless Internet Access to Real-Time Transit

Information." *Transportation Research Record: Journal of the Transportation Research Board*, 1791, 92-98.

Peng, Z. R., and Huang, R. (2000). "Design and development of interactive trip planning for web-based transit information systems." *Transportation Research Part C: Emerging Technologies*, 8(1-6), 409-425.

Yang, X., Wang, W., and Ma, W. (2000). "GIS-Based Public Transit Passenger Route Choice Model." *Journal of Southeast Univwrsity (Natural Science Edition)*, 30(6), 87-91.

Study on the Rational Size of the Box Girder Used in Cable-Stayed Bridge Based on ANSYS

YANG Xia-lin[1] ， SUN Xue-xian[2]，WU Ya-ping[3]，MAO Xiao-dong[4]

[1]Civil Engineering College, Lanzhou Jiaotong University, Lanzhou 730070,China;PH(86) 0931-4559336;email:cqlx06@163.com.

[2] Civil Engineering College, Lanzhou Jiaotong University, Lanzhou 730070,China; PH(86) 0931-4938054;email: sxx1955@163.com.

[3] Civil Engineering College, Lanzhou Jiaotong University, Lanzhou 730070,China; PH(86) 0931-4938532;email: wypsw@163.com

[4] Civil Engineering College, Lanzhou Jiaotong University, Lanzhou 730070,China; PH(86) 0931-4938532;email: mxd127@126.com.

ABSTRACT:

By using the structural analysis program ANSYS, finite element models are established based on a box girder with varying thickness of the bottom slab , thickness of the inclined web, inclination of the inclined web, thickness of the vertical web, and thickness of the top slab of cable-stayed bridge. In order to consider the effects of the adjacent zone out of the girder section, the internal forces of the two-end surface that were obtained by the horizontal shaft system analysis were exerted on each model. Also, the weight, cable force, and pre-stressed force including girder longitudinal, diaphragm transverse and inclined web vertical direction are considered. Based on the above, the three-dimensional stresses of the box girder with different working situation are analyzed. By the result of above static analysis, the reasonable proposals on thickness of the bottom slab and thickness of the inclined web and inclination of the inclined web and thickness of the vertical web and thickness of the top slab of cable-stayed bridge are proposed. Analysis shows that the stress distributions of main girder are reasonable when the bottom slab thickness is around 30cm, the inclined web thickness is around 30cm, the inclined web inclination is 150 ~152°, the vertical web thickness is around 40cm and the top slab thickness is around 22cm.

Key Words: cable-stayed bridge; box girder; finite element analysis; reasonable sizes.

1 INTRODUCTION

In recent years, a large number of cable-stayed bridges were designed with the main girder of good bending and torsion resistance properties, their sizes also gradually became light and slim. What should not be overlooked is that many existing cable-stayed bridges' main girder, in the construction stage and the use stage, particular in the use stage, experienced varying degrees of cracking. Based on a

bridge girder section's type and size, the cable-stayed bridge box girder space stress analysis method was used, combining the structural analysis program ANSYS. Five different thickness of the bottom slab, five different thickness of the inclined web, five different inclinations of the inclined web, five different thickness of the vertical web and four different thickness of the top slab for the main girder were analyzed by using the finite element analysis method. Thus, the rational box-size for the cable-stayed bridge was proposed.

2 FINITE ELEMENT ANALYSIS MODEL

In order to analyze the influence of various parameters on the stress distribution for the box girder, the finite element models are as follows: the original size of a bridge (the bottom slab thickness is 18cm), increases to 24cm, 30cm, 35cm, and 40cm;); the inclined web thickness increases to 24cm, 30cm, 35cm, and 40cm ; (the bottom slab thickness increases to 35cm; The inclination angle of bottom slab and inclined web is 149.40°), the inclination angle changes to 144.83° , 147.24° , 151.27° , and 152.96° , the inclination angle of inclined web changed with the width of bottom slab. The original size of a bridge (the bottom slab increases to 35cm, the inclined web increases to 30cm), the vertical web thickness increases to 30cm, 35cm, 40cm and 45cm and the original size of a bridge (the bottom slab increases to 35cm, the inclined web increases to 30cm, the vertical web thickness increases to 40cm), the top slab thickness increases to 30cm, 35cm, 40cm. 20 finite element models of the box girder were established for the main gird.

The stress analysis of space needed to choose a segment from the main girder, then the local stress analysis can be conducted. In general, when we analyze the local stress, we should first analyze the structure in a spatial structure as a whole, then choose the local segment as the analyzed object according to the Saint-Venant principle, which should meet the boundary displacement and the forcing state.

2.1 Structure and load

A bridge girder is a pre-stressed concrete structure. The box girder is a two-box single room with inclined web and inverted trapezoidal cross section, with the opening width of 13.25 m, the bottom slab thickness and web thickness of 18 cm, the top slab thickness of 22 cm, and the vertical web thickness of 25 cm, Figure 1 is the girder cross-section.

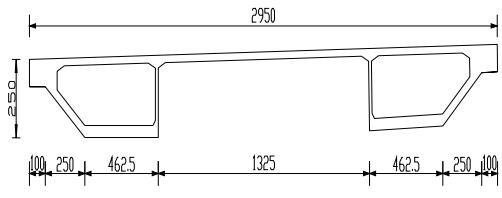

Fig1. Cross section of girder (cm)

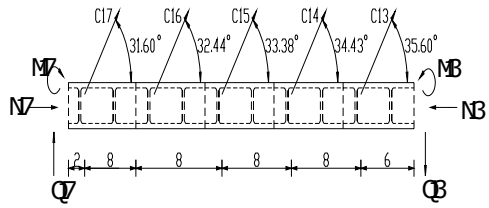

Fig2. Boundary force of girder（m）

As shown in Figure 2, we research the 40 m girder's spatial stress effect under the internal forces in the end, the cable force, self-weight, and pre-stressed force. The

internal force in the end and the cable force are based on analysis of the plane-frame, and are imposed on the girder as loads. The directions in Figure 2 are all positive.

2.2 The establishment of spatial finite element model

As seen from the cable-stayed bridge box girder structure, the cable-stayed bridge's box girder structure is more complex, so we select the 8-node hexahedral element, which can fit the structure better when meshing the structure.

The internal forces on the end of the girder, which was calculated from the plane beam element, and the internal forces applied on the girder by the stay-cable were applied on the corresponding position. To calculate facilitate, to minimize error, the axis forces were applied on the top slab, bottom slab, and the inclined web uniformly (scattered in individual nodes). The moment that was regarded as couple of forces, according to the principle of static equivalent, was applied on the structure. The role of the pre-stressed steel and the stay-cable were considered as the node force. The self-weight of the girder was also considered in the analysis.

3 THE RESULTS AND ANALYSIS

3.1 Comparative analysis of stress of box girder with different thickness of bottom slab.

As seen in the figure 3(a), with increasing bottom slab thickness, the main tensile stress in the bottom slab generated by different working conditions is equal at different positions. However, the maximum main tensile stress decreases gradually in bottom slab. At the same time, when the thickness is more than 30 cm, the value is lower than the tensile strength design value of C50 concrete. As seen in figure 3(b), with increasing bottom slab thickness, the absolute main compressive stress decreases gradually. At the same time, when the thickness is more than 30 cm, the value is lower than the compressive strength design value of C50 concrete. As seen in figure3(c), with increasing bottom slab thickness, the absolute main compressive stress in the vertical web decreases gradually and all of the compressive stress values are lower than the compressive strength design value of C50 concrete. As seen in figure 3(d), the main tensile stress distribution in the inclined web is the same. The value appears at the bottom zone in the inclined web, a zone at the junction of the inclined web, the bottom slab, and the transverse girder. However, when the thickness of the bottom increases, the value increases gradually. When the thickness changes from 18 cm to 30 cm, the maximum value show a decreasing trend. However, when the thickness of bottom slab increases to 35cm and 40cm, the maximum value again shows a clearly rising trend, at the same time, the maximum values are all higher than the stress strength design value of C50 concrete. As seen in figure 3(e), with increasing bottom slab thickness, the absolute value decreases gradually in inclined web. At the same time, when the thickness is greater than 30cm, the value can meet the requirement of the stress strength design value of C50 concrete. As seen in figure 3(f), the maximum main tensile stress in the inside of the solid rib appears at the center area when the bottom slab is different. When the value

changes from 18cm to 30cm, the maximum value shows a decreasing trend. When the value changes from 35cm to 40cm, the maximum value shows a rising trend again. Most importantly, when the bottom thickness is 30 cm, the maximum value is the relative minimum value. When the bottom thickness is 24cm and 35cm, the maximum value is basically the same. However, when the bottom slab thickness is 18cm and 40cm, the maximum value is greater than the tensile strength design value of C50 concrete.

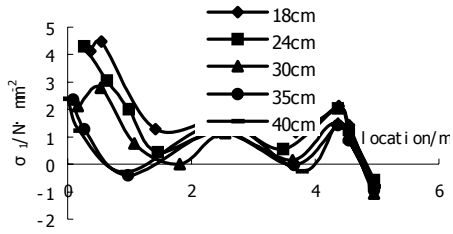

a. Main tensile stress of the bottom slab

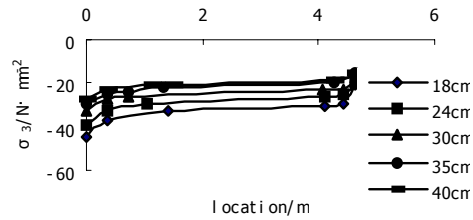

b. Main compressive stress of the bottom lab

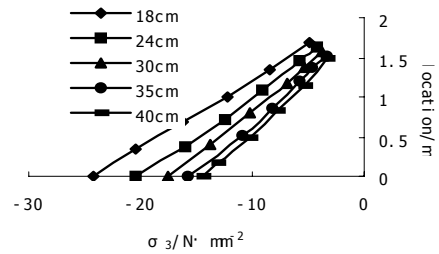

c. Main compressive stress of the vertical web

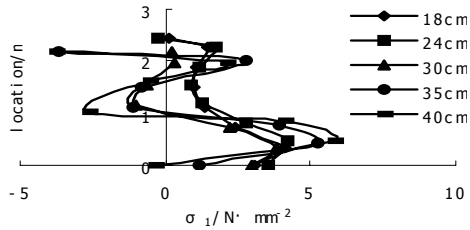

d. Main tensile stress of the inclined web

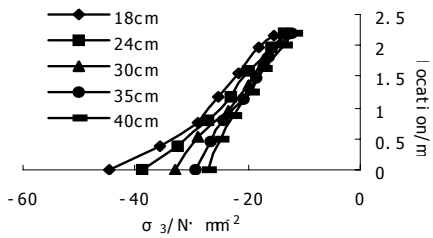

e. Main compressive stress of the inclined web

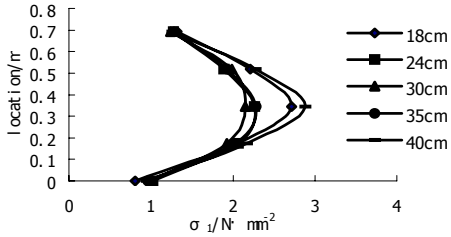

f. Main tensile stress of the solid rib

Fig3. Main stress distribution of box girder with different thickness of bottom slab

3.2 Comparative analysis of stress of box girder with different thickness of inclined web.

Three-dimensional stress distribution characteristics in various regions of the girder are mostly the same as above. In order to better understand the changes of stress for the girder with the different thickness of the inclined web, the stresses under different working conditions are shown in Table 1.

Table1 Peak stress (N • mm^{-2}).

Thickness (mm)	σ_1 *(bottom slab)*	σ_3 *(bottom slab)*	σ_3 *(vertical web)*	σ_1 *(inclined web)*	σ_3 *(inclined web)*	σ_1 **(solid rib)**
18	2.36	-22.01	-17.11	3.00	-28.23	2.28
24	2.13	-18.56	-17.01	1.37	-25.38	2.01
30	2.34	-17.99	-16.68	1.48	-24.63	2.09
35	2.62	-17.62	-16.73	1.83	-24.99	1.97
40	4.13	-18.48	-17.02	2.10	-23.91	1.50

3.3 Comparative analysis of stress of box girder with different inclination angles of inclined web

In order to better understand the changes of stress for the girder with different inclination angles of the inclined web, the stresses under different working conditions are shown in Table 2.

Table2 Peak stress ($N \cdot mm^{-2}$).

inclination angle (°)	σ_1 *(bottom slab)*	σ_3 *(bottom slab)*	σ_3 *(vertical web)*	σ_1 *(inclined web)*	σ_3 *(inclined web)*	σ_1 **(solid rib)**
144.83	2.52	-22.42	-15.84	2.25	-28.42	2.65
147.24	2.62	-21.28	-16.37	3.01	-27.28	2.27
149.40	2.36	-22.01	-17.11	3.00	-28.23	2.28
151.27	2.43	-21.74	-17.23	2.56	-27.74	2.50
152.96	2.10	-21.89	-17.19	2.04	-27.89	2.64

3.4 Comparative analysis of stress of box girder with different thickness of vertical slab.

In order to better understand the changes of stress for the girder with different thickness of the vertical slab, the stresses under different working conditions are shown in Table 3.

Table3 Peak stress ($N \cdot mm^{-2}$).

Thickness (mm)	σ_1 *(bottom slab)*	σ_3 *(bottom slab)*	σ_3 *(vertical web)*	σ_1 *(inclined web)*	σ_3 *(inclined web)*	σ_1 **(solid rib)**
25	2.34	-17.99	-16.68	1.36	-24.63	2.09
30	2.36	-18.26	-16.56	1.39	-24.68	1.82
35	2.18	-17.27	-17.09	1.48	-25.03	1.81
40	2.11	-17.53	-17.11	1.91	-25.39	1.87
45	2.03	-17.08	-16.43	1.81	-24.91	1.89

3.5 Comparative analysis of stress of box girder with different thickness of top slab

In order to better understand the changes of stress for the girder with different thickness of the top slab, the stresses under different working conditions are shown

in Table 4.

Table4 Peak stress (N • mm^{-2}).

Thickness (mm)	σ_1 *(bottom slab)*	σ_3 *(bottom slab)*	σ_3 *(vertical web)*	σ_1 *(inclined web)*	σ_3 *(inclined web)*	σ_1 **(solid rib)**
22	2.11	-17.53	-17.11	1.91	-25.39	1.87
30	3.36	-17.36	-17.72	2.70	-25.18	1.89
35	2.87	-18.27	-18.53	2.67	-25.93	1.42
40	2.70	-19.53	-19.16	2.79	-26.89	1.39

4 CONCLUSION

(1)It is necessary for the Cable-Stayed Bridge to have sufficient bottom slab thickness. However, the thickness should be controlled within a certain range.

(2) Every indicator is reasonable when the bottom thickness is about 30 cm, the inclined web thickness is about 30 cm ,the inclination angle of the inclined web is about 150 ~152° , the vertical web thickness is about 40 cm, and the top slab thickness is about 22 cm.

(3) The bottom slab and inclined web are extremely unfavorable; greater importance should be attached to them in the design phrase and the construction phrase.

(4) The cable-stayed bridge with the double-box single-room girder structure under loading has complex spatial characteristics, so it is impossible to analyze the structure mechanical characteristics accurately in detail, it is necessary to make space analysis for the structure.

ACKNOWLEDGEMENTS

This study is financially supported by National Natural Science Funds (50678076) and “Qing Lan” Talent Engineering Funds by Lanzhou Jiaotong University.

Author information: YANG Xia-lin(1970-),woman, associate professor,E-mail: cqlx06@163.com,

BIBLIOGRAPHY

XIANG Yi-qiang, FENG Shuo, WANG Jin-feng(2005). “Spatial Static Behavior Analysis of Long-Span P.C.Continuous Rigid-Frame Box Girder Bridge with Single Cell”. *Journal of Highway and Transportation Research and Developmen*, 22 (3):58-61.

YANG Xia-lin, LI Qiao, Ran Qi-shan(2006). “Three dimensional stress analysis of main box girder with twin-box single cross section used in cable-stayed bridge”. *China Journal of Highway and Transport*, 19(1): 71-74.

ZHOU Wei-dong, FANG Zhen-zheng(1999). “Spatial stress analysis of the cable anchorage zone in a PC tower”.*Tongji University Journal*, 27(2):203-206.

Xiang, Y.Q., Feng, S., and Wang, J.F. (2005). Spatial Static Behavior Analysis of Long-Span P.C.Continuous Rigid-Frame Box Girder Bridge with Single Cell. Journal of Highway and Transportation Research and Development, Vol. 22, No. 3, pp. 58 – 61.

Yang, X.L., Li, Q., and Ran, Q.S. (2006). Three Dimensional Stress Analysis of Main Box Girder with Twin-box Single Cross Section Used in Cable-stayed Bridge. China Journal of Highway and Transport, Vol. 19, No. 1, pp. 71 – 74.

Zhou, W.D., and Fang, Z.Z. (1999). Spatial Stress Analysis of the Cable Anchorage Zone in a PC Tower.Tongji University Journal, Vol.27, No. 2, pp. 203 – 206.

RESEARCH ON THE CRASHWORTHINESS OF TWO-LAYER THIN-WALLED STRUCTURES

XIAO Shoune[1], SHAN Qiyu[1,2], YANG Guangwu[1], CHEN Hanzhen[1]

[1]State Key Laboratory of Traction Power, Southwest Jiaotong University, Chengdu, 610063,China; PH(86)28-86466543;FAX(86)28-86466543; email:snxiao@swjtu.cn

[2]School of Mechanical Engineering, Southwest Jiaotong University, Chengdu, China; PH(86)28-86466541;FAX(86)28-86466543; email:Shanqiyu1984@126.com

Abstract

In order to design the appropriate crashworthy structure of a locomotive vehicle, the two-layer thin-walled structures were taken as research objects. The efficient non-linear explicit dynamic finite element analysis software, ANSYS/LS-DYNA, was adopted to research the energy absorption characteristics of the one-layer thin-walled structure and the two-layer, thin-walled structure. The results have shown that the evaluation parameters (the energy-absorbing efficiency, the buffer index) of energy absorption characteristics of two-layer, thin-walled structures are better than those of one-layer structures. An idea of using two-layer thin-walled structure as an energy-absorbing element of a crashworthy vehicle is put forward. The results of simulation on two-layer, thin-walled structures with different shapes have also shown that the dimensions of the inner-layer have effect on energy absorption characteristics.

Key words: *Crashworthiness, Thin-walled structure, Non-linear finite element*

1 Introduction

With the increase of train speed, train accidents have threatened safety of passengers and brought huge economic losses to railroads. After research about the history of railway accidents, we have found that these accidents can not be avoided even if many active protection technologies are used on the train. In order to protect the safety of passengers and reduce loss from accidents, many passive technologies were applied to high-speed trains. Many simulation and experiment research projects, which related to crashworthiness vehicle design and energy-absorbing device(Abramowicz,1984; Hanssen,2000; Karagiozova,2001; Scholes,1993), were carried out by researchers whose work mainly focused on energy absorption characteristics of one-layer, thin-walled structures. Because enormous energy will be generated in a high-speed collision, one-layer structures cannot meet energy-absorbing requirements. In this paper, we take two-layer, thin-walled structure as an energy-absorbing element and analyze its energy absorption characteristics through simulation.

2 Theoretical foundation

The collision problem of locomotive vehicle structure has many

characteristics, such as large displacement, large rotation, large deformation and large strain, and is affected by material constitutive relation, structural failure, frictional contact and other factors. After simulating the entire collision process by dynamic non-linear finite element method, we can obtain the deformation, speed, acceleration and stress and strain distribution of elements.

The collision problem of large deformation usually costs a lot of calculation time. In order to avoid solving large-scale simultaneous equations and improve accuracy and efficiency of calculation, an explicit algorithm is often chosen in analysis.

At the time of t_N, a semi-discrete form of deformation differential equation is expressed by the following equation (FANG, 2005):

$$M\ddot{q}_N = P_N - F_N, \qquad (1)$$

Where, M is lumped mass matrix, $\ddot{q}_N$ is acceleration vector, P_N is overall load vector, F_N is overall equivalent node force vector of element stress field.

A single-point integral algorithm is used in element calculation, and hourglass mode produced by single gauss integral method is controlled in the program.

Taking hourglass viscous damping for example, after adding it to Eq. (1), Eq. (1) is transformed to Eq. (2):

$$M\ddot{q}_N = P_N - F_N + H_N \qquad (2)$$

Where, H_N is the hourglass viscous damping vector of the structure.

Contacts inevitably exist in the collision process. And after introducing contact force F_C, Eq. (2) will be transformed to Eq. (3):

$$M\ddot{q}_N = P_N - F_N + H_N + F_C \qquad (3)$$

The explicit central difference method is adopted in time integral.

$$\dot{q}_{(N+1)/2} = \dot{q}_{(N-1)/2} + \Delta t_N \ddot{q}_N \qquad (4)$$

$$\dot{q}_{N+1} = \dot{q}_N + \Delta t_{(N+1)/2} \ddot{q}_{(N+1)/2} \qquad (5)$$

$$\Delta t_N = (\Delta t_{(N-1)/2} + \Delta t_{(N+1)/2})/2 \qquad (6)$$

Where, $\dot{q}_{(N-1)/2}$ is the node velocity vector at the time of $t_{(N\text{-}1)/2}$, $\dot{q}_{(N+1)/2}$ is the node velocity vector at the time of $t_{(N+1)/2}$, and q_N is the node displacement vector at the time of t_N.

3 Simulation methods of collisions in two-layer thin-walled structures

Two-layer cylindrical thin-walled structure belongs to a combined cylindrical shell, namely, cylindrical shells with different radiuses which are encased together. It has two failure forms under axial load, as shown in Figure 1.

For the first form, as shown in Figure 1(a), the distance between the inner and outer shells is large, regular axisymmetric deformation happens in the cylindrical shell, and the two shells do not interact in the process of compression deformation. For the second form, as shown in Figure 1(b), the distance between the inner and outer shells is small, the deformation of the two shells interplays after puckering happens, and collision characteristics of the two-layer structure change greatly due to interaction (JIA,2006).

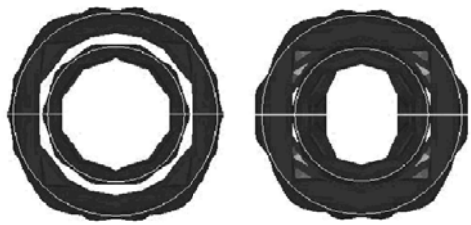

(a) Two-layer cylindrical shell without interaction (b) Two-layer cylindrical shell with interaction

Figure 1. Interaction between inner and outer shell in two-layer cylindrical shell.

3.1 Geometric model

For the analysis of two-layer cylindrical shell, its thickness is 1.5mm and length is 200mm. The diameter of outer shell is 75mm, and that of the inner is 65mm, 60mm, 55mm, 50mm and 45mm, respectively. In order to compare with energy absorption characteristics of two-layer cylindrical shell, a one-layer shell is analyzed, and its diameter is 75mm, 65mm, 60mm, 55mm, 50mm and 45mm, respectively.

3.2 Simulation method

A prescribed constant velocity is applied on a rigid plate which to used to crush the cylindrical shell. The bottom of the tubes are fixed to a stationary rigid plane in the whole process. Two types of contact are employed in numerical analysis. For the cylindrical shell itself, an automatic single-surface contact is adopted to take into account contact for itself during deformation, while an automatic node-to-surface contact is applied between cylindrical shell and rigid plate. The static friction coefficient and dynamic friction coefficient between all surfaces in contact are assumed to be 0.2 and 0.15, respectively.

4 Simulation results and comparison

Compression deformations are shown in Figure 2, including deformations of the two-layer cylindrical shell (its diameter of inner layer is 55mm, and that of outer layer is 75mm) and the one-layer cylindrical shell (its diameter is 55mm and 75mm, respectively). As shown in Figure 2, the number and size of the plastic hinge generated by the two-layer cylindrical shell under the axial load are different from that of the one-layer shell.

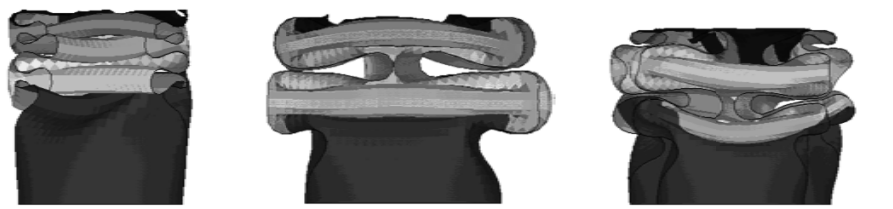

(a) Compression form of one-layer shell (its diameter is 55mm) (b) Compression form of one-layer shell (its diameter is 75mm) (c) Compression form of two-layer shell

Figure 2. Comparison form between one-layer shells and two-layer shell.

Energy-deformation curves are shown in Figure 3, and axial

force-deformation curves are shown in Figure 4. The energy absorbed by the two-layer cylindrical shell is higher than total energy absorbed by two one-layer shells. Compared to the one-layer shell, the axial force curve of the two-layer cylindrical shell is gentler, and the fluctuation of load is smaller in the distance of run from 40mm to 135mm. Axial peak force of two-layer cylindrical shell is also smaller than that of one-layer cylindrical shell.

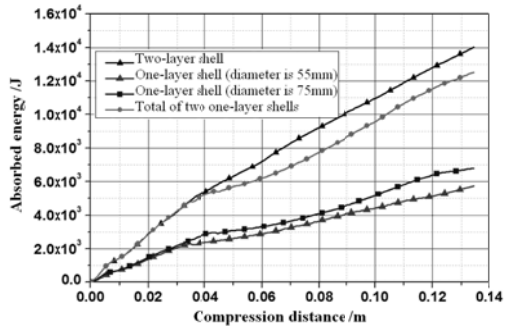

Figure 3. Energy-deformation curves.

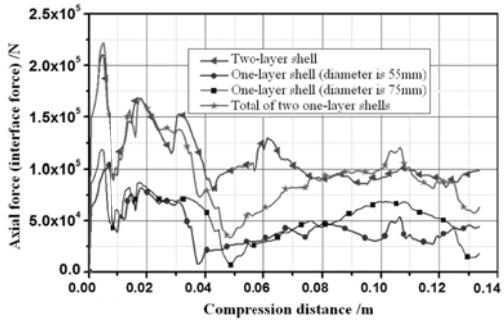

Figure 4. Axial force-deformation curves.

4.1 Comparison of energy absorption capacity

To evaluate energy absorption capacity of energy-absorbing element, we should consider not only total absorbed energy but also SEA (specific energy absorption, namely, absorbed energy per unit mass), because the level of absorbed energy is proportional to SEA. The simulation results are presented in Table 1 and Table 2.

Table 1. Comparison of SEA between one-layer cylindrical shells.

Energy absorption capacity	Diameter of single cylindrical shell /mm					
	45	50	55	60	65	75
Absorbed energy /J	5178	5469	5755	5983	6124	6808
Mass /g	332.80	369.74	406.70	443.68	480.66	554.6
SEA /J/g	15.56	14.79	14.15	13.48	12.74	12.28

Table 2. Comparison of SEA between two-layer cylindrical shells.

Energy absorption capacity		Diameter of two-layer shell (inner+outer) /mm				
		45+75	50+75	55+75	60+75	65+75
Sum of two one-layer shells	Absorbed energy /J	11986	12277	12563	12791	12932
	Mass /g	887.40	924.34	961.30	998.28	1035.3
	SEA /J/g	13.51	13.28	13.07	12.81	12.49
Two-layer shell	Absorbed energy /J	13493	13607	14018	13610	13297
	Mass /g	887.40	924.34	961.30	998.28	1035.2
	SEA /J/g	15.21	14.72	14.58	13.63	12.84
Comparison between sum of two one-layer shells and two-layer shell	Increase of absorbed energy /%	12.57	10.83	11.58	6.4	2.82
	Increase of SEA /%	12.51	10.84	11.55	6.4	2.80

From the results we can see that:

(1) For the one-layer shell, the SEA decreases with increase of the diameter of one-layer cylindrical shells (with the same thickness).

(2) The energy absorbed by the two-layer cylindrical shell is higher than total energy absorbed by two one-layer shells. Increased amplitudes for energy absorbed by two-layer cylindrical shells are as high as 6%~12.57%, except the two-layer cylindrical shell with an inner diameter of 65mm.

(3) The SEA of two-layer cylindrical shells is higher than that of one-layer cylindrical shells.

(4) The space between two shells affects length of the plastic hinge produced by the two-layer cylindrical shell, and that affects energy absorption capacity. The SEA of the two-layer cylindrical shell combined closely is higher than that of two-layer cylindrical shell combined loosely. In these two-layer cylindrical shells, energy absorbed by two-layer cylindrical shell, in which the diameter of inner shell is 55mm, is the highest; the second is that with the diameter of the inner shell of 60mm, the SEA decreases with the increase in diameter of the inner shell as well.

4.2 Comparison of buffer capacity

Buffer capacity, which is defined as a ratio between axial peak force and mean crash force, is an important index for evaluation of energy absorption characteristics of energy-absorbing element. If buffer capacity is small, peak force is relatively small, impact is relatively stable in the process of deformation, and the degree of damage to the passenger is relatively small too. The simulation results of peak force and buffer index are presented in Table 3 and Table 4.

Table 3. Axial force and buffer index of one-layer cylindrical shell.

	Diameter of two-layer shell /mm					
	45	50	55	60	65	75
Axial peak force /kN	94.8	97.9	103.6	106.9	110.9	118912
Mean crash force /kN	38.4	40.5	42.6	44.3	45.4	50430
Buffer index	2.47	2.42	2.43	2.41	2.44	2.36

Table 4. Axial force and buffer index of two-layer cylindrical shell.

		Diameter of two-layer shell (inner+outer)/mm				
		45+75	50+75	55+75	60+75	65+75
Sum of two one-layer shells	Axial peak force /kN	213.7	216.8	222.5	225.8	229.8
	Mean crash force /kN	88.8	90.9	93.1	94.7	95.8
	Buffer index	2.41	2.38	2.39	2.38	2.40
Two-layer Shell	Axial peak force /kN	195.0	203.2	210.5	219.5	226.6
	Mean crash force /kN	100.0	100.8	103.8	117.3	98.5
	Buffer index	1.95	2.02	2.03	1.87	2.30
Comparison between sum of two one-layer shells and two-layer shell	Decrease of axial peak force /%	8.78	6.30	5.40	2.82	1.39
	Decrease of buffer index /%	18.97	15.45	15.22	21.53	4.09

The simulation results show that:

(1) For the one-layer shell, the buffer index decreases with the increase in diameter of the one-layer cylindrical shell (with the same thickness), but the change is not evident.

(2) The peak force of the two-layer cylindrical shell is less than the sum of two one-layer cylindrical shells.

(3) The buffer index of the two-layer cylindrical shell is less than that of the one-layer cylindrical shell, in other words, buffer capacity of two-layer cylindrical shell is better than that of one-layer cylindrical shell.

5 Conclusions

(1) The energy absorbed by the two-layer cylindrical shell under axial load is more than the total energy absorbed by two one-layer shells. The SEA of the two-layer cylindrical shell is higher than that of one-layer cylindrical shell, and its impact performance is improved significantly.

(2) The axial peak force of the two-layer cylindrical shell is less than the sum of two one-layer cylindrical shells evidently.

(3) The buffer capacity of two-layer cylindrical shell is superior to one-layer cylindrical shell, which can improve control ability to overload.

Acknowledgements

This research is sponsored by Independent Research Topics of State Key Laboratory (2008TPL_T10), National Key Foundation Research Development Plan (2007cb714705), and University Doctor Academics Special Science Research Fund (20070613008).

References

Abramowicz W; Jones N. (1984). “Dynamic axial crushing of circular tubers”, *International of Impact Engineering*, 2(3), 263-281.

FANG Jiazhi, QIAO Qunying, CHANG Chongyi, etc.(2005). “Application of response surface method in impacting energy absorption of thin-walled structure”, *Journal of China Agricultural University*, 10(1), 81-85.

Hanssen A. G; Langseth M; Hopperstad O. S.(2000). “Static and dynamic crushing of circle aluminum extrusions with aluminum foam filler”, *Int J Impact Eng*, 2(4), 475-507.

JIA Dingzhi. (2006). “The study on an energy-absorbing and buffering of the layer-combined cylindrical shell and simulation”, Taiyuan: North University of China, 41-45.

Karagiozova D; Norman J. (2001). “Dynamic Effects on Buckling and Energy Absorption of Cylindrical Shells under Axial Impact”, *Thin Walled Structures*, 39, 583-610.

Scholes A; Lewis J. H. (1993). “Development of crashworthiness for Railway Vehicle Structures”, *Journal of rail and Rapid Transit*, 207 (F1), 1-16.

Effects of Roadway Lighting Level on the Pedestrian Safety

Huaguo Zhou[1], and Ping Hsu[2]

[1]Assistant Professor, Southern Illinois University, Edwardsville, Illinois, 62025, Phone: 618/650-2815, E-mail: hzhou@siue.edu.
[2] District Safety Engineer, the Florida Department of Transportation, Tampa, FL, 33612. E-mail: ping.hsu@dot.state.fl.us.

ABSTRACT

The level of roadway lighting is an important factor for the safety of roadways during the nighttime, especially for pedestrians. Past studies have shown that over fifty percent of pedestrian crashes occurred during nighttime. Most of these were fatal and severe injury crashes. These results make it clear that proper design and timely maintenance of street lighting will definitely help improve the safety of the roadway system. To evaluate the roadway lighting systems and maintain their functionality, it is essential to perform field lighting measurements. Currently, field measurements of roadway lighting systems are often conducted by handheld light meters at a short sample section of roadways. The evaluation of an entire corridor or a longer roadway section is difficult when using the traditional manual measurement methods. This study addresses this difficulty by developing a mobile lighting measurement system that can be used to collect massive lighting level data in a safe and efficient way.

In this study, a mobile lighting measurement system was developed and installed in a test vehicle to collect illuminance data along a corridor of U.S. 19 in Pinellas County, Florida. The night time pedestrian crash data were collected for a three year period. The preliminary study shows that the frequency of nigh time pedestrian crash at low lighting level segments is much higher than those segments with a high illuminance level.

CE Database subject headings: Traffic Safety, Pedestrian Safety, Roadway Lighting.

INTRODUCTION

Background

This paper summarize some preliminary results of a research project funded by the Florida Department of Transportation (FDOT) District 7 to collect all required data and to perform an evaluation of highway lighting levels on the State-maintained roadways within the District. Specifically, the main objective of this project is to measure the maintained illuminance levels in the roadway areas. This paper covers

the basic concepts of newly developed lighting measurement strategies and a case study on U.S. 19 to exam the relationship between the street lighting level and night time pedestrian crashes.

Problem Statement

Roadway lighting is one of the key elements of roadway system in regards to safety. A Federal Highway Administration study (1990) reported that, in the United States, nighttime crash rates are five times higher than daytime crash rates. More to the point, approximately 50 percent of the fatalities occur during the nighttime and only 25 percent of the vehicle miles are driven during the nighttime. These statistics clearly indicate that the improvements to nighttime driving environment might help reduce nighttime crash rates. In the past, many studies were conducted to investigate the impacts of installation of street lighting on roadway safety. Most studies indicated that roadway safety was positively impacted in the way that reduced the number of crashes, injuries, and fatalities.

Proper design and timely maintenance are two vital factors for street lighting systems to be effective and beneficial to road users. The design itself needs to consider many factors and requires expertise in many areas, such as civil, electrical, and lighting engineering. The newly installed system should be evaluated to assure that roadway lighting levels meets the design standards. Initial design might be perfect; however, as time passes, the system may not work as well as when initially installed. In order to maintain the effectiveness and functionality of street lighting systems after design, it should be inspected to assess how well the system is maintained.

Currently, roadway lighting levels are often measured with handheld light meters. After roadway lighting systems are designed, the design programs can establish a grid on the pavement surface and then use the estimated illuminance values at these points on the grid to determine the average value and the uniformity ratios (avg/min and max/min). To manually collect illuminance data using handheld light meters on all of the roadways in District 7 represents an enormous data collection task. This data collection effort would also put the people operating the light meters in the middle of the roadways during nighttime low-lighting conditions, creating a potential safety concern for both data collection personnel and other roadway users.

In order to address these concerns, CUTR proposed to develop new measurement strategies for collecting the lighting data in a manner that minimizes the risk exposure for the data collection personnel. The original idea is to measure the lighting level on a moving vehicle using a combination of lighting meters and Distance Measurement Instrument (DMI). The illuminance data recorded by a light meter will match the location data from GPS or DMI.

An additional area of concern to the District is maintaining adequate lighting levels in crosswalk areas for the safety of pedestrians. The Department has indicated a desire for research on street lighting levels that are adequate for the needs of the pedestrian. Similarly, to the work being done for the automobile, strategies also must be

developed to measure the light levels on pedestrian facilities in a manner that is safe and efficient.

LITERATURE REVIEW

Past studies, research projects, standards and guidelines related to the street lighting data collection, design and the evaluation of the roadway lighting systems were reviewed and summarized.

Lighting System Design

Design of a roadway lighting system is a joint effort of engineers from various areas of specialization. Gazzar *(2002)* divided the design process into four steps to help the designer come up with better decisions. The four design steps are described briefly as follows.

Step 1: An initial study should be conducted to identify the roadway elements and also specifications of the roadway. The design criteria of different elements require individual considerations. As an example, a pedestrian crosswalk area usually requires higher levels of lighting. Lighting level requirements also vary by the functional classification of roadways. One must acquire all the data related to the design area for an effective and efficient lighting system.

Step 2: Fixture and luminaire selection requires one to be familiar with detailed specifications of the equipment available in the market. It is impossible to review the technical specifications of all equipment on the market. One can simplify the process by determining the standards and the limitations. A good selection of fixtures and luminaire will make the remaining steps of the design process more convenient for the designer.

Step 3: The location of the fixtures and poles can be determined by use of readily available software for this purpose. CAD files of the roadway can be imported to the software and the process can be conducted. In addition, the software usually assists fixture selection by importing the electronic file which includes photometric characteristics of a fixture.

Step 4: Verification of the lighting design criteria can also be conducted by the design software. There are three design criteria considered for roadway lighting systems design, which are explained in the following subchapters.

Roadway Lighting Design Criteria

Illuminance, luminance, and small target visibility are three criteria for verification of roadway lighting design in the standard practice.

Illuminance

Illuminance is defined as the amount of light flux that falls on the surface at a certain distance from the light source. The standard units of illuminance used in practice are foot candle (English) and lux (Metric). The surface under consideration for

illuminance determination in roadway lighting is the pavement surface. Horizontal illuminance is used in the standard practice of roadway lighting design and evaluation.

The illuminance level at any point depends on the distance from the light source and luminous intensity of the light source. The value of illuminance can be determined by the inverse square method or using tables and charts developed by the manufacturers of luminaires. Each specific type of luminaire has its own chart and table for roadway lighting design. The inverse square method is often used to calculate the illuminance at definite points. The point must be located at a distance five times greater than the luminaire size. The equation to calculate the illuminance by the inverse square method is presented as Equation 1. Figure 1 shows the elements in Equation 1.

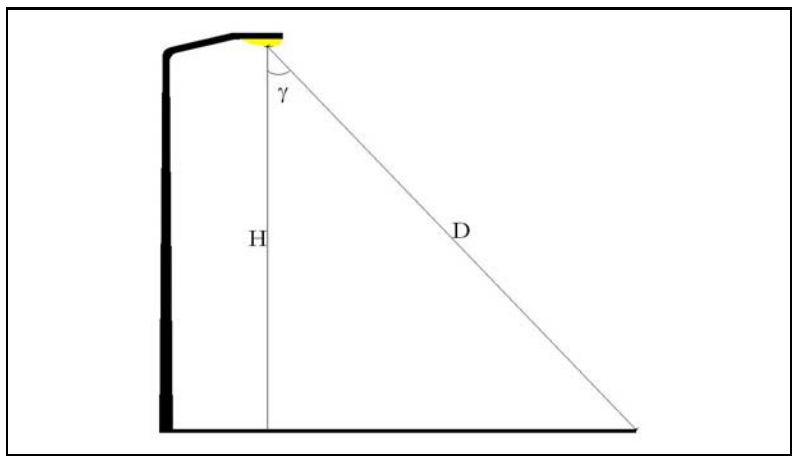

Figure 1. Inverse Square Method Variables.

$$E_h = \frac{I(\varphi,\gamma)\cos\gamma}{D^2} \qquad \text{Equation 1}$$

Where:

$I(\varphi,\gamma)$ = luminous intensity of the source in direction of the point in;
D = actual distance from light source the source in direction of the point in question;
H = vertical mounting height of the light source above horizantal plane;
φ = the angle from the light source reference axis to the point in question; and,
γ = the angle from the nadir of the light source to the point in question.

For horizontal plane, $Cos\,\gamma = H/D$, from which Equation 2 can be derived:

$$E_h = \frac{I(\varphi,\gamma)\cos^3\gamma}{H^2} \qquad \text{Equation 2}$$

Luminance

Luminance is another commonly used measurement of lighting level for the design and evaluation of roadway lighting systems. The American Association of State Highway and Transportation Officials (AASHTO) Roadway Lighting Design Guide *(2002)* defines luminance as a measure of the reflected light from the pavement surface that is visible to the motorist's eye. Determination of luminance requires consideration of reflective characteristics of the pavement. Equation 3 is used to calculate the value of luminance at a desired point. In addition, the luminance calculations and field evaluations are conducted based on two assumptions: (1) The observer is at a distance of 83.07 meters from the point in question; (2) The observer's eye level is 1.45 meters above the pavement. Based on these assumptions, the observers' direction of sight is one degree downward. The observer is located on a parallel line to the centerline of the roadway that passes through the point in question. The luminance value at a point can be calculated with the general Equation 3. The general equation must be modified based on the assumptions described earlier to calculate the luminance value at a desired point on the road surface.

$$L = \frac{1}{\pi} E_h q(\beta, \gamma) \qquad \text{Equation 3}$$

Where:

E_h = illuminance at the point in question, as defined in Equation 2.1 and
$q(\beta,\gamma)$ = the directional reflectance coefficient for angles of incidence β and γ.

Small Target Visibility

Small target visibility is a relatively new approach to improve the safety of drivers. American National Standard Practice for Roadway Lighting of Illuminating Engineering Society of North America *(1999)* (IESNA) included this method in its latest edition. The standard defines small target visibility as the visibility level of an array of targets on the roadway considering the following factors:

- The luminance of the targets
- The luminance of the immediate background
- The adaptation level of the adjacent surroundings
- The disability glare

Illumination Measurement and Safety Impacts

Evaluation of roadway lighting systems is an important task to ensure that the system works at the desired level. Evaluation methodology is usually selected based on the standards required for the lighting system. The timing of the evaluation is another factor to take into consideration. Initial evaluations are often conducted right after installation. The evaluation results will not be affected by some light depreciation factors such as dirt and aging of luminaires. However, evaluation of a system after years of operation will reveal the effects of light depreciation factors. In the literature

review, many guidelines were found for the design of roadway lighting systems. Many commercial software were especially developed for this purpose. However, few guidelines and standards are available for evaluation purposes.

In 1988, Zimmer developed "A Mobile Illumination Evaluation System" at the Texas Transportation Institute. The main purpose of the system was to collect illumination data for high mast lighting systems. The illumination method was selected for data collection. The system was installed in a test vehicle and illuminance measurements are taken by a light meter placed on top of the vehicle. Illumination data were taken on each lane of roadways to compute the system characteristics. The system developed for that study could collect data at reasonable speeds. However, the technology for lighting measurements and computers at that time were not well developed. Currently, the light meters are more accurate and the laptop computers are faster. For high mast lighting systems, luminaires are relatively higher than conventional roadway lighting. The measurements may not be affected by the height of the light meter sensor as in conventional roadway lighting measurements. The study also did not develop a methodology to convert the illuminance on the top of vehicles to six inches above the pavement.

A study conducted by Green et al. *(2003)* at the Kentucky Transportation Center of the University of Kentucky, investigated the relationship between illumination levels and nighttime crashes. Illumination data was collected with handheld light meters at the identified locations. The results of the study indicated that nighttime crashes were reduced by 45 percent after installing street lighting at the intersections. Additionally, the study included a survey of States related to their roadway lighting standards. The survey results showed that most States use the information from either AASHTO "An Informational Guide for Roadway Lighting" or "American Standard Practice for Roadway Lighting" (ANSI/IESNA RP-8-00) as their standards.

Three methods have been used to evaluate roadway lighting level. Illumination method is mostly used in field evaluation and recommended by national and state lighting design guidelines. An early study has indicated that the idea of developing a mobile illuminance measurement system is feasible. In addition, past studies showed that safety can be improved by adding or improving street lighting.

METHODOLOGY

Based on literature review, illuminance method is found to be the most suitable method for field evaluation of roadway lighting systems. Currently, illuminance data are manually collected by the use of handheld light meters. In this project, a mobile lighting measurement system will be developed to eliminate the risk of personnel and reduce the labor costs.

System Development

Before system development, it is essential to understand what kind of data is needed for collection. The results of literature review indicated that the illuminance is one of

the main criteria for evaluation of roadway lighting level. The illuminance method requires measurement of illuminance (lux or foot candle) values at some desired points. Collecting coordinates of desired points and corresponding illuminance data simultaneously and accurately is a challenging task. If both coordinates and illuminance data were collected separately, it would be difficult to match them. Due to the above reasons, it was necessary to develop a mobile measurement system that can collect both distance and illumination data at the same time. After considering safety and speed issues, it was decided that the system should be installed on top of a vehicle. The system installed in vehicle could collect illumination data at a desired distance interval and a reasonable speed of a test vehicle.

After the initial design, the project team determined the necessity of the following elements:

- Light Meter
- Distance Measurement Instrument (DMI)
- Laptop Computer
- Connections between the computer, light meter and DMI
- Software to collect, store and analyze data

DATA COLLECTION AND ANALYSIS

The study corridor is located along U.S. 19 (SR 55) in Pinellas County from River Watch Boulevard in North Pinellas County to 54th Avenue South spanning 32 miles. The U.S. 19 corridor in Pinellas County has more total pedestrian crashes than any other roadway within the county.

Crash Data

The datasets used for the study include: FDOT U.S.19 pedestrian crashes 2000-2005; FDOT District 7 pedestrian crashes 2000-2005; and FDOT district 7 crash data management system.

FDOT crash data includes only crashes occurring along the State Highway System and typically is limited to long form crash data which include the more sever crashes. As such, the crash data for this study do not include most minor “fender-bender’ crashes. Likewise, non-injury pedestrian crashes tend to be underreported. Crashes that occur on frontage roads along U.S. 19 are also included in the data set.

Three years of pedestrian accident data (2003-2005) were collected to adequately identify the corridor’s safety problems and evaluate the relationship between the lighting intensity and crash frequency. The hard copies of pedestrian crash record (2003-2005) were reviewed. There are a total of 199 pedestrian crashes.

Illumination Data

The illumination along the corridor was recorded using a developed mobile lighting measurement system, a combination of a light meter and a Distance Measurement Instrument (DMI). The illumination was recorded at 40 feet intervals on the most right side lane of U.S. 19.

Data Analysis

Along the 32 mile stretch of U.S. 19 in Pinellas County, according to the FDOT crash database, 105 pedestrian crashes of the total 199 pedestrian crashes during the six year period occurred at night. Also, only 18 of these 105 crashes occurred at locations without streetlights, and the remaining 87 crashes occurred at locations where streetlights were present. Therefore, the lighting conditions of the crash site locations were analyzed.

Figure 2 shows the frequency of crashes and lighting level as measured in lux. Illuminance is the amount of light reaching the roadway surface, measured in foot candles (lumens/ft2) or lux (lumens/m2).

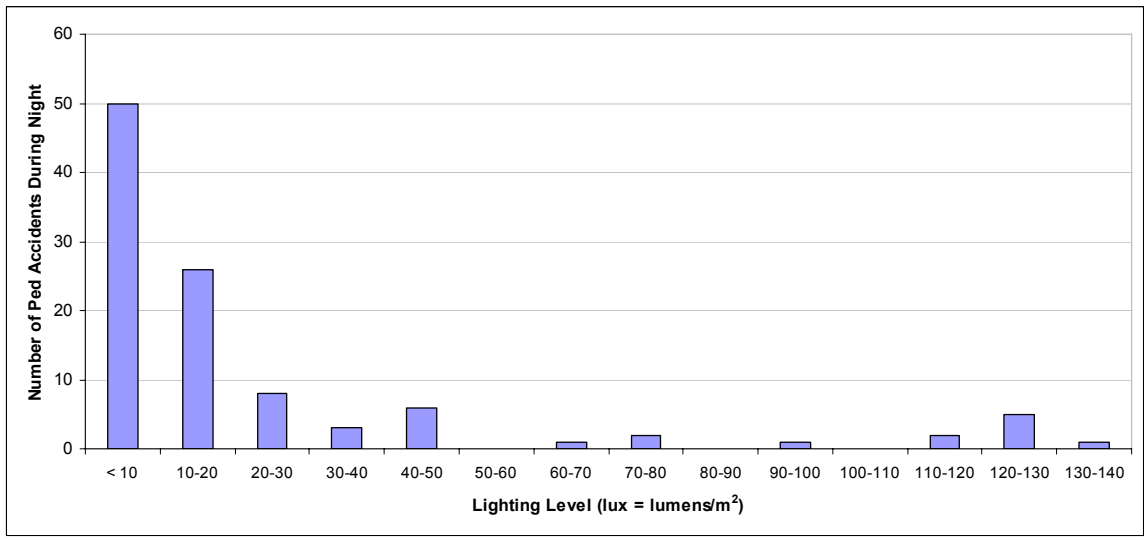

Figure 2. Number of pedestrian accidents at night for different lighting conditions.

The lighting level was measured using a handheld light-meter (EXTECH 401036) fixed to the top of a vehicle (about four feet above the pavement) moving at an average speed of 30 mph. The measurement was taken in the right lane of the roadway. As shown in Figure 8, lighting condition at 50 crash site locations was below 10 lux. According to the preliminary measurement of lighting level on U.S. 19, night time pedestrian crashes occur more often at lower lighting level conditions as compared to higher lighting level conditions.

CONCLUSIONS

The mobile lighting measurement system developed by this research can be used to collect massive light data in short periods of time. The new system will not only reduce the cost of the future data collection efforts, but also improve the safety of the data collection personnel. The preliminary research showed that there is a possible relationship between the night time crashes and roadway lighting level. The next phase of the project will collect the illuminance along 250 miles state highway. And also the crash data will be collected to investigate if there is a direct relationship between the lighting level and night time crashes.

ACKNOWLEDGEMENT

This study was funded by the Florida Department of Transportation, District 7. The authors also wish to acknowledge the contribution of their former colleague Mr. Larry Hagen and graduate student Fatih Pirinccioglu at the Center for Urban Transportation Research of the University of South Florida.

REFERENCES

American Association of State Highway and Transportation Officials (2002). *An Information Guide for Roadway Lighting,* Washington, D.C.

Federal Highway Administration, (1990), *The Relationship of Fixed and Vehicular Lighting to Accidents*, FHWA TS-90-028, Washington, DC.

Gazzar, M.G. El.(2002) *A Logical Approach to Lighting Design*. Dewberry Publications. Fairfax, VA

Green, E., Kenneth A., Barrett, R., Monica L. and Pigman, J.(2003) *Roadway Lighting and Driver Safety*. Kentucky Transportation Center. University of Kentucky. Lexington, KY

Illuminating Engineering Society of North America (1999*), American National Standard Practice for Roadway Lighting,* ANSI/IES RP-8-00.

Zimmer, R.A. (1988). "A Mobile Illumination Evaluation System." *Transportation Research Record 1172*. Transportation Research Board. Washington, D.C. 1988

Analysis of a New Combined Micropile Structure for Preventing Slope Slippage and Its Application in a Practical Project

S.G. Xiao[1], K.Cui[2], D.P. Zhou[3], and J. Feng[4]

[1]Department of Geotechnical Engineering, Southwest Jiaotong University, Chengdu 610031, P. R. China; PH (86-28) 8760-0836; email: xiaoshiguo126@126.com
[2]Department of Geotechnical Engineering, Southwest Jiaotong University, Chengdu 610031, P. R. China; PH (86-28) 8760-0836; email: cuikai80@hotmail.com
[3]Department of Geotechnical Engineering, Southwest Jiaotong University, Chengdu 610031, P. R. China; PH (86-28) 8760-0836; email: dpzhou@home.swjtu.edu.cn
[4]Department of Geotechnical Engineering, Southwest Jiaotong University, Chengdu 610031, P. R. China; PH (86-28) 8760-0836; email: fengjun4316@163.com

ABSTRACT

We discuss the combining of micropile substructures to produce a new retaining and reinforcement structure for slopes. Each substructure is an element comprising of several separated micropiles connected by a roof plate. The structure has the advantages of small pile length, easy and quick construction, operational safety, and low cost. It can be applied to a moderate or small slope or in landslide control projects. In particular, the structure is very suitable for dealing with project emergencies. According to the general load features of the structure, it is believed that the part of the structure above the slip surface of a landslide may be regarded as a single rigid frame under landslide thrust and that the part under the slip surface may be treated as an elastic axial bar model. In this way, internal forces of the structure and the required length of the anchoring section of the micropiles can be obtained. This information is used directly in practical design. Analysis shows that each micropile in the structure is mainly loaded by an axial force, but the roof plate is principally subject to a bending moment. The new structure and the analysis method proposed in this paper are successfully used in practice for a cutting slope in a Guangyuan–Bazhong expressway project in Sichuan Province, China, and the performance of the structure is verified.

Keywords: combined micropile structure, slope slippage, landslide thrust, rigid frame, internal forces of a structure

INTRODUCTION

This paper examines a structure that prevents slope slippage. The structure comprises of several micropiles connected by a roof plate to endure lateral load.

Many of these structures could be arranged along a slope strike with a set separation to resist landslide thrust. Each micropile in the structure has a slenderness ratio greater than 30 and a diameter no greater than 250 mm. Micropiles that are inserted into the ground by boring and pressed grouting usually have a diameter between 110 and 150 mm. The proposed structure has the advantages of small pile diameter, short construction time, high security for constructors, low cost, and flexible arrangement.

The concept of micropiles was first suggested by Fernando Lizzi in the 1950s (Tom et al., 2000). The piles were called root piles at the time and used to reinforce building foundations. The technology of small piles has since then been developed in America, France, Japan and China. Structures of micropiles that endure vertical loads have been widely discussed in previous works. However, there has been little research on structures bearing lateral forces (Duncan and Evans, 1994; Donald et al., 1995; Mokwa and Duncan, 2001; Thomas et al., 2004; Thompson and White, 2006). In China, a micropile structure with a top beam connection has been used for landslide reinforcement in recent years. However, the combining of the aforementioned micropile structures has scarcely been studied (Huang, 2001; Xie et al., 2001; Wang, 2005). Some works have examined the seismic response of micropiles under lateral forces by considering their dynamic characteristics (Kevin et al., 2004; Sung June Lee, 2004). Based on previous works, Chinese researchers preliminarily analyzed the action characteristics of beam-connected micropiles and discussed key points that should be addressed in project design (Ding, 2001; Ding and Wang, 2004). Shi and He (2005) reported a preliminary design approach that uses reticular micropiles connected by a top beam. The composite structure of reticular micropiles and soils is referred to as a reinforced soil wall. They determined the different states of bonding between micropiles and soils using an approximate model: a calculation model of a reinforced concrete beam. Feng et al. (2006) studied calculation methods for multiple micropiles connected by a top beam to reinforce a bedrock slope and proposed a new method for slope reinforcement.

Using existing research results, a new structure comprising of micropiles connected by a roof plate to prevent slope slippage is proposed in this paper. We present analysis of the structure and discuss engineering applications.

NEW MICROPILE STRUCTURE AND ITS RETAINING MECHANISM

New micropile structure. The new structure for preventing slope slippage presented here comprises of a roof plate and micropiles of grouting materials and reinforcements as shown in Figure 1. The grouting materials protect the reinforcements against corrosion. The roof plate assembles all elements and forms an integral system that can sustain pile stresses. The roof plate requires sufficient thickness, strength, rigidity, and durability. To ensure a reliable connection between the plate and piles, reinforcement hooks are fabricated at the top of the piles.

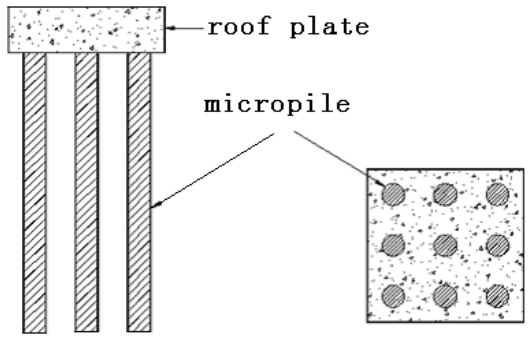

(a) Micropile structure (b) Roof plate profile

Figure 1. The new combined micropile structure.

Prevention of slope slippage and reinforcing mechanism. The ability of the micropile structure to resist sliding of the slope and maintain stability depends on the piles and surrounding rock–soil mass. For efficiency, the base of a micropile needs to be under the most likely to slip surface. The micropile–rock–soil complex, axial forces, and bending and shearing forces need to be considered.

(1) Micropile–rock–soil complex

The micropile structure passes through the potential sliding mass and is anchored in the stable bed below. During the grouting of micropiles under pressure, the micropile bodies push through the rock–soil mass and cement together loose broken grains. This can improve the mechanical properties of the rock–soil mass surrounding the micropiles and form a micropile–rock–soil complex that resists slope slippage. Micropiles act as a complex skeleton with good strength and rigidity. Thus, the micropile–rock–soil complex can constrain the deformation of the rock–soil mass between piles. The micropile structure plays an important role in this system. The micropiles transfer internal component stresses of the rock–soil mass and stabilize the stratum. The transferred stress is less concentrated as it is distributed more widely. This efficiently prevents slipping along the slip surface, and, therefore, the slope is stabilized.

(2) Axial forces

Under landslide thrust, the slender micropiles essentially bear axial forces (axial tension and compression) in anchoring the slope.

(3) Bending and shearing forces

Micropiles are subject to bending moments and shear forces due to the action of landslide thrust. However, these are not the controlling forces for slender pile bodies, i.e., the stability of a micropile is determined mainly by axial forces (tension and compression).

MECHANICAL ANALYSIS MODEL FOR THE MICROPILE STRUCTURE

We considered the simple example of a combined micropile structure having small elements. Each element comprises of nine micropiles (in three rows and three columns). Figure 2 shows that the columns are set along the slope strike direction (perpendicular to the landslide thrust direction). Assuming we are addressing the problem of plane strain, the vertical effects of the slope body on the structure are not considered. Supposing that load is distributed by the landslide thrust, the linear load distribution for one column of micropiles along the axial direction of the micropiles is:

$$q_0(x) = FL / H \tag{1}$$

where F is the landslide thrust per unit width (kN/m) calculated using the transfer coefficient method and physical mechanical parameters of the sliding mass and rock–soil mass, L is the spacing between two adjacent elements in the slope strike direction, and H is the height of sections of the micropiles above the slip surface.

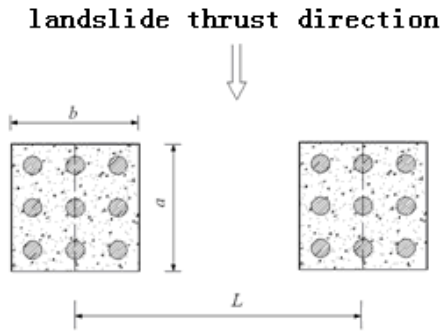

Figure 2. Layout of the combined structure.

The internal forces of the combined structure are determined as shown in Figure 3. The structure above the slip surface is simplified as a plane frame structure by considering the pile–rock–soil complex effect as shown in Figure 3(b). Note that all micropiles except that nearest to the slope top endure lateral force $q(x)$ as well as the extrusion force of the rock–soil mass between micropiles. Because of the complicated interaction between the micropile nearest to the slope top and the rock–soil mass, the extrusion force is neglected simply and conservatively for convenience in practical engineering application. Therefore, the combined structure above the slip surface is a simplified plane frame model as shown in Figure 4.

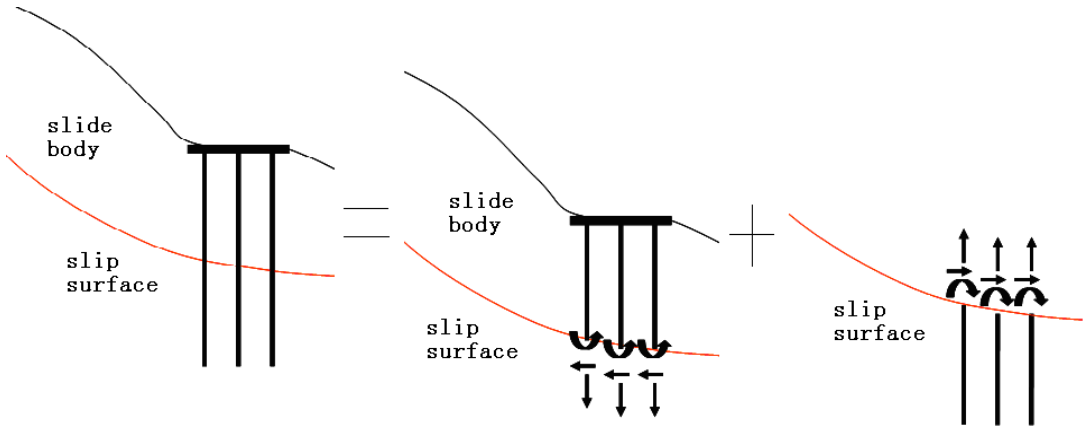

Figure 3. Analytical model of internal forces in the combined structure.

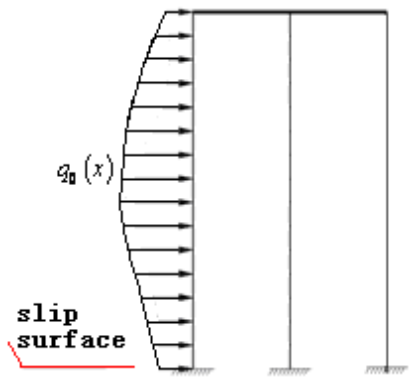

Figure 4. Simplified mechanical model of the upper part of the combined structure.

In calculating the load for the lower part of the structure shown in Figure 3(c), we considered an elastic axially loaded member after calculating the load for the upper part of the structure according to the important mechanical characteristics of the micropile and the retaining mechanism of the structure.

ANALYTICAL METHOD

Calculation of internal forces in the micropile body.

(1) Calculation for the upper part of the combined structure

Figure 5(a) is the graphical representation of calculated forces for the upper part of the plane frame structure according to the analysis model discussed above. Structural internal forces and retaining reactions are calculated using structural mechanics; the calculation process is not described here. The results are given in Figures 5(b) and (c).

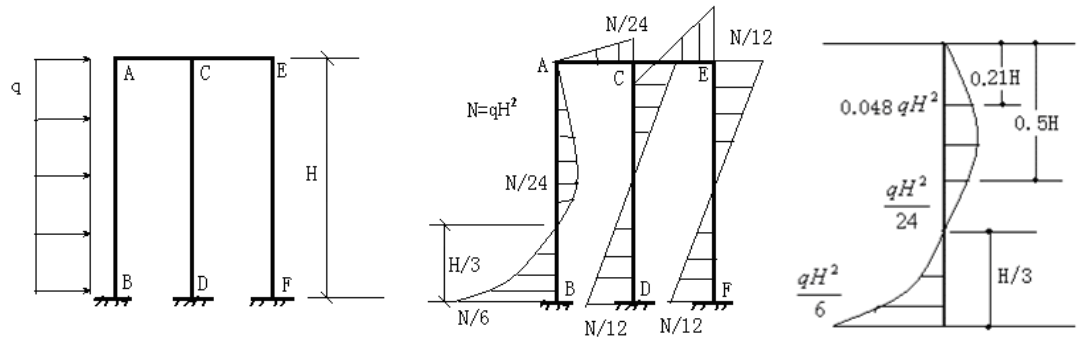

(a) Calculated graphical representation **(b) Bending moment** **(c) Moment detail for micropile AB**

Figure 5. Internal force calculations for the upper part of the combined structure.

(2) Calculation for the lower part of the combined structure

Internal forces in the lower part of the structure are calculated by considering an elastic axially loaded member. A uniform distribution of friction resistance between the lower pile and rock–soil mass is considered to simplify the calculation. The internal force calculation for the lower pile section is used mainly to determine the required length of the anchoring section. Details are described in the following section.

Determination of the anchoring section length and the full structure length. The method for calculating the anchoring section length is to first calculate the axial force, shear force, and bending moment on the slip surface after internal forces have been calculated for the upper part of the structure. The anchoring depth is determined from the tensile axial force. Whether the length of the free section produces the required compressed micropile stability should then be examined.

The calculation results show that the AB section is subject to the greatest tension. The anchoring section length l_a is determined from the ultimate skin friction of the rock–soil mass around the micropile below the slip surface:

$$l_a = F_{sp} \cdot P_{AB} / (\pi \cdot d \cdot \tau), \tag{2}$$

where F_{sp} is the design safety factor for friction between the injected cement paste and micropile, P_{AB} is the enduring tension for the AB section, d is the micropile diameter, and τ is the magnitude of the ultimate skin friction.

The compression stability of a micropile under pressure (EF section) with a larger slenderness ratio should be theoretically verified. The anchoring section must be longer than both l_a and the minimum anchorage depth for micropiles to work in an elastic state under compression. The anchoring section is usually embedded in stable

rock. Therefore, the compression stability of this section is suitable; however, the length of the anchoring section is generally controlled by tension conditions.

Moreover, soil mass around micropiles (sliding mass) has a smaller restriction effect on the pile body for the upper part of the structure. Therefore, the suitability of its length (i.e., length of the "free section") should be checked in light of stability of compressed bar. A suitable full pile length is then determined. The stability of the free section is calculated using the Euler formula:

$$F \le \frac{F_{cr}}{K} = \frac{\xi \pi^2 EI}{K\left(\mu l_f\right)^2}, \tag{3}$$

where F is the maximum axial force for the compressed micropile, F_{cr} is the critical compressive force according to the Euler formula, K is the design safety factor for the compressed micropile stability, ξ is a correction coefficient between 1.05 and 1.35, EI is the flexural rigidity equivalent, μ is the Euler length coefficient (with a value of 0.5 here), and l_f is the length of the free section.

Determination of the roof plate. The roof plate is a flexible member as shown in Figure 5(b). The upper side of the roof plate endures compression at the third span near the central section. The plate compresses the slope surface, so it is important that the pressure below the plate does not exceed the bearing capacity of the slope surface.

ENGINEERING EXAMPLE

The combined structure proposed in this paper was applied in a cutting slope project for an expressway (Guangyuan–Bazhong line, Sichuan, China). Figure 6 shows the cutting slope site K51 + 175. Table 1 lists the parameters of the slope according to a geological survey. Ultimate skin friction around pile in weakly weathered silt-sandy mudstone is 0.17 MPa, and compressive strength of the rock mass is 7.94 MPa.

The slope comprised of a typical thick layer of clay with a low liquid limit and a crushed stone stratum overlying bedrock. Potential slope failure was typically circular as shown in Figure 6. The design safety factor was taken as 1.25. The design horizontal thrust was calculated using the transfer coefficient method as 324 kN/m.

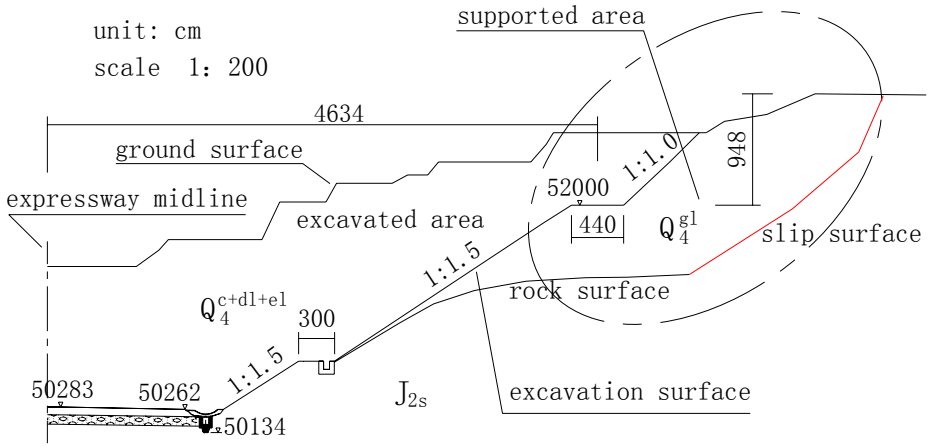

Figure 6. Cross-section of a cutting slope project (Guangyuan–Bazhong expressway, Sichuan, China).

According to characteristics of the slope, we chose a structure element comprising of nine micropiles (in three rows and three columns) connected by a roof plate as shown in Figure 7. The diameter of each micropile hole had a diameter of 130 mm and was injected with M20 cement mortar. Three 32 mm-diameter reinforcing bars were used for each micropile. The distance between two elements was 3 m, and the distance between two micropiles in the same element was 0.6 m in the sliding direction and 0.5 m perpendicular to the sliding direction. The roof plate had an overhang length of 0.2 m. According to the position of the most important potential slip surface, the free section length of the micropile body was determined as 6.6 m.

The used reinforcements had an ultimate tension capacity of 400 MPa and a strength of 320 kN. The equivalent elastic modulus and flexural rigidity of a single micropile were respectively 2.6×10^7 kN/m^2 and 364.5 kNm^2.

Table 1. Mechanical parameters of rock–soil mass in calculations of internal forces.

Stratum number	Rock mass or soil name	State	Bulk density (g/cm^3)	Cohesion (kPa)	Internal friction angle (°)	Allowable bearing capacity (MPa)
$Q_4^{c+dl+el}$	low liquid-limit clay including gravel	soft-hard plastic	2.0	15	10	0.20
Q_4^{gl}	crushed	medium	2.3	20	15	0.25

	stone including soil	density				
J_{2s}	silt-sandy mudstone	strongly weathered	2.36	-	-	0.30
		weakly weathered	2.53	-	-	0.80

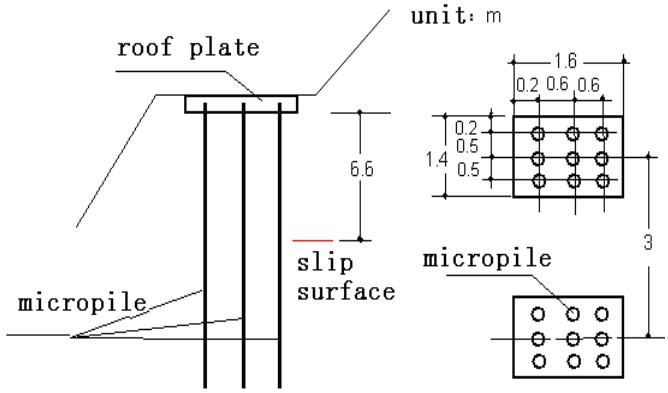

Figure 7. Preliminary design of the combined structure.

(1) Bending moment and axial force

The external load acting on the combined structure was $q = 324 \times 3 / 6.6 = 147.27$ kN/m. From Figure 5(b), the calculated bending moment for the upper part of the structure was $N = 6415.2$ kNm. The axial forces for AB, CD, and EF sections were then calculated as $P_{AB} = 890$ kN (tension), $P_{CD} = 445$ kN (tension), and $P_{EF} = 1335$ kN (compression).

(2) Roof plate calculations

The maximum tension reinforcement of one reinforcement Φ32 was $P_{AB} / 9 = 890 / 9 = 99$ kN < 320 kN. Thus, the reinforcement was suitable.

The admissible shear stress between the anchoring section and rock–soil mass was $\tau = 170$ kPa; F_{sp} was taken as 1.2. Following equation (2), $L_a = 5.2$ m. Therefore, L_a was taken as 5.4 m and the full length of the pile as 12 m.

The critical load of the compression bar for a free section length of 6.6 m was $P_{cr} = 1.2 \times 4\pi^2 EI / H^2 = 4\pi^2 \times 364.5 / 6.6^2 = 396$ kN, where the coefficient 1.2 was determined by considering the restriction effect of the surrounding soil mass on the micropile. Figure 8 is a sketch of the pressure applied to the soil mass and the EF section of the micropile by the CE section of the roof plate. The compressive force $Ps = 250 \times 0.84 = 210$ kN can be supported by the soil mass, while for the EF section, $P = 3 \times 396 + 210 = 1398$ kN > $P_{EF} = 1335$ kN. Thus, the requirement is met.

According to the results in Figure 5(b), the bending moment of the roof plate was $M = qH^2 / 24 = 147.27 \times 6.6^2 / 24 = 267.3$ kNm as shown in Figure 9.

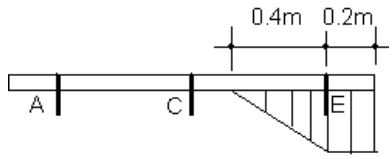

Figure 8. Sketch of pressure under the roof plate.

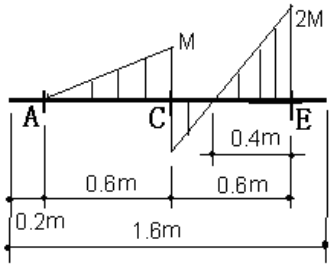

Figure 9. Bending moment of the roof plate.

CONCLUSION

This paper proposes a new type of light retaining structure. The structure is a combination of micropiles with a roof plate and is suitable for situations with small landslide thrust (≤ 500 kN/m). The combined structure brings the rock–soil mass together as one system to resist landslide thrust. Internal forces of the structure are calculated by dividing the structure into two parts. The upper part can be considered a frame structure under lateral landslide thrust, and the lower part can be considered an elastic axially loaded member. The micropiles of the combined structure bear mainly axial forces in contrast to the roof plate, and, thus, principally endure bending moments. The structure can be designed by considering the tension–compression stability of the pile body and the shallow stability of the slope body under the roof plate. The combined structure has been realized in practice for a cutting slope project of an expressway (Guangyuan–Bazhong line, Sichuan, China). The structure promises better application and socioeconomic benefits. To improve the approach, the interaction between micropiles and sliding mass needs to be considered in detail in further studies.

ACKNOWLEDGEMENTS

We are thankful to Communication Department of Sichuan Province, China for supporting our research funds.

REFERENCES

Ding Guangwen (2001). “Design method for treating a landslide with micropiles.”

West-China Exploration Engineering, (4), 15-17.

Ding Guangwen, Wang Xin (2004). "Application of micropiles combination structure in reinforcing landslide." Geotechinical Engineering Technology, (1), 47-50.

Donald, A. Bruce, Al F. Dimillio, Ilan Juran (1995). "A Primer on Micropiles." Civil Engineering, (12), 51-54.

Duncan, Evans (1994). "Lateral Load Analysis of Single Pile and Drilled Shafts." ASCE Journal of Geotechnical Engineering, 120(5), 1018-1033.

Feng Jun, Zhou Depei, Jiang Nan, etc. (2006). "A model for calculation of internal force of micropile system to reinforce bedding rock slope." Chinese Journal of Rock Mechanics and Engineering, 25(2), 284-288.

Huang Weiqin (2001). "Combined application of micro-piles in slope reinforcement." Chinese Journal of Rock Mechanics and Engineering, 20(Sup. 1), 1218-1220.

Kevin J. McManus, Guillaume Charton, and John P. Turner (2004). "Effect of Micro-piles on Seismic Shear Strain." ASCE Geo-Support, (3), 1-12.

M. J. Thompson and D. J. White (2006). "Design of Slope Reinforcement with Small-Diameter Piles." ASCE Journal of Advances in Earth Structures, 67-73.

Mokwa and Duncan (2001). "Laterally loaded pile Group effects and p-y Multipliers." ASCE Journal of Geotechnical Special Publication, (113), 728-742.

Shi Peidong, He Kaisheng (2005). "Origin, application, and development of small diameter piles (IV)." Geotechinical Engineering World, 8(7), 18-23.

Sung June Lee (2004). "Behavior of A Single Micropile in Sand Under Cyclic Loads." Doctor Dissertation of University of Illinois, Urbana.

Thomas, D. Richards, Mark Rothbauer (2004). "Lateral Loads on Pin Piles (Micro-piles)." ASCE Geo-Support, (1), 1-17.

Tom Armour, Paul Groneck, James Keeley, Sunil Sharma (2000). "Micropile Design And Construction Guidelines Implementation Manual Priority Technologies (PTP) Project." Publication NO.FHWA-SA-97-070. USA.

Wang Gongxian (2005). "Key technique in landslide control and its handling measures". Chinese Journal of Rock Mechanics and Engineering, 24(21), 3818-3827.

Xie Xiaohua, Liu Jifu, Pang Qisi (2001). "Application of micropiles in a landslide treating engineering." West-China Exploration Engineering, (2), 110-111.

Experimental Research on the Mechanical Parameter of Fly Ash Soil

Liu Han-bing[1], Li Chang-yu[2], Wei Hai-bin[3]

[1]Department of Road and Railway Engineering, Jilin University, No.5988, Renmin Street, Changchun City, China; PH (+86) 431-85095446; FAX (+86) 431-85095446;
[2] Department of Road and Railway Engineering, Jilin University, No.5988, Renmin Street, Changchun City, China; PH (+86) 13689818150; email: lchy79@163.com
[3] Department of Road and Railway Engineering, Jilin University, No.5988, Renmin Street, Changchun City, China; Corresponding Author email: weihb@jlu.edu.cn

ABSTRACT

In order to study the mechanical characteristics of fly ash soil, fly ash and silty clay were mixed according to the proportions 1:4, 1:2, and 1:1 by dry weight with the water content of 15%, 17%, and 19% to test the static characteristic of fly ash soil. The test results show that the compressive strength of fly ash soil (1:2) slowly decreases with the increase of water content and is greater than 150 MPa when the water content ranges from 15% to 23.5%; the deformation modulus of fly ash soil (1:2) decreases with the increase of water content, while still greater than 3 MPa; the compressive strength of fly ash soil with three kinds of lime soil ratio decrease with the increase of water content, but when lime soil ratio is 1:2, the compressive strength is greater than the others. Through the test of dynamical characteristics, we obtained that the dynamic strength of fly ash soil increases with the increase of confining pressure, and the dynamic strength, dynamic modulus, and shearing strength of the fly ash soil (1:2) are better than the others. The frost heave test shows that the amount of frost heave decreases with the increase of fly ash content, which performs strongly in the early stage of frost heave and is gradually stabilized later.

Key words: mechanical characteristics, fly ash, soil dynamic strength, the modulus of deformation, the amount of frost heave

INTRODUCTION

Northeast China belongs to seasonal frost zone. Subgrade in this area appears to have a moisture accumulation phenomenon in the freezing process under the influence of a negative temperature gradient. After freezing, the volume of accumulated water increases, which causes subgrade uplifting and pavement cracks, namely the frost heave phenomenon. When spring comes, the subgrade soil emerges from the cracks in the pavement caused by frost heave in the form of mud, forming frost boiling. It can be concluded that the water content of subgrade soil makes a great influence on its strength. The current control methods and measures are mainly

the improved reinforcement method and pharmacy method. Fly ash has been widely used in bases and subbases of highway engineering (Feng, 2002). Strength of pavement, especially asphalt pavement, mainly depends on the base, which requires the base material to have sufficient strength to bear the traffic load. According to the current research of home and abroad, there is no systematic analysis on the influence of water content on the nature of the soil engineering (Qi, 2005). The addition of random distribution fiber to fly ash can increase the anti-liquefaction strength of fly ash (A. Soominathan, 2002). Indoor freeze-thaw and freezing stability experiments of fly ash soil have been made to determine if the freeze-thaw resistance of fly ash soil is better than fly ash and soil individually by measuring the value of CBR, and if the freeze-thaw resistance of fly ash and soil is close. The information about the influence of water content on the strength of fly ash soil cannot be found.

Based on the experimental results of fly ash soil with different water content and different lime-soil ratios, this paper analyzes the influence of water content on static properties of fly ash soil, such as compressive strength and deformation modulus, as well as the influence of different lime-soil ratios on the dynamic properties and frost heave of fly ash soil. It can offer a theory to engineering design and the application of fly ash soil.

MATERIALS SELECTION AND SAMPLE PREPARATION

Materials selection. The total content of $SiO_2 + Al_2O_3 + Fe_2O_3$ of the test fly ash is 78.13% ~ 88.64%, and the content of SO_3 is 0.1% ~ 0.72%; the ignition loss of SO_3 is 1.0% ~ 5.26%. The test fly ash is Si-Al-type, with the nature of volcanic ash, appears fine and powdery when dry, feels soft and smooth, and looks like cement dust. Test soil is taken from Changchun city as representation. The physical properties of test materials are listed in Table 1. The mechanical properties of subgrade soil are directly related to water content and soil density. The change of the natural environment will change the water content of subgrade soil. This experiment mixed soil and fly ash with the ratios of 1:4, 1:2, and 1:1 by dry mass; each mixture was tested with water content of 15%, 17%, 19%, and 23.5%.

Table 1. Basic Physical Properties of Specimen.

Materials	Plastic Limit %	Liquid Limit %	Plasticity index %	Optimum water content %	Maximum dry density g/cm^3
Silty clay	22.4	34	11.6	12	1.92
Fly Ash		46.5		36.8	1.09

Sample preparation. The compactness of all samples was controlled by maximum dry density, and the maximum dry density was determined by the standard

compaction test. The preparation process of samples was as follows: mixing the fly ash and soil by dry mass, drying the test soil, crushing and sieving, stirring the mixture of fly ash and soil uniformly, and adding water to the mixture until the predetermined water content. Then the mixtures were maintained in a moist chamber for 24 hours and divided into three layers to be compacted by adopting a standard method.

For the static test, the height of the sample was 50 mm, and the diameter was 50 mm (shown in Figure 1). For the dynamic test, the height was 140 mm, and the diameter was 70 mm. All samples were sealed with plastic film and placed in the conservation box (temperature 20 ± 1°C, relative humidity 96 ± 2%) for 7 days (GB, 1999).

The equipment used in the static test was an YYW-2 strain-controlled, unconfined, compressive instrument produced by Nanjing soil instrument factory; the loading rate was controlled at 2.4 mm/min. The equipment used in the dynamic test was a DTC-306 multi-functional, electro-hydraulic servo dynamic triaxial apparatus made in Japan, shown in Figure 2.

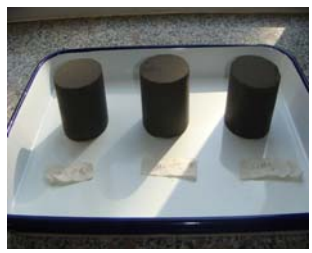

Figure 1. Samples of fly ash soil.

Figure 2. Dynamic triaxial apparatus.

STATIC PROPERTIES TEST OF FLY ASH SOIL AND ANALYSIS

Effect of fly ash content on the characteristics of fly ash soil. With confining pressure equaling 100 kP, 200 kPa, and normal temperature, the dynamic strength of silty clay is slightly higher than fly ash (ash to soil = 1:2). However, with the raising of confining pressure, the increase amplitude of dynamic strength of fly ash soil (ash to soil = 1:2) is greater than silty clay. Under certain conditions, dynamic strength decreases with the increase of destruction cycles, and it increases with the raising of confining pressure (Li, 2007). However, this paper is limited to the research that fly ash to soil = 1:2.

In this paper, plenty of indoor experiments were done to study the effects of different lime-soil ratios on the characteristics of fly ash soil. From Figure 3, it can be obtained that the compressive strength of three kinds of mix ratios with different water content decreases with the increase of water content. When water content is less than the optimum water content, the change of compressive strength with the variation of water content is greater when water content is greater than the optimum water content, the change of compressive strength with the variation of water content is less. However, the compressive strength of fly ash soil with fly ash to soil = 1:2 is greater than the other two cases, which is consistent with literature (Hu, 2002). It can be obtained that the deformation modulus of fly ash soil with water content of ω = 17% and ω = 23.5% decreases with the increase of fly ash content (see Figure 4); when water content reaches the optimum water content, ω = 19%, the deformation modulus of fly ash soil with fly ash to soil = 1:2 is smaller than the other two mix ratios. This shows that the fly ash content greatly influences the deformation modulus of fly ash soil.

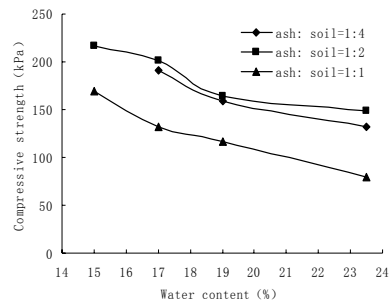

Figure 3. Water content and compressive strength.

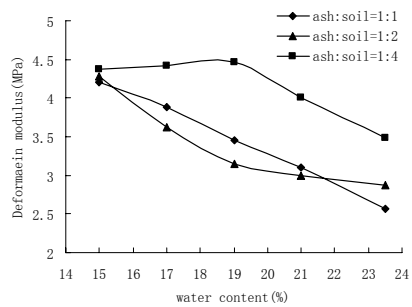

Figure 4. Water content and modulus.

Effect of water content on the strength of fly ash soil (1:2). Subgrade is the foundation of pavement; its wheel load resistance capacity mainly depends on the deformation resistance ability of the top surface of the subgrade under a certain stress level. It can be obtained from Figure 5 that the compressive strength of fly ash soil (1:2), as subgrade materials, changes slightly with the increase of water content. The

compressive strength of the ash soil with a water content within 15% ~ 23.5% is greater than 150 kPa. The optimum water content of the fly ash soil used in this experiment is 19%. From Figure 5, we can see that before the optimum water content the variation degree of the compressive strength of fly ash soil with water content is greater than after the optimum water content, which indicates that fly ash soil has good water stability. When fly ash as a subgrade material is compacted with the optimum water content, the increase of water content caused by other external factors will have less effect on the strength of the subgrade.

Effects of soil water content on the deformation modulus of fly ash (1:2). Based on test data, this paper calculated the deformation modulus corresponding to the limit stress state with different water content. Calculation results are shown in Figure 4. From Figure 4, it can be obtained that the deformation energy of the fly ash soil (1:2) decreases with the increase of water content. When water content changes from 15% to 19%, deformation modulus decreases by 28.67%; when the water content changes from 19% to 23.5%, the curve changes slightly; deformation modulus only decreases by 7.39%. It can be concluded that when water content is greater than the optimum water content, the deformation modulus changes slightly with the variation of water content, and the deformation modulus is greater than 3 Mpa.

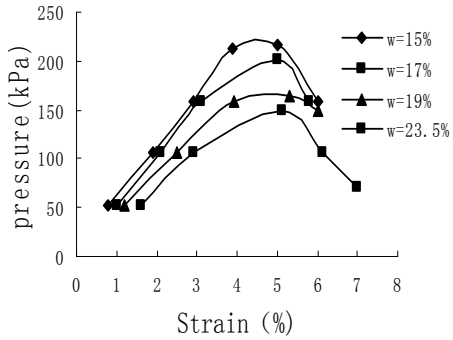

Figure 5. Curves of stress and strains.

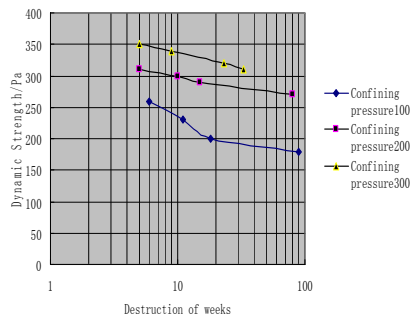

Figure 6. Dynamic shear stress and cycle numbers.

DYNAMIC PROPERTIES TEST OF FLY ASH SOIL AND ANALYSIS

The dynamic properties experiment was carried out with lime-soil ratios of 1:1, 1:2, and 1:4. The test load was applied with frequency f = 1Hz, confining pressure 100 KPa, 200 KPa, 300 KPa, in the form of sine wave. The adopted destruction criterion is ε_d = 5%. In order to draw the $\sigma_d - N_f$ curve, the ideal situation of testing points distribution is that the four points would fall in the range of the $4^{th} \sim 6^{th}$ cycle, $10^{th} \sim 15^{th}$ cycle, $20^{th} \sim 30^{th}$ cycle, and $50^{th} \sim 70^{th}$ cycle. After obtaining the dynamic stress corresponding to N_f = 10 from the $\sigma_d/2$ -lg N_f curve with confining pressure $\sigma_3 = 100$ KPa, 200 KPa and 300 KPa, the pull and push half-cycle stress circle can be drawn by taking consolidation pressure as the vertex and σ_d as the diameter. Then the index of sheer strength, i.e., cohesive force c_d, and internal friction angle φ_d can be obtained by drawing the envelope of failure stress circle. The experimental data are shown in Table 2.

In the dynamic modulus test, the confining pressure of 100 KPa and initial dynamic stress of 100 KPa is applied. After six times of vibration, the next dynamic stress is doubled. Then the dynamic strain (ε_d) in different stress (σ_d) levels are measured. The skeleton curve of $\sigma_d - \varepsilon_d$ is of hyperbola type; it can be described by the hyperbolic model of $\sigma_d = \varepsilon_d / (a + b\varepsilon_d)$. The value of a and b can be derived by the regression statistical analysis. Because the curve of $\sigma_d - \varepsilon_d$ is of hyperbolic curve type, the relationship between ε_d / σ_d and ε_d is linear. The intercept of the vertical axis is $\varepsilon_d / \sigma_d = 1 / E_0$, where E_0 is the initial dynamic elastic modulus. The test data are shown in Table 2.

It can be obtained from Table 2 that the dynamic strength of fly ash soil increases with the increase of the confining pressure. The dynamic strength, dynamic modulus, and shear strength with the lime-soil ratio of 1:2 are better than the other two ratios, which is because the amount of used fly ash increases with the increase of soil clay content and soil plasticity index. But when the amount is over a certain range, too much fly ash exists as free ash in the void of soil, which will lead to the decrease of fly ash soil strength.

ANALYSIS OF FROST HEAVE TEST OF FLY ASH SOIL

To measure the amount of frost heave of fly ash soil, the fly ash and soil were mixed with the ratios of 1:1, 1:2, and 1:4 and stirred with the optimum water content. Then the mixture was compacted and made to cylindrical specimen with the height of 10 cm and a diameter of 5 cm. For imitating the actual lateral force condition of road, the fly ash soil samples were applied with lateral confining pressure. The surrounding samples were kept under constant temperature, so the cold can transfer in the specimen from the top to the bottom. The amount of frost heave is measured by a dial indicator mounted on the top center of the specimen.

Table 2. Results Summary of Fly Ash Soil Dynamic Test.

Ratio of ash and soil	Failure strength of 10 cicles （KPa）			Dynamic modulus (MPa)	Cohesion (kPa)	Internal friction angle （°）
	100 kPa	200 kPa	300 kPa			
1：1	226	283	319	146.26	127.4	18
1：2	234	300	338	171.64	147.5	22
1：4	230	292	326	158.32	134.9	20

The experiment results indicate that the frost heave appears most evident in the early period of cooling (the process of phase transition of water in ash soil) and tends to be stable with the decrease of temperature. Under the same boundary conditions, the amount of the frost heave decreases with the increase of the content of fly ash.

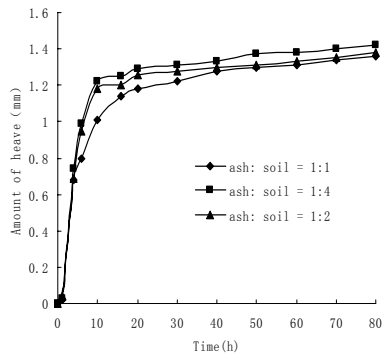

Figure 7. Relationships between the amount of frost heave and time.

CONCLUSION

(1) The compressive strength of the fly ash soil (1:2) changes slightly with the increase of water content. The compressive strength of the ash soil with a water content within 15% ~ 23.5% is greater than 150 kPa. When less than the optimum water content, the variation degree of the compressive strength of the fly ash associated to the change of the water content is greater than when it is over the optimum water content.

(2) When water content is greater than the optimum water content, the deformation modulus changes a little with water content variation; the deformation modulus is greater than 3 Mpa.

(3) The compressive strength with lime-soil ratios of 1:4, 1:2, and 1:1 decreases with the increase of water content. This shows that the fly ash content greatly influences the deformation modulus of fly ash soil.

(4) The dynamic strength of fly ash soil increases with the increase of confining pressure, dynamic strength, and dynamic modulus; the strength index with a lime-soil

ratio of 1:2 is better than the ratio of 1:1 and 1:4.

(5) The amount of frost heave decreases with the increase of fly ash content, which appears stronger in the early time of frost heave and gradually tends to stabilize later.

REFERENCES

A. Boominathan, S.Hari. Liquefaction strength of fly ash reinforced with randomly distributed fibers. *Soil Dynamics and Earthquake Engineering* 22 (2002): 1027-1033.

FENG Hai-ning, YANG You-hai, GONG Xiao-nan. Test research on engineering characteristic of fly ash. *Rock and Soil Mechanics*, 2002, 23 (5): 579-583.

GB/T50123-1999, Soil Test Method Standard.

Hu shan, Luan hai. The research on freezing stability of high-grade highway fly ash subgrade on seasonal frozen area, *Road*, 2002 (05): 53-57

Li chang-yu. Experimental research on dynamic properties of fly ash soil subjected to freeze-thaw cycles, Jilin University, 2007.

QI Ji-lin,CHENG Guo-dong. State of the art of influence of freeze-thaw on engineering properties of soils. *Advance in earth science*, 2005, 20 (8): 0887-08.

The Bearing Character of Bridge Piles in Karst Areas

KANG Hourong[1 2], ZHANG Xiedong[1], and LI Hong[1]

[1]School of Transportation, Wuhan University of Technology, 1040 Heping Road Wuchang, 430063,P.R.China; PH(027)86551193; FAX(027)86544875; email:khr165@vip.sina.com
[2]Department of Communications of Guizhou Province, 111 Yanan west Road Guiyang, 550003,P.R.China; PH(0851)5954761; FAX(0851)5992145; email:khr165@126.com

Abstract: This paper covers a project that conducted methods of self-balanced pile tests with three-dimensional numerical simulation analysis on effects of karst caves on the load capacity of bridge foundations located at hidden caves. Taking Nanpanjiang Bridge in Yunnan as a case study, it carried out static loading tests on No.1 Pier, No.2 pier and No.1 pile which foundations are free from caves. Then it adopted the finite element method to establish a cave-rock-pile foundation three-dimensional analysis model for systematically analyzing effects of top plates with different thickness and caves with different sizes and locations under different working conditions on the loading capacity of bridge foundations. Furthermore, soils having four different conditions surrounding piles under each working condition were also considered and analyzed. It was found that the distance between roof of the cave and pile tip was the main factor affecting the loading capacity of the pile foundation. The research results were successfully applied in evaluating loading the capacity of a pile foundation in Nanpanjiang Bridge in Yunnan. Thus, the research results improved utilization and reliability of roof of karst caves in highway construction.

Key words：*karst; pile; bearing character; numerical simulation*

A large-diameter grouting pile is embedded in the bedrock, whose hole is artificially or mechanically dug. It can fully use the pile strength and rock strength, and because it has good adaptability, high bearing capacity and can substantially reduce the cost, it is widely used around the world. Many experts and scholars at home and abroad have made a lot of work about it, but the bearing characteristics of the pile in karst areas is still lacking (Dengshan et al. 2002; Minghua et al. 2003)..

With Yunnan Nanpanjiang Bridge (Shenggen et al. 2004) as the background, through field tests and numerical analysis, this paper researched the pile bearing character, and on that basis, combining relevant research results at home and abroad, it put forward the evaluation method of pile bearing capacity in karst areas.

1 Nanpanjiang Bridge pile test

1.1 Project Profiles

Nanpanjiang Bridge is a prestressed concrete continuous rigid frame, whose 1#,2# pier is an artificially dug pile foundation, where rock distribution characteristics are as follows: Quaternary loose layer (artificially filled, red clay); cave packed with gravel soils, red clay; strongly weathering siliceous dolomite, loose rock structure; structure and fragmentation quartzite rock fragments, fragments of rock; medially weathering siliceous dolomite and quartzite, joint developed; lightly weathered siliceous dolomite, joint developed.

There is a cave of about 40% of the pile base area 1502.8m below the 2# pile, which extends southeast along of 18.4m, 9m width, and more than 20 meters high, vertical development, clay, gravel soil filled, loose structure, clay-like soft plastic, 1502.8 to 1497.58m without filling. A platform is first filled with gravel, which is grouted layer by layer, and then a masonry wall was built on the platform, pouring concrete to the design elevation.

To determine the pile bearing capacity and analyze the influence of karst on the pile bearing character, the paper selected the 2#pile of 1# pier and the 1#pile of 2# pier for a static load test. The parameters of the test piles are as follows.

Table 1. Test pile parameters.

Pile number	Pile diameter /mm	Pile Length /m	Distance from load box to the end of test pile /m	Estimated value of loading /KN
2# Pile of 1# pier (Test pile Z1)	2500	49.0	12	39800
1# Pile of 2# pier (Test pile Z2)	2500	40.0	15	39000

1.2 Analysis of the bearing capacity

1.2.1 Influence of Karst on pile bearing characteristics

The Q ~ S curve of Z1 pile is obviously steeper than that of Z2. The settlement of Z1 pile is far greater than that of Z2 pile under the same load (Figure 1).

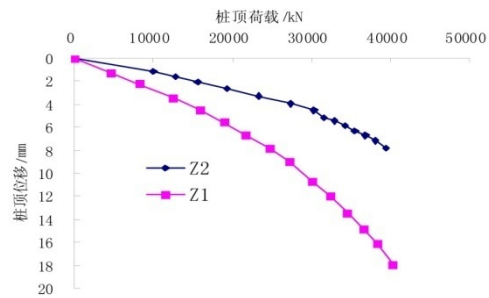

Figure 1. Q～S curve

The tip and the lower-part of the pile were selected for analysis to find the differences between Z1 and Z2. Figure 2 shows the relation between the average friction and relative displacement of Z1 tip, Z2 piles, which is fitted by hyperbola fitting method. From the experimental results, the average friction of Z2 pile is greater than the Z1 pile. From the fitting results, the critical displacement of Z2 pile is 4 mm when it shows maximum friction, and that of Z1 is 8 mm. But they have almost the same maximum friction. And for the lower-part of pile, the box load is supported by the lateral friction and tip resistance. Considering

that the tip resistance is small, especially considering the influence of karst, it is considered that the entire load on the lower-part of pile is taken by friction. The relation curves and the fitted curves are found and the results are as follows. From Figure 3, the measured value and the maximum value of the lower-part of the pile is greater than Z1, and Z1 need greater displacement than Z2 to show maximum friction.

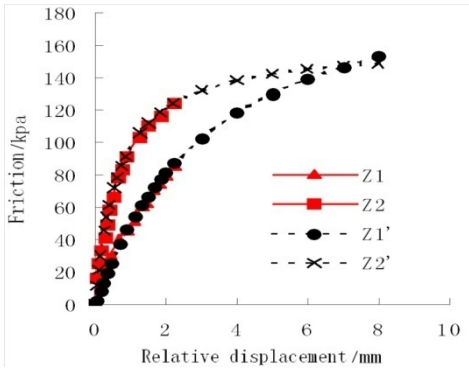

Figure 2. Average friction of pile tip and relative displacement. (The map dotted curve is fitting curve.)

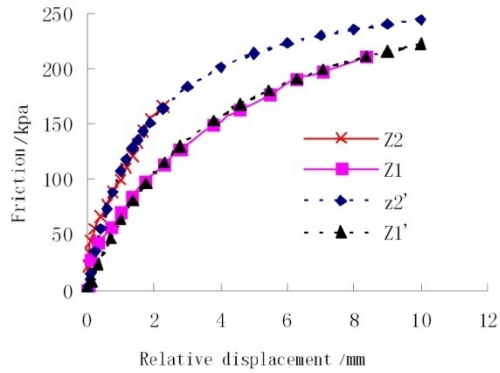

Figure 3. Average friction of the lower-part of pile and relative displacement. (The map dotted curve is fitting curve.)

1.2.2 Analysis of test results

It can be determined from these tests that karst mainly influences the lateral friction of the pile, and the entire pile will be affected. For the pile tip, it mainly affects the lateral friction and for the lower-part of the pile it will affect the entire pile. According to the test and research results, the pile-stress state of the pile end rock-soil friction will have a greater influence on frictional resistance around the pile. When the strength of the rock around the pile tip is low, not only will the lateral strength be reduced, but also the critical pile-soil displacement will increase. The two test piles selected have little difference in the rock around the piles. The main difference lies in that Z1 piles lie on the karst cave, where the filling materials have low strength, resulting in lower strength of the bearing layer, which is not conducive to the friction, and it is more obviously close to the pile tip. In addition, there is a free-face near the end of the pile tip where the rock strength is low compared with the Z2 pile. Pile axis forces gradually diffuse to the rock around the pile through piles of lateral friction, which make the rock more relaxed, deformation increased, and the performance will be more obvious down the pile, causing the low-part friction of Z1 pile to be lower than that of the Z1 pile, so the displacement of maximum friction of Z1 pile is larger than Z2 larger. The Z1 pile tip will be affected little by the cave, because there is a certain distance from the cave, but the displacement of the maximum friction will increase.

2 Influence of karst on pile bearing capacity

Using the finite element method (Shilong et al. 2005), the paper did numerical simulation analysis. First it anti-counted rock with axisymmetric model, concrete and rock characteristics and rock-pile friction contacts, and at the same time did the pile load bearing capacity self-balance experiment with the axisymmetric model. The load-displacement curves can be used to calibrate the model, from which parameters of the numerical model can be found. Secondly, the related axisymmetric model and the three-dimensional model are constructed, and their calculation results were compared, and 3D models were evaluated accordingly. Finally, a three-dimensional model was used to analyze the sensitivity of rock cave location and various rock types, as well as lateral friction and pile resistance.

2.1 Three-dimensional finite element model

In order to analyze the influence of the cave on the pile bearing capacity, based on the 2D axisymmetric model, a 3D finite element model of the pile-rock-cave was established to simulate the interaction, whose scale is similar to the 2D axisymmetric model. The 3D and 2D axisymmetric models have the same contact face, geometric profile, the same material properties, so they have the same load-deformation activity characteristics. Four displacement points were set up along the pile to detect the 3D model.

2.2 Sensitivity analysis of the influence of cave on pile bearing capacity

2.2.1 Calculation of working conditions

Based on the pile-rock-caverns 3D finite element model, having detected it, considering the influence factors of bearing capacity such as the thickness of the tip of the pile, diameter, elevation and eccentricity of the cave, different caves were set up to form various 3D models. Each factor has four models, for a total of 16 models. Meanwhile, in order to analyze the different influence of rock on the pile bearing characteristics, four different rock types were considered in each model.

In order to study and verify the sensitivity analysis conclusion, the cave was considered to be near the pile tip. At the same time the extreme state (where pile is fully embedded in the cave, having no rock supporting it) was also simulated.

A total of 16 working conditions were analyzed, considering the following factors.

(1) The cave lies beneath the pile and they have the same axes. The space from the cave to pile tip is a constant value, which is equal to the pile diameter. Cave diameter changes from where it is one times the pile diameter and its cross section is ten times that of the pile.

(2) The cave lies beneath the pile. The cave center iteration happens with the pile axes. The thickness from pile tip to the cave top changes from five times pile diameter to eight times pile diameter when the cave diameter is equal to five times pile diameter.

(3) The cave eccentric area beneath the pile. The space from the cave top to pile

is constant value, which is equal to the pile diameter. The eccentric distance from pile axes to cave center is one to six times cross-section.

(4) The cave eccentric area beneath the pile. The space from the cave tip to pile is a constant value, which is two times the pile diameter. The eccentric distance from pile axes to cave center is one to four times cross-section.

Cave is considered to lie beneath the pile, whose eccentric distance is equal to 2×D, diameter is equal to 5×D, the thickness from pile tip to the cave top is equal to 1×D, and their calculation models are showed in figure 4.

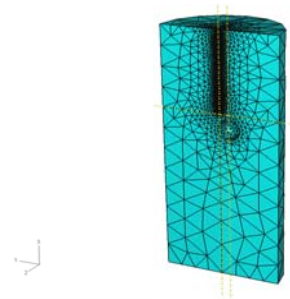

Figure 4. cave diameter of 5×D, thickness of 1×D, eccentric distance of 2×D

2.2.2 Analysis of sensitivity calculation results

Idealistic spherical cave will change the proportion of pile lateral friction and pile bottom bearing capacity to total bearing, When supposing the isotropic of rock pile with D-P plastic flow rules

When the influence factors of the cave on pile bearing capacity increases gradually, for example, the more the cave lies near the pile and the more the cave is big, simulation calculation shows that the load on the pile bottom reduces and the more load is on the interface of rock-concrete. Then, the influence of the roughness of pile-rock, the degree of fragmentation and weathering on the total bearing capacity will be greater than the case that there is no cave beneath pile.

(1) The influence of rock mechanical characteristics on the pile bearing characteristics mainly embodies that the relative changes in the pile carrying capacity and pile lateral friction, the rock pile-stress state of friction will have a greater impact on the lateral friction. When the elastic modulus of the rock around the pile reduce, not only will the pile tip bearing capacity relatively increase, but also the critical displacement of rock-pile will also increase, especially when the cave is located beneath the pile, the impact is more obvious.

(2) When the thickness from the cave to the pile is small (e.g. less than 1D), the ratio of the thickness to the span is less than 0.5, the pile bearing characteristics will be impacted. And with the ratio of the thickness to the span reduce, the proportion of pile tip bearing capacity to total bearing capacity increase, but the proportion of lateral friction to total bearing capacity will be reduced. When the thickness from the cave to the pile increases (e.g. the thickness is equal to 2D) with the same ratio of the thickness to the span, the pile tip bearing capacity in the case of large roof thickness is bigger than that in the case of small roof thickness, but the lateral friction in the case of large roof thickness is less than that in the case of small roof thickness. When the cave center deviates from the pile axes, the influence of cave on pile bearing characteristics will reduce.

(3) Although there is no obvious fact indicating that the bedrock produces

differential deformation, the lateral friction and the pile bearing capacity has changed. It can be seen from the calculation figure that the lateral friction-load slope increases with the diameter increase. Accordingly, the pile bearing capacity decreases. Hasson (1997) pointed out that lateral friction increases when the contact surface stress increases. In the initial loading phase, the displacement is small, as well as the pile - rock surface stress, because most of the load is transferred to the bedrock. When the load increases, displacement increases, the lateral friction plays a more important role in the pile capacity. For small diameter cave, for example, cave diameter is one to five times pile diameter, lateral friction will quickly reach 30% of the total load. Then the lateral friction percentage will be a little lower. The results show that when the lateral friction will achieve the maximum increase with the staggered motion of the rock - piles interface, the incremental load will be supported by bedrock. In the small load loading stage, the main load is supported by bedrock. Then the pile tip carrying capacity–load percentage curve will fall rapidly. Having slow down to the bottom, the pile tip bearing capacity-load percentage will have a some increases. However, the curve rebound increases with the increase of cave diameter. Accordingly, for a super large cave, e.g. 10 times pile diameter, it will delay the lateral friction-load curve peak time. In the sensitivity analysis, four factors the may have influence on the pile bearing capacity were selected. The results indicated that the distance from pile tip to cave top is a key factor of bearing and the diameter and eccentricity have little influence on the bearing.

2.2.3 Analysis when the cave is close to the pile tip

In order to study and verify the conclusions, it was simulated that the cave is close to the pile tip. At the same time the critical state of socketed pile (the distance of pile tip to cave top is equal to zero) is also simulated. The results are shown in Figure 5.

In Figure 5, the distance from the pile tip to cave top is 0D, 0.125D, 0.25D, and 0.375D, respectively, when the ideal spherical cave is close to pile tip.

P-S-curve indicated that the influence of cave-to-pile vertical displacement becomes obviously large when the cave is close to the pile, particularly in the case of one times the pile diameter, the pile bearing capacity becomes smaller, and the vertical displacement is increased under the same load.

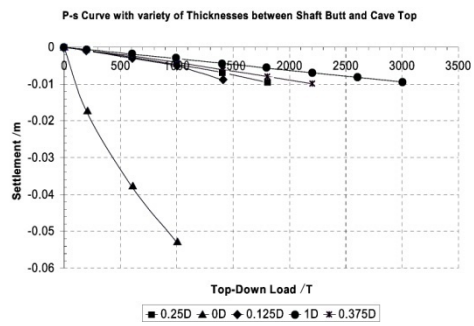

Figure 5. P-S curve of the distance from the pile tip to cave top is equal to 0-1D

3 Conclusions

Through static load tests and numerical analysis, the paper comes to the following conclusions:

(1) Under the same load, the pile settlement in the situation that the cave exists is far larger than that in the situation that the cave doesn't exist. The influence of karst on pile bearing characteristics mainly influences the lateral friction, and has an influence on the whole pile: it will mainly influence the critical displacement of upper pile and both the critical displacement and maximum friction in the lower segment of the pile.

(2) A cave will change the proportion of the lateral friction and pile tip bearing capacity to the total bearing capacity. The load borne by the pile tip will reduce, and the more load will be borne by the interface of rock-concrete when the cave is close to the pile tip and the cave diameter becomes large; Then pile-roughness of the rock, broken rock and weathering has a larger influence on the total capacity than the state that there is no cave.

(3) When the cave is near a pile, particularly in the range of 1D, the influence of the existence of the cave on the pile vertical displacement obviously becomes large. When the cave nears the pile tip, corresponding bearing capacity becomes small and the vertical displacement becomes larger under the same load. There is a close correlation between the displacement and the cave and the load. When the load is small, the differential displacement is also small, otherwise it will increase. In smaller diameter caverns, load - by the displacement is not obvious. When the cave becomes small, it has little influence on the load-displacement.

(4) Four possible influence factors were selected on the pile bearing capacity: thickness from the pile tip to the cave, cave diameter, cave eccentricity, cave depth when there is eccentricity. Analysis showed that the thickness from the pile tip to the cave top is a key factor of bearing capacity and the diameter and eccentricity has little influence on the bearing capacity.

REFERENCES

Dengshan, C., Bangmei, W. (2002). Study of Mechanism of Loading on Bored Pile in Karst District. Bridge Construction. No. 6, 2002, pp.16-19.

Minghua, Z., Tengfang, Y., Li, L., Desong, J. (2003). Computation Study on Safety Thickness of Bearing Rock Strata at Ends of Piles in Karst Region. Highway, No. 1, 2003, pp. 124-128.

Shenggen, H., Shilong, M., Weiming, G. (2004). Testing Study on Bearing Behavior of Piles for Nanpan River Great Bridge in Karst Area. Chinese Journal of Rock Mechanics and Engineering, Vol. 23, No.5, 2004, pp. 809-813.

Shilong, M., Drumm, E.C., Baoshan H., Wenbin, H., Gang, Z. (2005). Back-Calculation of Rock Socket Friction for Concrete Shafts in Karst. Carsologica Sinica, Vol. 24, No. 2, 2005, pp. 140-146.

The Analysis of Traffic Landscape from Users' Perspective: The Case of the Zhangjiang Tram

Li Na[1], Chen Xiaohong[2] and Xiong Wen[3]

[123] Room 337, Department of Transportation Engineering, Tongji University, 4800 Cao'an RD., Shanghai, 201804; PH (086)21-69584683;email:linayiqun@163.com

1 Abstract

The conventional studies of traffic landscape mostly focused on the aesthetical requirements from the designers' perspective. However, there has been a lack of concern and research from the users' perspective, which serves as the basis of traffic landscape design and construction. This paper, which is based on the tram construction project in Zhangjiang Area, Shanghai, explores the user's preference to traffic landscape. Users include drivers, passengers, pedestrians, and nearby residents. To explore the preferences for traffic landscape elements among different people in different districts, a survey was conducted to sample users' attitudes towards traffic landscape. The relative importance of various landscape elements can be simultaneously evaluated from this survey.

Keywords: traffic landscape, Zhangjiang tram, preference, landscape elements

2 Introduction

Streets, which serve as our indispensible links to the outside world, are also stages for traffic landscapes and must embody the features of both traffic and landscapes.

When referring to traffic landscape, vegetation or trees typically come to mind. Antupit regards vegetation/trees as the primary element that great streets must include (Antupit S. et al., 1996). But roadside vegetation is not the sole meaning of traffic landscape. Traffic landscape design includes both the design of streets in urban areas and their integration into the surrounding environment, namely comprehensive consideration of the alignment of roads, combination of buildings, public facilities, roadside vegetation and artistic exhibits such as sculptures and flowers (Xue An-shun et al., 2007).

Studies of traffic landscape in China focus mostly on aesthetical analysis from the designers' perspective. However, streets are not only thoroughfares but also community open spaces: public spaces that give shape to the city and provide people with places to meet, gather and transport themselves (Antupit S. et al., 1996). Thus, users' activities are vital constituent parts of roads. Traffic landscape design should meet users' needs. But designers' preference cannot represent the diverse preferences of users, particularly those of pedestrian and drivers. (Yang Liang-liang et al., 2007). It is generally recognized by landscape ecologists, environmental engineers,

environmental economists and sociologists around world that social factors play a very important role in landscape design. Public participation in decision-making and incorporation of human preferences, needs and activities in the management plans safeguard their continuation and success (Pavlikakis G.E. et al., 2006)

Researchers from various countries have investigated differences in preferences between cultural and sub-cultural divisions and ethnic groups. Factors such as personality, environmental orientation and educational background have also been reported to influence preference (Assenna Todorova et al., 2004). However, such studies are rare in China. The basic object of this paper is to explore the domestic landscape preference from users' perspective.

3 Backgrounds and Method

As a transportation mode, the modern tram has advantages of high-speed, low-noise, no exhaust pollution, and low construction and operating costs. It has become a popular construction program in China. The tram network in Pudong area, Shanghai is planned to be 63.0 kilometers in length, covering Lujiazui, Sanlin and Zhangjiang areas. The 8.8 km long section in Zhangjiang area is a test section. It is crucial to solicit and evaluate public opinion with the Zhangjiang Tram project because of the overhead contact system and the tram rail, which are expected to be the most likely elements to disrupt the traffic landscape.

Evaluating the beauty of certain landscape objectively and scientifically is very difficult because, while beauty is partially defined by environmental characteristics, it depends largely on individual judgment. Even when groups of people witness the same scene under the same conditions, they do not have the same impression of the landscape. A landscape is composed not only of what lies before the viewer's eyes but what lies within his head (Meinig D.W., 1976). The methods generally used for evaluating scenic beauty are cartographic representations, simulated assessments and questionnaire surveys (Antupit S. et al., 1996).

The investigation described in this paper was built around the landscape design challenges encountered in the tram construction program in Zhangjiang area, and respondents involved residents, local employees and students. The evaluation utilized questionnaires to obtain categorical information for the respondents, such as age, gender,(无) and occupation. Then, the respondents were shown three groups of simulated photomontages, exhibiting different types of landscape elements. The respondents gave their assessments according to their visual preference after gaining a direct impression of each group of images.

4 Investigation

4.1 General Situation

This survey was carried out on two days in April, 2008. A total of 285 respondents returned the questionnaires, but only 244 respondents provided complete

responses. The questionnaires were distributed in three functional districts in Zhangjiang: Zhangjiang Semiconductor Industry Park, the large Ziwei Road residential community and Zhangjiang university area, through which the planned tram line will pass. A smaller number of questionnaires were distributed outside Zhangjiang area. The number of completed questionnaires in these four sites is showed in Table 1.

Table 1.The amount of the questionnaires in four places.

Place	Frequency	%
Semiconductor Industry Park	62	25.4
University Area	90	36.9
Large residential community	57	23.4
Outside Zhangjiang area	35	14.3
Total	244	100.0

4.2 Basic information

Among all the respondents, 121 were males (49.6%) and 123 (50.4%) were females. A large number of technology- and capital-intensive industries are located in Zhangjiang area, with an employment base of approximately 90,000, which is much more than the area population of 24,000. Meanwhile, Zhangjiang university area includes several respected schools, including Fudan University and Shanghai University of T. C. M., with a combined enrollment of 80,000 students, which is nearly as large as the area employment base. The majority of the people who work and study in Zhangjiang are young or middle-aged. Of the survey respondents, 213 (87.3%) are 18-50 years old and 193 (79.1%) respondents have a college degree or higher. The occupation of respondents is summarized in Table 2 and their ages are summarized in Table 3.

The characteristics of the respondents are representative of the population in Zhangjiang area. Therefore the result of the survey should serve as a proxy for the preference of the people in Zhangjiang area.

Table 2.Occupation of respondents.

Occupation	Frequency	%
Student	109	44.7
Teacher	3	1.2
Factory operator	14	5.7
Office clerk	21	8.6
Technical personnel	48	19.7
Retiree	22	9.0
Other	27	11.1
Total	244	100.0

Table 3.Age of respondents.

Age	Frequency	%
<18	4	1.6
18-30	180	73.8
31-50	33	13.5
51-65	14	5.7
>65	13	5.3
Total	244	100.0

5 Analyses

5 Attention to traffic landscape

The survey includes six aspects of tram construction for respondents to assess the importance according to their own needs, on a ten-point rating scale, from "most important" (10) to "least important" (1). These aspects were improving street landscape, controlling construction cost, increasing travelling speed, improving comfort, reducing fares and preventing pollution. The descriptive statistics of the assessment results are shown in Table 4. Comparing the average scores using an F-test at a significance level of 0.05, the p-value is approximately 0, indicating that respondents' attitudes towards these six aspects differ significantly. The aspect with the highest mean (8.68) and lowest standard deviation (1.97) was "preventing pollution." Its Kurtosis was 4.29, indicating that people are generally very concerned about the issue. For the aspect of "improving street landscape," respondents give an average score of 7.57, in the middle of these six aspects. The results showed that respondents also pay some attention to street landscape, but less than pollution, comfort and fares.

Table 4.The importance of the aspects in tram construction.

Aspects	Mean	Std. deviation	Kurtosis
Preventing pollution	8.68	1.97	4.29
Improving comfort	7.97	2.04	0.53
Reducing fares	7.71	2.48	0.27
Improving street landscape	7.57	2.24	0.61
Increasing traveling speed	7.29	2.39	0.10
Controlling construction cost	5.54	2.73	-0.94

Comparing the scores given by males and females on improving street landscape, the results indicate that there is a difference in opinion between males and females. Female respondents (8.02) paid more attention to street landscape than males (7.11). The comparison of responses by gender is summarized in Table 5. While analyzing respondents of different ages, occupations, education backgrounds and in different survey places, there is no significant difference on their attitudes.

Table 5.T-test for scores of improving street landscape by gender.

Gender	Frequency	Mean	Std. deviation	t	df	Sig. (2-tailed)
Male	121	7.10	2.53	-3.25	217.34	0.001
Female	123	8.02	1.81			

5.2 Importance of street landscape elements

In the questionnaire, several common street landscape elements were listed, including some that have a close relation to tram systems, such as street vegetation,

road surface, and overhead contact system. The respondents were requested to select the most important elements that influence the street landscape from the list and then arrange the elements in importance priority.

Among the completed surveys, 84.4% included select street vegetation as one of the most important elements, which is a much higher frequency than any other elements on the list. This result confirms that quality vegetation is the highest priority for a great street (Antupit S. et al., 1996). Over half of the respondents also selected bus stops and public facilities as the most important elements, which are the two listed elements(删除) most often used by road users in daily life. The percentage selecting overhead contact system and tram rails, the two elements closely related to the tram system, was not very high. Respondents indicated paying little attention to these two elements, possibly because modern tram technology is advanced and less intrusive compared to the conventional tram and the aesthetics have been largely improved. It is also likely that, for many users, landscape elements such as quality vegetation or bus stop facilities can compensate for the disruptive landscape caused by tram construction. The results of the respondents' prioritization are summarized in Table 6.

Table 6.The selection of the elements according to their importance.

Landscape element	Frequency	%
Street vegetation	207	84.8
Bus stops	129	52.9
Public facilities (garbage bins, etc.)	123	50.4
Surrounding buildings	117	48.0
Lamp posts and poles	114	46.7
Road surface	101	41.4
Buses and vehicles	94	38.5
Overhead contact system	93	38.1
Tram rails	91	37.3
Creation of sculptures	69	28.3
Other	5	2.0

Comparing the highest priority element selected by the respondents in each of the four survey distribution sites shown in Table 7, most people still consider street vegetation to be the most important landscape element. In each of the Zhangjiang area sites, respondents identified overhead contact system and bus stop facilities as the next most important elements. This makes sense, since the bus stop is the most commonly used road facility for residents, students and workers in Zhangjiang, so people will pay more attention to this element. However, outside Zhangjiang area, respondents selected tram rail and surrounding buildings respectively, as the next most important, and at a higher rate than the other elements selected by the Zhangjiang sites. This may be caused by the fact that Zhangjiang is a newly-built

community with modern, low density buildings and wide roads. As such, it is likely that being in close proximity to buildings and rail will not bother the Zhangjiang population very much.

Table 7.The highest priority landscape element selected at four survey sites.

Survey Site		Industry Park	University Area	Large Residential Area	Outside Zhangjiang Area
Highest priority landscape element	Street vegetation	58.1%	51.1%	28.1%	60.0%
	Road surface	4.8%	3.3%	5.3%	2.9%
	Lamp posts and poles	1.6%	2.2%	3.5%	2.9%
	Public facilities (garbage bins, etc.)	6.5%	4.4%	7.0%	2.9%
	Overhead contact system	8.1%	10.0%	12.3%	2.9%
	Tram rails	4.8%	7.8%	3.5%	11.4%
	Creation of sculptures	3.2%	1.1%	8.8%	0.0%
	Buses and vehicles	3.2%	4.4%	10.5%	2.9%
	Bus stops	6.5%	8.9%	15.8%	2.9%
	Surrounding buildings	3.2%	6.7%	5.3%	11.4%

5.3 Photomontage simulations

During the survey, respondents were shown three groups of simulated photomontages exhibiting different types of landscape elements: vegetation，artistic exhibits;（删除） and tram components. The respondents gave their assessments on a ten-point rating scale, from “strongly like” (10) to “strongly dislike” (1), according to their visual preference. In order to reduce potential bias from surrounding elements, all three groups of photos were modified with photo software to apply the same backgrounds. The original photos of the vegetation and the sculptures and flowers were taken in Zhangjiang in 2007. Since the tram system in Zhangjiang is still under construction, the original photo of tram components was from a tram system in Spain.

●Vegetation

The first group of photos, shown in Figure 1, displays four types of roadside vegetation. As shown in Table 8, evaluation of the average scores for each type of vegetation using an F-test at a significance level of 0.05 results in a p-value of approximately 0. This indicates that respondents’ attitudes towards these various types of vegetation are significantly different. “Trees with lawn” (8.76) or “Trees

with hedges" (7.94) are strongly favored by respondents, while "no vegetation" ranked lowest among the choices.

Table 8.F-test for various vegetation types.

Vegetation types	Mean	Mean Rank
No vegetation	3.996	1.15
Only trees	4.998	2.00
Trees with hedges	7.945	3.24
Trees with lawn	8.758	3.60

F= 578.18, p=0.000

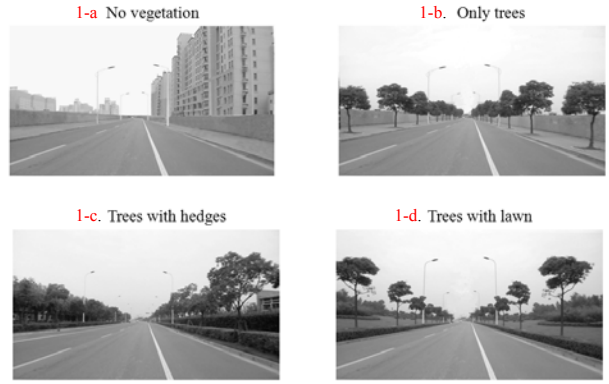

Figure 1.Street Vegetation.

●Artistic exhibits

The second group of photos, shown in Figure 2, displays four types of artistic exhibits. The respondents' attitudes towards these various types of exhibits were significantly different at a significance level of 0.05, as summarized in Table 9. Among them, "display of flowers" (8.615) was the most popular type.

Further comparing the scores of ordinary sculpture and colorful sculpture, respondents' attitudes towards these two exhibits were not significantly different. The Photo2-b of the colorful sculpture exhibit is the actual scene in Zhangjiang Semiconductor Industry Park. Changing the color of the sculpture does not change the preference of the respondents.

Table 9.F-test for various artistic exhibits.

Artistic Exhibit types	Mean	Mean Rank
No artistic exhibit	5.146	1.77
Ordinary sculpture	5.840	2.27
Display of flowers	8.615	3.71
Colorful sculpture	5.824	2.25

F= 331.03, p=0.000

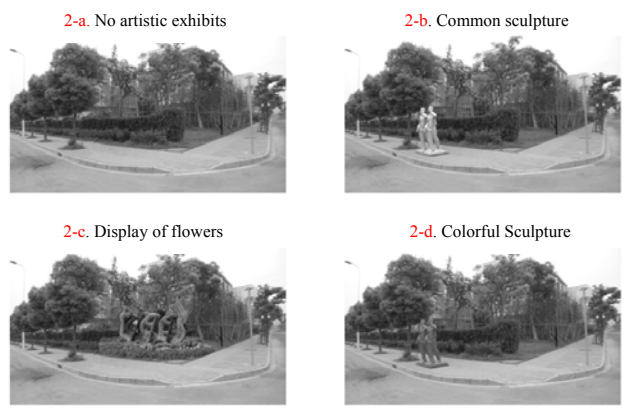

Figure 2.Artistic exhibits of sculpture or flowers

●Tram system components

The third group of photos, shown in Figure 3, displays four combinations of different overhead contact systems and road surfaces. Comparing the average scores using an F-test at a significance level of 0.05, as shown in Table 10, the p-value is approximately 0. This indicates that respondents' attitudes towards these four combinations of components were significantly different. The most preferred combination was grass road surface with no overhead contact system (8.14).

Cluster analysis of the assessment scores splits these four photos into two groups. Photos 3-a and 3-b, which depict a cement road surface, received lower scores than photos 3-c and 3-d, which depict a grass road surface. The results suggest people are more sensitive to road surface than overhead contact system, which is consistent with the results in shown in Table 6.

Table 10.F-test for various tram components.

Components		Mean	Mean Rank
Cement surface	With overhead contact system	4.750	1.55
	No overhead contact system	6.219	2.32
Grass surface	With overhead contact system	6.715	2.68
	No overhead contact system	8.142	3.45

F= 293.06, p=0.000

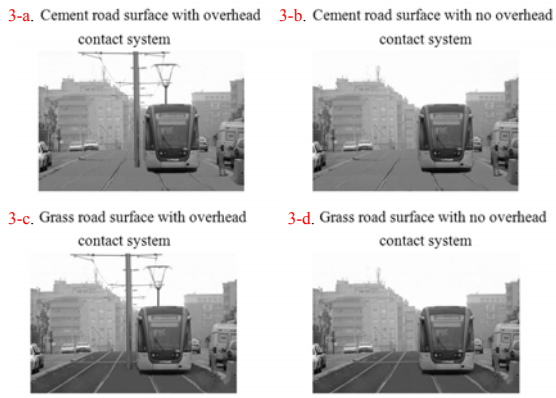

Figure 3.Landscape elements concerning tram.

6 Conclusion

This survey was carried out in three functional districts in Zhangjiang area and one place outside Zhangjiang, soliciting responses from residents, students and employees in Zhangjiang area, and learning the preference of these road users in order to provide some reference to the traffic landscape design in the tram construction program.

Results of the survey indicated that users were most concerned about pollution during construction of the tram project. Users also expressed concern about traffic landscape, but less so than pollution, comfort and fares. There is a notable difference in responses towards traffic landscape between males and females. Responses by females tended to focus more on improving traffic landscape. The findings showed no significant differences among people of different ages, occupation, education backgrounds and fore responses from different survey sites.

For the most important elements in traffic landscape, street vegetation received the largest number of responses, with bus stop and public facilities being the next

most often selected. The percentage of respondents selecting overhead contact system and tram rail, which were considered by the designers as the probable element influencing traffic landscape, was not very high. Comparing the results of the questionnaires of the four survey sites, respondents in Zhangjiang area tended to select street vegetation, bus station and overhead contact system as most important. However, respondents outside Zhangjiang area tended to select street vegetation, tram rail and surrounding buildings. This may be due in part to the fact that Zhangjiang is a newly-built community, with a low building density and wide roads, which lessens the influence of buildings and tram rails.

When comparing preferences for the particular types of street vegetation, trees with lawn or hedges were welcomed by the respondents. Options with only trees or with no vegetation were not popular. The most favored artistic exhibit was displays of flowers. The sculpture placed in Zhangjiang at present did not receive very favorable responses. Comparing the tram system components, the most popular combination was grass road surface with no overhead contact system. Respondents appeared to be more sensitive to the particular road surface than whether or not the overhead contact system was installed. As such, designers could give priority to road surface during planning.

References

Akbar K.F., W.H.G. Hale, A.D. Headley (2003). Assessment of scenic beauty of the roadside vegetation in northern England. *Landscape and Urban Planning* (J), 63:139-144

Antupit Stephen, Barbara Gray, Sandra Woods (1996). Steps ahead: making street that work in Seattle, Washington. *Landscape Urban Plan* (J), 35: 107-122

Assenna Todorova, Shoichiro Asakawa, Tetsuya Aikoh(2004). Preferences for and attitudes towards street flowers and trees in Sapporo, Japan. *Landscape and Urban Planning*(J), 69: 403-416

Meinig D.W. (1976). The beholding eye: ten versions of the same scene. *Landscape Architecture* (J), 1: 47-54

Pavlikakis G. E., Vassilios A. Tsihrintzis (2006). Perceptions and preferences of the local population in Eastern Macedonia and Thrace National Park in Greece. *Landscape and Urban Planning* (J), 77: 1:16

Xue An-shun, Shi Jing (2007). Analysis of landscape design of urban roads. *Shanxi Architecture* (J) , 33(27): 272-273

Yang Liang-liang (2007), Fu Ye. Corridor comparison and effects of "San'an" avenue in Beijing. *Journal of Capital Normal University (Natural Science Edition)* (J), 28(5): 71-75

Traffic Incident Acoustic Recognition Based on Wavelet Decomposition and SVM

Luo Xianglong[1] Wu Qisheng[2] Niu Guohong[3]

[1]School of Information Engineering, Chang'an University&School of Electronic and Information Engineering, Xi'an Jiaotong University, Central Section of the South 2nd Ring Road, Xi'an, 710064; PH(86)029-82334956; FAX(86)029-82334357; email: xlluo@chd.edu.cn.

[2]School of Electronic&Control Engineering, Chang'an University, Central Section of the South 2nd Ring Road, Xi'an,710064; PH(86)029-82334956; FAX(86)029-82334357; email:qshwu@chd.edu.cn.

[3]Xi'an Municipal Engineering Design&Research Institute, No.28,Zhuque Road, Xi'an,710068; PH(86)029-88421567; email:newgirl8074@yahoo.com.

ABSTRACT

Traffic incident automatic detection and recognition play an important role in traffic management and controlling. For the problems of automatic traffic incident detection and recognition, a method is proposed based on wavelet decomposition and support vector machine (SVM) with vehicle acoustic signals. Vehicle acoustic signals are decomposed with the wavelet analysis, and the power in different frequency is regarded as the different incident eigenvectors and also as training samples of SVM traffic incident classifier. By the processing of normal driving, braking and crash incident acoustic signals, the result shows that the proposed method is an effective method for automatic traffic incident detection and recognition.

Keywords: Wavelet decomposition；SVM；Traffic incident；Automatic recognition

INTRODUCTION

The traffic incident detection and identification is a hot research spot in the field of traffic management and controlling. The automatic detection and identification is especially concerned because of its low cost, not subject to weather restrictions, and high detection rate. Automatic incident detection (AID) methods can be divided into indirect and direct method. The indirect detection method determines traffic incident through abnormal traffic flow change, which is characterized by economic convenience. The vast majority of currently used methods belong to the indirect detection method, but its response time is too slow, and has a lag time. The direct detection method finds incident using video image processing technology, this method is "see" the traffic incident in fact, so the detection rate is far more than the indirect detection method, but it is subject to climate conditions, and intensive detection points and large capital are necessary(Jiang, 2001).

The traffic sound has always been looked as traffic noise, so generally people are extent to eliminate these noises. But in fact we can distinct different traffic incidents using special incident sounds. Then could directly "listen to" the incident

happenchance using vehicle sounds as the video image technology to "see" the incident? Harlow (Harlow, 2001) and S.Chen (Chen, 1997) has already begun such studies in this field, Xiong Lieqiang (Xiong, 2005) has proposed to detect traffic incident using vehicle acoustic and road vibration signals, Chen Qiang (2005) has verified the differences of vehicle crash with normal acoustic signals, as well as thunders through the simulation. However, these methods only show the feasibility through vehicle acoustic signals to detect traffic incidents, so the detection method based on vehicle acoustic signals need further study.

In this paper, the AID method is proposed based on wavelet decomposition and SVM using vehicle acoustic signals. The paper is organized as follows: in section 2, the feature extraction is introduced based on the wavelet decomposition, and the SVM method is reviewed. The experiment results are presented in section 3.

BACKGROUND THEORY

Feature extraction based on the wavelet decomposition. The feature selection is an important component on pattern classification since even the best classifier will perform poorly if the features used as inputs are not selected well. Meyer proposed a group of wavelet in1986, and the binary expansion and translation of proposed wavelets constitute standardized orthonormal bases in $L^2(R)$. Mallat (1998) presented the concept of multiresolution analysis in 1988, and gave a fast algorithm of wavelet transform-Mallat tower decomposition algorithm.

In this paper, the vehicle acoustic signal is divided into M bands by the wavelet decomposition, and the energy of each band is $E_i (i = 1, ..., M)$, then the feature vector can be obtained as follow:

$$T = \frac{1}{E_r}[E_1, E_2, \cdots, E_M] \tag{1}$$

Where $E_r = \sqrt{\sum_{i=1}^{M} E_i^2}$ is the root mean square (RMS) of the vehicle acoustic signal.

SVM. For a given training set, while there may exist many hyper-planes that separate the two classes, the SVM classifier is based on the hyper-plane that maximizes the separating margin between the two classes. Mathematically, this hyper-plane can be found by minimizing the following cost function:

$$J(w, \xi) = \frac{1}{2}\|w\|^2 + C\sum_{i=1}^{n} \xi_i \tag{2}$$

Subject to the constraints:

$$y_i[(w \bullet x_i) + b] \geq 1 - \xi_i, i = 1, 2, \cdots, n, \quad (x_i, y_i), i = 1, 2, \cdots, n, x \in R^d, y \in \{+1, -1\} \tag{3}$$

Where C is a user-specified, positive, regularization parameter, and $\xi_i > 0$ are slack variables.

The linear SVM can be readily extended to a nonlinear classifier by first using a nonlinear operator $\Phi(.)$ to map the input pattern into a higher dimensional space. In this condition, the constraints (3) can be written as:

$$y_i(w \bullet \Phi(x_i) + b) \geq 1 - \xi_i \quad i = 1, 2, \cdots n \tag{4}$$

Using the technique of Lagrange multipliers, one can show that a necessary condition for minimizing $J(w, \xi)$ in (2) is that the vector w is formed by a linear combination of the mapped vectors $\Phi(x_i)$, that is:

$$w = \sum_{i=1}^{n} \alpha_i y_i \Phi(x_i) \tag{5}$$

Where $\alpha_i \geq 0, i = 1, 2, \cdots n$, are the Lagrange multipliers associated with the constraints in (4).The SVM approach aims at constructing a classifier of the form:

$$f(x) = sign\{\sum_{i=1}^{n} \alpha_i y_i \Phi^T(x_i)\Phi(x) + b\} = sign\{\sum_{i=1}^{n} \alpha_i y_i K(x_i, x) + b\} \tag{6}$$

Where $K(x_i, x)$ is kernel function. Typical kernel functions have linear, polynomial, RBF and MLP (Hsu 2002, Oliver, 2002, and Millet-Roig, 2000).

EXPERIMENT

The type of the traffic incident is very complex, in this paper three types of acoustic signals of normal, braking and crash are analyzed, and normal driving (it is looked as an incident), braking incident and crash incident are identified truly. The sample frequency of acoustic signals is $11025HZ$. The time-domain waveforms of three different incident acoustic signals are shown in Figure 1, and theirs corresponding spectrum is shown in Figure 2. From Figure 1 and Figure 2, we can see that time-domain characteristics of three incidents have no obvious difference, in the frequency domain the energy of the normal driving is mainly concentrated in the lower frequency bands around $1500HZ$, and the energy distribution is more even in the entire low-frequency (see Figure 2a); the energy of the braking incident is mainly concentrated in about $500 \sim 1000HZ$ and $1500HZ$, and the energy is very small in low frequency band(see Figure 2b);for the crash incident, the energy is mainly concentrated in about $2500HZ$ .The spectral characteristics of three different incidents have obvious difference, so in this paper, the energy in frequency domain is looked as identification features.

Vehicle acoustic signals are divided into 6 layers by wavelet decomposition,

and the energy of various frequency bands is calculated separately. According to (1), 3 group 7-dimensional feature vectors can be obtained. Four samples are used training samples for each traffic incident, respectively. The normal driving incident is looked as one category, labeled as tag 1; the braking incident as a class, labeled as tag 2; the crash incident as a class, labeled as tag 3. A total of 12 sets of 7-dimensional feature vector are obtained, and these feature vectors are used as training samples to identify the traffic incident (see Table 1). Another six samples, which included the above-mentioned three types of incidents, each type has two samples, are used as the test samples for classification and identification. The feature

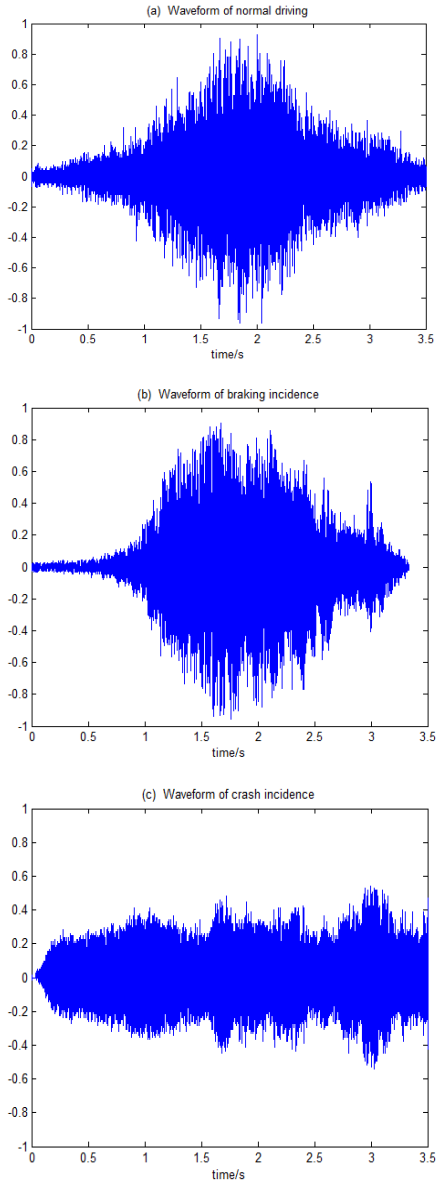

Figure 1. The time waves for three traffic incidents of vehicle acoustic signals(a)normal;(b)braking;(c)crash

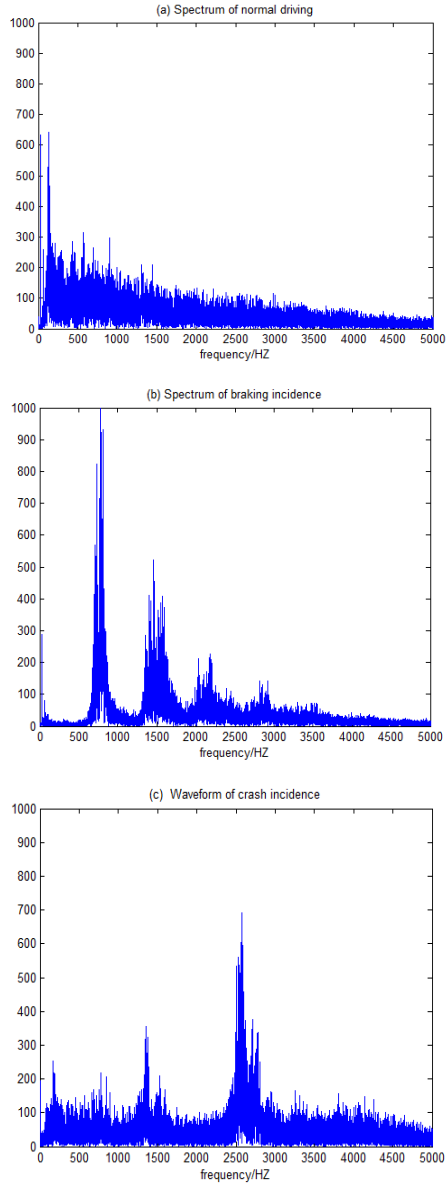

Figure 2. The frequency spectrums for three traffic incidents of vehicle acoustic signals(a)normal;(b)braking;(c)crash

Table 1. The training samples of traffic incidents classifier

No.	Feature vectors of the training samples	Tag	Incident type
1	0.1351 , 0.1678 , 0.1593 , 0.1594 , 0.1745 , 0.1245 , 0.0794	1	normal
2	0.1545 , 0.1352 , 0.1247 , 0.1463 , 0.1682 , 0.1557 , 0.1154	1	normal
3	0.1546 , 0.1365 , 0.1243 , 0.1483 , 0.1646 , 0.1575 , 0.1142	1	normal
4	0.1460 , 0.1662 , 0.1319 , 0.1455 , 0.1566 , 0.1276 , 0.1262	1	normal
5	0.0596 , 0.0167 , 0.0220 , 0.1156 , 0.2900 , 0.3594 , 0.1367	2	braking
6	0.0484 , 0.0122 , 0.0111 , 0.2110 , 0.3451 , 0.2497 , 0.1225	2	braking
7	0.0602 , 0.0137 , 0.0303 , 0.1922 , 0.2997 , 0.2492 , 0.1547	2	braking
8	0.0604 , 0.0099 , 0.0109 , 0.2139 , 0.3286 , 0.2530 , 0.1233	2	braking
9	0.0347 , 0.0532 , 0.1644 , 0.1452 , 0.1957 , 0.2507 , 0.1561	3	crash
10	0.0314 , 0.0578 , 0.1794 , 0.1265 , 0.1467 , 0.3035 , 0.1547	3	crash
11	0.0270 , 0.0617 , 0.1967 , 0.1484 , 0.1695 , 0.2668 , 0.1299	3	crash
12	0.0203 , 0.0586 , 0.1870 , 0.1391 , 0.1543 , 0.2835 , 0.1572	3	crash

Table 2. The recognition results of traffic incidents by SVM

Incident type	Feature vectors of the test samples	result
normal	0.1137 , 0.1694 , 0.1653 , 0.1539 , 0.1542 , 0.1311 , 0.1124	1
normal	0.1121 , 0.1632 , 0.1589 , 0.1540 , 0.1351 , 0.1635 , 0.1132	1
braking	0.0553 , 0.0159 , 0.0664 , 0.1124 , 0.2822 , 0.3210 , 0.1468	2
braking	0.0651 , 0.0166 , 0.0493 , 0.1072 , 0.2886 , 0.3239 , 0.1493	2
crash	0.0249 , 0.0638 , 0.1831 , 0.1673 , 0.2297 , 0.1979 , 0.1333	3
crash	0.0238 , 0.0657 , 0.1825 , 0.1632 , 0.2143 , 0.2075 , 0.1430	3

vectors of these six samples are input to traffic incident classifier set up above, the classification results are shown in Table 2, and the result is exactly the same as known traffic incidents.

CONCLUSION

In this paper, the AID method is proposed based on wavelet decomposition and SVM using vehicle acoustic signals. By the processing of normal driving, braking and crash incident acoustic signals, the result shows that the proposed method has good classification results, the algorithm is simple, and only fewer samples can achieve the classification requirements for automatic traffic incident detection and identification. But the type of traffic incidents is very complex, and the vehicle acoustic signal is prone to suffer from other environment noises, so traffic incident detection and identification need further study with a variety of types of vehicle acoustic signals.

REFERENCE

Chen Qiang(2005), "*Research on the Technology of Passive Acoustics Detection of Expressway Traffic Flow Characteristic Parameters*."Doctoral Thesis of Jilin University.

Chen S., Sun, Z. P., Bridge, B. (1997). "Automatic traffic monitoring by intelligent sound detection," *Proceedings of IEEE Intelligent Transportation Systems Conference*, Boston.

Harlow C., and Wang Y. (2001), "Automated Accident Detection," *Transportation Research Board Annual Meeting*, Washington DC.

HSU C W, LIN C J(2002). "A comparison of methods for multiclass support vector machines."*J.IEEE Transaction on Neural Networks*, 13(2),415-425.

Jiang Guiyan, Wen Huimin, Yang Zhaosheng(2001)."Design of Freeway Automatic Incident Detect ion System and Algorithm."*J. Journal of Traffic and Transportation Engineering*,1(1),77-81.

Mallat S G. *A Wavelet Tour of Signal Processing*(1998). Aca2demic Press, New York.

Millet-Roig J,Ventura-GalianoR, Chorro-GascoF J, Cebrian A(2000)."Support Vector Machine for Arrhythmia Discrimination with Wavelet Transform Based Feature Selection."*J.Computers in Cardiology*, 27(1),407-410.

Olivier Chapelle, Vladimir Vapnik, et al(2002). "Choosing multiple parameters for support vector machine."*J. Machine Learning,* 46(1), 131- 159.

Xiong Lieqiang, Shang Le, Gao Xiaohong(2005)."A Study of AID for Urban Expressway Based on Traffic Noise and Road Vibration."*J. Journal of Wuhan University of Technology (Transportation Science & Engineering)*, 9(2),238-241.

Gray-Periodic Extensional Combinatorial Model for Road Traffic Accidents in Cold Regions

Shi. An[1] and **Lilan.** Li[1,2]

[1]School of Transportation Science and Engineering, Harbin Institute of Technology, Harbin P.R. China, 150009; Tel/Fax (0451-86282116)
[2]School of Management, Harbin Institute of Technology, Harbin P.R. China, 150001; Tel/Fax (0451-86282116); e-mail：lililan@hit.edu.cn

ABSTRACT

Traffic accidents in cold regions have both general trends of change and periodic fluctuation due to the cyclical changes of the climate. Considering that Grey System Prediction Model can reflect the general trends of change visually, and Periodic Extensional Prediction Model mainly reflects the periodic fluctuation, the paper adopts the way of the Gray-Periodic Extensional Combinatorial Model to predict the traffic accidents in cold regions. This model considers both the development trends and periodic fluctuation of the traffic accidents. Finally an example analysis is given to fit and predict the road traffic accidents in cold regions, and the analysis results showed that the Gray-Periodic Extensional Combinatorial Model was suitable for the prediction of road traffic accidents in cold regions, and the fitting and prediction accuracy was much higher, which provides theory reference and practical basis for the traffic accident management and control in cold regions.

INTRODUCTION

Road traffic accidents are very serious under the snow and ice conditions in the cold regions. They are a huge threat to people's life and property. From a theoretical and objective perspective, road traffic accidents are predictable and preventable and have their own laws of development and characteristics. An effective prediction of traffic accidents can master the future development of the situation and rules（Jianming Ma et al. 2008）, and provide an important theoretical basis as well as reference data for road traffic accident mitigation.

At present, the study on the prediction of road traffic accidents is usually aiming at the general trends of change(K. Nikolopoulos et al.

2007；LIU Gang et al. 2007；MingzhiMao, et al. 2006；S.R. Singh 2007）. However, the occurrence of traffic accidents in cold regions has both general trends of change and periodic fluctuations because of the cyclical changes of the climate. Thus it makes the prediction model more uncertain and the prediction accuracy is reduced, and it also reduces the practical value of the prediction results.

Gray prediction of road traffic accidents (MingzhiMao et al. 2006) can discover and master the law of system development through dealing with the original data and building Grey models. The geometric figure of the prediction result is a relatively smooth curve, which can reflect the general trend visually. However, the fitting precision is poor for the data column of road traffic accidents which has greater volatility. While the periodic extensional prediction model can reflect the characteristics of cycle fluctuation commendably, it cannot reflect the characteristic of general trends of change. The more obvious that the general trends of change show, the lower prediction accuracy becomes. In fact, the gray prediction model has strong integration and penetration features for general models, so incorporating GM (1,1) model to the general model can enhance the prediction accuracy sharply. So for the data column of road traffic accidents which have the characteristics of general trends of change and cycle fluctuation, it should build the Gray-Periodic Extensional Combinatorial Model (REN Feng et al. 2007) to combine the two prediction methods. This can make up each other's deficiency and achieve good prediction efficiency.

The paper adopts the Gray-Periodic Extensional Combinatorial Model to predict the traffic accidents in cold regions. That is, building the Residual Periodic Extensional Model on the basis of general Grey Model GM(1,1), and restructuring new data sequence by extracting the dominant period, and stacking the different periodic values at the same time as the residual compensation of GM(1,1).

GARY-PERIODIC EXTENTIONAL COMBINATORIAL MODEL

Assuming that a certain behavioral sequence of the system (nonnegative) is: $X^{(0)} = (x^{(0)}(1), x^{(0)}(2), \cdots, x^{(0)}(n)) \quad x^{(0)}(k) \geq 0; \quad k = 1, 2, \cdots, n$

Build the GM(1,1) model of the $X^{(0)}$ sequence.

1) Calculate the 1-AGO sequence $X^{(1)}$ of $X^{(0)}$. we can get: $X^{(1)} = (x^{(1)}(1), x^{(1)}(2), \cdots, x^{(1)}(n))$, where $x^{(1)}(k) = \sum_{i=1}^{k} x^{(0)}(i), \ k = 1, 2, 3, \cdots, n$.

2) Make the quasi-smoothness test for sequence $X^{(0)}$.

$$\rho(k)=\frac{x^{(0)}(k)}{x^{(1)}(k-1)}$$

If $\rho(k)<0.5$, it will satisfy the smooth condition, and the sequence change is steady.

3) Calculate the mean-value generating sequence $Z^{(1)}$ of $X^{(1)}$.

$Z^{(1)}=(z^{(1)}(2),z^{(1)}(3),\cdots,z^{(1)}(n))\quad z^{(1)}(k)=0.5(x^{(1)}(k)+x^{(1)}(k-1)),\qquad k=2,3,\cdots,n$

Constructing matrix $Y=\begin{bmatrix}x^{(0)}(2)\\x^{(0)}(3)\\\vdots\\x^{(0)}(n)\end{bmatrix}$, $B=\begin{bmatrix}-z^{(1)}(2) & 1\\-z^{(1)}(3) & 1\\\vdots & \vdots\\-z^{(1)}(n) & 1\end{bmatrix}$

4) Make a least-square estimation for the parameters column $\hat{a}=[a,b]^T$.

$$\hat{a}=[a,b]^T=(B^TB)^{-1}B^TY\qquad \alpha=\frac{a}{1+0.5a},\qquad \beta=\frac{b}{1+0.5a}$$

5) Build the model.

$$\hat{x}^{(0)}(k)=(\beta-\alpha x^{(0)}(1))e^{-a(k-2)}$$

6) Calculate the simulated value of $X^{(0)}$.

$$\hat{X}^{(0)}=(\hat{x}^{(0)}(1),\hat{x}^{(0)}(2),\cdots,\hat{x}^{(0)}(n))$$

7) Accuracy test.

Calculate residual series $x'(k)$: $\qquad x'(k)=x^{(0)}(k)-\hat{x}^{(0)}(k)$

Calculate residual sum of squares:

$$s=X'^{T}X'=[x'(2),x'(3),\cdots,x'(n)]\begin{bmatrix}x'(2)\\x'(3)\\\vdots\\x'(n)\end{bmatrix}$$

Calculate average relative error: $\Delta=\frac{1}{n}\sum_{k=1}^{n}\Delta_k$, $\qquad \Delta_k=\frac{|x'(k)|}{x^{(0)}(k)}$

Build the periodic extensional model of residual sequence $x'(k)$.

1) Calculate the mean-generating function of sequence $x'(k)$.

$$\overline{x}_m(i)=(\sum_{j=0}^{n_m-1}x'(i+jm))/n_m;\qquad i=1,2,\cdots,m,\qquad 1\le m\le M$$

Where n is the length of the sample sequences, n_m is the greatest

integer that is smaller than n/m, M is the greatest integer that is smaller than n/2. Then we can get mean-generating function matrix:

$$\begin{bmatrix} \bar{x}_1(1) & \bar{x}_2(1) & \bar{x}_3(1) & \cdots & \bar{x}_M(1) \\ & \bar{x}_2(2) & \bar{x}_3(2) & \cdots & \bar{x}_M(2) \\ & & \bar{x}_3(3) & \vdots & \bar{x}_M(3) \\ & & & & \bar{x}_M(M) \end{bmatrix}$$

Make periodical continuation of mean-generating function $\bar{x}_m(i)$.

$$f_m(k) = \bar{x}_m(i), \quad k = i[\mathrm{mod}(m)], \quad k = 1,2,3,\cdots,n$$

Where mod represents congruence, $f_m(k)$ is the continuation function of the mean-generating function.

2) Extract the advantage period.

(1) Based on the basic principle of variance analysis, we can use the following formula to test whether sequence $x'(k)$ contains the period with the length of m.

$$F^{(m)} = (n-m)S^{(m)}/((m-1)S)$$

It satisfies the F-distribution with the freedom of $(m-1, n-m)$.

where $S^{(m)} = \sum_{i=1}^{m} n_i(\bar{x}_m(i)-\bar{x})^2$, $n_i = n/i, \bar{x} = (\sum_{i=1}^{n} x(i))/n, S = \sum_{i=1}^{m}\sum_{j=1}^{n_m}(x(i+(j-1)m)-\bar{x}_m(i))^2$

For a given confidence level α, if $F^{(m)} > F_\alpha(m-1, n-m)$, we think that $x(k)$ contains the period the length of which is m.

(2) Establish the advantage period with the length of m. That is,

$$S(m)/m = \max S(m)/m, \quad 2 \le m \le M$$

3) Generate the new sequence. Sequence $x'(k)$ subtracts the continuation function which is corresponding to the period m can generate a new sequence. That is,

$$x''(k) = x'(k) - f_m(k)$$

Then, from repeating steps 2 and 3, we can extract the other advantage period.

4) Superposition. $f(k)$ is the superposition value which is the superposition of the value from different cycles at the same time, $f(k) = \sum_{i=1}^{m} f_i(k)$. It is the periodic extensional model which is built by the period-superposition extrapolated method.

Calculate the fitted value of the gray-periodic extensional combinatorial model.

$$\bar{x}(k) = \hat{x}(k) + f(k)$$

EXAMPLE ANALYSES

Table 1 is the statistical result of traffic accident rates of a certain highway in China's northeast area, distributed monthly from 2002 to 2005. The road traffic accident rates show clear signs of the seasonal cycle of change and sustained upward trends, so it is applicable to the gray-periodic extensional combinatorial model.

Table 1. Monthly distribution of road traffic accident rates per 10 thousand vehicles (time/MV) from 2002 to 2005.

Year	Jan.	Feb.	Mar.	Apr.	May	Jun.
2002	0.7970	0.3108	0.8862	0.6636	0.9744	0.8530
2003	1.0065	0.4482	0.9697	0.6392	1.0352	0.9348
2004	1.2058	0.6055	1.1045	0.7436	1.0303	0.9841
2005	1.3293	0.8399	1.3425	0.7924	0.9754	1.1151
Year	Jul.	Aug.	Sep.	Oct.	Nov.	Dec.
2002	0.6485	1.0084	1.1025	0.5345	0.8775	1.0244
2003	0.7159	1.0672	1.2037	0.9399	1.0244	1.2427
2004	0.7355	1.0979	0.9882	0.9542	1.1880	1.0761
2005	0.9197	1.1186	1.4274	0.9745	1.2840	1.2561

Build GM(1,1) model and calculate the residual sequence. Assuming that the sequence of road traffic accident rates per 10 thousand vehicles is: $X^{(0)} = (x^{(0)}(1), x^{(0)}(2), \cdots, x^{(0)}(n)) \quad x^{(0)}(k) \geq 0; \quad k = 1, 2, \cdots, n$

Calculate the parameters column:

$$\hat{a} = [a, b]^T = [-0.0093, 0.7596]^T$$

$$\alpha = \frac{a}{1 + 0.5a} = -0.00934, \qquad \beta = \frac{b}{1 + 0.5a} = 0.763$$

The GM(1,1) model is: $\hat{x}^{(0)}(k) = (\beta - \alpha x^{(0)}(1))e^{-a(k-2)} = 0.771e^{0.0093(k-2)}$

It is an index model and reflects the general trend of change in the sequence. Table 2 shows the residual and fitting error of the GM(1,1) model. The GM(1,1)model reflects an overall upward trend. However, the fitting effect is poor and the model can't meet the prediction requirement because of the accident rate sequence which has cycle fluctuation and large amplitude. Therefore, we should combine the periodic extensional model to correctly reflect the dynamic characteristics of the road traffic accidents in the cold regions.

Build the Periodic Extensional Prediction Model of residual sequence. When m equals to 12，15，13, they are advantage periods,

so $f(k) = f_{12}(k) + f_{15}(k) + f_{13}(k)$ .Then the gray-periodic extensional combinatorial model of the accident rate per 10 thousand vehicles is as follows, $\bar{x}(k) = 0.771e^{0.0093(k-2)} + f(k)$. Table 3 is the fitting result of the model.

Accuracy Test. From table 3 we know that the residual sum of squares equals 0.05 and the average relative error equals 0.0273. Compared to the gray model, the gray-periodic extensional combinatorial model has a better fit precision wise and can satisfy the precision requirement. The fitting results of some individual data in the model are less than desirable, because the original data has large amplitude. If we can carry data transformation processing based on the characteristics of the data to reduce the amplitude at the practical application of the model, the model can get better results.

PREDICTIONS

Suppose k equals to 49,50,51,⋯,60, and substitute the values to the gray-periodic extensional combinatorial model. Table 3 shows the predictive value of road traffic accident rates per 10 thousand vehicles in 2006.

CONCLUSIONS

This study successfully applies the gray-periodic extensional combinatorial model to the dynamic prediction of road traffic accidents in cold regions which have both general trends of change and cyclical change characteristics. The model combines the advantage of Grey prediction and periodic extensional prediction, and develops new information based on the full use of historical data. By the example verification, the Gray-Periodic Extensional Combinatorial Model can reflect the various characteristics of road traffic accidents in the cold regions and have a good fit effect with the historical data. The model expands the application range of the Grey prediction. The prediction accuracy is improved to provide a scientific basis for developing effective road safety countermeasures.

Table 2. The fitting effect of Model GM(1,1).

Year		Jan.	Feb.	Mar.	Apr.	May	Jun.
2002	Measured value	0.7970	0.3108	0.8862	0.6636	0.9744	0.8530
	Fitting result	0.764	0.771	0.778	0.785	0.793	0.800
	Residual	0.0331	-0.4602	0.1080	-0.1219	0.1816	0.0528
	Relative error (%)	4	-148	12	-18	19	6
2003	Measured value	1.0065	0.4482	0.9697	0.6392	1.0352	0.9348
	Fitting result	0.854	0.862	0.870	0.878	0.886	0.895
	Residual	0.1525	-0.4138	0.0996	-0.2390	0.1488	0.0401
	Relative error (%)	15	-92	10	-37	14	4
2004	Measured value	1.2058	0.6055	1.1045	0.7436	1.0303	0.9841
	Fitting result	0.955	0.964	0.973	0.982	0.991	1.000
	Residual	0.2509	-0.3583	0.1317	-0.2383	0.0392	-0.0163
	Relative error (%)	21	-59	12	-32	4	-2
2005	Measured value	1.3293	0.8399	1.3425	0.7924	0.9754	1.1151
	Fitting result	1.068	1.078	1.088	1.098	1.108	1.118
	Residual	0.2617	-0.2377	0.2548	-0.3054	-0.1327	-0.0034
	Relative error (%)	20	-28	19	-39	-14	0

Year		Jul.	Aug.	Sep.	Oct.	Nov.	Dec.
2002	Measured value	0.6485	1.0084	1.1025	0.5345	0.8775	1.0244
	Fitting result	0.808	0.815	0.823	0.831	0.838	0.846
	Residual	-0.1592	0.1932	0.2797	-0.2961	0.0392	0.1782
	Relative error (%)	-25	19	25	-55	4	17
2003	Measured value	0.7159	1.0672	1.2037	0.9399	1.0244	1.2427
	Fitting result	0.903	0.911	0.920	0.929	0.937	0.946
	Residual	-0.1872	0.1557	0.2837	0.0113	0.0871	0.2967
	Relative error (%)	-26	15	24	1	9	24
2004	Measured value	0.7355	1.0979	0.9882	0.9542	1.1880	1.0761
	Fitting result	1.010	1.019	1.029	1.038	1.048	1.058
	Residual	-0.2742	0.0788	-0.0404	-0.0840	0.1401	0.0184
	Relative error (%)	-37	7	-4	-9	12	2
2005	Measured value	0.9197	1.1186	1.4274	0.9745	1.2840	1.2561
	Fitting result	1.129	1.139	1.150	1.161	1.172	1.183
	Residual	-0.2092	-0.0209	0.2773	-0.1864	0.1124	0.0735
	Relative error (%)	-23	-2	19	-19	9	6

Table 3. The fitting result and predictive value of the Model (time/MV).

Year		Jan.	Feb.	Mar.	Apr.	May	Jun.
	Measured value	0.7970	0.3108	0.8862	0.6636	0.9744	0.8530
2002	Fitting result	0.8206	0.3318	0.9131	0.6657	1.0011	0.8261
	Relative error (%)	-3	-7	-3	0	-3	3
	Measured value	1.0065	0.4482	0.9697	0.6392	1.0352	0.9348
2003	Fitting result	1.0109	0.4348	0.9361	0.6214	1.0139	0.9161
	Relative error (%)	0	3	3	3	2	2
	Measured value	1.2058	0.6055	1.1045	0.7436	1.0303	0.9841
2004	Fitting result	1.1839	0.5752	1.0868	0.7424	1.0544	0.9825
	Relative error (%)	2	5	2	0	-2	0
	Measured value	1.3293	0.8399	1.3425	0.7924	0.9754	1.1151
2005	Fitting result	1.2922	0.8567	1.4096	0.8399	1.0730	1.1597
	Relative error (%)	3	-2	-5	-6	-10	-4
2006	Predictive value	**1.2504**	**0.7657**	**1.3510**	**1.1077**	**1.4472**	**1.2764**
Year		Jul.	Aug.	Sep.	Oct.	Nov.	Dec.
	Measured value	0.6485	1.0084	1.1025	0.5345	0.8775	1.0244
2002	Fitting result	0.6704	1.0488	1.1202	0.5357	0.8533	1.0260
	Relative error (%)	-3	-4	-2	0	3	0
	Measured value	0.7159	1.0672	1.2037	0.9399	1.0244	1.2427
2003	Fitting result	0.6923	1.0462	1.1768	0.9378	0.9976	1.2696
	Relative error (%)	3	2	2	0	3	-2
	Measured value	0.7355	1.0979	0.9882	0.9542	1.1880	1.0761
2004	Fitting result	0.7311	1.1089	1.0218	0.9720	1.2093	1.0977
	Relative error (%)	1	-1	-3	-2	-2	-2
	Measured value	0.9197	1.1186	1.4274	0.9745	1.2840	1.2561
2005	Fitting result	0.9472	1.1745	1.3418	0.9355	1.2583	1.2310
	Relative error (%)	-3	-5	6	4	2	2
2006	Predictive value	**1.1249**	**1.5075**	**1.5832**	**1.0030**	**1.3250**	**1.5021**

REFERENCES

Jianming Ma, Kara M. Kockelman, Paul Damien. (2008). "A multivariate Poisson-lognormal regression model for prediction of crash counts by severity, using Bayesian methods." *Accident Analysis and Prevention*, 40, 964–975

K. Nikolopoulos, P. Goodwin, A. Patelis and V. Assimakopoulos. (2007). "A comparison of multiple regression with alternative forecasting approaches." *European Journal of Operational Research*, 180(1):

354-368

LIU Gang, ZHU Jin-fu. (2007). "Civil Aviation Accident Forecasting Based on Gray Metabolism Markov Model." *China Safety Science Joumal,* 17(5): 17-20

MingzhiMao, E. C. Chirwa.(2006). "Application of gray model GM(1, 1) to vehicle fatality risk estimation." *Technological Forecasting and Social Change*, 73(5): 588-605

REN Feng，LI Wei，DING Chao. (2007). "Load Forecasting Based on Gray-Periodic Extensional Combinatorial Model." *Power System Technology*, 31(24): 52-54

S.R. Singh.(2007). "A simple method of forecasting based on fuzzy time series." *Applied Mathematics and Computation*, 186(1): 330-339

A Multi-objective Decision Model of Traffic Rescue Service Site Location on Road

Gan Chai[1], Chengwei Fang[1], Jiaxiang Zhou[1], Shui Wan[1]

[1]Intelligent Transportation System Institute, Southeast University, P.O.BOX 210096, Nanjing, China; PH 13851446229; email: chaig@263.net, fangchengwei@163.com.

ABSTRACT

The optimization layout of rescue sites is the premise of implementing traffic resources dispatch and improving rescue efficiency. The multi-objective demands for locating rescue sites on roads cannot be easily satisfied with the traditional single-objective rescue facilities. Based on determined objects used for location, the model of multi-objective decision is proposed to provide suitable schemes of location of rescue sites on road. Integrating traditional models of location, such as p-medians, p-centers, maximum covering location and backup covering, the founded model of multi-objective locations satisfy quick response objects by minimizing the maximum rescue time, satisfy service efficiency objects by maximizing the covering demands and minimizing the total weighted time, and satisfy the demand-oriented objects of serious accidental rescue by maximizing the backup covering demands. Combined with analysis, for example, parametric programming is used to analyze the model, which shows that the model is feasible, and can be used as the theoretical basis for locating traffic rescue sites on roads.

0 INTRODUCTIONS

The study of road traffic accident focuses on preventative measures and rescue schemes. The preventative measures mainly include the investigation and renovation of accident black spots, improvement of road conditions, as well as the construction of road safety facilities. The rescue schemes mainly include the rescue association, the resources dispatch, and on-site rescue. Optimizing the location of traffic rescue service sites on roads, which belong to the preventive measures, has not been given enough attention in real works. Location of rescue sites mainly depends on the subjective judgment and experience from decision-makers, a lack of scientific basis. And scholars at home and abroad propose a number of classic models, such as collection covering location model, maximum covering location model, backup covering model, and p-medians and p-centers.

Collection covering location is used to identify the minimum number of facilities which can cover all the requirement sites. If there are limited funds, only P facilities can be chosen, and in this case, the process of maximum covering location is used to identify the location of each facility to maximize the population (or other indicators) of covered requirement sites. As the requirement sites, which are served a by

single facility, can hardly have been served in time under a congested situation, the backup covering model gives the backup covering scheme for requirement sites. Considering the efficiency of location, the p-median model minimizes the total weighted distance from the facilities to the requirement sites. Considering the fairness of location, the p-center model makes the maximum rescue time from the facilities to the requirement sites minimal. The research of reference literature [5, 6] to road-network-zoning essentially belongs to the p-center model. The above models belong to single-objective decision models. Each model extracts only one major factor from the amount of decision factors as the object of the decision of the location. However, for the location of road traffic rescue service sites, the decision-makers should consider the cost of rescue, the response time, the strength of demand, and other factors and integrate all the factors into the final decision. That is to say, the multi-objective location model of decision-making is strongly needed. Therefore, by identifying the objectives of location, this paper proposes the multi-objective model and the method of solution adapting to road traffic rescue service sites location and provides the theoretical basis for traffic rescue sites on roads.

1 THE DECISION OBJECTIVE OF RESCUE SITES LOCATION

For the road network itself, the proportion of serious traffic accidents is relatively small. Therefore, the fairness and efficiency principle should be taken into consideration in the process of location. The fairness principle requires each requirement site can be covered in the rescue time limit. If not all the sites can be covered, we should minimize the maximum rescue time. For different sites, the efficiency requirements are different. For the sites of high strength, the shortest journey time from the rescue service site is required. The fairness principle can be reflected in the collection of covering location and p-centers, and the efficiency principle can be reflected in maximum covering location and p-medians. In addition, due to the serious results of accidents, the rescue service sites should have the ability of backup covering for the requirement sites, so that when grave accidents happen they can be associated and take part in the rescue process, and the damage of the accident can be reduced as much as possible.

The efficiency, as well as fairness, should be reflected in the decision objective of traffic rescue sites location on road. Based on the rapid response or fairness, the first object requires the maximum rescue time from the rescue site to the requirement site minimized. Based on the accessibility and the efficiency of rescue site, the second object requires the amount of requirement of one-time-covering and minimizing the total weighted time from rescue-site to the requirement site. The third object is based on the consideration of backup covering, and it requires maximizing the amount of requirement of backup covering. But the object of the decision does not take the minimized cost into consideration because the fairness and efficiency principle need to identify the number of rescue sites—P beforehand, and the parameter P affects the cost directly.

2 THE MULTI-OBJECTIVE DECISION MODEL OF LOCATION

2.1 The definition of road network

The road network is defined as G= (V, E, A, T), where V is the set of nodes, the amount of nodes |V|=n, E is the set of arcs which connect each nodes, A is the set of weights and the weight of node I is defined as a_i, T is the set of travel times among the sites, t_{ij} is the travel time from rescue-site j to requirement site i. The set of requirement sites I=V, the set of candidate rescue-sites J=V.

2.2 The establishment of the model

We set the maximum rescue time as L, and the objective of minimizing the maximum rescue time requires L being minimized. If node I is covered in limit time T, then y_i=1， otherwise y_i=0. Using the efficiency objective requires the demand quantity of one time covering to reach to $\max \sum_{i\in I} a_i y_i$. If node I is covered by backup resource in limit time T, then u_i=1, otherwise u_i=0. The objective of reducing the damage degree requires the demand quantity of backup covering to reach to $\max \sum_{i\in I} a_i u_i$. Where the requirement site i is severed by the rescue site j, z_{ij}=1, otherwise z_{ij}=0. The quick respond objective requires the total weighted rescue time to reach to $\min \sum_{i\in I} a_i t_{ij} z_{ij}$. The rescue time for reaching the rescue site should be smaller than the maximum rescue time, namely $\sum_{j\in J} t_{ij} z_{ij} < L$. If a rescue service site is established at a candidate site j, then x_j=1 otherwise x_j=0. We set $N_i = \{j \mid t_{ij} \le T\}$ as the set of rescue service sites which could arrive at the requirement site i in the limit time T and p as the number of predefine rescue service sites.

Objective functions:

$$\text{Min } V_1 = L \quad (1) \qquad \text{Max } V_2 = \sum_{i\in I} a_i y_i \quad (2)$$

$$\text{Max } V_3 = \sum_{i\in I} a_i u_i \quad (3) \qquad \text{Min } V_4 = \sum_{i\in I} a_i t_{ij} z_{ij} \quad (4)$$

ST:

$$\sum_{j\in J} x_j = p \quad (5)$$

$$\sum_{j\in N_i} x_j - y_i - u_i \ge 0, \forall i \in I \quad (6)$$

$$u_i \le y_i, \ \forall i \in I \quad (7)$$

$$\sum_{j\in J} z_{ij} = 1, \forall i \in I \quad (8)$$

$$z_{ij} \le x_j, \ \forall i \in I, \forall j \in J \quad (9)$$

$$\sum_{j\in J} t_{ij} y_{ij} \le L, \forall i \in I \quad (10)$$

$$x_i, y_i, u_i, z_{ij} \in \{0,1\}, \ \forall i \in I, \forall j \in J \tag{11}$$

2.3 The explanation of model

The number of rescue sites p is guaranteed by constraint (5). Constraint (6) shows that not every requirement site can be covered within rescue time limit. Constraint (7) guarantees that the requirement site can be covered in second time only when it has been covered one time. Constraint (8) guarantees that every requirement site can be served by relevant rescue service sites. Constraint (9) guarantees that node j can serve requirement sites only when the rescue service site has been established at this node. The maximum rescue time L is defined in Constraint (10). Constraint (11) guarantees the values of variables are 0 or 1. Object (1) and Constraint (5), (9) and (10) guarantee to minimize the maximum rescue time (L) from rescue service site to requirement site. It is namely the p-centers, and incarnates the principle of fairness. Object (2) and Constraint (5) and (6) guarantee to maximize the demand of one time covering. It is namely the maximal covering model, and incarnates the principle of efficiency of system. Object (3) and Constraint (5), (6) and (7) named backup covering model guarantee to maximize the demand of backup covering in term of rescue time limit. Object (4) and Constraint (5), (8) and (9) guarantee to minimize the total weighted time from rescue service sites to requirement sites. It is namely the p-median and incarnates the principle of efficiency.

The above model with 4 objectives is a multi-objective decision model of location. The standard function of multi-objective decision is Min [V_1，$-V_2$，$-V_3$，V_4].

The multi-objective decision model of roads rescue service sites location proposed in this paper integrates the classical location models, such as collection covering location model, maximum covering location model, backup covering model, p-medians and p-centers.

3 THE SOLUTION AND ANALYSIS OF THE MODEL

The methods of solving multi-objective decisions are a flexible approach, in general, including Pareto optimality analysis, objective programming method, fuzzy multi-objective programming method, as well as parameters programming method and so on. Parameters programming method is simple and practical in solving multi-objective programming problems. When using the parameters programming method, multi-objective optimizing model can be converted into a single-objective parameters programming model in two ways: weighted method and constraint method. First, an effective solution is produced in each method. Then, by the way of parameter variation of single-objective linear programming, a group of effective solutions are produced. The constraint method is used to solve the model in this paper.

One of all K objects has been retained and optimized in the constraint method. And the rest K-1 objects, each of which subjects to an acceptable value, have been considered as constraints. By adding these constraints to the original constraint equations, the multi-objective optimization model is converted to a single-objective linear programming problem. By continually changing the acceptable value on the right

side of the constraint equation, a set of effective solutions can be obtained. In the above-mentioned multi-objective decision model, the target V4 is retained, and we make the objective V1, V2 and V3 to be constrained by the acceptable value α, β and γ on the right of each equation. Namely, $L \le \alpha$, $\sum_{i \in I} a_i y_i \ge \beta$ and $\sum_{i \in I} a_i u_i \ge \gamma$. There is a lower limit of α which is the rescue time calculated by p-centers. Both β and γ has an upper limit value. The upper limit value of β is calculated by maximal covering model and the upper limit value of γ is calculated by backup covering model.

A virtual road network of highways is established in Fig 1. The small circles in the network are the candidate rescue service sites and also the requirement sites. The number a_i in each circle is the weight of the requirement site. For example, 2（3） means the weight of Node 2 is 3. The number above each line means the travel time t_{ij} from one site to another. Set limit time of rescue T=7 minutes.

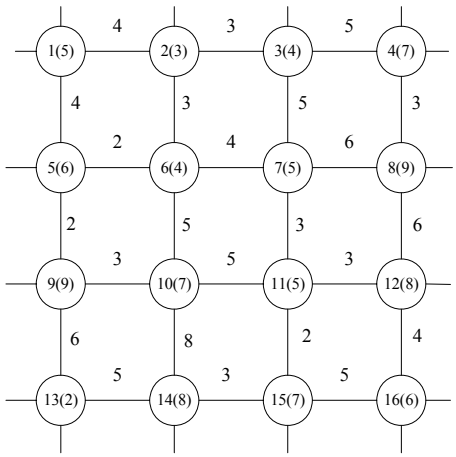

Figure.1 Example of virtual road network.

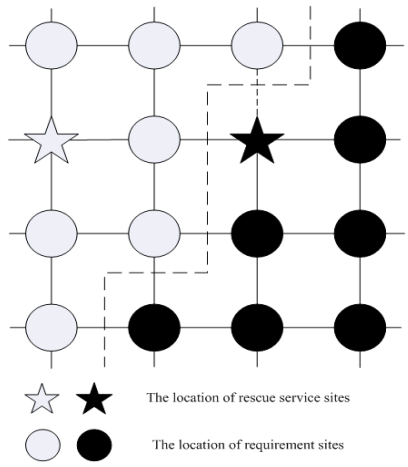

Figure.2 Schematic diagram of constrain method's result.

By calculating, we can see the rescue service sites are established at Node 5 and Node 7. Nodes 1, 3, 8, 10, 11, 12 and 15 can be covered by one time covering and Nodes 2, 5, 6, 7 can be covered by backup covering. The max rescue time is 10 minutes, and the requirement quantity of one time covering is 72, and the requirement quantity of backup covering is 18. The total weighted rescue time of this system is 471 minute. The rescue sites and their service objects are showed in Fig 2. The comparison of multi-objective location and single-objective location are made in Table 1.

It can be inferred from Table 1 that the result of p-centers and p-medians are the same, both of them chose Node 5 and 7 to establish rescue service sites. The total

weighted rescue time and the max rescue time of the system can be minimized simultaneously. In this case, however, the requirement quantity of backup covering is minimal. The maximum covering location realizes the goal that maximize the requirement of one time covering, but the total weighted rescue time and the max rescue time of the system are somewhat extended. The backup covering model makes the requirement quantity of backup covering maximized, but the total weighted rescue time and the max rescue time of the system, as well as the requirement quantity of one time covering are gravely extended. However, the multi-objective model of location is not better than any single-objective model in the performance, but by taking four objectives into consideration, decision-makers can make a reasonable trade-off among them.

Tab.1 The comparison results of multi-objective and single-objective model.

model	*location*	*V1*	*V2*	*V3*	**V4**
multi-object	5，7	10	72	18	471
p-medias	5，12	9	74	5	429
p-centers	5，12	9	74	5	429
maximal covering	6，12	10	78	10	441
backup covering	11，15	13	50	46	590

4 CONCLUSION

Rescue service sites location on roads is a multi-objective optimization problem. In this process of decision-making, both the fairness of location and the efficiency of sites should be considered, and sometimes, the backup covering of sites should also be taken into account. A multi-objective decision model proposed in the paper integrates the classic locating model, such as p-medians, p-centers, maximum covering and backup covering of traffic rescue site location on road. The objective weighted method and constrained method of parametric programming are adopted to solve the model, the solutions of the four classical location schemes are proposed, and an example of calculating the practical value of this multi-objective location model is shown. The multi-objective decision model is a determinate model that is unable to identify the number and the location of rescue vehicles under a crowded situation. Further study using random model and intelligent algorithms is needed to solve these problems.

BIBLIOGRAPHY

Church R, ReVelle C. “The maximal covering location problem.” *Papers of the Regional Science Association*, 32, pp: 101-108. (1974).

Cohon J L. “Multiobjective Programming and Planning.” New York：*Academic Press*. (1978).

Han Qiang. “The Simulated Annealing Algorithm of Multi-objective Emergency

Facilities Location." *Computer Engineering and Applications*, 43（30）, pp: 182-183. (2007).

Hogan K, ReVelle C. "Concept and Applications of Backup Coverage." *Management Science*, 32(11), pp: 1434-1444. (1986).

Hu Yu-da. (1990). "Practical Multi-objective Optimization." *Shanghai Science and Technology Press*. (1986).

Ines Kanoun, Habib Chabchoub, Belaid Aouni. "Goal Programming Model for Fire and Emergency Service facilities site selection." *MOPGP'06：7th Int. Conf. on Multi-Objective Programming and Goal Programming*. (2006).

John Current, Hokey Min, David Schilling. "Multi-objective Analysis of Facility Location Decisions." *European Journal of Operational Research*, 49（3）, pp: 295-307. (1990).

Konstaninos G Zografos, Konstaninos N Androutsopoulos, Geprge M Vasilakis. (2002). "A real-time decision support system for roadway network incident response logistics." *Transportation Research*, C, pp: 1-18. (1990).

Kostas G. Zografos, Teti Nathanail, Panos Michalopoulos. "Analytical Framework for Minimizing Freeway-incident Response Time." *Journal of Transportation Engineering*, 119（4, pp: 535-549. (1993).

Toregas C, Swain R, ReVelle C. "The location of emergency service facilities.", *Operations Research*, 19, pp: 1363-1373. (1971).

Yun Mei-ping, Yang Xiao-guang. "Improvement of Road Network Zoning Optimization Model for incident Management in Advanced Traffic Management Systems." *Journal of Highway and Transportation Research and Development*, 21（4）, pp: 73-76. (2004).

The Method of Road Safety Analysis Based on Two-dimensional Speed Difference

Liu Xingwang[1] and Wu Jingmei[2]

[1]Road Safety Research Center, M.O.C, Research Institute of Highway Ministry of Communications, NO.8 XiTuCheng Rd. Haidian District, Beijing 100088, China, PH (86) 10-6236 4459; FAX (86) 10-6236 3428; email: xw.liu@rion.cn
[2]Road Safety Research Center, M.O.C, Research Institute of Highway Ministry of Communications, NO.8 XiTuCheng Rd. Haidian District, Beijing 100088, China, PH (86) 10-6236 4459; FAX (86) 10-6236 3428; email: jm.wui@rion.cn

ABSTRACT

Human, vehicle and road are three essential factors in transport system, the coordination of system may be shown by the road-human, human- vehicle and vehicle-road. The traffic accident has the relations with the coordination of transport system under the condition of normal driving. The speed is the important index which may appropriately show vehicles' operation characteristics, and provide the relationship between human-road and vehicle-road. Each vehicle has an accelerating and decelerating moving speed in the two-dimension, and the speed has the relationship with road geometric, traffic and accident. Based on analyzing the speed and vehicles' operation characteristics, it is developed to use two-dimensional speed difference to show the rule between moving and safety, and then develop the road safety evaluation model and criterion for the horizontal alignment by using theory computing and actual accident investigation method.

INTRODUCTION

There are three important relationships in transportation system: road-human, human-vehicle and vehicle-road. The operating speed is a variable of system operation, which has the relationship with road geometric, transportation environment, driver expectation and vehicle conditions. So it is possible to evaluate the coordination of horizontal and vertical alignments based on vehicles' operating speed characteristic.

At present, the operating speed difference is commonly used to assess the coordination of horizontal and vertical alignments (TRB 1998, NCHRP 2003,FHWA 1999). The advantage of this method is simple and easy to use. The disadvantage is that it neglects the effect that the speed difference per unit time has on the traffic, also neglects the effect that the transition curve has on reducing the vehicles' speed

difference of road section. In addition, it can't show that the curve length has the influence on traffic safety. Therefore, it should be improved.

SAFETY ANALYSIS OF TRANSPORTATION OPERATION SYSTEM

It is important to understand the characteristic indexes of the transportation system in order to assess if the road transportation operation system is coordinated. The transportation operation system has three kinds of characteristic indexes. The first one includes the horizontal and vertical alignments characteristic indexes (slope spot, tangent straight slow spot, transition curve and curve included), the road surface condition changing characteristic indexes(super elevation, roadside width and friction coefficient included), and the apparent distance changing characteristic (distance road section providing, apparent distance changing and so on included). The second one includes some human of actual sensation, such as sigh distance spot, sensation changing spot, human's operation frequency. The third one includes vehicles speed changing path characteristic, vehicles acceleration path characteristic, and vehicles wheel path characteristic.

The practical experience shows that the horizontal and vertical alignments have obvious relations with the operating speed, which may respond the relations on the horizontal and vertical alignments inducing the driver; the driving sensation and operation time may be shown by the driver's most need time; the driving operation difficulty degree and the relations on vehicles conform to the route may be possible to be responded by the vehicles acceleration changing indexes. So it can appraise the system the safety based on operation speed and curve acceleration.

The important indexes and correlational dependence of road, human and vehicle are summarized in Table1.

Table1. Road-Human-Vehicle

Road	Human	Vehicle	Relationships	Indexes
Alignments	Sensation	Speed change	Alignment inducing the drive	Operation speed
Road surfaces	Respond time	Acceleration	Driving operation difficulty degree	Vehicles acceleration changing
Sight distance	Operation difficulty	Wheel	Vehicles conform to the route situation	Vehicles acceleration changing

SAFETY ASSESSING TECHNOLOGY OF CURVE ROAD SECTION BASED ON TWO-DIMENSIONAL SPEED DIFFERENCE

Operating speed model. Speed is one of most obvious index. The operating speed and the curve radius have a very close relationship. Many models have been developed to forecast the operating speed in domestic and other foreign countries (Karen S 2001, NCHRP 2003).

The roadway alignment affects driving speeds. There are some fixed operating speed characteristics at center and entrance of curve. Before analyzing horizontal and

vertical alignment coordination, we need carry on forecasting the operating speeds in the curve center and curve entrance. Considered the curve influence and unifying the former research results, the curve entrance operation speed and the curve center operation speed are shown in Table 2.

Table 2. Operation speeds in the Curve Center and Curve Entrance

Tangent length L (m), from $R_1 \rightarrow R_2$	Speed of vehicle entering curve R_2 （km/h）	Speed in curve R_1 （km/h）
L <100	$V_{85}=108.23-\frac{4508.06}{R_2}$	$V_{85}=108.23-\frac{4508.06}{R_1}$
100≤L≤ 500	$V_{85}=108.23-\frac{4508.06}{R_2}+L-100+(L-100)*0.01$	$V_{85}=108.23-\frac{4508.06}{R_1}$
L >500	108.23	$V_{85}=108.23-\frac{4508.06}{R_1}$

Analysis of two-dimensional speed difference. The speed changing along the curve was shown in Figure 1. While a vehicle goes through the alignment, the driver firstly notices the coming curve, then prepares for deceleration, then starts to decelerate at certain distance spot from the curve. The certain distance includes the part tangent and part curve, when the vehicles go to the curve center point (B), and finish the curve operation simultaneously the moving speed becomes 0 km/h at the curve vertical direction.

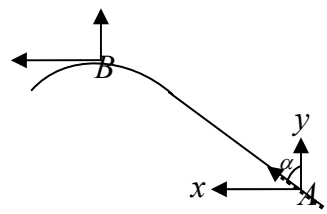

Figure 1. The Speed Changing along the Curve

From recent investigation statistics, it's discovered that vehicles usually decelerate at the 20 m point from the beginning of the curve, the curve length is shown by H(m), the circular curve length is L(m), the circular curve radius is R(m), the speed of starting to decelerate is V_0(m/s), the speed of arriving the mid-point of curve is V_1(m/s), the moving speed is from V_0 to V_1, the speed becomes 0 in the y direction, the corner is a, a is composed by the curve angle a_1 and the transition curve angle a_2, then:

$$\alpha = \alpha_1 + \alpha_2 \tag{1}$$

a_1 is just the curvature of curve:

$$\alpha_1 = \frac{L}{2R} \tag{2}$$

a_2 may be obtained from following:

$$\alpha_2 = \frac{A^2}{2\beta^2} \tag{3}$$

When the vehicle arrives the curve center point, the length is S (m) from A to B, then,

$$S = \frac{L}{2} + H + 20 \tag{4}$$

Supposed the vehicle do an uniform retarded motion from the deceleration spot to the circular curve beginning spot, and then do the uniform motion in the curve section, so the total time is M (s).

$$M = \frac{L}{2V_1} + 2\frac{H+20}{V_0 + V_1} \tag{5}$$

The changing rule that the deceleration difference changes with the time and the radian in the y orientation is:

$$\Delta V_S = \frac{\left|V_1 \sin(\alpha)\right|}{M \bullet \alpha} \tag{6}$$

The changing rule that the vehicle deceleration difference changes with the time and the radian in the circular curve in the y orientation is:

$$\Delta V_d = \frac{\left|2V_1^2 \sin(\alpha_1)\right|}{L\alpha_1} \tag{7}$$

The changing rule with the time and the radian changing rule in $L/2$ curve is the normal state changing rule for the curve, may be seen as a safety state rule. So, it takes the difference between the changing rule with the time and the radian in S and in $L/2$ to show the coordination of horizontal and vertical alignments, the influence and difficulty which the frontal alignments have the influence on the back alignments .The operation difficulty, the safety and the coordination may be expressed with following:

$$\Delta V_{Sd} = \frac{\left|V_0 \sin(\alpha)\right|}{M} - \frac{\left|2V_1^2 \sin(\alpha_1)\right|}{L} \tag{8}$$

Appraisal process and standard. According to above analysis, the connection standards between the curve and the curve, the straight and the curve are realized by:

$0.1 \leq \triangle V_b$. The connection standard between the curve and the curve is not good, it is easy to cause crash occur. The investigation statistics results show that these are the typical l short radius curve, and 152 in 213 accidents.

$0 < \triangle V_b \leq 0.1$. The connection standard between the curve and the curve is fare, it needs to take the traffic engineering measure to reduce the curve enter speed. The investigation statistics results show that these are 43 in 213 accidents.

$\triangle V \leq 0$. The connection standard between the curve and the curve is good, it is fit for driving. The investigation statistics results show that these are 17 in 213 accidents.

CASE STUDY

The above assessment method and the model are applied in a domestic two-level highway, the appraisal results are shown in Table 3.

Table 3. Application Results

Corner		R					Coordination
	6.41.26	1381	950.617	950.687	950.778	950.848	not good
40.45.41		150	951.048	951.098	951.155	951.205	good
	61.39.21	110	951.286	951.336	951.404	951.454	good
8.49.22		630	951.535	951.605	951.632	951.702	not good
	46.5.45	130	951.967	952.037	952.072	952.142	not good
68.7.50		190	953.697	953.122	953.277	953.347	not good
16.29.33		70	953.999	953.797	953.899	953.999	not good
	19.45.44	100	955.341	954.119	954.240	954.360	not good
	62.1.17	120	956.038	954.747	954.888	955.018	not good
17.10.21		130	956.430	955.411	955.485	955.555	not good

From the appraisal results, this method is helpful to design alignments improving the road safety.

CONCLUSIONS

1) A new assessment method and standard was developed to assess the curve coordination. The method overcomes the limitation by the speed difference method, and also makes the appraisal process to conform to the traffic operation.

2) The operating speed model used in the paper is a propositional model. It considers the driving behavior characteristic difference in various places. The operating speed should have the difference, which should fellow the local actual situation.

3) This method may further promote to be applied in highway design and safety evaluation.

REFERENCES

Transportation Research Board(1998), "Managing Speed: Review of Current Practices for Setting and Enforcing Speed Limits." *TRB Special Report* 254.

NCHRP(2003), "Geometric Design Consistency on High-Speed Rural Two-Lane Roadways." *NCHRP Report* 502.

FHWA(1999), " Evaluation of Design Consistency Methods for Two-Lane Rural Highways." *Publication No. FHWA-RD*-99-173.

Karen S. Schurr(2001) , "Relationship Between Design, Operation and Posted Speeds on Horizontal Curves on Rural Two-Lane Highways in Nebraska."*TRB 2001 Annual CD-ROM*.

NCHRP(2003), "Design Speed, Operation speed, and Posted Speed Practices." *NCHRP Report* 504.

Risk Evaluation for Highway Transportation of "Toxic Gas" Hazardous Materials - Based on a Back Propogation (BP) Neural Network

I.M.LIU, Kai-zheng[1] and C.O.LIU, Hao-xue[2]

[1]PH.D Student, School of Automobile, Chang'an University, Shannxi, Xi'an, 710064, PH (86)13669183672, email: liukaizheng_627@126.com
[2]Professor, School of Automobile, Chang'an University, Shannxi, Xian, 710064, PH (86)13201656581, email: liuhx@chd.edu.cn

Abstract: Risk evaluation models are developed to improve decision making regarding the safety of highway transportation of "toxic gas" hazardous materials. Based on ANN (Artificial Neural Network) theory and the Back Propogation (BP) method, a new risk evaluation model has been established utilizing the assessment indices of the inherent hazard of transported gas, the traffic accident rate of road sections and the population density of roadside areas. 12 road sections whose risk levels have been determined by a fuzzy synthetic evaluation model are used to train the network to an evaluation error less than 10^{-5}. Simulation results show that the proposed model in this paper improves on previous published models and has wide applicability.
Keywords: highway transportation; toxic gas; risk assessment; BP neural network

1 Introduction

Many types of hazardous materials are routinely and necessarily transported on roadway networks. One class of hazardous materials is the "Toxic Gas", which includes materials that are known to be poisonous or are assumed to be poisonous if exposed to human during transportation. Due to their importance in industrial uses, hazardous materials in the "Toxic Gas" category are frequently transported on highways. Analysis on more than 500 hazardous materials transportation accidents show that about 20% of them involves a gaseous hazardous material, and accidents involving the "toxic gas" category often lead to heavy casualty and serious pollution events because of their chemical properties. In order to avoid this kind of accidents and decrease the loss, researchers have studied "toxic gas" hazardous materials transportation and have established practical models for risk assessment, such as the fuzzy synthetic evaluation model, the time-varying risk evaluation model, and risk rank indices method(LIU Haoxue,2006;WEI Hang,2006; REN Changxing,2006). As many factors affect transportation safety and the transportation environment is complex, the methods above cannot always work efficiently because of limitations in the researcher's data availability. After analyzing the advantages and disadvantages

of those methods and considering characteristics and risk factors of road transportation for toxic gas, this paper introduces a new risk assessment model based on a BP neural network to enhance the level of evaluation.

2. Characters of BP Neural Network and Assessment Indexes Choosing

2.1 Characters of BP Neural Network

Assessment based on BP Neural Network (Error Back Propagation Network) has been shown to reduce the difficulties of dynamic optimization for multi-objective and variable-weight problems, and also removes the subjective factors during weight determination. Characteristics of knowledge memory and self-adaptation for a BP Neural Network make the combination of experience and new information possible, making it an effective method for risk assessment. A BP Neural Network is composed of an input layer, a hidden layer and an output layer, and its learning process is composed of signals' positive spread and error's converse spread (ZHU Daqi, 2006; GE Zhexue, 2007). Figure1 shows the structure of a BP neural network

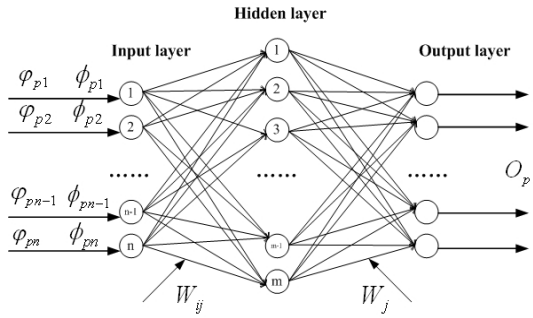

Figure 1. Structure of BP neural network (GE Zhexue, 2007)

Where, $\varphi_{p1},\varphi_{p2},...\varphi_{pn}$ are input values; $\phi_{p1},\phi_{p2},...\phi_{pn}$ are non-dimensional transformed values of training samples; W_{ij} is the connection weight from input node i to hidden node j;W_j is the connection weight from hidden node j to the output layer.

2.2 Choosing Indices

In consideration of the possibility and damage of accidents during transportation, the inherent hazard of the transported gas, the traffic accident rate, and the population density along the routes are defined as assessment indices. Assessment values of indexes are non-dimensional transformed by formula (1) as input vectors of the network. Where, r_i is the non-dimensional value of NO.i index , u_i is assessment value of NO.j index, u_{max} and u_{min} respectively are the highest and the lowest value of NO.i index in its range.

$$r_i = \begin{cases} 1, & u_i \le u_{\min} \\ \dfrac{u_{\max} - u_i}{u_{\max} - u_{\min}}, & u_{\min} < u_i \le u_{\max} \\ 0, & u_i > u_{\max} \end{cases} \quad (1)$$

(1). Traffic Accident Rate of Road Sections

Studies indicate that traffic accidents, vehicle and tank failure, bad condition of the road and weather are main causes for transportation accidents of hazardous materials. The major cause is traffic accidents, accounting for 80% of the cases. Many developed countries have conducted statistical research of hazardous materials transportation accidents. CCPS researched accidents in the USA from the 1980s to early 1990s and obtained authoritative data shown in table.1 which was cited widely. In the absence of pertinent data from China, and considering the present road traffic and infrastructure development in China is similar to the situation of the USA in the 1980s, the traffic accident rate for transport trucks on different road classes in table 1 was used for this model. The evaluated road section's traffic accident rate is determined as the assessment value of this index based on the road section's class and type.

Table1.Traffic accident rate on different highway classes (CCPS, 1995)

Highway type		Traffic accident rate of commercial vehicle(10^6km)
Area	Lane	
Rural	Two-lane	1.36
Rural	Multi-lane(undivided)	2.79
Rural	Multi-lane(divided)	1.34
Rural	Expressway	0.4
Urban	Two-lane	5.38
Urban	Multi-lane(undivided)	8.65
Urban	Multi-lane(divided)	7.75
Urban	Single lane	6.03
Urban	Expressway	1.35

(2). Inherent Hazard

Physical and chemical properties of the subject "toxic gas" material will affect the accumulating time of a toxic cloud or plume, the abreaction, and the severity of consequences, which means that magnitude of risk differs for gases of different properties. A common measure of gas toxicity available for most substances is the Lethal Concentration, or LC50. LC50, gas density and gas odor, are determined as relevant indices for inherent hazard evaluation. According to GB5044-85, the gases are assessed by the above parameters and given assessment values (see table2 and

table 3). The full mark is 50 and the 3 categories are weighed with 50%, 30% and 20% respectively. The inherent hazard evaluation value is the summation of the 3 categories.

Table2.Value of gas toxicity

LC_{50}	Classification			
	Serious toxic	High toxic	Mid toxic	Low toxic
$LC_{50}(mg/m^3)$	<20	20-200	200-2000	>20000
Assessment value	25	20	15	10

(3). Population Density of Roadside

People, livestock, agriculture, waters and nature reserves will be all threatened when leakage of toxic gas occurs (LIU Haoxue, 2006). Life is the first thing that should be considered in risk evaluation of accidents and human casualties directly affect any measurement of accident severity. Therefore, population density of the roadside is chosen to reflect the potential consequences of a given incident.

The model of the roadside should reflect the number of people exposed to a potential gas plume per unit area. The evaluation value is the product of population density of administrative regions where accident occurred and the outdoor exposure rate of those people .In this paper, exposure rate of people is determined as 20%, based on average outdoor working hours.

Table 3. Value of gas density and odor

Toxic gas density /air density	Assessment value	Smell type	Assessment value
>1.3	15	Pungent smelly	3
1.0-1.3	10	Mild	7
0.5-1.0	5	Smell less	10
<0.5	2		

3 Design and Training of the BP Neural Network

3.1 Design of the BP Neural Network

3 assessment indices are determined and vectors of (1,0,0,0),(0,1,0,0), (0,0,1,0) and (0,0,0,1)are used to denote the risk degrees of low, mid, high and highest. A network whose design parameters are shown in table 4 is established, and the amount of hidden units is determined by trials for finding the parameter achieving the smallest error.

Table 4. Designing parameter of BP neural network

Input units	Hidden units	output units	Training function	Learning function	Performance function	Learning error	Learning speed
3	7	4	traingdx	logsig	mse	10^{-5}	0.1

3.2 Training of BP Neural Network

(1). Determination of training samples

12 road sections whose risk levels have been previously identified by fuzzy synthetic evaluation model are used as training samples using non-dimensional transformed assessment values of the indices for each road section as inputs. Input values and expected output values are showed in table 5.

Table 5.Training samples of network

Number	Non-dimensional assessment value				Assessment result	
	Inherent hazard		Traffic accident rate	Population density		
1	CH_3Cl	0.4167	0.8693	0.9533	low	(1,0,0,0)
2	NH_3	1.0000	0.8707	1.0000	low	(1,0,0,0)
3	CO	0.7803	0.8707	0.8533	low	(1,0,0,0)
4	Cl_2	0.3750	0.8693	0.7100	mid	(0,1,0,0)
5	CO	0.7803	0.8693	0.8933	mid	(0,1,0,0)
6	H_2S	0.3750	1.0000	0.8567	mid	(0,1,0,0)
7	F_2	0.2083	0.3224	0.7167	high	(0,0,1,0)
8	Cl_2	0.3750	0.8693	0.8600	high	(0,0,1,0)
9	H_2S	0.4167	0.8693	0.8000	high	(0,0,1,0)
10	Cl_2	0.3750	0.8693	0.3867	highest	(0,0,0,1)
11	NO	0.0833	0.8693	0.0000	highest	(0,0,0,1)
12	N_2O_4	0.0000	0.0000	0.0167	highest	(0,0,0,1)

(2). Training of Network

To achieve better convergence and lower error, the paper takes 0.1 as learning speed, 100,000 as the largest learning time and 0.00001 as learning error. Matlab7.0 is used for training simulation of the network and the required error is achieved after 22502 iterations .Figure.2 is the error curve of training, which indicates that learning error is as low as 9.99885×10^{-6}.

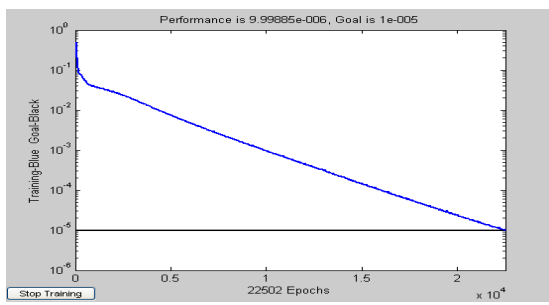

Figure2.error curve of network training

4 Application Case

To validate applicability of the model, 2 representative road sections are

selected for simulation.

NO. 1：An Kang section of 316 national highway is a 3-class two-lane highway in a rural area, the population density of roadside is 20 and the transported gas is SO_2. SO_2 is low-toxicity, pungently odorous, colorless and can be easily detected after leakage. This road section has low population density and serious human casualties can be avoided if protective measures will be taken in time. Considering these factors and accident records, it can be judged that SO_2 transportation on this road section is relatively low in risk but is not the best choice because of low road class.

NO.2: Gao Ling section of BaoTou-MaoMing expressway is a two-lane expressway in a rural area, population density of roadside is 315 and the transported gas is NO. NO will be oxidated to NO_2 in air, NO_2 is high-toxicity, pungent smelly brown gas. Although this road section is in good condition, high traffic volume and high population density make large scale evacuation difficult, with public panic and serious human casualties possible after leakage. So it can be judged that NO transportation on this road section is very high in risk.

Non-dimensional index values of NO.1and NO.2 road section can be calculated and are indicated in table6.

Table6.Evaluating value of road sections

Evaluating index	Index value		Non-dimensional index value	
	NO.1	NO.2	NO.1	NO.2
Inherent hazard	SO_2 33	NO 45	0.5833	0.0833
Traffic accident rate(/10^6km)	1.36	1.35	0.8893	0.8707
Population density(/km^2)	20	315	1.0000	0.0167

Inputting the non-dimensional value (0.5833 , 0.8893 , 1.0000) and (0.0833 , 0.8707 , 0.0167) into the BP Neural network model results in the outputs (0.0000,1.0000, 0.0000,0.0000) and (0.0012,0.0000,0.0013,0.9986)after simulation. This shows that the risk of SO_2 transportation on An Kang section of 316 national highway is medium and the NO transportation on Gao Ling section of BaoTou-MaoMing expressway is highest. The evaluating result output from the model matches the factual risk level of the two road sections.

5 Conclusions

1). This paper presents a risk evaluation model of highway transportation for “toxic gas” hazardous materials based on a BP neural network whose evaluating indices are the inherent hazard of gas, the traffic accident rate of the road section and the population density of the roadside. It improves on previous models that involved complex structures, fussy calculations and influence of subjective factors.

2). A BP network with 3 input units, 7 hidden units and 4 output units is established and its evaluation error reaches 10^{-5} after training. The trained network is used to simulate SO_2 transportation on An Kang section of 316 national highway and NO transportation on Gao Ling section in BaoTou-MaoMing expressway. Simulation results show that the model is short in calculating time, high in accuracy, and broadly applicable.

REFERENCES

Center for Chemical Process Safety (CCPS).(1995). *Guidelines for chemical transportation risk analysis* .New York

GE, Zhexue,and SUN, Zhiqiang. (2007). "Section 1: Basic for Neural Network: *Theory of Artificial Neural Network and* Realization by MATLAB R2007," Electronic Industry Press, Beijing, 1.1.1-1.1.3

LIU, Haoxue,and ZHOU,Xun.(2006)."Fuzzy synthetic evaluation model of transportation routes of dangerous goods," *Journal of Traffic and Transportation Engineering*, 6(2):80-82

REN,Changxing,and WU,Zongzhi.(2006)"Study on the risk rank indices of hazardous materials transportation" *Journal of Safety and Environment*, 6(4): 126-129

WEI,Hang,and Li,Jun,and PU,Yun.(2006). "Route Planning for Hazardous Materials Transportation in Time-varying Network" *Journal of Systems Engineering-Theory &Practice*, 10(10), 107-112

ZHU,Daqi,and SHI,Hui.(2006). "Section 1: Introduction. Principles and Application of Artificial Neural Network," Science Press, Beijing, 1.1-1.3

Study on Different Residual and Weight Coefficient in Model Updating of Bridge Structure

Li Jie [1], Huang Min-shui *[2], and Zhu Hong-ping [3]

[1] School of Environment and Civil Engineering, Wuhan Institute of Technology, 430073, 693 Xiongchu Avenue, Wuhan, Hubei, China; PH (86)27-87195166; email: wit613@mail.wit.edu.cn

[2] School of Environment and Civil Engineering, Wuhan Institute of Technology, 430073, 693 Xiongchu Avenue, Wuhan, Hubei, China; PH (86)27-87194698; email: huangminshui@tsinghua.org.cn (*Correspondence author)

[3] School of Civil Engineering and Mechanics, Huazhong University of Science and Technology, 430074, 1037 Luoyu Road, Wuhan, Hubei, China; PH (86)27-87542631; email: hpzhu@mail.hust.edu.cn

ABSTRACT

Relative merits of different residuals used in the construction of objective function and weight coefficients in single-objective function for structural model updating are investigated in this paper based on the improved genetic algorithm (IGA). Presently there are three residuals which are used mostly in finite element (FE) model updating: frequency residual, mode shape residual, and modal flexibility residual. Relative merits of the three residuals are analyzed through the simulation of a simply supported beam. Then, model updating is studied comparatively based on IGA. Frequency is the main characteristic parameter of bridge structure, which has high identification precision and should be used with priority. When there are several updating parameters, information should be complemented. If identification error of the mode shape is relatively less, the complement of the mode shape is feasible. In the end, through the analysis of weight coefficients for different residuals in single-objective function, it can be seen that the model updating performance is better when the frequency residual has a larger weight coefficient.

INTRODUCTION

In health monitoring of bridge structure, damage identification based on FE model updating is often used. Simplifying assumptions are widely adopted in FE modeling of a structure and the FE model is constructed based on highly idealized engineering drawings that may not accurately represent all of the physical aspects of an actual structure. When vibration testing is performed to validate the analytical model, inevitably the results, commonly natural frequencies, and mode shapes do not coincide with the expected results from the analytical model. These discrepancies originate from the uncertainties in simplifying assumptions of structural geometry and materials as well as inaccurate boundary conditions. The inaccurate factors mainly come from three aspects: model structure errors, model parameter errors, and model order errors (Mottershead and Friswell 1993). The problem of how to modify the analytical model based on dynamic measurements is the model updating in structural dynamics. That is to say, the purpose of FE model updating is to modify the mass, stiffness, and damping parameters of the analytical model in order to obtain better agreement between analytical and experimental results.

The Iterative method is often used in model updating. Its usual principle is to

quantize the discrepancies between analytical and experimental results through the construction of objective function and minimize objective function through the adjustment of updating parameters. Thus model updating is changed into an optimization problem. Consequently, whether model updating can be carried out successfully mainly depends on the accuracy of the model, quality of vibration testing, definition of the optimization problem, and calculation performance of the optimization algorithm.

In the paper, the relative merits of different residuals used in the construction of objective function and weight coefficients in single-objective function for model updating are investigated. The research results are validated though the simulation of a simply supported beam, it can be seen that model updating performance is better when frequency residual has a larger weight coefficient.

CONSTRUCTION TECHNIQUE OF OBJECTIVE FUNCTION

Model updating is changed into optimization problem as follows

$$\begin{aligned} &Min \quad f = f(x) \qquad R(x) = f_e(x) - f_a(x) \\ &S.t \quad \underline{x_i} \le x_i \le \overline{x_i} \qquad (i = 1, 2, ..., N) \end{aligned} \tag{1}$$

where f is the function of updating parameters which can be the stiffness matrix, mass matrix, mode shape, flexibility, or mode shape correlation, etc... f_e and f_a are the experimental and analytical natural frequencies, respectively. x_i and $R(x)$ represent the updating parameter and residual function, respectively. $\underline{x_i}$ and $\overline{x_i}$ are the lower limit and upper limit of updating parameters, respectively.

Taylor expansion of f at x_0 is as follows

$$f = f(x_0) + \sum_{i=1}^{N} \frac{\partial f}{\partial x_i} \cdot \Delta x_i \tag{2}$$

where N and Δx_i are the number and increment of updating parameters, respectively.

Equation (1) can be rewritten in matrix style

$$G \cdot \Delta x = R \tag{3}$$

where, $\Delta x = [\Delta x_1, \Delta x_2, \ldots, \Delta x_N]^T$, G is the Jacobian matrix, which consists of the partial derivative of modal parameters to updating parameter, and is often named as the sensitivity matrix.

In structural dynamics the eigen equation is as follows

$$(K - \lambda_i M)\phi_i = 0 \tag{4}$$

where K and M are the stiffness matrix and mass matrix, respectively. λ_i and ϕ_i are the eigen value and eigen vector, respectively.

Frequency residual. The most important residual for FE model updating in structural dynamics is the discrepancies between the analytical and experimental undamped eigen frequencies. The eigen frequency residual R_f is formulated as

$$R_f = \sum_{i=1}^{N} \left| \frac{\lambda_{ai} - \lambda_{ei}}{\lambda_{ei}} \right| \quad (i = 1, 2, ..., N), \quad 0 \le \left| \frac{\lambda_{ai} - \lambda_{ei}}{\lambda_{ei}} \right| \le UL \tag{5}$$

where, $\lambda_i = (2 \cdot \pi \cdot f_i)^2$, f_i is the eigen frequency to i-th mode. λ_{ai} and λ_{ei} are the analytical and corresponding experimental eigen values respectively, and UL is upper limit of error between the two eigen values. N refers to the number of identified eigen frequencies which are used in updating process..

Eigen frequencies can be measured and identified during vibration testing, which provide global information of the structure. They are indispensable quantities used in the updating process and have a favorable effect on the condition of the optimization problem. But the high-order natural frequencies are not measured as accurately as the low-order ones. An objective function with only a limited set of eigen frequencies is too poor of a basis for the definition of structural dynamic behavior. So other residuals are also necessary to form the full objective function for FE model updating.

Mode shape residual. Mode shapes contain spatial information about the dynamic behavior of structure. Therefore it is possible to be used as the residual with discrepancies in mode shape in the construction of objective function. Since structures are mostly measured under operational conditions, the in-operation modal testing makes use of the freely available ambient excitation caused by natural excitation sources on or near the test structure. As a result, the identified experimental mode shapes cannot be absolutely scaled, so the scaling and normalization of mode shapes obtained from vibration testing is an important issue, which is not standard in conventional model updating. In model updating, the modal assurance criterion (MAC) is often used in automatic pairing and comparing analytical and experimental mode shapes (Allemang and Brown 1982). The value of MAC is bound between 0 and 1, a value of 1 means a perfect correlation and a value of 0 indicates that the two modes do not show any correlation.

MAC is defined as

$$MAC_i = \frac{(\phi_{ai}^T \cdot \phi_{ei})^2}{(\phi_{ai}^T \cdot \phi_{ai}) \cdot (\phi_{ei}^T \cdot \phi_{ei})} \qquad (i = 1, 2, ..., N) \tag{6}$$

where ϕ_{ai} is the analytical eigen mode which has been paired with the j-th experimental mode ϕ_{ei}.

Mode shape residual is formulated as (Moller and Friberg 1998)

$$R_s = \sum_{i=1}^{N} \frac{(1 - \sqrt{MAC_i})^2}{MAC_i} \qquad (i = 1, 2, ..., N) \tag{7}$$

Modal flexibility residual. The flexibility matrix is defined as the inverse of the stiffness matrix as shown in Equation (8)

$$G = K^{-1} \tag{8}$$

where G and K are the flexibility matrix and stiffness matrix, respectively.

The inverse vibration representation of the flexibility matrix is as follows

$$G = \Phi \Lambda^{-1} \Phi^T = \sum_{i=1}^{n} \frac{1}{\omega_i^2} \phi_i \phi_i^T \tag{9}$$

where, $\Phi = [\phi_1, \phi_2, \cdots, \phi_n]$ is the mode shape matrix, ϕ_i is the mode shape to i-th mode, and $\Lambda = diag(f_i^2)$ is the modal matrix.

A method is developed to accurately estimate structural flexibility considering residual flexibility from forced vibration testing (Doebling 1995), in which the input of the system is known. For the case of known input, there is no problem in calculating the residual flexibility. As to ambient vibration testing, the input of the system is not measured. For the case of unknown input with measurements carried out only in certain locations, the situation is much more different and the calculation of residual flexibility is not so straightforward.

In general, the measured modes are typically those that are lower in frequency. The lower ones contribute the most to the flexibility. Therefore, a good estimate of the flexibility matrix may be obtained from only a few low-order frequencies and mode shapes at measured DOFs. Hence, the flexibility matrix becomes

$$G_{mm} = \Phi_{n_m} \Lambda_n^{-1} \Phi_{n_m}^T \tag{10}$$

where G_{mm} is the measured flexibility matrix, Φ_{n_m} is the measured mode shapes of the structure at measured DOFs, and Λ_n corresponds to the eigen values of measured modes.

In general, the modal flexibility error residual may be given by the expression

$$R_{flex} = \sqrt{\left\| G_{\exp} - G_{ana} \right\|_2} \tag{11}$$

where $G_{\exp}$ and G_{ana} are measured and analytical modal flexibility matrixs respectively at the measured DOFs (Yan *et al* 2004; Zhao and DeWolf 2002) .

IMPROVED GENETIC ALGORITHM (IGA)

Owing to the genetic algorithm (GA) with no restriction on continuous and differential characteristics of the optimization problem and with advantages in robust, global optimization, and capability of parallel processing, GA has become an important method to solve optimization problems. But simple genetic algorithm (SGA), which adopts uniform cross and mutation, tends to appear as the premature phenomenon in the evolutionary process, which could lead the GA to be trapped in the local solution and be unable to find the global optimum solution.

In this paper an improved genetic algorithm (IGA) is presented. Firstly, proportional selection combined with elitist strategy is adopted in selection (Fei *et al* 2006). Secondly, heuristic crossover and non-uniform mutation are taken in crossover and mutation (Tu and Lu, 2008). Finally, adaptive crossover and mutation probability are adopted to ensure the convergence of GA (Srinivas and Patnaik 1996), to make sure genetic iteration evolves to the global optimum solution and guarantee the diversity of population at the same time. The method overcomes the defects of a slow convergence rate and easily becoming stuck at a local optimum when SGA is applied in the health monitoring of bridge structure. It accelerates convergence greatly and ensures the finding of a global optimum solution.

SIMULATED SIMPLY SUPPORTED BEAM

The simply supported beam bridge is adopted in many bridges, so a simulated simply supported beam is studied in this paper. This aims at demonstrating a comparative research on the influence of different possible residuals on objective function for FE model updating. The simulated simply supported beam with a length of 6.4 m is presented (see Figure 1). The mass density and elastic modulus are 2500 Kg/m^3 and 3.2×10^{10} Pa respectively. Similarly, the area and moment of inertia of the

cross section are 0.05 m^2 and 1.66×10^{-4} m^4 respectively.

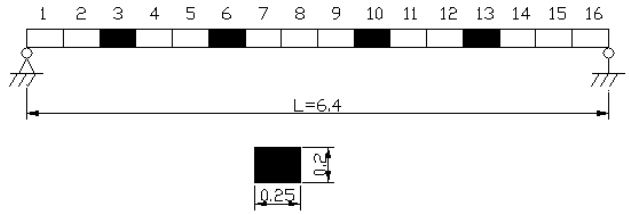

Figure 1. A simulated simply supported beam (m).

Comparative analysis of different residuals. In the paper, IGA is adopted to update the FE model. Evolution is terminated when the generation reaches 1000 or discrepancy between the analytical solution and optimum solution is less than 1e-8. Analytical modal analysis is first carried out to obtain analytical frequencies and mode shapes. To obtain the simulated experimental modal parameters, four damage locations are assumed in the beam (see Figure 1) in which the elastic modulus and moment of inertia of beam elements 3, 6, 10 and 13 are reduced by 30%, 40%, 20% and 30% respectively. The modal analysis is carried out again to obtain the assumed experimental modal parameters. The initial values of frequencies and corresponding errors are shown in Table 1. The maximum error that appeared in frequency is 7.41% and the minimum error is 3.41%.

Model updating of the undamaged beam is to correlate the modal parameters with the damaged beam and to identify the damage severity and location. Elastic modulus of individual elements is chosen as an updating parameter (UP). The number of UP is selected with respect to the numbers of modes considered for which two cases are considered:

Case 1. UP=4, where the elastic modulus of damaged elements 3, 6, 10 and 13 are selected as UP and number of UP is less than the mode number considered. It is the case that structural damaged locations are exactly known.

Case 2. UP=16, where the elastic modulus of all 16 elements are selected as UP and number of UP is equal to the mode number considered. It is the case that structural damaged locations are not known.

Three objective functions consisting of the frequency residual only, mode shape residual only, or modal flexibility residual only are studied independently, of which there are two cases depending upon number of UP.

From the results it can be seen that (see Table 1, Table 2 and Table 3)

1. Based on the frequency residual, IGA can accurately identify the severity of damage when UP=4, but IGA cannot accurately identify the severity and location of damage when UP=16.

2. Based on the mode shape residual, IGA can accurately identify the severity of damage when UP=4. IGA can accurately identify the location of damage when UP=16, but cannot accurately identify the severity of damage.

3. Based on the modal flexibility residual, IGA can accurately identify the severity of damage when UP=4. IGA can approximately identify the location of damage when UP=16, but cannot accurately identify the severity of damage.

Table 1. Results based on frequency residual before and after updating.

Mode	Initial FE model /Hz	Damaged beam /Hz	Error %	Updated value /Hz			
				UP =4	Error %	UP =16	Error %
1	7.922	7.462	6.16	7.462	0.00	7.460	-0.03
2	31.686	29.499	7.41	29.500	0.00	29.560	0.21
3	71.299	67.728	5.27	67.730	0.00	67.669	-0.09
4	126.780	118.150	7.30	118.150	0.00	118.260	0.09
5	198.160	191.630	3.41	191.630	0.00	191.280	-0.18
6	285.540	275.270	3.73	275.280	0.00	275.220	-0.02
7	389.060	368.310	5.63	368.310	0.00	367.970	-0.09
8	508.970	485.890	4.75	485.900	0.00	485.660	-0.05
9	645.620	618.120	4.45	618.110	0.00	618.380	0.04
10	799.490	759.930	5.21	759.930	0.00	759.560	-0.05

Table 2. Results based on mode shape residual before and after updating.

Mode	Initial FE model /Hz	Damaged beam /Hz	Error %	Updated value /Hz			
				UP =4	Error %	UP =16	Error %
1	7.922	7.462	6.16	7.467	0.06	6.855	-8.14
2	31.686	29.499	7.41	29.516	0.06	27.104	-8.12
3	71.299	67.728	5.27	67.754	0.04	62.225	-8.13
4	126.780	118.150	7.30	118.250	0.08	108.630	-8.06
5	198.160	191.630	3.41	191.690	0.03	175.700	-8.31
6	285.540	275.270	3.73	275.330	0.02	252.640	-8.22
7	389.060	368.310	5.63	368.460	0.04	337.960	-8.24
8	508.970	485.890	4.75	486.070	0.04	446.010	-8.21
9	645.620	618.120	4.45	618.380	0.04	567.610	-8.17
10	799.490	759.930	5.21	760.250	0.04	697.820	-8.17

Table 3. Results based on modal flexibility residual before and after updating.

Mode	Initial FE model /Hz	Damaged beam /Hz	Error %	Updated value /Hz			
				UP =4	Error %	UP =16	Error %
1	7.922	7.462	6.16	7.462	-0.01	7.460	-0.02
2	31.686	29.499	7.41	29.539	0.14	29.522	0.08
3	71.299	67.728	5.27	67.833	0.16	67.008	-1.06
4	126.780	118.150	7.30	118.210	0.05	120.430	1.93
5	198.160	191.630	3.41	191.700	0.04	189.140	-1.30
6	285.540	275.270	3.73	275.320	0.02	270.230	-1.83
7	389.060	368.310	5.63	368.520	0.06	370.110	0.49
8	508.970	485.890	4.75	486.140	0.05	483.240	-0.55
9	645.620	618.120	4.45	618.440	0.05	611.650	-1.05
10	799.490	759.930	5.21	760.440	0.07	757.220	-0.36

Overall, the updating performance is not good, so single-objective function based on different residuals and their weight coefficients are studied subsequently.

Weight coefficient for different residuals. There are few research reports on weight coefficient for different residuals in dynamic FE model updating. The

model updating problem is often formulated as an optimization problem in which the objective functions are built up into a single-objective function using weight coefficients. Standard optimization techniques are then used to find the optimum value of the parameters that minimizes the objective function. The results of optimization are influenced by weight coefficients, which are assumed. The choice of weight coefficients depends on model adequacy and uncertainty in the available measured data, which is not known in advance. Hence, the selection of weight coefficients is a very important task since the relative importance among the data is not so obvious, but very specific for each problem.

Different residuals are combined into a singleobjective function by using weight coefficients for each residual. The residuals should be weighted separately according to their importance and accuracy. At the same time engineering insight is needed to provide the correct weight coefficients. There are no strict and quick rules for the selection of weight coefficients since the relative importance in the criterion is not obvious and specific for each optimization problem. Then a method is necessary to solve the problem repeatedly by varying the values of the weight coefficients until a satisfactory solution is obtained (Grandhi and Bharatramv 1993). In this paper, the objective function is as follows

$$R = a \cdot R_f + b \cdot R_s + c \cdot R_{flex} \tag{12}$$

where R_f, R_s and R_{flex} are defined in equation (5), (7) and (11) and a, b and c are weight coefficients for R_f, R_s and R_{flex} respectively.

When FE model updating is carried out, three cases are considered:

Case 1. a=b=c.

Case 2. a=0.1, b=1, c=10.

Case 3. a=10, b=1, c=0.1.

From the results it can be seen that (see Table 4):

1. Objective function value is least in case 3, the maximum is -2.2e-05 and the minimum is -6.42e-06. It is largest in case 1, the maximum is -2.51e-03 and the minimum is -3.72e-03.

2. Frequency error is least in case 3, the maximum is 0.09 and the minimum is 0. It is largest in case 1, the maximum is 2.14 and the minimum is 0.

3. As for MAC error, there is no obvious difference in the three cases.

4. Stiffness reduction error is least in case 3, the maximum is 1.4 and the minimum is 0. It is largest in case 1, the maximum is 29.8 and the minimum is 0.

Table 4. Model updating based on different weighting coefficients.

Weighting coefficient	Objective function value		Frequency error %		*MAC* error %		Stiffness reduction error %	
	Max	Min	Max	Min	Max	Min	Max	Min
a=1,b=1,c=1	-2.73e-04	-8.89e-05	0.57	0	2.17	0.02	9.6	0
a=0.1,b=1,c=10	-2.51e-03	-3.72e-03	2.14	0	1.64	0.01	29.8	0
a=10,b=1,c=0.1	-2.2e-05	-6.42e-06	0.09	0	2.18	0.02	1.4	0

Through the comparative analysis of weight coefficient for different residuals in single-objective function, it can be seen that if the updating method is fixed, when frequency residual is assigned a larger weight coefficient, mode shape residual a

lesser, and modal flexibility residual the least, updating performance is best.

CONCLUSIONS

The following conclusions are drawn:

1. Model updating is carried out using different residuals and the best combination is recognized with the help of simulated case study. It is demonstrated that the combined objective function which consists of three residuals, namely the frequency residual, mode shape residual, and modal flexibility residual, with different weigh coefficient assigned to each of them, is recognized as the best one.

2. Through comparative analysis of weight coefficient for different residuals in single-objective function, it can be seen that if the updating method is fixed, when frequency residual is assigned a larger weight coefficient, mode shape residual a lesser, and modal flexibility residual the least, updating performance is best.

3. Successful updating of the simulated simply supported beam demonstrates that the cost of calculation is not too high. The method in this paper can be used in many applications of bridge structures like damage identification, health monitoring, and structural assessment and is of great theoretical and engineering value.

ACKNOWLEDGEMENTS

This research was sponsored by the National Natural Science Foundation of China (No.50608036, No.50778077).

REFERENCES

Mottershead, J. E., and Friswell, M. L. (1993). "Model updating in structural dynamics", *Journal of sound and vibration*, 167(2): 347-375.

Allemang, R. J., and Brown, D. L. (1982). "A correlation for modal vector analysis", *Proceedings of 1st International Modal Analysis Conference*, 110-116.

Moller, P. W., and Friberg, O. (1998). "Updating large finite element models in structural dynamics". *AIAA Journal*, 36(10), 1861-1868.

Doebling, S. W. (1995). "Measurement of Structural Flexibility Matrices for Experiments with Incomplete Reciprocity". *Ph. D. Thesis*, University of Colorado, Department of Aerospace Engineering Sciences.

Yan, A. M., Boe, P. De., and Golinval, J. C. (2004). "Structural damage location by combined analysis of measured flexibility and stiffness". *Proceedings of progress in structural engineering, mechanics and computation*, 635-640.

Zhao, J., and DeWolf, J. T. (2002). "Dynamic monitoring of steel girder highway bridge". *Journal of Bridge Engineering*, 7(6), 350-356.

Fei, Q. G., Li, A. Q., and Miao, C. Q.(2006). "Dynamic finite element model updating using meta-model and genetic algorithm", *Journal of Southeast university (English edition)*, 22(2): 213-217.

Tu, Z. G., and Lu, Y.(2008). "FE model updating using artificial boundary conditions with genetic algorithms", *Computers and structures*, 86(7-8): 714-727.

Srinivas, M., and Patnaik, L. M. (1996). "Genetic search: Analysis using fitness moments". *IEEE Transactions on knowledge and data engineering*, 8(1): 120-133.

Chang, C. C., Chang, T. Y. P., and Zhang, Q. W.(2001). "Ambient vibration of long-span cable-stayed bridge", *Journal of Bridge Engineering*, 6(1): 46-53.

Grandhi R. V., and Bharatramv G. (1993). "Multiobjective Optimization of Large -Scale Structures". *AIAA Journal*, 31(7), 1329-1337.

Study on a Passageway Location Model of Underground Expressway

Yucong Hu, Bingqiang Situ, Wenzhou Jin, Qin Liu

School of Civil Engineering and Transportation, South China University of Technology, Guangzhou, Guangdong, China, 510640; email:ychu@scut.edu.cn, email:benst2002@126.com, email:ctwzhjin@scut.edu.cn, liuqin85@126.com

ABSTRACT

An important consideration in underground expressway plan and design is how to locate passageways providing services. This paper develops a new model to address issues involving demand decay, share rate, and efficiency of passageway simultaneously. The model is built with the objective of maximizing efficiency; and an iterative algorithm using the network equilibrium model is developed to obtain the steady share rate and to determine passageway locations with the maximal efficiency. Finally, an example is presented to illustrate the flexibility and effectiveness of the model and algorithm. The results show that the algorithm can obtain the steady share rate, and get the model convergent. In addition, the passageway locations will be globally optimized.

INTRODUCTION

The academic research of underground expressway presently focuses on traffic capacity, traffic organization, management and control, and the estimation of the environmental influences on underground expressway (Thalheimer, 2004；Hirata et al.，2006). Few quantitative research work has been done on the network planning and passageways locating. This paper analyzes the factors that influence the passageway locations of the underground expressways and proposes a passageway location model. Incorporating the network equilibrium model and space network analysis, a new algorithm is developed with the objective of maximizing efficiency of passageway in the whole network.

ANALYSES ON FACTORS RELATING TO PASSAGEWAY LOCATIONS

In order to ensure the safety and efficiency, connecting the underground expressways with ground road in passageways is preferred at present stage. The passageway location model needs to be achieved by the transport facilities with a rational layout for the purpose of meeting the demand and guiding the spatio-temporal transfer of the demand finally. A demand curve (Hurst, 1972) reflected that the demand is decreasing with the increase of the distance between the demand point and supply location. Farhan and Murray (2006) advanced the location model for the first time, which simultaneously addressed the coverage range, partial regional service, and distance decay.

Comparing with the common location problem, the passageway location of underground expressway has two special aspects: intercommunity and

particularity. The intercommunity is related to decay of the demand caused by the distance; the particularity is the share rate of underground expressway， which is not entirely dependent on the capacity of the underground expressway or the serving capacity of passageway. Thus, the passageway location model of the underground expressway is affected by three major factors: the demand decay, share rate and efficiency of passageway. The objective of the model is to obtain the largest number of vehicles served in per unit time (i.e., achieving the maximal efficiency).

MODEL FORMULATION

For setting up the passageway location model, we have the following assumptions.

1) the road network comprised of the urban expressways and the main roads serve the vehicles within the moderate and long travel distance.

2) the passageway location is assumed to be set up in the intersection.

3) all vehicles on the road concentrate in the middle of the road at a moment; the middle point is the demand point o.

4) the most amount of demands on each road is the largest number of vehicles in the whole day; the demand is N_O.

5) each road in the district is considered to achieve the maximal requirement simultaneously. The extent of travel time and most demand which arisen from the vehicles' passing through from every demand point to the others are neglected here. This assumption is acceptable under the current congested circumstance of the urban network.

To model this problem, we define the notation as follows.

N_o total demand at point o in link a

N_{oj} demand served by passageway point *j* form N_o

A_j share rate of underground expressway in passageway point *j*

A_j^n share rate in passageway point *j* at the *n*th iteration

W_{oj} aggregate of paths of o-j pairs in the network

d_k^{oj} travel distance on the path *k* of *o-j* pairs

$\hat{d}_{oj}$ the shortest distance in all the paths of *o-j* pairs, where $\hat{\mathbf{d}} = (\ldots, \hat{d}_{oj}, \ldots)$

t_k^{oj} travel time (cost) on the path *k* of *o-j* pairs

$\hat{t}_{oj}$ the least travel time (cost) in all the paths of *o-j* pairs

where $\hat{\mathbf{t}} = (\ldots, \hat{t}_{oj}, \ldots)$

$t_a(\cdot)$ Travel time (cost) function on link *a*

x_a Flow of link *a*

$x_{ja'}^n$ Flow of underground expressway *a'* linked to passageway point *j* at the *n*th iteration

C_a Capacity of link *a*

A. Passage Location Model

First, we present two principles to distribute the expressways:

1) the expressway location needs to satisfy the demand of vehicle's middle and long distance travel; and

2) the level of underground expressway needs to be consistent with the ground roads.

The passageway efficiency V is defined as the number of vehicles served in per unit time. Therefore, two conditions need to be fulfilled. The first one is that the more demand of point o, the less travel time (cost) of o-j pairs; and the other one is that the passageway efficiency in one zone is the most in whole. The passageway location function is:

$$\text{Maximize } V = f(N, A, d, t), \tag{1}$$

where the demand decay function is described as $f(d) = e^{-\mu d}$ in the literature (Farhan and Murray, 2006; Hanson and Giuliano, 2004). Furthermore, μ is within the typical range of 0.5 to 2. The value of share rate A will be introduced in section B. Decision variable is defined as:

$$Y_{oj} = \begin{cases} 1 & \text{if } \hat{d}_{oj} \text{ is not less than the shortest distance of } o\text{-}other \text{ pairs,} \\ 0 & \text{otherwise.} \end{cases}$$

Now, the formulation is given as follows:

$$\begin{aligned} \text{Maximize} \quad V &= \max_j \left(\sum_o \frac{N_{oj}}{\hat{t}_{oj}} \times Y_{oj} \right) \\ &= \max_j \left(\sum_o \frac{N_o \times A_j \times e^{-\mu \cdot \hat{d}_{oj}}}{\hat{t}_{oj}} \times Y_{oj} \right), \end{aligned} \tag{2}$$

$$\begin{aligned} \text{subject to} \quad & \hat{t}_{oj} = \min_{k \in W_{oj}} \left\{ t_k^{oj} \right\} \forall o, j, k; \\ & \hat{d}_{oj} = \min_{k \in W_{oj}} \{ d_k^{oj} \} \forall o, j, k; \\ & Y_{oj} \in \{0,1\} \forall o, j; \\ & \sum_j Y_{oj} = p. \end{aligned} \tag{3}$$

t in the model is the sum of the impedances of each link in the path of *o-j* pairs, where the impedances are valued travel time (cost). BRP function is used to gain the travel time (cost) as follow:

$$t_a(x_a) = t_a(0) \left[1 + \alpha \left(\frac{x_a}{C_a} \right)^{\beta} \right] \quad \forall a. \tag{4}$$

The travel time (cost) t_k^{oj} on the path *k* of *o-j* pairs is given by

$$t_k^{oj} = \sum_a t_a \delta_{a,k}^{oj}. \tag{5}$$

The equation $\delta_{a,k}^{oj} = 1$ is feasible if the link *a* is on the path *k* of *o-j* pairs, otherwise,

$$\delta_{a,k}^{oj} = 0.$$

B. Share Rate Model

Function (1) refers to the share rate A of underground expressway. The equilibrium model could offer the distribution flow of link a. Hence, the share rate model is:

$$A_j^n = \frac{\sum_{a'} x_{ja'}^n}{O+D} \quad \forall j, a', n, \tag{6}$$

where a' represents an underground expressway.

A space network comprised of ground roads and underground expressways is constructed using the equilibrium model. Considering the service object, the characteristics, the traffic benefit and non-superposition of underground expressway into consideration, Figure 1 givens an example of constructing a network with underground expressway.

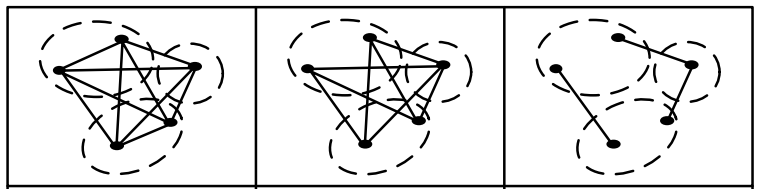

Figure 1. Process of constructing the space network

After several circles of iterative algorithm, the rate is steadied, and the result of passageway location model is optimized.

AN ILLUSTRATIVE NUMERICAL EXAMPLE

The network in Figure 2 is an illustrative numerical example. There are 4 zones and 36 links in this network. Each passageway points' IDs are shown in Figure 3. The demand point *o* is in the middle of each link. Symmetrical distributing randomly produces the amount of demands of points and zones. The shortest distance matrix $\hat{\mathbf{d}} = (\ldots, \hat{d}_{oj}, \ldots)$ and the minimal travel time (cost) matrix $\hat{\mathbf{t}} = (\ldots, \hat{t}_{oj}, \ldots)$ are determined using the Dijkstra algorithm. The application of the second iteration in zone is described as follow:

Input 1) the share rate (A=76.58%) which was the result of first iteration,

2) the demand of each demand point, the shortest distance matrix and the minimal travel time (cost) matrix in zone 1, as listed in Table 1,

3) the parameters μ=1, O_1=D_1=1635, and ε=0.1000.

First, these data is inputted into the model. Then the results show that the maximal efficiency is 644 and the optimized passageway point is No. 8. According to the same method, the maximal efficiencies and the optimized passageway points in other zones can be solved. Then, a new space network is built and its flow is distributed again, up to the new share rate that is obtained. Execute the iterative algorithm again until the result at the fourth iteration shows ε=0.0739, which follows

$\frac{\sqrt{\sum_j \left(A_j^{n+1} - A_j^n\right)^2}}{\sum_j A_j^n} \le \varepsilon,$. The iterative algorithm is finally stopped.

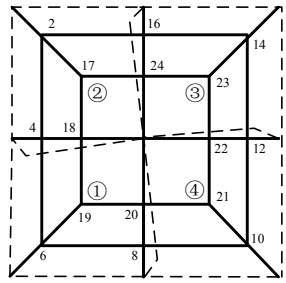

Figure 2. Network

Table 2 presents the results of iterative operations in each zone. Figure 3 illustrates the relationship between value of efficiency and passageway point in each iterative operation. All curves of the four zones are similar, which is explained as follow.

Table 1. Relative Data of Demand Point and Passageway Point

j / *O*	Shortest Distance				Minimum Travel Time (cost)				Dem-and
	6	8	19	20	6	8	19	20	
28	0.0401	0.24	0.15	0.27	1.59	10.48	167.77	15.27	564
29	0.2314	0.03	0.23	0.11	10.01	1.12	158.42	5.92	500
35	0.0974	0.29	0.21	0.33	4.46	13.35	170.64	18.14	594
36	0.1011	0.10	0.21	0.17	4.44	4.44	161.74	9.23	544
44	0.0601	0.25	0.05	0.17	123.31	132.20	123.31	136.99	493
45	0.2340	0.04	0.16	0.04	11.28	2.40	154.90	2.40	512
51	0.1691	0.26	0.06	0.18	245.15	236.26	78.97	231.47	464
52	0.1686	0.14	0.06	0.06	89.93	81.04	76.25	76.25	483
59	0.2868	0.14	0.18	0.06	56.17	47.29	194.00	42.49	518

Table 2. Results of Iterative Operation

Iterative ID	Zone ID	Maximal Efficiency	Optimization Passageway ID	Share Rate	ε
1	1	——	18	76.58%	——
	2	——	17	70.24%	——
	3	——	23	70.46%	——
	4	——	21	70.88%	——
2	1	644	8	43.59%	0.2127
	2	561	4	32.67%	
	3	639	16	45.22%	
	4	641	12	45.94%	
3	1	304	8	58.70%	0.1589
	2	246	4	47.21%	
	3	332	16	56.03%	
	4	391	12	58.25%	
4	1	497	6	66.89%	0.0739
	2	308	4	37.62%	
	3	357	16	65.51%	
	4	388	12	62.25%	

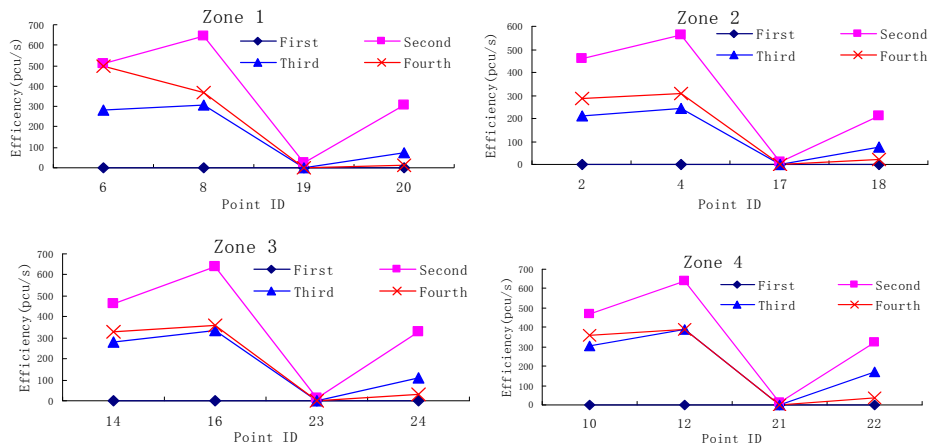

Figure 3. Curves of passageway efficiencies in each zone

1) the values of efficiency in No. 6 and No. 8 zones are larger than those in No. 19 and No. 20 zones in each iterative operation. It reveals that the passageway location model always chooses the optimal point from the points with a high probability. Since the values of efficiency of the points in poor locations are very small, these points are not selected.

2) the four curves tend to tranquilization in the middle level, which means the share rate of underground expressway tends to be steady.

3) the optimized point is No. 8 in the 2nd and 3rd curves, and the value of efficiency in No.6 zone is close to the values of No.8 gradually until it exceeds the No.8 in the fourth iteration. The result shows that the course of the travel time (cost)

tending to be steady has the potential to globally optimize the result of passageway location model.

CONCLUSIONS

This paper presented a new passageway location model of underground expressway. A share rate model and its solution algorithms for forming an underground expressway space network were also developed. In conclusion, firstly, if the number of demand, share rate, and travel time (cost) were known, the locations of passageway can be obtained by using these models. Secondly, since the value of efficiency changed with the steadying of share rate, this iterative algorithm can make the model convergent. Finally, the travel time (cost) also changed continually with the iterative operation. Therefore, the passageway locations of underground expressway are globally optimized.

REFERENCES

Farhan, B., and Murray, A. T. (2006). "Distance decay and coverage in facility location planning." *The Annals of Regional Sci.*, 40(2), 279-295.

Hanson, S., and Giuliano, G. (2004). *The geography of urban transportation*. M. 3rd ed. Guilford, New York.

Hirata, T., Yai, T., and Mahara, T. (2006). "Traffic Safety Analysis in Underground Urban Expressway Using Driving Simulation System MOVIC-T4." . *Transportation Research Board Annual Meeting*, 6-2184.

Hurst, M. E. E. (1972). *A geography of economic behavior: an introduction*. Duxbury, MA: North Scituate.

Thalheimer, E. S. (2004). "Reduction in city background noise due to relocation of artery traffic into underground tunnels." *The 2004 National Conference on Noise Control Engineering*, 406-416.

Zhang T., Zhao Y., Liu Y. et al. (2007). "Underground road function definition and analysis on its applicability in Shanghai." *Chinese Journal of Underground Space and Engineering*, 3(3), 406-410.

Optimum Choice for the Construction Management Plan Based on Entropy Weight

Yong-Fen Ruan[1] ; Jin-Ping Wang[1] ; Wang Dong[1] ; Mou jie[1]

[1]Department of Civil Engineering, School of Architecture, Science and Technology Institute of Kunming,Kunming,650224 China. Tel:+86-871-3801057;email: ryy64@yahoo.com.cn ; tumu380@yahoo.com.cn

ABSTRACT

According to engineering practice's experience and theoretical research, the evaluation index system of bridge construction organization design is established. Based on entropy theory, the optimum model for the design scheme of construction is set up. This model is established on indices of different schemes to build up a non-fuzzy judgment mathematical matrix and standardize it to calculate entropy, then these indices are applied in calculating entropy weight. Then we can calculate the attribute matrix and seek the ideal point. Finally we can get the best scheme by priority order degree of distance or nearness degree between all schemes and the ideal point. Examples show that the construction management plan selected based on the entropy theory has strong evaluating capability and is simple and effective. This method is instructional in all-around evaluations.

INTRODUCTION

A construction management plan in bridge engineering is a programmatic document of technology and economy for the general layout document of construction engineering (Mao Ze-Hua, 2004). It also plays a very important role in realizing scientific production management, ensuring quality, economizing resources and reducing costs of construction site. There are lots of factors which influence the tendering and bidding of construction management plans in bridge engineering. Often the decision-making scheme concerns a complex system that consists of multiple indices and multiple schemes. Therefore, it is very difficult to evaluate the scheme using merely objective function or the evaluation criterion. The most commonly used method in an evaluation process requires an expert grading method in which the proposal with the highest score wins the bid. The result of this method sometimes can't represent the actual situation of the evaluation object. The process of multi-index assessment method (Mao Ze-Hua,2004;Cai Xue-Feng,2004;Ruan Yong-Fen,2003) depend upon experts to give proper index weights which leads to higher randomicity and the loss of some useful information. Although the analytic hierarchy process (AHP) method is an effective tool for solving a multi-objective decision-making problem and is successfully applied in many fields of decision-making. But its evaluation matrix used a relatively lopsided judgment scale

(Xie Qian-Bo,1998). To deal with this complicated problem, this paper constructs an index system which influences the decision making of plans according to the actual situation, applying this entropy weight theory in the optimum choice evaluation of constructional organization design of bridge engineering and constructs a non-fuzzy judgment matrix based on the result of read and appraisal from the experts to select the best proposal.

PRINCIPLE OF ENTROPY WEIGHT DECISION-MAKING

The word "entropy" originates from the Greek language. Entropy is referred to as a measure of uncertainty. The bigger the information entropy is, the greater the degree of disorder and the smaller the effect; contrariwise, the smaller the information entropy is, the lower degree the extent of disorder and the bigger the effect. As weight, the entropy deducted through calculation using the evaluation matrix is not the important actual index in decision making or evaluation problems. Rather, the evaluation scheme set is given out, then every evaluation index value is confirmed. It is a coefficient with relative vehement extent under the competition condition (Tian Zhen-Qing,2002; Chen Li-Ming,2003; Qiu Yuan-Hua,2002) under situations when each types of evaluation index is confirmed and the evaluation scheme set is given.

Entropy

When entropy H ($p_1,p_2,\ldots,p_m$) satisfies three combinations below and consistency requirement, the entropy has only have one form.

If $$\mathrm{H}(\mathrm{p}_1,\mathrm{p}_2,\ldots,\mathrm{p}_\mathrm{n}) \le \mathrm{H}\left|\frac{1}{n},\frac{1}{n},\ldots,\frac{1}{n}\right| \quad (1)$$

$$H(p_1,p_2,\cdots,p_n) = H(p_1,p_2,\cdots,p_n,0) \quad (2)$$

$$H(S*T) = H(S) + H(S/T) \quad (3)$$

Then, entropy is defined as

$$H_n(X) = H_n(p_1,p_2,\cdots,p_n) = -k\sum_{i=1}^{n} p_i \log_2 p_i \quad (4)$$

Among p_i is the corresponding probability.

Suppose B' is a non-fuzzy judgment matrix.

$$B' = (b_{ij})_{m\times n} \quad (5)$$

Suppose $s_\mathrm{i} = \sum_{j=1}^{n} b_{ij}(i = 1,2\ldots n)$ is the sum of the elements in the k column, $f_{ij} = b_{ij} \big/ S_i$ can represent the probability of occurrence of the j element in the i result. Therefore the results of n types of calculations result of entropy are as follows:

$$H_i = -\sum_{j=1}^{i} f_{ij} \log_2 f_{ij}(i = 1,2,\ldots n) \quad (6)$$

Entropy weight

In evaluation problems which have *m* evaluation indices and *n* evaluation objects, the non-fuzzy judgment matrix B' is shown as follows:

$$B' = (b_{ij})_{m\times n} \tag{7}$$

$$b_{ij} = \frac{b'_{ij} - \min\limits_{j} b'_{ij}}{\max\limits_{j} b'_{ij} - \min\limits_{j} b'_{ij}} \tag{8}$$

After standardizing matrix B', we can get matrix B below

$$B = (b_{ij})_{m\times m} \tag{9}$$

Among it $b_{ij} \in [0,1]$

So the entropy which has m evaluation indices and n evaluation object is defined as:

$$H_i = -k\sum_{j=1}^{n} f_{ij} \ln f_{ij} \qquad i = 1,2,\cdots m \tag{10}$$

Among it $f_{ij} = \dfrac{b_{ij}}{\sum\limits_{j=1}^{n} b_{ij}}, k = \dfrac{1}{\ln n}$.

In order to make $\ln f_{ij}$ valid, it is commonly postulated that when $f_{ij} = 0$, $f_{ij} \ln f_{ij} = 0$.

In the evaluation which has *m* evaluation indices and *n* influence factors, the degree of influence of *i* assessment indices is entropy weight that can be calculated using following formulas.

$$\omega_i = \frac{1 - H_i}{m - \sum\limits_{i=1}^{m} H_i} \tag{11}$$

$$w = (\omega_i)_{m\times 1} \tag{12}$$

Among it, $0 \le \omega_i \le 1$, $\sum\limits_{i=1}^{m} \omega_i = 1$.

Evaluation process of entropy weight

1. Make sure that there are *n* schemes to be evaluated and *m* assessment indices in each of the evaluation scheme.

2. After standardizing the non-fuzzy evaluation, matrix $B' = (b_{ij})_{m\times n}$,

$B = (b_{ij})_{m\times n}$ can be derived.

3. Calculate entropy of every index H_i

4. Calculate attribute matrix $A = (b_{ij} \times \omega_i)_{m\times n} = (a_{ij})$

5. Seek ideal point $p^* = (p_1^*, p_2^*, \ldots, p_m^*)^T$

Among it: $$p_i^* = \max_j \left\{ a_{ij} \,|\, i = 1, 2\ldots, m; j = 1, 2\ldots n \right\} \tag{13}$$

6. Calculate distance

$$d_j^* = \sqrt{\sum_{i=1}^{m} (a_{ij} - p_j^*)^2}, j = 1, 2, \ldots, n \tag{14}$$

7. Calculate nearness degree.

$$T_j = 1 - \frac{\sum_{i=1}^{m} a_{ij} p^*{}_i}{\sum_{i=1}^{m} \left| p^*{}_i \right|} \tag{15}$$

Based on T_j value, the rank of the proposal can be decided and proposals of lower value will be considered first; if T_j is equal, then compare d_j^* value , consider proposal with lower value first.

APPLICATIONS

Its main bridge is a pre-stressed box-section continuous beam bridge. Five construction companies bid for the project. Each construction company produced a construction management plan based on the requirements of the bidding documents, then we have five schemes P_i(i=1,2,3,4,5). And then we used the main factors which influence the outcome to produce the system of evaluation. The index set used to evaluate the project is , C_J= (C_1, C_2, …,Cu_9) = {Construction plan and scheme C_1, measure on construction quality assurance C_2, safety guarantee C_3 , construction preparative working plan C_4,construction schedule and measure C_5, temporary electricity and heat supply C_6, measure on cost reduction C_7, schedule needing resource C_8 , overall construction site plan C_9} (Cai Xue-Feng,2004) nine experts were invited to score evaluation indices of every the construction management plan. Its result is in Table 1.

Table 1. Assessment result of construction planning design schemes

Constructional management plan schemes	1	2	3	4	5
Construction plan and scheme	85.5	93.5	89.5	96.7	82.5
Measure on construction quality assurance	81.5	85.1	84.3	86.5	87.9
Safety guarantee	82	86	85.3	84.3	85.9
Preparative working plan	89	80.4	80.5	80.5	90.8
Construction schedule and measure	90.5	85.7	89	82.7	86
Temporary electricity and heat supply	86.4	80.3	90	85	80.8
Measure on cost reduction	86.1	85.2	82.5	82.5	85
Schedule needing resource	80	82	80.6	80.7	90
Overall construction site plan	78	84	86	80	81.9

Then non-fuzzy assessment matrix is B'. After standardized and specification the matrix is B.

$$B' = \begin{bmatrix} 85.5 & 93.5 & 89.5 & 96.7 & 82.5 \\ 81.5 & 85.1 & 84.3 & 86.5 & 87.9 \\ 82 & 86 & 85.3 & 84.3 & 85.9 \\ 89 & 80.4 & 80.5 & 80.5 & 90.8 \\ 90.5 & 85.7 & 89 & 82.7 & 86 \\ 86.4 & 80.3 & 90 & 85 & 80.8 \\ 86.1 & 85.2 & 82.5 & 82.5 & 85 \\ 80 & 82 & 80.6 & 80.7 & 90 \\ 78 & 84 & 86 & 80 & 81.9 \end{bmatrix} \quad B = \begin{bmatrix} 0.2113 & 0.7746 & 0.4930 & 0 & 0 \\ 0 & 0.5625 & 0.4375 & 0.7812 & 1 \\ 0 & 1 & 0.825 & 0.575 & 0.975 \\ 0.8269 & 0 & 0.0096 & 0.0096 & 1 \\ 1 & 0.3846 & 0.8077 & 0 & 0.4231 \\ 0.6289 & 0 & 1 & 0.4845 & 0.0515 \\ 1 & 0.75 & 0 & 0 & 0.6944 \\ 0 & 0.2 & 0.06 & 0.07 & 1 \\ 0 & 0.75 & 1 & 0.25 & 0.4875 \end{bmatrix}$$

According to formula (10) we can get the entropy value of each evaluation indices in the Table 2.

Table 2. Entropy value for assessment indexes

Assessment indices	Construction plan and scheme	Measure on construction quality assurance	Safety guarantee	Preparative working plan
Entropy/H	0.7834	0.8317	0.8481	0.4638
Construction schedule and measure	Temporary electricity and heat supply	Measure on cost reduction	Schedule needing resource	overall construction site plan
0.8121	0.7083	0.6746	0.4934	0.7942

According to Table 3, use formula (11) to get attribute matrix A.

$$\omega_i = (0.0836,\ 0.065\ ,0.0586\ ,0.2070\ ,0.0725\ ,0.1126\ ,0.1256\ ,0.1956\ ,0.0795)^{\mathrm{T}}$$

$$A = \begin{bmatrix} 0.0177 & 0.0648 & 0.0412 & 0.0836 & 0 \\ 0 & 0.0365 & 0.0284 & 0.6498 & 0.065 \\ 0 & 0.0586 & 0.0484 & 0.0337 & 0.0572 \\ 0.1711 & 0 & 0.0020 & 0.0020 & 0.2070 \\ 0.0725 & 0.0279 & 0.0586 & 0 & 0.0307 \\ 0.0708 & 0 & 0.1126 & 0.0546 & 0.0058 \\ 0.674568 & 0.505926 & 0 & 0 & 0.0872 \\ 0 & 0.0391 & 0.0117 & 0.0137 & 0.1956 \\ 0 & 0.0596 & 0.0795 & 0.0199 & 0.0387 \end{bmatrix}$$

The ideal points

$$p^* = (0.0836,\ 0.065,\ 0.0586,\ 0.2069,\ 0.0725,\ 0.1126,\ 0.1256,\ 0.1956,\ 0.0795)^{\mathrm{T}}$$

The distance, nearness degree and priority order between each scheme and ideal point can be seen from table 3.

Based on the results, Scheme 4 is the best no matter if it is evaluated by priority order degree of distance or nearness degree.

Table 3. Optimums choice order for every scheme

Scheme	1	2	3	4	5
Distance	1.5310	1.6136	1.7726	1.3648	1.9010
Priority order according to distance	2	3	4	1	5
Nearness degree	0.7034	0.6434	0.6449	0.4741	0.8024
Priority order according to nearness degree	4	2	3	1	5

CONCLUSION

The consistency between the predicted values and the literature (Cai Xue-Feng, 2004) demonstrated the feasibility and correctness of the model. The entropy weight decision-making method can standardize different indexes which have different dimensions, physical implications and belong to different types. Its entropy can represent, to the fullest extent, the actual standard of different indexes and consists of the empirical evaluations from the experts; therefore the evaluation result has the combined advantage of subjective assessment and objective assessment. The entropy model of this passage not only consists of a clear concept and a logical theory, but also can be calculated easily using Excel. Meanwhile, it doesn't have disadvantages which include the usually objective way of fixing entropy weight and

the inclination of assessment result towards the average that results in low distinguishing rate. Therefore, due to the above advantages, it can be widely applied in engineering.

REFERENCES

Cai Xue-Feng, Li Ling, Zhu Qian(2004). "Application Research of Gray Correlation Method in Evaluation for the Design of Bridge Construction Organization." *Journal of Highway and Transportation Research and Development*, 21(10), 73-75.

Chen Li-Ming, Qiu Yuan-Hua(2002). "The Fuzzy Analysis in View of Entropy Coefficient for Influence Factor of Large Scale Project Decision Making." *Forecasting*, 22(3):65-57.

Mao Ze-Hua (2004). "Application of fuzzy decision method and analytic hierarchy process to evaluation programs of construction project public bidding." *Journal of Hefei University of Technology(Natural sciences)*, 27 (10), 4-9.

Qiu Yuan-Hua(2002). "Management Decision and Application of Entropy Theory", *Peijing: Machinic and Industry press*.

Ruan Yong-Fen, Ye Liao-Yuan(2003). "Determination of Deep Foundation Pit Supporting Scheme by Using the Gray System Theory and Method.", *Chinese Jouenal of Rock Mechanics and Engineering*, 22(7):1203-1206.

Xie Qian-Bo(1998). "Analytic Hierarchy Principium", *Tianjin: Tianjin University Press*.

Tian Zhen-Qing,Zhou Yue(2002). "The Certification of the fundamental properties of comentropy." *Journal Of Inner Mongolia Normal University(Natural Science Edition),*31(4):347-360.

Lane Change Behavior Character and Its Influence to Traffic Safety on Urban Roads

Y. Zhang [1], Q.Huang [2], M. Zhang [3] , and X. Yu [4]

[1]Traffic College, Northeast Forestry University, Harbin, HaPing Road 217; PH 0451-86549858; email: haitian8850@sina.com

[2] Department of Mechanical Engineering, Harbin Vocational & Technical College, Harbin, HaPing Road 217; PH 0451-86636743; email:qiuju99@163.com

[3]Traffic College, Northeast Forestry University, Harbin, HaPing Road 217; PH 0451-86636743; email: Zhangmin616@126.com

[4] Traffic College, Northeast Forestry University, Harbin, HaPing Road 217; PH 0451-86636743; email: yuxingsheng@163.com

ABSTRACT: This paper defined the quantitative relationship between the times of drivers' unauthorized lane changes and the times of traffic conflict by traffic conflict technology, then the influence coefficient of unauthorized lane change behavior. The concept of lane change frequent-degree is also given in this paper, then the influence of traffic safety from the characteristic of frequently changing lanes about taxi is analyzed and calculated.

INTRODUCTION

Lane changing is a behavior which frequently occurs when vehicles are operating, so there are many characteristics of lane changing on our country's urban roads. They influence traffic safety directly or indirectly (Mohamed et al, 2000). Analyzing the influence of these characteristics on traffic safety is useful for us to gain insight of these behaviors generating causes and regularity of outbreak then guide us to make scientific management methods to secure the traffic safety (Ioannis et al, 2002).

THE CONCEPT OF LANE CHANGE BEHAVIOR

Lane change behavior describes the combined course that drivers adjust and finish their drive strategies according to their driving character, the traffic

environment, such as surrounding vehicles' speed, gap and so on (Jerry et al, 2003). In fact, lane change is a kind of behavior that drivers demonstrate their decision by the way they drive vehicles. According to differences of advantage motivation, lane change behavior can be divided into obligatory and arbitrary lane change (Gipps, 1986). The former means there are definite lanes which drivers must change at a given area, such as ramps diverge and merge vehicles, mixed area, etc. The latter means that when the speed of the front vehicle is slow, the driver will change lanes to maintain a higher speed and more driving space.

LANE CHANGE BEHAVIOR CHARACTER ANALYSIS ON URBAN ROADS

In our country, urban roads have many vehicle types, large traffic flow and complex condition, drivers also have different physiological and psychological character, and the traffic environment influence make the drivers' expected speed limited (Wang et al, 2008), so lane change behavior has much character, such as unauthorized lane change, taxis frequently changing lane, forced lane change at ramp exit and entrance, contend for lane change at instable traffic flow and so on. These characteristics, especially unauthorized lane changes and taxis frequently changing lanes, severely influence the traffic safety.

Drivers' unauthorized lane change analysis

In this paper we investigated about 504 hours of traffic flow on 42 roads in various cities including Harbin, Beijing, Dalian, and Xian. We used the methods of video recording, questionnaires, etc. We got the figures by the date, see figure 1.

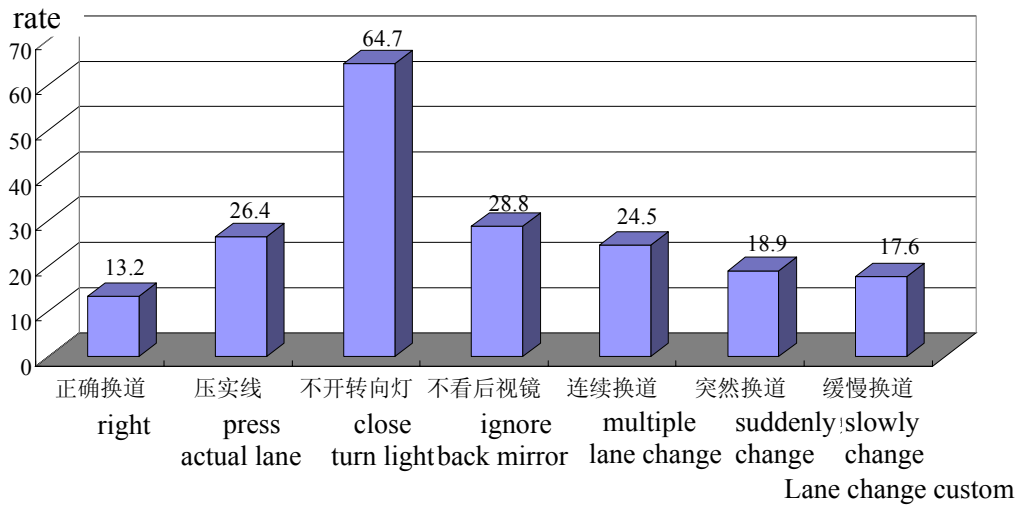

Figure 1 Drivers' lane change custom statistics

From Figure 1 we know that the majority of drivers have unauthorized lane change behavior. We also found that many drivers had several defective lane change customs at the same time. The real cause of unauthorized lane change behavior is that drivers cannot run at their desired speed (Thomas et al, 2005), and they always realize it by violation of regulation, so many drivers perform the defective lane change custom.

Taxis frequently changing lane analysis

In our country, vehicle types are complex, speed contrast is great, taxi drivers often get higher running speed by changing lanes frequently. We define lane change frequency degree K to describe this case, it is the ratio of all the lane change times of one type of vehicle and its traffic flow at specified road sections in one hour time.

$$K = \frac{T_t}{T_v} \tag{1-1}$$

In the formula, T_t means the total lane change times of this type of vehicle in an hour at this road-section, T_v means the traffic flow of this type of vehicle in an hour at this road section. If K is less than 1, several vehicles did not change lanes, if K is more than 1, several vehicles changed not only one lane at a time, the larger the K is the more frequent the lane changes.

There are many taxis on urban roads. The goal of taxis is to serve the passengers with optimum speed in a minimum amount of time, so the taxi drivers often attain higher speeds than the typical driver and always change lanes to attain their aim (Hiroshi, 2001). By calculations based on our investigation, we got the lane change frequency degree average value of several types of vehicles: taxis are 1.45, private vehicles are 1.14 and trucks are 0.86. Consequently, we know that the taxi's lane change frequency degree is larger than other types of vehicles, it agrees with the face.

The influence of drivers' unauthorized lane change to safety

In most cases, the lane changes which violate the regulation did not cause traffic accidents, but it made traffic conflicts(Hoong et al, 2003). We chose the roads which had the same traffic flow and calculated the average value by the investigation data, see table 1.

From this table we know that the more times unauthorized lane changes occur, the more times traffic conflicts with the same traffic flow. Referring to the foreign

calculation method of conflicts and accidents (Nishida, 1999; Sultan et al, 2001), this paper defined the relative value of unauthorized lane changes and got the relative coefficient average value of unauthorized lane change times to traffic safety.

Table 1 Statistic of unauthorized lane change and traffic confliction times (times/hour)

Average traffic flow (veh/h)	1870	2650	3750	4250
Average press real line	5	3	6	7
Average turn light close	24	27	19	23
Average ignore back mirror	7	6	3	4
Average suddenly changing lane	3	5	7	4
Average forced changing lane	8	7	12	10
Unauthorized lane change times	47	48	47	48
Traffic confliction times	39	45	49	54

Table 2 the influence coefficient of unauthorized lane change

Times of unauthorized lane change (time/hour)	<25	25~40	40~55	55~70
Coefficient of traffic safety influence	0.25	0.5	0.75	1.00

The influence of taxis frequently changing lanes for safety

When the taxi changes lanes, it will influence surrounding vehicles' speeds, and frequently changing lanes will influence the vehicles in adjacent lanes (Louid et al, 2005). So many taxies frequently changing lanes will at last influence the speed of the traffic flow, and make it in an unstable state, the unstable traffic flow is the highest traffic accident rate state. We give the condition of taxis frequently changing lanes, see figure 2.

Figure 2 Taxis frequently changing lanes

Taxis changing lanes frequently will make the probability of traffic conflicts grow (Li et al, 2002), this paper obtained the data from classical road-section in Harbin, Beijing, Dalian, Xi'an etc. we got the traffic flow of each road section at three time-intervals every day, and each road section we observed for three days, we recorded the condition of each road section by camera, then threatening the date by professional. By calculation and analysis we found that the conflicting times increased when the taxis changed lanes frequently, so the taxis frequency of changing lanes is an incipient fault which poses traffic safety of urban roads. We cannot give all the data in this paper because of the graphical limitations, so we gave some of data below, see Table 3.

CONCLUSION

Lane changing is a behavior which frequently occurs when vehicles are operating, so there are many characteristics of lane changes on our country's urban roads. They influence the traffic safety directly or indirectly. This paper defined the quantitative relationship between the times of drivers unauthorized lane changes and the times of traffic conflicts by traffic conflict technology, and then determined the influence coefficient of unauthorized lane change behavior. The concept of lane change frequency-degree is also given in this paper, then the influence to traffic safety from the characteristic of frequently changing lanes about taxis is analyzed and calculated. We hope this paper is useful for the theory of developing traffic safety technology and improving traffic safety management, and then improving the traffic environment and protecting traffic safety.

Table 3 The influence of taxis frequently changing lanes for safety

Road-section name	Time-interval	Total traffic flow (veh/h)	Taxi lane change frequence degree	Confliction (time)
Hexing Road	08:00-09:00	1215	1.27	24
Hexing Road	09:00-10:00	1237	1.19	21
Hexing Road	12:00-13:00	865	1.02	14
Hexing Road	13:00-14:00	883	1.06	16
Hexing Road	16:00-17:00	1225	1.26	28
Hexing Road	17:00-18:00	1241	1.13	24
Xuefu Road	08:00-09:00	1345	1.35	34
Xuefu Road	09:00-10:00	1384	1.42	38
Xuefu Road	12:00-13:00	788	1.05	17
Xuefu Road	13:00-14:00	810	1.10	19
Xuefu Road	16:00-17:00	1357	1.38	36
Xuefu Road	17:00-18:00	1372	1.44	39
Haping Road	08:00-09:00	1154	1.03	13
Haping Road	09:00-10:00	1225	1.08	9
Haping Road	12:00-13:00	758	1.14	12
Haping Road	13:00-14:00	793	1.17	8
Haping Road	16:00-17:00	1154	1.12	13
Haping Road	17:00-18:00	1225	1.07	9
Sandadongli Road	08:00-09:00	1322	1.27	29
Sandadongli Road	09:00-10:00	1331	1.35	33
Sandadongli Road	12:00-13:00	795	1.02	14
Sandadongli Road	13:00-14:00	814	1.12	16
Sandadongli Road	16:00-17:00	1328	1.29	35
Sandadongli Road	17:00-18:00	1337	1.36	36
Sangzhi Road	08:00-09:00	1236	1.35	31
Sangzhi Road	09:00-10:00	1268	1.42	36
Sangzhi Road	12:00-13:00	1104	1.03	17
Sangzhi Road	13:00-14:00	1142	1.08	20
Sangzhi Road	16:00-17:00	1326	1.46	37
Sangzhi Road	17:00-18:00	1332	1.51	41
……	…….	……	…….	….

REFERENCES

Mohamed A. Abdel-Aty, A. Essam Radwan. (2000). "Model traffic accident occurrence and involvement". *Accident Analysis and Prevention*, 32(5), 633-642

Ioannis Golias, Mstthew G. Karlaftis. (2002). "An international comparative study of self-report driver behavior". *Transportation Research Part F Traffic Psychology and Behaviour,* 4(4), 243-246.

Jerry L. Deffenbacher, David M. Deffenbacher, Rebekah S. Lynch, et al. (2003). "Anger, Aggression, and Risky Behavior: a Comparison of High and Low Anger Drivers". *Behavior Research and Therapy*, 41(6), 701-718

P. G. Gipps. (1986). "A model for the structure of lane-changing decisions". *Transportation Research Part B Methodological*, 20(5), 403-414

Wang Y. G., Pei Y. L., Zhao Y. D. (2008). "Vibration-based damage detection with structural modal characteristics". *The Baltic Journal of Road and Bridge Engineering*, 3(1), 21-28

Thomas Ayres, Li Li, Doris Trachtman, et al. (2005). "Passenger-side rear-view Mirror: driver behavior and safety". *International Journal of Industrial Ergonomics*, 35(2), 157-162

Hiroshi Ohno. (2001). "Analysis and modeling of human driving behaviors using adaptive cruise control". *Applied Soft Computing*, 1(3), 237-243

Hoong Chor Chin, Mohammed Abdul Quddus. (2003). "Applying the random effect negative binomial model to examine traffic accident occurrence at signalized intersection". *Accident Analysis and Prevention*, 35(2), 253-259

Yasushi Nishida. (1999). "Driving characteristics of the elderly: risk compensation of the elderly driving from the viewpoint of reaction behavior". *JSAE Review*, 20, 375-380

B. Sultan, M. McDonald. (2001). "The lane changing process: data analysis & modeling behavior". *Traffic Engineering Control*, 42(3), 202-207

Louid Tijerina. (2005). "Eye glance behavior of van and passenger car drivers during lane change decision phase". *Transportation Research Record*, 1937, 37-43

Li L.X, Wang F.Y. (2002). "The automated lane changing model of intelligent vehicle highway systems". *5th IEEE International Conference on Intelligent Transportation Systems*, Singapore, 216-218

Study on the Rules of Crash Distribution

X. Zhong [1], X. Chen [2], and Z. Wei [3]

[1] Chelbi Engineering Consultants, Inc. No. 20, Anyuan Road, 8 Floor - Xingyuan Talent Tower, Chaoyang District, Beijing, 100029, China; PH(+86-10)848986981; email: zhong_xiaoming@126.com
[2]Beijing Institute of Technology, Beijing, 100081, China; email: chenxue781@bjt.edu.cn
[3] Beijing University of Technology, Beijing 100124, China; PH(+86-10)848986981; email: weizhonghua@bjut.edu.cn

ABSTRACT

Traffic safety is a difficult problem around the world. It is desirable to analyze the crash distribution rules to reduce traffic crashes. However, extensive research is needed to support policy-makers and road safety engineers to make scientific decisions and to take effective measures in China. The objective of the paper is to reveal the distribution rules of crashes in China. Using statistics data, this paper discusses crash frequency and severity distributions by various factors, including temporal dimension, road factors (such as road classes or functions, geometric alignment, etc.), vehicles factors, and drivers' factors in details. The distributions of crash type and crash causes are also examined in the paper. A series of useful and interesting conclusions are available for domestic and overseas traffic policy-makers and road safety engineers.
Keywords: Traffic Safety, Crash Distribution, Crash type, Crash Characteristics

INTRODUCTION

Traffic safety is a serious problem around the world. Crashes have killed 1,462,223 people and injured 5,562,351 people in China since the 1990s (Data from the China Crash Data Annual Report 1990-2007). It is desirable to analyze the crash distribution rules to reduce traffic crashes (Alfonso 2001 and De 2002). However, few researchers，especially in China and some other underdeveloped regions，have performed extensive research to reveal the crash distribution rules (Li 2007, Mao 2007, and Meng 2008). The objective of the paper is to explore the characteristics and the crash distribution rules of crashes in China. First of all, the authors analyzed traffic safety trends then they discussed the rules of crash frequency and severity distributions by various factors, including temporal dimension, road factors (such as road classes or functions, geometric alignment, etc.), vehicles factors, and drivers' factors (such as

driving years). Finally, distributions of crash types and crash causes are examined in detail throughout the paper, followed by the conclusions. A series of useful and interesting rules are available from discussion. The conclusions and suggestions would give reference to domestic and overseas traffic policy-makers and road safety engineers.

CHARACTERISTICS OF CRASHES

Crash tendency and 24-hour distribution

Figure 1 shows the tendency of crash indexes from 1990 to 2007, and Figure 2 shows the characteristics of crash distributions during a 24-hour time period. The crash indexes increased from 1990 to 2003 and decreased from 2003 to 2007. The frequency of crashes was climbing in the daytime (from 7:00 AM to 20:00 PM) while was moving downward in the night (from 20:00 PM to the next day 7:00 AM). The characteristics of crash distributions during the 24-hour time period reflected the characteristics of traffic volume and drivers' physiological changes with time. The conclusion was similar to previous research (Walmman 2001 and Zheng 2006). At peak hours, the volume was larger, and the crash frequency also increased. In the afternoon, the drivers' capacities for work or vigorous activity are general lower than in the morning, and drivers are easily subjected to negative factors, such as fatigue and desertion, which is the reason why more crashes occur in the afternoon. Although there was less traffic volume at night and the crash rate was relative lower, the proportion of fatality crashes was higher due to driver error caused by bad judgment and weak visual nighttime capacities.

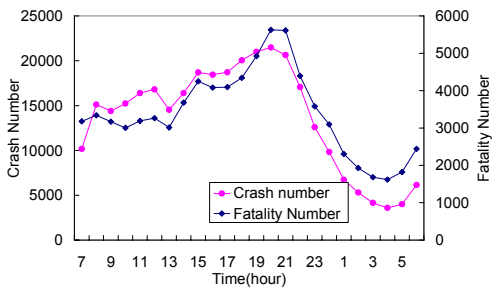

Figure 1. Crash index tendency.

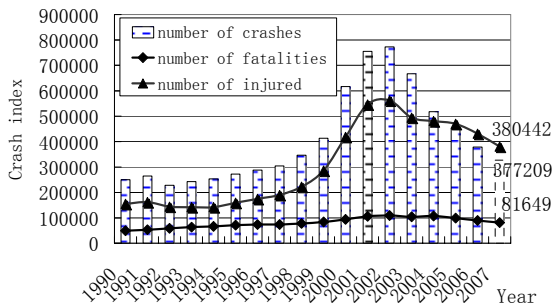

Figure 2. 24-hour crash distribution.

Distribution by roadway

Different safety performances appear on different technical classes and functional Roads (Hauer et al. 2004). Total highway mileage was 3,583,700 kilometers, where 60,271 deaths and 222,420 injuries were caused by 190,825 traffic crashes (accounted for 58.3% of the total number of crashes in 2007). And the city road mileage reached 329,800 kilometers, where 114,433 crashes (accounted for 35.5% of the total number of crashes in 2007) occurred and caused 17,431deaths and 127,271 injuries. In China, highways are divided into five classes: national highway, provincial highway, county

highway, countryside, and village roadway. From the statistical data shown in Table 1, it means that about 14 people would be killed by traffic crashes on an average 100 kilometers of national highway in a year. The average number was nearly nine deaths by crashes every 100 kilometers of provincial highway in a year. About two or three people would be killed by crashes every 100 kilometers of county highway in a year. The crashes that occurred on national highways and provincial highways were two to four times more severe than those that occurred on other roads. There may be two main reasons to explain this phenomenon. First, traffic volume on national highways and provincial highways is much heavier than on other roads. Second, multi-vehicle crashes are more common because of drivers' manipulative errors or illegal behaviors under complicated traffic conditions and deficient road safety facilities.

Compared with the crash frequency of highways, the number of crashes that occurred on city roads was larger than that on the provincial highway but smaller than that on the national highway. Heavy traffic volume and signal lamp would encourage lower speeds, which accounted for the low number of severe crashes. However, roads with mixed traffic volumes will increase the possibilities of crashes on the city roads.

Table 1. Crash distributions on different roads in 2007.

Roadway type	Crash Index in 2007					Crash Index on Average 100 Kilometers			
	No.of crashes	No.of deaths	No.of injuries	Economic losses RMB ($\times 10^4$ Yuan)	Miles (km)	No.of crashes	No.of deaths	No.of injuries	Economic losses RMB ($\times 10^4$ Yuan)
National highway	53039	20033	60841	46336.82	137100	38.69	14.61	44.38	33.80
Provincial highway	62782	20893	72180	2322.77	255200	24.60	8.19	28.28	0.91
County highway	47995	12982	57322	11721.97	514400	9.33	2.52	11.14	2.28
Countryside &Village roadway	20969	4850	25077	3540.44	2619900	0.80	0.19	0.96	0.14
City Expressway	17825	3427	19987	5257	329800	34.70	5.29	38.59	7.97
City Local Road	96608	14004	107284	21028					

Relationship between traffic safety and various traffic mode

Four traffic modes, including passenger cars, buses, trucks, and motorcycles, were the dominant modes involved in traffic crashes. The number of crashes involving cars and buses was twice as high as the number of crashes involving cars and trucks while the severity of crashes related to trucks was more serious than that related to passenger cars because heavy and light trucks with poor brake performance are usually driven while overloaded and with excessive speed. In addition, the number of crashes connected with driving non-motorized vehicles and foot passengers cannot be ignored, since 17,734 crashes resulted, 3,868 people died, and 16,794 people injured.

Distribution by safety performance of vehicle

Crashes often coincide with the dangerous situation of vehicles. But crash data

showed only 5 percent of the total crash number occurred while vehicles operated under suboptimal conditions. Compared with crash severity involving optimal performing vehicles, the severity involved with suboptimal vehicles was more serious, with 5 percent of the total crash number resulting in nearly 10% percent of the total fatalities.

Distribution by driving Years

Crashes are related to driver experience and road user consciousness to obey traffic laws. To some extent, years of driving experience correlates to fewer crashes. Figure 3 illustrates the relationship between driving years and crashes in 2007, which is similar to some researchers' conclusions (Walmman and Hastrom 2001 and Zhong 2007*)*. According to the statistical data in 2007, drivers with less than 3 driving years were involved in 33.72 percent of total crashes number and drivers with less than 5 driving years constituted more than 50 percent of the total number of crashes.

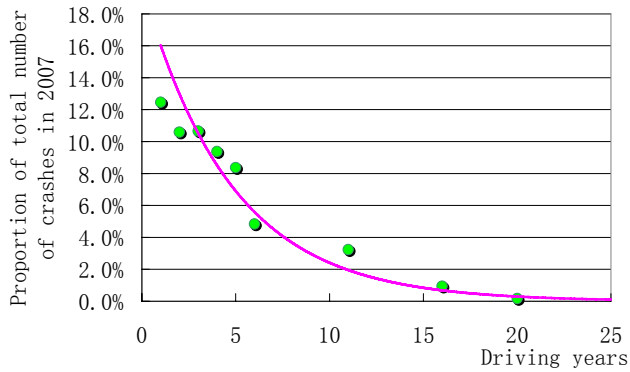

Figure 3. Relationships between the number of crashes and driving years.

As shown in the crash statistics data, a person's occupation may determine the likelihood of involvement in a crash. Peasants were involved in 100,659 crashes because of traffic law violations in 2007, which accounted for 30.76 percent of the total crash number. Individual proprietors answered for 18.71 percent of total crash number and 18.93 percent of total deaths, respectively. Most peasants and individual proprietors are less educated than other people in China. As a whole, crashes reflected the peace-breaker safety consciousness in China.

CRASH TYPE DISTRIBUTION AND CAUSE

Crash type distribution

Crash type was divided into 14 types, including side collision, head-on collisions, and rear-end collisions. Similar to crash types in other countries (Hauer et al. 2004 and Rune 2004), the above mentioned crash types were the most common three types according to the statistical data in 2007(Table 2). Side collisions were the most common and occurred on various types of roads. Head-on collisions usually took place

on Highway Class II and Class III. Rear-end collisions frequently appeared on freeways and highways. The most common three crash types on tangent segments were head-on collisions, side collisions, and rear-end collisions. The number of fatality crashes occurring on tangent segments was 68,231, which was the maximum number of fatalities on various alignments. Most collisions at tangent segments were connected with high speeds. Head-on collisions, overturned vehicles, and side collisions were the three common crash types at curve segments.

Analysis of causes of crashes

Drivers' illegal behaviors were responsible for 89.35 percent of the total crashes in 2007. The 292,343 crashes induced by drivers' illegal behaviors caused 73,510 fatalities and 344,552 injuries, accounting for 90.03 percent and 90.57 percent of total fatalities and total injuries, respectively. The five common drivers' illegal behaviors included: impeding safety driving behavior, disobeying the rule of giving way, speeding, driving with no license, and illegal driving on an opposite lane. The above five reasons caused 199,524 crashes, 48,416 fatalities, and 230,060 injuries, sharing by nearly 60 percent of total crashes number, total fatalities, and total injuries, respectively. The causes of crashes indicated that it takes efficient measures to monitor and administer the drivers' illegal behaviors together with driver education to improve road safety (Zhong and Wang 2006).

Table 2. Crash Type Distribution in 2007

Crash Type	Number of crashes		Number of deaths		Number of injuries		Property loss ($\times 10^4$ RMB Yuan)	
	%of total	Number	%of total	Number	%of total	Number	%of total	Number
Side collision	120547	36.84%	20966	25.68%	139601	36.69%	29617.09	24.71%
Head-on collision	92315	28.21%	23683	29.01%	111152	29.22%	27099.81	22.61%
Rear-end collision	38064	11.63%	12306	15.07%	44380	11.67%	29077.59	24.26%
Collision with Pedestrian	25282	7.73%	6188	7.58%	24854	6.53%	2438.92	2.03%
Sideswipe collision same direction	10448	3.19%	1856	2.27%	11377	2.99%	2702.32	2.25%
Overturned	8889	2.72%	4811	5.89%	15159	3.98%	8830.58	7.37%
Collision with fixed objects	7906	2.42%	2810	3.44%	8463	2.22%	8854.25	7.39%
Sideswipe collision opposite-direction	7039	2.15%	1241	1.52%	9399	2.47%	1847.38	1.54%
Roller and collision	4472	1.37%	2891	3.54%	2335	0.61%	582.78	0.49%
Collision with stopping vehicle	2617	0.80%	1201	1.47%	2881	0.76%	2774.76	2.31%
Falling from cliff	1678	0.51%	1419	1.74%	2781	0.73%	2000.43	1.67%
Fire	144	0.04%	34	0.04%	68	0.02%	1929.01	1.61%

Collision with Animal	78	0.02%	19	0.02%	71	0.02%	23.62	0.02%
Others	7730	2.36%	2224	2.72%	7921	2.08%	2099.86	1.75%
Total	327209	100.00 %	81649	100.00 %	380442	100.00 %	119878.40	100.00 %

CONCLUSIONS

This paper investigated traffic safety, and analyzed the characteristics and distribution of crashes in China. The main findings of the study can be summarized as follows:

1. In China, the general tendency of crash indexes has experienced a slight downward trend from 2004 to 2007. The number of crashes occurred at peak hours and more often in the afternoon.

2. The ratio of number of crashes occurring on highways and city roads was about 6 to 4 in 2007. The situation of traffic safety on national highways and provincial highways was much more serious than on the other roads. Higher priority should be given in treating high crash locations on national highway, provincial highway and city roads.

3. Passenger cars, trucks, and motorcycles were the main types of vehicles involved in crashes, and crashes reflected the peace-breaker safety consciousness in China.

4. The crash ratio declined for drivers with more years of driving experience. Drivers with less than 5 years of driving experience were more likely to be involved in crashes. Passengers, non-motorized vehicle drivers, pedestrians, and motorcycle drivers are all vulnerable to in crashes.

5. There are many reasons for crashes, but drivers' illegal behaviors are responsible for most crashes. Impeding safety driving behavior, disobeying the rule of giving way, speeding, driving with no license, and illegal driving on an opposite lane are the most common reasons for crashes.

REFERENCES

Alfonso, M. (2001). "Development of a potential for safety improvement index austroads." *Road Safety Audit 2nd Edition.* Sydney, New South Wales, Australia.

De, L., P., and Sayed, T. (2002). "Development of a road safety risk index." *Journal of the Transportation Research Board 1784*, TRB, National Research Council, Washington, D.C., USA.

Hauer, E., Council, F. M., and Mo, Y. (2004). "Safety models for urban four-lane undivided road segments." *83rd Annual Meeting of the Transportation Research Board (CD-ROM)*, National Research Council, Washington, D.C., USA.

Li, K. B., Li, S. Y., and Qian, H. B. (2007). "Study of the strategy of improving road traffic safety." *Transportation Science & Technology*, No. 2.

Mao, L. Z., Duan, L. R., Mao, E. R. (2007). "International comparison analysis on road traffic safety factors." *Journal of Transportation Systems Engineering and*

Information Technology, No.3.

Meng, X. (2008). "On elements of influencing road traffic safety," *Journal of Liao Ning Police*, Academy No. 4.

Ministry of Public Security P. R. (2008). "China Crash Data Annual Report1990-2007."

Rune, E. (2004). "To what extent is there bias-by-selection? Selection for road safety treatment in Norway." *the 83rd Annual Meeting of the Transportation Research Board (CD-ROM)*, National Research Council, Washington, D.C., USA.

Walmman, C. G., and Hastrom, H. (2001). "Friction measurement methods and the correlation between road friction and traffic safety." *A Literature Review. VTI 911A,* Linkoping, Sweden.

Zheng, A. W. (2006). "Current situation and improvement of road traffic safety in China." *Journal of Wuhan Uni. of Sci. & Tech. (Natural Science Edition),* Vol. 29, No. 1.

Zhong, X. M., and Wei, Z. H. (2007). "Traffic safety situation and suggestions of safety policy for China." *Proceedings of ICTCT Extra-Workshop in Beijing, China, April 2nd*.

Zhong, X. M.，Wang, H. Z., and Sun, (2006). "Study on new concepts of highway safety design." *85th Transportation Research Board Annual Meeting(CD-ROM）*, National Research Council, Washington, D.C., USA.

Quick Maintenance for Tunnel Lining Voids with Polymer Grouting Technology

XU Jianguo[1], WANG Fuming[2], WANG Bo[3]

[1]College of Environment and Hydraulic Engineering, Zhengzhou University, Zhengzhou, 450002, PH13598055897, email: Jianguoxu@zzu.edu.cn
[2]College of Environment and Hydraulic Engineering, Zhengzhou University, Zhengzhou, 450002, email: Wangfuming@zzu.edu.cn
[3]College of Environment and Hydraulic Engineering, Zhengzhou University, Zhengzhou, 450002, email: Wangbo@zzu.edu.cn

ABSTRACT

The tunnel is a permanent construction and the lining is a main part in the tunnel structure. So the quality of lining construction should affect the traffic safety. In order to maintain the existing void between initial lining and surrounding rock or in the secondary lining construction, ground-penetrating radar nondestructive testing technology and polymer grouting technology for maintenance of tunnels has been presented. First use ground penetrating radar to analyze the distress and voids in the tunnel lining. Then use ground penetrating radar to evaluate quality of the whole structure and determine the disease scope of the tunnel, maintain void region with polymer grouting technology. The field test results show that the use of polymer grouting technology can repair the tunnel distress, and provide an ideal manner for tunnel quick maintenance.

KEYWORDS: *Tunnel, Polymer Grouting, Ground-Penetrating Radar, Quick Maintenance*

1 INTRODUCTION

The tunnel is the permanent construction and the lining is a main part in the tunnel structure. So the quality of lining construction would affect traffic safety. At present, the lining manner is mainly the composite lining and the New Austrian Tunneling Method (NATM) is used for tunnel design and construction. The stage of construction can be divided into two partsy the composite lini and secondary lining. The secondary lining can be carried through when the surrounding rock is stabilized. The stressed state of the secondary lining is very complicated and there are many influence factors, such as surrounding rock grade, groundwater, tunnel burying depth, stiffness of initial supporting and construction time. Because of the influence

factors of construction technique, the tunnel lining void may appear in the position between initial supporting and secondary lining. In case of the existence of the asymmetry void in the secondary lining, the loose pressure and deformation pressure of surrounding rock can not be transmitted asymmetrical. The results of the disease are as follows—are as followeg, the loose pressure and deformation pressure of surrounding rock can not be transmin probability of failure, deformation and falling down of the secondary lining that affects traffic safety seriously. So it is very important to do the tunnel lining construction inspection and long-term traffic safety inspection.

Ground-penetrating radar is a new type of nondestructive instrument techniques (Jing et al. 2007). Characteristics of the instrument include handiness, high efficiency, high precision, high differentiate rate and hyper-shallow detection. Ground-penetrating radar can be used in every stage of tunnel building (You et al. 2007). At the operation and acceptance stage, it also can be used for building quality checking, such as the thickness of lining concrete, lining concrete cracks, tunnel lining voids and leakage. At the operation stage, the tunnel lining service condition can be detected with disease style, disease range and disease depth (Wang et al. 2007).

The common methods to deal with tunnel diseases (such as cracks, voids and leakage) are concrete grouting processes and the use of EAA epoxy material. The main shortcoming is poor maintenance results - only maintained for several months and the high cost of maintenance. The polymer grouting technology for quick tunnel maintenance can be used in concrete panel repairing and elevation (Liu et al. 2007). The achievement is remarkable and the application prospects good (Wang 2007).

2 CHARACTERISTICS OF POLYMER GROUTING TECHNOLOGY

Polymer grouting technology was presented for road and infrastructure maintenance in the 20th century. It has been applied popularly all over North America and Europe. In China polymer grouting technology has begun to be used in freeway maintenance. The critical technologies include polymer material and injection technology. Shallow injection technology is mainly used in void maintenance and elevation of concrete panels. Deep injection technology is mainly applied in base stabilization of road foundation courses and infrastructure.

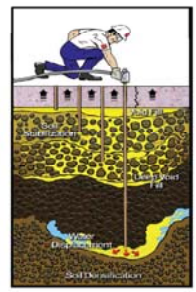

Figure1. Equipment for polymer grouting technology and operating sketch.

Polymer grouting technology has the following characteristics (Liu et al. 2007):

a. Stage of construction is short and less influences the traffic. By the use of polymer grouting maintenance technology, from equipment installation and injection to finishing the whole construction only needs several hours. Traditional methods need at lest several days or several weeks.

b. The polymer material expands rapidly when grouting (its volume is 10-20 times larger than the liquid material). Polymer material fills in the void and crash position automatically.

c. After expansion, the gravity load of the polymer material is only 10% as equivalent volume of grout and it has favorable elasticity.

d. The number of drilling holes is less than in traditional methods and the aperture dimension is also smaller, so it is does not destroy the structure.

e. The performance advantages of polymer material includes good water resistance, non-shrinkage, good durability and non-environmental pollution.

f. The whole injection process is finished under automatic inspection, saving time, saving labor and economy.

3 APPLICATION OF TUNNEL MAINTENANCE WITH POLYMER GROUTING TECHNOLOGY

3.1 Tunnel lining disease inspection with ground penetrating radar

After tunnel construction, besides the lining concrete surface, the inspection of lining quality mainly depends on construction record and experimental data. All these can't reveal the lining thickness and voids behind the lining. But by use of ground penetrating radar, this problem could be effectively solved.

Ground Penetrating Radar (GPR) is an electromagnetic technology that uses radio waves to inspect and scan the underground medium distributing (You et al. 2007), the unseen objective and underground interface. High frequency electromagnetism waves are transmitted with the type of wideband impulse across antenna. By the reflection and transmission of the objective, the waves are received by the receiver antenna. When the electromagnetism wave is transmitted in the medium, its transmission path, electromagnetism field intensity, and wave shape are

affected by the electrical properties and assemble form of the medium. According to the time domain wave collection, treatment and analysis, the underground interface, the spatial position and structural state of the objective can all be ascertained.

With the collection data of ground penetrating radar, the cross section can be obviously divided into three different horizontal layers (Figure 2). The in-phase axis of the reflection wave of the first layer is consentaneous and well-balanced. But the thickness is different which displays the lining thickness. The in-phase axis of most reflection waves of the second layer is inconsistent, the energy of the echo-wave decreases with the reduction of medium density. The disturbing of noise waves shows that there are several reflection waves of voids at grouting tamping section of concrete and surrounding rock.

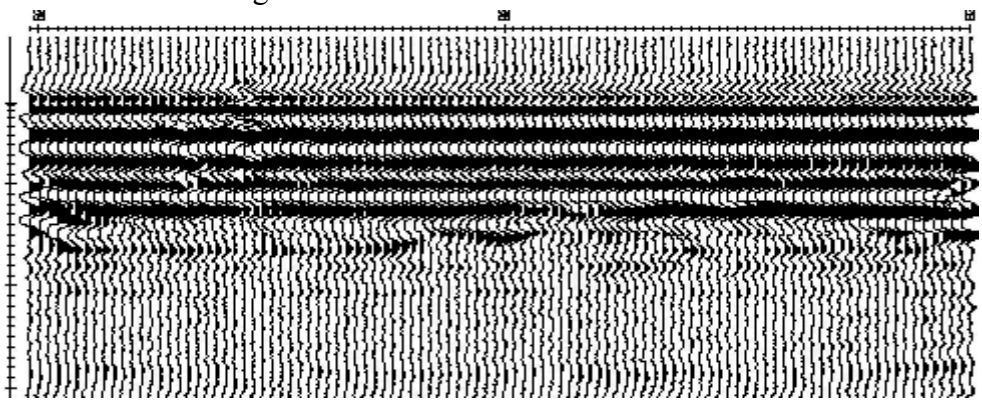

Figure 2. Cross section of ground-penetrating radar image.

The energy of echo-waves of the third layer is weak and the axis of reflection wave is consentaneous which show the full rock section. The surrounding rock cranny causes the noise waves in some section.

Generally, according to the radar imagines, the interface of the initial lining and the secondary lining, the lining and the surrounding rock could be distinguished. But if the dielectric constant of the initial lining of pneumatically applied concrete and the secondary lining formwork concrete is almost the same, the interface reflection wave of the initial lining and secondary lining isn't obvious. So the initial lining and the secondary lining can be regarded as the same layer.

The tunnel lining diseases are usually the voids and cracks between the initial lining and the secondary lining or between the initial lining and the surrounding rock. With these diseases, the radar imagines are abnormal. Figure 3 and Figure 4 show radar images of tunnel voids in the position of crown of arch and tunnel spandrel, respectively.

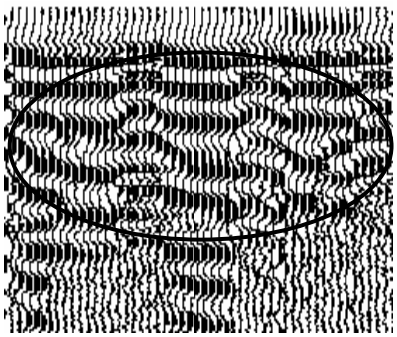

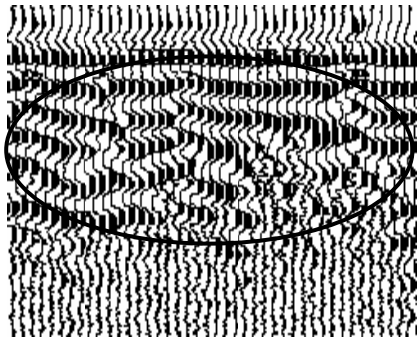

Figure 3. Radar imagine of crown of arch. Figure 4. Radar imagine of spandrel.

The collection GPR images of experimental locations is shown as Fig.5. The result shows that the image along with measure line 5meter-7meter is abnormal and there is a void at the interface of initial lining and surrounding rock. The polymer grouting is suggested to carry through for this section.

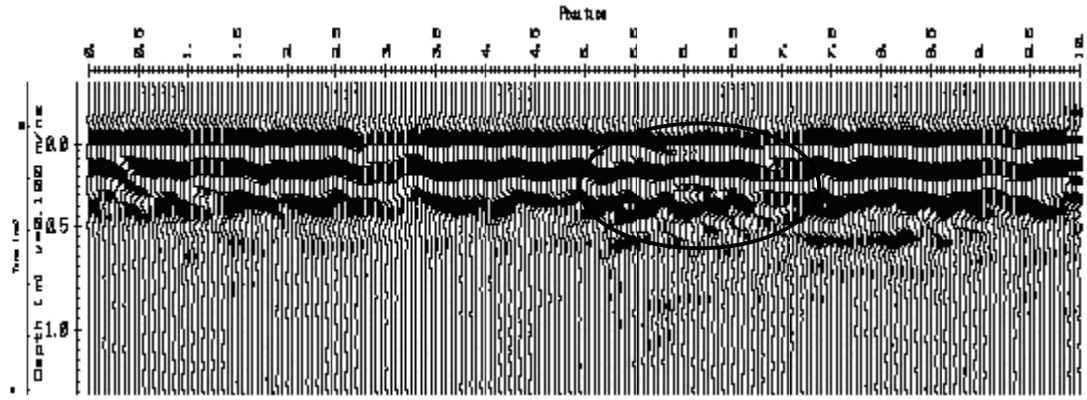

Figure 5. Ground penetrating Radar image of lining before grouting.

3.2 Quick maintenance of tunnel lining with polymer grouting technology

With the polymer grouting technology, a tunnel of a motorway is inspected with ground penetrating radar and polymer grouting maintenance for tunnel lining voids. The core drilling result after polymer grouting is shown as Figure 6. The polymer material overflows from another grouting bore when grouting (Figure 7).

Figure 6. Polymer grouting maintenance Figure 7. After polymer grouting.

After polymer grouting, ground penetrating radar is used to inspect the same section that has voids. A ground penetrating radar image after polymer grouting is shown as Figure 8. Comparing Figure 5 with Figure 8, it can be seen that in the two images the in-phase axis of reflection waves are basically the same. All these indicate that after polymer grouting the void is filled up.

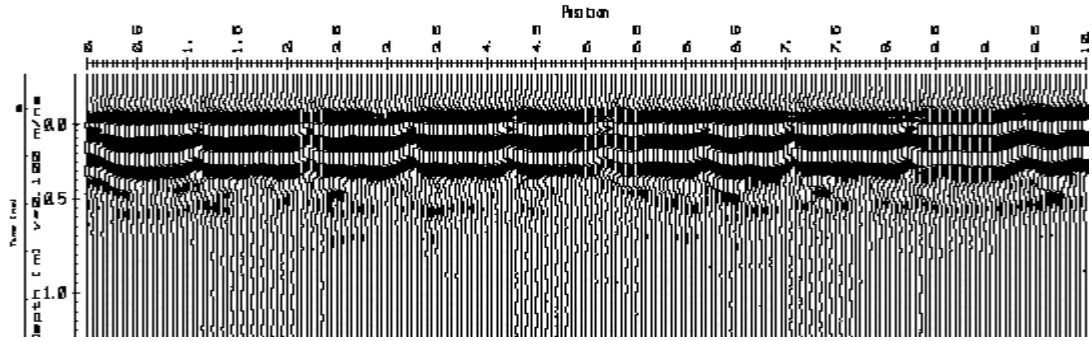

Figure 8. Ground penetrating radar image of lining after polymer grouting.

4 CONCLUSION

The ground-penetrating radar nondestructive testing technology and polymer grouting technology for maintenance of tunnel diseases has been presented. First, ground-penetrating radar is used to inspect the disease and voids in the tunnel lining. Then the void region repaired with polymer grouting repair technology. The test results show that by using polymer grouting technology the tunnel disease can be repaired, and this method is an ideal manner for tunnel quick maintenance.

REFERENCES

Jing, X. L., and Zhang, L. (2007). Application of GPR Technology in the Quality Detection of Railway Tunnel Liner. Chinese Journal of Engineering Geophysics, Vol. 4, No. 4, pp. 345-349.

Liu, Z. Y., and Wang, F. M. (2007). Application Research for Uretek Technology in Maintaining Pavement. Journal of Highway and Transportation Research and Development, Vol. 24, No. 11, pp. 46-48. (in Chinese)

Wang, D. X. (2007). Application of High Polymer Grouting in Rebuilding Old PCC Pavement. Science & Technology Information, Vol. 23, No. 5, pp. 393-393.

Wang, X. W., and Li, J. H. (2007). The Application of Surveying Radar Technology in the Quality Detection of Tunnel Lining. Journal of Chengdu University of Technology(Science & Technology Edition), Vol. 34, No. 3, pp. 354-358. (in Chinese)

You, G. M., and Liu, X. Z. (2007). Application of Ground Penetrating Radar to Geological Forecast for Expressway Tunnel Construction. Journal of Highway and Transportation Research and Development, Vol. 24, No. 8, pp. 92-95. (in Chinese)

Safe Spacing Research Based on the Theory of Cellular Automaton on Freeways in Foggy Weather

Q. Shi[1], Z. Huang[1]，and W. Liu[1]

[1]School of Mechanical and Automotive Engineering, Hefei University of Technology, 230009, Hefei, China；PH(0551) 2901338-2512；email：shiqing7081@sohu.com

ABSTRACT

The random disturbance parameter γ is introduced into the cellular automaton (CA) model of traffic flow to simulate the cases of car-stopping, hitting the car ahead, and other vehicular crashes occurring on the freeway. By analyzing the disturbance vehicles in the driving environment of different visibilities of foggy weather, the correlations of limited speed and the safe spacing for optimum visibility are developed. The safe spacing and average safe velocity of the vehicle under different visibilities are simulated and analyzed, thus providing the theoretical gist for freeway administrative departments to establish and implement the management strategies.

Keywords: Cellular Automaton; Visibility; Safe Spacing; Driving Security

INTRODUCTION

The frequency of accidents on the freeway in foggy weather is very high. When visibility is down to a certain critical value, the freeway must be closed. To assure the driving security on the freeway in foggy weather, it's necessary to take some corresponding measures such as road control, meanwhile it's important to keep appropriate velocity and inter-vehicle distance (Tang 2005).

Researcher has been conducted concerning safe driving during foggy weather conditions (Qi 2007). The research on the relationship between speed, inter-vehicle distance, and visibility is also helpful increasing safety on the freeway and reducing the length of closing time of the freeway.

The theory of cellular automaton is widely applied to the research on traffic flow. Its rules can be modified flexibly to consider various real traffic conditions. In this paper, the cellular automata are used to simulate the vehicles. Considering the poor visibility in foggy weather, drivers often slow down to ensure the safety. So the cases of traffic flow on freeway in foggy weather can be better simulated by the FI model of following car slow start (Schadschneider 1997). Through introducing the

random disturbance parameter γ in traffic flow, the paper simulates the unexpected cases of car-stopping, hitting the car ahead, and others in traffic stream. By analyzing the behaviors of disturbing vehicles under the conditions of different visibilities in foggy weather, we have developed the relationships between limited speed and safe spacing to the visibility. It can provide the theoretical gist for the freeway administrative departments to establish corresponding management measures.

THE RANDOM DISTURBANCE MODEL OF A FREEWAY IN FOGGY WEATHER

Cellular automaton is a dynamic system defined on a cellular space that consists of cells with discrete and finite states (Chopard and Droz 1998). The system evolves along the discrete time dimension according to certain partial rules. CA model in traffic flow uses the grids of one dimension lattice chain to simulate the vehicles on the road (Ja et al. 2007). The FI model of following car slow start can be depicted by the following definitions and rules (Benjamin at al. 1996).

A one-lane is expressed by the one-dimensional discrete lattice chain of L cells. Each cell can accommodate only one car traveling with velocity v that takes values ranging from 0 to $v_{\max}$. The car's behavior at the last time step has a great influence on the following car's behavior of speedup at this time step. So the parameter P_1, which is called the slow start probability of following cars in the acceleration rule, is used to describe the diversity of driving behavior of the following car affected by stopping behavior of car ahead. The evolvement rules of the FI model of the following car slow start using the random disturbance parameter γ are described as follows:

(1) The rule of acceleration

If $v_n(t-1)=0$ and $v_n(t)\le v_{\max}$, then with P_2 (random accelerating probability), $v_n(t)\to v_n(t)+1$; with $(1-P_2)$, $v_n(t)\to v_{\max}$. And when the car ahead accelerates, then the following car accelerates with probability P_1.

(2) The rule of deceleration

To avoid colliding with the car ahead, if $v_n(t)>gap$, then $v_n(t+1)\le gap$.

(3) The rule of randomization

Considering the actual driving behavior and the mentality factors of drivers, the cars with maximal velocity change their speeds with the probability P_3 (P_3 is the probability of car braking lingeringly) according to $v_n(t+1) = \max\{v_n(t+1)-1, 0\}$, while the other cars maintain their velocities.

(4) The random disturbance parameter γ

In order to simulate the disturbance of accidents or car stopping in the traffic stream, we choose the vehicles randomly as the disturbance in the simulation and introduce the random disturbance parameter γ as the probability of the disturbance occurrence. Then we simulate each visibility and safe spacing in the condition of various limitative speeds and analyze the states of the following cars whether they are safe under the condition of random disturbance.

(5) The update of vehicle's position

When the velocities of all cars are determined, the position evolving with the time is updated to be: $X_n(t+1) = X_n(t) + v_n(t+1)$

Here in the rules：

$v_{\max}$ ——the limit speed of the car;

$v_n(t)$——the velocity of car n at time t;

$X_n(t)$—— the position of car n at time t;

gap —— the spacing between car n and its preceding car.

In this model, the rule of acceleration reflects the characteristic that the driver wants to drive with the maximal value. The rule of deceleration reflects the behavior taken by the driver for avoiding colliding with the car ahead. The rule of randomization reflects the uncertainty of the driving behavior. The rule of random disturbance simulates the situation of vehicle stream on the freeway in foggy weather.

THE SIMULATION AND ANALYSIS OF SAFE SPACING

By the exertion of the random disturbance parameter in CA model and

analyzing the simulated results in different cases, the relationship between visibility, limitative speed, and safe space are developed.

The determination of parameters of the model

In the CA model, we take the length of the road as L=6.75 km, every cell lattice as c=7.5 m, then the number of lattices is N=900. For the different cases of visibilities, the maximum velocity and safe spacing are chosen crosswise. The process is simulated according to the FI model of following car slow start mentioned above. The number of the time steps that model runs and evolves every time is 10^4. The average velocity values of the last 10^3 steps are used to calculate the average statistic, and the single density point averages the statistic again with the results of 10 times simulation. To obtain the contrastive outcome, we choose 11 groups of data. Every index is listed in Table 1.

Table 1. The indexes of the CA model.

The value of every index of drafted test				The value of every index of test calculated with cell			
Visibility （m）	Drafted maximal speed (km/h）	Inter-vehicle distance a（m）	Inter-vehicle distance b（m）	Visibility （cell）	Drafted maximal speed (cell/s)	Inter-vehicle distance a（cell）	Inter-vehicle distance b（cell）
390	135	150	120	52	5	20	16
390	108	135	105	52	4	18	14
195	108	120	90	26	4	16	12
195	81	105	75	26	3	14	10
97.5	81	90	60	13	3	12	8
97.5	54	75	52.5	13	2	10	7
75	54	75	52.5	13	2	10	7
75	54	60	45	10	2	8	6
52.5	54	60	45	7	2	8	6
52.5	27	52.5	37.5	7	1	7	5
37.5	27	52.5	37.5	5	1	7	5

The analysis of the simulation process

As the FI model of freeway in foggy weather uses the random disturbance

parameter γ to simulate the probability of the traffic accidents or the behavior of car stopping, then the process of simulation introduces the accident rate (Konduri 2002) correspondingly to make the statistical analysis. The indexes are defined in terms of the following rules:

The accident of hitting the car ahead occurs in model when:

$$S_{stop} > S_{safe}$$

That is: when random disturbance appears with a certain probability γ and the braking distance of the following car is bigger than the safe distance, the accident of collision will happen. It's denoted as A_i (i is the frequency of accident). When the number of cars coming into the pileup is k, then we consider it as k-1 times accidents.

The accident rate on a freeway in foggy weather in this model is as follows:

$$P_A = A_n / \left(N_{vehicle} - 1 \right)$$

In the formula: P_A = the accident rate;

$N_{vehicle}$ = the total number of vehicles in car stream.

According to the definition of the accident rate, we analyze the simulated results contrastively. The process of that is as follows:

(1) On the condition of safe spacing, we obtain the values of traffic density or volume when the inter-vehicle distances are *a* and *b*, and calculate values of all indexes according to the values of traffic density and volume.

(2) To simulate with the traffic density ranging from 0 to 1 or the corresponding value of traffic volume, we get the accident rates in the simulation process when the inter-vehicle distances are *a* and *b*, respectively.

(3) Under the condition of unchanged accident rate, we can get the curves of safe spacing in different cases of visibility by varying the safe spacing.

According to the course of simulation, every group of data is analyzed and compared separately. Taking the first group of data for example, when the visibility is 52-cell, we introduce the random disturbance, which is the rate of car stopping. When a car stops or has an accident, the following cars' drivers will have the behavior of decelerating or stopping their cars. Under the conditions of different volumes (densities), we can calculate the possible accident rate according to the visibility of 52-cell and to the safe spacing of 20-cell and 16-cell.

Figure 1 shows the mutative relations of the provided safe spacing and

simulated safe spacing to the density when the visibility is 52-cell, which is 390 meters, and the random disturbance parameter γ is 0.2. From this figure, we can see that when the density is small, the accident rates at the safe spacing of 20-cell and 16-cell are both low, and the difference between them is very small. It indicates that the safe spacing can be shortened further at this density area. At the area of high density, the accident rate at the safe spacing of 20-cell and 16-cell are both very high, and the difference between them is small. But when the density is from 0.22 to 0.78, the accident rates at the safe spacing of 20-cell and 16-cell grow rapidly as density increases. We should formulate the density from 0 to 0.22 to reduce the occurrence of accidents on freeways.

Figure 2 represents the mutative relations of the provided safe spacing and simulated safe spacing to the density when the speeds are limited and the visibility of 52-cell and the disturbance degree γ of 0.2. The figure shows that the influence, which the magnitude of limitative speed has on the accident rate, is small whether it's at the area of low density or high, but the accident rate increases rapidly with the increase of the limitative speed.

Figure 3 shows the changes of the visibility and accident rate simulated under the condition of different disturbance degrees. The changing trends of the curves in the figure show that in the case of low density (k=0.2) the accident rate grows correspondingly to the increase of the disturbance degree, and that the accident rate increases rapidly when the visibility is poor. This shows a fact that the pileup accident occurs frequently in poor visibility areas, in other words, the occurrence rate of very serious accidents is rather high.

THE DETERMINATION OF LIMITATIVE SPEED AND SAFE SPACING

After comparing and analyzing the 11 groups of data and considering the drafted values of different visibilities in foggy weather, we can obtain management and control measures at different cases of visibility on the basis of enhancing the capacity (see Figure 3). Compared with the national standard, it can be seen that the simulated value in control and management scheme is slightly lower than that in the national standard (Yang and Wu 2003). But referring to the capacity, the simulated value of traffic capacity is a little higher than that in the national standard. As seen from the trend of the curves in Figure 4, when the visibility decreases, the velocity and the safe spacing decrease correspondingly; but as the length of the time of the driver's response to the stimulus becomes longer, the needed safe spacing of the

braking distance becomes longer.

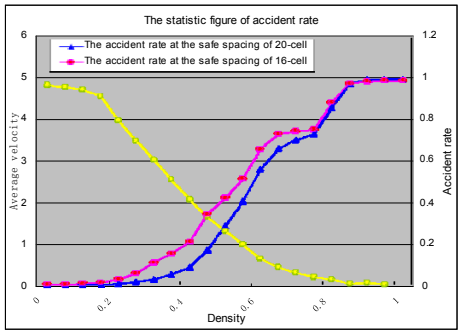

Figure 1. Accident rate with the visibility of 52-cell, γ =0.2 and v_{max} =5.

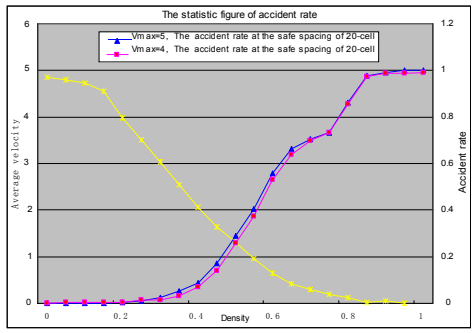

Figure 2. Accident rate when v_{max} =5 and v_{max} =4 at the visibility of 52-cell and γ =0.2.

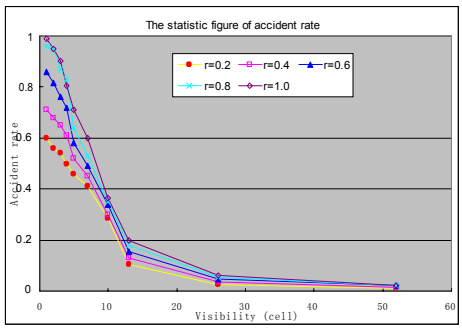

Figure 3. Accident rate when v_{max} =5 and k=0.2.

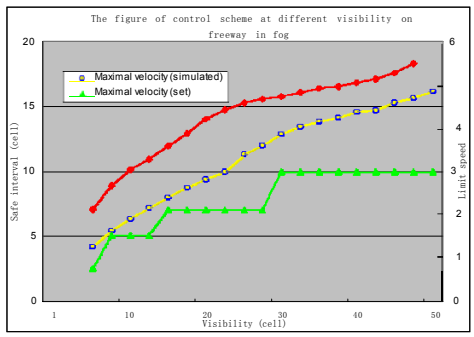

Figure 4. The speed and safe spacing at different visibility in foggy weather.

CONCLUSION

The paper analyzes the relationship between safe spacing, the average safe velocity, and the accident rate synthetically and provides the theoretical general idea of the management control for the traffic management department to enhance the capacity in foggy weather. We can derive the conclusions as follows from the results of the simulation strategies:

(1) To avoid accidents in foggy weather, we should formulate the density from 0 to 0.22.

(2) Under the precondition of maintaining traffic safety, the average safe velocity and the maximal volume at this speed derived from the simulation on the basis of the theory of CA have a great significance on enhancing the transportation

ability of the freeway in foggy weather and thereby enhancing the economic benefit of the freeway.

(3) The result obtained by the simulation scheme is just smaller than that set by the state, but comparing with the actual accident rate on the freeway in foggy weather, the rate in the simulation scheme is smaller. It shows that the incomplete management of opening-up is also the reason causing the accident on the freeway in foggy weather except for the factor of weather. It means that the administrative department should keep the safe spacing by improving their management. So, studying the passing frequency of cars on freeways in foggy weather can help by decreasing the accident rate even further.

ACKNOWLEDGEMENTS

This work was supported by National Natural Science Foundation of China (No. 70771036), the Natural Science Foundation of Anhui Province (No. 070416244).

REFERENCES

Benjamin, S. C., Johnson, N. F., and Hui., P. M. (1996). "Cellular automaton models of traffic flow along a highway containing a junction." *J. Phys*. A 29, 3119-3127.

Chopard, B., and Droz. M.(1998). *Cellular automata modeling of physical systems*, Cambridge University Press.

B. Ja，Z. Gao, K. Li, and X. Li (2007). *Models and simulations of traffic system based on the theory of cellular automaton*, Beijing, Science Press.

Konduri, Sravanthi (2002). "Statistical models for prediction of freeway incidents." *Proceedings of the International Conference on Applications of Advanced Technologies in Transportation Engineering*, 167-174.

Y. Qi, B. Liu, and Z. Guo (2007). "Safety management system for freeway in fog." *Journal of Tongji University (Natural Science)*, 35(1), 61-66.

Schadschneider, A., and Schreckenberg, M. (1997). "Traffic flow models with 'slow-to-start' rules." *Ann. Phys*. 6, 541-551.

J. Tang (2005). "Research on safeguard technology of freeway in fog." *Hefei: The Master Dissertation of Hefei University of Technology*.

P. Yang, and B. Wu (2003). *The traffic management and control,* Beijing, China Communications Press.

Simulation of Turning Stability Control for Two-Motor-Drive Electric Vehicle

Shaobo Xie[1], Cheng Lin[1], Peng Liu[1]and Xiaowei Zhang[1]

[1]National Engineering Laboratory of Electric Vehicle, Beijing Institute of Technology; No.5 Zhongguancun South Street, Haidian District, Beijing city, People's Republic of China, 100081; Email: 2201020133@163.com

Abstract

Two-motor-drive electric vehicles (TMDEVs) have developed significantly in recent years. An important residual problem for this vehicle type is how to coordinate the operation of the driving motors for stable vehicle handling. In order to improve the turning stability of TMDEVs a control scheme, based on the target slip rate of driving wheels, is proposed to distribute the torque of both motors. First a dynamic model of TMDEVs and the tire model are described. Second a control strategy based on the target slip rate using a slide mode control method is specified. Then a dynamic analysis and simulation are conducted. The results show the proposed strategy can make the driving tires achieve the target slip rate and improve the turning stability of this vehicle.

Key words: two-motor-drive, electric vehicle, turning stability control, target slip, dynamic simulation

1. Introduction

With current serious world resource and pollution problems more and more attention is being paid to the electric vehicle. The TMDEV which has no traditional power train and mechanical differential greatly simplifies the structure and enables the accurate controlling of drive motors, due to its characteristic high efficiency and quick response (Shin-ichiro Sakai, 1999). However, the existing problem is how to coordinate the operations of both motors to minimize the abrasion of tires and improve the handling and stability performance, especially when turning the vehicle. This paper proposes a new control scheme and identifies a successful dynamic simulation.

2. Seven degrees of freedom (7-DOF) vehicle model and tire model

The nonlinear vehicle model in the paper with rear wheel drive and front wheel steering includes longitudinal, lateral and yaw dynamics as well as four wheel rotational dynamics.

2.1. Vehicle model

The differential equation of vehicle motion is as follows:

$$m\cdot(\dot{u}-v\cdot\omega_r)=F_{y3}+F_{y4}-F_{y1}\sin\delta_f-F_{y2}\sin\delta_f-\frac{1}{2}C_D A\rho u^2$$

$$m\cdot(\dot{v}+u\cdot\omega_r)=F_{y1}\cos\delta_f+F_{y2}\cos\delta_f+F_{y3}+F_{y4}$$

$$I_z\cdot\dot{\omega}_r=a\cdot(F_{y1}\cos\delta_f+F_{y2}\cos\delta_f)-b\cdot(F_{y3}+F_{y4})+\frac{B}{2}\cdot(F_{y1}\sin\delta_f-F_{y2}\sin\delta_f)+\frac{B}{2}\cdot(F_{x3}-F_{x4})$$

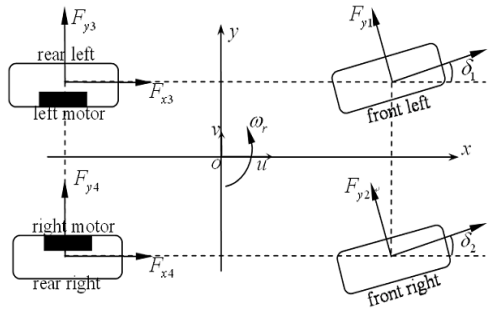

Figure 1. 7-DOF nonlinear vehicle model..

For a front steering vehicle, we assume: $\delta_1 = \delta_2 = \delta_f$, $\delta_3 = \delta_4 = 0$.

For the variation of the tire normal force, which has significant effects on the vehicle handling and stability performance, the tire normal model includes the load transfer due to the longitudinal and lateral accelerations (Farzad Tahami, 2003):

$$F_{z1} = \frac{amg}{2l} - \frac{\mathrm{m}a_x h}{2l} - \frac{ma_y h}{2\mathrm{B}} \qquad F_{z2} = \frac{amg}{2l} - \frac{\mathrm{m}a_x h}{2l} + \frac{ma_y h}{2\mathrm{B}}$$

$$F_{z3} = \frac{bmg}{2l} + \frac{\mathrm{m}a_x h}{2l} - \frac{ma_y h}{2\mathrm{B}} \qquad F_{z4} = \frac{bmg}{2l} + \frac{\mathrm{m}a_x h}{2l} + \frac{ma_y h}{2\mathrm{B}}$$

2.2 Tire model

The tire model has an important influence on the simulation of vehicle dynamics (R. Wade Allen, 2000), especially for large slip angles. The Gim tire model (Gim. G, 1990) was used for the dynamic simulation. This model describes the relationship between longitudinal and lateral forces, which is dependent on normal load F_z, longitudinal slip S_s, slip angle of every wheel α and the friction coefficient of road μ.

The slip angle for each wheel is defined as:

$$\alpha_1 = \delta_f - \arctan\left(\frac{v + a\omega_r}{u - \frac{B}{2}\omega_r}\right) \qquad \alpha_2 = \delta_f + \arctan\left(\frac{v + a\omega_r}{u + \frac{B}{2}\omega_r}\right)$$

$$\alpha_3 = \arctan\left(\frac{v - b\omega_r}{u - \frac{B}{2}\omega_r}\right) \qquad \alpha_4 = \arctan\left(\frac{v - b\omega_r}{u + \frac{B}{2}\omega_r}\right)$$

Longitudinal wheel slip rate can be described as: $s_i = \dfrac{\omega_i r - u_i}{\max(\omega_i r, u_i)}$, $i = (1,2,3,4)$

Lateral wheel slip rate is defined as:
$$\begin{cases} s_\alpha = |\tan\alpha|, & \text{During braking;} \\ s_\alpha = (1 - |s_i|)|\tan\alpha|, & \text{During driving;} \end{cases}$$

The longitudinal force:

$$F_x = C_s S_s l_n^2 + \mu_x F_z \left(1 - 3l_n^2 + 2l_n^3\right) \qquad S_s < S_{sc}$$

$$F_x = \mu_x F_z \qquad S_s \geq S_{sc}$$

The lateral force:

$$F_y = C_\alpha S_\alpha l_n^2 + \mu_y F_z \left(1 - 3l_n^2 + 2l_n^3\right) \qquad S_s < S_{\alpha c}$$

$$F_y = \mu_y F_z \qquad S_s \geq S_{\alpha c}$$

3. The control scheme for turning stability

The TMDEV has no traditional mechanical differential unit. On a straight road with a dry and flat surface, the left and right driving motors can be controlled with the same commands given by the vehicle center controller (Fig. 2). When the vehicle turns , however, the normal load of each wheel will be redistributed because of centrifugal forces and road conditions. Consequently the vehicle controller needs to coordinate the motor operation in order to reduce abrasion of the wheels and keep the vehicle stable for good handling and maneuvering performance. The turning stability control strategy can solve these issues well. Referring to the scheme (Yinghui Ge, 2005), this paper proposes a torque allocation control strategy (Fig. 3), which is based on the target slip rate of the driving wheels. The controluses the sliding mode controller.

The control model can be described as follows: When the vehicle makes a turn in a curve, the slip rate of the rear left wheel s_3^* is chosen as the objective slip rate. At the same time, considering the slip difference $\Delta s = K(Wr - \Delta\varphi)$ between both driving wheels due to the deflection motion, the slip rate of the rear right driving wheel $s_4^* = s_3^* - \Delta s$ can be evaluated. The vehicle controller gives commands to both driving motors, respectively, based on the target slip rate. The real slip rate of both driving wheels are s_3 and s_4, and $\Delta\varphi$ approximately equals to $\frac{\delta}{l}V$.

To eliminate the chattering phenomenon at the boundary layer, the controller structure uses the hyperbolic tangent function (Jalili-Kharaajoo.M, 2003) instead of a saturation function. The increments of the two motors can be shown as: $\Delta T_3 = K_3 \tanh(\Delta s_3)$, $\Delta T_4 = K_4 \tanh(\Delta s_4)$, K_3 and K_4 are the proportional coefficients. So the torque exerted on the motors is $T_3 = T^* + \Delta T_3$ and $T_4 = T^* + \Delta T_4$, T^* is the given torque by the accelerator pedal.

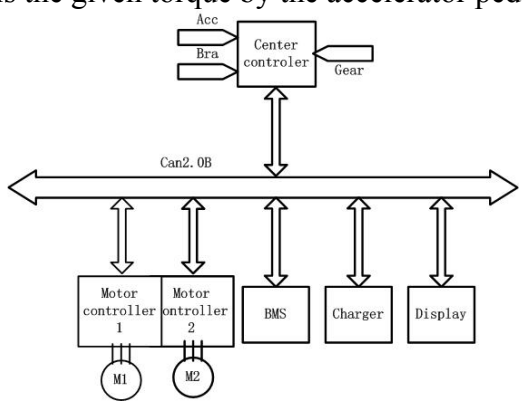

Figure 2. Vehicle control framework based on can bus

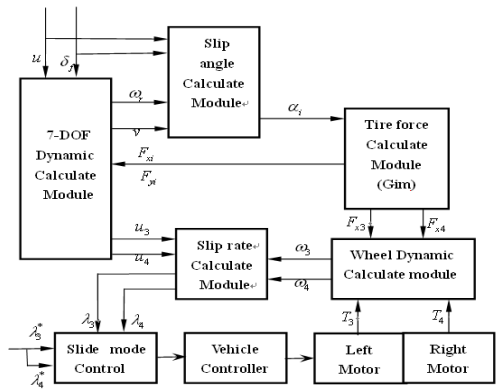

Figure 3. Block diagram of dynamic analyze and control

4. Simulation analysis

In this section two different simulations are carried out on the 7-**DOF** nonlinear

vehicle model platform, presented in the Section 2, to analyze and evaluate (Konghui Guo, 1991) the turning stability using a sliding mode control scheme based on the target slip rate. The first is a step maneuver and the second simulation is a single sinusoidal steering input. The initial longitudinal velocity is 20m/s and the initial torque of both motors is 210Nm. The target slip rate of the rear left wheel λ_3^* is 0.05. In all figures, the solid line represents the rear left wheel and the dashed represents the rear right wheel. The values of the vehicle parameter are listed in Table 1.

Table 1. Value of vehicle model parameters in simulation

Symbol	Value	Symbol	Value
m	$1818kg$	J_z	$3885kg.m^2$
a	$1.2m$	I_z	$1.6kg.m^2$
b	$1.5m$	C_f	$-18518N/rad$
L	$2.7m$	C_r	$-20658N/rad$
B	$1.52m$	K	0.05
h	$0.5m$	K_3	12
R	$0.32m$	K_4	15

4.1 Step maneuver

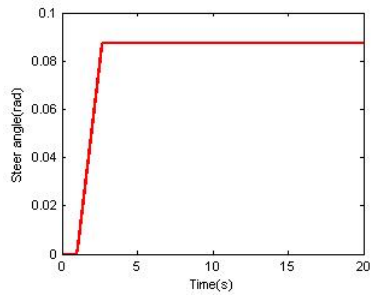

Figure4. The angle of the steering wheel on the step maneuver

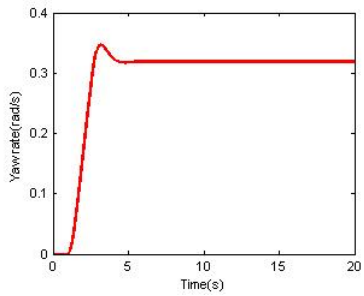

Figure5. Response of yaw rate

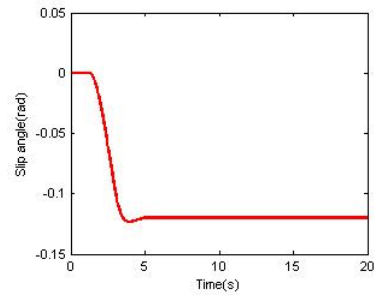

Figure 6. Side slip angle

In this section the steering angle is fixed after 1 sec (Fig. 4). The yaw rate and side slip angle arrive at the desired range in about 1.5 seconds (Fig. 5 and 6) and the vehicle is in a stable condition. The slip rate of both driving wheels fluctuate slightly at the target slip rate of 0.05 (Fig. 7) and the torque is distributed correspondingly (Fig. 8). The figure 9 and 10 show the velocity of the wheel center and the rotation of the right wheel is bigger than that of the left wheel to achieve the target slip rate and decrease the abrasion of the tires.

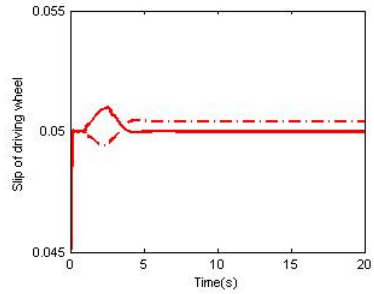

Figure 7. Slip rate of driving wheels

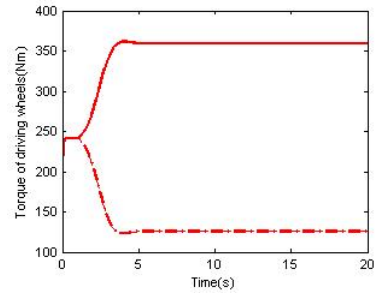

Figure 8. Torque of driving wheels

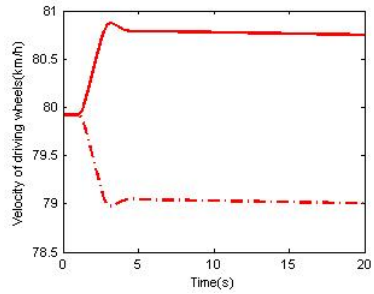

Figure 9. Velocity of driving wheel center

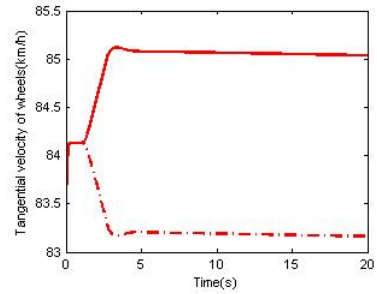

Figure10. Tangential velocity of driving wheel rotation

4.2 Sinusoidal steering input

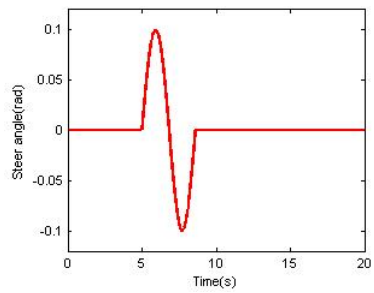

Figure 11. steering angle of single sinusoidal input

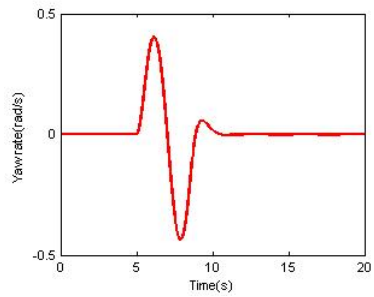

Figure 12. Response of yaw rate

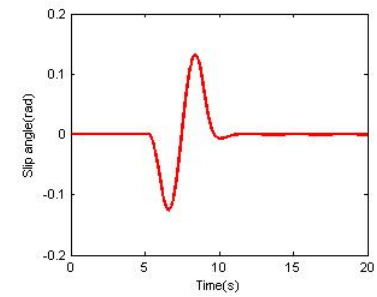

Figure 13. Side slip angle

In this section the steering angle is represented as a single sinusoidal curve with a cycle of 3.6 seconds (Fig. 11). The yaw rate and the side slip angle change correspondingly with the steering angle and the values are controlled within an acceptable range (Fig. 12 and 13). Figure 14 shows both driving wheels reach the demanded slip value of 0.05. It is noted that the tangential and wheel center velocity (Fig. 16 and 17) also act with the sinusoidal steering angle to reduce the abrasion of the tires and improve the turning stability.

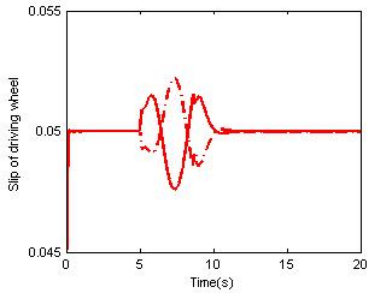

Figure 14. Slip rate of driving wheels

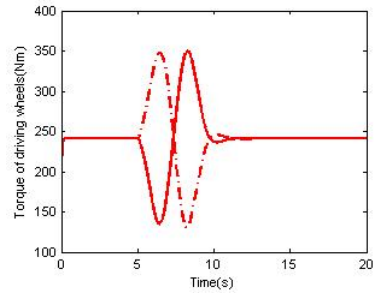

Figure 15. Torque of driving wheels

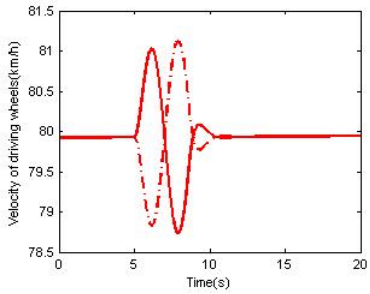

Figure 16. Velocity of driving wheel center

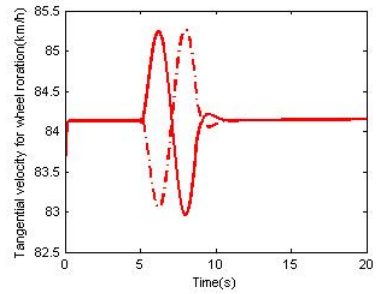

Figure 17. Tangential velocity of driving wheel rotation

5. Conclusion

In this paper, a 7 degrees of freedom nonlinear model of the rear-motored-wheel electric vehicle is demonstrated. The proposed model, based on a target slip rate, is simulated in a step maneuver and with a sinusoidal steering input. The result shows the control strategy can coordinate the torque demands of both wheels and achieve the desired slip rate to improve the turning stability of a two-motor-drive electric vehicle.

References

Farzad Tahami and Shahrokh Farhanghi (2003). Stability Assist System for a Two-Motor-Drive Electric Vehicle using Fuzzy Logic, *SAE paper*, 2003-01-1258.

Gim, G. and Nikravesh, P E (1990). "An Analytical Model of Pneumatic Tires for vehicle Dynamic simulations, Part 1: Pure Slips." *International journal of Vehicle Design,* 11(6), 589-618.

Jalili-Kharaajoo.M. and Besharati.F (2003). Sliding Mode Traction Control of an Electric Vehicle with Four Separate Wheel Drives. *Preceedings of the IEEE Conference on Emerging Technologies and Factory Automation,* vol. 2, 291-296.

Konghui Guo (1991). *Controllability and Stability of Vehicle.* Changchun, Jilin Science and Technology Publishing House.

R. Wade Allen, Thomas T. Myers, Theodore J. Rosenthal and David H. Klyde(2000). The Effect of Tire Characteristics on Vehicle Handling and Stability, *SAE paper*, 2000-01-0698.

Shin-ichiro Sakai, Hideo Sado and Yoichi Hori (1999). Motion Control in an Electric vehicle with four independently Driven In-Wheel Motors. *IEEE/ASEM*

transactions on Machatronics, 4(1), 9-16.
Yinghui Ge, Guangzheng Ni (2005). A Novel Electronic Differential Algorithm for In-wheel Motor Driven EV. *Automotive Engineering*, 27(3), 340-343.

The simulation analysis of passenger evacuation in one Metro station based on Exodus*

Y.F Ye[1], Q.F Hu[2] and H.W. Huang[3]

[1]Department of Geotechnical Engineering, Tongji University, Shanghai 200092, China, PH (86) 21-65982386, email: yyf0387@126.com
[2]Shanghai Institute of Disaster Prevention & Relief, Tongji University, Shanghai 200092, China, PH (86) 21-65983449, email: huqunf@tongji.edu.cn
[3]Department of Geotechnical Engineering, Tongji University, Shanghai 200092, China, PH (86) 21-65989273, email: huanghw@ tongji.edu.cn
*Supported by Hi-Tech Research and Development Program of China (2006AA04Z442)

ABSTRACT

In Shanghai, the Metro is a major part of a modern urban transit system. Essential to the safe operation of the metro station is the design for emergency evacuations. Based on the comparative study of different simulation theories and methods of group evacuation behavior, Exodus V4.06 and Smartfire V4.1 were employed to simulate the evacuation under different risks in one metro station in Shanghai. The computation result shows that people's distribution in the station has significant influence on the evacuation time and the exits used; the intervention on evacuation route, such as the proper guidance from the working staff, is essential to ensure the right choice of evacuation route, evacuation time saving, and personnel safety.

INTRODUCTION

The Metro, is an essential part of a modern urban transit system. It is a major transportation component because of its high speed, passenger volume, and little influence from the weather. However, due to their inherent properties there exists a great potential risk during metro and metro station operation,

A Metro station is a public facility with high passenger volumes and movement, generally situated underground. A relatively airtight area, there is a large space in the station with a relatively small number of exits which include a few ventilation shafts and several station passageways. Once a fire or other emergencies strike, there could be a considerable number of causalities as well as economic loss without proper evacuation procedures. For instance, in November, 1986, a fire (caused by technical failure) in the Kings Cross Station in London killed 32 and injured more than150 people. Also in March 1995, a poison gas attack in Japan's metro resulted in 12 deaths and about 5500 injuries. (Huang, 2008). The question of how to evacuate a large number of passengers and staff efficiently and safely when fire and other emergencies occur is a topic worth probing.

The evacuation is simulated using Building Exodus V4.0 using one metro station in Shanghai as a prototype. Assuming a fire strikes during the rush hour, the ensuing congestion and confusion during the evacuation is analyzed to determine the key issues, developing corresponding technical measures in an effort to provide references for the design of metro station evacuation and emergency plans.

DESIGN REQUIREMENTS OF EVACUATION IN METRO STATION

Time requirement of evacuation. According to the specification in item 19.1.19 of Code for Design of metro (GB 50157-2003) (NSCGPRC, 2003), and item 26.1.4 of Urban Rail Transit Design Standard (DGJ08-109-2004 (SPCS, 2003), the staircase, escalator and evacuation exits should be sufficient to evacuate all the passengers either on the trains or waiting on the platform as well as the Metro staff in 6 minutes in the event a fire breaks out during the rush hour.

Design requirement of evacuation performance. In fire engineering, the design criteria and specifications require that all people should be evacuated before fire develops fully threatening life. The mathematical description is as follows: (SHI, 2007)

ASET > RSET

ASET (Available Safety Egress/Escape Time) refers to the time from fire breakout to becoming life threatening; RSET (Required Safety Egress/Escape Time) refers to the time used from a fire breakout up to the completion of evacuation.

The evacuation time criterion in common use is shown in Figure 1.

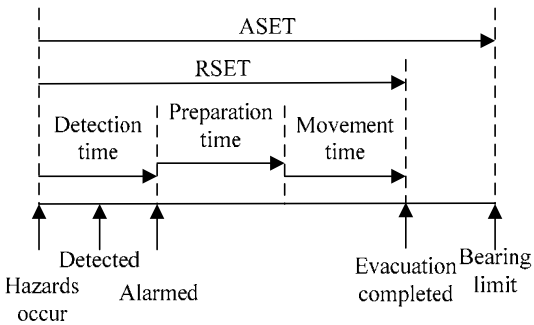

Figure 1 The basis of judgment of safety evacuation

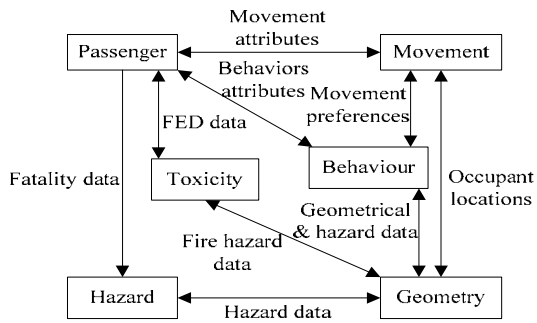

Figure 2 The Interaction of Building EXODUS sub-modules

INTRODUCTION OF BUILDING EXODUS AND SMARTFIRE

The EXODUS software was developed by FSEG (Fire Safety Engineering Group) of Greenwich University in Britain, and is composed of six interrelated sub modules, i.e. the building, people, motion, behavior, risk and toxicity as shown in Figure 2. EXODUS is capable of simulating evacuation in all types of buildings, referencing interpersonal relations in evacuation; the interaction of people and building; the mutual influence of people and the risk environment, thus making it a powerful tool in evacuation design, evaluation and research.

The SMARTFIRE software was also developed by the FSEG. It aims to make Fire Field Modeling techniques accessible to non-Computational Fluid Dynamics (CFD) experts. SMARTFIRE achieves these aims by integrating knowledge-based tools and techniques within many of the modules. SMARTFIRE provides a user friendly environment, together with modest computer requirements, which make Fire Field Modeling a practical and viable reality.

BRIEF INTRODUCTION TO THE METRO STATION IN SHANGHAI

The metro station in the Shanghai simulation covers an area of 10965m^2, with net length 197.36m, net width of standard section 17.10m. It is a two-storied

underground structure and the island style platform is located on the lower floor. The middle part of the platform is the public area, and there are 2 sets of stairs and escalators and one set of cross-zigzag staircase which connects with the station hall. The ends of the platform are the equipment rooms. The planar sketch of the platform is show in Figure 3.

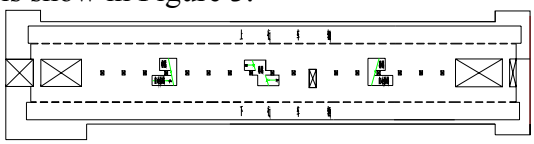

Figure 3 The planar sketch of the platform

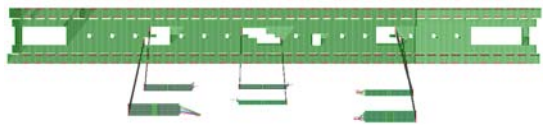

Figure 4 The geometrical model of the platform in the Building Exodus

THE SETTING OF DISASTER ENVIRONMENT

The evacuation under two different kinds of disasters in metro station is simulated and analyzed in this research.

1. Evacuation simulation under general circumstances: It is assumed that there exists an emergency (such as a bomb threat,), and one escalator has stop working; all the people are evacuated with or without the guidance of working staff.

2. Evacuation simulation under disaster: It is assumed that a small scale fire breaks out and all the passengers in the metro station need to be evacuated. According to Congling Shi et ale(SHI, 2006), there are few combustible materials in the station, i.e. 5kg petrol. Thus the simulation in this study is conducted under the assumption that there has been arson with 5kg petrol spilled in the metro station.

THE SELECTION OF PARAMETERS

Walking speed is classified into six scales in Exodus, namely out walk, walk, jump, crawl, going upstairs, going downstairs. The exact speed is listed: 1.2~1.5m/s, 1.08~1.35m/s, 0.96~1.2m/s, 0.24~0.3m/s. The speed of going upstairs and downstairs is quoted from the actual measurement in one metro station in Shanghai by Junchi Ma (MA, 2007), Table 1. In the simulation, the number of people to be evacuated is determined by the passenger flow in long-term period (2034). The worst case scenario would be 200 people on the platform, and 1321 arriving passengers on one train, for a total number of 1521 evacuees.

Table 1 The percentage and walking speed of passengers in the Shanghai metro station in terms of age and gender

Person types	Proportion (%)	Upstairs speed (m/s)	Downstairs speed (m/s)
Male (Aged 15 to 29)	24.5	0.54	0.81
Male (Aged 30 to 50)	25.0	0.50	0.69
Male (Aged 51 to 80)	2.5	0.41	0.54
Female (Aged 15 to 29)	24.0	0.51	0.60
Female (Aged 30 to 50)	22.0	0.47	0.53
Female (Aged 51 to 80)	2.0	0.39	0.39

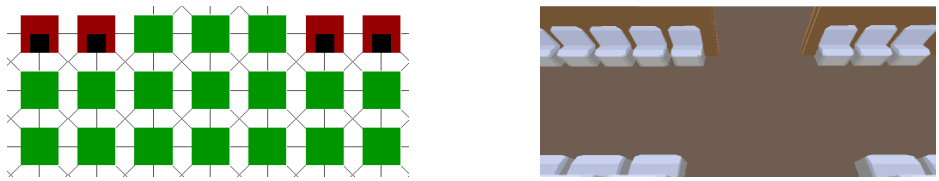

Fig.5 The schematic drawing of chair seat nodes in the model and effect drawing

THE COMPUTATION RESULTS AND ANALYSIS OF THE SIMULATION

A simulated computation geometrical model is set up according to the actual size as in Figure 4. Figure 5 shows the schematic drawing and effect drawing of the nodes of chair seats in the model. Figure 6 is the schematic drawing of the people distribution on the platform and the train before the evacuation.

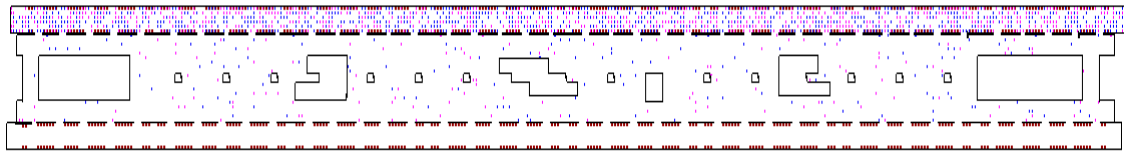

Fig.6 The schematic drawing of the person distribution on the platform

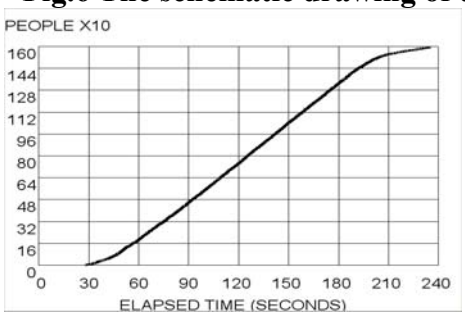

Figure 7 The curve diagram of escaped number against time in the first case under the general circumstances

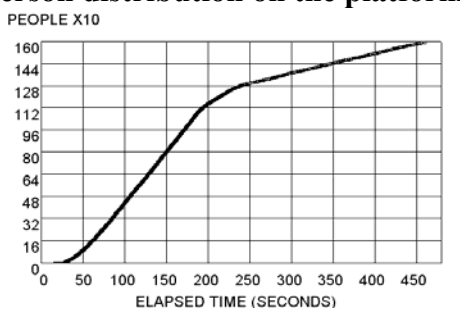

Figure 8 The curve diagram of escaped number against time in the second case under the general circumstances

1. The computation results and analysis of evacuation simulation under general circumstances is classified as follows:

a) In the first case, the 6 staircases in the public area are open to all the people being evacuated who choose the shortest flight route with no external intervention.

The computation results show that it takes 3 minutes and 55 seconds for everyone to be evacuated, as shown in Figure 7. The results are within the code requirements.

b) In the second case, the escalator on the right side of public area is considered closed; the other 5 staircases are open to everyone being evacuated with no external intervention. Item 26.3.3 of Urban Rail Transit Design Standard (DGJ08-109-2004) describes one escalator is likely to be broken down or under maintenance.

The results show that it takes 7 minutes and 30 seconds for everyone to be evacuated, as shown in Figure 8. The results do not meet code requirements. Analysis shows that people tend to choose the shortest flight and the staircase on the right side is heavily congested due to the fact that the escalator on the right side is not available (Figure 9). People using the right staircase are not aware that the middle and left

staircases are not being fully utilized.

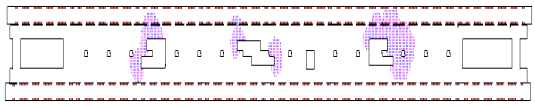

Figure 9 The distribution of people on the platform 2 minutes after the fire breaks out in Case (b) under the general circumstances

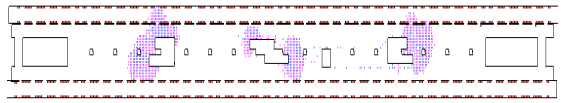

Figure 10 The distribution of people on the platform 2 minutes after the fire breaks out in Case (c) under the general circumstances

c) The third case is similar to the second one. In the third case, when one exit is congested, guidance and intervention is made from the working staff to change some people's flight route to fully use every exit.

Figure 11 shows the people distribution after a 2 minute intervention. The distribution of people in each exit is far more even than that of the second case (Figure 9). The simulation results show that it takes 5 minutes for everyone to evacuate, taking 2 minutes 30 seconds less than in the second case, thus fulfilling the requirement of the code.

2. The computation analysis results of evacuation under disaster is as follows:

In the disaster circumstances, the overall heat release of the fire is 40.3 MW, each second is 1.4MW on average. Assuming that the fire takes place near the pillar (the red part in Figure 11) between the right-side staircase in the middle area and the pillar, and the fire lasts for 1 hour. The fire is simulated by Smartfire 4.1. Figure 11 shows the plan sketch of the computation model. Figure 12 shows the temperature field of the section of Z axis according to the computation results.

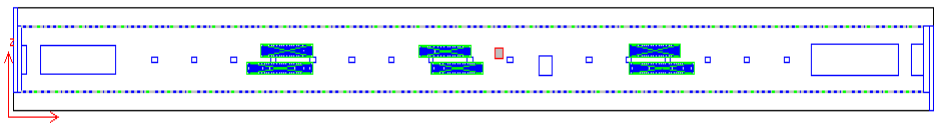

Figure 11 The planar sketch in the Smartfire calculation model

The computation result of Smartfire is introduced in the computation model of Exodus and correlated with the disaster situations in all the modules of Exodus. The computation result shows that the fire risk without heavy fog does not have significant influence on the evacuation result. In this case, with the guidance of working staff and the intervention of flight route, it takes 5 minutes 15 seconds for everyone to evacuate. The simulated result meets the requirements of the codes and no casualties occur in the evacuation.

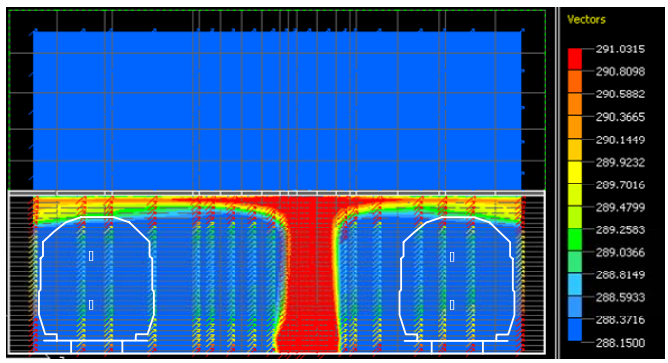

Figure 12 Temperature field in the along z-axis section where the fire breaks up

THE COMPREHENSIVE ANALYSIS OF SIMULATION

According to the analysis of computation results, time needed to evacuate under different circumstances are shown in Table 2.

It is shown from the analysis of different situations that the evacuation time in a metro station meets the requirements of the code. The safe evacuation training of the working staff, regular safety drills, in-time checking and updating of the fire fighting equipment can efficiently prevent major casualty accidents.

CONCLUSION

The conclusion drawn from the computation analysis is listed as follows:

1. Under different risks, people instinctively choose the shortest flight route. Without intervention of people's flight route, the time needed to evacuate is strongly influenced by the use of each exit and distribution of people in the metro station.

Table 2 Time needed to evacuate under different circumstance

Evacuation scene	General scene		Fire scene	
	Immediate evacuation	Immediate evacuation	Immediate evacuation	
Evacuation strategy	All stairs were open; No intervention to evacuation route	One escalator was shut down; No intervention to evacuation route	One escalator was shut down; The evacuation course was intervened	One escalator was shut down; The evacuation course was intervened
Evacuation time	3 minute 55 second	7 minute 30 second	5 minute	5 minute 15 second

2. In evacuation people intuitively choose the shortest route. Some of the exits might not be used at all, while others might be heavily congested. This phenomenon wastes precious time for people to escape. Therefore, intervention must be made to save time, for instance, the rational guidance and intervention from the working staff must be made when one exit is overcrowded.

3. It has been learned from the simulation analysis, that under general circumstances it takes 2 minutes 30 seconds less to evacuate everyone with proper guidance and intervention than without, saving 1/3 of the evacuation time. The result shows the importance of proper guidance.

4. The design of intervention on evacuation route ensures the even use of each exit in evacuation. Proper safety evacuation training of the working staff and rescuers, regular safety drills, in-time checking and updating of the fire fighting equipment can efficiently prevent major casualties.

5. Small scale fire with little fog has little influence on the evacuation. As item 26.5.3 of Urban Rail Transit Design Standard (DGJ08-109-2004) describes, the platform and station hall should be able to resist fire with 1.5MW. In this situation, with proper guidance of the working staff, evacuation can be completed in time.

REFERENCES

HUANG Hongwei, YE Yongfeng, HU Qunfang. (2008). "Analysis on the current situation of risk management on metro operation safety." *China safety science journal*, 18(7): 55-62. in chinese

MA Junchi. (2007). *Investigation and Simulation on Crowd Evacuation in Fire Disaster*. SHANG HAI: Tongji University, 2007.

Specifications of Project Construction of Shanghai. (2003). *DGJ08–109–2004 Urban rail transit design standard.* Shanghai, in Chinese

SHI Congling, ZHONG Maohua, LUO Yanping, et al. (2006). "Simulating Calculation and Analysis of Gasoline Arson Fires in Metro Compartment." *China Safety Science Journal*, 16(1): 32-36. in Chinese

SHI Congling, ZHONG Maohua, LIU Zhicheng, et al. (2007). "Performance-based design on occupant evacuation of elevated metro station in fires." *Journal of Safety Science and Technology*, 3(4): 11-15. in Chinese

The National StandardsCompilation Group of People's Republic of China. (2003). *GB 50157-2003. Code for design of metro*. Beijing：China Planning Press，2003. in Chinese

Research Of Company Freight Traffic Generation Prediction Models In High-Tech Park

Zheng Ke [1] and Zhang Yaping[2]

[1]Civil Engineering College, Fuzhou University, P.O.Box 350108, PH (+86)13763832018; email: zh99k@163.com
[2]School of Transportation Science and Engineering, Harbin Institute of Technology; P.O. Box 150090, PH (+86) 15846598208; email: zxlt0905@163.com

ABSTRACT

This paper applies the cluster analysis method to categorize the 17 sample companies in a high-tech park in terms of their workshop area. First of all, the annual freight traffic volume per unit workshop area has been used as the index to cluster the 17 sample companies into 4 groups. The results show that each group of companies produces the similar products. Secondly, the workshop area or site area of a company correlates well with its annually generated freight traffic. The regression analysis shows a linear correlation between the workshop area (or site area) of the company and its annual freight traffic volume. These models can be applied to predict the freight traffic volume for the planning high-tech park.

KEY WORDS

High-tech Park, Freight traffic volume, Regression analysis method, Cluster analysis method

INTRODUCTION

The freight transport constitutes an essential part of the transportation. Together with the passenger transport, the freight transport has become an important component of the urban transportation, which underlies the modern economic and social activities. The research abroad on the freight transport forecasting has started a long time ago. Gregory A. Godfrey and Warren B. Powell proposed the method of the adaptive estimation of the daily demands for the freight transportation using exponential smoothing-based methods (Gregory A. Godfrey, Warren B. Powell, 2000). Then Rodrigo A. Garrido and Hani S. Mahmassani addressed the method of forecasting freight transportation demand with the space–time multinomial probit model in the same year (Rodrigo A. Garrido, Hani S. Mahmassani, 2000). J. Enrique introduced a multi-modal supply–demand equilibrium model for predicting intercity freight flows (J. Enrique Fern_andez L., Joaqu ın de Cea Ch.,Alexandra Soto O., 2003). Peter Nijkamp and his team compared the family of discrete choice models and the neural network model, and the results showed that in general the predictive potential of neural network models is higher than that of discrete analysis (Peter Nijkamp, Aura Reggiani, Wai Fai Tsang, 2004). To meet the demand of recent development in freight transportation industry, Feng Xiao and Hai Yang who work in

Hong Kong University of Science and Technology proposed a game-theoretic model over a freight transportation network (Feng Xiao, Hai Yang, 2007)

The current research in China on the freight transport is relatively insufficient, especially on the freight transport problem of high-tech park. Wang Xiaokun and his team carried out the research on the characteristics and policies of the freight transport in central business district (Wang Xiaokun, Yang Dongyuan, Hu Xiaowen, 2006). Yang Longhai and his team have carried out the research on the forecasting model of freight transportation demand at port free trade zone (Yang Longhai, Zhang Xiqiao, Li Shejiao, Luo Zhaohong, 2007). Liang Chengwen studied the planning method of freight transport in big cities (Liang Chengw, Li Shaoyan, LiuWei, 2008). These above methods and results provide the good reference for this paper.

As we all known, High-tech Park is the cradle of high-tech companies. And the supply and demand goods traffic trips produced by the companies in High-tech Park constitutes a great fraction of the total traffic trips in high-tech park. Normally, there are at least tens of companies, or even more than one hundred companies in a park. And it is unnecessary and impracticable to survey every company in the park in order to find out the patterns of freight traffic trips. From the common sense, the companies whose production categories are similar will have the similar patterns of freight traffic trips. We came out with an idea that we can study the patterns of freight traffic trips in a park by analyzing and investigating the freight traffic trips' related data of some sample companies in the park. Therefore, we randomly picked 17 maturely developed companies as the sample companies for investigating and analyzing the high-tech parks in the city of Changsha in China. This paper establishes the traffic trip prediction model for each category of company after analyzing the freight traffic data of the 17 companies.

1DETERMINATION OF COMPANY ANNUL FREIGHT TRAFFIC VOLUME

The truck is the standard car type among all kinds of freight vehicles to contribute to the traffic volume. Standard parameters of a truck are as following: the normal load of 3~5 ton and the carriage volume of 5~8m^3. From the valid company questionnaires, we can obtain how much a normal-type wagon can load for the various productions and raw materials of the sample companies. So, the annual freight traffic volume of each company can be obtained based on them.

Furthermore, vacant driving can occur during the freight transport. According to the surveys of freight vehicles' load of 17 sample companies, the average vacant driving rate is about 30% among the freight transport in the park. Considering the vacant driving rate, the formula of converted companies' freight traffic volume is:

$$Q = Q_s /(1 - p) \tag{1}$$

Where Q_s represents actual number of car loadings of company's production and raw material; p represents vacant rate of the freight vehicles.

Based on the above analysis, the cruising data of 17 sample companies including their corresponding workshop acre, site acre and production category are shown in Table 1. Each company's annul freight traffic volume is also given by the conversions.

Table 1 annul freight traffic volume on company's unit workshop acre

Company number	Production category	Workshop acre (m^2)	Site acre (m^2)	Annual traffic volume (veh/year)	Annul traffic volume per unit workshop acre (veh/year·100m^2)
1	Cable	5000	12044	22317	446
2	E-apparatus	2183	9392	13759	630
3	Electrical source	2150	10753	4560	212
4	Machine	5736	16853	723	13
5	Rubber goods	2100	16000	2150	102
6	Light car fitting	5400	46800	5197	96
7	Cash register	3500	16668	2095	60
8	Material	6000	313020	26603	443
9	Chemical fiber	9000	66000	6625	74
10	Plastic	3200	11144	2566	80
11	Machine	10830	41840	1736	16
12	Medicine	800	6000	2479	310
13	Biology	924	8696	2909	315
14	Machine	22400	64000	3273	15
15	Electromechanic	30000	82000	8134	27
16	Battery	6800	17053	1004	15
17	Electronic	939	6743	2950	314

2 COMPANY ANNUL TRAFFIC VOLUME CLUSTERING ACCORDING TO WORKSHOP ACRE UNIT

2.1 Cluster method and calculation

Usually, the parameters such as "distance" and "similarity coefficient" are used to describe the extent how the samples are similar. In this paper, since there is only one index (variable) in each sample, it's proper to use "distance" to measure the samples' similarity. In the real computing, the formula (2) can be used to compute the distance between samples. That is:

$$d_{ij} = \left| x_i - x_j \right| \tag{2}$$

Where: d_{ij} represents absolute value distance between sample *i* and sample *j*; x_i and x_j are the value of index of sample number *i* and sample number *j*.

After deciding computing model of samples' distance, we still need to choose the method for specific cluster computing. Considering the conditions of the samples and their indexes in the real life, we decide to take the shortest distance cluster method.

This method defines the distance as the shortest distance among all the pairs between the two categories, and that is:

$$D_{KL} = \min_{i \in G_K, j \in G_L} d_{ij} \tag{3}$$

Where: D_{KL} represents the distance between category G_K and category G_L.

From the above cluster analysis and formula, the cluster result of 17 sample companies can be obtained as Figure 1.

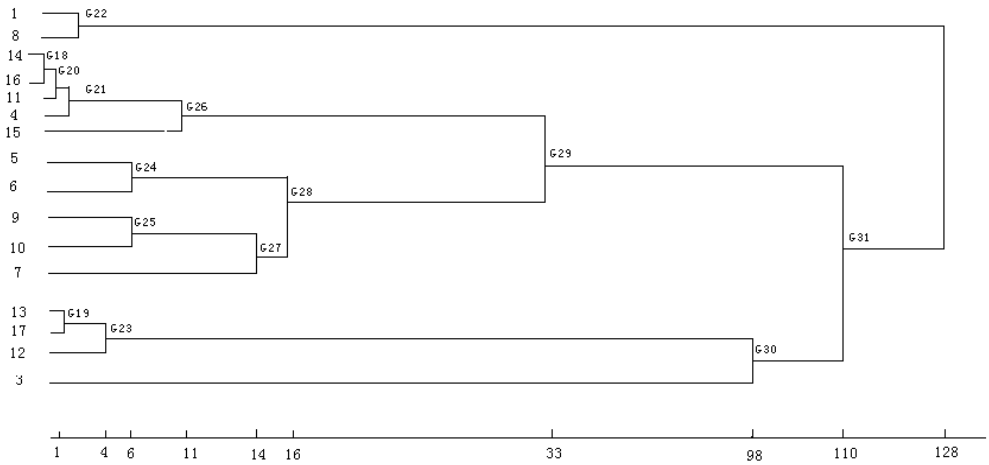

Figure1 Cluster tree figure of 17 sample companies according to freight traffic volume.

Notes: Vertical coordinate represents company number, horizontal coordinates represents the distance between categories.

2.2 The number of category ascertaining

The above cluster result provides how close samples are related to each other, but we still need to determine the number of samples in each category. So the parameter, R^2 statistic in cluster analysis, can be used to decide the number of the cluster category.

In cluster analysis, the expression of R^2 statistic is:

$$R^2 == \frac{\sum_{i=1}^{k} n_i (\bar{x}_i - \bar{x})^2}{\sum_{j=1}^{n} (x_j - \bar{x})^2} \tag{4}$$

Where: n represents the total sample number; k represents k kinds of categories the samples are merged to when clustering; n_i represents the sample number of

category G_i in k categories; $\bar{x}$ represents total gravity of the samples; $\bar{x}_i$ represents gravity of category sample; x_j represents the sample index.

According to formula (4), the value of R^2 corresponding to the cluster at each turn and the number of category can be calculated, as shown in Table 2.

Table 2 Relationship between clustering number and the value of R^2

Clustering	1	2	3	4	5	6	7	8	9	10	11	12
Cluster number	G_{18}	G_{19}	G_{20}	G_{21}	G_{22}	G_{23}	G_{24}	G_{25}	G_{26}	G_{27}	G_{28}	G_{29}
Integrating times	0	1	1	2	3	4	6	6	11	14	16	33
R^2	0.9996	0.9997	0.9997	0.9994	0.9988	0.9988	0.9990	0.9989	0.9982	0.9979	0.9963	0.9779

If we plot the times and the corresponding R^2 in Table 2 on a graph, we can see a turning point of the curve at 11 times, which can be used to decide the number of samples in the clustering category. From Table 2, at 11 clustering times, the cluster distance is 16veh/（year·100m^2)

According to this integrating distance, cluster tree in figure 1 is integrated, and the annul freight traffic volume per unit workshop acre produced by 17 companies in Table 1 can be divided to four categories. They are:G_{26}(4 machine manufacture, 11 machine manufacture, 14 machine manufacture, 15 electromechanical manufacture, 16 battery); G_{28} (5 rubber goods, 6 light car fitting, 7 cash register, 9 chemical fiber, 10 plastic); $G_{23,3}$ (3 electrical resource, 12 medicine, 13 biology, 17 electron); $G_{22,2}$ (1 cable, 2 E-apparatus, 8 material).

3 ESTABLISHMENT OF ANNUL FREIGHT TRAFFIC VOLUME PREDICTION MODEL OF EACH CATEGORY OF COMPANIES

Based on the four categories mentioned above, we can establish the regression model about annul freight traffic volume Q_n and company's workshop acre S_1. Taking the companies in G_{26} as an example: G_{26} consists of 5 companies with the numbers of (4, 11, 14, 15, 16). Table 1-1 already showed the annual freight traffic volume and workshop acre of the 5 companies. If we draw the data on the graph, we can see a linear trend of them and fit them with a linear line. With the mathematical theory of statistic, we can obtain linear regression model about Q_n and S_1. The linear regression models about Q_n and S_1 for other categories of companies can be established in a similar way, as shown in Table 3. Although the site acre is not as closely related to the production and raw material as the workshop acre, the acre of site is more commonly used than the workshop acre. Qualitatively, the company site acre is directly proportional to the workshop acre. So, the regression model about the site acre S_2 and the annual freight traffic volume of each category of companies is also established with the same method, as shown in Table 3.

Table 3 Regression model about company workshop acre, site acre and annul freight traffic volume of each category

Category	$G_{23,3}$	G_{26}	$G_{22,2}$	G_{28}
Regression model about S_1 and Q_n	$Q_n=1.43S_1$ - 1504	$Q_n=0.27S_1$ - 1126	$Q_n=3.29S_1$+ 6419 r=1.00	$Q_n=0.72S_1$ - 368
Regression model about S_2 and Q_n	$Q_n=0.39S_2$+ 100 r=0.90	$Q_n=0.11\ S_2$ - 2104 r=0.92	$Q_n=0.03S_2$+ 17714 r=0.76	$Q_n=0.09\ S_2$ - 1073 r=0.98

Notes: S_1, S_2 represents workshop acre and site acre of each company (m^2)

From Table 3-1, the variables Q_n and S_1, S_2 in most categories are interrelated well with the related coefficient r above 0.90 (r=0.90), except that company site acre and its corresponding annul freight traffic volume in category $G_{22,2}$ doesn't interrelate well. In general, the workshop acre is better interrelated to the annul freight traffic volume than the site acre.

4 APPLICATIONS

4.1 Application instance

We can analyze an application as following. The total area of the industrial estate in a high-tech park in Changsha is 2,985,192m^2. 11.89%(354,857m^2) of the area is $G_{23,3}$, 48.39%(1,444,483m^2) is G_{26}, 29.35%(876,210m^2) is $G_{22,2}$ and 10.37%(309,642 m^2) is G_{28}. According to the formula in Fig. 3-1, the annual freight traffic volume of the present area of every category estate and the total industrial estate can be calculated respectively: 138,494veh, 156,789veh, 44,000veh, 26,795veh and 366,078veh.

Let's assume that the total area of the industrial estate of a planning high-tech park is 6.06km^2. Assuming that the structure of the industrial estate doe not change, each category area can be calculated by the current proportion: the area of $G_{23,3}$ is 721,033.38m^2, the area of G_{26} is 2,934,466.38m^2, the are of $G_{22,2}$ is 1,779,842.7m^2 and the area of G_{28} is 628,857.54m^2. According to the formula in Fig.3-1, the annual freight traffic volume of each category estate and the total industrial estate can be calculated respectively: 281,303veh, 320,687veh, 71,109veh, 55,524veh and 728,623veh.

Based on the above analysis, the freight traffic volume caused by industrial estate in the high-tech park is considerably limited. The current industrial estate area (2.99 km^2) and the planning area (6.06km^2) can only generate the freight traffic volume of 1,003pcu and 1,996pcu respectively. The investigation of the present road network in the high-tech park show that even in the peak hours, the average traffic flow on the road network is only 0.1. And the freight traffic volume (converted to car traffic volume) only constitutes 21% of the total traffic. Therefore, the current road network has enough room for the planning high-tech park. The above analysis will be helpful when planning new high-tech parks.

5 CONCLUSIONS

For the companies whose production category is similar, their annul freight traffic volume produced per unit workshop acre is comparably close; and for the companies whose production category differs, their annul freight traffic volume produced per unit workshop acre also differs.

For the companies whose production category is similar, the workshop acre or site acre of the company correlates well with the annul freight traffic volume produced by the company, so a model can be established to predict the annul freight traffic volume of this category of companies.

After establishing the prediction model of the freight traffic volume, the freight traffic volume of the companies in a planning High-tech Park can be forecasted, and the model can offer the quantitative analysis for the network planning and traffic control in the park.

REFERENCES

Feng Xiao, Hai Yang. (2007). Three-player game-theoretic model over a freight transportation network, Transportation Research Part C 15, 209–217.

Gregory A. Godfrey, Warren B. Powell. (2000). Adaptive estimation of daily demands with complex calendar effects for freight transportation. Transportation Research Part B 34, 451-469.

J. Enrique Fern_andez L., Joaqu ın de Cea Ch.,Alexandra Soto O.(2003). A multi-modal supply–demand equilibrium model for predicting intercity freight flows Transportation Research Part B 37, 615–640.

Liang Chengw, LiShaoyan, LiuWei. (2008) A Study on Cargo Transportation Planning in Shenyang urden Quick Urbanizatio.Planners, Vol. 24, No. 1, 52-55.

Peter Nijkamp, Aura Reggiani, Wai Fai Tsang. (2004). Comparative modelling of interregional transport flows: Applications to multimodal European freight transport, European Journal of Operational Research 155, 584–602.

Rodrigo A. Garrido, Hani S. Mahmassani. (2000). Forecasting freight transportation demand with the space-time multinomial probit model.Transportation Research Part B 34, 403-418.

Wang Xiaokun, Yang Dongyuan, Hu Xiaowen. (2006). Freight Transportation Characteristics and Assessment of Policy in Urban Central Commercial District. Journal of Transportation Systems Engineering and Information Technology Vol. 6, No. 6,130-135.

Yang Longhai, Zhang Xiqiao, Li Shejiao, Luo Zhaohong. (2007). The Freight Traffic Demand Forecasting of Shenzhen Yantian Harbor Free Trade Zone. Urban Transport of China, Vol.5, No. 2, 51-54.

Bending Vibration Suppression of High Speed Railway Passenger Car Body

Caihong Huang[1], Jing Zeng, and Ren Luo

[1]Traction Power State Key Laboratory, Southwest Jiaotong University, Chengdu, 610031, China; PH (+86)13402834910; email: rainbow.huang@tom.com

ABSTRACT

Vertical dynamic response of a high speed passenger car considering elastic vibration has been investigated, in which car body is modeled as a simple uniform elastic Euler-Bernoulli beam with free ends. It is found that vibration in the elastic model is bigger than in the rigid one. In order to reduce the vertical flexural vibration, an effective and practical method is introduced, which is to paste free damping layers on the outside sheathing of the car body. The calculations show that it is a useful measure for improving the riding comfort of the high speed car. The thicker the damping materials attached, the better the ride comfort will be. But considering the weight it may introduce, only 3mm bitumen based damping materials is enough to get a satisfactory result.

INTRODUCTION

To increase train speed, railway vehicles have become increasingly lightweight in recent years. However, it decreases car body stiffness excessively, leading to serious bending vibration in the vertical direction and deteriorating the ride comfort (Takigami and Tomioka 2008). Therefore, it is important to investigate methods to reduce bending vibration with a view to improve riding comfort. Vibration characteristics of the rigid car body and elastic car body are discussed in this paper, the results of which show that first bending mode of vibration has a great influence on the riding comfort of a lightweight car body. To solve this problem, a simple and practical way is suggested which is to increase the structural damping by pasting free damping layers on the outside sheathing of the car body.

MODELING

Vertical model of the high speed car is given in Figure 1(a). It is considered as a rigid-flexible coupling system composed of wheelsets, bogie frames, car body, primary suspension and secondary suspension. The car body is modeled as a simple Euler-Bernoulli beam in consideration of only vertical vibration. The parameter values given in Appendix A are typical for a high speed car.

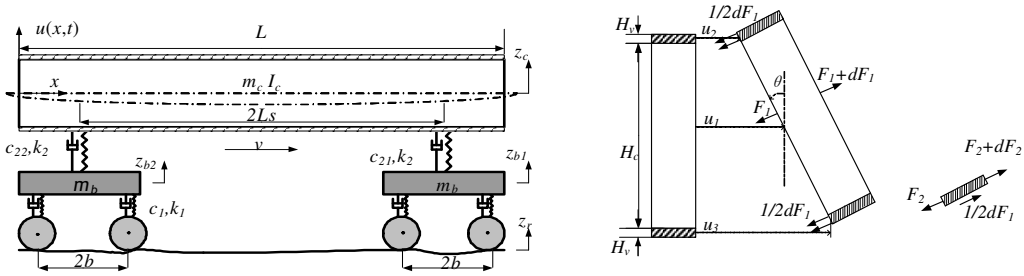

(a) Passenger car (b) Force and geometric relations

Figure 1. Passenger car model.

Assuming the car body as a uniform elastic beam with free ends (Zeng et al. 2007), equation (1) hold for the vertical displacement of vehicle systems.

$$\begin{cases} m_c\ddot{z}_c + \sum_{i=1}^{N} m_{zi}\ddot{q}_i + c_{21}[\dot{z}_c + \dot{u}(x_1,t) - L_s\dot{\theta}_c - \dot{z}_{b1}] + c_{22}[\dot{z}_c + \dot{u}(x_2,t) - L_s\theta_c - \dot{z}_{b2}] \\ \quad + k_2[2z_c - z_{b1} - z_{b2} + u(x_1,t) + u(x_2,t)] = 0 \\ I_c\ddot{\theta}_c - \sum_{i=1}^{N} m_{\theta i}\ddot{q}_i + c_{21}L_s[L_s\dot{\theta}_c - \dot{u}(x_1,t) + \dot{z}_{b1}] + c_{22}L_s[L_s\dot{\theta}_c + \dot{u}(x_2,t) - \dot{z}_{b2}] \\ \quad + k_2L_s[2L_s\theta_c + z_{b1} - z_{b2} - u(x_1,t) + u(x_2,t)] = 0 \\ m_b\ddot{z}_{b1} + 2c_1\dot{z}_{b1} + c_{21}[\dot{z}_{b1} - \dot{z}_c - \dot{u}(x_1,t) + L_s\dot{\theta}_c] + (2k_1 + k_2)z_{b1} \\ \quad - k_2[z_c + u(x_1,t) + L_s\theta_c] = c_1[\dot{z}_r(t) + \dot{z}_r(t-\tau_1)] + k_1[z_r(t) + z_r(t-\tau_1)] \\ m_b\ddot{z}_{b2} + 2c_1\dot{z}_{b2} + c_{22}[\dot{z}_{b2} - \dot{z}_c - \dot{u}(x_2,t) - L_s\dot{\theta}_c] + (2k_1 + k_2)z_{b2} \\ \quad - k_2[z_c + u(x_2,t) - L_s\theta_c] = c_1[\dot{z}_r(t-\tau_2) + \dot{z}_r(t-\tau_3)] + k_1[z_r(t-\tau_2) + z_r(t-\tau_3) \\ \ddot{q}_i(t) + \eta_i\omega_i\dot{q}_i(t) + \omega_i^2 q_i(t) = -m_{zi}\ddot{z}_c(t) + m_{\theta i}\ddot{\theta}_c(t) + \sum_{i=1}^{2} F_k(t)Y_i(x_k) \end{cases} \tag{1}$$

where:

$$\begin{cases} \omega_i = \dfrac{(2i+1)^2\pi^2}{4L^2}\sqrt{\dfrac{EI}{\rho A}} \\ Y_i(x) = A_iU_i(x) = A_i\left[ch\beta_i x + \cos\beta_i x - \dfrac{ch\beta_i L - \cos\beta_i L}{sh\beta_i L - \sin\beta_i L}(sh\beta_i x - \sin\beta_i x)\right] \\ \beta_i = \dfrac{(2i+1)\pi}{2L},\ \ A_i = 1/\sqrt{\rho A\int_0^L U_i{}^2(x)dx} \\ F_k(t) = -c_2[\dot{z}_c(t) + \dot{u}(x_k,t) + (-1)^k L_s\dot{\theta}_c - \dot{z}_{bk}(t)] - k_2[z_c(t) + u(x_k,t) + (-1)^k L_s\theta_c - z_{bk}(t)] \\ m_{zi} = \rho A\int_0^L Y_i(x)dx\ ,\ \ m_{\theta i} = \rho A\int_0^L (x - \dfrac{L}{2})Y_i(x)dx \\ \tau_1 = 2b/v,\quad \tau_2 = 2L_s/v,\quad \tau_3 = 2(b+L_s)/v \end{cases} \tag{2}$$

where: z_{b1}, z_{b2}, z_c, θ_c represent front frame translation, rear frame translation, carbody translation and pitching. $q_i(t)$ is modal coordinate of the car body flexible

deformation. $x_k=L/2-(-1)^k L_s$, k=1 (Front bogie), k=2 (Rear bogie). η_m is loss factor of car body in the m order modal.

VIBRATION MODE ANALYSIS

In order to investigate which modal is the main modal resulting in the car body elastic vibration, the vibration modal of the car is shown in Figure 2. Considering the track irregularities, amplitude frequency curve in the car body center under various conditions is given in Figure 3. Vibration in the elastic model is bigger than in the rigid one. Moreover, there exists resonance near 9.7Hz which is first bending mode of car body. Because there exists a vibration node of second bending mode in the car body center, it has little influence in the elastic vibration. As to the third vibration mode, it is contrary to the first mode in the center so it also has little influence in the elastic vibration in the center, only has influence in the high frequencies. So the first bending mode is the main mode which needed to be suppressed.

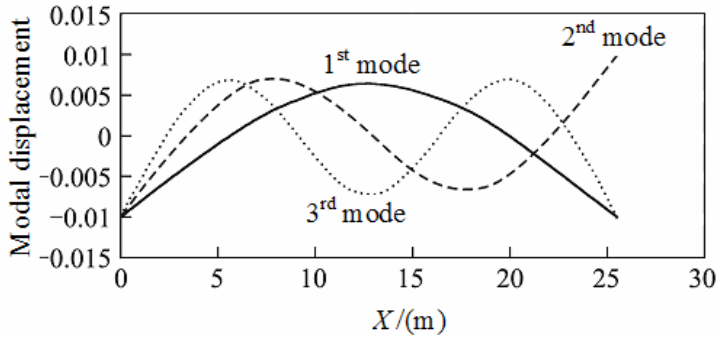

Figure 2. Vibration modal.

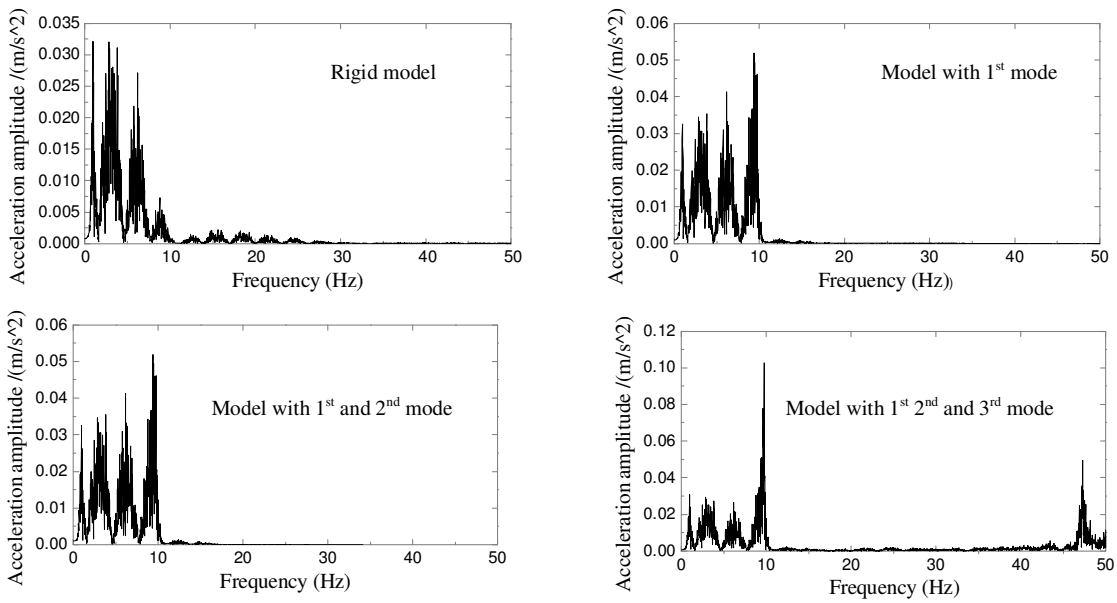

Figure 3. Vertical acceleration of car body center in the frequency domain

Vibration suppression with free damping treatment. As the natural frequency of the first bending mode of car body is the main reason contributing to the elastic vibration, free damping layers can be pasted on the outside sheathing of the car body to increase the internal damping to improving the riding comfort of the high speed car, as is shown in Figure 1.

The displacement field is based on the following hypothesis:

- Flexural vertical displacement field is the same in all parts of the section;
- There is no slip between the different materials;
- Shear stresses are ignored.

Because of the previous hypothesis, the strain energy per length is composed of two terms: traction-compression and flexure of the elastic and viscoelastic parts (Zhao et al. 1990). They have the following expressions:

$$W_{ext}{}^{i} = \frac{1}{2} E_i A_i \left| \frac{du_i}{dx} \right|^2 , \quad W_{fl}{}^{i} = \frac{1}{2} E_i I_i \left| \frac{d^2 y_i}{dx^2} \right|^2 = \frac{1}{2} E_i I_i \left| \frac{d\theta_i}{dx} \right|^2 \tag{3}$$

where, u_i、y_i and θ_i represents the longitudinal displacement、flexural displacement and rotating angle of material i respectively. Under the free damping layers treatment, $\theta_i=\theta$; E_iA_i represents tension stiffness，E_iI_i represents bending stiffness. If the relationship between θ and u_i is given, it is easy to calculate the total strain energy. Assuming θ is harmonic, namely $\theta=\underline{\theta} cos(\beta x)$. If the boundary effects is ignored, $u_i=R_i\theta$ can be got, Where, R_i is called tension effect.

Because the strain energy is different in the full wavelength, strain energy density must be got to calculate the loss factor.

$$W_{extm}{}^{i} = \frac{1}{\lambda} \int_0^{\lambda} W_{ext}\, dx = \frac{\beta}{2\pi} \int_0^{\frac{2\pi}{\beta}} \frac{1}{2} E_i A_i \left| \frac{du_i}{dx} \right|^2 dx = \frac{1}{4} E_i A_i R_i{}^2 \underline{\theta}^2 \beta^2 \tag{4}$$

$$W_{flm}{}^{i} = \frac{1}{\lambda} \int_0^{\lambda} W_{fl}\, dx = \frac{\beta}{2\pi} \int_0^{\frac{2\pi}{\beta}} \frac{1}{2} E_i I_i \left| \frac{d^2 y_i}{dx^2} \right|^2 dx = \frac{1}{4} E_i I_i \underline{\theta}^2 \beta^2 \tag{5}$$

A usual definition of damping is given by the ratio between the dissipated and the strain energies. So, Loss factor of car body with free damping layers is shown in Equation (6):

$$\eta_{\mathrm{m}} = \frac{\sum_{\mathrm{i}=1}^{3} \eta_{mi} (W_{extm}{}^{\mathrm{i}} + W_{flm}{}^{i})}{\sum_{\mathrm{i}=1}^{3} (W_{extm}{}^{\mathrm{i}} + W_{flm}{}^{i})} = \frac{\sum_{\mathrm{i}=1}^{3} \eta_{mi} (E_i A_i R_i{}^2 + E_i I_i)}{\sum_{\mathrm{i}=1}^{3} (E_i A_i R_i{}^2 + E_i I_i)} = \frac{\eta_{m1} (E_1 A_1 R_1{}^2 + E_1 I_1) + 2\eta_{m2} (E_2 A_2 R_2{}^2 + E_2 I_2)}{(E_1 A_1 R_1{}^2 + E_1 I_1) + 2(E_2 A_2 R_2{}^2 + E_2 I_2)} \tag{6}$$

R1 and R2 can be got by the force and geometric relations, as is shown in Figure 1(b).

As self-adhesive type of bitumen-based damping sheet is cheap and

convenient to be used especially to suppress large areas of the shell vibration, it is particularly suitable damping materials in the rolling stocks. Its dynamic characteristics are shown in Figure 5 (Zhang 1994).

To reduce the elastic vibration, two free damping layers are pasted on the outside of the car body. With the damping treatment, the relation between loss factor and thickness is shown in Figure 6.

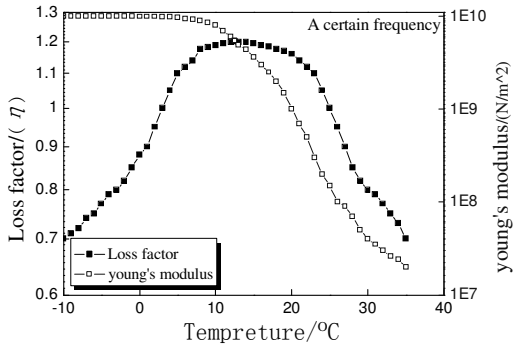

Figure 5. Dynamic characteristics.

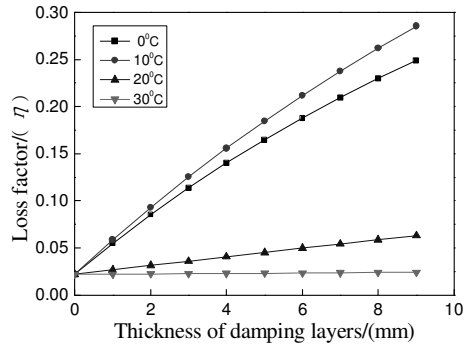

Figure 6. Loss factor and thickness.

As is shown in the picture, loss factor increases with the increase of the thickness. But considering the weight it may introduce, ride comfort running at the speed of 220km/h is analyzed in Figure 7. As is shown in Figure 7, 3mm is enough, namely, only 700kg is introduced in the weight.

Running at the speed of 220km/h and with a damping thickness of 2mm, the relationship between acceleration amplitude and frequency in the car body center is shown in Figure 8. The first bending vibration near 9.7Hz is suppressed successfully. In the normal temperature, a better result will be got, while in the high temperature it is not so effective.

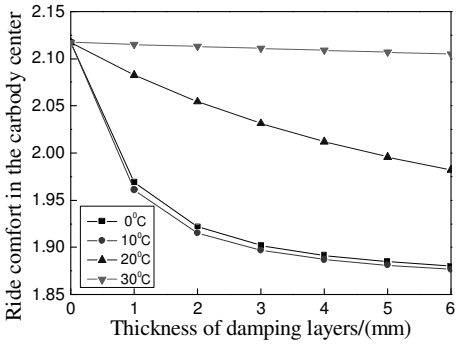

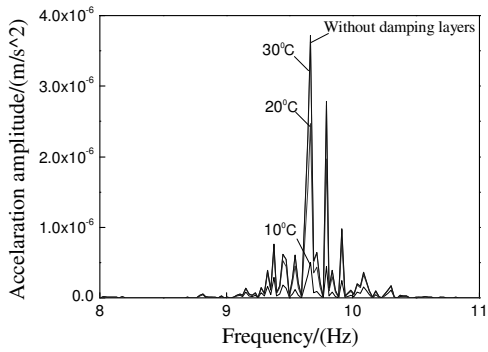

Figure 7. Ride comfort and thickness. Figure 8. Acceleration amplitude.

CONCLUSIONS

After careful analytic analysis and numerical calculating, the conclusions can be drawn as below:

(1) Vibration in the elastic model is bigger than in the rigid one, which is close to the real working condition.
(2) The first bending mode is the main mode which needed to be suppressed.
(3) The first bending vibration is suppressed successfully by the free damping treatment. In the normal temperature, a better result will be got, while in the high temperature it is not so effective.
(4) 3mm is enough, namely, only 700kg is introduced in the weight.

ACKNOWLEDGEMENTS

This work is supported by National Natural Science Foundation of China (No. 50823004), Most Special Fund from the Traction Power State Key Laboratory and Southwest Jiaotong University National Basic Research Program of China (973 Program) (No.2007CB714700)

Appendix A

Parameter values for a high speed car

Primary spring stiffness(k_1)	2000KN·m^{-1}	Mass of bogie(m_b)	2.3 t
Secondary spring stiffness(k_2)	600 KN·m^{-1}	Mass of vehicle(m_c)	40t
Primary damping(c_1)	50 KN·s·m^{-1}	Wheelbase($2b$)	2.5 m
Secondary damping(c_2)	75 KN·s·m^{-1}	Vehicle length(L)	25.5m
Distance between bogie centers($2L_s$)	18m	Body pitch moment inertia(I_c)	2500 t·m^2
Equivalent quality per length(ρA)	1.57 t·m^{-1}	Bending moment(EI)	5×10^6 KN·m^2

REFERENCES

Takigami, T. and Tomioka, T. (2008). "Bending Vibration Suppression of Railway Vehicle Carbody with Piezoelectric Elements." *Journal of Mechanical Systems for Transportation and Logistics*, 1(1), 111-121.

Zeng, J. and Luo, R. (2007). "Vibration Analysis of Railway Passenger Car Systems by Considering Flexible Carbody Effect." *Journal of the China Railway Society,* 29(6), 19-25.

Zhang, H. (1994). "Application of viscoelastic damping materials based on asphalt in the vibration and noise reduction." *Noise and Vibration Control*, 1(3), 31-37.

Zhao, J., Zhang S., and Dai, D. (1990). "Improving anti-vibration characteristics and reducing noise radiation of structural components of vertical lathe." *Design and Research*, 1(2), 15-18.

Analysis of Deformation Characteristics of Collision Vehicles Using Close-range Photogrammetry

Z-M. Tao[1] and Y-L. Pei[2]

[1]School of Transportation Science and Engineering, Harbin Institute of Technology, Harbin 150090, China; email: taozeming@163.com

[2]School of Transportation Science and Engineering, Harbin Institute of Technology, Harbin 150090, China; email: yulongp@263.net

ABSTRACT

Determining deformable location, size, and depth of vehicle is important during the process to reason a road accident. The use of close-range stereo photogrammetry in traffic accident scene investigations is vital for providing such information in more detail comparing with traditional methods. A case study is introduced to verify the method using the paralleling axis stereo vision theory, which provides accurate three-dimensional (3D) coordinates of the deformation-related feature points, and describes the location and the range of the vehicle deformation.

INTRODUCTION

Recording vehicle deformation parameters is important in traffic safety studies, in which the location and range of the vehicle deformation would be obtained for simulating the real accident site and determining the cause of the accident. It is a key element of traffic scene investigations, which involve deformation location, range, and depth. Close-range photogrammetry survey might provide the 3D coordinates of the collision part by recording the deformation location and range.

In related fields, a series of studies on improving traffic scene accident investigations using close range photogrammetry are carried out. One important element discussed in these studies is vehicle deformation measurement. In China, similar research papers are published. For example, Lu (2006) described a method for the reconstruction of vehicle deformation using self calibration, which is a valuable tool for measuring vehicle deformations. The research would continue enriching the theory. The paralleling axis stereo vision theory is adopted to conduct the photogrammetric survey of vehicle deformations. The deformation data are analyzed, the deformation feature locations are obtained, and the deformation depth is calculated.

CLOSE-RANGE PHOTOGRAMMETRIC THEORY

The main concept of close-range photogrammetric theory is to realize the measurement on a small scale model by simulating the eye function in the nature. The

core of close-range photogrammetry is to simulate the stereo vision and discussing the coordination transformation problems among different coordinate systems. Common 3D coordinate systems are revolved during the procedure. These systems are image coordinate system, camera coordinate system, and global coordinate system.

Image coordinate system. The image coordinate system is defined on the image, (u, v) is recorded by pixel unit, (x, y) is recorded by physical unit. O_1 is (x, y) system's origin, and is the intersection point of the camera optic axis and the image flat, x axis and y axis respectively parallels u axis and v axis. If O_1's coordinate is (u_0, v_0) in the (u, v) coordinate system and the relative physical coordinate is (dx, dy), the formula (1) is obtained

$$\begin{bmatrix} u \\ v \\ 1 \end{bmatrix} = \begin{bmatrix} \frac{1}{dx} & 0 & u_0 \\ 0 & \frac{1}{dy} & v_0 \\ 0 & 0 & 1 \end{bmatrix} \begin{bmatrix} x \\ y \\ 1 \end{bmatrix} \tag{1}$$

Transformation between camera and global coordinate systems. The origin of the camera coordinate system O_1 is at the camera's optic center, X_c axis and Y_c axis respectively parallels x axis and y axis, Z_c axis is the camera's optic axis, which is perpendicular to the image flat, the intersection point of the camera optic axis and the image flat is (x, y) system's origin O_1, OO_1 is the effective camera focus f. The global coordinate system is viewed as the application coordinate system, which shows the location of the real objects.

If (X_w, Y_w, Z_w, 1) is in the global coordinate system and (X_c, Y_c, Z_c, 1) is in the camera coordinate system, then their relationship is given by the formula (2), where R is the rotation matrix (3×3), $R = R_\alpha R_\beta R_\gamma$; T is a position vector, $T = (T_x, T_y, T_z)$

$$\begin{bmatrix} X_C \\ Y_C \\ Z_C \\ 1 \end{bmatrix} = \begin{bmatrix} R & T \\ 0 & 1 \end{bmatrix} \begin{bmatrix} X_W \\ Y_W \\ Z_W \\ 1 \end{bmatrix}, \tag{2}$$

Coordinate calculation using theory of parallel axis stereo vision. As shown in Figure 1, the image flats of C_l, C_r are i_L and i_R, and $I_l(u_l^0, v_l^0)$, $I_r(u_r^0, v_r^0)$ are the centres of i_L and i_R, where I_l is the origin of the coordinate system. The coordinates of P are (X, Y, Z), whose projection in the left image pixel coordinate system is P_l (x_l, y_l), in the right image pixel coordinate system is P_r (x_r, y_r), and baseline length is b.

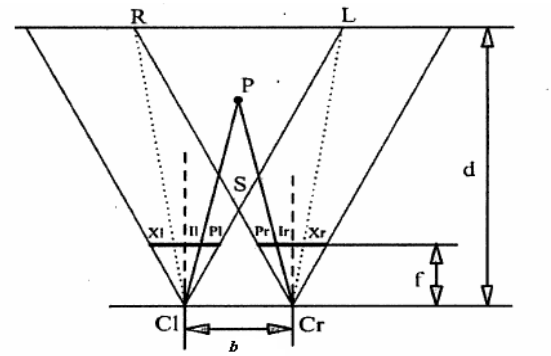

Figure 1. Parallel axis stereocopic vision

According to the perspective projection principle, then

$$\begin{cases} \dfrac{Z-f}{f}=\dfrac{X_l}{x_l}=\dfrac{Y_l}{y_l} \\ \dfrac{Z-f}{f}=\dfrac{X_r}{x_r}=\dfrac{Y_r}{y_r} \end{cases} \tag{3}$$

$$\begin{cases} \begin{pmatrix} x_l \\ y_l \\ z_l \end{pmatrix} = M \begin{pmatrix} X \\ Y \\ Z \end{pmatrix} + \begin{pmatrix} 0 \\ 0 \\ -f \end{pmatrix} \\ \begin{pmatrix} x_r \\ y_r \\ z_r \end{pmatrix} = M \begin{pmatrix} X \\ Y \\ Z \end{pmatrix} + \begin{pmatrix} b \\ 0 \\ -f \end{pmatrix} \end{cases} \tag{4}$$

Using the formulas (3) and (4), the formula of the parallel axis stereo vision can be obtained as

$$\begin{cases} X = b\dfrac{x_l}{x_l - x_r} \\ Y = b\dfrac{y_l}{x_l - x_r} \\ Z = \dfrac{bf}{x_l - x_r} \end{cases} \tag{5}$$

ELEMENTS OF COLLISION VEHICLE DEFORMATION ANALYSIS

There are many collision forms of road accidents, such as a vehicle hitting a pedestrian, a vehicle hitting a bicycle, a vehicle hitting a fixed object, and multiple vehicle collisions.. While the vehicle collides with another vehicle or object, since the motion inertia is blocked at the moment, vehicle deformation would occur. The location of the vehicle collision can be used to determine the accident cause. After stereo matching of close-range photogrammetry in road accident scene investigations,

the 3D coordinates of the vehicle deformation feature points will be calculated basing on the theory of close-range photogrammetry. Then, deformation analysis could be subsequently performed. The main analysis includes collision location analysis, collision deformation range and shape analysis, and collision deformation depth analysis.

Collision location analysis. The outcome of the collision location analysis may be applied to ascertain the relative touching position and the touching angle of the accident vehicles at the moment that the collision occurs. By choosing some deformation border characteristic points to perform the stereo matching and using the close-range photogrammetric coordinate transformation principle the 3D space coordinates of those points can be calculated. These coordinates are comparatively analyzed with the whole border of the vehicle to determine the collision location on the vehicle body and analyze the vehicle collision parts.

Collision deformation range and shape analysis. The size of accident vehicle deformation range depicts the size of the mutual bumping area where the accident vehicle deformation depth reaches the maximum. The deformable shape demonstrates the space distribution of the impact force at the collision moment. The deformation border characteristic points of the accident vehicle obtained by coordinate calculations can be jointed as a deformation boundary line, which can clearly describe the deformable range and shape of the accident vehicle.

Collision deformation depth analysis. The collision deformation depth of the accident vehicle demonstrates the degree of severity of the collision. It can reflect the degree of the collision action, together with the original stiffness of the collision parts. This has a significant input to the deformation model that determines the collision speed of the accident vehicle on the stiffness—deformation value. But only by measuring and calculating the 3D space coordinates of the deformation characteristic points by the close-range photogrammetry can the accident vehicle collision deformation depth data be determined. To determine these data, the following tasks should be undertaken: (a) choose the deformation characteristic points within the deformation range of the accident vehicle, (b) perform the close-range photogrammetric analysis and calculate the coordinates of the characteristic points using relative transformation, (c) select a fine vehicle that has the same type as the accident vehicle as the contrasting object, abstract the matching feature points, and obtain the corresponding coordinates by the same method, (d) change the two coordinate systems into one coordinate system, and (e) comparatively analyze the coordinates of each pair of characteristic points, and determine the average value of the deformation depths.

CASE STUDY

In a collision on some city road, a black car was crossing the main road of the city from the north to the south, while a red minibus was moving at full speed from the west to the east on the main road. The two vehicles bumped into each other, both drivers not paying enough attention. The black car crashed greatly and the red microbus head was damaged slightly. The black car's deformation is obvious and is representative. Thus, the black car is selected for the deformation analysis. Some stereo images are shot as shown Figure 2.

Figure 2. Stereo images of the black car involved in the accident

The vehicle deformation characteristic analysis process using close-range photogrammetry is as follows. First, the camera model calibration is accomplished (see Table 1), providing the camera model's inner elements. Then, the sign board is put down around the black accident vehicle, which will give the calibrating sizes and provide the self-definition coordinate on the scene. Subsequently, the model's outer elements are obtained at the same time. The stereo images are shot (see Figure 1). Making use of the stereo images, the matching coordinate data are abstracted with the help of the filter procedure and the stereo matching procedure. Finally, the coordinate system is changed into the defined coordinate system using the parallel axis stereo vision with the inner elements and the characteristic points' space coordinates are recomputed by the close-range photogrammetric coordinate calculation methods.

Table 2 is the result of the coordinate calculations, representing the space location of vehicle deformation characteristic point. The 3D data model (shown in Figure 3) demonstrates the space location and the shape of the vehicle deformation characteristic points. The fine vehicle of the same type as the accident vehicle is selected as a contrast. Noting the relative characteristic points in contrast with the accident vehicle deformation characteristic points, it applies the photogrammetric method to calculate the 3D coordinates of those points (see Table 3). Then, MATLAB was used to demonstrate the measurement results (Figure 4 displays the location of the contrasting fine vehicle feature points). Then, different coordinates are transformed into the same system, and every collision point's deformation depth is calculated (see Table 4). Finally, the average deformation depth is determined as 0.143 m.

Table 1. Calibration Result 1 of Experimental Camera in Pixel

Parameter	Value	Parameter	Value	Parameter	Value
f_x	3182.09930	y_0	675.02695	k_3	-0.00448
f_y	3482.59731	k_1	0.02297	k_4	0.02074
x_0	1562.23541	k_2	-0.70124	k_5	0.00000

Table 2. 3D Coordinates of Feature Points on the Damaged Car

Point	X(mm)	Y(mm)	Z(mm)	Point	X(mm)	Y(mm)	Z(mm)
1	307.113	1453.751	-20.774	5	163.448	1341.400	131.534
2	269.663	1403.867	48.321	6	237.411	1350.891	108.478
3	217.456	1431.945	20.937	7	298.640	1397.019	61.914
4	134.343	1380.188	109.096	8	338.549	1414.266	10.901

Table 3. 3D Reconstruction of Fine Car's Relative Points

Point	X(mm)	Y(mm)	Z(mm)	Point	X(mm)	Y(mm)	Z(mm)
1	471.792	2220.069	-172.307	5	537.433	2169.613	-44.982
2	578.533	2416.784	-256.309	6	504.163	2202.992	-14.866
3	669.260	2145.235	-195.825	7	450.166	2237.414	-7.364
4	564.641	2105.801	-112.813	8	393.212	2237.414	-45.684

Table 4. Feature Points' Deformation Depths of the Black Car

Point	Deformation depth (mm)	Point	Deformation depth (mm)
1	101.3156	5	82.4218
2	267.6018	6	33.6688
3	147.0593	7	149.6358
4	148.0080	8	215.4050

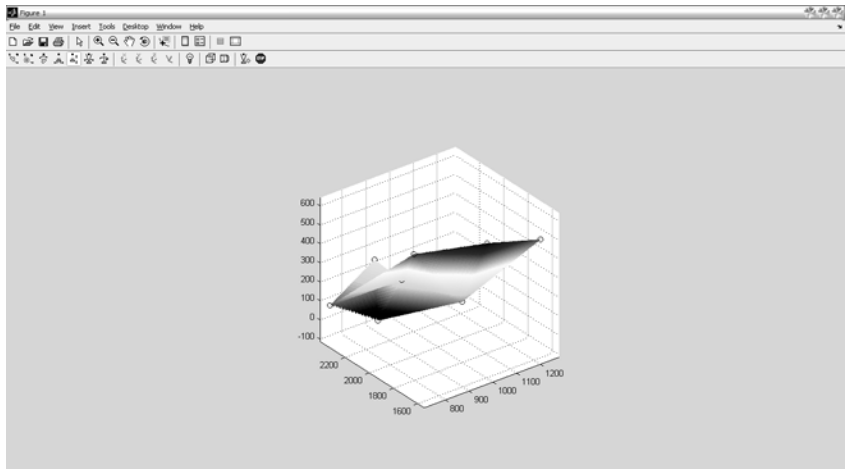

Figure 3. 3D reconstruction of damaged car's feature points

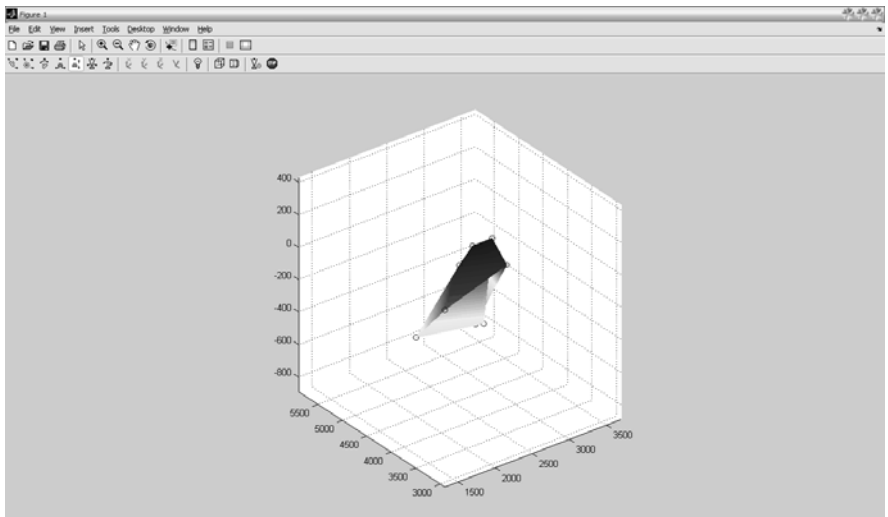

Figure 4. 3D reconstruction of fine car's relative points

This case study indicates that using the close-range photogrammetry for analyzing the deformation vehicle in the traffic accident scenes is feasible. This analysis can provide vehicle deformation space location and range description of the accident vehicle. This surveying pattern provides a new look at collision vehicle deformation studies.

CONCLUSIONS

Based on the coordinates of the 3D stereo images of the accident vehicle, it applies the photogrammetric principles to carry out the vehicle deformation characteristic point reconstructions and applies the relevant methods to perform the deformation analysis. This provided a new method to analyze the vehicle deformation that could describe in detail the vehicle deformation information about space position and deformation range.

ACKNOWLEDGEMENT

This research is supported by the National 863 High Technology Project (2007AA11Z231).

REFERENCES

Arnold, P. E. (2007). *Use of photogrammetry as a tool for accident investigation and reconstruction: A review of the literature and state of the practice*. Virginia Transportation Research Council, 530 Edgemont Road, Charlottesville, N.C.

Ghost, S. K. (1980). "Photogrammetry for police use: Experience in Japan". *Photogrammetric Engineering and Remote Sensing*. 46(3), 329-332.

International Congress and Exposition (1993). *Investigation into vehicle frontal impact stiffness, BEV and repeated testing for reconstruction*. Detroit, MI, 227-255.

Kerkhoff, J. F. (1985). "Photographic techniques for accident reconstruction". *Proceedings-Society of Automotive Engineers*. Detroit, MI, , 145-158.

Lu, G., Li, Y., and Huang, S. (2007). "A study on the modeling for three-dimensional reconstruction of crushed vehicle with self-calibration technique". *Automotive Engineering*. 29(2), 128-131.

Lu, G., Xu, H., Ma, S., and Li, Y. (2006). "Self-calibration three-dimensional reconstruction model of traffic accident photographs". *Journal of Traffic and Transportation Engineering*, 6(3), 109-113.

Scott, A. Cooner, P. E., Kevin, N., and Balke, P. E. (2000). *Use of photogrammetry for investigation of traffic incident scenes*. Texas Transportation Institute, The Texas A&M University System, College Station, Texas.

Fenton, S. and Ziernicki, R. M. Using Digital Photogrammetry to determine vehicle crush and equivalent barrier speed (EBS). *SAE International*, Paper 1999-01-0439.

Traffic Safety Evaluation of the 30 Provincial Capital in China Based on Principal Component Analysis

MA Sheqiang [1, 2], SHAO Chunfu [1], MA Zhuanglin [1] and LIU Dong [2]

[1]MOE Key Laboratory for Transportation Complex Systems Theory and Technology, School of Traffic & Transportation, Beijing Jiaotong University, Beijing 100044, China; PH (86) 10-51683665; Email: masheqiang@sina.com
[2]Traffic Management Engineering Department, Chinese People's Public Security University, P.O. Box 218-6, Beijing 102623, China; PH (86) 10-83901277; Email: masheqiang@sina.com

Abstract: In order to evaluate traffic safety level in the 30 provincial capital cities (except Lhasa) of China, the correlation between the number of traffic accident fatalities and social-economic factors were analyzed. It shows that the number of traffic accident fatalities in the provincial capitals cities of China is markedly correlative with the gross regional product (*GRP*), population, passenger traffic, and freight traffic. According to the correlation, six feasible evaluation indices were put forward, including fatalities per 100000 people population, fatalities per 100 million GRP, passenger traffic fatalness, freight traffic fatalness, fatalities per accident, and mortality of traffic accident. Then they were transformed into four uncorrelated principal components based on principal component analysis. Finally, the four principal components were used to estimate the evaluation score of traffic safety level for the 30 provincial capital cities. The 30 provincial capital cities were ranked by road safety level. The results show that the differences in road safety among the 30 provincial capital cities were comparatively distinct in 2006.

Key words: traffic safety; provincial capital; correlation; comprehensive assessment; principal component Analysis

1 Introduction

Traffic accident has become one of worldwide hazards. The number of traffic accident fatalities in China has ranked No.1 in the world since late 1980s even though it has been declining for 6 years since 2003. The total number of traffic accident fatalities was about 73,484 in 2008 in China. In China, traffic safety has become one attention-getting issue and reducing traffic accident fatalities is still positioned as one of top-ranking national policies. In particular, the provincial capital cities are where traffic safety issues are correspondingly serious in provincial regions. So improving the road traffic safety level for the provincial capital cities is very important in China.

The past experiences have proved that traffic safety evaluation is very important to search for key issues and improve the road safety level. Accordingly, many researchers have dedicated to find new methods for traffic safety evaluation, the remarkable research findings include the synthetic evaluation model (Liu Tao, 2005),

AHP method (Wu Yihu, 2006), evaluation model based on gray theory (Niu Huiyon, 2005), evaluation method based on the theory of fuzziness (Ning Shoude, 2003), evaluation method based on BP artificial network (Yang Tianjun, 2005), and comprehensive method (Peng Junlong, 2005). These models and methods are important for road safety evaluation. However, there are some limitations that restrict their further application. For instance, the correlations between the evaluation indices were neglected; and the weights and classification of evaluation indices were determined by the researcher's subjective experience and preferences.

Principal component analysis (*PCA)* method can transform correlative evaluation indices into uncorrelated principal components that are not confined by the user's subjectivity. This paper attempts to put forward the evaluation indices for the road traffic safety in the 30 provincial capital cities of China, and to evaluate their traffic safety level based on *PCA*. Finally, a precise ranking of the 30 provincial capital cities in 2006 was given based on traffic safety level.

2 Principle of principal component analysis

In general, when evaluation indices are more than two, some of them are likely correlated so that the information of evaluation indices is used repeatedly and the validity of the valuation is impaired. *PCA* can transform such evaluation indices into lesser-uncorrelated composite indices, and utilize the latter to synthetically evaluate road traffic safety without much loss of information.

When setting n evaluation objects and selecting p evaluation indices x_i, $n \times p$ data matrix X is constructed below.

$$X = \begin{bmatrix} x_{11} & x_{12} & \cdots & x_{1p} \\ x_{21} & x_{22} & \cdots & x_{2p} \\ \vdots & \vdots & \vdots & \vdots \\ x_{n1} & x_{n2} & \cdots & x_{np} \end{bmatrix}$$

where x_{ij} is the jth evaluation indices value of the ith objects, i=1,2...,n; and j=1,2...,p.

The matrix X can be transformed into matrix Y, where

$$\begin{cases} y_1 = l_{11}x_1 + l_{12}x_2 + \cdots + l_{1p}x_p \\ y_2 = l_{21}x_1 + l_{22}x_2 + \cdots + l_{2p}x_p \\ \vdots \\ y_m = l_{m1}x_1 + l_{m2}x_2 + \cdots + l_{mp}x_p \end{cases}$$

of which x_i and y_i are the columns of X and Y respectively, the principal components y_1, y_2, ..., y_m ($m \le p$) are those uncorrelated linear combinations whose variances are as large as possible.

The first principal component is the linear combination with maximum variance $Var(y_i)$, the second principal component is the linear combination with second maximum variance, etc. The primary task of *PCA* is to ascertain coefficient l_{ij}, then y_1, y_2, ..., y_m can be used to evaluate the objects as composite indices.

3 Selection of the evaluation indices

3.1 Correlations analysis

The evaluation indices must be measurable, comparable and uncorrelated. Before the selection of the evaluation indices, the correlation between the number of traffic accident fatalities and socio-economic factors is analyzed by the statistical data set over a 17-year period (1990-2006) of China. The Pearson correlation coefficients （R）range from 0.799 to 0.933, and the probabilities of significance (Sig.) are less than the level of significance 0.01 in Tab.1, the number of traffic accident fatalities is significantly correlative with population, *GDP*, passenger traffic, and freight traffic in China. To further validate such correlations, they are analyzed again based on the statistical data set of the 30 provincial capital cities in 2006. Likewise, such correlations as 0.500<R<0.936 and 0.005<Sig.<0.01 in Tab.2 are also significant, i.e. these socio economic factors impacting the traffic safety must be considered when selecting the traffic safety evaluation indices for the 30 provincial capital cities in China.

Tab.1 Correlation between traffic accident fatalities and social economic factors in China，1990-2006

	GDP	Population	Passenger Traffic	Freight Traffic
Pearson Correlation Coefficient（R）	0.821	0.933	0.883	0.799
Sig. (2-tailed)	0.000	0.000	0.000	0.000
Correlation is significant at the 0.01 level (2-tailed).				

Tab.2 Correlation between traffic accident fatalities and social economic factors of the 30 provincial capital cities in China, 2006

	GRP	Population	Passenger Traffic	Freight Traffic	Number of Traffic Accident
Pearson Correlation Coefficient（R）	0.845	0.701	0.500	0.893	0.936
Sig. (2-tailed)	0.000	0.000	0.005	0.000	0.000
Correlation is significant at the 0.01 level (2-tailed).					

3.2 Evaluation indices

Based on the aforementioned correlation analysis, the traffic safety evaluation indices are put forward for the 30 provincial capital cities in Tab.3, where the fatalities per passenger traffic and per freight traffic are used to indicate the average damage level of highway transportation; the fatalities per traffic accident indicates the average danger level of each accident; the mortality is the death proportion in all deaths and injuries of road traffic accidents.

Tab.3 Evaluation indices for traffic safety of the 30 provincial capital cities in China, 2006

Provincial	Fatalities	Fatalities	Fatalities per	Fatalities per	Fatalities per	Mortality

Capitals	per 100000 People	per 100 millions Yuan GRP	Passenger Traffic (persons per 10000 persons)	Freight Traffic (persons per 10000 tons)	Traffic Accident (persons per case)	(%)
Beijing	11.46	0.17	0.55	0.44	0.24	0.17
Tianjin	9.25	0.20	0.23	0.43	0.18	0.13
Shijiazhuang	3.08	0.14	0.02	0.27	0.35	0.25
Taiyuan	7.63	0.26	0.12	0.21	0.17	0.13
Hohhot	8.94	0.21	0.05	0.27	0.18	0.14
Shenyang	8.83	0.25	0.10	0.37	0.29	0.21
Changchun	8.41	0.36	0.12	0.67	0.18	0.15
Harbin	6.26	0.29	0.11	0.68	0.47	0.31
Shanghai	9.00	0.12	0.44	0.36	0.19	0.16
Nanjing	9.04	0.20	0.03	0.49	0.36	0.28
Hangzhou	13.94	0.27	0.04	0.64	0.16	0.12
Hefei	6.66	0.29	0.05	0.65	0.27	0.18
Fuzhou	9.67	0.36	0.06	0.98	0.16	0.12
Nanchang	6.10	0.25	0.08	0.74	0.39	0.27
Jinan	5.68	0.16	0.06	0.39	0.33	0.24
Zhengzhou	5.87	0.20	0.04	0.59	0.16	0.13
Wuhan	4.95	0.16	0.04	0.45	0.14	0.11
Changsha	7.40	0.26	0.05	0.43	0.19	0.14
Guangzhou	19.86	0.25	0.05	0.61	0.19	0.14
Nanning	7.93	0.61	0.06	0.88	0.24	0.15
Haikou	5.04	0.25	0.01	0.58	0.17	0.12
Chongqing	4.06	0.37	0.02	0.36	0.14	0.10
Chengdu	8.11	0.33	0.03	0.64	0.16	0.13
Guiyang	6.37	0.37	0.01	0.44	0.33	0.21
Kunming	7.99	0.34	0.06	0.42	0.13	0.10
Xi'an	8.19	0.42	0.07	0.55	0.17	0.17
Lanzhou	8.00	0.39	0.13	0.47	0.17	0.16
Xining	5.88	0.44	0.04	0.54	0.58	0.36
Yinchuan	11.61	0.50	0.07	0.77	0.19	0.14
Urumqi	8.87	0.27	0.08	0.21	0.23	0.16

4 Application of road traffic safety evaluation

(1) Constructing the sample matrix

The six evaluation indices in Tab.3 are regarded orderly as the *j*th evaluation indices for traffic safety of the 30 provincial capital cities in China. As the provincial capital cities, Beijing, Tianjin, Shijiazhuang ...Yinchuan and Urumqi are regarded orderly as the *i*th evaluation objects, i.e. x_{ij} is the *j*th evaluation indices value of the *i*th evaluation objects, the sample matrix $X=[x_{ij}]$ (i=1,2...,30; j=1,2...,6), where the

values of x_{ij} are shown in Tab.3, and x is the columns of X.

(2) Transforming X into standardization matrix $Z=[z_{ij}]$, where

$$z_{i,j}=\frac{x_{i,j}-\bar{x}_j}{s_j},\quad \bar{x}_j=\frac{\sum_{i=1}^{30}x_{i,j}}{30},\quad s_j^2=\frac{\sum_{1=1}^{30}(x_{i,j}-\bar{x}_j)^2}{29},\ i=1,2\ldots30,\text{ and } j=1,2\ldots6.$$

(3) Calculating correlation coefficient matrix R of the matrix Z, where

$$R=\begin{bmatrix} 1.0000 & 0.0474 & 0.2362 & 0.2165 & -0.2674 & -0.2588 \\ 0.0474 & 1.0000 & -0.3195 & 0.5347 & 0.0206 & -0.0404 \\ 0.2362 & -0.3195 & 1.000 & -0.1705 & -0.0721 & -0.0423 \\ 0.2165 & 0.5347 & -0.1705 & 1.0000 & 0.0412 & 0.0053 \\ -0.2674 & 0.0206 & -0.0721 & 0.0412 & 1.0000 & 0.9748 \\ -0.2588 & -0.0404 & -0.0423 & 0.0053 & 0.9748 & 1.0000 \end{bmatrix}$$

and $r_{ij}=\frac{\sum_{k=1}^{30}z_{kj}\cdot z_{kj}}{29}$, of which r_{ij} is the correlation coefficient between the ith and jth evaluation indices, i.e. $r_{ij}=r_{ji}$. R also is the covariance matrix of matrix X.

(4) Calculating the eigenvalues λ_i of R, where $\lambda_1=2.1222$, $\lambda_2=1.7138$, $\lambda_3=1.1310$, $\lambda_4=0.5839$, $\lambda_5=0.4259$, and $\lambda_6=0.0232$, in which $\lambda_1\geq\lambda_2\geq\cdots\geq\lambda_6>0$.

(5) Determining the number of principal components

When $\sum_{j=1}^{m}\lambda_j / \sum_{j=1}^{6}\lambda_j \geq 85\%$, the minimum m is the number of principal components, min(m)=4, and $\sum_{j=1}^{4}\lambda_j / \sum_{j=1}^{6}\lambda_j$ =92.6%>85%.

(6) Calculating the four principal component $y_1, y_2, \ldots, y_4$

$$y_i = z_i \times l_i$$

where l_i is the ith eigenvector of R, z_i is the columns of Z, and y_i is ith principal components.

$$y_1 = -0.3399z_1 + 0.0069z_2 - 0.1384z_3 - 0.0140z_4 + 0.6593z_5 + 0.6560z_6$$

$$y_2 = -0.1067z_1 - 0.6583z_2 + 0.4072z_3 - 0.6231z_4 - 0.0097z_5 + 0.0340z_6$$

$$y_3 = -0.6524z_1 + 0.0152z_2 - 0.6058z_3 - 0.3098z_4 - 0.2297z_5 - 0.2418z_6$$

$$y_4 = -0.6333z_1 - 0.3220z_2 - 0.6625z_3 - 0.1968z_4 + 0.0824z_5 + 0.1047z_6$$

Seen from the first principal component y_1, the weights coefficients of z_5 and z_6 are 0.6593 and 0.6560 respectively, they are bigger than others. This indicates that the fifths and sixth indices (Fatalities per Traffic Accident and Mortality) are more important than others for the 30 provincial capital cities in 2006.

(7) Calculating the evaluation score, the formula is as follows:

$$S = \sum_{i=1}^{4} (y_i \times \frac{\lambda_i}{\sum_{j=1}^{4} \lambda_j})$$

where *S* is the vectors whose *i*th element value is the evaluation score of the *i*th evaluation objects(shown in Fig.1, the 30 provincial capital cities are on the x-coordinate).

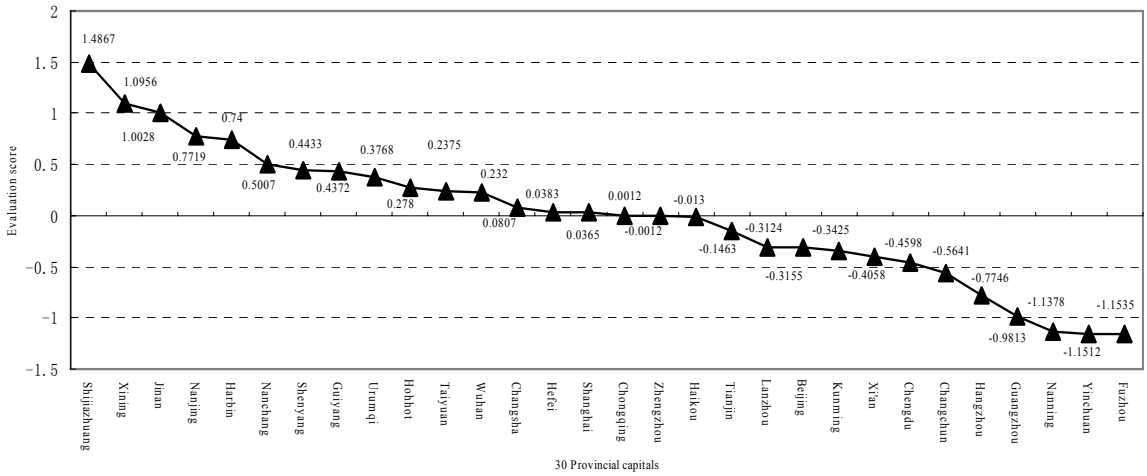

Fig.1 Sequence of traffic safety level for the 30 provincial capital cities in China, 2006.

5. Results analysis

As can be seen from Tab.3, the smaller are the values of theses evaluation indices, the better are the traffic safety level in the provincial capital cities. Thereby, for the 30 provincial capital cities, the larger are their evaluation score in Fig.1, the worse are their traffic safety level. It can also be seen from Fig.1 that the traffic safety levels in the 30 provincial capital cities were markedly discrepant, and the five best provincial capitals of traffic safety were Fuzhou, Yinchuan, Nanning, Guangzhou, and Hangzhou in 2006. The five worst provincial capital cities of road traffic safety were Shijiazhuang, Xining, Jinan, Nanjing, and Harbin in 2006. It indicates that the fatalities per traffic accident and mortality in the five worst provincial capital cities were higher than others, so reducing both is an effectual to improve traffic safety level in the five worst provincial capital cities.

6. Conclusions

Here, the conclusions can be provided as follows:

(1) In China, the traffic safety in the provincial capital cities is evidently correlative with socio-economic factors, expressly such as population, GRP, passenger traffic, and freight traffic, the selection of evaluation indices should focus on them.

(2) The differences in traffic safety level among provincial capital cities in China were comparatively distinct in 2006. The fatalities per traffic accident and mortality were the crucial evaluation indices for road traffic safety of the 30 provincial capital cities in China.

(3) Principal component analysis is one desirable means to evaluate road traffic safety.

Acknowledgment

The support from National Key Technology R&D Program (No. 2007BAK35B06) of China is gratefully acknowledged.

References

Liu T. and Li Y. (2005). "Synthetic Evaluation and Prediction Model of Road Safety Grade in Regional Road Network" *Journal of Tongji University(natural science)*, 33(3)：311-315.

Ning S.D., Shi P. and Liu F. (2008). "The Research on Road Rraffic Security Evaluation Based on the Theory of Fuzziness" *Mathematics in Practice and Theory*, 38(7)：109-116.

Niu H.Y.(2005). "Study on Safety Evaluation of Urban Road Traffic Based on Gray Theory" *China Safety Science Journal*, 15(9):92-95.

Peng J.L., Zhang Q.S. and Zhang X.M. (2005). "Highway Traffic Safety Assessment by Using a Comprehensive Method" J*ournal of Safety and Enviorment*,5(5):12-14.

Wu Y.H., Liu W.J. and Xiao Q.M.(2006). "AHP for Evaluating the Traffic Safety of a Highway" *Journal of Changsha University of Science and Technology (Natural Science)*, 3(2):7-11.

Yang T.J., Zhang X.C., Yang X.G. and Pan H.Z.(2005). "Research on the Evaluation of City Road Traffic Safety Based on BP Artificial Network" J*ournal of China University of Mining &Technology,* 34(1):37-40.

Study on Spatial Information Model and Database of Traffic Facilities Management System Based on ArcGIS

Y. WANG[1], S. DONG[1], H. KUI[1], T. GAO[2], H. YU[1], H. WANG[1], and Y. LIU[1]

[1]Traffic Environment Laboratory, Traffic &Transportation School of Jilin University, Jilin Changchun; Tel:043184049946; The corresponding author is KUI Hailin, E-mail: khl69@163.com.
[2]New Postcom Equipment Co.,Ltd; Tel:13811391187.

ABSTRACT

Space positioning information model and logic model of traffic facilities are established, by studying the internal organizational structure of Geodatabase model. On the basis of the data of Jilin province expressway, the spatial database is designed in detail with seamless integration of database management model, by analyzing the characteristics of spatial database of traffic facilities. The traffic management system is realized by secondary development of GIS, the software of which includes VB.NET, ArcGIS Engine and ArcSDE. The system implementation verifies the superiority of the GIS model, provides a scientific and efficient management tools for traffic facilities management.

INTRODUCTION

The goal of GIS is to provide a spatial framework within which to rationalize the application of the Earth's resources and provide decision support for the sustainable development of the human environment. In this course, the model of geographical objects need be made. Data Modeling, which can transfer the data of real world to useful data sets, plays an important role in the spatial database. Data modeling is applied in the field of GIS, which is spatial data modeling. Spatial data model, which describes the relation of the objects things by datamation of physical model, can simulate and abstract the objective geographic world perfectly on the aspects of spatial semantic and attribute semantic. Space positioning information model and logic model of traffic facilities are established, by studying the internal organizational structure of Geodatabase model. On the basis of the data of Jilin province expressway, the spatial database is designed in detail with seamless integration of database management model, by analyzing the characteristics of spatial database of traffic facilities. The traffic management system is realized by secondary development of GIS.

DESIGN OF SPATIAL DATA MODEL STRUCTURE

The spatial information model of the traffic facilities management system introduces GeoDatabase model, the internal organizational structure is shown in **Figure 1**.

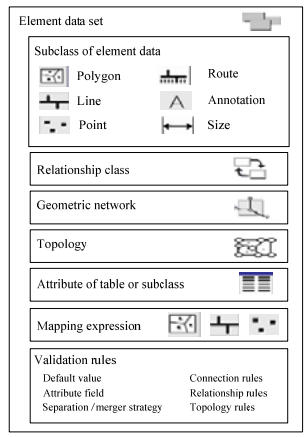

Figure1. Internal organizational structure of geodatabase model

Geometry characteristic, such as point, line and polygon, and the relationship of them are established by using ArcGIS new generation model, that is, GeoDatabase model, in the course of system developing, which is showed in **Figure 2**.

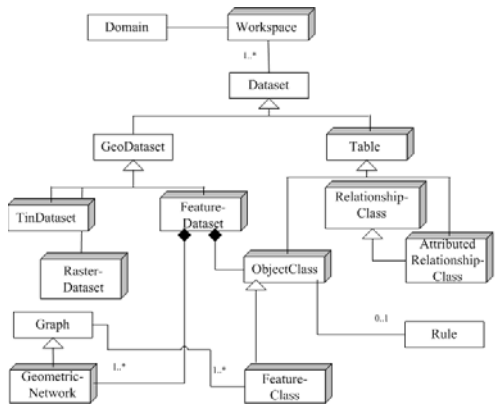

Figure 2 Logic model based on geodatabase

Spatial information model is multidimensional spatiotemporal model including spatial position, time and geographical spatial attribute. The information amount of the model is great, so the information of the model is massive data. The spatial information model, which should be organic dynamical model and satisfy the needs of the different scales, is the basis of GIS application system. On the basis of the main-ramp topology model of expressway, the spatial position information model is established, and the position of point and line, the main design objects of which include infrastructure, such as route, segmentation, toll station, sign, administration office, park plot and service area, and intercommunication ramp position. The spatial positioning model, which is showed in **Figure 3**, is established in the ArcInfo UML System with UML and model provided by ArcGIS. **Figure 4** shows the logic model of point infrastructure of expressway. In this model, the point event can be traffic accident points, facilities distributing points, vehicle position, and so on. The positions of these elements display the statistics and analysis results on the electronic map according to different topic demands, after these elements is positioned by using the corresponding the mileage poles number and the miles percentage of starting and

ending points on topological network being established.

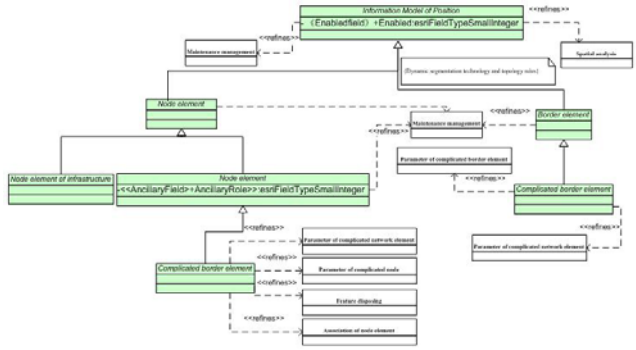

Figure 3. Spatial positioning information model

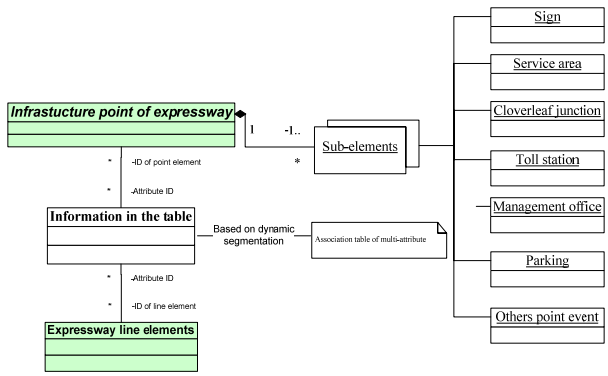

Figure 4 Logic model of traffic facilities

METADATA DESIGN OF SPATIAL DATABASE

Metadata is the data that describes data, that is, the description information about the data and information resource. Geographic metadata helps the users position, evaluate, obtain and use the geographic data by noting the content, quantity, quality, condition and other characters of geographic spatial data.

The system metadata table is design as **Table 1**.

Table 1 Traffic facilities layer information

Filed	Type	Size	Description
ID	Number	Long	serial number
Symbols Index	Number	Long	The index of feature display symbols
Symbol Size	Number	Long	The size of feature display symbols
. . .	. . .	. . .	. . .
Symbol color	Number	Long	The color of feature display symbols

There is a metadata table in every layer. The table of route metadata is shown

in **Table 2**. The table of traffic facilities metadata is shown in **Table 3**.

Table 2 Route metadata

Field	Type	Size	Description
ID	Number	Long	Record Number
Data set encoding	Text	50	Including the information of type
Route Name	Text	50	The name of real world
Name of Attribute Table	Text	50	

Table 3 Traffic facilities metadata

Field	Type	Size	Description
ID	Number	Long	Record Number
Data set encoding	Text	50	Including the information of type
Facility Name	Text	50	The name of real world
Name of Attribute Table	Text	50	

SYSTEM IMPLEMENTATION

Traffic management system calls ArcEngine, the latest research and development kit of ArcGIS, with VB.NET language. The system adopts the C/S architecture, that is, the clients run in 32-bit operating system of Windows XP or windows 2000, the system database is installed on a dedicated server, and the client accesses the system database through ArcSDE database engine. The general framework of system is shown in **Figure 5**.

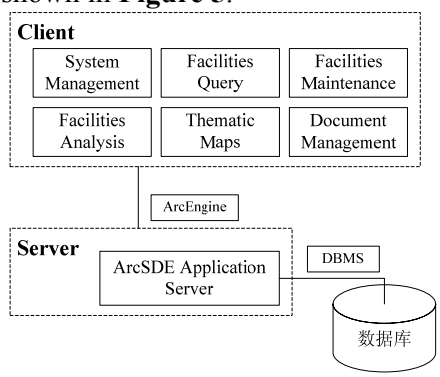

Figure 5. General framework of system

System developing uses the basic functional modules and related application modules of ArcGIS Engine. The basic module, which is a basic function class library, assemblies the ArcGIS Engine interface basically. This module is called by the

application module, after it forms function, on that time, a part of classes are inherited. This module being above of AO, call AO and reference the program set of AxMapControl, AxPageLayoutControl, AxToolbarControl, AxTOCContro, Carto, ControlCommands, DataSourceGDB, DataSourceRaster, Display, Geodatabase, GeoDatabaseDistributed, Geometry, MapControl, Output, PageLayoutControl, System, SystemUI, TOCControl, ToolbarControl, Utility, and so on. The system uses VB.NET language to call the background data through ArcSDE and achieves the query, retrieval and analysis of data. A part of codes are as follows:

```
Dim pPropSet As IPropertySet = New PropertySet
Dim pSdeFact As IWorkspaceFactory = New SdeWorkspaceFactory
With pPropSet
  .SetProperty("SERVER", Server)
  .SetProperty("INSTANCE", Instance)
  .SetProperty("DATABASE", Database)
  .SetProperty("USER", User)
  .SetProperty("PASSWORD", Password)
  .SetProperty("VERSION", version)
End With
openSDEWorkspace = pSdeFact.Open(pPropSet, 0)
```

The system interface is shown in **Figure 6**.

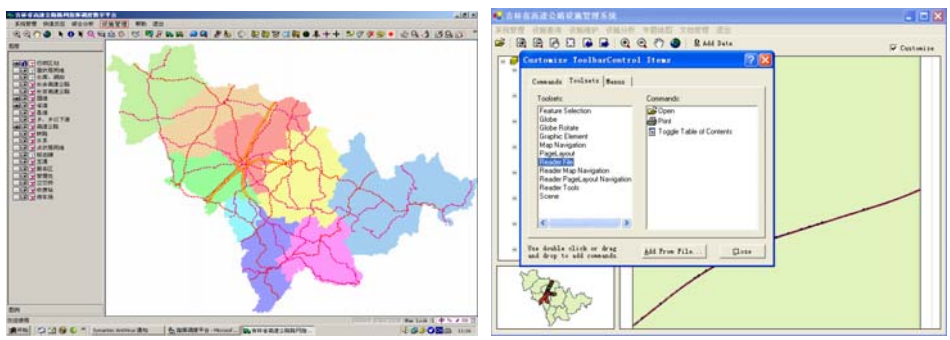

Figure 6. System interface

CONCLUSION

Space positioning information model and logic model of traffic facilities are established by studying the internal organizational structure of Geodatabase model. The spatial database is designed in detail with seamless integration of database management model, by analyzing the characteristics of spatial database of traffic facilities. The traffic management system is realized by secondary development of GIS, the software of which includes VB.NET, ArcGIS Engine and ArcSDE. The system, which provides the effective approach to improve the operating efficiency and service level of freeway for the traffic management departments of Jilin province, and plays an important role in promoting information and sustainable development of Jilin province traffic, is basis of realizing modernization, scientific and intelligent of freeway management. The system implementation verifies the superiority of the GIS model, provides a scientific and efficient management tools for traffic facilities management.

ACKNOWLEDGEMENT

This work is financially supported by the National Key Technology R&D Program（Grant No．2006BAJ18B02）.

BIBLIOGRAPHY

Seffino L A, Medeiros C B, Rocha J V,et al (1999). "WOODSS—A Spatial Decision Support System Based on Workflows". Decision Support Systems, 27, 105-123.

Ai lun (2004). "Data Modeling Basic Tutorial". Beijing: Tsinghua University Press.

Alonso G, Abbadi A (1994). "Cooperative Modeling in Applied Geographic Research". International Journal of Intelligent and Cooperative Information Systems, 3(1), 83-102.

HE Xiao-zhao, LI Qi, CHENG Ji-cheng (2003). "Study on Grid-based Spatial Information Models and Service". Geography and Geo-Information Science, 19(3), 60-63.

Alonso G, Hagen C. Geo-Opera (1995). "Workflow Concepts for Spatial Processes". Proceedings of Advances in Spatial Data-bases. Berlin/Heidelberg/NewYork: Springer Verlag, 238-257.

Marr A J, Pascoe R T, Benwell G L, et al (1998). "Development of a Generic System for Modeling Spatial Processes". Com-puters, Environment and Urban Systems, 57-69.

Peng cong (2005). "A Study on the Database of Monitoring and Scheduling System Based on GIS for Urban Public Traffic". Graduate School of Chinese Academy of Sciences, 17.

Weske M, Vossen G, Mederos C B (1998). "WorkflowManagement in Geoprocessing Applications". Proceeding of 6th ACM International Symposium Geographic Information Systems—ACMGIS'98. Washington, 88-93.

Zeng bin (2004). "Object Modeling and Geodatabase". ESRI China(Beijing) Training Center.

Expressway Data De-noised Approach Based on Wavelet Analysis

Z. Wang[1], J. Guan[1], J. Sun[2], J. Yu[1] and J. Liu[1]

[1]Beijing Stone Intelligent Transportation System Co. Ltd., Mail 2F, Xinsanyuan Office, NO.14 Zaojunmiao, Haidian District , Beijing, 100081, P. R. China; PH (010)6213-2676ext. 8506;FAX(010)6212-4578;email:greatpromise05@163.com
[2]Beijing Transportation Research Center , Mail Room 413, No 9, Xuanwu District, Beibinhe Road, Beijing, 100055, P.R.China; PH(010)6337-2641; FAX(010)6337-2715; email: sunjp@bjtrc.org.cn

ABSTRACT

Compared with traditional collection methods using detectors or sensors, floating-car data collection has advantages such as a broad coverage area, low cost installation and maintenance costs and little influence from external sources. Therefore, floating-car data is being broadly applied in traffic relative studies. Traffic original data usually contains some random components, which disturb the distinction of traffic status. The original data must be de-noised in order to filter these random components. This paper presents wavelet analysis to de-noise the original data from floating-car data collection. In this paper, the data from RTMS (Remote Traffic Microwave Sensor) collection is treated as true data. Traffic original data, from various ring mainlines of Beijing on various days, are processed through wavelet threshold de-noising. The experiment results show that de-noised data is better than the original data in terms of evaluation indexes. For example, MSE of the de-noised data can drop as low as 6.36% and the correlation coefficient can be increased by more than 1.18%.

INTRODUCTION

Compared with traditional collection methods using detectors or sensors, floating-car data collection has advantages such as a broad coverage area, low cost installation and maintenance costs and little influence from external sources. Consequently, floating-car data is being broadly applied in traffic relative studies (e.g. traffic dynamic forecasts and traffic congestion evaluation). Since data is collected via taxi-mounted GPS (Global Positioning Satellite System) units, the floating-car data is susceptible to drivers' individual behavior, and lane information can be indistinguishable from the floating-car original data. This leads to speed discretization of different lanes on the same road section. Also, the volatility of floating-car data is stronger than that of RTMS (Remote Traffic Microwave Sensor) data. To be sure of data accuracy, floating-car original data needs to be de-noised.

De-noising approaches in common use include MA (Moving Average) algorithm, exponential moving average algorithm, KF (Kalman Filter) algorithm, and etc (JIANG, 2004). They are mostly applied to the stationary and fixed-interval time series. Traffic measurements collected from floating-car systems are primarily spot speed, GPS location and time stamp. The reporting interval of traffic measurements is about 90s and is unsteady, so the traditional de-noising approaches are not effective for floating-car original data. Wavelet analysis, immune algorithms and spectral subtraction algorithms can be applied to de-noise real-time traffic data (CHEN, 2006). In this paper (CHEN, 2006), the decomposition level of wavelet analysis, which has a great effect on de-noising, is

not mentioned.

This paper first introduces the wavelet analysis and wavelet de-noising methods. In contract to wavelet de-noising methods, the acquiescent threshold de-noising is selected and the SNR (Signal-to-Noise Ratio) is used to determine the decomposition level of acquiescent threshold de-noising (FENG, 2005). For the purpose of de-noising effect evaluation, RTMS data is used as the true data and we use MSE (Mean Square Error) and the correlation coefficient as de-noising evaluation indexes. In this paper we use wavelet analysis to de-noise the floating-car original data from various Beijing ring mainlines on various days, and then de-noise the 5-min interval average speed (average speed calculation algorithm is illustrated in the paper HU Z W, 2008). In comparison to the correlation coefficient and MSE of the floating-car and RTMS data, the de-noising effect is significant. Due to the limitation of RTMS detector installation locations, this paper proposes the floating-car data de-noised approach be used only for urban expressways.

AN INTRODUCTION TO WAVELET ANALYSIS

Fourier transformation is usually applied to the non-linear time series. In the case of Fourier analysis, data is either in the time domain or in the frequency domain, but there is no direct relationship between the two. This means that in the frequency domain one can determine which frequencies appeared and how strongly they are present but not where (in the time domain) they appeared. To cope with this problem, a windowed Fourier transformation (WFT) can be used. It splits the input signal into different windows, which are then analyzed individually. The difficulty of this approach lies in the way the window borders must be handled.

The wavelet analysis solves this problem by dealing with the input signal at different scales or resolutions. On a large scale the focus is on rough features, i.e. trends, whereas on a small scale the focus is on minor features, i.e. noise. The general idea is to adopt a wavelet prototype function, called an analyzing wavelet or a mother wavelet. These functions are basics in the function space (Samant, 2000).

By viewing the traffic time series as a signal, wavelet analysis can separate the traffic time series into different resolution levels with different time scales. Thus, wavelet analysis is a technique that enables us to perceive traffic measurements in a third dimension.

THE PRINCIPLE OF WAVELET DE-NOISING

Given a signal x(t), we denote by dx(j, k)=<x, Ψj, k > the wavelet coefficients. The basis of the decomposition is generated from translated and dilated versions of the mother wavelet, Ψ0:

$$\Psi j, k(t)=2\text{-}j/2\,\Psi 0(2\text{-}jt\text{-}k) \qquad j=1\cdots J, \quad k\in Z \qquad (1)$$

The wavelet can be understood as the result of a cascade of quadrature-mirror low-pass and high-pass filters (g(n) and h(n), respectively), in which the output of the high-pass filter (the details of the signal) are wavelet coefficients at each scale j, while the output of the low-pass filter (the approximation of the signal) is filtered again iteratively. The principle of wavelet decomposition is shown in Figure 1.

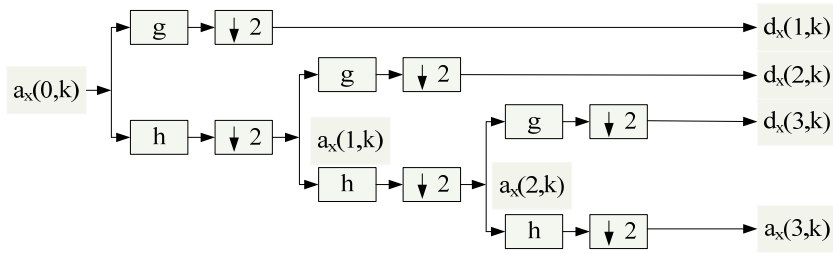

Figure 1. Wavelet de-noising for level 3 decomposition.

METHODS OF WAVELET DE-NOISING

Many de-noising methods based on wavelet analysis have been presented (SUN, 2005). They include the wavelet transform modulus maximum, wavelet correlation, wavelet threshold de-noising and wavelet translation invariant de-noising.

Wavelet threshold de-noising is the most widely used de-noising method among the four, due to its ability to obtain the approximate optimal estimation of original signal, fast computing and extensive adaptation. In the traffic time series, there are some abrupt data points that may be traffic events and jump points of traffic condition. They are essential for traffic prediction and traffic condition analysis. Wavelet threshold de-noising cannot change the traffic measurement characteristics, especially for jump points. When we deal with the real-time traffic time series, the de-noising method must be selected to quickly process data. Based on the above analysis, we apply wavelet threshold de-noising to de-noise the floating-car data.

DE-NOISING PROCEDURES

In floating-car time series, spot speed is an important measurement. Accordingly, floating-car speed time series data is taken for a one-dimension signal. The de-noising procedure of a one-dimension signal includes three parts: decomposition, threshold quantization and reconstruction of signal.

The first step is the decomposition of the one-dimension signal. The goal is to determine the wavelet decomposition level.

The second step is threshold quantization of the high-frequency coefficient dx(J,k). We select one threshold value to quantize the high-pass coefficient dx(j,k)(j=1…J) of each level (from the 1st level to the number N level).

The final step is the reconstruction of the one-dimensional signal according to the ax(J,k) and dx(J,k) (j=1…J).

DETERMINING THE WAVELET DECOMPOSITION LEVEL

SNR is a parameter that illustrates the amount of noise in signal and is defined as the ratio of signal power to the noise power corrupting the signal (HAN, 2007). Given the time series *y(t)* with noise *t*=1, 2,…, N, N is the length of time series. *y(t)=x(t)+w(t),* where *x(t)* is the time series of signal and *w(t)* is the added noise.

SNR is shown as in Equation 2:

$$SNR = 10\log 10\{\sum_{i=1}^{N}[y(t)-\bar{y}]^2 / \sum_{i=1}^{N}[y(t)-x(t)]^2\} \quad (2)$$

Where $\bar{y}$ is the mean of the time series *y(t)*. Generally, greater SNR means more

signal and less noise in the time series. If we select more decomposition levels to de-noise data, the available signal will be lost, leading to the reduction of SNR, more calculations and slower calculating speed. If a lower decomposition level is selected, the de-noising effect is not the best. But SNR of the time series cannot be decreased, so the wavelet decomposition level will have a large effect on the wavelet de-noising.

We applied the wavelet threshold de-noising to the road in the North Third Ring (from LianXiangqiao to Beijing Sports University) on 25 March 2008. We selected different wavelet functions and different decomposition levels to de-noise, and obtained the results shown in Table 1.

Table 1. Correlation coefficient and MSE of floating-car data and different wavelet function under varying decomposition levels.

Wavelet name	Decomposition level	Correlation Coefficient	MSE
db3	1	0.8571	245.770
db3	2	0.8550	247.588
db3	3	0.8607	252.403
db3	4	0.8614	254.339
db2	1	0.8570	247.579
db4	1	0.8532	248.577
db5	1	0.8524	248.164

From the above analysis for the same wavelet function under different decomposition levels, SNR is quickly dropped down by the increase of the decomposition level. For the same decomposition level, SNR is improved little by the increase of wavelet function. Wavelet db3 and decomposition level 1 have achieved the de-noising of original data.

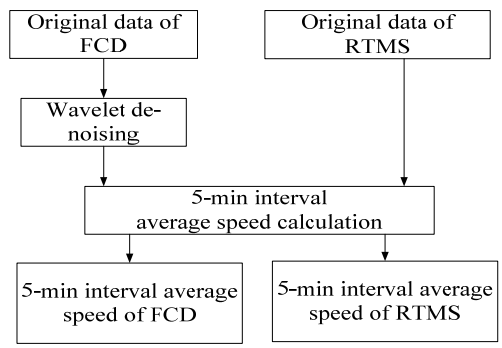

Figure 2. De-noising analysis process.

Process steps are as follows:

1）Floating-car original data is de-noised.

2）The five-minute interval average speed of RTMS data from the same day and road as the floating-car data is calculated.

3）After de-noising the floating-car original data, five-minute interval average speed is calculated and de-noised again.

4）The de-noising effect is evaluated.

This paper selected the correlation coefficient and MSE as the evaluation indexes. The floating-car and RTMS are two different kinds of data collection

technology, so there is inevitably systemic error between them. Still, the whole trend of traffic measurement from the two data collection technologies presents strong correlation. So using RTMS five-minute interval average speed as the true data, we respectively compared the correlation coefficient and MSE of the five-minute interval average speed of floating-car original data and that of the five-minute interval average speed of floating-car de-noised data. We must presuppose that the correlation between the two kinds of data, when collected on the same day, is strong. Otherwise, the data is not de-noised in this way.

EXPERIMENTAL RESULTS

For this paper, we selected mainlines in Beijing as experiment sites. Due to the limited space analyzed, this paper only introduces partial results. The selected road is located in the North Second Ring (from Gulouqiao to Andingmenqiao). First, we compared floating-car original data with floating-car de-noised data. The results are shown in Figure 3 and Figure 4. Most of the noise in the original data was separated. We applied an average speed calculation algorithm to calculate average speed based on the floating-car original data, floating-car de-noised data and RTMS data. We applied MA and wavelet to de-noise the five-minute interval average speed of the floating-car data. We contrasted the correlation coefficient and MSE between the floating-car average speed (data sets were floating-car original average speed, MA average speed and wavelet de-noising average speed) and RTMS average speed. In Figure 5, the correlation of the Wavelet de-noising average speed and RTMS average speed is strongest and the MSE is least. The experiment results show that de-noised data is better than the original data in terms of evaluation indexes, such as MSE, which for de-noised data can drop as low as 6.36% and can achieve a correlation coefficient above 1.18%. The acquiescent wavelet de-noising method can be applicable to the floating-car data so that random components of floating-car data can be filtered.

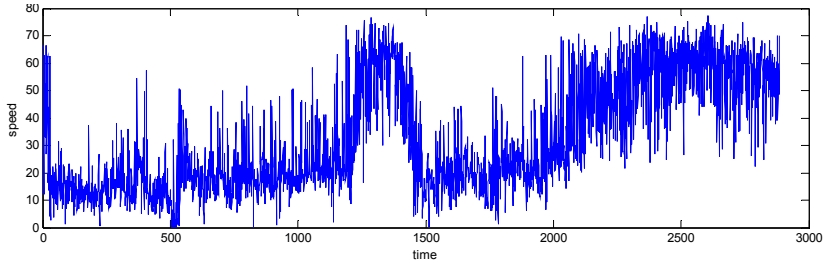

Figure 3. Original speed in North 2nd ring (from Gulouqiao to Andingmenqiao) on July 8, 2008.

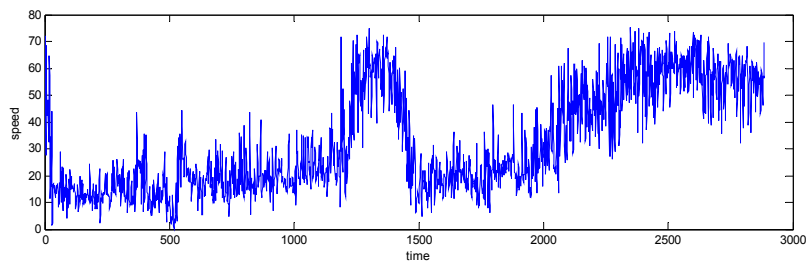

Figure 4. De-noised speed in North 2nd ring (from Gulouqiao to Andingmenqiao) on July 8, 2008.

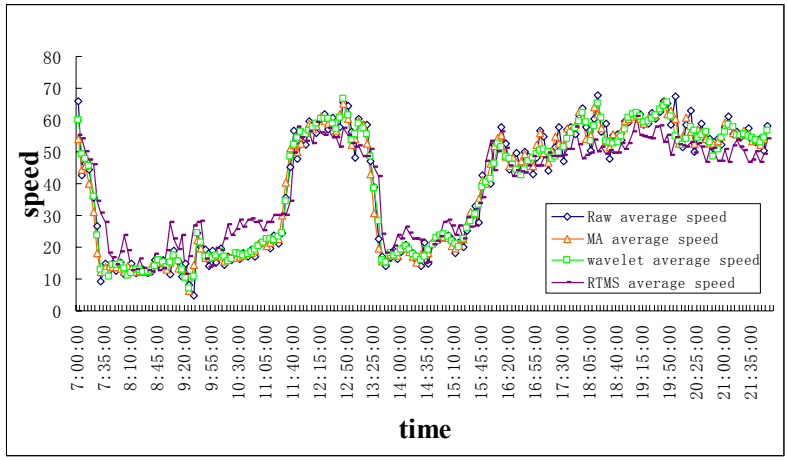

Figure 5. Comparison of average speed in North Second Ring (from Gulouqiao to Andingmenqiao) on July 8, 2008.

FUTURE WORK AND CONCLUSIONS

Floating-car data can cover every class of road in the urban environment. But for now, RTMS can only be installed on urban expressways. Therefore we de-noise the floating-car data on the expressway to contrast with data from RTMS. Through wavelet de-noising, the volatility of floating-car data is decreased and the correlation with RTMS becomes stronger. Thus, wavelet de-noising is applicable to floating-car data. Arterial traffic data is more complicated than expressway traffic data. Due to the limitation of RTMS installation conditions, we cannot obtain arterial traffic data from RTMS. In future work we intend to find an approach to de-noise arterial data.

ACKNOWLEDGEMENT

This work is supported by a grant from the National High-tech Research and Development Program of China (863 Program) (NO.2007AA11Z220 and NO.2007AA11Z212). Beijing Municipal Science & Technology Commission (NO.D07050600440704).

REFERENCES

Chen, S. Y., Wang, W., Li, W. Y. (2006). "Noise recognition and noise reduction of true -time traffic data." *Journal of Southeast University*, 322-325.

Feng, Y., Gao, G. R. (2005). "Self-adaptive determination of decomposition order in threshold de-noising method based on wavelet transform." *J .Wuhan Univ. (Nat. Sci. Ed.)*, 1-14.

Han, M., etc. (2007). "Prediction theory and method of chaotic time series." China WaterPower Press.

Hu, Z. W., Wen H. M., Sun J. P., Chen F. (2008). "Study on floating-car data system based on vehicle license plate recognition data."*4th China Annual Conference on ITS*, 834-840.

Jiang, G. Y. (2004). "Technologies and applications of the identification of road traffic conditions." China Communication Press.

Samant, A., Adeli H.(2000). "Feature extraction for traffic incident detection using wavelet transform and linear discriminant analysis." *Computer Aided Civil and Infrastructure Engineering*, 15(4), 241–250.

Sun, Y. K. (2005). "Wavelet analysis and application." China Machine Press.

Influence analysis of Deep Discount Policy on Public Transit Ridership

Yan Han[1], Hongzhi Guan[2], Xuejiao Fang[3]

[1]Key laboratory of Traffic Engineering, Beijing University of Technology, Beijing, 100124; PH (0863) 010-67391509; FAX (0863) 010-67391509; email: hanyan422@bjut.edu.cn

[2]Key laboratory of Traffic Engineering, Beijing University of Technology, Beijing, 100124; PH (0863) 010-6739190; FAX (0863) 010-67391980; email: hguan@bjut.edu.cn

[3]Key laboratory of Traffic Engineering, Beijing University of Technology, Beijing, 100124; PH (0863) 010-67396181; FAX (0863) 010-67391509; email: snowfish0815@eamils.bjut.edu.cn

ABSTRACT

To encourage the use of public transit modes and/or discourage the use of auto for the commuter trip, deep discount policy was provided and implemented in May 2006 in Beijing. To estimate responses of urban travelers to Deep Discount policy, the choice behavior survey was carried out in Beijing, including passengers' individual characters, trip behavior and their choices to railway and bus under certain conditions. And the influence factors of mode split are analyzed. Then traveler mode choice model considering different ticket ratio between railway and bus was established and the mode choice behavior are specified and estimated. The estimation results suggest that ticket cost and ticket cost ratio between bus and railway are the most cited factors in explaining ridership growth and shift. The conclusion will provide an analysis tool for an evaluation of the effectiveness of deep discounts actions. Also the result can provide the Deep Discount policy sustain for the increasing of the trip proportion of public traffic.

INTRODUCTION

As congestion in urban areas continues to worsen and expressway solutions become less effective, many local governments and communities are turning their attentions to public transit systems. To improve the trip proportion of public traffic, deep discount policy was provided and implemented in May 2006 in Beijing. To maximize the return on different improving methods in public transit systems, effective analysis tools are needed to determine transit ridership potential and the benefits of investments.

Foreign scholars paid attention to the relationship between transit ridership and trip fare, such as ticket cost, and did research about it early. Previous research concluded that travelers were more concerned about their travel cost such as ticket cost, trip time and etc(Zong.2005).People are willing to choose the mode which utility is the maximum and the influence of generalized cost on trip is more concerned in those researches (Ben-Akiva et al.1990).Travel cost is divided by the traveler's income to reflect the presumption that a traveler with a high income is less concerned about money cost than a traveler with a low income (Gillen.D.W. 1977). The generalized cost include time cost, currency cost, safety and reliability of the trip

were discussed. Distance ratio between railway and bus and coefficient factors such as rapid and comfort are considered in the design of ticket cost of Shanghai （Liu.2003). Transit Price Elasticity and Cross-Elasticity are provided during the research about the Transportation Elasticity. Several TDM strategies involve transit fare reductions. Commuter Transit Benefit programs，in which employers encourage and sometimes subsidize transit passes，are effective at increasing ridership. Deep Discount transit passes can encourage occasional riders to use transit more frequently. Shaw. J. (1997) in Many Campus Transport Management programs include free or discounted transit fares. Not all increased transit travel that results from fare discounts represents a reduction in automobile travel. A portion represents shifts from walking,cycling and ridesharing,or absolute increases in personal travel.

From the introduction above, we can see domestic and foreign scholars have not done study about ticket ratio between railway and public traffic according to mode choice behaviors. Existing ridership models,either long-range or short-term,are limited by both our understanding of the complicated decision-making processes of individual travelers and a lack of fundamental data. So it lacks a tool to do study about urban deep discount policy.

Public traffic ticket ratio can be divided into three levels: ratio between public traffic ticket and the value level of the society merchandise; ratio between different kinds of public traffic modes' ticket and ratio between bus systems. The two latter ticket ratios have great influence on the passenger proportion which is split by different transportation mode. During the determination of the ticket ratio, to maximum the social benefits, factors which should be considered are listed as the following(Chen Shuhong.2007):(1)Economic bearing capacity of the passenger(2)Competition factor between bus and railway (3)Government Economic policy.

In this paper, based on the choice behavior survey in Beijing, the influence factors of mode split were analyzed. Then traveler mode choice model considering different ticket ratio between railway and bus was established and the mode choice behavior was discussed. The conclusion will provide an analysis tool for an evaluation of the effectiveness of deep discounts actions that encourage the use of public transit modes and/or discourage the use of auto for the commuter trip.

MODEL CHOICE BEHAVIOR SURVEY AND ANALYSIS

Survey Summary

The survey in this paper was conducted in Beijing in October 2005.The subject of this survey was the revealed preference of public traffic users under Deep Discount policy. Consider capacity of the mass transit is invariable whether the value of ticket changes, and there are N identical commuters who can either travel by bus or by railway（Hai-Jun Huang.2002）.

The survey consisted of three parts, of which only two are relevant to this

study. One part concerned respondents' household characteristics such as age, gender, education, occupation, family size, number of family workers, car possession and income level. The other part yielded information about the respondents' potential trip mode choices in different hypothetical choice situations which includes travelers' choice under different ticket ratio such as 1:1, 1.5:1, 2:1and 3:1.

The survey takes the mode of quiz face to face. Railway in route1, 2, 13, Batong and 12 paralleled bus routes with different service level, geographic position the characteristics surrounded were considered. A total of 776 respondents were selected.

In addition, because the trip behavior may be different in weekday and weekend (Guan Hongzhi et al.2003), so the survey for behavior was conducted respectively on weekday and weekend.

Analysis on Survey Results

Trip fare is one of important factors which influence the trip mode choice. The stated preference of users between bus and railway under different ticket ratio were asked in the survey (Yao Liya et al.2003). Using the investigate datum, the proportion of travelers selecting railways and buses were given.

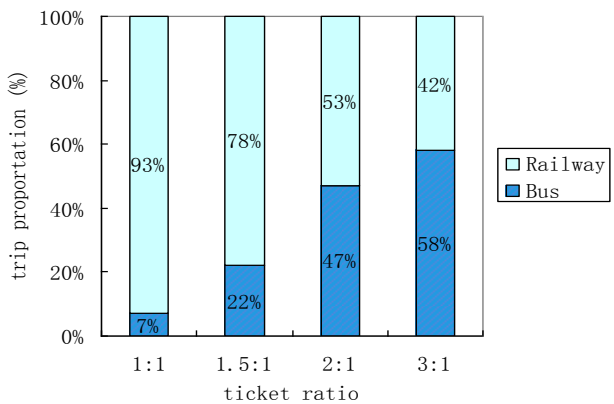

Figure 1. Travel Mode Choice under Different Ticket Ratio

As shown in Figure1 , that the proportion of travelers selecting railways and buses are closely equal which indicates that the traffic volume can be distributed reasonably by adjusting the ticket ratio between railway and bus.

CHOICE MODELS

Model Specifications

Logit model was used as following in this paper （Guan Hongzhi. 2003):

$$P_{in} = \frac{e^{V_{in}}}{\sum_{j \in A_n} e^{V_{jn}}} \qquad (1)$$

where： P_{in} = probability of a traveler n choosing the project i

V_{in} = deterministic component of utility i for user n (fixed item)

A_n= aggregate of the choice project of traveler n

The choice projects aggregate A is supposed as follows:

A= {i=1(bus), i =2(railway)}

Then, the mode choice Logit model can be modeled as:

$$P_{1n} = \frac{1}{1+e^{-(V_{1n}-V_{2n})}} \quad (2)$$

$$P_{2n} = 1 - P_{1n} = \frac{e^{-(V_{1n}-V_{2n})}}{1+e^{-(V_{1n}-V_{2n})}} \quad (3)$$

$$V_{1n} - V_{2n} = \theta_1 + \theta_2 X_{1n2} + \theta_3 X_{1n3} + \theta_4 X_{1n4} + \theta_5 X_{1n5} + \theta_6 X_{1n6} + \theta_7 X_{1n7} + \theta_8 X_{1n8} \quad (4)$$

Where:

V_{1n}=deterministic component of utility for user n from choosing bus (fixed item);

V_{2n} =deterministic component of utility for user n from choosing railway (fixed item);

θ_1=constant;

$\theta_2 \ldots\ldots \theta_8$= parameters to be estimated;

X_{1n2}= traveler n's age1;

X_{1n3}=traveler n's age2;

X_{1n4}=traveler n's income1;

X_{1n5}=traveler n's income 2;

X_{1n6}, X_{1n7} ,X_{1n8}=ticket raito1（1.5:1)、ticket ratio 2（2:1)、ticket ratio 3（3:1)；

X_{1n9}= traveler n's fare.

Variable Filtration and Grouping

Using the survey datum, the influence of the travelers' household characteristics and trip characteristics on trip mode choice are analyzed through crosstabs chi-square test, the result is listed as shown in Table 1.

Table 1. Value of Chi-Square and Correlation of Influencing Factors

Test value	Gender	Age	Occupation	Income	Purpose	Car Possession	Ticket ratio
Chi-squared Value	6.933	18.831	31.405	39.216	18.846	2.518	139.110
Correlation	0.008	0.002	0.000	0.000	0.004	0.113	0.000

As shown in Table 1, gender, age, occupation, income, and trip purpose have marked influences on the results of trip mode split, and the effect of car possession is not significant to choice modes. Variables filtration and grouping were decided as following by correlation analysis:1)Gender is divided into Male and Female;2)Age is divided into three groups: Age1 is between 18 and 35 years old,Age2 is between 35 and 55 years old and age3 is others;3)Occupation is divided into three groups: Occupation1 is official, manager; Occupation2 is engineering and technical personnel, office clerk, workers, professional undergraduate and Occupation3 is others;4)Income

is divided into three groups:Income1 is below 800 RMB/month, Income2 is between 800 and 3000 RMB/month and Income3 is over 3000 RMB/month; 5)Purpose is divided into two groups:Purpose1 is work, business, recreation and Purpose2 is others.

Calibration of Model

Using the logit model and survey datum, mode choice model is proposed as shown in Table 2 and test of the model of mode split is given in Table 3.

According to the statistic analysis, age, income, ticket ratio, and trip fare are chosen as the independent variables of the mode choice model based on ticket ratio. The absolute values of t-statistics of age1, age2 income1, income2, ticket ratio1-3 are all higher than 1.96 at a 5 percent confidence level, which indicates that these seven influential factors are significant for the choice probability.

The coefficients of age1and age2 are positive, meaning that these two factors have positive effect on the mode choice.

The coefficients of income1 and income2 are both negative, which means income has negative effect on the mode choice. The higher the income is, the lower the choice probability of bus is as opposed to railway. The absolute coefficient of income2 is higher than income1, and it can be considered that with the upgrade of the people's income level, the demand of trip such as punctuality, comfortable and convenient performance will become higher than before.

The coefficients of Ticket Ratio1（1.5:1）、Ticket Ratio1（2:1）Ticket Ratio1（3:1）are positive, meaning that these three factors have positive effect on the mode choice. That is to say, the higher the ticket ratio between railway and bus is, the less the travelers are likely to choose the railway as opposed to bus.

And the coefficient of the trip fare is negative, meaning that it has negative effect on the mode choice. The higher the trip fare is, the less the travelers are likely to choose the railway.

The goodness of fit parameter ρ^2 and goodness-of fit index adjusted by freedom $\bar{\rho}^2$ of the model are 0.2595 and 0.2427 respectively, which implies that the forecast veracity of the model is satisfied and the precision of this model is high.

Table 2. Model of Mode Split

	Mode model	Parameter value	t value
	Constant	-4.0407	-4.3445
	Age1（18~35）	1.8523	2.5103
	Age2（35~55）	2.3634	3.0269
Discrete Variables	Income1（￥800-3000/month）	-0.4956	-2.5148
	Income2（>￥3000 / month）	-1.3279	-5.6545
	Ticket Ratio1（1.5:1）	1.4536	4.4146

	Ticket Ratio2（2:1）	2.5817	8.0649
	Ticket Ratio3（3:1）	3.0997	9.5952
Continuous variables	Fare	-0.0706	-1.74

Table 3. Test of Model of Mode Split

Model test	Sample size	L(0)	L($\hat{\theta}$)	-2[L(0)- L($\hat{\theta}$)]	ρ^2	$\bar{\rho}^2$
value	776	-537.882	-500.153	279.14	0.2595	0.2427

According to the calibration result of the model listed in the table 2, the probability of each traveler choosing bus and railway can be given. During the mode split of the traffic planning, if the probability value is larger than 0.5, suppose that traveler is likely to choose the trip mode. The total probability of travelers choosing between railway and bus can be calculated respectively and the passenger volume ratio is also given corresponding to the ticket ratio.

CONCLUSIONS

Based on survey data and BL model, mode choice model corresponding to ticket ratio between railway and bus was established. Conclusions following can be obtained by analyzing the model: Gender, age, income, trip fare and ticket ratio have marked influences on the results of trip mode split, and the effect of car possession is not significant to choice modes. On the basis of combination of variable factors, the variables that should be used in the model were determined and the model of public traffic mode split is presented in this paper. The relationship of trip fare, ticket ratio and mode split can be studied, which provided a base for adjusting the structure of public traffic by using the deep discount policy. The forecast veracity of the model is satisfied and the precision of this model is high.

ACKNOWLEDGEMENTS

Financial support provided by the National Natural Science Foundation of China (Grant No. 50678004) is acknowledged. The author would like to thank one anonymous referee for his (her) helpful comments and suggestion, which improved the content and composition substantially.

REFERENCES

Ben-Akiva, M., & Morikawa, T. (1990). Estimation of switching models from revealed preferences and stated intentions. Transportation Research A, 24, 485−495.

Chen Shuhong. (2007). Study on Relation of Fare Ratio between Rail Transit and Routine Bus System, Master Dissertation of Beijing University of Technology (2007):34-40

LIU, G.. (2007) A Behavioral Model of Work-trip Mode Choice in Shanghai. China Economic Review18 (2007) 456–476

Gillen, D.W. (1977) .Estimation and Specification of the Effects of Parking Costs on Urban Transport Mode Choice.. Journal of Urban Economics, Vol. 4 (1977) pp. 186–189.

Guan Hongzhi.(2004). Disaggregate Model —A Tool of Traffic Behavior Analysis [M].Beijing: China Communications Press, 2004

Guan Hongzhi, Liu Lanhui.(2003).Survey and Analysis of Parking Behavior in Metropolitan Business Quarter, JOURNAL OF BEIJING POLYTECHNIC UNIVERSITY, 2003, 29[1]: 47~50. （in Chinese）

Hai-Jun Huang. (2002). Pricing and logit-based mode choice models of a transit and highway system with elastic demand. European Journal of Operational Research 14 (2002) 562–570

Shaw, J. Minimum Parking Requirements in Midwestern Zoning Ordinances." Paper presented at the Transportation Research Board 76th Annual Meeting, January12–16, 1997, Washington, D.C., Preprint No. 97-0405.

Yao Liya, Guan Hongzhi, Yan Hai. (2007).The Effects of Fare on Traffic Structure and Mode Split Model, JOURNAL OF BEIJING UNIVERSITY OF TECHNOLOGY, 33(8): 47~50.（in Chinese）

Zong Fang.(2005).Study on Activity -based Travel Time and Mode Choice Models [D] Changchun: Jilin University , 2005（in Chinese）

Design and Validation of Wireless Dynamic Testing System for Bridge Based on the 941B Type Vibration Sensor

Li Zhonglong[1], Zhang Lianzhen[1], Zhu Xiaodi[2], Gu Hongjiang[2] and Jiang Zitian[3]

[1] School of Transportation Science and Engineering, Harbin Institute of Technology, Harbin 150090, China;
[2] Liaoning Province Communications Science Research Institute, Shenyang, 110015, China;
[3] Communication Research Center; Harbin Institute of Technology; Harbin 150001; China

Abstract

In order to ensure the safety of the bridge operation, Structural Health Monitoring (SHM) or regular tests should be carried out. SHM or regular tests are very important for large structures such as suspension bridges, cable-stayed bridges, cross-ocean bridges, towers, and so on. Much more attention have been paid to some advanced technologies for SHM or regular tests. In order to collect signals wirelessly in civil engineering structure monitoring, a Wireless Dynamic Testing System was designed by modularization and system method, which combines bridge structure detection technique, computer technology, modern sensor technology, wireless communication, and system technology. The wireless testing system consists of a master station and several substations. The master station is composed of a control center subsystem and a data transmission subsystem. The substation is composed of a data transmission subsystem and a gathering subsystem. The software system consists of controlling, data, and Single Chip Microcomputer processing. Finally, the wireless measurement system is tested by a field test of the Sifangtai Cable-stayed Bridge.

Key word: Structural Health Monitoring; Wireless transmission; Bridge detection tests; Data acquisition; Vibration sensor

Bridge structures have to withstand vehicle load, crowd load, wind load, earthquakes, and so on. When any of the loads mentioned above is working on bridges, it would cause effects such as impact and vibration, which is becoming a major issue in the design, computation, construction, operation, repair, maintenance, and management of bridges. Therefore dynamic tests should be carried out on bridges.

Traditional tests use the wired method, which requires a long time to obtain the information needed and is therefore inefficient. To address such problems, a wireless dynamic testing system is proposed which adopts the wireless data transmission method to acquire structural vibration information data and uses software programming to analyze the signals for the intrinsic rules of the bridge vibration. Thus dynamic characteristics of bridge structures can be evaluated.

1 Study and design of the wireless dynamic testing system

The wireless dynamic test system based on the 941B vibration sensor is mainly composed of a master station and some far-end substations. The master station is composed of a control center and a data transmission module subsystem. The far-end substation is composed of a data transmission module subsystem, a data acquisition subsystem, and a vibration sensor. The data acquisition subsystem is composed of a front-end amplification and filtering module, an analog-digital conversion module, a voltage module, and the smallest single-chip system. The structure of the whole wireless dynamic testing system is shown in fig. 1.

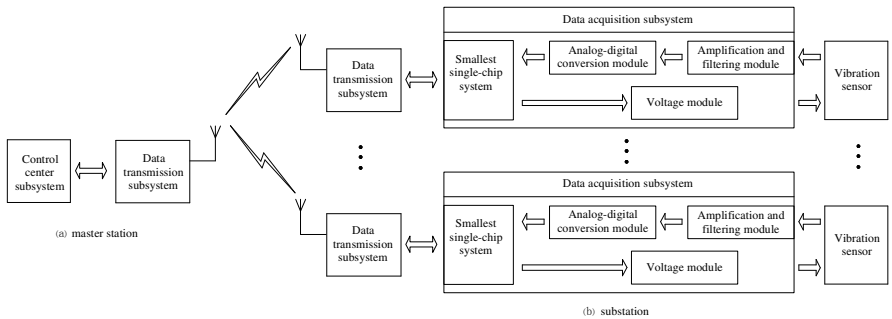

Fig. 1 Structure of Dynamic Wireless measurement system

The dynamic testing system uses a computer as the control center, completing all data acquisition subsystem instruction andsends with data processing. The data transmission module subsystem completes the receiving and dispatching control of the wireless signal from the wireless channel equipments; it may carry on the essential transformation and the pretreatment to the sensor signal. Each data acquisition unit establishes 2 or 3 sensors.

2 Design of collecting subsystem of wireless dynamic measuring system

The data collecting subsystem of the dynamic system which connects sensor units and a single chip computer-controlling module consists of a front filtering amplifying circuit, a single chip computer-controlling module, data collection, and a radio frequency module.

By the controlling orders sent from the master station, it can realize filtering of the simulated signals outputted by the vibration pickup and adjustment of the amplification factor under the control of the single chip microcomputer. This way data is collected and then sent to the radio frequency module for wireless transmission which can enhance the measuring precision of the system and simplify post data processing.

2.1 Design of front filtering amplifying circuit

The amplifying function and filtering function of the front filtering amplifying circuit are performed by a simulation device and integrators. The magnification can be altered by changing the resistance in the simulation amplifying

circuit. As for the simulation integrator circuit, satisfying filtering effects can be obtained through proper change of capacitance and resistance. The selection of filtering and amplifying parameters can be achieved by adding some simulation switches.

2.2 Design of single chip computer controlling module

The single chip computer-controlling module is one of the most important parts of the collection joints in the dynamic testing system. It commands the rest parts of the circuit to work together to guarantee all functions of the data collecting joints are being carried out properly. The single chip computer-controlling module is the smallest system of a single chip computer and consists of a MCS-51 single chip computer, an address latch unit, and an 8255 program general parallel interface chip. The dynamic data collection requires long-time without interruption. Meanwhile, the speed of serial ports between the single chip computer-controlling module and radio frequency module is restricted, which leads to overabundant data and thus great storage depth is required. Therefore each circuit is extended with a data memory device in the design.

Firstly, the address code is applied on the address input terminal of the RAM chip, the corresponding memory unit is chosen, and then the writing operation can be carried out. Then the datum written is put in the datum bus line. The patch selection signal and writing signal are added, which opens the tri-gate to make the transferred datum enter into the input circuit and sent to the bit line of the memory cell in order to be written in the memory unit.

Secondly, the main chain controlling element supplies power, with the voltage between 0 and 5V, but the simulation signal voltage range of the dynamic system is between -5V and +5V, requiring its main chain controlling element to supply a voltage of $\pm$5V. The AD transferred chip used in datum collecting nodes of the dynamic system is the AD7807 produced by the BB Company. By using the internal reference voltage as the working reference voltage, the voltage range of 0 to 5V is determined. Because the voltage of the input simulation signal is between -5V and +5V, the simulation signal must be handled properly before being sent to the AD7807 transferred chip. The treatment methods taken in this system design is: first, a resistor divider is taken to change the voltage range from between $\pm$5V to between $\pm$2.5V; second, let the simulation signals pass thorough a reverse proportion operational circuit with 1 time amplification in turn to render a 180 degrees discrepancy between the output simulation signal and the input simulation signal; third, this signal and a -2.5V voltage signal are applied to the input terminal of a reverse input summation circuit, which would generate a simulation signal with the voltage between 0 to +5V at the output terminal as expressed. By sending this signal to the AD translator, the sample of the input simulation signals could be

finished in the AD7807.

Finally, some addresses and control lines are extended and distributed. Datum memory is added for each circuit signal in the design and an 8255 is added to meet the needs of the data memory for a 19-bit address. The datum bus line is connected with the 8255 datum terminal for a single chip computer to read the data easily.

2.3 Design of data collection and radio frequency module in bridge wireless dynamic testing system

The radio frequency module of the data collection node of the dynamic system requires that acquisition of data and transmission of data be in sync, which means that after each data acquisition, the data acquired needs to be sent to the main station through a wireless channel. This demands the data frame of the communication protocol to be sent in the sampling clearance. In addition, the power amplifier of the data collection node must be kept on open status during the sampling in order to send the data frame, because it needs 5ms to activate the power amplifier. As for the dynamic system, data collection and transmission are alternately appearing, if the power amplifier were turned off after each time of transmission, then it would take 5ms longer each time during the new transmission. This would not only cause too frequent on and off of the power amplifier, but also reduce the using life. Moreover, when the sampling speed is high, activation time would impede the data frame transmission during the sampling interval.

3 Study and design of communication protocol of bridge wireless dynamic testing system

3.1 Study and design of communication protocol of bridge dynamic system

The sampling rate of the dynamic system is 200Hz. The length of data collection is 10 min long each time after receiving the command of data collection. If all the collection data are stored in the SCM and sent to the main station together after the collection is finished, it would render a very large transfer delay and influence the real-time property of the system. Besides, secondary stations need to collect large data memories and this doubtlessly raises the system cost. In order to avoid such problems, every time when finishing a collection, the data collected could be sent to the main station immediately during sampling intervals.

The sampling rate of the dynamic system is 200Hz, namely, the sampling interval is 5ms while the serial rate of SCM is 19.2kbps, which means if all 5ms were used to send data information, only 12 bytes at the most could be transmitted. In addition, the running of the SCM and the delay of the data collection circuit are all time-costly, so the length of the data frame sent during the sampling interval must be less than 12 bytes. Based on the preliminary estimation, the running of the SCM and the delay of the data collection circuit together cost less than 1ms, so

theoretically, as long as the data frame length is less than 10 bytes, the SCM would achieve data collection and transmission in the sampling interval and meanwhile get ready for the next data collection.

In the communication protocol of the dynamic system, the frame length is fixed to 8 bytes, and the serial sending time must be less than 3.4ms. The information frame of the dynamic system is divided into a descending frame and an upstream frame. The descending frame is sent from the main station and used to control the secondary station; the upstream frame is sent from the secondary station and used to send the collection data back to the main station. The details are introduced below:

In this article, we define the communication link from the main station to the secondary station as the descending link while the communication link from the secondary station to the main station is the upstream link. The system adopts a parallel communication style with a rate of 57.5kbps. Both the descending and upstream link use the same uniform frame format and are in support of the ARQ function. The communication flow chart of the system is shown in Fig.2.

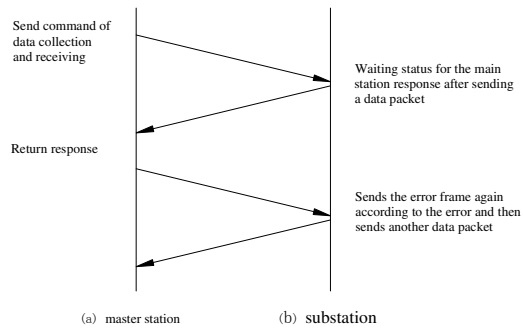

Fig. 2 Communication Process

As soon as the main station gives the command of data collection, the secondary station that receives the command begins to collect the data and sends them back to the main station. To be specific, in the secondary station 4 data and a control dictate compose a data frame, then 8 data frames compose a data packet. After each transmission of the data packet, the secondary station enters into the status of waiting for the main station response. Meanwhile, the main station unpacks the received data packet and checks them, then sends the error drafts back to the secondary station. The secondary station then sends the error frame again according to the error drafts, and then sends another data packet. If the error draft shows no error, the secondary station will send another data packet immediately. In the whole data collection process, the main station could stop the work of the secondary station by sending the stop command.

3.2 communication frame format

The length of the communication frame is 18 bytes and the frame format is

shown in Fig.3.

0x7E	LEN	Dadd	Sadd	TYPE	CONTENT	CHK

Fig. 3 Frame format

0x7E is the first byte, which means the start of the communication frame and is called the frame head.

LEN is the second byte, which is the length of the communication frame. In order to set up radio equipment conveniently, the uplink frame has the same length with the downlink frame. The length of the communication frame is 18 bytes.

Dadd is the third byte, which is the destination address. The master station's address is set to 0x00 while 0xFF is the broadcast address. Each master station could have 254 secondary stations, thus the secondary station address ranges from 0x01 to 0xFE.

Sadd is the forth byte and the source address, which shows the source of the communication frame.

TYPE, the fifth byte, is the type-frame type selection address and its definition is shown in Table 1.

Table 1 TYPE-frame type selection

downlink frame		uplink frame	
The command frame of the first sensor in data Acquisition	0x01	The data-frame of single node	0x01
The command frame of the second sensor in data Acquisition	0x02	The data-frame of multiple nodes	0x02
The command frame of itinerancy between two nodes	0x03	The data-frame of retransmitting ARQ	0x03
The command frame of ending secondary station	0x04	The frame of terminating data Acquisition	0x04
The responsive frame of master station	0x05		
The command frame of being enable to report data	0x06		

CONTENT specifies the content of the communication frame and is part of the frame from the sixth byte to the seventeenth byte. Its length is 12 bytes and a more detailed introduction would be discussed in the following chapters.

CHK is the eighteenth byte and represents the checking byte, adopting the first LEN-1 bytes' summation of all the bytes in the frame except CHK.

4 Field test of Sifangtai Cable-stayed Bridge in Harbin

4. 1 Field test of Sifangtai Cable-stayed Bridge in Harbin

Tests were carried out on the Sifangtai Cable-stayed Bridge in Harbin in May, 2008 by the wireless dynamic testing system. The distance between the master station and secondary station was 100m, and the additional attenuation was 25dB. The testing procedure from the master station to the secondary station was normal and the return time tested is consistent with the estimation, which proved that data acquisition and transmission time of the communication channel are in accordance with design specifications.

4. 2 Results and analysis of the laboratory tests

For the purpose of validating the reliability and accuracy of the system, a comparison of data between the theoretical values and the acquired data obtained by the INV306 dynamic signal acquisition and analysis device, made by the Beijing Oriented Vibration and Noise Research Institute, was carried out.

The fundamental frequency estimated theoretically of the Sifangtai Cable-stayed Bridge is 0.297Hz. Actually measured from the mid-span section in stiffening girder, the vertical fundamental frequency actually measured was 0.352Hz after data processing and analysis by the INV306. The fundamental frequency measured and analyzed by the wireless dynamic testing system was 0.35Hz, which is close to both the result measured by the current equipment and the theoretical value. It proves that the wireless dynamic testing system can be applied to data acquisition from the vibration-pick-up device, and to wireless date transmission. What's more, its accuracy meets engineering requirements and thus it is suitable for application in practical engineering.

Conclusions

Based on vibration sensors, the design of the data transmission module of the wireless dynamic testing system and the corresponding communication protocol realizes reliable and effective data transmission. This system has been successfully applied in strain-gauging of an actual large-scale bridge structure and it has been proven to be theoretically correct and technically feasible with many advantages such as high accuracy, network, high reliability, easy operation, affordability, friendly interface, and so on. It also has positive and initiative consequences on the exploitation of wireless testing in bridge structures

On the whole, the wireless testing system can overcome many insufficiencies of the wired method of data acquisition with obvious efficiency in bridge detection and health monitoring. Thus it has practical significance and application prospects.

BIBLIOGRAPHY

Casciati Fabio,Faravelli Lucia.Borghetti Fausto. Wireless links between sensor-device control stations in long span bridges[c].Conference on Smart Systems and Nondestructive Evaluation for Civil infrastruct- ures: California, USA, 2003 : 1-7

Ding Libo, Zhang He, Li Haojie, et al. Design and implementation of a small-size wireless data acquisition system[A]. Instrumentation and Measurement Technology Conference[c], Proceedings of the 19th IEEE, 2002, 1(5): 21-23.

Gao, R.X. and Hunerberg, P.Design of a CDMA-based wireless data transmitter for embedded sensing[c]. Instrumentation and Measurement, IEEE Transactions on , Volume: 51 , Issue: 6 , Dec. 2002:1259-1265.

Huang Qiao,Li Zhonglong, Sha Xuejun , Xu Yubin. Sensor-Based on the wireless measurement system for bridge.China: 200510009685.x, July, 2005.

Jerome Peter Lynch, Kincho H. Law, anne S. Kiremidjian,etal.A wireless modular monitoring system for civil structures[c]. IMAC-XX: A Conference on Structural Dynamics.Los angeles,California, 2002: 1-6.

Application of Fractal Theory in Pavement Surface Texture Measurement

Yuan Yan[1] , Lai Anxing[2] , Que Yun[3]
[1]College of Civil Engineering of Fuzhou University, Fujian, PH (86)0591- 22865353; FAX (86) 0591-22865355; email: yanecho@163.com
[2]College of Civil Engineering of Fuzhou University, Fujian, PH (86)0591- 22865353; FAX (86) 0591-22865355; email: laxan@126.com
[3]College of Civil Engineering of Fuzhou University, Fujian, PH (86)0591- 22865353; FAX (86) 0591-22865355; email: queyun_2001@tom.com

ABSTRACT

This paper presents a non-contact method measuring asphalt pavement surface texture based image processing technology and fractal theory to overcome the deficiencies of conventional volumetric method. The pavement surface texture images are acquired using ordinary CCD camera. Then fractal analysis on contour of gray level, which is extracted from binary image by target segmentation at adaptive threshold value and edge detection, is made. A fractal dimension of contour of gray level, scale-independent, is determined.

This study comprises field tests and laboratory tests. A regression equation of FDC and MTD measured by sand patch test is built, and a statistical correlation based on a good coefficient of determination (R^2) for the data is obtained in the preliminary results. It is observed that the FDC decreases with the MTD. At last, the possibility of replacing volumetric by this measurement in the practical application is discussed.

KEY WORDS: Surface texture measurement; Fractal dimension; Digital image processing; Contour of gray level; Mean texture depth.

1. RESEARCH BACKGROUND

It is widely recognized that pavement surface texture influences many different pavement–tire interactions, including friction, interior and exterior noise, splash and spray, rolling resistance, and tire wear (Henry, J. J. 2000). Different texture characteristics have different effects on tire-pavement interactions. As a result, much attention has recently been focused on the measurement and evaluation of surface texture characteristics for transportation safety and ride quality.

There are several different methods for quantifying surface texture. Two commonly used methods are the mean texture depth (MTD) and the mean profile depth (MPD). The MTD is determined using the traditional volumetric method (commonly referred to as the “sand patch test”) whereas the MPD is determined using laser technology at highway speeds. A known volume of sand material is spread properly on a pavement surface to form a circle, and the MTD is then

computed by dividing the known volume of sand by the calculated average of four equally spaced diameters of the circular patch. Even though the reproducibility (40%) of the sand patch test is poor, it is the most common means to measure texture as the reference "ground-truth" standard throughout the world, since there is a great deal of past research (Gerardo, W. F., 2003). The MPD is a statistic computed by analyzing 102 mm segments of the collected profile data that acquired from modern high-speed vehicle-mounted laser-based measuring devices or new portable devices such as the Circular Texture Meter (Jcbarrantes, 2007).

However, even with experienced, skilled operators, the sand patch method takes some time to perform, and is normally done in live traffic conditions with varying levels of traffic control (Gransberg, D.D, 2005, Pidwerbesky. B, 2006). And laser measurements commonly have relatively accurate test results but expensive cost. Moreover, MPD is scale-dependent and the sampling length, the sampling spacing and the instrument resolution, etc. affect the result strongly.

2. RESEARCH OBJECTIVES AND METHODOLOGY

The purpose of this research is to evaluate whether a practical method of pavement surface texture measurement using digital image processing, incorporating fractal theory could be developed. This is accomplished by comparing the results obtained using the sand patch method. The objectives of the research are to develop:

- An accurate, repeatable method of measuring texture to replace the sand patch method;
- A fast, safe method of measuring texture to reduce the operator risk associated with road surface texture measurement and minimize disruption to traffic;
- To find the most effective and scale-independent parameters to estimate texture roughness.

In this regard, it is necessary to determine a parameter to quantify the roughness of surface texture. In surface sciences, the fractal analysis approach is based on concept of self similarity of surface at different scales. Its advantage is that it is insensitive to the structural details, and the structure is characterized by single descriptor, the fractal dimension D. It provides information on the degree of complexity of different surface topographies. Moreover, recent statistical comparison of relevant roughness parameters reveals that the fractal dimension is the most relevant parameter to describe the surface topography (D. Risovi´c, 2008). The objective parameter selected to quantify the surface texture roughness is fractal dimension of contour of gray level (FDC) of each image due to self-similarity of surface texture of asphalt pavements statistically. Here, FDC is defined as roughness of contour of gray level, whose physical meaning is asphalt mixture without voids of pavement surface. In some way, the FDC quantifys the capacity of asphalt mix without voids filling with space of section plane.

Evaluation of surface texture roughness based image analysis by fractal theory is obtained in three main steps:

•Image acquisition: Digital images were taken in the fields and in the lab and sand patch tests are taken in the same location as the images. Pavement surface real texture information was acquired using ordinary charge-coupled device (CCD) camera.

•Image processing and analysis: Some suitable image processing methods are taken to improve primitive image. Then contour of gray level was extracted from binary image by target segmentation at adaptive threshold value and edge detection and FDC, scale-independent, was determined for each 'ring'.

•Regression analysis: The 'ring' FDC is statistically correlated with their corresponding sand patch measurements using some regression techniques and the coefficient of determination (R^2 value) as the objective measure of correlation. The output is a regression equation that describes the best fit of a curve that represents the relationship of the change in FDC with respect to the change in MTD.

3. EXPERIMENTAL PROCEDURES

This study comprises field tests and laboratory tests. Field tests are conducted on the two different types of 6 asphalt pavements existed (coarse-graded HMA&fine-graded HMA) whereas laboratory tests simulated newly constructed SAC type of asphalt pavements. It's necessary to take images before and after the sand patch tests so that the latter determined the size of the former. In the fields, images are taken on the shoulder, wheel path and the area between the wheel-paths. In the lab, 20 standard samples manufactured by wheel rolling method furnished with surface space for both image taking and sand patch tests.

3.1DIGITAL IMAGE ACQUISITION AND PROCESSING

Standardized image acquisition method is carefully designed and carried out. In this regard, the experiment must maintain fixed focal length and fixed tilt of camera. With these constrains met, constant lighting is not needed due to a camera self-adjustment (Stemprok, R., 2000). In this study, each image was taken vertically above the surface texture at a height of about 20cm in the whole experiments.

The acquired images are taken some suitable image processing techniques to improve primitive image quality including resizing, noise reduction, contrast enhance and so on. And the images are converted into black and white images called gray-scale images.

Then images of contour of gray level are extracted from binary image by target segmentation at adaptive threshold values and edge detection. How to choose an adaptive threshold value for target segmentation of each gray image is considered as a key step. Each image has a most adaptive value for target segmentation in the preliminary experiment. There are usually two peaks in the density histogram of a

gray image of pavement surface texture (Mao, L.H., 2005). In a result, the valley between two peaks is considered as the most adaptive value for converting a gray image into a binary image. And the differential edge detection was used for feature extraction from binary images. These images of contour of gray level furnish the input for fractal dimension calculation and the opportunity to relate the roughness analysis of visual output using fractal dimension value with a physical measurement taken at the same location as the images.

3.2 IMAGE FRACTAL DIMENSION ESTIMATION

In the image analysis paradigm, fractal dimension measurements are used to estimate and quantify the complexity of form, shape or texture of objects (Bruno, O. M., 2008). Although various algorithms exist for computing fractal dimension for digital imaging, this study was based on the box-counting. As can be seen, the box-counting method is one of the most popular methods to estimate fractal dimension because of its easily operating.

The box-counting method is based on the number of boxes $N(\varepsilon)$ of size ε required to fill the entire area of an image. To changing the size of ε means that the number of boxes, $N(\varepsilon)$, also changes. In other words, the smaller the size of ε, the greater the number of boxes, while the larger the size of ε, the fewer the number of boxes $N(\varepsilon)$.The box-counting method defines the fractal dimension of an object by the expression below (Voss, R.F., 1988). The procedures of fractal analysis are shown in Figure 1.

$$D = \frac{\log N(\varepsilon)}{\log (1/\varepsilon)}$$

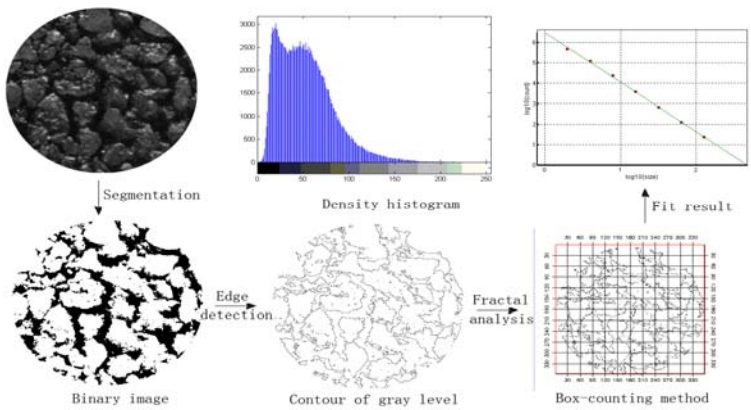

Figure 1. Flowchart of the fractal analysis

4. RESULTS AND DISCUSSION

4.1 CORRELATION BETWEEN FDC AND SAND PATCH TEST RESULTS

The first task is the investigation of the relation between the two indices, i.e. FDC and MTD. A comparison of FDC and MTD on the fine-graded HMA pavement

is shown in Figure 2. One can see that the FDC decrease with the MTD and the satisfactory textures show lower FDCs. Other types of mixture show the same tendency with the fine-graded HMA pavement.

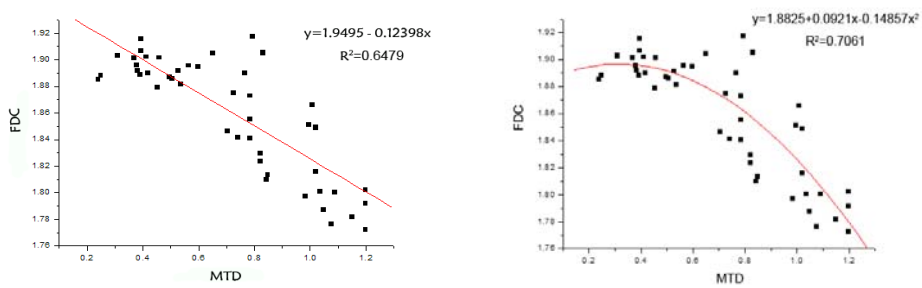

Figure 2. Relationship between MTD and FDC (Fine-graded HMA)

Table 1. Results of Regression Analysis (FDC = f (MTD))

Places	*Mix types*	*Forms*	*Transform equations*	R^2
Field	Coarse-graded HMA	Linear	y= 1.948-0.125x	0.7661
		Polynomial	y= 1.906-8.942x-0.085x^2	0.7869
	Fine-graded HMA	Linear	y=1.949-0.123x	0.6479
		Polynomial	y= 1.882+0.092x-0.148x^2	0.7061
Lab	Stone asphalt concrete (SAC)	Linear	y=2.089-0.235x	0.7232
		Polynomial	y=1.8581+0.257x-0.256x^2	0.7375

Table 1 summarizes the results of the analysis investigated for two forms of regression: linear and polynomial. It also shows the coefficients of determination (R^2) for each of the transforms. The correlation of data between the two indices relies upon the accuracy of position location to ensure that texture as measured with the method corresponds to the exact same spot used for the sand patch results. It is noted that the values obtained are not relative high, but these values could be considered as quite satisfactory since there is an amount of different methods for fractal dimension estimation of images. And it appears that the coefficients of determination (R^2) for polynomial regressions are higher than for linear regressions, which means the FDC deceases not so fiercely when the MTD is small enough(Fine-graded HMA 0.6, Coarse-graded HMA 0.7, SAC 0.8, respectively). According to the results of the applied regression analysis (see table1), the best fit is achieved for the correlation between FDC and MTD.

4.2 EFFECT OF SURCFAE TEXTURE DEPTH ON FRACTAL DIMENSION

In general, the fractal dimension of surface texture is postulated to be proportional to the fracture surface roughness. However, it is observed that the FDC decreased with the MTD. Figure 3 illustrates the reason of this ‘abnormality’.

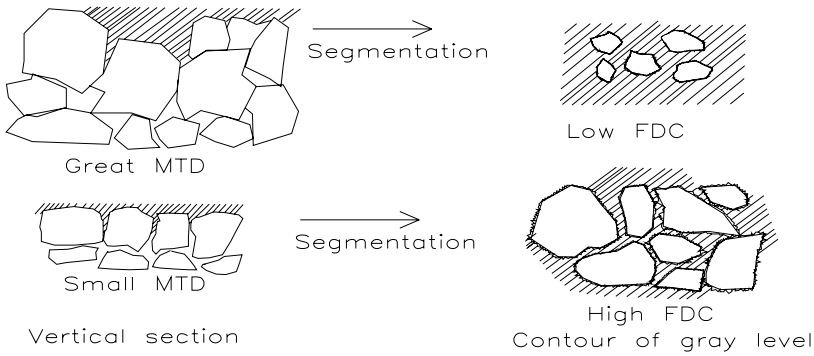

Figure 3. Schematic diagram of result analysis

Segmentation extracted the target (asphalt mixture) from the background (voids) while contour of gray level is gained by edge detection. When MTD of surface texture is great, it's obvious that there are more voids for filling with sand material. As a result, the target is relative less and the FDC was low. In reverse, when MTD is small, the contour of gray level is so complex and irregular that the FDC is high. That's to say, the FDC quantifying the roughness of contour of gray level represented the capacity of asphalt mixture without voids filling with the space of surface plane.

In summary, it can be concluded that surface texture can be measured simply and quickly by using the CCD camera. There is a negative correlation between the FDC and the MTD of surface texture closely and the correlation is proved to be quite good in the aforementioned cases. If image taking methods are standardized and regressions of each type of asphalt pavement between MTDs and FDCs are built, one can predict the MTD of surface texture by images easily based on regression equations rather than obsolete sand patch tests or expensive laser apparatus.

5. CONCLUSIONS

Many useful conclusions can be drawn from the research at this point. First, the literature supports the need for an accurate and reproducible method to measure surface texture. Measuring surface texture by the digital image processing technique and fractal theory can overcome the deficiencies of conventional volumetric method. The main results of the present case study highlighted a number of aspects and findings, which could be summarized in the following:

- The correlation between the FDC determined and the MTD obtained from sand patch test in this study was found to be quite satisfactory.
- Fractal dimension of contour of gray level could quantify the roughness of surface texture in some way. But high fractal dimension of pavement surface textures show low magnitude in depth.
- The results of the trials clearly demonstrated that the merger of digital image processing and fractal theory measurements is possible and the potential to

successfully replace the sand patch test with a camera is high.

However, this study only deals with image-based surface texture analysis in two-dimension (2D) scope, so the real texture (3D images) cannot be reconstructed. Also no correlations with mixture performance are carried out in this study. The next logical stage is to correlate FDC against standard measurements of surface friction. This would then allow this potentially powerful technology to give engineers a fast and inexpensive means to measure surface friction and that information to maintain and ensure the safety of public roads.

6. ACKNOWLEDGEMENT

The authors would like to thank Fujian education department and Fuzhou University (2007-XQ-22) for supporting this research (JA07012, 2007-XQ-22).

7. REFERENCES

Bruno, O. M., etc, (2008). "*Fractal dimension applied to plant identification*", Information Sciences , 23 January.

Gerardo, W. F., etc, (2003). "*Pavement Surface Macrotexture Measurement and Application",* TRB 2003 Annual Meeting CD-ROM, Virginia Tech Transportation Institute.

Gransberg, D.D., etc,(2005). *"Measuring Chip Seal Surface Texture with Digital Imagery",* 2005 Transit New Zealand International Conference on surface Friction for Roads and Runways, Christchurch, New Zealand.

Henry, J. J. (2000). *NCHRP Synthesis 291, "Evaluation of Pavement Friction Characteristics"*, TRB, National Research Council, Washington, DC.

Jcbarrantes, (2007). "*Chapter 2 – Surface Characteristics",* MTAG Volume II – Rigid Pavement Preservation 2nd Edition, Caltrans Division of Maintenance.

Mao L.H., (2005). "*Road image segmentation*", A Dissertation Submitted to Southeast University for the Academic Degree of Master of Engineering.

Pidwerbesky. B, Waters, J. (2006). "*Road surface texture measurement using digital image processing and information theory"*, Land transport New Zealand Research Report 290.

Risovi´c, D., etc, (2008). "*Inferring fractal dimension of rough/porous surfaces- a comparison of SEM image analysis and electrochemical impedance spectroscopy methods*", Applied Surface Science, doi:10.1016/j.apsusc.

Stemprok, R., etc, (2000). "*Calculated Roadway lighting error and Measurement of Visibility with CCD devices*", Proceedings of the symposium of commission International De L'Eclaire,(CIE), Divison 4 and 5 meeting,Toronta,Canada.

Voss, R.F. (1988). "*Fractals in nature: from characterization to simulation"*, in: H.-O. Peitgen, D. Saupe (Eds.), The Science of Fractal Images, Springer-Verlag, New York.

Research on Application of Externally Prestressing for Simple-continuous Bridge

Sheng Kejian[1,2], Li Rongda[1], Wang Zonglin[1]

1. School of Transportation Science and Engineering of Harbin Institute of Technology , 150040, harbin

2. Civil Engineering Department of Heilongjiang Institute of Technology , 150050, harbin

ABSTRACT: The joint style of the connecting section is one of the key problems of the simple-continuous system. The cost of bridge structure, the difficult degree of construction, and the performance of application are all determined by its joint style. In this paper, a new joint style, that is, applying externally pre-stressing for the connecting section, has been proposed based on the theories of externally pre-stressing systems and post-continuous technologies at home and abroad. Firstly, by using the finite element analysis software "ANSYS", the nonlinear full-stage simulations on test beams are carried out. The cracking behavior, deflection variation, bending moment redistribution of test beams, and the ultimate loading capacity of continuous beams are investigated emphatically. Secondly, the result of numerical analysis have been verified by corresponding indoor experiments. Finally, some suggestions on structure design are put forward.

Key words: simple-continuous system; externally pre-stressing; nonlinear full-stage simulation; ultimate loading capacity; numerical analysis

INTRODUCTION

Presently, multi-span middle span-length bridges constitute a large proportion of highway bridges. A new construction method, "simple-continuous", was invented based on the integration of the advantages of the simply supported beam in prefabrication production and continuous supported beam in mechanical property. The joint style of the connecting section is one of the key problems of the simple-continuous system. The engineering cost of the bridge, progress, a difficult degree of construction, and the performance of application are all determined by its joint style. The R.C. joint and post-tensioning P.C. joint are the major joint styles in the simple-continuous system bridge presently. However, the usual cracking in bridge decking of the R.C. joint often affects the service performance and durability of structure. At the same time, The post-tensioning P.C. joint has also some obvious defects, such as higher cost, complex construction procedures, a web plate with large size to accommodate pre-stressed tube, a long construction period, especially in a

frozen area, and so on. With the daily increase in the construction of simple-continuous system bridges, the application of this system will be limited in some degree because of high costs, a long interval period, and complex construction caused by singleness of the joint style.

So far, studies on the joint style of simple-continuous system had been done at home and abroad by some researchers. In late the 1990's, as a part of the National Union Highway Research Plan, the Construction Technology Laboratory (CTL) carried out the studies on this joint and achieved a conclusion that the positive moment created by the time effect will lead to the connecting section cracking. In England, Clark and Sugie had a study on the positive and negative moment connecting method of the prefabricated beam in the late 1990's. They suggested that no creep and contraction effects should be considered and the resistance moment of 700kN.m should be designed in joint for the span length of 20~36m. Nebraska University invented two ways to keep prefabricated beams connected, i.e. the reinforced screw bolt joint and pre-tensioned tendons joint. Owing to the simple construction procedure and lower structure cost, the measures had been applied successfully in 10th Street Viaduct in Lincon City in 1993 and had also been applied in other countries.

However, the present design of prefabricated members for simple-continuous structure was carried out fully according to the relative regulations of the simply supported beam and continuous beam, lacking special technical standards and without considering the natural characteristics of this system. Recently, the significant value of the externally pre-stressing structure has been confirmed in China and many kinds of studies have been carried out. Applying externally pre-stressing technology in joint can reduce the size of the web plate, the weight of prefabricated beams, and can eliminate the embedded tube and grouting so as to accelerate the construction process, which will be of significant value to cold regions in Northern China.

DESCRIPTION OF PROBLEM

As we all know, structural system transition is a key procedure of the simple-continuous system construction. The essence of this method is the pouring of connecting concrete and tensioning of externally pre-stressing tendons for negative moment. Under the ultimate state, stress of externally pre-stressing tendons can be written as

$$\sigma_p = \sigma_{pe} + \Delta\sigma_{pu} \tag{1}$$

where σ_{pe} is the effective pre-stressing force, and $\Delta\sigma_{pu}$ is the increment of the pre-stressing force under the ultimate state.

The increment of pre-stressing force will be created due to the deformation of concrete for an externally pre-stressing structure in service. Excessive tensioning

control stress may make the real stress approach to the ultimate strength of the material, eventually, brittle failure taking place. On the other hand, the use of externally pre-stressing tendons for the connecting section will induce the alteration of rigidity and internal force of the structure. However, it is infeasible that the problem mentioned above can be computed by a special equation. Therefore, studying the rules of sectional rigidity alteration, stress increment of pre-stressing tendons, and redistribution of internal force on an externally pre-stressing joint will play an important role in the design and construction of the simple-continuous bridge. Therefore, this paper focuses on the study of applying externally pre-stressed technology in the joints of simple-continuous structures based on the post-continuous technologies and externally pre-stressing theories at home and abroad. The nonlinear analysis on the finite element model of testing beams and experiments are the major contents in this paper.

DESCRIPTION OF ANALYTICAL MODEL

The purposes of numerical analysis are to calculate deflection alteration, stress increment of pre-stressing tendons, and redistribution of internal force on a testing-beam model. The analytical model is designed by means of simulating a testing beam which is 2×3.5m simple-continuous structure, with the span-depth ratio of 11:7. The material of the model adopts the strength design value of "Specifications of Design for Concrete Structure (GB 50010-2002)" and rational concrete constitutive equations.

Cube compressive strength standard value of concrete $f_{cu,k}$=38.5Mpa, singe axle compressive strength f_{cd}=18.4Mpa, singe axle tensile strength f_{td} =1.65Mpa, shear force transition coefficient of open crack β_c=0.3, shear force transition coefficient of closure crack =0.95, Young's modulus E_c= Mpa, Poisson's ratio υ_c= 0.2, and tensile stress release coefficient T_c = 0.6.

The equation for the ascending branch of a single axle stress-train curve originates from GB 50010-2002, and the equation for the descending branch of the single axle stress-train curve adopts the Hongnestad method. The stress-strain relationship is expressed in the form

$$\sigma_c = f_c[1-(1-\frac{\varepsilon_c}{\varepsilon_0})^n] \qquad (\varepsilon_c \le \varepsilon_0) \qquad (2)$$

$$\sigma_c = f_c[1-0.15(\frac{\varepsilon_c-\varepsilon_0}{\varepsilon_{cu}-\varepsilon_0})] \qquad (\varepsilon_0 < \varepsilon_c \le \varepsilon_{cu}) \qquad (3)$$

According to GB 50010-2002, the computation results are n=2,ε_0 = 0.002, ε_{cu}=0.0033. The curve mentioned above will be fitted by a series of data points, adopting the multi-linear isocline strengthening model (MISO). The diagram in Fig.1

shows the stress-train curve of concrete, it should be noted that the Young's modulus input is the initial elastic modulus.

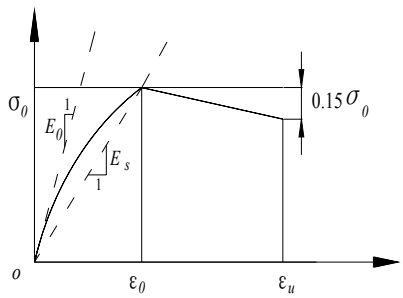

(a)

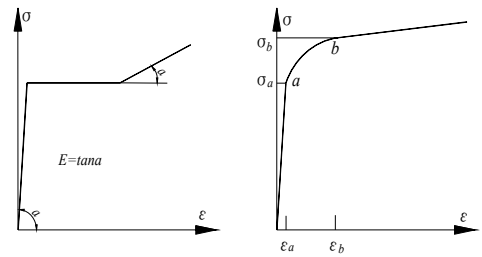

(b)

Fig.1. Concrete Stress-Train Curve

Fig.2. Reinforcement Stress-Train Curve

The stress-strain curve of simple reinforcement can be divided into three sections: elastic stage, yield stage, and strengthening stage. Fig.2(a) shows the bilinearity following and strengthening model of simple reinforcement. The stress-strain curve of pre-stressing tendons can also be divided into three sections: elastic stage, softening stage, and succeeding stage. Fig.2(b) shows the multi-linear following and strengthening model of simple reinforcement. The stress-strain curve obtained by testing data is furnished by the following function

$$\sigma = \frac{\sigma_b \varepsilon_b - \sigma_a \varepsilon_a}{\varepsilon_a - \varepsilon_b} + \frac{\varepsilon_a \varepsilon_b (\sigma_a - \sigma_b)}{\varepsilon(\varepsilon_b - \varepsilon_a)} \qquad (4)$$

The separated finite element model applying externally pre-stressing technology with ANSYS is shown in Fig.3., where the SOLID65 element, LINK8 element , and LINK10 element are adopted for concrete, simple reinforcement, and pre-stressing tendons respectively; the bonding and slipping between concrete and reinforcement are neglected.

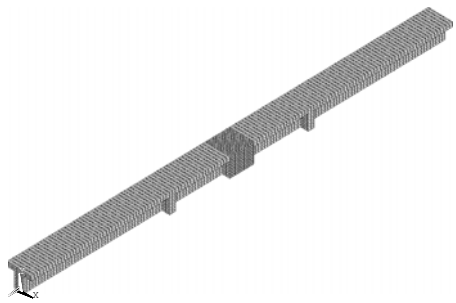

.

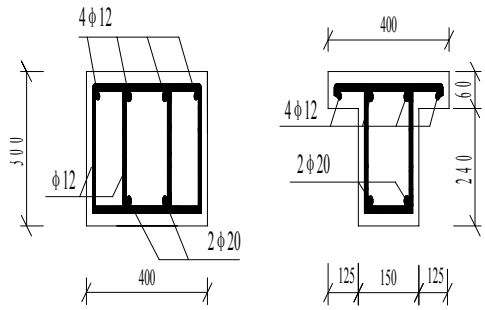

Fig.3. Finite Element Model

Fig.4. Sectional Constitution

The purposes of testing are to research the deflection alteration, stress increment of pre-stressing tendons, and redistribution of internal force on the

testing-beam. The concrete grade of the testing-beam is C40, longitudinal reinforcement adopts Φ20 and Φ16 reinforced bars, hooping reinforcement adopts a ϕ10 plain steel-bar, and externally pre-stressing tendons adopts $\phi^j 15$（7ϕ5）strands. The testing beam is a 2×3.5m simple-continuous structure, its span-depth ratio is 11:7. Fig.4. shows the sectional size and reinforcement layout. Loading layout of the testing beam in a laboratory is shown in Fig.5. Pressure sensors are adapted to measure and adjust bearing opposite force. Straight through pressure sensors are installed at the ends of strands to acquire the stress increment of strands. Using strain gauges to measure the strain of the mid-span and internal bearing and using the dial indicator to measure the displacement of bearings, and beam body, angle of rotation. The step stress scheme is accepted, the gradation of each step is 10kN and persistent time of each step is 20 minutes. When the test is being carried out, the cracking should be observed and the cracking load, bearing opposite force, displacement, and strain are all read carefully. Increasing the load up to the beam failure fully, the crack distribution rule and failure pattern of the beam can be observed.

Fig.5. Experiment Layout of Testing Beam

COMPARATION ANALYSIS OF NUMERICAL COMPUTATION AND TEST RESULTS

Analytical results of Rigidity

By comparing the results of numerical computation and the indoor test, as shown in Fig.6, the load-deflection curve of an externally pre-stressing beam can be divided into three stages: elastic stage before cracking, elastic stage after cracking, and nonlinear ultimate state stage. Approximately, the cracking load is 62.5 kN and the ultimate load is 242.8 kN. Therefore, the “three fold-line rigidity reduction model” applying elastic theory is feasible to compute the deflection of the mid-span for simple-continuous bridge.

Analytical results of stress increment of prestressing force

The relative movement between externally pre-stressing tendons and concrete will take place except for in the anchoring and deflecting areas so that the deformations of them aren’t coordination. The plain deformation analysis method is

also unfit for the computation of the ultimate stress of pre-stressing tendons. Consequently, the stress increment during the test can be acquired only by total deformation of the structure. The diagrams in Fig.7 shows the comparative results of numerical computation and the indoor test. As a result, the stress increment of externally pre-stressing force can be approximately computed by numerical analysis.

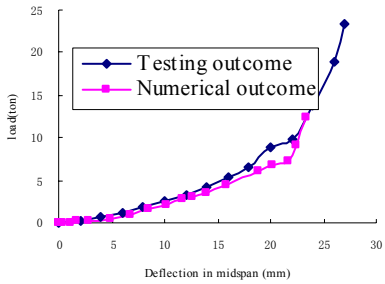

Fig.6.Load-Deflection Curve in Midspan

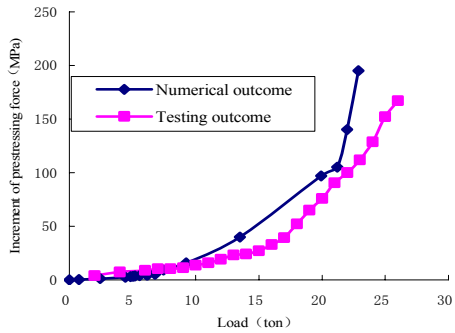

Fig.7. Increment of Prestressing Force-Load Curve

Analytical results of internal force redistribution

After entering into the elastic-plastic stage, the structural rigidity distribution and sectional mass axis are all altered so that the internal force will be also change. The study on internal force redistribution of continuous beams can help analyze the performance under loading, cracking, and deformation rules of continuous beams. Applying the results of internal force redistribution to design continuous beams can make full use of the material strength. Diagrams in Fig.9 report the rule of internal force redistribution of the simple-continuous bridge, where M_2 and M_2' are the internal bearing moments by testing and numerical computation respectively, M_1 and M_1' are the mid-span moments by testing and numerical computation respectively. To make the illustration explicit, viewing the M_2/M_1 as a variable(M_2'/M_1' =1.85) to analyze the moment redistribution rule is performed in Fig.10. With the cracks at the mid-span developing, the rigidity of this section will descend gradually, the moment will also transfer from the mid-span to internal bearing. Thus, M_2/M_1 will rise as the load increases in the Load- M_2/M_1 curve. When cracks in the internal bearing occur, the relative rigidity of this section begins to decrease, and the decreasing speed is higher than that of the mid-span section. Therefore the moment in the internal bearing begin to transfer from the internal bearing to the mid-span. M_2/M_1 will decrease as the load increases in the Load- M_2/M_1 curve.

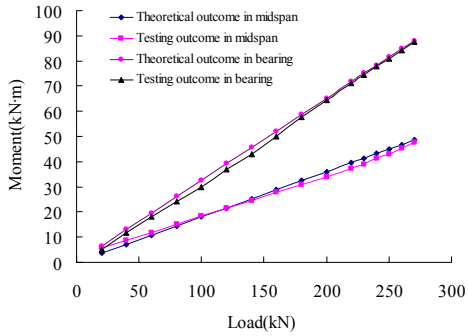

Fig.8. Load－Moment Curve

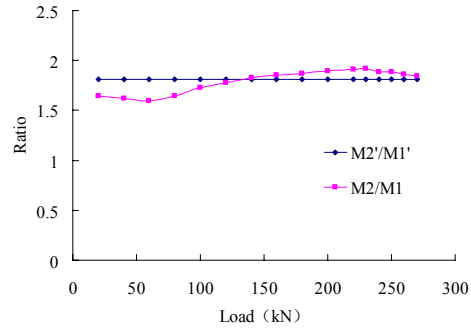

Fig.9. Load－M_2/M_1 Curve

CONCLUSION

This paper proposed the following conclusions by carrying out the theoretical analysis and experimental research on the mechanical performance of the externally pre-stressing force joint for the simple-continuous bridge.

The "Three fold-line rigidity reduction model" can be applied to compute the deflection of the mid-span for simple-continuous bridges according to elastic theory. Therefore, a simple and effective method has been obtained to the further studies on the externally pre-stressing force joint for simple-continuous bridges.

By the comparing and analyzing the results of numerical computation and an indoor test, the hypothesis that the stress increment of externally prestressing force can be approximately computed by numerical analysis has been verified.

The moment redistribution rule after the cracking of he control section was obtained by the comparing and analyzing the results of numerical computation and an indoor test, which will play an important role in reinforcement computation and sectional design of simple-continuous bridge.

Bibliography

Wang Zonglin.(2001). Ultimate State Analysis of Externally Prestressed Concrete Bridge, Ph. D Dissertation of Harbin Institute of Technology, pp. 27-69.

Murray,D.W.et al.(1979). Concrete Plasticity Theory for Biaxial Stress Analysis, ASCE Journal of the Engineering Mechanics Division, Vo1.105, No. EM 6, pp.989~1006.

Anand, S.C. et al.(1980). Constitutive Relations and Solution Schemes in Plastic Analysis, ASCE, Journal of the Engineering Mechanics Division, Vo1.106 ,No. EMI, pp.21~36.

Ottosen, N.s.(1980). Nonlinear Finite Element Analysis of Concrete Structure, Rrso National Laboratory, DK-400 Rockslide, Denmark May 1980, pp.102~108.

Buyakozturk, O.et al(1993), Constitutive Modeling of Concrete in Finite Element

Analysis, Computers and Structures Vol. 21, No.3, pp.581~610.

Alkhairi F M, Naaman AE.(1993). Analysis of externallyly prestressed with unbolded internal or externally tendons ,Journal of Structural Engineering , ASCE , Vo 1.119 (9), pp. 2680~2700.

Nihal Ariyawardena.(2000). Presstressed Concrete with Internal or Externally Tendons Behaviour and Analysis, Ph. D Dissertation of The University of Calgary, Canada , pp.45~48.

Virlogeux, M.(1998). Nonliear Analysis of Externallyly Prestressed Structures, Proceedings of the FIP Symposium, Jerusalem, Sept. 1998, pp.216~220.

Panos M. Pardalos,H. Edwin Romeijn,Hoang Tuy.(2000). Recent developments and trends in global optimization,Journal of Computational and Applied Mathematics, Vo1.124,pp.209～228.

Jasbir S. Arora.(2002).Methods for discrete variable structural optimization, Recent Advances in Optimal Structural Design, pp.1～40.

Amir Mirmiran,Siddharth Kullkarni,Reid Castrodale,Richard Miller.(2001). Nonlinear Continuity Analysis of Precast & Prestressed Concrete Girders with Cast-in-place Decks and Diaphragms,PCI Journal,2001,(5),pp.60～80.

Restraint Efficacy Analysis and Structure Optimization for the Design of Airplane Metal Chocks

Li Fuhai[1], Gu Hongbin[1] and Yao Hongyu[2]

[1]College of Civil Aviation, Nanjing University of Aeronautics and Astronautics, 29 Yudao Street, Nanjing, Jiangsu Province, 210016, P.R.China; PH(8625)84893501; FAX(8625)84891289; email: lifh@mail.castc.org.cn, ghb@nuaa.edu.cn
[2]Department of Safety Research, Center of Aviation Safety Technology of CAAC, 24 Jia Xibahe Beili, Chaoyang District, Beijing, 100028, P.R.China; PH(8610)64473073; FAX(8610)64473072; email: yaohy@mail.castc.org.cn

Abstract

The restraint failure of airplane wheel chocks is one of the most important reasons for accidental airplane movements and the ground accidents in civil aviation. The calculation formula of wind lift force on airplanes is set up according to the running time-speed-load test data of a B737-800 on the ground. The finite element mechanical radial tire model is set up based on the Mooney-Rivlin constructive model according to the outline deformation test data of airplane tires under different loads. The restraint efficacy and failure modes of statically indeterminate chocks are studied by ANSYS based on the chocks' working conditions, and the new parameter of pushing coefficient is put forward to evaluate the restraint efficacy. In the end, an optimized design scheme is presented for B737-800 metal chocks. The numerical analysis shows that the optimized chock can better match the airplane tires under different loads and can exert more restraint efficacy.

Keywords: *airplane, chock, restraint efficacy, failure mode, structure optimization*

1 Introduction

Wheel chocks are the most common ground support equipment used to restrain airplanes from moving and colliding with other objects such as aerobridges while the airplanes are parked on parking aprons without mooring and engine power (SAE 2002).

However, in recent years the restraint failure of wheel chocks has been blamed for some ground accidents which have led to unexpected huge amounts of property loss. According to our surveys at 12 domestic airports, it was found that those events resulted from the nonstandard design and incorrect usage of wheel chocks (CASTC

2008). This paper aims at providing the solution to the accidental airplane movement and the ground accidents caused by the restraint failure of metal wheel chocks.

2 Radial tire simulation model

Airplane tires are elastomeric and their outlines change in shape and size under different airplane weights. Suppose that the origin is located at the contact point between the parking apron surface and the theoretical tire, the x-axis points to the airplane's tail along the fuselage's length and the y-axis is vertically upward. Table 1 shows the bottom outline deformation test data of B737-800 main wheel tires under airplane basic empty weight (BEW) and takeoff weight (TOW).

Table 1. Deformation test data of tire outlines.

BEW(35140kg)		TOW(46940kg)	
Abscissa(m)	Ordinate(m)	Abscissa(m)	Ordinate(m)
0.000	0.000	0.000	0.000
0.203	0.013	0.218	0.013
0.243	0.026	0.257	0.026
0.270	0.039	0.283	0.039
0.292	0.052	0.300	0.052
0.315	0.064	0.319	0.064
0.352	0.096	0.363	0.096
0.382	0.128	0.391	0.128
0.409	0.160	0.421	0.160
0.430	0.192	0.435	0.192

The finite element mechanical radial tire model can be set up according to the test data of table 1 and the two-term Mooney-Rivlin constructive model which can better simulate the small and middle deformations. The strain energy formula of the Mooney-Rivlin model is as follows (ANSYS 2002):

$$w = c_{10}(\bar{I}_1 - 3) + c_{01}(\bar{I}_2 - 3) + \frac{1}{D}(J-1)^2 \qquad (1)$$

where c_{10} and c_{01} are the material constants characterizing the material deviatoric deformation, $\bar{I}_1$ and $\bar{I}_2$ are the first and second deviatoric strain invariants, J is the determinant of the elastic deformation gradient and D is the material incompressibility parameter. Figure 1 shows the finite element tire model under airplane BEW. It can be seen that the tire bottom is flat due to the airplane weight.

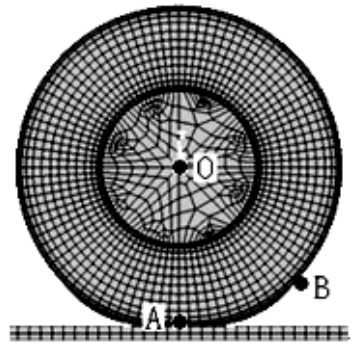

Figure 1. Radial tire model.

3 Wind forces on surface airplane

The wind lift force on an airplane with wing-flap 0 approximately equals the lift force on the same airplane with wing-flap 5 during the early running time. Although the calculated value by this means is a little larger than the actual one, the value is conservative and safe for the analysis of chocks. Figure 2 shows the running time-speed-load test data of B737-800 with wing-flap 5.

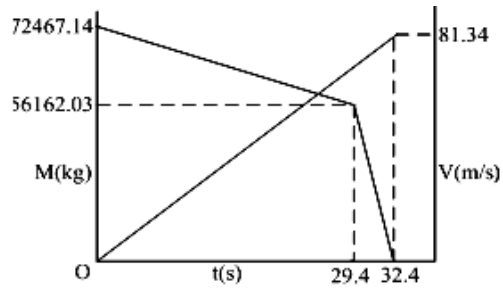

Figure 2. Running time-speed-load test data.

From figure 2 the following equations can be set up,

$$\begin{cases} L = K_L t \\ K_L = \dfrac{\left[\left(M_0 - M_R\right) g\right]}{t_R} t \\ V = K_V t \\ K_V = \dfrac{V_T}{t_T} \\ t_T = t_R + 3 \end{cases} \qquad (2)$$

where L is the wind lift force on an airplane, V is the wind speed, K_L and K_V are the lift force slope and speed slope relative to the running time, respectively, the

subscript labels T and R stand for Takeoff and Rotate, respectively, M_0 and M_R mean the initialization mass and the mass at the Rotate time, respectively.

From equations (2), the following formula used to calculate L can be induced:

$$L = 2164.92V \qquad (3)$$

The wind push force can be calculated by the following formula used to calculate the push force on a plane parked on a ship in high wind conditions (AVIC 1994),

$$P = 6331A\left(\frac{V}{100}\right)^2 \qquad (4)$$

where P is the wind push force, A is the airplane aerodynamic projective area which is vertical to the wind direction. As for the B737-800, A is 38.37 ㎡(CASTC 2008).

The airplanes must be moored when the wind speeds exceed the upper speed limits specified for their stability. The minimum speeds specified for airplanes to be moored in high wind conditions are the maximum speeds under which they can be parked stably and do not move with installed chocks, without parking brakes applied and mooring (Boeing 2005) . Table 2 shows the upper wind speed limits for the B737-800 (Hainan Airlines 2003) and the maximum wind lift and push forces calculated by formulas (3) and (4).

Table 2. Maximum wind lift and push forces on airplanes.

Surface condition	Maximum wind speed(m/s)	Lift force(N)	Push force(N)
Dry	15.43	33404.72	5783.57
Wet	10.29	22277.03	2572.14

4 Restraint efficacy of metal chocks

Metal chocks usually have the structures of linear elements and have two arc-shaped steel tubes pressed by tires, so their mechanical models are statically indeterminate and the restraint efficacy is affected by the spatial positions of those two tubes. A sample of forces on a metal chock is shown in figure 3.

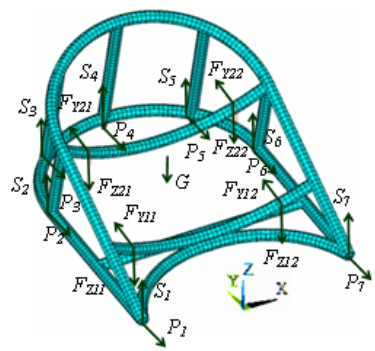

Figure 3. Forces on a metal chock

G is the chock's gravity force. F_{Y11} and F_{Y12} are the push forces on the lower tube, F_{Y21} and F_{Y22} are the push forces on the higher tube from the tire. F_{Z11} and F_{Z12} are the press forces on the lower tube, F_{Z21} and F_{Z22} are the press forces on the higher tube from the tire. F_{Y1} is the resultant force of F_{Y11} and F_{Y12}, F_{Y2} is the resultant force of F_{Y21} and F_{Y22}. F_{Z1} is the resultant force of F_{Z11} and F_{Z12}, F_{Z2} is the resultant force of F_{Z21} and F_{Z22}. F_Y is the resultant force of F_{Y1} and F_{Y2}. F_Z is the resultant force of F_{Z1} and F_{Z2}. S and P stand for the support forces and friction forces on the chock spikes from the ground, respectively.

An airplane usually weighs tens of tons or more, and therefore the lower tubes of metal chocks must be on the parking apron surface to gain the best mechanical conditions for bearing the pressure of the airplane tires. The center point of the tire is defined as point O and its projective point at the surface is defined as point A. The contact point between the tire and the chock is defined as point B. The angle between Line OA and Line OB shown in Figure 1 is defined as the working angle of the lower tube or higher tube. It is known by testing that the smallest working angle of the lower tube is 0.44 rad at which the lower tube locates at the boundary of the contact area between the tire and the parking apron surface. The restraint efficacy of metal chocks can be analyzed when the higher tube's position varies and the pushing coefficient is defined as F_Y divided by F_Z shown in table 3.

Table 3. Pushing coefficient of different move distances.

Move distance(m)	F_{Y1}(N)	F_{Z1}(N)	F_{Y2}(N)	F_{Z2}(N)	F_Y(N)	F_Z(N)	F_Y/F_Z
0.000	99	397	2665	3985	2764	4383	0.63
0.003	269	1363	2360	3641	2629	5004	0.53
0.006	464	2548	1832	3287	2296	5836	0.39

According to the friction self-locking principle, a chock can not be pushed away if the pushing coefficient is smaller than the friction coefficient between the chock and the apron surface. The abscissa represents the higher tube move distance along the radius outwards, the ordinate represents the pushing coefficient shown in Figure 4 when the higher tube's working angle is 0.79 rad and the apron surface is dry.

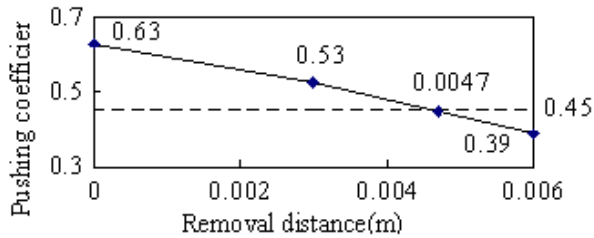

Figure 4. Pushing coefficient of different move distances.

It can be concluded that the pushing coefficient decreases with the increasing move distance of the higher tube. When the higher tube's working angle is 0.79 rad and the distance is 0.006m, the pushing coefficient is 0.39 which is smaller than the friction coefficient of 0.45. In such a case, the chock can not be pushed away by the tire. The intersection abscissa can be calculated and it is 0.0047m. In the same way, the move distances can be calculated when the higher tube's position varies and the apron surface is wet. It can be concluded that the higher tube should locate outside the left boundary of the strip region with shadow lines in Figure 5. However, the lower tube can be pressed and pinched by the tire and the chock can not be removed if the higher tube is too far away from the right boundary. The working region of the higher tube can be worked out based on the above analysis and it is the strip region.

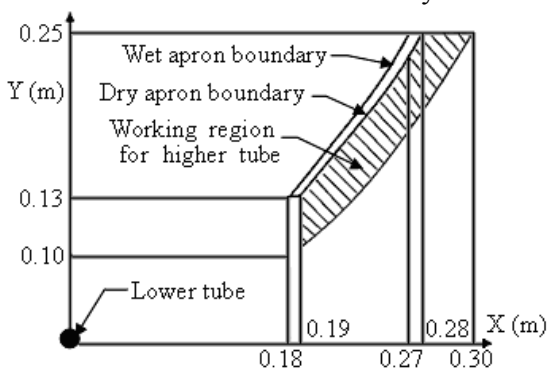

Figure 5. Higher tube working region.

5 Structure optimization design of metal chocks

According to the Figure 5, an optimized design scheme is presented for the B737-800 metal chocks. The finite element mechanical models of a radial tire and a metal chock are shown in Figure 6. The diameter and wall thickness of steel tubes are 0.026m and 0.003m, respectively, and the chock's safety coefficient of the whole structure strength is 1.51 for B737-800 airplanes with the maximum takeoff weight.

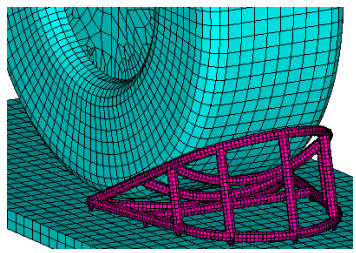

Figure 6. Finite element mechanical models

6 Results discussion

Airplane tires have air-supported membrane structures which are usually more complex than solid ones. The tire model in Figure 1 is set up based on the deformation test data of the tire bottom. The model can be more accurate if it is set up based on the whole tire deformation test data under more different airplane weights.

The working region of the higher tube can also be worked out if the tube moves outwards along the horizontal axis. However, the calculation process is a little more complex because the higher tube's working angle varies.

7 Conclusions

The method for analyzing airplane chocks' restraint efficacy is concise and applicable. So far the research results of this paper have been taken as the basis to draft the technical specification for civil airplane wheel chocks.

References

ANSYS, Inc. (2002). "Hyperelasticity." *Advanced analysis with ANSYS seminar during the 2002 user's conference*, http://ansys.net/papers/nonlinear/conflong_hyperel.pdf.

Boeing Co. (2005). "Section 10: Parking mooring, storage and return to service." *Boeing 737-600/700/800/900 aircraft maintenance manual*, part II, 10.11-10.21.

Center of Aviation Safety Technology of CAAC (CASTC) (2008). "Technical report of research work for restraint efficacy of wheel chocks", 2-11.

China Aviation Industry Corporation (AVIC) (1994). "Section 4.6: Load calculation." *Design standard for mooring airplane fuselage (HB-7082-94)*, 4.6.1-4.6.2.

Hainan Airlines Co. Ltd. (2003). "Instruction for mooring in high wind conditions." *Technical advisory (2003-MULT-008)*.

Society of Automotive Engineers (SAE) (2002). "Wheel Chocks." *Aerospace information report (Air4905)*.

The Comparison of Three Getting Signal Control Delay Video Methods at Signalized Intersection

Hui-ling Zhang[1, 2]，Ke-ping LI [1]，Hong-bo QIAN [1]，Gui-min SU [1]

[1]. School of transportation engineering Tongji University Shanghai 201804, China; PH (086) 021-6958; email: huilingz@126.com
[2]. Transport School Chongqing Jiaotong University Chongqing 400074, China; PH (086) 021-33626318; email: huilingz@126.com

ABSTRACT

The paper studies three video detection methods，and present the methods' detection theory. The instantaneous stopping detection method can obtain vehicles' stopping delay. The semiautomatic software detection method can use the video generated from the camera to retrieve vehicles' stopping and accelerating delay. This method however cannot obtain the total delay that includes the accelerating, stopping and decelerating delays. The double section video method sets two areas at a proper situation and obtains the signalized control delay. Using manually collected exact delay, the paper analyses the accuracy of these three video methods. It is proven that the instantaneous stopping detecting method can get about 70% accuracy, the semiautomatic software detecting method 82%, and the double section video detecting method can get more than 90% accuracy.

INTRODUCTION

Delay times at a signal controlled intersection are one of the most important parameters to estimate the control method's effect. It can be defined as the delay time produced by the signal control. For the intersection, the delay time means the extra time that the vehicle spends when passing the intersection. Previous methods for intersection delay include the steady-state theory, fixed number theory, transition function curve method and other classical arithmetic. These methods assume that the arriving vehicle rate and the capacity are not change in a period of time (Quan, 1989). The TRANSYT system just considers the stopping delay. The system assumes that the average arriving traffic flow is known and does not changed in a period of time, which does not consider the vehicle lane's function. In the HCM2000, vehicle dispersing and the upstream intersection's impact is considered in the delay model. The relative research in China focuses on the model parameter's calibration and the relation between delay time and other parameters, such as saturation, lane's function and so on.

The paper describes three video methods to extract the parameters at signal controlled intersections. The video method can get the relative parameters on-line, which does not depend on the model.

VIDEO DETECTOR THEORY

Instant Stopping Delay Method

The instant stopping delay method comes from the gap aviation

photographing method. It records the number of stopped vehicles in per frame and then adds the total number of stopped vehicles in a period of time (Ran, 2007). It is similar to the dot-sample method.

According to the description, at the random time t, every vehicle has the instant stopping delay. If the vehicle is running, the value of $D_i(t)$ is 0, and if the vehicle is stopped, the value is 1. This is shown in equation (1):

$$D_i(t) = \begin{cases} 1 & \text{If the vehicle stopping;} \\ 0 & \text{If the vehicle not stooping;} \end{cases} \quad (1)$$

So, in the period time of T, the total stopping delay can be calculated as:

$$D_{\sum}(T) = \sum_{i=1}^{n} D_i(t) \quad (2)$$

In the formula n is the frame counts in the period time of T.

One of the most difficulties in this method is to judge the vehicle's state. Mitsuru gives three methods to deal with the problem, including the gap method, the moving method, and the manual method. In China, during the red phase, a driver who is on the approach lane will pass the intersection if he/she thinks the space between his/her vehicle and the front vehicle is large enough. Considering that fact, the speed is used to judge the vehicle's state. In SimTraffic, 3.0 m/s is used as the threshold. This choice however does not fit the stopping delay definition. In this research, we choose 0.216km/h as the threshold speed.

Semi-automatic Detection Method Based on the Software

Showing as Fig.1, semi-automatic detection method chooses the stop time effected by the red signal as its first observing time (t_1' in Figure 1) and the time when the vehicle passes the stop line as its second observing time (t_2' in Figure 1).

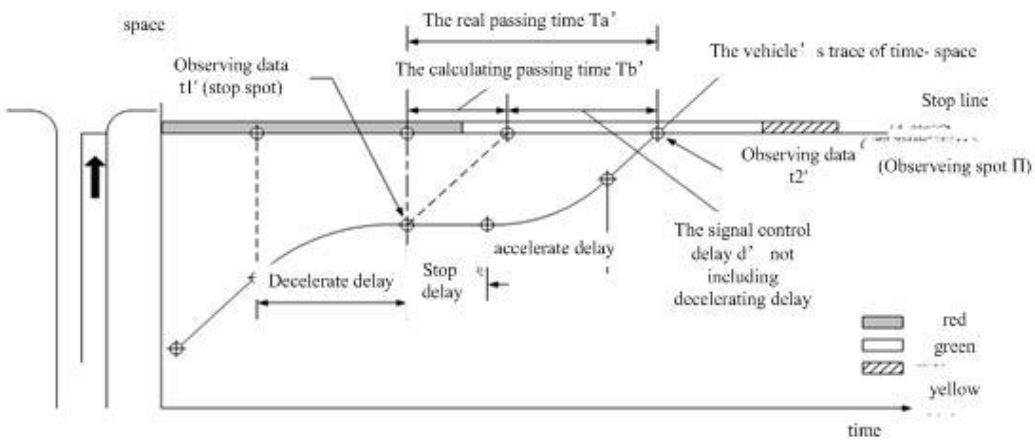

Figure 1 Semi-automatic detection method observe spot sketch map

The signal control delay variable d can be calculated as:

$$d = d' + d_{dc} \quad (3)$$

In equation (3), d' is the delay that the vehicle drives from the stop location to the stop line（s）; and d_{dc} is the vehicle's deceleration delay for blocked (s).

The variable d' can be calculated as:

$$d' = T_a' - T_b' \quad (4)$$

In equation (4), T_a' is the time that the vehicle drives from the stop location to the stop line (s); and T_b' is the calculated value that the vehicle travels from the stop location to the stop line using its normal speed（s）.

The variable T_a' can be calculated by:

$$T_a' = t_2' - t_1' \quad (5)$$

In equation (5), t_1' and t_2' 's meaning are showing in Figure1.

The variable T_b' can be calculated by:

$$T_b' = \frac{D' \times 3.6}{v} \quad (6)$$

In equation (6), D' is the distance between the vehicle's stop location and the observing location II（m）; and v is the vehicle's normal speed.

The deceleration delay variable d_{dc} can be calculated by:

$$d_{dc} = \frac{v}{a \times 3.6} \quad (7)$$

In equation (7), v is the normal average speed（km/h）; and a is the vehicle's average deceleration (m/s^2)，which should be measured in the field.

Double Section Video Detecting

The double section video detection method places two virtual detectors to extract the intersection traffic parameters. The first detector is placed on the stop line to record the vehicle's departure time. The second detector is placed far from the stop line. It aims to record the vehicle's approach time. The distance between the two detectors is 50-100 m. It can vary according to the camera height and the traffic saturation. How cameras can be set up is shown in Figure. 2. In this paper, the detector length is chosen as 15 m. The width can be set according to the number of lanes.

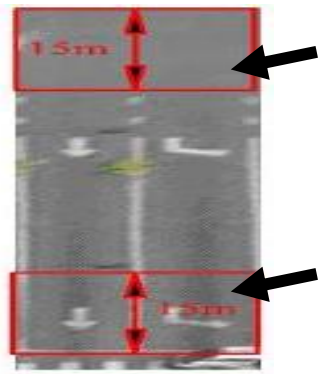

Figure2. The sketch map of the virtual detector setting

Because each vehicle is tracked from entering to leaving, the system can record the entering time and leaving time automatically. So the signal controlled delay time can be easily calculated as shown in Figure 3.

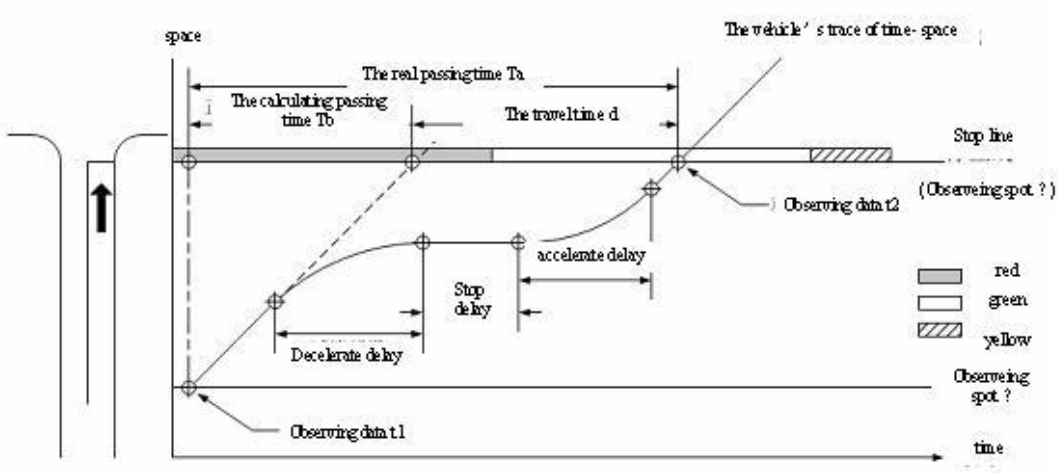

Figure 3. The sketch map of double section method

When the vehicle passes the far stop line detector, the time is recorded automatically (t_1 in Figure 3). Then the vehicle is tracked until it arrives at the stop line detector at , time t_2 in Figure 3. As a result, the actual travel time time that the vehicle spends at the approach road T_a can be calculated by:

$$T_a = t_2 - t_1 \qquad (8)$$

Assume that T_b is the time that the vehicle passing the space between the two detectors using its normal speed. The value of T_b can be calculated by:

$$T_b = \frac{D \times 3.6}{v} \qquad (9)$$

In equation (9), D is the distance between the two virtual detectors（m. Then the signal controlled delay d can be calculated by:

$$d = T_a - T_b \qquad (10)$$

COMPARISON AMONG THE METHODS

For the same video that comes from signal control intersection in Shanghai, the three methods are used for extracting the parameters. The manually collected data are used as the ground-truth. The comparison results are show in Table 1.

Tab le 1. The Comparison Results of the Three Video Detection Methods

cycle	Instant stopping delay method		Semi-automatic detection method		Double section method		Manual stat. data	
	Delay time （s）	Traffic flow(v/c)	Delay time （s）	Traffic flow(v/c)	Delay time （s）	Traffic flow(v/c)	Delay time （s）	Traffic flow(v/c)
1	12.35		25.01	12	24.40	14	22	14
2	7.6		18.49	17	14.53	15	13	15
3	11.67		30.94	7	27.40	9	22.56	9
4	38.5		50.72	8	44.79	6	48.17	6
5	26.75		52.63	11	46.76	11	43.08	12
6	18.88		48.67	8	32.82	9	31	9
7	9.3		84.01	11	58.964	11	62	10
8	38.25		58.67	14	51.71	12	49	12
9	40.92		70.13	9	57.19	8	55	8
10	23.1		52.31	8	43.97	10	39	10
Average error	40.41%		29.44 %	16.18%	9.27%	2%		

*The traffic flow is record as the number of vehicles in per cycle.

From the Table 1, the following conclusions can be made:

(1) The instant stopping delay method can estimate the stopping delay, but cannot estimate the control delay. Also, the method cannot estimate traffic flow.

(2)The semi-automatic detection method can measure the delay that includes the acceleration delay and stopping delay. In the software, the deceleration delay is added through the model to calculate the signal control delay. However this has to be done manually.

(3) The double section video detection method can estimate the signal control delay and traffic flow automatically. However the method requires strict conditions on the height and location of the camera. In addition, the camera has to face down and be placed securely.

(4) As showing in Table 1, for the same video, the instant stopping delay

method can estimate the stopping delay and captures about 60% of the signal control delay. The semi-automatic detection method estimates the signal control delay and other traffic parameters, but it has just 70% accuracy on delay and 83.82% accuracy on traffic flow. The double section video detection method can estimate the parameters as the semi-automatic detection method. The delay error is less than 10% and the traffic flow accuracy is more than 95%.

CONCLUSIONS

The video technology has been widely used in transportation. The paper described three video detection models that are deduced according to their respective detection theories. Using a test example, it is shown that the instant stopping delay method can estimate stopping delay. The semi-automatic detection method has fewer requirements in setting the camera, but it has to be done manually. The double section video detection method can estimate the parameters with high accuracy, but it has strict requirements in setting the camera.

ACKNOWLEDGE

This work was supported by a grant from the National High Technology Research and Development Program of China（No. 2007AA11Z221），Chongqing Natural Science Foundation(No. CSTC 2008BB6345).

REFERENCES

Quan Y S.(1989). “Urban Traffic Control”.Beijing: China Communication Press.

Ran Q W, Yang J G, Wang Z A, et al.(2007) “ Instantaneous Stop Delay Detection Based on Video ”. *Journal of Xi’an Jiaotong University*. 41（6）：692-696.

Saito M., Walker J., Zundel A..(2001) “Use of image analysis to estimate average stopped delays per vehicle at signalized intersections”. Washington, DC. TRB 2001： 106-113.

TRB (2000). “HCM 2000 [S/CD]”. Washington DC : National Research Council.

Enhancing Immersion through Adjusting Parameters of Vehicle Driving Simulator

Zhou Xiaobo[1] Zhu Shunying[2] Wang Hong[3] Liu Bing[4]

[1]Master Student, Dept. of Traffic Engineering, Wuhan University of Technology，430063，1040 Heping Ave., Wuchang, Wuhan, Hubei, China; Tel: +86-13163370732; E-mail: zwhc84@126.com.
[2]Professor, Dept. of Traffic Engineering, Wuhan University of Technology，430063，1040 Heping Ave., Wuchang，Wuhan, Hubei, China; Tel: +86-13995680983;E-mail: zhusy2001@163.com.
[3]Associate Professor, School of Transportation, Wuhan University of Technology, 430063, 1040 Heping Ave., Wuchang,Wuhan, Hubei, China; Tel: +86-027-62597390; E-mail: wanghong2004317@sina.com.
[4]Master Student, Dept. of Traffic Engineering, Wuhan University of Technology，43006，1040 Heping Ave., Wuchang，Wuhan, Hubei, China. Tel: +86-13871475997，E-mail: lbjiaotong@126.com.

ABSTRACT

Virtual scenes shown on vehicle driving simulator displays are somewhat different from reality, leading to a poor sense of immersion. In order to enhance the immersion techniques of vehicle driving simulators, this paper suggests two ways to make the size of the object shown on the display much more like the real object: by adjusting the parameters of the virtual camera and location of driver's eyes. The paper also analyzes the process of translation from an initial three-dimensional model to a two-dimensional image on the display. The process includes observing, projecting, and scaling the object. We also create a process by which to measure driver vision which entails observing and projecting transformation. Based on the relationship of the analyzed processes, an optimal model is established by adjusting parameters of the virtual camera, including the focus, the visual angle and the image resolution, and by adjusting the location of the driver's eyes. Parameters can be optimized based on the model, which will greatly increase the immersion function of vehicle driving simulators.

Key words: vehicle driving simulator; immersion; parameters of a virtual camera; location of driver's eyes

INTRODUCTION

Vehicle driving simulators are used widely in transportation research and practice. The vehicle driving simulators with arc-shaped channels or multi-channel displays produce much better immersion, interaction, and imagination; however, such simulators are too expensive to be used prevalently, so the simulators used for training are almost always single-channel display. The display size, virtual camera parameters, and location of the driver's eyes in single-channel simulators affect virtual scene immersion and the driver's perception of the scene. If any of these parameters are unreasonable, the displayed image will appear dissimilar to the real object, weakening the simulator's immersion function. Some scholars have researched the relationship between the virtual scene size and the display size, the

location of driver's eyes, and the parameters of virtual camera. Christopher D. Wickens (2002) mentioned in his research about Spatial Awareness Biases that if there is a change in the size of display or the geometric field of view (GFOV), the stand point of virtual camera, or even the location of observer's eyes, it will change both the location and size of the image mapped onto observer's eyes. Woodrow Barfield (1995) studied the relationship of the GFOV and spatial performance, stating that if one reduces the GFOV, the image mapped onto our eyes becomes larger. Ronald R.Mourant (2007) found that the GFOV can affect the driver's judgment about velocity. The GFOV relates to the visual angle of virtual camera: if the angle becomes larger (the focus becomes smaller), the image of the object will be enlarged and the object will appear closer to observer; if the location of driver's eyes is changed, the appearance of the observed object will change too. This leads to a series of changes that include the intersection of the line-of-sight with the display and the image size in driver's eyes. To enhance the sense of immersion, this paper proposes an adjustment in the parameters of the virtual camera and the location of driver's eyes in order to compensate for the fact that immersion is affected by the display size.

APPROACHES TO ENHANCE IMMERSION IN DRIVING SIMULATORS

Foley J D (1987) and Bryson S (1993) mentioned that there are many factors affecting the sense of immersion in virtual reality, such as display size, resolution, focus, etc. Summarizing their points, there are three ways to enhance the immersion of the driving simulator:

(1) Changing the display size. Larger images provide larger fields of view.

(2) Changing virtual camera parameters. The virtual camera parameters include the visual angle of the camera, camera focus, and image resolution.

(3)Changing the location of driver's eyes. Proper location makes the driver feel comfortable.

Since the technology of arc-shaped channels and multi-channel displays has been fully developed, this paper will not discuss the first method, but rather address the other two methods.

THE PROCESS OF SHOWING IMAGES ON THE DISPLAY

There are three steps that transform an original model from the three-dimensional world into a two-dimensional image shown on the display. These are observing transformation, projecting transformation, and scaling transformation (Xiang, 2008).

OBSERVING TRANSFORMATION.

We suppose that there is a world coordinate system (WC) $O-XYZ$, place the object models into the WC, and then establish another coordinate system called the camera coordinate system (or viewing coordinate system, VC for short) $O_c-X_cY_cZ_c$. The origin of the VC is the center of virtual camera $O_c(x_c, y_c, z_c)$, as shown in Figure1.

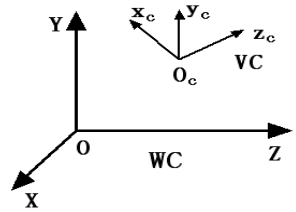

Figure1. Observing transformation

Translation and rotation are two necessary processes when transforming the coordinate of a point from the WC to the VC. Assume there is a point $P_w(x_w, y_w, z_w)$ in the WC, the point located at $P'(x_c, y_c, z_c)$ in the VC, the expression of transformation matrix is shown as follows:

$$\because\ x_c,\ y_c,\ z_c,\ 1)^T = \begin{bmatrix} R_c & t_c \\ 0^T & 1 \end{bmatrix} (\ x_w,\ y_w,\ z_w,\ 1)^T = M_{co}(\ x_w,\ y_w,\ z_w,\ 1)^T \tag{1}$$

Where R_c is a 3-by-3 unit orthogonal matrix, t_c is a three-dimensional translation vector, $0^T = (0\ \ 0\ \ 0)$, M_{co} is a 4-by-4 matrix (Kajita,2007; Zhang, 2008). Since M_{co} is determined by the relative position of the camera to the WC, it is called outside parameters matrix of virtual camera.

PROJECTING TRANSFORMATION. The projecting transformation is quite similar to the imaging process of a virtual camera on a single-channel driving simulator. The camera can be as simplified as a pinhole camera model (Zhang Mao-jun, 2001). Assume $P_i(x_i\ \ y_i)$ is the image coordinate of $P'(x_c, y_c, z_c)$ in the VC, the process of projecting transformation can be written as

$$k_c \begin{bmatrix} x_i \\ y_i \\ 1 \end{bmatrix} = \begin{bmatrix} f_c & 0 & 0 & 0 \\ 0 & f_c & 0 & 0 \\ 0 & 0 & 1 & 0 \end{bmatrix} \begin{bmatrix} x_c \\ y_c \\ z_c \\ 1 \end{bmatrix} = p \begin{bmatrix} x_c \\ y_c \\ z_c \\ 1 \end{bmatrix} \tag{2}$$

Where, k_c is a scale factor, f_c is the focus of the virtual camera optical system, p is called perspective projecting matrix.

The basic unit of the image is a pixel, but the unit of the transformation above is physical, thus we should translate the physical unit to pixel. Suppose that each pixel on X and Y axis occupies dx and dy of length measured by physical unit separately, the origin of the physical coordinate system is (u_0, v_0) in pixel coordinate system (see Figure.2).

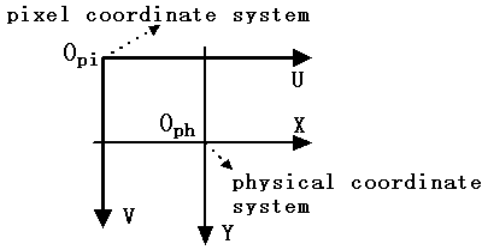

Figure2. Unit transformation

The unit transformation in the image can be expressed as

$$\begin{bmatrix} u \\ v \\ 1 \end{bmatrix} = \begin{bmatrix} \frac{1}{dx} & 0 & u_0 \\ 0 & \frac{1}{dy} & v_0 \\ 0 & 0 & 1 \end{bmatrix} \begin{bmatrix} x_i \\ y_i \\ 1 \end{bmatrix} \tag{3}$$

Then the perspective projecting can be deduced as

$$k_c \begin{bmatrix} u_i \\ v_i \\ 1 \end{bmatrix} = \begin{bmatrix} a_x & 0 & u_0 & 0 \\ 0 & a_y & v_0 & 0 \\ 0 & 0 & 1 & 0 \end{bmatrix} \begin{bmatrix} x_c \\ y_c \\ z_c \\ 1 \end{bmatrix} = M'_{ci} \begin{bmatrix} x_c \\ y_c \\ z_c \\ 1 \end{bmatrix} \tag{4}$$

Where, $a_x = f_c/dx$, $a_y = f_c/dy$ are measure factors on u , v axis separately, they are called the normalized focus. a_x, a_y, u_0, v_0 are related with inside parameters of virtual camera, so they are called inside parameters of camera.

SCALING TRANSFORMATION. The image in the camera should be scaled to show on the driving simulator display, the process is shown as follows:

$$\begin{bmatrix} u_d \\ v_d \\ 1 \end{bmatrix} = \begin{bmatrix} a(2f_c)^{-1}\cot(\frac{\theta_h}{2}) & 0 & 0 \\ 0 & b(2f_c)^{-1}\cot(\frac{\theta_v}{2}) & 0 \\ 0 & 0 & 1 \end{bmatrix} \begin{bmatrix} u_i \\ v_i \\ 1 \end{bmatrix} = M_{c\to d} \begin{bmatrix} u_i \\ v_i \\ 1 \end{bmatrix} \tag{5}$$

Here, we denote a as the length of display, b as the width, and θ_h as the horizontal geometric field of view, θ_v as the vertical geometric field of view., (u_d, v_d) is pixel coordinate of P on the image. The matrix $M_{c\to d}$ can be factored as $M_{c\to d} = M_d M_c$.

Where, $M_d = \begin{bmatrix} a & 0 & 0 \\ 0 & b & 0 \\ 0 & 0 & 1 \end{bmatrix}$ and $M_c = \begin{bmatrix} (2f_c)^{-1}\cot(\frac{\theta_h}{2}) & 0 & 0 \\ 0 & (2f_c)^{-1}\cot(\frac{\theta_v}{2}) & 0 \\ 0 & 0 & 1 \end{bmatrix}$

Actually, M_d is related with the size of display and is called the parameters matrix of display; M_c is related with the focus and visual angle of virtual camera.

Since M_c and M'_{ci} are the matrixes that relate to the parameters of virtual cameras, they can be composed to one matrix $M_{ci} = M_c M'_{ci}$, M_{ci} is called as the inside parameters matrix of virtual camera.

The process that translates the point $P_w(x_w, y_w, z_w)$ in the WC to be the point $P_d(u_d, v_d)$ on the display, where the unit is pixel is shown as

$$k_c(u_d, v_d, 1)^{\mathrm{T}} = M_d M_{ci} M_{co} (x_w, y_w, z_w, 1)^{\mathrm{T}} \tag{6}$$

Where, k_c is a scale factor, M_d is parameters matrix of display; M_{ci} is inside parameters matrix of virtual camera; M_{co} is outside parameters matrix of virtual camera.

A SIMPLIFIED IMAGING MODEL FOR DRIVER'S EYES

The process by which an object is mapped onto the eyes is much too complicated, but we can observe the intersection of the line-of-sight with the display when we observe a virtual object as the point that will be crossed with the object imaged in eyes. Likewise, the observing transformation and projecting transformation information are required, but scaling transformation can be neglected in the driver's observation process.

We can designate an eye coordinate system (EC) whose origin is the location of driver's eyes. Similarly, the observing transformation matrix of driver's eyes is $M_{eo} = \begin{bmatrix} \mathrm{R_e} & t_e \\ 0^T & 1 \end{bmatrix}$. It is called the outside parameter matrix of the eyes.

Suppose the coordinate of the object is $P_e(x_e, y_e, z_e)$ in the eye coordinate system; the equation of display surface is $z = z_d$; and the display center is on the z axis. Driver sight intersects the display at $P_d(x_d, y_d, z_d)$. Therefore the parametric equation of the line of sight is

$$x = x_e t, \quad y = y_e t, \quad z = z_e t \tag{7}$$

Since $z_d = z$, so $t = \frac{z_d}{z_e}$, then we can compute that $x_d = \frac{z_d}{z_e} x_e$, $y_d = \frac{z_d}{z_e} y_e$.

If we use an equation to express the imaging process in eyes as

$$k_e \begin{bmatrix} x_d \\ y_d \\ z_d \end{bmatrix} = \begin{bmatrix} z_d & 0 & 0 & 0 \\ 0 & z_d & 0 & 0 \\ 0 & 0 & 1 & 0 \end{bmatrix} \begin{bmatrix} x_e \\ y_e \\ z_e \\ 1 \end{bmatrix} = M_{de} \begin{bmatrix} x_e \\ y_e \\ z_e \\ 1 \end{bmatrix} \tag{8}$$

Here, k_e is a scale factor too.

Similarly, the unit of intersection in the display is physical, it needs to be translated to a point with the pixel unit. The translation matrix is

$$M_d^{'} = \begin{bmatrix} \frac{1}{dx_d} & 0 & u_d \\ 0 & \frac{1}{dy_d} & v_d \\ 0 & 0 & 1 \end{bmatrix} \tag{9}$$

We denote dx_d, dy_d as physical length of each pixel on image that projected to display on X, Y separately. So the whole process is show as

$$k(u_d', v_d', 1)^{\mathrm{T}} = M_d' M_{de} M_{eo} (X_w, Y_w, Z_w, 1)^{\mathrm{T}} \tag{10}$$

CALIBRATING PARAMETERS

Based on the above analyses, the coordinate deviations of the intersection and the point on the display can be expressed by a vector

$$M' = k(u_d, v_d, 1)^{\mathrm{T}} - k(u_d', v_d', 1)^{\mathrm{T}} \tag{11}$$

Since the scale factor k_c is related with depth of the object in the VC, k_e is

related with depth of the object in EC , and usually the origin of the VC approaches the origin of the EC, suppose that $k = k_c \approx k_e$, so (11)can be replaced by

$$M' = k(M_d M_{ci} M_{co} - M_d^{'} M_{de} M_{eo}) \begin{pmatrix} X_w & Y_w & Z_w & 1 \end{pmatrix}^T \quad (12)$$

Define M as : $M = (M_d M_{ci} M_{co} - M_d^{'} M_{de} M_{eo})$

Now the main challenge is to make (12) small enough. Obviously, the factor $k \neq 0$ and $\begin{pmatrix} X_w & Y_w & Z_w & 1 \end{pmatrix}^T$ is variable, so we have to reduce M to achieve this. The problem therefore becomes an inequality-constrained minimization problem. The objective function can be abbreviated as $\min \| M \|$. $\| M \|$ is the normal number of M and the constraints are $\theta_h - \theta_{h\min} \geq 0$, $\theta_v - \theta_{v\min} \geq 0$, $z_d > 0$. Here $\theta_{h\min}$ and $\theta_{v\min}$ are the minimum horizontal and vertical visual angle respectively, its value can be given prior under different conditions, $z_d > 0$ show that the eyes must keep a respectful distance from the display.

So the problem can be written as

$$\begin{aligned} &\min \| M \| \\ &s.t. \theta_h - \theta_{h\min} \geq 0 \\ &\theta_v - \theta_{v\min} \geq 0 \\ &z_d > 0 \end{aligned} \quad (13)$$

Now we can change the inside parameters of camera and the location of driver under the constraints, and the immersion will be enhanced when changing the parameters.

DISCUSSION AND CONCLUSION

To solve the problem that single-channel displays affect the immersion factor in driving simulators, this paper established an optimum model by adjusting the virtual camera's parameters and the location of driver by analyzing computer graphics and the process of imaging in eyes.

Compared to enlarging the display or bending the display to an arc-channel, the method stated in this paper costs much less. If the parameters are optimum, some experiments can be done with simple display that will reduce the cost. Furthermore this method can enhance the immersion factor even if done with a multi-channel or arc-channel display. According to our analysis, the location of driver's eyes is an important factor affecting the immersion process that has been neglected by other literature. However, the method in this paper locates the driver in different experimental environments in order to enhance the immersion.

The model is based on driving simulators with single-channel display. When used on vehicle driving simulators with multi-channel and arc-channel display, it must be modified since the processes by which images are displayed are very complex. This will be addressed in future research, and we will do our best to verify and perfect the method stated in the paper through experimentation.

ACKNOWLEDGMENTS

This work was supported by the National Natural Science Foundation of China (NO. 50778142).

REFERENCES

Bryson S(1993). "Implementing virtual reality." *ACM SIGGRAPH*, Course notes 43:1~49.

Christopher D. Wickens(2002). "Spatial Awareness Biases." *Technical Report AHFD-02-6/NASA-02-4*.

Foley J D(1987). "Interfaces for advanced computing.".*Scientific American*, Oct. 83~90.

Ronald R .Mourant, Najla Ahmad, Beverly K, Jaeger, Yingzi Lin(2007). "Optic flow and geometric field of view in a driving simulator display." *DISPLAYS 28* (2007)145-149.

Shuuji Kajita, Hirohisa Hirukawa, Kazuhito Yokoi, Kensuke Harada(2007) "Humanoid Robots." *Tsinghua University Press*, 15-59.

Woodrow Barfield, Claudia Hendrix, Ove Bjorneseth(1995). "Spatial performance with perspective displays as a function of computer graphics eyepoint elevation and geometric field of view." *Applied Ergonomrcs* Vol 26. No. 5. 307-314.

Xiang, Zhi-gang(2008). "Computer Graphics with OpenGL." *Tsinghua University Press*, 125-141.

Zhang, Guang- jun(2008). " Vision Measurement." *Science Press ,*131-136.

Zhang, Mao- jun(2001). "Virtual Reality System." *Science Press*, 122-156.

A calculation method for the information utility of traffic guide signs

Zhu Li-li[1], SHI Jian-jun[2] and Chen Xin-dong[3]

[1]Beijing Key Lab of Transportation Engineering, Beijing University of Technology, Beijing 100124, China, PH (010)67395425; email: zhulili@emails.bjut.edu.cn
[2]Beijing Key Lab of Transportation Engineering, Beijing University of Technology, Beijing 100124, China, PH (010)67392991; email: jjshi@bjut.edu.cn
[3]Center of Tunnel and Underground Engineering, Beijing Jiaotong University, Beijing 100044, China, PH (010)51468747; email:07121567@bjtu.edu.cn

ABSTRACT

In this paper, we make use of informatics-based methods, establishing a calculation technique to measure the utility of a traffic sign's information for drivers. Additionally, some simple analyses are carried out to determine the usefulness of certain information for drivers who need different types of information.

KEYWORDS

traffic guide sign, information, utility

1 PREFACE

As a traffic management tool, the function of the traffic sign is transmit information to drivers. The relationship between traffic signs and drivers is that of information source to receiver. At present, some achievements have been made in the study of traffic sign information. These studies mainly focus on calculating the volume of information transmitted by traffic signs (Liu Xi, 1999; Cao Peng, 2006), and on evaluating the usability of the signs (Chen Guo-long, 2007), etc. However, it is necessary to improve the utility of traffic signs if we want to ensure that a traffic sign's information is adequately transmitted to the driver. Informatics offer an effective way to measure a traffic guide sign's usefulness.

2 THE CONTROL ROLE OF INFORMATION AND GENERAL INFORMATION MEASURE MATHOD

2.1 THE CONTROL ROLE OF INFORMATION

In the case of traffic systems, information is a statement about the contents of a thing (or system) communicated to the outer world as the system adapts to the external environment. Feeding such adaptations to the external environment, then, this exchanged content makes information an expression set for the specific location of the space in which a thing exists. This information resource reduces driver uncertainty about the status of the thing or system, while differential rule out other uncertainties.

"Control" is an adjustment process meant to overcome any uncertain status in

the system. In such adjustment processes, the system develops so as to move toward a fixed status. “Control” means that system behavior develops in a certain way, while “information” communicates the system's development status as selected by control and information both reflect the system’s increased activity toward negentropy.

2.2 GENERAL CALCULATION METHOD FOR INFORMATION VOLUME

The probabilistic information of a single case removed is the statistical uncertainty of information sink. A formula about the entropy of a discrete source formula proposed by Shannon as shows below (Piao Chang-gen, 2004, *Foundations of Systematology*):

$$H = -K\sum_{i=1}^{n} p_i \log p_i \qquad (2\text{-}1)$$

Where K is a plus constant. H is the measurement about information, choice and uncertainty, termed as the entropy of the probability set $p_1, p_2, \cdots, p_n$. When the logarithmic base is *2*, the K value takes *1*, the units of information amount is *Bit* (abbreviation for *Binary Digit*). This is a general way of representing a method for measuring the amount of an information source.

3 TYPES OF THE INFORMATION OF TRAFFIC GUIDE SIGNS

Generally, the traffic managers need to communicate two types of information: management information and service information, as shown in Figure 1(Shao Hai-peng, 2007). Traffic signs and directions in our study focus on service-oriented information. Their function is to provide travelers with the road network surrounding their current locations and/or urban (or regional) center, landmark buildings, key place names, as well as direction, distance information and so on. This enables drivers to position themselves within the road network, and it provides a reference point so as to assist, travelers in their decision-making.

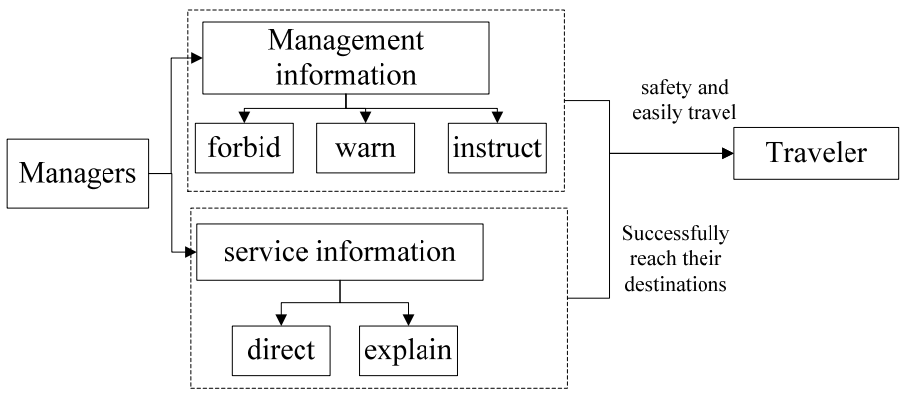

Figure1. Travel information classification and its role

4 CALCULATION METHOD FOR THE INFORMATION UTILITY OF

TRAFFIC GUIDE SIGNS

4.1 ASSUMPTIONS ON THE TARGET OF TRAFFIC GUIDE SIGNS

For the general traffic participants studied in this paper, we made the following assumptions:

a) The drivers are not absolute strangers to the road traffic, but know the basic regional situation (such as it can be found on maps). They are familiar with the surrounding environment, recognizing the important landmarks in the region;

b) For different road signs, drivers know their destinations;

c) Drivers have a basic knowledge of traffic and can understand the content of road signs.

Based on the assumptions above, we calculated the utility of guide information needs for different drivers respectively.

4.2 CALCULATION METHOD FOR THE INFORMATION UTILITY OF TRAFFIC GUIDE SIGNS

With respect to guide signs, the sign is located in a place of discrete probability of source; that is, it communicates self-contained information known as the source self-information. There are *n* types of elements in this source, (Chinese characters, letters, shapes, colors, numbers, images and symbols, etc.). Each element contains its own self-information $H(X_i)$(Zhou Yin-qing, 2006, *Foundations of Information Theory*).

The probability space for element X_i is as follows:

$$\begin{pmatrix} X_i \\ P \end{pmatrix} = \begin{pmatrix} x_1 & x_2 & \dots & x_j & \dots & x_{M_I} \\ p(x_1) & p(x_2) & \dots & p(x_j) & \dots & p(x_{M_i}) \end{pmatrix}$$

So, the self-information of guide sign H can be calculated by formula (4-1):

$$H = \sum_{i=1}^{n} H(X_i) = \sum_{i=1}^{n} \sum_{j=1}^{M_i} - p(x_j) \log p(x_j) \quad (i=1,\ 2, \cdots\cdots\ n,\ j=1,2 \cdots\cdots M_i) \text{(4-1)}$$

Among the information of guide sign, as for element i

$$p(x_1) = p(x_2) = \wedge = p(x_{M_i}) = \frac{1}{M_i},$$

so, formula 4-1 equals to (4-2):

$$H = \sum_{i=1}^{n} H(X_i) = \sum_{i=1}^{n} \log M_i \qquad (i=1,2, \ \cdots\cdots n) \qquad \text{(4-2)}$$

Where: H ——The total information volume of information source;

X_i ——element i in information source;

M_i ——status Number of element i ;

$p(x_j)$ ——the probability of the status j for an element of information source;

n ——types of elements contained in information source, including characters, letters, shapes, colors, numbers, images and symbols.

As for the information volume contained in every element of a traffic guide sign, Yung-Ching Liu (Yung-Ching Liu 2005) has presented a calculation method for each element. For instance, in the case of Arabic numerals, each number transmits 3.3 bits of information; in the case of sign-shape, 8 kinds of shapes can be used in traffic signs (*Road Traffic Signs and Markings GB5768-1999*) and each shape transmits 3bit information In this way, we can calculate the total amount of self-information contained in each guide sign.

For traffic sign users, the amount of information obtained from the sign is limited; they can not make full use of all the information contained in the sign. Here, we divide all the information on the signs into two parts: some elements ($X_a, a \in (0, k \le n)$) can provide users with certain information, and the information contained in these elements can be fully absorbed by users, Other sign elements($X_b, b \in (0 \le k, n)$) only enable users to reduce some uncertainties; they can help somewhat in reaching the destination, but do not provide exact information. Therefore, the information that the sign users get from traffic sign H' is supposed to composed by two parts, as shown in (4-3)：

$$H' = \sum_{a=1}^{k} \log M_a + \left[\sum_{b=k}^{n} \log M_b - \sum_{b=k}^{n} H(Y; X_b) \right] \quad (0<a<k<b<n) \tag{4-3}$$

therein： $H(Y; X_b) = \sum_{j=1}^{M_j} - p(Y; x_j) \log p(Y; x_j)$,

where： H' ——information obtained by sign users;

Y ——the case of get the destination;

$p(Y; x_j)$——determine the probability of case Y after realized the status j of element b ;

$H(Y;x_b)$—— priori information of element *b* for users.

The other symbols keep the same meaning as mentioned above.

Easily approve that $H' \le H$.

Defining η is the utility of traffic guide signs. It equals the ratio of information that the sign users get and self-information of information source, as shown in (4-4):

$$\eta = \frac{H'}{H} \tag{4-4}$$

From the above analysis we can see: $0 \le \eta \le 1$.

4.3 THE UTILITY OF INFORMATION ANALYSIS FOR DIFFERENT TYPES OF DRIVERS

1) Drivers who are completely familiar with the local traffic environment

These drivers do not need the information on the sign at all. The guide sign is superfluous, so they get no information from the guide sign, the utility $\eta = 0$.

2) Drivers who are fairly familiar with the local traffic environment

Such drivers are fairly familiar with the local traffic environment, but could still use the help of outside information to arrive their destination. The information amount they obtain is not 0, the utility $0 < \eta < 1$.

Consider as a point of analysis the driver who only needs directional information to arrive at the destination. According to the rules in *Road Traffic Signs and Markings GB5768-1999*, there are, on average, 4 kinds of direction on signs, the information represented on one sign therefore being $H = \log 4 = 2bit$, After the drivers have obtained the information from the signs, the posterior probability becomes *1/2* for the direction of destination. The information obtained equals $H' = H - \log 2 = 1bit$, so the current utility of guide signs is $\eta = 1/2$. The calculation method for other, more complicated situations is similar.

3) As for those drivers who are completely unaware of the local traffic environment and can receive all the sign information, they can make full use of the information on signs, so, the utility $\eta = 1$.

Up to now, this section describes the calculation method for the information utility of traffic guide signs, and we have analyzed the information utility for different types of drivers.

5 CONCLUSIONS

The value of information utility for traffic guide signs is a key indicator for evaluating the design and usability of road signs. In this paper, made use of some informatics research to create a calculation formula for standardizing the utility of guide sign information, and we have analyzed the information utility for different types of drivers. What should therefore be recognized is that the three main types of drivers have different needs at different locations, so the main information type of guide signs should also be different. Different partial information should be provided for drivers who have different information requirements. In this way can improve the utility of guide signs, thus saving materials and resources used for the production of signs.

REFERENCES

Cao Peng, Wu Wen-jing, Juan Zhi-cai (2006). "Study on Drivers' Comprehension of Traffic Signs Based on Information Measurement." *Journal of Highway and Transportation Research and Development*, 23(9), 118-120.

Chen Guo-long (2007). *Study and Evaluation on the Information's Usability of Traffic Guide Signs*. Jilin University, Jilin, China.

Liu Xi, Zhang Kan (2003). "Quantitative evaluation methods for road traffic signs," *Chinese Journal of Ergonomics*, 9(4), 23-26.

Piao Chang-gen (2004). *Foundations of Systematology*, Shanghai Lexicographic Publishing House, Shanghai, China.

Road Ttraffic Signs and Markings GB5768-1999 (1999), Standards Press of China, Beijing, China.

Shao Hai-peng, Dong Hai-qian(2007). *A Better Usage of Traffic Info-Terms in Traffic Management*, Urban Transport of China, 5(6),19-22..

Yung-Ching Liu (2005). "A simulated study on the effects of information volume on traffic signs, viewing strategies and sign familiarity upon driver's visual search performance," *International Journal of Industrial Ergonomics*, 35, 1147–1158.

Zhou, Yin-qing (2006). *Foundations of Information Theory*, Beijing University of Aeronautics and Astronautics Press, Beijing, China.

Safety Evaluation Methods of Road Traffic Based on Gray Cluster Theory

L. Wei[1] and Z. Guan[2]

[1]Associate Professor, MOE Key Laboratory for Urban Transportation Complex Systems Theory and Technology, School of Traffic and Transportation, Beijing Jiaotong University, 100044, PH: (010)51688344, email: wly105@sohu.com.

[2]Master Student, School of Traffic and Transportation, Beijing Jiaotong University, 100044, PH: (010)51689121, email: moyn007@163.com.

ABSTRACT

This article analyzes the characteristics and the applicability of the gray cluster theory, taking the traffic statistics of Jiangsu, Jilin, Beijing, Chongqing and Gansu as examples, and arriving at the conclusions that the road traffic safety levels of Beijing and Chongqing are relatively higher, the level of Jiangsu is ordinary, while the levels of Jilin and Gansu are relatively lower. This paper, aiming at road traffic safety assessment based on the gray cluster theory, explores the analysis thread and research steps, as well as analyzes the reasonableness of the results. What's more, the authors propose their own ideas on the selection of the evaluation indicators, the determination and processing of whitening values of different gray classes. In addition, this paper also carries on the forecast to this theory's application prospect and the trend of development.

Keywords: Traffic safety evaluation; gray cluster theory; evaluation indicators; whitening function

INTRODUCTION

Gray system theory (Niu 2005) takes the uncertainty system as the research objects, mainly withdraws the valuable information from the generation and development of the known information in order to correctly understand and evaluate the system operation behaviors. In the road traffic system, the happening of the accidents may be random and casual, and some traffic data are also inconvenient to be collected and sorted. Therefore, there may be a number of uncertain factors in the road traffic system. Accordingly an area's road traffic system may be regarded as a gray system (Yue et al., 2005). In the safety evaluation process, sometimes there is no need to have access to all statistical indicator data. In accordance with the gray cluster thought, evaluating the overall level of road traffic safety in a certain gray class can be realized through screening, processing, extending, and expanding of part of the available information, with the combination of the qualitative and quantitative analysis.

The gray cluster theory can be used to consider the multi-factor influences of the evaluating indicators, and reflect the road traffic safety conditions accurately through the determination of the primary factors. Else, the evaluation method can carry out a comprehensive analysis from the horizontal or the vertical angle, which means it can assess the road traffic safety situation in the different areas or in the same area during the different periods dynamically. Above all, the gray cluster theory has broad applicability and significant guiding effect in the practical work.

As a result, this article has a research on the road traffic safety evaluation method based on gray cluster theory, with the traffic accidents statistic data of five representative and typical districts: Jiangsu, Jilin, Beijing, Chongqing, and Gansu.

ANALYSIS THREAD

Gray cluster theory is applied to road traffic safety evaluation, while combined with the specific characteristics of road traffic system out of a comprehensive consideration. The analysis and the research may be carried on according to the following steps:

(1) Explicating the objects. Determine the number of the evaluating objects, indicators and the gray classes. In this step, the selection of the evaluating indicators is a key link. The indicators based on the road traffic system should be able to fully reflect the level of the security and the severity of the accidents. In order to fully take the consequences of the accidents and the extent of the impacts relevant to the mobile car retention quantity, highway mileage et al. into account, as well as evaluate the level of road safety reasonably from the aspects of quantity (frequency) and quality (severity), we use the indicators of the relative accidents rate for research: the indicators of mortality per 10 thousand vehicles (persons per 10 thousand vehicles), death/injury ratio (%), the number of serious accidents per 100 thousand kilometers.

(2) Giving out the original sample matrix D. If we calculate and evaluate the actual indicators data directly, it will easily make the concept unclear and the comparison difficult, since each indicator has a different dimension and changing range. Therefore, it's necessary to deal with the data to obtain non-dimension matrix D'. In this article, the non-dimension matrix generates from Equation 1, the values of which are varied between 0 and 1.

$$x = \frac{d - d_{\min}}{d_{\max} - d_{\min}} \tag{1}$$

While the processed values of each evaluating indicator change from low to high, the nature displays from superiorly to poorly.

（3）Determining the whitening values of each gray class. The whitening values of each gray class could be determined through drawing the cumulative frequency curve and then obtaining the characteristic values corresponding to the cumulative frequency of the gray class. However, because this method determines the whitening values of each gray class on basis of the selected sample data, it makes the final

results only comparable among the samples. If we select different sample data when carrying out road safety evaluation, the evaluation criteria established will be different also, which makes the results of the evaluation fail to be comparable. Therefore, some scholars have suggested that the whitening values of each gray class can be obtained from the related normative standards or experts' advices, in order to unify the evaluation standard (Liu Yongqing, Li Wenquan, 2006). Urban Road Traffic Management Evaluation Index System is a set of evaluation indicator systems synthesized, in which the situations of the cities vary from the scale, the development phase, the demand characteristic, and the traffic management points. This article will refer to this system's classification situation and then determine the evaluation standard of different indicators and different gray classes.

(4) Determining the gray whitening function of each gray class. The gray whitening function $f_{jk}(x_{ij})$ describes the "preferred" level of the value in the corresponding range. "i" stands for the evaluation object, "j" stands for the evaluation indicator, and "k" stands for the evaluation gray class.

(5) Calculating the cluster coefficients. It conforms to the Equation 2:

$$\eta_{jk} = \frac{\lambda_{jk}}{\sum_{j=1}^{n} \lambda_{jk}} \tag{2}$$

"η_{jk}" stands for the cluster coefficients while the indicator j belongs to the gray class k, "λ" stands for the characteristic value—corresponding whitening value.

(6) Carrying on the cluster to the object. First, determine the cluster value of each gray class of each indicator using Equation 3:

$$\sigma_{ik} = \sum_{j=1}^{n} f_{jk}(x_{ij}) \bullet \eta_{jk} \tag{3}$$

Secondly, fix the final cluster value according to the Equation 4:

$$\sigma^{*} = \max(\sigma_{ik}) \tag{4}$$

Finally, determine the safety situation hierarchy of each object.

APPLICATION EXAMPLE

Basic data

This article takes Jiangsu, Jilin, Beijing, Chongqing and Gansu as examples, and then evaluates their levels of road traffic safety through gray cluster method. These five representative districts are different from geographical locations, natural conditions, and levels of economic development.

In 2007, the related traffic data of each district are shown in Table 1.

Table 1. Basic data（2007）

District	Mobile Car Retention Quantity（10 thousand cars）	Highway Mileage（km）	Traffic Accidents Death（persons）	Traffic Accident Injury（persons）	Serious Accidents Number（accidents）
Jiangsu	330	133732	5884	18617	12
Jilin	110	85445	1870	8099	10
Beijing	278	20754	1182	6257	0
Chongqing	145	104705	1218	11893	9
Gansu	53	100612	1548	4286	11

(**Note:** The data of Traffic Accidents Death, Traffic Accident Injury and Highway Mileage are obtained from 2008 China Statistical Yearbook. The data of Mobile Car Retention Quantity are referred to National Economy and Social Development Statistical Bulletin of different areas in 2007. The data of Serious Accidents Number are obtained from the Brief on the 2007 National Road Traffic Accidents promulgated by the Ministry of Public Security.)

Application of Gray Cluster Evaluation

(1) Calculate the indicators of mortality per 10 thousand vehicles, death/injury ratio, and the number of serious accidents per 100 thousand kilometers in the five districts according to the basic data listed in Table 1. From these calculations the sample matrix D is obtained as follow (see Matrix 1). Then, deal with the data in the matrix D to obtain the non-dimension matrix D' (see Matrix 2) according to the Equation 1.

(2) The evaluation standard will be classified as grade 1,2,3,4,5 in accordance to the Urban Road Traffic Management Evaluation Index System (2007), which reflects that the safety level changes from high to low. The whitening values of each gray class are listed below (see Matrix 3).

Since the whitening values of each gray class of each evaluating indicator differ a lot, it should be dealt with the equivalent non-dimensional treatment according to the Equation 1 with the sample data, in order to ensure comparability with the sample matrix. The results of the standardization are shown in Matrix 4.

$$\begin{vmatrix} 17.83 & 31.61 & 8.96 \\ 17.00 & 23.09 & 11.76 \\ 4.25 & 18.89 & 0.00 \\ 8.40 & 10.24 & 8.57 \\ 29.21 & 36.12 & 10.89 \end{vmatrix} \quad (1) \qquad \begin{vmatrix} 0.544 & 0.826 & 0.762 \\ 0.511 & 0.497 & 1.000 \\ 0.000 & 0.334 & 0.000 \\ 0.166 & 0.000 & 0.729 \\ 1.000 & 1.000 & 0.926 \end{vmatrix} \quad (2)$$

(**Note:** The rows express in turn: mortality per 10 thousand vehicles, death/injury ratio, the number of serious accidents per 100 thousand kilometers; the lines express in turn: Jiangsu, Jilin, Beijing, Chongqing, Gansu.)

$$\begin{vmatrix} 8 & 12 & 16 & 20 & 32 \\ 9 & 15 & 20 & 25 & 30 \\ 1 & 4 & 8 & 12 & 16 \end{vmatrix} \quad (3) \qquad \begin{vmatrix} 0.150 & 0.310 & 0.471 & 0.631 & 1.112 \\ 0.029 & 0.184 & 0.377 & 0.570 & 0.764 \\ 0.085 & 0.340 & 0.680 & 1.020 & 1.361 \end{vmatrix} \quad (4)$$

(**Note:** The rows express in turn: grade 1,2,3,4,5; the lines express in turn: mortality per 10 thousand vehicles, death/injury ratio, the number of serious accidents per 100 thousand kilometers. The data of The Number of Serious Accidents per 100 Thousand Kilometers are calculated in light of the classification of the number of the serious accidents mentioned in the Urban Road Traffic Management Evaluation Index System and the average highway mileage of different districts.)

If we determine the whitening values of each gray class by drawing the cumulative frequency curve, we can derive the curves shown in Figure 1. By the figure, we can find that except for the limitation mentioned above, this method cannot be effectively used in cluster evaluation to derive the characteristic values precisely through regression analysis, while the amount of the sample is small and the dispersion degree is large.

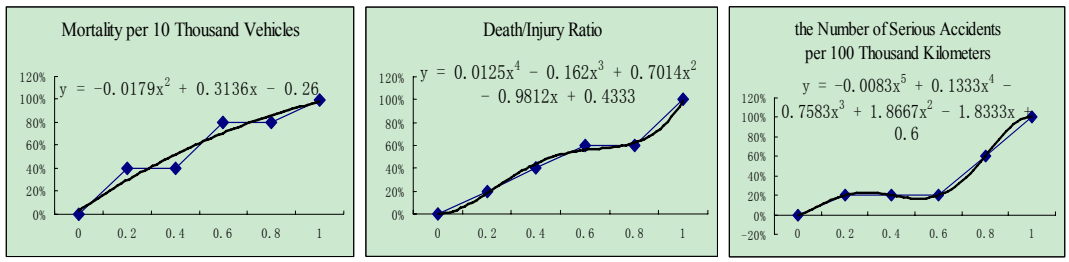

Figure 1. Cumulative frequency curve

(3)The classic gray whitening function is studied in this article. The models are listed below (see Equations 5-9)

$$f_1(x) = \begin{cases} 1 & x > \lambda_1 \\ \dfrac{\lambda_2 - x}{\lambda_2 - \lambda_1} & \lambda_2 \le x \le \lambda_1 \\ 0 & x < \lambda_2 \end{cases} \quad f_2(x) = \begin{cases} 0 & x > \lambda_1 \\ \dfrac{x - \lambda_1}{\lambda_2 - \lambda_1} & \lambda_2 \le x \le \lambda_1 \\ \dfrac{\lambda_3 - x}{\lambda_3 - \lambda_2} & \lambda_3 \le x < \lambda_2 \\ 0 & x < \lambda_3 \end{cases} \quad f_3(x) = \begin{cases} 0 & x > \lambda_2 \\ \dfrac{x - \lambda_2}{\lambda_3 - \lambda_2} & \lambda_3 \le x \le \lambda_2 \\ \dfrac{\lambda_4 - x}{\lambda_4 - \lambda_3} & \lambda_4 \le x < \lambda_3 \\ 0 & x < \lambda_4 \end{cases}$$

$$f_4(x) = \begin{cases} 0 & x > \lambda_4 \\ \dfrac{x - \lambda_3}{\lambda_4 - \lambda_3} & \lambda_4 \le x \le \lambda_3 \\ \dfrac{\lambda_5 - x}{\lambda_5 - \lambda_4} & \lambda_5 \le x < \lambda_4 \\ 0 & x < \lambda_5 \end{cases} \quad f_5(x) = \begin{cases} 0 & x > \lambda_4 \\ \dfrac{x - \lambda_4}{\lambda_5 - \lambda_4} & \lambda_5 \le x \le \lambda_4 \\ 0 & x < \lambda_5 \end{cases}$$

Table 2. The cluster coefficients

	1	2	3	4	5
Mortality per 10 Thousand Vehicles	0.57	0.37	0.31	0.28	0.34
Death/Injury Ratio	0.11	0.22	0.25	0.26	0.24
Number of Serious Accidents per 100 Thousand Kilometers	0.32	0.41	0.45	0.46	0.42

First, calculate the cluster coefficients conforming to the formula (see Table 2).

Then, calculate the cluster values of grade 1 to 5 according to models 5 to 9 in light of the relationships between the sample values and characteristic values (see Table 3).

Table 3. Cluster values of each district

District	1	2	3	4	5
Jiangsu	0	0	0.510	0.239	0
Jilin	0	0	0.354	0.665	0
Beijing	0.890	0.049	0.194	0	0
Chongqing	0.623	0.037	0.385	0.066	0
Gansu	0	0	0.124	0.398	0.261

(4) Calculate the final cluster value according to Equation 4, and then finally determine the safety situation hierarchy of each object. In conclusion, in 2007, Jiangsu: $\sigma^* = 0.510$, the safety level is in grade 3; Jilin: $\sigma^* = 0.665$, grade 4; Beijing: $\sigma^* = 0.890$, grade 1; Chongqing: $\sigma^* = 0.623$, grade 1; Gansu: $\sigma^* = 0.398$, grade 4.

Evaluation Results

On basis of the analysis of the evaluation results, we come to a conclusion: the road traffic safety levels of Beijing and Chongqing are relatively higher, Jiangsu is ordinary, while Jilin and Gansu are relatively lower. It is concluded from the traffic accidents statistical data that the evaluation results in general conform to the reality. The results could support the road safety management departments for decision-making and have a certain reference value.

With the analysis process and evaluation results, we find that: (1) the distribution of the values of the indicators will affect the cluster coefficients. This kind of difference has something to do with the selection of the functions and the indicators. (2) Different indicators should be chosen for different evaluation purposes. In the daily traffic safety management process, we should consider different factors from the humans, vehicles, roads, environment and management, and establish a multi-level evaluation indicator system to make the evaluation results more comprehensive. (3) We should take the timeliness and applicability of the norms into full consideration as there may be some limitations with the development of the society.

PROSPECT

Along with a more widespread application of the gray cluster theory in the road

traffic safety evaluation, some experts and the scholars have made some tentative plans for improvements to the traditional model. For instance, the improvement to the determination method of the whitening values of each gray class which is mentioned in Section 3 changes the pattern of traditional methods. Moreover, several scholars have made some improvement to the whitening function. In theory, the sample values after dealing with the whitening functions should change rapidly as the differences between the sample values and characteristic values of certain gray class increase. However, the classical whitening function value changes stably, which would not obtain the best cluster effect. The function should be improved to be expressed in the form of an exponential function (Tian et al., 2007). Because the exponential function has the characteristic of interval monotonicity and the existence of the limitation, it is quite appropriate to take it as whitening function. In addition, the gray cluster theory is also widely combined with other theories, such as AHP and neural network technology et al. The application fully displays the characteristic of each theory and evaluates the level of the road traffic system more objectively.

CONCLUSION

Referring to the present research situation and improvement opinions of the gray cluster theory, this article chooses the classical cluster steps for the analysis and comparison of the road safety assessment, and proposes its own understandings on how to select and identify the evaluating indicators. For the determination of whitening values of each gray class, the article opts for the classification provided by "Urban Road Traffic Management Evaluation Index System", which could break through the limitations of the sample data to improve the objectivity and the comparability of the assessment. The authors put forward their own ideas on the treatment of obtaining non-dimensional whitening values, using the equivalent approach to the sample indicators' to maintain the consistency of membership and ensure the standardization. What's more, the article analyzes the influencing factors of the results, such as choice of objects, determination of standards, expressions of the function et al., which have certain significance on the safety management work.

ACKNOWLEDGEMENTS

The work in this paper is funded by the project, National Key Technology R&D Program (2007BAK35B06).

REFERENCES

Brief on the 2007 National Road Traffic Accidents. (2007).

China Statistical Yearbook. (2008).

Liu, Y., Li, W. (2006). "Improvement for road traffic safety gray clustering evaluation method". Urban Traffic, 4(3):58-61.

National Economy and Social Development Statistical Bulletin. (2007).

Niu, H. (2005). "Study on safety evaluation of urban road traffic based on gray theory". China Safety Science Journal, 15(9):91-95.

Tian, F. (2007). "Evaluation of traffic safety based on improved grey clustering method". Transportation Science& Technology, 2:68-70.

Urban Road Traffic Management Evaluation Index System. (2007).

Yue, X. (2005). "Traffic safety analysis and evaluation of Fuzhou city". Journal of Fujian Agriculture and Forestry University (Natural Science Edition), 15(9):91-95.

Road Traffic Control Information and Traffic Resource Analysis System

ZHANG Hui[1], YANG Zhongzhen[2], JIANG Yonglei[2], KANG Haigui[1]

[1] Department of Civil Engineering, Dalian University of Technology, Dalian, 116023, China; TEL/FAX (411) 8470-9517; email: hgkang@dlut.edu.cn
[2] College of Transport Management, Dalian Maritime University, Dalian, 116026, China; TEL/FAX (411) 8472-6756; email: yangzhongzhen@263.net

Abstract: This study aims to develop a system to manage road traffic control information and analyze traffic resources. In this system road traffic control information is represented as objects, such as points, lines, or regions, in GIS while the specifications of them are stored in the attribute table of the objects. Moreover, GU (Graphic User) interfaces are developed to process, edit, query, display, and print the information. Based on road networks and the relevant traffic control information, a road traffic resource analysis system is developed.

INTRODUCTION

GIS (Geographical Information System) is a computer application system to collect, process, analyze, and display spatial data and transmit data in different systems, locations, and users. GIS is extensively used in many fields, such as transport management, urban planning, and real estate marketing (Zhang *et al*, 2003). GIS-T is a computer system that can collect, store, manage, analyze, and handle spatial and traffic information. It is the extension of GIS in transportation and an integration of GIS technology to analyze and process transportation information.

The rapid urbanization and motorization in China has shortened the cycle time for urban road supply and demand. Since the existing road system cannot meet the demand, the urban road networks are being improved continuously and the traffic control system, including traffic signals, signs and marks, lanes, and one-way roads, is being frequently adjusted. During the construction of new or improved roads, infrastructure construction sites often occupy a portion of an existing road and significantly affect the efficiency of the overall road network. Therefore, how to collect, manage, and update the dynamic information and analyze traffic resources with this information has become a subject of significant interest. Based on a GIS platform, this study develops a system to manage road traffic control information and analyze traffic resources dynamically and visually. It has been implemented and used by the police from the urban traffic branch.

Many applications of GIS in the field of transportation can be found. For example, the road network model system of GuangDong is used to edit, analyze, and

display highway network data of GuangDong province (Wang, *et al*, 2001). The LanZhou urban traffic information system can not only display the locations of video monitors but also analyze congestions and display the congested locations. The GuangDong highway network model system is based on a 1:500,000 map scale. Using the same method, the LanZhou system represents roads and intersections with lines and points, respectively, in GIS. In both systems, the road information is inputted manually and information relating to traffic controls and construction sites cannot be positioned accurately. Moreover, spatial data in the system differs from the actual situation due to the use of small-scale maps (Yang *et al*, 2000).

To overcome the problems, we use a 1:2500 map scale for the spatial information resource and polygon objects of MapInfo to represent roads and intersections. As a result, spatial information such as the width or length of a road or the area of the intersection can be obtained directly. Since traffic control information and construction sites can be recorded into polygons of roads and intersections, traffic resources can be analyzed accurately with the spatial analysis of GIS. However, it is obvious that the traditional line-point network topology method cannot be applied here. In order to analyze traffic resources and release real-time information, a new network topology method that can analyze the spatial relationship between the polygons of intersections, roads, and the direction of roads has been developed.

SYSTEM STRUCTURE

As shown in Figure 1, the system consists of data models and GU interfaces. Data models refer to layers in the MapInfo database. There are several layers, including the road layer, the intersection layer, the traffic mark layer, the traffic sign layer, and the layers of current construction sites, future construction sites, and construction history.

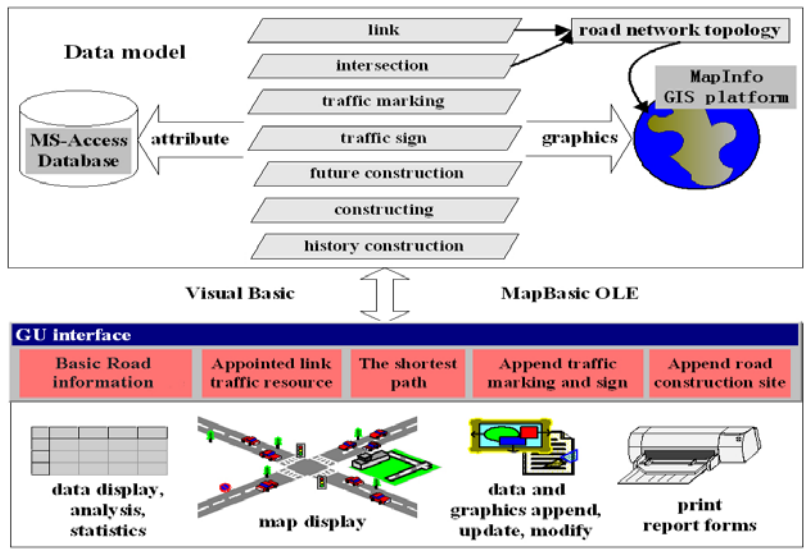

Figure1. System Framework

Layers of roads and intersections are the bases. Polygons here correspond to links or nodes of the road network, but with the same shape as the actual ones. Users can measure the area, width, and length of an intersection or road and can also know its spatial location. The traffic mark layer contains all traffic control marks on the pavement and they have the same shapes and XY-coordinates as the actual ones. The traffic sign layer contains all traffic control signs beside or above the roads. Layers of current and future construction sites and construction history record all construction sites that may affect road traffic based on the dates of establishment of the construction sites and construction activity. GU interfaces are developed with MS-VB that can be used to analyze, display, input, update, and modify attribute and graphic data. It also contains the interfaces of the basic road information, the inquiry, the statistics of traffic control information, the traffic marks and signs, the construction site appending, and the shortest path search and display. With them, users can manage and query various road traffic control information visually.

SYSTEM DESIGN AND REALIZATION

Data Model

As the basic data platform, the road and intersection layers are the first two data models. They are established based on a 1:2000 digitized map. Roads and intersections are polygons in MapInfo. Since the digitized map can vividly reflect the actual urban topography, these polygons completely contain the spatial attributes of the urban road network. In order to establish the network topology structure automatically, a road polygon must start from the adjacent intersection when creating a road in the database. Then, topology analysis of the road network can be carried out with spatial calculations in MapInfo as follows:

Step 0: Number the objects in the road and intersection layers respectively. Put the serial numbers of them into a field of the attribute table (Table 1).

Step 1: Fetch each object in the road layer and find objects in the intersection layer that intersect with each road object. As Figure 2 shows, intersections *i and, j* are two ends of roadway *k*. In terms of network topology, it can be said that roadway *k* starts from (and ends at) intersection *i* and ends at (also starts from) intersection *j*. This is done by judging which intersection the road polygon starts from

Step2: Find one-way roads manually and record them in the attribute table as shown in Table 1 (Ren *et al*, 2003)

Step3: Calculate the coordinate strings of road *k* (k：$(1，x_1,y_1)，\ldots，(n，x_n,y_n)$), and intersection *j*（$j$：$(1，x_1,y_1)，\ldots，(m，x_m,y_m)$）to get the XY-coordinate $(q，x_q,y_q)$ of the first intersecting point between the road and the road ending intersection. Calculate the road length with coordinate string（$\boldsymbol{k}$：$(1，x_1,y_1)，\ldots，(q，x_q,y_q)$）and road width with coordinate string（$\boldsymbol{k}$：$(1，x_1,y_1)$，$(n，x_n,y_n)$）. Record the length and width in the attribute table.

Table 1 Roadway Attribute Table

Link ID	Start point	End point	Direction	Length	Width
K1	***l***	***i***	1（single）	***d1***	***w1***
K2	***i***	***j***	0（two）	***d2***	***w2***

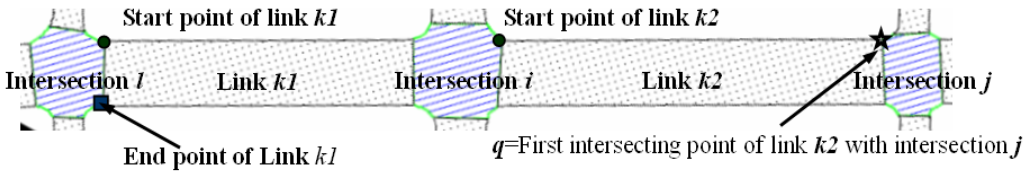

Figure 2. Road Network Topology

The traffic sign layer records the location and attributes of traffic control signs on both sides of the road. The traffic mark layer records the location, shapes, and attributes of traffic control marks painted on the pavement. The attributes include the name, number, type, and installation time. The traffic sign and mark layers are established annually. Thus, at the beginning of each year the system will create new layers and store the old ones automatically. Construction information along a road is stored in three layers, which records current ones, future ones, and the history of the constructions, respectively. A construction site is represented with a polygon and polygons are painted with different colors to display the characteristics of the project. Information about the construction site such as name, nature (water, electricity or gas), starting date, ending date, responsible person, and number of the occupied lanes is stored in the attribute table.

Figure 3 shows a part of the data model in the system. Two construction sites (electricity and gas projects), traffic signs along the roadway, zebra stripes, the lane, center line, and several traffic flow orientation arrows can clearly be seen. All of them are essential to analyzing traffic resources. For example, the shortest path search algorithm cannot find the correct path unless the “left-turn restriction”, a “construction site on the road”, and a “one-way road” are taken into account.

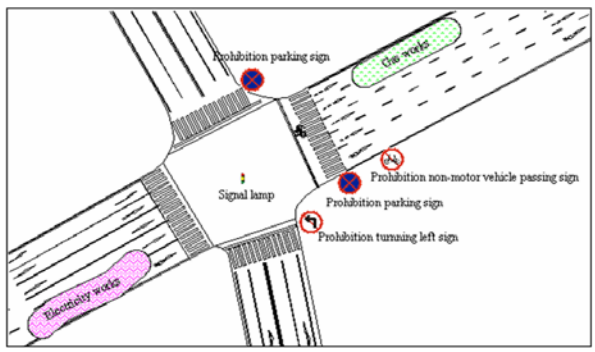

Figure 3. Data Model in the System

Data Model Management System

The data model management system consists of several GU interfaces, which

are supported by MS-VB and MapBasic derived programs. With GU interfaces, users can query, calculate, analyze, display, and print information. In addition, the system also offers tools for users to add new data into the models.

In the basic road information system, simple or complicated inquiries can be done. For example, after the name, width, service level, or direction code is given, the spatial location and detailed descriptions of the corresponding roads can be found. Furthermore, after a road is picked up in GIS, its relevant traffic information will be displayed as shown in Figure 4. A total of 207 traffic signs are available in the traffic sign library. When it is necessary to add a new traffic sign in a data model, the user just needs to point to a site in GIS and select the identification number (ID) of the traffic sign according to the prompt and a new sign will be created automatically. With the same method, the user can add traffic marks in a designated location. A total of 20 kinds of traffic flow orientation arrows, 2 kinds of zebra stripes, 2 kinds of car lanes, and 2 kinds of center lines are available in the marks library.

In the construction site input system, after the user draws a line in a position and inputs the name, starting and ending dates, responsible person, and the width of the area, as shown in Figure 5, a new construction site will be added. The system stores and manages it according to the starting date. If the date is in the past, a buffer of the line will be created in the current construction site layer. Otherwise the buffer will be created in the future construction site layer. Since construction site data changes everyday, the system can update and transfer data among the three layers automatically.

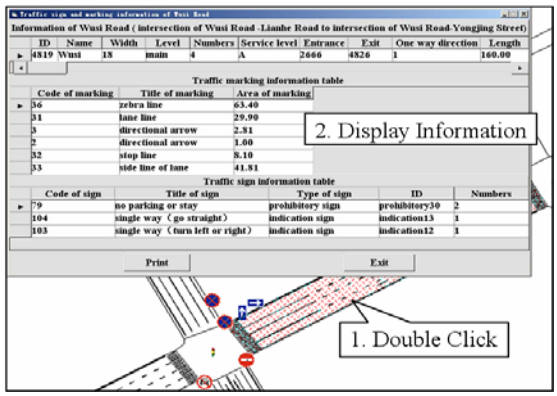

Figure 4. Shows Information for a given Road

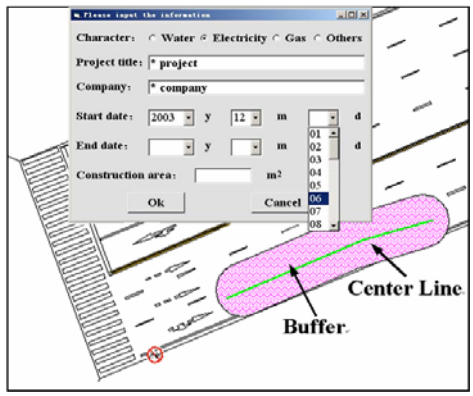

Figure 5. Adding a Construction Site

A tool in GIS is created to do this when the system is started. After the system begins to work, the tool will decide if there are projects in the future construction layer that will start according to the entered dates. If there are projects currently starting, the system moves the data from the future construction layer to the current construction layer. Then the tool will decide if there are projects in the current construction layer that will be finished according to the entered dates. If there are projects currently ending, the system will ask the user to confirm it and move the data from the current construction layer to the construction history layer. If the user

does not confirm the construction ending according to the entered date, the system will ask for an updated ending date.

ROAD TRAFFIC RESOURCE ANALYSIS

Road traffic resource analysis includes road surface condition analysis, the shortest path analysis, vehicle routing, and traffic resource distribution. Since the system stores lots of relevant road traffic information, the accuracy and validity of a traffic resource analysis based on the system can be guaranteed. The shortest path searching method should be the subject of more detailed research to ensure it properly takes into account the many relevant factors. It is reasonable to think that besides signal controls, travel speed and turn restrictions are the main factors affecting the travel time of a path (LU *et al*, 2003). Within a temporary equilibrium, the travel time of each road is stable. For example, the travel time of a road does not change during the rush hour on weekdays. However, if there is a construction site on the road, the travel time will become longer. Therefore, although in a temporary equilibrium, the shortest path does change when there are new construction sites or turn restrictions. Therefore, an indicated shortest path might indeed not be the actual shortest path (ZOU *et al*, 2002). Based on the information about road and traffic control in the database and the Dijsktra algorithm, we developed a method that can take the effects of construction sites and turn restrictions on travel time into account during the shortest path search.

Since a left-turn restriction cannot be considered in the Dijsktra algorithm, it has to be put into the network topology. Traditionally, an intersection with a left-turn restriction is separated into several nodes and then roads are connected to the nodes according to the actual situation as shown in Figure 6. This method increases the number of nodes and links in the network. If the road network is large and there are many left-turn restrictions, it will increase the calculation time greatly. Moreover, since a road network in our system is represented as a polygon, it is difficult to partition an intersection into several polygons. A method, in which the ID of the left-turn exit-link of an approach is recorded in attribute table, was developed.

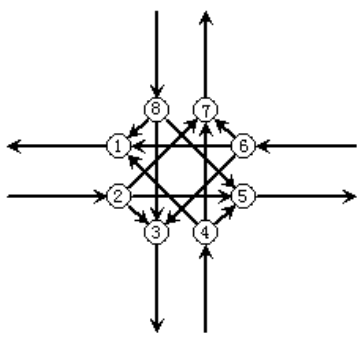

Figure 6. Actual Connection of an Intersection

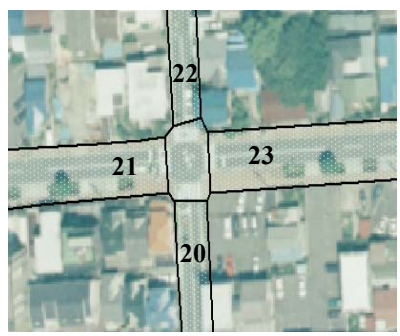

Figure 7. Exits of a Left Turn Restriction Approach

As Figure 7 shows, suppose the left-turn in approach 20 is restricted and its exit-links are roads 21, 22, and 23. In that case, we record 21 in the field of

"Left-Turn Restriction" of record 20. This can be done either by a manual or an automatic method. The automatic process supported by the GIS spatial analysis function is described as follows.

1) As Figure 8 shows, the process is creating a rectangle that is double the size of the minimum bounding rectangle of the intersection polygon and calculating the XY-coordinates of the vertex of the rectangle to get ($1,X_1,Y_1$), ($2,X_1,Y_2$),($3,X_2,Y_2$), ($4,X_2,Y_1$).
2) Next, it creates lines from the CentroID of the intersection to CentroIDs of roads, then judges which side of the rectangle intersects with the line from the CentroID of the intersection to the CentroID of road 20 to obtain point 5 (which is the same as point 1) and point 4, the remaining point with the bigger ID. Here point 1 remains.
3) Finally, it decides which line intersects with side 1-2 to get a line from the CentroID of the intersection to the CentroID of link 21. Then it knows link 21 is the exit link for a left-turn off road 20.

Since not all approaches are left-turn restricted, the program will not be run for all roads in the network. What we should do is to overlay the traffic marks layer onto the road layer to find roads that contain left-turn restriction marks and run the program for these roads. The overlay can also be done by a program and the two programs can be integrated into one tool.

After the above work, in the Dijsktra algorithm, if the field of "Left-Turn Restriction" of the current road is not zero, then the travel time of the forward link with its ID equal to that number will be given a large value such as 100 hours.

Construction on the road may affect road capacity and thus extend the travel time. Since delays happen only when road capacity is under severe traffic flow, traffic flows on roads should be taken into account when analyzing the effects of the construction sites on the shortest path. The traffic flows are the results of traffic assignments in static equilibrium (Lu, 1997). In the condition of a road without a construction site, equilibrium traffic flow q_a on road a can be calculated with the Franc-Wolf algorithm and road capacity C_a can be calculated based on road width. Then road traffic time can be calculated with the BPR (Bureau of Public Road) function while considering the construction sites. As Figure 9 shows, there is a construction site, which is l meters long, W meters wide on road 23 and road 23 has n lanes in one direction which are w meters wide. Therefore, its travel time is as follows.

$$t_{23} = t_{23}(0)\left\{(1+\alpha\left(\frac{q_{23}}{C_{23}}\right)^{\beta})\times\frac{L-l}{L}+(1+\alpha\left(\frac{q_{23}}{C_{23}\times\dfrac{w\times n-W}{w\times n}}\right)^{\beta})\times\frac{l}{L}\right\}$$

Here t_{23}=actual travel time, q_{23}=traffic flow on the road, C_{23}=link capacity,

L=length of the road (meters, obtained from the link layer), α, β=parameter (α=0.045, β=4), $t_{23}(0)$=road travel time for a speed not restricted by the effects of the construction site.

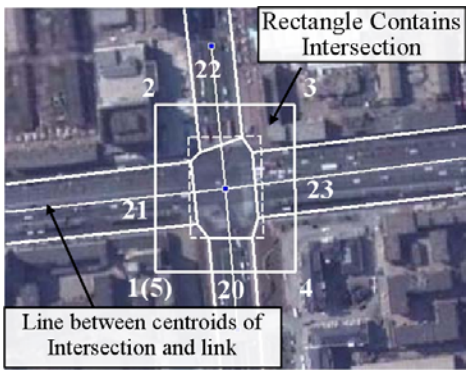

Figure 8. Automatic Judge Exit of Left Turn

Figure 9. Overlap of Link with Construction Site

We compiled programs with C# and MapBasic for the above situation and the Dijsktra algorithm and installed the programs into two front ground interfaces. Users can easily search the shortest path between intersections with these interfaces. This shortest path takes both left-turn restrictions and construction sites in the road network into account.

SUMMARIZATION

With the above method we developed a road traffic control information system based on a MapInfo database. It advanced the standardization, digitalization, and modernization of road traffic information management. The system functioned well and improved the efficiency of the Police Office responsible for traffic management. However, since the system was developed by the GIS technique as a stand-alone terminal application, it is not suitable for an office network and open information sourcing. Our future research will focus on upgrading the system with the Web-GIS technique to give remote clients the ability to visit the system via the Internet.

REFERENCES

LU H.P. (1997). Theory and Methodology of Traffic Planning, *Tsingh University Press*, Beijing, China.

LU S., LU H.P. (2003). Analysis of Influencing Factors on Urban Travel Speed, *Journal of Highway and Transportation Research and Development*, V 20, N 1, 89-92.

REN G., WANG W. (2003). Techniques of Processing Link-Direction Issues in Traffic Analysis Software, *Journal of Highway and Transportation Research and Development*, V 3, N 3, 117-120.

WANG J. *et al* (2001). Construction and Application of Highway Network Model System - An Application base on ARC/INFO, *2001 ESRI China's User Conference*, Beijing.

YANG Z.S., LIU H.H. (2000). Research on the Application of Geographic Information System to Transportation Planning and Management, *Journal of Highway and Transportation Research and Development*, V 17, N 2, 30-32.

ZHANG H.S. *et al* (2003). Application Analysis of Geographical Information System for Intelligent Transportation Systems, *Journal of Transportation System Engineering and Information Technology*, V 3, N 3, 34-37.

ZOU X.D., ZHENG S.F. (2002). Optimal Path Algorithm for Road Network with Traffic Capacity Limits, *Journal of Highway and Transportation Research and Development*, V 19, N 4, 82-84.

Research on the crashworthiness optimization of curved-road concrete barriers

LEI Zhengbao[1]，LIU Lan[1]，PENG Zuo[2]，HOU Shijing[2]

[1] Engineering Research Center of Catastrophic Prophylaxis and Treatment of Road & Traffic Safety, Ministry of Education, Changsha University of Science and Technology, P.O. Box 410004, Changsha, P.R.China; PH(+86)731-5258627; FAX(+86)731-5258646; email: doclei@qq.com

[2]Key Laboratory for Highway Engineering, Ministry of Education, Changsha University of Science and Technology, P.O. Box 410004, Changsha, P.R.China; PH(+86)731-5258630; FAX(+86)731-5258646; email: hjs8671917@qq.com

ABSTRACT

In order to optimize the crashworthiness of curved-road concrete barriers in which the curve-road radius is 400 meters, based on the NJ concrete barrier, a “vehicle-curve road-barrier” integration model is established. The six cross-section parameters of concrete barriers are regard as factors, five levels for each factor. The optimal results are obtained using the orthogonal experimental design methods. The $L_{25}(5^6)$ orthogonal table is used for the simulation test arrangement, the SPSS statistical package is used for the variance analysis of simulation results. Subsequently, using the optimal results, based on the foundation shape of the NJ concrete barrier, a "vehicle-curve road-barrier” integration model including the foundation of concrete barrier is established. Simulation results show that the integrity of the concrete barrier stays intact, and the assumption of "the concrete barrier bottom node fix" used in orthogonal experimental design is practicable and the foundation shape of the NJ concrete barrier can be used directly in curved-road concrete barriers. Finally, the forces and stresses acting on the concrete barrier during the collision between vehicle and barrier is computed. A reinforcement project of curved-road concrete barriers is suggested.

KEYWORDS

transportation engineering, concrete barrier, orthogonal experimental design, collision, the reinforcement project

1 INTRODUCTION

China's traffic accident death toll has been the highest in the world for more than 10 years. Most expressways and the highways has had installed various forms of barriers, setting up the appropriate special rails is in response to major traffic accidents, but unfortunately, the existing rails are based on the straight path. Research on the curved-road is scarce. Barriers used on straight roads has been installed on curved roads, whether or not it is right has not been clearly answered,

and there are not related explanations and justifications in the existing curved-road design specifications (Zhang Jing, Bai Shufeng, Shi Hongxing, etc.,2007). In China, the curved-road network of highways substantial occupies a large proportion, less than 100 meters on average one out of corners. Curved roads is the main source of serious accidents, and road condition improvement is a huge project which needs not only putting in a lot of manpower, material and financial resources, but also much time. Obviously, study of the curved-road barrier is more realistic compared to improving road conditions.

2 FINITE ELEMENT MODEL

2.1 THE BASIC SPECIFICATIONS

Collision conditions (Lei Zhengbao, Zhou Pingyan, Yan Haiqi, etc., 2006): crashworthiness level SS, the mass of bus 18 t, the collision velocity 80 km/h, and the collision angle 20°.

Road design using ultra-high 8% with radius curve of 400m. Busses will be handled as a rigid body, and only the outline of the bus, height of mass center, inertia, weight and other parameters are considered. Parameters are shown in Table 1.

In the bus locations outside the front axle are used to establish coordinates: X-axis parallel to the bus longitude, Y-axis parallel to the bus width, Z axis parallel to the direction of the height of the bus. The coordinates of bus mass center: XC = 3250mm, YC = 1250mm, ZC = 1390mm; bus moment of inertia at the center of mass: I_{zz} = 62586000, I_{yy} = 62586000, I_{xx} = 22897200.(Liu Lan, 2008).

Table 1. Specifications

Exterior dimensions(L×W×H)	12×2.5×4m
F / R track base	2/1.8m
F/R Suspension system	1.5/ 4m
wheel base	6.5m
Minimum Groundclearance	0.350m
Tire radius	0.5mm
Curb vehicle weight	9120 kg
Total Weight	18000 kg

Coefficient of friction between bus and ground is set at 0.7, between buses and rails are set at 0.2; bus collision barrier time 1.5s (Lei Zhengbao, Xie Yuhong, Li Haixia, 2005).

2.2 MESH

Rigid material models are used for the bus and road, bus material parameters: density 7.87kg/dm^3, Young's modulus E =2.0×10^{5}MPa, Poisson's ratio 0.27; road material parameters: density 2.5kg/dm^3, Young's modulus E =3.5×10^{4}MPa, Poisson's ratio 0.25; mesh with the thickness of 1 mm, by 2-point-integral Belytschko-Tsay shell element, shell size were admitted to 50mm, the smallest shell size is 30mm, the element warping angle $\leqslant$ 25° ,and element interior angle $\geqslant$25° . the bus model include 115165 quadrilateral elements, 140 triangle elements, 119757 nodes; road

model containing 73500 quadrilateral elements, 9 triangular elements, 74150 nodes.

Constant-stress flexibility elements and Brittle_Damage material models are used for the barrier. Barrier material parameters: mass density 2.5kg/dm^3, Young's modulus E=3.0×10^{4}MPa, Poisson's ratio 0.20, stretching limit 3MPa, shear limit 14.5MPa, fracture toughness 14.9×10^{-3}kg/mm^2, viscous Parametric 0.72MPa/s, yield stress 29MPa. Then we obtain the "vehicle–curve road–barrier" integration vehicle-road system dynamics finite element model. It is clear that as long as the modified section parameters of the barrier are according to the above steps, we can get the corresponding " vehicle–curve road–barrier" integration system dynamics finite element model.

3 BARRIER CROSS-SECTION PARAMETERS OPTIMIZATION

According to orthogonal experimental design, we get the possible combinations of barrier cross-section parameters to set up "vehicle–curve road–barrier" integration dynamics finite element model one by one using the modeling method above. LS-DYNA software is used to simulate the tests, then achieve the optimal results using SPSS software (Lei Zhengbao, Yu Jinxiu, YAN Haiqi, etc., 2007).

3.1 FACTORS AND LEVEL

Barrier cross-section shape control by the six variables (factors) (Figure 1).

Each factors set five levels (table 2), The $L_{25}(5^6)$ orthogonal table is appropriate.

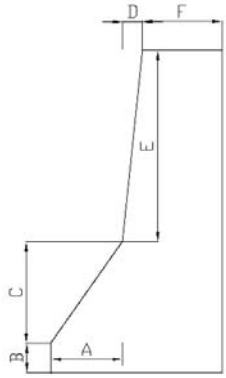

Figure 1. Factors

Table 2. The level of factors (mm).

factor / level	A	B	C	D	E	F
1	125	45	150	50	400	100
2	175	50	200	60	475	150
3	225	65	250	70	550	200
4	275	75	300	80	625	250
5	325	80	350	90	700	300

3.2 THE RESULTS AND ANALYSIS

According to Table 2, based on orthogonal L_{25} (5^6) provided by the combination of tests, and simulation tests carried out 25 times, each factor and test results are shown in Table 3. From Table 3 we know: the 25th test's results are good. Table 4 gives us an orthogonal intuitive analysis results. Table 4 shows that the greater the difference between extreme., the greater the change that the numerical factor in the trial within the scope of change will lead to in tests, so the difference between extremes is the largest one of the factors affecting the level of the test results of the

biggest factors, that is the most important factor. Thus, under the influence of primary and secondary level to arrange the result is: C> B> E> F> A> D.

Tab. 3 experiment result（mm, H.O.RW: height of rear wheel）

Factor / No.	A	B	C	D	E	F	H.O.RW	Barrier height
1	125	45	150	50	400	100	1407	595
2	125	50	200	60	475	150	1041	725
3	125	65	250	70	550	200	952	865
4	125	75	300	80	625	250	1429	1000
5	125	80	350	90	700	300	1306	1130
6	175	45	200	70	625	300	1220	870
7	175	50	250	80	700	100	1499	1000
8	175	65	300	90	400	150	1685	765
9	175	75	350	50	475	200	2143	900
10	175	80	150	60	550	250	942	780
11	225	45	250	90	475	250	1370	770
12	225	50	300	50	550	300	1083	900
13	225	65	350	60	625	100	1620	1040
14	225	75	150	70	700	150	1052	925
15	225	80	200	80	400	200	951	680
16	275	45	300	60	700	200	1202	1045
17	275	50	350	70	400	250	2249	800
18	275	65	150	80	475	300	843	690
19	275	75	200	90	550	100	1383	825
20	275	80	250	50	625	150	852	955
21	325	45	350	80	550	150	2075	945
22	325	50	150	90	625	200	1418	825
23	325	65	200	50	700	250	1296	965
24	325	75	250	60	400	300	1442	725
25	325	80	300	70	475	100	738	855

Table 4. The average of rear wheels lift height (D.B.E: difference between extreme).

factor / level	A	B	C	D	E	F
1	1227.0	1454.8	**1092.4**	1356.2	1546.8	1329.4
2	1497.8	1458.0	1178.2	1249.4	**1187.0**	1341.0
3	**1215.2**	1239.2	1223.0	**1242.2**	1287.0	1333.3
4	1265.8	1489.8	1227.4	1319.4	1307.8	1457.2
5	1393.8	**957.8**	1878.6	1432.4	1271.0	**1138.8**
D.B.E	282.6	532.0	786.2	190.2	359.8	318.4

Table 4 also shows that various factors, the optimal level for the portfolio: A3B5C1D3E2F5, that is, A=225mm, B=80mm, C=50mm, D=70mm, E=475mm, F=300mm. As this group has no arrangement in Table 3, which shows that orthogonal table lists the 25 groups with not only the best can be seen with the results, but it also can be inferred that the results may be a better match. In order to verify such an inference, it is also necessary with this group of simulation tests.

When significant level α =0.05, the results of variance analysis are shown in Table 5. The paper use the test out of the design methods, so error analysis can only take the relative error, classifying the factors corresponding to the minimum variance as errors.

Table 5 shows that factor C and B are significant factors, should choose their level best, the others can be based on the need to consider their level of choice.

Table 5. Test significance

factor	Error SS	Def	Mean square	F ratio	F	significance
A	298144.640	4	74536.16	2.387	6.390	
B	1018822.640	4	254705.66	8.157	6.390	*
C	2009633.440	4	502408.36	16.089	6.390	**
D	124908.640	4	31227.16	1.000	6.390	
E	363830.240	4	90957.56	2.913	6.390	
F	367744.290	4	91936.07	2.944	6.390	

D.B.E	124908.64	4	31227.16			

4 THE SIMULATION FOR OPTIMAL RESULTS

To prove the above results and identify the optimal solution, it is needed for intuitive analysis of the optimum combination A3B5C1D3E2F5, that is, A=225mm, B=80mm, C=150mm, D=70mm, E=475mm, F=300mm, Fig.2 to Fig.4 for the height change in the bus simulation results.

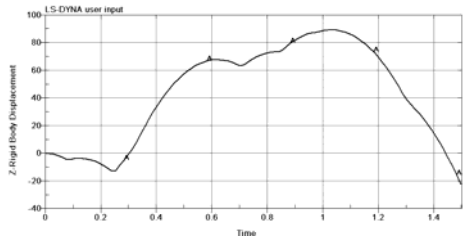

Figure 2. Height of the bus mass center.

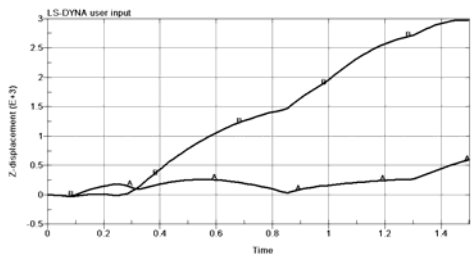

Figure 3. Height of the left and right front wheel.

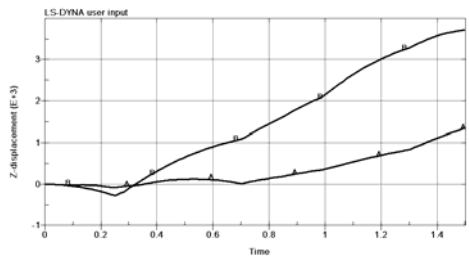

Figure 4. Height of left and right rear wheel.

Clearly, the optimal combination A3B5C1D3E2F5 can not stop the bus from running out of barrier. The wheel near the barrier at the end is raised to a height of 1400 mm, significantly more than the maximum height of the barrier. Figure 5 shows that the bus goes out of concrete barrier rails and flies in to the space outside.

By all appearances, the optimal combination A3B5C1D3E2F5 does not lead to optimal results. According to the general principles of orthogonal design, the best simulation test results from 25 groups should be chosen. The 25th group is better compared to simulation results in other groups. The 25th group simulation results are shown in Figure 6 to Figure 9.

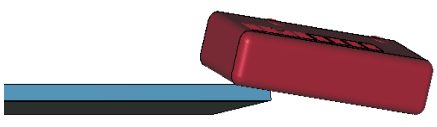

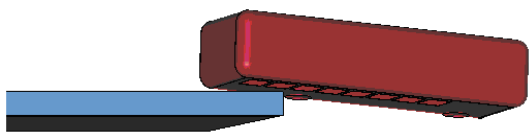

Figure 5. Bus goes out of the barrier. Figure 6. Bus rolls over inside of the barrier.

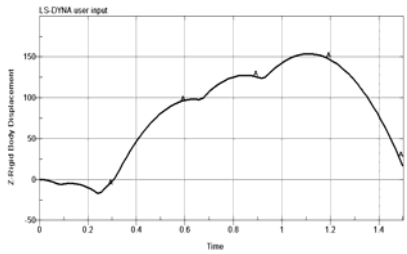

Figure 7. Height of mass center

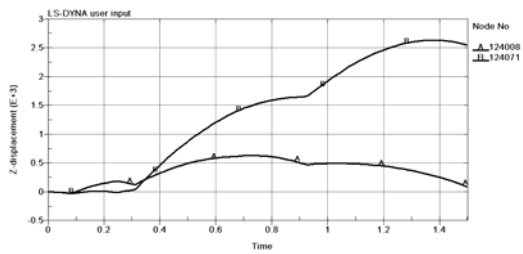

Figure 8. Height of left & right front wheel.

Figure 6 – Figure 9 indicate that the bus has completely rolled over, but did not run out of barrier. Figure 9 shows that the wheel near the barrier rises to a height of 738 mm, while the overall height of the barrier is 855 mm. Thus, the optimal is the 25th group result.

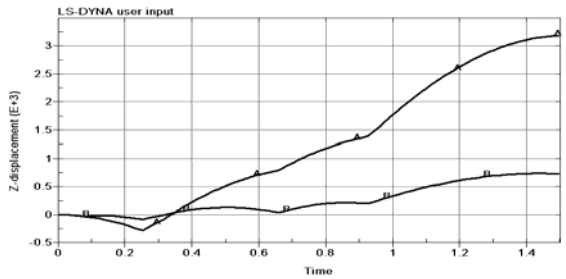

Figure 9. Height of left & right rear wheel.

5 BASE FOR THE DESIGN AND REINFORCEMENT

In the simulation above, the base has not been adopted, an assumption of "barrier at the bottom fixed nodes" is used before it was proved. The reinforcement project in the concrete barrier is also a key question in design.

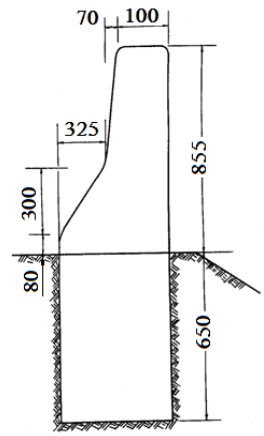

Figure 10. Barrier base

5.1 CURVE-ROAD BARRIERS BASE AND FINITE ELEMENT MODEL

The curved-road barriers finite element model is based on the use of the standardized road side of concrete embedded lock base, in accordance with Figure 10, and the basis for cross-section at the bottom line extends down to 650 mm. This barrier has the section size as follows: 430mm×650mm. Barriers and foundation are poured together locked in embankment road, embedded in the soil.

Road model reference Table 6, taking into account the barrier base width of 495mm, the depth of foundation set for 1500 mm.

Table 6. Material parameters for the road base.

NAME	MAT	Thickness (mm)	Young's modulus(MPa)	Poisson's ratio	Density (t/mm3)
Surface	*MAT_ELASTIC	150	1200	0.25	2.5E-9
Base layer	*MAT_ELASTIC	300	800	0.25	2.4E-9
Pad layer	*MAT_ELASTIC	200	600	0.25	2.3E-9
Ground layer	*MAT_ELASTIC	1500	40	0.40	1.8E-9

5.2 BASE DESIGN

From the simulation results, the barrier is not separated from the foundation, the road embankment is not separated from the soil during vehicle impact, and the base has not been overturned by vehicle. The simulation results show that the base of the straight road is applicable to a curved road (Figure 11 and Figure 12).

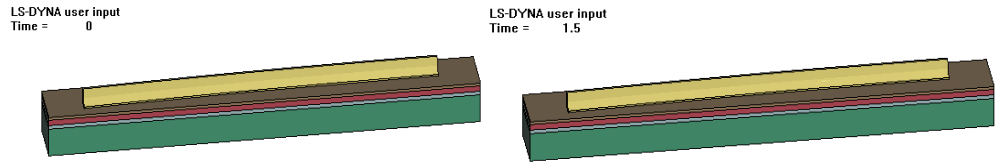

Figure.11 Barrier and its base at t=0s. Figure 12. Barrier and its base at t=1.5s.

Clearly, the barrier integrity intact, the foundation has played its due role for the fixed barrier. In other words, orthogonal experimental designs on the assumption of "barrier at the bottom fixed nodes" are practical.

5.3 REINFORCEMENT PROJECT

From the simulation output, t =0.72s when the rear of the bus collides with the barrier the biggest barrier stress occurred. The maximum stress reached 121.764MPa, as shown in Figure 13. Maximum stress element numbered 204,154, located in the place where barrier and its base connected, is shown in Figure 14.

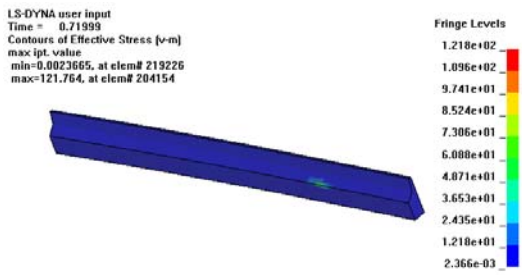

Figure13. Max stress on barrier in simulation.

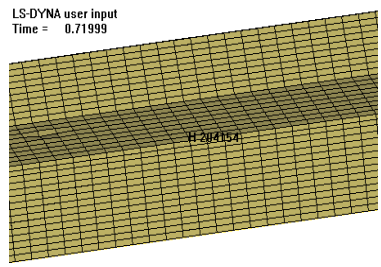

Figure 14. Location of max stress element.

From the entire process of the collision, the stresses are no more than 30MPa, except at t=0.72S when the stress is too large.

The barrier stress analysis finds the weak cross-section in the barrier, the maximum stress, and provides reference for reinforcement. The reinforced steel bars are calculated based on the collision force, then reinforced area and the reinforcement project can be determined. According to the results output the biggest barrier collision force reached 287190 N (see Figure 15).

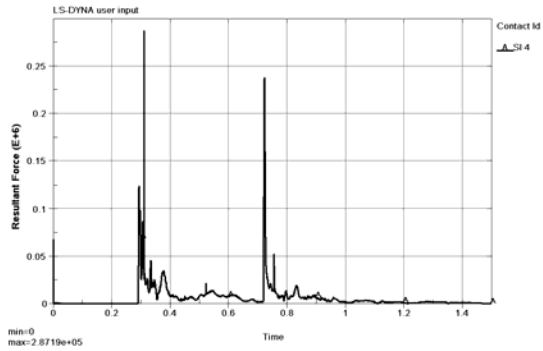

Figure 15. Max force on the barrier.

There have been two kinds of very mature reinforcement options in straight concrete barriers:

Option I, a reinforcement program for general cases: configuration 8 φ12 vertical steel bars and spacing 34cm φ 6 stirrups, in the special position was reinforced.

Option II, an enhanced reinforcement program: Configuration 4 φ 16 & 6 φ12 vertical steel and spacing 34cm φ 8 stirrups, it is also reinforced in a special place.

Concrete is an elastic-plastic material; moreover, force in vehicle collisions is entirely non-linear. In the vehicle collision process, the back wall will have great tensile stress, while the stress in the internal wall is very small, so we must allocation the vertical steel bars along the contour lines.

The steel bars can guarantee that the entire concrete barrier withstands the impact force 287190N, as long as the overall area of the steel bars is more than 1367.6mm^2 which has a tensile strength of 210N/mm^2.

Comparing two types of concrete barrier reinforcement options, we can see that the area of vertical steel bars is only 904.32 mm^2 in the reinforcement program for the general option, less than the requirements of 1367.6mm^2, which does not meet the requirements.

The area of vertical steel bars is 1482.08 mm^2 in the enhanced reinforcement program, more than the required 1367.6mm^2, and so it is able to meet the requirements.

Therefore, the enhanced reinforcement project in straight concrete barrier can be directly used for reinforcement of curved-road concrete barriers, namely: configuration 4 φ16 & 6 φ12 vertical steel and spacing 34cm φ 8 stirrups, as is used for reinforcement in special places.

6 CONCLUSION

(1) Increasing the height of the concrete barrier is an important way to protect busses from going over the barrier, and a reasonable cross-section of the concrete barrier design parameters can control the accident inside the barrier.

(2) the optimal cross-section parameters of curve-road concrete barrier is: A=325mm, B=80mm, C=300mm, D=70mm, E=475mm, F=100mm.

(3) the six cross-section parameters of the curved-road concrete barrier have the following priorities: C> B> E> F> A> D.

(4) when the significant level $\alpha = 0.05$, C and B are significant variables, and should choose their best levels (that is, B=80mm, C=300mm), whereas the other four variables can be considered based on their needs.

(5) the assumption of "barrier at the bottom of fixed nodes" used in orthogonal experimental designs are practical. The NJ-based form of concrete barrier has good stability, and can be used directly in curved-road.

(6) the enhanced reinforcement project in straight concrete barrier can be directly used for reinforced project of curve-road concrete barrier, namely: configuration 4 φ16 & 6 φ12 vertical steel and spacing 34cm φ 8 stirrups, as is used for reinforcement in special places.

ACKNOWLEDGMENTS

The project supported by the National High Technology Research & Development Program of China.(2006AA11Z224) , Hunan province science & technology program (2008CK3074) and Changsha City Science & Technology Program (K0802090-11) are gratefully acknowledged.

REFERENCES

Lei Zhengbao, Xie Yuhong, Li Haixia. (2005). The Crashworthiness of Structure with Large Displacement and Large Deformation. National University of Defense Technology Press, Changsha, Hunan.

Lei Zhengbao, Zhou Pingyan, Yan Haiqi, etc.(2006). Finite element model for crashworthiness study of vehicle crash barrier system. China Safety Science Journal, 16(8):9-16.

Lei Zhengbao, Yu Jinxiu, YAN Haiqi, etc. (2007). Research on interrupted type of concrete guardrails using orthogonal design. Journal of Vibration and Shock. 26(7):13-17.

Liu Lan. (2008). The reseatch on new technology of barrier, the thesis for the degree of master of engineering,.

Zhang Jing, Bai Shufeng, Shi Hongxing, etc.(2007). Dynamic numerical simulation and experiment for vehicle and curved concrete barriers crash. China Journal of Highway and Transport, 20(1): 102-106.

HIGYWAY ACCIDENTS ANALYSIS WITH PANEL DATA MODEL

T. Xu[1], X. Sun[2], Y. He[3], C. Xie[4]

[1]Key Lab of transportation Engineering, Beijing University of Technology, Beijing, 100124, P.R.China. Emailannabelxu@163.com

[2]Professor, Key Lab of transportation Engineering Beijing University of Technology, Beijing，100124, P.R.China .Email:xdsun@bjut.edu.cn

[3]Assistant Professor, Key Lab of transportation Engineering Beijing University of Technology,Beijing, 100124, P.R. China;Email:ylhe@bjut.edu.cn

[4]Yangzhou Transportation Management Bureau,Yangzhou 225002, P.R.China, Email: xcr110@126.com

ABSTRACT

The total mileage of highways in China has ranked the second in the world and traffic accidents have become a potential safety problem, which threaten people's lives. Panel data model as a new tool is introduced to analyze crashes. Panel data, which combines cross-sectional and time-series characteristics, allows researchers to construct and test realistic behavioral models that cannot be identified using only cross-sectional or time-series data. This paper introduces the modeling process of fixed effects model and random effects model. These models are applied to the Jingjintang Highway. Variables are divided into four categories including roadway variables, traffic variables, indicator for different areas, and accidents variable. The two models' results are compared and the fixed-effects model was chosen to describe the relationship between accidents and other factors after the Hausman test. The fixed effects model was chosen since it could identify unobserved factors and segments with high safety risks. Panel data model as a new statistical tool will be widely used in the transportation analysis field.

Keywords: Traffic Safety; Accidents Analysis; Panel Data Model; Fixed-effects; Random-effects

INTRODUCTION

According to government statistics (Ministry of Communications, 2006), China's highway mileage reached 3,350,000 kilometers in 2006, ranking the second in the world and people travel more conveniently than before. However, road traffic safety situation continues to deteriorate in recent years. Traffic accidents and the associated economic loss are an incredible social and economic burden on the nation.

This paper introduces panel data models to traffic accidents analysis, which can overcome a simple time-series model or data model cross-section. In this paper,

Jingjintang Highway is divided into 64 subsections according to road conditions and each subsection was considered as a panel. Fixed effect and random effect models were developed and the Hausman test results showed that the individual fixed-effects model is more reasonable to describe highway traffic accidents.

LITERATURE REVIEW

The earlier models for crash prediction were developed using ordinary or normal linear regression, such as multiple linear regression, Poisson regression, and negative binomial regression (Montella, 2008). Panel data analysis is a more recent method for analyzing speed limit policy. Greenstone (2002) used linear fixed effects panel models to track yearly fatality rates in all 50 states from 1982 to 1990. He concluded that fatality rates rose by 30% on rural interstates and fell by 17% on urban non-interstates. Noland (2002) examined the traffic safety effects of roadway infrastructure improvements using fixed-effects negative binomial regressions with panel data from over 14 years. Noland concluded that engineering design improvements have not been effective in reducing fatalities and injuries.

PANEL DATA METHODOLOGY

Model description

Panel data refers to two-dimensional data, consisting of a cross-sectional variable and a time-series variable (Xie 2005). Typical structure of panel data is as shown in Figure 1:

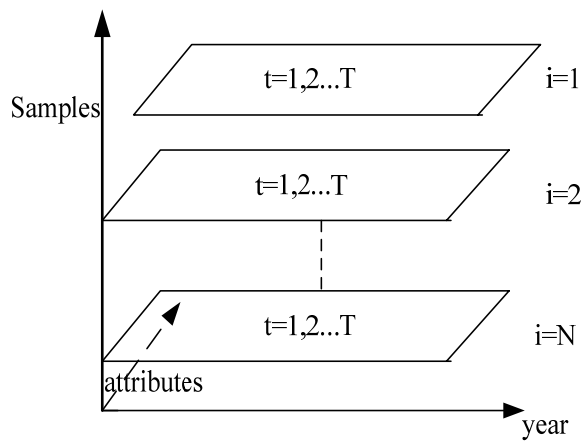

Figure 1. Structure of panel data

Panel data model often contains more data and reduce the co-linearity relationship between explanatory variables. Panel data permits identification of variations across individual roadway segments and over time. Accommodation of observation-specific effects also mitigates omitted variables bias. There are two standard model types that are appropriate for panel data, fixed and random effects models. The specification of fixed effects (FE) linear model is as shown in Equation 1.

$$y_{it} = x_{it}^{'}\beta + \alpha_i + \varepsilon_{it} \quad \text{i=1,2,3...N and t=1,2,...T} \qquad (1)$$

Where ε_{it} is an error that varies across both segments and time periods. α_i is the time-invariant with fixed effect specific to roadway segment i; it can be estimated by the following formula:

$$a_i = \overline{y_i} - \hat{\beta}'_{FE}\,\overline{x_i} \tag{2}$$

Where $\overline{y_i}$ is the number of crashes on segment i over T time periods, $\overline{x_i}$ is the vector of average values of the explanatory variables for segment i over T time periods, and β'_{FE} is the least squares dummy variable (LSDV) estimator.

The specification of a random effects (RE) linear model is as follows:

$$y_{it} = x'_{it}\beta + \mu_i + \varepsilon_{it} \tag{3}$$

Where μ_i is the random effect specific to roadway segment i and ε_{it} is an error that varies across both segments and time periods.

Linear fixed effects models can be estimated using a least squares dummy variable model. Linear random effects models can be estimated using a generalized least squares (GLS) approach, by assuming an appropriate distribution for random effects.

Hausman Test

The choice of specification generally depends more on whether correlations exist between omitted variables and the included explanatory variables. Both FE and RE model forms were estimated here and which estimates should be used in practice are decided after the Hausman test was performed (Alberto M., 2005). The following is the chi-squared statistic:

$$W = \chi^2[\mathrm{K}-1] = [\hat{\beta}'_{FE} - \hat{\beta}_{RE}]'\,\hat{\psi}^{-1}[\hat{\beta}_{FE}' - \hat{\beta}_{RE}] \tag{4}$$

Where $\psi = Var[\hat{\beta}'_{FE} - \hat{\beta}_{RE}] = Var[\hat{\beta}'_{FE}] - Var[\hat{\beta}_{RE}]$, β'_{FE} is the LSDV estimator for the FE panel model, and $\hat{\beta}_{RE}$ is the GLS estimator for the RE panel model.

MODEL DEVELOPMENT

Data preparation

- **Crashes Collection**

Data for this study were collected from different sources. It consists of crashes from January 2002 to December 2005, AADT, passenger cars percentage, large truck percentage and travel speed. There were totally 3784 crashes recorded.

- **Traffic flow data**

There are 23 loop detectors installed underneath pavement to monitor traffic flow for both directions along this freeway. Five traffic flow data items can be extracted from the detectors including speed of large vehicles, speed of small vehicles, volume of large vehicles, volume of small vehicles, and occupation rate. Minimum time interval for original data from detector was one minute. In order to make cluster analysis, the whole freeway was divided into sixty-four subsections according to road characteristics and data was grouped at one-hour interval. The percentage of large vehicles ranged from 21% to 77%. Variables are summarized as shown in Table 1.

Table 1 Traffic data statistics results

Variables	MAX	MIN	MEAN
Crashes per year	109.00	.00	11.0000
AADT	37286.25	4648.37	5616.78
Large vehicles percentage	0.45	0.09	0.24
Section length (km)	10.00	0.50	2.29
Average_angle	56.00	d0.00	24.68
Average_slope	1.62	0.00	0.3563774
Rural or city	City -Rural		

A linear panel data model can be specified as in Equation 5.

$$Accident_{it} = (Segment_length_i)\ \exp(\alpha_{it}\beta_1(X_1)\beta_2(X_2)\beta_n(X_n)\varepsilon_{it}) \quad (5)$$

$$ln(Accident_{it} / Segment_length_{it}) = \alpha_{it} + \beta_1(X_1) + \beta_2(X_2) + ... + \beta_n(X_n) + \varepsilon_{it} \quad (6)$$

Where $Accident_{it}$ is number accidents to occur on section i over the period and the performance of ln(x) makes sure that $Accident_{it}$ is negative integer. $Segment_length_i$ is length of section i. X_i is a $n\times1$ vector containing the values of crash i of p explanatory variables, β_i is a $n\times1$ vector of regression coefficients.

Model process

Fixed model prediction is predicted using least squares dummy variable as Table 2.

Table 2 Least squares regression results

Ln（ACC/Length）	Coef.	Std.Err	t	p
volume	.0001121	9.79e-06	11.44	0.000
Truck_percent	-2.273556	0.5359399	-4.24	0.000
City_rural	0.6786234	0.1302167	5.21	0.000
Cons	0.2274454	0.1717774	1.32	0.187

Prediction results with GLS method is as shown in Table 3.

Table 3 Random effect-model regression result

Accident_ratio	Coef.	Std.Err	T	P vaule
volume	0.0000844	9.91e-06	8.47	0.000
truck_percent	1.4666674	.4986217	3.01	0.003
intercharge	0.7993095	0.1767222	3.41	0.001
City_rural	0.602429	0.1508033	5.88	0.000
Cons	0..24359	0.1568766	1.55	0.12

Hausman test

The Hausman specification test compares the fixed versus random effects under the null hypothesis that the individual effects are uncorrelated with the other variables in the model. Table 4 compares the fixed effect and random effect models.

Table 4 Hausman Test result

	(b)	(B)	(b-B)	sqrt(diag(V_b-V_B)
	fixed		Difference	S.E.
volume	0.000035	0.0000844	-0.0000494	.0000747
Truck_percent	0.2417662	1.4666674	-1.2249012	3.09099
intercharge	0.3777045	0.7993095	-0.421605	
City_rural	0.518205	0.602429	-0.084224	8.636169
Test: Ho: difference in coefficients not systematic			Prob>chi2 =	0.0000

In table 4, P>0 indicates that a random effect model produces biased estimators, violating one of the Gauss-Markov assumptions; so the fixed effect model is preferred. Sigma_u is not significantly greater than sigma_e, so $\theta = \frac{\sigma_\mu^2}{\sigma_\mu^2 + T\sigma_\alpha^2}$ does not approach 1. Estimation with random effect model will produce larger deviations.

Final model explanation

The parameters estimation for fixed model (7) using LSDV are as shown in

Table 5

$$ln(Accident_{it} / \hat{Segment_length_{it}}) = 0.000035 * volume_{it} + 0.2417662 * truck_percent_{it} +$$
$$+0.5158295 * \text{intercharge}_{it} + 0.6324561 * city_rural_{it} + \alpha_i$$
$$\Rightarrow Accident_{it} = Segment_length_{it} * e^{(0.000035 * volume_{it} + 0.2417662 * truck_percent_{it} + 0.581332 * city_rural_{it} + \alpha_i} \quad (7)$$

Table 5 Parameters for panel data model

$\hat{\beta}_1$	$\hat{\beta}_2$	$\hat{\beta}_3$	$\hat{\beta}_4$	$\hat{\alpha} = \sum_{i=1}^{64} \hat{\alpha}_i$
0.00035	0.2417662	0.5158295	0.6324561	1．913
$\hat{\alpha}_1 = 3.889064$	$\hat{\alpha}_2 = 2.406556$	…	$\hat{\alpha}_{63} = 0.7513168$	$\hat{\alpha}_{64} = 0.2509566$

According to the final model, we can see that from 2002 to 2005, increasing traffic volumes, interchange area, percentage of large vehicles and differences of regions are contributing factors for accidents. For highways in plain areas such as Jingjintang, design features are not the main factors for accidents. Meanwhile, we can also find that intercepts of sections with high accidents is more than 2 or 3, while the common road is less than 1. Sections with high accidents can easily be identified by intercepts statistics.

CONCLUSIONS

Although the previous model uses a large number of statistical regressions, they all ignored fixed differences among road subsections. This paper presents panel data application in the highway accident analysis process, which aims to address the inadequate sample size, multi-colinearity problems. Fixed effect model and random effect model were developed respectively using data from Jingjintang Highway. Hausman test results show that individual fixed model is more suitable than random effect model for expressway accidents prediction and analysis. Furthermore, intercepts of different cross-section can help to quickly distinguish between a high accidents sections road and common sections. Panel data model as a new econometric tool is very effective, especially for the existence of regional differences in the traffic analysis.

ACKNOWLEDGEMENT

This project speed limit and control technologies for highways is supported by West Transportation Construction Foundation of China under Grant 2007 318 223 33-01.The author would like to thank supervisor Dr. Sun for advice and Key Lab of Transportation Engineering, Beijing University of Technology for providing data. Also, give thanks to graduate students who collected data.

REFERENCES

China Road Traffic Safety Blue Book (2006), the Ministry of Communications Highway Institute of Science and Technology People's Transportation Press, November,2007

Montella, A., M.Lamberti (2008) ,Crash Prediction Models for Rural Motorways, TRB 2008 Annual Meeting CD-ROM, Washington D.C.

Greenstone, M. (2002). A reexamination of resource allocation responses to the 65-mph speed imit. Economic Inquiry, 40(2), pp. 271-278.

Noland, R. B. (2003). Traffic fatalities and injuries: The effect of changes in infrastructure and other trends. Accident Analysis and Prevention, 35(4), pp. 599-611.

Xie S., Zhu, H., Advanced Econometrics (2005), Fudan University Press , 2005,5

Figueroa, A. (2005), Speed factors on four-lane highways in free-flow conditions, the 84th Annual Meeting of the Transportation Research Board, TRB 2005 Annual Meeting CD-ROM, Washington D.C.

The Impacts of Differential Speed Limits On Speed

LIU Shicui[1] SUN Xiaoduan[2] HE Yulong[3] HOU Shuzhan[4]

[1]Key Lab of Transportation Engineering, Beijing University of Technology, Beijing, 100124, P.R.China .Email:liushicui1984@emails.bjut.edu.cn

[2]Professor, Key Lab of transportation Engineering Beijing University of Technology, Beijing, 100124, P.R.China .Email:xdsun@bjut.edu.cn

[3]Key Lab of transportation Engineering Beijing University of Technology ,Beijing， 100124, P.R.China . Email: ylhe@bjut.edu.cn

[4]Key Lab of transportation Engineering Beijing University of Technology, Beijing, 100124, P.R.China. Email:hshu@ emails.bjut.edu.cn

ABSTRACT

Design speed is generally used as a basis for determining the post speed limits in China. Therefore the fixed value becomes the post speed for the whole road. Because of the big difference in operational characteristics between cars and trucks, this method is clearly inappropriate, considering the effects of Differential Speed Limits (DSL) are controversial. This paper expatiates the advantages and disadvantages of DSL, using hypothesis testing and analysis of variance methods (ANOVA) to analyze the difference of 15th percentile speed, 85th percentile speed, mean speed, speed variance, speed limit compliance between DSL and USL (uniform speed limit). Finally, consider truck mixed rate and traffic volume as variables to establish a linear regression model between speed limit differences and speed statistical indicators.

Keywords: differential speed limits; transportation safety; speed differences; 85th percentile speed

INTRODUCTION

Solomon (1964) conducted a study of more than 10,000 accident-involved drivers and their vehicles speed on a highway of 600km length, and found that the probability of being involved in a crash per vehicle-mile followed a function of vehicle speeds which followed a U-shaped curve. The study found that collision rates was lowest when vehicles travel around average speed, with the increase of speed and mean speed, and the probability of being in a crash increased whenever vehicles traveled at higher or lower than the average speed. Garber and Gadirau (1998) found that collision rates increased with the increasing speed variance. So in order to lower collision rate, speed variance should be decreased. However in recent years, studies have shown that the relationship between accident and speed is not significant. Collision rate relates to variation of vehicle speeds, and vehicles overtaking and

overtaken will be frequent when variation of vehicle speeds is large, which is prone to result in high collision rates. So, speed differences should be dropped as well rather than to only drop speed to lower collision rate.

DSL

Differential speed limit means that according to the operational safety and operation management of different types of vehicles, differential speed limits are imposed on cars and trucks.

There is no consistent recognition of the effect of differential speed limit. Some researchers support DSL, but others object. The supporters of DSL argue that it would increase the probability of crashes between trucks and other types of vehicles if trucks are traveling at a relative high speed. And because of the larger dimension of trucks, the supporters also concern that truck needed more time and a longer distance to decelerate to a complete stop than other types of vehicles if to travel at the same speed. Therefore, a lower speed limit was advised to be imposed on trucks. But the opponents of DSL argued that trucks and other types of vehicles should adopt USL (uniform speed limits), the reason is that, firstly, a truck driver has a greater sight distance than the passenger car driver because of the higher position in a truck, which made truck drivers have enough time to decelerate to complete stop. Secondly, the opponents of DSL also contended that differential speed limit might increase the variation of vehicle speeds and speed differences, and result in higher frequency vehicles overtaking and overtaken which might increase the probability of certain types of crashes.

Many researchers do studies on the effect of DSL (differential speed limit) on mean speed, operating speed, speed variance and other speed statistics indicators, but have not conclude consistent conclusion. Hall and Dickinson (1974) found that the speed variation can be brought about by enforced differential truck speed limits. J.R. Esterlitz and H.M. Baum [4] found that average car speeds were 1.3 mi/h less in states with differential limits and were statistically significantly different, average truck speeds were 2.7 mi/h less in the states with the 10 mi/h differential limit, and this difference was also statistically significant. Harkey, David L and Ruben Mera (1994) stated that mean speed of cars traveling on interstate highway systems was not affected by different speed limits. Other researchers expounded the advantages and disadvantages of DSL (differential speed limit) and also put forward some valuable suggestions.

DATA ANALYSIS

Uniform speed limit scheme is adopted on Yuqian Expressway of Chongqing

province, that cars and trucks have uniform speed limit of 100 km/h. Yusui Expressway of Chongqing province adopts differential speed limit scheme, 100km/h for cars and 80km/h for trucks, this paper collects and analyzes speed data of two different speed limit scheme on linear segment of road section which have similar road geometry conditions.

Classification of vehicle types

MetroCount5600 is used to collect data. MetroCount ARX Classification Schemes divide vehicles into 12 types, but JTG B01-2003 [6] divides vehicles into 3 types, it is obvious that these two classification schemes are not consistent. Convenience for the study, this paper combines two classification schemes, using wheelbase of 3.8 meter as classification criteria, and divide vehicles into cars (wheelbase less than or equal to 3.8 meter) and trucks (wheelbase no less than 3.8 meter).

Speed statistical indicators analysis

This paper using hypothesis testing and analysis of variance methods to comparative analysis the difference of 15^{th} percentile speed, 85^{th} percentile speed, mean speed, speed variance, and speed limit compliance between DSL and USL. The ANOVA results are as follows:

Table 1. ANOVA

	car		truck		total vehicle	
Statistics	F	Sig.	F	Sig.	F	Sig.
15^{th} percentile speed	1.08	0.304	21.477	0	12.461	0.001
85^{th} percentile speed	1.204	0.278	61.456	0	2.737	0.105
mean speed	1.642	0.207	48.027	0	5.676	0.022
Standard deviation	0.284	0.597	35.977	0	0.008	0.931
compliance	2.262	0.14	6.337	0.016		

1）Speed statistical indicators of cars

The results of ANOVA indict that 15^{th} percentile speed , 85^{th} percentile speed, mean speed, speed variance, compliance of speed limit of cars have no statistically significance between roads with DSL and USL. These two different speed limit schema impose the same speed limit on cars, therefore, no significant effect of differential speed limit on cars speed.

2）Speed statistical indicators of trucks

The result of ANOVA indicate that 15^{th} percentile speed, 85^{th} percentile speed,

mean speed, speed variance, and compliance of speed limit of trucks exist difference, and difference is also statistically significant. The trucks speeds over 24 hours (see Figure 1~4) can conclude that 15th percentile speed, 85th percentile speed and speed standard deviation of trucks with DSL are obviously lower, the compliance of speed limit of trucks with DSL are basically lower than those with USL. In other words, imposing lower speed limit on trucks decreases operating speed of trucks, and can also conclude that DSL do not increase the variation of trucks, but make the distribution of trucks more centralized.

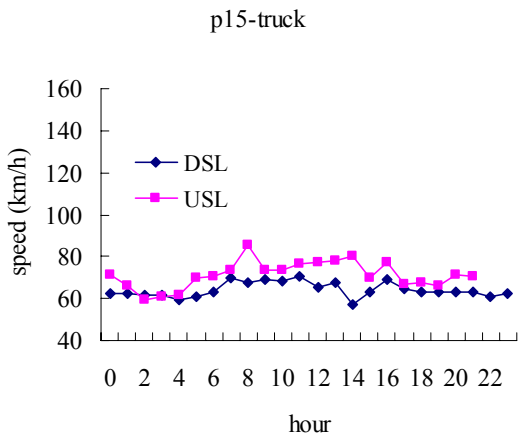

Figure 1. 15th percentile speed

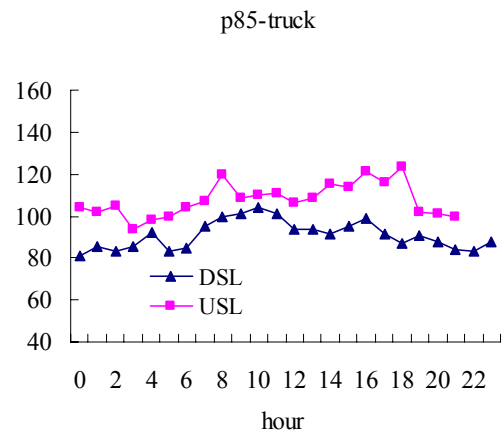

Figure 2. 85th percentile speed

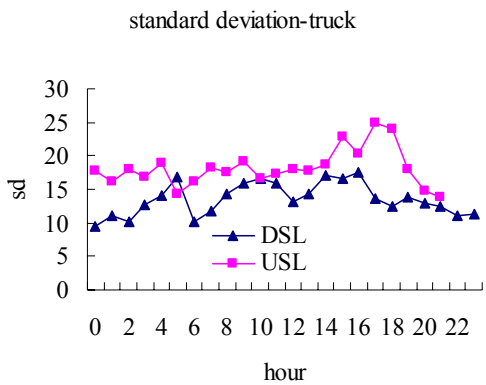

Figure 3. Standard deviation

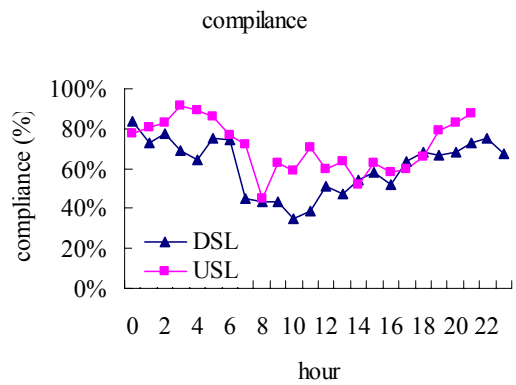

Figure 4. Compliance comparison

3）Speed statistical indicators of total vehicles

The 15th percentile speed, mean speed has significant difference, but 85th percentile speed, speed variance has no significant difference. That is to say differential speed limit affects the total vehicles speed. The effect of DSL on vehicle

speed variance and operating speed is not obvious.

Speed differences analysis

From the analysis, it can conclude that DSL has little effect on cars speed, but has a remarkable effect on truck speed, imposing a lower speed limit on trucks may result in speed statistical indicators of trucks to decrease, and increase speed differences between cars and trucks, it can also affect the variation of vehicle speeds. Correlation analysis (see Table 3) results indicate that speed limit differences resulting from different speed limit schema correlate with operating speed differences between cars and trucks, mean speed differences between cars and trucks, and speed standard deviation, three statistical indicators which increase with speed limit differences. DSL might increase speed differences, and also increase the variation of vehicle speeds, this mostly occurs because imposing a lower speed limit on trucks affect truck speed.

Table 2. Correlation

correlation	dif_p85	dif_mean	Sd
dif_sl	0.865	0.848	0.668

The relationship between speed limit differences and operating speed differences, speed limit differences and mean speed differences, speed limit differences and speed standard deviation need to be further determined. Preliminary study considers truck mixed rate and traffic volume as variables, and use SPSS software Linear Regression-Stepwise method to do regression analysis. Finally, truck mixed rate and traffic volume were excluded because of some reasons. The linear regression results are as follows.

Table 3. Linear regression

linear regression results	R	R^2
dif_p85=0.951dif_sl+24.686	0.865	0.749
dif_mean=0.671dif_sl+21.541	0.848	0.72
sd_total=0.198dif_sl+23.534	0.668	0.446

Where: dif_sl is speed limit difference between cars and trucks; dif_p85 is operating speed differences between cars and trucks; dif_mean is mean speed differences between cars and trucks; sd_total is standard deviation of total vehicles;

CONCLUSIONS AND RECOMMENDATIONS

- There is no consistent conclusion of the relationship between differential speed limit and transportation safety, so more research is needed for further

determination. Differential speed limit considers performance differences of different vehicle types, and might improve the safety operation condition of some type of vehicles. However, vehicle classification is a problem for implement differential speed limit.

- Differential speed limit might increase speed differences between cars and trucks, and might effect the variation of vehicle speeds. It will be very effective if the speed limit method of different vehicle types and lanes is combined. Speed limit by lane is a type of speed management that sets different speed limit value on different lanes. Speed limit signs are always installed on portal framed supports or are located nearby overpasses. The overhead of the speed limit sign indicates the below lane's speed limit. Another method is to paint words or markings on road surface in order to convey speed limit information.

ACKNOWLEDGEMENT

This research was conducted at the Beijing University of Technology and was funded by the Western Region Transportation Science and Technology Projects under Grant: 200731800027.

REFERENCES

D. Solomon (1964). "Accidents on Main Rural Highways Related to Speed, Driver, and Vehicle". Washington,D.C., Federal Highway Administration

N.J. Garber and R. Gadiraju (1998). "Speed Variance and Its influence on Accidents", AAA Foundation for Traffic Safety, Washington, DC.

J.W. Hall and L.V. Dickinson (1974). "An Operational Evaluation of Truck Speeds on Interstate Highways", Dept. Of Civil Engineering, University of Maryland.(1974)

J.R. Esterlitz, H.M. Baum, P.L. Zador, and M. Penny (1990). Different Speed Limits for Cars and Trucks: Do They Affect Vehicle Speeds?, Insurance Institute For Highway Safety, Arlington, VA.(1990)

Harkey, David L. and Ruben Mera (1994). "Safety Impacts of Different Speed Limits on Cars and Trucks", US Department of Transportation, Federal Highway Administration, Publication No.FHWA-RD-93-161 .

Ministry of Transport of the People's Republic of China. Technical Standard of Highway Engineering (JTG B01-2003).China Communications Press. 2004

Study on the Influence of Coarse Aggregate on the Pavement Performance of Road Cement Concrete

Shen Ai-qin[1] Xiong Jian-ping[2] He Jun-hui[3] Liu Tai-jun[4]

([123]Key Laboratory for Special Area Highway Engineering of Ministry of Education,Chang'an University,Xi'an 710064,Shanxi,China;[4]Shan'xi Provincial Communication Construction Group,Xi'an 710075,Shan'xi,China)

Abstract:

This paper presents a lab study on the influence of coarse aggregate on the pavement performance of road cement concrete. The result shows that influence degree of every technological property of coarse aggregate affect road concrete differently. The lithology of coarse aggregate will not lead to the obvious fluctuation of the pavement performance of road concrete. The flexural tensile strength of broken pebble stone road concrete is 40% lower than that of crushed stone concrete. The nominal maximum aggregate size of coarse aggregate has significant effect on the pavement performance, and it should be no more than 26.5mm when it's used on high level road. The decreasing amplitude of flake content to the pavement performance of road concrete is bigger than that of needle content. The crashing value of coarse aggregate has very significant effect on the flexural tensile strength of road concrete, so its content should be controlled.

Key words:

Road Engineering ; Road Cement Concrete ; Coarse Aggregate; Pavement Performance ; Influence Rules

Introduction

Coarse aggregate is an important part of road cement concrete. It forms the backbone structure of the road cement concrete. The technological property and the amount of coarse aggregate have very significant influence on the pavement performance of the road cement concrete (Shen, 2004; Neville, 1983; Mindess et al, 2004).

The climate condition and traffic situation of the areas where the cement concrete pavement is used in our country are very different. Under the different environmental situations and road load levels, the traditional method that chooses coarse aggregate using the strength only is not enough. It's against the performance-based road cement concrete design theory. Therefore this paper systematically analyzes the relation between the technology performance of the coarse aggregate and the pavement performance of road cement concrete. It puts forward the technology index of the road cement concrete which can meet different load levels and climate conditions. It provides scientific basis for improving the related technology standards.

1. Raw Meaterials

The Experiment uses the "Qinling" 425# ordinary Portland cement from Shanxi Yao Country cement plant. Fine aggregate is a river sand with fineness modulus 2.6, belonging to medium sands. Coarse aggregate is a limestone and broken pebble stone.

The main technology performance parameters are shown in table 1.

Table 1 the main technology performance of coarse aggregate

Aggregate spices	Crashing value%	Needle and flake%	Sturdiness %	Mud content %
Limestone	15.6	4.3	4.2	0.4
Broken pebble stone	32.4	8.3	6.1	0.3

2. Experiment Design

Considering the comprehensive influence of coarse aggregate key technology performance parameters and material composition on the pavement performance of road cement concrete simultaneously, and considering the interactive influence of water cement ratio, unit water use and other factors on the experiment ,we developed the detailed mixture ratio of road cement concrete design as shown in table 2.

Table 2 the design of mix proportion for the road cement concrete

Nominal maximum aggregatesize /mm	Water consumption /(kg/m^3)	Water cement ratio			Coarse aggregate /(kg/m^3)	Fine aggregate /(kg/m^3)
		0.40	0.42	0.44		
		cement content/(kg/m^3)				
31.5	145	363	345	330	1350	683
19						
31.5	150	375	357	341		
19						
31.5	155	388	369	352		
19						
31.5	160	400	381	364		
19						

3. Experimental Results and Analysis

The road cement concrete is confected using the designed scheme of mix proportion in table 2. The effect of coarse aggregate on pavement performance of road cement concrete is shown through analyzing the following aspects.

3.1 Variety of Coarse Aggregate (Broken Stone and Broken Pebble Stone)

The workability of fresh concrete and the 28d mechanical strengths of hardened concrete are tested and presented in in table 3.

Table 3 The result of workability and mechanical strength

	Limestone gravel			Broken pebble stone		
Water cement ratio	Slump /mm	Compressive strength/MPa	Flexural tensile strength/MPa	Slump /mm	Compressive strength /MPa	Flexural tensile strength/MPa
0.40	31	44.8	6.28	46	42.2	4.88

	32	48.1	7.05	44	37.4	5.32
	32	43.5	6.25	49	41.8	4.94
	35	42.6	5.89	45	44.0	5.26
0.42	28	45.7	6.08	31	44.4	4.81
	24	45.1	5.94	34	39.0	4.54
	24	46.0	6.33	36	43.6	4.97
	29	39.9	5.86	37	42.5	4.83
0.44	19	42.3	5.32	23	35.0	4.95
	20	42.5	5.35	27	41.7	4.99
	17	42.9	5.34	25	40.6	5.07
	19	37.9	5.12	29	37.0	4.46

(1)The slump of broken pebble stone road cement concrete is 50% greater than that of the broken stone road cement concrete. And when the water cement ratio is certain, as the unit water use increases, the magnitude of increase of slump of broken pebble stone road cement concrete is more than that of broken stone road concrete.

(2) The compressive strength of broken pebble stone concrete is generally lower than that broken stone concrete. And it still can meet the technology demand of road concrete. But under the same mixture proportion, the flexural tensile strength of broken pebble stone road concrete is generally 10~30% lower than that broken stone road concrete. The type of aggregate has great effect on flexural tensile strength of road concrete.

(3) The compressive strength and flexural tensile strength ratio of broken pebble stone concrete is greater than that broken stone concrete. It is disadvantageous to the road cement concrete whose main mechanical control index is flexural tensile strength and anti-fracture ability. Because broken pebble stone has many un-broken natural smooth surface, its bond strength with cement mortar is weaker than broken stone that lead to its flexural tensile strength decrease (Lee, 2002; Du, 1996). Otherwise, the strength of aggregate is so low that it makes the compressive strength and flexural tensile strength ratio of broken pebble stone a little high.

So, the type of coarse aggregate has a significant effect on the workability and flexural tensile strength of road concrete. High grade highway should choose broken stone first.

3.2 Needle and Flacke Particles

Needle and flacke particles of limestone from Shanxi Jingyang are picked out by a standard instrument method, and mixed in the aggregate that doesn't contain needle and flake particles with different proportions. With such aggregate, the road cement's mechanical performance test results are shown in table 4.

Table 4 The mechanical strength of different needle and flake particle content

Flake content/%	Compressive strength/MPa	Flexural tensile strength/MPa	Needle Content /%	Compressive strength/MPa	Flexural tensile strength/MPa

	7d	28d	7d	28d		7d	28d	7d	28d
0	38.3	46.0	5.18	6.34	0	38.3	46.0	5.18	6.34
5	37.2	45.4	5.13	6.22	5	38.0	45.9	5.35	6.37
10	36.0	44.9	4.85	6.08	10	37.6	46.5	5.12	6.20
15	35.4	43.7	4.40	5.45	15	37.9	45.7	4.81	5.86
20	35.0	42.5	3.76	4.52	20	37.4	45.5	4.55	5.12
25	33.9	40.1	3.53	4.07	25	35.4	43.1	4.22	4.73

The test results in table 4 show that, needle and flake particle content on the compressive strength of road concrete has smaller effects. Even if the needle and flake particle content is more than 20%, the compressive strength of concrete decreases only about 4%. Adding needle and/or flake aggregate, the trend of flexural tensile strength of road concrete is decreasing. But it has been noticed that the flake particles of road concrete have more effects on flexural tensile strength than the needle particles. When the particle content is more than 15%, the flexural tensile strength of road concrete decreases as much as 14%. And when flake content is higher, the extent of decreasing is larger.

Above all, it can be seen that if the needle and flake particles are too much, it would reduce the unitary performance of road concrete. For different grades of road, its content should be strictly controlled. The relevant recommended values are shown in table 5.

Table 5 Suggestion on limited values of needle and flake particles content of coarse aggregate

The highway grade		Expressway, first class and second class highway	Third class and forth class highway
Suggested value of this study	Needle content/%	＜9	＜12
	Flake content/%	＜6	＜8

3.3 Nominal maximum aggregate size

Different nominal maximum sizes of coarse aggregate are used to make road concrete, the test results from testing its workability and mechanical strength are shown in table 6.

Table 6 The mechanical strengths of different nominal maximum aggregate size

	31.5			26.5			19.0		
Water cement ratio	Slump /mm	Compressive strength /MPa	Flexural tensile strength /MPa	Slump /mm	Compressive strength /MPa	Flexural tensile strength /MPa	Slump /mm	Compressive strength /MPa	Flexural tensile strength/ MPa
0.40	42	41.5	5.49	34	51.2	6.58	32	48.1	7.05
	47	47.0	5.87	37	45.9	6.48	32	43.5	6.25

	51	50.1	6.25	50	48.2	6.22	48	42.6	5.89
0.42	36	50.3	5.90	28	44.8	6.01	24	42.1	5.94
	39	47.6	5.59	26	42.2	5.73	24	46.0	6.33
	40	45.6	5.41	31	44.7	5.67	29	39.9	5.86
0.44	21	41.1	5.05	20	42.1	5.41	20	42.5	5.35
	25	42.6	4.93	19	40.7	4.92	17	42.9	5.34
	28	40.4	4.65	22	37.5	4.54	19	37.9	5.12

Analyzing the data of table 6, from the perspective of workability we can see that, when the coarse aggregate nominal maximum particle size increases, the slump of new road concrete increases. This shows that increasing the maximum nominal particle size is conducive to improving the road concrete's workability. But it will also make the segregation and bleeding of concrete even more serious. Therefore, choosing nominal maximum particle size still needs comprehensively considering other proportions of concrete. The increase of nominal maximum particle size makes the overall compressive strength of road concrete increase on the overall, but lowering the flexural tensile strength. As can be seen from the experimental data, compared with the largest nominal diameter of 31.5mm, the using of nominal maximum size of the coarse aggregate 19.0mm is easier to prepare a road concrete with higher flexural tensile strength.

The suggested values of road concrete's coarse aggregate nominal maximum size that meet the different highway levels are shown in Table 7.

Table 7 Suggested values of broken stones' nominal maximum size in road concrete

The highway grade		Expressway, first class highway	Second class highway and others
The suggested values of nominal maximum aggregate size/mm	Recommended range	≤26.5(19.0～26.5 are the best)	≤31.5
	Specification regulated data	≤31.5	

3.4 Crushing value

In order to make the test representative, we nation widely selected 10 kinds of different origin prepared gravel road concrete. The test results of their workability and the mechanical strengths are shown in table 8.

Table 8 The mechanical strength of road concrete with different crushing value

Kinds	NO.	Crushing value/%	Slump/mm	Compressive strength/MPa	Flexural tensile strength/MPa	Splitting strength/MPa
Ordinary road concrete	y1-1	12.2	33	49.6	6.42	4.22
	y1-2	14.3	31	50.3	6.61	4.27
	y1-3	15.6	29	43.1	5.37	3.54

	y1-4	15.6	34	47.3	6.22	4.18
	y1-5	18.8	32	45.8	6.01	3.97
	y1-6	21.5	31	46.2	5.89	3.82
	y1-7	23.5	30	44.8	5.7	3.91
	y1-8	25.1	33	44.5	5.65	3.69

(1)When the crushing value of coarse aggregate increases, the compressive strength, the flexural tensile strength and cleavage strength of road concrete will decrease. Linear correlation exists between the two, but the influence of flexural tensile strength is obviously superior to compressive strength.

(2)As can be seen from the data in the table, when the crushing value index is less than 20%, the flexural tensile strength can easily reach 5.5 MPa. It meets the requirements of strength of high-level highway. But when the crushing value index is more than 30% , the flexural tensile strength can hardly reach 5.0 MPa.

(3)Considering the test results in previous sections, the relationship between the crashing value of aggregate and the flexural tensile strength can be referred in table9.

Table 9 The correspondence relation of crushing value and flexural tensile strength

Crushing value（%）	0～20	20～25	25～30	＞30
Flexural tensile strength （MPa）	＞6.0	5.7～6.0	5.1～5.7	＜5.0

4. The suggested technology standard values of coarse aggregate for road concrete

The test analysis above established a correlation between the key technological property of coarse aggregate and pavement performance of road concrete. Ensuring mechanical performance according to different road grades and climate conditions, the suggested values for aggregate are shown in table 10.

Table 10 The suggested values in technical standard of coarse aggregate

The highway grade / Items		Highway, first class highway	The second class highway and the third,fourth highway which has the antifreeze demand	The third,fourth highway and substandard highway
Nominal maximum aggregate size		≤26.5（19.0～26.5optimum）	≤31.5	≤31.5
Crushing value /%	Broken stone	＜20	＜25	＜30
	Broken pebble stone	＜22	＜24	＜26

Needle and flaky particle content	Needle	＜9	＜9	＜12
	Flaky	＜6	＜6	＜8

5. Conclusions

(1)The workability of broken pebble stone concrete is better than that of broken stone concrete. But its flexural tensile strength is 30% less than that of broken stone concrete. Therefore, it is better to use broken stone as coarse aggregate for high level highways.

(2)The influence of needle particle content on road concrete's pavement performance is similar to the influence of flaky particle content, but the influence degree is small . Needle particle content should not exceed 20%.

(3)Flaky particles have significant influence on flexural tensile strength of road concrete. When the flaky particle content is more than 15%, the flexural tensile strength of road concrete may decrease by 14%.

(4)Through the mechanical strength tests of road cement concrete with eleven different crashing values of coarse aggregate nationwide, the crashing value has very significant effect on flexural tensile strength. Its value should be controlled.

References

A. M. Neville. (Translated by Lee, G. J), *Property of concrete*, China Architecture & Building Press, 1983

Du, Q. Y. Study on the influence of aggregate on strength of concrete, Yunnan Building Material, 1996.4

Lee, L. *The influence of surface characteristic of coarse aggregate on strength of concrete,* Technology of Highway and Transport, 2002.4

Shen, A. Q, *Cement and cement concrete*, China Communications Press, Beijing, China, 2004.4

Sidney Mindess，J.Francis Young，David Darwin. (Translated by Wu, K. R), *Concrete,* Chemical Industry Press, Beijing, China, 2004

Research on the Competitiveness of China's Ports

B. Liu[1] and C. Liu[2]

[1]School of Economics and Business Administration, Dalian Maritime University; Dalian, P.R.China, 116026; email: bl403881@hotmail.com
[2]Business School, Shandong University at Weihai; Weihai, P.R.China, 264209; email: lcenjoy@tom.com

ABSTRACT

To understand the actual situation of a port, it should be observed from different perspectives; to evaluate the actual situation of a port, we should use a number of measurement indicators. Take this as a starting point, this paper first introduces the background and reasons for writing. Secondly, it simply describes the competitiveness of our ports and more specifically presents the method of studying the integrated competitiveness of our ports. At the same time, it classifies our ports according to their competitive characteristics, which is the innovation point of the paper. Thirdly, it analyzes the comprehensive competitiveness index ranking of Chinese ports, describes the changes between 2007 and 2006, and identifies a few representative ports on the list, analyzing their various indicators, strengths and weaknesses in detail. Lastly, it sums up the characteristics of Chinese ports based on the previous expressions and gives corresponding policies and recommendations.

1 INTRODUCTION

A nation doesn't have competition ability in all aspects, but it has core competitiveness in a certain aspect, so as to promote the development of other related industries. The competitiveness of our ports directs the competitiveness of our country, and the competitiveness of the country is a source of national strength. The economic development process of China is powerful proof: in the past 30 years of opportunity and development, China has been focusing on building coastal port cities and trying hard to make them hubs of international resources and cradles of technological innovation. It also reveals the law of economic development in light of new economic theory to make the competitive ports take a positive role in promoting the economic development of China. As a result, it is necessary for us to rank the competitiveness of ports of our country. On one hand, this can reflect the present development condition of our ports, and identify their existing problems and constraints; on the other hand, this can also unearth their potential and offer corresponding policies and recommendations, in order to give the ports freer rein to promote China's economic development and further enhance national strength

further in such areas.

2 LITERATURE REVIEW

At present, the domestic and overseas research on port competitiveness is divided into two categories. The first category establishes indexing systems to study port competitiveness. Huang Jianyuan and Yan Yixin (2004) have designed a comprehensive evaluation system of port container transportation competitiveness in China including the indexes such as operational efficiency and cost and expense. Cullinane (2005) has made an analysis of the relative competitiveness of Shanghai and Ningbo, which are the two adjacent container ports. He evaluates the service needs based on the fact that the two ports have the same hinterland, and he analyzes the current supply capacity and future expansion plans at length, ultimately evaluating the relative competitiveness of Shanghai and Ningbo in terms of price and service quality. Li Shitai (2006) establishes an index system that contains four aspects of producing elements: operation and management ability of port, demand condition, and relative supporting industry. There are numerous similar studies in our country, but their selections of index and the methods of quantification are not perfect. They are more limited for contrasting the indexes one by one, and they don't give the overall evaluation and ranking of port competitiveness.

The second category of existing research establishes comprehensive evaluation models to study port competitiveness. The analytic hierarchy process (AHP) is the main method used to determine the weight of index system, and models are constructed to evaluate port competitiveness comprehensively. Scholars such as Ji Yongbo (2005) have established the comprehensive evaluation model of port competitiveness on the basis of a fuzzy optimization model. Expert such as Wang Chunying (2006) have used the method of entropy and weight value to determine the evaluation weight of ports evaluation index to establish the multi-grade fuzzy comprehensive evaluation model. This model helps to analyze the factors of port competitiveness qualitatively, but some indexes are difficult to quantify, and their weights are difficult to determine accurately, which in turn makes it difficult to prove evaluation results.

The common characteristic of these two kinds of research is the lack of application and countermeasures to study ports on the basis of systematic theories. Therefore, they have little reference value for improving the competitiveness of our ports. Based on this, this paper establishes a more scientific index system from five aspects such as the natural conditions of port, the investment trends, the increasing rate of throughput, the assignment capacity of port, and the financial condition of port, which together make up for the shortcomings of comparing a single index other than a comprehensive competitiveness study from the previous research. This paper

establishes the evaluation model of comprehensive competitiveness of port based on the factor analysis method. First, it improves upon the existing theories of AHP and fuzzy evaluation, which have difficulty determining highly accurate evaluation results. Second, it reveals the main factors affecting port competitiveness and it improves the index system and method of evaluating port competitiveness. Finally, it makes an illustrative analysis of the 25 domestic and offers policies to improve the port competitiveness of our country.

3 DETERMINANT OF INDEX SYSTEM OF PORT COMPETITIVENESS

3.1 Definition of port competitiveness

According to the general definition of competitiveness and different, more detailed explanations from academia, and in combination with the characteristics of the port industry, this paper defines port competitiveness as the ability and opportunity that a port enterprise has to provide high-quality and low-price service for relative enterprises and industries in the competitive market environment, so as to achieve the maximum value of port enterprises. The essence of competitiveness is a kind of ability, which at a superficial level is the ability to allocate and utilize the resource advantages that competitors cannot, and at a more fundamental level is the ability to integrate various resources organically, which are the elements of the enterprises. Competitiveness relying solely on natural resources at a certain point in time cannot last long; however, poor resources can also create competitiveness through efficient processes of conversion. Core competitiveness is the organic synthesis of various techniques, skills, and knowledge, the ability to combine internal coordination with overall cooperation comprehensively, and it penetrates the whole organizational process and delivery value. Core competitiveness is the source of creating competitive advantages for enterprise. All world-famous enterprises have unique specialties in product development, technology innovation, management method, marketing, and trademark or customer service. Port competitiveness embodies the following aspects: the first is the customer value, which is a key element of the core benefits that customers care about; the second is the advantage of difference, which highlights their uniqueness in the competition, which is difficult or costly for competitors to imitate; the third is ductility, which exploits new products or services to meet customers' needs and has the vitality of lasting development.

3.2 Definition of index system

According to the above principles, we chose 13 indicators including five aspects: natural conditions, growth rate of throughput, investment trends, operational capacity, and financial status of the port. Natural conditions reflect the geographic location and the channel depth of ports. Growth rate of throughput reflects the

number of goods shipped in and out ports, which are loaded and unloaded. Investment trends reflect the ability to attract capital to ports. Operational ability reflects the efficiency of loading and unloading and the situation of warehousing and storage of ports. The financial situation reflects the solvency, operation, profitability and growth of ports. Table 1 shows the index system in detail:

Table 1. Evaluation Index System of Port Competitiveness.

1st level	2nd level	Name of variables
natural conditions	port draught	X_3
	the number of Bridge Crane	X_2
	Berth	X_1
	location advantage	X_{14}
growth rate of throughput	growth rate of port container throughput	X_5
	growth rate of port cargo throughput	X_6
investment trend	foreign direct investment	X_9
	total investment	X_{10}
operational capacity	routes	X_7
	handling rate	X_4
	utilization of berth	X_{13}
	amounts of berthing	X_8
financial position	total profit	X_{11}
	total asset	X_{12}

The data used in this paper is collected and arranged through surveying "China traffic yearbook in 2007" and the data from questionnaires of various samples of ports.

4 EVALUATION OF PORT COMPETITIVENESS BASED ON FACTOR ANALYSIS

This paper uses factor analysis to evaluate and sort comprehensive competitiveness of ports. We can utilize factor analysis to concentrate with less data and use several practical factors to reflect main information of plenty original data.

4.1 KMO inspection and Bartlett test results of ball degrees

KMO is 0.737 in this study, which is evidence of fitting for factor analysis. The Sig that Bartlett test results of ball degrees gives is 0.000, which demonstrates that the data comes from normal distribution, so it is suitable for factor analysis.

4.2 Evaluating the score and sorting

The score of each factor, the score and the taxis of comprehensive competitiveness are presented in Table 2.

Table 2. List of Monomials and Comprehensive Rank of Ports.

The rank of total score	port	Total score	F1	F2	F3
1	Shanghai	114.38	159.98	-107.67	109.39
2	Tianjin	64.14	86.03	-84.72	110.69
3	Shenzhen	41.18	45.46	6.16	57.08
4	Qingdao	40.06	45.42	-11.79	69.28
5	Ningbo-zhoushan	36.71	39.29	12.28	50.17
6	Yingkou	30.57	32.00	-43.20	107.76
7	Nanjing	26.46	31.88	0.00	25.93
8	Tangshan	24.29	27.00	6.30	29.60
9	Guangzhou	24.19	22.34	2.06	60.41
10	Qinhuangdao	21.60	21.67	-17.81	66.81
11	Suzhou	20.90	19.72	6.96	43.78
12	Xiamen	20.53	17.94	20.23	35.77
13	Yantai	18.73	14.01	10.08	55.89
14	Dalian	18.72	17.66	8.39	36.80
15	Rizhao	18.06	17.90	-12.59	54.43
16	Wuxi	17.06	15.55	17.72	24.96
17	Lianyungang	15.76	9.63	22.96	42.64
18	Dandong	14.01	11.70	-4.78	49.07
19	Zhanjiang	11.18	6.73	10.00	38.12
20	Nantong	10.33	5.70	11.07	36.06
21	Zhongshan	9.50	3.67	9.08	43.43
22	Wuhan	8.81	6.17	0.77	33.28
23	Jinzhou	6.86	-0.15	10.07	43.43
24	Huanghua	6.85	1.77	6.58	36.36
25	Quanzhou	6.52	-0.30	14.90	36.00
26	GroupofFuzhou	6.27	-1.81	16.63	40.72
27	Wuhu	5.57	0.63	8.68	30.33
28	GroupofWenzhou	5.38	-2.38	14.15	39.86
29	Haikou	5.01	0.43	6.51	29.63
30	Shantou	4.58	-0.65	8.31	30.31
31	Zhuhai	3.37	-5.25	12.87	41.87
32	Chongqing	3.35	-3.50	8.99	36.20

Note: Although the scores of competitiveness of many ports are negative, this does not mean the competitiveness of those ports is negative, which is due to the result that the author has standardized the data in the whole process of analysis; it therefore represents the relative competitive level of each port only.

4.3 Result analysis

According to the analysis of the characteristics of the comprehensive competitiveness of China ports, we list separately the most efficient port, the most international port, the most aggressive port, the most innovative port, the most governmental port and the most private port. Such a method of classification analysis is a new event in the industry. It has a profound, extensive and practical significance, coinciding with the purpose of the research. It is good for ports "to understand their own competitive position, dig their own advantages, develop their superiority and avoid their weaknesses, improve themselves, and establish effective investment, financing, innovation and development strategies in competitive market." Next, we will introduce specifically the prior six ports from the China port competitiveness ranking in 2006 and 2007. Their rankings have since changed, but the ports maintain the same competitive characteristics.

(1) The most efficient port: Shenzhen Port

Shenzhen Port depends on the developed Pearl Delta, Macau, and Hong Kong, and it has a vast economic hinterland and advantageous geographical location. Its international shipping capacity is increasing gradually, its infrastructure is improving gradually, its service level continues to improve, and its price advantage is very obvious. Shenzhen Port has become the major hub in the comprehensive transportation system of China, especially its developing container business, which makes it the container hub of south China. In 2007, the container throughput of Shenzhen Port reached to 13.70%, and its cargo throughput reached 13.65%. Because of its excellent benefits, full potential, timely economic growth, and strong ability to provide service to customers, Shenzhen port is worthy of being deemed the most efficient port of China ports in 2007.

(2) The most international port: Shanghai Port

Shanghai Port penetrates the Yangtze River Golden Waterway in the west, and it is located in the main channel of China. A developed economic hinterland, strong support of national policies, and superior conditions of the capital market enable it to accumulate labor, capital, technology, resources, information and technology rapidly, and give it competitive advantages. In 2007, the growth rate of container throughput of Shanghai Port reached 20.41% and the growth rate of cargo throughput reached 4.19%. Although serious environmental pollution of environment, poor capital operation, lack of management levels, and poor earnings potential still restrict its further development, it can make full use of its own advantages to reorder itself, and to realize the transformation from large port to strong port, and to maintain the status of China’s international port.

(3) The most aggressive port: Guangzhou Port

Guangzhou Port is located in the center of the Pearl River Delta whose

export-oriented economy is the most active in China, which has obvious location advantage. Although there are some geographical flaws, the use of Nansha deep-water wharf compensates for these shortcomings, allowing Shenzhen Port to grow over time from river port to harbor port. In 2007, its growth rate of container throughput reached 38.21%, and its average growth rate of container throughput was 41.4% between 2005 and 2007. Guangzhou Port is the Chinese port with the highest berthing rate, the most frequent shipping, the largest batches, the most complex waterways and the most intense competition. Its goods are adequate, its cash flow is abundant, its business is adjusted timely and its port construction is active and steady, so Shenzhen Port is deserved the title of most aggressive port in 2007.

(4) The most innovative port: Qingdao Port

The biggest advantage of Qingdao Port is its natural deepwater waterway; among the other ports its condition is unquestionably superior. It continues to offer the three qualities of "blue sky, clear water, green land" and it has built a wall for wind and dust prevention at an internationally advanced level at present. Relying on scientific and innovative management, the port promotes the "second" era of handling and production strongly. All of the above are its unique aspects. In 2007, the growth rate of container throughput of Qingdao Port reached 22.05%, and the growth rate of cargo throughput reached 17.78%. Because of the urgency consciousness, the port has created an innovative approach to the Chinese "1>2", and it has achieved good results. Therefore, Qingdao Port is worthy of the most innovative port in 2007.

(5) The most governmental port: Tianjin Port

Tianjin Port is located in the intersection of Beijing-Tianjin urban belt and Bohai Sea Rim Economic Circle, which is the nearest port to North and Northwest China among the Bohai Sea Rim Ports, and it is one of the busiest and the fastest developing ports in the northern coastal area of China. Under the support of the government and the guidance of its policies, the complete supporting facilities, the efficient customs clearance process, the positive financial innovation and the plentiful cash flow, this port's core competitiveness has improved greatly, and they will further consolidate as a central logistics hub. In 2007, the growth rate of container throughput of Tianjin Port reached 19.36% and its growth rate of cargo throughput reached 18.02%, so it became known as the most governmental port of China in 2007.

(6) The most private port: NingboZhoushan port

Ningbo–Zhoushan Port boasts the advantage of a joint venture with Sinopec, integrating port resources and improving production efficiency, which makes its oil transit remain very competitive; five kinds of goods structures are increasingly reasonable so that cargo throughput maintains a sustainable growth rate of 12.53

percent; container throughput ranks fourth in terms of coastal ports with the growth rate as high as 31.32 percent. Personalized service makes Ningbo–Zhoushan Port stand among consignors in Europe, Thailand, Malaysia and Singapore, and makes the personality of "taking the Four Seas" of Ningbo's private economy widely known. Ningbo-Zhoushan Port will continue to compete with Shanghai Port in the ship-owner market, and enhance cooperation with the international shipping giant, increasing efforts to develop container routes to attract the world's top 20 largest shipping companies to open routes in Ningbo Port. The "benchmarking strategy" of Ningbo–Zhoushan Port also wins endless business opportunities for itself. Therefore, Ningbo–Zhoushan Port was honored as the Chinese private port in 2007.

5 CONCLUSION

(1) The investment in ports is increasing and the throughput continues to rise

In 2007, the investment in ports continued to increase as it has in recent years, and it appears that the trend of multiple developments, which includes central, local, state-owned enterprises, private enterprises and foreign enterprises namely, and the state-owned enterprises are the leaders of investment. Port investment is mainly distributed in docks, waterways, loading and unloading equipment, information, stack of goods and transportation system, etc. Its strengths are the construction of the infrastructure and information of ports and improvements in loading and uploading and handling ability. It shows that the facilities our ports are improving overall gradually, and their comprehensive ability is strengthening as a whole. In 2007, the cargo throughput of all our ports completed 6410 million tons, which is 15.1 percent larger than in 2006. The domestic trade cargo throughput completed 4561 million tons, which is 15.3 percent larger than in 2006; the growth rate is 1.9 percent faster than in 2006, and it is the first time that the growth rate of domestic trade cargo throughput exceeded foreign trade cargo throughput; The container throughput broke through 100 million cases in 2007. Although the growth of port throughput slowed, the total throughput increased greatly. Coal, oil, minerals and container are still the main contributors to port throughput.

(2) The ports profit overall, but efficiency must improve

The growth of China's economy, the improvement of the management level of ports, and the high efficiency of port productivity contribute to the overall profits of ports in 2007. Compared with the history, the overall profits of ports show great progress. However, compared with the international ports, it is too far behind them. This suggests that the assets of our port enterprises must grow dramatically, but efficiency doesn't grow with the same frequency, which shows that distortions exist in the asset structures of our port enterprises and the structure of port-vicinity industrial zones, which need to be resolved.

(3) Exert the function of port engine, and promote the benefits of regional integration

Port integration is intended to utilize natural port conditions and layout, to integrate port resources according to the economic development of ports and the economy development of their hinterlands, to optimize the port configuration and to exert the function of port engine. When we make port integration among areas, we should consider both the differences of cultural backgrounds of ports and the interest needs of special group of local government. Forever, we could reduce the resistance of integration and achieve the complementary advantages of the regions of ports.

(4) The ports step toward capital market, and their degree of internationalization deepens

In 2007, more and more port enterprises listed in internal and external of China, which demonstrates that the capital consciousness of our port industry is increasing and China's ports are stepping into capital market gradually; it also marks the beginning of modern enterprise management of our ports. Internationalization is the inevitable choice of Chinese ports, which is illustrated by the development process of Shanghai Port. However, acting as the environment is a complete and integrated strategy. At present, it is too early for China's ports internationalize, but we should seize the opportunity of port development, and plan to promote the internationalization of our ports in good time.

(5) The development of ports prompts the development of port-vicinity industrial zone, the differences of regional economics bring the economics characteristics of ports

In 2007, the port engine promoted the further development of port-vicinity industry, which shows that China's economy is becoming more and more mature. Depending on local resources and seizing the opportunity to transform world industries, we have built the port-vicinity industrial chains which adapt international markets in the Pearl River Delta and the Yangtze River Delta, and the industrial areas and city groups around the Bohai region are spreading toward the port-vicinity area. At the same time, the development of regional economies differs, and that brings regional development characteristics to port development. In different areas, the development of ports shows differences. Among each economic belt, the advantage of a port engine appears, and specialization and diversification exist at the same time.

(6) The port construction emerges as an inflection point, port competitiveness confronts with new challenges

The construction of China's ports emerges as an inflection point, and the ports that were once in the secondary position are raised to an important position. The traffic industry is developing with resource-saving and environmentally-friendly

objectives, and it promises new challenges to competitiveness; constructing and improving the comprehensive transportation system puts forward new aims for port layout; building port projects, which mainly rely on continental and marine hinterlands, brings innovative thinking to the forefront. Constructing ports and waterways under complex conditions also poses new challenges to port competitiveness.

REFERENCES

Cullinane, K.P.B, Wang, T., and Cullinane, S.L. (2005). "Container Terminal Development in Mainland China and its Impact on the Competitiveness of the Port of Hong Kong" *Transport Reviews*, 24(1), 33-56.

Huang, J., and Yan, Y. (2004). "The Design Scheme Of Comprehensive Evaluation Index System Of Container Transportation Competitiveness Of Ports" *Transportation management*, 26(9), 8-10.

Ji, Y., Su, P., and Han, J. (2007). "The Application of Fuzzy Optimization Model in Evaluating Comprehensive Competitiveness Of Container Port In Container Ports Competitiveness Evaluation Of Comprehensive Application." *Port & waterway scientific research*, (4), 3-6.

Li, S. (2006). "The Research of Effecting Factors, Analysis And Evaluation Of Port Core Competitiveness" *The economics of special zone*, (7), 327-328.

Wang, C., Xiao, P., and Xiao, L. (2006). "The Application Of Fuzzy And Comprehensive Evaluation Method Of Entropy In Evaluating Port Competitiveness" *The Waterway and Port*, 27 (2), 131-134.

Equilibrium Model of Trip Modes in Road Traffic and Orientation of Charge Policy

Linlin Wu [1] Qifen Zha [2] Jianyi Liu [1]

1School of Business Administration, Jiangsu University, Zhenjiang,212013, PH (86) 511-88792088; FAX (86) 511-88792188; email: llwu@ujs.edu.cn
2 School of Finance Economics, Jiangsu University, Zhenjiang, 212013

ABSTRACT

In the adjacent urban trip modes, car and bus are the most prevalent means of transportation. Based on the practical situation that transport bottlenecks are frequently caused in the urban traffic and working on the premise that both of the two trip modes have access to the same traffic route and intervene with each other, this paper develops a model for transport bottlenecks. The paper analyses the differences of the generalized travel cost between car and bus. It deduces and compares the change of traffic flow and travel costs of car and bus under static and dynamic charge policies. This paper deepens our understanding of the issues on these two competitive systems. Based on the analysis, the paper concludes that from the perspective of sustainable development, the government should guide passengers to change their trip modes and should implement the policy of dynamic fees to promote the sustainable development in urban areas.

KEY WORDS: *model of transport bottlenecks; equilibrium model; transport fees*

INTRODUCTION

Based on the current situation in China, highway trips are more popular for passengers traveling between adjacent cities. In highway trips, cars and buses are usually run by the same route of mixed operations. Thus, it is relatively complicated to establish an equilibrium model of trip modes to be consistent with the practical traffic situation, which also provide the basis for enacting traffic policies from the perspective of sustainable development.

There is extensive research on calculating traffic expenses, pricing, and charges in recent years. After Vickrey presented the mathematical model for endogenesis time election for the first time, some efforts such as Tabuchi (1993) and Arnott (1990, 1995) made contributions on the basis of passengers' traffic time and expenses. Friesz (1983) and Norbert (1994) worked on the pricing issues of various traffic modes in the market economy. Scholars such as Ferrari P. (2002) and Bellei G. (2002) studied the pricing issues of highway trip from many perspectives. Evans (1987, 1990) elaborated the operation condition of public transportation in the competition mechanisms from the perspective of macro economy, but failed to build mathematical models to analyze the operation condition. Other researchers (Huang, 1995 &1998); Si, 2001;, and Chen, 2005) have built relative mathematical models

and worked on the above issues in different ways. However, the above papers have not investigated on how to simulate vehicles' traveling on the highway and how to charge the vehicles especially under the practical circumstances that cars and buses travel by the same route. This turns out to be important to promote the sustainable development of the transportation system.

SETTING UP RESEARCH CONDITIONS

Suppose that two adjacent metropolitan cities are namely a satellite city W and a central city Z respectively; there is no rail traffic between them. Passengers have to choose the highway trip. In the mean time, cars and buses travel by the same route. There is a bottleneck along the highway (Suppose it is a tunnel) with a capacity that m vehicles can pass through it per unit time. There is a toll station on the way from *W* to *Z*. *N* passengers go to work from the satellite city to the central city every morning, among whom N_2 passengers go by car and N_2 passengers go by bus. All the passengers expect to arrive at the central city at a certain time t_D. Normal traveling time of cars from *W* to *Z* is H_c and that of buses is H_b. Furthermore, t_0 is the departure time of cars from *W* to *Z* when cars are expected to arrive at the destination at t_D.

MODEL OF TRANSPORT BOTTLENECKS

Cars' Travel Expenses. When the departure rate of cars from *W* to *Z* exceeds the traffic capacity of the bottleneck m, it is inevitable that cars have to wait in line. Suppose $u(t)$ is the departure rate at a certain time t, and $q(t)$ is the queue length at time t, we can get $dq(t)/d(t) = u(t) - m$.

Traffic expenses of cars which depart at time t may be represented as following:

$$C_{c(t)} = \begin{cases} \alpha_c(H_c + q(t)/m) + \beta_c\left[t_D - (t + H_c + q(t)/m)\right] + F_{c(t)} + R_c & t \le t_0 \\ \alpha_c(H_c + q(t)/m) + \gamma_c\left[(t + H_c + q(t)/m) - t_D\right] + F_{c(t)} + R_c & t > t_0 \end{cases} \quad (1)$$

In the above equation, $C_{c(t)}$ is the generalized travel cost for passengers by car who depart at time t. α_c is the time cost coefficient of passengers. H_c is the normal travel time. β_c is the bonus coefficient （β_c<0） when passengers go to work earlier . $F_{c(t)}$ is the fee for roads and bridges at time t which is imposed by the toll station. R_c is the fee for fuels. γ_c is the punishment coefficient when passengers are late for work. According to the result of Small's investigation (1982) and the research of Smith (1984)，we may have $\gamma_c > \alpha_c > \beta_c$.

Buses'Travel Expenses. Likewise, the generalized travel cost for passengers by bus who depart at time t may be represented as following:

$$C_{b(t)}=\begin{cases}\alpha_b(H_b+q(t)/m)+\beta_b\left[t_D-(t+H_b+q(t)/m)\right]+P_b+R_{(t)} & t\le t_0\\ \alpha_b(H_b+q(t)/m)+\gamma_b\left[(t+H_b+q(t)/m)-t_D\right]+P_b+R_{(t)} & t>t_0\end{cases} \quad (2)$$

In the above equation, $C_{b(t)}$ is the generalized travel cost for passengers by bus who depart at time t. α_b is the time cost coefficient of passengers. β_b is the bonus coefficient （β_b<0）when passengers go to work earlier . P_b is the ticket fare for buses. $R_{(t)}$ is the congestion fee caused by physical contacts when passengers depart at time t. γ_b is the punishment coefficient when passengers are late for work. Likewise, we may have $\gamma_b>\alpha_b>\beta_b$.

Bottleneck Equilibrium Model. When all the passengers can arrive at the destinations at time t by means of the two traffic modes, passengers usually will not change their modes. Suppose that t_c^1 is the departure time of the first passenger who travels by car. and the traffic expenses should be:

$$C_c^1=\alpha_c H_c+\beta_c(t_D-t_c^1)+F_{c(t_c^1)}+R_c \quad (3)$$

Suppose that t_c^z is the departure time of the last passenger, and then the traffic expenses should be:

$$C_c^z=\alpha_c H_c+\gamma_c(t_c^z-t_D)+F_{c(t_c^z)}+R_c \quad (4)$$

Suppose that H is the specified time intervals in which buses commute.

$$t_c^z-t_c^1=\left[N_1+(t_c^z-t_c^1)/H\right]/m \quad (5)$$

When traffic modes are in equilibrium, all the passengers have the same traffic expenses, and we may have

$$\begin{cases}t_c^1=t_D+(F_{c(t_c^1)}-F_{c(t_c^z)})/(\beta_c+\gamma_c)-\gamma_c N_1 H/(mH-1)(\beta_c+\gamma_c)\\ t_c^z=t_D+(F_{c(t_c^1)}-F_{c(t_c^z)})/(\beta_c+\gamma_c)+\beta_c N_1 H/(mH-1)(\beta_c+\gamma_c)\\ \\ C_c^z=\alpha_c H_c+\dfrac{(F_{c(t_c^1)}-F_{c(t_c^z)})\gamma_c}{\beta_c+\gamma_c}+\dfrac{\beta_c\gamma_c HN_1}{(mH-1)(\beta_c+\gamma_c)}+F_{c(t_c^z)}+R_c\end{cases} \quad (6)$$

According to the practical situation in China, the toll stations between cities aim to charge fees for the construction of public highway, and the fixed amount of money they charge depends on different models of cars. Thus, $F_{c(t_c^1)} = F_{c(t_c^z)}$.

So we may have

$$C_b^1 = \alpha_b H_b + \beta_b (t_D - H_b - t_b^1) + P_b + R_{(t)}^1 \quad (7)$$

$$C_b^z = \alpha_b H_b + \gamma_b (t_b^z + H_b - t_D) + P_b + R_{(t)}^z \quad (8)$$

Suppose that the approved passenger load of bus is A, and the bus departs on time. H stands for the specified time intervals in which buses commute. We may have

$$\begin{cases} t_b^1 = t_D - H_b - \dfrac{\gamma_b N_2 H / A}{\beta_b + \gamma_b} \\ t_b^z = t_D - H_b + \dfrac{\beta_b N_2 H / A}{\beta_b + \gamma_b} \\ C_b = \alpha_b H_b + \dfrac{\beta_b \gamma_b N_2 H / A}{\beta_b + \gamma_b} + P_b + R_{(t)} \end{cases} \quad (9)$$

In the above equations, C_b stands for the traffic expenses of passengers by bus.

HIGHWAY TOLLING STRATEGIES

In order to relieve traffic congestions and change the present pricing mechanism, the measures such as increasing the static charges and implementing dynamic charges are the first choices. Suppose the fee F_z is added to reduce passengers by car. Some passengers by car will necessarily change their mode and travel by bus. As a result, the traffic congestions are relieved.

Dynamic pricing aims to optimize the operation of public highways between the two adjacent cities. Thus, no vehicles need to wait in queues. Under this condition, during the period $[t_c^1, t_c^z]$, both of the departure rate and reach rate should be $u(t) = m$. Thus, passengers by car may adopt such a dynamic pricing strategy:

$$F_{c(t)} = \begin{cases} C_c - \beta(t_D - H_c - t) & t \le t_0 \\ C_c - \gamma(t + H_c - t_D) & t > t_0 \end{cases} \quad (10)$$

Based on the analysis of policies of static and dynamic pricing, we may have the conclusion that static pricing may enable passengers to change their travel modes and increase the number of passengers who travel by bus. Dynamic pricing, however,

changes the time distribution of cars, which reduces cars' and buses' waiting times on the road. Thus, from the perspective of sustainable development, the transportation management authority should combine static pricing with dynamic prcing and should enhance buses' departure frequency to promote the sustainable development of the area. The passengers are then advocated to choose public traffic modes and the traffic congestion can be relieved. At this moment the pricing strategy should be:

$$F_{c(t)} = \begin{cases} C_c - \beta(t_D - H_c - t) + F_z & t \le t_0 \\ C_c - \gamma(t + H_c - t_D) + F_z & t > t_0 \end{cases} \qquad (11)$$

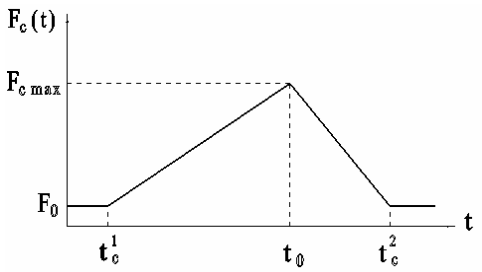

Figure1.The relationship curve of pricing strategies and time

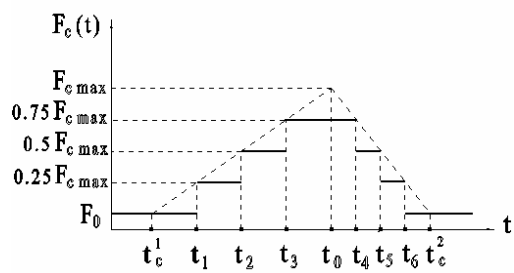

Figure2. The strategy of pricing in different periods

According to Equation（11）, the relationship between the amount of charge and time is shown in Figure 1. As the amount of dynamic charges is a continuous function of time, it requires advanced techniques to implement. However, we may approximate the optimal dynamic strategies by means of adopting staircase pricing strategy. As shown in Figure 2, though it can not eliminate waiting completely, the staircase pricing strategy can relieve traffic congestion and is easy to operate.

CONCLUSION

Trips between adjacent cities in China are very common. The passenger flow to and from work between the satellite city and the central city has already drawn many researchers' attention. This paper simulates the most common traffic modes between adjacent cities and provides basis for developing traffic policies from the perspective of the area's sustainable development. This paper however does not introduce the influence into the model analysis of when passengers who travel by car change their traffic modes. In this case, the number of buses will be greatly increased which may lead to traffic congestion. These issues will be studied in subsequent papers.

ACKNOWLEDGMENT: The authors wish to thank the support by the humanities and social science fund of National Ministry of Education（07JA910003）and the science and technology fund of Zhenjiang City（SH2005058）.

REFERENCES

Arnott, R, De Palma, A., and Lindsey, R.(1990). "Departure time and route choice for the morning commute." *Transportation Research, Part B,* 24, 209-228

Bellei, G., Gentile, G., and Papola, N.(2002). "Network pricing optimization in multi-user and multi-modal context with elastic demand." *Transportation Research,* Part B, 36, 779-798.

Chen, K., and Luo, X.(2005). "Game-theory of reasonable ticket price for urban railway transport." *Journal of Changan University (Natural Science Edition),* 25(4), 52-55. (in Chinese)

Evans, A.(1987). "A theoretical comparison of competition with other economic regimes for bus services." *Journal of Transport Economics and Policy,* 21 (1), 7-36

Evans, A.(1990). "Competition and the structure of local bus markets." *Journal of Transport Economics and Policy,* 24(3), 255-281

Friesz, T.L , and Harker, P.T.(1983). "Multicriteria Spatial Price Equilibrium Network Design: Theory and Computational Results." *Transportation Research,* Part B, 17(5), 411 - 426.

Ferrari, P.(2002). "Road network toll pricing and social welfare." *Transportation Research Part B,* 36 (5), 471-483.

Huang, H.J., and Yang, H.(1996). "Optimal variable road-use pricing on a congested network of parallel routes with elastic demand." *Transportation and Traffic Theory,* edited by Lesort J-B. Eisevier Science Ltd, 479-500

Huang, H., Bell, M.G.H. and , Yang, H.(1998). "Pricing and model split in a competitive system of mass transit and highway." *Journal of Management Sciences in China,* 1 (2),17-23. (in Chinese)

Huang, Y. and, Zhou J..(2004). "Fare competition between highway and public transport." *Journal of Southeast University (Natural Science Edition),* 34(2), 268-273. (in Chinese)

Norbert, O.(1994). *Urban Travel Demand Modeling: From Individual Choice to General Equilibrium*. *A Wiley - Interscience Publication ,* John Wiley & Sons , INC, 112 - 203.

Small, K.A.(1982). "The scheduling of consumer activities: Work trips." *American Economic Review ,* 74, 467-479

Smith, M.J.(1984). "The existence of a time-dependent equilibrium distribution of arrivals at a single bottleneck". *Transpn Sci,* 18, 385-394

Si, B., and Gao, Z. .(2001). "Optimal Model and Solution Algorithm for Passenger Ticket Pricing under the Condition of Multimodal Transportation." *Chinese Journal of Management Science,* 9 (1), 55-62.

Tabuchi, M.(1993). "Bottleneck congestion and modal split." *J. of Urban Economics,* 34, 414-431

Vickrey, W.S.(1969). "Congestion theory and transport investment." *American Economic Review ,* 59, 251-261

Analysis of the Influence of Emergent Incident on Expressways by Simulation

M. Li,[1] W. Jin,[2] and S. Fang[1]

[1] Key Laboratory of Road and Traffic Engineering of the Ministry of Education, School of Transportation Engineering, Tongji University, Shanghai, China; PH (021) 69584649; email: momijido004@sina.com

[2] Department of expressway traffic police, Jiaxing, Zhejiang, China; PH (0573) 82875625; email: cjl-002@163.com

ABSTRACT

This paper studies on the emergent incident's influence on expressway network. According to the survey about expressway network of Yangtze River Delta region, the paper defines a basic unit of expressway network. In order to evaluate how the incident influences the expressway, this paper has developed an evaluation indicator, the delay increase. To compare the different influences of different types of incident, this paper addresses several factors which affect evaluation indicator, including flow, duration of incident, and type of the influence. Establish the simulation model of expressway network and do the simulation experiment about the various affecting characteristics of the incident by using traffic simulation software AIMSUN. Use the simulation results to analyze the influence of the incident on the network through specific data. On this basis, study the relationship between flow of vehicle, duration of incident and delay increase and develop a function model about it. This paper also gives the application of the simulation data and function model in practice.

Keywords: Expressway; Incident; Simulation experiment; Delay increase

INTRODUCTION

At present in China, the construction of the highway network of the Yangtze River Delta region has reached a high level. The density of the road network is quite large. However, in the field of expressway management, it still hasn't a complete system either in theory or practice. Especially when the incident happens, it is hard to deal with the case timely and efficiently. Although there are some contingency plans, the plans themselves often have been made by experience. The lack of scientific theories in emergency rescue has become a serious problem. For the management of the expressway, the treatment of the incident is one of the most important parts. In order to treat the incident timely, effectively, and reasonably, the primary mission is to find out how the various emergency incidents influence the expressway. Give the influence an assessment so as to find the better measure of rescue.

The study of this subject both in China and abroad focuses on the expressway emergency response in varies situations (Elvey and John 2003).. The relative research includes detection of the incident, setting up a framework for emergency rescue, and building the system of incident rescue (X. Wang et al.2005). These researches have noted the main features of the incident and the assessment indicators of it on expressway. However, the most current domestic research is based on theoretical analysis and building of framework, lacking the application of specific data. Thus caused few study result to be directly usable in practice. The reason is understandable—it is difficult to obtain the relative data on expressway, especially under emergency. Meanwhile, the study of incident rescue by simulation experiment is hardly seen. Lack of suitable simulation software which can be used to simulate the incident is the main problem. In order to research the influence of incident on expressway while the relative real data can be hardly attained, the use of traffic simulation software is practical and reasonable. The core of the traffic simulation software is its car-following model and lane-changing model. As long as the parameters of these models are defined, the simulation can be completed to find the large number of target data which is used to do the analysis. This paper uses simulation experiment to analyze the influence of incident since the allowed deviation of model parameters will not affect the trend in the experiment result.

THE CHARACTERISTICS OF THE INCIDENT AND EXPRESSWAY NETWORK

According to the investigation of expressway networks in Yangtze River Delta region, the incident on expressway can be divided into two parts, predictable and unpredictable events. The predictable events are usually stipulated in the ordinance and rarely occur. So it has little influence on expressway. This paper will mainly focus on unpredictable events which could also be separated into two parts, traffic accident and inclement weather.

The influence of incident on expressway can be attributed to the influence on section and lanes when doing a simulation experiment. Whether it is a traffic accident or inclement weather, the influence can be attributed to the temporary closure of lanes, sections or section speed limit. The difference only lies in the duration of lane closure, the range of it, etc.

With the development of expressway in the Yangtze River Delta region, the region has been gradually improved into a network. According to the investigation, the incident on expressway will only influence its own section mostly; few times will the cross expressway be affected and there is almost no affect to the parallel expressway. The radiation scope of the incident is not significant. Only large areas of inclement weather will influence the entire expressway network. If there is an incident, police will often use the parallel expressway or ground road nearby to do the traffic diversion. Parallel expressway is more preferred because the use of ground

road diversion will cause greater impact on the road, drivers are often unfamiliar with it, and there also exists some organizational problems. To sum up, this paper gives a definition of basic unit to expressway network. The network is composed by three expressways two of them are parallel and the other crosses them (see Figure 1). All the expressway networks can be divided into a basic unit, and to study the incident influence in a basic unit.

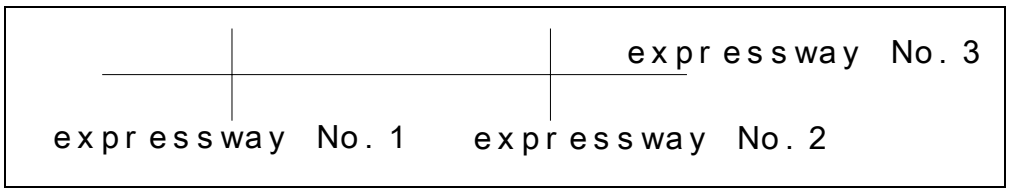

Figure1 Basic unit of expressway network

SIMULATION MODEL

Calibrate the model parameter. Whether the simulation results are meaningful and consistent with the reality is related to the calibration of model parameter. The paper calibrates the parameter on the basis of investigative data. It includes the basic parameters of the expressway network, car type and behavior, etc. It should be noted that the car-following model and lane-changing model in traffic simulation software AIMSUN is the GIPPS model (AIMSUN 6 User's Manual 2008)..

Choose the expressway network for simulation. This paper chooses three expressways named Huhang (No.1), Hangpu (No.2), and Zhajiasu (No.3) in Zhejiang province as the basic unit of expressway network to do the simulation experiment. The general location of these expressway are shown in Figure 1. All the section parameters are calibrated according to them.

SIMULATION EXPERIMENT

Select the evaluation indicator and its influencing factors. This paper develops a new evaluation indicator to evaluate the influence of incident — the total delay increase in expressway network. The delay of a car means the actual time spent to pass the section minus the time needed in free flow condition (the minimum time needed). Then total delay means the sum of delays of all the cars. The evaluation indicator shows the delay increase compared to the normal condition, also means to show the total delay increase caused by the incident.

This paper considers the following three variables as influencing factors on the evaluation indicator.

- Flow in the section: Using 1000~2400veh/h as the scope of simulation. Every 200veh/h as an interval.
- Duration of incident: Using 20~120sec as the scope of simulation.
- Type of influence: Single lane closure, section closure, section speed limit.

The experiment use different combinations of variables to find out its influence

on the evaluation indicator. The experiment has been designed in three parts.

The first part of the experiment: standard test. Since when the traffic flow reaches a certain value, it will not be the free flow anymore. Delay will generate, so delay in the normal condition should be known as the reference of the incident condition.

The second part of the experiment: relationship between flow, duration, and delay increase. This part assumes that there is an incident happening in expressway No.3 and the right lane of its section is closed. Conduct the simulation experiment by only changing the flow in the section and duration of the incident. Since the incident may cause some delay increase in other two cross expressways, sum up the delay increase in all three expressways and get the value of evaluation indicator. The flow changes from 1000 to 2400veh/h, and duration of incident changes from 20 to 110min. There are in total 80 different experiments, part of the results are shown in Table 1.

Table 1 Relationship between flow, duration, and delay increase

Actual Flow （veh/h）	Duration (min)	Delay Increase (min)	Actual Flow （veh/h）	Duration (min)	Delay Increase (min)
1029	20	177	1029	70	487
1029	30	279	1029	80	560
1029	40	333	1029	90	631
1029	50	307	1029	100	662
1029	60	328	1029	110	760

The third part of the experiment: different types of influence in the section. This part assumes that there's an incident in expressway No.3, and section is closed or speed is limited. Do the experiment with different flows and durations, part of the results is shown in Table 2.

Table 2 Experiment data of different type of influence

Actual Flow （veh/h）	Duration (min)	Type of influence	Delay Increase (min)
1029	30	Section closure	11204.93
1029	60	Section closure	42767
1029	60	Speed limit 60km/h	8661
1029	60	Speed limit 80km/h	2150
1029	90	Speed limit 60km/h	12463
1029	90	Speed limit 80km/h	3110

RESULT ANALYSIS

The second part of the simulation experiment assumes that there is an incident happening in the expressway and caused the right lane of its section to close. This kind of incident happens quite typical in the expressway. The relation between flow,

duration of incident and delay increase is shown in Figure 2 according to simulation data.

From the chart, it can be concluded that the delay increase caused by incident and the flow have an exponential relation. When the flow is relatively low, duration of the incident has little contribution to the delay increase. When flow is beyond 1500veh/h, the influence of duration on delay increase becomes more and more obvious. This means that there exists a mutation point of delay increase. Incident duration will have little influence when flow is lower than the value of the mutation point. According to the simulation result, the value of the mutation point is a little bit lower than the half value of the section capacity.

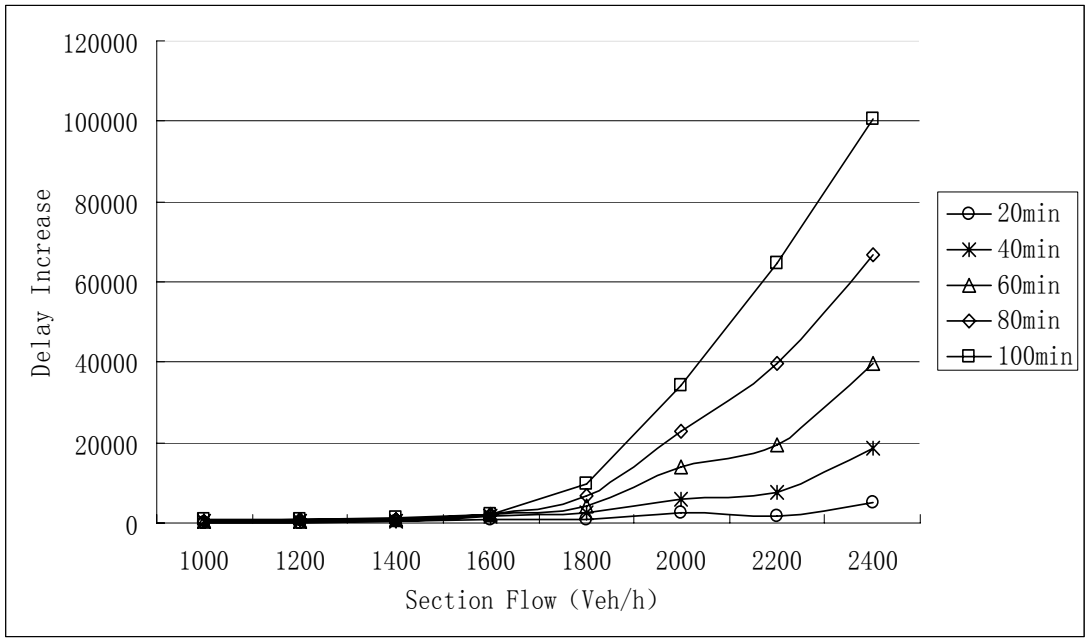

Figure 2 Simulation data about delay increase

In terms of duration, if the flow is kept unchanged, the relationship between duration and delay increase is approximately linear. With the increasing of the duration, the increasing of delay increase became much faster. The reason is that with the increasing of the duration, the influential area in the section expanded. When duration is long, delay will be generated even when the car is still far from the position of the incident.

Analyzing the results of the third part of the simulation experiments, it is obvious that the section closure or speed limit will caused a quite a large delay increase compared to the second part of the simulation experiment.

THE FUNCTION OF DELAY INCREASE

From the second part of the experiment, the relationship between flow, duration and delay increase under the typical incident can be regressed as a function.

According to the analysis above, the function is supposed as in Equation 1.

$$D = e^{aQ + bT + c} \quad (1)$$

Where D is delay increase, Q is flow, T is duration and a, b, c are coefficients in need to be regressed. This paper uses the software SPSS to do the linear regression after using the log function on both sides. The results are shown in Table 3 and Table 4.

Table 3 Model Summary

Model	R	R Square	Adjusted R Square	Std Error of the Estimate	Change Statistics				
					R Square Change	F Change	df1	df2	Sig F Change
1	0.97	0.941	0.94	0.4541	0.941	614.409	2	77	0.000

Table 4 Coefficients

Model		Unstandardized Coefficients		Standardized Coefficients	t	Sig.
		B	Std Error	Beta		
1	c	-0.426	0.247		-1.725	0.089
	a	0.040	0.000	0.888	32.086	0.000
	b	0.250	0.020	0.391	14.117	0.000

From the table, the regression function is calculated as $D = e^{0.004Q + 0.025T - 0.426}$, and the Sig F Change is 0.000. That means the regression model is effective and parameters are obvious. Since the function is regressed, it can be used to calculate the delay increase caused by the typical emergent incident.

CONCLUSION

This paper defined a basic unit of expressway network as the suitable research extent of the influence of incident and a new evaluation indicator to analyze the influence. From the specific simulation data, it can be seen that flow in the section will have the greatest contribution to the delay increase under emergency, especially when the flow is beyond the half value of the section capacity. Since a specific simulation result was found in different types of incident, it can be used to analyze real rescue measures at the indicator of delay increase. When under inclement weather, whether the section should be closed (will cause delay) or just limited in speed (may cause accident and then also cause delay) can be analyzed from specific data so that the better measure can be chosen. The regression model of the delay increase is mainly used to do traffic diversion under emergent incident. When several diversion paths can be chosen, regress each delay model from them and analyze the best diversion measures by calculating the total delay increase under the different

diversion flows.

ACKNOWLEDGMENTS

This work is supported by the National High-tech Research and Development Program (863 Program), under the Grant 2007AA11Z233.

REFERENCE

X. Wang, J. Xiao, and M. Wang (2005). Analysis of the Current Emergency Rescue Situation of the Freeway Traffic Accidents in our Country. Journal of ZhongYuan institute of technology, 16(5), 22.

Gong, X., Tang, S., and Z. Wang (2002). Survey on freeway traffic flow modeling. Journal of Traffic and Transportation Engineering.2(1),74.

Elvey, R. and M. John (2003). Emergency Traffic Management. Paper prepared for presentation at the Work Zone Safety Session of the 2003 Annual Conference of the Transportation Association of Canada St. John's, Newfoundland and Labrador. P. Eng.

Microsimulator and Mesosimulator in AIMSUN 6 User's Manual (2008). Software Manual, TSS-Transport Simulation Systems, S.L.

Optimization of Regional Traffic Structure from the Perspective of Sustainable Development

Linlin Wu[1], Qifen Zha[2], and Jianyi Liu[1]

[1]School of Business Administration, Jiangsu University, Zhenjiang,212013, PH (86) 511-88792088; FAX (86) 511-88792188; email: llwu@ujs.edu.cn
[2] School of Finance Economics, Jiangsu University, Zhenjiang, 212013

ABSTRACT

Under the situation of meeting the regional transport needs, we will minimize the social transportation cost to optimize the transport structure, which accords with regional sustainable development. From the perspective of industrial economics, this article analyzes the external costs arising from land use, energy consumption, environmental pollution, traffic safety and other factors of different transport modes. This article also establishes the social cost models which are based on the internalization of external costs. By comparing different modes of economic transport costs, it proposes some recommendations for transport structure optimization to meet the requirements of maximizing social welfare and provides a basis for the transport network planning, adjustment and policy-making.

1 INTRODUCTION

The traditional structural optimization of traffic is mainly based on time efficiency, making the shortest travel time the main objective of optimization. However, if we are only concerned with time efficiency, this will surely give rise to the corresponding energy and resource consumption, and environmental pollution, which will lead to unsustainable development in many regions or countries. Thus scholars have begun to pay attention to the sustainable development of traffic means. Saidur (2007) and Ifue (2007) have studied the relationship between transportation and energy from the perspective of resource control. Barney (1991) and Rumelt (1984, 1987) have discussed energy consumption and control of transportation development from the perspective of energy consumption and land control. The domestic scholar Lu Huapu (2004) has also explored the problem of optimal structure of traffic.

In fact, regardless of the perspective, the key to exploration of traffic optimization is whether it can meet the traffic demand as well as realize the social minimum costs of the entire transportation. If it can reach this requirement, then the traffic structure has reached the goal of optimization. Therefore, the problem of the total social cost is the key to the traffic structural optimization. If we include the external costs such as environmental pollution, resource consumption, and energy consumption in the transport costs as well as minimize the region's overall social

cost, and we accordingly put forward the program of structural optimization of the traffic, then all mentioned above is not only beneficial in terms of sustainable transport development, but also in terms of social sustainable development as a whole.

Economic characteristics of transportation, from the aspect of the transport infrastructure, have more obvious positive externalities due to the property of the quasi-public goods. However, when transport entities (transport companies, private car owners) are providing transport services, society is responsible for pollution, noise, traffic accidents and other external costs. The negative externalities are more obvious, especially with the emergence of congestion. The objective and accurate definition of the economic external characteristics of various transport means is not only the notion of the social costs, but also the realization of the structural optimization of traffic.

2 ANALYSIS OF THE EXTERNAL ECONOMICS OF TRANSPORTATION

2.1 The analysis of the positive externalities about the transportation

The positive externalities of the transport industry are mainly manifested in railways, roads, ports and other transport infrastructure provisions. On one hand, transportation has provided substantial economic and social benefits, which enables the specialization of production, large-scale economic development, economic globalization and the convenience for the mobility of population. As a result, people can enjoy a greater quality of life and more employment opportunities. On the other hand, the traffic transportation increases land values of surrounding real estate and promotes the development of the interrelated industries. It also makes difficult to ask the non-equipment users for return and therefore prevents the outflow of the effects. From a general view, the positive externality of the construction of fundamental transportation facilities always overruns its negative internality. However, its positive externality is limited, as people can turn the external effect into its own income actively and then realize its internality spontaneously.

2.2 The external analysis of transportation

The external analysis of transportation displays its impact on sustainable development, which occurs when providing its service. The negative effects caused by transportation can not be directly measured by money, but they are apparent in the form of external costs, such as traffic jams, pollution, traffic accidents and ecological destroy. In 2001, the direct loss due to traffic accidents reached to 3,088 billion RMB and the loss of pollution reached 1230 million RMB. This kind of analysis also proves that the cost of maintaining transportation is more than the cost people have spent. Among different kinds of transportation activities, the negative external cost of transportation can be divided into: safety costs, environmental costs, and resource costs.

As to the calculation of the external cost, we can make a qualitative evaluation

by way of TELF. We can also make a quantitative evaluation by way of effect-fare. The research of the external cost of transportation in China has been the first step, so we do not have fully comprehensible datum on transportation, and therefore we cannot get the external datum on transportation based on the actual situation of China. Here we can determine something from the outcomes of European countries, which are listed below:

Figure 1. The external cost of different transportation in European countries.

	The transportation of customers			The transportation of goods			
Kinds of Transportation	Highway	Railway	Airline	Highway	Railway	Airline	Water-way
External Cost	50.7	11.6	4.6	57.8	11.5	18.8	14.1

3 THE SOCIAL COSTS MODEL OF TRANSPORT

3.1 The social costs model of various transports

Based on the generalized cost analysis, we can calculate the transportation of various forms of transport social cost. The relationship of social costs, private costs (internal costs), as well as external costs is:

$$C_i = C_i^I + C_i^O \tag{1}$$

In the equation: C_i represents the social costs; C_i^0 represents internal costs; C_i^0 represents external costs (C_i^0 positively expresses the performance of the external income and negatively expresses the performance for the external costs).

Private costs are present in the internal market system. In the transportation industry, private costs include some pre-investment and operation of the process of traffic with the cost of change. It can be expressed as:

$$C_i^I = C_{i0} + K_i^1 Q_i = C_{i0} + K_i^1 NS \tag{2}$$

In the equation : C_{i0} expresses pre-input costs of the i kind traffic mode; K_i^Iexpresses traffic cost correlation coefficient; Q_i expresses traffic volume of the i kind way; N expresses the number of people or things (1000 people or tons); S expresses distance (km).

The calculation of external costs we can derive from Table 1 is:

$$C_i^O = K_i^2 NS \tag{3}$$

The social costs of various modes of transportation:

$$C_i = C_{i0} + K_i^1 NS + K_i^2 NS \tag{4}$$

$$C_i = C_{i0} + (K_i^1 N + K_i^2 N)S \tag{5}$$

3.2 Various modes of transport social cost analysis and comparison

1. Before the external costs are not recorded

Because external costs are not credited to the former, $C_i = C_i^I$, then

$$C_i = C_{i0} + K_i^1 NS \tag{6}$$

According to China's railways, highways, airports and shipping terminals in the corresponding construction standards, as well as the traditional transport standard-price system for railways, highways, aviation, and water transportation, if we make $C_i = C_j$ (i, j representing different transport modes), it can calculate their respective distance of these several modes transportation in the same transportation costs.

2. After credited to the external costs

According to type (5), the same order $C_i^* = C_j^*$, K_i^2, will be substituted for different coefficient from Table 1.It can calculate that their distance at transport costs are equal.

Comparing the costs, we can find that compared with railway transportation, road, water and air transportation, the relative economic distance is shortened. Especially in road transport, the advantages of relative distance are lost. This is because the external costs of rail transport are the smallest and road transport is the largest in this mode of transport.

4 STRUCTURAL OPTIMIZATION OF TRAFFIC STRATEGY

Any product of the existence of external costs can reflect the needs of society, but it also shows the production of producers does not reflect the needs of society, nor can it guide and achieve optimal allocation of social resources through the price mechanism. Therefore, the government should make transportation cost price fully reflect all society and choose the lowest cost of transportation for society according to various transportation characteristics, specifically including the following aspects.

4.1 Through adjustment of taxation to achieve the preparation of market-oriented transportation.

Taxation is an effective means of internalizing external costs. Various modes of transportation cost analysis show that as long as the government can impose tax matching with the external costs in different modes of transport, it will achieve the internalization of external costs of transportation. From the social point of view, there is no loss of social welfare. The social costs have been fully responded to, thereby correcting the market failure, and guiding the social optimal distribution of resources.

4.2 Adjust the composition of the structure of integrated transport systems.

Due to the existence of external costs, current highway transportation and railway transportation are not objective responses to their social costs. In fact, through the analysis of the third part of this article we can see the economics of road

transport are even shorter than imagined. Therefore, the government in the macro transport planning will reduce the cost of railway traffic on society. For long distance transportation of construction, the government should use the rail transit advantages of speed and social costs. For short distance transportation of construction, the government should use the highway advantages of flexibility, considerate and to a certain extent having the smallest social costs. We should support the development of road transport; at the same time, water transport and air transport are beneficial supplements. As far as meeting the traffic demand in the circumstances, it will achieve the smallest social costs.

4.3 Implement different infrastructure investment policies to provide the basis for the traffic structure optimization.

According to different possibilities of the transportation infrastructure internalization of external benefits, we should implement different investment policies. For the expressway, and inter-city railway infrastructure construction, because of their external costs it is relatively easy to internalize and through the appropriate fees ease congestion product characteristics, we can pass to invest financing of civil construction. But for most quasi-public goods belonging to the infrastructure, the government should make an investment. According to the World Bank, the route index for commercial is 2.4; it has a strong commercial infrastructure, but the rural commodity index for highways is 1, basically pure public goods. To the pure public goods by market mechanism is very difficult; it must rely on the government funds. So, for the internalization of external benefit in relatively difficult infrastructures, such as rural, county-level highways, and inland waterways construction, the government should focus on investment, through optimizing infrastructure, in order to realize transportation structure optimization.

4.4 Appropriate support water transportation, optimizing structure of transportation.

Based on the mode of transportation analysis and comparison in external costs, we can find that the external waterway transport costs far less than highway transportation and slightly more than the railway transportation. In a certain range, waterway transport has its advantages, and therefore appropriate development of water transportation is necessary. However, our country's investment in waterway transportation has been fixed at 5% - 7% of the total social costs. This relative share of investment is too small. Therefore, the investment in the inland waterways and shipping docks could increase supplying capacity of water transportation. To a certain extent, it would eliminate or alleviate traffic jams, freight traffic structure, and optimize pressure, reducing traffic and transportation of the total social cost.

5 CONCLUSION

Through the analysis of the characteristics of transportation economy, we can see external economies and diseconomies also exist in transportation. An effective

way of avoiding the external costs of transport like land use, energy cost, pollution is for the government, according to the transportation economic characteristics, to devise accurate traffic development strategies and tax adjustments. Through policies and internalization of external costs, improvements will be made in the reasonable allocation of resources, eliminating market failure, so as to meet traffic requirements, use all the means of transportation to their cost advantage and realize the transportation of lowest total social lowest and traffic structure optimization goals.

REFERENCES

Barney, J.(1991). "Firm resources and sustained competitive advantage." *Journal of Management,* 17, 99-120.

Glaister, S.(1997). "Deregulation and privatization: British experience." *Recent Developments in Transport Economics,* Ginesde. Rus, Chris. Nash. Ashgate Publishing Limited.

IFUE. (2007). *Transport energy consumption and emissions in China*. Heidelberg: IFUE.

Karlsruhe, Zurich, Paris.(2004). "External costs of transport: up date study." *The International Union of Railways (UIC)*.

Lu, H., Wang, J., and Zhang, P..(2004). "Urban transport structure optimization based on energy consumption." *Tsinghua Univ (Sci-Tech),* 44(3), 383-386.

National Bureau of Statistics of China. (2002). *Chinese statistical yearbook: 2002*. Beijing: China Statistics Press.

Rumelt, R. P.(1984). "Toward a strategic theory of the firm." *Competitive Strategic Management,* Lamb R (ed). Prentice—Hall: Englewood Cliffs, NJ. 556-570.

Rumelt, R. P.(1987). "Theory, strategy, and entrepreneurship." *The Competitive Challenge,* D. J. Teece (ed). *Ballinger*: Cambridge, MA. 137-158.

Saidur, R., Sattar, M. A., Masju, K. H. H., et. al. (2007). "An estimation of the energy and energy efficiencies for the energy resources consumption in the transportation sector in Malaysia." *Energy Policy,* 35, 4018-4026.

Wang, Y., and Lu, H. (2004). "Integrated model of urban land-use and modal split based on sustainable development." *Tsinghua Univ (Sci-Tech),* 44(9), 1240-1243.

Xia, S., Yang, J., and Yang, Z. (1995). *Outline of systems engineering,* Beijing: Tsinghua University Press.

Ye, W., and Zhen, H. (2004). "The Internalizing of Waterway Transport and the Constitution of Related National Policies." *China Soft Science Magazine,* 9, 32-37.

Performance Evaluation of Waterproof Bond Layer Materials Based on Grey Target Theory

YU Xin[1]

[1]Transportation College of Hohai University, 1# Xikang Road, Nanjing, China, PH (086)25-83784668; FAX (086) 25-83784668; email:Hhu_yuxin@163.com

ABSTRACT

To compare the performance of Waterproof bond layer materials on concrete bridge deck, combined with Taipu bridge, laboratory tests were carried out to common materials such as hot spray SBS modified asphalt, SBS modified emulsified asphalt, asphalt rubber SAMI and a typical professional waterproof coating. The comprehensive performances of above materials were analyzed based on grey target theory. The results showed that the optimal cost-effective one is asphalt rubber SAMI, followed by hot spray SBS modified asphalt, SBS modified emulsified asphalt. The typical professional waterproof coating are relatively poor.

Key Words: Waterproof bond Layer, Grey Target Theory, Performance Evaluation, Asphalt rubber SAMI

INTRODUCTION

Waterproof bond layer is important to bridge deck pavement . Field investigation showed that the overwhelming majority distresses such as rutting and shoving are related with the shear damage of waterproofing bond layer. Combined with Taipu Bridge on Husuzhe expressway, the paper compared the performance of different materials commonly used in China. Laboratory tests were carried out and results were analyzed based on grey target theory. Last, the paper recommended the optimal cost-effective material. The results provide a reference for selecting waterproof bond layer material.

MATERIAL TECHNOLOGY REQUIREMENTS AND TEST METHODS

Bridge Deck pavement works in harsh temperature conditions, so pavement material should have good high temperature stability and low temperature toughness to prevent the bridge deck pavement from distresses such as flowing, deforming and cracking. Usually, high temperature performance is evaluated with glass specimen surface flowing temperature test and low-temperature tender test is carried out to evaluate low temperature performance.

Studies have shown that shear strength and bond strength are the most important indicators of waterproofing bond layer material. Shear strength is usually evaluated with shear test and the bond strength is evaluated with pull-out test.

In addition, anti-construction damage and watertight are also important performance of waterproofing bond layer materials. They are evaluated with anti-breaking test for the former and high-pressure leakage test for the latter.

Table 1 shows part of the technology requirements and test methods of waterproof bond layer materials in Jiangsu Province of China mainly for the coating and structural materials because the membrane-type material is seldom used.

Table1. Technology requirements and test methods of Coating and structural waterproofing bond layer material

Test type		**Test condition**	**Test** methods
Physical indicators	Flexibility, ℃	-15℃	JC 408-1991 **6.6**
	Heat resistance, ℃	160℃	JC 408-1991 **6.7**
Road Performance	Bond strength （25℃），MPa	0.2	Φ10cm Composite sample 10mm/min Loading speed, electric drawing instrument
	Shear strength （40℃），MPa	0.4	Φ10cm Composite sample，10mm/min，Loading speed, electric shear instrument
	Impermeability	0.3MPa，30min Impermeable	High-pressure leakage test
	anti-construction damage performance	Impermeable in 0.3Mpa water pressure	Anti-breaking test, High-pressure leakage test

INDOOR PERFORMANCE TEST RESULTS

First, different materials were selected. Then, laboratory tests were carried out. The test results are shown in table 2 (Yu et al. 2008).

For asphalt rubber SAMI, the usage amount is 2.0~2.5kg/m^2 with the usage amount of gravel being 7~8kg/m^2.The usage amount of hot spray SBS modified asphalt is 1.8~2.0kg/m^2 with the usage amount of gravel being 7~8kg/m^2 .The usage amount of SBS modified emulsified asphalt is 0.7~0.9kg/m^2 with the usage amount of gravel being 5~7 kg/m^2. For the typical coating material, the usage amount of the bottom material is 0.5～0.52kg/m^2 with the amount of 1# and 2# high viscosity material being 0.95～1.0kg/m^2.

Table 2. Different waterproof bond layer material properties

Material Pilot project	SBS modified asphalt	Asphalt rubber SAMI	coating material	SBS modified emulsified asphalt
High Temperature Performance Test	150℃	150℃	140℃	150℃
Low Temperature Performance Test	-20℃	-20℃	-20℃	-20℃
Shear strength	0.37MPa	0.60MPa	0.37MPa	0MPa
Bond strength	0.88MPa	0.91MPa	0.74MPa	0.89MPa
Anti-aging	77.3%	88.4%	0%	93.0%

performance				
Impermeability	impermeable	impermeable	impermeable	permeable
Cost（rmb/m^2）	11.0	16.5	8.0	5.0

GREY TARGET THEORY

According to test results above, we can see different materials differ in different performance aspects. The paper tried to optimize the best material of comprehensive performance with Grey Target theory. Grey Target analysis method is a kind of grey relation analysis theory that is used on process mode sequence, which selects the more optional unit by comparing the bull's-eye degree (Deng et al. 1998; 2002). The steps of establishing the basic model of Grey Target theory are as follows:

①The establishment of grey mode

Grey mode is a kind of indicator sequence. It is a key factor sequence of a solution about a project.

$$\omega_i = (\omega_i(1), \omega_i(2), \cdots, \omega_i(n)),$$

$$\forall \omega_i(k) \in \omega_i \Rightarrow k \in K = \{1,2,\cdots,n\}, \quad i \in I = \{1,2,\cdots,m\}$$

Among which, ω_i is the sequence of multi-polarity indicators, $\omega_i(k)$ is the data of I mode and k indicator； $K = \{1,2,\cdots,n\}$ is the distribution of indicators;

$\exists k^*, s^* \in K \Rightarrow POL\omega_i(k^*) \neq POL\omega_i(s^*)$， That is, any two indicators do not have the same polarity; $\omega(k) = (\omega_1(k), \omega_2(k), \cdots \omega_m(k))$ is called the K indicator mode sequence, referred to as K-indicator sequence.

②Establishment of the standard mode

For $\omega_i = (\omega_i(1), \omega_i(2), \cdots, \omega_i(n))$

$\forall \omega_i(k) \in \omega_i \Rightarrow k \in K = \{1,2,\cdots,n\}$ $i \in I = \{1,2,\cdots,m\}$

$\omega(k) = (\omega_1(k), \omega_2(k), \cdots \omega_m(k))$， $\forall \omega_i(k) \in \omega(k) \Rightarrow i \in I = \{1,2,\cdots,m\}$；

The $POL(\max), POL(\min), POL(mem)$ are named as the maximum value polarity, the minimum value polarity, moderate value polarity respectively, then

when $POL\omega(k) = POL(\max)$, $\omega_0(k) = \max_i \omega_i(k), \omega_i(k) \in \omega(k)$;

when $POL\omega(k) = POL(\min)$, $\omega_0(k) = \min_i \omega_i(k), \omega_i(k) \in \omega(k)$;

when $POL\omega(k) = POL(mem)$, $\omega_0(k) = u_0$（Specified value）,or $\omega_0(k) = \underset{i}{avg}\, \omega_i(k)$, $\omega_i(k) \in \omega(k)$, then the sequence $\omega_0 = (\omega_0(1), \omega_0(2), \cdots \omega_0(n))$ was the standard model.

③Grey target transformation (Deng Julong et al. 2002)

If $T\omega_i(k) = x_i(k)$， $T\omega_i(k) = \dfrac{\min\{\omega_i(k), \omega_0(k)\}}{\max\{\omega_i(k), \omega_0(k)\}}$ (1)

T is the Grey Target Transformation， $x_i(k)$ is the unified measure Transform value.

④Grey relation factor sets and grey relation differences information space conversion

grey relation factor sets: $@_{GRF} = \{x_i \mid i \in I, x_i = T\omega_i, \omega_i \in @_{INU}\}$

grey relation differences information space: $\Delta_{GR} = (\Delta, \zeta, \Delta_{oi}(\max), \Delta_{oi}(\min))$,

$$\begin{gathered} \Delta = \{\Delta_{oi}(k) \mid i \in I = \{1,2,\cdots,m\}, k \in K = \{1,2,\cdots,n\}, \\ \Delta_{oi}(k) = |x_o(k) - x_i(k)| = |1 - x_i(k)|, x_o(k) \in x_o \Rightarrow x_o = T\omega_o\} \\ \zeta = 0.5, \\ \Delta_{oi}(\max) = \max_i \max_k \Delta_{oi}(k) = \max_i \max_k |1 - x_i(k)| \\ \Delta_{oi}(\min) = \min_i \min_k \Delta_{oi}(k) = \min_i \min_k |1 - x_i(k)| \end{gathered} \tag{2}$$

⑤Calculation of the bull's-eye factor (Deng Julong et al. 1987):

$$\gamma(x_o(k), x_i(k)) = \frac{\min_i \min_k \Delta_{oi}(k) + 0.5 \max_i \max_k \Delta_{oi}(k)}{\Delta_{oi}(k) + 0.5 \max_i \max_k \Delta_{oi}(k)} \tag{3}$$

⑥Calculation of the bull's-eye degrees:

$$\gamma(x_o, x_i) = \frac{1}{n} \sum_{k=1}^{n} \alpha_k \gamma(x_o(k), x_i(k)) \tag{4}$$

α_k is the weight coefficient in the above formula.

MATERIAL SELECTION BASED ON GREY TARGET THEORY

This Grey Target analysis project is named "Bridge Deck Pavement Waterproof Bond Layer Material Evaluation." Four kind materials were used. The test results of these materials are shown in table 2. According to the project type, the paper established a standard mode that included six performances in the list, and took economic value into account. To highlight shear strength and economic value, the weight of the two coefficients were set 1.1 while the weight of the other were set 1.0.

The material optimized should have relatively higher and lower temperature stability. The former target was set 160C and the latter was -20C according to research. The highest test values were elected for the shear strength and bond strength as target. They were 0.60MPa and 0.91MPa respectively. The anti-aging properties were set at 93% as target in the same way. To facilitate analysis, for waterproof performance, impermeable is set as 1 and permeable as 0. For economic value, set the market average cost as target, which is 10.12RMB / m^2. The analysis process is as follows (Li et al. 2008):

①Established original series with the results in table 3.

Table.3 The original series for Grey Target analysis

Material / Comparison factors	$\omega_1(k)$ SBS modified asphalt	$\omega_2(k)$ Asphalt rubber SAMI	$\omega_3(k)$ Coating material	$\omega_4(k)$ SBS modified emulsified asphalt
$\omega_i(1)$ High Temperature	150	150	140	150

Performance（℃）				
$\omega_i(2)$Low Temperature Performance（℃）	-20	-20	-20	-20
$\omega_i(3)$Shear strength（Mpa）	0.37	0.60	0.37	0
$\omega_i(4)$Bond strength（Mpa）	0.88	0.91	0.74	0.89
$\omega_i(5)$Anti-aging performance（%）	77.3	88.4	0	93.0
$\omega_i(6)$ Impermeability	1	1	1	0
$\omega_i(7)$cost（rmb/m^2）	11.0	16.5	8.0	5.0

②Grey Target Transformation

Based on formula 1, transform table 3 to table 4.

standard mode $\omega_o = (160, -20, 0.6, 0.91, 93, 1, 10.12)$， and $T\omega_o = x_o = (1,1,1,1)$

Table.4 The data after Grey Target transformation

	$T\omega_1(k)$	$T\omega_2(k)$	$T\omega_3(k)$	$T\omega_4(k)$
$T\omega_i(1)$	0.937	0.937	0.875	0.937
$T\omega_i(2)$	1.00	1.00	1.00	1.00
$T\omega_i(3)$	0.62	1.00	0.62	0.00
$T\omega_i(4)$	0.97	1.00	0.81	0.98
$T\omega_i(5)$	0.83	0.95	0.00	1.00
$T\omega_i(6)$	1.00	1.00	1.00	0.00
$T\omega_i(7)$	0.92	0.61	0.79	0.49

⑶Grey relational difference information space

First, identify differences information collection Δ, then transform table 4 to table 5 based on formula 2.

Table.5 Differences information collection

	$\Delta_{o1}(k)$	$\Delta_{o2}(k)$	$\Delta_{o3}(k)$	$\Delta_{o4}(k)$
$\Delta_{0i}(1)$	0.063	0.063	0.125	0.063
$\Delta_{0i}(2)$	0.00	0.00	0.00	0.00
$\Delta_{0i}(3)$	0.38	0.00	0.38	1.00
$\Delta_{0i}(4)$	0.03	0.00	0.19	0.02
$\Delta_{0i}(5)$	0.17	0.05	1.00	0.00
$\Delta_{0i}(6)$	0.00	0.00	0.00	1.00
$\Delta_{0i}(7)$	0.08	0.39	0.21	0.51

According to Table 6, the grey relational difference information space is as follows:

$$\Delta_{GR} = (\Delta, \zeta, \Delta_{oi}(\max), \Delta_{oi}(\min))$$

$$\Delta = \{\Delta_{o1}, \Delta_{o2}, \Delta_{o3}, \Delta_{o4}, \Delta_{o5}, \Delta_{o6}\}, \zeta = 0.5$$

For the test material: $\Delta_{oi}(\max) = 1$, $\Delta_{oi}(\min) = 0$

④Calculated bull's-eye factor with formula 3 with the results in table 6.

Table.6 Bull's-eye factor value

	$\gamma(x_o(k), x_1(k))$	$\gamma(x_o(k), x_2(k))$	$\gamma(x_o(k), x_3(k))$	$\gamma(x_o(k), x_4(k))$
$\gamma(x_o(1), x_i(1))$	0.89	0.89	0.80	0.89
$\gamma(x_o(2), x_i(2))$	1.00	1.00	1.00	1.00
$\gamma(x_o(3), x_i(3))$	0.57	1.00	0.57	0.33
$\gamma(x_o(4), x_i(4))$	0.94	1.00	0.73	0.96
$\gamma(x_o(5), x_i(5))$	0.75	0.91	0.33	1.00
$\gamma(x_o(6), x_i(6))$	1.00	1.00	1.00	0.33
$\gamma(x_o(7), x_i(7))$	0.86	0.56	0.70	0.50

⑤Calculated bull's-eye degrees with formula 4 with the results in table 7.

Table.7 Bull's-eye degrees

Material	SBS modified asphalt	Asphalt rubber SAMI	Coating material	SBS modified emulsified asphalt
Bull's-eye degrees	0.88	0.93	0.75	0.73

According to the analysis results, among the test materials, rubber asphalt SAMI has the highest bull's-eye coefficient. In other words, in accordance with the analysis value, asphalt rubber SAMI has the most optimal performance, followed by hot spray SBS modified asphalt, the SBS modified emulsified asphalt and coating material is fairly.

CONCLUSION

During the Taipu bridge Deck construction, four materials for waterproof bond layer commonly used in China were tested. According to the test data, the paper evaluated the comprehensive performance of the materials based on grey target theory. The conclusion showed that, taking economic and performance value into account, the most optimal cost-effective material is asphalt rubber SAMI, followed by hot spray SBS modified asphalt, and SBS modified emulsified asphalt. The typical professional waterproof coating is relatively poor.

REFERENCE

Deng Julong (1987).Grey systems basic method [M]. Wuhan. Science and Technology Press of Huazhong University.

Deng Julong (2002).Grey theoretical foundation[M]. Wuhan. Science and Technology Press of Huazhong University.171～195.

Yu Xin, Li Yingtao et al(2008).Cement concrete bridge deck Asphalt pavement defects prevention and treatment technology research. Jiangsu Provincial

Communications Department Project.

Probabilistic Pedestrian-Vehicle Conflict Micro-Model in Non-Signal Controlled Multi-Lane Segments

S. Lu, S. Fang, and S. Zheng

Key Laboratory of Road and Traffic Engineering of the Ministry of Education, School of Transportation Engineering, Tongji University, Shanghai, China; PH (021) 69584649; email: lusiwenwinner@163.com

ABSTRACT

To analyze the safety problem of a pedestrian crossing the street in a non-signal controlled multi-lane segment, the traffic conflict probabilistic micro-models of multiple lanes are developed under conditions of entirely unsafe gap perception in accordance with traffic conflict technology. The model considers the effect of multiple lanes, vehicle volume, and width of lane on the pattern to pedestrians crossing. The numerical results of two-way four-lane traffic conflict probabilistic micro-models are calculated by means of Monte Carlo method. According to the delay level of pedestrians, the evaluation index based on the 90% confidence interval of conflict probability is set up in order to assess the safety of pedestrian crossing streets and optimally establish the pedestrian crossing facilities in segment.

INTRODUCTION

In recent years, the pedestrian traffic accident rates on urban roads have been generally increasing, and the safety of these pedestrians' lives have been seriously threatened when they cross the streets. Especially, the problem caused by pedestrians crossing no-signal controlled multi-lane segment gets more and more prominent. According to the theory of traffic conflict, accidents between pedestrians and vehicles usually result from traffic conflict. Therefore, many researchers hope to analyze the safety problem in pedestrians crossing the street in terms of traffic conflict theory. Based on regression analysis, Javid (2004) has developed the model that describes the relationship between the number of pedestrian-vehicle conflicts and the volume of vehicles and pedestrians; PEI Yu-long (2007) has chosen braking distance for vehicles as the standard of judging conflict severity in order to define the hazard degree of pedestrian crossing streets. However, these researches could not explain the principle of pedestrian-vehicle conflict such as the physical movement characteristic of pedestrian-vehicle conflict. Furthermore, they did not consider the psychological response of crossing pedestrian too much and ignore the influence of the randomness of traffic conflict and the numbers of lanes on the safety level of pedestrian crossing

streets.

Consequently, considering the pedestrians crossing characteristic, this paper develops the theoretic micro-model of multi-lane pedestrian-vehicle conflict probability and the evaluation index of risk for pedestrians crossing a no-signal controlled multi-lane segment in order to evaluate the safety level of pedestrians crossing the street in this segment.

DEFINITION OF PEDESTRIAN-VEHICLE CONFLICT

Based on the contradiction caused by movement of pedestrian and vehicle in a time and space resource aspect, the pedestrian-vehicle conflict is defined as the occurrence of collision between pedestrians and vehicles in a multi-lane road segment when they approach to a certain degree in the range of time and space without any trend to change their initial movement state. The affected area of the conflict is the whole lane width where vehicles run.

DEFINITION OF PEDESTRIAN'S SAFE GAP PERCEPTION

When crossing street in no-signal controlled segment, the pedestrian usually judges the running status of vehicle flow. If the arrival time headway of an approaching vehicle is a less than safe gap, the pedestrian may think it not safe enough and decide to wait aside instead of going across. While the arrival time headway of approaching vehicle is more than the safe gap, he will think it safe and go across. This process is defined as safe gap perception. But if a pedestrian still goes across the street, ignoring the danger when the arrival time headway is less than safe gap, it is considered that he has not perceived safe gap. According to this definition, the value of safe gap for pedestrian crossing the different lanes including the non-motorized lane is put forward.

$$T_i^c = t_r^p + t_{i+1}^p = t_r^p + \frac{i \bullet D + W_{nv}}{V^p} \qquad (1)$$

Where T_i^c indicates the value of safe gap for the pedestrian crossing the vehicle flow in lane i; t_r^p indicates the response time needed for a pedestrian crossing the vehicle flow; D indicates the width of the vehicle lane; V^p indicates the pedestrian crossing speed; t_{i+1}^p indicates the time taken to cross the lane i by the pedestrian; W_{nv} is the width of non-motorized lane.

DEVELOPMENT OF PEDESTRIAN-VEHICLE CONFLICT PROBABILISTIC MODEL IN TWO-WAY MULTI-LANE SEGMENT

According to the definition of safe gap for pedestrians, once a pedestrian goes across a street after safe perception, it does not happen that he conflicts with the approaching vehicle because the arrival time needed for the approaching vehicle is more than that needed for the pedestrian crossing this lane. Once a pedestrian goes

across the street without safe perception, the conflict will probably occur in the process of crossing. It indicates that in fact the pedestrian-vehicle conflict is mainly caused by pedestrians crossing without any safe perception. Meanwhile, the principle of pedestrian-vehicle conflict in one-direction close lanes is the same to that in the opposing far lanes. Accordingly, this paper has mainly researched the situation that pedestrian conflicts occur with one-way approaching vehicle flow (see Figure 1).

When pedestrian who wants to go across the non-signal controlled multi-lane segment has waited longer than what he could endure most or he has something emergent to do, he often directly goes across the street even if the arrival time headway is less than the value of safe gap. Therefore, entirely unsafe gap perception can be defined as that in the process of a pedestrian crossing, the arrival time headway of approaching vehicle in every lane is less than the value of the safe gap.

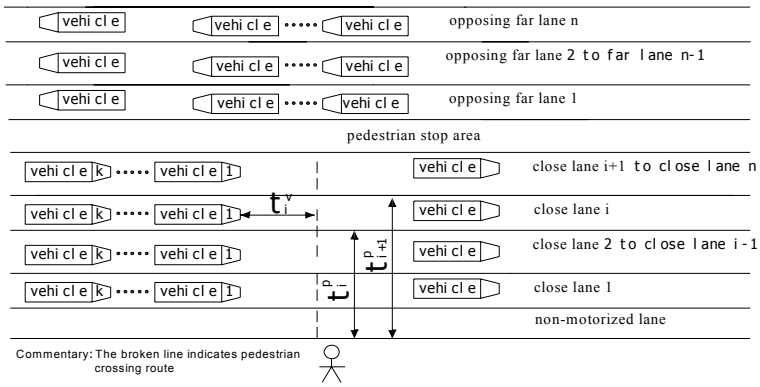

Figure 1. Process of pedestrian-vehicle conflict in lane i.

It is the most dangerous for pedestrians to cross the street in this situation. Meanwhile, no matter how the arrival time headway of a non-motorized vehicle is, the pedestrian always goes across the street. Therefore, the influence of the non-motorized vehicle on pedestrian-vehicle conflict can be ignored. The pedestrian-vehicle conflict probabilistic model is obtained under condition of entirely unsafe gap perception. The details are as follows:

The conditional probability of conflict between the pedestrian and the first approaching vehicle in lane i entirely without any safe gap perception is

$$P_i(C_1|B)=\frac{P[(\bigcap_{g=1}^{n} t_g^{v1}<T_g^c)\bigcap(t_i^p<t_i^{v1}<t_{i+1}^p)]}{P(\bigcap_{g=1}^{n} t_g^{v1}<T_g^c)}=\frac{P(t_i^{v1}<T_i^c\bigcap t_i^p<t_i^{v1}<t_{i+1}^p)}{P(t_i^{v1}<T_i^c)} \quad (2)$$

Where t_g^{v1} indicates the arrival time headway of the first approaching vehicle in lane g when pedestrian starts to cross the street (see Figure 1); n indicates the total number

of one-way lanes; $B=\left\{\bigcap_{g=1}^{n} t_g^{v1} < T_g^c\right\}$ indicates that the arrival time headway of the first approaching vehicle in every lane is less than the value of safe gap; $C_1=\left\{t_i^p < t_i^{v1} < t_{i+1}^p\right\}$ indicates that the pedestrian-vehicle conflict occurs when the first vehicle approaches to the conflict spot.

At the same time, when the arrival time headway of first approaching vehicle is $t_i^{v1} < t_i^p$ in lane i, the pedestrian will probably conflict with the certain following vehicle. Since at first the pedestrian begins to pass through the time headway of the first vehicle that is less than safe gap, it can be considered reasonably that he could choose to go across any arrival time headway of the following vehicle in lane i. In this situation, if the pedestrian walking to the edge line of lane i conflicts with the certain following vehicle, the time and space of both sides absolutely satisfy the condition of $\left\{0 < t_v^{'} < t_{i+1}^p - t_i^p\right\}$. Therefore, $C_2=\left\{0 < t_v^{'} < t_{i+1}^p - t_i^p \bigcap t_i^{v1} < t_i^p\right\}$ indicates that after the first vehicle has passed, the pedestrian conflicts with the certain following one in lane i. Thus, at the moment, the conditional probability of conflict is:

$$P_i(C_2|B)=\frac{P[(0 < t_v^{'} < t_{i+1}^p - t_i^p \bigcap t_i^{v1} < t_i^p)\bigcap_{g=1}^{n} t_g^{v1} < T_g^c]}{P(\bigcap_{g=1}^{n} t_g^{v1} < T_g^c)}=\frac{P(0 < t_v^{'} < t_{i+1}^p - t_i^p \bigcap t_i^{v1} < t_i^p)}{P(t_i^{v1} < T_i^c)} \quad (3)$$

where $t_v^{'}$ indicates the time needed for the certain following vehicle to reach the conflict spot after the first one has passed in the same lane.

Thus, under the situation of pedestrian's entirely unsafe gap perception, the conditional probability of conflict in lane i is:

$$P_i(C|B)=P_i(C_1|B)+P_i(C_2|B) \quad (4)$$

Meanwhile, the non-conditional probability of pedestrian-vehicle conflict in lane i is:

$$\begin{aligned} &P_i(C\bigcap B)=P_i(C_1\bigcap B)+P_i(C_2\bigcap B) \\ &=P[(\bigcap_{g=1}^{n} t_g^{v1} < T_g^c)\bigcap(t_i^p < t_i^{v1} < t_{i+1}^p)]+P[(0 < t_v^{'} < t_{i+1}^p - t_i^p \bigcap t_i^{v1} < t_i^p)\bigcap_{g=1}^{n} t_g^{v1} < T_g^c] \end{aligned} \quad (5)$$

In the process of pedestrian crossing streets, the total conditional probability and total non-conditional probability in one-direction close lanes are respectively:

$$NCP_{total}=1-\prod_{i=1}^{n}[1-P_i(C\bigcap B)] \quad (6) \quad \text{and} \quad CP_{total}=1-\prod_{i=1}^{n}[1-P_i(C|B)] \quad (7)$$

Where NCP_{total} is the total non-conditional probability; CP_{total} is the total conditional probability.

CASE ANALYSIS

Identification of model parameter. According to relevant research results from home and abroad (ZHOU,1987; LU, 2007;) . The model parameters are decided as follows: width of vehicle lane is valued as 3.75 meters; width of non-motorized lane is valued as 2 meters; width of marginal strip is valued as 0.25 meters; speed of pedestrian crossing conforms to parameters $N(1.5, 1)$ normal distribution, $V_{pmin} = 0.5m/s$, $V_{pmax} = 4.5m/s$; In most cases, the arrival time headway of vehicle t_v conforms to parameters λ negative exponential distribution, and response time of pedestrian t_r^p conforms to LN（0.17, 0.194）lognormal distribution, the unit is second.

Calculating method. The probabilistic value of pedestrian-vehicle conflict is difficult to achieve through common integration formula because the model contains many random variables. Therefore, the Monte Carlo method widely applied in the engineering field is used to calculate the probabilistic value of conflict through the production of a random number to meet the conditions of above variables.

Conflict probability in two-way four-lane segment. According to the model of pedestrian-vehicle traffic conflict probability in multi-lane segment developed as above, the probability of pedestrian-vehicle conflict in an urban two-way four-lane segment has been taken as an example to explain the application of model above.

Assuming that the vehicle volume in every close lane at the same direction is equal in terms of factual situation, the numerical calculation results of pedestrian-vehicle conflict probability in **two-way four-lane segment** have been listed in Table 1. It can be found that traffic non-conditional conflict probability increases with vehicle volume under condition of entirely unsafe gap perception. But the total conditional probability increases slowly with vehicle volume, especially in one-way two opposing far lanes because the width of the non-motorized lane has not effect on the pedestrian-vehicle conflict in the opposing far lanes. Furthermore, the conflict probability value is on a higher level. It almost accords with the actual situation. Consequently, it is proved that the main reason causing pedestrian-vehicle traffic conflict is that the pedestrian crosses the street without any safe gap perception (including the error of safe gap perception) by means of theoretical method.

Table 1. Conflict probability in Two-Way Four-Lane Segment

Vehicle volume in one lane（vehicles/h）	200	300	400	500	600	700
Total conditional probability in close lane（%）	69.55	73.23	74.12	76.92	78.56	80.85
Total non-conditional probability in close lane（%）	8.35	14.39	19.94	26.61	32.55	38.99
Total conditional probability in close lane（%）	84.38	86.05	87.12	87.94	88.89	89.86
Total non-conditional probability in close lane（%）	6.74	13.10	19.95	27.23	34.48	41.49

EVALUATION OF SAFETY LEVEL OF PEDESTRIAN CROSSING IN NON-SIGNAL CONTROLLED SEGMENT

In the actual situation where the pedestrian is not willing to wait for a long time under condition of the large traffic volume in a no-signal controlled segment, pedestrian usually tends to make a compromised choice that he can make safe perception in some lanes and doing nothing in other lanes. At the same time, based on the above theoretical analysis, it can be affirmed that when pedestrian is crossing the multi-lane segment, the occurrence of pedestrian-vehicle conflict is not influenced by other lanes but only relates with the arrival time headway of the vehicle in this current lane. The conflict probability corresponds to conditional probability. Consequently, half of total conditional conflict probability under condition of entirely unsafe gap perception $p=CP_{total}/2$ can be used to indicate the total conditional conflict probability on condition that pedestrian crosses the street with safe gap perception for just a part of all the lanes. In the situation, this kind of total conditional conflict probability between pedestrians and vehicles is more likely to reflect the actual safety level of a pedestrian crossing in this segment.

According to the characteristic of traffic conflict in road segment, it can be considered that the number of conflicts between pedestrians and vehicles in this segment conforms to binomial distribution just as $C\sim B(m, p)$. where m indicates the number of pedestrian crossing times in one direction within a given period of time (two people and more crossing together is defined as one time), $p=CP_{total}/2$； m is regarded as the number of pedestrian crossing time with safe gap perception for only a part of all the lanes, and can be written as $m=\alpha M$. Where M indicates the actual total number of times that pedestrians crosses the street, and α indicates the control proportion of total pedestrian crossing times in this way , which is related with the delay in the process of pedestrian crossing. The more the delay time is, the more the proportion of the way that pedestrian forces to cross the unsafe gap will be (YANG, 2007). The details of the method are as follows:

$$\bar{t}=\int_0^{T_{\max}^c} t\lambda_v \mathrm{e}^{-\lambda_v t}\,dt \tag{8}$$

$$d_p=\frac{1-f}{f}\bar{t}=\frac{1-e^{-\lambda_v T_{\max}^c}}{e^{-\lambda_v T_{\max}^c}}\bar{t} \tag{9}$$

$$\alpha=\begin{cases}0.6 & d_p>40s\\ 0.5 & d_p\in(20,40]s\\ 0.4 & d_p\le 20s\end{cases} \tag{10}$$

Where d_p indicates the pedestrian's average delay time corresponding to different volumes; T^c_{max} indicates the maximum safe gap corresponding to average pedestrian crossing speed in one direction; λ_v indicates the total average arrival

rates of vehicle flow in one direction; $\bar{t}$ indicates the average pedestrian waiting time when the arrival time headway is less than maximum safe gap; *f* indicates the probability that the arrival time headway is more than maximum safe gap.

However, when the value of m is large enough, the random variable can be obtained according to the central limit theorem of binomial distribution:

$$Z \approx \frac{C - mp}{\sqrt{mp(1-p)}} \qquad (11)$$

It nearly conforms to standard normal distribution $N(0, 1)$ (when $m \to \infty$).

Based on the assumption and discursion as above, the 90% fractile of total conditional conflict probability under condition of making safe gap perception for only a part of lanes can be used as the control standard of danger level in the process of pedestrian crossing. The detail critical values are as follows (ZHOU, 2001):

$$C_{\text{upper}} = mp + u_{1-\frac{\partial}{2}}\sqrt{mp(1-p)} \quad \text{and} \quad C_{\text{lower}} = mp - u_{1-\frac{\partial}{2}}\sqrt{mp(1-p)} \qquad (12)$$

Thus, Equation 12 has shown that once the actual number of pedestrian-vehicle conflict is more than the critical value, the proportion of the way that the pedestrian forces to cross the unsafe gap can overpass the control rate α given by the delay level of pedestrian. Therefore, according to highway black-spot qualitative control method (GUO, 2002), the danger level is high in this segment and the reasons should be analyzed immediately and relevant measures should be taken when the number of pedestrian-vehicle conflicts is more than C_{upper}; when the number of conflicts is in the range of [C_{lower} , C_{upper}], the danger level is normal and a tracking observation should be taken and some measures should be adopted according to the fact; when the number of conflicts is lower than C_{lower}, the danger level is low and the safety level in this segment is high enough.

According to the method above, the specific case analysis in this paper is as follows: assuming that when pedestrians cross the street during rush hours in two-way four-lane no-signal controlled road segment, the relevant data are: when the total vehicle volume of one-way two close lanes is 1100 vehicles/h and the number of times of a pedestrian crossing is 120 times in an hour and the number of conflicts in close lanes is 36. According to Table 1 and the formula as above, it can be calculated out that $\alpha = 0.5$, and in one-direction close lanes, the critical number of conflicts are respectively C_{upper}=30 and C_{lower}=17. Therefore, it can be judged that the dangerous status of a pedestrian crossing the close lanes is high and relevant measures should be taken; as to the evaluation of safety level for pedestrian crossing the opposing far lanes, the same method could be used.

CONCLUSIONS

Based on the principle of pedestrian-vehicle traffic conflict and pedestrian's

perception of safe gap, the micro-model of multi-lane pedestrian-vehicle conflict probability has been developed, which contains the influence factors such as the lane number, vehicle volume, width of lane. Meanwhile, combined with the delay level in the process of pedestrian crossing and based on the 90% of pedestrian-vehicle conflict probability, the evaluation index of risk level has been put forward in order to provide theoretic foundation for the evaluation of pedestrian crossing safety level in a no-signal controlled segment.

REFERENCES

Guo Z.Y., and Fang S.E. (2002). Road Safety Engineering, China Communication Press, Beijing, 2002.

Javid. (1991). Applying Conflict Technique to Pedestrian Safety Evaluation. ITE Journal, Vol. 61, No.3, pp. 21.

Lu S.W., and Fang S.E. (2007). The Calculation Method of the Average Critical Gap When the Pedestrians Cross the Vehicle Flow. Proceeding of the 7th International Conference of Chinese Transportation Professionals, pp. 553-557.

Pei Y.L. (2007). Study on Hazard Degree of Pedestrians Crossing Based on Traffi c Conflic. Journal Harbin Institute of Technology, Vol.39, No.2, pp. 285-289.

Yang X.G. (2007). Application of Different Pedestrian Cross Pattern to No-Signal Controlled Segment. Journal of Tongji University (Natural Science), Vol35, No.11, pp. 1466-1469.

Zhou W. (2001). Traffic Conflict Identification of Road Accident Blackspots. China Journal of Highway and Transport, Vol.13, No.1, pp. 81-86.

Research on Simulation of Train Tracing Operation Based CBTC

Z. Ma[1]， X. Chai[2] and L. Chong[3]

[1]College of Urban Railway Transportation，Shanghai University of Engineering Science, 333 Longteng Road, Shanghai 201620, China; PH(21)6779-1160; FAX(21) 6779-1163; email: maziyan@163.com
[2]College of Urban Railway Transportation，Shanghai University of Engineering Science, 333 Longteng Road, Shanghai 201620, China; PH(21)6779-1161; FAX(21) 6779-1163; email: cxdyj@163.com
[3]College of Urban Railway Transportation，Shanghai University of Engineering Science, 333 Longteng Road, Shanghai 201620, China; PH(21)6779-1171; FAX(21) 6779-1163; email: liquidpaopao077@163.com

ABSTRACT

This paper analyzes the system structure and technical character of the Communication Based Train Control (CBCT), and introduces the prototype of train tracing operation simulation in CBTC. The control model of train tracing operation in CBTC is established by analyzing the process of train operation, the logical control and the principle of moving block. There is a simulating algorithm of train tracing operation control, which is based on the concept of Moving Block (MB) and the technology of computer simulation. This simulation system is realized to trace several trains through VC++.

INTRODUCTION

The train control technology based track circuit was adopted in the traditional railway transportation signal system. The development of the modern train control system followed the trend of CBTC, which represents direction of the development of the modern railway signal system. The CBTC system realizes many functions, such as real time bi-communication between trains and the wayside with fast speed and sufficient capability, Automatic Train Protection (ATP), Automatic Train Operation (ATO), Automatic Train Supervision (ATS), and so on. The CBTC strongly ties with the MB, which has no fixed block. However, the CBTC can modify the section length according to the train operation status and can move with the train operation. The MB has improved railway transportation efficiency by making train operation more secure and by enabling short tracing intervals between trains. Due to limited time and funding, it is not possible to conduct field experiments of all combinations of parameters. Establishing a CBTC system enables simulation of train tracing operations. Simulation is particularly useful for understanding extreme cases which are very difficult to simulate through field experimentation. Additional parameters that can be tested through simulation include tracing intervals between trains, calculating the least distance of the train tracing, optimizing train organizing in CBTC lines, increasing density of train operation, and strengthening

transportation capability of the lines.

THE STRUCTURE OF THE CBTC SYSTEM

The CBTC system is a wireless signal system used to locate trains. The train operation control takes advantage of the concept of MB. In The CBTC system, the vehicle on-board controller detects and calculates the train position and reports to the wayside system by bi-directional communication. The wayside system sends a "moving authorize" signal to the train according to the train's speed, position and other factors.

The CBTC system consists of ATS, DSU, ZC, VOBC, and DCS, etc. The structure of the CBTC system is illustrated in Figure1.

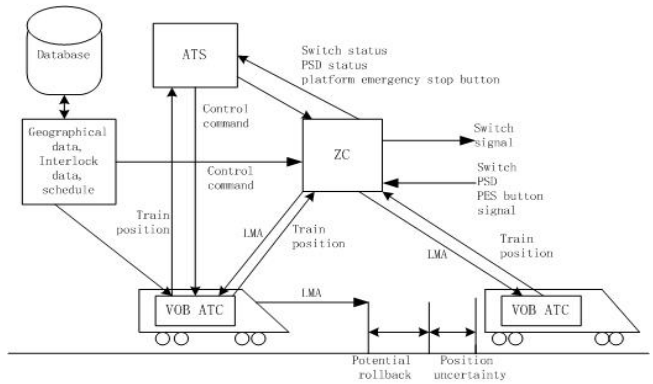

Figure 1. The Structure of the CBTC.

The principle of the train operation. The ZC timer makes judgments that authorize the moving train (speed or distance) according to geographical data, train position, route status, emergency stop button, PFD status, and other factors. This authorization to move signal is sent to the designated train.

The train is controlled by the authorization to move signal. Information, such as the train position and other factors is sent to ZC and ATS.

Wayside equipment supervising. The ATS can offer an MMI (Man Machine Interface) and send operation control commands to the ZC. The ATS gets the information, such as switch status, signal status, PSD status, platform emergency closing, etc., from each centralized station and displays it on the MMI.

The ZC receives the control command and sends a logical judgment to the control switch, the signal, and other equipment in the wayside control unit.

Train supervising. The concerned parameter is input into the ATS MMI and sends the operation command to the designated train. When the train information is changed, the information is automatically sent to the ATS. The information covers train number, train position, and others. The ATS information is displayed in the MMI when it is received. Then, the vehicle on-board ATC will process the command and judge whether the command should be implemented or not. If the command is to be implemented, the train operation control is started.

Vehicle on-board controller. The vehicle on-board controller will use database information to locate the train position by detecting the wayside response.

The vehicle on-board controller communicates between the ATS and the ZC through the DCS to report the train position and status. Then, the control command is sent to the controller.

The principle of MB. The CBTC system can control the train tracing interval by MB. In the traditional track circuit system, the moving authorize signal is limited by the unit of the track circuit section. In the CBTC system, the moving authorize signal is determined in a more precise way. The safe distance between two trains is determined by the current speed of the two trains, train positions, the capability of the train's brakes, obstacle characters, and other dynamic data. The main purpose of the MB system is to reduce the distance between running trains and improve the overall transportation capability. This can be achieved by improving the precision of the trains' positional locations and by increasing the frequency of sending moving authorize signals. Of course, ensuring safe operation to avoid injury is the foundation for all of these improvements and methods.

When the train is running, the train's speed status, position status and other information is sent to the wayside system by a communication network. The wayside system calculates the longest train braking distance and assures that there is no compromise of the safe protection distance. This is the MB section. The principle of MB is illustrated as Figure 2.

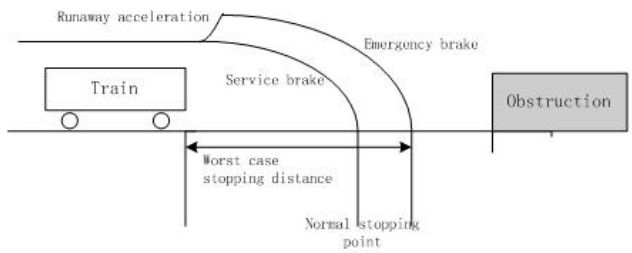

Figure 2. The principle diagram of Moving Block.

THE SIMULATING MODEL OF TRAIN OPERATION CONTROL

The prototype of the CBTC simulation train tracing system is established on the structure of the CBTC system and the principle of the MB.

The ATS's main function is to create the lines and depots illustration and create the operation control function. It can also be used to supervise and control wayside equipment and trains.

Vehicle on-board ATC includes TOD and train data. The TOD is the display system of the driver operating unit. It displays information, such as the current speed, permitted speed, maximum speed, train position status and others. The TOD is used to show the current operation status of the train, provide drivers with the control interface for braking, opening doors, and to perform other operations. It can also be used to send train control commands. The train data consists of train status data and train control command, which includes the operations of the TOD and the ATS. The train dynamic data is sent to the corresponding modules of trains to create the function of the train operation simulation.

The function of the ZC consists of station control, interlock control, and computer moving authorization. The station control includes station hold, station skip, emergency close, and so on. The interlock includes route setting, interlock logic to cancel, and other operations. The moving authorization can calculate the current speed and distance according to ATP protection logic.

The data from the lines and the wayside equipment includes: signal proportion, such as switch, signal, section, emergency station close, PSD, and so on. The line topology includes the relationship between the system platform management parts and depot data.

The train simulation operation is the function of the VOBC. The train simulation operation can simulate train operation, such as, depot leaving, section entry, station entry, station stop, station exit, turning back, depot entry and so on. Train simulation operation generates the information and sends it to the ZC. The information is used to calculate the next moving authorization signal and to display on the interface of the TOD and the ATS.

The simulating model of train operation control is established on the foundation of the prototype of the CBTC system. The distance of train tracing is determined by the distance of moving section, the maximum speed of train running, and the braking performance in the worst instance.

$$L=V^2/(2B) \qquad (1)$$

In the above formula: V is the maximum speed of the train; B is the train braking rate.

The initialization is conducted in the train operation simulation. First, the initial position of the train is determined. This position is the beginning of the section. Each section on the lines is separated into ΔS=25m. When the train is virtually running within ΔS, the time that train takes on each ΔS will be measured.

When all the trains overpass all the ΔS within the current section, this represents that the train head has moved into the next section. Using the same method, we separate the next section into ΔS as the current section; the train runs on the ΔS virtually repeating the above process until the train stops. The process of train operation is described in Figure 3.

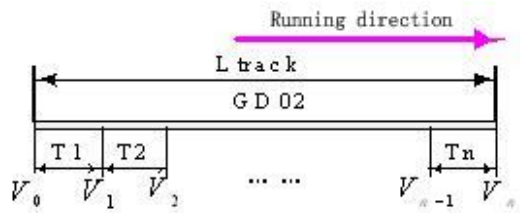

Figure 3. The simulating of the CBTC train operation process.

The process of a train running on the ΔS and the time, T, of a train staying on the ΔS is calculated per the following formula.

$$\Delta S_i = V_{i-1} T + \frac{a_i T^2}{2} \qquad (2)$$

In the above formula: ΔSi is the No.i ΔS of the current section; Vi-1 is

entrance speed of the train running on the No.i ΔS of the current section; a_i is the acceleration of the train running on the No.i ΔS of the current section.

When the train starts up, the entrance speed is V0 = 0 m/s on the current ΔS. The time of the train running on the ΔS can be calculated using Equation (2). The entrance speed on the ΔS can be calculated according to the following formula. It is the entrance speed on the next ΔS.

$$Vi = V_{i-1} + a_i T_i \qquad (3)$$

In the above formula: V_i is the exit speed of the train running on the No.i ΔS of the section; V_{i-1} is the entrance speed of the train running on the No.i ΔS of the current section; a_i is the acceleration of the train running on the No.i ΔS of the current section; T is the time of the train running on the No.i ΔS of the section.

The total distance of the train running on the No.i ΔS of the current section is calculated using the following formula.

$$S_{run} = \sum_{i=1}^{n} \Delta S_i \qquad (4)$$

In the formula: ΔS_i is the No.i ΔS of the current section.

SIMULATION OF TRAIN TRACING OPERATION

In the simulation system, several trains can be simulated in the tracing operation mode at the same time. The simulation control clock is set; the thread is started; and one train is dispatched from the list of trains by rank. Then, the simulating train operation will be processed in the thread. The arithmetic and the flow of the train operation simulation are illustrated in Figure 4.

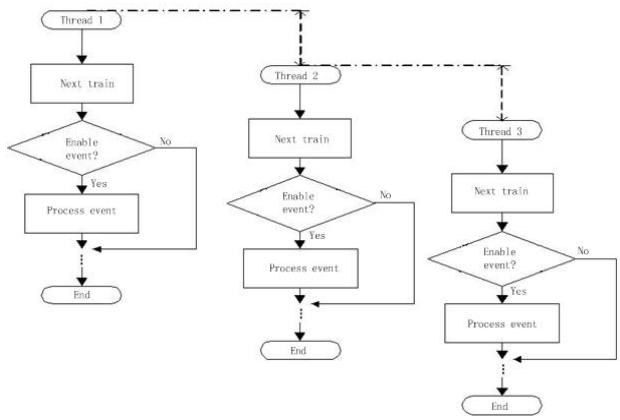

Figure 4. The arithmetic and flow of the train operation simulation.

In the simulation operation, one thread simulates one train operation in one simulating clock; the train operation in the section is tagged by the time that the train runs in the section. It counts from entrance time to exit time.

In the course of designing and programming the simulation system, the ATS and the ZC are set in one module and the train simulating operation and vehicle on-board operation are set in another module. The ATS, the ZC, and the vehicle on-board ATC system use UDP to realize real-time communication by the

network.

The simulating system is created using the VC++ programming language. The simulating control interface of the ATS and the TOD is illustrated in Figure 5.

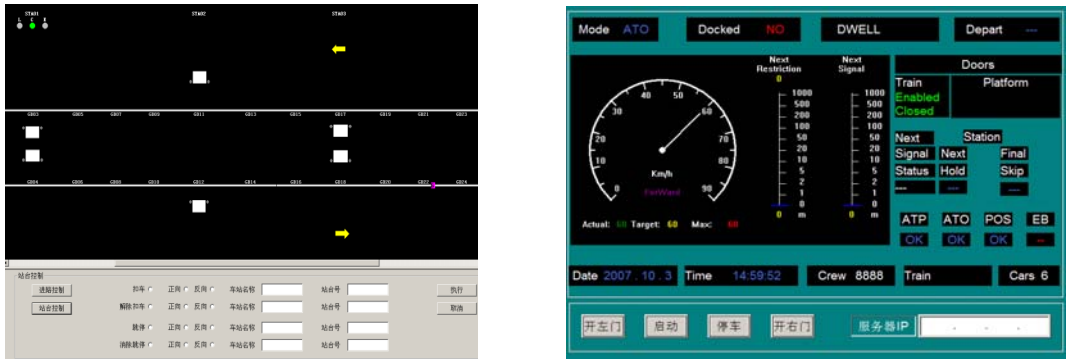

(a) ATS control interface (b) TOD interface

Figure 5. Simulating control interface.

CONCLUSION

Many lines in China have adopted the CBTC, which is an advanced railway transportation signal system. The performance parameters in this paper are provided from the corresponding company and organization. This thesis aims to establish a simulation model of a train tracing operation in the framework of the CBTC system. The model includes designing simulation arithmetic, creating a simulation system by programming, and performing simulation tests that focus on train tracing operation. In an actual railway transportation system that includes dispatching and organizing, there is more uncertainty caused by trains breaking down, and the need to manage passengers. These conditions also affect train operations. Additional effort to include these factors into a simulation system needs to be done.

REFERENCES

Huang, Z., and Sun, J. (2007).“Study on simulation algorithm of metro train operation,” *Electric Locomotives & Mass Transit Vehicles*, 45-49.

Armin, Z, and Gnter, H. (2003). “A train control system case study in model-based real time system design,” *International Parallel and Distributed Processing Symposium,* Washington IX: IEEE Computer Society,118-126 .

Lu, F., and Song, M. (2006). “Model and Simulation for Tracking Interval Control of Subway Trains,” *Information and Control* , 644-647.

Ma, Z. (2007). “Application of Wireless Ethernet in ATC System,” *Microcomputer Information* , 23(31)33-35.

Liu, H., and Mao, B. (2005). “Study on Tracking Operations Between Trains of Different Block Modes and Simulation System,” *Journal of the China Railway Society,* 120-124.

Kan, S. (2007). “Design of Monitor Software Based On Interface Program of Emulational Board,” *Microcomputer Information* , 23(31)190-193.

Research on Rapid Curing Technology of Lime-flyash-cement Stabilized Macadam

CHEN Yuanzhao[1] LI Zhenxia[1] WANG Xuancang[1]

[1]School of Highway, Chang'an University, P.O. Box 745, Xi'an, ST Middle Segment of South 2nd Ring Road; PH (+86)029-82334836; FAX (+86) 029-82334836; email: cyz740513@163.com

Abstract : In order to solve the problem of long curing time and long construction time of projects, the early strength of lime and fly-ash stabilized macadam can be increased by applying the proper amount of cement. First, compressive strength, cleavage strength and compression rebound modulus of lime-fly ash-cement stabilized macadam are tested systematically applying standard curing (T: 20±2°C, RH: ≥95%) and high-temperature curing (T: 60±2°C , RH:≥95). Secondly, a relationship curve between strength and curing age is found by applying four different regression models. Thirdly, strength gain relationship between high temperature curing and standard curing is achieved. So, the 180-day strength by standard curing can be determined from the strength cured by high temperature curing. Fourthly, the microstructure of samples is observed and analyzed systematically by applying electron microscope scanning. By the way of high temperature curing, not only can the microstructure of it be improved, but also the curing time can be shortened. Therefore, design parameters and major control index of ratio design for the lime-fly ash-cement stabilized macadam base course construction can be confirmed rapidly.

Key words: road engineering , lime-fly ash-cement stabilized macadam, rapid curing , standard curing , electron microscope scanning , design parameters .

1 Introduction

Lime-fly ash stabilized macadam is the inorganic binder stable material used for highway base and subbase layers. However, there are so much gravel and little bonding in the lime-fly ash stabilized macadam mixture that the bond force is not enough. In lime-fly ash-cement binder using the appropriate content cement, not only the will bond force be enhanced, but also the early strength of the binder will be improved, which indicates the superiority of the mixture. Furthermore, higher gravel content is beneficial to improving early strength of the mixture and anti-cracking properties, which can solve many problems, such as construction rolling, maintenance of the base, early opening to traffic and so on (SHA Aimin, 2003). And last, using fly-ash in road construction can realize waste utilization, which is beneficial for environmental protection.

At present, a rapid curing method has to be found to shorten the curing time of the semi-rigid base for the short project construction period. So the design parameters and major control index of construction mixture ratio design for the

lime-fly ash-cement stabilized macadam base course construction can be conformed rapidly. The paper adopts high-temperature curing as rapid curing method. The strength increasing rule relationship for the lime-fly ash-cement stabilized macadam, between high temperature curing and standard curing is achieved through experimental study. Then, the long term strength, cured by standard curing methods, can be determined from the strength which is gained by high temperature curing.

2 High-temperature curing study scheme for Lime -fly ash-cement stabilized macadam

(1) The 180-day compression rebound modulus and cleavage strength are chosen to be the design parameters and the main control index of construction mixture ratio design for lime-fly ash-cement stabilized macadam, cured by standard curing (T 20±2°C, RH≥95%).

(2) According to the compressive strength of lime-fly ash-cement stabilized macadam, cured by high-temperature curing(T 60±2°C, RH≥95%), the strength increasing rule for it is analyzed. Then, the strength-age regression equation and the value of design parameters can be confirmed.

(3) The comparative analysis of microstructure observation for lime-fly ash-cement stabilized macadam is carried out, whose compressive strength, cured by high-temperature curing, is equal to the 180-day compressive strength, cured by standard curing. The strength increasing rule of lime-fly ash-cement stabilized macadam, cured by two curing condition, is studied in nature. Then, the feasibility that high-temperature curing can shorten the curing age of lime-fly ash-cement stabilized macadam is validated (HE Siguo, CHU Hong&LUO Xiaogang, 2002).

3 Physical and mechanical properties tests for the mixture

3.1 basic properties test for the mixture

(1) Cement adopts “Qinling” composite Portland cement produced by Qinling Cement Company, Yaoxian, shaanxi. Indices are shown in Table 1.

Table 1. Indices of the cement

item	3d strength/MPa		28d strength/MPa		initial setting time/s	final setting time/s	stabi-lity	fine-ness /%
	flexural strength	compressive strength	flexural strength	compressive strength				
test value	5.4	22.3	9.1	40.6	18960	24000	quali-fied	5.4

(2) Lime adopts high quality calcareous hydrated lime , grade I or grade II, produced by Fuping, shaanxi. Indices refer to Table 2.

(3) Fly ash adopts dry fly ash produced by the Second Thermal Power in Huxian. Indices refer to Table 3.

(4) Macadam adopts high quality limestone macadam produced by Jingyangkou town. Indices refer to Table 4, and gradation refers to Table 5.

Table 2. Physicochemical properties of the lime .

item	CaO/%	MgO/%	amount of sieve residue/%	
			0.71mm	0.125mm
test value	59.7	3.0	0.32	11.08

Mix proportion test results of lime-fly ash-cement stabilized macadam refer to Table 6.

Table 3. Physicochemical properties of the fly ash .

item	SiO_2 /%	Al_2O_3 /%	Fe_2O_3 /%	loss on ignition /%	fineness/%	
					sieve residue for 0.3mm	sieve residue for 0.075mm
test value	48.8	27.5	6.2	6.2	2.7	26

Table 4. Indices of the macadam .

item	crushing value/%	mud content/%	apparent density/(kg/m^3)
10mm ~ 30mm	19.8	0.339	2740
5mm ~ 10mm	—	0.292	2698
0 ~ 5mm	—	—	2776

Table 5. Gradation of the macadam .

ballast grain size	mass fraction through different sieve pore /%							
	31.5	19	9.5	4.75	2.36	1.18	0.6	0.075
10 ~ 30mm	100	79.8	1.2	0.5	0	0	0	0
5 ~ 10mm	100	100	95.2	44.1	5.7	2.9	0	0
0 ~ 5mm	100	100	100	99.7	84.4	63.9	39.6	8.7

Table 6. Mix proportion test results of Lime-fly ash-cement stabilized macadam .

mix proportion	heavy compaction		specimen shaping		
	maximum dry density /(kg/m^3)	optimum water content/%	dry density /(kg/m^3)	water content /%	compa-ction/%
cement: lime: fly ash: macadam =2:6:14:80	2050	9.7	2010	9.7	98

3.2 Compressive strength , compression rebound modulus and cleavage strength test s

Compressive strength, cleavage strength and compression rebound modulus test results, cured by standard curing, are shown in Table 7.

Table 7. Compressive strength , cleavage strength and compression rebound modulus test results under standard curing .

age /d	compressive strength/MPa	cleavage strength /MPa	compression rebound modulus/MPa
7	2.21	0.32	-
28	3.37	0.40	852
90	6.24	0.86	1268
150	7.56	1.11	1605
180	8.22	1.24	1771

3.3 Strength increasing rule relationship analysis for samples cured by standard curing and high-temperature curing .

Refer to Figure 1 for the trendline line for unconfined compressive strength increasing with age, cured by high-temperature curing.

It can be seen from Figure 1, rate of compressive strength gained before 14d is large, and then it gains more slowly after 14d. It also can be seen from Table 7 and Figure 1, that the 28d compressive strength value under high-temperature curing, 8.25MPa exceeds 8.22MPa, 180d compressive strength value under standard curing.

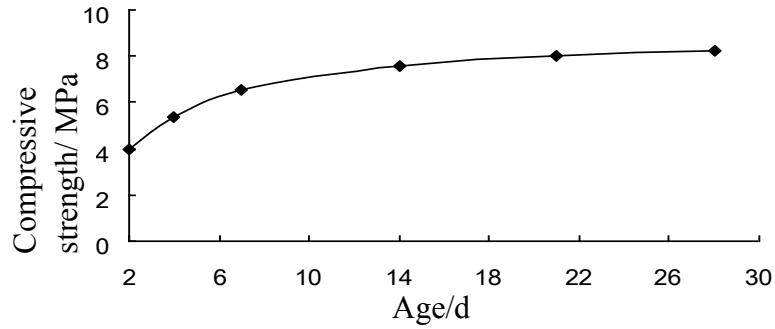

Figure 1. Tendency line for unconfined compressive strength increasing with age under high-temperature curing .

Curve fitting for logarithmic curves, power function curves, hyperbola and S curves is carried out by applying SPSS software. Large-variability test data is eliminated in order to ensure the consistency of the growth tendency line with the actual situation. Refer to Table 8 for the concrete fitting data.

Based on the curing test results of lime-fly ash-cement stabilized macadam, regression calculation applying the logarithmic method, power function method, hyperbola method, S curve method and strength growth tendency line under high-temperature curing, the 150d and 180d strength values under standard curing can be calculated applying the regression formula. The relationship curve equation

(refer to Table 9) between age and strength under high-temperature curing, corresponding time for the strength value, cured by high-temperature curing, is equal to stipulate age strength value under standard curing.

Table 8. Compressive strength and fitting data with different models by high-temperature curing .

age /d		2	4	7	14	21	28	correlation
test values /(MPa)		3.95	5.4	6.58	7.54	8.01	8.25	-
regressio –n value	logarithmic method	4.21	5.34	6.25	7.38	8.04	8.51	0.981
	power function method	3.83	5.70	6.75	7.56	7.85	8.00	0.946
	hyperbola method	4.29	5.18	6.03	7.28	8.13	8.79	0.953
	S curve method	3.63	5.92	6.91	7.57	7.79	7.90	0.986

According to the compressive strength growth tendency of lime-fly ash-cement stabilized macadam, cured by high-temperature curing, and corresponding relation with the age for standard curing, the conclusions are as follows:

(1) Under the high-temperature curing condition, the compressive strength of lime-fly ash-cement stabilized macadam increases with the increase of curing age. Compressive strength increases rapidly along a straight line before a certain curing age, and after that age, compressive strength increases slowly, even stops, and fluctuation phenomena for the strength takes place, too. During the hardening period, the internal pressure stresses of stabilized materials cause it. During the hydration process, the compressive strength increases with the development of hydrate. But the hydrate goes on hydrate, and its volume increases, which causes internal pressure, even break the covering film. Under certain conditions, tiny split defects may take place in the stabilized material, or a bladder is formed caused by an external hard shell strength formed rapidly. Strength is damaged by them. Strength goes on increasing with the development of hydrate. However, tiny split defects and bladders increase with the development of hydrate, too. Tiny split defects and bladders will do harm to the internal structure on a certain level, which arouse fluctuation phenomenon of the test value at the critical time (WANG Long, MENG Shutao&XU Quanliang, 2006).

Table 9. Relationship between unconfined compressive strength (abbre viation Rc) and age (abbreviation t) under high -temperature curing .

regression method	curve equation between R_c and t under high- temper -ature curing	corre la-tio n coeff ic-ien t	150d		180d	
			R_c under standa d curing /MPa	age for high temper at-ure curing /d	R_c under standar- d curing /MPa	age for high-tem -perature curing /d
Logarithmic method	$R_c = 1.631 \ln t + 3.077$	0.981	7.85	19	8.22	24
power function method	$R_c = 3.556t^{0.272}$	0.946	7.85	18	8.22	22
hyperbola method	$R_c = 8.226 - 9.187/t$	0.953	7.85	24	8.22	-
S curve method	$R_c = e^{(2.136-1.585/t)}$	0.986	7.85	21	8.22	-

(2) The test regression results show that regression coefficients of cleavage strength and compression rebound modulus are larger applying the logarithmic method, power function method and S curve method and strength growth tendency line under high-temperature curing. Regression variability is less, and regression effect is more noticeable. Compared with the power function method and S curve method, the regression effect applying the logarithmic method is better, and is more suitable to the growth law of cleavage strength and compression rebound modulus increasing with the curing age. Therefore, logarithmic method is put forward to use.

4 Microstructure observation comparative analysis of lime-fly ash-cement stabiliz ed macadam cu red by high -temperature curing and standard curing

Samples of the maximum curing age under high-temperature curing are chosen to carry out microstructure analysis. Samples under standard curing for 180d are chosen, too. See to Figure 2 and Figure 3 for images of the microstructure of lime-fly ash-cement stabilized macadam (2:6:14:80) under different curing condition and curing age.

It can be seen from Figure 2 and Figure 3 that the microstructure under high-temperature curing for 21d is denser. Defects, such as holes, tiny cracks and bubbles almost do not exist. Hydration gels, produced by hydration reaction and pozzolanic reaction of lime and fly ash, almost cover up the whole sample, and the surface of the sample seems more smooth. Plenty of holes, cracks and bubbles take place in the sample cured by standard curing for 180d. These defects spread widely, and the crack is wide and runs through the whole sample. Crystals and aggregate have not been

cemented completely by hydration gel material, and lots of gaps exist between them.

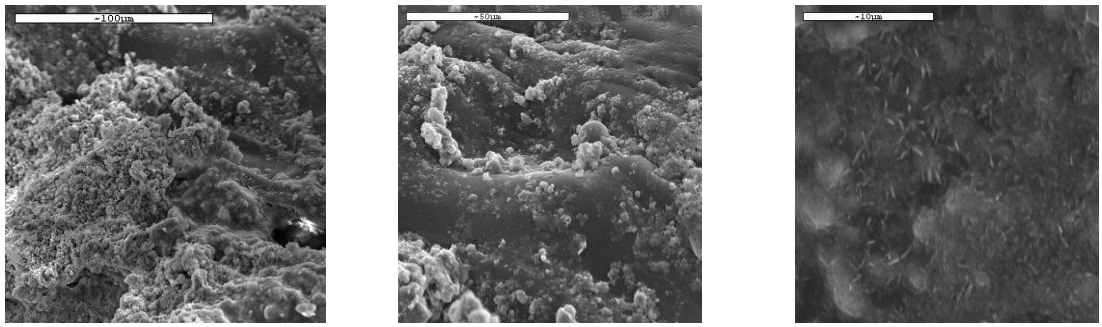

(a) amplification1000 times (b)amplification1500 times (c)amplification3000 times

Figure 2. Microstructure cured by high -temperature curing for 21d.

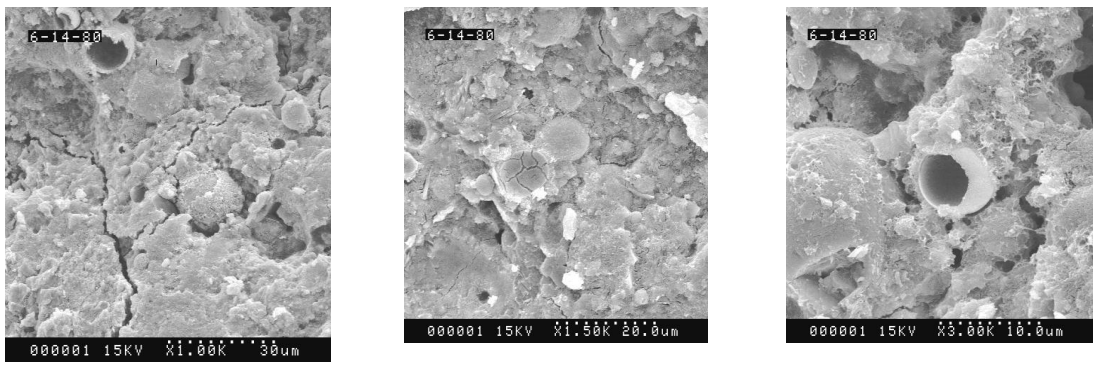

(a) amplification1000 times (b) amplification1500 times (c)amplification3000 times

Figure 3. Microstructure cured by standard curing for 180d.

From the above observation analysis, it is clear to see that the sample microstructure, cured by high-temperature curing for 21d, is denser than that of cured by standard curing for 180d. And the structure is better. Conclusively, the sample microstructure cured by high-temperature curing grows more rapidly and better. And there are no visible defects in lime-flash-cement stabilized macadam, such as holes, microcracks and bubbles. The holes become smaller, and the structure becomes more symmetrical, compact and complete when applying high-temperature curing. Connection performance and the early strength of stabilized material are improved. The conclusion can be drawn from microstructure observation contrast cured by two curing method and macroscopic strength value analysis. The microstructure of lime-flash-cement stabilized macadam can be improved by applying high-temperature curing. The early strength can be increased, and the curing age can be shortened. The engineering design needs can be met. It is feasible to shorten the curing age of lime-flash-cement stabilized macadam through high-temperature curing (JIANG Zengguo& ZHAO Yuan, 2005).

5 Conclusions

(1) By adopting high-temperature curing as a rapid curing method for lime-fly ash-cement stabilized macadam, strength increasing rule relationship of it between high-temperature curing and standard curing is found out through test. According to the relation, strength for the long age cured by standard curing can be determined by that of short age cured by high-temperature curing.

(2) Strength increasing rule analysis for lime-fly ash-cement stabilized macadam, cured by high-temperature curing, is carried out applying regression analysis methods for mathematical statistics. The compressive strength-age regression equation and the value of design parameters for lime-fly ash-cement stabilized macadam are confirmed. The corresponding curing age for high-temperature curing is determined by the strength through standard curing.

(3) Change in the microstructure with curing age of lime-fly ash-cement stabilized macadam, cured by high-temperature curing, is observed and analyzed applying electron microscope scanning. The strength increasing rule for rapid curing is studied and explained. The comparative analysis of microstructure observation for lime-fly ash-cement stabilized macadam is carried out, whose compressive strength, cured by high-temperature curing, is equal to the 180-day compressive strength, cured by standard curing. The strength increasing rule of lime-fly ash-cement stabilized macadam, cured by two curing condition, is studied. The results indicate that microstructure of lime-flash-cement stabilized macadam can be improved applying high-temperature curing. The early strength can be increased, and the curing age can be shortened. The engineering design need can be meet. It is really feasible to shorten curing age of lime-flash-cement stabilized macadam by high-temperature curing.

References

HE Siguo, CHU Hong&LUO Xiaogang.(2002).“Application Research on Construction Method for Shortening Curing Period of Semi-rigid Base.” Highway, 10, 21-25.

JIANG Zengguo&ZHAO Yuan.(2005).“Mechanism and Optimal Application of Chemical Additives for Accelerating Early Strength of Lime-fly Ash Stabilized Soils.” Journal of Wuhan University of Technology (Materials Science Edition), 20(3), 110-112.

SHA Aimin.(2008).“Material Characteristics of Semi-rigid Base.” China Journal of Highway and Transport, 21(1), 1-5.

WANG Long, MENG Shutao&XU Quanliang.(2006).“Study on the Design Parameter of Graded Macadam Base.” Journal of Highway and Transportation Research and Development, 23(8), 22-27.

Experimental research on shear connectors' stress of composite beam bridge under complex stress condition

Zhang Shibo[1], Wang Ronghui[2], Zhang Junping[3], Gong Lingling[4]

[1]School of Civil Engineering and Transportation, South China University of Technology, Guangzhou, 510640,China, FAX (+86) 020-83825575; Email: bridge007@sogou.com
[2]State Key Laboratory of Subtropical Building Science, School of Civil Engineering and Transportation, South China University of Technology, Guangzhou, 510640, China, PH (+86) 020-87564820;Email:rhwang@scut.edu.cn
[3]School of Civil Engineering, Guangzhou University, Guangzhou, 510006, China
[4]School of Civil Engineering and Transportation, South China University of Technology, Guangzhou, 510640,China, Email: 279260600@qq.com

ABSTRACT

In order to study the mechanical properties of shear connectors for a composite beam under complex stress conditions, two 1:2 reduced-scale model tests with different types of shear connectors are conducted. These models are designed base on a real composite beam bridge in Guangzhou. Comparative analysis about the relative slipping on the steel-concrete interface of the rigid shear connector model and flexible shear connector model under the same boundary conditions is studied in detail. Responses of two types of shear connectors under three different load cases are also compared. The model test results show that the ultimate bearing capacity of concrete is the key factor of relative slipping on the steel–concrete interface and differences between rigid and flexible shear connectors are large. It is useful as references for future research and designs of shear connectors in composite beams.

1 INTRODUCTION

The steel-concrete composite beam bridge is an advantageous bridge style because it takes full advantage of both steel's tensile properties and concrete's compression properties. These two materials are connected by shear connectors in order to transfer shear force on the interface between the steel beam and concrete slab. Good performance of the shear connectors can allow the steel beam and concrete slab bear the load together. Different shear connector types and arrangements afford different shear resistance, which dominates the relative slipping between the steel beam and concrete slab and affects the bearing capacity of the composite beams (Zhan YL, 2006).

The shear bearing capacity of shear connector is easy to calculate (Nie JG, 1999), but the withdrawal capacity of the shear connectors often requires experimental research to be done because it is difficult to be solved with the general mechanical method (Fang ZZ, 2002). Studies on various issues concerning

experimental research on shear connectors have been reported. Dennis Lam et.al (D.Lam, 2005) proposed an effective numerical model using the finite element method to simulate the push-off test and performed parametric studies to investigate variations in concrete strength and shear stud diameter. Cem Topkaya et.al (Cem Topkaya, 2002) proposed a new push-out test to study the composite shear stud strength at early concrete ages. Test results revealed that shear transfer is achieved at very early concrete ages. Ellobody E and Young B (E. Ellobody, 2006) studied the structural performance of shear connection in composite beams with profiled steel sheeting; an accurate and efficient nonlinear finite element model was developed to study the behavior of headed stud shear connectors welded through-deck. Kim YH et.al (Kim YH, 2006) performed a series of push-out tests to evaluate the performance of several existing shear connectors. Results show that the perforated shear connector with flange head is superior to existing shear connectors such as a general headed stud, perfobond, etc. It is efficient as a rigid shear connector. Kim HY (Kim HY, 2006) investigated the behavior of steel-concrete composite bridge decks with perfobond ribs through push-out, full-scale flexural, and deck-to-girder connection tests. Test results confirmed the effect of perfobond ribs.

Mechanical properties of shear connectors for the composite beam under complex stress condition are studied in detail through two model tests. The models are designed based on a prototype of the three spans of the pre-stressed steel-concrete composite beams bridge in Guangzhou with the main span length of 50+70+60m. Load–Relative slipping behavior and the shear capacity of the shear connector in composite beam are obtained from the experimental model test including three different load cases: horizontal loading, vertical loading, and a combination of horizontal loading and vertical loading. The results presented in this paper are useful as references for future research and designs of shear connectors in composite beams.

2 MODEL DESIGN

Two model tests are conducted. One uses shear studs as the shear connector, which is labeled Model 1, the other uses profiled sheeting as the shear connector, which is labeled Model 2. Design parameters of the two models are the same except the structural type and arrangement of the shear connector. In these two models, the section of steel box girder is 1000 mm high, 2000 mm long, and 850 mm wide. The section of the concrete slab is 2000 mm long and 4250 mm wide. The base of the steel box girder and the top of the concrete slab were connected by an embed bolt. Materials of the model adopt 16Mnq steel, C60 concrete, and HRB335 reinforced bar (JTG D62, 2004). Vertical plans of the model and loading device are shown in Figure 1. The geometric and physical similarity relation between the model and prototype is listed in Table 1.

Table 1 Geometry and physical similarity ratio (model/ prototype)

item	size	material parameter	load	stress	strain

similarity ratio	1/2	1/1	1/4	1/1	1/1

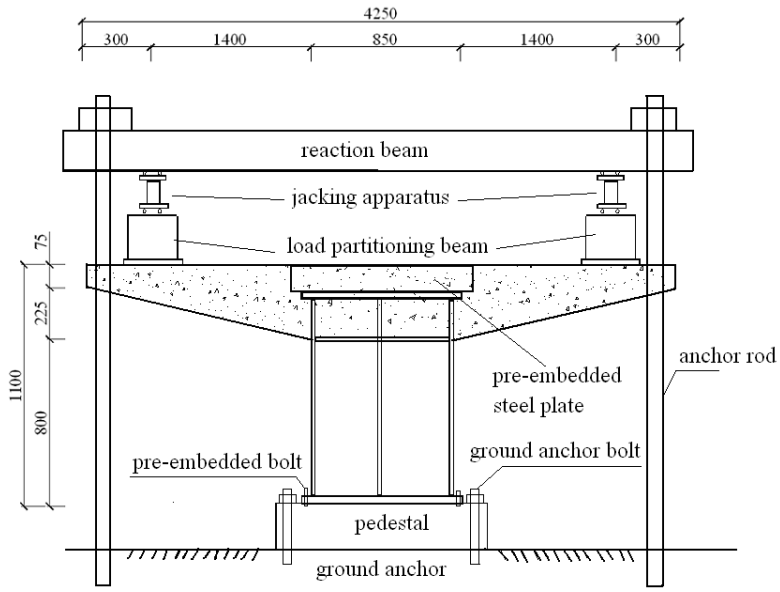

Figure.1. Vertical plan of model and loading device

2.1 Shear connector arrangement

In Model 1, the arrangement of shear studs, which are 11mm diameter×60 mm long, is 5 rows and 10 lines with the grid of 200×200mm. In Model 2, the arrangement of profiled sheeting, which is 50mm long×4.5 mm thickness, is 3 rows and 7 lines with the grid of 300×300mm. Both of the two models have the same steel ratio of the shear connector. The areas of the two kinds of shear connector are: $A_n = 4751.7mm^2$ and $A_c = 4725.0mm^2$, respectively, so it can be considered equal.

2.2 Loading procedure

There are three kinds of load cases in the model test: horizontal loading, vertical loading, and a combination of horizontal and vertical loading. For horizontal loading, the load applied to the studs model has no specific direction, but the load applied to the profiled sheeting model is specified from the direction of the mouth of the channel beam. The horizontal load of the two models is loaded from 0kN to 100kN gradually. For vertical loading, there are five loading steps from 0kN to 50kN at every 10kN and the loading is repeated three times. For the combination of horizontal and vertical loading, the horizontal load of the two models is stabilized at 100kN and the vertical load of the two models is loaded from 0kN at a separation of 10kN until the models fail.

2.3 Measuring-point arrangement

Six strain gages are affixed on the surface of the concrete slab, six high performance reinforcement meters are affixed on the surface of the reinforced bars, and eight strain gages are affixed on the surface of horizontal baffle of steel box

girder in each model. Moreover, fifty BTM strain meters are affixed on the shear studs in Model 1 and forty-two 120-3AA strain gages are affixed on the profiled sheeting in Model 2.

3 SUMMARY AND DISCUSSION OF THE RESULTS

3.1 The strain of shear connector

Shear connectors are divided into 5 rows (labeled 1# and 2#... 5# from left to right) and 10 lines (labeled 1L and 2L... 10L from front to back) in Model 1 and are divided into 3 rows (labeled 1#, 2#, 3# from left to right) in Model 2. The test results and discussions are as follows:

(1) Under horizontal loading, the regularity of the axial strain of shear studs can be found (see Figure.2) in Model 1. The axial strain of shear studs of the first line (nearly the loading point) is bigger than that of the rest, it decreases from the first line to the fifth line. The rest (far) can be neglected. The regularity of the axial strain of profiled sheeting cannot be found in Model 2 because the value of the strain is very small.

(2) Under vertical loading (no larger than 50kN), shear studs of the #1 and #5 rows are in tension while that of rows #2～#4 are in compression in Model 1. The profiled sheeting of the #1 and #3 rows are in tension while that of the #2 row is in compression in Model 2. The axial strains of two kinds of shear connectors has linear relationship with the load, but the value of that is very small (see Figure.3).

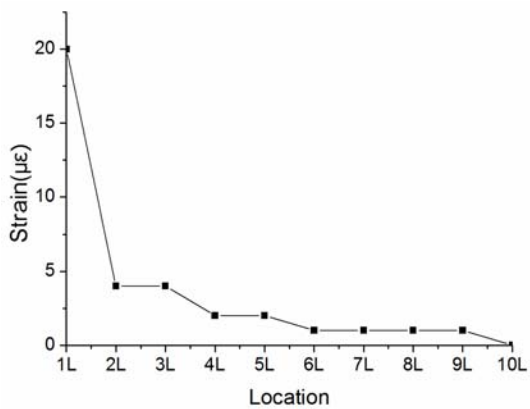

Figure.2. The average axial strain of shear studs under horizontal loading in each row

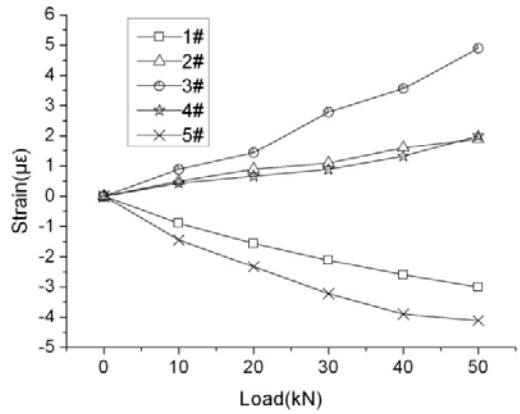

Figure.3. The average axial strain of shear studs under vertical loading in each row

(3) Under the combination of horizontal and vertical loading, when the horizontal load is stabilized at 100kN and about 80kN of the vertical load is applied to shear studs in Model 1 while about 110kN vertical load is applied to the profiled sheeting in Model 2, tiny cracks appear on the concrete.Then the stress of the shear connector increases rapidly. Finally, all shear connectors are in tension.

(4) Under the combination of horizontal and vertical loading, when the horizontal load is stabilized at 100kN and before the vertical load reach 100kN, the

strain of the two kinds of shear connectors increase slowly at the beginning of destruction. The axial stress of profiled sheeting does not exceed 18.0 MPa and the axial stress of shear studs is between 5.0 MPa and 34.0 MPa when the model has destructed (see Figure.4 and Figure.5).

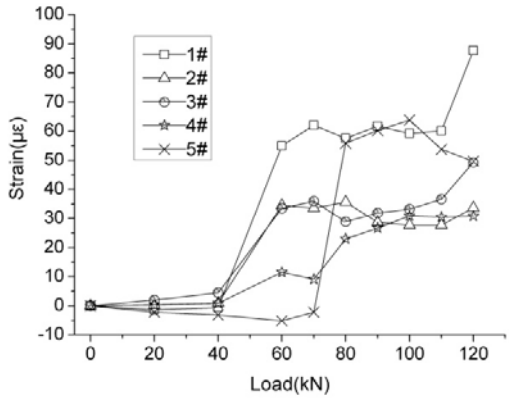

Figure.4. The average axial strain of shear studs under horizontal and vertical loading in each row

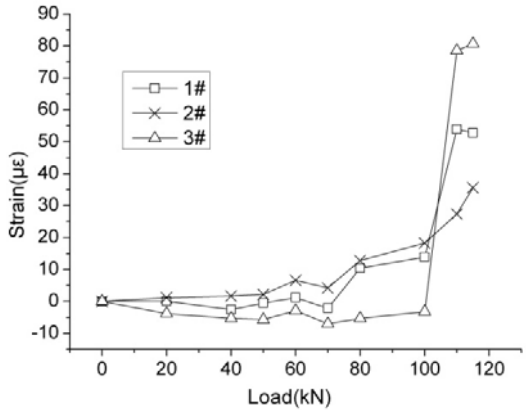

Figure.5. The average axial strain of profiled sheeting under horizontal and vertical loading in each row

3.2 Test results of relative slipping on the steel-concrete interface

Under horizontal loading, the relative slipping between the concrete slab and box girder is very small. When horizontal loading is up to 100kN, the relative slipping on the steel-concrete interface is 0.18 mm in Model 1 and 0.15 mm in Model 2. A linear relationship between the relative slipping and the load is shown on the Load-relative curve in two test models. Moreover, there are no obvious cracks and the slipping can recover when the load is removed. Figure.6 presents the relationship curve between the load and the relative slipping in Model 2.

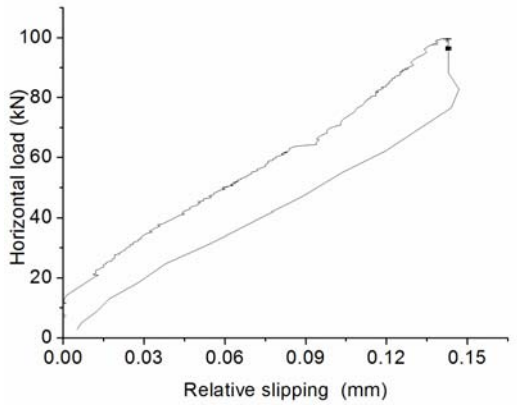

Figure.6. Load-relative slipping curve (model 2)

4 CONCLUSIONS

This paper takes the three spans of the continuous composite beams bridge in Guangzhou as a background and conducts experimental research on two 1:2 reduced-scale test models with different shear connectors. The main conclusions are as follows:

(1) The ultimate bearing capacity of reinforced concrete is the key factor to the relative slipping on the steel-concrete interface under complex stress conditions, and the relative slipping increases rapidly after concrete cracks.

(2) Both rigid and flexible shear connectors can effectively resist load, but the model of profiled sheeting has better slip resistant performance and recovery performance compared to the model of shear studs. The main reason is that profiled sheeting has a stronger restriction to concrete for its big stiffness when the strength of concrete is close to the ultimate strength.

(3) Under 100kN horizontal loading, the relative slipping is 0.18 mm on the steel-concrete interface in Model 1 while the relative slipping is 0.15 mm in Model 2. It indicates that the rigid shear connector can reduce the relative slipping on the steel-concrete interface under the same load.

(4) In the same steel ratio of the shear connector, the withdrawal resistance of profiled sheeting is greater than that of shear studs while the axial stress of profiled sheeting is smaller than that of shear studs.

REFERENCES

Cem Topkaya, Yura Joseph A. Williamson Eric B. (2002) "Composite shear stud strength at early concrete ages." *Journal of Structural Engineering*, 130(6), 952-960.

D.Lam, Ellobody E. (2005). "Behavior of headed stud shear connectors in composite beam." *Journal of Structural Engineering*, 131(1), 96-107.

E. Ellobody, Young B. (2006). "Performance of shear connection in composite beams with profiled steel sheeting." *Journal of Constructional Steel Research*, 62(7), 682-694.

Fang ZZ, Zheng ZQ (2002). "Experimental study on the prestressed steel-concrete composite continuous beams with different degree of shear connection." *Journal of Fuzhou University (Natural Sciences Edition)*, 343-348, (in Chinese).

Kim HY, Ju JY. (2006). "Experimental investigation on behaviour of steel-concrete composite bridge decks with perfobond ribs." *Journal of Constructional Steel Research*, 62(5), 463-471.

Kim YH, You SK, Jung JH. et al. (2006). "An experimental study on the shear behavior of perforated shear connector with flange head." *Fracture and Strength of Solids Vi*, Pts 1 and 2, 306-308, 1349-1354.

Ministry of Communications of the People's Republic of China. (2004). "JTG D62—2004 Code for design of highway reinforced concrete and prestressed concrete bridges and culvert." *China Communications Press*, Beijing.

Nie JG, Tan Y, Wang HQ (1999). "Strength of stud shear connectors in composite steel HC beams." *Journal of Tsinghua University (Science and Technology)*, 94-97, (in Chinese)

Zhan YL, Zhao RD, Mao XM (2006). "Comparison of the loading capacity of shear connectors in steel-concrete composite structures." *Building Science Research of Sichuan*, 16-19, (in Chinese).

A Retrograde Vehicle Detection Method Based on the 0ptical Flow Field

Zhao You-ting Li Xi-ying Wang Zhen-bo

Zhao You-ting, Graduate, Intelligent Transportation Research Center, Sun Yat-sen University, Guangzhou 510275, China, Phone:13826032419, E-mail: chuanganqiyuanli@163.com

Li Xi-ying, Associate Professor, Intelligent Transportation Research Center, Sun Yat-sen University, Guangzhou 510275, China, Phone:13570060699, E-mail: stslxy@mail.sysu.edu.cn

Abstract : Vehicles generally run at high speeds on the highway, so the presence of retrograde vehicles on the road greatly increases the probability of traffic accidents. In view of this situation, we introduce a new macro-method to detect retrograde vehicles based on optical flow. Our approach mainly uses pyramids with the Lucas-Kanade motion estimation method, which greatly reduces computational complexity. Since the flow of traffic is regular and physically measurable, its optical flow field is also orderly and regular, allowing the optical flow vector to accurately reflect the velocity of traffic flow. Experiments show that retrograde vehicles on the highway can be well detected by finding abnormal changes in the optical flow field.

Key words : retrograde vehicle, optical flow field, image pyramids

1. Introduction

In recent years, rapid economic development and swift growth in the number of vehicles has contributed to an exponential increase in traffic density and congestion. Subsequently, the rate of traffic incidents rises year after year. Retrograde vehicles on the highway are particularly vulnerable to dangerous traffic situations like congestion, accidents, and so on. There is an urgent need to detect retrograde vehicles automatically, quickly, and accurately.

There are two ways to detect retrograde vehicles: one is based on indirect data (non-video) and the other uses video. Video-based methods have been widely used in recent years, typically as difference algorithms between consecutive frames (Lipton et al., 1998; Wang Ning, 2005). This method uses the time difference between pixels of two or three successive frames in an image sequence. It extracts the range of motion and the direction of the moving objects by selecting a threshold to then identify the retrograde vehicle. Non-video based methods are also used widely, such as the algorithm of retrograde vehicles based on wireless sensor networks (Akyildiz et al., 2002; Zhao Dian-kui, 2007). Wireless networks detect the deformation of a magnetic field that follows the movement of vehicles, thereby sensing their direction.

Optical flow method belongs to the field of moving-object detection based on

video images. Its advantages are obvious - the background of the video is not required in advance; the calculation results depend only on the relative motion of the consecutive frames; and it avoids interference from complex environments, thereby enhancing the reliability and accuracy of detection. At present, this method is widely used by researchers to detect and track moving objects (Li Xi-ying, Ni Guo-qiang, 2002), however it is rarely used to detect traffic incidents. Aiming at the identification of retrograde vehicles on the highway, this paper presents a new detection method based on the optical flow field. Experiments show that this method can directly obtain the figure of the retrograde vehicles, and the retrograde vehicles can be well detected by finding abnormal changes in the optical flow field.

2. Lucas -Kanade Motion Estimation using Pyramids

2.1 Introduction of the Optical Flow Method

The concept of optical flow was first proposed by Gibson in 1950. Optical flow is the distribution of apparent velocities of movement of brightness patterns in sequential images. The optical flow field is the surface motion of image patterns. Research of the optical flow method seeks to determine the movement of each pixel according to its time-domain variation and the relativity of the pixel intensity in sequential images. Currently, there are many methods which have been proposed for computing optical flow. By examining basic theory and mathematical methods, Barron (Barron et al., 1994) and others divided optical flow technology into four types: gradient-based methods, region-based matching methods, energy-based and phase-based techniques. Compared to the other four techniques, the original gradient-based constraint is superior because it has simple principles and low computational complexity. Accordingly, this paper chooses the Lucas-Kanade method, which is based on gradient (Lucas BD, Kanade T, 1981), to calculate the optical flow field of images in a traffic scene.

The Lucas-Kanade method uses partial information from the image to calculate optical flow. Assume that the optical flow remains unchanged within a small neighborhood Ω of the image, the optical flow-v in each small spatial neighborhood Ω can be obtained by minimizing:

$$\sum_{m\in\Omega} W^2(m)(\nabla I * v + \frac{\partial I}{\partial t})^2 \tag{1}$$

where

$$\nabla I(m) = (I_x, I_y)^T \tag{2}$$

W(m) denotes a window function that gives more influence to constraints at the center of the neighborhood than those at the periphery. $V=(u,v)^T$ is the optical flow vector within a small spatial neighborhood Ω, its dimension is the pixel/frame. I is

the gray of the point (x,y) in the image. The abbreviations Ix、Iy and It are the partial derivatives of image gray with respect to x, y and time, respectively.

For n-points m_i at a single time t, the solution to (1) through weighted least-squares is given by:

$$A^T W^2 Av = A^T W^2 b \tag{3}$$

where:

$$A = (\nabla I(m_1),..., \nabla I(m_n))^T \tag{4}$$

$$W = diag(W(m_1),..., W(m_n)) \tag{5}$$

$$b = -(\frac{\partial I(m_1)}{\partial t},..., \frac{\partial I(m_n)}{t})^T \tag{6}$$

The solution to (3) is $v=(A^TW^2A)^{-1}A^TW^2b$, which is solved in closed form when A^TW^2A is nonsingular, since it is a 2*2 matrix:

$$A^T W^2 A = \begin{bmatrix} \sum W^2(m) I_x^2(m) & \sum W^2(m) I_x(m) I_y(m) \\ \sum W^2(m) I_x(m) I_y(m) & \sum W^2(m) I_y^2(m) \end{bmatrix} \tag{7}$$

where all sums are taken over points in the neighborhood Ω.

2.2 Representation of the Image Pyramid

The Lucas-Kanade algorithm has simple principles, low computational complexity, and it can attain exact optical flow field. But it also has limitations in its application. For example, it only applies to small image motion, requiring that moving objects offset in less than one pixel between consecutive frames. To address this situation, we use the layered structure and multi-resolution characteristics of an image pyramid to set the moving object's dynamic extension at different image resolution levels.

Image pyramids, which can be built by several methods, are often used for multi-resolution display. This paper uses the most simple sub-sampling method, namely, for a N * N image (N is the integer power of 2, N = 2n, n is an integer). The pyramids at each level are created by applying a filter to the images and selecting alternative rows and columns, where the pixels of such selections can constitute a N/2*N/2 image. In other words, it can acquire a miniature of the original image via two-dimensional sub-sampling. If continued, the original image can be reduced to a 1*1 image. Each image with a greater subscript is smaller than its predecessor in size therefore creating a pyramid data structure. In light of our actual needs for this paper, we have selected a 4-level pyramid structure. Seen in Figure 1, the highest resolution level of the pyramid is the original image, which is also the first level of the image.

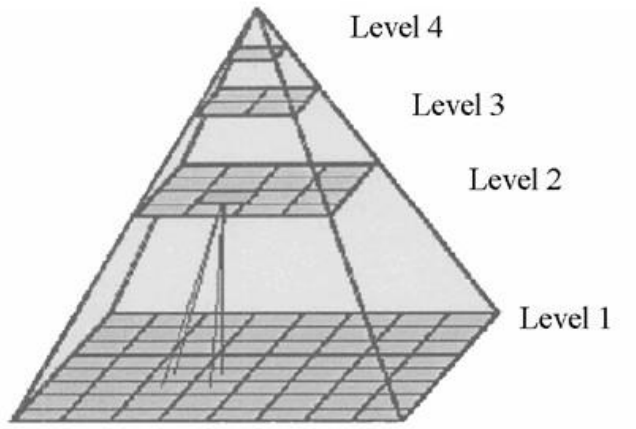

Figure 1. Image pyramid st ructure

While using pyramids, the lower high-resolution level can be used to analyze details, and the higher low-resolution level can be used to analyze larger objects. Consequently, the motion can initially be estimated at lower resolution, and then further estimates can be made more accurately from top to bottom. In the experiments, a four-level image pyramid is used. First, calculate the fourth level's optical flow field. Second, estimate the optical flow field of the third level by amending that of the fourth level. Step by step, the first level's optical flow field can be obtained. As there is an abundance of motion information in the first level, this level's optical flow field is selected for analysis.

2.3 The algorithm Based on Hierarchical Optical Flow Field

After attaining the 4-level image pyramid, it can calculate the optical flow field through multi-resolution pyramid data structure, use the following algorithm:

(1) Compute simple LK at highest level;

(2) At level i:

- Take flow u_{i-1}, v_{i-1} from level i-1
- Bilinear interpolate it to get u_i^*, v_i^* matrices of twice resolution for level i
- Multiply u_i^*, v_i^* by 2
- Compute f_t from a block displaced by $u_i^*(x,y)$, $v_i^*(x,y)$
- Apply LK to get $u_i'(x,y)$, $v_i'(x,y)$ (the correction in flow)
- Add corrections: $u_i = u_i' + u_i^*$, $v_i = v_i' + v_i^*$

(3) Repeat Step 2, until able to calculate the first level's optical flow field.

Figure 2 (a) is the two successive frame images; the above figure is the first frame, and the following figure is the second frame, after 1/25 second. In the figure, the left side of the vehicles is normal, and the right side is considered retrograde; Figure 2 (b) is the final optical flow field calculated by the 4-level pyramid.

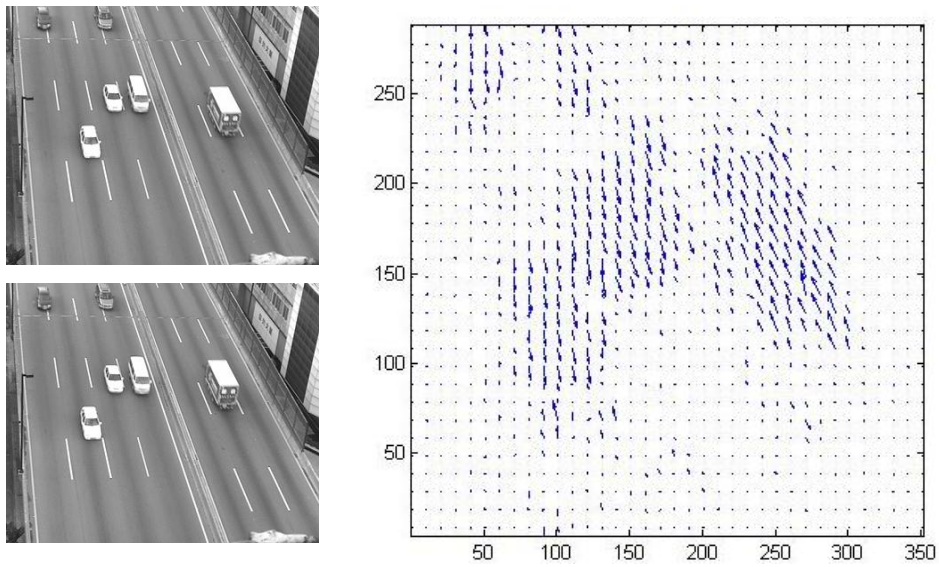

(a) two successive frame images (b) Optical Flow field of Image Pyramid

Figure 2. Lucas-Kanade Motion Estimation using Pyramids

3. Retrograde Vehicle Detection

A typical character of the retrograde vehicle is that it travels in the opposite direction of the normal one. Therefore, in the case of the retrograde vehicle, the common process is to detect the vector direction of the optical flow field to find anomalies. Comparing Figures 2(a) and Figure 2(b), one sees that the vector direction of optical flow for normal vehicles and retrograde vehicles coincide with the actual direction. In order to distinguish vehicle direction accurately and automatically, the whole optical flow angle is divided into 15 regions, so that every 24° becomes one region. The steps taken to make out the direction are as follows: First, compartmentalize all optical flow vectors into the above 15 regions. Second, locate the region within the range of 0° to 180° that has the maximum optical flow vector number, and designate this as the normal vehicle region. Third, locate the region within the range of 180° to 359° that has the maximum optical flow vector number, and designate it as the retrograde vehicle region. Finally, use a certain threshold to limit the reverse region. If the reverse region area is too small, it is considered to be non-existant and vice versa.

Figure 3 shows the results of the retrograde vehicle detection. Figure 3 (a) is the original optical flow field calculated above. Figure 3 (b) is the further processed optical flow field based on a 15-region division. In the figure, the region marked with "*" is the optical flow vector of the normal vehicles, and the region marked with "o" is the optical flow vector of the retrograde vehicles. Figure 3 (c) is the final image of moving object detection based on clustering algorithms. In the figure, the blue region

2 is the retrograde vehicle region. That is, when the blue region 2 is obtainable, there are retrograde vehicles in the traffic scene.

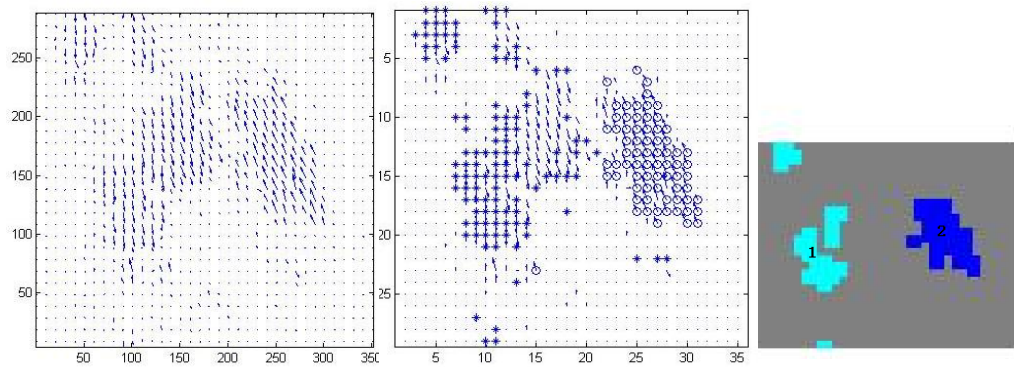

(a) (b) (c)

Figure 3. Retrograde vehicles detection results based on the optical flow field

4. Conclusion and Prospect

Experimental results show that when the retrograde vehicle region is large enough, the method mentioned in this article does well in detecting retrograde vehicles. Therefore, this method illustrates a good prospect of application and extension in the field of automatic detection technology. But this technology still has limitations, such as the large amount of time required for calculation. Further research will investigate how to improve the operational efficiency of the existing method, and how to enhance the method's capabilities in order to deal with more types of road conditions. In addition, video-based data is a precondition for vehicle detection based on the optical flow field. Though video equipment is not yet prevalent on all highways, its installation is an inevitable trend of the future, providing a good application foundation for the optical flow method.

References

Akyildiz I F,Su W,Sankarasubramaniam Y, et al. (2002). "Wireless Sensor Networks: A Survey." Computer Networks, 38 (4): 393-422.

Barron M, Fleet D J, Beauchem in S S. (1994), "Performance of Optical Flow Techniques." International Journal of Computer Vision , 12(1): 43-47.

Lucas B D, Kanade T. (1981), "An Iteractive Image Registration Technique with an Application to Stereo Vision." Proceedings of the 7th International Joint Conference on Artificial Intelligence, Vancouver: 674-679.

Lipton A,Fujiyoshi H, Patil R. (1998), "Moving Target Classification and Tracking from Real-time Video,".Applications of Computer Vision, 12, 8-14.

Li Xi-ying; Ni Guo-qiang (2002)."Optical Flow Computation of Infrared Image." Infrared and Laser Engineering, 31(3):189-193.

Wang Ning (2005), "Video Vehicle Tracking and Traffic Incidents Detection". Master degree thesis, Shanghai Jiao Tong University, Shanghai, China.

Zhao Dian-kui (2007), "Highway Traffic Emergency Auto-Detection Using Wireless Sensor Network." Master degree thesis, Dalian University of Technology, Dalian, China.

Research on A Risk Analysis System of Vessel-Bridge Collision

FU Tao[1], WANG Junjie[1], ZHANG Junjian[1]

[1]Department of Bridge Engineering, Tongji University, Shanghai, 200092, China; PH (086) 021- 65983116-2708; email: greenvillage_17@163.com

Abstract: Due to the construction of bridges crossing inland waterways, straits and gulfs, as well as the rapid development of vessel transportation, collisions between vessels and bridges occur frequently which leads to great concern about the safety of bridges crossing navigation channels. Thus, it becomes vital to analyze the risk of vessel-bridge collisions. In the paper, a risk analysis system of vessel-bridge collision is proposed which mainly includes an assessment database system, a probability of vessel-bridge collision assessment, a module for anti-collision resistance calculation of the pier, a probability of collapse assessment, a consequence assessment system, an auxiliary decision-making system as well as a risk disposition system. The key contents of every subsystem are represented. This system can provide a guide for vessel-bridge collision design and assessment.

Key words: vessel-bridge collision; risk analysis; reliability theory;

1. Introduction

With the development of economy in the world, a large number of bridges crossing inland waterways, straits and gulfs are constructed or in the planning phase. The numerous bridges bring generous economic profit while influencing vessel transportation significantly. According to statistical data, vessel-bridge collision accidents occurred more than 100 times in the past several decades, which caused enormous casualties, property loss, and environmental destruction (Geng, B, 2007). Vessel collisions with bridges occurred frequently in the past and will likely continue to occur in the future. The catastrophic events force researchers and officials to take a closer look at the frequency of vessel collisions and methods to prevent further accidents from occurring. It has become a more and more of a concern to carry on vessel-bridge collision risk analysis rationally in practice.

2. Risk analysis system of vessel-bridge collision

In view of the severity of vessel-bridge collisions, some research work has been developed by a number of researchers all over the world in the recent years. The research is either specific projects (e.g. Great Belt Bridge Project in Denmark and New Sunshine Skyway Bridge in America) or general design guidelines of bridges (e.g. AASHTO 1991, AASHTO LRFD 1994 and Eurocode 1.2.7). In AASHTO LRFD, a vessel-bridge collision is considered as a risk event which provides three vessel collision design methods, namely, Methods I, II, and III, including determination of the vessel design, a collision probability analysis, a calculation of collision force, and a bridge protection design, etc. Only the collision force has been taken into account in the highway or railway design code of China with no mention

of collision risk which needs to be farther developed.

The vessel-bridge collision risk R which mainly includes the probability P of bridge against vessel impact and possible consequences C can be written as follows:

$$R = P \times C \tag{1}$$

In the paper, a complete vessel-bridge collision risk analysis system is proposed with inclusion of the following parts: assessment database system, module for probability of collision assessment, module for anti-collision resistance calculation of pier, module for probability of collapse assessment, consequence assessment system, auxiliary decision-making system, and risk disposition system. Figure1 illustrates the composition of a risk analysis system of vessel-bridge collision.

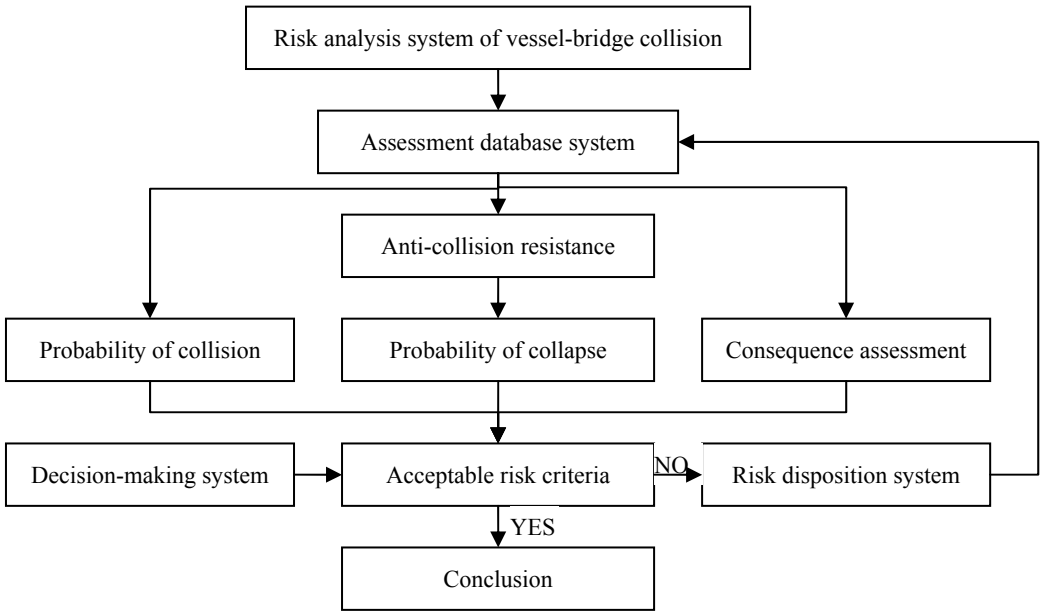

Figure1. Risk analysis system of vessel-bridge collision

2.1 Assessment database system

The probability calculation of vessel-bridge collision involves a great deal of information including: bridge navigable clearance, waterway condition and natural environment in bridge area, information about vessels transiting the waterway, etc. A database should be set up for risk analysis according to classification. The other modules of the system transfer the data from the database and then write the result into the database after calculation. The database also has the function of data management and query. Assessment of the database system includes the following several sub-databases:

(1) Basic information in the database includes the name of the bridge, bridge type, span arrangement, etc. (2) Navigation information in the database includes the span clearance, navigation density, geometry of the waterway, water depth at location of bridge piers, sailing path of vessel, etc. (3) In the vessel information database, the vessels are divided into ship, barge, and fleet with the parameters of deadweight tonnage, draft, and displacement of no-load and full-load, width, length, and height of

the vessel, etc. (4) The natural environment information in the database includes the angle of current, and the annual average velocity of current, water level, wind direction, etc. (5) The accident information in the database of vessel-bridge collision. (6) Active and passive protection measures information database.

2.2 Probability of vessel-bridge collision assessment

The statistical analysis method and mathematical model method are applied in calculating the probability of a vessel-bridge collision. The statistical analysis method may encounter difficulties because of the discontinuity and incompleteness of data. Regarding the mathematical model method, some typical models have been put forward, mainly including the IABSE Model (O.D.Larsen, 1993), the AASHTO Model, the Eurocode Model, the Kunz Model (C.U.Kunz, 1998) etc.

The vessel track, vessel location and accident rate per voyage unit are taken into account by the Kunz Model and Eurocode Model. Both of them are appropriate for research in progress and mechanism of accident while inconvenience in application.

The probability of aberrancy and geometric probability are considered in the AASHTO Model and the IABSE Model. The probability of aberrancy in the IABSE Model is mainly based on observation data while a formula is proposed to calculate the probability of aberrancy in the AASHTO Model with consideration of correction factors with bridge location, vessel traffic density, and current velocity. With respect to geometric probability, the AASHTO Model uses a normal distribution to account for it which is applied extensively at present compared with the IABSE Model.

The correction factors used in the AASHTO LRFD code are just a few of the many different variables that determine whether a bridge will suffer a collision. Other variables such as wind, visibility conditions, navigation aids and human error have a strong influence on the probability of a collision but they are not directly included in the AASHTO LRFD code as they are considered to be difficult to be quantified. However, if any one of these is particularly significant at a given channel and bridge location its influence on the results would not be ignored.

In the paper, a new concept about the probability of a vessel-bridge collision assessment is proposed. The district of upstream and downstream can be divided into small areas. The probability of a collision of each area can be calculated according to the method used in seismic risk analysis, and then the key problems are to determine the principles of area division. The total probability of collision is the superposition of each area.

2.3 Calculation module for anti-collision resistance of pier

The nonlinear characteristics of concrete and reinforcement should be considered in the calculation of anti-collision resistance. P-Y curve is used to describe the pile-soil interaction. The structural internal force can be obtained by finite element method. The pile is considered to be destructed while the section under horizontal force exceeds the limit bending ability. According to the failure mode, resistance is the horizontal force while the main compressive stress of the section exceeds the

allowable value while increasing the horizontal force progressively.

2.4 Probability of collapse assessment

With respect to the probability of collapse analysis, only the AASHTO LRFD code and the Eurocode propose the methods to calculate it by now. The AASHTO LRFD code which addresses the probability of collapse is developed by Cowiconsult based on studies performed by Fujii and Shiobara using Japanese historical damage data on vessels colliding at sea (Fujii, Y. and Shiobara, R, 1978). The damaged data of the bridge is based on the observations of damages between vessel-vessel collisions, while there is little accurate damage data of bridges during vessel-bridge collisions. It proposes a method to calculate the probability of collapse based on the relationship of the anti-collision resistance of a pier and the vessel impact force, if the anti-collision resistance, H, is greater than the vessel impact force, P, the probability of collapse will be zero. As the H/P ratio decreases, the probability of collapse remains low until the ultimate lateral pier strength becomes less than one-tenth of the vessel impact force. From then on, small reductions in the H/P ratio cause the probability of collapse to increase quite sharply.

While the approach recommended by the AASHTO code for the calculation of probability of collapse can often provide reasonable answers, some of its shortcomings can be addressed: (1) It comes from empirical data of vessel-vessel collisions rather than vessel-bridge collisions; (2) It is not derivate based on a strict theory of probability; (3) It can not cover various components of the bridge. In fact, once a bridge suffers a ship collision, the calculation of the probability of collapse is a complicated problem, which is a function of many variables. It depends on the randomness of the vessel impact force as well as the characteristic of the structure. Recognizing the shortcomings of the AASHTO code, a new concept of probability of collapse assessment is proposed based on reliability theory. The bridge safety condition can be expressed by a reliability index through the relationship between impact force probability distribution and anti-collision resistance probability distribution, and the limit state equation of a bridge can be set up. Then the failure probability is calculated based on reliability theory. Obviously the anti-collision resistance varies with material properties of the concrete, steel reinforcement and soil, water level, and impact angle. The anti-collision resistance of a pier can be written as $R(\eta,\Delta,\theta)$, where η, Δ, θ denote material properties, water level and impact angel respectively. The vessel impact force can be expressed as $P(v, DWT)$, where v and DWT denote impact velocity, and deadweight tonnage of vessel respectively. Then the limiting condition equation can be formulated as:

$$G(X) = R(\eta,\Delta,\theta) - P(v, DWT) \tag{2}$$

As $R(\eta,\Delta,\theta)$ is implicit functions, it should be calculated by FEM to obtain the

function value. Three methods are applied to calculate the failure probability, as seen in Figure 2. After determining the probability distributions of parameters, the failure probability can be obtained based on reliability theory which can reflect the risk level of vessel-bridge collision more accurately.

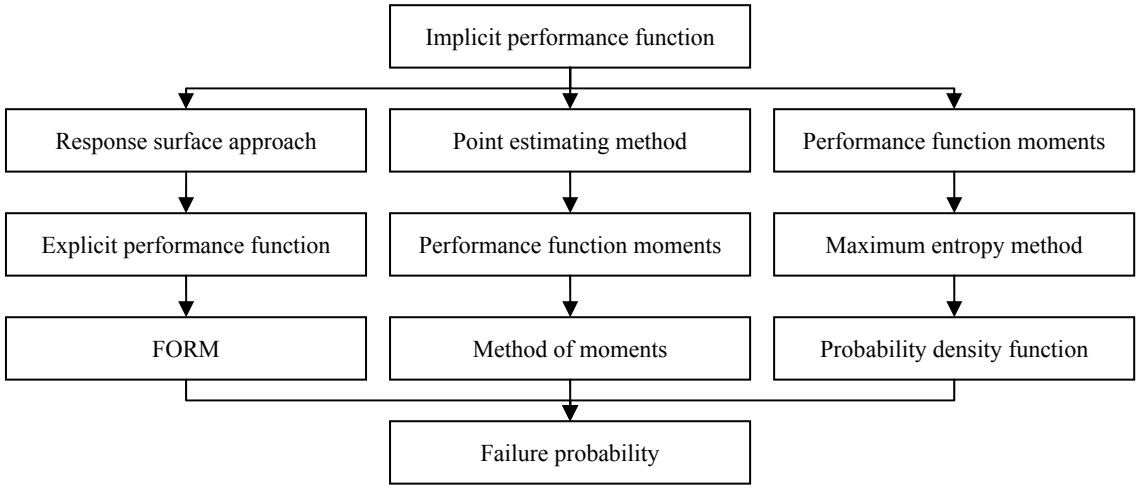

Figure 2. Flow chart of probability of collapse analysis.

2.5 Consequence assessment system

Regarding to consequences assessment about vessel-bridge collision, it can be divided into direct consequences and indirect consequences. The direct consequences mainly include bridge loss (e.g. reconstruction cost, bridge benefit loss etc), user's loss (e.g. casualty cost, vehicle and goods cost etc) as well as vessel loss (e.g. salvage and repair cost etc). The direct consequences mainly include traffic delay loss, environmental loss and society loss.

Some of the consequences are difficult to measure financially. How to quantize the consequences is still a subject to be researched further.

2.6 Auxiliary decision-making system

The key problem of an auxiliary decision-making system is to determine the acceptable risk criteria. The determination of acceptable risk criteria is a complicated problem involving technology, economy, politics, and culture. At present, the methods to determine acceptable risk criteria mainly include: the ALARP principle, the F-N Diagram, Risk matrix, PLL value, etc.

Eurocode recommends minimum values for the reliability index according to different classes of structure. In the AASHTO LRFD code, bridges are categorized as either "critical" or "regular". For a bridge classified as "critical", the annual frequency of collapse must not be greater than 0.0001 while the required annual frequency of collapse for a bridge designated as "regular" must be no larger than 0.001. Acceptable risk criteria of the AASHTO LRFD code is used world-wide in vessel-bridge collision risk assessment.

The vessel-bridge collision accident may cause loss. High acceptable risk criteria imply high initial cost. The owners should balance the cost and benefit to determine

the acceptable risk criteria. How to determine suitable acceptable risk criteria according to an actual situation is still a subject to be studied.

2.7 Risk disposition system

As for the bridge discontent with the acceptable risk criteria, measures must be taken to reduce a vessel-bridge collision risk. Three kinds of measures can be applied to decrease the risk of a vessel-bridge collision: (1) Limitation of vessel velocity; (2) Modification of bridge design; it mainly includes change of span arrangement, foundation type and channel width, increasing of the reinforcement ratio, etc. (3) Anti-collision device design; it contains active protection design and passive protection design. Active protection design refers to reasonable measures to avoid a collision between a vessel and a bridge which mainly includes set navigational remarks, perform sailing route regulations, assign sailing warning regions, pilotage for special vessels, AIS for vessels and VTS in the bridge area. Regarding the bridges with a high risk level, the protection structure that should be adopted mainly include: artificial island fenders, steel boxed cofferdam fenders, group-pile fenders, attachment structures, sand-filled and capsule structures, gravity pendulum structures ,etc.

3. Conclusions

(1) The risk assessment of vessel-bridge collision is a complicated subject which refers to many influence factors. In the present paper, a risk analysis system of vessel-bridge collision is developed with seven subsystems with a definition of the relationship among them.

(2) A new concept with consideration of more influence factors for calculating the probability of a vessel-bridge collision is put forward based on seismic risk analysis. Because of the shortcomings in the calculation of the probability of collapse, a reliability-based method is proposed which can reflect the risk level of a vessel-bridge collision accurately.

(3) Some problems which need to be further researched are represented, including: how to quantize consequences of a vessel-bridge collision, how to make reasonable risk criteria, and the effects of measures for reducing a vessel-bridge collision risk.

References

C.U.Kunz. (1998). “Ship Bridge Collision in River Traffic, Analysis and Design Practice.” *Ship Collision Analysis.*

Fujii, Y., and Shiobara, R. (1978). “The Estimation of Losses Resulting from Marine Accidents.” *Journal of Navigation.*

Geng, B. (2007). “Safety Assessment of Bridges Due to Vessel Impact.” *Ph.D. thesis of Tongji University.*

O.D.Larsen. (1993). “Ship Collision with Bridges.” *IABSE Structural Engineering Documents.*

Methods of Setting Maximum Speed Limits on Freeways

Guozhu Cheng and Yulong Pei

School of Transportation Science and Engineering, Harbin Institute of Technology, P.O.Box 202, Harbin, 150090; PH(86)451-86282832; FAX(86)451-86282832; email:guozhucheng@126.com, yulongp@263.net

ABSTRACT

Using the ideas of multi-objective optimization, the paper brought forward the maximum speed limit methods based on efficiency, safety, economic and comfortable quality of freeways. The maximum speed limit value under the conditions of at-grade straight lines section, free traffic flow, good pavement and weather was taken as a basic value. Minimizing the sum of time cost and fuel consumption cost were taken as the objective function. The death rate of accidents and passenger's comfortable quality that met corresponding allowed range was taken as constraint conditions. The basic value of the maximum speed limit calculation model was established based on minimum generalized operating costs of vehicles. A mathematical method of extremism solution was adopted to obtain the basic values. At last, it was given that basic values according to different design speeds and different vehicle types.

INTRODUCTION

Freeways are the most important component of highway networks, and how to realize its function of efficiency, safety, economics and comfortable quality is always one of the key subjects for all segments of the society. In order to guarantee realizing the above functions of freeway, the method of setting maximum speed limit has been usually adopted to manage freeway. Practice has proved that reasonable speed limits can promote increased efficiency, safety, economic and comfortable level of freeways, however, inappropriate speed limits will result in the opposite results. Now, being restricted to finance, technology and conception, the management level of freeways have been generally low speed limits, but standards of setting still lack theoretical results as technical support in China. This paper studied the method of setting maximum speed limits that embodies the system's dynamic characteristic of freeways to provide gist for speed management of freeway.

METHOD

Basic method. Freeway's operation should realize four objects. They are efficiency, safety, economic and comfortable ride quality. However, there is mutual conditionality between them. Under the condition of free flow, operation speed is higher, efficiency is higher but safety and comfortable quality will decrease. Therefore it is the basic thought to determine reasonable maximum speed limit values that multi-objective optimization method is adopted to look for the best relationship among efficiency, safety, economic and comfortable quality.

Method of setting maximum speed limit. Multi-objection optimization method was adopted to study and give objective functions and constraint conditions.
The key meeting objective functions and constraint conditions were defined as the

fiducial value of the maximum speed limit. It means the maximum speed limit value under ideal conditions. Ideal conditions include design speed of 120km/h, at-grade straight lines sections with free flow, good pavement and weather.

The fiducial value of the maximum speed limit should be given according to vehicle type. The fiducial value determined by the method of this paper is for cars. The trucks' fiducial value, it can be obtained by contrasting their observed operation speed data. Furthermore, it can be calculated through the ratio of design speed for freeways with other design speeds. For curved sections, sloped sections, constrained flow, damaged pavement and bad weather conditions, the fiducial value should be corrected.

OBJECTIVE FUNCTIONS AND CONSTRAINT CONDITION

Objective functions Drivers can be divided into three types, they are adaptive, conservative and hazardous (Zhou Wei, 2001). Adaptive type drivers should be the research focus when determining the fiducial value of the maximum speed limit. Time cost was caused by operation speed being less than speed under ideal conditions. Time cost function was defined as equation (1).

$$C_{\mathrm{t}} = \frac{G}{365 \times 8} \times E \times Q \times (\frac{L}{v} - \frac{L}{v_i}) \tag{1}$$

Where, C_{t} is time cost of passengers on freeway. G is GDP per person. E is mean carry coefficient (persons/veh); Q is traffic volume(veh/d) ; L is the length of freeway(km). v is operation speed(km/h). v_i is speed under ideal condition(km/h).

2.1.2 Fuel Consuming Cost Function

Fuel consuming data had been surveyed on the Cheng-yu Freeway, Kun-yu Freeway, Kun-qu Freeway, Jing-shi Freeway and Tai-jiu Freeway. The model relationship between speed and fuel consuming volume of at-grade straight line section was established by regression.

$$F = 0.0013 v_{\mathrm{t}}^2 - 0.2518 v_{\mathrm{t}} + 22.497 \tag{2}$$

Where, F is fuel consuming volume per 100km(liter/100km)。

According to equation (2), economic speed of at-grade straight line section v_{e} can be calculated to be 97km/h, and corresponding minimal fuel consuming volume $F_{\min}$ equal to 10.3liter/100km. The fuel consuming cost function was defined in equation 3.

$$C_{\mathrm{g}} = (0.0013 v^2 - 0.2518 v + 22.497) \cdot \frac{L}{100} P_{\mathrm{g}} \cdot Q_{\mathrm{d}} \qquad v > v_{\mathrm{e}} \tag{3}$$

Where, C_{g} is fuel consuming cost(yuan) ; P_{g} is gas price(yuan/liter) ; Q_{d} is traffic volume per day (veh/d) ; v_{e} is economic speed(km/h).

Supposing the power of time cost and fuel consuming cost is same, generalized running costs of vehicles was defined as the sum of them. Objective function was defined in equation 4.

$$\min(C) = \min(C_{\mathrm{t}} + C_{\mathrm{g}}) \tag{4}$$

Constraint conditions of safety. According to the data of NCSS，the death rate of traffic accidents is proportional to four power of speed grads (Du 2002). The

relationship between them can be seen in equation 5. When speed exceeds 114.24km/h, the probability of death caused by accident is 100%.

$$I_{\text{Death}} = (\frac{\Delta v}{114.24})^4 \tag{5}$$

Where, I_{Death} is death rate of traffic accident (%). Δv is speed grads, i.e. the difference of vehicle's speed and mean speed (km/h).

The maximum speed limit should assure that the death rate of traffic accidents is less than the accepted value. Based on this principle, the constraint condition of safety was defined as equation 6.

$$\begin{aligned} I_{\text{Death}} &= 6E-07(v_{\text{h}}-\bar{v})^4 + 6E-17(v_{\text{h}}-\bar{v})^3 - 1E-14(v_{\text{h}}-\bar{v})^2 \\ &+ 3E-13(v_{\text{h}}-\bar{v}) < [I_{\text{Death}}] \end{aligned} \tag{6}$$

Where, v_{h} is the maximum speed limit value (km/h). $\bar{v}$ is the mean speed(km/h). $[I_{\text{Death}}]$ is the accepted value of the death rate of traffic accidents (%).

Constraint conditions of comfortable quality. It is important that how to increase comfortable quality of road traffic (Lu Nan, 2005). Interrelated study has given the relationship between R.M.S. of acceleration (a_{w}) and person's sense through test of taxi with 1.3L exhaust volume (seen table 1). Data of speed and a_{w} are be listed in table 2 (Huang Yi, 2005).

The relationship model between them can be obtained by regression as shown in equation 7.

$$v = 0.048 a_{\text{w}}^{0.5425} \tag{7}$$

Table 1.The Relationship between the R.M.S. of acceleration and Person's sense

a_{w}(m/s^2)	People's Sense
<0.32	comfortable
0.32~0.68	comfortable relatively
0.68~0.80	uncomfortable relatively
0.80~1.60	uncomfortable

Table 2. Survey Data of Speed and a_{w}

speed(km/h)	a_{w} (m/s^2)	speed(km/h)	a_{w} (m/s^2)
30	0.287	80	0.490
40	0.345	90	0.551
50	0.475	100	0.584
60	0.442	110	0.614
70	0.467	120	0.644

The relationship between speed and comfortable quality can be obtained according to table 1 and equation 7. It can be seen from table 3 that passengers will be uncomfortable when speed exceeds 132km/h and the uncomfortable quality will increase sharply when speed exceeds 179km/h. The maximal threshold value of comfortable relatively was regarded as the constraint condition of comfortable quality. It was described in equation 8.

$$v_{\text{h}} \leq 132\text{km/h} \tag{8}$$

PARAMETERS CALIBRATION

Parameter of time cost functions. According to economic statistic data

promulgated by National Bureau of Statistics of China, GDP per person was determined as 23220 yuan per person per year.

Table 3 The Relationship between speed and passengers' comfortable quality

speed(km/h)	Passengers' Comfortable Quality
$v \leq 32$	comfortable
$32 < v \leq 132$	comfortable relatively
$132 < v \leq 179$	uncomfortable relatively
$v > 179$	uncomfortable

According to interrelated study (Feng 1993), the proportion of cars will be greater and will reach 90% in 2020. It has been predicted that the average seats in cars will reach 8.77 in 2020 and the carry ratio will be 80%. Therefore, the mean carry coefficient E can be calculated to be 7.016 person per car.

According to the current status of automobiles in China, the design value of the maximal speed is 160~200 km/h (Shen 2006). A medium sized car with good capability was selected as a representative vehicle type in this paper. Its ideal speed was determined by mean value of design speed given in literature (Shen 2006), i.e. v_i equal to 180km/h.

Average operation speed. According to surveyed operation speed data on Freeway of Harbin city, average operation speed of cars is 109.1km/h and that of trucks is 81.1 km/h at at-grade straight line section.

Accepted death rate of accident. According to the number of traffic accidents, the death toll and mortality rate of partially developed countries and China (Pei 2004), it can be found that the U.K. is the developed country with the lowest accident death rate, which is 1.5%. France is the developed country with the highest accident, which is 6.4%. In China, the accident death rate reaches 23.6% and is higher than that of developed countries. The maximum value of developed countries' death rate of accident was regarded as accepted death rate of accident in this paper, i.e. $[I_{\text{Death}}]$=6.4%. The maximum speed corresponding accepted death rate of accident can be obtained (seen table 4). Constraint condition of safety is give according to data of table 4.

$$\begin{cases} \text{car}: \quad v_{\text{hb}} \leq 127.3\text{km/h} \\ \text{truck}: \quad v_{\text{hb}} \leq 99.3\text{km/h} \end{cases} \tag{9}$$

Table 4.The Maximum speed corresponding to accepted accident death rate

vehicle type	car	truck
accepted accident death rate (%)	6.4	6.4
corresponding speed grads(km/h)	18.17	18.17
average operation speed(km/h)	109.1	81.1
corresponding maximum speed (km/h)	127.3	99.3

Gas price. According to data promulgated on Chemical Net of China, gas price i.e. Pg equal 4.88 yuan per liter.

KEY OF MODEL

Solution method. According to time costs and fuel consumption cost

functions, the key of fiducial value can be described as the minimum key in equation 10.

$$f(v) = \mathrm{a}v^2 - \mathrm{b}v + \frac{\mathrm{c}}{v} + \mathrm{k} \qquad (\mathrm{a},\mathrm{b},\mathrm{c} > 0) \tag{10}$$

Looking for differential coefficient of equation 10, equation 11 can be obtained.

$$f'(v) = 2\mathrm{a}v - \mathrm{b} - \frac{\mathrm{c}}{v^2} \tag{11}$$

When differential coefficient of $f(v)$ equals zero, the minimum key of equation 10 can be obtained.

$$2\mathrm{d}v^3 - \mathrm{e}v^2 - \mathrm{f} = 0 \tag{12}$$

Equation 13 is the exclusive real key of equation 12. Speed calculated by equation 13 is the key of the car's fiducial value of maximum speed on the freeway.

$$\begin{aligned} v = {} & \frac{1}{6\mathrm{d}}[54\mathrm{d}^2\mathrm{f} + \mathrm{e}^3 + 6\mathrm{d}\sqrt{3\mathrm{f}(27\mathrm{d}^2\mathrm{f} + \mathrm{e}^3)}]^{\frac{1}{3}} + \\ & \frac{\mathrm{e}^2}{6\mathrm{d}}[54\mathrm{d}^2\mathrm{f} + \mathrm{e}^3 + 6\mathrm{d}\sqrt{3\mathrm{f}(27\mathrm{d}^2\mathrm{f} + \mathrm{e}^3)}]^{-\frac{1}{3}} + \frac{\mathrm{e}}{6\mathrm{d}} \end{aligned} \tag{13}$$

Optimal key of model. The sum of the car's time cost and fuel consuming cost is defined as $f(v)$.

Making $f'(v) = 0$, then

$$2.6\mathrm{E}\text{-}05P_g v^3 - 2.518\mathrm{E}\text{-}03P_g v^2 - \frac{G \cdot E}{2920} = 0 \tag{14}$$

According to equation 14 and above calibrated model parameters, equation 15 can be obtained.

$$\begin{aligned} \mathrm{d} &= 2.6\mathrm{E}\text{-}05 \times P_{\mathrm{g}} / 2 = 6.344\mathrm{E}\text{-}05 \\ \mathrm{e} &= 2.518\mathrm{E}\text{-}03 \times P_{\mathrm{g}} = 1.229\mathrm{E}\text{-}02 \\ \mathrm{f} &= G \times E \ / 2920 = 55.792 \end{aligned} \tag{15}$$

According to equation 15 and equation 13, the model key can be obtained, *v is* equal to 124.99km/h. This key is bigger than economic speeds and smaller than ideal speeds but meets the constraint conditions. Thus, it can be regarded as the optimal model key.

Determination of fiducial value. Fiducial value of the car's maximum speed limit on the freeway, with a design speed of 120km/h, can be determined that v_{hbc} equals to 125km/h according to the above optimal model key.

The fiducial value of a truck's maximum speed limit can be calculated according to equation 16.

$$v_{\mathrm{hbt}} = \frac{\overline{v}_{\mathrm{t}}}{\overline{v}_{\mathrm{c}}} \times v_{\mathrm{hbc}} \tag{16}$$

Where, v_{hbt} is the fiducial value of a truck's maximum speed limit, $\overline{v}_{\mathrm{c}}$ is the average operation speed of cars and $\overline{v}_{\mathrm{t}}$ is the average operation speed of trucks.

Then fiducial value of a truck's maximum speed limit can be obtained that v_{hbt} equal to 95km/h. The fuducial value for freeways with other design speeds can be calculated by equation 17.

$$v_{\text{hb-}d} = \frac{v_d}{120} \times v_{\text{hb}} \tag{17}$$

Where, $v_{\text{hb-}d}$ is fiducial value of maximum speed limit corresponding freeway with different design speed (v_d equal to 120km/h, 100 km/h, 80 km/h and 60km/h). They are listed in table 5.

Table 5. The maximum speed limit fiducial value of freeway

design speed(km/h)	calculated value(km/h)		suggested value(km/h)	
	car	truck	car	truck
120	124.99	92.92	125	95
100	104.17	82.47	105	85
80	83.33	65.97	85	65
60	62.50	49.48	65	50

CONCLUSION

The multi-object optimization method of setting maximum speed limits was put forward based on efficiency, safety, economic and comfortable quality. The definition and suggested value of the fuducial value of maximum speed limits were given. It can provide reference gist for setting reasonable speed limit value in China.

ACKNOWLEDGMENT

This research was supported by Specialized Research Fund for the Doctoral Program of Higher Education (200802131013).

REFERENCES

Du, B. Y.(2002). "Expressway traffic accident and matrix of vehicle speed." *Journal of Highway and Transportation Research and Development*, 19(6), 116-118.

Feng, X. N., and Wang M. Y. and Shi B. L.(1993). "Traffic and Transport Volume Conversion Methodology Study." *Journal of Highway and Transportation Research and Development*, 10(3), 53-60.

Huang, Yi.(2005). "Research on vibration comfort of taxi driver." *Dissertation of Chongqing College of Transportation*, Chongqing.

Lu, N., and Shao, C.F.(2005). "An evaluation model for comfort degree of traffic design." *Road Transportation and Safety*, 5(5), 14-17.

Pei, Y. L., and Wang, W.(2004). "Road Traffic Accident Cause and Countermeasures." *Science Press*, Beijing, 5.

Shen, J., and Wang. J., and Ling J. S.(2006). "Discussion on Definition Supplement of Vehicle Maximum Speed." *Special Automobile*, (12),1-4.

Zhou, W., and Wang, B. G.(2001). "Theoretical study about road section capacity." *Journal of Traffic and Transportation Engineering*, (2), 92-98.

Study On The Carrying Capability Of Preplanned Regional Earthquake Evacuation Corridor Based On Macro-simulation

Yang Wang [1], Zhijie Li [2], Jing Cao [3], Xiaokuan Yang [4]

[1]Key Laboratory of Traffic Engineering in Beijing, Department of Civil Engineering, Beijing University of Technology; P.O. Box 100124, Ping Le Yuan100, Chao Yang District, Beijing; email: wangyang8265@emails.bjut.edu.cn
[2]Department of Civil Engineering, Beijing University of Technology; P.O. Box 100124, Ping Le Yuan100, Chao Yang District, Beijing; email: lzj@emails.bjut.edu.cn
[3]Key Laboratory of Traffic engineering in Beijing, Department of Civil Engineering, Beijing University of Technology; P.O. Box 100124, Ping Le Yuan100, Chao Yang District, Beijing; email: caojing@bjut.edu.cn
[4]Key Laboratory of Traffic Engineering in Beijing, Department of Civil Engineering, Beijing University of Technology; P.O. Box 100124, Ping Le Yuan100, Chao Yang District, Beijing; PH (010) 67391678; email: xiaokuan@hotmail.com

ABSTRACT

All over the world, earthquakes have been broken up more frequently than ever before. The huge disaster of an earthquake challenged the capability of government to handle an emergency. The emergency evacuation corridor planning will be more significant for restoration of a disaster area. This paper proposes a methodology for the research on carrying capability of a regional earthquake evacuation corridor based on macro-simulation to prove the availability and rationality of a predetermined regional earthquake evacuation plan. The proposed approach includes three processes: 1) Estimate the evacuation demand of the earthquake affected area and estimate traffic volume of each link and node of roadway network; 2) Confirm the OD-pairs based on the location of shelters and the preplanned direction of evacuation; 3) build up the earthquake evacuation network through the macro-simulation software, OREMS, as well as input the outcome of procedure 1) and 2). Evaluate the carrying capability of the preplanned regional earthquake evacuation corridor through evacuation clearance time and average evacuation speed which are the output of OREMS. In the end, the proposed approach was employed in the Beijing case and proved the availability and rationality of the Beijing earthquake evacuation corridor planning.

1 INTRODUCTION

The earthquake in Wenchuan, in the Sichuan province, has challenged the capability of Chinese government to handle an emergency. The emergency evacuation corridor planning will be more significant for rescue and restoration of

the disaster area. The data collected from the earthquake in Tangshan has show that the survival rate has a significant relationship with evacuation time (see Table 1).

Table 1. Relationship Between Evacuation Time And Survival Rate

Evacuation Time	Survival Rate
Half an hour	95%
One day	81%
Two days	53%
Three days	36.7%
Four days	19%

The earthquake evacuation corridor was different from traditional transportation systems that serve the normal traffic demand for are two reasons. First, subway and railroad may be damaged during an earthquake. Even though the facilities are still there, they cannot be used for evacuation for safety considerations. Second, due to limited capacity and the constraints of geographic conditions, ferries or helicopters are seldom considered in the process of an evacuation plan. Therefore, surface transportation systems look much more flexible and sustainable. It is evident that surface transportation systems are very important for earthquake evacuation. It is necessary for all levels of government to preplan an earthquake evacuation corridor and evaluate the availability and rationality of a regional earthquake evacuation corridor planning.

At present, there are two main aspects about emergency evacuation technology: 1) research on methodology of emergency evacuation planning, 2) research on management strategies of emergency evacuation traffic. Evacuation planning includes three aspects such as: evacuation demand estimate, evacuation distribution estimate, and evacuation-related traffic assignment. Current practice in hurricane evacuation demand estimation involves the estimation of the total evacuation demand in the first step, followed by the estimation of its temporal distribution in the second. A study (Haoqiang Fu, 2007) proposed two ways of estimation of hurricane evacuation demand. Participation rate models are the primary method to estimate evacuation demand and response curves are used for the temporal distribution. The sequential Logit model is the other way to provide estimates of dynamic disaggregate travel demand for hurricane evacuation. The study demonstrated the superiority of the sequential Logit model over the traditional two-step method in modeling hurricane evacuation travel demand. Evacuation distribution estimation also involves aggregative model and disaggregative model (Guangxiang Cheng, 2008). However, there still was no case study to prove the accuracy of these two models.

In general, evacuation efficiency can be improved by setting up the programming model to optimize the destination and route assignments in the network. An evacuation assignment model could be classified into two categories: static and

dynamic, according to the evacuation demand and impedance function that can be either time-dependent or not (Elise Miller-Hooks, 2008). The dynamic assignment model can not only be used in evacuation planning but also used in improving the management strategy of evacuation traffic (Heng Wei, 2008)(Yue Liu, 2008). Due to the fact that the dynamic evacuation traffic assignment model needs a more high-powered computer, it is hard to apply this model in the actual urban road network.

Although there has been some research on management strategy of emergency evacuation traffic, this research is focused on the effectiveness of a single strategy in the situation of hurricane evacuation (Virginia P. Sisiopiku, 2007)(Brian Wolshon, 2007). There is still lack of case studies on the carrying capability of an earthquake evacuation corridor. This paper proposes criterion for selecting the earthquake evacuation road, the methodology for searching availability and the rationality of earthquake evacuation corridor planning.

2 PRINCIPLES AND METHODOLOGY

2.1 Principle in the Selection Of Earthquake Evacuation Corridor

According to the relative rule of law, an earthquake evacuation corridor must be provided with high-capacity and high anti-seismic ability. The selection principle of an earthquake evacuation corridor involves five aspects: 1) safety and flexibility; 2) high capacity; 3) integrate with urban network planning; 4) convenient for surveillance; 5) adaptable either during normal conditions or emergencies.

2.2 Methodology Of Assess The Carrying Capability Of Earthquake Evacuation Corridor

Macro-simulation Model (OREMS)

After an earthquake, the most important mission is to transfer people to the shelter as soon as possible through the preplanned earthquake evacuation corridor. This paper used the macro-simulation model (OREMS) that is based on the UE (User Equilibrium) principle to optimize the earthquake evacuation procedure. This objective model could be mathematically described as follows.

$$\text{Objective:} \quad \min Z(x) = \sum_a \int_0^{x_a} t_a(\omega) d\omega$$

$$\text{S.T.} \quad \sum_k f_k^{rs} = q_{rs} \quad \forall r,s$$

$$f_k^{rs} \geq 0 \quad \forall k,r,s$$

$$x_a = \sum_r \sum_s \sum_k f_k^{rs} \delta_{a,k}^{rs} \quad \forall a$$

$$t_a(x_a) = t_a^0 \left[1 + \alpha \left(\frac{x_a}{C_a} \right)^{\beta} \right]$$

Where, $Z(x)$:the objective function, is the sum of the integrals of the link performance functions;

x_a :flow on link a, vehicle;

$t_a(x_a)$:impedance function, minute;

t_a^0 :travel time on link a in free speed, minute;

f_k^{rs} :flow on path k connecting O-D pair r-s, vehicle;

q_{rs} :flow rate between origin r and destination s, veh/hr;

$\delta_{a,k}^{rs}$:indicator variable; $\delta_{a,k}^{rs} = \begin{cases} 1 & \text{if link } a \text{ is on path } k \text{ between O-D pair } r\text{-}s \\ 0 & \text{otherwise} \end{cases}$;

C_a :capacity of link a, veh/hr;

α, β :pending coefficient;

Algorithm of Optimization Model

The macro-simulation model of an earthquake evacuation traffic assignment is a nonlinear programming model with linear constraints. The convex combination algorithm is especially useful for determining the equilibrium flows for transportation networks. The algorithm itself, when applied to the solution of the UE problem, can be summarized as follows:

Step0: Initialization. Perform all-or-nothing assignment based on $t_a = t_a(0), \forall a$. This yields $\{x_a^1\}$. Set counter $n = 1$.

Step 1: Update. Set $t_a^n = t_a(x_a^n), \forall a$.

Step 2: Direction finding. Perform all-or-nothing assignment based on $\{t_a^n\}$. This yields a set of flows $\{y_a^n\}$.

Step 3: Line search. Find α_n that solves $\min_{0 \le \alpha \le 1} \sum_a \int_0^{x_a^n + \alpha(y_a^n - x_a^n)} t_a(\omega) d\omega$

Step 4: Move. Set $x_a^{n+1} = x_a^n + \alpha_n (y_a^n - x_a^n), \forall a$.

Step 5: Convergence test. If convergence criterion are met, stop (the current solution, $\{x_a^{n+1}\}$, is the set of equilibrium link flows); otherwise, set $n = n + 1$ and go to step 1.

Through the convex combination algorithm, we can find the best solution of the evacuation traffic assignment model. The outputs of the macro-simulation model (OREMS) include evacuation time and speed. The availability and rationality of a preplanned earthquake evacuation corridor could be assessed by these simulation results.

3 CASE STUDY

3.1 Objective Evacuation Network

"Statistics Yearbook Of Beijing 2004" shows that the population density in the central district of Beijing was 42 times more than the average population density in the entire city of Beijing. This data implied that the central district of Beijing a

higher threat of earthquakes. In this paper, the central urban area is identified as the study area, such as Dongcheng, Xicheng, Chongwen, Xuanwu district. According to the aforementioned selection principal of an earthquake evacuation corridor, identified 13 east-west, 12 north-south main street and 3 expressway in the 3rd ring to make up an earthquake evacuation corridor.

3.2 Earthquake Evacuation OD

Beijing statistics shows that cars per capita is 0.2. Automobile occupancy should be 4 persons/vehicle during an earthquake evacuation. The capacity of buses used in earthquake evacuation is 180 persons/bus. The bus should be converted to the car equivalent. The conversion coefficient is 2.5. Based on the above rules, the earthquake evacuation demand expressed as the number of the car equivalent (see Table 2).

Table2. Earthquake Evacuation Demand In Central District Of Beijing

District	Population (million)	Evacuation Demand (vehicle)
Dongcheng	0.69	139917
Xicheng	0.83	168306
Xuanwu	0.61	123694
Chongwen	0.41	83139
Total	2.54	515056

In accordance with the relative rules about the emergency shelter planning, recommended area per capita of earthquake emergency shelters was 2.0m^2. The planning earthquake shelters include all parks and stadium in the central district of Beijing. The capacity constrain of shelter also expressed as the number of equivalent car. (see Table 3)

Table 3. The Capacity Constrain Of Earthquake Shelter

District	Park	Green Area (m^2)	60% Green Area (m^2)	Capacity (person)	Capacity (pcu)
Dongcheng	7	1318798	791278.8	395638	80224
Xicheng	7	1400906	840543.9	420270	85220
Xuanwu	4	449244	269546.4	134772	27327
Chongwen	4	2349379.5	1409627.7	704813	142920
Other	11	3535938.5	2121563.1	1060777	215101
Total	33	9054266	5432559.9	2716270	550792

3.3 Validation Analysis of Carrying Capability

After setting up the evacuation network and inputting the evacuation demand OD by the OREMS, the objective area was divided into four quadrants by the Chang

Avenue and the middle Axial Road (Figure1 and Figure2). This paper adopts two evacuation strategies, one-way and contra-flow, to evacuate people to the shelter (Figure 3).

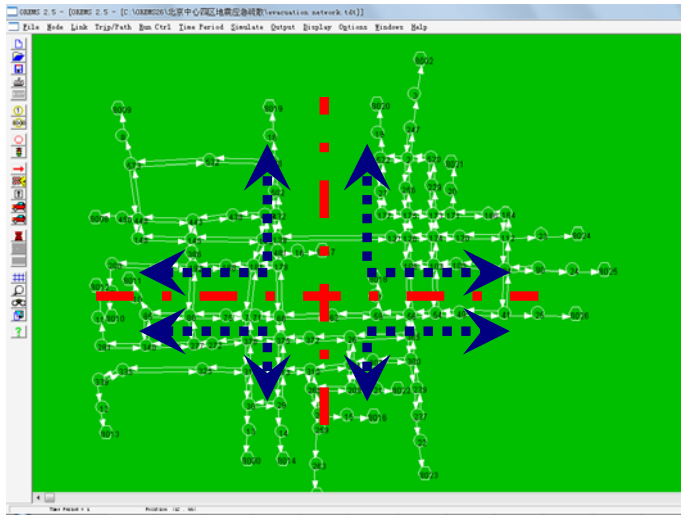

Figure 1. Earthquake Evacuation Direction.

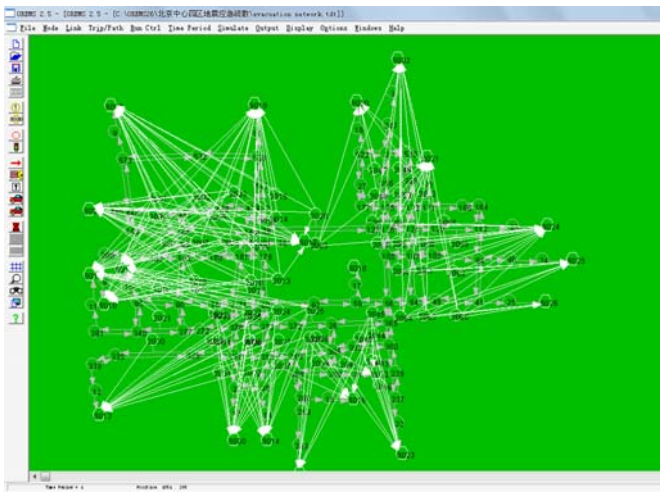

Figure 2. Evacuation Demand Distribution.

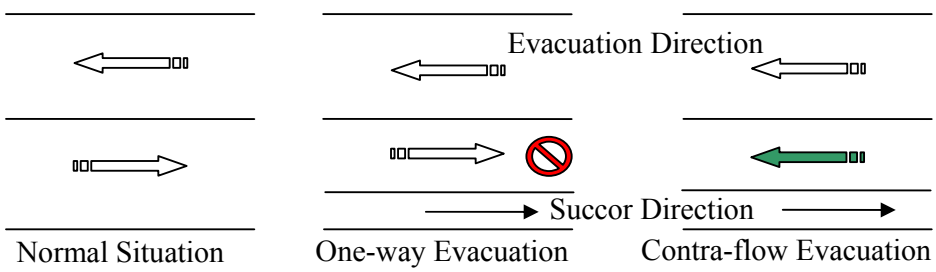

Figure 3. One-way Evacuation and Contra-flow Evacuation.

After applying the macro-simulation model, the result of the analysis of the carrying capability of an earthquake evacuation corridor is show in Table 4.

Table 4. Analysis Result of Carrying Capability of Evacuation Corridor

Evacuation Strategy	Evacuation Time	Average Evacuation Speed
One-way Evacuation	4:02 hours	24.6 mile/hour
Contra-flow Evacuation	2:33 hours	32.7 mile/hour

The output of OREMS shows that the carrying capability of an earthquake evacuation corridor, based on the selection principle, fulfills the earthquake evacuation demand. For the same network, a contra-flow evacuation strategy would significantly improve the evacuation efficiency. The time spent on evacuating 95% of the population was shortened from 2 hours and 45 minutes to 1 hour and 35 minutes. According to the data shown in Table 1, the preplanned earthquake evacuation corridor based on the selection principle could reduce the loss of life caused by an earthquake.

Although a contra-flow evacuation strategy could achieve a positive evacuation result, three important things should be accomplished before an actual evacuation is executed: 1) venue for community to get on evacuation vehicles must be preplanned; 2) the traffic management person has to assign the key intersection to regulate the evacuation traffic. 3) the traffic in the reverse lanes need to be cleared up before a contra-flow evacuation begins. The evacuation time obtained from the proposed methodology does not include mobilization time. Forecasting the length of the mobilization time needs further research. The publicity about evacuation is also important for the success of an earthquake evacuation.

4 CONCLUSION AND FUTURE STUDY

This paper puts forward a set of principles to select a suitable earthquake evacuation corridor and proposes a methodology for the research on the carrying capability of a regional earthquake evacuation corridor, based on macro-simulation to prove the availability and rationality of a preplanned regional earthquake evacuation corridor. In the end, the proposed approach was employed in the Beijing case study and proved the availability and rationality of the Beijing earthquake evacuation corridor planning. There are still some inadequacies in this paper. Such as, this paper does not consider the effect by the time-dependent variation of evacuation demand, and, does not take into account access capacity constraints in the earthquake shelter . Therefore, there leaves much to be improved in future studies.

REFERENCES

Haoqiang Fu. “Static vs. Dynamic and Aggregate vs. Disaggregate: A Comparison between Practice and Research in Hurricane Evacuation Travel Demand Modeling.” Annual Meeting of the Transportation Research Board,

Washington, D.C. 07-0646. (2007)

Guangxiang Cheng, Chester G. Wilmot. "A Destination Choice Model for Hurricane Evacuation." Annual Meeting of the Transportation Research Board, Washington, D.C. 08-0840. (2008)

Elise Miller-Hooks. "The Maximal Dynamic Expected Flows Problem For Emergency Evacuation Planning." Annual Meeting of the Transportation Research Board, Washington, D.C. 08-2924. (2008).

Heng Wei, Qing-An Zeng, Hong Hu. "Integrated Urban Evacuation Planning Framework for Responding to Man-Made Disasters over Surface Transportation Network." Annual Meeting of the Transportation Research Board, Washington, D.C. 08-1112. (2008).

Yue Liu, Gang-Len Chang, Ying Liu. "A Corridor-based Emergency Evacuation System For Washington D.C.: System Development And Case Study." Annual Meeting of the Transportation Research Board, Washington, D.C. 08-0674. (2008).

Virginia P. Sisiopiku. "Application of Traffic Simulation Modeling for Improved Emergency Preparedness Planning." Journal of Urban Planning and Development. Vol. 133, No. 1, March 1, 2007.

Brian Wolshon, Emile Marchive. "Emergency Planning in the Urban-Wildland Interface: Subdivision-Level Analysis of Wildfire Evacuations." Journal of Urban Planning and Development. Vol. 133, No. 1, March 1, 2007.

The Analysis of Traffic Flow State on Foggy Expressway Based on Fuzzy Clustering

WANG Jianjun[1], XIE Chenfeng[2], CHANG Zhenwen[2], ZHANG Jingjing[2]

[1] Key Laboratory for Special Area Highway Engineering of Ministry of Education, Chang'an University, Xi'an 710064, PH029-82334850; FAX029-87818191 email:wjjun16@163.com

[2] School of Postgraduate, Chang'an University, Xi'an 710064, PH029-82334850; email:xie_1225@yahoo.com

Abstract : Traffic flow state is a vague concept. It can not be measured off in different traffic flow states by using a specific index, which is in line with the fuzzy clustering characteristics. The Fuzzy C-Means (FCM) algorithm is used to analyze the traffic flow state in fog and non-fog periods in terms of a large amount of data of speed, density, and volume. The traffic flow state is classified into three, four, and six categories, respectively. By comparing and analyzing the traffic flow state in the two periods, results show that the regularity in fog is more obvious than that in non-fog. The traffic flow state in the fog period can be well described by four categories.

1. Introduction

In an intelligent traffic guidance system, the real-time traffic data and the historical traffic data are usually merged together in order to make the best estimate of road traffic flow at the moment. The identification of a traffic flow state should be based on the category of an existing state. While in different weather and road conditions, the traffic flow state may change dramatically even if the volume has not changed (Daniel and Matthew, 1983). It is necessary to study the flow states separately under different weather conditions, especially in rain, snow, and fog. The classification of a traffic flow state on a general road has been studied (CHEN, 2005; JING and MENG, 2007). The author studies the traffic flow state in fog to provide a basic theory for an intelligent traffic guidance system of the expressway.

2. The definition and classification of fog

Fog is the hydrometeor near ground, which is an aerosol system composed of the tiny water droplets or ice crystals suspended in the air. The existence of fog reduces visibility. If the visibility of target is down to less than 1000 meters, there is hydrometeor in the air near the ground that is called fog (PAN and JIANG, 2006).

3. Data Acquisition and Processing

3.1 data selection

The influence of volume on traffic flow classification is minimal. At the same volume, the state may be diametrically opposed (CHEN, 2005). For example, when the volume is zero, it may be a free or a congested flow. In addition to volume, speed and density is a linear relationship, each of them can be able to reflect the variation of a traffic flow state intuitively (Daniel and Matthew, 1983). As the speed increases, the

traffic flow state becomes better. Speed is one of the most important parameters of the drivers. The state continues to deteriorate with density increasing, so density is more concerned by administrators (JING and MENG, 2007). For reasons given above, the speed and density are selected as a basic parameter to judge the flow state.

3.2 data investigation location and time

In this paper, the data was collected from January 2002 to September 2008 on Zhanglong (Zhangzhou-Longyan) and Longchang (Longyan-Changting) expressway. The data includes visibility that is lower than 300m in fog and higher than 1000m in non-fog.

3.3 data preprocessing

Because the units of the speed and density are inconsistent, the collected data of speed and density should be standardized on the premise that their influence on a traffic flow state is equal, as shown in formula (1).

$$x'_{ik} = \frac{x_{ik} - \bar{x}_k}{s_k} \qquad (1)$$

When k = 1, k is for density; when k = 2, k is for speed; x_{ik} is the raw data of speed or density; $\bar{x}_k$ is the mean; s_k is the variance; x'_{ik} is the standardization. In order to compress standardized data between 0 and 1, we use the method based on the standardization of range as shown in formula (2). $x'_{k\max}$ is the maximum; $x'_{k\min}$ is the minimum.

$$x''_{ik} = \frac{x'_{ik} - x'_{k\min}}{x'_{k\max} - x'_{k\min}} \qquad (2)$$

4. Fuzzy clustering algorithm

Clustering is a process that distinguishes and classifies things according to certain requirements and rules. Traditional clustering analysis is a hard classification with the quality of either this or that. It has an uncertainty description of sample to clusters on fuzzy clustering (GAO, 2004). Traffic flow state is a very vague concept. There are no specific indicators to separate two different states, which is in accordance with the characteristics of fuzzy clustering. Thus, this paper analyzes the traffic flow state by using fuzzy clustering.

More attention is focused on the research to clustering analysis method based on the objective function. The Fuzzy C-Means (FCM) clustering algorithm is one of the most perfect. The objective function of the FCM algorithm is described as follows:

$$J_m(U, P) = \sum_{k=1}^{n} \sum_{i=1}^{c} (u_{ik})^m (d_{ik})^2$$

Where U is the dividing matrix; P is the clustering center vector; u_{ik} is membership that the data of No. k belongs to the clustering center of No.i, $u_{ik} \in [0,1]$;

$(d_{ik})^2$ is Euclidean distance between sample x_k and the clustering center of No. i; m is a weighted index (JING and MENG, 2007).

The steps are as follows:

Initialization: give a cluster c and set stop threshold ε of iteration; initialize clustering center $P^{(0)}$; set iteration counter b=0.

Step1. Calculate or renew dividing matrix $U^{(b)}$ by using the following formula:

$$u_{ik}^{(b)} = \left\{ \sum_{j=1}^{c} \left[\left(\frac{d_{ik}^{(b)}}{d_{jk}^{(b)}} \right)^{\frac{2}{m-1}} \right] \right\}^{-1}$$

Step2. Renew the clustering center $P^{(b+1)}$ by using the following formula:

$$p_i^{(b+1)} = \frac{\sum_{k=1}^{n} (u_{ik}^{(b+1)})^m . x_k}{\sum_{k=1}^{n} (u_{ik}^{(b+1)})^m} \quad , i=1 , 2 , \dots , c;$$

Step3. If $\| P^{(b)} - P^{(b+1)} \| < \varepsilon$, output U and P; otherwise set b = b + 1 , turn to the first step.

5. The classification of traffic flow state

There are different classifications of a traffic flow state because of the road conditions and traffic guidance systems. Free flow, transition flow, and congested flow is usually described as the traffic state (JIANG, 2004). In China, the service level that describes the road traffic flow operating conditions is classified into four categories on each class of highway. The density and speed is the standard of classification (CHEN and YAN, 2003). The United States Highway Capacity Manual (HCM) classifies the service level of the urban main road into six categories from A to F by using average overall speed as a grading index (Javy and Norman, 2000). In this paper, the traffic state in fog and non-fog is classified into three, four, or six categories in accordance with the usual classification, the highway service level in China, and the United States HCM service level. There is a comparative analysis to the traffic flow state of different categories and periods.

The data of speed and density between 0 and 1 in fog and non-fog is obtained by using the method based on the standardization of range on formula (1) and (2). Then, the data is classified and processed by using FCM algorithm in MATLAB.

5.1 The traffic flow state is classified into three categories

After 21 iterated operations, the objective function value of a traffic flow state in fog reached 4.5677; after 33 iterated operations, the objective function value of a traffic flow state in non-fog reached 8.536214. Their accuracy were 10^{-5} as the condition of control. The Clustering results are shown in Table 1.

Table 1. The Clustering Results of Three Traffic Flow States.

Categories	Clustering center of fog		Clustering center of non-fog	
	Density (cars. $km^{-1}.lane^{-1}$)	Speed($km.h^{-1}$)	Density (cars. $km^{-1}.lane^{-1}$)	Speed($km.h^{-1}$)
State I	6.5605	70.0381	3.4166	82.7641
State II	9.2635	61.0643	10.6355	68.2015
State III	16.2558	50.5954	5.6575	55.0227

The three categories of clustering density and speed data in fog and non-fog were measured by plotting the density on the abscissa and speed on the ordinate on Figure 1 and Figure 2. The conclusions are shown as follows:

(1) Traffic flow state is gradually transit from free to congestion as the density increases and speed decreases. The clustering center of three traffic flow states is nearly in a straight line. The approximate boundary of speed between free flow (state I) and transition flow (state II) is 64 km/h, but between transition flow and congested flow (state III) is not clear because of wide fluctuations of speed. The boundary of density among the three traffic flow states is not clear.

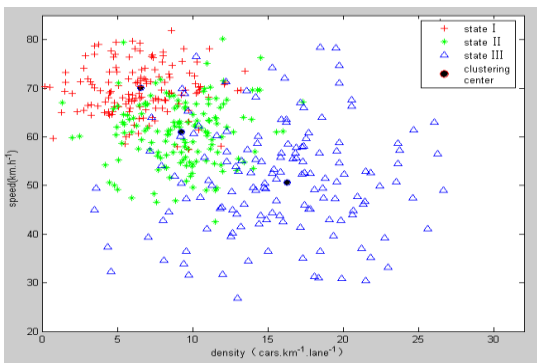

Figure 1. Three traffic flow states in fog.

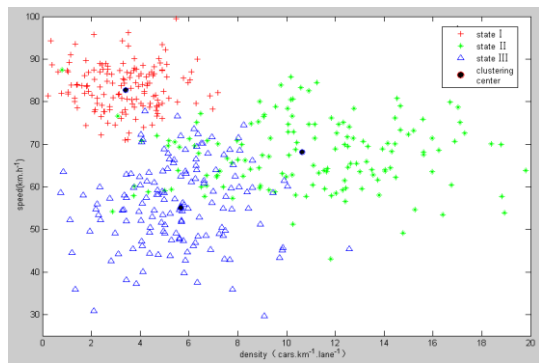

Figure 2. Three traffic flow states in non-fog.

(2) In a non-fog period, the traffic density does not increase as the speed decreases. The density of the transition flow is higher than the congested flow. The clustering center of three traffic flow states shows as a triangle on Figure 2. The clustering center of transition flow is the farthest from the origin, that is to say the volume of the transition flow is much larger than that of the congested flow and slightly larger than that of free flow.

(3) The speed of the clustering center in non-fog is higher because the speed has a wider distribution. In a non-fog period, the free and congested flow density of the clustering center is higher. The speed data is dispersed, which made the result different from in fog by using FCM algorithm.

(4) The three traffic flow states show strong significant correlation, so the density and speed data of fog period as classified into three categories is reasonable.

Because the range of speed variation in non-fog is much wider than that in fog, three categories do not comparatively show the characteristics of traffic flow state.

5.2 The traffic flow state is classified into four categories

After 25 iterated operations, the objective function value of a traffic flow state in fog reached 4.1352; after 64 iterated operations, the objective function value of a traffic flow state in non-fog reached 5.876359, their accuracy was 10^{-5} as the condition of control. The Clustering results are shown in Table 2.

Table2 . The Clustering Results of Four Traffic Flow States .

categories	Clustering center of fog		Clustering center of non-fog	
	Density (cars. $km^{-1}.lane^{-1}$)	Speed($km.h^{-1}$)	Density (cars. $km^{-1}.lane^{-1}$)	Speed($km.h^{-1}$)
Ⅰ	6.4240	72.6385	3.2194	83.8083
Ⅱ	8.8615	64.4835	14.7145	70.5079
Ⅲ	12.5367	55.177	8.9775	58.5605
Ⅳ	15.7721	47.4290	10.8866	52.0220

The four categories of clustering density and speed data in a fog and non-fog period were measured by plotting the density on the abscissa and speed on the ordinate on Figure 3 and Figure 4. The conclusions are shown as follows:

(1) The traffic flow state shows strong significant correlation when classified into four categories in fog. The lower the speed is the higher the density is. The clustering center of the four traffic flow states is nearly in a straight line.

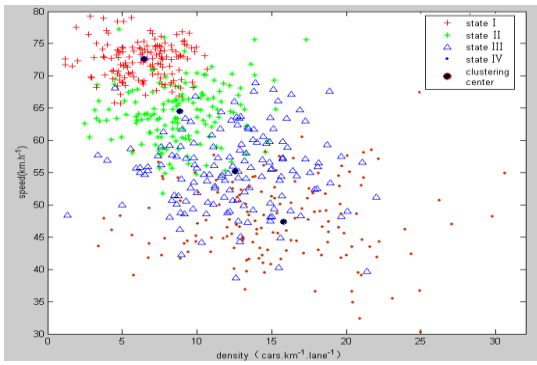

Figure 3. Four traffic flow state s in fog.

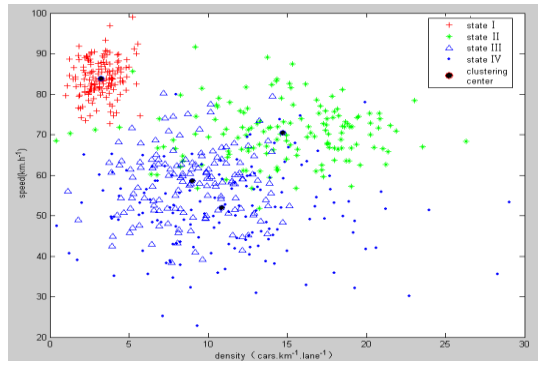

Figure 4. Four traffic flow states in non-fog.

(2) The mingled data of the three categories is classified into the extra traffic flow state by the comparison of Figure 2 and Figure 4. In this way, the state Ⅰ, Ⅲ and Ⅳ have more obvious regularity . The volume of state Ⅱ is the largest and the highway capacity gets the maximum use out of it.

(3) The speed of clustering a center in non-fog is higher than that in fog, which is harmonious with our perceptual intuition. The density of a clustering center in non-fog is almost smaller than that in fog.

(4) The four traffic flow states in fog show strong significant correlation. Making detailed analysis on the traffic flow state by classifying them into four

categories is favorable to understand.

5.3 The traffic flow state is classified into six categories

After 53 iterated operations, the objective function value of a traffic flow state in a fog period reached 3.4536; after 57 iterated operations, the objective function value of a traffic flow state in a non-fog period reached 3.011431, their accuracy was 10^{-5} as the condition of control. The Clustering results are shown in Table 3.

Table3 . The Clustering Results of Six Traffic Flow States .

categories	Clustering center of fog		Clustering center of non-fog	
	Density (cars. $km^{-1}.lane^{-1}$)	Speed($km.h^{-1}$)	Density (cars. $km^{-1}.lane^{-1}$)	Speed($km.h^{-1}$)
Ⅰ	5.8432	74.3105	3.06145	85.5535
Ⅱ	7.1675	68.1437	7.0753	77.0277
Ⅲ	13.6269	60.1605	5.0805	70.8625
Ⅳ	10.8374	55.9393	10.4561	66.0724
Ⅴ	18.6135	50.2905	9.2151	59.7655
Ⅵ	15.6269	47.3190	12.7775	52.5495

The six categories of clustering density and speed data in a fog and non-fog period were measured by plotting the density on the abscissa and speed on the ordinate on Figure 5 and Figure 6. The conclusions are shown as the follows:

(1) As shown in the Table 3, the speed of a clustering center in non-fog is higher than that in fog. The density of a clustering center in fog and non-fog mingled with each other, but the maximum density in fog is much higher than that in non-fog.

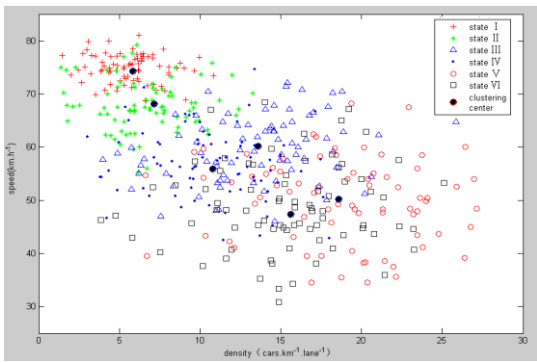

Figure 5. Six t raffic flow states in fog.

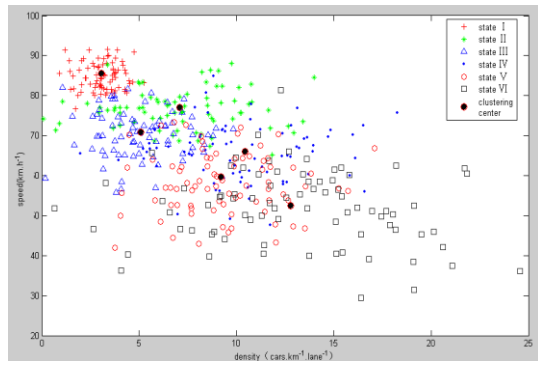

Figure 6. Six traffic flow states in non-fog.

(2) The density of state Ⅰ, Ⅱ, Ⅲ, Ⅴ and Ⅰ, Ⅱ, Ⅳ, Ⅵ in fog is smaller with the increasing of the speed. But the volume of state Ⅲ and Ⅴ are obviously larger than state Ⅳ and Ⅵ That is equal to classify the traffic flow state into six from density, speed and volume.

(3) The traffic flow state Ⅰ, Ⅲ and Ⅴ in non-fog have linear relationships, the same to the state Ⅰ, Ⅱand Ⅳ. The state Ⅵis the transition flow to the state Ⅳand Ⅴ.

(4) The consistent traffic of all states is carefully described by classifying the traffic flow state of fog and non-fog into six categories.

6. Conclusion s

Traffic flow state in fog has its particularity that reflects at the classification of the traffic flow data on the same road by using FCM algorithm. The traffic states in fog are much different from that in a non-fog mostly because of the different speed in the two periods. In a fog period, drivers are more cautious and the speed variation of the vehicle is smaller, which makes traffic flow states more regular than in non-fog. By increasing the classification, the description of traffic flow states in fog and non-fog are more detailed. The traffic flow state should be classified according to the requirements, especially in fog. The traffic flow state as classified into four categories is appropriate, not only to put emphasis the regularity of traffic flow, but also overcome the disadvantage of too much classification.

It should be noted that this study only evaluated a traffic flow state by using the speed and density and suppose the two indicators have the same influence on a traffic flow state. Deciding whether the two indicators influence on a traffic flow state is different and how to determine the weights would be required for an intensive study.

Acknowledgement s

This work is supported by the National High Technology Research and Development Program of China under Grants No.2007AA11Z248.

References

CHEN Dewang (2005). “Classification of Traffic Flow Situation of Urban Freeways Based on Fuzzy Clustering”. Beijing, Journal of Transportation Systems Engineering and Information Technology. 5 (1), 62-67.

CHEN Kuanming, Yan Baojie (2003). “Dao Lu Tong Xing Neng Li Fen Xi”. Beijing, China Communications Press. 39-40.

Daniel L. Gerlaugh and Matthew J. Huber, Translator: Jiang Huang etc. (1983) “The Traffic Flow Theory”. Beijing: China Communications Press.19-27.

GAO Xingbo (2004). “Analysis and Application of Fuzzy Clustering”. Xi’an, Xi Dian University Press.49-601.

Javy Awan, Norman Solomon etc (2000). “Highway Capacity Manual 2000”. The TRB Committee on Highway Capacity and Quality of Service

JIANG Guiyan (2004). “Technologies and Applications of the Identification of Road Traffic Conditions”. Beijing, China Communications Press. 49-55.

JING Peng, MENG Xianghai (2007). “Traffic Flow Situation during Snow Melt Period Based on Fuzzy Clustering”. Journal of Northeast Forestry University . 35(4), 46-49

PAN Xiaodong, JIANG Hong (2006). “Cause and Security Countermeasures of Traffic Accident in Foggy Expressway”Beijing, Communications Standardization Issue. 158.

Research on the Impact of Divers' heart rate on Longitudinal Slope of Freeway Tunnel

Zhao Jianyou[1]， He Cao[1] and Shi Yanni[1]

[1]Automobile Institute of Chang'an University, P.O. Box: 567 City: Xi'an, Shanxi, 710064, PH：（029）82334069; FAX (029)82334069 Email: jyzhao@chd.edu.cn

ABSTRACT

This paper researched the longitudinal slope of a tunnel from the driver's psychological view, and analyzed the heart rate changes in different drivers. According to the measured data, we established the quantitative model between the driver's physiological and psychological response by an increased heart rate, and the longitudinal slope of the tunnel and running speed with a regression analysis. This model proved capable of describing the response of drivers driving through the contrast between field data and model calculated data. Finally, we calculated a safe slope of the tunnel and security pace value according to the model.

INTRODUCTION

With high-grade freeways extended to the western region, there have been an increasing number of tunnels, and some of these formed tunnel groups. The so-called tunnel groups are a number of tunnels which the distance of two tunnels is less than 2km under normal circumstances (design speed is 80 km/h)) (ZHOU Zhong-ye et al. 2008).Tunnel groups change the driving environment frequently in a short period, it brings great impact on drivers either psychologically or physiologically and it can become a security risk; at the same time, the tunnel alignment will also have a certain impact on the drivers. The restriction on the slope by traditional theory is mainly based on the power of the vehicles. Uphill, the traditional theory is only concerned about how much the car can climb up the slope, and does not take the subjective factors of people described and the state when the drivers are climbing the slope into consideration sufficiently(ZHANG Sheng-rui et al 2007). The tunnel belongs to the bottleneck section of the road net of the highway, so light traffic accidents may also affect the operational efficiency of the entire road network. Therefore, it is necessary to carry out studies about the impact physiologically and psychologically on the drivers according to the tunnel longitudinal slope in order to improve the safety of the operation of the tunnels.

EXPERIMENTAL DESIGN

Experimental object. Choose 5 male and 3 female drivers with different ages and different driving experiences as the Experimental object. Considering the high rate of accidents on the road, do not choose the new drivers with less than 3 years experience, and input the drivers' information in Table 1. Before the test we must make sure the

drivers should have enough sleep, avoid food and drugs which can influence the heart rate such as smoking, drinking tea, wine, and coffee, and avoid strenuous exercises.

Experimental Equipments. (1)Experimental car, FORD TRANSIT. (2)KF-2 Physiological Detector, Record the driver's ECG Database (Display sensitivity:10mm/mv, Error≤±5%, Scanning velocity :25mm/s, Error≤±10%), Breathing wave（Precision≤±5%），Body temperature（Error±5%），Galvanic Skin Reflex(GSR)(Error≤10%),and the Physiological parameter about the body moves the change intensity.

Table 1. The information of drivers.

Drivers NO.	1（M）	2（M）	3（M）	4（M）	5（M）	6（F）	7（F）	8（F）
Age	25	26	37	39	56	38	39	52
Driving age	3	6	10	22	32	10	7	15
Familiarity with the test section	Unfamiliarity	Familiarity	Unfamiliarity	General	Familiarity	Unfamiliarity	General	Unfamiliarity

Experimental Routes. Choose the section from the Bridge of ZhiFang (K42+800) to the export of Qinling tunnel NO.1 (K64+827) as the uplink and downlink experimental route, the speed limit of all the uplink route is 80km/h, and the speed limit of all the downlink route is 60km/h. There are 22 tunnels in this section (Shaanxi Provincial Highway Survey and Design Institute. 2007); the longitudinal slope of the tunnel is in Table 2 and Table 3.

Table 2. The distribution of down-steam's longitudinal slope for grade line.

Downlink tunnel NO.	01	02	03	04	05	06	07	08	09	10	11
Longitudinal slope of Tunnel（‰）	25.8	45	43	28	45	45	45.02	29	37	45	35.41
Downlink tunnel NO.	12	13	14	15	16	17	18	19	20	21	Zhifang
Longitudinal slope of tunnel（‰）	26.5	27.22	20.2	40	40	21.35	16.5	29	38.13	38.13	23

Table 3. The distribution of up-steam's longitudinal slope for grade line.

Uplink tunnel NO.	Zhifang	21	20	19	18	17	16	15	14	13	12
Longitudinal slope of Tunnel（‰）	22.13	28	28	37	37	16.5	25	25	42	20	20

Uplink tunnel NO.	11	10	09	08	07	06	05	04	03	02	01
Longitudinal slope of Tunnel （‰）	32.91	25.82	35.41	35.5	26	30	30	45	43	38	46

Experimental Procedures. Test for 10 minutes' the static heart rate as a normal heart rate before driving and compare with the dynamic heart rate in the following test of driving. When arriving at the experimental route, make sure the driver wears the physiological detector and record the time of entering the car as the start of the test. When collecting the electrocardiosignal read the instant velocity and record the time manually under special circumstances (e.g. the time of entering the tunnel hole and the time of exiting, or overtaking another vehicle, etc.).When the test is finished, get out of the car and record the time. The test requests that the recording time of the manual and physiological detector are the same, so as to make sure all the data is synchronous.

EXPERIMENTAL DATA ANALYSIS

We can get the sample data of all variables through Statistics Theories and general knowledge excludes some abnormal data, then build a regression model about the heart rate, velocity, Longitudinal slope of the Tunnel by the theory of regression analysis.

It could not fully reflect the influence of the longitudinal slope of the tunnel to drivers by comparing the increase of the drivers' heart rates because of the differences of each driver. So we used the increased rate of heart rate. A drivers' heart rate in calm is shown in Table 4. The increased rate of heart rate = (the heart rate in driving-the heart rate in calm)/ the heart rate in calm. Research shows that the drivers will be nervous when the heart rate increases more than 20% and the drivers will be frightened when it increases more than 40% (Huang Xi-ting .1988; ZHAO Jian-you. 2003).

Table 4. Drivers' average heart rate in calm.

Drivers NO.	1(M)	2(M)	3(M)	4(M)	5(M)	6(F)	7(F)	8(F)
Average heart rate in calm （Times/min）	61	67	70	72	62	65	52	79

The comparison of different drive speed and increased heart rate in different drivers. The different mental status, driving experiences and driving technologies, performance in different driving behaviors, and mental experiences will certainly be different. In order to facilitate the problem, compare the 5 male drivers' average with the 3 female drivers' average.

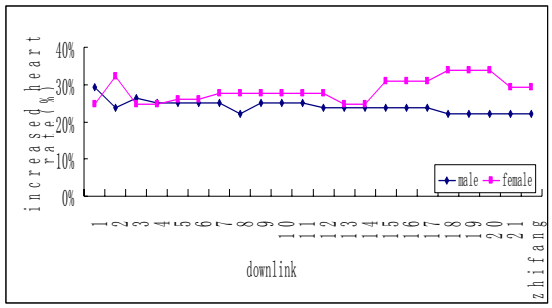

Figure 1. Male and female drives' speed distribution in downlink.

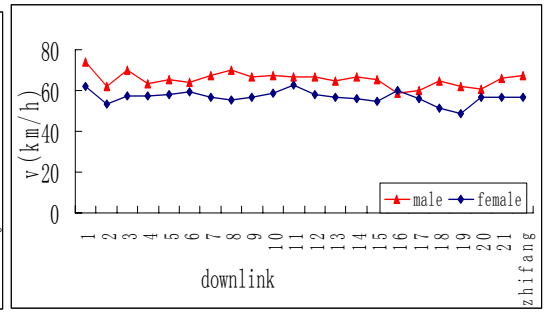

Figure 2. Male and female drives' increased heart rate in uplink.

Figure 1 and Figure 2 show male and female drivers' speed and increased heart rate in down-steam, so we can get the conclusion that male drivers have a higher speed and a lower heart rate than a female, while female drivers' have a lower degree of psychological stress than males in downlink.

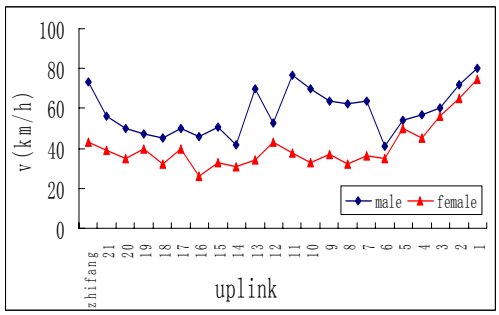

Figure 3. Male and female drive' speed distribution in downlink.

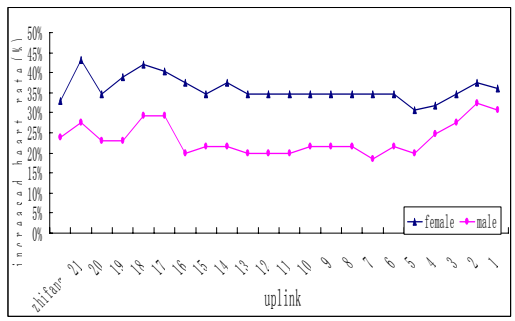

Figure 4. Male and female drives' increased heart rate in uplink.

Figure 3 and Figure 4 show male and female drivers' speed and increased heart rate in uplink, so we can conclude that male drivers have a higher speed and lower increased heart rate than females, while female drivers have a lower degree of psychological stress than males in uplink too.

Contrasting the information of drivers, we can get the reasons that lead to it: the average driving age of male drivers is more than females so they have much more driving experience; in addition, the extent of familiarity is deeper than females, and it indicates that male drivers' psychological qualities are better than females' in the tunnel groups of the freeway section, they can tackle the changing road conditions easily, and the drastic changes of heart rate can not happen. On the other hand, it also shows that the expectation of velocity of male drivers is much higher and they can not feel too much tension with high speed and complex road sections.

Built a Relation Mode between Longitudinal slope for Grade Line, Drive Speed and Increased Rate of Heart rate. According to the measured data, established the quantitative model between driver's physiological and psychological response by an increased heart rate, and Longitudinal slope of tunnel and running speed with regression analysis. The measured data of the uplink and downlink are shown at the

Table 5 and Table 6 respectively.

Table 5. The corresponding date of longitudinal slope of tunnel, running speed and the increased heart rate when downlink.

Longitudinal slope of tunnel i（‰）	23	38.13	38.13	29	16.5	21.35	40	40	20.2	27.22	26.5
Running speed v（km/h）	55	57	58.2	56.8	57	57.4	59.8	60.8	61.6	60.4	60
The increased rate of heart rate n（%）	32	28	23	38	23	24	30	30	30	32	32
Longitudinal slope of tunnel i（‰）	35.41	45	37	29	45.02	45	45	28	43	45	25.8
Running speed v（km/h）	63.8	63.2	61.8	63.2	61.8	60.2	60.6	59.2	63.4	54	59.6
The increased rate of heart rate n（%）	30	33	35	33	30	32	25	35	32	27	37

Table 6. The corresponding date of longitudinal slope of tunnel, running speed and the increased heart rate when uplink.

Longitudinal slope of tunnel i（‰）	22.13	28	28	37	37	16.5	25	25	42	20	20
Running speed v（km/h）	72	62	56	62	62	45	22	38	30	70	53
The increased heart rate n（%）	37	33	40	31	32	31	28	32	32	27	29
Longitudinal slope of tunnel i（‰）	32.91	25.82	35.41	35.5	26	30	30	45	43	38	46
Running speed v（km/h）	77	70	64	62	64	35	50	45	76	75	75
The increased heart rate n（%）	27	28	28	27	27	28	27	27	30	34	22

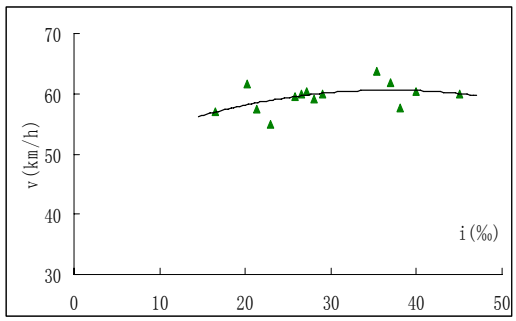

Figure 5. The regression curve of the longitudinal slope of the tunnel and running speed at downlink

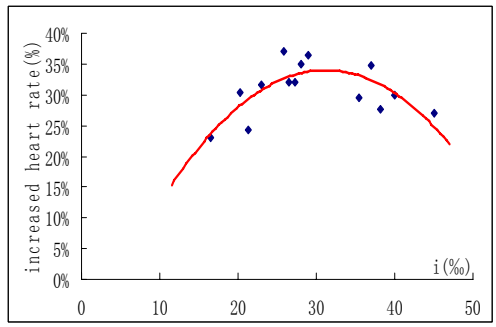

Figure 6. The regression curve of the longitudinal slope of the tunnel and Increased heart rate at downlink

The regression mode of figure 5: $v = -0.0088 i^2 + 0.6463i + 48.689$

Model applicable scope: $0<i<5\%$

The correlation coefficients of mode: $R=0.23$

The regression mode of figure 6: $n=-0.0005 i^2 +0.03i-0.1281$

Model applicable scope: $0<i<5\%$

The correlation coefficients of mode: R=0.75

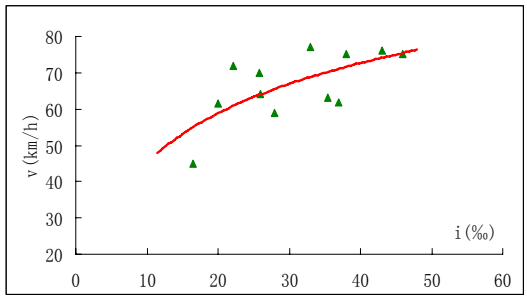

Figure 7. The regression curve of the longitudinal slope of the tunnel and running speed at uplink

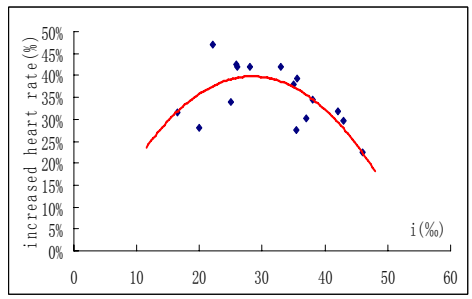

Figure 8. The regression curve of the longitudinal slope of the tunnel and increased heart rate at uplink

The regression mode of figure 7: v=19.929Ln (i)-0.8655
Model applicable scope: 0<i<5%
The correlation coefficients of mode: R=0.67

The regression mode of figure 8: $n=-0.0006i^2+0.0321i-0.0579$

Model applicable scope: 0<i<5%
The correlation coefficients of mode: R=0.72

Figure 5 and 7 shows that the whole distance of downlink section is more than 20km at the test section with the slope between 0 and 5%,the drivers usually brake to slow down the speed because of 60km/h's limiting at downlink, and in the uplink the speed limit is 80km/h the driver usually accelerate, so the speed of upraise is much higher than that of down, Figure 6 and 8 shows that when the longitudinal slope of tunnel' s range is 0~5%, with increasing angle of the longitudinal slope of the tunnel the increased heart rate first increases, then decreases, the angle of the longitudinal slope of the tunnel is about 3% when the increased heart rate is max.

Contrast the data of measured increased heart rate with the data of calculated value (the average of downlink and uplink), and get 22 groups data, as Figure 9 showed, the maximum error of model calculations is 15.32%, the least error is 0.05%, the average error is 6.34%, Through the comparison, we can regard as the precision of model calculations is much better and it can reflect the changes of increased heart rate in driving.

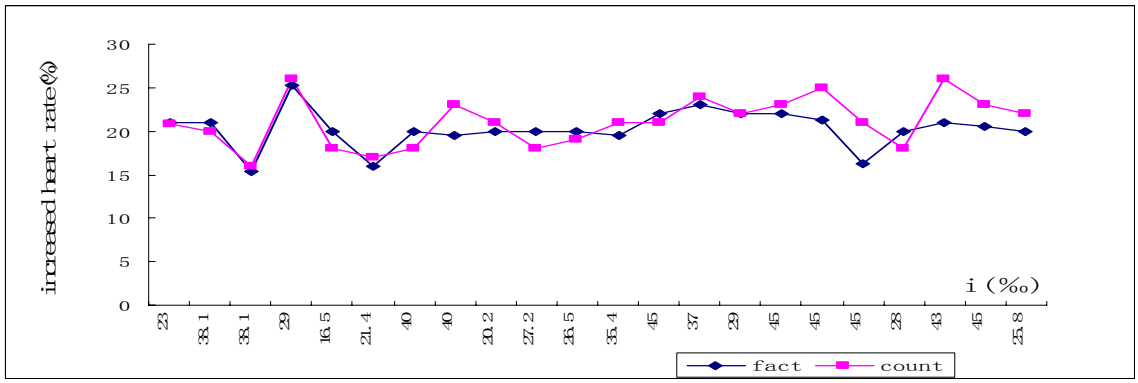

Figure 9. The comparison of the tested and model calculations of the increased heart rate.

THE SAFE SLOPE OF THE TUNNEL AND SECURITY PACE VALUE

The Safe Slope. According to the highway tunnel design codes, the longitudinal slope of the tunnel should be no less than 3‰ and no more than 30‰, to be limited by the topographical condition it can be appropriately increased, but no more than 40‰ (WANG Shu-ling et al 2007).

The related research indicated that the increased heart rate is not surpasses 40%, otherwise the driver's psychological overload is vulnerable to accidents, when the increased heart rate is 40% of the marginal value, take it into regression equation we can know that the max of the longitudinal slope of the tunnel at uplink is 30‰, it indicates that the longitudinal slope of the tunnel at downlink is corresponding to the design standard. Similarly we can known the max of the longitudinal slope of tunnel at uplink is 27‰, so the safe slope of the tunnel value at uplink is 27‰.

The Security Pace. Take the marginal value of slope into the regression mode of the longitudinal slope and velocity, we can see that the security pace value at downlink is 60.2 km/hand the security pace value at uplink is 73.7km/h.

CONCLUSION

Though the test of practical driving, the paper makes a study about the effects of the longitudinal slope of the tunnel on the heart drivers and velocity, the conclusions are as follows:

(1) Male drivers have higher speed and lower increased heart rate than female but increased heart rate is lower than female.

(2) The expectation to velocity of male drivers is much higher than female, and in the high velocity and complex road section they can maintain a stable heart rate.

(3) According to the measured data, the quantitative model that established between driver's physiologically and psychologically response by increased heart rate and the longitudinal slope of the tunnel and running speed have high precision and

can reflect the changes of increased heart rate in driving.

(4) The max of the longitudinal slope of the tunnel at uplink is 27‰, at downlink is 30‰; Security pace value at downlink is 60.2 km/h and the security pace value at uplink is 73.7km/h.

REFERENCES

ZHOU Zhong-ye, LIAO Zhi-gao, LIU Ben-min, GUO Zhong-yin. (2008). Analysis of Traffic Property and Safety in Freeway Tunnel Group. Computer and Communications.Vol.26, No.1, 2008, pp.27-30

ZHANG Sheng-rui, MA Zhuang-lin, SHI Qiang. (2007).Distribution characteristics and countermeasures of traffic accidents in expressway tunnel group. Journal of Chang an University (Natural Science Edition).Vol.27, No.1, 2007.pp.63-66

Shaanxi Provincial Highway Survey and Design Institute. (2007).National Trunk (GZ40) Eleanor ~ estuarine habitat in Shaanxi floods Huxian Meiyukou ~ Yangxian tree clearance above the highway construction design .Xi'an

Huang Xi-ting (1988). Experimental Psychology guidance. People's Education Press.

ZHAO Jian-you. (2003). Automobile driver action behavior at traffic accident moment. Journal of Xi an Highway University.Vol.23, No.4, 2003, pp.91-93

WANG Shu-ling, CHEN Jin-chuan, LIU Xiao-ming, RONG Jian. (2007). Research on Safety Slope Grade Based on Driver's Psychological Response. Journal of Highway and Transportation Research and Development.Vol.24, No.2, 2007, pp.126-130

A Study on Cable-removing Scheme of the Cable-stay System of the Zhijing River Bridge

WEI Jianjun[1] and CHEN Nianhe[2]

[1]School of Architecture and Civil Engineering, China University of Mining &Technology, P.O. Box 221008, Xuzhou, China; Department of Civil Engineering, Xuzhou Institute of Architectural Technology, Xuzhou, China.PH(86)516-83889549; email:weijjbridge@163.com

[2]Department of Civil Engineering, Xuzhou Institute of Architectural Technology, Xuzhou, China; PH(86)516-83889549; email: chennianhe@xzcat.edu.cn

ABSTRACT

The Zhijing River Bridge is a CFST arch bridge in Hubei province. The limitations are more cables, as the angles of some cables are very small and made cable adjusting difficult in construction. The Iterative optimization method with once-tension principle and alignment controlled by pre-cambers is introduced into the alignment control and cable-force calculation of the erection stage. All cables should have been removed after the arch rib closure in the original design, but in the latter hoisting construction, the early cable force and elevation were influenced seriously and the inner force of main arch rib became uneven. The influence by the time, order and method of cable-removing are calculated in the optimization process and the new cable-removing schemes are brought forward. In that, part of the cables removed before closure, and they are analyzed and compared to each other, and then a best scheme with easier control is determined.

INTRODUCTION

The cableway erection without supporting frame is always used in the construction of arch bridge, and later the method is developed with jack inclined drawn and steel wires buckled-hanged, and applied widely in the erection of long span concrete-filled steel tubular arch bridge. Because the prestress wire is used as buckle cable in the cable-stay erection of steel arch ribs, the line of arch rib become relatively easy to control.

In the erection of long-span arch bridge, the coordinate and cable force of each segment is continuously changing. For every segment fixed with bolts, the line of arch rib and cable force unfit for usually adjust. The line of arch rib direct affects the accuracy of rib closure. Hence, the time sequence and method of remove cable make impact on the line and internal force of arch ribs. Therefore, it is necessary to analyze the remove cable scheme and carry on optimization, compare and choose.

PROBLEM BACKGROUND

Zhijing River Bridge is a concrete filled steel tube arch bridge in the Hu-Rong West Expressway in Hubei province. The span of main arch crosses the degree as 430 meters. Fig.1 shows a photograph of the bridge. Each arch rib of the bridge is divided into 30 segments for the limits of construction space and transport conditional. Double-rib assembled in the deck of the bridge span and hoistinged together. The oblique-draw-buckle-hanged system consists of 10 major segments and each segment divide into 3 parts that slinged with 4 cables which anchored to juncture pier at one end and through steel beam to the arch rib at the other.The concrete block is poured on the cap of juncture pier as anchor beam to Subject to all of the construction load by cable. As a matter of convenience for construction and allay expenses,the double juncture piers as buckle pier for its body is high and the double abutment as anchor beam.Because single longitudinal slope and the inconsistent elevation of juncture piers on both sides, the height of buckle point and cable angle are unconformability.The quantity of calculation analysis is enlarged and the line control become inconvenient.The layout of cable-stay system is showed on Fig.2.

Figure 1. Photograph of the Zhijing river bridge, Hubei, China.

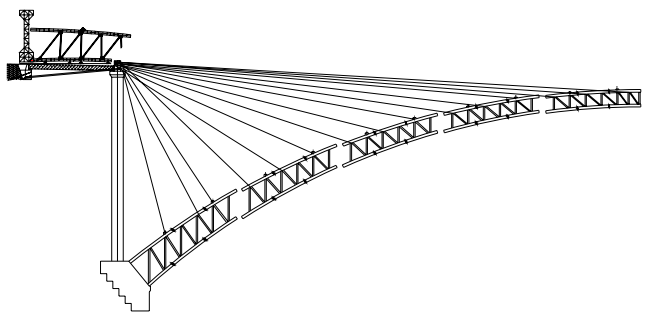

Figure 2. Layout of cable-stay system.

In the actual construction, the line of arch ribs consistent with the design by adjusting the cable. The cable-stay system of this bridge has more cables with small angle, which add more difficulty on cable adjusting. Further more, adjust arch rib

line with these cables must be difficult and dangerous. It needs to look for a optimization method for line adjustment.

MATHEMATICAL OPTIMIZATION METHOD

To find out the best path to erect the arch rib, optimization calculation theory is loaded into the forward iteration analysis calculation. Base on the space finite element analysis of the arch bridge, the cable force is deduced reversely via optimization theory. Buckling cable force taken as design variable, the displacement and stress of the arch rib taken as state variable. Through setting appropriate objective function, the optimal cable force of each segment in the erection is obtained. The line of arch bridge after construction matches the design expectation, and the inner force of the structure in the optimal state after construction. Function approximation optimization method is called zero-order method for the dependent variable is used instead of partially derivative in the principle. The relationship between objective function and variables method is set up via least square and curve fitting. The principle is achieved through a few design variable sequences to calculate the objective function and then obtained the least-squares between all data points.

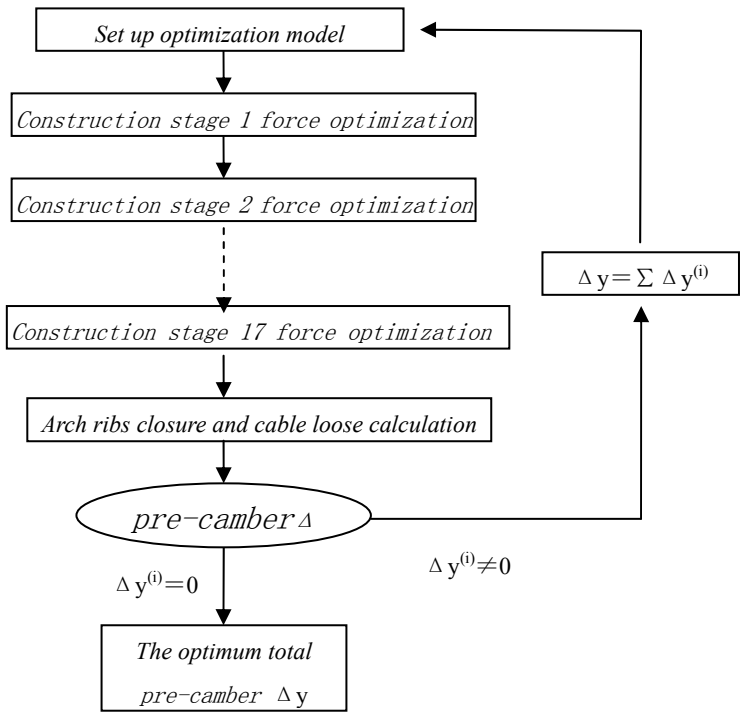

Fig 3.Optimization process of cable force.

Base on the principle of pulling rib to place with cable once tension, the calculation ruler be order as follows: the cable force adjusting is carried out once in the arch rib fixing with buckle cable and not to be adjusted until the closure of ribs and unlock cables, but the cable of Z1、Z2 have another construction stage for cable

force adjusting respectively. Each construction stage has an independent optimization circle. After optimization cycles same times as construction stages, all cable forces in every stage can be obtained. Because there is one group cable forces to be optimized in both sides respectively, two variables for optimization are set in each calculation phase. The stress of steel arch rib and the displacement of cable point in the lifting are set as state variables. The objective function is the absolute displacement summation of new additive cable points in both sides and other cable points displacement needn't to be controlled.

The line control target of steel ribs can be described as: the control line=manufacture line(arch line + pre-cambers)-deflection curve of hingeless arch bridge with dead load. The optimization process of cable force is shown in Fig 3.

CABLE REMOVE SYSTEM ANALYSIS AND SELECTION

The problem of original proposal

All buckle cables will be removed after rib closure in the original program. In the cable-stayed system, the fastening-tower is replaced by juncture pier. The cable in the vicinity of midspan approach horizon and the horizontal angle of Z5 on both sides only are 3.095 ° and 0.795 °.More temporary cable not be remove before closure make the more trouble for cable adjusting in the follow construction stage. With the cantilever length increase, the cable force gradually digressed and the elevation deflection of control point enhanced in the early stages.

Determination of the new program

The time sequence and method of remove cable after ribs closure will affect the line and inner force of arch ribs. It is necessary to adjust the original remove cable program and develop a new convenience construction control program. The calculation results of original program show that the cable force, deviation of control points and stress of control section are the largest in the large cantilever. The cable force of Z1, Z2, L5, L6 in early stages are only 79%, 69%, 72%, 76% of its early rally and L5, L6 hold a very small force. In the erection program, the deviation in the L / 4 of arch rib is larger than others.

Based on the above analysis, the cable adjusting scheme should focus on the four group cables. There is five schemes for selection.

Scheme 1: Z1 cable removal;

Scheme 2: Z2 cable removal;

Scheme 3: L5, L6 cables removal;

Scheme 4: Z1, Z2 cables removal; and

Scheme 5: Z1, L5 and L6 cables removal.

Above five schemes were calculated of the arch ribs in the biggest bracket state via above optimization method. The optimization cable force, the vertical deviation of arch rib node and steel rib stress of control section are obtained and

showed in the table 1 and table 2.

Table 1. Cable Force Before Closure (tonf).

scheme	Z1cable	Z2cable	L5cable	L6cable	Z3cable	L7cable	L8cable	Z4cable	L9cable	L10cable	Z5cable
initial force	*61.78*	*99.27*	*48.30*	*47.72*	*60.38*	*64.62*	*70.42*	*89.27*	*99.18*	*110.52*	—
origial scheme	49.09	68.73	34.63	36.06	47.10	52.46	61.00	80.54	92.04	105.83	163.37
scheme 1	—	71.89	35.86	37.02	48.16	53.44	61.82	81.42	92.96	106.78	160.97
scheme 2	52.86	—	38.87	39.49	50.91	55.94	63.83	83.44	94.96	108.76	171.40
scheme 3	51.79	76.97	—	—	51.04	56.07	63.89	83.45	94.90	108.62	183.85
scheme 4	—	—	40.42	40.70	52.25	57.17	64.84	84.53	96.09	109.93	169.25
scheme 5	—	80.66	—	—	52.34	57.27	64.90	84.54	96.04	109.81	181.51

Table 2.Control Section Stress of Arch Rib Before Closure (MPa).

	scheme	arch spring	L/8	L/4	3L/8
top boom	origial scheme	-86.821	-42.153	-4.573	-12.730
	scheme 1	-74.750	-45.841	-5.222	-12.623
	scheme 2	-69.129	-39.987	-13.071	-15.973
	scheme 3	-73.626	-37.988	-19.796	-18.762
	scheme 4	-54.413	-43.935	-14.133	-16.026
	scheme 5	-59.827	-41.797	-20.760	-18.773
lower boom	origial scheme	-11.733	-33.250	-73.161	-44.864
	scheme 1	-18.273	-30.429	-72.521	-44.970
	scheme 2	-22.961	-33.570	-64.808	-42.865
	scheme 3	-20.398	-35.628	-60.392	-40.982
	scheme 4	-30.599	-30.530	-63.711	-42.874
	scheme 5	-27.649	-32.747	-59.391	-41.020

Program selection

Compare the results we can see that the deviation and stress in the scheme 1 to 5 have great improvement to original program. In the scheme 4 and 5, the deflection of arch rib nodes is only about half of the original and the peak stress has been largely reduced. Therefore, scheme 4 and 5 will be the more satisfactory adjustment programs in the deflection and stress of arch ribs.

The cable force is vital control factor in the erection construction. If some cable force bigger than others, the variance of inner force of cable-stay system will be enhanced and the construction risk enlarges. Compare the cable force of every scheme before ribs closure we can see that all cable force did not exceed their early rally, but the cable force of Z5 to increase above 10% in the scheme 3 and 5.

Because the force of Z5 cable is the largest and dangerous, and not be allowed to increase too much, the scheme should be excluded. Scheme 1 should be excluded for the unobvious adjust effect. Therefore, scheme 4 is the ideal cable remove program.

CONCLUSION

It is effectively on adjusting the line and the adverse stress of arch ribs that removes some cables that exert negative impact on line and inner force of arch ribs before closure. The defect of line control via adjusting pre-camber that cable tensioned once in place can be overcome to some extent. The method has much better operability and safety. In the concrete implementation, the cables are completely loosed instead of demolition for lowering risk and improving safety reserves. Only some aspects of remove cable scheme are analyzed. It is a complex problem that remove cables affect the arch ribs line and inner force of steel tube in different construction stages and the problem need to be further thorough research.

BIBLIOGRPHY

CHEN, Baochun(1999).“Design and construction of concrete-filled steel tubular arch bridge.” *People traffic publishing company*, Bei jing.

XU J. (2000).”Construction control theory of long span bridge.” *People traffic publishing company*, Bei jing.

ZHANG J., ZHENG J., QIN R. (2002). “Calculation method for optimizing the installation process of CFST arch bridge.” *Bridge Construction,* Jan. 1,52—58

ZHENG J. (1999). “The closure technique of long span RC arch bridge.” *China highway transact*ion, Dec. 1:42—49.

ZHOU S., JIANG L. and ZHENG Z. (2000).”Simulate Calculation study of cable-stayed force for arch bridge segmental construction. ”*Chonhqing jiaotong university transaction,* Mar.8—12.

ZHOU S.,CAI J.and XIONG H. (2001).“Calculation of force in control cable for arch segment erection with one time jacking cable method.” *Engineering Mechanics,* Dec.

Design Theory for speed control by using constant edge rate

Liu Bing[1], Zhu Shunying[2], Wang Hong[3], Xia Jing[1], Sun Qinmei[1]

[1]Doctoral student, Dept. of Traffic Engineering, Wuhan University of Technology，430063，1040 Heping Ave. , Wuchang,Wuhan, Hubei, China; Tel: +86-13871475997; E-mail: lbjiaotong@126.com.

[2]Professor, Dept. of Traffic Engineering, Wuhan University of Technology，430063，1040 Heping Ave., Wuchang，Wuhan, Hubei, China;Tel: +86-13995680983;E-mail: zhusy2001@163.com.

[3]Associate Professor, School of Transportation, Wuhan University of Technology, 430063, 1040 Heping Ave., Wuchang,Wuhan, Hubei, China; Tel: +86-027-62597390; E-mail: wanghong2004317@sina.com.

Abstract

Edge rate is the important source for a driver's speed perception. This paper briefly introduces the concept of edge rate, the theory for a driver's speed perception and control which are based on the edge rate, and an application effect of edge rate in foreign and domestic autos. According to the concept of edge rate and Newton's equation of motion, the speed control design model, which is based on the assumption that the driver maintains the constant edge rate with the comfortable deceleration rate, is deduced. By using the 3DMAX, the edge rate experiment videos that car moving on the highway are made, 260 stimulation of Subjectively Equal Speed experiments are designed by using the Forced-Choice Method, through 6 males and 2 females' experiment results, the experiments results show that driver's speed perception value is the largest when the edge rate is 8HZ, but the difference between 8HZ and 16HZ is litter, considering driver's speed perception value is the largest when the edge rate is 12HZ under the fog environment, then 12HZ is selected as the reasonable value. According to experiment result, the edge rate spacing for controlling the speed from 120km/h to 90km/h is calculated.

Key words: Driver; Speed Perception; Speed Control; Edge Rate; Design Theory

1. Introduction

About 1/3 of road traffic accidents for fatal collisions were related to speeding in the United States. The study of traffic experts in Australia showed that the accident rate increased 2 times as speed increased 5km/h when speed exceeds 60 km/h, and the severity of the accident increases exponentially. So how to effectively control the speed and its difference is a key to reducing the total number and the severity of accidents. The process for a drivers control speed is divided into four stages as the speed information perception, judging it, making a decision, and acting. During the speed information perception stage, more than 90 percent of the information comes from the visual system, of which edge rate is an important source for a driver's speed perception. This paper focuses on the theory and method about a driver's speed perception and control from the perspective of edge rate.

2. Speed control measure by using constant edge rate

2.1 The definitions of edge rate

Edge rate is the number of the optical elements passing across an observer's

visual field in unit time (Christopher, 2003). If an observer knows the ground-texture spacing, speed can be estimated from the edge rate. When the edge rate increases (ground-texture spacing decreases), the observer's perception speed increases.

When driving through constant spacing texture, with speed v, which length is S, T_X is the spacing between texture elements，the number of elements in length S is $n = S/T_x$， transverse time $t = S/V$， according to the concept of edge rate we can get ER=V / T_X, where，ER is the edge rate.

2.2 Application of edge rate in deceleration

ATSSA (2006) have paved horizontal lines with diminishing spacing on an export ramp. Two months later, the 85 percent speed reduced by 24 percent, the total collision number reduced by 43 percent, MassSAFE (2004) found that the speed can be significantly reduced by paving the cross-sectional lines on the entire lane in the mode of gradually reducing the spacing between the two adjacent cross-sectional lines. The cross-sectional lines or the edge line paved on the lane is a form of expression of the edge rate. From the above we can see that the edge rate can be used for reducing speed. For the "unconscious" application of edge rate, three design concepts were adopted, which are the constant spacing, diminishing spacing by stage, diminishing spacing by every marking, and both tridimensional edge rate and planar edge rate were used. Yet, so far there is no relevant theory and method for practice guidance. In theory, an edge line with diminishing spacing is ideal, which can guarantee that the edge rate passing through the driver's visual field keeps increasing or is constant and tempts the driver to decelerate continuously and achieve a more effective slowdown. For the edge line with constant spacing, the edge rate passing through the driver's visual field will decrease as the speed reduces, producing a false impression that speed is decreasing, which may lead the driver to accelerate. Therefore, the slowdown effect of an edge line with constant spacing is restricted, which has been confirmed in a touch test (Whltney, 2003). In this paper, research was made on the theory and design method about edge line for speed control, with the edge rate keeping constant during the uniformly retarded motion course.

3. Design theory of edge rate density

3.1 Constant edge rate design model with comfortable deceleration rate

Design principle：The driver maintains the constant edge rate with the comfortable deceleration rate. Then if the driver does not reduce speed，the decreased spacing will result in increasing edge rate which will compel the driver to reduce speed. According to the concept of edge rate，when a vehicle arrives at the nth edge line, the time is t，then $ER = n/t$， $t = n/ER$；according to Newton's equation of motion，the following equation are deduced, which are shown as following：

$$x_n = \frac{1}{2} a t^2 + v_0 t = \frac{1}{2} a (\frac{n}{ER})^2 + v_0 \frac{n}{ER} \quad (1)$$

$$v_n = v_0 + a \frac{n}{ER} \quad (2)$$

Where, x_n is the position of the nth edge line, v_0 is the initial speed, a is a comfortable deceleration rate, v_n is the instant speed when a vehicle arrives at the n_{th} edge line.

3.2 Reasonable edge rate

Theoretically speaking, the larger the edge rate is, the larger the driver's perception speed will be. However, the human vision has the character of Critical Flicker Frequency. When the marking spacing reduces to a certain value, people will tend to regard the discontinuous line as a continuous straight line, which will lead to the underestimation of speed. So it is necessary to carry on research to the reasonable edge rate density. Using the 3DMAX, videos of a simulated car moving on the highway are made with different edge rates, then psychophysical experiments are conducted to measure the influence that edge rate has on speed perception.

(1) Index of the driver's perceived speed

The experiment takes the SSES (Shen, 2005) (Stimulation of Subjectively Equal Speed) as an index to measure the driver's perceived speed. The meaning of SSES is that the subject feels the speed of SSES with comparison stimuli is the same as the speed of standard stimuli. So if the SSES is lower than the speed of standard stimuli, the driver underestimates speed with the scenery condition of standard stimuli, and vice versa.

(2) Experiment procedure

Forced-Choice Method (Frank, 2006) is selected to measure SSES.

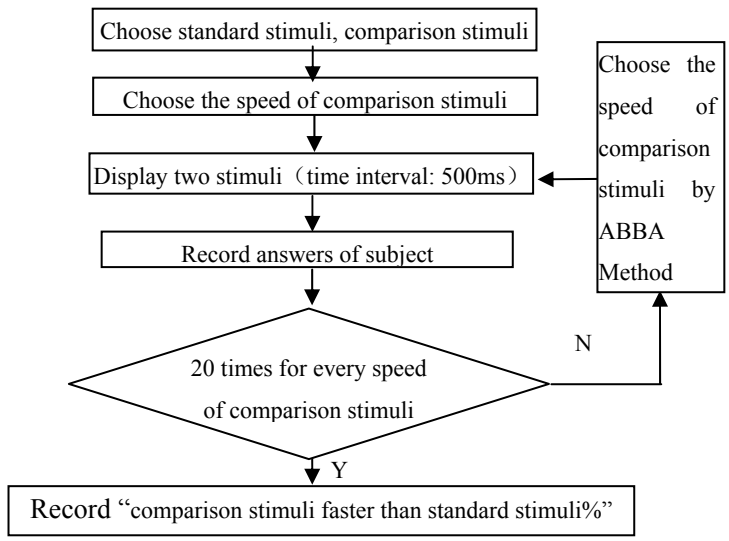

Figure 1.Process of the speed-comparison experiment

The standard stimuli are the videos with different speed (100km/h，120km/h，140 km/h，160km/h is chosen in the experiment) and different edge rates (2、4、8、16HZ is chosen in the experiment); the comparison stimuli are the videos of a standard freeway in China, with the speed range of 90km/h~220km/h; the speed step-rate is 10km/h. So the total comparison scenarios are 260 groups of Subjectively Equal Speed experiments (4×5×13). Every comparison scenario is carried out twenty times by every participant. The experiment adopts multi-level ABBA method to control deviation (Ruud, 2005). The form is shown in Table 1.

Table 1. The form of multi-level ABBA.

The display order of comparison stimuli	Front	behind	behind	Front
Speed of comparison stimuli	Increase	decrease	decrease	Increase

According to the experimental result, "faster%" was taken as a horizontal axis,

physical speed of comparison stimuli was taken was vertical axis, then speed $v50\%$ was obtained by a method of linear interpolation –then it is SSES.

(3)Experiment scenarios

The scene of the road is made according to the relevant norm of highway design in China: Two-way, four lanes of roads, the width of each lane is 3.75m, the width of the hard shoulder is 3.5m, the width of the line of demarcation of each lane is 15cm, the length of each marking is 6m, the distance during two markings is 9m, such as figure 2a. The standard scene has altered spacing λ of the line of demarcation of a lane (such as figure 2b), edge rate $ER = v / \lambda$.

a b

Figure 2. Experiment scenario (a is standard stimuli, b is comparison stimuli).

(4) Participants

There were 8 participants (6 men and 2 women, 4 men and 1 woman among them hold the driving license.) took part in the experiments. They were naïve as to the purposes of the experiment; the eyesight or corrected eyesight of them is no less than 1.0.

(5) Results

Participants' average value of SSES is summarized as shown in Fig. 3 X-Y1（real line）. Through the single-factor analysis of variance we get $F = 6.22 > F_{0.01}(10,54)$, which indicates that edge rate has significant effect on the driver's speed perception. Considering the difference of physical speeds, we select the ratio between perceived speed and physical speed to reflect the physical speed's influence on perceived speed, as Fig. 3 X-Y2 shown (dashed line). The ratio>1 indicates the scenery condition of standard stimuli results in underestimation of speed, and vice versa.

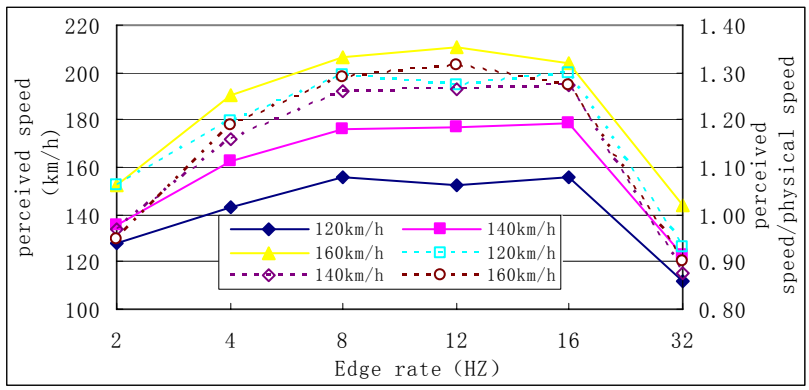

Figure 3. The relationship of SSES/physical speed, edge rate and physical speed.

(6)Discussion

Looking at Figure 3, we find that drivers exhibit 3 overall characters under 3 different speeds:

A. When the edge rate is 2HZ drivers not manifest overestimation effect, they even

underestimated speed when speeds are 140km/h and 160km/h, this phenomenon is associated with the frequency of a conventional lane demarcation line passing across an observer's visual field. The real line of conventional lane demarcation line is 6m，the spacing between adjacency lines is 9m, so the frequency that a lane demarcation line passes across an observer's visual field is $ER = v_0/(3.6\times 15) = v_0/54$，when speeds are 120km/h, 140km/h and 160km/h respectively, the edge rate of lane demarcation lines are 2.22, 2.59 and 2.96HZ respectively. In the above situation, if the edge rate is smaller than 2 then the driver will underestimate speed. As a result, when we utilize the edge rate to reduce speed, the edge rate value should be larger than the frequency of a conventional lane demarcation line passing across an observer's visual field.

B. When the edge rate is in the range of 4~16HZ, the subjects overestimate the speed and the overestimation becomes larger as the edge rate increases, however, the difference in perception speed between different drivers is subtle when the edge rate is in the range of 8~16HZ. With the ANOVA, we find: when the edge rate is 12HZ, the Standard Deviation is the smallest; the subjects are most sensitive to the perception of speed when the edge rate adopts the value 12HZ.

C. When the edge rate increases to 23HZ, drivers underestimate speed. This phenomenon is associated with the eye's Critical Flicker Frequency, when the flicker frequency increases to some degree, people will perceive flicker as an absolutely steady or successive light, but not as flicker, which is the flicker fuse phenomenon. Critical Flicker Frequency (CFF） indicates the stimuli flicker frequency when flicker fuse phenomenon appears. Different people have different CFF, but people's CFF is about 20～55HZ usually (David, 2007). When the edge rate is 32HZ, the influence of CFF will result in the driver's underestimation of speed.

According to the above analysis, 8~16HZ is the reasonable interval of the edge rate, and when we carry out the same experiments in a fog environment, the results indicate the driver's perceived speed is largest when the edge rate is 12HZ. Aiming at making the design of the edge rate can be applied into wider road environments, we select 12HZ as the reasonable value of the edge rate.

4. Case Study

4.1 Design of edge rate spacing

According to the judgment of comfortable deceleration rate by AASHTO (2001) (American Association of State Highway and Transportation Officials), we choose -3.0m/s^2 as a comfortable deceleration rate, when the initial speed is 120km/h and the governor's expectation speed is 90km/h we choose $ER = 12HZ$, the ratio between a real line and a blank of edge of the line is 9:6. According to equation(1) and (2) we can calculate the position of the edge line and the speed when the driver arrives at nth the edge line, the spacing is the different value between positions of the adjacenct edge line, as shown in Table 2.

Table 2. Spacing value.

No	Position （m）	Speed （km/h）	Spacing （m）	No	Position （m）	Speed （km/h）	Spacing （m）	No	Position （m）	Speed （km/h）	Spacing （m）
0	0.00	120.00	2.77	14	37.19	109.50	2.53	28	70.97	99.00	2.28
1	2.77	119.25	2.75	15	39.71	108.75	2.51	29	73.26	98.25	2.27
2	5.52	118.50	2.73	16	42.22	108.00	2.49	30	75.52	97.50	2.25
3	8.26	117.75	2.72	17	44.71	107.25	2.47	31	77.77	96.75	2.23
4	10.97	117.00	2.70	18	47.19	106.50	2.46	32	80.00	96.00	2.21

5	13.67	116.25	2.68	19	49.64	105.75	2.44	33	82.21	95.25	2.20
6	16.35	115.50	2.66	20	52.08	105.00	2.42	34	84.41	94.50	2.18
7	19.02	114.75	2.65	21	54.51	104.25	2.40	35	86.59	93.75	2.16
8	21.67	114.00	2.63	22	56.91	103.50	2.39	36	88.75	93.00	2.14
9	24.30	113.25	2.61	23	59.30	102.75	2.37	37	90.89	92.25	2.13
10	26.91	112.50	2.60	24	61.67	102.00	2.35	38	93.02	91.50	2.11
11	29.51	111.75	2.58	25	64.02	101.25	2.34	39	95.13	90.75	2.09
12	32.08	111.00	2.56	26	66.35	100.50	2.32	40	97.22	90.00	2.07
13	34.64	110.25	2.54	27	68.67	99.75	2.30				

4.2 Verification of rationality

We made an experimental video with the spacing as shown in Table 2, and then let 8 participants judge the moving mode of the vehicle. Every judgment has 3 options: uniform motion, acceleration motion, deceleration motion, and each participant carries out 10 judgments. From the experiment we find： under the design mode of keeping the edge rate constant the number of times for uniform motion, acceleration motion, and deceleration motion is 50, 17, 13, while the uniform motion and acceleration motion accounts for 83.6 percent. The result indicates the design of the edge rate gets a favorable effect.

ACKNOWLEDGMENTS

This work was supported by NSFC (NO. 50778142), and the course of the experiment was supported by the Engineering Research Center of Transportation Safety, ministry of Education.

References

AASHTO, (2001). American Association of State Highway and Transportation Officials. “A Policy on Geometric Design of Highways and Streets”.

ATSSA, The American Traffic Safety Services Association, (2006). “Low Cost Local Road Safety Solutions”, 25~28.

Christopher. D.Wichens, Justin Hollands. (2003). “Engineering Psychology and Human Performance”, East China Normal University Press. 193~196.

David Carmel，Pascal Saker，Geraint Rees，Nilli Lavie，(2007). “Perceptual load modulates conscious flicker perception”，Journal of Vision, 7(14), 2.

Frank Jäkel, Felix A. Wichmann. (2006). “Spatial four-alternative forced-choice method is the preferred psychophysical method for naïve observers”, Journal of Vision , 6(11), 1307~1322.

MassSAFE, (2006). “Report on Passive Speed Control Devices”, University of Massachusetts 139 Marston Hall, 4~7.

Ruud G.J., Gerard P. Van Galena, Majken Hulstijnb, Wouter H. and Gijs Bloemsaat，(2005). “Muscular co-contraction covaries with task load to control the flow of motion in fine motor tasks”，Biological Psychology，68(3)， 331-352.

Shen Haoming, Yoshifumi Shimodaira, and Gosuke Ohashi. (2005). “Speed-Tuned Mechanism and Speed Perception in Human Vision”，Systems and Computers in Japan, 36(13), 1718–1727.

Whltney, Westwood and Goodal, (2003). “The influence of visual motion on fast reaching movements to stationary object”, Nature, Hun 19, 869~872.

Optimization of Dynamic Dispatching Decisions of Local Wagon-flows in Terminal with IRTS

HU Zuoan[1] and YAN Yusong[2]

[1]College of Traffic and Transportation, Southwest Jiaotong University; P.O. Box 259, Chengdu, 610031, China; PH (086) 028-86465966; email: zuoanhu@163.com
[2]College of Traffic and Transportation, Southwest Jiaotong University; P.O. Box 259, Chengdu, 610031, China; PH (086) 028-86465966; email: yanyusong@263.net

ABSTRACT

For the dispatching decision of wagon-flows in railway terminals, the transferring wagon-flows should be primary, and the local should support the transferring. The allocation of local wagon-flows into outbound trains is drawn from the dispatching decision results of transferring wagon-flows in the terminal. A mixed-integer programming model with the minimization of stopping time for the local wagons in the terminal is built for determining dispatching decision of the local wagon-flows. Because of the timing requirements for dynamic dispatching and the characteristics of the model, an improved genetic algorithm is presented. Finally, one example is presented to validate the ideas, model and algorithm.

INTRODUCTION

The wagon-flows in a railway terminal come from the arterial railroads, and return to them. The organization of wagon-flows on the arterial railroads is global and primary. The organization of wagon-flows in the railway terminal is local and subordinate. The latter should be subject to the needs of the former, and both should cooperate with each other. During the process of the wagon-flows dispatching decision in the railway terminal, various wagon-flows are layered, which means that the transferring should be managed. The local should support the transferring.

On the basis of the above fundamental analysis and the complexity and uncertainty of wagon-flows organization, the dispatching decision of various wagon-flows in a railway terminal should be solved step by step (Yan, 2001). Three problems should be sequentially solved. The first is the dispatching decision of the transferring, and at its core is to decide assembling content and wagon-flows source of the outbound trains. On the basis of the above, the second is making further dispatching decisions on the local wagon-flows with a focus on their allocation. The third is to decide the organization plan of transship trains.

At present, the combination of the transferring and local wagon-flows is seldom considered. Furthermore, the majority is static, and dynamic dispatching decision is seldom studied (Niu, 2001; Wang, 2002). So, the dynamic dispatching

decision of the local wagon-flows in a railway terminal with IRTS is studied on the basis of the optimization result of the transferring wagon-flows dispatching decision.

The group number and quantity of the wagon-flows that are allocated into the outbound trains are drawn from the dispatching decision results of transferring wagon-flows, which are supplied by the local wagon-flows. The research is conducted for the dispatching decision of the local wagon-flows based on the condition that the loading quantity is bigger than the unloading.

MODELS

The start time for dispatch is T_s, and the end time is T_e.

In the periods of dispatching, the number of inbound trains is n, and their arriving time is T_i^{dd}. These trains are made up of the following three parts: wagon-flows that are waiting for marshalling in the switchyard at the beginning of dispatching, which can be regard as an inbound train; trains that are waiting for technical operation or being operated at the beginning; and trains that will reach the terminal in succession during the periods of dispatching.

In the periods of dispatching, the number of outbound trains is m, and their departing time is T_j^{cf}.

k ($k = 1,2,\cdots K$) is the group number of the departing wagon-flows, which is distinguished by the destination for heavy wagons and by the sorts for empty wagons.

Through the optimization of the transferring wagon-flows dispatching decision, FBM_j is drawn and denotes the quantity of the local wagons allocated into the outbound trains j.

Among the inbound train i in the period of dispatching, the quantity of the end heavy wagons is DZM_i. After unloading, these heavy wagons are loaded again and formed the number k group of wagons whose quantity is DZM_{ik}. Their operating time is t^z. The quantity of these heavy wagons allocated into the outbound train j is q_{ijk}.

Among the inbound train i in the period of dispatching, the quantity of the end empty wagons is DKM_i. After loading, the quantity of the No. k group of wagons is DKM_{ik}. Their operating time is t^k. The quantity of these heavy wagons allocated into the outbound train j is p_{ijk}.

At the beginning of dispatching, the end wagon-flows can depart after being operated for some time. According to the operating time, these end wagon-flows can be divided into L sorts (The wagon-flows which will be operated for the same time are the same sort), the quantity of every sort of the wagons is YZM_l, and the No. k group of wagons is YZM_{lk}. Their operating time is t_l^{yz}. The quantity of these wagons allocated into the outbound train j is s_{ljk}.

β_{ijk}, β'_{ijk} and β_{ljk} are Boolean variables. β_{ijk} is 1 if the local wagons from the end heavy wagons among the inbound train i that are allocated into the outbound train j accord with the assembling groups number 0 otherwise. β'_{ijk} is 1 if the wagons from the end empty wagons among the inbound train i that are allocated into the outbound train j accord with the assembling groups No, 0 otherwise. β_{ljk} is 1 if the wagons from the No. l sort that are allocated into the outbound train j accord with the assembling groups number0 otherwise.

α_{ij}, α'_{ij} and α_{lj} are Boolean variables. α_{ij} is 1 if the local wagons from the end heavy wagons among the inbound train i that are allocated into the outbound train j accord with meeting time, 0 otherwise. α'_{ij} is 1 if the wagons from the end empty wagons among the inbound train i that are allocated into the outbound train j accord with the meeting time, 0 otherwise. α_{lj} is 1 if the wagons from the l sort that are allocated into the outbound train j accord with the meeting time, 0 otherwise.

The optimization model of dynamic dispatching decision of local wagon-flows in terminal with IRTS is the following:

$$\min f = \sum_{i=1}^{n}\sum_{j=1}^{m}\sum_{k=1}^{K}\left(q_{ijk}+p_{ijk}\right)\left(T_j^{cf}-T_i^{dd}\right)+\sum_{l=1}^{L}\sum_{j=1}^{m}\sum_{k=1}^{K}s_{ljk}\left(T_j^{cf}-T_s\right)$$
$$+\sum_{i=1}^{n}\left(DZM_i+DKM_i-\sum_{j=1}^{m}\sum_{k=1}^{K}\left(q_{ijk}+p_{ijk}\right)\right)\left(T_g-T_i^{dd}\right)$$
$$+\sum_{l=1}^{L}\left[YZM_l-\sum_{j=1}^{m}\sum_{k=1}^{K}s_{ljk}\right]\left(T_g-T_s\right) \quad (1)$$

s.t.

$$q_{ijk}\le M\beta_{ijk}\ ,\ p_{ijk}\le M\beta'_{ijk}\ ,\ s_{ljk}\le M\beta_{ljk} \quad (2)$$

$$\sum_{j=1}^{m}q_{ijk}\le DZM_{ik}\ ,\ \sum_{j=1}^{m}p_{ijk}\le DKM_{ik}\ ,\ \sum_{j=1}^{m}s_{ljk}\le YZM_{lk} \quad (3)$$

$$q_{ijk}\le M\alpha_{ij} \qquad T_i^{dd}+t^z\le T_j^{cf},\ \alpha_{ij}=1,\ \text{otherwise}\ \alpha_{ij}=0$$
$$p_{ijk}\le M\alpha'_{ij} \qquad T_i^{dd}+t^k\le T_j^{cf},\ \alpha'_{ij}=1,\ \text{otherwise}\ \alpha'_{ij}=0$$
$$s_{ijk}\le M\alpha_{lj} \qquad T_s+t_l^{yz}\le T_j^{cf},\ \alpha_{lj}=1,\ \text{otherwise}\ \alpha_{lj}=0 \quad (4)$$

$$\sum_{k=1}^{K}\left(\sum_{i=1}^{n}\left(q_{ijk}+p_{ijk}\right)+\sum_{l=1}^{L}s_{ljk}\right)\le FBM_j \quad (5)$$

q_{ijk}、p_{ijk}、$s_{ljk}\ge 0$ and integer (6)

Above, $i=1,2,\cdots n$, $l=1,2,\cdots L$, $j=1,2,\cdots m$, $k=1,2,\cdots K$

Expression (1) denotes the objective function. Expression (2) denotes the constraints of the wagon-flow groups number. Expression (3) denotes the constraints

of the quantity of the wagons. Expression (4) denotes the constraints of the meeting time. Expression (5) denotes the constraints of the number of every outbound train.

IMPROVED GENETIC ALGORITHMS

The dynamic dispatching decision model of local wagon-flows in railway terminals is a nonlinear large-scale combinatorial optimization one. The complexity of the problem is NP-Hard. Because of the validity of genetic algorithm in solving these problems, it is used to solve the model.

According to the characteristics of the model, the integer code is used. The variable q_{ijk} , p_{ijk} and s_{ljk} are regarded as genes that directly make up a chromosome, so the length of the chromosome is entirely decided by a combination of the number of variables q_{ijk} , p_{ijk} and s_{ljk} .

The method of penalty function is used to deal with the constraints, so that the problem is transformed into an unconstrained optimization problem. The fitness ratio of every individual is:

$$\varepsilon_l = \frac{F_{\max} - F_l}{F_{\max} - F_{\min}} \tag{7}$$

To prevent the best individual from being eliminated, a strategy is used that combines the methods of fitness ratio and the best individual preserved.

The self-adaptive genetic operators P_c and P_m are calculated by the following formulations:

$$P_c = \begin{cases} P_{c1} - \dfrac{(P_{c1} - P_{c2})(\varepsilon' - \varepsilon_{avg})}{\varepsilon_{\max} - \varepsilon_{avg}}, & \varepsilon' \geq \varepsilon_{avg} \\ P_{c1}, & \varepsilon' < \varepsilon_{avg} \end{cases}$$

$$P_m = \begin{cases} P_{m1} - \dfrac{(P_{m1} - P_{m2})(\varepsilon_{\max} - \varepsilon)}{\varepsilon_{\max} - \varepsilon_{avg}}, & \varepsilon \geq \varepsilon_{avg} \\ P_{m1}, & \varepsilon < \varepsilon_{avg} \end{cases} \tag{8}$$

In the above formulations, $\varepsilon_{\max}$ is the maximum fitness ratio, ε_{avg} is the average of every generation, ε' is much more maximum between two individuals that will be crossed. ε is the fitness ratio of mutated individuals. P_{c1} and P_{m1} are bigger crossover and mutation ratios. P_{c2} and P_{m2} are smaller.

AN ILLUSTRATIVE EXAMPLE

Various data for some terminals are shown as the following tables. For the parameters of genetic algorithm, population_size N is 80, P_{c1} is 0.8, P_{c2} is 0.3, P_{m1} is 0.08, P_{m2} is 0.01, and the maximum number of generation T is 300. The

algorithm is programmed with c++, and runs on a portable computer with T2050. Until generation 287, the best result is drawn.

CONCLUSIONS

In this paper, the dispatching decision of the local wagon-flows in the railway terminal is studied. An optimization model is constructed and a rapid algorithm is designed. An idea for innovation of our railway operation organization based on informed decision making is introduced. But the idea is validated simply in the thesis, which is far removed from the practical application. Further research should release the constraints step by step in order to fully reflect the actual conditions.

Table 1 Inbound Trains.

inbound train	arrival time	Heavy	Empty	assembling 1	2	3	4	5
1	12:00	0	0	50	33	22	50	18
2	12:00	6	0	17	0	10	0	13
3	12:10	5	10	18	0	11	0	0
4	13:29	4	7	0	12	0	23	0
5	13:45	0	6	0	36	0	4	0
6	13:57	2	9	14	0	21	0	0
7	14:11	5	6	0	14	0	21	0
8	14:30	2	4	0	0	40	0	0
9	14:45	1	0	0	16	0	19	10
10	15:00	5	0	0	17	0	14	10
11	15:35	0	4	18	0	16	0	8
total		30	46	117	128	120	131	59

Table 2 Outbound Trains.

outbound train	departing time	group	outbound train	departing time	group
1	13:35	4	7	15:37	2
2	13:50	1，3	8	16:00	1，3
3	14:20	1	9	16:40	1，3
4	14:55	2，4	10	17:20	2，4
5	15:16	1，3	11	17:45	5
6	15:25	2，4			

Table 3 Operation Time (min).

operation	time	operation	time
arriving	30	sending	30
disassembling	25	taking	30
assembling	25	unloading	150
departing	30	loading	150
double	210		

Table 4 Local Wagon-flows Allocated into Outbound Trains.

outbound train	number	group	outbound train	number	group
1	0	4	7	10	2
2	0	1，3	8	11	1，3
3	0	1	9	0	1，3
4	11	2，4	10	0	2，4
5	10	1，3	11	0	5
6	11	2，4			

Table 5 End Wagon-flows at the Beginning of Dispatching.

sort	1	2	3	4	5	total	operating time(min)
1	0	6	0	8	0	14	80
2	10	8	2	0	0	20	100
3	0	0	3	6	0	9	130
4	4	4	0	7	0	15	180
5	0	5	0	0	1	6	210
6	0	2	1	0	0	3	300

Table 6 Heavy Wagons Number after Operation.

inbound train	number after double operation					total	number after loading					total
	1	2	3	4	5		1	2	3	4	5	
1	0	0	0	0	0	0	0	0	0	0	0	0
2	0	6	0	0	0	6	0	0	0	0	0	0
3	4	0	1	0	0	5	5	3	2	0	0	10
4	0	0	0	2	2	4	0	0	4	3	0	7
5	0	0	0	0	0	0	4	0	0	0	2	6
6	0	0	0	2	0	2	0	3	0	6	0	9
7	0	1	4	0	0	5	1	0	5	0	0	6
8	2	0	0	0	0	2	0	2	0	0	2	4
9	1	0	0	0	0	1	0	0	0	0	0	0
10	0	2	0	3	0	5	0	0	0	0	0	0
11	0	0	0	0	0	0	0	4	0	0	0	4
total	7	9	5	7	2	30	10	12	11	9	4	46

Table 7 Optimization Result.

outbound train	transferring	local	total
1	46/4	0	46
2	24/1、22/3	0	46
3	46/1	0	46
4	33/2、2/4	6/2、5/4	46
5	10/1、26/3	10/1	46
6	12/2、23/4	8/2、3/4	46
7	36/2	9/2	45
8	14/1、21/3	4/1、5/3	44
9	1/1、45/3	0	46
10	15/2、31/4	0	46
11	46/5	0	46

ACKNOWLEDGEMENTS

This research is supported by the National Natural Science Foundation (60674007).

REFERENCES

He, S., Song, R., and Chaudhry, S. (2003). An integrated dispatching model for rail yards operations [J]. *Computers & Operations Research*, 30, 939 – 966.

Hu,Z.. (2009).Optimization of wagon flows organization in terminal with intelligent railway transportation system [D]. South West Jiaotong University Doctor thesis, Chengdu.

Niu, H., and Hu, A. (2001). Nonlinear 0-1 programming model and algorithm for traffic organization in railway junction terminal [J]. *Journal of the China Railway Society*, 23(3), 8-12.

Wang, C. (2002). Study on wagon-flow allocating problem in a marshalling station by using calculating method on-table [J]. *Journal of the China Railway Society*, 24, (4), 1-5.

Yan, Y., and Zhu, .. (2001). Study on models of wagon flow's dispatching decision in railway terminal [J]. *Journal of the China Railway Society*, 23 (1), 9-12.

Laboratory Evaluation of the Warm Mix Asphalt Performance in Liaoning

Yang Yanhai[1] and Zhang Huaizhi[1, 2] and Wu Yaodong[1]

1 Communication Research Institute of Liaoning Province, Key laboratory of Expressway Maintenance Technology of Ministry of Transportation, Number 81, Wencui Road, Dongling District, Shenyang, Liaoning Province, China Post Code: 110015, PH (024)24512416
2 Tongji University, Key Laboratory of Road and Traffic Engineering, Ministry of Education, No.4800 Cao An Road, Jia Ding District, Shanghai, China Post Code: 201804
Yang Yanhai Email: yangyanhai168@126.com
Zhang Huaizhi Email: huaizhi.zhang@163.com
Wu Yaodong Email: vpwyd@163.com

ABSTRACT

In this study, temperature of mixing under the condition of construction decreased by more than 20℃ through adding the Sasobit modifier into mixes. Rutting test, bending test at low temperature, fatigue test and dynamic modulus test were conducted to evaluate the performance and mechanical characteristics of the asphalt mixes adopting LH90# base asphalt, LH90#+3%Sasobit modified asphalt, LH90#+3%SBS+3%Sasobit modified asphalt and LH90# + 4%SBS modified asphalt respectively. It was induced that the dynamic stability and dynamic modulus increased notably and the anti-deformation ability at high temperature enhanced for the mixtures with 3%Sasobit, the crack resistance at low temperature and fatigue resistance ability decreased for the mixtures with LH90#+3%Sasobit and increased for the mixtures with SBS modified asphalt +3%Sasobit.

Key words: road engineering, warm mix asphalt, Sasobit, fatigue, dynamic modulus

1. Introduction

Hot mixed asphalt has been widely utilized in pavement construction and at the mixing and paving procedures, binders and aggregates will be heated up to 145°C-170°C and 150°C-220°C respectively, and then mixed at greater than 160°C. The mixes will maintain the temperature of 135°C-185°C, afterward be paved at over 125°C and grinded at over 120°C. Such high temperature not only speeds up asphalt aging and reduces the service life of mixes but also leads to consume a large amount of energy and increase the emissions of CO, CO2, SO2 and NOx (Pinchin Environmental Limited Air & Noise Group, 2005). This is also not in harmony with the strategy of sustainable development of China.

To solve these problems the WMA (warm mix asphalt) technology is employed that the temperature of mixing and paving are between HMA and cold mixed asphalt and performances of mixture attain the requirements of HMA. Furthermore, the decrease in emissions represents a significant cost savings (Hampton,

T., 2005). In this study for the WMA used in Liaoning, performances at high and low temperature, the anti-water ability and anti-fatigue ability were investigated.

2. Original Materials

In this study, mineral materials were produced in Xiaotun, a town of Liaoyang City in Liaoning province, and original binders were Liaohe 90# base asphalt and the modified asphalt with SBS.

The process of warm mixing was attained by an additive, in particularly, branded Sasobit®. It is a kind of hard wax, which has a molecule chain comprising 40~115 of carbon atoms. The density is 0.94 g/cm^3 at 25°C, the viscosity is 0.012Pa·s at 135℃ and the melting point is 115℃. As temperature is less than the melting point, Sasobit forms the net crystalloid structure and this may add the stability of asphalt and enhance the anti-rutting ability of mixes. It has been testified that Sasobit will distribute uniformly in asphalt by simply mixing at high temperature compared with some other modifiers, such as PP, SBS. In this study, the optimum Sasobit content in asphalt was 3 %(Zhang Y. et al., 2006).

3. Mix Design

Marshall Method was used and grade size AC-13 was adopted because WMA is mainly used in surface layer .Sieve results for mineral materials were shown in Table 1 and the grade curve was shown in Figure 1.

Table 1. Sieve results of mineral materials

Aggregate	Passing for below sieve sizes(mm)/%									
	16.0	13.2	9.5	4.75	2.36	1.18	0.6	0.3	0.15	0.075
13.2～16	100.0	0.0	0.0	0.0	0.0	0.0	0.0	0.0	0.0	0.0
9.5～13.2	100.0	96.3	4.3	0.0	0.0	0.0	0.0	0.0	0.0	0.0
4.75～9.5	100.0	100.0	100.0	3.8	1.2	0.0	0.0	0.0	0.0	0.0
2.36～4.75	100.0	100.0	100.0	97.0	9.9	0.3	0.0	0.0	0.0	0.0
1.18～2.36	100.0	100.0	100.0	100.0	99.6	1.7	0.0	0.0	0.0	0.0
0～1.18	100.0	100.0	100.0	99.2	97.6	84.4	51.6	19.0	6.4	1.6
Filler	100.0	100.0	100.0	100.0	100.0	100.0	100.0	98.8	94.9	82.9
Synthetic grade	100.0	97.0	82.5	50.2	30.4	24.2	16.9	10.6	8.1	6.6
Up limit	100	100	85	68	50	38	28	20	15	8
Down limit	100	90	68	38	24	15	10	7	5	4

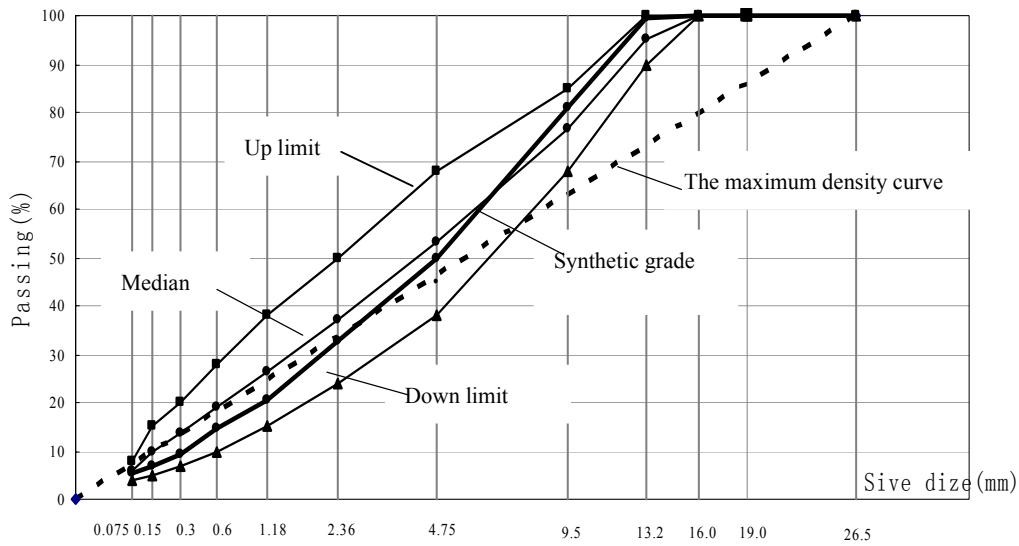

Figure 1. Grade curve for AC-13

Density results of aggregates were shown in Table 2 and the ratios of aggregates was show in Table 3.

Table 2. Density results of aggregates

size	water absorptive rate /%	Apparent specific density /γ_a	Bulk specific density /γ_b
16～19mm	0.22	2.740	2.723
13.2～16mm	0.19	2.738	2.724
9.5～13.2mm	0.31	2.737	2.714
4.75～9.5mm	0.39	2.746	2.717
2.36～4.75mm	0.55	2.750	2.709
1.18～2.36mm	0.91	2.741	2.675
0～1.18mm	0.63	2.741	2.694
Filler	—	2.826	2.826

Table 3. Aggregate ratios

Mineral materials	9.5～13.2	4.75～9.5	2.36～4.75	1.18～2.36	0～1.18	Filler
Ratio /%	20	31	18	8	17	6

Marshall Test was conducted to decide the optimum asphalt content after the optimum grade had been determined. Specimens were prepared by standard method and the density, VV, VMA, VA, VFA and flow value and Marshall Stability were measured. Finally, the optimum asphalt aggregate ratio was determined as 4.5%.

4. Performance tests of WMA

Four types of binder, i.e., LH90# base asphalt, LH90#+3%SBS, LH90#+3%SBS +3%Sasobit and LH90#+4%SBS, were used and the performance tests of mixes at high and low temperature, water stability test, anti-fatigue test and dynamic test for mixes with the four types of binder were carried out. It was shown that the mixing temperature for mixes added Sasobit in decreased by 20℃ (Yang

Yanhai et al, 2008).

4.1 Rutting test

The dynamic stability DS (time/mm) at 60℃ was used to express the performance of mixes at high temperature and the test results were shown in Table 4.

Table 4. Compare of rutting test results

Binder size		Deformation at 45min/mm	Deformation at 60min/mm	DS /(number/mm)	Average DS /(number/mm)
LH90#	1	9.764	10.010	550	440
	2	7.864	9.781	329	
LH90#+3%Sasobit	1	3.001	3.476	1326	1234
	2	3.394	3.946	1141	
LH90#+3%SBS +3%Sasobit	1	2.219	2.402	3438	3700
	2	1.696	1.855	3962	
LH90#+4%SBS	1	2.067	2.233	3795	3424
	2	2.647	2.853	3052	

It was indicated that the asphalt LH 90#+3%Sasobit contributed largely to the stability of mixes at high temperature in contrast to LH90#, in particular, the DS increased by 180% but was still very small in contrast to the SBS modified asphalt; for LH90#+3%SBS+3%Sasobit and LH90#+4%SBS, the former added 8% more than the latter to the high temperature stability. Consequently, it was concluded that Sasobit effectively increased the stability of mixes at high temperature and this influence was more remarkable for base asphalt.

4.2 Bending tests at low temperature

The bending tests at low temperature were conducted to evaluate the anti-cracking performance of WMA. The failure strain at -10℃ was used as the analytical index and the results were sketched in Figure 2 .

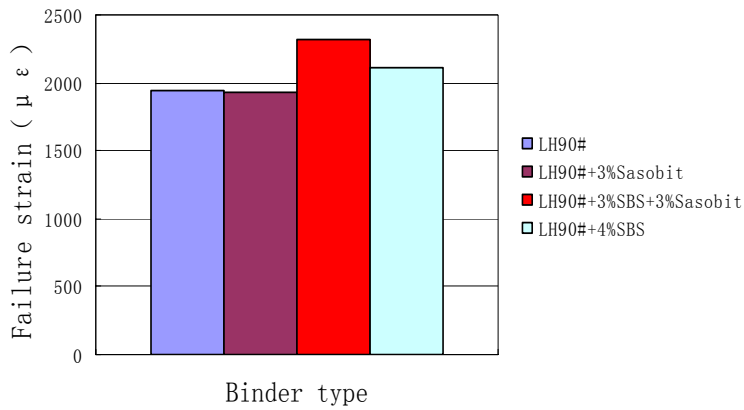

Figure 2. Failure strains for different types of binder

Observations from Figure 2 indicated that the failure strains maintained the same level for LH90#+3%SBS and LH90#; the failure strain for LH90#+3%SBS+3%Sasobit increased by 9.8% in contrast to LH90#+4%SBS. Therefore, it was concluded that Sasobit applied a positive effect on the modified asphalt but influenced little on the base asphalt on the performance of mixes at low temperature.

4.3 Water stability tests

Two indexes, strength and residual stability, were used to evaluate the water stability of WMA . The relevant test results were listed in Table 5 and Table 6.

Table 5. Indirect tensile test results

Binder type	Tension strength /MPa		TSR /%
	-	After frozen and threw	
LH90#	0.6812	0.5933	87.09
LH90#+3%Sasobit	0.7168	0.6004	83.76
LH90#+3%SBS+3%Sasobit	0.6178	0.5602	90.67
LH90#+4%SBS	0.6416	0.5879	91.63

Table 6. Marshall Test results

Binder type	Marshall stability /kN		Residual stability /%
	In water for 30min	In water for 48h	
LH90#	9.48	8.20	86.5
LH90#+3%Sasobit	11.27	9.51	84.35
LH90#+3%SBS+3%Sasobit	14.36	12.77	88.9
LH90#+4%SBS	13.8	12.64	91.6

From table 5 and table 6, it was indicated that Sasobit decreased the water stability but still met the requirements of relevant standards no matter for the base asphalt or for the modified asphalt.

4.4 Fatigue Tests

Fourth points bending beam fatigue test was used to analyze the fatigue performance of mixes under the condition of controlled strain (Graham C. et al, 2005). The test results were drawn in Figure 3.

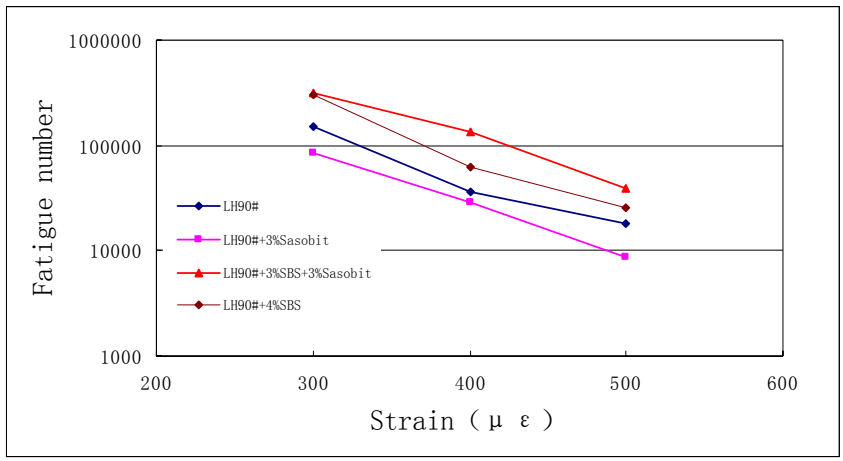

Figure 3. Relationship between strain and fatigue number for different types of binder

From figure 3, Sasobit had a positive action to the SBS modified asphalt but had a negative action to the base asphalt (LH90#) on the fatigue performance.

4.5 Dynamic modulus tests

Mixes are subjected to dynamic load in reality and the dynamic modulus of mixes has a close relationship with service performance of mixes. In the study, the size of specimens was 150mm×100mm(height×diameter), produced by coring from coarse specimens with the size of 150mm×170mm.the continuous half-sinusoidal load and no confining press was subjected, test temperature was 15℃ and 45℃, test frequencies were 0.01Hz, 0.1Hz, 0.2Hz, 0.5Hz, 1Hz, 2Hz, 5Hz, 10Hz, 20Hz, and 25Hz. The test results were shown in Figure 4 and Figure 5.

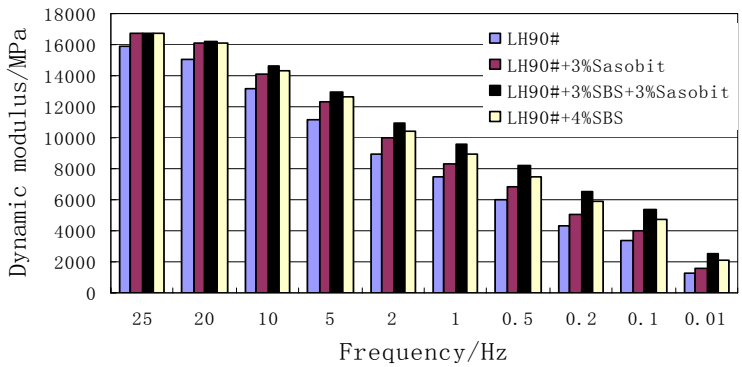

Figure 4. Dynamic modulus with frequency at 15℃

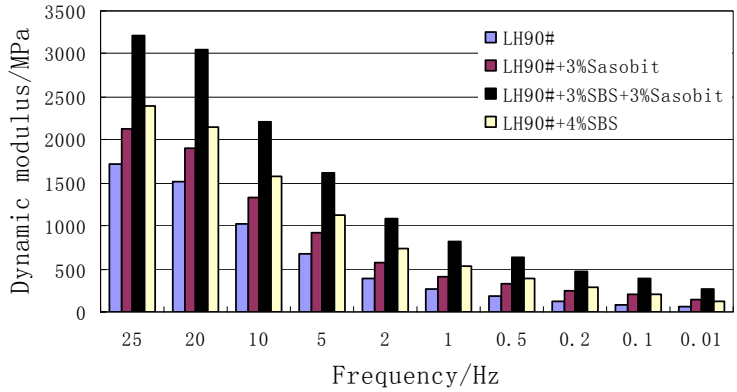

Figure 5. Dynamic modulus with frequency at 45℃

Observations from Figure 5 and Figure 6 indicated that Sasobit contributed much more to dynamic modulus of mixes at 45℃ than at 15℃. This also verified the good performance of anti-rutting of Sasobit.

5. Conclusion

As the binder was added into 3% Sasobit,

(1) the temperature of mixing decreased by 20℃,

(2) and the dynamic stability increased significantly.

(3) Sasobit had a positive effect on the SBS modified asphalt but had a negative effect on the base asphalt on the anti-cracking ability and fatigue performance of Mixes.

(4) The dynamic modulus of WMA with Sasobit advanced remarkably and this enhanced the stability of mixes at high temperature.

Bibliography

Graham C.H., Brian D.P. (2005), Evaluation of Sasobit for Use in Warm Mix Asphalt, NCAT Report 05-06, 2005.

Hampton, T. (2005), "U.S. Studies Warm-Mix Asphalt Methods: NAPA, European Producers to Sponsor Laboratory Research Effort." http://enr.construction.com/products/newproducts/archives/030428.asp, Accessed August 30, 2005.

Pinchin Environmental Limited Air & Noise Group (2005), Report for a Combustion Gas Emission Testing Program and the Miller Aggregate Resources Facility in Brechin, Ontario. Report, October, 2005.

Yang Y.H., Liu X.D., Wu Y.D. (2008), "Study on Performance of Asphalt and Implement of Warm Mixing Based on Sasobit", Journal of Highway and Transportation and Development, Vol. 25, No.4, April, 2008.

Zhang R., Huang X.M., Zhao Y.L. (2006), "Study on the new asphalt mixes additive Sasobit". Journal of China & Foreign Highway,Vol.26, No.2, April, 2006.

Model of High Speed Railway Wheel Ovalization

Xueshan Zhang[1], Xinbiao Xiao[2] and Xuesong Jin[1]

[1] School of Civil and Safety Engineering, Dalian Jiaotong University, P.O. Box398, Dalian China, ST16028; PH (086) 411- 84106755; email: zxs@djtu.edu.cn
[2]National Traction Power Laboratory, Southwestern Jiaotong University, Chengdu, China, ST 610031; PH (086) 28- 87634355; email: xinbiaoxiao@163.com

ABSTRACT

Periodic non-roundness of railway wheels causes various vehicle-track coupling system dynamic responses, which has a detrimental influence on both the track and vehicle components. In order to guarantee safety and stability, and to minimize costs for repair and maintenance, it is desirable to determine a range for acceptable roundness values and to detect, remove, and repair out-of-roundness wheels in time. This paper analyzes the problem of out-of-round railway wheels that are in service and creates categories for non-roundness of railway wheels. A calculation method using long wavelength to determine periodic non-roundness is proposed. In addition, a new mathematical model is put forth to numerically simulate wheel ovalization, which is called the second order periodic non-roundness of the wheel. Wheel ovalization is converted to track geometric irregularity as system excitation in the traditional way. In the numerical simulation, the dynamic model of a half railway vehicle coupled with a tangent track is employed, in which elliptical railway wheels are considered in the calculation of the wheels and the rails in rolling contact. Using this new numerical method investigates vehicle-track coupling system dynamic responses including lateral and vertical displacement of wheelsets and the vehicle, and lateral and vertical vibration acceleration of the track at different phase angles of the two side wheels of the same wheelset. These responses are compared with those of the traditional model. The numerical results show that the discipline and frequency of dynamic responses are accordant; however, the amplitude and the phase of lateral dynamic responses are different. It is concluded that the traditional track geometric irregularity excitation model does not truly simulate the effect of periodic wheel ovalization on vehicle-track coupling system dynamic behavior. The new model is more accurate and reasonable.

0 INTRODUCTION

Wheel out-of-round (OOR) phenomena have been widely found in railway traffic [1]. The non-roundness of railway wheels causes various on vehicle-track coupling system dynamic responses, which has a detrimental influence on both the track and vehicle components. Now that the range of modern high speed trains has become higher and newer building substructures have become “stiffer,” measurements show that small radius deviations have enlarged rapidly of some

typical OOR shapes.

Therefore, in order to minimize costs for repair and maintenance and to meet noise legislation, there is a large economic incentive for detecting and replacing non-round wheels promptly. Also, it is desirable to investigate the cause of OOR wheels in order to identify suitable countermeasures.

Regarding these problems, many published papers have reported relevant results including the dynamic influence and development mechanism of OOR (Ahlbeck, D. R., 1987; Barke, D. W., 2005; Jenkins, H. H., 1974; Johansson, A., 2003; Meinke, P., 1999; Meywerk, M.. 1999; Morys, B., 1997; Morys, B., 1999; Nielsen, J. C. O., 2000; and Newton, S. G., 1974). The studies by Jenkins, et al., and Newton and Clark are contributions in experimental detection and numerical simulation of OOR that have played a significant role in the early understanding of OOR wheels. A literature survey written by Nielsen, J. C., O. and Johansson, A., (2000) discussed 1) impact loads present on the Northeast Corridor high-speed track in North America (Ahlbeck and Hadden), 2) research on periodic OOR on ICE trains in Germany (Zacher and Pallgen), 3) experiments on the Gotthard line (UNRA, an international workgroup), and 4) another experimental and theoretical investigation of periodic OOR (Werner). A series of numerical methods for predicting OOR are put forward by foreign scholars. Meinke, P., and Meinke, S., adopted rigid body dynamics in combination with a wear model in predicting longer-wavelength non-roundness considering the rotor dynamics of high-speed wheelsets. Morys, et al., have investigated a rigid body model of an ICE carriage on an elastic track model. Johansson, A., and Nielsen, J.C.O., et al., have carried out full-scale experiments, analyzed causes of different types of OOR wheels, simulated the influence of OOR on wheel/rail vertical contact force and track dynamics responses, put forward wavelength-fixing mechanisms of periodic OOR, and proposed the development of periodic OOR wheel profiles.

However, mathematical models simulating periodic OOR wheels have not been generally known thus far. In this paper, a new mathematical model is put forward to numerically simulate wheel ovalization. It provides the theoretical foundation to conduct further research on the mechanisms that cause the development of periodic OOR. It also provides the foundation for determining the range of out-of-roundness which is beneficial to detect, repair, and remove non-round wheels promptly.

1 PROBLEM OF OUT-OF-ROUND RAILWAY WHEELS

Imperfections on wheel tread are basically divided into two types: defects along part of the wheel circumference, and defects around the complete wheel circumference. These are both regarded as types of wheel OOR. The former includes imperfections such as wheelflat, spalling, etc. Figure 1 shows these two common types of local OOR wheels which mainly result from braking thermal damage and rolling contact fatigue.

The latter includes wheel corrugation and wheel polygonalization. This type of OOR has a periodic radical irregularity around the wheel circumference.

The first four orders of periodic polygonalization of railway wheels are depicted in Figure 2.

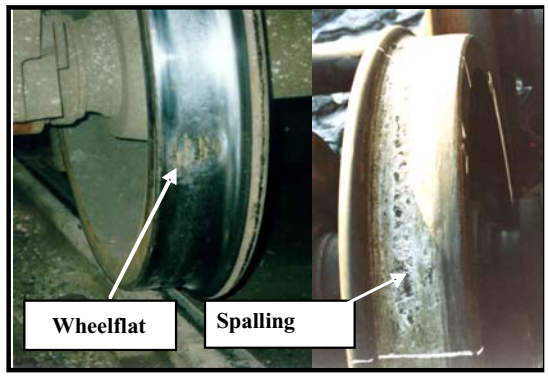

Figure 1. Non-roundness of wheelflat of railway wheels.

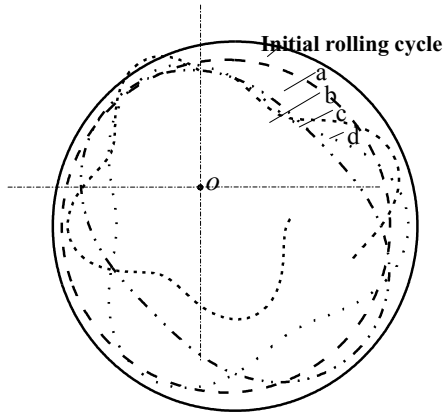

Figure 2. Periodic polygonalization and spalling.

The deformed circular **a**, **b**, **c**, and **d** are defined as firs, second. third, and fourth order polygonalization, respectively. The latter three polygonalizations are probably caused by initial small irregularity development over long-time wear, but the exact causes are not entirely understood. Periodic non-roundness includes irregularities for which it can be clearly seen that one OOR order dominates, as sketched in Figure 2, whereas it is difficult or impossible to determine a dominating OOR order when the wheel OOR falls into non-periodic non-roundness. Wheel OOR generation and development mechanisms are considerable complicated.

Periodic railway wheel OOR presents serious problems for rail transportation, of which the most severe is wheelsets hunting along the rail. It not only affects vehicle running stability and safety, but it may also result in long-wavelength rail corrugation, as depicted in Figure 3.

When wheelsets hunting run at high speed, high-frequency lateral wheel/rail contact vibrations will occur at wheelsets hunting peaks, which leads to short-wavelength rail corrugation (Jin X.S.,2006). If wheelsets hunting go on for a long time, wheel flange root and wheel tread trail will wear relatively severely, resulting in the origin of dents wear or wave wear along the wheel tread, as shown

in Figure 4. Region A and region B correspond to the contact plane of the wheel flange root and the wheel tread trail, respectively, where dents are generated. It should be emphasized that there are other reasons that dents are generated.

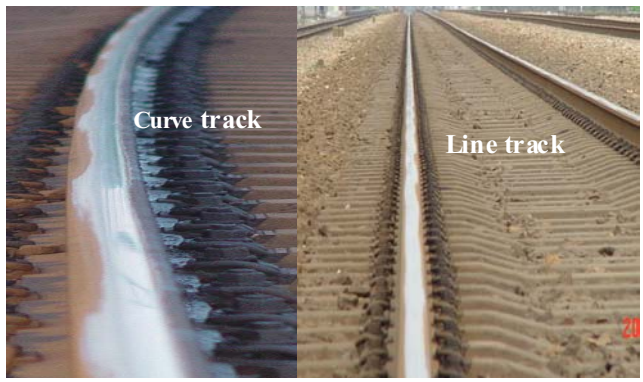

Figure 3. Rail corrugation resulting from wheelset.

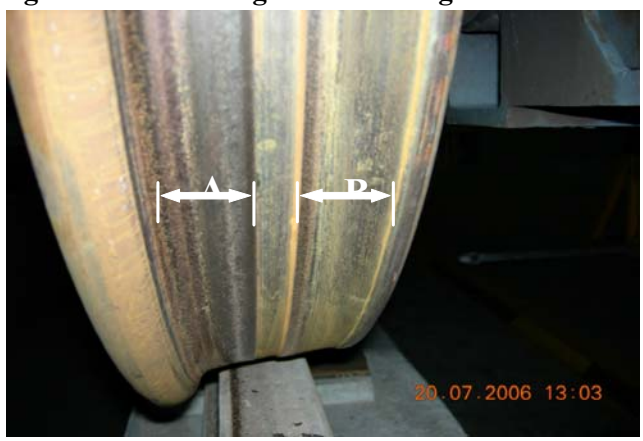

Figure 4. Dents wear of railway hunting.

2 DYNAMIC MODEL OF VEHICLE-TRACK

In order to investigate the influence of ovalization on vehicle-track coupling system dynamic responses, a vehicle-track spatial coupling dynamics model is applied, based on the theory of Zhai. The half-passenger car considered is equipped with a bogie with two wheelsets and double suspension systems. The calculation model of the half-passenger car and the track is shown in Figure 5.

The key part of modeling vehicle-track coupling dynamics is the wheel/rail contact calculation model which has a direct influence on the precision and the speed of the computing analysis. In this paper, the normal forces of wheel-rail are calculated by a Hertzian nonlinear contact spring with a unilateral restraint; the creep forces of wheel-rail are decided by the nonlinear creep theory of Shen. The creepages and creep forces are concerned with the parameters of contact geometry of the wheel/rail. It is emphasized that the rolling circle is elliptical, and not ideal circle. Vehicle-track coupling system dynamic responses are solved with new explicit integration methods, and initial conditions and boundary conditions are referred to in the literature (Jin, X.S., 2006).

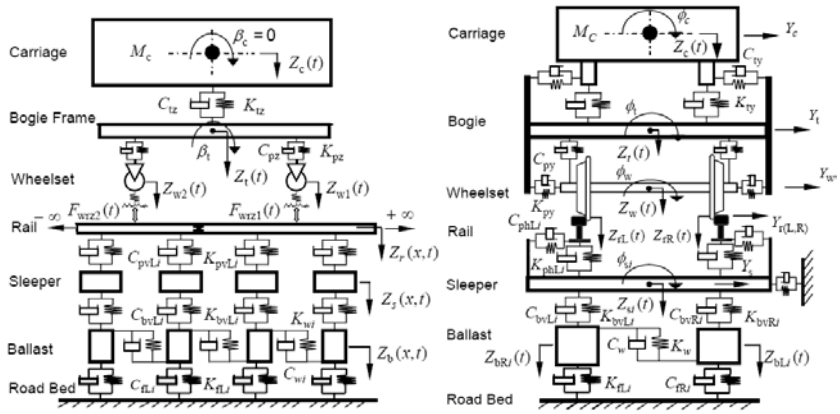

(a) Elevation (b) Side elevation

Figure 5. Coupled vehicle-track model.

3 MODEL OF WHEEL OVALIZATION

Considering the irregularity of the wheel circumference, the traditional method naturally converted it to track geometric irregularity as system excitation, where if the two side wheels of the same wheelset are in the same phase, high/low irregularity of the track is adopted to simulate the case. If the two side wheels are in different phases, tortuous irregularity of track is applied to simulate the case. In this paper, a new mathematical model is put forth to numerically simulate wheel ovalization, in which instant rolling radii of wheels are considered as a function of time. According to this method, the parameters of contact geometry of the wheel/rail are calculated. The instant rolling radii can be expressed as

$$r(t)=\frac{ab}{\sqrt{a^2\sin^2\theta(t)+b^2\cos^2\theta(t)}} \qquad (1)$$

where, a, b is the length of the semi-major, semi-minor axis of ovality, respectively, $\theta(t)$ is the angle between the initial contact radius of the elliptical railway wheel and the horizontal axis at t time, as depicted in Figure 6, and calculated from Equation (2)

$$\theta(t)=\theta(t-1)+\omega\Delta t \qquad (2)$$

where, ω is the rotational velocity of the wheel, and Δt is the time step length of integration. The corresponding program has been compiled, which modifies the elliptical wheel initial nominal contact radius at each time step, and the parameters of the contact geometry of the wheel/rail are obtained.

The model of the second order periodic OOR wheel is described in Equations (1) and (2) and illustrated in Figure 6. The two side wheels of the same wheelset are frequently asymmetrical. In this paper, we consider the general condition, and assume that the two side wheels of the same wheelset are asymmetrical, that is, there is phase angle difference Φ, as shown in Figure 7. The difference between the length of the semi-major axis and the semi-minor axis is defined as the ovalization extent.

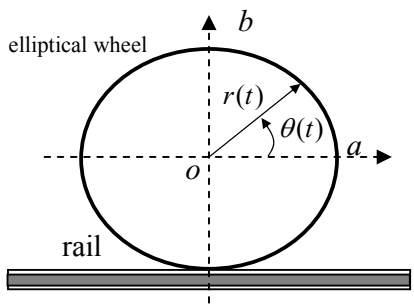

Figure 6. Model of railway wheel.

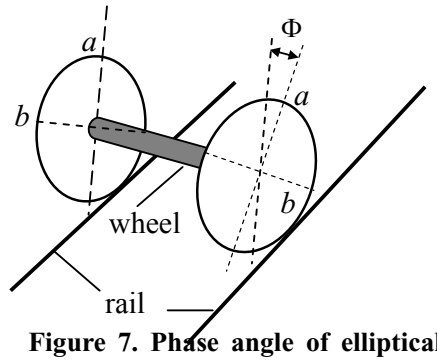

Figure 7. Phase angle of elliptical railway wheels.

4 NUMERICAL RESULTS AND DISCUSSION

A certain China high speed railway vehicle is used and the main parameters are as follows: LMa wheel tread, wheel radius 457.5mm, 60kg/m rail. Values of other parameters of the vehicle and the track are listed in Appendix E and attached list 7 of literature (Zhai, W.M., 2002). The vehicle runs on a tangent track without any excitement. The following two cases are calculated: Case 1 corresponds to the condition that only the two side wheels of the leading wheelset are in different phases, and Case 2 corresponds to the condition that the two side wheels of the trailing wheelset are also in different phases. The phase angle difference Φ of the same wheelset changes from $\pi/12$ to π.

For brevity, only parts of the results of the two cases are plotted. When the vehicle speed is 200km/h, the phase angle difference of the two side wheels of the same wheelset is $\pi/12$ and the ovalization extent is 1mm. The numerical results of the new and traditional models are produced. Figures 8(a) and 8(b) show the vehicle lateral and vertical displacement, respectively. Figures 9(a) and 9(b) show the leading wheelset lateral and vertical displacement, respectively. Figures 10(a) and 10(b) show the left track lateral and vertical vibration acceleration of the leading wheelset, respectively.

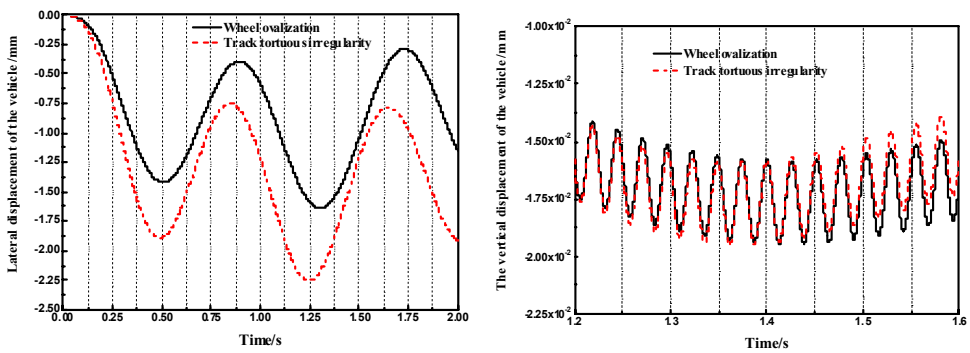

(a) Vehicle lateral displacement (b) Vehicle vertical displacement

Figure 8. Vehicle lateral and vertical displacement.

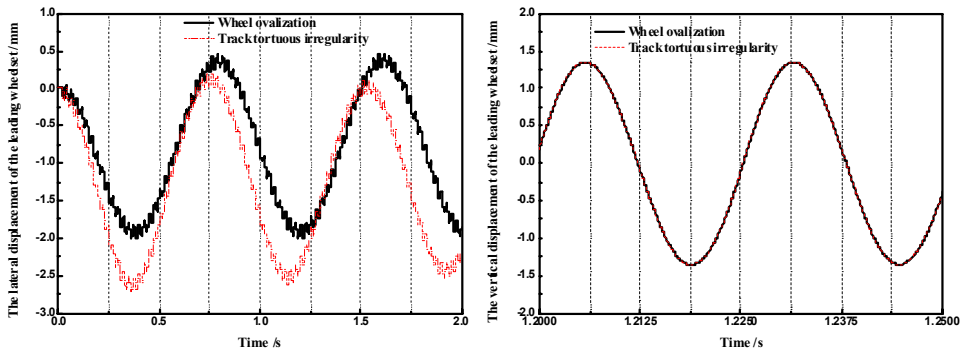

(a) Wheelset lateral displacement (b) Wheelset vertical displacement

Figure 9. Leading wheelset lateral and vertical displacement.

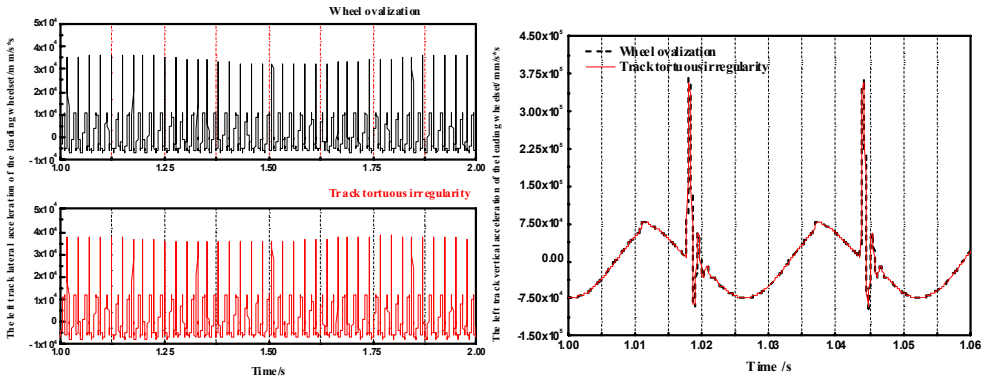

(a) Track lateral vibration acceleration (b) Track vertical vibration acceleration

Figure 10. Track lateral and vertical vibration acceleration.

Observing Figure 9(a), we easily find an interesting phenomenon in that the current case wheel ovalization induces in larger wavelength equal amplitude lateral hunting movement of wheelsets, whose oscillation frequency is 1.2Hz; and wavelength is about 46m. The high-frequency equal amplitude periodic vibration shown in the figure is relevant to the second order periodic non-roundness of wheels directly, its oscillation cycle depends on ovalization wavelength and high-frequency vibration frequency is about 38.7Hz. Results of other phase differences considered also indicate that different degree hunting movements of wheels which deviate from the track center appear. Therefore, at some special conditions, wheel ovalization will cause long-wavelength lateral hunting of wheelsets. Further research on the situation of wheelset hunting is required.

5 CONCLUSIONS AND PROSPECT

The calculation method of long wavelength periodic non-roundness is proposed, and a new mathematical model is put forth to numerically simulate

wheel ovalization. Vehicle-track coupling system dynamic responses are investigated, including lateral and vertical displacement of the vehicle and wheelsets, lateral and vertical vibration acceleration of the track at different phase angles of the two side wheels of the same wheelset. These are compared with that of the traditional track geometric irregularity model. The numerical results show that the discipline and frequency of dynamic responses are accordant; however, amplitude and phase of the lateral dynamic responses are different. It is concluded that the traditional track geometric irregularity excitation model does not truly simulate the effect of periodic wheel ovalization on vehicle-track coupling system dynamic behavior. The new model is more accurate and reasonable.

High speed railway wheel ovalization causes various vehicle-track coupling system dynamic responses including lateral hunting, which aggravates the running character, and even decreases the service time of both the track and vehicle components. Therefore, further investigation need to be done to explore the formation and development mechanisms of OOR in order to instruct railway traffic on-site detecting and repairing.

ACKNOWLEDGMENTS

This project was supported by the Foundation of Ministry of Railways of China (No. 2008 J001-A) and the Open Foundation of National Traction Power Laboratory (No.TPL0803).

REFERENCES

Ahlbeck, D. R. (1987). “A study of dynamic impact load effects due to railroad wheel profile roughness.” Proceedings of 10th IAVSD Symposium, Prague, CSSR, 13～16.

Barke, D. W., Chiu, W. K. (2005). “A Review of the Effects of out-of-round Wheels on Track and Vehicle components.” *IMechE Journal of Rail and RapidTransit*，219 (F)：151～175.

Jenkins, H. H., and Stephenson (1974). “The effect of track and vehicle parameters on wheel/rail vertical dynamic forces.” *Railway Engng J*, January，2～16.

Jin, X.S, Xiao, X.B., Wen, Z.F., Wang, K.Y. (2006). “Effect of sleeper pitch on rail corrugation at a tangent track in vehicle hunting.” In：Proceeding of 7th International Conference on Contact Mechanics and Wear of Rail/Wheel Systems，Brisbane，Australia. September 24-26. Institute of Materials Engineering Australasia Ltd，179～188.

Johansson, A. (2003). “Out-of-Round Railway Wheels－literature survey, field tests and numerical simulations.” Licentiate Thesis，Sweden.

Meinke, P., and Meinke, S. (1999). “Polygonalization of wheel treads caused by static and dynamic unbalances.” *J. Sound Vibr*., 227(5), 979-986.

Meywerk, M. (1999). “Polygonalization of railway wheels.” *Arch. Appl. Mechanics*, 62(9), 105-120.

Morys, B. (1999). “Enlargement of out-of-round wheel profiles on high speed trains.” *J. Sound Vibr*., 227(5), 965-978.

Morys, B., and Kuntae, H.B. (1997). "Simulation analysis and active compensation of the out-of-round phenomena at wheels of high speed trains." *In Proceedings of World Congress on Railway Research*, Florence, Italy, Nov., 95-115.

Newton, S. G.., and Clark, R. A. (1974). "An investigation into the dynamic effects on the track of wheelflats on railway vehicles." *J. Mech. Engng Sci.*，21 (4)：287～297.

Nielsen, J.C.O. and Johansson, A. (2000). "Out-of-round railway wheels－A Literature Survey." *IMechE Journal of Rail and Rapid Transit*，214 (F)：79～91.

Zhai, W.M. (2002). "Vehicle-Track Coupling Dynamics[M](Second Edition). Beijing: China Railway Publishing House.

From Time Based Speed Series to Behavior Sequence: The Transformations and Applications of VTDR Data

Zhenfeng He and Zhenzhi Huang

School of Mathematics & Computer Science, Fuzhou University, Fuzhou, Fujian, China, 350108, email: hezhenfeng@yahoo.com.cn, zhenzhi.huang@gmail.com

ABSTRACT

Vehicle Traveling Data Recorders (VTDRs) have been universally installed on fixed-route intercity buses, and the data collected is growing rapidly. It becomes urgent to utilize VTDR data to give drivers and managers some helpful feedbacks. Two novel representations of VTDR data: Location Based Speed Series (LBSS) and Behavior Sequence (BS) are presented for the analysis of these data. The data gathered directly from VTDR is Time Based Speed Series (TBSS), which defines the speeds at different time points. The fixed intercity route makes it feasible to covert a TBSS to an LBSS, which defines the speeds at different locations. BS is then proposed to extract the dynamic information, such as the speed change pattern at a segment of an LBSS. For converting an LBSS to a BS, a Background Based Symbolization (BBS) approach is presented. Based on the background of an average speed curve, five typical behavior patterns are defined. During the BBS process, each length-fixed segment of an LBSS is labeled as one of the five patterns, and the consequent pattern sequence is a BS. A simple example is presented to illustrate the transformations. The applications of LBSS and BS are illustrated with the analysis of FuQuan Highway data. The LBSS is effective in the evaluation of the driving behavior at Xiangsiling Tunnel. And BS is more suitable in mining sequential patterns than those symbolized by Symbolic Aggregate Approximation (SAX).

INTRODUCTION

Vehicle Traveling Data Recorders (VTDRs), also known as In Vehicle Data Recorders (IVDRs), are onboard devices to record many valuable states of vehicles, such as speed, brake, lights etc. (As speed is the most important state parameter, we will only discuss the transformation of speed series.) There have been some approaches to track the use of VTDR, its positive effects are proved (Toledo 2008), and various types of feedbacks are even expected by the drivers (Roetting 2003).

For the past years, China has been promoting the installment of VTDR on passenger vehicles. Now most intercity passenger vehicles have been equipped with VTDR, and the data collected are growing rapidly. It becomes urgent to analyze the data to give helpful feedbacks. Yet, we haven't seen any report focused on the analysis of VTDR data gathered from passenger vehicles. Here we'll explore the nature of passenger vehicles' running records, and transform them into two new representations: the Location Based Speed Series (LBSS) and Behavior Sequence

(BS). The transformation process will be further illustrated with a simple example. And the usage of these representations will be also provided.

THE VTDR DATA FROM PASSENGER VEHICLE

Scheduled passenger service is important for China's intercity bus transportation system, many scheduled buses run between each pair of neighboring cities each day. For example, there are about 70 passenger vehicles run from Fuzhou to Quanzhou over regular routes every day (most of them go through the 161 kilometers long FuQuan Highway). The data used here are all on FuQuan Highway (from Fuzhou to Quanzhou), collected by Fujian Minyun Transportation Company.

VTDR are not required to fit GPS (Global Position System) by China's National Standard GB/T19056-2003, and most of the VTDR equipped by Minyun are not with GPS. So there's no location info in the data gathered. Yet, the extraction of location information is feasible. As the route of a passenger vehicle is usually predefined, the location of a vehicle can be inferred based upon the distance it has run: if a vehicle has run about 26.5km from Fuzhou Highway Entrance, it would be at Xiangsiling Tunnel (a 400m long tunnel in the highway); if it has run 161km, it should be near the Quanzhou Highway Exit.

The intrinsic location information in fixed-route vehicle data, such as passenger vehicles, enables the comparison between different driving processes without the interference of changeable road condition. We can make a road as "background", and the comparison is only between the driving behaviors under the same "background". That is, compare driving sequences based upon the location. For example, we will compare the behavior of different driving processes at a specified high crash risk location, such as the Xiangsiling Tunnel. And we will not try to directly compare the driving behavior at a specified time point, such as 20 minutes after driving on Fuquan Highway. Since the vehicle would be at different locations after 20 minutes of driving, where the road conditions could be quite different, which would complicate the comparison of driving behaviors.

THE REPRESENTATIONS OF THE DATA

Time Based Speed Series (TBSS). The data gathered by VTDR is a TBSS, $V_T=(v_1, v_2, \ldots v_n)$ where v_i is the speed at time point t_i, and $t_1<t_2<\ldots<t_n$. Many VTDR record speed at a fixed interval, so we can suppose $c=t_{i+1}-t_i$, where c is a constant.

Location Based Speed Series. An LBSS $V_L=(v_1, v_2, \ldots v_n)$, Where v_i is the speed at location l_i. The location can be defined as the distance from the entrance of the Highway, so they are comparable; suppose $l_1<l_2<\ldots<l_n$. To simplify the data analysis task, the interval between consecutive locations is set to a constant $l=l_{i+1}-l_i$.

For a TBSS, it is easy to compute the location L_k at time point t_k:

$$L_k = \int_0^{t_k} v dt \approx \sum_{i=1}^{k} v_i * c \qquad (1)$$

In Equation 1, the interval between neighboring time points is c.

So we get Crude LBSS (CLBSS) $V_{CL}=(v_1, v_2, \ldots v_n)$, where v_i is the speed at location L_i. For a CLBSS, the distance between neighboring locations L_{i-1} and L_i is $\Delta_i = v_i * c$. When v_i changes, Δ_i will change accordingly. To convert a CLBSS to an LBSS, an interpolation process is necessary.

Behavior Sequence. LBSS defines the speeds at different locations, but it does not consider the relations between neighboring locations. So LBSS only provides a static view of a driving process.

From a dynamic point of view, a driving process is actually a sequence of speed-changes. Different driving behaviors may result in the same speed-change, and we cannot decide driving behaviors only based upon the speed-change. But there are close relationships between driving behavior and speed-change. Therefore we can suppose a speed-change signifies a driving behavior, and a speed-change sequence becomes a behavior sequence.

There are unlimited forms of the speed-change. Yet, to enable the driving behavior analysis, the number of behavior forms should be limited. Only five typical speed change patterns are considered. They are presented in Figure 1: the bold line is the average speed at each location, and the thin line is the real speed for the driving process in analysis. Compared with the average speed curve, a vehicle can be:

(1) Low Speed (Run at a speed that is less than the average) (Pattern A, Figure 1a);
(2) Deceleration (Pattern B, Figure 1b: the speed curve crosses the average speed curve, and the speed is bigger than the average speed at the left of the cross-point, lower than the average speed at the right of the cross-point);
(3) Vibrate around the average speed (Pattern C, Figure 1c);
(4) Acceleration (Pattern D, Figure 1d: contrary to pattern B),
(5) High speed (Patter E: which is contrary to pattern a, Figure 1e).

A small sliding window is usually employed to segment a time series; we can divide an LBSS into a set of subsequences by this approach. Based upon the five patterns presented, we can decide the behavior pattern of each subsequence one by one. So the Behavior Sequence could be extracted. As the average speed curve plays a background role in the symbolization process, the process is named as a Background Based Symbolization (BBS) process.

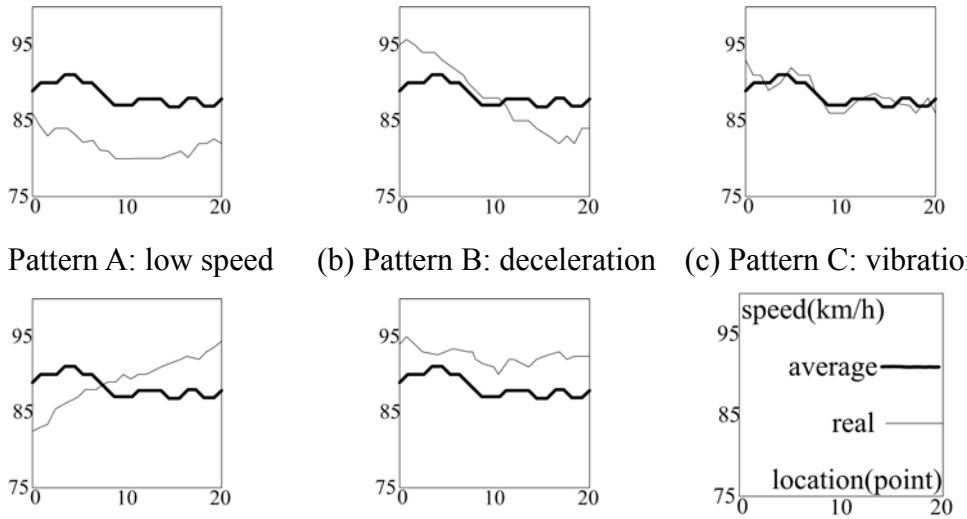

(a) Pattern A: low speed (b) Pattern B: deceleration (c) Pattern C: vibration

(d) Pattern D: acceleration (e) Pattern E: high speed (f) Notation

Figure 1. Five patterns of speed change comparing to the average speed curve

THE TRANSFORMATION OF SPEED SERIES

We will illustrate the transformation process with a short time series V_T=(0,3,5,7,10,11,13,15,16,18,19,20,19,17,15,12,9,5,3,2,0) as shown in Figure 2. The length of V_T is 21. It is recorded every one second, and the unit of speed is m/s (meter per second). During the short period, the vehicle has run 219 meters.

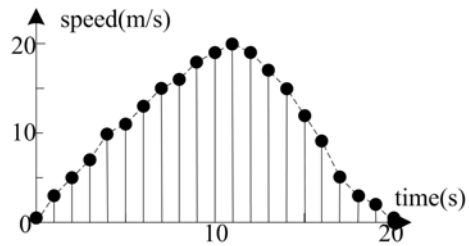

Figure 2. The original TBSS

If the location at the beginning is 0, the location at other time points can be computed by formula (1). So V_T is converted to a CLBSS (Figure 3).

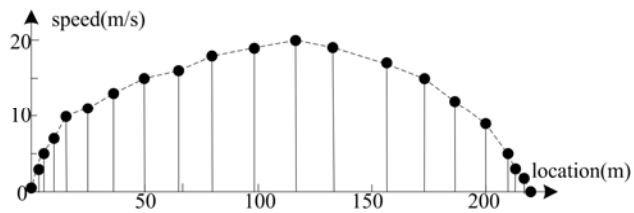

Figure 3. CLBSS (an LBSS directly converted from TBSS)

The next step is the interpolation process. Suppose the target LBSS defines speed for every 10 meters, then we should compute the speeds at location 0, 10, 20, 30, …, 200, 210, 220. And the CLBSS in figure 3 becomes an LBSS (Figure 4).

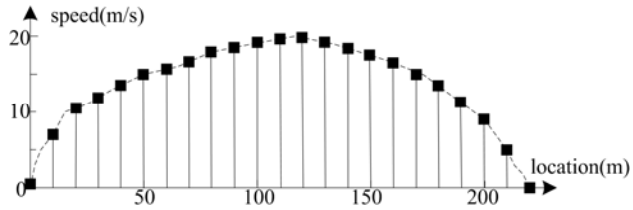

Figure 4. LBSS after interpolation

Now, considering the background information (Figure 5), the background is the average speed for each location, which is represented by a solid line.

The behavior pattern is the speed change pattern in a small location window. Suppose the length of the window is 40 meters, using the patterns defined in Figure 1, we can get the corresponding BS as: EBADBA.

It should be stressed that the pattern is a "relative pattern". The speed change should be studied with the background information (the average speed curve). For example, in the second window (location 40-79m), the speed is actually increasing. But compared with the average speed curve, the speed has changed from "above average" to "below average". So this is a "relative deceleration" process, and the speed-change pattern should be Pattern B. As the road condition can influence a driver's behavior significantly, absolute speed is relatively meaningless. On the other hand, average speed summarizes the general behavior of many driving processes; the comparison with average speed curve would be more meaningful.

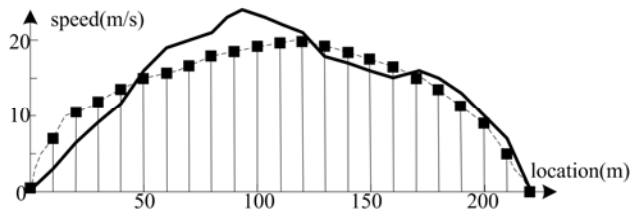

Figure 5. LBSS with the background info

APPLICATIONS OF THE TWO REPRESENTATIONS

Location based behavior analysis. As an LBSS specifies the speed based on location, it enables us to focus our attention on some sensitive locations. Based upon a Box-and Whisker Diagram (Huang 2008) that displays the speed at different locations near the Xiangsiling Tunnel (from Fuzhou to Quanzhou), it is obvious that the speed is more dispersive just before entering the tunnel, where outliers are crowded. This suggests that this area is a relatively high-risk area. The conclusion conforms to actual observation: two accidents involve five vehicles just happened on this range on August 8th, 2008, among which two of the vehicles are passenger vehicles. Clearly, the location based behavior analysis could provide the needed feedbacks for road designers and transportation risk analyzers. There are other interesting usages for LBSS, such as the extraction of general patterns (Huang 2008).

Behavior pattern analysis. Base upon the BS, it is easy to mine sequential patterns. As sequential patterns may present the connections between consequent behaviors (Hand 2001), it can help us to understand a driver's behavior at higher level, and to do some sort of short-term predications.

To evaluate the BS, we shall compare it with the sequence symbolized by SAX(Symbolic Aggregate Approximation) (Lin 2003) The symbolization process of SAX does not consider the background information. Table 1 lists the top 8 sequential patterns mined from two types of sequences (ordered by support rate).

Table 1. The top 8 sequential patterns mined based on BS or SAX

Order	Based on BBS	Based on SAX
1	<3,5,5>	<3,3>
2	<5,5,5,5>	<3,4>
3	<3,3,3>	<5,5>
4	<5,3,1>	<4,3>
5	<1,1,1,3>	<1,1>
6	<3,1,1,1>	<3,2>
7	<5,5,3>	<4,4,4>
8	<1,1,1,1,1,1,1>	<2,3>

For SAX approach, the symbols 1-5 are the levels of speed, with 1 the lowest and 5 the highest speed (breakpoints are based on Gauss distribution) (Lin 2003). For BBS approach, the symbols 1-5 are patterns presented in Figure 1. Clearly, the patterns mined from the sequence by SAX symbolization approach are very short (mostly comprise of 2 items only) and not interesting (usually represent a simple speed change). While the patterns mined from the BS are relatively longer and interesting: <5,3,1> is a deceleration process, a very long sequence <1,1,1,1,1,1,1> suggests that a driver is more likely to keep at a relatively lower speed for a comparatively longer distance.

CONCLUSION

We have presented the different representations for fixed-route vehicle data collected from VTDRs. We can extract the speed curve based upon the location-change pattern to get an LBSS; and a BS can be got by a background based symbolization approach. Both the LBSS and the BS are proved to be effective. A different representation may provide us with a more informative view on a given dataset. In the future, we would try other representations of VTDR for mining the passenger vehicle data efficiently and precisely. Upon the representations presented, we would further explore other usages.

ACKNOWLEDGE

Fujian Youth Innovation Foundation (2006F3075) supports this paper.

REFERENCES

Hand, D., Mannila, H., and Smyth, Padhraic.(2001). *Principles of Data Mining*, The MIT Press. Cambridge, Mass.

Huang, Z., and He, Z. (2008). "A novel approach to extract speed pattern from VTDR data", *Proceedings of the International Conference on Intelligent Computation Technology and Automation (ICICTA 2008)*, Volume 2, 209-214

Lin, J., Keogh, E., Lonardi, S., and Chiu, B. (2003). "A Symbolic Representation of Time Series, with Implications for Streaming Algorithms", In Proc. of the 8th ACM SIGMOD Workshop on Research Issues in Data Mining and Knowledge Discovery.

Roetting, Matthias., Huang, Y., McDevitt, J., and Melton, David. (2003). "When technology tells you how you drive—truck drivers' attitudes towards feedback by technology", *Transportation Research Part F*, 6, 275-287.

Toledo, T., Musicant, O., and Lotan, T. (2008). "In-vehicle data recorders for monitoring and feedback on drivers' behavior", *Transportation Research Part C*. 16(3) 320-331

Road Safety in Sections under Mixed Flow Traffic Environment

Sisi Liu[1] Xiaoduan Sun[2] Yulong He[3]

[1]The College of Architecture and Civil Engineering, Beijing University of Technology, Beijing, 100124; PH 010-67393982; email: cherry644446@emails.bjut.edu.cn
[2]Civil Engineering Department, University of Louisiana, Lafayette, LA 70504; PH 337-482-6514; FAX 337-482-6688; email: xsun@louisiana.edu
[3]The College of Architecture and Civil Engineering, Beijing University of Technology, Beijing, 100124; PH 010- 67396176; email: ylhe@bjut.edu.cn

ABSTRACT

Mixed traffic is a significant feature of Chinese traffic flow on urban street network, which is also a major cause of traffic congestion and frequent traffic accidents. In sections where motor vehicles and non-motor vehicles moving in same direction without separation, they would interfere with each other. This interference has serious impact on the capacity of sections, and simultaneously increases the accident risk. This paper analyzed the data through the method of probability theory and statistics, and got the result that "the number of non-motor vehicles and the lateral distant between motor vehicles and non-motor vehicles are both interference factors aroused by non-motor vehicles". Finally, non-motor vehicles' disturbance model to the motor vehicles were set up based on data analysis and proved to be correctly. The research provided a theoretical and basis to the traffic safety management under the mixed traffic environment.

KEYWORDS: Mixed traffic flow; Traffic safety; Road condition; Urban transport

INTRODUCTION

As a big country with large number of non-motor vehicles, the mixed traffic is the most important reason of the traffic congestion in the major cities of our country, and the accidents caused by mixed traffic showed year-on-year growth trend (Study on Road Traffic Delay Caused by Non-Motorized Vehicle, 2004).. Urban transport in China has a significant more number of bicycles than other developed countries, and there is no isolation or discrete barrier between motor vehicle and non-motor vehicle lanes in sections. Due to the different characteristics in their respective share of road space and operating speed between motor vehicle and non-motor vehicle, non-motor vehicles affect the speed of motor vehicles a lot, which caused serious traffic congestion even blockage and led to China's general low urban road vehicle operating speed and relatively high traffic accident rate. Therefore, the operation and safety research under the conditions of mixed traffic sections has a practical significance.

NON-MOTOR VEHICLE'S INFLUENCE OF MOTOR VEHICLE ANALYSIS IN SECTIONS

In roadway sections, the interference from non-motor vehicle to motor vehicle is mainly the lateral interference. The degree of interference depends on two factors: the number of non-motor vehicles in the lateral, and the lateral distance between them (IMPBMVT, 2006). Based on the video capturing of the traffic flow data collection methods, these two factors were utilized to carry out quantitative analysis of the impact.

In support of this thesis research, Jiaodadonglu Road in Haidian District was selected for data collection. To obtain representative data, data were collected during the afternoon peak hours (17:30-18:30) of the two business days (April 7, 2008 and April 21, 2008, which is both Monday). The chosen section is on a two-way road, which has mixed traffic. There are two motor vehicles lanes with the width of 3.5m and one non-motor vehicles lane with the width of 3m. Observation points are located at both ends of the bridge across the street, as shown in Figure 1. The labeled size in Figure 1 is the distance got in data acquisition.

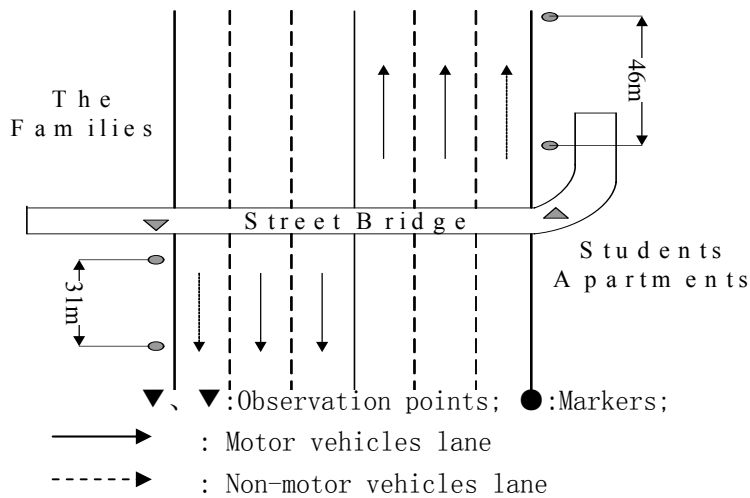

Figure 1. Section schematic of Jiaodadonglu Road

Upon completion of filming, the video was firstly transferred into computer, and then the samples were processed. 368 groups of samples were collected; the data items include motor vehicle speed, the number of non-motor vehicles in lateral side of motor vehicles and the distance between them. Through the data collected the following two relationships were obtained:

(1) Relationship between the speed of motor vehicles and the number of non-motor vehicles in lateral side

The distribution of the speed of motor vehicle and the number of non-motor vehicles in lateral side is as shown in Figure 2. From the figure, one can generally see that with the number of non-motor vehicles increasing, the motor vehicle speed has a

downward trend. These two can consider having a linear relationship, that is, with the increase in the number of non-motor vehicles, motor vehicle speeds linearly decline.

(2) Relationship between the speed of motor vehicles and the lateral distance with the non-motor vehicles

The relationship between the speed of motor vehicles and the lateral distance with the non-motor vehicles is shown in Figure 3. This relationship can also be regarded as a similar linear relationship, that is, the speed of motor vehicles increase as the lateral distance between them raised.

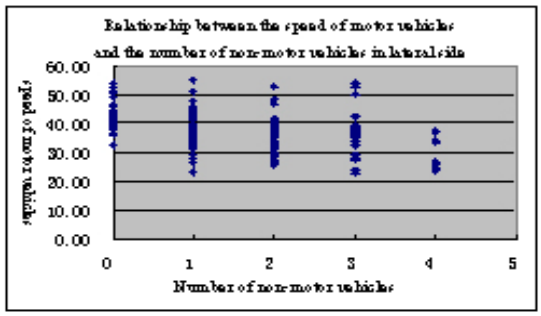

Figure 2. Relationship between the speed of motor vehicles and the number of non-motor vehicles in lateral side

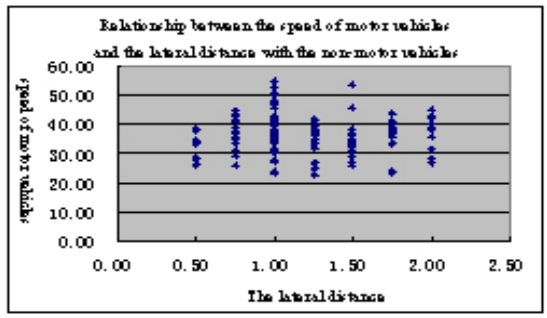

Figure 3. Relationship between the speed of motor vehicles and the lateral distance with the non-motor vehicle

NON-MOTOR VEHICLE INTERFERENCE MODELS

From the above Scatter, the speed of motor vehicles, y, the number of non-machine, x1, and the vehicle lateral distance, x2, are similar to a linear relationship. First, we assume that y and the two independent variables x1, x2 has a linear correlation, establish a dual linear regression equation, and then return to test whether the effect of the equation was significant (Probability statistics and random process,2000)According to data collected, then:

$$y = b_0 + b_1 x_{i1} + b_2 x_{i2} + \zeta_i$$

From a representative data including 25 groups, the least squares estimation of

$$28.96b_1 + 0.39b_2 = -104.3$$
$$0.39b_1 + 4.44b_2 = 5.13$$

b0, b1, b2 can be obtained. The following are the two equations derived:

$$b_1 = -3.62, \qquad b_2 = 1.47 \qquad b_0 = \bar{y} - b_1\bar{x}_1 - b_2\bar{x}_2 = 45.48$$

Solution of this equation is:

Therefore, the obtained regression equation was

$$\hat{y} = 45.48 - 3.62x_1 + 1.47x_2$$

The b1， b2 in equation both has a clear meaning. For b1, the speed of motor vehicles will reduce 3.62 km / h for each non-motor vehicle.; For b2 = 1.47, it can be expressed as that the lateral distance between non-motor vehicles and motor vehicles for each additional 1m, motor vehicles will increase the speed of 1.47 km / h.

The equation previous described is under the assumption that there is a linear relationship among them, it is necessary to carry out the linear regression significant testing. The linear regression test of significance tests whether regression coefficients b1， b2 are all zero. If they are all zero, there is no significant linear relationship. If not all zero values, there is a significant linear relationship. To this end, the proposed null hypothesis is:

H_0： $b_1=b_2=0$

Here use the F statistic to test the hypothesis H0, the expression for

$$F=\frac{S_R/m}{S_S/(n-m-1)}, where \mathrm{S_R},\ \ S_S$$

$$S_T=\sum y_i^2-25\bar{y}^2=875.29, S_R=b_1l_{1y}+b_2l_{2y}=385.11$$

$$S_\tau=S_T-S_R=875.29-385.11=490.10$$

Thus, the observed value of the test F statistic is

$$F=\frac{S_R/2}{S_\varepsilon/(25-2-1)}=8.64$$

Given significant level α = 0.01, from the F distribution table has,

$$F_{1-\alpha}(m,n-m-1)=F_{1-0.01}(2,22)=5.72$$

Because of F = 8.64> 5.72 = F1-0.01 (2, 22), we should reject H0. Therefore, the number of non-motorized vehicles and the lateral distance has significant linear affect at the speed of the vehicle at the level of α = 0.01. Thus, these two factors have significant effect on the speed of motor vehicles.

IMPROVEMENTS

In light of the fact that the situation of mixed traffic will exist in our country for a long time, the paper integrates the safety research and analysis above under the conditions of mixed sections of road, and presents the following countermeasures:

(1) Separate the motor vehicles from non-motor vehicles (Urban Transport of China, 2007). On urban roads of China, the mixed traffic of motor vehicles and non-motor vehicles occurred in the absence of physical isolation on the road. Motor vehicles and non-motor vehicles travel in the same lane when they travel in the same direction. The speed difference between them and the unstable of non-motor vehicles are the two major reasons of the interference to motor vehicles. Setting up physical isolation between motor vehicles and non-motor vehicles, that is, to separate non-motor vehicles from the space, can fundamentally solve the problem of the mixed

traffic conflict on road that has no physical isolation. It will fundamentally solve the security issues that brought by mixed traffic.

(2) Plan a reasonable road network for non-motor vehicles. According to the existing road conditions and traffic policy, build non-motor vehicles path at different levels with different functions in the city, and form a non-motor vehicles path system. This can not only achieve motor vehicle and non-motor vehicle traffic diversion, provide safe, comfortable and efficient environment for non-motor vehicles, but also reduce interference to motor vehicles in section and improve the operating efficiency of motor vehicles at the same time.

(3) Set up crosswalks pavement marking and traffic islands. If pedestrians and non-motor vehicles randomly cross the street, there must have conflict with motor vehicles on the road, which endanger the safety of non-motor vehicles at the same time will also affect the normal traffic. Cross the street at a location where has prevailing crosswalk line or traffic island is much safer than there is none. The better the traffic management facilities across the street, the less the danger is. Crosswalks line and traffic islands installed to protect the safety and control traffic order can have a significant impact.

(4) Improve the roadway lighting (Road Safety, 2004). When vehicles traveling on the road, in the context of the background surface brightness, the first thing that a driver sees is the outline of the object, and then they decide whether it is necessary to take appropriate measures. Therefore, it is necessary to make the road and obstructions on road have sufficient brightness to ensure traffic safety. Rational arrangement of lighting can not only make vehicle drivers see the front of the road and the obstacles, but also be beneficial to the removal of the side to see whether there is any non-motorized traffic. Therefore, it could prevent collisions caused by drivers who failed to see the non-motor vehicle.

(5) Limit the speed of motor vehicles. When the volumes of non-motor vehicles lanes are high, they often overflow into adjacent motor vehicles lane. as the non-motor vehicles form of arbitrariness, as well as the different speed between motor vehicles and the non-motor vehicles, rear-end conflict can easily occur between them. For slowdown conditions, the greater the initial velocity, the longer brake stopping distance, the greater the possibility of rear-end collision. Non-motor vehicles always inserted into the motor vehicles when there is a gap. The size of the gap depends on the rider. If he chooses a smaller gap insertion, then the brake stopping distance of the motor vehicle behind will not be enough, causing an accident. Non-motor vehicles traffic during peak hours is high, which makes management difficult. Therefore, limiting motor vehicle speed is an effective means of reducing the rate of conflict between them.

(6) Enhance the traffic laws and safety education (Urban Roads Bridges & Flood Control, 2004). An important element of accident prevention is comprehensively improving the quality of the traffic safety of participants. Accident prevention should

start with the nursery for the safety of the system on education. During the different levels of education before high school, students should mandatorily receive traffic safety education, which can help them establish the concept of traffic law, road safety, traffic safety, good ethnics, and the ability to obey traffic law from the beginning. Traffic safety education targeting different groups from all levels of society should adopt different approaches and methods.

CONCLUSIONS

For the serious situation of mixed traffic in China, the paper investigated a sample roadway segment and built a regression model of non-motor vehicle interfering with motor vehicles with regression analysis parameters. The paper obtained the following conclusions: In a section of mixed traffic between non-motor vehicle and motor vehicle, the number of the non-vehicles and the spacing between them not only have a significant influence on speed, but also lead to the road traffic safety factors which should not be ignored. For these two factors, paper proposed a series of traffic management countermeasures to improve traffic operation and safety, which have certain theoretical significance and practical application value.

REFERENCES

Wang Mingwen. Study on Road Traffic Delay Caused by Non-Motorized Vehicle. Beijing University of Technology, 2004:18-20.

Yuanqiang Zhou and Yuzo Akatsuka. A Study on Characteristics of Bicycle Traffic under Mixed Traffic on a Road Segment in Beijing China. Proceedings of the International Symposium on Non-motorized Transportation Beijing， May23-25，1994：195-200.

Yuli Pan and H.R. Kerali. Effect of Nonmotorized Transport on Motorized Vehicle Speeds in China. Transportation Research Record, No.1695：35-51.

Guan Hongzhi; Chen Yanyan; Liu Xiaoming; Ren Futian An Analysis Model for Mixed Traffic Flow on Street. Journal of Beijing University of Technology, 2001,27(1):12-15.

Long Xiaoqiang and Yan Qipeng. Liquid inner-friction model about non-maneuverable lane interference with motor lane. China Journal of Highway and Transport, 2002,15(1):100-102.

Zang Xiaodong; Tang Yuanhong; Zhang Xianjun. Former analysis of side interference for mixed traffic. Technology & Economy in Areas of Communications,2000,2(3):54-55.

Guan Hongzhi; Wang Mingwen; Chi Hongbo. Study on Road Traffic Delay Caused by Bicycle for Mixed Traffic Stream. Journal of Beijing University of Technology, 2005,31(3):281-283.

Jia Shunping; Peng Hongqin; Yin Xiangyong. Analysis of Bicycles Friction Interference on Motor Vehicles Driving in Mixed Traffic. Journal of Beijing

Jiaotong University,2006,30(6):1-5.

Song Na. The interference model of Pedestrian and bicycle to motor vehicle traveling (IMPBMVT). Beijing Jiaotong University, a master's degree thesis, 2006.3: 26-81.

Shao Haipeng; Yang Xiaoguang; Dong Haiqian. A Study on Improvement of Streets Traveled by Mixed Traffic. Urban Transport of China, 2007.1(5):83-87.

Luo Xiaohui. Measure for Comprehensive Handling of Urban Non-Motor Vehicles. Urban Roads Bridges & Flood Control, 2004.1(1):5.

Pei Yulong. Road Safety. Beijing: China Communications Press, 2004.

Tao Zhixing. Research on Characteristics of Mixed Vehicle-bicycle Traffic Flow on Road Section. Jilin University, a master's degree thesis, 2006.2:36-38.

Zhang Zhiyong. Study on the City Road Traffic Safety Management. Southwest Jiaotong University, a master's degree thesis, 2003.4.

Ning Le’ran. Study on the City Road Traffic Safety Management. Beijing: Chinese People's Public Security University Press, 2006.

Shao Zufeng. Road safety traffic management technology. Beijing: Chinese People's Public Security University Press, 2006.

Zhang Fuyuan; Guo Shaojian. Probability statistics and random process. Beijing: Beijing university of aeronautics &astronautics Press，2000.

Analysis on Vehicle No-sideslip Single Side Skid Equivalent Frictional Coefficient

Yongheng Yue[1], Qiang Zhao[1], Qingdong Xia [2]

[1]Traffic College, Northeast Forest University, 150040, Hexing Road 26th, Harbin, China; PH (086)8219-2617; email:yueyyh@126.com, email: Zhaoqiang@nefu.edu.cn
[2]Traffic Police Bureau Accident Department, 150001, Fushu Road 144th, Harbin, China; PH(086)8666-4272; email:xqdsir@163.com

ABSTRACT

Road frictional coefficient is a key factor to calculate the vehicle pre-impact speed in traffic accident analysis. Statistical data show that no-sideslip single side skid cases often occur in traffic accident. The traditional method adopts simple vehicle two-dimensional dynamic model to compute the equivalent frictional coefficient. This model can not accurately reflect vehicle dynamic state. This paper established a three-dimensional dynamic model of the vehicle driving, derived the no-sideslip single side skid equivalent frictional coefficient formula according to vehicle real conditions, and presented the ultimate expression of no-sideslip single side skid equivalent frictional coefficient. Experiment results show that the above analysis is rational and accurate.

INTRODUCTION

Road frictional coefficient is a key factor to calculate the vehicle driving speed. It relates to some factors such as tire pressure, ground state, and vehicle driving speed and so on (Bradley, et.al. 2004). In some traffic accidents, when a vehicle brakes non-synchronically at its four wheels, its equivalent frictional coefficient is different from that of the synchronal braking case. So it is unsuitable to compute the pre-impact speed using the parameters in synchronal braking frictional coefficient. This paper established three-dimensional dynamic model of the vehicle driving, derived a no-sideslip single side skid equivalent frictional coefficient formula according to vehicle real conditions, and presented a final expression of no-sideslip single side skid equivalent frictional coefficient.

ESTABLISHMENT OF DYNAMICAL MODEL

Introduction of classical vehicle single axis skid dynamical model

. Considering a vehicle's four tires with the same braking, the frictional force formula is as follow: $F = mg\varphi$, Where φ is road frictional coefficient and m is the vehicle mass, and g is gravity acceleration.

As to the vehicle single axis braking, there are forces working on vehicle as Figure. 1.

Li has fully analyzed the process of calculating equivalent frictional

coefficient of the vehicle single axis skid and presented the equivalent frictional coefficient formula as follow (Li).

$$\varphi_e = \frac{\varphi_1 - \lambda_x(\varphi_1 - \varphi_2)}{1 - \lambda_z(\varphi_1 - \varphi_2)} \quad (1)$$

Where φ_1 is fore axis frictional coefficient. φ_2 is back axis frictional coefficient. λ_x is the ratio of between mass center and fore axis distance to two axis distance, $\lambda_x = l_1/L$. λ_z is the ratio mass center height to two axis distance, $\lambda_z = z_c/L$.

According to the above formula, when a Jetta^{TM} car brakes, fore axis brakes

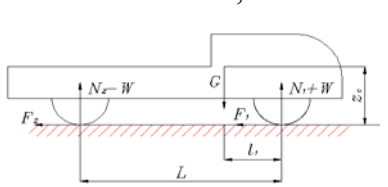

Figure 1. Single axis skid tow-dimensional force

and back axis keeps free, its which equivalent frictional coefficient is 0.495; Contrarily back axis brakes and fore axis keep free, its which equivalent frictional coefficient is 0.36. The value of equivalent frictional force will be affected by different skid state, and then the calculating result of equivalent frictional force will affect on vehicle driving speed, which further affects traffic accident survey results.

Analysis of equivalent frictional coefficient of no-sideslip single side skid.

No-sideslip single side skid vehicle often occur in traffic accidents. When vehicle single side brakes, but the other side is free. Traditional calculation method of equivalent frictional coefficient of no sideslip single side skid is $\varphi_e = \varphi/2$, but it exits a large error between analyzed pre-impact speed and real pre-impact speed.

Force model of no-sideslip single side brake vehicle.

First we research on left side skid vehicle force model. It is shown as following Figure 2, which is three dimensional force model, because traditional two dimensional force model can not reflect on real state.

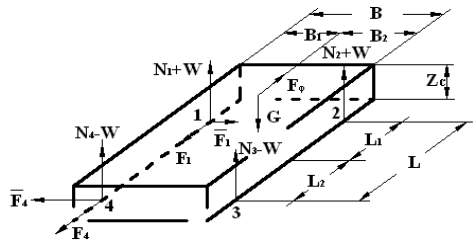

Figure 2. No-sideslip left skid dynamic

For the above model, when vehicle driving, the upright force of ground working on four tires should be first solved, but this force model is statically indeterminate. To approximate the model, we assumeed that vehicle driving four tires force model is simple as shown in Figure 3 and Figure 4.

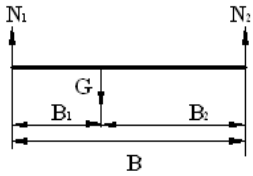

Figure 3.vehicle fore projective force

Based on Figures 3 and 4 the force equations can be given as : $N_1 + N_2 = x$; $N_3 + N_4 = y$.

Setting model force equation as: $y \cdot L_2 = x \cdot L_1$, $x + y = G$.

We have

$$N_1 + N_2 = G(1-\lambda_x) \quad (2)$$

$$N_3 + N_4 = G\lambda_x \quad (3)$$

Vehicle fore projective force model is defined as follow Figure 4.

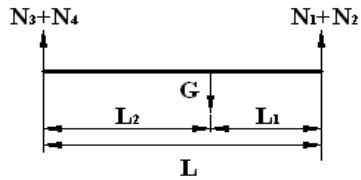

Figure 4. vehicle side projective force

Setting model force equation as: $N_1 \cdot B_1 = N_2 \cdot B_2$; $N_1 + N_2 = G(1-\lambda_x)$.

We have

$$N_1 = G(1-\lambda_x)(1-\lambda_B)\ ; \quad N_2 = G\lambda_B(1-\lambda_x) \quad (4)$$

Same as analysis method, we have

$$N_3 = G\lambda_x\lambda_B\ ; \quad N_4 = G\lambda_x(1-\lambda_B) \quad (5)$$

where N_4 is defined coordinates center, setting dynamic balance equation and moment balance equation:

$$\overline{F}_4 = \overline{F}_1 \quad (6)$$

$$F_1 + F_4 = F_\varphi \quad (7)$$

$$N_1 + N_2 + N_3 + N_4 = G \quad (8)$$

$$GL_2 + F_\varphi z_c = (N_1 + w)L + (N_2 + w)L \quad (9)$$

$$G \cdot B_1 = (N_2 + w)B + (N_3 - w)B \quad (10)$$

$$\overline{F}_1 \cdot L = B_1 \cdot F_\varphi \quad (11)$$

Setting frictional force equation of N_4 point and N_1 point as:

$$\overline{F}_1^{\,2} + F_1^2 = \varphi^2 (N_1 + w)^2 \quad (12)$$

$$\overline{F}_4^{\,2} + F_4^2 = \varphi^2 (N_4 - w)^2 \quad (13)$$

According to the above equation, we can deduce as:

$$a_1\varphi_e^4 + a_2\varphi_e^3 + a_3\varphi_e^2 + a_4\varphi_e + a_5 = 0 \quad (14)$$

where $a_1 = \frac{1}{4} + \frac{B_1^2}{L^2} - \frac{z_c^2\varphi^2}{2L^2}$; $a_2 = \frac{\varphi^2 z_c(1-\lambda_B)}{2L} - \frac{\varphi^2 z_c(1-\lambda_x)(1-\lambda_B)}{L}$;

$$a_3=\frac{\varphi^2(1-\lambda_B)^2(1-2\lambda_x)}{2}+\frac{\varphi^4(1-\lambda_B)^2 z_c^2}{4L^2}-\varphi^2(1-\lambda_x)^2(1-\lambda_B)^2;$$

$$a_4=\frac{\varphi^4 z_c(1-\lambda_B)^3(1-2\lambda_x)}{2L};\quad a_5=\frac{\varphi^4(1-\lambda_x)^4(1-2\lambda_x)^2}{4}。$$

Formula (14) is used to calculate equivalent frictional coefficient of vehicle in no sideslip left side skid. If we have car structure parameter, we can solve the equivalent frictional coefficient of vehicle in no sideslip left side skid by Matlab software.

Modification of theoretical frictional coefficient

Braking time of liquid skid vehicle is 0.2s from zero to vehicle max skid force(Xu). When vehicle skid force arrives at max value, v_1, skid force changing is shown as Figure 5. In the traffic accidence, theoretical frictional coefficient is used to calculate and analyze vehicle driving speed of before traffic accidence, but the calculated vehicle driving speed does not agree with real vehicle driving speed. This error comes into being for omitting 0.2s effect from v_0 to v_1 of skid force.

Analyzing and amending relation between computed fricational coefficient in the traffic accident and theory frictional coefficient

The skid force model is described as follow:

$$F=kt\ ,\ t\in(0,0.2] \tag{15}$$

where φ is theoretical frictional coefficient, m is vehicle mass, g is gravitational accelerate.

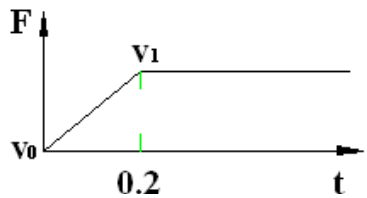

Figure 5. Skid force curve when braking

We can also deduce $k=\frac{\varphi mg}{0.2}$ and $0.1\varphi g=v_0-v_1$.

In general, based on tire marks at the scene, we are to investigate the pre-impact vehicle velocity in traffic accident. This formula is defined as follow: $v=(2g\varphi S)^{0.5}$,where g is gravitational accelerate, φ is frictional coefficient, S is tire marks of traffic accident vehicle.

Hence,

$$v_1=(2g\varphi S)^{0.5} \tag{16}$$

$$v_0=\left[2g(\varphi S+\varphi_1\Delta S)\right]^{0.5} \tag{17}$$

where ΔS is vehicle driving distance at 0.2s, φ_1 is equivalent frictional coefficient within the ΔS range.

From Equations 16 and 17, we can obtain

$$\sqrt{\varphi_e} = \sqrt{\varphi} + \frac{0.1\varphi g}{\sqrt{2gS}} \tag{18}$$

According to the above formula, we can determine the relation between computed frictional coefficient and theoretical frictional coefficient, and we apply computed frictional coefficient to calculate accident vehicle driving speed which is accordant with practical vehicle driving speed.

EXPERIMENT

We completed an experiment test on Aug. 8, 2008, and obtained some real testing data of no-sideslip left side skid. The experiment equipments include: CTM-2002 (non contact laser velometer), tapeline, and a Jetta™ car.

CTM-2002 is shown in Figure 6. It can record the vehicle skid speed and distance. But we want to analyze and calculate the vehicle pre-brake speed to use visible tire marks in traffic accident, so we must use amended theoretical frictional coefficient. Figures 7, 8 and 9 presented the installing and debugging process. The testing data are as shown Table 1.

Figure 6. CTM-2002c non-contact velometer

Figure 7. Installing of CTM-2002c on Jetta™ car

Figure 8. Debugging of CTM-2002c on Jetta car

Figure 9. In-car debugging of CTM-2002c

Table 1. No-sideslip Left Skid Testing Data

Num	Skid speed	Skid distance	Equivalent frictional coefficient
1	5.56m/s	3.5m	0.45
2	5.2m/s	3.2m	0.43
3	5.8m/s	4.3m	0.4
4	6.6m/s	5.2m	0.43
5	7.2m/s	5.3m	0.5

According to the above five group of testing data, we can obtain that the average value of single side skid equivalent frictional coefficient is 0.442, and average skid distance is 4.3m. By the no-sideslip single side skid equivalent friction coefficient Equation 14 and Jetta car parameters in Table 2, we can derive theoretical equivalent frictional coefficient, which is 0.3905.

Table 2. Jetta^{TM} car construction parameters

Jetta^{TM} car construction parameters	index
Axis distance	2.48m
Tire distance	1.46m
Mass center to fore axis distance	1.04m
Mass center to left side distance	0.6m
Mass center high	0.5m
Frictional coefficient	0.75

By amending Equation 18, we derived amended theoretical equivalent friction coefficient; the amended value is as follow:

$$\varphi_e = \left(\sqrt{\varphi} + \frac{0.1\varphi g}{\sqrt{2gS}} \right)^2 = \left(\sqrt{0.3905} + \frac{0.1 \times 0.3905 \times 9.8}{\sqrt{2 \times 9.8 \times 5.3}} \right)^2 = 0.4388$$

Tabel 3 shows the errors of single side skid equivalent frictional coefficient theoretical value and testing equivalent frictional coefficient value by experiment, the equivalent frictional coefficient by tradition method.

Table 3. Error Analysis

Absolute error	Testing data: 0.442(left) 0.2374(right)	tradition value: 0.375
Amended theoretical value of left side skid: 0.4388	0.72%	14.5%
Amended theoretical value of right side skid: 0.2372	0.84%	58%

From error analyzing table one can see that the amended theoretical value of vehicle no sideslip left side skid almost equals with testing data by experiment. But the absolute error between equivalent frictional coefficient by tradition method and testing data by experiment is much bigger, as is 14.5%. However, the right side

tradition friction coefficient error are surprisingly as high as 58% and this error could not be tolerance.

CONCLUSION

We put forward the new model of No-sideslip single side skid equivalent frictional coefficient formula, and then, amend this model. This new model is right by experiment data analyzing. By different conditions road friction coefficient, we can also calculate No-sideslip single side skid equivalent frictional coefficient applying to the model in this paper, so this model can justly and objectively calculate No-sideslip single side skid vehicle pre-impact driving speed in the accident.

Research result of this paper can support traffic police officers justly and objectively deal with traffic accident, thus it has significance meaning.

ACKNOWLEDGE

This paper is supported by Heilongjiang province Education Bureau Project under grant No.11523006 and North East Forest University foundation under grant No 07013.

REFERNCES

Bradley E. Heinrichs, Boyd D.Allin, James J.Bowler, Gunter P.Siegmund. (2004). "Vehicle speed affects both pre-skid braking kinematics and average tire /roadway friction."Accident Analysis and Prevention 36. 829-840.

Li jiang. Traffic Aaccident Mechanics. China Machine Press.

Xu yigang. Road traffic accident new theory. Sandong people public house.

Discussion on Methods of Traffic Routes' Alignment Survey and Application of Principle of Least Squares

Liang Yubao[1] He Baoxi[1] Liu Shaotang[2] Ma Qianli[1]

[1]Department of Surveying and Land Information, Henan University of Urban Construction, Pingdingshan, Henan Province , China , 467044; email: lyb2003218@163.com
[2]Henan Institute of Engineering, Zhenzhou, Henan Province, China , 451191

ABSTRACT

Traffic route's alignment survey is among the important works required in location survey stage. This paper concisely introduces both conventional and contemporary techniques of traffic route's alignment survey. It also analyzes and discusses the question that while traffic route's alignment survey is being conducted by conventional diagrammatic method (or called offset method), how to improve the accuracy of diagrammatized centerline stations' coordinate parameters for staking-out by the principle of least squares to reduce the workload of repeatedly threading, checking on and adjusting the laid-out centerline stations. Finally, the authors draw the conclusion that the laid-out traffic route's center line stations based on staking-out coordinate parameters obtained by the principle of least squares are able to satisfy the required tolerance of location survey of traffic route's centerline stakes.

Key Words: traffic route, alignment, surveying method, least squares

1. INTRODUCTION

Alignment survey, one of the important works required in traffic route's location survey stage, is a process of staking out preliminarily-designed centerline in field. Its fundamental task is to stake out intersections, a series of straight lines separated by certain distances and directions of the centerline proposed by a plan.

In alignment survey, method used to acquire staking-out coordinates of centerline stations includes analytical method and diagrammatic method. With analytical method, coordinates of centerline stations (including starting point, ending point and intersections etc.) are provided by designing calculations, and these stations are staked out later in field by polar coordinate method and included-angle method. On the other hand, diagrammatic method means to take measurements of coordinates of centerline stations for staking-out directly from strip map or aerial map and lay out these stations by diagrammatic method. Analytical method always provides higher level of accuracy compared with diagrammatic method.

The reason for analytical method's higher level of accuracy is that the available staking-out data are provided by the designing plan and thus no contradiction exists

between them. On the other hand, the reason for diagrammatic method's lower level of accuracy is that the deviation of diagrammatized coordinate parameters of centerline stations for staking-out is too large to ensure the laid-out stations are precisely in one straight line and therefore it is necessary for surveyors to repeatedly thread, check and adjust the laid-out center line stations (Zhang Kunyi 1999).

2. BRIEF INTRODUCTION ON METHODS OF TRAFFIC ROUTE'S ALIGNMENT SURVEY

Along with the rapid development of surveying techniques, especially the widely application of EDM instruments and total stations, the methods for alignment survey of traffic route have been improved greatly. The GPS RTK technique will be applied more extensively in alignment survey of traffic route and its construction.

2.1 Methods of Alignment Survey with Conventional Techniques and Instruments

Methods of alignment survey with conventional techniques and equipments include analytical method and diagrammatic method. Here the conventional instruments and equipments refer to theodolites, steel type and range finders.

In analytical method, the centerline of traffic route and coordinates of intersections of centerline straight segments (or any point) are both determined by designing plan. Therefore the lengths and directions of lines from traverse stations to centerline straight segments' intersections (or any point) can be inversely calculated from coordinates of laid-out traverse stations so that intersections of centerline straight segments can be laid out with polar coordinate method.

Diagrammatic method enables (Gong 1992) coordinates of intersections of centerline straight segments (or any point) to be taken directly from strip map or aerial map, and then laid out in field by polar coordinate method with inversely calculated lengths and directions of lines from traverse stations to centerline straight segments' intersections (or any point) and (2)centerline stations to be laid out in field by diagrammatic method (or called offset method) with staking-out offset parameters which have been diagrammatized directly from strip map or aerial map, such as d_4, d_5 (see Fig.1).

2.2 Methods of Alignment Survey with Modern Techniques and Instruments

(1) Application of Total Station in Alignment Survey of Route

Total station consists of electronic theodolite, electro-magnetic range finder, and micro-processor and is able to perform functions of measuring angles, distances, and elevations. Besides its function of measuring angle or distance as an electronic theodolite or electro-magnetic range finder respectively, total station supported by its program modules is able to accomplish the procedure of three-dimensional coordinate surveying, laying-out surveying, RDM and REM etc.

Based on designed coordinates of intersections of centerline straight segments (or any point), the location survey of traffic route can be carried out by applying total station's function of laying out coordinates. On the other hand, the distance between two adjacent intersections of centerline straight segments and included angle between two intersected centerline straight segments can be inversely calculated from formerly designed coordinates of intersections of centerline straight segments so that the location survey of traffic route is able to be accomplished by applying included-angle method and total station's function of laying out angles and distances.

Directly diagrammatized coordinates of centerline straight segments' intersections from strip map or aerial map can also be laid out by applying total station's function of laying out coordinates. Because of the lower accuracy of diagrammatized coordinates, it is necessary to thread, check and adjust the laid-out stations and then locate them by intersecting straight segments of centerline.

(2) Application of GPS RTK in Alignment Survey of Route

GPS RTK is developed from real-time dynamic differential techniques in phase measurement of carrier wave. It is able to provide three-dimensional coordinate in designated coordinate system of stations with centimeters accuracy. In RTK surveying, reference station conveys both their measurements and coordinates of themselves via data link to mobile station besides receiving data from reference station via data link. Mobile station collects GPS observational data and processes differential measurements real-timely to gain location measurements of centimeters accuracy.

The flow of work of alignment survey by GPS RTK is approximately as the following: firstly, make preparations of laid-out data; secondly, set up RTK reference station at known points and start GPS receiver to ensure differential signals are sending off from reference station; then start GPS receiver at mobile station, and with RTK setting to alignment surveying mode conduct alignment survey by selecting proper method.

Before, during and after staking-out traffic route, it is advisable for surveyors to perform necessary checks at known points.

Alignment survey by GPS RTK is composed of office work and field work. The former mainly includes designing centerline straight segments for later staking-out in GPS electronic field book with formerly designed coordinate data of intersections of centerline straight segments, starting and ending points of curves, centers and radii of circles. The latter includes locating the designed route in field with GPS RTK set to alignment surveying mode.

When applied in route's alignment surveys, especially for long traffic routes, RTK technique has unique advantages compared with conventional surveying techniques, which include (a) being handled expediently and operated flexibly. With

RTK technique, alignment survey can be conducted either consecutively or to start from any position of a route at any moment. This is convenient for several instruments to be operated jointly; (b) being direct-viewing, clear-displaying and convenient. The designed route can be displayed directly on RTK operating screen and the operator can lay out the points accordingly; (c) demanding less workers and thus resulting in higher efficiency; (d) measurements can be checked on in real time so the reliability of measurements is enhanced. Beware to check on positions of known points at any moment during alignment survey; (e) the errors of measurements are not cumulative and disseminative thus results in a higher standard of accuracy (Zhang Xiao et al. 2007).

3. APPLICATION OF LEAST SQUARES IN ALIGNMENT SURVEY OF ROUTE BY DIAGRAMMATIC METHOD

3.1 Procedure of Laying-out Centerline Stations Diagrammatically

Procedures or steps to be followed in laying-out centerline stations by diagrammatic method include

(1) diagrammatizing staking-out parameters, such as coordinates and offsets from designing plan;

(2) laying-out centerline stations in field by polar coordinate method or offset method;

(3) threading, which is equivalent to adjusting staked-out stations which have been displaced by errors stemming from diagrammatizing and laying-out back into the designed straight line;

(4) locating the intersections. The straight segments of centerline determined by preceding methods are checked to assure their validity. If they are extended, adjacent straight segments will intersect and an intersection is acquired. Therefore intersections of route's centerline straight segments are located. See Fig.1.

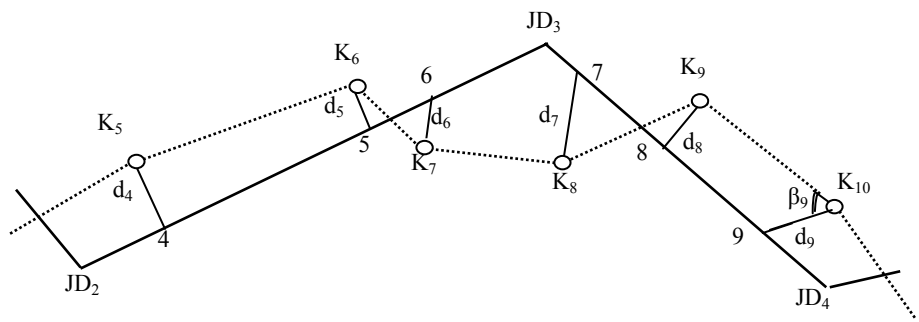

Figure 1.Sketch of alignment survey by diagrammatic method (or called offset method).

Note: In the above figure, JD_2, JD_3 and JD_4 are intersections of centerline straight

segments of route and K_5、K_6 are traverse controls . d_4、d_5、β_9 are parameters for diagrammatizing.

While centerline stations are laid out either by polar coordinate method (see point 9 in Fig.1) or by offset method (see point 4, 5 and 6 in Fig.1), the diagrammatized pairs of coordinates X and Y of centerline stations, such as point 4, 5, 6, 7, 8, and 9, can be determined by applying formerly solved parameters. Because of the effects of errors stemming from diagrammatizing and laying-out, the obtained centerline stations are not in line and the displacements are large enough to guarantee repeatedly threading, checking on and adjusting the laid-out centerline stations. By extending the adjusted centerline straight segments, the intersections such as JD_2, JD_3 and JD_4 are established. This procedure is discussed in most of the present surveying textbooks (Ji Binde et al. 2002).

3.2 Procedure and Thread in Applying Principle of Least Squares

(1)Being centerline straight segments designed from strip map, JD_2 JD_3, JD_3 JD_4 are diagrammatized as coordinates of point 4, 5, 6 and point 7, 8, 9 respectively. See Fig.1. Take these diagrammatized coordinates for observational values, because point 4, 5, 6 and point 7, 8, 9 are in line respectively.

(2)List condition equations respectively for these two centerline segments in accordance with geometry features of three points in every centerline segment

$$\hat{\alpha}_{56} - \hat{\alpha}_{54} = 180^0 ; \ \hat{\alpha}_{89} - \hat{\alpha}_{87} = 180^0 .$$

(3)Solve the above condition equations with principle of least squares so that obtain the optimum estimations of centerline stations. Lay out these centerlines stations by polar coordinate method.

(4) Accuracy verification.

3.3 Steps in Applying Principle of Least Squares

3.3.1 Set up Condition Equation Model

Based on diagrammatized coordinate observational values, list condition equations about adjustments

$$\hat{\alpha}_{56} - \hat{\alpha}_{54} = 180^0 \tag{1}$$

$$\hat{\alpha}_{89} - \hat{\alpha}_{87} = 180^0 \tag{2}$$

Suppose adjustments of coordinate $\hat{\mathrm{X}} = \mathrm{X} + V_X$, $\hat{\mathrm{Y}} = \mathrm{Y} + V_Y$. So that

$$\arctan\frac{(y_6+v_6)-(y_5+v_5)}{(x_6+v_6)-(x_5+v_5)} - \arctan\frac{(y_5+v_5)-(y_4+v_4)}{(x_5+v_5)-(x_4+v_4)} - 180^0 = 0 \tag{3}$$

$$\arctan\frac{(y_9+v_9)-(y_8+v_8)}{(x_9+v_9)-(x_8+v_8)}-\arctan\frac{(y_8+v_8)-(y_7+v_7)}{(x_8+v_8)-(x_7+v_7)}-180^0=0 \quad (4)$$

Where $\hat{\alpha}$ stands for azimuth of straight line; $\hat{X}$, $\hat{Y}$, X, Y stand for adjustments and measurements of diagrammatized coordinates; and V_X, V_Y stand for corrections of diagrammatized coordinates coordinates (Wuhan University Geodesy Adjustment Group 2005).

3.3.2 Solution of Condition Equations to Obtain Corrections

(1) Linearization of Condition Equations

From equations 3 and 4, we know that condition equations are nonlinear. Expand them by method of Taylor series, omitting quadratic term and terms after it. The following equations are obtained by rearrangement

$$\rho''(\frac{\Delta Y_{56}^0}{(S_{56}^0)^2}-\frac{\Delta Y_{54}^0}{(S_{54}^0)^2})V_{X_5}-\rho''(\frac{\Delta X_{56}^0}{(S_{56}^0)^2}-\frac{\Delta X_{54}^0}{(S_{54}^0)^2})V_{Y_5}- \quad \rho''\frac{\Delta Y_{56}^0}{(S_{56}^0)^2}V_{X_6}+\rho''\frac{\Delta X_{56}^0}{(S_{56}^0)^2}V_{Y_6}+\rho''\frac{\Delta Y_{54}^0}{(S_{54}^0)^2}V_{X_4}-$$

$$\rho''\frac{\Delta X_{54}^0}{(S_{54}^0)^2})V_{Y_4}+W_1=0 \quad (5)$$

$$\rho''(\frac{\Delta Y_{89}^0}{(S_{89}^0)^2}-\frac{\Delta Y_{87}^0}{(S_{87}^0)^2})V_{X_8}-\rho''(\frac{\Delta X_{89}^0}{(S_{89}^0)^2}-\frac{\Delta X_{87}^0}{(S_{87}^0)^2})V_{Y_8}-\rho''\frac{\Delta Y_{89}^0}{(S_{89}^0)^2}V_{X_9}+\rho''\frac{\Delta X_{89}^0}{(S_{89}^0)^2}V_{Y_9}+\rho''\frac{\Delta Y_{87}^0}{(S_{87}^0)^2}V_{X_7}-$$

$$\rho''\frac{\Delta X_{87}^0}{(S_{87}^0)^2})V_{Y_7}+W_2=0 \quad (6)$$

They are linear condition equations where ρ'' --206265"; ΔX^0, ΔY^0 stand for computed increments of X coordinate and Y coordinate from diagrammatized coordinates; S^0 stands for approximate corresponding side length computed from diagrammatized coordinates; and misclosure

$$W_1=\alpha_{56}^0-\alpha_{54}^0-180^0;\ \ W_2=\alpha_{89}^0-\alpha_{87}^0-180^0$$

Where α^0 stands for approximate value of straight line's azimuth reversely calculated from diagrammatized coordinates.

(2)Solution of Linear Condition Equations by Method of Least Squares

From linear condition equations 5 and 6, we know that the two equations contain twelve unknown variables and have indefinite solutions. It is a mathematical

problem of solving function's extremum with conditions for surveyors to solve V from function $V^T PV = \min$. Basic equations are established and solved with the following result

$$\mathrm{V} = -QA^T (AQA^T)^{-1} W \tag{7}$$

where Q stands for covariance factor of measurements and adopts the value of I (suppose diagrammatized coordinates are independent); A stands for Coefficient matrix of condition equations; and W stands for misclosure of condition equations.

After corrections being solved, the most probable value (or adjusted value) of observed coordinates can be obtained as the following

$$\hat{\mathrm{X}} = X + V_X \; ; \quad \hat{\mathrm{Y}} = Y + V_Y \; .$$

(3)Accuracy Estimation

Root mean square error of unit weight (RMSE)

$$\hat{\sigma}_0 = \sqrt{\frac{V^T PV}{r}} \tag{8}$$

Accuracy of adjusted value of diagrammatized coordinates

$$\hat{D}_{\hat{L}} = \sigma_0^2 (Q - QA^T (AQA^T)^{-1} AQ), \tag{9}$$

where P stands for weight of measurements , and adopts the value of I ; r stands for the number of condition equations; $\hat{D}_{\hat{L}}$ stands for variance-covariance matrix for adjusted value of diagrammatized coordinates.

3.4 Example for Demonstration

Diagrammatized coordinates of the three points on each straight segment of traffic route's centerline are shown in Table1. Adjusted coordinates based on least squares methods are listed in Table 1 (Liang Yubao et al. 2008).

Table 1. Data sheet of diagrammatized coordinates of traffic route stations.

Station number	Diagrammatized coordinates (m)		Station number	Diagrammatized coordinates (m)	
	X	Y		X	Y
4	3740500.0	38434719.3	7	3740000.0	38436364.0
5	3740413.5	38435000.0	8	3739500.0	38436986.5
6	3740259.5	38435500.0	9	3739312.5	38437220.0

Related data are calculated and then substituted into linear condition Equations 5 and 6. After rearranging, we get

$$-1.835V_{X_4} - 0.566V_{Y_4} + 1.932V_{X_5} + 1.726V_{Y_5} - 3.768V_{X_6} - 1.160V_{Y_6} - 29.8'' = 0$$

$$-2.014V_{X_7} - 1.618V_{Y_7} + 7.385V_{X_8} + 5.930V_{Y_8} - 5.371V_{X_9} - 4.312V_{Y_9} - 27'' = 0$$

Solve the above condition equations, then we get

$$\underset{6\ 1}{V_x} = \left[V_{x_4}, V_{x_5}, V_{x_6}, V_{x_7}, V_{x_8}, V_{x_9} \right]^T = \begin{bmatrix} -2.10 \\ 2.22 \\ -4.33 \\ -0.38 \\ 1.39 \\ 1.01 \end{bmatrix} cm \qquad \underset{6\ 1}{V_y} = \left[V_{y_4}, V_{y_5}, V_{y_6}, V_{y_7}, V_{y_8}, V_{y_9} \right]^T = \begin{bmatrix} -0.65 \\ 1.98 \\ -1.33 \\ -0.30 \\ 1.11 \\ -0.81 \end{bmatrix} cm$$

Accuracy estimation can be performed by the following steps.

From Equation 8, root mean square error of unit weight

$$\hat{\sigma}_0 = \sqrt{\frac{V^T PV}{r}} = \sqrt{\frac{39.3}{2}} = \pm 4.43 cm.$$

From Equation 9, accuracy of adjusted value and location error of diagrammatized coordinates are computed and shown in Table 3.

Table 2. Data sheet of diagrammatized coordinates of traffic route stations by least squares.

Station number	Diagrammatized coordinates (m)		Station number	Diagrammatized coordinates (m)	
	X	Y		X	Y
4	3740499.979	38434719.293	7	3739999.996	38436363.997
5	3740413.522	38435000.019	8	3739500.014	38436986.511
6	3740259.457	38435499.987	9	3739312.510	38437219.992

Table 3. Data sheet of accuracy of adjusted value of diagrammatized coordinates of traffic route stations by least squares

Station number	accuracy of adjusted value of diagrammatized coordinates (cm)		Error in station location (cm)	Station number	accuracy of adjusted value of diagrammatized coordinates (cm)		Error in station location (cm)
	σ_X	σ_Y	σ		σ_X	σ_Y	σ
4	±4.13	±4.40	±6.03	7	±4.36	±4.38	±6.82
5	±4.09	±4.16	±5.83	8	±3.49	±3.84	±5.19
6	±2.97	±4.31	±5.23	9	±3.96	±4.13	±5.72

Regulations for highway surveying specified tolerance of deviation of stake locations for high order highway's centerline stakes as followings: in longitudinal direction, S/200 +0.1m (S stands for location measurements of centerline stakes, in meters); in transverse direction, 10cm (China Ministry of Communications 1992).

Take half the tolerance of deviation of centerline stake locations for tolerance of RMSE in lengthwise and transverse directions of centerline stake locations, i.e.

$$\sigma_{\mathrm{L}} = \frac{1}{2} \times 10 = \pm 5\mathrm{cm}; \qquad \sigma_{\mathrm{T}} = \frac{1}{2} \times 10 = \pm 5\mathrm{cm}$$

So that tolerance of RMSE of centerline stake locations

$$\sigma_{\mathrm{C}} = \sqrt{\sigma_{\mathrm{L}}^2 + \sigma_{\mathrm{T}}^2} = \sqrt{5^2 + 5^2} = \pm 7.07\mathrm{cm}$$

4. CONCLUSION

The following conclusion can be drawn from the above discussions:

If the designed coordinates of intersections of route's centerline straight segments are known, surveyors can conduct alignment survey for traffic route by either conventional surveying techniques or contemporary surveying techniques. The choice depends on actual situation. If the coordinates of intersections of route's centerline segments have not been designed, surveyors may directly diagrammatize coordinates from strip map or aerial map, and conduct alignment survey for traffic route by diagrammatic method (or offset method). When using diagrammatizing method, beware to diagrammatize coordinates of at least three evenly distributed centerline stations for each centerline segment. Then eliminate contradictions within diagrammatized coordinates and work out the optimum estimation by applying method of least squares.

From estimated accuracy of adjusted value of diagrammatized coordinates, we can see that location accuracy of diagrammatized coordinates which have been handled by method of least squares is within the range of tolerance of RMSE of centerline stake locations specified by regulations($\sigma_{\mathrm{C}} = \pm 7.07\mathrm{cm}$). Therefore surveyors can directly apply this method in laying out centerline stakes, such as starting point, ending point and intersections of centerline's straight segments without any troubles of repeatedly threading, checking on and adjusting the laid-out centerline stations. The related complicated computational process conforms to strong regularity and can be handled by computer programs that can be operated conveniently and practically.

In brief, this paper concisely introduces both conventional and contemporary techniques of traffic route's alignment survey. It also analyzes and discusses the question that while traffic route's alignment survey is being conducted by conventional diagrammatic method (or called offset method), how to improve the accuracy of diagrammatized centerline stations' coordinate parameters for staking-out by principle of least squares in order to reduce the workload of repeatedly threading, checking on and adjusting the laid-out centerline stations. Finally, the authors draw the conclusion that the laid-out traffic route's centerline stations based on staking-out coordinate

parameters obtained by principle of least squares are able to satisfy the required tolerance of location survey of traffic route's centerline stakes.

REFERENCES

China Ministry of Communications (1992). Compilation of Regulations on Highway Reconnaissance, People's Communication Press, Beijing.

Ji Binde, and Shao Zixiu (2002). Engineering Survey, Survey and Mapping Press, Beijing.

Liang Yubao, Wei Liang, and Zhao Xiaoyan (2008). Discussions on Application of Principle of Least Squares in Alignment Survey for Route, Engineering Reconnaissance, (07):52-54.

Wuhan University Geodesy Adjustment Group (2005). Error Theory and Surveying Adjustment, Wuhan University Press，Wuhan.

Zhang Kunyi(1999). Traffic Civil Engineering Survey, People's Communication Press, Beijing.

Zhang Xiao and Zhao Fenglei (2007). Application and Discussion of Alignment Survey in Midline Project of China's South-to-North Water Diversion, Yangtze River, 2007.(10):91-92.

A Study on Speeding Driving Based on Expected Speed

Chen Hu[1] ,SUN-Xiaoduan[2], Liu-Shicui [3]

[1]Key Lab of Transportation Engineering ,Beijing University of Technology, Beijing, 100124, P.R.China. Email: chenhu@emails.bjut.edu.cn
[2] Key Lab of transportation Engineering Beijing University of Technology. Beijing. 100124, P.R.China. Email: xdsun@bjut.edu.cn
[3]Key Lab of Transportation Engineering, Beijing University of Technology, Beijing, 100124, P. R. China. Email: liushicui1984@emails.bjut.edu.cn

ABSTRACT:

In the recent years, in china, speeding is one of the most serious road traffic violations and is one of the main reasons that cause road traffic accidents. In 2007, the road traffic accident fatalities caused by speeding account for 14.06% of the total, ahead of the main reasons for the accident, so the treatment of speeding is the main task of the traffic control department. This article, from the point of view of expected speed of driver, studies the mechanism of its formation, and establishes the relationship model between speeding rate and traffic volume through the measured data in the field. The model can help traffic control department to identify road sections and time sections in which speeding happens very often. That will allow police to focus on control and improve law enforcement efficiency and reduce the cost of law enforcement.

Key words: *expected speed, speeding rate, traffic volume, enforcement efficiency*

1.The harm of speeding driving

The speeding driving is described that the speed of the automobile driving on the road exceeds the specified speed. The implementation of the road traffic safety regulation arcticle 45 provides (Huang Changjie, 2004): the speed of motor vehicle driving on the road shall not exceed the speed limit marked on the traffic signs and lines. Without any speed limit mark on the road, motor vehicle's maximum speed shall not exceed the following speed limit: if without road central line, 30km/h on the urban road and 40km/h on the highway; if there is only 1 driveway in each direction, 50km/h on the urban road and 70km/h on the highway. Arcticle 78 prescribes: the driving speed on each driveway on the expressway should be marked, what's more, the maximum speed shall not exceed 120km/h.

The ultimate purpose of speed limit is to guarantee the safety of driving, but according to the PRC's road traffic accident statistics annals (Traffic Management Bureau in Ministry of Public and Security, 2008)[1] reported that there are 327209 traffic accidents ranking above common accident in the whole country in 2007, resulting in 81649 deaths, 380442 injured, and direct property loss 1.199 billion yuan.

And the accidents, deaths, injured population and direct property loss resulting from speeding driving separately account for the total 10.23%,14.06%,9.63% and 11.22%, further more, speeding driving is located in the forefront of all kinds of causes. The following figure 1 illustrates the distribution of the traffic fatality accident reasons. From the figure, we can directly see that the deaths caused by speeding driving arranges in second, only inferior to the reason of other influencing factor, above all, far more than other illegal behavior causing death. The road traffic accident statistics annals also reports that the speed driving, converse driving and illegal meeting are the main accident reason, and there are 244 fatality accidents with 3 deaths each time and 33 with more than 5 deaths resulting from speeding driving, respectively accounting for the total 16.7%, 12.6%; that resulting from converse driving respectively accounting for the total 9.7%, 13.8%; that resulting from illegal meeting respectively accounting for the total 7.1%, 10.5%. Obviosly, speeding driving is one of the most serious road traffic illegal activities, also one of the primary causes of road traffic accidents. Therefor it is the main contents of law enforcement for traffic management department in the past, present and future to tackle speeding driving.

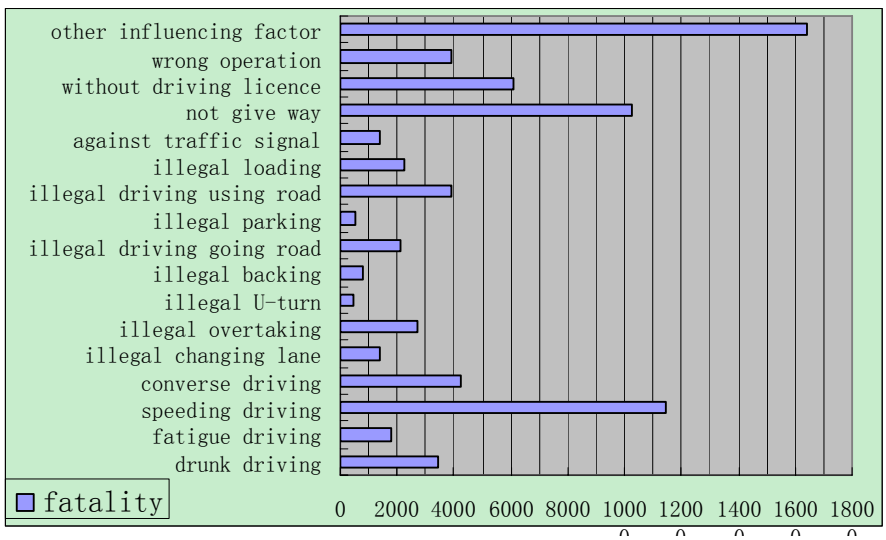

Figure 1 distribution of the traffic fatality accident reasons with driver in 2007.

2 The analysis of the formation process of speeding

2.1 The definition of expected speed

Expected speed refers to the driver hopes to achieve a highest “safe” speed without or generally without the influence of other motor vehicle (Ou Jushang, 2006). Here the meaning of “safe” speed is just the specific driver consider a kind of safe driving speed from individual mentally, but not the real meaning of road traffic safety speed. From the formation process of expected speed, it is a target speed which drivers get after considering all kinds of factors such as road condition, traffic condition, vehicle performance, climate condition and so on. It is going to have an effect on vehicle actual operation speed. Obviously the different individual driver has

different standard to the formation of "safe" speed, and so the expected speed is also different. From the aspect of psychology (Jin Zhifu, 2004), the process of formation can be divided into 4 stages: initially identification, adjustment, confirmation, and maintenance. It is a continuous cycle process, as shown in figure 2.

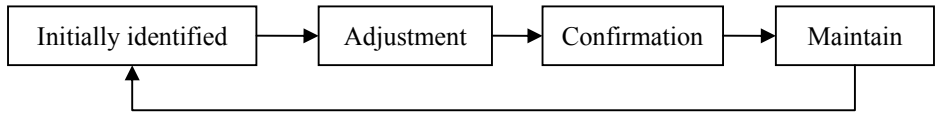

Figure 2 The formation process of expected speed.

2.2 Mechanism of speeding driving formation

According to the above driving behavioral analysis, in the driving process, the vehicle drivers continuously collect the information of road alignment, pavement condition, traffic flow, natural climate and so on, and analyse the information in order to identify the expected speed. At last, the analysis result is distributed to hands or feet to control the speed of vehicle, then the driver continuously adjust the vehicle speed in a safe range in the light of information obtained. On the contrary, if driver has carried on the wrong analysis in various stages, and the correction ability don't prompt play a role, speeding will happen. Therefore, speeding driving may exist in following svevral stages owing to wrong judgment or incorrect operation.

1) Not get comprehensive information in the stage of obtaining traffic information. The drivers don't obtain comprehensive traffic information in time, so they make incomplete analysis and judgment only on the basis of partial information, thus resulting in wrong analysis result and speeding driving. For example, the driver did not see speed limit sign and line because of the lack of concentration, thus the actual speed of vehicle exceeds the speed limit.

Make wrong analysis and judgment in the stage of analysis and judgment of traffic information.

2) The drivers make wrong analysis and judgment. This is due to the decline of driver's ability to analyze and judge temporarily. Fatigue driving, drunk driving, sudden illness or lack of driving experience and other factors may cause the driver's ability to reduce, and can't do correct analysis and judgment base on the obtained traffic information, which lead to the expected speed higher than safet driving speed, thus result in speeding.

3) Do wrong operation in implementation stage. The drivers obtain comprehensive and true traffic information in the stage of obtaining traffic information, and do correct analysis and judgment about this traffic information, and also output correct instruction to executive organ, but executive organ make an error in the implementation of instruction because it did not follow the enter instruction. That results in the actual speed of vehicle exceeding the safe driving speed. This is

mainly due to the driver's lack of experience and good psychological quality.

4) Drviers' correction ability does not play a role in time. At the aforementioned every stage, if drivers' correction ability can play a role in time, the speeding driving can be prevented. On the contrary, after the drivers making wrong analysis and judgment, driver's correction ability doesn't play a role in time, so the vehicle's driving speed exceeds the safe speed. The primary reason is that drivers are absent minded, fatigue driving, driving under the influence of alcohol, inexperience, paroxysmal sickness and so on.

3. The relationship between speeding rate and traffic volume in expressway

Expressway's speeding rate and traffic volume have the direct relation (Pei Yulong et al, 2004). Thinking from the direct-viewing angle, we usually believe that along with the increase of traffic volume, the freedom of vehicle driving falls, so the possibility of speeding reduces. But in actual data analysis process, author discovered that when traffic volume was small, the speeding rate increased along with traffic volume increase; when traffic volume was more than a critical value, the speeding rate reduced along with traffic volume increase. Next this problem will further explain through a concrete measured road section.

Yuyi expressway in Chongqing

Yuyi expressway is a expressway from Chongqing to Yi'chang in Hubei province. The entire line is 266 kilometers. Yuyi expressway has three sections, which respectively are Chongqing to Chang'shou, chang'shou to liang'ping, liang'ping to wan'zhou. One half is old (section of Chongqing to Chang'shou, open in 2000), the other half is newly built (sections of chang'shou to liang'ping and liang'ping to wan'zhou, open in 2003). There are two lanes in each direction in old section and three lanes in each direction in new sections. The new sections is obviously better than the old in road alignment and pavement condition, therefore speeding driving is very serious in new sections. The design speed of Yuyi expressway is 80 km/h and there is only one speed limit value 80 km/h on the entire line. The examination spot we choosed was a straight line segment, in the direction of leaving Chongqing. The grade is 0.5% and the examination period is 24 hours. The data collected is grouped for every hour. Table 1 lists the statistic analysis.

Carrying on the regression analysis with the data in above table, we obtained the quadratic curve relation between speeding rate and traffic volume per lane. The relation model as follows:

$$SR = 14.409 + 0.667Q - 0.002Q^2 \qquad (1)$$

Where SR——speeding rate（%）;

Q——traffic volume（pcu/h/lane）

The model is showing that with the increase of traffic volume, the speeding rate doesn't always reduce, but the speeding rate is increasing first and then reducing. So traffic management department could focus on control when speeding rate is very

high, and thus improve law enforcement efficiency. Figure 3 is the relation curve figure between speeding rate and traffic volume.

Table 1 statistic analysis between speeding rate and traffic volume in Yuyi expressway

Time	Traffic volume /pcu	Speeding vehicle /pcu	Traffic volume per lane/(pcu/h/lane)	Speeding rate /%
0	128	53	42.67	41.41
1	113	39	37.67	34.51
2	76	19	25.33	25.00
3	80	28	26.67	35.00
4	94	23	31.33	24.47
5	99	34	33.00	34.34
6	185	114	61.67	61.62
7	528	434	176.00	82.20
8	650	548	216.67	84.31
9	769	623	256.33	81.01
10	747	607	249.00	81.26
11	598	459	199.33	76.76
12	426	316	142.00	74.18
13	568	433	189.33	76.23
14	582	474	194.00	81.44
15	571	445	190.33	77.93
16	553	431	184.33	77.94
17	470	387	156.67	82.34
18	357	258	119.00	72.27
19	377	284	125.67	75.33
20	340	232	113.33	68.24
21	281	170	93.67	60.50
22	195	107	65.00	54.87
23	195	101	65.00	51.79

4 conclusion

This article explains the formation process of speeding driving from the aspect of expected speed, and further carry on regression analysis with actually measured data. At last, the relation model is obtained, which provides a theoretical basis for controlling speeding driving behavior. But also there are some problems. Because of the sample size, whether the model is universal or not is still needs further study; for different expressways, the influencing factor of inflexion point on the model curve needs to be further discussed.

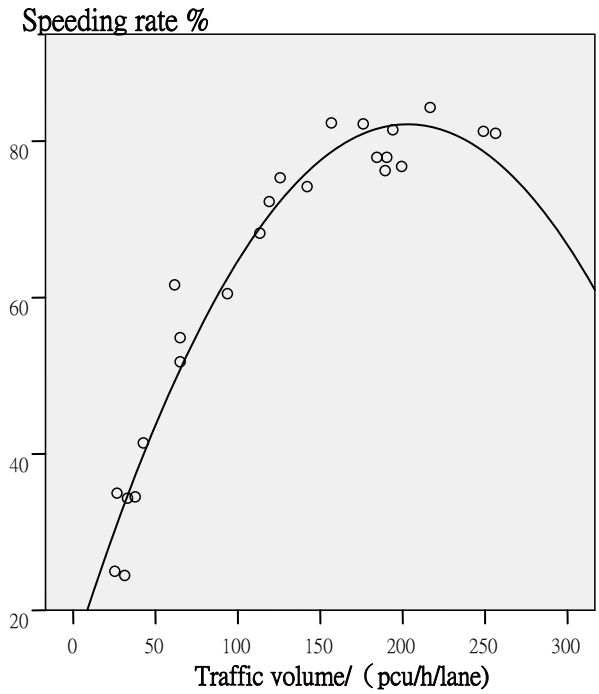

Figure 3 the relation curve between speeding rate and traffic volume in Yuyi expressway

REFERENCES

Huang Changjie (2004). The implementation of the road traffic safety regulation. BeiJing. China Communications Press

Traffic Management Bureau in Ministry of Public and Security (2007). The PRC's road traffic accident statistics analysis

Ou Jushang (2006). Countermeasure analysis of the vehicle's travelling over speed limit. Journal of Transportation Engineering and Information, volume: 4, issue:4

Jin Zhifu. Traffic psychology (2004). Beijing: China People Public and Security University Press,2004

Pei Yulong,Wang Wei. (2004). Road traffic accident causes and prevention countermeasures. Beijing: Science Press

Vehicle Tracking from Videos Based on Mean Shift Algorithm

Xiong Chang-Zhen[1] Pang Yi-Gui[1] Li Zheng-Xi[1] Liu Ya-Li[1] Li Ying-Hong[1,2]

[1]Laboratory of Intelligent Transportation System, North China University of Technology Beijing 100144; PH: 010-88802861-802; email: {xczkiong & pygncut}@163.com
[2] School of Information and Engineering, University of Science and Technology Beijing, Beijing 100080; PH: 010-88802226; email: lyh427@ncut.edu.cn

ABSTRACT

Vehicle tracking is one of the essential tasks in a video-based Intelligent Transportation System. A novel method for vehicle tracking is proposed in this paper. First, we analyze the disadvantages of the traditional parameterized model and compare them to the merits of the nonparametric model. Then the mean shift algorithm is deduced by using kernel density estimation in multi-dimensional space. Its convergence is proven using a simple method. In order to overcome the disadvantages of the original mean shift algorithm, this paper proposes an adaptive template and a kernel weights selecting method. The new method accelerates the convergence speed of the algorithm. When we apply this adaptive method, the experimental results show that the proposed method performs well with video-based vehicle tracing.

INTRODUCTION

The mean shift algorithm (Cheng, 1995) is derived from the density gradient of probability distribution which was first proposed by Fukunaga (1975). Due to the complexity of the feature space, it is hard to use a common parameter model to estimate the distribution of the feature space in a computer image (Duda, 2001). But this approach is promising when used in nonparametric estimation. While inadequate in the sample distribution, the density distribution can be directly described by samples in nonparametric estimation. Meanwhile it can be used to analyze any feature space. The kernel estimator mentioned in the paper (Cacoullos, 1966) is a frequently used nonparametric estimation function. Though conditions for traditional parameter estimation are very strict, the distribution model of the feature space can be known in advance. However, the distribution should be estimated approximately, according to the samples, and a traditional parameter estimation method may lead to a large error in the data. Our approach, using nonparametric estimation can overcome these shortcomings. Thus this paper proposes a novel vehicle tracking method based on a nonparametric estimation.

Nonparametric density estimate functions (Parzen,1962, Rosenblatt,1956) have been used widely in object tracking, image segmentation, information fusion and so on (Fashing and Tomasi, 2005; Li and Tang, 2008; Minwoo Park, 2008; Tao, 2008; Li, 2008). Usually, a histogram is considered to be the simplest nonparametric estimate in many cases. In addition, the kernel density estimation and the neighborhood estimation are also regarded as being types of nonparametric estimation. The kernel density estimate is the most common nonparametric density estimation. The most commonly used kernel functions include the Gaussian kernel function, the Polynomial kernel

function, the Sigmoidal kernel function, and so on. The advantage of using nonparametric technology is that it does not require a priori knowledge, but only requires the taking of samples. Thus it is has been widely used in object tracking (Z. Li and Tang, 2008; Park, 2008; P. Li, 2008).

MEAN SHIFT ALGORITHM

Definition 1:Let $k(x)$, $x \in [0,+\infty)$ be a positive function and monotone decreasing, if it satisfies

$$\int_0^{\infty} k(x)dx < +\infty \quad , 0 < k(0) < +\infty \tag{1}$$

Then $k(x)$ is a kernel function (e.g. $k(x) = e^{-x}$). The Gaussian kernel is the most commonly used kernel function. It is here defined as $k(\| x - x_c \|) = \exp(-\| x - x_c \|^2 / (2\delta^2))$, where x_c is the kernel center, and δ is a parameter used to modulate the radial range of the kernel.

Definition 2: Let $k(u)$ $u \in (-\infty,+\infty)$ be a measurable Borel function (X. Liu, 2001), for a given constant h_n ($h_n > 0$) and a data set $s = \{x_i, i = 1...n\}$ (where n-dimensional space), if the corresponding kernel function is $k_h(x)$, then the density function $f(x)$ at the point of x can be estimated as

$$f_n(x) = \frac{1}{n}\sum_{i=1}^{n} k(x - x_i) = \frac{1}{nh_n}\sum_{i=1}^{n} k(\frac{x - x_i}{h_n}) \tag{2}$$

Here $k(\cdot)$ is the kernel function and x is the center of the kernel. If the samples are adequate, the estimated density function can infinitely approximate the real density function. However, in multi-dimensional space, the point x can be represented by a vector and it has $\| x \|^2 = x^T x$. Correspondingly, the kernel function $K(x)$ mentioned in (1) became a multi-variable kernel function (also named under Radial symmetry kernel function), where $K(x) = ck(\| x \|^2)$ and $k(x)$ is the profile function of $K(x)$, $x \geq 0$ and c is a normalized constant. In d -dimensional Euclidean space R^d , if $k_\Sigma(x)$ is the kernel function, then the probability density can be defined as

$$\hat{f}(x) = \frac{1}{n}\sum_{i=1}^{n} k_{\Sigma_i}(x - x_i) \tag{3}$$

Here

$$k_{\Sigma_i}(x - x_i) = c_{k,d,i}\left|\Sigma_i\right|^{-1/2} K(\Sigma_i^{-1/2}(x - x_i)) = c_{k,d,i}\left|\Sigma_i\right|^{-1/2} k(\| x - x_i \|^2_{\Sigma_i}) \tag{4}$$

And here, $\| x - x_i \|^2_{\Sigma i} = (x - x_i)^T \Sigma_i^{-1}(x - x_i)$ is Manhatton distance, and Σ is the bandwidth of the matrix. A different sample point has a different effect on the kernel function, thus (2) can be refined as

$$\hat{f}(x) = \sum_{i=1}^{n} w_i k_{\Sigma_i}(x - x_i) \tag{5}$$

Where w_i is the weight at the sample point x_i, and it has $\sum w_i = 1$, $w_i \geq 0$. Thus the density function of $f(x)$ is obtained:

$$\hat{f}(x) = \sum_{i=1}^{n} w_i c_{k,d,i} |\sum_i|^{-1/2} k(\|x - x_i\|^2_{\Sigma_i}) \tag{6}$$

Here $\sum_i$ ($d \times d$ dimension) is the sample covariance. In order to reduce the calculation, it uses $\sum_i = diag(h_1^2 .....h_d^2)$ or $\sum_i = h^2 I_d$. Substitute $\sum_i = h^2 I_d$ to (6), the kernel density estimation of the function becomes

$$\hat{f}(x) = \frac{c_{k,d,i}}{n^d} \sum_{i=1}^{n} w_i k(\left\| \frac{x - x_i}{h_n} \right\|^2) \tag{7}$$

In order to obtain the largest data density distribution zone, the density gradient estimation can be used. The kernel density gradient is equivalent to the partial differential with the variable x in (6). Then we have

$$\nabla \hat{f}(x) = 2c_{k,d} \sum_{i=1}^{n} w_i \sum_i^{-1} \sum_i^{-\frac{1}{2}} k'(\|x - x_i\|^2_{\Sigma_i})(x - x_i) \tag{8}$$

Let $g(x) = -k'(x)$, then

$$\nabla \hat{f}(x) = 2c_{k,d} \sum_{i=1}^{n} w_i \sum_i^{-1} \sum_i^{-\frac{1}{2}} k'(\|x - x_i\|^2_{\Sigma_i})(x - x_i) = 2\sum_{i=1}^{n} w_i \sum_i^{-1} \sum_i^{-\frac{1}{2}} g(\|x - x_i\|^2_{\Sigma_i}).m_{\Sigma_{i,g}}(x) \tag{9}$$

Equation (9) contains two parts. The second part is defined as the mean shift vector: $m_{\Sigma_{i,g}}(x) = \sum_{i=1}^{n} w_i x_i \sum_i^{-1} |\sum_i|^{-\frac{1}{2}} g(\|x - x_i\|^2_{\Sigma_i}) / \sum_{i=1}^{n} w_i \sum_i^{-1} |\sum_i|^{-\frac{1}{2}} g(\|x - x_i\|^2_{\Sigma_i}) - x$ (10)

From definition 2, we know that $g(x)$ is the profile function of the $G(x)$, and it has $G(x) = g(\| x \|^2)$. Let

$$\hat{f}_{\Sigma i,g}(x) = 2\sum_{i=1}^{n} \hat{w}_i |\sum_i|^{-1/2} g(\|x - x_i\|^2_{\Sigma_i}) \tag{11}$$

Where $\hat{w}_i = w_i \sum_i^{-1}$, then we have

$$m_{\Sigma i,g}(x) = \nabla \hat{f}(x) / 2\hat{f}_{\Sigma i,g}(x) \tag{12}$$

Obviously, $m_{\Sigma i,g}(x)$ is direct proportion to $\nabla \hat{f}(x)$. This indicates that the kernel center always shifts to the largest spatial density of the samples. Now suppose that the target center x is initialized as x_0. It iterates j times, the centre point shifts to x_j. Then the iterative formula at the time $j+1$ is

$$x_{j+1} = x_j + m_{\Sigma_{i,g}}(x) = \sum_{i=1}^{n} w_i x_i \sum_i^{-1} |\sum_i|^{-1/2} g(\|x - x_i\|^2_{\Sigma_i}) / \sum_{i=1}^{n} w_i \sum_i^{-1} |\sum_i|^{-\frac{1}{2}} g(\|x - x_i\|^2_{\Sigma_i}) \tag{13}$$

$w_i = 1/n$ is used in many papers (Parzen, 1962; Rosenblatt,.1956; Xue,1993; Fashing and Tomasi, 2005), but this is not reasonable. This is because different distances between the sample points would produce different effects on the object. Thus this paper proposes a novel method, using an adaptive weight algorithm. The weight is

$$w_i = \exp(\lambda[1 - (x_i - y_j)^2 / \sigma_j^2])/n, \text{ and } \sum_{i=1}^{n} w_i = 1 \tag{14}$$

Where λ is a normalized coefficient and it has

$$\sigma_j^2 = \frac{1}{n}\sum_{i=1}^{n}(x_i - y_j)^2 \tag{15}$$

For $\forall \varepsilon > 0$, if $\| m_{\sum i,g}(x) \| < \varepsilon$, the mean shift vector is obtained. Thus the program ends the iteration. As is well known, the convergence is very important to an algorithm. In this part, the convergence of the mean shift algorithm is proven. From the theorem 5.59 in the paper (Liu-gen, 2001), the kernel function is derivative at almost every point. That is to say, the Lebesgue measure is zero at the un-derivative points. If the definition of the un-derivative points is added, then $k'(x)$ exists in the whole definition domain of the kernel function $k(x)$. From the definition 2 of $k(x)$, $k(x)$ the monotone decreases and where larger than zero, at almost every point it is $k'(x) \le 0$. According to (6), the following result is obtained

$$\nabla \hat{f}(x) = 2c_{k,d} w_i \left|\sum_i\right|^{-\frac{1}{2}} k'(\left\|x - x_i\right\|^2_{\Sigma_i}) \sum_i^{-1}(x - x_i) \tag{16}$$

$$\text{Let} \quad Z_i(x) = -2c_{k,d} w_i \left|\sum_i\right|^{-\frac{1}{2}} \sum_i^{-1} k'(\left\|x - x_i\right\|^2_{\Sigma_i}) = 2c_{k,d} w_i \left|\sum_i\right|^{-\frac{1}{2}} \sum_i^{-1} g(\left\|x - x_i\right\|^2_{\Sigma_i}) \tag{17}$$

This shows that where $Z_i(x)$ is a positive definite matrix, then the density gradient becomes

$$\nabla \hat{f}(x) = \sum_{i=1}^{n} Z_i(x) x_i - \sum_{i=1}^{n} Z_i(x) x \tag{18}$$

Thus the mean shift vector is

$$m_{\sum i,g}(x) = [\sum_{i=1}^{n} Z_i(x)]^{-1} \sum_{i=1}^{n} Z_i(x) x_i - x \tag{19}$$

And the iterative algorithm is obtained

$$y_{j+1} = [\sum_{i=1}^{n} Z_i(y_j)]^{-1} \sum_{i=1}^{n} Z_i(y_j) x_i \tag{20}$$

If $\sum Z_i(y_j)$ is irreversible, then it has $y_{j+1} = y_j$. Thus it has $y_{j+1} = y_j$ only if $\nabla \hat{f}(x) = 0$. If it has $y_{j+1} \neq y_j$, then the direction of the vector moving is also the gradient direction according to (17)-(20). Thus the shift series moves towards to the increasing direction of the function value. We will prove that the shift series is rigidly increasing in the following part.

According to the definition of the kernel function, $k(x)$ is a bounded function. And $\hat{f}$ is also a bounded function according to (4-6). Thus $\hat{f}(y_j)$ is also a bounded function. In order to prove the convergence of $\hat{f}(y_j)$, we only need to prove $\hat{f}(y_j)$ monotonically increases when $j = 1,2,3\cdots$. The following results can be easily obtained (and the detailed derivation is omitted)

$$\hat{f}(y_{j+1}) - \hat{f}(y_j) \ge \sum_{i=1}^{n} c_{k,d} w_i \left|\sum_i\right|^{-1/2} g(\| x - x_i \|^2_{\Sigma_i}) \| y_{j+1} - y_j \|^2_{\sum_i} \tag{21}$$

When $y_{j+1} \neq y_j$, it has $\hat{f}(y_{j+1}) - \hat{f}(y_j) > 0$ from $g(x) \ge 0$. Thus for any given j, it satisfies $\hat{f}(y_{j+1}) - \hat{f}(y_j) \ge 0$. That is to say $\hat{f}(y_j)$ is strictly increasing. The monotonous series is a definitely bounded convergence, thus $\hat{f}(y_j)$ is convergent and $\hat{f}(y_{j+1}) - \hat{f}(y_j)$ converges to zero. $\| y_{j+1} - y_j \|$ is convergent from (20). Thus $\{y_j \mid j = 1,2,3....\}$ is a Cauchy series and convergent.

OBJECT TRACKING BASED ON MEAN SHIFT ALGORITHM

The basic tracking method is to find the best match between the objects from a video sequence. Suppose that the center of the candidate region of one object is y and the histogram in that candidate region can be expressed as

$$p(y,\sum_q)=\{\ \hat{p}_u(y,\sum q)_{u=1.....m}\ \} \tag{22}$$

where u is the eigenvalue which expresses a feature of the histogram that has $\sum \hat{p}_u(y,\sum q)=1$. The probability density function that belongs to u is

$$\hat{p}_u(y,\sum_q)=c\sum_{i=1}^{N_{\sum q}} K_{\sum q}(y-x_i)\delta[b(x_i)-u] \tag{23}$$

Where c is a normalization factor. If the distribution feature of the target model can be expressed as

$$\hat{q}_u=C\sum_{i=1}^{N_{\sum q}} k(\|\mathbf{x}_i^*\|^2)\delta[b(\mathbf{x}_i^*)-u] \tag{24}$$

The similarity between $\hat{q}_u$ and $p(y,\sum_q)$ can be measured by Bhattacharyya distance J_B, where $J_B=-\ln[\int \hat{q}_u p(y,\sum)]^{1/2}du$ (Maggio, 2005). To make J_B get the minimum value is equivalent to making $\int[\hat{q}_u p(y,\sum)]^{1/2}du$ get the maximum value. According to the discrete character of pixels, it has

$$\rho(\hat{q}_u,\hat{p}(y))=\sum_{u=1}^{m}\sqrt{\hat{q}_u p(y,\sum_q)} \tag{25}$$

If the image is in RGB color space, the degree of similarity in each subspace is described as

$$\hat{p}_t(y,\sum_q)=c\sum_{i=1}^{N_{\sum t}} K_{\sum q}(y-x_i)\delta[b(x_i-u_t)]\ t\in\{R,G,B\} \tag{26}$$

Then it has $\hat{p}(y)=\hat{p}_R(y,\sum_q)\times\hat{p}_G(y,\sum_q)\times\hat{p}_B(y,\sum_q)$. Thus the original template information can be described as $\hat{q}_u=\hat{q}_{u_R}\times\hat{q}_{u_G}\times\hat{q}_{u_B}$, where $\hat{q}_{u_t}$ is the color component information calculated by (24). In (25), the series can be expressed as using Taylor series expansion at $(y,\sum q)$

$$\rho(\hat{q}_u,\hat{p}(y))\approx\sum_{u=1}^{m}\sqrt{\hat{q}_u p(y_0,\sum_q)}+c\sum_{i=1}^{N_{\sum q}} w_i K_{\sum q}(y-x_i) \tag{27}$$

Here
$$w_i=\sum_{u=1}^{m}\sqrt{\hat{q}_u/p(y_0,\sum_q)}\delta[b(x_i)-u] \tag{28}$$

To maximize $\rho(\hat{q}_u,\hat{p}(y))$ is to obtain the second type maximum. It is surprising that to obtain the second type maximum we can deduce the Mean Shift vector, thus the mean shift algorithm can ensure the best match between templates of the objects.

According to Lindeberg theory (Bretzner and Lindeberg, 1998), the normalized density function of $\hat{f}(x)$ can be defined with the parameter r as $\hat{f}_r(x)$, and it satisfies

$$\hat{f}_\gamma(x)=|\sum_i|^{\frac{\gamma}{2}}\hat{f}(x)=\frac{1}{n}|\sum_i|^{\frac{\gamma}{2}}\sum_{i=1}^{n}k_{\Sigma_i}(x-x_i)=\sum_{i=1}^{n}w_i c_{k,d,i}|\sum_i|^{\frac{\gamma-1}{2}}k(\|x-x_i\|^2_{\Sigma_i}) \tag{29}$$

Computing the partial derivative of $\hat{f}_r(x)$ with Σ_i, then it obtains

$$\partial\hat{f}_\gamma(x)/\partial\sum_i=\frac{\gamma\text{-}1}{2}\hat{f}_\gamma(x)\sum_i{}^{-1}-\sum_{i=1}^{n}w_i c_{k,d,i}|\sum_i|^{\frac{\gamma-1}{2}}\varphi \tag{30}$$

$$\partial \hat{f}_\gamma(x)/\partial \Sigma_i = -\frac{\gamma-1}{2}\hat{f}_\gamma(x)\Sigma_i^{-1}[\frac{2}{\gamma-1}\psi - \Sigma_i]\Sigma_i^{-1} \quad (31)$$

Where $\varphi = k'(\|x-x_i\|^2_{\Sigma_i})(x-x_i)^T\Sigma_i^{-2}(x-x_i)$

$$\psi = (\sum_{i=1}^{n} w_i c_{k,d,i}|\Sigma_i|^{\frac{\gamma-1}{2}} k'(\|x-x_i\|^2_{\Sigma_i})(x-x_i)^T(x-x_i))/\hat{f}_\gamma(x) \quad (32)$$

And γ is a constant between zero and one. In (31), the changed value $\Delta\Sigma_i$ can be obtained by $2\psi/(r-1)-\Sigma_i$. $\Delta\Sigma_i$ and $\partial\hat{f}_\gamma(x)/\partial\Sigma_i$ are directly proportional according to (26). This ensures that the mean shift algorithm can find the best match between templates. Thus the adaptive iterative algorithm that uses the bandwidth Σ_i is $\Sigma_{i+1}=2\psi/(\gamma-1)$ .Thus the tracking algorithm can be implemented as follows: first, calculate $m_{\Sigma i,g}(x)$ and w_i , then assign $m_{\Sigma i,g}(x)$ to x , return to the first step until $\|m_{\Sigma i,g}(x)-x\|<\varepsilon$. Here, ε is a given error.

EXPERIMENTAL RESULTS

In order to verify the efficiency of the proposed method, many real-time traffic surveillance videos were tested on the VC++6.0 platform. Figure 1, Figure 2 and Figure 3 display tracking a white car, a red car, and a black car respectively. In these experiments, the algorithm adopted the adaptive kernel histogram. For the statistical characteristic of the adaptive kernel histogram, the mean shift algorithm achieved both faster convergence speed and higher sensitivity. Thus it fulfilled the needs of a real-time tracking environment. However, the histogram may vary even while tracking the same car at different times. This is because tracking a moving car in different scenes may capture different initial information at each different initial time. But our adaptive mean shift algorithm can effectively track the same car in different scenes. In the experiment, the algorithm can track the moving vehicle traveling between 10 and 130 km per hour. In Figure 1, the white car has a speed of 20 km per hour. In Figure 2, the red car is traveling at 100 km per hour. Figure 4 shows the results of multiple vehicles being tracked at the same time, where the moving speed ranges from 90 to 120 km per hour.

Figure 1. One white car tracking result.

Figure 2. One red car tracking result.

Figure 3. One black car tracking result.

Figure 4. Multi vehicles tracking results.

CONCLUSION

A mean shift algorithm is a non-parameter estimation method based on a density gradient. It can converge to a stable point of a recent probability density function. So a mean shift algorithm can be used in video tracking. In video tracking based on mean shift algorithm, the bandwidth of the kernel has a significant impact on the estimated results. This is because the mean shift kernel bandwidth not only determines the quantity of the samples which involve in the iterative algorithm, but also reflects the size of the tracking window. However, in many papers, the kernel bandwidth is determined by the initial tracking window, and does not change during the whole tracking procedure. This can result in a great location error. Thus this paper proposes the changed-scale adaptive tracking algorithm, where the kernel bandwidth is adaptively adjusted. So the change of the kernel bandwidth is directly proportional to the gradient of the kernel density function.

Thus this new method overcomes the disadvantage of the original mean shift algorithm by using the adaptive bandwidth and weights. This proposed method accelerates the convergence speed of the algorithm. The adaptive method is effectively applied to video-based vehicle tracking. And the vehicles tracked in our experimental results have shown that the new algorithm performs well in video-based tracking.

ACKNOWLEDGEMENTS

This paper was partly funded by the Scientific Research Common Program of the Beijing Municipal Commission of Education (KM200910009001) and PHR(IHLB).

REFERENCES

Bretzner, L. and Lindeberg, T. (1998). "Feature tracking with automatic selection of spatial scales", *Computer Vision and Image Understanding,*71(3): 385-392.

Cacoullos, T. (1966). "Estimation of a multivariate density". *Annals of the Institute of Statistical Mathematics*, vol.38(2), pp.179-189.

Duda, R.O., Hart, P.E., and David, G. (2001). *Pattern Classification,* 2nd edition. John Wiley & Sons, New York.

Fashing, M. and Tomasi, C. (2005). "Mean Shift Is a Bound Optimization", *IEEE Transactions On Pattern Analysis And Machine Intelligence*, Vol. 27(3),pp. 471-474.

Fukunaga, K. and Hostetler, L.D. (1975). "The estimation of the gradient of a density function, with applications in pattern recognition". *IEEE Transactions on Information Theory*, 21(1):pp.32--87.

Li, P. (2008). "An Adaptive Binning Color Model for Mean Shift Tracking", *IEEE Transactions On Circuits And Systems For Video Technology* ,Vol. 18(9),pp.1293-1299.

Li, Z., Tang Q.L., and Sang, N. (2008). "Improved mean shift algorithm for occlusion pedestrian tracking", *Electronic Letters*, Vol. 44,(10), pp.622-623.

Maggio, E. and Cavallaro, A. (2005). "Hydrid particle filter and mean shift tracker with adaptive transition model". *Proc. of IEEE Signal Processing Society Interna-*

tional Conference on Acoustics, Speech, and Signal Processing (ICASSP), Philadelphia, PA, USA.

Park, M., Liu, Y., and Collins, R.T. (2008). "Efficient Mean Shift Belief Propagation for Vision Tracking", *Proc. of CVPR* :pp.1-8.

Parzen, E. (1962). "On estimation of a probability density function and mode". *Annals of the Institute of Statistical Mathematics*,Vol.33(3), pp.1065-1076 .

Rosenblatt, M. (1956). "Remarks on some nonparametric estimates of a density function". *Ann. Math. Stat*, vol. 27(3), pp.832-837.

Tao, W., Jin, H., and Zhang, Y. (2007). "Color Image Segmentation Based on Mean Shift and Normalized Cuts", *IEEE Transactions On Systems, Man, And Cybernetics—Part B: Cybernetics*, Vol. 37(5),pp.1382-1389.

Xue, C. X. (1993). *Real function theory and functional analysis*. Beijing:Higher Education Press, pp. 187-188, (in Chinese).

Xue, L., and Pan, M. (2001). "Strong convergence rates of the double kernel estimates of conditional density", *Chinese Journal of Engineering Mathematics*. vol.18 (1), pp. 89-93.

Yizong Cheng. (1995). "Mean Shift, Mode Seeking, and Clustering", *IEEE Transactions on Pattern Analysis and Machine Intelligence*, vol. 17(8), pp. 790-799.

The Evaluation of Micro-benefit on Highway Construction Investments

CHEN hong [1] and TIAN Yujia[2] and XIAO Dianliang[3] and WANG Fengxia[4]

[1]Traffic Engineering Department, Highway College, Chang'an University, P.O. Box 487, Shaanxi Xi'an, 710064; PH :86-29-82334432; email: hongchen82@126.com
[24]Traffic Engineering Department, Highway College, Chang'an University, P.O. Box 487, Shaanxi Xi'an, 710064; PH&FAX:86-29-82334886; email: sean8205@126.com
[3]China Academy of Transportation Sciences, Ministry of Communications, No.240 Huixinli, Chaoyang District,Beijing,100029, China; email: sean8205@163.com

ABSTRACT

Based on the principles of investment management, this paper analyzes the content of statistical indicators of investment benefit in highway construction, and establishes a relevant index system. Finally, it employs fuzzy comprehensive evaluation methods to evaluate the micro-benefit of a highway construction project in Shaanxi Province tests the feasibility of evaluation index systems. The results indicate that this method could have strong maneuverability and practicability.

INTRODUCTION

While the global financial crisis has impacted the Chinese economy, it has providing an economic "lubricant" for its transportation infrastructure. In order to boost domestic demand and promote sustained growth, the Chinese Government has proposed a business encouragement policy with the investment of 4000 billion yuan by the end of 2008. At the same time, the Ministry of Transport is also planning a investment plan of 5 trillion yuan in 3-5 years, in which the vast majority of funds are used for highway construction. These measures are intended to achieve maximum investment returns with minimal input, which is the common goal of any investment activity (Yuan et al. 2001). Setting up a complete system of statistical indicators with investment benefits is necessary in order to adapt to the increasing investment in highway construction and the rapid development of highway transportation. Thus, in order to attain the goal of investment in highway construction, in this article the system of statistical indicators on investment benefits is established to study the evaluation of investment micro-benefit in highway constructions.

THE MICRO-BENEFIT EVALUATION INDEX SYSTEM

The Connotation of Statistical Indicators of Investment Efficiency. Investment benefit is an aspect of the relationship between the effective results of an investment and labor, namely the relationship between highway construction input

and output (Zhou et al. 1998). From the input perspective, investment activities have three main details: funds, materials and manpower. The output of highway construction investment activities is mainly displayed by new fixed assets and new engineering benefits.

The calculation of various indexes through comparing investment input and output and construction represents concrete forms of investment efficiency. Investment efficiency is a broad category, but can be divided into investment economic efficiency, investment social efficiency and investment environment efficiency. This paper primarily studies investment economic efficiency. The investment efficiency index must reflect economic efficiency and the contrast relationship between the output and input of the highway construction process. Namely, the investment efficiency index must be the opposite index rather than the gross index.

There are various indexes reflecting the economic benefit of investment. When considering the characteristics of the highway construction process and, in order to adapt to the needs of investment classification management according to the economic benefit of investment, it is important to divide investment benefit indexes into micro and macro categories. This paper mainly studies micro investment benefit evaluation.

The Determination of Micro-benefit Evaluation Indexes. Considering comprehensive, comparability, and operability principles, the following premise is investigative, universal, and covers all aspects of investment efficiency. It also reflects different information in that it determines microscopic evaluation index systems according to the different stages of highway project construction, as follows:

Construct prior microscopic evaluation efficiency index. The evaluation of prior construction in investment benefits primarily reflects controls over the investment decision-making as a feasibility study, (exploration design as well as the design progress). This paper chooses a project decision-making periodic rate and the design cycle rate. When applying the project decision-making periodic rate, the computed value should be 0 if the benefit is good. If not, explain prophase work plan is not accurate enough. When applying the project design cycle rate, the actual design cycle in the actual work should be stipulated in the contract design cycle. The value of the project design cycle rate should be near 0. If not, the contract is not practical enough or there are some problems with design work. The preparatory work and the quality of design are hard to guarantee.

Microscopic investment efficiency indicators in complete period. For the benefit of the project construction period, it reflects on the achievements of investment namely new project efficiency, quality, etc, Selected index is as follows:

The investment accomplishment ratio should have an optimal value of 100%.The project benefit accomplishment ratio value is between 0~1. From this numerical size we can see the construction section of project. The value is close to 1, the project close to completion. ③The accumulated fully funded ratio should reflect the progress of the project. With the capital progressively in place, the value should increase gradually from 0 to 1. If unplanned factors such as a rise in materials' price occurs and the extended construction period results in accumulated funds that are more than the total amount of the plan, the value is more than 1. For the project plan accomplishment ratio, check the implementation of the project with the index. The optimal value should be at 100%. An excellent project ratio reflects the quality of project construction. Only good quality can ensure good benefits. The optimal value is 100%.

Microscopic investment benefit indexes for completed period. Completed period means the project is completely consigned for use. Define unit mileage construction cost ratio and construction period ratio to reflect the benefit variation of this stage. Unit mileage construction cost rate should reflect the bias between actual cost and investment plan in unit mileage of a single project. It is convenient for project managers to analyze investment cost saving or waste. The optimal value is near zero. The construction period variation refers to the deviation degree between the actual construction period and the national project unified quota period, or designed and planned schedule. The actual construction period is more or less than the planned construction period .The optimal value should be nearby 0. However, this does not mean that a shorter time is better. A too-short time period will not guarantee quality. Too long will affect the investment benefit.

A structure drawing of the above-mentioned indexes and investment benefit in each construction process is shown in Figure 1.

THE EVALUATION METHOD OF INVESTMENT MICRO-BENEFIT

In order to enable management and decision-making that will precisely assess and analyze the investment effectiveness based on the above established index system of the investment micro-benefit in highway construction projects, a comprehensive evaluation of investment effectiveness must be carried out by synthesizing all of the gained statistical information of the investment. In this paper we apply the Fuzzy Comprehensive Evaluation method to comprehensively evaluate the investment micro-benefit in a highway construction project by making a comparison with the same period (Ma et al. 2005). The concrete steps of evaluation are as follows:

Ascertain the set of comment grade $V=(v_1,v_2,v_3,v_4,v_5)$.The set of comment grade is expressed as five grades: bad, below average, average, above average and

good with v_1、v_2、v_3、v_4 and v_5.

Construct the evaluation index system (general goal criterion index).

Corresponding to the established evaluation index system above, the hierarchical structure of evaluation is made up as follows.

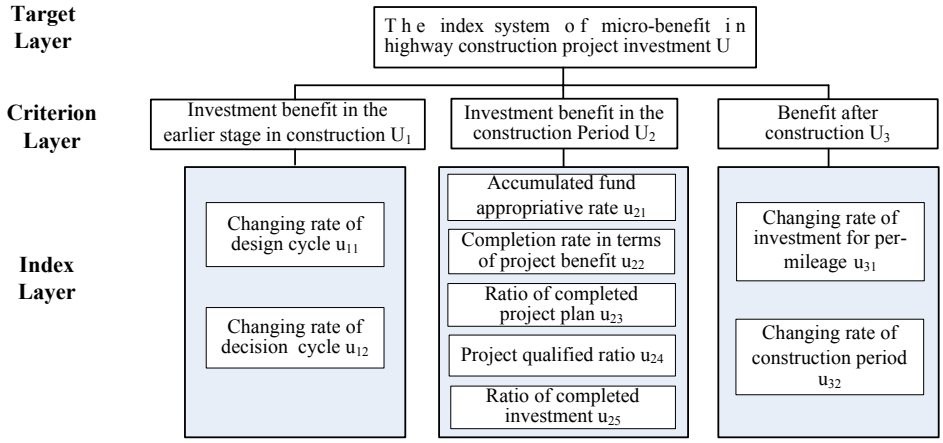

Figure 1.The Hierarchical Structure of Evaluation Indexes of Micro-Benefit.

Ascertain weighing. Ascertain the weighing vector A_t(t=1、2、3) about the bottom layer of index relative to criterion layer, and the weighing vector A about criterion layer relative to the overall goal. Each weighing vector is shown as A_1(a_{11}, a_{12}), A_2(a_{21}, a_{22}, a_{23}, a_{24}, a_{25})，A_3(a_{31}, a_{32})，A(a_1,a_2,a_3). This article determines weights using AHP and constructs the judgment matrix subjectively by multiple comparisons among indexes, then deals with figure and consistency tests according to judging matrix. From there, the relative importance weights of each indicator can be concluded.

Ascertain the grade of membership function of each level according to the content and its number range of each index.

For each index value under each criterion layer, ascertain its vector of membership degree R_{tj} (t=1,2,3;j=1,2,3,4,5);

For each criterion, construct the matrixes of membership degree R_t=(R_{t1}，R_{t2},….) by its membership vector, and solve the vector of membership degree B_t= A_t • R_t of each index;

Construct the matrixes of membership degree R=[B_1, B_2, B_3]of each criterion about overall goal by B_t, and solve the vector of membership degree B=A • R；

Solve the fuzzy evaluation value W=B·V^T of project investment effectiveness, in which V^T=(20，40，60，80，100) is the set of comment grade and W is single value. We can evaluate the quality by comparing W value of evaluation objects to comment grade.

Table 1. The Criterion of Grade and Comment.

Criterion	0～20	20～40	40～60	60～80	80～100
Comment Grade	bad	below average	average	above average	good

Use the above method for highway construction projects to evaluate the micro-benefit of investment for highway construction projects. Make certain the level and position of effectiveness is according to the evaluation scores of investment performance for construction projects.

EXAMPLE ANALYSIS

By using 2002 for the evaluation base year, this article takes Yulin-Jingbian expressway in Shaanxi province as an evaluation project to count and evaluate its investment performance. YuJing expressway is the first desert highway (134.174km) with 1.817 billion yuan in its project budgetary estimate. The project started in December 15, 1999 and ran until late September 2003. The practical project ran ahead 40 days of its planned duration of 39 months.

Determine the index weight. At the start of the evaluation, five experts were asked to determine the evaluation matrix according to the relative importance between the various indicators. The evaluation matrix included too many indicators to list.. For more details see references (Chang'an University, 2006).The forms judged by each experts were collated, and each expert's individual weight vectors of sub-indicators and indicators were calculated using AHP. Then the average weight vectors were worked out to educe the weight matrix A_1,A_2,A_3 of indicators strata and the weight matrix A of criterion strata.

A_1 = (0.29, 0.71) A_2 = (0.09, 0.17, 0.17, 0.50, 0.07)

A_3= (0.333, 0.667) A = (0.137, 0.625, 0.238)

In order to ensure the horizontal comparability of investment returns between different construction projects, each evaluation index weight adopts a unified standard.

Evaluation result. After working out the relative weight of each index, the evaluations of estimate, which reflect the different construction phases of the project investment efficiency were calculated. The final evaluation result W is shown in Table 2.

Table 2. The Evaluation Result of investment efficiency of Yujing Expressway.

Project Name	**Composite Scores**	**Total Comment**
Yulin-Jingbian Expressway	88	good
Each Index Name	**Actual Value of Index**	**Comment**
Changing rate of decision cycle	0.3333	below average

Changing rate of design cycle	-0.25	good
Accumulated fund appropriative rate	0.7401	above average
Completion rate in terms of project benefit	1	good
Ratio of completed project plan	——	——
Project qualified ratio	0.8065	good
Ratio of completed investment	1.0004	good
Changing rate of investment for per-mileage	-0.2685	good
Changing rate of construction period	-0.037	good

From the project evaluation results we can see that the overall investment performance of Yujing expressway is excellent, and the evaluation of sub-indicators in each phase of pre-construction, construction and construction completed are good or above average**.** The results indicate that the project not only shows good benefit in the pre-decision making and design aspects, but also in the organization and management of the construction process.

CONCLUSIONS

(1) Based on the analysis of the effective statistical indicators in highway construction investment, and according to the different construction phases of highway projects, this article sets up an evaluating index system of the investment micro-benefit in highway construction projects.

(2) Using the theory of fuzzy comprehensive evaluation combined with qualitative and quantitative analysis, the investment micro-benefit evaluation model in terms of a highway construction project is established. Finally, examples demonstrate the interoperability and practicability of the method to enhance the scientific and objective features of decision-making.

(3) To improve the evaluation system, the concrete usage should also be included. Some issues such as membership grade should be resolved gradually in follow-up studies in order to improve the reliability of the method.

REFERENCES

Chang'an University (2006).Highway Construction Investment Returns System of Statistical Indicators, 2003.

Ma, R., and Liu, Y. (2005).Weight value determination method of highway construction comprehensive evaluation. Journal of Traffic and Transportation Engineering, Vol. 25, No. 2, 2005, pp. 110-112.

Yuan, J., and Zhu, W. (2001). Study on Post-Evaluation of Highway Construction Projects. Highway, Vol.53, No. 6, 2001, pp. 63-69.

Zhou, W., and Wang, X. (1998).Road Economics and Management.China Communication Press, Beijing,1998.

Noise Source Identification and Noise Reduction of a Double Crank Four Ring-Plate-Type Cycloid Reducer

B. Yang [1], Y. Liu[2] and X. Zhang[2]

[1]School of Mechanical Engineering, Dalian Jiaotong University, P.O. Box 343, Dalian China, ST116028; PH(086) 411-84106584; email:yangbing@djtu.edu.cn
[2]School of Traffic and Transportation Engineering, Dalian Jiaotong University, Dalian China, ST116028

ABSTRACT

A double crank four ring-plate-type cycloid reducer is a new drive that has high load capacity and high transmission efficiency. The vibration and noise tests of the reducer prototype are completed using the HEAD acoustics multi-channel noise test and analysis system. The noise distributing laws of the reducer surface at different rotational speeds and different loads are obtained. The main noise sources of the reducer are identified as the noise: 1) generated by involute spur gears when they mesh; 2) generated by the four ring-plates and cycloidal gear; and 3) radiated by the cylinder block vibration because of internal excitements. The relevant noise reduction measures are proposed for each of these noise sources. The experiment results show that noise reduction is achieved.

INTRODUCTION

A cycloidal pinwheel drive provides many advantages, including low volume, light weight, a high reduction ratio and high efficiency. The double crank four ring-plate-type cycloid reducer driven by three gears requires no output unit and the stiffness of the output shaft is high. The tumbler bearings are placed outside the gear, instead of inside the gear as in the traditional cycloid planetary drive. Hence, the size of the bearings is no longer restricted. The double crank four ring-plate-type cycloid reducer is able to transfer larger torques than a typical planetary cycloid drive. So, it is a new drive with large value of research and development (He W.D., 2000; Li L.X., 2005; Li X., 2004). However, it generates great noise, as does other machinery, that causes great harm to workers' health. So, noise reduction research is very urgent. The vibration and noise tests of the reducer prototype are completed using the HEAD acoustics multi-channel noise test and analysis system. The characteristics of the vibration and noise are obtained and the noise sources are identified. The paper also identifies appropriate noise reduction measures.

NOISE SOURCE IDENTIFICATION

Test contents.

The vibration and noise tests of the reducer prototype are completed using the

HEAD acoustics test and analysis system in an ordinary laboratory. Two noise test points and ten vibration test points were positioned in the test procedure. The location of the test points is shown in Figure 1. In order to grasp the noise distributing laws of the reducer, four different speeds and four different loads were selected. The four rotational speeds are 500 rotations per minute, 750 rotations per minute, 1000 rotations per minute and 1500 rotations per minute, respectively. The four loads are 25%, 50%, 75% and 100% of the full load, respectively.

Figure 1. Location of the test points.

Calculation of noise and vibration frequency generated by the reducer.

Noise and vibration frequency generated by involute spur gears.

The meshing frequency of gears can be expressed as

$$f_n = \frac{nz}{60} \tag{1}$$

where n is the gears speed and z is the teeth number of the gears.

The shaft frequency can be expressed as

$$f_s = \frac{n}{60} \tag{2}$$

The actual meshing frequency can be expressed as (He Yunru,1998)

$$f = lf_n \pm mf_s \tag{3}$$

where l and m are arbitrary integers. L is high harmonic frequency and m is the sideband number of modulation frequency when it is equal to shaft frequency. The teeth number of involute spur gears is 78, so the meshing frequency and the shaft frequency can be calculated by (1) and (2) shown in Table 1.

Noise and vibration frequency generated by ring-plates and cycloidal gear.

The teeth number of pin wheel in the ring-plate is 78. The noise and vibration frequency generated by ring-plates and cycloidal gear when they mesh can also be calculated using (1) and (2). The results are shown in Table 2.

Table 1. Frequency of involute spur gears.

rotational speed (r/min)	f_n(Hz)	f_s(Hz)
500	650	8.33
750	975	12.5
1000	1300	16.67
1500	1950	25

Table 2. Frequency of ring-plates and cycloidal gear.

rotational speed (r/min)	f_n(Hz)	f_s(Hz)
500	291.67	8.33
750	437.5	12.5
1000	583.3	16.67
1500	875	25

Test results and analysis.

Vibration frequency spectrum analysis.

Figure 2 shows the vibration frequency spectrum diagram of acc1 test point and Figure 3 shows the vibration frequency spectrum diagram of acc2 test point at 500 rotations per minute. The frequency spectrum diagrams of the other points are not given here due to limited space.

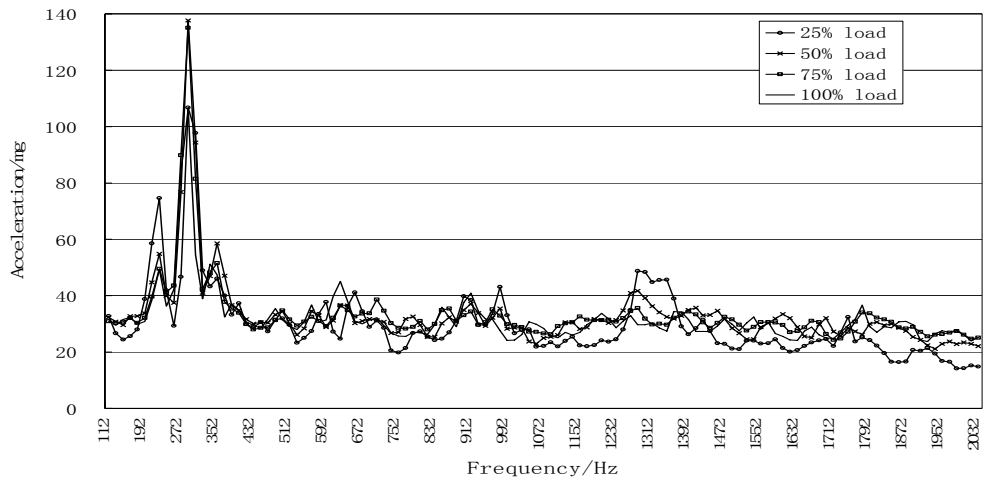

Figure 2. Acc1 spectrum diagram of different loads at the speed of 500r/min.

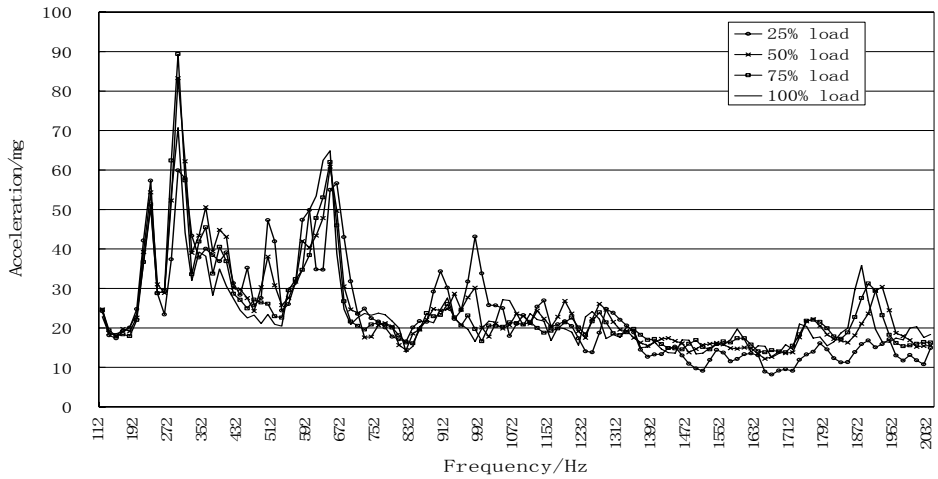

Figure 3. Acc2 spectrum diagram of different loads at the speed of 500r/min.

When the rotational speed is certain, the laws of vibration acceleration curves are roughly consistent with the changing of load. The peak frequencies are basically the same, but the peak values vary. In general, there are two frequency-bands. One is near 224Hz and the other is near 288 Hz at 500 rpm. For two frequency-bands, one is near 244Hz and the other is near 464 Hz at 750 rpm. For three frequency-bands, one is near 288Hz , one is near 608Hz ,and one is near 1296 Hz at 1000 rpm.

Noise frequency spectrum analysis.

Figure 4 shows the noise frequency spectrum diagram of mic1 test point at 500 rotations per minute. From the diagram, we can conclude that there are two frequency-bands. One is near 288Hz and the other is near 624 Hz at 500 rpm. And 288 Hz is the meshing frequency of ring-plates and cycloidal gear. From (3), we can determine that the third-order band below of the involute spur gears is 624Hz. The noise generated by involute spur gears when they mesh is larger than that of ring-plates and cycloidal gear at the speed of 500 rpm. And,the noise generated by ring-plates and cycloidal gear is larger than that of involute spur gears at the speed of 750 rpm and at the speed of 1000 rpm.

Main noise sources.

There are mainly two noise sources inside the reducer. One is the noise generated by ring-plates and cycloidal gear when they mesh and the other is the noise generated by involute spur gears when they mesh. The noise generated by involute spur gears is the main source at lower speed, while the noise generated by ring-plates and cycloidal gear is the main source at higher speed.

Acc1 and acc2 is symmetrical layout, so the frequency their spectrum diagram should be basically consistent in theory. However, their frequency spectrum diagrams

are very different actually, because the four ring-plates are not balanced. The four ring-plates do high-speed eccentric movement when they work. It is not possible to make the four ring-plates identical so the four ring-plates are not balanced.

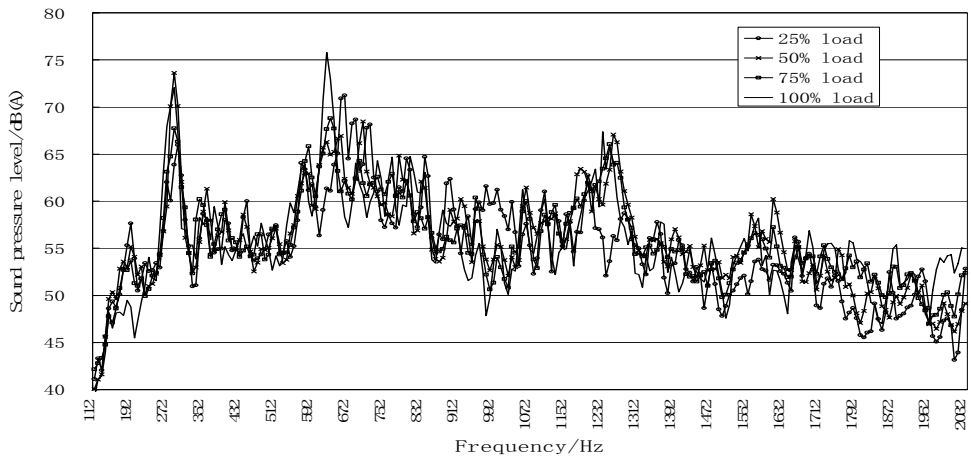

Figure 4. Mic1 spectrum diagram of different loads at the speed of 500r/min.

The resonance happens when the natural frequency of a component part is close to the exciting frequency. The exciting frequencies of the reducer mainly contain vibration frequencies generated by involute spur gears and vibration frequencies generated by ring-plates and cycloidal gear and their side-band frequencies. Test results show that the natural frequency of cylinder block is close to the exciting frequency so the resonance occurred. So the noise radiated by the cylinder block vibration is very large (Bao, J.H., 2005; Guo, W.Q., 2008; Qi J. Z., 2007).

NOISE REDUCTION MEASURES

In order to reduce the noise, the following measures can be adopted:

Damping ring.

Damping rings should be installed in the internal groove of the gear flanges. Damping rings decrease the gear damping from three aspects: systematic damping, structural damping and material damping. The vibration and noise would decrease after the use of damping rings.

Ring-plate reconstruction.

The inertia moment is smaller with the decrease of the ring-plate quality. So the ring-plate quality should be reduced as much as possible.The four ring-plates should be made identical as far as possible. Improving the accuracy of manufacturing and installation of ring-plates could also reduce the vibration and noise.

Cylinder block reconstruction.

The original cylinder block thickness is 12mm. The cylinder block thickness

should be 16mm after calculating in order to prevent resonance,. Test results show that the noise peak value of mic1 is reduced by 4.1 dB(A).

CONCLUSIONS

Double crank four ring-plate-type cycloid reducer is a new drive that has high load capacity and high transmission efficiency. The characteristics of the vibration and noise are obtained after the vibration and noise tests. The noise sources are identified. The experiment results show that the better effect of vibration and noise reduction is achieved.

ACKNOWLEDGEMENTS

We are grateful for the support provided by the National Science Foundation of China (No 50175011).

REFERENCES

Bao, J.H., and He, W.D. (2005). " Finite element analysis of cylinder block of crank ring-plate cycloid reducer." *Journal of Dalian Railway Institute*, 26(1):38-40.

Guo, W. Q., and Liu, Y. (2008). "Modal analysis of cylinder block of crank ring-plate cycloid reducer." *Noise and Vibration Control*, 28(3):29-31.

He, W.D., and Li, X. (2000). " Study on double crank ring-plate-type cycloid drive." *Chinese Journal of Mechanical Engineering*, 36(5):84-88.

He, Y. R. (1998). "Mechanism analysis and control of vibration and noise produced by gears and gearbox." *Vibration,Measurement and Diagnosis*, 18(3):221-226.

Li, L. X., and Li X. (2005). "Experimental study of double crank ring-plate-type pin-cycloidal gear planetary drive." *Journal of Dalian Railway Institute*, 26(1):1-4.

Li, X., and He, W. D.(2004). "A new cycloid drive with high-load capacity and high effiencey." *ASME Journal of Mechanical Design*, 126(4):683-686.

Qi, J. Z., and Meng, X. J. (2007). "Modal analysis on the ring of three-ring reducer based on ansys." *Journal of Hebei Polytechnic University* (Natural Science Edition), 29(4):56-58.

Analysis Model for Operating Speed on Two-lane Secondary Highway

Dianliang Xiao[1] and Yujia Tian[2]

[1]China Academy of Transportation Sciences, MOC, No.240 Huixinli, Chaoyang District,Beijing,100029, China; PH:86-10-58278205; email: sean8205@163.com.
[2]Traffic Engineering Department, Highway College, Chang'an University, Mailbox 487, Shaanxi Xi'an, 710064; PH :86-29-82334886; email: sean8205@126.com

ABSTRACT

In order to improve traffic safety and reduce the rate of traffic accidents on the flat curve of two-lane highway, this paper studied the operating speed of vehicle in straight line and little radius. Through the speed experiment, we collected the speed that vehicle traveled on a flat curve, and then ensured the critical radius of the two-lane highway. Finally, the paper established the modeling of the element of flat curve and speed, the element of flat curve and side friction factor coefficient. The model can be applied in safety evaluate of two-lane secondary highway in our country. The improvement is considerable.

INTRODUCTION

The geometric alignment of highway directly influences traffic safety and transportation operational efficiency. From the distribution of traffic accident on two-lane secondary highway (Du, 2002), we confirm that the horizontal curve sections especially minor radius of curve sections are concentrated with traffic accidents. Therefore, the master curve with the safety inherent in the relationship between the radius of the horizontal curve safety design and safety sections of both curves remediation is of great significance. Through many field surveys and analyses of the curve section of the vehicle at speed laws, a small radius curve segments operating speed and the radius of model was set up, and our country two-lane secondary highway curve radius of the critical value was derived. The future safety of Horizontal Curve design standards to provide basic information and research methods were also set up.

DATA ACQUISITION

The scope of this research is to study horizontal curves when we collect experimental data. Based on the research in the past, we select horizontal curve sections which have curve radius between 125m and 800m on secondary highway (Chang'an University 2005). Experimental times are from 9:00 to 11:00 in the morning and 15:00 to 17:00 in the afternoon. In order to ensure the accuracy of speed observed value, the minimum number of vehicles (sample size) using the

following formula to compute.

$$n = (\frac{\sigma K}{E})^2 \qquad (1)$$

In the equation, n- the minimum number of sample size, E- allowable error of speed observed value, K- confidence level, general selection 95% of confidence level ,that is k=1.96

Under traffic free flow condition, we set the speed measuring radar gun at straight line segment of entering the curve, mid-point of curve and line segment of leaving the curve. The data were used for measuring uninterrupted operating speed of vehicles. At the same time we recorded the situation of vehicle operation using DV cameras, recorded the travel time, and to calculate the speed of the vehicles. The layout of experimental apparatus is shown in Figure 1.

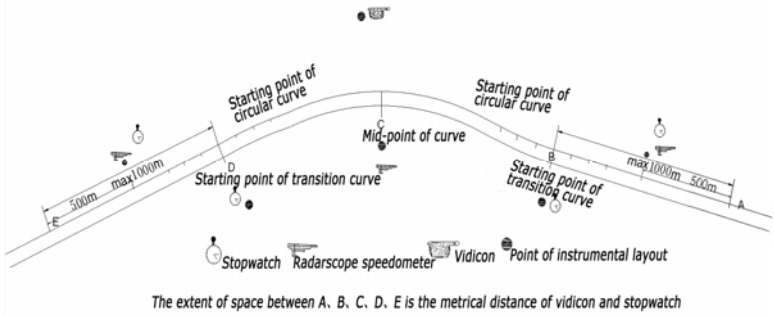

Figure 1. The Layout Schematic Diagram of Experimental Apparatus

DATA ANALYSIS

Data analysis for operating speed of line segment

In order to calibrate operating speed of motor-car and medium truck adjacent straight-line segments on two-lane secondary highways, we surveyed speeds of straight-line segments which adjacent minor radius of curve sections on Qinghai-Tibet Highway, Yanhu Highway, Meitai Highway and Fuhe Highway. The operating speeds collected were entered into SPSS. The speed histograms are shown in Figures 2 and 3, one can see the speed largely followed a normal distribution.

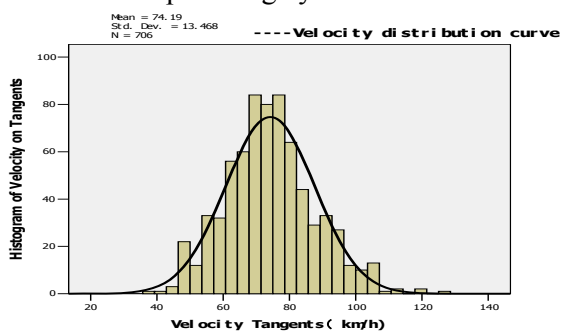

Figure 2. Speed Histogram for Straight-line Segment of Adjacent Curve (Motor car)

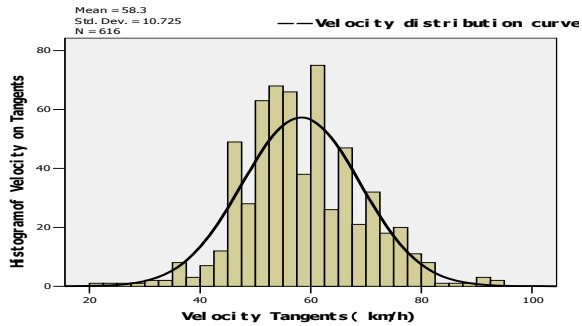

Figure 3.Speed Histogram for Straight-line Segment of Adjacent Curve (Medium truck)

Through analyzing operating speed data, we obtained the characteristic speed for motor-car and medium truck of straight-line segment on two-lane secondary highway.

Motor car: $V_{85\%}$=89km/h，$V_{50\%}$=73km/h；Medium truck: $V_{85\%}$=67km/h，$V_{50\%}$=50km/h

Data analysis for operating speed of minor radius of curve sections

Generally speaking, for the vehicles traveling on a curve, along with the transition curve - enter the curve - leaving curve, there will have a process of slowing to enter - maintaining stability – accelerating away. This article analyzed the change of vehicle speed before and after entering the curve based on the condition of different drivers at the same radius curve to driver. The author selected the minor radius of curve with radius of 200m, 300m and 500m, unfolds the effects of speed changes on traffic safety with different radius of curves.

(1) When the curve radius R = 200m, the distribution maps of operation law for motor car and medium truck as shown in Figures 4 and 5.

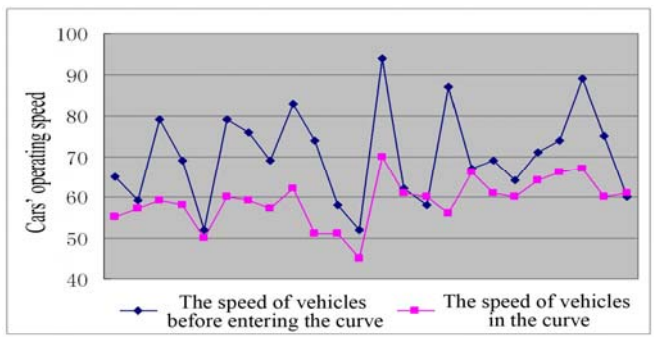

Figure 4. Speed Diagram of Motor car (R=200m)

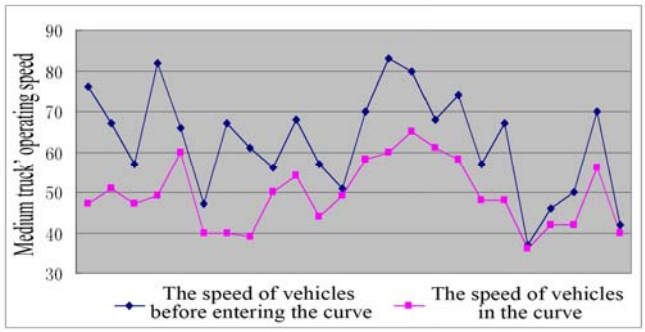

Figure 5.Speed Diagram of Medium truck (R=200m)

Figure 4 shows the situation of operating speed for motor car at a radius R=200m section of curve. The range of speed difference is -2 - 31km/h between before and after entering the curve, and the average of speed difference is 13.7 km/h. The bigger the speed is before entering the curve, the greater change of speed difference after entering the curve, only when the speed at 60km/h or so, the change of speed after entering the curve is not obvious. Figure 5 reflects the situation of operating speed for different medium trucks at a radius R=200m section of curve. The range of speed difference is 1 - 33km/h between before and after entering the curve, and the average of speed difference is 13.1 km/h. Compared with the motor car, the speed differences of medium truck are larger, and trucks have different deceleration. For medium trucks, the operating speed is about 50km/h when the curve radius is 200m.

(2) When the curve radius R =300m, the operation law of vehicles are basically the same as R = 200m.

(3) When the curve radius R = 500m, the distribution maps of operation law for motor car and medium truck as shown in Figures 6 and 7.

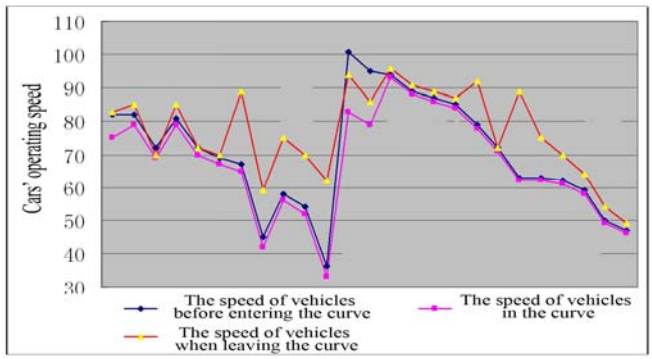

Figure 6. Speed Diagram of Motor Car (R=500m).

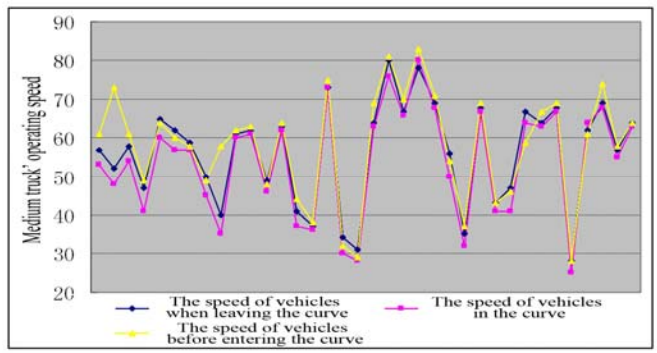

Figure 7. Speed Diagram of Medium Truck (R=500m)

Figure 6 shows the situation of operating speed for motor car at a radius R=500m section of curve. The range of speed difference is 1 - 18km/h between before and after entering the curve, and the average of speed difference is 3.08 km/h. The change range of speed difference is 1 - 29km/h between exit the curve and within the curve. It shows that the motor cars are accelerated when exiting the curve, and the exit speed is greater than the speed before entering the curve. Figure 7 shows the situation of operating speeds for medium trucks at a radius R=500m section of curve. The range of speed difference is -2 - 6km/h between before and after entering the curve, and the average of speed difference is 2.53 km/h. We can see that the changes of speed differences for medium trucks at a radius R = 500 meters have not been obvious before and after entering the curve. These results mean that the curves whose radius R = 500m are regarded as straight line when drivers of medium truck through it.

Based on the above analysis, we obtained some rules for vehicle operation of small radius of curve sections.

- There will have a process of slow to enter - maintain stability - accelerate away from when vehicles through the curves.
- The smaller the curve radius, the greater changes of speed difference between enter the curve and within the curve.
- The change process of vehicles speed before and after the centre of curve approximately showed a quadratic curve.
- The operating speed of vehicles increased with the increase of curve radius, and the range of motor cars speed increases is greater than that of medium trucks.

MODEL

According to the related research results about highway (Helmut et al.1995; Nicholas, 2001) vehicles run within the Horizontal Curve with less than the value of critical curve radius R_0 (critical radius is the radius when the curve radius is larger than this value, the running state of vehicles consistent with the straight line), and

the relationship between operating speed and curve radius can be expressed by power function. The model curve of "operating speed-radius" reflects the relationship between operational status of vehicles and the curve radius. Based on this theory, the model of vehicle operating speed which fit the actual situation in China is selected as follows:

$$V_{85\%} = aR^b \qquad (2)$$

Where: $V_{85\%}$ - 85 percentile speed, km/h; R - circular curve radius, m; a, b - model parameters.

Survey data were from some horizontal curves with radius of 200m, 250m, 300m, 400m, 500m, 600m and 650m on the two-lane secondary highway with the design speed of 80km/h, highway width of 11~15m, flat grade, and good or very good pavement condition without distresses. Based on the systemizing and analysis of the operating speed on the curve, the value of vehicles' operating speed, $V_{85\%}$, can be concluded and shown in Table 1. Its operating speed and the model of curve radius are shown as Equations 3 and 4. And the operating speed and the regression chart of curve radius are shown in Figures 8 and 9.

Table 1. The $V_{85\%}$ Value of Vehicles on the Horizontal Curve with Small Radius.

Radius of horizontal curve(m)	$V_{85\%}$ of cars(km/h)	$V_{85\%}$ of medium trucks(km/h)
200	64.0	44.5
250	67.0	46.8
300	73.0	53.0
400	79.0	57.9
500	84.0	66.4
600	88.0	68.8
650	90.0	69.0

The operating speed model for motor cars:

$V_{85\%} = 13.016R^{0.300}$, R^2=0.995 (3)

The operating speed model for medium trucks:

$V_{85\%} = 5.245R^{0.402}$, R^2=0.981 (4)

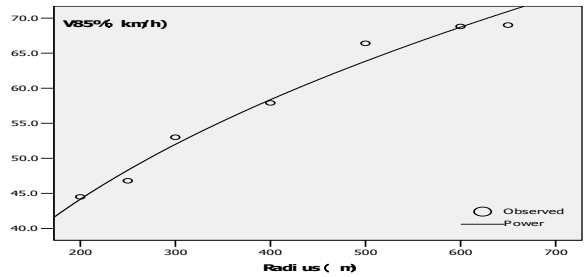

Figure 8. $V_{85\%}$ and Curve Radius Regression Chart (Motor Car)

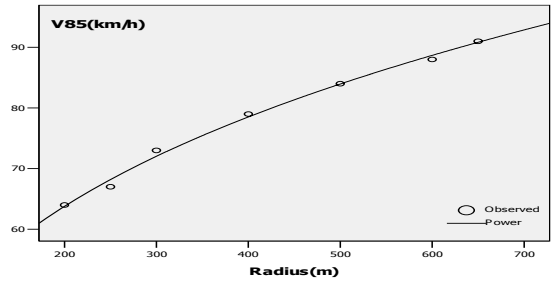

Figure 9. $V_{85\%}$ and Curve Radius Regression Chart (Medium Truck)

Because of the different performances on various vehicle types, the corresponding critical radius must be different at the same highway classification. A number of survey data have shown that, compared with the other models, critical radius of motor car is the biggest on highway at all levels. The critical radius of motor car for the secondary highways is 610m, and the critical radius of curves with small radius of medium truck is below 550m. The survey data revealed that, when vehicles entrance the horizontal curve with the radius R> 600m, the changes of vehicle speed are random and have no necessary connection to horizontal curve among these taken samples. Therefore, taking R_0=610m as the critical radius is reasonable.

CONCLUSIONS

(1) We have studied the characteristics of speeds of vehicles on straight line segment of two-lane secondary highway in China (motor car $V_{85\%}$＝89km/h, $V_{50\%}$ =73km/h; medium truck $V_{85\%}$＝67km/h，$V_{50\%}$=50km/h), and the operation law of motor car and medium truck on straight line segment and curve section with small radius.

(2)The models of operating speed and curve radius on curve section with small radius of two-lane secondary highway for motor cars and medium trucks are established. The model of operating speed for motor car is $V_{85\%} = 13.016R^{0.300}$, and the model of operating speed for medium truck is $V_{85\%} = 5.245R^{0.402}$.

(3)In this paper, the critical radius R_0=610m of curves with small radius of two-lane secondary highway in China is proposed.

REFERENCES

Chang'an University(2005). Research on the key technologies of two-lane highway construction in the western regions, April 2005.

Du Xinquan(2002). Situation analysis and countermeasure research on road safety in western China. Highway Transportation Abstracts, Vol. 7, No. 11, 2002, pp. 29-31.

Helmut T Zwahlen, Jin Yong Park(1995).Curve Radius Perception Accuracy as Function of Number of Delineation Devices(Chevrons).Transportation Research Record 1495, 1995, pp. 99-106.

Nicholas J.Garber(2001). The effect of speed and geometric characteristics on crash frequency for two-lane highway. CD-ROM, Pre-Print of the 80th Transportation Research Board Annual Meeting.

Study on the Method for Calculating Ship Squat in the Restricted Channel

ZHENG Zhong-Yi[1], GANG Long-Hui[2] and LI Hong-Xi[3]

[1] Navigation College, Dalian Maritime University, P.O. Box 110126, Dalian, PH (0411)-84728381; email: dlzzyi@sina.com

[2] Navigation College, Dalian Maritime University, P.O. Box 110126, Dalian, PH (0411)-81224238; email: ganglh@yahoo.com.cn

ABSTRACT

Safety is essential for the great ship which are sailing in the restricted channel, by estimating the squat and the Under Keel Clearance (UKC) correctly. This paper conducted the study on the method for calculating the squat in restricted channel. While the ship is sailing in the restrictive channel, the squat is affected by ship boundary layer. In this paper, hydrodynamic theory and flat boundary layer theory were applied to put forward the approximate formula to calculate ship boundary layer. Considering the impact of ship boundary layer, the method of squat calculating was put forward. Finally, the method was verified by real ship data.

KEYWORDS: Squat, Restrictive Channel, Boundary Layer, Hydrodynamic Theory

1 BACKGROUND

When the ship is navigating in the restricted channel, the phenomenon will appear such as increasing of the draw, squat of the ship, or decreasing of Under Keel Clearance (UKC). Incorrect estimating of squat will lead to a series of maritime accidents, e.g. aground, grounding, out of control etc. It can be seen that the correct estimation on ship squat is significant to ensure the safety of the ships navigating in the restricted channel.

At first, theoretical analysis was used into the research of ship squat. Havelock (1939) used ship wave-making theory to study the squat of ship in the unrestricted water. This research did not consider the effect of the water depth on the squat. Constantine (1961) considered the water depth and put forward that hydrodynamic equation of one dimension should be applied to study the water flow around the hull in the shallow and confined channel. But he assumed that the speed of water flow was stationary. Afterward, some researches also studied the squat based on the previous results, such as Tuck (1966), Taylor (1970) etc.

The other way to research the ship squat was the experimental method. This method achieved the squat by simulating ship moving and exactly measuring, and then finding the relationship between the squat and the related factors. Theses researches included Hooft (1974), Huuska (1976), ICORELS (1980), Norrbin (1986), Millward (1990), Eryuzlu (1994), Soukhomel (2002). The research of ship squat in our county was behind other developed countries.

Although lots of results were obtained, few has mentioned the effect of fluid boundary layer on the ship squat. This paper analyzed the affect of restricted channel and fluid boundary layer on the ship squat. The hydrodynamic theory and flat boundary layer theory were applied to deduce the equation for calculating the ship boundary layer and squat.

2 SHIP SQUAT IN THE RESTRICTED CHANNEL

While the ship is navigating in the restricted channel, it displaces large amount of water and a blank field appears behind the poop of the ship. At the same time when the water surrounds the ship flows to fill the blank field, the water level at the side of the ship decreases. So the position of the ship also decreases. The decreasing distance is called "squat".

2.1 THE AFFECT OF THE RESTRICED CHANNEL ON THE SQUAT

In the open water, there was enough water to fill the blank field in the poop, so the squat was slight. But in the restricted channel, the amount of water was limited because of the restriction of the width and height of the restricted channel. So the water moving to the poop came from the bottom and the sides of the ship. The phenomenon increases the extent of the ship squat.

2.1 THE AFFECT OF THE SHIP BOUNDARY LAYER ON THE SQUAT

(1) Ship Boundary Layer

Boundary layer was provided by L.Prandtl (1904), a Germany scientist. Boundary layer is defined as a thin fluid layer at the surface of the object, in which the speed of the fluid increases from zero to the same speed around the water.

While ship is moving in the water, a boundary layer is established around ship. The width of the layer varies large by gradually changing, showed as Figure 1.

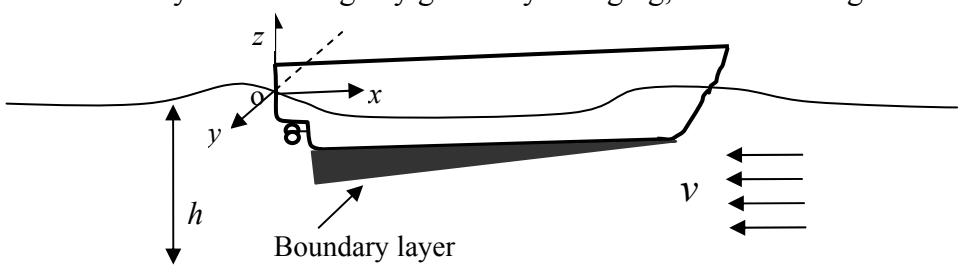

Figure 1. Draft of ship boundary layer

(2) Affect of the Ship Boundary Layer on the Squat

In the hydrodynamic theory, Bernoulli equation of constant and incompressible fluid is:

$$\frac{v^2}{2}+\frac{p}{\rho}+gz=\text{Constant} \tag{1}$$

Where, v is the speed of the fluid; $v^2/2$ is the kinetic energy of fluid per unit mass; p/ρ is the pressure of the fluid, at the surface, p/ρ=0; z is the height of the water lever; and gz is the potential energy of the fluid per unit mass.

Equation (1) describes the potential energy per unit mass of the fluid is constant at the same water level. Based on this, the Bernoulli equation of the water line *AB* in Figure 2 is

$$\frac{v_A^{\ 2}}{2} + gz_A = \frac{v_B^{\ 2}}{2} + gz_B = \text{Constant} \tag{2}$$

The points, *A* and *B,* were at the same waterline, and located at the middle and front of the ship respectively since the surface, p/ρ=0.

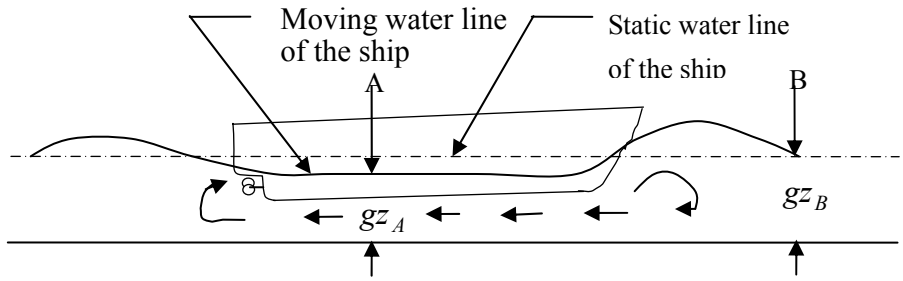

Figure 2. Energy components about the moving water line of the ship

The continuous equation of incompressible fluid is

$$Sv = \text{Constant} \tag{3}$$

Here, *S* is the cross-sectional area of the passing water. At the A and B,

$$S_A v_A = S_B v_B = \text{Constant} \tag{4}$$

Because of the existence of the ship hull, $S_A < S_B$. Regarding to the equation (2) and (3), $v_A > v_B$, $v_A^{\ 2}/2 > v_B^{\ 2}/2$, $gz_A < gz_B$. So it is known that the cross-sectional area of the passing water decreases due to the existence of the ship boundary layer and the squat increase further.

3 CALCULATING OF THE SQUAT IN THE RESTRICTED CHANNEL

3.1 CALCULATION OF THE WIDTH OF THE SHIP BOUNDARY LAYER

Based on the boundary theory, the width of the ship boundary layer is:

$$\delta(x) = 0.37x\,\mathrm{Re}_x^{-\frac{1}{5}} \tag{5}$$

Here, $\delta(x)$ is the width of the ship boundary layer and it varies with *x*. Re_x is Reynolds number which is formulated as:

$$\mathrm{Re}_x = \frac{vx}{\upsilon} \tag{6}$$

υ is the coefficient of moving sticky of fluid.

$$S_0 v = (S_0 - S(x))v', \qquad v' = \frac{S_0 v}{S_0 - S(x)} \tag{7}$$

So the width of the ship boundary layer is

$$\delta(x) = 0.37x^{\frac{4}{5}}(\upsilon)^{\frac{1}{5}}\left(\frac{S_0 v}{S_0 - S(x)}\right)^{-\frac{1}{5}} \tag{8}$$

3.2 CALCULATION OF THE SHIP SQUAT

Any point *x* at the ship, the cross-sectional area of the passing fluid $A(x)$ is

$$A(x) = S_0 - S_1 - S_2 - S_3 \tag{9}$$

S_0 is the cross-sectional area in channel, $S_0 = Bh$, B and h is the width and height of the channel; S_1 is the cross-sectional area of the ship hull under the water surface; S_2 is the variant area around ship hull, $S_2 = [B - b(x)]\zeta$, $b(x)$ is the width of ship hull under the water, ζ is the variation of water surface around the hull; S_3 is the area of the boundary layer, $S_3 = [2T + b(x)]\delta(x)$, T is the draw. After exchanging, $A(x)$ can be formulated as follows:

$$A(x) = Bh - S_1(x) - [B - b(x)]\zeta - [2T + b(x)]\delta(x) \tag{10}$$

Because of $v'(x) \cdot A(X) = v \cdot S_0$, $v'(x)$ is the function of v, if $v'(x) = \tilde{q} \cdot v$, then

$$\tilde{q}\{1 - \frac{S_1(x)}{S_0} - [1 - \frac{b(x)}{B}]\frac{\zeta}{h} - \frac{[2T + b(x)]\delta(x)}{S_0}\} = 1 \tag{11}$$

At any waterline of the surface, $g\zeta + \frac{1}{2}(\tilde{q}\, v)^2 = \frac{1}{2}v^2$, and at the waterline around hull, $\frac{P}{\rho} + gz + \frac{1}{2}(\tilde{q}U)^2 = \frac{1}{2}v^2$, it is know that the pressure of the fluid P can be described by:

$$P = \rho g(\zeta - z) \tag{12}$$

The pressure of water affecting on the ship is equal to the gravitation of the ship itself. The gravitation of the ship also is equal to its displacements:

$$\rho g\Delta = \iint -P dS' \cdot \hat{z} \tag{13}$$

Δ is the displacement of the ship, S' is the total areas of the hull under water; $\hat{z}$ is the vector on the axis z.

Divergence theorem was applied to exchange the equation (13), then

$$\rho g\Delta = \iint -\nabla P \cdot \hat{z} dv = \iiint \rho g dV \tag{14}$$

Where $dV = dxdya$ is the capacity of the ship under water. It is assumed that the squat in the middle of the ship is *s* (Figure 3). Then at any point on the ship, the squat is:

$$\sigma(x) = \frac{2 \cdot s \cdot x}{L} \tag{15}$$

Where L is the length of the ship. At any point *x*, the decrease and the increase of cross-sectional area of the hull under water is $b(x)\zeta(x)$ and $b(x)\sigma(x)$ respectively.

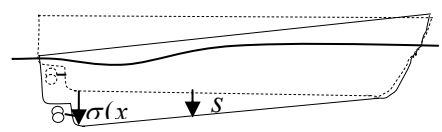

Figure 3. Draft of the Ship

The displacements of the ship is constant whether the ship is moving or not:

$$\int_0^L b(x)\sigma(x)dx - \int_0^L b(x)\zeta(x)dx = 0 \tag{16}$$

After the transformation, the ship squat is:

$$s = \frac{L\int_0^L b(x)\cdot\zeta(x)\cdot dx}{2\int_0^L x\cdot b(x)\cdot dx} \tag{17}$$

The maximum squat is:

$$S = \frac{2\cdot s\cdot L}{L} = 2\cdot s = L\frac{\int_0^L b(x)\cdot\zeta(x)\cdot dx}{\int_0^L x\cdot b(x)\cdot dx} \tag{18}$$

4 REAL DEMONSTRATIONS

The real data of the ship, Wigley, was selected to verify the proposed method. The width of hull and the cross-sectional area of hull under water are described by:

$$b(x) = b_{\max}[1-\frac{(2x-L)^2}{L^2}] \tag{19}$$

$$S(x) = \frac{2}{3}T\cdot b(x) = \frac{2}{3}T\cdot b_{\max}[1-\frac{(2x-L)^2}{L^2}] \tag{20}$$

The parameters of the restricted channel is

$L = 200m$, $b_{\max} = 40m$, $T = 9m$, $v = 5m/s$, $B = 80m$, $h = 12m$;

$S_0 = Bh = 960$; $F_h = \frac{v}{\sqrt{gh}} = \frac{5}{\sqrt{10\times 10}} = 0.46$; $b(x) = 40[1-\frac{(x-100)^2}{10000}]$,

$S(x) = 240[1-\frac{(x-100)^2}{10000}]$. If the temperature of the water is 10º, $\upsilon = 1.306\times 10^{-6}$.

The calculated results of the squat by using different methods were listed in Table 1.

Table1. Calculated results of the squat

	Considering the boundary layer	Without consideration of boundary layer	Soukhomel model
The maximum squat (m)	1.188	1.078	1.09
UKC (m)	1.812	1.922	1.91

Regarding to Table 1, it is clear that the squat is maximal and the UKC is minimal by using the method with the consideration of the ship boundary layer.

5 CONCLUSIONS

This paper studies the method for calculating the ship squat in the restricted channel. Firstly, the paper analyzed the effect of the ship boundary layer and the restricted channel on the squat. Then hydrodynamic theory and flat boundary layer theory were applied to deduce the calculating equation of the ship boundary layer and the ship squat in the restricted channel. Finally, the real ship data was used to verify the method. The compared analysis demonstrated that the result calculated by the method provided in this paper is compiled to the actual case.

ACKNOWLEDGEMENT

This study is funded by the foundation (200CB417215).

REFERENCES

Constantine, T. (1961). "On the movement of ships in restricted waterways." J. *Fluid Mech.*.

Dai R., Jia ., Sun L. (2002). "Research on vessel squat measurement." *Journal of Traffic and Transportation Engineerin*, vol.2 (2), 59-62.

Eryuzlu, N E., YL.Cao, F.D'Agnolo. (1994). "Underkeel requirements for large vessels in shallow waterways." *28th International Navigation Congress*, PIANC, Sevilla, 17-25.

Hooft J D. (1974). "The behaviour of a ship in head waves at restricted water depths." International Shipbuilding Progress, 21(244), 367-390.

Huuska O. (1976). "On the evaluation of underkeel clearances in finish waterways." *Helsinki University of Technology Ship Hydrodynamics Laboratory*, Otaniemi, Report no.9.

Liu Z., Xia G., Wang F.(1995). "Real Estimation of Squat in the Restricted Channel.". *Journal of Dalian Maritime University*, vol.21 (4), 9-13.

Millward, A. (1990). "A preliminary design method for the prediction of squat in shallow water." *Marine Technology*, 1990, 27(1), 10-19.

Norrbin N H. (1986). "Fairway design with respect to ship dynamics and operational requirements." *SSPA Maritime Consulting Research Report,* No.102, Sweden.

Overseas Coastal Area Development Institute of Japan. (2002). *Technical standards and commentaries for port and harbor facilities in Japan*.

Report of Working Group IV. (1980). PIANC Bulletin NO.35, Supplement. ICORELS(International Commission for the Reception of Large ships).

Tuck E O. (1966). "Shallow water flows past slender bodies." *J. Fluid Mech.*, 81-95.

Tuck E O. & Taylor, P J. (1970). "Shallow water problems in ship hydrodynamics. " *8th Symp.Naval Hydro.ONR*, Washington DC.1,627-659.

A STUDY ON DRIVER'S DYNAMIC VISUAL CHARACTERISTICS

SONG Fei[1], YANG Xiao-kuan[2]

[1]Transportation Research Center, Beijing University of Technology, Beijing, China; Tel: (86)13426252060; Email: songfei@emails.bjut.edu.cn
[2]Professor, Transportation Research Center, Beijing University of Technology, Beijing, China; Tel: (8610) 6739-1678; Fax: (8610) 6739-2991;
Email: xiaokuan@bjut.edu.cn

ABSTRACT

The driver's visual characteristics and road safety are closely related. Previous studies show that 80% of the divers' information of the road is obtained by their eyes. Therefore, the visual characteristics are closely related to driving operations. In this paper, on the basis of the theoretical analysis at home and abroad before, dynamic visual characteristics research about two different categories of drivers (professional and non-professional drivers) in real-world road environment have been explored. In the research, eye tracking system was used to study regularity of fixation duration and the perspective distribution. Two kinds of drivers were compared and conclusion of distribution visual feature had been made. It was found from this study that the driving experience had an obvious effect on the drivers' eye movement characteristics. It was concluded from the study of perspective distribution that the drivers' concern on the vicinity was more than the objects in a distance. The findings from this study will assist the design of roadway, satisfy drivers' driving request, and make the roadways safer.

Key words: dynamic visual characteristics, visual tracking, eye tracking system

INTRODUCTION

Drivers always capture the traffic information by their eyes when they are driving on the road. Drivers' visual characteristics have a direct impact on road safety. During driving, 95% information received by drivers is dynamic visual information (Ma Y. et al. 2006). As a result, it is very necessary to study the drivers' dynamic visual characteristics and its impact on traffic safety. Drivers at home and abroad have been required to have good visual characteristics, but this inspection is carried out at the static state (Geoffrey U. et al. 2002). In this paper, the result is based on the investigation on the real road conditions. Comparison of the professional and non-professional drivers was made. Finally, the drivers' dynamic visual characteristics and its variation regularity were summarized.

DRIVERS' DYNAMIC VISUAL CHARACTERISTICS

The drives' vision when they are driving is called dynamic vision. The visual

characteristics can be affected by some influential factors (Zhao B. 1988): the driver's age and status, road environment, the relative velocity, the illumination, and color of target, etc. The information captured by drivers is very complex. And it affects drivers' decision making and other road users' safety. Thus, it's necessary for us to study the dynamic visual characteristics of drivers. In this paper, the process of drivers' visual perception was studied. Driver's dynamic visual characteristics were analyzed and described. Another focus of this paper is on some influential factors of the drivers' visual characteristics, such as the individual differences (e.g. driving experience) among drivers and road environment.

DATA COLLECTION

In this study, Smart-Eye Pro. eye tracking system was used as an observation instrument (see Figure 1) to conduct experiment. The instrument is a system which consists of four parts (Smart Eye AB. 2007): an infrared light source from the camera, a scene camera, a image and data processing host, and a software which can track and measure eye movement characteristics of the drivers. The system can make real-time status tracking of drivers' movement, such as the driver's head position, eye sight and eye closure. Its output is the corresponding original data. The eye movement experiment was conducted for both professional and non-professional drivers in different conditions, from which the data of drivers' visual behavior can be obtained.

Drivers' eye movement during driving is a complex process. Considering the characteristics of system's data collection and making reference to data of similar studies, the following data were taken as evaluation criteria (Fan H. et al. 2007): the drivers' fixation distribution, the average fixation duration, and the perspective distribution.

Data for this study were collected on the typical suburban roads and urban roads in Nanjing. The investigations were made in sunny days and non-holidays as well. The objects of investigations were professional and non-professional drivers.

Figure 1. Eye tracking system and running interface in Smart-Eye Pro

DATA PROCESSING AND ANALYSIS

Eye tracking system recorded data including the numbers of experimental data points, the coordinates of trajectory points, and so on. These data were used after reprocessing. The data of the drivers' fixation distribution and the values of horizontal or vertical perspective are obtained. The features of dynamic visualization of drivers

could be observed and analyzed by experiments.

- **Variations of drivers' fixation points**

The fixation of a driver is the instantaneous point which the driver fixes on. The process of eye movement can be directly described by fixation distribution (see Figure 2). For different drivers, the fixations are different.

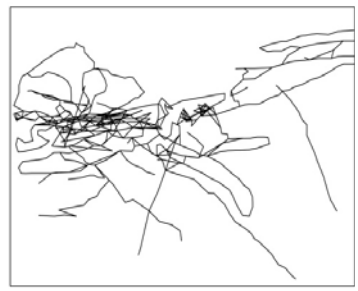

Figure 2. The driver's fixation distribution

Variation on horizontal direction

The variations on horizontal direction were analyzed based on the path types and the driving experience (see Figure 3).

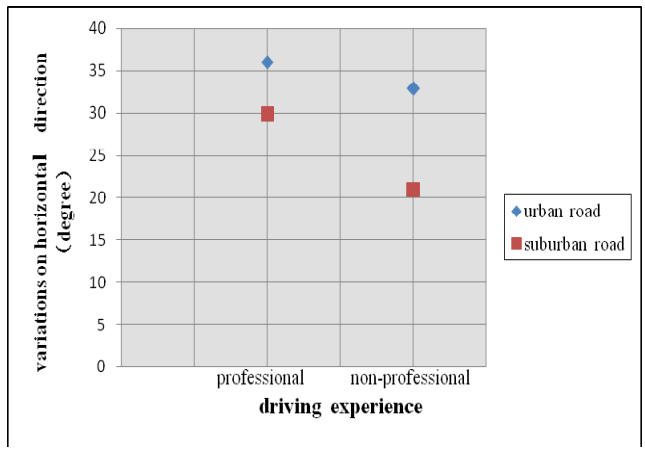

Figure 3. Chart of variations on horizontal direction

Compared with suburban roads, all drivers on urban roads have a large change in the horizontal direction of fixation points. The reason for this is the complexity of traffic information. When driving on the urban road, drivers are affected by vehicles which are in front of, in opposite direction and on the left lane. At the same time, non-motorized vehicles and pedestrians crossing the street also have some impacts on the driving behaviors. Drivers are in a condition with so much information that they need to watch wider. However, the situation is different on the suburban roadways where traffic volume is relatively low.

Due to the fact that non-professional drivers do less information search on both sides of the road, their scope of visual search is smaller than that of professional drivers. There is obvious difference between two types of drivers when they're on suburban roads. It's difficult for non-professional drivers to get the information on

roadsides when they drive on suburban roads with a high volume of heavy vehicles. As a result, the non-professional drivers' scope of visual search is smaller.

Variation on vertical direction

The variations on vertical direction were analyzed based on the path types and the driving experience (see Figure 4).

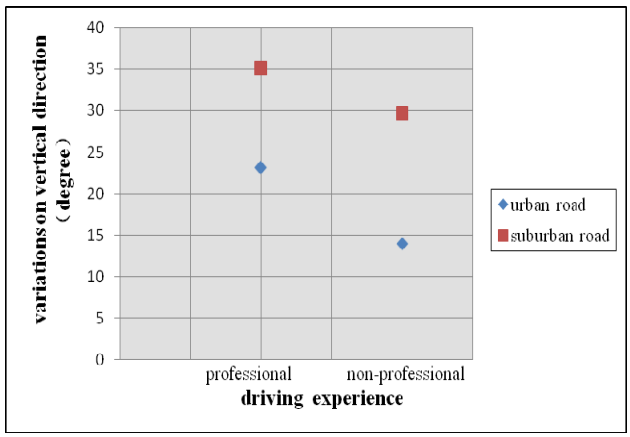

Figure 4. Chart of variations on vertical direction

According to the figure, in different types of roadways, all drivers have obvious differences on the level of vertical visual search. Compared with urban roads, drivers' fixation on suburban roads changed a lot. Due to the fact that drivers don't have enough time to look around, the situation exists when driving on urban roads. At this point, driving experience seems very important.

Although they have the same change trend, compared with professional drivers, non-professional drivers' level of vertical visual search is obviously lower. The reason for this situation is that non-professional drivers are not familiar with the road condition. They couldn't prepare for the signal indication in advance and so on.

Table 1. Variations of drivers' fixation points on different kinds of road

Road types	urban roads		suburban roads	
Driving experience	professional	non-professional	professional	non-professional
Variation on horizontal direction（degree）	36.0	33.0	29.9	20.9
Percentage(compared with professional drivers)	8.3%		30.1%	
Variation on vertical direction(degree)	23.1	14.0	35.2	29.7
Percentage(compared with professional drivers)	39.4%		15.6%	

Through the table, it can be seen that different types of drivers have different characteristics of the dynamic vision on urban roads and suburban roads. The driver on urban roads pays more attention on both sides of the road than the vehicle in front of. Through analysis, it is found that the level of non-professional drivers' visual search is significantly lower than professional drivers'. This is due to the fact that non-professional drivers are lack of driving experience. They couldn't obtain the information accurately, such as traffic signals and signs.

Nowadays, there're more and more non-professional drivers on roads, as the status of them the traffic flow will be great influenced. Road conditions and the facilities should be designed more desirable for these drivers.

- **The average fixation duration**

The average fixation duration was analyzed, which based on the path types and the driving experience (see Table 2).

Table 2. The average fixation duration of drivers on different kinds of road (seconds)

Road types	urban roads		suburban roads	
Driving experience	Professional	non-professional	professional	non-professional
The average fixation duration(seconds)	0.258	0.271	0.323	0.317
Percentage(compared with professional drivers)	5.0%		1.9%	

The experiment showed that the average fixation duration of drivers on urban roads were shorter suburban roads. The complexity information of the urban road leads the driver to spend less time to observe and judge them.

Take these two kinds of drivers for comparison, the non-professional driver's fixation duration is longer than professional driver. Then, conclusion can be made that non-professional driver needs more time to make reactions, which indicates that they will take more time to recognize and judge traffic information than the professional driver.

This message will help the traffic planners and engineers. They can design the traffic signals and signs in such a way to meet requirements of non-professional drivers.

- **Perspective distribution (horizontal direction) change**

The perspective change refers to the driver's eye rotation changes while driving. Normally, when a driver is observing an important target or dealing with some abnormal information, his/her eyes will be significantly changed in angular velocity.

Distribution of fixation regions in horizontal zone

In this study, drivers' visual field was divided into three regions with regard to different roadways (see Figure 5).

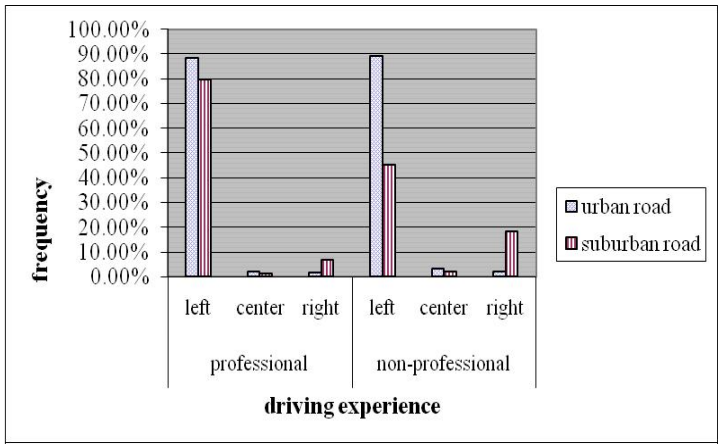

Figure 5. Chart of distribution of fixation regions in horizontal zone

Figure 5 shows that drivers gaze at the left side more frequently than central region and the right side. The frequency of professional drivers on either side doesn't change a lot. For non-professional drivers, there's a significant change. They gaze at the left side of the road more often while driving on the urban road. However, they pay more attention on the right side of the suburban road. The reason is that during investigation, the experiment vehicle run on the leftmost traffic lane, which is different from normal situation.

Some of non-professional drivers always keep slow speed even there aren't many vehicles. As the result, they always are overtaken by others. When they are overtaken, they watch the vehicles on left lanes. However, they still don't keep paying attention to the left lanes even if there aren't so many cars.

Distribution of fixation angles in horizontal direction

After analyzing the fixation angles of drivers in different types of roadways, some results were received (see Figure 6).

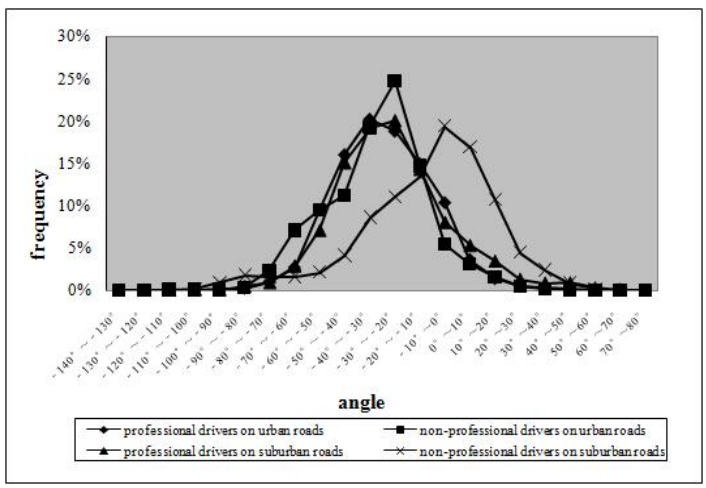

Figure 6. Chart of distribution of fixation angles in horizontal direction

The results show that drivers on the different road sections have the similar distributions. For two types of drivers, the distributions of fixation angles in horizontal direction are both the normal distributions, with all peak points being located on the left of angle 0°. As can be seen from the chart, the professional driver's search scope is larger than the non-professional driver.

Due to the differences between two kinds of drivers, the cognitive ability of non-professional drivers should be carefully considered in the design of roadways. The traffic signals and signs should be designed and installed properly for drivers, especially for non-professional drivers. The results from this study look good for improvement of the roadway safety and efficiency.

CONCLUSION

This paper investigates drivers' dynamic visual characteristics by means of eye tracking system. Corresponding experiments were conducted in the real road conditions to collect necessary data. Based on the data analysis and comparison some conclusions related to regularities of professional and non-professional drivers on fixation distribution, the average fixation duration and the perspective distribution have been reached.

From this study it is found that the road environment has great impact on the drivers' dynamic visual characteristics, especially on the non-professional drivers. During driving, the driver's eye drift to the front and left anterior. Apart from that it is observed that the non-professional driver needs more time to gain the traffic information and their ability of reacting any events is inadequate.

The other finding from this study is that driving experience has a great influence on driving behaviors, including the dynamic visual characteristics. As the number of the non-professional driver increases, it is necessary to improve the location of traffic signs and the environment, because it will enhance safety as well as improve the efficiency of roadways. This paper may have significant contribution to roadway's design and management.

BIBLIOGRAPHY

Fan H., Huang Q., and Lu J. (2007). "The Person's Vision-eye Movement System in the Research of Transportation [J]." *Road Traffic & Safety*.

Geoffrey U., Chapman P., Bowden K., and Crundall D.(2002). "Visual search while driving: skill and awareness during inspection of the scene [J]." *Transportation Research Part F*, 5(2), 87-97.

Ma Y., and Guo Y.(2006). *Study on Drivers Visual Search Pattern Based on Analysis of Eye Movements [M]*. Chang'an University.

Smart Eye AB.Smart-Eye Pro User manual. (2006). Gothenburg, Sweden.

Zhao B. (1988). "Driver's Dynamic Visual Characters and its Effects." *Journal of Highway and Transportation Research and Development*.

STUDY OF HYDRODYNAMIC PRESSURE ON THE CYLINDRICAL PILE-CAP PIER IN DEEP WATER SUBJECTED TO SEISMIC ACTION

LIU Haopeng[1], SONG Bo[2], ZHANG Guoming[3]

[1]School of Civil and Environmental Engineering, University of Science and Technology, Beijing, Beijing 100083, China; email: liuhaopeng19860531@163.com
[2]School of Civil and Environmental Engineering, University of Science and Technology Beijing, Beijing 100083, China; email: songbo@ces.ustb.edu.cn
[3]School of Civil and Environmental Engineering, University of Science and Technology Beijing, Beijing 100083, China; email: iwalk@qq.com

ABSTRACT

In the present paper，study on the influence of hydrodynamic pressure on a 40-meter deep pile-cap pier was made on the basis of the engineering project of the Yangtze River Bridge #3 in Nanjing. Hydrodynamic pressure of the pile-cap pier was evaluated using a three-dimensional finite element model proposed for investigating the dynamical behavior of the pile-cap pier during earthquake in deep water. Two models of the pile-cap pier were proposed for the cases under the conditions with and without water, respectively. The hydrodynamic pressure along the pile caps has increased from top to bottom, and coupling effects would not be ignored in the design of deep-water piers. The numerical results were compared with those from a shaking table experiment, showing a good agreement with each other, especially in the displacement results and mode analysis of the structure.

Keywords: Numerical Analysis, Hydrodynamic Pressure, Shaking-Table Test, Dynamic Response, Earthquake

INTRODUCTION

Since the 21st century, sustained development of bridge construction in China has pulled many long-span bridges into our sights, including the design of the Sutong Bridge (with a main span of 1088m), the Stonecutters Bridge in Hong Kong (the main span is 1018m), and Zhoushan Island Bridge program in which the Xihoumen Bridge is expected to be built with a main span of 1650m.

In general, construction of bridges above deep rivers and sea are challenged by deep water. Some regions of rivers and seas are 80m deep, with the deepest up to 120 m. The effect of waves and fluid on bridge piers is obviously expected very important. Analysis of interaction between piers and water has to account for coupling effects. Solid under the action of fluid will produce deformation or movement, which in turn imposes an impact on the movement and stress of water. This process can be modeled by means of coupled equations, with unknowns to describe fluids and solids, respectively, and the solution domain covering both the fluids and solids. Morison

proposed to calculate the wave force using the Morison equations in 1950 (Morison 1950). However, since the equations include the nonlinear terms, numerical modeling and application of spectrum method for the seismic response of bridge structures becomes more difficult. Goto and Kotsubo used the Westergaard method to analyze a cylinder on the hydrodynamic pressure and found that the Westergaard solution is better for a short cylinder rather than a slender one (Goto H. et al. 1965). Yuan Yinchun discussed how the nonlinear items in the Morison formulas contribute to the seismic response of ordinary bridge pile and pier structure, and simplified the calculation of seismic response of bridges. Zhang Hailong indicated that the hydrodynamic pressure had a significant impact on the seismic response of bridge pier structures, and he suggested to incorporate the effect of hydrodynamic pressure into seismic design (Zhang et al. 2007). Zhang Guoming conducted a study on deep-water piers to compare the methods of hydrodynamic pressure computation due to earthquake between the anti-seismic bridge codes employed in Japan and in China, and analyzed the similarities and differences of the hydrodynamic pressure computations in the two codes (Zhang et al 2008)..

As opposed to the experimental study of wave forces, dynamic test of underwater structure, especially shaking table experiments in water, is rarely conducted both domestically and internationally. Lai Wei and Wang Junjie carried out a shaking table experiment on the underwater pile-group foundation, and analyzed the interaction between seismic response of that foundation subjected to hydrodynamic pressure and interaction of water and structure under different seismic wave levels (Lai et al. 2007). Zhang Guoming took the Third Nanjing Yangtze River Bridge as a benchmark project, and designed and setup a pile-cap pier model testby using the similar principles with the scale factor of 1:50. A shaking table test was completed by loading and seismic wave from Tianjin area in two cases of model: the one around water and the one without water.

SIMULATION OF DYNAMIC BEHAVIOR OF PIERS IN DEEP WATER

Nanjing Yangtze River Bridge No. 3, which is shown in Figure 1, an important part of the national highway connecting Shanghai and Chengdu, is located in the upper reaches of Nanjing Yangtze River. The total length of the traffic line is 15.6km, along which the cable-stayed bridge has a total length of 1288m with a main span of 648m. Figure 1 also shows the twin towers that are composed of steel box girders, which have double cable-plane with the south pier foundation reaching the depth of 50m below zero. This investigation mainly focuses on the hydrodynamic pressure of the south pier.

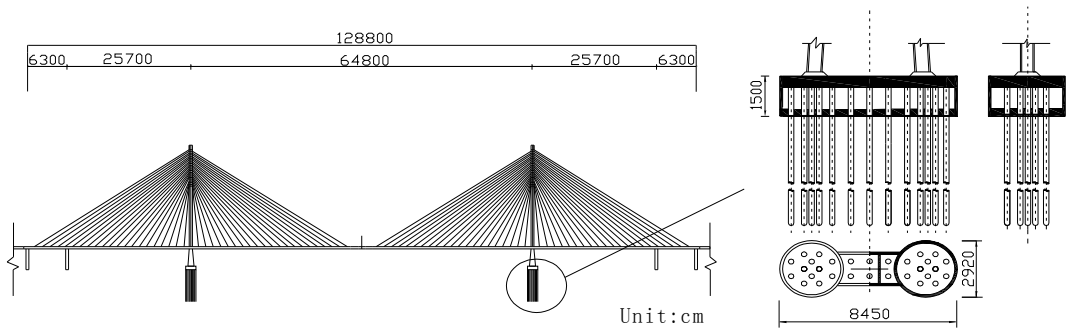

Figure 1. Nanjing Yangtze River Bridge No.3 and its south pier

Since the fluid--structure interaction induces fluid-solid coupling effect and the Nanjing Yangtze River Bridge No.3 is supported by piles with more than 50% of their lengths in earth layers, some assumptions are introduced, including that the interface of piles and soil is rigidly jointed. Across the direction of flow, the dumbbell-shaped foundation is symmetric, so only one circle pile cap foundation is selected for research. Figure 2 shows Solid5 element and Fluid142 element, which are respectively used to simulate concrete units and water unit. In the finite element method, fluid model should be established first, and then the solid model. The fluid-solid coupling tags（also known as FSI）are imposed on the interface of fluid-solid. In this investigation, two models are established, as shown in Figure 2: one for the piles without water in the surrounding area, and the other for piles in the water, in an effort to compare mechanical properties of the piles in the water and in anhydrous state. It should be noted that the fluid elements need to be analyzed within a rigid wall, so a "sink" is built to contain the piles and water.

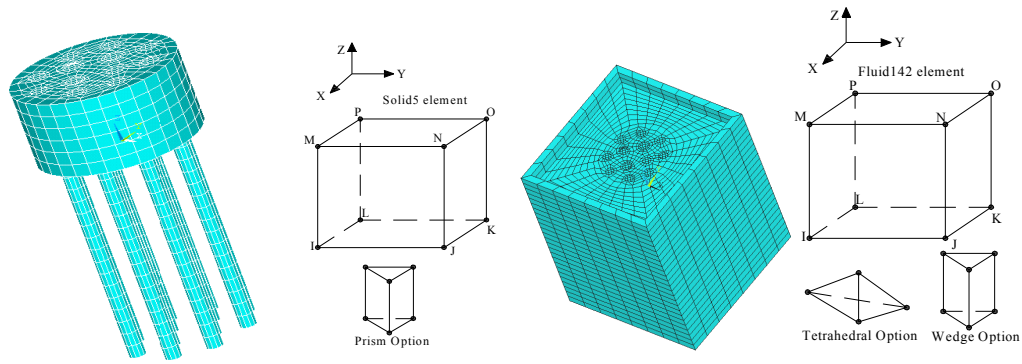

(a)Model of piers and Solid5 element (b)Model of water and Fluid142 element

Figure 2. Model discretization

Regarding the boundary conditions, the bottom of the piles without water is fixed while the topp part is pressed with uniformly distributed load to consider the effect of upper load; the same is true to the piles in the water, while the grid container is also fixed.

The finite element model is analyzed with the imposed boundary conditions. Analysis of the model refers to dynamic characteristics and seismic response. Results

of the first four vibration frequencies and subsequent vibration figures are listed in Table 1.

Table 1. Results of natural vibration

Order	1	2	3	4
Frequency(Hz)	0.293	0.556	4.029	4.601
Period(s)	3.413	1.798	0.248	0.217
Vibration mode	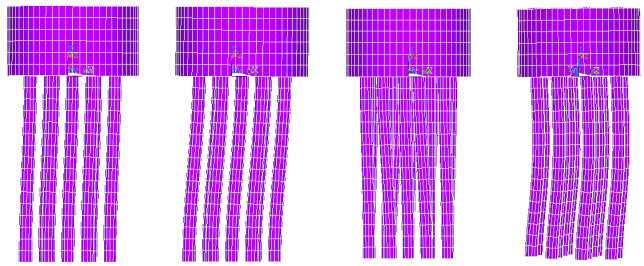			

An earthquake acceleration-time record does not accord with a defined function, but rather a series of time-varying random pulse, and vibration modes and frequencies change so much that there is without any model to discribed it. Thus, the solution to the dynamic equation is not available unless seismic waves are given versus time △T(time step) for numerical simulation. Then the basic integral equation dynamic movemet of the structure during each time step can be resolved. Finally, the structure displacement, velocity, acceleration and internal forces will be obtained.

Considering the site characteristics, seismic waves have been adjusted according to relevant principles. Tianjin seismic waves (Figure 3) were input,,with a peak acceleration of 244.62galand the main cycle of 0.55s. Frequency range of these seismic waves are wider than others, so they are more suitable for seismic design; over years they have been used as a typical example from a major earthquake.

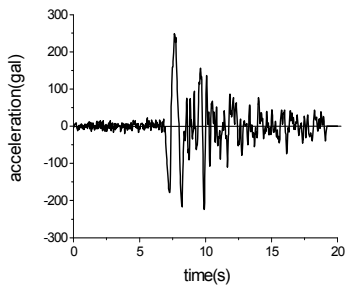

Figure 3. The acceleration-time curve of curve of seismic waves from Tianjin

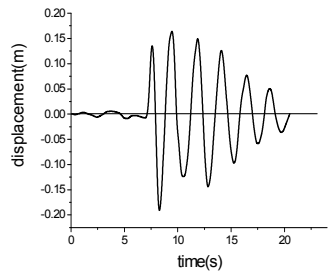

Figure 4. The Displacement-time node 4964

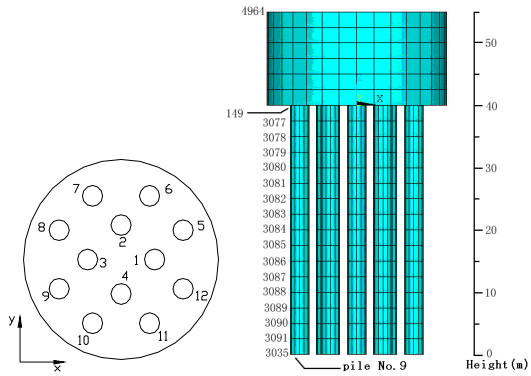

Figure 5. Location of piles and key nodes in pile cap

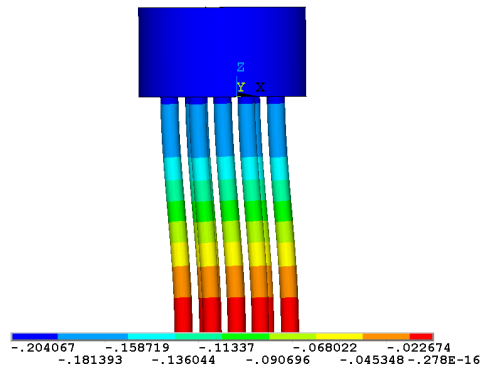

Figure 6. Nephogram of displacement in x direction

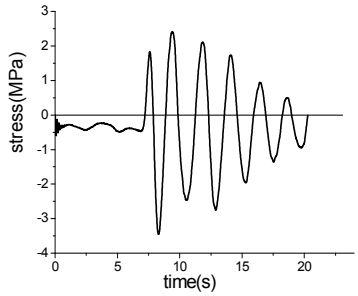

Figure 7. Stress-time curve of node 3035

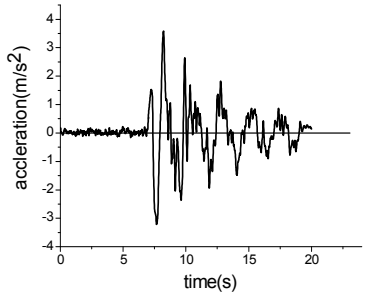

Figure 8. Acceleration-time curve of node 4964

Figure 4 is the ANSYS simulation of the displacement of node 4964 in the pile caps. This point is on the boundary of the top face of the cap as shown in Figure 5. Time-curves from the figure show the maximum displacement is 0.191m, and the cloud chart of this moment for the whole pile-cap pier is shown in Figure 6. The entire cap is basically in the translational state, while the displacement of piles increases from the bottom to the top gradually. In the whole process of the interaction, the largest compressive stress is 3.45 MPa, which appears at node 3035, as shown in Figure 5, at the bottom of the pile at the moment of 8.35s, which is not exactly consistent with the appearance of the largest displacement. And the largest tensile stress is 2.41 MPa at the moment of 9.43 s. Stress-time curve of node 3035 is shown in Figure 7.

ANSYS can not directly give the acceleration-time curve. However, after taking derivatives of the displacement twice, the acceleration-time curve of the node 4964 is shown in Figure 8, with the peak acceleration of 3.53m/s^2 at the moment of 8.20s, a little earlier then the maximum displacement and stress.

EXPERIMENTAL STUDY OF DYNAMIC BEHAVIOR OF PIERS BY SHAKING TABLE TEST

Test of interaction between water and piers mainly consists of shaking table test and vibration site test. Since shaking table test features in high repeatability and feasibility and is easy to control experimental process, it has been used by more and more researchersas a tool for analysis of solid-fluid coupling. In last several years,

with development of similarity theory and advances of anti-seismic test technology, shaking table test became the popular way to study structural dynamic problems.

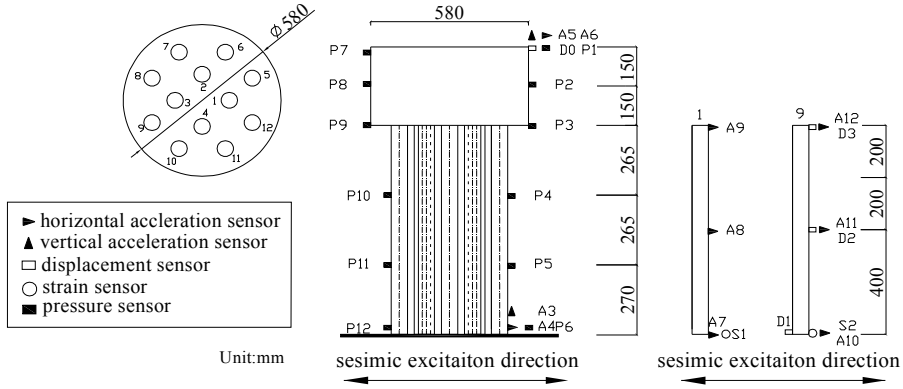

Figure 9. Layout of the testing facilities

South pier cap of Nanjing Yangtze River Bridge No. 3 is dumbbell-shaped, with a dimension of 84m (along the bridge)×29m (longitudinal to the bridge) and its thickness 7.5m. Its concrete cover is 4.6m thick. Each circle part consists of a total of 30 bored piles, and each of them is 3m in diameter and 120m in length at the deepest area. The bearing stratum is a weathering mudstone layer. South pier foundation and pile cap layout is given in Figure 9. Similarity factors are decided by the size of shaking table and the experimental model. The size of the shaking table is 1.5m × 1.5m, while the prototype diameter of the pile caps is 30m, so similarity factor is 1:50. Other similarity factors are listed in Table 2. Measuring points of the experimental model are located as shown in Figure 9. Seismic waves from Tianjin were selected for the experiment, which is the same as the waves used for numerical simulation. Thus comparisons can be made to evaluate the two methods mentioned above. A collection is made to evaluate water pressure of test piles, which is distributed at the pier elevation as shown in Figure 10, from Figure 10, hydrodynamic pressure on the pile caps has increased from top to bottom, below the height of 40cm the increase in water pressure slows down.

COMPARISONS OF RESULTS FROM NUMERICAL ANALYSIS AND SHAKING TABLE TEST

A comparison is made between the numerical and experimental results. The model similarity factor for the natural frequency is 33.5, and the expected value of natural frequency in numerical way is 6.72/33.5=0.201Hz. The test results are in good agreement with the simulation results, as shown in Table 3.

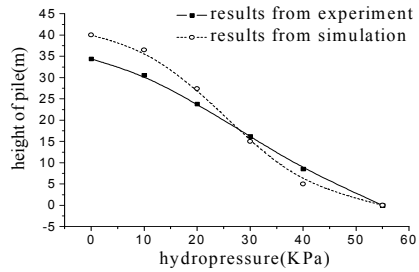

Figure 10. Comparison in hydrodynamic pressure

Table 3. A comparison of two methods

Physical Quantity	Similarity factor
Length	$S_l = 1/50$
Elastic modulus	$S_E = 6.87$
Density	$S_\rho = 6.87$
Acceleration	$S_a = 1$
Stress	$S_\sigma = S_E = 6.87$
Strain	$S_\varepsilon = S_\sigma / S_E = 1$
Inertia force	$S_F = S_E S_l^2 = 2.75\text{e}{-3}$
Water pressure	$S_P = S_l = 0.02$
Moment	$S_M = S_E S_l^3 = 5.5\text{e}{-5}$
Frequency	$S_f = S_l^{-1}\sqrt{S_\rho / S_E} = 33.5$
Time	$S_t = S_l\sqrt{S_E / S_\rho} = 0.03$
Displacement	$S_u = S_l = 0.02$

Table 2. List of similarity factors

	Numerical way	Experimental way
Vibration mode	1	1
Natural frequency(Hz)	0.210	6.72
Max-displacement(cm)	19.4	0.388

From Figure 8, the numerical simulation shows the peak displacement at the top is 19.1cm, as opposed to the experimental result of is 0.388cm. With displacement similarity factor 0.02, the expected value of peak displacement in numerical simulation is 0.388/0.02=19.4cm, which is in a good agreement with the actual result. The occurance of the largest displacement and the largest compressive stress does not coincide, just as the numerical simulation indicates. And also, the largest tensile stress comes up after the largest compressive stress, which is just like the simulation way. For the hydrodynamic pressure, which is shown in Figure 10, however, there is an obvious difference in pressure-height curve between the two methods, such as the pressure at the pile bottom by the experiment is 35kPa as compared to 40kPa in the simulation, the difference may be due to the fact that boundary conditions vary in different methods. But both curves basically follow the same trend.

CONCLUSIONS

In this investigation, with the Nanjing Yangtze River Bridge No.3 as the engineering benckmark, a finite element model of pile foundation was proposed to explore fundamental dynamical behavior of the pile-cap pier during an earthquake in

deep water. A comparison was made between the numerical and the experimental results. The numerical outcome match well with those from the experiment, especially in the displacement and mode analysis of the structure.

Actually, the water domain near the analysis boundary should have been considered infinite. In this paper, only part of the water was taken into account. Also we introduced other simplifications, such as the pile length and the structure material, which should be further investigated. On the other hand, the model test is only limite to the elastic stage of the structure, the elastic-plastic stage will be considered in the future research.

REFERENCES

Garritsma, IR.J. (1957). "Experimental determination of damping added mass and added mass moment of inertia for a ship model." *I.S.P.*, 14(38):505~519.

Goto, H., and Toki, K. (1965). "Vibration characteristics and a seismic design of submerged bridge piers." *Pro. 3rd world conf. on earthquake eng,* New Zealand, II.

Lai, Wei, and Wang, Junjie (2006)."The shaking table test for submerged bridge pier." *Earthquake Engineering and Engineering Vibration*.

Olson, L.G., and Bathe, K.J. (1983). "A study of displacement based fluid FE for calculating frequencies of fluid and fluid-structure systems." *Nucl. Engrg Des*., 76:137~151.

Liu, Zhenyu, and Li, Qiao (2008)."Additional Hydrodynamic Pressure on Rectangular Hollow Piers in Deep Water Due to Earthquake." *Journal of Vibration and Shock*. (?)

Morison, J.R, O'Brien, and M P, Johnson J.W. and Schaaf, S.A. (1950). "The force exerted by surface wave on piles." *Petroleum Transactions*, AIME,189:149~154.

Tanaka, Hudspeth R.T. (1988). "Restoring forces on vertical circular cylinders forced by earthquake." *Earthquake engineering and structural dynamics*, 16:99~119.

Wu, J.S., andHsieh M. (2001). "An experimental method for determining the frequency-dependent added mass and added mass moment of inertia for a floating body in heave and pitch motions." *Ocean Engng*, 28：417~438.

Zheng, Shixiong (1998)."The Effects of the Fluid-structure Interaction Seismic Response of Bridge Piers." *Bridge Construction*. (?)

Zhu, Shisong (2006)."Research on Seismic Response of the Second Danjiangkou Bridge Considering Water Effect." *Journal of WuhanUniversity of Technology*.

Influencing Factors Contributing to Rear-end Collisions on Highways: PCA Based Investigation and Findings

H. Jun[1], H. Xu[2], Y. Pei[3] and H. Ji[4]

[1] School of Transportation Science and Engineering, Harbin Institute of Technology, P.O. Box 2525, 202 Haihe Rd. Harbin 150090, China, PH (86) 451- 8628 2117; FAX (86) 451-8628 2116; email: junhaimin@163.com
[2] School of Transportation Science and Engineering, Harbin Institute of Technology, P.O. Box 2525, 202 Haihe Rd. Harbin 150090, China, PH (86) 451- 8628 2117; FAX (86) 451-8628 2116; email: stedu@126.com
[3] School of Transportation Science and Engineering, Harbin Institute of Technology, P.O. Box 2526, 202 Haihe Rd. Harbin 150090, China, PH (86) 451- 8628 2832; FAX (86) 451-8628 2832; email: yulongp@263.net
[4] School of Transportation Science and Engineering, Harbin Institute of Technology, P.O. Box 2525, 202 Haihe Rd. Harbin 150090, China, PH (86) 451- 8628 4775; FAX (86) 451-8628 4775; email: jihai1986@163.com

ABSTRACT

Taking the 2003-2005 highway accident data surveyed from Hada Highway and Hashuang Highway into consideration, rear-end collisions are divided into two patterns: rear-collisions and stationary object collisions. The principal analysis identified the impact level of different factors on two types of rear-end collisions. Then, significant impact factors are detected and identified by charting analysis and clustering research. The final investigation result indicates that fatigue, excessive speed, unsafe following distance, congestion et al, are main impact factors on rear collision accidents. However, excessive speed, fatigue, illegal parking, et al, have a significant effect on the occurrence of stationary object collisions, which provide a reference for highway management departments.

INTRODUCTION

Highways, as a modern transport infrastructure, play an important role in the development of society and economics, with the merits of huge traffic flow, high speed travel, well-equipped and comfortable traffic environment, et al, which leads to its high efficiency in supporting industrial development and improvement (Button et al, 2000). However, automobiles are becoming popular with urban families and becoming a need for enjoying the convenience of modern life directly brought by technological development. Severe social problems such as heavy traffic congestion, environmental pollution, and traffic accidents have become one of the central and heated issues accompanying the increase of automobiles, leading to traffic accidents that especially attract the world's attention (Hamada et al, 2006).. In China, for instance, it has been officially announced that more than one million people lost lives in traffic accidents in 2003, in which random rear-end and side-swiping collisions,

caused by an insufficient following gap and braking distance, covers about one-third of the total accidents.

To cope with this problem, a program on Intelligent Transportation Systems (ITS) has been proposed to increase road efficiency and decrease the negative effect of accident-related factors and countermeasures. Both administrative and technology measures, have also been adopted to investigate the causes and probability of traffic accidents. During the research, the rear-end collision was considered the main accident pattern on highways and its occurrence was considered to be a key idea affecting investigation results and result implications, especially rear-end and side-wiping collisions. Therefore, the research, with wide recognition, contributes to smooth traffic flow control, accident prevention and traffic safety administration.

ACCIDENT TYPE CLASSIFICATION

According to accident patterns, highway rear-end collisions are divided into two types, including rear collision, characterized by the collision between the front of the following vehicle and the rear of the leading vehicle (Davis et al, 2006). The other is the stationary object collision, which occur between the front of the following vehicle and the rear of the stationary parked vehicle. Based on this definition, accidents surveyed from Hada Highway and Hashuang Highway from 2003 to 2005 were classified into two types, as listed in Table 1 and Table 2.

Table 1. Rear-end Accident Pattern Distribution on Hada Highway

Accident Patterns	Accident Number (Times)		Death (P)		Injury (P)		Economic loss (×10^4Yuan)	
	Hd	Hs	Hd	Hs	Hd	Hs	Hd	Hs
Rear-end collisions	46	55	37	33	46	35	97.70	144.85
Stationary Object collisions	6	7	4	3	10	6	5.80	10.42

The equivalent number of accidents (Neyens et al, 2007) is introduced to analyze the seriousness of different patterns of highway accidents.

$$ER_i = K_1 F_i + K_2 J_i + R_i \quad (1)$$

where ER_i is the equivalent number of the ith rear-end accident. K_1 is the weight of dead persons in the ith rear-end accident. K_2 is the weight of injured persons in the ith rear-end accident. F_i is the statistical number of dead person in the i^{th} rear-end accident. J_i is the statistical number of the injured person in the i^{th} rear-end accident. R_i is the accident number of the i^{th} rear-end accident.

For the sake of simplicity, the weight k_1 of the dead person is considered 2.0 and the corresponding injured k_2 is 1.5 (Garcia et al, 2006). From Table 1, the equivalent numbers of each rear-end accident pattern on Hada Highway are obtained as ER_1=189, ER_2=29 and the result is the same for Hashuang Highway, ER_1=173.5 and ER_2=22. Therefore, rear-end collisions are the main cause of highway accidents.

PRINCIPAL COMPONENT ANALYSIS METHOD

To distinguish the degree of impact of the above-mentioned factors for highway rear-end collisions, the principal component analysis method which transfers a few indicators into some main indicators, is used to analyze the influence degree (Wang et al, 2008). According to its working theory, the calculation process is divided into the following six steps.

The statistical accident data is recorded as

$$X=\begin{bmatrix} X_1 \\ X_2 \\ \vdots \\ X_3 \end{bmatrix}=\begin{bmatrix} x_{11} & x_{12} & \cdots & x_{1p} \\ x_{21} & x_{22} & \cdots & x_{2p} \\ \vdots & \vdots & & \vdots \\ x_{n1} & x_{n2} & \cdots & x_{np} \end{bmatrix} \tag{2}$$

For $(i=1,2,\cdots,n;\ j=1,2,\cdots,p)$, initial accident data is standardized by Z-score as $x_{ij}^{*}=(x_{ij}-\bar{x}_j)/\sigma_j$, which means value $\bar{x}_j=\sum_{t=1}^{n}x_{tj}/n$, $\sigma_j^2=\frac{1}{n-1}\sum_{t=1}^{n}(x_{ti}-\bar{x}_j)^2$. Thus, for $(i=1,2,\cdots,n;\ j=1,2,\cdots,p)$, correlation coefficient matrix R is defined as $R=(r_{ij})_{p\times p}$, here $r_{ij}=\frac{1}{n-1}\sum_{t=1}^{n}x_{ti}^{*}\bullet x_{tj}^{*}$.

If the given values comply with $\lambda_1\ge\lambda_2\ge\cdots\ge\lambda_p\ge 0$, $a_1,a_2,\cdots,p$ is the corresponding orthogonal unit eigenvector, then the i^{th} PCA of vector X is defined as $Z_i=a_i^{t}X$, where Z_1 is named as the first principal components of investigated vector. Contribution rate of PCA is determined by $G(m)=\sum_{i=1}^{m}\lambda_i/\sum_{i=1}^{p}\lambda_i$. According to the analysis result, accident causes could be investigated.

ACCIDENT IMPACT DETERMINATION BY PCA

The purpose of analyzing the impact factors is to make the quantitative analysis of the relationship between each factor and the occurrence probability of rear-end collision and detect the main factors, which will provide a research basis[9].

Rear-end accidents. Four indictors of rear-end collisions on Hada Highway and Hashuang Highway are surveyed ranging from 2003 to 2005. The results are obtained by principal components analysis method as

Eigenvalues and eigenvectors are λ_1 =3.7192, λ_2 =0.1783, λ_3 =0.0762, λ_4 =0.0263. The eigenvector of λ_1 is Z_1 =(0.5002, 0.5164, 0.4984, 0.4845). Supposing m=1, then the contribution rate of PCA can by calculated by model (3)

$$G(1)=\sum_{i=1}^{m}\lambda_i/\sum_{i=1}^{p}\lambda_i=0.9298>80\% \tag{3}$$

The result is more than 80% and indicates the feasibility of characterizing the four indicators with a comprehensive one. The impact force of each factor can be judged by model (4), where X_i is the standardized accident data as in Table 3.

$$Z_1 = 0.5002X_1 + 0.5164X_2 + 0.4985X_3 + 0.4845X_4 \quad (4)$$

For the analysis of impact factors of stationary vehicle collisions, the result is obtained by PCA as shown in Table 4.

Table 3. Evaluation of Impact Factors for Rear-end Collision

Impact factor	Number (X_1)	Dead toll (X_2)	Injuries (X_3)	Economic losses (X_4)	(Z_1)
Over-speeding	2.046	1.638	2.157	0.866	3.36
Drunk driving	-0.535	-0.648	-0.728	-0.609	-1.26
Fatigue driving	1.822	2.360	1.926	2.729	4.41
Overloading of trucks	-0.199	-0.046	0.310	0.735	0.39
Overcrowding	-0.535	-0.527	-0.612	-0.708	-1.19
Illegal overtaking	-0.648	-0.647	-0.612	-0.597	-1.25
Illegal parking	-0.872	-0.647	-0.728	-0.736	-1.49
Unsafe following distance	0.587	0.194	0.079	0.339	0.60
Illegal lane-changing	-0.648	-0.647	-0.612	-0.692	-1.30
Brake misconduct	-0.311	-0.527	-0.381	0.009	-0.61
Vehicle effect	0.812	0.795	0.541	-0.012	1.08
Road condition	-0.872	-0.647	-0.728	-0.736	-1.49
Environmental factor	-0.648	-0.647	-0.612	-0.588	-1.25

Table 4. Evaluation Data of Impact Factors for Stationary Vehicle Collisions

Impact factor	Number (X_1)	Dead toll (X_2)	Injuries (X_3)	Economic losses (X_4)	(Z_1)
Over-speeding	2.777	1.391	3.149	2.943	5.191
Drunk driving	-0.462	-0.512	-0.359	-0.440	-0.883
Fatigue driving	1.388	2.344	0.809	1.134	2.782
Overloading of trucks	-0.462	-0.512	-0.359	-0.440	-0.883
Overcrowding	-0.462	-0.512	-0.359	-0.440	-0.883
Illegal overtaking	-0.462	-0.512	-0.359	-0.440	-0.883
Illegal parking	0.462	1.391	-0.359	0.329	0.864
Unsafe following distance	-0.462	-0.512	-0.359	-0.440	-0.883
Illegal lane-changing	-0.462	-0.512	-0.359	-0.440	-0.883
Brake misconduct	-0.462	-0.512	-0.359	-0.440	-0.883
Vehicle effect	-0.462	-0.512	-0.359	-0.440	-0.883
Road condition	-0.462	-0.512	-0.359	-0.440	-0.883
Environmental factor	-0.462	-0.512	-0.359	-0.440	-0.883

IMPACT FACTOR DETERMINATION

The purpose of analyzing the impact factors is to make the quantitative analysis of impact factors on rear-end collisions with the calculation result of evaluation indicators, which will provide the basis to determine the relationship

between each factor and the occurrence probability of rear-end collisions (Dzianis et al, 2008).

Using charts and cluster analysis methods to choose the impact factors behind the accident, then the main impact factors can be identified. The chart method is more commonly used with the simple, direct, easy to understand features. Impact factors acquired by principal component analysis are sorted according to size, then drawn from the evaluation index chart, as shown in Figure 1, and Figure 2. Design elements are divided into three types according to curve trend, then 0 and 2 are chosen as thresholds.

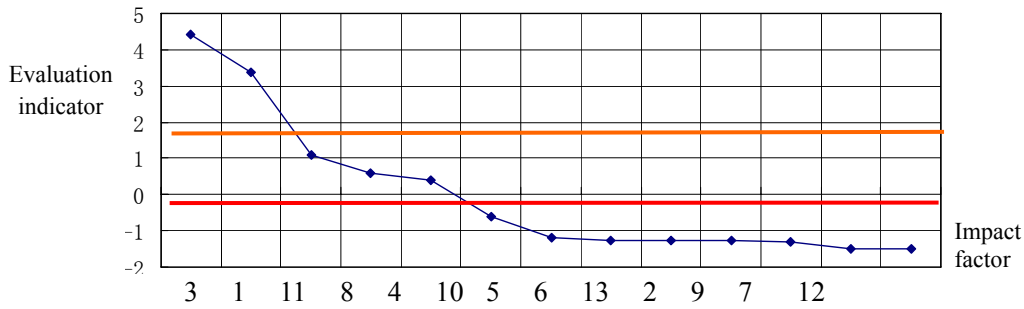

Figure 1. Index of impact factor on rear-end collision

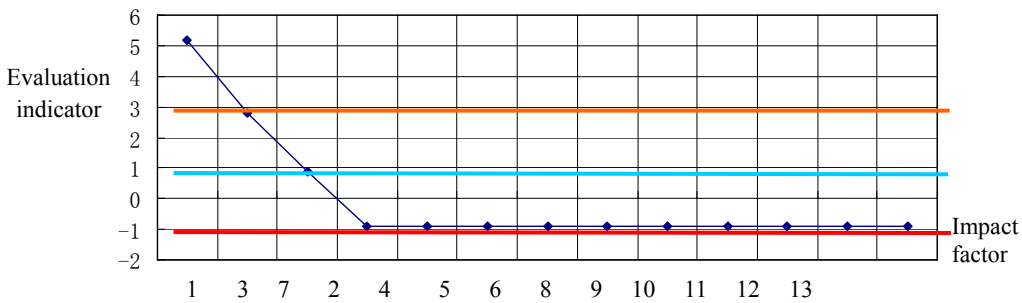

Figure 2. Index of impact factor on stationary vehicle collision

The basic idea of clustering analysis is to classify each research object in a category and combine the two that are more similar with each other, then calculate the distance and similarity between the new category and other categories. This process continues until all objects classified in a category. With SPSS, Figure 3 shows the result of the clustering analysis.

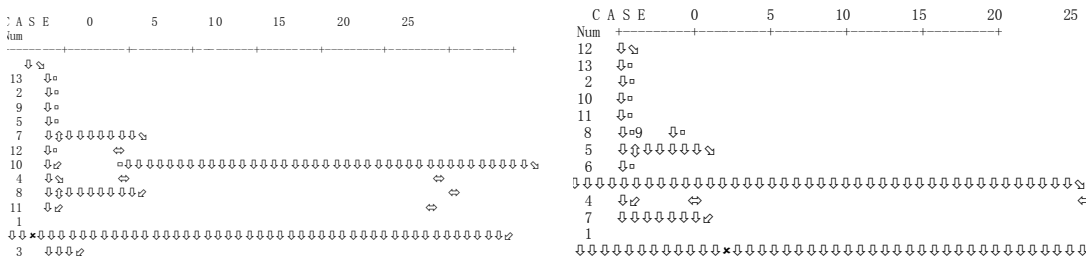

a) Rear-end collision b) stationary vehicle collision

Figure 3. Hierarchical clustering results by PCA

DISCUSSION AND CONCLUSION

The indicators are investigated to analyze the impact factors on rear-end accidents and stationary vehicle collisions by PCA. By chart analysis, three types are acquired. The first is fatigue driving and over-speeding, and the second includes vehicle factors, unsafe following distance, overloading of trucks, improper braking, passenger overloading, illegal overtaking, environmental factors, drunk driving, illegal lane-changing and road conditions.

With clustering analysis, three types are also acquired. The first is fatigue driving and over-speeding and the second is vehicle factors, unsafe following distance, and overloading of trucks. Then the third includes improper braking, passenger overloading, illegal overtaking, environmental factors, drunk driving, illegal lane-changing and road conditions. The analysis result indicates they are consistent. According to the comprehensive analysis, the outstanding five impact factors are chosen as fatigue driving, over-speeding, vehicle factors, unsafe following distance and vehicle overloading.

ACKNOWLEDGEMENT

This research work was partially supported by the National Scientific Foundation of China under grant number 50778056. The authors also wish to thank the editors and reviewers of ICCTP 2009 for their assistance during this project.

REFERENCES

Hamada, M. (2006). Analysis of traffic accident trends in Japan and predictions for the future. *Review of Automotive Engineering*, 27(1), 145-150

Button, N. P; Reilly, P. M. (2000). "Uncertainty in incident rates for trucks carrying dangerous goods". *Accident Analysis & Prevention.*, 32(6), 797-804

Davis, G. A; Swenson T. (2006). "Collective responsibility for highway rear-ending accidents?: an application of probabilistic causal models". *Accident Analysis & Prevention*, 38(4), 728-736

Neyens, D. M.; Boyle, L. N. (2007). "The effect of distractions on the crash types of teenage drivers". *Accident Analysis & Prevention*, 39(1), 206-212

Garcia A, Martin A, Paez J. (2006). "Analysis of the driver's workplace in coaches related to passive safety". *International Journal of Vehicle Design*, 42(1-2), 134-153

Wang, Y. G.; Pei, Y. L.; Zhao, Y. D. (2008). "Vibration-based damage detection with structural modal characteristics". *The Baltic Journal of Road and Bridge Engineering*, 3(1), 21-28

Dzianis, K.; Ivan, L.; Kornelija, R. (2008). "Implementation of experimental research in road traffic: theory and practice". *The Baltic Journal of Road and Bridge Engineering*, 3(2), 101-108

Nagai, M. (2006). "Enhancing safety and security by incident analysis using drive recorders". *Review of Automotive Engineering*, 27(1), 9-15

Passenger Transport Demand Prediction for Newly-Built Regions

Zhang Maomin[1] and Liu Yisheng[2]

[1] School of Economics and Management, Beijing Jiaotong University, Beijing 100044, China, No.3 of Shangyuan Residence, Haidian District, Beijing 100044, China; PH (86) 10- 5168 7163; FAX (86) 10-5168 7163; email: zmm0033@163.com
[2] School of Economics and Management, Beijing Jiaotong University, Beijing 100044, China, No.3 of Shangyuan Residence, Haidian District, Beijing 100044, China; PH (86) 10- 5168 8218; FAX (86) 10-5168 8218; email: bslys@263.net

ABSTRACT

The index of generalized traffic demand is proposed from the property of trip time and space. Considering the factors of trip mode, trip distance, trip velocity, and a generalized traffic demand, a model is developed which can weigh the size of traffic demand per hour. The corresponding general traffic demand model of transportation model is developed according to the characteristics of motor vehicles and pedestrians. The paper uses a given city as an example and the generalized traffic demand model correlative to the impact factor is developed and the relation between traffic demand and factors is analyzed. The paper presents the countermeasures decreasing the urban transportation problem using an average case analysis. From the conclusion, the two most obvious factors which affect the majority of general traffic demand are the structure of activity patterns and the average trip velocity. An increased proportion of bus transit and commuter transportation are the most obvious factors to decrease total car trip. Increased speed of private car use is the most obvious factor to decrease the total car trip.

INTRODUCTION

Running mode of transport accounts for a total area of the road and the actual existence of the road space within a certain time and space are in general used as the indicators to measure city passenger transport demand and supply (Yao et al, 2005). Previous research on the traffic demand was discussed as to the number of standard cars in peak hours at the actual road network in a certain period of time. Scale indicators are: peak-hour traffic, mixed traffic generation, and non-motorized traffic generation, such as production. Traffic demand studies have not fully considered travel distance and travel speed (Karst et al, 2004; Ryan et al, 2003),, a single volume of traffic generation can not measure the characteristics of traffic demand, such as travel speed, trip distance etc. (Wang et al, 2008).

Louis presented the concept of consumption of time and space in his research on capacity of road network(Boamet et al, 2001).. Based on capacity of road network, road length and effective travel time which compose road resources have attributes of time and space consumption. In this paper, the study is also based on the consideration of the traditional static traffic demand to promote completion of a

resident's trip. Generalized traffic demand will describe it as the traffic generation with a certain number of travel speed travel distance per unit of time. This paper provides a good combination point for analysis on traffic demand and traffic supply, not only can the efficiency of city transport systems be analyzed to provide a basis to urban transport policy making, but it also can be used as an important part of transportation demand management.

GENERALIZED TRAFFIC DEMAND MODEL

Research Method. Traffic production includes traffic generation and traffic attraction. Traffic process can be described as generation unit and attraction unit accomplish the given traffic distance through stated traffic methods and definite speed. Previous research focused on each part step-by-step, no research took traffic process as traffic demand production. Researching and optimizing the characteristics of urban traffic demand generation can adapt limited roadway system resources (Giulio et al, 2005).

In general, pedestrian flow and vehicle flow are quite heavy. For the given city, the gross of traffic generation is fixed in a period of time, but the distribution effect is decided by different kinds of speed, distance and varying traffic modes. From the space-time demand property of traffic generation, generalized passenger transport traffic demand is raised; it is considered as the amount that is produced by diversified traffic mode and converted to equivalent car. This amount has definite traffic speed and traffic time properties. When urban roadway space-time resources are limited, the effect is different. Research on traffic demand optimization not only optimizes and controls its effect, but also puts forward a new idea for traffic research in large cities.

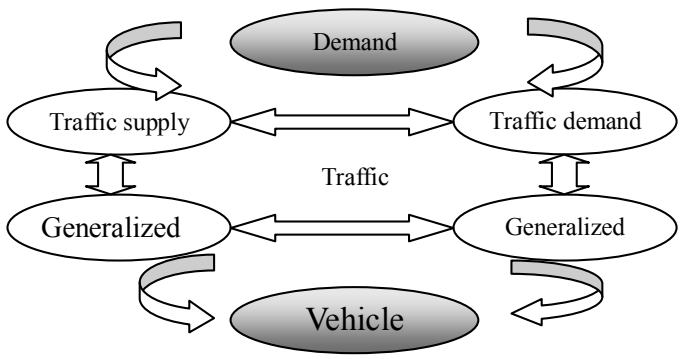

Figure 1. Traffic demand vehicle circulation efficiency analysis

In the city roadway system, the traffic unit includes vehicles, non-vehicles and pedestrians. When vehicle and non-vehicle use road resources, pedestrians usually use the walking system. Compared with the vehicle system, the walking system uses limited road resources. This paper considers traffic demand produced by the walking system alone. In the passenger transport structure, the transfer from pedestrian traffic mode to others should be calculated by founded models.

Vehicle demand model. The framework of our urban passenger transport is

quite complex. In general, different cities have different frameworks and different traffic mode proportions. Using a large city as a research object in this paper, vehicles are classified as: bus, commuter cars, car, private car and taxi. The production of urban traffic demand relates the traffic gross and intensity, the total traffic quantity of the *i* kind traffic model is $Q_{Mi} = P \cdot Y \cdot P_i \cdot D_i$.

Where, Q_{Mi} is the total traffic quantity of the i^{th} kind traffic model, person-time．km; P is the total urban passenger transport quantity, person-time; Y is traffic intensity, time/(person．day); M_i is traffic model, except walking traffic; P_i is the traffic proportion of the i^{th} kind traffic model, $\sum_i P_i = 1$; D_i is the average traffic distance of the i^{th} kind traffic model, km.

Then in the road system, the total traffic quantity means the summation of all kinds of traffic model, except walking, and is defined as $Q = P \cdot Y \sum P_i \cdot D_i$. Traffic quantity in unit time relates to urban scale, urban development degree and so on, calculated method: $Q_t = Q / T$.

This index reflects the traffic demand in unit time. In general, this index has the same rule with the resident traffic which changes following time. In peak hours, this index affects urban traffic demand directly, and can be obtained by stating the traffic data in a different period of time(Yam et al, 2000). In order to accomplish this, traffic needs some kind of traffic mode with a stated speed and must complete the traffic within the traffic distance. Owing to traffic should use some road resources in urban traffic systems and the walking traffic uses fewer resources than vehicles. For research convenience, this paper researches the walking system separately: $VEH_i = K_i / C_i$

Changing different traffic mode passenger transport quantity into equivalent car, then generalized passenger transport demand measure model:

$$M = PEO \cdot Y \sum_i \frac{P_i \cdot D_i \cdot K_i}{C_i \cdot V_i \cdot T} \qquad (1)$$

where, M is Generalized total passenger transport demand, veh/min-1; C_i is the average patronage of No. *i* transportation, people; V_i is the average trip speed of No. *i* species mode of transportation, km/h; k_i is vehicle model converted coefficient.

The meaning of generalized passenger transport demand of per unit time is the multiplication of the various traffic generated equivalent amount of car travel with the product of the sum of travel time. Vehicles must occupy some space resources of the road network. This model has the same dimensionless approach as the generalized road network capacity, if the generalized traffic demand is assigned to the road network, and we can analyze the operational efficiency of motor vehicles traffic in the city road network.

Supposing $a_i = D_i K_i / C_i V_i$, the type of number *i* traffic relationship with the traffic demand is calculated as follows:

$$M_i = a_i P_i + \frac{(1-P_i)P_1 a_1}{1-P_0} + \cdots + \frac{(1-P_i)P_{j-1} a_j}{1-P_0} + \cdots \frac{(1-P_i)P_{j+1} a_{j+1}}{1-P_0} + \cdots + \frac{(1-P_i)P_n a_n}{1-P_0}$$

$$= a_i P_i + \frac{(1-P_i)}{1-P_0} \sum_{j \neq i} P_j a_j \qquad (2)$$

N is the passenger transport form of the quantity, p_i is the proportion of type number i transport mode for the mode of transportation in the status quo, it can be seen that the impact of the volume demand in various ways is different. Order $b_i = P_i D_i K_i / C_i$, so the average trip speed and demand model:

$$M_i = b_i / V_i + \sum_{j \neq 1} b_j / V_j \qquad (3)$$

This indicator reflects the level of city traffic load. On the whole, the volume demand increases as the speed decreases, but with different modes of travel, the extent of the impact is different. When a certain mode of travel's travel speed is 0, the traffic demand is considered infinite; when road traffic jams occur, consider the local traffic demand as infinite. Vehicles parked in the road system occupy time and space resources, but without travel.

Foot traffic demand model. Traveling by walking uses a shorter distance, and speed is comparatively stable. So, as a separate model to study, use the above analysis methods to set up the foot traffic system demand model:

$$M_p = PEO \cdot Y \frac{P_p \cdot D_p}{T \cdot V_p} \qquad (4)$$

Where, p_i is the traffic-sharing ratio of walking, %; D_i is the average trip distance of foot traffic, km; V_i is the average travel speed of foot traffic, km / h.

Foot traffic through the walking system provides an analysis of the total supply. The current problem of the walking system in our country is the Humanized Design of the foot traffic system which enhances the level of the motor city but reduces the proportion of trips by foot traffic.

EXPERIMENT TEST

Taking a certain city as an example, the model application is analyzed and the data from the 2004 year's investigation results is used. The data of passenger traffic structure, average travel time, average travel distance, et al. have been shown as Table 1. As the city is not building a rail transit system, the value of this index is 0.

Based on the model in Table 1, traffic demand output and speed is set up. In the model of traffic mode, assume that certain traffic mode is changed, and the relative proportion of other is unchanged. The calculation result is shown in Table 2. Model results show the unit of quantity but the numerical magnitude only expresses the change law of demand but not mean actual value.

Table 1. Statistics of Basis Data

Traffic mode M_i	Public bus M_1	Commuter bus M_2	Official car M_3	Private car M_4	Taxi M_5	Rail transit M_6	Bicycle M_7
Proportion P_i (%)	0.428	0.106	0.166	0.062	0.037	-	0.200
Travel distance D_i (km)	12.4	6.9	13.8	14.7	14.3	-	3.4
Travel speed V_i (km/h)	25	28	30	30	28	-	10
Passenger Capaity C_i (P)	72	40	3	3	2.5	200~1000	1
Vehicle conversion coefficient K_i	2	2	1	1	1	-	0.2

Table 2. Vehicle Out-driving Demand Model

Traffic mode	Public bus M_1	Commuter bus M_2	Official car M_3
Travel speed model	1.4753/v	0.3657/v	7.6544/v
Traffic mode model	-1084.3p+1092.9	-688.1p+697.7	-456.3p+594.3
Traffic mode	Private car M_4	Taxi M_5	bicycle M_7
Travel speed model	3.0576/v	1.3607/v	-
Traffic mode model	-371.8p+518.8	-331.2p+491.4	-409.4p+579.4

As can be seen from Figure 2 (a), when the proportion of one certain traffic mode increased, the total demand decreased. The demand of various modes changed sensitivity from big to small followed by the order: public bus, commuter bus, official car, private car, taxi. With the proportion of public transport, when commuter traffic increased, generalized traffic demand reduced significantly. The reason is that the quantity of passengers transported by public bus and commuter bus is large so that the total number of travelers per capita road resource is less.

Figure 2 (b) shows that the traffic demand of different traffic modes will decrease with its average speed increasing. And in the social vehicles, when the travel speeds of official cars and private cars increases, obviously the generalized traffic demand reduces. Therefore, the official cars and private cars in city traffic occupy the largest proportion of the composition.

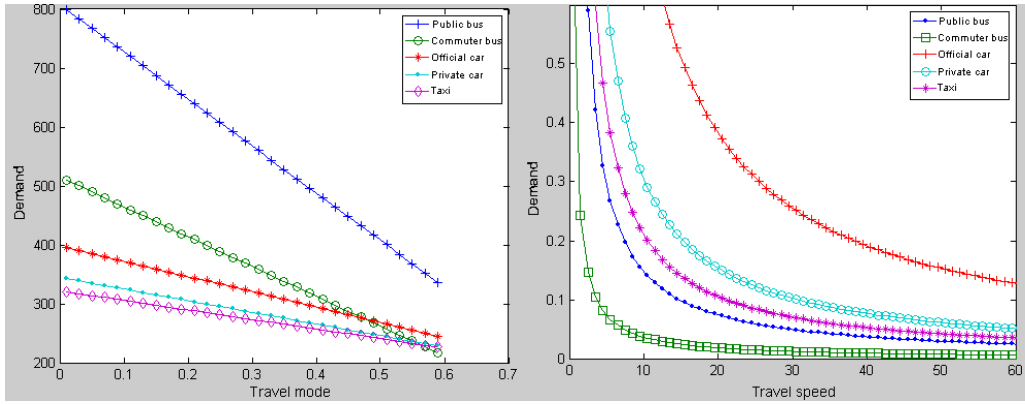

a) Traffic mode **b) Velocity**

Figure 2. Total demand change with different conditions

By the equation (4), we can see that when the average travel distance increases, the demand increases, but for a specific city, the spatial average travel distance of various traffic modes will not vary much in general. In the analysis of this factor, by increasing the accessibility of various travel modes, the individual travel residence time in the road resource will be decreased in order to reduce the total production of generalized traffic demand.

CONCLUSIONS

Through traffic generated by the process, a broad indicator of the traffic demand is presented, and the corresponding measurement model determined. Through analyzing the relationship between a variety of factors and the demand generated, the most obvious factors influencing generalized urban passenger traffic demand are: the structure of the proportion of passenger traffic and motor vehicle travel speeds, in which the increase ratio of buses and commuter cars lead to a reduction of the most obvious travel; community bus vehicles' and private cars' increased speed is equivalent to a reduction in car travel. This analysis of major cities in the process of traffic demand not only provides a basis to urban transport development policy making, but also analyzes the efficiency of a city's transport system.

ACKNOWLEDGEMENT

This research work is partially supported by National Key Technology R&D Program of China under granted number 2006BAJ18B01.

BIBLIOGRAPHY

Yao, E. J. and Takayuki M. (2005). "A Study of an Integrated Intercity Travel Demand Model". *Transportation Research Part A: Policy and Practice*, 39(4), 367-381

Karst, T. G. and Bertvan W. (2004) "Accessibility evaluation of land-use and transport strategies: review and research directions". Journal of Transport Geography, 12(4), 127-140

Ryan, S. and Throgmorton J. A. (2003). "Sustainable transportation and land development on the periphery: a case study of Freiburg, Germany and Chula Vista, Califomia". *Transportation Research Part D: Transport and Environment*, 8(1): 37-52

Boamet, M. and Crane R. (2001). "The Influence of Land Use on Travel Behavior Specification and Estimation Strategies". *Transportation Research Part A: Policy and Practice*, 35(9): 823-845

Wang, Y. G.; Pei, Y. L. and Zhao Y. D. (2008). "Vibration-based damage detection with structural modal characteristics". *The Baltic Journal of Road and Bridge Engineering*, 3(1), 21-28

Giulio, E. C. and Stefano, D. L. (2005). "Multilayer feedforward networks for transportation mode choice analysis: An analysis and a comparison with random utility models". *Transportation Research Part C: Emerging Technologies*, 13(2), 121-155

Yam, Richard C.M.; Whitfield, Richard C. and Chung, Raymond W. F. (2000). "Forecasting traffic generation in public housing estates". *Journal of Transportation Engineering*, 126(4), 358-361

The Method to Identify Black Spots of Long Highway Tunnel

Zhuanglin MA[1], Chunfu SHAO[2], Shengrui ZHANG[3], Juan ZHANG[4]

[1]Zhuanglin MA, MOE Key Laboratory for Transportation Complex Systems Theory and Technology, School of Traffic & Transportation, Beijing Jiaotong University, Beijing 100044, China; PH(86)10-5168-3665; email: 06114185@bjtu.edu.cn
[2]Chunfu SHAO, MOE Key Laboratory for Transportation Complex Systems Theory and Technology, School of Traffic & Transportation, Beijing Jiaotong University, Beijing 100044, China; PH(86)10-5168-8344; email: cfshao@center.njtu.edu.cn
[3]Shengrui ZHANG, School of Highway, Chang'an University, Xi'an 710064, Shanxi, China; PH(86)29-8233-4255; email: zhangsr@chd.edu.cn
[4]Juan ZHANG, MOE Key Laboratory for Transportation Complex Systems Theory and Technology, School of Traffic & Transportation, Beijing Jiaotong University, Beijing 100044, China; PH(86)10-5168-7145 email: y4zhangjuan@126.com

ABSTRACT

According to the characteristics of traffic accidents of long highway tunnel, this paper proposes a method to identify black spots based on improvable accident of tunnel environment. On the basis of the relationship of traffic accident and long highway tunnel system components, including the driver, the vehicle and the tunnel environment, accidents are classified into seven categories, and this paper only considers four categories relating to tunnel environment. The degree of membership of each accident in the tunnel environment component is used to represent the ability of accidents by tunnel environment improvement. Each accident is weighted by its ability. Then, the method of the equivalent of accident frequency and accident rate is used to identify black spots. Finally, the Kaoyishan tunnel in Beijing-zhuhai freeway in China was applied to analyze black spots using this method. The results show that the proposed method is useful to improve the safety of long highway tunnel.

KEY WORDS Traffic safety; Long Highway Tunnel; Black Spots; Tunnel Environment;

INTRODUCTION

The sustainable fast economic development in China for the past 10 years has greatly inspired the construction of new highways particularly long highway tunnels. Long highway tunnels play an important role in developing highway networks and the number of long highway tunnels in China has continually increased rapidly over past several years. Long highway tunnels have some advantages, such as reducing vehicle-miles of travel, saving travel time, reducing the emissions, and so on.

Therefore, the construction of long highway tunnel has brought large social and economical benefit. However, as a special structure type, the transportation environment in highway tunnel makes the tunnel section as black spots (Amundsen and Ranes, 2000; Luo, et al., 2006; Zhang, et al., 2007). Consequently, for the agency of tunnel management, it is an economical and effective way to identify black spots, analyze the causes of accidents and propose safety improvement measures. Especially, when the funding is limited, it is beneficial to improve the safety in black spots of long highway tunnels.

Many identification methods of black spots were proposed by researchers domestic and abroad, such as accident frequency method, accident rate method, matrix method, equivalent number of total accidents method, quality control method, the critical rate method, accident cumulative frequency curve method, and so on. (Pei and Wang, 2004). Recently, many researchers proposed some new methods, such as the identification method based on traffic conflict technique, the equivalent of accident frequency and accident rate method, outstanding factor method, fuzzy evaluation method, improved quality control method, and so on (Zhou and Luo, 2000; Zhu and Lu, 2002; Liu, et al., 2003; Shao, et al., 2004; Pei and Ding, 2005; Pei and Dai, 2005; Pei, 2006). However, since black spots include many accidents that cannot be avoided by road improvements, thus the location identified by these methods may not be truly accident-prone locations from a highway agency's point of view.

Accidents caused by three components of highway tunnel system or any of these components or a combination of them shown in Figure 1: the driver, the vehicle and the tunnel environment. From the view of tunnel management, drivers and the vehicles contributed little while the tunnel environment contributed mostly to accidents. Therefore, the identification of black spots should be related to identify the factors contributing to accidents in the tunnel environment.

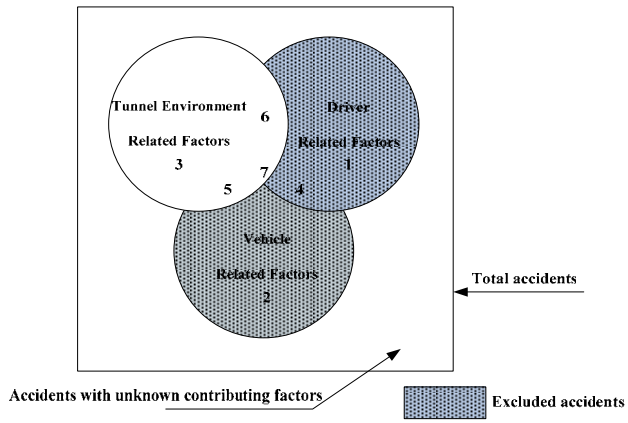

Figure 1. Classification of accidents according to causes

The work reported in this paper describes a method to identify black spots

based on an assessment of factors that contribute to accidents in long tunnels. Accidents that do not belong to the tunnel environment group are excluded from the identification of black spots. Then the equivalent of accident frequency and accident rate method is used to identify black spots. Finally, the Kaoyishan tunnel in Beijing-zhuhai freeway in China is used to analyze black spots by the method.

IDENTIFICATION METHOD OF BLACK SPOTS

The basic idea of identification method is to classify accidents by the contribution to accidents according to their patterns and contributing factors into one of the three groups in the tunnel system or a combination of these groups. Accidents that do not belong to the tunnel environment group are excluded from the identification of black spots. Then the equivalent of accident frequency and accident rate method is used to identify black spots. The steps for the identification method of black spots in this paper can be described as follows:

Step 1. The equivalent of accident frequency related to tunnel environment of each accident was calculated.

Step 2. The equivalent of accident frequency and accident rate related to tunnel environment of each section was calculated.

Step 3. The average equivalent of accident frequency and accident rate related to tunnel environment of the whole long highway tunnel was calculated.

Step 4. The upper limit of the equivalent of accident frequency and accident rate related to tunnel environment at a 0.05 significant level was calculated.

Step 5. The equivalent of accident frequency and accident rate of each section compared the upper limit at a 0.05 significant level. If both the equivalent of accident frequency and the equivalent of accident rate are not less than the upper limit at a 0.05 significant level, the section is identified as black spots.

Calculation of the equivalent of accident frequency related to tunnel environment

Firstly, accident data were analyzed and sorted, and accident data related to tunnel environment were only considered according to the classification shown in Figure 1, named category 3, 5, 6 and 7.

Secondly, according to the influence of the accidents severity on society and individual, the accident severity is calculated by giving a certain weight to deaths and injuries, and the formation was as follows:

$$ER_{ij} = W_j(K_1 F_{ij} + K_2 J_{ij} + 1) \quad (1)$$

where ER_{ij} is the equivalent of accident frequency related to tunnel environment for jth traffic accident in section i; W_j is the weights of jth traffic accident related to tunnel environment; F_{ij} is the fatalities of jth traffic accident related to tunnel

environment in section i; J_{ij} is the injuries of jth traffic accident related to tunnel environment in section i; K_1 and K_2 are the weights of fatal and injured accident.

Calculation of the average equivalent of accident frequency and accident rate related to tunnel environment

For all the selected sections, the formation of the equivalent of accident frequency and accident rate of t years in section i were as follows:

$$ER_i = \sum_{j=1}^{m} W_j (K_1 F_{ij} + K_2 J_{ij} + 1) \quad (2)$$

$$ER_{fi} = \frac{ER_i \times 10^6}{365 \times t \times L_i \times AADT} \quad (3)$$

where ER_i is the equivalent of accident frequency related to tunnel environment in section i; m is the number of accidents occurred in t years in section i; ER_{fi} is the equivalent of accident rate related to tunnel environment in section i; t is the statistical time; L_i is the length of section i; $AADT$ is annual average daily traffic volume of tunnel.

According to the equivalent of accident frequency and accident rate of different section, the formation of the average equivalent of accident frequency and accident rate were as follows:

$$ER_m = \frac{1}{n} \sum_{i=1}^{n} (ER_i / L_i) \quad (4)$$

$$ER_{fm} = \frac{\sum_{i=1}^{n} ER_i \times 10^6}{365 \times t \times \sum_{i=1}^{n} L_i \times AADT} \quad (5)$$

Where ER_m is the average equivalent of accident frequency related to tunnel environment; n is the number of sections; ER_{fm} is the average equivalent of accident rate related to tunnel environment.

Determination of black spots

According to quality control method, the upper limit of the equivalent of accident frequency and accident rate were calculated based on the average equivalent of accident frequency and accident rate at a 0.05 significant level. The formations are listed below:

$$\overline{ER_m} = ER_m + k \times \sqrt{\frac{ER_m}{M} + \frac{1}{2M}} \quad (6)$$

$$\overline{ER_{fm}} = ER_{fm} + k \times \sqrt{\frac{ER_{fm}}{M} + \frac{1}{2M}} \quad (7)$$

where, $\overline{ER_m}$ is the upper limit of the equivalent of accident frequency related to tunnel environment; $\overline{ER_{fm}}$ is the upper limit of the equivalent of accident rate related to tunnel environment; k is the statistical constant (1.96); M is the number of vehicles through tunnel in statistical time. According to matrix method, the equivalent of

accident frequency and accident rate were combined to identify black spots in this paper. The equivalent of accident frequency and accident rate of different sections were compared to the upper limit of the equivalent of accident frequency and accident rate. If ER_i is not less than $\overline{ER_m}$ and ER_{fi} is not less than $\overline{ER_{fm}}$, the section i is identified to black spots.

EXPERIMENTAL RESEARCH

The proposed method was applied to empirical analysis at Kaoyishan tunnel in Beijing-Zhuhai freeway in China. Kaoyishan tunnel is a two-way tunnel, and the study scopes of the left line and right line are ZK144+644~ZK147+825 and YK144+666~YK147+815. In this paper, the weights of fatal accidents K_1 and injure accident K_2 are equal to 2 and 1.5 separately. The weights related to tunnel environment are shown in Table 1(Ma, 2004).

Table 1. The weights related to tunnel environment

Category	Weights	Value
3	The weights related to tunnel environment	0.49
5	The weights related to vehicle and tunnel environment	0.32
6	The weights related to driver and tunnel environment	0.14
7	The weights related to driver, vehicle and tunnel environment	0.05

In this paper, 0.2km is taken as the standard length. Traffic accidents occurring in Kaoyishan tunnel during 2003-2004 were considered, and the equivalent of accident frequency and accident rate related to tunnel environment of different sections were calculated. Then, according to Equation (4) and (5), the average equivalents of accident frequency and accident rate related to tunnel environment were calculated, which were 2.52 times per kilometer and 0.12 times per million vehicle-miles respectively. Finally, the upper limit of the equivalent of accident frequency and accident rate were also calculated, which were 3.23 times per kilometer and 0.29 times per million vehicle-kilometers. Therefore, if ER_i is not less than 3.23 and ER_{fi} is not less than0.29, the section i is identified to black spots, and the situation of black spots are shown in Table 2.

Table 2. Black spots of Kaoyishan tunnel

Location	Length (km)	Accident frequency	Injured	Killed	ER_i (km)	ER_{fi}(/ million vehicle-kilometers)
ZK146+044~K146+244	0.2	1	0	2	8	0.38
ZK146+825~K147+025	0.2	4	3	0	10	0.47
ZK147+425~K147+825	0.4	6	3	0	8.4	0.4
Summation	0.8	11	6	2	8.6	0.41

CONCLUSION

For different analysts, key components of researches are different, so the identification of black spots is also different. In terms of the agency of tunnel

management, black spots in long highway tunnel should be located where traffic accidents occurred intensively due to the deficiencies of tunnel environment. Therefore, this paper attempts to propose a new method to identify black spots based on tunnel environment. The identification of black spots is the first step in the tunnel-safety-improvement project, and the further study will focus on analyzing the cause of accidents occurred in long highway tunnel and proposing improved measures for black spots accordingly.

ACKONWLEDGE

This paper was supported by the research projects sponsored by the National Key Technology R&D Program of China (No. 2007BAK35B06).

REFERENCES

Amundsen F H and Ranes G. (2000). "Studies on traffic accidents in Norwegian road tunnels." *Tunnelling and underground space tencnology*, 15(1): 3-11.

Liu Z.Q., Gong Z. and Cai D. (2003). "Identification for road accident-prone locations." *Journal of Traffic and Transportation Engineering*, 3(2): 120-123.

Luo Y. P., Gao G. F. and Wu H. L. (2006). "Study on fuzzy evaluation system of traffic safety in highway tunnel." *Journal of Shijiazhuang Railway Institute*, 19(3): 75-79.

Ma Z. L. (2006). *Analysis on traffic accident and preventive countermeasures in freeway tunnel*, Chang'an University, Xi'an.

Pei Y. L. and Wang W. (2004). *Research on the cause and countermeasures of road traffic accidents*, Science Press, Beijing.

Pei Y. L. and Dai T. Y. (2005). "Fuzzy evaluation method to distinguish black spot." *Journal of Highway and Transportation Research and Development*, 22(6): 121-125.

Pei Y. L. and Ding J. M. (2005). "Outstanding factor method to black spot differentiation." *China Journal of Highway and Transport*, 18(3): 99-103

Pei Y. L.(2006). "Improvement in the quality control method to distinguish the black spot of the road." *Journal of Harbin Institute of Technology*, 38(1): 97-100.

Shao C. F., Xian K. and Qin L. Y. (2004). "An approach for space relation model of road traffic accidents based on GIS." *2004 Beijing International Intelligent Traffic Forum: Safety and Smooth Flow of Traffic, Chinese People's Public Security University Press, Beijing.*

Zhou W. and Lu S. G. (2000). "Traffic conflict identification of road accident black spots." *China Journal of Highway and Transport*, 13(1): 81-86.

Zhu X. L. and Lu B. K. (2002). "Identification of accident prone location." *Journal of Xinjiang Agricultural University*, 25(1): 63-66.

Zhang S. R., Ma Z. L. and Shi Q. (2007). "Distribution characteristics and countermeasures of traffic accidents in expressway tunnel group." *Journal of Chang'an University (Natural Science Edition)*, 27(1): 63-66.

Study on the Relationship of Traffic Flow Complexity and Traffic Conflict on Urban Road

XU Zhihong, CHEN Xuewu, Zhang Meikun

School of Transportation, Southeast University, Nanjing Jiangsu 210096, China; email: spray147@163.com

ABSTRACT

In order to quantitatively describe the complexity of the traffic flow system, this paper analyzes the traffic flow complexity on a road based on introducing statistical complexity and its properties. Taking traffic flow on three typical road sections in Nanjing, by comparing and analyzing the relationship between traffic flow complexity and traffic conflict rate on different sections, the paper draws out the regression model of traffic flow complexity and traffic conflict rate. The results show that: The characteristic complexity is an effective measure of the random and non-linear systems and the relevance between traffic flow complexity and non-serious traffic conflict rate is better enough to measure and analyze the traffic flow complexity, which brings a new idea in studying the complexity of traffic system.

KEYWORDS

Traffic flow complexity; Traffic conflict rate; Statistical complexity; Regression analysis

INTRODUCTION

A traffic system is an open and complex giant system and at the same time is a dynamic non-linear composite system. In cities especially in urban centers, traffic systems often show such characteristics that are complex and non-linear. As one element of the traffic system, traffic flow also shows a non-stationary, complexity, and is non-linear. Therefore non-linear analysis methods may help to better reveal the characteristics and mechanism. In recent years, with the development Lempel-Ziv algorithm, it is possible to quantify the complexity of traffic engineering through approximate entropy and statistical complexity methods.

Statistical complexity was first proposed by Lopez-Ruiz in 1995. The paper analyzes the traffic flow complexity on the road based on introducing statistical complexity and its properties. Take traffic flow on three typical road sections in Nanjing, by comparing and analyzing the relationship between traffic flow complexity and traffic conflict rate on different sections, draw out the impact of traffic conflict rate on the complexity of traffic flow in order to provide new ideas in studying the complexity of traffic systems.

STATISTICAL COMPLEXITY

Currently the depiction of characterization of traffic flow system complexity, fractal dimension, Lyapunov exponent and the measure entropy characteristic quantities etc. are usually adopted. These characteristic quantities can partly depict the complexity of the system, but they are facing two problems in the application: 1) the calculation of these characteristic quantities requires a long time series, the measured data is very difficult to meet their requirements; 2) these methods can only draw out the complexity criterion, but cannot do comparison between different locations, different time slots of the traffic flow system, that is to say, those methods can only resolve the problem of whether or not the system is complex but cannot resolve the problem of the extent the complexity of system arrivals. Therefore, it is necessary to realize the comparable measure of the complexity of traffic flow system. In this paper, I introduce the statistical complexity of nonlinear dynamic theory which is put forward in recent years to try to measure the complexity of traffic flow based on such a theory.

Foundation of the statistical complexity is information theory, which is mainly used to study how the shannon entropy of continuous expansion subsystem converges to the entropy density of whole system which is a measure of components of system regularity.

Assuming a discrete random variable Y with N-state y, the $P(Y)$ is the probability when random variable Y equals y, then the statistical complexity C is

$$C(Y) = H(Y)D(Y) \tag{1}$$

$$H(Y) = -\sum P(Y)\log_2 P(Y) \tag{2}$$

$$D(Y) = \sum 2\left[P(Y) - \frac{1}{N}\right] \tag{3}$$

Where: H is information entropy; D is the non-equilibrium item which shows the dispersion between Probability $P(Y)$ and the uniform distribution.

In C expression, the contributions that randomness and disorder make to the complexity of the statistics are considered, but $H(Y)$ and N are relevant, while the $D(Y)$ and N are not relevant, thus the contribution of which are in different ways, so the calculation of statistical complexity with formula (1) is not so unreasonable.

Based on what has been shown above, Feldman etal. [8] use the information distance of non-equilibrium distribution $P(Y)$ and balanced distribution $P(\hat{Y})$ in place of the non-equilibrium $D(Y)$ of formula (1), and give a modified formula:

$$DFC(Y) = \sum P(Y)\log_2 \frac{P(Y)}{P(\hat{Y})} = \sum P(Y)\log_2 \left[NP(Y)\right] \tag{4}$$

Where： DFC is the extensive quantity.

Thus, the calculation formula of statistical complexity has been modified to

$$C(Y) = H(Y)DFC(Y) \qquad (5)$$

For systems with complete rules and orders, it has $H(Y) = 0$, $C(Y) = 0$; for complete White Noise system, it has $P(Y) = \frac{1}{N}$, $DFC(Y) = 0$, $C(Y) = 0$. The advantages of formula (5) are: it meets the boundary conditions of order and randomness, and can clearly measure such chaotic system as neither completely random nor completely orderly, which makes it more scientific to depict the complexity of the system and less data are required. But it also has two disadvantages: 1) when calculating the complexity of two-dimensional array, they are required to be changed into a higher dimensional array firstly, which is rather complicated and excessively fine-grained; 2) Measurement is established on statistical significance so that some minor structural complexity of the system will inevitably get neglected.

According to the model checking, when samples are taken between 400~ 1000, complexity tends to be stable, and the complexity values of white noise within the system and the cycle of systematic statistical errors are very small, thus there exists a great gap compared to the statistical complexity of the chaotic regional logistics and the Henon system which shows statistical complexity meets the boundary conditions of order and randomness, and can be used to express the complexity of a nonlinear structure well.

MEASUREMENT OF TRAFFIC FLOW COMPLEXITY

Headway is used to calculate the complexity of traffic flow, because headway can reflect a large amount of information such as the traffic volume, speed and traffic density etc., and is also easy to investigate.

Collection of Traffic Flow Data

The following investigation locations were chosen: Nanjing Taiping North Road (R1), Beijing East Road, (R2) and the Zhujiang Road (R3). The investigation times are Wednesday's 8:00-9:00 (morning peak MP) ,10:00-11: 00 (morning platy MN) ,12:00-13: 00 (noon peak NP) ,15:00-16: 00 (noon platy NN) ,18:00-19: 00 (evening peak EP) and 20:00-21: 00 (evening platy EN), from above 18 series of Headway times are received, the sample volume is 500. Not only Headway but also the corresponding traffic conflicts are investigated. Figure 1 shows headway investigated from the R1 road mining sections of MP time.

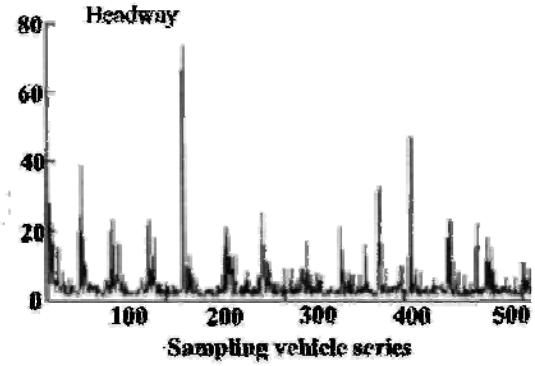

Fig 1. Variation of time-distance of sampling vehicle.

Measurement Based on the Statistical Complexity

In Combination with 30 traffic flow sequences from the result of the survey, we measured them by the statistical complexity method; the results are shown in Figure 2.

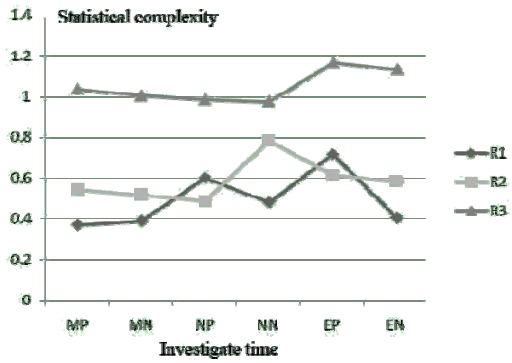

Fig 2. Statistical complexity of three roads.

As can be seen from the chart:

（1） The peak of complexity of the traffic flow in various sections are almost in the peak periods, but as traffic flow increases to a certain extent, it becomes gradual and orderly, the complexity gradually becomes smaller.

（2） The complexity of Zhujiang Road is the largest. Taiping North Road and Beijing East Road are similar, which is related to the road hierarchy, traffic flow composition and traffic volume. Zhujiang Road is a residential road located the central area of electronic distribution in Nanjing, traffic composition flow is rather complicated, on which the cross-section is a piece of board, and traffic flow is more seriously out of order. Taiping North Road and Beijing East Road are arterial roads, and channelization facilities are perfect, relatively speaking, traffic flow is in order, that is, complexity is relatively small.

（3） Complexity values are much greater than the cycle system and the white noise that illustrates traffic flow system is neither cyclic nor a completely

random system, but it is a dynamic system with a non-linear structure , moreover the non-linear structure can generate chaos.

REGRESSION ANALYSIS

Traffic Conflict Rate

Traffic conflicts are divided into serious conflicts and non-serious conflicts.

The traffic conflict on the section is mainly relevant with the traffic volume and the length of the sections, so the traffic conflict rate of each section is different in different time.

$$I = \frac{C}{Q \times H} \qquad (6)$$

$$I = I' + I'' \qquad (7)$$

Where: I is traffic conflict rate, I' is traffic non-serious conflict rate, I'' is traffic serious conflict rate, C is traffic conflicts, Q is traffic volume, H is the length of the sections.

Tab.1 traffic conflict rate of each section.

	MP		MN		NP		NN		EP		EN	
	I'	I	I'	I	I'	I	I'	I	I'	I	I'	I
R_1	4.53	5.49	3.98	4.63	4.34	5.35	5.36	6.33	6.95	7.89	3.12	4.07
R_2	6.78	7.87	5.76	6.45	6.54	7.52	7.29	8.03	8.76	10.51	4.55	5.42
R_3	11.85	13.54	9.56	10.79	10.89	11.72	8.25	9.51	13.43	14.89	7.89	9.26

Modeling

A regression analysis of the traffic flow complexity of three sections and the corresponding traffic conflict rate wereperformed using SPSS software. After fit, the complexity of traffic flow of the sections and traffic non-serious conflicts rate have better relevance.

$$C = 4.891I'^2 + 0.080I' + 4.511 \qquad (8)$$

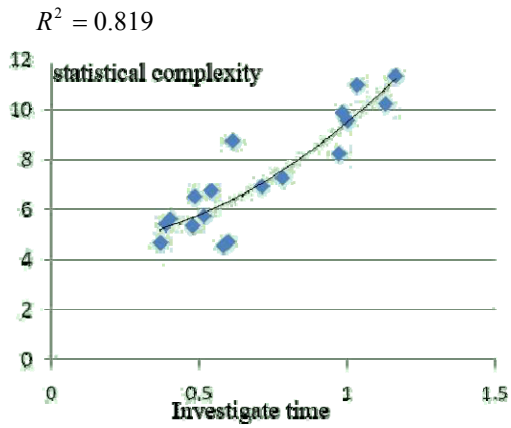

Fig3. Regression of traffic flow complexity and non-serious traffic conflict rate.

It was indicated that complexity of traffic flow and the corresponding sections of the serious traffic conflict rate are poor as shown by regression analysis. On the one hand, the source of serious conflict data collection is much less than the non-serious conflict data and it is difficult to draw out the correlation between them because in a short period of time it is difficult to observe a serious conflict. On the other hand because the complexity is used to measure the randomness of traffic flow, to a large extent, a serious conflict is determined by man-made factors or road facilities.

A regression analysis was made about complexity of traffic flow and the corresponding traffic conflict rate. The correlation coefficient is $R^2 = 0.759$, which can meet the demand. The formula is as follows:

$$C = 0.002I^2 + 0.118I - 0.089 \qquad (9)$$

From what has been analyzed above, we can see that non-serious traffic conflict rate and the complexity of traffic flow are directly proportional, but the increased rate is gradual. In practical applications we can analyze the factors which impact traffic flow complexity through comparison of non-serious conflict rates to compare with different complexity of traffic flow, and achieve a fundamental understanding about characteristics of the traffic flow.

CONCLUSIONS

1) Complexity of Traffic flow systems and chaotic systems are closer which shows traffic flow systems are highly stochastic, with non-linear structure and may produce chaos.

2) The peak of complexity of traffic flow of various sections are almost in the peak periods, but as traffic flow increases to a certain extent, it becomes gradual and orderly, complexity gradually becomes smaller.

3) Non-serious traffic conflict rate and the complexity of traffic flow are well correlated. In practical application we can analyze complexity of different traffic flows through comparison of non-serious conflict rates.

ACKNOWLEDGEMENTS

The author greatly thanks Chen Xue-wu for all exciting discussions about models of traffic forecasts and for her careful reading of this article. This work has been supported by the National Science and Technology Support Program of China (2006BAJ18B07).

BIBLIOGRAPHY

HE Guo guang; MA Shou feng; FENG Wei dong. Preliminary study of fractals of traffic flow[J]. China Journal of Highway and Transport,2002,15(4):82-85.

ADDISONPS,LOWDJ. A Novel Nonlinear Car-following Model[J]. Chaos, 1998,

8(4):791 - 799.

NAIRAS, LIUJC, RILETTL, etal. Non-linear Analysis of Traffic Flow [C]/ /IEEE. Proceeding s of the 4th Intelligent Transportation Systems. Oakland IEEE, 2001: 681-685.

Yao Rong-han; Wang Dian-hai. Entropy models of inhabitant trip distributions and parameters calibration[J]. Journal of Traffic and Transportation Engineering, 2005,5(4):106-110.

LIU Feng-tao; HE Guo-guang. Complexity Measure of Traffic Flow Based on Approximate Entropy and Statistical Complexity[J]. China Journal of Highway and Transport,2007,20(4): 108-112.

SI Bing-feng; SUN Zhuang-zhi; ZHAO Xiao-mei. Mixed Traffic Network Flow-Split Model Based on Stochastic User Equilibrium[J]. China Journal of Highway and Transport, 2006,19(1):93-98.

ZHOU Yong-hua. Mechanism and Approach of Traffic Flow Predictive Control [J]. China Journal of Highway and Transport,2007,20(1):107-111.

FELDMANDP,CRUTCHFIELDJP. Measures of Statistical Complexity: Why[J]. Physics LettersA,1998,238(3):244-252.

Control and Monitoring of Surface Subsidence for Shallow Tunnel under Existing Railway

Wang Xinzheng[1] and Xing Liying[2]

[1]School of Civil Engineering, Nanyang Normal University, Nanyang 473061, P.R.China; PH 13525696713; email: wxz791023@126.com
[2]School of Civil Engineering, Nanyang Normal University, Nanyang 473061, P.R.China; PH 13782165330; email: xly19854525@126.com

ABSTRACT

Shallow tunnel may inevitably disturb ground soils during the construction. process, The disturbance will certainly produce different levels of surface subsidence, and thus it will cause some unfavorable influence on the safety of construction and surrounding structures. Therefore, it's necessary to determine the control index of surface subsidence scientifically and reasonably, which can relieve, eliminate and avoid the unfavorable impact. The underground passage of Changchun railway station in the south and north squares lies in the soft soil layer, and was dug through the station yard, and thus its construction is very difficult. In the construction process, firstly, a suitable strict control and monitoring system is designed to detect the surface subsidence. Then the collected data from the monitoring system is analyzed and fed back, and the construction is dynamically managed. Finally the construction work is ensured to keep on going smoothly and safely.

Key words：*existing railway; shallow tunnel; surface subsidence*

With the rapid development of our economy, the urban traffic becomes increasingly busy. Many crossings of highway and railway need to be replaced by overpasses, and mainly underground excavation form or culvert advancing into hole form. When a tunnel under the railway is excavated, it will inevitably cause some disturbances to its adjacent structures, and the disturbance will lead to the rail irregular operations. Meanwhile as the train passes the place, it will produce impact force, and increase the surface subsidence.It turns out great vulnerabilities of the system. Therefore, it is vital to study the surface subsidence of the shallow tunnel. Alleviation of the surface subsidence is of great significance to ensure the safe operation of railway and the tunnel construction. .

A BRIEF DESCRIPTION OF THE PROJECT CONSTRUCTION

The project introduction

The underground passage under the north and south squares of the Changchun station is about 274m long, heading north from LiaoNingLu, and stop at the Changchun freight station, including a main channel, a building connecting the south and north hall, and the escalator section. Construction of the south and north hall part adopts the cut and cover method, and the main channel adopts the subsurface excavation method, with the mileage from DK0+063.279 to DK0+218.679, and its span approximately equal to 155.4m. The subsurface excavatione is supported with a structure of two columns and three arches. Middle part for pedestrian passage is 8 m wide, and both sides of the commercial development zone are 3m wide. The total excavation is 16.2 m wide, the excavation is 7.3 m deep, and the tunnel has a largest covering of 5 meters. The main channel crosses Changchun station yard 14 strands

operation orbits and part of hump lines, also four passenger platforms and four postal channels; In construction area, the underground pipelines distribute densely, which made the construction environment very complex.

The construction method

The station goes through the shallow soft soil stratum, and large spanned. Thus the shallow depth excavation edge hole method is adopted, with its main construction procedures shown in Figure 1. The entire construction sequential is described as follows, firstly carry on the tunnel edge hole's excavation support construction using the short steps obligate core method. The distance between the upper and the lower steps is 5 m apart, and each excavation is 0.5 m. Then the excavation of left pilot tunnel is performed after the right side hole's initial support closed 5 m long, excavate the core cave after the left side hole's initial support closed 5 m long, using the short steps core soil with CD reserved method. The right and the left sections of upper step are apart from 5 m, in the middle adding up temporary support by I_{16} beam, and the distance between the upper and the lower steps is 5 m. After the whole section excavation is done, the secondary lining is to be installed together, carry on the two sides span's second lining, then break the initial supporting of two sides hole, and carry on the lining of the middle arch, in order to becoming an organic whole with the two sides span second lining, eventually dismantle the rest of initial supporting of both sides hole and the second lining slab. As soon as finish two sides span lining, begin the sides decorate construction. The middle arch's decoration is carried on after completing the midspan vault lining.

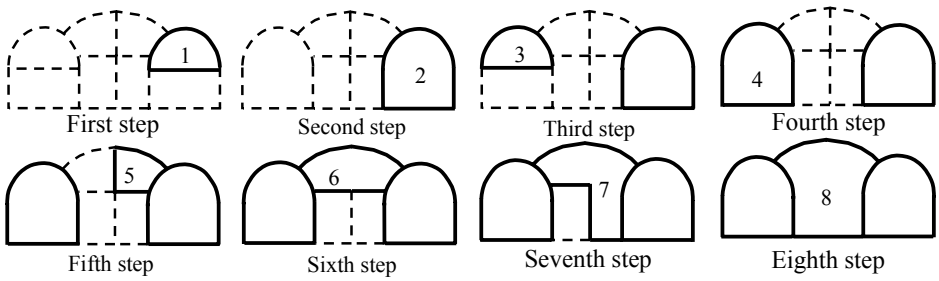

Figure1. edge hole construction's step schematic diagram

MONITORING MEASUREMENT

Definition of settlement control benchmark

The harmful settlement must be controlled in the shallow tunnel construction. The most important problem is how to setup the settlement control benchmark, and use the control benchmark to monitor the existing building above ground、surface subsidence in the construction process under the guidance of the theoretical analysis, and subsequently manage tunnel construction based on the monitoring data.

The horizontal surface subsidence may adopt the normal probability curve to analyze, which was proposed by Mexico scholar Peck and British scholar Reilly. When excavated single hole equation is as follow:

$$S = S_{\max} \exp\left(-\frac{x^2}{2i^2}\right) \qquad (1)$$

In the equation, x stands for the distance measured from tunnel center, S *is* the surface subsidence of the point with distance x from the tunnel center, S_{max} is the

maximum settlement, and *i is* the coefficient of the width of the settled tank.

The building foundation types and its stiffness directly affect the building deformation, which is caused by the surface subsidence. And different foundation types have different adaptabilities to the foundation deformation.

Table 1. The allowable surface subsidence of the channel construction

Section equivalent radius(m)	Coating thickness (m)	Internal frictional angle(°)	Bath setting width coefficient（mm）	Allowable computed settlement (mm)			
				Underground	pipeline	Postal channel	Railway line
7.11	5.0	19	6.78	86.7		66.2	13.6

The main channel at Changchun station crosses 14 strands operation orbits and part of hump lines , also four passenger platforms and four postal channels. If the same benchmark is used, it would be conservative in some areas, and non-conservative in others. Therefore, the control standard of different type buildings should be set up separately. The allowable maximum differential settlement should meet their safety needs to the best in their engineering practice. The allowable surface subsidence benchmark is shown in Table 1, which meets the normal requirement of underground pipelines, underground postal channels and railways.

Design of the monitor measuring system

In connection with the engineering practice of the tunnel at Changchun station, the surface subsidence is measured at every 5 ~ 15 m of a measurement section as shown in the measurement layout. There are 11 ~ 15 points at each section, and 2 monitoring sections at the four postal channels at the north and south sides, setting up the surface subsidence measuring-points at the canopy pillars, which is shown in Figure 2. The measuring-points of vault sink and headroom are placed for every measurement section of 5-15 m, and each measurement section has three vault sink points and three headroom convergence lines. The measuring-point arrangement is shown in Figure 3.

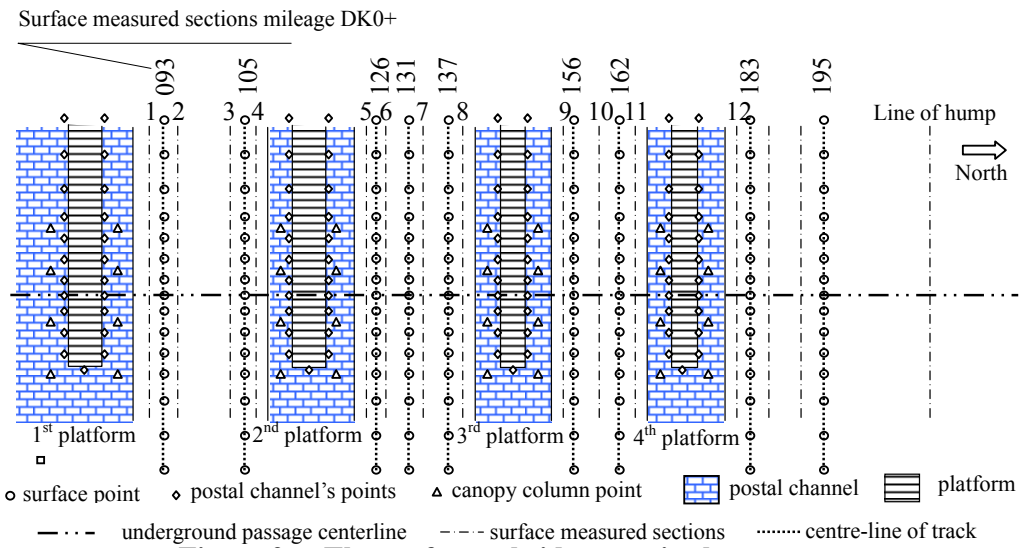

Figure 2. The surface subsidence point layout

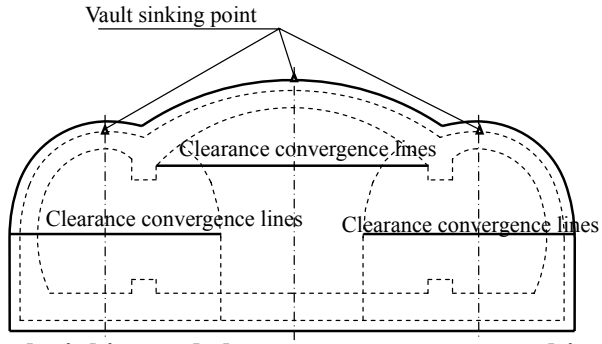

Figure 3. The vault sinking and clearance convergence multipoint arrangement

SUBSIDENCE CONTROL MEASUREMENT DURING THE CONSTRUCTION

Construction measures for the rail traveling soil stratum

When the passage crosses the railway, some auxiliary measures are adopted to reduce the surface subsidence, in order to keep the subsidence of the railway base within the permitted range. To maintain the normal operation of the railway, a big pipe is grouted ahead of preliminary support, anarch radial grouting is applied to the small catheter to reinforce the soil stratum, and locks are added up at the arch foot and on the lateral brace.

Construction measures for railway postal channels stratum

The underground passage crosses the railway postal channel four times. When passing through the channel, the benching tunneling method is applied, with the construction principle of "short footage, quick closure, and strong support." Because the postal channel has only a 1.5 m of headroom, some auxiliary measures are adopted. For instance, a preliminary support is provided by densely grouting the small catheter, the reinforced postal channel bottom and the tunnel vault soil are grouted , in order to ensure the safety of the vault soil and channel, fast going through the area.

Technique of Buckling the rail reinforcement

Because the shallow tunnel construction causes substantial surface subsidence, which will make the rail track distortion, and affect the train's passage. To ensure the train's moving unaffected, the reinforcement technique of beam buckling rail is feasibly adopted to strengthen the track structure, in an attempt of maximizing the line's overall stability in order to prevent the collapse that is potentially caused by the tunnel construction. In addition, in order to eliminate the track distortion caused by the excessive subsidence, variations of the surface subsidence is monitored for the three tunnel construction stages: pre-precipitation and with the edge hole supporting completed, the middle hole supporting completed, and the entire project completed.

CONSTRUCTION EFFECT AND DATA MONITORING

Monitor processing and data analysis

Surface subsidence

The measured data indicates that the maximum surface subsidence, with its value of 60.26 mm at the eighth point at the center channel, occurred at the section of DK0+195. The surface subsidence records at the transverse sections of DK0+183 and DK0+195 are plotted in Figure 4. The maximum surface subsidence is 24.7 mm,

of the postal channel occurred at the eighth point of the fourth platform south of 4# postal channel. The surface subsidence at the 1st and 2nd platform of the postal channel is shown in Figure 5. Here give the surface settlement and time curve of a maximum surface subsidence, 1st platform's canopy 4# column point surface subsidence time curve is shown in Figure 6.

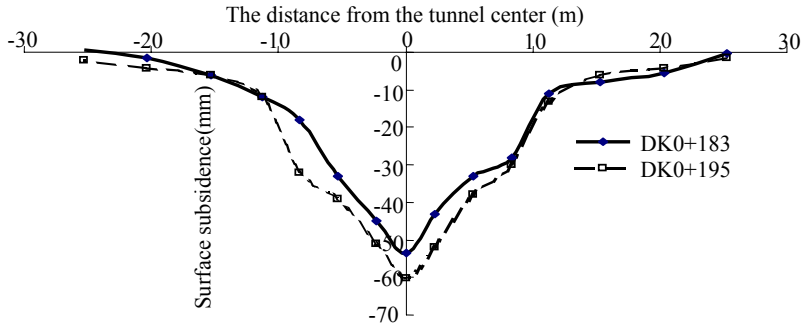

Figure 4. DK0+183, 195 measurement sections surface subsidence's transverse curve

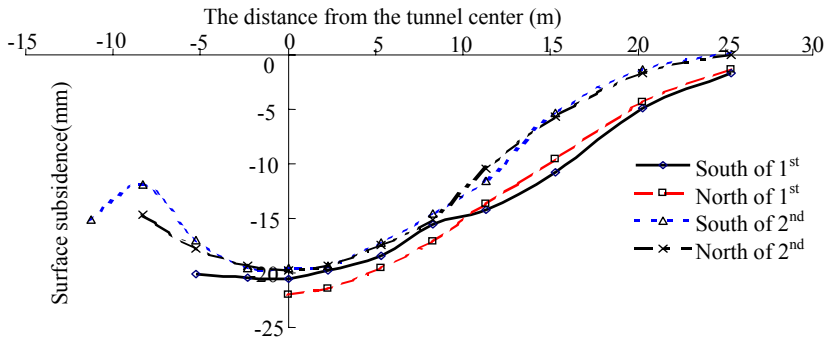

Figure 5. 1st and 2nd platform postal channel sections surface subsidence's transverse curve

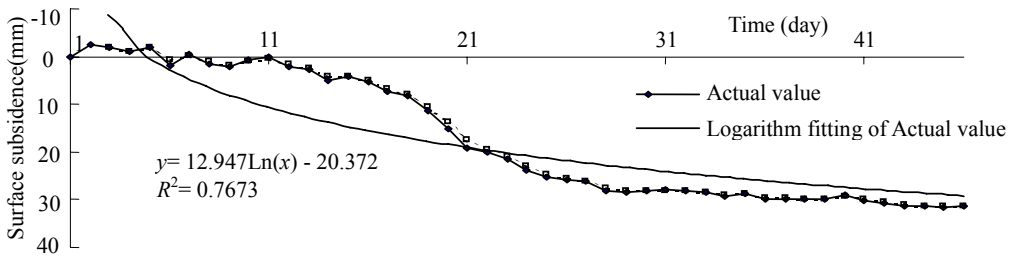

Figure 6. 1st platform's canopy 4# column point surface subsidence's time curve

Vault settlement and headroom convergence

Due to the two columns-three arche structure for the underground passage, every vault settlement's and every headroom convergence's measurement section also has three vault sink points and three lines, which are set with every hole's excavation. The vault settlement time curves of DK0 + 093 section center hole、east hole 、west hole are shown in Figure 7~9.

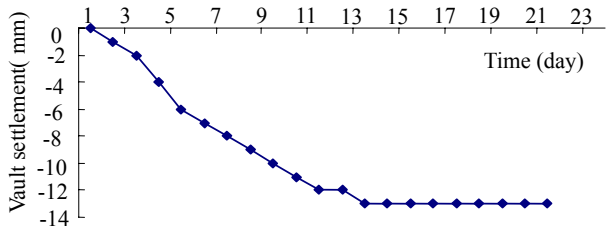

Figure 7. DK0 + 093 section center hole's vault settlement time curve

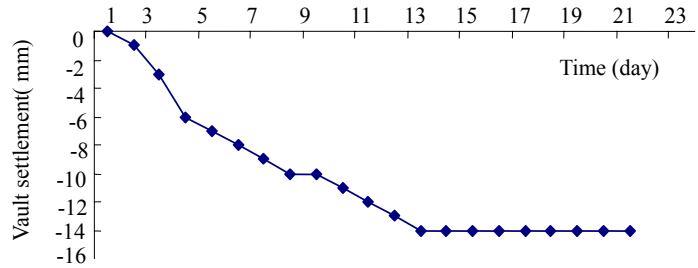

Figure 8. DK0 + 093 section east hole's vault settlement time curve

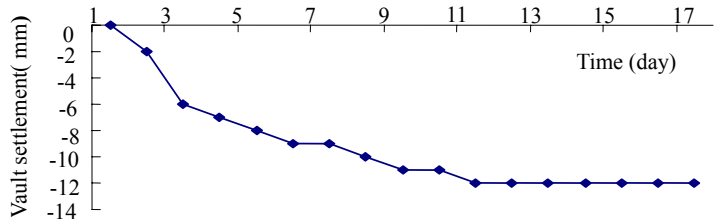

Figure 9. DK0 + 093 section west hole's vault settlement time curve

The vault settlement and headroom convergence are smaller than the surface subsidence. Because the vault measuring-points are built-in after the excavation, there is no vault prophase displacement.

Effect of the implementation

Monitoring of the construction process indicates that the subsidence of channel center is between 38.25 mm and 60.26 mm, with its maximum of 60.26 mm occurring at the DK0+195 section. The measured settlement is in the allowable range. Current track surface subsidence is limited to 13.6 mm. Based on the subsidence requirement, the construction will become extremely difficult, or the engineering cost will be greatly increased.

In consideration of the ground track and bed maintenance characteristics, and the monitoring results of track deformation, the tunnel builder should apply the rail buckling reinforcement to the original rail, and perform in stages the construction work, fill the ballast and keep a good maintaining job for the track base to limit that maximum settlement of rail top surface less than 13.6 mm, and make the railway work normally.

CONCLUSION

1) Construction of the underground passage of Changchun station strictly follow the construction requirements, which read "pipe advancement, strict grouting, short excavation, strong support, quick sealing and frequent measurement". A series of plans are implemented to effectively minimize the surface subsidence, and ensure the safety and stability of the above and underground structures. These plans are integrated with the long shed-pipe and pre-grouting with tubule for preliminary support. After the short-step excavating two edge holes then center hole with the short steps core soil with CD reserved method, reinforcing the stratum of rails and postal channels, buckle rail reinforcing, sorting out the rail in stages and so on.

2) Settlement measurement plays an important role in the shallow tunnel construction. According to the monitoring feedback , the observational management can be employed for the construction work. If the monitoring data exceeds the standard or alerting value, the construction scheme should be timely adjusted, and the supporting reinforcement measure should also be rectified to ensure the construction process undisturbed.

BIBLIOGRAPHY

Fan, Wenxing (2006). “Control and Analysis of Settlements in Subway Tunneling with Shallow Excavation.” *Municipal Engineering Technology*， 24,398-401.

Liu, Hui (2002). “Application of Shallow Underground Excavation Method and Shield Driving Method for Urban Subways.” [*Journal of Railway Engineering Society*56 -57.

Shi, Zhongheng, Zhang, Mi and Wang, Xinjie (1997). “Design and Construction of Underground Railway.” Shanxi Science and Technology Publishing House， Xian, 69-75

Voids Classification Standard for Cement Concrete Pavement Slabs Based on Service Life

Sheng Zeng[1] and Jia Xu[2]

[1]Professor, School of Traffic and Transportation Engineering, Changsha University of Science and Technology, P.O. Box 7, Changsha, Hunan, 410076, P. R. China; (86) 731-2309896; zszs35@sohu.com

[2]Graduate Student, School of Traffic and Transportation Engineering, Changsha University of Science and Technology, P.O. Box 7, Changsha, Hunan, 410076, P. R. China; (86) 731-2309896; jilinxujia@sina.com

ABSTRACT

Based on calculation of load stresses at both the middle of the longitudinal joint and the slab corner with various degrees of voids between the slab and the base layer, critical loading load transfer location of slab with voids could be analyzed. According to these data, we have analyzed the effect of voids beneath cement concrete pavement service life. In addition we came out with a void classification standard. Our research shows that, once the pavement has been void, as the void is expanding, the maximum loading position would transfer from the middle of the longitudinal joint to the corner. When the void size L_v is larger than 0.7m, the boundary of void area and no void area becomes the most unfavorable load position. So our void classification standard is as follow: slight degree void when L_v is 0～0.4m, moderate degree when L_v is 0.4m～0.7m and severe degree when L_v is larger than 0.7m.

KEYWORDS

Pavement engineering; cement concrete pavement; void; classification standard; service life

INSTRUCTION

In engineering, common judgment methods to determine the existence of void mainly include the falling weight deflectometer (FWD), the ground penetrating radar, and acoustic-vibration method and so on. Voids can also be judged by empirical methods. It is proposed that all the deflection values, which are more than 0.2mm, are identified as the slabs containing voids by the Chinese national standard. Establishing a division standard for the void grade is very important to evaluate the CCP slab void accurately. Therefore, we put forward the division standard of the CCP void beneath based on the fatigue life influence coefficient ε in order to guide the actual treatment of slab void (Chen, 2008) (Huang, 1993) (Wang et al., 2008).

THE FATIGUE LIFE INFLUENCE COEFFICIENT ε

The fatigue life influence coefficient ε is defined as the ratio of residual

fatigue life between void and no-void. We establish the division standard of CCP void beneath by analyzing ε. We give research on the load stress in the middle longitudinal edge and in the slab corner under different void sizes, as well as the most unfavorable loading position transfer law of concrete slab (Zhao, 2004).

LOAD STRESS IN THE MIDDLE LONGITUDINAL EDGE UNDER VOID SLAB CORNER

We assumed different slab corner void sizes in ANSYS and calculated the maximum load stress in the middle longitudinal edge. We have established calculation model of elastic half-space concrete slab. Void isosceles triangle region is set up in the slab corner, and the right-angle is L_V. The influence of the void beneath on slab loading stress is not obvious, which can be omitted in the structure calculations by analysis (Han et al., 2006) (Luo et al., 2001) (Zhou et al., 2004).

Comparing the void with no-void under the maximum load stress, we define the void stress correction coefficient ε_σ as follows:

$$\varepsilon_\sigma = \frac{\sigma_y}{\sigma_w} \tag{1}$$

Where: σ_y is the maximum load stress under the void (MPa); σ_w is the maximum load stress under no-void (MPa).

The calculation of ε_σ in the middle longitudinal edge under slab corner void is shown in Figure 1. We can see a better relationship between ε_σ of Winkler and void size. Regression formula can be expressed as follows (Zhou et al., 2007):

$$\varepsilon_\sigma = 1.85e^{-\frac{L_v}{3.525}} - 0.816 \tag{2}$$

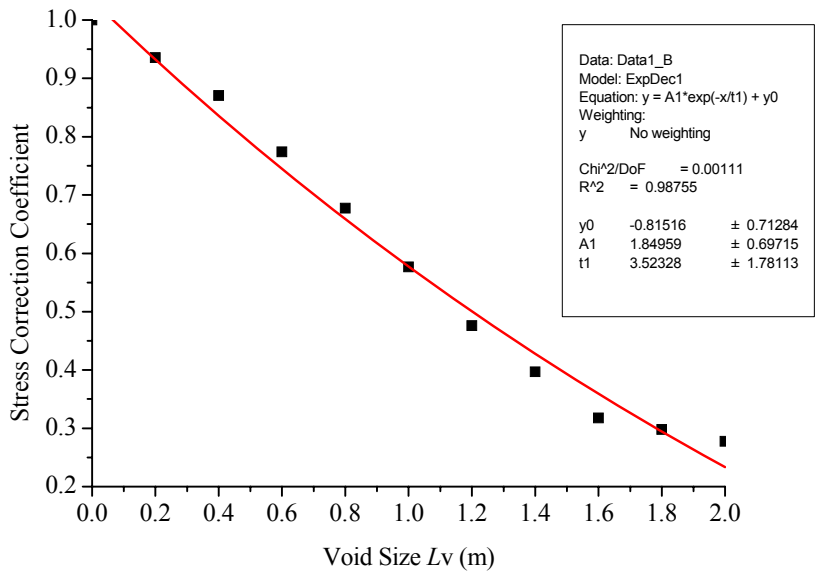

Figure 1.The fitting curve of load stress in the middle of the longitudinal joint in different void size.

LOAD STRESS OF THE SLAB CORNER LOADING POSITION UNDER VOID

When the slab corner void appears, the void regions can be approximated as an isosceles triangle, and the triangle AOB is shown in Figure 2. Assumed that the void critical section AB is fixed，OB and OA are unrestrained, the flexural stress of void critical section AB can be obtained by formula (3) subject to standard single axle load .

$$\sigma_{lj} = \frac{3\pi pa^2}{h^2 L_V}(L_V - 2a) \tag{3}$$

Where: σ_{lj} is the max flexural stress of single standard axle load in the critical section *AB* (MPa); *p* is the load pressure, taken 0.7 MPa.

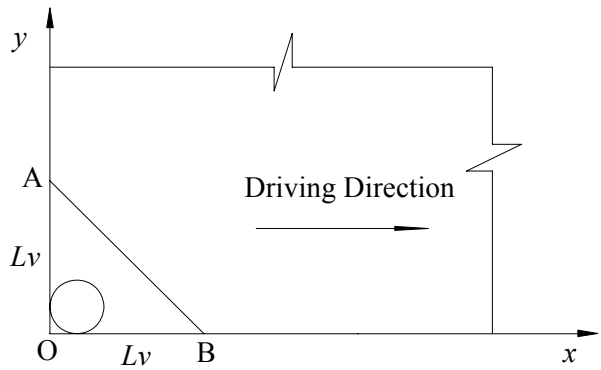

Figure 2.The critical load position in the void region.

We calculated different sizes of void σ_{lj} with a slab thickness of 0.25m. The results are shown in Figure 3. We can find that the flexural stress in the void critical section increases gradually with increase of the void size.

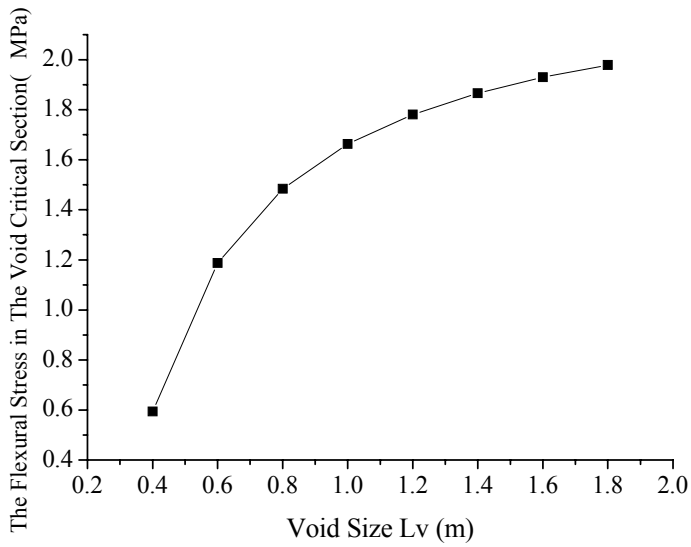

Figure 3.The flexural stress in void critical section.

Figure 4 compares the stress in the critical section of the slab corner void and the stress in the middle longitudinal edge (foundational response modulus k =200MN/m^3). As it is shown in the figure, we can know that when the slab corner void size $L_v \leqslant 0.7$m, all the maximum flexural stress in the section on AB is less than or close to that in the middle longitudinal edge under the standard axle load 1.325MPa. When $L_v > 0.7$m, it is more than 1.325MPa (Tang, 1992) (Tan et al., 2003).

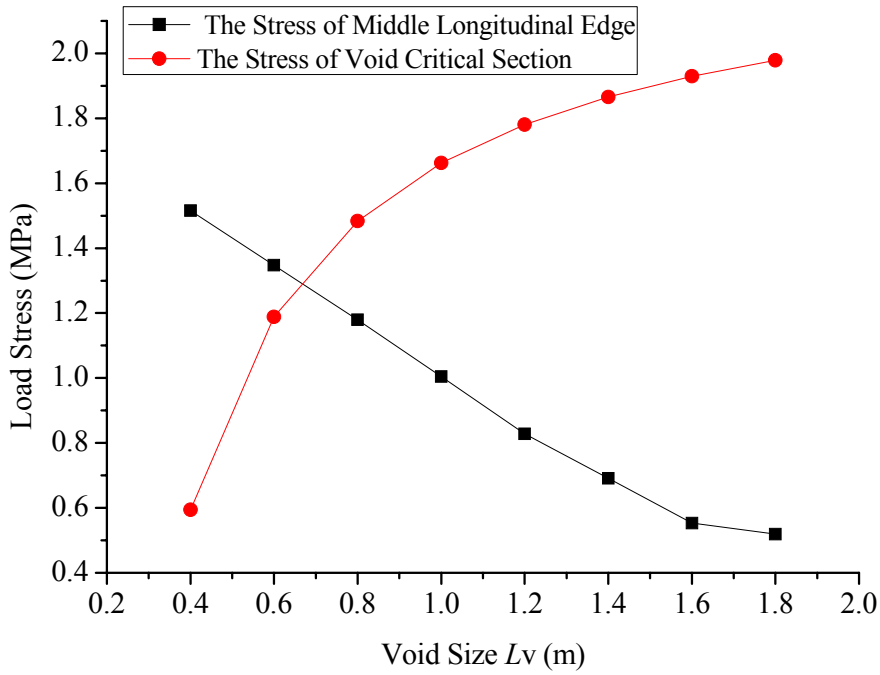

Figure 4.The transfer of critical loading position under the void slab corner.

CALCULATION OF VOID SLABS FATIGUE LIFE AND CLASSIFICATION STANDARD

The fatigue life of void concrete slabs N_f can be calculated based on the fatigue damage equation in "Concrete Pavement Design Specification" (JTG D40-2002). We can obtain N_f using formula (4). The results are shown in Table 1.

$$N_f = 10^{12.26-12.978\frac{\sigma}{f_m}} \tag{4}$$

Where: N_f is the effect numbers of cumulative standard axle loading when fatigue damage; σ is flexural tensile stress (Temperature stress is not taken into account in this paper); f_m is the flexural strength, taken 5 MPa.

Table1.The Calculated Results of Service Life.

Void Size L_v (m)	0.4	0.6	0.8	1	1.2	1.4	1.6	1.8
N_f (10^6)	211.38	577.98	255.93	87.80	43.37	26.10	17.80	13.28

Comparing N_f under void and no-void, we can get the fatigue life influence coefficient ε. The result is shown in Figure 5.

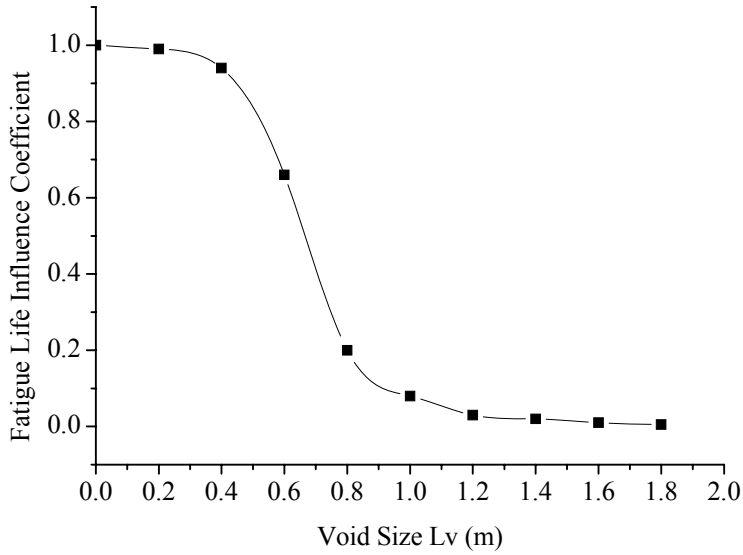

Figure 5. ε in different void size.

We can see from Figure 5 that ε reduces obviously with increase of voids at the slab corner. When void size increases to 0.4m, the trend of curve become downward significantly, and fatigue life also reduces. Then it needs to use reinforcement processing immediately, or else it will present early rupture. When the void size reaches 0.8m, ε will drop to 0.1m. As a result of critical loading position transferring to slab corner, concentration stress will be in void slab critical sections. Void size continues to increase, and curve drops to flat. However, fatigue life influence coefficient ε has been reduced very slightly at that time. Since L_V=0.7m is the critical void size of the critical loading position transferring, in view of this we can define that L_V=0.4m and L_V =0.7m are the division boundaries of void grade. According to the analysis above, we can establish the classification standard of the CCP void, as shown in Table 2.

Table 2.The Void Classification Standard of Cement Concrete Pavement.

Void Size in the Slab Corner L_V (m)	0～0.4	0.4~0.7	>0.7
Void Classification	Slight	Moderate	Severe

CONCLUSIONS

1. The modified coefficient of void stress under the loading in the middle longitudinal edge can be represented as an exponential attenuation function for the void slab corner. The stress in the middle longitudinal edge reduces as the void size increases, which indicates that the critical loading position of slab beneath transfers rapidly to the slab corner.

2. When the void size L_V>0.7m, the boundary of the void and no-void region in the slab corner becomes the most disadvantageous location. As a result of repeated loading, fracture will occur with the limiting fatigue stress. It impacts the service life of the pavement slab.

3. According to the analysis, the void size L_V=0.4m and L_V=0.7m should be the division boundaries of the void classification.

ACKNOWLEDGMENTS

The support and assistance from Dr. Yaping Zhang, Dr. Jian Zhao, Hongyi Yang, Xiaojun Zeng, Jiahui Zheng, Xianyong Gan, and Zhencun Li are much appreciated.

REFERENCES

Chen, D.H. (2008). "Field experiences with RDD and overlay tester for concrete pavement rehabilitation". *Journal of Transportation Engineering–ASCE* January: 24-33.

Han, X., Chen, S.J., Zhong, L., et al.(2006). " Review for void detective methods of the concrete pavement". *Journal of Chongqing Jiaotong University* (*Natural Science*), 25(4): 73-76.

Huang, Y. H. (1993). "Pavement analysis of rigid pavements with pumping". Purdue University, West Lafayette, Ind. 1993.

Luo, Q. X., Fu, X. and Song, R. X. , et al. (2001). "Impact-echo method and testing system for detecting internal defects and thickness of concrete structure". *Highway*, (3): 55-58.

Tang, B. M. (1992). "Detection of void beneath the rigid pavement slab". *China Journal of Highway and Transport*, 5(1): 40-44.

Tan, Z. M., Yao, Z. K., and Liu, B. Y. (2003). "Thermal stress analysis of two-layered concrete slabs". *China Journal of Highway and Transport*, 16(2): 10-12.

Wang, Q., Wang, X. C., and Wang C. H. (2008). "Differentiation of the cavity beneath cement pavement slab based on deflection difference and pumping height". *Journal of Highway and Transportation Research and Development*. 25(12): 84-87.

Zhao, M. C. (2004). "Analysis of the effect of the cavity beneath cement concrete pavement slabs on life span". *Journal of Highway and Transportation Research and Development*. 21(2): 1-4.

Zhou, W. X., Sun, L. J., and Kan, S.N. (2004). "A Study on Void Underneath Slab of Joint Concrete Pavement and Slab Jacking Treatment". *Highway*, (12): 194-199.

Zhou, Y. M, Tan Z. M, and Liu B. Y. (2007). "Loading stress in cement concrete pavement slab with void underneath". *Journal of Tongji University* (*Natural Science*), 35(3): 341-345.

Design of 3D Virtual Simulation and Evaluation System for Road Traffic Signs

Jiang haifeng，Zhang zhiyong，Chen jian，Fang zhengpeng

Research Institute of Highway Ministry of Transport, P.O. Box 100088, City, BeiJing; PH (010) 62359799; FAX (010)62370567; email: hf.jiang@rioh.cn
Key Laboratory of Road Safety Ministry of Transport, P.O. Box 100088, City, BeiJing; PH (010) 62359799; FAX (010)62370567; email: zy.zhang@rioh.cn, cj.chen@rioh.cn, zp.fang@rioh.cn

ABSTRACT

A three-dimensional (3D) virtual simulation system was developed in this paper for reappearance of the visibility and validation of road traffic signs. The system combined subjective and objective evaluation methods to reconstruct and optimize traffic signs design. Based on the system perspective of driver-vehicles-road, a 3D interactive simulation model was proposed and developed, including driver functional model, vehicle type select model, vehicle generation model, 3D road scene, and road network building model. This system has solved the shortages of static testing method and the complicated problems of dynamic testing method. And this system has provided a straight forward and reliable on-line analysis and simulation platform for pre-design, post-optimization and transformation work for road traffic signs system.

Keywords: Road, Traffic Signs, Virtual Simulation, Visibility, Safety Evaluation, 3D

1 INTRODUCTION

Road traffic sign is one of the important traffic safety infrastructures, which is to protect the safety of road transportation (Ministry of Science and Technology Highway, 1999, Chu 2005). Past research showed that most traffic accidents happened on some sections of highway where traffic signs are not visible and not properly designed. In recent years, a three-dimensional transportation network has formed with the rapid development of highway construction. In reality, the service level of traffic signs has lagged far behind. The common problems include no design standard, improper visibility, and so on (see Fig 1).

Figure 1. The Actual problems of traffic signs

Presently there are two evaluation methods for the visibility and validation of

[1]road traffic signs. One is static laboratory testing method, the other is real dynamic vehicle testing methods. Static laboratory testing method is in the lab room. Although the process of the method is very simple and easy to implement, test results do not entirely reflect the influence factors, such as during driver recognition of road traffic signs, he must be affected by the moving vehicle at high speed. Real dynamic vehicle testing method is to test the visibility and validation for traffic signs in actual vehicle, and this method is implemented on highway. So its testing results most accord with realities. But the testing process is in a typical road environment can not fully cover common road environments in reality. The task of the testing method is heavy and the cost of the testing method is very high (Chu, 2005) As a result, a comprehensive evaluation for traffic signs visibility and validation is developed based on virtual reality techniques (VR), which not only solve all kinds of traffic problems recently in our country but also is an import way to optimize the design of traffic signs [3].

2 ANALYSIS OF TRAFFIC SIGNS VISIBILITY IMPACT FACTORS

The primary characteristics of traffic signs is Easy-visibility and understandable. In order to realize the evaluation and optimization the visibility and validation for road traffic signs, we should study some crucial factors which impact drivers' visibility on traffic signs. Based on the system perspective of driver-vehicles-road, we can divide these factors into subjective and objective factors, as is shown in table 1. These factors are interactive each other, which make the qualitative and quantitative evaluation for road traffic signs very complicated (Yi, 2004).

Table.1 Influencing Factors

Influencing Factors		Specific Index
human	driver	Sexual ，, age, driving skills, etc
vehicle	speed	Driver seat high, eye height and speed
road	Road characteristics	Road width, linear, slope, etc
environments	weather	Rain, snow, fog light
Physical Characteristics of traffic signs	design	shape, color, symbols, characters and size, fonts, spacing, and stroke thickness of traffic sign
	set	Distance from lane center, height, order, tilt angle set model

2 DESIGN OF SYSTEM FUNCTION MODELS

After Specific the subjective and objective factors of road traffic signs, some function models of system has been designed separately in this paper, based on five

Supported by : West Transportation Construction Technology Projects (2004 318 223 33-10)

aspects such as driver, vehicle, roads, environments and traffic signs, physical characteristics.

2.1 DRIVER: FUNCTION DESIGN OF DRIVER MODELS

Driver function models are designed mainly from perspective, visual distance and eye height of driver. There a lot of factors influence driver identify traffic signs information, including driver's seat, Vehicle rear-view mirror and the front of the vehicle former perspective and so on. So considering these factors, the driver function models designed in this paper have some special functions, such as the driver can adjust his view angel, also can control keyboard (up, under, left and right, etc.) to make the vehicle speed up, slow down or turning.

2.2 VEHICLES: VEHICLE GENERATION AND TYPE SELECT MODELS

By using of Multi-Agent techniques, dynamic behavior models of vehicle have been designed. This model can control vehicle's driving behavior according to the setting parameters. And vehicle control rules of travel speed and direction are established. Such as speed up, slow down or turn (Chen, 2007). The function setting interface for vehicle type and driver's view angel is shown in figure 2.

Figure 2. Setting Interface for Vehicle Type and Driver's View Angel

2.3 ROAD: 3D ROAD NETWORK AND ENVIRONMENT MODEL

Through this model we can quickly and easily building a 3D road network scene by using data of road linear mapping and road design information. These data is mainly from field mapping, Google earth and aviation pictures. Through interactive dialogue interface, these data can be input into the computer. Function model including as follows:

1. Road models

This model can generate a road automatically and some properties of road can be set conveniently by users interactive with setting interface. The properties of road including soil road shoulder, road surface, hard shoulder, center isolating marked line, roadbed slope, drainage, road side of isolation facilities, road surface materials, surface slope, the number of lanes, lane width, safety barrier, outline of the signposts

and other safety devices (Yang, 2005). The alignment and surface construction interface of road as shown in Figure 3.

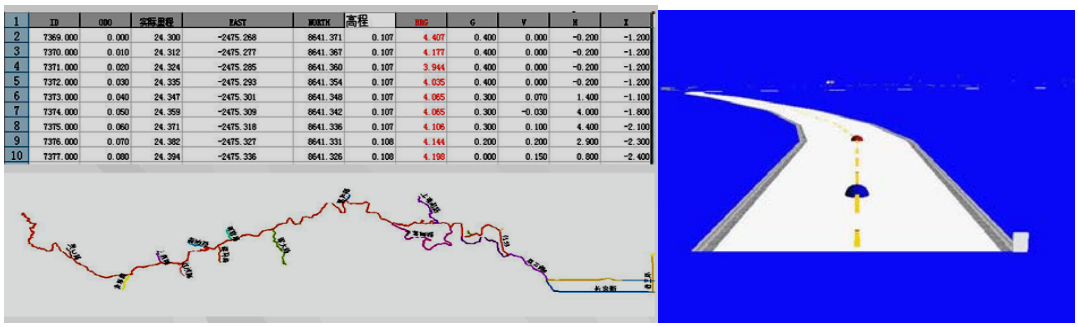

Figure 3. Interface for road alignment and road surface construction

2. Road intersection model

Grade intersection model is an independent model, which can describe the situation of two roads or more than two roads crossing. Such as grade intersection model and 3D-intersection model. User can through mouse and keyboard select intersection's type. Road cross in the intersection can connecting automatically after the intersection type selected.

3. Bridge and tunnel models

Bridge and tunnel models are also designed as Independent unit. The length, width and height of bridge and tunnel can be input into the computer by keyboard. Then the road surface properties can be generation automatically. Lighting and traffic safety facilities can be seated accurately. And the seated position of bridge and tunnel can be layout through mouse.

4. Simulation model of road Scene

The simulation model of road scene provides users some function menus. Through these menus users can be selected vary kinds of scenes to form a simulation road. The simulation effect of road scene as is shown in figure 4.

Figure 4. Simulation effect of road scene

3 3D-DIMENSIONAL MODELS DYNAMIC DESIGN OF TRAFFIC SIGNS

3D-dimensional models of traffic signs are designed dynamically for four

major kinds of road traffic signs (warning signs, ban signs, indication signs and guide signs). The functions of these traffic signs models mainly include location, type selection, support pattern, dynamic editing for traffic signs size and information. 3D-dimensional models of traffic signs dynamic design structure is shown in Figure 5.

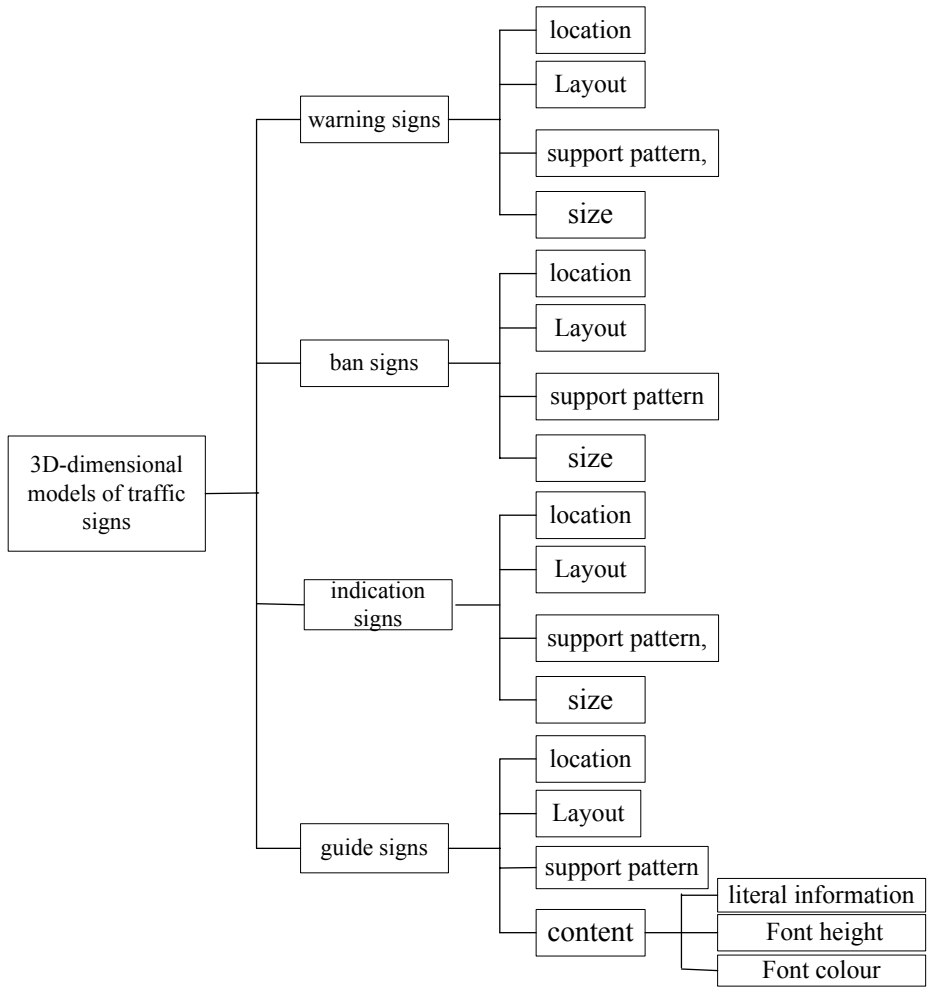

Figure 5. The structure of 3-Dimensional models for traffic signs

The Function implementation steps of traffic signs 3D-dimensional models as follows:

1. Firstly, after determined the location of traffic signs, user can place a selected traffic signs on the road surface through a mouse click or enter mileage of road.

2. Select a kind of layout for traffic signs by traffic menus.

3. Select a kind of support pattern for traffic signs by traffic menus. This model provides some common support patterns. Such as pillar pattern, single cantilever pattern, dual cantilever pattern, door frame pattern and attached pattern. And traffic sign board can automatically position at proper location on the road. Then, according to the traffic information determines the size of traffic signs board.

4. Finally, based on the job completed, users can edit traffic signs' information dynamically and real-timely.

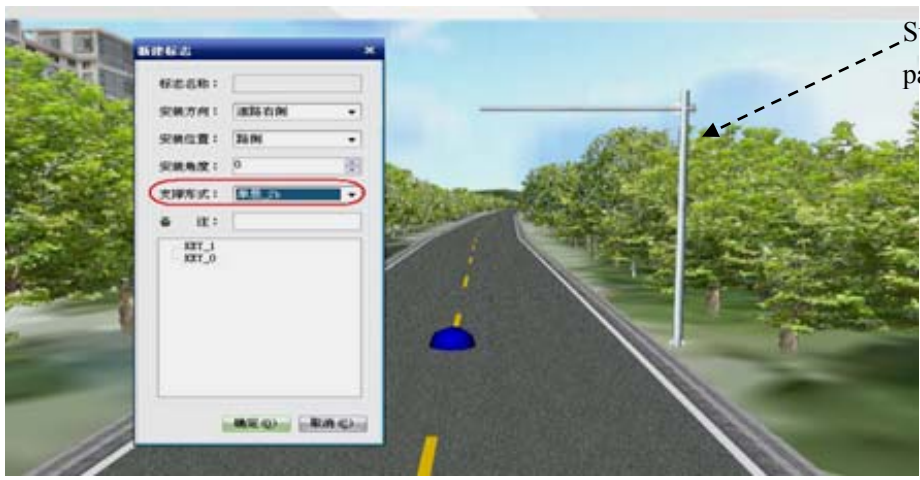

Figure 6.Traffic signs support pattern select interface

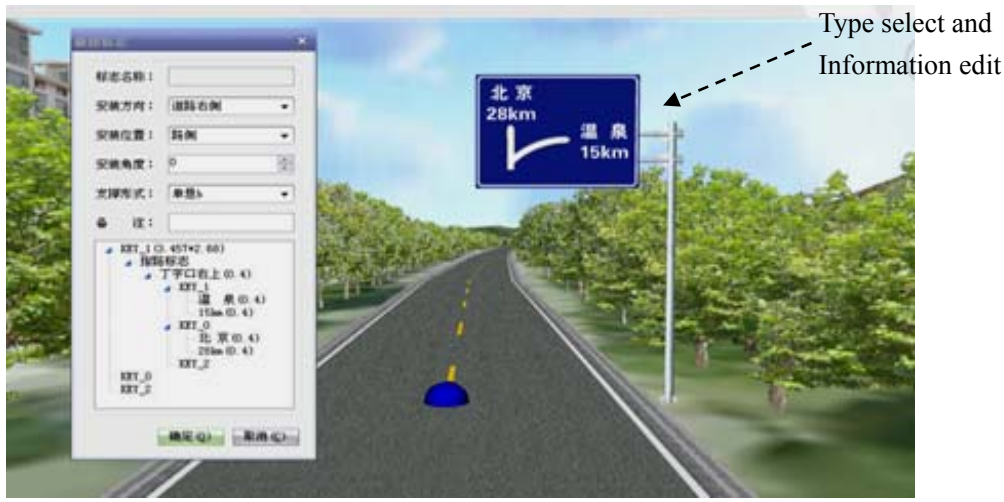

Figure 7.Traffic signs type select and information edit interface

As is shown in figure 6 and figure 7, the install location, support pattern, install angel, type and content information of traffic signs can be designed dynamically and modified real-timely on the road sides.

4 EVALUATION METHODS AND INDEX OF TRAFFIC SIGNS

Based on the 3D road network model, traffic signs model and vehicle model are completed above; we can evaluate the visibility and validation of traffic signs in accordance with the evaluation methods and index. The evaluation methods take into account objective index and subjective index. Due to different traffic signs have different functions; evaluation methods should according to the main function of different type traffic signs to classify and to establish. For example directional traffic

signs and guide traffic signs emphasize understandability, warning traffic signs and prohibition traffic signs emphasize validity.

For example established evaluation index for directional traffic signs and guide traffic signs as follows:

1. Running time. Evaluator departs from the starting point until the evaluators found the test traffic signs. This period counted as the running time of the evaluator.

2. Error rate. Calculation method is shown in formulate 1. Error understanding number divided by total number of evaluations of a certain sample evaluators we can calculate error rate. The total number of evaluations is the sum of the error understanding number and the proper understanding number of evaluation. That is,

$$\text{Error rate} = \frac{\text{error understanding number}}{\text{The total number of evaluations}} \times 100\% \quad (1)$$

Considering environment impact on the visibility of traffic signs, this system has developed some function models to set and display sun light, rain, snow and fog weather features, which will to ensure the authenticity and validity of evaluation results. The 3D virtual simulation system for road traffic signs has been applied in Men-Tou ditch of 109 National Road. The section of evaluation function simulation interface as shown in Figure 7. Visibility and validation of road signs and markings on the Men-Tou ditch of 109 National Road has been evaluated by subjective evaluation methods. By these methods, about ten bad visibility and improper-set traffic signs and markings have been found on the road. These traffic signs can easily leads to various types of traffic accident. And finally, these traffic signs and markings have been improved by Traffic Management Department. This is helpful to ensure the traffic safety on the road.

Fig.7 evaluation function simulation interface of 109 national road

5 CONCLUSIONS

Based on human factors, a set of 3D virtual simulation platform was developed for traffic safety. And the 3D interactive modeling and simulation was developed for drivers, vehicles and road. This system can assist Pre-evaluation and Post assessment of the visibility and actual implementation for various traffic signs on classified highway. The evaluation results can help reduce the unreasonable and unscientific traffic signs design scheme. In theory, the 3D virtual simulation platform developed in this paper will enrich and improve the existing traffic signs research results.

REFERENCES

Chen T., Wei L. (2007). "Driver-vehicle-road virtual simulation with interaction mode", *J. Journal of Chang an University (Natural Science Edition)*27 (1): 67-71.

Chu X., Yan X., and Zhang X., Li H. (2005). "Design of a Virtual Testing System for the Visibility of Road Signs and Markings", *J. Journal of Wuhan Automotive Polytechnic University* .27 (4) :135-138.

Ministry of Science and Technology Highway editor-in-chief (1999). *Compilation of road traffic engineering standards and criterion GB5768-1999: 1*, M. Beijing: Publishing house of People's traffic.

Yang H., Xu J., Li J.(2005). "Evaluation of highway route design based on computer simulation", *J. China Journal of Highway and Transport*, 18 (1):14-18.

Yi T., and Xiong J.(2004). "Development and Application of Microcosmic Traffic Flow Simulation System Based on Virtual Reality", *J. Computer Simulation, Simulation*. 21 (5):148-150190.

Using VISSIM to Calculate the Capacity of Urban Expressway Interchange

X. Zang[1,3] and W. Zhou[2]

[1]Beijing Key Lab of Traffic Engineering, Beijing University of Technology, Beijing, 100022, China; email: zxdzxdzxd69@yahoo.com.cn
[2]Research Institute of Highway Ministry of Communications, Beijing, 100088, China; email: Zhw59@hotmail.com
[3]School of Civil Engineering, Guangzhou University, Guangzhou, 510006, China

ABSTRACT

Traffic flow at urban expressway interchanges is unique, and researchers have used the VISSIM simulation model to calculate the capacity of such interchanges. In this paper, in order to calibrate and validate VISSIM, the measures of effectiveness (MOE) are put forward, the confidence intervals of parameters chosen in the VISSIM are calculated, and then the factors in the interval are fine tuned to meet the accuracy of MOE, which is the percentage of error between the simulated and observed values. At last, the capacity of an urban expressway interchange in Guangzhou is calculated based on the proposed method. The validation results show that the approach to calibration and validation is feasible.

INTRODUCTION

An interchanges is a key joint of urban expressways. It determines the capacity of connecting urban expressways, and it may become the bottleneck if its operation is unreasonable. At present many urban interchanges in China become quite congested, so it is necessary to study the capacity of urban expressway interchanges. But how to define the interchange capacity is difficult because there is not a general concept of interchange capacity. In this paper, we define the concept as the maximum volume of traffic that an interchange can serve under the definite conditions. This concept must be different from the capacity of weaving area, merge area, diverge area, or basic section area.

The urban expressway interchange is a complex traffic system. Generally, there are diverging, weaving, and merging areas in one interchange, and the traffic flow is greatly disturbed.. It is difficult to analyze the traffic flow characteristics using statistical and theoretical methods to calculate the capacity of an interchange (Zhou et al. 2007). Using computer simulation to calculate the capacity is feasible because the computer simulation has repeated characters, real-time characters, continued characters and easily controlled characters (Zhong et al. 2006). It can simulate the traffic flow under different conditions and analyze the vehicle characteristics, driver characteristics, traffic flow characteristics, and so on. This paper will calculate the capacity of an urban expressway interchange based on VISSIM after calibration and

validation.

THE TRAFFIC FLOW CHARACTERISTICS

There are various types of interchanges on urban expressways. Their lane numbers and traffic composing and geometrical conditions are different, and their capacity values are different, too. In diverging, s or weaving, or merging areas, the traffic flow is disturbed. The traffic flow in the weaving area is disturbed by that in the diverging area, and the traffic flow in the merging area is disturbed by the weaving area. This occurs because the distance between the diverging area and weaving area or between the weaving area and merge area is too short, and the vehicles cannot return to their natural condition after being influenced, and its time headway distribution is not determined.

Figure 1 is an illustration of time headway distribution, and it is drawn based on the actual survey data from an urban expressway interchange in Guangzhou city. From Figure 1, we can see that with the increased distance from the end of the weaving area to the start of the merge area, the mean time headway decreases, but traffic flow volume increases. This occurs because in the weaving area, the straight running vehicles will change lanes from the outside to the inside lane to avoid the disturbance. The vehicle volume in the outmost lane is low, and after the weaving area, many vehicles change lanes from the inside lane to the outmost lane.

Moreover, the distribution of time headway in the outmost lane in the merge area does not accord with the exponential distribution, M3 distribution, or Erlang distribution, but alterable parameters WEIBULL distribution. All these distributions demonstrate that the traffic flow characters in interchange are different from those in another place, for example in the base segment or merge area of an expressway. So we must consider these characters and build feasible calibrating methods when we calibrate the VISSIM.

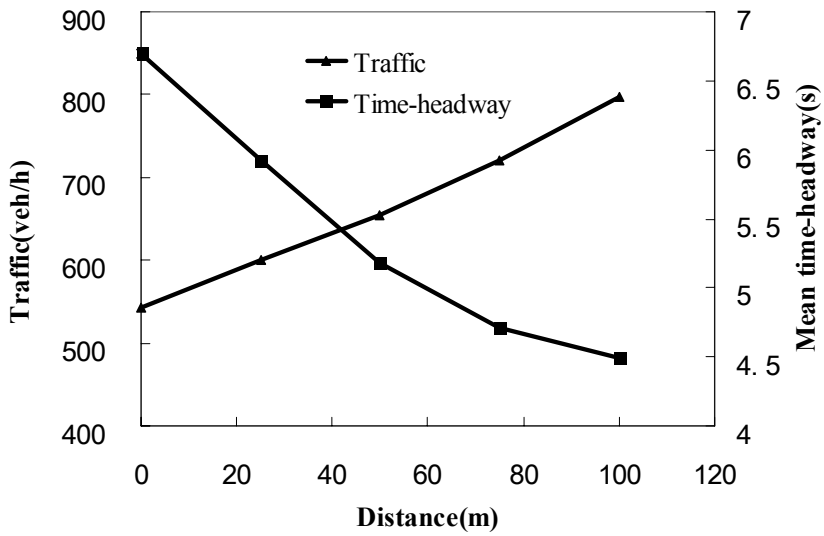

Figure 1. The relations of traffic and time headway with distance.

CALIBRATION of VISSIM

The meaning of calibration. Calibration is the adjustment of parameters in a model so as to represent local conditions (Cohen, 2004). The reliability of any simulation software depends on its ability to produce results close to reality (Liu et al. 2008). The process of determining whether the simulation model is close enough to the situation being simulated is generally achieved through an iterative trial-and-error process involving calibration of the model parameters, comparing the model to the actual system behavior, and using the discrepancies between the two to improve the results until the accuracy is judged to be acceptable (Hourdakis, et al. 2003).

Selection of calibration parameters. In VISSIM, there are many parameters, including fixed parameters and adjustable parameters. The fixed parameters include road condition factors and controlled condition factors, for example, lane width, curve radius, gradient, and so on. The adjustable parameters include driver character factors, lane change time, minimum time-headway, and so on(Sun et al. 2007). The fixed parameters can be obtained by survey, and the adjustable parameters need research and are analyzed based on the record and data surveyed. In interchanges, because traffic flow characteristics are particular, the greatest difference from other facilities is the driver characteristic, so we choose the emergency stop distance, expected lane change distance, minimum time-headway, observed front vehicle, additional safety distance, and minimum and maximum acceleration as the main calibration parameters.

The measures of effectiveness (MOE) and the goodness of fit measure. In an interchange, the measures of effectiveness must express the traffic flow characters synthetically, so the variables chosen for MOE aretotal time, interzone mean velocity, and traffic volume in the downstream of mainline. The goodness of fit measure calculates the difference between the simulated and observed values(Merritt, 2003). The test measure is as follows:

$$P = \frac{V_S - V_O}{V_O} \times 100\% \qquad (1)$$

Where p is the percentage of error between the simulated and observed values, V_S is the simulated value of all the MOE, and V_O is the observed value of all the MOE.

The confidence interval of the MOE. After much research and analyzing the survey data, researchers concluded the following: the emergency stop distance is related to velocity, a driver's reaction time, and the friction of the road surface. The expected lane change distance is shorter than the other area because the traffic flow in interchange is disordered, and the driver is more cautious than in other facilities. The minimum time-headway within an interchange is smaller than that in the other facility because the drivers are tensional, and they do not want be stopped but to go through the interchange sequentially. According to the actual survey data, the researchers calculate the 95 percent confidence interval of above factors. The value is shown in Table 1. The value of calibration parameters should be within the interval.

Table 1. The 95% cConfidence interval of calibration parameters.

Parameters	Diverge area		Weaving area		Merge area	
the emergency stop distance(m)	18	21	16	19	18	21
expected lane change distance(m)	135	165	130	160	132	162
the minimum time-headway(s)	0.9	1.2	0.9	1.2	0.9	1.2
additional safety distance(m)	1.5	2.5	1.5	2.5	1.5	2.5
minimum acceleration(m/s^2)	-1	-1.2	-1	-1.2	-1	-1.2
maximum acceleration(m/s^2)	-4	-4.6	-4	-4.6	-4	-4.6

Methodology for practical calibration. In VISSIM, there are too many parameters and the calibration is very difficult. Many scholars consider that the calibration process is an optimization problem (Chu, 2004). Many methods have been used, for example, genetic algorithm, the gradient approach algorithm, genetic simulated annealing algorithm. For interchanges, using the methods above will not be feasible because the traffic flow states are varied, and the calibration result is not unique. That is to say there will be many different combinations for calibrating factors by only the optimizing method. The calibration result in one condition may be not fit for every condition. We must then calibrate VISSIM by combining the actual data with optimization methods. The steps are as follows:

1) Survey the calibration parameters chosen above in the interchange.

2) Analyze the confidence intervals as calculated in Table 1.

3) Program based on the circular calculation algorithm.

4) Adjust the parameters in the confidence interval to meet the target that the $P < 5\%$ after an iterative trial-and-error process.

5) Adjust the other parameter except the parameters at step 4 if the target of step 4 cannot be achieved.

6) Validate the calibrated VISSIM based on the data that is different from the data used for calibrating, but it should be the same as the traffic conditions. Detail is included in the next chapter.

7) Calculate the capacity of an interchange by using a calibrated VISSIM.

VALIDATION OF VISSIM

Validation is a comparison of the measures of effectiveness as computed by a model and as observed in field data under the same traffic flow conditions. In order to ensure the validity of the calibrated VISSIM, the data used for validation must be different from the data used for calibration. The measure of goodness-of-fit we used for evaluating the calibrated simulation model is the Mean Percentage Error (MAPE), which can be calculated by:

$$MPE = \frac{1}{n}\sum_{i=1}^{n}((M_{oi} - M_{si}) / M_{oi}) \qquad (2)$$

Where M_{oi} is the observed values, M_{Si} is the simulated values, and n is the minimum number of replications for the required accuracy. It is calculated by:

$$N = (\frac{st_{a/2}}{uE})^2 \quad (3)$$

Where u and s are estimates of the mean and standard deviation of the MOE, E is the required accuracy, $t_{a/2}$ is the critical value of the t-distribution at significance level a. If $MPE < 5\%$, we can use the calibrated VISSIM to predict the capacity of an urban expressway interchange.

A SIMULATION EXAMPLE

According to the steps above, we calculated the capacity of an urban expressway half-cloverleaf interchange in Guangzhou city. The circumstance is as Figure 2, which was plotted according to the GPS data. The parameters calibrated are as Table 2, and the processes are as the section of **Methodology for practical calibration**. The validated results of MOE are shown in Figure 3 (only given a demonstration of interzone mean velocity, the others is elided). In Figure 3, the interzone mean velocity is the mean velocity from the beginning of the weaving area to the beginning of the merging area, which begins in lane 1 under the different traffic conditions. Figure 3 shows that the change of velocity in the interchange is violent, and the chaos is serious. And one line is the actual data line, the other line is the simulation data line. The difference between the two lines shows the calibrating effect. From Figure 3 we can see the two lines are very close, so the calibrated VISSIM is effective. Then based on the calibrated VISSIM, we calculate the capacity of an interchange in a single direction in KEYUN road is 7490 (pcu/h) (total 4 lanes) under the conditions that the ratio of weaving volume to total volume is 15 percent, the ratio of diverging volume to total volume is 10 percent, and the ratio of merge volume to total volume is 10 percent. In an interchange, the traffic characteristics are complex, and too many factors influence the capacity of the interchange. So the researchers' conclusion only fits particular conditions. However, the method to calibrate the VISSIM is helpful when studying the interchange capacity extensively.

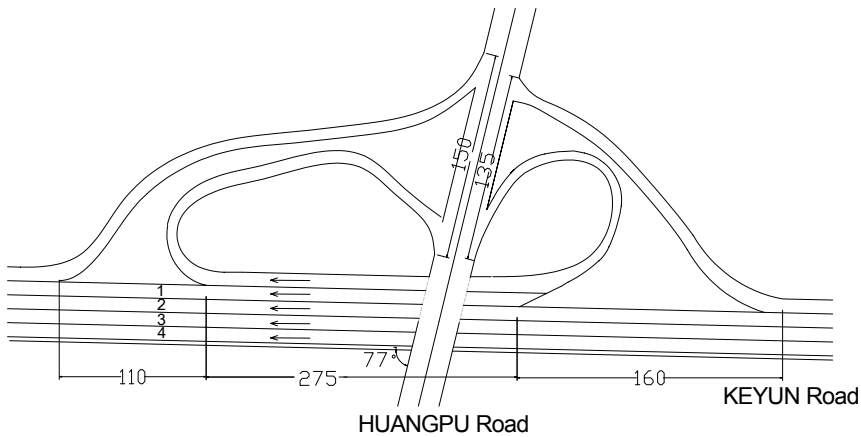

Figure 2. The circumstance of interchange chosen.

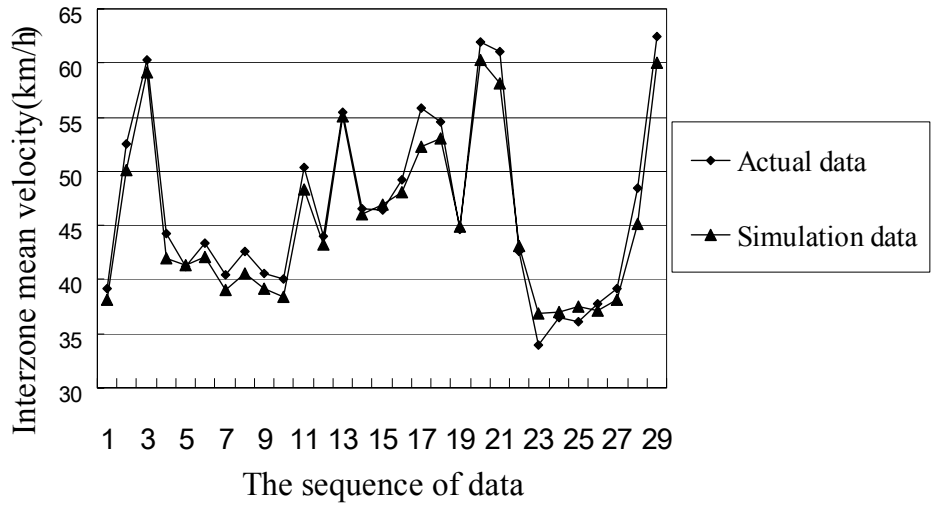

Figure 3, The comparison between the actual data and simulation data.

Table 2. The value of MOE calibrated.

Parameters	Diverge area	Weaving area	Merge area
the emergency stop distance(m)	20	17	20
expected lane change distance (m)	145	135	135
the minimum time-headway(s)	1.05	1.05	1.05
additional safety distance(m)	2	2	2
minimum acceleration(m/s^2)	-1.1	-1	-1
maximum acceleration(m/s^2)	-4.2	-4.2	-4.2

CONCLUSIONS

The study shows that the calibration of VISSIM at an interchange is different from that in other facilities because the traffic flow characteristics are particular. In order to calibrate the parameters in VISSIM, we make certain the confidence interval is based on the actual data surveyed, then the parameters are tuned to satisfy the goodness of fit best. If the accuracy cannot be obtained, then tune the other parameters slightly. The simulated results demonstrate that this calibrating method is feasible, and the accuracy is sufficient. However, the interchange models are varied in different nations or districts, and the traffic characteristics are also different. It is difficult to ascertain the universal interchange capacity, so the research results in this paper are limited. The calibrating method is also fit for other kinds of interchanges.

In this paper, six parameters are calibrated, but many parameters concerning vehicles are not calibrated. More research is needed in capturing all the vehicle parameters.

REFERENCES

Merritt, E. (2003). "Calibration and validation of CROSIM for Swedish road traffic conditions." The 83rd TRB Annual Meeting, CD-ROM.

Hourdakis, J., Panos, G., Michalopoulos, and Kottommannil, J. (2003). "A practical procedure for calibrating microscopic traffic simulation models." Transportation Research Board 2003 Annual Meeting. CD-ROM.

Chu, L. Y., Liu, H. X., Oh, J., andRecker, W. (2004). "A calibration procedure for microscopic traffic simulation." Transportation Research Board 2004 Annual Meeting. CD-ROM.

Liu Ying, Li Keping, Zhang Zhenhua (2008). "The approach to calibration and validation of traffic simulation model in urban expressway." East China Highway J. 169, 88-89.

Cohen, S. L. (2004). "An approach to calibration and validation of traffic simulation models." Transportation Research Board 2004 Annual Meeting. CD-ROM.

Sun J.n,Yang, X. ,and Liu H. (2007). "Study of microscopic traffic simulation model systematic parameter calibration." J. of system simulation. 19(1), 48-50.

Zhong, L., Rong, J, Sun, X. ,and Ren, F. (2006). "Capacity of weaving sections of urban expressway obtained with a simulation method." J. of Highway and Transportation Research and Development. 23(4), 88-93.

Zhou, J.,and Shao, C. (2007). "Capacity analysis of urban interchange using simulation method." J. Road Traffic and Safety. 7(2), 36-41.

RGB Based Crowded Pedestrian Counting In Red Light Time

G. Y. Zhang[1, 2] ,Q.Zhao[1], Z.W. Luo[1],H.Wei[3]

[1]Shanghai Super Star Industrial Development Co., Ltd (Fu Dan University Post-Doctor Station), 11th Floor, Shanghai Science & Technology Tower, No.285, Jian Guo Road West, Shanghai, P.R.C, PH (86-21)-64452140; FAX (86-21) 64452125; email: zhaoqiang1@gmail.com
[2]Shanghai Finance University, Shanghai, 201209; email: zhanggy@shfc.edu.cn[3]Fudan University, Shanghai, 200433; email: weihui@fudan.edu.cn

ABSTRACT

During the red-light time, when pedestrians walk to the zebra line, the presence between pedestrian and vehicle is one of the main problems for pedestrian counting. Common approaches including edge detection, histogram of gradient, and segmentation based on histogram of intensity gradient are not feasible. After the review of the general pedestrian counting methods, a new algorithm for pedestrian counting from the crowd RGB picture is proposed in this paper. Firstly, using the sequential frames with differential color threshold as based templates of human head and shoulder detection for preliminary counting db3 wavelet is used for retrieving the features. and K-mean cluster is used for the centroid detection of feature points clusters. Additionally, the track of centroid is used for the filtering of pedestrians not walking towards the camera. The algorithm is applied in pedestrian alerting system of Eshan Road and Dongfang road in Shanghai. In 1000 alerting events, the error is below 22% and the related analysis result is presented.

1. INTRODUCTION

Pedestrian detection and counting in urban traffic is one of the key issues in Intelligent Traffic System (ITS) and traffic safety research. Based on the background subtraction methods in the image process, Single Edge Detection (Haritaoglu,1998), Histogram of Oriented Gradient(Dalal,2005), and Intensity Histogram base Region Division methods(Michael Girard,1985) were used in single frame based pedestrian detection and counting. For the sequential frames of video stream, it is proposed to use Biology Movement (Shafique, 2005), self-adapt background subtraction (Nixon.,1999), etc. methods for pedestrian contour retrieve and recognition. These methods were not feasible in crowded scenario. One method to solve this problem in current research is to detect, retrieve, and track the feature points of human head and face, thususe these data for pedestrian counting. Viola (2001) proposed the traditional

technique of base human-face detection . The method can be used in real time detection. However, the application of Adaboost classifier in his method requires large number of face pictures for positive and negative classifier training.

The key point of this project is not to recognize and match; hence, it proposed a new human counting algorithm for crowded scenario during day period based on RGB pictures showing in the following sections

2. SYSTEM FRAMEWORK

Based on the region-detail synthesis, the detection sequence is shown in Figure 1: Pedestrian contour →Face region→Face feature points→Centroid of feature points→Moving direction.

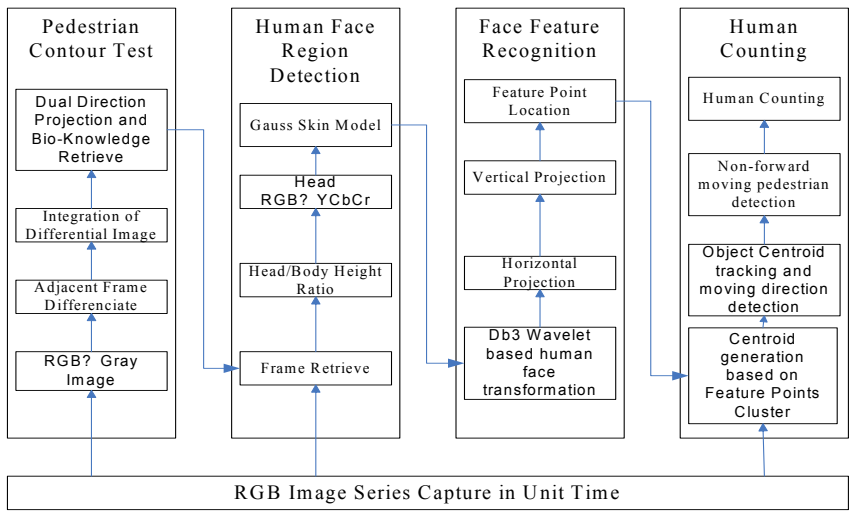

Figure 1. Statistic of Pedestrian Red Light Violation in a Crowded Scenario

3. ALGORITHMS FOR PEDESTRIAN STATISTIC IN RED LIGHT TIME

3.1 Gray-level Image Differentiation based Pedestrian Contour Detection

Different with the conventional background subtraction method, the algorithm applied here only record the moving objects in the camera scene. Roadside camera is setup facing zebra line vertically; the *i*th frame can be presented as:

$$f_i(u,v) = f_{P_i}(u,v) + f_{V_i}(u,v) + f_{B_i}(u,v) + f_{N_i}(u,v), i = 1,2,3,\cdots$$

Where,(u,v)-pixel coordinates, $f_i(u,v)$-gray level of point(u,v), $f_{Pi}(u,v)$-gray level of pedestrian in the frame, $f_{Vi}(u,v)$-gray level of vehicles, $f_{Bi}(u,v)$-gray level of background image, $f_{Ni}(u,v)$-gray level of image noise, follow zero mean Gauss Distribution.The *j*th differential frame can be written as:

$$I_j(u,v) = \left| f_{i+1}(u,v) - f_i(u,v) \right|, i = 1,2,3,\cdots, j = 1,2,3,\cdots$$

Where $I_j(u,v)$ is the difference of two adjacent frames, when the sample time closing to zero, $f_{Bi}(u,v)=f_{Bi+1}(u,v)$. In a frame sequential with M images, the sum of M-1 differential frames is:

$$I_{\Sigma}(u,v)=\sum_{j=1}^{M-1}I_j(u,v)=\sum_{i=1}^{M}\left|f_{P_{i+1}}(u,v)-f_{P_i}(u,v)\right|+\sum_{i=1}^{M}\left|f_{V_{i+1}}(u,v)-f_{V_i}(u,v)\right|+\sum_{i=1}^{M}\left|f_{N_{i+1}}(u,v)-f_{N_i}(u,v)\right|$$

Where the background is subtracted and the left is the block information of pedestrian, vehicle tracks, and point noise under Gauss distribution. The erosion process is used to eliminate the point noise with minimum damage to block information, the result is image $I'_{\Sigma}(u,v)$. The vertical projection of pedestrian moving track maybe present as:

$$V(u)=\sum_{v=1}^{H}I'_{\Sigma}(u,v),u=1,2,\cdots,W$$

Where, W-image width, H-image height, V-the histogram with multi-peak values, *x*–the number of pixel values, which correspondent to the pedestrian number, use the α (decide by M) *W_p (pedestrian width) region on both sides of peak value to estimate the vertical track of pedestrian, it gives *x* regions. S_k stands for the *k*th vertical region for the projection of histogram in vertical direction.

$$S_k(v)=\sum_{u=a_k}^{b_k}I'_{\Sigma}(u,v),v=1,2,\cdots,H$$

Where, a_k-the start point of *k*th vertical region, b_k-the end point of *k*th vertical region. S_k-the histogram close to square wave, use the distance from start point of square wave to β (decided by M)*H_p(Average Height of Pedestrian) as the horizontal region estimation of the *k*th pedestrian's track, the descending side of square wave is not used here considering the occlusion of vehicles in the scene. Hence, after the projection of the eroded image, any pedestrian contour of the original images is located within the rectangle area decided by the projection results.

3.2 Gauss Skin Color Model in YC_bC_r Space

Considering the both presence of human, vehicles during the red-light scenarios, based on the pedestrian contour location, the human head, body height ratio is used for the detection of human face in the head/shoulder region, which only keeps the pedestrians facing the camera and counts the pedestrian numbers accurately being tracked.

Using Gauss Skin model and YCbCr space (Phung, 2002) to divide the estimated human face region. Since the captured image is in true color, the RGB conversion to YCbCr can be achieved by the following equation:

$$\begin{bmatrix} Y \\ C_b \\ C_r \end{bmatrix} = \begin{bmatrix} 16 \\ 128 \\ 128 \end{bmatrix} + \frac{1}{256} \begin{bmatrix} 65.481 & 128.553 & 24.966 \\ -37.797 & -74.203 & 112 \\ 112 & -93.786 & 18.214 \end{bmatrix} \begin{bmatrix} R \\ G \\ B \end{bmatrix}$$

The statistic result shows the skin color of human face is within the certain region. The center of this distribution can be calculated by the samples. The mean and variance of the distribution are calculated as follows:

$$\mu = [156.56 \quad 117.43], C = \begin{bmatrix} 160.13 & 121.143 \\ 121.143 & 299.46 \end{bmatrix}$$

The similarity of one pixel to the skin is counted base on its distance to this center, as follows:

$$P(C_r, C_b) = \exp(-0.5(x-\mu)^T C^{-1}(x-\mu)), x = [C_r \quad C_b]^T$$

The empirical result showing a good result may be achieved using 0.65 as the threshold in image binarization:

$$F(u,v) = \begin{cases} not & P(C_r, C_b) > 0.65 \\ yes & P(C_r, C_b) \le 0.65 \end{cases}, \quad u,v \text{ is pixel coordinate within the head region}$$

3.3 Human Face Feature Recognition and Locating with Wavelet

The separated face region data need to be distilled for real time based tracking, the feature based recognition, and location is used here based on the wavelet methodology (Satyanadh, 2004). Assuming we have 2D scatter signal of human face image $\{X_{m,n}\}_{m,n \in Z} \in Z$, with $C_{0,m,n}=X_{m,n}$, the wavelet based deduction is:

$$\begin{cases} C_{j,m,n} = (H \otimes H)(C_{j+1})_{m,n} = \sum_{k,l} C_{j+1,k,l} h_{k-2m} h_{l-2n} \\ D^1{}_{j,m,n} = (H \otimes G)(C_{j+1})_{m,n} = \sum_{k,l} C_{j+1,k,l} h_{k-2m} g_{l-2n} \\ D^2{}_{j,m,n} = (G \otimes H)(C_{j+1})_{m,n} = \sum_{k,l} C_{j+1,k,l} g_{k-2m} h_{l-2n} \\ D^3{}_{j,m,n} = (G \otimes G)(C_{j+1})_{m,n} = \sum_{k,l} C_{j+1,k,l} g_{k-2m} g_{l-2n} \end{cases}$$

Where, H and G equal to the low/high frequency filter of db3 wavelet in Daubechies group. D^1 is the vertical direction wavelet parameter, D^2 is the horizontal direction wavelet parameter, *and D3* is wavelet parameter on diagonal direction.

The details in vertical edge of original frame is well remained after the second layer wavelet transformation in high frequency image, which may efficiently recognize human face features such as eyes, nose, and mouth, the location of these features may be easily calculated with the integral of horizontal/vertical gray level projection.

3.4 Fuzzy Based K-Mean Clustering

The tracking of pedestrian requires the identification of one pedestrian with his feature points; here the Fuzzy K-Mean methodology is used to locate the centroid of pedestrian face feature points in original frame, for pedestrian identification. FKM algorithm gives out the cluster centroid within the human face feature points clustering process.

3.5 Tracking

The empirical result shows that most of the pedestrian walks through the zebra lines with a constant speed, and the adjacent frames got minor difference. The binary principle to tell the centroid of ith frame ($u_{i,k}$,$v_{i,k}$) in the i+1 frame ($u_{i+1,l}$,$v_{i+1,l}$) belongs to the same pedestrian is:

$$d = \sqrt{(u_{i+1,l} - u_{i,k})^2 + (v_{i+1,l} - v_{i,k})^2}, k = 1,2,\cdots, l = 1,2,\cdots, sign(d) = \begin{cases} 1 & d \le \delta \\ 0 & d > \delta \end{cases}$$

Where δ is decided by the sample frequency and pedestrian moving speed.

Sample M frames in unit time, the *k*th pedestrian moving direction can be:

$$Direction = \begin{cases} \text{moving towards the camera} & v_{M,k} - v_{1,k} > 0 \\ \text{moving away form the camera} & v_{M,k} - v_{1,k} < 0 \\ \text{moving vertically to the camera facing direction} & v_{M,k} - v_{1,k} = 0 \end{cases}$$

4. APPLICATION AND ANALYSIS

The algorithm is applied in pedestrian alerting system at Eshan Road and Dongfang road inShanghai. In one thousand alerting events, the error is below 22%. An example is presented here. 15 frames (768×576 pixels) are processed per second. Figure 2 listed the original RGB image series.

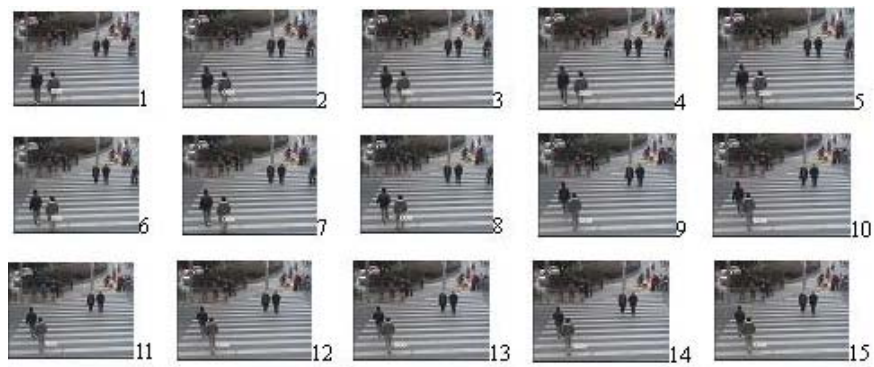

Figure 2. Original image series

Figure 3 showed the sum of 14 gray differential frames..and Figure 4 showed the pedestrians' contours of the original imageslocated within the rectangle area

Figure 3. The sum of 14 gray differential frames

Figure 4. The result of pedestrians' contour detection

The result of the point locations by face feature for the 15th original image is shown in Figure 5. By obtaining the face feature points of 9 sequent original frames, the clustering result is shown in Figure 6. The number and the direction of the men moving forward the camera can be detected easily.

Figure 5. The face feature point location

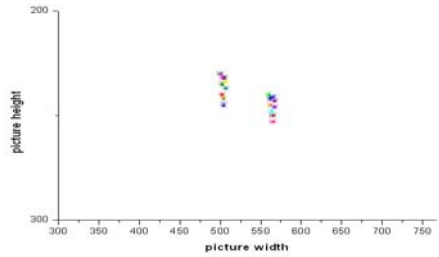

Figure 6. The clustering result

5. Conclusion and Future Work

After the review of the general pedestrian counting methods, a new algorithm for pedestrian counting in crowd RGB picture is proposed in this paper. The algorithm is applied in pedestrian alerting system of Eshan Road and Dongfang road in Shanghai. A perfect result is obtained. The new algorithms and research approach for night period will be developed in the future work.

REFERENCES

Dalal N,Triggs B.(2005). Histograms of oriented gradients for human detection[C]. IEEE International Conference on Computer Vision and Pattern Recognition,2005, I:886- 893.

Haritaoglu I, Harwood D , Davis L S. (1998). A human body part labeling system using silhouettes [J].Fourteenth International Conference on Pattern Recognition, 1998(1):77- 82.

Girard M., Maciejewski A. A.(1985). Computational modeling for the computer animation of legged figures [J] .ACM SIGGRAPH'85 , Proceedings,1985, 7:263-270.

Nixon M.S., et al.(1999). Automatic gait recognition in BIOMETRICS personal

identification in networked society[J]. Kluwer Academic, 1999:231-249.

Paul Viola, Michael Jones.(2001).Robust Real-time Object Detection. In Proc.of IEEE Workshop on Statistical and Computational Theories of Vision,.

Phung S. L., Chai D. and Bouzerdoum A.(2002). A Novel Skin Color Model in YCbCr Color Space and Its Application to Human Face Detection[C]. ICIP 2002.

Satyanadh G, Vijayan A.(2004).Face detection technique based on rotation invariant wavelet features. International Conference on Information Technology: Coding Computing, ITCC, v2, International Conference on Information Technology: Coding Computing, ITCC 2004: 157-158

Shafique K,Shah M.(2005).A noniterative greedy algorithm for multiframe point correspondence [J]. IEEE Trans on Pattern Analysis and Machine Intelligence, 2005, 27(1): 51-65.

Impact of Posted Speed Limits on Operating Speed in Urban Expressways

H. Wang[1], X. Sun[1], B. Li[1], and Y. He[1]

[1] Beijing Key Lab of Transportation Engineering, Beijing University of Technology, P.O.Box 100124, 100# Pingleyuan, Chaoyang District, Beijing; PH (86) 67391597; FAX(86) 67391597; email: wanghuarong@emails.bjut.edu.cn

ABSTRACT

The relationship between posted speed limits and operating speed is one of the main factors in determining appropriate speed limits in a speed zone. In this research, 19 sites were randomly selected from the 3rd, 4th, and 5th Express Ring-Road in Beijing, and the spot speed and headway data were collected at these sites. Then, free-speed data were reduced from the original data, and the 85th percentile speeds were computed as each site's operating speed. Deviation analysis of operating speed at the 3rd and 4th site shows that there were no obvious distinctions between these two types of road facilities. The regression analysis of posted speed limits and operating speed shows that there exists a strong linear relationship between these two speed terms. The percentage of operating speed exceeding posted speed limits increases with the speed limit value. The relationships between speed limits and operating speed established here may be expected to provide some quantifying basis for transportation agencies to set posted speed limits in speed zones. Results of this study may help the Department of Transportation and its districts quantify the speed limits and provide more objective insights for setting speed limits.

Keywords: posted speed limits; operating speed; deviation analysis; regression analysis

INTRODUCTION

According to the Fatality Analysis Reporting System (FARS) released by the National Highway Traffic Safety Administration (NHTSA) in the U.S., over one third of all fatal crashes in the years from 1988 to 2006 were related to speeding, that is, exceeding the posted speed limit or traveling too fast for the existing conditions (NHTSA 2006). In China, 10.2 percent of all fatal crashes were related to speeding in 2007 (TMRI 2008). Speed management is a very important tool for improving road safety. Posting speed limits as one of the speed management practices is often understood as a tool to control vehicle speeds and to mitigate accident risks referred to crash statistics. The final report on speed management (Milliken et al. 1998) stated that current approaches for setting speed limits in the U.S. consist of two main methods: maximum statutory speed limit and speed zoning. In determining a legislated speed limit, such factors as design speed, vehicle operating speed, crash history, and enforcement experience are taken into consideration. While the 85th percentile speed under a free-flow condition is the most decisive factor used in setting speed limits in speed zones, the numeric value of a speed limit may be adjusted by

additional factors such as crash rate, roadside development, and roadway geometry, parking, and pedestrian level. The speed limit setting practices in China mainly consider the design speed of certain roadways, ignoring the fact that most drivers have an understanding of a reasonable speed and operate their vehicles at a speed they consider appropriate for the roadway geometry and environment regardless of speed limits. Initially, it is necessary to discover the relationship between posted speed limits and operating speed in China. Here, several segments located in the 3rd, 4th, and 5th Urban Express-Ring Road of Beijing were selected to collect field speed data and speed limits information in October 2007 to make following research.

SPEED DATA COLLECTION

Site Selection Criteria

Here, sites were selected based on the following criteria:

- Sites were selected to represent a basic segment, that is, a reasonable distance from accesses, ramps, and weaving sections to prevent speed data from having any immediate influences by such features.
- Sites were selected to provide a good typical location where speed limit signs could be easily recognized.
- Sites were selected to make sure there was no automated enforcing instrument, such as photo radar, in use.

With these sites selection criteria, a hypothesis was made: drivers of these sites select their speed based only on the speed limits signs and their perception of the driving environment. Accordingly, there were 8, 3, and 8 sites, respectively, selected from the 3rd, 4th, and 5th urban Express Ring-Road of Beijing.

Data Treatment and Reduction

The raw video traffic flow data were exported from Autoscope 2004 to Microsoft Excel and saved as event data. The information includes detecting time, lane, speed, and vehicle length. The 85th percentile speed (a renowned operating speed representation and the primary basis to set speed limits) should be measured under free-flow conditions (NHTSA 2006). A number of studies defined the free-flow speed as similar to selecting those vehicles that have a substantial headway and are not impeded by other vehicles or other factors. It is usual to set a minimum headway between vehicles in the traffic flow of 3 seconds to measure free speed, but a time gap of at least 4 seconds is preferable (Geneva 2008). Here, a time gap of 4 seconds was selected as free speed. In this research, the proportion of truck, bus, or other large vehicle is little than 5 percent, so large vehicles were ignored, and only passenger cars were considered. Then, 8,198 free speeds were reduced from 22,475 originally collected data of 19 different sites during this study. The detailed information of each investigating site, such as posted speed limits, original sample size, and free-speed sample size was shown in Table 1.

ANALYSIS AND RESULTS

Operating Speed

As mentioned above, the 85th percentile speed is a renowned representation of operating speed. Accordingly, we extracted each free-speed sample's 85th percentile speed using the statistical method as each site's operating speed. Table 2 presents a summary of the site statistics, including the mean, standard deviation (SD), maximum and minimum speed, and 85th percentile speed. The site No. in Table 2 corresponds to that in Table 1.

Table 1. Information of investigating sections.

Investigating Location	Site No.	Posted Speed Limits /kph	Original Sample Size	Free-speed Sample Size
3rd Urban Express Ring Road	1	80	349	264
	2	80	592	326
	3	80	375	241
	4	80	1245	234
	5	80	1478	173
	6	80	379	230
	7	80	588	336
	8	80	331	258
4th Urban Express Ring Road	9	80	832	326
	10	80	744	365
	11	80	561	341
5th Urban Express Ring Road	12	100	2758	763
	13	100	1574	199
	14	100	1112	342
	15	100	800	347
	16	100	2592	582
	17	100	2550	880
	18	100	2150	1049
	19	100	1465	942

Making contrast between posted speed limits value in Table 1 and the 85th percentile speed value in Table 2, it can be seen that almost all of the 85th percentile speeds exceed its corresponding posted speed limits. The relationship between posted speed limits and 85th percentile speed will be investigated later in depth.

Relationship between Posted Speed and Operating Speed

Deviation Analysis

As shown in Table 1, the posted speed limit at the sites we selected from the 3rd and 4th Express Ring-Road was 80 kph, and we formulated a regression analysis without separating these two parts. To discover whether there are obvious distinctions among a sample's distribution from these two sites, we formulated a deviation

analysis about the 85th percentile speed of the 3rd and 4th Express Ring-Road. The deviation analysis results are shown in Table 3.

The *p* value in the last column of Table 3 is 0.8658 and greater than 0.05, which means that there are no obvious differences between the mean values of the 85th percentile speed in the 3rd and 4th sites. The result shows that the operating speed data obtained from the 3rd and 4th Express Ring-Road can be seen as one sample, thus we can make a regression analysis.

Table 2. Summary statistics for investigating sites.

Site No.	Mean/kph	SD/kph	Min./kph	Max./kph	85th percentile speed/kph
1	85.14	18.49	30	156	98
2	93.88	21.38	37	146	110
3	100.03	16.77	54	156	110
4	73.48	15.75	36	147	87
5	85.3	18.62	35	146	101
6	75.53	10.57	58	140	86
7	70.35	11.88	44	115	80
8	63.32	15.08	22	128	77
9	85.42	14.52	55	147	98
10	84.21	14.37	30	144	98
11	76.83	13.40	40	141	89
12	93.64	21.19	42	152	117
13	99.73	13.07	68	142	112
14	85.19	15.59	50	130	105
15	80.73	16.93	41	151	102
16	83.29	19.08	24	150	106
17	113.4	18.94	71	166	130
18	94.44	19.53	47	158	113
19	86.16	19.10	28	154	105

Table 3. Deviation analysis.

Origin of Deviation	Degree of freedom	Sum of Sq	Mean of Sq	F value	Pr (>F)
Factor	1	4.12	4.12	0.0302	0.8658
Residual	9	1227.88	136.43	—	—
Sum	10	1232.00	—	—	—

Regression Analysis

It is generally acknowledged that 85th percentile operating speeds exceed posted speeds (Parker 1997). Many of these reports have also demonstrated that the 50th percentile operating speed either is near or exceeds the posted speed limit (Fambro et al, 1997). Figure 1 illustrates the differences between rural two-lane highways and suburban/urban (S/U) roadways in the U.S. (Fitzpatrick et al. 2003). It can be seen from Figure 1 that 85th percentile speeds of urban and suburban roadways exceed existing posted speed limits more often than rural arterials in the U.S. As stated in part 1, little research was conducted on the relationship between operating speed and posted speed limits in China. Figure 2 is drawn by the data obtained from each site's posted speed limits in Table 1 and its corresponding 85th percentile speed in Table 2. It can be seen from Figure 2 that when the posted speed limits increase from 80 kph to 100 kph, the percentage of 85th percentile speeds exceed the posted speed also increase, i.e., increasing from 91 percent to 100 percent.

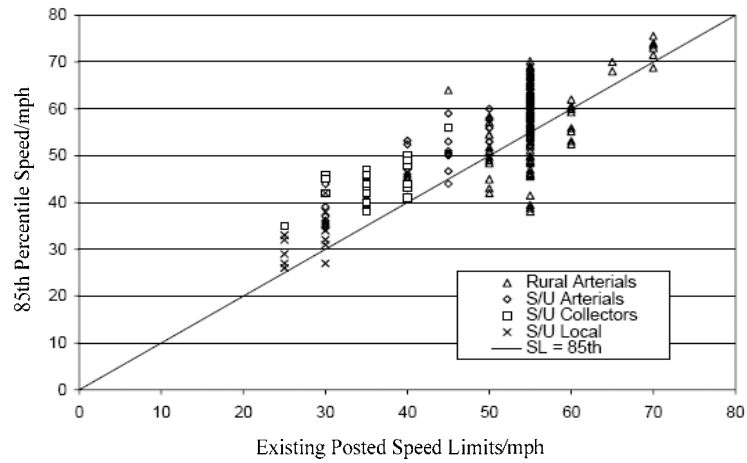

Figure 1. 85th percentile speed versus posted speed from NCHRP, Texas, and FHWA data.

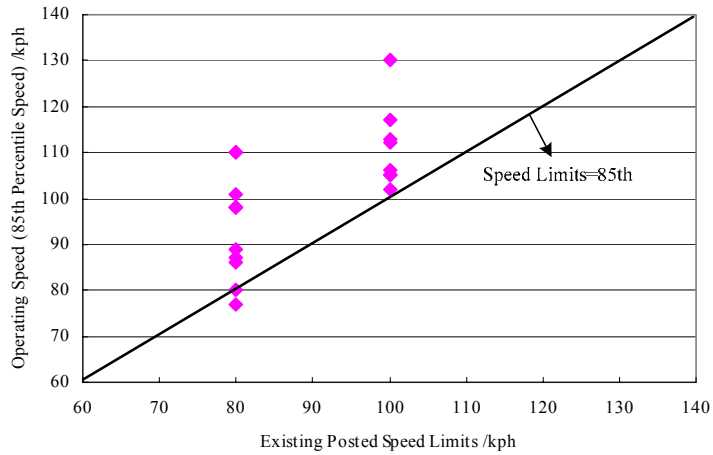

Figure 2. 85th percentile speed versus posted speed in Beijing Express Ring-road.

The linear regressing analysis results between 85th percentile speed and existing posted speed limits obtained by statistical R programming are shown in Table 4. From Table 4, we can draw the linear relationship between 85th percentile speed and posted speed limits as following: $y = 0.8625x + 25$, Where x is existing posted speed limits and y is 85th percentile speed.

The R square of equation (1) is 0.4321. In Table 3, x variable's P-value is little than 0.01, which means that there is strong linear relationship between 85th percentile speed and posted speed limits. This result is identical to the conclusion drawn from the NCHRP Report 504.

Table 4. Linear regression results between 85th percentile speed and existing posted speed limits.

	Coefficients	Standard error	t-Statistic	P-value	Lower 95%	Upper 95%
Intercept	25	21.33768	1.171636	0.257503	-20.0186	70.01858
x Variable	0.8625	0.239828	3.596325	0.002227	0.356507	1.368493

DISCUSSION

It can be seen from Figure 2 that among 19 investigating sites, only one site's operating speed is below its posted speed value. According to the speed limits setting guidelines of speed zone, does this mean that existing speed limits are not reasonable and should be raised? However, it was doubtful that all speed limits on the urban highways where the numerical value of speed limits are lower than the operating

speed must be raised (Park 2003). Numerous studies of travel speeds on rural interstate highways have shown that 85th percentile speeds increased when speed limits were raised and then continued increasing. The 85th percentile is not a stationary point. It is rather a moving target that increases when speed limits are raised. If speed limits are raised to meet a current 85th percentile speed, a higher new 85th percentile speed will soon result. As noted before, raising speed limits also requires considering other factors such as traffic safety and enforcement level, which should be investigated independently in detail.

CONCLUSIONS AND RECOMMENDATIONS

It would be possible to develop mathematical models for other classes of roadways, such as limited-access freeways and rural two-lane highways based on the approach proposed in this research to investigate the relationship between their operating speed and posted speed limits. In order to find the relationship of these two speed variable's relationship more appropriately, periodic investigations on the effects of newly set speed limits on operating speed and safety are necessary. Moreover, the investigating sites should be added to collect data including most types of roadway and various level of posted speed limits information in later research, thus providing a good basis for other related research.

ACKNOWLEDGEMENTS

This research was conducted at the Beijing University of Technology and was funded by the Western Region Transportation Science and Technology Projects under Grant: 200731800027.

REFERENCES

Fambro, D. B., Fitzpatrick, K., and Koppa, R. J. (1997). "Determination of stopping sight distances." NCHRP Report 400, Transportation Research Board, Washington, D.C.

Jaehyun Park (2003). "Modeling of setting speed limits on urban and suburban roadways." Ph.D. Dissertation, University of South Florida.

Fitzpatrick, K. (2003). "Design speed, operating speed, and posted speed practices." NCHRP Report 504, TRB, National Research Council, Washington, D.C.

Milliken, G. M. (1998). Managing speed: review of current practice for setting and enforcing speed limits." Special Report 254, TRB, National Research Council, Washington, D.C.

NHTSA. Traffic Safety Facts 2006. (2006). National Center for Statistics & Analysis, Report DOT-HS-810-837. U.S. Department of Transportation.

Parker, Jr., M. R. (1997). "Effects of raising and lowering speed limits on selected roadway sections." Final Report, Publication No. FHWA-RD-92-084, Federal Highway Administration, Washington, D.C.

Traffic Management Research Institute (TMRI) of the Ministry of Public Security of the People's Republic of China. (2008). Annual Traffic Accidents Statistical Report 2007. (in Chinese)

Nonparametric Analysis of Timely Distribution of Traffic Crash

Zhang Yaping[1], Lan Xiang[2], Zheng Ke[3], Liu Lihua[4] and Yaoxu[5]

[1]School of Transportation Science and Engineering, Harbin Institute of Technology, Harbin, China; P.O. Box 150090, PH (+86) 15846598208; email: zxlt0905@163.com

[2]School of Transportation Science and Engineering, Harbin Institute of Technology, P.O. Box 150090; email: lanxiangkkkk@163.com

[3]Civil Engineering College, Fuzhou University, Fuzhou, China; P.O. Box 350108; email: zh99k@163.com

[4]Department of Municipal Engineering, Henan University of Urban Construction, Pingdingshan, China; P.O. Box 467044; email: liulihuaalicia@126.com

[5]Harbin Urban Planning and Design Research Institute, Harbin, China; P.O. Box 150010; e-mail: hrbyao@163.com

ABSTRACT

Compared with parametric analysis method, nonparametric method is more robust and widely used. In order to make different safety policy of various kinds of time and reduce traffic crashes, this paper wisely and reasonably uses nonparametric tests models, such as Mann-Whitney, and Shapiro-Wilk, to analyze traffic crash date. After testing of normality, this paper discusses timely distributions of traffic crashes --hourly, monthly and yearly distributions of traffic crash data by nonparametric tests. So some right models for suitable timely distribution are given. Finally, analysis of related crashes data in America and China is carried out.

Keywords: nonparametric analysis, timely distribution, traffic crash

INTRODUCTION

Many countries invested so much money, human resources, and advanced equipments to study traffic crashes, especially driving fatality (Richard A. Retting et al., 2003; Dominique et al., 2008; Wen et al., 2005). It is necessary to take great effort to reduce the number of crashes and improve the environment of traffic safety (Marc Graudry and Sylvain Lassarre, 2000). So far, there are some shortcomings of parametric statistical approaches and models. For example, when using parametric test, some presuppositions, such as independently observation, normality of population, consistent standard of population and so on, should be met. If the data is not appropriate for parametric approaches, it is reasonably to consider using nonparametric method and models rather than parametric ones (S, Siegel, 1986; Brian et al., 2002). The reason why some nonparametric statistics is suitable for some situation is that they are not stringed by presupposition of parametric (i.e., they

are more freely). In addition, nonparametric analysis is unique for interval data of crashes (W.J Conover, 2006). In order to make some safety policies and regulations for different timely distributions of crashes, it is clearly that the law and characteristics of hourly, daily, monthly and yearly crashes distribution ought to be studied.

APPROPRIATE NONPARAMETRIC METHODS FOR TIMELY DISTRIBUTION OF CRASHES

It is reasonable to consider using nonparametric statistic model to analyze timely distribution of crashes (Pei Yulong and Wang Wei, 2007). Timely distribution of traffic crashes is the statistic characteristic during different time. It is commonsense that variation of characteristic of traffic fluid is big within different hour, day, month, or year. The location, climate, traffic infrastructure and culture would affect the crashes. Sometimes, in order to make sure that the average number of monthly crashes has changed, it is usually to use the t test, which is a kind of parametric method, to test the difference (Shen Feimin and Zhang Ronggui, 2006). If the data is appropriate for parametric approach, it is wisely to considering using parametric ways. However, in the real observed data, there is seldom situation fit the requirement of parametric ways. So it is reasonably considering usage of nonparametric method. In addition, some situations that would be discussed below are fit to apply three nonparametric tests of crashes. Mann-Whitney test is the first one. It is effective to test the difference of average and median of crashes, particularly deviation of them is so small that even expert in this field have no confidence to get conclusion from his experience. And it is used fitly for test for effectiveness of some safety improvement, which has been made before. Secondly, Cox-Stuart test can be used to detect the trend of two groups. So it is quite reasonable to apply to test the trend of the crashes in two years or months. Finally, One sample χ^2 test can be used for test the random distribution of crashes in different phrases. The basic idea is that when the null hypnosis is right, observation and expectation are very closing to each other,

$$\chi^2 = \sum_{i=1}^{k} \frac{(o_i - e_i)^2}{e_i} \tag{1}$$

Where o_i stands for the number of item i observation;

e_i stands for the expectation of item i when null hypnosis H_0 is right;

$\sum_{i=1}^{k}$ stands for the sum of all item.

NONPARAMETRIC ANALYSIS OF TIMELY DISTRIBUTIONS

A. Normality fitness and standard deviation test

It is necessary to take some normality fitness and standard deviation test

before analysis of data of crashes. The reason is that the parametric test is more powerful and more information from data then nonparametric test. That is mean parametric method is the first choice. This paper collects alcohol-related crash fatalities of 52 states from 2006 to 2007 in the U.S.A (A Brief Statistical Summary, 2008).It is easier to decide whether the sample fit to the normality from a Quantile-Quantile (QQ) Plot. QQ Plot is a kind of scatting one, in which quantile of standard normal is the horizontal axle and value of the sample is the vertical axle (Huang yan and Wu ping, 2005). If the data distribute around a line in QQ plot (see Figure1), then sample is fit to the normal distribution. In addition, P-values of Shapiro-Wilk and Kolmogorove-Smirnov are smaller than 0.01(significance level). In sum, this alcohol-related crash fatality cannot satisfy the requirement of parametric method. It is wisely to considering using nonparametric ways.

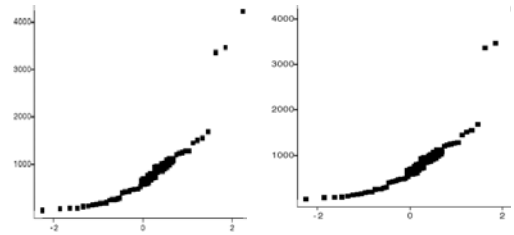

Figure 1 QQ plots of alcohol-related crash fatalities of 52 states in the USA from 2006 to 2007

***B.* Nonparametric Analysis of hourly Distribution of Traffic Crash**

Table 1 is the hourly distribution of crashes in Heilongjiang China since 2006 to 2007. Based on roughly estimation, it seems that the hourly crash distributions of highways are different. In order to demonstrate the hypnosis, Mann-Whitney test was used and processes are as followed.

Table 1 Hourly distribution of crashes in Heilongjiang China (2006-2007)

Phrase / Year	0~2	2~4	4~6	6~8	8~10	10~12	12~14	14~16	16~18	18~20	20~22	22~24
2006	132	122	230	522	625	610	748	859	888	894	730	374
2007	156	130	236	519	689	642	656	837	900	825	783	343

1) Null hypnosis--H_0: the hourly crash distributions in Heilongjiang from 2006 to 2007 are almost same. Alternative hypnosis H_1: the hourly crash distributions of crashes in Heilongjiang are different;

2) Method: It is used by the Mann-Whitney bilateral test, because date is from different independent samples (2006 and 2007), small samples (only 12 phrases), and ordered scale of measurement;

3) Significance level: $\alpha < 0.05$;

4) Statistical value: $T = \sum_{i=1}^{12} R(x_i)$.

Where $R(x_i)$ is the rank of the random variables and T is the sum of rank of the random variables;

5) Rejection region: because of two-tailed test, when H_0 is satisfied, one-tailed p-value<0.025;

6) Inference: the paper using Statistical Assistant System (SAS) to process the data, the result showed that P-value>0.05. This p-value suggested that from material that is collected there is no reason to reject the null hypnosis and accept H_0: the hourly crash distributions in Heilongjiang from 2006 to 2007 are almost the same.

***C*. Nonparametric Analysis of monthly Distribution of Traffic Crash**

Table 2 is the statistical monthly distribution of crashes in Heilongjiang in China from 2006 to 2007. From estimation, it seems that the monthly crash distributions are trend to rise. In order to infer the trend, Cox-Stuart test was used and processes are the same as followed. Firstly, pair the random variables as (x_1, x_{1+c}), (x_2, x_{2+c}), (x_3, x_{3+c}),…, $(x_{n'}, x_{n'+c})$, Where $c = (n'+1)/2$, n' is the number of reordered variables; If $x_i < x_{i+c}$, then use "+" stand for the paired random variable; If $x_i > x_{i+c}$, then use "-" stand for the paired random variable. It is reasonablely to use the Cox-Stuart test, because date is from different independent samples (from 2006 to 2007), small samples (only 12 months), and ordered scale of measurement. At last, the result showed that T=8, P-value>0.05 (n=12, p=1/2, T=8). This result suggested that there is no reason to reject the null hypnosis from material collected and it had to accept H_0: the monthly crash distributions will trend to rise in 2008.

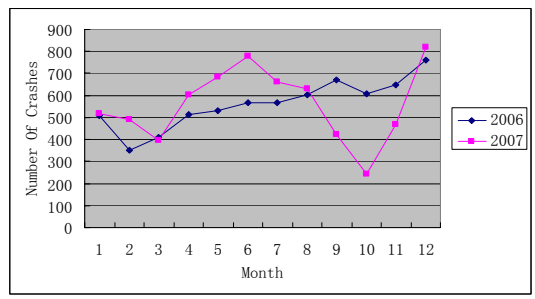

Figure 2 Curve of number of crash in Heilongjiang, China (2006-2007)

Table 2 Monthly distributions of crashes in Heilongjiang, China (2006-2007)

Month / Year	1	2	3	4	5	6	7	8	9	10	11	12
2006	508	351	408	514	532	567	566	603	669	609	647	760
2007	519	489	397	601	683	777	660	629	425	245	470	821

***C*. Nonparametric Analysis of yearly Distribution of Traffic Crash**

Figure 3 is a histogram of alcohol-related crash fatalities from 2003 to 2007 of 52 states in the U.S.A. From the Figure 2, it is suitable to use nonparametric methods. The yearly alcohol-related crash fatalities from 2003 to 2004 of 52 states in the U.S.A are different. In order to demonstrate the hypnosis, Mann-Whitney test were used and processes are as followed.

1) Null hypnosis--H_0: the yearly alcohol-related crash fatalities from 2003 to 2004 of 52 states in the U.S.A remain almost same or had the decreasing trend. Alternative hypnosis –H_1: the yearly alcohol-related crash fatalities from 2003 to 2004 of 52 states in the U.S.A had a rising trend;

2) Method: it is used by the Mann-Whitney bilateral test, because date is from different independent samples (52 states in the U.S.A), small samples (only 52 states compared with themselves), and ordered scale of measurement.

3) Significance level: $\alpha < 0.05$;

4) Statistical value: $T = \sum_{i=1}^{52} R(x_i)$, where $R(x_i)$ is the rank of the random variables, T is the sum of rank of the random variables.

5) Rejection region: because of one-tailed test, when H_0 is satisfied, one-tailed p-value<0.05.

6) Inference: the result shows that T=-11.76 (P-value <0.05), this result indicates that the yearly alcohol-related crash fatalities from 2003 to 2004 of 52 states in the U.S.A has a rising trend.

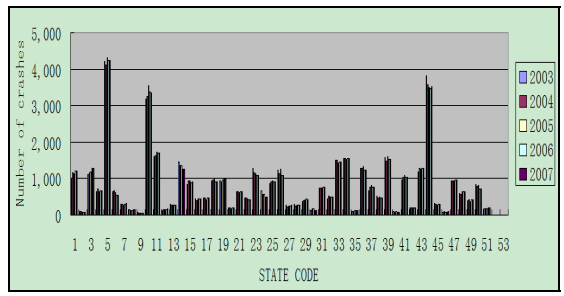

Figure 3 Histogram of alcohol-related crash fatalities of 52 states in the U.S.A

In fact, Department of Transportation Administration in America had realized the trend and made great effort to reduce the number of crashes in whole country in 2005. The result of statistic crashes is declining compared with past two years (2003 and 2004). In addition, universities and training agents provided some programs to make the youths and drivers realize the great hazard of driving after drinking alcohol. Finally, in order to predict the trend of crashes in 2008, the paper used result of crashes statistical 2006 and 2007. Mann-Whitney test were used and processes are the result showed that T=-0.1031, (P-value>0.05). That meant that management of crashes in the U.S.A is successful and the trend of crashes would be declining.

CONCLUSIONS

This paper reviews parametric test and nonparametric method and models. In some situation, nonparametric statistical is suitable because they are more freely. Three nonparametric models, such as Mann-Whitney test, Cox-Stuart test and so on, are used in timely distribution of crashes. Secondly, the paper uses Mann-Whitney

test for the yearly alcohol-related crash fatalities from 2003 to 2004 of 52 states in the U.S.A, a result shows that this result indicated that the yearly alcohol-related crash fatalities from 2003 to 2004 of 52 states in the U.S.A had a rising trend. In fact, Department of Transportation in America had realized the trend and made great effort to reduce the number of crashes in whole country since 2005. The result of statistic crashes was declining compared with past two years (2003 and 2004). In addition, universities and training agents provided some programs to make the youths and drivers realize the great hazard of driving after drinking alcohol. Finally, the paper predicts the trend of crashes in 2008 through analysis of the yearly alcohol-related crash fatalities from 2006 to 2007 of 52 states in the U.S.A. Result meant that management crashes in the U.S.A in 2008 would be declining. Although nonparametric analysis is very useful, there are still some drawbacks and restrains for its prevailingly use in crashed analysis. In addition, it is significantly robust, but it would lose some power of test.

REFERENCES

A Brief Statistical Summary. (2008). Published by the Mathematical Analysis Division Department of Transportation. *http: //www-nrd.nhtsa.dot.gov/cats/listpublications*

Brian L. Smith, Billy M.Willianms, R. Keith Oswals. (2002). Comparison parametric and Nonparametric Traffic Volume Forecasting, *Transportation Research Part C*. Emerging Technologies, 10(4): 303-321.

Dominique Lorda, Peter Young, Jin Park. (2008). Investigating the effects of fixed and varyin g dispersion parameters of Poisson-gamma models on empirical Bayes estimates. *Accident Analysis and Prevention*, 40, 1441-1457.

Huang yan, Wu ping. (2005) Application of SAS. *Machinery Press.*

Marc Graudry, Sylvain Lassarre. (2000). *Sructural Road Accident Models.*, PERMON, 225~235

Pei yulong, Wang wei.(2007). Cause and prevention for traffic crashes. *Science Press*

Richard A. Retting, Helen B., Weinsteinb, Mark G. Solomon. (2003) Analysis of motor-vehicle crashes at stop signs in four U.S. cities. *Journal of Safety Research,* 34, 485–489.

Shen feimin, Zhang ronggui (2006). Cause and prevention for traffic crashes,*Transpo -rtation Press*.

S. Siegel. (1986) Nonparametric Statistic.*Science Press*

Wen Cheng, Simon P. (2005) Washington. Experimental evaluation of hotspot identi fication methods. *Accident Analysis and Prevention* 37, 870–881.

W. J Conover.(2006). Practical nonparametric statistic. *Post and Telecom Press*

Evaluation of Fire Risk at Highway Tunnels

HUANG Jing[1], REN Shao Yun[1], ZHANG Wei[2]

[1]Department of Fire Command, The Armed Police Academy, Lang fang，Hebei Province 065000, P.R. China. Phone: +86-316-2068566; Email: hjlinda@126.com
[2]School of Chemistry and Materials, Lang fang Normal University, Lang fang，Hebei Province 065000, P.R. China. Phone: +86-316-2069711; Email: zhangwei_friends@163.com

ABSTRACT

The purpose of this study is to prevent and reduce fire at highway tunnels. This paper systematically analyzes the influence factors for the safety system of highway tunnels, establishes a risk assessment model for tunnel fire based on analytic hierarchy process and multi-grade fuzzy evaluation, and introduces a risk factors assessment system for tunnel fire in details. Using this model, the risk of a specific highway tunnel fire has been assessed. The research results show that this evaluation method is in accordance with the actual situation. Therefore the model is recommended to put into practical applications.

1 PREFACE

With the rapid development of Chinese economy and improvement of people's daily lives, all sorts of highway tunnels have been built and China has become a country which owns the world's top highway tunnels both in scales and in distance. Consequently the numbers and frequencies of tunnel fire accidents appear to rise yearly, resulting in huge losses of life and property. In order to prevent and reduce the occurrence of fire, risk analysis and evaluation are essential to identify the potential hazards and take corresponding measures to improve the safety levels of these traffic tunnels. Due to the diversities of the hazards which may lead to a fire and the ambiguous interactions among them, Analytical Hierarchy Process(AHP) and Fuzzy Comprehensive Evaluation Method are introduced for comprehensive risk evaluation on the highway tunnel fire, to facilitate a quantitative description of the impacts of these factors on tunnel safety.

2 SETUP OF RISK ASSESSMENT SYSTEM OF TUNNEL FIRE

2.1Establishment of assessment index system

Tunnel fires are usually caused by a number of factors that interact each other. The four main influence factors are: (1) Vehicle. To a large extent a tunnel fire is caused by this factor, therefore checking dangerous vehicles and limiting them into the tunnels is essential to prevent fires. (2) Fire safety management system. The safety responsibility system, the fire evacuation plan and the periodic inspection are the best ways to reduce fire hazards. (3) Fire protection facilities. Completed fire

detection and alarm system, appropriate fireproof structures and emergency ventilation system are very helpful to prevent fire escalating in its early stage. (4) Tunnel structure. Tunnel wall and internal combustion properties have important influence on flame control. Each primary factor above consists of several secondary indices for assessment as shown in table 1.

Table 1. Risk assessment index system for highway tunnel fire.

	Primary Indices	Secondary Indices
Highway tunnel fire risk assessment index system U	Vehicle （U_1）	Fire caused by vehicle crash（U_{11}）
		Flammable loads on fire（U_{12}）
		Vehicle electrical equipment on fire（U_{13}）
		Vehicle braking equipment on fire（U_{14}）
	Fire safety management system （U_2）	Fire safety responsibility system（U_{21}）
		Fire safety awareness （U_{22}）
		Fire safety training（U_{23}）
		Fire evacuation plan（U_{24}）
	Fire protection facilities （U_3）	Automatic fire detection and alarm system （U_{31}）
		Sprinkler systems（U_{32}）
		Hydrant system（U_{33}）
		Smoke control systems（U_{34}）
		Lighting Systems（U_{35}）
	Tunnel structure （U4）	Tunnel construction（U_{41}）
		Tunnel fire safety evacuation facilities （U_{42}）
		Tunnel wall decoration（U_{43}）
		Tunnel Design（U_{44}）

2.2 Weight determination of each assessment index

AHP is applied for weight determination, which compares the indices in pairs on a scale of 1 to 9 to set judgment matrix and calculate its maximum eigenvalue and eigenvector, and then obtain relative weights of the indices in a certain level related to their corresponding indices in upper level, to form a set of weighted aggregative index numbers. The detailed calculation procedure is shown below:

2.2.1 Setting judgment matrix A.Calculation of geometric mean of each row in the judgement matrix

$$\overline{\omega}_i = \sqrt[n]{\prod_{j=1}^{n} a_{ij}} \qquad i=1,2,3,\ldots,n \qquad (1)$$

2.2.2 Normalized $\overline{\omega}_i$

$$\omega_i = \frac{\overline{\omega_i}}{\sum_{j=1}^{n} \omega_j} \qquad i,j=1,2,3,\ldots,n \qquad (2)$$

$\omega=[\omega_1, \omega_2, \ldots, \omega_n]^T$ which is the eigenvector.

2.2.3 Calculation of the maximum eigenvalue

$$\lambda_{max} = \sum_{i=1}^{n} \frac{(A\omega)_i}{n\omega_i} \qquad (3)$$

2.2.4 Consistency check

Consistency test is based on：

$$CR = \frac{CI}{RI} \qquad (4)$$

which，$CI = \frac{\lambda_{max} - n}{n-1}$，RI is the average random consistency index. When CR<0.1, the matrix has satisfactory consistency. The results shown in table 2~6

Table 2. Matrix A and weight of index

A	*B*	*C*	*D*	*E*	*Weight*	**Consistency check**
B	1	2	2	3	0.429	λ_{max} =4.115
C	1/2	1	1	2/3	0.214	CI=0.046
D	1/2	1	1	2/3	0.214	CR=0.058<0.1
E	1/3	3/2	3/2	1	0.143	Meet Requirements

Table 3. Matrix B and weight of index

B	B_1	B_2	B_3	B_4	*Weight*	**Consistency check**
B_1	1	3	2	5	0.473	λ_{max} =4.172
B_2	1/3	1	2	4	0.258	CI=0.057
B_3	1/2	1/2	1	4	0.202	CR=0.063<0.1
B_4	1/5	1/4	1/4	1	0.067	Meet Requirements

Table 4. Matrix C and weight of index

C	C_1	C_2	C_3	C_4	*Weight*	**Consistency check**
C_1	1	4	1	3	0.403	λ_{max} =4.117
C_2	1/4	1	1/2	1/2	0.109	CI=0.039
C_3	1	2	1	3	0.339	CR=0.043<0.1
C_4	1/3	2	1/2	1	0.149	Meet Requirements

Table 5. Matrix D and weight of index

D	D_1	D_2	D_3	D_4	D_5	*Weight*	**Consistency check**
D_1	1	2	2	1	3	0.300	λ_{max} =5.117 CI=0.039 CR=0.043<0.1 Meet Requirements
D_2	1/2	1	1	1/2	3/2	0.150	
D_3	1/2	1	1	1/2	3/2	0.150	
D_4	1	2	2	1	3	0.300	
D_5	1/3	3/2	3/2	1/3	1	0.100	

Table 6 Matrix E and weight of index

E	E_1	E_2	E_3	E_4	*Weight*	**Consistency check**
E_1	1	1/2	1	2	0.222	λ_{max} =4.172
E_2	2	1	2	4	0.111	CI=0.057
E_3	1	2	1	1/2	0.222	CR=0.063<0.1
E_4	1/2	4	2	1	0.444	Meet Requirements

3 FUZZY COMPREHENSIVE EVALUATIONS

3. 1Establishment of the comment set of evaluation indicator

As per the scientific standard of the Ministry of Public Security （2001BA803B02－09），fire hazards are categorized into five levels for severity evaluation. In this paper the hazardous indices leading to tunnel fire are also categorized into five levels to form a comment set *V*. And *V* = { light risk V_1, low risk V_2 , ordinary risk V_3 , high risk V_4 , severe risk V_5 }。For a centesimal grading system, V_1 = 95, V_2 = 85, V_3 = 70, V_4= 50, V_5 = 30.

3. 2Single factor fuzzy evaluation

Single factor fuzzy evaluation evaluates all kinds of factors within evaluation indicators. The function of membership grade is established based on the requirement of evaluation indicators and evaluation standard, then the membership grade of evaluation schemes are given for evaluation indices. Finally, the membership grade matrix is obtained by combination of each single factor. The single factor fuzzy evaluation of tunnel fire risk is determined by expert panel, in another word, membership grade matrix R_i of all factors in U_i.

$$R_i = \begin{bmatrix} r_{i11} & r_{i12} & r_{i13} & r_{i14} & r_{i15} \\ \vdots & \vdots & \vdots & \vdots & \vdots \\ r_{ij1} & r_{ij2} & r_{ij3} & r_{ij4} & r_{ij5} \end{bmatrix} \qquad (5)$$

3. 3Multi-grade fuzzy comprehensive evaluation

Many factors that may induce tunnel fire are ambiguous, and these factors can be divided into many layers. A single-grade comprehensive evaluation often results in relatively small numerical values in the fuzzy evaluation matrix due to too many factors being involved. In this situation, it is hard to sort various factors in a preferential order and unlikely to obtain a meaningful evaluation result. However, multi-grade fuzzy comprehensive evaluation with stepwise approaches is able to highlight the main factors without eliminating other factor, therefore its evaluation results can reflect the overall features of the objects being assessed.

$$B = A \cdot R \qquad (6)$$

A---Weight sets of evaluation indicator; "·"--- Fuzzy operator;

R---Matrix of membership degree.

3.4 Example

3.4.1 Establishment of evaluation matrix

Taking a highway tunnel for an example, an evaluation matrix R_i of membership degrees is setup based on every evaluation indicator graded by 10 experts according to the level of evaluation indicator. The grades of the primary index 'fire safety management (U2)' are shown in Table 7.

Table 7

Evaluation indicator	Weight	Level of evaluation indicator				
		V_1	V_2	V_3	V_4	V_5
U_{21}	0.473	4	3	2	1	0
U_{22}	0.258	3	2	3	1	1
U_{23}	0.202	2	3	2	2	1
U_{24}	0.067	2	3	3	2	0

And the evaluation matrix of fire safety management is

$$R_2=\begin{bmatrix}0.4 & 0.3 & 0.2 & 0.1 & 0.0\\ 0.3 & 0.2 & 0.3 & 0.1 & 0.1\\ 0.2 & 0.3 & 0.2 & 0.2 & 0.1\\ 0.2 & 0.3 & 0.3 & 0.2 & 0.0\end{bmatrix}$$

Similarly：$$R_1=\begin{bmatrix}0.3 & 0.3 & 0.2 & 0.2 & 0.0\\ 0.2 & 0.3 & 0.1 & 0.3 & 0.1\\ 0.3 & 0.2 & 0.2 & 0.2 & 0.2\\ 0.2 & 0.2 & 0.3 & 0.2 & 0.1\end{bmatrix}$$

$$R_3=\begin{bmatrix}0.3 & 0.3 & 0.2 & 0.1 & 0.1\\ 0.4 & 0.2 & 0.2 & 0.2 & 0.0\\ 0.3 & 0.3 & 0.3 & 0.1 & 0.0\\ 0.2 & 0.3 & 0.2 & 0.2 & 0.1\\ 0.2 & 0.2 & 0.3 & 0.1 & 0.1\end{bmatrix}$$

$$R_4=\begin{bmatrix}0.3 & 0.3 & 0.2 & 0.2 & 0.0\\ 0.3 & 0.2 & 0.3 & 0.1 & 0.1\\ 0.2 & 0.3 & 0.2 & 0.2 & 0.1\\ 0.2 & 0.2 & 0.3 & 0.2 & 0.1\end{bmatrix}$$

3.4.2 **Multi-grade fuzzy comprehensive evaluation**

For many risk evaluation objects of highway tunnel fire, ordinary addition and multiplication model is chosen for calculation to obtain reasonable evaluation results. One-grade fuzzy evaluation is shown as following.

$B_2=A_2 \cdot R_2=$（0.292，0.289，0.226，0.149，0.045）

Similarly：

$B_1=A_1 \cdot R_1=$（0.247，0.273，0.181，0.226，0.073）

$B_3=A_3 \cdot R_3=$（0.275，0.275，0.225，0.145，0.080）

$B_4=A_4 \cdot R_4=$（0.233，0.244，0.255，0.189，0.079）

By considering the evaluation matrix B_i of each primary indicator U_i as its one-grade evaluation result, the risk evaluation matrix B of tunnel fire is obtained through two-grade fuzzy comprehensive evaluation of $R=(B_1, B_2, B_3, B_4, B_5)^T$, as shown below:

$$R=\begin{bmatrix}R_1\\ R_2\\ R_3\\ R_4\end{bmatrix}=\begin{bmatrix}0.247 & 0.273 & 0.181 & 0.226 & 0.073\\ 0.292 & 0.289 & 0.226 & 0.149 & 0.045\\ 0.275 & 0.275 & 0.225 & 0.145 & 0.080\\ 0.233 & 0.244 & 0.255 & 0.189 & 0.079\end{bmatrix}$$

Two-grade fuzzy comprehensive evaluation is listed as following:

$$B=A\cdot R=(0.429, 0.214, 0.214, 0.143)\begin{bmatrix}0.247 & 0.273 & 0.181 & 0.226 & 0.073\\ 0.292 & 0.289 & 0.226 & 0.149 & 0.045\\ 0.275 & 0.275 & 0.225 & 0.145 & 0.080\\ 0.233 & 0.244 & 0.255 & 0.189 & 0.079\end{bmatrix}$$

=（0.261，0.273，0.211，0.187，0.069）

3.4.3 Evaluation of fire hazard level

The risk evaluation score for highway tunnel fire is calculated based on the linear weighted average model, and the fire hazard level is determined thereafter as a recommendation reference for appropriate safety measures .

$$F = \sum_{i=1}^{5} b_i \times e_i = 95\times0.261+85\times0.273+70\times0.211+50\times0.187+30\times0.069=74.19$$

The fire hazard of the highway tunnel falls in the category of 'ordinary risk'. In this situation, fire can be triggered by any problem in certain links, and the corresponding safety measures shall be taken to eliminate fire hazards.

4 CONCLUSIONS

Fire hazards can be revealed and fire can be consequently reduced via nonscheduled fire safety evaluation of highway tunnels. By using analytic hierarchy process and fuzzy comprehensive evaluation, fire hazards of highway tunnel can be comprehensively assessed from all aspects of their influence factors, which is helpful for the relevant department to take certain safety measures to reduce the risk of fire.

BIBLIOGRAPHY

Pei X J(2000). "Estimation method and the application on experts' grade." *J. Harbin Railway Science & Technology*., (1):32-35.

Wang Z X(2003). "Basic research of road tunnel safty" *J. Underground Engineering and Tunnels.*,(1):2~5.

Xin J,Xia D Y(2006). "Fuzzy Synthetic Evaluation for Fire Risk of University Campus Dormitory."*J. Journal of The Chinese People's Armed Police Force Academ.*，*22(5)23*-25.

Yang R X, Chen X F(2002). "Traits of long road tunnel fire and its fire prevention design basic reseach"*J. Profl Fire Prevention Science and Technology.* ,(5):50-52.

Yang L B, Gao Y Y(2002). "Fuzzy Math Principle and Its Application." *J. Huanan Science and Technology University Press,* Guang Zhou.

Zeng X P , Qiu J, Li J N(2007) "Study on Expressway Tunnel Safety Evaluation Method."*J. Technology of Highway and Transport*，Oct(5):85-87

Wang Y(2005)，. "Study on the Safety Evaluation on System and Method of Urban Traffic Tunnel " *Master. Safety Technology and Engineering.*

Chen J X, Luo Y B, Jiang J C(2006) "The safety assessment of a road tunnel."*J. Modern Tunnelling Technology.*, 43(4)68-71.

The Analysis of Rural Road Safety and Its Strategies

Sun Feng

College of Transport and Vehicle Engineering; Shandong University of Technology; Zibo 255049; China; Email: sunfeng0904@sina.com

ABSTRACT

This paper presents the main features of traffic accidents on rural roads by detailed statistical analysis of traffic accidents, modes of vehicles, time, driver behaviors and other related factors about traffic accidents occurred on Huantai County rural roads from 2005 to 2007. The root causes of accidents were obtained by applying traffic engineering principles to the current situation of rural road construction and transport development. This paper proposed strategies to reduce deaths and injuries resulting from traffic accidents on rural roads from the aspects of traffic management system, safety education, safe facilities, vehicle management, etc., which will be applied to the field of traffic safety management on rural roads.

INTRODUCTION

With the rapid development of China's rural economy, the demand for transport of both passengers and cargoes has been on the increase. It is also true for the rural road mileage and its traffic flow. However, traffic accidents on rural roads have been increased year by year. So how to take effective measures to improve China's rural road safety has become an urgent issue in the field of traffic safety. At present, researchers mainly concentrate on studying the safety of freeways, highways and urban roads. But few studies on the safety of rural roads have been made. Since rural roads greatly differ from them in road conditions, transport components, characteristics of transport participants' travel, it is significant to propose effective strategies to reduce deaths and injuries resulting from traffic accidents through analyzing the characteristics of rural road accidents and deeply studying the problems about traffic safety existing on rural roads. This paper has put forward several countermeasures based on the deep study of the problems about rural road traffic safety by taking Huantai County rural roads in Zibo as an example.

CURRENT SITUATION OF TRAFFIC DEVELOPMENT

Rural roads mileage. With the rapid development of industry and agriculture in Huantai County, the demand in transportation is growing, the construction of county and township roads is being accelerated, and the traffic mileage is also growing rapidly. Based on statistics of 2008, the total mileages of county roads and township roads in Huantai County are 139.388km and 190.756km respectively. According to the 11th Five-Year Plan of the Rural Roads in Huantai County (2005), Huantai County will rebuild five county roads covering 36.6km, seven township roads which are 58.4 km long and three tourism roads with the length of 25.5km, and build 14-kilometre-long new township road by 2010.

Motor vehicles and drivers. In recent years, the number of motor vehicles and drivers is increasing steadily. The details are clearly set out in Table1. Table1 shows that the growth rate of motorcycles has slowed down, however, the possession of

motorcycles still account for the largest quantity. There are 62658 motorcycles, which constitute 73.6% of all motor vehicles possession. Meanwhile, the number of people who own private cars is on the rise with the fantastic development in economy in rural areas in China. In 2007, the increased number of cars accounted for 40.7% of all the new vehicles. With the rapid increase of private cars, the growth of drivers appears to be accordingly accelerating.

Table 1. Quantity of New Motor Vehicles and Drivers .

Year	Trailer	Oversize vehicle	Car	Motorcycles	Quantity of drivers	Growth rate
2003	58	196	1912	6472	52192	——
2004	71	308	1877	6107	53075	1.69%
2005	55	135	2149	5619	54117	1.96%
2006	122	191	2638	4239	55009	1.65%
2007	188	310	3082	3940	58127	5.67%

Passenger and cargo transportation . From Table2, it can be seen that in recent years, transportation volume of both passenger and cargo in Huantai County is increasing rapidly, especially in 2007, its transportation volume of passenger increased by 143% compared with 2006. The transportation volume of cargo in 2007 was up 342% over the previous year (HCSY, 2002~2007).

Table 2. Transportation Volume of Passenger and Cargo in Huantai County .

Year	Transportation volume of passenger (million passenger)	Passenger miles (million passenger-kilometer)	Transportation volume of cargo (million ton)	Rotation volume of freight transport (million ton-kilometer)
2002	476.0	17703	309.0	26083
2003	438.0	17151	343.0	30815
2004	433.0	16750	387.0	35643
2005	378.0	17010	358.0	36398
2006	842.0	35057	426.0	46600
2007	1534	85279	2487	206159

Analysis of current situation . Through the above statistics, it can be seen that Huantai county road mileage, number of motor vehicles and drivers, and transportation volume of both passenger and cargo are in a period of rapid growth. But, it is worthwhile to note that in the light of the experience of foreign countries, it is also a period of sharp increase in traffic accidents (Mao Li-zeng and Duan Li-ren, 2007).

STATISTICS AND ANALYSIS OF TRAFFIC ACCIDENTS

Overview on rural road traffic accidents . This paper analyses the 609 traffic accidents occurring on the rural roads in Huantai County, Zibo City between 2005 and 2007. Figure1 presents that there is an increasing tendency for the traffic

accidents which happened on rural roads in Huantai County between 2005 and 2007.

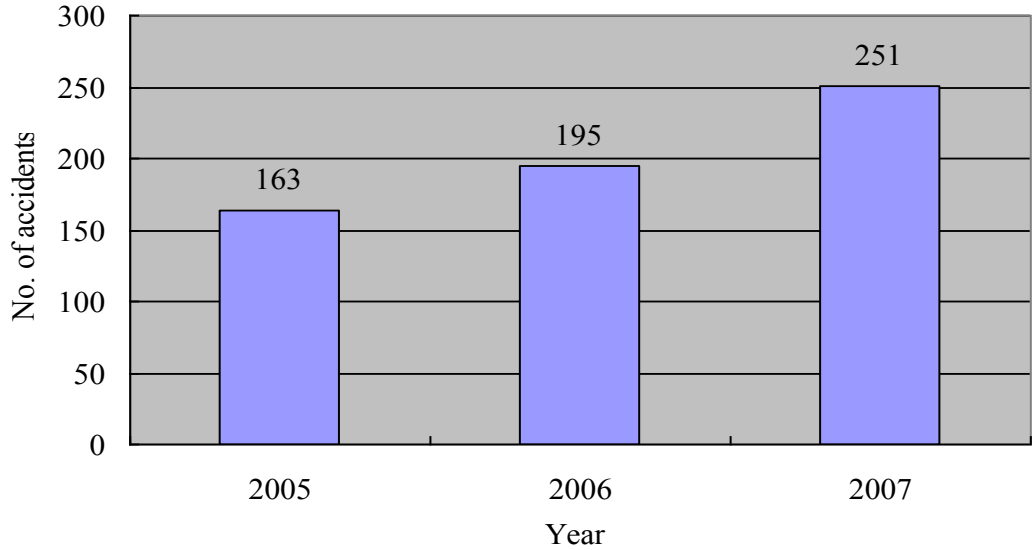

Figure1 . The Traffic Accidents Happened on the Rural Roads in Huantai County (2005~2007).

Time distribution of traffic accidents and number of deaths. From Figure2, we can see that a high number of traffic accidents on rural roads mainly happen between 15:00 and 22:00, and the most of the accidents involved death happen at night, where 18:00~21:00 is the critical point and the deaths during this period account for 31.1% of all deaths. This means that it is prone for the accidents to happen at night, which not only brings about high accident risk but also involves serious injury or loss of life. Sleepiness is now recognized as being a significant accident causation factor at night. Research has shown sleep-related crashes tend to occur at night and to be more severe due to higher impact speeds. They tend to involve drivers who are at work or driving company cars (Maycock, 1996, 1997) and younger male drivers (under-30) are particularly at risk (Reyner et al, 2001).

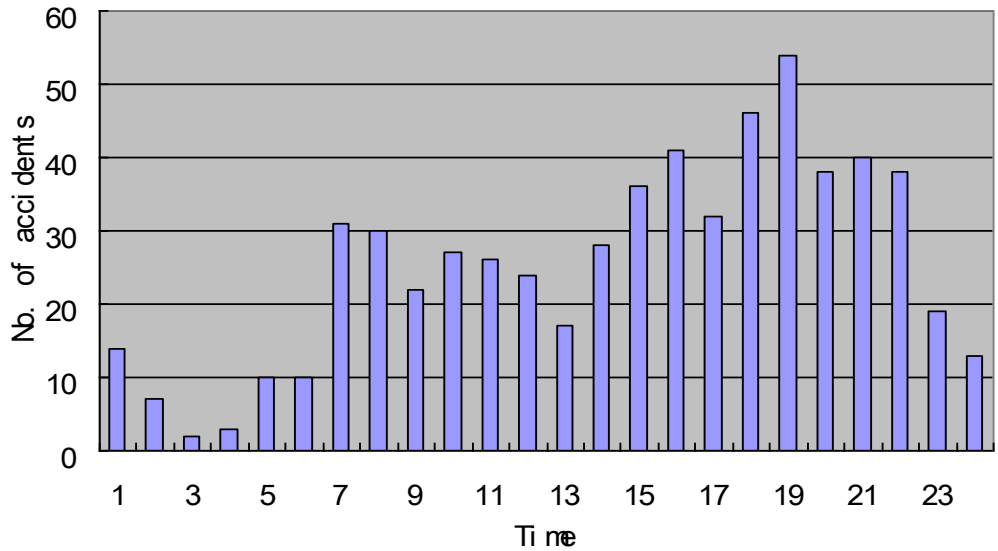

Figure 2. Time Distribution of Traffic Accidents on Rural Roads

Distribution of types of vehicles involved in traffic accidents. Table 3 shows

the proportion of vehicles involved in road accidents. It can be seen that the proportion of two-wheeled motor vehicles involved in accidents is considerably the largest, which accounts for 31.48% of rural accidents. It is mainly the inadequacy of buses that results in the high level of motorcycle ownership in the rural townships, accounting for 73.6% of all motor vehicle ownership. Through the analysis of motorcycles that contributed to accidents, we concluded that the motorcyclists who drive without a license account for 43.07% of accidents, the illicit motorcycles account for 15.66% and driving under the influence of alcohol account for 15.66%, which is attributable to the motorcyclists' poor safety awareness and the backward management system for motorcycles. The second most common vehicle involved in traffic accidents is the car, which is reported in 21.64% of rural accidents.

Table 3. List of Vehicle Types Involved Traffic Accidents on Rural Roads.

Vehicle type	No. of traffic accidents	Percentage
Two-wheeled motor vehicle	288	31.48%
Car	198	21.64%
Truck	130	14.21%
Pick-up	65	7.10%
Three-wheeled motor vehicle	61	6.67%
Medium-size truck	57	6.23%
Farm vehicle	53	5.79%
Tractor	31	3.39%
Medium-size car	23	2.51%
Large bus	9	0.98%

Distribution of types of drivers' violation involved in traffic accidents. Through qualitative surveying over traffic accidents happened on rural roads in Huantai County between 2005 and 2007, we concluded that the proportion of driving without a license, the illicit motorcycles, failing to look properly and driving under the influence of alcohol is the higher, taking 23.84%、14.08%、13.64% and 9.76% respectively in terms of the relative importance of all the drivers' violation contributed to rural accidents.

ANALYSIS OF PROBLEMS ABOUT TRAFFIC SAFETY

Based on the above qualitative survey, along with current situation of Huantai County transportation, the paper points out various road safety problems existing on rural areas of Huantai County, which is also prevalent in rural areas in China.

Rural communities' low awareness of traffic safety. Rural communities' traffic safety awareness is relatively low, for instance, it's not uncommon for peasants not to watch out for cars when crossing the road and not to dodge the other vehicles when going around the curves in the road. It is quite common for the motorcyclists to violate traffic regulations, mainly include driving without a license, not wearing protective helmets, speeding, driving under the influence of alcohol, and so on.

Relatively backward public transportati on. In rural areas, the development of public transportation is relatively backward, which makes the rural communities

inconvenient to travel out, so more and more families purchase agricultural vehicles, electric bicycles, motorcycles to meet the demand of production and livelihood. However, the poor management of vehicles in rural areas indicates that there exist potential safety hazards.

Imperfect traffic safety infrastructure . While rural roads are gradually increasing, the traffic safety infrastructure is not perfect, such as traffic signs are not sufficient, road traffic markings are not conspicuous and improvement and maintenance of roads is not in time which causes damage to rural roads. In addition, the inadequate street lights especially in the areas through rural village, result in the high incidence of accidents late in the afternoon.

Weak supervision on rural roads. The rural road has the characteristics of multipoints and large size, but at present its supervision is very weak. So far it is administered only by traffic department. As rural traffic becomes complicated, traffic police's supervision on the rural roads will be constrained by the shortage of police.

Backward in management system of motor vehicle and driver. As the number of private cars increases , the number of novice drivers is rising quickly. However, the novice drivers are a vulnerable road user group and prone to traffic accidents because of their inexperienced driving skills and lack of driving experience. By surveying the traffic accidents between 2005 and 2007 in Huantai County, it is found that the accidents caused by the drivers with driving experience under 3 years are about 35.1% of all the traffic accidents.

COUNTERMEASURES TO IMPROVE RURAL ROAD SAFETY

Based on the above problems concerning the rural road safety, this article puts forward the most effective countermeasures to improve the rural road safety.

Clarify responsibility and strengthen rural road safety. According to the Highway Law and Law on Road Traffic Safety, the township (town) people's government is in charge of the construction and maintenance of rural highway, and the road traffic safety management department takes in charge of rural highway traffic safety. They have to perform administrative duties, attach great importance to road traffic safety management and add the rural road traffic safety management to the agenda under the unitary leadership of the county government.

Publicize traffic safety of rural road and create a good atmosphere . All the township (town) people's governments with relative departments should initiate education campaign about Law of The People's Republic of China on Road Traffic Safety, and widely publicize the related knowledge about traffic safety. The theme of traffic safety publicity is "safety comes first while traveling" and its purpose is to popularize knowledge about traffic safety and educate people by taking serious accidents as an example to improve rural communities' road safety and law-abiding awareness.

Accelerate the development of bus. Accelerating bus developments of urban and rural integration can make bus extend to rural areas, provide facilities for rural communities to travel out and reduce their cost of travel out, which can restrict the increase of motorcycles at essence and gradually reduce the proportion of traveling out by motorcycles.

Develop and perfect transport facilities. Accelerate the development of traffic safety facilities on rural highways to guarantee orderliness and safety the traffic.

While a highway is under new construction, renovation or expansion, traffic safety facilities should be designed, constructed and tested at the same time. Further more, it is necessary to improve lamp lighting facilities on the rural roads, especially in the areas through rural village and town.

Increase the number of traffic police and guarantee expenditure. Ensure the normal operation of traffic management through enriching traffic police, and all the township people's governments should guarantee expenditure of traffic police, improve infrastructures including vehicles and telecommunications and provide high technology equipments to relieve traffic police's pressure from work and effectively solve the problem of insufficient traffic police.

Strengthen administration of agriculture vehicles and motorcycles. The traffic administrative department and agricultural machinery department shall join efforts and closely cooperate with each other while acting in accordance with the division of their functions and duties, to strengthen the administration of agriculture vehicles. It is essential to organize rural police stations to participate in specialized administration of motorcycles.

Step up evaluation and administration of drivers. It is helpful to introduce traffic safety information system about vehicle drivers to record drivers' traffic violations, their traffic scores for breaking rules and regulations, traffic accident conditions. The records about drivers' traffic safety can offer the reference for employers to recruit drivers and insurance company to handle the insurance business. In addition, it is also essential to strengthen the evaluation and administration of driver training school, standardize the teaching process, and ensure the novice drivers to possess the quality of safety driving.

CONCLUSION

In this paper, by detailed statistics of rural road traffic accidents occurred in Huantai County from 2005 to 2007, combing the current situation of rural road construction and transport, the root causes of the accidents are concluded. Based on the above analysis, this paper proposed strategies to reduce deaths and injuries resulting from traffic accidents on rural roads from the aspects of traffic management system, safety facilities, transport development, etc., which will be applied to the field of traffic safety management on rural road.

REFERENCES

Huantai County Statistic Yearbook (HCSY). (2002~2007). Huantai Statistics Department, Zibo, China.

Mao Li-zeng, Duan Li-ren. (2007). "International Comparison Analysis on Road Traffic Safety Factors". Journal of Transportation Systems Engineering and Information Technology. 7 (3), 111~117.

Maycock G (1996). "Sleepiness and driving: The experience of UK car drivers". Journal of Sleep Research, 5, 229-237.

Maycock G (1997). "Sleepiness and driving: The experience of heavy goods vehicle drivers in the UK". Journal of Sleep Research, 6, 238-244.

Pennoni, C.R. (1992). "Visioning: The future of civil engineering." J. Profl. Issues in Engrg. Educ. And Pract., ASCE, 118 (3), 221-233.

The 11th Five-Year Plan of the Rural Roads in Huantai County. (2005). Huantai Road Transport Department, Zibo, China.

A Traffic Accident Reconstruction Study on Continuous Collision of Three Cars

YU Qiang[1],WEI Lang[2] and CHEN Tao[3]

[1]School of Automobile, Chang'an University, Xi'an, 710064, China; PH (86) 029-82334315; FAX (86) 029-82334476; email: qiangyu@chd.edu.cn
[2]School of Automobile, Chang'an University, Xi'an, 710064, China; PH (86) 029-82334471; FAX (86) 029-82334476; email: qch_1@chd.edu.cn
[3]School of Automobile, Chang'an University, Xi'an, 710064, China; PH (86) 029-82334475; FAX (86) 029-82334476; email: chentao@chd.edu.cn

ABSTRACT

This paper analyzes the characteristics of three cars continuous collision accidents by dividing them into different processes. The relation model between vehicles during the impact process is established, and the physical models of each vehicle before and after the impact based on principles of kinematics are established. In this way, according to the stop location, stop states of the vehicles as well as the marks left on the road, the whole movement process of three-car continuous collision and any transient movement state of each car are computed and reconstructed by using reverse analytical calculation method.

1. INTRODUCTION

A great deal of research work of issues recurrence for simulated traffic accident at home and abroad has been done and brought some results so far. The more representative one was the car on car collision accident simulation recurrence research in 1995 by Xi'an Highway University and Japan Automobile Research Institute (WEI, 2000a). Later, they also did the further research for the two cars in a collision after collision occurring in the second issue, established the analytical calculation model, and validated the correctness of the model through examples (WEI, 2000b,WEI, 2000c).But the analysis, calculation, as well as recurrence technology for many vehicles involved in collisions in a row are still in a blank state. This type of traffic accidents takes a large proportion of total. As a result, this thesis does research on three consecutive car collision pattern and reproduction technology in the traffic accident.

In the continuous collision of three cars, the movement states of vehicles are different, and the analytical methods used in the process of analysis and solution also vary. Therefore, this article studies the accident patterns of the car A and B collision, and then car B and C collision, and car B didn't not lose the stability after the first collision.

2. THE MODEL ESTABLISHMENT

Collision process in accordance with the above-mentioned characteristics of its movement can be divided into five phases. The dynamic models involved in the five stages include: vehicle lateral dynamics model; vehicle vertical dynamic model; tire dynamic model and vehicle dynamic model of the collision process. These

models don't take roll-over accident into consideration. Next the models mentioned above will be separately established.

2.1 Vehicle longitudinal and lateral dynamics model

Simplified vehicle longitudinal and lateral dynamics model in the process of movement is shown in Figure 1. XOY in the map is the coordinate system fixed on the ground, $\xi o\gamma$ is the coordinate system fixed on the vehicle's centroid, and ξ is the driving direction. Thus obtained:

$$\delta_m m\dot{V}_{o\xi} = F_{HL\xi} + F_{HR\xi} + F_{FL\xi}\cos\delta + F_{FR\xi}\cos\delta - F_{FL\upsilon}\sin\delta - F_{FR\upsilon}\sin\delta - F_R - F_L \quad (1)$$

$$m\dot{V}_{o\gamma} = F_{HL\gamma} + F_{HR\gamma} + F_{FL\upsilon}\cos\delta + F_{FR\upsilon}\cos\delta + F_{FL\zeta}\sin\delta + F_{FR\zeta}\sin\delta \quad (2)$$

$$\begin{aligned} m\rho_0^{\,2}\dot{\omega} = {} & (F_{FR\upsilon} + F_{FL\upsilon})\cos\delta L_V - (F_{HR\gamma} + F_{HL\gamma})L_H + (F_{HR\gamma} - F_{HL\gamma})\frac{S_H}{2} \\ & + (F_{FR\zeta} + F_{FL\zeta})\cos\delta\frac{S_F}{2} + (F_{FR\upsilon} - F_{FL\upsilon})\sin\delta\frac{S_F}{2} + (F_{FR\zeta} + F_{FL\zeta})\sin\delta L_V \end{aligned} \quad (3)$$

The meaning of symbol above formulas is in Figure 1.

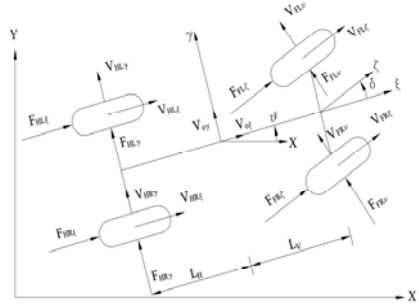

Figure 1.Vehicle dynamics model (longitudinal and lateral).

2.2 Vehicle vertical dynamics model

Simplified vehicle vertical dynamics model in the process of movement is shown in Figure 2. The resultant vertical vehicle dynamic model equation is:

$$\begin{aligned} m\ddot{z}_2 = {} & -C_{2FR}(z_{2FR} - z_{1FR}) - D_{2FR}(\dot{z}_{2FR} - \dot{z}_{1FR}) - C_{2FL}(z_{2FL} - z_{1FL}) - D_{2FL}(\dot{z}_{2FL} - \dot{z}_{1FL}) \\ & - C_{2HR}(z_{2HR} - z_{1HR}) - D_{2HR}(\dot{z}_{2HR} - \dot{z}_{1HR}) - C_{2HL}(z_{2HL} - z_{1HL}) - D_{2HL}(\dot{z}_{2HL} - \dot{z}_{1HL}) \end{aligned} \quad (4)$$

$$m_{1FR}\ddot{z}_{1FR} = C_{2FR}(z_{2FR} - z_{1FR}) + D_{2FR}(\dot{z}_{2FR} - \dot{z}_{1FR}) - C_{1FR}(z_{1FR} - z_{0FR}) \quad (5)$$

$$m_{1FL}\ddot{z}_{1FL} = C_{2FL}(z_{2FL} - z_{1FL}) + D_{2FL}(\dot{z}_{2FL} - \dot{z}_{1FL}) - C_{1FL}(z_{1FL} - z_{0FL}) \quad (6)$$

$$m_{1HR}\ddot{z}_{1HR} = C_{2HR}(z_{2HR} - z_{1HR}) + D_{2HR}(\dot{z}_{2HR} - \dot{z}_{1HR}) - C_{1HR}(z_{1HR} - z_{0HR}) \quad (7)$$

$$m_{1HL}\ddot{z}_{1HL} = C_{2HL}(z_{2HL} - z_{1HL}) + D_{2HL}(\dot{z}_{2HL} - \dot{z}_{1HL}) - C_{1HL}(z_{1HL} - z_{0HL}) \quad (8)$$

$$\begin{aligned} J_Y\ddot{\psi} = {} & C_{2FR}(z_{2FR} - z_{1FR})L_F + D_{2FR}(\dot{z}_{2FR} - \dot{z}_{1FR})L_F + C_{2FL}(z_{2FL} - z_{1FL})L_F \\ & + D_{2FL}(\dot{z}_{2FL} - \dot{z}_{1FL})L_F - C_{2HR}(z_{2HR} - z_{1HR})L_H - D_{2HR}(\dot{z}_{2HR} - \dot{z}_{1HR})L_H \\ & - C_{2HL}(z_{2HL} - z_{1HL})L_H - D_{2HL}(\dot{z}_{2HL} - \dot{z}_{1HL})L_H + ma_x h_g \end{aligned} \quad (9)$$

$$\begin{aligned} J_X\ddot{\varphi} = {} & C_{2FR}(z_{2FR} - z_{1FR})\frac{S_F}{2} + D_{2FR}(\dot{z}_{2FR} - \dot{z}_{1FR})\frac{S_F}{2} - C_{2FL}(z_{2FL} - z_{1FL})\frac{S_F}{2} \\ & - D_{2FL}(\dot{z}_{2FL} - \dot{z}_{1FL})\frac{S_F}{2} + C_{2HR}(z_{2HR} - z_{1HR})\frac{S_H}{2} + D_{2HR}(\dot{z}_{2HR} - \dot{z}_{1HR})\frac{S_H}{2} \\ & - C_{2HL}(z_{2HL} - z_{1HL})\frac{S_H}{2} - D_{2HL}(\dot{z}_{2HL} - \dot{z}_{1HL})\frac{S_H}{2} - G_a a_y h_g \end{aligned} \quad (10)$$

The meaning of symbol above formulas is in Figure 2.

2.3 Tire dynamics model

The analytic analysis of vehicle lateral dynamics model is related to wheel

lateral force. The wheel lateral force is not only related to the wheel-side angle, but also is related to the tire characteristics and vertical loads on the wheels. In order to take into account the analytical precision of analysis and to calculate the workload of the two factors, in this option of analysis by using the Fiala tire model. The mathematical expression of the model:

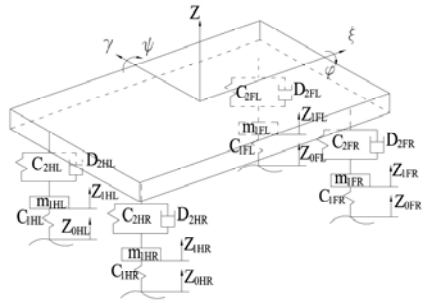

Figure 2.Vehicle dynamics model (vertical).

$$C_y = k_y W L_R^{\,2} / 2 \tag{11}$$

$$\phi = C_y \tan\alpha / F_Z \tag{12}$$

$$\phi_0 = \phi - \phi^2/3 + \phi^3/2 \tag{13}$$

$$F_Y = \phi_0 \mu F_Z \tag{14}$$

Where k_y -Fetal crown lateral rigidity of imprinted Tire Rubber unit surface area; L_R -Imprinted Tire length; W -Imprinted Tire width; α -Tire declination; μ -Ground attachment coefficient; F_Z -Vertical wheel load.

2.4 Dynamics model in the collision process

Instantaneous states of the collision of two vehicles are shown in Figure 3. Two vehicles in the collision process are in line with the law of conservation of momentum, so two vehicles dynamics model in the collision process are obtained(that is, the model whit the relationship between speed and angular velocity of two cars before and after collision) ,which are as follows:

$$m_A(V_{g\eta A} - V_{q\eta A}) + m_B(V_{g\eta B} - V_{q\eta B}) = 0 \tag{15}$$

$$m_A(V_{g\tau A} - V_{q\tau A}) + m_B(V_{g\tau B} - V_{q\tau B}) = 0 \tag{16}$$

$$m_A\rho_A^{\,2}(\omega_{gA} - \omega_{qA}) + \tau_A m_A(V_{g\eta A} - V_{q\eta A}) - \eta_A m_A(V_{g\tau A} - V_{q\tau A}) = 0 \tag{17}$$

$$m_B\rho_B^{\,2}(\omega_{gB} - \omega_{qB}) + \tau_B m_B(V_{g\eta B} - V_{q\eta B}) - \eta_B m_B(V_{g\tau B} - V_{q\tau B}) = 0 \tag{18}$$

The meaning of symbol above formulas is in Figure 3.

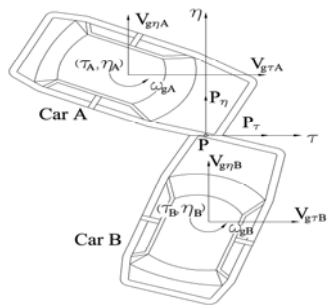

Figure 3.Vehicle impact dynamics model.

3. ANALYSIS OF MOVEMENT PROCESS

As in the accident analysis, the movements of the vehicles are based on the location of the vehicle stopped, and the stop state of vehicles on roads, marks left by the vehicles, as well as marks left in the collision process on the vehicle and on the roads, using reverse analytical method of calculation to obtain. Therefore, modeling and analysis process with the reverse resolution process consistent.

3.1 Simulation phase V

After the collision of car B and C, it is confirmed that two vehicles in the collision instant location from the ground traces and traces of vehicle collisions in the collision. When the collision after the end, car B and C is in a state of freedom of movement and, ultimately, is stopped. Taken use of vehicle lateral dynamics model, vehicle Vertical dynamics model, As well as relations between the two coupling, and taking the tire dynamic model into account, According to car B, car C parking location and state; the ground marks of movement process and the location of instantaneous parameters of vehicle collision, it is confirmed that the car B's and car C's centroid velocity and angular velocity of rotation in the end of collision through the reverse analysis method.

In the calculation process, this paper chooses the coordinate of the car B stopped location as the initial point of iterative calculation. At this time as a vehicle in a static state, by setting the corresponding initial parameters, this paper chooses the coordinate of the car B stopped location as the termination point of iterative calculation. Carry out iterative calculation by using vertical dynamics equation and horizontal dynamics equation. At the end of iterative process, calculated car B's speed and the rotation angular velocity at the beginning of this movement, It is also the car B's speed and the rotation angular velocity at the ending the moment of collision $V_{g\eta B}$, $V_{g\tau B}$ and ω_{gB}.

Taking use of the completely similar process, car B's speed and the rotation angular velocity at the ending the moment of collision $V_{g\eta C}$, $V_{g\tau C}$ and ω_{gC} are calculated.

3.2 Simulation phase IV

The collision process of car B and C by using the collision dynamics model above is calculated. As mentioned earlier, this paper only discusses the case of car B does not lose stability after the first collision in a three car collision course. Therefore, car B was in a controllable state before the second collision, when the rotating angular velocity of car B was $\omega_{qB} = 0$. Similarly, car C was also in a controllable state before the second collision, when the rotating angular velocity of car C was $\omega_{qC} = 0$.From substituting these conditions as well as the previous step calculate of car B's and car C's speed and angular velocity $V_{g\eta B}$, $V_{g\tau B}$, ω_{gB}, $V_{g\eta C}$, $V_{g\tau C}$ and ω_{gC} in the moments after the collision into the collision dynamics model, the velocity $V_{q\eta B}$, $V_{q\tau B}$, $V_{q\eta C}$, $V_{q\tau C}$ of car B and C before the collision can be calculated.

3.3 Simulation phase IIV

This phase includes three parts, which are: the movement of car A after the

first collision to stop state; the movement of car B before the second collision and the normal movement of car C before the collision. Separately calculate here.

3.3.1 Simulation of car C's movement before the collision

Car C was completely controllable before the collision. According to the situation of the ground traces, it is estimated whether the driver has taken braking measures before the collision, by which the values of simulation variables are determined. When braking measures absence: $F_{FL\zeta} = F_{FR\zeta} = F_{HR\xi} = F_{HL\xi} = 0$; when there is braking measures: $F_{FL\zeta} = \mu F_{FLZ}$, $F_{FR\zeta} = \mu F_{FRZ}$, $F_{HL\xi} = \mu F_{HLZ}$, $F_{HR\xi} = \mu F_{HRZ}$;the car C's instantaneous velocities before collision which are calculated by the previous step, $V_{q\eta C}$, $V_{q\tau C}$, are chosen as the initial value in the iterative calculation $V_{q\eta C0}$, $V_{q\tau C0}$. The collision location coordinates are chosen as the initial point of the iterative calculation, choose a key point coordinates on the vehicle trajectory by road signs as the end point of the iterative calculation, iterative calculate by lateral dynamics equation and vertical dynamics equation, finally get car C's instantaneous movement state value before the collision.

3.3.2 Simulation of car B's movement before the second collision

As already mentioned above, this paper discusses car B at the controllable state from the first collision to the second collision. According to the situation of the ground traces, whether the driver had taken braking measures between the two collisions of car B is estimated, by which the values of variables of this simulation process are determined. The car B's instantaneous velocities before the second collision which calculated by the Previous step, $V_{q\eta B}$, $V_{q\tau B}$, are chosen as the initial value in the iterative calculation $V_{q\eta B0}$, $V_{q\tau B0}$. This thesis chooses the second collision location coordinates as the initial point, choose the first collision location coordinates as the end point of the iterative calculation, iterative calculate by lateral dynamics equation and vertical dynamics equation, finally get car B's each instantaneous movement state value from the first collision to the second collision and the instantaneous movement state value after the first collision.

3.3.3 Simulation of car A's movement after the first collision

After the first collision of car A, two vehicles' instantaneous locations are determined from the ground traces and traces of vehicle s' collisions in the collision. Car A was in a freedom movement state after the collision, And, ultimately, is stopped. Car A's parking location and status are taken as the initial iteration point, take the ground marks of the movement process and the instantaneous location parameters of the vehicle collision into account, iterative calculate by lateral dynamics equation and vertical dynamics equation, finally get car A's instantaneous centroid velocity and angular velocity of rotation after the first collision.

3.4 Simulation phase

The collision process of car A and B is calculated by using the collision dynamics model above. As car A and B are in controllable states before the first collision, the rotation angular velocity of car A and car B are zero at this time, that is $\omega_{qA} = 0, \omega_{qB} = 0$. Substituting these conditions, as well as instantaneous speed and angular velocity of car A and car B $V_{g\eta A}$, $V_{g\tau A}$, ω_{gA} and $V_{g\eta B}$, $V_{g\tau B}$, ω_{gB} ,which are

calculated by the previous step into the collision dynamics model, the speed of car A and B before the collision $V_{q\eta A}$, $V_{q\tau A}$, $V_{q\eta B}$, $V_{q\tau B}$ can be calculated.

3.5 Simulation phase

Car A and C are in the controllable states before the collision. According to the situation of the ground traces, it is estimated whether the driver has taken braking measures before the collision, by which the values of simulation variables are determined. This article chooses the car A's and car B's instantaneous velocities before collision which are calculated by the previous step at the same time $V_{q\eta A}$, $V_{q\tau A}$, $V_{q\eta B}$, $V_{q\tau B}$ as the initial value in the iterative calculation $V_{q\eta A0}$, $V_{q\tau A0}$, $V_{q\eta B0}$, $V_{q\tau B0}$. This paper chooses collision location coordinates as the initial point of the iterative calculation, chooses a key point coordinates on the vehicle trajectory by road signs as the end point of the iterative calculation, iteratively calculates by lateral dynamics equation and vertical dynamics equation, and finally get car A's and car B's instantaneous movement state value before the collision.

4. CONCLUSION

This paper chooses one form to research on recurrence technology on the basis of the analysis in the three car collision process. First of all, the whole process is divided into five stages by its movement characteristics. Then, it establishes dynamics equations of each stage, and gives the boundary conditions for analysis and calculation of each stage. Finally, by taking use of reverse analytical method for calculation, it acquires the ideas of cars' movement states in the whole collision process and calculation process of three vehicles involved collisions, and provides a theoretical foundation of recurrence technology study in three car collision accident.

5. ACKNOWLEDGEMENT

The project is supported by national science and technology supporting program of China (No. 2007BAK35B01).

REFERENCES

WEI L.(2000a). "Establishment of error bounds for the main effect factor in car to car collision model." *China Journal of Highway and Transport,* 13(1), 109-113.

WEI L., Chen Y., and Hirotoshi I.(2000b). "A study on simulation model for car to car crash and their second impact in traffic accidents." *Automotive Engineering,* 22(1), 38-41,61.

WEI L., Chen Y., and Hirotoshi I.(2000c). "An experiment research on the car to car collision." *Automotive Engineering,* 22(4), 256-261.

Study on the Preventive Maintenance Time for Asphalt Pavement

Ying Ronghua, Wu Ting, Wang Lijuan and Hou Zhaoguang
(School of Traffic and Transportation Engineering, Changsha University of Science & Technology)

Abstract: Through the MTS of mid-point trabecular bending fatigue test about asphalt mixture, a fatigue life equation is obtained, and the relationship between the fracture length and N/N_f is analyzed. Based on this, we determine the fatigue life of asphalt pavement under standard axle load combined with the actual road conditions and fatigue failure is predicted quantitatively. Aimed to the law of fatigue damage of the asphalt pavement performance, the asphalt pavement preventive maintenance time has been studied, and we suggest a method to determine the best preventive maintenance time in the asphalt pavement based on the fracture length.

Key words: Preventive Maintenance; MTS of Trabecular Bending Test; Fatigue Life; Fracture Length; Maintenance Time

1 Introduction

In recent years, how to prevent and delay the emergence of diseases in high-grade highway has been paid great attention by our highway worker. However, we usually carry out the maintenance and repair after the roads are broken, it is easier to identify and determine the timing of maintenance and repair, but the preventive maintenance is that taking measures when the roads is still in good condition, which makes pavement preventive maintenance face a difficult issue, that is, the timing of the preventive maintenance? (Yu, 1993)

Before carrying out the preventive maintenance, the trend of the pavement damage must be made clear; because the asphalt pavement structure is always under the circulating effect of traffic and temperature loads, and its destruction is mainly fatigue failure. In this paper, the timing of preventive maintenance in asphalt pavements is put forward based on fatigue failure.

2 Fatigue test of asphalt mixture with large stone (LSAM)

Gradation is determined as follows through the optimization:

Table2.1 Mineral aggregate gradation

Gradation	31.5	26.5	19.0	16.0	13.2	9.5	4.75	2.36	1.18	0.6	0.3	0.15	0.075
	90	76	55	48	41	31	26	14.5	10.5	7	5	3.5	1.5

Use the Marshall method to determine that the optimum asphalt content of dense framework structure of LSAM is 4.1%.

In this paper, during the fatigue study, apply the material testing machine of MTS for the LSAM, and use the repeated bending load fatigue test of mid-point loading with the sample size of 50.0mm × 63.5mm × 381mm.

According to the results of bending fatigue test, and the corrected fatigue equations of asphalt mixture are:

$$N_f = 3612434(\frac{1}{\sigma})^{1.8237} \quad (5\text{Hz}) \tag{2.1}$$

$$N_f = 1220113(\frac{1}{\sigma})^{2.056} \quad (10\text{Hz}) \tag{2.2}$$

$$N_f = 420318(\frac{1}{\sigma})^{2.1036} \quad (50\text{Hz}) \tag{2.3}$$

Through observing the cracks, correlation formulas of crack length with N / N_f are obtained, and the correlation coefficients are more than 0.98.

3 The service life prediction of asphalt pavements based on fatigue test

3.1 Asphalt pavement structure

In order to estimate the fatigue life of asphalt pavement, it is necessary to analyze the structure of asphalt pavement to obtain internal stress distribution of asphalt pavement under loading. Taking into account the actual situation and the analysis convenience, this paper selects a typical asphalt pavement structure to analyze:

Upper layer	AC-13	1600 Mpa	μ=0.25
Lower layer	AC-20	1400 Mpa	μ=0.25
LSAM		μ=0.25	
Semi-rigid Base	lime-fly ash concrete	850Mpa	μ=0.35
Soil Base		40Mpa	μ=0.35

3.2 Prediction of fatigue life of asphalt pavements

Through fatigue life equation (2.3), carrying out the standard axle load conversion using standard load of BZZ-100, tire pressure of 0.707MPa, load radius of 10.65cm, distance of double round of 31.95cm, and static modulus used in the structure design system in our country.

In this study, calculate the layer bottom tension stress of base course in the above pavement structure by BISAR procedure under the standard axle load. The results are as follows:

In the pavement structure, tensile stress of large stone asphalt stabilized macadam base of 12cm is 0.13946Mpa, which is substituted in the fatigue life equation (2.3) to attain the action times of approximately 6.9×10^7 in the entire fatigue life.

If the daily average action times of standard axle load N_1 = 18000 times / d in such a typical flexible base asphalt pavement structure with an average annual growth rate of 6%, 6 lanes and lane coefficient of 0.4, the service life is 18 years in accordance with the formula $N_e = \frac{N_1[(1+\gamma)^t - 1]\times 365}{\gamma}\eta$

.

3.3 The prediction based on fatigue failure

By observing the cracks in fatigue test, we can see that crack length is related to N / N_f, in accordance with the formula with maximum correlation coefficient to quantitatively predict the fatigue failure of asphalt pavement, and the formula is as follows (Zheng, Zhou, Zhang, 2003):

$$y = 56.461x^{5.9221}$$
$$R^2 = 0.987 \tag{3.1}$$

When $N / N_f = 0.5$, and the service life is 18 years in the above typical structure under the standard loading, the crack length is about 0.93mm by using the formula (3.1), in other words, at

the ninth year of pavement usage, we can see that the cracks appear according to the test, and the crack length of each year can be predicted by the formula (3.1).

4 Determination of the timing of the preventive maintenance based on fatigue failure

In this paper, because fatigue failure is one of the main damage types of asphalt pavement, we quantitatively determine the indicator of maintenance timing. Because fatigue crack length and speed change with the age of road changing, until the cracks have reached a certain level, the road enters into the severely failure state, in accordance with laboratory test integrated with decay condition of practice pavement to determine that the indicator of maintenance timing for fatigue failure is the crack length, then apply the method of cost-effectiveness ratio to determine the maintenance timing of the road condition after preventive maintenance.

In this paper, the example in the former chapter is used to determine the timing of preventive maintenance.

(1) The preventive maintenance scheme

Because this paper is to study the maintenance timing selection, so select slurry seal as the only maintenance measure.

(2)Road condition indicator

By the formula (3.1) we can obtain the length of fatigue cracks in different road condition, so select the crack length as the road condition indicator. In order to simulate the failure condition of the practical pavement, according to the entire pavement service life of 18 years, converse the relationship between N / N_f and fatigue cracks to the crack length of each year that is:

$$Y=2*10^{-7}*e^{1.3645x} \tag{4.1}$$

Making the maintenance timing in accordance with the road condition attenuation law: at the 5th, 6th, 7th and 8th year, the pavement crack length of practical pavement is respectively 0.00796mm, 0.02812mm, 0.08175mm and 0.20602 mm.

(3) The lowest acceptable level

The lowest acceptable level of performance index (Dong, Sun and Peng, 2005) when taking preventive maintenance measures is the maximum or minimum limits of the Y-axis of performance index when calculating the effect area, to the performance index curve which decreases with the age of road growing, lowest acceptable level of the performance index is the lower limit, the area over the lower limit of performance indicators will not be counted as part of the effect when calculating the effect area. According to the test results, we can see that when the crack length is 20mm, the failure rapidly increases, so we can determine the crack length of lowest acceptable level is 20mm. The figure is as follows:

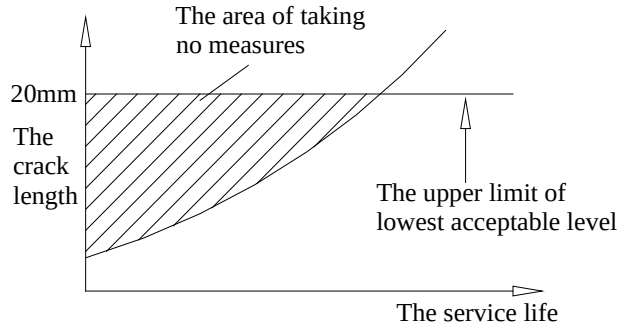

Figure4.1 The lowest acceptable level

(4) The decay condition of pavement cracks after preventive maintenance

According to the changes of the decay curves of pavement condition after preventive maintenance provided in the reference (Ren, 2006), the decay curves after micro surfacing are as follows through similarity analysis in this article:

Table4.1 Performance curve equations after taking preventive maintenance measures

The age of road when taking preventive maintenance measures	The decay curve equations of crack length
5	$y=2*10^{-7}e^{1.6818x}$
6	$y=2*10^{-7}e^{1.3154x}$
7	$y=2*10^{-7}e^{1.3933x}$
8	$y=2*10^{-7}e^{1.6039x}$

(5) The age to the lowest acceptable level

Table4.2 The age of road achieving to the lowest acceptable level when taking maintenance measures at different timing

The decay curves	The x value to the lowest acceptable level	The age of road to the lowest acceptable level
$y=2*10^{-7}e^{1.3645x}$	13.5	13.5
$y=2*10^{-7}e^{1.6818x}$	11.00	16.00
$y=2*10^{-7}e^{1.3154x}$	14.00	20.00
$y=2*10^{-7}e^{1.3933x}$	13.22	20.22
$y=2*10^{-7}e^{1.6039x}$	11.48	19.48

(6) The calculation of the effectiveness index

$$DRR = S_1 - S_0 = \frac{(P_B - P_D)}{q} - \frac{(P_B - P_A)}{p}$$

By $PJ = PB - PC$ and we can obtain the performance jump and reduction of deterioration rate as follows:

Table4.3The parameters of effectiveness model

Maintenance year	P_A	P_B	P_C	P_D	p	q	PJ	DRR
5th	0	0.00796	0.0000002	19.410845	5	11	0.0079598	1.762307
6th	0	0.02812	0.0000002	19.470981	6	14	0.0281198	1.384089

7th	0	0.08175	0.0000002	19.922058	7	13.22	0.0817498	1.489101
8th	0	0.20602	0.0000002	19.989926	8	11.48	0.2060198	1.697584

From the results of calculating the effectiveness index we can see that: at the 8th year the performance jump is the best, at the 5th year the effect of reduction of deterioration rate is the best.

(7)Maintenance effect

1) Calculating the effect area when maintenance measures are not taken

When preventive maintenance measures are not taken, the integral area of the performance curve which has reverse tendency is as follows:

$$AREA_{+} = \int_{x_0}^{x_1}(UBC - EQ_{DN}) = \int_{0}^{13.5}(20 - 2\times10^{-7}\, e^{1.3645x})dx = 253.697$$

2) The calculation of the effect area after maintenance measures are taken

As can be seen from Table 4.2, in the first scheme the road reaches the lowest acceptable level of preventive maintenance measures at the service life of 16 (computed from the 5th year)years (which is the first year to achieve minimum acceptable), so we use 16 years as the analysis period. Calculate the effect area in accordance with maintenance measures as follows:

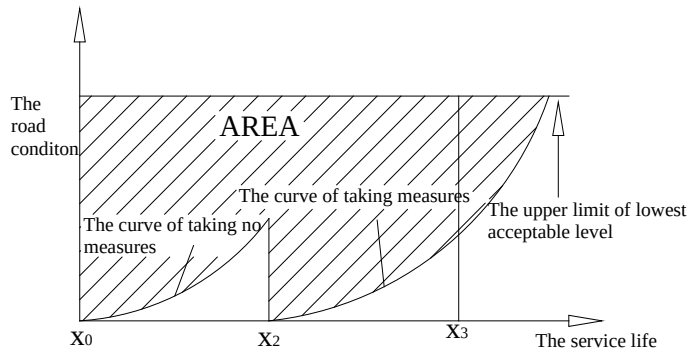

Figure4.2 Determination of the area of performance index

$$AREA_{PT(+)} = \int_{x_0}^{x_1}(UBC - EQ_{DN}) + \int_{0}^{(x_2 - x_1)}(UBC - EQ_{PT}) \qquad (4.2)$$

Table4.4 The calculation of the effect area after maintenance measures are taken

The age of road when taking preventive maintenance measures（year）	5	6	7	8
Effect area	319.397	319.978	319.934	319.814

3) The calculation of effect

There are four maintenance schemes in which taking the maintenance measure of micro-surfacing at the age of 5, 6, 7and 8 years, the effect area of each scheme is calculated in terms of Figure 4.2.

Calculating the effect according to the following formula:

$$BE = (AREA_{BE})/(ARER_{DN-TOT})\times100\% \qquad (4.3)$$

Table4.5 Results of effect calculating after taking the preventive maintenance measures

The age of road when taking preventive maintenance measures（year）	5	6	7	8

Effect（%）	26.897	26.126	26.109	26.062

(8) Maintenance cost

1) Costs of preventive maintenance measure

Because we are to make the cost analysis of the maintenance item in this highway, and the initial construction costs are the same, we can assume that the initial construction costs are zero, only the costs of preventive conservation measures are different. Based on local experiences and quota calculation, thickness of micro-surfacing of domestic modified asphalt is 1cm with its costs of 296,750 million yuan / km.

2) Pavement residual value

Calculate the pavement residual value at the end of the analysis period according to the ratio of residual life to its service life.

$$SV = (1 - \frac{L_A}{L_E})C_r \tag{4.4}$$

For the first scheme, its service life is 11 years computed in accordance with its performance index decay equation of road condition and the lowest acceptable level, at the end of the analysis period it has been used for 10 years. According to the calculation model set up by the above formula the pavement residual value of the first scheme is:

SV= (1-10/11)*29.675=2.6977million yuan

For the second scheme, its service life is 14 years, and at the end of the analysis period it has been used for 9 years, thus its residual value is as follows:

SV= (1-9/14)*29.675=10.5982million yuan

For the third scheme, its service life is 13.22 years, and at the end of the analysis period it has been used for 8 years, thus its residual value is as follows:

SV= (1-8/13.22)*29.675=11.7174million yuan

For the forth scheme, its service life is 11.48 years, and at the end of the analysis period it has been used for 7 years, thus its residual value is as follows:

SV= (1-7/11.48)*29.675=11.5805million yuan

3) Calculating cost present value

Costs can be calculated by the present value, cost present value of PC is computed as follows:

$$\text{PC} = \sum_{t=1}^{n} (CO)_t \ (\text{P/F,i,t}) \tag{4.5}$$

In the four schemes of this article, the expenditure at different times during the analysis period is conserved to the present value according to the discount coefficient (let the first year as the datum year), and the discount rate is7%.

The calculation results are shown in Table 4.6.

Table4.6 Calculation Table of cost present value

Time of taking preventive conservation	Preventive maintenance costs (million yuan/km)	Residual value (million yuan/km)	Total cost (million yuan/km)
5	21.1579	0.7874	20.3705

6	19.7737	3.0935	16.6802
7	18.4801	3.4202	15.0599
8	17.2711	3.3802	13.8909

Note: The total cost = Preventive maintenance costs - Residual value

(9) Determination of the best maintenance timing

According to the increment method, the calculating results of cost-effectiveness ratio are in Table 4.7.

Table4.7 Cost-effectiveness ratio

Time of taking preventive conservation	Effect（%）	Total cost (million yuan/km)	Cost-effectiveness ratio （%）
5	25.897	20.3705	0.01271
6	26.126	16.6802	0.0157
7	26.109	15.0599	0.01734
8	26.062	13.8909	0.01876

From Table 4.7, we can see that when taking the measure of micro-surfacing at the pavement life of 8 years, the cost-effectiveness ratio of preventive maintenance measure is the biggest, just look at the effect, at the 6th year is the best, just look at the total cost, at the 8th year is least; at the 5th year the effect is the least and the costs is the most, so it is excluded. Then optimize plan according to the increment method optimization program: comparing the latter two options, costs are increased by 11,690 yuan / km but the effect is only increased by 0.047%; then comparing the schemes of the 8th year and the 6th year, the costs are increased by 27,111yuan/km but the effect is only increased by 0.064%, so it is considered that the increase of the effect is less, finally the best maintenance timing is to take the maintenance measure at the 8th year.

5 Conclusion

In this paper, we obtain the law of fatigue damage by interior trabecular fatigue test to determine that the maintenance timing indictor of the fatigue failure is the crack length, then using the method of cost- effectiveness ratio to calculate the best timing of preventive maintenance. However, there still exist some problems and deficiencies, requiring further study.

References:

Dong Ruikun, Sun Lijun, Peng Yong (2004). Discussion on the Method of Determining the Timing of Preventive Maintenance of Asphalt Pavement [J]. China Safety Science Journal, Vol.3, No.14,2004, pp.31-35.

Dong Ruikun, Sun Lijun, Peng Yong(2005). Indexes for Timing of Asphalt Pavement Preventive Maintenance (PPM) Based on Pavement Functional Performance [J]. Chinese Journal of Underground Space and Engineering, Vol.2, No.1, 2005, pp.292-295.

Ren Yong (2006). Study on the Preventive Maintenance Time for Asphalt Pavement Based on Life Cycle Cost [D]. Master Degree thesis of the road and railway engineering department in Chang'an University, 2006, pp.60.

Zheng Jianlong, Zhou Zhigang, Zhang Qisen (2003). The Anti-crack Design Theory and Method of the Asphalt Pavement. Beijing: China Communications Press, 2003, pp.13-17.

Wavy Road Elevation Measurement Based on the Principle of Inertia

Han Y. [1]and H. Wang[2]

[1]State Key Laboratory of Automotive Safety and Energy, Tsinghua University, Beijing 100084, China;
School of Automobile, Chang'an University, Xi'an 710064, China; PH 13228055890; Email: hanhany@gmail.com
[2]School of Electronic & Control Engineering, Chang'an University, Xi'an 710064, China; PH 13759964041; Email: huanhwang@163.com

ABSTRACT

Precision Level is widely used to measure road elevation. The measuring process needs several cooperating people to complete. The measuring error is not easily to be controlled due to the artificial influence. A wavy road elevation measurement method is proposed in this paper based on the principle of inertia. This equipment mainly consists of a gyro, a three-axis accelerometer and a photoelectric encoder. When moving on the road at a high speed, it can real-timely measure the running speed and the pitch angle of the car, from which the road elevation can be obtained by data processing. The advantage of this method is simple, high speed and easy to achieve, it can be applied to measure the wavy road elevation.

KEYWORDS: road elevation; inertia; gyro; three-axis accelerometer

INTRODUCTION

Elevation refers to the distance along the plumb line direction from a point to the absolute base, which is always called the absolute elevation and short for elevation (RUMMEL R et al. 1998). Elevation is one of the elements which determine the location of terrestrial points. At present, the most commonly used methods to measure the elevation are the leveling (YANG Jun-zhi et al. 2008) and trigonometric leveling (YE Jian-hua**,** 2006). The leveling can calculate the elevation by using the equipment providing the level of sight (such as LEVEL) to measure the height difference between two terrestrial points; whereas trigonometric leveling obtains the height difference through the observation of the zenith distance (or elevation angle) and the horizontal distance between two points. Compared with the leveling, the trigonometric leveling is easy to observe, free from restrictions on terrain conditions, and is the basic method to obtain elevation. However, in geodesy, effects of the earth bending and atmospheric vertical refraction must be considered since the length of side is long.

To improve the accuracy of elevation measurements and reduce the difficulty, a simple and reliable wavy road elevation measurement method is proposed based on the principle of inertia.

WORKING PRINCIPLE OF SYSTEM

The main parts of this equipment are a gyro, a three-axis accelerometer and a photoelectric encoder. When moving on the road at a high speed, it can real-timely measure the running speed and the pitch angle of the car, from which the road elevation can be obtained by data processing.

Gyro

Gyroscope (GUO Su-yun, 2006) is a device to sense and maintain the direction, which is designed based on the theory that angular momentum is undiminished. The gyros have two characters: one is inertia or rigidity, and the other is precession that the detection system only uses. The precession of the gyros produces inertia when the gyroscope rotor rotates at a high speed. It helps rotation axis of the gyroscope rotor maintain a fixed direction in space and prevent and antagonize any forces which may change the direction of rotor at the same time.

Install one gyroscope in the inspection car and make sure that the rotation axis of the gyroscope rotor is consistent with the forward direction of the car. When the gyro is energized, the output voltage is proportional to the changing rate of the angular velocity. Based on this principle, when the inspection car is running on the road, gyroscope can real-timely measure the angle (θ) between the forward direction of the car and the horizontal direction according to changes of its own rotating angular velocity. As shown in Figure 1.

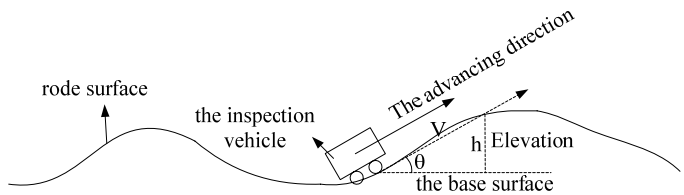

Figure 1. Working Principle of System

Three-axis Accelerometer

When the inspection car is stationary or running with no changes in the direction, the gyroscope rotor is stationary or uniformly running and the output value of the gyro is zero. This, however, prevents the device from measuring the pitch angle of the car, for which we have introduced three-axis acceleration (MENG Wei-guo, 2007)

to make up for this deficiency. Name the three axis of the three-axis accelerometer: A-axis, B-axis and C-axis. When installing, make sure that one of the three axis of the acceleration is consistent with the forward direction of the car (say A-axis). When the inspection car is stationary or running with no changes in the direction, the components of the gravitational acceleration at A axis, B axis and C axis will be measured by the three-axis acceleration, so that the angle between the direction of the gravitational acceleration and A-axis (that is, the forward direction of the car) will be obtained, from which the initial pitch angle (θ_0) of the car can be gained. As shown in Figure 2.

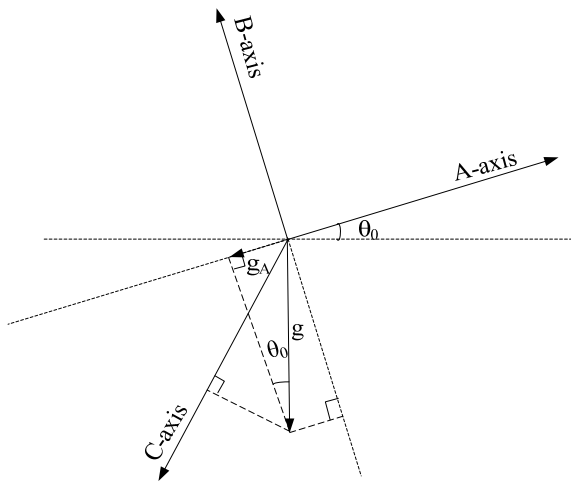

Figure 2. Principle of three-axis accelerometer

Photoelectric Encoder

With real-time pitch angle of the car, the elevation of the pavement can be measured as long as the real-time speed of the car is known. To that end, the speed of car will be obtained by the photoelectric encoder. Photoelectric encoder is a device used to measure the speed and it is classified as single-output encoder and dual output encoder (Yang Wen-yuan. 1994). A single-output encoder is used in the system, and the single-output means that the encoder output is a set of pulses. The photoelectric encoder is installed at an appropriate location of the inspection car. Through accumulating the number of the output pulses during a period, the speed signal could be gained (ZHAO Yan, 2003).

DATA PROCESSING

The Obtaining of Detect car's Pitch Angle

Suppose an inspection car is running with changes in the direction. The pitch angle of the car is θ_0 at a time t_0, and the pitch angle is θ, when the time reaches t_1. Assuming that the variable quantity of gyroscope rotor's angular velocity is ω from the time t_0 to t_1, the pitch angle θ will be obtained from the following formula (1):

$$\int_{t_0}^{t_1} \omega dt = \theta \qquad (1)$$

Equation 2 is an alternative of Equation 1 provided (t_1- t_0) is small enough.

$$\theta = \theta_0 + \omega(t_1 - t_0) \qquad (2)$$

In the calculation, θ_0 corresponds to the initial state of the pitch angle, which is hard to get by reading the gyroscope output when the inspection car is stationary or running without changes in the direction. However, it can be obtained by reading the output of the three-axis acceleration. Three axis of the acceleration are perpendicular to each other, which compose a three-dimensional coordinates system. From Figure 2, assuming that the component of gravitational acceleration (g) at A-axis reading from the three-axis acceleration is g_A, the relationship between gravitational acceleration and pitch angle is expressed as follows:

$$g \sin \theta_0 = g_A \qquad (3)$$

So, by combining formula (2) and (3), the pitch angle of the inspection car at any time can be obtained.

The Obtaining of Inspection Car's Speed

Assuming that the circumference of the inspection car's wheel is L and the number of the output pulses of the photoelectric encoder is N, when the wheel finishes one revolution. When a pulse signal is captured, the progressive journey (s) of the inspection car will be obtained by the formula (4) as follows:

$$s = L / N \qquad (4)$$

The pulse signals are put into the microcontroller which is set to run with interrupts. By recording the time (T) and signal number (n) between two interrupts, speed of the car will be obtained by the formula (5) as follows:

$$V = \frac{L \times n}{N \times T} \qquad (5)$$

The Obtaining of Elevation

With the speed and pitch angle of the car, elevation could be calculated by choosing a base surface. From Figure 1, the base surface where the inspection car

begins to run is selected as the base level. Hence, road elevation could be obtained by the following formula (6):

$$h = \int V \sin\theta dt \qquad (6)$$

EXAMPLES OF VERIFICATION

Vehicle-mounted surface measurement has been carried out on two roads by using the algorithm in this paper and the results are compared with those measured by the leveling. The results are plotted in Figure 3 and 4 (blue curve for the Leveling measurement results, the green curve for the results of this method of measurement).

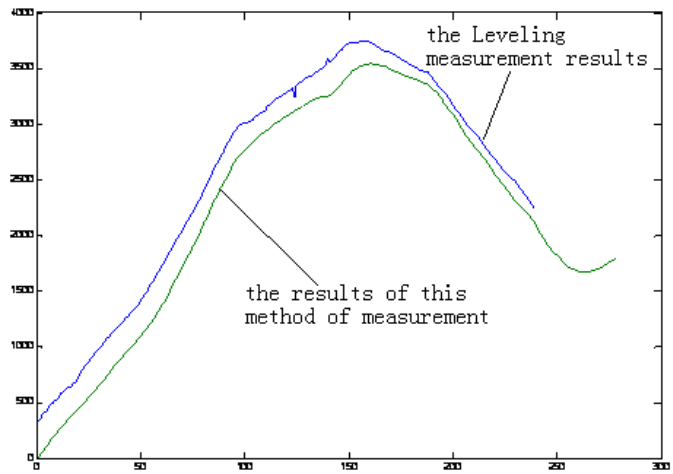

Figure 3. Comparison Result 1 (Horizontal axis: Length - m, Vertical axis: Height - mm)

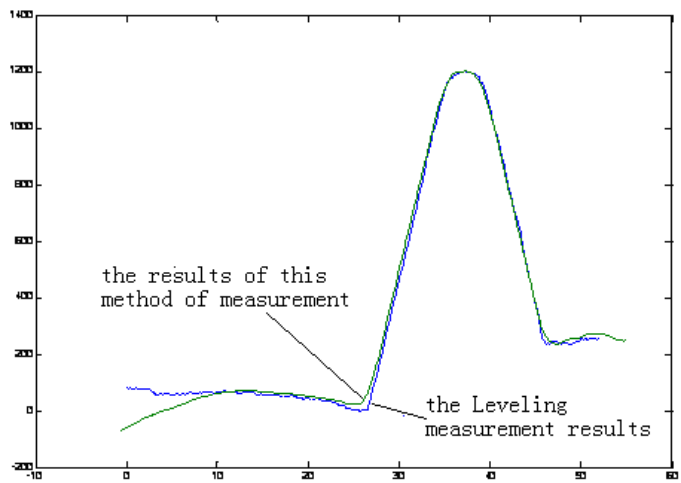

Figure 4. Comparison Result 2 (Horizontal axis: Length - m, Vertical axis: Height - mm)

Therefore, it shows that the road pattern measured by this method is close to the facts and available, and that the overall measurement error is less than 5%. However, if the road is flat and with little wave, the measurement error is big enough when little angle is measured, for the reason that the accuracy of the angular rate measured by the selected MEMS gyroscope is limited. According to this situation, it can improve the measurement accuracy by choosing high-precision fiber optic gyro sensor.

CONCLUSION

A wavy road elevation measurement method based on the principle of inertia is proposed in this paper. The technical innovation point of this method is using the most advanced gyroscope to measure pitch angle of car real-timely as well as using three-axis gyroscopes to compensate for the acceleration that can not be detected when the gyroscope rotor is stationary or uniform running. This method only requires the car running on the road to be measured. The elevation could be measured through data processing. The method is simple, quick and easy to achieve. Since the accuracy of the angular rate measured by the selected MEMS gyroscope is limited, the measurement error is big enough when little angle is measured, so the equipment can be applied only to measure the big wavy road elevation. How to use it in the road where is flat and with little wave needs to be further studied.

REFERENCES

Guo, S. Y. (1996). The theory of gyroscope in inertial navigation system.. *Defense Industry Press*, Jul. (1).

Meng, W. G. (2007). Characteristics of three axis accelerometer ADXL330 and its application. *International Electronic Elements,* (02).

Rummel, R., Teunissen, P. (1998). Height Datum Definition, Height Datum Connection and the Role of the Geodetic Boundary Value Problem .*Bulletin Geodesique*, 624, 62(4) :477-498 .

Yang, W. Y. (1994). Photoelectric encoder classification and its applications. *Instrument Technique and Sensor,* (01).

Ye, J. H. (2006). A general talk about total station apparatus triangulated height measurement. *Journal of Guangxi University (Natural Science Edition)*, S1

Yang, J. Z. and Zhang, R. (2008). Current Development Situation of the Precise Leveling Rulers. *Bulletin of Surveying and Mapping*, (12).

Zhao, Y.(2003). The Research of Speed Measurement Method With Encoder. Graduate University of Chinese Academy of Sciences (Changchun Institute of Precision Machinery and Physics).

Investigation of Relationship between Level of Service and Safety

Xuesong Wang, Hangfei Lin, and Xiaohong Chen

School of Transportation Engineering, Tongji University, Shanghai, China 201804; PH (86) 21-69583946; FAX (86) 21-65982897; email: wangxs@tongji.edu.cn

ABSTRACT

While it is generally agreed that operational conditions have an effect on traffic safety, their relationship has not been well defined at a level of detail that adequately supports operation and planning performance measurements. Signalized intersections are the most complex locations on the roadway network, and they are vital to the efficiency and safety of transportation systems. Based on the data collected at 164 four-legged signalized intersections in the State of Florida, this study investigated the relationship between level of service (LOS) and safety at signalized intersections. The LOS was calculated for three time periods: a.m. peak, midday, and p.m. peak. The crash count data models were applied to fit crash frequency models for total crashes in order to investigate LOS and safety relationship. Overall, the LOS indicator is a significant factor for predicting crash occurrence at intersections. However, the models show that the operational condition itself (by only including the LOS indicator) is not sufficient to predict the safety status. LOS "D" is a desirable level which is associated with less total crashes.

Keywords: operational condition, safety status, level of service (LOS), signalized intersections

INTRODUCTION

Signalized intersections are the most complex locations on the roadway network, and they are vital to the efficiency and safety of transportation systems. Level of service (LOS) is a measure of operational condition for speed and travel time, freedom to maneuver, traffic interruptions, comfort, and convenience (HCM, 2000). Researchers believe that operational condition has an effect on safety. On the other hand, safety is an integral part of intersection operations, which in turn will affect operational condition of signalized intersections. However, the relationship between operation and safety is not clear. Congestion might reduce the number of crashes because of lower speed on congested roads. In some cases, crash statistics show that the number of crashes is reduced when the road is less congested.

At signalized intersections, there is a clear relationship between traffic volume and crash frequency. Higher volumes usually correspond to a larger number of crashes because the probability of a crash occurring is generally greater when there are more vehicles (Hauer et al., 1988; Wang and Abdel-Aty, 2007; Wang and Abdel-Aty, 2007). However, higher volumes do not definitely equate to increased congestion, and there is little research on the relationship between intersection operational conditions and safety (Persaud & Nguyen, 1998). Because safety is not explicitly considered in operational measures to define LOS, beginning with HCM 1994, "safety" was removed from the LOS definition (Zhang & Prevedouros, 2003). The objective of this study is to investigate the relationship between LOS and safety at signalized intersections. Crash data at Signalized intersections and other intersection-related information were collected. The LOS was calculated. The crash frequency modeling technique was applied in this study to facilitate the analysis.

LITERATURE REVIEW

Only a few studies investigated the relationship between safety performance and various LOS measures for signalized intersections. Persaud and Nguyen (*1998*) explored the relationship between LOS and safety for four-legged signalized intersections. Data from rural areas in Ontario, Canada were used. These consisted of a sample composed of 107 four-legged signalized intersections and 970 associated crashes over 6 years (1988-1993). Only a.m. and p.m. peak period data were considered in the analysis. It was assumed that two peak periods did not differ much in model parameters. The required intersection peak hour average stopped delay, capacity, and LOS were calculated using the Highway Capacity Software (HCS) based on HCM 1994. Two sets of models were estimated for the analysis: one that uses flow and delay as variables and the other uses LOS as a categorical variable. The analysis suggested that the best models for these two sets are those having separate calibrated parameters for a signalized intersection's major and minor flows. They found that the expected number of accidents during the peak periods is larger for LOS D and E than it is for LOS B and C.

Hall and Polanco de Hurtado (*1992*) inspected 445 urban signalized intersections in Albuquerque, New Mexico, and selected about 260 for the analysis. Crashes from 1987 to 1989 were included for those occurring at intersection and intersection-influenced locations (i.e. occurring within 200 ft of an intersection), and then converted to crash rate. Weekday one-hour peak period intersection volumes from 1989-1990 were used for calculating LOS and v/c ratios using the procedures from HCM 1985. The 60-minute peak hour periods considered were morning (beginning either at 7:15 or 7:30 a.m.) and afternoon (beginning at 4:30 p.m.). They found that accident rate exhibited a small but positive correlation with the amount of traffic entering the intersection. However, the authors concluded that equations developed for estimating accident rates as a function of v/c had such high standard errors that they could not be used for any practical purpose. This could be due to the use of accident rate and ordinary linear regression for intersection safety analysis (Hauer, 2002).

It can be noted that some common limitations can be encountered when trying to explain the LOS-safety relationship. Persaud and Nguyen (*1998*) recommend the

use of larger data sets for this type of analysis in future studies. Furthermore, crash rate is still being used, as well as linear regression when analyzing it (Hall and Polanco de Hurtado, *1992*). The investigation of how operational conditions affect safety is still at the exploratory phase.

DATA PREPARATION

The study was based on a sample of 164 regular four-legged signalized intersections in Orange and Hillsborough Counties of Central Florida. The intersections are located in suburban areas. The data collected for the selected intersections include signal timing, 24-hour approach volume, turning movement count, intersection geometry design features, and crash data. Both counties have turning movement count for the selected intersections for three time periods: a.m. peak, p.m. peak, and midday.

Levels of service (LOS) and related operational measures, i.e. delay, lane group capacity, and volume to capacity ratio (v/c), were calculated for the selected intersections using the Highway Capacity Software (HCS), which is based on the 2000 version of the Highway Capacity Manual (HCM, 2000). The study considers three time periods (a.m., midday, and p.m.). The process started by entering the required geometric design features into the software, which include the number of out-flowing lanes and receiving lanes for all approaches, whether these are shared or exclusive, and queue storage lengths for each approach. These main features were determined with aerial imagery captured by GoogleTM Earth and verified with the information in the intersection's respective signal timing plan. Other input data considered were traffic volumes and peak hour factors (PHF). These were calculated on each approach based on the available turning movement counts and the peak 15-minute volumes for each time period.

Collisions over 6 years (2000 - 2005) were collected for the selected intersections from the Crash Analysis Reporting (CAR) system maintained by the Florida Department of Transportation (FDOT) Safety Office. Crashes included are those occurring "at intersection" or "intersection-related".

METHODOLOGY

Negative Binomial regression provides a common tool for modeling cross-sectional count data like crash frequencies at signalized intersections (Poch and Mannering, 1996). In this study, for each selected intersection, there are observed crash frequencies for three time periods. Multiple observations on the same intersection are most likely to be correlated because of the common unobserved characteristics of intersections. Generalized Estimating Equations (GEEs) provide an extension of generalized linear models (GLMs) to the analysis of clustered data, which account for the temporal correlation among the repeated observations for a given intersection. GEE comes from specifying a known function of the marginal expectation of the dependent variable as a linear function of covariates, assuming that the variance is a known function of the mean, and specifying a "working" correlation matrix for the observations for each intersection (Zegeer et al., 2008). GEE is proved to be a promising modeling approach for temporal or clustered crash frequencies. Lord and Persaud (*2000*) applied GEE for a 6-year period of data for 868 four-legged

signalized intersections. Wang et al. (*2006*) and Abdel-Aty and Wang (*2006*) conducted temporal and spatial analysis for signalized intersections.

MODELS FOR TOTAL CRASHES

Crash frequencies of the selected intersections were extracted and plotted by LOS of the entire intersection for a.m. peak period as shown in Figures 1. The figure shows that more congested intersections correlate with higher frequency of collisions. For the a.m. peak, the highest number of crashes occurred at intersections with LOS F.

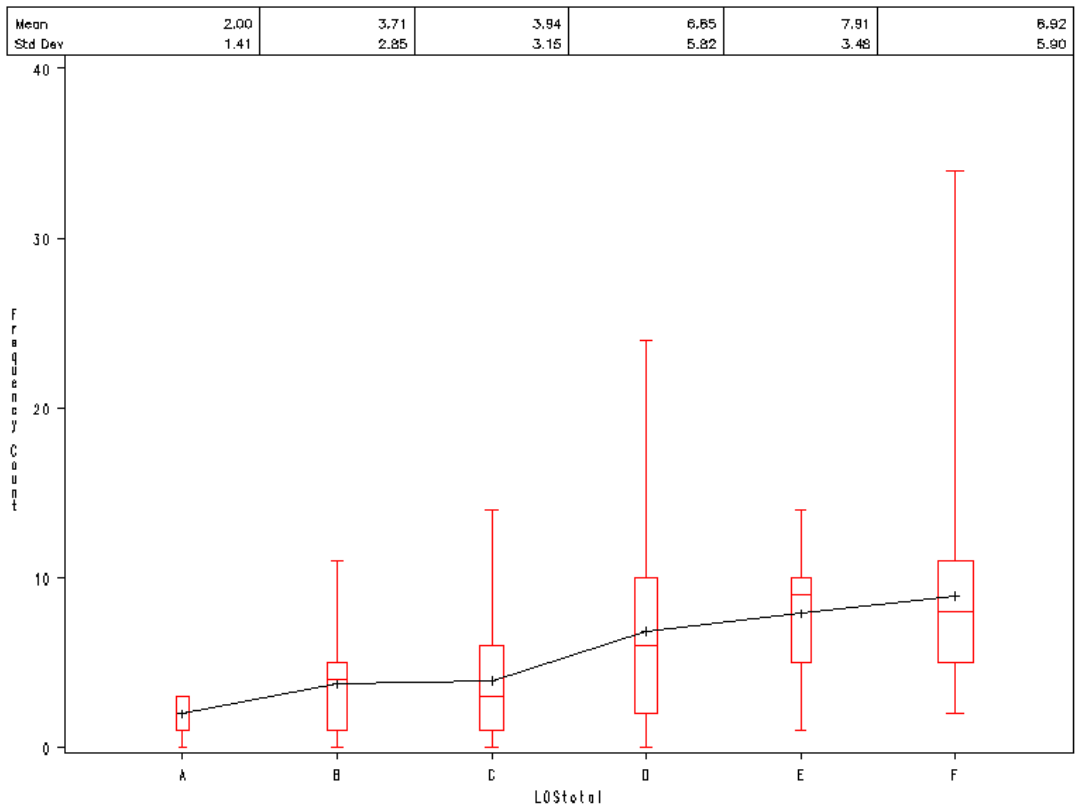

Figure 1. Crash frequency distribution by LOS in a.m. peak

GEE Negative Binomial regression was used for fitting the total crashes in the a.m. peak, midday, and p.m. peak periods (see Table 1) to account for temporal correlation among the repeated observations for a same intersection. In Model 1, total crashes in each time period were fitted by only including LOS indicators, which were treated as categorical variables. Compared to the base case (LOS A), the positive coefficients and low p-values indicate that worse LOS conditions are significantly correlated with more crashes. In addition to LOS indicators, Model 2 included intersection traffic flows, geometric design features, as well as traffic control and operational features. The LOS indicators are still significant in the model 2.

Table 1 Models for Total Crashes

	Model 1 LOS indicator only model			Model 2 Full model		
Parameter	**Coef.**	**S. E.**	**P-value**	**Coef.**	**S. E.**	**P-value**
Intercept	1.0921	0.2332	<.0001	-3.4194	0.7972	<.0001
Intersection LOS for the time period						
F	1.1678	0.2389	<.0001	0.6868	0.2633	0.0091
E	1.1491	0.2465	<.0001	0.7874	0.264	0.0029
D	0.8437	0.2395	0.0004	0.5571	0.2562	0.0297
C	0.8028	0.2354	0.0006	0.6492	0.2486	0.009
B	0.46	0.2357	0.051	0.4561	0.2489	0.0668
A	0	0		0	0	
Time period						
PM Peak				0.2576	0.0632	<.0001
Midday				0.2418	0.0558	<.0001
AM Peak				0	0	
Logarithm of average volume for the time period on major road				0.4093	0.0728	<.0001
Logarithm of average volume for the time period on minor road				0.2708	0.0514	<.0001
Left-turn lane offset on minor road						
With positive offset				-0.2738	0.1482	0.0646
Zero offset				-0.3734	0.1501	0.0129
Negative offset				0	0	
Speed limit on minor road				0.011	0.0057	0.0541
Skid resistance at intersection				-0.0229	0.0088	0.0092
County						
Orange				-0.4432	0.0751	<.0001
Hillsborough				0	0	
Scale	1.0325			1.0757		
Model Assessment (Cumulative Residual)						
Number of intersections	164			164		
Observations per intersection	3			3		
Maximum Absolute Value	11.4368			5.2267		
P-value	0.0002			0.4311		

Lin et al. *(2002)* proposed a Cumulative Residuals method based on the cumulative sums of residuals for checking the model overall goodness-of-fit. For a GEE model, the distribution of the stochastic processes under the assumed model can be approximated by the distribution of certain zero-mean Gaussian processes whose realizations can be generated by simulation. Each observed residual pattern could then be compared with a number of realizations from the Gaussian process. A p-value larger than 0.20 indicates that the null distribution in Kolmogrov-type supremum test is not violated (*2002*). Model 1 has a large Maximum Absolute Value (11.4368) and a

small p-value (0.0002) for the Cumulative Residuals test; this indicates that the model's overall goodness-of-fit is not acceptable and that only using LOS for modeling crash frequency is not sufficient. On the other hand, Model 2 has a relatively small Maximum Absolute Value (5.2267) and a large p-value (0.4311). Incorporating additional parameters had the desired effect of improving the model's overall goodness-of-fit.

Similar to the box-plots in Figure 1, Model 1 crash frequency increases as LOS deteriorates. However, in Model 2, LOS "E" is the worst situation since it has the highest positive coefficient among the LOS parameters. LOS "D" is significantly better than LOS "C", "E", and "F" in terms of safety. As expected, the model predicts that the p.m. peak experienced more crashes than other periods. As a measure of exposure, higher traffic volumes on major and minor roadways are significantly associated with more crashes; this indicates that under the same operational level intersections with higher traffic volumes will have more crashes. It was found that providing zero or positive offset on minor roads reduced total crashes. Joshua and Saka (*1992*) pointed out that the minimum value of the offset can be zero, but cannot be a negative value in practical design, which would results in unsafe conditions. A higher speed limit on minor roadways is associated with more crashes (coef. = 0.011; p-value = 0.0541). An interesting finding in the model indicates that both positive and zero left-turn lane offsets have a significant benefit in safety. It was also found that the sign of the coefficient for the skid resistance at intersection is negative as expected, which means that higher skid resistance is associated with fewer crashes.

SUMMARY AND DISCUSSION

The crash frequency models show the following relationship between the operational condition and safety:

- Overall, LOS indicator is a significant factor for predicting crash occurrence at signalized intersections. However, the models with only LOS indicator are not significant. It shows that the operational condition itself is not sufficient to predict the safety of signalized intersections.
- Generally, as congestion increases, the crash frequency increases. However, there is a desirable level LOS "D" associating with less total crashes. At LOS "D", operational condition produces a desirable balance between safety and congestion. This phenomenon is obscured when the LOS indicator is used as the only predictor in the models or by only looking at crash frequency distribution trends among different LOS levels.
- The time period factor, with three levels in this analysis, i.e., a.m. peak, midday, and p.m. peak, is significant in the models for total crashes. It indicates that the crash mechanism is different in different times of a day.
- Average delay was tested as a continuous variable but it was found to be insignificant. A six-level LOS indicator is better than average delay in the crash frequency models. It indicates that the relationship between crash frequency and average delay is not linear. The unit change of delay at different congestion levels does not have the same effect on safety. This is shown by the different coefficients for LOS indicators.

Acknowledgements

This study is supported by the Program for Young Excellent Talents in Tongji University (1600219099).

REFERENCE:

Abdel-Aty, M., and Wang X. (2006). "Crash Estimation at Signalized Intersections along Corridors: Analyzing Spatial Effect and Identifying Significant Factors." *Transportation Research Record: Journal of the Transportation Research Board, No. 1953,* Transportation Research Board of the National Academies, Washington, D.C. 98–111.

Hall, J. W., and Polanco de Hurtado M. (1992). "Effect of Intersection Congestion on Accident Rates." *Transportation Research Record, No. 1376,* Transportation Research Board of the National Academies, Washington, D.C. 71–77.

Hauer, E. (2002). *Observational Before-After Studies in Road Safety*. Pergamon.

Hauer, E., J. C. N. Ng, and Lovell J. (1988). "Estimation of Safety at Signalized Intersections." *Transportation Research Record, No. 1185,* Transportation Research Board of the National Academies, Washington, D.C. 48–61.

Lord, D., and Persaud, B. (2000), "Accident Prediction Models With and Without Trend: Application of the Generalized Estimating Equations (GEE) Procedure." *Transportation Research Record, 1717.* 102–108.

Persaud, B., and Nguyen T. (1998). "Safety Considerations in Capacity Analysis." *Third International Symposium on Highway Capacity*. Copenhagen, Denmark, 817–831.

Poch, M., and Mannering F. (1996). "Negative Binomial Analysis of Intersection-Accident Frequencies." *Journal of Transportation Engineering,* 122. 105–113.

Transportation Research Board. Highway Capacity Manual, 4th edition. (2000). Washington D.C.: National Research Council.

Wang, X. and Abdel-Aty, M. (2007). "Right-Angle Crash Occurrence at Signalized Intersections." *Journal of the Transportation Research Record*, 2019, 156-168.

Wang, X., and Abdel-Aty, M.(2008)."Modeling Left-Turn Crash Occurrence at Signalized Intersections by Conflicting Pattern." *Accident Analysis & Prevention*, 40. 76-88.

Wang, X., Abdel-Aty, M and Brady P. (2006). "Crash Estimation at Signalized Intersections: Significant Factors and Temporal Effect." *Transportation Research Record: Journal of the Transportation Research Board, No. 1953,* 10–20.

Zegeer, J. D., Vandehey, M, Blogg, M., Nguyen, K., and Ereti, M. (2008) *NCHRP Report 599: Default Values for Highway Capacity and Level of Service Analyses.* Transportation Research Board of the National Academies, Washington, D.C.

Zhang, L., and Prevedouros, P. D. (2003), "Signalized Intersection LOS that accounts for Safety Risk." *TRB 82nd Annual Meeting Compendium of Papers*. CD-ROM. Transportation Research Board of the National Academies, Washington, D.C.

Research and Application of Graphic-attributes Integration Based on Web GIS in Aviation Accident Investigation

SUN Rui-shan[1], YUAN Ding[2] and XIE Zi-nan[3]

[1]Research Institution of Civil Aviation Safety, Civil Aviation University of China, Tianjin, china, 300300; PH (86) 022-24092593; FAX (86) 022-24957940; E-mail: sunrsh@hotmail.com

[2]Research Institution of Civil Aviation Safety, Civil Aviation University of China, Tianjin, china, 300300; PH (86) 022-24094252; FAX (86) 022-24957940; E-mail: yuan825ding@hotmail.com

[3]Aviation Accident Investigation Center(AAIC), Civil Aviation Administration of China, Beijing, china, 100028; PH (86) 010-64280968; FAX (86) 010-64280968; E-mail: sxiezn@mail.castc.org.cn

Abstract

With the development of computer science and geographic information system (GIS), the graphic-attributes integration system which depends on graphic data and structured data is applicable to aviation accident investigation. Combined with graphics, text and multimedia, Web GIS technology is the core content of Web GIS graphic-attributes integration system. This article is on the basis of clarifying the concept of Web GIS graphic-attributes integration, and introduces the characteristics and framework of system of Web GIS based on B/S mode, and focuses to discuss the function integration, implementation process and key techniques, which provides a guarantee for analyzing aviation accidents.

1. Introduction

The traditional GIS can't meet the requirement of information management due to lack of the consideration of the information media's diverse feature. Hence, it is necessary to create a MIS based on the graphic-attributes integration, leveraging visualization to manage and make a decision (Yao, Jan., 2008). This article introduces a way of leveraging on Web GIS technology as well as the advantage of GIS to the geo-spatial data management, to solve the problem of lacking data integrity of the accident investigation. It realizes the consolidation of graphic-attributes integration under network and provides a display platform of 3-D information for the aviation accident investigation.

2. Web GIS based on B/S Mode

GIS is a system of access, store, query, consolidation, analysis which can also display the geo-spatial data and the related information (Yao, May, 2008). Accident investigation needs to refer to the terrain landform, airport, road, architecture, land, etc. It provides the evidence to determine the accident site and causes through a technology of graphics processing, mapping and visualization.

2.1 Web GIS definition

The Web GIS is a GIS system based on Internet and Client Application, running under Internet WWW protocol. It uses Web pages as users' interface. From

any WWW dot, the user can browse and access the data, index, and analyze, it makes the user be able to interact。

2.2Web GIS features

The traditional GIS has many disadvantages, like high development cost, inefficient operation and multi-accessing net bottleneck, it is difficult to ensure the integrity and also hard to operate and release. Table1 list the advantages of Web GIS based on B/S, comparing with the traditional GIS：

Table 1.The comparison of the two different GIS.

	Traditional GIS	Web GIS
Development Cost	High	Low
Response Time	Slow	Fast
Platform of Client Cerver	Weak	Powerful
User Interface	Simple	Rich
Tools of the Development and Support	Rich	Rich and Widely Used
Typical Platform and Product	ArcGIS, MapInfo,...	Google Earth, World Wind(NASA), UrMap,...

3. The function of Web GIS graphic-attributes integration

3.1 The conception of Web GIS graphic-attributes integration

Various sources needed to be collected in the aviation accident investigation, which includes wreckage and data of the accident site and all kinds of photos, flight data, satellite images, aerial photos, geographic data, AIP data, etc(ICAO,2001). Although the information needed to be examined varies, it can be categorized into graphic data and structured data, in which the graphic data can be divided into image and vector data. Web GIS graphic-attributes integration system refers to seamless integration between the graphics and structured information based on computer technology, then access to and develop the information, display and input between graphics and structured data can be achieved in this system(CHENG, 2008). It makes the image match the vector data in the accident investigation, and then incorporate with the structured data like flight data, which not only overcomes the drawback of simply dependent on the vector data applied to accident analysis, but connects more information.

3.2 The function integration

The accident reconstruction technology based mainly on flight data recordings, cockpit voice recordings, radar data, witness information involves many aspects of accident investigation, including field investigation, causes analysis, accident rating determining, safety recommendations, etc. It can mark related information on the flight path (Li, 2007). According to the thinking of Web GIS graphic-attributes integration, the accident reconstruction includes accident site reconstruction and digital AIP charts.

3.2.1 Accident site reconstruction

An overall description should be made in the accident investigation to determine and mark the first impact point between the aircraft and obstacle (terrain) and main scattered objects in follow-up track and flight path. It also determines the basic state of the aircraft wreckage and reconstructs the accident site by photos and

videos for the scene of accident. This system which makes the landform of accident site as background can describe wreckages by legends and localize them by latitude & longitude. Reconstruction of the site involves several steps as shown in Table 2:

Table 2. Five steps in reconstruction of the accident site.

Step Number	Contents
Step.1	Establish the wreckage legend library
Step.2	Use latitude & longitude to determine wreckage distribution, finish reconstruction and define for wreckage point object
Step.3	The position and size of wreckage legends are fit for accident site by rotating and conducting scaling
Step.4	Define the first impact point, the main scattered objects in flight path and other significant features
Step.5	Finish the reconstruction of wreckage distribution on accident site

3.2.2 The application of digital AIP charts

The Figure.1 is a schematic drawing according to actual air traffic control of an airport. Located in the runway at both ends of the oval-shaped surfaces are holding areas which are defined by IAP; Lines are routes; English letters are designators and names which represent radio aids; Numbers are channel frequency. This three dimensional demonstration platform takes the real airport terrain landform as background, overcomes the drawback of simply dependent on the vector data applied to express information, and adopts image combining vector data to intuitively reflect the departure/arrival procedures which need to follow during take off and land. Moreover, it can use Web GIS latitude & longitude timely to define (refresh) information of the marked point, and promptly reflect the deviation. In this way, it is facilitate to investigator for position of the accident site and the process of anomaly.

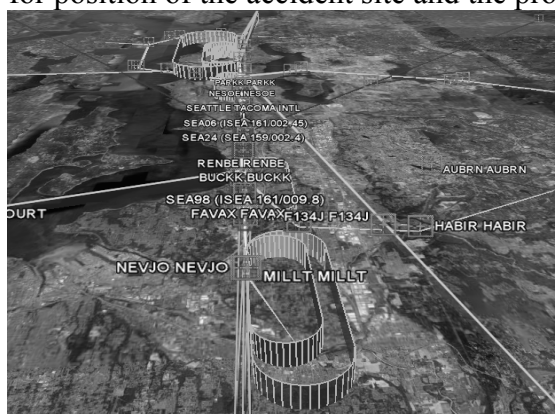

Figure.1 Digital AIP charts.

4. Implementation of system and key technique

4.1 Implementation of graphic-attributes integration

4.1.1 Introduction of Google Earth

Traditional GIS data uses two-dimensional platform to display. It can not rotate, nor show the depth of field, and sometimes can not distinguish the different colors (SUN, 2007). Therefore, we can not observe the crash point from different angles, nor can different levels are set up to analyze the flight path, so the visual part of the target has been greatly constrained. Google Earth provides global landform and

3D data, and creates the conditions for three-dimensional dynamic display.

4.1.2 KML language

KML(Keyhole Markup Language), developed by Google, is standard data based on XML grammar and file format which is used to describe and preserve the geographic information such as points, lines, planes, 3D models etc.

The functions can be illustrated as follows:

1. Distinguish locations with legends and marks
2. Designate clear visual angles for each view to set up different close-ups
3. Designate description based on easy HTML grammar for each feature, and support hyperlinks and embedded pictures.
4. Load KML file from local or remote network address dynamically.
5. When the Google Earth client view changes, send automatically view information to the specified source server and obtain useful information.

4.1.3 Expression and function of data of KML in Google Earth

Google Earth provides global physiognomy, and adds different layers in Google Earth by creating KML files to integrate display of graphics and structured data. Table 3 introduces six types of display provided for adding GIS data in Google Earth：

Table 3. Six kinds of data type for the addition in Google Earth.

Data Type	Application
Placemark	Locate what you want to search
Path(Lines)	Depict route, flight path and other related segments
Polygon	Outline the contours and shape features
GroundOverlay	Use the local information affixed to the corresponding region
ScreenOverlay	Match with GroundOverlay to describe position
3D Data	Set 3D model to directly show geographic images

Geo-spatial data model only deals with real entities and graphic images in coding. The thought of graphic-attributes integration should not only match images and vector data on the information platform of accident investigation, but also add structured data to the KML marked points, which include the property name, type and related flight parameter. KML uses kml, Document, Folder, Placemark as a root tag of KML file to organize information and inherits the implementation of geographical expansion of the target property value.

4.2 Data management

This Figure 2 shows the framework of Google Earth system development which is based on B/S. This mode takes Google Earth server as a center, and establishes Http transmission protocol of the three-tier. The first one: Google Earth Browser layer, it can provide map browsing and three-dimensional demonstration platform, and also output the interactive final query results between users and server. The second, Google Earth Server layer, it stores plenty of GIS data, including images, KML files, etc. This server also responds to the users' requests and simultaneously executes the related inquiry operation and data communication. The third one, User Server layer, it not only publish can the map and additional GIS data, display them on Google Earth Browser by user application software, but also may read those data from the application software and save it in user server.

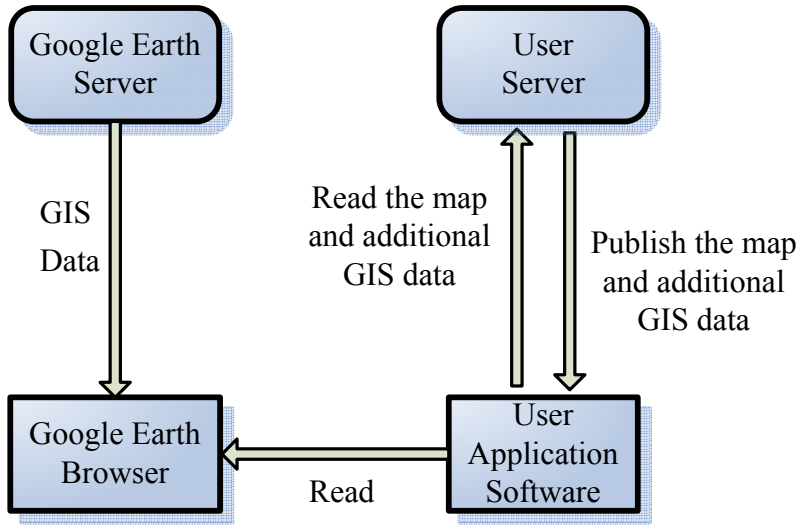

Figure 2. The general framework of Google Earth system development.

The graphic-attributes integration system involves graphic data, entity attribute, and photos, files, video, audio and other multimedia data. This technology must firstly deal with how to carry out the centralized management of various data. With the rapid development of object-oriented relational database technology, all of the commercial databases, such as oracle, SQL Sever, provide support for large binary object type to meet the feature that the spatial data dynamic growth in non-structure, which make it possible for the spatial data to save in relational database. Figure 3 shows the mode of object—relational database management, it makes geo-spatial data and their attribute mixed in the background large-scale relational database to manage them uniformly (Wu,2002).

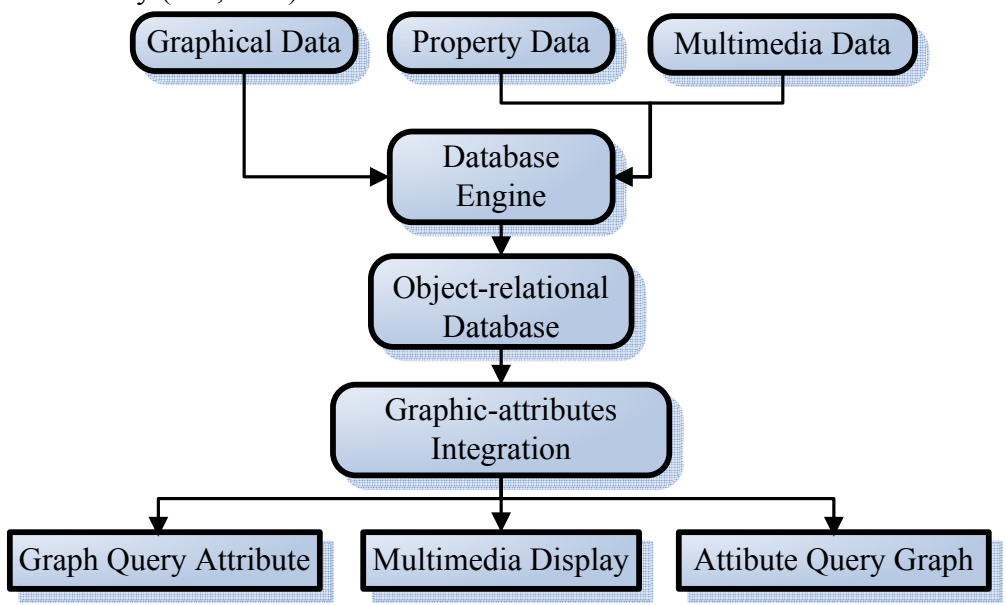

Figure 3. Object-relational database management mode.

5. Conclusions

This article presents a new design of Web GIS graphic-attributes integration system for aviation accident investigation, and discusses the major technologies of the function integration, implementation process, data management model. The system creates a platform enabling multi-layer, three-dimensional, visual display of information, and combines GIS graphic data and structured data, and therefore realizes real "graphic-attributes integration". With the rapid development of computer technology and GIS, further theoretical research and practical development is in great demand, so as to better fulfill the demand of aviation accident investigation.

References

CHENG R., WANG D., YI J..(2008). "Application of GIS-based Information system with the Integration of Graphic Data and Text in Land Resources Management."*Imaging technology*, No.4

ICAO Annex 13 Aircraft Accident and Incident Investigation. (Jul, 2001). "*International Civil Aviation Organization*." 5-1~5-5

Li C., Zhao Z., Zhao J. (2007). "Computer Aided Analysis System for Flight Accident Investigation." *Journal of computer-aided design & computer graphics*,Vol.19, No.1

SUN Y., MAO Z., CHEN M., WANG W., Mao X. (2007). "Application of Google Earth in Light Buoys Monitoring System." *Journal of traffic & computer*, Vol.25, No.6

Wu X. (2002). "Principles and methods of geographic information system." *Publishing House of Electronics Industry*, Beijing, 94-97

YAO Y. (2008). "Research on graphics and document integration of information management system based on GIS." *Technological development of enterprise*,Vol.27, No.1

YAO Y., ZHU J., XUE L.(2008). "Application and Research of Web GIS in Meteorological Telecommunication Information System." *Computer engineering*, Vol.34, No.10

Study and Implementation on JPEG Image Enhancement System of Tire Mark

CHEN Tao[1], WEI Lang[2]

[1]Key Laboratory of Automotive Transportation Safety of Ministry of Communications, Chang'an University, Xi'an 710064, China; PH (086) 029-82334475; FAX (086) 029-82334476; email: chentao@chd.edu.cn
[2]School of Automobile, Chang'an University, Xi'an 710064, China; PH (086) 029-82334471; FAX (086) 029-82334476; email: qch_1@chd.edu.cn

ABSTRACT:
Tire mark intelligent identification and comparison is a key procedure in determining and tracing the violating vehicles at traffic accident scene survey, but in some cases the acquired JPEG image is hard to recognize due to the low contrast and the nonuniform background brightness. This paper puts forward image enhancement algorithm based on the JPEG decoder and develops a software system by Visual C++6.0 for this purpose. The histogram equalization (HE) and adaptive histogram equalization (AHE) are used to improve the global and local image brightness and contrast individually in image enhancement algorithm. The application results show that this system is effective to tire mark image enhancement, which lays the foundation for intelligent comparison and identification of tire mark.

INTRODUCTION

Tire mark is important evidence in accident investigation. It can be used to presume the impact locations and driver's behaviors as well as vehicles' heading, minimum speeds before the collision, and post collision trajectories, etc., in accident reconstruction. Especially, it can be used to identify the possible tire involved and reduce the scope of vehicles' investigation in the case of hit-and-run accidents. In practice, tire marks can be recognized by investigators or policemen using a simple skill such as the vehicle heading from the drivers' description, the position of the stopped vehicles and the tire-marks etc. Being a high complexity of accident scene such as multi-cars accident, and new and old tire marks irregularly distributed on the roadway. Therefore, it is necessary to develop an intelligent identification system to aid the traffic accident investigation and analysis. The evidences mainly resulted from JPEG image of tire mark taken by DC at accident scene. It is very important to acquire good quality images, but in practice a significant percentage of acquired images are of poor quality due to some environmental factors or user's body condition. The poor quality images of tire mark cause that many details may be ignored. Therefore, it is a great help to develop an image enhancement algorithm of tire mark to improve quality of accident appraisal.

Image enhancement algorithms have been designed to process a given image so the results are better than the original image for their applications or objectives [Jae, 1999]. Image enhancement has as main task to improve the visual quality of an

image from the human perspective. It uses several techniques, such as histogram equalization, contrast stretching, and slicing, that were initially developed for grayscale images. However, several attempts have been made to generalize the aforementioned techniques to color images. The generalization has been proven to be rather complicated due to the various color models and the relationships between the color components.

IMAGE ENHANCEMENT OF TIRE MARK

JPEG decoder of tire mark image

The JPEG image standard is by far the most popular method for storing and exchanging photographic image files. The term 'JPEG' actually covers a wide range of related methods developed by the Joint Photographic Expert Group in the late 1980s. JPEG includes standards for both lossless and the more common lossy compression, as well as progressive rendering techniques for encoding images to be sent over slow transmission lines (such as the Internet).

JPEG is a popular image compression standard, representative of discrete cosine transform (DCT) methods used in many image and video compression algorithms. JPEG includes a variety of techniques, but baseline sequential color decoding is by far the most popular and is the technique considered in this implementation. JPEG can be compressed with different quality factors (Price1999).

In JPEG compression, pixels are usually represented using 8-bit luminance (Y) and red (Cr) and blue (Cb) chrominance component values. The basic unit of compression is an 8x8 set of component values. Because the human eye is most sensitive to luminance, it is typical to sample the Y value four times for every chrominance pair. The original image is divided into minimum-coded unit (MCU) regions, where each MCU includes all component blocks necessary to reconstruct that region. In the typical case with down sampled chrominance values, each MCU would contain four luminance blocks and two chrominance blocks representing a 16x16 pixel region in the original image. MCUs are processed from left to right and top to bottom to reconstruct the image. When compressing, each block is DCT transformed into the frequency domain, and the frequency values are quantized to reduce the information, with many of the higher frequency coefficients becoming zero. The coefficient values are zigzag ordered to maximize runs of zeros, and the values are run-length and Huffman encoded.

The decode flow (see Figure 1), begins by reading the header information to determine the JPEG type and the number and composition of MCUs. Tables needed for decoding and dequantization are read in. The remaining stream contains the compressed values for all the MCUs in left-right, top-bottom order. As the stream is read in, the values are Huffman decoded and expanded to recover each MCU's coefficients. Because of the Huffman codes, the amount of bits required to be read from the stream varies between MCUs. Each 8x8 block within the MCU is scaled by the appropriate array of quantization values, and then run through an inverse DCT

transform to recover an approximation of the original Y, Cr, or Cb component values. Once all component blocks have been recovered, the chrominance values may need to be upsampled, and each YCrCb pixel is converted to RGB representation.

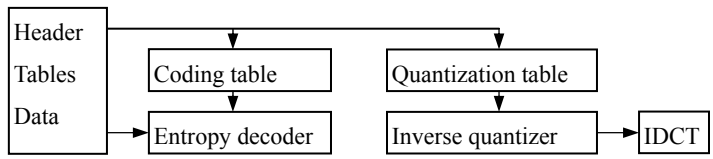

Figure 1. The JPEG decoder

Brightness and contrast enhancement of tire mark image

The image enhancement of tire mark includes brightness correction and contrast optimization adjustment. Equalization of color images can be realized by applying the grayscale image equalization method separately to the Red, Green and Blue components of the RGB color values of the image. Still, it should be noted that applying the same method on the Red, Green, and Blue components of an RGB image may yield changes in the image's color balance since the relative distributions of the color channels change as a result of applying the algorithm. Brightness and contrast enhancement includes: linear stretch, histogram equalization (HE), adaptive histogram equalization (AHE) (Sherrier1987), and multi-scale enhancement (Jian, 1994) and etc. This paper adopts the HE for the global brightness and contrast enhancement, and AHE for local tire mark.

The HE algorithm is used to image handling, and its expression is as follows:

$$cdf(v) = round(\frac{cdf(v) - cdf_{\min}}{(M \times N) - cdf_{\min}} \times (L-1)) \quad (1)$$

Where $cdf(v)$ is the equalization value of cumulative distribution function;

$cdf_{\min}$ is the minimum value of the cumulative distribution function; and

M × N gives the image's number of pixels and L is the number of grey levels used.

$cdf(v)$ is defined by:

$$cdf(v) = \sum_{j=0}^{i} p(x_j) \quad (2)$$

Where $p(x_j)$ is the probability of an occurrence of a pixel of level i in the image.

AHE is a local enhancement technique mapping based on small overlapping areas of an image. There are the cases in which it is necessary to enhance details over small areas in an image. In AHE rectangular, sub image of an input image is first defined. Histogram of that block is obtained and Histogram Equalization function is determined. Finally, processed sub images are represented together with bilinear interpolation (Gonzalez, 2002).

A description of the function algorithm implemented for AHE follows (Kearfott, 1996). First, a contextual region of size k pixels is used to define a neighbourhood centered ground some given pixel. The local histogram of gray levels, h(n), is then determined. The rank is computed at the center pixel for a region I having size by k using:

$$r(i) = \sum_{n=0}^{k} h(n) \tag{3}$$

The set of ranks is normalized so that $0.0 < r'(i) < 1.0$. A value of the enhancement factor, $0.0 < A < 1.0$, is chosen for stretching the maximum and minimum toward the ends of gray level distribution function.

The enhanced pixel value, $g(x,y)$, is obtained from the following, which yields a nearly uniform histogram of output image:

$$g(x,y) = [r'(i) * (i_{\max} - i_{\min}) + i_{\min}] * A \tag{4}$$

Where the derived local maximum and minimum, i_{max} and i_{min}, are specified for the contextual region. For an entire image, composed of an array of perceivable gray values, one computes the expected information that any pixel contains, or the image entropy, from:

$$H = -\sum_{x=0}^{M} p(x) \log_2 p(x) \tag{5}$$

Where *P(x)* is the probability of occurrence of intensity x in the image, with $0 < x < M$, where M is the maximum gray level. It has been shown that the information content and entropy are maximized when all signal levels are equiprobable.

Brightness and contrast adjustment of tire mark image

In Microsoft visual c++6.0, brightness and contrast adjustment of tire mark image can be realized by matrix transformation, see the equation (6) and (7).

$$[R_B] = [R][T_B] \tag{6}$$

$$[R_C] = [R][T_C] \tag{7}$$

Where $[R_B]$ is modified brightness matrix; $[R_B] = [R_B \quad G_B \quad B_B \quad A_B \quad 1]$, $[R_C]$ is modified contrast matrix; $[R_C] = [R_C \quad G_C \quad B_C \quad A_C \quad 1]$; $[R] = [R \quad G \quad B \quad A \quad 1]$; b is the brightness; c is contrast.

$$[T_B] = \begin{bmatrix} 1 & 0 & 0 & 0 & 0 \\ 0 & 1 & 0 & 0 & 0 \\ 0 & 0 & 1 & 0 & 0 \\ 0 & 0 & 0 & 1 & 0 \\ b & b & b & 0 & 1 \end{bmatrix} \quad [T_C] = \begin{bmatrix} c & 0 & 0 & 0 & 0 \\ 0 & c & 0 & 0 & 0 \\ 0 & 0 & c & 0 & 0 \\ 0 & 0 & 0 & 1 & 0 \\ 0.5(1-c) & 0.5(1-c) & 0.5(1-c) & 0 & 1 \end{bmatrix}$$

IMPLEMENTATION AND RESULTS

The JPEG image enhancement of tire mark (JIETM) is one of the most important parts of the intelligent identification of tire mark. The functional flow chart of the JIETM system is shown in Figure 2. Since the system is an independent

software which can't be dependent on any other software, such as Photoshop, CorelDraw … etc, it is developed by using Microsoft Visual C++6.0. It consists of JPEG decoder, brightness correction and contrast enhancement, brightness and contrast adjustment and JPEG save (encoder).

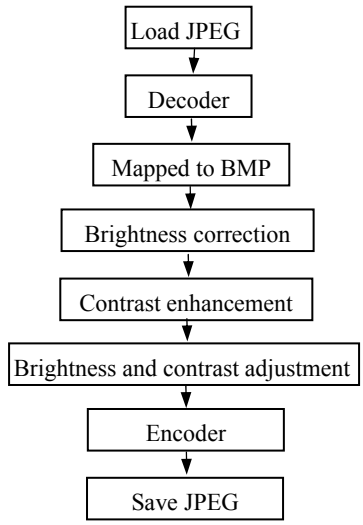

Figure 2. Flow chart for image enhancement of the tire mark

To verify the effectiveness of the proposed method and robust of developed system, experiments were performed with many JPEG image with nonuniform brightness levels and low contrast levels from the actual accident scene. Figure 3 shows handling results of an image obtained from the real accident scene located in Sichuan province by applying the software. The results show that the software gains the better visual effect both in global range and local image. According to the application results of many other images, it is found that the software has high practicality and effectiveness in improving incorrect exposure, but in some cases, when the pavement texture color and tire mark had no significant difference, it is hard to remarkably improve the image quality.

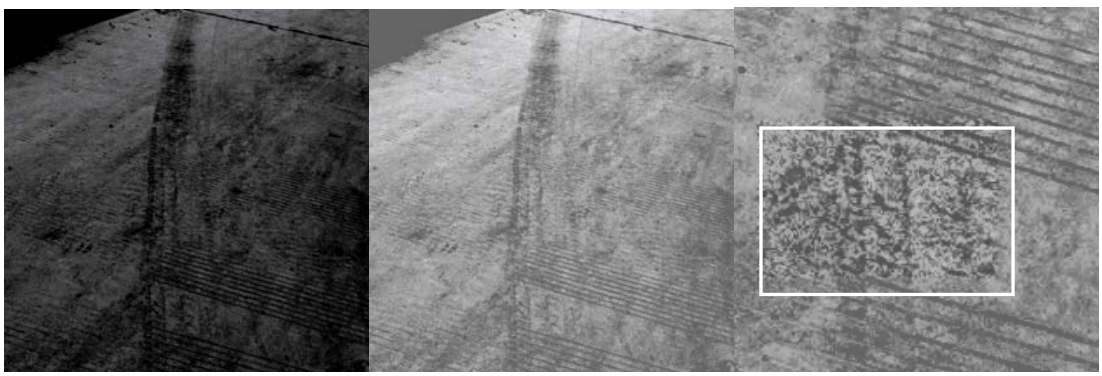

(a) Original. (b) Brightness correction. (c) Contrast enhancement.

Figure 3. Test image of tire mark on accident scene

CONCLUSION

In this paper, a computer implementation based on visual c++6.0 has been presented for image enhancement of tire mark. It deals with JPEG images by decoder and encoder, determines the brightness and contrast of image by HE and AHE algorithms, and adjusts the pixel by matrix transformation. The global adjustment is performed by HE algorithm, and local adjustment can be executed by AHE algorithm. The results show that the system produces good visual effect with shorter time consuming, and the method proposed using HE and AHE has achieved the better performance for low contrast and nonuniform brightness images. The system lays the foundation for intelligent identification and comparison of tire mark, and can be applied directly to handling color JPEG photos taken in the accident scene. But, the system is only effective in some case because of the difference of road surface and interference from other mark. In the future, and in order to achieve better effects, the different enhancement algorithms should be studied.

ACKNOWLEDGEMENT

The project is supported by national science and technology supporting program of China (No. 2007BAK35B01).

REFERENCES

Gonzalez, R.C.and Woods R.E. (2002). *Digital Image Processing 2ed*. Prentice Hall.

Jian L; HEALY D. M, WEAVER J. B. (1994), "Contrast enhancement of medical images using multiscale edge representations", *Opt. Engng*. 33 (7): 2151–2161.

Jae S. Lim (1999). "Two-Dimensional Signal and Image Processing", *Prentice-Hall, Englewood Cliffs*, NJ.

Kearfott K. J., Lin S. Y., Yakoubian J. S. (1996). "Preliminary evaluation of adaptive histogram equalization for digital mammography". *Australian Nuclear association 9th pacific basin nuclear conference*, Sydney.

Price J. R, Rabbani M (1999). "Biased reconstruction for JPEG decoding". *IEEE Signal Processing Lett*, 6: 297- 299.

Sherrier R. H. and Johnson G. A. (1987), "Regionally adaptive histogram equalization of the chest", *IEEE Trans. Med. Image*, 6(1):1–7.

Analysis of Characters and Causes of Road Traffic Accident Migration

JIAO Chengwu[1], YANG Manjuan[1] and HAO Yubo[2]

[1]The Fifth Division, Department of Traffic Engineering, Research Institute of Highway (RIOH), MoT, 8 Xitucheng Rd, Beijing, China; PH (8610) - 62360341; FAX (8610) 62363428; email: cw.jiao@rioh.cn, mj.yang@rioh.cn

[2]Xilinguole League Research Institute of Highway, 18 Nadamu St, Xilinhot City, Inner Mongolia Autonomous Region, China, PH (86479) - 8866947; email: hyb0327@163.com

ABSTRACT

There is a phenomenon of traffic accident migration in the highways after used for some period, especially those that have been improved for traffic safety. In order to make sure the hypostasis and causes of the phenomenon, the character of this phenomenon was analyzed and induced, based on the investigation of traffic accident data of 5 years occurring in a freeway in South China. Then the possible causes of traffic accident migration were researched. And some potential causes of traffic accident migration was analyzed by studying accident causes and analyzing the variation of infrastructure and safety measurements of the freeway.

INTRODUCTION

The accident migration is a phenomenon which is found when accident data was statistically analyzed along a highway. The phenomenon was a puzzle whether the measurements of traffic safety improvement adopted in a black spot positively impacted the traffic safety of the whole highway. The accident migration was suggested that may indeed exist after intersections were converted to multiway stop control (Persaud, 1986). A migration of accidents from one location to another was distinctly found as an effect of adding an additional non-standard mixed-flow lane to a freeway in a restriping and reconstruction projects (Levine et al, 1988). And a potential for accident migration was showed through micro-simulation to application of variable speed limits on I-4 in Orlando, Florida (Abdel-Aty et al, 2006).

There were two viewpoints about the causes of the accident migration. One was that the statistical analysis deviation caused the phenomenon of accident migrations. Some researchers found there was a bias in the before and after comparison of accident frequencies in sites due to impropriety of the process of dividing the whole highway into some sections by a kind of rules (such as equidistance). The bias and its causes was proved by presenting a new probabilistic hypothesis and analysis of simulation result (Maher, 1987). And a bivariate negative binomial model was established to explain traffic accident migration (Maher, 1990).

The other was that the driver's risk compensation effect caused the accident

migrations. The drivers escaped from the potential threat of traffic accident owing to the safety improving measurements in the sites the measurements bringing into effect. And consequently they would be less aware of the dangerous during driving. The reduction of vigilantness may continue for a long distance and increase the risk of traffic accident in neighborhood sections of the sites, which is called the risk compensation. On the basis of this, the authenticity of accident migrations was verified and the scope of the migrations was researched (Boyle et al, 1984).

Although some evidences and research have proved the presence of accident migration, and its causes were analyzed, there is still some controversy over whether or not this effect actually exits. And there are no established techniques yet available to estimate such a effect for a particular site (PIARC, 2003). In this paper, new cases of accident migration were presented and their character and causes were analyzed based on road traffic accident data in China.

GENERAL INFORMATION ABOUT THE G4 FREEWAY

The G4 National Freeway is an important and busyness highway corridor from North China to South China. The section which was discussed was about 109 kilometers long in South China. There are many sharp turns, long and abrupt longitudinal gradients, grand bridges and long tunnels in the section when it goes through the natural calamitous mountain area of South China, which caused the high risk of traffic accident, macroscopically.

Table 1. Design Guide Line of The Section of The G4 Freeway.

Design Guide Lines	Unit	Value	
		Hilling Terrain	Mountain Terrain
Design Speed	km/h	100	80
Subgrade Width			
Entirety	m	24.5	23.0
Separate	m	2×12.5	2×11.75
Least Radius of Horizontal Curve	m	1000	500
Maximal Longitudinal Gradient	%	2	5
Least Radius of Vertical Curve			
Protruding	m	10000	8000
Concave	m	12611	8000

The section is a bidirectional freeway with four lanes. different criteria is adopted in hilling terrain segments (from K0 to K13 and from K85 to K109) and mountain terrain segment (from K13 to K85) of the section. The design guide lines of the two kind of terrain was shown as Table 1. The section was open to traffic in April, 2003. And two phases traffic safety improvement projects were implement in 2004 and 2005 because of severity of traffic accident.

BLACK SPOTS ANALYSIS

More than 2200 traffic accident have occurred during the period from April,

2003 to December, 2007 in the section of the G4 freeway. And there are 557 severe traffic accident one of which leads at least one death or three grievous bodily harm. Based on analysis on spatial distribution of the severe traffic accident, the black spots of the section were found by means of cumulative relative frequency (Pei Yu-long, Wang Wei, 2004).

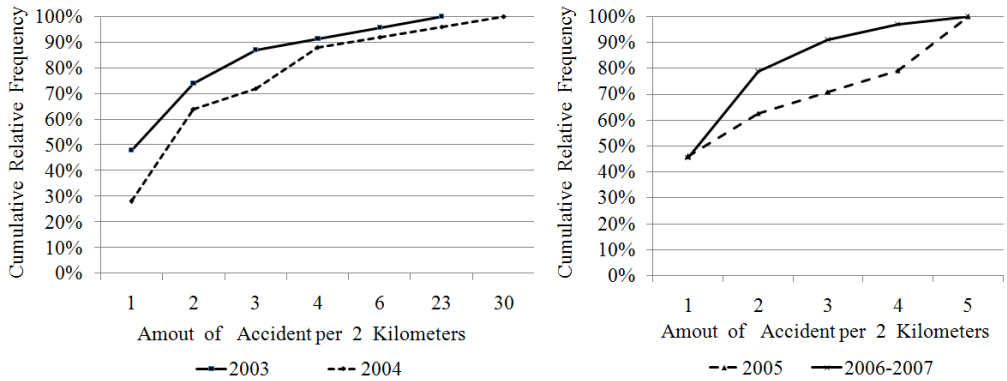

Figure 1. Cumulative relative frequency curves (downwardness).

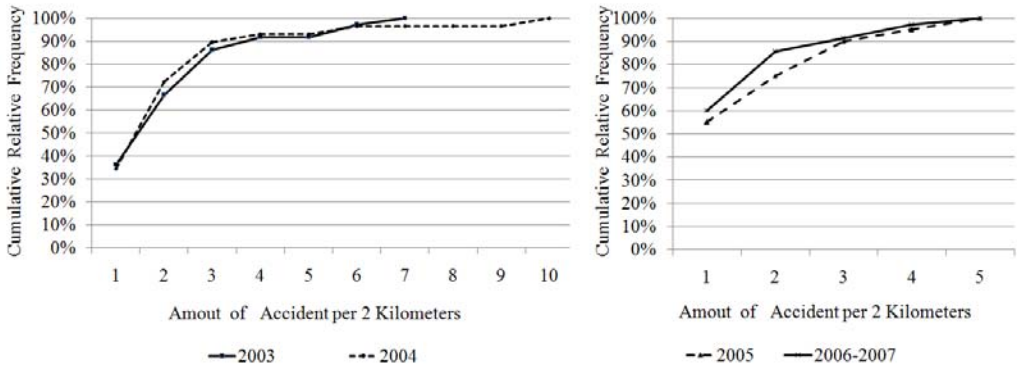

Figure 2. Cumulative relative frequency curves (upwardness).

Table 2. Number of Black Spots.

Period	Direction	Criteria	Number of black spots
2003	downwardness	3	6
	upwardness	3	11
2004	downwardness	4	7
	upwardness	3	7
2005	downwardness	5	9
	upwardness	3	5
2006-2007	downwardness	3	3
	upwardness	3	5

The accident data was disparted into two parts by different direction of upwardness (from South to North) and downwardness (from North to South). The traffic accident occurring frequency was counted in the freeway segment per 2 kilometers. Then the cumulative relative frequency curves was drawn every year

from 2003 to 2007 by counting the frequency of sites where the amount of accident was the same (seeing Figure 1 and Figure 2). The year of 2006 and 2007 were considered as one period of time for the safety improvement projects were accomplished in 2005.

The threshold filtering black spots was confirmed, according to cumulative relative frequency curves. The sites where the amount of accident was equal to or more than the value in the inflexion of the curves or in the point of cumulative relative frequency being greater than 85% (seeing Table 2).

CHARACTER ANALYSIS OF THE ACCIDENT MIGRATION

A kind of chart can be drawn to describe the spatial relationship of black spots in different periods by labeling the black spots with a coordinate of mileage (x axle) where the sits located and year (y axle) when the sits were considered as a black spot. And the size of the points in the chart represents the amount of accident occurring in the site. This kind of chart was drawn according to analysis of black spots of the two directions in order to find the phenomenon of accident migration (seeing Figure 3 and Figure 4).

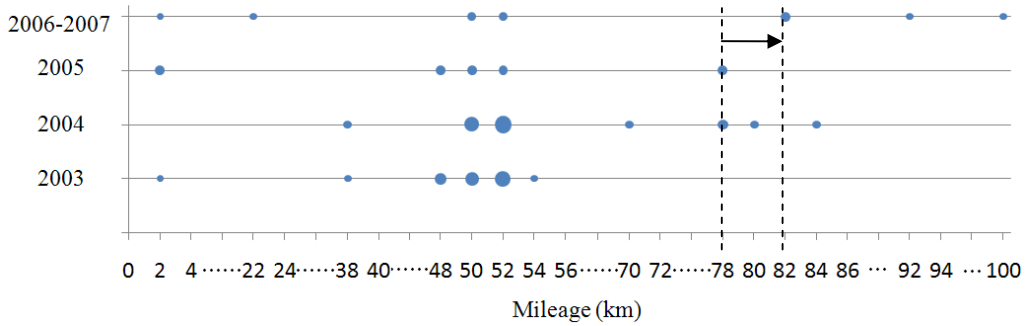

Figure 3. Spatial relationship of black spots (downwardness).

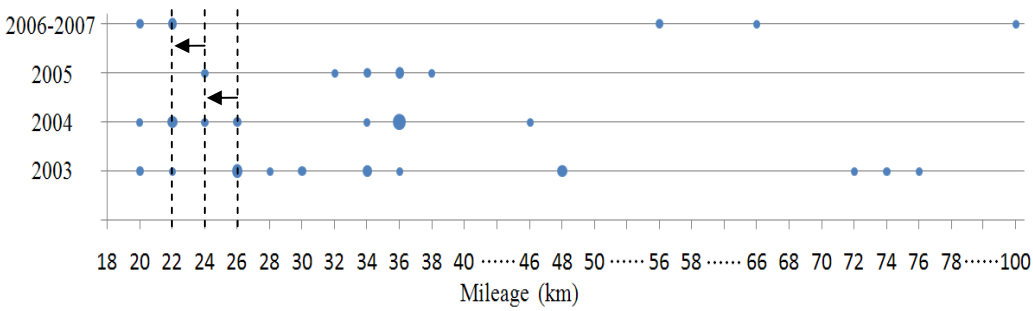

Figure 4. Spatial relationship of black spots (upwardness).

By analyzing spatial relationship of black spots, an accident migration from the segment of K76 - K80 to that of K80 - K82 can be found after the safety improvement of 2005 in downward direction. And an accident migration can be found in the segment of K20 - K26 in upward direction.

The downward Segment of K76 - K82. A spatial relationship of accident

which occurred in the downward segment of K76 - K83 was drawn by labeling the actual mileage of the accident, by which a more accurate spatial relationship was described (seeing Figure 5). So accident congregating in the segment of K77 - K79, especially nearby the site of K78, can be found in 2004 and 2005. Contrastively, there was only one accident occurring in site of K78 during the two years period from 2006 to 2007. And the four accident occurring in the site of K82 (where severe accident seldom occurred before 2006) indicate a new black spot during the period from 2006 to 2007. So the accident migration can be concluded from the segment of K77 - K79 to that nearby K82.

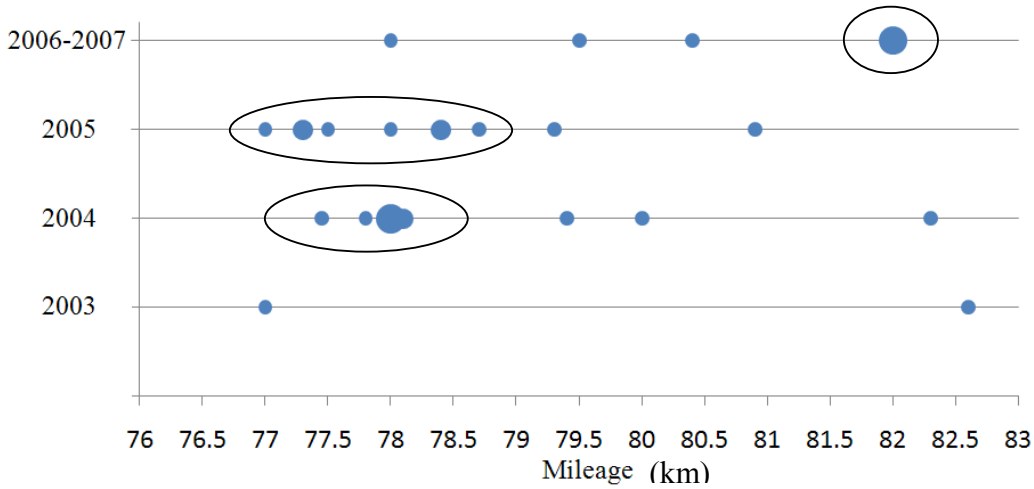

Figure 5. Spatial relationship of accident (downward Segment of K76 - K82).

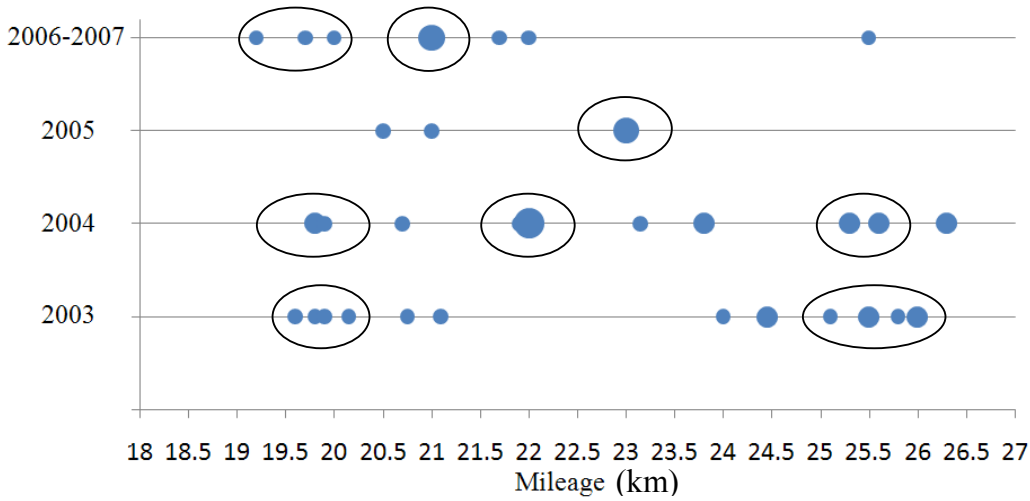

Figure 6. Spatial relationship of accident (upward Segment of K20 - K26).

The upward Segment of K20 - K26. There was a seeming macroscopical trend which the accident-congregating sites migrated from the segment of K25 - K26 to north (direction of mileage decreasing). But the segments of accident

congregating during the period from 2006 to 2007 were also site where accident congregate in 2003 and 2004 (seeing Figure 6). So it was unable to conclude the existence of accident migration from segment of K25 - K26 to that of K20 - K21.

CAUSES ANALYSIS OF THE ACCIDENT MIGRATIONS

The design and safety improvement countermeasure of the segment of K76 - K82 and K20 - K26 was investigated in order to find the causes of the migration perhaps occurring in the two sites. And the character of migrations was defined farther by analyzing the causes.

The downward Segment of K76 - K82. There are two tunnels in this segments with horizontal curves. The first tunnel located in the segment of K76 - K78 is more than 2,100m long with the alignment combined with two curves whose radius is 1,900m and 1,000m respectively and one straight line about 800m long. There was about 16 rear-end accident occurring in the tunnels because of the bad sight distance and overspeed according to analysis of the accident data. Speed control devices, sight guidance device and enhancing enforcement of police were implemented in the process of safety improvement projects during the period from 2004 to 2005. Then little accident occurred in this tunnel in 2006 and 2007. However, there is another tunnel in the segment of K81 - K82 which just locates in the lower reaches of the first tunnel. The alignment of the second tunnel is also combined with two curves whose radius is 2,300m and 1,560m respectively. Four accident occurred in the second tunnel in 2006 and 2007. Contrastively no severe accident occurred in the second tunnel before 2006.

So the accident migration from the segment of K77 - K79 to that nearby K82 can be explained by the theory of the risk compensation.

The upward Segment of K20 - K26. There is a continuous long downgrade just in upper reaches of this segment which is more than 10km long with average gradient of 3%. On the one hand, the accident occurring in this segment was mainly due to brake heat fade and lose control of vehicles impacted by the continuous long downgrade. Truck escape lanes and service zone were rebuild at the end of the continuous long downgrade during the process of safety improvement in 2005. On the other hand, there is a long straight line from K20 to K22 and the average gradient of downgrade in this segment is almost 4%. Partly because of the existence of the long steep downgrade straight line, there was rear-end accident in almost every years during the period from 2003 to 2007, and there was more than 10 accident in the segment at the end of the long straight line (nearby K20) during the past 5 years, according to the analysis of accident data.

So it was different of the main causes of accident occurring in the segment of K25 - K26 and that of K20 - K22. And the causes of accident occurring in the segment of K20 - K22 had existed before the safety improvement implement.

Therefore it was difficult to define the accident migration from the segment from segment of K25 - K26 to that of K20 - K21, although the traffic was also impacted by the continuous long downgrade in upper reaches of K26.

CONCLUSION

A case of traffic accident migration was presented based on freeway accident data in China. The phenomenon of accident migration was found by means of drawing and analyzing a kind of chart of spatial relationship of accident. And the facticity of two accident migrations was analyzed and distinguished.

Causes analysis of the accident migrations was done by comparing the accident data before and after the safety improvement effort and analyzing the alignment of the freeway. It was proved important that paying more attention to the segment of lower reaches when traffic safety of a site was improved according to the case of accident migration.

The existence of accident migration was proved again according traffic accident data in China. However, the causes of the accident migration, for example risk compensation, still need to be approved by some research based on direct data.

ACKNOWLEDGMENT

The authors thank the Scientific Innovation and Personnel Developing Projects of Research Institute of Highway, MoT, China for its sponsoring.

REFERENCES

Abdel-Aty, Mohamed; Dilmore, Jeremy; Hsia, Liang (2006). "Applying variable speed limits and the potential for crash migration." Safety Data, Analysis, and Evaluation, Transportation Research Record, n 1953, 21-30

Boyle, A. J. ; Wright, C. C.(1984) "Accident 'migration' after remedial treatment at accident blackspots". Traffic Engineering & Control, 25(5), 260-267

Levine, Douglas W. (Univ of California); Golob, Thomas F.; Recker, Wilfred W (1988). "Accident migration associated with lane-addition projects on urban freeways." Traffic Engineering & Control, 29 (12), 624-629

Maher, M. J. (1900). "A bivariate negative binomial model to explain traffic accident migration." Accident Analysis & Prevention, 22(5), 487-498

Pei Yu-Long, Wang Wei (2004). "Research on the causes and countermeasures of road traffic accidents". Science Press, Beijing, 4.3.8

Persaud, Bhagwant N (1986). "Safety migration, the influence of traffic, volumes, and other issues in evaluating safety effectiveness – some findings on conversion of intersections to multiway stop control." Transportation Research Record, 108-114

PIARC Technical committee on road safety (C13) (2003). "Road safety manual" Part 2, Chapter 8, 298-299

A Time-varying Route Optimization Model for Urban Hazmat Transportation

Wang Yunpeng[1], Sun Wencai[1], Li Shiwu*[1], Sun Weiyuan, Tian Jingjing[1], Wang Haiwei[1], Wang Hui[1], Chen Yi[1], Cao Gang[1]

[1]Traffic Environment Laboratory, Traffic &Transportation School of Jilin University, Jilin Changchun.

*[1]The corresponding author: Li Shiwu, Tel:043185095086, Email:shiwu@jlu.edu.cn

ABSTRACT

In order to arrange the route of hazmat transportation reasonably and reduce the harm brought by hazmat accidents, influencing factors including transportation cost, environmental risk, rescue capability, road accident risk, population risk, and traffic condition in hazmat transportation under time-varying conditions are analyzed. The urban road network in Changchun city was selected as the research object, an optimum model of transportation route under time-varying conditions was established based on ArcGIS and evaluated and analyzed using real data. The results show that the route optimized under time-varying conditions of the model is reasonable, and the graphics description is valuable for supervisors.

Key words: *Hazmat transportation, Urban road network, Route optimization, Time-varying, ArcGIS*

0 INTRODUCTION

In recent years, with the increasing of hazmat transportation volume year by year, traffic accidents related to it have also been increasing. Because the hazmat traffic accidents happen often accompanied by disasters (leakage, combustion, explosion, poisoning, etc.) so that the after effects and influence are serious. Therefore, the scientific and reasonable measures of hazmat transportation in all aspects of management are very necessary, while route optimization is the most important part of hazmat transportation.

From the existing research (Miaou et al. 1991), most of the hazmat transportation routes optimizations are single-objective, just for transportation costs, distance, time and risk etc., and the hazmat transportation is reduced to the shortest route problem (Revelle et al. 1991; Sung et al. 2000), and the majority are focused on the theoretical analysis (Wu et al. 2004), and less practical (Wang et al. 2009).

In this paper, a route optimization model of hazmat urban transportation under the time-varying conditions is created based on a GIS platform.

1 MODELING

1.1 Analysis of modeling target

Generally, in hazmat transportation, three of the most typical objectives are considered: cost, risk and equity.

1.2 Analysis of influencing factors

The influencing factors include transportation cost, environmental risk, rescue capability, accident risk, population risk, and traffic conditions. The first three do not have time-varying characteristics, while the latter three do.

- Transportation Cost - includes two elements: distance and time.
- Environmental Risk - the harm of hazmat transportation accidents to the surrounding environment.
- Rescue Capability - evaluated by the distance between the accident location and the surrounding rescue facilities.
- Accident Risk - The accident risk value of hazmat transportation route is the sum of all of the sections of the road. The accident rate is different at different times of the day.
- Population Risk - There is no obvious difference among the threats brought by the hazmat leakage to the separate individuals in the region within a certain distance. Therefore, the spots with dense population are chosen as the centers in this paper, sub-divided into three different regions according to the different distances, named as buffer that is the high-concentration zone (zone 3), the middle-concentration zone (zone 2), low-concentration areas (zone 1), concentration is changed with distance. When section of road lies in the 1,2,3-class buffer zone, risk of population exposure is low, middle and high separately.
- Traffic Condition – Forbidden pass or restricted pass etc. in technology or by law, as well as traffic jams, delay etc. need to be considered in route choice of hazmat transportation.

1.3 A Time-varying Route Optimization Model

$$R = \left[\sum_{c=1}^{n_c} \left[w_c \sum_{cf=1}^{n_{cf}} w_{cf} s_{cf} \right] \right] \tag{1}$$

where c is risk type; n_c is the number of risk type; w_c is the percent weight of c; cf is the factor of c type; n_{cf} is the number of the factor of c type; w_{cf} is the percent weight of the factor of c type; s_{cf} is the level of the percent weight of the factor of c type.

Formula (2) is comprehensive cost at the time-varying conditions, where,

w_f is the weight of each factor.

$$Cost_{t_m,route} = w_{tra_cost} \times F_{TC}\begin{Bmatrix} t_l_{t_m,route} \\ t_t_{t_m,route} \end{Bmatrix} + w_{acc} \times F_{AR}\left\{r_a_{t_m,route}\right\} + w_{pop} \times F_{PR}\left\{r_p_{t_m,route}\right\}$$
$$+w_{entir} \times F_{ER}\left\{r_e_{route}\right\} + w_{succor} \times F_{RC}\left\{s_c_{route}\right\} + w_{traffic} \times F_{TC'_{t_m,route}} \quad (2)$$

Get the optimal route of urban hazmat transportation under the time factor, as:

$$Route_{t_m}^{opt} = \min Cost_{t_m,route} = \min \sum_{t_m,arc} Cost_{t_m,arc} \times arc \quad (3)$$

$Cost_{t_m,route}$ is the comprehensive cost of hazmat transportation route at t_m time segment; $Cost_{t_m,arc}$ is the comprehensive cost of road section at t_m time segment; $Route_{t_m}^{opt}$ is the optimal route of hazmat transportation route at t_m time segment; t_m is the period of the time hazmat vehicle run in ; $m = 1,2,\cdots\cdots,24$; arc is 0 or 1.

2 APPLICATION AND EVALUATION OF THE MODEL

2.1 Assumption and the initial conditions of data

The accident statistical data from the traffic police department are regarded as an objective reflection of the actual accidents; section of road is the object in the calculation of accident risk analysis, and the range of the road section is defined in [0, 5] km ; only the delay of a typical intersection is analyzed.

- Accident risk - Hourly distribution of yearly road traffic accidents is based on the statistical urban accident data from the traffic command center in Changchun City, as shown in Figure 1:

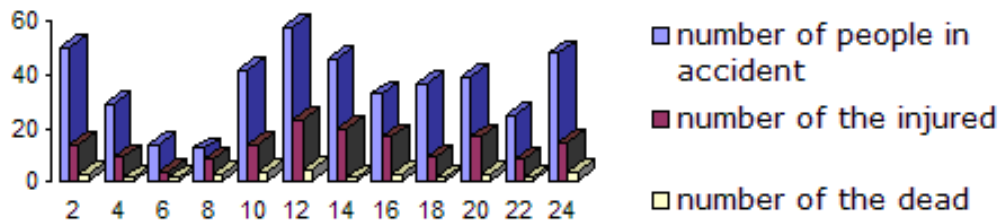

Figure 1. Hourly distribution of yearly road traffic accidents.

The frequency of historical accidents that happened in a certain period of time is regarded as the modifying coefficient of the accident risk.

$$risk_acc_{t_m,route} = \sum_{t_m,arc} (a_{t_m,arc} \times acc_prob_{arc} \times acc_level_{arc} \times leak_prob_{arc}) \times arc \quad (4)$$

where, t_m is the time period of hazmat transportation vehicle，$m = 1, 2, \cdots\cdots, 24$；$A_{t_m}$ is the number of accidents occurred in the period of time t_m；$risk_acc_{t_m, route}$ is the accident risk of hazmat transportation in the period of time t_m.

- Population Risk - The schools, malls, restaurants and recreation grounds are chosen to be analyzed, and the population distribution of such location is shown in Figure 2. Here, 10:00~14:00 is selected as period T1 (malls and restaurants as the main consideration); 14:00~18:00 as period T2 (malls and schools as the main consideration); and 20:00~24:00 as period T3 (recreation grounds as the main consideration) to analyze the transportation route.

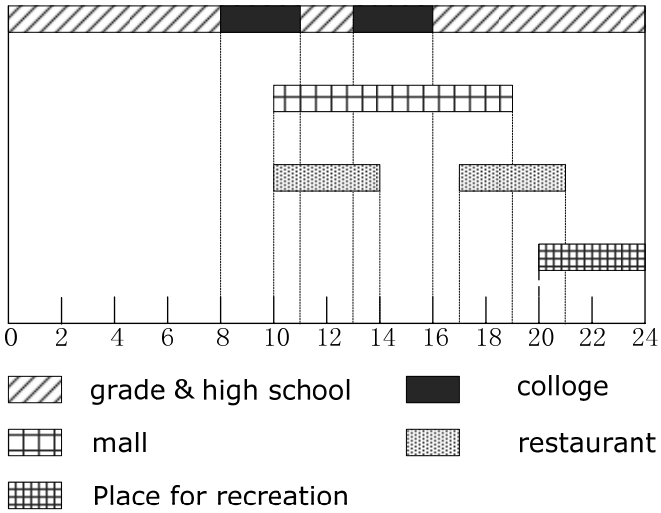

Figure 2. The period of high-density population distribution.

- Traffic Condition - In this paper, Gongnong Square is chosen as a typical intersection. Representative data is obtained via point-sample observation.
  The total waiting time: $T = 297 \times 15 = 4605\ Veh.S$ (5)
  The average waiting time on the entrance road per vehicle:

$$T_{wait} = {}^{4605}\!/_{469} = 9.8\ S \quad (6)$$

  Others waiting time is zero.

2.2 Weighting Factors

The weights are calculated by the way of the expert marking，as shown as Table 1.

Table 1. Weighting factors.

Influencing Factors	Layered Index	Weight
Traffic Condition	Time	0.144
	Distance	0.176
Accident Risk	/	0.230
Population Risk	/	0.193
Environmental Risk	/	0.097
Rescue Capability	Hospital	0.064
	Fire Protection	0.038
	Police	0.058

2.3 Time-varying Route Optimization

The crossing of Jilin road and the East Ring Road is selected as the origination of the transportation，the crossing of Huolinhe Road and West Ring Road as the destination. The analysis results based on the GIS are shown as figure 3~5.

- The route analysis in period of T_1
- The route analysis in period of T_2
- The route analysis in period of T_3

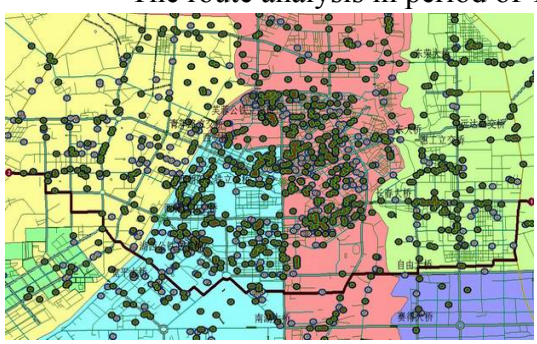

Figure 3. Route in period of T_1.

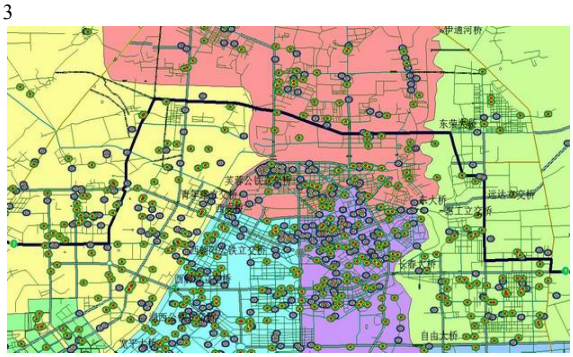

Figure 4. Route in period of T_2.

- The route analysis in period of T_2

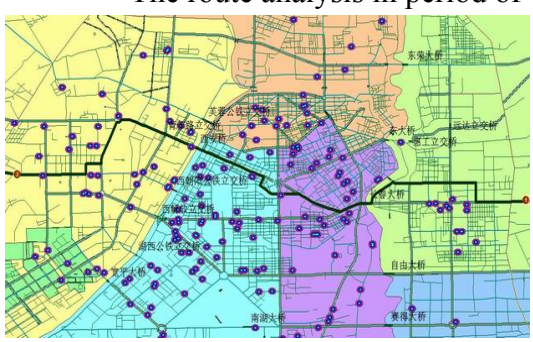

Figure 5. Route in period of T_3.

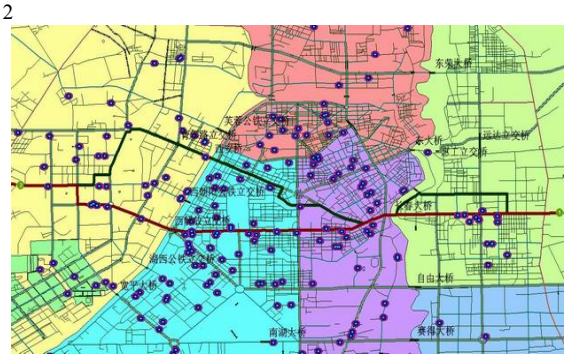

Figure 6. The contrast A(T_1)& B

2.4 Evaluation of the Route Optimization Result

Assume that A is the route of the model, B is the shortest route. The above result comes from the integrated evaluation, but in reality, the route choice is generally made by transportation cost, so that most of the drivers choose the shortest distance route, the contrast is as follows (Figure 6 through Figure 8).

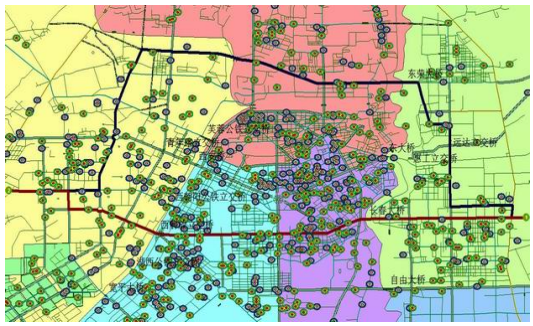

Figure 7. The contrast A(T_2)& B

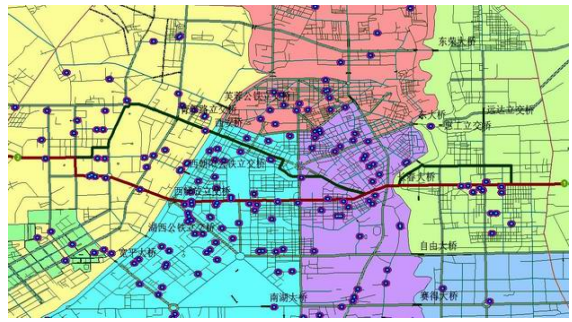

Figure 8. The contrast A(T_3)& B

The result of the contrast analysis can be summarized from Table 2, as follows:

- The number and the risk degree of the high-density population region that A goes through are both much less than B.
- Although B is less than A in distance, the integrated cost of B is obvious.
- Hazmat transportation has strong time-varying characteristics.

Table 2. Index contrast between the shortest route and the route of the model.

Period of time	T_1		T_2		T_3	
Index	Integrated Cost	Distance	Integrated Cost	Distance	Integrated Cost	Distance
Shortest Route	98.25	15598.26	74.23	15598.26	57.33	15598.26
Route of the Model	48.03	18172.49	55.06	21941.17	23.53	16868.98
Multiple / Difference	2.10	2574.23	1.39	5342.91	2.52	1270.71

3 CONCLUSION

In this paper, a route optimization model of urban hazmat transportation under the time-varying conditions is created and evaluated by real data. In the model, the integrated influence of multiple factors is regarded as the final target. The results show that hazmat transportation has strong time-varying characteristics; the model is valuable for supervisors, and the practicability and maneuverability in the route

choice of urban hazmat transportation will be improved.

ACKNOWLEDGEMENTS

This work is financially supported by the National Natural Science Foundation of China (No50878094) and Jilin Provincial Science & Technology Key Program (No. 20065007) and the National Key Technology R&D Program (No. 2006BAJ18B02).

REFERENCES

Miaou S. P., Chin S. M. Computing k-shortest path for spent nuclear fuel highway transportion[J]. European Journal of Operational Research, 1991, 53: 64-80.

Revelle, C., Cohon, J., Shobrys, D. Simultaneous siting and routing in the disposal of hazardous wastes[J]. Transportation Science, 1991, 25(2): 138-141.

Sung, K., Bell, M. G. H., Seong, M., Park, S. Shortest paths in a network with time dependent flow speeds[J]. European Journal of Operational Research, 2000(121): 32-39.

Wang Yun-peng，Sun Wen-cai etc. Study on the Model of Optimum Route for Hazardous Material Transportation in Urban based on ArcGIS[J]，Journal，2009, 39(1): 45-49.

Wu Zongzhi, Duo Yingquan, Liu Mao, et al. A study on the methods of risk assessment of hazardous materials during road-transportation[J]. Journal of Basic Sience and Engineering, 2004, 12: 36-44.

A Speed Limit Model of Vehicle for Urban Road Hazmat Transportation

WANG Yunpeng[1], SUN Wencai[1], LI Shiwu*[1], LI Gunan, TIAN Jingjing[1], WANG Hui[1], CHEN Wanji[1]

[1]Traffic Environment Laboratory, Traffic and Transportation School of Jilin University, Jilin Changchun.

*[1]The corresponding author: Li Shiwu, Tel:043185095086, Email: shiwu@jlu.edu.cn

ABSTRACT

For problems in the process of limiting speed of a vehicle for urban road, safety benefits and traffic benefits are regarded as the assessment indicator, and a decision-making model of speed limit optimization is proposed. Combined with the characters of hazardous material transportation, the model is revised based on AHP and fuzzy comprehensive evaluation methods, a speed limit model of vehicles for urban road hazardous material transportation is established and verified via the real vehicle. The results show that the dispersion degree of vehicle speed running at the speed from speed limit model is obviously reduced, and the model has a significant feasibility and practicality.

Key words: *Hazardous material transportation, urban road, speed limit*

1 INTRODUCTION

Velocity is an important factor to induce road traffic accidents. For the transportation of hazardous material, excessive speed is the main reason leading to transport accidents (Guo et al. 2006); and because of the specificity of the transportation of hazardous material, reasonable speed limits is essential for ensuring their safety (Suo et al. 2005).

As seen from the existing research, there are few studies on running speed for urban roads, and the factors are not considered across-the-board (Watanatada et al. 1987; Leisch et al. 1977); speed limit is unreasonable, and there are few quantified models for speed limits (Abishai et al. 2000); I have not yet found the research on speed limits for the transportation of hazardous material.

Based on the AHP and the fuzzy logical reasoning, for the social benefits and traffic benefits, a speed limit model for urban hazmat transportation is created in this paper, which provides an effective way to decrease the accident rate.

2 THE ESTABLISHMENT OF A SPEED LIMIT MODEL OF URBAN HAZMAT TRANSPORTATION

2.1. The speed limit model for general goods transportation

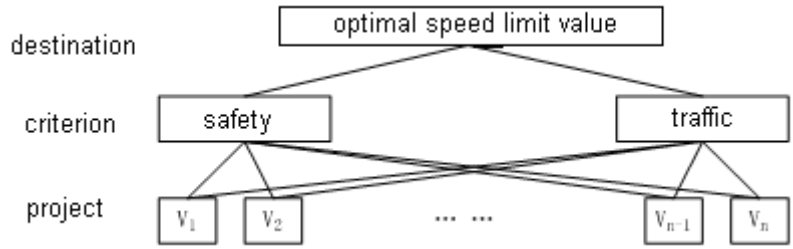

Figure 1. Optimal speed limit model.

2.1.1. The weight of criterion layer to destination layer

The weight of "safety benefits" and "traffic benefits" in the process of determining speed limit usually depends on type of road function, road location and the development level of the region along the road. The weight $\omega^{(2)} = [\alpha_1, \alpha_2]^T$ of "safety benefits" and "traffic benefits" is obtained in different statuses of traffic via Delphi.

2.1.2. The weight of project layer to criterion layer

- The determination of the project layer to weight of "safety benefits" - the weight of project layer on the "safety benefits" is obtained through calculation of authority vector $\omega_1^{(3)}$.
- The determination of the project layer to weight of "traffic benefit" - the weight of project layer to the "traffic benefit" is obtained through the calculation of the weight vector $\omega_2^{(3)}$.

2.1.3. The weight of project layer to destination layer

The combined weight ω of project layer to destination layer is used to indicate the membership degree of speed included in speed domain.

$$\omega = \left[\omega_1^{(3)}, \omega_2^3\right]^T \cdot \omega^{(2)} \tag{1}$$

2.2. The speed limit model for hazmat transportation

2.2.1. The indicator system for evaluating environment of hazmat transportation

The evaluation indicator system model for transportation environment impacts on safe speed of the hazmat transportation. As shown in Figure 2.

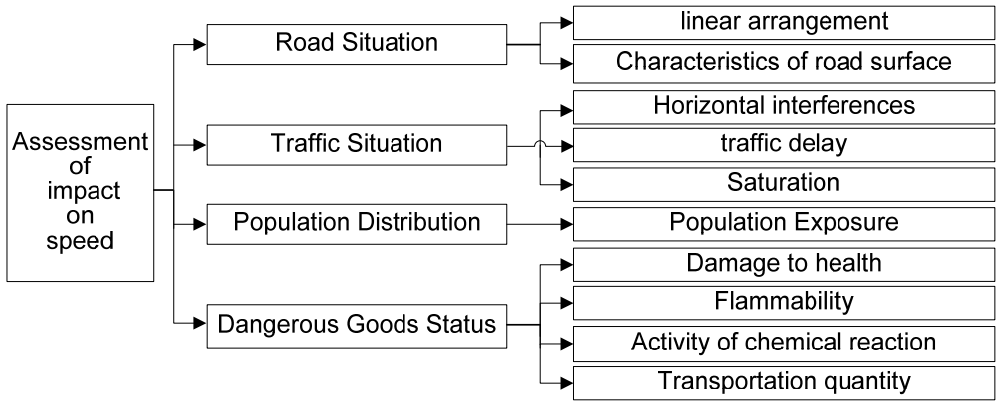

Figure 2. Evaluation indicator system.

2.2.2. The determination of weight of indicator

(1) Evaluation method

- Delphi method - Based on the Delphi method, this paper carries out that the qualitative evaluation indicator is converted into the quantitative. According to the evaluation system of impact on speed of hazardous material transportation, the Expert Opinion form is made.
- Fuzzy overall evaluation method

(2) Weight Calculation

According to the returned expert opinion form, the specific evaluation scores are determined, and then the weight of each indicator is calculated via AHP.

①Starting from road situation, traffic situation, population distribution, hazmat status, via the consulting experts' opinion for three rounds, finally the scorings of above three key factors are calculated, and it shows that they distribute at 3,8,5,6.

②Calculating the geometric mean of all elements of the same line of Judging matrix, $\varpi = (0.5791,1.5444,0.9652,1.1583)^{T}$

③ϖ_i Normalization，$W = (0.1364,0.3636,0.2273,0.2727)$

By referring to experts' advice, the following assessing grade and revising coefficients are determined, as shown as Table 1.

Table 1. Assessing grade and revising coefficient of transportation environment.

Scoring	Description	Coefficient
100-85	Almost no risk	1.0
75-85	Little risks	0.9
60-75	Heavy risks	0.7
60	Transportation prohibited	0.0

3 APPLICATION OF SPEED LIMIT MODEL OF URBAN HAZMAT TRANSPORTATION

In this paper, Yatai Street (an express road) in Changchun city is selected as the route. There are residential areas, schools, commercial areas, etc. along the road, so the traffic condition is complex. Divide the road into different sub-sections.

3.1 Speed limit of general goods transportation

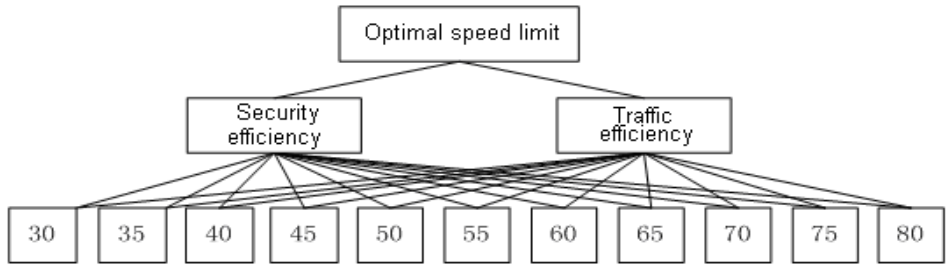

Fig 3. Decision-making model for determining speed limit of Yatai Street.

Through the questionnaire survey among experienced drivers, 80 questionnaires were collected, including 46 taxi groups, 24 private cars groups, and 10 other groups. The decision-making model for the optimal speed limit is built as shown in Figure 3:

(1) Determination of the weight of "safety benefit" and "traffic benefit" to decision-making of speed limit $\omega^{(2)} = \begin{bmatrix} 0.75 \\ 0.25 \end{bmatrix}$

(2) Determination of the normal speed membership degree of each speed

The normal speed subjection degrees are calculated, as shown as Table 2:

Table 2. Normal speed membership degree of each speed.

Speed km/h	30	35	40	45	50	55	60	65	70	75	80
Membership Degree	0.24	0.25	0.84	0.79	0.93	0.64	0.63	0.14	0.11	0.01	0.01

(3) The weight $\omega_1^{(3)}$

$$\omega_1^{(3)} = (0.0519,0.0546,0.1831,0.1721,0.2022,0.1393,0.1366,0.0301,0.0246,0.0027,0.0027)$$

(4) The weight $\omega_2^{(3)}$

$$\omega_2^{(3)} = (0.0495,0.0578,0.0661,0.0743,0.0826,0.0909,0.0992,0.1074,0.1157,0.1239,0.1322)$$

(5) Combined weight of project layer to destination layer

$$\omega = \left[\omega_1^{(3)}, \omega_2^{3}\right]^T \bullet \omega^2 \tag{2}$$

(6) The optimal speed limit

Integrated weight of speed is included in the speed field $V=\{30,35,40,...,80\}$, as shown as Table 3. The weight of 50 km/h is highest. Therefore, the optimal speed limit of Yatai Street is 50 km/h.

Table 3. Integrated **weight of every speed (km/h).**

Speed	30	35	40	45	50	55	60	65	70	75	80
Weight	0.04	0.04	0.14	0.13	0.15	0.11	0.10	0.02	0.02	0.00	0.00

3.2 Speed limit of hazmat transportation

Take a 10t LPG truck as an example. According to experts' advice, marks of the first section are shown in Table 4.

According to the evaluation of the hazmat status, the fuzzy assessing matrix of hazmat status is as follows,

$$Q_n = A_n \bullet [Q_{n1} \quad Q_{n2} \quad Q_{n3} \quad Q_{n4}]^T \tag{3}$$

$$Q_1=[0.3864 \quad 0.3134 \quad 0.1431 \quad 0.1570],\ Q_2=[0.1678 \quad 0.2461 \quad 0.1778 \quad 0.4083]$$

$$Q_3=[0.2924 \quad 0.3698 \quad 0.1581 \quad 0.1798],\ Q_4=[0.6292 \quad 0.2434 \quad 0.0159 \quad 0.1116]$$

Table 4. Evaluation of the first section.

Indicator for different layer	Assessment			
	Best	Better	Good	Bad
Reasonability of linear arrangement	0.6	0.2	0.2	0.0
Characteristics of road surface	0.7	0.2	0.1	0.0
Horizontal interferences	0.6	0.3	0.1	0.0
Traffic delay	0.4	0.4	0.2	0.0
Saturation	0.4	0.4	0.2	0.0
Population Exposure	0.3	0.2	0.3	0.2

According to the experts' advice, the weight W of the evaluation Q are as follows,

$$W_1=100 \quad W_2=80 \quad W_3=60 \quad W_4=40$$

$$S_{\text{authority}} = \sum_{j=1}^{5} q_j \bullet W_j \tag{4}$$

$$S_{\text{authority1}}=78.5808,\ S_{\text{authority2}}=63.4661,\ S_{\text{authority3}}=75.4959,\ S_{\text{authority4}}=87.8033$$

Combining with the evaluation level and revising coefficients in Table 3, speed

limits for every subsection for hazmat transportation are established as: 45 Km/h, 35 Km/h, 45 Km/h, 50 Km/h.

3.3 Result analysis

(1) "Consistency Test" evaluation

As shown in Figure 4, the speed limit and the overall trend of speed and average speed of every section are consistent. It shows that the speed limit is reasonable.

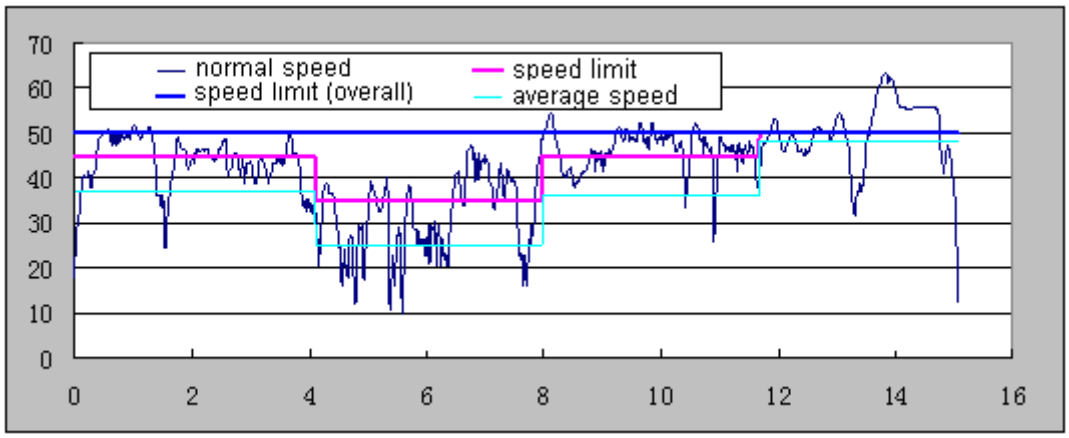

Figure 4. Speed comparison chart excluding the impact of the road intersection.

(2) Evaluation of the variance and standard deviation of speed

The various parameters of speed before and after amending of the sections are shown as Table 5. When the speed limit is implemented, each subsection and the overall standard deviation gets better except for the fourth section (influenced by traffic lights). Namely, the frequency and amplitude of speed decline. For hazmat transportation, both impact and risk decline.

Table 5. The statistical data of the speed with 95 percent confidence.

Subsection	First		Second		Third		Fourth		Overall	
variance	133	117	127	81	221	82	85	129	209	145
standard deviation	12	11	11	9	15	9	9	11	15	12
average	37	36	25	22	35	28	48	39	34	30
survey	397	413	549	533	375	355	256	312	1578	1614

4 CONCLUSION

The results show that: the dispersion degree when the car runs at the speed from speed limit model is obviously reduced, and the model has a significant feasibility and practicality.

ACKNOWLEDGEMENTS

This work is financially supported by the National Natural Science Foundation of China(No. 50878094) and Jilin Provincial Science & Technology Key Program (No. 20065007) and the National Key Technology R&D Program (No. 2006BAJ18B02）

REFERENCES

Abishai Polus, Kay Fitzpatrick, Daniel B.Fambro. “Predicting Operating Speeds on Tangent Sections of Two - Lane Rural Highways,” The 79th Annual Meeting Transportation Research Board Washington DC, January 2000.

Guo Wei, et al. Statistical Analysis of Urban Hazardous Chemistry Goods and Countermeasures. Environmental Pollution and Prevention, 9, 2006, 28(9).

Leisch J.E. and Leisch J.P.. New concepts in Design Speed Application. In Transportation Research Record 631, TRB, Washington, D.C.,1977.

Suo Zhang, et al. Speed Analysis of Road Traffic Accident. Traffic Standardization & Traffic and Safety, 156.

Watanatada, T. et al. Vehicle Speeds and Operating Cost, Model for Road Planning and Management. The Johns Hopkins University Press, Baltimore and London, 1987.

Risk Assessment of Road Operation Environment Under Atrocious Weather Condition

Ma Yan[1], Guo Zhong-yin[2], Guo Hua[3] and Xu Yong-gang[4]

[1]School of Transportation Engineering, Tongji University, Ph. D Candidate, Shanghai PRC, 201804, PH (021)6958-5413; email: mayan007@163.com
[2]School of Transportation Engineering, Tongji University, Professor, Shanghai PRC, 201804, PH (021)6958-5413; email: Zhongyin@tongji.edu.cn
[3]East China Brach of Beijing E-hualu Info Technology Co., LTD, Engineer, Shanghai PRC, 200092, PH (021)3362-6771, email: guohua1997@126.com
[4]School of Transportation Engineering, Tongji University, Ph. D Candidate, Shanghai PRC, 201804; The Rail Transit Project Construction Headquater of Ningbo Muncipality, Engineer, Ningbo PRC, 315000, email: xyg@zj165.com

ABSTRACT

Based on the influence of road operation safety under atrocious weather, a risk assessment research is presented from four aspects (i.e. climate environment, road condition, traffic environment, road maintenance and repair) to analyze the risk grade of road facilities operation environment. According to the operation environment analysis, the paper establishes a set of evaluation indexes and evaluation criterion for risk assessment of road operation environment. At the end, the lowest evaluative criterion of road operation environment is given to improve the design of road facilities and intensify operation environment safety of basic road facilities.

1 INTRODUCTION

Road facilities are an important carrier of highway transportation in our country. However, the geological and ecological environment in our country is very complex. Many meteorological disasters such as rainstorms, flooding, drought, cold damage and snow disasters occur frequently on interlaced highway line (Yuchun Yao et al. 2004). The disaster climate causes the road operation environment to be worse and influence the road facility's function and vehicle safety.

Vehicle travel safety depends largely on the security of the road operation environment. Road operation environment includes climate environment, road environment, transportation environment and management environment. Disaster climate has different influences on the road, traffic and management environment. Therefore, research of risk assessment of road operation environment under atrocious weather conditions has the important meaning in guaranteeing the operation safety of road facility and the vehicles.

2 RISK ANALYSIS OF ROAD OPERATION ENVIRONMENT UNDER

ATROCIOUS WEATHER CONDITIONS

The road operation environment is subject to many factors. Under the disaster weather's influence, adverse weather (rain, snow, freezing, etc.) have many disadvantageous impacts on the roadbed and road surface. Landslides and mud-rock flows caused by meteorological disasters will damage the road structure. Therefore, carrying on the real-time monitoring of inclement weather and geological environment is conducive to make the safeguard mechanisms respond promptly, thus improving the road operation environment security.

At the same time, the structural design of roads and the reasonableness of the geometric conditions are the basic premise to ensure the road operation environment safety. Evaluation of the road alignment, line-of-sight, roadbed, pavement performance will help us to determine the anti-risk level of road facilities. On the other hand, rain, snow, fog and other adverse weather conditions disturb the normal operation of traffic flow and cause traffic jams, traffic disruption, even lead to traffic accidents and seriously affect the operation of road traffic safety. When disaster weather occurs, prompt clean-up, maintenance and rehabilitation of the road infrastructure is very important to protect the road facility function and improve road operation environment safety.

In this paper, the risk assessment of road operation environment is researched from four aspects including the natural environment monitor condition, the road condition evaluation, risk degree of traffic environment and road administration maintenance situation.

3 RISK ASSESSMENT OF ROAD OPERATION ENVIRONMENT UNDER ATROCIOUS WEATHER CONDITIONS

3.1 Assessment of Climatic Environment Monitoring

Climatic environment monitoring mainly includes the meteorological condition monitoring and the geological condition monitoring. The function of meteorological condition monitoring lies in the prompt, accurate monitoring of heavy weather. The geological condition monitoring involves the real-time monitoring of the roadbed, road surface and the side slopes in special areas where disasters occur frequently so we can strengthen the prevention of the geological disasters region, draw a plan of pre-disaster early warning and rapid post-disaster recovery repairs to improve the road operation safety.

Climatic environment monitoring puts emphasis on the preparation, availability and emplaced rationality of the meteorology and the geological condition monitoring equipment. Through the environmental monitoring equipment, we can gather exhaustive information of meteorology, geology and natural environment of the road facility. According to the results of data processing, preliminary plans can be made to improve road operation environment safety.

Assessment indexes

1. Meteorological and geological condition monitoring facilities equipped
2. Monitoring equipment layout
3. Monitoring equipment intact ratio
4. Harmonization with road management and maintenance

Assessment contents

1. Establish at least one set of climatic environment monitoring equipment (CEME) on the main line at each road. The quantity and installation location of the CEME should be reasonably selected at the place where weather disasters frequently happened.
2. Establishment suggestion, related department implementation plan, progress report and effect evaluation of the climatic environment monitoring audited by an expert group no less than twice per year.
3. Regular maintenance of CEME should be implemented to ensure the equipment is in good condition and the rate of effectiveness more than 90%. At the same time, the effectiveness and intact rate of CEME set in disaster-prone sections is 100%.
4. The information (including rain, snow, fog and other weather information, landslides, mud-rock flows and other geological disasters information) detected by CEME is timely and accurate available to the road management department, which play a role in early warning and prevention to ensure the road facilities safety.

Assessment requirements

Review and check the index. The related base data of CEME, the recommendations of the expert group, implementation plans of the relevant department and the effect evaluation data of the equipment should be provided (Dianye Zhang et al. 2005).

Assessment grade

Judge the corresponding level by determining the number of indicators which can meet the requirements based on the materials. Assessment grades are shown in Table 1.

Table 1. Assessment grade of climatic environment monitoring situation

Assessment grade	Ⅰ	Ⅱ	Ⅲ	Ⅳ
U_1 Index	Meet 4 requirements [85，100）	Meet 3 requirements [70,85）	Meet 2 requirements [55，70）	Meet 1 requirements [0，55）

Assessment standard of climatic environment monitoring situation

In the process of road construction, there are many differences in funding, technology and management, so the selection and layout of CEME is impossible to achieve the optimal standard. When the request cannot be satisfied, the road operation environment safety may be affected to a certain extent. Therefore, reference to past research results and experts' evaluation, the minimum standard of climatic environment monitoring situation is presented to ensure the road operating environment safety.

Minimum standard: Meet at least three assessment contents to achieve the second-level assessment criteria.

3.2 Risk assessment of road facility environment

The quality of road facilities environment depends on the level of road design and completeness of road related facilities. The level of road design standards has a direct impact on the safety of road operating environment. Under the effect of a weather disaster, a bad alignment or road structure design will bring the result of overall poor road quality, easy damage to the roadbed and pavement and difficulty of repairing. Therefore, a good design of road alignment, roadbed and pavement should be made to enhance the anti-risk ability of road facilities.

Reasonable road safety facilities can improve the road capacity, reduce traffic accidents and the incidence of secondary accidents, save economic cost, alleviate the degree of drivers' fatigue and improve the level of road service. So it is very important in the safety of road operating environment.

Assessment indexes

1. Risk of road alignment
2. Status of roadbed
3. Status of pavement
4. Road safety facilities equipped

Assessment contents

1. Assessment of road alignment risk: Include the combination of horizontal and vertical alignment, sight distance, resultant gradient, curve radius, drainage, etc (PRCMOT 2004). Evaluate the proportionality and rationality of alignment according to the relevant technical standards;
2. Assessment of roadbed status: Include roadbed height, section type, drain etc. Evaluate the intension and stability of the roadbed according to the relevant technical standards;
3. Assessment of pavement status: Including pavement structure, crown gradient, drain, skid resistance, etc. Evaluate the intension, skid resistance and stability of pavement according to the relevant technical standards;
4. Road safety facilities equipped: Include signage and marking, protection and separation, anti-glare, abduction, lighting and emergency assistance and so on. Select and lay out facilities according the requirement of highway engineering

evaluation standards by quality inspection. The facilities settled on the whole road should have the ability of defending bad environment; The highway department should master the facilities status of each road in a timely way and solve the problems quickly.

Assessment requirements

Review and check the index. The relative data of road design, landform and geology data along the road, and in the particular data of the facilities should be provided.

Assessment grade

According to the relevant technical standards, judge the corresponding level by determining the number of indicators which can meet the requirements based on the materials. Assessment grade is shown in Table 2.

Table 2. Assessment grade of road environment

Assessment grade	Ⅰ	Ⅱ	Ⅲ	Ⅳ
U_2 Index	Meet 4 requirements [85，100）	Meet 3 requirements [70,85）	Meet 2 requirements [55，70）	Meet 1 requirements [0，55）

Risk assessment standard of road facility environment

In the process of road design, there are many differences in funding, technology and geology conditions, so the design of road and facility is impossible to achieve the optimal standard. When the request cannot be satisfied, the function of road corollary facilities may be affected. Therefore, reference to past research results and experience, the minimum standard of road facility environment risk is presented to ensure the road operating environment safety.

Minimum standard: Meet at least three assessment requirements, achieve the second-level assessment criteria.

3.3 Risk assessment of traffic environment

The traffic environment is an important influencing factor in road traffic operation safety. Under the influence of weather disasters, the traffic accident event's occurrence frequency is high. The seriousness of the incident and traffic flow status impacts the traffic capacity, the real-time safety and the travel time over the road facility. Through analysis and evaluation of the traffic state, spatial influence and duration under the influence of the weather disaster, the safety of the traffic environment can be determined.

Assessment indexes

1. Traffic state
2. Spatial influence scope

3. Duration

Assessment contents

The operational status of traffic flow was judged based on the traffic volume, travel speed, traffic density, lane occupancy rates and other traffic parameters under influence of a weather disaster. Suggested values of traffic state assessment are listed in Table 3. In order to protect the traffic environment safety, the status of traffic flow should be unblocked.

Table 3. Suggested values of traffic state assessment

Grade	Traffic status
I	Free traffic flow, excellent state
II	Non-free traffic flow, unblocked state
III	Non-free traffic flow, traffic congestion state
IV	Traffic interruption

According to the road sections and road network connectivity, accessibility and capacity, spatial influence scope of traffic incident can be determined. Suggested values of spatial influence scope are listed in Table 4. In order to ensure the road connectivity, influence scope should be limited in small area.

Table 4. Suggested values of spatial influence scope assessment

Grade	Spatial influence scope
I	Only one or two lane blocked, good connectivity and accessibility
II	Partial lane blocked, good connectivity
III	Partial section or road network traffic blocked, bad accessibility
IV	Large-scale road network line blocked, road network traffic interruption

The impact of the Road Traffic Incident can be reasonable judged according to traffic events duration. Suggested values of duration are listed in Table 5.Traffic events' duration should be less than 3 hours to resume the traffic flow operation.

Table 5. Suggested values of duration assessment

Grade	Duration
I	Less than 1 hour
II	2～3 hours
III	4～8 hours
IV	More than 8 hour

Assessment requirements

Review and check the index. The related data of traffic state parameters, the recommendations of the expert group, implementation plans of the relevant department and the effect evaluation data of the equipment should be provided.

Assessment grade

Judge corresponding level by determining the number of indicators meeting the requirements based on the materials. The Assessment grade is shown in Table 6.

Table 6. Risk assessment grade of traffic environment

Assessment grade	Ⅰ	Ⅱ	Ⅲ	Ⅳ
U_3 Index	Meet 3 requirements [85，100）	Meet 2 requirements [70,85）	Meet 1 requirements [55，70）	Meet 0 requirements [0，55）

Assessment standard of traffic environment

In the process of road operation, there are many differences in local land form, physiognomy, climatic conditions and volume of traffic flow, so the assessment of the traffic environment is impossible to achieve the optimal standard. When the request cannot be satisfied, the road operation environment safety may be affected to a certain extent. Therefore, reference to experts' evaluation, the minimum standard of traffic environment is presented to ensure the road operation environment safety.

Minimum standard: Meet at least three assessment requirements, achieve the second-level assessment criteria.

3.4 Assessment of road management environment

Road routine maintenance and rapid repair are important to ensure the normal operation of road traffic under disaster condition. Besides the road routine maintenance, there should be stored necessary materials, machinery and equipments on important road section where climatic and geological disasters often happened.

Assessment indexes

1. Road maintenance, repair material and mechanical facilities equipped
2. Road maintenance staff equipped
3. Effective rate of routine maintenance

Effective rate of routine maintenance =

$$\frac{The\ \ number\ \ of\ \ road\ \ facility\ \ maintenance}{The\ \ number\ \ of\ \ road\ \ facility\ \ damage}$$

Daily maintenance work includes roadbed, road surface maintenance and road disaster prevention and so on. The assessment of highway maintenance quality may refer to《Highway evaluate standard by maintenance quality inspection》(JTJ 075-94)。Suggested values of daily maintenance effective rate are listed in Table 7.

Table 7. Suggested values of daily maintenance effective rate

Grade	Ⅰ	Ⅱ	Ⅲ	Ⅳ
Acceptable range	＞0.8	0.8～0.6	0.6～0.4	≤0.4

Effective rate of rapid repair after disaster

$$\text{Effective rate of rapid repair} = \frac{The\ \ time\ \ required\ \ for\ \ road\ \ repair}{The\ \ average\ time\ \ required\ \ for\ \ road\ \ repair}$$

Rapid road repair work after a disaster includes field cleaning, troubleshooting and repair of the roadbed, road surface, slope, etc. The definition of the repair completion is at least one lane that will allow buses or trucks to pass in case of an emergency situation (Zhang Yi et al. 2007). Suggested values of the effective rate are listed in table 8.

Table 8. Suggested values of repair effective rate after disaster

Grade	Ⅰ	Ⅱ	Ⅲ	Ⅳ
Acceptable range	≤0.4	0.4～0.8	0.8～1.2	＞1.2

Assessment contents

1. Establish at least a road maintenance station on the main line for each road. The outfit rate of road maintenance, repair material and mechanical facilities set in the disaster-prone section is 100%.
2. Highway maintenance staff has to master the maintenance knowledge and skills, each person should be provided with the necessary maintenance equipment and accept effective management.
3. Effective rate of routine maintenance may not be lower than the middle class which is shown in table 7.
4. Effective rate of rapid repair after a disaster may not be lower than the middle class which is shown in table 8.

Assessment requirements

Review and check the index. The related data of road maintenance and repair equipment, the recommendations of the expert group, implementation plans of the relevant department and the effect evaluation data of the equipment should be provided.

Assessment grade

Judge corresponding level by determining the number of indicators which can meet the requirements based on the materials. Assessment grade is shown in Table 9.

Table 9. Assessment grade of manage environment situation

Assessment grade	Ⅰ	Ⅱ	Ⅲ	Ⅳ
U_4 Index	Meet 4 requirements [85，100）	Meet 3 requirements [70,85）	Meet 2 requirements [55，70）	Meet 1 requirements [0，55）

Assessment standard of the road management environment

In the process of road maintenance and repair, there are many differences in funding, technology and management, so road maintenance and repair is impossible to achieve the optimal standard. When the request cannot be satisfied, the road operation environment safety may be affected to a certain extent. Therefore, refer to experts' evaluation, the minimum standard of road management environment is presented to ensure the road operating environment safety.

Minimum standard: Meet at least above two assessment requirements, achieve the third-level assessment criteria.

4 CONCLUSION

By assessing four aspects of road operation environment including climate, road, transportation and administration, it provides road facilities with such functions as early warning before accidents, feedback under emergency and rapid repair after the disaster, so the operating security of the highway is greatly improved (Yan Ma et al. 2007).

1. Function of early warning: According to the evaluation of meteorological and geological environment monitoring, each monitoring facility not only makes prediction and determination timely and correct, but also identifies and warns of the potential for catastrophic weather and road accidents.
2. Function of feedback: By risk analysis and assessment of road running environments, it determines the weakness during road design, analyzes deficiency in transportation management and control under catastrophic weather environments, and feeds back road and traffic information immediately, so as to provide the reference for fundamental research on road operation security.
3. Control function: Once the road traffic is blocked under catastrophic weather, it is able to respond rapidly, sets down a series of measures including recovery service, traffic control and guidance, coordinates and allocates personnel, materials and so on, aiming at repairing the road, opening up the congested traffic and ensuring the normal road traffic operation.

REFERENCE

Dian-ye Zhang (2005). The Evaluation system of road traffic safety management. China Communications Press, January 2005.

Ministry of Transport of the People's Republic of China (PRCMOT) (1996), Technical Specification of Highway Maintenance, No.: JTJ 073-96.

Ministry of Transport of the People's Republic of China (PRCMOT) (2004), Technical Standard of Highway Engineering, No.: JTG B01-2003.

Yan Ma, Hua Guo (2007). Study on Freeway Travel Safety Ensuring System under Unfavorable Weather Condition. The 3rd China Annual Conference on ITS.

Yuchun Yao, Lingkan Yao, Yuanxun Wang (2004), Analysis on Road Disaster and Its

Effect on Environment in Mountain Area. Journal of Catastrophology. Vol.19, pp.16-20.

Zhang Yi, Xiaofen Guo, Jinhui Li (2007), Combinatorial optimization algorithm of rapid road repair and material distribution after disaster. Journal of Traffic and Transportation Engineering. Vol.l7, No.2, 2007, pp.118-121.

Study on Accident Reconstruction Model Based on Reverse-reasoning Method

ZHENG Lili[1], DING Tongqiang[1*], XI Jianfeng[1], SUN Jian[2], LI Jiang[1]

[1] College of Transportation, Jilin University, P.O. Box 130022, Changchun, PH (+86) 0431-85095705; FAX (+86) 0431-85095370; email: zlldtq1024@163.com
[2] Intellectual Property Office of Jilin Province, P.O. Box 150031, Changchun, PH (+86) 0431-82752930; email: dtq8@163.com

ABSTRACT: The article researches on the theory and practice of two-vehicle central collisions and two-vehicle eccentric impacts (collisions), proved that all kinds of complex two-dimensional collisions can transform into one-dimension collisions with theory analysis. Secondly, the article introduces collision parameters k and μ, established a vehicle speed model with a momentum equation and a momentum matrix equation, eliminated affection of impulsive force distributing coefficients by quadratic optimizing, and established accident reconstruction model of two-vehicle collision based on reverse-reasoning method, realized two calculate modes. Finally, the method was found to be effective and feasible by validating with actual cases. We also find that the two basic hypothesis of traffic accidents had effects on accident reconstruction, which need to be researched and optimized in the future.

KEY WORDS: traffic accident, accident reconstruction, reverse-reasoning method, accident dynamics

0. INTRODUCTION

Traffic safety is a major problem of national economy and society stability. Our country is facing the problem of traffic accidents, and how to deal with these traffic accidents is an important task. As a key point, since accident reconstruction involves reason analysis and responsibility cognizance of each accident, it can also improve the efficiency of dealing with traffic accidents.

1. THE CORE IDEA OF REVERSE-REASIONING METHOD

The kernel crash analysis method applied all over the world nowadays is the simulation method which is also called the positive-reasoning method. This method calculates the vehicle speed after crashing and simulates slipping and turning processing after crashing assuming a vehicle speed before crashing (Bruce et al. 1995). However the disadvantage of this method is avoiding solving a moment recovery factor of the universal face-to-face crash, and the disadvantage is the unknown vehicle speed and many parameters need to be assumed, and the stopping position after crashing is needed to be determined by simulating again and again (Daogao et al. 2005). Therefore the use of this method is often limited because of scarcity of initial computing parameters and time required to be spent on the simulation.

Facing the problem above, the universal face-to-face crash was transformed to a point-to-point crash, and the reverse-reasoning method was used for accident reconstruction. According to trails of vehicle slipping and turning after crashing, the reverse-reasoning method solves vehicle speed just after crashing and vehicle speed just before crashing. This method agrees with the form of traffic accidents better and can avoid solving for the moment recovery factor as well. And the parameters needed in computing for this method are far less than that in positive-reasoning method and are more easily obtained (Ward et al. 1999). Computational complexity in this method is better than that in positive-reasoning method. So reverse-reasoning method is more advantageous for simplifying computing and rapidly analyzing traffic accidents.

2. TWO-VEHICLE NON-CENTRAL AREA COLLSION TRANSFORMED INTO POINT COLLISION

In real life, the collision part of a traffic accident is not a particular point but an entire area (Knneth 1999). Take whichever O, the effect point, on the collision area , which at the same time needs a collision force-couple M. That is to say, besides P_n and P_x which act on O, it also needs M. Therefore a moment regain coefficient k_m is added when establishing an equation. When translating the effect line of normal momentum force for a distance e, it will absorb the collision force couple, thus the area-to-area crash was transformed to a point-to-point crash (Figure 1).

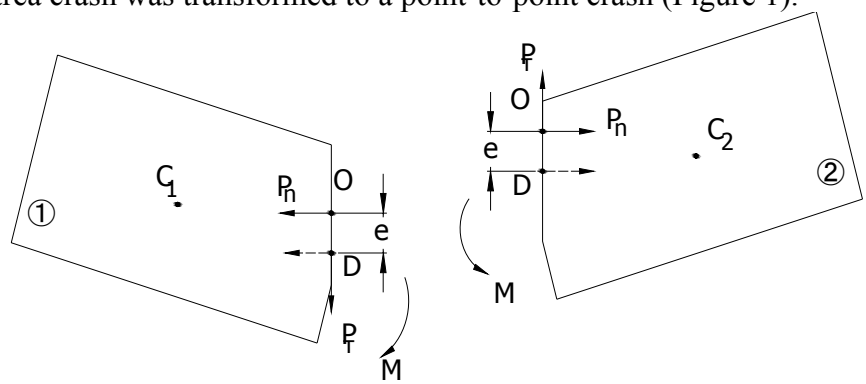

Figure 1. Sketch map of area collision transformed into point collision

3. ACCIDENT RECONSTRUCTION MODEL OF TWO-VEHICLE NON-CENTRAL COLLISION

3.1 Three Sets of Rectangular Coordinate system are Needed in Two-vehicle Non-central Collisions

The main characteristic of the non-central collision is that when the vehicles slide after collision, both translatory movement and rotation happen (WRA 2003). In order to establish the vehicle plane motion dynamic equation, three sets of rectangular coordinates are needed, as shown in Figure 2.

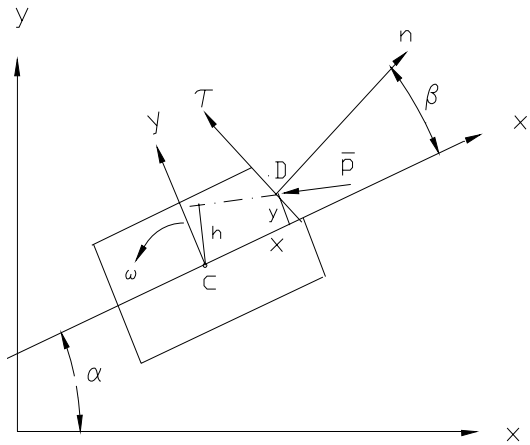

Figure 2. Three sets of rectangular coordinate system in Reverse-reasoning Method

(1) Vehicle body coordinate system XCY. Take vehicle body barycenter C as the origin of the coordinates, the vehicle body longitudinal axis as X, rotating the X axis 90° anticlockwise gets the Y axis. This vehicle body coordinate system is mainly used to ascertain the coordinate position of the collision point D compared to the barycenter.

(2) Normal coordinate system nDτ in the collision area. Take the collision area normal as n axis, 90° anticlockwise is τ axis. This collision-area normal coordinate is mainly used to decompose the collision momentum to the normal momentum P_n and tangential momentum P_x, and establish an equation along the normal and tangential directions, respectively.

(3) Earth-fixed coordinate system XOY. Usually take the direction of the accident-vehicle traveling path as the X axis, 90° anticlockwise is the Y axis, the origin O could be uncertain. The fixed coordinate system is mainly used to describe the driving parameters such as velocity, acceleration, skidding distance, and the direction angle between the two vehicles.

3.2 The Model of Two-vehicle Non-central Collision

The effect point of the collision momentum is known, so it is called a point-to-point collision. Figure 3 describes the collision pressure of both vehicle 1 and vehicle 2.

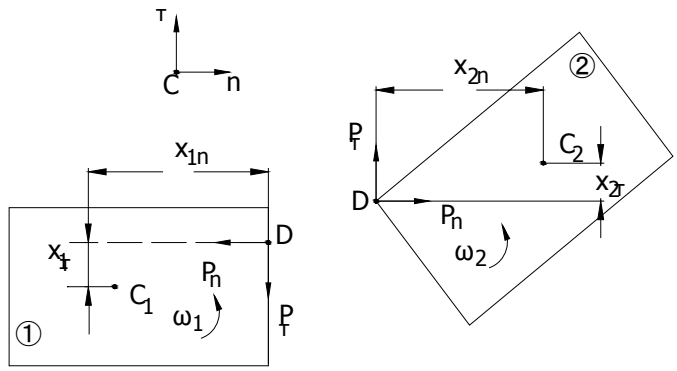

Figure 3. The force diagram of the non-central collision

Make the masses of the two vehicles as m_1 and m_2, the rotating inertia around the barycenter as J_1 and J_2 . The respective components of the two vehicles' speed before and after the collision in the normal coordinate are v_{1n}, $v_{1\tau}$, v_{2n}, $v_{2\tau}$ and v_{10n}, $v_{10\tau}$, v_{20n}, $v_{20\tau}$. The rotating angular velocities are ω_{10}, ω_{20} and ω_1, ω_2. Applying the impulse theorem and impulsive moment theorem and introducing an elastic recovery coefficient κ and a tangential fiction coefficient μ on the collision point D, then the accident reconstruction model is established:

$$[A_0]\{X_0\} = [A]\{X\} \tag{1}$$

Where:

$$\{X_0\} = [v_{10n} \quad v_{10\tau} \quad v_{20n} \quad v_{20\tau} \quad \omega_{10} \quad \omega_{20}]^T \quad \{X\} = [v_{1n} \quad v_{1\tau} \quad v_{2n} \quad v_{2\tau} \quad \omega_1 \quad \omega_2]^T$$

$$[A_0] = \begin{bmatrix} m_1 & 0 & m_2 & 0 & 0 & 0 \\ 0 & m_1 & 0 & m_2 & 0 & 0 \\ \frac{m_1 x_{1\tau}}{2} & -\frac{m_1 x_{1n}}{2} & -\frac{m_2 x_{1\tau}}{2} & \frac{m_2 x_{1n}}{2} & J_1 & 0 \\ -\frac{m_1 x_{2\tau}}{2} & \frac{m_1 x_{2n}}{2} & \frac{m_2 x_{2\tau}}{2} & -\frac{m_2 x_{2n}}{2} & 0 & J_2 \\ \mu & -1 & \mu & -1 & 0 & 0 \\ k & 0 & -k & 0 & -k x_{1\tau} & k x_{2\tau} \end{bmatrix} \quad [A] = \begin{bmatrix} m_1 & 0 & m_2 & 0 & 0 & 0 \\ 0 & m_1 & 0 & m_2 & 0 & 0 \\ \frac{m_1 x_{1\tau}}{2} & -\frac{m_1 x_{1n}}{2} & -\frac{m_2 x_{1\tau}}{2} & \frac{m_2 x_{1n}}{2} & J_1 & 0 \\ -\frac{m_1 x_{2\tau}}{2} & \frac{m_1 x_{2n}}{2} & \frac{m_2 x_{2\tau}}{2} & -\frac{m_2 x_{2n}}{2} & 0 & J_2 \\ \mu & -1 & \mu & -1 & 0 & 0 \\ -1 & 0 & 1 & 0 & x_{1\tau} & -x_{2\tau} \end{bmatrix}$$

3.3 Parameter Optimization of Reverse-reasoning Method

In order to enhance the reliability of the computed result, it needs to optimize some computed parameters in the accident reconstruction model.

3.3.1 Position Optimization of Collision Point

Take the initial collision point as the center, choose 5 points respectively along the two areas of the normal and tangent in the collision area as compute positions, 0.05m between every two points. According to the known model formula of the angular acceleration before the collision, use a computer to do circle calculations. Taking the minimum angle between the initial velocity direction and the known vehicle longitudinal direction before collision as the rule, compare the corresponding direction error of each calculation in order to find the minimum direction. Thus using the final result can get a collision position which is the prime collision point after adjustment.

3.3.2 Direction Optimization of Area Collision

Taking the initial normal of the collision area as norm, choose 5 directions respectively both clockwise and anticlockwise, with 2° between every two directions. Similarly, use the computer to do circle calculations according to the known model formula of the angular acceleration before the collision. Then taking the minimum angle between the direction of the initial velocity and the known angle of the vehicle longitudinal axis before collision as the rule, compare the corresponding direction error of each calculation to find the minimum direction. Thus using the final result can get a normal which is the best direction normal.

4. THE VERIFICATION OF THE TRAFFIC ACCIDENT CASE

The time of the case : 2004/04/16/14:45

The location of the case: The intersection of Pudong road and Suzhou north street in Changchun

Case outline：Jeep(1) driven along the Pudong road from east to west collided with truck(2) driven from south to north.

Inspection of the scene: As figure 4 shows, The roads are plane and straight with a good line of sight and bituminous pavement. The weather was sunny and there was no signal light in the intersection. The right front corner of truck (2) bumped into the left front area of jeep (1), both were damaged seriously. The data of the scene investigation is showed in figure 5.

Figure 4. General picture of accident (from west to east)

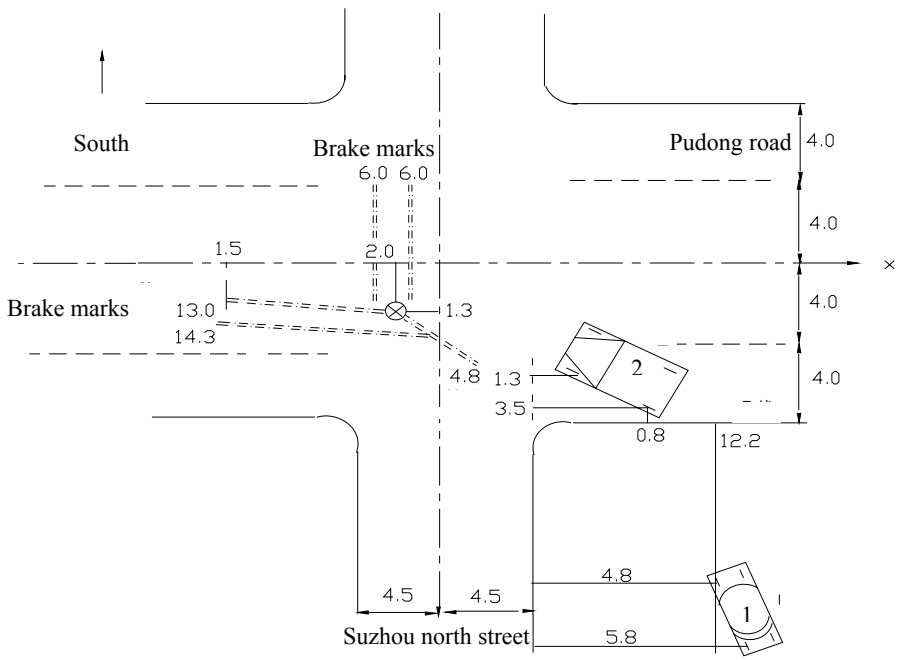

Figure 5. Scene of the two-vehicle collision on the intersection

The Collision Morphological Analysis and Reconstruction Calculation: This case should be processed as a general two-dimensional point collision because two vehicles crashed in the crossing and both were hit on the corner, which made them both rotated in a large angle. Take the Pudong road from east to west as the X axis,

jeep(1) as vehicle 1, truck(2) as vehicle 2. The calculated parameters of this case are showed in Table 1.

Table 1. Calculated parameter of two-vehicle collision on the intersection

Calculated Parameters	Jeep (1)	Truck (2)	Calculated Parameters	Jeep (1)	Truck (2)
Vehicle Quality (kg)	2330	2500	Slip direction angle(o)	-55	-41.8
Tread(mm)	1575	1410	Vehicle longitudinal axis angle before collision(o)	-2.2	-90
Wheelbase(mm)	2850	2515	Vehicle longitudinal axis angle after parking(o)	-68.5	-151
Collision point coordinates X(cm)	142.5	180	Equivalent Friction coefficient	0.58	0.7
Collision point coordinates Y(cm)	78	-70	Angular velocity before collision (degree/second)	0	0
Length of brake marks after collision(m)	22.7	10.5			

The calculate results before collision are as follows:

$v_{10} = 69.5(km/h)$, $v_{20} = 66.8(km/h)$

Drive speed calculation: The two results are initial collision speed rather than the drive speed before braking. We should calculate drive speed of the two vehicles before braking according to the length of the brake marks, because the two vehicles both braked before collision.

The length of brake marks before collision of Jeep1 is 14.3m, its collision speed is v_{10}=69.5 (*km/h*) =19.3 (*m/ s*). The drive speed v_1 before braking can be calculated as:

$$v_1 = \sqrt{v_{10}^2 + 2g\varphi_1 S_1} = \sqrt{(19.3)^2 + 2 \times 9.8 \times 0.7 \times 14.3} = 23.9(m/s) = 85.7(km/h)$$

The length of brake marks before collision of truck2 is 6.0m, its collision speed is v_{20} = 66.8(*km/h*)=18.5(*m/s*). The drive speed v_2 before braking can be calculated as:

$$v_2 = \sqrt{v_{20}^2 + 2g\varphi_2 S_2} = \sqrt{(18.5)^2 + 2 \times 9.8 \times 0.7 \times 6.0} = 20.6(m/s) = 74.3(km/h)$$

5. CONCLUSIONS

The paper confirms the validity and the feasibility of Reverse-reasoning Method by reconstruction of a real traffic accident. At the same time, it also discovered that the premise ("two basic hypotheses" of collisions) of its application influences the calculation accuracy, which should be further studied and optimized. Meanwhile, in view of the increasing severity of China's traffic safety situation, the author believes that it can help to enhance effectiveness, fairness and accuracy in traffic accident processing, and to propose transportation safety managing countermeasures if China independently researches and develops the traffic accident reconstruction model and applied software which agree with China's national condition.

ACKNOWLEDGEMENT

The authors thank the National Natural Science Foundation of China (Grant No. 50808093) and Postdoctor Science Fund of China (Grant No. 20070411000) for financial support.

REFERENCES

Bruce W. Main and Eric A. Kno. (1995). A New Application of Camera Reverse Project in Reconstruction Old Accident. SAE 950351, 136-142.

Daogao We, Keqiang Li. (2005). Research on the precise calculation and control strategy of front wheel toe-in of vehicles. IEEE International Conference on 14-16 Oct. 2005, 12-14.

Knneth S Baker. (1999). Traffic Collision Investigation. Northwestern University, 102-106.

Ward. D, Bertram. T, Hiller. M. (1999). Vehicle dynamics simulation for the development of an extended adaptive cruise control. IEEE/ASME International Conference on19-23 Sept. 1999, 730 – 735.

World Road Association(WRA). (2003). Road Safety Manual. Piarc technical committee on road safety, 216-225.

Evaluation Study of the Median Markings in Undivided Highway Tunnels

Guo Fengxiang [1], Xiong Jian [1], Liu Hongqi [2], Wan Huasen [1], Qin Yaqin [1]

[1] Faculty of Transportation, Kunming University of Science and Technology, China, 650224. PH（86）871-3801150, FAX（86）871-3802259, E-mail: xjebox@163.com
[2] Traffic Engineering Supervision &Testing Center, M.O.C. 8Xitucheng Rd, Beijing, China. 100088, PH:（86）10-62355709, FAX（86）10-62356515, E-mail: hq.liu@rioh.cn

ABSTRACT

This paper details research undertaken by the simulation laboratory at Faculty of Transportation, Kunming University of Science and Technology. The aim of this research is to compare the relative effectiveness of three kinds of median markings in undivided highway tunnels. The sample of the tunnels was selected from a real road in a mountainous area in Yunnan province as a test course and was reconstructed by computers on the driving simulator. Forty subjects participated in the experiment and the data were collected from the experiments. The study found consistently superior results for the Warning poles that can fall down and resume set on the centre of the undivided highway tunnel in comparison to common road markings and the enhanced visibility road markings in various measures of driving behavior. Questionnaires also give a higher evaluation for the Warning poles.

1 INTRODUCTION

With the increase in the number of tunnels, highway tunnels security issues are becoming increasingly apparent and attract more attention. Yunnan province is located in the mountains and there are a lot of undivided highway tunnels which have high risk of accidents. So many safety ensuring methods were designed for them.

The purpose of this research is to evaluate two kinds of median markings as well as a common road marking in undivided highway tunnels by using a driving simulator. One of the median markings is made of enhanced visibility quadrangles with a common road marking (see Figure1), (termed as ‘Visual marking’), another is Warning poles sitting on the center of the undivided highway with common markings in the tunnel (see Figure2). When vehicles hit these special warning poles, they fall down and subsequently resume (termed as ‘Warning poles’).

In order to reach the objective, experiments were organized based on Driving Simulator technology to obtain the behaviors of the vehicles passing through the tunnels. The speed, and its standard deviation, the track lateral position, and its standard deviation were used in the experiments to analyze and evaluate these three kinds of markings（Kay Fitzpatrick et al. 2000）. The purpose of the experiments is to see which markings help make the vehicles go smoothly and straightly.

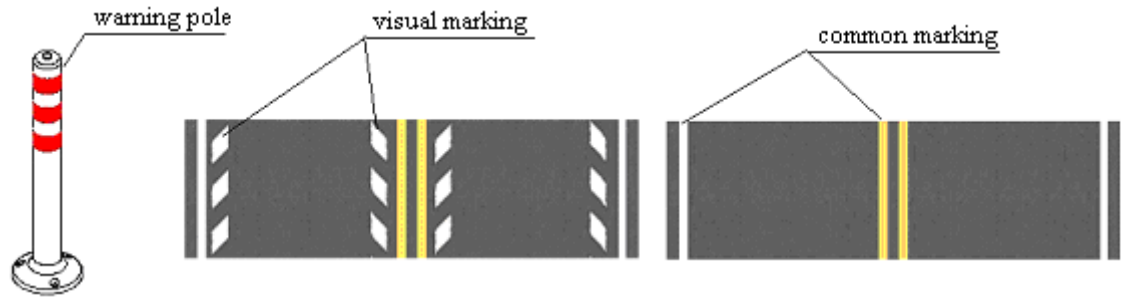

Figure1. Pattern of three median markings

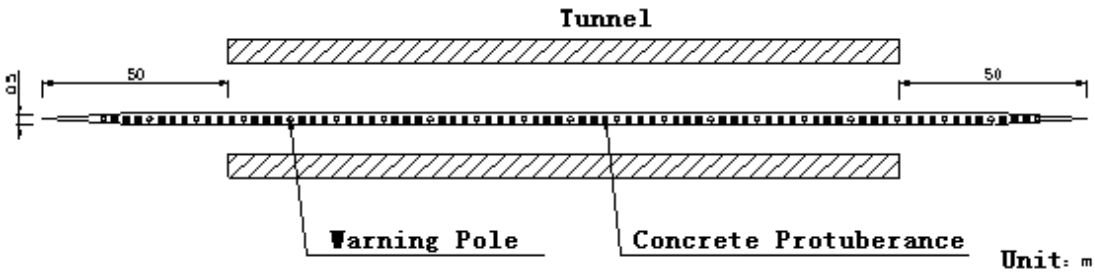

Figure2. Placement method for the warning pole in the tunnel

2 METHOD

To carry out the experiments on the Driving Simulator, it was first necessary to create a virtual experimental scenario exactly based on the sample road section (Berssenbrügge et al. 2006). Afterward, subjects (test drivers) were selected and trained to fit to the simulator (Nancy E. Laurie 2004). Before starting, preliminary testing and calibration are required to make the rig work well and the parameters of the vehicle dynamical model match with actual ones（Mats Lidström, 1998）. Finally, formal experiments were carried out and the data were collected. For further analysis and evaluation all parameters acquired from the simulator had to be treated and elaborated with respect to the exact position of the vehicle along the test course.

The driving simulator

The driving simulator (KMRTDS) was set up in the simulation laboratory at Faculty of Transportation, Kunming University of Science and Technology, which consists of following five subsystems: the computer system with an elaborate mathematical model of the vehicle, a visual scene creation system, the projection system which presents the visual environment on a 120-degree wide screen, a digital sound system, and a full scale cab with real operation room. The driving simulator is controlled by a platform in a control room, and all the experiments can be controlled for given conditions.

Experimental Scenario

The sample roadway was selected from a section of G213 (The National highway in China) located in a Yunnan province mountainous area. There were three tunnels in the 4-km long sample section, which were named T1, T2 and T3, and

similarly three kinds of markings were named M1, M2 and M3, respectively. The experimental scenarios are shown in table 1.

Table 1. Experimental Scenarios

Experimental Scenarios	The first tunnel(T1)	The second tunnel(T2)	The third tunnel(T3)
Scenario1	The first tunnel equipped with Warning pole (T1+M1)	The second tunnel equipped with Visual marking (T2+M2)	The third tunnel equipped with common marking (T3+M3)
Scenario2	The first tunnel equipped with Visual marking (T1+M2)	The second tunnel equipped with common marking (T2+M3)	The third tunnel equipped with Warning pole (T3+M1)
Scenario3	The first tunnel equipped with common marking (T1+M3)	The second tunnel equipped with Warning pole (T2+M1)	The third tunnel equipped with Visual marking (T3+M2)

Traffic flows were set in these three experimental scenarios, which were free flow and set on the opposite lane to avoid affects on drivers, but there were some cars in front of the subject in the driving lane with a higher speed so as not to affect driver's choice of speed.

a. The entrance to the tunnel **b. In the tunnel**

Figure 3. Experimental Scenario

Subject

In total, 40 subjects were selected with age from 28 to 48, 25 males, 15 females and all with driving experience over three years. Each subject participated in all the experiments based on above three scenarios.

Procedure

Before the experiments the driving simulator and its functions were

introduced to the subjects and preliminary tests were conducted to make them familiar with the simulator. After the experiments a questionnaire was required to be make as compensation.

The experiment data were collected from the vehicle dynamical model from each driver. The speeds of the vehicle and the track positions along the road were the main parameters for the study. Since all the collected parameters were with respect to time, they were transferred into location-based data so as to analyze a case at the site of the road. The data transformation can be figured out by locating every position of the moving vehicle on the test course as a coordinate system. Consequently the speed and other parameters of the vehicle were accurately located along the test course (speeds versus location).

3 DATA ANALYSIS AND EVALUATION

Data Analysis

Based on 40 drivers' data in the test course, an analysis gives rise to some results regarding the three kinds of markings.

Figure 4 shows the test result of the sample tunnel (1.78km long). From the figure it can be seen that the trends of mean speed profile of the three markings were nearly same and at the entrance and exit of the tunnel the speeds slow down under any marking condition.

Figure 4 also shows the standard deviations of the speed along the course. To clarify, entering, inner, and exit were set as three special segments for analyzing points. Table 2 shows the mean standard deviations at each segment. It can be seen in the table that at the entering and exit segments of the tunnel the speed deviations show little difference for the three markings, but at the inner segment the speed deviation for the common marking is much greater than warning poles and visual markings, and between warning poles and visual markings the former is smaller.

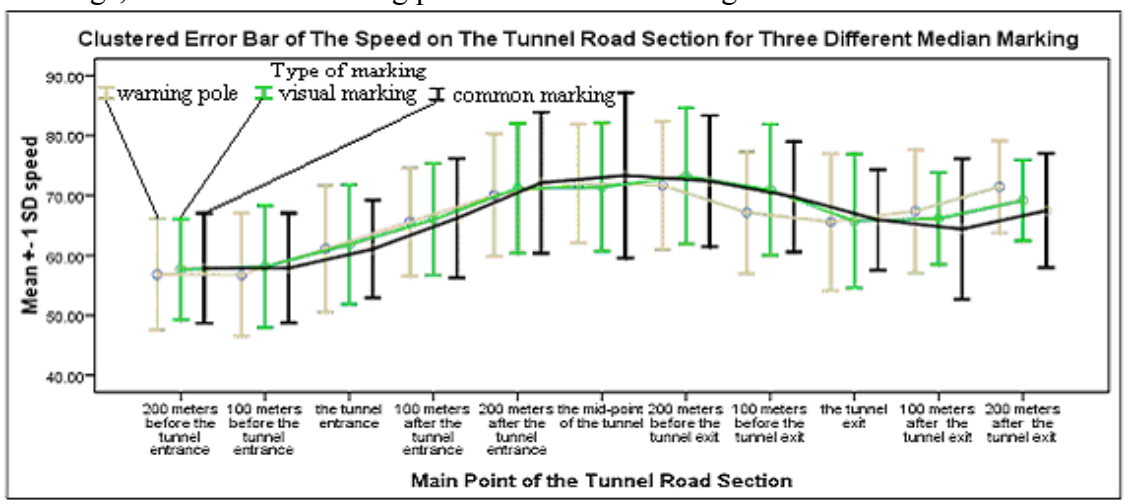

Figure 4. Clustered Error Bar of the Speed on the Tunnel Road Section for Three Different Median Marking

Table 2. The mean speed deviations on entering, inner and exit segment of the tunnel

Type of marking	Entering segment	Inner segment	Exit segment
Warning poles	9.49	9.90	9.82
Visual marking	9.78	10.70	9.57
Common marking	9.03	13.33	8.84

Like speed deviation, deviation of track lateral position along the test path and special segments are shown in Figure 5 and Table 3. From the figure, it can be seen that for the warning poles the mean distance between track and road center line is greater than visual marking and common marking. This means the vehicles in this case are each trying to avoid conflict with on-coming cars.

In addition the data of the table shows that the deviation of track lateral position in the warning poles condition is always greater than the others' at entering, inner and exit segment. The standard deviation of track lateral position shows how much a driver is able to maintain a constant track lateral position. In other words it is a surrogate of how much a driver 'weaved' along the road. Generally speaking, the less the deviation is, the better the vehicle's behavior (Tim Horberry et al. 2004).

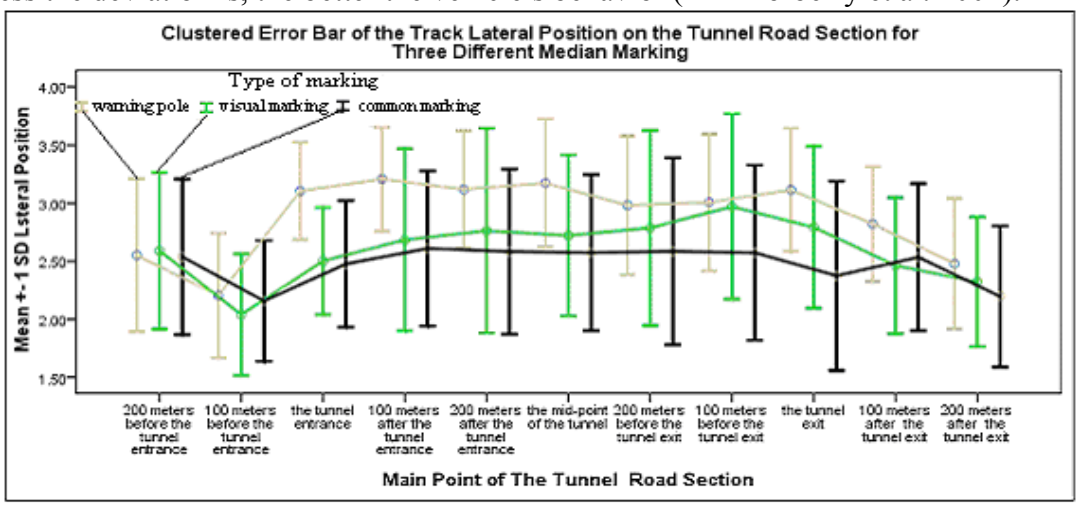

Figure 5. Clustered Error Bar of the Track Lateral Position on the Tunnel Road Section for Three Different Median Marking

Table3. The mean Track Lateral Position deviations on entering, inner and exit segment of the tunnel

Type of marking	Entering segment	Inner segment	Exit segment
Warning poles	0.55	0.53	0.53
Visual marking	0.66	0.77	0.68
Common marking	0.64	0.73	0.70

Note: The Track Lateral Position was the distance between road center line and track of the car.

4 CONCLUSIONS

- The three kinds of median marking in the tunnel have little impact on the speed of vehicles passing through the tunnel.
- Compared with visual markings and common markings, the warning poles make the vehicles go along a smoother and straighter path in the tunnel.
- The track lateral distance from road center line is greater than two others, so it is easer for the vehicle to avoid conflict with opposite cars.

5 ACKNOWLEDGMENT

This study was supported by the open fund from Key Laboratory of national highway traffic safety technology center. We also obtained the highway database from Yunnan Highway Design and Research Institute. To everyone involved, we express our sincere gratitude.

6 REFERENCES

Berssenbrügge and Bauch (2006) “A Night Drive Simulator for the Evaluation of a Predictive Advanced Front Lighting System” Information & Communication Technology, ICTCT 06′ITI 4th International Conference on Volume, Issue, 10-12 Dec. 2006.

Kay Fitzpatrick, Mark D. Wooldridge etc（2000） ‘Alternative Design Consistency Rating Methods for Two-Lane Rural Highways’ U.S. Department of Transportation PUBLICATION NO. 99-172, 30-31

Mats Lidström, （1998）“USING AN ADVANCED DRIVING SIMULATOR AS A DESIGN TOOL IN ROAD TUNNEL DESIGN”. Transportation Research Board, 77th Annual Meeting, Washington, D.C, Paper No. 980135.

Nancy E. Laurie and Shuping Zhang (2004) “An evaluation of alternative Do Not Enter signs: failures of attention” Transportation Research Part F 7 151–166.

Tim Horberry and Janet Anderson.（2004） “A Driving Simulator Evaluation of Enhanced Road Markings”. Australasian Road Safety Research, Policing and Education Conference.

The Numerical Analysis of Sound and Vibration from a Tire by FEM and BEM

Liang Chang [1], Wang-Xin Xiao [2] and Wei-Ping Xie [1]

[1] School of Civil Engineering and Architecture, Wuhan University of Technology, Wuhan 430070, China; email: changbing130@163.com

[2] Research Institute of Highway, Ministry of Communications, Beijing 100088, China; email: wx.xiao@rioh.cn

ABSTRACT

Numerical analyses of sound and vibration from the 225/50R17 smoothing radial tire, excited by surface load, have been carried out by using the FEM software, ANSYS, and the BEM software, SYSNOISE. The displacement frequency response of the tire which is respectively excited by radial contact force, tangential contact force and lateral contact force are calculated by using FEM. Then, the radiated sound power, radiation efficiency, and the directivity of sound in far field are given by using BEM in which the velocity boundary condition, are transformed from nodal displacements of FE modal.

INTRODUCTION

Sound radiation from a vibrating tire is a complex subject not only because of generation mechanisms, but also because the propagation of sound from the source to recipient is extremely complicated, which has attracted many scholars. Most research has been carried out experimentally and numerically, few aimed at radiated sound power, radiation efficiency, and the directivity of sound in far field.

Eberhardt [Eberhardt, A.C., 1981] concluded that sidewalls are not independent vibration radiators and that the contributions to emitted sound are about 10dB lower from the sidewalls than the tread. These conclusions are supported by Doan et al [Doan V.Q., Brackin D., Nishihata S. and Sauerzapf J., 1995], who considered side wall vibration as the most significant noise mechanism in the dominating frequency band 500-1000Hz. Ruhala [Ruhala, Richard, J., 1999] suggested that the sidewall region near the contact patch radiates more efficiently than the structural wave response along the tread band. Ulf Sandberg [Sandberg, Ulf and ejsmont, Jerzy A., 2002.] believed the tread band and the sidewall both contribute significantly to the radiation and also that belt resonance is the reason why the peak around 1kHz is observed in tire/road noise spectra for smooth or circumferential-grooved tires. R.A.G. Graf [R. A. G. GRAF, C.-Y. Kuo, A. P. Dowling and W. R. Graham., 2002] experimentally and numerically investigated the horn effect directivity. Some studies about tire/road noise directivity are summarized by Ulf Sandberg [Sandberg, Ulf and ejsmont, Jerzy A., 2002.], none of which can characterize clearly sound directivity resulting from tire vibration.

In this paper, the radiated sound power, radiation efficiency, and the directivity of sound in far field are studied. First, displacement frequency response of a smoothing tire which is respectively excited by radial contact force, tangential

contact force, and lateral contact force are calculated by employing finite element software ANSYS. Then, nodal displacements of FE modal are extracted and input into boundary element software SYSNOISE to calculate sound quantity. Some conclusions have been drawn from the numerical results.

NUMERICAL MODELS

Finite element model. Both the structure of the tire and the material at each part are complex, and the dynamic analysis on tire is emphasized in this paper. Three parts of a tire: the tread compound, the steel belt and the carcass ply are considered in order to highlight the computational efficiency and reduce the working load. Material parameters at each part are as follows: tread compound, ρ =1280 kg/m^3, EX =9.6×10^{6}N/m^2, $PRXY$ =0.49; steel belt, ρ =1500 kg/m^3, EX =1.1×10^{7}N/m^2, EY =1.3×10^{10}N/m^2, EZ =1.7×10^{7}N/m^2, $PRYZ$ =0.36; carcass ply, ρ =1100 kg/m^3, EX =2.94×10^{8}N/m^2, EY =1.5×10^{7}N/m^2, EZ =1.5×10^{7}N/m^2, $PRYZ$ =0.43. The tire is fixed at the wheel rim. Radial force, tangential force, and lateral force are respectively applied on the contact surface where tire and road meet. Because the vertical pressure at the leading edge is higher than that at the trailing edge [Sandberg, Ulf and ejsmont, Jerzy A., 2002], and both the tangential force and lateral force are proportional to vertical contact pressure. It is, therefore, assumed that the magnitude of the exciting force is linearly decreasing along the circumference from the leading edge to the trailing edge. Both the calculation frequency range is 10~1000 Hz, with the step of 10 Hz, aand the sound radiated from the tire vibration are nearly concentrated on the frequency range lower than 1000 Hz.

The ground contact length L =20cm and the tire contact width B =18cm are respectively determined by these two empirical formulas [Zhuang Jide, 1995]:

$$L = 2D\left(\frac{\delta}{D}\right)^s \tag{1}$$

and

$$B = B_0(1 - e^{-t\delta}) \tag{2}$$

where $\delta = c_1 \dfrac{W^{0.85}}{S_0^{0.7} D^{0.43} p^{0.6}} K_0$ is the deformation of the tire along the radial direction on the contact surface; c_1 is a parameter related to tire design, c_1=1.15 for a bias tire and c_1=1.5 for a radial tire, W is the load applied on tire (daN), D is the tire outside diameter (cm), S_0 is the tire width (cm), p is the inflation pressure (100kpa), $K_0 = 15\times10^{-3} \times S_0 + 0.42$.

Boundary element model. Boundary element mesh is obtained through the FEM software, ANSYS, and the BEM software, SYSNOISE data interface technology. The velocity boundary condition is established by inputting displacement frequency response results which are acquired from FEM. Then,

the calculation of the partial acoustic quantity is carried out by BEM. Air density is 1.225 kg/m^3 and the sound velocity in the air is 340 m/s.

NUMERICAL RESULTS AND CONCLUSIONS

Figure1, Figure2 and Figure3 show BEM calculation results of radiated sound power, radiation efficiency, and directivity for a vibrating tire excited by radial force, tangential force and lateral fore respectively..

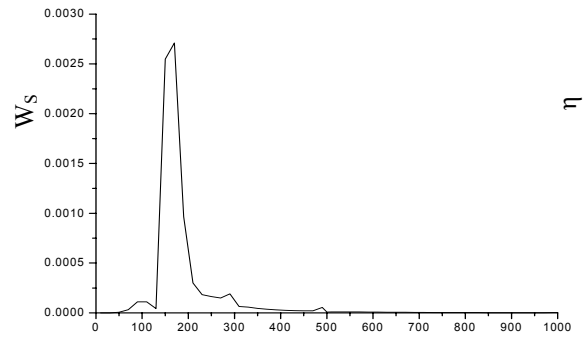

(a) Radiated sound power

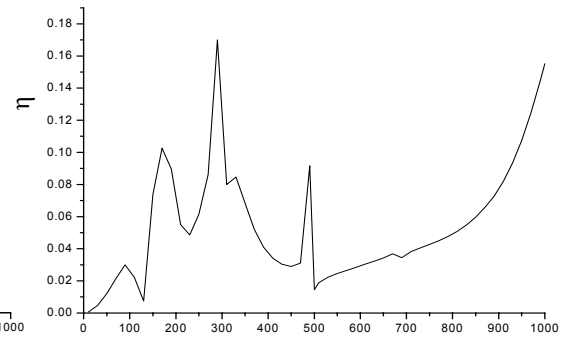

(b) Radiation efficiency

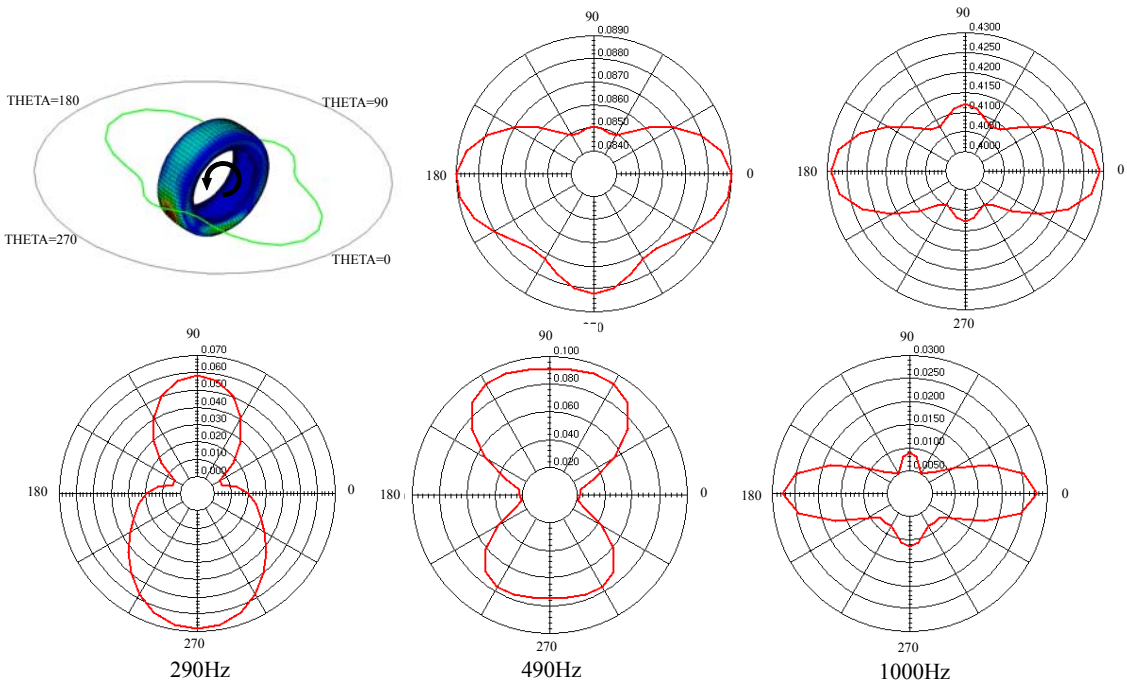

(c) Directivity of sound in far field

Figure 1. BEM calculation for a vibration tire excited by radial force.

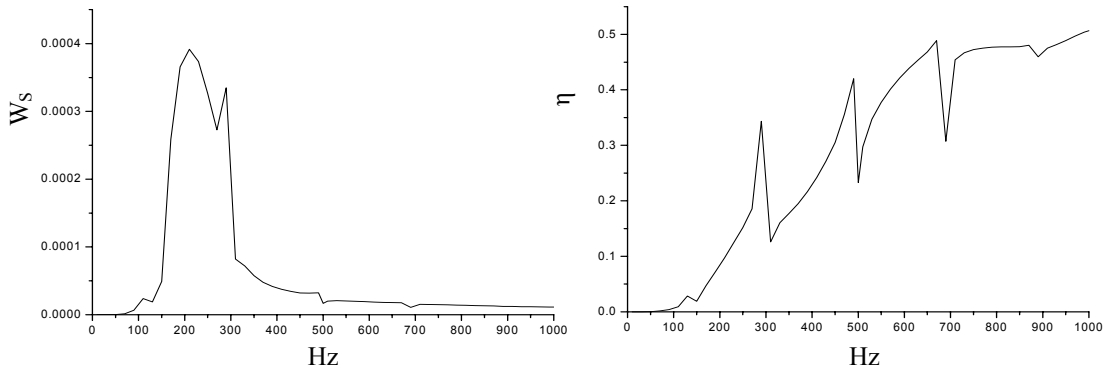

(a) Radiated sound power (b) Radiation efficiency

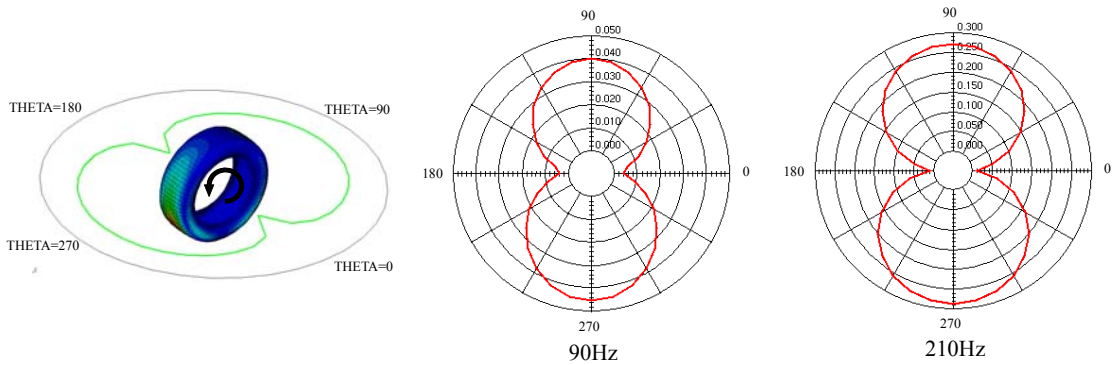

(c) Directivity of sound in far field

Figure 2. BEM calculation for a vibration tire excited by tangential force.

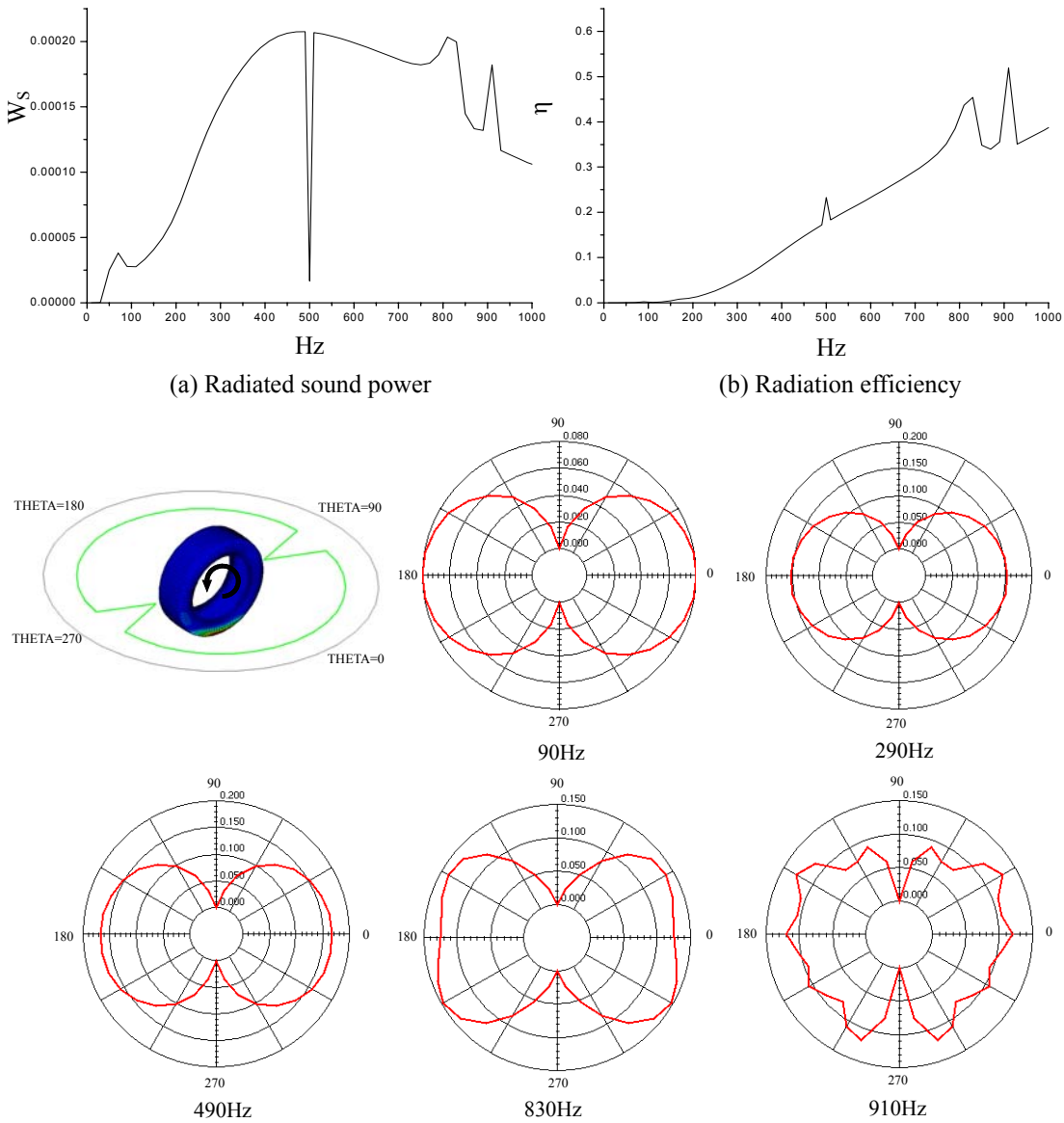

(a) Radiated sound power (b) Radiation efficiency

(c) Directivity of sound in far field

Figure 3. BEM calculation for a vibration tire excited by lateral force.

In Figure1, it is concluded that the peak value for radiated sound power of a vibrating tire excited by radial force occurs at 170Hz. Radiated sound power at a low frequency is higher than that at a medium frequency. At a low-frequency (10~500Hz), there are three peaks for radiation efficiency; however, at a medium-frequency (500~1000Hz), the radiation efficiency increases gradually. At different frequencies, the directivity of sound in far field shows different shapes. Sound levels are not substantially higher in the front and rear than that at the sides; although, levels may be lower, and the directivity of sound becomes complex with

increasing frequency.

In Figure2, it is concluded that the peak value for radiated sound power of a vibrating tire excited by tangential force occurs at 210Hz. Radiated sound power at a low frequency is also higher than that at a medium frequency. The general tendency of radiation efficiency increases with increasing frequency. Sound levels are higher in the front than in the rear and the sides.

In Figure3, it is concluded that the radiated sound power of a vibrating tire excited by lateral force distributes in a wide frequency range. The general tendency of radiation efficiency increases with increasing frequency. Sound levels are higher at the sides than in the front and rear, and the directivity of sound become complex with increasing frequency.

ACKNOWLEDGEMENT

The financial aid from the National Natural Science Foundation of China under grant NO.50708085 and NO.50678141 is gratefully acknowledged.

REFERENCES

Eberhardt, A.C. (1981). "An experimental and analytical investigation of the vibration noise generation mechanism in truck tires." *Report No DOT-HS-805-868, U.S.* Department of Transportation, Washington, DC, USA.

Doan V.Q., Brackin D., Nishihata S. and Sauerzapf J. (1995). "Investigation into the influence of tire construction on coast-by noise." *Tire Science and Technology.* 23(2), 96-115.

Ruhala, Richard, J. (1999). "A study of tire/pavement interaction noise using near-field acoustical holography." *PhD Thesis,* Penn State University, Dep. of Acoustics, State College, PA, USA.

Sandberg, Ulf and ejsmont, Jerzy A. (2002). "Tire/road noise reference book." Informex, SE-59040 Kisa, Sweden (www.informex.info).

R. A. G. GRAF, C.-Y. Kuo, A. P. Dowling and W. R. Graham. (2002). "On the horn effect of a tire/road interface, part 1: experiment and computation." *Journal of Sound and Vibration,* 256(3), 417-431.

Zhuang Jide. (1995). "Automobile tire." *Beijing Institute of Technology Press,* Beijing.

Technology Research on the Vehicle Collision Accident Self-alarm System

TIAN Zhe-Wen[1] XU Jia-Qi[2] FENG Qian[3] LEI Shuai[4] MEI Xiao-Ming[5]

[1]School of Automobile, Wuhan University of Technology, Zip Code：430070, Wuhan City, Hubei Province; TEL: 13294133999; FAX: 027-87859247; E-mail: tzw0290@163.com
[2]School of Automobile, Wuhan University of Technology, Zip Code：430070, Wuhan City, Hubei Province; TEL: 13296638063; FAX: 027-87859247; E-mail: andy_adm@126.com
[3]School of Automation, Wuhan University of Technology, Zip Code：430070, Wuhan City, Hubei Province; TEL: 15927233435; E-mail: 59935320@qq.com
[4]School of Automobile, Wuhan University of Technology, Zip Code：430070, Wuhan City, Hubei Province; TEL: 13477080767; FAX: 027-87859247; E-mail: 378490632@qq.com
[5]Dongfeng Motor Co., Ltd, Wuhan City, Hubei Province

ABSTRACT

Based on vehicle collision safety technology, GPS technology and mobile communication technology, this paper offers a person-free operating Vehicle Collision Accident Self-alarm System. The thesis introduces the principle and the structure of the system, and offers the solution of the self-alarm. The system can solve problems in which the drivers or passengers injured in the vehicle collision accident can't alarm by themselves or they can alarm but don't know their accurate location. The system will alarm automatically in a timely manner.

KEYWORDS: collision accident; self-alarm; GPS; mobile communication; solution

1. INTRODUCTION

With the explosive development of the automotive industry and the increasing volume of automobiles, with cars going faster, traffic accidents are growing rapidly. If a car has a serious collision, the crew in the car cannot call for help by themselves because of shock, coma or their movement limitations; or they can alarm but don't know where they are. These factors can seriously delay rescue and cause unnecessary death. The thesis offered by this paper utilizes vehicle collision technology, GPS technology and mobile communication technology to devise a person-free operating Vehicle Collision Accident Self-alarm System ("The System" for short). This system can smooth over the faults of traditional manual alarm systems, and can efficiently solve the problems mentioned above. After the collision accident, the system can trigger the alarm system, locate the vehicle accurately then send information to the rescue service station, so the rescuers can act quickly which can reduce the death rate.

2. THE PRINCIPLE AND STRUCUTRE OF THE SYSTEM

2.1 The Principle

When a car meets a serious collision, the Airbag System will inflate the airbags, meanwhile, the inflation signal will also be sent to the ECU of the System; the mounted GPS Action Athena can receipt the signal from satellites to compile the current geographical information and then save it into the RAM of the mounted terminal; the communicating module will load the information and format a SOS short message (including the current geographical information of the vehicle) which is going to be sent to the Long-range Service Center; the servers contact with the vehicle and determine whether they need rescue.

2.2 Structure

The System is formed with Independent Power Supply, Airbag Module, GPS Signal Receiver, Electronic Control Unit, Communicating Module, and Fault Self-test Module. The parts inside the dotted line rectangle of Figure 1 are the formation of the Mounted Terminal.

(1) Airbag Module: This module is the standard configuration, so we don't need to design it in the System. The System only collects the ignition signal as a trigger signal.

(2) GPS Signal Receiver: Receipts the satellite signal timely, vehicle location identification, combined with existing electronic navigation software can achieve precise positioning vehicles.

(3) Electronic Control Unit (ECU): Control the modules work coordinately. Judge whether there is an ignition signal so as to control whether the System works or not. It collects the location data; edits distress message itself, and send the communication instruction to the communication module. Communication Module: Send distress messages to the Service Center according to the instruction of ECU; receive voice call and two-way call.

(4) Independent Power Supply: Can supply the whole System after the main power supply of the automotive break down.

(5) Fault Self-test Module: Can diagnostic the fault of the mounted terminal.

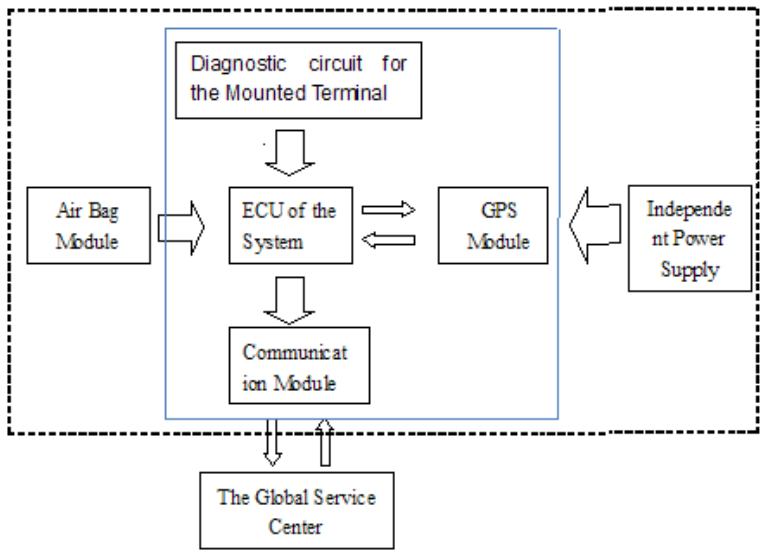

Figure 1. Structure of the System.

3. SYSTEM HARDWARE DESIGN

The design of The System mainly includes GPS Signal Receiver, Electronic Control Unit, Communication Module and Independent Power Supply.

3.1 GPS Signal Receiver

The GPS Signal Receiver can transform, amplify, and process the received navigation signal, so as to get the accurate location of the vehicle, then transmit the signal to the ECU. The System adopts a Chang-Tian GR-85 GPS Module from Taiwan China to get the original positioning data. Its structure is shown in Figure 2.

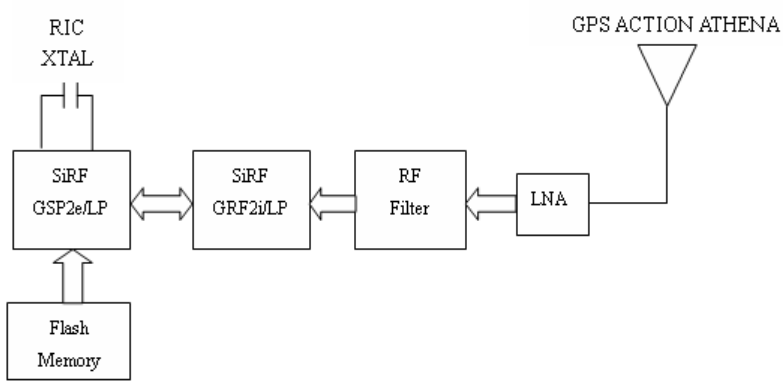

Figure 2. Structure of GR-85

3.2 Mounted Electronic Control Unit

The System adopts the embedded system which is timely, with high reliability and efficiency. The CPU of S3C44B0X is the 16/32-bit ARM 7TDMIRISC Processor (66MHz) with ARM7TDMI integrated Thumb code compression, on-chip ICE breakpoint debugging support, and a 32-bit hardware multiplier. S3C44B0X expands on a full range of common peripheral devices based on the ARM7TDMI core, which can greatly reduce the system circuitry in addition to the components outside the processor configuration, thereby allowing the cost of system to a minimum.

3.3 Communication Module

The System adopts GPRS Net as the communication platform, which has high transmission rate, high frequency utilization, almost zero error-bit rates, supporting multiple network protocols, and supports roaming.

The System uses the GPRS SIM300C module. The client model of the SIM300C system connector (60 pins) is IL-312-A60P-VF-A. This system connector is the interface between the SIM300C module and applications which mainly provides interfaces for the external power supply, RS-232 Serial Port, SIM Interface and Audio Interface.

Users can complete the operations to the module by AT commands through the serial interfaces provided by SIM300C, and can also access the internet by the GPRS functions offered by the module (GPRS network support required).

The module supports an external SIM card, and can be connected directly to a 3.0V or 1.8V SIM card. The module can monitor and automatically adapt to the type of the SIM card used. The designed circuit of the SIM card connection is shown in Figure 3.

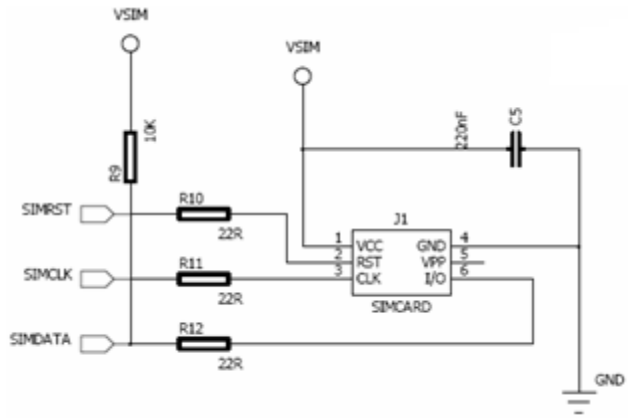

Figure 3. SIM card circuit

3.4 Power Supply

The Power Supply mainly provides power for the Communication Module, GPS Signal Receiver, the ECU, etc. In order to guarantee the reliability of the System, there is also a standby power supply. In this part, we only design the power supply to the Communication Module. Since the pulse emit can cause rapid changes of current consumption, the power supply must provide instantaneous peak current. Table 1 shows the reference value of current in different states.

Table 1. Reference value of current in different states.

Communication Status	Current (typical)
Free mode	4mA
In communicating(Circuit-switched mode, 1 slot receive, 1 slot emit)	250mA
In communicating(GPRS mode, 1slot receive, 2 slots emit)	500mA
In communicating－peak current	1700mA
GPRS mode, 3 slots receive, 2 slots emit	560mA
GPRS mode, 4 slots receive	125mA
Power-off	50uA

The Communication Module supply voltage range is 3.3V~ 4.6V, and the power supply should have 2A peak current output capacity. The 12V automotive power supply is regulated by the regulator chip MIC29302BU, and regulates to 3.3V~ 4.6V to properly operate the SIM300C module. When the DC supply voltage is lower than 3.3V, the module will switch to the standby power supply automatically, and in order to ensure the stability of the power supplied to the module, a regulator capacitor should be added to the input end of the power supply to the module, to stabilize the supply voltage for the module during the transmission.

The standby power supply is a Li-ion battery pack with a rated voltage between 3.6V~ 3.9V. It will be auto-charged when the voltage is lower than 3.6V, and stop charging when over 3.95V. The standby power supply does not need to supply power under normal operating conditions.

4 THE SELF- ALARM SOLUTION SCHEME

In order to alarm rapidly and efficiently, the geographical location, frequency of the SOS messages sent, the number calling from the Service Center and the time for waiting for the reply should be analyzed and processed. The location of the car is divided into three levels “A”, “B” and “C”, according to the GPS positioning information and the related electronic maps; level A for the traffic flourishing region; level B for the region whose traffic condition is over the average; level C for the traffic least developed region. We define “A” for the Good condition, “B” for the Medium condition and “C” for the Poor condition. The higher the level the lower frequency the alarm messages send. Starting with sending the collision signal, if there are no feedback calls from the service center with the passage of time, the alarm signal sending frequency will increase. That is to say, at the early stage, the lower sending frequency requires fewer alarm service resources; if there is still no feedback call when it reaches a certain period of time, raise the alarm signal frequency to call the greatest attention of the service station. The service station should carry out the voice calls to the car as soon as they receive the alarm messages. If there is still no reply after several calls, the service station will start rescuing.

The related parameters are defined as follows: the Mounted Terminal operation delay is t; the total number of alarm signal sending is n_1; the time interval between each message is T_c; the time for waiting for the feedback call is T_{cw}; the receiving and feedback delay is T_1; the voice calling delay is T_d; the time for waiting for the reply is T_s; the fixed time for waiting the reply is T_{s0}; the waiting time after hang up is T_w; the total number of voice calls is N_c; the fixed largest number of the voice calls is N; the voice calls can be connected is defined as Y=1, otherwise is Y=0; “Replied” is defined as R=1, otherwise is R=0. Enquiring if needing rescue, define Yes; if no, define No; the total communicating time is defined as T.

Step1 The Mounted Terminal will wait after sending the alarm message. If Tcw>Tc, then repeat Step 1.

Step2 If Tcw≤Tc, and there is a voice call, then stop sending alarm messages.

Step3 When Nc≤N,

1) If Y=1, then wait for the reply, the waiting time is Ts0:

a. If Ts > Ts0, and R=0, then hang up, wait time interval Tw, repeat Step3;

b. If R=1, then enquire instead of calling again; if Yes, then rescue, if No, hang up.

2) If Y=0, then hang up, wait a time interval Tw, repeat Step 3.

Step 4 If Nc>N, then judge to be Yes.

Step 5 Good:N=5. Medium:N=4. Poor:N=3. Tc＝10sec,Ts0＝30sec,Tw＝20sec.

Step 6 The total communicating time is $T \le t + (n1 - 1) \times Tc + T1 + Nc \times Td + (Nc - 1) \times Tw + Ts0 \times Nc$.

This scheme gives consideration to both cost and reliability of the whole system. It can help the Service Station work efficiently through the defined levels of the traffic condition. The flow-process diagram of the above tactics is shown in Figure 4. The System consists of the Self-Test subroutine, the Airbag Monitoring subroutine and

the Alarm Signal Sending and Feedback subroutine.

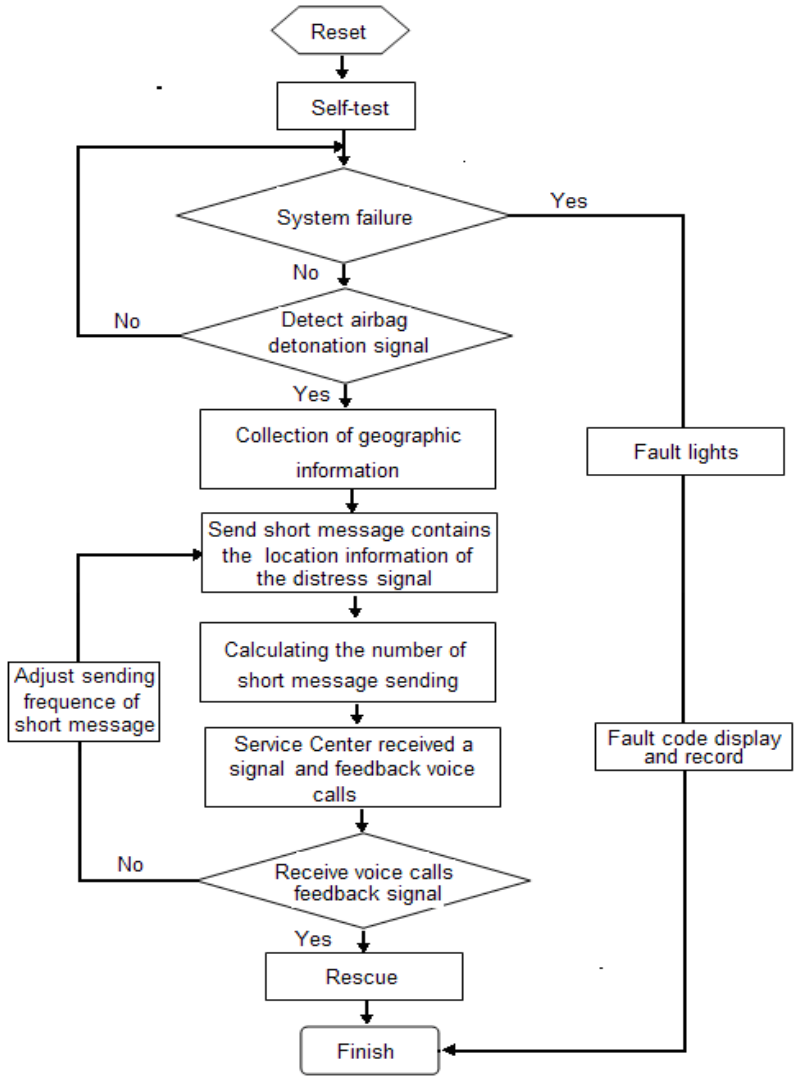

Figure 4. The flow-process diagram of theSystem software

5 SUMMARY:

Based on the study introduced above and design of the The System principles, we can solve the hard problems posed by some collision accidents in which the vehicle crew cannot alarm manually. This can shorten the rescue time and thereby reduce death rates and property loss. This study of the technology has great potential to improve the vehicle accident alarm system. The System still has some GPS satellites signal dead zones and the mobile communication signals, so in order to solve this problem, we still need more in depth study into alarm tactics.

BIBLIOGRAPHY:

Bin Chen, De-Hua Li, Xun Yao (2005-6). “The design and implementation based on GPRS technology scalable vehicle monitoring system.” *Computer Application Research*，175-178

Xiao-Feng Lu，Heng-Li Lu，Fang-Qin Zhang (2005). “The design and application of GPRS and GPS information in the automotive service system.” *Micro-computer Information*，Vol.21 No 3，188－190

Walt Moore (2004). “CONNECTOR SYSTEM FOR MOBILE DEVICES”，*Product design & development*，000(m6)E15-E15

Gu-Shan Zou，Yan-Guang Tsai，Kai Shi，Tao Wang, “The design and application based on the ARMGPRS Self-Navigation-System Terminal.” *Computer Application Research*，2005-9，201-202

Research on Pedestrian Safety under Rapid Development of Motorization

Wang Shuling[1], Liu Zhili[2], Guo Jifu[3] and Chen Yanyan[4]

[1]Beijing Transportation Research Center, Room411,No.9 Beibinhe Road, Xuanwu District, Beijing, 100055, P. R. China; PH (86) 10-63372730; FAX (86) 10-63372715;E-mail: wangsl@bjtrc.org.cn

[2] Integrated Transport Research Center of China , School of Traffic and Transportation, Beijing Jiaotong University, No.3, Shangyuancun, Handian District, Beijing, China PR,100044; E-mail:liuzhili@jtys.bjtu.edu.cn

[3]Beijing Transportation Research Center, Room416,No.9 Beibinhe Road, Xuanwu District, Beijing, 100055, P. R. China;
PH 86-10-63372702; FAX86-10-63372704;E-mail: guojf @bjtrc.org.cn

[4]Beijing University of Technology ,Transportation Research Center
No.100, Pingleyuan Chaoyang District, Beijing 100022, P. R. China
PH86-10-67391860; FAX 86-10-67391509; E-mail: cdyan@bjut.edu.cn

ABSTRACT

Walking is one of the important traffic modes in Beijing central city, and should be given sufficient attention. This paper, through a large of field survey and literature review, analyzed and summarized the difficulties faced by walking traffic, including traffic infrastructure, traffic environment and pedestrian safety awareness and such issues under the rapid development of motorization and trip demand. A series of ensured measures were listed at the end to improve walking environment.

KEY WORD: Walking, Pedestrian Safety, Traffic Environment, Motorization

1 BACKGROUND

Along with the fast development of Chinese economy and motorization, there are 0.17 billion motor vehicles in China (0.127vehivle/person) by the end of June of 2008. Beijing, as the capital of china, motor vehicle grows rapidly in recent years, the traffic congestion has become an obstacle in Beijing development process. In order to deal with the serious traffic congestion, the vehicle lane is widened increasingly, while the walk space is sharply invaded. The conflict between motor vehicle and pedestrian become more and more and correspondingly the hidden accidents and real traffic conflicts have aroused the society's attention.

The <World Report on Road Traffic Injure Prevention>has point out the traffic accidents and death number will increase largely in middle and low income countries between the year 2000 and 2020. If we do not take the adequate measures, by the end of 2020, the road traffic injury will become the third reason for the global disease and injuries. Walking, as the necessary traffic mode to connect public transport trips, is a part of "New Beijing Transport System". Therefore it is needed to protect pedestrian right of way and provide a safe and comfortable traffic environment for walking to

perfect Beijing traffic.

2 DEVELOPMENT OF MOTORIZATION IN BEIJING

Beijing economy has kept continuously rapidly incensement since 2000, the year average increase rate is over 10 percentage. In 2007, the GDP had reached 935.5 billion, increasing 13.3% comparable with 2006. Now Beijing development is influenced by the international finance crisis, but with the China national, and Beijing Municipal government's high attention, Beijing economy will still keep about 8% yearly growth in the future

According to related reference, when GDP per person is over 3000 dollars, the vehicle amount will enter a swift growth period. In 2008 Beijing average GDP per person has reached 9000 dollars. The rapid growth of economic and the high living standard lead to a higher request to the traffic journey conformability; the car enters the ordinary citizen family rapidly.

In recent years, Beijing vehicle amount increases about 10% every year. By the end of 2008, Beijing vehicle grossed to 3.5 million, among them, the personal car is 2.3 million. The vehicle number per thousand persons is 207(Beijing Transportation Research Center, 2009). This symbolizes that Beijing entered the fast motorization "the automobile time", the car entering the ordinary family will soon achieve.

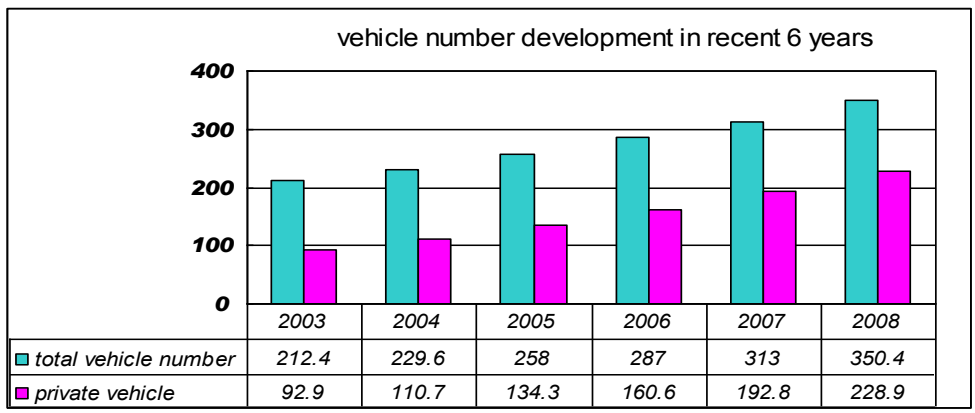

Figure 1 vehicle number development in recent years .

3 TRAFFIC ENVIRONMENT OF BEIJING

3.1 Air Environment

The vehicle rapidly growth has brought a series questions for the urban development, the most serious problem is the urban air pollution. Statistics show that 40-60% of suspended particle, 80% of hydrocarbons (HC) and 70-80% of nitrogen oxides (NOX) of Beijing air come from vehicle exhaust (Environmental Defense Fund, 2009). Beijing has taken a lot of measures to deal with the polluted environment, and the air quality has already improved in recent years, but there are still some index can not attain the standard. The pedestrian walks on the road, exposure in automobile exhaust with high concentration. It endangers people's health directly.

3.2 Traffic Infrastructure

The fast development of vehicle leaded to a more serious traffic congestion in Beijing. In order to alleviate it, more and more road space is occupied by motor vehicle, the walking and bicycle lane is continuously invaded, traffic infrastructure for walking does not consider pedestrian's demand, lead inconvenience and hidden conflict for pedestrians. To be noticed, this paper pays attention in Beijing central city, the suburban is out of consideration.

1) Sidewalk width insufficient

Some roads do not set sidewalk, passenger and motor vehicle mix in the same space. Some artery roads sidewalk width is less than 1 meter, during the peak hour passengers have to enter motor vehicle roadway, which extremely easy to cause traffic accident.

Beixiange street

Changshunjie street

The west ring road

Figure 2 Pictures of unreasonable sidewalk

2) Barrier on Sidewalk

Since a long period of time, there are no co-ordinate arrangements and the effective management of sidewalk. The sidewalk space is illegally occupied by different uses, such as municipal facilities, vehicle parking, bicycle running and parking, shopping and etc. those facilities and obstructs brought inconvenience and difficulties to pedestrian especially for the old, young, sick, disabled people and pregnant women

The investigation shows that 76% pedestrians disagree vehicle parking on the sidewalk; 81% pedestrians approve to widen sidewalk especially at the bus station (Beijing Municipal Institute of Planning and Design, Beijing Transportation Research Center, 2008.12)

3) Incomplete crossing facility

Pedestrian crossing facilities include crosswalk, overpass and underpass; it is a necessary part of walking system. The unreasonable interval of crossing facilities, vehicle interference, excessive overpass and underpass, over wide vehicle lane and etc, all those are for a goal, that is to provide high speed for motor vehicles. But what's for the pedestrian? They have to go up or down to cross a 8 or 10 vehicle-lanes street. For them the ground crossing is the best.

The investigation shows that 57% pedestrians feel crossing is inconvenient, only 5% pedestrian feel good for current crossing condition. The reason for inconvenience

is: detours too far (34%), the vehicle not give way to pedestrian (33%), overpass and underpass (24%) and too wide vehicle street (Beijing Municipal Institute of Planning and Design, Beijing Transportation Research Center, 2008.12).

4) Poor pavement and inconvenience for disabled people

Except for the new building roads, most of existing sidewalks and crossing facilities do not comply with disabled passing standard. The disabled people can not travel.

3.3 Traffic Accidents

Pedestrian, without any protection, is the vulnerable road user compare with vehicle driver. Once the pedestrian and vehicle conflict, the injured even dead must be the pedestrian. According to the statistics, pedestrian accounts for 25% of death in recent 20 years; it is the major vulnerable group (Duan Liren, 2006).

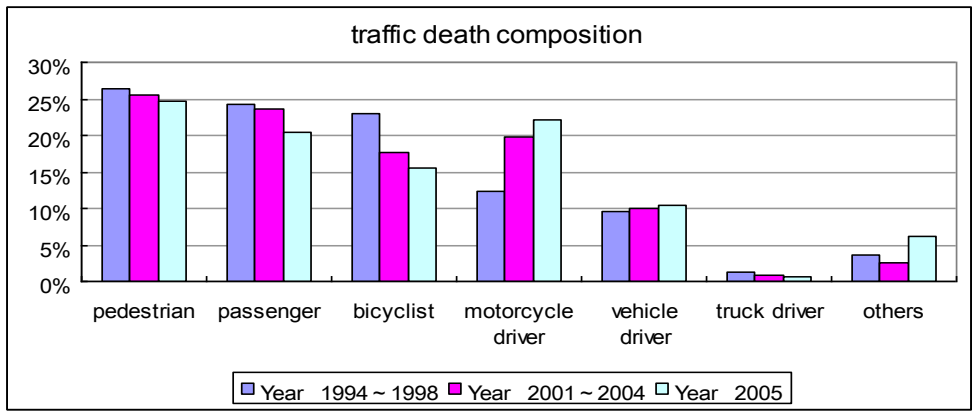

Figure3 Traffic Death Composition in China

4 DEVELOPMENT TREND OF WALKING

In order to alleviate the increasingly traffic congestion problem, Beijing government and many non-government organizations (NGO) carry out a number of activities to encourage less driving and more using public transport, bicycle and walking. 16th to 22nd of September 2007, Beijing held the first “China Urban Public Transport Week and Car Free Day” activity. And the activity continues. The theme of “car free day” of 2008 is “Human Street”.

After the successful Olympics. “Human Traffic” “High-tech Traffic” and “Green Traffic” become the strategic goal in the future of Beijing traffic development history. Walking, as an important component of the cityscape, reflects the fair, human and sustainability of Beijing traffic. It is an important component to build "New Beijing Transport System," and it will play an important role in integrated transport system in Beijing.

Whether the government or NGO have actively encouraged people to adopt green travel mode, walking is one of the most important component. Beijing walking policies should be to advocate walking and to implement walking priority. Beijing will provide a safe, smooth, convenient and comfortable walking environment for all

pedestrians including the disabled groups.

5 IMPROVEMENT MEASURES FOR WALKING SYSTEM

Europe's transport policy has been to encourage people to walk. In 1988, the European Parliament passed the "European Charter on the Rights of Walking." It brought forwards people should walk and ride in search of fun, and more attention should be pay to children, the elderly and disabled with their right. Those countries and regions developed a complete planning and construction guidelines; carried out scientific and careful designs; took the corresponding supporting policies; promoted government departments, business organizations and the public to participate actively at the same time.

The Olympic Games is an opportunity to arouse the Government and the public pay more attention to traffic and walking environment. Since 2000 Beijing has been improving the traffic environment continuously. Beijing is abolishing the vehicle parking on the sidewalk. Nearly 100 thousands trails piles have been hammered in the sidewalk since 2006, and it effectively prevents the vehicle entering walking space. More refuge islands have been settled along the roads and at the intersections; and the signal design became to consider pedestrian demand more. Beijing are changing pedestrian traffic environment gradually. But comparing with the successful pedestrian plan and walking system construction, there still is a big gap between Beijing and other developed cities. It is proposed from the following aspects to continue increasing pedestrian traffic environment in the future

Right of Way

The allocation of road space should consider all traffic participants; take into account the interests of all participants to implement safety first. One group’s benefit should not based on prejudicing to other groups’ benefits, especially vulnerable groups such as the sick and elderly. So it is necessary to plan the road space for pedestrian according to current design standards and guidelines, combined with the actual needs of pedestrians including traffic direction and volume; to design the sidewalks with reasonable width, continuity, separated, and green.

Pedestrian crossing safety facilities

The crossing facility’s type and location should be closely consistent with walking system of the residential areas, commercial areas, railway stations, recreational squares; and become an integrated complete system of city walking system to meet the actual needs of pedestrians. The ground crossing is the best choice for pedestrians, especially for the elder and disabled people. So when the construction is permitted, the priority belongs to the ground crossing facility, next is overpass and finally is underpass. To be notice, the refuge island and enough signal time for pedestrian should be guaranteed for the ground crossing.

Vehicle speed control

Studies show that pedestrians have 90% chance of survival when collisions with motor vehicle speed less than 30km/h; if collision vehicle speeds faster than 45km/h,

pedestrians have only less than 50% chance of survival (World Band, World Health Organization, 2004). Therefore, to lower motor vehicle speed is an important measure to improve pedestrian's safety at intersection.

According to the data of Beijing intersection vehicle speed investigation at night, the average speed and 85% speed respective are 42.3km/h and 58.75km/, they are both generally higher than the safe speed for pedestrian. So it is necessary to use of speed limited signs, hump, road alignment design, traffic management, signal control and other means to reduce the vehicle speed near the sidewalk and pedestrian crossing path.

Pedestrian safety education:

In addition to the engineering-related measures, it is indispensable to strengthen public traffic law's education and increase their safety awareness. There is no mandatory rule for pedestrian traffic safety education, so many pedestrians lack safety awareness, and behave out-of-order, which is one of the main causes of traffic accidents. The effective education and publication will improve road safety for all traffic participants.

Air quality improvement:

On one hand, new motor vehicle is request to apply higher emission standard. And the existing dirty vehicle is being accelerated out of use. On the other hand, the Government adopts the traffic demand management measures to lead reasonable motor vehicle use, effective reducing emissions and energy consumption. Through the rational use of motor vehicles, it is helpful to reduce the impact of exhaust to pedestrians.

6 CONCLUSIONS

Walking system as an important part to construct "Human Traffic, High-tech Traffic and green Traffic", along with the development of public transport and green travel activities, it will become a necessary way of daily trips. Therefore safe and comfortable walking environment become hot needs of citizens. Improve the walking environment includes air quality and traffic facilities. Through the guide use of motor vehicles, increasing pedestrian safety publicity and education, ensuring the right of way for pedestrians and other related human traffic facilities, Beijing will gradually improve the walking environment and build a pleasant city for all traffic participants.

7 REFERENCES

Beijing Transportation Research Center (2009). Beijing traffic operation report 2008.

Environmental Defense Fund (2009). Green commuting-Beijing Report 2008.

Beijing Municipal Institute of Planning and Design, Beijing Transportation Research Center(2008). Pedestrian and Bicycle Report.

Duan Liren (2006). Love life, Take care of the vulnerable road users--the Road Safety Problem Summary.

World Band, World Health Organization(2004). World Report on Road Traffic Injure Prevention.

Gradually Rolling Prediction of the Use-level of Road Network Based on BP Neural Network

ZHANG Tao, HOU Xiang-shen，LI Xin-kai，JING Hai-min，ZHENG Bing-qian[1]

([1]School of Transportation Science and Engineering, Harbin Institute of Technology, Harbin 150090, P.R. China, Tel: 13009725535, 0451-86284663, Email: zt-touchsky@163.com)

ABSTRACT

The use-level of road network prediction is the key for making a good plan of pavement maintenance. Traditional methods used for the use-level of road network prediction have some limitations. It is difficult for traditional prediction models to set up multi-parameter equations and predict many factors' changes. The precision is low, particularly in dealing with massive data of road networks. A neural network has certain advantages to predict the change of road network service's level. In this paper, a prediction model based on the Back-Propagation Neural Network (BP neural network) was established to predict use-level of a road network. China's road-related standards divide the use-level of road networks into *5* levels, so *5* state vectors were defined in the BP neural network. The status of a large number of roads over the years was turned into a *5*-dimensional time series. The BP neural network was built on the MATLAB software platform. Many methods were used to improve prediction precision, such as Bayesian methods, repeat training, and so on. The prediction method was ameliorated too. Combined with factual data of road conditions in Tianjin, through the comparison of direct prediction and gradually rolling prediction, the results showed that gradually rolling prediction offered a better prediction precision and was more applicable to use in the use-level of road network prediction. Using gradually rolling prediction, this paper predicted and analyzed the changes of the use-level of road network in Tianjin.

INTRODUCTION

The use-level of a road network mainly refers to the proportion that road sections of different states possess. The changes of the use-level of road network are very complicated due to the attenuation of road performance, road network maintenance and many other factors. The traditional model is hard to predict. In this paper, a neural network model was set up to predict ratio-changes of different levels (excellent, good, medium, hypo-medium, bad) of the overall road network status (strength coefficient and roughness). Prediction results could be used to help a road management department master the status and development trends of pavement performance, facilitate decision-making of short-term and long-term road network maintenance and make financial optimization.

Traditional models mainly use Deterministic Model (Empirical Regression,

etc.) and Probabilistic Model (Markov Model, etc.) to study the pavement performance (Yao Zu-kang, 1993), such as Finland Model, Norway Model, AASHTO Model, IDAHO state Model, S-type Model (Cheng Yu-zhu, 2007), and so on. In China, the Empirical Regression model is used in Guangdong, Tianjin and Beijing. The Deterministic Model is used in Jiangxi Province. A General Deterioration Equation for pavement performance was put forward by SUN Li-jun, LIU Xi-ping from Tongji University in 1995 (Sun Li-jun, Liu Xi-ping, 1995), etc. At present, most of these studies are carried out against a road section. It is difficult for the traditional prediction model to set up a multi-parameter equation and predict many factors' change. The precision is low. Therefore, studies about the use-level of road networks are so few that road management departments can not directly assess the entire road network status. BP neural network (BP network for short) can resolve the highly complex problem of nonlinear systems with the ability to dynamically update data, and be able to reverse the propagation of the error to correct model continuously (Ge Zhe-xue, Sun Zhi-qiang, 2007). So, many scholars at home and abroad use the BP network model to study pavement performance. For instance, Bing Wen-shan from Harbin University of C.E. & Architecture (HIT for now) (Bing Wen-shan, 2000), Xie Xu-fei from Harbin Institute of Technology (HIT) (Xie Xu-fei, 2004), Zhou Wen-xian from Tongji University (Zhou Wen-xian, 2006), used BP networks to set up different prediction models; J.D. Lea abroad used a BP network in South African to analyze and forecast road data. Good results had been obtained (J.D.Lea, 1999).

Based on previous studies, this paper makes use of the neural network toolbox in MATLAB for programming. A prediction model based on a BP neural network for predicting the change of the use-level of road network was established. The Prediction method was improved too. Combined with factual data of road conditions in Tianjin, comparing and analyzing prediction results, this paper could provide a reference for road network's maintenance decision-making.

ESTABLISHMENT OF A BP NETWORK MODEL

The structure of a BP network is composed of an input layer, hidden layer and output layer. When a study sample is provided to the network, neuron activation-value transfer input data from the input layer (no transfer-function) to the first hidden layer. The hidden layer deals with the information from the upper layer, and then passes on to the next layer until neurons in the output layer get the network's input-response. BP algorithm is applied to amend connection-weights layer by layer. BP network's structure shape is shown in Figure 1.

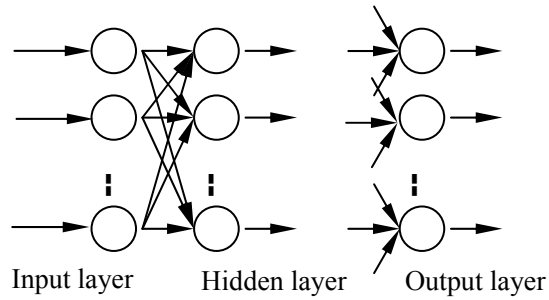

Figure 1. BP network structure.

The decay process of road performance is continuous. Data reflecting road status will form a time sequence (serial relations) (Xie Xu-fei, 2004). It is assumed that there are *q* road sections or routes with the same pavement structure in an area under the same traffic level, historical conditions of *TS* time step of one performance form *q* state sequences separately (Figure 2 (a)). The road sections between each other are not affected, so sequences could be designed as a serial relationship (Figure 2 (b)).

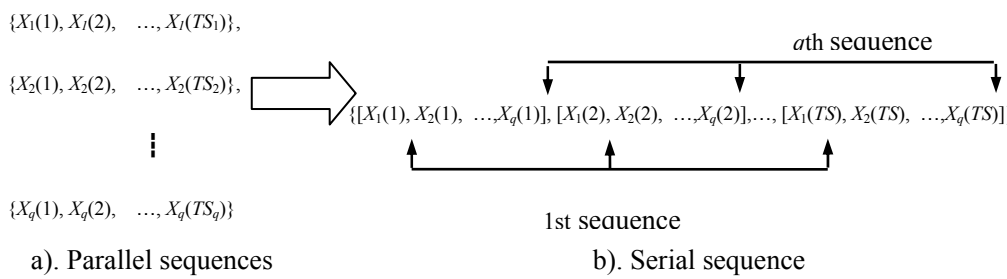

Figure 2. Sequences of data-state.

Performance evaluation levels are generally divided into *5* levels in existing norms of highway industry, which corresponds to *5*-dimensional state space. So in parallel sequence (Figure 2 (a)), state vector of the *t*th step in the *i*th sequence is: *Xi (t) = [xi1 (t), xi2 (t), xi3 (t), xi4 (t), xi5 (t)] T*. The more road condition sequences that are known, the greater the *TS* time step is, and the more comprehensive the information is. This data structure is conducive for the model's continuous updating. Considering a *2*-year recursive-chain network, which means inputs include state of the past and current year, and output includes state of the next year, the sample is: *([X (t-1); X (t)], X (t +1))* . In this paper, MATLAB software was used as a platform to offer neural network toolbox for programming. The flow of data processing in the BP network is shown in Figure 3.

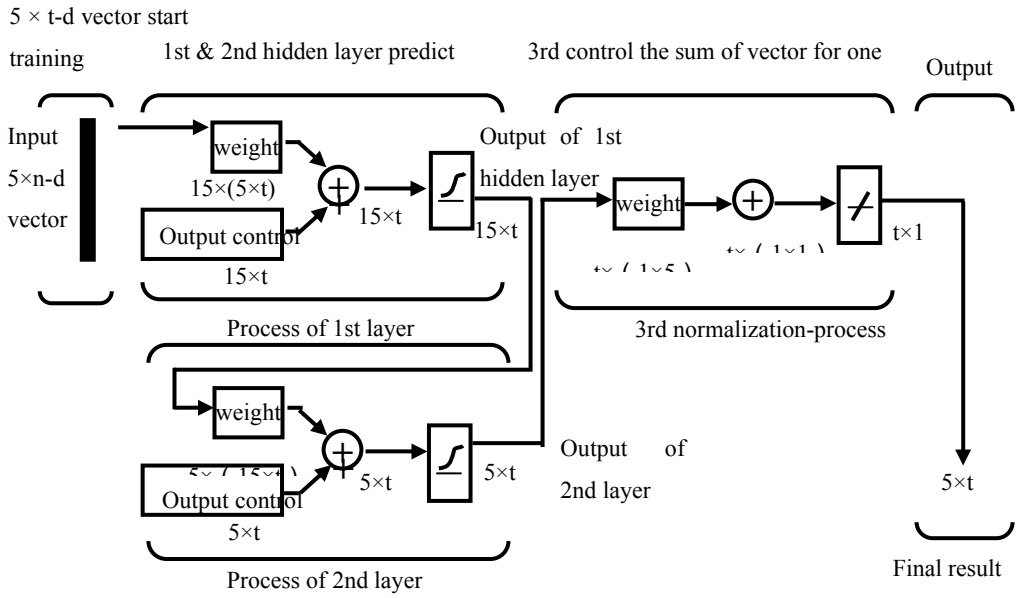

Figure 3. Information of Data-transmission.

In Figure 3, *5 × t(n)*-d means *5 × t(n)*-dimensional. *n* expresses number of years of known data, *t* expresses prediction cycle.

Many methods were used to improve prediction precision. Using Bayesian Methods could determine the best regular parameters to conquer the over-fitting problem. Re-initialization or re-training several times made the greatest degree of local minimum close to the overall minimum. Training stopped (validation stop) when training times increased to a scheduled value.

IMPROVEMENT OF PREDICT METHOD

Previous BP network prediction models support direct prediction. Results of *t*-years forecast are obtained directly. The longer the prediction cycle, the greater the prediction error. Compared to direct prediction, gradually rolling prediction model changed prediction method to improve prediction accuracy, fitting to do further analysis. Comparison of two kinds of prediction methods is shown in Figure 4.

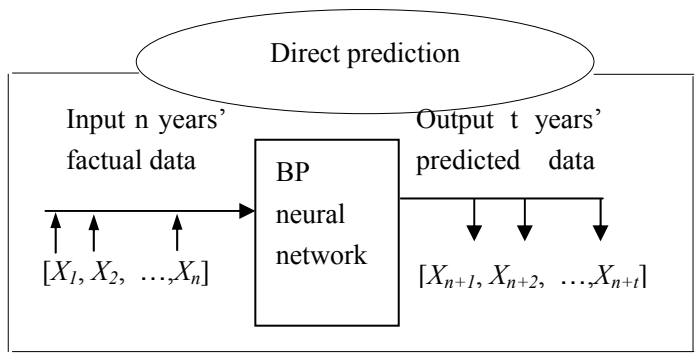

a). Direct prediction flow chart

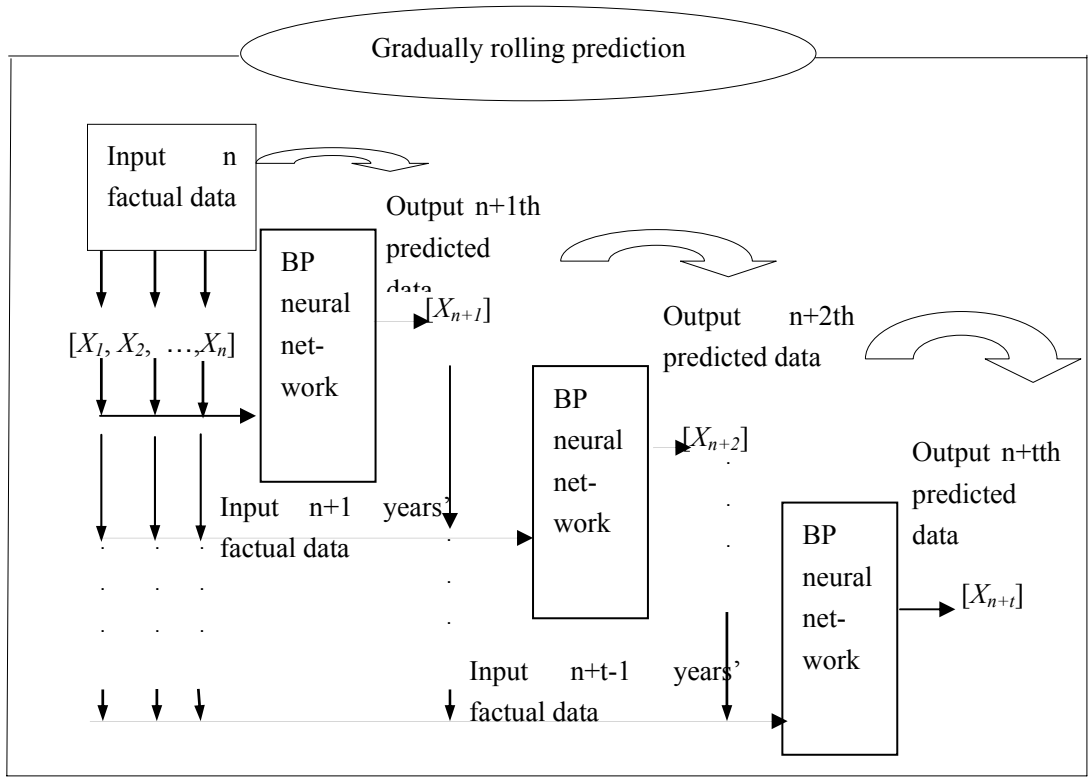

b). Gradually rolling prediction flow chart

Figure 4. Flow chart of 2 prediction models.

DATA PROCESSING OF ROAD NETWORK

In order to compare the two models, analyses of changes of SSI (structural strength index) are presented combined with the data over the years in Tianjin. At present, "Technical specifications for maintenance of highway Asphalt Pavement" (JTJ073.2-2001) divides SSI of asphalt pavement into *5* levels (Table 1).

Table 1. Evaluation criterion of SSI, (" technical specifications for maintenance of highway Asphalt Pavement "(JTJ073.2-2001)).

Criterion	Highway grade	Excellent	Good	Medium	Hypo-medium	Bad
SSI	Expressway, first class highway	≥1.0	0.83 ~ 1.0	0.66 ~ 0.83	0.5 ~ 0.66	< 0.5

Considering each criterion's requirements, 5-dimensional state space is defined as I = [1 ~, 0.83 ~ 1, 0.66 ~ 0.83, 0.5 ~ 0.66, 0.5 ~ 0]. Historical data of SSI were collected by the road management department. Data with high discreteness were deleted and those that met the requirements were divided into 5 parts (excellent to

bad) through I. The ratio of each part in the total was calculated. Taking year 2001 for example, in the whole road network, SSI of the excellent part takes 40 percent. Treated data compose a network state vector sample set. Using the final BP network model and 2001-2006 year's data, adjusting the time step and prediction cycle, 2007 year's predicted value was obtained. Then on the basis of 2001-2007 year's data (2007's data was a predicted value), 2008 year's predicted value was obtained, followed to 2009. After a normalization-process, the actual data and predicted values are shown in Figure 5.

COMPARISON OF PREDICTION RESULTS

The prediction results of the gradually rolling prediction model established by BP network are shown in Figure 5. Under the present maintenance program, the road network's SSI would continue the change law of previous years. Road sections which belonged to "Excellent" level would be more than 60% of total road network in 2007. With time passing, the sections belonging to the "Excellent" level would drop to about 40% in 2009, "Good" and "Medium" levels remained the same level, while the "hypo-medium" and " bad" level's share dropped in 2007, but increased to 25% and 15% in 2009.

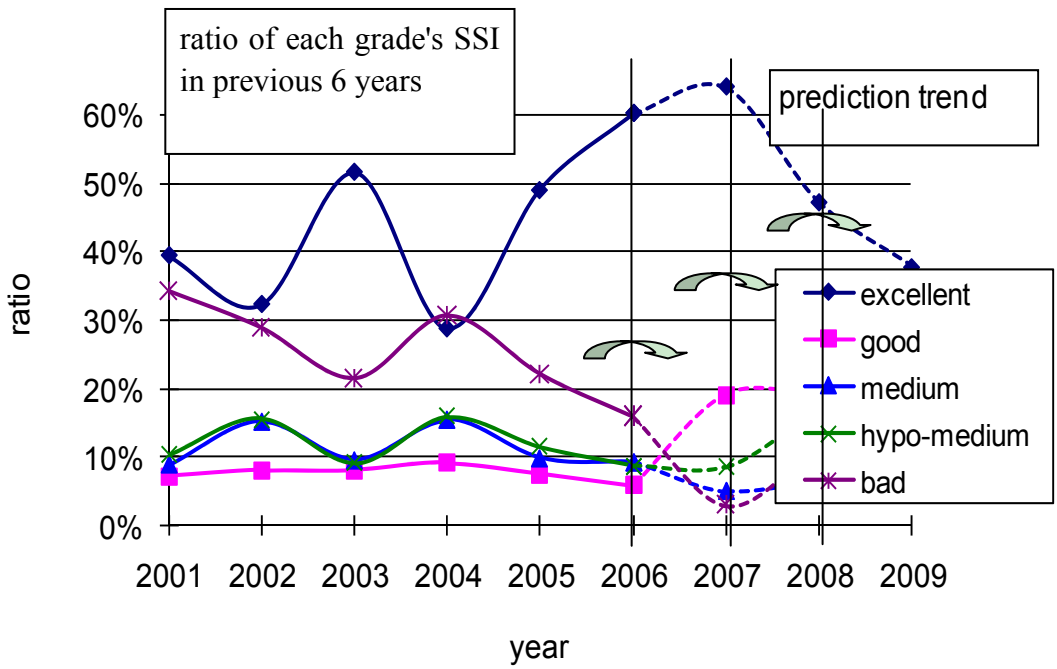

Figure 5. Network SSI gradually rolling prediction.

On the basis of the prediction data, Table 2 compares the errors generated by gradually rolling prediction and direct prediction.

Table 2. Comparison of 2 prediction errors of overall road network SSI.

SSI's grade	Grade range	Prediction value		Direct error relative		Rolling error relative	
		2007	2008	2007	2008	2007	2008
Excellent	1 ~	0.64	0.47	16%	22%	-12%	7%
Good	0.83 ~ 1	0.19	0.19	-12%	-12%	-12%	-9%
Medium	0.66 ~ 0.83	0.05	0.06	2%	0%	6%	5%
Hypo-medium	0.5 ~ 0.66	0.09	0.17	-12%	-14%	1%	-7%
Bad	0 ~ 0.5	0.03	0.10	7%	3%	17%	5%

From Table 2, the error of gradually rolling prediction was smaller than of direct prediction. The error in 2008 had become especially more uniform. No larger error appeared in individual level. This result could help management department not deviate from the original target when making long-term planning for maintenance. A guide was given. No error analysis was presented in 2009 since factual data was absent.

CONCLUSION

A prediction model of the use-level of road network was set up by neural network theory, conquering the limitations of the traditional prediction model. Gradually rolling prediction improved the BP neural network's prediction algorithm. Prediction precision had been improved greatly compared to direct prediction. Using the neural network model, the prediction results of the use-level of road network could help management departments make pavement maintenance decision-making more detailed and comprehensive.

REFERENCES

Bing Wen-shan. (2000). BP Network algorithm of the prediction of pavement condition index [J]. JOURNAL OF HARBIN UNIVERSITY OF CIVIL ENGINEERING AND ARCHITECTURE. 33(3):107~110.

Cheng Yu-zhu. (2007). Introduction of the model to predict asphalt pavement performances [J]. SHANXI ARCHITECTURE. 33(1):289~290.

Ge Zhe-xue, Sun Zhi-qiang. (2007). Neural network theory and the realization of MATLABR2007 [M]. Beijing: Publishing house of electronics industry.

J.D.Lea. (1999). Neural network for performance prediction on unsealed roads. Road & Transportation Research [J]. March.

(JTJ073.2-2001), "technical specifications for maintenance of highway Asphalt Pavement " [S].

Sun Li-jun, Liu Xi-ping. (1995). General Deterioration Equation for Pavement Performance [J]. JOURNAL OF TONGJI UNIVERSITY. 23(5): 512~518.

Sun Li-jun. (1997). Structural Behavior Study for Asphalt Pavement [M]. Shanghai： Tongji University Press.

W.O.Hadley. (1994). SHRP~LTPP Overview: Five-year Report[R]. SHRP-P-416.

Xie Xu-fei. (2004). Prediction Probabilistic Model of Pavement Performance Based on BP Neural Networks [D]. Harbin Institute of Technology master's thesis.

Yao Zu-kang. (1993). Pavement management system [M]. Beijing: China Communications Press.

Zhou Wen-xian, Li Ming-li, Sun Li-jun. (2006). Portland Cement Concrete Pavement Performance Prediction Model Based on Improved Neural Network [J]. JOURNAL OF TONGJI UNIVERSITY (NATURAL SCIENCE) . 34(9):1191~1195.

Identification of Hazardous Locations Based on Integrated Highway Safety State Analysis

WANG Yan[1] and GUO Zhongyin[2]

[1]Road Safety Research Center, Research Institute of Highway, Ministry of Transport, China, No.8 Xitucheng Road, Haidian District, Beijing; PH (010) 62378943; FAX (010) 62363428; email: whj98741@126.com

[2]School of Transportation Engineering, Tongji University, China, No. 1239 Siping Road, Shanghai; PH (021) 69585723; FAX (010) 69585723; email: zhongyin@mail.tongji.edu.cn

ABSTRACT

Identifying hazardous locations for an in-depth safety analysis and potential safety improvement is one of the key functions of any safety management program. This paper proposes a new method that overcomes the weakness of the current methods. In the proposed method, the integrated highway safety state is analyzed to identify hazardous locations. Three models correlating accident rate, traffic flow characteristics and road facility features are studied and the different risk levels are proposed. Then the integrated highway safety state is defined and two forms are adopted to describe the integrated highway safety state, which are the vector form and the single synthetic form. By analyzing the intrinsic relation among accident data, traffic flow characteristics, road facility features and highway safety, the procedure for identifying hazardous locations using highway safety state has been developed. This method can be used to identify potential hazardous locations and prioritize safety improvement programs which is fundamental to allocate resources under limited budget conditions.

BACKGROUND

Road safety problem worldwide. More than 3,500 people are killed in road crashes and 137,000 more are injured or disabled every day worldwide. In China, more than 600 people are killed and more than 45,000 injured daily, and road traffic fatalities in China are predicted to increase to almost half a million per year by 2020 unless urgent action is taken. Beyond the loss of human life, poor road safety has an enormous economic impact. Annual direct and indirect costs have been estimated at between $12 to 21 billion, approximately 1.5 percent of China's GDP. As part of a systematic approach to road safety, involving safer road user, safer vehicles and safer road, identifying hazardous locations can help address this crisis and save thousands of lives.

Potential for the new way of identifying hazardous locations. Most of the current methods for identifying hazardous locations depend on accident statistics,

thus a significant collision history must exist before hazardous locations are identified and the success of the identification process is governed by the quality of accident data. Unfortunately in many jurisdictions in China, the quantity and quality of collision data is far from enough to reflect the safety level correctly and efficiently due to the lack of a properly detailed and unified methodology to gather data. In addition, the potential hazardous locations can not be identified before the occurrence of accidents so that proactive countermeasures can not be taken to prevent the collision. To help mitigate this problem, the more recent studies try to develop methods that Identify hazardous locations not only based on collision statistics, but the analysis of traffic flow characteristics and road facility features. On the basis of the relevant research works, this paper proposes a new method that overcomes the weakness of the current methods.

DESCRIPTION OF HAZARDOUS LOCATIONS

Characteristics of hazardous locations. Generally, the accident rate in hazardous locations is higher than other safer locations. Most of the previous researches focus on using accident rate to measure risk level. However, accidents may not happen seriously in short period for the sake of careful driving, very low volume or other reasons.

Traffic flow characteristics have much to do with safety. From the macroscopical point of view, stable and free traffic flow contributes to high level of safety, while the turbulence of traffic flow leads to more accidents (Koornstra M. J., 1992). From the microcosmic point of view, if the driver can run at the expected speed and lane, without need to change lane frequently, there is less possibility for them to make mistakes leading to accidents. On the contrary, in the unsafe traffic flow condition, it's difficult for drivers to achieve their expectation so that they have to follow the foregoing car at the unstable speed and even change the lane frequently. Unsafe traffic flow often exists in hazardous locations.

Road facilities, including pavement, signs and markers etc., are the important components of driving environment. Obviously, facilities with good safety performance contribute to high level of safety. Facilities in hazardous locations often have some features unable to satisfy safety request. For example, the alignment is not continuous so that drivers have to accelerate and decelerate suddenly, or some signs provide wrong information to road users so that drivers can't make right decisions in time. All these cases will lead to higher possibility that accidents happen.

Risk estimation index of hazardous locations. By analyzing character of hazardous locations, risk estimation index can be put forward, which consists of three indices defined as accident rate (AR), traffic flow risk (TR) and road facility risk (FR).

Accident Rate, i.e. the accident number occurring on a certain segment per kilometer per year, reflects the risk level quantitatively from post-accident aspect.

Three kinds of driving behaviors can be found in a certain traffic flow

condition: free driving, car-following driving and lane-changing driving. In the low-volume traffic condition, speed tends to be higher, leading to high-speed risk. While in the high-volume traffic condition, drivers have to follow the foregoing cars or change the lane, leading to car-following risk and lane-changing risk. Traffic flow risk is the sum of the three kinds of risks mentioned above. Each kind of risk is modeled based on the speed of each vehicle and the following vehicle and the distance between them (ZHANG Xiao-dong *et al.,* 2006).

Many road facility features impact safety, and facility risk is defined to measure the extent to which facilities offer protection from accidents. According to the research works on safety effect of facility features, the most important factors affecting safety were selected to determine road facility risk, including alignment consistency, sight distance, skid resistance, signs, markings, roadside, etc. (Montella A., 2005).

Obviously, traffic flow risk and road facility risk can be estimated before accidents happen, so they can reflect the risk level from pre-accident aspect.

RISK ESTIMATION MODELS OF HAZARDOUS LOCATIONS

With respect to risk estimation models, previous studies have provided valuable insight regarding the methodologies formulated for road safety analysis, including historical accident data averages, predictions based on statistical models, results from before-and-after studies, and expert judgments made by experienced engineers. Each of these methods, if used alone, has significant weaknesses. On the contrary, there is an advantage to combining elements of each of these methods (Athanasios P. Chassiakos *et al.*, 2005). Due to the difference among three risk estimation indices, the corresponding risk estimation models have been established separately using different mathematical theories.

Risk estimation model based on AR. So far, there has been an established consensus among road traffic safety researchers that a non-linear, non-Gaussian relationship exists between traffic exposure and safety (Kononov J. *et al.,* 2003). This relationship is reflected by the Safety Performance Functions (SPF), which is calibrated for various classes of roads. Safety Performance Function provides a realistic estimate of expected accident frequency per unit of traffic exposure over a unit of time for various types of roads.

Based on substantial empirical evidence derived from observing safety performance of various roads over extended time periods as well as work of other researchers, the following understanding of relationship between safety and exposure has emerged. Accident rates decline when AADT reaches certain threshold endemic to a particular facility in a specific environment. This understanding suggests a choice of underlying function which would reflect this phenomenon. The following model form for SPF is usually employed.

$$E\{y\} = X^{\beta_0}(1 + \beta_1 X + \beta_2 X^2 \cdots) \tag{1}$$

Here, E{y} is the annual number of accidents expected to occur on a segment of road, X is the independent variable (AADT), and β are parameters to be estimated. With the Poisson distribution assumption of accident, the model parameters were estimated by the maximum-likelihood method.

$$\because \mu \in Poisson \therefore E(y) = \mu \ , \ Var(y) = \mu \tag{2}$$

$$P(x = y_i) = \frac{\mu_i^{y_i}}{y_i!} e^{-\mu_i} \tag{3}$$

$$L(\mu_P) = \prod_{i=1}^{n} \left(\frac{\mu_i^{y_i} e^{-\mu_i}}{y_i!}\right) \tag{4}$$

$$Ln(L) = \sum_{i=1}^{n} (y_i \ln \mu_i - \mu_i - \ln y_i!) \tag{5}$$

Where,

μ- Estimated number of accidents on roadway segment over a period of a year

y_i - Observed number of accidents on roadway segment over a period of a year

$L(\mu_P)$- Poisson likelihood function

Take 4-lane freeway for example, on the basis of the accident data in selected 4-lane freeways in China, the Safety Performance Function for 4-lane freeway has been established, shown in figure 1. The accident data and the highway data used in the model were collected from department of public security and highway bureaus. When collecting the accident data, the highways were divided into several segments according to road features, and then the accident rate for each segment was analyzed.

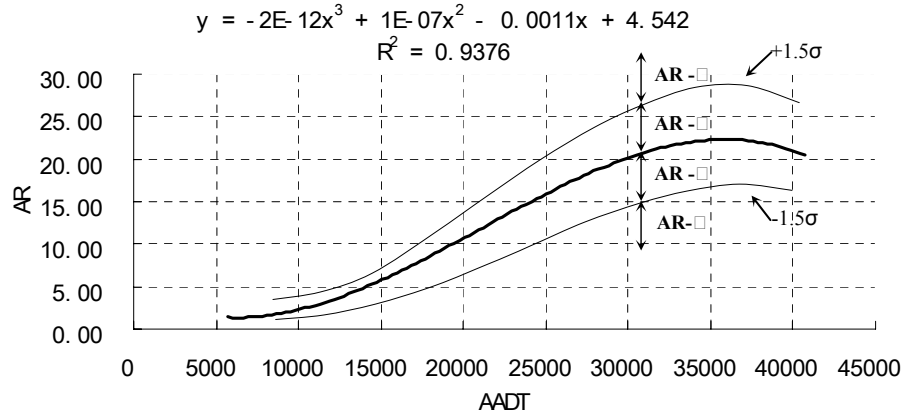

Figure 1. SPF for 4-lane freeway.

The level of safety predicted by the SPF represents normal or expected number of accidents at a specific level of AADT, and then the degree of deviation from the norm can be stratified to represent specific levels of risk. The delineated boundary line is located 1.5 standard deviations from the mean. Four levels of risk (LOR) can be proposed shown in figure 1, and the qualitative description is presented in Table 1.

Table 1. Qualitative Description of LOR based on AR.

Level of risk	Qualitative description
AR - I	Low potential for accident reduction
AR - II	Better than expected safety performance
AR - III	Less than expected safety performance
AR - IV	High potential for accident reduction

Risk estimation model based on TR. Thanks to the development of image identification technology, it's possible to get the speed and position information of vehicles in traffic flow from the visual record in the near future. In this paper, the traffic flow condition was simulated and the parameters for calculating TR were collected automatically by using traffic simulation software VISSIM. The values of TR at different levels of traffic volume were calculated and then the relationship between traffic flow risk and traffic volume has been established by applying regression analysis, shown in Figure 2.

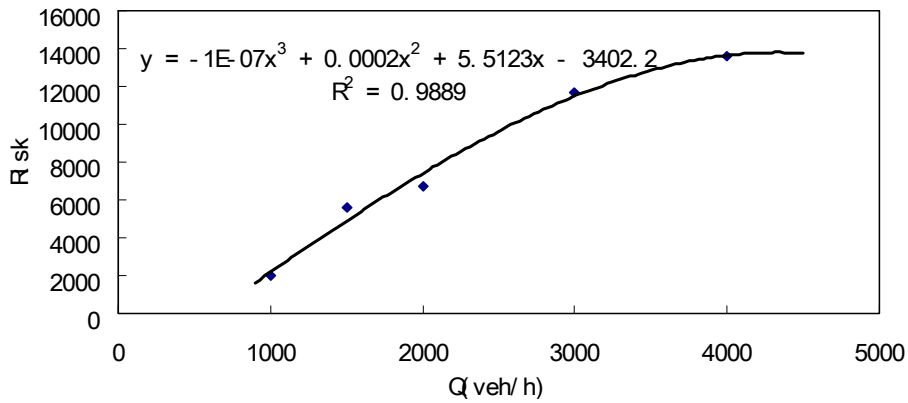

Figure 2. Regression model between traffic flow risk and traffic volume.

Similar to SPF, the value of traffic flow risk predicted by the regression model above can represent normal level of safety at a specific traffic volume, so the degree of deviation from the norm can be stratified to represent specific levels of risk. The delineated boundary line is located 1.5 standard deviations from the mean. Four levels of risk (LOR) can be proposed and the qualitative description is presented in Table 2.

Table 2. Qualitative Description of LOR based on TR.

Level of risk	Qualitative description
TR - I	Very low level of risk in traffic flow
TR - II	Low level of risk in traffic flow
TR - III	High level of risk in traffic flow
TR - IV	Very high level of risk in traffic flow

Risk estimation model based on FR. The risk estimation model based on FR was established by applying the fuzzy set theory. The facility features that affect highway safety have been hierarchically divided, and fuzzy judgment matrix has been

established on the basis of known accident relationships, shown in Table 3 (Lamm R., 1999). Then fuzzy comprehensive judgment is made to assess the risk of facilities features, obtained through weights and memberships of different facility feature. The relative weights were determined by professionals in the field of road safety using the hierarchical analysis method. The scores assigned to each facility feature result from field inspections and estimations by professionals and the trapezoid membership function was selected to determine the membership of each facility feature to different safety level.

Table 3. Fuzzy Judgment Matrix of FR.

Facility feature	Level of Facility Risk			
	FR-I	FR-II	FR-III	FR-IV
alignment consistency(ΔV)	<5km/h	5~10 km/h	10~20 km/h	≥ 20 km/h
sight distance	≥ 2.1SSD	1.6~2.1 SSD	0.75~1.6 SSD	<0.75SSD
skid resistance	≥ 0.50	0.50 ~ 0.40	0.40~0.30	<0.30
sharp curve warning sign	0~3	3~6	6~8	8~10
overtaking line	0~3	3~6	6~8	8~10
roadside	0~3	3~6	6~8	8~10
Excessive density of uncontrolled accesses	0~3/km	3~6/km	6~10/km	>10/km

According to the fuzzy judgment to the risk estimation of facility features, four levels of risk based on FR have been proposed and the qualitative description of each level is shown in Table 4.

Table 4. Qualitative description of LOR based on FR.

Level of Risk	Qualitative description
FR-I	Risk of facility features is very low, no need for improvement
FR-II	Risk of facility features is low, improve when capital is enough
FR-III	Risk of facility features is high, need improvement
FR-IV	Risk of facility features is very high, eager for improvement

HIGHWAY SAFETY STATE (HSS)

HSS Vector. According to risk estimation result, the Highway Safety State (HSS) can be determined by three attributes: accident rate, traffic flow risk, facility risk. Each of them reflects the risk level from different angle. To define the integrated highway safety state, the vector form is recommended. AR, TR and FR were selected as elements of the HSS vector. As discussed before, each element of HSS vector has four grades shown in Table 5, so there are 64(4×4×4) kinds of safety state in all.

Table 5. Grades of elements of HSS vector.

Grade	AR	TR	FR
1	AR-I	TR-I	FR-I
2	AR-II	TR-II	FR-II
3	AR-III	TR-III	FR-III
4	AR-IV	TR-IV	FR-IV

The HSS vector can be represented in the following form.

$$HSS_i = \left(AR_j, TR_k, FR_m\right) \quad (i=1, 64; j, k, m=1, 4) \tag{6}$$

Single synthetic index of HSS. The vector form can present the detailed information of highway safety state, so it helps to diagnose safety problems and select treatments. However, it's easy to compare the risk level of different locations and prioritize the improvement projects using the single synthetic index. Both of them are useful in highway safety management.

Nonlinear dimensionless analysis was adopted to convert original values of AR, TR and FR to standard values. Then the single synthetic index of HSS is defined as follows.

$$HSS_i = a_1 f(AR_i) + a_2 f(TR_i) + a_3 f(FR_i) \tag{7}$$

Where

AR_i, TR_i, FR_i —— the original value of AR, TR and FR in section *i*;

$f(AR_i), f(TR_i), f(FR_i)$—— the standard value of AR, TR and FR determined by dimensionless analysis in section *i*;

a_1, a_2, a_3 ——the weight determined by professionals using hierarchically analytical method.

The nonlinear dimensionless analysis method is described as follows:

$$f(x) = \begin{cases} e^{\frac{x - x_{\min}}{x_{\max} - x_{nin}}} & x > x_{\min} \\ 0 & x \le x_{\min} \end{cases} \tag{8}$$

Where

$x_{\max}$, $x_{\min}$ - the maximum value and the minimum value of index, determined as 3 standard deviations from the mean based on statistical analysis of index values.

It is important to point out that the weight for each index is changeable according to the quality of accident data, traffic flow data and facility data. The higher the quality of data, the more the weight of corresponding index is. What's more, the weight should be different at different locations.

IDENTIFICATION OF HAZARDOUS LOCATIONS USING HSS

Before identifying hazardous locations, highways should be divided into several homogenous sections according to traffic volume and road facility features. Then the integrated safety analysis mentioned above should be implemented on each section, and the risk level of each section will be estimated.

By analyzing the intrinsic relation among accident data, traffic flow characteristics, road facility features and highway safety, comments for highway safety state can be described as follows: the location with all three indices in grade 1,

i.e. *HSS*=(1,1,1), is the best state of highway safety; the location with all three indices in grade 1 or grade 2, such as *HSS*=(2,1,2), can be regarded as safe location; the location with any of the three indices in grade 3 or grade 4, such as *HSS*=(3,1,2), has potential safety problem; the location with all three indices in grade 4, i.e. *HSS*=(4,4,4), is the worst state of highway safety.

More specifically, the location with TR in grade 3 or grade 4, such as *HSS*=(2,4,2), need improvement treatments on traffic flow, such as speed restriction. While the location with FR in grade 3 or grade 4, such as *HSS*=(2,1,4), need improvement treatments on road facility, such as changing alignment, setting warning signs. As for the location with AR in grade 3 or grade 4 but TR and FR in grade 1 or grade 2, such as *HSS*=(4,1,2), the safety problem on this location is probably caused by other factors such as driver error, vehicle broken, instead of traffic flow and road facility problems.

To prioritize the improvement projects, the hazardous locations can be compared using the single synthetic index of HSS, the higher value of HSS means the more dangerous location.

Compared to previous methods, the advantage of the method studied in this paper is that the potential hazardous locations where not many accidents happened but traffic flow risk or facility risk is high can be identified, so the necessary treatment can be implemented to prevent large number of accidents occur in the near future. Furthermore, by considering traffic flow and facility features besides accident data, the method allows more effective and fair identification of hazardous locations, especially in places where accident data collection is disadvantageous.

CONCLUSION

Through analyzing the character of hazardous locations, risk estimation index and risk estimation models for hazardous locations have been studied. Based on the integrated highway safety state analysis, the new method discussed in this paper allows more effective and fair identification of potential hazardous locations compared to the previous methods. It also provides a priority for safety improvement programs which is fundamental to allocate resources under limited budget conditions.

Due to the limitation of the quantity and quality of accident data, traffic flow data and facility data, the risk estimation model discussed in this paper need be revised in the future as the data collection getting more advantageous, but this method provides a new way to do safety analysis which is more valuable than the model itself.

REFERENCES

Athanasios P. Chassiakos, Christina Panagolia, Dimitrios D. Theodorakopoulos. (2005). “Development of Decision-Support System for Managing Highway Safety.” *Journal of Transportation Engineering,* 131(5), 364-373.

Koornstra M. J. (1992). “The Evolution of Road Safety and Mobility.” *IATSS Research,* 16(2), 129-148.

Kononov J., Allery B. (2003). "Level of Service of Safety: Conceptual Blueprint and Analytical Framework." *Transportation Research Record No. 1840,* Washington, D.C., 57-66.

Lamm R., Psarianos B., Mailaender T., Choueiri E.M., Heger R., Steyer R. (1999). *Highway Design and Traffic Safety Engineering Handbook*. McGraw-Hill, New York, U.S.A.

Montella A. (2005). "Safety reviews of existing roads: a quantitative safety assessment methodology." *Transportation Research Record*, Washington D.C., 62-72.

ZHANG Xiao-dong, GUO Zhong-yin, GAO Jian-ping, JIANG Rui. (2006). "Safety analysis method on freeway on-ramp merging area". *Journal of Chongqing Jiaotong University*, 25(1), 99-106.

Analysis of Crowd Behavior in Route Choice Based on Dynamic Programming

Jiang Xiaobei [1], Xiong Hui [2], Guo Hongwei [3]

[1]Department of Transportation Engineering, Beijing Institute of Technology, Beijing 100081, China; PH (49) 89-289 15420; email: yougaduras@163.com
[2]Department of Transportation Engineering, Beijing Institute of Technology, Beijing 100081, China; PH (86)10-68915579-202; FAX (86)10-68914582-16; email: xionghui00@mails.tsinghua.edu.cn
[3]School of Traffic and Transportation, Beijing Jiaotong University, Beijing, 100044, China; PH (49) 89-289 15420; email: yougaduras@163.com

ABSTRACT

Pedestrian security has been becoming increasingly important in urban traffic because of the explosion and intensive activities of urban population. Considering the complexity of crowds' behavior, it is necessary to analyze the characteristics of the crowd and the law of crowds' route choice.

The macro and micro characteristics data were obtained from video observation at the study sites and the researchers' survey, including the flow rate, speed, density of the crowd, etc. Based on the analysis of the relationship between speed and density of the crowd, a crowds' route choice model was derived according to the basic theory of dynamic programming by dividing the route choice process into different stages, selecting the state/decision variables, analyzing the recurrence relation and the expression of the optimal value function. The model was verified by the field data collected in observations and the comparison between the calculation results and field data shows the model proposed can accurately describe the pedestrian route.

The model provides a mathematic method of the crowds' simulation. And the understanding of pedestrian behavior would help to improve the level-of-service of pedestrian traffic facilities in planning and design.

INTRODUCTION

Because of the complex behavior patterns of a crowd and the weakness of the traffic facilities, it is necessary to analyze the characteristics of the crowd, the law of crowd pedestrians' movement and the route choice behavior for developing effective prevention measures and reducing the risk.

The number of models for the crowd pedestrian behavior increases rapidly. A

great deal of research has been devoted to investigate crowd traffic. Besides the analysis of the characteristics of pedestrians, multidisciplinary theories have been widely adopted to develop pedestrian models. The cornerstone models for crowd were rooted in the traditional fluid mechanics models first put forward by L. F. Henderson (1971). In his model, the pedestrians at low density were seen as gas molecules and pedestrians at high density (crowd) were seen as liquid ones. Also in the 1970s Henderson (1974) had compared measurements of pedestrian flows with Navier-Stokes equations with considerable success. The analysis of the crowd was extensively evolved on the basis of Henderson's theory during the next 20 years. His phenomenological fluid-dynamics approach had been improved and mathematically founded by Helbing in the 1990s (1991, 1995) and this model was closely related to some gas-kinetic traffic models (I. Prigogine and R. Herman, 1971; S. L. Paveri-Fontana 1975) and fluid-dynamics (B. S. Kerner and P. Konhäuser 1993, 1994; D. Helbing 1995). Afterward the "microscopic" approaches for the vehicular traffic, series models for the pedestrian motion in microsphere had been proposed including the social force model (D. Helbing,1995) and the CA model in late 1990s (M. Fukui,1999; Blue and Alder 1998,1999). The former was accomplished through the interaction between pedestrians and environment, and described the "forces" as a measure for the internal motivations of the individuals to perform certain actions. The social force model is capable of describing the self-organization phenomena in pedestrian traffic. The latter was proposed based on the Nagel-Schreckenberg (1992) model which was used to model vehicular transportation. The pedestrians in this model were regarded as certain cellular and the movement was along the network of the system. And it modeled the pedestrians' movement and decision making behavior within a built environment. The CA model could offer a simulation of autonomous individuals and the interaction among them. It's also another trend for the development of pedestrian traffic.

Comprehensively, the microscopic models for the crowd pedestrian can be divided into two kinds, discrete models and continuous models. Each kind receives a great deal of interest for its evolution and both of them apply to pedestrian traffic research.

DATA COLLECTION

State boundaries for the pedestrians

The Level-of-Service (LOS) for pedestrian facilities is considered a measurement of validity by which pedestrians can determine the quality of service, including the number of pedestrians per unit area, walking speed which can be reached, the possibility, safety and comfort when pedestrians take some actions like over-taking and crossing, etc. (CHEN, 2003). From the five ranks of LOS, rank C

and below are chosen for the crowd state considering the pedestrian traffic state and the mental feeling. The author's survey aims to the crowd pedestrians in the states in which the unit area is under $2m^2/p$ and the pedestrian walking speed is under 1.0m/s. The hall of the Information Teaching Building in Beijing Institute of Technology was chosen for this study.

Method for data collection

Considering the high freedom of pedestrian movement and the experience with pedestrian traffic observation, a video data collection method with data conversion has been adopted for the field study. According to the video images, the micro/macro pedestrian data can be obtained and analyzed, and a "video-recording—image-processing—data-collecting procedure" is chosen for the data collection. A pedestrian track data collection program, developed by Mr. Sun in Tsinghua University, is used for converting the pedestrian track information into traffic data.

Observing parameters

Walking speed for individual pedestrians

In video observation, pedestrian position is fixed by each frame and a set of successive position points run in a series. Recording the coordinates of a certain pedestrian in the first frame and the coordinates after n ($n \geqslant 2$, even number are better) frames, the average walking speed is the rate of movement per unit time.

During the observation process, because the instantaneous speed in one point can hardly be measured. As a result, assuming n as 2, we consider the average walking speed as the spot speed.

Crowd speed

The concept of crowd speed in this study is defined as the time-mean speed at a certain point and it's the average spot speed of several pedestrians measured at a given point in unit time. It's also used for analyzing the relationship between crowd speed and density.

Crowd density

Crowd density means in the crowd region, the number of pedestrians per unit area (p/ m^2).

DATA ANALYSIS

According to the pedestrian position information obtained by the pedestrian track data collection program, the plane track and the plane coordinates of the pedestrian can also be obtained after coordinate transformation. The traffic parameters are then analyzed as follows:

Pedestrian walking speed

According to the statistical analysis of 545 samples, the average crowd

pedestrian speed is 0.660m/s, and the standard deviation is 0.32. Figure 1 illustrates the distributions of crowd pedestrians' walking speed. The speed distribution histogram indicates that the distributions of walking speed follows normal distribution, the same as the distribution of the pedestrian speed in sidewalks (Xiong Hui,2007) and crossing speed in crosswalks (Jiang Xiaobei, 2008).

Distribution of crowd density

During the process from the sudden increase of pedestrian flow to the evacuation of the crowd, there is a stable distribution of the crowd density in the observation area under a steady pedestrian flow. The statistic histogram of the crowd density is given by Figure 2. Figure 3 shows the high-density area, medium-density area and the low-density area are steadily in certain positions.

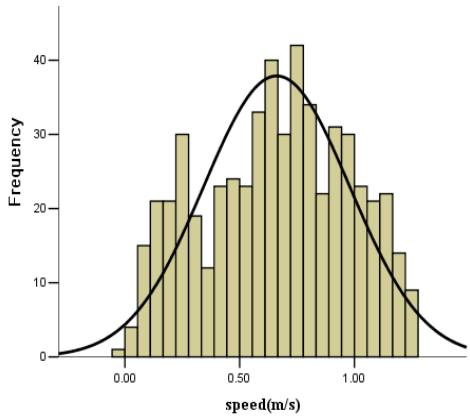

Figure 1. Walking speed distribution density

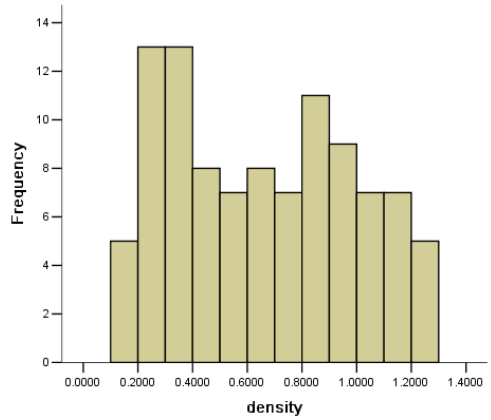

Figure 2. Statistic histogram of crowd

A conclusion from Figure 3 is that the high-density appears near the exits where the moving space for the pedestrian is extremely small, closing to static pedestrian occupancy area; the lower density appears to be decreasing with the larger distance to the exits.

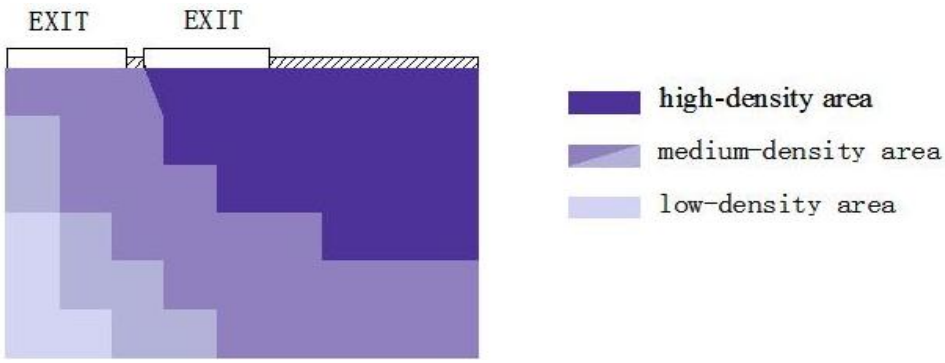

Figure 3. Stable distribution of the density

Relationship between crowd density and walking speed

The relationship between the average spot speed in a certain area in a frame and the density in this area can be expressed in Figure 4. In the classical pedestrian traffic research, the relationship between crowd density and walking speed is always described as linear relationship or exponential relationship. From the observation, an exponential relationship is chosen for fitting the relationship between crowd density and walking speed. The expression of curve in Fig.4 is y = 1.74839e-1.42192x. (R^2=0.807).

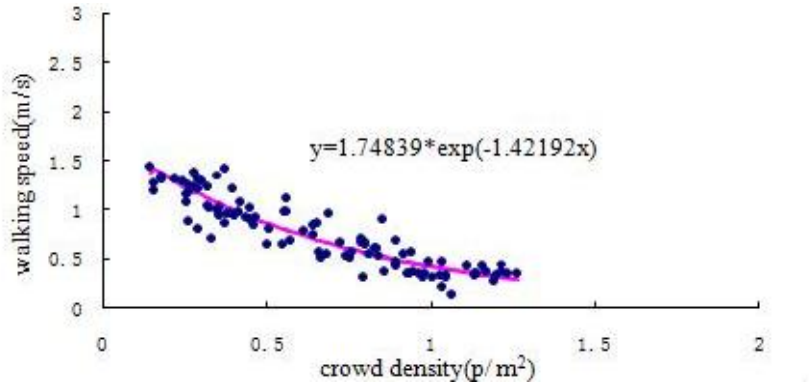

Figure 4. Relationship between crowd density and walking speed

ROUTE CHOICE MODEL BASED ON DYNAMIC PROGRAMMING

A decision making behavior for route choice

According to the node which is the current position of the pedestrian, the impedances of each path will be compared; consider a walking habit to choose one path. Then the pedestrian decides on another node and path. By inference, connecting all the nodes and paths, the final walking route from the origin to destination is formed.

Obviously the pedestrian will make an instantaneous decision when another node will be chosen. Route choice behavior can be judged as decision-making behavior for the position of each node in the whole route, and it is Markov decision processes (Hu Dihe, 1983). The cost is generally measured by the walking distance or time. In field observation, the length of walking time is the main consideration in the pedestrian's route choice.

Model set- up

Simulating for pedestrian walking environment

There are two methods for environment simulating: network system and plane coordinate. Both two are selected for the study. From the observation, the crowd density is between $3p/m^2$~$4p/m^2$, so in this situation occupancy area per pedestrian is about $0.25m^2$ and each grid is designed by 0.5m×0.5m, shown in Figure 5. At the same time, each node is set by a corresponding coordinate for the model calculation. The network is oriented in a plane coordinate system. Assume

each pedestrian will be in one node on the network after a certain state, and the pedestrian takes the link of the node (side/diagonal of the grid) as a certain walking path in a state.

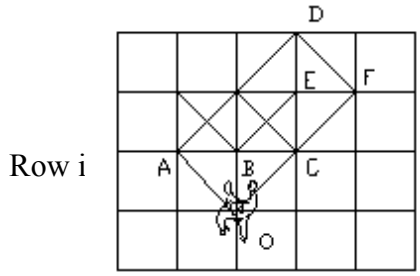

Figure 5. Network of the walking environment

Selecting the state and decision variables

According to the basic theory of dynamic programming, the state and decision variables should be defined for the route choice process. The process state variables with non-aftereffect are chosen to describe the pedestrian traffic state: the coordinate of the node (pedestrian position) (x_{ij}, y_{ij}) and the walking speed (v'_{xij}, v'_{yij}) in this state.

A pedestrian chooses the route with the shortest walking time, as a result, the time of the route is determined as the decision variable. In the network, excluding three nodes behind node $N_{i,j}$ (because in the crowd state, pedestrians can hardly go backward), there are 5 adjacent nodes corresponding with node $N_{i,j}$. If the pedestrian is now at node $N_{i,j}$, the 5 paths in front and the paths at sides will be considered.

Analyzing the recurrence relation and the expression of the model

Regarding the route from origin O to destination D as a state-transfering chart for a finite states system, each node as a certain state, then the arc (the link of every two nodes) is directed from state s_k to state s_{k+1}, corresponding with transfer $s_{k+1} = V_k(s_k, u_k)$. And the length of the arc equals the cost of transfer ($t_k(s_k,u_k)$), that is the walking time of the path.

The definition of objection function is given by

$$T_k = \sum_{m=k}^{n-1} t_m(s_m, u_m)$$

It represents the sum of the state transfer cost for all the following subprocesses, that is, the walking time from the current state to the final state

(pedestrian reaches the destination), and sufficient to satisfy:

1) a quantity function defined for the whole process and the following subprocesses;

2) $T_k(s_k, u_k, s_{k+1}, u_{k+1} \cdots) = \Psi_k[s_k, u_k, T_{k+1}(s_{k+1}, u_{k+1} \cdots)];;$

3) $\Psi_k(s_k, u_k, T_{k+1})$ is monotonic as its variable T_{k+1},

where $t_m(s_m,u_m)$ denotes the objection function of state m, and the recurrence relation is given by $T_k = t_k(s_k, u_k) + T_{k+1}$.

The optimal value function can be deduced by

$$f_k(s_k) = \min T_k = \min[t_k(s_k, u_k) + T_{k+1}] = \min\left(\frac{L_k(u_k)}{V_{i,j}(s_k)} + T_{k+1}\right)$$

where $L_k(u_k)$ denotes the length of the path (side/diagonal of the grid) when taking the decision u_k; $V_{i,j}(s_k)$ denotes the walking speed from state k to state k+1.

The function means that in state s_k the pedestrian makes the decision u_k so as to get a minimum walking time for the following state. Reversing backward from the destination, at any state of the process the walking time from the node to the destination is the shortest. And the calculation of the optimal value function is the whole time for a certain pedestrian to walk through the crowd area.

MODEL VERIFYING AND CONCLUSION

Model Verifying

Based on the equation of the crowd density-speed curve in Figure 4, the average walking speed in each density can be calculated and the paths in the network (side/diagonal of the grid) can also be gained. According to the model, the minimum walking time for the pedestrian is worked out from the optimal value function, and the route can be derived by linking all the nodes of the optimal decisions. Figure 6 describes the routes a_1/a_2, c, d chosen separately by pedestrians from origin A, C and D to destination EXIT.

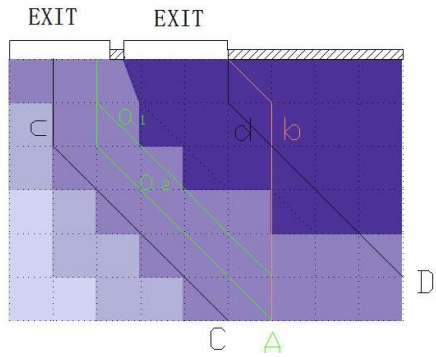

Figure 6. Routes chosen by pedestrians from origin A, C, and D to destination EXIT

The model was verified by the data collected in the field observations. Most tracks of the route from origin A (a bilaterally 0.25m) to the EXIT were between a_1 and a_2. The average walking time among 41 available samples that chose this route is 6.30s, compared with the average walking time derived from the model 6.36s, the error is 0.96%. Another 38 samples were chosen for validating the route d. The average walking time in the observations is 7.50s, compared with the average walking time derived from the model 7.39s, the error is 1.46%. Comparison between field data and calculation results shows that the route choice model proposed in the paper can accurately describe the pedestrian route.

CONCLUSION

The modeling of the crowded pedestrian route choice behavior provides the simulation of the crowd by using a mathematical method. The understanding of pedestrian behavior can help to improve the level-of-service of pedestrian traffic facilities. Due to the restriction of the survey conditions, limited field investigators, etc., the samples in other density zones, especially in the density close to the maximum limit density, were not obtained in this survey. For further studies, it's meaningful to take other density states into account.

REFERENCES

Blue, V. J. and Adler, J. L. (1998). "Emergent fundamental pedestrian flows from cellular automata microsimulation". Transportation Research Record, 1644: 29

Proceedings of the 14Th International Symposium on Transportation and Traffic Theory, Jerusalem, Israel, 235. (1999). Bi-directional emergent fundamental pedestrian flows from cellular automata microsimulation . Blue, V. J. and Adler, J. L.

Chen, Kuan-min and Yan, Bao-jie. (2003). Analysis of Road Traffic Capacity. China Communications Press, Beijing.

Fukui,M. and Ishibashi, Y. (1999). "Self-organized phase transitions in cellular automaton models for pedestrians". J. Phys. Sco. Jpn. 68, 2861-2863.

Fukui,M. and Ishibashi, Y. (1999). "Jamming Transition in Cellular Automaton Models for Pedestrians on Passageway". J. Phys. Soc. Jpn, 68,3738-3739.

Helbing, D. (1995). "Improved fluid-dynamic model for vehicular traffic".Phys. Rev. E51, 3164-3169.

Helbing, D. and Molnár, Péter. (1995). "Social Force Model for Pedestrian Dynamics". Phys. Rev. E 51: 4282-4286.

Henderson, L.F. (1971). "The statistics of crowd fluids". Nature, 229,381-383.

Henderson, L.F. (1974). "On the fluid mechanics of human crowd motion". Transportation Research, Vol.8, 509-515.

Hu, Dihe. (1983). Markov Process in Denumerable Status. Wuhan University Press, Wuhan.

Jiang, Xiaobei and Xiong, Hui. (2008). A Study on the Pedestrian Crossing Capacity at Signalized Intersection. 10th International Conference on the Applications of Advanced Technologies in Transportation, Athens,

Kerner, B.S. and Konhäuser, P. (1993). "Cluster effect in initially homogenous traffic flow". Phys. Rev. E 48(4) 2335-2338.

Kerner, B.S. and Konhäuser, P. (1994). "Structure and Parameters of Clusters in Traffic Flow". Phys. Rev. E, Vol. 50, No. 1, 54-83.

Nagel, K. and Schreckenberg, M. (1992). "A Cellular Automaton Model for Freeway Traffic", Journal de Physique I, 2: 2221-2229.

Paveri-Fontana, S. L. (1975). "On Boltzmann-Like Treatments for Traffic Flow: A Critical Review of the Basic Model and an Alternative Proposal for Dilute Traffic Analysis". Transportation Research, Vol.9, 225-235.

Prigogine, I. and Herman,R. (1971). "Kinetic Theory of Vehicular Traffic". American Elsevier, New York Chap. 4, p.42.

Xiong, Hui. Lv, Jian. Jiang, Xiaobei. Li, Zhenshan. (2007). Pedestrian Walking Speed, Step Size & Step Frequency from the Perspective of Gender and Age: A Case Study in Beijing, China. Proceedings of Transportation Research Board 86th Annual Meeting, Washington, D.C.

Vehicle Dynamics Model in Two-dimension Collision Accident

Cao Yi[1], Pei Yu-long[2] and Xiang Wen-sen[3]

[1] School of Transportation Science and Engineering, Harbin Institute of Technology, P.O. Box 2526, 202 Haihe Rd. Harbin 150090, China, PH (86) 451- 8628 2832; FAX (86) 451-8628 2832; email: caoyi820619@yahoo.com.cn
[2] School of Transportation Science and Engineering, Harbin Institute of Technology, P.O. Box 2526, 202 Haihe Rd. Harbin 150090, China, PH (86) 451- 8628 2832; FAX (86) 451-8628 2832; email: yulongp@263.net
[3] School of Transportation Science and Engineering, Harbin Institute of Technology, P.O. Box 2526, 202 Haihe Rd. Harbin 150090, China, PH (86) 451- 8628 2832; FAX (86) 451-8628 2832; email: xiangwensen0115@163.com

ABSTRACT

In order to provide a basis of vehicle velocity calculation and microcosmic analysis of accidents, this paper investigates a vehicle dynamics model in two-dimension collision accidents. Two-dimension collision accidents are classified into two categories: two-dimension centripetal collision and two-dimension non-centripetal collision. The vehicle dynamics models are also set up. By using reconstruction analysis software of road traffic accident, named PC-Crash, simulation experiments have been carried out for the two accident categories. Without considering the instances of double or multiple collisions, the result of experiments indicates that the model calculation results are similar with the simulation results using software, which validates the efficiency of proposed method.

INTRODUCTION

With the rapid development of the world's automobile industry, motor vehicle dynamic performance is getting higher and higher. The results show that vehicle collision accidents occupy more than 2/3 of the gross of road traffic accidents, and the two-dimension collision accident is one of the most familiar accident forms among vehicle collision accidents.

The definition of a two-dimension collision accident is that the accident vehicles only do translation and yaw movement in the same plane before and after impact, without rolling, flying and moving along with the road side slope. In this paper, the vehicle dynamics model for a two-dimension collision accident is set up in accordance with the principle of dynamics. By using this model, the vehicle's pre-impact velocity can be calculated according its post-impact velocity. Moreover, PC-Crash has been applied to validate the vehicle dynamics model.

KINETICS THEORY OF VEHICLE TWO-DIMENSION COLLISIONS

Elastic restitution coefficient of vehicle impact. The coefficient which is used to distinguish elastic or plastic impact is called the elasticity restitution coefficient (Pei Y. L. 2006).

By making the accident's impact point as the origin of coordinates, the coordinates system called $nD\tau$ can be set up. The normal and tangential elasticity restitution coefficients of vehicles can be defined as e_n and e_τ.

$$e_n = \left| \frac{(v_{2n} - v_{1n}) - (\omega_2 x_{2\tau} - \omega_1 x_{1\tau})}{(v_{20n} - v_{10n}) - (\omega_{20} x_{2\tau} - \omega_{10} x_{1\tau})} \right| \tag{1}$$

$$e_\tau = \left| \frac{(v_{2\tau} - v_{1t}) - (\omega_2 x_{2n} - \omega_1 x_{1n})}{(v_{20\tau} - v_{10\tau}) - (\omega_{20} x_{2n} - \omega_{10} x_{1n})} \right| \tag{2}$$

Relationship between plasticity deformation and effective impact speed. International studies have done lots of frontal and rear-end impact experiments for some cars whose engines are proposed. The definition of the effective impact speed and the relationship between it and plasticity deformation of cars has been found in the last reference (Zhang. X. Y. et al. 2007).

HYPOTHESIS OF COLLISION ACCIDENT

For expediently setting up the vehicle collision dynamics model, there are several hypothesis. (1) Because of the short impact time, the position of the vehicle can be considered the same during the course of the vehicles' impact. (2) Because of the vehicles' huge impulsive forces at the moment of impact, the influence of other familiar forces can be neglected.(3) Because of the energy loss, the kinetic energy theorem and energy conservation law are not suitable to academic analysis.

VEHICLE TWO-DIMENSION COLLISION DYNAMICS MODEL

Two-dimension centripetal collision of vehicles. The kind of impact that one impact impulsive force of a vehicle goes through another vehicle's center of mass is called centripetal collision. It can be considered that vehicle A and vehicle B are occurring at centripetal collision point O. The case can be shown in Figure 1.

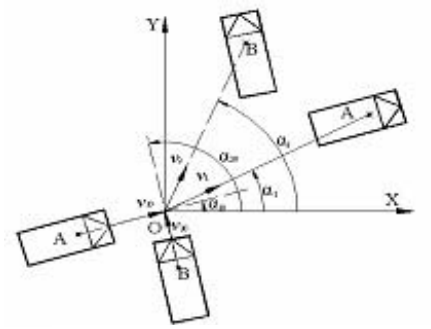

Figure 1. Two-dimension centripetal collision.

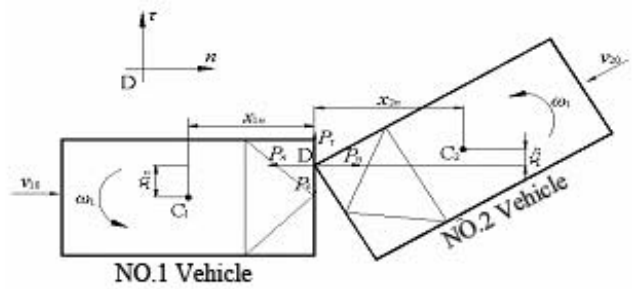

Figure 2. Two-dimension non-centripetal collision.

According to momentum conservation law, formulas (3) and (4) can be shown as flowing. By using the relationship between effective impact speed and plasticity deformation depth, the model can be set up as:

$$m_1 v_{10} \cos\alpha_{10} + m_2 v_{20} \cos\alpha_{20} = m_1 v_1 \cos\alpha_1 + m_2 v_2 \cos\alpha_2 \quad (3)$$

$$m_1 v_{10} \sin\alpha_{10} + m_2 v_{20} \sin\alpha_{20} = m_1 v_1 \sin\alpha_1 + m_2 v_2 \sin\alpha_2 \quad (4)$$

$$29.25 x_1 \cos\alpha_{10} = \frac{m_2}{m_1 + m_2}(v_{10}\cos\alpha_{10} - v_{20}\cos\alpha_{20}) \quad (5)$$

$$29.25 x_1 \sin\alpha_{10} = \frac{m_2}{m_1 + m_2}(v_{10}\sin\alpha_{10} - v_{20}\sin\alpha_{20}) \quad (6)$$

Two-dimension non-centripetal collision of vehicles. The prominent character of the vehicle non-centripetal collision is that the vehicle not only translates but also turns after impact. The movement parameters of vehicles are shown in Figure 2. The model can be constructed by using the definition of normal and tangent elasticity restitution coefficients combined with the momentum theorem and the theorem of moment of momentum. This model can be expressed in matrix form.

$$[A_0][V_0] = [A][V] \quad (7)$$

where $[A_0] = \begin{bmatrix} m_1 & 0 & 0 & m_2 & 0 & 0 \\ 0 & m_1 & 0 & 0 & m_2 & 0 \\ -m_1 x_{1\tau} & m_1 x_{1n} & I_1 & 0 & 0 & 0 \\ 0 & 0 & 0 & -m_2 x_{2\tau} & m_2 x_{2n} & I_2 \\ e_n & 0 & -e_n x_{1\tau} & -e_n & 0 & x_{2\tau} e_n \\ 0 & e_\tau & -e_\tau x_{1n} & 0 & -e_\tau & e_\tau x_{2n} \end{bmatrix}$, $[A] = \begin{bmatrix} m_1 & 0 & 0 & m_2 & 0 & 0 \\ 0 & m_1 & 0 & 0 & m_2 & 0 \\ -m_1 x_{1\tau} & m_1 x_{1n} & I_1 & 0 & 0 & 0 \\ 0 & 0 & 0 & -m_2 x_{2\tau} & m_2 x_{2n} & I_2 \\ -1 & 0 & x_{1\tau} & 1 & 0 & -x_{2\tau} \\ 0 & -1 & x_{1n} & 0 & 1 & -x_{2n} \end{bmatrix}$,

$[V_0] = [v_{10n} \quad v_{10\tau} \quad \omega_{10} \quad v_{20n} \quad v_{20\tau} \quad \omega_{20}]^T$, $[V] = [v_{1n} \quad v_{1\tau} \quad \omega_1 \quad v_{2n} \quad v_{2\tau} \quad \omega_2]^T$

It can be known that the post-impact velocities should be calculated first according to brake mark formulas. Then, the pre-impact velocities can be determined.

VALIDATION OF THE VEHICLE COLLISION DYNAMICS MODEL

This part's content will use road traffic accident simulation reconstruction analysis software PC-Crash to do vehicle impact simulation experiments. Therefore the dynamics model in two-dimension centripetal collisions and two-dimension non-centripetal collisions can be validated.

The validation of dynamics model in centripetal collision. By using the road traffic accident simulation reconstruction analysis software, PC-Crash, six vehicle centripetal collision simulation experiments are carried out. The courses of these experiments are shown in Figure 3.

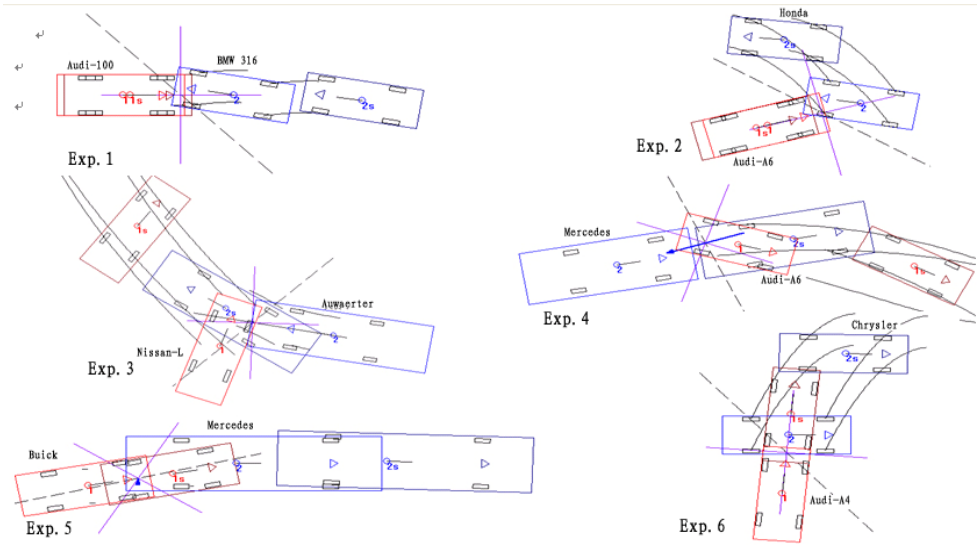

Figure 3. Two-dimension centripetal collision experiments by PC-Crash.

The original data is listed in Table 1. The results of simulation calculation and the model of two-dimension centripetal collision are shown in Table 2.

Table 1. Original Experiment Data in Centripetal Collision.

Experiment data	Exp.1	Exp.2	Exp.3	Exp.4	Exp.5	Exp.6
No.1 vehicle's name	Audi-100	Audi-A6	Nissan-L	Audi-A6	Buick	Audi-A4
No.2 vehicle's name	BMW	Honda	Auwaerter	Mercedes	Mercedes	Chrysler
1 vehicle's mass(kg)	1385	1430	1637	1430	1715	1430
2 vehicle's mass(kg)	1355	1140	8987	5460	6270	1660
Deformation (m)	No.1 front 0.42	No.1 front 0.47	No.2 front 0.05	No.1 tail 0.47	No.2 tail 0.45	No.1 front 0.46
Post-impact v_1 (km/h)	1.61	2.32	50.28	54.67	13.92	22.82
Post-impact v_2 (km/h)	30.05	30.15	30.85	55.67	37.78	32.80
No.1 direction (°)	0.00	-165.02	131.2	-6.75	4.44	84.92
No.2 direction (°)	6.77	126.55	160.09	9.55	4.19	67.13

Table 2. Experiment Results and Model Calculation.

Calculation results	Exp.1		Exp.2		Exp.3		Exp.4		Exp.5		Exp.6	
	Exp	Mod	Exp	Mod	Exp	Mod	Exp	Mod	Exp	Mod	Exp	Mod
Pre-impact v_{10} (km/h)	60.0	59.8	40.0	40.4	70.0	70.2	40.0	37.8	80.0	79.0	60.0	59.4
Pre-impact v_{20} (km/h)	30.0	29.6	70.0	71.2	40.0	39.4	60.0	60.5	20.0	20.1	10.0	8.4
No.1 direction (°)	0.0	2.8	15.0	13.0	70.0	78.7	-15.0	-15.9	10.0	8.0	85.0	83.1
No.2 direction (°)	170.0	178.0	170.0	170.3	170.0	179.5	10.0	9.4	0.0	0.1	0.0	-6.8

Validation of dynamics model in non-centripetal collision. By using PC-Crash, four times of vehicle non-centripetal collision simulation experiments have been done. The courses of these experiments are shown as Figure 4.

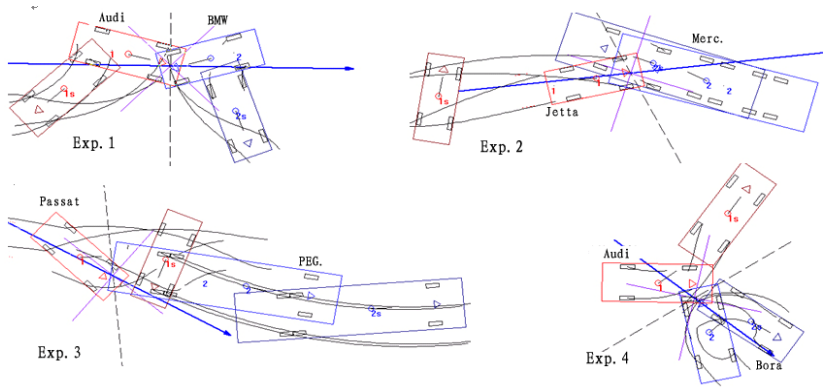

Figure 4. Two-dimension non-centripetal collision simulation by PC-Crash.

Table 3 shows the simulation input data. Results of simulation and calculation results of the model of two-dimension non-centripetal collisions are listed in Table 4.

Table 3. Original Experiment Data in Non-centripetal Collision.

Experiment data	Exp.1		Exp.2		Exp.3		Exp.4	
	No.1	No.2	No.1	No.2	No.1	No.2	No.1	No.2
Name	Audi	BMW	Jetta	Merc.	Passat	PEG.	Audi	Bora
Mass(kg)	1560	1395	930	11045	1455	7460	1250	1385
x_{in}(m)	-1.81	1.75	-1.56	3.47	-1.53	6.23	-1.58	0.64
$x_{i\tau}$(m)	0.52	0.31	-0.25	-0.4	0.93	-0.52	0.71	-1.61
v_{in}(km/h)	-22.43	11.05	-57.62	-17.56	39.48	50.16	24.45	11.83
$v_{i\tau}$(km/h)	-11.75	-18.25	-1.89	8.81	1.18	-12.78	17.71	10.18
ω_i(rad/s)	-4.95	3.93	2.64	-0.33	-2.85	0.80	4.64	-8.64
e_n	0.170		0.350		0.050		0.580	
e_τ	0.190		0.004		0.600		0.320	

Table 4. Results of Experiments and Model Calculation.

Calculation results	Exp.1				Exp.2			
	No.1 Vehicle		No.2 Vehicle		No.1 Vehicle		No.2 Vehicle	
	Exp	Mod	Exp	Mod	Exp	Mod	Exp	Mod
Name of vehicle	Audi		BMW		Jetta		Merc.	
v_{in}(km/h)	48.30	48.76	-67.61	-68.56	78.78	77.37	-28.98	-28.94
$v_{i\tau}$(km/h)	-12.94	-12.25	-18.12	-17.68	13.89	13.15	7.76	7.55
ω_i(rad/s)	0.00	0.21	0.00	0.26	0.00	0.05	0.00	0.01

Calculation results	Exp.3				Exp.4			
	No.1 Vehicle		No.2 Vehicle		No.1 Vehicle		No.2 Vehicle	
	Exp	Mod	Exp	Mod	Exp	Mod	Exp	Mod
Name	Passat		PEG.		Audi		Bora	
v_{in}(km/h)	96.59	85.51	39.39	41.17	59.09	61.37	-20.00	-21.48
$v_{i\tau}$(km/h)	-25.88	-24.24	-6.95	-7.82	-10.42	-11.15	34.64	36.23
ω_i(rad/s)	-3.00	-2.31	0.00	0.09	1.00	1.18	-2.00	-1.34

CONCLUSIONS

Without considering the case of more times impacts, the calculation results of the models are similar to PC-Crash. The results of simulation experiments indicate that the maximum relative error between the results of model calculations and software reconstruction is 11.15%. Therefore, it can be believed that the vehicle dynamics model in two-dimension collisions can comparatively accurately calculate the pre-impact velocity of the vehicles according to post-impact velocity of vehicles.

ACKNOWLEDGEMENT

This research is supported by the National High Technology Research and Development Program of China (2007AA11Z231).

REFERENCES

Dan A. Fittanto, Jordi Puig. “Utilizing a genetic algorithm to optimize vehicle simulation trajectories: determining initial velocity of a vehicle in yaw”. *2000 SAE Automotive Dynamics and Stability Conference*, 2000, Troy

Huang J. G. (2004). “Kinetic analysis and research on reconstruction of road traffic accident”. *Master Dissertation of Fu Zhou University*, 2-6

Li J., Ni H. D., Jin T. M. (1999). “Mechanical classification & model of two-dimension impact accidents”. *Journal of Highway and Transportation Research and Development*, 16(2), 74-77

Li J., Jin T. M., Ni H. D. (2000). “Traffic accident mechanics”. *China Machine Press*, Beijing, 104-128

Pei Y. L. (2006). “Road traffic safety”. *China Communication Press*, Beijing, 8-9

Raymond M. Brach, R. Matthew Brach. “Review of impact models for vehicle collision”. *SAE International Congress and Exposition*, 1987, Detroit: 3-7

Szydlowski, Wieslaw M., Jenkins, P. E. (1993). “Modeling of a sliding phase in accident reconstruction”. *SAE Special Publications*, 946, 35~40

Zhang. X. Y., Jin X. L., Qi. W. G., et al. (2007). “Reconstruction of the traffic accident based on deformation of the key points”. *Journal of Shanghai Jiaotong University*, 41(2), 238-243

Vehicle Trajectory Model in Two-dimension Collision Accidents

PeiYu-long[1], Cao Yi[2] and Ai Jun[3]

[1] School of Transportation Science and Engineering, Harbin Institute of Technology, P.O. Box 2526, 202 Haihe Rd. Harbin 150090, China, PH (86) 451- 8628 2832; FAX (86) 451-8628 2832; email: yulongp@263.net
[2] School of Transportation Science and Engineering, Harbin Institute of Technology, P.O. Box 2526, 202 Haihe Rd. Harbin 150090, China, PH (86) 451- 8628 2832; FAX (86) 451-8628 2832; email: caoyi820619@yahoo.com.cn
[3] Applied Foreign Language College, Heilongjiang University, 74 Xuefu Rd., Harbin, China, ST 150080; PH (86) 451-8660 8114

ABSTRACT

This paper provides a basis for vehicle movement trajectory reconstruction in two-dimension collision accidents and accidents disposal. On the basis of studies of predecessors, a different method of impact point named Area Method is put forward. By the statistical analysis of vehicle structure parameters, the moment of inertia calculation formula circling vehicles' center of mass is improved as well as vehicle movement trajectory model. The trajectory error indexes have also been set up. By using the movement trajectory model of the accident vehicle, the trajectories of accident vehicles for some accident cases have been reconstructed. By using the trajectory error indexes, the reconstruction results of the model and the tire marks at the scene have been contrasted and analyzed. The result of analysis indicates that the calculation results of model and the tire marks at the scene are similar, which validates the efficiency of this proposed method.

INTRODUCTION

With the rapid development of the world automobile industry, more and more vehicles have been equipped with ABS. Additionally, the influences of the weather and road makes tire marks of vehicles in collisions more and more illegibile. The vehicle movement trajectory model in two-dimension collision accidents can calculate the movement trajectory of vehicles, according to the final resting position of the accident vehicles. The model has significant guidance meaningful for reconstruction analysis and to judge the liability in collisions.

KINETICS ANALYSIS OF ACCIDENT VEHICLE

Coordinate systems. XOY coordinate system is riveted at earth. *x*O'*y* riveting at the vehicle's center of mass is a relative coordinate system. $\xi_{i,j}O''\eta_{i,j}$ are 4 relative coordinate systems which are riveted at the centers of 4 tires (Figure 1).

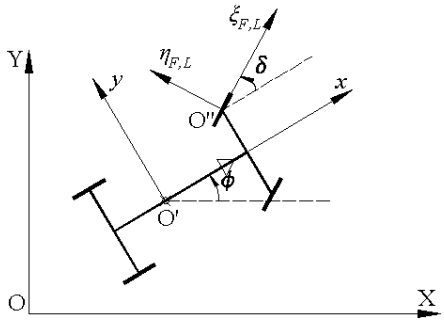

Figure 1. The coordinate systems of kinetics analysis.

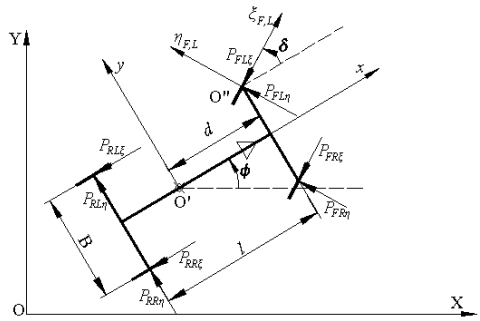

Figure 2. The mechanics analysis of vehicle.

Movement analysis of accident vehicle. The movement of an accident vehicle in a two-dimension plane can be regarded as the translation in *x*O'*y* coordinate system and the revolution about basic point O' of accident vehicle relative to *x*O'*y*.

Forces composition of accident vehicle. The vehicle can be supposed as a vehicle with 4 tires. When the vehicle is under the condition of not only turning but also braking, the forces of the vehicle in the two-dimension plane are shown as in Figure 2. Then, the resultant of forces and moment of the vehicle can be obtained. The calculation formula can be seen in the second reference. However, the longitudinal and transverse force of each tire can be calculated by the GIM Types-Ground model (Wei L. 1992).

HYPOTHESIS OF VEHICLE MOVEMENT TRAJECTORY MODEL

For setting up the vehicle movement trajectory model in a two-dimension collision accident, a hypothesis is demanded.

(1) Only forces and moment from the ground are applied to the vehicle body.

(2) Movements of the vehicle is in the same plane of the road surface.

(3) Movement trajectory of the vehicle at the moment of impact can be ignored.

(4) Its law of mass distribution and geometrical parameters are invariable.

CONSTRUCTION OF VEHICLE MOVEMENT TRAJECTORY MODEL

Form of movement trajectory model. The movement trajectory formula in the plane of the accident vehicle can be set up by using backward difference and middle difference formulas just as formula(1).

$$\begin{cases} v_X(t+\Delta t)-v_X(t)=\Delta t\cdot\dfrac{\sum P_X}{m} \\ v_Y(t+\Delta t)-v_Y(t)=\Delta t\cdot\dfrac{\sum P_Y}{m} \\ \omega(t+\Delta t)-\omega(t)=\Delta t\cdot\dfrac{\sum M}{I_Z} \\ \mathrm{X}(t+\Delta t)-X(t)=\Delta t\cdot\dfrac{v_X(t+\Delta t)+v_X(t)}{2} \\ Y(t+\Delta t)-Y(t)=\Delta t\cdot\dfrac{v_Y(t+\Delta t)+v_Y(t)}{2} \\ \phi(t+\Delta t)-\phi(t)=\Delta t\cdot\dfrac{\omega(t+\Delta t)+\omega(t)}{2} \end{cases} \quad (1)$$

where $v_X(t), v_Y(t), \omega(t)$——re t moment, the velocity component at the direction of OX,OY(m/s) and the yaw angular velocity about center of mass(rad/s);

$\sum P_X, \sum P_Y, \sum M$——component of vehicle's resultant of forces in the direction of OX, OY (N) and the resultant of moments of the vehicle about mass center (N·m);

$X(t), Y(t), \phi(t)$——at t moment, horizontal and longitudinal coordinate of vehicle's centre of mass(m) and the yaw angular displacement of vehicle(rad).

Confirmation method of position of vehicle's center of mass. Hypothesis: (1) The vehicle's centre of mass and gravity are the same point. (2) The vehicle's mass is symmetric about longitudinal axes of the vehicle. Therefore, the position of vehicle's center of mass can be measured by using the gravity method.

Confirmation method of position of impact point. By using two rectangles, that is $A_1A_2A_3A_4$ and $B_1B_2B_3B_4$, the accident vehicles can be described as shown in Figure 3 and Figure 4.

If B_2 is in the rectangle $A_1A_2A_3A_4$, the area summation of triangles $A_1A_2B_2$, $A_2A_3B_2$, $A_3A_4B_2$ and $A_3A_4B_2$ must equal the area of $A_1A_2A_3A_4$. If B_2 is out, the area summation of the 4 triangles must be greater than the area of $A_1A_2A_3A_4$. So, whether and where vehicles are impacting can be distinguished by the area calculation.

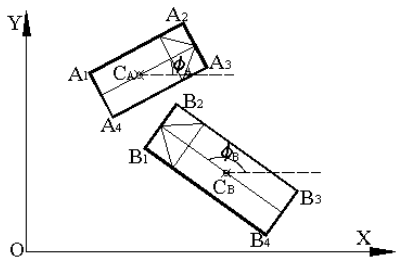

Figure 3. A and B vehicle do not impact

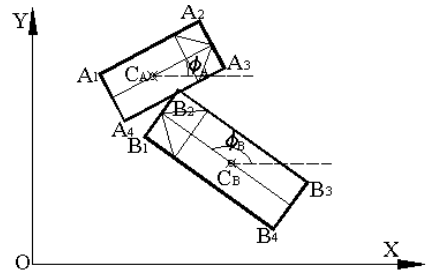

Figure 4. A and B vehicle impact

Vehicle's moment of inertia about the center of mass. Vehicles are classed into three categories which are car, truck and passenger. The data of wheel base, track-axle, mass and moment of inertia of 3 kinds of vehicles have been collected and analyzed. Therefore, the formulas of three kinds of vehicles' moment of inertia can be

expressed as following.

$$I_{Z car} \approx \frac{B \cdot L}{2.595} \cdot m \qquad (3)$$

$$I_{Z\ passenger} \approx \frac{B \cdot L}{1.110} \cdot m \qquad (4)$$

$$I_{Z truck} \approx \frac{B \cdot L}{1.640} \cdot m \qquad (5)$$

VEHICLE'S SPECIAL POINT SELECTED AND COORDINATE SETTING

The vehicle's special points selected in paper include 4 contact points between tires and ground which are E_1, E_2, E_3, E_4 . According to the coordinates of the centroid and the geometric parameters of the vehicle, the coordinates of the special points can be calculated easily (Cao Y. 2007).

ERROR INDEX OF ACCIDENT VEHICLE'S TRAJECTORY

The calculation coordinates of contacting point between the tires and ground can be denoted as (x_i, y_i), i=1,2,3……n. The actual coordinates of the vehicle's tires' braking marks can be denoted as (X_j, Y_j), j=1,2,3……m.

The absolute error of trajectory's length can be defined as ΔL, as follows.

$$\Delta L = \left| \sum_{j=1}^{m-1} \sqrt{(X_{j+1} - X_j)^2 + (Y_{j+1} - Y_j)^2} - \sum_{i=1}^{n-1} \sqrt{(x_{i+1} - x_i)^2 + (y_{i+1} - y_i)^2} \right| \qquad (6)$$

The relative error of the trajectory's length can be defined as L_E, as follows.

$$L_E = \left| \frac{\sum_{j=1}^{m-1} \sqrt{(X_{j+1} - X_j)^2 + (Y_{j+1} - Y_j)^2} - \sum_{i=1}^{n-1} \sqrt{(x_{i+1} - x_i)^2 + (y_{i+1} - y_i)^2}}{\sum_{j=1}^{m-1} \sqrt{(X_{j+1} - X_j)^2 + (Y_{j+1} - Y_j)^2}} \right| \qquad (7)$$

The maximum of the trajectory deviation can be defined as R_{max}, as follows.

$$R_{\max} = \max_{i=1,2,\ldots n} [\min_{j=1,2,\ldots m} \sqrt{(x_i - X_j)^2 + (y_i - Y_j)^2}] \qquad (8)$$

The relative biased error of trajectory can be defined as R_E, just as following.

$$R_E = \frac{10 \cdot \sum_{i=1}^{n} [\min_{j=1,2,\ldots m} \sqrt{(x_i - X_j)^2 + (y_i - Y_j)^2}]}{n \cdot \sum_{j=1}^{m-1} \sqrt{(X_{j+1} - X_j)^2 + (Y_{j+1} - Y_j)^2}} \qquad (9)$$

The scientific measure method is that by using all 4 error indexes of trajectory, the characters of length and deviation can be analyzed intuitively.

CASE ANALYSIS

General situation of the accident. The front of a specialty truck collided with the right rear of a taxi. The accident scene is shown as Figure 5 and Figure 6.

Figure 5. Accident scene (from south to north in view)

Figure 6. Accident scene (from north to south in view)

Reconstruction result of the trajectory model. The impact point of this accident can be regarded as origin *O*. According to the reconnaissance at the scene, the specialty truck's data is x_1=-1.0537m, y_1=-0.6636m, φ_1=-0.0224rad. The taxi's data is x_2=2.2196m, y_2=-5.8627m, φ_2=-1.3798rad. By using trajectory model, the trajectories can be obtained and shown as Figure 7.

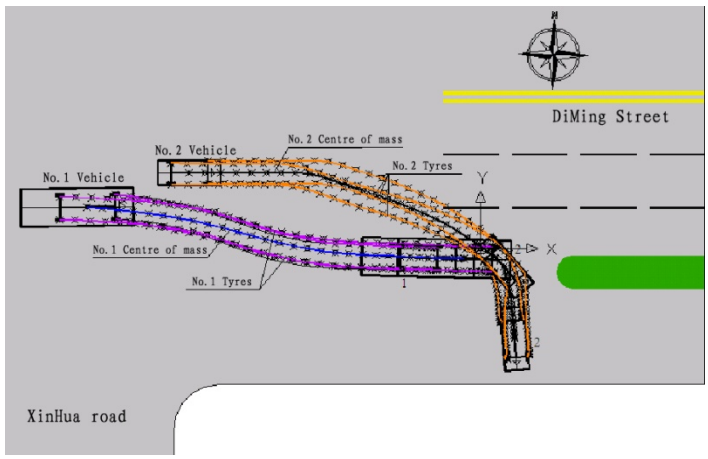

Figure 7. Reconstruction result of trajectory model in collisions case

The error analysis of calculation result of trajectory model. By contrasting the calculation result of the vehicle movement trajectory model with the marks of vehicle's tires left at the accident scene, the calculation errors of model can be discussed. Calculation results of errors are listed in Table 1.

From Table 1. we can see that the L_E of the left-back wheel of the taxi is largest that is 8%. There are 5 other two-dimension accident cases that have been analyzed in this research. The errors are all less than ±10%.

Table 1. Calculation Errors Result of Accident Vehicles

Error analysis	No.1 Vehicle (The specialty truck)		No.2 Vehicle (The taxi)
	Left-front wheel	Right-front wheel	Left-back wheel
ΔL(m)	0.21	0.48	0.28
L_E(%)	0.83	2.00	8.00
R_{max}(m)	0.30	0.27	0.25
R_E(%)	4.60	4.50	3.26

CONCLUSION

Without considering the case of twice impacts or more times impacts, the calculation result of the vehicle movement trajectory model in two-dimension collision accident is similar to the marks of vehicle's tires left at the accident scene. Therefore, it can be believed that the vehicle movement trajectory model in two-dimension collision accidents is valid.

ACKNOWLEDGMENT

This research is supported by National High Technology Research and Development Program of China (2007AA11Z231).

REFERENCE

Brach R. M. (1992). "Trajectory animation on a personal computer". *SAE Special Publications*, 907, 53-59

Cao Y. (2007). "Study on trajectory reconstruction model of the vehicle in two-dimension collision accident". *Master Dissertation of Harbin Institute of Technology*, 41-42

Hu Y. Z., , Li Y. B., Zhang W. (2003). "Method of vehicle trajectory model in traffic accident reconstruction". *Computer simulation*, 20(10), 96-98

Huang J. G. (2004). "Kinetic analysis and research on reconstruction of road traffic accident". *Master Dissertation of Fu Zhou University*, 2-6

Li J., Ni H. D., Jin T. M. (1999). "Mechanical classification & model of two-dimension impact accidents". *Journal of Highway and Transportation Research and Development*, 16(2), 74-77

Pei. J. P., Yuan. Q., Hu. Y. Z., et al. (2002). "Method of trajectory model in vehicle impact accident reconstruction". *Transactions of the Chinese Society of Agricultural Machinery*, 33(5), 23

Wei L. (1992). "An analysis of vehicle dynamic simulating tire model used in collisions accidents". *Journal of Xi'an Highway University*, 19(2), 73-76

Analysis of Runway Incursion in Civil Airport Based on Bayesian Network

Gao Yang[1] and Li Yang[2]

[1]Research Institution of civil Aviation Safety, Civil Aviation University of China, Tianjin, china, 300300; PH (86) 022-24092582 FAX (86) 022-24957940; E-mail: gycauc@hotmail.com

[2]Research Institution of civil Aviation Safety, Civil Aviation University of China, Tianjin, china, 300300; PH (86) 022-24094252 FAX (86) 022-24957940; E-mail: liyangmickey@gmail.com

ABSTRACT

At present, runway incursions have the greatest impact on runway safety, and it is also the most frequent cause of flight incidents. In order to prevent incidents of runway incursion, and to find the factors that induce these incidents, a Bayesian Network (BN) model is used to explore the relationship and interaction mechanism among those factors that cause runway incursion. It overcomes deficiencies attributed to the limitation of the sample capacity, and reveals the interaction law among human, aircraft, environment and management factors. It will provide a reliable technique to scientifically improve airport safety management, and further reduce accident rates.

0 Introduction

At present, it is a worldwide recognition that the runway incursion is one of the most unsafe incident types in the world [Gao Yang. 2008]. ICAO (International Civil Aviation Organization) defines runway incursions as: Any occurrence at an aerodrome involving the incorrect presence of an aircraft, vehicle or person on the protected area of a surface designated for the landing and taking off of aircraft [ICAO Annex 14 AERODROMES.1999]. In brief, when an aircraft, vehicle or person accidentally enters the runway being used by other aircraft taking off or landing, the runway incursion will happen.

With the rapid growth of civil aviation industry in our country, runway incursions occurs frequently [Huo Zhiqin. 2006]. A study by the Transportation Department in Canada shows that if the increase of traffic volume in an airport is 20%, then the possibility of runway incursions will increase 140%. While the growth of the traffic volume and the increase of the capacity of the airport are leading to higher stresses in airport safety, runway incursion may be more likely to occur. By 2020, the number of civil aviation airports in China will reach 244, and 97 new airports have been built since 2006[Scott A.Shappell. 2000]. In order to meet the requirements of growing airport capacity, the airport layout will be more complex. In addition to inappropriate design airport, signs and lighting, the airport safety situation will be more complex. Consequently, the occurrences of runway incursion will increase. Furthermore, the potential human errors make the uncertainties develop into a catastrophic accident possible.

The consequence of runway incursion may be catastrophic. Except for 911, the

most severe aviation accident is caused by runway incursion in human aviation history. In 1977, Nally archipelago Turner Reeve in Spain, two B-747 airplanes collided with each other and 583 people died. On April 30th, 2008, two planes fully loaded with fuel conflicted on the runway of Dalian airport (i.e. runway invasion), and the safety of the crew and passengers on the plane were threatened. To this end, how to carry out statistical analysis and study of runway incursion to mitigate running-related risks has become an imminent task in the safety of civil aviation.

There is still no systematic research about runway incursions in our country. In order to understand the trends and conditions of runway incursions which have happened in China, to explore the interaction mechanism of inducing factors, and to further establish effective preventive measures, the author will use a Bayesian network model to analyze the data of runway incursions. Applying the Bayesian network model in the study of runway incursions will not only be able to overcome insufficient data brought by limited sample space, but also can built up a relatively precise mathematical model to obtain a certain accuracy of the statistical properties. Coupled with a strong logical reasoning ability, Bayesian networks can be convenient in practical application and also has a good operability.

1 Review of Research Status

From the author's available research materials, the analysis of runway incursion incidents generally use Severity analysis, Failure analysis, Fault tree and Fault tree analysis etc. These methods can only carry out a brief description and qualitative analysis of the incidents. The typical methods which can identify the failures of equipment and hardware systems are failure mode, effects, and criticality analysis (FMECA) and failure mode and effects analysis (FMEA). But the severity of fault and probability of occurrence are from the experts' experience, limited to a single failure mode, and neglects threats brought by external changes. The Fault tree and Event tree are also common measures. Both are difficult to use the conditional probability calculation, which simply assumes relationships between the nodes are independent, and only can make an approximate description. "Bow" analysis (Bow Tie Analysis) incorporates the two methods together. On the one hand, it is used to identify hazards and determine the measures taken for prevention before the event;on the other hand, it is used to assess the effectiveness of remedial measures to achieve prevention after the event. However disadvantages of these two methods still remain, and ultimately they can not give precise results.

The Bayesian network model inherits the advantages of these methods, but also makes up for their shortcomings. First, the Bayesian network model assumes that the conditions between the nodes are independent, so we only need to consider the limited variables related to the variables. The solution of difficult questions can be simplified, and also a feasible solution of a complex runway incursion question can be obtained. Second, the inference principle of the Bayesian networks is based on the probability theory, and the conditional probability calculation method. The model is in line with reality, the result of the calculation is relatively accurate. Finally, Bayesian networks have the characteristic of the independent conditions, the author is just concerned with the local network diagram that are made up of the nodes, and these nodes are adjacent to each other. In the calculation we can calculate the

probability of occurrence of nodes according to the relevant status of known nodes. The mutual relationship between factors has been fully taken into account, so the calculated result will have a strong persuasion [Zhang Chao.2005].

Early in 1991, the FAA (Federal Aviation Administration) announced the first plan to prevent runway incursions. After that, Canada, Australia and other countries have also started research on runway incursions. In 2001, the ICAO began to conduct a special study of runway incursions.

With the rapid growth of air transport volume, the possibility of runway incursion increases more quickly than the growth in traffic volume. The United States aviation system is the world's most advanced and normative system, the results of its operation can represent the universal trend of civil aviation industry in a certain extent. Over the past 20 years, with traffic growth, the number of runway incursions happening at airports in the United States took an upward trend. It soared by a straight line from 186 times in 1988 to 336 times in 2002. After 2002, the occurrences of runway incursions have been controlled are in a stable trend thanks to the American effective runway safety actions in recent years.

From 2002 to 2006, the numbers of the airport runway incursions incidents in our country are as follows: in 2002 the number of runway incursions was 8, 10 times in 2003, 11 times in 2004, and 18 times in 2005. It can be seen that, in recent years, the number of runway incursions in our country have an overall upward trend. In addition, the low accident rate in the high-risk characteristic of runway incursion suggests that airport safety can not merely consider the issues happening, so analysis of runway incursion in civil airport based on Bayesian network seems particularly important.

2 Establish the model of runway incursion

2.1 Data sources and collating

Based on the analysis and research of 1000 domestic and foreign (domestic 475, overseas 525) runway incursions, 17 kinds of induced factors of runway incursions have been acquired, namely: crossing runway, coordination failures between controllers, obstructive communications, incorrect implement of repeat procedures, the use of non-standard terminology, long or complex controller instruction, controller fatigue, non-standard runway holding position sign or lights, pilot workload, pilot distraction, weather conditions, complicated airport layout, unfamiliarity of the airport, controller workload, inexperience of controller, indiscipline controller, controller distraction.

2.2 Establish the structure chart of Bayesian network

Because the inter-relationships exist among inducing factors of runway incursions, the author can not only classify as person, machines, environment, and management factors. Therefore, the author uses an heuristic search algorithm to set up the optimal structure chart of the Bayesian network. First of all, assume that the node set of the parent node is an empty set, and then add to the node that will turn the results of parent nodes into a biggest probability. This process will go on until the probability of the parent node can no longer be increased, so a possible network structure can be obtained. If this algorithm continues to be repeated, in this condition we can find out a number of possible network structures. By sorting the probability of

the network structure, the optimal Bayesian network structure can be identified, as shown in Figure 1.

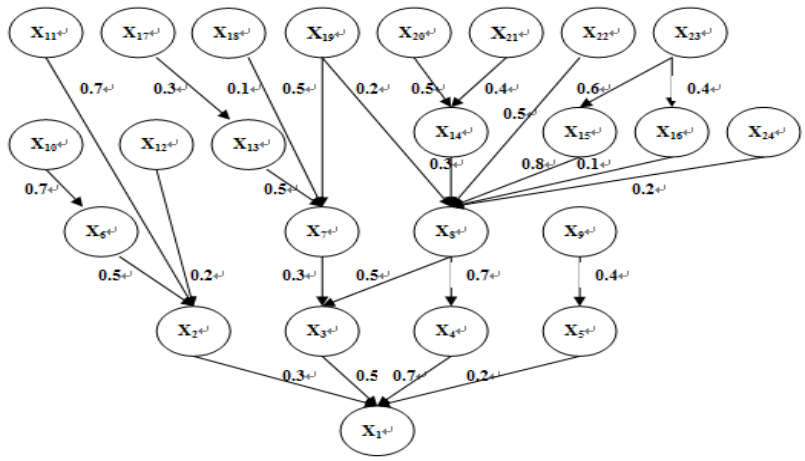

Figure 1. Causal relationship chart of runway incursions

The factor that may lead to runway incursions is known as the surface factor, that is without the arrow point to the figure; vice versa, the factor with the arrow point is the latent factor. Surface and latent factors are shown in Table 1 below.

Table 1. Surface Factors and Latent Factor Classification Table

Latent factors	Surface factors
X_2: Equipment factor	X_1: Runway Incursion
X_3: Human factor	X_9: Bad Weather Conditions
X_4: Management factor	X_{10}: Complicated Airport Layout
X_5: Environmental factor	X_{11}: Obstructive Communications
X_6: Crossing runway	X_{12}: Non-standard Runway Holding Position Sign or
X_7: Pilot Error	X_{17}: Pilot Workload
X_8: Controller Error	X_{18}: Unfamiliarity of airports
X_{13}: Pilot Distraction	X_{19}: Coordination Failures between Controllers
X_{14}: Inexperience of	X_{20}: Long or Complex Controller Instruction
X_{15}: Controller Distraction	X_{21}: Indiscipline Controller
X_{16}: Controller Fatigue	X_{22}: Incorrect Implement of Repeat
	X_{23}: Controller Workload
	X_{24}: The Use of Non-standard Terminology

2.3 Calculation Parameters

The above model can be described as B (D, P), D constitutes of a set of nodes for variable X = (X_1, X_2, ... X_{24}); P is composed of the parameters set of the Mean (u_1, u_2, ... u_{24}), conditional variance (v_1, v_2, ... v_{24}) and degradation coefficients ($b_{ij} \mid j < i$) (given in Figure 1). Obtained from 100 incidents of statistical data, the values of b_{ij} in

Figure 1 are given; $b_{ij} = p_{ij}*u_i/u_j$, p_{ij} are the correlation coefficients of X_i and X_j. Because on the base of $u_i = 0$, the variables have to obey normal distribution; based on the implicit factors of uncertainty, and its conditional variance v_i has a smaller value, when X_i for the implicit factors, so that $v_i = 10^{-5}$; and when X_i factors for the surface, so that $v_i = 1$. To calculate person, machine, environment, and management, four latent factors parameter values, and data curves are shown in Figures 2 and 3.

The mean values changes in the latent factors reflect the degree of change. It can be seen that among the person, machine, environment and management curves, the human factors have the most significant fluctuations which means that runway incursions has the most important impact, and is most vulnerable to accidents, then followed by equipment factors, management factors and environmental factors.

The reduction of the variance factors showed that the transition from a state of uncertainty gradually moves toward a state of certainty of latent factors. Herein, in order to avoid the occurrence of runway incursions the likelihood of improvement should be done first on the equipment factors, followed by management factors, environmental factors and human factors.

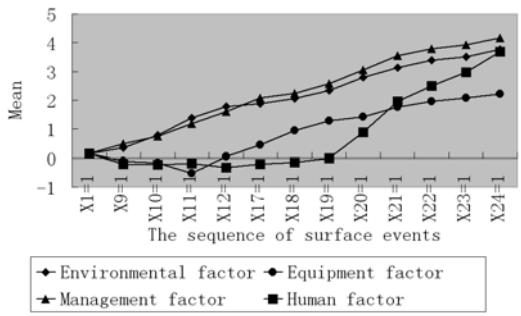

Figure 2. Mean

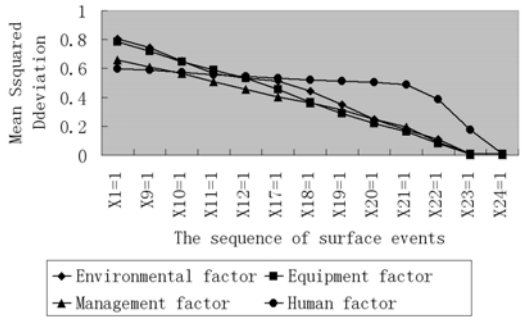

Figure 3. Mean squared deviation

2.4 Result Analysis

The results of parameters showed above manifest the human factor has great impact on the runway incursion. The human factor calculation results are interpreted in Table 2. Similarly, the calculation results of management factors, equipment factors and environmental factors can be drawn, which are not listed here considering the length limitation of this paper.

3. Conclusion

Based on Bayesian network model analysis and research on the influencing factors of runway incursion, the results showed that:

1. The application of the Bayesian network model can analyze runway incursions from the surface factors and latent factors. After that, a relatively precise result can be obtained. The results can provide some references for runway incursion prevention in our countries;

2. The analysis results show that the human factor plays the most important role in runway incursion incidents. The civil aviation system should emphasize the professional skills of personnel while comprehensively considering all the factors involved, and make a rational remedial plan.

Table 2. Calculation Results of Human Factors

Acquired data	Mean	Mean squared deviation	Description
Initial data	0	1.476	
X_1=1 runway incursion	0.159	0.597	Mean increases while mean squared deviation decreases, so human factors may lead to the occurrence of runway incursions
X_9=1	-0.189	0.558	Both mean and mean squared deviation decreases, so the possibility of runway incursions caused by environmental factors decrease
X_{10}, X_{11}, X_{12}=1	-0.324	0.546	Both mean and mean squared deviation decreases, so the possibility of runway incursions caused by Equipment factor decrease
X_{17}, X_{18}, X_{19} =1	-0.002	0.514	Mean increases while mean squared deviation decreases, so the possibility of runway incursions caused by Pilot Error increase
X_{20}, X_{21}, X_{22}, X_{23}, X_{24}=1	3.689	0.01	Mean increases while mean squared deviation decreases, so ATC Controller Error lead to the occurrence of runway incursions

References：

Gao Yang, Li Yang. (2008) "Analysis and Prediction of Runway Incursion Base on ARIMA Model." *China Safety Science Journal.* 11（18）：25

Huo Zhiqin, Lou Fan. (2006) "Statistic Analysis on Accidents and Incidents in the Last Decade in China Civil Aviation." *China Safety Science Journal.* 12：65~71

ICAO Annex 14 AERODROMES.(1999). VOLUME I AERODROME DESIGN AND OPERATIONS,THIRD EDITION.

Lou Fan, Chen Xiaojia, Gu Bichong. (2005) "Formation mechanism analysis of aviation calamity based on Bayesian networ." *Journal of Beijing University of Aeronautics and Astronautics.* 31(8)：934~938

Scott A.Shappell, Douglas A.Wiegmann. (2000) "The Human Factors Analysis And Classification System(HFACS)." Office of Aviation Medicine Washington, DC 20591.2000.02

Zhang Chao, Ma Cunbao, Hu Yunlan, Xu Jiadong. (2005) "On Quantitative Analysis of Fault Tree Based on Bayesian Network." *Journal of Projectiles, Rockets, Missiles and Guidance.* 235~237

Investigation of the Relationship between Red-Light-Running Frequencies and Intersection Features

Yiyi Cai,[1] Xuesong Wang,[1] and Xiaohong Chen[1]

[1]School of Transportation Engineering, Tongji University, P.O. Box 201804, Shanghai; PH (86) 21-69583946; FAX (86) 21-65982897; email: caiyiyi_2006@yahoo.com.cn

ABSTRACT

Red-light running is a complex problem. There is no simple reason to explain why drivers run red lights. The purpose of this study is to improve understanding of the red-light running and its relationship with the intersection features so that efficient countermeasures can be developed to improve intersection safety. Five large four-legged signalized intersections in Orange County in Central Florida, U.S., were selected. Data collected for these intersections include intersection features and red-light-running violations in 2006 and 2007. Red-light-running violations were modeled at the approach level using Generalized Estimating Equations (GEE) with Negative Binomial as the link function to account for site correlation among the data. The following factors were identified that have significant contributions to red-light-running frequencies: traffic flows to which the conflicting traffic belongs, the number of through lanes on the conflicting approach and speed limit of conflicting approach, and yellow time of a near-side approach.

Keywords: red-light running, intersection features, relationship, Generalized Estimating Equations (GEEs)

INTRODUCTION

Red-light running is one of the primary causes of crash occurrence at signalized intersections. There are three primary crash types (right-angle, left-turn, and rear-end crashes) related to it. According to the estimates given by the Federal Highway Administration (FHWA) in U.S., in 2003 there were nearly 206,000 red-light-running crashes at intersections, resulting in 176,000 injuries and 934 fatalities.

Red-light running is very complex. There is no simple reason to explain why drivers run red lights. This study is going to improve the understanding of red-light running and its relationship with the intersection features, and develop efficient countermeasures.

In China, few researchers focus on this area. Wang et al. (2006) did some research and found that rational signal phases and red-light-running violation camera systems decreased red-light-running behaviors. In the U.S., Bonneson et al. (2001; 2004) systematically analyzed the red-light-running problem. He raised approaches to identify problem locations, and found that red-light-running was related to approach volume, yellow intervals, speed limit etc. using a generalized linear regression technique. Most of the previous studies investigated factors influencing red-light-running violations based on the intersection level. Considering that there are discrepancies in the traffic and geometry features among approaches of an intersection, modeling the total number of red-light-running violations may obscure the real relationship between red-light running and intersection features.

The objective of this study is to investigate the significant factors of intersection features influencing red-light-running frequencies based on the approach level. Since disaggregating intersections into approaches will introduce correlation among observations from the same intersection, GEEs with Negative Binomial as the link function that account for the site correlation were used.

DATA PREPARATION

Five large four-legged signalized intersections in Orange County, Central Florida, U.S., were selected. Geometric designs (i.e., number of lanes, median types, angle of intersecting approaches, etc.) were observed from Google™ Earth (2008). Traffic flows from 2004 to 2007, signal controls, and operational features (i.e., speed limit of each approach, etc.) were collected. Red-light-running data from December 2006 to February 2007 were retrieved from the Traffic Engineering Office in Orange County. Daily average red-light-running frequencies were used in this study.

Both red-light-running frequencies and intersection features were assigned to corresponding approaches. At approach level, each intersection has four observations, defined as entering, near-side, opposing, and far-side approach in the clockwise view

(Wang et al. 2007). For instance, eastbound traffic is at the near-side approach if the observation site is northbound, as shown in Figure 1. The summary statistics are presented in Table 1. Only summary statistics for entering approaches are included in this table.

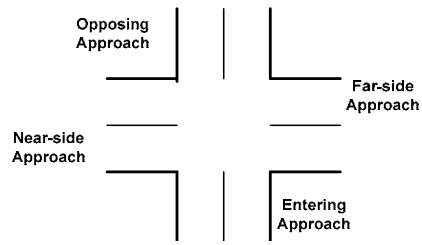

Figure 1. Illustration of entering approach, near-side approach, opposing approach, and far-side approach.

METHODOLOGY

As shown in Table 1, red-light-running frequencies at signalized intersections are non-negative, discrete, over-dispersed count data. There are several methodologies for count data modeling. MLRs and Poisson distribution methods are two approaches used in early studies. MLRs, requiring the variables to be independent, could not overcome the problem of multi-collinearity of the explanatory variables. Poisson distribution is not suitable for modeling over-dispersed data. The Negative Binomial modeling approach, which is an extension of Poisson regression modeling, is a common tool for modeling cross-sectional count data.

However, disaggregating intersections into approaches may introduce site correlation among observations from the same intersection. Using Negative Binomial regression leads to invalid statistical inference, due to incorrect test statistics and standard errors based on the unspecified variance (Wang et al. 2008). Generalized Estimating Equations (GEEs), as an extension of generalized linear models (GLMs), account for the correlation of repeated observations from one intersection (Zeger et al. 1986).

The red-light-running frequency model at approach level was fitted by using the GEEs with the Negative Binomial as the link function. The GENMOD procedure in the SAS software was used to estimate the model. Since all five intersections selected have left-turn protections, red-light-running and left-turn red-light-running were modeled.

MODELING THROUGH RED-LIGHT-RUNNING

There are two conflicting patterns related to through vehicles running a red light. One is the red-light-running vehicle conflicting with vehicles from crossing

approaches (near-side and far-side approaches). The other is rear-end conflict resulting from red-light running related actions, when the front vehicles stop abruptly before a red signal while following vehicles hit the rear of the front ones.

In order to investigate significant intersection factors related to the conflicts, the red-light-running rates of vehicles traveling in the through lanes were modeled in the approach level as shown in Table 2.

It has been found that the logarithm of the product of the conflicting through flows is the most appropriate functional form for the models at approach level. It shows to be significant in the GEEs model. The negative sign of the estimates, different from previous studies (Bonneson et al. 2001), indicates that a large amount of AADT of conflicting through traffic does not necessarily increase the red-light running frequencies.

Table 1. Data summary statistics for the approach level models.

Variable	Mean	Min	Max	Variance	SD
Total number of through lanes on entering approach	2.3	1	3	0.43	0.66
Total number of left-turn lanes on entering approach	1.50	1	2	0.26	0.51
Total number of right-turn lanes on entering approach	0.75	0	1	0.20	0.44
Division on entering approach	4.33	0	14	15.69	3.96
Left-turn protection on entering approach(*1 if "permitted"; 2 if "compound"; 3 if "protected"*)	3	3	3	0	0
Speed limit on entering approach(*mph*)	44.25	35	50	11.25	3.35
Angle of eastbound and southbound(*degrees*)	91.60	81	105	62.57	7.91
All red time on entering approach(*sec*)	1	1	1	0	0
Yellow time on entering approach(*sec*)	4.29	4	4.7	0.02	0.13
Entering approach through AADT(*vehicles*)	13713	2855	34053	76446444	8743
Entering approach left-turning AADT(*vehicles*)	4099	1518	10424	5423394	2329
Entering approach right-turning AADT(*vehicles*)	3570	1077	6735	3354667	1832
Red-light-running frequency of through lanes on entering approach	272	58	709	38110	195
Red-light-running frequency of left-turn lanes on entering approach	209	44	438	18643	137

The number of through lanes on entering and crossing approaches has a negative effect on red-light running. The larger number of through lanes is associated

with larger through volumes and longer crossing distance. From the psychological perspective, drivers are less likely to violate a red indication at wide intersections (Bonneson et al. 2004).

The speed limit on an entering approach and on a far-side approach has been identified to be significant, but they have different effects. The speed limit on the entering approach has a positive effect on the red-light violations, which is reasonable, for drivers at a high speed may underestimate the time it takes to cross the intersection. It is interesting to find speed limit on far-side approach decreases drivers' red-light behaviors. Drivers may take a conservative action when they feel dangerous crossing the intersection.

Yellow time has been found to influence red-light frequencies. The longer yellow time, which means longer clearance time, will reduce the possibility of running a red light.

Table 2. Significant factors of red-light-running model.

Parameter	GEE		
	Coef.	**s.e.**	**p-value**
Intercept	14.6163	1.919	<0.0001
Logarithm of the product of the through movements on entering and crossing approaches	-0.4553	0.102	<0.0001
Number of through lanes on entering approach			
>2	-0.1922	0.0786	0.0144
<=2	0	0	-
Number of through lanes on crossing approaches			
6	-0.9341	0.063	<0.0001
4,5	-0.4877	0.0802	<0.0001
2,3	0	0	-
Speed Limit on entering approach(mph)			
50	0.7962	0.1006	<0.0001
45	1.275	0.1081	<0.0001
35	0	0	-
Speed Limit on far-side approach(mph)			
50	-1.8853	0.0665	<0.0001
45	-0.8885	0.099	<.0001
35	0	0	-
Yellow time on near-side approach(sec)			
4.7	-0.3845	0.1503	0.0105
4.3	0	0	-
4	0	0	-

MODELING LEFT-TURN RED-LIGHT-RUNNING

In a signalized intersection, left-turn traffic may collide with traffic flows from different directions. Wang et al. (2007) classified left-turn crashes into nine patterns based on vehicle maneuvers at the approach level after analyzing 197 four-legged signalized intersections over six years. Among all patterns of left-turn crashes, pattern 1, shown in Figure 2, accounts for the highest proportion (72.5 percent), and pattern 2 in Figure 3 is the second common pattern (14.1 percent).

Figure 2. Conflicting patterns of left-turn red-light-running.

In the future, to understand the relationship between intersection characteristics and left-turn vehicles running a red light, GEE models with Negative Binomial regression as the link function were fitted.

The first three significant factors shown in Table 3 indicate that the logarithm of the product of the conflicting through flows is the most appropriate functional form. The negative sign of the impact of left-turn movements on the entering approach and through movements on the near-side approach on red-light running shows that an increase of AADT of conflicting traffic flows does not necessarily increase the frequency of the red light running. It is consistent with the conclusion above.

The crossing distance of left-turning vehicles is represented by the number of through lanes on the opposing and approach. A higher number of through lanes on the opposing side, which means the crossing distance is larger, is correlated with fewer red-light-running frequencies; while a higher number of left-turn lanes on the entering side and through lanes on the near-side approach is correlated with more red-light-running frequencies. Appearance of left-turn lanes increases the violations.

The speed limit on the near-side approach has been identified to be positively significant in the model. Higher posted speed limits generally produce frequent occurrences of red-light-running vehicles.

Table 3. Significant factors of left-turn red-light-running model.

Parameter	GEE		
	Coef.	s.e.	p-value
Intercept	5.9982	0.6851	<0.0001
Logarithm of the product of the left-turn movements on entering approach and through movements on opposing approach	0.6142	0.1891	0.0012
Logarithm of the product of the left-turn movements on entering approach and through movements on far-side approach	0.9686	0.1732	<0.0001
Logarithm of the product of the left-turn movements on entering approach and through movements on near-side approach	-1.8355	0.2327	<0.0001
Number of left-turn lanes on entering approach	1.1183	0.1208	<0.0001
Number of through lanes on opposing approach			
>2	-0.8191	0.065	<0.0001
<=2	0	0	-
Number of through lanes on near-side approach	0.4117	0.0658	<0.0001
Speed limit on near-side approach			
50	1.2061	0.7858	0.1248
45	1.0994	0.356	0.002
35	0	0	-

CONCLUSION

This study explored the safety effects of intersection features on red-light-running frequencies. Generalized Estimating Equations (GEE) with Negative Binomial as the link function have been used to model the relationship between them.

In the models, it is found that: (1) the logarithm of the product of the conflicting through flows is the most appropriate functional form for the models. The frequency of red-light-running is related to the traffic flows to which the conflicting traffic belongs rather than the sum of the traffic flows. In addition, a large amount of AADT of conflicting traffic flows does not necessarily increase the frequency of the red light running. (2) For geometric design features, number of red-light-running entering approach lanes and through lanes on conflicting approach are the significant variables. Long crossing distance decreases the red-light-running frequencies; designing left-turn lanes could probably increase the violations. (3) As for speed limit and signal control, the speed limit of the conflicting approach was found to be

significant in both models; in the through traffic model, speed limit of the entering approach and yellow time on the near-side approach are also significant. Maintaining a longer yellow signal time will decrease red-light-running frequencies.

In conclusion, compared to the intersection level models, dividing red-light-running into two types on the approach level allows us to better understand contributing factors of intersection features. Intersections selected here are common four-legged ones, so the conclusion can be widely used for other signalized intersections. It also provides an analyzing framework for investigating the red-light-running problem in China.

REFERENCES

Bonneson, J., and Zimmerman. K. (2001). "Review and evaluation of factors that affect the frequency of red-light-running." Publication FHWA/TX-02/0-4027-1, Washington, D.C., Federal Highway Administration.

Bonneson, J., and Zimmerman. K. (2004). "Identifying and treating locations with a red-light-running problem." Publication FHWA/TX-05/0-4196-2, Texas Transportation Institute.

Bonneson, J., and Zimmerman, K. (2004). "Development of guidelines for identifying and treating locations with a red-light-running problem." FHWA/TX-05/0-4196-2, Texas Transportation Institute.

Google Earth Homepage. Google Inc. http://earth.google.com. Accessed (July 17, 2008).

Wang, J. M. (2006). "Research of red Llght violation at signalized intersections in developing cities." Central South Highway Engineering, 31(4), 123-130.

Wang, X., and Abdel-Aty, M. (2006). "Temporal and spatial analyses of rear-end crashes at signalized intersections." Accident Analysis and Prevention, 38 (6),1137-1150.

Wang, X., and Abdel-Aty, M. (2007). "Right-angle crash occurrence at signalized intersections." Transportation Research Record: Journal of the Transportation Research Board No. 2019. TRB, National Research Council, Washington, D.C., 156-168.

Wang, X., and Abdel-Aty, M. (2008). "Modeling left-turn crash occurrence at signalized intersections by conflicting patterns." Accident Analysis and Prevention, 40 (January (1)), 76-88.

Zeger, S., and Liang, K. (1986). "Longitudinal data analysis for discrete and continuous outcomes." Biometrics, 42, 121-130.

Effects of Sunlight Glare on Drivers' Psychophysiological Characteristics

GAO Han [1, 2] and PEI Yulong[1]

[1]School of Transportation Science and Engineering, Harbin Institute of Technology, P.O. Box 150090, 202 Haihe Road, Nangang District, Harbin, P.R. China; PH (86) 451- 86282832; FAX (86) 451- 86282832; email: yulongp@263.net
[2]Liaoning Provincial College of Communications, P.O. Box 110122, 102 Shenbei Road, Shenbei New District, Shenyang, Liaoning, P.R. China; PH (86) 24-89708483; FAX (86) 24-29870046; email: gh1963@126.com

ABSTRACT

The road traffic accidents often occur when one or several links are imbalanced in the dynamic system, which comprises persons, cars, roads and environment. As a special natural phenomenon, sunlight glare makes drivers discomfort. Acting on drivers' eyes, sunlight glare changes drivers' visual condition and affects drivers' judgment on traffic environment. In this paper, the applicability of drivers' psychophysiological indexes under the sunlight glare condition was analyzed. The indexes include heart rate, skin temperature, galvanic skin response and respiration. By use of multi-channel psychophysiological instrument, a lot of practical experiments have been made on roadway. The impact on drivers' psychophysiological indexes generated by sunlight glare was also analyzed. In the end, some quantitative models of drivers' psychophysiological characteristics under the influence of sunlight glare were built with the regression analysis and numerical fitting method.

KEYWORDS: traffic safety, sunlight glare, psychophysiological characteristics

INTRODUCTION

Driving motor vehicle is a very complex Human-Machine interaction procedure, which requires drivers to collect information necessary momentarily, screen all the information rapidly to make correct judgment and response.

From cognition to response, drivers commonly go through three stages: perception, judgment, and response. Perception is the time needed to detect and identify the road information. At this stage, if the objective identified under traffic environment is of low stimulation intensity to sense organs, low contrast to environment, or drivers encounter temporary barriers of sensory function, this will make drivers ignore or misjudge road information, and sometimes cause traffic accidents occur.

Sunlight radiating drivers' eyes affects drivers' vision obviously and produces uncomfortable feelings. Therefore, the ability to perceive driving condition will be affected. Because psychophysiological responses to environmental stimulus are different among different individuals, it is necessary to measure drivers' psychophysiological indexes on roads and analyze the effects of sunlight glare and building the impact models in order to provide theoretical basis for evaluating driving environment and analyzing drivers' behavior characteristics.

PSYCHOPHYSIOLOGICAL INDEXES SELECTION

Indexes commonly used for representing drivers' psychophysiological characteristics are: heart rate (HR), skin temperature, electromyography (EMG), electroencephalogram (EEG), galvanic skin response (GSR), blood pressure (BP), and respiration (RSP). Due to the limitation of the experimental devices and the uncertainties of data sampling, of these indexes, EMG, EEG and BP were not considered in this research.

While driving vehicles, the mutation of light environment may cause the adaptive problem of eyes and the corresponding psychological reactions, such as the decline of the vision and recognition speed. Furthermore, the driver's mood may be affected, for instance, dizziness, upset mood irritability, depression, physical weakness and so on. These impacts will lead drivers being unresponsive. Traffic accidents often occur under these conditions.

TEST AND ANALYSIS

Experimental scheme. NeXus-10 was used for field experiement for this study. It is a ten channel physiological monitoring and biofeedback platform that utilizes Bluetooth 1.1 class 2 wireless communication and flash memory technologies. The advanced technology preamps enjoy independent 24 bit A-D converters per channel with DC coupled amplifiers allowing DC to 800 Hz (-4dB) recording including EEG, ECG, EMG, EOG.

Test is conducted for four days between June 19th and June 24th (5:00am–6:00am, 9.30am-10.30am and 5:00pm–6:00pm), in 2007.

Testing indexes included HR, skin temperature, GSR and RSP. Testing locations include the Zhongshan Road, Changjiang Road and Huashan Road in east-west Harbin city. Meanwhile, video cameras were used to record the road information in the test procedure.

Data Acquisition and analysis. In theory,the impacts of sunlight glare are different under different road conditions. In the test, NeXus-10 were used to record drivers' HR, skin temperature, GSR and RSP to measure the impacts of sunlight glare for different road conditions.

According to the statistical analysis of test data, drivers increased heart rate and psychological stress under sunlight glare environment. Heart rate increased by

about 10 times/min than normal average.The other indexes were changed, too. So sunlight glare is an important factor affecting drivers' behavior. Certainly, heart rate is also connected with other factors such as drivers' attention, mental status, age and sex. This article mainly focuses on the changes of psychophysiological characteristics caused by sunlight glare.

INFLUENCE MODELS

Based on the analysis of experimental data, the corresponding quantitative influence models were developed as follows.

HR model. Based on experiment data, HR fluctuates along a straight line: y=72.5, without sunlight glare. But with sunlight glare, it fluctuates according with cubic curve (see Figure 1). Under sunlight glare condition, the curve fitting model of HR is derived as the following equation:

$$y=71.152-0.05x+0.33x^2-0.11x^3$$

where y represents the value of HR with sunlight glare (*times/min*), x represents the influencing time (*s*).

The fitting degree of curvilinear is 0.992, which illustrates the fitting degree is better for describing the drivers' heart rate changes under the impact of sunlight glare.

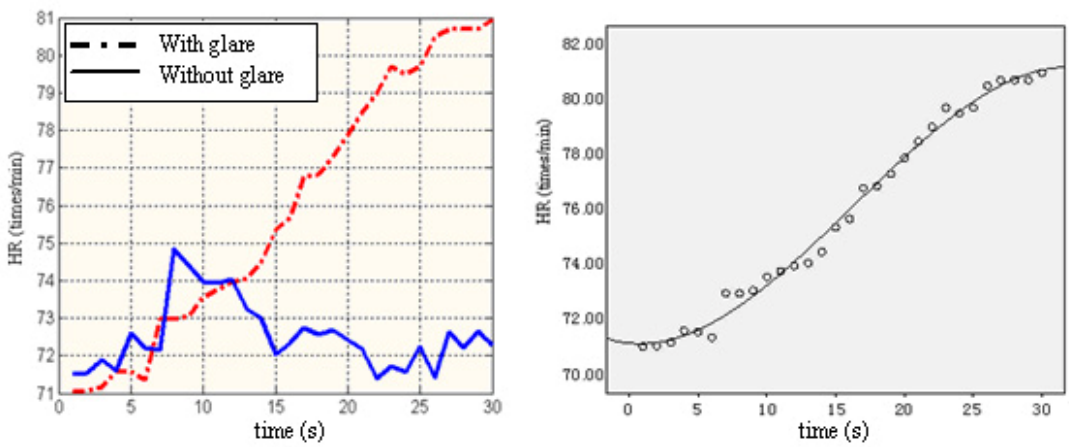

Figure 1. HR and curve fitting

Skin temperature model. There is a noticable impact of sunlight glare upon skin temperature(see Figure 2). Analyzing test data, the skin temperature is between 32.37°C and 32.42°C with average of 32.40°C under non sunlight glare condition and the fluctuation is little; under sunlight glare condition, the skin temperature is between 31.34°C and 32.44°C with average of 31.60°C and skin temperature fluctuation becomes more intense than the fluctuation under non sunlight glare condition.

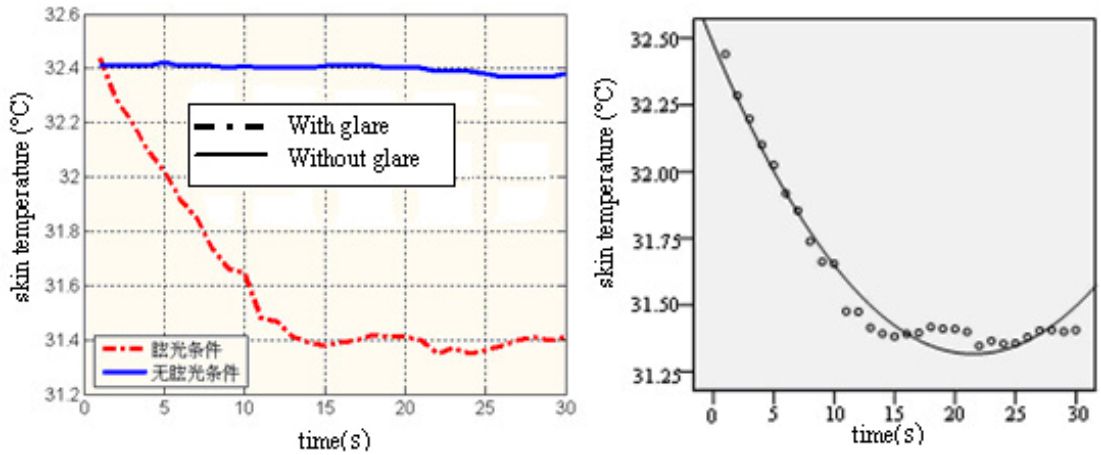

Figure 2. Skin temperature and curve fitting

Based on experiment data, skin temperature fluctuates along a straight line: y=32.4, without sunlight glare. But with sunlight glare, it fluctuates according with the trend of quadratic curve. Under sunlight glare condition, the curve fitting model of skin temperature is derived as the following equation:

$$y=0.003x^2-0.108x+32.479$$

where y represents the value of skin temperature with sunlight glare (°C), x represents the influencing time (s).

The fitting degree of curvilinear is 0.973, which illustrates the fitting degree is better for describing the driver's skin temperature change under the impact of sunlight glare.

GSR model. The impact of sunlight glare upon GSR is significant (see Figure 3). The results of data analysis showed thatthe GSR is between 6.950*mv* and 7.760*mv* with average of 7.181*mv* under non sunlight glare condition and the fluctuation is little; on the contrary, the skin temperature is between 7.450*mv* and 9.770*mv* with an average of 8.939*mv* and GSR fluctuation becomes more intense than the fluctuation under non sunlight glare condition.

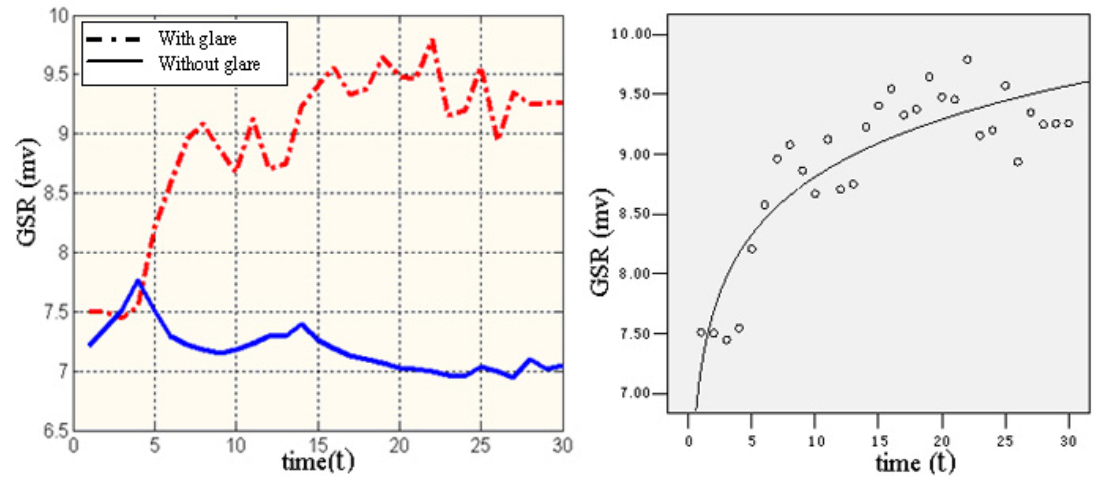

Figure 3. GSR and curve fitting

Based on experiment data, GSR fluctuates along a straight line: y=7.2, without sunlight glare. But with sunlight glare, it fluctuates between 8.5*mv* and 9.5*mv* and accords with logarithm curve. The curve fitting model for GSR under sunlight glare condition is derived as the following equation:

$$y=7.211+0.695ln(x)$$

where y represents the value of GSR with sunlight glare (*mv*), x represents the influencing time (*s*).

The fitting degree of curvilinear is 0.784, which illustrates the fitting degree is better for describing the drivers' GSR change under the impact of sunlight glare.

RSP model. There is a significant impact of sunlight glare upon RSP (see Figure 4). The results of data analysis showed that the RSP is between 1039.15*ml* and 1044.92*ml* with an average of 1041.32*ml* under non sunlight glare condition and the fluctuation is little. On the contrary, the RST is between 1040.27*ml* and 1051.58*ml* with an average of 1048.09*ml* and RSP fluctuation becomes more intense than the fluctuation under non sunlight glare condition.

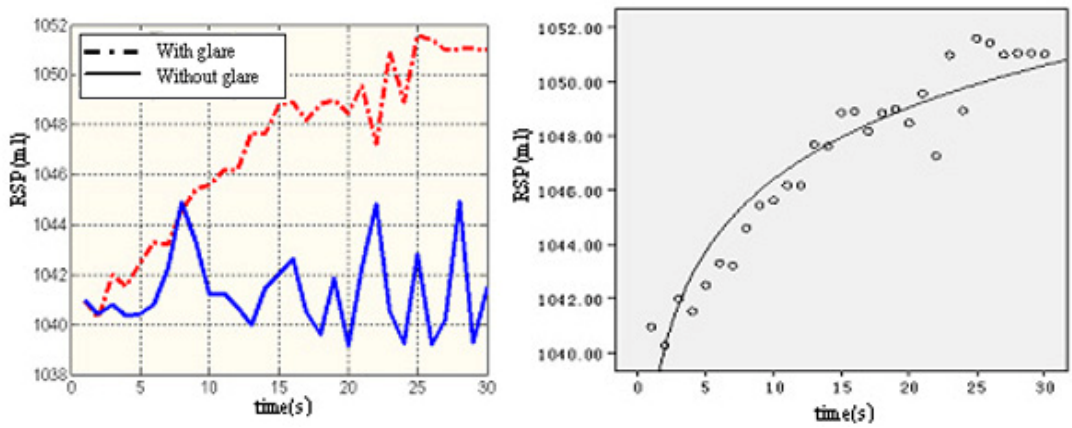

Figure 4. RSP and curve fitting

Based on experiment data, the curve fitting model for RSP under sunlight glare condition is derived as the following equation:

$$y=1037.566+3.831ln(x)$$

where y represents the value of RSP with sunlight glare (ml), x is the same as above.

The fitting degree of curvilinear is 0.890, which illustrates the fitting degree is better for describing the drivers' RSP change under the impact of sunlight glare.

CONCLUSION

In this paper, quantitative models were derived based on the experimental data to measure drivers' psychophysiological indexes including HR, GSR, skin temperature and RSP under sunlight glare condition. The measurement of these psychophysiological indexes can be used for evaluating the safety level under different driving environment.

Since the experimental data were collected from sedan drivers, these

quantitative models cannot be applied for other type of vehicle drivers. In order to find more accurate relationship between driving conditions and drivers' psychophysiological indexes, further study should be done.

BIBLIOGRAPHY

Klein S A. (1977). "Calculation of Monthly Average Insolation on Tilted Surfaces", *Solar Energy*,19 (4), 325~329.

Nazzal, A. (2005). "A new evaluation method for daylight discomfort glare", *International Journal of Industrial Ergonomics*, 35 (4): 295-306.

Pan X., YANG Z., Zhu Z.. (2005). "Relationship between Variation of Drivers' Heart Rate and Systolic Blood Pressure and Curvature Radius of Mountainous Highways", *Journal of Tongji University*, 33 (7): 900-903.

Tang D.. (2006). "Research on the Relationship of Driver s Physical and Mental Reaction, and Road Linetype", *Southeast universit*y, 16~26.

Evaluation of Road Traffic Safety Based Improved Fuzzy-AHP Method

Hu Liwei[1, 2], Pei Yulong[3], Qiu Zhuo[4] and Liu Ze[4]

[1] School of Transportation Science and Engineering, Harbin Institute of Technology, P.O. Box 2526, 202 Haihe Rd. Harbin 150090, China, PH (86) 451- 8628 2832; FAX (86) 451-8628 2832; email: liweihukm@sina.com

[2] Faculty of Transportation Engineering Kunming University of Science and Technology, Kunming 650224, China, PH (86) 871- 3802 298; FAX (86) 871- 3802 298; email: liweihukm@sina.com

[3] School of Transportation Science and Engineering, Harbin Institute of Technology, P.O. Box 2526, 202 Haihe Rd. Harbin 150090, China, PH (86) 451- 8628 2832; FAX (86) 451-8628 2832; email: yulongp@263.net

[4] School of Transportation Science and Engineering, Harbin Institute of Technology, P.O. Box 2525, 202 Haihe Rd. Harbin 150090, China, PH (86) 451- 8628 2116; FAX (86) 451-8628 2116; email: xiaoqiuzhuo@163.com, liuze365@126.com

ABSTRACT

An improved Fuzzy-AHP method is proposed in this paper for evaluation road traffic safety, based on the traditional AHP method. Several main indexes of road traffic safety were summarized and (0.1~0.9) scale method was used to determine the importance of each evaluation index. The weight of each index was confirmed through adopting a fuzzy consistent matrix, queuing all indexes according to their importance, and adopting a measure of accident prevention according to this. At the same time this verified the effectiveness and rationality of the method.

INTRODUCTION

Road traffic accidents not only directly threaten road users' safety resulting in enormous economic losses, but also seriously affect the normal operation of the road traffic system, reducing the transport efficiency of society greatly and causing a huge waste of social resources. To implement road safety measures, a comprehensive evaluation of the road safety situation including an understanding and grasp of the level of its safety and security posture, and study the distribution laws and the cases of road traffic accidents (Liu Y. T. 2004). To determine the reasonable safety evaluation index system through the AHP method, first draw up the weights of the indexes, then draw up the perfect road traffic safety improvement programs and

accident prevention measures. These are the theoretical basis and practical foundation upon which to reduce the rate and severity of accidents and to improve traffic safety. Therefore, in order to meet the growing requirements of high accuracy, this paper uses an improved Fuzzy-AHP method to evaluate the road traffic safety issue.

SET UP THE IMPROVED FUZZY-AHP MODEL

We used the (0.1 ~ 0.9) scales method in the improved Fuzzy-AHP method; that is to say using five scales (0.1, 0.3, 0.5, 0.7, 0.9) to determine the relative importance between the same level indexes. Model set up steps are as follows：

a) Set up the comparative judgment matrix $F = (f_{ij})_{n\times n}$, according to general AHP regulation. (0.2, 0.4, 0.6, 0.8) can be considered the medium value of the above-mentioned adjacent judgments.

The measurement results are complementary by such scales, and the elements of matrix $F(f_{ij}$ and $f_{ji})$ have the following properties: $0<f_{ij}<1$、$f_{ij}+f_{ji}=1$、$f_{ii}=0.5$.

b) Transform the complementary judgment matrix into the fuzzy consistent matrix: $P = (p_{ij})_{n\times n}$.

So that p_i, p_j, respectively, are the of sum rows, columns of the comparative judgment matrix F, that is: $p_i = \sum_{j=1}^{n} f_{ij}$, $p_j = \sum_{i=1}^{n} f_{ij}$ $i,j=1,2,\ldots,n$ (1)

Where $p_{ij} = p_i - p_j / 2(n-1) + 0.5$ $i,j=1,2,\ldots,n$ (2)

P matrix meets the consistency condition, so it isn't needed to carry out the consistency test, and the complementary judgment matrix P transformed into the reciprocal matrix: $A = (a_{ij})_{n\times n}$, $a_{ij} = p_{ij} / (1 - p_{ij})$ or $a_{ij} = p_{ij} / p_{ji}$. (3)

And a_{ij} meet $a_{ij}>0$, $a_{ji}=1/a_{ij}$, $a_{ii}=1$, $i,j=1,2,\ldots,n$

c) Use normalizing aggregation method for priorities to obtain weight vector of judgment matrix: $Q = \{q_1, q_2, ..., q_n\}^T$ and $q_i > 0, \sum_{i=1}^{n} q_i = 1$.

Because of reciprocal comparison matrix A satisfies the conditions of complete consistency, $a_{ij}=a_{ik}a_{kj}$. , we can obtain: $a_{ij} = \frac{1}{n}\sum_{k=1}^{n} a_{ik}a_{kj}$ $i,j,k=1,2,\ldots,n$ (4)

The a_{ij} has the following characteristics according to the properties of the coincidence reciprocal comparison matrix: $a_{ij} = q_i / q_j$ $i,j=1,2,\ldots,n$ (5)

Separately on both sides of equation (4) for i, j sum was:

$$\sum_{i=1}^{n} a_{ij} = 1/q_j \qquad i,j=1,2,\ldots,n \text{ and } \sum_{j=1}^{n} a_{ij} = q_i \sum_{j=1}^{n} 1/q_j \qquad i,j=1,2,\ldots,n \tag{6}$$

We can obtain: $$\sum_{j=1}^{n} a_{ij} = q_i \sum_{j=1}^{n} \sum_{i=1}^{n} a_{ij} \qquad i,j=1,2,\ldots,n \tag{7}$$

After finishing get: $$q_i = \sum_{j=1}^{n} a_{ij} \Big/ \sum_{j=1}^{n} \sum_{i=1}^{n} a_{ij} \qquad i,j=1,2,\ldots,n \tag{8}$$

Then we obtain the weight vector matrix Q of the matrix A.

APPLICATION IN THE ROAD TRAFFIC SAFETY EVALUATION

The principle of indexes' selection. It is very important to select reasonable evaluation indexes to the correct or not of evaluation model. So in the process of the indexes' selection, such principles should be followed: scientific, reliable, comparable, measurable, qualitative with quantitative analysis, etc.

Set up the evaluation index system. For evaluation indexes system of road traffic safety, four criteria layers are set ranging from road's basic conditions C_1, road environment, road management C_3 to road accident C_4, which has geometric alignment S_1, road Conditions S_2, intersection facility S_3, lane Width S_4, sight distance S_5 and security protection facility S_6, traffic signs and marking S_7, drainage facility S_8, lighting facility S_9, Others S_{10}, and road maintenance S_{11}, management system S_{12}, management tools S_{13} and accident quantity S_{14}, death toll S_{15}, injury number S_{16}, for each criteria layer (Shen F. M.et al. 2007) (Pei Y. L.,et al. 2004).

Set up the comparative judgment matrix. According to the (0.1 ~ 0.9) scales of the improved Fuzzy-AHP model, we have analyzed the expert evaluation results with the fuzzy mathematics theory, found the relative importance of indexes, then assessed the relative importance of indexes in the matrix.

a) The comparative judgment matrix: In this paper, we produced the indexes, the evaluation matrix, and distributed the domestic industry 9 experts to score. Experts compared and determined the essentiality of the T-C layer indexes and C-S layer 16 indexes based on the score criteria and their practical experiences, and got the T-C comparative judgment matrix (Table 1) and C-S comparative judgment matrix (Table 2) through collating the score values of all the experts.

b) Transformation the complementary judgment matrix into the fuzzy consistent matrix: The matrix 2 and 3 (Table 1 and 2) are converted to the fuzzy consistent matrix according to the equation (1) and (2), as shown in Table 3 and 4. $C_{ij}(1) + C_{ji}(1)=1$ (i, j=1, 2, 3, 4) is got by above matrix vector obviously.

c) Transform the complementary judgment matrix into the reciprocal matrix: Although the matrixes 3 and 4 (Table 3 and 4) meet the consistency requirement, they are complementary. So, in order to guarantee the independence of data, to avoid

mutual influence and get the veracious weight vector of indexes, we must convert matrixes 4 and 5 into the reciprocal matrix, as shown in Table 5 and 6.

Table 1. T-C comparison matrix

$T^{(0)}$	$C_1^{(0)}$	$C_2^{(0)}$	$C_3^{(0)}$	$C_4^{(0)}$
$C_1^{(0)}$	0.5	0.7	0.7	0.6
$C_2^{(0)}$	0.3	0.5	0.5	0.5
$C_3^{(0)}$	0.3	0.5	0.5	0.4
$C_4^{(0)}$	0.4	0.5	0.6	0.5

Table 3. T-C fuzzy consistent matrix

$T^{(1)}$	$C_1^{(1)}$	$C_2^{(1)}$	$C_3^{(1)}$	$C_4^{(1)}$
$C_1^{(1)}$	0.500	0.620	0.653	0.573
$C_2^{(1)}$	0.380	0.500	0.533	0.453
$C_3^{(1)}$	0.347	0.467	0.500	0.420
$C_4^{(1)}$	0.427	0.547	0.580	0.500

Table 2. C-S comparison matrix

$C_1^{(0)}$	$S_1^{(0)}$	$S_2^{(0)}$	$S_3^{(0)}$	$S_4^{(0)}$	$S_5^{(0)}$	$C_2^{(0)}$	$S_6^{(0)}$	$S_7^{(0)}$	$S_8^{(0)}$	$S_9^{(0)}$	$S_{10}^{(0)}$
$S_1^{(0)}$	0.5	0.6	0.5	0.7	0.6	$S_6^{(0)}$	0.5	0.5	0.8	0.6	0.7
$S_2^{(0)}$	0.4	0.5	0.4	0.6	0.4	$S_7^{(0)}$	0.5	0.5	0.8	0.7	0.7
$S_3^{(0)}$	0.5	0.6	0.5	0.7	0.5	$S_8^{(0)}$	0.2	0.2	0.5	0.3	0.4
$S_4^{(0)}$	0.4	0.4	0.4	0.5	0.4	$S_9^{(0)}$	0.4	0.3	0.7	0.5	0.5
$S_5^{(0)}$	0.4	0.6	0.5	0.6	0.5	$S_{10}^{(0)}$	0.3	0.3	0.6	0.5	0.5
$C_3^{(0)}$	$S_{11}^{(0)}$	$S_{12}^{(0)}$	$S_{13}^{(0)}$	—	—	$C_4^{(0)}$	$S_{14}^{(0)}$	$S_{15}^{(0)}$	$S_{16}^{(0)}$	—	—
$S_{11}^{(0)}$	0.5	0.5	0.4	—	—	$S_{14}^{(0)}$	0.5	0.4	0.5	—	—
$S_{12}^{(0)}$	0.5	0.5	0.4	—	—	$S_{15}^{(0)}$	0.6	0.5	0.6	—	—
$S_{13}^{(0)}$	0.6	0.6	0.5	—	—	$S_{16}^{(0)}$	0.5	0.4	0.5	—	—

Table 4. The C-S fuzzy consistent matrix

$C_1^{(1)}$	$S_1^{(1)}$	$S_2^{(1)}$	$S_3^{(1)}$	$S_4^{(1)}$	$S_5^{(1)}$	$C_2^{(1)}$	$C_2^{(1)}$	$S_6^{(1)}$	$S_7^{(1)}$	$S_8^{(1)}$	$S_9^{(1)}$
$S_1^{(1)}$	0.50	0.57	0.48	0.60	0.53	$S_6^{(1)}$	0.50	0.47	0.68	0.58	0.61
$S_2^{(1)}$	0.43	0.50	0.42	0.52	0.46	$S_7^{(1)}$	0.53	0.50	0.71	0.61	0.64
$S_3^{(1)}$	0.52	0.58	0.50	0.61	0.55	$S_8^{(1)}$	0.32	0.29	0.50	0.39	0.43
$S_4^{(1)}$	0.40	0.48	0.39	0.50	0.44	$S_9^{(1)}$	0.42	0.39	0.61	0.50	0.53
$S_5^{(1)}$	0.47	0.54	0.45	0.56	0.50	$S_{10}^{(1)}$	0.39	0.36	0.57	0.47	0.50
$C_3^{(1)}$	$S_{11}^{(1)}$	$S_{12}^{(1)}$	$S_{13}^{(1)}$	—	—	$C_4^{(1)}$	$S_{14}^{(1)}$	$S_{15}^{(1)}$	$S_{16}^{(1)}$	—	—
$S_{11}^{(1)}$	0.50	0.50	0.44	—	—	$S_{14}^{(1)}$	0.50	0.40	0.48	—	—
$S_{12}^{(1)}$	0.50	0.50	0.44	—	—	$S_{15}^{(1)}$	0.60	0.50	0.58	—	—
$S_{13}^{(1)}$	0.56	0.56	0.50	—	—	$S_{16}^{(1)}$	0.52	0.42	0.50	—	—

Table 5. Reciprocal judgment matrix

$T^{(2)}$	$C_1^{(2)}$	$C_2^{(2)}$	$C_3^{(2)}$	$C_4^{(2)}$
$C_1^{(2)}$	1.000	1.632	1.885	1.344
$C_2^{(2)}$	0.613	1.000	1.143	0.829
$C_3^{(2)}$	0.531	0.875	1.000	0.724
$C_4^{(2)}$	0.744	1.206	1.381	1.000

Table 6. Indexes weight matrix

$C_1^{(2)}$	$S_1^{(2)}$	$S_2^{(2)}$	$S_3^{(2)}$	$S_4^{(2)}$	$S_5^{(2)}$	$C_2^{(2)}$	$C_2^{(2)}$	$S_6^{(2)}$	$S_7^{(2)}$	$S_8^{(2)}$	$S_9^{(2)}$
$S_1^{(2)}$	1.00	1.33	0.94	1.44	1.13	$S_6^{(2)}$	1.00	0.90	2.17	1.38	1.56
$S_2^{(2)}$	0.75	1.00	0.71	1.08	0.85	$S_7^{(2)}$	1.11	1.00	2.45	1.53	1.74
$S_3^{(2)}$	1.06	1.41	1.00	1.53	1.20	$S_8^{(2)}$	0.46	0.41	1.00	0.65	0.74
$S_4^{(2)}$	0.65	0.92	0.65	1.00	3.21	$S_9^{(2)}$	0.72	0.65	1.53	1.00	1.13
$S_5^{(2)}$	0.89	1.17	0.83	1.27	1.00	$S_{10}^{(2)}$	0.64	0.57	1.35	0.89	1.00
$C_3^{(2)}$	$S_{11}^{(2)}$	$S_{12}^{(2)}$	$S_{13}^{(2)}$	—	—	$C_4^{(2)}$	$S_{14}^{(2)}$	$S_{15}^{(2)}$	$S_{16}^{(2)}$	—	—
$S_{11}^{(2)}$	1.00	1.00	0.79	—	—	$S_{14}^{(2)}$	1.00	0.67	0.92	—	—
$S_{12}^{(2)}$	1.00	1.00	0.79	—	—	$S_{15}^{(2)}$	1.50	1.00	1.38	—	—
$S_{13}^{(2)}$	1.27	1.27	1.00	—	—	$S_{16}^{(2)}$	1.08	0.72	1.00	—	—

d) Weight vector matrix: Through calculation of equation (4) ~ (8), we can get the weight vector matrix (Table 7) of all layers indexes.

Table 7. Indexes weight matrix

Criteria layer		Scheme layer							
Index	Weight	Index	Weight	Index	Weight	Index	Weight	Index	Weight
C_1	0.347	S_1	0.208	S_6	0.255	S_{11}	0.306	S_{14}	0.279
C_2	0.212	S_2	0.157	S_7	0.284	S_{12}	0.306	S_{15}	0.418
C_3	0.185	S_3	0.221	S_8	0.118	S_{13}	0.389	S_{16}	0.303
C_4	0.256	S_4	0.230	S_9	0.182	—	—	—	—
—	—	S_5	0.184	S_{10}	0.161	—	—	—	—

We can get the relative importance of the indexes from the weight vector matrix 8 (as in Table 7), then we realign the indexes of the criteria layer (as in C layer) and the scheme layer (as in S layer) of the comprehensive evaluation of road traffic safety. So the new matrixes are as follows: C= {C_3, C_2, C_4, C_1}, S= {S_8, S_2, S_{10}, S_9, S_5, S_1, S_3, S_4, S_6, S_{14}, S_7, S_{16}, S_{11}, S_{12}, S_{13}, S_{15}}, Figure 1 and Figure 2 show the weight dispersion of C layer and S layer respectively.

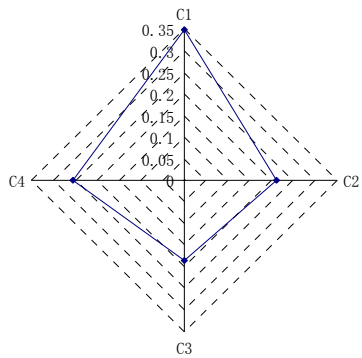

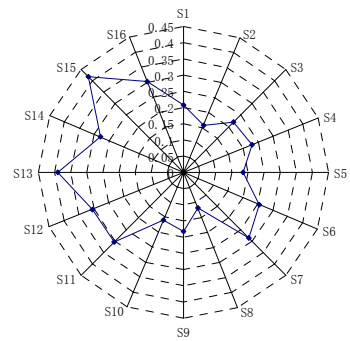

Figure 1. C layer weight dispersion **Figure 2. S layer weight dispersion Result**

From the sequencing results, we can find that the sequence of the sequencing of the sixteen indexes (As S layer or called micro evaluation layer) is inconsistent when compared with the sequencing of the macro evaluation indexes (as in C layer), but the general trend can be able to find the law. For instance, the weight of the road accident is very big in C layer, and the death toll is biggest in S layer, so we can say that the happenstance of accident is the absolute evaluation standard to test the road traffic safety level regardless of the macro evaluation or micro evaluation.

CONCLUSION

Through the study of a comprehensive evaluation of road traffic safety based on an improved Fuzzy-AHP method, we set up the road traffic safety comprehensive evaluation model. This improved model offers a simple and effective tool for solving the road traffic safety evaluation problem of many indexes.

ACKNOWLEDGEMENT

The study was supported by the National High-tech Research and Development Program (863 Program) under Grant No. 2007AA11Z231.

REFERENCE

Liu Y. T. (2004). "Manual of traffic safety", China Communications Press, 140-147

Synthesis of safety research related to traffic control and roadway elements. Report FHWA-TS-82-232. U.S. Department of Transportation, Washington, D.C., 1982

Xu Z. S., Wu Y. Y., Da Q. L. (2004). "Improved normalizing rank aggregation method for priorities", Journal of Southeast University, 34(4): 518-522

Shen F. M., Zhang R. G. (2007). "The forecast and prevention of road traffic accidents". *China Communications Press*, 150-159

Pei Y. L., Wang W. (2004). "Road traffic accident causes and preventive measures", *Science Press*, 99-107

Road Traffic Safety Micro-evaluation Based on Bayes Theory

Dai Leilei [1], Pei Yulong [2], and Ping Shaohua[3]

[1] School of Transportation Science and Engineering, Harbin Institute of Technology, P.O. Box 2525, 202 Haihe Rd. Harbin 150090, China. PH (86) 451- 8229 1584; FAX (86) 451-8628 2832; email: alei_9935@126.com
[2] School of Transportation Science and Engineering, Harbin Institute of Technology, P.O. Box 2526, 202 Haihe Rd. Harbin 150090, China. PH (86) 451- 8628 2832; FAX (86) 451-8628 2832; email: yulongp@263.net
[3] School of Transportation Science and Engineering, Harbin Institute of Technology, P.O. Box 2525, 202 Haihe Rd. Harbin 150090, China. PH (86) 451- 8628 4785; FAX (86) 451-8628 2832; email: pingshaohua_hit@126.com

ABSTRACT

Road traffic safety evaluation plays an important role in the traffic safety research. The traditional safety evaluation methods are mostly based on historical accident data, which belong to the macroscopical level and have obvious defects in traffic safety management. To realize the road traffic safety micro-evaluation, the paper established accident Probability Density Function (PDF) by using Kernel Density Estimation (KDE), proposed Accident Probability Prediction (APP) model based on Empirical Bayes (EB) method for considering the impact of accident location characteristics and historical data. The paper also established the method for road traffic safety micro-evaluation by adopting Traffic Accident Probabilities of Equivalent ten thousand Cars (TAPEC) indicator, and a comparative evaluation was conducted by the proposed method against cumulative frequency curve method. Through analyzing accident data collected from the G301, the results show that the proposed method is more reliable and can access to the transformation priorities of potentially dangerous road sections. So it can provide theoretical basis for checking the dangerous sections and improving accident prevention and response.

INTRODUCTION

Traditional safety evaluation models are mostly based on a large number of historical accident data that have limitations. The estimated values obtained by these models may not fit a specific condition. Therefore, the safety evaluations based on the traditional models sometimes cannot be applied for a single point. They are good for a set of points. And the evaluation results are mostly after the accidents happened.

In contrast, the probability evaluation model based on Bayes can identify the vulnerability of the traffic system and determine the accident probability of the road sections. Consequently it can rank the hazardous location by calculating the accident probability. Miaou S. P. (2003) studied the differences between the Bayes and the EB

method, and calibrated the parameters of these models; Persaud B.(1999) compared EB function with other conventional functions, and verified the efficiency of EB function for predicting the accident. Zheng H. (2008) constructed the indexes to estimate the road-side safety and the approaches based on Bayes theory to assess the road-side safety; Sun G. (2005) argued that multivariate regression EB-based approach could be used to estimate the safety levels of road sections.

Based on the above analysis, the paper proposes the Bayes-based APP model as the road traffic safety evaluation method by using TAPEC as indicator, to assess the road safety in a microscopic perspective and developed guidelines for transportation agencies to identify the potential hazardous road segments.

ACCIDENT PROBABILITY PREDICTION BASED ON BAYES THEORY

The EB method that combines the theoretical values with and the historical data is applied in the paper to add the influences of accident location characteristics and the dynamic traffic flow. The APP model is established as the following three steps:

1. Summarize the historical accident data and build up the distribution of the PDF to fit the probability distribution of the accident.
2. Set up a posteriori probability model of the accident prediction based on the accident probability density distribution function, to predict the probability of the traffic accidents in a particular traffic state.
3. Use the accident data of the study road sections, considering the impacts of the historical accident data, transform the prior prediction into posterior prediction of the probability distribution based the EB method.

Due to the incertitude of the accident, it is hard to obtain the PDF of the traffic accident. KDE can be infinitely close to the true sequence of a sample density function, which could be seen as a good approximation of the sequence. So KDE is applied in the paper to establish the accident PDF, which can be expressed as:

$$\hat{f}_h(x) = \frac{1}{Nh}\sum_{i=1}^{N} K(\frac{x - X_i}{h}) \tag{1}$$

Where $\hat{f}_h(x)$ is the PDF based on KDE, $K(\cdot)$ is the kernel function and the paper adopts Epanechnikov kernel function which can be expressed as formula (2), h is the window breadth parameter of the KDE model which can be expressed as formula (3), N is the number of the sample.

$$K(u) = \begin{cases} \frac{3}{4}(1-u^2) & if\,|u| \le 1 \\ 0 & otherwise \end{cases} \tag{2}$$

The h is so important for the KDE function that it will affect the resolution of results. If it is too large, the results will be too smooth to cover up the data's trend,

otherwise the model will produce excessive noise. So the optimal selection method which was proposed by Silverman in 1986 is applied in the paper as following:

$$h = 0.9n^{-1/5} \min(s, R/1.34) \tag{3}$$

Where n is the number of observation data, S and R is the standard deviation and quartile of X respectively.

There is a special approach to get x in the KDE model, dividing X into N due to the difference of the maximum and minimum of it, which can be expressed as:

$$x_i = X_{\min} + (X_{\max} - X_{\min})i/N \ , \ i = 1 \cdots N \tag{4}$$

The accident probability density distribution model can be obtained by putting (2) into (1), which can be expressed as follows:

$$\hat{f}_h(x) = \frac{3}{4Nh}\sum_{i=1}^{N}[1-(\frac{u_i}{h})^2] \ , \quad \left|\frac{u_i}{h}\right| \le 1 \tag{5}$$

Where u_i is the sample spacing that is $u_i = x_i - X_i$.

We use E_p denotes the APP result, and the PDF for predicting traffic accident based on EB method is as follows:

$$E_p = w \times \hat{f}_h(x) + (1-w) \times P(A) \tag{6}$$

Where w is the weight, $w = 1/[1 + Var(x)/E(x)]$, $E(x)$ is the sample mean of the accident probability at a certain period time of the similar road sections, $Var(x)$ is the sample variance of the accident probability at a certain period time, $P(A)$ is the accident probability by statistical analysis of historical observed data.

ROAD TRAFFIC SAFETY MICRO-EVALUATION BASED ON ACCIDENT PROBABILITY

Obtaining the probability of traffic accidents is important for predicting the state of road safety in advance. By sorting accident probability and setting the identification threshold of dangerous road sections, we can identify potentially dangerous road sections, and we can also access the transformation priorities of potentially dangerous road sections, ensure the full use of limited fund for potential safety risks.

For validating the evaluation results and comparing with the Cumulative Frequency Curve Method (CFCM), the paper adds the impact of the traffic accident severity, and adopts the Equivalent Traffic Accidents Number (ETAN) indicator.

$$ETAN = TAN + 9.5F + 3.5J \tag{7}$$

Where, TAN is the number of accidents-happened road sections, F is the number of accident deaths, J is the number of accident injuries.

Accident Probability Evaluation Method (APEM) adopts the TAPEC as evaluation indicator, the formula is as follows:

$$TAPEC = \frac{E_p}{Q} \times 10^4 \tag{8}$$

Where E_p is the prediction probability of accidents, Q is the two-way traffic volume of road sections.

By calculating the above two evaluation indicators, the paper proposed the identification threshold of accident-prone and potentially dangerous road sections: CFCM uses the inflection point of cumulative curve as identification threshold, where APEM applies the accident probability value to identify dangerous road sections, so as to implement the micro-evaluation of road safety.

CASE STUDIES

G301 is an important trunk road of National Trunk Highway Network, by collecting 1999~2003 traffic accident data of Heilongjiang Province K621~K747 sections, selects 194 effective pieces from 233 collected accident data, and the by-stake accident distribution of ETAN is shown in Figure 1.

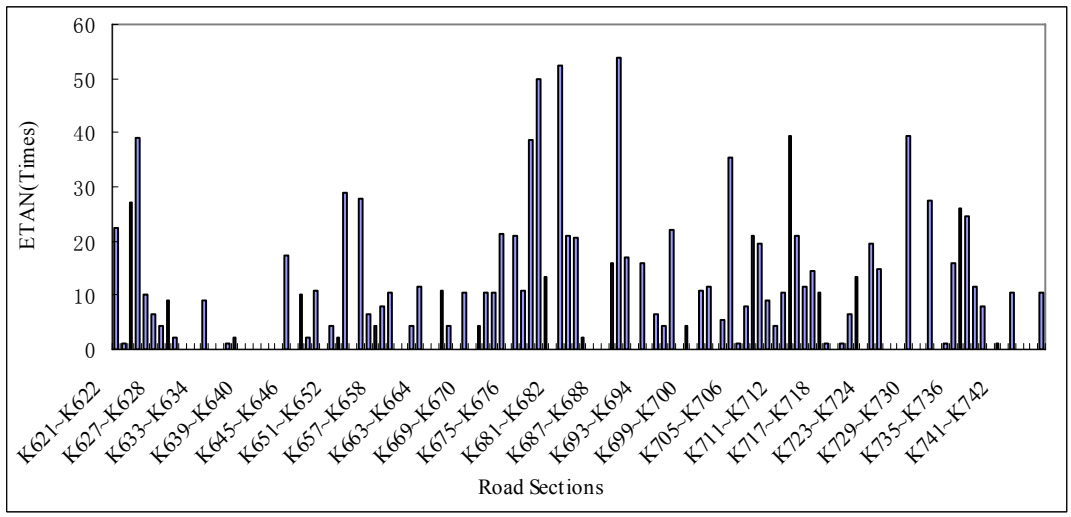

Figure 1. Statistical ETAN distribution of G301 K621 ~ K747 sections

The mathematical model of CFCM is shown in Figure 2, the relationship between ETAN and cumulative frequency curve fit parabola, through its derivation, and the ETAN inflection point reached 41.9. As 0.95 level of cumulative frequency was adopted in the paper, and the identification threshold of ETAN is 35.5.

As 1999~2002 is the base year and 2003 is the predicted year based on Bayes theory. Eviews 5.0 statistical analysis software is applied to plot the KDE-based probability distribution for predicting accident (see Figure 3), the relationship between number of accidents and accident probability is a single peak curve, and the APP results based on EB method are shown in Figure 4. Considering related factors, the probability criterion threshold of potentially dangerous sections is set to 0.05.

The comparative results of CFCM and APEM are shown in Table 1. The gray shaded areas are the same identified sections. It is show that both methods have good consistency, but the identified results of APEM slightly better than CFCM because

traffic flow and location characteristics are considered, and a relatively conservative threshold is adopted in the former. In addition, according to the size of the accident probability of dangerous road sections, the paper sorting road sections in accordance with the severity and give the several top sections of the potential danger.

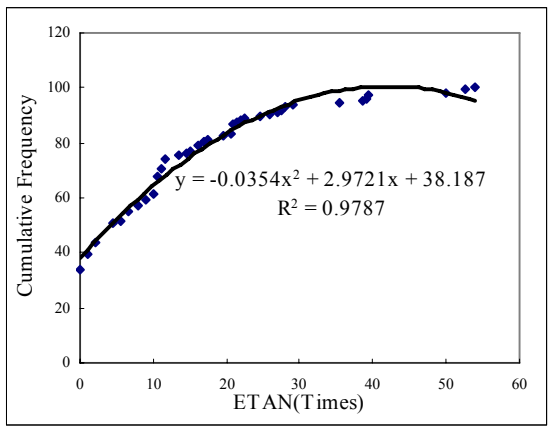

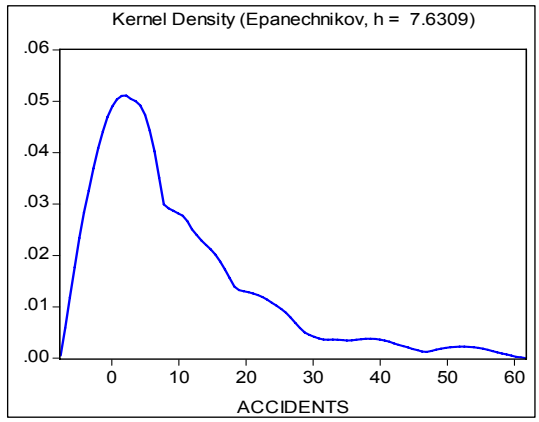

Figure 2. Cumulative curve of ETAN **Figure 3. Accident probability prediction**

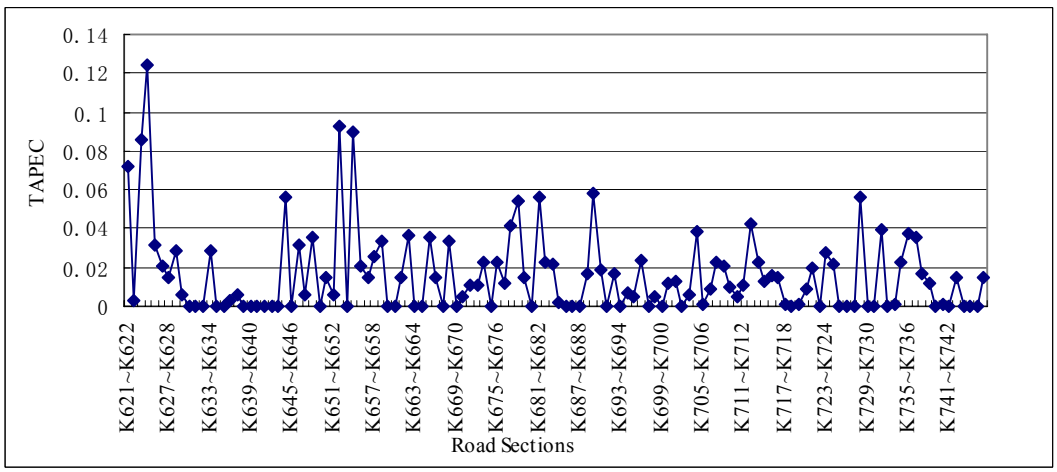

Figure 4. Results of accident probability evaluation

Table 1. The Comparative Results of CFCM and APEM

Sections order	CFCM accident-prone	CFCM ETAN	APEM potential danger	APEM TAPEC
1	K689~K690	54	K624~K625	0.124275
2	K681~K682	52.5	K652~K653	0.092414
3	K678~K679	50	K654~K655	0.089236
4	K712~K713	39.5	K623~K624	0.086054
5	K728~K729	39.5	K689~K690	0.058091
6	K624~K625	39	K728~K729	0.056533
7	K677~K678	38.5	K681~K682	0.056478
8	K704~K705	35.5	K644~K645	0.055808
9			K678~K679	0.053788

The statistical results show that accident-prone sections identified by CFCM accounted for 6.3 percent of the total mileage, and cumulative ETAN of them accounted for 29.3 percent of the total number, the ETAN on average is 46.3 times per kilometer (overall average is 9.5 times per kilometer). The potential danger sections identified by APEM accounted for 7.1 percent of the total mileage, and the TAPEC on average is 0.075 per kilometer (overall average is 0.016 per kilometer).

CONCLUSIONS

In the paper, accident probability density distribution is set up through the use of KDE function, while considering the impacts of accident location characteristics and historical statistics. The probability of accident prediction model is also set up based on EB method through the use of TAPEC indicator, and finally the road traffic safety micro-evaluation method is constructed by using APEM. Case study results show that APEM has a high reliability compared with CFCM, which identify potential hazards of the road sections, meanwhile it can access the transformation priorities of potentially dangerous road sections, so as to provide theoretical basis for accident prevention and response.

ACKNOWLEDGEMENT

The study was supported by the National High-tech Research and Development Program (863 Program) under Grant No. 2007AA11Z231.

REFERENCES

Pei Y. L. (2006). Road Traffic Safety. China Communication Press, Beijing, pp. 225-255.

Miaou, S. P., Lord D. (2003). Modeling Traffic Crash-flow Relationships for Intersections: Dispersion Parameter, Functional Form, and Bayes versus Empirical Bayes Methods. Transportation Research Record, 1840, pp. 31-40.

Persaud, B., Lyon, C., Nguyen, T. (1999). Empirical Bayes Procedure for Ranking Sites for Safety Investigation by Potential for Safety Improvement. Transportation Research Record, 1665, pp.7-12.

Zheng H., Li C. C., Liu Y. (2008). A Roadside Safety Evaluation Method Based on Bayesian Network. Journal of Highway and Transportation Research and Development, Vol. 25, No. 2, pp.139-144.

Sun G. P. (2005). Study on Identification Method of Road Hazardous Locations. Master Dissertation of Beijing University of Technology, pp. 57-67.

Jun-Seok Oh, Cheol Oh, Stephen G. Ritchie, et al. (2005). Real-time Estimation of Accident Likelihood for Safety Enhancement. Journal of Transportation Engineering, Vol. 131, No. 5, pp. 358-363.

Tang C. C., Zhang T. J., He Y. (2008). Road Safety Assessment. China Communication Press, Beijing, pp. 254-260.

Fang S. E., Guo Z. Y., Yang Z. (2001). A New Identification Method for Accident Prone Location on Highway. Journal of Traffic and Transportation Engineering, Vol. 1, No. 1, pp. 90-94.

Impact Analysis of countdown device on transit priority signal control

Li Ke-ping[1], Dong Yu-pu[2] and Qian Hong-bo[3]

[1]School of Transportation Engineering, Tongji University, Shanghai, Cao'an 4800; PH (086) 13641660290; email: keping_li@vip.163.com.

[2]School of Transportation Engineering, Tongji University, Shanghai, Cao'an 4800; PH (086) 13585790976; email:dongdong805@hotmail.com.

[3]School of Transportation Engineering, Tongji University, Shanghai, Cao'an 4800; PH (086) 13761162522; email: qhb0123456@sina.com.

ABSTRACT: This paper studies the restriction of countdown devices to the location of detectors and the response interval of red truncation by simulating different countdown situations using VISVAP programming software on VISSIM platform on the basis of theoretical analysis. It pointed out that, by shortening the countdown time of the transit stage and bringing the detector forward, the state of transit is more stable in the lower reaches of the detector which assures the validity of green extension; by shortening the countdown time of the non-transit stage the response interval is extended which improves the effect of red truncation; the travel time is 23% and 37% shorter under 5s countdown and non-countdown than at 15s countdown. So the countdown device should be used as little as possible or not at all; it is suggested to set at 5s when it is obligatory.

Keywords：countdown device; transit priority; signal control

1 INTRODUCTION

A bus has the characteristics of carrying more people than cars, using less space, having high efficiency, saving energy and being environmentally friendly; it will reflect the idea of sustainable development better and be the only way to solve traffic problems of the city.

Bus priority is being carried out in all of the country. The bus priority signal control contains different varieties; there are passive, active and real-time priorities. But in recent years, the traffic countdown devices have been widely used in many cities of our country. The existing literature (Wang Yan 2006, Yu Xuan, 2008) have discussed traffic safety and efficiency problems which come along with countdown devices. This paper has no comments about that. In order to implement the bus priority development

strategy, improve speed and service level of public transport, the writer will mainly analyze the impact analysis of the countdown device on active transit priority signal control and gives reasonable control recommendations in the section which will implement the bus priority strategy to set the countdown device.

2 ACTIVE BUS PRIORITY

Signal active priority strategy provides priority service for special buses based on detection information of the bus or priority claim that the vehicle/system has issued. It detects buses in the traffic flow and modifies signals for them directly. The active priority contains strategies as shown below: green extension, red truncation and compressing non-bus stage to bus stage and so on. Buses are orientated by selected detectors in the system, which is the basis for modifying green extension and red truncation. When the detected bus arrives during the red stage, the green stage of the other directions will be ended ahead of schedule to start up the green stage for the bus early by using early green strategy, as shown in Figure 1 (Chen-Fu Liao, Gary A. Davis(2006)). When the detected bus arrives between the green stage, the green display time of this direction will be extended using green extension strategy, as shown in Figure 2.

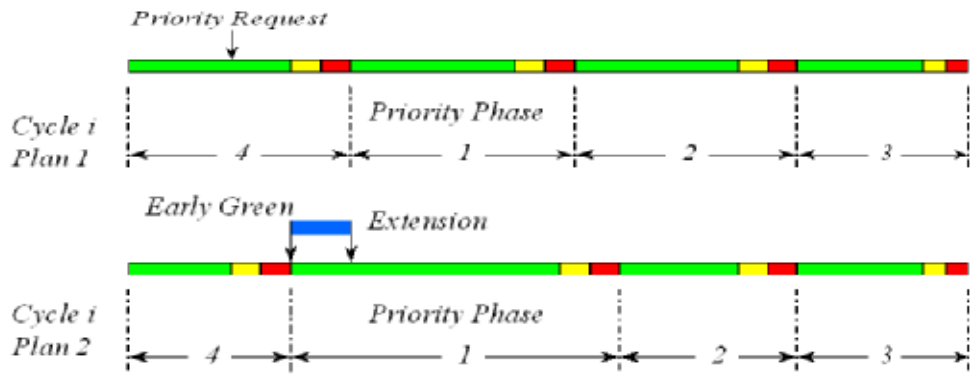

Figure 1. Signal Priority Control – Early Green/Red Truncation.

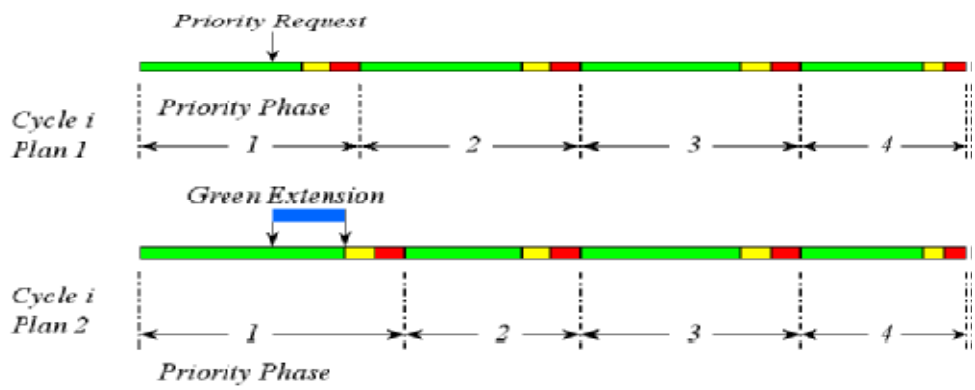

Figure 2. Signal Priority Control – Green Extension at Priority Phase.

3 IMPACT ANALYSIS OF COUNTDOWN DEVICES ON EARLY GREEN AND GREEN EXTENSION

3.1 Green extension

(1)Definition

Suppose a bus is arriving at the intersection, and will go through at the end of the current signal phase, while it cannot pass with its normal speed in the remaining green time. In that case, we can appropriately extend the green time to ensure that the bus can pass through the intersection in this signal phase. This kind of bus signal priority strategy is called “Green extension”.

(2)Location of detectors

1) Fundamental principles analysis

Because of the operating characteristic of signal controllers, once the stage closing signal of this phase is given (i.e. the vehicle countdown begins, or the pedestrian green flash begins), the end time of the current signal phase is completely determined, thus signal controllers cannot respond to a green extension claim. Consequently, detectors should be located at a far enough distance from the stop line.

Figure 3 reveals the relationship between the corresponding claim section of green extension/early green strategy and the stage closing signal, under the condition that the detection point is L distant from the stop line.

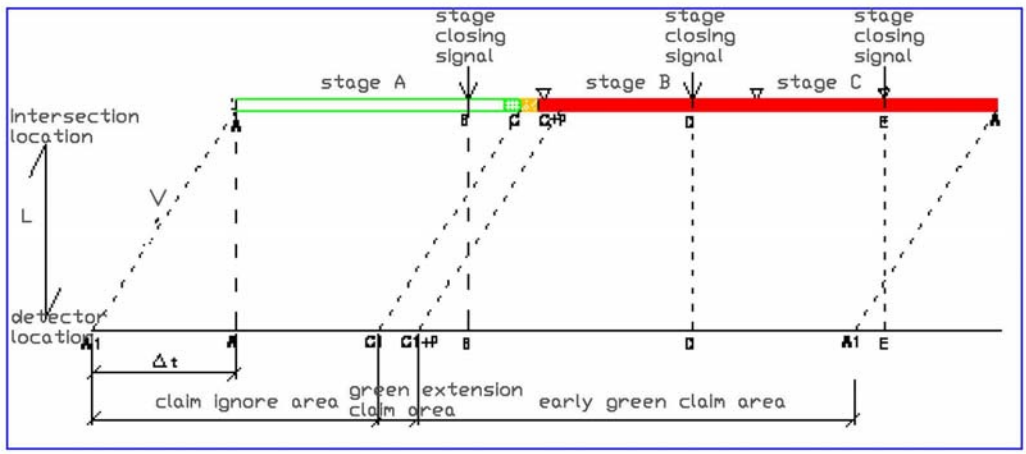

Figure 3. Bus signal priority claim section.

In the green extension/early green strategy showed in Figure 3, three claim sections are mentioned:

Claim ignore section - Buses detected in this section will not be given priority; they can across the intersection in the normal signal phase without stopping.

Green extension claim section - Buses detected in this section cannot across the intersection in the normal signal phase without stopping, but they can pass through when extended green time is given.

Early green claim section - Buses detected in this section cannot pass through the

intersection in the normal signal phase without stopping; they need to wait for the next green time for passage. But we can advance the green time to reduce the buses' waiting time.

As illustrated in Figure 4, if the detectors are located overly close to the stop line, or the stage closing signal is given too early, the green extension claim section will disappear.

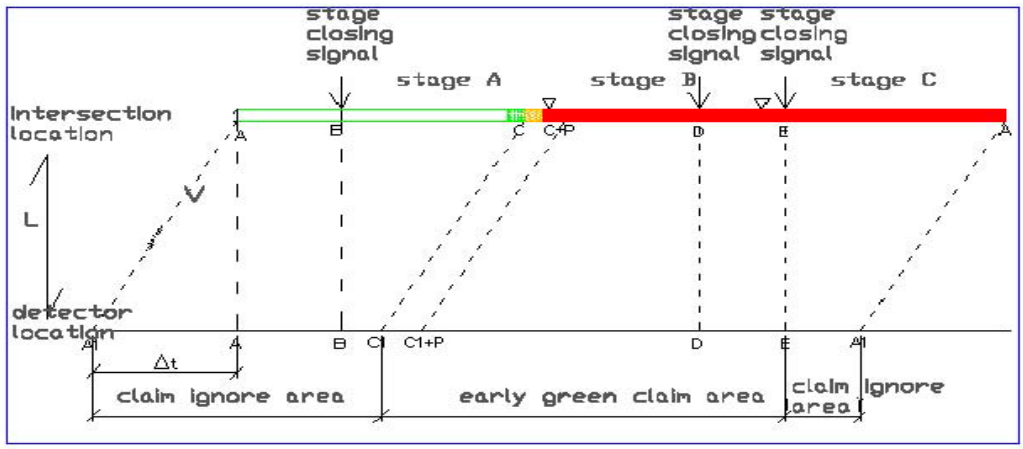

Figure 4. Impact of countdown device on claim section.

If the phase closing section is too long, the original "green extension claim section" C1-C1+P will lag behind B, then the "green extension claim section" will disappear; we cannot extend the green time. In such a case, we may increase the value of L, i.e. transfer the detect points to the upstream; or we may shorten the stage closing section, making sure that C1+P is before B, to keep the "green extension claim section".

2) Conclusion

Assume the distance between transit priority claim detector and the intersection is L, the vehicle speed is V and the closing period of priority claim of stage A is TA. From these analyses, we can see that the requirement to implement the green extension strategies of stage A are as follows: L/V>TA.

Or described in words as: The minimum distance between the transit priority claim detector and the stop line should be the travel distance with speed V during the closing period.

Also in order to ensure there is a certain period of "green extension claim section", the best distance between transit vehicle detector and the stop line is L=(TA+P)*V.

Or described in words as: The travel distance with speed V during the stage closed period and the additional P seconds, shown in Figure 5.

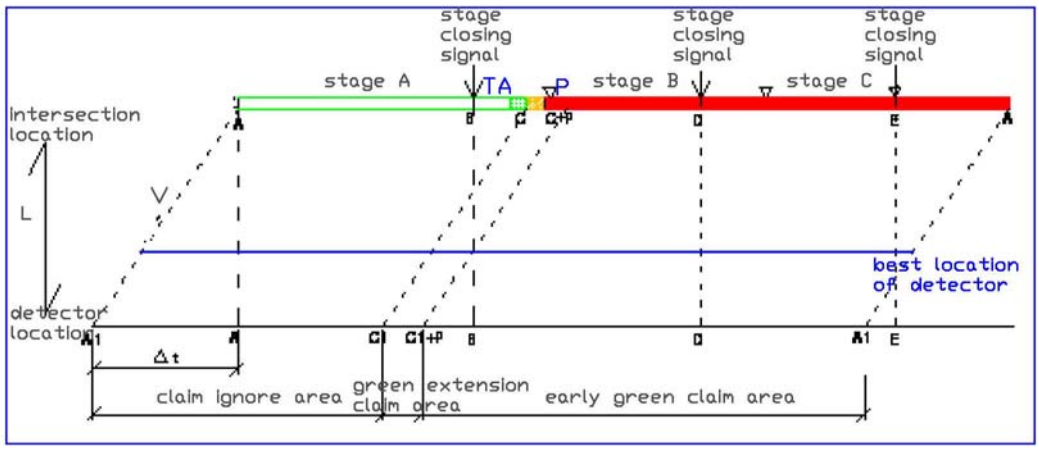

Figure 5. The best location of the detector.

These are the following conclusions:

1) Increasing the distance between the detectors and the stop line, which is L, can avoid the situation that "green extension" strategy can not be used happening. But if the value of L is too large to estimate the travel time, vehicles may not be able to enjoy the signal priority. Therefore, under the condition of meeting these requirements above, the value L should be as small as possible, which is L= (TA+P)*V.

2) If the detector is fixed, and the stage closing period is long, then "green extension" strategy may not be validated. Then shortening the countdown time can avoid it. Especially because the distance between intersections in Shanghai is generally short, it is suggested to shorten the countdown time if conditions allow.

3.2 Early green

(1)Definition

There are buses arriving at the end of the current stage and they are going to get across the section in this stage, but even if we have extended the green time of this stage, the buses are not certified to across the intersection according to their normal speed during the extra green time, or the buses arrive during red stage, then the green signal of claimed stage will be started in advance to get the buses across the intersection early.

(2)Location of detector

If green extension and early green are used together, then their detectors can be the same to save budget.

If early green is used separately, then the detectors are appropriate to set at the stop line, because buses can spring the detectors when they queue at the stop line. The analysis of impact of early green to detectors can also be seen in "3.1 green extension".

(3) Early green responding section

Accordingly, early green claim section is contained in the three claim sections,

which can be divided into responding section and non-responding section. Because of the characteristics of the signal controlling device, once the green countdown starts, the signal plan cannot be modified to start the green signal for bus stage early even the buses are detected during this time. So the early green responding section is shortened which results in the implement effect being discounted. The early green responding section is displayed as below.

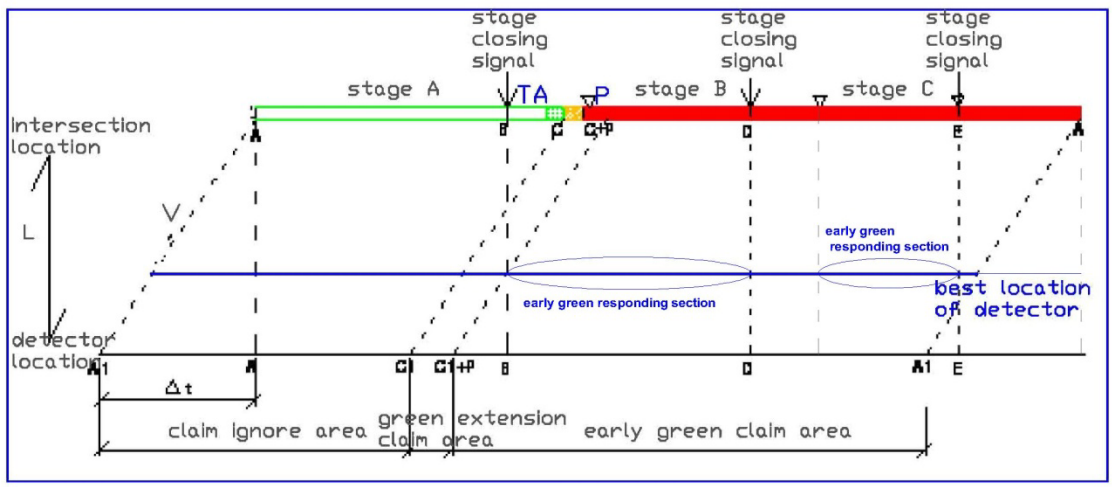

Figure 6. Early green responding sections

4 INSTANCE ANALYSIS

The theory mentioned above is validated on the VISSIM platform of PTV Corporation.

Section of North Cheng Du road and West Nan Jing road (Figure 7) under the south-north expressway of Shanghai was selected to be analyzed. Different countdown options were simulated using VISVAP software of VISSIM to analyze the impact to travel time of buses, shown in Table 2 and Figure 8.

There are three options (15s countdown, 5s countdown and non-countdown) being simulated at this section, under the condition that maximal green extension is 15s (P=15s), speed of the bus is measured at 18 KM/H, location of the detectors must be 150m, 100m, and 75m upstream of the stop line. Locations of the detector under different countdown times are shown in Table 1.

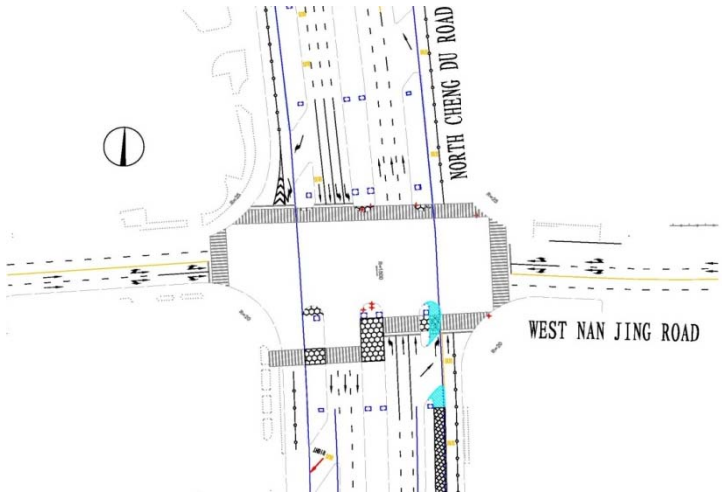

Figure 7. layout of Section of North Cheng Du road and West Nan Jing road .

Table 1. Locations of the detector under different countdown times.

countdown time (s)	15	5	non-countdown
location of detector (m)	150	100	75

Table 2. Travel time of buses under different countdown times.

	15s countdown	5s countdown (just main road)	5s countdown	non-countdown
travel time of buses (s)	58.7	56.5	45.1	37.2

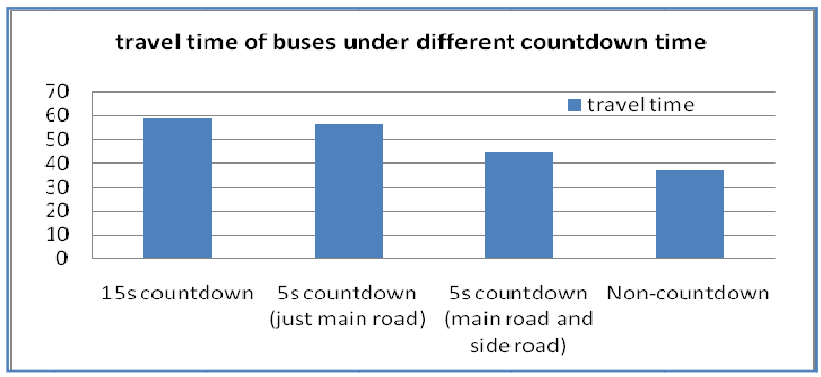

Figure 8. travel time of buses under different countdown time

The travel time is 23% and 37% shorter under 5s countdown and non-countdown, respectively, than 15s countdown. There are conclusions as below:

- The travel time of buses from detectors to stop line is difficult to forecast

when the distance between the detector and stop line is too long, in some cases green extension strategy will be invalidated. If the countdown time is shortened, then the location of the detectors can be moved forward where the state of the buses will be more stable.

- Green countdown of non-bus stage restricts the early green strategy. Because of the characteristics of the signal controlling device, once the green countdown starts, the signal plan can not be modified to start the green signal for the bus stage early even if the buses are detected during this time. So the early green responding section is shortened which results in the intended effect being discounted.
- Travel time of buses is reduced with the reduction of countdown time.

5 CONCLUSIONS AND RECOMMENDATIONS

1) Shortening the countdown time of the bus stage and advancing the location of detectors confirms the validity of green extension strategy because the state of buses is more stable downstream of the detector.

2) Shortening the countdown time of the non-bus stage enhances the intended effect of early green strategy because the early green responding section is increased.

3) From the analysis above we can see that the countdown device has a great restriction to bus priority strategy. So it should not be or less used at the section which will apply active bus priority strategy. It is suggested to set at 5s when it is obligatory.

4) This paper just simulates sections with bus lanes; actually, it will be more complicated when the non-bus lane, bicycles and pedestrians are considered. They are pending further study in the future.

6 ACKNOWLEDGEMENT

This work is supported by Doctoral Fund of Ministry of Education of China (Grant No. 20070247068) and national natural scientific foundation (Grant No. 50808140).

REFERENCES

Chen-Fu Liao, Gary A. Davis (2006).” *BUS SIGNAL PRIORITY BASED ON GPS AND WIRELESS COMMUNICATIONS PHASE I - SIMULATION STUDY*”, Minnesota, 3.4

WANG Yan, YANG Xiao-guang.” Discussion on Setting Traffic Signals with Counting down Display Unit at Intersection Based on Traffic Safety”. *China Safety Science Journal*, 16(3):55-59.

Yu Xuan.” *A RESEARCH ON INTERSECTION SIGNAL SECURITY AND CONTROL*”, 32-44

DRIVING SIMULATION STUDY OF TRAFFIC FLOW CHARACTERISTICS OF THE CLIMBING LANE ON A TWO-LANE RURAL ROAD

Qin Yaqin[1],Xiong Jian[1],Liu Hongqi[2], Guo Fengxiang[1] and Wan Huasen[1]

[1]Faculty of Transportation Engineering, Kunming University of Science and Technology, Kunming, Yunnan 650224, China, PH (86) 871-3802259; FAX (86) 871-3802259; email: xjebox@163.com

[2] Traffic Engineering Supervision &Testing Center, Ministry of Communications, Xitucheng Rd, Beijing, 100088, China. PH (86) 10-62355709, FAX (86) 10-62356515; email: hq.liu@rioh.cn

ABSTRACT

The climbing lane is a benefit to traffic safety through changing the traffic flow characteristics of the highway and avoiding overtaking maneuvers. This study was conducted by means of a driving simulator experiment to examine the effects of a climbing lane on an upgrade of an existing two-lane rural highway in Yunnan province. To construct and improve the fidelity of traffic flow scenarios on the driving simulator, simulated traffic flows under two special traffic volumes with and without the climbing lane were obtained from VISSIM. Thirty-two subjects were selected to drive on the test road in the driving simulator. On the basis of the simulation results, comparison evaluations of speed and track lateral position of the test vehicle along the section with and without climbing lane were conducted. In addition some simulation experiments from VISSIM were done to find the threshold of traffic volume for the setting of climbing lane. The result shows that there is a higher and steady speed after setting a climbing lane under different given traffic volumes. Moreover, it reduces conflicts with cars from the opposite direction. But this benefit will be reversed with the increase of traffic volumes.

INTRODUCTION

The climbing lane is a lane added on an uphill grade for use by trucks, long vehicles and heavy vehicles with speeds significantly reduced by grade. Current "Highway Engineering Technical Standards" in China provides that the freeway and highway should be set up with a climbing lane along the uphill when the slope is more than 4 percent. The climbing lane can make cars pass the truck and other slowly moving vehicles quickly. This will not only reduce the travel time, improve the mean speed and level of service of this section, but also avoid overtaking maneuvers. This can benefit traffic safety. The study results of Abishai Polus and Israel Reshetnik

(1987) showed that the climbing lane on upgrades could provide substantial flow benefits - reduction in delay and in passenger-car platooning- with implications for better safety.

Generally, the principal methods to study climbing lanes are ground test or pure software simulation. Werner Briton and Andrea Bressler (2004) focused on the derivation of capacities and traffic flow characteristics for freeway upgrades by methods employing empirical investigations based both on microscopic measurements and continuous traffic monitoring as well as on microscopic simulation. Sun Jiafeng and Zhou Ronggui (2006) simulated the average speed and delay on the climbing lane on a long upgrade under different traffic flows by simulation software. In this paper, driving simulator experiments had been done in order to study the effects of traffic characteristics with and without the climbing lane. The climbing lane for the experiment comes from a specific upgrade section of a real two-lane rural highway in Yunnan province.

EVALUATION INDEX

Indexes to evaluate the effect with and without the climbing lane may generally be categorized into two types. One is an objective index such as the traffic characteristics data, and the other is a subjective index such as the driver's assessment of his own condition. The objective index included speed, acceleration, road capacity, level of service, track lateral position and braking operation, etc. In this study, we selected the speed and track lateral position as indexes. The track lateral position is the displacement of the vehicle's track from the road center line (RCL: the middle line of the two-lane without the climbing lane).

EXPERIMENTAL PROGRAM

Driving simulation experiments were arranged to evaluate the effect of the climbing lane. The experiments were accomplished by subjects at four driving simulation scenarios with and without the climbing lane setting. All the data were collected directly from the driving simulator, and based on the data the comparison evaluations of the test track were investigated.

Equipment. The main equipment in the experiment is a full-size advanced driving simulator (KMRTDS) set up in the simulation laboratory at Faculty of Transportation, Kunming University of Science and Technology, which is comprised of six subsystems including driving cab system, control system, vehicle dynamic model system, visualized system, traffic simulation system and sound system. KMRTDS provides researchers a scientific tool to study road traffic and transportation under controlled experimental conditions. It allows researchers to create any visual data and scenario to study traffic problems in the surrounding design, special experiment and real world situations. By controlling the performances of driving vehicles, traffic flow, pedestrians' behavior and other environmental factors,

simulation experiments can be implemented and test data can be collected. With the optimized image processing speed of above 30 frame/s, and the calibration for the speed and visual, KMRTDS can ensure the real-time operation of the system and the fidelity of the experimental scene.

Another study tool is VISSIM, a microscopic simulation tool for traffic flow which describes vehicle performance and driver behavior in a very detailed manner. It provides the driving simulator traffic flow for the experiments

Test track and virtual scene. Figure 1 shows the structure design of the test track. The test site was a double two-lane rural highway at Xiaomo highway in Yunnan province. The length of the climbing lane was 650 meters, and the slope was 5 percent. The main lane width was 3.75 meters with a 3.5-meter-wide climbing lane on the right. The test track is divided into five sections including the entrance forward section (EFS), Climbing entrance section (CENS), Climbing parallel section (CPS), Climbing exit section (CEXS) and exit backward section (EBS). The layout of these five sections can be seen in Figure 2.

The traffic flow in the virtual scene was generated by VISSIM after some calibration work, and then was introduced to the test track by the interface software of VISSIM and KMRTDS. The traffic composition included cars, heavy vehicles and motorcycles with the proportion of 44%：44%：12%. The traffic volumes of 500pcu/h and 600pcu/h were selected as the simulation flow to the two main lanes, and the heavy vehicles were only allowed to enter the climbing lane.

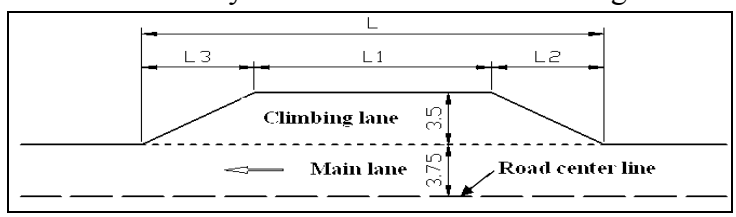

Figure 1. Structure design of climbing lane.

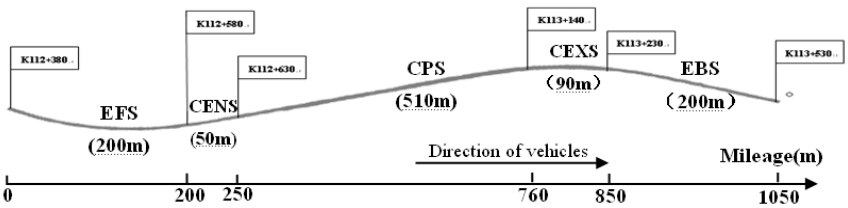

Figure 2. Layout of five sections of the test track.

Subjects. The subjects (test drivers) composition included 27 men and 5 women drawn from corporations in Kunming city with age ranging from 28 to 58 years. They were experienced drivers with at least two years of driving experience. No speed limit was set on the test road section, but subjects were asked to drive at the speeds they normally expected to.

Procedure. Figure 3 shows the view of the virtual scene in the experiment. To

carry out the experiment on KMRTDS, the steps followed were:

- Create two virtual test tracks exactly based on sample road section with and without the climbing lane.
- Build the simulation scenarios with traffic flows of 500 and 600pcu/h.
- Train the subjects to fit to the simulator. Before starting, preliminary test and calibration were required to make the parameters match with the real world.
- Carry out the experiments and collect the data.
- Require subjects to finish the questionnaire.
- For further analysis and evaluation all data acquired from the KMRTDS had to be treated with respect to the exact position along the test course.

Figure 3. View of the virtual scene of the test track outside and inside KMRTDS.

DATA ANALYSIS AND RESULTS

Based on 32 subjects' data in the test track from KMRTDS, we analyzed the indexes of speed and track lateral position. In the following description, we defined F1 and NF1 as the test scenarios with and without the climbing lane when traffic volume was 500pcu/h, and F2 and NF2 corresponding with traffic volume of 600pcu/h.

Profiles of indexes. The profiles of mean speed and track lateral position in four scenarios (F1, NF1, F2, and NF2) are shown in Figure 4 and Figure 5. Here we can see a comparison of mean speeds which are shown in Figure 4. It is obvious that the mean speed for cases F1 and F2 with the climbing lane is faster than the speeds at cases NF1 and NF2 without the climbing lane. It means that the speed can be improved after the setting of the climbing lane.

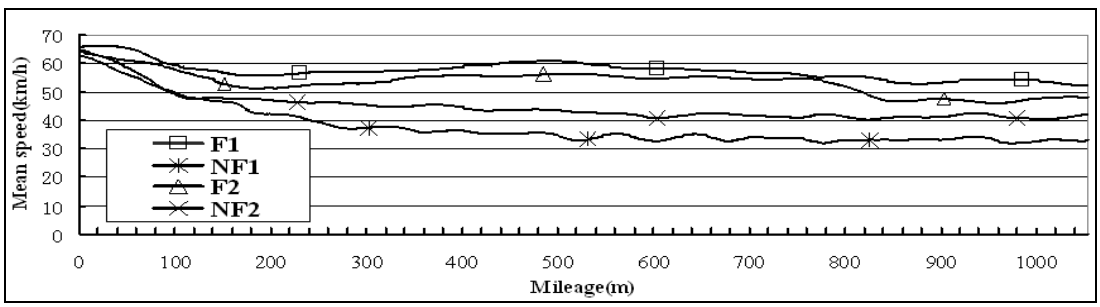

Figure 4. Profiles of mean speed of test track in four scenarios.

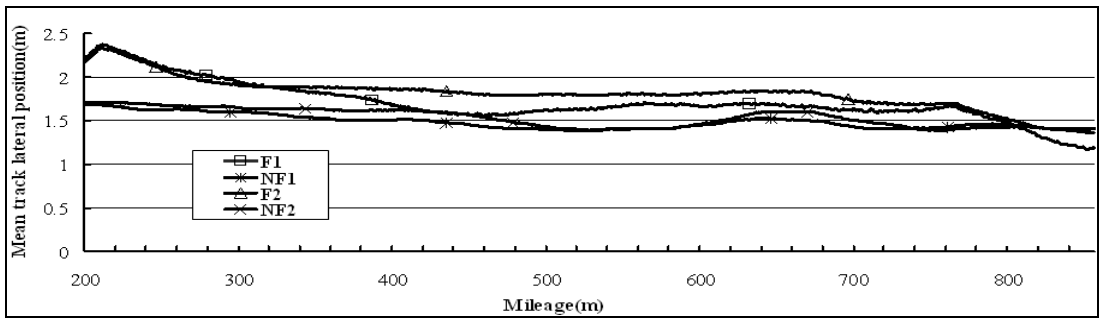

Figure 5. Profiles of mean track lateral position of test track in four scenarios.

In Figure 5, we draw the profile of track lateral position in three middle sections (CENS, CPS and CEXS sections, which length is from 200m to 850m,). We can know that the track lateral position (F1, F2) with climbing lane is further from RCL than that (NF1, NF2) without the climbing lane. These show that the setting of the climbing lane can improve the traffic characteristics and safety under these traffic volume conditions.

Analysis for middle sections. For further analysis, the mean and standard deviation of indexes were calculated at three middle sections (CENS, CPS and CEXS). Figure 6(a) shows the mean speeds with the climbing lane at these sections are faster than those without the climbing lane. The speed at F1 and F2 accelerated at CPS section, while at NF1 and NF2 decelerated all along. The standard deviations of mean speed at CENS and CPS are nearly same, while that at F2 at CEXS are greater than others. The reason is the more heavy vehicles will enter the main lane at CEXS with the traffic volume increased, which would influence the car in the main lane, thus made a greater wave of speed.

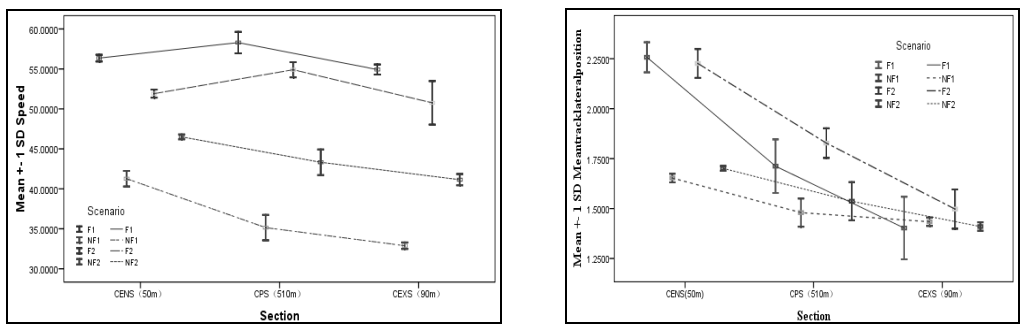

a) speed b) track lateral position

Figure 6. Chart of clustered error bar of speed and track lateral position of three special sections in four scenarios.

Similarly, the mean track lateral position with the climbing lane at CENS and CPS sections are larger than those without the climbing lane, while those are nearly equal at CEXS (see Figure 6(b)). This means the setting of the climbing lane would make the vehicles deviate further from RCL. Figure 6(b) also displays the standard

deviation of track lateral position with the climbing lane were bigger than those without the climbing lane. This means the setting of the climbing lane would improve the variation of the car in the lane. Although Homburger Wolfgang S. (1987) had concluded the merging area at the terminals of climbing lanes on two-lane roads do not present a hazard of major proportions, we concluded that the CEXS with the climbing lane was a hazard area under the two traffic volumes because of their larger standard deviation of track lateral position and higher speed.

Statistic analyses of indexes for whole test track. Mean, standard deviation and Std. error mean of speed and track lateral position in the whole test track (distance is from 0m to 1050m) for each scenario were calculated. The group statistics results are presented in Table1 and Table 2. The results from Table 1 show the mean speed of the whole test track with the climbing lane is higher than that without the climbing lane, while the standard deviation is smaller. This displays the speed is faster and speed consistency is better after the setting of the climbing lane under 500pcu/h and 600pcu/h.

Table 1. Group Statistics of speed.

Scenario	Mean（km/h）	Std. Deviation（km/h）	Std. Error Mean
F1	54.8938	7.95911	.19004
NF1	42.5553	10.61505	.25346
F2	52.0310	7.45993	.17812
NF2	47.9049	8.53911	.20389

Table 2. Group Statistics of track lateral position.

Scenario	Mean（m）	Std. Deviation（m）	Std. Error Mean
F1	1.710700	.2338593	.0091237
NF1	1.486700	.0809144	.0031568
F2	1.811975	.1834159	.0071557
NF2	1.531465	.1073676	.0041888

In Table 2, the standard deviation of mean track lateral position in the whole test track with climbing lane are greater than those without the climbing lane, which means the further from RCL and the less hazard from the opposite main lane.

Analysis with VISSIM. In order to find out the threshold of the traffic volume for setting climbing lane, VISSIM simulation experiments have been implemented. In the same test tracks as the driving simulation experiment, the mean travel times, mean speed and average delay per vehicle had been measured in the VISSIM simulation experiments under four kinds of traffic flow. The traffic volumes are set as 600, 1000, 1300 and 1600 pcu/h separately. Measured results are shown in Table 3. In table 3 and table 4, the scenarios CL and NCL means with and without the climbing lane.

Table 3. VISSIM simulation results with and without climbing lane

Traffic volume	600 pcu/h		1000 pcu/h		1300 pcu/h		1600 pcu/h	
Scenario	NCL	CL	NCL	CL	NCL	CL	NCL	CL
Mean travel time (s)	51.6	51.7	53.2	54.8	54.7	73.0	56.1	179.1
Mean speed (km/h)	46.6	46.4	45.1	43.8	43.9	32.8	42.7	13.4
Average delay per vehicle (s)	2.7	2.8	4.3	5.9	5.8	24.2	7.2	130.4

It can be seen from Table 3 that the mean travel time and delay of test track with the climbing lane of 1000 pcu/h is a little greater than those without the climbing lane. So the setting of the climbing lane has no influence on the road traffic characteristics. While the mean travel time and delay increased remarkably with 1600 pcu/h, the mean speed decreased rapidly. In this case, the traffic flow characteristics deteriorated rapidly. A further VISSIM simulation with climbing lane under traffic volume of 1200, 1300, 1400 and 1500 pcu/h separately had been done to find out the threshold of traffic volume. The simulation results are shown in Table 4. It can be seen from Table 4 that when the traffic volume exceeds 1300pcu/h, the mean travel time and delay increase all along with the mean speed decreases rapidly. In this case the volume of 1300pcu/h has approach to the saturated one.

Table 4. VISSIM simulation results for the test track with climbing lane.

Traffic volume （pcu/h）	1200	1300	1400	1500	1600
Scenario	CL	CL	CL	CL	CL
Mean travel time (s)	58.3	73.0	93.8	174.8	179.1
Mean speed (km/h)	40.6	32.9	25.5	13.8	13.4
Average delay per vehicle (s)	9.6	24.2	45.1	125.4	130.4

CONCLUSIONS

- When setting a climbing lane, the mean speed of vehicles increased and speed standard deviation decreased in the whole test track under the given traffic volumes.
- The traffic flow characteristics will be improved efficiently under lower traffic volumes after setting the climbing lane. But it will become the reverse case when traffic volume approaches saturation.
- In the exit of the climbing lane, the heavy vehicles will impact the cars in the main lane, and it will become serious with increased traffic flow.

ACKNOWLEDGEMENT

This study was supported by the open fund from Key Laboratory of National Highway Traffic Safety Technology Center. We also obtained the highway database

from Yunnan Highway Design and Research Institute. To everyone involved, we express our sincere gratitude.

REFERENCE

Abishai Polus, and Israel Reshetnik (1987) "Impact of passing-climbing lanes on traffic flow on upgrades." *Transportation Research Part A: General,* 21(6), 401-410.

Homburger, Wolfgang S.(1987) "Analysis of safety at upgrade terminals of climbing lanes on two lane highways." *Transportation research record,* 1987, 27-36.

Sun Jiafeng and Zhou Ronggui. (2006) "The influence and adjust of operating evaluation index of climbing lane on two-lane rural highways." *Journal of highway and transpotation research (Application technology),* 2006(4), 84-86.

Werner Briton and Andrea Bressler(2004) "Traffic flow on freeway upgrades" *Transportation research record, TRB 83rd Annual Meeting in January 2004,* 112-121.

A Safety Protection Technology System on Highway Roadside in China

LI Yang[1] MA Rongguo[1] NIU Yuxin[1] WANG Longfei [1]

1 Department of Traffic Engineering, School of Highway, Chang'an University, 710064, Xi'an, China, PH (86)29-82334856; email:dorothy06@gmail.com (LI Yang); mrg@chd.edu.cn (MA Rongguo); xinxin8286@qq.com (NIU Yuxin); choseoner002@gmail.com (WANG Longfei).

Abstract: In order to reduce the rate of roadside accident and help engineers make an informed decision or take the most effective measures in highway roadside safety improvement program, the authors put forward the roadside safety protection technology system (RSPTS) that suited to the actual situation to deal with the typical roadside safety problems appearing in China. RSPTS is built in accordance with a priority of active guidance, appropriate protection and timely security, including the technologies to prevent vehicles from leaving the road out of the lane (active guidance technology), to reduce the collision and rollover accident rate, and to alleviate the severity of roadside accidents. The potential benefit of this study is to reduce the roadside accident rate, in particular to alleviate the severity of the serious traffic accidents which can result in many injuries and deaths.

Key words: *Roadside traffic accidents; Safety tolerant design; Roadside safety protection technology system*

1 Introduction

With the rapid economic and social development, highway traffic safety has become a worldwide problem to be solved. According to the statistics, China is the largest traffic accidents country in the world by the end of 2008. The indicators of traffic accidents from 2001 to 2008 in China are shown in table1. Based on statistic data which were provided by the Administration Ministry of Public Security White Paper, about 12% deaths were caused by the roadside accident from 2001 to 2007, which is only account for 8% of the total highway accidents. About 70% traffic accident occurred in the secondary highway or lower grade highway and about 30% of total crashes are roadside crashes.

According to statistics, roadside safety problems in low grade are prominent. Lack of protective facilities, insufficient of crash protection, the configuration of protective facilities and hidden danger of slope and ditch evoked large amount of serious accidents. Thus, in allusion to the typical roadside safety problems appearing in China, the roadside safety protection technology system (RSPTS) is proposed in this paper. RSPTS is aimed to reduce the roadside accident rate, as well to alleviate the severity of traffic accidents.

Table 1. The indicators of traffic accidents from 2001 to 2008 in China.

year	Traffic accidents (ten thousand)	Death (ten thousand victims)	Injury (ten thousand people)	Property loss (billion rmb)
2001	75.5	10.6367	57.10	30.9
2002	77.3	10.90	56.20	33.2
2003	66.7507	10.4372	49.4174	33.7
2004	56.7753	9.9217	45.1810	27.7
2005	45.0254	9.8738	46.9911	18.8
2006	37.8781	8.9455	43.1139	14.9
2007	32.7209	8.1649	38.0442	12.1
2008	26.5204	7.3484	30.4919	10.1

2 Analysis of the roadside safety situation and problems in China

Roadside Safety problem of China is becoming increasingly serious, in particular in the mountainous area. The problems are mainly existed in the 100,000 kilometers low grade highway (Kan Weisheng 2007). The general problems are summarized as follows:

(1)The level and type of safety facilities can not match the roadside characteristics. The protective performance and reliability of facilities can not meet the actual requirement. A road section without security protection facilities or lack of protection is shown in figure1.

(2)Due to the large population and the shortage of land resources, there is no guarantee for the clear zone in China (see figure2).

(3)By using the high embankment, the design of the ditch and slope is not standardized, which makes the driver suffered a potential safety risks (see figure3).

(4)The column of traffic signs and the light poles are set inside clear zone, and the breakaway supports were hardly set and used (see figure4).

(5)There a lack of special guardrail terminal and transition treatment.

(6) No a clear specification for the work zones protection.

Figure 1. Lack of guardrail protection.

Figure 2. Dangerous road shoulder.

Figure 3. Dangerous wide ditch.

Figure 4. Untreated Rigid bridge Pier.

3 The leitmotiv and the framework of RSPTS

3.1 The leitmotiv description of RSPTS

Because traffic accidents are caused by the interaction among drivers, vehicles, highways, and environment, it is impossible to totally avoid the accidents. RSPTS is proposed in accordance with principles of active guidance for minimizing the injury extent and appropriate protection. Tolerance design concept is integrated into RSPTS, at the same time environmental protection and harmonious disposal should be taken into consideration (Li Yang 2008). Three leitmotivs of RSPTS are as follows:

(1) To prevent the vehicles run off the road and intrusion into the roadside region.

(2)To decrease the occurrence probability of collisions in circumstances of vehicle shave run off the road.

(3) RSPTS is devoted to alleviate the severity of roadside accidents.

3.2 The framework structure of RSPTS

It is necessary to stick to the three leitmotivs above to pay attention to the protection of clear zone and the reasonable installation of guardrail and the proper treatment to road shoulder, slope and ditch. The specific RSPTS system structure is shown in figure 5.

4 Active roadside safety guidance technologies

Active guidance refers to a benign interaction between driver and highway which was realized by installation of traffic safety facilities and improvement of the highway traffic environment. During the information interactive process, traffic environment has played an “active” role of guide to prevent vehicles from running out of the road, so as to lower the decrease the accident occurrence probability (David, J2005).From a technical point of view, the elimination of potential safety risk depend on the correct installation of deceleration vibration marking, contour marking and chevron alignment sign and so on to warn the driver keep driving inside the road (Avinoam Borowsky 2009). The specific roadside safety active guidance technology is shown in table2:

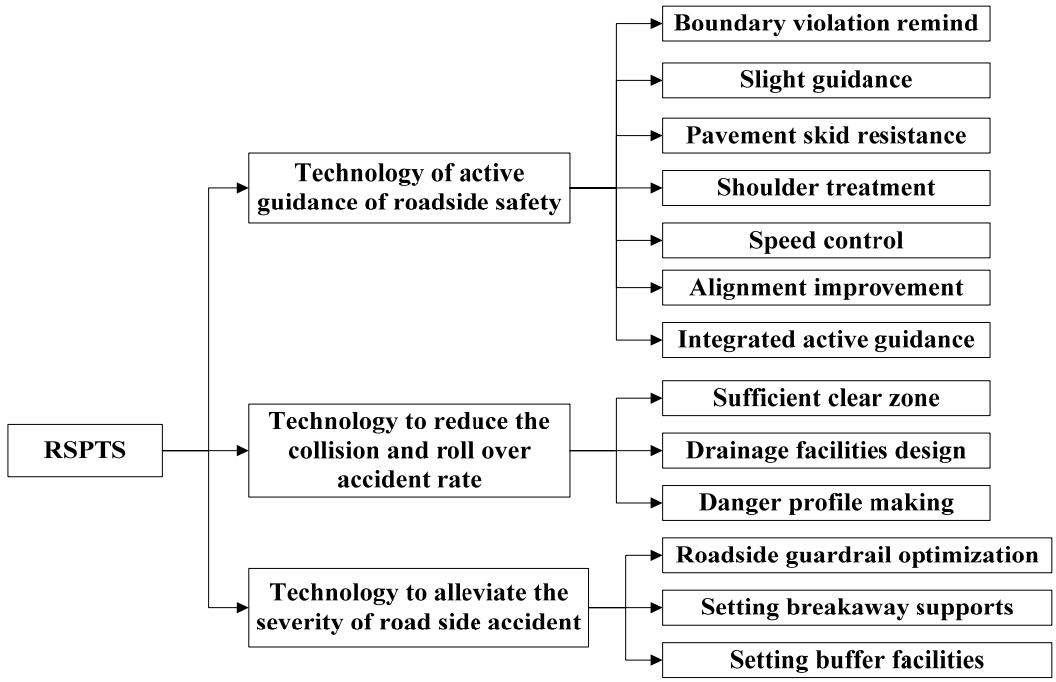

Figure 5. The specific RSPTS system structure

Table 2. Roadside safety active guidance technology

Technical measures	Instructions
Sight guidance	Setting the contour marking rationally
	Setting the chevron alignment sign rationally
	Setting the warning pier
Boundary violation remind	Setting the vibration marking
Pavement skid resistance	Using anti-sideslip wheel belt
	Increase pavement structural depth
	Laying special pavement
Shoulder treatment	Widening and hardening the shoulder
	Set the shoulder vibration zone
	Ensuring maintenance of shoulder
Speed control (Fred annering2009)	Setting deceleration facilities
	Setting the speed limit sign and marking
	Speed feedback sign
	Visual and mental deceleration facilities
Alignment improvement	Applied operating speed theory and alignment improvement for black pot and the sections of negative linear combination
Integrated active guidance	Applied comprehensive prevention for the roadside dangerous segment

5 Collision and rollover rate reduction technologies

The technology to reduce the collision and rollover rate is shown in table3:

Table 3. Roadside safety active guidance technology

Technical measures	Instructions
Sufficient clear zone	Embankment slop design
	Cutting Slope design
	Treatment of dangerous object
Drainage facilities design	Tolerance side slop design
	Traversal culvert design
Danger profile marking	Setting warning sign on the front of dangerous object
	Brushing the reflecting paint or film

6 Accident severity mitigation technologies

6.1 Optimal design of the roadside guardrail

(1) Guardrail end treatment

The tremendous acceleration which caused by a sudden brake will be a great risk and harm to the passengers, at the same time, the guardrail terminal is likely to cut into the vehicle body or make the vehicle roll-over. Hence, it is necessary to deal with the guardrail end so as to decelerate the vehicle speed and alleviate the severity of the serious traffic accidents (see figure6).

Figure 6. Abduction guardrail end and breakaway and buffer guardrail end.

(2) Guardrail transition treatment

The transition treatment should be taken on the different stiffness and type guardrails to maintain the continuity of intensity guardrail and also to prevent the occurrence of accidents in the discontinuous guardrails pot. The stiffness transition is ensured and the large Stiffness guardrails are avoided to become the roadside obstacle object, two examples are shown in figure7.

Figure 7. Guardrail transition treatment.

6. Installation of buffer facilities

Because vehicles need to shut on the expressway passageway and intersection also the entrances of separate type subgrade section, the accidental probability is higher than general road section. Except for dealing with the guardrail end in the dangerous trigone zone, it is necessary to set the buffer facilities such as anti-collision barrels in front of the trigone zone (see figure8).Many actual cases proved that the severity of accidents will evidently alleviated by setting buffer facilities (Fred Mannering, 2009).

6.3 Installation of breakaway support

Application of the breakaway support is very sparse in China, so it is effective to set the breakaway support to improve the roadside problem. With the development of economy and more and more regard to life, it is believed that the breakaway support will be extensively applied to play a role in life protection.

Figure 8. Setting the anti-collision barrels in front of the trogon zone

7 Conclusion

(1) RSPTS is established aiming at the leitmotiv of active guidance and minimize the injury extent and appropriate protection, which is suitable for the state situation and conform to the actual roadside safety problem in China.

(2) The suitable proposal of the types of safety facilities according to the actual situation is provided by RSPTS. This systemic technology can help engineers to make an informed decision or take the most effective measures in highway roadside safety

improvement program.

(3) Due to the incomplete data collection and other aspects, many factors which are involved in the roadside safety have not expounded in RSPTS. The relation between roadside safety and the geometric alignment, the composition of traffic volume should be discussed further in the systematical construction of RSPTS.

Acknowledgement

This study is funded by the "China's 863 Plan"—"Analysis for traffic accident in Expressway network under road environment (2007AA11Z248). " Special thanks are also given to the anonymous paper reviewers.

References

Avinoam Borowsky, David Shinar, Yisrael Parmet (2008). "Sign location, sign recognition, and driver expectancies" Transportation Research Part 11 : 463-464

David,J (2005). "Clear zone requirements based on horizontal sight distance considerations" Transportation Research Part A 35 : 391- 411

Fred Mannering (2009). "An empirical analysis of driver perceptions of the relationship between speed limits and safety" *Transportation Research Part F*12 : 103-104

Li Yang (2008). "Highway Roadside Safety Technology and Application" Master's degree paper of Chang'an University: 18-24

Kan Weisheng, Li Chengcheng, Tang Junjun (2007). "Corresponding Countermeasures on roadside safety problems", Highway, 3 : 97-100

Study on Pedestrian Safety and Countermeasures in Crosswalks around Campus——Case Study at Ludong University in Yantai

GU Jiuchun MU Chunyan WANG Liangshen LIU Kening SUN Jing

College of Transportation Engineering, Ludong university, P.O. Box 264025, Yantai Shandong Province, China; PH (+86) 13645359106; email: gujiuchun@163.com

Abstract : Crosswalk safety around many universities in China is increasingly getting worse. In order to come up strategies and measures for pedestrian safety around campuses, as a case study this paper investigated the road traffic and pedestrian's crossing characteristics in crosswalk around Ludong University. In addition, illegal crossing road behavior of pedestrians was surveyed and analyzed in details. As the conclusion, the paper summarized the strategies grouped into demand management, supply management, education and enforcement for improving the pedestrian safety at crosswalk, which might be useful to improve pedestrian's safety in crosswalk around campus in China.

Key words: *Pedestrian Traffic; Campus; Pedestrian safety; Countermeasures*

1 INTRODUCTION

With the rapid growth of higher education of China, the high student enrollment and large sizes of many college campuses have made walking a common and convenient mode of transportation. Almost all of students walk for most or all of their trips around campus. However, the interaction with vehicle traffic presents potential conflicts and hazards to pedestrians around campus. In most universities, the growing out-of-campus activities of students createa clash with autos, whether they live in the main campus or in secondary campuses. Therefore, pedestrian safety has become a concern for the universities in China.

In order to provide a safe pedestrian environment, we draw our cases from three crosswalks in front of gates of Ludong University (Figure 1). These cases are relevant because of their potential to foreshadow development in other universities in China. As an example this paper investigated the road traffic characteristics and pedestrian's crossing characteristics in crosswalk, and illegal crossing road behavior of pedestrians was surveyed and analyzed in details. At last, this paper discusses three safety countermeasures that can be applied to provide a safe environment around campus.

2 OVERVIEW OF TRAFFIC ENVIRONMENT

The environment around Ludong university campus comprises a mix of pedestrian environments. The west gate and south gate face Hongqi arterial and 500 meters apart from each other. The arterial, which is a two-way six-lane, 40 meters width and 60km/h speed limit major road on the south side of Yantai, also separates the campus into north part and south part and there is an overpass between two parts.

The east gate faces Qingnian arterial that is the same characteristics of Hongqi road (Figure 1). The university registers more than 20,000 students who need to cross road to get to and from bus stop or other out-campus areas, so the crosswalks in three gates are problematic because these roads have characteristics that make them hostile to pedestrians. Risks in the pedestrian environment are so serious that they made the news in Yantai. For instance, a February 2008 article in webpage (http://www.jiaodong.net), described that five students were clashed by car within three-day period at front of three gates crosswalks.

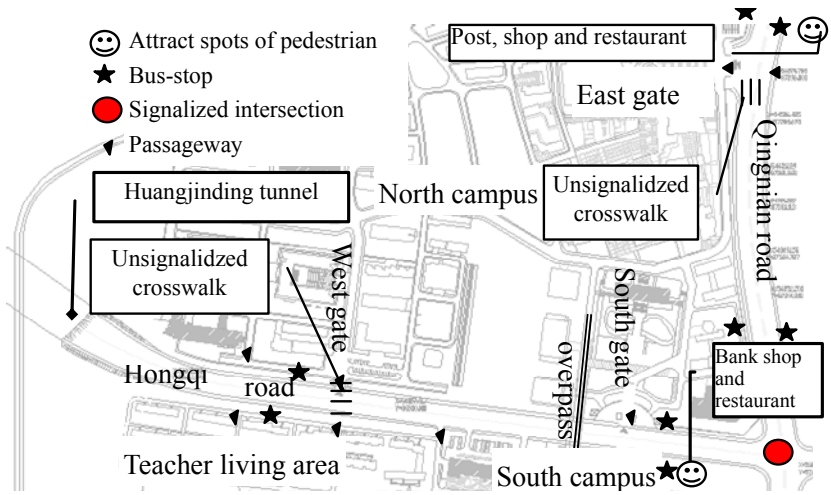

Figure 1. The illustration of traffic survey around Ludong University

3 VEHICLE DATA SURVEY AND ANALYSIS

In order to show the impact of volume and speed on pedestrian's safety, we employed the traffic stream characteristics analysis around three gates of Ludong University. Data was all collected on May 27, 2008 during the peaking hour.

The survey indicates the morning PHV of Hongqi road was 3678pcu/h, Qingnian road was 3820pcu/h and the evening peak hour volume approximately was equal. We can say that pedestrians would have to wait long time for an available gap to cross.

Spot speed data was collected using a laser speed gun at two locations in 20 meters apart from west gate and east gate crosswalk during the morning peak-hour period. The survey shows that approximate 4-15% drivers didn't obey the speed limit (60km/h), and approximate 6 percent vehicles traveled at speeds over 70 km/h which was 10 km/h over the posted speed limit. So it is necessary to provide a supervise device to increase speed limit compliance.

4 PEDESTRIAN TRAFFIC CHARACTERISTICS AT CROSSWALK

4.1Pedestrian traffic volume survey

The two crosswalks in survey are unsignalized crosswalks whose upstream vehicles arrival is discrete. Opposite the west gate around crosswalk, it is the teacher living area, and opposite the east gate around crosswalk, there is public community,

including post office, bus stops and shops (Figure 1). Most of students there walked across the road for daily living trip purposes in the observation period. The survey includes one-hour period in AM peak hours and normal hours. Figure 2 shows that the demands for pedestrians crossing were very concentrated. In figure 2(b), the violation of crossing outside of crosswalks is obvious.

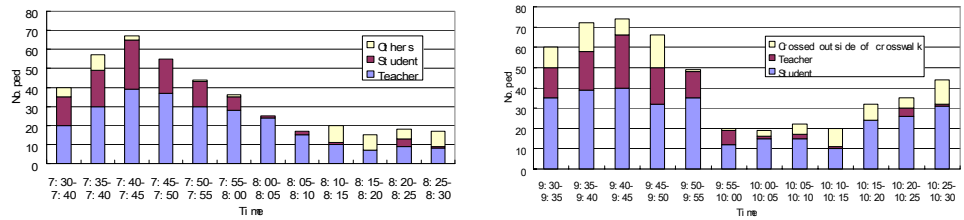

(a) (b)

Figure2.Pedestrian volume histograms at west gate(a)and east gatecrosswalks(b)

4.2 Pedestrian speed and waiting time

4.2.1Pedestrian speed in two crosswalks

The on-site survey shows that pedestrian speed on the west gate is 1.52 m/s, and 1.40m/s for the east gate respectively. For the different survey periods, it is time for working and studying at the west gate crosswalk, most of pedestrian trip purposes are about attending class in haste at a higher speed, comparing to go out of campus for traveling and shopping at a lower speed at the east gate crosswalk. Moreover, a proportion of pedestrians make acceleration in midway, mostly after midline, so there needs a calming environment. For the east gate crosswalk, the pedestrians usually cross the road with linked arms and walk together in groups and they walk in a lower speed than other categories. The reason results from most pedestrians of this type walking and chatting, and writing short message, with less caution on purpose, sometimes calling and having earphones, as previous study presented (SHI Jiangang,2007; XI Jianfeng,2006). In addition, students are easily aroused the attention by surroundings that make students easy targets for clash while crossing.

4.2.2 Waiting time

Table 1 shows the statistic of waiting time when pedestrians are on roadside and midline. In observation, few pedestrians took adventure and most pedestrians yielded to vehicle, the condition that vehicle yielding to pedestrian did not appear, when the waiting time is more than 40s, the percent of running across in risk is higher. In east gate crosswalk, the rate of risk type and impatient pedestrians are rather high and these walkers take shorter gap to carry out walk course, which can interpret as vehicle restrict pedestrian personal characters in walking. So related countermeasures should be used to reduce waiting time and give the vulnerable road user priority.

Table 1. Statistics of pedestrian waiting time

Index	West gate crosswalk	East gate crosswalk
Maximum roadside waiting time (sec)	43.31	50.47
Maximum midline waiting time (sec)	34.87	46.32
Mean of roadside waiting time(sec)	9.65	11.33
Mean of midline waiting time(sec)	6.56	7.48

4.3 Students safety perceptions analysis

Because of the old crosswalk in front of south gate being replaced by overpass 15 meters apart, in order to understand the causes of students illegal crossing better, the campus-wide opinion surveys for students were conducted to collect and analyze users' safety perceptions after traffic environmental changing. Survey questionnaires were distributed to some affiliated people (rough 500 students, 382 participants who returned valid surveys (male: 40%, female: 60%)). Coincidentally over 80% of respondents in this survey are those who indicated "time saving and convenient" or "unaware of erased crosswalk marking" or "accustomed to crossing behavior" (Figure 3(a)). In addition to questionnaire surveys, field pedestrian behavior data was collected by south gate on-site observation and individual interviews (male: 20, female: 20). Some of the causes of still crossing including having an urgent matter, time saving and convenient, custom formerly crossing, lack of management and lucky-me attitude and so on. The results presented in Figure 3(b) indicate about 30% of the pedestrians crossing using the old crosswalk. The interview violation causes result is in good agreement to the questionnaire.

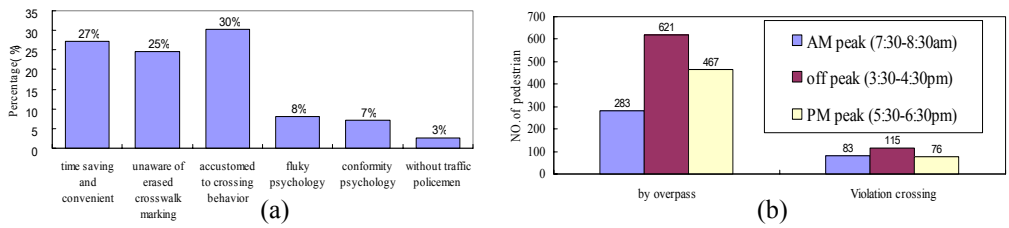

Figure 3. Reasons for pedestrian violation by questionnaire (a) and number of crossing statistics (b) at south gate

5 DESIGN STRATEGIES FOR IMPROVED SAFETY

From the analysis of upper materials, the field studies reveals several risk factors. The travel habit doesn't change with road environment variation, which causes higher accident rate at the beginning of traffic through. The peak traffic flows are heavy and few gaps for pedestrians crossing, and the vehicle can be fast, which makes crossing dangerous for pedestrians. There are additional hazards for pedestrians who were illegal to cross the road anywhere. Barriers to prevent pedestrians' crossing may be fully successful. The bridge doesn't design to integrate with bus stop. The environment of current designs for pedestrian travel on roads around Ludong University does not fully address students' crossing necessities.

These failures to accommodate pedestrians do not deter their presence but do put them at risk.

5.1 Pedestrian traffic demand management

Traffic demand management plans can be grouped into three categories: elimination, separation, and crosswalk coordination with bus stops (Jarice D. Rodriguez-Seda, 2008). The elimination of conflicts between pedestrians and vehicles is achieved by (1) separation of pedestrians and motorists with iron barriers along Hongqi road on central-line, which helps to channel pedestrians to crosswalks, overpass and discourage jaywalking. (2) Providing overpass for pedestrian crossings between two campuses.

The best practice is to install push button actuated pedestrian lights at west gate and east gate crosswalks and signalized crosswalk provides significantly lower pedestrian crash rates compared with before unsignalized crosswalk. Figure 4 shows the before photograph (a) and after photograph (b) of the studied crosswalks.

(a) unsignalized

(a)closed gate due to risk

(a) without barrier

(b) push button signal

(b)guide pedestrian to overpass

(b)metal fence along road

Figure 4. Illustration of studied spot photograph before and after

Crosswalk locations need to be coordinated with bus stops to guide pedestrians toward the crosswalk (C.McAndrews, 2008; Jarice D. Rodriguez-Seda, 2008). Such as a limited-access transit stop that is integrated with overpass for student riders who cross the street at south gate and we also adjusted bus stops at other gates of campus.

5.2 Supply management

The supply management strategies implemented around campuses consisted of the following: right of way markings and treatments; signages to guide pedestrians to crosswalks; using of speed-calming markings and contrasting marking color and texture. The supply management makes drivers more aware of the presence of crosswalk and slow vehicle speed. (Huang, H.F, 2000; Jarice D. Rodriguez-Seda, 2008; Karkee G.J, 2006) Furthermore, an appropriate coordination between pedestrian crossing locations and campus entrances would guide pedestrians to crosswalks and would prevent putting them at a place that does not have a crosswalk.

5.3 Education and enforcement

At first, we ignored students' traffic safety education at the beginning of traffic through on Hongqi and Qingnian road, which caused some pedestrians' accidents, so we take some traffic safety education strategies. We use freshman week to promote traffic safety during new employee orientation sessions (as presented by Jarice D. Rodriguez-Seda, 2008), such as visiting the traffic environment around campus , distributing pedestrian traffic safety brochures and providing freshman traffic safety class. We also established a safety student union to carry some programs focusing on improving traffic awareness. Furthermore, the student union concentrates efforts at the beginning of each semester to discourage jaywalking by writing "name-banner". Law enforcement measures are needed to complement education and all universities crosswalks should reinforce jaywalking enforcement on a regular basis and provide supervise devices to increase speed limit compliance and reduce red-signal violation rate at crosswalk.

6. CONCLUSIONS AND RECOMMENDATION

This paper summarizes some of strategies and measures to improve pedestrian safety at crosswalks around campus. The purpose of the paper is to provide examples of the techniques being implemented around Ludong university campuses that could be used by other campuses in China. As the conclusion, the strategies are grouped into demand management, supply management, education and enforcement. According to the results, there are some specific recommendations about crosswalk around campus: (1) Providing the convenient, comfortable pedestrian bridges and underpass around university, most importantly the co-location of pedestrian overpass and bus stops may improve its usage; (2) installing pedestrian push-button signal, (3) installing supervise devices to discourage the violation of traffic law, (4) providing traffic violation calming facilities, and (5) carrying out a freshman education campaign to promote traffic safety.

This paper presents some of strategies implemented around Ludong Universities, but road situation of each campus is different; it is recommended to seek techniques that are proven to work in a similar setting.

ACKNOWLEDGEMENTS

The authors wish to acknowledge the financial support to this research by the planning of traffic management system of Yantai project (grant number 2008L283).

REFERENCES

McAndrews C., E. Deakin, A. Celis.(2008). "Strategies for Improving Pedestrian Safety: Cases from Jalisco and Michoacán, México." TRB 87th Annual Meeting CD-ROM, 2-15.

Huang, H.F. and Cynecki, M.J.(2000). "Effects of Traffic Calming Measures on Pedestrian and Motorist Behavior." In Transportation Research Record, No. 1705, TRB, National Research Council, 26-31.

Jarice D. Rodriguez-Seda, Rahim F. Benekohal, Rita Morocoima-Black. (2008). "Pedestrian, Bicycle and Vehicle Traffic Conflict Management in Big TEN University

campuses." TRB 87th Annual Meeting CD-ROM, 2-11.

SHI Jiangang, CHEN Yanyan, REN Futian and RONG Jian.(2007). "Research on pedestrian behaviors and traffic characteristics at unsignalized midblock crosswalk:a case study in Beijing."TRB 86th Annual Meeting CD-ROM,2-14.

XI Jianfeng, LI Jiang, WANG Zhaofei, TAN Shan.(2006). "Study on pedestrian characteristics and crossing facilities in crosswalks around campus." Proceedings of the 6th International Conference of Transportation Professionals 2006, Dalian, China, 687-693.

Enhancing Airport Security and Place Marketing with Spider Web Networking

Li-Yen Hsu

Department of Aviation Management, China Institute of Technology, Taiwan, 312;
T/Fax: (886) 3-5717426; email: liyenhsu@cc.chit.edu.tw

ABSTRACT

To strengthen airport wireless services and security, optimal-degree spider-web networks are prototyped in both cellular communication and supervisory control and data acquisition (SCADA) networks. This paper provides details about a study of network information transmission to establish dual surveillance and mutually-independent-hamiltonian-path (MIHP) performance to benefit coping with detection-unavailability, radio interference, and multipath effects. Using sequential order, integrative connectivity, and reliability, SCADA networks can also improve maintenance, environmental control, and service-oriented images because the networks allow real-time parallel sensing, systematic fault-tolerance, and integrative management in area perspectives. Such configurations can offer integrated response capabilities even if the SCADA networks of two paths are destroyed.

INTRODUCTION

The examination of casino surveillance systems, where more than eight cameras may be required to monitor a game table, helps us to recognize that the line-of-sight environment can be dynamic, and unexpected faults can exist. However, the traditional approach to traffic surveillance employs the use of only one or two cameras that are installed in the middle of a section of road; such an approach cannot provide left- or right-side views of vehicles in the left- or right-hand traffic system. Thus, accidents may happen because the sightline is unavailable (Hsu, 2008a, b).

Contemporary terrorists' activities often relate to airports and may happen at any time, from any position, and even concurrently. For the landside of airports, monitored vehicles can be hidden by other vehicles. For the airside, landing/departing planes also can be involved in accidents related to failures of communication or surveillance, which can be improved by supporting a parallel mechanism. Such

mechanisms already exist in airsides, for example, the cooperative unit of two practical fault-tolerant radars or radar with multiple affiliated sensors (e.g., the advanced airport-surface-detection-equipment radar, ASDE-X) is applied to counter issues like blind spots, false images, or repair requirements. However, airports' network performance can be further improved.

For invisible applications such as radio frequency identification (RFID), dual surveillance can help counter material interference (information transmission covered by materials like metal or water) using a method similar to that used to counter sightline unavailability, and it can help deal with frequency interference or multipath effects by analyzing acquired data related to different positions and time sequence using mutually independent hamiltonian paths (see MIHP in next section). Analogically, the cooperative function of parallel surveillance is similar to that of the cooperation between the two eyes or two ears of a human being that compare images derived from (slightly) different positions or times. Moreover, a series of such dual-surveillance could be located along the path at blind-spot concerned positions to get parallel and thorough recordings as the diagnostic tool. Such parallelism is recommended in a critical/dynamic environment. Specifically, it is placed along the path, probable at exterior or interior positions, which can be integrated as an area-based resilient supervisory control and data acquisition (SCADA) network system (Hsu, 2008b). In addition, cellular communications, global positioning systems (GPS), and geographic information systems (GIS) can be integrated naturally to further strengthen responding capability.

A mathematical, optimal-degree, dual-surveillance-based spider-web network prototype, SW(m,n) (see next section) is proposed for airports and their neighboring areas for both wireless/heterogeneous SCADA networks on paths (Figure 1(a)) and interference-free oriented cellular communication (Figure 1(b)) (Hsu, 2008a, b). For both the airside and the landside, such a SCADA network that has fault tolerance and an order (properties of 1-edge hamiltonian and 1p-hamiltonian, see next section) for promoting maintenance efficiency/effectiveness is addressed. Such networks can be adapted to accommodate surveillance modes such as surveillance of both forward and backward directions and for accommodating the SCADA operation when one lane of a path is under maintenance. Moreover, such networks are scalable; i.e., they have the flexibility to extend a path or survey area to meet future requirements.

MATHEMATICAL PRELIMINARIES

Communication networks are usually illustrated by graphs in which nodes represent processors and edges represent links between processors. Let G=(V,E) be a

graph if V is a finite set and E is a subset of {(a,b) |(a,b) is an unordered pair of V}. A path is delimited by $(x_0,x_1,x_2,\ldots x_{n-1})$. A path is called a hamiltonian path if its nodes are distinct and span V. A cycle is a path of at least three nodes such that the first node is the same as the last node. A cycle is called hamiltonian cycle or hamiltonian if its nodes are distinct except for the first node and the last node, and if they span V. A bipartite graph G = (V,E) is a graph such that $V=A\cup B$ and E is a subset of {(a,b)| $a\in A$ and $b\in B$}; if G-F remains hamiltonian for any F={a,b} with $a\in A$ and $b\in B$, then G is 1_p-hamiltonian. A graph G is 1-edge hamiltonian if G-e is hamiltonian for any $e\in E$; moreover, if there is a hamiltonian path between any pair of nodes {c,d} with $c\in A$ and $d\in B$, then the bipartite graph G is hamiltonian laceable.

The spider web network, SW(m,n), is the graph with the node set {(i,j)| $0\leq i<m$, $0\leq j<n$}, where m and n are positive integers with m, n being even, such that (i,j) and (k,l) are adjacent if they satisfy one of the following conditions: (1) i=k and $j=l\pm1$; (2) j=l and k=i+1(**mod** m) if i+j is odd or j=n-1; (3) j=l, k=i-1(**mod** m) if i+j is even or j=0. The configuration of SW(m,n) is shown in Figure 1. SW(m,n) is proved 1-edge hamiltonian if $n\geq4$; 1_p-hamiltonian if $n\geq4$ (Hsu & Kao, 2007; Kao & Hsu, 2005a). Thus, the fault-tolerance engaged in is systematically based. Moreover, SW(m,n) are hamiltonian laceable if $n\geq4$ (Kao & Hsu, 2005b), see Figure 1(a).

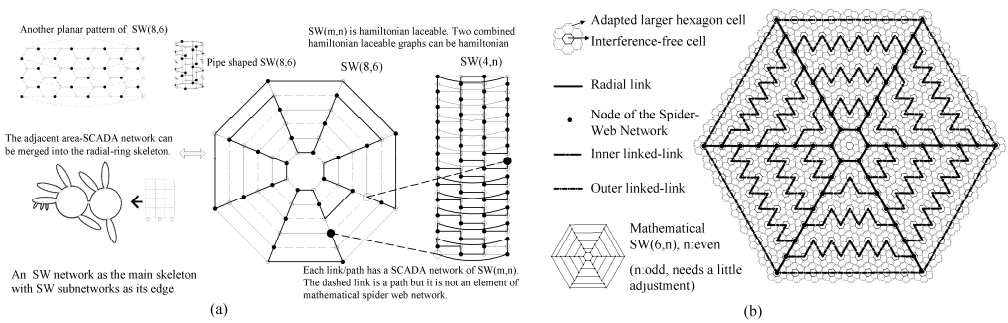

Figure 1. Spider-web network applications. (a). area based SCADA networks, (b). interference-free oriented cellular communication networks – SW(6,n).

The number of links connecting a node is called the degree; a network regularly having smaller degree is generally economical (Stojmenovic, 1997). Two hamiltonian paths, $P_1=(u_1, u_2,\ldots,u_{n(G)})$ and $P_2=(v_1,v_2,\ldots,v_{n(G)})$ of G from u to v, are independent if $u=u_1=v_1$, $v=u_{n(G)}= v_{n(G)}$, and $u_i\neq v_i$ for every $1<i<n(G)$. A set of hamiltonian paths, $\{P_1,P_2,\ldots,P_k\}$, of G from u to v, are mutually independent if any two distinct paths in the set are independent from u to v (Teng et al., 2006). Researches discovered that SW(m,n) has the performance of MIHP between any pair of bipartite nodes, and such a performance can be extended from SW(4,n), $n\geq4$; two pairs of MIHPs have been studied for SW(6,n) (Figures 2, 3) (Hsu, 2008a, b). There

are three horizontal extensive shapes (Figures 3(a)). Similar attributes can often be found between the cases with corresponding MIHP performance (Figure 3(b)).

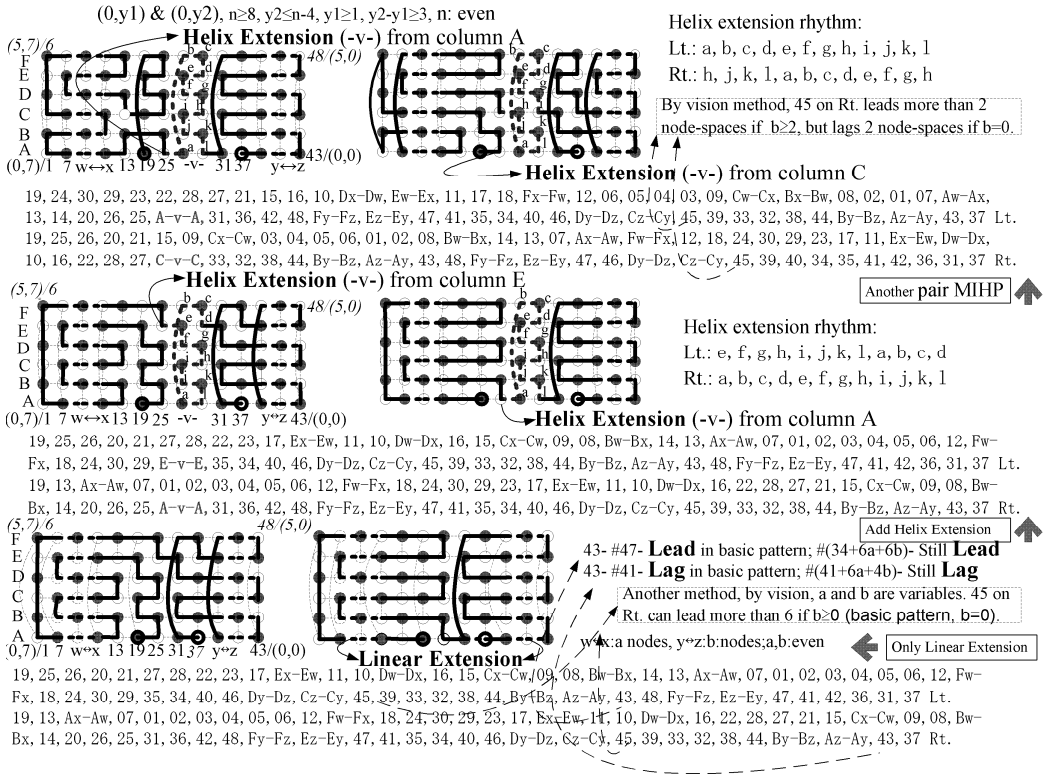

Figure 2. Concept diagram for proving dual-pair MIHP in SW(6,n).

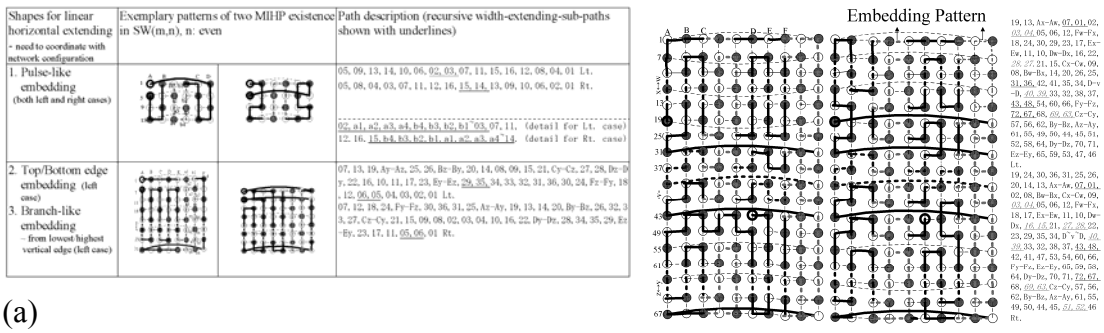

(a)

(b)

Figure 3. Horizontal extensive MIHP in SW(m,n). (a). three basic horizontal extensive shapes and their examples, (b). a typical MIHP pattern in SW(m,n).

SIGNIFICANCE

Reliable parallelism supports network performance. False detections may happen for many reasons such as multipath effects, node or link (transmission) faults, and a combination of the two. After configuring adaptable dual-surveillance as a basic detection-availability platform, systematic fault-tolerance, connectivity, and management efficiency enhances detection-availability. Furthermore, a diagnostic

performance MIHP can be established to analyze time-series related adversary conditions using independent, alternative, time-series recordings for data mining or diagnosing problems. This is similar to physicians employing independent alternatives and time-series records to diagnose a disease. In addition, the MIHP parallelism can offer inherent dynamic authorization/authentication during routine operations when alternative sequences offer corresponding meanings (Hsu, 2008a).

Benefit both passenger and freight transportation. Mobile commerce (m-commerce) can be improved through the use of the proposed wireless communication networks with data integrity and reliability; moreover, aiding the disabled or the elderly can be improved (Hsu & Cho, 2006). The detection-availability for applying RFID, which has emerged especially in logistic processing, can be more assured. The execution of MIHP-related authentication/authorization can also be initiated via RFID, and active RFID can be better reauthorized to deal with privacy issues.

Resilient area-based management system. The hamiltonian laceability can help flexibly integrate individual SCADA networks along paths, including interior paths, to area-based SCADA networks. If such networks can be adapted to an inherent "spider-web" skeleton (Figure 4), then they can have the performance of spider-web; i.e., offering responding capabilities even after two paths of a SCADA network have been seriously compromised.

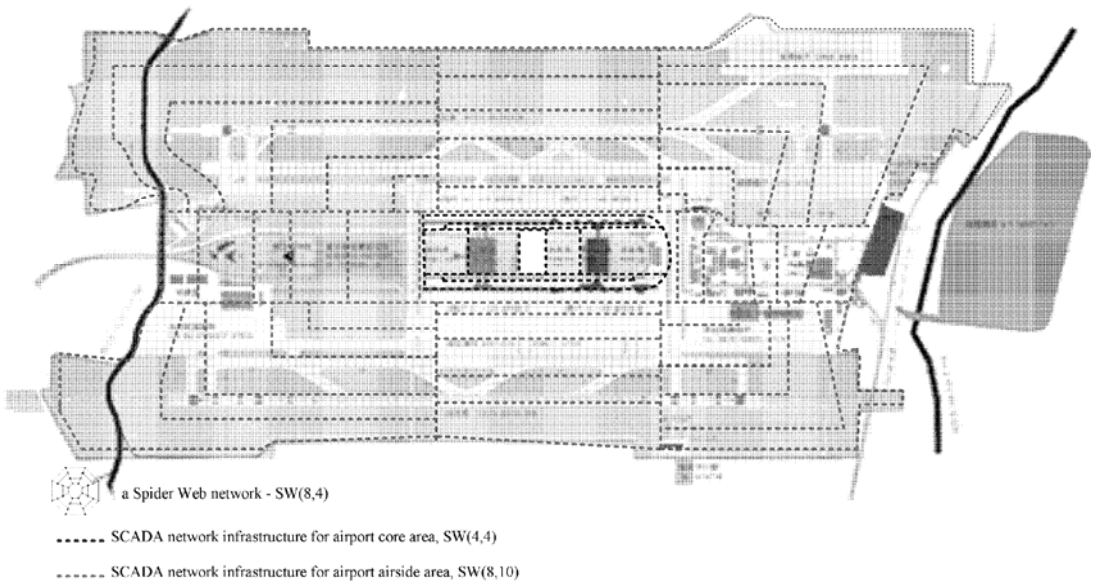

Figure 4. A SCADA network proposal for Taoyuan airport, Taiwan.

CONCLUSION

Communication is essential for airport. To improve airport services and security, network prototypes such as SW(m,n), which can provide detection availability, maintenance efficiency, and optimal degree, offer robustness and data integrity for both cellular communication and wireless/heterogeneous SCADA networks. Radial-ring spider-web configurations are prototyped for interference-free cellular telecommunication and are adaptively applied to develop area SCADA networks composed of dual-surveillance based subnetworks along paths with its advantages, including fault-tolerance, parallel processing, dynamic authentication/authorization, detection-availability, and/or countering the multipath effects of radio. Moreover, such configurations can offer integrated response capabilities even after the SCADA networks of two paths have been destroyed.

REFERENCES

Hsu, L.-Y. (2008a). "Developing critical/dynamical area security with dual-surveillance/radial-ring configured networks." *IEEE Conference on Technologies for Homeland Security*, Printing House, Boston, 240-245.

Hsu, L.-Y. (2008b). "Networking dual-surveillance/dual-pair-tele-paths for critical urban areas." *Journal of Southeast University - English Edition*, Southeast University, Nanjing, 114-119.

Hsu, L.-Y., & Cho, H.-J. (2006). "Developing generalized honeycomb torus networks for sustainable parking structures in the globalizing age." *Proceedings of Security and Management '06, CSREA,* Bogart, GA, 266-271.

Hsu, L.-Y., & Kao, S.-S. (2007). "Extending security/sustainability through pervasive spider web networks in urbanism." *Proceedings of Security and Management '07,* CSREA Press, Bogart, GA, 230-235.

Kao S.-S., & Hsu, L.-H. (2005a). "Spider web networks: A family of optimal, fault tolerant, hamiltonian bipartite graphs." *Comput. Math. Appl.,* 160(1), 269-282.

Kao, S.-S., and Hsu, L.-H. (2005b). "Hamiltonian laceability of spider web networks." *Chung Yuan Journal (Taiwan),* 33(1), 1-10.

Stojmenovic, I. (1997). "Honeycomb networks: Topological properties and communication algorithms." *IEEE Trans. Parallel Distrib. Syst.,* 8, 1036-1042.

Teng, Y.-H., Tan, J., Ho, T.-Y., and Hsu, L.-H. (2006) "On mutually independent hamiltonian paths." *Comput. Math. Appl.,* (19) 4, 345-350.

Dynamic Responses of a Magnetically Levitated Vehicle in a Crosswind

Jian-Jun Wu[1] and Xiao-Hong Shi[1]

Key Laboratory of Mechanics on Disaster and Environment in Western China (Lanzhou University), Ministry of Education, Lanzhou, Gansu 730000, China; PH (86) 931-8914240; FAX (86) 931-8912229; email: wujjun@lzu.edu.cn

ABSTRACT

The dynamic responses of a magnetically levitated vehicle (maglev) in a crosswind are studied because the action of the wind field is one of the main factors affecting the stability and safety of the maglev at high speeds. First, a model of the maglev system is established to represent four vehicle motions: heave, sway, pitch and roll. Then based on the steady and incompressible Navier-Stokes equation and $K-\varepsilon$ turbulent model, the aerodynamic characteristics of the maglev are numerically simulated by the finite element method to validate the model and algorithm suggested in this paper. Finally, numerical analyses are performed on the dynamic behavior of the vehicle in both steady and fluctuating crosswinds. It is shown that the stability of the maglev is greatly influenced by the wind velocity and its fluctuating component. Additionally, the variation of the maglev's dynamic response to wind velocity and its fluctuating component are described.

INTRODUCTION

The maglev is a new tool in high speed ground transportation. Due to its higher speed, lower friction, reduced noise, improved energy consumption and comfortable ride, the maglev system is becoming the focus of transportation worldwide (Cai et al., 1994; Zheng et al., 2000; Zhao et al., 2001; Wu et al., 2004). It is a nonlinear and multidimensional system, in which the dynamic stability of the vehicle at high speeds is highly sensitive to external disturbances. Therefore much attention has been directed to potential safety problems in recent years. Previous research focused only on the effects of guideway deformation and irregularity on the maglev, neglecting the influence of the wind field. In fact the wind field, especially the crosswind component, is one of the main factors affecting the stability and safety of the maglev. Thus it is necessary to study the aerodynamic characteristics and dynamic behavior of the maglev high speeds.

Cherchas (1979) suggested that the aerodynamic effects include longitudinal resistance and lateral force induced by crosswinds, which should be taken into consideration of the dynamic disturbances suffered by the maglev system. Garg and Barrows (1981) established a two-degree-of-freedom model of a maglev subjected to crosswind gusts in which vehicle motion was limited to sway and yaw. Their numerical simulations showed that aerodynamic drag and side tumbling moment

increased with vehicle speed. The aerodynamic drag, lift and pitching moment of a maglev subjected to longitudinal wind at different traveling speeds were numerically analyzed by Li et al. (2004) using the finite volume method. The influences of the suspension air gap on these aerodynamic forces were calculated, showing that suspension air gap had little effect on aerodynamic drag, but had much more significant effect on the lift force of the maglev.

Based on the above studies, a model of the maglev system is developed to represent four vehicle motions: heave, sway, pitch and roll. Then to validate the model and algorithm, the numerical simulations of the aerodynamic characteristics in a crosswind are compared with experimental results. Finally, the dynamic behavior of the vehicle in both steady and fluctuating crosswinds is discussed.

DYNAMIC MODEL OF A MAGLEV IN A CROSSWIND

Dynamic equations of the maglev system

As shown in Figure 1, the maglev system is composed of a car body and four maglev bogies. The maglev bogies are linked to the car body by vertical and transversal springs and dampers. Taking the car body's center of mass as the origin, a coordinate system is established with x, y, z axes as shown in Figure 1. The corresponding elastic coefficients and damping coefficients are denoted by k_z and c_z of the vertical springs, and k_y and c_y of the transversal springs, respectively. The car body and four maglev bogies all move with four degrees-of-freedom, which are denoted by z_c, y_c, ϕ_c and θ_c for the car body, and z_{bi}, y_{bi}, ϕ_{bi} and θ_{bi} for the i^{th} maglev bogie, where the subscript i is the index of the maglev bogie. The other notations of the maglev system in Figure 1 are listed in Table 1.

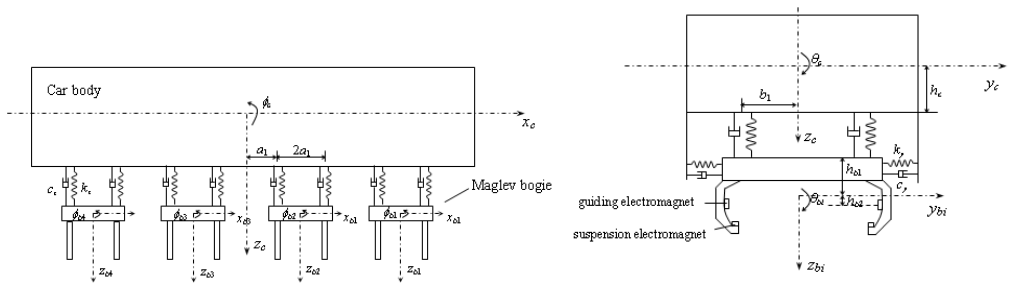

(a) Side view (b) Rear view

Figure 1. Schematic diagram of the maglev system.

Table 1. Notations of the maglev system.

Notation	Physical meaning	Value
m_c	Mass of car body (kg)	3.90×10^4
m_b	Mass of maglev bogie (kg)	6.60×10^2

Notation	Physical meaning	Value
I_{cy}	Car body's moment of inertia in pitch (kgm^2)	1.75×10^6
I_{cx}	Car body's moment of inertia in roll (kgm^2)	6.46×10^4
I_{by}	Maglev bogie's moment of inertia in pitch (kgm^2)	5.50×10^2
I_{bx}	Maglev bogie's moment of inertia in roll (kgm^2)	5.80×10^2
h_c	Distance between car body's center of mass and its bottom (m)	1.5
h_{b1}	Distance between maglev bogie's center of mass and its top (m)	0.4
h_{b2}	Longitudinal distance between maglev bogie's center of mass and that of guiding electromagnet (m)	0.1
a	Length of suspension electromagnet (m)	0.4
b	Width of suspension electromagnet (m)	0.1
c	Length of guiding electromagnet (m)	0.2
d	Width of guiding electromagnet (m)	0.05

The electromagnet and reaction plate of the guideway comprise a closed magnetic circuit through a control system. The electromagnetic force F is given by

$$F = \frac{\mu_0 N^2 A}{4}\left(\frac{i_0 + i}{\delta_0 + \delta}\right)^2 \tag{1}$$

in which i_0 is the current related to the control goal δ_0, i is the bias of the control current, δ_0 is the control goal of the air gap, and δ is the bias of the suspension air gap to δ_0. μ_0, A and N are respectively magnetic permeability in vacuum, pole area of the electromagnet, and number of turns in the coil.

In the maglev system, the controlling law of the guide control system is the same as that of the suspension control system, which is given by

$$i_z = G_{1z}\delta_z + G_{2z}\dot{\delta}_z, \quad i_y = G_{1y}\delta_y + G_{2y}\dot{\delta}_y \tag{2}$$

where G_{1z} and G_{2z} are displacement and velocity feedback control gains of the suspension electromagnet, and G_{1y} and G_{2y} are displacement and velocity feedback control gains of the guiding electromagnet.

According to Newton's second law and angular momentum theorem, the following dynamic equations describing the maglev system's four-degree-of-freedom motion are obtained:

Heave: $$m_c\ddot{z}_c + \sum_{i=1}^{4}\sum_{j=1}^{2}\sum_{k=1}^{2} F_{2z}(i,j,k) + F_L = 0 \tag{3}$$

Sway: $$m_c\ddot{y}_c + \sum_{i=1}^{4}\sum_{j=1}^{2}\sum_{k=1}^{2} F_{2y}(i,j,k) - F_D = 0 \tag{4}$$

Pitch: $$I_{cy}\ddot{\phi}_c - \sum_{i=1}^{4}\sum_{j=1}^{2}\sum_{k=1}^{2} L(i,j)F_{2z}(i,j,k) = 0 \quad (5)$$

Roll: $$I_{cx}\ddot{\theta}_c + b_1\sum_{i=1}^{4}\sum_{j=1}^{2}(F_{2z}(i,j,2) - F_{2z}(i,j,1)) - h_c\sum_{i=1}^{4}\sum_{j=1}^{2}\sum_{k=1}^{2} F_{2y}(i,j,k) - M_m = 0 \quad (6)$$

Here F_L, F_D and M_m represent the lift force, the side force and the rolling moment, respectively, of the car body subjected to a wind field. $F_{2z}(i, j, k)$ and $F_{2y}(i, j, k)$ represent vertical and horizontal components of the second suspension force, respectively, in which i is the index of the maglev bogie, numbered 1 through 4 from right to left. j =1(2) represents the front (back) end of the maglev bogie, and k =1(2) represents the left (right) side of the maglev bogie. They are respectively given by

$$\begin{aligned} F_{2z}(i,j,k) = k_z[z_c - L(i,j)\phi_c + Ls(j)\phi_{bi} + (-1)^k(b_1\theta_c - b_1\theta_{bi})] \\ + c_z[\dot{z}_c - L(i,j)\dot{\phi}_c + Ls(j)\dot{\phi}_{bi} + (-1)^k(b_1\dot{\theta}_c - b_1\dot{\theta}_{bi})] \end{aligned}$$

$$F_{2y}(i,j,k) = k_y(z_c - z_{bi} - h_c\theta_c - h_{b1}\theta_{bi}) + c_y(\dot{z}_c - \dot{z}_{bi} - h_c\dot{\theta}_c - h_{b1}\dot{\theta}_{bi})$$

Additionally, $Ls(k)$=(13-4i-2j) a_1 represents the force arm of the j^{th} second suspension force of the i^{th} maglev bogie on the car body's pitch. For i =(1, 2, 3, 4) and j =(1, 2), $Ls(k)=(-1)^{k+1}a_1$.

For the bogie, dynamic equations can be written as follows:

Heave: $$m_b\ddot{z}_b(i) - \sum_{j=1}^{2}\sum_{k=1}^{2} F_{2z}(i,j,k) + \sum_{j=1}^{2}\sum_{k=1}^{2} F_{1z_add}(i,j,k) = 0 \quad (7)$$

Sway: $$m_b\ddot{y}_b(i) - \sum_{j=1}^{2}\sum_{k=1}^{2} F_{2y}(i,j,k) + \sum_{j=1}^{2}[F_{1y}(i,j,2) - F_{1y}(i,j,1)] = 0 \quad (8)$$

Pitch: $$I_{by}\ddot{\phi}_b(i) + Ls(k)\sum_{j=1}^{2}\sum_{k=1}^{2} F_{2z}(i,j,k) - Ls(k)\sum_{j=1}^{2}\sum_{k=1}^{2} F_{1z_add}(i,j,k) = 0 \quad (9)$$

Roll: $$I_{bx}\ddot{\theta}_b(i) + b_1\sum_{j=1}^{2}[F_{2z}(i,j,2) - F_{2z}(i,j,1)] + b_1\sum_{j=1}^{2}[F_{1z_add}(i,j,2) - F_{1z_add}(i,j,1)] = 0 \quad (10)$$

Here $F_{1z_add}(i, j, k)$ represents the change of electromagnetic force in heave, expressed by

$$F_{1z_add}(i,j,k) = \frac{\mu_0 N^2}{4}a(b - |\delta_y(i,j,k)|)\left(\frac{I_{0z} + i_z(i,j,k)}{\delta_0 + \delta_z(i,j,k)}\right)^2 - \frac{\mu_0 N^2}{4}ab\left(\frac{I_{0z}}{\delta_0}\right)^2$$

in which $\delta_z(i,j,k) = z_{bi} - Ls(k)\phi_{bi} + (-1)^k b_2\theta_{bi}$, $i_z(i,j,k) = G_{1z}\delta_z(i,j,k) + G_{2z}\dot{\delta}_z(i,j,k)$.

$F_{1y}(i, j, k)$ represents the change of electromagnetic force in sway, expressed by

$$F_{1y}(i,j,k) = \frac{\mu_0 N^2}{4}c(d - |\delta_z(i,j,k)|)\left(\frac{I_{0y} + (-1)^k i_y(i,j)}{\delta_0 + (-1)^k \delta_y(i,j)}\right)^2$$

in which $\delta_y(i,j) = y_{bi} - h_{b2}\theta_{bi}$, $i_y(i,j) = G_{1y}\delta_y(i,j) + G_{2y}\dot{\delta}_y(i,j)$.

Equations (3)-(10) above constitute the dynamic equations of the maglev system.

Wind field equation

The wind field is described by the following equations of turbulent kinetic energy k, turbulent kinetic energy dissipation rate ε, wind speed u and relative pressure p.

Continuity:
$$\frac{\partial u_i}{\partial x_i} = 0 \tag{11}$$

Momentum:
$$\frac{\partial}{\partial x_i}\left(u_i u_j\right) = -\frac{1}{\rho}\frac{\partial p}{\partial x_i} + \left(\mu + \mu_t\right)\frac{\partial^2 u_i}{\partial x_j \partial x_j} \tag{12}$$

Turbulent kinetic energy:
$$\rho u_j \frac{\partial k}{\partial x_j} = \frac{\partial}{\partial x_j}\left[\left(\mu + \frac{\mu_t}{\sigma_k}\right)\frac{\partial k}{\partial x_j}\right] + \mu_t \frac{\partial u_i}{\partial x_j}\left(\frac{\partial u_i}{\partial x_j} + \frac{\partial u_j}{\partial x_i}\right) - \rho\varepsilon \tag{13}$$

Turbulent kinetic energy dissipation rate:
$$\rho u_j \frac{\partial \varepsilon}{\partial x_j} = \frac{\partial}{\partial x_j}\left[\left(\mu + \frac{\mu_t}{\sigma_\varepsilon}\right)\frac{\partial \varepsilon}{\partial x_j}\right] + C_1 \frac{\varepsilon}{k}\mu_t \frac{\partial u_i}{\partial x_j}\left(\frac{\partial u_i}{\partial x_j} + \frac{\partial u_j}{\partial x_i}\right) - C_2 \frac{\rho\varepsilon^2}{k} \tag{14}$$

where u_i (i=1, 2, 3) is the speed component, μ_t is the turbulent viscosity coefficient given by $\mu_t = \rho C_\mu k^2/\varepsilon$, C_μ is an empirical constant, and σ_k and σ_ε are Prandtl numbers corresponding to turbulent kinetic energy and the turbulent kinetic energy dissipation rate. C_1 and C_2 are empirical constants, ρ =1.225 kg/m^3 is fluid density, and μ =1.7894$\times 10^{-5}$ N/m^{2}s is kinetic viscosity. Launder and Spalding (1974) suggested that C_μ=0.09, σ_k=1.0, σ_ε=1.3, C_1=1.44, and C_2=1.92.

Boundary conditions

The maglev car body is subjected to a steady wind field, which is assumed to be a large volume with length, width and height, respectively, taken as 130, 100 and 50 times the width of the car. The modeled wind field dimensions and position of the vehicle within are displayed in Figure 2. Taking the car body's center of mass as the origin, the coordinate system shown in Figure 2 is established, in which the x axis is parallel to the wind, the y axis is vertical, and the z axis is parallel to the length of the car body. Length, width and height of the car are a_c, b_c and h_c; average wind velocity is U; vehicle velocity is V; and p is relative pressure.

Boundary conditions of the modeled wind field volume are given by

$$\begin{cases} x = -30b_c : u_x = U, u_y = u_z = 0 \\ x = 100b_c : p = 0 \end{cases} \qquad \begin{cases} y = -\left(h_c/2 + r\right): \quad u_x = u_y = u_z = 0 \\ y = 50b_c - \left(h_c/2 + r\right): u_x = u_y = u_z = 0 \end{cases}$$

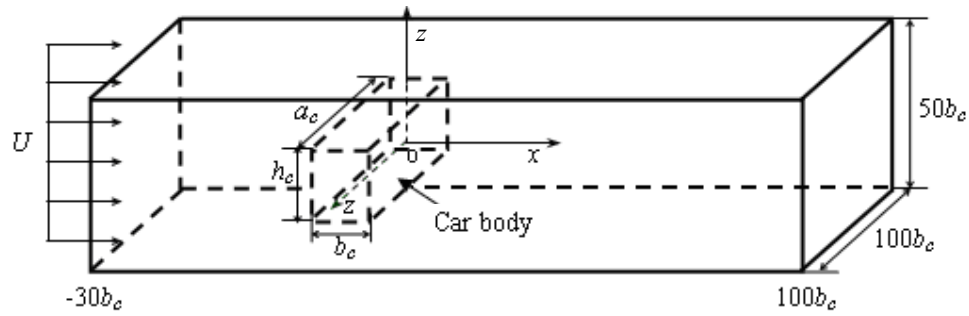

Figure 2. Modeled wind field dimensions and maglev position within.

Boundary conditions of the surface of the maglev are given by

$$\begin{aligned} &-b_c/2 \le x \le b_c/2,\ y = -h_c/2; \quad -b_c/2 \le x \le b_c/2,\ y = h_c/2; \\ &x = -b_c/2,\ -h_c/2 \le y \le h_c/2; \quad x = b_c/2,\ -h_c/2 \le y \le h_c/2: \end{aligned} \quad u_x = u_y = 0,\ u_z = V$$

Based on the above fundamental wind field equations combined with the boundary conditions, the side force, lift force and side overturning moment are obtained by the finite element method.

To verify the effectiveness of the wind field algorithm, vehicle parameters taken from Li (2003) are used to simulate the side force F_D of the vehicle in a crosswind by the finite element method. Then the coefficient of side force C_D is obtained from F_D through the following equation:

$$C_D = \frac{F_D}{(1/2)\rho_a a_c h_c U^2} \tag{15}$$

where ρ_a is air density. The results calculated from Equation (15) are listed in Table 2 with the experimental results given by Li (2003), in which the volume of the car body is 2.1m×0.472m×0.353m.

Table 2. Comparison of the coefficients of side force.

Wind velocity	10 m/s	20 m/s	30 m/s
Experimental results given by Li (2003)	0.45	0.42	0.38
Numerical results in this paper	0.42	0.38	0.36

It can be seen that the numerical results in this paper coincide with the experimental results given by Li (2003) very well, further justifying the method of modeling the wind field suggested by this paper.

Description of fluctuating wind

The fluctuating wind is simplified into White noise, described by

$$U(t) = \sum_{k=1}^{N(T)} Y_k \delta(t - \tau_k) \tag{16}$$

where Y_k are independent random numbers with uniform distribution. $N(T)$ is a random

Poisson distribution with uniform increments of λ_0.

NUMERICAL SIMULATION AND RESULTS DISCUSSION

The side force, lift force and side overturning moment of the maglev are calculated in varying crosswind speeds by the model and algorithm given in the last section. Then the dynamic behavior of the maglev in the crosswind is analyzed by the Runge-Kutta-Merson method.

Dynamic response of the maglev in a steady crosswind

With constant control gains, that is G_{1z}=1.42×10^3, G_{2z}=1.0, G_{1y}=1.0×10^3, and G_{2y}=14.2, the vehicle moving at 50m/s is subjected to steady crosswind speeds of 0m/s, 10m/s, 15m/s and 20m/s. The dynamic response of the maglev is shown in Figure 3.

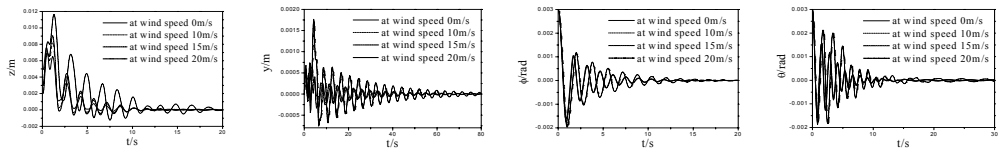

(a) heave (b) sway (c) pitch (d) roll

Figure 3. Maglev dynamic response in a steady crosswind of varying speeds.

It can be seen that the amplitude of all motions increases with increasing wind velocity. In other words, the stability of vehicle becomes worse, and the time needed to regain stability becomes longer. When wind velocity is less than 15m/s, the influence of the crosswind on every motion of the vehicle is relatively small, which can be neglected. When wind velocity reaches 20m/s, the influence of the crosswind on every motion of the vehicle is greater, requiring specific attention in practical engineering.

Dynamic response of the maglev in a fluctuating crosswind

When the vehicle moving at 50m/s is subjected to a steady and/or fluctuating crosswind of 15m/s, the dynamic responses of the maglev are as shown in Figure 4. It is shown that the influence of a fluctuating crosswind on heave, pitch and roll motion is quite feeble. However, the dynamic response in sway motion of a maglev subjected to a fluctuating crosswind is more pronounced than that of a vehicle subjected to a steady crosswind. Therefore, the influence of a fluctuating crosswind field on the maglev's dynamic stability is relatively significant for sway motion.

When the vehicle moving at 50m/s is subjected to a fluctuating crosswind with speeds of 10m/s, 15m/s or 20m/s, the dynamic response of the maglev is as shown in Figure 5. At windspeeds below 20m/s, it is obvious that the influence of a fluctuating crosswind on every motion of the maglev is quite feeble, which can be ignored. However, when the speed of the fluctuating crosswind reaches 20m/s, the

influence on dynamic stability is relatively significant for all four motions.

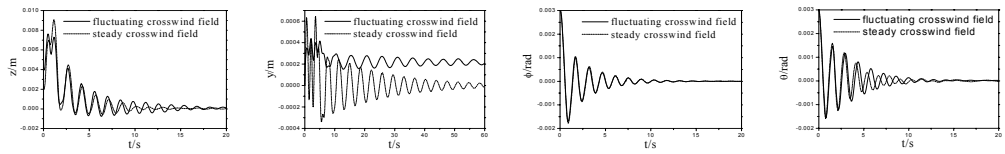

(a) heave (b) sway (c) pitch (d) roll

Figure 4. Comparison of maglev dynamic response to a steady and/or fluctuating crosswinds of 15m/s.

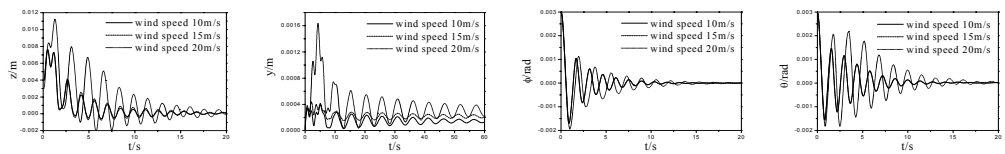

(a) heave (b) sway (c) pitch (d) roll

Figure 5. Comparison of maglev dynamic response to a fluctuating crosswind of varying speeds.

CONCLUSIONS

Based on a four-degree-of freedom model of a maglev system subjected to a crosswind of varying speeds with and without a fluctuating component, numerical analyses are conducted on the vehicle's dynamic response to understand the dynamic stability of a high-speed maglev. The main results are as follows:

(1) For a vehicle traveling at constant speed, the influence of a steady crosswind on all four vehicle motions is quite small when the wind speed is less than 15m/s. This is also true for the influence of a fluctuating crosswind. However, when the speed of a fluctuating crosswind reaches 20m/s, the influence of the crosswind on the dynamic stability of each vehicle motion is relatively significant.

(2) The influence of a fluctuating crosswind on maglev dynamic stability is significantly stronger than that of a steady crosswind.

(3) Whether the maglev is subjected to a steady crosswind or fluctuating crosswind, the sway component of motion will exhibit the most influence by the crosswind action.

ACKNOWLEDGEMENTS

The authors would like to express their sincere appreciation to the funding from the Program for New Century Excellent Talents in University (NCET-04-0979).

REFERENCES

Cai, Y., Chen, S. S., Rote, D. M., Coffey, H. T. (1994). "Vehicle/guideway interaction for high speed vehicles on a flexible guideway." *Journal of Sound and Vibration*, 175(5), 625-646.

Cherchas, D. B. (1979). "A dynamic simulation for a high speed magnetically levitated guided ground vehicle." J*ournal of Dynamic System, Measurement, and Control, Transaction of the ASME*, 101, 223-229.

Garg, D. P., and Barrows, T. M. (1981). "Modeling and dynamic response of maglev vehicle subjected to crosswind gusts." *Journal of Dynamic System, Measurement, and Control, Transaction of the ASME*, 103, 251-258.

Launder, B. E., and Spalding, D. B. (1974). "The Numerical Computation of Turbulent Flows." *Computer Methods in Applied Mechanics and Engineering*, 3, 269-289.

Li, R. X., Liu, Y. Q., Zhai, W. M. (2004). "Numerical analysis of aerodynamic force in longitudinal and vertical direction for high-speed maglev train." *Journal of the China Railway Society*, 25(1), 8-12 (in Chinese).

Li, Y. L. (2003). *Nonlinear Three-dimensional Coupling Vibration of Wind-Vehicle-Bridge System*, Southwest Jiaotong University, Chengdu.

Wu, F. Y., Gao L., Wei Q. C. (2004). "Dynamic effect of structural characteristics of elevated guideway on maglev system." *Engineering Mechanics*, 21(4), 144-149 (in Chinese).

Zhao, C. F., Zhai, W. M., Cai C. B. (2001). "Maglev vehicle/elevated-beam guide-way vertical coupling dynamics." *Journal of the China Railway Society*, 23(5), 27-33 (in Chinese).

Zheng, X. J., Wu, J. J., Zhou, Y. H. (2000). "Numerical analyses on dynamic control of five-degree-of-freedom maglev vehicle moving on flexible guideways." *Journal of Sound and Vibration*, 235 (1), 43-61.

Research on the Design of Inner Horizontal Surface of the Airport

SUN Rui-shan[1], ZHANG Li-xin[2] and ZHAO Hong-yuan[3]

[1]Research Institution of civil Aviation Safety, Civil Aviation University of China, Tianjin, china, 300300; PH (86) 022-24092593; FAX (86) 022-24957940; E-mail: sunrsh@hotmail.com

[2]Research Institution of civil Aviation Safety, Civil Aviation University of China, Tianjin, china, 300300; PH (86) 022-24094112; FAX (86) 022-24957940; E-mail: elen840803@yahoo.com.cn

[3]Department of Airport, Civil Aviation Administration of China, Beijing, china, 100710; PH (86) 010- 64092804; FAX (86) 010- 64019967; E-mail: hy_zhao@caac.gov.cn

ABSTRACT

The inner horizontal surface is mainly used to protect the space for a visual circling approach. The radius and height of the inner horizontal surface is described in The Convention on International Civil Aviation Annex 14-Aerodromes and Airport Services Manual Part 6: Control of Obstacles. However, they could not guarantee the space specified by another criterion, Procedures for air Navigation Services: Aircraft Operations. Vol. II, Construction of Visual and Instrument Flight Procedures (ICAO Doc. 8168-OPS/611). Urban construction was also restricted. This paper focuses on this problem and a method is given to consummate the obstacle limitation requirements of the airport.

1 Introduction

The obstacle limitation surfaces of the airport are vital to the limitation of obstacles around the airport and aircraft safety while taking off, climbing, approaching and landing so that aircraft can carry out their flight procedures. The requirements for obstacle limitation surfaces are based on the purpose of the runway, such as take-off or landing, and types of approach. But for all kinds of the runways, inner horizontal surface, conical surface, approach surface and transition surfaces shall be established. The inner horizontal surface is mainly used to protect the space for visual circling approaches(GAO Jin-hua,2000).

The notice about airport clearance protection issued by General Administration of Civil Aviation of China in 1995 had definitely pointed out that any units or individuals who construct building or facilities in the airport clearance region must be approved by the airport authorities, and then report to the departments of local urban construction planning for approval(CAAC,1995). Due to the influences from flight procedure design, aircraft performance, meteorological conditions and navigation equipment, in practice, the limitation of the obstacle height should be consulted by the airport authorities and navigational fairs management department. It needs to be further studied how to design the obstacle limitation surfaces to comply with the airport obstacle limitation criterion and maximally satisfy the needs of construction around the airport while not affecting the flight procedures. According to

the calculation of visual circling radius and obstacle clearance height (OCH), the paper makes an analysis and research on the inner horizontal surface design.

2 Standards related to airport inner horizontal surface design

There are many references involved in the airport clearance. The main bases in the design of the inner horizontal surface are International Civil Aviation Annex 14-Aerodromes (Annex 14) and Procedures for air Navigation Services: Aircraft Operations. Vol. II, Construction of Visual and Instrument Flight Procedures (ICAO Doc. 8168-OPS/611). There is some illustration in Airport Services Manual Part 6: Control of Obstacles. In China, the design requirements for inner horizontal surface in Civil Airport Airfield Technical Standards (MH5001-2006) strictly observe the related norms of Annex 14. In other countries, the designs of inner horizontal surface are also based on Annex 14, and slightly modified according to the actual conditions. For instance, an inner horizontal surface radius divide in UK CAP168 was defers to the main runway and subsidiary runway and the pattern of the surface is circular or just like a racetrack lies on the length of the runway whether more than 1800m(CAA,2001).

2.1 The main parameters standards of inner horizontal surface

The main parameters in inner horizontal surface design are radius and height, which are precisely defined in Annex 14 and Airport Services Manual Part 6 (see Table 1)(ICAO,2004;ICAO,1983). The inner horizontal plane is about 45m higher than the established airport elevation. From the average elevation of the centers on the strip ends of the runway, two circular arcs centered at the middle points of the two ends of runway are obtained with given radii. Then an approximate ellipse is formed by the tangency of the two straight lines parallel to the midline of the runway and the two circular arcs. (see Figure 1). The inner horizontal surface also can be simplified as a single circular when it as being to protect airspace for visual circling prior to landing at shorter runway with a lower velocity. For multi-runway airports, the constructed method was the same (see Figure 2).

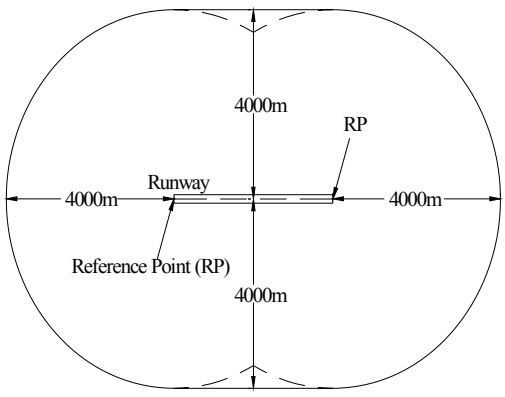

Figure 1. Inner horizontal for code number 4.

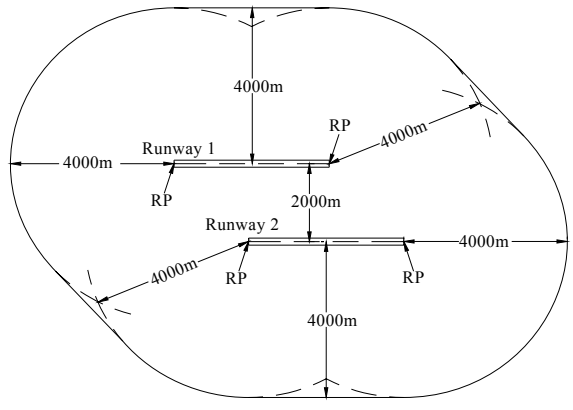

Figure 2. Composite inner horizontal for two parallel code number 4.

Table 1. Dimensions and slopes of inner horizontal surface.

Surface and dimension		Runway classification									
		Non-instrument				Non-precision approach			Precision approach category		
		Code number				Code number			I		II or III
									Code number		Code number
		1	2	3	4	1,2	3	4	1,2	3,4	3,4
Inner Horizontal	Height	45	45	45	45	45	45	45	45	45	45
	Radius	2000	2500	4000	4000	3500	4000	4000	3500	4000	4000

2.2 The visual circling area scope definition

The purpose of setting inner horizontal surface is to protect airspace for visual circling prior to landing. The visual circling area is the area in which obstacle clearance shall be considered for aircraft circling and the size varies with the category of the aircraft(ICAO,2006) To define the scope of the area, draw an arc from the centre of the threshold of each available runway with a radius $\overline{R}$ appropriate to the aircraft category, and then from the extremities of the adjacent arcs draw lines tangent to the arcs and connect the tangent lines at the last. For a multi-runway airport, the runways which are not available to Category E aircraft can be ignored if the calculation is about the area of Category E aircraft. The radius $\overline{R}$ can be calculated as follows:

$$\overline{R} = 2r + d$$

In this formula, r is the turning radius. The wind speed should be considered when calculated. d is the flying distance of aircraft in 10 second when there is no wind. OCH for visual circling area varies with the category of the aircraft either (see Table 2). The OCH is the sum of the altitude of the highest obstacle in the area and minimum obstacle clearance (MOC). Maximizing OCH for a visual circling approach, final approach and missed approach is the one for a visual circling approach.

Table 2. MOC and OCA/H for visual circling approach.

Aircraft category	A	B	C	D	E
Minimum obstacle Clearance (m)	90	90	120	120	150
Lower limit for OCH above aerodrome elevation (m)	120	150	180	210	240

3 Defects in airport inner horizontal surface design

According to Airport Planning and Environmental Protection (authors are QIAN Bing-hua and ZHANG Yu-fen), the initial design of the inner horizontal surface is based on the requirement identified by visual circling approach procedures. For instance, the inner horizontal surface for code number 4, whose radius is 4000m and height 45m, is to ensure that both sides of a light aircraft on the runway to fly over 150m high visual approach procedures and the MOC is 105m(QIAN Bing-hua,2000).

3.1 Research on the height of inner horizontal surface

Airport Planning and Environmental Protection does not illuminate the exact category of the light aircraft, in line with the OCH during final approach and missed approach, for Category A aircraft, the procedure needs MOC 90m when flying height is 120m, which means obstacles in this area are necessary to control the heights below 30m and the height of the inner horizontal should be designed as 30m. If there is an obstacle, whose altitude is between 30m and 45m, existing in this area the procedure of the visual circling approach will debug and the OCH is the sum of the obstacle height and the MOC 90m. Similarly, Category B, C, D and E aircraft can be calculated based on Table 2 and the conclusion is no influence to the procedure for Category B aircraft and higher when the height of the inner horizontal is 60m.

For the design of inner horizontal height there are some details worthy of our attention. The following case in an article in which the author engaged in related work shows the problem to a certain extent and the following brief analysis will be carried out.

The elevation at the threshold of runway 14 in Yichang Three Gorges Airport is 205m and runway 32 is 190m, height difference is 15m. In the inner horizontal surface near the transitional surface, two chimneys, whose heights are 249m, 44m higher than the elevation of runway 14, 59m over runway 32, penetrate through the inner horizontal seriously(SONG De-kuan,2000).

If the height of the inner horizontal surface is 60m, the problem in this case would not emerge, but because the obstacles are chimneys, the influence to the airport clearance is not only limited to the height, but also dust emission, which must be strictly controlled. There is an obvious problem in this case that the height difference of the runway 14/32 two thresholds is a little larger. According to the description in Civil Airport Airfield Technical Standards (MH5001-2006), the elevation of the inner horizontal shall be equal to the average elevation of the mid-point of the two thresholds(MH5001,2006). It is unreasonable using the average here because the evaluation can not identify the obstacle which penetrates through the inner horizontal surface established for runway 32 since its elevation is 240m in this case.

The calculation of the inner horizontal radius is not only impacted by the category of the aircraft, but also takes into account the elevation of the airport. For Category A aircraft, the required visual circling area is no more than a radius of

4000m except Tibet Qamdo Bangda Airport which elevation reaches to 4334m, and plain airports do not exceed 3000m. It is large enough to protect the light aircraft visual circling approaching with 4000m radius, but not for Category B aircraft and much heavier aircraft.

With regard to the calculation of the radius, the interpolation can be used to obtain the conversion factor k for the conversion of indicated airspeed (IAS) to true airspeed (TAS) based on airport elevation.

$$k = k_0 + \frac{(k_1 - k_0)}{500} \times (H - H_0)$$

In this formula, H is the airport elevation; assume a temperature of ISA+15°C and check the table to find out the value of k_0 and k_1 so as to get the value of k and calculate the TAS with the following formula. The calculation of the radius $\overline{R}$ refers the previous paper.

$$TAS = k \times IAS$$

Considering the calculation accuracy, this paper uses Excel to calculate the radii of visual circling area in Yichang Three Gorges Airport, Beijing Capital International Airport, Kunming Wujiaba Airport and Tibet Qamdo Bangda Airport. The computed result is shown in Figure 3. The calculation results reveal that plateau airports need much larger radii for protection than plain airports and the standards of radius without distinguishing by elevation become the potential hazard. Only for plain airports, such as Beijing Capital International Airport, the radius can not ensure the safety for aircraft flying frequently like B737 and A320 which are Category C.

	D	E	F	G	H	I	J	K	L	M
1		Aircraft category	Max speeds for visual circling (km/h)	IAS→TAS (km/h)	aerodrome elevation (m)	wind speed (km/h)	k	turn rate (° /s)	Radius(r) of turn (m)	**Radius for visual circling (m)**
2	Yichang Three Gorges Airport	A	185	191.68109	205	46	1.0361	3	1260.9373	**3054.3222**
3		B	250	259.0285	205	46	1.0361	2.4141501	2010.9269	**4741.3774**
4		C	335	347.09819	205	46	1.0361	1.8732841	3339.7775	**7643.7167**
5		D	380	393.72332	205	46	1.0361	1.6746544	4179.0199	**9451.7158**
6		E	445	461.07073	205	46	1.0361	1.4522325	5557.1553	**12395.063**
7	Beijing Capital International Airport	A	185	190.08343	35	46	1.0275	3	1252.4615	**3032.9325**
8		B	250	256.8695	35	46	1.0275	2.4313593	1982.5609	**4678.6481**
9		C	335	344.20513	35	46	1.0275	1.887173	3290.7993	**7537.724**
10		D	380	390.44164	35	46	1.0275	1.6872464	4116.8762	**9318.3125**
11		E	445	457.22771	35	46	1.0275	1.4633228	5473.2406	**12216.558**
12	Kunming Wujiaba Airport	A	185	208.487045	1895	46	1.127	2.8936034	1399.7382	**3378.607**
13		B	250	281.73925	1895	46	1.127	2.2468611	2321.5196	**5425.6483**
14		C	335	377.530595	1895	46	1.127	1.738681	3876.9038	**8802.5037**
15		D	380	428.24366	1895	46	1.127	1.5527558	4860.9205	**10911.407**
16		E	445	501.495865	1895	46	1.127	1.3450048	6478.5398	**14350.124**
17	Tibet Qamdo Bangda Airport	A	185	236.857794	4334	46	1.2803	2.6033738	1729.226	**4116.3902**
18		B	250	320.0781	4334	46	1.2803	2.0115505	2896.4294	**6681.9646**
19		C	335	428.904654	4334	46	1.2803	1.5505946	4874.4801	**10940.362**
20		D	380	486.518712	4334	46	1.2803	1.3828332	6128.9375	**13609.316**
21		E	445	569.739018	4334	46	1.2803	1.1959362	8194.2422	**17971.093**

Figure 3. Calculation of radius for visual circling with Excel

4 Recommendations for inner horizontal surface design

These recommendations are based upon the calculations and analysis above.

(1) The height of the inner horizontal surface should be increased to 60m. This figure is designed for B737 and A320 which are Category C used for short-haul and medium-haul flights. These two models are most frequently used in China. The visual circling procedure of Category B aircraft and aircraft which are heavier will not be affected if the obstacles are lower than 60m. Aircraft of Category A which are usually used for general aviation are not considered for their low usage frequency, so that city construction will not be affected.

(2) The radius of the inner horizontal surface should be increased to 5000m. Though the additional 1000m will not make any difference in protection level, another 2000m gained in the expansion of the conical surface at 5% grades can give basic protection to the visual circling procedure of Category C aircrafts. The calculation of radius should be based on the data of the particular airport. This result is just a reference.

(3) The altitude of one threshold is much different from another in some runways. In this case, the calculation should make use of the data of both thresholds. The obstacles should not be higher than the lower surface in the overlap region.

5 Conclusions

This paper focuses on the design of inner horizontal surface. Recommendations are given to adjust the design parameters through the calculation and analysis, so that the requirements of the airport clearance, flight procedure and the development of the urban construction can be maximally satisfied.

References

CAAC.(1995) "The notice about airport clearance protection" *General Administration of Civil Aviation of China*.

Civil Aviation Authority.(2001) "CAP168 Licensing of Aerodromes"

GAO Jin-hua, WANG Wei.(2000)."Airport Engineering" *Publishing House of Tianjin Science and Technology*, Tianjin. 54~59

ICAO (1983). "Airport Services Manual (Doc 9137), Part 6" *International Civil Aviation Organization*.

ICAO (2004). "Annex 14 Volume I: Aerodrome Design and Operation" *International Civil Aviation Organization*. 4-1~ 4-9

ICAO (2006). "Procedures for Air Navigation Services:Aircraft Operations.Vol.II.Construction of Visual and Instrument Flight Procedures" *International Civil Aviation Organization*. I-4-7-1~ I-4-7-3

Industry Standard of the People's Republic of China.(2006). "Civil Airport Airfield Technical Standards (MH5001-2006)",27~32

QIAN Bing-hua, ZHANG Yu-fen.(2000). "Airport Planning and Environmental Protection" *Publishing House of China Construction Industry,* Beijing. 82~92,87

SONG De-kuan.(2000). "Preliminary Discussion on the Ward of Airport Clearance and Approach-and-landing Flight Safety" *National Flight Technology and Safety Symposium, Aviation Society of China*, 133~137

Grey Relational Analysis Method of Main Reasons of Road Traffic Accidents

Xi Jianfeng[1], Wang Shuangwei[2]*, Zhou Na[2], Gao Yan[3], Ding Zhenglin[3]

[1]Transportation College of Jilin University, P.O. Box 130022, Changchun, PH (+86) 0431-85095705; FAX (+86) 0431-85095705; email: xijf@yeah.net
[2]Physics College of Northeast Normal University, P.O. Box 130022; Changchun, PH (+86) 0431-85099748; FAX (+86) 0431-85099748; email: wangsw77@163.com
[3]Traffic Management Research Institute of the Ministry of public Security, P.O. Box 214151, Wuxi, PH (+86) 0510-85505861; FAX (+86) 0510-85505861; email: gaoyan20022002@126.com

ABSTRACT：

Road traffic accidents are caused by many factors, which could be considered as the grey system with the characteristics of complexity, imperfect information, and non-definition. To quickly analyze the main factors contributing to traffic accidents, the grey relational analysis method is presented. In that, the grey relational degree and the grey relational order of each traffic accident factor are calculated, while the relative significance of each influence factor for traffic accidents is determined. So, the main reasons for traffic accident are specifically identified. According to a study of 2000 traffic accidents in one city in Northeast China between 2005 and 2007, the relational degree of weather is analyzed by using the grey relational analysis method when the amount of traffic accidents are looked upon as the decision attribute. The first three factors, and corresponding relational degree, are snowy (0.8587), cloudy (0.8491), and rainy (0.7877), respectively.

KEY WORDS: grey relational analysis, traffic accident, accident reason

INTRODUCTIONS

Based on a large amount of road traffic accident data used to deeply analyze the rules of the regional road traffic accidents, the influencing factors and reasons, we are able to extract useful information from a large amount of data to provide a basis for prevention countermeasures of road traffic accidents. So, some scholars have applied data mining methods such as rough set theory, association rules, and neural networks to analyze the main factors of traffic accidents and their significance (Li 2006; Yao 2005; Wu 2005).

In this paper, road traffic accidents are regarded as a complex, incompletely informational, inaccurate grey system. The grey relational analysis method is applied to analyze the influencing factors and degree of the road traffic accidents.

THE BASIC PRINCIPLES OF THE GREY RELATIONAL ANALYSIS

The grey system theory focuses on the "small sample", "poor information" uncertainty questions which can not be solved by probability and statistics and fuzzy math. The basic idea of the grey relational analysis is based on the geometry form similarity of the sequence curve to determine whether their relation is close or not. If the curve is close, the relational degree between the corresponding sequences is greater and vice versa (Deng 2002). Figure 1 shows the accident frequency of three kinds of vehicles in a place from 1993 to 1998, which can simply explain the important relationship between the grey relational degree and the degree of attribute values.

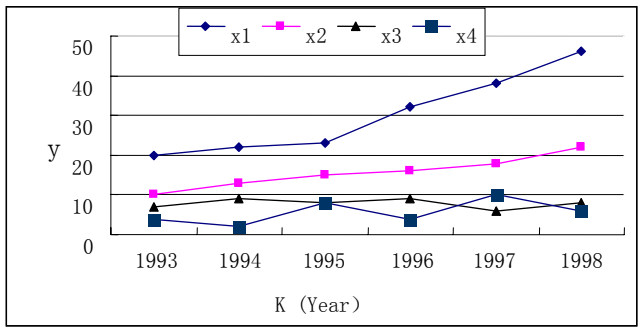

Figure 1. The accidents frequency of three kinds of vehicles.

In Figure 1, X1 is the curve of the decision-making attribute, which represents the total number of traffic accidents in the location of the study each year. X2, X3, X4, respectively, represent the number of accidents under the conditions of the three kinds of vehicle each year. From Figure 1, X2 and X1 have the most similar shape of the decision-making attribute curve, so the relational degree between X2 and X1 is the largest, while the impact of X2 is the largest too. In other words, in three transport modes X2 is the main influencing factor of the traffic accidents in the area.

PUTTING FORWARD THE METHOD

In this paper, we make use of the grey relational analysis to analyze which one of a number of the attribute values relating the road traffic accidents is most likely to affect the result of traffic accidents. The process of the method is shown in Figure 2.

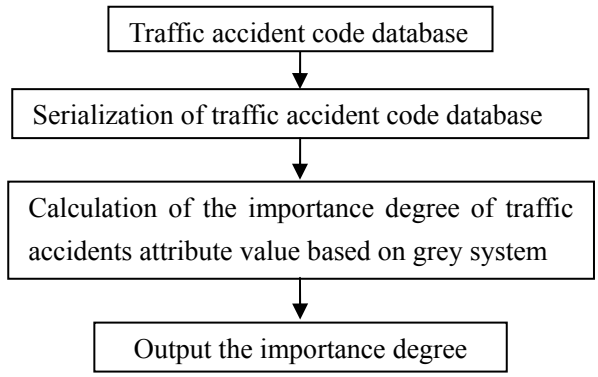

Figure 2. The process of grey relational analysis method of the causes of road traffic accidents.

THE SERIALIZATION OF TRAFFIC ACCIDENT DATA

In traffic accident data, the number of deaths can express the accident severities, the frequency can express how often the accidents happen, so this data can be directly used for relational analysis. In order to achieve this goal, this study uses the number of deaths of the traffic accidents as the sequence number, and the number of accidents or loss of property as a sequence of grey numbers. For example, assume that the number of accidents is 5876, 298, 187, 123, 45, 16, 7, when the corresponding deaths is 0,1,2,3,4,5,6, respectively. Then the sequence is:

$$X_1(k) = \{5876,\ 298,\ 187,\ 123,\ 45,\ 16,\ 7\} \quad (1)$$

Because the computer can not deal with the array variable in which the sequence number is zero, so here 1 is the beginning of the serial number. We put $X_1(k)$ as the decision-making attribute sequence. When we intend to study the relationship between the weather and the accident death number, we use the number of traffic accidents corresponding to the death number under different weather conditions as the behavior sequences. For example, the number of accidents is 876, 49, 27, 13, 7, 3, 0, which corresponds to the death number of 0, 1, 2, 3, 4, 5, 6, respectively. Then the sequence is:

$$X_2(k) = \{876,\ 49,\ 27,\ 13,\ 7,\ 3,\ 0\} \quad (2)$$

We put the sequence of $X_2(k)$ as one of the attribute values of the weather condition (sunshine). Similarly, we can get the other attribute values sequence of $X_3(k)$ (cloudy), (rain), $X_5(k)$ (snow), $X_6(k)$ (fog) and $X_7(k)$ (others). So, we can establish a sequence database when look at the means of the behavior sequences above as the grey number matrix.

CALCULATING THE IMPORTANCE DEGREE OF THE TRAFFIC ACCIDENT ATTRIBUTE VALUES

Traffic accident generalized grey relational analysis includes absolute grey relational degree, relative grey relational degree and general relational degree (Li 2006; Liu 1997).

(1) Calculate the traffic accident absolute grey relational degree ε_{0i}:

1. starting point of zero image;
2. calculate ｜s0｜, ｜si｜, ｜si-s0｜;

$$\begin{aligned} |s_0| &= \left|\sum_{k-2}^{n-1} x_0^0(k) + \frac{1}{2}x_0^0(n)\right| \\ |s_i| &= \left|\sum_{k-2}^{n-1} x_i^0(k) + \frac{1}{2}x_i^0(n)\right| \end{aligned} \tag{3}$$

$$|s_i - s_0| = \left|\sum_{k-2}^{n-1}(x_i^0(k) - x_0^0(k)) + \frac{1}{2}(x_i^0(n) - x_0^0(n))\right| \tag{4}$$

3. solve the value of the absolute grey relational degree

$$\varepsilon_{0i} = \frac{1 + |s_0| + |s_i|}{1 + |s_0| + |s_i| + |s_i - s_0|} \tag{5}$$

(2) Calculate the relative grey relational degree γ_{0i}

Grey relative degree is the quantitative characterization of the variation rate relative to the starting point of the sequences of X_0 and X_t. If the variation rate of X_0 and X_t is closer, γ_{0i} is bigger and vice versa. Calculation steps are below:

1.Initial image;
2.starting point of zero image;
3.calculate ｜s0｜, ｜si｜, ｜si-s0｜;

$$\begin{aligned} |s_0| &= \left|\sum_{k-2}^{n-1} x_0^0(k) + \frac{1}{2}x_0^0(n)\right| \\ |s_i| &= \left|\sum_{k-2}^{n-1} x_i^0(k) + \frac{1}{2}x_i^0(n)\right| \end{aligned} \tag{6}$$

$$|s_i - s_0| = \left| \sum_{k-2}^{n-1} (x_i^0(k) - x_0^0(k)) + \frac{1}{2}(x_i^0(n) - x_0^0(n)) \right| \quad (7)$$

4. calculate the value of the relative grey relational degree

$$\varepsilon_{0i} = \frac{1 + |s_0| + |s_i|}{1 + |s_0| + |s_i| + |s_i - s_0|} \quad (8)$$

(3) Calculate the value of the traffic accident grey general relational degree

$$\rho_{0i} = \theta\varepsilon_{0i} + (1-\theta)\gamma_{0i} \quad (9)$$

So, the process of the calculation of the grey general relational degree is shown as Figure3.

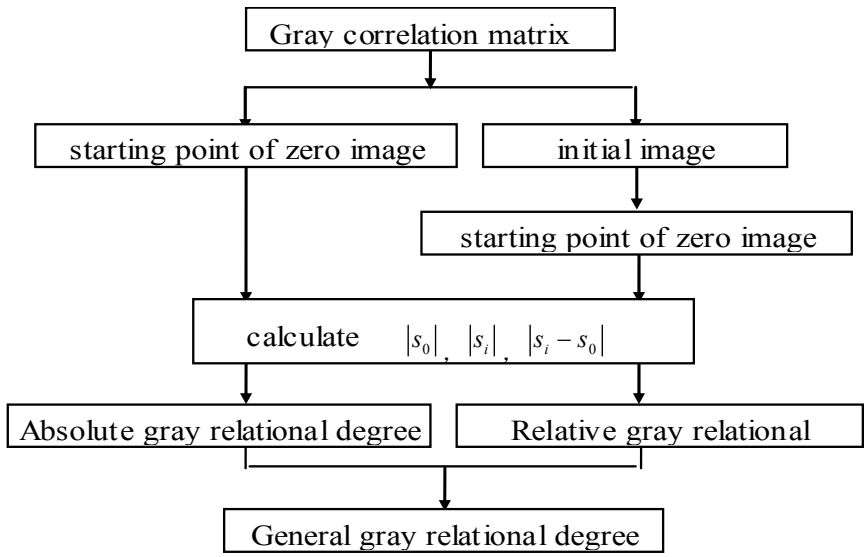

Figure 3. The process of the calculation of the general grey relational degree

5 THE CASE STUDY

Choosing data for 2000 traffic accidents in one region of Northeast China as the analysis object and mapping the traffic accident code database for serializing database, we can do the grey relational analysis case using Matlab software.

Taking the number of deaths as the decision-making attribute, the value of the death number 1, 2, 3, 4, 5, 6 is the behavior sequence. The corresponding total number of accidents of the death number is called $Y(i)$ （$i = 1,2,3,4,5,6$）, in which the corresponding total number of accidents of each attribute j is called $X_j(i)$ （$i = 1,2,3,4,5,6$）. Then we can get the correlation matrix.

(1) After analyzing the relational degree of transport modes, the results are

found as shown in Table 1:

Table 1. The order of relational degree of transport modes.

attribute	motor vehicle	non-motor vehicle	transit trip	walking	others
general relational degree	0.8598	0.7750	0.9011	0.9580	0.7508
importance	3	4	2	1	5

(2) After analyzing the relational degree of improper behavior, the results as Table 2.

Table 2. The order of relational degree of improper behavior.

attribute	illegal behavior	serious improper behavior	improper behavior	pedestrian improper behavior
general relational degree	0.8637	0.7813	0.8878	0.7703
importance	2	3	1	4

(3) After analyzing the relational degree of weather, the results as shown in Table 3.

Table 3. The order of relational degree of weather.

attribute	sunny	cloudy	rainy	snow	others
general relational degree	0.7295	0.8491	0.7877	0.8587	0.6480
Importance	4	2	3	1	5

From Table 1 to Table 3, pedestrian, improper behavior and snow are the primary factors for traffic accidents. So pedestrian is not only the accident reason, but is also the victim in the severity traffic accident. Many accidents which can be effectively avoided are caused by illegal behavior. Snow is also a quite important influencing factor for accidents. In a word, the analysis results are corresponding to the mixed traffic, the weakness of safety consciousness and concepts of drivers' obeying the law, and the long winter period in Northeast China.

6 CONCLUSION

We can accurately get the primary causes of traffic accidents from the massive traffic accident data available by using the relational analysis method based on grey system theory. For Northeast China, especially in winter, the education of vehicle drivers and pedestrian, and the surveillance of the illegal activities are key effective actions for preventing traffic accidents. But the value of general relational degree in the case is quite close (such as snow (0.8587), cloudy (0.8491)). Whether

their influence to traffic accident have obvious difference should be further investigated.

ACKNOWLEDGEMENT

The authors thank the "11th Five-Year" National Science and Technology Project Foundation of China (Grant No. 2007BAK35B01) for financial support.

REFERENCES

Deng Ju-long. (2002). Grey Theory Basis.Wuhan: Huazhong University of Science & Technology Press, 2002.

Li Jia, Zhu Shunying, Zhang Qiming, Xiang Hongyan.(2006). Traffic Accidents Reasons Analyzed with Innovated Gray Association Degree. Technology of Highway and Transport, 2006, pp. 114-116.

Liu Si-feng, GUO Tian-bang, DANG Yao-guo. (1997). Gray System Theory and Application. Beijing: Science Press, 1997.

Yao Zhi-sheng, Shao Chun-fu, Long De-lu. (2005).Cause Analysis of Traffic Accidents on Road Block Spots Based on Rough Set Theory. China Safety Science Journal, Vol. 15, No. 12, 2005, pp. 107-109.

Wu Hao. (2005). “Data Mining of the Road Traffic Accident Based on Association Rules”. Changchun: Department of Communications Engineering, Jilin University, June 2005.

Study on Fuzzy Neural Network Model of Vehicle-Bicycle Conflicts at Grade Intersection Based on Failure Tree Analysis

Ying-hui LIANG[1]，Xing-qiang ZHANG[2]

[1] Master Student, MOE Key Laboratory for Urban Transportation Complex Systems Theory and Technology, Beijing Jiaotong University, 100044, Beijing, China; PH (010) 51465309; Email: 07121280@bjtu.edu.cn

[2] Associate Professor，MOE Key Laboratory for Urban Transportation Complex Systems Theory and Technology, Beijing Jiaotong University, 100044, Beijing, China; PH (010) 51687138; Email: zhangxingqiang@jtys.bjtu.edu.cn

ABSTRACT

The bicycle safety problems at urban grade intersection should be regarded in China. Firstly, according to the amount of conflicts and the degree of danger, the vehicle-bicycle conflicts at a four-leg intersection are classified into 3 groups using the fuzzy clustering theory, and the interference between the through bicycles and the right-turn vehicles in the adjacent lane is used as the case study. The failure tree model of bicycle traffic safety is built and the main reasons for vehicle-bicycle conflict are explained from two aspects: the minimal cut set and the structural importance. Secondly, based on the failure tree analysis results, the fuzzy neural network model of vehicle-bicycle conflicts at grade intersections is built, the analysis results show that the reasons causing bicycle traffic conflict at grade intersections can be well analyzed and evaluated using the fuzzy neural network model.

Keywords： intersection; bicycle; traffic conflict; failure tree; fuzzy neural network

1 INTRODUCTION

Vehicle-bicycle conflicts are one of the most important features at urban grade intersections in China. It is essential to give an embedded study on the severity and the influence of traffic safety at grade intersection. Qian Dalin (2006) established the decision-making model of right-turn vehicles passing through the through bicycles; Liu Xiaoming (1997) established the traffic conflict probability distribution model and the safety evaluation standard at grade intersections; Jing Chunguang (2004) analyzed the vehicle-bicycle conflict situation in the mixed-traffic environment, and set up the critical value of left-turn bicycle flow for the phase setting. But the researchers paid less attention to the relation between the vehicle-bicycle conflict reasons and the conflict types. So in this paper, the fuzzy cluster method is used to analyze the vehicle-bicycle conflict seriousness. Then the failure tree of through bicycles and right-turn motor vehicle conflicts is set. Finally, using the minimal cut set of the failure tree as the input stylebook, and the vehicle-bicycle conflict fuzzy neural network prediction model is established, the analysis results show that the prediction model may well forecast vehicle-bicycle conflicts.

2 FUZZY CLUSTER ANALYSIS OF VEHICLE-BICYCLE CONFLICTS

The vehicle-bicycle conflicts at intersections may be divided into 5 types (see Figure 1) and look the conflict types which have the most account and the most dangerous as the object to study Based on the statistical vehicle-bicycle conflict quantities TC and the equivalent weight traffic amount of vehicle and bicycle MPCU at Ganjiakou intersection (see Table 1), the vehicle-bicycle conflict ratio TC/MPCU is regarded as the evaluated index. Ten conflict points are regarded as the evaluation set $X=(X_1, X_2, X_3 \ldots X_{10})$, the conflict danger degree X_K is divided into three kinds of type: lower danger, danger, higher danger.

Table 1. TC / MPCU at 10 conflict points.

	7:30-7:50	7:50-8:10	8:10-8:30
1 north A	0.0155	0.0185	0.0312
2 north B	0.0127	0.0157	0.0097
3 north C	0.3323	0.3072	0.2315
4 north D	0.1753	0.2389	0.1913
5 north E	0.2471	0.2253	0.2321
6 west A	0.0102	0.0105	0.0061
7 west B	0.0135	0.0150	0.0103
8 west C	0.2461	0.3890	0.2042
9 west D	0.0911	0.0795	0.0673
10 west E	0.0795	0.0673	0.0541

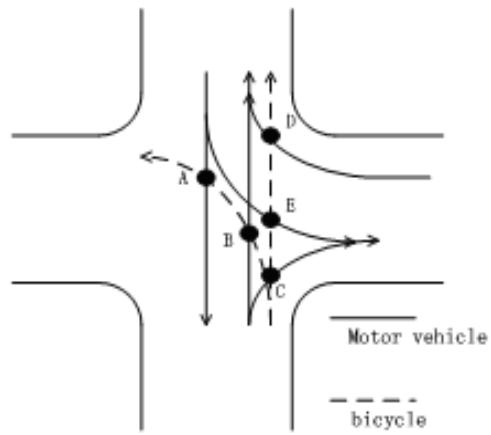

Figure 1.Vehicle-bicycle conflict types.

The fuzzy cluster analysis result (see Table 2) indicates that the interferences between the through bicycles and the right-turn vehicles are the most representative and the most dangerous. So the conflicts between the through bicycles and the right-turn vehicles are regarded as the research object in this paper.

Table 2. The fuzzy cluster analysis result of the vehicle-bicycle conflicts.

The grading of danger	the low danger	danger	the high danger
The number of conflict	1、2、6、7	9、10	3、4、5、8

3 FAILURE TREE ANALYSES

Three two-phase signaled intersections are taken as the example studies, according to the data from the video, the main reasons for the conflict between through bicycles and right-turn vehicles are shown in Figure 2. Based on the reason analyses, the failure tree is described in Figure 3. In the failure tree, the meaning of the letters is as follows:

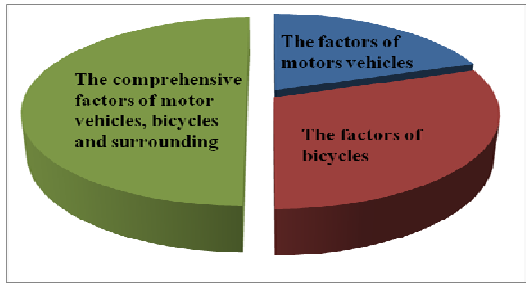

Figure 2. Vehicle-Bicycle Conflict factors.

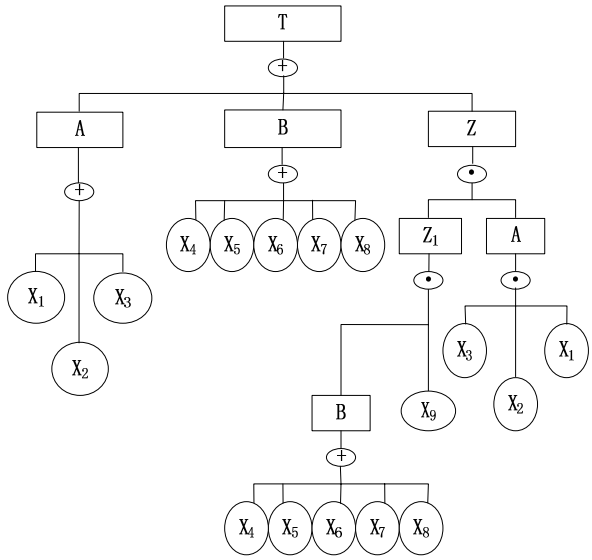

Figure3. The vehicle-bicycle conflicts failure tree.

T: through bicycles and right-turn vehicle conflict;

A: motor vehicle factors; B: bicycle vehicle factors; Z: the comprehensive factors of circumstance, motor vehicles and bicycles; Z_1: the condition of bicycle flow is not perfect;

X_1: right-turn motor vehicles occupy the bicycle lane; X_2: right-turn motor vehicle speed is excessively fast; X_3: right-turn motor vehicles don't avoid the through bicycles; X_4: bicycle speed is excessively fast when passing through the intersection; X_5: bicycles stop over parking line; X_6: bicycles go through intersection at random; X_7: bicycles pass through at a red light; X_8: bicycles run conversely; X_9: bicycle volume is excessively heavy when there is a green light.

By analyzing the minimal cut set of the failure tree, 13 minimal cut sets of the conflicts between through bicycles and right-turn motor vehicles in the adjacent lane are found. Based on the failure tree theory, the number of conflict patterns is 13.

$K_1=\{X_1\}$; $K_2=\{X_2\}$; $K_3=\{X_3\}$; $K_4=\{X_4\}$; $K_5=\{X_5\}$; $K_6=\{X_6\}$; $K_7=\{X_7\}$; $K_8=\{X_8\}$; $K_9=\{X_1X_2X_3X_4X_9\}$; $K_{10}=\{X_1X_2X_3X_5X_9\}$; $K_{11}=\{X_1X_2X_3X_6X_9\}$; $K_{12}=\{X_1X_2X_3X_7X_9\}$; $K_{13}=\{X_1X_2X_3X_8X_9\}$.

4 VEHICLE-BICYCLES CONFLICT FUZZY NEURAL NETWORK MODEL

In this paper, the relations between all kinds of factors and the traffic conflicts occurring at the intersection in Beijing are analyzed and forecasted, and the traffic conflict forecast model, based on fuzzy discursion of the neural network, is put forward. According to the video collection, the stylebooks may be determined.

Training stylebook 1: the through bicycles from north and the right-turning motor

vehicles on adjacent-lane motor vehicles at Ganjiakou intersection;
Training stylebook 2: the through bicycles from south and the right-turning motor vehicles on adjacent-lane vehicles at Ganjiakou intersection;
Training stylebook 3: the through bicycles from east and the right-turning motor vehicles on adjacent-lane vehicles at Ganjiakou intersection;
Training stylebook 4: the through bicycles from east and the right-turning motor vehicles on adjacent-lane vehicles at Fuchengmen intersection;
Training stylebook 5: the through bicycles from south and the right-turning motor vehicles on adjacent-lane vehicles at Fuchengmen intersection;
Training stylebook 6: the through bicycles from north and the right-turning motor vehicles on adjacent-lane vehicles at Fuchengmen intersection;
Testing stylebook 1: the through bicycles from west and the right-turning motor vehicles on adjacent-lane vehicles at Zhanlan road intersection;
Testing stylebook 2: the through bicycles from east and the right-turning motor vehicles on adjacent-lane vehicle at Zhanlan road intersection
Testing stylebook 3: the through bicycles from south and the right-turning motor on adjacent-lane vehicle at Zhanlan road intersection

The vehicle-bicycle conflict model at grade intersections is the system of neural network-driven fuzzy reasoning of the vehicle-bicycle conflicts. The structure of the fuzzy neural model is shown Figure 4, where: X is the input variable, Y is the output variable, g_j is the output variable of network NN_j, μj is the fitness of each network, R=3.

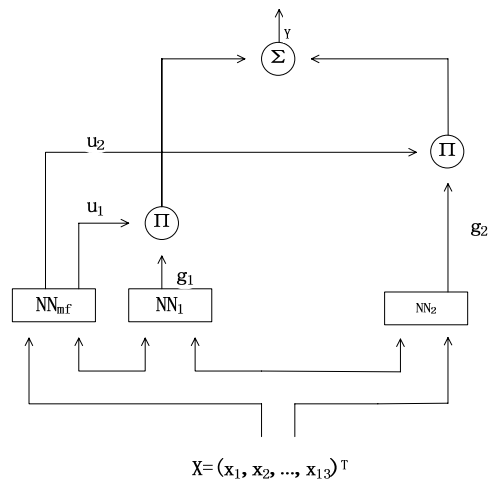

Figure4. The conflict fuzzy NN model

There are 3 neural networks in the vehicle-bicycle conflict fuzzy neural network model: the network NN_1, NN_2, the output numbers of conflict "y" which has two fuzzy rules in conclusion part. While the network NN_{mf} has given the fitness "μ_j" which include the two fuzzy rules corresponding to the input variable "p". The output variable "y" is decided by the formula (1)

$$y = \sum_{j=1}^{R} \mu_j \bullet g_j \qquad (1)$$

The vehicle-bicycle conflict fuzzy NN model adopts the BP model, the transfer function is sigmoid, and the output layer of network NN_j adopts the linear function. The concrete step as follows:
Step 1: To divide the input variable and the output variable into two parts properly. One part is training network whose training stylebooks are 1.2.3.4.5.6; another is the

testing network whose testing stylebooks are 7.8.9.

Step 2: Using clustering method cluster the input stylebooks. The first group contains 1.3.6; the second group contains 2.4.5, each cluster has a fuzzy rule, so this model has two fuzzy rules.

Step 3: The network NN_{mf} is made up of four input variables and two output variables. The learning stylebook is defined as follows: if the input pi of the training stylebook is clustered as the S group, then the S group training rule is followed. （S=one or two）

Step 4: The network NN_s corresponds to the article S rule corresponding to the S group divided in the second step, so the input stylebook in the S group is the learning stylebook of network NN_s. Avoiding excessive network learning, we can introduce the rule function as follows:

$$I_s = \frac{n_c}{n_i^s + n_c} \sum_{i=1}^{n_i^s} \{y_i - g_s(x_i)\}^2 + \frac{n_i^s}{n_i^s + n_c} \sum_{i=1}^{n_s} \{y_i^s - \mu_s(x_j) \bullet g_s(x_i)\}^2 \qquad (2)$$

Where: n_c is the account of testing stylebook, n_i^s is the account of stylebook in the S group, y_j^s is the output stylebook in the S group corresponding to the input variable p_j . When Is takes the minimum in the network NN_s , it can stop.

Regarding the reason sets, p_1 p_2 p_3 p_4 p_5 p_6 p_7 p_8 p_9 p_{10} p_{11} p_{12} p_{13}, which are contained in the minimal cut set of the failure tree as the input variables, y is the network conflict account output. The vehicle-bicycle conflict fuzzy neural network reasoning system established is shown in Figure 5.

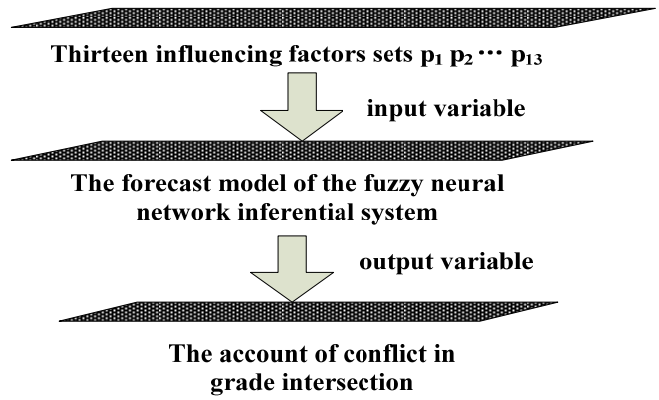

Figure5. Fuzzy neural network reasoning system

Table3. The data of conflict stylebook at intersection

Minimal cut set		1	2	3	4	5	6	7	8	9	10	11	12	13	14
Training stylebook	1	7	3	7	2	2	2	1	3	3	7	4	1	2	27
	2	16	1	3	3	3	3	0	3	7	9	3	2	2	34
	3	9	4	16	5	4	4	4	3	7	2	25	2	3	62
	4	2	2	9	3	6	5	0	6	13	4	9	4	6	49
	5	7	3	6	2	7	4	1	6	10	3	13	8	5	54
	6	3	2	11	4	3	5	2	4	9	6	12	7	5	48
Testing stylebook	1	6	3	8	2	4	3	1	3	8	2	19	2	5	43
	2	5	2	6	1	6	2	2	4	12	3	11	2	5	42
	3	4	3	7	3	5	3	2	5	10	4	12	3	6	44

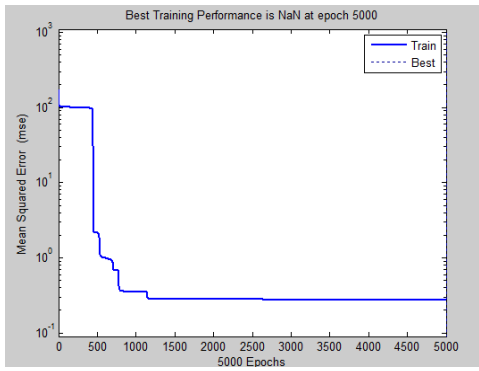

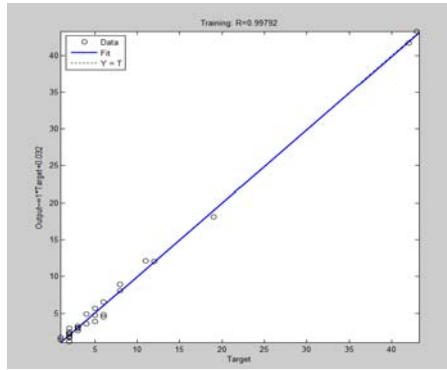

Figure6. Output error of the model. **Figure7. Output fitness of the model.**

The error training result and the target fitness are shown as Figure 7 and Figure 8, and the forecast results are shown in Table 4. The actual and the forecasted value match well. For example, the opposite error is 0.00599% for the first testing stylebook which shows that the model can better analyze the relation of the conflict reasons and the conflict accounts.

Table 4. Comparison between the actual value and the forecast value.

Number of testing stylebook	①	②	□
actual value(times)	43	42	44
the forecasted value(times)	43.2579	41.6871	43.7568
opposite error（%）	0.00599	0.00745	0.00553

5 CONCLUSIONS

(1) The fuzzy cluster analysis results indicate the conflict between through bicycles and right-turning motors is the most representative at grade intersection.

(2) The failure tree analysis results show that the minimal cut sets of the conflict between through bicycles and turning motor vehicles has thirteen patterns.

(3) The fuzzy neural network model of the vehicle-bicycle conflicts at grade

intersections is established, and the analysis results indicate that combination of the failure tree and fuzzy neural network can better analyze the relation of the conflict reasons and the conflict accounts.

6 REFERENCES

Qian Dalin, Huangdi (2006). "The Study on the Decision Behavior about Right-turning Motor Crossing the Straight-running Bicycles at the Signalized Intersection." [J] Systems Engineering Theory & Practice. Vol.26 (5): pp64-66.

Liu Xiaoming, Duan Hailin (1997). "Failure Analysis on Safety Assessment Method for Traffic Conflicts at Level Crossing and its Improvement [J]." China Safety Science Journal. Vol.3 (1): pp49-53.

Jing Chunguang, Wang Dianhai (2004). "Analysis and Dealing Method to Conflict of Mixed Traffic at Typical Intersection." China Civil Engineering Journal.Vol.37 (6): pp97-100.

Yin Hongbin (1999). "Use the fuzzy neural network to forecast the loss of traffic accident of highway." Journal of Highway and Transportation Research and Development. Vol.16 (3): pp57-62.

Ge Zhexue, Sun Zhiqiang (2007). "*The theory of neural network and the realization of Matlab R2007*". The publishing company of Electronic Industries.

Research on the Prediction Model of Traffic Accidents Using the Least Square Support Vector Machine

Zhang Wei-hua, Sun Qian and Sun Hao

School of Mechanical and Automotive Engineering, Hefei University of Technology, Hefei 230009, china; PH (86)-0551-2901338 EXT 2512; FAX (86)-0551-2903450; email:ahweihua@163.com

ABSTRACT

This paper analyzes the advantages of the least square support vector machine in the prediction of traffic accidents, decided the set of input vectors and output vectors and then established the model of prediction of traffic accidents by the use of the least square support vector machine. During the course of predicting, the related data of nationwide traffic safety from 1953 to 2006 was divided into the training set and the testing set and was simulated by the use of MATLAB7.0. The specific parameters of the model were gained by the training of the least square support vector machine. The testing set data was predicted. Predictive errors were calculated and compared with the prediction results of the support vector machine model. Simulation results represented that the model of prediction of traffic accidents based on the least square support vector machine had lower computational cost and higher predictive accuracy than the neural network prediction model and the support vector machine model.

INTRODUCTION

Recently our country's basic construction installation approached perfection. The substantial increase of automobiles owned and passenger turnover quantity impelled economic development, while it also brought negative impacts such as the problem that the traffic accident rate is at a high level should be urgently solved.

Generalizing and analyzing the related data of traffic safety in former years and then finding the internal laws of the traffic accident occurrence, at last forecasting the future conditions of traffic accident occurrence could provide related basis for policies of the traffic management department and have important significance.

Traffic accident prediction methods are many such as regression model methods, analysis hierarchy process (Yuan Wei, 2007) and so on. The flaws of those methods are that the models could not voluntarily adjust based the data differences when data regression and therefore prediction results are not precise enough. At present the methods which have a voluntary adjustment function are widely used for regression forecasts such as neural network models. However, the neural network model depends on the quality and quantity of learning data and could not dominate

convergence excessively; therefore prediction speed and effect are not perfect.

The support vector machine (hereinafter shortened as SVM) is a kind of realization method in the application of statistics theory that can solve the practical problems of small sample size, nonlinearity, high-dimension, local minimum (Vladimir N.Vapnik, 1999; Kim,2003) and so on by the use of a structural risk minimization standard based on risk minimization. Compared with the standard SVM, the least square support vector machine (hereinafter shortened as LS-SVM) regression performances are better and the calculation results are more precise. LS-SVM has a very obvious advantage of possessing the road traffic safety.

This paper establishes the traffic accident prediction model by the use of LS-SVM and gained the simulation results in order to validate the result by the use of related data of nationwide road traffic safety from 1953 to 2006.

LS-SVM PREDICTION MODEL OF TRAFFIC ACCIDENT

The choice of input vectors set and output vectors set. The reasons for road accident occurrence are various and therefore have randomness. People, vehicles, road conditions are the basic factors that influence road traffic safety. This paper chose nationwide highway mileage, motor vehicle population, population, passenger turnover volume and freight turnover volume as the input vectors set of accident prediction model by the integrative analysis of road, people, vehicle and environment factors.

The output vector that reflects the level of traffic safety sufficiently, therefore has three characteristics (GuoYing-shi, 2006): measurability, representativeness, comparability. This paper used three synthetic evaluation indexes including number of deaths, number of injured and number accidents in order to evaluate the traffic safety level.

The establishment of the LS-SVM traffic accident prediction model. For the known data vectors $\{x_j, y_j\}_{j=1}^{N}$ in N years (this paper used the relevant data from 1953 to 2006), input vector set $x_j = \{x_j^1, x_j^2, x_j^3, x_j^4 x_j^5\} =$ {highway mileage, motor vehicle population, population, passenger turnover volume and freight turnover volume}, as $x_j \in R^5$. The output vector set is the evaluation indexes of number of deaths, number injured and number of accidents as $y_j \in R$.

$$y_j = f(x_j) + e_j \qquad (1)$$

Where $f(x_j)$ is fitting value, e_j is deviation of fitting value and practical value.

Defining nonlinear mapping $\varphi(\cdot)$, relative data of nonlinear in (1) is mapped

from original space to character space $(\varphi(x_1),\varphi(x_2),\cdots\varphi(x_N)$, original nonlinear model is translated into linear model of character space，as LS-SVM model ：

$$f(x_j)=w^T\varphi(x_j)+b \qquad (2)$$

Where w, b are parameters which need to be identified in the model.

The parameters which need to be identified in (2) are processed by the use of the structural risk minimum standard：

$$R=\tfrac{1}{2}\left\|\vec{w}\right\|^2+\gamma * R_{emp} \qquad (3)$$

Where γ is regularization parameter, R_{emp} is the loss function.

Based on the prediction model of LS-SVM traffic accidents, loss function is chosen quadratic error as $e_j^{\ 2}$ in objective function, expression of optimal estimation function is：

$$J=\min\frac{1}{2}\vec{w}^T\vec{w}+\gamma\sum_{j=1}^{N}e_j^{\ 2} \qquad (4)$$

The constraint condition is:

$$y_j=w^T\varphi\left(x_j\right)+b+e_j\ \ j=1,2,\cdots,N \qquad (5)$$

From lagrangian function solution (4)，by the basis of KKT condition (Flake, 2002; Deng Nai-yang, 2004), the partial derivative of the lagrangian function is deduced ：

$$\vec{w}=\sum_{j=1}^{N}\alpha_j\varphi(\vec{x}_j);\ \ \sum_{j=1}^{N}\alpha_j=0$$

$$\alpha_j=\gamma e_j;\ \ \vec{x}^T\varphi(\vec{x}_j)+b+e_j-y_j=0 \qquad (6)$$

The kernel function is defined by the basis of Mercer condition (Zhang Xue-gong, 2000). This paper chose the Gauss radial machine kernel function ：

$$K(x,x_i)=\exp\left\{-\frac{\left\|\vec{x}_j-\vec{x}_v\right\|^2}{\sigma^2}\right\} \qquad (7)$$

Where $\left\|\vec{x}_j-\vec{x}_v\right\|^2=\sqrt{\sum_{k=1}^{5}(x_j^k-x_v^k)^2}$， σ is the kernel width.

（7）is substituted into（6），the optimization problem is translated into the solution of a linear equation：

$$f(\vec{x}_v)=\sum_{j=1}^{N}\alpha_j\exp\left\{-\frac{\left\|\vec{x}_j-\vec{x}_v\right\|^2}{\sigma^2}\right\}+b \qquad (8)$$

Where： $\vec{x}_j$ is input data vector of the training year, $\vec{x}_v$ is input data vector of the testing year. $f(\vec{x}_v)$ is the output vector set.

The prediction model of the LS-SVM traffic accidents has been established. The output vectors of the prediction model of the number of deaths, number injured and number of accidents are different. The parameters α_j and b are calculated and then the prediction model is obtained.

TESTING THE PREDICTION MODEL OF LS-SVM TRAFFIC ACCIDENTS

The input vector set is the nationwide highway mileage, motor vehicle population, population, passenger turnover volume and freight turnover volume (data source is national statistics bureau databases), the output vector set is the set of three indexes death number, injured number and accident number from 1953 to 2006.

The normalization of whole data. The determined input and output data obtain 8 aspects, such as data unit and order of magnitude are different. If the original data are used directly, it might appear that the data in the wide scale submerges the variational data in the smaller scale and therefore the accuracy of prediction result is reduced. The calculation of the Gauss radial machine kernel function involves the vector inner-product, so excessive value might cause difficult calculation and then influence the calculation efficiency of the whole model. Based on the above analysis, 8 aspects of the data are normalized.

$$A_i^{/} = \frac{A_i}{\|A\|_2} = \frac{A_i}{\sqrt{A_1^2 + A_2^2 + \cdots + A_i^2}} \qquad (9)$$

Where $\|\cdot\|_2$ is 2-norm of vector.

LS-SVM death number prediction simulation testing. Input data and output data in 1970, 1971, 1980, 1981, 1990, 1991, 1999, and 2000 are extracted from the total samples as a testing set; the other data are the training set. They are trained and tested respectively.

Vector machine regularization parameter C and RBF kernel function parameter σ^2 should be validated in LS-SVM. This paper validated the parameter value by the cross validation method (Li Xiao-yu, 2005; Han Liu, 2004). The training set was divided into 3 parts. Samples square sum of error were calculated and validated by 3-fold cross-validation, then two of them were used to train, the other one was used to validate. The appropriate value selections were determined by the basis of the model performance on the validation set.

Make sure $C = 1500$, $\sigma^2 = 0.7$. Through training the LS-SVM, parameters

α_j and b are obtained, where $b=0.6923$, α_j are seen as in Table 1.

Table 1. Death number prediction mode α_j value.

Year	1953	1954	1955	1956	1957	1958	1959	1960	1961	1962	1963	1964
Value	-5.13	-0.05	3.71	-1.86	1.57	-3.32	-1.46	7.73	-16.97	31.09	5.73	-6.79
Year	1965	1966	1967	1968	1969	1972	1973	1974	1975	1976	1977	1978
Value	-29.20	-25.95	22.65	16.85	15.44	-15.69	-25.94	7.48	-11.44	37.15	37.31	-49.50
Year	1979	1982	1983	1984	1985	1986	1987	1988	1989	1992	1993	1994
Value	-1.50	8.71	43.12	-97.87	47.87	15.14	-25.62	63.00	-65.09	22.77	-2.75	-17.43
Year	1995	1996	1997	1998	2001	2002	2003	2004	2005	2006		
Value	11.41	-9.73	-15.52	7.45	0.00	1.22	-0.34	0.94	0.93	0.39		

Figure 1 is the training curve of LS-SVM death number prediction model, where the red* broken line is actual output and the blue hollow circle real line is the fitting output. The training calculation time was 0.0150s, while the average of training error was 0.0664.

Substitute parameters α_j and b into（8）to gain the death number prediction model. The prediction death numbers in1970, 1971, 1980, 1981, 1990, 1991, 1999, and 2000 were gained by the use of the known prediction model. Figure 2 is prediction relative error of LSSVM death number prediction model, the average of prediction error is 2.99%.

Table 2. The comparison among the death number prediction of BP, SVM, LS-SVM.

	Calculation time (s)	Average error of prediction (%)
BP	38.375	3.52
SVM	0.3	3.03
LS-SVM	0.015	2.99

Comparing the final values of death number prediction with the practical values, the prediction results of BP neural network prediction model and SVM traffic accident prediction, and the comparative results are seen as Table 2 and Figure 3.

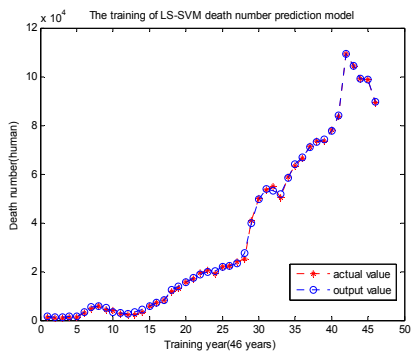

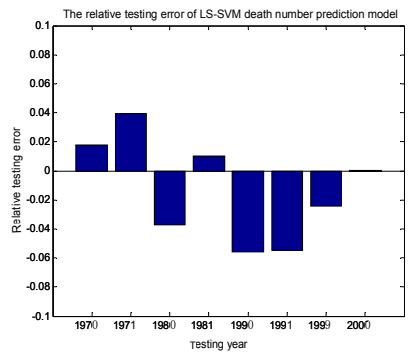

Figure 1. The training of LS-SVM death number prediction model.

Figure 2. The relative testing error of LS-SVM death number prediction.

In figure 3, fuchsine fork character real line is practical, blue * broken line is testing output of BP prediction model, black hollow dot-and-dash line is testing output of SVM prediction model, green + double linework is LS-SVM output.

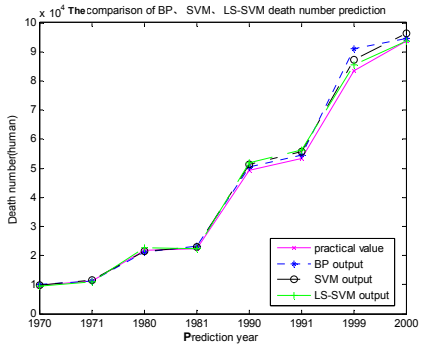

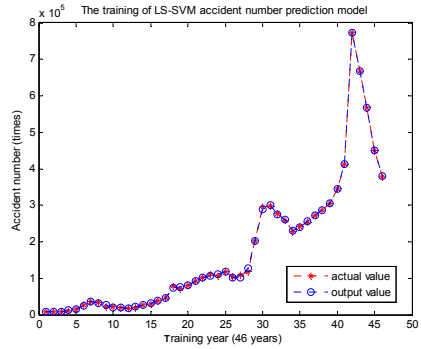

Figure 3. The comparison of BP, SVM, LS-SVM death number prediction

Figure 4. The training of LS-SVM accident number prediction model.

SVM accident number prediction simulation testing. Make sure $C = 16000$, through training LS-SVM, the parameters α_j and b are obtained. Where $b = 0.3637$， α_j are seen as Table 3.

Figure 4 is the training curve of the LS-SVM accident number prediction model, where the red* real line is actual output and the blue hollow broken line is fitting output. The average of relative training error is 0.0249.

Substituting parameters α_j and b into（8）is to gain accident number prediction model. Prediction average error is obtained as 3.09% by use of the established prediction model. Figure 5 shows the relative error of LS-SVM accident number prediction model.

Comparison of the final values of the accident number prediction with practical values, prediction results of the BP neural network prediction model and SVM traffic accident prediction, and the comparative result are seen in Table 4 and Figure 6.

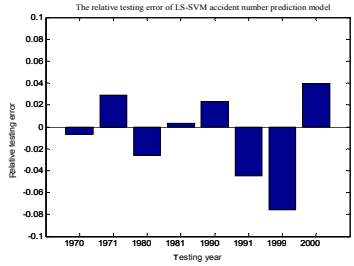

Figure 5. The relative testing error of LS-SVM accident number prediction model.

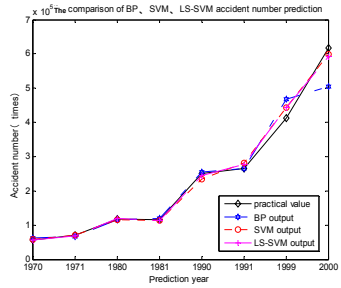

Figure 6. The comparison of BP, SVM, LS-SVM accident number prediction.

Table 3. Accident number prediction model α_j value.

Year	1953	1954	1955	1956	1957	1958	1959	1960	1961	1962	1963	1964
Value	12.02	10.94	5.58	-95.21	43.75	79.20	33.66	85.26	-177.27	85.53	18.89	12.12
Year	1965	1966	1967	1968	1969	1972	1973	1974	1975	1976	1977	1978
Value	-106.60	5.20	-139.57	90.99	71.91	136.59	-340.69	89.78	-33.40	30.80	353.55	-268.42
Year	1979	1982	1983	1984	1985	1986	1987	1988	1989	1992	1993	1994
Value	-73.15	94.38	377.39	-495.46	-168.98	259.70	20.63	73.45	-96.55	0.33	-45.07	89.27
Year	1995	1996	1997	1998	2001	2002	2003	2004	2005	2006		
Value	-54.09	33.37	-54.50	31.94	-1.16	3.76	-2.42	1.54	1.00	-0.11		

In figure 6, the black + character real line is the practical value, the blue square character double linework is the testing output of the BP prediction model, the red hollow broken line is the testing output of the SVM prediction model, and the cyan dot-and-dash line is the LS-SVM output.

Table 4. The comparison of the accident number prediction of BP, SVM, LS-SVM

	Calculation time (s)	Average error of prediction (%)
BP	0.3	4.12
SVM	14.015	3.84
LS-SVM	0.17	3.09

LS-SVM injured number prediction simulation testing. Make sure $C = 30000, \sigma^2 = 1.3$. Through training the LS-SVM, the parameters α_j and b were obtained, where $b = 0.5085$, α_j is seen as shown in Table 5.

Figure 7 is the training curve of injured number prediction model, where the red* real line is actual output and blue hollow broken line is the fitting output. The average of the relative training error is 0.0495.

Substituting parameters α_j and b into (8) is to gain the injured number

prediction model. The average of the prediction error is 3.19% and is gained by the testing of the established prediction model. Figure 8 is the relative error of the LS-SVM injured number prediction model.

Comparing the final values of injured number prediction with the practical values, the prediction results of BP neural network prediction model and SVM traffic accident prediction, the comparative results are seen as Table 6 and Figure 9.

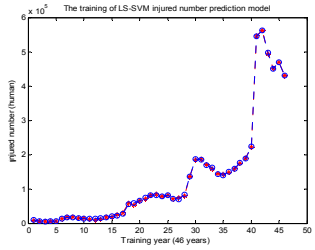

Figure 7. The training of LS-SVM injured number prediction model.

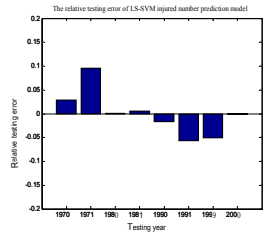

Figure 8. The relative testing error of LS-SVM injured number prediction model.

Table 5. Injured number prediction model α_j value.

Year	1953	1954	1955	1956	1957	1958	1959	1960	1961	1962	1963	1964
Value	1.12	11.18	19.51	-68.47	17.49	-86.21	80.07	-8.96	-79.65	380.94	-67.60	-2.68
Year	1965	1966	1967	1968	1969	1972	1973	1974	1975	1976	1977	1978
Value	-241.32	10.05	-192.54	228.35	118.71	138.73	403.77	-762.89	403.77	-208.70	314.84	506.99
Year	1979	1982	1983	1984	1985	1986	1987	1988	1989	1992	1993	1994
Value	-442.23	-176.15	88.89	564.92	-703.32	-104.21	264.98	-9.61	189.19	-234.67	136.45	-210.90
Year	1995	1996	1997	1998	2001	2002	2003	2004	2005	2006		
Value	183.71	-42.90	-1.35	-56.05	37.39	-0.73	2.50	-2.10	1.72	1.30		

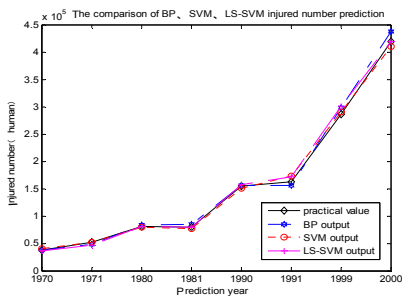

Figure 9. The comparison of BP, SVM, the LS-SVM injured number prediction

Table 6. The comparison among the injury number prediction of BP, SVM, LS-SVM

	Calculation time (s)	Average error of prediction (%)
BP	7.312	4.27
SVM	0.4	3.39
LS-SVM	0.16	3.18

In Figure 9, the black + character real line is the practical value, blue square character double linework is the testing output of the BP prediction model, red hollow broken line is the testing output of SVM prediction model, and the cyan dot-and-dash line*character is the LS-SVM output.

CONCLUSION

This paper constructs traffic accident prediction model by the use of LS-SVM, chooses highway mileage, motor vehicle population, population, passenger turnover volume and freight turnover volume as the input vectors set, death number, injured number and accident number as the output vectors set, and then makes a simulated testing based the related data of nationwide traffic safety from 1953 to 2006.

The simulated result indicates the model which this paper establishes has the follow advantages:

(1) Training speed is fast, prediction efficiency is high.

LS-SVM generalizes training problem into the solution of linear equation. Not like the standard SVM, quadratic form programming problem should be solved. Because the solution of linear equation is easier and faster than quadratic form programming problem, the solution algorithm of LS-SVM is easy. The prediction model of traffic accident which is established by the use of LS-SVM has faster calculation and higher efficiency besides the advantages which standard SVM dealing with nonlinear equation has.

(2) The prediction result of model is precise.

LS-SVM, as branch of SVM, could study the structure of problem model automatically based risk minimum principle, so the complexity and structure of model could be adjust continuously by the change of just one control parameter to ensure the stability and accuracy when prediction model of traffic accident training and testing.

REFERENCES

Deng Nai-yang, Tian Ying-jie etal.(2004). The new method in data excavation [M].”Beijing: Science Press, 32-65.

Guo Ying-shi, Yuan Wei, Fu Rui.(2006). “Research on Characteristics of Assessment Indexes for Road Safety [J]. ”*Journal of Highway and Transportation Research and Development,* (5):102-105.

Han Liu, Ding Liu, Gang Zheng etal.(2004). “Research on natural gas load forecasting based on support vector regression [J].” *In :Proc. of WCICA’2004*, 3591-3595.

Kim Kyoung-jae.(2003). “Financial time series forecasting using support vector machines [J]. ” *Neurocompuetring*,307-319.

Li Xiao-yu, Zhang Xin-feng, Shen Lan-sun.(2005). “A Selection Means on the Parameter of Radial Primary Kernel Function [J].” *Chinese Journal Electronics,* (12A) :2459-2463.

Vladimir N.Vapnik.(1999). “2006An overview of statistical learning theory [J].” *IEEE Transactions on Neural Networks*,10(5) :988-999.

Flake G W, Lawrence S.(2002). “Efficient SVM Regression Training with SMO［J］.” *Machine learning*, 1(11):271-290.

Yuan Wei, Fu Rui, Guo Ying-shi, Han Wen-li.(2007). “Prediction model of death toll

resulted from road traffic accidents [J].” *Journal of Traffic and Transportation Engineering,* (4):112-115.

Zhang Xue-gong.(2000) “Introduction to Statistical Learning Theory and Support Vector Machines [J]. ” *Acta Automatica Sinica*, 26(1) :32-42.

Study of Anti-slide Pile Composed of Arch and Truss Structure Based on FEM

Chenglin HAN[1], Xiedong ZHANG[2], and Liang YIN[3]

[1]School of Transportation, Wuhan University of Technology, Wuhan, 430063; PH 13476299581; FAX (86) 027-86544875; email: 05han@163.com
[2]School of Transportation, Wuhan University of Technology, Wuhan, 430063; PH 18971012118; FAX (86) 027-86544875; email: zhangxd@189.cn
[3]Jiangsu Province Communication Planning and Design Institute Co.; Ltd.; Nanji-ng, 210005; PH 15926289776; FAX (86) 027-86544875; email: yin_whut@163.com

ABSTRACT

In order to deal with the application problems of anti-slide pile, a new structure type of anti-slide pile called Anti-slide Pile System Composed of Arch and Truss Structure is put forward. By applying the FEM software MIDAS/CIVIL, one landslide treatment engineering example was designed to compare the top displacement with the two other kinds of conventional piles, single-row anti-slide pile, and double-row anti-slide pile in a straight line under the same forces. The results demonstrated that the displacement of this new kind of pile on the top is much smaller than the two other kinds of conventional piles. The distribution of the deformation is also more rational and controlled easily. After examined by ANSYS, Anti-slide Pile System Composed of Arch and Truss Structure is feasible, and the global stiffness of the anti-slide pile is increased significantly so that the top displacement of the pile is decreased significantly. Therefore, this new kind of pile has a wide application in landslide treatment engineering.
Keywords: Anti-slide pile, MIDAS/CIVIL, ANSYS, displacement, global stiffness

INTRODUCTION

Landslide that endangers the safety and stability of highway engineering is one of the most common styles of highway disasters. As an efficient engineering measure of landslide treatment, anti-slide pile is currently used largely in landslide treatment. However, the top displacement of the conventional anti-slide pile is too large and leads to the slop failure. According to the application and problems of anti-slide pile in highway landslide treatment, a new structure type of anti-slide pile called Anti-slide Pile Composed of Arch and Truss Structure System is put forward. By using the finite element method, the analytical results show that this new kind of anti-slide pile is completely feasible.

The Birth of Anti-slide Pile Composed of Arch and Truss Structure. Currently, there have been many kinds of structure types of anti-slide pile accommodating to highway characteristics. As for the treatment of the slope engineering, the anti-slide pile is set under the bottom of the landslide on the stable sliding and geological structure surface. Although most of the treatments are successful, there are also many problems. Greater safety reserve leads to the economic wastes. At the same time, from the aspect of the displacement and the internal force of the pile, many are greater. To increase the capability of the pile and to lower the displacements of the top as well as strengthen the stability of the pile, this paper puts forth a new kind of Anti-slide Pile Composed of Arch and Truss Structure.

Anti-slide Pile Composed of Arch and Truss Structure. The plan of Anti-slide Pile Composed of Arch and Truss Structure is circular with locking beams combined among the piles in order to increase the overall stiffness of the structure by making full use of the arch and reducing the displacement of the top of each pile as shown in Figure 1 and Figure 2.

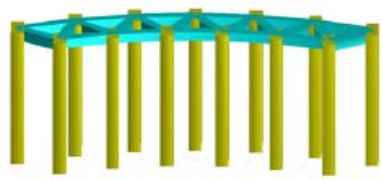

Figure 1. The structure model of anti-slide pile.

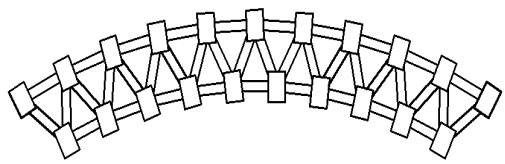

Figure 2. The layout plan of anti-slide pile.

This new kind of anti-slide pile is based on the advantages of mechanical characteristics of the arch and truss structure. The axis of the arch is circular so that the horizontal force, which is perpendicular to the way of the sliding, will exist when the arch is encountered by the thrust of the slide .At the same time, the geological conditions will be good to adapt to the horizontal force. If not, the link is also set between the two sides as shown in Figure 3.

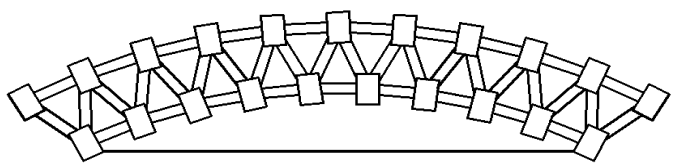

Figure 3. The layout plan of anti-slide pile with link.

Description and Design of the Engineering Sample. This paper selects the fourth slope of the HuRongXi national highway (K177 + 000-K178 + 400), which are key projects in China. The slope in this sample is like a sector (22 m × 140 m × 170 m) that has a narrow front-end and a broad tail. The volume is almost 523,600 m^3. This paper designed and calculated the single and double-row linear pile and Pile Composed of Arch and Truss Structure in order to compare the results with each other.

Single-row Straight Anti-slide Pile. In the fourth sliding slope, there are thirteen straight piles, and its section is 2,500 mm x 1,500 mm, while the spacing is 2,500 mm. The length of the pile is 28,000 mm of which 10,000 mm remains in the consolidation stage shown in Figure 4 and Figure 5. After simulated and solved by FEM software MIDAS/CIVIL, the results show that the maximum top displacement of the pile is 110 mm. It demonstrates that this straight pile is not feasible because of the large deformation on the top and will most likely slide again.

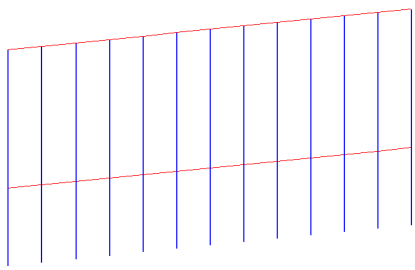

Figure 4. The model of single-row pile.

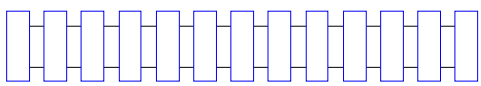

Figure 5. The layout plan of single-row.

Double-row Straight Anti-slide Pile. Getting rid of one pile in the single-row pile to enlarge the stiffness in the double-row Straight Anti-slide Pile is modeled and analyzed in MIDAS/CIVIL as shown in Figure 6 and Figure 7; however, the space increases to 4,500 mm. The results show that the top displacement is 40 mm, which is smaller than single-row Straight Anti-slide Pile.

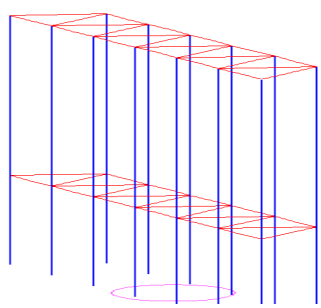

Figure 6. The 3D model of double-row pile.

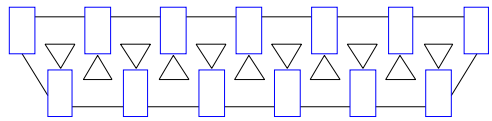

Figure 7. The layout plan of double-row pile.

Anti-slide Pile Composed of Arch and Truss Structure. The layout plan of this new kind of anti-slide pile is a circular arch that looks like the arch. According to the fourth slide, the design parameter value is in Table 1.

Table 1. Parameter value of the anti-slide pile.

Parameter	Inside Diameter	Outside Diameter	Included angle	Cross Section
Value	33800 mm	37100 mm	4°	2,500 × 1,500 mm^2

Modeled and analyzed in MIDAS/CIVIL as shown in Figure 8 and Figure 9, the results show that the top displacement is 9 mm, which is much smaller than double-row Straight Anti-slide Pile. Thus, the analysis of the model concluded that Anti-slide Pile Composed of Arch and Truss Structure has many advantages compared to other straight anti-slide piles, such as mechanical behavior, the distribution of the internal force, and top displacement.

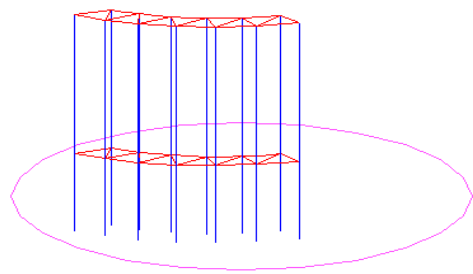

Figure 8. The 3D model of the new pile.

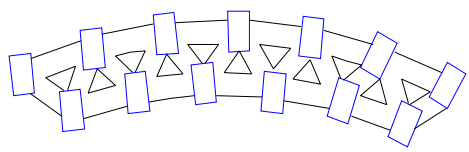

Figure 9. The layout plan of the new pile.

Checked by ANSYS10.0 (STRUCTURE). For verification the accuracy of the results above, the model and design were also analyzed in general FEM software ANSYS in order to optimize the design parameter value. To display the deformation of the pile and the soil, the 3D model would be more effective. Single-row and double-row Straight Anti-slide Pile and Anti-slide Pile Composed of Arch and Truss Structure were modeled by using the bottom to top element method.

Next, grids were generated in the way of manual and free method with quadrangle and triangles shown in Figure 10. In order to deduce the influence of stress concentration, the mesh was subdivided, especially at the key regions. At the bottom of the pile, the DOFS are all fixed in the direction of x, y, z, and at the sliding area, the direction of y was set. To simulate the force between the soil and piles, 733300N/M^2 was applied on the area of xz.

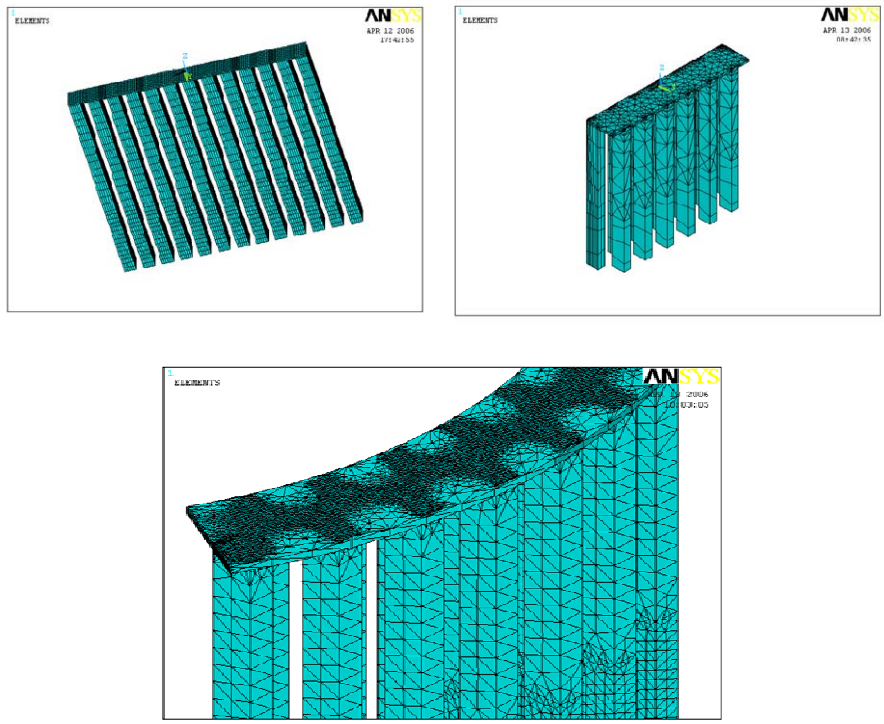

Figure 10. The mesh partition model of the piles.

After solved in ANSYS, the result shown in Figure 11 was obvious by observing the displacement contour map. By comparative analysis, Anti-slide Pile Composed of Arch and Truss Structure has the smallest displacement in the direction of y on the top of the piles as shown in Table 2.

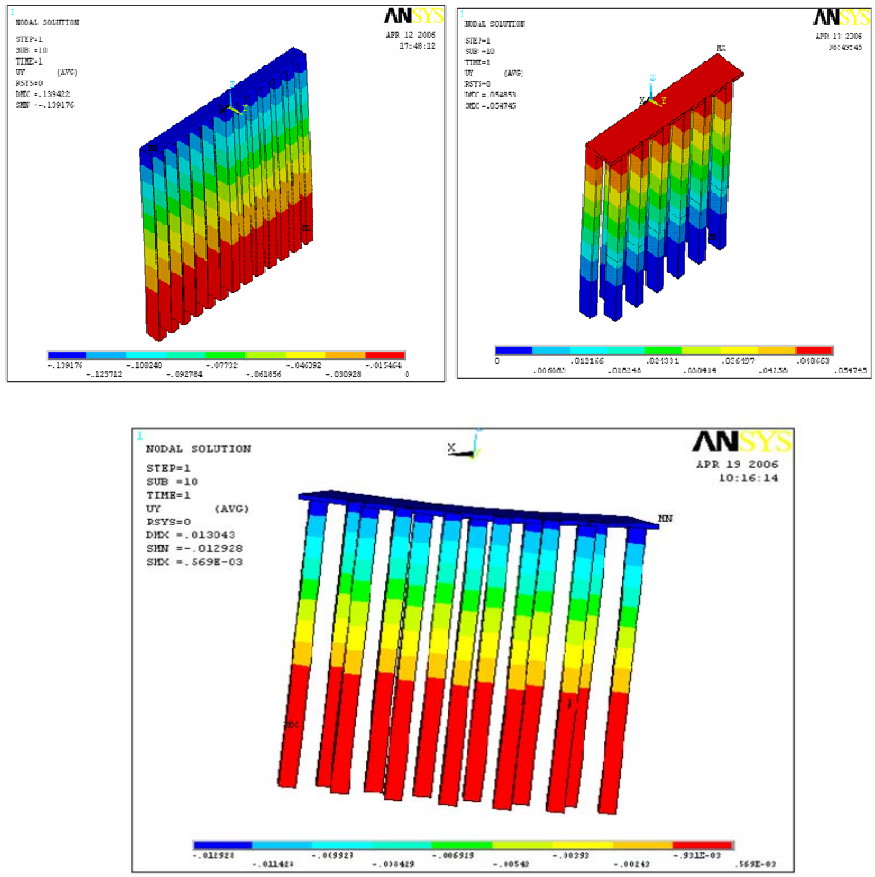

Figure 11. The displacement isoline of three kinds of piles.

As is shown in Table 2, the displacement of Anti-slide Pile Composed of Arch and Truss Structure has fallen remarkably when comparing to the other two kinds of piles. The top displacement of the double-row pile (55 mm) declined by 60% to the single-row pile (139 mm), but the new pile is more than 76% than that of the double-row pile. The distribution of the deformation along the new kind of the pile is more rational and smaller than the other side. With the existing arch and truss structure, the overall stiffness of the new pile increased so the deformation was lower than the other two conventional piles. At the same time, the turn of the arch and the pile on the top was restricted with a rigid joint in order to resist the overturn of all and create greater stability.

Table 2. The comparison of the displacement on the top of the piles.

Software	Single-row pile	Double-row pile	The new pile
MIDAS	100 mm	40 mm	9 mm
ANSYS	139 mm	55 mm	13 mm

CONCLUSION

The Pile Composed of Arch and Truss Structure has been developed and acknowledged by the FEM software MIDAS/CIVIL and ANSYS. The main conclusions are as follows: Firstly, by taking advantages of the arch and truss mechanical property to increase the overall stiffness, the planout of the pile, which is a circular arc, is reasonable and decreases the deformation of the slope. Secondly, due to considering the pile-soil effects in 3D space, the distribution of deformation along the new pile and the displacement on the top are much smaller than the conventional piles. Thirdly, the position of the new pile is diversified based on the local terrain and the geological condition for the purpose of using the advantages of the arch and truss. Fourthly, the cost of the pile, which is constructed by reinforced concrete, will greatly be reduced because of the smaller deformation accordingly. So the new pile has a wonderful prospect in highway slope treatment engineering.

BIBLIOGRAPHY

LI Haiguang (2004). *New type supported retaining structure design and project examples*, Beijing, China.

OU Xiangping and QIU Hongsheng (2004). *A research paper about the slippery stability evaluation of HURONG expressway in KI77 + 000-K17 8 + 400*, WuHan University of technology, China.

SI Xiaojing (2005). *Study on Program of Anti-Sliding Pile Analysis and Calculation*, JiLing University, China.

Analysis the Influences of Fatigue on Driver's Behavior Characteristics

Y. Ma,[1] Y. Pei[1], and Y. Wang[1]

[1]School of Transportation Science and Engineering, Harbin Institute of Technology, P.O. Box 2525, Harbin, 150090; PH (86) 0451-86282832; FAX (86) 0451-86282832; email: mayanlihit@163.com, yulongp@263.net, wangyaqiao@163.com

ABSTRACT

This paper explores the influences of fatigue on a driver's sensation, judgment, and operating characteristics. Researching the effects of fatigue on driving has great significance for the prevention and reduction of the accidents caused by fatigue. By analyzing the influences of fatigue on driving, different methods of experimental psychological testing and investigation fatigue can be used to research the driver's sensation, judgment, and operating characteristics under different degrees of fatigue., and confirm the relationship between the driving fatigue degree and the driving characteristics evaluation after testing the indicator. This research determines the value of appraisal indicators on driving characteristics under different degrees of fatigue. The findings provide the reference basis for the related departments to constitute or revise the rules of driving time.

Keywords: fatigue degree; experimental psychology; indicator of driving characteristics; continuous driving time

INTRODUCTION

Driver fatigue easily leads to erroneous driving behavior. According to statistics, 40~70 percent of traffic accidents is due to driving fatigue (Jian 2002). In those accidents, the ones caused by perception fatigue accounted for 40.1 percent, and the accidents caused by judgment fatigue accounted for 41.5 percent. Perception and judgment fatigue of the drivers are the main reasons for accidents (Williamson and Boufous 2006). To research the impact of fatigue on drivers, propose the measurements from the aspect of technology and management are very necessary for reducing traffic accidents caused by driving fatigue. Based on the road traffic conditions, use the methods of Experimental Psychology Testing and subjective fatigue investigative methods, research the impact of fatigue on indicators of a driver's perception, and research judgment and operating characteristics after continuously driving. Analyze the changing rules of the evaluation indicators;

determine indicator's value and its evaluation degree on driving characteristics under different fatigue levels. Provide the reference basis for the related departments to constitute or revise the rules of driving time.

THE INFLUENCE ANALYSIS OF FATIGUE ON DRIVING SAFETY

Driver fatigue might easily lead to a decline in perception, judgment, and vehicle operation after long periods of driving time, and it could definitely increase the risk of traffic accidents occurring. Driving fatigue can be divided into three phases that are perception, judgment, and operation. These three phases of fatigue may impact traffic safety in different ways (Harbluk et al. 2007). Figure 1 shows the influences of driving fatigue on safety.

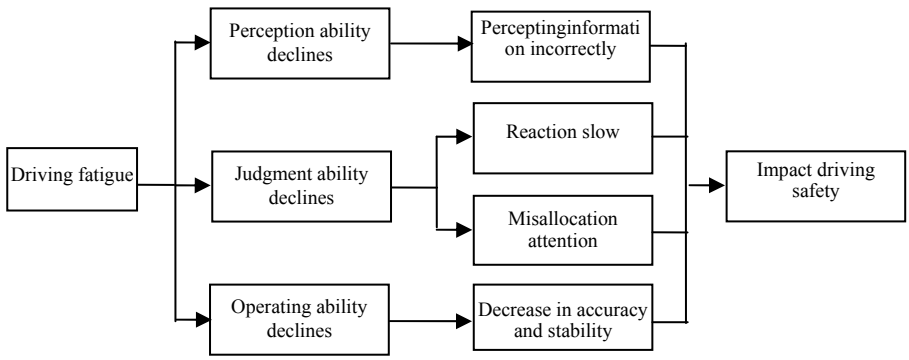

Figure 1. Influence of fatigue on driving safety.

TESTING OF FATIGUE ON DRIVING CHARACTERISTICS

Evaluation indicators of driving characteristics and experimental apparatus

Choose the experimental apparatus that can measure indicators accurately and conveniently to the best of our abilities. Compared with others, select the Experimental Psychology equipment produced from Beijing University Laboratory, shown in Table 1 (Ma and Pei, 2009).

Experimental design

The selection of survey sample

According to the smallest sample size calculation results (Summala et al. 1998), 40 drivers with good health and no history of traffic accidents were selected, among those 32 male drivers and 8 female drivers with an average age of 37 with an average driving experience of 18.2 years. Each driver should accept at least two experiments. Researchers tested a total number of 120 samples.

Table 1. Testing indicators and instruments.

Categories	Evaluation indicators	Experimental equipment
Perception	Depth perception difference	Depth perception test instrument
	Speed perception difference	Speed perception test instrument
Reaction and judgment	Choice reaction time	Visual reaction time instrument
	attention appointment	Attention appointment instrument
Operating	Number of correct optical number response	Attention appointment instrument
	Number of wrong judgment in action	Action judgment instrument

Experimental site

The experimental road is Sui-man Highway, and the section is Harbin-Daqing, which has a design speed of 120km/h. On Daqing-Qiqihar the design speed is100km/h. The traffic flow on these highways is basically in a state of freedom, so the impact of vehicle and environmental factors will be reduced. The testing vehicles were all cars.

The testing method and program

Researchers used psychological equipment to test the driver's perception, judgment, and operating characteristics in order to analyze the evaluation indicators of driving characteristics and to record the driver's subjective feeling of fatigue at the same time. Subjective fatigue is divided into five degree with the first being the most sober, and the last one is presented the highest sleepiness.

THE RELATIONSHIP BETWEEN FATIGUE AND EVALUATION INDICATORS OF DRIVING CHARACTERISTICS

Correlation analysis between fatigue and evaluation indicators

Delete the incomplete, unstable, and abnormal data and determine the available sample is 108. Calculate the correlation coefficient of variables based on the correlation analysis method of Spearman (Summala et al. 1998, Patten et al. 2006) shown in Table 2. The subjective fatigue degree can reflect the fatigue character more accurately.

The analysis of the influence of driving fatigue on driving characteristics

The influence of driving fatigue on the ability of depth reception

Researchers test the ability of depth perception on drivers with different degrees, of fatigue and analyze the relationship between fatigue degree and depth perception. Figure 2 shows these results. From Figure 2, we can see that there are

significant differences in the ability of depth perception of drivers who are experiencing fatigue to those who are not under the influence of fatigue. As fatigue increases, a driver's depth perception decreases.

Table 2. Relationship between subjective fatigue degree and testing indicators.

Testing indicators	Samples	Subjective fatigue degree	
		Correlation coefficient *R*	Significant level *P*
Depth perception	108	0.683	< 0.01
Speed perception	108	0.755	< 0.01
Choice react time	108	0.728	< 0.01
Attention appointment	108	-0.795	< 0.01
Correct operation number	108	-0.777	< 0.01
Disoperation number	108	0.779	< 0.01
driving time	108	0.875	< 0.01

The influence of driving fatigue on the ability of speed perception

The relation between fatigue degrees and the ability of speed perception of drivers is shown in Figure 3. With the increase of fatigue degree, the ability of speed perception is decreased significantly. Fatigued drivers perceive their driving speed as higher than the actual speed they are traveling. The ability of perceived speed difference of drivers in fatigue status is higher than those who are in non-fatigue status.

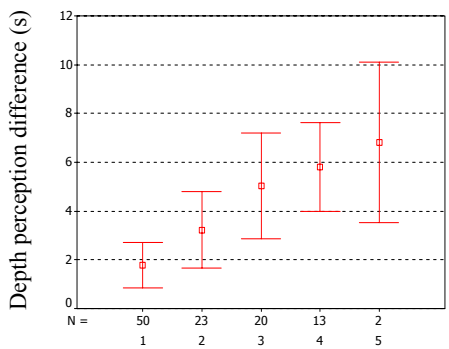

Figure 2. Relation between fatigue degree and depth perception difference.

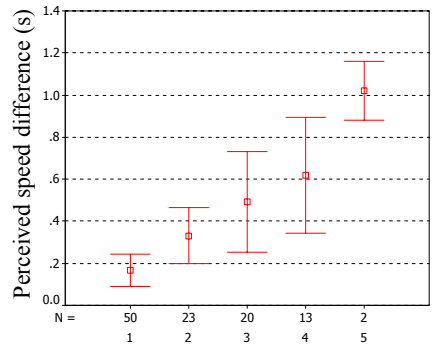

Figure 3. Relation between fatigue degree and perceived speed difference.

The influence of driving fatigue on ability of reaction

The relation between fatigue degrees and the ability of reaction of drivers is shown in Figure 4. From Figure 4, we can see that there are significant differences in the ability of drivers to react to different situations. The ability of fatigued drivers to react is significantly lower than those who are in non-fatigue status. As the fatigue degree increases, the ability of a driver's reaction decreases.

The influence of driving fatigue on ability of attention appointment

The relation between fatigue degrees and the ability of attention appointment of drivers are shown in Figure 5. From Figure 5, we can see that there was a negative correlation between the attention appointment of drivers and fatigue degree. With the increasing of fatigue degree, the ability of reaction is decreasing obviously, and there are significant differences in the ability of attention appointment under different status.

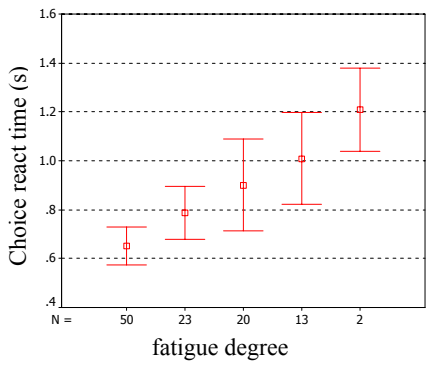

Figure 4. Relation between fatigue degree and choice react time.

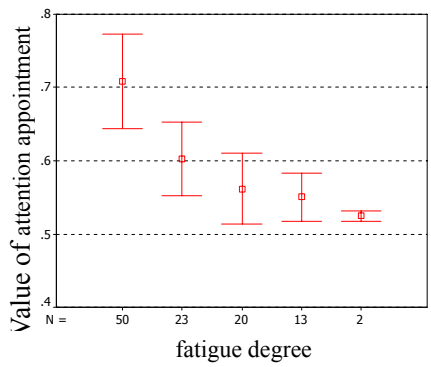

Figure 5. Relation between fatigue degree and attention appointment.

The impact of driving fatigue on correct operation number of light reaction

The relation between fatigue degrees and the ability of correct operation number of light reaction of drivers are shown in Figure 6. From Figure 6, we can see that with the increasing of fatigue degree, the correct operation number of drivers in the unit time is decreasing obviously. It is more accurate for non-fatigue drivers to complete an operation.

The impact of driving fatigue on the ability of operation judgment

The relation between fatigue degrees and the ability of operation judgment of light reaction of drivers is shown in Figure 7. From Figure 7, there are obvious differences on the ability of operation judgment of drivers. When they are in the states of fatigue, the number of disoperation decreases.

According to the method of fuzzy clustering analysis, determine the synthesis evaluation classification of driving characteristics (Ma 2007). Table 3 shows the result.

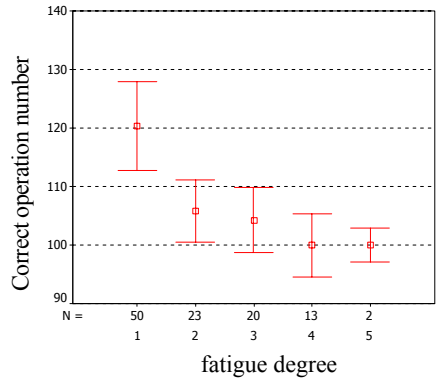

Figure 6. Relation between fatigue degree and correct operation number.

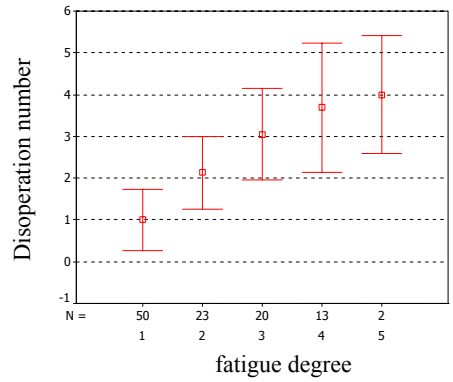

Figure 7. Relation between fatigue degree and disoperation number.

Testing indicators	Subjective fatigue degree				
	1	2	3	4	5
Driving time (min)	80	115	190	210	240
Depth perception (mm)	1.593~2.174	3.061~4.162	4.039~6.607	4.489~10.511	8.534~36.366
Speed perception (s)	0.149~0.194	0.303~0.393	0.430~0.701	0.634~1.236	0.897~2.291
Choice react time(s)	0.632~0.679	0.760~0.837	0.858~1.058	1.039~1.411	1.143~2.734
Attention appointment	0.689~0.727	0.578~0.619	0.527~0.577	0.512~0.563	0.487~0.589
Correct operation number	117.4~122.2	104.2~107.97	99.26~104.87	91.34~103.66	94.59~125.41
Disoperation number	0.78~1.18	2.08~2.64	2.65~3.85	3.45~7.55	5.32~16.71
Synthesis indicators value	0.93	0.85	0.67	0.51	0.37
Synthesis classification	Excellent	Good	General	Bad	Worse

As is shown in Table 3, the drivers' perception, choice, and operation characteristics are impacted by fatigue degree; there are obviously differences between single and synthesis evaluation classification under the same fatigue degree. If degree of subjective fatigue is between 1 and 2, the synthesis evaluation classifications of driving characteristics is in the state of good, with the increase of the fatigue degree, the synthesis evaluation classifications of driving characteristics drop gradually. When the fatigue degree is at 4, the synthesis evaluation classifications of driving characteristics is in the state of bad, and the drivers may make mistakes on speed perception, choice, and operation, all of which could easily lead to a traffic accident.

CONCLUSION

A driver's subjective can be used as driving fatigue evaluation indicators; With the increase of continuous driving time, the degree of subjective fatigue of the driver is increasing, and the general level of driving characteristics decreases gradually; When the fatigue degree is 4, the driver's driving characteristics are in a poor state, the speed of perception and ability to react are incorrect. The research of fatigue on driver's perception, judgment, and operating characteristics would provide a reference for determining continuous time and improving the regulations of driving safety.

ACKNOWLEDGMENT

This research was supported by the Research Fund for Postdoctoral Science Foundation of Heilongjiang Province of China and the Doctoral Program of Higher Education (200802131013).

REFERENCES

Williamson, A. and Boufous, S. (2006). "A data-matching study of the role of fatigue in work-related crashes." *Transportation Research Part F:* Traffic Psychology and Behavior. Corrected Proof, Available online 8 December 6(2): 211~215

Patten, C. J. D. and Kircher, A. (2006). "Driver experience and cognitive workload in different traffic environments." *Accident Analysis and Prevention.* 38(5): 887-894.

Summala, H., Lamble, D. and Laakso, M. (1998). "Driving experience and perception of the lead car's braking when looking at in-car indexes.. *Accident Analysis and Prevention*. 30(4): 401-407.

Jian, J. (2002). "Evaluation of driving fatigue mechanism and feedback selecting

model." Chengdu: College of Traffic and Transportation, *Southwest Jiaotong University*.

Harbluk, J. L., Noy Y. I. (2002) "An on-road assessment of cognitive distraction: impacts on drivers' visual behavior and braking pPerformance." *Accident Analysis and Prevention*. 39(2): 372-379.

Ma, Y., and Pei, Y.. (2009). "Influences of continuous driving time on test indicators of driving characteristics." *China Journal of Highway and Transport.* 22(1): 84-88.

Ma, Y.. (2007). "Study on characteristics of driving and its countermeasures to road safety." Harbin: School of Transportation Science & Engineering, Harbin Institute of Technology, 2007.6.

Dilemma Zone Modeling using Yellow-Onset Vehicular Trajectory Data

Heng Wei[1] and Zhixia Li[2]

[1]Art-Engines Laboratory, Department of Civil and Environmental Engineering, University of Cincinnati , P.O. Box 210071, Cincinnati, OH 45221-0071, USA; PH (513) 556- 3781; FAX (513) 556-2599; email: heng.wei@uc.edu
[2]Art-Engines Laboratory, Department of Civil and Environmental Engineering, University of Cincinnati, Cincinnati, OH 45221-0071; PH (513) 484- 2991, USA; email: lizx@email.uc.edu

ABSTRACT

Dilemma zone is dynamically featured both in location and length at signalized intersections. This study presents a proof-of-concept development of the innovative methodology for characterizing the dynamics of dilemma zones using video-capture techniques. With availability of ground-truth video and extracted vehicle trajectory data, various dilemma zone contributing factors, such as vehicle type, speed at the onset of yellow indication, onset acceleration/deceleration, dilemma zone behavior (pass or stop), yellow duration, and arrival type can be identified and/or quantified. More importantly, the study quantitatively distinguishes and models the risky zone and option zone, both of which constitute a dilemma zone under varied speeds and yellow durations. The paper demonstrates a significant advancement in dilemma zone data analysis and modeling, which provides a solid basis for further research on modeling the dynamics of dilemma zones and loop detectors placement for dilemma zone protection problems in the future.

INTRODUCTION

Among all possible factors contributing to vehicle collisions at high-speed signalized intersections, the yellow phase dilemma is one of the major problems that have not been fully solved yet. A dilemma zone (DZ) is defined as a roadway segment within which a vehicle approaching an intersection during the yellow interval can neither safely clear the intersection, nor stop comfortably at the stop line (Gazis et al, 1960). As is illustrated by Figure 1.a, the DZ is formed due to the minimum safe stopping distance (X_c) being longer than the maximum yellow clearance distance (X_0).

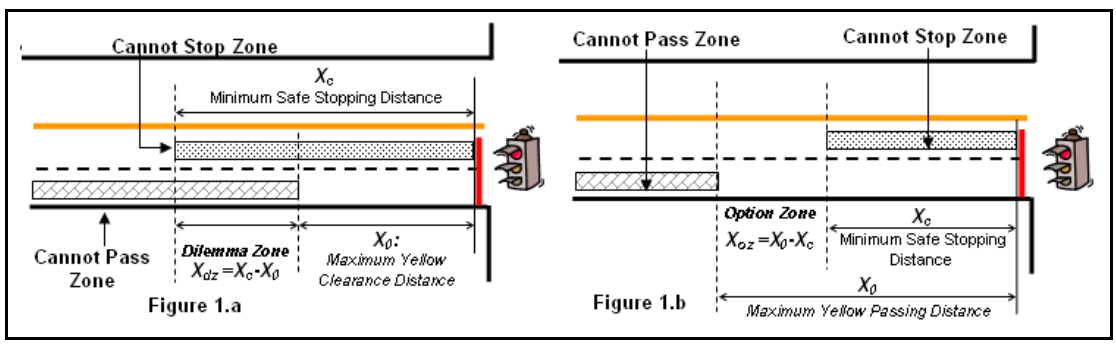

Figure 1. Formation of Dilemma Zone and Option Zone.

With existence of DZ, the drivers are exposed to a potentially hazardous condition in which a rear end accident may occur if the leading vehicle stops abruptly during the yellow interval. An angle accident may occur if the driver attempts to cross the intersection at the onset of the red interval (Pant et al., 2005). The concept of DZ along with its mathematical model, the GHM model, is further applied in the handbooks of the Institute of Transportation Engineers (ITE, 1982) for determining the safe yellow change interval. Although it is assumed that the DZ can be eliminated ($X_0 \geq X_c$) when the yellow interval is calculated based on the ITE formula (ITE, 1982), more and more researchers (Saito et al., 1990; Koll et al., 2004) now agree that even when $X_0 \geq X_c$, drivers within the range between X_c and X_0 at the yellow onset still experience indecisiveness (dilemma) about whether to pass or to stop. This range is known as the option zone (OZ), as illustrated by Figure 1.b, and has been proved to be a potential cause of intersection crashes as well.

Both DZ and OZ are dynamically featured in location and length (Moon and Coleman, 2002; Chang and Liu, 2006). This dynamics is caused due to varying drivers' aggressiveness upon seeing the yellow indication, and can be reflected by the varying values of contributing factors, such as the driver's perception-reaction time (PRT), and the acceleration/deceleration rate. Traditionally, the locations of the DZ and OZ are determined based on theoretically estimated values of these contributing factors (Pant et al., 2005; FHWA, 2006), which have been proved to be incapable of representing the DZ/OZ dynamics, and yield inaccurate DZ/OZ locations. Recently, Chang and Liu (2006) used *fixed spatial-point* trajectory data to facilitate studying the dynamic features of dilemma zone. They computed the DZ lengths based on the GHM model by using the average values of the contributing factors obtained from the trajectory data. It is a big advance in modeling the dynamic dilemma zone using trajectory data. But, computing the DZ lengths with those average factor values is still hard to reflect the DZ dynamics as well as the exact DZ locations.

This research demonstrates a novel method that uses *time-based* yellow-onset trajectories to model the dynamic dilemma zones. A video-capture-based software program VEVID (Vehicle Video-Capture Data Collector) is developed by the authors (Wei et al, 2005) to extract high-resolution (up to 30 frames per second) *time-based* trajectory data at the yellow onsets. It enables obtaining the vehicle's speed and distance from stop line at the exact instant when the signal indication changes from green to yellow. With the availability of the yellow-onset trajectories, the dilemma zone model can be calibrated based on the real driving behaviors, and reflect the exact locations of the dynamic DZ and OZ.

NEW UNDERSTANDING AND MODELING OF DILEMMA ZONE

In GHM model, the yellow interval is supposed to be used for clearing vehicles through the entire intersection (including the width of the intersection). However, based on field observations, when a driver perceives the yellow indication, he/she does not consider whether he/she could clear the intersection completely during the yellow interval. Actually, his/her concern is whether he/she could pass the stop line before the onset of the red indication. Therefore, in this study, the intersection width and vehicle's length are not considered when calculating the maximum yellow passing distance X_0.

Also, results from previous studies indicate that the values of dilemma contributing factors are not constant but vary at different approach speeds: the deceleration rate for stopping increases as the approach speed increases (Moon et al., 2003; Gates et al., 2007); the acceleration rate for passing decreases as the approach speed increases (Gazis et al., 1960); and the perception-reaction time (PRT) of drivers decreases as the approach speed increases (faster drivers reacts more quickly) (Gates et al., 2007).

Based on these understandings, the GHM model can be modified into the following equations:

$$X_c(V_0) = V_0\delta_{stop}(V_0) + \frac{V_0^2}{2 \cdot a_{stop}(V_0)} \quad (1)$$

$$X_0(V_0) = V_0\tau + \frac{1}{2}a_{pass}(V_0) \cdot [\tau - \delta_{pass}(V_0)]^2 \quad (2)$$

Where, V_0 = vehicle's approach speed (ft/s);
$X_c(V_0)$ = minimum stopping distance at speed V_0 (ft);
$X_0(V_0)$ = maximum yellow passing distance at speed V_0 (ft);
$\delta_{stop}(V_0)$ = minimum PRT for safe stopping at speed V_0 (s);
$a_{stop}(V_0)$ = maximum deceleration rate for stopping at speed V_0 ft^2/s);
$\delta_{pass}(V_0)$ = minimum PRT for safe passing at speed V_0 (s);
$a_{pass}(V_0)$ = maximum acceleration rate for passing at speed V_0 (ft^2/s);
τ = duration of the yellow interval (s).

As discussed earlier, both OZ and DZ are actually two types of yellow dilemma zones while they have different characteristics. DZ is a risky zone (RZ) that retains a hazardous chance for a vehicle happening to be located within this zone to run red, because the yellow duration is insufficient for the vehicle to safely pass the stop line while not sufficient distance for the vehicle to stop before the stop line. While not as risky as the DZ, the OZ potentially causes the driver's hesitation in the decision-making process when deciding whether stop or pass. Therefore, the dilemma zone is defined in this paper as a general concept and it is composed of risky zone and option zone, which are referred to DZ and OZ discussed in the previous section of the paper. The length of the RZ can be modeled by Equation (3), when $X_c > X_0$, while the length of the OZ can be modeled by Equation (4), when $X_0 > X_c$.

$$L_{RZ}(V_0) = X_c(V_0) - X_0(V_0) = V_0\delta_{stop}(V_0) + \frac{V_0^2}{2 \cdot a_{stop}(V_0)} - \{V_0\tau + \frac{1}{2}a_{pass}(V_0) \cdot [\tau - \delta_{pass}(V_0)]^2\} \quad (3)$$

$$L_{OZ}(V_0) = X_0(V_0) - X_c(V_0) = V_0\tau + \frac{1}{2}a_{pass}(V_0) \cdot [\tau - \delta_{pass}(V_0)]^2 - [V_0\delta_{stop}(V_0) + \frac{V_0^2}{2 \cdot a_{stop}(V_0)}] \quad (4)$$

According to the equations, it is obvious that the location of the dilemma zone is highly related to the contributing factors: $\delta_{stop}(V_0)$, $a_{stop}(V_0)$, $\delta_{pass}(V_0)$, and $a_{pass}(V_0)$. In order to determine appropriate values of these factors which reflect the real-world driving behaviors, field observations need to be conducted. And, the observed

yellow-onset trajectories can be used as ground-truth data to calibrate the dilemma zone model.

DATA COLLECTION AND TRAJECTORY EXTRACTION

The intersection of OH-4 and Seward Rd is selected as the case study site (see Figure 2), where the speed limit is 50 mph and the yellow interval is 4.5 seconds on the OH-4 approaches. In order to guarantee the full coverage of the dilemma zone, two camcorders were placed at the right of way of the eastbound OH-4 at 300 ft and 500 ft from the stop line, respectively. They were synchronized before videotaping. Totally, 6.5-hour period of traffic operation was videotaped at this location.

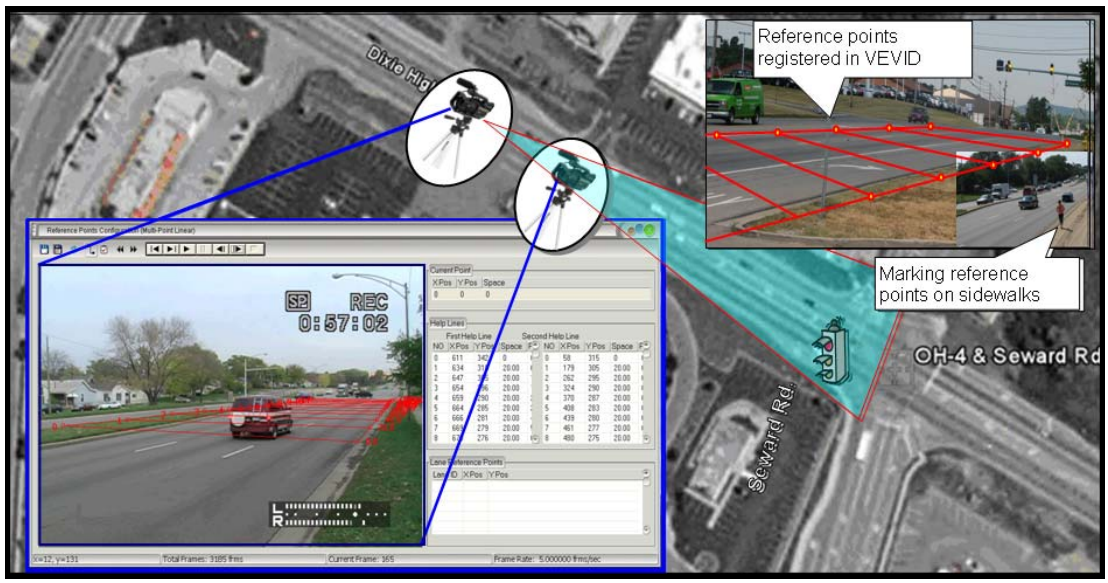

Figure 2. Video Data Collection and Trajectory Data Extraction.

In field, reference points were set up from the stop line to the position of the camcorder at a fixed spacing of 20 ft along the curbs of both sides. They were used for VEVID to convert the screen-measured distance into the real world distance (Wei et al, 2005). A chalk was used to mark those points on the curbs, and then a surveyor stepped on each mark for a short while (e.g., 5 seconds). All these actions were recorded by the camcorder.

In office, the video was played back, and the reference points were recognized and registered into the database of VEVID by identifying the surveyor's feet locations when he stepped on the marks in the video, as shown in the top-right corner of Figure 2. In VEVID, the video can pause at each exact yellow onset, and real world yellow-onset distance from the targeted vehicle to the stop line can be obtained by simply clicking the mouse over the contacting point between the rear tire (or front tire) and the pavement. With this distance, the yellow onset speed can be derived by dividing the distance interval between the frame of yellow onset and the preceding frame by the time interval. (e.g., time interval between two consecutive frames at the frame rate of 30 fps is 1/30 second).

Besides the yellow-onset distance and speed, the acceleration rate for passing and the deceleration rate for stopping were also derived and recorded. The drivers'

PRTs for stopping were recorded as well by counting the time elapsed from the yellow onset to the instant when the illumination of the brake light is observed.

During each yellow interval, only the last-to-pass (excluding those run-reds) and the first-to-stop vehicle in each through lane were targeted for extracting the trajectory data, because only these vehicles directly contribute to the formation of dilemma zone. Totally, 522 qualified vehicle samples were obtained.

MODEL CALIBRATION WITH TRAJECTORY DATA

In order to obtain the ground-truth data for the model calibration, observed yellow-onset trajectories of the first-to-stop and last-to-pass vehicles are respectively plotted on coordinate systems with the yellow-onset speed on the vertical axis and the yellow-onset distance from the stop line on the horizontal axis. Then, the ground-truth profiles of the observed minimum stopping distance X_c' and observed maximum yellow passing distance X_0' are mathematically modelled by performing regression analysis on those samples with the closest stopping distances and the furthest passing distances at various speeds, as illustrated by Figure 3 and Figure 4. The resulted relationship between X_c' and V_0 and the relationship between X_0' and V_0 can be expressed by the following equations.

$$X_c' = 0.0337V_0^2 - 0.3142V_0 + 145 \quad (5)$$
$$R^2 = 0.968$$

$$X_0' = 0.0675V_0^2 - 2.0076V_0 + 250 \quad (6)$$
$$R^2 = 0.9001$$

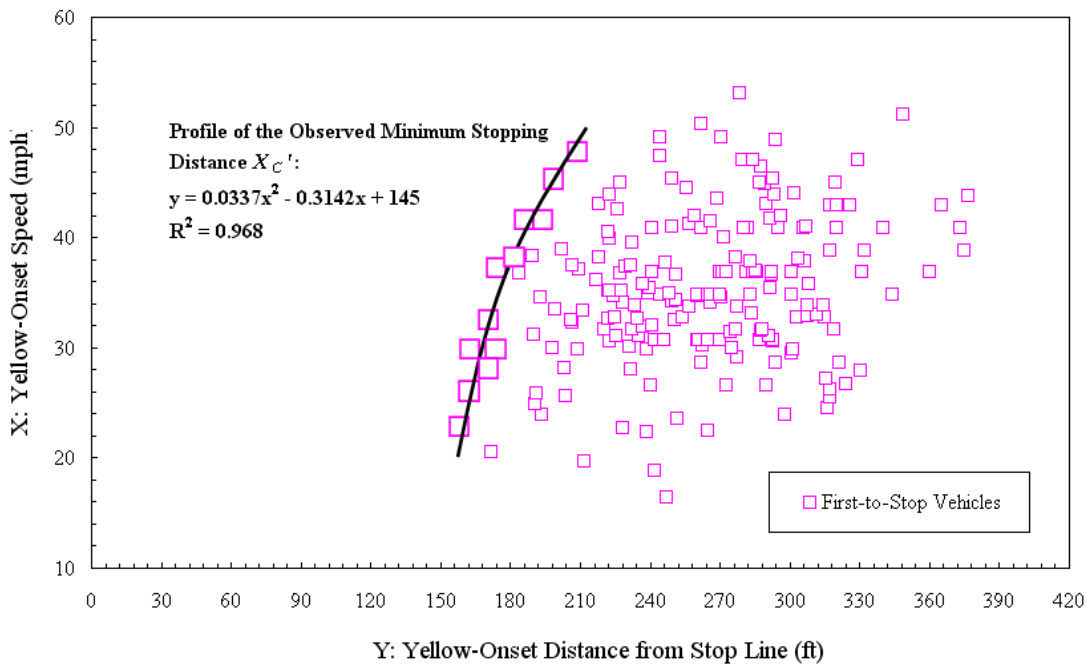

Figure 3. Yellow-Onset Trajectories and Regression Model *of* X_c'.

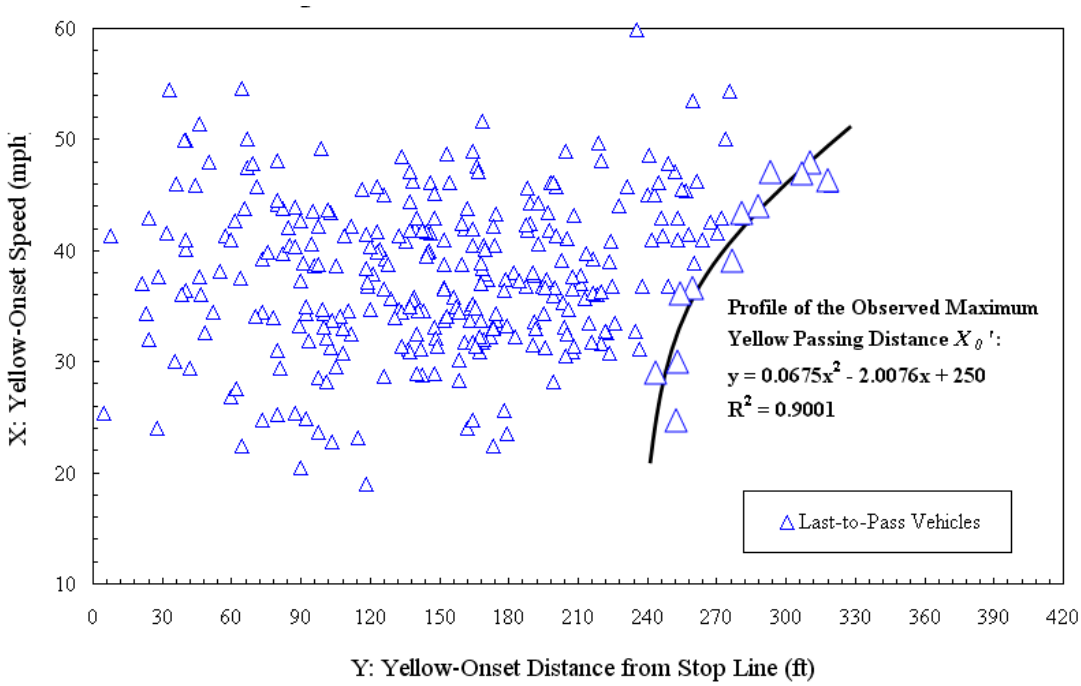

Figure 4. Yellow-Onset Trajectories and Regression Model *of* X_0'.

With the availability of the ground-truth profiles of X_0' and X_c', a process of trial-and-fit method is then employed for calibrating the X_0 and X_c models, as illustrated by Figure 5. Appropriate values of the contributing factors are obtained through fitting the modelled X_c and X_0 values (based upon Equations (1) and (2)) to the ground-truth X_0' and X_c' values (based upon Equations (5) and (6)) at each given speed.

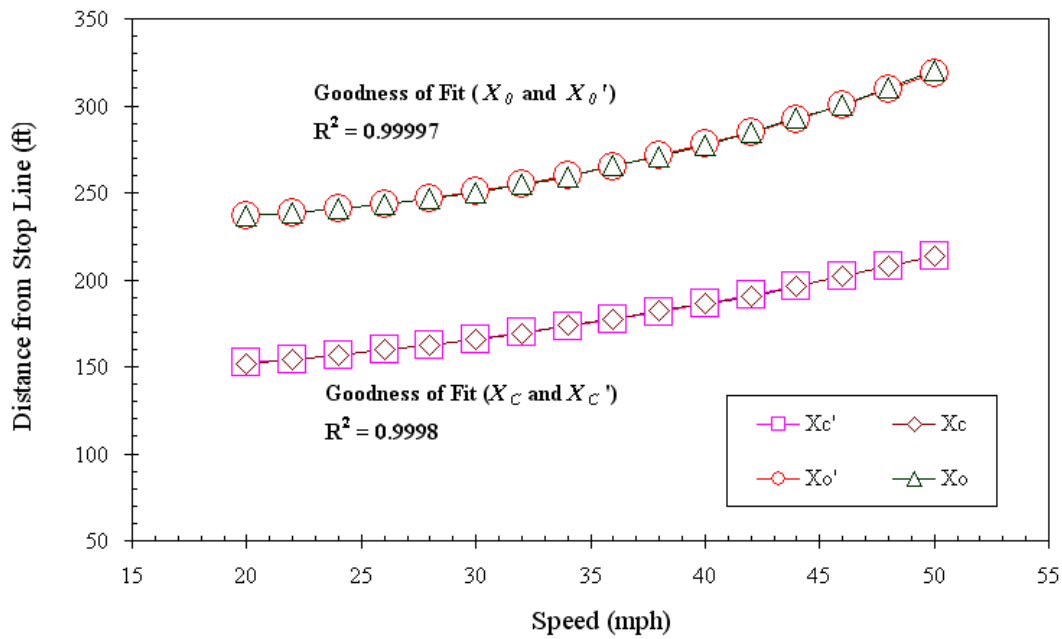

Figure 5. Model Calibration using the Trial-and-Fit Method

Note that during the calibration process, values of the contributing factors are guaranteed satisfying the following constrains: the deceleration rate for stopping increases as the approach speed increases; the acceleration rate for passing decreases as the approach speed increases; both PRTs for stopping and passing decrease as the approach speed increases; and all values of the contributing factors are within the observed ranges.

The goodness-of-fit analysis shows that the correlation coefficient R^2 is 0.9998 between the profiles of X_c and X_c', while the number is 0.9997 between the profiles of X_0 and X_0'. Both R^2 values indicate a good fitting. Through the model calibration, appropriate values of $\delta_{stop}(V_0)$, $a_{stop}(V_0)$, $\delta_{pass}(V_0)$, and $a_{pass}(V_0)$ at various speeds are obtained and shown in Table 1.

Table 1. Calibrated Values of the Contributing Factors.

V_0 (mph)	$\delta_{stop}(V_0)$ (s)	$a_{stop}(V_0)$ (ft/s^2)	$\delta_{pass}(V_0)$ (s)	$a_{pass}(V_0)$ (ft/s^2)
20	0.6	-3.2	0.505	13.01
22	0.595	-3.86	0.5	11.67
24	0.59	-4.55	0.495	10.21
26	0.585	-5.28	0.49	8.91
28	0.58	-6.09	0.485	7.68
30	0.575	-6.89	0.48	6.48
32	0.57	-7.72	0.475	5.36
34	0.565	-8.54	0.47	4.31
36	0.56	-9.45	0.465	3.36
38	0.555	-10.29	0.46	2.46
40	0.55	-11.18	0.455	1.67
42	0.545	-12.07	0.45	0.98
44	0.54	-12.91	0.445	0.23
46	0.535	-13.72	0.44	-0.34
48	0.53	-14.55	0.435	-0.89
50	0.525	-15.35	0.43	-1.12

DEVELOPMENT OF DILEMMA ZONE LOOKUP CHART

Based on the calibrated dilemma zone model, a dilemma zone lookup chart can be simply developed for practical use. It provides a convenient tool that identifies whether the risky zone or the option zone exists, and what the location and length of the dilemma zone are, for a specific speed and under a certain yellow duration. Figure 6 is the dilemma zone look-up chart developed based on the factor values in Table 1.

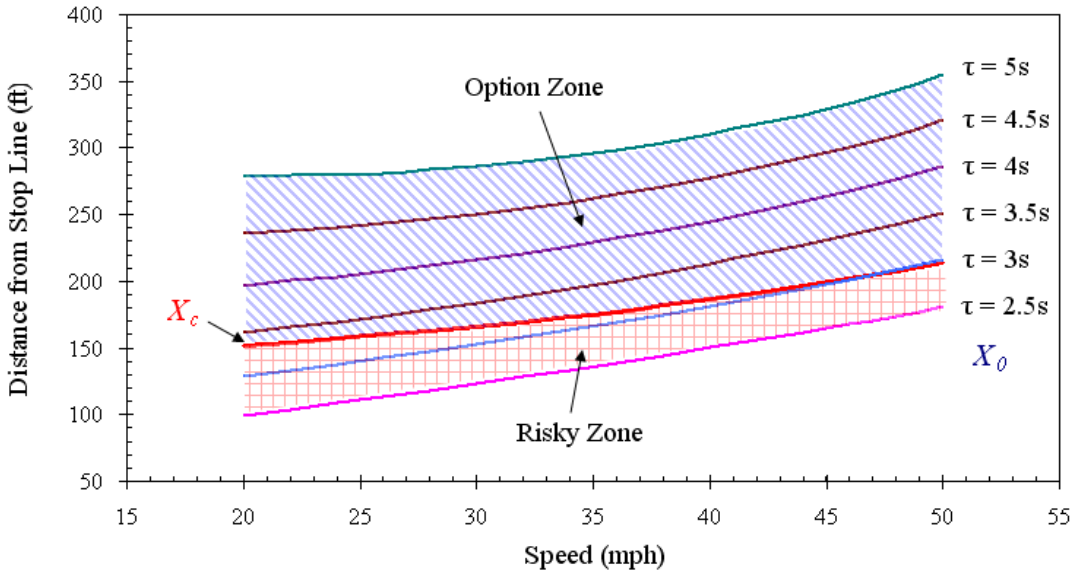

Figure 6. Dilemma Zone Lookup Chart.

In Figure 6, there is only one X_c profile, because the value of X_c does not change with the yellow durations according to Equation (1). For a specific speed and a certain yellow duration, a risky zone exists when the X_0 profile is under the X_c profile; otherwise, an option zone exists. It also indicates from the chart that the length of option zone becomes longer as the yellow duration increases, while the length of risky zone becomes shorter as the yellow duration increases. Both of the findings are in accordance with the results of previous studies (Saito et al, 1990; Koll et al, 2004).

CONCLUSION

This study conducted a proof-of-concept development of an innovative methodology for modelling the dynamic dilemma zones using video-capture techniques and time-based trajectory data. Contributing factors calibrated from the field-observed trajectory data well reflect the dynamic yellow-dilemma-related driving behaviors in the reality. As a result, the developed dilemma zone lookup chart provides a convenient tool for identifying the real location and length of dilemma zone, and is suitable for practical use. The methodology provides a solid basis for further research on the optimal placement of loop detectors for dilemma zone protection in future.

REFERENCES

Chang, G., and Liu, Y. (2006). "Interrelations Between Crash Rates, Signal Yellow Times, and Vehicle Performance Characteristics: Phase II." *Report MD-06-SP508B4B*, Maryland State Highway Administration, MD.

Federal Highway Administration (FHWA) (2006). *Traffic detector handbook 3rd Edition*.

Gates, T.J., Noyce, D.A., Laracuente,L., and Nordheim, E.V. (2007). "Analysis of Driver Behavior in Dilemma Zones at Signalized Intersections."

Transportation Research Record No. 2030, Transportation Research Board of the National Academies, Washington, D.C., 29-39.

Gazis, D., Herman, R., and Maradudin, A. (1960). "The problem of the amber signal light in traffic flow." *Operations Research*, 8(1), 112-132.

Institute of Traffic Engineers (ITE) (1985). *Transportation and Traffic Engineering Handbook*, Prentice Hall.

Koll, H., Bader, M., Axhausen, K.W. (2004). "Driver's behavior during flashing green before amber: a comparative study." *Accident Analysis and Prevention*, 36 (2), 273–280.

Moon, Y., and Coleman III, F. (2002). "Dynamic dilemma zone based on driver behavior and car-following model at highway-rail intersections." *Transportation Research – Part B*, 2002.

Moon, Y., Lee, J., and Park, Y. (2003). "System Integration and Field Tests for Developing In-Vehicle Dilemma Zone Warning System." *Transportation Research Record No. 1828*, Transportation Research Board of the National Academies, Washington, D.C., 53-59.

Pant, P. D., Cheng, Y., Rajagopal, A., Kashayi, N. (2005). "Field Testing and Implementation of Dilemma Zone Protection and Signal Coordination at Closely-spaced High Speed Intersections." *Report FHWA/OH-2005/006*, Ohio Department of Transportation, OH.

Saito, T., Ooyama, N., Sigeta, K. (1990). "Dilemma and Option Zones, the Problem and Countermeasures-characteristics of Zones, and a New Strategy of Signal Control for Minimizing Zones." *Proceedings of the Third International Conference on Road Traffic Control*, London, 137-141.

Wei, H., Meyer, E., Lee, J., Feng, C.E. (2005). "Video-Capture-Based Approach to Extract Multiple Vehicular Trajectory Data for Traffic Modeling." *ASCE Journal of Transportation Engineering*, 131(7), 496-505.

Evaluating the Impacts of Ramp Configurations and Influential Factors on Freeway Exit Ramps

Hongyun Chen[1], and Jian John Lu[2]

[1] Ph.D Candidate, Center for Urban Transportation Research (CUTR), University of South Florida, CUT 100, 4202 E. Fowler Ave, Tampa, FL, 33620, Phone: (813)9747882,Fax: (813)974-9755 Email: hchen5@mail.usf.edu

[2] Professor, P.E., Department of Civil and Environmental Engineering, University of South Florida, 4202 E. Fowler Ave. ENB118, Tampa, FL, 33620, Phone: (813)9745817, Fax: (813)974-2957 Email: lu@eng.usf.edu

ABSTRACT

The primary objective of the study is to evaluate safety performances of different exit ramps used in Florida. More specific, the research objectives include: (1) to evaluate the impacts of different ramp configurations on safety performance; and (2) to identify the different factors contributing to the crashes happening on the exit ramp sections. 389 sites were investigated throughout Florida by four ramp configurations, diamond, out connection, free-flow loop and parclo loop. Cross-sectional comparisons and crash predictive model were used to quantify the impacts. The result shows that the out connection ramps appear to have the lowest average crash. The predictive model indicates that replacing an out connection exit ramp with a diamond, free-flow, and parclo loop will increase crashes counts by 26.90%, 68.47% and 48.72% respectively. This study will help transportation decision makers develop technical guidelines governing the selection of the optimum design on freeway exit ramps.

Keywords: Exit Ramp, Configuration, Generalized Regression Model, Safety Performance

INTRODUCTION

Freeways provide the primary transportation networks by achieving the highest functional hierarchy of highway systems by design purposes. The AASHTO Green Book (A Policy on the Design of Geometric Highways and Streets) (ASSHTO 2004) defines the design standards on the highway facilities such as the ramps, interchanges and frontage roads. In order to accommodate high traffic demands of safety on freeways, exit ramps and secondary crossroads, designing proper handlings of freeways and ramps are essential in the highway systems. Also, the crash is a direct index on safety evaluations. The wide variety of site geometric conditions, traffic volumes, highway types, and design layouts could eliminate or increase conflict points at some degrees while crashes related to conflict points at some levels. Successful managements on the exit ramp sections could obtain benefits on economics and gain satisfactions on safety improvements. The newest instruction is the ITE "Freeway and Interchange Geometric Design Handbook" edited by Joel (2006). The handbook focuses on geometric and operational characteristics of

freeways and interchanges. The book recognized that geometric design procedures for freeways and interchanges may vary. It also provides the evidence that is valued as an accompaniment of the AASHTO Green book (ASSHTO 2004), the Highway Capacity Manual (HCM 2000), and Traffic engineering Handbook 5th Edition (Pline 1999). "Ramp Management and Control Handbook" (FHWA 2006), aims to manage ramp policies, strategies and technologies as to improve safety on the exit ramp and the influential areas.

Several types of exit ramps are used for traffic to exit freeways; however, the impacts of exit ramp types on the safety performance have not been well studied or documented until recently and little focus has been put on the safety issues in the State of Florida as well. So this study would conduct comprehensive crash comparisons and analyses on freeway exit ramp sections. The results will help transportation decision makers develop tailored technical guidelines governing the selection of the optimum exit ramps and the related factors to be used on freeway exit ramp sections. Since the limit work that has been performed, a few tentative conclusions could be drawn. Moreover, the various influential factors on the safety performance at entire exit ramp sections need to be revised since previous studies have a few limitations. Lord and Bonneson (2005) calibrated predictive models for different ramp configurations at 44 selected sites. The ramp design configurations addressed in this study included diagonal ramps, non-free-flow loop ramps, free-flow loop ramps, and outer connection ramps. The non-free-flow (parclo flow loop) ramp experienced twice as many accidents as other types of ramps. Bauer and Harwood (1998) modeled the Negative Binomial regression model on the entire ramp section as well and concluded that diamond ramp have slight less crash frequency comparing to other ramp types when other influential variables remain constant. At the same year, Khorashadi (1998) used another method known as ANOVA test to forecast the relationship among ramp configurations, geometry parameters and crash frequencies. This study found that the geometric elements had much weaker impacts than the ramp configurations.

It is obvious that few studies consider the following two issues in the safety effects, widening and ramp terminal treatments. Widening in this study is defined as the number of lanes changing after the pointed nose or in the middle of the entire ramp. The definition of ramp terminal treatments in "Ramp Management and Control Handbook" is those can be implemented at ramp/arterial connections as to better manage traffic exiting the ramp facility. Diverse terminal control strategies have the potentials to affect operations on the exit ramp and adjacent arterials. Accordingly, different terminal control designs or different combinations of terminal designs might have various powers on the safety aspects of entire ramp sections.

The objective of the study is to evaluate safety performances of different exit ramps used in Florida and nationals. The research objectives can divide into two parts. The first one is to evaluate how the impacts of different exit ramp types on the safety performance of freeway exit ramps. The second one focuses on identifying the different factors contributing to the crashes happening on the ramp sections. The four different configurations and other parameters on the entire exit ramp sections are

examined as well to find their effects on the safety features for the entire ramps. Base on the result in this study, it would be a way to judge what kind of geometric, traffic, and combinations of the correlated conditions have the best safety performance on the freeway diverge sections and entire exit ramp sections. Four widely used configurations in United States are identified in the study. They are defined as diamond exit ramps, out connection exit ramps, free-flow loop exit ramps and parclo loop exit ramps. From Figure 1-A to Figure-D illustrate the four ramp configurations which describe the shape of ramps in simplified modes.

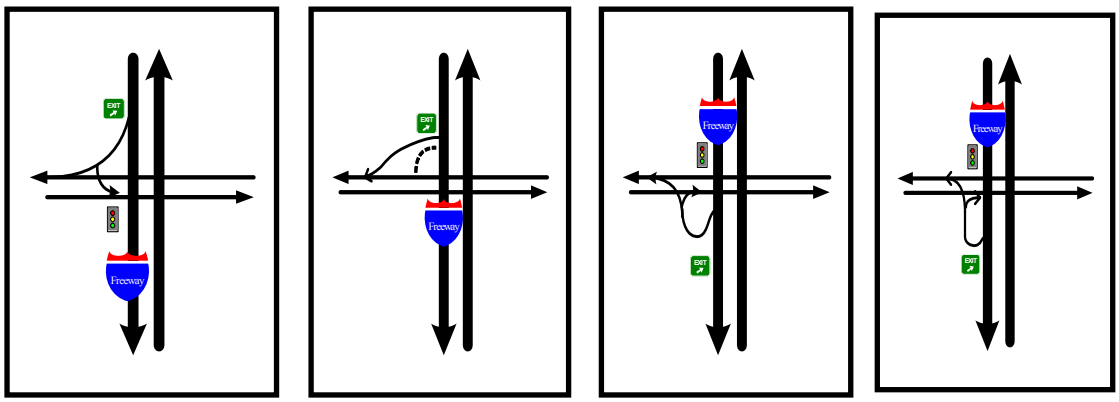

A. Diamond Loop **B. Outer Connection** **C. Free-flow Loop** **D. Parclo**

FIGURE 1 Typical Four Exit Ramp Configurations

Figure 1-A is a diamond exit ramp which is a one-way road with both left and right turnings at terminals. Figure 1-B is an out connection exit ramp which only supplies the single turn at the ends of exit ramps. Figure 1-C and 1-D are two classic loop ramps that make at least 270 degrees of turning movements to the secondary roads. Free-flow loop ramps are designed as full cloverleaf ramps with or without collector or distributor roads on the ramp segments. The parclo loop exit ramp is a partial cloverleaf ramp which has a preference to provide an arrangement setting the right exiting vehicles.

METHODOLOGY and DATA COLLECTION

Crash Data

Crash frequencies or crash rates are two indicators that are generally used in the safety studies to compare different treatments. The resource of the noticed crashes is only from police long form crash report which describes specific features for each crash. In this study, crash rate is defined as crashes per million vehicles per vehicle miles traveled for a specific section. Crash rates are used as a criterion for more truthful for segments under the same geometric and traffic conditions to narrow the impacts of these important factors. The crash rate, r, for a particular freeway segment can be calculated in the following formula:

$$r = \frac{1{,}000{,}000 \times A}{365 \times T \times V \times L} \quad (1)$$

Where, r = crash rate at a freeway segment (crashes per million vehicles per mile); A= number of report crashes (crashes per year); T= number of years; V= average daily traffic volume (vehicles per day); L= length of the freeway segment (miles).

Cross-Sectional Comparison Approach

The cross-sectional comparison analysis is satisfactory to provide adequate and reasonable consequences. In this study, cross-sectional comparison was conducted to measure exit ramp sections with four configurations. On the basis of the collected crash data, statistical analysis was conducted to quantitatively evaluate the safety impacts of different exit ramp types. Hypothesis tests are utilized to test whether the observed differences of the selected variables such as mean values between two or more groups have significantly variation in a statistical term. The average crash number and crash rate from one type to another one were examined if they are significantly different. At a 90% confidence level, T-test is used as follows:

$$t_0 = \frac{\overline{X}_1 - \overline{X}_2}{\sqrt{s_p^2(\frac{1}{n_1} + \frac{1}{n_2})}} \quad (2)$$

Statistical Predictive Model

In order to identify the factors that contribute to the crashes and quantify the effects on crashes at selected sites, generalized linear models are used for modeling crashes at selected segments. Generalized linear models are the expansion forms of the classical linear regression models. The classical linear regression model assumes that the dependent variable is continuous and normally distributed with a constant variance. Numerous previous studies have suggested the use of Poisson models or Negative-Binomial (NB) Models for modeling crash data. If the linear predictor is a linear function of the explanatory variables, the fitted crash prediction model takes the functional form as below:

$$\mu_i = \exp(\beta_0 + \beta_1 x_{i1} + \beta_2 x_{i2} + ... + \beta_k x_{ik}) \quad (3)$$

Where, β_0, β_1,…β_k = coefficients of explanatory variables;x_{i1}, x_{i2}, … …x_{ik} = explanatory variables. Two parameters are often used for evaluating the goodness-of-fit of a generalized linear model, the scaled deviance (SD) and the Pearson's χ^2.

Data Collection

The crash frequency is related to the segment length since different distances might have different effects on the number of crashes when other situations are equal. The entire ramp section is the length of the exit ramp itself. The definition means that the painted nose is the beginning of exit ramp and the end of terminals is the closing stages for the exit ramp. Figure 2 present the ramp segment lengths for four ramp configurations as mentioned above. From the four figures, four bold lines added to each one illustrate the study field for ramps.

Figure 2-A. Diamond Exit Ramp Segment Length

Figure 2-B. Out Connection Exit Ramp Length

Figure 2-C Loop Exit Ramp Segment Length

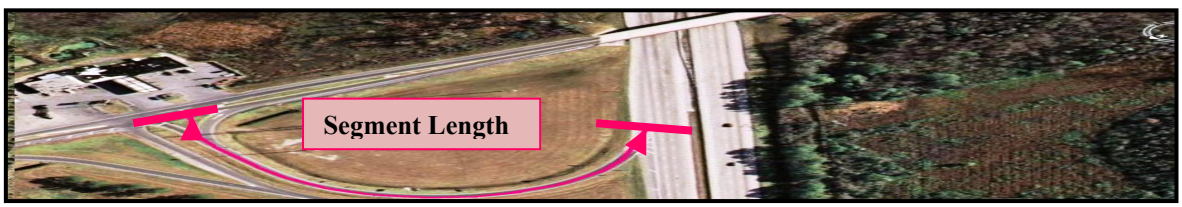

Figure 2-D. Parclo Loop Exit Ramp Segment Length

FIGURE 2. Exit Ramp Segment Lengths for Four Ramp Configurations

DATA ANALYSIS

As mentioned previously, the cross-sectional comparisons were conducted to compare the effects of the four ramp configurations on the safety performance of the exit ramp sections respectively. A total of 389 sites with 247sites for diamond ramps, 93 sites for out collection ramps, 26 sites for free-flow loop ramps, and 23 sites for parco loop ramps were categorized. A total of 2520 crashes were stated for the entire segments for three years from 2004 to 2006. The sites were grouped for four configurations simply named as D (Diamond), O (Out-connector), F (Free-flow Loop) and P (Parclo Loop). The average crash frequencies for the four groups are 2.20, 2.32, 2.21 and 1.00 crashes per site per year. Summary statistics for average crash frequency and average crash rate by four exit ramp configuration groups were given in Table 1. The average crash frequencies indicate the parclo loop group has the less average crash frequency, however the average crash rates point out that the out

connection group has the best safety performance while considering the ramp volume and ramp length. The average crash rate is more reliable as it eliminates the impacts of different ramp volumes and ramp distances. The free-flow loop group has more potential crashes in terms of the maximum average crash rate comparing to the others.

The average crash rate for the free-flow loop group is almost 162%, and 69% more than the out connection group and the diamond group. This result shows different ramp configurations might influence the exit ramps in different ways and the free-flow ramp would have more chances to occur crashes. The conclusion is consistent with previous studies. In the past researches (Bauer and Harwood 1998, Joe. et. al 1999), diamond ramps had the best safety performances comparing to other ramp configurations. But the out connection ramps have less average crash rate than the diamond ramps. This might be the reason that the out connection ramps are widely used as the freeway interchanges that have high design standards than normal exits. These improved standards might be better sign locations before and after the entrances of exit ramps, better road conditions, or less variations along the exit ramps. For the loop exits, parclo loop ramps reported 16.7% less average crash rate than free-flow loop ramps.

Table 1 Summary of Average Crash Frequency and Crash Rate

	Crash Frequency				Crash Rate			
Type	D	O	F	P	D	O	F	P
No. of Sites	247	93	26	23	247	93	26	23
Total Crashes	544	216	57	23	544	216	57	23
Average Crash	2.20	2.32	2.21	1.00	3.47	2.24	5.86	4.88
SD.	2.46	3.44	2.20	1.09	6.35	3.89	8.33	8.9
Median	1.33	1.33	2	0.67	1.86	0.85	2.16	2.20
Max	11	22	8	4	77.11	22.25	37.28	41.51
Min	0	0	0	0	0	0	0	0

Table 2 Statistical Hypotheses Tests

Crash Type	Statistics for Two Mean Tests: 90%					
	D:O	D:F	D:P	O:F	O:P	F:P
Frequency	NO	NO	YES	NO	YES	YES
Rate	YES	YES	NO	YES	YES	NO

The average crash frequency and crash rate for each population were tested at a 90% confidence level. Table 2 listed all the results for the hypothesis tests. The comparison of the average number of crashes for the diamond exit ramps and the out connection exit ramps showing “D:O” is significantly different at 90% confidence level, listing “YES” in the table. For the crash rate, the out connection exit ramps have significant difference to the other three configurations. The out connection ramps have the least average crash rate so that it has the best safety performance among the four configurations at 90% confidence level. The free-flow ramps have the highest average crash rate and the hypothesis tests documented this configuration is more dangerous than the diamond and out connection.

Crash Predictive Model

The crash prediction model was developed to identify the factors that contribute to the crashes reported at selected exit ramp segments. Considering the available data source, a total of 388 observation sites were included in the model. One site did not have ramp design speeds which were believed significantly important to crashes. The dependent variable of the model is the average crash frequency per year reported at selected exit ramp sections. 19 independent variables were initially considered when building the crash prediction model. The crash modeling starts from a Poisson model. For an adequate model, the scaled deviance and Pearson's χ^2 divided by the degrees of freedom shall be close to one. In this study, the Pearson's χ^2 divided by the degrees of freedom was found to be 5.84, indicating the fact that the crash data are overdispersed and NB models shall be used. Stepwise regression method was used to select independent variables in the model. 8 variables were not found to be statistically significant. The best model contains 11 independent variables. The regression results of the best model are given in Table 3. The scaled deviance and Pearson's χ^2 divided by the degrees of freedom are 1.18 and 1.06 which are reasonably close to one, indicating the fact that the model is adequately fitted. The final equation of the model is:

$$Y = \exp(-1.0721 - 0.2253 X_1 + 0.4392 X_2 + 0.2973 X_3 - 0.2608 X_4 - 0.0062 X_5 + 0.6861 X_6 + 0.3679 X_7 + 0.2470 X_8 - 0.0978 X_9 + 0.0129 X_{10} + 0.0580 X_{11}) \quad (4)$$

Where, Y = expected average crash frequency in an exit ramp section (crashes/year), X_1 = 1 if the site has an out connection exit ramp, 0 others; X_2 = 1 if the site has a free-flow loop exit ramp, 0 others; X_3 = 1 if the site has parclo loop exit ramp, 0 others; X_4 = Length of the entire exit ramp (mile); X_5 = Number of lanes on the ramp sections; X_6 = 1 if the number of lanes widening after the entrance of exit ramps, 0 no; X_7 =Upstream distances between exit ramp terminal and first intersection (mile); X_8 = ADT per year in thousands on exit ramp sections; X_9 = Ramp shoulder width (mile); X_{10} =Post speed limit on mainline (mph); X_{11} = Post or suggested speed limit on exit ramp sections (mph).

Table 3 Regression Results for Crash Prediction Model for Exit Ramp Sections

Criteria for Goodness of Fit				
Criteria	DF	Value	Value/DF	
Deviance	375	441.8539	1.1783	
Scaled Deviance	375	441.8359	1.1783	
Pearson Chi-Square	375	397.9857	1.0613	
Scaled Pearson	375	397.9857	1.0613	
Log Likelihood	3221.6867			
Analysis of Parameter				
Parameter	Coefficient	S. Error	χ^2	Pr >
Intercept	-1.0721	0.8577	0.6089	0.11

Out-connect exit ramp	-0.2253	0.1577	0.0837	0.05
Free-flow loop exit ramp	0.4392	0.2428	0.9150	0.07
Parclo loop exit ramp	0.2973	0.2897	0.2704	0.09
Length of entire ramp	-0.2608	0.3117	0.3502	0.04
Number of lanes on exit ramp	-0.0062	0.1477	0.2833	0.03
Widening	0.6861	0.1466	0.9732	<0.0
Secondary Upstream	0.3679	0.1689	0.6990	0.02
ADT in thousands on ramp	0.2470	0.0860	0.4155	0.00
Should width	-0.0978	0.0775	0.0540	0.02
Post speed limit on mainline	0.0129	0.0093	0.0311	<0.0
Post or suggested speed limit	0.0580	0.0133	0.840	<0.0
Dispersion	1.1143	0.0993		

All selected independent variables were statistically significant with a 90% confidence level. The coefficients of the model show that the crash counts at exit ramp sections increase with the mainline lane number , ramp ADT, post speed limit both on mainline sections and ramp sections, distances from ramp terminals to the first upstream intersection, and widening, but decrease with the ramp length, the exit ramp lane number, and ramp shoulder type. With the increase of number of lanes on the exit ramp sections, the situation is different from diverge areas. Since more number of lanes on the ramp sections might diminish vehicle distributions on the ramp sections which are particular transition from freeway sections to the secondary roads. The desperation of vehicles would diminish conflict points on the ramp section. With longer ramp length, the impacts of freeway diverge areas and secondary cross roads would be minimal, so fewer crashes would occur comparing to those short distance ramps. With larger should width, drivers have more flexible spaces while dangerous situations happened especially for loop exit ramps that need more space to avoid angle and sideswipe crashes.

ADT exit ramp sections would increase the opportunities occurring crashes. It is consistent with previous studies. Post speed limits both on mainline and ramp sections have positive influences on the crashes. Since ramp speed is much lower than freeway segments, such as 25-40 mph, drivers would continually maintain high speed on the ramp section while the post speed limit is high; however usually ramp sections did not have a high design standard comparing to freeways. This would mistake drivers so that chances of having potential crashes would rise. Another two positive variables are the widening conditions and distance from ramp terminals to first upstream intersection. It is institutive that widening would cause more merging or diverging maneuvers which were generally the main reasons of happening crashes. The coefficient of distance from ramp terminals to first upstream intersection is 0.3679 which has a significant increase in crash frequency while the increasing the distances. It means if the intersection is far away the ramp terminals, it would raise the chances of happening crashes. If the intersection is nearby the ramp terminals, more attentions would paid at those intersection areas as most drivers are more sensitive to intersections than the normal driveways or roadways.

The coefficients for the three indicator variables have different signs, indicating the fact that the site with the out connection exit ramp has the least numbers of crashes. This conclusion is consistent with the result of our cross-sectional comparison. Based on the model, the sign of out connection exit ramp is negative. It can concluded that replacing a diamond exit ramp with an out connection exit ramp, will reduce crashes in the sections by exp (0.2253)-1=26.90%. However, replacing a diamond exit ramp with a free-flow loop ramp and a parclo loop ramp will increase crash counts at exit ramp by exp (0.4392)-1=56.86%, and exp (0.2973)-1= 35.62%. Thus, we can calculate the increasing percentages for replacing an out connection exit ramp with 68.47% and 48.72%. While only concerning on the loop exit ramp, replacing a parclo loop exit ramp with a free-flow loop exit ramp would increase crash counts by exp (0.4392-0.2973)-1=15.66%.

CONCLUSION

A total of 389 exit ramp sites were collected, 247 sites for the diamond exit ramps, 93 sites for the out connection ramps, 26 sites for the free-flow loop ramps and 23 sites for the parclo loop ramps. Summary of safety evaluation were given in following conclusions:

1) The average crash rates on four ramp configurations show that the out connection group has the best safety performance. The free-flow loop ramp is more dangerous in terms of the greatest average crash rate comparing to others.
2) The signs of the coefficients in the model indicate that the crash counts at exit ramp sections increase with the mainline lane number, ramp ADT, post speed limit both on mainline sections and ramp sections, distances from ramp terminals to the first upstream intersection, and widening, but decrease with the ramp length, the exit ramp lane number and ramp shoulder type.
3) The coefficients for ramp configurations indicate the fact that the site with the out connection exit ramp has the least numbers of crashes. Based on the model, replacing an out connection exit ramp with a diamond exit ramp, a free-flow loop ramp and a parclo loop ramp will increase crashes at exit ramp sections by 26.90%, 68.47%, and 48.72%. For the loop exit ramp, replacing a parclo loop exit ramp with a free-flow loop exit ramp would increase crashes by 15.6%.

The study provided technical specifications for transportation agencies to develop tailored guidelines or practical design instructions. Transportation engineers, researchers and investigators would benefit from the study as well. The results of this study would help transportation decision makers select the optimal exit ramp types and design combinations in our freeway mainline segments.

Reference

A Policy on Geometric Design of Highways and Streets, (2001). American Association of State Highway and Transportation Officials, Washington, DC.

Bauer K.M, Harwood D.W., (1998). Statistical Models of Accidents on Interchange Ramps and Speed-Change Lanes. FHWA-RD-97-106.

Bared J., Giering L.G., Warren L.D., 1999. Safety of Evaluation of Acceleration and Deceleration Lane Lengths. ITE Journal, 50-54.

Batenhorst R.A., Gerken J.G., (2000). Operational Analysis of Terminating Freeway Auxiliary Lanes with One-Lane and Two-Lane Exit Ramps: A Case Study. Mid-Continent Transportation Symposium 2000 Proceedings.

Bared J., Powell A., Kaisar E., Jagannathan R., 2005. Crash Comparison of Single Point and Tight Diamond Interchanges Sources. Journal of transportation Engineering, American Society of Civil Engineers, p 379-381.

Bonneson A., (2005). Calibration of Predictive Models for Estimating the Safety of Ramp Design Configurations. Transportation Research Record 0912, TRB.

Bruce,N.J., Wael A. and Juan R., (1998), Truck Accidents at Freeway Ramps: Data Analysis and High-Risk Site Identification, Journal of Transportation and Statistics, , pp. 75-92.

Cirillo J.A. Dietz SK., Beatty R.L., (1969). Analysis and Modeling of Relationships between Accidents and the Geometric and Traffic Characteristics of the Interstate System. Federal Highway Administration.

Garber N., Fontaine M., (1999). Guidelines for Preliminary Selection of the Optimum Interchange Type for a Specific Location. VTRC-99-r15.

Highway Capacity Manual. (2000). Transportation Research Board, National Council, Washington D.C.

Hunter M., Machemehl R. and Tsyganov A., (2000). Reevaluation of Ramp Design Speed Criteria: Summary Report, Center for Transportation Research, University of Texas at Austin, No. 1732-S.

Janson B.N., Awad W., Robles J., (1998). Truck Accidents at Freeway Ramps: Data Analysis and High-Risk Site Identification. Journal of Transportation and Statistics, 75-92.

James L. Pline. Traffic Engineering Handbook 5th Edition (1999), Institute of Transportation Engineers

Joanne C.W. Ng and Tarek S., (2004), Effect of geometric design consistency on road safety, Canadian Journal of Civil Engineering 31, no2 218-27.

Juan Carlos Munoz, and Carlos Daganzo, (2000), Experimental Characterization of Multi-lane Freeway Traffic Upstream of an Off-ramp Bottleneck, UCB-ITS-PWP-2000-13.

Khorashadi A., (1998). Effect of Ramp Type and Geometry on Accidents. FHWA/CA/TE-98/13, California Department of Transportation.

Keller,J., Abdel-Aty M., and Brady A. P. (2006). Type of Collision and Crash Data Evaluation at Signalized Intersection, ITE Journal

Kristen L., Sanford B., and Mark,R. V., (2002).Improving the Identification, Analysis and Correction of High-Crash Locations, ITE Journal

Leisch, Joel P, (2006). Freeway and Interchange Geometric Design Handbook, Institute of Transportation Engineers

Lord D., Bonneson A. J., (2005). Calibration of Predictive Models for Estimating Safety of Ramp Design Configurations. Transportation Research Record,

1908, 88-95, Transportation Research Board of the National Academies, Washington, D.C.

Leonard S. and William R.M, (1972). Optimal Ramp Control for Incident Response, Research and Training in Urban Transportation, Urban Mass Transportation Administration of the Department of Transportation, Britain.

Maher, M.J., Summersgill, I., (1996). A comprehensive methodology for the fitting of predictive accident models. Accident Analysis and Prevention 28, 281–296.

McCartt A.T., Northrup V.S., Retting R.A., (2004). Types and Characteristics of Ramp-Related Motor Vehicle Crashes on Urban Interstate Roadways in Northern Virginia. Journal of Safety Research, 35, 107–114

Resende P., and Benekohal R.F., (1997). Effects of Roadway Section Length on Accident Modeling, Proceedings on Traffic Congestion and Traffic Safety in the 21st Century, pp. 403-409

Sarhan M. Hassan Y., and Abd E. H., (2006). Design of Freeway Speed Change Lanes: Safety-Explicit Approach, TRB, Washington, D.C.,

Tom H. M., Garrett B., Thomas M. W. and Neal R. H., (2006). Safety Performance of Two-Way Stop-Controlled Expressway Intersection, ITE Journal

Uncertainty Analysis of Collision Velocity in Motor Vehicle Crashes Using an Evidential Reasoning Algorithm

R. Shen[1], J. Ai[2], and Y. Pei[3]

[1] School of Transportation Science and Engineering, Harbin Institute of Technology, P.O. Box 2525, 202 Haihe Rd., Harbin, China, ST 150090; PH (86) 451-8628 2832; FAX (86) 451-8628-2832; email: ssunqq@yahoo.cn
[2] Applied Foreign Language College, Heilongjiang University, 74 Xuefu Rd., Harbin, China, ST 150080; PH (86) 451-8660 8114
[3] School of Transportation Science and Engineering, Harbin Institute of Technology, P.O. Box 2526, 202 Haihe Rd. Harbin, China, ST 150090; PH (86) 451-8628 2832; FAX (86) 451-8628 2832; email: yulongp@263.net

ABSTRACT

The confirmed pre-impact velocity is the base of accident reconstruction and responsibility identification. The uncertainty of pre-impact velocity calculation is defined as the warp between the result of accident reconstruction and fact, caused by the error from measurement and estimation, or some unknown information. To deal with this problem, a fuzzy rule-based evidential reasoning algorithm is employed in pre-impact velocity calculation. Taking certain influencing factors into consideration, referring variables are taken as the sub-attributes of the pre-impact velocity. The process is building a multiple hierarchical structure model presented with an evidential reasoning algorithm. The quantitative sub-attributes can be calculated with aggregating different degrees, and combined degrees of belief and uncertain belief of all the sub-attributes for the calculation to the pre-impact velocity through evidential reasoning algorithm. The results show that this algorithm is applicable to analyze the calculation results of collision velocity. And uncertainty analysis of accident reconstruction is significant and essential.

INTRODUCTION

Accident reconstruction is important when analyzing an accident and confirming who is responsible for the accident. The reconstruction process is often influenced by some uncertain factor. For example, in the spot measurement, the surveyors need to measure some parameters with instrumental and qualitative estimation, mainly involving geometric parameters, environmental parameters, motion parameters, vehicle parameters, anthropometric parameters, and experimental parameter,. Because of the error from measurement and estimation, the difference

between the result of accident reconstruction and fact comes out, which is defined as uncertainty.

For road accident identification, the pre-impact velocity confirmed is one of the important factors for the analysis of road accidents, which is the basis of responsibility identification. Sometimes the special value of pre-impact velocity is not necessarily a concern. The range of pre-impact velocity confirmed is perhaps enough. Therefore, the analysis of uncertainty is brought on the further perceivable lay. On the basis of the uncertain degree estimation, the result of velocity estimation would be suitable to actual circumstances under the same unknown condition.

In this paper, attention is focused on the problem of the effect of referring parameter variables on pre-impact velocity with uncertainty.

UNCERTAIN PARAMETER ANALYSIS WITH CLASSICAL MODELS

There are several methods to use when calculating the pre-crashing speed, namely momentum equation, kinetic energy theorem, energy conservation, to list a few. By the energy-work equivalence principle, after vehicles collide, the vehicles' separation speeds were determined using McHenry-Marquard's theoretical-empirical dependencies, derived from the energy-work equivalence principle. In the model, the frictional impulses are ignored. In the post-crash movement, two vehicles remain in contact with the ground[1]. Vehicles' angular velocities at separation follow as:

$$\omega_j^{(sep)} = \operatorname{sgn}\Delta\varphi_j \cdot \sqrt{\frac{\mu_j \cdot g \cdot \Delta\varphi_j{}^2}{(I_j/(m_j \cdot L_j)) \cdot \left|\Delta\varphi_j\right| \cdot (1-f_j) + (s_j/1.7)}} \tag{1}$$

Where j is the number of the vehicle, $\Delta\varphi_j$ the total angle of rotation in post-impact motion (rad), μ_j the friction coefficient, g the gravity coefficient, 9.81(m/s^2), I_j the moment of inertia (kg m^2), m_j the real mass(m), L_j the wheel base (m), f_j the coefficient of post-impact motion drag (from 0 for all wheels freely rotating to 1 for all wheels locked), and s_j the distance between center of gravities (CGs) of vehicles' impact and rest position (m)[1]. Speeds of vehicles' CGs at separation follow as:

$$v_j^{(sep)} = 1.7 \cdot \left[\frac{\mu_j \cdot g \cdot \left|\Delta\varphi_j\right|}{\omega_j^{(sep)}} - \frac{I_j \cdot \left|\omega_j^{(sep)}\right| \cdot (1-f_j)}{m_j \cdot L_j} \right] \quad (j=1,2) \tag{2}$$

In the article, the example is chosen from literature [1], in order to have a comparison analysis. By the momentum conservation, not take into account the restitution coefficient and sliding energy loss during crash process. Therefore, angular velocities at impact are 0[1]. The principle of momentum conservation follows as:

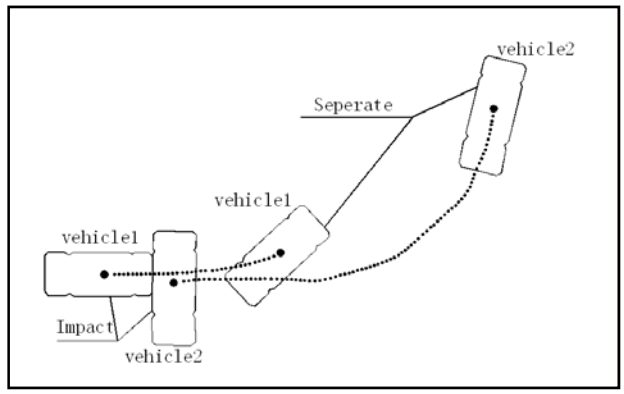

Figure 1. Two vehicle collision hint.

$$m_1 v_1^{(imp)} \cdot \sin(\alpha_1^{(imp)} - \alpha_2^{(imp)}) = m_1 v_1^{(sep)} \cdot \sin(\alpha_1^{(sep)} - \alpha_2^{(imp)}) + m_2 v_2^{(sep)} \sin(\alpha_2^{(sep)} - \alpha_2^{(imp)})$$

(3)

Throughout the formulas (1), (2), and (3), the impact velocities are functions referring some variables, following as:

$$v_j^{(imp)} = z(\mu_1, I_1, m_1, f_1, s_1, \mu_2, I_2, m_2, f_2, s_2, \alpha_1^{(sep)}, \alpha_2^{(sep)}, \alpha_1^{(imp)}, \alpha_2^{(imp)}) \quad (j=1,2) \qquad (4)$$

As can be easily noticed, formula (4) is complicated for referring independent variables. The uncertainty of pre-impact velocity is brought on by all the uncertainty of these referring independent variables. Because of the variety of the independent variables, if we cannot deal with the information redundancy brought on by the referring variables and the relativity among the variables, the uncertainty may be beyond its rational range. Therefore, we need to choose a valid method to deal with.

EVIDENTIAL REASONING ALGORITHM

In the article, the evidential reasoning algorithm based Dempster-Shafer was used to measure the uncertainty of the pre-crash velocity. This method can solve the problem of the redundancy and relativity between the independent variables.

Define the top attribute of pre-impact velocity expressed by *E*. *E* has *L* (*L=14*) sub-attributes (referring independent variables), and *L* attributes are quantitative and associated with the top attribute of pre-impact velocity, which is expressed by a set: $E = \{e_1, e_2, \ldots, e_i, \ldots, e_L\}$.

Due to different sub-attributes with different dimensions, the description of different sub-attributes needs to be aggregated into a comparable index for uncertainty calculation. Therefore, the notion of assessment grade is brought in. In short, it is acceptable for the assessments of an attribute to be distributed among different grades. And a set of grades with a degree of belief structure is employed in assessing an attribute.

Let *H* represent the set of the assessment grades of an attribute, $H=\{H_n,$

n=1, ……, N }. In this article, N is set to be 5, the description as H_1={smallest}, H_2={smaller}, H_3={average}, H_4={large}, and H_5={largest}.

$$B=\{\beta_n, n=1, \ldots\ldots, N\}, 0\le\beta_n\le 1, \ \sum_{n=1}^{N}\beta_n \le 1 \ \text{ and } \ \beta_H = 1-\sum_{n=1}^{N}\beta_n \tag{5}$$

B is defined as the set of degrees of belief about which an attribute is assessed to be H, while β_H is defined as the uncertain degree of belief for the attribute.

$S(E)=\{(H_n, \beta_n), n=1, \ldots, N\}$ represents that top attribute E is assessed to grade H_n with degree of belief β_n, n=1, …, N. While β_H is defined as the belief of unassigned to any individual grade after all the N grades have been considered. The tenet of evidential reasoning algorithm is to aggregate the sets of grades with degree of belief of all sub-attributes, in order to calculate the belief degree with grades of top attribute, including the belief degree of uncertainty.

For a sub-attribute e_i, $B_i=\{\beta_{n,i}, n=1, \ldots\ldots, N\}$ is used to represent its assessment. Therefore, $S(e_i)=\{(H_n, \beta_{n,i}), n=1, \ldots, N\}(i=1, \ldots\ldots, L)$. For all sub-attributes, the numeric value of an assessment can be transformed to the set of equivalent grades.

Let $h_{N,i}$ be the largest feasible value and $h_{1,i}$ the smallest. That is a large value $h_{n+1,i}$ is larger to a smaller value $h_{n,i}$. Suppose a value $h_{n,i}$ for a sub-attribute is judged to be equivalent to a grade $H_n(n=1,\ldots\ldots, N)$. Then a value h_j on e_i is represented to a grade set with degrees of belief by using the following formulae [3].

$$\beta_{n,i} = \frac{h_{n+1,i}-h_j}{h_{n+1,i}-h_{n,i}} \ \text{ and } \ \beta_{n+1,i} = 1-\beta_{n,i}, \text{ if } h_{n,i}\le h\le h_{n+1,i} \tag{6}$$

$$\beta_{k,i} = 0 \quad \text{for } k=1, \ldots\ldots, N \text{ and } k\ne n, n+1 \tag{7}$$

$$S(e_i(h_j))=\{(h_{n,i}, \beta_{n,i}), n=1, \ldots\ldots, N\} \tag{8}$$

In this paper, pre-impact speed was taken as the top attribute. Table 1 shows 14 sub-attributes.

Let ω_i be the weight of the sub-attribute e_i in the assessment to top attribute E and $0\le\omega_i\le 1$, $\sum_{i=1}^{L}\omega_i = 1$.

$$m_{n,i}=\omega_i\beta_{n,i} \qquad (n=1, \ldots\ldots, N;\ i=1, 2, \ldots\ldots, L) \tag{9}$$

$$m_{H,i} = 1-\sum_{n=1}^{N} m_{n,i} \qquad (i=1, 2, \ldots\ldots, L) \tag{10}$$

Let $m_{n,i}$ be the basic probability mass representing the degree to which the ith sub-attribute e_i supports the hypothesis that top attribute E is assessed to the grade H_n.

$m_{H,i}$ is the remaining probability mass unassigned to any individual grade after

all the N grades have been considered for assessing the top-attribute. $m_{H,i}$ can be broken down into two parts, which are $\overline{m}_{H,i}$ and $\widetilde{m}_{H,i}$ [4].

Table 1. Hierarchical structure of pre-impact velocity with influencing factors.

Top attribute	Sub-attribute	Weight	Numerical value
	Friction coefficient μ_1	0.10	[0.6, 0.8]
	Moment of inertia I_1	0.08	[1187, 1587]
	Mass m_1	0.09	[960, 1020]
	Post-impact motion drag coefficient f_1	0.06	[0.6. 0.8]
	Distance between CG in initial and final positions s_1	0.07	[5.8, 6.2]
	Friction coefficient μ_2	0.10	[0.6, 0.8]
	Moment of inertia I_2	0.08	[1677, 2077]
	Mass m_2	0.10	[1090, 1250]
	Post-impact motion drag coefficient f_2	0.06	[0.4, 0.8]
$v_1^{(imp)}$	Distance between CG in initial and final positions s_2	0.07	[14.1, 14.5]
	Direction of vector of vehicle 1 impact velocity $\alpha_1^{(imp)}$	0.04	[-2.0 , 2.0]
	Direction of separation velocity vector $\alpha_1^{(sep)}$	0.04	[-2.37 , 3.63]
	Direction of vector of vehicle 1 impact velocity $\alpha_2^{(imp)}$	0.04	[-2.0 , 2.0]
	Direction of separation velocity vector $\alpha_2^{(sep)}$	0.04	[-1.32 , 4.68]

$$\overline{m}_{H,i} = 1 - \omega_i \quad \text{and} \quad \widetilde{m}_{H,i} = \omega_i \left(1 - \sum_{n=1}^{N} \beta_{n,i} \right) \quad (i=1, 2, \ldots\ldots, L) \tag{11}$$

To obtain the combined degrees of belief of all sub-attributes, $E_{I(i)}$ is firstly defined as the subset of the first i sub-attributes as follows:

$$E_{I(i)}=\{e_1, e_2, \ldots, e_i\} \; i \in [1, \mathrm{L}] \tag{12}$$

Let $m_{n,I(i)}$ be a probability mass defined as the degree to which all the i attributes in $E_{I(i)}$ support the hypothesis that the E is assessed to the grade H_n; let $m_{H,I(i)}$ be the remaining probability mass unassigned to individual grades after all the sub-attributes in $E_{I(i)}$ have been assessed. The relationships (13) and (14) are obviously constructed when i=1.

$$m_{n,I(1)} = m_{n,1} \qquad for\ n=1, 2, \ldots\ldots, N \tag{13}$$

$$m_{H,I(1)} = m_{H,1} \tag{14}$$

Then, based on the above definition and limits, the deduction of an evidential reasoning algorithm can be followed as[4][5]:

$$m_{n,I(i+1)} = K_{I(i+1)} [m_{n,I(i)} m_{n,i+1} + m_{H,I(i)} m_{n,i+1} + m_{n,I(i)} m_{H,i+1}] \quad (n=1, 2, \ldots\ldots, N) \tag{15}$$

$$m_{H,I(i)} = \widetilde{m}_{H,I(i)} + \overline{m}_{H,I(i)} \quad (i=1, 2, \ldots\ldots, L) \tag{16}$$

$$K_{I(i+1)} = \left[1 - \sum_{t=1}^{N} \sum_{\substack{j=1 \\ j \neq t}}^{N} m_{t,I(i)} m_{j,i+1} \right]^{-1} \tag{17}$$

$$\overline{m}_{H,I(i+1)} = K_{I(i+1)} \overline{m}_{H,I(i)} \overline{m}_{H,i+1} \tag{18}$$

$$\widetilde{m}_{H,I(i+1)} = K_{I(i+1)} [\widetilde{m}_{H,I(i)} \widetilde{m}_{H,i+1} + \overline{m}_{H,I(i)} \widetilde{m}_{H,i+1} + \widetilde{m}_{H,I(i)} \overline{m}_{H,i+1}] \tag{19}$$

Where K is the disturbed coefficient in the D-S theory, in the special evidential reasoning algorithm, and $K_{I(i+1)}$ is defined as a normalizing factor.

In summary, after all L assessments have been aggregated, the combined degrees of belief of all sub-attributes for assessment back to attribute E calculated by

$$\beta_n = \frac{m_{n,I(L)}}{1 - \overline{m}_{H,I(L)}} \qquad (n=1, 2, \ldots\ldots, N) \tag{20}$$

$$\beta_H = \frac{\widetilde{m}_{H,I(L)}}{1 - \overline{m}_{H,I(L)}} \tag{21}$$

SOLUTION AND COMPARISION ANALYSIS

In order to use the evidential reasoning approach to calculate the speed and its uncertainty, some numeric values need to be normalized first to eliminate the possible adverse influences coming from different sizes of various variables.

Throughout the calculation of the evidential reasoning approach, the result from the algorithm is the set of beliefs with different degrees. Therefore, we should set up certain functions to describe the speed.

In the case study, the speed function is set up to be a linear function with $v(H_1)$=67, $v(H_2)$=77, $v(H_3)$=87, $v(H_4)$=97, and $v(H_5)$=107. The speed function can be also set up in another nonlinear form.

The fact that the expected value of vehicle 1 speed obtained in evidential reasoning approach calculations (82.8-95.6km/h) is closer to the real value (87.7 km/h), and the uncertain degree of the speed is 0.125, therefore, the minimum value of vehicle 1 speed is 82.8 km/h, and the utmost value is 95.6km/h. If choosing the average one, the value is 89.2km/h.

Compared to the calculation results of Wach and Unarski (2007), the results are shown in the Table 2. As can be seen, the different calculation results of pre-impact speed due to the precision of the vehicle's final position obtained in literature [1]. In classical calculations and PC-Crash software, the result of speed is separately 86.8km/h and 84.0km/m, which is also closer to 87.7km/h [1]. Therefore, using the evidential reasoning algorithm calculates reasoning results in a relatively brief way, and the results are credible. Last but not least, a variety of factors are

generally considered with evidential reasoning algorithm, which is valuable. Based on the reasoning weight confirmed, the obtained result is due to the reasoning weight of the sub-attribute.

Table 2. Calculation results of pre-impact speed of vehicle 1 with different model.

classical model	PC-Crash	evidential reasoning algorithm	Monte carlo simulation (precision of position)
86.8km/h	84.0km/m	82.8km/h (minimum value) 95.6km/h (maximum value) 0.125 (uncertain degree)	76-91 km/h (10%) 68-101 km/h (20%) 58-112 km/h (30%)

CONCLUSIONS

The appropriate way to obtain the uncertainty of the pre-impact is to apply a reasoning decision method. Although some method is used, the solution process is based on the probability of distribution analysis, and the sensitivity analysis is given.

Applying the evidential reasoning approach for the solution of the pre-impact is reasonable and creditable, which gives the results as the distribution of probability density with different degrees and uncertainty.

The result is credible and valuable, and can be as the basis for responsibility identification. The uncertainty calculation is valuable and necessary, but we can also choose another method to calculate the uncertainty, or considering other influencing factors.

AKNOWLEDGEMENTS

The project is supported by the National High Technology Research and Development Program of China (863 Program) under Grant No. 2007AA11Z231. The authors would like to express their gratitude to the sponsors.

REFERENCES

Wach, W amd Unarski, J. (2007). "Uncertainty of calculation results in vehicle collision analysis." *Forensic Science International*, 167(2-3), 181-188.

Wach, W. and Unarski, J. (2006). "Determination of vehicle velocities and collision location by means of Monte Carlo simulation method." *Special Publication Accident Reconstruction SP-1999*, SAE Paper No. 2006-01-0907.

Liu, J., Yang, J. B., Wang, J., et al. (2004). "Fuzzy rule-based evidential reasoning approach for safety analysis." *International Journal of General System*, 33(2), 183-204.

Yang, J. B., and Xu, D. L. (2002). "On the evidential reasoning algorithm for multiple attribute decision analysis under uncertainty." *IEEE Transactions on System,*

Man and Cybernetic—Part A: Systems and Humans, 32(3), 289-304.

Yang, J. B. (2001). "Rule and utility based evidential reasoning approach for multi-criterion decision analysis under uncertainties." *European Journal of Operational Research*, 131(1), 31-61.

Choice of Reasonable Longitudinal Gradient at Alignments of Mountain Highways Based on Driver's Physiological Reactions

Xian-Qiang Ren[1], Jian-Yi Liu[2] and Song Gao[3]

[1] School of Automobile and Traffic Engineering, JiangSu University, Xuefu Rd. Zhenjiang 212013, China, PH (86) 536-3822 873; FAX (86) 536-3822 818; email: zhanglip0503@163.com

[2] School of Automobile and Traffic Engineering, JiangSu University, Xuefu Rd. Zhenjiang 212013, China, PH (86) 536-3822 873 ; FAX (86) 536-3822 818; email: bjliujianyi@163.com

[3] School of Transportation Engineering, Shandong University of Technology, Zhangzhou Rd. Zibo 255049, China, PH (86) 536-3822 873; FAX (86) 536-3822 818; email: gaosong@sdut.edu.cn

ABSTRACT

This paper studies the relationships of various vertical grades at longer slope mountainous terrain highways on the driver's heart rate. This paper analyzes the vertical grade effects by measuring the driver's heart-rate and the vehicle speed using the auto-recording heart-rate instrument and motive GPS respectively. The research results suggest that the profile grade at the long slope alignment should not be more than 5% for mountain highways and signing improvements which may reduce accidents in such terrains.

INTRODUCTION

In many highways in mountain areas, there are greater elevation changes and sharp horizontal curves because of the terrain and poor economic conditions. Probably traffic accidents are often caused by vehicles running on such highways due to brake destruction while braking in extreme conditions. Usually these situations have become a challenge for highways in the mountainous areas of Western China. In current conditions, the design norms must be strictly controlled to reduce the traffic accidents in consideration to the concept of 'taking humans as the basis and the tolerant design'. Therefore, it becomes increasingly important to research the reasonable design parameters of the alignment of the highways in terms of the roadway safety, the driver's comfort and other aspects.

The safe highways not only have good alignments but also meet the need of the driver's comfort. The psychological pressure and the physiological burden on the driver must be controlled at a minimal level (Liu Z. Q., Gong Z., Cai D., 2003). The experiments of the reasonable profile grade at long slope alignment of mountain highways is based on the driver's physiological reactions with the variance of heart-rate and the vehicle speed as the quantification indexes to evaluate the design parameters of the alignment. By making driving experiments in different sections of the mountain highways at various grades, the experiment results are used to study relationships between the driver's heart-rate, the vehicle

speed, and the longitudinal gradient of the long slope alignment. This paper advances some auxiliary parameters of the profile grade design based on the driver's psychological and physiological burdens.

EXPERIMENT INSTRUMENT AND METHODS

Drivers suffer from the physiological burden as well as the psychological burden. The commonly-used research methods of the driver's physiological burden include flicker fusion frequency, the variance in heart rate, the variance of blood pressure, the variance of ElectroEncephaloGraph (EEG), change in respiratory rate, dispersion of skin potentials, and eye movements. The experiment research shows that it is feasible and effective to use the variance of heart rate as an evaluation index of a driver's psychological pressure in driving (Pan X.D., 2001, 2003).

In order to show the relationship between the heart rate and the highway alignment, this experiment uses the variance of heart rate and the free vehicle speed as the evaluation index. The variance of heart rate is the dispersion of the mean of the driver's heart rate in the process of driving experiment and that of driver's heart rate prior to the experiment. When the variance in heart rate is 5 to 10 P/min, it shows that the driver's psychological and physiological burdens are normal. Free vehicle speed refers to the idea that the driving speed is decided by the driver's feeling, thus avoiding the driver's psychological and physiological burdens caused by limiting the driving speed. When the free vehicle speed of the driver exceeds the limit of this highway's design speed, it indicates that there exists some potential safety problem in this section of the highway.

Instruments used in the experiment and data collection: (1) The motive GPS (Global Position System) instrument is used to measure the driver's location (longitude and latitude), vehicle speed and time, etc. Portable computers are used to record and store the data measured using GPS (Ashley S., 2003)

(2) Auto-recording heart rate instrument, "Century 3000" made in USA is used to monitor and measure the information of the driver's heart rate, and it is convenient and stable for measuring the variance of the heart rate during driving.

Highways and time of experiment: This experiment selects some mountain highways of low design speed, complicated driving conditions and obvious end long slopes in order to make clear the impact of the long slope alignment of the mountain highways on the driver' s psychology and physiology. Ten sections of B-grade road were selected, which include most longitudinal gradients of 0~7%. All the sections in this road are typically those where traffic accidents often occur. In order to reduce the influence of the weather, temperature and humidity, the experiments were conducted in early spring and in dry weather.

Vehicle and driver choice: A seven-seat microbus was used for the experiment. Considering the representativeness of drivers' experience and age, six male drivers at all age groups old, middle-aged, and young were the drivers of the experiment.

THE PROCESS OF THE EXPERIMENT

Experiment purpose: This experiment is intended to gain the parameters at the long slope alignment of mountain highways, the data of the variance of the driver's heart rate and vehicle speed by recording the drivers' behavior in different slope alignments of the mountain highways. This data is used to evaluate whether the longitudinal gradients are within reasonable tolerance.

Experiment theory: The psychology of the drivers on the long slope alignment of mountain highways may have different degrees of strain as they meet different longitudinal gradients at the long slope section, and their heart rates can quantitatively reflect this kind of strain. The driver's vehicle speed and location (longitude and latitude) at different times can be measured by the motive GPS. the design parameters of the number of kilometer stakes and the profile grade in the experiment highway can be obtained by changing the coordinates of longitude and latitude, and consulting the design documents of the alignment of this experiment section (Ashley S., 2003; Dornhemima, 2004). Drivers' heart rates at different times can be measured by the auto-recording heart rate instrument. Part of the experiment data after they are arranged and disposed are shown in Table 1. The following analyses and researches are all based on this experiment data after they are arranged and disposed.

Table 1. Part of the Experiment Data After Arranged and Disposed

Kilometer stake number	Arriving time (h:m:s)	Vehicle speed (km/h)	Profile Grade, I (%)	Variance of heart rate, H (P/min)
K1530	8:10:02	53.5	2	8
	8:10:47	57	3	7
K1531	8:11:27	68	5.5	12
K1532	8:11:45	50	1.5	8
	8:13:32	55.5	6	14
K1533	8:13:48	38	7	20
K1534	8:15:26	66	4.5	9
	8:15:58	64	4.2	8
K1535	8:16:48	62	3.5	7
	8:17:26	53	2.2	9

ANALYSIS AND DISCUSSION

From the experiment data, the vehicle speed (V) and the mean heart rate (H) increases when the drivers drive on the different longitudinal gradient (i) at long slope alignment.

The distribution discrete points (i,V), (i, H) are shown in Figure 1, and Figure 2. By using the MATLAB software and the theory of nonlinear least mean square problem (Wei L., Gao L. M, Yu Q., et al., 2004) the fitting equation of discrete points (i,V),(i, H) is derived. The fitting equations are shown in Table 2 and fitting curves are shown in Figure 3 and Figure 4.

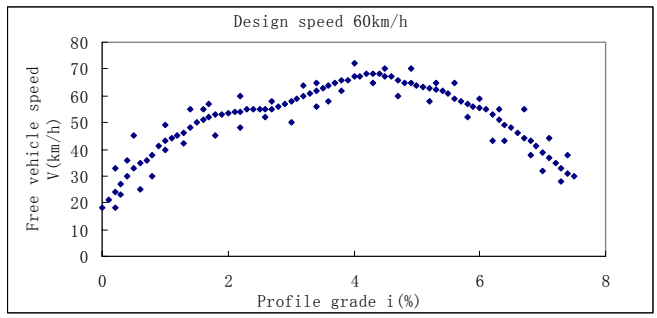

Figure 1. Discrete-points（i，v）distribution.

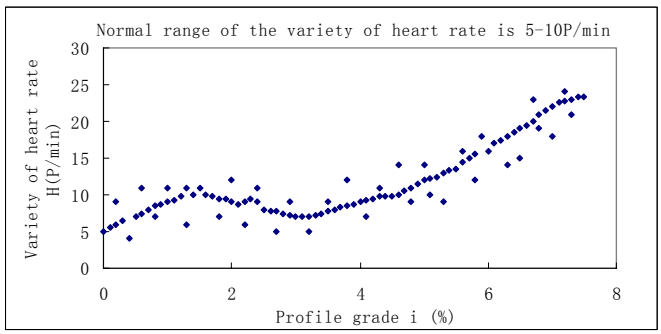

Figure 2. Discrete-points（H，v）distribution.

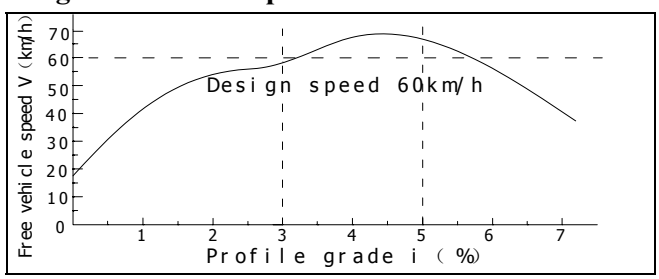

Figure 3. Fitting relation of i and V.

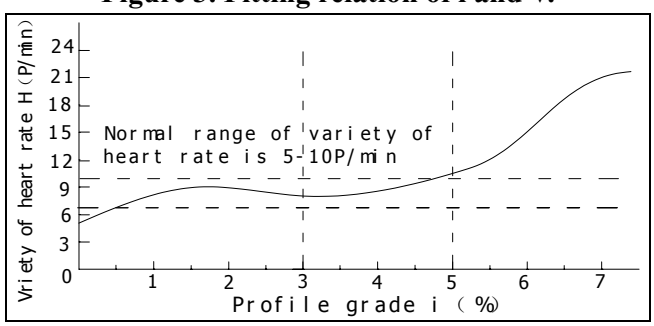

Figure 4. Fitting relation of i and H.

When the driver drives on the different longitudinal gradient at the long slope alignment of mountain highways, a quantitative analysis of the above fitting equations derived are presented in Table 2. The fitting curves in Figures 1 through 4 demonstrate the following:

(1) When $i \le 3\%$, the vehicle speed has a sharp increase and the psychological stress of the driver also slightly increases because of effect of vehicle's gravity divided in the direction of the longitudinal slope. At this moment,

the driver doesn't brake, but he is very careful, so driving at such section was usually safe.

(2) When $3\% < i \le 5\%$, the driver's heart rate may increase because the longitudinal gradient at this alignment becomes bigger, but as the driver brakes, his strain is eliminated. However, the acceleration caused by the vehicle gravity divided in the direction of the longitudinal slope becomes large, so the vehicle speed also becomes larger. At that time, the phenomena of overtaking and over speeding will easily occur. In the investigation of traffic accidents on this highway, overtaking and over speeding are the main reasons to cause accidents. Therefore, warning signs of "No overtaking" and "No over speeding" must be set up in these sections, and some of the crucial sections should become slowing-down belts.

(3) When $i > 5\%$, the driver's psychological stress has a sharp increase because he has to brake to overcome the ever-increasing acceleration. Though the vehicle slows down to some degree, the brake's temperature increases because of continual braking, which causes the brake to fail to work, and accidents usually occur for this reason. So the longitudinal gradient at the long slope section of mountain highways should not be more than 5%.

Table 2. Fitting equation of free vehicle-speed (V), heart-rate increasing number (H) and longitudinal gradient (i).

Fitting equation of V and i	$v = 0.75i^3 - 8.5i^2 + 31.75i + 18$	$i \le 3\%$
	$v = -1.5i^3 + 13i^2 - 26.5i + 60$	$3\% < i \le 5\%$
	$v = 1.1i^3 - 20.9i^2 + 116.6i - 133$	$i > 5\%$
Fitting equation of H and i	$H = 0.33i^3 - 2.5i^2 + 3.2i + 5$	$i \le 3\%$
	$H = 0.1i^3 - 1.75i^2 + 11.65i - 15$	$3\% < i \le 5\%$
	$H = 1.67i^3 + 25i^2 - 151i + 306.7$	$i > 5\%$

CONCLUSION

The following conclusion is drawn on the basis of the study of the relationships between the driver's heart-rate, operating speed, and the longitudinal gradient of the long slope alignment of the mountain highways. These study recommendations could be used as a reference to design mountainous highway alignments and be used by the highway managers.

(1) The longitudinal gradient at the long slope alignments of mountain highway should not be more than 5%.

(2) Clear signs of "No Overtaking" and "No Over Speeding" must be set up at the long slopes of 3% to 5% to improve the management of the present highways.

REFERENCES

Ashley S. (2003). "Next-Generation GPS". *Scientific American*, 289(3), 64

Dornhemima. (2004). "GPS launch rate to grow". *Aviation week and Space Technology*, 161(11), 56-59

Liu Z. Q., Gong Z., Cai D. (2003). "Identification for road accident-prone locations". *Journal of Traffic and Transportation Engineering*, 3(2), 120-123

Pan X. D. (1998). "Studies on evaluation of geometrical design of forest roads by driver's psychological and physiological response-alignment description of forest roads in mountain areas and variation systolic blood pressure". *Journal of Japanese Forestry Society,* 80(3), 143-150

Pan X. D. (2001). **"**The application of body information technology on road and traffic environment and safety evaluation". *China Journal of Highway and Transport*, 14(s), 109-111

Wei L., Gao L. M, Yu Q., et al. (2004). "Fuzzy evaluating model of driver's road safety perception". *Journal of Traffic and Transportation Engineering*, 4(1), 102-105

Impacts of Road Sight Distance on Safe Driving Conditions

Xian-Qiang Ren[1], Jian-Yi Liu[2] and Song Gap[3]

[1] School of Automobile and Traffic Engineering, JiangSu University, P.O. Box Xuefu Rd. Zhenjiang 212013, China, PH (86) 536-3822 873; FAX (86) 536-3822 818; email: zhanglip0503@163.com
[2] School of Automobile and Traffic Engineering , JiangSu University, P.O. Box Xuefu Rd. Zhenjiang 212013, China, PH (86) 536-3822 873 ; FAX (86) 536-3822 818; email: bjliujianyi@163.com
[3] School of Transportation Engineering, Shandong University of Technology, P.O. Box Zhangzhou Rd. Zibo 255049, China, PH (86) 536-3822 873; FAX (86) 536-3822 818; email: gaosong@sdut.edu.cn

ABSTRACT

It is very important to have enough sight distance to ensure drivers drive safely on the road. Enough sight distance will give the driver enough time to judge the changes of road's direction and gradient accurately and then choose the correct driving line to avoid hitting rolling stocks and roadblocks or park the vehicle down on the emergency parking places at state of emergency. Based on the principle of the vertical curve design, this paper discusses the safe driving conditions on highways and doing research on the impacts of road sight distance. Combined with safety evaluation for one expressway, this paper proposes some reasonable recommendations for black spot treatment.

PREFACE

Highway safety analysis is the evaluation on planning, studying, designing achievement of highway and its affiliated facilities or on potential factors of the traffic safety. One of the key factors in evaluation is the level and the vertical sight distance. It is very important to have enough sight distance when drivers drive safely. Enough sight distance will give the driver enough time to judge the changes of road's direction and gradient accurately and then choose the correct driving line to avoid hitting rolling stocks and roadblocks or park the vehicle down on the emergency parking places at state of emergency (Harold Peterfeso. 1998).

There are many factors which influence stopping sight distance, such as dark plane bending on the road (it has the obstacle in the curve), crest vertical curve in vertical section and sag vertical curve below separate grade crossing. Carrying on the road vertical surface geometric design, we should pay attention to optimum composition of plane curve and vertical curve and avoid composition of dark plane bending and vertical curve, bright plane and crest vertical curve. When algebraic differences of gradients are big, their combination will give such feeling that drivers

give up smooth slope and shortcut and deliberately climb slope and turn around. This paper discusses the relationship among the design length of vertical curve, stopping sight distance and algebra difference of grades and the conditions which road alignment design should be reached for making sure driving safely.

FORMULAS OF STOPPING SIGHT DISTANCE

Crest vertical curve. In designing crest vertical curve, the smallest length of vertical curve should be satisfied with the demand of sight distance in order to drive safely. According to the relationship of the length of vertical curve and stopping sight distance, two cases will be discussed in the following (Zhang Yu-hua.2002) .

(1)Length of curve less than stopping sight distance ($L<S_T$)

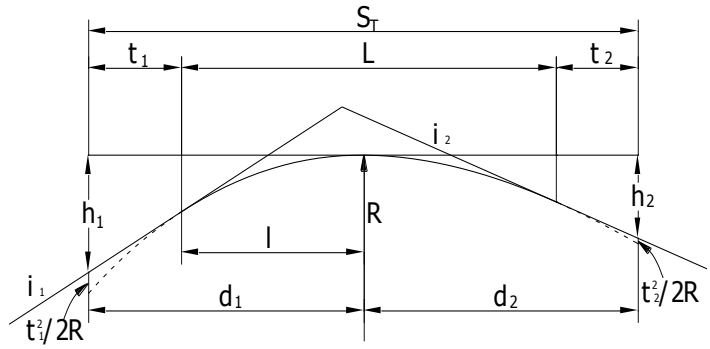

Figure 1. L<ST in crest vertical curve .

According to the Figure 1 and the length of sight distance $s_T = t_1 + L + t_2$, combined with vertical curve design formula, it can be gained as follows:

$$s_T = \frac{(\sqrt{h_1} + \sqrt{h_2})^2}{\omega} + \frac{L}{2} \qquad (1)$$

i_1: Grade of the tangent on the start point of vertical curve; measured in percent of slope; assigned to uphill grades in plus values and minus values in downhill grades

i_2: Grade of the tangent on the end point of vertical curve

ω: Algebraic difference of gradients ($=i_2-i_1$); measured in percent of slope

L: Length of vertical curve

s_T : Stopping sight distance

h_1, h_2: A value of 1.20m is usually taken as the eye level height above the road surface for an observer sitting in the vehicle and a value of 0.10m to an object height [3], which means h_1 will be 1.20m and h_2 will be 0.10m.

(2)Length of curve greater than or equal to stopping sight distance ($L \geq S_T$)

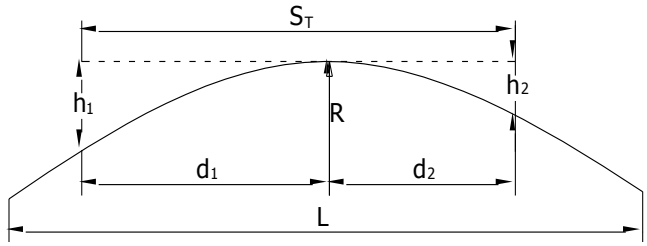

Figure 2. $L \geq ST$ in crest vertical curve .

The formula is derived from the Figure 2 and the length of sight distance $s_T = d_1 + d_2$, combined with vertical curve design formula as follows:

$$s_T = \sqrt{\frac{2L}{\omega}}(\sqrt{h_1} + \sqrt{h_2}) \qquad (2)$$

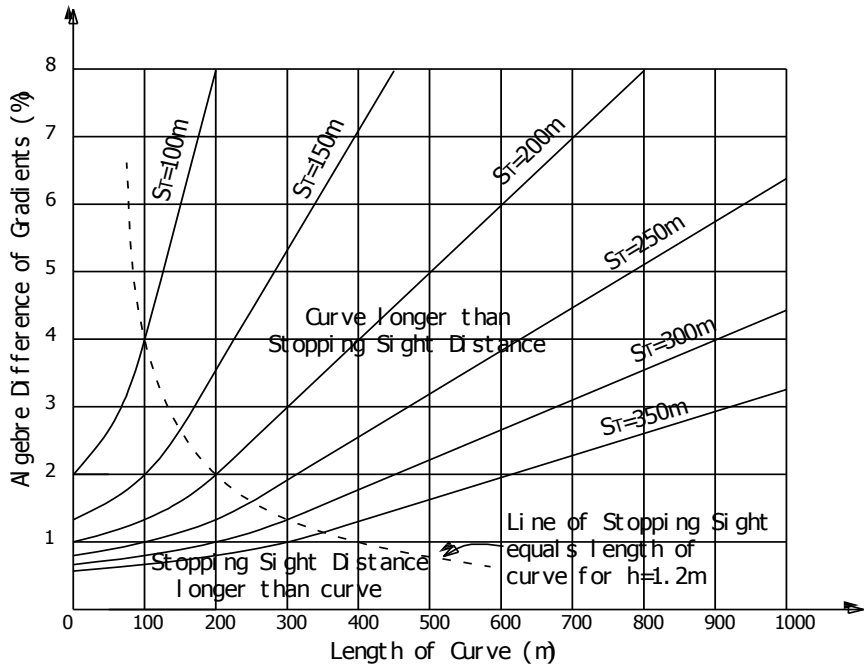

Figure 3. relationship among stopping sight distance, curve lengths and algebraic difference of gradients in crest vertical curve .

According to formulas (1) and (2), relationship among stopping sight distance, curve lengths and algebraic difference of gradients in crest vertical curve (Ioannis Taiganidis. 1998) is shown in Figure 3.

Comparing with the above two situations and combining with Figure 3, we can see that the impacts of formula (2) are greater than formula (1). So we should regard comparison between the calculation sight distance of formula (2) and the standard value as effective control. If calculation value is greater than or equal to the standard value, it meets the requirements.

Sagvertical curve. Designing minimum length of sag vertical curve should meet two requirements: first, ensuring traffic safety at night- adequate distance before lighting; second, ensuring sufficient distance for travel under the overpass. This paper mainly discusses the former.

There are two situations in the following discussion.

(1)Length of curve less than stopping sight distance ($L<S_T$)

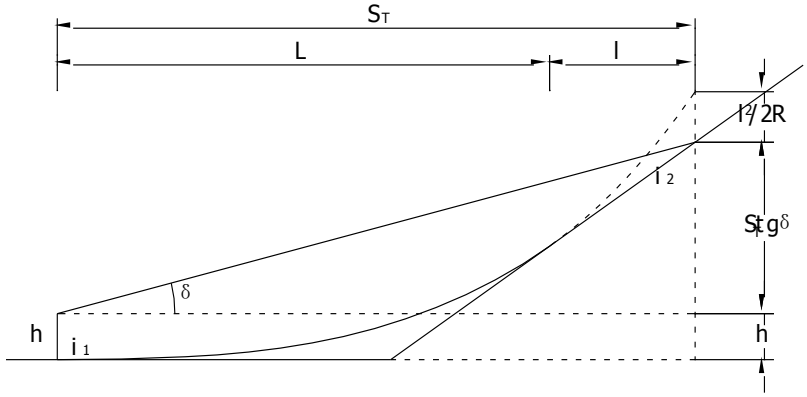

Figure 4. $L<S_T$ in sag vertical curve .

Shown in Figure 4, stopping sight distance and vertical curve design formula acquiring the formula as:

$$h + s_T tg\delta = \frac{\omega(2S_T - L)}{2} \qquad (3)$$

h: Height of lights of cars before, taken 0.75 m

δ: Beam spread angle of lights of car before, taken 1.5 degree[3].

(2)Length of curve greater than or equal to stopping sight distance ($L \geq S_T$)

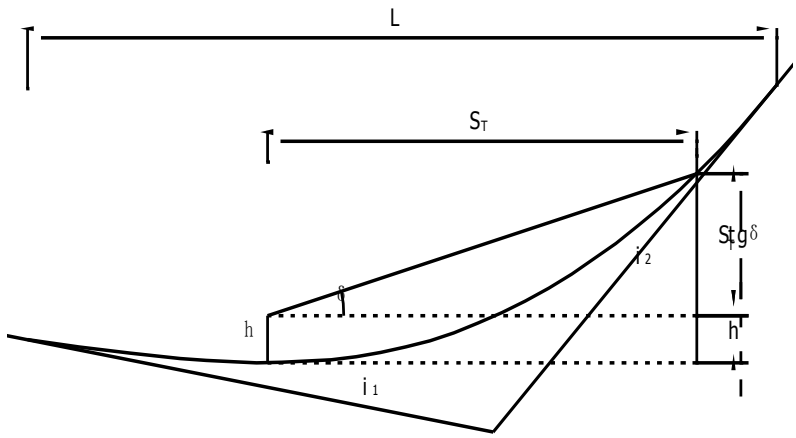

Figure 5. $L \geq S_T$ in sag vertical curve .

$$h + s_T tg\delta = \frac{S_T{}^2\omega}{2L} \qquad (4)$$

From the Figure 5, it can be gained as follows:

According to formulas (3), (4), figure 6 can be used to describe the

relationship among stopping sight distance, curve lengths and algebraic difference of gradients.

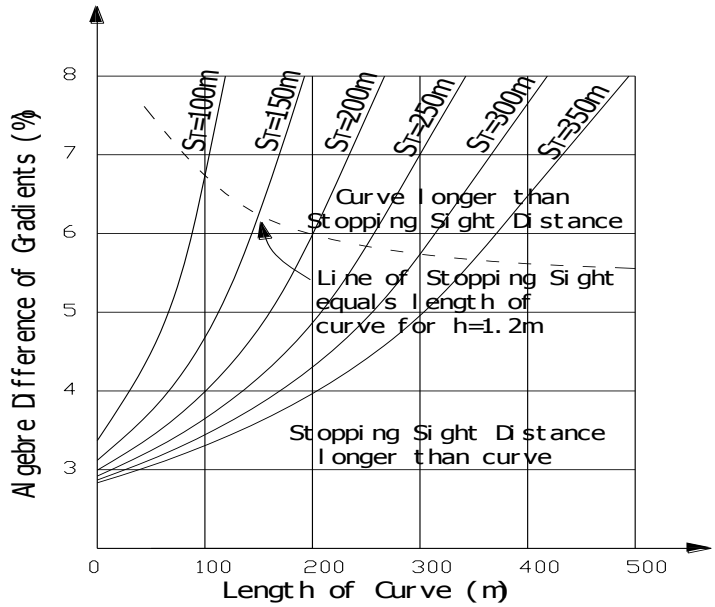

Figure 6. relationship among stopping sight distance, curve lengths and algebrai c difference of gradients .

Comparing with the above two situations and combining with Figure 6, we can see that the impacts of formula (4) is greater than formula (3). So we should regard comparison between the calculation sight distance of formula (4) and the standard value as effective control.

Result analysis. (1) Figure 3 and Figure 6 visually reflect the relationship among stopping sight distance, curve lengths and Slope. Under the proposed design of length of curve, we can directly determine whether the design meets the requirements of stopping sight distance or not from the Figure as long as slope is unchangeable.

(2) The relationship between algebra difference of grades and length of curve should be in one-to-one proportion while stopping sight distance is unchangeable. The bigger ω is, the longer the curve needs, the better it is for slope-climbing and at the same time it could avoid bumping at high speed because of shorter curve.

(3) When ω is invariable, the longer S_T is, the greater L will be. As a result, the curve becomes smoother and vision of racing driver is much wider than before, which means the driving will be safer and more comfortable.

(4) When design of length of curve and stopping sight distance do not meet the requirements because the terrain and environment factors are restrained.

APPLICATION

The study is conducted on a highway segment that is the major component of

national highway network planning. The total length is 199.334 km, and it was finished in October 2003. According to statistics, the rate of traffic accident is 7.81 times per km on the road during 2004. Based on the frequent traffic accidents and increasing traffic volume, the departments have decided to implement safety assessment for this section of road and then combining with the results present reform suggestion, finally confirm the implementation of identified six lanes extension design program. Contents of assessment mainly aim at types of traffic accidents, analysis of traffic flow characteristics, speed continuity, vertical-linear design quality, test of stopping sight distance, ultra-high road, sub grade drainage, interchange design and bridges and tunnels quality test. The results show that a full range of accident-prone section of the road presents big potential safety problems in ensuring driving distance, using the level and the vertical linear indicators and traffic engineering facilities and so on, while the lack of stopping sight distance is an important cause on certain sections of the high incidence of accidents.

This Application shows a section of the linear design indicators and distribution of the incident. In consecutive uphill and downhill sections, accident rate is 8.95 times per km from south to north, while 9.33 times per km from north to south. In light of the formulas (1), (2), (3), (4), and combining with Figure 3 and Figure 6, the results showed some of the vertical sight distance can not meet the requirements. The largest line-of-sight designed in this section is 140 m, instead of the standard value of 160 m. It is obvious that the lack of sight distance is the important cause of resulting in traffic accidents.

CONCLUSION

The majority of road traffic accidents are related to speeding and lack of sight distance. In order to guarantee the vehicles travel safety, we can test whether the alignment design is smooth and continuous, and whether sight distance meets the requirements by utilizing the perspective drawing, curvature chart, and the slope chart. If conditions are restrained on one section of road and alignment or sight distance can not meet requirements of design standard, we can take traffic engineering control measure to ensure the road traffic safety as much as possible.

REFERENCES

Harold Peterfeso. (1998). “Stopping Sight Distance Design manual”. Washington State Department of Transportation , (65), 1-9.

Zhang Yu-hua. (2002). “Surveys and Designs for Highway”. China Communications Press , 73-79.

The Ministry of Communications of the People's Republic of China. Technical Standard of Highway Engineering (JTG B01-2003) (2003), China Communications Press, 16-18.

The Most Informative Site. Engineering, Integrated Publishing (The Most

Informative Site on the Internet): Chaper 11 Horizontal and Vertical Curves.

Ioannis Taiganidis. (1998).” Aspects of Stopping Sight Distance on Crest Vertical Curves”. Journal of Transportation Engineering , (7), 12-16.

A Study on Multifactorial Prediction Model for the Road Traffic Accidents

LIU Zhao-hui

Key Laboratory of Mine Disaster Prevention and Control of Ministry of Education, College of Resources and Environmental Engineering, Shandong University of Science and Technology, Qingdao 266510, China, PH (86)-532-80681350;
email: liuzhaohuijlu@126.com

Abstract

Disharmony of various factors in road system is one of important reasons that cause traffic accidents. In order to study how traffic accidents are influenced by various road factors, it is required to transform traditional linear prediction models into non-linear prediction ones. Considering above-mentioned problems, multifactorial model for road traffic accident prediction based on Grey-Radial Basis Function (RBF) neural networks is put forward by combining virtues of Grey theory that aim at handling "poor" information and weaken undulation of data sequence together with the superior capability of neural networks of adapting non-linear information. Finally, the results of a case study demonstrate that the combined model can effectually overcome the shortcoming that current prediction models only consider influence of one factor on the traffic accidents. The proposed models can also improve efficiency of system modeling and precision of the prediction.

Keywords: Traffic safety; Grey system prediction; Radial basis function (RBF) neural networks; Multifactorial prediction model

1. Introduction

Influencing factors of actual road system are various and complex that have characteristics of grey, uncertain, fuzzy and random. The issue of how to mathematically model the relationship of influence factors and prediction index based on qualitative cognition is a very interesting and worthwhile research field.

Owing to the characteristics of the road systems, obtaining the complete information for the system model under limited techniques and limited space-time condition are difficult or sometimes impossible, namely, the system is in a "poor" information condition. Grey system theory can effectively improve utilization rate of available information, which provides potential tool for analyzing and disposing "poor" information system. But grey dynamic modeling theories have drawbacks that are weak in parallel computation , self-organizing and self-adaptive capability (DENG 1990; LIU etc.1999). However, parallel distributing capability of neural network formed by learning, self-organizing and non-linear dynamics has the predominance on disposing mode information that is difficult to express by language. Nevertheless, neural network also has "black box" weakness (Robert etc.1998;

S.Massoud Amin.1998). Therefore, method of combining grey system theory with neural network theory is considered, which combines the advantages of grey theory that improves utilization rate of available information and the capability of neural network that disposes of non-linear adaptability information, to solve traffic accident prediction problem affected by various road factors (LIU 2007).

2. Methods

2.1. Grey System Prediction Models

The Grey System Prediction can effectively forecast multifactor system. Its basic idea is to build Model GM (1, N) for relationship of traffic accident and various influence factors, and to build Models GM (1, 1) for each influence factors respectively, which constitutes the Grey System Prediction Model for forecasting the system (DENG Julong.1990; LIU Sifeng etc.1999).

Grey differential equation of Model GM (1, N) is as fallows:

$$x_1^{(0)}(k) + az_1^{(1)}(k) = \sum_{i=2}^{N} b_i x_i^{(1)}(k) \tag{1}$$

The parameters matrix is elicited according to least-squares algorithm, computation equation as follows:

$$\hat{a} = [a, b_2, b_3, \cdots, b_N]^T = (B^T B)^{-1} B^T Y \tag{2}$$

Approximate Time Response Sequence of grey differential equation of Model GM (1, N) is as fallows:

$$\hat{x}_1^{(1)}(k+1) = \left(x_1^{(1)}(0) - \frac{1}{a} \sum_{i=2}^{N} b_i x_i^{(1)}(k+1) \right) \cdot e^{-ak} + \frac{1}{a} \sum_{i=2}^{N} b_i x_i^{(1)}(k+1) \qquad \mathrm{k} = 1, 2, \cdots, \mathrm{n} \tag{3}$$

Prediction values of the original data sequence $X_1^{(0)}$ are obtained by Inverse Accumulating Operation according to formula (4).

$$\hat{x}_1^{(0)}(k+1) = \alpha^{(1)} \hat{x}_1^{(1)}(k+1) = \hat{x}_1^{(1)}(k+1) - \hat{x}_1^{(1)}(k) \qquad \mathrm{k} = 1, 2, \cdots, \mathrm{n} \tag{4}$$

When N is equal to 1, Model GM (1, N) is same as Model GM (1, 1), so computation processes for Model GM (1, 1) are elided.

Residual Test and Posterior Variance Test are used for precision tests of the Grey System Prediction Models.

2.2. RBF neural network model

The RBF neural network has characteristics that are well approximation

precision, quick convergence speed and can't get stuck in a local minimum, etc., which can effectually overcome the shortcomings of BP neural networks.

The architecture of the RBF neural network is presented in Figure 1。The network consists of three layers: an input layer, a single layer of nonlinear processing neurons, and an output layer. The transfer function of the hidden layer is radial basis and the transfer function of the output layer is pure linear function. In practical applications, the most widely use of RBF is the Gaussian RBF.

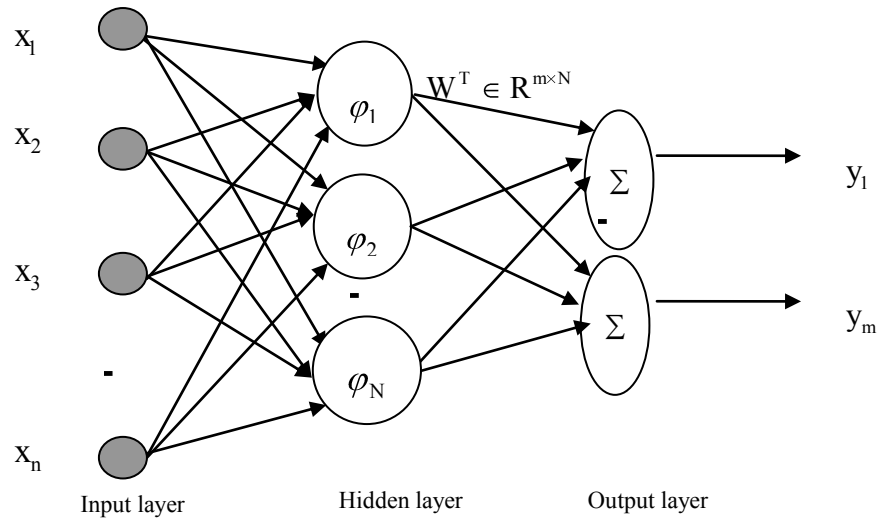

Figure 1. The RBF NN architecture .

Because of the length limit for papers, for particulars, refer to the literature (Fredric M. Ham, Ivica Kostanic.2003).

3. Grey -RBF neural networks combined prediction model

Assigning a weight to each prediction models is one of key problems of the combined prediction model. This paper confirms the weighs vector w_n according to optimization combined prediction method (LIU Zhaohui.2007).

Optimization combined weights vector is obtained by

$$w_n = \frac{E_n R_n}{R_n^T E_n R_n} \tag{5}$$

where $E_n = (c_{ij})_{n\times n}$ is a prediction error information matrix in which $c_{ij} = \sum_{t=1}^{N} e_{it} e_{jt}$

and R_n is a n dimension column vector with elements are all 1s.

If the combined prediction structure consists of two prediction methods, optimal combined weights coefficient are given by

$$w_1 = \frac{c_{22} - c_{12}}{c_{11} + c_{22} - 2c_{12}} \quad , \quad w_2 = \frac{c_{11} - c_{12}}{c_{11} + c_{22} - 2c_{12}} \tag{6}$$

Combined prediction value can be obtained by the Combined Prediction Model that is given by

$$\hat{y}_{ct} = \sum_{i=1}^{2} w_i \hat{y}_{it} = w_1 \hat{y}_{1t} + w_2 \hat{y}_{2t} \qquad t = 1, 2, \cdots, N \tag{7}$$

where $\hat{y}_{ct}$ is the combined prediction value, $\hat{y}_{1t}$ is the prediction value of the Grey System Prediction Model, $\hat{y}_{2t}$ is the prediction value of the RBF neural network model, w_1 is a weight assigned to the Grey System Prediction Model and w_2 is a weight assigned to the RBF neural network model.

4. Case study

On the basis of 19 factors that affect road traffic safety in literature (LIU Zhaohui.2007), which has been already given an order according to the weights value, three primary factors of alignment combination, safeguard facilities and sight distance are utilized to achieve multifactorial road traffic accidents forecasting based on Grey-RBF neural networks. Quantificational data of the road influence factors of certain high-grade highway are shown in Table 1.

Table 1. Original data sequences of road influence factor s.

$X_i^{(0)}$	Input data					Target data	
	2000	2001	2002	2003	2004	2005	2006
equivalent accident number $X_1^{(0)}$	187	213	232	195	176	162	167
alignment combination $X_2^{(0)}$	0.056	0.061	0.062	0.049	0.044	0.041	0.046
safeguard facilities $X_3^{(0)}$	0.386	0.453	0.493	0.625	0.671	0.671	0.758
sight distance $X_4^{(0)}$	4.695	4.863	4.871	4.938	4.915	4.883	4.880

In order that put original data in same range, initialization method is adopted to preprocess the data. By calculating, the simulation data of the Grey System Prediction Model are obtained, which is shown in Table 2.

Table 2 . Comparison the simulation data of the Grey System Prediction Model with the original data .

Sequence number	Original data	Simulation data	Residual error	Relative error
2	1.139	1.070364	0.068636	0.060260
3	1.241	1.314466	-0.073466	0.059199
4	1.043	1.112541	-0.069541	0.066674
5	0.941	0.976977	-0.035977	0.038233

Precision test's results of the Grey System Prediction Model conform to the requirements of precision grade (LIU Zhaohui.2007) which demonstrates the Grey System Prediction Model, can be used to forecast. Prediction results for the equivalent accident number are obtained by inverse initialization that shown in Table 4.

This paper adopts function newrbe() provided by MATLAB7 neural networks toolbox to design and train RBF networks. Function sim() is adopted to simulate prediction, function norm() is used to measure simulation degree of prediction value and original data. Utilizing characteristic of RBF network with the structure of self-adapted determine, the output is no relationship with initial weights, etc. to realize prediction of RBF neural networks on traffic accident numbers.

According to determinate network input factors (road influence factors) and output factor (equivalent accident number), data during 2000 to 2004 are adopted as the training samples of the network and data during 2005 to 2006 are adopted as the extrapolated testing samples of the network that are shown in Table 1 completely. By normalization operation, input data are transformed into sensitive area of input function. The sensitive area is interval 0, 1.

The Function newrbe() can automatically select neuron numbers of the hidden layer and produce a RBF neural network with zero error on training vectors. When input vectors and goal vectors are obtained, only the spread parameter 'SPREAD' for the hidden layer needs to be factitiously adjusted (note: each bias in the hidden layer is set to 0.8326/SPREAD in practical application), which determines an optimal value for the problem. Let SPREAD equal to 0.1, 0.2, …, 1.0, respectively, the approximate errors of the network are shown in literature (LIU Zhaohui.2007). When SPREAD is equal to 0.3, the prediction error of network is minimized by trial calculations (LIU Zhaohui.2007). Finally, by inverse normalization operation, prediction results of the RBF neural networks are obtained and prediction result of SPREAD=0.3 is used as final prediction value, which is shown in Table 3.

Table 3. Results o f inverse normalization operation of RBF.

SPREAD values	2005	2006	SPREAD values	2005	2006
spd=0.1	202.51	202.44	spd=0.6	177.16	182.84
spd=0.2	169.86	170.52	spd=0.7	234.91	232.33
spd=0.3	157.76	163.11	spd=0.8	201.29	217.47
spd=0.4	154.75	163.34	spd=0.9	179.48	209.67
spd=0.5	177.82	180.14	spd=1.0	163.18	204.78

Weights of each prediction model that constitute the combined prediction model are elicited by formula (6), namely $w_1 = 0.207$ and $w_2 = 0.793$. The combined prediction results calculated by formula (7) are shown in Table 4.

Table 4. Results of the Grey -RBF neural networks combined prediction for the equivalent accident number .

Year	Prediction values of the Grey system prediction	Prediction values of the RBF neural networks	Prediction values of the Grey-RBF neural networks combined prediction
2005	168	158	160
2006	159	163	162

According to the principle and the usage of integrated evaluation for prediction method, four indices are adopted to prove prediction effect of the combined prediction model that the results of evaluation are shown in Table 5. It indicates that the four indices of Grey-RBF neural network combined prediction all surpass those of grey system prediction and RBF neural networks prediction, which sufficiently demonstrates preponderance of the combined prediction method in the multifactor prediction of road traffic accidents.

Table 5. Evaluation on the effect of the combined prediction .

Prediction method	Mean absolute error	Mean absolute percent error	Theil coefficient	validity
Grey System Prediction	7.000	0.042	0.022	0.952
RBF neural networks prediction	4.000	0.024	0.012	0.975
Grey-RBF neural networks combined prediction	3.500	0.021	0.010	0.978

5. Conclusions

(1) The multifactorial prediction model for the road traffic accidents based on Grey-RBF neural network is put forward in this paper, which provides a new practicable solution for predicting the multifactor time sequence.

(2) The Grey System Prediction (GSP) not only synthetically considers the

influence of various road and environment factors on predicted frequencies of the road traffic accidents, but also can overcome the shortcoming of model GM(1, 1) that only aims at certain sequence of the complex road system to forecast. The RBF neural network prediction not only can effectually overcome the shortcomings of BP neural networks, such as long training time, slow convergence speed and prone to getting stuck in a local minimum, but also can obtain a good prediction effect even if the sample data isnot sufficient and can deal with instable data to a certain extent.

(3) The analysis results of this case study demonstrate that the combined model can effectually and accurately reflect future development trend of the traffic accidents in a complex road system affected by various factors.

References

DENG Julong. (1990). Grey System Theory tutorial. Wuhan, Huazhong University of Science and Technology Press, 1-428.

Fredric M. Ham, Ivica Kostanic. (2003). Principles of Neurocomputing for Science & Engineering. China Machine Press, 140-165.

LIU Sifeng, GUO Tianbang, DANG Yaoguo. (1999). Grey System Theory and Application. 2th Edition. Beijing: Science Press, 1-270.

LIU Zhao-hui. (2007). A Study on Comprehensive Evaluation for the Traffic Safety of High-Grade Highways and Multifactorial Prediction Model for the Traffic Accidents. Doctoral paper of Jilin University, 92-155.

Robert J, Schilling James, Carroll J. (2001). Approximation of nonlinear systems with radial basis function neural networks. IEEE, Transactions on Neural Networks, 12(1): 21-28.

S.Massoud Amin, E.Y. Rodin, etc.(1998). Traffic prediction and management via RBF neural nets and semantic control. Computer-Aided Civil and Infrastructure Engineering, 13: 315-327.

Case Studies for Shaking Table Tests on Seismic Soil-Pile Group-Bridge Structure Interaction in Liquefiable Ground

Liang Tang[1], Xianzhang Ling[1], Pengju Xu[1], Xia Gao[1], and Liquan Wu[2]

[1]Institute of Subgrade and Protection Engineering, Harbin Institute of Technology, P.O. Box 150090, City, Harbin, P.R.China; PH (86) 451- 86284876; FAX (86) 451-86282205; EMAIL: hit_tl@163.com

[2]School of Civil Engineering and Architecture, Zhejiang University of Science and Technology, P.O. Box 310023, City, Hangzhou, P.R. China; PH (86) 571-85070518; FAX (86) 571-85070518; EMAIL: wuliquan1966@163.com

ABSTRACT

This paper documents two shaking table test studies that characterized the key features of seismic soil-pile group-structure interaction systems involving the low-cap pile group and elevated-cap pile group in liquefiable ground. The shaking table tests were performed using the laminar shear box with depth of 2 m and plan dimensions of 2 m and 1.5 m. The base in both tests was excited by three different El Centro earthquake events. Some representative results were especially presented to study how cap type affected seismic response of bridge pile-column pier in liquefiable ground. It showed from the tests that seismic performance of low-cap pile group was better than that of elevated-cap pile group in liquefiable ground. Low-cap pile group presented to weaken more acceleration response of the pile especially in the upper pile parts when the sand layer hadn't been liquefied or liquefied incompletely, however elevated-cap pile could amplify acceleration response of the pile.

INTRODUCTION

One of the major sources of earthquake-induced damage to the piles was the occurrence of soil liquefaction, and the significance of liquefaction-related damage to the piles had been clearly demonstrated in strong earthquakes (Finn et al. 2002; Abdoun et al. 2002). Shaking table tests were often expected to provide reliable predictions of the performance of geotechnical systems during major seismic events. Shaking table tests had become an effective method to investigate and solve seismic problems of bridge piles in liquefied ground, so it had attracted much attention from the scholars at home and abroad recently, and the significant progress in this field had been made in Japan and America (Boulanger et al. 1999). Elevated-cap pile group was often applied in bridge engineering, and low-cap pile group which could reduce the vibration of bridge superstructure and improve the mechanical characteristics of bridge piles was widely used in bridge engineering (Fujii et al. 1998; Isemoto et al. 1998). Unfortunately, however, there was currently only limited information available regarding the seismic response of pile group with low cap and elevated cap of bridge in liquefiable ground. In this study, two shaking table tests for seismic soil-pile group-structure interaction in liquefiable ground with the same soil structure were completed to study acceleration characteristics of bridge pile-column pier in different types of pile cap including low cap and elevated cap.

FACILITIES AND TEST CONDITION

Shaking table tests were performed in the State Key Laboratory for Disaster Reduction in Civil Engineering, Tongji University, Shanghai, China, using MTS shaking table facility. The dimension of the table was 4 m×4 m, and the maximum payload was 25, 000 kg. The laminar shear box with 2 m high, 1.5 m wide and 2 m long (shaking direction) was designed and fabricated by Wu X.P. (Wu et al. 2002). Moving parts of the shear box approximately weighed 0.7 tons. This was typically 5% of the weight of the whole test model including the box. The shear box was designed to be sufficiently light compared to the weight of the test model. Therefore, the shear box produced nearly one-dimensional wave propagation fields, i.e. free-field conditions (Ling et al. 2004). The same soil profiles in both tests consisted of two horizontal soil layers. The test sand with a non-uniformity coefficient of 3.0, mean particle diameter of 0.32 mm, specific gravity of 2.72, maximum void ratio of 0.96, minimum void ratio of 0.57 and maximum diameter of 2 mm was obtained from Shanghai in China. The sand wasn't washed and was placed into the laminar shear box, partially filled with water in advance, using a free fall method for the saturated sand layer. No compaction efforts were made to densify the sand layer. The height of the lower sand layer with average void ratio of 0.8, relative density of about 51% and factor of permeability of about 0.0035 cm/s prepared was 1.6 m. This method for the desired saturated sand had been successfully used in the previous model studies by Ling X.Z. et al (Ling et al. 2004; 2005). The upper layer of 0.3 m thickness was normally consolidated reconstituted silty clay for the "model clay". The model clay had liquid and plastic limits of LL45 and PL28, and the plasticity index of PI 17. Also note the water table was approximately at the soil interface between the upper and lower soil layers to ensure the sand layer was completely submerged. The dimension of low-cap pile group and elevated-cap pile group was also presented in **Figure** 1. The piles, cap and column pier were modeled with fine-aggregate concrete and galvanized fine iron wires. All the bars embedded in the model structure were replaced by galvanized iron wire with different diameter and had the same bar mark "Φ". The vertical reinforcement for a pile with 80 mm diameter consisted of 9 Φ2 bars evenly distributed around a circle with a diameter of 70 mm and the confinement for the vertical steel was provided by Φ1 bar spirals with a pitch of 20 mm especially with a pitch of 10 mm within the range of 600 mm of the piles near the cap. A 5 mm concrete cover of the piles was maintained to protect the reinforcement bars. The vertical reinforcement of the pier with 160 mm diameter consisted of 32 Φ2 bars evenly distributed around a circle with a diameter of 150 mm and the confinement for the vertical steel was provided by Φ1 bar spirals with a pitch of 20 mm especially with a pitch of 10 mm within the range of 150 mm of the pier near the cap. A 5 mm concrete cover of the pier was still maintained. The concrete from the material specimen tests had an average 28-day compressive strength of 8.5 MPa. The top of the pier carried a mass of 360 kg to represent the inertial effect of bridge superstructure in both tests. **Figure** 1 shows the details of the soil-pile-structure systems. The container bases were excited by three El Centro earthquake events as the representative ground motion input, summarized in **Table** 1. Event B was the input shaking table motion with time scaling factor of $\sqrt{10}/1$. Events C and D were the earthquake events respectively with the peak amplitude of 0.15 g and 0.5 g without time scaling. Each shaking event was separated by an amount of

time that exceeded the time required for full dissipation of excess pore water pressure.

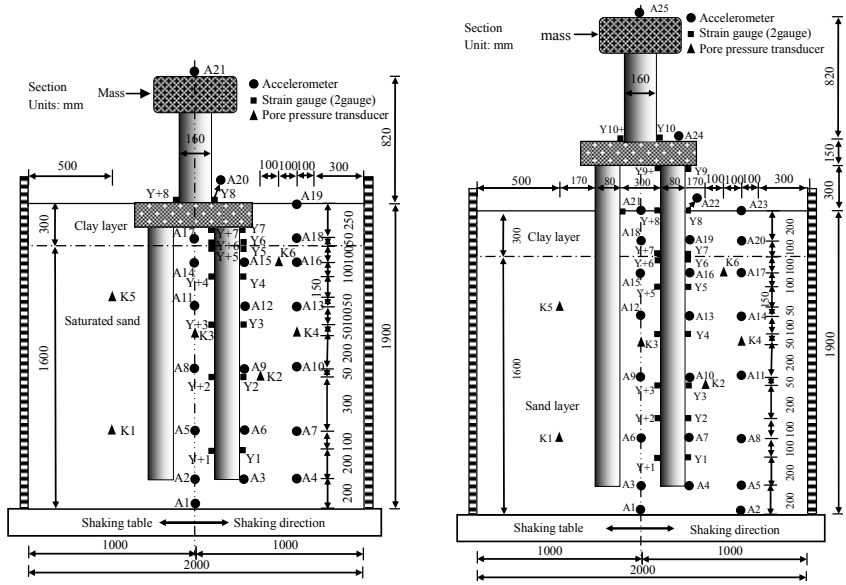

(a) test one (b) test two

Figure 1. Schematic figure of whole test system.

Table 1. Suite of shaking events.

Event	Motion	A_{max} base input (g)
A	White noise	0.002
B	Scaled El Centro earthquake (NS)	0.15
C	El Centro earthquake (NS)	0.15
D	El Centro earthquake (NS)	0.5

TYPICAL PHENOMENA

The law of excess pore pressure ratio in the sand almost remained uniform in both tests, so the results of pore pressure ratio in test one were adopted to explain the test phenomena. The time histories of the pore pressure ratio in the sand from test one is shown in **Figure** 3. Since the peak pore pressure ratio of the sand layer increased evidently bottom-up but less than 0.3, what's more, the sand layer hadn't liquefied and the structural damage of the soil was not serious, the ground surface and the column pier in both tests vibrated slightly in events B. In both tests the upper sand layer liquefied slightly; a little water perspired in the ground surface in event C. The vibration amplitude and the frequency of the column pier in both tests relatively decreased a little in event C compared with that in event B, which resulted from these factors including the peak pore pressure ratio of the sand decreasing bottom-up, the peak pore pressure ratio in the sand almost exceeding 0.6 and the weakened ability to transmit the soil vibration with the gradual development of sand liquefaction.

From both tests in event D the peak pore pressure ratio of the sand layer tended to decrease while the peak pore pressure ratio reached or exceeded the required pore pressure ratio for liquefaction (0.75-1.0); in addition, its duration

ranged from 30 s to 50 s, as a result, the sand layer liquefied completely and then the sand boil and waterspouts occurred strongly and lasted for a long time; the settlement of ground surface ranged from 4 cm to 6 cm; some wide cracks appeared near the pile heads and some cracks also were observed on the piles near the soil depth of about 1000 mm which indicated that the inertial effect and seismic soil-pile interaction all had significant effect on dynamical performance of the piles in liquefied ground. However, when the input shaking acceleration reached the peak in event D the piles around the soil interface broken off which led to the collapse of the superstructure, what's worse was that the big fracture region (transverse crack) appeared around the soil interface ranging from 20 cm to 50 cm and most of the main steel bars in the piles were pulled to snap which suggested that the breakage of the piles mainly occurred during soil liquefaction and the breakage region gradually expanded with the development of soil liquefaction. This was despite the fact that a large safety factor was employed in the design of bridge piles, but many case histories of their damage and failure in liquefied soil still happened. These results also suggested that low-cap pile was easier to obtain seismic demand than elevated-cap pile, so it was worthy to be recommended to adopt low-cap pile in liquefiable ground region.

Figure 2. Test phenomena.

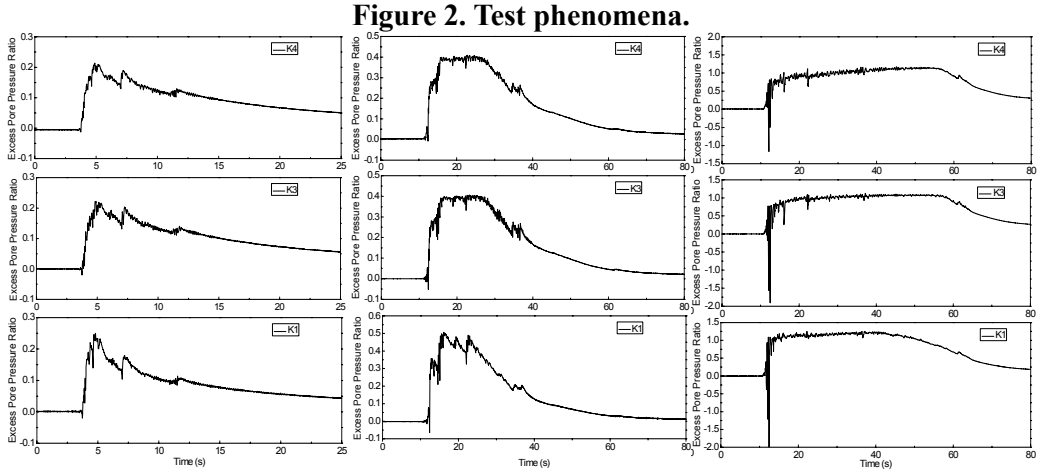

(a) event B (b) event C (c) event D

Figure 3. Time histories of pore pressure ratio in test one.

ACCELERATION **RESPONSE** OF PILE-PIER

The magnification factor of the peak acceleration is defined as the ratio of the responded peak acceleration to the input peak acceleration. The peak acceleration magnification factor and the peak acceleration of the pile-column pier in tests one and two are presented in **Figure** 4 to **Figure** 6 in three different events; the datum in the brackets from the figures was the peak acceleration time of the pile (Unit: s) and the peak acceleration time of the pile group-column pier from tests one and two was almost consistent with the peak time of the input earthquake motion in three different earthquake events. Since in events B and C the sand layer hadn't liquefied or partly liquefied, the negative effect of soil liquefaction on the pile didn't occurred, the cap fixed in the clay layer had strong constraint effect on the pile head and the soil layer effectively restricted the pile body, but the soil-pile kinetic interaction was not evident, the peak acceleration and the magnification factor of the peak acceleration of low-cap pile trended to decrease bottom-up. Considering the incomplete liquefaction of the sand which was the same with that in test one and the constraint of the soil to the pile being effective, the soil-pile kinetic interaction wasn't also remarkable in events B and C, the peak acceleration and the peak acceleration magnification factor of the lower parts of the pile from bottom to top trended to decrease; however, elevated-cap pile was affected more by the inertia effect from the superstructure and the elevated-cap, so the peak acceleration and the peak acceleration magnification factor progressively increased on the upper parts of the pile. The soil had strong constraint effect on the pile and had powerful ability to transmit the vibration in event B, so the acceleration of both elevated-cap pile and low-cap pile in the soil had the attenuation effect on the input earthquake motion, on the contrary, the acceleration of elevated-cap pile above ground surface appeared to have amplification effect caused by inertia effect from the superstructure and the elevated-cap. The acceleration response of the lower part of the pile (below 700 mm) had amplification effect while the response of the upper part of the pile appeared damping effect on the input earthquake motion in test one under event C. The acceleration of the pile from test two manifested that the input earthquake motion were amplified with varying degree in event C. It's concluded that low-cap which effectively constrained the pile head especially in the upper segment of pile could decrease acceleration response of the pile much when the sand layer wasn't liquefied or liquefied incompletely; On the contrary, high-cap had the weak constraint effect on the pile head and could amplify acceleration response of the pile for the lack of the lateral support; the acceleration response of the pile was remarkably controlled by the cap type on the upper pile while it was dominated more by the soil constraint on the lower part of the pile. Since the sand layer liquefied completely in test one in event D, the soil-pile kinetic interaction and the inertial effect from the superstructure began to appear, the magnification factor of the peak acceleration of the pile revealed that the input earthquake motion was amplified more; the peak acceleration and its magnification factor of the pile gradually increased bottom-up, and the decrease of the acceleration was observed only around the soil interface. The acceleration response of the pile and column pier in test two under event D distorted for the pile broken down around the soil interface.

The peak acceleration and its magnification factor of the pile were bigger in

event C than in event B for the same test, which suggested that the pile responded more intensely to 0.15g El Centro earthquake wave and had no relation to the cap type, however, the peak acceleration and its magnification factor of the pile were relatively small on the pier top according with the phenomenon of the small vibration amplitude of the column pier under 0.15g El Centro earthquake event. These showed that the sand layers softened more evidently and the constraint from the soil to the pile tended to become weaker in the prototype earthquake wave (last for a longer time) than the scaled earthquake wave with the same amplitude.

The soil structure for tests one and two was destroyed slightly in events one and two; the ability to transmit vibration was still strong for the soil while the structure was constrained firmly by the soil, what's more, the peak acceleration of the column pier increased gradually bottom-up and the input earthquake motion was amplified evidently presenting the acceleration of the pier top. However, the peak acceleration of the column pier on low-cap pile decreased in event D, the peak acceleration of the pier top didn't increase because the ground liquefied completely but decrease reversely, and the magnification factor was smaller than that in events one and two, for which the explanation might be that the ability of the sand layer to transmit vibration weakened and the liquefied sand represented the damping action. Note that at present seismic design of bridge piles didn't take into account the advantageous effect that the liquefied sand layer could attenuate the earthquake wave, so it was worthy of further study. Elevated-cap pile group was broken so that peak acceleration of the pier top was very large in event D.

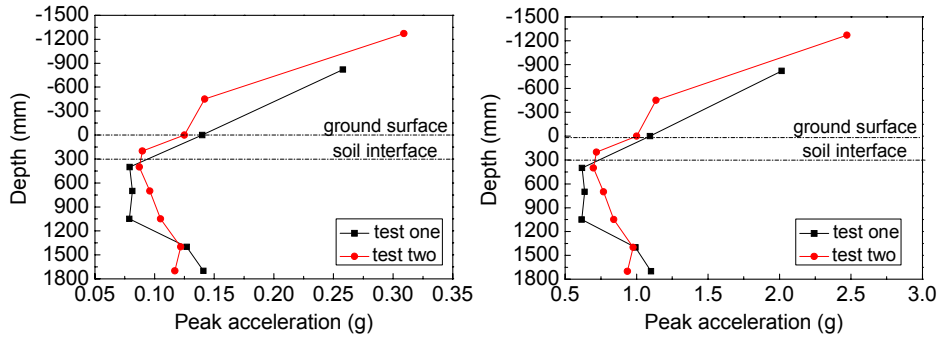

Figure 4. Peak acceleration of the pile and pier in event B.

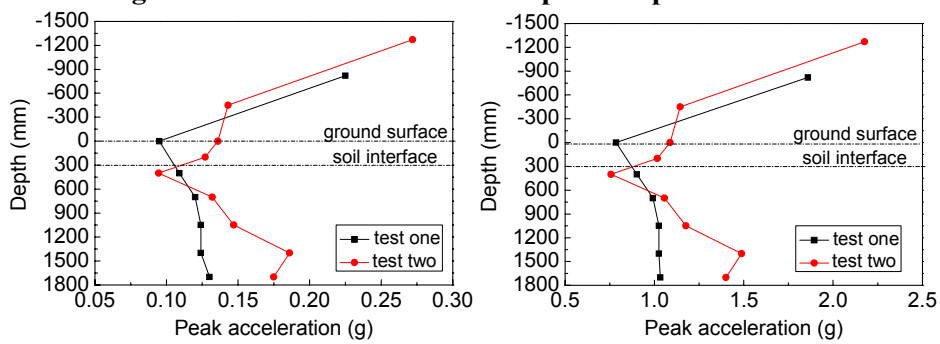

Figure 5. Peak acceleration of the pile and pier in event C.

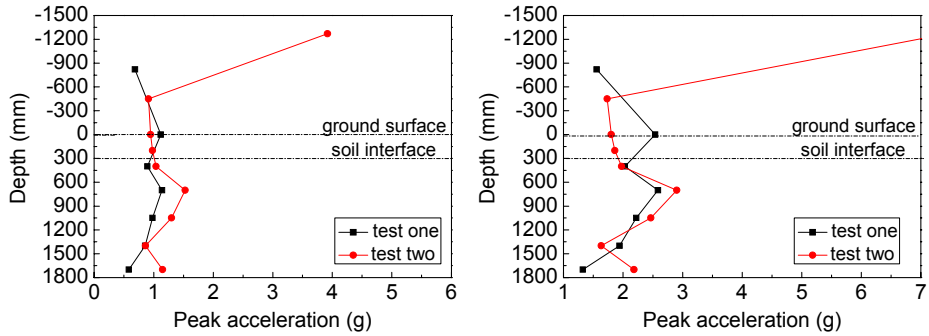

Figure 6. Peak acceleration of the pile and pier in event D.

The acceleration response of the pier top was mainly determined by rotation stiffness of the ground, translation stiffness and deformation stiffness of the structure. The peak acceleration and its magnification factor of the pier top were larger in test two than in test one which caused a larger displacement of the pier top in test two than in test one under events one and two, as a result, it would have a negative effect on the whole stability of the structural system and indicated that elevated-cap pile group was more helpful to amplify the acceleration of the pier top compared with low-cap pile. Considering the similar input earthquake motion, the same structure material and the nearly uniform structure displacement component in both tests, these were mainly because the low-cap was fixed in the clay layer so the rotation stiffness of low-cap pile group was larger, but the switch component and the translation component would be relatively small, however the rotation stiffness of elevated-cap pile group was smaller and the switch component and the translation component was relatively larger.

CONCLUSIONS

Compared with elevated-cap pile group, low-cap pile group was easier to satisfy seismic requirement of bridge piles in liquefiable ground.

When the sand layer didn't liquefy or partly liquefied, low cap obviously decreased the acceleration of the pile especially the upper pile segment; but elevated cap more played a role in amplifying the acceleration of the pile; the acceleration of the upper pile was significantly influenced by the cap type while the acceleration of the lower pile segment was more controlled by the restraint of the soil layer.

Whether the pile type was low cap and elevated cap or not the peak acceleration of the column pier gradually increased bottom-up and the acceleration of the pier top exhibited to amplify the input shaking acceleration evidently when the ground liquefied incompletely. The peak acceleration of the pier top on low-cap pile decreased a little as the ground liquefied completely, in addition, the peak acceleration of the column pier decreased gradually bottom-up.

ACKNOWLEDGEMENTS

Funding was provided by three National Natural Science Foundation of China (No.90815009, No.50378031 and No.50178027) and the shaking table tests were implemented in State Key Laboratory for Disaster Reduction in Civil Engineering in China. These supports are gratefully acknowledged.

REFERENCES

Abdoun, T., and Dobry, R. (2002). Evaluation of Pile Foundation Response to Lateral Spreading. Soil Dynamics and Earthquake Engineering. Vol. 22, 2002, pp. 1051-1058

Boulanger, R.W., Curras, C.J., Kutter, B.L., and et al. (1999). Seismic Soil-Pile-Structure Interaction Experiments and Analyses. Journal of Geotechnical and Geoenvironmental Engineering. ASCE. Vol. 125, No. 9, 1999, pp. 750-759

Finn, W.D.L, and Fujita, N. (2002). The Piles in Liquefiable Grounds: Seismic Analysis and Design Issues. Soil Dynamics and Earthquake Engineering. Vol. 22, 2002, pp. 731-742

Fujii, S., Isemoto, N., Satou, Y., and et al. (1998). Investigation and Analysis of A Pile Foundation Damaged by Liquefaction during The 1995 Hyogoken-Nambu Earthquake. Soils and Foundations. Special Issue on Geotechnical Aspects of the January 17. 1995 Hyogoken-Nambu Earthquake. No. 2, 1998, pp. 179-192

Ling, X.Z., Wang, C., and Wang, C. (2004). Scale Modeling Method of Shaking Table Test of Dynamic Interaction of Pile-Soil-Bridge Structure in Ground of Soil Liquefaction. Chinese Journal of Rock Mechanics and Engineering. Vol. 23, No. 3,2004, pp. 450-456

Ling X.Z., Wang L.X., Wang D.S., and et al. (2005). Study on Large-Scale Shaking Table Proportional Model Test of The Dynamic Property of Foundation in Unfree Ground of Liquefaction. China Journal of Highway and Transport. Vol. 18, No. 2, 2005, pp. 34-39

Imamura, S., Hagiwara, T., Tsukamoto, Y. and et al. (2004). Response of Pile Groups Against Seismically Induced Lateral Flow in Centrifuge Model Tests. Soils and Foundations. Vol. 44, No. 3, 2004, pp. 39-55

Wu, X.P., Sun, L.M., Hu, S.D., and et al. (2002). Development of Laminar Shear Box Used in Shaking Table Test. Journal of Tongji University. Vol. 30, No. 7, 2002, pp. 781-785

CT Scan o n Frozen Roadbed Soil under Dynamic Triaxial Test Condition of Beilu River Section, Qinghai -Tibet Railway of China

WANG Lixia[1], LING Xianzhang[2], ZHANG Feng[2], PU Yibin[3] and WU Liquan[4]

[1]Jilin Institute of Architecture and Civil Engineering, P.O. Box 130021, City, Changchun, P.R. China; PH (86) 431-85935001; FAX (86) 431-85916258; email: wanglixiaql@163.com
[2]Institute of Subgrade and Protection Engineering, Harbin Institute of Technology, P.O. Box 150090, City, Harbin, P.R. China; PH (86) 451-86282576; FAX (86) 451-86282576; email: Xianzhang_ling@263.net
[3]State Key Laboratory of Frozen Soil Engineering, CAS, P.O. Box 150090, City, Lanzhou, P.R. China; email: wanglixiaql@163.com
[4]School of Civil Engineering and Architecture, Zhejiang University of Science and Technology, P.O. Box 310023, City, Hangzhou, P.R. China; PH (86) 571-85070518; FAX (86) 571-85070518; email: wuliquan1966@163.com

ABSTRACT

As an effective scanning method with no damage, the CT scanning technique is used more widely in studying the dynamic deformation of frozen soil. Aiming at stability and dynamic deformation of frozen soil, the structural change before and after a dynamic tri-axial test, failure type and their main affecting factors of frozen soil taken from roadbed of Qinghai-Tibet Railway are discussed from microstructure according to CT scanning results. It indicates that water content, temperature and confining pressure are the main affecting factors. Change of density, strength and modulus during dynamical deformation decreases with an increase of water content and confining pressure, similarly the changes of the microstructure and structure. When temperature decreases, density, strength and modulus decrease rapidly, but the microstructure and structural changes decreases. When axial dynamic strength decreases, degradation of density, strength, modulus changes from large to small at the beginning and then from small to large, but structure change and demagnification are the reverse of that. The dynamic failure type of the frozen soil depends on the composite in condition of higher water content and lower temperature, but belongs to loose expand and border cracking when water content is lower, belongs to equally expand type when confining pressure or temperature is higher, belongs to composite and uniform expand type when confining pressure is lower and water content is higher, and belongs to loose failure type when confining pressure is higher and water content is lower. To frozen soil, these CT scanning results and recognition not only benefit the study pf stability and dynamic deformation, but also provide important data for further dynamic characteristics studies and establishing dynamic deformation models.

INTRODUCTION

CT scanning is a reliable detection method for the dynamic performance and deformation structural study of frozen soil (Pu et al 1995, Ma et al 1995, Liu et al 2002, Sun et al 2005, Ling et al 2003, Xu et al 2005). At present, according to

structural change of dynamic deformation of frozen soil, some research has completed many testing and theoretical studies of failure mechanisms (Ling et al 2003). Stability and dynamic deformation of Qinghai-Tibet Railway roadbed, based on low temperature dynamic tri-axial test condition, structural change, failure type and their main influence factors, are discussed from microstructure of CT scanning and some beneficial results are achieved.

MEASURING INTRODUCTION

The test was conducted in the State Key Laboratory of Frozen Soil Engineering CAS of China. An MTS-810 material testing machine with automatic numeric control and collection system was used to perform low temperature tri-axial testing. The CT scanning instrument was Siemens SOMATOM plus X-ray spiral CT machine with differentiating rate 0.35 mm×0.35 mm, least distinguish volume 0.12mm3(layer thick 1mm) and reduced density differentiating rate 0.3%(3Hu). These tests satisfied Standard for soil test method (GB50123/T-99), Code for Measurement Method of Dynamic Properties of Subsoil (GB50269/T-97), and German Siemens Corp. standard method (C1-015.208.05.03.02).

CT scanning included testing the same transect of the same specimen before and after dynamic tri-axial test in order to compare the changes. Also, the testing transects are modified to normalize the test data and eliminate error from differences in layer and size before and after the test. CT data is calculated by the Housfield formula, $ME=1000(\mu-1)$. in which, μ is the mass absorption coefficient, determined by clustering regression analysis of CT scanning results of several samples and was modified according to water content. Generally, only the main correction terms are considered in soil tests. The CT number is calculated approximately by $ME=1000[1-A(RD-S)](\mu-1)$, in which S represents the standard specimen diameter; R represents the equivalent diameter of the real specimen; D represents the average density of the soil; A represents a correction coefficient for the specimen.

Silty clay was sampled from the roadbed of the Beilu River section of Qinghai-Tibet Railway. Its plastic limit is 16.4%, liquid limit is 27.9%, dry density is 1.8g/cm^3(Wang et al 2005). For comparison of the results, standard specimen (62mm diameter, 125mm high) were batch made by the artificial frozen method using remolded silty clay. First, soil was made with water content of 13%, 18% and 23%, respectively. Then, in order to ensure its water content and homogeneous structure, setting the soil aside without evaporation for at least 6 hours. Thirdly, dies were filled and compacted layer by layer to the design dry density. After molding it was quickly frozen for about 48 hours at -30°C. After demolding and set aside for 24 hours with constant temperature of testing condition, the specimens were consolidated for 2 hours in the low temperature pressure cell of the tri-axial testing machine.

TESTING RESULTS

CT scanning results before dynamic tri-axial test. Data of CT scanning before low temperature tri-axial testing show that initial water content affects mass absorption coefficient of frozen soil to X rays directly. For instance, when the water content is 18% (DQ kinds of frozen soil), $\mu=1.304$. When the water content is 23%

(NO kinds of frozen soil), μ =1.167. To DQ kinds of frozen soil, CT number ME=1662.51, average square difference SD=141.73. To NO kinds of frozen soil, CT number ME=1512.91, average square difference SD=133.12. It can be concluded that the former possesses finer and closer structure, higher strength and larger modulus which is consistent with testing results of dynamic strength and dynamic shearing modulus of frozen soil. On CT photos, black represents high density, white represents low density and gray distribution represents uniformity of structure. So, from Figure 1, DQ kind of frozen soil is much finer and closer. This can be explained that water content of DQ kind of frozen soil is equal to the optimum water content (18%) and is easily compacted. From CT photos, it can also be found that structural characteristic of NO kind of frozen soil is weaker and compaction density is lower, and some black strip and plaque are distinctively visible.

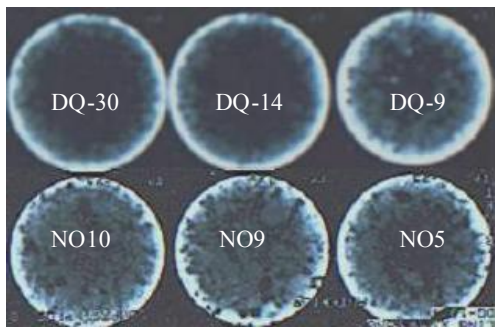

Figure 1. CT photos of frozen soil specimen transect before dynamic tri -axial test.

Comparison of CT scanning results. Through transect CT scanning parameters before and after dynamic tri-axial test, mean CT number increment and square deviation increment were calculated. Then the bar graphs were drawn to describe the relationship between water content, confining pressure, negative temperature, and axial dynamic load with two increments. According to these relationships, CT photos and common optics photos of dynamic deformation of soil specimen, some recognition on the effects of water content, confining pressure, negative temperature and axial load to dynamic deformation is achieved.

(1) Water content

After dynamic tests, the mean CT number increment increases greatly and are all negative when water content increases from 13% to 23% as shown in Figure 2. It indicates that the decrease in density, strength and modulus due to dynamic deformation becomes less. When water content increases from 13% to 23%, square deviation has a big decrease, and as the latter increases the former decreases. It indicates that the change of micro deformation mechanism and structural demagnification of frozen soil with higher water content changes less, but for deformation mechanism and structural demagnification, lower water content soil has bigger value. As shown in Figure 3, specimens with water content of 23% belong to composite failure. From the inner part to the edge, the structure changes gradually. Specimens with water content of 13% loose expand and border cracking type of failure. Structure of the inner part is fine and close, but in the border, there are wide

cracks. From Figure 4, which is from common optics photos, specimens with water content of 23% compress in the axial direction and expand in the diameter direction without any visible cracking. But, specimens with water content of 13% have distinctive shearing cracks. To sum up, water content deeply affects deformation, failure mechanism and structural change of frozen soil.

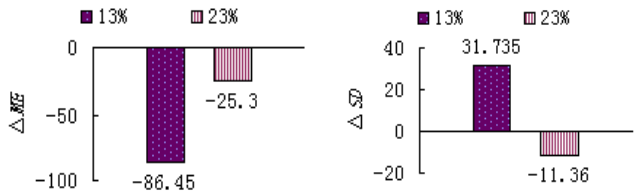

Figure 2. Bar graphs of CT data for frozen soil at varying water content .

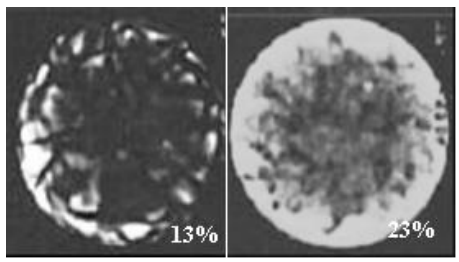

Figure 3. CT photos of frozen soil specimen transects after dynamic tri -axial test .

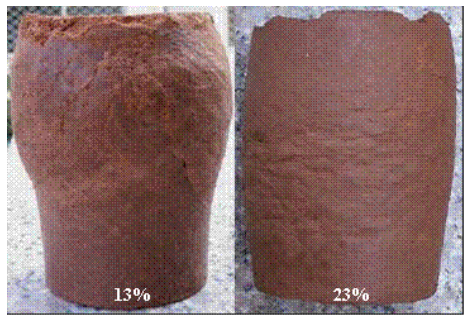

Figure 4. Photos of frozen soil specimens after dynamic tri -axial test.

(2) Confin ing pressure

As shown in Figure 5, confining pressure increases from 1MPa to 1.5MPa, mean CT number increment and square deviation increment both increase and remain negative. It indicates that the decrease in density, strength and modulus of frozen soil due to dynamic deformation becomes less as confining pressure increases. Higher confining pressure gets along with far less decrease of density, strength and structural characteristics. Under a confining pressure of 1.5MPa, the structure of the soil is finer and closer, and strength and modulus of it are higher compared with under a confining pressure 1.0MPa. This law is consistent with testing results of dynamic strength, maximum dynamic shearing modulus of frozen soil (Dynamic strength and maximum dynamic shearing modulus under confining pressure 1.5MPa are higher than that under confining pressure 1.0MPa).

As CT photos show in Figure 6, under confining pressure 1.0MPa and

1.5MPa, specimens show a type of uniform expand failure. From the inner part to the border, the failure effect becomes more serious. Structural characteristics change gradually. The inner part is fine and close, but in the border, there are wide cracks. From Figure 7, common optics photos, specimens under confining pressure 1.0MPa and 1.5MPa both have shearing cracks. Consequently, confining pressure affects deformation, failure mechanism and structural change of frozen soil to some extent, and significantly to failure mechanism.

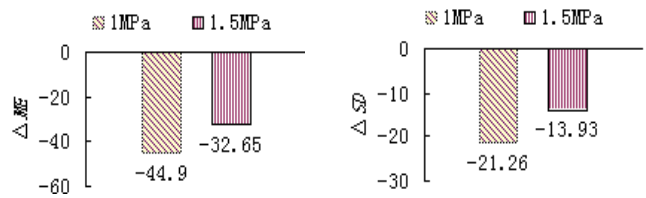

Figure 5. Bar graphs of CT data for frozen soil at varying confining pressure .

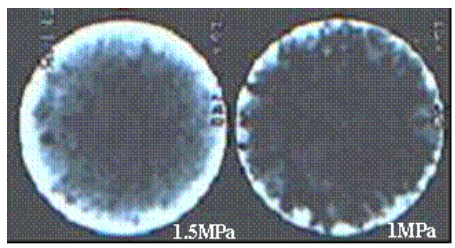

Figure 6. CT photos of frozen soil specimen transect after dynamic tri -axial test .

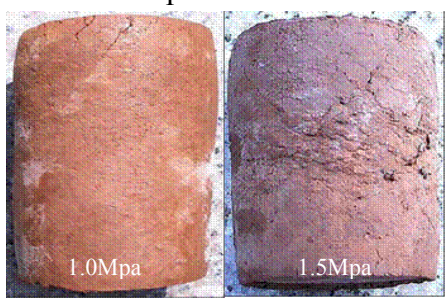

Figure 7. Photos of frozen soil specimens after dynamic tri -axial test.

(3) Negative temperature

As shown in Figure 8, temperature decreases from -2°C to -12°C, and mean CT number increment decreases and is less than zero. It indicates that the decrease of density, strength and modulus of frozen soil due to dynamic deformation becomes larger as temperature decreases. Square deviation increment (△SD) increases and remains negative. Lower negative temperature goes along with a far less decrease of density, strength and structural characteristics. That is to say, structural change and demagnification of frozen soil decreases with negative temperature drops down. This point fits the testing result that the stability of higher-temperature frozen soil is weaker than that of lower-temperature frozen soil well. Furthermore, change law of △ME and △SD with negative temperature can reflect the softening transform of the deformation mechanism. As CT photos show in Figure 9, at -2°C, small deformation

and large compact density of the inner part, loose structure and wide cracks of the border indicates an expand type of failure. At -12°C, similar structure and deformation of the transect, a little large compact density of the inner part, serious failure and many wide cracks indicate a composite type of failure. From Figure 10, common optics photos, specimens at -2°C failure due to compression at axial direction and expand in diameter direction, but at -12°C, there is no obvious deformation and failure characteristic.

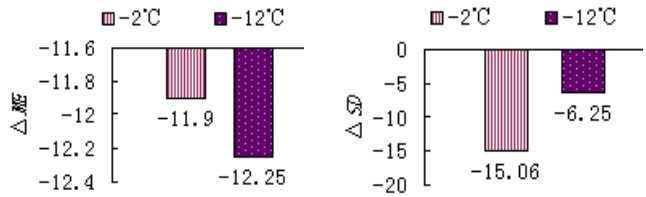

Figure 8. Bar graphs of CT data for frozen soil at varying low temperature .

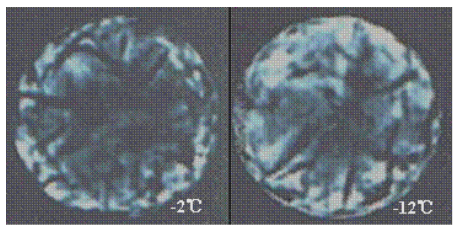

Figure 9. CT photos of frozen soil specimen transect after dynamic tri -axial test .

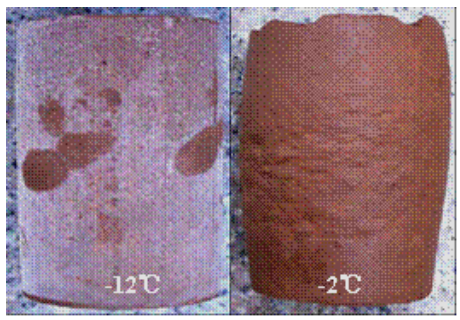

Figure 10. Photos of frozen soil specimens after dynamic tri -axial test.

(4) Intensity of axial dynamic load

As shown in Figure 11 and Figure 12, in the condition of confining pressure of 1MPa and water content of 23%, axial loads of 5.5MPa , 5MPa , 4.5MPa and 1.0MPa are applied successively. After the test, the mean CT number increment is negative and changes from increase to decrease. Square deviation increment is negative also, but changes from decrease to increase. It indicates that, along with decrease of dynamic load, a decrease in density, strength and modulus changes from large to small, then, to large, but the decrease of structural characteristics and demagnification change from small to large, then, to small. In condition of a confining pressure of 2MPa and water content of 13%, the law is similar except less change value. As CT photos shown in Figure 13, in condition of the confining pressure of 1.0MPa and water content of 23%, micro-characteristics of uniform deformation are obvious. The inner part of the transect exhibits a consistent deformation along with fine and close structure, but in the border, serious failure has

taken place. In the condition of a confining pressure of 2.0MPa and water content of 18%, the failure belongs to the loose type, and micro characteristics of integral failure are obvious. Structure of the whole section is dense with wide cracks. From the inner part to the border, failure effects becomes more serious. From Figure 14, common optics photos, plastic deformation is obvious in the condition of a confining pressure of 1MPa and water content 23%. But, shearing cracks, axial compression and expansion in diameter direction is obvious in condition of confine pressure 2MPa and water content 18%. It should be said that intensity of axial dynamic load can affect to dynamic deformation characteristics, failure mechanism and structural change to a degree, but it will be more significant when it is analyzed in combination with other factors.

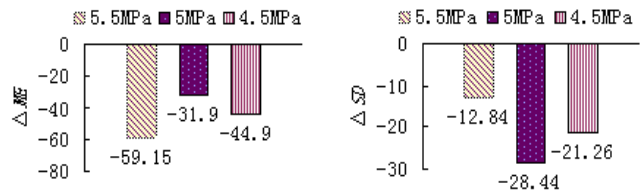

Figure 11. Bar graphs of CT data for frozen soil specimen at varying axial dynamic stress (1MPa, 23%).

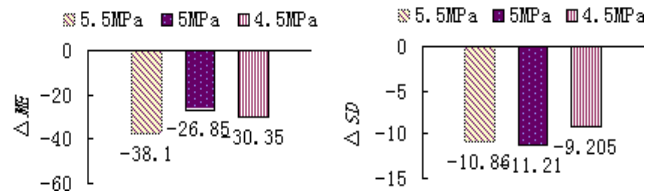

Figure 12. Bar graphs of CT data for frozen soil specimen at varying axial dynamic stress (2MPa, 18%).

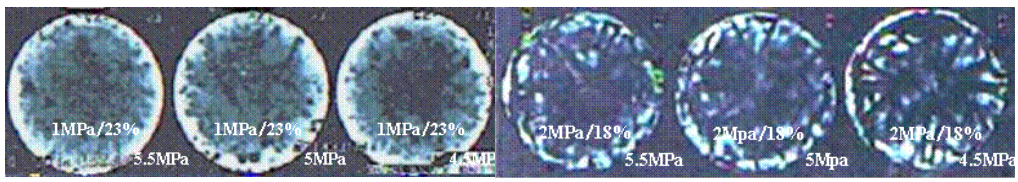

Figure 13. CT photos of frozen soil specimen transects after dynamic tri -axial test.

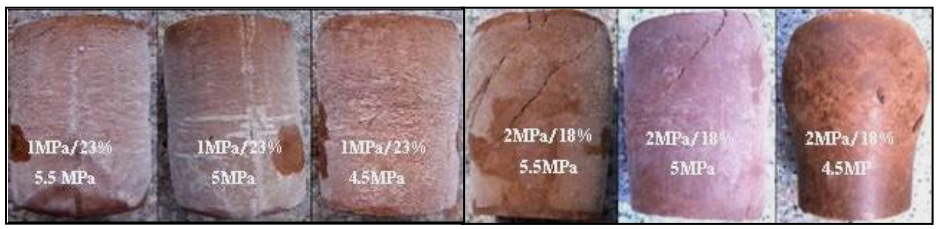

Figure 14. Photos of frozen soil specimens after dynamic tri -axial test.

CONCLUSIONS

(1) Water content, negative temperature, confining pressure and axial load are

all main affecting factors of dynamic deformation structure change and failure type.

(2) In low temperature dynamic tri-axial testing condition, change of density, strength and modulus during dynamical deformation decreases with increasing of water content and confining pressure, similar to change of microstructure and structure.

(3) With temperature decreasing, change of density, strength and modulus decrease rapidly, but the structural change and degrade of demagnification decreases.

(4) With axial dynamic strength decreasing, degrade of density, strength and modulus changes from large to small at beginning and then from small to large, but structure change and demagnification are the reverse of that.

(5) Dynamic failure type of the frozen soil belongs to composite in the condition of high water content and lower temperature, but belongs to loose expand and border cracking when water content is lower, belongs to uniform expand type when confining pressure or temperature is higher, belongs to composite and uniform expand type when confining pressure is lower and water content is higher, and belongs to loose failure type when confining pressure is higher and water content is lower.

ENDING WORDS

With rapid building and development of civil engineering in cold regions, dynamic performance and dynamic stability of frozen soil have taken great attention. CT scanning technique on frozen soil deformation and destroy are well developed, it provides an effective method for study dynamic performance, deformation structural change, failure type and affecting factors. On the base of many scholar's instructive study, using CT scanning technique, aiming at frozen silty clay taken from roadbed of Beilu River section of Qinghai-Tibet Railway, structural change of dynamic deformation, type of failure and its affecting factors interaction under low temperature are studied, especially reference (Xu et al 2005), supplemental testing item of micro mechanism and failure type under axial dynamic load are performed, some beneficial recognition are achieved.

ACKNOWLEDGMENTS

This study is supported by the Natural Science Found of China (Grant No. 50678055 and 50538030), the State Key Laboratory of Frozen Soil Engineering Open Found of China (Grant No. SKLFSE200402), the Doctor Subject Special Scientific Found of China (Grant No. 20070213076), and the Supported and Guidance Plan Found of Zhejiang Province, China (Grant No. 2008C23019).

REFERENCES

Liu Z. L, Li H. S., Zhu Y. L. (2002). "Damage characteristics and micro-crack damage measurement of frozen soil under uni-axial compression." Journal of Dalian University of Technology, 42(2):223-227.

Ling X. Z., Xu X. Y., Qiu M.G. (2003). "Study on CT scanning of Harbin frozen silty clay before and after dynamic triaxial test." Chinese Journal of Rock Mechanics and Engineering , 22(8): 1244-1249.

Pu Y.B., Wu Z.W. (1995). "CT mathematical equation of CT experiment on frozen soil." Journal of Glaciology and Geocryology , 17(supp.): 135-139.

Sun X.L., Wang R, Hu M.J.(2005). "Meso-scopic mechanism analysis of deformation properties of frozen silty clay under triaxial shear." Acta

Mechanica Solida Sinica, 26(1):62-66.

Wu Z.W., Ma W.(1995). "Monitoring the change of structures in frozen soil in uniaxial creep process by CT." Journal of Glaciology and Geocryology, 19(1): 52-57.

Wang L.X., Ling X.Z., Xu X.Y.(2005). "Comparison of dynamic and static triaxial test on frozen silty clay of Qinghai-Tibet Railway." Chinese Journal of Geotechnical Engineering, 27(2):202-205.

Xu C.H., Xu X.Y., Shen X.D.(2005). "Study on residual strain of frozen soil and CT analysis under cyclic loading of variable amplitudes." Rock and Soil Mechanics, 26(4):572-576.

Freeze-Thaw Stability of Slopes in Seasonally Frozen Regions of the Northeast China

WANG Lina[1], LING Xianzhang[1], ZHANG Feng[1], GAO Xia[1], and WU Liquan[2]

[1]Institute of Subgrade and Protection Engineering, Harbin Institute of Technology, P.O. Box 150090, City, Harbin, P.R.China; PH (86) 451- 86282120; FAX (86) 451-86282116; email: wlnyongji@126.com

[2]School of Civil Engineering and Architecture, Zhejiang University of Science and Technology, P.O. Box 310023, City, Hangzhou, P.R. China; PH (86) 571-85070518; FAX (86) 571-85070518; email: wuliquan1966@163.com

ABSTRACT

The finite element analysis is used to investigate the effects of initial water content, freezing temperature and freeze-thaw layer thickness on the stability of the thawing slope in a seasonally frozen region of Northeast China. The finite element method with shear strength reduction technique is used to evaluate the stability of slopes under the freeze-thaw processing. The numerical results indicated that the slope stability decreases with increasing initial water content, debasing freezing temperature, increasing freeze-thaw layer thickness and thawing depth. Initial water content has the biggest influence on the slope stability. The above results enrich the investigations on the freeze-thaw stability of slopes in the seasonally frozen areas and provide the instructions for engineering practice controlling the freeze-thaw stability of slopes.

INTRODUCTION

China ranks third among the biggest four frozen soil countries of the world, and the area of seasonally frozen soil is $5.14\times10^6 km^2$. The engineering, such as road, construction, water conservancy, power station and mine are extensively distributed in the seasonally frozen regions. Especially in recent years, with the executing of the strategic of the western development and promoting the northeast, infrastructure of seasonally frozen regions will be more developed. Nevertheless, freeze-thaw hazard is becoming one of the primary problems restricting the engineering construction, and urgent need to be studied and solved. At the present time, the stability of slope and landslide control in unfrozen regions is investigated deeply, and plentiful and substantial results are obtained. Because the stability of slope in seasonally frozen regions is affected by more factors, such as repeated freeze-thaw, than in unfrozen regions, up to now, there are few studies of slopes in seasonally frozen regions and the data is dispersion(Harris et al 2000, LIU, H. J. et al 2006, Simonsen et al 2002, NIU, F. J., et al 2002, SHAN, W., et al 2008). Natural slope and manmade slope are distributed in the topical seasonally frozen soil distributed in most regions of the

Northeast China, and freeze-thaw stability becomes the important hidden danger of engineering construction. In view of the above content, according to the stable control problem of the slope in seasonally frozen regions of China's Northeast, the finite element analysis is used to investigate effects of initial water content, freezing temperature and freeze-thaw layer thickness on the freeze-thaw stability of the slope, thus to develop investigations of freeze-thaw stability in seasonally frozen regions.

FINITE ELEMENT ANALYSIS

Condition simplification. Because of the complication of the frozen soil, for simplification, some hypothesizes are as follows:

(1) Soil is assumed to the isotropic homogeneous material. The Northeastern China seasonally frozen region locate at the inner of Song-liao basin, where natural terrain fluctuates small and quaternary sedimentary changes small, soil is the material of isotropic homogeneous in the same slope, thus the simplification is basically reasonable.

(2) Hydrodynamic pressure and hydrostatic pressure of ground water are not considered, and there is not water supply and excretion of the boundary. Freeze-thaw failure and landslide occur in spring thawing period. There is no infiltration or infiltration content is little because of non-rainy season in spring thawing period, together with groundwater circulation usually occurs below freeze-thaw surface, so the effects of the ground water on freeze-thaw stability of the slope can be neglected.

(3) Soil is equitable freezing and thawing.

(4) Calculation model is simplified as plane strain problem because the dimension of cross section is much smaller than vertical section.

Relation of stress-strain. The shear strength of soil is the key factor of evaluating slope stability, and soil slope will be failure when maximum shear stress reaches failure limit. Based on this, the ideal elasto-plastic model based on Mohr-Coulomb yield criterion is adopted.

Definition of safety factor. The safety factor of the slope is defined as

$$F_s = \frac{\tau_f}{\tau_M} \tag{1}$$

where F_s=safety factor, τ_f=actual shear strength and τ_M=maximum shear strength at failure.

Introducing Mohr-Coulomb yield criterion, the safety factor can be expressed as

$$F_s = \frac{c + \sigma_n \tan\varphi}{c_c + \sigma_n \tan\varphi_c} \tag{2}$$

where c is the actual cohesion; φ is the actual friction angle, c_c is the cohesion at failure, φ_c is the friction angle at failure and σ_n is the actual normal stress component.

The parameters c and $\tan\varphi$ are reduced by the same proportion until the slope failure, so the safety factor can be further expressed as

$$F_s = \frac{c}{c_c} = \frac{\tan\varphi}{\tan\varphi_c} \tag{3}$$

In the paper, evaluation criteria for the stability of the slope are synthetically

considered between plastic zone transfixion and displacement mutation of characteristic notes.

Calculation model and mesh generation. The concrete application of the numerical analysis on freeze-thaw stability of slopes is described based on a highway cut slope in a seasonally frozen region of China's northeast. The slope with a height of 20m and a gradient of 1:1 is analyzed with a two-dimensional finite element mesh, as shown in Figures 1 and 2. Calculation region is divided into two regions, frozen region and unfrozen region. The boundary condition of displacement constraint is adopted in the paper, that is, horizontal displacements are restricted at right and left boundaries and the vertical and horizontal displacements are restricted at the lower boundary. Based on the principle of virtual work, element matrix is formed, and total stiffness matrix is assembled by the direct stiffness method. Hooke's law is used to solve element stress.

Physical and mechanical parameters. The physical and mechanical parameters of the frozen soil, thawing soil and unfrozen soil are listed in Table 1.

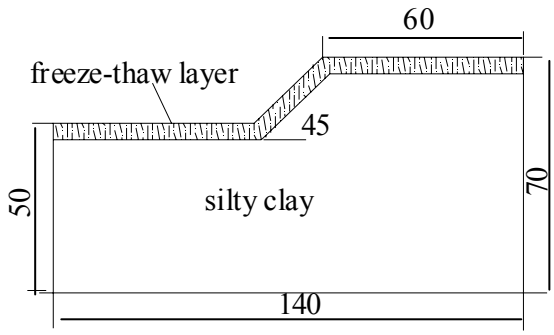

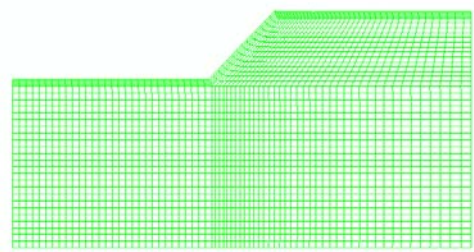

Figure 1. Profile sketch of slope (unit: m). **Figure 2. Partition scheme of slope.**

ANALYSIS OF INFLUENCE FACTORS

The practice shows that the primary factors affecting the stability of slope in seasonally frozen region are initial water content, freezing temperature and freeze-thaw layer. Based on the above example, the factors affecting freeze-thaw stability of slope are analyzed by the Finite Element Method (FEM).

Influence of initial water content. In order to investigate the influence of initial water content on the stability of the slope with different thawing depth (h), conditions are shown in Table 2.

Figure 3 depicts the relationship between safety factor and initial water content at different thawing depth (h). When h is constant, the safety factor of the thawing slope decreases with the initial water content increasing, that is, stability of the slope decreases. When $h \leq 1$m, there are less effects of initial water content on stability of the slope. Nevertheless, when $h \geq 1.5$m, there are obvious effects. When W_0 is constant, the safety factor of the thawing slope decreases with the thawing depth increasing. Especially when the initial water content exceeds 14%, the freeze-thaw stability of slope decreases rapidly with increasing the thawing depth.

Table 1. Physical and Mechanical Parameters of the Soil.

Type	Water content (%)	Unit weight (kN/m^3)	Elastic modulus (MPa)	Poisson ratio	Cohesion (kPa)	Friction angle (°)	Tem per-ature ℃
Thawing soil	11.80	18.00	5	0.38	15.20	28.70	-3
	11.80	18.00	5	0.38	15.10	28.67	-5
	11.80	18.00	5	0.38	15.00	28.64	-7
	11.80	18.00	5	0.38	14.80	28.63	-10
	11.80	18.00	5	0.38	14.50	28.60	-15
	13.06	18.20	5	0.38	12.93	28.49	-3
	14.17	18.38	5	0.38	11.02	28.40	-3
	15.40	18.58	5	0.38	9.52	28.21	-3
	16.80	18.80	5	0.38	7.74	28.10	-3
Unfrozen soil	-	17.00	6	0.35	28.00	30.00	-
Frozen soil	-	18.00	30	0.32	40.00	28.00	-

(**Note**：'-'signs that the temperature in thawing soil is the freezing temperature before the frozen soil thawing)

Table 2. Calculation Parameters of Different Conditions.

Condition	Initial water content (W_0)	Maximum of active layer (Z)	Freezing temperature (T)
A1	11.80%	2m	-3℃
A2	13.06%	2m	-3℃
A3	14.17%	2m	-3℃
A4	15.40%	2m	-3℃
A5	16.80%	2m	-3℃

The above results show that there are greater effects of initial water content on the stability of slope during the freeze-thaw process. The reason is that the volume of soil water rises during the freezing process, filling the gap of soil particles, promoting soil particles moment, and induce changes of soil structure, and hence make intensity change. As increasing of initial soil water content during the freezing process, the water migration to freezing front increases, and lead to more intensive change of soil structure. If the water can not discharge promptly when active layer soil melts, the mechanical parameters of melted soil would decrease significantly, and make stability

of melted slope decrease. Therefore, the freeze-thaw stability of slope decreases with increasing the initial water content and thawing depth. The relationship between safety factor and initial water content of slope of all the ice melting is linear descending, as shown in Figure 4.

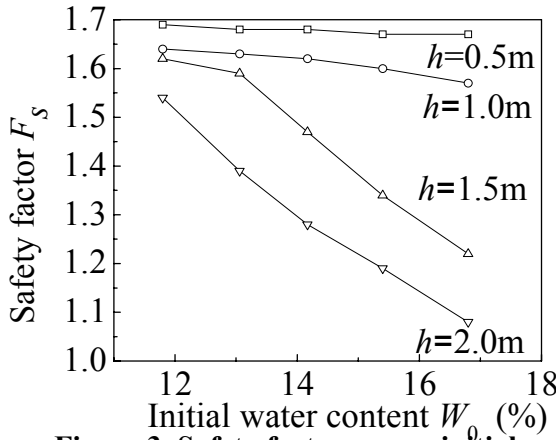

Figure 3. Safety factor versus initial water content at different *h*.

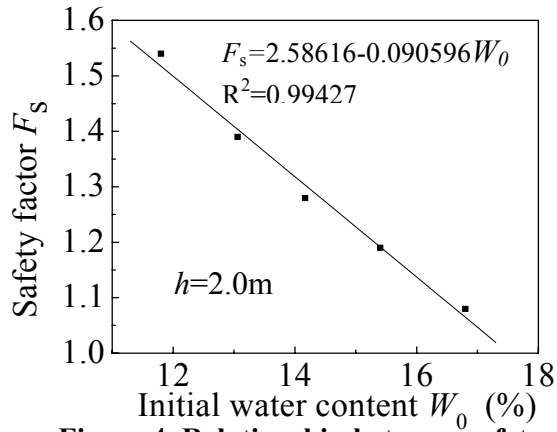

Figure 4. Relationship between safety. factor and initial water content.

Influence of freezing temperature. Freezing temperature affects the freezing rate and unfrozen water content after stably frozen, consequently affects the frozen-thawed soil structure. The mechanical properties of the frozen-thawed soil change with the different freezing temperature. In order to study the effects of freezing temperature on the stability of the slope with different thawing depth, the following five conditions are selected, that is, T=[-3, -5, -7, -10, -15]℃. Other parameters see condition of A1.

Figure 5 shows the relationship between safety factor and freezing temperature at different thawing depth. When h is constant, the safety factor of the thawing slope decreases with the freezing temperature decreasing, that is, stability of the slope decreases. When h≤1.5m, there are less effects of freezing temperature below -10℃on stability of the slope. When T is constant, the safety factor of the thawing slope decreases with the thawing depth increasing.

The above results show that there are certain effects of freezing temperature on the stability of slope. During the freezing process, temperature gradient of freezing temperature field increases with the freezing temperature decreased, which make the water freeze quickly at peak surface and the Mass and energy balance is destroyed, thus unfrozen water migrates to freezing surface quickly. Soil water content and structure are changed by freezing temperature, and induce the decrease of shear strength of thawing soil, consequently the stability of slope is decreased. Figure 6 shows the relationship between safety factor and freezing temperature when thawing depth is equal to freeze-thaw depth is linear descending.

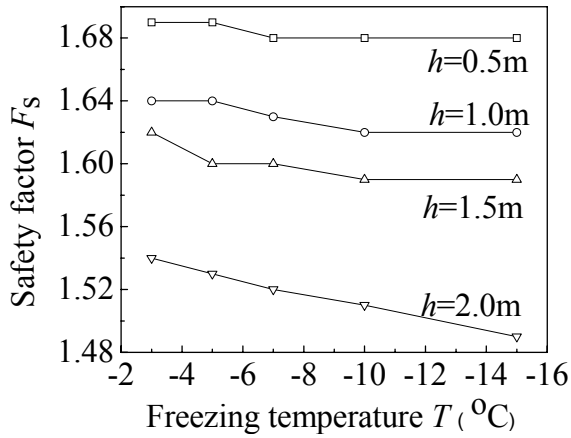

Figure 5. Safety factor versus freezing temperature.

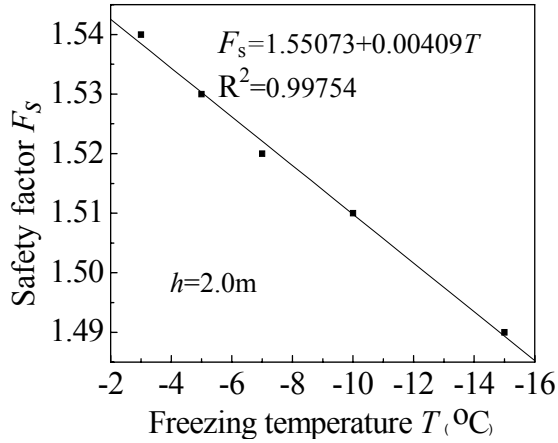

Figure 6. Relationship between safety factor and freezing temperature at different *h*.

Influence of freeze-thaw layer. In order to investigate the effects of seasonally freeze-thaw layer on the stability of the slope, the following five conditions are selected, that is, Z=[0.0, 0.5, 1.0, 1.5, 2.0]m. Others parameter see Table 3.

Table 3. Calculation Parameters of Different Conditions

Condition	Active layer (m)	Thawing depth (m)
H=20m β=45° W_0=11.8% T=-3℃	0.0	0.0
	0.5	0.5
	1.0	1.0
	1.5	1.5
	2.0	2.0

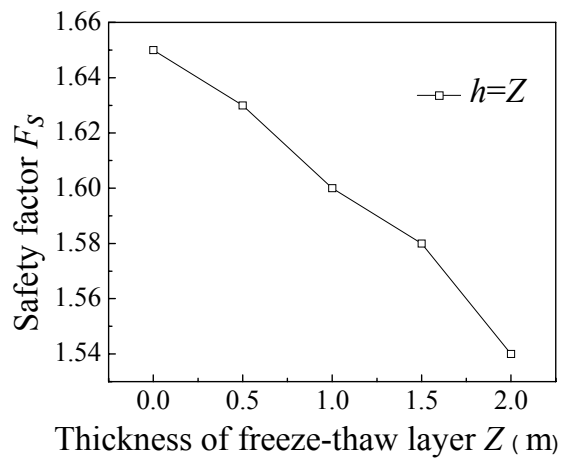

Figure 7. Safety factor versus thickness of freeze-thaw layer at *h*=*Z*.

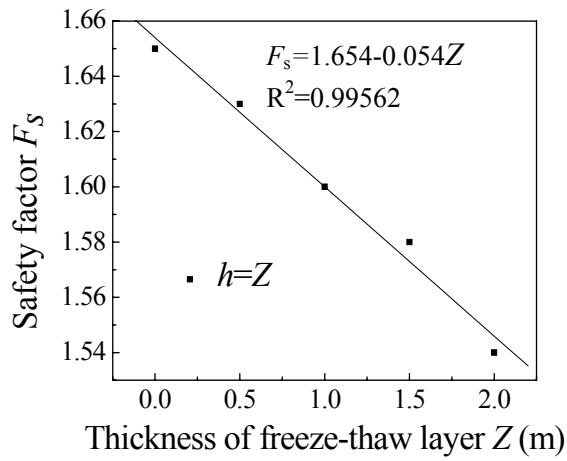

Figure 8. Relation between safety factors and thickness of the freeze-thaw layer.

Figure 7 depicts the relationship between safety factor and thickness of active layer when thawing depth is equal to active layer. The safety factor of the thawing slope decreases with the active layer increasing, that is, stability of the slope

decreases. Because the mechanical parameters of soil decrease during freeze-thaw process, the downslide trend of slope is apparent with the thawing depth decreased, and the stability of slope decreases.

Figure 8 shows the relationship between safety factor and thickness of active layer when thawing depth is equal to freeze-thaw depth. Linear descending relationship between safety factor and thickness of active layer is obtained.

CONCLUSIONS

The following conclusions are obtained:

(1) Freeze-thaw stability of the slope decreases with increasing initial water content, reducing freezing temperature, increasing freeze-thaw layer thickness and thawing depth.

(2) The relationships between safety factor and initial water content freezing temperature and freeze-thaw layer are all linear descending, and the fit formulas which can predict the freeze-thaw stability of slope in seasonally frozen region are obtained.

ACKNOWLEDGMENT

This study is supported by the State Key Laboratory of Frozen Soil Engineering Open Found of China (Grant No. SKLFSE200402), and the Supported and Guidance Plan Found of Zhejiang Province, China (Grant No. 2008C23019).

REFERENCES

Harris, C., Lewkowicz, A.G. (2000). "An analysis of the stability of thawing slopes." *Canadian Geotechnical Journal*, 37:449-462.

LIU, H. J., WANG, P.X. (2006). "Stability analysis of loss of stability caused by freeze and melt of earthen side slopes of highways." *Journal of Harbin Institute of Technology*, 38(5):764-766.

NIU, F. J., CHENG, G. D., XIE, Q. (2002). "Study on instability of slopes in permafrost regions of Qinghai-Tibet High Plateau." *Proceedings of the 5th International Symposium on Permafrost Engineering*, Yakutsk: Permafrost Inst. SB RAS Press, 192-197.

Simonsen, E., Janoo, V. C., Isacsson, U. (2002). "Resilient properties of unboundroad materials during seasonally frost conditions." *Journal of Cold Regions Engineering*, 16(1):28-50.

SHAN, W., LIU, H. J., YANG, L., et al. (2008). "Study of regularity of variation of water content in shallow layer of soil road cutting slopes in seasonally frozen-ground region." *Rock and Soil Mechanics*, 29:335-340.

Stability and Reinforcement Methods of a High Slope at the Hang-Yong Natural Gas Pipeline in China

WU Liquan[1], ZHANG Feng[2], LING Xianzhang [2], YU Huoming[3], CHEN Tianhong[1], and LIU Wei[1]

[1]School of Civil Engineering and Architecture, Zhejiang University of Science and Technology, P.O. Box 310023, City, Hangzhou, P.R. China; PH (86) 571-85070518; FAX (86) 571-85070518; email: wuliquan1966@163.com
[2]Institute of Subgrade and Protection Engineering, Harbin Institute of Technology, P.O. Box 150090, City, Harbin, P.R. China; PH (86) 451-86282576; FAX (86) 451-86282576; email: fzhang_hit@163.com
[3]Zhejiang Engineering Prospecting Institute, P.O. Box 315012, City, Ningbo, P.R. China; email: yhm62103@163.com

ABSTRACT

Based on the elastic-plastic finite element method and limiting equilibrium theory, this paper focuses on the high slope stability and analyses the influence by the work environment and strength of the high slope structural plane at Hang-Yong Natural Gas Pipeline in China. The numerical results reveal that this high slope is in the ultimate equilibrium state and it maybe occurs to rapidly slide when it is in heavy rainfall condition; Draining the groundwater level and infusing slurry on the weak structural plane could improve the stress condition and advance emergency capacity inside slope; and the slope safety coefficient may reach 1.61 integrating the two methods proposed. However, it must adopt other engineering method to reduce the tensile damage at after-edge of slope. All above studies are significant for supplying the basis references to reinforcement methods and monitoring the high slope in safety.

INTRODUCTION

This engineering slope locates at an inclined ramp in Yinzhou county, Ningbo City of China, along the Hang-Yong Natural Gas Pipeline. In history, this slope had three landslips happen in the direction of E140°S, which landslide body fissure distributes at after-edge and two sides and leading edge, the figure of after-edge is an approximately vertical arc and northern and southern side is an arc as a whole. The first landslide happened in 1956 and could not be researched cause of long time, the second landslide happened in 1995 with a 2.0-4.0m high of posterior wall and a superficial layer 2000m^3 cubage of slide slope, and the third landslide happened in April 2005 with a 0.5-1.6m high of posterior wall, which several fissures with a 2-5cm width occurred in slope body firstly, the fissures became obviously and wider subsequently, last the slope happened to slide at leading edge with a small capacity 300m^3.

At present, this side slope is creeping deformation, and it may occurs to rapidly slide in the condition of heavy rainfall according to the site exploration, which could

directly pose hazard on the adjacent Hang-Yong Gas San-Shan Station and it's pipelines without effective reinforement in time, and it could lead to unmeasurable economic losses and aftermath. Therefore, this paper study and estimates the high slope's stability based on the elastic-plastic finite element method and limiting equilibrium theory, and the different reinforcement methods are calculated and analyzed to provide the guiding datum to reinforcement scheme and safety monitor subsequently.

ENGINEERING GEOLOGY SURVEY AND SLIDE GENESIS

This slope developed on the erosion - abrasion hilly area. The direction of the hill is South-North direction and the gradient is about 20°-30°. The exposed stratum is composed of the gravel silty clay (Q_4) and the ignimbrite (J_3x). Moreover, three structural planes with a 1-3 lines in per meter and 0.5-15 meter extension are developed in this area.

There is a weak structure plane in the slope body according to the drilling data and fissure feature. As is shown in Figure 1, this slope could be subdivided into three parts: the lower part is the anti-slide portion with 30 meters length, which failure face is gentle and weak interlayer in intensive weathered bedrock, there are tensile and fanlike fissure at edge. The middle part is the main slide portion with 40 meters length, which failure face dip angle is changeable from 7° to 40° and it is the contact face between intensive and weak weathered bedrock. The upper part is the pull-type slide portion with 25 meters length, which the fissure is tensile and the slide plane is the contact face between intensive (native soil) and weak weathered bedrock.

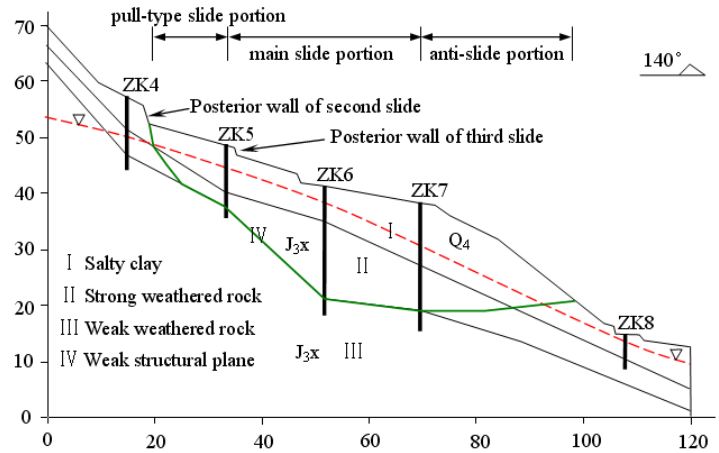

Figure 1. Engineering geology map of slope (unit: m).

Many factors lead to incipient fault in this slope. The first is the thicker native soil (maximizing 20 meters) with a weak machnical property. The second is the heavy rainfall increasing the rock-soil gravity and the saturated slope matter softening the native soil layer and intensively weathering bedrock and the mechanical strength of structure face. Moreover, the human engineering practice, such as chronically irrational quarrying and excavation slope for road in the slope leading-edge, has posed incipient fault on the slope destabilization.

STABILITY ANALYSIS

Constitutive model and mechanical parameters. Using the finite element ZZYFEM2005 to analyze the slope stability (Zhang et al 2007, Zhu et al 2008,Yu and Zhu 2004), which the slope materials are assumed to be an isotropic body and the calculation model is simplified to be a plane strain. As is shown in Figure 2, the calculation range is 120m×70m, and the horizontal placement is zero at two sides, and the vertical placement is zero at lower boundary. There are 3706 quadrilateral unit with same parameter and 3602 node points in this model. It adopts the Goodman contact face and the nonlinear elastic model for constitutive relation at structural plane in slope body, and the ideal elastic-plastic model in other material constitutive relation, and the Drucker-Prager yield criterion for rock mass. The physical mechanics parameters are listed in Table 1. Most of them are determined by the engineering geology exploration results, consulting the structural deterioration and degree of weathering in rock body and the similar other engineering parameters (Ye 1991).

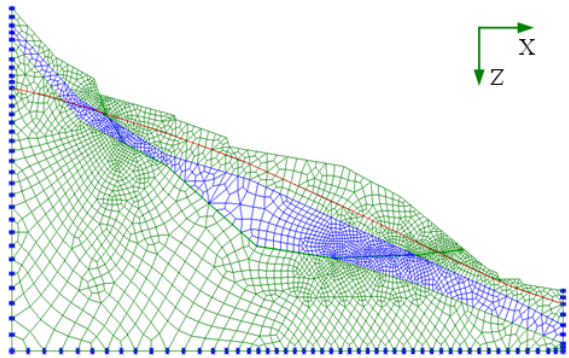

Figure 2. Finite element mesh of slope in nature condition (unit: m).

Table 1. Mechanics Parameters of Slope Materials.

	Condition	Elastic modulus MPa	Poisson ratio	Unit weight kN/m^3	Cohesion kPa	Friction angle °	Shear stiffness kN/m	Normal stiffness kN/m
I	N	8.0	0.30	18.5	250	28	—	—
	S	7.5	0.30	21.5	220	25	—	—
II	N	600	0.35	22.5	750	30	—	—
	S	580	0.35	23.0	700	28	—	—
III	N	657	0.35	24.5	830	35	—	—
	S	650	0.35	25.0	800	32	—	—
IV	N	—	—	21.5	23	12	4810	41600
	S	—	—	22.0	12	9	4000	38900

Note: "N" represents the natural condition, and "S" represents the saturated condition.

Slope safety factor. The global slope safety factor is equal to the ratio between anti-slide force and slide force at structure face for the rocky slope containing weak structure face (Ling and Cai 2002, Li et al 2003, Zheng et al 2005). It utilizes the finite element program to calculate the stress at joints in weak structure face to establish the

integral slope safety factor F_s, which overcomes the shortcoming that the bottom force at rock-soil strip is not the real stress in limiting equilibrium theory.

$$F_s = \frac{\sum_{i=1}^{N} T_{fi}}{\sum_{i=1}^{N} T_i} = \frac{\sum_{i=1}^{N} \left(c_i + \sigma_{ni} . \tan \varphi_i \right) A_i}{\sum_{i=1}^{N} \tau_{si} A_i} \tag{1}$$

Where N represents the slide numbers in slide body, T_i represents the slide force of No.i slide plane along slide direction, T_{fi} represents the anti-slide force of No.i slide plane along slide direction and A_i represents the area of No.i slide plane after taking out tensile region.

Stability analysis. It obtains any point's stress, yielding approach and state through the finite element calculation in natural condition in this slope. The maximal shear stress nephogram is shown in Figure 3. It displays that the maximal shear stress foamats the concentrated zone nearby the built-in point of structural plane and it emerges in saturated intensive weathered bedrock. Moreover, the unidirectional tension failure appears at the after-edge of slope surface as is shown in Figure 4, which it coincides with site exploration; and the slope is in ultimate equilibrium state because the integral safety factor of slope is 0.97. The stress in concentrated zone of maximal shear stress is increasing in complete saturation state than natural satae cause of locally abundant precipitation rain fall, here the slope in a destabilizing state becase the interface betwwen soil and rock is obvious and safety factor of slope is 0.90.

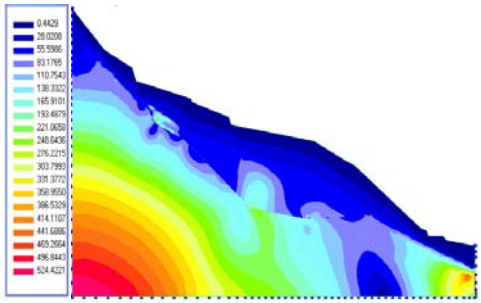

Figure 3. Nephogram of $\tau_{\max}$ in nature condition.

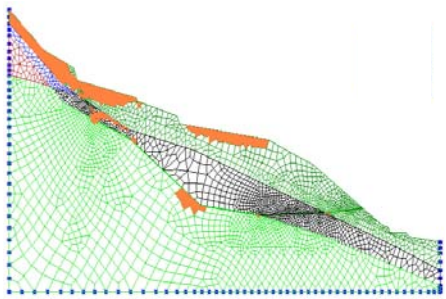

Figure 4. Distribution of yield zone in nature condition.

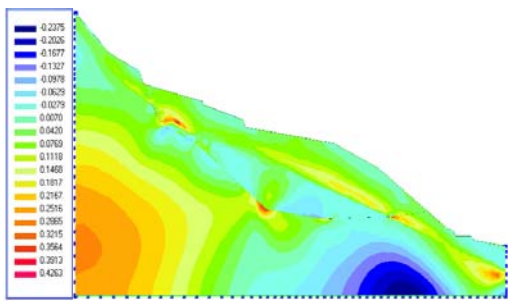

Figure 5. Nephogram of η in nature condition.

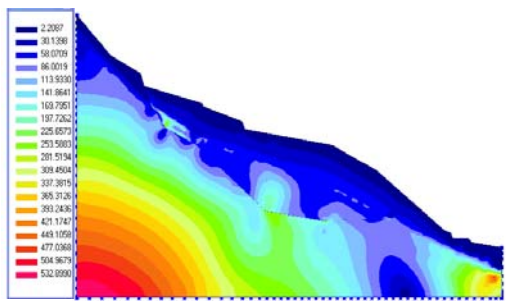

Figure 6. Distribution of $\tau_{\max}$ in saturated condition.

ANALYSIS OF DIFFERENT REINFORCEMENT METHODS

Draining groundwater level. The mainly treating methods are setting

drainage system, draining the groundwater level and decreasing infiltration flow to display the strength of structural plane and rock-soil body for the high slope with higher groundwater level and structure face. The maximal shear stress and approaching degree of yield is displayed in Figure.7 in condition of the groundwater level under the entire structural plane; which the range of stress concentrated zone decreased and the maximal shear stress cut down comparing with it in natural state; the approaching degree of yield reduced too and the maximal approaching degree of yield of slope body unit is close to 0.27. Here the slope safety factor is 1.26 and 0.29 higher than it in natural state and it increased the slope emergency capacity.

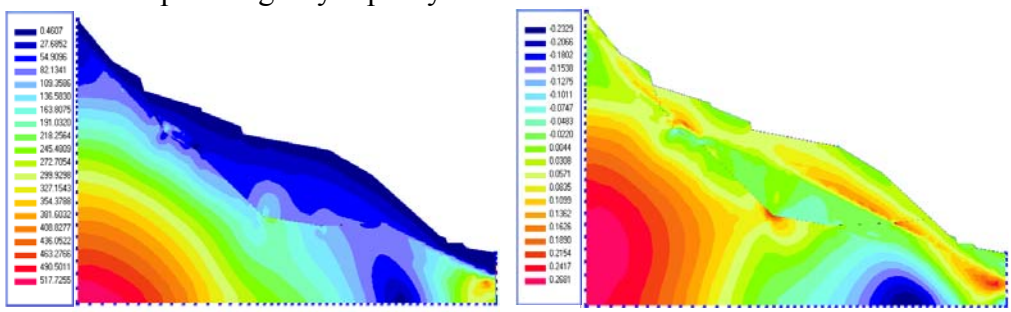

Figure 7. Nephogram of τ_{max} and η under drained slope (Fs=1.26).

Infused slurry of structure plane. The infused slurry is common in slope reinforcement, which infused slurry with High pressure could increase the strength indexing of structure face utilizing existing drilling hole. Table 2 lists the calculation parameter of this slope after infusing slurry. The maximal shear stress and approaching degree of yield are displayed in Figure 8 through finite element method calculation, which the maximal shear stress decrease and the approaching degree of yield reduce comparing with it in natural state; the integrating safety factor is 1.29, therefore the entire slope stability is enhanced effectively.

Table 2. Mechanics Parameters of Structure Face after Infusing the Slurry.

Type	Unit weight kN/m^3	Cohesive kPa	Friction angle °	Shear stiffness kN/m	Normal stiffness kN/m
Natural structure plane	22.0	30	15	4810	41600
Saturated structure plane	22.5	16	12	4000	38900

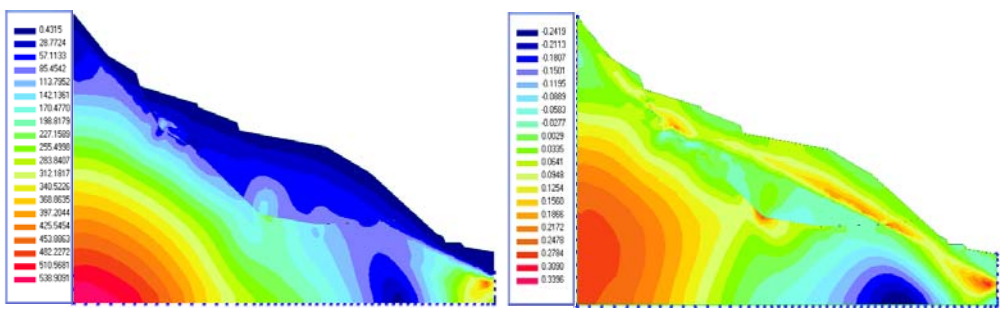

Figure 8. Nephogram of τ_{max} and η under infused slurry slope (Fs=1.29).

Draining groundwater level and infusing slurry slope body. The maximal shear stress and approaching degree of yield are displayed in Figure 9 after integrating

lowering groundwater level and infusing slurry in slope body. Comparing with it in natural state, the distribution condition of maximal shear stress is improved largely and the stress concentrated zone is reduced greatly, meanwhile it displays a uniform sandwich and the approaching degree of yield declines (the maximal is 0.26), here the integrating safety factor is 1.61.

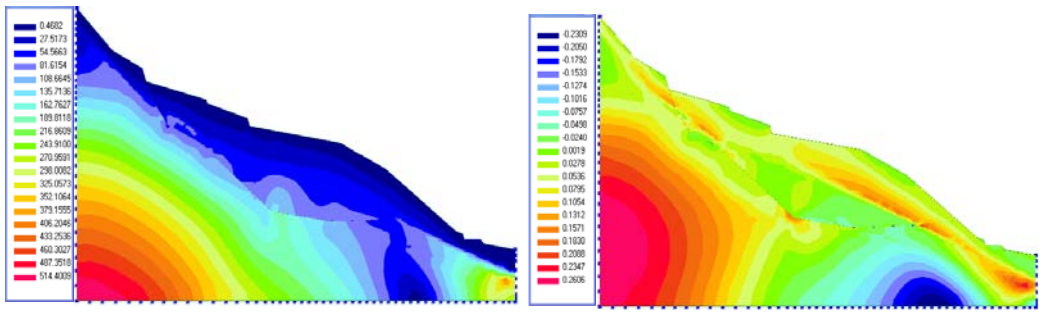

Figure 9. Nephogram of τ_{max} and η under infused slurry and drained slope (Fs=1.61).

Results comparison. Table 3 lists the results of contrast among anti-slide force, slide force and slope safety factor at structural plane in different engineering condition, which the slide force simultaneously increases along with the anti-slide force addition at the structural plane. The different is that the anti-slide force increase more rapidness than the slide force with completely saturated state exceptions. Therefore it could ensure the slope stability when the safety factor of slope gradually increases in engineering condition ③, ④ and ⑤

Table 3. Comparison between Slide Force and Anti-Slide Force in Different Engineering Conditions.

Engineering condition	Engineering condition description	Anti-slide force (kN)	Slide force (kN)	Safety factor
①	Natural condition	4335	4484	0.97
②	Completely saturated condition	4483	4941	0.90
③	Draining grounder water lever	5994	4761	1.26
④	Infusing slurry on structure plane	6188	4810	1.29
⑤	Combine the ③ and ④	7498	4643	1.61

CONCLUSIONS

Taking the high slope along Hang-Yong Natural Gas Pipeline as an example, the stability is analyzed through finite element numeric calculation at structural plane in different engineering condition, results display that it has the vital significance for the strength of structure face and work environment to integrating slope stability. Main conclusions are concluded as follows:

(1) This high slope is in ultimate equilibrium state and creep deformation stage at present, which it may occurs to rapidly slide when it is induced by disadvantage factors, especially the continuously heavy rainfall leading to completely saturated condition. therefore it may imperil the safety of gas line and job facilities at the slope leading edge.

(2) Strength of structure face is the main factor to affect the slope stability. The slope safety factor arrives at 1.25 when the groundwater drains to keep the level beneath structure face and the structure face is in natural state; and the integrating slope safety factor reaches 1.29 after infusing slurry to improve the strength of structure face, and the slope safety factor hits a peak of 1.61 integrating above two methods. The three choice schemes could improve the stress condition inside slope and greatly increase the anti-slide force, which it effectively increases the integrating safety of high slope and adds the emergency capacity.

(3) Three proposed reinforcement methods above could not eliminate the tensile failure at after-edge of slope face, and it must complement other reinforcement engineering, such as vegetative cover, to improve the tensile strength of superficial soil and prevent failure enlargement at after-edge and rainwater infiltration that it could affect the integrating safety of high slope.

ACKNOWLEDGMENT

This study is supported by the Supported and Guidance Plan Found of Zhejiang Province, China (Grant No. 2008C23019).

REFERENCE

Li, T.C., Lu, Z.L., Yao W.M., et al. (2003). "Finite element iteration method for stability safety factor of slopes against sliding." *Chinese Journal of Rock Mechanics and Engineering*, 22(3): 446-450.

Ling, X. Z., Cai, D. S. (2002). "Rock mass mechanics." *Harbin: Harbin Institute of Technology Press*.

Ye, J. H. (1991). "Mechanical properties of rocks." *Bejing: China WaterPower Press.*

Yu, N., Zhu, H.H. (2004). "Research on design and computation method of shield tunnel liningsin complex stratigraphic conditions." *Industry Construction*, 34(4):57-60.

Zhang, B.L., Zhu, Z.Y., Ling, X.Z., et al. (2007). "Research of reinforcement plan for red mud dam and the construction processes to emulation analysis." *Rock and Soil Mechanics*, 28(6):1280-1284.

Zheng, H., Tian, B., Liu, D.F., et al. (2005). "Definitions of safety factor of slope stability analysis with finite element method." *Chinese Journal of Rock Mechanics and Engineering*, 24(13): 2225-2230.

Zhu, Z.Y., Ling, X.Z, Wang, X.Q. et al. (2008). "Simulation analysis of construction process of a high rock slope stabilization." *Journal of Harbin Institute of Technology (New Series)*, 15(2): 188-193.

Stability of Slope with the Weak Structural Plane Based on 2-D Nonlinear Finite Element Method

ZHANG Feng[1], WU Liquan[2], LING Xianzhang[1], ZHU Zhanyuan[1,3], and WANG Lina[1]

[1]Institute of Subgrade and Protection Engineering, Harbin Institute of Technology, P.O. Box 150090, City, Harbin, P.R. China; PH (86) 451-86282576; FAX (86) 451-86282576; email: fzhang_hit@163.com
[2]School of Civil Engineering and Architecture, Zhejiang University of Science and Technology, P.O. Box 310023, City, Hangzhou, P.R. China; PH (86) 571-85070518; FAX (86) 571-85070518; email: wuliquan1966@163.com
[3]Information and Engineering Technology College, Sichuan Agricultural University, P.O. Box 625014, City, Ya'an, P.R. China; PH (86) 835-8268909; FAX (86) 835-8268909; email: zhuzyuan910@163.com

ABSTRACT

To overcome the disadvantages of the limit equilibrium method and the finite element method on evaluation the stability of slope with the weak structural plane, the elastic-plastic finite element method, the Goodman joint element and the limit equilibrium method are utilized together, and two concepts, that are the joint element safety factor and the node yielding degree, are introduced to evaluate the slope stability with the weak structural plane, and the correspond calculation codes are programmed. Finally, a man-made slope case is analyzed to validate the numerical model and program codes. The stress, strain, displacement, the node yielding degree of the slope and the force of weak structural plane are calculated by elastic-plastic finite element method, and the element safety factor of the slope with the weak structural plane are calculated with the limit equilibrium method. That numerical results are agree well with the engineering fact indicates the program coded are reliable, and the proposed numerical model and two introduced concepts can not only consider the influence of the relation of stress and strain on the slope stability, but also evaluate the stability of the slope with single stability factor of safety which is well known in geotechnical engineering. All of above are meaningful to evaluated the slope stability and provide a new and simple numerical approach.

INTRODUCTION

With development of economic and society, more and more man-made slope are created. For example, natural slopes are excavated to construct the roads, railways, dams and other projects in mountainous area. Therefore, stability evaluation of engineering slope is very necessary and significant for protecting these projects keep in safety and from disasters. During the past three decades, many researches have been studying on the stability of slope, and have achieved many fruits. The limit equilibrium method (LEM) has still been playing the most important role in the slope

stability analysis (Duncan 1996, Chen 2003). It is able to provide a safety factor of a slope without the knowledge of the initial conditions with the result that the LEM is favored by many engineers, although the LEM does not consider the relation of stress-strain of geo-materials. Recently, as the many particular advantages of the finite element method (FEM) over the limit equilibrium method, especially the development of the numerical simulation technology, the finite element method has achieved a greater attention and increasing applications in the slope stability analysis (Zhang et al 2007, Zhu et al 2008, Tan et al 2008). However, using the FEM to ensure the safety factor for engineer is difficult and can not instruct the engineering practice. Fortunately, the strength reduction FEM are proposed and developed (Zhao et al 2003, Zheng et al 2004), the safety factor can present by reducing the strength parameters continuously until meeting some convergence criteria(Griffiths et al 1999, Zheng et al 2004, Fang et al 2008), but the calculation process is complex and the results are subjective.

Therefore, to overcome the disadvantages of the LEM and FEM, a simple approach, combining the LEM and the FEM, are introduced based on the nonlinear stress-strain relation and the Goodman joint element to establish the numerical simulated model, and the corresponding codes are programmed based the Fortran Language to evaluate the stability of slope with the weak structural plane. The joint element safety factor and the node yield degree are introduced to evaluate the slope stability. Finally, a case is analyzed to validate the numerical model and the program codes.

THEORY OF SLOPE STABILITY

Elastic-plastic relation of stress-strain. Most mechanics behaviors of geo-materials are nonlinear. It is well recognized that stress-strain relations do not remain linear, even for the low stress levels. So the elastic-plastic model is used to describe the relation of the stress and the strain for the geotechnical material. Slope stability nonlinear FEM usually adopts perfect elastic-plastic model, whose increment form is,

$$\{d\sigma\} = \left[D_{ep} \right] \{d\varepsilon\} = \left[D_e - D_p \right] \{d\varepsilon\} \tag{1}$$

Where: $d\sigma$ is the stress increment, $d\varepsilon$ is the strain increment, $[D_e]$ is the elastic matrix, $[D_p]$ is the plastic matrix, and $[D_{ep}]$ is the elastic-plastic matrix.

For the perfect elastic-plastic materials, the elastic-plastic matrix $[D_p]$ could be calculated as,

$$D_p = \frac{[D]\left\{\frac{\partial g}{\partial \sigma}\right\} \left\{\frac{\partial f}{\partial \sigma}\right\}^T [D]}{A + \left\{\frac{\partial f}{\partial \sigma}\right\}^T [D]\left\{\frac{\partial g}{\partial \sigma}\right\}} \tag{2}$$

Where: A is a parameter to present the material hardening. For the perfect elastic-plastic model, A is equal to 0. While adopting associated flow rule, $g \equiv f$ =0.

Simulation of weak structural plane. Using the Goodman joint element to simulate the weak structural plane of slope, and do not consider the coupling effect between the normal and the tangential. Its increment form could present as:

$$\begin{Bmatrix} d\tau_s \\ d\sigma_n \end{Bmatrix} = \begin{bmatrix} k_s & 0 \\ 0 & k_n \end{bmatrix} \begin{Bmatrix} du_s \\ du_n \end{Bmatrix} \tag{3}$$

Where: $d\tau_s$ is the shear stress increment, $d\sigma_n$ is the normal stress increment, k_s is the shear stiffness of the weak structural plane, and k_n is the normal stiffness of the weak structural plane.

Node yielding degree. The weak structural plane is one of the sensitive influence factors on the slope stability. However, that whether the slope body is yield and generate a new sliding plane is easily ignored if only consider safety condition of the weak structure plane. Therefore, using the node yielding degree to present the process of node enter into yield state (Yu and Zhu 2004). For the Drucker-Prager criterion, the node yielding degree is:

$$\eta = \frac{\alpha I_1 + \sqrt{J_2}}{k} \tag{4}$$

Where: $\alpha = -\sin\varphi \Big/ \left(\sqrt{3} \cdot \sqrt{3 + \sin^2\varphi}\right)$, $k = -c \cdot \sin\varphi \Big/ \sqrt{3 + \sin^2\varphi}$, I_1 is the first invariant of stress tensor, and J_2 is the second invariant of stress deviator tensor. If the yielding degree is greater than or equal to 1.0, the node meets the yield state. Otherwise, the node is the normal state.

Joint element safety factor of slope. According the limit equilibrium theory, the global safety factor of soil and rock slope with weak structural plane is equal to the ratio that the total resisting shear force divide by the shear force on structure plane (Li et al 2003, Zheng et al 2005). Through the finite numerical analysis to achieve each element stress of the structural plane, and the joint element safety factor F_s^i is,

$$F_s^i = \frac{T_{fi}}{T_i} = \frac{c_i + \sigma_{ni} . \tan\varphi_i}{\tau_{si}} \tag{5}$$

and the global safety factor of slope F_s is,

$$F_s = \sum_{i=1}^{n} F_s^i \tag{6}$$

Where: n is the total number of slip planes element, F_s^i is the element safety factor, T_i is the shear force along the shear direction on the i^{th} slip plane element, T_{f_i} is the resisting shear force along the shear direction on the i^{th} slip plane element, and F_s is the global safety factor of slope

Based the above numerical theories of slope stabiliy, the codes to simulate the slope stability are programmed. The stress, displacement, node yield degree and the element safety factor can gain through these codes to evaluate the slope stability.

STABILITY ANALYSIS OF SLOPE

Engineering geology of slope. This engineering slope case is locates at a slanting hillside along the Hangzhou-Ningbo natural gas pipeline of China. In history, this slope has taken place three severe slides, the main sliding direction is about N140°E, the surface sliding split mainly is the tensile and shear splits distributing on posterior edge, both sides and front edge of the slope, the sliding posterior edge boundary is about vertical arced, the north and south side is nearly arced.

Figure 1 shows the engineering geology profile of slope case. The profile direction is about N140°E, and the gradient of slope is 20°-30°. According to the geology exploration, the slope stratum contains the salty clay (Q4) and the ignimbrite (J_3x). The groundwater level is about 4m-10m. In slope, a weak structural plane (i.e., $\overline{ABCDEF}$) through the salty clay and the strong weathered rock appears in the slope foot. Influenced by the rainfall, the surface of slope appeared many tensional fractures, therefore, to protect the natural gas pipeline and the road from destroyed by the landslip, the stability of this slope need to evaluate.

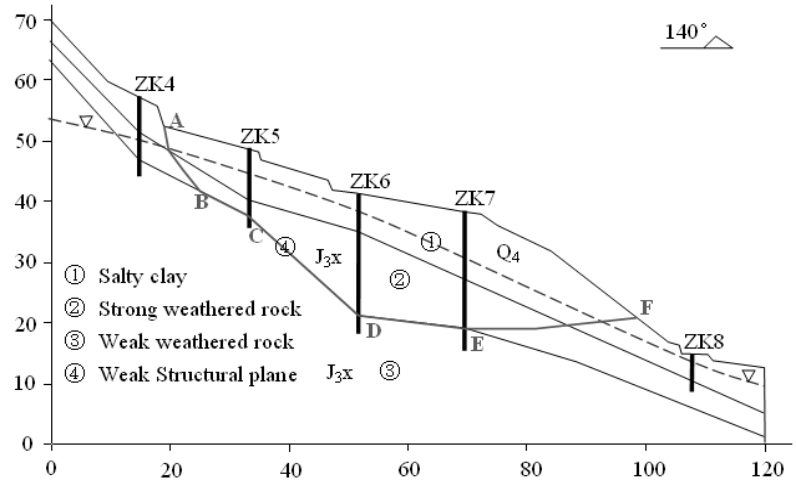

Figure 1. Engineering geology profile of slope (unit: m).

Numerical model. The geotechnical materials of this slope are assumed to the homogeneous body and the numerical model is simplified to two-dimension the plane strain problem. As is shown in the Figure 2, the calculation geometry of the finite element model is 120m in length and 70m in height, the displacements of

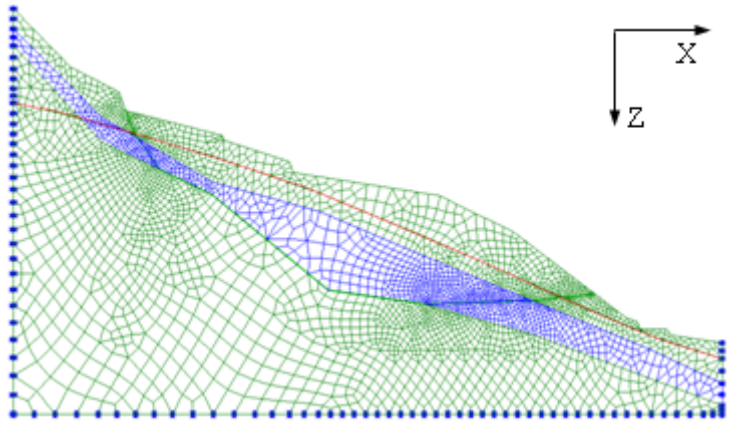

Figure 2. Finite element mesh of slope in natural conditon (unit: m).

horizontal and the vertical direction are zero. The geometry model is subdivided into 3706 isoparametric quadrilateral elements and 3602 nodes. The soil and the bed rock are used the ideal elastic-plastic model, and the structural plane in slope is simulated by Goodman joint element. Additionally, the Drucker-Prager strength criterion is adopted in this model.

According to the parameter test experiments, the physical and mechanical parameters of the geotechnical materials in this model are listed in Table 1, and part mechanical parameters are got by the back analysis (Zhang et al 2008) or reference (Ye 1991)

Table 1. Mechanics Parameters of Slope Materials.

NO.	State	Elastic modulus MPa	Poisson ratio	Unit weight kN/m^3	Cohesion kPa	Friction angle °	Shear stiffness kN/m	Normal stiffness kN/m
①	N	8.0	0.30	18.5	250	28	—	—
	S	7.5	0.30	21.5	220	25	—	—
②	N	600	0.35	22.5	750	30	—	—
	S	580	0.35	23.0	700	28	—	—
③	N	657	0.35	24.5	830	35	—	—
	S	650	0.35	25.0	800	32	—	—
④	N	—	—	21.5	23	12	4810	41600
	S	—	—	22.0	12	9	4000	38900

Note: “N” represents the natural condition, and “S” represents the saturated condition.

NUMERICAL RESULT AND ANALYSIS

Through the program codes, the stress, strain, displacment, node yielding degree and element safety factor are gained to evluate the slope stability. Figure 3 shows the maximum shear stress nephogram of slope in nature condition. Note that most zones of the maximum shear stress distribute on its rules, but influnced the structural plane, three concentration zones are formed near the the structural plane,

and the maximum shear stress can approach to 214kPa.

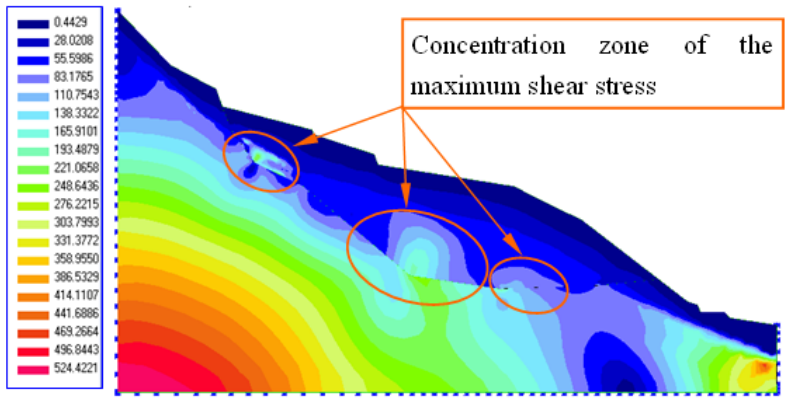

Figure 3. Nephogram of maximum shear stress of slope in nature condition.

Figure 4 shows the nephogram of yielding degree of slope in nature condition. Note that the largest yielding degree of slope is only 0.426, and the area is not reach into the yield state. However, because of the soil strengh is lower than bedrock strengh, the potential sliding surface is developed on the boundary plane betweent the saturated soil and the weathered rock, it should be give an greaer attention on reinforcement the slope.

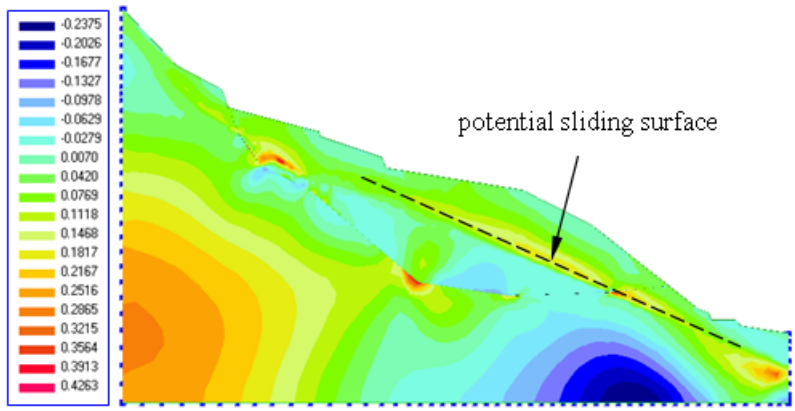

Figure 4. Nephogram of the yielding degree of slope in nature condition.

To reflect the force distribution on the weak structural plane, Figure 5 shows the force distribution of the weak structural plane along the element from A to F. Note that the resisting shear force and the shear force are positive correlation and maximum shear force approach to 236kN happed on element No.55. On the most elements, the shear force is equal to the resisting shear force, and most of element safety factor are greater than 1.0 too. However, the safety factor from No.0 to No.50 are less than 1.0, especially on the element from No.40 to No.55 (i.e., from point C

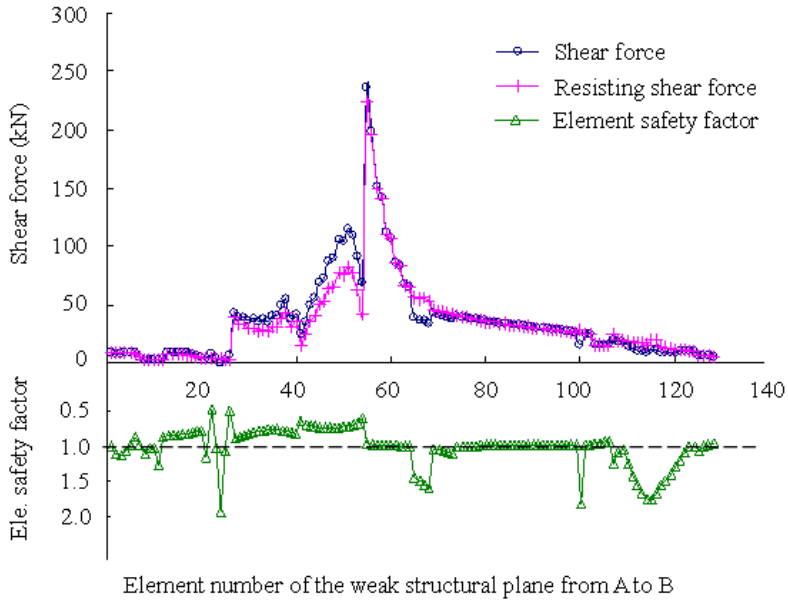

Figure 5. Force and element safety factor of the weak structural plane.

and point D), the shear force is greater than the resisting shear force.

Therefore, the main unsteady reason of this slope is that the resisting shear force can not resist the shear force on the No.12 to No.55. One of good approach to keep the slope in safety is improving the resisting shear force of these elements. Moreover, Numerical reslult shows that the total shear force of the structural plane is 4484kN, and the total resisting shear force is 4335kN, the resisting shear force can not resist the shear fore, and the entire safety factor of slope is 0.97, so the slope is at limit equilibrium state, this result is in good agreement with the actual phenomenon of the case slope, which verifies the reliability and rationality of the numerical model and program code.

CONCLUSIONS

Based on the 2-D nonlinear finite method and limit equilibrium method, the numerical simulation model proposed in this paper and its program code are verified by the slope case, it shows that:

(1) The proposed numerical simulation model can overcome the disadvantage of limit equilibrium method and the finite method. The stress-stain relations of the geo-materials are considered and the global safety is provided for engineer design.

(2) The program codes are reliability and rationality to evaluate the slope stability with the weak structural plane. Using this method can not only calculate the element safety factor, but also give the element shear force and resisting shear force. Moreover, the potential sliding surface is easly presented by the nephogram of the yielding degree.

(3) The proposed numerical simulation model and the program codes are able to evaluate the similarly slope stability, which give an insight on evaluation the slope stability and meaningful for reinforcement the slope.

ACKNOWLEDGMENT

This study is supported by the Supported and Guidance Plan Found of Zhejiang Province, China (Grant No. 2008C23019).

REFERENCES

Chen, Z.Y. (2003). "Soil slope stability analysis: theory, methods and programs." *Beijing: China Water Power Press*, 533-560.

Duncan J. M. (1996). "State of the art :limit equilibrium and finite element analysis of slope." *Journal of Geotechnical Engineering*, ASCE, 122(7): 577-596.

Fang, J. R., Xu, Z. X., Zhuang, X. Y. (2008). "Appraisal and analysis of three-dimensional slope stability based on elastoplastic FEM." *Rock and Soil Mechanics*, 29(10):2667-2652.

Fang, J. R., Xu, Z. X., Zhuang, X. Y. (2008). "Appraisal and analysis of three-dimensional slope stability based on elastoplastic FEM." *Rock and Soil Mechanics*, 29(10):2667-2652.

Griffiths, D.V., and Lane, P.A.(1999). "Slope stability analysis by finite elements." *Geotechnique*, 49(3): 387-403.

Li, T.C., Lu, Z.L., Yao W.M., et al.(2003). "Finite element iteration method for stability safety factor of slopes against sliding." *Chinese Journal of Rock Mechanics and Engineering*, 22(3): 446-450.

Ling, X.Z., Zhang F., Zhu Z.Y., et al.(2008). "Estimating mechanics parameters of rock mass based on improved genetic algorithm." *Chinese Control and Decision Conference, CCDC, Yantai*, 4608-4612.

Tan, X.H., Wang, J.G. and Wang, Y. (2008). "Nonlinear finite element analysis of slope stability." *Rock and Soil Mechanics*, 29(8):2047-2050.

Ye, J.H. (1991). "Handbook of rock mechanical parameter." *Beijing: Press of water and power*, China.

Yu, N., Zhu, H.H. (2004). "Research on design and computation method of shield tunnel liningsin complex stratigraphic conditions." *Industry Construction*, 34(4):57-60.

Zhang, B.L., Zhu, Z.Y., Ling, X.Z, et al. (2007). "Research of reinforcement plan for red mud dam and the construction processes to emulation analysis." *Rock and Soil Mechanics*, 28(6):1280-1284.

Zhao, S.Y., Zheng, Y.R., Deng, W.D. (2003). "Stability analysis of jointed rock slope by strength reduction FEM." *Chinese Journal of Rock Mechanics and Engineering*, 22(2):254-260.

Zheng, H., Tian, B., Liu, D.F., et al. (2005). "Definitions of safety factor of slope stability analysis with finite element method." *Chinese Journal of Rock Mechanics and Engineering*, 24(13): 2225-2230.

Zheng, Y.R., Zhao, S.Y. (2004). "Application of strength reduction FEM to soil and rock slope." *Chinese Journal of Rock Mechanics and Engineering*, 23(19):3 381-3388.

Zhu, Z.Y., Ling, X.Z, Wang, X.Q. et al. (2008). "Simulation analysis of construction process of a high rock slope stabilization." *Journal of Harbin Institute of Technology (New Series)*, 15(2): 188-193.

Vibration Characteristics of Permafrost Embankment Induced by Passing Trains in Qinghai-Tibet Railway in Winter

ZHU Zhanyuan[1,2], LING Xianzhang[2], WANG Lina[2], ZHANG Feng[2], CHEN Shijun[2] and WU Liquan[3]

[1]Information and Engineering Technology College, Sichuan Agricultural University, P.O. Box 625014, City, Ya'an, P.R. China; PH (86) 835-8268909; FAX (86) 835-8268909; email: zhuzyuan910@163.com
[2]Institute of Subgrade and Protection Engineering, Harbin Institute of Technology, P.O. Box 150090, City, Harbin, P.R. China; PH (86) 451-86282576; FAX (86) 451-86282576; email: xianzhang_ling@263.com
[3]School of Civil Engineering and Architecture, Zhejiang University of Science and Technology, P.O. Box 310023, City, Hangzhou, P.R. China; PH (86) 571-85070518; FAX (86) 571-85070518; email: wuliquan1966@163.com

ABSTRACT

The vibration characteristics of embankment induced by passing trains in the Qinghai-Tibet railway were investigated, and the effects of vibratory load of train on soil-in-ice layer were quantitatively evaluated, based on the self-programming software of vehicle-track-embankment dynamic coupled system. The results indicate that: (1) the maximum dynamic compressive stress induced by locomotives is apparently higher than that by trailers. (2) Vibrational energy of the embankment top surface concentrates on the interval from 0.5Hz to 10Hz, and dominant frequency of soil-in-ice layer top surface is within 3Hz; (3) The phenomenon of stress concentration emerging in ballast at rail supporting position is apparent, and the distribution of maximum dynamic compressive stress of roadbed surface is in the shape of saddle. (4) Vibratory load of train has main effect on embankment in an ellipse-shaped zone about 6m under sleeper. (5) The maximum dynamic compressive stress level of soil-in-ice layer top surface induced by trailers is about 16.7~19.8% that of embankment top surface, and negative exponential function is used to fit the attenuation relationship of embankment dynamic compressive stress versus depth. (6) Embankment vibration displacement is predominant in the vertical direction, and the dynamic displacement of soil-in-ice layer top surface can be neglected. The conclusions are the reliable theoretical basis for engineering design and safety analysis of Qinghai-Tibet railway operation.

INTRODUCTION

With the opening to traffic of Qinghai-Tibet Railway, China scientific academia has made significant progress in the world problem of road building engineering in permafrost regions. Currently, dynamic performance of embankment with frozen layers and simulation of geothermal field mechanism have been further researched by domestic and foreign scholars, and great achievements has been

obtained (Cheng 2005, Wu et al 2002, Ling et al 2002, Wang et al 2005, Zhu et al 2007, etc). However, road construction work in permafrost regions is still the world wide difficult problem, for the disease rate of route is 30% approximately. The permafrost engineering reliability evaluation of Qinghai-Tibet railway is a complicated work under the trend of global temperature rising, thus the question is whether subgrade vibration deformation can meet demand of railway normal operation and disease rate is less than 15%. Accordingly, the characteristics of embankment vibration induced by passing trains in the Qinghai-Tibet railway were investigated, and the effect of train vibratory load on soil-in-ice layer was quantitatively evaluated in the paper, based on the embankment structure of the Beiluhe test section in the permafrost region along Qinghai-Tibet Railway and the self-programming software of vehicle-track-embankment dynamic coupled system. The results are the reliable theoretical basis for engineering design and Qinghai-Tibet railway operation safety evaluation.

DYNAMIC FINITE ELEMENT ANALYSIS MODEL

Test section situation. The Beiluhe test section is in the arid climate region of the Qinghai–Tibet Plateau. The mean annual air temperature in the region is −5.2℃, and the highest temperature gets up to 23.2℃, and the lowest temperature is -37.7℃. The frozen period lasts about 7 to 8 months, from September to April next year (Niu et al 2002), and the maximum thickness of snow cover is 14 cm. From state key laboratory of frozen soil engineering of Chinese Academy of Sciences, the following data is obtained: the depth of permafrost table is 2 to 3 m, and the mean annual ground temperature is -2.0 to -1.0℃ in the test secton; the soil consists of fine sand, silty sand, gravel sand, clay, mudstone and sandstone; the section locates in basically stable low temperature district according to the secondary zonation, where subsoil ice is extraordinarily enriched and soil-in-ice layer is continuous distribution. The route of the section, adopting 50 kg seamed steel rail, 1800 sleepers of type II per kilometer and 450mm thick ballast, is slightly curved single-line in service, with the curvature radius of approximate 1000 meters.

Calculation model. The embankment with heat pipe situated at DK1137+700, with 3.5m height and 11.3m width of top surface, has been adopted as subject investigated. Subgrade profile and geological condition can be seen in Figure 1 and Table 1. Afterwards, the calculation of static and dynamic analysis is conducted by self-programming software (ZL-RNTLM). Two-dimensional finite element plane strain model of sleeper-ballast-embankment-field system is shown in Figure 2, which has 12697 joints, 125277 quadrilateral elements and 10 beam elements. The calculation width of each side of foundation extends to 31m, and the calculation depth is 30m. The viscous boundary is adopted, in addition time histories of interaction force of track and sleeper are used as train vibratory loads acting on beam elements of sleeper, which is shown in Figure 3.

Constitutive relation and parameters selection. Equivalent linearization model is employed in finite element analysis. The calculation parameters of ballast, roadbed surface layer, embankment fill, and the strata are listed in Table 1, based on dynamic triaxial test of frozen soil under transportation loads and literature data of frozen soil dynamics at home and abroad. The beam element of sleeper is linear elastic and its

Elastic Modulus E is 30GPa. Section area and moment of inertia of the beam element below the track are $0.04585m^2$ and $1.59\times10^{-4}m^4$, respectively, and those of intermediate regime of the beam element are $0.0339m^2$ and $7.639\times10^{-5}m^4$, respectively.

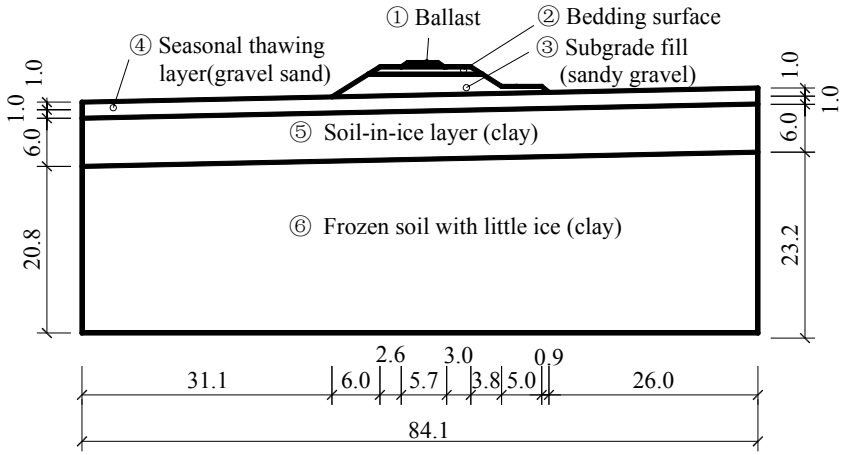

Figure 1. Profile and strata structure of subgrade (units: m).

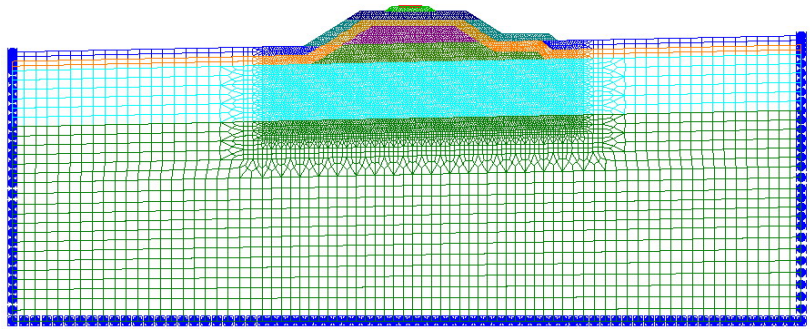

Figure 2. Finite element model of sleeper-ballast-embankment-field system.

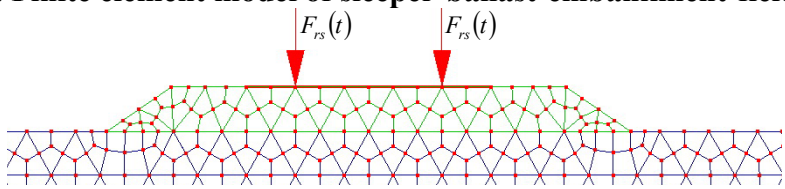

Figure 3. Beam element of sleeper and input of load.

SIMULATION OF TRAIN VIBRATORY LOAD

Dynamic analysis model of vehicle-track shown in Figure 4 is a coupled system, which is composed of vehicle model, track model and wheel-rail coupled model. The vehicle model is a multi-freedom vibrating system constituted by multiple vehicles, bogie, wheelset, secondary spring and damping shock absorber. The track model is infinite Euler beam model supported by three-layer elastic system. Three-layer mass-spring-damper system is used to simulate sleeper, ballast and embankment. Then the software ZL-TNTLM of vehicle-track coupled dynamic system is programmed based on the model. Afterwars dynamic emulation analysis on the section DK1137+700 in Qinghai-Tibet Railway is conducted by the self-compiling program under the coupled pulse excitations of mileage vertical profile irregularity and broad rail gap (10 mm). The incentive curve of sleeper nearby

Table 1. Calculation Parameters of Roadbed Filling and Strata Structure

Soil layer	ρ g/cm^3	μ	$G_{d\max}$ MPa	soil dynamic parameters	shear strain γ_d (10^{-4}) 0.05	0.1	0.5	1	5	10	50	100
①	2.00	0.30	286	α_G	0.999	0.999	0.994	0.989	0.945	0.896	0.632	0.462
				λ	0.004	0.006	0.019	0.030	0.075	0.090	0.110	0.120
②	1.95	0.22	586	α_G	1.000	1.000	0.997	0.995	0.975	0.950	0.793	0.656
				λ	0.010	0.014	0.027	0.037	0.072	0.095	0.175	0.217
③	1.90	0.24	536	α_G	1.000	0.999	0.997	0.995	0.973	0.948	0.784	0.644
				λ	0.005	0.007	0.017	0.024	0.055	0.078	0.166	0.216
④	1.80	0.31	276	α_G	0.999	0.999	0.993	0.987	0.936	0.880	0.594	0.422
				λ	0.006	0.009	0.021	0.031	0.074	0.106	0.208	0.252
⑤	1.60	0.35	320	α_G	1.000	0.999	0.995	0.989	0.948	0.902	0.647	0.478
				λ	0.054	0.065	0.097	0.115	0.171	0.201	0.277	0.306
⑥	1.80	0.35	269	α_G	0.999	0.997	0.985	0.971	0.870	0.770	0.400	0.250
				λ	0.082	0.099	0.149	0.177	0.261	0.303	0.388	0.411

Note: ρ is natural density; μ is poisson ratio; $G_{d\max}$ is maximum dynamic shear modulus; α_G is dynamic shear modulus ratio; λ is damp ratio.

the broad rail gap is obtained, as shown in Figure 5, when the train K917, with the dynamic marshalling of two diesel locomotivs NJ2 and four trailer YZ25T, passing by at the speed of 94 km/h.

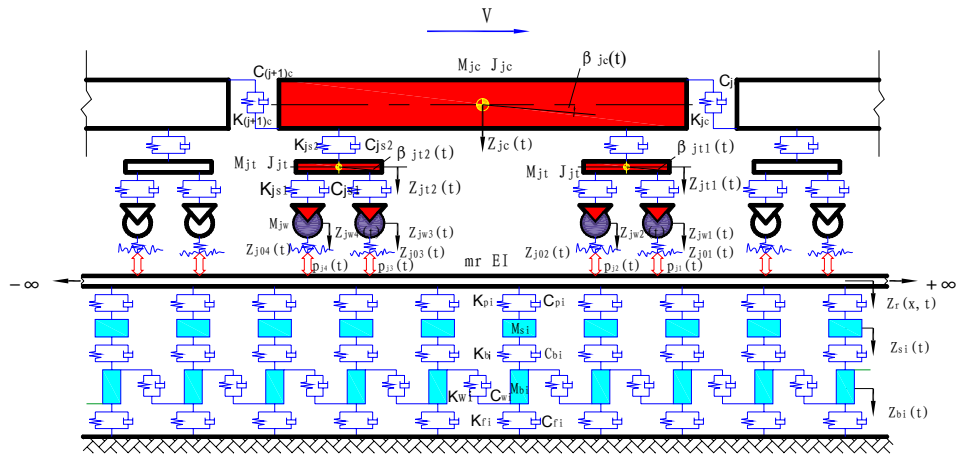

Figure 4. Two dimensional dynamic model of vehicle-track.

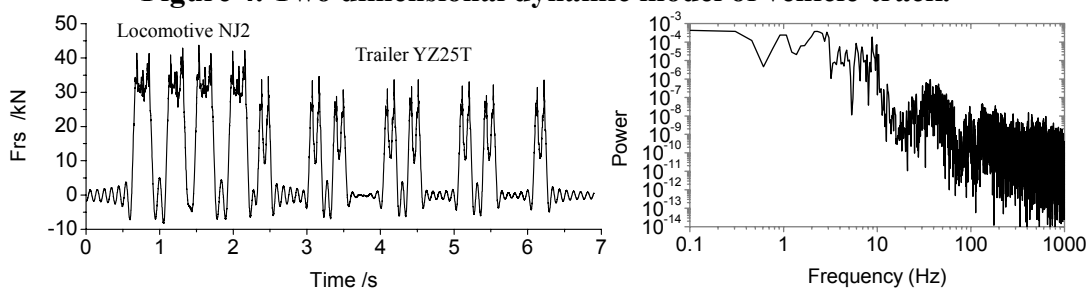

Figure 5. Time history and frequency analysis of the force exerted on sleeper.

RESULTS ANALYSIS

The vibration response analysis of the permafrost embankment induced by trains in winter is carried out by the finite model of sleeper-ballast-embankment-field system depicted in Figure 3, and by exerting the load time history shown in Figure 5 on sleeper. Figure 6 shows the time history and spectrum analysis of the subgrade dynamic compressive stress σ_{dz}, and H is distance to the bottom of sleeper. Note that maximum dynamic compressive stress of subgrade surface is 48.2 kPa during locomotives passing by, apparently bigger than 27.3kPa during trailers passing by; the vibration peaks of the embankment top surface appear as bogies passing by, and also occur near the sleeper action rate *f*, i.e. 46.9Hz, and its dominant frequency is within 10Hz; the subgrade vibration attenuates with the depth increasing, and high frequency component at soil-in-ice layer top surface disappears, aferwards the vibration dominant frequency is within 3Hz due to energy dissipation and filtering action of ground.

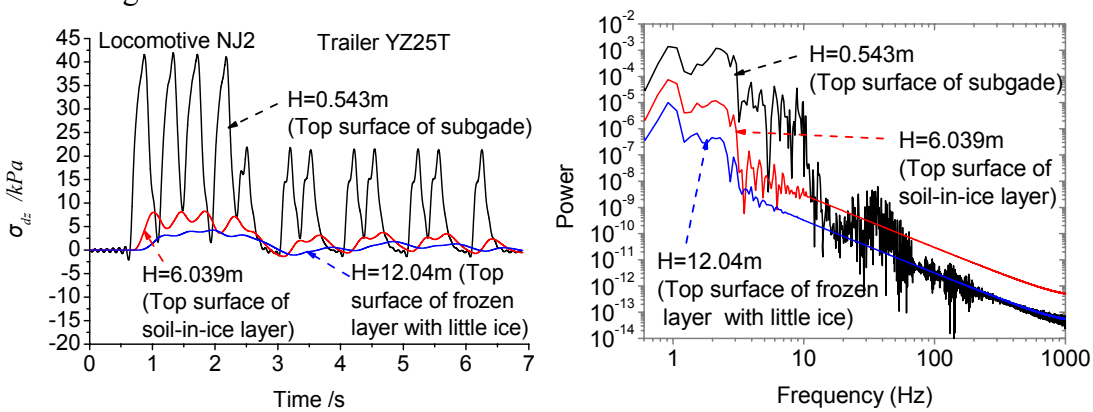

Figure 6. The time history and frequency analysis of subgrade dynamic compressive stress (K917, V=94km/h).

The distribution of subgrade dynamic compressive stress $\sigma_{dz\max}$ induced by train traffic is shown in Figure 7, which shows that: stress concentration of the roadbed near rail is apparent, the distribution of maximum dynamic compressive stress of roadbed surface is in the shape of saddle, and the main vibratory response of embankment is in an ellipse-shaped zone about 6m depth under the sleeper; maximum dynamic compressive stress of the soil-in-ice layer top surface induced by locomotive is 9.56kPa, which is 19.8% that of subgrade surface; maximum dynamic compressive

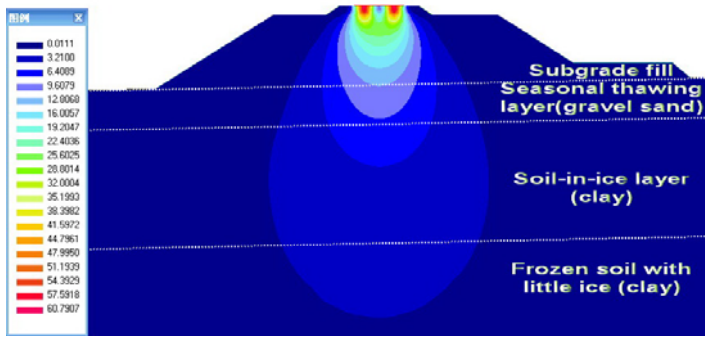

Figure 7. Maximum subgrade dynamic compressive stress (locomotive, K917, V=94km/h, units: kPa).

stress of the soil-in-ice layer top surface induced by trailer is 4.57kPa, which is 16.7% that of subgrade surface and the negative exponential function is used to fit the attenuation relationship of embankment dynamic compressive stress versus depth.

The distribution of maximum dynamic elastic displacement during train traffic is depicted in Figure 8 and Figure 9. Therein from Figure 8, it can be seen that the maximum horizontal dynamic displacement is symmetrically distributed in the subgrade profile, and predominant at the ballast near the rail supporting place and roadbed close to the brim of sleeper, and from Figure 9, the maximum vertical dynamic elastic displacement mainly focus on the ballast near the rail supporting place and the roadbed surface. It is demonstrated that embankment vibration displacement is prominent in the vertical direction, and the maximum horizontal displacement of ballast surface is 0.006mm and the vertical one is 0.244mm, however, the maximum vertical dynamic displacement of soil-in-ice layer surface is 0.000868mm, which is about 0.36% that of roadbed surface and can be negligible.

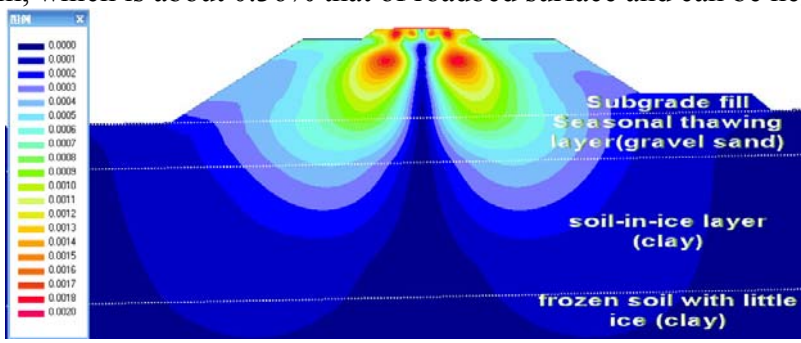

Figure 8. Maximum horizontal dynamic elastic displacement (units: cm).

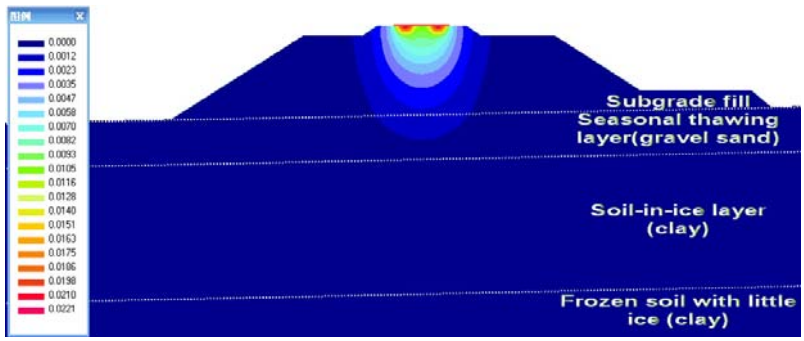

Figure 9. Maximum vertical dynamic elastic displacement (units: cm).

CONCLUSIONS

According to analysis of vibration response of the permafrost embankment induced by passing trains in the Qinghai-Tibet railway based on the established finite element model of sleeper-ballast-embankment-field system and the self-programming software of vehicle-track-embankment coupled dynamic system. The conclusions can be drawed as follows:

1) The maximum dynamic compressive stress induced by locomotives is apparently higher than that by trailers, and peaks are always appearing as bogies passing by. Vibrational energy of the embankment top surface is predominant between 0.5 Hz to 10Hz, and dominant frequency of soil-in-ice layer top surface is within 3 Hz.

2) Vibratory load of embankment from trains is mainly in an ellipse-shaped zone about 6m depth under sleeper. The phenomenon of stress concentration in the ballast close to sleeper is apparent, and the distribution of maximum dynamic compressive stress of roadbed surface is saddle in shape, and the maximum dynamic compressive stress of soil-in-ice layer top surface induced by passing trailers is about 16.7-19.8% that of roadbed top surface. The attenuation relationship of embankment dynamic compressive stress versus depth can be fitted by negative exponential function.

3) Embankment vibration displacement is mainly prominent in the vertical direction, and the dynamic displacement of soil-in-ice layer top surface is very small and can be neglected.

ACKNOWLEDGMENTS

This study is supported by the Natural Science Found of China (Grant No. 50678055 and 50538030), the State Key Laboratory of Frozen Soil Engineering Open Found of China (Grant No. SKLFSE200402), the Doctor Subject Special Scientific Found of China (Grant No. 20070213076), the A Project Supported by Scientific Reserch Fund of SiChuan Provincial Education Department of China, and the Supported and Guidance Plan Found of Zhejiang Province, China (Grant No. 2008C23019).

REFERENCES

Cheng, G. D. (2005). "A subgrade cooling approach for the construction of Qinghai-Tibet Railway." *Cold Regions Science and Technology*, 42: 169-176.

Cheng, G. D. (2005). "Permafrost studies in the Qinghai-Tibet plateau for road construction." *Journal of Cold Regions Engineering*, ASCE, 19(1): 19-29.

Ling, X. Z., Xu, X.Y., Qiu, M.G. et al.(2002). "Ultrasonic experiment study on dynamic elastic mechanical indexes of frozen silty clay." *Proceedings of the 5th International Symposium on Permafrost Engineering*, 38-42.

Ma, W., Liu, R., Wu, Q.B.(2008). "Monitoring and analysis of embankment deformation in permafrost regions of Qinghai-Tibet Railway." *Rock and Soil Mechanics*, 29(3):571-578.

Niu, F.J., Zhang, J.M., Zhang, Z.H.(2002). "Engineering geological characteristics and evaluations of permafrost in Beiluhe testing field of Qinghai-Tibetan railway." *Journal of Glaciolgy and Geocryology*, 24(3): 264-269.

Wang, L.X., Ling, X.Z.(2005). "Study on differentiate criteria of earthquake breakage of frozen subgrade." *Chinese Journal of Rock Mechanics and Engineering*, 24(4): 638-642.

Wu, Q.B., Liu, Y.Z., Zhang, J.M., et al.(2002). "A review of recent frozen soil engineering in permafrost regions along Qinghai-Tibet Highway." *Permafrost and Periglacial Process*, 13: 199-205.

Zhu, Z.Y., Ling, X.Z., Hu, Q.l. et al.(2007). "Experimental study on dynamic strain rate of frozen soil from railway embankment of Qinghai-Tibet railway in China." *Chinese Journal of Geotechnical Engineering*, 29(10): 1472-1476.

Zhu, Z.Y.(2009). "The subgrade vibration response and the vibration-subsidence prediction of the frozen soil in Qinghai-Tibet railway," *Doctor Degree Dissertation, Harbin: Harbin Institute of Technology.*

Reliability Analysis of Cable-stayed Bridge under Reaction of Seldom Occurred Earthquake

LI Feng-chen[1], ZHANG Li-na[2], WANG Da-peng[3], YANG Ze-ping[4], and YANG Ou[5]

[1]East China Institute of Technology, Ph.D., Fuzhou, JX 344000 China; email: fcli_1980 @163.com
[2]East China Institute of Technology, M.E., Fuzhou, JX 344000 China; email: zlnlfc2008@sina.com
[3]School of Civil Engineering, Harbin Institute of Technology, Ph.D., Harbin 150090, China; email: wdp791028@163.com
[4]East China Institute of Technology, M.E., Fuzhou, JX 344000 China; email: zpyang@ecit.edu.cn
[5]School of Civil Engineering, Harbin Institute of Technology, Ph.D., Harbin 150090, China; email: ouyang@hit.edu.cn

Abstract: Because of the importance of seismic engineering, a practical cable-stayed bridge under the earthquake reaction is analyzed. The dynamic calculation model of the large-span cable-stayed bridge is created by ANSYS. The reaction of the bridge and the stay cable under seldom occurred earthquake is analyzed. The rationality of its design is checked. The results demonstrate that the failure of the dropped beam in superstructure and the shear failure of the bridge tower and pier can not occur under the seismic design grade specified by seismic code. The emergency capacity of the cable is enough in the safety standards. The results demonstrate that the design of the large-span cable-stayed bridge is reasonable.
Key words: cable, cable-stayed bridge, earthquake, dynamic model, seismic grade

1 Introduction

China is a country with much threatening earthquake. Especially, a terrible earthquake of 8 grade stroke Wenchuan in the Sichuan Province on May 12, 2008. The number of death people is up to 69,136 and 17,686 people is missing. The total direct losing of economy reaches 8,451 hundred billions substantially. This terrible earthquake brings huge injury into the body and spirit of every Chinese people. In the Wenchuan earthquake, all of main lines of communication and lifeline engineering are damaged completely, including highway, bridge, railway, and so on, which makes it very difficult to develop rescue behavior. Because of the importance of bridge engineering in economy and traffic, the response rule of these engineering under seldom occurred earthquake and the rationality of their seismic protection are paid more attention by seismic researchers from many countries (Irvine H. M., 1981; Cremona C., 2003).

Because of the importance of seismic engineering, a practical cable-stayed bridge under the earthquake reaction is analyzed. The reaction of the bridge and the

stay cable under seldom occurred earthquake is analyzed (Matteo J, Deodatis G and Billington DF, 1995). Several failure forms under seldom occurred earthquake, including bending failure, shear failure, the failure of the dropped beam and bearing damage are studied. The seismic design of the large-span cable-stayed bridge is checked (Faber M. H., Enelund S. and Rackwitz R., 2003).

2 Finite Element Model of Cable-stayed Bridge

2.1 General condition of engineering

The bridge system can be seen in Figure.1. The main part of bridge is a cable-stay bridge with single tower and two planes of cables. Every span is 40, 108, 16, 26m. The structure system consists of piers, tower and beams, and the connection among these components are fixed. The tower presents fold line with straight top and inclined lower side. The height of tower on the top of the bridge cover is 50m. On vertical elevation of tower, the inclined lower side is 30m high with 12° inclination angle, and the straight top is 20m high. The transverse form of tower presents reverse Y shape. The main beam of main span has the cross section with double triangle box-shaped and ribbed plate. The cables of main span are distributed in half sector and double cable plates. The distance of adjacent cable is 8m. The steel wire of cables is galvanized with the diameter of 7mm, and has high strength and low laxity. The standard strength of steel wire is 1,670Mpa. The cables on the right side of tower are numbered from A1 to A11. The cables on the left side of tower are numbered from B1 to B3. The serial number of cables and piers are showed in Figure 1.

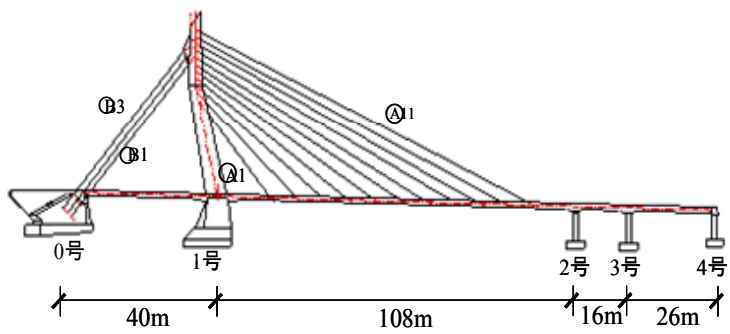

Figure 1. Elevation view of cable-stayed bridge.

2.2 Finite Element Model using ANSYS

2.2.1 Material Property and Element Selection

The main body of cable-stayed bridge consists of main beam, stayed cables and tower. Material properties of every component are shown in Table 1. In the modeling process of ANSYS, 3D solid element “SOLID65” is used for reinforcement concrete. Shell element “SHELL63” is used for steel plate. Linear element “LINK10” is used for cables.

Table 1. Material properties.

Material	Young's modulus/Pa	Poisson ratio	Density/(kg/m^3)	Component
Steel	2.1×10^{11}	0.3	7850	Stayed cables
Steel	2.1×10^{11}	0.3	7800	Upper tower
Concrete C50	3.45×10^{10}	0.1677	2550	Main beam、Tower、Tower piers
Concrete C30	3.0×10^{10}	0.1677	2550	Bridge piers

2.2.2 Finite Element Model and Boundary Condition Simulation

The model of the whole bridge is set up by the material properties and elements in Table 1. The connection of bridge piers and the ground is assumed to be fixed connection. The connection parts between tower and main beam are poured together by concrete. The structure in the anchoring region of cables is sophisticated, so that cable elements are set up by natural nodes on tower and beam. The finite element model of upper tower, No.1 bridge pier and lower tower is shown in Figure 2.

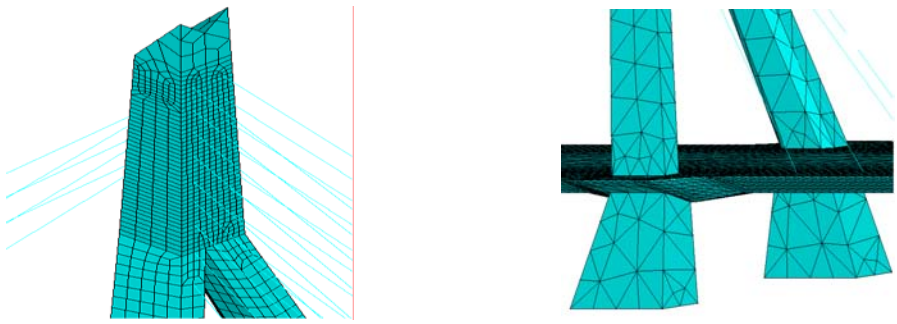

(a) Upper tower model (b) No.1 Bridge pier and lower tower model

Figure 2. Finite element model.

3 Modal Analysis of Cable-stayed Bridge

The frequencies and modals are analyzed by ANSYS. The modal extraction method is subspace iterative method. The former six natural frequencies are shown in Table 2. The former six modals are shown in Figure 3.

Table 2. Former six natural frequencies (unit: Hz).

First (vertical)	Second (transverse)	Third (vertical)	Fourth (transverse)	Fifth (torsion)	Sixth (torsion)
1.5362	3.3074	3.5428	3.9731	5.2880	5.4872

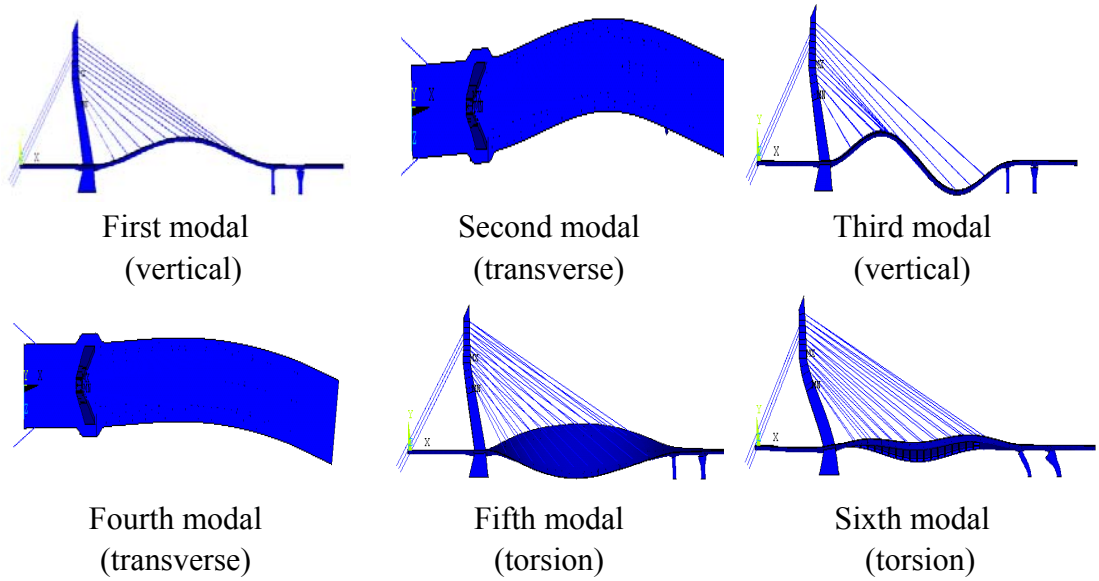

Figure 3. Former six modals.

4 Time History Response Analysis

For this cable-stayed bridge, the intensity of ground earthquake is 7 degree. There is no liquefiable soil layer. The soil in this field belongs to middle hard soil. The sort of building field belongs to II class. El-centro ground motion acceleration record is used to calculate the response of the bridge under seldom occurred earthquake along longitudinal input (Cremona C., 2003).

4.1 Response of Lower Structure

The damage of bridge during earthquake often occurs from lower structure. Especially, the damage of bridge piers may lead to the drop of the beam. The damage model of high pier often presents bending form. The damage model of short pier often presents shear form. The height of this bridge is 8m, and the core of piers is solid. So the piers do not belong to high pier. The time history curves of shear stress for tower pier and the base of No.2 bridge pier are shown in Figure 4.

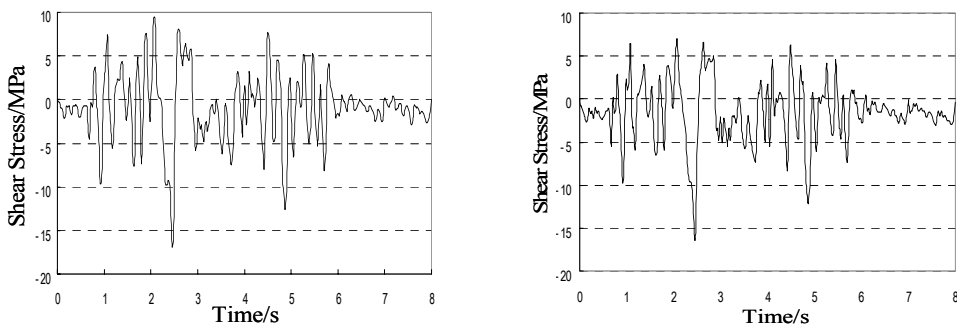

(a) Tower pier (b) No.2 Bridge pier

Figure 4. Time history curves of shear stress.

It can be seen from Figure.4, time history curves of shear stress for tower pier and the base of No.2 bridge pier are similar, and their peak values are nearly equal. The maximum shear stress is about 17MPa, which is far less than the design stress. The results demonstrate that lower structure meets the seismic acquirements.

4.2 Response of Upper Structure

The time history curves of acceleration for the middle of bridge deck and the middle of tower are shown in Figure 5. It can be seen that the acceleration of the middle of bridge deck is enlarged with 3 times, and the acceleration of the middle of tower is enlarged with 10 times, which are both in the normal range.

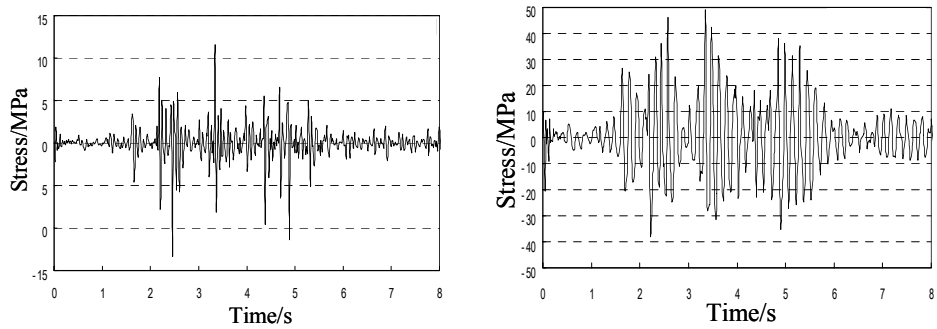

(a) Middle of bridge deck (b) Middle of tower

Figure 5. Time history curves of acceleration for middle of bridge deck and middle of tower.

4.3 Response of Cables

Because the bridge is symmetric along longitudinal direction and the earthquake is also input along longitudinal direction, the analysis for cables only focus on one side. The time history curves of cable stress for several representative cables, A1 and B1, are shown in Figure 6.

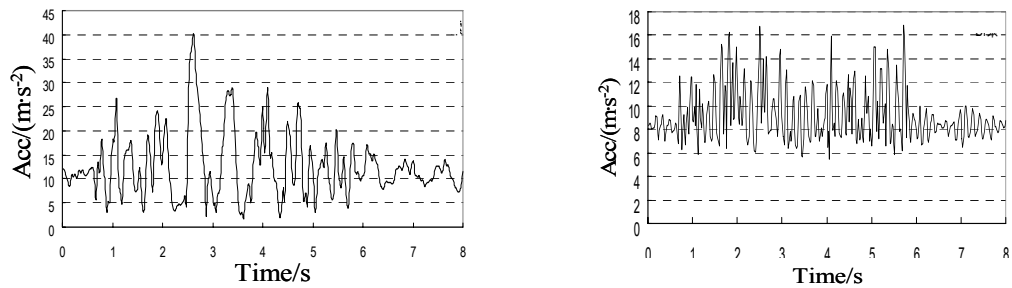

(a) Cable A1 (b) Cable B1

Figure 6. Time history curves of cable stress for cable A1 and B1.

Through the analysis for cables A1 to A11 and B1 to B3, it can be seen that the time history curves of cable stress for all 14 cables are nearly consistently, the amplitude values all fluctuate up and down the initial cable stress, and the peak

values nearly emerge at the same time. The maximum of cable stress emerges on cables A6 and A7, the cable stress of which are 41.0MPa and 42.2MPa, respectively, but both of them are far less than the standard strength of 1,670MPa.

5 Conclusions

The finite element model for a practical cable-stayed bridge is set up. The time history response analysis under El-centro earthquake excitation is carried out. Some analysis results, including time history of shear stress for lower bridge piers, time history of acceleration for upper bridge deck and time history of cable stress are obtained. Some conclusions are summarized as following:

(1) The shear stress curves of tower pier and bridge pier under longitudinal earthquake excitation present correspondence, and the difference of values is minimal. It shows that tower pier and bridge pier bear the earthquake response averagely, the design of which is reasonable.

(2) The damage model of upper structure is the failure of the dropped beam. The maximum displacement of bridge deck is in the safe range. The enlarged multiple of acceleration is normal. The maximum of cable stress is far less than the standard strength.

(3) This cable-stayed bridge will be safe under seldom occurred earthquake.

References

Cremona C (2003). "Probabilistic approach for cable residual strength assessment." *Engineering Structures*, 25, 377-384.

Faber M. H., Enelund S. and Rackwitz R. (2003). "Aspects of parallel wire cable reliability." *Structural Safety*, 25, 201-225.

Irvine H. M. (1981). "Cable Structure." *The Massachusetts institute of technology press*, Cambridge, MA.

Matteo J., Deodatis G. and Billington D. F. (1995). "Safety analysis of suspension-bridge cables: Williamsburg Bridge." *Journal of Structural Engineering*, ASCE, 120(11), 3197-3211.

The Key Technology of 'One Road One Line with Straight Driving' Public Transportation System

Zhiyong Guo[1], Wei Wang[2], and Xuewu Chen[3]

[1]Transportation College, Southeast University, Nanjing, China, 210096; PH (86) 25-51579094; or Transportation College, Wuhan University of Technology, Wuhan, China, 430064; PH (86) -27-86565741; email: guozyy1972@163.com
[2]Transportation College, Southeast University, Nanjing, China, 210096; PH (86) 25-83794101; email: wangwei@seu.edu.cn
[3]Transportation College, Southeast University, Nanjing, China, 210096; PH (86) -25-83794101; email: chengxuewu@seu.edu.cn

ABSTRACT

The paper suggests a new mode of public transportation system, called "One Road One Line with Straight Driving", in order to save residents' travel time and improve bus agencies' operation efficiency. After analyzing the implication and characteristics of the "One Road One Line with Straight Driving" mode, this paper develops the framework for the new mode. It also discusses the key technologies of the framework, including the analysis of passenger flow, the technology integrating the layout of network and bus stops, the technology integrating intelligent public transportation dispatching and bus priority signal control among others.

Keywords: public transportation system, One Road One Line with Straight Driving Mode, key technology

INTRODUCTION

Practices in China show that the strategies of public transportation priority are in line with the actual conditions of urban and transportation development in China. The traditional public transportation modes in China have some shortcomings, which lead to relatively low share of public transportation as indicated in Table 1 and Table 2.

In this context, the paper suggests a new mode of public transportation system, called "One Road One Line with Straight Driving." The key technologies involved in this new mode include the technology integrating the layout of network and bus stops, the technology integrating intelligent public transportation dispatching and bus priority signal control, among others.

Table1. Current transit service in some cities in China

	Nanjing (04)	Bengbu (02)	Changed (07)	Suzhou (02)	Huzhou (04)	Weifang (06)	Yangzhou (2003)	Changzhou (2004)
Share of transit (%)	29.82	23.31	27.58	6.44	6.31	8.08	4.31	8.39
Network density (km/km^2)	2.81	1.17	1.54	1.58	1.70	5.07	1.87	1.49
Line overlap factor	—	3.07	3.51	2.76	2.7	3.14	5.0	3.1
Coverage rate (%)	73	70.5	73.6	89.26	—	—	69.7	55

Table2. Dissatisfactions reported by transit users (%)

Dissatisfaction	Nanjing (02)	Bengbu (02)	Changed (07)	Suzhou (02)	Huzhou (04)	Weifang (2006)	Yangzhou (03)	Changzhou (04)
Too crowded in vehicle	29.70	32.37	27.00	26.25	14.50	28.78	35.10	12
Unpunctual	19.40	12.95	12.60	19.55	21.27	16.05	46.25	8
Long time of waiting	18.20	9.53	10.00	20.08	27.31	24.40	38.50	30
High price	2.60	10.80	28.70	6.02	3.99	3.39	3.14	25
Bad service attitude	7.60	7.93	7.60	5.45	12.81	14.01	11.30	8
Inconvenience	9.30	16.67	12.20	21.67	15.11	11.74	18.20	8
Others	13.20	8.75	1.90	0.98	5.02	1.63	7.10	9

IMPLICATION OF ϴNE ROAD ONE LINE WITH STRRAIGHT DR IVING" MODE

In the new public transportation mode called "One Road One Line with Straight Driving", in principle, only one bus line will be assigned to one road or street, and the bus is operating along the road without turning at intersections, which makes the bus network consistent with road network. In this new mode, bus stations are set near the stop lines of intersections to improve the efficiency and convenience of the transfer system: on one hand, it facilitates the seamless connection between bus lines with different directions; on the other hand, it ensures that passengers can arrive anywhere with no more than one time transfer. Meanwhile, the technologies of intelligent public transportation dispatching and transit signal priority are used to coordinate the signal plans in a way that that the signal lights switch to red when buses make stops on the corresponding approaches, and thus improve the efficiency of the overall system.

Comparing with the tradition mode called "central urban area focus mode", the new mode has the following characteristics:

Firstly, there is only one bus line set assigned to one road or street, and the buses run along each road without turning at intersections in the new mode (in particular cases, two bus lines may be assigned to the same segment of a road). Therefore bus line overlap factor is near one, and the transit network is consistent with the road network. The configurations of bus lines depend on the demand of transit users, and the layout of transit network that covers basically all roads and streets in the city. The resulting new mode decreases the bus line overlap factor, and thus reduces bus queues, which advances the efficiency of road utilization.

Secondly, all bus stops on one road serve only one bus line, and the arriving

interval of the bus is constant. Therefore, compared to the traditional modes, the new mode will help to reduce bus queues, the corresponding waiting time and transfer time of passengers on bus stops, and thus improves level of service.

Thirdly, there are several available paths with one time transfer for transit passengers to make the flow distribution more balanced. As a result, the phenomenon existing in the traditional mode, in which routes in arterial road are crowed while others are smooth, will be avoided.

Fourthly, buses run along roads without turning at intersections in the new mode. This characteristic helps to eliminate the conflicts between the buses and the other vehicles, and ensure that the buses will arrive evenly at intersection. Meanwhile, traffic management strategies that improve transit efficiencies, such as transit signal priority and arterial coordination control, can be easily implemented under this new mode.

Fifthly, bus delays due to signal control can be significantly reduced in the new mode. Stochasticity of transit travel is then decreased and one could expect more accurate travel time prediction. Moreover, it is much helpful for developing advanced passenger information system and dynamic bus assignment system.

THEORETICAL FRAMEWORK OF ϴNE ROAD ONE LINE WITH STRAIGHT DRIVING'MODE

The theoretical framework of the new mode includes the following components: (1) the adaptability of the new mode, (2) analysis of passenger flow, (3) layout of network and bus stops, (4) transit signal priority, (5) intelligent public transportation dispatching, etc.

Facilitated by the research on the network layout and design models of bus traffic systems, the adaptability analysis is intended to construct the new bus traffic network mode called "One Road One Line with Straight Driving" based on urban form and road network. The new pattern provides technological support to macroscopic decisions. By SP investigation, the passenger flow analysis of the new pattern is fundamental to design the layout of network and bus stops, and the security operations. The layout design of network and bus stops is the key work in the urban public transportation system of the new pattern. While the design of facilities for transit signals priority and intelligent public transportation dispatching ensure the efficient operation of the system. The theory framework of the new mode is shown in Figure 1.

THE KEY TECHNOLOGIES OF ϴNE ROAD ONE LINE WITH STRAIGHT DRIVING'MODE

The adaptability and match analysis technology of the new mode.

Research on adaptability and match analysis technology of the new mode includes the following three aspects:

(1) Based on the implication of the new mode and the requirements for road transport infrastructure, a matching model that deals with the urban form, typical

road network structure and the new mode of public transport system is established, and its adaptation is evaluated. Moreover, the level of implementing the new mode (e.g., full, local or single-line operation) is explained.

(2) Based on the idea of "active public transit", research includes: a) to ensure the efficient and equitable bus trips, a double-layer optimization model of urban road network density is developed, and the technology and method to analyze road network density for typical network layout (Grid, radiation ring) are studied; b) in the new mode, road planning and design technologies which meet the needs of public transport network and stop layout(e.g., the layout of the road section and the geometric design), are studied.

The passenger flow analysis technology of the new mode.

(1) The SP survey method and the data analysis technology are used to understand individual travel behavior. These methods and technologies include the investigation report and form design, survey methods, database establishment, and the analysis of statistical characteristics of residents' trip chaining behavior.

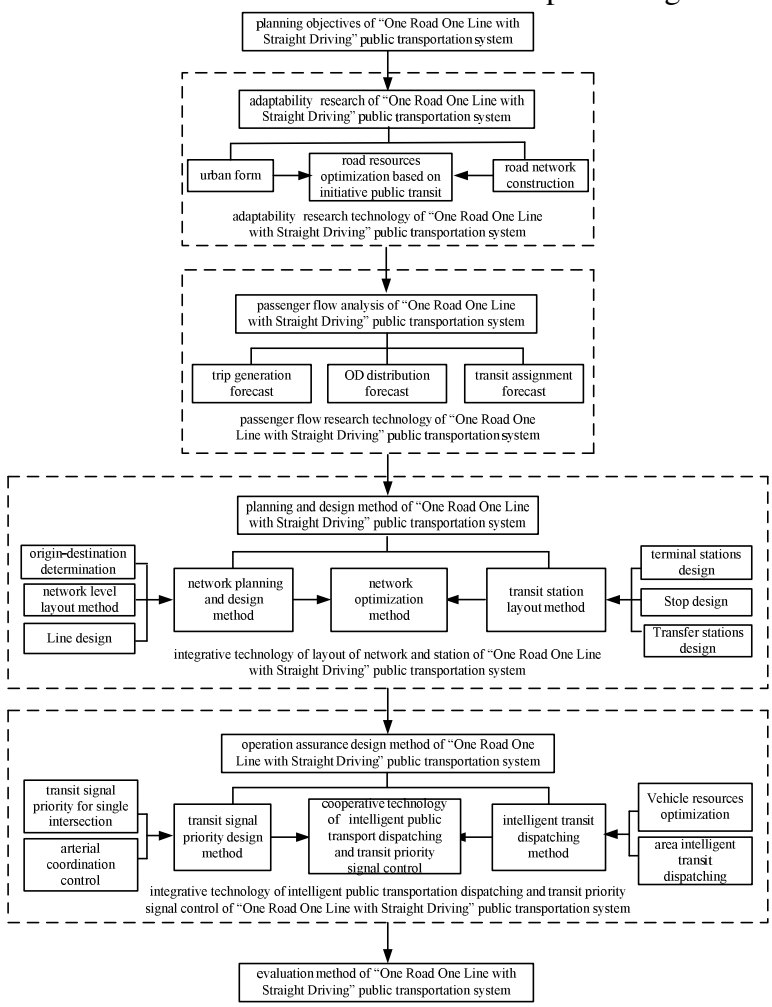

Figure1. Theory research framework of the new mode

(2) The influence of the new mode on travel characteristics (such as trip purposes, modes used, and trip distribution) and their change patterns are studied given the conditions of a highly information based society. A forecasting method of urban travel demand is proposed as the basis to forecast travel demand for public transport.

(3) An activity-based demand forecast model of the new mode is developed, with the emphasis on individual travelers' behavior. The demand forecasting model is composed of the following elements:

a) The utility functions that are constructed as an activity-based generation-mode split model using the factors from the above studies;

b)The utility functions and the corresponding algorithms that are developed to capture the destination choice behavior as an activity-based distribution model (Nageswar 2001); and

c) The demand forecasting model for transfer passengers.

(4) Distribution technologies for bus passenger flows of the new mode are researched. The details are as follows:

a) A multi-path probabilistic distribution model of bus route choice with a single transfer is established to ensure efficient travel and convenient transformation, and a corresponding rapid algorithm is proposed. This distribution model is based on the demand forecast for bus passenger flows. The characteristics of bus passenger flows (e.g., destination, walk time, departure interval, transfer time, and line grading), and the route choice behavior for residents taking public transport are considered in the model; and

b) Meanwhile, to ensure efficient travel and convenient transformation, a model and the corresponding solution algorithm for transfer passenger flows are developed to minimize the transfer times, considering the travel choice behavior of public transport.

Integration of network layout and stop design.

The technologies developed include:

(1) Grading technology for bus lines. Based on the passenger flow allocation of public transport, the land use, road configurations and traffic conditions along lines are analyzed to establish a fuzzy-cluster analysis model of hierarchy evaluation for the bus lines of the new mode;

(2) The bus lane design. Based on the distribution characteristics of vehicles on different grades of bus lines, the models are developed to represent the speed-flow relationships for buses and social vehicles driving on different roads and under traffic conditions. In the new mode, the design techniques for bus lanes of different grades are studied, focusing on lane type, section layout, and geometric design.

(3) The integrative design of bus stop layout and intersection channelization. Based on the arrival and parking characteristics of vehicles at bus stops near intersections, collector-distributor characteristics of passenger flows, and the size and

channelization design of intersections, an integration technology of the location, type and geometric design of bus stops and intersection drainage are studied in order to reduce the transfer space of social vehicles and pedestrians when passing through intersections (Yang 2007).

(4) Optimization and design of transfer nodes. Based on the demand forecast of transfer passenger flows, the grade and road conditions of bus transfer routes, and the level and scale of transfer nodes for public transport are determined. The integrative design of transfer nodes and crossing facilities is proposed, and the corresponding technical standards for the transfer node design are developed.

Integration of bus priority and the scheming of operation.

(1) Bus Priority control technology. Bus Priority control technology is a key measure to improve the operational efficiency of public transport. The corresponding research includes:

a)The fuzzy self-adaptive signal control based on Agent technology for single intersection is studied (Wadjas 2003) to minimize the delay of buses with straight line;

b)The coordination control technology based on content control theory for main bus lines is studied in order to realize the "non-blocking" run of high-grade bus lines and the optimal efficiency of bus passenger flow,; and

c)The regional coordination control model and the algorithm for public transport are developed based on Multi-Agent technology.

(2) Intelligent technology of bus dispatching. The studies include:

a) Bus travel time prediction. Based on ITS, GIS, vehicle location, wireless communication etc, the real-time operating data of buses is collected. Then, a dynamic model for bus travel time prediction is developed;

b) The optimization model of start timetable for bus lines. An optimization model of start timetable is developed with the passenger demand as the input data. This model is to find the optimal solution of start timetable under the objective of maximizing the weighted average of bus passenger satisfaction and bus enterprise satisfaction. The start interval and the fleet size are used as constraints; and

c) The dispatching model based on demand analysis of bus passenger flows in the new mode. The optimization model of timetable with the largest consistency of bus lines (Ceder 2001) is studied to minimize the waiting time for transfer passengers. Dispatching optimization and regional coordination model of start time for bus lines are studied using game theory and an approximate global optimization algorithm.

(3) Active coordination of scheduling for main bus lines and signal control for intersections. In order to reduce the signal delay at intersections along the way, the active coordination of scheduling for main bus lines and signal control for intersections is studied according to the match degree of vehicle dispatching and

signal control synergies at intersections,. The green wave control for buses is implemented to ensure their accessibility.

CONCLUSION

With its high efficiency and service level, the new mode proposed in the paper is able to enhance the attractiveness of public transport and meet the travel demand of residents. Therefore, it demonstrates a bright future of application. The establishment of the proposed framework and the discussion of key technologies point out the direction for in-depth studies.

REFERENCES

Ceder, A., et al(2001). "Creating Bus Timetables with Maximal Synchronization. " *Transportation Research Part A*, 38:913-928.

Chen Xuewu, Li Wenyong(2006). "Research and Implementation on Initiative Public Transit Network Plan." *Journal of Wuhan University of Technology*, 30(1):9-12.

Nageswar Jonnalagadda, Joel Freedman, William A. Davidson, et al. Development of a Microsimulation Activity-Based Model for San Fransisco－Destination and Mode Choice Models[EB/CD]. Paper presented at the 80th Annual Meeting of the Transportation Research Board, Washington, D.C., 2001.

Wadjas, Y., and P. Firth. Transit Signal Priority along an Arterial Using Advanced Detection. In Transportation Research Record 1856, TRB, National Research Council, Washington, D.C., 2003, pp.220-230.

Yang Longhai, Li Lilan, Zhong Shaopeng. Research on the location of bus stops upstream the approach at signalized intersections. *Journal of Harbin Institute of Technology*, 2007, 39(2):292-295.

Research on Urban Public Transit Dispatching System based on Real-time Prediction and Game Theory

Wen Hui-ying [1] Cheng Gong [2] Li Peng-fei [3]

[1]Wen Hui-ying, School of Civil Engineering and Transportation, South China University of Technology, Guangzhou 510640; PH(86) 13600066536; email: hywen@scut.edu.cn

[2]Cheng Gong, School of Civil Engineering and Transportation, South China University of Technology, Guangzhou 510640; PH(86)13265033589; email: 42270648@qq.com

[3]Li Peng-fei, School of Civil Engineering and Transportation, South China University of Technology, Guangzhou 510640; PH(86)15918772812; email: scutlpf@gmail.com

Abstract

Considering the complexity and uncertainty of urban public transit, a dispatching system based on real-time prediction and game theory is proposed in this paper. After the real-time passenger flow data is obtained, the vehicles' passenger load rate for several consecutive time intervals is predicted, the preliminary dispatching strategies for bus lines or subway lines will be proposed. Then game theory is applied to find the best dispatching strategies for different lines. Finally, the efficiency and flexibility of each station, line and whole urban public transit system can be improved to a higher level.

1. INTRODUCTION

In recent years, urban public transit problem has become one of the most important problems which have obvious impact in daily life. Urban public transit has shown such characteristics as complexity and uncertainty, and cannot make prompt response to time-variant passenger demand. In order to improve the adaptive capacity and operational efficiency of urban public transit system, some domestic experts and scholars have done a lot of research and presented some important results. But how to implement it in practical application is still not clear, and more research needs to be conducted.

2. PROJECT OF URBAN PUBLIC TRANSIT DISPATCHING SYSTEM

2.1. Dispatching targets of the system

The urban public transit includes bus, subway and taxi. Both bus and subway are operated regularly in time schedule and route, and they have large transport capacity,; taxies have no specified stations and fixed routes, and they only can carry a little proportion of passengers flow. The investigation about service capabilities of different transit tools shows that more than 90% passengers choose bus or subway. So, bus system and subway system are chosen as dispatching targets of this system.

2.2. Components and structure of the system

It is appropriate to use a multi-level structure to describe a urban public transit dispatching system. Dispatching center should be set up in the city's traffic management center; subway system and bus system should also set up their own management centers in order to operate and dispatch bus lines or subway lines in their levels（see Figure 1）.

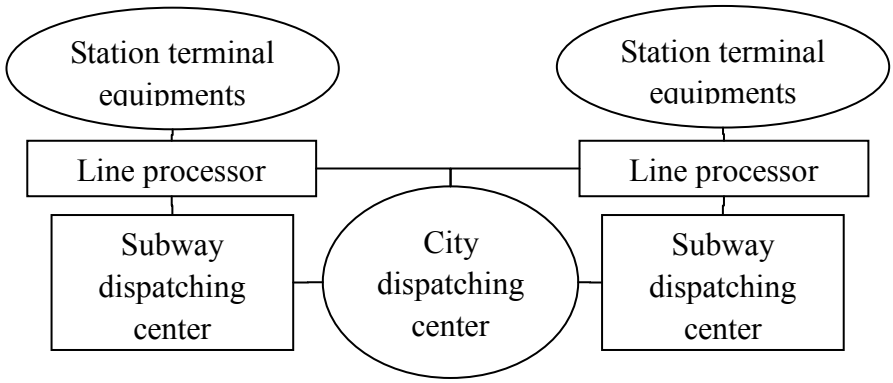

Figure 1. Structure of urban public transit dispatching system

2.3. Components of line processor and their function

Line processors are playing a key role in urban public transportation dispatching system(Xiangyong Yin et al. 2000). They compute rational strategies according to different goals, capacities and given data（see Figure 2）.

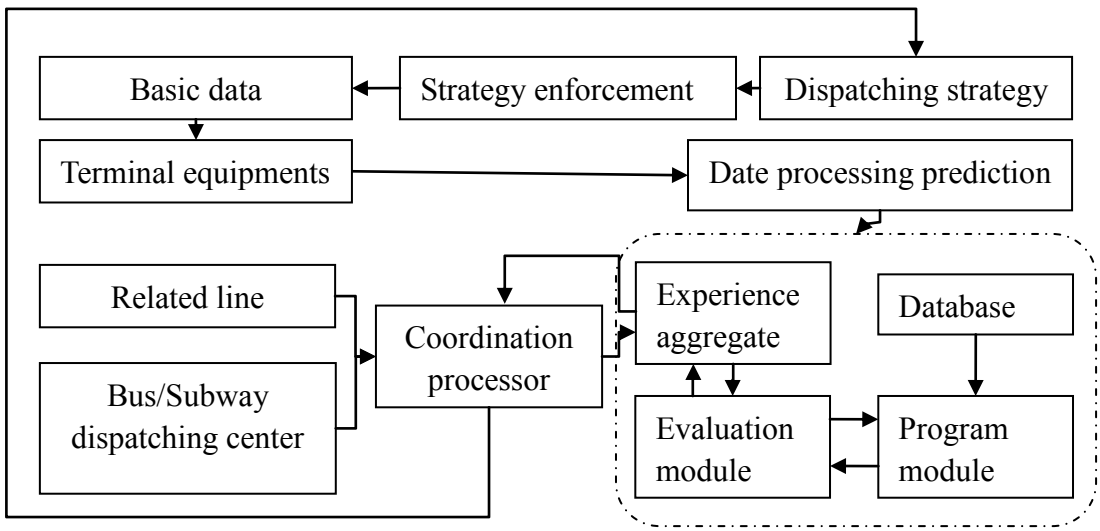

Figure 2. Structure of line processor

The passenger flow data are collected by the detectors installed in buses and stations, and the data are sent to the line processor. The processor makes a prediction based on the obtained data; the current adopted operating strategy can be updated. According to the processed data, program module processes all the data and calibrate a set of new parameters, thus a new optimal dispatching strategy of this line will be figured out.

3. GENERATING AND CO ORDINATING OF DISPAT CHING STRATEGY

3.1. Strategy targets and data obtaining

The goal of dispatching strategy is to find appropriate departure frequencies of bus or subway lines. The departure frequencies must be suitable for the different passenger transport requirements and capacities of stations.

The passenger flow data can be obtained by registered equipments or monitoring facilities which were installed in vehicles or at stations (Sun Zeyu et al. 2005). For buses, it's appropriate to install some radio-frequency radiation recorder sets near its front door and back door, so the number of passengers who get into and off the bus can be recorded easily at every service station.

3.2. Formulating process of line dispatching strategy based on real -time prediction

Considering that the passenger demand of a station is often reflected in the vehicles' passenger load rate when they are going to leave the station, a prediction of passenger load rate is conducted to provide the basis for finding the optimal strategy.

The passenger flow data of each station is detected by corresponding installed equipments and sent to line processor in real-time (HAN Yin et al. 2003). The processor uses the following method to deal with those obtained data and figure out an appropriate departure frequency for each line.

(1) Expression of passenger load rate. The passenger capacity of vehicles is termed as Z, number the stations is denoted as j (j=1,2,3,…,n) , and vehicle index is represented as i (i=1,2,3,…,n). U_{ij} and D_{ij} are used to denote the number of passengers who get into and get off the vehicle i at the station j. So the passenger load rate r_{ij} can be expressed as:

$$r_{ij} = \sum_{c=1}^{j} (U_{ic} - D_{ic}) / Z \qquad (1)$$

(2) Prediction of passenger load rate. In fact, it needs a period of time for one prepared vehicles to go into service. And passenger demands of each station changes with time, so a strategy achieved only based on the current situation does not work for the situation at the oncoming time intervals, therefore the procedure of strategy searching must be integrated with prediction.

The delay time of strategy is termed as T, and the passenger load rate r_j^* at T time later in station j can be predicted based on the recently obtained data of passenger load rate in station j. $Q(r_j)$ is adopted to represent the data aggregation j of the recently obtained passenger load rate, and the rate of station j after T time is:

$$r_j^* = g[Q(r_j), T] \qquad (2)$$

In the above equation, $g[Q(r_j),T]$ is a predicting function expression about passenger load rate r_j and time T.

(3) Computation procedure of departure frequency of a line

① It is supposed that the maximum allowed passenger load rate of vehicles is r_{max}. If $r_j^* \geqslant r_{max}$, the current departure frequency should be updated in order to make it adapt to passenger demands. $\overline{r_j}$ is used to denote the average passenger load rate of station j in the past Δt time, supposing that current departure frequency is H, and T time later the optimal departure frequency of station j is (LIU Chuang et al. 2008).:

$$H_j^* = f_1(r_j^*, \overline{r_j}, H) \qquad (3)$$

Here, $f_1(r_j^*, \overline{r_j}, H)$ is a function, and $r_j^*, \overline{r_j}, H$ are its parameters.

② If $\overline{r_j} \leq r_j^* \leq r_{max}$,then let $H_j^* = H$; If $r_j^* \leq \overline{r_j}$,then let $H_j^* = f_2(r_j^*, \overline{r_j}, H)$, $f_2(r_j^*, \overline{r_j}, H)$ is another function.

(4) Coordinating of different departure frequencies According to step (3), the obtained departure frequencies of different stations which belong to a same line are different from each other, so the frequency data must be coordinated and the more reasonable departure frequency of the whole line should be figured out.

$H_j^*(j = 1,2,3,\ldots, n)$ is the obtained frequencies of each station, and the importance of different stations can be considered by ordering different priority coefficients like $P_j(j = 1,2,3,\ldots, n)$ .Line processor coordinates a set of H_j^* until a rational frequency H^*can be computed, and the following should be met:

$$P_j^* \geq P_j(j = 1,2,3,\ldots, n) \mid H^* \qquad (4)$$

3.3. Holistic dispatching strategy based on Nash -balance of game theory

Optimization of one bus line or subway line doesn't mean higher efficiency and capability of the whole public transit system. A single station is often shared by several lines, and each station has one specified capacity limit; on the other hand, the number of spare vehicles has a limit as well. Because of these, it's possible that the departure frequencies of some lines can not be allowed in the same time.

Dispatching strategy of one line might have some impact on that of others and be affected by them, therefore, a line processor should consider other processor's possible strategies. So different processors exchange their information with each other and coordinate all strategies according to game theory, and a situation of Nash-balance might be reached.

3.3.1. Coordination model

The line processors are the main participators of coordinating process, the aggregate of them is termed as C; the aggregate of each processor's information is

denoted as I; S is the aggregate of all possible strategies; U is objective function. It means the efficiency and capability of the whole system and includes several targets such as reasonable departure frequencies of each line, moderate passenger load rate of vehicles, and acceptable schedule for each station.

The coordinating process can be defined as F={C,I,S,U}. During the process, each line processor chooses proper strategies from strategy space S according to its own information, and tests each other with strategies of other line processors. Through continuous coordinating, a Nash-balance can be reached and all parties' interests can be met in a accepted extent, the balance situation must be able to meet these conditions:

$$r_{min}^{k} \le r_{ij}^{k} \le r_{max}^{k} \qquad (5)$$

$$\sum_{1}^{k}\sum_{1}^{m} i \mid \forall t \le M \qquad (6)$$

$$\sum {}_{j} H_{k}^{*} \mid \forall t \le H_{j\max} \qquad (7)$$

r_{min}^{k}, r_{max}^{k} are the allowed minimum value and maximum value of passenger load rate of line K; $\sum_{1}^{k}\sum_{1}^{m} i$ is the sum of running vehicles of all lines, M is the number of all available vehicles; $\sum {}_{j} H_{k}^{*}$ is the sum of frequencies of all lines in station j, $H_{j\max}$ is the maximum service capacity of station j.

3.3.2. Coordination program

(1) Under normal situations, each line operates buses according to its normal schedule, line processor record the passenger load rate of vehicles which departs in a past T time period of time from each station, then the rate after in each station can be predicted;

(2) If some stations' predicted passenger load rates are out of the allowed range, then adjust the frequency of the line according to the established regulations. After figuring out a new strategy, the processor sends a coordination request to others who have close relations with it;

(3) Receiving the request, each of those processors makes response immediately, and a temporary coordination group is established and starts finding Nash-balance;

(4) If Nash-balance can be reached, coordinating strategy would be established based on the balance, each line could define its dispatching method, the coordinating process come to an end; if the balance can't be found out, processors will send coordination requests to dispatching center;

(5) Computers of different dispatching center make response, coordinate all the possible strategies, if Nash-balance can be reached, then each line determines its

frequency; if not, the coordination request will be sent to the city dispatching center;

(6)Computers in city dispatching centers coordinate different strategies and try to find Nash-balance, if it is reached, then lines of bus and subway will adjust their operation conditions; if not, a widely accepted sub-optimal dispatching order must be sent down directly.

4. URBAN PUBLIC TRANSPOR T DISPATCHING SYSTEM SIMULATION AND APPLICATION

In Figure 3, supposing that the number of passengers who get on buses in each station comply with passion distribution; the departure interval of each line is 15 T (30 minutes); the delay time capacity of each station is 30 vehicles per hour; the number of spare bus is big enough; the allowed passenger load rate is within the range (0.3, 1.3), and linear regression model is adopted to predict the passenger load rates. A simple computer program was written in order to simulate the dispatching system (Adamsli A et al. 1998;Moazzem Hossain et al. 2000).

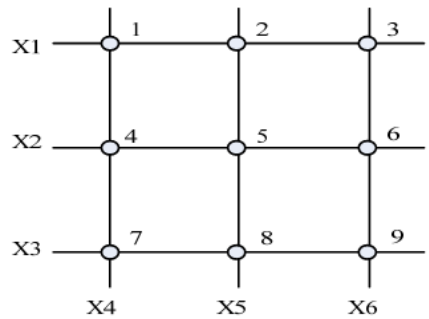

Figure 3. Bus lines and its stations

It's obvious that this urban public transit dispatching system can enhance the flexibility of lines and operation efficiency of vehicles, moreover, this system can also improve stations' capacity, and finally improves the service level of whole public transit system (see Figure 4).

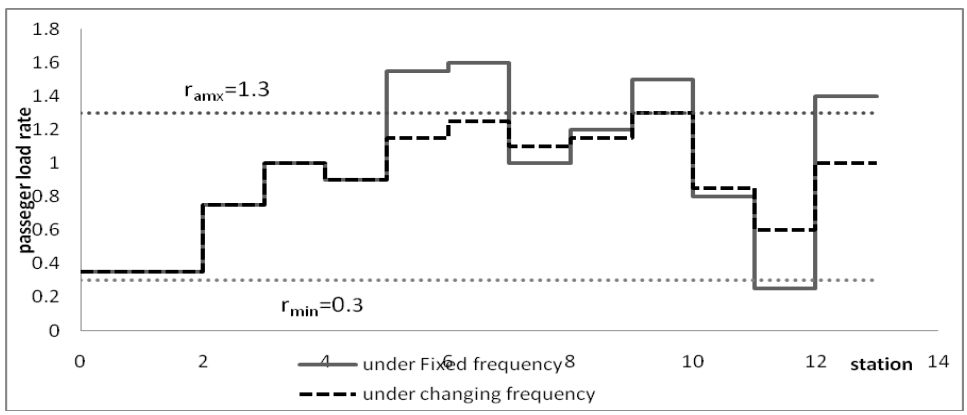

Figure 4. Comparison of passenger load rate

Through the investigation for one bus line which is dispatched by fixed frequency in Guangzhou, the passenger load rate is as follows(see Table 1); with the urban public transportation dispatching system, we adjusted the frequency and the

passenger load rate as follows (see Table 1):

Table 1. The data of passenger load rate

Station	1	2	3	4	5	6	7	8	9	10	11	12	13	14
Fixed frequency	0.3	0.7	1.0	1.3	1.6	1.6	1.5	1.2	1.5	0.8	0.7	0.5	0.3	0.2
Changing frequency	0.3	0.8	0.9	1.1	1.2	1.3	1.2	1.3	1.3	1.2	1.1	1.0	0.8	0.5

From the data, the urban public transit dispatching system reduces the passenger load rate during the rush hour, and enhances the average passenger load rate (see Table 2). The system can enhance the flexibility of lines and operation efficiency of vehicles.

Tab le 2. Comparison of passenger load rate

Station	Fixed frequency	Changing frequency
Average load rate	0.94	1.01
Rush hour load rate	1.49	1.27

5. CONCLUSION

This paper proposes an urban public transit dispatching system based on real-time prediction and game theory. On the basis of the obtained passenger flow data, line processors are used to process the data and make predictions, and the elementary dispatching strategy is obtained. Then game theory is applied to coordinating the strategies and an optimized dispatching strategy for whole public transit system is obtained. The simulation result shows that the capacity and flexibility of each station, line and whole public transit system can be improved.

REFERENCES

Adamsli A, Turnau A(1998). Simulation support tool for real-time dispatching control in public transport. Transport Reasearch C , 32:73-87

HAN Yin, YANG Zhao-sheng, HU Jiang-ming (2003).Study on Basic Data Forecast Method of Public Transport Intelligent Dispatching System. Journal of Highway and Transportation Research and Development , 20(3):140-143

LIU Chuang, YAO Jia, JIANG Li-wei.(2008). The Research of Real-time Network Optimization Models and Methods about Public Transport Intelligent Dispatching System. Journal of Jiamusi University(Natural Science Edition) , 26(1):53-55

Moazzem Hossain, Mir Zahid'Hasan (2000).Simulation of Bus Operation under Mixed Traffic Conditions, Proceedings of ICTTS'2000, 441-448

Sun Zeyu, Wang Bingfeng (2005). Intelligent Transportation system base on GSMSMS. Journal of Changchun University of Science and Technology, 1(4):135-135

Xiangyong Yin, Hongqin Peng.(2000). The Development of Public Transportation

Dispatching Platform Based on Expert System. Traffic and Transportation Studies,845-850

INDIVIDUAL AND POPULATION LEARNING IN ROUTE CHOICE BEHAVIOR OF DRIVERS: EXPERIMENT AND MODEL

PU Liang[1], GUAN Hong-zhi[1], LU Zi-xu[2], HUANG Shan[1], FANG Jia[1]

[1]Key Laboratory of Traffic Engineering, Beijing University of Technology, 100124, Beijing
[2]China IPPR International Engineering Corporation, 100089, Beijing

ABSTRACT

This paper carries out four sessions experiment upon drivers' route choice behavior, which aims to study drivers' decision rules under complete information and incomplete information, Historical (H) and No Historical (NH) conditions. With the theory of learning in games as a tool, this study compares experimental data across sessions, and proceeds to construct a population-level model and an individual-level model of the drivers' choice behavior based on a recursive and updated belief set. The paper also measures the influence of various information conditions and drivers' previous experience on their route choice behavior. It's found that learning is a prevalent phenomenon in the process of drivers' decision-making, and the effect of learning remarkably depends on payoff differences between alternative routes, even when a driver may not have a clear idea of travel time of other options. It has been shown by experiment that experience and information exert their important influence on drivers' choice behavior, although they fail to accelerate convergence to network equilibrium. A driver will become more sensitive to payoff differences when he gains experience and holds complete information of alternative routes. The experienced drivers can more accurately perceive traffic conditions, consequently the frequency of switch between routes is greatly reduced. There exist considerable differences in the effect of complete information among drivers due to their different learning rules. This paper classifies drivers in terms of their different learning rules, and explores the influence of a variety of information and traffic conditions on drivers' learning behavior.

KEY WORDS: *learning; games; experience; information; route choice behavior*

1 INTRODUCTION

Traffic network equilibrium should be interpreted as an idealized condition. The traffic flow of any route or the whole network could be calculated by traffic assignment theory and stochastic utility theorem if the traffic network can eventually converge to that equilibrium (Liu, 2001; Shao, 2004; Lu, 2006). However, it raises two questions of network equilibrium. Firstly, network equilibrium is based on the assumptions that the drivers hold complete information about traffic network, and

that drivers' choice behavior depend on full rationality and identical decision rules, while those assumptions may not be satisfied by actual conditions. Secondly, those traffic network equilibrium models can only show the final status of network equilibrium but not the whole process. In fact, network equilibrium arises as the long-term outcome of a learning process in which the drivers are influenced by incomplete information in addition to their bounded rationality. Therefore, it is essential to know drivers' learning processes and decision rules in actual conditions so as to understand traffic network equilibrium.

Games theory researchers have fruitfully studied the learning processes of bounded rational players over time. Cournot (1897) assumed that players will choose a best response to what they most recently observed; Maynard Smith, Price (1973, 1974) and Brown (1951) respectively developed evolutionary model and fictitious play model to explain learning phenomenon. Cross (1983), Roth and Erev (1995) proposed reinforcement model and the concept of cumulative payoffs to simulate players' choice behavior. Weibull (2006) systematically summarized and perfected evolutionary game theory. Crawford (1995) interpreted data from coordination games using player-specific belief sets. Cheung and Friedman (1997) estimated a weighted fictitious play model on individual-level data from four games, including hawk dove, stag hunt, buyer seller and battle-of-the-sexes. Boylan and El-Gamal (1992) explained learning behaviors in coordination games and dominance-solvable games with fictitious play model and cournot dynamics; they found fictitious play model fit data better. Camerer and Ho (1999) developed an experience-weighted attraction model on the basis of experiments. Stähl (2001) studied players' learning process on decision rules.

In these years, some researchers attempted to use the theory of learning in games to explain route choice behavior of drivers so as to improve traditional theory. Li Zhen-long (2003) made an analysis of route choice behavior of drivers under guide information based on evolutionary game model. Wu Bing and Li Lin-bo (2006) analyzed traffic congestion phenomenon using evolutionary game approach.

So far, there are few quantitative analysis of route choice behavior based on the theory of learning in games. This study carries out four sessions experiment upon drivers' route choice behavior. Comparing experimental data across sessions, the paper proposes a population-level model and an individual-level model of the drivers' choice behavior based on a recursive and updated belief set. This paper also discusses the influence of various information conditions and drivers' previous experience on their route choice behavior.

2 LEARNING MODELS

2.1 POPULATION-LEVEL LEARNING MODEL

At present, an extensively used approach in the analysis of population learning phenomenon is the evolutionary model. The basic idea of this model is based on the assumption that the percentage of a population that uses a strategy

changes proportionally with relative payoff advantage of that strategy. This paper proceeds to construct a population-level learning model of the driver's choice behavior also based on the evolutionary approach.

Suppose there are *n* independent routes between O and D in a traffic network. The user cost function of each route is defined as:

$$C_i = A_i + B_i v_i, (i = a, b, \cdots, n) \tag{1}$$

Where A_i = the minimum user cost of route *i*,

B_i = the traffic flow parameter. It's inversely proportional to the capacity of route *i*,

v_i = the traffic flow. The total traffic flow Q of the whole networks is calculated by adding together all v_i.

According to the evolutionary approach, let $Q_i(t)$ represent the number of drivers' choosing route *i* in period *t*, so the percentage of drivers' choosing this route in period *t* is $P_i(t)=Q_i(t)/Q$. In this time period, the payoff to using route *i* and the average payoff in the population are defined as $u_i(t)$ and $\bar{u}(t)$, respectively. The rate of the percentage changes of drivers choosing route *i* is:

$$\frac{dP_i(t)}{dt} = [u_i(t) - \bar{u}(t)] \bullet P_i(t) \tag{2}$$

If we allow the lagged relative payoff advantage of route *i* to affect the driver's choice in period *t*, we obtain the following equation:

$$\frac{dP_i(t)/dt}{P_i(t)} = \frac{P_i(t+1) - P_i(t)}{P_i(t)} \tag{3}$$
$$= \alpha_0 + \alpha_1(u_i(t) - \bar{u}(t)) + \alpha_2(u_i(t-1) - \bar{u}(t-1)) + \cdots + \alpha_k(u_i(t-k+1) - \bar{u}(t-k+1)), (k = 1, 2, \cdots)$$

Where, α_0 = a constant, it captures the drift toward route *i*,

α_k = the weight parameter placed on relative payoff advantage in period *t*-*k*+1.

Based on equation (3), we will discuss these questions about the population learning in the following sections:

1. Whether a significant correlation exists between the percentage changes of drivers choosing a route and relative payoff advantage of that route?
2. Whether historical relative payoff advantages have lagged effects on drivers' choice behavior, and how long is the duration of these effects?
3. How various information and traffic conditions influence drivers' population learning behavior?

2.2 INDIVIDUAL-LEVEL LEARNING MODEL

Different from population-level learning model, which places more emphasis on the tendency of population learning behavior, the individual-level learning model attempts to make some predictions about how specific individuals will change what they do. There are considerable differences in predictions about the choice behavior of individuals due to different explanations about cognitive and thinking processes.

The reinforcement model assumes a player always receives "reinforcements" which are proportional to his realized payoff. Cournot dynamics assumes the strategy played last period by others will be played again. The fictitious play model weights all previous observations equally. The weighted fictitious play model counts recent experiences more than distant ones. Because of the lack of study on individual driver's learning behavior, this paper attempts to measure the weights placed on current and lagged experiences directly, rather than using the above-mentioned models.

Suppose there are also n independent routes between O and D in a traffic network. The user cost function of each route is same as in equation (1):

$$C_i = A_i + B_i v_i, (i = a, b, \cdots, n)$$

The parameters are the same as the above.

Each individual makes decisions based on his perception of potential payoffs due to the lack of precise understanding about the choice of the others and the traffic conditions.

In this paper, the perceived payoff function $G_i(t)$ of route i before a driver makes a choice in period t is defined as:

$$G_i(t) = \beta_0 + \beta_1 u_i(t-1) + \beta_2 u_i(t-2) + \cdots + \beta_k u_i(t-k), (k = 1, 2, \cdots) \quad (4)$$

Where, β_0 = a constant, it captures the drift toward route i,

β_k = the weight parameter placed on lagged realized payoff of this driver in period t-k+1

According to stochastic utility theorem, the driver will choose routes with higher perceived payoffs more frequently. The probability of a driver choosing route i in period t is:

$$P_i(t) = \frac{e^{G_i(t)}}{\sum_{j \in N} e^{G_i(t)}}, (i, j \in N) \quad (5)$$

Based on equation (5), we will discuss these questions about individual learning behavior in the following sections:

1. Whether previous experiences can affect the choice of individual drivers?
2. Whether there are differences among drivers in effectively memory length and the attitude toward previous experiences?
3. How do various information conditions affect different types of drivers?

3 EXPERIMENTS

We ran four sessions experiment upon drivers' route choice behavior. Subjects were 22 undergraduates at Beijing University of Technology. The experimental traffic network are comprised of two independent routes, where route a is shorter with lower capacity, and on the contrary, route b is longer and having higher capacity. Subjects made choices between two routes and chose optimal decision based on their

realized payoffs until achieve network equilibrium. Table 1 contains the information and traffic conditions in each session:

Table 1 Information and traffic conditions in each session

session	information used to making a choice			traffic conditions	
	received payoff in last period	received payoffs in all period	unchosen payoffs (forgone payoffs) in last period	First BPR Function	Second BPR Function
1	√			√	
2	√	√		√	
3	√	√			√
4	√		√	√	

The first session experiment intends to simulate drivers' choice behavior in an unfamiliar traffic network. In this session, after each choice, subjects got feedback only about their received payoff in last period. The second and third session experiments attempt to explore drivers' decision-making in a more familiar traffic network. For this purpose, subjects were told their received payoffs in all periods of each session. The fourth session experiment aims to study drivers' choice behavior if they hold complete information about received payoffs and forgone payoffs. In addition, we set a different BPR function in session 3 in order to detect subjects' response under different traffic conditions, and moreover, the marginal cost caused by one unit vehicle in session 3 is higher than other sessions.

The experiments overcame the challenge which is how to transmit information to each subject respectively. We did this by using questionnaires on which the received payoff information in last period were provided. Based on this information, each subject made a decision about which route to choose in the next period. After that, subjects wrote their choices on the questionnaires and handed them in. We calculated payoff of each route according to the number of subjects' route choice, and then, we feedback this information to each subject by a new questionnaire again. In session 2 and session 3, besides the information from these questionnaires, subjects could also record their received payoffs in each period of this session on a paper. In session 4, subjects could get feedback about their received payoffs and forgone payoffs after each period through questionnaires.

4 MODELS SPECIFICATION

4.1 POPULATION-LEVEL MODEL SPECIFICATION

Because there are only two alternative routes in our experiments, we can calculate the change in the percentage of drivers choosing route a in period t to discuss the population-level learning process. According to equation (3),

$$\frac{P_a(t+1)-P_a(t)}{P_a(t)} = \alpha_0 + \alpha_1(u_a(t)-\bar{u}(t)) + \cdots + \alpha_k(u_a(t-k+1)-\bar{u}(t-k+1)), (k=1,2,\cdots) \quad (6)$$

Where, $P_a(t)$ = the percentage of drivers choosing route a in period t,

$u_a(t)$ = the payoff to choosing route a in period t,

$\bar{u}(t)$ = the average payoff in the population in period t, $\bar{u}(t)=P_a(t)u_a(t)+P_b(t)u_b(t)$,

k = the order of lags.

We use Ordinary Least Squares (OLS) to estimate equation (6) because it is a multiple linear regression model and $P_a(t)$, $u_a(t)$, $\bar{u}(t)$ in this equation can be derived from experimental data.

It is calculated as:

$$\min\sum_{t=1}^{T}\frac{P_a(t+1)-P_a(t)}{P_a(t)}-\left[\alpha_0+\alpha_1(u_a(t)-\bar{u}(t))+\cdots+\alpha_k(u_a(t-k+1)-\bar{u}(t-k+1))\right] \quad (7)$$

Allowing for the order of lags k is unknown, we estimate equation (6) at different value of k, and then select a reasonable model according to the estimated results.

4.2 INDIVIDUAL-LEVEL MODEL SPECIFICATION

Similarly, we can analyze the change in the probability of a driver choosing route a or b to explore the individual-level learning process. According to equation (5), the probability of a driver choosing route a or b in period t can be written as

$$P_a(t)=\frac{e^{G_a(t)}}{e^{G_a(t)}+e^{G_b(t)}}=\frac{1}{1+e^{G_b(t)-G_a(t)}}=\frac{1}{1+e^{\beta_0+\beta_1\Delta u(t-1)+\cdots+\beta_k\Delta u(t-k)}} \quad (8)$$

and

$$P_b(t)=1-P_a(t) \quad (9)$$

respectively. Where, $\Delta u(t)$ is a function of the payoff differences, $\Delta u(t) = u_b(t)- u_a(t)$.

The forgone payoff of a driver in period t is defined as his average payoff to choosing that route previously, except in the fourth session experiment. Furthermore, we classified the individuals into four groups in terms of their changes in frequency of switch (shown in table 2). We estimated an individual-level learning model for each group respectively.

Table 2 The changes in the frequency of switch across different groups

group	frequency of switch in session 2 or session 3 than the ones in session 1		frequency of switch in session 4 than the ones in session 1	
	reduce	almost unchanged or increase	reduce	almost unchanged or increase
1	√		√	
2	√			√
3		√	√	
4		√		√

We estimate equation (8) using Maximum Likelihood Estimation (MLE). The likelihood function for the sample is obtained from:

$$\max \quad L = \prod_{i=a} P_a(t) \prod_{i=b} (1 - P_a(t)) \tag{10}$$

Similarly, we estimate equation (10) at different value of *k,* and then select a reasonable model according to the estimated results and Akaike Information Criterion (AIC).

AIC is a function that is used to determine the order of lags *k*. The value of AIC function of equation (10) can be obtained as follows.

$$AIC(k) = -\frac{\ln L}{n} + \frac{k}{n} \tag{11}$$

Where, ln*L* = the value of maximized log-likelihood function, i.e. the logarithm of equation (10),

n = the size of calibration samples.

When the order of lags *k* is increasing, the first term in equation (11) will decrease because of the improvement of goodness-of-fit, whereas the second term will increase due to a more complicated model. According to AIC, the value of *k* that can minimize equation (11) is the reasonable order of lags.

5 RESULTS

5.1 RESULTS OF POPULATION-LEVEL MODEL

We estimated population-level learning model using EViews5.0. Table 3 contains OLS estimates of population-level learning model. P values are reported in parentheses.

Table 3 Estimates of population-level learning model

session	k				
		α_0	α_1	α_2	MA(1)
1	k=1	1.069 (0.0013)	0.153 (0.0005)	-	-
		R-squared	Adjusted R-squared	Durbin-Watson stat	F-statistic
		0.596	0.567	1.817	20.644 (0.0004)
		α_0	α_1	α_2	MA(1)
2	k=2	1.187 (0.0050)	0.418 (0.0001)	0.147 (0.0850)	-
		R-squared	Adjusted R-squared	Durbin-Watson stat	F-statistic
		0.790	0.752	1.940	20.689 (0.0002)
		α_0	α_1	α_2	MA(1)
3	k=1	1.292 (0.0155)	0.088 (0.0000)	-	0.859 (0.0344)
		R-squared	Adjusted R-squared	Durbin-Watson stat	F-statistic
		0.744	0.697	1.907	15.999 (0.0006)
		α_0	α_1	α_2	MA(1)
4	k=1	1.151 (0.0004)	0.223 (0.0000)	-	0.699 (0.0365)
		R-squared	Adjusted R-squared	Durbin-Watson stat	F-statistic
		0.869	0.847	1.898	39.795 (0.0000)

Durbin-Watson (DW) statistics is a measure, which is used to test for serial correlation in the residuals of a time series regression model under the classical linear model assumptions. The value of DW will be close to 2 when the assumption of no serial correlation is valid. However, when k=1, the values of DW derived from population-level data in session 3 and session 4 are 1.219 and 1.037 respectively, significantly less than 2. It means that, the residuals in these two sessions may suffer

from positive serial correlation. Then, we found that autocorrelation cutoffs after order one and partial correlation is trailing according to the correlogram of residuals (shown in Figure 1). Thus, we introduce moving average process of order one (MA(1)). Then, the more reasonable models are obtained.

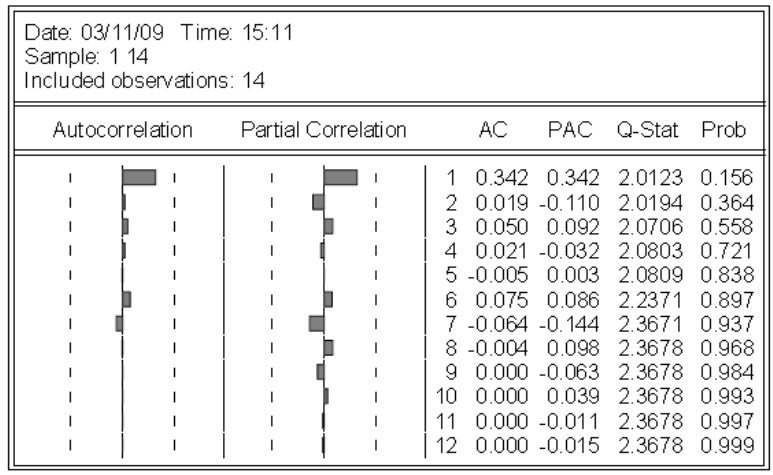
Date: 03/11/09 Time: 15:11
Sample: 1 14
Included observations: 14

Autocorrelation	Partial Correlation		AC	PAC	Q-Stat	Prob
		1	0.342	0.342	2.0123	0.156
		2	0.019	-0.110	2.0194	0.364
		3	0.050	0.092	2.0706	0.558
		4	0.021	-0.032	2.0803	0.721
		5	-0.005	0.003	2.0809	0.838
		6	0.075	0.086	2.2371	0.897
		7	-0.064	-0.144	2.3671	0.937
		8	-0.004	0.098	2.3678	0.968
		9	0.000	-0.063	2.3678	0.984
		10	0.000	0.039	2.3678	0.993
		11	0.000	-0.011	2.3678	0.997
		12	0.000	-0.015	2.3678	0.999

Figure 1 The correlogram of residuals before introducing MA(1) into session 3 (k=1)

From Table 5, we can find that the percentage changes of drivers' choosing a route remarkably depends on the relative payoff advantage of that route, even when a driver may not have a clear idea of travel time of other options.

The increase in α_1 and the goodness-of-fit for experimental data in session 2 shows that subjects pay more attention to payoff differences as they become more familiar with the traffic network. Moreover, they also have a longer memory in this session. Their choice behavior is influenced by their received payoffs of last two periods. The aforementioned changes imply that the subjects tend to switch cautiously in general (shown in Table 4). The decrease in the frequency of "trembles" (the switch from the higher payoff route to the lower one) indicates that subjects can more accurately perceive traffic conditions in this session.

The decrease in α_1 as well as the increase in the frequency of switch in session 3 shows that the subjects adjust themselves to changed traffic conditions.

The estimators in session 4 embody the influence of complete information. The increase in α_1 reflects that subjects are more sensitive to the changes of payoff differences. However, the length of memory remains unchanged. In this session, the frequency of switches decreases, at the same time, the frequency of "trembles" remains practically unchanged. It indicates that the effect of complete information differs from individual to individual. In the following discussion, we can find considerable differences through the analysis of individual-level model.

Table 4
The speed of convergence and the frequency of switches in each session

session	the number of choices lead to convergence	total frequency of switch	frequency of "trembles"(wrong switch)
1	17	113	28
2	17	95	18
3	15	113	-
4	16	97	24

5.2 RESULTS OF INDIVIDUAL-LEVEL MODEL

We specified individual-level learning model using Gauss9.0. The results are given in Table 5 and P values appear in parentheses.

Table 5 Estimates of individual -level learning model

group	session	β_0	β_1	β_2	Hit Ratio	McFadden R-squared
1	1	-0.803	0.198	-	80.00	0.196
		(0.1150)	(0.0677)			
	2	-5.041	1.201	-	96.67	0.583
		(0.0318)	(0.0461)			
	3	-3.266	0.201	-	92.31	0.478
		(0.0005)	(0.0043)			
	4	-3.045	0.122	-	93.33	0.115
		(0.0503)	(0.4738)			
2	1	0.473	0.302	-	86.67	0.433
		(0.5310)	(0.1692)			
	2	0.177	0.141	0.055	57.14	0.151
		(0.7865)	(0.3335)	(0.6474)		
	3	0.625	0.068	0.030	75.00	0.268
		(0.4693)	(0.1722)	(0.6000)		
	4	1.048	0.015	-	73.33	0.006
		(0.0815)	(0.7498)			
3	1	-4.302	0.132	-	93.33	0.270
		(0.0955)	(0.2727)			

	2	-0.799 (0.3088)	0.159 (0.3736)	-	78.57	0.069
	3	-0.746 (0.2511)	0.005 (0.8050)	-	69.23	0.004
	4	-2.681 (0.0135)	0.017 (0.8563)	-	93.33	0.005
4	1	0.641 (0.4669)	-0.004 (0.9402)	-	66.67	0.000
	2	0.402 (0.4492)	-0.003 (0.9662)	-	60.00	0.000
	3	-0.139 (0.8056)	0.003 (0.8622)	-	46.15	0.002
	4	-1.053 (0.1006)	0.078 (0.2406)	-	60.00	0.100

From Table 5, we can find considerable differences between groups on their decision rules and their attitude toward information and previous experiences.

The individuals in group 1 can be regarded as strictly empiricists. They are highly sensitive to the changes of the payoff differences in all sessions. The frequency of switch can be greatly reduced when these drivers gain experience and hold complete information of alternative routes. Thus, the learning model fits their data fairly well.

The drivers in group 2 are counted as skeptical empiricists. They show sensitivity to payoff differences as well as a longer memory. However, they attach great more importance to realized payoffs of alternative routes than perceived payoffs. They will switch between routes more frequently once they get to know this information.

The subjects in group 3 are described as perverse players. They are slower in learning than former two groups even aware of the payoff differences. They tend to make a choice according to impressions on traffic network.

The drivers in group 4 prefer to make a decision randomly. They have frequent switches in all sessions due to their indifference to payoff differences. So the goodness-of-fit of the learning model is worse. Nevertheless, a steady decrease in β_0 reflects these subjects are less willing to choose route a which capacity is lower.

Table 6 The frequency of switch across different groups

session	the frequency of switch of			
	group 1	group 2	group 3	group 4
1	40	19	21	33
2	14	8	31	42
3	26	22	28	37
4	12	35	11	39

6 CONCLUSION

In this paper, we proceeds to construct a population-level model and an individual-level model of the drivers' choice behavior based on experimental data. These models succeeded in capturing some aspects of behavior observed in a variety of experimental environments. Specifically,

1. A significant correlation exists between payoff differences and drivers' choice. Therefore, the model based on the theory of learning in games can fit well with the data from population-level and individuals of some groups.

2. The payoffs of last two periods can exert their significant influence on drivers' choice behavior.

3. Although gaining experience and holding complete information of alternative routes fail to accelerate convergence to network equilibrium, the experienced drivers can more accurately perceive traffic conditions, consequently the frequency of switch between routes is reduced.

4. There are considerable differences between different types of drivers on their decision rules and their attitudes toward information and previous experiences.

Despite these successes, we do not believe that our models have captured all important aspects of learning process of drivers. This learning process is complicated and diversified, and we still know very little about it. We hope that we'll have a chance to improve our models some day so as to make it more reasonable.

REFERENCES

Boylan, R. T. and El-Gamal (1992). "Fictitious Play: A Statistical Study of Multiple Economic Experiments." *Games and Economic Behavior*, 5, 205-222.

Brown, G. (1951). "Iterated Solution of Games by Fictitious Play." *Activity Analysis of Production and Allocation.* Wiley, New York, 377-380.

Camerer, C. and Ho, T. H. (1999). "Experience-Weighted Attraction Learning in Normal Form Games." *Econometrica*, 67, 827-874.

Cheung, Y. W. and Friedman, D. (1997) "Individual Learning in Normal Form Games: Some Laboratory Results." *Games and Economic Behavior*, 19, 46-76.

Cournot, A. (1897). *Researches into the Mathematical Principles of the Theory of Wealth*. Macmillan, New York.

Crawford, V. (1995). "Adaptive Dynamics in Coordination Games." *Econometrica*,

63, 103-144.

Cross, J. G. (1983). *A Theory of adaptive Economic Behavior*. Cambridge University Press, New York/London.

Li Zhen-long (2003). "A study of route choice behavior of drivers based on the evolutionary game under the condition of traffic flow guidance." *Journal of transportation system engineering and information technology*, 3(2), 23-27.

Liu Can-qi (2001). *Advanced traffic planning*. China Communications Press , Beijing.

Lu Hua-pu (2006). *Theory and method of transportation planning(second edition)*. Tsinghua University Press, Beijing.

Maynard Smith, J and Price, G. R. (1973). "The Logic of Animal Conflict." *Nature*, 246: 15-18.

Maynard Smith, J. (1974). "The Theory of Games and the Evolution of Animal Conflict." *Journal of Theoretical Biology*, 47: 209-21.

Roth, A. and Erev, I. (1995). "Learning in Extensive Form Games: Experimental Data and Simple Dynamic Models in the Intermediate Term." *Games and Economic Behavior*. 8, 164-212.

Shao Chun-fu (2004). *Traffic planning*. China Railway Publishing House, Beijing.

Stähl, D. O. (2001). "Population rule learning in symmetric normal-form games: theory and evidence." *Journal of Economic Behavior and Organization*, 45, 19-35.

Weibull, J. W. (2006). *Evolutionary game theory*. Shanghai People's Publishing House, Shanghai, 40-56.

Wu Bing and Li Lin-bo (2006). "Evolutionary dynamic analysis of traffic congestion." *China journal of highway and transport*, 19(3), 106-110.

Research on a generalized cost model for optimization of Ningbo-Zhoushan ports' collection and distribution system

W. Liu[1], H. Pan[2], and X. Pi[3]

[1]Ph.D. Candidate, Tongji University, Department of Urban Planning, Shanghai 200092, China; email: liuweiwei915@gmail.com
[2]Professor, Tongji University, Department of Urban Planning, Shanghai 200092, China; email: hxpank@online.sh.cn

ABSTRACT

This paper reviews the generalized cost model and analyzes the makeup of generalized cost, calculated as the monetary operating cost, travel time cost and externality cost, which together form a linked cost function. The transfer cost function was built by applying queuing theory. Finally, the model was applied to the case of Ningbo-Zhoushan port's optimization, testing the veracity and effect of the generalized cost model.

1. INTRODUCTION

Currently, many defects exist in the theory of optimization of ports' collecting and distributing systems. The primary problem is the lack of a cost model that accounts for different goods and transportation modes and the lack of a freight network optimization model that accounts for multi-modal transportation.

A cost model is key to traffic assignment. The narrowly-defined cost function considers only the journey time spent by vehicles; while the generalized cost function consists of various network-service-level related factors, such as travel expense, time value, and the degree of reliability of transport.

Most research on transport cost models has concentrated on urban transport networks, whose main research object is passenger transport. Therefore, the cost function of regional freight network has been paid less attention, and existing literature is mainly confined to highway networks, lacking cost function research on integrated transportation networks.

If the narrowly-defined cost function, with time as the only variable, is applied to urban traffic assignment, there would be no big error. However, if it is used in regional freight networks, the time alone can not accurately reflect the service level of a freight network; therefore, regional freight network assignment without consideration of generalized cost will cause a larger deviation.

2. GENERALIZED COST MODEL

Among all kinds of generalized costs, money and time spent are the two most important factors. Hence, the generalized cost model in this paper includes the monetary operating cost, travel time cost and other external costs.

2.1 Link Generalized Cost Model

2.1.1 Monetary Operating Cost

The unit operating cost is concerned with type of good, transport mode and distance. Once product type and the transport mode have been confirmed, the unit operating cost is a function of transport distance. There are usually two ways to calculate the monetary operating cost: a calculation can be based on a freight tariff or on a regression method. The latter is often used. Through a series of fittings, there is generally a linear relationship between the unit of freight T and the mileage of L. The regression equation is as follows:

$$T_{1i} = aL_i + b$$

Where T_{1i}: monetary operating cost of transport mode I (yuan/ton)
L_i: transport length (km), a,b: regression parameters

2.1.2 Travel Time Cost

Travel time cost is also a form of travel impedance that is usually applied in urban road networks. The most representative models are the BRP model, the TRRL model, and the Davidson model (Branston). The travel time cost model of a port's collecting and distributing system differs markedly from the traditional model of city roads.

Highway travel time cost model

In highway systems, BPR function (Bureau of Public Roads) is most commonly used. BPR function takes into account the impact of traffic load on travel time, but does not account for intersection delays, non-motorized vehicles and other factors. It is suitable for regional inter-city road network, such as the highway part of a port's collecting and distributing system. The highway travel time cost is given by the expression: $t = t_0\left[1 + \alpha(\frac{V}{C})^{\beta}\right]$

Where t_0 : the free flow time(hr), V: the traffic volume (pcu/hr)

C: the capacity of the highway (pcu/hr), α, β: model parameters.

Railway travel time cost model

Based on the assumption that no more than two trains can meet at the same time on a single-track railway line, the conditions of driving too close to the front train, or a conflict between opposite directions, does not exist; that is, there is no congestion effect. Double-track railway travel time cost is given by the expression:

$t = \frac{L}{Sp}$ where L: the railway length (km), Sp: railway's average speed (km/hr)

The operation of a train running on single-track railway is more complex than on double-track railway. To ensure safe train operation, some mandatory requirements such as station blocking and interlocking, must be met for single-track railway. This paper suggests a polynomial nonlinear function similar to BPR function (Guelat) to calculate the single-track railway travel time cost.

$\tilde{t} = t_0\left[a + bV + c(\frac{V}{Cap})^d\right]$ Where V : train carriages on single-track railway (carriage/ hr); *Cap*: the capacity of the railway section(carriage/ hr)
t_0: the free flow time of the railway section(hr), *a,b,c,d*: model parameters

Waterway travel time cost model

There is generally no congestion in water transport. As a result, the time spent depends on the ship's average speed. The waterway travel time cost is given by the expression: $t = \frac{L}{Sp}$

Where *L*: the navigation length (km), *Sp*: ship's average speed (km/hr)

2.1.3 Other External Costs

Presently there is no common method to calculate external costs of all transport modes. The most practical way is to combine the existing results of transport economics and use the empirical data.

Table 1. Unit External Cost of Railway and Highway.

External cost (units)	Railway	Highway
cents / tonne-kilometers	0.054	0.394
yuan / tonne-kilometers	0.004212	0.03073

2.2Transfer Generalized Cost Model

2.2.1 The Concept and Classification of Freight Transfer Hubs

Freight transfer hubs are the intersections of two more transportation routes and the integrated facilities offering transfer, store and clearance services (Shen 2005).

Table 2. The Classification of Freight Transfer Hub.

Freight transfer hub		Transfer way	Hub type	Physical infrastructure
Land-land transfer hub	Highway transfer hub	highway ↔ highway	Single-mode	Lorry changing station
	Railway transfer hub	railway ↔ railway	Double-mode	Railway marshal yards
	Highway-railway transfer hub	highway → railway railway → highway	Double-mode	Inland integrated transport hub
Land-water	Water transfer hub	waterway ↔ waterway	Single-mode	Inland and

Freight transfer hub		Transfer way	Hub type	Physical infrastructure
transfer hub		highway → waterway		coastal harbor
	Water-land transfer hub	railway → waterway waterway → highway waterway → railway	Double-mode	
Other transfer hub: Airport, special commodity transfer and so on				

This paper focuses on double-mode hubs, at which goods transfer between different transport modes (hubs with → in the above table).

2.2.2 Generalized Cost Model of Highway-railway Transfer Hub

According to system theory and queuing theory, as well as transport process in transfer hubs, a highway-railway transfer hub can be regarded as a complex queuing service system. Such a queuing service system is composed of three interrelated subsystems (an arrival, a detention and a departure subsystem).

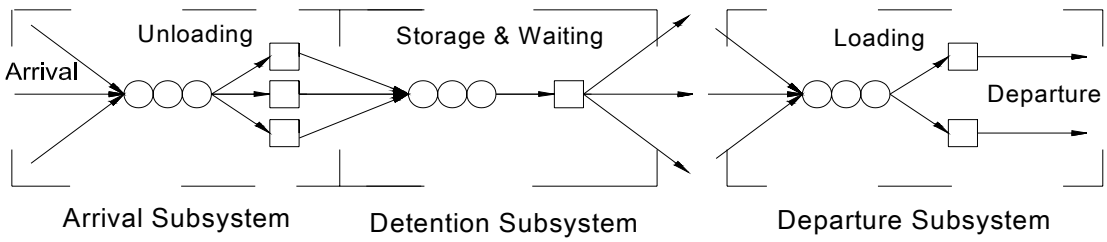

Figure 1. Highway-railway Transfer Hub Queuing System.

Monetary operating cost in a transfer hub includes handling and storage costs, while the travel time cost in a transfer hub is mainly the waiting time including unloading time, detention time and loading time.

For long-term freight network planning, residence time is much more than loading and unloading time. Thus at the strategic level, residence time can be only considered that the entire system as an approximate [M/M/1] queuing system. The generalized cost equation of a highway-railway transfer hub is as follows:

$$S_t = \theta_1 T_m + \theta_2 T_t = \theta_1 \times \rho + \theta_2 \cdot (VOT + \lambda) \cdot \left(\frac{Ser_t}{1 - V_t / CAP_t} \right), \quad Ser_t = \frac{lp}{CAP_t}$$

Where T_m: average monetary operating cost at transfer hub t

T_t: average residence time cost at transfer hub t

ρ : unload and load fee at transfer hub t (yuan/ton, yuan/TEU)

λ: storage fee at transfer hub t (yuan/ton·day, yuan/TEU·day)

V_t : throughput at transfer hub t, Ser_t : average service time at transfer hub t
CAP_t : the capacity of transfer hub t, l_p : the time length of the planning period

2.2.3 Generalized Cost Model of Land-water Transfer Hub

The process of a land-water transfer hub can be interpreted by Figure 2.

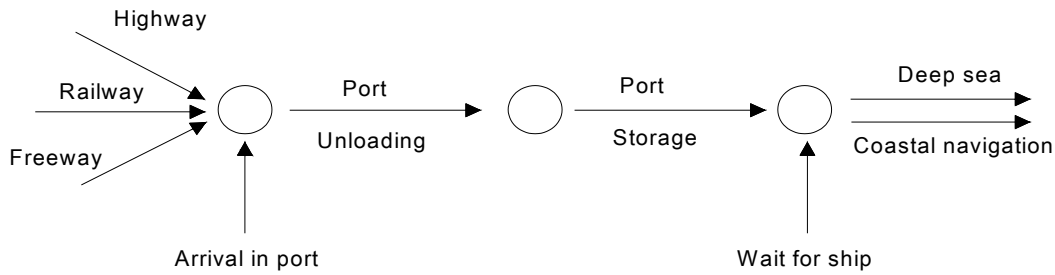

Figure 2. The Diagram of Land-water Transfer Hub.

The generalized cost of a land-water transfer hub consists of a port service fee and the delay time cost. The port service fee also contains the cost of customhouse and cargo survey besides cartage and storage charge, which have specific charge criteria at a port.

At the condition of **highway → waterway** and **railway → waterway**, the waiting time is more dominant than loading and unloading time and service time. Waiting time is determined by the frequency of carriers, and equal to half of headway. The average waiting time is given by the expression:

$$T_t = \frac{1}{2} \times \frac{L_p}{N} \times \max\left\{1, \left(\frac{V_{boat}}{N}\right)\right\}$$

where V_{boat} : port cargo carriers required, N: the ship sail frequency; l_p : the time length of the planning period

At the condition of **waterway → highway**, if sufficient cargo gathering, then time waiting for truck do not need. The total time cost at port are loading and unloading time and service time, that is $T_t = t_z + t_s$ where T_t : average residence time cost; t_z: loading and unloading time, t_s:other service time.

At the condition of **waterway → railway**, average residence time can be calculated according to ***five scheduled train*** plans (location-fixed, line-fixed, train-fixed, time-fixed, price-fixed).

$$T_t = \frac{1}{2} \times \frac{L_p}{N} \times \max\left\{1, \left(\frac{V_{train}}{N}\right)\right\}$$

where V_{train} : train carriages needed for port cargo; N : the ***five scheduled train*** frequency; l_p : the time length of the planning period.

3. OPTIMIZATION MODEL OF PORTS COLLECTING AND DISTRIBUTING SYSTEM

3.1 Multimode Multiproduct Network Optimization Model

A port's collecting and distributing system contains not only a transfer hub, but also a variety of transport modes. Generally speaking, optimization of a port's collecting and distributing system is a kind of multimodal multiproduct network optimization problem (INRO Consultants). The objective function is to minimize the cost of freight transportation on the port's collection and distribution network. The generalized cost contains both link cost and transfer cost, which have been modeled in chapter 2. The following objective function F(v) can therefore be formulated:

$$F = \sum_{p \in P} \left(\sum_{a \in A} s_a^p(v) v_a^p + \sum_{t \in T} s_t^p(v) v_t^p \right)$$

$$\text{S. T. :} \quad \sum_{k \in K_{od}^{m(p)}} h_k = g_{od}^{m(p)} \quad h_k \geq 0,\ k \in K_{od}^{m(p)} \quad o \in O,\ d \in D,\ p \in P$$

Where N: a set of modes, A: a set of links, T: a set of transfers, M:a set of transport mode; $K_{od}^{m(p)}$: a set of path conveying product p from O to D

v_a^p: the flow of product p on link a, v_t^p: the flow of product p on transfer t

s_a^p: generalized cost of product p on link a, s_t^p: generalized cost of product p on transfer t, g_{od}^p:the demand of product p from O to D, h_k: flow of link k, $k \in K_{od}^{m(p)}$

3.2 Application and Test

We applied the model to the Ningbo-Zhoushan port transportation optimization to check the veracity and effect of optimization in the near future. If the test is in line with the accuracy requirements, then it can be applied to future multimode multiproduct network analyses.

Table 3. Transport Flow Distribution on Collecting and Distributing System.

Transport mode & link			Traffic flow		error (%)
			Calculated	Observed	
Highway	Trunk network	Hangzhou-Ningbo	33846	36590	7.5%
		Ningbo-Wenzhou	20997	19734	6.4%
	Channel for port	Luoxia Road	21450	24000	10.6%
		Jiangnan Highway	14300	18215	21.5%
		Tongtu Highway	31250	27000	15.7%
		National Highway 329	19250	17610	9.3%
Railway	Trunk line	Xiaoshan-Ningbo	40301	36712	9.8%
	Branch line	Zhenhai branch railway	8055	8493	5.5%
		Beilun branch railway	12343	12877	4.1%

Through the traffic flow comparison between calculated volume and observed volume on some important network sections, the average error rate of the results is around 10%, which within the threshold for precision.

4. CONCLUSION

Based on previous research, this paper attached importance to the generalized cost model—the core content in multimode multiproduct network optimization. By analyzing the constitution and indicators of generalized cost, a new generalized cost function model was established. The application in a practical project verified the model's feasibility and precision.

REFERENCES

Branston, D. (1976). "Link capacity functions: A review." *Trans. Res. J.*, 10, 223-236.

Bureau of Public Roads. (1964). *Traffic assignment manual*, U.S. Dept. of Commerce, Urban Planning Division, Washington D.C.

Guelat, J., and Florian, M. (1990). "A multimode multiproduct network assignment model for strategic planning of freight flows." *Transp. Sci.*, 24(1), 25-39.

INRO Consultants. (2000). *Stan User's Manual* , Montréal.

Shen, Z., and Den, X. (2005). *Transportation Engineering* (Second Edition). China Communications Press, Beijing.

Assessing Performance of Public Transit Network Using Network-Based Accessibility Measures

LU Fangqiang[1] and CHEN Xuewu[2]

[1]School of Transportation, Southeast University, Si Pai Lou 2#, Nanjing, China, 210096; PH (86) 13951823554, email: lufangqiang@seu.edu.cn
[2]School of Transportation, Southeast University, Si Pai Lou 2#, Nanjing, China, 210096; PH (86) 025-83795643; email: chenxuewu@seu.edu.cn

ABSTRACT

Accessibility is a fundamental concept in transportation analysis and planning. Typically, accessibility refers to the 'ease' of reaching opportunities for activities and services can be used to evaluate the performance of a transportation system. In this paper, Utility-Based (UB) accessibility measures derived from the combined travel demand model are used to assess the performance of public transport network. Network-based accessibility measures using a combined travel demand model that is consistent with random utility theory are established. By using travel time and ticket fees via bus as the measures, accessibility between any two bus stops is described from the user's perspective. An example is provided in this paper to examine the effect of this method. The results indicate that the accessibility measures proposed in this paper are capable of measuring the degree of bus stop accessibility to assess the public service.

INTRODUCTION

To be accessible or not to be accessible seems to be the questions these days. Public transport network plays a crucial role in providing persons with sufficient access to their destinations via bus. Yet, traditional public transport planning often neglects this important role the public transport networks play and limits its focus on the efficiency of the public transport system itself. In future, accessibility should be given more weight in land use and transport decisions. Accessibility planning is a key area of transport policy. However, accessibility is often misunderstood, poorly defined and poorly measured construct. Finding an operational and theoretically sound concept of accessibility is quite difficult and complex (Karst, 2004; Thomas, 2008). Indeed improved access to bus services is a major aspect of integrated transport strategy. The importance of access to public transport in order to access local services has been identified by several studies (Zhao, 2005; Cheng, 2007).

This paper makes a review of UB accessibility measures; this is followed by the introduction of accessibility based measure that used to analysis public transport network. Then, an example is provided to examine the effect of this method.

Conclusions and future research are given in the final section

UB ACCESSIBILITY MEASURES REVIEWED

Accessibility is frequently measured as a function of the available opportunities moderated by some measure of impedance. Despite the popularity of the concept, accessibility has historically been measured in different ways depending on the context of the applications. UB accessibility measures interpret accessibility as the outcome of a set of transport choices. Utility theory addresses the decision to purchase one discrete item from a set of potential choices, all of which satisfy essentially the same need, and can be used to model travel behaviors and the (net) benefits of different users of a transport system.

An initial approach is based on random utility theory using the denominator of the multinomial logit model, also known as the logsum, as an accessibility measure, assuming that an individual p assigns a utility to each possible destination j in a specific choice set and chooses the alternative that maximizes his/her utility. The logsum serves as a summary measure, indicating the desirability of the full choice set (Ben-Akiva and Lerman, 1979):

$$A_i = \frac{1}{\lambda} \ln \sum_{j \in J_p} e^{\lambda u_{pj}} \tag{1}$$

where λ is a travel cost sensitivity parameter and u_{pj} is measured utility.

Utility is derived at the individual or homogeneous population group level, and travel costs (i.e. travel time and ticket fee) can be regarded as the index.

MEASUREMENT OF NETWOEK-BASED ACCESSIBILITY

Description of the public transport network. In general terms, the role of public transport planning is to ensure the satisfaction of a certain demand for person movements with different trip purpose, at different times of the day, given a public transport system with a certain operation capacity. The public transport network itself can be seen as made up of nodes (stop locations) and lines (bus lines).

Consider a set of stop locations N ($n \in N$), a set of bus lines L ($l \in L$), and a set of bus routes S ($s(l) \in S$). Following Ren (2007), bus route is defined as a section between every two bus stops of one bus line in this paper. In very general terms the public transport network can be represented by: $G = (N, S, L)$.

In this section, we illustrate a simple public transport network (two bus lines: L1 has 5 stop locations from 1 to 5; L2 has 3 stop locations from 1 to 3) to make the concept of bus route understandable as depicted in Figure 1.

As can be seen from Figure 1, every two stops can only have 1 bus route from one line, while it is feasible to have more than 2 bus routes from different bus lines. We can get 10 bus routes from Line 1 and 3 bus routes from Line 2. Based on the definition of bus route, if there are n stops in a line, the number of the bus route can be calculated by: $n(n-1)/2$.

When passengers aboard the bus they can only get off at their destination, viz. they should not get off half-way. Therefore, after determining the number of transfer times, the set of passenger routes (bus route or the combination of bus routes) K between any two bus stops can be got, such as the set of passenger routes between stop1 and 4 include $S_3(L_1)$ and $S_{13}(L_2)-S_8(L_1)$.

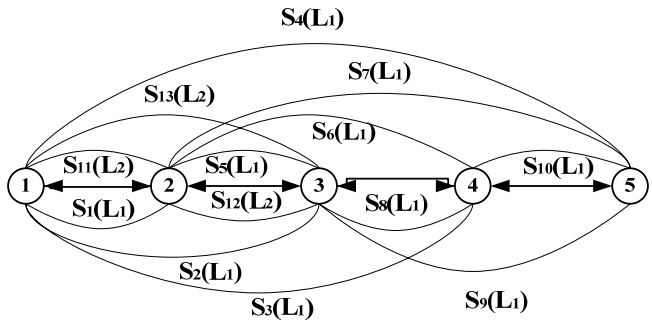

Figure 1. A simple public transport network with two bus lines.

Model formulation. This section introduces the model of UB accessibility. In terms of conceptualization, the model considers accessibility a property of stop locations, based on detailed measurements of UB accessibility derived from random utility theory. In this paper, we assume that different individuals value the attractiveness of the bus stop locations differently and no more than 1 time of transfer via bus.

Given the number of potential travelers taking passenger route from origin i to destination j per unit time d_{pij}. The probability expression can be derived as follows:

$$\frac{d_{pij}}{d_{ij}} = P_{p|ij} = \frac{e^{\beta_k U_p}}{\sum_{k \in K} e^{\beta_k U_k}} \qquad \forall i, j, p \tag{2}$$

Where d_{ij} is the amount of passengers from stop location i to j; β_k is the parameter in the combined travel demand model; U_k is the expected received utility of passenger route choices.

In this paper, the utility measure is adopted to quantify the accessibility between any two bus stop locations that is consistent with random utility theory used in the combined travel demand model described above. Ben-Akiva and Lerman (1979) defined the accessibility measure derived from random utility theory as follows:

$$A = E\left(\underset{k \in K}{Max}\, U_k\right) \tag{3}$$

For an individual, accessibility was defined as the expected value of maximum random utility of alternative k in choice set K. Moreover, two

important properties for accessibility were proved: a. monotonicity with respect to choice set size; b. monotonicity with respect to the systematic utilities. The first property implies that any addition to a person's choice set leaves the individual no worse off than before the addition. The second property implies that the measure of accessibility does not decrease if the systematic utility of any of the alternatives in the choice set increases.

With the two important properties, accessibility measures can be determined to assess the performance of public transport network. For example, under a certain abnormal event, the capacities of bus routes in the network may be significantly degraded, making them not attractive to some bus users. This will reduce the size of the choice set (i.e., smaller number of alternative passenger routes). Under the first property, the accessibility measure for route choice should not increase due to the unattractiveness (or unavailability) of some degraded routes. Furthermore, due to congestion caused by the reduced number of available passenger routes, according to the second property, the accessibility measure should not increase.

In addition, if the random variable is assumed to follow a Gumbel distribution, the accessibility measure will have a closed-form expression. Let $V_k = U_k + \varepsilon_k$ and $U_k = E(V)$, where ε_k is a Gumbel random variate. The measure defined in Eq.(3)becomes:

$$A = E\left(\underset{k\in K}{Max} U_k\right) = \frac{1}{\beta}\ln\sum_{k\in K} e^{\beta U_k} \tag{4}$$

Thus, by using the expected received utilities given in Eq.(2), the accessibility measure of any two bus stops is defined as follows:

$$A_{ij} = \frac{1}{\beta_k}\ln\sum_{k\in K} e^{\beta_k U_k} \tag{5}$$

Assessment procedure. In this section, a assessment procedure is provided to compute the accessibility measures and to perform the bus stop accessibility analysis. The steps are briefly summarized as follows:

Step1: Numbered bus stops, bus lines, bus routes.

Step2: Confirming the set of K of any two bus stops.

Step3: Using Eq.(2) to obtain the utility of passenger route choices.

Step4: Using Eq.(5) to get the accessibility measures of any two bus stops.

Step5: Report the results of the assessment analysis.

AN EXAMPLE

Taking the public transport network shown in Figure 2 as an example, this paper examined the effect of this method on assessing the performance of public transport network.

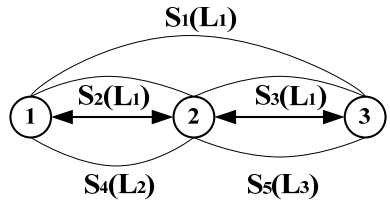

Figure 2. A simple public transport network with three bus lines.

The amount of passengers from stop location i to j (d_{ij}) were listed in Table 1.

Table 1. Bus OD matrix of public transport network.

OD	1	2	3
1	0	45	15
2	45	0	25
3	15	25	0

The travel time t_s of five bus routes were listed in Table 2. The waiting time t_w was assumed to be 2.5 minutes in this paper. The travel time t_k of a bus route k can be calculated by $t_k = t_w + \sum_m t_s$. The fixed travel cost c_k on a bus route k can be calculated by $c_k = m \times 1$ ￥, where m is the number of bus routes (1 or 2).

Table 2. The travel time of bus routes.

S	S_1	S_2	S_3	S_4	S_5
t_s (min)	5	3	2	2.5	2

Accessibility measures of any two bus stops can be computed using Eq.(2) and Eq.(5). Table 3 shows the results of accessibility measures.

Table 3. Accessibility measures for any two bus stops.

A_{ij}	1	2	3
1	0	0.56	0.78
2	0.56	0	0.64
3	0.78	0.64	0

As can be seen from Table 3, the value of accessibility has a positive relationship with the number of passenger routes and the amount of travel time. The higher value of accessibility, the more attractive of the bus service to the passengers. It is indicated that the accessibility proposed this paper can be used to assess degree of bus accessibility and evaluate the performance of the public transport service.

CONCLUSIONs AND FUTURE STUDY

This paper has presented a network-based accessibility measures for

assessing the degree of bus accessibility to evaluate the public service. The method employed a combined travel demand model formulated. Taking a simple public transport network as an example, this paper examined the effect of this method. It is indicated that accessibility has a positive relationship with the number of passenger routes and the amount of travel time. Improving the accessibility of public transport will be an effective policy to improve the public transport service and increase the passenger volume. In this paper, we just present the method of assessing the degree of bus stop accessibility to evaluate the public service. A case study may be needed to verify the effectiveness of the method.

ACKNOWLEDGEMENTS

This research has been supported by the project of "The Decision Theory And Technology Study On Urban Bus Rapid Transit System Planning" (NO. 20070286011) and "2008 Suzhou Technical exclusive program-Railway transportation program." (No. ZXJ0804).

REFERENCES

Ben-Akiva,M., and Lerman,S.R.(1979). "Disaggregate travel and mobility choice models and measures of accessibility". In D.A.Hensher&P.R.Stopher(Eds.), Behavioural travel modeling, London:Croom-Helm, 654–679.

Cheng, C.X., Zhang, W.C., and Chen J. (2007). "Evaluating the Accessibility about Beijing's Subways in 2008 Based on Spatial Syntax" GEO-INFORMATION SCIENCE, 9(6), 31-35.

Karst, T.G., and Bert, v. W. (2004). "Accessibility evaluation of land-use and transport strategies:review and research directions." *Journal of Transport Geography*, 12, 127-140.

Ren, H.L., and Gao, Z.Y. (2007). "Research on Bi-level Model and Solution Algorithm for Dynamic Transit Design Problem." Systems Engineer-Theory & Practice, 5, 82-89

Thomas, S. (2008). "How to plan for regional accessibility?" *Transport Policy*, 15,127-137.

Zhao, S.Z., and Kuang, X.(2005). "An Evaluating Index of Accessibility for Urban Public Transit network Based on TransCAD" *Journal of Transportation Systems Engineering and Information Technology*, 5(2), 55-58.

Modeling Study of Coal Allocation and Distribution Plan Based on Graph Theory and Fuzzy Optimization Method

Xian Liang[1], Wang Hui[2] and Zhang Jin[3]

[1]School of Electrical Engineering, Southwest Jiaotong University, Mailbox 691, Chengdu, 610031, China; PH (+86)13880644313; email: xianliang85@163.com
[2]College of Logistics, Southwest Jiaotong University, Chengdu, 610031, China; PH (+86)13550136054; email: angelwyh1220@163.com
[3]College of Logistics, Southwest Jiaotong University, Chengdu, 610031, China; email: zhjswjtu@263.net

ABSTRACT

For a long time, mismatched distribution has spatially existed between the production and consumption of coal resources in China. The current situation of allocating and transporting coal from the northwest of China to the rest of the country to meet demand will continue for a long period of time. In this paper, the example of the allocation and distribution (A&D) of coal in Shanxi Province is presented, and a model is set up for research. Since coal transport is particular and the parameters in the transport process are hard to quantify, a model based on fuzzy theory was used to get the primary A&D plan. Then, the relevant coal A&D network was built by using graph theory, and a detailed coal transport network was set up through non-linear programming modeling. Finally, a numerical example is provided to validate the effectiveness and advantage of the proposed model using MATLAB.

Keywords: Allocation; graph theory; fuzzy model; non-linear programming

INTRODUCTION

For a long time, coal, as China's basic energy source, has accounted for more than 70% of the production and consumption of disposable energy. It is predicted that China will require 2 to 2.6 gigatons of coal until 2010. Even up to 2020, coal consumption will account for about 60% in the energy consumption structure. However, mismatched distribution has always spatially existed between the production and consumption of coal resources in China. The current situation of allocating and transporting coal from northwest China to the rest of the country to meet demand will continue for a long period of time. Coal from Shanxi Province has a very important position in China. According to authority statistics, over the past 30 years, Shanxi has cumulatively produced over 9 gigatons of coal, which accounts for 30% of the total output of coal in China, and has cumulatively allocated and distributed 7 gigatons of coal, which accounts for 80% of amount of

coal traded in the national inter-provincial network. The export of Shanxi coal accounts for 70% nationwide as well. To solve the issue of national energy consumption, the allocation and distribution of coal from Shanxi to the rest of China appears essentially significant. Although rapid and drastic changes are taking place in vehicles for railway and road, coal allocation and distribution are still very severe and difficult problems. Meanwhile, economic development calls for more resources and short-term solutions. Therefore, it appears extremely important to transport coal faster and more safely at less cost. As indicated in some studies of the distribution status quo of coal in China (Gao 2008), coal transport is the key to the whole national economic development.

FUZZY MODEL OF COAL ALLOCATION AND DISTRIBUTION

Suggestions on Modeling

The establishment of a coal transportation network requires the collaboration of the entire coal supply chain. Coal mining enterprises should build cooperative relationships among various transport companies, especially railway transport departments. Coal mining enterprises should consider railway transport capacity when drawing up supply and marketing plans, and then determine coal supply and production plans. Meanwhile, transport departments should consider the supply plans of the coal mining plants as well to ascertain transport A&D plans. Information sharing set up by this means can guide the modeling of a coal A&D plan. With the rapid development of the global market and economy, flexibility has to be considered as important to competitiveness in an increasingly intense competitive environment (Pujawan 2004). Effective control of supply chain flexibility can enhance the business performance of a company (Kumar et al. 2006).

Fuzzy Model

As for the influencing factors in the transport process, it is difficult to quantify these factors and obtain precise data. For instance, the parameters of road capacity should be expressed by using fuzzy numbers to truly reflect the actual road transport capacity. As a result, fuzzy analysis on road networks and fuzzy classification of roads are of very important and practical significance for transport optimization decision-making in both peacetime and during disasters, especially for coal bulk cargo, which has more uncertainty. The concept of a fuzzy set was introduced (Zadeh 1965) as a mathematical method of representing vagueness and imprecision in actual problems. An interactive fuzzy goal programming technique was presented (Abd et al. 2006) for multi-objective transportation problems (MOTP). Li and Lai (2000) improved a fuzzy approach to MOTP. Pramanik and Roy (2006) solved the fuzzy goal programming approach with crisp and fuzzy coefficients for MOTP .

Assume $\widetilde{G}(V,E)$ denotes the entire fuzzy transport network; $f(v)$ denotes

the matrix of traffic flow through the transport network; $\widetilde{\mu}_D(f(v))$ denotes membership function of $f(v)$; R denotes a collection of all accesses from one coal supply point to one demand point in Shanxi; $\widetilde{F}$ and $\widetilde{C}_{ij}$ respectively denote target value and degree of membership of road capacity; V denotes the definite value of maximal flow; $\mu_F(v)$ denotes the degree of membership of demand quantity. According to fuzzy decision principle, the fuzzy transport model was proposed as following:

$$\max \mu_D(f(v)),\ \widetilde{\mathrm{D}} = \bigcap_{\forall r_{ij} \in R} \widetilde{C}_{ij} \cap \widetilde{F}$$

i.e., $$\widetilde{\mu}_D(f(v)) = \wedge \widetilde{\mu}_{r_{ij}}(C_{ij}) \wedge \mu_F(v) \quad \forall r_{ij} = R$$

Assume G(V,E) denotes the basic network abstracted from the coal transport network. The solving model of fuzzy transport optimal flow was obtained as the following:

$$\begin{cases} \max f(v) \\ \max \widetilde{\mu}_D f(v) \end{cases},\ \sum f_{ij} - \sum f_{ji} = \begin{cases} 0 & i \neq s,t \\ v & i = s \\ v & i = t \end{cases} \qquad i \to j, i \leftarrow j$$

$$0 \le f_{ij} \le \widetilde{c}_{ij},\ D = \bigcap \widetilde{C}_{ij} \cap F,\ \forall r_{ij} \in R$$

where R denotes one route from s to t, and F denotes fuzzy constraint of the maximal flow.

The optimal flow of the fuzzy problem can be solved according to the proposed model. The model can sufficiently reflect uncertainty in practice because it more realistically abstracts the coal transport system.

NON-LINEAR MODEL OF COAL ALLOCATION AND DISTRIBUTION

Streamlined-Formed Network Based on Graph Theory

Assume there is a directed network *G(V,E)*, as shown in Figure 1.

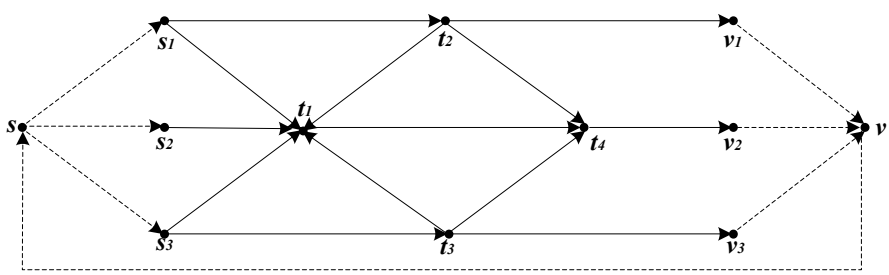

Figure 1. Coal A&D network.

To clearly denote the function of every node in the figure, s_i is used to denote each coal-producing area in Shanxi; t_i denotes each coal transfer stop or transport hub; and v_i denotes each coal demanding area. The directed arcs indicate the transport capacity of railway, highway, or waterway. In terms of coal nature and the practical situation, coal is transported to the provinces and cities mostly by railway in China. In the network, two virtual nodes (i.e., source and convergence) are set, and s denotes the coal source point; v denotes the coal convergence point. The directed arc ss_i is assumed to denote the process of transferring coal from underground to ground; arc v_iv denotes the coal consumption process; arc vs is a nominal one that makes the whole transport network connected. The cost is different according to different ways of transport; thus, assume that the transport costs of railway, highway, and waterway are definite in different areas.

The network constraint conditions are as follows:

1) Coal supply constraint: $s(s,s_i)$ denotes coal output in the producing area in the research year, and then freight quantity $f(s,s_i)$ meets $f(s,s_i)\geq 0$, $f(s,s_i)\leq s(s,s_i)$.

2) Coal demand constraint: $v(v_i,v)$ denotes the coal demand quantity in the demand area, which meets $0 \leq v(v_i,v) \leq f(v_i,v) \leq s(v_i,v)$.

3) Through-capacity constraint of coal transfer stop: Assume coal transport capacity of the existing line remains unchanged, and $t(ij)$ denotes through-capacity of existing coal on the transfer line, so the constraint of transport capacity $f(ij)$ at transfer stop is: $0 \leq f(ij) \leq t(ij)$.

Parameters Setting

T the T year of planning period, $T \in [1,15]$, let T=0 denote the year of 2000

S the supplying area, $S \in [1, \mathrm{M}]$, M is a definite integer

D the demand area, $D \in [1, \mathrm{N}]$, N is a definite integer

A the number of general road sections

B the number of coal road sections, $B \in [1, \mathrm{K}]$, K is the sum of the coal road sections

β transport effectiveness

L(B) the length of Section B

P(T,B) the coal transport cost (yuan/ton-km) of Section B in the T year; for instance, P(0,1)=0.15 denotes the coal transport cost of Section 1 in the year of 2000 is 0.15 yuan per ton-km

C(T,A) the coal through capacity (million ton) of Section A in the T year; for instance, C(0,1)=10 denotes the coal through capacity of Section 1 in the year of 2000 is 10 million ton

BS(B,S) the matrix of coal road Section B with the beginning of supply area S, BS(B,S)=1 when B is related to S; else BS(B,S)=0

BD(B,D) the matrix of coal road Section B with the end of demand area D, BD(B,D)=1 when B is related to D; else BD(B,D)=0

BA(B,A) the matrix of coal road Section B related to general road section A, BA(B,A)=1 when B passes through A; else BA(B,A)=0
$MX_1(T,S)$ the output of soft coal in supply area S in the T year
$MX_2(T,S)$ the output of blind coal in supply area S in the T year
$MY_1(T,S)$ the consumption of soft coal in supply area S in the T year
$MY_2(T,S)$ the consumption of blind coal in supply area S in the T year
$NY_1(T,D)$ the demand of soft coal in demand area D in the T year
$NY_2(T,D)$ the demand of blind coal in demand area D in the T year
$LQ_1(T,B)$ the freight quantity of soft coal in coal Section B in the T year
$LQ_2(T,B)$ the freight quantity of blind coal in coal Section B in the T year
$DF_1(T,D)$ the gap of soft coal in demand area D in the T year
$DF_2(T,D)$ the gap of blind coal in demand area D in the T year
$PVD_1(T,D)$ the penalty coefficient of soft coal in demand area D in the T year
$PVD_2(T,D)$ the penalty coefficient of blind coal in demand area D in the T year

Function Determination

The objective function of minimizing the total cost was given as follows:

$$\min\ f(T) = \sum_{B=1}^{K} \mathrm{L}(B)\mathrm{P}(T,B)\left[\mathrm{LQ}_1(T,B) + \mathrm{LQ}_2(T,B)\right]$$
$$+ \sum_{D=1}^{K}\sum_{B=1}^{K}\left[\mathrm{PVD}_1(T,D)\mathrm{DF}_1(T,D) + \mathrm{PVD}_1(T,D)\mathrm{DF}_2(T,D)\right]$$

where the supply constraints are $\sum_{B=1}^{K} \mathrm{BS}(B,S)\mathrm{LQ}_1(T,B) \le \mathrm{MX}_1(T,S) - \mathrm{MY}_1(T,S)$

and $\sum_{B=1}^{K} \mathrm{BS}(B,S)\mathrm{LQ}_2(T,B) \le \mathrm{MX}_2(T,S) - \mathrm{MY}_2(T,S)$; the transport constraint is

$\sum_{B=1}^{K} \mathrm{BA}(B,A)\left[\mathrm{LQ}_1(T,B) + \mathrm{LQ}_2(T,B)\right] \le \mathrm{C}(T,A)$; the demand constraints are

$\sum_{S=1}^{M}\sum_{B=1}^{K} \mathrm{BS}(B,S)\mathrm{BD}(B,D)\cdot\beta\mathrm{LQ}_1(T,B) + \mathrm{DF}_1(T,D) \le \mathrm{NY}_1(T,D)$ and

$\sum_{S=1}^{M}\sum_{B=1}^{K} \mathrm{BS}(B,S)\mathrm{BD}(B,D)\cdot\beta\mathrm{LQ}_2(T,B) + \mathrm{DF}_2(T,D) \le \mathrm{NY}_2(T,D)$; another constraint is $\mathrm{LQ}_1(T,B), \mathrm{LQ}_2(T,B), \mathrm{DF}_1(T,D), \mathrm{DF}_2(T,D) \ge 0$.

Numerical Example

Taking T=1, for instance, select 3 coal supply areas, 6 demand areas, 6 coal road sections, and 4 general road sections. Statistical value was given in the following matrices and Table 1.

$$BS(B,S)=\begin{bmatrix}1&0&1&0&1&0\\0&1&1&0&0&0\\1&0&0&1&0&1\end{bmatrix},\ BA(B,A)=\begin{bmatrix}1&0&1&1&1&0\\1&1&0&1&0&1\\0&1&1&0&1&1\\0&0&1&0&1&0\end{bmatrix},\ BD(B,A)=\begin{bmatrix}1&1&0&1&0&1\\0&1&1&0&1&0\\1&0&0&1&0&1\\1&0&1&0&1&0\\0&1&1&0&1&0\\1&0&0&1&0&1\end{bmatrix}$$

Table 1. Value of Each Parameter (mt: millon ton).

mt \ S	1	2	3
$MX_1(1,S)$	20	10	5
$MX_2(1,S)$	15	10	5
$MY_1(1,S)$	4	1	0.8
$MY_2(1,S)$	2	1	0.4

mt \ D	1	2	3	4	5	6
$NY_1(1,D)$	3	4	5	4	2	1
$NY_2(1,D)$	2	3	1	2	4	3

mt \ A	1	2	3	4
$C(1,A)$	10	8	12	9

D	1	2	3	4	5	6
$PVD_1(1,D)$	-0.01	-0.012	-0.01	-0.008	-0.005	-0.006
$PVD_2(1,D)$	-0.01	-0.011	-0.009	-0.007	-0.008	-0.005

The optimal result calculated by MATLAB is shown in Table 2.

Table 2. Optimal Result Calculated by MATLAB (mt: millon ton).

mt \ B	1	2	3	4	5	6
$LQ_1(1,B)$	3.15	3.48	2.52	4.33	2.67	2.85
$LQ_2(1,B)$	1.78	2.41	1.78	2.73	4.32	2.22

CONCLUSION

This paper proposes the fuzzy model, which primarily solves the problem of optimizing decision-making of the fuzzy transport network. The model reflects uncertainty of the transport process when it was actually operated. A further A&D network model was set up using correlative graph and non-linear theory. Since the model results in several matrix relationships and relevant data related to coal transport, a transport plan can be optimized by using relevant mathematical software to calculate the transport amount of each coal road section only if above-mentioned data are available. Finally, the feasibility and effectiveness of the proposed simple-operated model were validated. The paper concentrates on initial modeling, referring less to algorithms used in later calculations. The model will integrate with detailed algorithms to develop a more complete and practical coal A&D plan in further study in the future.

ACKNOWLEDGMENTS

We would like to take this opportunity to express our sincere gratitude to our supervisor, Zhang Jin, Dean of College of Logistics at SWJTU for his kind assistance and valuable suggestions in the process of our writing.

REFERENCES

Abd, E. W. F., and Lee, S. M. (2006). "Interactive fuzzy goal programming for multi-objective transportation problems." *Omega*, 34(2),158–166.

Gao, Y. (2008). "A study on trunk coastal routes of coal transportation in China," 14-16.

Kumar, V., Fantazy, K. A., and Kumar, U. (2006). "Implementation and management framework for supply chain flexibility." *Journal of Enterprise Information Management*, 19(3), 303-319.

Li, L., and Lai, K. K. (2000). "A fuzzy approach to multiobjective transportation problem." *Computers and Operations Research*, 27(1), 43–57.

Pramanik, S., and Roy, T. K. (2006). "A fuzzy goal programming technique for solving multi-objective transportation problem." *Tamsui Oxford Journal of Management Sciences*, 22(1), 67–89.

Pujawan, I. N. (2004). "Assessing supply chain flexibility: a conceptual framework and case study." *International Journal of Integrated Supply Management*, 1(1), 79-97.

Zadeh, L. A. (1965). "Fuzzy sets." *Information and Control*, 8(3), 338–353.

A Comprehensive Bus Line Evaluation Method Based on Fuzzy C -means Cluster ing Algorithm

Chen Suping, Chen Xuewu, Yang Min

School of Transportation, Southeast University; Room 1513, QunYingLou, No.35, JinXiangHe Road, Nanjing 210018, China; email: csp1983@163.com

ABSTRACT

Analyzing and appraising the operational situation of bus lines is an important basis on which bus companies can adjust bus lines and establish operation schedules. However, at present, the assessment of bus lines lacks accurate and scientific methods. This article proposed to use a Fuzzy C-means clustering algorithm to comprehensively analyze the structural difference and operational effects of bus lines. By comparing the evaluation indexes of each line, those with similar structure and operational effects were classified into one category, each with its own unique structural and operational characteristics. Based on this, the algorithm was applied to the operational situation of the public transit system in Changzhou city. As a result of the evaluation process, suggestions to optimize the transit system are proposed.

Key words : Fuzzy C-means Clustering; cluster factor; comprehensive evaluation

INTRODUCTION

The evaluation of the operational effects of bus lines is important to bus companies. Through compiling, analyzing, and researching daily operations data, representative content can be obtained, providing a basic understanding of the bus lines' management state and operational quality, which can provide a reliable basis for determining policy orientation. However, the kinds of data to be analyzed and the evaluation of bus lines still lack scientific and accurate methods.

Clustering analysis means classifying things according to the similarity degree of their properties. Individuals in same class have high homogeneity and individuals in different classes have high heterogeneity (Bezdek 1976). In recent years, clustering analysis method obtained a widespread application in public transportation domain, Liu Xiao; Li Mohan (Xiao, 2004) evaluated the public transit network's service level of the residents' zones in Dandong city using Fuzzy clustering analysis method. Li Yuhua(Yuhua 2004) applied grey clustering analysis to evaluate the service level of the public transit system in Qingdao city. In its master degree thesis, Li Hong Tao (Hongtao 2005) proposed a GIS based Clustering Analysis of Urban public traffic network service level. The above clustering methods mainly focus on the entire transit network, stressing in evaluation to the entire transition system, but lacking evaluation of concrete bus lines.

This paper presents the use of the Fuzzy C-means clustering algorithm on the appraisal of concrete public bus lines. First, the bus lines' evaluation index system was determined, and then the clustering algorithm was used to classify the bus lines into different categories. Each line's operational characteristics were analyzed separately, and scientific suggestions were provided for the bus companies' operations dispatch.

BASIC PROCESS OF PUBLIC BUS LINES' SYNTHETIC EVALUATION

In the evaluation of the public bus line, three levels were involved: line layout level, line facility level, and line operation level. The layout level includes line alignment, etc., and must be considered unified in the road network's construction. The facility level includes bus allocation and stop locations of each line; this is mainly related to passenger flow distribution and can be reflected from indexes such as the line's passenger flow volume, average stop spacing, etc. The operation level is related to service level indexes such as average travel speed, punctuality rate, and passenger comfort. A synthetic evaluation of bus lines should include indexes from the above three aspects; the appropriate evaluation methods were used to conduct omni-directional analysis of the lines.

PRINCIPLE AND STEP OF FUZZY C -MEANS CLUSTERING ANALYSIS

Principle of Fuzzy C-means Clustering Analysis

Clustering analysis is a method based on "like attract like." Input samples' classified attributes are not known beforehand, but an automatic classification is applied to the samples using the "similarity" or "distance." between them. The fuzzy clustering analysis method, which was proposed by Bezdek (1981), considers the boundary's fuzzy characteristics between different classes. Its computed result is superior to other taxonomic approaches (Wei 2002). The principle of Fuzzy C-means clustering analysis is as follows (Xinbo 2004):

(1) The input sampled data set for X, $x_{ij} \in X$ is the sample attribute data value, $1 \leqslant j \leqslant p$. n is the sample number, and p is the sample attribute number. Fuzzy C-means clustering's goal is to make the objective function J_m the smallest.

$$J_m(U,V) = \sum_{k=1}^{n}\sum_{i=1}^{c}(u_{ik})^m(d_{ik})^2 \qquad (1)$$

Where c is the clustering number; n is the sample number; $U=[u_{ik}]$ is the fuzzy classification matrix; $V=(V_1, V_2, \ldots, Vc)$, V_i is the clustering center of the ith class. $(d_{ik})^2=(X_k-V_i)^2$, which (X_k-V_i) is the distance between vector X_k and V_i. It is generally taken the Euclidean distance as the distance of (X_k-V_i), that is $\| X_k - V_i \| = \left[\sum_{j=1}^{p}(x_{kj} - V_{ij})^2\right]^{1/2}$, $m \in (1, \infty)$ is the weight of the index.

(2) Seeking the minimum of J(U,V) according to the clustering criterion, so

$$\begin{cases} \min\{J(U,V)\} = \min\left\{\sum_{k=1}^{n}\sum_{i=1}^{c}(u_{ik})^m (d_{ik})^2\right\} = \sum_{k=1}^{n}\left\{\min[\sum_{i=1}^{c}(u_{ik})^m (d_{ik})^2\right\} \\ \sum_{i=1}^{c} u_{ik} = 1 \end{cases} \tag{2}$$

(3) Solving the problem by using the Lagrange multiplier method,

$$F = \sum_{i=1}^{c}(u_{ik})^m (d_{ik})^2 + \lambda\left(\sum_{i=1}^{c} u_{ik} - 1\right) \tag{3}$$

(4) Optimality conditions are as follows:

$$\begin{cases} \dfrac{\partial F}{\partial \lambda} = \left(\sum_{i=1}^{c} u_{ik} - 1\right) = 0 \\ \dfrac{\partial F}{\partial u_{ik}} = \left[m(u_{ik})^{m-1}(d_{ik})^2 - \lambda\right] = 0 \end{cases} \tag{4}$$

(5) According to step (4), we get:

$$u_{ik} = 1 / \left[\sum_{j=1}^{c}\left(\frac{d_{ik}}{d_{jk}}\right)^{2/(m-1)}\right] \tag{5}$$

$$V_i = \sum_{k=1}^{n}(u_{ik})^m X_k / \sum_{k=1}^{n}(u_{ik})^m \tag{6}$$

From the above inferential reasoning process, if the data set X, clustering number c, and the weight of the index m are known, we can determine the best fuzzy classified matrix and the clustering center by (5) and (6). Therefore, the optimized questions can be solved by using an iterative algorithm.

Steps of Fuzzy C-means Clustering

According to the principle of fuzzy C-means clustering, the concrete steps for carrying on fuzzy C-means clustering analysis by iterative algorithm are as follows:

Step 1: Assign the clustering number c, $2 \leqslant c < n$; choose the form of d_{ik}; assign the weight of the index m, $1 \leqslant m < \infty$.

Step 2: Initializing $U^{(0)}$, the sum of the elements in each column should be 1; set the iteration number l=0.

Step 3: Compute the c clustering centers $\{V_i^{(l)}\}$ by using formula (6).

Step 4: Update $U^{(l)}$ to $U^{(l+1)}$ by using formula (5) and $\{V_i^{(l)}\}$.

Step 5: Compare $U^{(l)}$ and $U^{(l+1)}$, if $\| U^{(l+1)} - U^{(l)} \| \leqslant \varepsilon_L$, , then stop the iteration; otherwise, return to step 3, l=l+1.

SYNTHETIC EVALUATION OF BUS LINES IN CHANGZHOU CITY

Choosing the Clustering Factors of Bus Lines

The following factors should be considered when choosing the public bus lines' clustering factors: The chosen indexes should be representative and can reflect the structural properties and operational effects of the research objects (JPTC 2008). To guarantee that this method has strong versatility, the chosen indexes should be able to be collected and computed easily. Based on the above principles, all the bus lines' evaluating indicators were classified and analyzed. Deferring to the principles of generality, coordination, comprehensibility, objectivity and usability, six indexes in three aspects were considered as the bus lines' evaluation indexes, as shown in Figure 1.

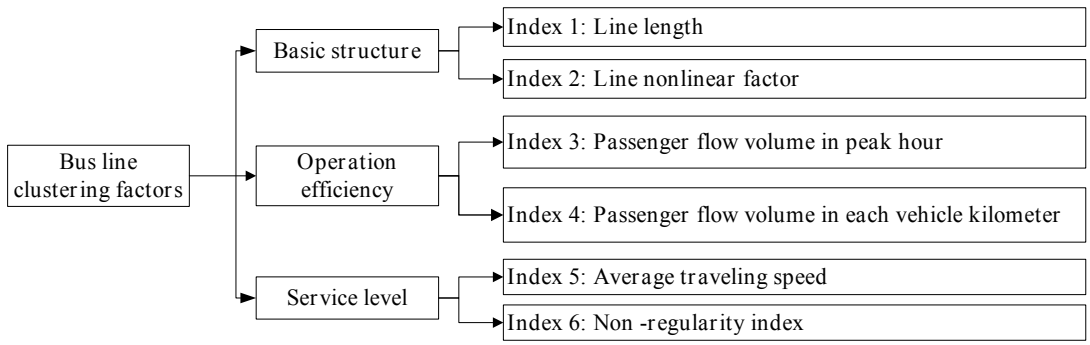

Figure 1. Bus line clustering factors .

After designating the clustering factors, statistical data for 35 bus lines were analyzed and computed. The value of the clustering factors is shown in Table 1.

Table1. Value of Clustering Factors of Surveyed Lines.

Bus Lines	Index 1	Index 2	Index 3	Index 4	Index 5	Index 6
1	10.50	2.52	1737	7.39	13.59	0.33
…	…	…	…	…	…	…
901	12.10	1.65	1273	5.26	18.82	0.25
902	6.80	1.30	918	6.75	13.51	0.20
B13	12.90	1.49	3195	6.72	21.19	0.20

Normalization of Bus Lines Clustering Factors

As shown in Table 1, the differences in dimension and magnitude of the clustering factors are very large, so the data must first be normalized. Otherwise, it is easy to highlight the indexes with high magnitude, but this reduces, even neglects, indexes with small magnitude (Zhouyang 2005). Therefore, the indexes were normalized; the results are shown in Table 2.

Table2. Normalized Bus Line Clustering Factors .

Bus Lines	Index 1	Index 2	Index 3	Index 4	Index 5	Index 6
1	0.10	1.00	0.13	0.66	0.12	0.50
…	…	…	…	…	…	…
901	0.13	0.42	0.08	0.45	0.33	0.37
902	0.02	0.19	0.04	0.60	0.11	0.30
B13	0.15	0.32	0.29	0.60	0.43	0.30

Fuzzy C-means Clustering Analysis

After the clustering factors were determined, the appropriate index weight m and cluster number c were selected. Bezdek (2002) determined that m=2 was the most meaningful from the physical interpretation, so we let m=2. For cluster number c, c=2, c=3 and c=4 were selected to classify the bus lines. After computation, the results were compared with the public bus lines' actual operation situation in Changzou city, and it was found that dividing into four categories was most appropriate. The classified members and distance matrix are shown in Table 3 and Table 4.

Table 3. Classified Members .

Category	Bus Lines
1	14, 23, 25, 56, 902, 812, 813, 81
2	1, 5, 7, 8, 16, 20, 29, 30,33, 38, 201, 259, 302, 901, 811
3	15, 17, 18, 35, 57, 68, 328
4	3, 6, 9, 11, 12

Table 4. Distance Matrix .

Category	1	2	3	4
1	0	0.993	0.957	0.303
2	0.993	0	0.804	1.156
3	0.957	0.804	0	0.944
4	0.303	1.156	0.944	0

Clustering Analysis Results

The Category 4 bus line operation efficiency is best; passenger flow volume is large, and line length is generally short, so this kind of bus line is most efficient in all categories. After investigation, it was found that this kind of bus line was located in the passenger flow corridor of Changzhou city, so the passenger flow volume of these lines is the largest. However, for the Category 4 lines, the service level is bad, and the average traveling speed is slow.

As is shown in Table 4, the Category 1 lines are closest to the Category 4 lines, so it has something in common with the Category 4 line, for example, large passenger flow volume and high efficiency. The Category 1 lines mainly connect the central urban area and the adjacent districts, and their service level is much higher than the Category 4 lines. The main reason is that the line nonlinear factor is smaller and alignment is smoother.

The Category 2 lines' length and passenger flow volume are moderate, and their efficiency is inferior to the Category 1 and Category 4 bus lines. The primary cause is because the Category 2 lines are generally built on collector streets and belongs to inferior skeleton bus lines.

Category 3 bus lines' length is generally much longer; the average line length is usually more than 30 kilometers, and their operation efficiency is lowest. The alignment of these lines usually starts from the center of the city and extends to the urban marginal areas. Their main task is to satisfy the travel demand of the city boundary residents who need to travel to the downtown area.

Through the above analysis, unified with each kind of line alignment, some pertinence measures were proposed, as shown in Table 5.

Table 5. Optimization Measures of Bus Lines.

Measures	Concrete Contents
1	Reduce the line overlap factor on main streets to avoid too many bus lines competing for passengers and disturbing each other.
2	Try to establish as many stops as bus bays to reduce the delay of vehicles in and out of the stops.
3	Shorten or cut lines that are too long to improve operation efficiency.
4	Enhance transit priority measures in center districts to reduce delay and improve vehicle traveling speed.

CONCLUSION

In view of the problem that current public bus line evaluations lack scientific and accurate methods, this article proposed to use a fuzzy C-means clustering algorithm principle to appraise and analyze bus lines. Concrete evaluation steps and key questions were presented. The method was applied to evaluate 35 bus lines' operations situation in Changzhou city. Each category of lines was analyzed, and optimized suggestions were given. The article proposed some reference meanings for bus companies to adjust bus lines and establish a dispatch schedule.

ACKNOWLEDGMENT

The authors wish to acknowledge the Doctoral Program of Higher Education of China (20070286011), China Sustainable Energy Program of the Energy Foundation (G-0803-09882), and Suzhou Integration Program of MRT and Surface

Transportation (ZXJ0804).

REFERENCES

Bezdek, J. C. (1976). "A physical interpretation of fuzzy ISOdata." IEEC Trans. SMC, 6(3), 387-390.

Hongtao, L. (2005). "Based-GIS clustering analysis of urban public traffic network service level." Xi'an University of Architecture and Technology.

JPTC. (2008). "Technical report of BRT operation and network optimization of bus system object in Jinan." Jinan Public Transportation Company.

Wei, W. (2002). "Chapter 12: Clustering analysis of urban transit network" Urban Public Transit Planning and Management. Science Press, Beijing.

Xiao, L. (2004). "Cluster analysis of Dandong City′s networks service in public traffic" J. Journal of Liaoning Institute of Technology, 24(2), 45-46.

Xiaoling, G. (2003). "The application of fuzzy cluster analysis in transportation planning" J. Transportation and Computer , 23(123), 80-83.

Xinbo, G. (2004). "Chapter 4: Clustering analysis." Fuzzy Clustering Analysis and Its Application. Xidian University Press, XI'an, 4.1-4.3.

Yuhua, L. (2004). "Comprehensive evaluation of urban public transport based on gray clustering method" J. Journal Harbin Univ. Sci. & Tech.,, 9(6),76-78.

Zhouyang, L. (2005). "The application of fuzzy clustering analysis in opening passenger dedicated line." J. Journal of Yuncheng university, 20(5), 39-41.

A Nonlinear Model for Decision-Making for Container Slot Chartering & Allocation under Liner Shipping Alliance

Ji-hong Chen and Hong Zhen

College of Communications and Transport, Shanghai International Shipping Institute, Shanghai Maritime University, P.O. Box 1290, Shanghai, China, 200135; PH (86) 21-65853850 ext. 8038; email: cxjh2004@163.com

ABSTRACT

The development of strategic alliances is very important to the liner industry. Liner shipping companies can benefit significantly from cooperating with shipping alliance members. This paper proposed a nonlinear model for container slot chartering & allocation under liner shipping alliance, which can help planners make better scheduling decisions for their fleets and routes under alliance agreement, and estimate shipping system costs more accurately. The proposed model pursued an optimal scheduling strategy for liner shipping company under shipping alliance agreement. The results showed that slot chartering under shipping alliance has outstanding advantages for shipping companies to lower their system costs, offset route capacity, and ensure the completion of freight tasks among others.

INTRODUCTION

Liner shipping alliance has been developed particularly rapidly these years. Alliance members can cooperate in the form of slot chartering, to take advantage of economies of scale. Slot chartering (Phties M. Panayides 2003) is a specific way for the shipping alliance members to share their shipping resources (Ji-hong Chen et al. 2008). It means that according to the alliance agreement, both parties cooperate by the sale of container slot and in a way that one party is to sell while another is to buy. In this way, shipping companies do not completely rely on their own ships (Hua-An Lu et al. 2006). Instead, they do their shipping business by leasing certain number of container slots from other shipping alliance members.

Many linear optimization models have been developed to identify the liner shipping routes (Phties M. Panayides 2003), fleet planning (Ji-hong Chen et al. 2008), transportation network (Hua-An Lu et al. 2006), etc in the literature. However, there are some defects in the models in terms of their practical applications. This paper is intended to develop a nonlinear model as a decision-making tool to determine slot chartering and allocation under containerized liner shipping alliance. Moreover, the paper uses LINGO software to solve the optimization model for a sample problem.

TRADITIONAL LINEAR OPTIMIZATION MDEL FOR LINER SHIPPING FLEETS & ROUTES (Model Ⅰ)

The optimization model is developed as below:

$$\text{Min} \quad Z_0 = \sum_i \sum_j c_{ij} x_{ij} + \sum_j \delta_j u_j \tag{1}$$

s.t.

$$\sum_j \frac{1}{n_{ij}} \le m_i \tag{2}$$

$$\sum_i N_i x_{ij} + u_j = Q_j \tag{3}$$

$$x_{ij} \ge 0; \quad u_j \ge 0; \text{ integer} \tag{4}$$

Model Ⅰ is a linear model developed for route planning and slot allocation for liner shipping company (Gang Zhao 1997), without considering shipping alliance agreement. The explanation for the model and parameters can be referred to model Ⅱ.

NONLINEAR OPTIMIZATION MODEL FOR SLOT CHARTERING (MODEL Ⅱ)

$$\text{Min} \quad Z = \sum_{\forall i \in S} \sum_{\forall j \in R} c_{ij} x_{ij} + \sum_{\forall j \in R} \delta_j u_j + \sum_{\forall k \in H} \sum_{\forall j \in R} \omega_{kj} e_j q_{kj} \tag{5}$$

s.t.

$$\sum_{\forall j \in R} \frac{1}{n_{ij}} x_{ij} \le m_i \qquad \forall i \in S \tag{6}$$

$$\sum_{\forall j \in R} \frac{1}{p_{kj}} \omega_{kj} \le l_k \qquad \forall k \in H \tag{7}$$

$$\sum_{\forall i \in S} N_i x_{ij} + \sum_{\forall k \in H} q_{kj} \omega_{kj} + u_j = Q_j \qquad \forall j \in R \tag{8}$$

$$\omega_{kj} \ge \omega_{kj}^d \quad \forall k \in H; \forall j \in R \tag{9}$$

$$\omega_{kj} \le \omega_{kj}^u \quad \forall k \in H; \forall j \in R \tag{10}$$

$$q_{kj} \ge q_{kj}^d \quad \forall k \in H; \forall j \in R \tag{11}$$

$$q_{kj} \le q_{kj}^u \le M_k \quad \forall k \in H; \forall j \in R \tag{12}$$

$$\omega_{kj} \le M Y_{kj} \quad \forall k \in H; \forall j \in R \tag{13}$$

$$q_{kj} \le M Y_{kj} \quad \forall k \in H; \forall j \in R \tag{14}$$

$$\omega_{kj} q_{kj} > M(Y_{kj} - 1) \quad \forall k \in H \; ; \forall j \in R \tag{15}$$

$$Y_{kj} \in \{0,1\} \tag{16}$$

$$x_{ij} \, , \; \omega_{kj} \, , \; q_{kj} \, , \; u_j \geq 0 \;\; \text{and integer} \;\; \forall i \in S \; ; \forall k \in H \; ; \forall j \in R \tag{17}$$

DESCRIPTION OF THE MODEL

In model Ⅱ, formula (5), (8) and (15) show that the model is a nonlinear model. Explanation of the parameters and formulas for model Ⅰ is almost the same as model Ⅱ. Explanation for the models is as follows.

Symbols and sets. i: symbol for the ships of the shipping company ; k: symbol for cooperative ships; j: symbol for liner shipping routes; S: a set for all the ships of the liner shipping company; H: a set for all the cooperative ships; R: a set for all the liner shipping routs.

Decision variables. x_{ij}: the number of consecutive voyages for ship i on route j in the planning period; ω_{kj}: the number of cooperative consecutive voyages for cooperative ship k on route j in the planning period; q_{kj}: the number of slots (TEU) for chartering, from cooperative ship k on route j for each consecutive voyage; u_j: un-carried TEU of the shipping company on rout j in the planning period; Y_{kj}: binary variables ($Y_{kj} \in \{0,1\}$).

Parameters. c_{ij}:transportation cost of ship i on route j for a consecutive voyage; δ_j:opportunity cost for each TEU(twenty equivalent unit) on route j; e_j: slot charting cost of one TEU for cooperation, paid to the cooperative company; m_i: the number of ship i; l_k : the number of cooperative ship k; n_{ij}:maximum consecutive voyages for ship i on route j in the planning period; p_{kj}:maximum consecutive voyages for cooperative ship k on route j in the planning period; N_i:capacity (TEU) of ship i; M_k: capacity (TEU) of cooperative ship k; Q_j: forward shipment (TEU) of the shipping company in route j in the planning period; M: a very big number ($M \to \infty$).

Formulas. Formula (5) means the total system cost for the shipping company should be minimized; formula (6) and (7) show that number of ships or cooperative ships assigned should be no more than the number of available ships; formula (8) means the ships and the cooperative ships assigned for slot chartering should finish the carrying tasks; formula (9) and (10) show minimum & maximum limits for cooperative consecutive voyages of cooperative ship k on route j in the planning period; formula (11) and (12) show the range of the available slots for chartering for each cooperative consecutive voyage of cooperative ship k on route j; with the help of Y_{kj} (binary variables), formula (13) through (15) show, if there is

or no cooperative voyage, there will be or no container slots for chartering; formula (16) and (17) show the ranges for decision variables.

ALGORITHM FOR THE MODEL

Much effective algorithm for the nonlinear models has been offered by the scholars. A particle swarm optimization algorithm for nonlinear integer programming (Shang Gao et al. 2007) and a penalty interior-point method for nonlinear programming (Yi-rong Yao et al. 2008) were effective and helpful. When the model involves many variables, we often deal with it with the help of the related computer software, such as MATLAB and LINGO. The paper will process the example with the help of LINGO software.

APPLICATION OF THE MODEL

We assume two shipping companies (company A and company B) in a shipping alliance will cooperate in form of slot chartering. According to the alliance agreement, shipping company A can rent container slots from company B for each voyage in 4 container shipping routes, and for each cooperative voyage, the largest number of slots for chartering from each ship of company B is 1000TEU. Company A has three types of ships: 5 Ship1 (6000TEU), 8 Ship2 (3400TEU), and 8 Ship3 (2000TEU). For cooperation, company B offers three kinds of ships: 6 Ship Ⅰ (6000TEU), 6 Ship Ⅱ (5000TEU), and 8 ShipⅢ(4000TEU). The planning period is a quarter of a year. Other specific data can be got from Table1~3.

Table 1. Largest number of voyages for each ship in each route.

Company/Ship/Route		Route 1	Route 2	Route 3	Route 4
	Ship1	3	2	3	1
Company A	Ship2	4	3	3	2
	Ship3	5	5	5	2
	Ship Ⅰ	3	2	1	3
Company B	Ship Ⅱ	3	4	2	3
	ShipⅢ	5	5	5	2

Table 2. Largest number of cooperative voyages for ships of company B in each route (ω_{kj}^{u}).

Ship/Route	Route 1	Route 2	Route 3	Route 4
Ship Ⅰ	2	3	2	3
Ship Ⅱ	4	3	3	4
ShipⅢ	6	5	7	7

Table 3. Costs for one consecutive voyage or one TEU for company A (ten thousand USD).

Cost/Ship/Route		Route 1	Route 2	Route 3	Route 4
Transportation Cost for a Consecutive Voyage	Ship1(6000TEU)	100	110	120	140
	Ship2(3400TEU)	80	90	100	100
	Ship3(2000TEU)	60	80	80	90
Slot Chartering Cost (per TEU)		0.08	0.05	0.07	0.06
Opportunity Cost (per TEU)		0.3	0.125	0.2	0.175

Planning and routing without slot chartering. For the situation with no cooperation under shipping alliance, the results of planning and routing ships of Company A with model Ⅰ were obtained from LINGO software as shown in Table 4.

Table 4. Total number of consecutive voyages & total cost (ten thousand USD) of shipping system for Company A in the planning period.

Ship/Route	Route 1	Route 2	Route 3	Route 4	Total cost
Ship1 (6000TEU)	6	2	3	1	
Ship2 (3400TEU)	0	0	0	16	9110
Ship3 (2000TEU)	2	34	1	1	

Decision-making for slot chartering. With model Ⅱ and the help of LINGO software, the optimization results of Decision-making for slot chartering for Company A are in Table 5 and Table 6.

Table 5. Number of consecutive voyages and total cost of shipping system ($1,000) for Company A under shipping alliance

Ship/Route	Route 1	Route 2	Route 3	Route 4	Total cost
Ship1 (6000TEU)	7	3	3	0	
Ship2 (3400TEU)	0	0	0	16	6885
Ship3 (2000TEU)	0	26	0	9	

Table 6. Total number of cooperative voyages & number of slots for chartering

Ship/Route		Route 1	Route 2	Route 3	Route 4
ω_{kj}	Ship Ⅰ	0	3	0	3
Total Number of	Ship Ⅱ	0	4	0	4
Cooperative Voyages	ShipⅢ	0	3	0	7
q_{kj}	Ship Ⅰ	0	1000	0	1000
Number of Slots(TEU) for	Ship Ⅱ	0	1000	0	1000
Chartering for each Voyage	ShipⅢ	0	609	0	1000

Comparing Table 5 with Table 4, we can see that the total cost of the shipping system of Company A decreases significantly. System cost was reduced to 6885 from 9110, which represents 24.4% of decrease. These results indicate that slot chartering under shipping alliance has outstanding advantage for shipping companies to reduce their system costs.

CONCLUSION

Integration of global logistic systems has already had a significant impact on international shipping services (Chin-Shan Lu et al. 2007). Strategic alliances between liner shipping companies provide a whole new stage along with a flexible managing method for the carriers (Hua-An Lu et al. 2006). Co-operative activities such as joint fleet, slot exchange, slot charter, share of port usage etc., have been widely operated in the contemporary liner industry. Slot chartering is the fundamental and also the most effective form of cooperation for shipping alliance.

This paper proposed a nonlinear optimization model for ship scheduling and slot chartering under shipping alliance. The proposed method can help planners make better scheduling and routing decisions under alliance agreement constraints. Meanwhile, it can make more accurate estimates system costs, freight voyages, and cooperative voyages in liner service route planning. The proposed model pursues an optimal scheduling strategy to reduce system cost. Moreover, the experimental results of a case study show that the proposed model can perform as a good decision support tool to improve the management performance for liner shipping alliance members.

REFERENCES

Chin-Shan Lu, Kee-hung Lai, and T.C.E. Cheng (2007), "Application of structural equation modeling to evaluate the intention of shippers to use Internet services in liner shipping", European Journal of Operational Research 180(2),845–867.

Gang Zhao (1997). "Analysis and Improvement on the Vessel Allocation Model of Liner Service", Journal of Systems Engineering 12(1), 80-86.

Hua-An Lu, James Cheng, and Tai-Shen Lee(2006). "An Evaluation of Strategic

Alliance in Liner Shipping-An Empirical Study", Journal of Marine Science and Technology 14(4), 202-212.

Ji-hong Chen, Hong Zhen, and Bei-hua Zong (2008). "Improved Vessel Allocation Model of Liner Shipping and Its Application for Slot Chartering under Shipping Alliance", Journal of Transportation Systems Engineering and Information Technology 8(3),120-125.

Phties M.Panayides (2003). "Competitive strategies and organizational performance in ship management", Maritime Policy and Management 30(2),123-140.

Shang Gao, and Jing-yu Yang (2007). "Particle Swarm Optimization Algorithm for Nonlinear Integer Programming", Microcomputer Applications 28(2),126-130.

Yi-rong Yao, and Lian-sheng Zhang (2008). "A Penalty Interior-Point Method for Nonlinear Programming", Chinese Journal of Contemporary Mathematics 29(2),151-158.

Study on the Model of Hub Location under Earthquake Conditions

Shi An [1], Lei Ye[2], Candong Wang[3]

[1]School of Transportation Science and Engineering, Harbin Institute of Technology, Heilongjiang Harbin 150090, China; PH 13351113338; email: anshi@21cn.com

[2]School of Transportation Science and Engineering, Harbin Institute of Technology, Heilongjiang Harbin 150090, China; PH 15846595966; email: moran.aaa@163.com

[3]School of Transportation Science and Engineering, Harbin Institute of Technology, Heilongjiang Harbin 150090, China; PH 13704506385; email: wangcandong5@163.com

ABSTRACT

Hubs play a significant role in the transport of emergency supplies after earthquakes. To ensure that transport and incident management operate efficiently under earthquake conditions, this paper presents a model for hub location suitable for the conditions of earthquakes. Taking the characteristics of road networks and freight transportation under the condition of earthquakes into account, the minimum of total supplies' reliable transit time under the service time constraints of kinds of supplies is the objective function of hub location under earthquake conditions. A surcharge is introduced in the cost function for those o/d pairs that were not being delivered to on time. The cost of waiting time due to congestion and the cost of reliable traveling time are considered. A Simulated Annealing algorithm was developed to solve the model. The algorithm has been tested in randomly-created networks. The results show that when a situation of congestion occurs, the proposed algorithm enables better solutions to be found.

Key words: model of hub location under the condition of earthquake; operations research; reliable transit time; surcharge overtime; waiting time due to congestion

INTRODUCTION

The catastrophe of a destructive earthquake put tremendous pressure on the urban transportation hub. On one hand, great damage is caused to the transportation infrastructure; on the other hand, the transportation of emergency rescue teams and supplies into the affected areas put tremendous pressure on the hub. Hub location can satisfy the demands of people and material transportation in the relief effort, and determine the operation of emergency rescue, evacuation, and withdrawal, as well as urban renewal.

Therefore, in urban development construction, taking special traffic demand under earthquake conditions into consideration for hub location should be synchronized with overall urban planning.

HUB LOCATION RESEARCH

Since O'Kelly (1986) presented the findings of his studies on hub location, many researchers have centered their efforts on the hub location problem. Campbell (1994) presented a linear model for the p-hub location problem. Later, Skorin-Kapov et al. (1997) developed an expression to simplify the problem. Aykin (1995) proposed an algorithm to solve the problem of locating p hubs. O'Kelly et al. (1998) developed a model called FlowLoc. Ebery et al. (2000) studied the hub location problem of multi-distribution and capacity constraints. Kara and Tansel (2002) studied the p hub location problem of mono-distribution. The research of domestic hub location can be classified into two categories: the two-stage method of hub location (Zhang et al. 2001; Yuan et al. 1991), and the application of AHP (Yan and Wang 1999 Guo and Yan 1997) and Fuzzy Theory (Liu and Yan 2006) to hub location evaluation.

The research of hub location domestically and abroad addressed normal situations, but did not take into consideration the needs of special transportation under earthquake conditions when they discuss the problem of hub location.

DEFINING THE PROBLEM

The traffic-attracting nodes in emergency relief are affected regions and planning refuges; traffic-generated nodes include designated relief supplies reserve centers and posts of rescue teams. Transportation of emergency relief supplies have a weak economy and are strongly time-sensitive; thus, hub location under earthquake conditions is a problem of optimizing the hub sites to minimize total supplies reliable transit time under the service time constraints of the kinds of supplies. In this paper, the following assumptions are made:

Cargo passes through one or two hubs to complete its transport.

- Economies of scale are taken into account.
- Supply delivery under earthquake conditions has time constraints.
- When cargo arrives at a busy hub, a queuing phenomenon can occur.
- A devastating earthquake causes serious damage to the connectivity of road networks. Reliable transit time is corrected by the connectivity reliability of road networks.

OPTIMAL LOCATION OF HUBS UNDER EARTHQUAKE CONDITIONS

This paper presents a model for hub location based on Aykin's model (1996). The specific model is:

$$\sum_{i}^{Min}\sum_{k}\sum_{t}\sum_{j}\sum_{a}(W_{i,j}^{a}+C_{f}^{a}WT_{i,j}^{a})(\beta T_{i,k}+\alpha T_{k,t}+\beta T_{t,j})V_{i,k,t,j} \tag{1}$$

$$C_{f}^{a}=\begin{cases}0, & if\left(T_{i,k}+T_{k,t}+T_{t,j}+\omega_{k}+\omega_{t}\right)\le T_{Max}^{a}\\ C_{f}^{a}, & if\left(T_{i,k}+T_{k,t}+T_{t,j}+\omega_{k}+\omega_{t}\right)>T_{Max}^{a}\end{cases}$$

$$s.t. \quad \sum_{k}\sum_{t} V_{i,k,t,j} = 1 \quad \forall i,j \tag{2}$$

$$\sum_{k} Y_k = \sum_{l=l_1}^{l_4}\sum_{k} Y_k = p_1 + p_2 + p_3 + p_4 = p \tag{3}$$

$$\sum_{i\neq k}\sum_{\substack{l\neq k \\ h\neq k}} \left(V_{i,l,h,k} + V_{k,l,h,i}\right) \le M\left(1 - Y_k\right) \quad \forall k \tag{4}$$

$$\sum_{\substack{l\neq k \\ h\neq k}} (V_{k,k,h,t} + V_{t,h,k,k} + V_{t,t,h,k} + V_{k,h,t,t}) + \sum_{\mathrm{h}} (V_{k,h,h,t} + V_{t,k,h,k}) \le M(2 - Y_k - Y_t) \quad \forall k \neq t \tag{5}$$

$$\sum_{k} Z_{i,k} = 1 \quad \forall i \tag{6}$$

$$\sum_{t}\sum_{j} V_{i,k,t,j} \le \left(N - p + 1\right) Z_{i,k} \qquad \forall i,k \tag{7}$$

$$\sum_{i}\sum_{k} V_{i,k,t,j} \le \left(N - p + 1\right) Z_{j,t} \qquad \forall t,j \tag{8}$$

$$V_{i,k,t,j}(T_{i,k} + T_{k,t} + T_{t,j}) \le T_{Max} \quad \forall i,k,t \tag{9}$$

$$\begin{aligned} &\sum_{i}\sum_{t}\sum_{j} \left(V_{i,k,t,j} W_{i,j}\right) \le CHub_k \quad \forall k \\ &\sum_{i}\sum_{t\neq k}\sum_{j} \left(V_{j,t,k,i} W_{j,i}\right) \le CHub_k \quad \forall k \end{aligned} \tag{10}$$

$$Z_{i,j}, V_{i,k,t,j}, Y_k \in \{0,1\} \quad \forall i,k,t,j \tag{11}$$

Where,

$W_{ij} = \sum_{a=1}^{q} W_{i,j}^{a}$ - cargo flow from *i* to *j*, $WT_{i,j}^{a}$ is load of cargo *a* from *i* to *j* which is not on time

C_{f}^{a} - surcharge of cargo *a* due to not on time

$\omega_k = \dfrac{1}{\mu_k - \lambda_k}$ - queuing time spent in hub *k*, λ_k、μ_k are arrival rate and service rate of *k* hub

T_{Max}^{a} - maximum delivery time of cargo *a*

α / β - factor of scale economy between hubs/between hub and non-hub

$T_{m,k} = t_{m,k} \cdot \psi_{m,k}$ - reliable transit time between node *m* and node *k*, $\psi_{m,k}$ is connectivity reliability

$V_{i,k,t,j}$ - when the cargo going from *i* to *j* passes through hubs *k* and *t*, $V_{i,k,t,j}=1$; otherwise, 0

$Z_{i,k}$ - if the *i*-node is assigned to hub *k*, $Z_{i,k}=1$； otherwise, 0

Y_k^l - when the k-node is a l tape hub, $Y_k^l=1$; otherwise, 0

$Y_k = \sum_{l=l_1}^{l_4} Y_k^l$ - when the *k*-node is a hub, $Y_k^l=1$; otherwise, 0

p - number of hubs
M - a very high number
$CHub_k$ - capacity of hub k

SOLUTION ALGORITHM

To solve the problem of hub location, a simulated annealing algorithm based on Aykin's1995 was developed.

Initial Solution

When seeking the initial solution, all nodes in the network are considered hubs. Therefore, each node is assigned to itself. The total cost is calculated with this solution. In each loop, the cost of the solution of closing down one of the hubs in the network is calculated, and the hub that represents the least increase in cost is closed.

Improvement of the Initial Solution

In this stage, exchanges are made between those nodes that are hubs and those that are not. Finally, the greatest money-saving changeover is selected in accordance with the following equation for estimating savings:

$$U_{t,r} = \max_{k \in H} \left\{ R_{k,r} \right\} \tag{12}$$

Where

$R_{k,r}$ - estimated saving when substituting hub k for node r.

The amount of cargo goes from hub k to l:

$$I_{k,l} = \sum_{\{i/Z_{i,k}=1\}} \sum_{\{j/Z_{j,l}=1\}} \left(W_{i,j} + \mathrm{C}_f W T_{i,j} \right) \tag{13}$$

The savings achieved when hub k is replaced by the node r is:

$$R_{k,r} = \sum_{\{i/Z_{i,r}=1\}} O_i (T_{i,k} - T_{i,r}) + \sum_{\{i/Z_{i,r}=1\}} O_i (T_{k,i} - T_{r,i}) + \sum_{\substack{q \in K \\ q \notin r}} (I_{r,q}) \alpha (T_{k,q} - T_{r,q}) + \sum_{\substack{q \in K \\ q \notin r}} (I_{q,r}) \alpha (T_{q,k} - T_{q,r}) \tag{14}$$

Where

O_i - total cargo originating at node i
D_i - total cargo arriving at node i,
$Z_{i,k}$ - if node i is assigned to hub k, $Z_{i,k}$=1; otherwise, $Z_{i,k}$=0

Since $U_{t,r}$ is an estimate of the savings involved and is its lower limit, in some cases the result could be a negative value. However, on updating the assignation of nodes to hubs, the switching of node r to a hub is a good choice. Because of this, the algorithm calculates the probability of acceptance. The exchange between r and t is calculated in the following function:

$$P(accept \quad at \quad \Delta) = \begin{cases} e^{-\Delta/T}, & if \quad U_{r,t} \geq 0 \\ 1, & if \quad U_{r,t} < 0 \end{cases} \tag{15}$$

$\Delta = U_{t,r}/$ evaluation of the objective function for the best known solution (16)

If $U_{t,r}<0$, it is always recommendable to make this change; once $U_{t,r} \geq 0$, a random number ω is generated, which is compared with the value of the probability of accepting the change. If $\omega < P(accept \quad at \quad \Delta)$, the switchover between *r* and *t* will be made. The cooling function is

$$T_n = T_{n-1}{}^{v} \tag{17}$$

Where

T_n - temperature value for the loop *n*

v - cooling parameter

To relax congestion in the hub, the flow of cargo in the network is balanced. First, the quantity of cargo that passes through each hub is calculated using Eqs. (10) and (11). Next, the hubs where the nominal capacity is exceeded and those where the amount of cargo is not below their nominal capacity are identified. The necessary re-assignations are made to reduce the cargo going through those hubs where the nominal capacity is being exceeded. To reduce congestion in an *h* hub, the ($Z_{i,h}$=1) *i*-node nearest to a non-congested *k* hub is selected from all the *h* hub's assigned nodes, and the *i* assignation is changed using ($Z_{i,h}$=0; $Z_{i,k}$=1).

COMPUTATIONAL RESULTS

The model was evaluated in 10 randomly-created networks of 52 nodes each. The load matrices and the distance were also generated at random. The problem of locating three hubs was solved for each situation. The delivery time was 24 hours, and 10 hours were available for transporting and handling the cargo at hub. The tests conditions can be seen in Table 1.

Table 1. Characteristics of the Hubs.

Capacity	Rate of Service	Under Capacity		Over Capacity	
		Rate of Arrival	Time in Hub	Rate of Arrival	Time in Hub
10	13	12	1	12.44	1.8
10	13	12	1	12.7	3.4
15	19	18	1	18.44	1.8
15	19	18	1	18.7	3.4

It is assumed that the cargo that is not delivered within the delivery time has an additional cost of 20% over that which is delivered in time. The results obtained with Aykin's algorithm were compared with the results obtained from the same problems but introducing the task of balancing the assigning of nodes. The results are compared in Table 2.

Table 2. Results for Problems of Different Time Consumed at Hub.

ω = 3.4	Improvement %				ω = 1.8	Improvement 改善%			
	CHub＝10		CHub＝15			CHub＝10		CHub＝15	
Experiment	*PSIT*	*LSIT*	*PSIT*	*LSIT*	Experiment	*PSIT*	*LSIT*	*PSIT*	*LSIT*
1	10.2	9.8	27.2	28.3	1	-2.1	-2.3	6.1	6.7
2	2.1	1.7	10.4	10.2	2	0.4	-0.2	3.9	3.3
3	4.2	4.3	12.4	12.4	3	-2.2	-2	6.8	6.9
4	0.8	1.1	10.5	11.1	4	-2.4	-2.2	3.6	3.7
5	2.5	3.1	23.2	23.7	5	2.8	2.5	5	5.1
6	46.3	46.8	46	46.5	6	11.6	12.1	13.9	14.5
7	1.3	1.2	16.7	17	7	-1.7	-2	5.9	5.7
8	6.3	6.5	16.8	16.8	8	-0.8	-1.1	0.1	-0.1
9	5.3	5.5	38.2	39.2	9	-8.4	-8.3	-2.6	-2.9
10	8	8.6	17.4	17.9	10	0.6	-0.1	3.8	3.4

$PSIT_b$ and $PSIT_0$ are the number of pairs served in time with and without balancing nodes assignation separately. $LSIT_b$ and $LSIT_0$ are the load served in time with and without balancing nodes assignation separately.

$$\%\ improvement\ PSIT = \left(\frac{PSIT_b - PSIT_0}{PSIT_0} \right), \%\ improvement\ LSIT = \left(\frac{LSIT_b - LSIT_0}{LSIT_0} \right) \quad (18)$$

It can be seen that when the additional waiting time at the hub due to congestion is long, balancing the assignation of node offers very satisfactory results, because the increase in the distance the cargo travels is compensated for by the decrease in the time spent waiting at the hub.

To study the consequences of balancing out the assignation of nodes, the total cost of the solution was broken down into travel cost, distance surcharge, and congestion surcharge .These values were calculated for each of the problems. Table 3 shows the averages for the 10 problems in each case.

Table 3. Change in Components of Cost Controlling Overload in Hubs.

Test	% Mean Improvement			
	Capacity	Cost Due to Distance	Cost Due to Congestion	Total Cost
△	10	-1.51	2.06	0.55
ω=2.4	15	-1.53	4.71	3.18
△	10	-1.41	0.48	0.48
ω=1.8	15	-1.19	1.15	1.15

It can be seen from the results that, in all cases, the cost of late deliveries due to distance increases on balancing the assignation of nodes, while the cost of late delivery through congestion is reduced. It can also be seen that, on average, the total cost of the solution improves.

CONCLUSIONS

This study takes the standard of service into account when locating hubs under earthquake conditions and considers that each hub has limited capacity. The standard of service is measured according to the amount of cargo to be served within the delivery time and to the number of o/d pairs to be served on time. The objective function considers three factors: (1) the cost of transport between each o/d pair and the cost arising from not delivering the goods within the agreed time limit; (2) the surcharge generated when cargo makes too long a journey; and (3) the cost created by cargo that is delivered late because it spent too much time at the hub. The model introduces a delivery time restriction to solve the issue of urgent delivery characteristics under earthquake conditions, which controls the waiting time due to congestion at the hub effectively; in this way the model allows the problem of hub location under earthquake conditions to be solved by reducing congestion at the hubs and ensuring delivery on time.

The methodology used to improve the initial situation is simulated annealing. The cooling function used is the traditional one. By testing in randomly created networks, when a situation of congestion occurs, the proposed algorithm enables the total delivery time to decrease, and the number of pairs and supplies served in time to increase. The proposed algorithm enables better solutions to be found, thereby fitting the problem of hub location under earthquake conditions.

REFERENCES

Aykin, T. (1995). "Networking policies for hub-and-spoke systems with application to the air transportations system." *Transportation Science*,29, 201-221.

Campbell, J. F. (1994). "Integer programming formulations of discrete hub location problems." *European Journal of Operational Research,* 72, 387-405.

Ebery, J, Krishnamoorthy, M., Ernst, A., and Boland, N. (2000). "The capacitated multiple allocation hub location problem: Formulations and algorithms." *European Journal of Operational Research,* 120, 614-631.

Guo, X., Xu, S., and Yan, G. (1997). "Decision method for stations arrangement of highway transport hub.: China Journal of Highway and Transport, 10(3), 83-88.

Liu, Y., and Yan K. (2006). "Fuzzy multi-criteria decision-making method in planning of transport hub." Journal of Huazhong University of Science and Technology·Urban Science, 23(2), 63-66.

O'Kelly, M.E. (1986). "The location of interacting hub facilities." *Transportation Science*, 20(2), 92-106.

O'Kelly, M.E., and Bryan, D. L. (1998). "Hub location with flow economies of

scale." *Transportation Research B*, 32, 605-616.

Rodriguez, V. (2002). "Metodologi a para determinar la ubicacio de hubs con capacidad limitada." Tesis doctoral, Tecnun, Universidad de Navarra, San Sebastian.

Skorin-Kapov, D., Skorin-Kapov, J., and O'Kelly, M.E. (1997). "Tight linear programming relaxations of uncapacitated p-hub median problems." *European Journal of Operational Research*, 94, 582-593.

Yan, Q., and Wang, Z. (1999). "Application of AHP to the general planning of yard and station of highway main hub." *Journal of Southwest Jiaotong University*, 34(2), 223-227.

Yuan, H., and Lu, H. (2001). "Study on model and method of comprehensive transportation terminal planning." *Journal of Highway and Transportation Research and Development*, 18(3), 101-105.

Zhang, J., Ren, F., and Qiu-sheng, X. (1991). "Approach to location selecting of urban passenger transfer center." *Journal of Beijing Polytechnic University*, 17(4), 21-25.

Empirical Correlation Analysis of Parking Arrival and Departure Rates for Urban Parking Facilities

Jun Chen[1] Huanhuan Chao[2] Hua Bai[3]

[1] School of Transportation, Southeast University, 2 Sipailou, Nanjing, China, ST 210096; PH (86) 25-83795641; FAX (86) 21-83795641; email: chenjun@seu.edu.cn

[2] Wu xi Communications Industry Group Co., Ltd. Wuxi, China, ST 214031; email: zhaohh-211@163.com

[3] School of Transportation, Southeast University, 2 Sipailou, Nanjing, China, ST 210096; PH (86) 25-83794213; FAX (86) 21-83795641; email: bh_birch@163.com

ABSTRACT

To improve the effects of urban parking facilities' management and control, this paper collected 10 hours data consecutively on parking arrival and departure rates from one off-street park in central Nanjing city in China and sets the time series marshal as an interval of 15 minutes. Autocorrelation functions and partial correlation functions are set up to describe the relationship among the parameters such as parking arrival rate, parking departure rate, and parking actual occupancy. A Granger causality test model was used to analyze the three characteristics mentioned above. Conclusions were drew that, in specific time sections, the lagged parking arrival rates can affect the value of the current parking departure rate and occupancy rates of valid parking berths distinctly, while the lagged parking departure rates can greatly affect the value of current occupancy rates of valid parking berths. Finally, forecasting models of parking arrival and departure rates were set up based on correlation analysis, and the results show that these models demonstrate promising performance for modeling parking arrival and departure rates.

Keywords: parking arrival rates, parking departure rates, correlation analysis, forecasting model.

INTRODUCTION

With the rapid development of the Chinese economy and car ownership, the problem of the supply-demand imbalance of parking facilities in urban centers has become severe. Parking arrival and departure rates reflect dynamic parking demand, which is of important guiding significance for the optimal setting and management for parking facility. The existing literature (Chen Jun et al. 2007; Jeffrey F.Paniati. 2007; Guan Hongzhi et al. 2005; Yan Hai et al. 2005) on parking

arrival and departure rates emphasize influencing factors and behavior characteristics of drivers; the correlation between arrival and departure rates and the utilization ratio of parking facilities are rarely researched, which are important research issues of this paper.

EXPERIMENTAL INVESTIGATION APPROACH OF SHOT-TIME PARKING ARRIVAL AND DEPARTURE RATES

To get shot-time variation characteristics of parking arrival and departure rates, this study investigates the Bai-nao-hui underground parking located on Zhujiang Road in the city centre of Nanjing. The approach is to record the parking arrival and departure rates from the electronic toll systems of parking lots and statistically analyze each 15 minutes to meet the research precision. In Figure 1, the time series is set as the x-coordinate and the arrival and departure rates (veh/15min) are set as the y-coordinate.

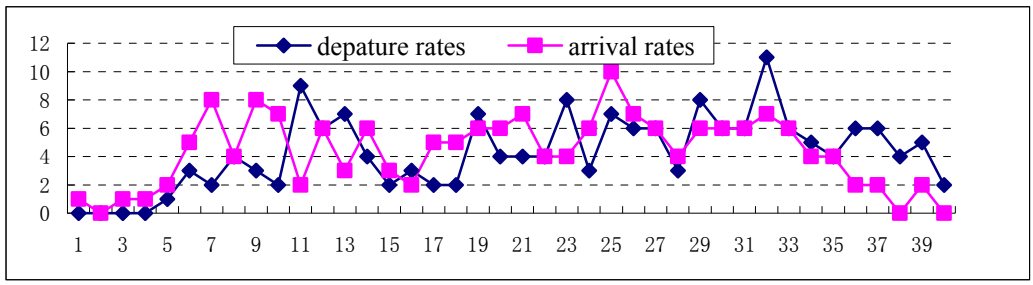

Figure 1. Distribution of parking arrival and departure rates at 15 minute intervals.

EXPERIMENTAL DATA AND CORRELATION ANALYSIS OF SHOT-TIME PARKING ARRIVAL AND DEPARTURE RATES

This paper treats the trend of parking arrival and departure rates as a set of random variable $\{y_t\}$ depending on time period t. The autocorrelation functions and partial correlation functions (William H.K et al. 2006) are expressed as:

$$r_k = \frac{\sum_{t=k+1}^{T}(y_t - \bar{y})(y_{t-k} - \bar{y})}{\sum_{t=1}^{T}(y_t - \bar{y})^2} \tag{1}$$

$$\phi_k = \begin{cases} r_1, & k = 1 \\ \dfrac{r_k - \sum_{j=1}^{k-1}\phi_{k-1,j} r_{k-j}}{1 - \sum_{j=1}^{k-1}\phi_{k-1,j} r_j}, & k > 1 \end{cases} \tag{2}$$

where r_k is the autocorrelation coefficient of the current value of parking arrival rates (departure rates) and the value before time k; ϕ_k is the partial correlation coefficient of the current value of parking arrival rates (parking departure rates) and the value before time k, the partial correlation of lagging k

steps is the coefficient of y_{t-k} when regression of $y_{t-1} \ldots y_{t-k}$ by y_t; T is value of the time series (for the 10-hours investigation, the time interval is 15 minutes, so T=40); $\bar{y}$ is the sample mean; $y_t, y_{t-1}, \ldots y_{t-k}$ is the variable set based on time series t.

Based on the time series data, the results of the autocorrelation coefficient and the partial correlation coefficient of parking arrival and departure rates in 15min analyzed by software Eview5.0 (Yi Danhui. 2002) are shown in the figures below.

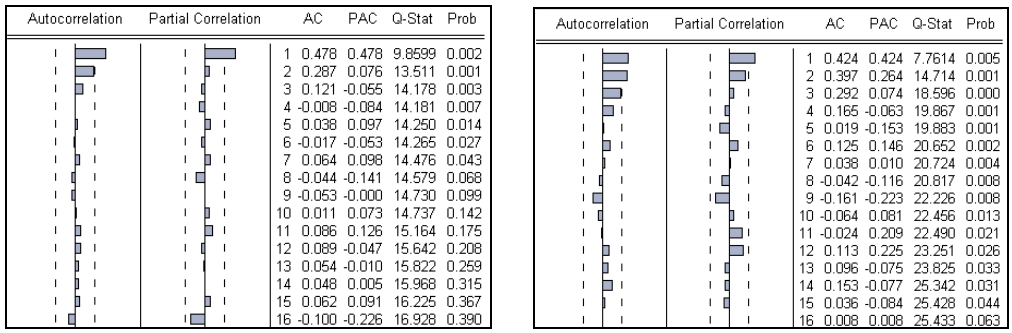

(a) **(b)**

Figure 2. Autocorrelation coefficient and partial correlation coefficient of parking arrival rates (a) and departure rates (b).

Several explanations are necessary: (1) If the value of the autocorrelation (partial) coefficient lies within the boundary of two dashed lines marked in Figure 2, there would be no significant difference between significance level reached at 95% and that of 0; (2) AC and PAC denotes, respectively, the result of the autocorrelation coefficient and the partial correlation coefficient; Q-Stat and Prob denote the Q statistic and the probability of series independence test.

As a result, there is notable correlation between the arrival and departure rates at 15min and in the adjacent time interval than that in the other time interval.

For the further study of variation characteristics of parking arrival and departure rates, three indexes were selected to study the correlation characteristics, which are parking arrival rates, parking departure rates, and occupancy rates of valid parking berths. The correlation characteristic formula can be expressed as:

$$r_{xy}(l) = \frac{c_{xy}(l)}{\sqrt{c_{xx}^2(0) c_{yy}^2(0)}} \quad l = 0, \pm 1, \pm 2 \cdots \tag{3}$$

$$c_{xy}(l) = \begin{cases} \sum_{t=1}^{T-l} (x_t - \bar{x})(y_{t+l} - \bar{y}) / T & l = 0,1,2,3 \cdots \\ \sum_{t=1}^{T+l} (y_t - \bar{y})(x_{t-l} - \bar{x}) / T & l = 0,-1,-2 \cdots \end{cases} \tag{4}$$

where $r_{xy}(l)$ is the cross correlation coefficient of time series $\{x_t\}$ $\{y_t\}$ under

lagging time l; $\{x_t\}$ and $\{y_t\}$ are the values of pair wise correlation coefficients among parking arrival rates, parking departure rates, and occupancy rates of valid parking berth. The other parameters are the same as above.

Based on the time series in Figure 1, the results of cross correlation among parking arrival rates, parking departure rates, and occupancy rates of valid parking berths analyzed by software Eviews5.0 are shown as follows.

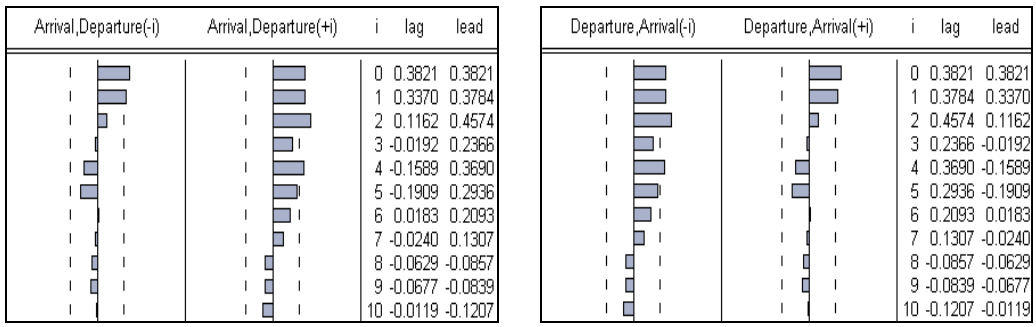

(a) **(b)**

Figure 3. Cross correlation of parking arrival-departure rates (a) and departure-arrival rates (b).

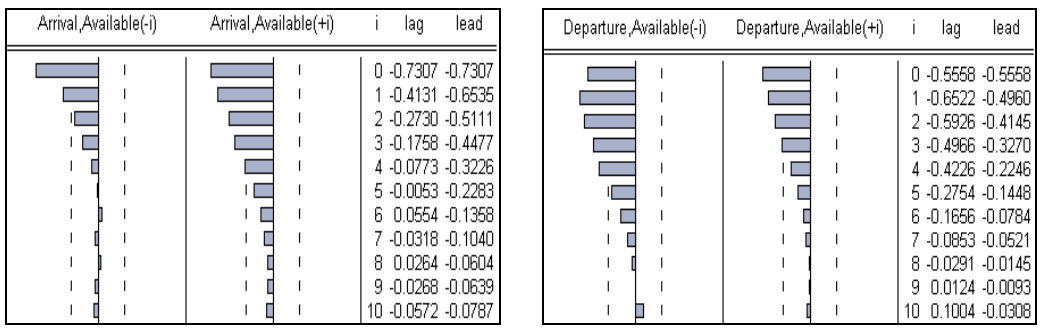

(a) (b)

Figure 4. Cross correlation of parking arrival rates- berth available rates(a) and parking departure rates- berth available rates(b).

Note: -i presents lagging time i; +i presents leading time i.

As shown in the figures, (1) there was a positive correlation between parking arrival rates at time t and parking departure rates form time t-1 to time t+5; (2) parking departure rates at time t are positively correlated with parking arrival rates from time t-1 to time t-5 and that in time t+1; (3) significant negative correlation was observed among parking arrival rates at time t and occupancy rates of valid parking berths at time t-1, and from time t+1 to t+4; (4) there is a negative correlation between parking departure rates at time t+1 and occupancy rates from t-4 to t+3.

CAUSALITY TESTS OF RELATED CHARACTERISTICS

The literature (Jenkins 1968; Jian 2004) shows that causality cannot be determined, although there is a certain correlation between two series. If series $\{x_t\}$

is useful to the series $\{y_t\}$ prediction, there is a remarkable Granger causality relationship from series $\{y_t\}$ to $\{x_t\}$, which means it meets the causality test. The test formula for whether series $\{x_t\}$ causes series $\{y_t\}$ is expressed as follows:

$$y_t = \alpha_0 + \alpha_1 y_{t-1} + \cdots + \alpha_l y_{t-l} + \beta_1 x_{t-1} + \cdots + \beta_l x_{t-l} \quad (5)$$

where α_0 , α_1 …, α_l are the regression coefficients; F statistics is Wald statistics with joint hypothesis. The joint hypothesis is $\beta_1 = \beta_2 = ...\beta_l = 0$, which means there is no causality relationship between $\{x_t\}$ and $\{y_t\}$ according to the Granger causality test.

Using the test equation above, the causality relationship of parking arrival rates and parking departure rates Lag=1~40 is tested separately. The results show that when lag=1~9, the variety of parking arrival rates can cause changes in parking departure rates, and changes in parking departure rates can cause changes in parking arrival rates. This means that parking arrival rates in the past 1~9 periods affect the current parking departure rates.

FORECASTING MODEL OF PARKING ARRIVAL AND DEPARTURE RATES BASED ON CORRELATION ANALYSIS

Based on the 30 samples of 40 pieces of 15-minute periods in Figure 1, the prediction time series model can be made by regression, expressed as follows:

$$y_t = -4.5281x_{t-1} + 7.5985 - 0.4584y_{t-1} + \varepsilon_t - 0.5088\varepsilon_{t-2} - 0.9851\varepsilon_{t-4} \quad (6)$$

$$z_t = -6.6854x_{t-1} + 0.2565y_{t-6} + 6.8123 - 0.7925z_{t-5} + \varepsilon_t - 0.9777\varepsilon_{t-9} \quad (7)$$

where y_t is parking arrival rates at time t (pcu/15 min); z_t is parking departure rates at time t (pcu/15 min); x_{t-1} is occupancy rates of valid parking berths at time t-1; y_{t-1} is parking arrival rates at time t-1; y_{t-6} is parking departure rates at time t-6; z_{t-5} is parking departure rates at time t-5; and ε_t is the random disturbance at time t .

Using the prediction model from formulas (6) and (7), the comparison between the prediction value and the actual value can be obtained by predicting the parking arrival rates and departure rates from periods 31 - 40 as follows.

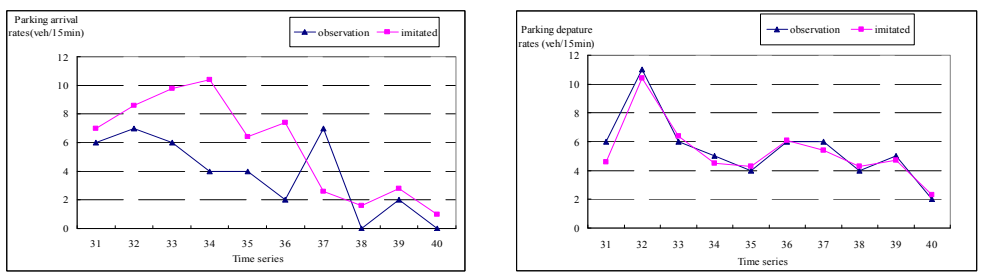

(a) **(b)**

Figure 5. Comparison between prediction value and actual value of parking

arrival rates (a) and departure rates (b).

The results shown in Figure 5 indicate that the prediction model based on correlation analysis can reflect the trend of parking arrival rates and fits well to the departure rate in different periods at actual parking lots.

CONCLUSION

By investigating parking arrival and departure rates on work days, the time series was set as intervals of 15 minutes and then autocorrelation, cross correlation, and causality of the time series were analyzed. The main conclusions are as follows:

(1) Current parking arrival and departure rates are distinctly autocorrelated with the two adjacent parking arrival and departure rates and are distinctly partial correlated with one adjacent parking arrival and departure rate.

(2) The parking arrival rate of the previous time can evidently affect the parking departure rate, while the parking departure rate does not influence the parking arrival rate.

(3) The parking arrival rate of the previous time evidently affects the occupancy rate of valid parking berths, while the occupancy rate of valid parking berths has little influence on the parking arrival rate.

(4) The parking departure rate of the previous time can evidently affect the occupancy rate of valid parking berths, and the occupancy rate of valid parking berths can also affect the parking arrival rate.

(5) Prediction models based on correlation analysis demonstrate promising performance for modeling parking arrival and departure rates. Results mentioned above provide technical support for the association study of parking arrival and departure rates.

ACKNOWLEDGMENT

This research is supported by National High-tech R&D Program (863 Program: 2008AA11Z201); National Key Technologies R&D Program (2006BAJ18B01); The Program for New Century Excellent Talents in University of China (NCET-07-0176).

REFERENCES

Chen Jun, Zhou Zhiyong, Mei Zhenyu etc.. (2007). *Urban parking facility planning and guidance information technique*. Southeast University Press. Nanjing.

Danhui, Y. (2002). *Data analysis and Eviews application.* China Statistics Press, Beijing.

Guan Hongzhi, Yao Yonngsheng. (2005). “A choice model of the length of parking time in CBD.” *Journal of Highway and Transportation Research and Development,* 22(11),144-158.

Hai, Y., Xiaoguang, Y., and Baojie, Y. (2005). "Parking choice model study for special events." *China Journal of Highway and Transport*, 18(2), 90-93.

Jenkins, G. M., and Watts, D. G.. (1968). *Spectral analysis and its applications.* Holden Day, San Francisco.

Jian, Z., and Zinai, L. (2004). "Applicability of the Granger causality test". *Journal of Tsinghua University (Science and Technology)*, 44(3), 358-361.

Lam, W. H. K., et al. (2006). "Modeling time-dependent travel choice problems in road networks with multiple user classes and multiple parking facilities." *Transportation Research Part B,* 40, 368-395.

Paniati, J. (2007). "Advance parking management systems: A cross-cutting study." U.S. Federal Highway Administration.

Transit Network Optimization Method Based on BRT Attracting Region: A Case Study of Changzhou

Zimu Li, Xuewu Chen, and Xiaoqing Liu

School of Transportation, Southeast University; No.35, JinXiangHe Road, Nanjing, Jiangsu Province, PRC, 210008; PH: (86) 15850552234; email: mzzm414@163.com

ABSTRACT

There are two approaches in common transit network optimization (TNO) research: if only adjusting routes, the network may lack integration; otherwise, network adjusting would reduce the operability. To overcome these problems, this paper proposed a TNO method based on research in City of Changzhou. First, bus routes in BRT attracting regions were found and classified according to their position relationship, influence extent and function split. Then optimal schemes of each route were generated using some optimization methods. Second, the concept of key nodes was proposed for the first time. The network was rebuilt by expectation line search. Optimal schemes were established after schemes were screened. Finally, schemes comparison was conducted according to the optimal objective function and the optimum solution was determined. The method was applied for BRT No.2 in City of Changzhou. The results show that the passenger flow volumes are greatly increased.

Keywords**:** *transit network optimization*, *BRT*, *route classification*, *key node*, *network integration*

1 INTRODUCTION

Due to serious urban traffic congestions in China, public transportation systems become increasingly important. Normal bus systems have several disadvantages, such as the limited capacity, slow speed, poor accuracy, etc. Thus, the normal bus systems cannot provide enough capacity and level of service for urban transportation needs. MRT and LRT are now being built in some cities. BRT becomes an important option because it can be the skeleton of public transportation and fill the incapability of MRT and LRT. However, the normal bus network and the BRT system are interrelated. Thus, the normal bus network needs to be optimized in order to increase the benefit of BRT. In addition, the convenience of transit passengers needs to be maintained

2 MAJOR BACKGROUNDS IN THIS PAPER

(1) BRT attracting region

BRT attracting region is a continuous public transit attracting region based on each station of BRT, where passenger collecting-distributing and flow volume are

high. The immediate service radius may range from 500m to 800m. A median value of 650m is suitable according to its function and level of service (Zhang, 2007).

(2) Overlap station and overlap section

An overlap station has the same name with a normal bus stop or nearby stops (e.g. less than 100m). The number of overlap stations is noted as T. We define the section of normal bus route between the first and the last overlap station as one overlap section of this normal bus route with $T \geq 2$. Number (N) is a classification parameter. An example can be seen in Figure 1.

(3) Node, key node and node expectation line

Nodes include (i) road network intersections, (ii) transit stations and stops, and (iii) original stations and destination stations of BRT and normal buses. Key nodes are locations where a route must pass. They are usually near important passenger collecting-distributing areas such as traffic hubs, residential areas, schools, hospitals, etc. The basic location of a bus route can be obtained by linking its key nodes according to their spatial locations. A node expectation line is a line that connects key nodes and some optional nodes of a route, and represents the expectation location of this route.

3 TRANSIT NETWORK OPTIMIZATION METHOD

3.1 Summarization of transit network optimization method

The TNO Method has three parts. The flow chart of it is shown in Figure 2.

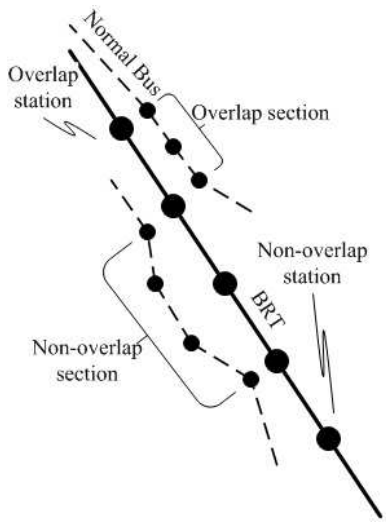

Figure 1. Overlap stations and overlap sections

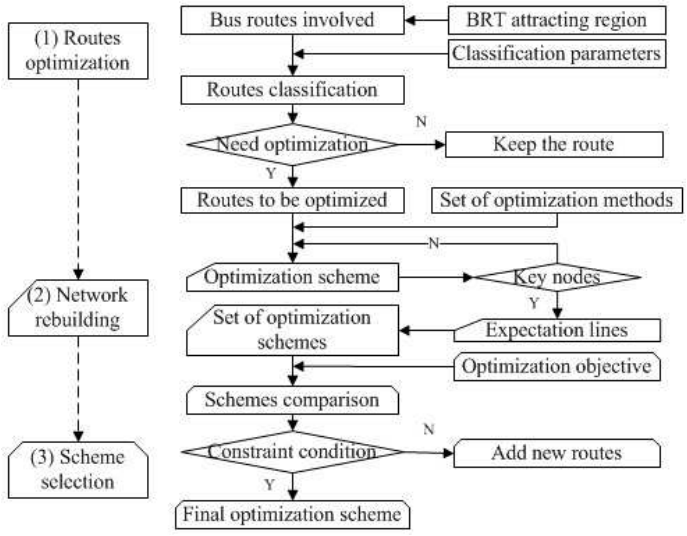

Figure 2. Flow chart of TNO method based on BRT attracting region

3.2 Routes Optimization

3.2.1 Routes classification

(1) Classification by position relationship

There are three types of routes (see Table 1) after classification. The parameters are amount of overlap stations (N) and overlap sections (T). An overlap route usually has some similar sections with BRT and needs more improvements. A cross route usually crosses the BRT corridor and needs less improvements. The other routes are usually unnecessary to be improved.

Table 1. Classification by position relationship

Classification	Name	Parameters
I	Overlap-route	$N \geq 1$, and $T \geq 2$
II	Cross-route	$N = 0$, and $T \geq 1$
III	Other-route	$N = 0$, and $T = 0$

(2) Classification by influence extent

The classification parameters are p and T (see Table 2). $p = \sum l_N / l_{BRT}$, where l_N is the length of an overlap section and l_{BRT} is the total length of BRT route. A competition route may impact operations and passenger collecting-distributing of BRT. An assistant route has benefits for BRT and needs optimization to release their capacity and increase transfer volume.

Table 2. Classification by influence extent

Classification	Name	Parameters
A	Competition-route	$p \geq 20\%$, or $T \geq 4$
B	Assistant-route	$0.5\% \leq p < 20\%$, or $2 \leq T < 4$
C	Unrelated-route	$p < 0.5\%$, or $T \leq 1$

(3) Classification by function split

Routes after optimization have different functions for BRT, which are the basis of the classification (see Table 3). A branch route is a part of BRT system that serves important areas which are insufficiently serviced by the BRT corridor. A feeder route has origin or destination stations in BRT attracting regions.

Table 3. Classification by function split

Classification	Name	Function
a	Branch-route	Supporting the BRT mainline
b	Feeder-route	Normal bus connected to BRT
c	Generic-route	The other independent routes

3.2.2 Optimization judgment

The judgment parameters are *P*, *L*, and *S*. *P* is the overlap stations' proportion in all stops of a normal bus route whose number is *t*, i.e. $P = T / t$; *L* is the length of the longest overlap section; and *S* is the distance between normal bus stops and BRT stations which are in the same overlap station. *S* should be compared with the average riding distance of BRT, which is noted as *D*. Values in Table 4 are for cities where BRT is the main skeleton of public transportation. Once one parameter is not optimal, the route needs to be optimized.

Table 4. Critical values of optimization judgment parameters

Parameters	Values need optimization	
	Urban district	Suburban district
L	$L > 0.5\ D$	$L > 0.8\ D$
S	$S > 50$m	$S > 80$m
P	$P > 60\%$	

3.2.3 Set of optimization methods

I-A, I-B and II-B (there is no II-A routes) routes' optimization are usually easier than the other types. The methods are shown in Table 5. Every route that needs to be optimized has been processed by several optimization methods, where each method includes several optimization schemes. The methods can also be used together. For example, we can extend a route's original station while adjusting its destination station.

Table 5. Set of optimization methods

Method	Explanation	Route types
Adjusting	Adjusting stop spacing and route location	I-A, I-B, II-B, others
Extending	Extending certain operation section	I-A-a, I-A-c, I-B, II-B
Truncation	Cutting off certain operation section	I-A, I-B, II-B-c
Revocation	Cancelling the operation of a route	I-A-c

3.3 Network rebuilding

3.3.1 Determination of key nodes

Key nodes play a crucial role in determining a bus route's direction and location. The methods to determine key nodes include Manual Approach, System Analysis and Market analysis Project (Chua and Silcock, 1982, and Chua, 1984), which focus on the existing routes and emphasize the application of experience. Otherwise, the final scheme will greatly vary from the present network and will be difficult to be implemented.

3.3.2 Establishment of node expectation lines

The establishment of node expectation lines is based on route searching, in an attempt to obtain optional nodes that can connect contiguous key nodes. The set of node expectation lines is determined using searching results and needs to satisfy the following conditions:

$$l_{min} \le l \le l_{max}$$
$$= l / d \le \ _{\max}$$

where l is the length of expectation lines; l_{min} and l_{max} are minimum and maxinum values of length of bus routes (km); and d is the straight distance between the origin and destination of expectation lines. Usually, l_{min} = 5km, l_{max} = 15km, and $_{\max}$ = 1.4 (Urban road traffic planning and designing standard, 1995).

3.3.3 Set of optimization schemes

Each optimization scheme of a route to be optimized should be compared with the nodes expectation lines of this route. Then screening schemes that can meet the constraint conditions is taken to establish set of optimization schemes.

3.4 Scheme selection

3.4.1 Optimization objective

The objective is to decrease competition routes, optimize assistant routes and increase BRT passenger flow volume (PFV). The PFV of BRT mainline and branch routes and transfer volume need to be increased.

$$\max f = \sum_{i \in R} f_{\mathrm{m}}(i) + \sum_{\in R} f_{\mathrm{a}}(i) + \sum_{\in i \ R} f_{\mathrm{b}}(i) + \sum_{\in \ i \ R} f_{\mathrm{c}}(i)$$

s. t.

$$X \le X_{\max}$$
$$e(i) \le e_{\max}(i)$$
$$q(i) \le q_{\max}(i)$$
$$r_a \ge r_b$$

$f_{\mathrm{m}}(i)$ is the PFV of the ith BRT mainline (person/day); $f_{\mathrm{a}}(i)$ is the PFV of the ith BRT branch route ; $f_{\mathrm{b}}(i)$ and $f_{\mathrm{c}}(i)$ are the transfer PFV from the ith feeder route and the ith generic route; X and X_{max} are transfer ratio and maximum transfer ratio; $e(i)$ and $e_{max}(i)$ are PFV of the ith cross section of BRT (Chen, 2002) and the maximum value of it (person/hour); $q(i)$ and $q_{max}(i)$ are PFV of the ith node of BRT and the maximum value of it (person/hour); r_a (r_b) is the covered area rate after (before) the optimization process; and r_a needs to be higher than r_b to avoid service blank.

3.4.2 Schemes comparison and selection

Set of route optimization schemes (R) was obtained after routes optimization and network rebuilding are finished. Steps of schemes comparison and selection are as follows.

Step1. Select the first route optimization scheme of each route from *R*, and establish original optimization scheme M_0;

Step2. Input related data (include OD matrix, route information, time value, etc.), and calculate M_0 to obtain the original solution;

Step3. Select the *j*th route optimization scheme of the *i*th route to establish optimization scheme M_{ij}; and

Step4. Calculate M_{ij} to find the optimum solution.

4 CASE STUDY OF CHANGZHOU

The length of mainline of BRT No. 2 is about 21km, and there are 2 origin and destination stations and 23 couples of stops. The classification of the routes to be optimized in BRT attracting region are shown in Table 6.

Table 6. Classification of routes to be optimized

Classification	I-A-a	I-A-b	I-A-c	I-B-a	I-B-b	I-B-c	II-B
Counts	2	2	1	1	2	4	9

A BRT network with one mainline and three branch routes was established by using the TNO method based on BRT No. 2 attracting region (see Figure 3). Nine routes were mainly optimized with one route truncation. Other routes were optimized mainly by adjusting the distance from BRT overlap stations to assistant operation of BRT (see Figure 4). With appropriate operation dispatching, the daily PFV of the mainline of BRT No. 2 after the optimization process was 80,000 persons by forecasting in TransCAD. The PFV is increased by about 25%. The optimization's benefit is significant.

Figure 3. Optimization BRT network

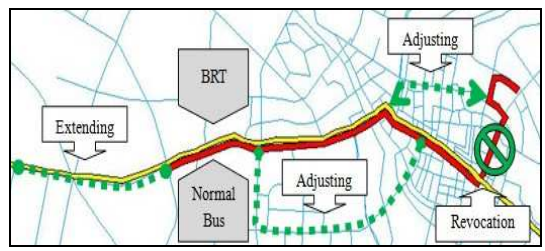

Figure 4. Optimization schemes

5 CONCLUSIONS AND RECOMMENDATIONS

The method proposed in this paper conducts the optimization step by step, increasing the optimization flexibility. The comparison and selection of scenario analysis can be done for different optimization objectives. Disadvantages, such as difficult to implement caused by many theoretic optimization and inconvenient trip of residents, can be avoid. of the current transit network and operation efficiency are increased which has been confirmed by Changzhou Public Transport Company. The convenient and safety problem caused by the increasing of transfer times can be solved by seamless integration of stations.

The method focuses on BRT network with single mainline. The parameters in

classification of routes are usually physical facilities. In future research, we will analyze large transit networks with multiple BRT mainlines. The structure of the method and the parameters of classification need to be adjusted. The algorithm will be improved for the application in cities with more complex circumstances.

ACKNOWLEDGEMENTS

This research is supported in part by the Research Fund for the Doctoral Program of Higher Education of China (20070286011), China Sustainable Energy Program of the Energy Foundation (G-0803-09882) and Suzhou Integration Program of Rail Transit and Ground Transportation (ZXJ0804).

REFERENCES

Chen, X. W. (2002). "Section 7: Urban mass rail transit system planning method." *Urban public transport system planning method and management technology*, Wang W, Yang X. M. and Chen X. W., Beijing, 7.2.3.

Chua, T. A. and Silcock, D. T. (1982). "The practice of British bus operators in planning urban bus services." *Traffic Engineering and Control*, Vol. 23: 66-70.

Chua, T. A. (1984). "The planning of urban bus routes and frequencies: a survey." *Transportation*, Vol. 12(2): 147-172.

Urban road traffic planning and designing standard (1995), *MOHURD*.

Zhang, S. J. (2007). "BRT system network planning theory." *Study on urban BRT system planning theory and method*, Beijing Jiaotong University, 4.3.3

Efficiency Evaluation of Urban Transit Terminals Based on the Cloud Model

Shijun Yu[1] Yingshun Liu[2] and Yongneng Xu[3]

[1] Vehicle & Transportation Department, Nanjing University of Science & Technology, Nanjing 210094, P. R. China; Tel.: 86-25-84315833; email: fishte@163.com (corresponding author)
[2]Vehicle & Transportation Department, Nanjing University of Science & Technology, Nanjing 210094, P. R. China; Tel.: 86-25-84315833; email: yingshun@mail.njust.edu.cn
[3]Vehicle & Transportation Department, Nanjing University of Science & Technology, Nanjing 210094, P. R. China; Tel.: 86-25-84315833; email: x780906yn@163.com

Abstract：The urban transit terminal plays a significant role in urban transportation system for passenger distribution and transfer. Transfer efficiency is regarded as a key factor of urban transit terminal operational performance which reflects level of service. Thus, efficiency evaluation of urban transit terminal is important to measure the level of service improvement. First, influence factors of terminal transfer efficiency are analyzed and the corresponding evaluation index system is proposed. Then, based on the cloud model, a comprehensive evaluation model for the transfer efficiency of urban transit terminal is investigated. In this evaluation model, fuzzy and random qualitative concepts are integrated; uncertainty expressions are mapped to different cloud particles; variations of the weight are mapped to mathematical expectation of clouds; and the efficiency of urban transit terminal transfer is evaluated synthetically. Finally, an applicative example is used to show that the evaluation model is efficient and effective.

Key words: urban transit terminal, transfer efficiency, evaluation, cloud model

1. Introduction

An urban transit terminal is part of very large urban transportation service systems. The transit terminal plays an important role in urban transportation system for passenger distribution and transfer.

Kwon and Kwon (2003) studied the impact of the effective use of the coefficients in park and ride facilities. Beimborn et al. (2003) investigated public transport services on coefficients, such as accessibility and connectivity. Shih et al. (1997) developed a synchronous transfer Interval travel design model. Bates(1978) treated the existing transport system to improve the transfer facilities, and he suggested that transfer facilities must be more efficient to encourage passengers to use the transfer. Ye and Tan (1998) analyzed the problems of urban rail transit transfer and made some suggestions. Wang and Li (2003) analyze and deduce the

mean transfer time formula, present some measures on other transportation transfer, and keep track of them in full coordination to attract more passengers. Many other studies also examine urban passenger transfer problems (Qin, 2003; Du, 2005; Wu, 2005). The research of urban transit terminal is mainly concentrated on the choices of transfer modes and transfer facilities planning. Evaluation of urban transit terminal transfer efficiency did not receive enough attentions. At present, researches focus on transfer facilities' effectiveness and many issues impact transfer facilities in major cities, including transfer facilities, location, size and configuration.

Transfer efficiency is regarded as a key factor of urban transit terminal operational performance which reflects level of service. Thus, measuring the efficiency of urban transit terminals is very important. In this paper, a cloud-model-based method is introduced to evaluate efficiency of urban transit terminals.

2. Cloud model and uncertainty illation

2.1 Concept of cloud model

The cloud model is an uncertainty conversion model between some qualitative concepts expressed with linguistic words and their relative quantitative values. Let U as a domain comprising accurate numbers, whose accorded qualitative concept is $\tilde{A}$. For any given element X in the domain, there is a random number having stable tendency $y = \mu_{\tilde{A}}(x)$, which is called certainty degree of x for $\tilde{A}$. The distribution of y in domain is called the cloud model, or the cloud in a simpler name. The cloud consists of a number of cloud drops, each of which presents one point projected from qualitative concept to numeral domain. For its every realization, the cloud model can denote the certainty degree of the point, reflecting some qualitative concept.

The cloud is identified by three digital characteristics, E_x (expected value), E_n (entropy) and H_e (hyper entropy), which express the quantity feature of qualitative concept.

The algorithm of generating the cloud is called the cloud generator, which includes forward cloud generator, condition X cloud generator, condition Y cloud generator and backward cloud generator. When the cloud drops are produced by the digital characteristics of cloud, the cloud generator is called forward cloud generator; when cloud's three digital characteristics (E_x, E_n, H_e) and the special value x_0 are given, the cloud generator is called condition X cloud generator; when cloud's three digital characteristics(E_x, E_n, H_e) and the special value μ_0 are given, the cloud

generator is called condition *Y* cloud generator; if a group of cloud drops(x_i , μ_i) satisfying normal distribution to be specimen is given and the three digital characteristics(E_x , E_n , H_e) of cloud model are known, we call this backward cloud generator. Condition *X* cloud generator and condition *Y* cloud generator are the basis of conducting uncertainty illation by cloud model. By integrating the forward cloud generator and the backward cloud generator, the conversion between qualitative words and quantitative values can be achieved at any moment.

2.2 Uncertainty illation based on cloud model

The formal description of a qualitative rule is: if *A* then *B*. *A* and *B* are cloud objects, denoting language value. The cloud generator is the basis of conducting uncertainty illation by cloud model. Connecting a condition *X* cloud generator and a condition *Y* cloud generator can yield a single rule generator. Figure1 presents the schematic diagram about single rule generator. In the figure, CG_A denotes condition *X* cloud of the input language value *A*. CG_B denotes condition *Y* cloud of the output language value *B*. When we input some special value x_0 to activate CG_A, CG_A produces a group of figures μ_i (μ_i reflects the corresponding qualitative rule's activation intensity), and pipes into CG_B, this figure μ_i controls CG_B to produce a group of random drops (y_i , μ_i). It needs a brief account that the cloud drop and output produced by generator are not only one and uncertain, so it can achieve uncertainty illation.

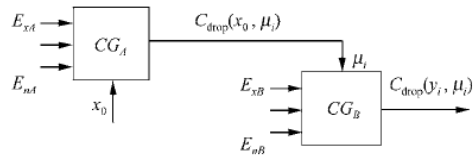

Figure1. Single rule generator

3. Description of evaluation factors with cloud model

3.1 Evaluation factors

Three criteria are taken into account in the evaluation: convenience, comfort and safety. Each criterion consists of several factors, which are shown in Table 1.

3.2 Description of evaluation factors

The evaluation standard of every evaluation factor is according to the knowledge of experts respectively. A qualitative and fuzzy language is used to express a certain numerical range.

Table 1. Evaluation factors

Convenience	Comfort	Safety
Total walk time	Climate control	Police protection
Total time in system	Area per person	Emergency response
Route travel times	Rest room facilities	Entry control
Total delay	Avoid crowding	Emergency egress
Queue length	Waiting areas	Safe walking
Flow conflicts	Cleanliness, sanitation	Surfaces
Connectivity	Esthetic design	Lighting
Directional information		
Service reliability		
Consumer services		

For example, the evaluation standard "shorter, short, common, long, longer" in factor "total walk time" is according to the time spend by walk in the transfer process. The evaluation standard of the factor "queue length" is according to the length of queue. So do others.

The five qualitative concepts of the evaluation standard of the factor "total walk time (unit in second)" are expressed with cloud model in time field as follows:

$$D_{A_1} = \begin{cases} 1, & x \in [0,60] \\ D(60,60/3,0.05), & \text{others} \end{cases}$$

$$D_{A_2} = D(120,60/3,0.05)$$

$$D_{A_3} = D(180,60/3,0.05)$$

$$D_{A_4} = D(240,120/3,0.05)$$

$$D_{A_5} = \begin{cases} D(360,120/3,0.05), & \text{others} \\ 1, & x \in [360,\infty) \end{cases}$$

4. Evaluation based on the cloud model and correlation analysis

4.1 Data preparation

First, we use the cloud model to express the factor's evaluation standard of transfer efficiency. The cloud model was discussed in Section 2.

Before analyzing the relation between transfer efficiency and evaluation factors, we can translate the uncertain factor conditions into quantitative impact.

By using the factor "total walk time" as an example, we can establish the qualitative illation rule by the knowledge of expert as follows:

1) if total walk time is "shorter", then impact value is "higher";

2) if total walk time is “short”, then impact value is “high”;
3) if total walk time is “common”, then impact value is “common”;
4) if total walk time is “long”, then impact value is “low”; and
5) if total walk time is “longer”, then impact value is “lower”.

The five qualitative concepts of the rule’s rear are expressed with the cloud model in impact value fields as follows:

$$D_{B_1} = D(90,15/3,0.05)\,; D_{B_2} = D(70,15/3,0.05)\,; D_{B_3} = D(50,15/3,0.05)\,;$$

$$D_{B_4} = D(30,15/3,0.05)\,; D_{B_5} = D(10,15/3,0.05)$$

Using the cloud of the rule’s front to drive forward cloud generator, we can obtain a group of distance figures, then determine theirs average to be the input of condition X cloud generator, and count the certainty degrees of the five qualitative concepts of the rule’s front respectively. Finally, we can determine the maximum μ_i.

If the *i-th* rule in rule-base is activated, the activation intensity is μ_i. After using the single rule generator to generate output, we select the output to be this factor’s impact value. When calculating the output by using the algorithm of condition Y cloud generator, we choose the plus or the minus by corresponding whether the input is of up or down. When $x < E_{xA}$, we choose the minus, while if $x > E_{xA}$, we choose the plus. According to survey data we can get samples to establish the rules. The form of samples data is shown in Table 2.

Table 2. Samples data

Factors	Terminal 1	Terminal 2	Terminal 3	Terminal 4	Terminal n
Total walk time	97.20	76.73	63.25	86.26	…
Total time in system	87.52	80.34	70.80	68.43	…
Route travel times	96.13	87.38	76.15	91.43	…
Total delay	85.08	84.70	80.43	72.99	…
Queue length	96.12	95.26	86.98	68.10	…
Flow conflicts	96.24	93.99	95.99	79.30	…
Connectivity	73.78	70.36	84.69	66.04	…
Directional information	94.54	91.28	91.55	69.39	…
Service reliability	73.78	70.36	84.69	52.29	…
…					…

4.2 Calculating weights by correlation analysis

First, we must normalize the reference data, compare data, then calculate weights of transfer efficiency factors according to the following formula:

$$\zeta_i(k) = \frac{\min_i \min_k |x_0(k) - x_i(k)| + \zeta \max_i \max_k |x_0(k) - x_i(k)|}{|x_0(k) - x_i(k)| + \zeta \max_i \max_k |x_0(k) - x_i(k)|}$$

$$r_i = \frac{1}{n}\sum_{k=1}^{N} \zeta_i(k)\,; w_i = \frac{r_i}{\sum_{k=1}^{n} r_i} \times 100$$

where x_i is impacting value; $\zeta_i(k)$ is the correlation coefficient x_i to x_0 in moment *K*; ζ is distinguished coefficient, usually chosen between 0 and 1; r_i is the correlation degree of each transfer efficiency factors; and w_i is the weight of each transfer efficiency factors.

After calculating, the weight of transfer efficiency evaluation factors is shown in Table 3.

Table 3. Weight of transfer efficiency evaluation factors

Index	Weight	Index	Weight	Index	Weight
Convenience	**47.62%**	**Comfort**	**19.05%**	**Safety**	**33.33%**
Total walk time	11.22%	Climate control	15.51%	Police protection	14.75%
Total time in system	10.10%	Area per person	13.20%	Emergency Response	16.39%
Route travel times	7.86%	Rest Room Facilities	14.85%	Entry control	11.48%
Total delay	12.35%	Avoid crowding	16.50%	Emergency egress	13.11%
Queue length	13.47%	Waiting Areas	14.03%	Safe walking	18.03%
Flow conflicts	8.98%	Cleanliness, sanitation	14.36%	Surfaces	13.93%
Connectivity	7.86%	Esthetic Design	11.55%	Lighting	12.30%
Directional information	7.63%				
Service reliability	10.66%				
Consumer services	9.88%				

By analyzing the weight of factors, we can find which factors effect transfer efficiency significantly and must be improved. With the weight of factors, the comprehensive evaluation of transfer efficiency also can be obtained.

5. Conclusion

The analysis of the variability of factors which impact on the transfer efficiency of urban transit terminals may provide useful insights on the strengths and weaknesses of a given transportation terminal service and recognize qualitative attributes that need special attention. This research focused on the transfer efficiency of urban transit terminal performance and employed the cloud model to assess the

quality implications of the variability of the efficiency with respect to the transit terminal systems.

In conclusion, this research demonstrates how factor analysis and cloud model may be used to analyze the variability of transfer efficiency and how the results and findings of this process may contribute to policy and decision making. The urban transit terminal operators and authorities may include these methods in their quality-control programs in order to facilitate the formulation of short- and medium-term action plans. Depending on the aim and nature of a survey and the level of detail of the collected data, this proposed approach may assist in operational adjustments related to service frequencies, network expansion, facilities configuration, network coverage and many others.

References

Bates, E G. (1978). "A study of passenger transfer facilities", *Transportation Research Record,* 662.

Beimborn, E. A., Greenwald, M. J., and Jin, X. (2003). "Transit accessibility and connectivity impacts on transit choice and captivity." *80th Annual Meeting of the Transportation Board*, Washington, DC.

Du, C., and Jiang, Y. (2005). "Connection of urban rail transit with other public transportations." *Urban Rapid Rail Transit*, 18 (3): 45-49 (in Chinese).

Li, D., Wang, S., Li, D., et al. (2002). "Theories and technologies of spatial data mining and knowledge discovery." Geomatics and Information Science of Wuhan University, 27(3):221-233.

Li, D.. (2005). "Artificial intelligence with uncertainty." National Defense Industry Press, Beijing.

Kwon, Y. J., and Kwon, Y. I. (2003). "Elements for the effective use of park-and-ride facilities in the Seoul metropolitan areas, Korea," *80th Annual Meeting of the Transportation Board*, Washington, DC.

Qin, Y., Yan, K. and Zhao, T. (2003). "A study on the change system of urban synthetic passenger transport system." *Journal of Changsha Communications University*, 16 (2): 67-72 (in Chinese).

Shih, M., Mahmassani, H.S., and Baaj, M. H. (1997) "Trip assignment model for timed transfer transit systems." *76th Annual Meeting of the Transportation Board*, Washington, DC.

Wang, Q. P., and Li, F. (2003). "On the coordination of switching non-rail transport modes to rail transport modes in urban passenger traffic system." *Journal of Xi an University of Architecture &technology*, (2): 136-150(in Chinese).

Wu, Y., and Zhang, X. (2005). "The transfer with bus system and counter measurements of urban mass transit." *Urban Rail Transit*, 25(8): 19-21.

Ye, X., and Tan, F. (1998). "The transfer and lighter in urban public transport." *Urban Mass Transit*, 3:22-25 (in Chinese).

Travel mode choice in large cities of China based on loss aversion theory

ZHOU Xuemei[1] MENG Yan[2] DI Di[3]
[1] School of Transportation Engineering, Tongji University, China, zhouxm @ mail. tongji.edu.cn
[2]Transportation and Traffic College, Jilin University, China, rachelmeng 2004 @ sina. com
[3] School of Transportation Engineering, Tongji University, China, didi 02121226 @ 163.com

Abstract

Public transportation priority development is a basic policy to solve the problem of travel of Chinese people. Firstly, the author Analysis the means of urban traffic and their characteristics in China, then point the factors affecting their choice and the method professors used to study. Secondly, using the traffic survey analysis, prepare the questionnaire to determine factors which are important to the choosing of travel mode. Thirdly, construct the main factors related variables and passenger travel will of the asymmetric response model with multiple linear regression method. Finally, through the analysis of the status quo of China's urban traffic and passengers will travel model of asymmetric response, and from policy implementation, technical standards and the law-making, give some suggestions improve urban transportation system structure, improve the urban living environment, and ease urban traffic.

1. Introduction

With the steady development of the national economy, urban traffic development is rapid in our country, the large and middle scale cities have had a complete transportation system basically. However, the growth of vehicle's quantity and the increase of road course are uncoordinated, so residents' normal journey is difficult and discommodious seriously (Benartzi et al. 1995).

Li Linbo and Wu Bin (Li Linbo et al, 2003) pointed travelers can make their own choice from time, expense and environment, traffic modes can be chose and so on. And they make a quantitative analysis on factors influenced residents' travel choice. Li Min's (Li Min, 2004) activity-based behavioral analysis mainly studied on people's travel behavior characteristics and the choice characteristics. Zhou Xuemei(ZHOU Xuemei et al, 2007)based on Stated Preference Survey, individual characteristic and travelers intentions criteria are discussed and the effects of public transit choice are derived, Travel mode choice model is established on the basis of the surveyed data of Cixi in China. Zong Fang(Zong Fang et al, 2007) built a travel mode choice model based on the Logistic model and analyzed the effect of the policy of encouraging application of the

public traffic system on the travel modes of the inhabitants. Abdellaoui (Abdellaoui et al. 2007) analyzed mode choice behavior for suburban trips in the Grand Canary island using mixed revealed preference (RP)/ stated preference (SP) information.

2. Travel Mode Categories in Large Cities and Their Affective Factors

Researching on urban traffic travelers' choices makes an extremely vital role in grasping the present situation of urban traffic (Tversky et al. 1992), forecasting the trend of mass transit development and proposing effective measure for public transportation priority.

At present stage of our country, there are five urban travel modes as followed: the public transportation, the urban rail traffic, the taxi, the sedan and other travel mode such as the motorcycle, the bicycle as well as the ambulation. The large-scale city has a complete municipal transportation system generally.

The transportation characteristic influence mainly means in a journey intrinsic property, factors influenced to travelers' travel mode selection (Bateman et al. 1997). There are the trip purpose, the running time, the distance, the expense, comfortableness, the security, the time reliability as well as transfers the number of times and the waiting time and so on.

The paper chooses the price, the time reliability, the travel time, the security and comfortable as essential factors. And based on this, a questionnaire is established, uses 5-point Likert-type scale. The analysis obtains, the journey expense, the time reliability, the travel time are the most important factors The concrete information as the ***Table 1*** shows.

Table 1.Questionnaire survey second partial information statistics

	The least important(1)	The less Important(2)	Indefinite(3)	The more Important(4)	The most Important(5)
Price	0	0	0	46.03%	53.97%
Punctuality	0	1.02%	1.97%	46.01%	51%
Travel time	0	4.88%	12.07%	43.25%	39.80%
Safety	0	9.89%	13.74%	39.01%	37.36%
Comfortable	2.20%	25.82%	39.01%	18.68%	14.29%

3. Empirical Analysis of Travel Mode Choice in a Large City

3.1. Model Assumptions

According to the actual situation, in order to simplify the model, the assumptions are as follows:

- Within the research period, residents' travel modes are fixed.
- City has a Sound urban transport system.
- No considering of short-distance travel.
- Personal attributes do not affect travel mode.

3.2. Model Specification

We use the following set of variables to specify the function: price (P_i), schedule (S_i), time(T_i). These variables represent attractiveness of a transport mode and, as shown in previous empirical studies, all of them affect residents' choice directly. The price (P_i) is the representative of the amount of costs of a certain transport mode passengers choose, such as fares, prices, parking fees and other costs; schedule (S_i) represents the on time character of a certain transport mode, such as bus, subway Operation plans in accordance with the time running on time; time (T_i) represents the time of a transport mode need to reach their destinations, to compare different means, we assume that each mode is exactly the same travel routes.

Assuming passengers only choose one mode of transportation, the v_i Function can be written as follows:

$$\begin{aligned} v_i = \alpha_i &+ \beta_1 (PGAIN_i + \lambda_P PLOSS_i) \\ &+ \beta_2 (SGAIN_i + \lambda_S SLOSS_i) \\ &+ \beta_3 (TGAIN_i + \lambda_T TLOSS_i) \end{aligned} \quad (1)$$

P_i is the price or cost of one mode of transportation i at present, S_i is punctuality of the mode of transportation, T_i is the time need of the mode of transportation. P_r represents market price. If $P_i \leq P_r$, $PGAIN_i = P_i - P_r$, and $PLOSS_i = 0$; If $P_i \geq P_r$, $PLOSS_i = P_r - P_i$, and $PGAIN_i = 0$. Similarly, if the punctuality of the mode of transportation i equal to or exceed (better than) the reference point ($S_i \geq S_r$), then $SGAIN_i = S_i - S_r$, and $SLOSS_i = 0$. On the other hand, if the punctuality of the mode of transportation i is lower (inferior to) than the reference point ($S_i < S_r$), then $SLOSS_i = S_i - S_r$, and $SGAIN_i = 0$. So does the T_i.

3.3. Model

According to the statistical data of survey questionnaire, 182 valid, we select the bus, subway, taxi, car and other transport to study(the number of people were 58,51,33,26,14 respectively). Other type of transport is only 0.77 percent, and various factors affects loss aversion.

Because a market share of any transport mode can theoretically range from zero to one only, we utilize the following binary logit function to model a transport mode's market share as

$$S_i = \frac{1}{1 + e^{-v_i}} \quad (2)$$

According to the survey data, we get four functions respectively as follow. Here we take ***bus*** as an example.

$$\begin{aligned} v_{BUS} = -0.727 &+ 0.695(PGAIN + 1.889 PLOSS) \\ &+ 0.344(SGAIN + 3.279 SLOSS) \\ &+ 0.788(TGAIN + 1.346 TLOSS) \end{aligned} \quad (3)$$

According to (3), $\beta_1 = 0.695$, $\lambda_P = 1.889$.

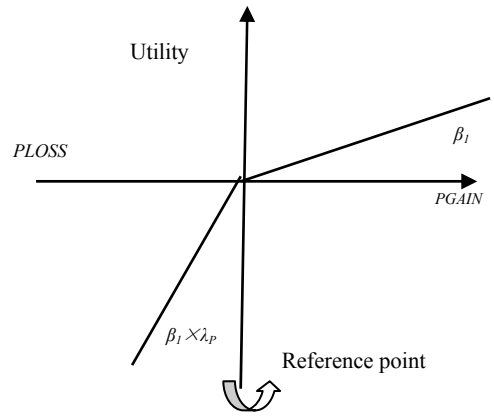

Figure1. Slopes reflecting loss aversion of the price of bus

The relationship can be draw from the price impact of the loss aversion slope map as shown in ***Figure 1***.

Taking into account of the definition of punctuality of any transport mode, subway is always punctual. No punctuality loss aversion effect on subway (the loss is neutral). Therefore, $\boldsymbol{\beta_2 = 0}$. Parameters of other functions, such as the relationship of subway, taxi and car with the loss aversion of the price, schedule and time are list in ***Table 2***, with there test results.

Table2. Parameters of functions

v_i	α_i	β_1	λ_p	β_2	λ_s	β_3	λ_T
bus	-0.727	0.695	1.889	0.344	3.279	0.788	1.346
	0.000	0.018	0.000	0.042	0.001	0.001	0.001
subway	-0.904	1.144	1.767			0.785	1.912
	0.000	0.043	0.000			0.048	0.011
taxi	-1.403	0.344	2.587	0.477	3.071	0.232	5.134
	0.000	0.027	0.000	0.000	0.000	0.037	0.000
car	-1.724	0.448	2.083			0.352	2.946
	0.000	0.448	2.083			0.024	0.000

3.4. Model Testing

To judge the goodness of the models, we use the adjusted R2 values. Its value obtained directly from the computer output with software SPSS15.0 (Yoshinori Suzuki et al. 2001), we calculate the adjusted R2 for each model by the following formula:

$$Adjusted R^2 = 1 - \frac{\sum_i \left(S_i - \hat{S}_i\right)^2 / (m-p)}{\sum_i \left(S_i - \overline{S}_i\right)^2 / (m-1)}$$

Where $\hat{S}_i$ is the predicted value of $\overline{S}_i$, the arithmetic mean of S_i, m is the total number of sample size used for parameter estimation, and p is the number of parameters estimated. The results can be seen in ***Table 3***.

Table3. Test results of functions

model	R	R Square	Adjusted R Square	Std. Error of the Estimate
bus	0.970	0.940	0.912	0.18162825
subway	0.897	0.805	0.753	0.42499817
taxi	0.987	0.973	0.960	0.09447970
car	0.976	0.953	0.932	0.11959297

3.5. Estimation and Analysis

We learn from the attractive function of every travel mode that the loss parameters of loss is larger than that of gain, with price, time and schedule (that is ***PLOSS>PGAIN***, ***SLOSS>SGAIN***, ***TLOSS>TGAIN***). According to the concept of loss aviation in Behavioral Economics (Köbberling et al. 2005), it shows that residents more sensitive with loss than gain. Take bus transport mode for example, if the price (mainly referring to the fare) fell 75 percent, according to calculation formula related above the number of bus travel up to 85, an increase of 46.55 percent; if travel time and punctuality and in the 75 percent, the choice may be drawn bus number 89 and 84 respectively, an increase of 53.45 percent and 44.83 percent. These shows that price, travel time and punctuality are all important to residents who choose bus to travel. In turn, more than 50 percent price increase will cause more residents travel by bus originally change to by subway.

To sum up, passengers who choose bus are more sensitive to punctuality, travel time and the gain of price. However, the price of subway is more sensitive to its punctuality and travel time. Though fast is the main advantage of taxi, when traffic become worse, the choice of taxi passengers will change to travel by subway possibility. Those who travel by car are sensitive to the loss aviation of price significantly. These tell us that we can take various strategies with different transport mode respectively to help passengers choose public transportation.

4. Strategies to Improve Public Transport Attractive

According to the model we point out strategies from three aspects as follows.

4.1. Policy measures

- Increase the social promotion; raise the traffic awareness of all the people.
- Improve the public transport system and its internal level. Improve the public
- Continue to develop urban rail transport vigorously.
- Improve public transport service quality.
- Control the use of cars.

4.2. Technology Strategies

- Public transport Operation priority
- Pricing Scientifically.
- Pricing in accordance with the law.
- Establish a rational mechanism of price subsidies.

5. Conclusions

In the use of the concept of loss aversion in economics, in light of China's large city transport development status and characteristics of the existing mode of travel, the article analysis the affecting factors and their role, and then point out that price is an important factor for every choice, the increase of travel time and the on time loss aviation will decrease the attraction of subway severely, also worse the traffic, worse the car's attraction, in the face of high prices its advantages would not exist. Sound public transport system is a major factor for residents to choose it. Besides strengthening the transportation infrastructure construction, government also can put forward some policies from the implementation of policies, technical standards and the law-making, to improve urban public transport to attract residents, and promote public transportation into a priority situation, and eventually achieve a high ratio of public travel, optimize urban transportation system structure, improve the urban living environment, ease city traffic.

6. Acknowledgments

The research partly supported by National Basic Research Program of China (973 Program: 2006CB705500)

7. References

Abdellaoui, Mohammed, Han Bleichrodt, and Corina Paraschiv. (2007). "Measuring Loss Aversion under Prospect Theory: A Parameter-Free Approach," Management Science 53, 1659–1674.

Bateman, Alistair Munro, Bruce Rhodes, Chris Starmer, and Robert Sugden(1997),"A Test of the Theory of Reference-Dependent Preferences," Quarterly of Economics, 112(May), 479-505.

Benartzi, Shlomo, and Richard H. Thaler. (1995). "Myopic Loss Aversion and the Equity Premium Puzzle," Quarterly Journal of Economics 110, 73–92

Köbberling, Veronika, and Peter P. Wakker. (2005). "An Index of Loss Aversion," Journal of Economic Theory 122, 119-131.

Li Linbo, Wu bing. Psychological factors affect travel mode choosing(2003). Journal of Jiaotong University,11(3),27-31.

Lin Min. Analysis of Activity-based Residential Travel Behavior (2004). Jilin University.

Tversky, Amos, and Daniel Kahneman. (1992). "Advances in Prospect Theory: Cumulative Representation of Uncertainty," Journal of Risk and Uncertainty 5, 297–323.

Yoshinori Suzuki, John E. Tyworth, Robert A. Novack.Airline market share and customer service quality: a reference dependent model (2001).Transportation research Part A 35,773-788.

Zong Fang,Juan Zhi-cai (2007). Activity-based travel mode choice model and analysis on traffic demand management. Journal of Jilin University (Engineering), 37(1), 48-53.

ZHOU Xuemei, ZHANG Xianzun, YANG Xiaoguang, LAO Yunteng (2007). Travel Mode Choice-Based Prediction of Public Transit Demand. Journal of Tongji University (Natural Science), 35(12), 1625-1631.

Topological Properties of Public Transport Networks: A Temporal Perspective

Xiao-Yong Yan [1] and Ming-Sheng Wang [2]

[1]Key Laboratory of Traffic Safety and Control in Hebei, School of Transportation Engineering, Shijiazhuang Railway Institute, Shijiazhuang, Hebei Province, China 050043; PH (0311) 8793-6413; FAX (0311) 8793-5516; email: yanxy@sjzri.edu.cn

[2]Key Laboratory of Traffic Safety and Control in Hebei, School of Transportation Engineering, Shijiazhuang Railway Institute, Shijiazhuang, Hebei Province, China 050043; PH (0311) 8793-5276; FAX (0311) 8793-5276; email: wangmsh@sjzri.edu.cn

ABSTRACT

In this paper, we present an empirical analysis of the topological properties of PTN based on the bus networks data of Shijiazhuang from 1996 to 2008. As a result, we find that the PTN is a small-world, accelerated growing network and a hybrid between a scale-free and a random network. To explain the results, we propose a simulation model based on accelerated growth and nonlinear preference rules to show a possible evolutionary mechanism for PTN. Numerical simulations show that the model performs well in reproducing basic topological properties of the real-world PTNs. The results can help us to understand the evolution mechanism of PTN as well as other evolving transportation networks.

INTRODUCTION

Recent years have witnessed an upsurge in the study of complex systems that can be described in terms of networks (Boccaletti et al. 2006). Public transport networks (PTN) can be mentioned as an important example of these evolving complex networks. There has been a substantial amount of interest in the topological properties and evolutionary processes of PTNs among researchers in different scientific fields (Sienkiewicz and Holyst 2005; Gao et al. 2005; Lu and Shi 2007; Xu et al. 2007; Ferber et al. 2009). These studies made careful analysis of various PTN instances using empirical, simulational, and theoretical tools and revealed the general features of PTN such as small-world, scale-free, and hierarchically-organized. However, most of these studies viewed networks from a static perspective, so it was difficult to capture and explain the evolution mechanism of PTN.

In this paper, we will use complex network theory to analyze the topological properties of PTN from a temporal perspective. An empirical analysis

of PTN based on the bus networks data of Shijiazhuang from 1996 to 2008 is presented first. The results indicate that the PTN is a small-world, accelerated growing network, and its evolution is governed by both random and preferential attachment. Based on the empirical survey, we propose a simulation model that captures the PTN's time evolution. Finally, numerical results are presented to demonstrate the effectiveness of our model.

The set-up of the paper is as follows: in the next section we provide an empirical analysis of the topological properties of the PTNs in Shijiazhuang; in the third section we describe our model for PTN evolution; in the fourth section we compare the major topological properties of simulated and real-world PTNs; discussion and conclusions are given in the last section.

EMPIRICAL ANALYSIS

The empirical study object in this research is the historical data of bus networks of Shijiazhuang from 1996 to 2008, which is provided by the Shijiazhuang Public Transport Corporation. As the bus network is appreciably changing in one-year intervals, we expand interval for 4 years and chose 4 sets of data, which are 1996, 2000, 2004 and 2008.

Usually the PTN can be described by three different topological representations: space L, space P, and space C (Sienkiewicz and Holyst 2005; Ferber et al. 2007). In space P, the network consists of nodes representing bus stops, and an unweighted edge between two nodes exists if there is a direct bus route that links them. In our analysis, we are interested in features of the PTN as measured when represented in space P, because it can better describe the accessibility and convenience of PTNs (Xu et al. 2007). Using this topological representation, the main statistical topological properties of PTNs are calculated and shown in Table 1.

Table 1. Statistical Topological Properties of PTNs of Shijiazhuang in 4 Years.

Year	R	N	E	M	$<k>$	$<l>$	$<C>$	u
1996	44	500	6472	18.23	25.89	2.24	0.86	0.23
2000	70	696	12326	20.39	35.42	2.30	0.80	0.32
2004	86	899	18341	21.24	40.80	2.35	0.78	0.39
2008	104	1033	22027	21.96	42.65	2.38	0.77	0.42

R: number of routes; N: number of nodes; E: number of edges in Space P; M: mean number of stops per route; $<k>$: average degree of nodes, a node's degree k in space P is the number of its neighbors; $<l>$: average path length; $<C>$: average clustering coefficient, the clustering coefficient C is defined as the probability that two neighbors of any given node are also neighbors of each other; u: parameter of the stretched exponential distribution.

To get a deeper understanding of the topological properties of PTNs, we give a detailed analysis of their degree distributions. The degree distribution $p(k)$ gives the probability that a selected node has exactly k links. Another way of presenting degree data is to make a plot of the cumulative distribution function $P(k)$, which can reduce the noise in the degree data (Boccaletti et al. 2006). Figure 1 shows the cumulative node degree distribution of PTNs.

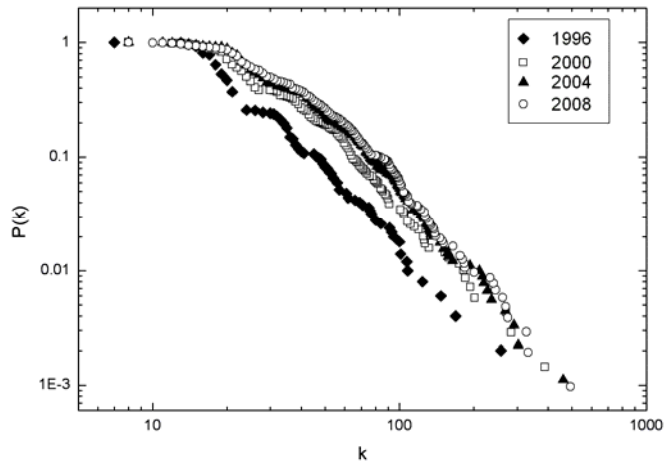

Figure 1. Cumulative degree distribution in log-log scale.

From Table 1 and Figure 1, we can find at least three nontrivial characteristics of PTN:

1. PTN is a small-world network. The high average clustering coefficient and small average path length show that PTN has small-world features. This has been revealed by many previous researchers (Sienkiewicz and Holyst 2005; Gao et al. 2005; Xu et al. 2007).

2. PTN is an accelerated growing network. The average degree <k> of PTN increases with time, which means that the number of edges grows faster than the number of nodes. This is a main characteristic of an accelerated growing network and has been found in some social networks of collaboration (Barabási et al. 2001).

3. PTN is a hybrid between a scale-free and a random network. The degree distribution of PTN represents a transition from power-law to exponential decay with time and can be well fitted with the stretched exponential distribution (Zhou et al. 2005). The cumulative distribution function of stretched exponential distribution is $P(k) = \exp(-(k/A)^u)$, in which u is a nonnegative parameter smaller than one. The borderline u=1 corresponds to the usual exponential distribution and u=0 to the power-law. It is well known that the exponential distribution can occur for evolving networks when nodes are attached completely randomly and power-law when attached preferentially to nodes with high degree (Barabási and Albert 1999). The increasing parameter u reveals that the PTN is evolving from scale-free network to a random one.

SIMULATION MODEL

To reproduce the major topological properties of empirical PTNs mentioned above, we propose a simulation model in this section. In our model, the PTN is built in an iterative fashion, each time repeating and reusing the elements generated in the previous steps as follows:

Step 1: The simulation PTN starts from an initial route with m stops which are fully connected. Set t=0.

Step 2: A new route with (m-1)q(t) new stops and m-(m-1)q(t) "old" stops which are chosen from the existing stops is added to the PTN. Here we define $q(t)=t^{-a}$, in which a is a parameter and determines the speed of growth of new stops. The rule of selecting the old stops is using a nonlinear preference rule with probability $p \propto k^b / \sum_i k_i^b$, where k denotes degree of an old stop, i denotes all existing stops, b is a parameter and b>0. Similarly, all of the stops in this route must be fully connected.

Step 3: Set t=t+1 and repeat Step 2 until R routes are created.

This model is very similar as compared with some evolution models of collaboration networks (Ramasco et al. 2004; Chang et al. 2007). The principal difference of our model is that the ratio of new stops declines with time and the selection of old stops follows a nonlinear preference rule. This can be explained as follows: When the PTN's scale is small, the main aim of developing a new route is to enlarge the service area of PTN, so most stops of the newly-developed routes are new. On the other hand, a few "old" stops be connected directly each other to ensure the convenience of PTN. As a result, the small-scale PTN usually has a star-like structure with a tiny number of stops, called hubs, which have a large number of links. New routes connect preferentially to these hubs and the PTN appears to be scale-free. But with increase in network size, there are a large number of routes crossing in more than one hub to enhance the accessibility and efficiency of the PTN and it evolves to a more random network. We think this model should be capable of capturing the key evolution mechanism of real-world PTNs.

NUMERICAL RESULTS

To check the validity of our model, we present a numerical experiment to compare the simulation results of the model with the empirical data on PTNs of Shijiazhuang. Table 2 and Figure 2 show some of the results.

Table 2. Numerical Results of the Simulation Model.

R	*N*	*E*	*M*	<*k*>	<*l*>	<*C*>
44	453	7038	19.97	31.07	2.07	0.85
70	717	12884	20.05	35.94	2.14	0.81
86	901	17763	20.88	39.43	2.18	0.80
104	1073	21910	21.74	40.84	2.25	0.79

The model's parameters: a=0.17; b=1.3; m is a random number with a Gaussian distribution centred at 20.

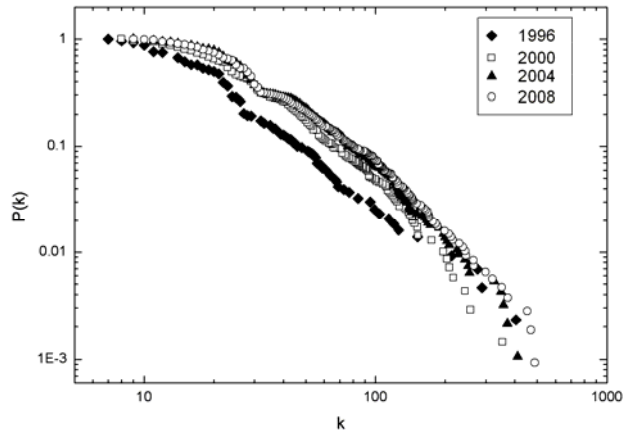

Figure 2. Cumulative degree distribution of simulation PTNs.

From Table 2, we can see that the simulation PTN also has a high average clustering coefficient, a small average path length, and a gradually increasing average degree. Figure 2 shows that the degree distribution of simulation PTNs represents a transition from power-law to exponential decay with time. Comparing Table 1 and Figure 1, it is apparent that the simulation results of our model are capable of reproducing the major topological properties of empirical PTNs.

CONCLUSION

The PTN represents a prototype of complex evolving networks. By mapping the PTNs of Shijiazhuang from 1996 to 2008, we infer the dynamic and structural mechanisms of this complex system. The empirical measurements allow us to uncover the time evolution of the topological properties of PTN. The results indicate that the PTN is a small-world, accelerated growing network and that the network evolution is governed by both random and preferential attachment. Also, we propose a simple model that captures the PTN's time evolution based on accelerated growth and nonlinear preference rules. The numerical experiments show that the model is capable of reproducing the major topological properties of real-world PTNs. The results and methodologies presented in this paper could be useful for a systematic study of other complex evolving transportation networks as well, such as railway, airport and logistics networks.

REFERENCES

Barabási, A.L., and Albert, R. (1999). "Emergence of scaling in random networks." *Science*, 286 (Oct.), 509-512.

Barabási, A.L., Ravasza, E., and Vicsek, T. (2001). "Deterministic scale-free networks." *Physica A*, 299(3-4), 559-564.

Boccaletti, S., Latora, V., Moreno, Y., et al. (2006). "Complex networks: Structure and dynamics." *Physics Reports*, 424(4-5), 175-308.

Chang, H., Su, B. B., Zhou, Y. P., and He, D. R. (2007). "Assortativity and act degree distribution of some collaboration networks." *Physica A*, 383(2), 687-702.

Ferber, C., Holovatch, T., Holovatch, Y., and Palchykov, V. (2009). "Public transport networks: Empirical analysis and modeling." *The European Physical Journal B*, 68(2), 261-275.

Gao, Z. Y., Wu, J. J., Mao, B .H., and Huang, H. J. (2005). "Study on the complexity of traffic networks and related problems." *Journal of Transportation Systems Engineering and Information*, 5(2), 79-84.

Lu, H. P., and Shi, Y. (2007). "Complexity of public transport networks." *Tsinghua Science & Technology*, 12(2), 204-213.

Ramasco, J. J., Dorogavtsev, S. N., and P-Satorras, R. (2004). "Self-organization of collaboration networks." *Physical Review E*, 70: 036106.

Sienkiewicz, J., and Holyst, J. A. (2005). "Statistical analysis of 22 public transport networks in Poland." *Physical Review E*, 72: 046127.

Xu, X.P, Hu, J.H., Liu, F., and Liu, L. S. (2007). "Scaling and correlations in 3 bus-transport networks of China." *Physica A*, 374(1), 441-448.

Conventional Bus Stop Capacity in Peak

Haijian Bai[1], Wenquan Li[2] and Ruijuan Dong[3]

[1]School of Transportation, Southeast University, Nanjing, China, 210096, PH 86-25-83791011; Email: baihaijian0000@163.com.
[2]School of Transportation, Southeast University, Nanjing, China, 210096, PH 86-25-83795647; Email: wenqli@seu.edu.cn.
[3]Institute of Transportation Engineering, Hefei University of Technology, Hefei, China, 230009, PH 86-551-2901338-2512; Email: dongruijuan95@163.com.

ABSTRACT

Congestion often occurs at bus stops during peak hours, since traffic flow and service frequency are very high near bus stop. Based on research of road traffic flow, the capacity model of bus stop is built in two steps after analyzing the operation rules in-out bus stop during peak hours. First, the formula of bus stop physical facility capacity is established. The formula of maximal arriving rate (bus stop capacity) is then solved based on obtaining the state equation's parameters by the analysis method of birth-death process. The numerical capacity tables of different berths anddwell time are calculated using Matlab. In addition, curve fitting formula is deduced from the table for application convenience, which provides a preference for the bus stop building and planning. Finally, a numerical example in City of Nanjing is presented to describe the method.

OVERVIEW

The importance of developing public transportation systems was widely realized by most cities in world. However, some problems still exist when the bus routed network is planned, such as underestimation of bus stop capacity during peak, hours. Bus stops are often operated normally in light traffic, while the congestion in bus stop will occur during peak hours due to the increasing bus frequency, road traffic flow and limitation of in-out bus stop. These problems result in inefficient use of buses and influence the traffic in adjacent lanes. Therefore, it is beneficial to study the bus stop capacity during peak hours.

The current literature on the bus stop capacity has two problems. First, the studies emphasize on network and route volumes, while the single bus stop capacity is not sufficiently investigated. Second, although the bus flow is lower than the capacity, the queue congestion often occurs around the bus stop during peak hours. The research on the bus stop capacity is studied in a TCRP (Transit Cooperation Research Program) report and other references (Bai and Li, 2007; TCRP, 2003; Hamdouch and Lawphongpanich, 2008; Zhao et al., 2008). Although the model parameters and estimation values are found in these references, the stop capacities during peak hours and light traffic are not appropriately addressed. The calculated capacity of bus stop is often smaller than factual one during peak hours, which results in congestions even if the bus flow is lower than the capacity. Thus, an appropriate approach needs to

consider the traffic flow characteristics during peak hours. Under the condition of analyzing the bus operational characteristics at out-line stop and on-line bus stops, this paper establishes the birth-death formula of vehicle operations at bus stop. Additionally, the formula of conventional bus stop capacity during peak hours is proposed..

MODEL ANALYSIS OF CONVENTIONAL BUS STOP

Conventional bus stops can be classified out-line and in-line bus stops. The advantages of out-line bus stop include lower influence to vehicles on adjacent lanes and lower probability to form bottleneck near bus stop. However, the capacity of the out-line stop is smaller than one of the in-line stop. Because of the stochastic dwell time, the phenomemon of in-out bus stops in advance complicates the stop operations. But during peak hours, there is little different operational characters between on-line and out-line bus stop. Considering the limitation of *M/M/1* and *M/M/S* queue system, this paper models bus stop as a birth-death process (Zhu and Shu,2006). We first discusss bus stop as a whole birth-death system and then discuss the birth-death status parameters.

The delay of buses are very slight in the case of no queue in bus stop when the arriving rate is lower than capacity. When the queue occurs in bus stop, the bus flow will increase to physical facility capacity. There is little probability for bus to change lane during peak hours when the passed bus number is close to the physical facility capacity. Assum that k berths in bus stop and k buses are coming in bus stop immediately after it is clear. The passed bus number will be stable in physical facility capacity as queue occurring. However, the delay of stop operations will be increased because of queue. The longer the queue is, the greater the delay is . The bus stop is the key location of delay on bus line, which must be restricted in an appropriate range. The bus arriving rate is lower than the capacity in reference (Bai and Li, 2007) whose value is close to the physical facility capacity. However, the bus queue is often long, which influences the service level of bus stop and operation efficiency of line. Therefore, it is not suitable for physical facility capacity or capacity of ideal condition as evaluation criterion. The queue delay must be considered in capacity evaluation criterion. This paper proposes a method to calculate the conventional bus stop capacity in given delay level during peak hours. The bus arriving rate in this condition just embodies the service level of the bus stop.

We can adopt in-line bus stop as prototype to deduce the formula of conventional bus stop capacity during peak hours. Based on the analysis of bus stop operations, physical facility capacity formula is constructed. Physical facility capacity is the output rate when the bus arriving rate is input rate. The state equation of birth-death is established. The queue probability of buses is selected as the congestion index of bus stop. The inequality, is deduced in order that bus arriving rate in different berth bus stop needs to meet in condition of given delay index. The maximum bus arriving rate equals the conventional bus stop capacity during peak hours.

MODEL OF CAPACITY DURING PEAK HOURS

Assuming k berths in the bus stop, the bus arriving rate of a line to the bus stop is λ, which is input rate of birth-death system. Then let deceleration time of incoming bus be t_j, average service time of boarding and alighting be t_d, bus safe reflecting time-headway be t_a. g and c indicate the green time and cycle next intersection respectively, B_f be physical facility capacity, B_c be bus stop capacity during peak hours. The physical facility capacity can be established using formula (1) according to the operation analysis of bus stop.

$$B_f = \frac{3600 \cdot k \cdot (g/c)}{t_j + t_d(g/c) + (k-1)t_a} \tag{1}$$

Where, $(k-1)t_a + t_j$ represents the whole deceleration time of k buses; Hence, the output rate of birth-death system is formula (2).

$$\mu_i = \begin{cases} \dfrac{3600 \cdot i \cdot (g/c)}{t_j + t_d(g/c) + (i-1)t_a} & i = 1,2,\ldots k \\ \dfrac{3600 \cdot k \cdot (g/c)}{t_j + t_d(g/c) + (k-1)t_a} & i = k+1, k+2,\ldots \end{cases} \tag{2}$$

The state equations of birth-death can be deduced as following (3-4). When no buses are in bus stop ($i = 0$), the state equation is:

$$\mu_i P_1 = \lambda P_0 \tag{3}$$

If there are i buses in bus stop, the state equation is:

$$\lambda P_{i-1} + \mu_{i+1} P_{i+1} = (\lambda + \mu_i) P_i \tag{4}$$

where P_i = probability of i buses coming simultaneously， $i = 0, 1, 2\ldots$.

According to formula (3-4), formula (5) can be deduced.

$$P_i = \begin{cases} \dfrac{\lambda^i}{\prod_{j=1}^{i} \mu_j} P_0 & i \le k \\ \dfrac{\lambda^i}{B^{i-k} \prod_{j=1}^{k} \mu_j} P_0 & i > k \end{cases} \tag{5}$$

where $\sum_{i=0}^{k} P_i + \sum_{i=k+1}^{\infty} P_i = 1$.

We can establish the formula of P_0 at k berths bus stop as following (6-8).

$$P_0(1) = \frac{B_f - \lambda}{B_f} \tag{6}$$

$$P_0(2) = \frac{(B_f - \lambda)\cdot \mu_1}{u_1 \cdot (B_f - \lambda) + B\lambda} \tag{7}$$

$$P_0(k) = \frac{(B_f - \lambda)\cdot \prod_{i=1}^{k-1} \mu_i}{(B_f - \lambda)\cdot \sum_{i=0}^{k-2} \lambda^i \prod_{j=i+1}^{k-1} \mu_j + B_f \cdot \lambda^{k-1}} \qquad k = 3,4,5,6... \tag{8}$$

where $P_0(k)$ indicates the probability of 0 bus arriving rate in k berths bus stop. Let the allowed bus queue probability be α, formula (9) is:

$$P_i(i \le k) \ge 1 - \alpha \tag{9}$$

By the corresponding formula (5-8) with different number of berths into formula (9), we can obtain the bus arriving rate inequality as following formula (10-12).

$$1 - \left(\frac{\lambda}{B_f}\right)^2 \ge 1 - \alpha \qquad k = 1 \tag{10}$$

$$\frac{\left(B_f \mu_1 + B_f \lambda + \lambda^2\right)\cdot (B_f - \lambda)}{{B_f}^2 \mu_1 + B_f \cdot \lambda \cdot \left(B_f - \mu_1\right)} \ge 1 - \alpha \qquad k = 2 \tag{11}$$

$$\frac{\left(B_f \cdot \sum_{i=0}^{k-1} \lambda^i \prod_{j=i+1}^{k-1} \mu_j + \lambda^k\right)\cdot (B_f - \lambda)}{B_f \cdot \sum_{i=0}^{k-2} \lambda^i \prod_{j=i+1}^{k-1} \mu_j \cdot \left(B_f - \lambda\right) + {B_f}^2 \cdot \lambda^{k-1}} \ge 1 - \alpha \qquad k = 3,4,5,6... \tag{12}$$

Choosing the corresponding formula in (10-12) according to given number of berths, we can calculate allowed maximum of bus arriving rate, which corresponds to bus stop capacity in peak.

CALCULATION RESULTS AND CURVE FITTING FORMULA

According to formula (2), physical facility capacity is calculated as follows. Tables 1 and2, with *g/c*=0.5, compare with capacity in TCRP. The suggested values of related parameters are calculated as follows: number of berths is 1~7, dwell time is 20~90*s*, $t_j = 5s$, and $t_a = 3s$.

Table 1 （*g/c*=0.5）Conventional bus stop physical facility capacity （*bus/h*）

Dwell time	20	25	30	35	40	45	50	55	60	65	70	75	80	85	90
1	120	103	90	80	72	65	60	55	51	48	45	42	40	38	36
2	200	176	157	141	129	118	109	101	95	89	84	79	75	71	68
3	257	230	208	189	174	161	150	140	132	124	117	111	106	101	96

4	300	272	248	229	212	197	185	173	164	155	147	140	133	127	122
5	333	305	281	261	243	228	214	202	191	182	173	165	158	151	145
6	360	332	309	288	270	254	240	227	216	206	196	188	180	173	166
7	382	355	332	311	293	277	263	250	238	227	217	208	200	192	185

It is reasonable to select bus queue probability α=15% according to the research of bus operation state in TCRP. Conventional bus stop capacity during peak hours, B_c, is determined from formula (10-12) by MATLAB 7.0, as following Table 2 and Figure 1.

Table 2 （*g/c*=0.5）Conventional bus stop capacity in peak（*bus/h*）

Dwell time	20	25	30	35	40	45	50	55	60	65	70	75	80	85	90
1	35	31	28	25	23	21	20	19	17	16	15	15	14	13	13
2	69	63	57	53	49	46	43	41	38	36	35	33	31	30	29
3	97	89	83	77	72	68	64	61	58	55	53	50	48	46	45
4	119	111	103	97	92	87	83	79	75	72	69	66	64	61	59
5	137	129	121	115	109	104	99	94	91	87	83	81	78	75	73
6	152	144	136	129	123	118	113	108	104	100	97	93	90	87	85
7	164	156	149	142	136	130	125	120	116	112	109	105	102	98	95

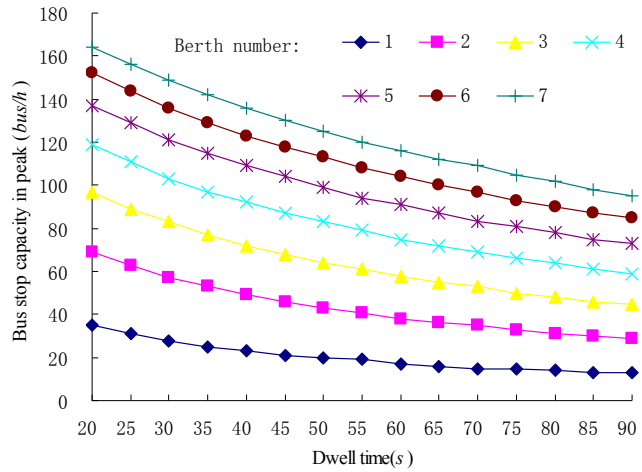

Figure 1. Bus stop capacity curve in peak in different dwell time (*g/c*=0.5)

Formula (10-13) is very complicated. Hence, a curve fitting formula 13 is obtained according to table 2. The correlation coefficients are over 0.9.

$$B_c\left(g/c=0.5\right)=\begin{cases}0.1114t_d^{\,2}-3.2435t_d+37.07, & k=1\\ 0.1701t_d^{\,2}-5.4178t_d+72.815, & k=2\\ 0.2017t_d^{\,2}-6.7769t_d+101.94, & k=3\\ 0.2059t_d^{\,2}-7.387t_d+124.54, & k=4\\ 0.2121t_d^{\,2}-7.833t_d+143.53, & k=5\\ 0.2081t_d^{\,2}-8.0017t_d+158.74, & k=6\\ 0.1878t_d^{\,2}-7.7902t_d+170.73, & k=7\end{cases} \tag{13}$$

A NUMERICAL EXAMPLE

The example station is located at Beijing East Road in City ofNanjing named Beijihuitang station. Investigation was conducted during the period of 5:30 to 6:30. The basic data is following. The example station is 25 meters to next intersection. 13 lines park in the bus stop, which has 4 berths. g/c=80/154=0.519, and t_d=32s. The mean bus arriving rate is 138 *bus/h.* First of all, physical facility capacity B_f=244 *bus/h* can be calculated by formula (1). Then we can obtain capacity in peak B_c=106 *bus/h* by formula (6-13). Observe that the actual bus volume is lower than physical facility capacity because of 244>138. Also observe that the bus queue probability is over 60%. Then we compare capacity during peak hours to actual bus volume, 106<138. Saturation is 138/106=1.3>1. Bus stop is supersaturated, which is confirmed by actual status of the station.

The authors believe that frequent congestion will occur if the physical facility capacity in alighting traffic is used as the design basis of bus stops. The congestion will result in lower service level of bus lines and influence the vehicles of adjacent lanes seriously. Then capacity in existing method is close to physical facility capacity. It is not suitable to take capacity in existing method as a criterion during bus stop planning and designing. This paper proposes a numerical model based on the given probability, which is close to actual capacity of bus stop during peak hours and is suitable to be reference in planning and designing of bus stop. However, the research of different between in-line stops and out-line stops is insufficient in the new capacity model, which will be investigated in the future.

ACKNOWLEDGE

The work is supported by the National High Technology Research and Development Program of China (No.2007AA11Z210) and the National Key Technology Research and Development Program (No.2006BAJ18B03).

REFERENCES

Bai, H., and Li, W. (2007). “Calculation process research of routine bus-stop routes capacity.” *J. Journal of Southeast University(Natural Science Edition)*, 37(6), 1077-1080.

Transit Cooperative Research Program (TCRP). (2003). "Report 100: Transit capacity and quality service manual 2nd edition." *Washington D C*, 4.1-4.109.

Hamdouch, Y., and Lawphongpanich, S. (2008). "Schedule-based transit assignment model with travel strategies and capacity constraints." *J. Transportation Research Part B: Methodological,* 42(7-8), 663-684.

Zhao, X., and Gao, Z., and Li, K. (2008). "The capacity of two neighbour intersections considering the influence of the bus stop." *Physica A: Statistical Mechanics and its Applications*, 387(18), 4649-4656.

Zhu, Q., andShu, X. (2006). "Characteristic numbers and their probability meaning of two kinds of birth and death processes." *J. Applied Mathematics A Journal of Chinese Universities (Ser.A),* 21(3), 311-320.

Inhabitant Trip Behavior Similar to Quantum Transition

Rong-Han Yao[1] and Dian-Hai Wang[2]

[1] Lecturer, Center for Transportation Research, Dalian University of Technology, Dalian 116024 China; PH (086) 411-84707761; email: cyanyrh@yahoo.com.cn
[2] Professor, College of Transportation, Jilin University, Changchun 130022 China; PH (086) 431-85095857; email: wangdianhai@sohu.com

ABSTRACT
Trip mode transfer is a behavior of inhabitant in the process of adjusting their trip mode. The behavior is similar to the transition of quantum. In this paper, trip mode transfer and quantum transition were compared. According to the quantum transition theory, three linear imitation models and a polynomial imitation model were built. The models were applied via 1990 NPTS (Nationwide Personal Transportation Survey) data from U.S. and 2001 CCTS (Changchun Trip Survey) data from the city of Changchun, China. The results indicate that the relations between income difference and number of transferring levels, trip distance difference and number of transferring levels, and trip distance difference and income difference are all linear and the function between trip distance difference and income difference fits quadratic and higher polynomials of which the constant items are zero when one trip mode transfers to others. The proposed models can reveal the rules of change of trip mode sharing rates.
Key Words: trip behavior; trip mode transfer; quantum transition; energy level

INTRODUCTION
Inhabitant reorganization is a universal phenomenon arisen from inhabitant adjusting their travel behavior when economy developing, land use changing or level of living improving etc. The phenomenon sometimes brings on recombining trip distributions. Adjusting travel behavior is usually adjusting trip modes. The adjusting mostly relies on inhabitant income. Generally speaking, inhabitant will adjust trip mode properly when choosing it with income increasing, such as converting bicycle into motorcycle or bus, transforming bus into taxi or diverting taxi to private car etc. The behavior often makes trip distance increase accordingly. In addition, with increase of income, people are pursuing life quality with high standard, such as capacious space, neat surrounding or trip comfort etc. However, the restriction of city planning and land use and the discommodity of layout of old city zones make the standard difficult to realize at the city center. According to the rules of city construction, the kind of zones commonly locates at the periphery of city. When inhabitant income increases to a certain value, it is possible to choose dwelling place renewedly. When choosing

dwelling place, inhabitants have tendency to choose the areas away from the city center. That is to say, trip distance of inhabitant increases. This is one major cause of city extension ceaselessly, which is also related to trip mode transfer.

A topic relative to trip mode transfer is modal split or mode choice. It is an important part of the traditional four-step procedure for transportation planning applications. Many researchers developed various models based on random utility maximization theory or maximum simulated likelihood method to analyze individual or household travel behavior, such as the logit model (Bhat 2000; Li et al. 2002), the mixed logit model (Bhat and Sardesai 2006), and the nested logit model (Dissanayake and Morikawa 2002) etc. Lately, some scholars described travel mode choice via neural network (Xie et al. 2003; Celikoglu 2006). The achievements have significant influences on predicting trip distributions or traffic assignment. They pay attention to individual or household behaviors of not adjusting but choosing trip mode.

Some scholars presented the macroscopic descriptive model of inhabitant distribution based on the probability density model of electron occurring out of nucleus (Wang et al. 1996; Wang et al. 2007). In the model, an inhabitant is regarded as an electron, and a household, work location or shopping center is looked upon as a nucleus, inhabitants go the motion round the nucleus with a certain radius. Since the factor of income was rarely considered in the conventional trip distribution models, some researchers gave the electron energy model of trip distribution by comparing the similarity of energy level transition in the quantum mechanics theory and the increase of inhabitant trip distance (Qu et al. 2003). These results have an important significance to trip distribution prediction, but the subject of trip mode transfer did not be referred. However, the applied quantum mechanics theory has a referenced value to studying trip mode transfer. The theory indicates that quantum transition will occur when electron energy increases to a certain value; that is, electron transfers from a lower energy state to a higher energy state and the radius of motion of electron going round the nucleus increases accordingly. The characteristics of quantum transition are very similar to the characteristic of trip mode transfer. That is to say, the inhabitant behavior of adjusting trip mode is similar to quantum transition.

In the paper, the similarity of trip mode transfer and quantum transition is analyzed in detail. The trip mode transfer models are given on the basis of energy level transition theory. The models are explained by 1990 NPTS (Nationwide Personal Transportation Survey) data from U.S. and 2001 CCTS (Changchun Trip Survey) data from the city of Changchun, China.

Basic Principle

Similarity of Phenomena. The quantum transition theory assumes that an electron will transit to the final state with higher energy level from the original one with lower one after absorbing a photon; it will release a photon after transiting to the final state with lower energy level from the original one with higher one. For trip mode transfer, an inhabitant will change his trip mode with lower quality (e.g. slower speed) to higher quality (e.g. quicker speed) after his income increases; he will have to alter his trip mode with higher quality (e.g. quicker speed) to lower quality (e.g. slower speed) after his income decreases.

The similarity between trip mode transfer and quantum transition is as follows (Yao and Wang 2007). The first is income and electron energy. The chosen trip mode by an

inhabitant lies on his income. This is similar to the one that the chosen movement track by an electron depends on its energy. The second is the trip distance and track radius. A great deal of statistical data showed that the reachable trip distances are different for various trip modes. Then the trip distance can be a token of relevant trip mode. Similarly, the radius is a token of electron movement track. The third is trip mode quantization and electron track quantization. The category of trip modes is limited and discrete. Trip modes can be numbered by using natural number according to energy (e.g. speed) order. This is similar to the quantum characteristic of electron track. The electron only moves in some discrete tracks. The last one is trip mode transfer and quantum transition. When the income of an inhabitant increases, he/she will choose a trip mode with higher quality (e.g. quicker speed) to realize further trip distance. On the contrary, when the income decreases, he/she will have to choose a trip mode with lower quality (e.g. slower speed) and only realize closer trip distance. Similarly, when the energy of an electron increases, it will transition to a track with higher energy and movement radius is also longer; when its energy decreases, it will transition to a track with lower energy and movement radius is also shorter.

Trip* Mode *Transfer Model. Based on the quantum mechanics theory, electron energy is composed of the kinetic energy of motion of electron going round the nucleus in a circle and the potential energy of the system. Let us only consider the potential energy and suppose that trip distance (regarding household, work location or shopping center as trip origin or destination) is a token of the potential energy. For a average sense, trip distance is farther when inhabitant income is higher.

In the Bohr theory of hydrogen atom (Zhou 1998), a basic equation is

$$E_n = E_1 / n^2 \tag{1}$$

where n is primary quantum number and an integer, and E_1 and E_n are energy of electron which locates at the first and nth stationary state trajectories, respectively.

The relation between the primary quantum number and radius of electron away from the atomic nucleus is $n^2 = r_n Z / \alpha_1$. For hydrogen atom, $Z = 1$, and Eq.(1) becomes

$$E_n = \alpha_1 E_1 / r_n \tag{2}$$

where r_n is the radius of the nth stationary state orbit at which electron locates, and α_1 is the radius of the first Bohr orbit which is a stationary state orbit of electron in hydrogen atom away from the nucleus nearest.

According to Eq.(2), we have

$$r_n - r_m = \alpha_1 E_1 (E_m - E_n) / (E_n E_m) \tag{3}$$

In the Bohr theory, the zero (maximum value) of potential energy locates at infinite away from the atomic nucleus;the potential energy of electron at each energy level is negative. When the potential energy of electron is greater, the attraction power between electron and nucleus is less, namely the ability of electron escaping the nucleus is larger. But trip distance and inhabitant income are all positive in the process of trip mode transfer. In Eq.(3), α_1 and E_1 are constants, then

$$\Delta r = \beta \Delta E / (E_n E_m) \tag{4}$$

where $\Delta r = r_n - r_m$ is the radius difference between two energy levels; $\Delta E = E_n - E_m$ is the energy difference between two energy levels; $\beta = -\alpha_1 E_1$ is a

positive parameter.

In Eq.(4), the radius difference is directly proportional to the energy difference, and inversely proportional to the product of the energies. It is a ternary nonlinear function. The parameter β is difficult to be calibrated. In fact, the three variables are not unattached. Furthermore, the radius difference depends more on the energy difference. As a result, Eq.(4) can be rewritten as a unitary nonlinear function:

$$\Delta r = f(\Delta E) \tag{5}$$

According to the above similarity, the trip mode transfer model is

$$\Delta D = f(\Delta I) \tag{6}$$

where ΔD is trip distance difference; ΔI is income difference.

MODEL REVISION

Energy Level Analysis. Table 1 lists the income and trip distance for the different trip modes obtained from 1990 NPTS and 2001 CCTS data. From Table 1, the energy levels of trip mode in U.S. and Changchun city are walk, bike, school bus, private vehicle, rail/subway and bike, bus, autocycle, car from the lowest to the highest.

Table 1. Income and trip distance for different trip modes

	Trip Mode	Walk	Bike	School Bus	Private Vehicle	Rail/Subway
NPTS	Income ($10^4\times$dollars)	2.501	2.9741	3.0659	3.2658	3.3393
	Trip Distance (miles)	2.5522	3.1472	5.2837	7.735	12.7907
	Trip Mode	Bike	Bus	Autocycle	Car	
CCTS	Income ($10^3\times$yuans)	1.1616	1.3734	1.6	2.076	
	Trip Distance (km)	2.0544	3.9679	4.4962	5.8674	

Linear Imitation Formulas. Table 2 lists the number of transferring levels, income difference and trip distance difference obtained from 1990 NPTS and 2001 CCTS data. From Table 2, any two of the income difference, trip distance difference and number of transferring levels follow a linear relation, namely:

$$\Delta I_n = \gamma_1 n + \varphi_1 \tag{7}$$

$$\Delta D_n = \gamma_2 n + \varphi_2 \tag{8}$$

$$\Delta D_n = \gamma_3 \Delta I_n + \varphi_3 \tag{9}$$

where ΔI_n and ΔD_n are income difference and trip distance difference when transferring n levels; $\gamma_1, \varphi_1, \gamma_2, \varphi_2, \gamma_3, \varphi_3$ are constants.

Table 2. Number of transferring levels, income difference and trip distance difference

	Number of Transferring Levels	1	2	3	4
NPTS	Income Difference ($10^4\times$dollars)	0.2096	0.3767	0.565	0.8384
	Trip Distance Difference (miles)	2.5596	4.9421	7.4131	10.2384
	Number of Transferring Levels	1	2	3	
CCTS	Income Difference ($10^3\times$yuans)	0.3048	0.5705	0.9144	
	Trip Distance Difference (km)	1.271	2.1707	3.813	

Polynomial Imitation Formula. Eq.(6) is a nonobjective function and its concrete expression is not clear yet. However the trip distance difference can be imitated as a polynomial of the income difference, namely

$$\Delta D = a_0 + a_1 \Delta I + a_2 \Delta I^2 + \cdots + a_n \Delta I^n \tag{10}$$

where $a_0, a_1, a_2, \cdots, a_n$ are unknown coefficients.

Figure 1 illustrates the relations between the trip distance difference and the income difference for one trip mode transferring to others obtained from 1990 NPTS and 2001 CCTS data. From Figure 1, the curves all traverse the origin of coordinate and are all nonlinear, namely $a_0 = 0$ and $n \geq 2$ in Eq.(10).

MODEL APPLICAION AND RESULTS

Linear Models. Table 3 indicates the correlative coefficient of the linear trip mode transfer model via 1990 NPTS and 2001 CCTS data. From Table 3, the correlation coefficients of the linear imitation models are all greater than 0.98. It is showed that the income difference and the trip distance difference are linearly correlated to the number of transferring levels; and the trip distance difference is linearly correlated to the income difference. Furthermore, their linear correlation is very strong.

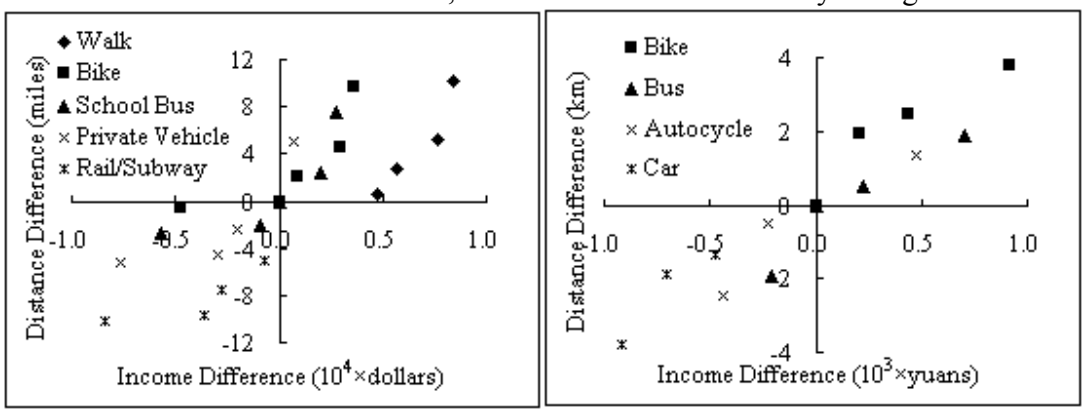

(a) NPTS (b) CCTS

Figure 1. Curves of one trip mode transferring to others

Table 3. Correlative Coefficient of Linear Imitation

Relations	Number of Levels and Income Difference		Number of Levels and Distance Difference		Income Difference and Distance Difference	
Data	NPTS	CCTS	NPTS	CCTS	NPTS	CCTS
Correlative Coefficient	0.9930	0.9973	0.9992	0.9861	0.9970	0.9957

Polynomial Model. Table 4 indicates the correlative coefficient of the polynomial trip mode transfer model via 1990 NPTS and 2001 CCTS data. From Table 4, the correlation coefficients of the quadratic and cubic polynomial imitation models are all greater than 0.90 and 0.96 respectively; and the correlation coefficients of the biquadratic polynomial imitation models are all equal to 1.00. It is showed that the function relation between the trip distance difference and the income difference fits the quadratic and higher polynomials of which the constant items are zero; the imitation effects of the biquadratic and higher polynomials have no difference.

Table 4. Correlative Coefficient of Polynomial Imitation

	Polynomial	Walk	Bike	School Bus	Private vehicle	Rail/Subway
NPTS	Quadratic	0.9676	0.9675	0.9604	0.9066	0.9539
	Cubic	0.9789	0.9747	0.9627	0.9687	0.9767
	Biquadratic	1.0000	1.0000	1.0000	1.0000	1.0000
	Polynomial	Bike	Bus	Autocycle	Car	
CCTS	Quadratic	0.9844	0.9648	0.9797	0.9858	
	Cubic	1.0000	1.0000	1.0000	1.0000	
	Biquadratic	1.0000	1.0000	1.0000	1.0000	

CONCLUSIONS

The quantum mechanics theory describes the quantum transition behavior in the microscopic world. The trip mode transfer is a behavior of inhabitants adjusting trip modes in the macroscopic world. The two phenomena are similar. In this paper, their common points were analyzed. Based on the quantum transition principle, the trip mode transfer model was presented. The linear and polynomial imitation formulas were given via the NPTS and CCTS data. The results showed that the relation of any two among income difference, trip distance difference and number of transferring levels is linear; the function between trip distance difference and income difference fits quadratic and higher polynomials of which the constant items are zero for one trip mode transferring to others.

The contribution of this paper is to reveal the similarity between trip mode transfer and quantum transition, to describe the trip mode transfer rules via survey data, to establish the trip mode transfer models according to the quantum transition theory, and to explain the micro-phenomenon in the macroscopic world. It is valuable for trip distribution and modal split, and useful to explain inhabitant reorganization phenomena. Therefore, it may provide new perspectives to urban planning and urban traffic planning of developing cities.

ACKNOWLEDGEMENTS

This paper is supported by the projects (Nos. 50808035 and 2006CB705505). The authors appreciate the National Natural Science Foundation of China and the Ministry of Science and Technology of China.

REFERENCES

Bhat, C. R. (2000). “Incorporating observed and unobserved heterogeneity in urban work travel mode choice modeling.” *Transportation Science*, 34(2), 228-238.

Bhat, C. R., and Sardesai, R. (2006). “The impact of stop-making and travel time reliability on commute mode choice.” *Transportation Research Part B*: *Methodological*, 40(9), 709-730.

Celikoglu, H. B. (2006). “Application of radial basis function and generalized regression neural networks in non-linear utility function specification for travel mode choice modelling.” *Mathematical and Computer Modeling*, 44(7-8), 640-658.

Dissanayake, D., and Morikawa, T. (2002). “Household travel behavior in

developing countries: Nested logit model of vehicle ownership, mode choice, and trip chaining." *Transportation Research Record*, (1805), 45-52.

Li, Q., Ooeda, Y., Matsunaga, C., and Sumi, T. (2002). "Identifying the determinants of commuting travel mode choice from daily commutation behavior." *Memoirs of the Faculty of Engineering*, *Kyushu University*, 62(4), 191-206.

Qu, Z. W., Liang, C. Y., and Wang, D. H. (2003). "Research on simulation of inhabitant trip distribution based on electronic energy." *Journal of Transportation Systems Engineering and Information Technology*, 3(4), 48-52.

Wang, D. H., Jing, C., and Yao, R. H. (2007). "Electron cloud model of residential trip distribution." *Acta Phys*. *Sin*., 56(7), 3642-3648.

Wang, D. H., Yang, Z. S., and Lei Y. L. (1996). "Research on the inhabitants distribution model by simulation electron cloud." *Systems Engineering-Theory & Practice*, (7), 71-74.

Xie, C., Lu, J. Y., and Parkany, E. (2003). "Work Travel Mode Choice Modeling with Data Mining: Decision Trees and Neural Networks." *Transportation Research Record* 1854, 50-61.

Yao, R. H., and Wang, D. H. (2007). "Trip mode transfer model by simulating quantum jump." *Journal of Traffic and Transportation Engineering*, 7(3), 111-115.

Zhou, S. S. (1998). *Atomic Physics (Revised Edition)*. East China Normal University Publisher, Shanghai, China.

Study and Simulation of Behavioral Decision-Making Model of Through Bicycles Passing Vehicles at Signalized Intersection

Xing-qiang ZHANG[1], Shen WANG[1], Ying-hui LIANG[1]

[1] MOE Key Laboratory for Urban Transportation Complex Systems Theory and Technology, Beijing Jiaotong University, 100044, Beijing, China; PH (010) 51687138; Fax (010) 51688344; Email: zhangxingqiang@jtys.bjtu.edu.cn

ABSTRACT: Interferences between vehicle flow and non-vehicle flow at a grade intersection are mainly induced by the crossing behavior between bicycles and vehicles. In this paper, according to the conflict danger degree, vehicle-bicycle conflicts at a 4-leg intersection are classified into 3 groups using the fuzzy cluster theory; the behavior of through bicycles crossing right-turn motor vehicles on neighboring lanes is used as the case study. The factors affecting the crossing behavior are analyzed, including the bicycle speed before crossing and the acceptable Gap. Then a decision-making model describing bicycle crossing behavior is built by the logistic regression model. Finally, based on the model, the Multi-Agent simulation system of the through bicycle crossing right-turn motors is built, the simulation results show that the behavioral decision-making model is reasonable, and the simulation system is validated.

Keywords: bicycle; intersection; crossing behavior decision-making model; simulation

1 INTRODUCTION

In Chinese urban traffic, vehicle-bicycle conflicts at intersections are one of the most important factors to traffic jam and safety. So analyzing bicyclist microscopic behaviors and establishing the bicycle-motor interaction model are necessary to study the mixed traffic characteristics and to find an effective method for resolving the mixed traffic problem. Based on the boundary gap theory, Wu (2004) established the acceptable gap probability model when a bicyclist passing through vehicles at a signalized intersection. Xu (2006) studied the distributed rules of left-turn bicycles passing through vehicles and established models between left-turn bicycles and through vehicles. Researchers pay more attention to the bicyclist behaviors, but bicyclist behavior simulation is sparse at signalized intersections. In this paper, various bicycle behaviors are examined based on data collected at two typical intersections in Beijing: the Ganjiakou intersection and the Fuchengmen intersection. According to the conflict danger degree, the vehicle-bicycle conflicts at a 4-leg intersection are classified using the fuzzy cluster theory. Then speed distribution and cyclist acceptable gap at signalized intersections are analyzed in order to establish microscopic behavior model of bicyclist passing through motor. Finally, using the software NetLogo, an agent based microscopic model is established to simulate the

behavior of bicyclists passing through vehicles.

2 FUZZY CLUSTER ANALYSIS OF VEHICLE-BICYCLE CONFLICT

Based on the quantity and danger degree, the vehicle-bicycle conflicts at intersections are classified using the fuzzy cluster theory. Fuzzy cluster target function can be expressed as:

$$\min F(U,V,W) = \sum_{\mathrm{h}=1}^{c}\sum_{j=1}^{n}\{u_{hj}^{2}[\sum_{i=1}^{m}[w_i(x_{ij}-v_{ih})]^2]^{\frac{a}{2}}\} \quad , \qquad (1)$$

where: $X=(X_1,X_2,\cdots X_n)$ is the value swatch set; $V=(V_1,V_2,\cdots V_n)$ is the cluster center matrix; $W=(W_1,W_2,\cdots W_n)$ is the characteristic weight sector of V; $U=(u_{kj})$ is the subordinate grade membership matrix; $\alpha=2$ is the least squares optimized rule. The matrix U and the sector W should accord with the restriction conditions, respectively:

$$0\le u_{hj}\le 1;\ \sum_{\mathrm{h}=1}^{c}u_{hj}=1;\ 0<\sum_{j=1}^{n}u_{hj}<n \ \text{ and } \sum_{\mathrm{i}=1}^{m}w_i=1;\ 0\le w_i\le 1 \qquad (2)$$

The vehicle-bicycle conflicts at intersections may be divided into 5 types (see Figure 1). Based on the statistical vehicle-bicycle conflict quantities TC and the equivalent weight traffic amount of vehicle and bicycle MPCU at the Ganjiakou intersection (see Table 1), the vehicle-bicycle conflict ratio TC/MPCU is regarded as the evaluated index. Ten conflict points are regarded as the

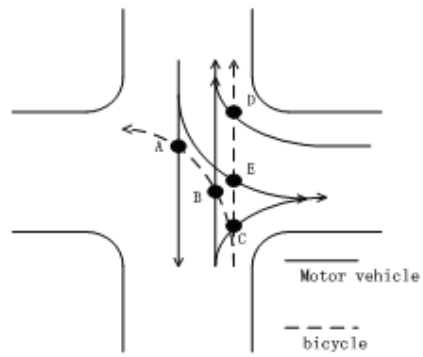

Figure 1. Vehicle-Bicycle Conflict Types

evaluation set X=(X_1、X_2、X_3……X_{10}), the conflict danger degree XK is divided into three kinds of type: lower danger, danger, higher danger.

Table 1. Vehicle-Bicycle Conflict Ratio TC / MPCU at Ganjiakou Intersection

Ganjiakou Intersection	7:30-7:50	7:50-8:10	8:10-8:30
1. North A	0.0155	0.0185	0.0312
2. North B	0.0127	0.0157	0.0097
3. North C	0.323	0.3072	0.2315
4. North D	0.753	0.2389	0.1913
5. North E	0.471	0.2253	0.2321
6. West A	0.102	0.0105	0.0061
7. West B	0.135	0.0150	0.0103
8. West C	0.461	0.3890	0.2042
9. West D	0.911	0.0795	0.0673
10. West E	0.795	0.0673	0.0541

Using Matlab, the fuzzy cluster results showed that the higher danger conflict types are 3, 4, 5, 8 (see Table 1), which indicates that the conflicts between through bicycles and right-turn vehicles on the adjacent lane are the most dangerous and representative. So the conflicts between the through bicycles and the right-turning motors are the main focus in this paper.

3 PASSING THROUGH DECISION-MAKING MODEL

Based on the collected data, the average bicycle speed is 3.47m/s and follows a normal distribution. The speed is clearly affected by the intersection type: 4.18m/s at the Fuchengmen intersection and 3.14m/s at the Ganjiakou intersection. Speed is less affected by sex of the bicyclist. The bicycle acceptable also follows a normal distribution and the average value is 2.71s (see Figure 2).

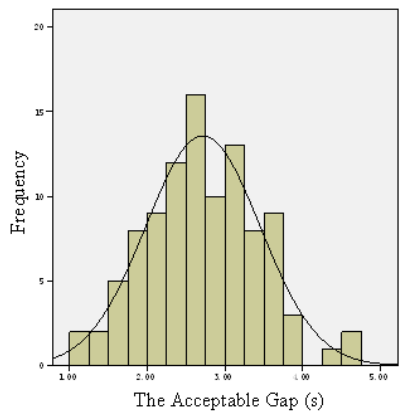

Figure 2. Distribution of the Accepted Gap

In this paper, we assume that each bicyclist independently selects the acceptable gap. Furthermore, bicycles will not affect each other. As a result, 4 factors: the front motor type, the following motor type, sex of the bicyclist, and whether the bicycle is parked or not, are selected to check the relation of the acceptable gap by the Levene's method (see Table 3). The results show that the primary factor of the acceptable gap is the following motor type; the other factors are subordinate.

Table 3. Levene's Test

Levene's Check		Cyclist sex	Front motor	Following motor	Parking or not
Equal variances test	*F* value	0.936	0.577	0.760	0.631
	P value	0.336	0.449	0.385	0.429
T test	*T* value	1.400	-0.798	0.641	-0.072
	P value	0.165	0.427	0.523	0.943

The logistic regression theory is adopted to establish the decision-making probability model. Assuming that the acceptable gap is 1 and the refused gap is 0. A hundred groups of passing through data and 44 groups of refusing data are analyzed. The acceptable Gap model of the through bicycles passing through the right-turn motors may be expressed as:

$$P = \frac{1}{1 + \frac{1}{\exp(\beta_0 + \beta_1 * v + \beta_2 * Gap + \beta_3 * l)}}. \qquad (3)$$

Here: $\beta_0, \beta_2, \beta_3, \beta_4$ are regression coefficients; Gap is the gap distance; v is the followed motor speed; l is the type of followed motor, 0 is car and 1 is truck.

Variables are imported into the model using the step regression method based on the score test. The resulting acceptable probability model can be expressed as:

$$\mathrm{P} = \frac{1}{1 + \frac{1}{\exp(1.157 - 1.233 * \mathrm{v} + 0.556 * Gap - 1.724 * l)}} \qquad (4)$$

The actual frequencies and the forecast frequencies are compared with the "Hosmer –Lemeshow" parameters which are obtained using the Pearson Method. The compared results show that the statistical parameters follow the "g-2" distributing, which indicates that the decision-making model is reasonable. The forecast results and the actual results are shown in the Table 4. The correct ratio is 76.2%, in which the correct ratio of the accepted passing through samples is 90.0% and the refused passing through samples is 44.2%. The decision-making model may well forecast the crossing behavior of through bicycles and right-turning motor vehicles on the neighbor lane.

Table 4. Classification Tab. of Gap Choice Model

		The forecasted results		
		Passing through or not		Correct ratio
		0	1	
Passing through or not	0	19	24	44.2
	1	10	90	90.0
Totally				76.2

4 MULTI-AGENT SIMULATION

In this paper, intersection traffic agent's hierarchy consists of two layers: traffic unit agent and traffic environment agent (see Figure 3). The traffic unit agent is further divided into three layers: the motor agent, the bicycle agent and the pedestrian agent. The bicycle agent and the motor agent include 6 sub-structures; each sub-structure has separated behavior and interact each other in order to simulate traffic conditions realistically.

In communicating information among sub-structures, the bicycle roadway shift decision is defined as that front bicycle's speed is lower than the following bicycle and the following bicycle's speed is lower than 50% of the maximal speed. A Bicyclists selects randomly one roadway and judges whether there are other bicycles in front of him/her. If this is not the case, a roadway shift will appear.

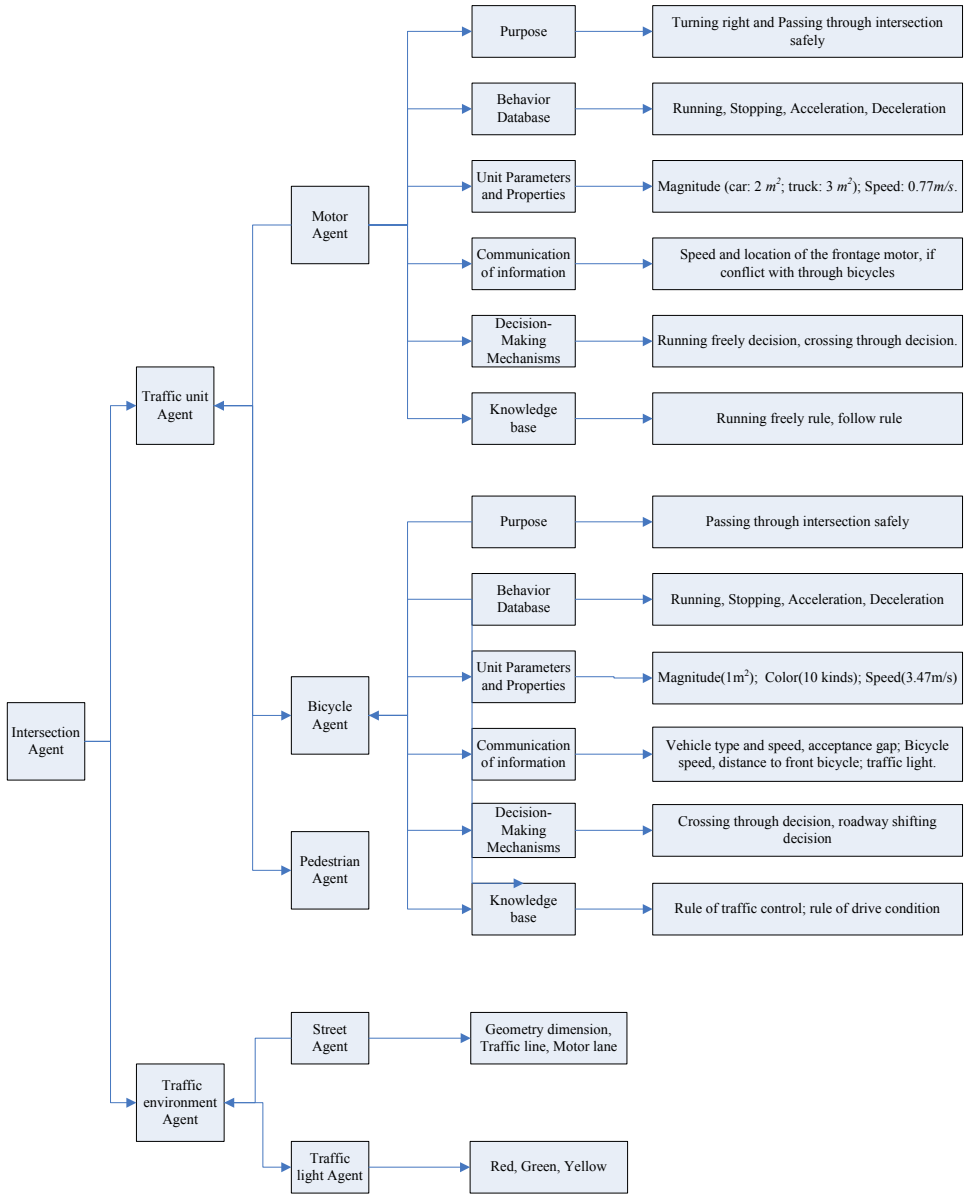

Figure 3. Structure of the intersection Agent

The bicycle passing through decision is made according to the decision-making probability model. If the probability is less than P, the bicyclist will refuse to pass through motor vehicle. Otherwise, the bicyclist will pass through.

By establishing the intersection agent model, the simulation for through bicycles passing right-turning vehicles is implemented based on the software called NetLogo (see Figure 4 for the simulation interface). The simulation interface is shown in Figure 5. In total, 109 observed samples were used to analyze the frequency distribution; the results show that the bicycle average speed is 2.77m/s, which is consistent with the former data.

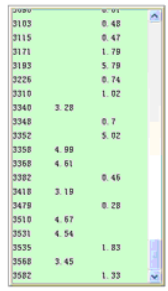

Figure 4. Simulation Interface

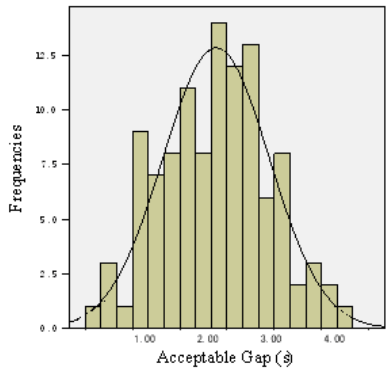

Figure 5. The Accepted Gap

5 CONCLUSIONS

(1) At intersections, bicycle speeds follow a normal distribution. The mean speed is 3.47m/s and the variation is 0.99. Intersection type plays an important role to the speed distribution. The acceptable gap also follows a normal distribution. The mean gap is $\mu = 2.71$ s and the standard deviation is $\sigma = 0.73$ .The following vehicle type plays an important roles to the acceptable gap.

(2) The decision-making model of through bicycles passing right-turn vehicles is established and validated; the forecast accuracy rate reaches 76%.

(3) The micro-simulation model for the through bicycle passing the right-turn vehicles is established based on multi-agent; the simulation results show that the model proposed in this paper works properly.

6 REFERENCES

Wu, J., and Huang, L. (2004). "The Behavior of Cyclists and Pedestrians at Signalized Intersections in Beijing." *Journal of Transportation Systems Engineering and Information Technology*, 4(1), p105-114.

Xu, L., and Wang, W. (2006). "Analysis of Influence of Left-turn Non-motors in Signalized Intersection." *China Journal of Highway and Transportation*, 19(1), p89-92.

Li, J. and Jiang, G. (1995). "The Application of Photogrammetric technique to Traffic Accident Reconstruction." *China Journal of Highway and Transportation*, 8(1), p39-41.

Quan Yu, and Shi, J. (2006). "Frame of Micro Traffic Flow Simulation System Based on Agent." *Computer Simulation,* 23(1), p210-214.

AN OPTIMIZATION MODEL FOR BUS RAPID TRANSIT

Bo Yan[1], Yonglei Jiang[1], Bin Yu[1], Zhongzhen Yang[1]
[1]College of Transport Management, Dalian Maritime University, Dalian, 116026, China; TEL/FAX (411) 8472-6756; email: yangzhongzhen@263.net

Abstract: This paper develops a new model, aiming to maximize the efficiency of bus rapid transit (BRT) system (i.e. maximize direct-through travelers on unit length of BRT route). Since the problem is NP-hard, a heuristic algorithm, based on ant colony optimization, is developed. With a numerical test from Dalian City, China, the effectiveness of the model and the algorithm is examined.

Keywords: BRT; optimization; ant colony optimization

1 Introduction

High-quality transit service is considered as an effective way to attract travelers away from private car trips toward the transit use in congested metropolitan areas. Bus Rapid Transit (BRT) is an innovative transportation system, which combines the quality of rail transit and the flexibility of buses. BRT often operates on exclusive transit ways with high-capacity and high-speed vehicles. Since many features of BRT are similar to light rail transit (LRT), BRT may be considered to be able to improve transit service through incorporating favorable operational characteristics of rail-based transit systems. Referring to rail transit route planning, BRT routes need to cover large transit demand corridors which can provide enough travelers.

Planning BRT routes is similar with arterial transit route network design. Transit network design has been an important problem in urban transportation planning. There have been many successful studies on transit network planning over the past several decades. Ceder and Wilson (1986) introduced three-step method (trip assignment, planning routes and departure interval) into the design of network of public bus routes. Hasselstrőm (1981) presented a two-step model to optimize routes and frequency simultaneously. Wang (2001) developed a model aiming to maximize direct travelers. Yang et al. (2007) presented an optimization method of public bus network, which can efficiently obtain the trade-off between route length and the number of direct travelers and improve the efficiency of optimization. Recently, some studies have been completed on BRT route planning. Bai et al. (2007) optimized the BRT routes using tabu search algorithm and tested the model and the algorithm by simulation. Fan and Pan (2007) study the application of genetic algorithm on intelligent transport systems scheduling of vehicles. Sun et al. (2007) focus on BRT headway and scheduling combination optimization with genetic algorithm. An et al. (2008) employed particle swarm optimization to solve a set of

bi-level programming models to find a feasible solution for the BRT network design problem. All the aforementioned studies stimulated us to develop a heuristic algorithm to optimize the routes of BRT.

The purpose of this paper is to extend the model of Yang et al. (2007) to design BRT routes. The objective of this study aims to maximize direct transit trip density, which is related to the direct transit demands and the length of the route. Some network optimization problems are NP-hard, which is difficult to be solved using traditional techniques. In this paper, ant colony algorithm is used to solve the optimization model.

1 Optimization Model

Among existing studies, the direct traveler approaches are practical and convenient. They aim to maximize the number of the direct travelers under the length constraint or set the route along the shortest path. Maximization of the number of direct travelers may cause the bus routes in the network to be extremely long, whereas the latter limits the number of alternative routes and then damages the optimizing quality. Moreover, in both cases mentioned above, the route directions might not coincide with travelers flow directions. To overcome these problems, we choose the maximum direct traveler density as the optimal objective, that is, the maximum number of travelers per unit length. As a bus route is composed of the stops and the road segments it covers, the optimization problem is hereby equivalent to finding the corresponding stops and road segments. Here, N denotes the stop collection; and A denotes the collection of road segments. All of the alternative bus routes, the sub collections of A, are denoted as S = {SOD}. Then, if not considering the loop route, the bus network optimization model is as follows:

$$\max \quad D_{od} = \frac{P_{od}}{L_{od}}$$

$$s.t. \quad \begin{cases} L_{min} \le L_{od} \le L_{max} \\ od \in F \\ q_{od}^{x} \le 1.5 \\ m \ne n \qquad \forall m, n \in S_{od} \\ \forall l_{gh} > 0.8km \end{cases} \tag{1}$$

where

$$x_{ij} = \begin{cases} 1 & \text{i, j are consecutive on Planning BRT routes;} \\ 0 & \text{else.} \end{cases}$$

D_{od} = direct traveler density of the route starting from O and ending at D;

o= origin stops;

d=destination stops;

F=collection of origin and destination stops;

pi j = the number of direct travelers between stops i and j

$P_{od} = \sum_{g \in N} \sum_{h \in N} p_{gh} x_{gh}$ =the number of direct travelers from original stop i to destination stop j;

l_{gh} = length of the road section between g and h, usually l_{gh}=0.8~1.2km;

$L_{od} = \sum_{g \in N} \sum_{h \in N} \Delta_{gh} l_{gh} x_{gh}$ =if the length of BRT routes is too short, it will add the turnover time and affect the speed advantage of BRT. Hence, the length constraint of BRT routes is relaxed as $10km \le L_{od} \le 25km$;

$$\Delta_{gh} = \begin{cases} 1 & \text{g, h are consecutive on Planning BRT routes;} \\ 0 & \text{else.} \end{cases}$$

q_{od}^{x} = nonlinear rate, because usually buses with large capacity is adopted in BRT routes, if the value of nonlinear rate is too large, the operational speed will be affected.

m, n= the middle stops of candidate routes. This constraint aims to control the route trend, which means one route should pass through the one stop twice or more.

2 Algorithm Design

2.1 *Ant Colony Optimization introduction*

The ant colony optimization (ACO)algorithm is a probabilistic technique for solving computational problems which can be reduced to finding good paths through graphs. ACO was firstly introduced by Dorigo (1992) and has been used to find the solutions for many difficult combinatorial optimization problems. In ACO, artificial ants build solutions by moving on the problem graph. During the process they deposit artificial pheromone on the graph in such a way that future artificial ants can build better solutions. Due to positive feedback rule, the ACO possesses powerful ability in searching better solutions for combinatorial optimization problems.

2.2 *Transition rules*

The moving of ants is according to certain rules instead of unconscious. First, ants can only move through feasible neighbor nodes, which suggest that many nodes are unavailable for the ant moving. For example, the nodes which have been visited are unavailable in the optimization problem of BRT routes. The transition rules are as follow: the ant chooses available nodes according to the probability of each available node. The method of choosing probability of node j for the ant k at the node i is as follows:

$$P_{ij}(k) = \begin{cases} \dfrac{\tau_{ij}^{\alpha} \times \eta_{ij}^{\beta}}{\sum_{h \notin tabu_k} \tau_{ih}^{\alpha} \times \eta_{ih}^{\beta}} & j \notin tabu_k \\ 0 & others \end{cases} \tag{2}$$

Here, ： the intensity of which reflects the prior experience of the ants at this searching, and also means the total pheromone which cumulated during the running process of the ants; ： visibility, the value of which is obtained by solving a greedy

algorithm of an original problem; it only considers the local and encourages the ants to search for the local optimized routes; , : the pheromone heuristic factor and the visibility heuristic factor; $tabu_k$: the setting of unavailable nodes of the ant k.

2.3 *Pheromone Refreshing Strategy*

According to the transition rules, an ant can construct a solution of an original problem. For example, a solution means that the ant has searched a BRT route between original node and destination one. Then, the quantity of pheromone of each segment will be refreshed by the formula (3):

$$\tau_{ij}(t+1) = \rho \times \tau_{ij}(t) + \sum_{k=1}^{p} \Delta \tau_{ij}^{k} \tag{3}$$

Where is the remaining coefficient of pheromone (0, 1); p: the scale of ants; $\Delta\tau_{ij}^{k}$: The pheromone increment when the ant k is on line (i, j) in one loop.

To improve the efficiency of updating pheromone, ant-weight strategy (Yang et al. ,2007) is used to compute the pheromone increment, which can integrate the global and local information of the search. Specifically, the updating strategy of the increased pheromone is as follow:

$$\Delta\tau_{ij}^{k} = \begin{cases} \dfrac{Q}{f^{k}} \times \dfrac{f^{k} - f_{ij}}{(n-2)f^{k}} & \text{if link}(i,j) \text{ on the } k_{th} \text{ route} \\ 0 & \text{otherwise} \end{cases} \tag{4}$$

where Q= a constant, f^{k} = the direct traveler density of route k, f_{ij} = the direct traveler density on link (i, j), n = the number of the stops along route k (n>2).

The strategy for updating the increased pheromone consists of two components: the first is global pheromone increment Q/f^{k} related to the direct traveler density of route k; and the second one is local pheromone increment $(f^{k} - f_{ij})/((n-2)f^{k})$ based on the contribution of link (i, j) to route k. Thus, the update strategy ensures that the assigned pheromone increments are directly proportional to the direct traveler density. The more favorable of the link/route, the more pheromone increment is allocated to, and the more accurate directive information is provided to the later search. Meanwhile, by adjusting the pheromone assigning method for the links of current optimal path automatically, the algorithm can facilitate more delicate searches in the next cycle in a more favorable area. This helps to improve the learning capacity of the algorithm from past searches, and enhance the efficiency.

3 Case Studies

In order to examine the feasibility and validity of our model and algorithm, the main urban zone of Dalian City is used in our case study. The area of Dalian City is 180 km^2 with 89 bus routes and 3004 bus stops. ACO is implemented to search the routes with largest direct traveler density for BRT routes and the result is shown in Figure 1.

To validate the designed BRT route, transit passenger assignment is

implemented on the networks with or without BRT routes, respectively. The result is shown in Figures 2 and 3.

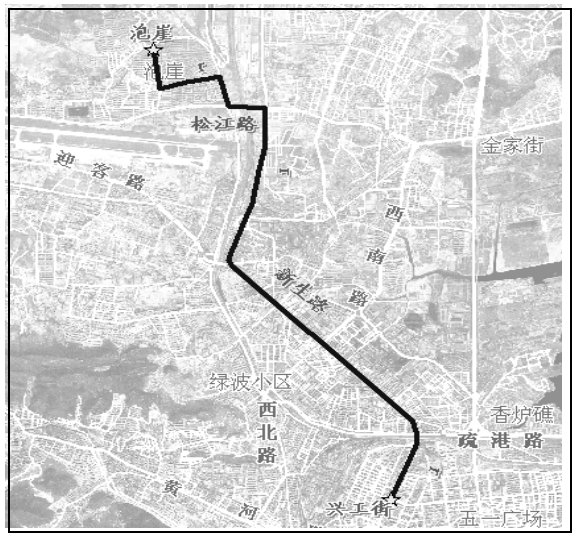

Figure 1. the Resulting BRT Routes

Figure 2. Distribution Result without BRT Routes

Figure 3. Distribution Result with BRT Routes

Because of its advantages such as the speediness, large capacity and so on, travelers flow is collected on the BRT route; and the flow of the bus routes near the BRT route is decreased significantly. It is necessary to change the public bus routes in the service area of BRT routes. With BRT routes, the total time of trip of residents decreases from 10.08 to 9.98. This is because that the BRT route is built along the public corridor, where the dense travelers flow is collected. Moreover, it employs public special bus lane to ensure fast operating speed. All these attribute to the decreased trip time.

4 Conclusions

This paper presents an optimization model of BRT routes which aims to maximize the density of direct travelers flow. This model has the objectives of minimizing transfer times and maximizing traveler flow of unit, by satisfying the constraints of the length of routes and nonlinear coefficient. An ACO based on the coarse-grain model is designed to solve the model. Finally the validity of the model and algorithm is examined in the case study. The result indicates that the model developed here can be used to optimize the routes of BRT effectively.

References

An, J., Teng J., and Meng L. Y. (2008), "A BRT Network Route Design Model." *Proceeding of the 11th International IEEE Conference on Intelligent Transportation Systems* Beijing, China, October 12-15.

Bai, Z. J. and He G. G. (2007). "Study on simulation optimization of bus rapid transit networks system based on Tabu search algorithm." *Computer Engineering and Applications*, 43(17): 226-229.

Ceder A., and Wilson, N. H. M. (1986). "Bus network design." *Transportation Research*. Part B**,** 20B (4):331–44

Dorigo, M. (1992), "Optimization, learning and natural algorithms." *Politecnico di Milano*, Italy.

Fan, Q. S., and Pan, W. (2007). "Application research of genetic algorithm in intelligent transport systems scheduling of vehicle." *Computer and Digital Engineering*, 35(5): 34–35.

HasselstrŐm, D. (1981). "Public transportation planning - a mathematical programming approach." *G teborg: University of G teborg*.

Sun, C. J., Zhou, W., and Wang, Y. Q. (2008), "Scheduling combination and headway optimization of bus rapid transit." *Journal Of Transportation systems Engineering And Information Technology*, 8(5), 61-67.

Wang, W., Yang, X. M., and Chen, X W (2001). "Planning method and management technology of urban public transportation system." Beijing: *Science Press*.

Yang, Z. Z., Yu, B., and Cheng C. T (2007). "A parallel ant colony algorithm for bus network optimization." *Computer-Aided Civil and Infrastructure Engineering*, 22, 44–55.

A Model of Mixed Land Use and Trip Production by BP Neural Network

Yue Zhao[1], Chunfu Shao[2], Zhihua Xiong[3]

[1]MOE Key Laboratory for Transportation Complex Systems Theory and Technology, School of Traffic & Transportation, Beijing Jiaotong University, Beijing 100044, China; PH(86)10-5146-5442; email: kitsnail1108@sina.com
[2]MOE Key Laboratory for Transportation Complex Systems Theory and Technology, School of Traffic & Transportation, Beijing Jiaotong University, Beijing 100044, China; PH(86)10-5168-8344; email: cfshao@center.njtu.edu.cn
[3]MOE Key Laboratory for Transportation Complex Systems Theory and Technology, School of Traffic & Transportation, Beijing Jiaotong University, Beijing 100044, China; PH(86)10-5168-8344; email: xiongzhihua@jtys.bjtu.edu.cn

ABSTRACT

Due to the drawbacks of existing trip production forecasting model, this paper develops a model of mixed land use and trip production using back-propagation neural network, which has the advantages of non-linear relation mapping. In the first place, contemporary researches on the relationship between mixed land use and trip production in China and oversea countries are reviewed to provide helpful groundwork. Then, based on the theory of neural network, the major mixed land-use factors and network structure are proposed. Furthermore, the model is verified and applied using existing data. The result shows that the forecasting model has relative high precision, which proves its good maneuverability as well as theoretical advantages. At last, the future research directions are discussed.

Key Words: mixed land use; land use index; trip production; BP neural network

INTRODUCTION

In recent years, academics and engineers worldwide have paid special attention on traffic demand forecasting as the basis and core content of transportation planning. The traditional travel demand forecasting method, well known as the four-stage planning method, is composed of trip production, distribution, model split and traffic assignment. In this method, the reliability of the trip production forecasting method, the first stage of the four-stage method, will directly affect the precision of the following three stages (Zheng et al. 2007). In addition, urban land use and traffic are linked and mutually affect each other (Yang et al. 2006). From the viewpoint of transportation planning, traffic demand results from land use and different land-use patterns determine trip production, forms of distribution, and to some extent, transportation structure. The capacity of road facilities cannot satisfy demand when land use is unreasonable or exploited too intensely. On the other hand, from the perspective of land use, transportation development would change urban structure and land-use patterns (Chen et al. 2004; Zheng et al. 2007).

Contemporary researches on the bearing between urban mixed land use and trip production in China and oversea countries could be divided into two categories, namely the mathematical models and artificial experience models (Lu, et al., 2008). Mathematical models, such as the trip generation rate models, classification generation rate models, regression analysis models, and classification regression analysis models, forecast trip production by setting up a mathematical model to represent the correlation between land-use influence factors and transportation (Badoe and Miller, 2000; Chen, et al., 2004; Yang, et al., 2006). However, the issues of mathematical models lie in: (1) the process is too complicated since practical operation requires large amounts of data; (2) the ways to calibrate weight parameters cannot be unified; and (3) the accuracy of prediction is limited.

Furthermore, the artificial neural network method, which has been successfully applied in various fields and Back-Propagation network (for short, BP network) in particular, is the most suitable method to predict trip production among other network models (Dougherty, 1995). The advantage of BP network in trip production forecasting include: (1) its non-linear mapping between input and output aggregate with a simple realization process; (2) no need to be aware of the internal structure of the system; (3) what is necessary to do is to simulate the system by studying existent samples; and (4) it can significantly cut the precision caused by inaccuracy of data and parameters (Pei et al. 2004). Meanwhile, trip production of mixed land use has its own characteristics and there are disparities in different land-use combinations. Hence, BP network as a simple and high precision method can be used in this field.

The work demonstrated in this paper starts with the discussion of the major mixed land-use factors. Then, a model of mixed land use and trip production is developed using the BP network. In summary, this paper is aimed to improve the performance of traditional prediction methods, to simplify the planning process and to enhance the prediction efficiency and accuracy of original models.

MIXED LAND-USE INDICES

The chief land-use indices factors and social economical character factors are the main elements that impact trip production (Lu et al. 2008). In a mixed land use area, the former includes different characteristics and combinations of land use, and the latter includes level of population, level of economic development, accessibility of transportation, vehicle population, etc (Clay et al. 2006). This paper mainly discusses major mixed land-use indices (e.g., the characteristics of land use, the intensity of land exploiting, the degree of mixed land use and the location factor), since they are the main influential factors of trip production and all other indices could be indicated by them.

Character of land use. Land use with different characteristics can lead to different trip production patterns (Yang et al. 2006). For instance, trip production patterns deriving from ten major categories of land-use forms in China vary from

each other. Characteristics of land use can be digitized as the indicator of functional community, which is described by the largest proportion of land area code of the community.

Intensity of land exploiting. The intensity of land exploiting directly determines the volume that urban traffic system could support. Regardless of the characteristics land use (e.g., residence or commercial space), it is believed that the higher the intensity is, or the greater the occupancy is, the larger travel demand would be generated (Chen et al. 2004).

Floor area ratio (FAR), also known as building density, is an important technology index that reflects intensity of land exploiting. FAR equals the building area divided by land area. It is widely believed that the greater the FAR the more intensive the land use is.

Degree of mixed land use. This index refers to a particular region with a variety of land uses. Trip production of a mixed land use community should not be taken as the summation of the productions from every single characteristic of land use simply because mixed land use has its own characteristics and varies by different land-use combinations. Therefore, this paper uses diversity index (H), dominance index (D), and evenness index (E) referred to definition in biology to describe this index as follows.

(1) Diversity index H describes the quantity and complexity of land use types and also reflects the proportion of each type. This index will increase when the differences between the ratios of land-use types are minimal. The formation of Shannon-Weiner diversity index function, which is a commonly used expression, is stated as follows:

$$H=-\sum_{k=1}^{n} P_k \ln(P_k) \tag{1}$$

Where: P_k represents the proportion of kth type of land from the total area; n represents number of types. For a given n, diversity index number will reach maximum as $H_{max}=\ln(n)$; if the proportion of each type is equal, $P_k=1/n$.

(2) Dominance index D demonstrates discrepancy of maximum and actual value of diversity index, and illustrates the degree of one or several other types that dominate the whole extent. The formation, Simpson's index function, is as follows:

$$D = H_{max} + \sum_{k=1}^{n} P_k \ln(P_k) \tag{2}$$

(3) Evenness index E, also known as Pielou index, describes even degree of distribution of types and the formation is as follows:

$$E = \frac{H}{H_{max}} \tag{3}$$

Location factor. The advantages of urban land use largely depend on the

location characteristics. Since travel will be greatly affected by it, location factor index is recommended to reflect the impact (Shi et al. 2005). Location factor is composed of the aggregated economic benefits, transport accessibility and the standard of infrastructure and environmental quality. Therefore, in the process of evaluation, we should consider the geographical locations, the level of economic development and the transport accessibility of a mixed land use area as whether it empnasizes on the development of industrial zones or the approach to the edge of bloc, highways, large shopping malls, hospitals, schools, tourist attractions, car parks, public transportation hub, the station, railway stations, etc., and then give different levels to communities.

Take Beijing as an example, areas that approach to "two axis, two band and multi-center "can be digitized as 3; area that approach to six high-ranking industrial function districts, including Zhongguancun Technology Zone, CBD, Beijing Economic Technological Development Area (Yizhuang), Shunyi Near the Airport Industrial Park, the Olympic Center Area and Beijing Financial Street, can be digitized as 2; area that approach to hospitals, shopping malls, parks and parking lots can be digitized as1; and others as 0.

MODELLING

Model structure. In order to develop a model with both operability and theoretical value, this paper sets up a three-layer BP network model which is a one-way transmission of forward network including input, hidden and output layers (Shmueli et al. 1996).

Based on the analysis above, the indicators of functional community, FAR, diversification index (H), dominance index (D), evenness index (E) and location factor are selected as input neurons.

In the process of model development, the symbole p, which is defined as the number of neurons in hidden layer, is crux since it will directly affect the effectiveness of the model, but there's no accurate theoretical or methodological explanatation. Some researchers use formations: $\sum_{i=0}^{n} c_p^i \rangle k$ or $p = \sqrt{n+q} + a$, where n represents the number of input neurons, q represents the number of output neurons and a represents a constant between 1 and 10, to calculate p (Feisi Technology Research and Development Center 2005).

Output neurons are trip production of community in morning and evening peak hours. The corresponding proposed analysis model is shown as Figure 1.

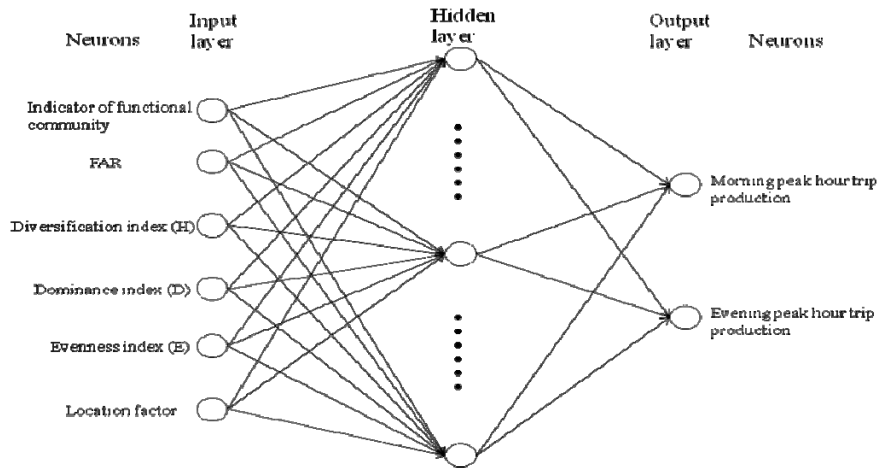

Figure 1. Model of mixed land use and trip production by proposed model

BP neural network model can be realized through many programs. This paper uses toolbox of Matlab to accomplish it.

Firstly, the model is trained by using the 30 existing samples of mixed land use areas in Beijing, which include residence land use Wangjing region, business land use CBD, industrial land use Jiuxianqiao and foreign affairs land use embassy region since these blocks are typical representatives of mixed land use.

Secondly, select 50% of data randomly as training samples and the remaining 50% as test samples. Set the number of input neurons to 6, training frequency to 10000, training error goal to 0.1, and suitable number of hidden layer to 5. Training error curve is shown in Figure 2.

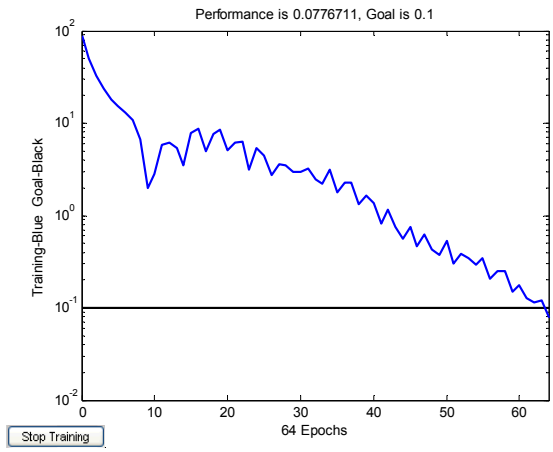

Figure 2. Training error curve of the BP neural network

According to practical operation, the speed of convergence for this model is relative fast. The model is repeatedly trained and modified until the precision results meet the requirement. The output and the estimation errors are shown in Table 1. The results indicate that the prediction error of the trip productions in mornings and evenings are 1.86% and 2.82% respectively, which is acceptable.

Table 1. Model Application Results

Peak hours	Model output (frequency/hour)	Actual value (frequency/hour)	Absolute error (frequency/hour)	Relative error (%)
7:00-8:00	2576	2625	-49	1.86
18:00-19:00	2207	2146	61	2.82

CONCLUSION

The bearing between mixed land use and trip production is a complicated non-linear mapping which BP network is skilled in. The work in this paper analyzes the indices that impact trip production directly and summarizes the major indices that are relevant to mixed land-use ones. Meanwhile, the model is developed to integrate the advantages of BP network and correlation between mixed land use and trip production. According to the characteristics of neural networks, there are some improvable aspects in this paper. One of the most important respects lies in the black-box operation of network that restrains the modification of hidden layer number, training algorithm and studying frequency. Therefore, future study will need to focus on ameliorating model structure and parameters automatically according to the input parameters and output results in order to improve operability and precision of the model.

ACKNOWLEDGE

This paper is supported by the National Basic Research Program of China (No.2006CB5505).

REFERENCES

Badoe D. A., Miller E. J. (2000). "Transportation–land-use interaction: empirical findings in North America, and their implications for modeling". *Transportation Research Part D: Transport and Environment*, 5(4),235-263

Chen P; Li J. and Zou Z. Y. (2004). "Discussing Again on Forecast of Traffic Demand Combined with Land Use". *Journal of Huazhong University of Science and Technology (Urban Science Edition)*, 21(1), 73-75

Clay M. J., Johnston R. A. (2006). "Multivariate uncertainty analysis of an integrated land use and transportation model: MEPLAN". *Transportation Research Part D: Transport and Environment*, 11(3), 191-203

Dougherty M. (1995). "A review of neural networks applied to transport". *Transportation Research Part C: Emerging Technologies*, 3(4), 247-260

Feisi Technology Research and Development Center. (2005). "Theory in neural network and Matlab 7 application". *Publishing House of Electronics Industry*, 99-108

Lu H. P. (1998). Theory and Method in Transportation planning. *Tsinghua University Press*, 92-108

Lu H. P, Zhou Q. and Xu W. (2008). "A Neural Network Model for Trip Generation Forecasting". *Journal of Transportation Engineering and Information*, 6(2), 6-11

Pei Y. L., Wang X. N. (2004). "Traffic impact forecast model based on the BP network". *Journal of Herbin Institute of Technology*, 36(8), 1034-1037

Shi F., Wang W. and Lu J. (2005). "Improvement and Conclusion about Resident Trip Generation". *Urban Transport of China*, 3(1), 43-46

Shmueli D., Salomon I., Shefer D. (1996). "Neural network analysis of travel behavior: evaluating tools for prediction". *Transportation Research Part C: Emerging Technologies*, 4(3), 151-166

Yang L. Y., Shao C. F., Liu Z. L., et al. (2006). "A Study on Mechanism of Interactions between Urban Transportation and Land-Use". *Urban Transport of China*, 4(4), 21-25

Zheng J., Lu H. P. (2007). "Study on the Impacts of Urban Land Use on Travel Demand". *Central South Highway Engineering*, 32(2), 175-179

Assessment Methodology for Road Network Travel Time Reliability under Ice and Snowfall Conditions

Junqiang Leng [1,2], Yaping Zhang [2] and Yuquan Leng [3]

[1]School of Automobile Engineering, Harbin Institute of Technology. Weihai, China, 264209. email:lengjunq@tom.com
[2]School of Transportation Science and Engineering, Harbin Institute of Technology. Harbin, China,150090. email: zxlt0905@163.com
[3]School of Marine Engineering, Harbin Institute of Technology. Weihai, China, 264209. email: lengyu.nan@163.com

ABSTRACT

Travel time reliability is considered as an important index on the reliability of a road network. The objective of this article is to study the impact of ice and snowfall on the travel time reliability. For this purpose, the link travel time ISB-BPR (Ice and Snowfall Based- Bureau of Public Roads) model is proposed, which is based on the conventional BPR (Bureau of Public Roads) model and scale functions are added to the corresponding parameters of BPR. To follow the characteristics of route choice, SUE (stochastic user equilibrium) is adopted in this study. We develop an assessment methodology, which integrates sensitivity analysis of SUE and Monte Carlo simulation to evaluate the travel time reliability. The ISB-BPR model and the algorithm are applied to a hypothetical small road network and results are presented. The results show that travel time level of service and intensity of ice and snowfall have the most significant impact on the travel time reliability.

Keywords: road network, travel time reliability, ice and snowfall, ISB-BPR model

INTRODUCTION

Road network has always been regarded as the lifeline of human beings. Especially the recent earthquakes in Sichuan province and the ice and snowfall disaster in the south of China are vivid reminders of the severe impacts on the transportation network and people life. Road network stability and reliability is a subject of great practical importance to traffic planners and engineers involved in network design and traffic management and control（Al-Deek and Emam, 2006）. Travel time reliability is one of the important parameters of road network reliability. It plays an increasingly important role in effectively describing the traffic operation performance and environmental protection concerns in urban areas, as expressed by the traffic flows, LOS and other attributes (Chen et al. 2002, Chen and Skabardonis, 2003). The travel time reliability information may be spread to travelers and commuters to help them decide on departure time and provide them with possible optimal alternative routes.

At present, the reliability research is mainly directed against the day to day recurrent traffic congestion. A classic example of nonrecurring congestion study is the network reliability under adverse weather conditions of rains (Lam et al. 2008). Although numerous accomplishments have been achieved in this area, so far, few studies have focused on road network reliability under ice and snowfall conditions, which will be studied in this research.

LINK TRAVEL TIME MODEL

In previous research, the BPR model was widely used in travel time reliability estimation. With the influence of ice and snowfall, the visibility and pavement friction will be reduced. As a result, the BPR model is not applicable to this condition. To calibrate and capture the actual functional relationship between the adverse effects and link travel time, a new link travel time model is proposed on the basis of the conventional BPR model. This is named as Ice and Snowfall Based-Bureau of Public Roads (ISB-BPR) model. It can be written as:

$$T_i(x_i, I) = g_{it}(I)t_i + \beta t_i(\frac{x_i}{g_{iC}(I)C_i})^n .$$

Here x_i and C_i , respectively, are the traffic demand and capacity on link i; t_i is the free-flow travel time on link i, which is a deterministic parameter; T_i is the travel time on link i; β and n are parameters in the conventional BPR function; $g_{it}(I)$ and $g_{iC}(I)$ are the scaling functions on free-flow travel time and link capacity, respectively, where *I* denotes the intensity of ice and snowfall. The scaling functions should satisfy the following conditions:

(1) $g_{it}(I)$ is a monotonous increasing function;

(2) $g_{iC}(I)$ is a monotonous decreasing function;

(3) When $g_{it}(I) = 1$ and $g_{iC}(I) = 1$ implying that there is no ice and snowfall, ISB-BPR will be BPR.

In this study, the ISB-BPR model is adopted. Since C_i is a random variable, so is T_i . For simplicity, let $g'_{iC}(I) = 1/\ g_{ic}$, $g_{it}(I)$ and $g'_{iC}(I)$ follow normal distributions expressed as:

$$g_{it}(I) \sim N(\mu_i^t, (\delta_i^t)^2)$$
$$g'_{iC}(I) \sim N(\mu_i^c, (\delta_i^c)^2)$$

It should be pointed out the actual distributions should be calibrated by observed field traffic data. The link travel time forms a probability distribution. Its mean can be determined as:

$$E[T_i] = t_i E[g_{it}(I)] + \beta t_i x_i^n E[g'_{ic}(I)]E\left(\frac{1}{c_i^n}\right)$$

The link capacity of each link forms different probability distributions, which can be obtained by Mellin transformation. In this study, the link capacity adopts normal distribution. The mean of the travel time on link *a* can be determined as:

$$E[T_i] = t_i \mu_i^t + \beta t_i x_i^n \mu_i^c \frac{\left(1-\theta_i^{1-n}\right)}{\overline{c}_i^n (1-\theta_i)(1-n)}, n \neq 1,$$

$$E[T_i] = t_i \mu_i^t + \beta t_i x_i \mu_i^c \frac{\ln \theta_i^{-1}}{\overline{c}_i (1-\theta_i)}, n = 1.$$

Here θ_i denotes the capacity use efficiency of link *i* on the worst ice and snowfall

conditions, $0 < \theta_i < 1$. In the theoretical research, the link capacity lower bound is $\theta_i \bar{c}_i$. The value of θ_i is different for each link; $\bar{c}_i$ is the design capacity of link *i*.

TRAVEL TIME RELIABILITY

Link Travel Time Reliability. Travel time reliability is the probability that a trip will arrive at its destination within a given period at a certain level of service. In this article, link travel time reliability is defined as the probability that the expected travel time at degraded capacity caused by ice and snowfall is less than the link free-flow travel time plus an acceptable threshold. It can be written as:

$$R(T_i) = P(T_i < t_i(1+\delta))$$

Where, δ is acceptable travel time threshold. For example, the parameter β in the ISB-BPR function is 0.1, hence the upper travel time threshold will be the free-flow travel time plus the acceptable time or 110% of the free flow travel time.

Path Travel Time Reliability. The road network is composed of links. Its reliability depends on all links reliability and how they are connected. For example, the following statement is false: "If all of the links in a system have 95% reliability at a given time, then the reliability of the system is 95% for that time."（Al-Deek and Emam, 2006）.

Generally, path is composed of links with the connection in series. Reliability of links connected in series can be written as:

$$P_k = \prod_{i \in A} P_i \quad , \quad \forall k \in K_{st}$$

Where , A is the links set of path k between OD pair *st.* In fact, OD pair *st* has one more paths; P_i and P_k, respectively, are the travel time reliability of link *i* and path *k*. If there are *m* paths between OD pair *st,* then OD pair reliability can be written as:

$$P_{st} = 1 - \prod_{k=1}^{m} (1 - P_k)$$

Where , P_{st} is the travel time reliability of OD pair *st*.

TRAFFIC ASSIGNMENT MODEL

As the network complexity and randomness of the traffic conditions , road users can not be fully aware of the real-time information. The path choice is stochastic. Consequently, Stochastic User Equilibrium (SUE) may be applied to modeling the traffic assignment as follows:

$$\min Z(f) = \frac{1}{\theta} \sum_{s,t} \sum_{k} f_k^{st} \ln\left(f_k^{st}\right) + \sum_{i \in A} \int_0^{x_i} t_i(w, y_i) dw$$

$$s.t. \qquad \sum_k f_k^{st} = q_{st}, \forall s, t$$

$$f_k^{st} \geq 0, \forall s, t$$

$$x_i = \sum_{s,t} \sum_{k} f_k^{st} \cdot \delta_{i,k}^{st}, \forall i$$

Where, k is the set of paths; f_k^{st} is the traffic volume on path k between OD

pair st; A is the set of links; x_i is the traffic volume on link i;

$$\delta_{i,k}^{st} = \begin{cases} 1 & if \quad i \quad belongs \quad to\ path \quad k \\ 0 & otherwise \end{cases}$$

SOLUTION ALGORITHM

Sensibility analysis and Monte Carlo simulation are adopted in this paper. Sensibility analysis is used to solve SUE. Monte Carlo as a test tool is used to simulate the traffic condition and calculate the reliability. The link capacity C_i and demand pattern parameters q_{st} are all random variables. Due to the absence of observed field data, it is assumed that they all follow the normal distributions. Here, the random variety generation (RVG) proposed by Chang (Chang et al. 1994) is used to generate the distribution. The flowchart of the algorithm is shown in figure 1.

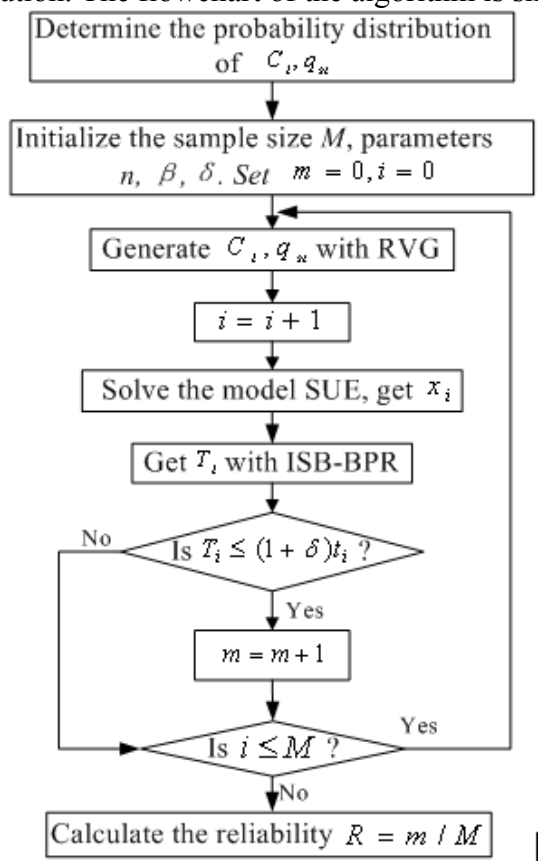

Figure 1. The flowchart of algorithm

NUMERICAL EXAMPLE

Simulation Settings. The purposes of the numerical example are to illustrate the ice and snowfall effects on road reliability and the application of the proposed model and solution algorithm. An example of a small hypothetical road network is studied as shown in figure 2. This network consists of four zones, six nodes and eight links, where zones 1, 2 are trip origin zones and zones 5, 6 are destination ones. The link data is shown in table 1. The forecast levels of hourly average snowfall intensity

are: light snowfall ($\leq 2.4mm/24hour$), normal snowfall ($\leq 4.9mm/24hour$), amber snowfall ($\leq 9.9mm/24hour$) and red snowfall ($\geq 10.0mm/24hour$). Therefore, the snowfall intensity may be assumed as depth of snowfall. The base traffic demands are respectively $q_{15}=20$ pcu/min, $q_{16}=30$ pcu/min, $q_{25}=20$ pcu/min and $q_{26}=20$ pcu/min. The link travel times are calculated from the ISB-BPR formula with $\beta=0.15, n=4$.

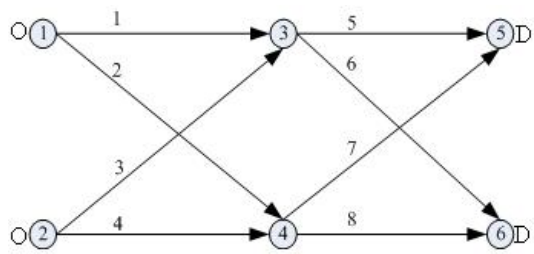

Figure 2. The test road network

Table 1. The link data of network

Link	t_i	C_i	$g_{it}(I)$	$g_{iC}(I)$
1	7	45	exp(0.09I)	exp(-0.04I)
2	8	45	exp(0.09I)	exp(-0.04I)
3	8	45	exp(0.09I)	exp(-0.04I)
4	7	45	exp(0.09I)	exp(-0.04I)
5	8	45	exp(0.09I)	exp(-0.04I)
6	9	45	exp(0.09I)	exp(-0.04I)
7	9	45	exp(0.09I)	exp(-0.04I)
8	8	45	exp(0.09I)	exp(-0.04I)

Monte Carlo simulation method and the software of Matlab7.0 are used to develop a procedure to estimate the reliability of travel time under different level of service, traffic demand and link capacities degradation. The procedure is shown in Figure 1.

Simulation Results and Analysis. In simulation, we assume that random variables c_i and q_{st} follow norm distributions. Table 2 and table 3 show that the estimated means and standard deviations of random variable resulting from the 4000 Monte Carlo simulations are very close to the theoretical values.

Table 2. Statistical value of capacities

Link	Theoretical		Estimate	
	Mean	Std.	Mean	Std.
1	45	8	45.0698	8.0321
2	45	8	44.9471	7.9864
3	45	8	45.1261	7.9646
4	45	8	44.9801	8.0932
5	45	8	45.0429	8.0165
6	45	8	44.9714	8.0619
7	45	8	45.1254	8.0441
8	45	8	44.9953	7.9269

Table3. Statistical value of OD demand

OD pair	Theoretical		Estimate	
	Mean	Std.	Mean	Std.
1-5	20	5	20.0292	4.9496
1-6	30	5	29.9282	5.0449
2-5	20	5	20.1187	4.9907
2-6	30	5	29.9233	4.9793

To illustrate the effects of level of services on the reliability, the following scenarios are simulated. For simplicity, we set the snowfall intensity $I=2.4$. Due to

space limitations, only portions of the tables are listed here. Table 4 is the reliability of link 1 at different service levels of travel times. Table 5 is the reliability of OD pair 1-5.

Table 4. Reliability of link 1 at different δ

δ	0.1	0.2	0.3	0.4	0.5	0.6	0.7	0.8	0.9	1.0
R	0	0	0.7610	0.9460	0.9765	0.9898	0.9938	0.9965	0.9965	0.9968

Table 5. Reliability of OD 1-5 at different δ

δ	0.1	0.2	0.3	0.4	0.5	0.6	0.7	0.8	0.9	1.0
R	0	0	0.9563	0.9980	0.9997	0.9999	1.0000	1.0000	1.0000	1.0000

To illustrate the effect of the snowfall intensity on the reliability, four scenarios of OD pair 1-6 under different snowfall intensities are simulated and the results are shown in Figure 3. From the figure, it can be seen that both travel time level of service and snowfall intensity are important factors in reliability analysis of a road network. The higher the snowfall intensity, the lower the travel time reliability. With the decrease of travel time requirements (i.e. δ increases), the reliability becomes higher. On the other hand, higher service levels result in lower reliability.

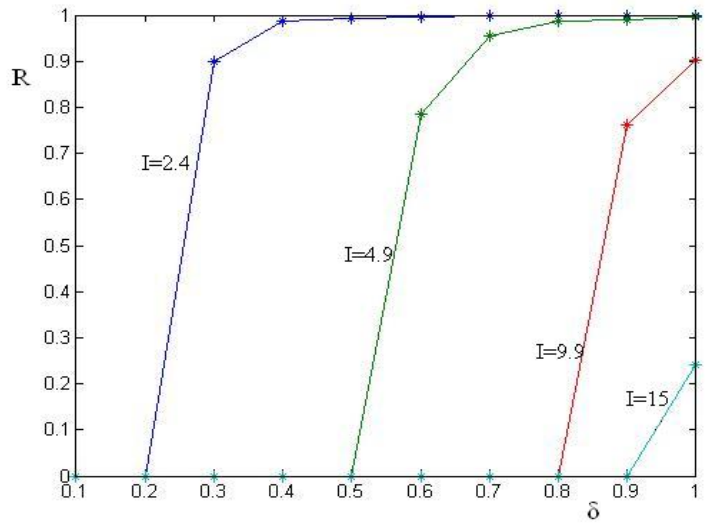

Figure 3. The effect of the snowfall intensity on the travel time reliability

CONCLUSIONS

This paper proposed the link travel time model of Ice and Snow Based- Bureau of Public Roads (ISB-BPR) model, which is based on the classical Bureau of Public Roads (BPR) model. SUE is used for the traffic assignment. We developed an assessment methodology, which integrates sensitivity analysis of SUE and Monte Carlo simulation to evaluate the travel time reliability. A numerical case study was also provided to demonstrate the practicality of the proposed model and the efficiency of the solution algorithm. Although only a small size road network was tested and normal probability distributions were adopted in this paper, the method has potentials to be extended to large-scale networks and other adverse weather conditions. It is useful for the planning and performance improvements of a road network.

REFERENCES

Al-Deek, H., and Emam, E.B. (2006). ”New Methodology for Estimating Reliability

in Transportation Networks with Degraded Link Capacities." *Journal of Intelligent Transportation Systems*, ,10(3), 117-129.

Chang, C.H., Tung, Y.K., and Yang, J.C. (1994). "Monte Carlo simulation for correlated variables with marginal distributions." *Journal of Hydraulic Engineering* 120(3), 313-331.

Chen, A., Ji, Z., and Recker, W.W. (2002). "Travel time reliability with risk-sensitive travelers." *Transportation Research Record*, 1783, 27-33

Chen, C., Skabardonis, A., and Varaiya, P. (2003) "Travel-time reliabilityas a measure of service.", *Transportation Research Record*, 1855, 74-79

Lam, Hu, S., Agachai. (2008). "Modeling impacts of adverse weather conditions on a road network with uncertainties in demand and supply". *Transportation Research Part B*, 42, 890-910.

Multi-section Short-term Traffic Flow Prediction Based on Multi-Dimensional Time Series

Gangliang Chen[1] and Lin Cheng[2]

[1]Transportation College, Southeast University, Nanjing 210096, China; TEL: (86)15850550322; email: cgl2802@126.com
[2]Transportation College, Southeast University, Nanjing 210096, China; TEL: (86)025-83795649; email: gist@seu.edu.cn

ABSTRACT

Time series has already been widely utilized in the field of traffic flow prediction from the viewpoints of both theoretical exploration and practical implementation; however, the current research mostly limited to the one-dimensional time series and single section predictions. The objective of this paper is to use the multi-dimensional time series to forecast the multi-section short-term traffic flow. The correlation analysis of the multi-section traffic flow parameters (e.g. traffic volume) is firstly conducted to identify several sections with high correlation. Then, these road sections are treated as a whole to perform the threshold regression multi-dimensional time series short-term traffic flow forecasting. Finally, Comparative analysis between the multi-section and single section (ARIMA model) scenarios is presented to demonstrate the efficacy and robustness of the proposed methodology. Computational results indicate that applying the multi-dimensional time series to forecast the multi-section short-term traffic flow is more precise and robust than the single section approach.

KEY WORDS: Short-term Traffic Flow Prediction; Multi-Dimensional Time Series; Multi-section; Correlation Analysis; Threshold Regression

1 INTRODUCTION

Short-term traffic flow prediction is the key of the ITS, and it is also the major foundation of the traffic information service, traffic control and induction. While the current research of short-term traffic flow prediction is mostly focused on the filed of single-section, the research on the multi-section shot-term traffic flow prediction is very little involved. Many traffic detectors are installed on the highway and urban expressway, which can obtain the real time traffic information. Applying the dynamic analysis technology to the history and real-time data for the quick analysis, real-time prediction and judgment, it can improve the effectiveness of traffic control and induction. All these information can supply strong technical support for the traffic information service, travel induction, traffic incident detection, traffic management and the remission of traffic congestion of highway and urban expressway (Yiannis Kamarianakis et al. 2005). Therefore, the multi-section research on the short-term traffic prediction is of much practical significance. This paper is mainly on utilizing the multi-dimensional time series to forecast the multi-section short-term traffic flow.

2 TRAFFIC FLOW DATA CORRELATION ANALYSIS

Before the prediction, we utilize the correlation analysis to identify the study object of multi-section. The main propose of correlation analysis is to obtain the correlation degree of the multi-section's traffic data. According to the correlation degree, some of sections which have the relative strong correlation degree are divided into the same group. As a result, the whole road sections are divided into several groups. This paper introduces a method which is called Multidimensional Scaling (MDS) to analysis the multi-section data (Zhu Jianping et al. 2006).

2.1 The fundamental principle of MDS

The problem which MDS can be solved is following: Identify the expression in the low dimension space when the n objects' mutual similarity (or distance) is given. In order to minimize the change brought by the dimension reduction, the new expression should be "matching in gross". Every object in the multi-dimension space is a point, so the distance and similarity of the points are highly similar. That is to say two similar objects in the multi-dimension space have the relative closer distance; otherwise the dissimilar have further distance.

2.2 The application of MDS in correlation analysis of multi-section traffic flow data

In order to make the correlation analysis more accurate, it is essential to do some pretreatment for the raw data (identification, rejecting and restoration of error data), and then we obtain the processed data of Remote Traffic Microwave Sensor (RTMS) from RT008 to RT013 during the October 15th 2007 to October 29th 2007 between 7:30 ~ 8:30 interval 5-minute. The sections which are installed the RTMS are marked as Section 1, Section2,…,Section 6, which are shown in the **Figure 1**.

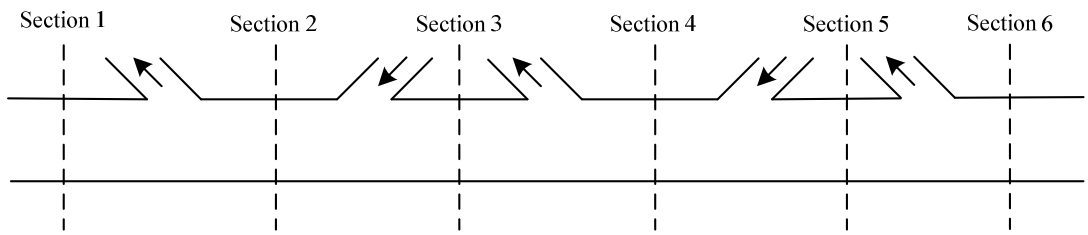

Figure 1. Chart of Road Cross-sections Where Traffic Sensors Locate

As the data of 6 sensors we get is during the 15 days, so firstly average the data of peak hour of the 15 days, thus we get the average value of the 15 days' value in peak hour. Utilizing these average value, the correlation degree of every section can be calculated, the larger of the degree, the stronger of the correlation. The original data matrix composed by these correlation degree can be adapted the MDS to make further study.

With the help of Multidimensional Scaling tool box in the software of SPSS, we can analyze the 6 sections' data with the method of MDS to determine their relevance. Confined to article length constraints, only two-dimensional perceptual mapping (coordinates perceptual mapping) is shown in **Figure 2**.,where Case1，case2，…，case6 are Section 1, Section2, …Section 6 respectively.

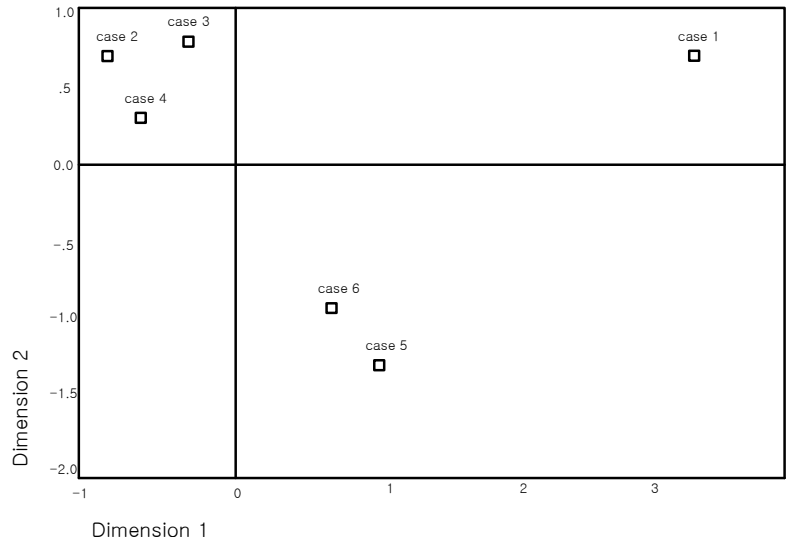

Figure 2. Derived Stimulus Configuration of Traffic Flow of 6 Road Cross-sections

From the figure above we can see that, among these 6 Sections, Section 2, Section 3, Section 4 are in the first quadrant, and the distance between each other is close, therefore, they will fall into one category, as a whole to be studied; Section 1 is more further form than the other sections, thus classified it as a separate category to be studied; and Section 5, Section 6 in the fourth quadrant, a relatively close distance between each other and therefore Section 5, Section 6 classify as a category to be studied. In that case, according to their degree of correlation, the original six sections will be divided into three groups: the first group is Section 1; second group is Section 2, Section 3, Section 4; the third group is Section 5, Section 6.

3 TRAFFIC FLOW PREDICTION MODEL AND METHOD

Assume that $X_{\mathrm{p}}(t)$ is p-dimensional time series, and it has n group of observations, marking it as:

$$X_{\mathrm{p}}(t)=\begin{bmatrix} x_{11} & \cdots & x_{1n} \\ \cdots & \cdots & \cdots \\ x_{p1} & \cdots & x_{pn} \end{bmatrix}$$

Yet the general, support that there are $m \cdot p$ threshold variables and any of these variables corresponds to l+1 threshold values, and m is order. There are $\sum_{ii=0}^{m \cdot p} C_m^{ii} \cdot p$ combinations for every group threshold values of $m \cdot p$ threshold variables, and thus m-order multi-dimensional time series of threshold auto-regressive model can be defined as (Jin Juliang et al. 2000):

$$X_{\mathrm{p}}(t)=\begin{cases} \sum_{i=1}^{m} B_1^{(i)} X_p(t-i)+ b_{1,0} & R\in (r_0, r_1] \\ \sum_{i=1}^{m} B_N^{(i)} X_p(t-i)+ b_{N,0} & R\in (r_{l-1}, r_l] \end{cases} \tag{1}$$

Where $X_{\mathrm{p}}(t)=\begin{bmatrix} x_1(t) \\ \cdots \\ x_p(t) \end{bmatrix}$, $B_k^i=\begin{bmatrix} b_{11,k}^{(i)} & \cdots & b_{1p,k}^{(i)} \\ \cdots & \cdots & \cdots \\ b_{p1,k}^{(i)} & \cdots & b_{pp,k}^{(i)} \end{bmatrix}$, $X_p(t-i)=\begin{bmatrix} x_1(t-i) \\ \vdots \\ x_p(t-1) \end{bmatrix}$, $r_j=\begin{bmatrix} r_{1,j} \\ \vdots \\ r_{m\cdot p,j} \end{bmatrix}$

$R=\begin{bmatrix} x_1(t-i) \\ \vdots \\ x_p(t-1) \end{bmatrix}$, $r_0<r_1<\cdots<r_l$, $N=l\sum_{ii=0}^{m\cdot p}C_{m\cdot p}^{ii}$, $i=1,2,\cdots,m$, $k=1,2,\cdots,N$

Sometimes it only uses p variables to predict the anterior g variables of multi-dimensional time series ($g \le p$), and this can be achieved by deleting p-g line of model (1) (Yang Weiqing et al. 1992), and the new model is:

$$X_{\mathrm{g}}(t)=\begin{cases} \sum_{i=1}^{m}B_1^{(i)}X_{p-q}(t-i)+a_{1,0} & R\in(r_0,r_1] \\ \sum_{i=1}^{m}B_N^{(i)}X_{p-q}(t-i)+a_{N,0} & R\in(r_{l-1},r_l] \end{cases} \tag{2}$$

For the equation (1), introducing the half polynomial:

$$\varphi_+=\begin{cases} \varphi & \varphi>0 \\ 0 & \varphi\le 0 \end{cases} \tag{3}$$

And thus the equation (1) can be transformed as:

$$X_p(t)=\sum_{i=1}^{m}B_1^{(i)}X_p(t-i)+c_{1,0}+\sum_{i=1}^{m}\sum_{j=1}^{l}A_j^{(i)}(X_p(t-i)-r_j)_+ \tag{4}$$

Correspondingly equation (2) can be transformed as:

$$X_g(t)=\sum_{i=1}^{m}B_1^{(i)}X_{p-q}(t-i)+d_{1,0}+\sum_{i=1}^{m}\sum_{j=1}^{l}A_j^{(i)}(X_{p-q}(t-i)-r_j)_+ \tag{5}$$

Where $A_k^{(i)}=\begin{bmatrix} a_{11,k}^{(i)} & \cdots & a_{1p,k}^{(i)} \\ \cdots & \cdots & \cdots \\ a_{p1,k}^{(i)} & \cdots & a_{pp,k}^{(i)} \end{bmatrix}$, $k=1,2,\cdots,N$

For the equation (1) (4) and equation (2) (5), it is not difficult to prove the equivalence between them (Yan Huasheng et al. 1994).

Introduce the screening technology of independent variable for the equation (4) and equation (5), and thus it can set up the threshold regression model of multi-dimensional time series. If the threshold variable's value is not selected in the final regression equation, that is to say to sub-merge the corresponding subsections, which indicates impact of the threshold variable and its value on the dependent variable is not significant. At this point, we have obtained the universal modeling program of threshold regression model of multi-dimensional time series.

4 EMPIRICAL RESEARCH

Peak-hour traffic volume is the most representative traffic volume of one-day, and it is also the most difficult prediction target, therefore chose the peak-hour as prediction research object, not only can test the prediction ability of threshold auto-regressive model of multi-dimensional time series, but also is full of practical significance. Select the second group of sections in correlation analysis, which is Section 2, Section 3 and Section 4, and take traffic volume data of these three

sections during the October 15, 2007 to 29 between 7:30 ~ 8:30 interval 5-minute as a study object; set order *m*=3, select the max and min value of the above estimating factors at one time. To each estimating factor, we could use the method of adding by 0.1 unit from the minimum value until it reach the max value of the related estimating factor, so that we could finish the conformation of threshold variable and the related threshold value. We utilize the method of 4 factors optimal subset regression to establish the multi-dimensional time series threshold auto-regressive model of peak hour traffic volume (take time period of 7：45~8：00 as an example):

$$x_{2,t} = 1.2(x_{2,t-1} - 13)_+ - 0.3(x_{3,t-2} + 5)_+ + 0.7(x_{3,t-3} - 6)_+ - 0.6(x_{4,t-2} + 7)_+ + 3 \quad (6)$$

$$x_{3,t} = -1.3(x_{3,t-1} - 5)_+ + 0.9(x_{3,t-2} - 2)_+ + 0.5(x_{4,t-1} - 4)_+ - 0.8(x_{4,t-2} - 9)_+ + 8 \quad (7)$$

$$x_{4,t} = -1.3(x_{3,t-1} - 14)_+ + 1.2(x_{3,t-3} - 13)_+ - 0.8(x_{4,t-1} - 9)_+ - 0.3(x_{4,t-2} - 5)_+ + 5 \quad (8)$$

In equation (6) to (8), $x_{2,t}$ 、 $x_{3,t}$ and $x_{4,t}$ separately represent the peak hour t moment's value of detector 2, detector 3 and detector 4. According to the definition of half polynomial, when the estimated factor is higher or lower than some threshold value, the relation between the estimated factor and the estimated object will be changed. In order to detect that whether the time series model is through the test of significance or not, we do the calculation of equation (6) to (8), and the F value is 5.8, 6.4 and 5.6 respectively, which all exceed the F significance text of $\alpha = 0.05$. These results indicate that the multi-dimensional time series threshold autoregressive model of the peak-hour traffic volume through a significant test.

Compared with the prediction and measured value of the peak hour, and the results are shown in **Figure 3**, where abscissa is time series, from 7:30-8:30 every five minutes for an interval time-series; ordinate is traffic flow, and lines are the measured and prediction traffic flow, and unit is vehicles per 5 minutes.

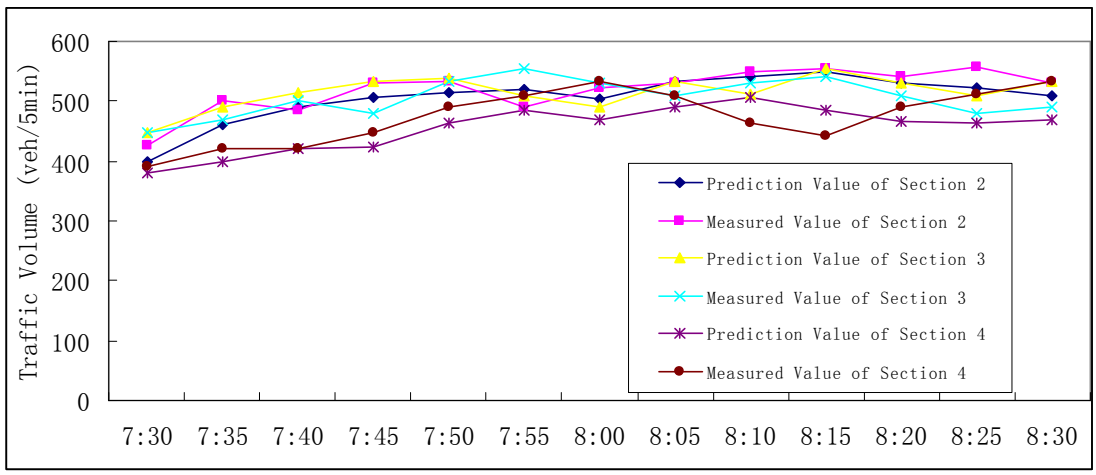

Figure 3. Prediction Values and Measured Values of Traffic Volumes from Road Cross-sections 2-4

From the fitting degree of prediction and measured values in figure 3, the cross-section values of prediction are consistent with the observed trend of traffic. Every moment's difference of the dashed line and solid line is the prediction error, and from the chart we can see the qualitative observation floating area of the each sectional predictive value is small.

In order to study quantitatively the effects of multi-section prediction, we do

the prediction of these 3 sections utilizing the single-section time series method (Autogression), and compared the results with this paper's. We adopt the Mean Absolute Percentage Error (MAPE) and Mean Absolute Percentage Error (MAD) as the comparative indicators of the prediction error, for these two indexes can reflect the difference between measured and prediction values more comprehensive.

Table 1. Error of Two Forecasting Methods of Time Series

		MAPE	MAD
Multi-section	Section 2	8.31%	11.27
	Section 3	9.75%	10.34
	Section 4	8.47%	11.16
Single-section	Section 2	15.36%	17.64
	Section 3	13.09%	14.68
	Section 4	16.56%	15.21

From the analysis results, compared with the single-section method, the multi-section method is more accurate than the single-section method, not only in the aspect of MAPE, but also the MAD.

5 CONCLUSION

This paper brings the thought of correlation analysis on multi-section traffic flow parameter, and utilizes the MDS to make the correlation analysis. It divides the road sections into several groups whose members are strongly related to each other, and determines the research object. Under the background of bringing the half multinomial, this paper conducts a new expression of threshold regression model of multi-dimension time series. What's more, according to the new expression, we put out a series new normal project of modeling. From the similarity of peak hour traffic measurement and test result, those three model all have several threshold, and the regression threshold model has a good capacity of similarity and estimating, and it has a broad application future and it is useful for further research and test.

REFERENCE

Jin Juliang, Yang Xiaohua, Jin Baoming Ding Jing(2000). Application of Threshold Regressive Model to Predicting Annual Runoff. Journal of Glaciology and Geocryology. Vol. 22, No. 3, 2000, pp. 230-234.

Yang Weiqing, Gu Lan(1992). Time Series Analysis and Dynamic Data Modeling. Beijing: Beijing Industrial College Press.

Yan Huasheng, Cao Jie(1994). Method of Building a Multivariate Threshold Regression model. Scientia Atmospherica Sinica. Vol. 18, No. 2, 1994, pp. 194-199.

Yiannis Kamarianakis and Poulicos Prastacos(2005). Space-time modeling of traffic flow. Computer & Geoscience. Vol. 31, No. 2, 2005, pp. 119-133.

Zhu Jianping (2006). Practical Multivariate Statistical Analysis. Science Press.

Research on the Characteristics of Time Headway Distribution in Expressway Weaving Section of Type A

Xue Changlong[1] and Zhao Jiaqi[2] and Pei Yulong[3]

[1]Jilin Provincial Highway Construction Bureau, Mail Stop No. 2518, Jiefang Rd., Changchun City, Jilin Prov., China 130021; PH (86) 431-83444920; FAX (86) 431-83444985; email: xuechanglong@126.com
[2]Department of Maths, School of Basic Science, Changchun University of Technology, Mail Stop No. 17, Yan'an Rd., Changchun City, Jilin Prov., China 130012; PH (86) 431-85716486; email: scorpiozhao@yahoo.com.cn
[3]School of Transportation Science and Engineering, Harbin Institute of Technology, P.O.Box 2526, 202 Haihe Rd., Nangang Dist., Harbin City, China 150090; PH (86) 451-86282832; email: yulongp@263.net

ABSTRACT

Traffic flow shows unique characteristics in expressway weaving sections and time headway distribution is usually changed by traffic flow in weaving sections. In order to represent the inherent features of time headway distribution in expressway weaving sections, we use the advanced traffic detection instruments to collect the data of expressway weaving sections of type A in Beijing, Guangzhou and Shanghai. Based on the data processing and analysis with several commercialized tools such as Video Trace, MetroCount and NC-97, and applying probability theories to analyze those data by different lanes and sections, we found the practical distribution mostly obeys displaced negative exponential distribution and Cowan M3 distribution, shows dynamic rule of time headway distribution in expressway weaving sections, changing along with the traffic volume of passing certain section. Finally, this rule is proven by fitting technique of χ^2 and test of goodness.

INTRODUCTION

Weaving section is part and parcel of entire expressway system, and the characteristics of time headway distribution in weaving sections are also crucial to estimate capacity. The movements of vehicles on ramps and vehicles in mainline always lead to the turbulence of traffic stream, speed reducing, delay increasing and bottleneck. At the same time, because traffic volume of both mainline and ramp is higher on expressway, operation feature of traffic flow on expressway is different from that on freeway, such as merging, weaving and so on. So it is significant that we study the characteristics of time headway distribution on expressway weaving section.

It will lead to time headway redistributing in weaving location if

the number of entering vehicles from ramp changes (Li Wenquan et al. 2003). In order to obtain characteristics of time headway distribution in expressway weaving sections under conditions of different lanes and volumes, we conducted the regression analysis based on a large number of field data related to time headway statistic distribution of type A weaving sections which are typical in most of the cities.

DATA COLLECTION AND PROCESSING

Recently, we chose several typical expressway routes and collected a large number of practical data from all parts of expressway system in the cities of Beijing, Guangzhou, Shenzhen, Shanghai, Tianjin, Shenyang and Harbin. Here, several advanced traffic detection tools were used to collect data of weaving sections, and the tools include American NC-97 portable traffic counter, Australian MetroCount 5600 vehicle classification system, Chinese Video Trace™ VT2100R detection system and all weather digital video cameras. When put in practice, digital video camera was fixed so high that can easily observe the whole weaving area (Yan Baojie 1994). At the same time, according to their functions, other equipments were arranged in pairs or groups to collect data. The duration time of data collection for each site was 12 hours continuously, from 6:00a.m. to 6:00p.m., in order to fit the least demand number of statistic analysis and make the collected data more representative. The equipments installed in research site were shown as below (see Figure 1).

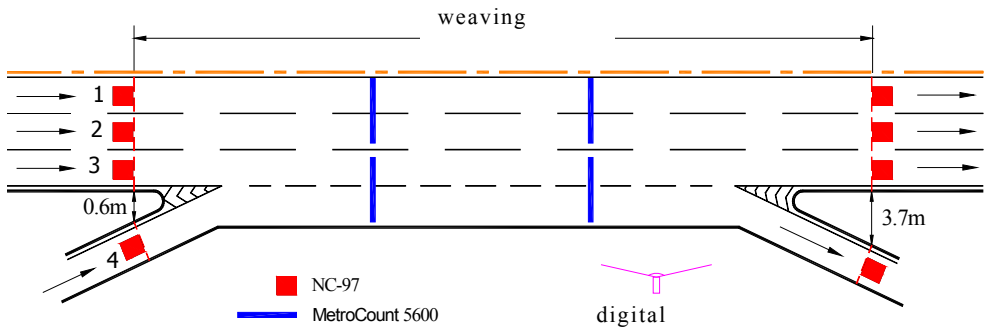

Figure 1. Sketch of equipments laying.

For the data processing, the data collected by MetroCount 5600 and NC-97 were preprocessed with the data processing systems themselves, and the Video Trace™ VT2100R calibrated the basic parameters required from the traffic flow data collected by digital video camera. Based on the observation and analysis, we found the current expressway traffic stream always arrived by the manner of motorcade and usually went and stopped when traffic volume was close to saturation, which implied that the state of traffic flow could have dramatic change within a short time period. Hence, 1 minute is adopted as data aggregation time period to represent the macroscopic characteristics of traffic flow,

operation state in different periods and LOS corresponding in expressway weaving sections.

CHARACTERISTICS ANALYSIS OF TIME HEADWAY DISTRIBUTION

Time headway indicates a time interval when two continuous vehicles pass through a certain point in the same travel direction (China Academy of Highway and Transport 1998). The characteristics of time headway distribution in expressway weaving sections should be analyzed with befitting distribution models, then its distribution rule can be obtained. For modeling, a number of studies have been done by researchers throughout the world. At present the representative models mainly include negative exponential distribution, displaced negative exponential distribution, Cowan M3 distribution and K-rank Erlang distribution (Nathan Gartner et al. 1998).

Due to the close correlation between time headway distribution and traffic volume, we made time headway data regressed by different lanes and volumes with several distribution models mentioned above. Now one weaving section on the North third Ring Road in Beijing was taken as an example. The actual time headway distributions of different lanes and three segments, entrance sites, interweaving sites and exit sites were shown in the following (see Figure 2).

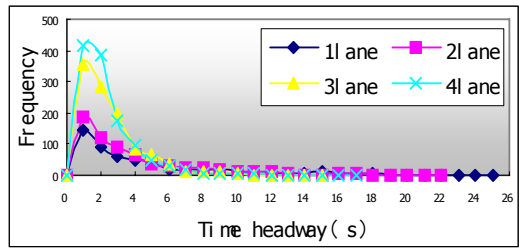

(1). Entrance site.

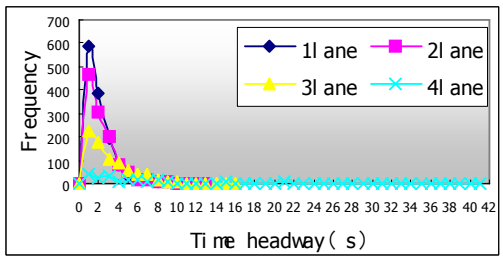

(2). Interweaving site.

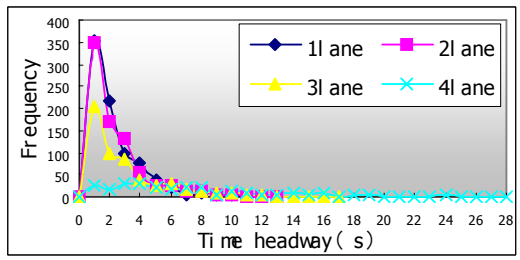

(3). Exit site.

Figure 2. Actual time headway distributions of weaving sections.

As shown in Figure 2, actual time headway distributions of both lane 1 and lane 2 are closer at the same site, so are those of both lane 3 and lane 4. While, at different sites, changing trend of time headway distributions of both lane 1 and lane 2 is similar, so is that of both lane 3 and lane 4. The reason is that main stream vehicles which are going to exit to ramp will have to merge into the most-right lane of mainline

actually before they start to run into weaving section, the main stream vehicles which are not going to weave section mostly use middle lanes or most-left lanes. Only a few main stream vehicles exit to ramp from weaving section to most-left lanes by time after several times of lane changing.

Time headway distributions of each lane at different sites have been regressed nonlinearly. The regression quality of theoretic distribution to actual distribution was verified by the fitting method of χ^2 at the marked level of 0.05 (see Table 1).

Table 1. Time headway distribution and checkout every lane in weaving section.

Regression models				negative exponential distribution		displaced negative exponential distribution		Cowan M3 distribution		Erlang distribution			
										2 rank		3 rank	
χ^2 checkout				χ_o^2	χ_t^2	χ_o^2	χ_t^2	χ_o^2	χ_t^2	χ_o^2	χ_t^2	χ_o^2	χ_t^2
lane、observation sites、volume(veh/h)、results	1	entrance site	537	113.805	21.026	17.255	19.675	151.096	27.587	264.816	18.307	539.115	16.919
				×		✓		×		×		×	
		interweaving site	1347	508.734	14.067	2781.78	9.488	2.606	16.919	503.623	9.488	1142.59	7.815
				×		×		✓		×		×	
		exit site	836	281.042	14.067	596.977	9.488	13.642	16.919	214.955	9.488	508.201	7.815
				×		×		✓		×		×	
	2	entrance site	660	121.694	19.675	9.057	18.307	69.657	24.996	221.547	15.507	516.862	14.067
				×		✓		×		×		×	
		interweaving site	1157	398.386	14.067	664.551	9.488	7.013	18.307	295.61	9.488	546.906	7.815
				×		×		✓		×		×	
		exit site	791	264.428	14.067	615.878	9.488	12.868	18.307	262.462	9.488	608.443	7.815
				×		×		✓		×		×	
	3	entrance site	1072	323.51	15.507	127.172	11.07	14.08	18.307	197.264	11.07	404.596	9.488
				×		×		✓		×		×	
		interweaving site	775	174.197	18.307	10.587	14.067	85.497	23.685	146.846	14.067	363.726	12.592
				×		✓		×		×		×	
		exit site	541	210.496	15.507	10.198	12.592	312.517	24.996	349.622	11.07	625.385	9.488
				×		✓		×		×		×	
	4	entrance site	1192	415.003	15.507	455.388	11.07	17.844	18.307	270.603	11.07	568.537	9.488
				×		×		✓		×		×	
		interweaving site	226	42.476	21.026	10.169	21.026	114.885	26.296	107.717	21.026	220.768	18.307
				×		✓		×		×		×	
		exit site	267	54.709	22.362	16.278	21.026	94.378	27.587	31.618	21.026	87.525	18.307
				×		✓		×		×		×	

(Note: χ_o^2 =the value of observation; χ_t^2 =the value of theory; ×=refuse; ✓=accept.)

The regression results indicate that time headway distributions in expressway weaving section of type A are as dynamic variation between displaced negative exponential distribution and Cowan M3 distribution with different traffic volumes. Moreover, dynamic distributions of time headway of both lane 1 and lane 2 are usually the same changing characteristics, so are those of both lane 3 and lane 4.

χ^2 TEST OF TIME HEADWAY DISTRIBUTIONS

It is required that there should be some methods to estimate the regression quality when theoretic distribution is compared to actual data distribution. χ^2 test is usually used in traffic engineering at present. Under the condition of the least data required, firstly, the method needs to estimate distribution parameters, then to determine theory frequency with the assumed theoretic distribution model and figure out χ^2 value of actual observation data, finally to verify whether the assumed theoretic distribution model is acceptable or not at the marked level of 0.05. The following example is to analyze time headway distribution of lane 1 at interweaving site in the weaving section mentioned above including 1346 samples.

Parameters of Actual Observation

$$M = \frac{\sum_{i=1}^{12} f_i t_i}{\sum_{i=1}^{12} f_i} = \frac{2246}{1346} = 1.6686$$

$$D = \frac{\sum_{i=1}^{12} f_i t_i^2}{N-1} - \frac{\left(\sum_{i=1}^{12} f_i t_i\right)^2}{N(N-1)} = \frac{7164.5}{1345} - \frac{2246^2}{1346 \times 1345} = 2.54$$

$$\lambda = \frac{1}{M} = \frac{1}{1.6686} = 0.5993$$

χ^2 Test

The assumed theoretic distribution models are negative exponential distribution, displaced negative exponential distribution, Cowan M3 distribution and K-rank Erlang distribution, which are verified respectively by the method of χ^2. The verified result is acceptable when Cowan M3 distribution is assumed. The test process is as follows:

Let the least time headway of traffic flow equal to one second,

t_m=1s, then the ratio of the vehicles whose time headway are bigger than t_m over all vehicles is:

$$\alpha = e^{-0.55(q\text{-}0.025)} = e^{-0.55(1347/3600\text{-}0.025)} = 0.8253$$

$$\lambda = \frac{\alpha q}{1 - t_m q} = \frac{0.8253 \times 1347/3600}{1\text{-}1 \times 1347/3600} = 0.4934$$

Where, q= average arriving rate of traffic flow (pcu/s), λ= shape parameter.

So the Cowan M3 distribution model is:

$$p(h \geq t_i) = 0.8253 e^{-0.4934(t_i\text{-}1)}$$

The theoretic frequency is $F_i = 1346\left[p(h \geq t_i) - p(h \geq t_{i+1})\right]$. According to the rule of χ^2 test, F_i of samples in each group must not be less than 5. If F_i is less than 5, those samples will not be merged into near groups until F_i of the new group is more than 5.

Then $$\chi_o^2 = \sum_{i=1}^{10} \frac{f_i^2}{F_i} + \frac{\left(\sum_{i=11}^{12} f_i\right)^2}{\sum_{i=11}^{12} F_i} - N = 1347.9824 + \frac{4}{6.41804} - 1346 = 2.606$$

DF=11-2=9, α=0.05, After looking up the distribution table of χ^2 we can get $\chi_{0.05}^2 = 16.919$.

$\chi_o^2 < \chi_t^2$. The assumed theoretic distribution model is accepted, and so the actual data at this site obey Cowan M3 distribution.

According to the same reason, others' time headway distributions of each lane at correspondence site are verified. The test results are shown in the above table (see Table 1).

CONCLUSION

Weaving operation of vehicles could lead to new distribution of time headway in weaving sections and form dynamic distribution characteristic. After analyzing the practical data in detailed, we found that time headway distribution in expressway weaving section of type A could be well regressed with displaced negative exponential distribution and Cowan M3 distribution. At the same time other actual data of the same type weaving sections, such as East third Ring Road south farming exhibition pedestrian bridge in Beijing and Inner Ring Road B near railway station in Guangzhou, were analyzed with the same methods. We draw the conclusion that time headway distributions in expressway

section are as dynamic variation as different traffic volumes at different sites. If volume is less than 250 veh/h, time headway will obey negative exponential distribution; if volume is between 250 veh/h and 750 veh/h, time headway will obey displaced negative exponential distribution; if volume is between 750 veh/h and 1500 veh/h, time headway will obey Cowan M3 distribution.

There are unique characteristics of traffic flow in expressway weaving sections. This analysis provides fundamental research for further study on capacity of expressway weaving sections, reasonable planning of expressway, and traffic management.

REFERENCES

China Academy of Highway and Transport. (1998). "Traffic engineering manual." *China Communications Press,* Beijing, 381-382.

Li Wenquan, Wang Wei, and Zhou Ronggui. (2003). "Headway Characteristics of Lane 1 on Expressway Merge Area." *Journal of Highway and Transportation Research and Development,* 20(1), 114-117.

Nathan Gartner, Carroll J. Messer, and Ajay K. Rathi. (1998). "Traffic Flow Theory." *Transportation Research Board.*

Yan Baojie. (1994). "Traffic Research & Analysis." *China Communications Press,* Beijing, 104-106.

An Improved Ant Colony Algorithm for Placing-in and Taking-out of Wagons in Branch-shaped Sidings

Guo Qianqian[1] Ni Shaoquan[2] Li Chengbing[3] Chen Dingjun[4]

[1]College of Traffic and Transportation, Southwest Jiaotong University, Chengdu Sichuan, 610031, China; PH (+86) 028-87634680; email: gqq6330312@163.com
[2]College of Traffic and Transportation, Southwest Jiaotong University, Chengdu Sichuan, 610031, China; PH (+86) 028-87600706; email: shaoquanni@163.com
[3]College of Traffic and Transportation, Southwest Jiaotong University, Chengdu Sichuan, 610031, China; email: bingbingnihao2008@126.com
[4]College of Traffic and Transportation, Southwest Jiaotong University, Chengdu Sichuan, 610031, China; PH (+86) 028-87600706; email: chen-dingjun@163.com

ABSTRACT. The key of placing-in and taking-out operations of wagons is how to select a rational sequence, which is hard to solve. According to the analysis of characteristics of placing-in and taking-out operations of wagons in branch-shaped private sidings, we construct Hamilton graph of this problem, and convert this problem into searching Hamilton loop of minimum weight. In this paper, we present an improved ant colony optimization (ACO) algorithm for such a problem. The proposed ACO algorithm has several features, including introducing upper and lower bounds to the values of pheromone trail, and applying local search and modified global search strategy. The improved algorithm is experimented on branch-shaped sidings problem with 6 nodes and shows its advantage over conventional ant colony algorithm. For the large scale branch-shaped sidings problems, this proposed algorithm can save much time.

1 Introduction

Placing-in and taking-out wagons operation is an important task in large railway freight stations and some technical stations. Selecting a rational procedure of placing-in and taking-out operation, nonproductive detention time of wagon in the railway stations can be reduced and wagon turn-round can be accelerated. Therefore, many earlier researchers have carried out research on problem of placing-in and taking-out of wagons. Gao and Yang (1981) solves the problem of optimization of the orders of placing and taking-out of wagons on station with the shortest route in graph theory. Wang (1996) proposes three optimized targets and gives an optimization method for taking-out after placing-in of wagons in non-through trains. Yu and Li (2002) consider the problem as a typical traveling salesman subject, and solve it with heuristics-saving algorithm. Yang et al. (2008) proposes a chromosome presentation and realizes the genetic algorithm for the problem.

This paper is concerned with the problem of placing-in and taking-out of

wagons in branch-shaped sidings. The objective is to minimize the total time that a locomotive spends going to every private sidings. We firstly construct Hamilton graph of the problem, then find the Hamilton loop with minimum weight by means of an improved ant colony algorithm, which introduces mutation and crossover operators of genetic algorithm into basic ant colony algorithm.

The remainder of the article is organized as follows. Construction of Hamilton Graph is described in Section 2. The proposed ACO algorithm is presented in Section 3. Computational results of test problems are provided and discussed in Section 4. Section 5 summarizes the conclusions of this study.

2 Construction of Hamilton Graph

In this paper, we mainly discuss placing-in and taking-out operations of wagons in branch-shaped private sidings. The key problem is how to minimize the time a locomotive spends going to every special line. To construct the model, we firstly simplify constraints that are shown as follows: (1) One locomotive; (2) Every special line has two turnouts; (3) The number of cars that will be placed-in and taken-out is known. (4)The time the locomotive spends going to every special line is determined.

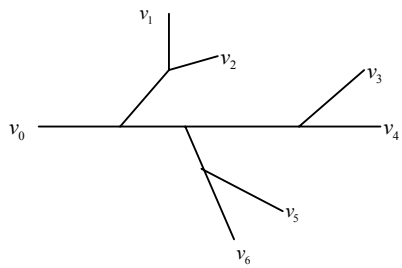

Figure 1. The special lines on branch-shaped sidings

As shown in Figure 1, v_0 which represents the station at the start node. $v_1 \sim v_6$ are leaves of the special line. In Figure 2, Hamilton loop of branch-shaped sidings is shown, the weight of edge (v_i, v_j) is equal to the time that the locomotive goes from v_i to v_j $(i, j = 0,1,2,3,4,5,6)$ .The problem of placing-in and taking-out of wagons is searching Hamilton loop with minimum weight.

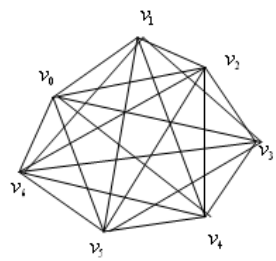

Figure 2. Hamilton loop of branch-shaped sidings

In fact, the problem of Hamilton loop is a well-known traveling salesman problem (TSP). TSP is a paradigmatic NP-hard combinatorial optimization problem, so it is hard to get an accurate result with traditional mathematical method. With the rapid development of computer, modern intelligent algorithms, such as genetic algorithm, simulated annealing algorithm, and ant colony algorithm, have successfully solved TSP. In this paper, we proposed the improved ACO algorithm for placing-in and taking-out operations of wagons in branch-shaped sidings.

3 The proposed ACO algorithm

Ant Colony Optimization (Dorigo M.,1997, ACO) is inspired by the foraging behavior of real ants, which can be described as follows. Real ants have the ability to find the shortest path from a food source to their nest without using visual cues. Instead, they communicate information about the food source by producing a chemical substance, called pheromone, laid on their paths. Since the shorter paths have a higher traffic density, these paths can accumulate a higher amount of pheromone. Hence, the probability of ants following these shorter paths will be higher than the longer ones.

ACO is one of the meta-heuristics for discrete optimization. It has been successfully applied to a large number of combinatorial optimization problems, including traveling salesman problems (Dorigo M.,1997), vehicle routing problems (Bullnheimer B.,1999) and quadratic assignment problems (Gambardella L.M.,1999), which have shown competitiveness with other meta-heuristics.

The ACO algorithm proposed in this paper is basically the ACS version (Dorigo M., 1997), but it introduces the feature of a minimum pheromone value and a maximum pheromone value from"max-min-ant system" (Stützle T., 2000, MMAS).

To make the algorithm more efficient and effective, we employ two distinctive features, including introducing mutation and crossover operators of genetic algorithm. Before elaborating on these features, we present our ACO algorithm as follows:

Step 1: Parameter initialization. Let the initial pheromone trail $\tau_{ij}(0) = C$ (C is constant); Let m be the ant number; Let n be the number of node, where m=n-1.

Step 2: Main loop. In the main loop, each of the m ants constructs a solution. This loop is executed for the maximum iteration $N_{c\max} = 100$.

Step 2.1: Constructing a solution by each ant. A set of artificial ants is initially created. Each ant starts with a node other than node v_0 and then successively appends a node to the partial solution until a feasible solution is constructed. In choosing the next node j , the ant applies the following state transition rule:

$$j = \begin{cases} \arg \max_{u \in allowed_k} \left\{ [\tau_{iu}(t)][\eta_{iu}(t)]^{\beta} \right\} & if \ q \le q_0 \\ S & otherwise \end{cases}$$

Where $\tau_{iu}(t)$ is the pheromone trail associated with node u to node i at time t; $\eta_{iu}(t)$ is the heuristic desirability at time t; β is the parameter which determines the relative importance of the heuristic information; $allowed_k$ is the set of feasible components, q is a random number uniformly distributed in [0,1], and q_0 is a parameter $(0 \le q_0 \le 1)$ which determines the relative importance of exploitation versus exploration. If $q \le q_0$, node j with maximum value is behind node i; otherwise, node j is chosen according to S. The random variable S is selected according to the probability:

$$p_{ij}^{k}(t) = \begin{cases} \dfrac{[\tau_{ij}(t)]\ [\eta_{ij}(t)]^{\beta}}{\sum_{u \in allowed_k} [\tau_{iu}(t)]\ [\eta_{iu}(t)]^{\beta}} & if \ j \in allowed_k \\ 0 & otherwise \end{cases}$$

Step 2.2: Local update of pheromone trail. To avoid premature convergence, a local trail update is performed. This is achieved by the following local updating rule:

$$\tau_{ij}(t+1) = (1-\xi)\tau_{ij} + \xi\tau_0 \qquad \text{where} \quad \xi \in (0,1]$$

Step 2.3: Local search. When each of m ants complete a solution, we select the best solution and suboptimal solution of this iteration. In our algorithm, we execute mutation and crossover operators of genetic algorithm into best solution and suboptimal solution of this iteration. Finally, we evaluate the best solution.

Step 2.4: Global update of pheromone trail. The global updating rule is applied after each ant has completed a feasible solution .The following rule is applied to the best solution which is found in Step 2.3. If edge (v_i, v_j) belongs to the best solution, then

$$\tau_{ij}(t+n) = (1-\rho)\tau_{ij}(t) + \rho\Delta\tau_{ij}(t)$$

where ρ ($\rho \in (0,1]$) is a parameter representing the evaporation of pheromone. The amount $\Delta\tau_{ij}(t) = 1/L_{best}$, where L_{best} is the global best solution. In order to prevent the solution from falling into a local optimum that results from the pheromone evaporating to zero, we introduce a lower bound and upper bound to the pheromone trail value by letting $\tau_{\max} = 5\tau_0$ and $\tau_{\min} = \frac{1}{5}\tau_0$.

Step3: When the cycle number $N_c \geq N_{c\max}$, the circulation is stopped and the results are put out; otherwise, turn to step 2.

4 Computational experiments

To verify the performance of the algorithm, the problem on branch-shaped sidings with 6 nodes is conducted. The running time that the locomotive goes from v_i to v_j is shown in Table 1 $(i, j = 0,1,2,3,4,5,6)$ .The algorithm is coded in MATLAB7.0 and implemented on a Pentium IV 3.0 GHz PC. The parameters are as follows: $N_{c\max} = 100$, $\xi = 0.1$, $\rho = 0.1$, $\beta = 5$, $q_0 = 0.9$ .The optimal route was v_0-v_3-v_2-v_1-v_4-v_5-v_6-v_0, and the total time is 190 min. In conventional ACO algorithms, the local search is executed once for every iteration，but our algorithm applies the local search whenever a better solution is found. Moreover, our approach requires only about 33% of the computation time as compared to the conventional approach. For the large scale branch-shaped sidings problems, this proposed algorithm can save much time.

Table.1 The running time between v_i to v_j

$d(v_i,v_j)$ v_j / v_i	v_0	v_1	v_2	v_3	v_4	v_5	v_6
v_0	-	35	20	25	40	30	35
v_1	35	-	15	50	45	65	70
v_2	20	15	-	25	45	50	55
v_3	25	50	25	-	65	45	40
v_4	40	45	45	65	-	35	45
v_5	30	65	50	45	35	-	10
v_6	35	70	55	40	45	10	-

5 Conclusions

In this paper, we have presented an ACO algorithm for placing-in and taking-out operations of wagons in branch-shaped private sidings. The developed algorithm has some distinctive features, including applying local search and modified global search strategy, and these features make the algorithm very effective and efficient. For the large scale branch-shaped sidings problems, this proposed algorithm can save much time.

Acknowledgements

This study was supported by National Natural Science Foundation of China (No. 60776826).

References

Bullnheimer, B., Hartl, R..F., and Strauss, C. (1999). "An improved ant system algorithm for the vehicle routing problem." Annals of Operations Research. (89):319-328.

Dorigo, M., and Gambardella, L. M. (1997). "Ant colony system: a cooperative learning approach to the traveling salesman problem." IEEE Transactions on Evolutionary Computation. (1),53–66.

Dorigo, M., and Gambardella, L. M. (1997). "Ant colonies for the traveling salesman problem." BioSystem.43(1),73–81.

Dorigo, M., and Stützle, T. (2002). "The ant colony optimization metaheuristics: algorithms, applications, and advances." International Series in Operations Research&Management Science. Dordrecht: Kluwer; 251 – 285.

Gambardella, L. M., and Dorigo, M. (1999). "Ant colonies for the quadratic assignment problem." Journal of Operational Research Society,(50),167 – 176.

Gao zi, and Yang Minglun (1981). "The Optimization of the Orders of placing and Taking-out of Wagons on Station with Tree-type Industrial Sidings." Journal Of Southwest Jiaotong University, (3),64-69

Shi Hongguo, Peng Qiyuan, and Guo Hanying (2005). "An Algorithm by Using Hamilton Graph to Resolve Wagons' Placing-in and Taking-out on Branch shaped Sidings. " China Railway Science,26(2),132-135.

Wang Ciguang (1996). "A Study on Placing-in and Taking-out of Wagons on Branch-Shaped Sidings." Journal Of Southwest Jiaotong University, 31(6),675-678.

Yu Shaohe，and Li Xiamiao (2002). "The Model of Placing-in and Taking-out for Working Wagons and the Calculation Method." Railway Transport and Economy, 24 (12),46-48

Yang Yungui, Wang Ciguang, and Xue Feng (2008). "Study on genetic algorithm for railway placing-in and taking-out of wagons in branch- shaped private siding." Computer Engineering and Applications, 44(12), 210-211.

A Study on Vehicle Trip Distribution Forecasting Based on BP Neural Network

MENG Xiang-hai[1], LIU Qing[2], DU Ying-chun[3] and LU jian[4]
[1] School of Transportation Science and Engineering，Harbin Institute of Technology, Heilongjiang Harbin 150090; Professor; email: mengxianghai100@126.com
[2] School of Transportation Science and Engineering，Harbin Institute of Technology, Heilongjiang Harbin 150090; email: liuqing864@163.com

ABSTRACT

Trip distribution is an important step of the four-phase method in transportation demand forecasting. It is affected by many factors. First, factors influencing vehicle trip distribution are analyzed and the results show that location potential, traffic impedance, trip production, and trip attraction play an important role. Second, an aggregation scale factor of the traffic zone is evaluated by fuzzy algorithm and the zone accessibility is calculated, and then, the location potential that is determined by the aggregation scale factor and zone accessibility is obtained. Third, traffic impedance based on travel time is determined based on analyzing the influences of traffic flow discontinuation, bicycles, pedestrians, and width of lanes. Finally, the trip distribution forecasting model based on the BP neural network which takes location potential, traffic impedance, trip production, and trip attraction as input parameters and the result of trip distribution as output parameters is established. The test shows that the forecasting result fits well with the survey data. Thus, the BP neural network model can be used for trip distribution forecasting with high prediction accuracy.

KEY WORDS: trip distribution; BP neural network; location potential; impedance function

FACTORS INFLUENCING VEHICLE TRIP DISTRIBUTION

The factors influencing vehicle trip distribution are complicated and various, so it is necessary to apply the modern technology which can supply an effective method for further improving prediction accuracy. Therefore, the BP neural network is used for vehicle trip distribution forecasting. For vehicle trip distribution, it is influenced by the location of the traffic zone, road condition, interference of non-motorized vehicles and so on. Trip production, trip attraction, the location potential of the traffic zone and traffic impedance are considered and finally determined as the factors influencing vehicle trip distribution. Among them, the trip production and trip attraction have been obtained in trip generation forecasting. Thus, it just needs to describe the location potential and determine the traffic impedance.

DESCRIBING LOCATION POTENTIAL OF TRAFFIC ZONE

The location potential refers to the attracting capability of people activity,

which is affected by economic and geographical position and the geographical position of traffic. The location potential of the traffic zone is determined and calculated by an aggregation scale factor and zone accessibility. An aggregation scale factor of the traffic zone is divided into seven grades (see Table 1) and evaluated by fuzzy algorithm. Zone accessibility is the attraction ability of the traffic zone, and can be calculated by the formula as follows:

$$A_i = \sum_{j=1}^{n} (P_j / d_{ij}) \tag{1}$$

Where, A_i is the accessibility of zone *i*; P_i is the local population of zone *i*; and d_{ij} is the distance between zone *i and* zone *j*.

Table 1. Aggregation Scale Factor of the Traffic Zone.

Grade	1	3	5	7	9	11	13
Description	Worst	Worse	Bad	Medium	Good	Better	Best

TRAFFIC IMPEDANCE FUNCTION OF VEHICLE TRIP BASED ON TRAVEL TIME

Traffic impedance reflects the convenience of travel between each pair of traffic zones. For vehicle trip distribution, travel time is chosen as the traffic impedance which can reflect not only the distance between two traffic zones but also the practical road traffic condition.

The characteristics of mixed traffic flow on urban roads determine that the travel time of a basic section is affected by many factors and needs to be corrected. First, the theoretical calculation of running speed is established based on the relationship among three parameters in traffic flow theory. Second, this theoretical model is modified according to the influences of traffic flow discontinuation, bicycles, pedestrians and the width of lanes. Finally, the calculation method of average running speed is proposed, and then travel time is obtained.

When the road facility condition is constant, the average running speed on a section is related to the traffic volume and traffic density on road. Travel time *t* is obtained by means of comparing the relationship among three parameters and calculated by the formulas as follows:

$$t = L / V \tag{2}$$

$$V = V_m / 2 \pm \sqrt{V_m{}^2 / 4 - Q V_m / K_m} \tag{3}$$

$$V_m = \eta_1 \eta_2 \eta_3 \eta_4 V_a \tag{4}$$

$$K_m = \eta_1 \eta_2 \eta_3 \eta_4 n / (l + l_0) \tag{5}$$

Where L is the length of the road; V is running speed; Q is traffic volume; V_m is the free flow speed; K_m is the jamming density; η_1 is the correction coefficient of discontinuous flow; η_2 is the correction coefficient of a bicycle; η_3 is the correction coefficient of a pedestrian; η_4 is the correction coefficient of lane width; V_a is design speed; n is the number of unidirectional vehicle lanes; l_0 is the average clear distance between two cars on a blocked section which can select 1.5m; l is the average vehicle length.

BP VEHICLE TRIP DISTRIBUTION FORECASTING

Selection of a neural network model. **A** neural network model mainly includes a perceptron neural network, linear neural network, radial basis function network and BP neural network. The factors influencing vehicle trip distribution are nonlinear mapping relationships with vehicle trip distribution, so a BP neural network and radial basis function network are suitable for the research object based on the characteristics of a neural network model. So a BP neural network is chosen for vehicle trip distribution forecasting, and the suitable model is established according to the forecasting precision.

Input and output of network. Input parameters of a network include vehicle trip production, vehicle trip attraction, location potential of a traffic zone, and traffic impedance. The output parameter is vehicle trip distribution of each traffic zone.

The study area is Liaoyang of Liaoning Province. Based on the 56 traffic zones divided in the World Bank loan project, the vehicle trip generation data of 20 relatively stable traffic zones during the year 2005 is selected as the data sample for building a network model. Network performance is determined by network generalization. The network generalization is not tested by data of a training set but by the other data. So in the experimental design, the vehicle trip generation data of 20 traffic zones is divided randomly into two parts. One part is used as a training sample and the other part is used as a testing sample. Based on the formula (1-5) and the collection date, vehicle trip production, vehicle trip attraction, location potential of a traffic zone and traffic impedance of the 20 traffic zones of Liaoyang city in 2005 can be obtained (show in Table 2 and Table 3 respectively).

Selection of network structure and learning parameter. **A** three-layer BP network can reflect any n dimensional to m dimensional mapping relationship, so this example adopts the three-layer BP network with one hidden layer. The number of input layer neurons is 4, namely vehicle trip production, vehicle trip attraction, location potential of a traffic zone, and traffic impedance. The number of output layer neurons is 1, namely vehicle trip distribution. The transfer function of the hidden layer adopts the bipolar tansig function and the transfer function of the output layer adopts the linear purelin function. The values of network

learning parameter are as follows: the target of prediction accuracy, the maximum training times, and the initial learning rate is 0.002, 20000 and 0.01, respectively.

Table 2. Location Potential and Trip Generation

No.	Location potential	Vehicle trip attraction	Vehicle trip generation	No.	Location potential	Vehicle trip attraction	Vehicle trip generation
1	1.00	4410	4589	11	1.00	4410	4589
2	1.13	7209	5889	12	1.13	7209	5889
3	1.08	4447	4708	13	1.08	4447	4708
4	1.13	6396	7135	14	1.13	6396	7135
5	1.12	6963	7277	15	1.12	6963	7277
6	1.14	7078	7729	16	1.14	7078	7729
7	1.16	10181	9206	17	1.16	10181	9206
8	1.11	5399	4753	18	1.11	5399	4753
9	1.08	5944	5578	19	1.08	5944	5578
10	1.13	8392	6869	20	1.13	8392	6869

Table 3. Traffic Impedance. (Units: min)

No.	1	2	3	4	5	6	7	8	9	10	11	12	13	14	15	16	17	18	19	20
1	0	18	28	0	17	18	22	25	23	20	17	18	16	29	17	20	17	30	22	25
2	18	0	67	18	33	13	21	18	21	27	19	25	23	67	21	12	11	22	13	10
3	27	17	0	27	26	18	15	20	18	36	20	24	61	47	22	50	31	13	12	16
4	22	19	17	0	35	20	26	19	23	30	40	29	25	128	42	26	24	15	19	18
5	16	20	45	16	0	20	21	20	23	11	43	20	23	24	20	23	21	28	21	20
6	19	14	15	19	20	0	14	17	62	21	25	62	74	27	21	18	20	22	18	7
7	27	14	17	27	19	58	0	13	15	30	31	21	33	24	26	20	16	17	22	5
8	26	20	31	26	20	17	15	0	18	25	26	27	24	30	30	22	12	15	10	16
9	20	18	20	20	19	24	14	14	0	20	1	25	30	40	18	25	25	7	14	21
10	11	48	41	11	17	21	12	20	20	0	23	18	19	27	20	20	18	9	28	22
11	18	18	30	18	14	21	30	26	1	13	0	17	64	26	23	22	16	18	23	14
12	20	33	36	20	22	21	23	58	48	14	20	0	18	43	18	32	23	24	22	16
13	17	26	28	17	21	28	23	26	28	17	19	23	0	17	15	21	11	15	17	19
14	25	22	43	25	22	27	29	37	1	25	27	72	35	0	24	21	16	20	13	4
15	25	23	27	25	20	18	24	28	30	57	26	18	15	21	0	15	19	22	10	20
16	15	14	18	15	24	20	19	24	25	49	31	25	37	18	18	0	23	23	12	13
17	19	11	30	19	20	20	15	12	24	18	16	23	12	17	18	22	0	12	11	19
18	29	21	12	29	27	22	16	15	8	10	19	22	14	19	22	14	10	0	16	6
19	21	17	15	21	22	17	21	11	13	27	22	21	16	12	12	23	12	17	0	18
20	23	10	15	23	19	10	7	15	18	6	20	12	18	6	21	12	18	5	20	0

The determination of hidden layer neuron and model training. The number of hidden layer neurons is determined by a trial calculation based on the consideration to the network's learning ability and learning rate. Considering the input layer neuron is 4, the forecasting result of the network is analyzed when the number of hidden layer neurons separately chooses 2 to 10. In this paper, the values

of hidden layer neurons are all carried out with repeated and large training, and finally the global optimal solution of a BP network is chosen. The network forecasting error of a training sample is seen in Table 4. The average absolute error mae and mean square deviation mse are referenced for comprehensive evaluation of a network forecasting result. The training method of each network structure is a LM algorithm.

Table 4. Comparing the Forecasting Errors of Different Neuron Hidden Layers.

Number of hidden layer neuron	Mae	Mse	Network convergence rates
2	0.0560	0.00199	205
3	0.0553	0.00198	23
4	0.0535	0.00192	13
5	0.0549	0.00195	8
6	0.0543	0.00193	7
7	0.0547	0.00198	4
8	0.0548	0.00193	4
9	0.0546	0.00195	5
10	0.0541	0.00193	7

The result of selecting the number of hidden layer neurons is that when the number of hidden layer neurons is 4, the network forecasting is the best with an average absolute error of 5.35％ and a mean square deviation of 0.0192. It meets the prediction accuracy after 13 steps of training. Thus, a three-layer BP neural network for vehicle trip distribution forecasting is established.

Model testing. The testing sample is the second group including ten traffic zones. Based on the established BP neural network, the vehicle trip distribution of the ten traffic zones is forecasted and compared with the survey date (see Figure 1).

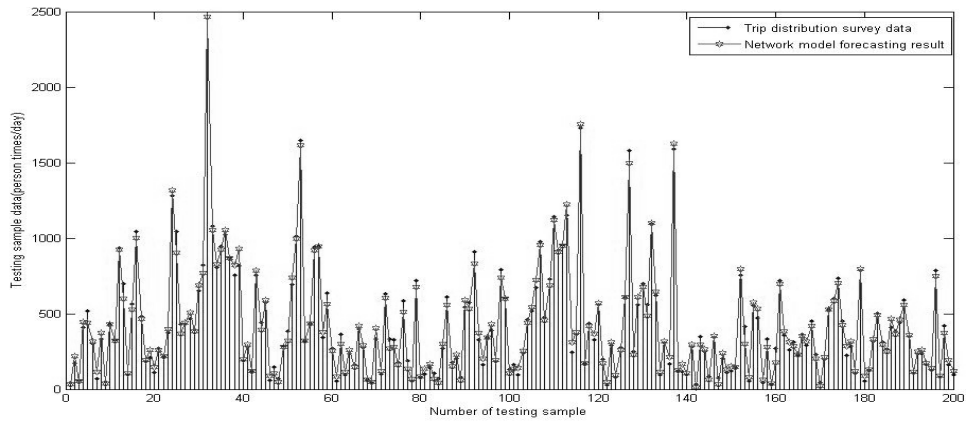

Figure 1. Comparison of model forecasting result with survey data.

Based on the comparison, it can be seen that the result of vehicle trip production and vehicle trip attraction forecasted by the established BP neural network are equal of 84824 person times/day, which is the same as the survey data. The established model meets the boundary condition that trip production and trip

attraction should be equal. The average absolute error of testing a sample forecasting result by a BP neural network is 4.91%, which shows that the prediction accuracy is high. Therefore, the established BP neural network has a high prediction accuracy for vehicle trip distribution forecasting and can be used for trip distribution forecasting.

CONCLUSION

Due to the complexity of data acquisition in the research process, only location potential of traffic zone and travel time are considered as the influencing factors of vehicle trip distribution model. More influencing factors can be taken into consideration in the subsequent research. The network model adopts the most widely used BP neural network, and other neural network models also have a wide scope of application, so other neural networks can be adopted in future research. Aiming at the study of vehicle trip distribution , other trip distribution patterns are the same and can be studied and discussed by similar methods in future research. In the process of establishing traffic impedance functions, travel time is influenced by many factors and local actual situations are suggested to be analyzed because cities with different grades are influenced by different factors. Besides, travel time is considered as traffic impedance in this paper, and traffic impedance is suggested to be calculated synthesizing the distance, expense, and other influencing factors.

BIBLIOGRPHY

Erramilli, V., Crovella, M, and Taft, N. (2006). An Independent Connection model for Traffic Matrices. Tech. Rep. 2006-022, Computer Science Dept. , Boston University, Boston, MA, USA.

HU Jinbin, TANG Xuqing. (2004). BP algorithm and its application in artificial neural network. Information Technology.

LI Xuhong. (1997). Research of Urban Traffic Distribution Forecasting Model. Journal of southeast university.

LIU Wei. (2006). Research on the Application of TransCAD in Forecasting Highway Traffic Distribution.

WANG Wei, ZHANG Guihong. (1992). Research on Impedance Function of Urban Streets. Journal of Chongqing Jiaotong University.

WU Jia-you, LIU Shu-hong. (2003). Research on forecasting model of new blocks. Journal of Chongqing Jiaotong University.

WU Yuhang, CHENG Shanshan, PAN Yuli. (2001). Study on Prediction Model of Travel Time Costs. Journal of Highway and Transportation Research and Development.

ZHUANG Yan, LI Shen. (2005). Study on the Link Traveling Time Function for Urban Road Based on TransCAD. Communications Standardization.

Bus Service Frequency Multi-objective Optimal under Snowy Day

Wang, Jian[1], Hu, Xiaowei[2] and Hu, Chunbin[3]

[1]School of Transportation Science and Engineering, Harbin Institute of Technology, No. 202, Haihe River Road, Nangang District, Harbin, Heilongjiang Province, PRC, 150090: PH (86) 13030092006; email: wang_jian@hit.edu.cn
[2]School of Transportation Science and Engineering, Harbin Institute of Technology, No. 202, Haihe River Road, Nangang District, Harbin, Heilongjiang Province, PRC, 150090: PH (86) 13936646128; email: hxwhit@163.com
[3]China Academy of Urban Planning & Design, No.9 Sanlihe Road, Beijing, PRC, 100037: PH (86) 13466796732; email: huzhou3407@163.com

ABSTRACT

A snowy day has a great impact on vehicles, road capacity, and drivers' behavior. Drivers may drive at slower speeds to obtain the longer perception times and stopping distances. Snow can reduce bus ridership, lengthen bus driving times, and dwell time, and increase bus operation costs and ridership's waiting time. Public transit service frequency determines passenger waiting times, and thus the time exposed to snow. This paper analyzes the passenger waiting time cost, in-vehicle time cost, fuel consumption cost, and bus vehicle cost, then takes the minimal bus line total system cost as the goal, establishing a bus service frequency multi-objective optimization model. Analysis of the relationship between frequency associated with the vehicle average running speed and financial subsidy, using examples to verify the effectiveness of the multi-objective optimization model, can optimize the bus frequency on a snowy day and improve bus service satisfaction.

1 INTRODUCTION

A snowy day will increase the city road network performance variability, to a large extent determining the city's road traffic conditions and road safety situation. In general, snow influences almost every aspect of transit service, such as reducing transit ridership, increasing vehicle running and dwell times, and increasing operation costs. In Zhan Guo et al. (2007) analysis, bus service frequency determines passenger waiting times and the time exposed to adverse weather. Total travel time might be lengthened due to slower speed and longer dwell time at stations. Hofmann and O'Mahony's (2005) study considered the impact of adverse weather on bus performance such as ridership, frequency, and travel time variability.

This paper first analyzes the passenger's time cost, and company operation costs, then takes the minimal bus line total system cost as the goal, establishing the bus service frequency multi-objective optimization model, and using examples to verify the effectiveness of the model. The relationship between frequency associated with the vehicle average running speed and financial subsidy is analyzed.

2 BUS SERVICE FREQUENCY OPTIMIZATION MODEL

Bus frequency optimization is a complex process. Providers (companies) want a longer frequency to reduce variable costs, and passengers request a more efficient service (i.e. high frequency) to reduce the waiting time cost. Therefore, to reduce companies' cost means increasing passengers' cost, and vice versa. This will only minimize the cost of companies and passengers to gain the greatest social benefits. Based on this idea, this article has taken into consideration the passengers' time value and companies' operating costs. Minimizing the bus line system's total cost (including passenger's time cost and company's operation cost) as the optimization goal establishes the bus service frequency multi-objective optimization model.

2.1 Model assumption. It is necessary to carry out the following assumptions:

1) At the optimization time period, all buses on the road drive at the same average speed;
2) Ignoring occasional accidents causes traffic jams on the bus lines;
3) All buses are not allowed to transcend and overtake bus station;
4) All buses operating on the line are the same models, and the capacity is sufficient;
5) Passengers at station will not wait too long to leave.

2.2 The analysis of bus running time

The bus running time $t_{k,k+1}$ from station k to $k+1$ can be stated as follow:

$$t_{k.k+1} = \frac{l}{v_b} + \frac{v_b}{2}\left(\frac{1}{a_a} + \frac{1}{a_d}\right) + t_s = \frac{l}{v_b} + t_{sd} \tag{1}$$

Here l is the distance between stations (this paper uses average distance, m); v_b is the average speed of bus drive on road (m/s); a_d is the deceleration speed (m^2/s); a_a is the acceleration speed (m^2/s); t_s is the average bus stop time (s); t_{sd} is the delay of bus dwell at bus station (s). Here the impact of intersection factors on bus running is ignored.

2.3 The analysis of passenger's time cost

Anthony A. Saka (2001) focused on the bus running time and divided it into acceleration and deceleration time, stop time, the waiting time at the signal intersection, smooth run-time, and other delays. Martin Lowson (2004) divided passenger trip time into walk time, wait time, in-vehicle time and transfer time. Based on the above research, this paper divides passenger time cost into passenger waiting time cost and in-vehicle time cost (including bus running time and the delay due to bus stations). According to passengers' psychological characteristics, passengers prefer stay a few minutes in the bus than to wait one minute at bus station; therefore, passengers waiting time value and in-vehicle time value are different.

2.3.1 Passenger waiting time cost

Each passenger has a different waiting time, but waiting time is closely related to bus departing interval. With random passenger arrivals at the station, the average waiting time can be assumed to be half of the departing interval, which is the average waiting time of passengers:

$$t_1 = L_b \cdot P \cdot (h/2) \tag{2}$$

Here h is the bus departing interval under optimization interval (s); L_b is the length of bus line (m); P is the bus passenger demand at unit length (person/m).

Supposing bus passenger waiting time per unit time value is λ_1 (Yuan/s), and then passenger waiting time cost under optimization time interval is:

$$C_1 = \lambda_1 \cdot t_1 = \lambda_1 \cdot L_b \cdot P \cdot (h/2) \tag{3}$$

2.3.2 Passenger in-vehicle time cost

Passenger in-vehicle time cost including passenger in bus running time and the delay due to bus stations. Passenger in bus running time t_{21} is determined by the average distance and the average vehicle speed, which can be expressed as:

$$t_{21} = L_b \cdot P \cdot (L_c/v_b) \tag{4}$$

The delay due to bus stations t_{22} can be expressed as:

$$t_{22} = L_b \cdot P \cdot \frac{L_c}{l} \cdot \left[\frac{v_b}{2} \left(\frac{1}{a_a} + \frac{1}{a_d} \right) + t_s \right] = L_b \cdot P \cdot \frac{L_c}{l} \cdot t_{sd} \tag{5}$$

Here L_c is the average distance of passenger (m).

Supposing passenger inner-bus time per unit time value is λ_2 (Yuan/s), and then passenger in-vehicle time cost is:

$$C_2 = \lambda_2 (t_2 + t_3) = \lambda_2 \cdot L_b \cdot P \cdot \frac{L_c}{l} \cdot \left(\frac{l}{v_b} + t_{sd} \right) \tag{6}$$

2.4 The analysis of Bus Company's operating cost

In the analysis of bus passenger's time cost in this section, consider Bus Company's interests and analyze Bus Company's operating cost, which includes the bus fuel cost C_3 and bus vehicle cost C_4.

Fuel consumption is different when the bus drives in the normal status and stops at the station, and therefore divides bus fuel cost C_3 into two parts: bus normal driving fuel consumption costs and bus stops fuel consumption costs. Supposing bus normal driving fuel consumption per unit time value is λ_{31} (Yuan/s), each time bus stops fuel consumption per unit time is λ_{32} (Yuan per unit time).

$$C_3 = \lambda_{31} \cdot \frac{L_b}{v_b} \cdot \frac{t}{h} + \lambda_{32} \cdot \frac{L_b}{l} \cdot \frac{t}{h} \tag{7}$$

Bus vehicle cost C_4 includes vehicle depreciation, maintenance, driver wages, and other costs; bus vehicle cost per vehicle is λ_4 (Yuan per vehicle)

$$C_4 = \lambda_4 \cdot (t/h) \tag{8}$$

2.5 The foundation of bus service frequency optimization model

Bus line total system cost can be divided into passenger's time cost and company's operation cost. This section takes the minimal of passenger's time cost and company's operation cost as the goal, establishing bus service frequency multi-objective optimization model. The optimization model's objective function is:

$$\min C = \min\left(C_1 + C_2 + C_3 + C_4\right) \tag{9}$$

Here C is the bus line total system cost, which can be expressed as follows:

$$C = C_1 + C_2 + C_3 + C_4 = \lambda_1 \cdot L_b \cdot P \cdot \frac{h}{2} + \lambda_2 \cdot L_b \cdot P \cdot \frac{L_c}{l} \cdot \left(\frac{l}{v_b} + t_{sd}\right) + \lambda_{31} \cdot \frac{L_b}{v_b} \cdot \frac{t}{h} + \lambda_{32} \cdot \frac{L_b}{l} \cdot \frac{t}{h} + \lambda_4 \cdot \frac{t}{h} \tag{10}$$

When the distance between stations is larger than the acceleration distance and the deceleration distance, the expression is as follows:

$$l \geq \frac{v_b^2}{2a_a} + \frac{v_b^2}{2a_d} \tag{11}$$

To gain the best service frequency $f = t/h$, and minimize the bus line total system cost, taking order partial differential on h:

$$\frac{\partial C}{\partial h} = \frac{1}{2}\lambda_1 \cdot L_b \cdot P - \frac{t}{h^2} \cdot \left(\frac{L_b \cdot \lambda_{31}}{v_b} + \frac{L_b \cdot \lambda_{32}}{l} + \lambda_4\right) = 0 \tag{12}$$

$$\Rightarrow h = \sqrt{2t \cdot \left(\lambda_{31} \cdot l \cdot L_b + \lambda_{32} \cdot v_b \cdot L_b + \lambda_4 \cdot v_b \cdot l\right) / \left(\lambda_1 \cdot v_b \cdot P \cdot l \cdot L_b\right)}$$

From formula (12) can find the effect factors of bus service frequency, the average speed of bus drive on road v_b, the bus passenger demand at unit length P, the distance between stations l and the optimization time interval t. To analyze a bus line departing interval of working day, can divide the working day into different optimization time interval, considering the bus passenger demand at unit length P, to solve for corresponding departing interval.

If $t = 3600s$, $\lambda_1 = 0.025$ Yuan/s, $\lambda_{31} = 0.1$ Yuan/s, $\lambda_{32} = 3$ Yuan per unit time, $\lambda_4 = 8$ Yuan per vehicle, $P = 0.15$ person/m, $l = 600m$, $L_b = 12000m$, then find the relationship between bus departing interval h and the average speed of bus drive on road v_b is: $h = 418.2v_b^{-0.39}$.

If $t = 3600s$, $\lambda_1 = 0.025$ Yuan/s, $\lambda_{31} = 0.1$ Yuan/s, $\lambda_{32} = 3$ Yuan per unit time, $\lambda_4 = 8$ Yuan per vehicle, $v_b = 6m/s$, $l = 600m$, $L_b = 12000m$, then find the relationship between bus departing interval h and the bus passenger demand at unit length P is: $h = 253.65P^{-0.5025}$.

3 THE DISCUSSION OF BUS FREQUENCY OPTIMIZATION MODEL

3.1 The average speed of bus drive on road v_b

On snowy days, for the lower sliding friction coefficient, the braking distance is extended. It is necessary to increase the spacing and reduce the driving speed, which increases the traffic delay. Markku and Heikki (2007) in Finland's study found that vehicle speed will be 6-7 km/h (1.6-1.9 m/s) reduction under adverse weather; Joseph et al. (2001) found when snow begins, speeds decrease by 30%.

Vehicle speed is decided by the vehicle's dynamic performance and road conditions. According to the vehicle traction force formula $Z_\varphi \varphi = Ggf + Ggi + C\rho AV^2$

and vehicles structure formula $Z_\varphi = Gg\left(d + h_g i\right)/L$, Z_φ is the pressure between the driving wheel and ground surface; φ is the adhesive coefficient between tires and ground surface; G is car body weight; g is acceleration of gravity; f is rolling resistance; i is road gradient; C is car streamlined coefficient; ρ is air density; A is cars' windward area; V is cars' running speed; d is distance from car center of gravity to drive shaft; h_g is the height of car center of gravity; L is wheel base.

The maximum speed that a vehicle can reach is determined by car weight and the adhesive coefficient between tires and the ground surface. Under snowy conditions, the adhesive coefficient between tires and the ground surface decreases and the maximum traction force decreases as well. Meanwhile, the ratio of the free-flow speed in the two different conditions can be calculated as:

$$\frac{V_s}{V} = \left(\left(\frac{d + h_g i}{L}\varphi_s - f_s - i\right)\Big/\left(\frac{d + h_g i}{L}\varphi - f - i\right)\right)^{1/2} \tag{13}$$

Take the structural parameters of a certain type of bus as an example. $L = 5.7m$, $h_g = 0.6m$ and $d = 4.8m$. In normal conditions, $\varphi = 0.5$, and $f = 0.02$. If no measure is taken in snowy conditions, $\varphi_s = 0.2$, $f_s = 0.03$. Substitute all the data into the formula (12), and then obtain the ratio V_S / V =58.33%.

3.2 The discussion of government financial subsidy

However, on snowy days due to the impact of the adverse weather factor which extends passengers wait time and in-vehicle time, in formula (10) in order to achieve minimum bus line total system cost can only increase departing interval to reduce Bus Company's operating cost. This is contrary to the actual survey when passengers were complaining about longer departing interval. Peter Tisato (1998) suggested that bus subsidy is favorable for public transport's option value. Here considering financial subsidy, is how to optimize the bus frequency under snowy day, access better bus services and improve passenger's bus service satisfaction.

Supposing under optimization time interval t, the subsidy of a departing bus is λ_5 (Yuan per bus), then the government financial subsidy C_5 is:

$$C_5 = \lambda_5 \cdot (t/h) \tag{14}$$

Then formula (10) can be expressed as:

$$\begin{aligned} C &= C_1 + C_2 + C_3 + C_4 - C_5 \\ &= \lambda_1 \cdot L_b \cdot P \cdot \frac{h}{2} + \lambda_2 \cdot L_b \cdot P \cdot \frac{L_c}{l} \cdot \left(\frac{l}{v_b} + t_{sd}\right) + \lambda_{31} \cdot \frac{L_b}{v_b} \cdot \frac{t}{h} + \lambda_{32} \cdot \frac{L_b}{l} \cdot \frac{t}{h} + \lambda_4 \cdot \frac{t}{h} - \lambda_5 \cdot \frac{t}{h} \end{aligned} \tag{15}$$

And formula (12) becomes:

$$\begin{aligned} &\frac{\partial C}{\partial h} = \frac{1}{2}\lambda_1 \cdot L_b \cdot P - \frac{t}{h^2} \cdot \left(\frac{L_b \cdot \lambda_{31}}{v_b} + \frac{L_b \cdot \lambda_{32}}{l} + \lambda_4 - \lambda_5\right) = 0 \\ &\Rightarrow h = \sqrt{2t \cdot \left(\lambda_{31} \cdot l \cdot L_b + \lambda_{32} \cdot v_b \cdot L_b + \left(\lambda_4 - \lambda_5\right) \cdot v_b \cdot l\right) / \left(\lambda_1 \cdot v_b \cdot P \cdot l \cdot L_b\right)} \end{aligned} \tag{16}$$

If $t = 3600s$, $\lambda_1 = 0.025$ Yuan/s, $\lambda_{31} = 0.1$ Yuan/s, $\lambda_{32} = 3$ Yuan per unit time, $\lambda_4 = 8$ Yuan per vehicle, $P = 0.15$ person/m, $l = 600m$, $L_b = 12000m$, in

normal situation $v_b = 6m/s$, under snow situation $v_b = 4m/s$, under this situation keep the primary departing interval, it needs $\lambda_5 = 100$ Yuan per bus.

4 CONCLUSIONS

We can draw these conclusions:

1) The relationship between bus departure interval and the bus passenger demand at unit length is an inverse proportion. According to the increasing passenger demand, departure interval will diminish and frequency increase.

2) The relationship between bus departure interval and the average speed of the bus drive on road is an inverse proportion. With the decline of average speed, passenger in-vehicle time cost will increase; in order to reduce bus line total system cost, the departing interval must be increased.

3) For the impact of snow, extending passengers wait time and in-vehicle time, passengers complain about the vehicle delay and hope to increase the frequency. So to the solution is to introduce subsidy into bus line total system cost, to optimize the bus frequency on snowy days, reform public transport services and improve bus service satisfaction.

ACKNOWLEDGMENTS

This research is supported by National Natural Science Foundation of China (Project No. 70673016 and 70503008), and Heilongjiang Postdoctoral Science Foundation funded project (Project No.LBH-Q06060). This work was performed at the National Center of Technology, Policy and Management, Harbin China.

REFERENCES

Guo, Zhan; Wilson, Nigel H.M.; Rahbee, Adam. (2007). "The impact of weather on transit ridership in Chicago." *Transportation Research Record,* Vol. 2034.

Hofmann, Markus, and O'Mahony, Margaret. (2005). "The impact of adverse weather conditions on urban bus performance measures." *8th International IEEE Conference on Intelligent Transportation Systems,* September 13-16, 2005, Conference Center MessezentrumWienNeu, Vienna, Austria.

Lowson, Martin. (2004). "Idealised models for public transport systems." *International Journal of Transport Management,* 2, 135-147.

Perrin Jr., Joseph; Martin, Peter T.; Hansen, Blake G.. (2001). "Modifying signal timing during inclement weather." T*ransportation Research Board 80th Annual Meeting,* January 7-11, Washington, D.C. Paper No. 01-3233.Kilpelainen, Markku; Summala, Heikki. (2007). "Effects of weather and weather forecasts on driver behaviour." *Transportation Research Part F,* 10, 288-299.

Saka, Anthony A.. (2001). "Model for determining optimum bus-stop spacing in urban areas." *Journal of Transportation Engineering,* 127(3), 195-199.

Tisato, Peter. (1998). "Service unreliability and bus subsidy." *Transportation Research Part A,* 32(6), 423-436.

Capacity Model of Low Channeling Roundabout Based on Vehicle Arrival Characteristics

Dong, Ruijuan[1], Zhang, Weihua [2] and Bai, Haijian [3]

[1,2]School of Mechanical and Automotive Engineering, Hefei University of Technology, Hefei, Tunxi Road NO.193, 230009; PH (86) 0551-2901338 EXT 2512; FAX (86) 0551-2903450; email: dongruijuan95@163.com
[3]School of Transportation, Southeast University, Nanjing, 210096; TEL: 13505179676; email: baihaijian000@163.com

ABSTRACT

This paper first studied the relationship between vehicle arrival rate and loop flow of roundabouts and finally established the capacity linear model with vehicle arrival rate and proportion of left turn vehicles as the independent variable based on analyzing the change relation of roundabout capacity which varies with loop flow in gap-acceptance theory. Compared with the gap-acceptance theory model, the new model has the following advantages: model can easily be calculated, parameters can easily be obtained. In the last part, the roundabout maximum traffic capacity was defined according to the characteristics of its self-adjustment of traffic flow and was acquired by using the new model. Thus the new model can provide more practical references for planning design of roundabouts.

INTRODUCTION

Various calculating models of non-signal-controlled roundabout capacity are mainly based on three theories. One model is the blending theory model with the maximum capacity of interwoven section of the roundabout. The capacity model, which was established based on the blending theory, was widely applied in early periods. The second model which is currently widely used analyzed the largest number of vehicles entering the loop in various road and traffic conditions based on the gap acceptance theory. The third model is the regression model which reflects the relationship between the roundabout's capacity and the vehicle arrival rates. This model has poor adaptability, so different types of intersections model are difficult to unify.(Bo Chun-yu,2002; Ren Fu-tian;2001; Ruili Wang,2002;Xie Jun,2007)

The calculating model which was proposed by domestic experts (Xiang Qiaojun, 2000) for the capacity of the low channeling roundabout based on the theory of gap acceptance theory applied more widely. However, this model has some shortcomings in computation complexity and parameter determination, such as loop flow and the ratio of free vehicles flow at loop lane. Moreover the maximum capacity of the roundabout is not easy to compute. The roundabout has a self-adjustment function. The roundabout capacity depends on that the number of vehicles entering into the loop is equal to the largest number of vehicles entering into the loop. Therefore, it is crucial to solve the equilibrium points between the capacity

and the vehicle arrival rate for the calculation of the roundabout capacity. But the gap-acceptance model is very difficult to solve the equilibrium point. Hence, this paper tried to establish more practical model for the capacity formula of low channeling roundabout and solve the maximum capacity is very important based on the gap acceptance model.

CAPACITY MODEL BASED ON GAP-ACCEPTANCE THEORY

The models of gap-acceptance theory change with the number of loop lanes. The capacity calculating models of sub single-loop and double-loop lanes are separately established by domestic experts Xiang Qiaojun, etc.

The capacity of single-loop roundabout is:

$$C_e = 3600 \times \frac{\alpha q_r e^{-\lambda(t_c - t_m)}}{1 - e^{-\lambda t_f}} \tag{1}$$

Where, C_e is the capacity of the roundabout, *pcu/h;* t_m is the minimum headway, *s;* t_f is the follow up time of the vehicle at loop, *s*; t_c is the critical gap time (the minimum time of the vehicle passing through the loop and entering into the loop), *s*; q_r is the loop vehicle flow, *pcu/h;* α is the proportion when the headway of loop vehicles are greater than or equal to t_m (the proportion of free flow at loop); $\lambda = \alpha q_r /(1 - q_r t_m)$.

Left and right approach capacities are divided into by Double-loop roundabout capacity which are analyzed respectively. The right approach capacity is the same as the total single-loop roundabouts. The total capacity of double-loop roundabout is:

$$C_e = 3600\left[\frac{q_r e^{-\lambda'(t_c - t_m)}}{1 - e^{-\lambda' t_f}}\left(1 - \frac{2q_{r1}q_{r2}t_m}{q_{r1} + q_{r2}}\right) + \frac{\alpha_2 q_{r2} e^{-\lambda_2(t_c - t_m)}}{1 - e^{-\lambda_2 t_f}}\right] \tag{2}$$

Where, C_e is the capacity of the roundabout, *pcu/h;* q_{r1}, q_{r2} are respectively vehicle flow inside and outside the loops, *pcu/s*; α_1, α_2 are respectively free flow proportions inside and outside the loops; $\lambda' = \alpha_1 q_{r1} / (1 - t_m q_{r1}) + \alpha_2 q_{r2} / (1 - t_m q_{r2})$.

CAPACITY MODEL BASED ON VEHICLE ARRIVAL CHARACTERISTICS

The loop flow is the key factor for the roundabout capacity in the gap-acceptance theory model, so it is necessary to establish the relationship between the loop flow and vehicle arrival characteristics before establishing the capacity model based on vehicle arrival characteristics. The loop vehicle flow q_r is the mean flow in four conflict point sections (see Fig.1). Each section's loop flow is equal to the sum of its left side approach flow direction and its opposite approach left turn flow direction (It is assumed that all of the arrival vehicles can enter and through the intersection). Therefore, the mean flow in four conflict point sections is:

$$q_r = q(1/4 + \beta_L / 4) \tag{3}$$

Where, q is the total vehicle arrival rate of roundabout, *pcu/s*; β_L is the

proportion of vehicles which are turning to the left.

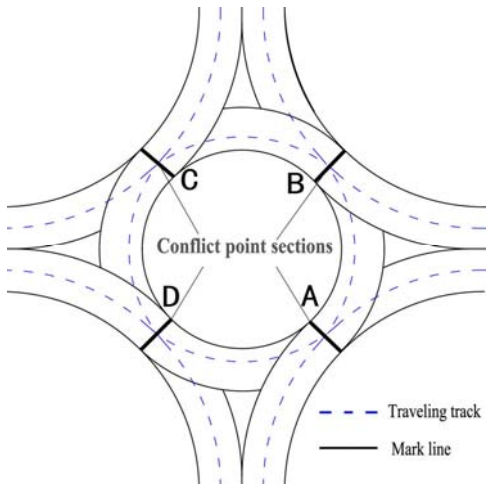

Figure 1. Schematic Diagram of Conflict Point Sections

From plenty of investigation and relating literature (Chen Kuan-ming, 2003), in Formula 1 and 2, the suggested values of related parameters are calculated according to the standard car as follows: $t_m = 2s$，$t_c = 6s$，$t_f = 3s$. In theory, various combinations of α and q_r can achieve, but α will constantly decrease with the increase of q_r. According to literature review and field investigation, the value range of α with change of q_r is given (see table 1，Xiang Qiaojun, 2000). Thus in the light of the Formula 1, roundabout traffic capacity can be calculated correspondingly at different loop flow.

Table 1. Value Range of q_r and α

q_r, *pcu/h*	<500	500～600	600～800	800～1000	1000～1200
α	1	0.9	0.8	0.7	0.6

The roundabout capacity can be calculated on the basis of Formulas 1 and 2. According to Formula 3, loop flow can be replaced by vehicle arrival rates and the proportion of left turn vehicles. Thus, we can calculate and acquire the roundabout capacity under the condition of different arrival rate and proportion of left-turn vehicles (see Table 2).

Table 2. Capacity at Different Arrival Rates and Proportion of Left Turn Vehicles

a. Single-Loop Roundabout （*q*, *pcu/h*）

	q=1000	q=950	q=900	q=850	q=800	q=750	q=700
β_L=0.05	826	843	861	879	897	915	934
β_L=0.10	809	827	846	865	883	902	921
β_L=0.15	792	812	831	850	870	889	909
β_L=0.20	776	796	816	836	856	877	897
β_L=0.25	759	780	801	822	843	864	885

β_L=0.30	743	764	786	807	829	851	873

b. Double-Loop Roundabout （*q* , *pcu/h*）

	q=1600	q=1550	q=1500	q=1450	q=1400	q=1350	q=1300
β_L=0.05	1525	1549	1573	1597	1622	1646	1671
β_L=0.10	1478	1502	1528	1553	1579	1605	1631
β_L=0.15	1431	1457	1483	1510	1537	1564	1591
β_L=0.20	1386	1413	1440	1467	1495	1523	1552
β_L=0.25	1341	1369	1397	1426	1454	1483	1513
β_L=0.30	1298	1326	1355	1385	1414	1444	1475

According to calculation results of Table 2, we can calculate the difference between roundabout traffic capacity and vehicle arrival rate changes with vehicle arrival rates and the proportion of left turn vehicles. (see fig.2).

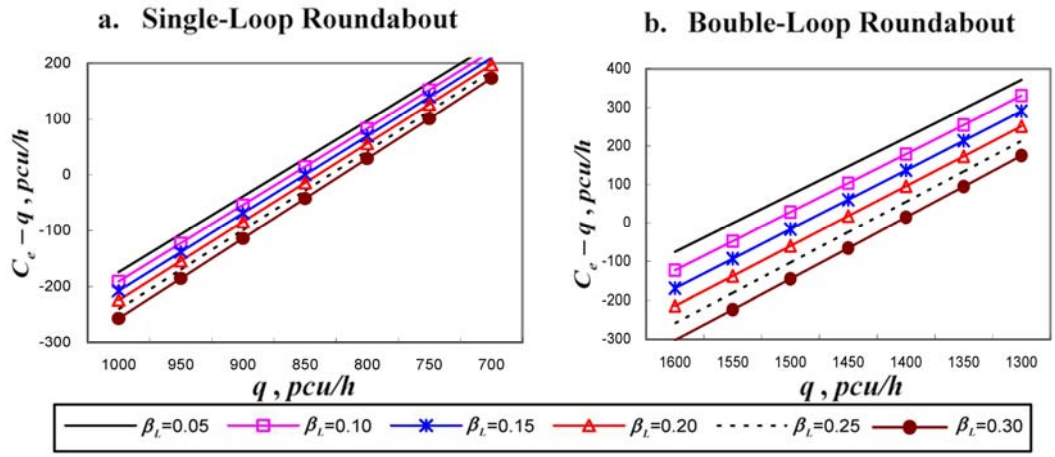

Figure 2. Relation Graph of q and $C_e - q$ about No-Signal Roundabout

The Fig. 2 can be drawn: A linear relationship holds between the q and $C_e - q$ about no-signal roundabout. The formula of the relationship between C_e, q and β_L can be established by using the linear regression method. Using the calculation data of Table 2, we obtain the fitting formulas 4 and 5, and the correlation coefficients of fitting formula are over 0.9.

The capacity of a single-loop roundabout is:

$$C_e = 1187.019 - 0.345q - 0.295q\beta_L - 36.076\beta_L \quad (4)$$

The capacity of a double-loop roundabout is:

$$C_e = 2319.063 - 0.468q - 0.315q\beta_L - 188.94\beta_L \quad (5)$$

Formulas 4 and 5 are acquired by regressive analysis of the formulas 1 and 2, but more simple forms of expression. Moreover, the change law of roundabout capacity with vehicle arrival rates and the proportion of left turn vehicles becomes more visual. In addition, the regression linear model is easier to solve.

THE MAXIMUM ROUNDABOUT TRAFFIC ROUNDABOUT CAPACITY

The new model can clearly reflect that the roundabout capacity depends on the vehicle arrival rate. The larger the vehicle arrival rate, the smaller the capacity

and vice versa. When the differences between capacity and vehicle arrival rate are positive, the capacity is still surplus. But the surplus carrying capacity has no practical significance because no more vehicles arrive and enter the loop. With the vehicle arrival rate increases, the surplus value of capacity begins to reduce to zero while the utilization ratio of the roundabout reached the maximum. If at this time the vehicle arrival rate increases further, the capacity becomes less than vehicle arrival rate, as well as the surplus value is negative while the roundabout begins to be crowded, or even blocked. Thus, when the capacity equals the vehicle arrival rate, the capacity value reached the maximum. The capacity which was obtained through the equilibrium point is defined as the roundabout maximum capacity. The maximum capacity is analyzed considering various roundabout correction coefficients.

The roundabout capacity model based on the gap-acceptance theory is modified properly in "Analysis on the Capacity of Urban Road" (Chen Kuanming, 2003). Correction coefficients and correction method are as follows:

$$F_L = 1.14 - 0.92\beta_L \quad (6)$$

$$F_R = 0.76 + 1.60\beta_R \quad (7)$$

Where, F_L, F_R are respectively the correction coefficients of left and right turn vehicles; β_R is the proportion of right vehicles turn.

Based on the above correction coefficients and Formulas 4 and 5, making the C_e equal to q, we can calculate the maximum roundabout capacity at different proportion of left and right turns (see table 3).

Table 3. Maximum Capacity at Different Proportions of Left and Right Turns

a. Single-Loop Roundabout （*pcu/h*）

	β_L=0.00	β_L=0.05	β_L=0.10	β_L=0.15	β_L=0.20	β_L=0.25	β_L=0.30
β_R=0. 00	669	661	653	645	637	629	622
β_R=0. 05	739	730	721	713	704	696	688
β_R=0. 10	810	800	790	781	771	762	753
β_R=0. 15	880	869	859	848	838	828	819
β_R=0. 20	951	939	927	916	905	895	884
β_R=0. 25	1021	1008	996	984	972	961	949
β_R=0. 30	1091	1078	1065	1052	1039	1027	1015

b. Double-Loop Roundabout （*pcu/h*）

	β_L=0.00	β_L=0.05	β_L=0.10	β_L=0.15	β_L=0.20	β_L=0.25	β_L=0.30
β_R=0. 00	1200	1183	1166	1149	1132	1116	1100
β_R=0. 05	1327	1307	1288	1270	1251	1234	1216
β_R=0. 10	1453	1432	1411	1391	1371	1351	1332
β_R=0. 15	1580	1556	1534	1512	1490	1469	1448
β_R=0. 20	1706	1681	1656	1632	1609	1586	1563
β_R=0. 25	1832	1805	1779	1753	1728	1703	1679
β_R=0. 30	1959	1930	1902	1874	1847	1821	1795

Table 3 can be drawn: no-signal roundabout capacity depends on its proportion of left and right turns. When the proportion of left and right turns lies between 0%~30% and the vehicle arrival rate of single-loop roundabout is more than 620~1090 *pcu/h*, its capacity would be less than the vehicle arrival rate. This will cause large delays and even traffic jams. Therefore, the single-loop roundabout is suitable for less than 620~1090 *pcu/h* vehicle arrival rates. The double-loop roundabout is suitable for less than 1100~1960 *pcu/h* vehicle arrival rates.

CONCLUSION

The paper first studies the relationship between vehicle arrival rates and loop flow of roundabouts. Then, based on the gap-acceptance roundabout capacity model, the simplified regression model is established on the basis of vehicle arrival rates and proportion of left turn vehicles as the independent variable. Compared with the gap-acceptance theory model, the new model has the following advantages: the model can easily be calculated and parameters easily be obtained. Finally, this paper obtains the maximum capacity and the adaptation range of traffic arrival rates by the use of the regression model.

The regression model is obtained based on the gap-acceptance model of the low channeling roundabout, and therefore only applicable to the low channeling roundabout. If the loop lane has a right turn lane, the right turn vehicles need not to drive intertwined with straight and turning left vehicles at the loop. Thus, the calculated maximum capacity is the maximum capacity of the straight and left turn vehicles. The roundabout capacity model needs to be further studied under the conditions of more than two loop lanes.

REFERENCES

Bo Chun-yu, Cui Hai-liang, etc. (2002). "A Study on Service Capacity of Roundabout" *J. Journal of Huazhong University of Science and Technology (Nature Science)*, 30(5), 47-49.

Chen Kuan-ming, Yan Bao-jie.(2003). "The Analysis on Capacity of Urban Road.". *China Communications Press*, Bei Jing, 8.1-8.4.

Ren Fu-tian, Yang Feng, etc. (2001). "Capacity Analysis of Roundabout in Beijing." *J. Technology of Highway and Transport*, 18(3), 64-66.

Ruili Wang, Heather J. Ruskin. (2002). "Modeling Traffic Flow at a Single-Lane Urban Roundabout" *Computer Physics Communications*, 147, 570–576.

Xiang Qiao-jun, Wang Wei, etc. (2000) "The Model Construction of Low Channeling Roundabouts'Capacity and It's Application." *J. Technology of Highway and Transport*, 17(1), 42-45.

Xie Jun, Yan Bao-jie, etc. (2007). "Theory Model of Circular Intersection Traffic Capacity in Urban." *J. Journal of Chang'an University (Natural Science Edition)*, 27(4), 76-78.

The Reasonable Distance of Unsignalized Crosswalks based on Traffic Flow, Stability and Efficiency

Zhu Shunying[1], Xia Jing[2], Wang Hong[1], Liu Bing[3]

[1]School of Transportation, Wuhan University of Technology, 430063, 1040 Heping Ave., Wuchang, Wuhan, Hubei, China; PH: +86-13995680983; E-mail: zhusy2001@163.com.

[2]Deptartment of Traffic Engineering, Wuhan University of Technology , 430063 , 1040 Heping Ave. , Wuchang, Wuhan, Hubei, China; PH: +86-13971264545; E-mail: xiajingjt@126.com.

[3]Deptartment of Traffic Engineering, Wuhan University of Technology, 430063, 1040 Heping Ave. Wuchang, Wuhan, Hubei, China. PH: +86-13871475997, E-mail: lbjiaotong@126.com.

Abstract

The distance of midblock crosswalks directly influences traffic flow stability and operating efficiency. Considering the present situation of urban transportation in China, the reasonable distance of midblock unsignalized crosswalks was studied combined with the characteristics of vehicle traffic flow and pedestrian flow. In the peak hour traffic environment, eleven kinds of pedestrian crossing distance were designed (150m~400m, gap is 25m) in simulation model Vissim. Data of average speed time series, vehicular delay and pedestrian delay under time scales of 1s, 5s and 10s were obtained. The largest Lyapunov index of average speed time series was used to identify the influence of crosswalk distance over vehicle traffic flow stability. Vehicular delay and pedestrian delay were utilized to reflect the relationship among the distance of midblock crosswalks, vehicle flow efficiency and pedestrian crossing efficiency. This research takes the midblock management mechanism into consideration, balances the relationship among traffic flow stability, efficiency and pedestrian efficiency, and puts forward the recommended midblock crosswalk distance.

1 Introduction

Crossing is the main passage which pedestrians use to cross the street, and it also is an important component of Urban Transportation Facilities. It forms an Interaction System with the traffic flow and influence each other. Some scholars have studied the mutual interference between traffic flow and pedestrian on the crossing. Based on the behaviors of drivers and pedestrians crossing the street, Aronsson (2007) analyzed the impact of a single crosswalk on vehicle speed. Bastian (2007) set up the evaluation framework about the single crosswalk and vehicle traffic flow. Kaseko (2004) used Vissim to simulate the situation of pedestrian crossing on urban main roads, which reflected the influence of a single crosswalk on vehicle speed. But the above research all started from the angle of single crosswalk and did not get involve the distance of a continuous crosswalk. Research analyzed the effect of crosswalks on traffic flow from vehicular delay and pedestrian delay, which makes the evaluation lack all-sidedness. At present, confirmation about the distance of

crosswalks mainly depends on experience, some scholars(Yang, 2003 & Zhai, 2004) realized the tolerable walking distance of pedestrians according to different road functions, and then proposed the corresponding distance recommendation value. Only several researches had studied rational distance, such as the study of Lu(2002). In view of this, this paper plans to adopt the method of Computer Simulation, study the relationship between the distance of crosswalks and traffic flow from two aspects of traffic flow stability and efficiency, and finally confirm a rational value.

2. Traffic flow stability and efficiency

2.1 Definition and measurement of traffic flow stability

Traffic flow stability is an important index of measuring the running quality of traffic flow. If the traffic flow is stable, generally it is in an uncrowded and unblocked state of highway density section, speed fluctuations are orderly within the rational range. When it was interfered with by environment, it has a relatively strong ability to resume the original stable state. If the traffic flow is unstable, the density and speed at different times will be in disorder, which makes the efficiency of the traffic flow and traffic safety level reduced. Therefore, traffic flow stability is an important index of evaluating rationality of traffic facilities.

The paper uses the largest Lyapunov index λ_1 of average vehicle speed time series to reflect traffic flow stability. λ_1 is one of the common values reflecting chaos motion characteristic. λ_1 is a kind of index that can measure the average divergence and convergence of neighboring trajectory. Whether it is greater than zero or not can be regarded as a standard to judge whether the time series are in chaos(Lv, 2002), its value also indicates the system's chaotic degree. If $\lambda_1 > 0$, system is certainly chaos, an unstable condition(Zhu, 2008). When $\lambda_1 < 0$, the vector system in the direction of the movement is stable, the system's movement is in a certain predictable and orderly condition .The system is stable. This paper uses VISSIM simulation system to obtain average vehicle speed time series under different time scale, and then makes use of this sequence's largest Lyapunov index to distinguish the influence of crosswalk distance on vehicle flow stability.

2.2 Definition and measurement of efficiency

Pedestrians on crosswalks as an exterior interference will influence the operational efficiency of traffic flow. This paper uses vehicular delay and pedestrian crossing times to measure the influence of crosswalk distance on traffic efficiency. The equally lost time for vehicular delay and each vehicle passing the crosswalk is used to measure the influence crosswalk distance on the traffic efficiency. Pedestrian crossing time is the sum of time from the longitudinal sidewalk to the crosswalk and the time it takes a pedestrian to go through. Generally speaking, pedestrians will choose the crosswalk that is nearer them while conducting crossing behavior, usually the most disadvantageous crossing position is in the midpoint between two neighboring crosswalks. Here is an assumption that pedestrians uniformly distributed on both sides of road and pedestrian speed is constant. The paper approximately assumes that pedestrian embarks from the pedestrian crossing $d/4$ position moving toward this crosswalk, then street, and pedestrian crossing time is as follows:

$$t = t_1 + t_2 = d/(4 * v_p) + t_2 \qquad (1)$$

Where, t ——Pedestrian crossing time; t_1 ——Time of pedestrian along the longitudinal sidewalk arriving at the beginning of the nearest crosswalk; t_2 ——The time of pedestrian passing the crosswalk, can be provided from VISSIM simulation; d ——Distance of crosswalks, 150~400 m, gap is 25m; v_p ——Walking speed of pedestrian.

3. The simulate experiment of pedestrian flow and vehicle flow interaction

3.1 experiment scenes

The experiment adopts simulation software of VISSIM (4.1 edition) of Germany PTV Company. VISSIM is a discrete, random urban road micro-simulation software with (1/10) as time step long. It is based on the city traffic and the public transport simulation model, among them vertical sports of vehicles are adopted "psychology-physiology following model"; it can be set up with several parameters for example, vehicle parameter, traffic parameter, road parameter etc., also can imitate the reappearance the real road traffic conditions to the maximum extent. The simulation method can provide long time serial on different time scales, and avoid the restriction of surveying the data of traffic flow.

3.1.1 The characteristic of highway section

According to national standards of P.R.C.Code for transport planning on urban roads (GB-50220-1995), this paper adopts 1km long in total, six lanes of a two-way main road straight line sections as experiment section, and the width of the lane is 3.5 m, longitudinal slope for 0, width of crosswalk on lane are designed according to urban road design specification, priority rules of the crosswalk and lane are set up according to Mohamed S Kaseko(2004).11 kinds distance of crosswalk have been designed in the experiment (150m~400m, gap is 25m). In addition, in VISSIM, set up the corresponding data collector and road evaluation in order to get average speed, vehicular delay and pedestrian crossing time.

3.1.2 Parameter input

Choosing a model workday after field investigation, find the vehicle flow of peak hour in Peace Road in Wuhan city of China is 3000pcu/h, at the same time also survey traffic generation and attraction amount of crossing pedestrians are 800 persons/(hour*direction) in 1km of sections. According to the research of Wang(2007), we set up total cumulative frequency curve of pedestrian crossing. Vehicle speed on arterial highway is set up as 40~60km/h, the pedestrian average speed is 1.15m/s. The difference distance of crosswalks will cause its quantity to change; therefore under different distances the pedestrian flow on the crosswalk is different. The paper supposes that the pedestrian reaches the crosswalk equally, and the road section on both sides will establish the guard rail to force pedestrians to observe the traffic regulations, then under each distance of crosswalk, pedestrians flow on each are equal under every distance of crosswalk. According to the measured data, calculate the unidirectional pedestrian attraction quantity in each hour is 0.8 person /m, in view of crosswalk distance is different, obtains that crosswalks on the 1km main road can attract the length of D pedestrian crossing quantity, then calculate total pedestrian attraction quantity Q in the 1km section.

$$D=[\mathrm{int}(1000/d)+1]\square d \qquad (2)$$

$$Q = 0.8D = [\text{int}(1000/d)+1]\times 0.8d \text{ (person/(hour*direction))} \quad (3)$$

$$Q' = Q/\text{int}(1000/d) \text{ (person/hour/direction)} \quad (4)$$

Where, Q—The total attraction quantity of pedestrian,

Q'—The unidirectional crossing quantity of pedestrian on each crosswalk.

In VISSIM, the quantity of pedestrians crossing in the experimental section in VISSIM is in accordance with Q'.

3.1.3 Simulation parameter

At the initial stage of simulation, the vehicles are not distributed uniformly, vehicle flow parameters record are infidelity, so 400 seconds is regarded as the starting point of data recording. In the experiment, different simulation time-periods are selected, and different intervals are set up, thus output data under different time scales 1s, 5s and 10s are obtained. In each situation, four different random numbers are chosen, their averages are calculated in order to dispel the randomness of the experimental data after getting the data separately in simulations of each kind of situation.

3.2 Experimental results

3.2.1 Influence of distance on stability

From the simulation experiment, obtain time series of average vehicle speed under each distance of crosswalk and under different time intervals of 1s, 5s and the 10s, then get the largest Lyapunov index λ_1 through compiling programs in Matlab, see Figure 1.

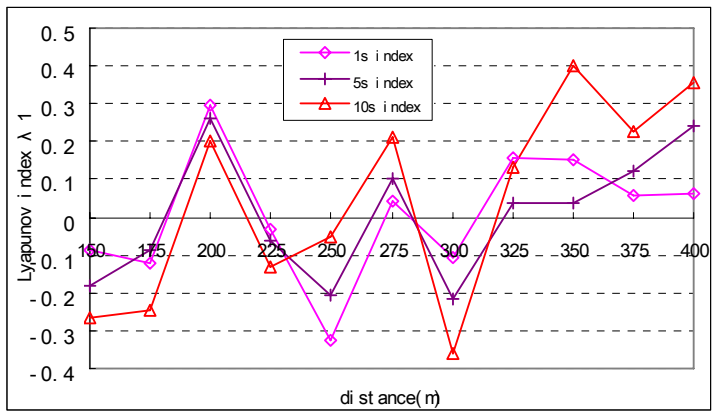

Figure 1. Lyapunov index λ_1 under different distance

It indicates that eleven types of distances are having remarkable effects on stability (p-value<0.01) to carry on variance analysis to data of Figure 1.As seen in Figure1, when the distance is 150m, 175m, 225m, 250m, 300m, λ_1 are negative, this shows that its traffic flow is stable; λ_1 of the remaining six types of distance are all positive, the traffic flow is in chaos. From Figure.1 also seen that λ_1 under different time scales is self-similarity, which indicates that it is reasonable to use chaos thought to judge crosswalk distance.

It indicates that eleven types of distances are having remarkable effects on vehicular delay and pedestrians crossing time of (p-value<0.01) after carrying on

analysis of variance to Figure 2 data. Seen from Figure 2, with the increase of crosswalk distance, the average speed shows the downward parabola trend change on the whole, when the distance is 250m, average speed is the largest, secondly are 275m and 300m. At the 150~250m, average speed increases with increased distance. Under the distances of 300~400m, average speed reduces with increased distance.

3.2.2 Influence of distance on efficiency

The vehicular delay and pedestrian crossing time have been shown in Figure 2, the vehicular delay of 250m is minimum. At the distance of 150~250m, vehicular delay reduces slightly with increased distance. Begin from 325m, vehicular delay increases sharply with increased distance, at distance of 350m~400m, the increasing degree slows down, delay at 400m is the maximum, and the whole curve presents the parabola with upward line. Pedestrian crossing time at 150m is the minimum, and at 400m is the maximum. It increases with the increased distance, and presents linear change on the whole.

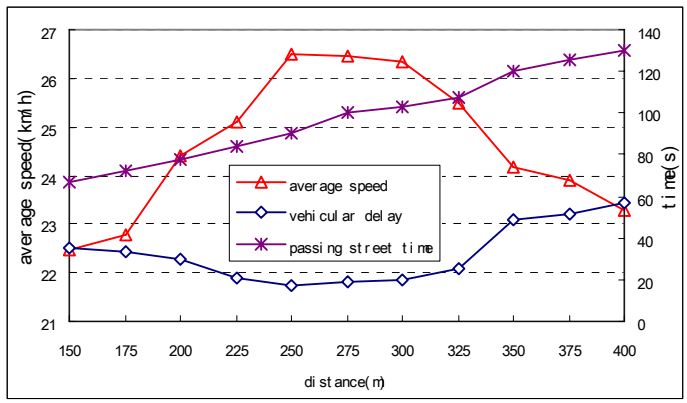

Figure 2.Average speed under different time scale and vehicular delays and passing street time of pedestrians under different distances

4 Discussion and analysis

The main road as an important component in urban road network and can be divided into two kinds: traffic and service. While studying crosswalk distance on main road, first analyze road management function of these two types of main roads, then based on the demand of traffic flow stability, vehicle operating efficiency, and pedestrian efficiency a reasonable value is determined.

The traffic main roads view the function of "passing" of a motor vehicle as the main purpose, give consideration to other traffic modes; generally speaking, it mainly relies on fast traffic. While confirming its distance of the crosswalk, should first make it meet the demand of traffic flow stability and vehicle operational efficiency, and then meet the demand of pedestrian efficiency, causes them to be most optimally balanced. The main service roads emphasize the function of "reaching", rely mainly on living service function, and pay attention to the services of different traffic modes. On the crosswalk of the service main road, the right of way of vehicles and pedestrians are equal; the distance should simultaneously meet stability, vehicle efficiency and pedestrian efficiency.

According to road management functions of traffic and service main roads, different weights of stability, vehicle efficiency and pedestrian efficiency of traffic

and main service roads are given respectively, they are 0.4:0.4:0.2 and 1/3:1/3:1/3. The stability index λ_1 and efficiency index (vehicular delay and pedestrian crossing time) are all cost indexes. Here stipulates that for each index the minimum value is 100 points, the maximum value is 0 point. According to different weights, the comprehensive scores under eleven types of distances are calculated separately, the results as shown in Figure 3.

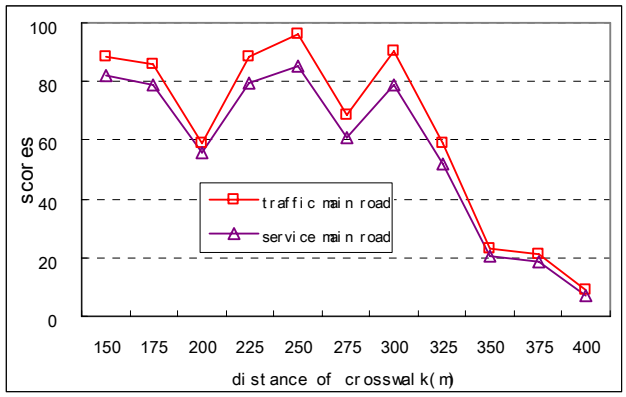

Figure 3.Weight ratios of stability vehicle efficiency and pedestrian efficiency of traffic and service main roads are respectively 0.4:0.4:0.2 and 1/3:1/3:1/3

In Figure 3, the comprehensive score of 250m is the largest. It can well meet the demand of traffic and service main road to stability and efficiency; therefore the recommended crosswalk distance on main road is 250m.

Acknowledgement

This work was supported by a grant from the Major State Basic Research Development Program of China (973 Program) (No.2005CB724205) .

Reference

Aronsson,Karin F.M., Bang,Karl L.(2007). Speed characteristics of urban streets based on driver behavior studies and simulation including pedestrian movements.TRB2007.

Bastian Jonathan Schroeder. (2007). A Framework for Evaluating Pedestrian-Vehicle Interactions at Unsignalized Crossing Facilities in a Microscopic Modeling Environment.TRB2007.

Mohamed S Kaseko, Ganesh J.Karkee. (2004). Development of a Midblock Pedestrian Crossing Simulation Model Using VISSIM.trb,2004

Yang Xiaoguang. (2003). Manual of Urban Traffic Design[M].Beijing:China Communication Press.

Zhai Zhongmin.(2004). Road traffic optimized organization[M].Beijing:China Communication Press.

Lu Jian, Ye Huiqiong, Yao Donglei. (2002). Reasonable distance of pedestrian crossing facilities[J]. Journal of Traffic and Transportation Engineering, 12.

Lv Jinhu,Lu Jun-an,Chen Shihua.(2002). Chaotic Time Series analyse and Its Applications[C]. Wuhan: Wuhan University Press.

Zhu Shunying, Wang Hong, Xiang Hong yan. (2008). Parameter and traffic incident dynamic foremost method. [M]. Nanjing: Southeast University Press.

National standards of P.R.C.Code for transport planning on urban road

(GB-50220-1995) [S]. State Technical Supervision Bureau and the Ministry of Construction of P.R.C.

Wang Fang. (2007). Study on Characteristics of Pedestrian Flow on Unsignalized Crosswalks and Its Application[D]. Jilin University master graduation thesis.

Study on the Green Traffic Planning System of New Rural Communit ies

Li Chang-hong[1, 2] and Liu Cong-hong[1]

[1]Institute of Architecture, Tianjin University, Tianjin 300072, China; Email: work_98@126.com
[2]Department of Urban Planning and Architecture, Tianjin Institute of Urban Construction, Tianjin 300384, China

ABSTRACT

In this era of socialist countryside construction, lack of consideration for local residents, vehicles, and community roads in new rural community planning leads to unsustainable development. Green transportation systems that are appropriate for production and living should be developed for rural communities. Traffic Calming techniques can be used to optimize the road network and reduce the negative impact of motor traffic. By analyzing the case of Baodi, Tianjin, this study suggests how to build an appropriate scale, orderly, safe, comfortable and low energy consumption green transportation system and create a scientific, healthy, and sustainable new rural community development.

1. INTRODUCTI ON

Transportation is a key problem that can deeply affect the quality of human lives especially in residential communities. A new chapter was written in the 11th Five-Year Plan (China, 2006) with the major historic task of building and urbanizing the new socialist countryside. However, the theoretical study of transportation planning comparatively lags behind rapid construction. In designing and planning new-rural communities, lack of consideration of three elements of transportation, including local residents, traffic vehicles, and community roads (Boulter, 1999), leads to unsustainable development of the transportation planning system.

The purpose of this research is to build a green transportation system by means of using Traffic Calming techniques, such as reducing the turning radius, setting the bottleneck speed, and improving the road marks to optimize the road network in new rural communities and reduce the negative impact of motor traffic, creating a safe and pleasant environment.

2. BACKGROUND S

2.1 Green Transportation

Green transportation advocates that stress on the traffic organization should be put on the pedestrians in the road space, reducing the negative impact of motor traffic to the maximum limit to create pleasant, livable, and sustainable communities (Kallberg and Ranta, 2000). This idea is similar to the opinion of New Urbanism that encourages resolution of traffic problems on the basis of the comfortable distance of pedestrians in the neighborhoods (Yang dong-feng, 2007).

2.2 Traffic Calming

2.2.1 History of Traffic Calming

In the USA, traffic calming as a method to design roads and road networks to physically enforce lower driving speeds and to reduce traffic volumes, started as early as 1928 with an experimental neighborhood design in Radburn (Bagby , 1980). In the late 1960s, this idea was further implemented in Europe with the development of the SCAFT guidelines in Sweden, promoting the development of residential areas accessed by a system of ring roads. The technologies of traffic calming have been widely accepted in the neighborhoods of advanced countries (Webster, 1998, 2000).

2.2.2 Tendency of Techniques

Traditional traffic calming consists of four sections: (i) vertical deflections, (ii) horizontal deflections, (iii) volume deflections, and (iv) traffic signs deflections. The purpose of traffic calming schemes is to lower the speed of automobile into 30～40 kilometers per hour and achieve an enjoyable environment of safe streets. However, the studies in practice indicate that the traditional techniques have some flaws, such as averting the traffic pressure from one neighborhood to another, producing a limited effect on lowing transportation by a single technique (Silke, 1996). The tendency of techniques in the field is in the direction of regional and synthetic study.

3 METHODOLOGY

3.1 Site Selection

The study has been carried out in Majiadian which is located in the south district of Baodi in Tianjin. The distance is 8 kilos away from Baodi district and 60 kilos away from Tianjin city. The project of the new rural community is the promoter region for living, which be situated on east of one branch, south to the 5th Road, west to the 18th Road, north to the 4th and east to the 19th Road, the area of construction land is 7.51 hectares (Figure1).

Figure 1 Site Selection

3.2 Specific Schemes

3.2.1 Foundation of Green Transportation

The design of the community was aimed at building a green transportation system which is orderly, accessible, ecological, and low consumption. The road network adopted community-level "community-level road, group-level road, foot-level road", which is made of two cross roads-A and B, one ring road-C. The width and the form of the road-network is shown in Figure 2.

Figure 2 Scheme of Green Transportation

3.2.2 Improvement of Schemes

There are two more effective and acceptable traffic calming devices follow to optimize the schemes: Speed Bumps and Speed Humps.

(i) Speed Bumps

Speed bumps are raised pavement areas across a roadway and generally have a height of 3 to 6 inches with a length of 1 to 3 feet. These are typically found on private roadways and parking lots and do not tend to exhibit consistent design parameters from one installation to another. A bump causes a driver significant discomfort at typical residential speeds and generally results in vehicles slowing to 5 mph or less at the bump. At high speeds, bumps tend to have less overall vehicle impact because the suspension quickly absorbs the impact before the vehicle body can react (Bos and Dijkstra, 1998).

(ii) Speed Humps

Speed humps are raised areas in the roadway pavement surface extending transversely across the travel way. Sometimes called pavement undulations or sleeping policemen, speed humps normally have a maximum height of 3 to 4 inches with a travel length of approximately feet (Carsten, 1998). Within typical residential speed ranges, humps create a gentle vehicle rocking motion that causes some driver discomfort and results in most vehicles slowing to 15 mph or less at each hump and 25 to 30 mph between properly spaced humps in a system (Watts, Stait, Godfrey, Chinn and Layfield, 2002). At high speeds, the hump can act as a bump and jolt the vehicles suspension and its occupants or cargo.

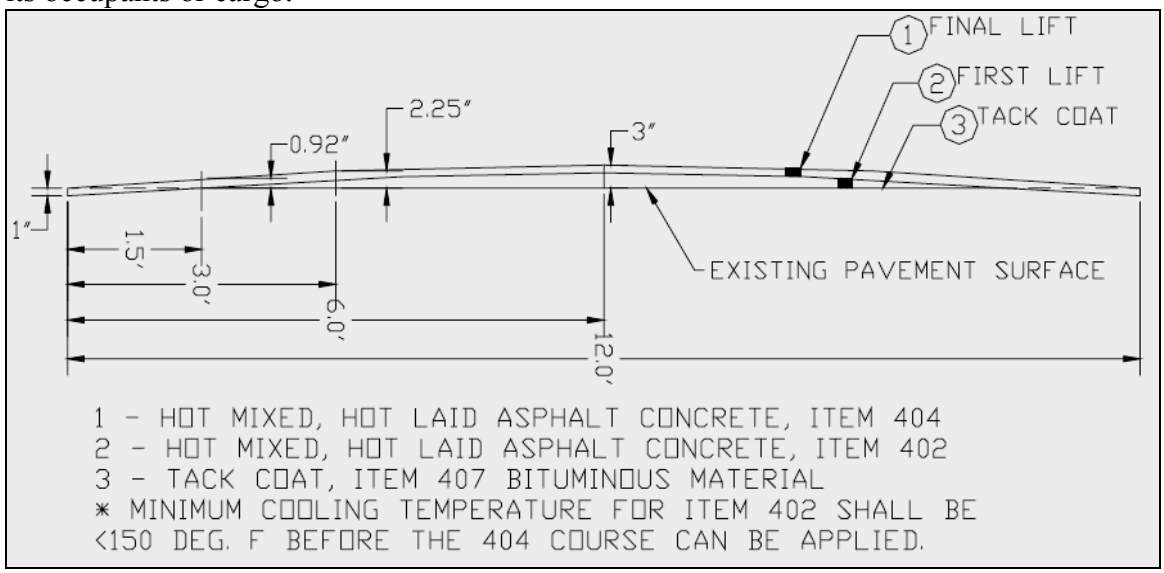

Figure 3 Speed Hump

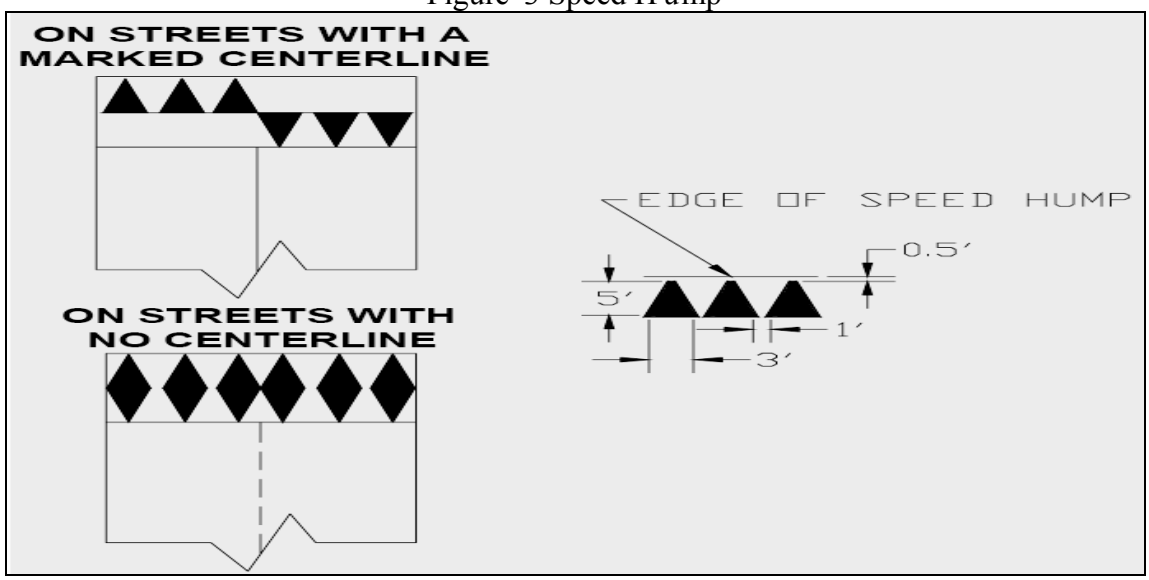

Figure 4 Speed Humps – Shark Teeth (Marking) Detail

4 ANALYSIS

Through simulated experiments, the results indicate that after using the traffic techniques the environment of the community has been greatly improved. The road network is constructed to very high standards, almost completely straight over more than 0.3 kilos, with pavement width in excess of 7 meters and with wide verges. Problem areas reported include: A relatively recent increase in traffic volumes; High speed on the road; A large percentage of heavy vehicles using the road; High noise levels emanating from the road; Accidents occurring on the road. The data below reveals that the important functions of speed bumps and humps applied in the scheme.

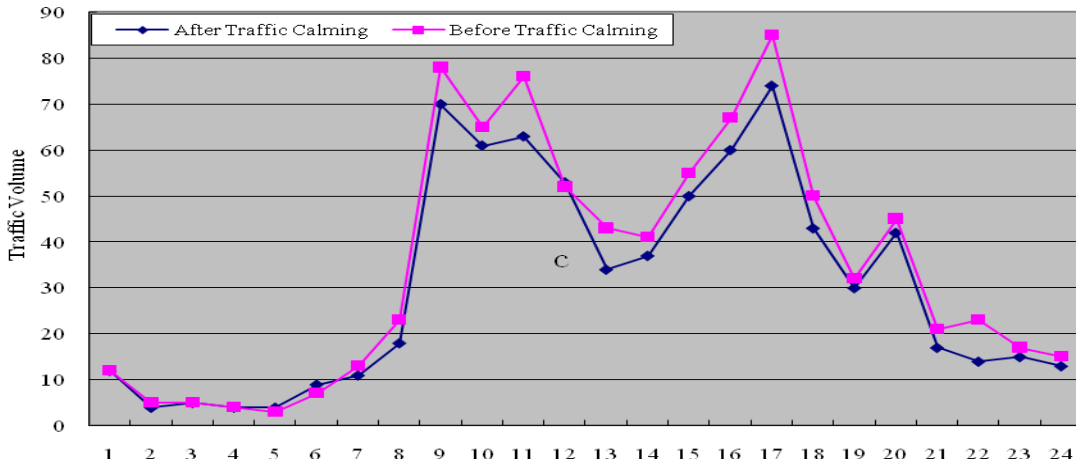

Figure 5 Total Traffic Volume

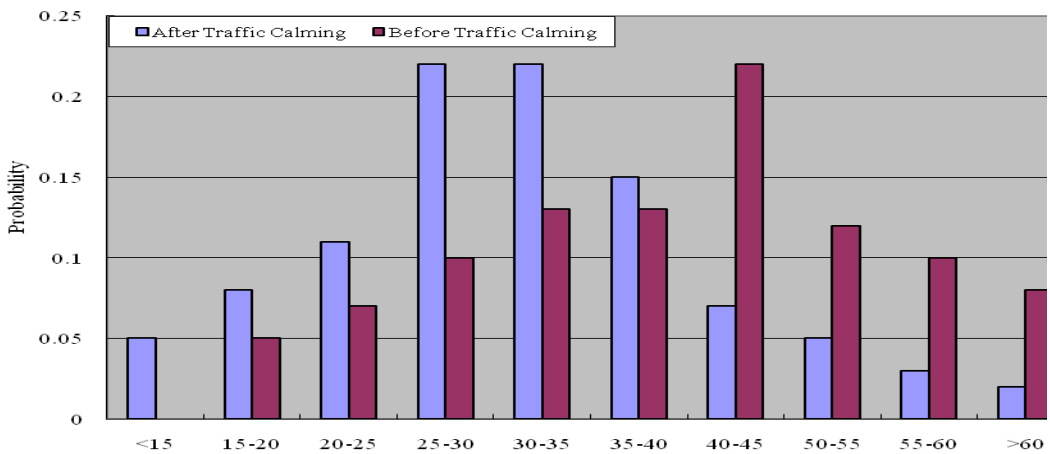

Figure 6 Percentage of Vehicles in Speed Classes

5. CONCLUSIONS

This literature review has shown that traffic calming is an effective and economical tool in planning green transportation in new rural communities to reduce vehicle speed, noise, and road accidents. It puts forward to build an appropriate scale, orderly, safe, comfortable, and low energy consumption of green system to realize the scientific, healthy, and sustainable development of new socialist rural communities.

REFERENCES

Bagby G (1980). "Effects of Traffic Flow on Residential Property Values" Journal of the American Planning Association, Vol. 46, No. 1, 88-94.

Bos J M J and A Dijkstra (1998). "Road safety effects of small-scale infrastructural measures with emphasis on pedestrian safety". SWOV-report A-98-17. SWOV, Institute for Road Safety Research. Leidschendam.

Boulter P G (1999). "Remote sensing of vehicle emissions near two traffic calming measures in Gloucester". TRL Report 307. Transport Research Laboratory, Crowthorne.

Carsten O, (1998). "Intelligent speed control "could cut accidents by 35%"Traffic Engineering and Control. July/August 1998.

Clarke A (1994). "Traffic Calming, Auto-Restricted Zones and Other Traffic Management Techniques: Their Effects on Bicycling and Pedestrians." National Bicycling and Walking Study, No. 19. FederalHighway Administration. Washington DC

Kallberg V P and S Ranta (2000). "Impacts of urban speed-reducing measures." 2nd international symposium on highway geometric design in Mainz, Germany 14-17 June 2000.

Proctor S (1991). "Accident reduction through area-wide traffic calming schemes." Traffic Engineering & Control. 1991-12. Pg. 566-571. Printerhall limited. London.

Silke E (1996). "Traffic calming blocks way for winter maintenance." Surveyor 10/10/96.

Watts G R, Stait R E, Godfrey N S, Chinn L and Layfield R E, (2002). "Development of a novel traffic calming surface 'Rippleprint". TRL Report TRL545, Transport Research Laboratory, Crowthorne

Webster D (1998). "Traffic calming – public attitude surveys: A literature review." TRL Report 331. Transport Research Laboratory, Crowthorne.

Webster DC (2000). "Traffic Calming – Literature search on the design and performance of traffic calming measures" TRL Report 439. Transport Research Laboratory, Crowthorne.

Yang dongfeng(2007). "New Trend of World New-town Development since1990."Areal Research and Development, Vol. 26, No. 6, 18-22.

Predicting Methods of Trip Modal-split Based on Structural Model

Zhuping[1] ZHOU, Gang[2] REN, Wei[2] WANG
[1]Jiangsu Provincial Key Laboratory of Transportation Planning and Management Southeast University Nanjing, 210096, China,PH: +86-13770953687; email: jzp19850926@163.com
[2]School of Transportation, Southeast University, Nanjing, 210096, China.

Abstract: The passenger traffic mode split is the result of the integrated effect among various factors, which are interrelated and mutually independent as well as interacted and mutual restrictive. In order to analyze the motivation of traffic structure, the influence mechanism of different factors should be analyzed comprehensively to figure out the basic caustic relationship between each factor. The structure model of system engineering modeling method will be applied to clarify the logical relationship between different factors. Furthermore, the mode split prediction method based on the structure model of various factors will be set up by fitting survey data. The result of the case analysis with less errors illustrates this method is easily applicable and of great value.

Introduction

The commonly forecasting model in trip mode split includes the diversion curve model, probability model, regression model etc. In the last few years, Chinese researchers placed an emphasis on trip mode split which meets the requirement of sustainable development, while the foreign study varies widely: Schmocker *et al.* studied modal split by the different attributes(gender, age, profession etc) of the travelers with different selection characteristics(Schmocker *et al.* 2008), Bergstrom *et al.* discussed the influence mechanism of external factors such as natural conditions, architectural environment, urban form and so on(Bergstrom 2003; Robert, 2002); in addition, Thogersen *et al.* analyzed the traffic mode structure in one certain city or area(Thogersen, *et al.* 2006; Goran, *et al.* 2006).

The inherent law of change in traffic structure would be ignored on the condition of only analyzing the regression equation between mode split and its related factors. The system structure model which was first introduced by Professor John N. Warfield (the United States, 1973), is widely used to analysis social, economic, environmental, management systems (Haijun, 2006; Benjamin *et al.*, 2006) for system planning. Transportation system involves many different elements. Consequently, some indirect relationship should be introduced to clarify the relationships between various elements, and the structural model should first be established, then forecast traffic modal split step by step.

Factors for mode split

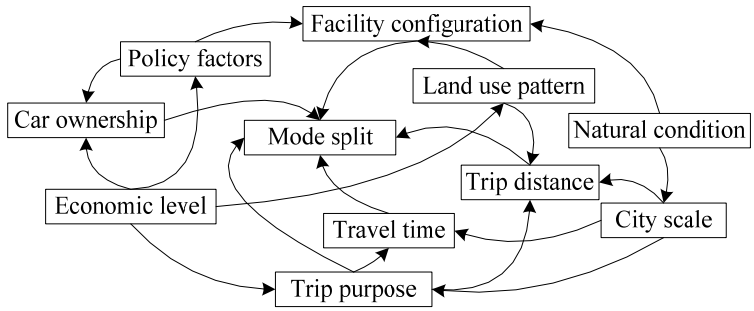

Fig.1 Causality among Influencing Factors of Trip Mode Split

Structural model building

The corresponding computation for the relationship between the influencing factors (in Figure 1) would be performed by establishing a multi-level hierarchy model (Dong, 2007; Shangyun, 2004).

0.1 Causal relationship matrix calculation

0.1.1 Adjacency Matrix building

First, define variable symbols and numbering as follows: V_1-mode split, V_2-trip distance, V_3-travel time, V_4-trip purpose, V_5-traffic facilities configuration, V_6-private vehicle ownership rate, V_7-policy factors, V_8-economic level, V_9-urban form, V_{10}-city scale, V_{11}-natural conditions.

Then set up the adjacency matrix, which is denoted by R, and describe the direct relationship between every two factors in the system. The elements of $\mathbf{R}$ is defined as:

$$\gamma_{ij} = \begin{cases} 1 & \text{accessible from } V_i \text{ to } V_j \\ 0 & \text{no route between } V_i \text{ and } V_j \end{cases} \quad (1)$$

0.1.2 Accessibility matrix calculation

Accessibility matrix, which describes the factors accessible degree of the system through a certain length of path, can be obtained by certain computing with the sum of adjacency matrix and unit matrix. Simplifying assumptions are:

$$\mathbf{R}_1 = (\mathbf{R}+\mathbf{I})^1, \quad \mathbf{R}_2 = (\mathbf{R}+\mathbf{I})^2, \quad \ldots \mathbf{R}_n = (\mathbf{R}+\mathbf{I})^n \quad (2)$$

It could be calculated to $(\mathbf{R}+\mathbf{I})^p = (\mathbf{R}+\mathbf{I})^{p+1}$ in turn with application of the rules of Boolean algebra. Take matrix $\mathbf{R}$ to operation in accordance with such rules to get:

$$\mathbf{R}^2=\mathbf{R}^3=\mathbf{M}=\begin{bmatrix} 1&0&0&0&0&0&0&0&0&0&0 \\ 1&1&0&0&0&0&0&0&0&0&0 \\ 1&0&1&0&0&0&0&0&0&0&0 \\ 1&1&1&1&0&0&0&0&0&0&0 \\ 1&0&0&0&1&0&0&0&0&0&0 \\ 1&0&0&0&0&1&0&0&0&0&0 \\ 1&0&0&0&1&1&1&0&0&0&0 \\ 1&1&1&1&1&1&1&1&1&0&0 \\ 1&1&0&0&1&0&0&0&1&0&0 \\ 1&1&1&0&1&0&0&0&0&1&0 \\ 1&1&1&0&1&0&0&0&0&1&1 \end{bmatrix} \quad (3)$$

0.1.3 Accessibility Matrix decomposition

Accessibility matrix decomposition consists of the following steps: first, demarcate the region, and then decompose inter-level. Decomposition algorithm can be described as follows: constitute an accessible set $X(V_i)$ with the factors relevant to V_i, the factors

which can arrive V_i will compose an antecedence set $Y(V_i)$. The mathematical relationship is stated as formulation (5):

$$X(V_i)=\left\{V_j \in W / m_{ij}=1\right\},\quad Y(V_i)=\left\{V_j \in W / m_{ji}= \right. \tag{4}$$

Where W is node set of all the factors, m_{ij} is the correlation degree of node i and j (value 1 or 0).

Set up a new set defined as the common set T, which contains all the factors V_i that the intersection of accessible set and antecedence set is equivalent to the antecedence set.

$$T=\left\{V_i \in X(V_i) \bigcap Y(V_i)=Y(V_i)\right\} \tag{5}$$

Then the accessible set, antecedence set, as well as the intersection of these can be found on the basis of known matrix M, as shown in Table 1. For inter-level decomposition, conditions can be seen in formulation (7):

$$X(V_i) \bigcap Y(V_i)=X(V_i) \tag{6}$$

Available from Table 1, only the element 1 satisfy this requirement, confirm $L_1=\left\{V_1\right\}$ being the first level, then remove the element 1 from the table, continue the calculation, the second level is educed to be $L_2=\left\{V_2, V_3, V_5, V_6\right\}$. Similarly, calculate the third level and the fourth level. Upon that, rearrange the row vector of the matrix according to the order of $\{1,2,3,5,6,4,7,9,10,8,11\}$, and then in accordance with the above order rearrange the column vector to obtain the shifted accessibility matrix $\mathbf{M}'$:

$$\mathbf{M}'=\begin{bmatrix} 1&0&0&0&0&0&0&0&0&0&0 \\ 1&1&0&0&0&0&0&0&0&0&0 \\ 1&0&1&0&0&0&0&0&0&0&0 \\ 1&0&0&1&0&0&0&0&0&0&0 \\ 1&0&0&0&1&0&0&0&0&0&0 \\ 1&1&1&0&0&1&0&0&0&0&0 \\ 1&0&0&1&1&0&1&0&0&0&0 \\ 1&1&0&1&0&0&0&1&0&0&0 \\ 1&1&1&1&0&0&0&0&1&0&0 \\ 1&1&1&1&1&1&1&1&0&1&0 \\ 1&1&1&1&0&0&0&0&1&0&1 \end{bmatrix} \tag{7}$$

0.2 Establish multi-level hierarchy model

We minus identity matrix from the shifted accessibility matrix $\mathbf{M}'$. From the definition of accessibility, knowing that: ①V_2, V_3, V_5, V_6 the second level only the first level V_1, namely $V_2 \to V_1$, $V_3 \to V_1$, $V_5 \to V_1$, $V_6 \to V_1$; ② then remove the column and row which V_1 is in to establish the relationship between the second and third level. We can see that the third level has V_4, V_7, V_9, V_{10}, whose mutual influence relationships are $V_4 \to V_2$, $V_4 \to V_3$, $V_7 \to V_5$, $V_7 \to V_6$, $V_7 \to V_5$, $V_9 \to V_2$, $V_9 \to V_5$, $V_{10} \to V_2$, $V_{10} \to V_3$, $V_{10} \to V_5$; ③ remove rows and columns which $V_2 V_2$, V_3, V_5, V_6 are in to know V_8, V_{11} existing in the fourth level, that is $V_8 \to V_7$, $V_8 \to V_9$, $V_{11} \to V_9$. Based on the foregoing analysis, can establish a four-level hierarchical model as Figure 2:

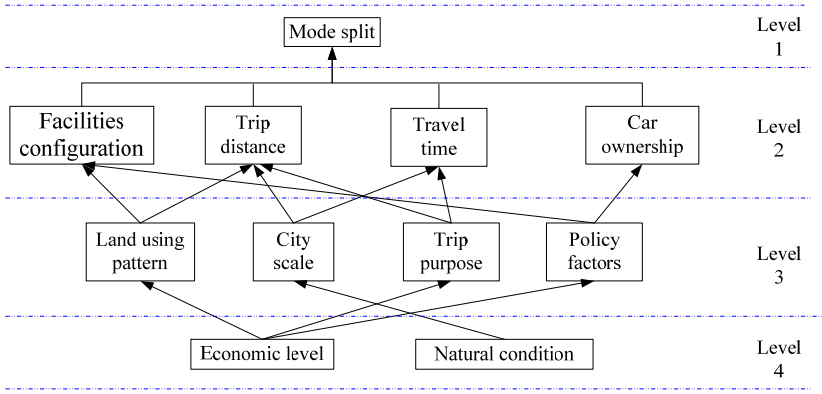

Fig.2 Structural Model for Influencing Factors of Trip Mode Split

1 The mode split prediction method

1.1 The indicators of variable factors

Based on the relevant research data (Crane 2000; Shangyun 2004; Haixiao 2005; Haifeng 2006), the variable factors indicators can be determined as follows:

①Urban form C: Urban form can be described by urban planning disciplines: select the compact degree as quantitative indicator for the urban form as formula (9).

$$C = A / \pi R^2 \tag{8}$$

Where A is the area of built-up section of the city. πR^2 is the area of the smallest circumcircle of the city.

②City scale S: With the view to integrity and comprehensiveness, the urban population is taken for indicator.

③Trip purpose I: In this paper, indicators for the trip purpose is defined as:

$$I = I_{\text{elastic}} / I_{\text{non-elastic}} \tag{9}$$

Where I_{elastic} and $I_{\text{non-elastic}}$ are proportions of elastic travel and non-elastic travel (work, school and backhaul) respectively.

④Policy factor P: We classifies policy in accordance with the strength for public transport priority shown in Table 1, demonstrating reference data of each type of cities for quantify.

Tab.1 Policy Intensity of Prioritize Public Transportation

Policy of prioritize public transportation	Very large	larger	general	little	none
value	0.75～1	0.5～0.75	0.25～0.5	0～0.25	0

⑤Transport facilities configuration R: Road network density as the analysis is selected as R indicator.

⑥Private vehicle ownership rate O

⑦Travel time T: Select the average travel time-consuming of the traffic survey data.

⑧Trip distance: Most of the domestic cities estimate the trip distance through the average travel time-consuming and travel speed of different traffic modes, as formulation (10).

$$D = \sum_i T_i V_i f_i \tag{10}$$

Where T_i is the average travel time-consuming of traffic mode i; V_i is the average travel

speed of traffic mode i(V_i of walking, bicycle, bus, car is 3.6, 9, 14.4, 27km/h respectively); f_i is the split rate of traffic mode i.

⑨Mode split rate M : Mode split rate could access from the trip survey data directly.

1.2 Mathematical modeling for all levels

The basic data in this paper is from transportation school of Southeast University, including different sizes and patterns cities. Taking into account that the complicated natural conditions is difficult to quantify, it started from the third level.

1.2.1 Relation between the second level and the third level

Set up the relationship between trip distance D and urban form C, city scale S, trip purpose I ; as well as between travel time T and city scale S, travel purpose, the relationship between transport facilities configuration R and urban form C, policy P; and between private vehicle ownership rates O and policy P.

① Data Fitting $D = F_1(C, S, I)$

$$D = 7.853\times10^{-2}\sqrt{S} + 0.157C - 0.208\exp(I) + 2.269 \quad (R^2 = 0.736) \tag{11}$$

Where, D is trip distance (km); S is city scale (million people).

We use the square of the adjusted correlation coefficient value (Adjusted R Square) to evaluate the model, which is known as model precision coefficient, namely, R^2 's closer to 1, the model's more accurate.

② Data fitting $T=F_2(S, I)$

To S, I, Use logarithmic and exponential function to fit respectively:

$$T = 3.580\ln(S) - 1.386\exp(I) + 7.676 \quad (R^2 = 0.853) \tag{12}$$

Where, T is travel time, other parameters are ditto.

③ Data fitting $O=F_3(P)$

$$O = -70.418P^4 + 127.3P^3 - 70.814P^2 + 14.661P - 0.1207 \tag{13}$$

④ Data fitting $R=F_3(C, P)$

Use composite exponential to fit to C, while to P, use the form of exponential function. Following formula reveals the fitting results:

$$R = -9.25\times10^{-2}\exp(\exp((C - 0.211)/0.432)) + 2.942\times10^{-2}P^{-1.974} + 5.987 \tag{14}$$

Where, C, P are the same as above.

1.2.2 Relation between the second level and first level

Set up relationship between mode split M and transport facilities configuration R, trip distance D, travel time-consuming T, private vehicle ownership rate O.

① Walk-split data fitting $M_\alpha = F_4(R, D, T, O)$

$$M_\alpha = -0.476R - 7.265D + 0.274T - 13.942O + 55.757 \quad (R^2 = 0.893) \tag{15}$$

Where, M_α is the walk-split rate (%),other parameters are ditto.

Judging form formulation (15), trip distance influences the walk-split rate most strongly, hence, it could be an important consideration to select the walk mode in microcosmic scale.

②Bicycle-split data fitting $M_\beta = F_4(R, D, T, O)$

$$M_\beta = 3.190R + 14.518D - 1.458T - 3.458O + 19.195 \quad (R^2 = 0.967) \tag{16}$$

Where, M_β is bicycle split rate (%).

③Public transport-split data fitting $M_\gamma = F_4(R,\ D,\ T,\ O)$

$$M_r = -2.694R - 5.682D + 1.126T + 6.247O + 12.540 \quad (R^2 = 0.926) \qquad (17)$$

Where, M_r is the public transport vehicles split rate (%).

The travel time plays most roles in public transport split.

④Car-split data fitting $M_\omega = F_4(R,\ D,\ T,\ O)$

$$M_\omega = 0.219R - 1.741D + 0.216T + 10.337O + 6.594 \quad (R^2 = 0.903) \qquad (18)$$

Where, M_ω is the car split rate (%).

1.3 Model validation

Model validation is to verify the goodness of fit of built model, reality system and testing whether the model can reflect the characteristics and changing rule of reality system or not. We used survey data from Weifang city to validate the built model, the good forecasting results in Table 2 show practical value of the proposed method.

Tab.2 Prediction accuracy of mode split forecasting results

	Predictive value	Survey data	Error rate		Predictive value	Survey data	Error rate
M_α	23.96	21.72	10.17%	M_r	8.94	8.08	9.62%
M_β	52.37	55.82	-6.18%	M_ω	14.76	14.38	2.64%

2 Conclusions

From the view of data analysis, factor contribution rate was used in the model to estimate the influencing effects of motor vehicle population, trip distance, road traffic facilities, travel time on trip mode split. The analysis results can provide theoretical basis for trip mode structure policy.

It is a new attempt to build the hierarchical structure model for modal split, which comprehensively considers all aspects of influencing factors in the transportation system. Moreover, calculation results which are the factual manifestation of traffic structure in this city, can be a great help for policymakers to grasp the traffic structure in a macro level and plan the further transportation more profoundly. However, accuracy decision coefficients (R Square) in parts of formulations are not as high as expected, indicating a certain gap with actual situations, so the pioneer work can be traced to solve these problems.

Acknowledgments

This work is supported in part by Project supported by National Natural Science Foundation of China（NO. 50738001), and National Key Basic Research Program (NKBRP, NO. 2006CB705500) and Application Innovation Program of the Ministry of Public Security of China (No. 2007YYCXJSST043).

References

Bergstrom A., Magnusson R. “Potential of transferring car trips to bicycle during winter”. Transportation Research Part A 37 (2003) 649–666

Benjamin S. Blanehard), Wolte J.Fabrycky. *Systems Engineering and Analysis*,3rd Ed. Tsinghua University Press. 2006

Crane，R. “The Influence of Urban Form on Travel: An Interpretive Review”. Journal of Planning Literature，Vol.15（1），2000，p3-23.

DONG Zhaojun. *System Engineering and Operational Research*. National Defense

Industry Press, 2007.
Goran VUK, Christian Overgaard Hansen. "Validating the passenger traffic model for Copenhagen". Transportation (2006) 33: 371—392
Haifeng LI. Study on the Urban Form, Traffic Pattern and Resident Traffic. Southeast University Doctor Degree Dissertation，2006.3
Haijun ZHANG. Generation and Research of System Structural Modeling. Master degree thesis of harbin engineering university. 2006.4
Haixiao MAO. Research on Person Trip Charateristics of Chinese Citizens. Master degree thesis of beijing polytechnic university. 2005.3
Robert Cervero. "Built environments and mode choice: toward a normative framework". Transportation Research Part D 7 (2002) 265–284
Schmocker Jan-Dirk, Mohammed A, *et. al*. "Mode choice of older and disabled people: a case study of shopping trips in London". Journal of Transport Geography, 2008, 16, p257–267.
Shangyun CHEN. Study on Development Strategies and System Structure of Passenger Traffic in Metropolises of China. Southwest Jiaotong University Doctor Degree Dissertation，2004.2
Thogersen J. "Understanding repetitive travel mode choices in a stable context: A panel study approach". Transportation Research Part A 40 (2006) 621–638.

A Multi-class Multi-modal Combined Model for TDM Measures Evaluation in Large Scale Urban Transportation Network

ZHANG Tianran[1,2], YANG Dongyuan[1], YANG Chao[1] and ZHAO Yali[1]

[1]School of Transportation Engineering, Tongji University, Shanghai 201804, China
[2]Shanghai City Comprehensive Transportation Planning Institute, Shanghai 200040, China, PH (86) 21-62792285, email: zhangtianrantj@163.com

Abstract: A multi-class multi-modal combined modal split and traffic assignment model is formulated by variational inequality. It is used to evaluate the effects of Travel Demand Management (TDM) measures quantitatively in large scale urban transportation system. Three algorithms, i.e., Generalized Partial Linearization, Method of Successive Averages, and Constant Weight are compared. The convergence results show that the proposed algorithm is competent for practical application. Sixteen pure and combined TDM measures, such as cordon-based congestion charge, Park and Ride, fuel pricing, bus fares decrease, and bus exclusive lanes construction are tested quantitatively using the comprehensive transportation network of Huizhou, Southern China. The evaluation focuses on the sensitivity of public transport fares, the competition between taxi and rail transit, the effect of bus exclusive lanes, the different effects of cordon-based congestion charge and parking charge as well as the demand of Park and Ride under different parking charge.

1 Introduction

In recent years, with rapid economic and social development, metropolises in China are confronting difficulty balancing the restriction in road space resources and the increasing demand of motorization. The government realizes that great efforts should be made to develop public transportation and implement suitable TDM to construct sustainable urban transportation systems. To evaluate TDM, network model needs to have two critical capabilities, i.e. the capability to model the different behavior by heterogeneous travelers to the TDM in multi-modal transportation network and the capability to model various TDM measures simultaneously. The heterogeneity or multiclass means that people with different value of time (VOT) or different trip purpose will have different preferences of travel time and cost. Ignoring heterogeneity of VOT may cause serious errors in travel demand prediction and policy evaluation. On the other hand, combined models can reflect the interaction of multi-modal transportation system. Florian, Wu and He (2000) formulated the problem as a variational inequality, which is the most detailed multiclass, multimodal combined model. Kaneko, et al. (2001) estimated the impact of Area License Scheme with multi-class combined modal split and assignment model in the Bangkok Metropolitan Area. Boyce and Marshall (2002) had collaborated in the implementation and application of three combined models for the Chicago region for evaluating policy alternatives. There is much literature about this topic but we lack the space here to introduce the research. This paper concerns the travel behavior of multi-class users under TDM measures. Nine modes including pure modes, such as Private car, Taxi, Bus (with Bus exclusive lane), Rail, and combined modes, such as

P&R, Taxi & Rail, Bus & Rail are considered in the model. The interaction among different traffic flows, i.e., car, bus and freight, are modeled as asymmetric traffic assignment problem. The multi-modal vehicles such as trucks and buses are treated as vehicles instead of passenger car unit, As a result, the Jacobian of general cost is asymmetric. This is different with multi-modal traffic assignment model in current commercial software such as EMME/2 and TransCAD. The uniqueness of the asymmetric traffic assignment is guaranteed by special link travel time function. It works well in several large scale urban transportation networks.

2 Model formulation and algorithms

2.1 Travel behavior assumption

(1) Multiclass users

The mixed logit form directly corresponds to the situation, in which VOT and underlying utility coefficients for travel time and cost are assumed randomly distributed, rather than deterministic. We assume travelers have different VOT and submit to the lognormal distribution and classify it to the discrete set. The mean VOT of each class is calculated by

$$\overline{v}_i = \int_{v_{i-1}}^{v_i} vf(v)dv \Big/ \int_{v_{i-1}}^{v_i} f(v)dv,\ \forall i = 1,2,...,I \tag{1}$$

where v is the VOT, $f(v)$ is the VOT's probability density function of lognormal distribution.

(2) Route choice in multimodal network

The probability of choosing route k on condition that for user class i with their own VOT, from zone r to zone s by mode m, is given by

$$\Pr(k \mid i,r,s,m) = \exp\left(-\theta_1 C_{rs,k}^{i,m}\right) \Big/ \sum_k \exp\left(-\theta_1 C_{rs,k}^{i,m}\right) \tag{2}$$

where $C_{rs,k}^{i,m} = t_{k,rs}^{i,m} + p_{k,rs}^{m} / v_i$ is the general cost composed by time and monetary cost, $t_{k,rs}^{i,m}$ is the travel time of path k by mode m between OD pair (r, s) for user class i, $p_{k,rs}^{m}$ is the monetary cost of path k by mode m between OD pair (r, s) for user class i. v_i is the mean VOT of user class i. θ_1 is the diversion parameter of route choice.

(3) Modal choice

Probability of choosing mode m on condition that for user class i, from zone r to zone s, is given by,

$$\Pr(m \mid i,r,s) = \exp\left[-\theta_2\left(V_{rs}^{i,m} + S_{rs}^{i,m}\right)\right] \Big/ \sum_m \exp\left[-\theta_2\left(V_{rs}^{i,m} + S_{rs}^{i,m}\right)\right] \tag{3}$$

where $S_{rs}^{i,m} = -\ln\sum_k \exp\left(-\theta_1 C_{rs,k}^{i,m}\right)(1/\theta_1)$ is the inclusive cost of route choice, $V_{rs}^{i,m}$ is the component of mode choice cost except from travel cost between OD pair (r, s). θ_2 is the diversion parameter of mode choice.

2.2. Model formulation

The model is formulated as a variational inequality problem

$$\sum_{r,s,k,i,m}\left[C_{rs,k}^{i,m}(\mathbf{f}^*) + \frac{1}{\theta_1} f_{rs,k}^{i,m*} \ln\frac{f_{rs,k}^{i,m*}}{q_{rs}^{i,m*}}\right]\left(f_{rs,k}^{i,m} - f_{rs,k}^{i,m*}\right) + \sum_{r,s,i,m}\left[\frac{1}{\theta_2} q_{rs}^{i,m*} \ln\frac{q_{rs}^{i,m*}}{q_{rs}^{i*}} + q_{rs}^{i,m*} V_{rs}^{i,m}\right]\left(q_{rs}^{i,m} - q_{rs}^{i,m*}\right) \geq 0 \tag{4a}$$

s.t.

$$\sum_m q_{rs}^{i,m} = q_{rs}^{i}, \forall i, r, s \tag{4b}$$

$$\sum_k f_{rs,k}^{i,m} = q_{rs}^{i,m}, \forall r, s, i, m \tag{4c}$$

$$x_a^{i,m} = 1/voc_m \times \sum_{rs,k} f_{rs,k}^{i,m} \delta_{a,k}^{i,m,rs}, \forall i, m, a \tag{4d}$$

$$x_a^m = \sum_i x_a^{i,m}, \forall m, a \tag{4e}$$

$$q_{rs}^{i,m} \geq 0, f_{rs,k}^{i,m} \geq 0, x_a^{i,m} \geq 0, t_a^m(x_a^m) > 0, \frac{\partial t_a^m(x_a^m)}{\partial x_a^m} > 0, \theta_1 > \theta_2 > 0, \forall i, m, r, s, k, a \tag{4f}$$

where voc_m is vehicle occupancy (person-trip/vehicle-trip) for mode m, q_{rs}^{i} is OD trips of user class i sum of all mode. $q_{rs}^{i,m}$ is OD trips of user class i with mode m. $f_{rs,k}^{i,m}$ is the path flow(trips). $x_a^{i,m}$ is vehicle flows of user class i on link a of travel mode m. x_a^m is flows on link a of mode m. $\delta_{a,k}^{i,m,rs} = 1$ if path k between OD pair (r, s) by mode m user class i includes link a, and 0 otherwise. $C_{rs,k}^{i,m}(\mathbf{f})$ is route general cost function where $\mathbf{f}$ is the vector of flows of all physical vehicle type. We assume there are interactions between modes in this model. For different physical type of vehicles (multi-modal), the Jacobian of general cost function is asymmetric. The uniqueness of model solution is related to the form and parameters of link travel time function. We use a special type of link travel time function and the calibrated parameters can guarantee the uniqueness solution of x_a^m. For example, the route general cost of cars (private car and taxi) in class i is

$$\text{GCost(car,i)} = \sum_{a \in MiniPath} \left[t_a^{car}(\mathbf{x_a}) + (toll_a + fuel \times length_a)/(voc_{car} \times v_i) \right] \tag{5}$$

where

$$t_a^{car}(\mathbf{x_a}) = t_a^{car,0} \left[1 + \alpha_{car} \left(\left(x_a^{car} / C_a^{car} \right)^{\beta_{car}} + \gamma_{car} \left((x_a^{HGV} + F_a^{bus}) / C_a^{car} \right)^{\beta_{car}} \right) \right] \tag{6}$$

and $t_a^{car,0}$ is the car's free flow travel time in link a, $x_a^{car} = \sum_i \left(x_a^{i,car} + x_a^{i,taxi} \right)$ is total flow of private cars and taxies with different VOT. v_i is VOT of class i. x_a^{HGV} is the freight vehicle flows in link a, F_a^{bus} is the bus flow, C_a^{car} is the capacity, $toll_a$ is the toll of link a, $fuel$ is the fuel cost of one kilometer for cars and $length_a$ is the length of link a. It is worthwhile to remark that the link travel time function can reflect the level of service (LOS) of each mode in different congestion conditions. When the road is not congested, the LOSs' for different modes are considerably different. For example, cars will have higher speed than buses when the road is not congested. Similarly, the link travel time of freight vehicles is defined as

$$t_a^{HGV}(\mathbf{x_a}) = t_a^{HGV,0} \left[1 + \alpha_{HGV} \left(\left((x_a^{HGV} + F_a^{bus}) / C_a^{HGV} \right)^{\beta_{HGV}} + \gamma_{HGV} \left(x_a^{car} / C_a^{HGV} \right)^{\beta_{HGV}} \right) \right] \tag{7}$$

The necessary condition for $\nabla_a^{car,HGV}$ (Eqs.8) to be positive definite is that $0 < \gamma_{car} \cdot \gamma_{HGV} < 1$. The parameters in Eqs. (6) and (7), i.e., α_{HGV}, β_{HGV}, γ_{HGV}, α_{car}, β_{car}, γ_{car}, are calibrated and have a good fit of mixed traffic. Details are given in Zhang's PhD dissertation (2008).

$$\nabla_a^{car,HGV} = \begin{bmatrix} \dfrac{\partial t_{car}}{\partial x_{car}} & \dfrac{\partial t_{car}}{\partial x_{HGV}} \\ \dfrac{\partial t_{HGV}}{\partial x_{car}} & \dfrac{\partial t_{HGV}}{\partial x_{HGV}} \end{bmatrix} \tag{8}$$

The uniqueness of the model solution $x_a^{i,m}$ can't be guaranteed because we cannot expect the travel disutility vector appearing in the variational inequality (4) to be strictly monotone even though all the link travel cost functions are strictly monotone. So in this model, we attempt to test the multi-model asymmetric traffic assignment and multi-class traffic assignment simultaneously in large scale network. The uniqueness characteristic of solution (x_a^m and $x_a^{i,m}$) is demonstrated in large scale networks. Kuhn-Tucker conditions for this problem lead to fore-mentioned travel behavior assumption. In order to simplify the model, we change formula (4a) as determinate route choice, i.e. $\theta_1 \to \infty$.

$$\sum_{r,s,k,i,m} C_{rs,k}^{i,m}(\mathbf{f}^*)\left(f_{rs,k}^{i,m} - f_{rs,k}^{i,m*}\right) + \sum_{r,s,i,m}\left[q_{rs}^{i,m*}/\theta_2 \ln q_{rs}^{i,m*}/q_{rs}^{i*} + q_{rs}^{i,m*}V_{rs}^{i,m}\right]\left(q_{rs}^{i,m} - q_{rs}^{i,m*}\right) \geq 0 \tag{9}$$

2.3.Algorithms and convergence criterion

We use the generalized partial linearization (GPL) and simplified diagonal method to solve variational inequality problem (4).

Step0: Initialize the multi-modal multi-class travel cost as zero for each OD pair. Each link has zero flow. Set n=0;

Step1: Calculate the minimal cost $C_{rs}^{i,m}(n)$ and the modal split $e_{rs}^{i,m}(n)$. Do all or nothing assignment for multi-modal multi-class trips and update travel cost;

Step2: Do all or nothing assignment for multi-modal multi-class trips and obtain the subsidiary link flow solution $y_a^{i,m}(n)$. Set iteration number n=n+1;

Step3: Find the best combined search direction $\lambda(n)$ for $\min F\left[q_{rs}^{i,m}(n+1), x_a^{i,m}(n+1)\right]$

$$F\left[q_{rs}^{i,m}(n+1), x_a^{i,m}(n+1)\right] = \sum_{m,a}\alpha_m \int_0^{x_a^m(n+1)} t_a^m(x_a^1(n),\ldots,x_a^{m-1}(n), w, x_a^{m+1}(n),\ldots,x_a^{|M|}(n))dw \tag{10}$$

$$+\sum_{i,m,a} x_a^{i,m}(n+1)p_a^m/v_i + \frac{1}{\theta_2}\sum_{i,m,r,s} q_{rs}^{i,m}(n+1)\ln\frac{q_{rs}^{i,m}(n+1)}{q_{rs}^i} + \sum_{i,m,r,s} q_{rs}^{i,m}(n+1)V_{rs}^{i,m}$$

Step4: Convergence test. If not convergent, update the link flows and go to Step 1, otherwise terminate.

In Step 3, in finding the search direction $\lambda(n)$, the diagonal method is used. So the other mode's flows of objective function are fixed by last iteration. It is easy to use bi-section linear search method to find the optimal search direction $\lambda(n)$

$$\begin{aligned} \frac{d}{d\lambda}F\left[q_{rs}^{i,m}(n+1), x_a^{i,m}(n+1)\right] &= \sum_m \alpha_m \times \sum_{i,a}\left[y_a^{i,m}(n) - x_a^{i,m}(n)\right] + \sum_{i,m,a}\left[y_a^{i,m}(n) - x_a^{i,m}(n)\right] \times p_a^m/v_i \\ &+ \frac{1}{\theta_2}\sum_{i,m,r,s}\left\{\left[e_{rs}^{i,m}(n) - q_{rs}^{i,m}(n)\right] \times \ln\frac{q_{rs}^{i,m}(n) + \lambda(n)\left[e_{rs}^{i,m}(n) - q_{rs}^{i,m}(n)\right]}{q_{rs}^i} + \left[e_{rs}^{i,m}(n) - q_{rs}^{i,m}(n)\right]\right\} \\ &+ \sum_{i,m,r,s}\left[e_{rs}^{i,m}(n) - q_{rs}^{i,m}(n)\right]V_{rs}^{i,m} = 0 \end{aligned} \tag{11}$$

It has been generally understood that the weights yielded by the line search step of the above algorithms may be replaced by predetermined weights, based on the properties of the Method of Successive Averages (MSA). This method may become useful when no objective function $F[\mathbf{q}, \mathbf{x}]$ is available. The weights $\lambda(n)$ generally

applied with MSA are 1/n. Computational experiences revealed that using Constant Weights (CW), instead of MSA, may yield a substantially improved result (Sheffi, 1985). The values of 1/n in MSA are replaced by Constant Weights $\bar{\lambda}$.

In Step 4, the general convergence criterion we test in large scale network is

$$RGap = \frac{\sqrt{\sum_{i,m,a}(x_a^{i,m(n+1)} - x_a^{i,m(n)})^2}}{\sum_{i,m,a} x_a^{i,m(n)}} + \frac{\sum_{r,s}\sum_{i,m} q_{rs}^{i,m(n+1)} \mid q_{rs}^{i,m(n+1)} - q_{rs}^{i,m(n)} \mid}{\sum_{r,s}\sum_{i,m} q_{rs}^{i,m(n)}} \tag{12}$$

However, this convergence criterion is not so suitable for MSA algorithms and it is better to calculate the recent three iteration's value (Sheffi, 1985). This will require a considerable memory in practice. We give MSA Revised criterion (Noriega and Florian, 2007) as following

$$RGap = \frac{\sum_{a}\sum_{i,m} x_a^{i,m(n+1)} \times C_a^{i,m}(x_a^m) - \sum_{r,s}\sum_{i,m} MRC_{r,s}^{i,m(n+1)} \times q_{rs}^{i,m(n+1)}}{\sum_{r,s}\sum_{i,m} MRC_{r,s}^{i,m(n+1)} \times q_{rs}^{i,m(n+1)}} + \frac{\sum_{r,s}\sum_{i,m} q_{rs}^{i,m(n+1)} \mid q_{rs}^{i,m(n+1)} - q_{rs}^{i,m(n)} \mid}{\sum_{r,s}\sum_{i,m} q_{rs}^{i,m(n)}} \tag{13}$$

where $MRC_{r,s}^{i,m}$ is the minimal general cost of OD pair (r, s) for class i using mode m.

2.4. Convergence performance in case study

We realize the model's algorithm with VC++ coding and use a personal computer with Intel Pentium(R)D 2.8GHz CPU, 1GB memory to test it in a large scale network in Huizhou, southern China. There are 269 Traffic Analysis Zones, 13,006 road links and 65 bus lines related to the road network, 4,122 road nodes, 102 rail links and 49 rail stations, 2,600 centroid connectors and transfer links. There are 735,774 total motorization trips and 65,650 freight vehicle trips in a typical peak hour. According to the stated preference survey, the VOT distribution was estimated by mixed logit model. We divide the personal trips into five classes by Formula 1. In Huizhou's study, we considered multi-modal system foregoing. Some algorithm tips of multi-modal shortest path are available in Zhang's PhD dissertation (2008).

The relative gap decreased stably both by GPL and MSA methods as shown in Fig. 1. Generally, MSA Revised relative gap is larger than the value using Formula 10. It takes about one hour to research 0.01. Although CW methods work well in Boyce's separable multi-class combined mode (Boyce and Bar-Gera, 2003), in our case, it has no stable solution because there is no convergence after a long calculation. Fig. 2 shows that relative gap decreased at first, but moved up and down for a long time. It could not be decreased to 0.15. So in an asymmetry traffic assignment, CW may not work well. Note: we received the same result by testing this method in another large scale network of Shenzhen, with 491 Traffic Analysis Zones and about 13,000 links.

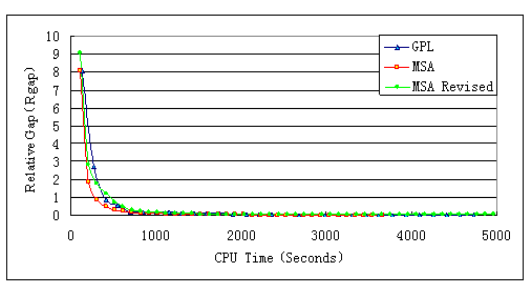

Figure 1. Convergence performance of GPL and MSA methods

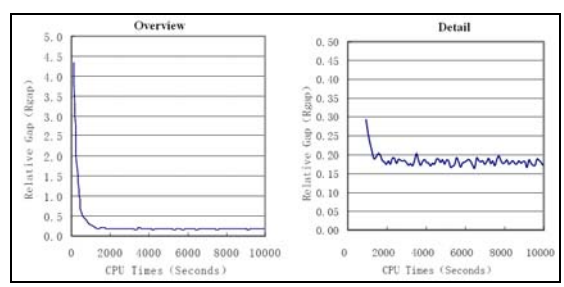

Figure 2. Convergence performance of CW method

3 TDM measures evaluation

We test 16 pure and combined TDM measures such as cordon based congestion charge, bridge's charge, parking charge, Park and Ride, fuel pricing, public transportation fares decrease, bus exclusive lanes construction, transfer time decreased and truck regulation. We set 17 scenarios, No.1 means no TDM measures (basic scenario) and No.2 to No.17 mean 16 pure and combined TDM measures. The detail of each TDM measure is listed in Tab. 1. The spatial position of Park and Ride, Cordon based Charge, Bridge Tolling, and Parking Charge are given in Fig. 3. The bus exclusive lanes are given in Fig. 4. There are abundant results such as different traveler classes having different travel behaviors under the TDM measures, car users changed their routes or use other transportation mode, and so on. For the limitation of the paper's length, we focus on following four themes.

Table 1. TDM measures test in Huizhou City

Measures	Measure Descriptions
1	Base scenario without TDM measure
2	Uniform bus fare 2 Yuan (mile based fare in basic scenario)
3	Increase 40% bus frequency in main corridor based on Measure 2
4	Free parking of P+R
5	Uniform Rail fare 3 Yuan
6	Combined Measure 2 and 5
7	Increase fuel fare
8	Bridge tolling: 10Yuan for cars and 15 Yuan for freight vehicles
9	Cordon based charge
10	Combined Measure 8 and 9
11	Combined Measure 10 and 12
12	Parking charge
13	Combined Measure 4, 6 and 10
14	Decrease the transfer time between bus and rail
15	Bus exclusive lanes setting
16	Combined Measure 4, 10 and 15
17	Measure 6 and some bridges do not allow freight vehicles pass

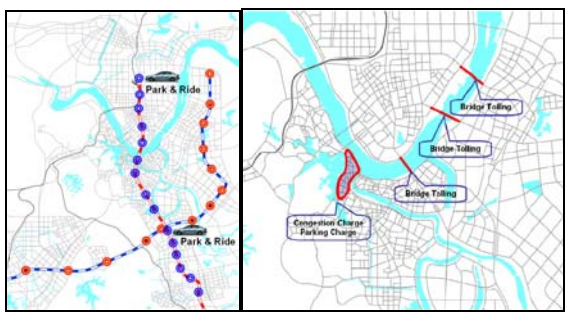

Figure 3. P+R, congestion charge, parking charge and bridge tolling position

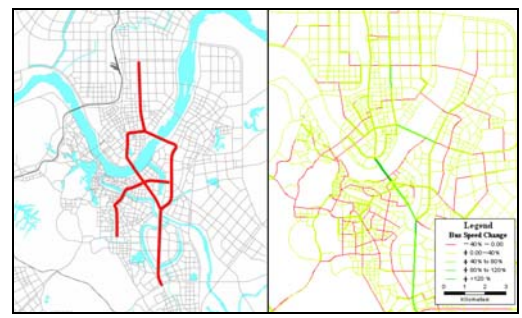

Figure 4. Bus exclusive lanes speed change before and after the TDM Measure

(1) Sensitivity of public transportation fares and the relationship between rail and taxi. When the bus fare decreased, more people will use the bus. Interestingly, the car's mode share does not obviously decrease. That means the mode share of public

transportation doesn't obviously increase. When bus users increased, the bus will become more congested. The result shows that bus and rail combined mode share greatly decreased when we use measure No.2 (see in Fig. 5). In many models, combined transfer modes are not considered. So these models may tell policy decision makers that the decreased bus fare will have a good effect on public transportation priority strategy. This is somewhat misleading. In fact, the new equilibrium leads to the more costly combined mode because of public transportation congestion. Now by using measure No.3 (meanwhile increase the frequency of buses in the main corridor), the bus congestion is alleviated and the increasing bus flow leads to private car congestion. Although the bus and rail combined mode share still decreased, policy makers will be gratified that the car mode share is decreased. When the rail fare decreased, there is a considerable decrease of private car and taxi users. This is mainly because the in-vehicle congestion of mass transit rail is not as obvious as bus. In many big Chinese cities, rail planning and construction are following the fashion. Taxi operators worry about the market of taxi users after the rail construction. In Huizhou's study, however, the combined mode share of taxi and private car transfer to rail is increased. Although the pure taxi users are decreased, taxi operators still can do their business well. The reason for this is there are only three rail lines in Huizhou and have no network scale effect. If rail fare deceased in a city with an accessible rail network, the result may be reversed. Nevertheless, rail fare decrease will reduce the private car usage if the rail is not so congested. From the model's test, we concluded that combined measures such as decreasing the fares of bus and rail simultaneously and increasing bus frequency, will lead to modal share shift more effectively (see in Fig. 5).

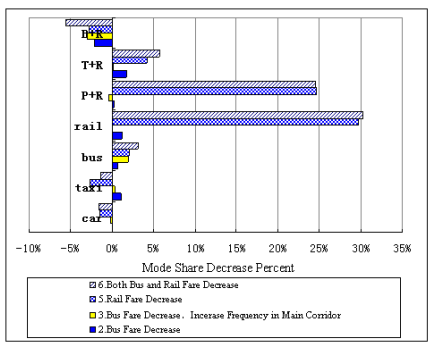

Figure 5. Modal share under the TDM measures of public transportation fare decrease

(2) The effect of bus exclusive lane. In many big Chinese cities, public transportation priority policies are very important and the bus exclusive lane setting is one of most popular measures. Using TDM measure No.15, the 28km bus exclusive lane's average flow density increased 540trips/km·h (see in Fig. 6). It seems that the public transportation priority policy works well by this measure. In fact, the total car users decreased only 126 trips. This is a lesson to decision makers who plan the bus exclusive lane blindly. When we set special lanes for buses, private cars will change their routes in order to minimize their travel time. In our multi-modal variational inequality model, the bus speed is affected by the flow of other vehicles such as private cars. This is very realistic and leads to more road congestion

in the bus lines with no exclusive lanes (see in Fig. 4). The decreasing of total buses' level of service in non-exclusive lanes leads to disutility of bus users. So it is important to plan a certain scale of bus exclusive lane networks and the private cars will have no way to change their routes. Until then, the new equilibrium will lead car users to use other modes.

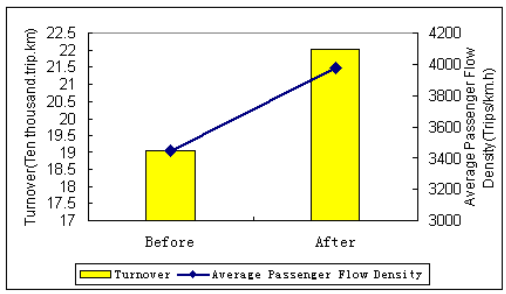

Figure 6. Passenger flow in bus exclusive lanes before and after the TDM Measure

(3) Comparing the effects of cordon-based congestion charge and parking charge. In order to compare the effects of cordon-based congestion charge and parking charge, we set them in the same area which contains four Traffic Analysis Zones (see Fig. 3). In the charging zone, the parking charge works more effectively than cordon-based congestion charge but has the reverse result in the whole city. Cordon-based congestion charge mainly affects through traffic and arrival traffic from non-charging areas to charging areas. Parking charge mainly influences the entire charging area's arrival traffic. The effect of route and modal change of private car users depends on the range of charging areas and the spatial distribution of travel demand. In the case study, congestion charge takes more effect on big volume through traffic and has restrained the car users more effectively than parking charge in the entire city, but it has reverse results in the parking charge area (see Fig. 7). Policy makers may choose combined TDM measures to control the target traffic.

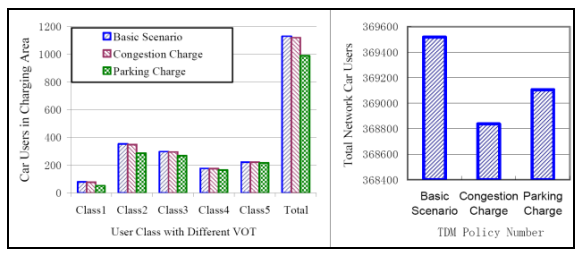

Figure 7. Comparing the effect of congestion charge and parking charge

(4) Park and Ride demand analysis. In our model, P+R demand is analyzed in multi-modal network. We also considered the P+R station choice behavior. If more than two P+R stations are available, the travelers will choose the station that minimizes their total general cost. Many factors like parking fare, rail fare, transfer time and the congestion of center area, affect the traveler to choose this mode. Our model is competent for considering these factors. In our model test, the parking fare is very sensitive. TDM measure No.4 is free parking charge. The total demand of P+R is twice the basic scenario. If we decrease the rail fare simultaneously in TDM

measure No.13, the demand increased more obviously. Using push and pull--combined policies will be more effective. Policy makers should consider the parking price, parking station land use pricing and the benefit of park operator comprehensively.

4 Conclusions

This paper uses a multi-class multi-modal network equilibrium model with combined modal split and route choice model to test various combined TDM measures in Huizhou City. Although further validation needs to be done for the model, this paper gives policy decision makers some valuable conclusions.

(1) Although bus fare decreases encourage people to use pure bus mode, passengers taking the combined mode with rail may be decreased because of the bus in-vehicle congestion. Combined measures such as decreasing the fare of bus and rail simultaneously and increasing bus frequency, will lead to modal share shift more effectively. Rail fare decrease will result in less use of pure taxi and private cars. But the combined mode between taxi and private car to rail may increase if the rail network has no scale effect. (2) Bus exclusive lanes will increase the passenger flow density on them. Meanwhile, cars will change their route to save time, thus decreasing the service of common buses. Consequently, the total modal share of bus can't obviously increase. So it is important to plan a certain scale of bus exclusive lane networks. (3) Cordon-based congestion charge mainly affects the through traffic and arrival traffic from non-charging areas to charging areas. Parking charge mainly influences the whole charging area's arrival traffic. The effect of route and modal change of private car users depends on the range of charging areas and the spatial distribution of travel demand. (4) Whether P+R mode works well depends on many factors like parking fare, rail fare, transfer time and the congestion of center areas. Using push and pull--combined policies will be more effective.

Acknowledgement

This research is supported by the Key National Natural Science Foundation of China (Grant No: 50738004), China National High-Tech Research and Development Project (863 Project) (No. 2007AA11Z206) and Program for New Century Excellent Talents in University (NCET-08-0406).

References

Bar-Gera, H., and Boyce, D. (2006). "Solving a Nonconvex Combined Travel Forecasting Model by the Method of Successive Averages with Constant Step Sizes." *Transportation Research Part B*, 37, 351-367.

Boyce, D., and Marshall, N. (2002). "Travel Forecasting for Alternative Scenarios for 2030 with a Multiclass Combined Model." *Transport Chicago*, Chicago.

Florian, M., Wu, J. H., and He, S. (2000). "A Multi-Class Multi-Mode Variable Demand Network Equilibrium Model with Hierarchical Logit Structures." *Proceedings of Seminar F, Behavioural Modelling, European Transport Conference*, Volume P441, 211-224.

Kaneko, Y., Fukuda, A., Srisurapanon, V., and Oda, T. (2001). "Estimation of the Impact of Area License Scheme with Multi-class User Equilibrium Model." *Journal of Eastern Asia Society for Transportation Studies*, 4(2), 277-291.

Noriega, Y., and Florian, M. (2007). "Algorithmic Approaches for Asymmetric Multi-Class Network Equilibrium Problems with Different Class Delay Relationships." in Press.

Sheffi, Y. (1985). *Urban transportation networks: equilibrium analysis with mathematical programming methods*, Englewood Cliffs: Prentice-Hall Inc.

Zhang, T. R. (2008). "Research on Travel Demand Management Policies Evaluation Based on Transportation Network Equilibrium Theory." PhD dissertation, Tongji University.

Nonlinear Analysis of Prestressed Steel Box Beams

Yanmin Jia

College of Civil Engineering, Northeast Forestry University, Harbin, No.26, Hexing Road, Xiangfang District, Harbin, Postcode:150040, China; Tel: 86- 0451-82191377; Email: yanminjia2008@126.com

ABSTRACT

Post-tensioning using high-strength cables or tendons can be effectively used to increase the load carrying capacity of steel structure. In this paper, a nonlinear analytical model is formulated for the elastic behavior of a simply supported steel box beam with curved prestressing tendons. The governing differential equation prestress and serve load are derived using the self-equilibrium principle and the principle of minimum potential energy, respectively. The effects of design parameters such as prestressing force, and tendon area on working load and deflection of the steel box beam are studied.

Key words: Prestressed Steel Box Beam; prestressing tendon; self-equilibrium principle

1. Fundamental Equation

The prestressed steel beam shown in fig. 1(Jia Yanmin et al. 2003)，the prestressing was anchored only at the ends with seven uniformly spaced intermediate connections deviators. The saddles are placed at specific locations along the steel beam to create different profiles of the tendons.

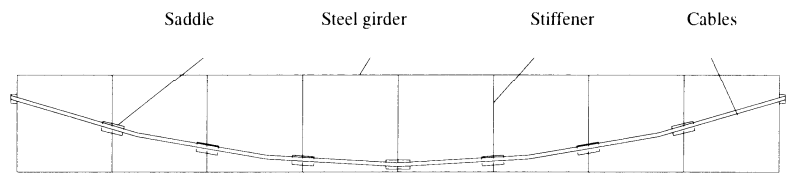

Fig. l Construction of prestressed steel beam

Tendons were provided for the prestressing, during the post-tensioning and under the loading process, the tendons remain in curve, and they could have displacement compatible with the steel beam at the saddle connection points in vertical direction, and there is a relative movement between the tendons and the steel beam along the tendons length.

As prestressed steel beam carries not only external loads, but also longitudinal compression force from prestressing tendons, it is reasonable to analyze them as bean-columns(Ni Yuanzheng et al. 1998). However, as the force in the tendons changes with the deflection of the beam and the external loads, it makes the

prestressed steel beams different from normal beam-columns; it is necessary to analyze the prestressed steel beam specifically.

There are two phases for prestressed steel box beam in the whole procedure (Vincenzo Nunziata. 1999). The first phase is the application of the prestressing force to them, and second one is the application of the external load. We try to perform nonlinear analysis for these two stages. The governing differential equations were derived and solved.

The fundamental assumptions of this analysis method are:

1. Plane surface is maintained;
2. Deformation of the steel box beam due to shear force is negligible;
3. Tendon's strain is considered uniformly distributed throughout the entire tendons.

2. Governing differential equation

2.1 prestressing

After applying tension to the tendons with jacks and tightening them, the steel beam must have upward deflection. The self-equilibrium system would be formed between steel beam and tendons, shown in Figure 2.

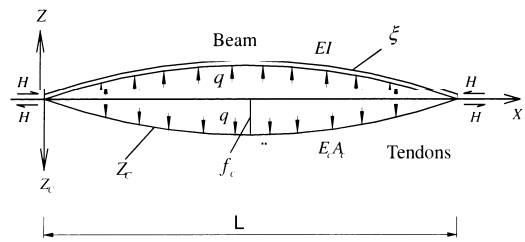

Fig.2 The self-equilibrium state of prestressed steel beam

Based on principal equilibrium, we can get self equilibrium equation of prestressed steel beam on prestressing phase:

$$EI\frac{d^4\xi}{dx^4}+H\frac{d^2\xi}{dx^2}+H\frac{d^2z_C}{dx^2}=0 \qquad (1)$$

Where: E is modulus of elasticity of steel beam; I- moment of inertia of steel beam section; H is the initial horizontal tendons force of tendons，ξ is the upward curve of steel beam was produced by prestressing force H; z_c is the curve of tendons (profile in the steel beam), its distance of mid-span is f_c ; q is equivalent uniform load that was unloading portion of self weight of steel beam.

2.2 loading

In the loading phase, assuming external uniform load is *Q*, $Q = q+p$, the tendons is in contact with the saddle at the tendons bend, but there is assumed to be no friction between the tendons and saddle (Bilal M. Ayyub et al. 1990), the deflection due to shear force of tendons and steel beam is considered negligible, and the tendons strain is considered uniformly distributed throughout the entire beam (Pisanil M A et al. 1996). Tendons were provided for the prestressing, As a result the tendons remain in curve during the loading process, so that they could have displacement compatibly with the steel beam at these connection points in vertical direction during the loading process.

Based on self -equilibrium phase, under acting uniformly external loading *p*, curve of displacement of beam and tendons w was produced shows in fig.3

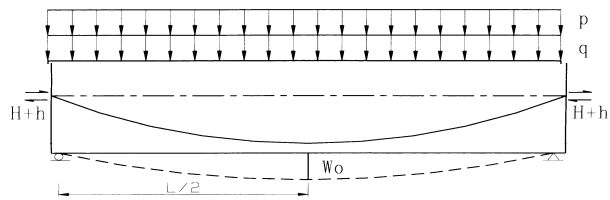

Fig.3 Calculation diagram of the prestressed steel girder under applied loading

In this case, *H* is the initial tendon force, *h* is tendons force increment. W_o is displacement of mid-span of steel beam by applying external load.

2 .3Governing differential equation

The prestressed steel beam was analyzed with the principle of minimum total potential energy. Since shear strain value of beam is small，the value of shear strain energy is negligible. Considering the strain energy of tendons and flexural strain energy of steel beam and loading potential energy, the total potential energy equation of the prestressed steel beam can be written

$$\pi = V_1 + V_2 + V \qquad (2)$$

Where: V_1 is strain energy of tendons; V_2 is flexural strain energy of steel beam; *V* is loading potential energy.

Based on the principle of minimum potential energy, this energy is at a stationary position when an infinitesimal variation from such position involves no change in energy. By differentiating π with respectively to $\delta \Pi = 0$ and considering arbitrariness of δw and $\delta w'$, we can get follow equation. The governing differential equation for prestressed steel beam on loading phase is derived

$$EIw^{IV} - (H + \frac{h}{2})w'' = p + \frac{h}{2}z_C'' \qquad (3)$$

3. Comparison of Predictions and Measurements

In order to investigate the fundamental mechanical behavior of prestressed steel beam, 1/10 -scale, 4m long specimen were constructed using the Q235 steel plates. One is normal steel box, The other is the steel box beam with curved prestressed tendon. The tendons are the low-relaxation, 15.2 mm diam，seven-wire stranded tendons with an ultimate stress of 1,860 MPa. Both specimens have the same box cross section, shown in fig. 4. The specimens for both were subjected to a similar quasi-static test.

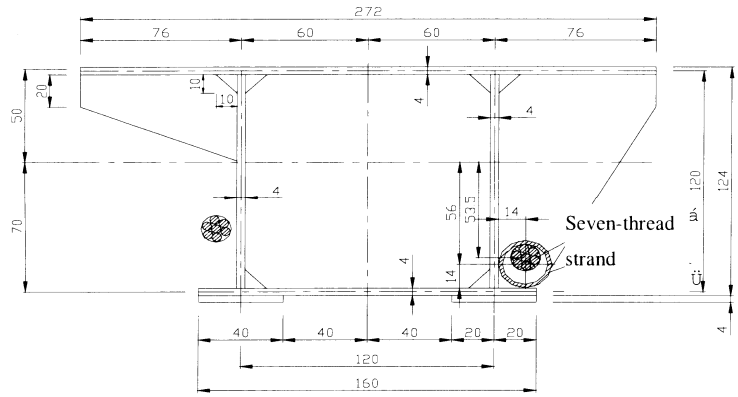

fig. 4. Diagram of the steel girder model

The normal specimen was tested with distributing load that were applied distributing load along the centerline of the beam and point load at the mid-span. The distributing load value is 2.5knlm and the point load value is 10kN. After applying pre-stressing force H=82.5kN，the pre-stressed specimen was tested using the same load with the normal specimen.

The comparisons of the calculated values and the test results of deflection that was produced by prestressing force are shown in Table 1.

Table 1 the bottom plate strains on mid-span and 1/4 span（μ ε）

Item	Distributing load（2.5kN/m）						Point load（10kN）					
	L/2			*L/4*			*L/2*			*L/4*		
	Measure	Calculation	Error	Measure	Calculation	Error	Measure	Calculation	Error	Measure	Calculation	Error
Steel beam	219.3	232.4	5.79%	168.0	174.3	3.70%	440.2	445.5	1.17%	213.7	222.75	4.23%
Prestressted steel beam	194.8	205.7	5.03%	147.8	152.3	3.05%	392.8	397.5	1.2%	185.7	193.31	4.1%
Improvement %	12.58	13.58		13.67	14.45		12.06	12.07		15.07	15.22	

Under the same test load，bottom plate strains on mid-span and 1/4 span of the prestressed steel beam is small than normal steel beam. The prestressing force can improve condition of mechanics on steel beam, reduce tension stress on bottom plate, and increase capacity of resistant fatigue.

4. Conclusions

The theory analysis and experiment expression as follow：

I. It can improve mechanics behavior of steel beam to apply prestressing force on steel beam.

2. The increasing stiffness for steel beam is directly proportional to the prestressing force H，and is inversely proportional to the square of the span length for the beam.

REFERENCES

Bilal M. Ayyub, A. Ibrahim. (1990) Posttensioned Trusses:Analisis and Design. Journal of Structural Engineering , Vol. 116, No. 6, June 1990, pp. 1491-1506,

Jia Yanmin, Gai Bingzheng, Zhang Yinge, Ni Yuanzheng. (2003), Theoretical analysis and experimental study of prestressed steel girders. Engineering Mechanics. Vol. 20, No.3, 2003, pp. 161–166. (in Chinese)

Ni Yuanzheng,.(1998). A new type of steel box girder bridge with prestressed tendons. Civil Engineering Journal. 1998，Vol. 31, No. 1, pp. 44–51 (in Chinese)

Pisanil M A. (1996). Numberical model for external prestressed beams. Structural Engineering and Mechanics, Vol. 4, No. 2, pp.177–19

Vincenzo Nunziata, (1999). Prestressed Steel Structures. XVII Congresso C.T.A. Costruire in Acciaio: Struttura E Architettura, Napoli, 3 - 5 October 1999

Algorithm of PFE and Its Application in Shenzhen Urban Transport Simulation System

LIN Tao[1] CUI Xiaotian[2]

[1]Tongji University; The School of Transportation Engineering, Room No.423, Shanghai, 201804, P.R.China; e-mail: lint@sutpc.com

[2]Tongji University; The School of Transportation Engineering, Room No.423, Shanghai, 201804, P.R.China; e-mail: cxt@sutpc.com

ABSTRACT

This paper introduces the OD matrix adjustment, especially the development and application for PFE. In the second part, the logical structure and core module algorithms are deeply analyzed and discussed. Finally, a data fusion model that combines sensor data and FCD is designed according to the fact in Shenzhen. With the core of PFE, the model is applied in Shenzhen Urban Transport Simulation System.

1 BACKGROUND

1.1 History of OD matrix adjustment

The OD matrix adjustment, which by using observed link volumes to estimate and adjust OD matrices, can be implemented for online urban traffic management and offline transportation planning applications. In 1980, Van Zuylen and Luis Willumsen pioneered a famous algorithm to deal with the OD matrix adjustment. After that, many scholars, such as Bell, M.G.H, Spiess, H., Chen Y., Yang H., Codina E. and Barcelo J., continuously improved the static OD matrix adjustment. However, most researchers estimated average OD movements by referencing to observed link volumes over a relatively long modeling period. Thus, the fluctuated nature of link flows and OD movements over the analysis period is not taken into consideration.

During the 1990s, the dynamic traffic assignment (DTA) and dynamic OD matrix adjustment gained increasing attention because they were gradually proving to be more useful tools for ITS, which asks for a dynamic approach of assigning the flows for detailed time slices within the modeling period. On the basis of static and dynamic OD matrix adjustment or path flow estimation, some assignment softwares were available for real-time analyses and simulation. Professor Bell from University of Newcastle upon Tyne initiated the development of a bi-level mathematical programming formulation for adjusting OD trip matrices that dynamically reproduced the observed traffic volumes[2]. Led by Professor Bell, the simulation team successfully developed a tool named PFE (Path Flow Estimator). The PFE has been subsequently integrated into the MONET (by Siemens) and VISUM-ONLINE (by PTV AG) as the key component for the matrix estimation mechanism. Both the MONET and VISUM-ONLINE are suitable for the analysis of real time traffic conditions for traffic information system (TIS).

1.2 Development of PFE

Through applying the PFE (Path Flow Estimator), the assignment syntheses and revised traffic volumes and travel times on the network. This information can be adopted for on-line and off-line applications in ITS. Given data from traffic detectors and other forms of sensors, path flows, and travel times are inferred on the basis of a LOGIT path choice model. The LOGIT model and the link cost functions allow the delays incurred by congestion to be taken into account. The most significant paths in the network are generated by an approximate steepest descent column generation method. A time-dependent PFE is formulated to better represent the transitory overloads situations that characterize congested conditions.

As a powerful tool, the PFE is widely used to support traffic studies (including traffic assessments, traffic impact studies, mode and route choice studies, etc.) as well as the real-time traffic condition monitoring and short-term traffic forecasts in the ITS applications. It was directly and indirectly taken into practice in Berlin, Hamburg, London, York, Athens, Turin, Lyon, Toulouse and Stockholm.

2. ALGORITHM OF PFE

2.1 Logical structure of PFE

The PFE uses two types of input data: static and dynamic. The output consists of path flows, path travel times, unmeasured link flows, link travel times, and OD flows. The input and output are shown in Figure 1:

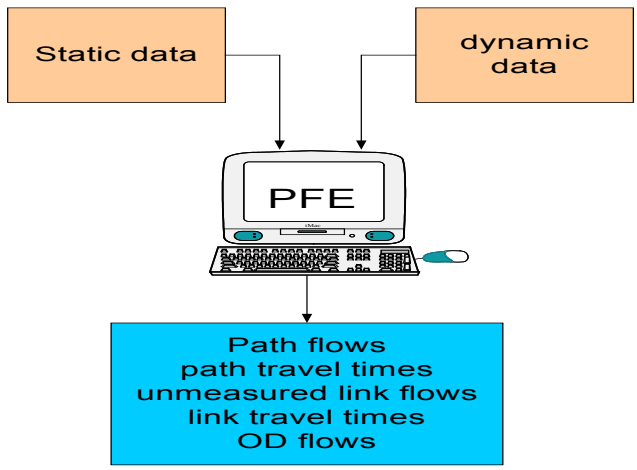

Figure 1: Input and Output of PFE

For ITS operations, there are two approaches used in online application of PFE: event-driven and time-driven. For activity we mean an action or a set of actions that have to be accomplished to perform certain operations within the system. The messages showed in the diagram can be any kind of signals useful to exchange information between two systems. The following figures show the two suggested approaches.

The event-driven solution requires the presence of a program manager in charge of scheduling the various activities. The following actions may take place in the system:

- The program manager sends a message to PFE notifying that the dynamic data for the current time slice are ready.

- PFE activates a filter program that reads the data necessary from the whole database, processes those data and writes the new dynamic files in PFE format into its file system. When finished, it sends an acknowledgement to PFE.
- PFE then operates and produces the results to be written into its file system. When terminated, it sends a message to the manager that results are ready for dispatch for further analyses.

The event-driven approach has several advantages. It is fully centralized so the program manager can change the scheduling of activities according to different scenarios. It is faster because the manager activates the necessary modules as soon as possible and, also, can alter the length of time slices according to the traffic conditions. It is also more reliable because the program manager, being familiar with the various modules, may encounter a faulty situation and take rapid actions accordingly. If any difficulty is found for any reason, the operator would only need to alert the program manager operating the relevant modules.

The time-driven solution is relatively simpler. In this case, PFE activate the filter at fixed time intervals and when the pre-processing phase is finished it elaborates the data. This approach is easier to

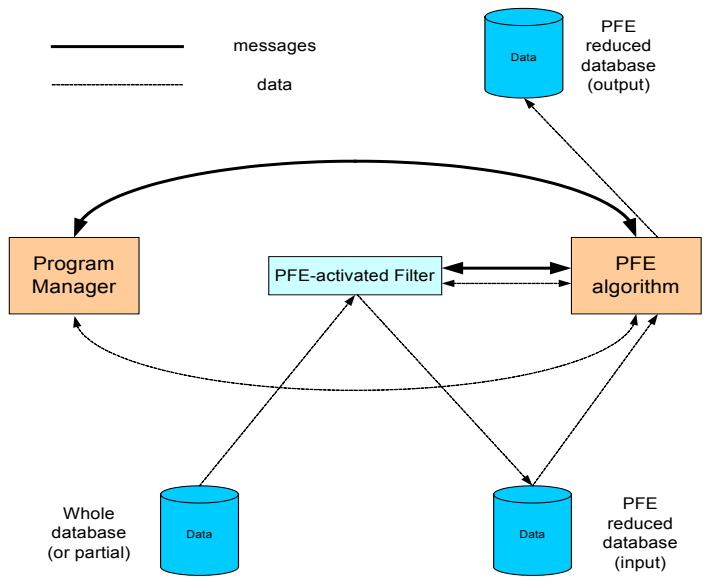

Figure 2: Event-driven PFE structure

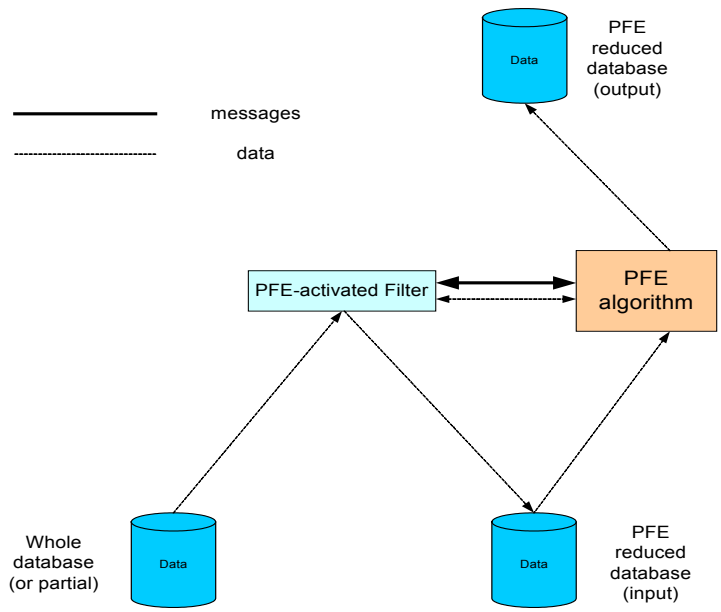

Figure 3: time-driven PFE structure

implement and more robust. The only requirement is to maintain “alive” status of the PFE program. Also it might be the only possible solution when the system is split over different computers.

2.2 Core Algorithm of PFE

Bell （2005）suggests two approaches for estimating the split fractions. In the first approach, which might be suitable for single intersections or small networks, it is assumed that the fastest vehicle between each O-D pair reaches its exit within one time interval and the slowest vehicle does not stay on the network for more than one interval. This is to say, all the vehicles enter and exit the networks in one interval. Each exit volume for an estimation interval h is then expressed as a convex combination of two terms. The first term represents the exit volume measured in the previous interval h-1. The second term represents the sum of all the OD flows departing during interval h that are headed towards the exit under consideration. Formally,

$$y_j(h) = (1-\alpha_j) y_j(h-1) + \alpha_j \sum_i b_{ij} q_i(h)$$

where $y_j(h)$ is the volume measured at exit j during interval h, $q_i(h)$ the entering volume at origin I during interval h, b_{ij} the unknown proportion of $q_i(h)$ headed towards exit j and α_i a travel time ”dispersion” parameter also to be estimated.

The second approach allows for vehicles to stay on the network for a pre-fixed number of intervals m with the fastest vehicle still taking within one time interval to traverse the network. For m=3, each exit volume is specified as follows:

$$y_j(h) = \sum_i b_{ij0} q_i(h) + \sum_i b_{ij1} q_i(h-1) + \sum_i b_{ij2} q_i(h-2$$

where b_{ijk} is the unknown proportion of traffic from entrance i destined for exit j with a travel time, when truncated, of exactly k intervals.

In both approaches, constrained weighted least squares are used to obtain estimates of the split fractions and additional travel-time dispersion parameters. While Bell's models offer some relaxation of the simplifying assumptions regarding travel times that characterize earlier approaches, a key limitation is that both split fractions and travel time dispersion parameters are assumed to be constant over time. The model, therefore, does not estimate a time varying split fraction, instead, it attempts to “refine”its previous estimate of the split fractions during each interval.

3. APPLICATION FOR PFE

3.1 Structure of SUTSS

With the rapid progress of information technology development and the requirements of making the transport system more efficient and the travelers being better informed for their planning of their travel arrangement, ITS are widely used to meet the above requirements for urban areas, in particular the central area with unstable traffic conditions.

Due to the rapid growth in car ownership and economic activities, Shenzhen, like other world-class cities, faces the difficulties of severe traffic congestion and related environmental impacts. As recommended in the Shenzhen Integral Transport Planning, among the traffic relaxation measures proposed, an ITS assignment called Shenzhen Urban Traffic Simulation System has been proposed to tackle the traffic related problems. SUTSS is the first phase for the development of an intelligent transport information platform for planning and public information service purposes. The traffic simulation system is considered the heart of the intelligent transport information platform for Shenzhen. The SUTSS consists of five components: a network and a communication subsystem, a data collection subsystem, a core traffic simulation subsystem (including macro, meso, and micro levels) and a service subsystem to provide supporting traffic information for planning and policy-making purposes. As a huge system, the major challenge is to develop a transport information platform to meet the framework of integrating the four subsystems mentioned above.

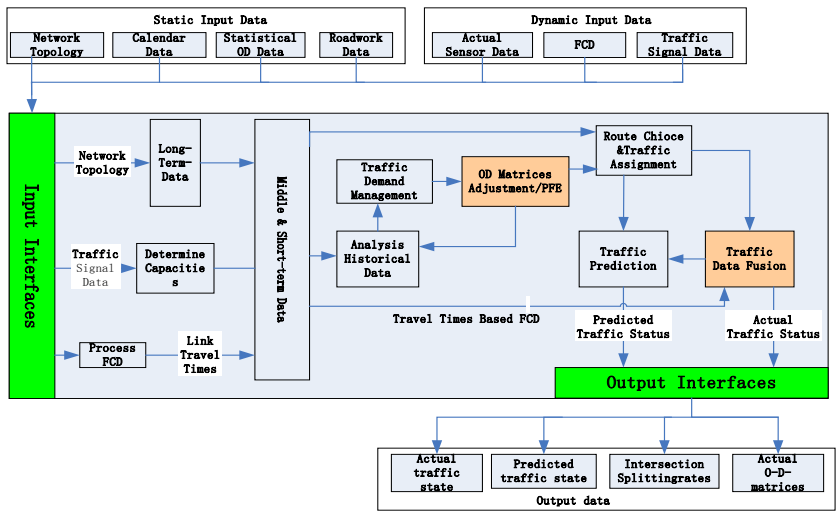

Figure 4: Data Flow Chart in SUTSS

3.2 Location optimization

The PFE algorithm estimates or adjusts an origin and destination matrix from traffic counts. The dynamic data that PFE needs is observed traffic volume at fixed locations and traffic control time slice setting. A Greedy-like algorithm [4] tries to maximize the information benefit (with respect to typical flow patterns) by adding

gradually further detectors. The goal of this procedure is to satisfy the following criteria:

(1) Observe as many paths as possible;
(2) Hit as much traffic as possible;
(3) Avoid unnecessary linear dependencies;
(4) Defined places with respect to variable message signs;
(5) Strategically important hot spots in terms of congestion;
(6) Highly occupied intersections;
(7) Traffic planning relevant spots;
(8) Local knowledge.

3.3 Visualization of PFE with FCD Enhanced

The task of PFE, with its ability of completing the traffic dataset for the observed links, is vital for the short-term forecast of traffic conditions. By making reference of the historical traffic data and the OD matrix, it could be suitable for event planning and operations. It is also worth noting that due to the synthetic nature of link speeds and travel time output from the assignment algorithm, the resultant time and speed are more dependable on the speed-flow relationship adopted for the model. With the availability of the floating car data (FCD), (Shenzen has a fleet of 6,000 taxis equipped with GPS), positioning data is constantly transmitted to their control centers. It is planned to complement the fixed detector, the FCD information will be used for the enhanced analyses of link traffic conditions (i.e. speed and travel time). An additional usage of the FCD is also planned for the recalibration/update of the speed flow relationship under different loading conditions; the corresponding traffic volume will come from the observations of the traffic detectors.

As Fig.4 shows, the fusion between FCD and PFE results expands the cover scope and improves the veracity of traffic information, so that more exact and entire visualization becomes possible. This is the advantage of fusion over each system.

REFERENCE

Bell, M.G.H (2002). “The estimation of an origin destination matrix from traffic counts.” *Transportation Science* 17, 198-217.

Bell, M.G.H (2005). “The real time estimation of origin-destination flows in the presence of platoon dispersion.” *Transportation Research*, 25B, 115-125

Van Zuylen, H. and Willumsen, L.G. (2004). “The most likely trip matrix estimated from traffic counts.” *Transportation Research* 14B, 281-293.

Yang, H.and Zhou, J. (2006).“Optimal Traffic Counting Locations for Origin-Destination Matrix Estimation.” *Transportation Research B*,32B (2): 109-126.

The Applied Research on Forecasting Cargo Volume Of Northeast Economic Zone by System ic Dynamics

Shuzhi Zhao[1] Tonghe Ni[2] and Yonggang Zhu[3]

[1]Department of Transportation Planning and Management, Transportation and Traffic College, Jilin University, 130025, ChangChun, (PH) 0431-85095086, E-mail: zszcy01@sohu.com

[2]Department of Transportation Planning and Management, Transportation and Traffic College, Jilin University, 130025, ChangChun, (PH) 0431-85095086, E-mail: nile1949@yahoo.com.cn

[3]Department of Transportation Planning and Management, Transportation and Traffic College, Jilin University, 130025, ChangChun, (PH) 0431-85095086, E-mail: zhuyonggang777@163.com

Abstract

This paper researches the northeast economic zone, analyzes the impact factors of cargo, establishes the relationship between various factors and cargo by linear regression through the AHP, determines the weight of various factors, forms the systemic dynamics model on forecasting cargo volume in northeast economic zone, and proves the validity of the model through error analysis. In addition, the paper does a forecast for the cargo volume of the northeast economic zone 2011 to 2015, and its results can provide references for integrative transportation in northeast economic zone.

Key words : Systemic Dynamics Cargo Volume Forecast

It is necessary to lay down a scientific plan of regional integrative transportation with the development of regional economic integration. Therefore, forecasting the cargo volume can provide reliable evidences for this plan correctly.

This paper is based on the northeast economic zone covering Heilongjiang, Jilin, Liaoning province and some Inner Mongolia Autonomy, such as HuLunBeier City, Xingan league, Tongliao City, Chifeng City and the east XinLinGele league. The paper establishes some systematic dynamics models with some factors of cargo in northeast economic zone, so as to reflect the relationship between various factors and cargo systematically and dynamically, thus forecasting the cargo of northeast economic zone in an effective way. Generally speaking, it plays an important role for realizing and promoting transportation in efficiency and benefit, further more, making old northeast industry area prosper.

1. The relativity analysis of cargo volume and influential factors

1.1 The influential factors of cargo volume

Cargo volume is influenced by many factors, and the influential degrees are different, too. Among them the development of primary, secondary and tertiary productions have the most important influence on cargo volume. In addition, the

growth of consumer demand and fixed asset investments in society will continue to promote the cargo volume. Therefore, the study chooses a number of important socio-economic indicators for researching influential factors of cargo volume (FT). Such as, PIGDP (the value-added of the primary industry), SIGDP (the value-added of the secondary industry), TIGDP (the value-added of the tertiary industry), PL (population), PCDI (per capita disposable income), and FAT (the total social investment in fixed assets). Through such analysis, the development tendency of cargo can be reflected on influential factors overall.

1.2 The analysis of linear regression about cargo volume and influential factors

The research is based on northeast economic zone, adopting the statistical date from 1998 to 2006, and establishing the relevant mathematical model. Among, TCDI means total disposable income in the zone. The original cargo volume and influential factors are shown in the following table 1.

Units is 10000 tons, 100 million Yuan, 10000 people and Yuan respectively.

Table 1 . Table of cargo volume and factor s in Northeast Economic Zone.

Year	FT	PIGDP	SIGDP	TIGDP	PL	PCDI	TCDI	FAT
1998	185933.2	1554.86	4144.46	3142.85	11719.6	3377.94	3958.80	2381.82
1999	193712.1	1486.87	4458.92	3439.53	11773.4	3513.62	4136.71	2503.90
2000	195662.7	1454.52	5125.97	3933.84	11837.3	3655.57	4327.20	2845.01
2001	195573.5	1562.19	5382.75	4425.28	11865.5	3973.38	4714.61	3224.90
2002	198960.3	1691.28	5761.02	4927.86	11888.8	4443.95	5283.31	3687.25
2003	202255.8	1511.36	6548.66	5513.97	11906.7	5050.90	6013.96	4611.11
2004	217595.4	2212.54	7480.32	6318.46	11925.6	5588.31	6664.38	6187.88
2005	235134.0	2476.95	9361.05	7181.59	11953.7	6272.57	7498.07	8892.64
2006	257425.0	2700.07	11132.61	8193.46	11991.3	7081.58	8491.70	11768.30

From the above, it analyzes the relationship between cargo and those factors, there are the value-added of the primary industry, the value-added of the secondary industry, the value-added of the tertiary industry, total disposable income and the total social investment in fixed assets. From the analysis are the following formulas:

FT_1=122870.81+46.63PIGDP (R^2=0.918,SF=4.81E-5)

FT_2=144017.79+9.87SIGDP (R^2=0.978,SF=4.55E-7)

FT_3=141422.78+12.95TIGDP (R^2=0.914,SF=5.67E-5)

FT_4=129558.83+14.02TCDI (R^2=0.924,SF=3.62E-5)

FT_5=172587.14+7.14FAT (R^2=0.990,SF=3.08E-8)

From the testing results of parameter, the determinant parameters of regression models ‘R Square’ are all over 0.9. It shows that each influential factor has a close relationship with cargo volume. Every regression model ‘Significance F’ is lower

than 0.001, which shows that each regression formula is worthy of remark. And it illustrates that the models can reflect the relationship between influential factors and cargo volume accurately (Zhao 2008).

2. The definition of influential factor extent

On the basis of analyzing the deep relevance between cargo and influential factors, this research defines the degree of every influential factor by AHP and expert investigation.

2.1 The establish ment of the hierarchical structural levels

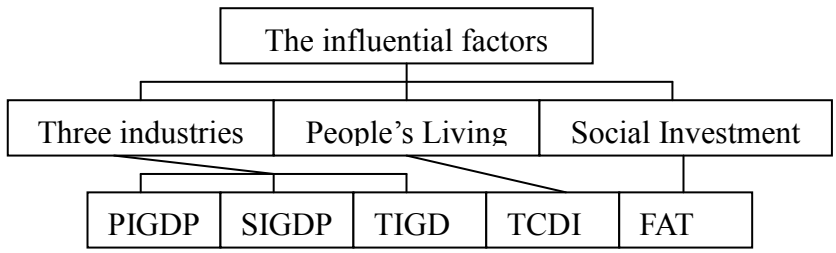

Figure 1. Figure of AHP structure

2.2 The Con formation of the estimate matrix

It applies expert investigation method to design question form, and define the correlation degree of adjacent hierarchical factors in the hierarchical structure according to the statistical survey result, so as to construct the estimate matrix of important degree on influential factors.

	PIGDP	SIGDP	TIGDP	TCDI	FAT
PIGDP	1	1/5	1/2	2	3
SIGDP	5	1	4	8	9
TIGDP	2	1/4	1	3	4
TCDI	1/2	1/8	1/3	1	2
FAT	1/3	1/9	1/4	1/2	1

Figure2. Figure of estimate m atrix

So it can get the maximal eigenvalue λ_{max} and characteristic vector v: $\lambda_{max} = 5.0746$.

$v = [0.1926 \quad 0.9223 \quad 0.3067 \quad 0.1132 \quad 0.0736]$

2.3 The c onsistent testing of estimate matrix

Consistent index $CI = \frac{\lambda_{max} - n}{n-1} = 0.01865$, and when n=5, RI=1.12 through looking over tables. thus, the stochastic consistency rate $CR = \frac{CI}{RI} = 0.0167 < 0.1$, illustrates that the estimate matrix passes the consistency testing. After incorporating the characteristic vector, it can get $w = [0.1197 \quad 0.5734 \quad 0.1907 \quad 0.0704 \quad 0.0458]$.

3. The establi shment of cargo volume forecast model.

3.1 The causality chart of cargo volume forecast system

It establishes the causality chart of cargo in northeast economic zone to reflect the relationship of cargo volume and every influential factor objectively through system analysis in the chart. The positive sign means that variable increases the source variable increase ,the variable increase vice verse variable, look at figure 3.

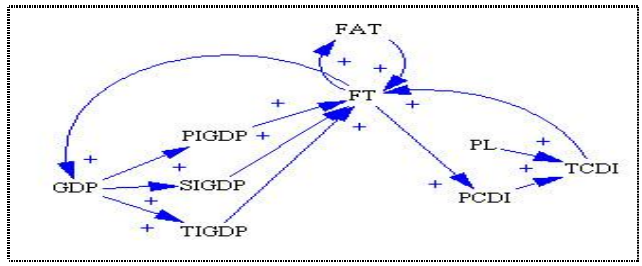

Figure3. Figure o f causal relationship in cargo forecast system

3.2 The establishment of systemic dynamic model

On the basis of studying the relationship between every influential factor and cargo volume, the systemic dynamic model is established. In this model , 'va' means the added value of a variable, 'rate' means the increase percent of a variable, and 'w' means the degree of a variable. In Figure 4, it is the systemic dynamic model of cargo volume in northeast economic zone (Wang 2004).

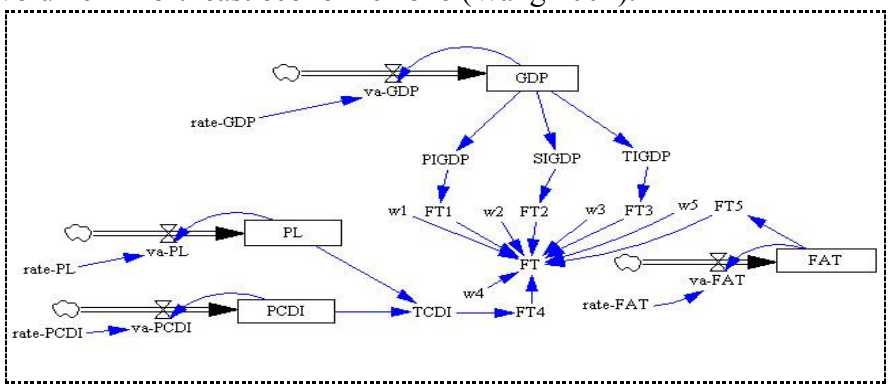

Figure4. Model figure of cargo forecast system

It describes the relationships among the factors by DYNAMO language. In the model, L is the level equation, R is the rate equation, and A is the assistant equation. In addition, the letter K means current, letter J means a moment ago , and letter L means future. DT means the time length between J and K or between K and L.

L GDP.K=INTEG(+"va-GDP.JK"); R "va-GDP.JK"=GDP.J*"rate-GDP.JK";
A FT1.K=122870.81+46.63PIGDP.K; A FT2.K=144017.79+9.87SIGDP.K
A FT3.K=141422.78+12.95TIGDP.K; L PL.K=INTEG(+"va-PL.JK")
R va-PL.JK=PL.J*"rate-PL.JK"; L PCDI.K=INTEG("va-PCDI.JK")
R "va-PCDI.JK"=PCDI.J*"rate-PCDI.JK"; A TCDI.K=PCDI.K*PL.K/10000
A FT4.K=129558.83+14.02TCDI.K; L FAT.K=INTEG(+"va-FAT.JK")
R "va-FAT.JK"=FAT.J*"rate-FAT.JK"; A FT5.K=172587.14+7.14FAT.K
A FT.K=FT1.K*w1+FT2.K*w2+FT3.K*w3+FT4.K*w4+FT5.K*w5

4. The forecast of cargo volume in northeast economic zone.

4.1 Model test

(1) The a nalysis of fitting degree

On the basis of actual cargo volume data in northeast economic zone from 1998 to 2006, the paper does the fitting degree analysis for the systemic dynamic forecast model which have been established. In order to get the emulational results of cargo volume on the past nine years and figure out the relevant error between actual value and emulational value, VENSIM software is applied. See Table 2.

Table 2 . Error analysis of cargo forecast result .

Year	Cargo volume （ ten thousand ton ）		Opposite error （%）
	Actual value	Emulational value	
1998	185933.2	183440.0	-1.34
1999	193712.1	188492.0	-2.69
2000	195662.7	194159.0	-0.77
2001	195573.5	200518.0	2.53
2002	198960.3	207655.0	4.37
2003	202255.8	215668.0	6.63
2004	217595.4	224670.0	3.25
2005	235134.0	234786.0	-0.15
2006	257425.0	246158.0	-4.38

The opposite error between forecast value and actual value can be seen in the above charts, it is less than 7%.The emulational result reflects the cargo development basically. So this model can be used to forecast cargo volume in future.

(2) Average value testing for data collectivity

Through analyzing, cargo volume data in the past years are normal distribution. First, it defines the original date of cargo volume $x_1 \sim N(\mu_1, \sigma^2)$ and emulational data $x_2 \sim N(\mu_2, \sigma^2)$, furthermore, x_1 and x_2 are reciprocal independent, and $n_1 = n_2 = 9$. $\overline{x_1}$ and $\overline{x_2}$ are the average values of data ,and s_1^2 and s_2^2 are the variances of data. Under the level of $\partial = 0.05$, the otherness of average values are as

follows.

Supposed $H_0: \mu_1 = \mu_2$ and $H_1: \mu_1 \neq \mu_2$, do the 't' testing for the two swath data.

$\overline{X_1} = 212039.87$, $S_1^2 = 538010395.86$, $\overline{X_2} = 214013.25$, $S_2^2 = 407024453.36$. Coalescence variance is $S_W = 472517424.61$, and inspection value is $|t| = 0.18156 < t_{0.025}(16) = 2.1199$. So, it can't refuse H_0. Under the level of $\partial = 0.05$, there is no distinct otherness between the average values of original date and emulational data.

(3) Variance testing for collectivity dat a

.Under the level of $\partial = 0.05$, the otherness of variance values are as follows.

Supposed $H_0: \sigma_1^2 = \sigma_2^2$, $H_1: \sigma_1^2 \neq \sigma_2^2$,do the 'F' testing .The inspection value is F=1.188. $F_{0.975}(8,8) = 0.2257 < F = 1.188 < F_{0.025}(8,8) = 4.43$. So it can't refuse H_0. Under the level of $\partial = 0.05$, there is no distinct otherness .

It shows that there is no distinct otherness between the swatch data through the testing of the average and variance. The emulational data can stand for the development tendency of actual cargo volume. The model is in effect, so it can be used to forecast the cargo volume recently.

4.2 The forecast of cargo volume

It applies the systemic dynamic model and VENSIM software to account unborn result of cargo volume. It shows Table 3 as follows.

Table 3 .Forecast result s of cargo in future (Unit: 10000 tons)

Year	2011	2012	2013	2014	2015
Forecast value	328414	351649	377885	407532	441064

See from Table 3, the cargo volume in northeast economic zone will keep increasing during the twelfth plan. In the zone, it can reach over 3 billion tons in this 2010, and it will reach over 4.4 billion tons in 2015.

5. Conclusion

The paper studies the influential factors of cargo volume from systemic dynamics. It establishes the systemic dynamics model to forecast cargo volume in the future. Compared with those foregoing methods, systemic dynamics model considers more influential factors, and adopts quantitative calculation methods to analyze the cargo development tendency objectively. It also reflects the dynamic influence from impact factor development on cargo volume development, meanwhile, it validates the practicality and effectiveness by VENSIM software.

References

Wang, Qipan, System Dynamics. (1994). Tsinghua University Press, Beijing.
Zhao, Shuzhi, Transportation Economic Analysis. (The Second Edition). (2008). China Communications Press, Beijing.

A Study on the Location Selection of Public Traffic Transfer Hub Based on Improved Particle Swarm Algorithm

Lin Lifan[1], Zhang Weihua[1], Hu Jinxin[1] and Sun Qian[1]

[1]School of Mechanical and Automotive Engineering, Hefei University of Technology, Hefei 230009, China; PH (86)-0551-2901338 EXT 2512; FAX (86)-0551-2903450; email:linlifan2008@163.com

ABSTRACT

Location selection of public traffic transfer hubs is the key of urban public traffic planning. In this paper, according to the characteristics and requirements of public traffic transfer hubs, optimum objects and corresponding constraints are presented and a mathematical model of location selection is established. Then, improved Particle Swarm Algorithm, which has a higher success ratio on searching the optimal solution than Particle Swarm Algorithm, is used to compute the proposed model. At last, the application of algorithm is analyzed and the result proves that this method can effectively solve the problem of public traffic transfer hub location selection.

INTRODUCTION

As the key nodes of urban traffic system, public traffic transfer hubs are an important contact aspect of many kinds of passenger traffic modes-switch which links out-city traffic to in-city traffic and public transport to private transport and so on. Usually, a number of public transport lines and a variety of transportation modes, such as buses, trams, metro, taxi, etc., converge on the public traffic transfer hub, which not only has the basic function of passenger conversion/massing, but also outfits many kinds of working organizations and the multi-purpose architectural complexes to serve passengers. Practice shows that the quality of urban public traffic transfer hubs has a great effect on the city public transport service levels and road traffic system.

At present, much research regarding public traffic transfer hubs only took the one-fold problem of location selection itself into account. They didn't pay more attention to the problem of the hub's influence on surrounding roads and the passenger flow. Based on the previous statement, this paper sets up a location selection model with which the public traffic transfer hub and the net of surrounding roads can be optimized at the same time and then uses the improved particle swarm algorithm for solving the model calculation.

MODEL FOUNDATION

When a new public traffic transfer hub is built, it will bring a mass of traffic flow which can lead to more traffic congestion on its surrounding roads. This is

called counteractive of hub to the traffic network (Liu 2003). This kind of counteractive will impel some departments of city governments to widen some old pavement sections or new pavement sections. It will bring changes of traffic networks. In that case, the cost of traffic network ameliorating and the change of passenger flow should be considered. The first objective is the minimum cost. Another is the maximal management capability of passenger flow. Thus, a double-objective location selection model can be established as follows.

$$\min Z = \sum_{i=1}^{M}\sum_{r=1}^{n} b_{ir}\theta_{ir} + \sum_{a=1}^{m} c_a(\varphi_a) \tag{1}$$

$$\max E_i = \sum q'_{rs}\delta^i_{rs} \tag{2}$$

$$s.t. \quad q'_{rs} = q_{rs} + \sum_{i=1}^{M}\theta_{ir}p_{ir} + \sum_{i=1}^{M}\sum_{j=1}^{M}\theta_{ir}\theta_{js}u_{ij} \tag{3}$$

$$\theta_{ir} = \begin{cases} 1, & \text{hub 'i' in section 'r'} \\ 0, & \text{otherwise} \end{cases} \tag{4}$$

$$\delta^i_{rs} = \begin{cases} 1, & \text{when the shortest path between 'r' and 's' pass through 'i'} \\ 0, & \text{other conditions} \end{cases} \tag{5}$$

$$M \subset K \quad n \tag{6}$$

$$\varphi_a \geq 0, \quad 1 \quad m \tag{7}$$

$$1 \leq i \quad M, \quad 1 \quad K \tag{8}$$

The first objective of the model is the minimum cost of the hub construction and the surrounding road expansion. The second objective of the model is the minimum distances between the hubs and the nodes where the passenger flow is large in the service area. It is the transfer gross that has a much closer relationship with the indicators of the hub, so the model's second goal is the greatest distribution intensity of the hub's passenger flow. In the formula, n expresses that the target region is divided into n traffic communities; M expresses that M transportation hubs are proposed to be built in the target region; b_{ir} is the cost of land and construction when hub is located in the district of r; $\theta_{ir} \in \{0,1\}$, $\forall i \quad r \quad R$. Matrix θ is the location solution of multi-hubs; φ_a is the expansion volume of road section a; $c_a(\varphi_a)$ is the expansion construction cost of road section a; E_i is the passenger flow distribution intensity indicator of the alternative hub; q_{rs} is the passenger flow

distribution matrix OD between n districts before the hub's construction ; q'_{rs} is the OD passenger flow volume between the point r and s in OD after the construction of the hubs; p_{ir} is the distribution volume of the passenger flow from the hub i to the district r ; u_{ij} is the distribution volume of the passenger flow from the hub i to the hub j .

In order to reduce the difficulty in arriving at a solution, this paper uses the multi-objective linearity weighted algorithm (Hua 2007) to turn the double-objective optimization problem into the single-objective optimization problem. The objective function changes to:

$$\min g = \alpha Z - \beta E_i \qquad (9)$$

Among the above expressions, α 、 β are the weighted coefficients.

And: $\alpha + \beta = 1, 0 \le \alpha \le 1, 0 \le \beta \le 1$

IMPROVED PARTICLE SWARM ALGORITHM

PSO algorithm is similar to other evolutionary algorithms; the potential solution of each optimization problem is a "particle" in the search space. Each particle has an adaptive value which is decided by the optimized function and a velocity which decides the direction and distance to fly. Particles follow the current optimal solution to search in solution space. PSO is initialized as a group of random particles (random solutions), then finds the optimal solution through the iteration (Yu, 2008). In each iteration, the particle updates itself by tracking the two "extremes". The first is the optimal solution found by the particle itself, and this becomes the individual extremum; the other extremum is the optimal solution currently found by the whole group, and this extremum is a global extremum. Each particle updates their locations according to the following formula:

$$v_{id}^{k+1} = \omega v_{id}^{k} + c_1 Rand_1 (pbest_{id}^{k} - x_{id}^{k}) + c_2 Rand_2 (gbest_{d}^{k} - x_{id}^{k}) \qquad (10)$$

$$x_{id}^{k+1} = x_{id}^{k} + v_{id}^{k+1} \qquad (11)$$

In the expression: k is the times of iteration. v_{id}^{k} is the d dimension speed of particle i which in kth iteration. x_{id}^{k} is the d dimension location of particle i which is in kth iteration.

$Rand_1$ 、 $Rand_2$ are random numbers between 0 and 1. ω is the inertia weight coefficient. $pbest_{id}^{k}$ means the best location which particle i reached. $gbest_{id}^{k}$ means the best location which particle i will reach in global area. c_1 、 c_2 are the speedup coefficient. Their extent is （0~4）(Wang, 2004). And the degree of self-inherit and inherit from excellent individual is decided by them.

By analyzing, it is known that the larger inertia weight is in favor of the overall exploration at the initial stage of algorithm, while the smaller is in favor of the local optimization in the late evolution. Local minimum jumped out by adjusting the size of ω. Studies in literatures (Shi 1998; Trelea, 2003; Naka 2003) have shown that the parameter ω has a decisive effect on the astringency of the algorithm. If ω linearly decreases with the iterative process of the algorithm, the global search and local search capabilities of the particles can be weighed, and the algorithm performance and high search efficiency can be significantly improved. In this paper, based on the strategy of Linearly Decreasing Weight (Linearly Decreasing Weight PSO, LDWPSO) proposed in paper (Shi, 1998), a particle swarm method with a dynamic change in the inertia factor is applied, namely:

$$\begin{cases} \omega = \omega_{\max} - (k / k_{\max})^2 & 1 \le k \le k_{\max} / 2 \\ \omega = \omega_{\min} + (1 - k / k_{\max})^2 & k_{\max} / 2 < k \le k_{\max} \end{cases} \quad (12)$$

Specific calculation steps are as follows:

*Step*1 : N groups even-distributed random variables $X_i^{(0)}(x_{i1}^{(0)}, x_{i2}^{(0)}, \cdots, x_{ij}^{(0)}, \cdots, x_{ip}^{(0)})$ which fit the constraint condition were created from the extent [0,1] of every optimized variable simply marked as $X_i^{(0)}$, $i = 1, 2, \cdots, n$, $j = 1, 2, \cdots, p$. In addition, the $gbest_d$ (the best location in global area), $V_i^{(0)}(v_{i1}^{(0)}, v_{i2}^{(0)}, \cdots, v_{ij}^{(0)}, \cdots, v_{ip}^{(0)})$ and $pbest_{id}$ were initialized.

*Step*2: Calculate the objective function numerical value. The corresponding function value $g(X_i^{(0)})$ was solved by the use of the starting value $X_i^{(0)}$ from *Step*1 into the objective function.

*Step*3: Comparing the objective function value of each particle with $pbest_{id}$ which it reached. If the objective function value is better than $pbest_{id}$, it should be kept as the current best location. Otherwise, it should be kept as the $pbest_{id}$.

*Step*4: Select the particle which has the least objective function value and compare it with $gbest_d$. If it is better than $gbest_d$, it should be kept as the global best location. Otherwise, it should be kept as the $gbest_d$.

*Step*5: Solve the speed and location of change particles with the expression （10)、(11)、(12)．

*Step*6: Evolutional iteration. The paper gets the new particle $X_i^{(1)}$ from *Step*5 and solves the objective function value, and then turns the algorithm into *Step*3 and begins the next best location operation. It repeats this process up to

the termination condition (To reach the largest number of iteration or the optimal position of particle swarm adapting to meet the minimum target).

SIMULATION APPLICATION

The planning of the public traffic transfer hubs in the Hefei High-tech Zone is used as an example. According to investigations on the status of the traffic flow and road network, the paper divides the community into 27 traffic sections (as shown in Figure 1). Now we need to choose the location for five bus centers. That is: $n = 26$, $M = 5$. With four phase methods of transport planning, the bus passenger flow OD distribution matrix of the traffic community is predicted. The construction cost of the site is ascertained according to the relative proportions of the city regional land prices and the proposed site scales. The cost of road expansion and reconstruction depends on the status of the road network and predicted traffic flow.

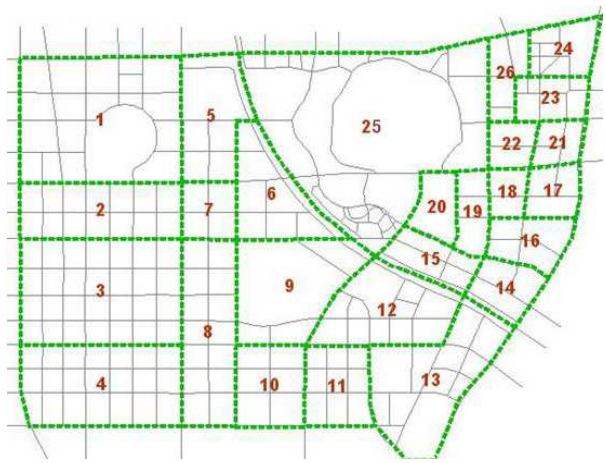

Figure 1. Cell division of the traffic map

The results of the improved particle swarm algorithm are compared with the basic PSO algorithm in order to verify the actual results. Related parameters are set as follows: particle number N=30, iteration number $k_{\max} = 250$, the inertia weight $\omega_{\min} = 0.4$, $\omega_{\max} = 0.9$, learning factor $c_1 = c_2 = 2.0$. With basic particle swarm optimization solved, the mean value is 375.82, the rate of the successful search for the optimal solution is 46%; while using improved particle swarm algorithm, the mean value is 369.05, the rate of the successful search for the optimal solution is 65%. By comparison, obviously it is not difficult to find out that improved particle swarm algorithm is much better at solving the problem than the basic particle swarm optimization.

Five transit hub locations identified by improved particle swarm algorithm are shown in Table 1, and the iterative process of the algorithm is shown in Figure 2.

In Figure 2, the turbulence line expresses the average target value of all the current particles, and the solid line expresses the iteration of the current optimal target.

Table1. The Results of the Location Parameter Table

	X coordinate	Y coordinate	Function value	Cell service
Hub for high-tech zones	51.3	14.6	303.7	4，8，9，10，11
Science city hub	6.2	47.5	289.2	1，2，3
Chief district Hub	80.9	25.5	355.1	12，13，14，15，16，19，20
Simon transfer hub	37.4	70.3	481.5	5，6，7，25
Hefei west railway Station hub	105.1	46.7	416.7	17，18，21，22，23，24，26

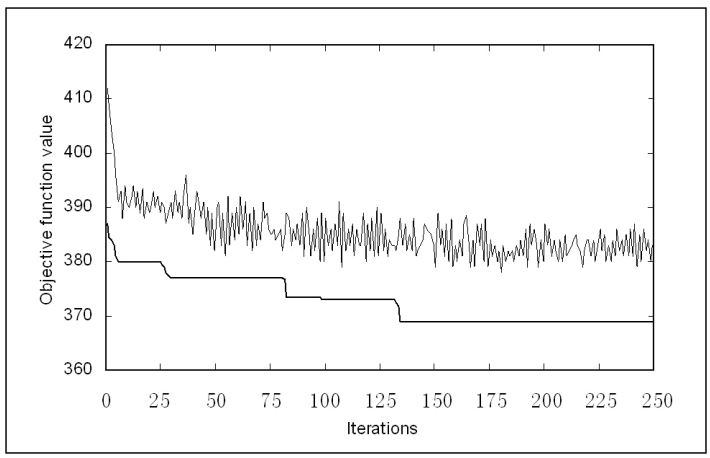

Figure 2. Algorithm Iterative Process Chart

CONCLUSION

In this paper, a theoretical model for public traffic transfer hub planning and location selection is presented to urban transport system. It considers the distribution intensity of passenger flow and the total cost of roads expanding and hub building. Then the paper uses the improved particle swarm algorithm to solve the model. The real example of public traffic transfer hub which is laid out in Hefei High-tech Zone proves the accuracy and usage of this model. It provides an effective method for the location selection of urban public traffic transfer hubs.

REFERENCES

Hua, Guo-wei; Yang, Feng-mei; Lai, Kin Keung.(2007). “Two Bi-objective Optimization Models for Competitive Location Problems [J].” Systems Engineering—Theory & Practice,(1)：99-106

Liu, Can-qi.(2003). “Model of Simultaneously Optimizing the Transport Pivot Siting and Network Design and Its Algorithm[J].” Journal of Highway and Transportation Research and Development, 20(3)：113-116

Naka, S; Genji, T; Yura, T et al. (2003). “A hybrid particle swarm optimization for distribution state estimation [J]. ” IEEE Tans Power Syst, 18(1):60-68

Shi, Y; Eberhart, R. (1998). “Particle swarm optimization [C].” IEEE International Conference of Evolutionary Computation. Anchorage, Alaska: IEEE Press.

Trelea, I C.(2003). “The particle swarm optimization algorithm: convergence analysis and parameter selection [J].” Inform Process Lett, 85(6):317-325

Wang, Junwei; Wang, Dingwei. (2004). “Experiments and analysis of inertia weight of particle swarm optimization [J].” Proceedings of International Conference on Service System and Service Management, 655-659

Yu, Guang-bin; Gui-xian, L.I., JIN Xiang-yang ,BAI Yan-wei. (2008). “Modified particle swarm dynamic process neural network and its application [J]. ” Journal of Jilin University (Engineering and Technology Edition), 38(5)：1141-1145

Region Public Transportation Timetable Optimization Based on Node and Line's Wait Analysis

SUN Wen-xia[1], SONG Ti[2], MA Li-xia[2]

[1]School of Management, Tianjin University, Tianjin 300072, China
[2]School of Civil Engineering , Hebei University of Technology , Tianjin 300132, China; sunwenxia@hebut.edu.cn

Abstract
Based on the thinking of balanced transport capacity and transport volume, this paper puts forward a regional bus dispatching method that suggests adjustments to transport capacity in multi-lines in order to achieve resource sharing and transport capacity sharing. The node and line's wait of public transportation network are analyzed in detail during regional bus dispatching processing in this article. The waiting factor is defined and the wait computational method is given in this paper. The capacity of the bus station is analyzed in detail. Based on this, this paper established the corresponding mathematical model taking the total wait time of the regional network as the main goal. The heuristic algorithm is used to carry on the solution to the model. This model effectively realizes that when the total wait time of simultaneous arrivals at transfer nodes is the greatest, the passenger in the network needs to transfers from one line to another line with the shortest standby period. This paper puts forward a regional public transportation timetable Optimization based on node and line's wait analysis.
Keywords: Traffic engineering; Bus regional dispatching; Heuristic algorithm; Synchronous transfer; Wait; Bus timetable

1. Introduction

Transit planning is a multi-objective problem where the user's and operator's interests conflict. The usual practice for the regulating authorities consists of imposing lines with given route configurations and frequencies so as to secure a certain level of coverage in time and space, while the operator then adjusts the line run departure times so as to match its employment resources in an economic manner. Consequently, transfer synchronization receives little concern. Transfer synchronization is a crucial element of service quality, and it is entirely dependent on departure time setting. The shortest flexible characteristics of traditional bus line timetables leads to vehicles remaining idle at off-peak periods and insufficient in peak periods. Based on the thinking of balanced transport capacity and transport volume, this paper recommends regional bus dispatching methods with adjustments made in transport capacity in multi-lines in order to achieve resource sharing and transport capacity sharing.

Valerie Guihaire and Jin-Kao Hao (2009) present a global review of the crucial strategic and tactical steps of transit planning: the design and scheduling of the network. They first exhibit the context and the goals of strategic and tactical transit planning. Following the objective of maximizing the number of direct travelers, Pape et al. (1992) present a heuristic method for the transit network design problems. The higher the frequency of bus stops on a route, the better the accessibility, but the

lower the travel speed. Murray (2003) studies two variations of this problem. The problem of simultaneous transit line configuration and passenger line assignment is dealt with by Guan et al. (2003). An aggregated meta-heuristic approach to the transit network design problem is considered by Zhao and Gan (2003), Zhao and Ubaka (2004) and Zhao and Zeng (2006) with the objective of minimizing the number of transfers and optimizing route directness while maximizing service coverage. Yu etal. (2005) developed an ant colony based optimization model for bus network design that aims at achieving minimum transfers and maximum passenger flow per unit length with route length and directness constraints.

Many specialists and scholars at home and abroad have extensively studied the regional bus dispatching problem. In 1992, Voss put forward network design formulations in schedule synchronization in order to reduce passenger wait time at transfer stations. In 1999, Magede Dessouky elaborated real-time control techniques of synchronous transfer; Ceder and Wilson , Shi Qin formulated maximum synchronicity of bus timetables in a given bus line network, thus enabling the passenger who in the network needs to transfer to another line to have the shortest standby period. Yang Xiaoguang etc. (2003) studied two bus lines' transfer problems. However, in these papers, the nodes and lines' wait time in the public transportation network are of equal rank. These papers didn't embody different significant degrees of various lines and nodes. For this reason, in this paper, we will present a definition of line and node's wait factor and assign the weight to line and node in model.

2. Definition of wait

2.1 Definition of node wait.

The objective of the synchronous transfer problem is to allow as many vehicles as possible to arrive at the same time at the transfer transit station. In order to obtain a quantification relationship, we establish the following assumption before creating the model: frequency of bus line is constant; suppose bus line operation is performing well and the running speed and cut-off interval is stead fastness; bus drivers don't overtake in all lines; running stop in bus line is determinate; the traffic flow and vehicle and operational condition of line is relatively stabilized; the need of passenger is not influenced by departure frequency and is also relatively stabilized.

Considering transfer stations in public bus networks, its wait coefficient is determined by passenger transfer volume at the station. α_n is the ratio of the passenger transfer volume at n node to the total passenger volume set down and picked up at n node .

$$\alpha_n = 2 \times Volume_n / TotalVolume_n \qquad (1)$$

Where, $Volume_n$ =the passenger transfer volume at n node; $TotalVolume_n$ = the total passenger volume set down and picked up at n node.

Because of different geographical positions of nodes, the transfer passenger volume is different. For example, nodes located as urban hinge, syntaxes multi-bus lines, are important nodes. Transfer passenger volume is great at those nodes and the wait time at the nodes is greater than others. We should give top priority to arrange

bus meetings at those nodes in order to promote the combined efficiency of passenger transfer and reduce the total bus waiting tone at the node.

2.2 Definition of bus line wait time.

We can allocate wait time in terms of departure intervals. For those buses where the departure interval is comparatively large the interval between pervious and latter bus is comparatively large. There is little probability to meet other buses; if passengers miss the previous bus, he or she must wait a long time to ride the latter bus. Short departure interval bus line has a high departure frequency which increases ride probability. The significance of synchronous arrival is greater for the long departure interval line than short departure interval. Define the line's wait time, which is the maximum value of least departure interval of all bus line, as unit 1. Let us introduce the notation:

$H_{\max k}$=Maximum departure interval of line k ; $H_{\min k}$=Minimum departure interval of line k ; β_k =the value of weight factor of lines; the value of weight factor of other lines is the ratio of least departure interval to the maximum departure interval.

$$\beta_k = H_{\min k} \Big/ H_{\max k} \tag{2}$$

3. Definition of station capacity.

Station capacity, C_n, is the maximum number of vehicles that can stop at the station at the same time. The perfect state of synchronous transfer is number of vehicles matched with station capacity.

$$C_n = \frac{L_n + d_s - 2d_e}{l + d_s} \tag{3}$$

$$C_n \le \frac{vt + d_s + l - l_d}{l + d_s} \tag{4}$$

Where, L_n =the length of stabling zone at node ; d_s = longitudinal safe distance between two stop vehicles ; l = length of vehicle; d_e= safe distance between bus and endpoint ; l_d= distance between back door and front door of bus; v = speed of travel; t = cut-off interval.

4. Creation of model

4.1 Constraints and assumptions

We define the following variables:

T =planning time quantum ; t =continuous time in the period $[0,T]$; M =total number of lines in a bus network ; N =the amounts of change nodes in bus network ; X_{ki} =outgoing time of ith bus services in kth line in T period ; F_k =the amount of departure of kth line in planning period ; R_n =the capacity of nth node ; T_{kn} = bus running time from starting point to nth node in line k, if bus of k line doesn't stop nth node, $T_{kn} = -1$;

D_{kiqjn}=binary variable, its value is 1 if i[th] vehicle in line k meet j vehicle in q line at n node, otherwise 0 ; D_{kitn}=binary variable, i[th] vehicle in k bus line arrives at n node at t moment , $D_{kitn}=1$ 。

4.2 Set up model

Based on node and line wait factor, regional bus dispatching optimization model aimed at maximum synchronous transfer rate is as follows:

$$f(z)=\max \sum_{n=1}^{N}\sum_{k=1}^{M-1}\sum_{i=1}^{F_k}\sum_{q=k+1}^{M}\sum_{j=1}^{F_q}\alpha_n D_{kiqjn} \tag{5}$$

$s.t$

$$X_{k1}\le H_{\max k} \quad , \quad 1\le k\le M \tag{6}$$

$$X_{kF_k}\le T \quad , \quad 1\le k\le M \tag{7}$$

$$H_{\min k}\le X_{k(i+1)}-X_{ki}\le H_{\max k} \quad , \quad 1\le k\le M, 1\le i\le F_k-1 \tag{8}$$

$$Y_{nt}=\sum_{n-1}^{N}\sum_{i=1}^{F_k} D_{kitn} \tag{9}$$

$$Y_{nt}\le C_n \tag{10}$$

In the above model, the meaning of objective function (5) is: the total wait is greatest in network, that is to say, buses of the larger wait bus line synchronous arrival has top priority at larger wait nodes. Constraint condition (6) will ensure that the interval from the starting time of T period to the first departure time is not more than the maximum departure interval. Constraint condition (7) will ensure that the departure time of the last vehicle comes within planning time. Constrain condition (8) indicates the restrictions of departure interval. Constraint condition (9) Y_{nt} denotes the number of vehicles at n node at t moment; Constrain condition (10) will ensure the arrival vehicle quantity is no more than station capacity.

5. Solution Approach

The algorithm flow chart in this paper is illustrated in Figure 1. Computational Experimentation gives **the** computational process in detail.

6. Computational Experimentation

In some regions, there are 3 unidirectional bus lines and 6 double action bus lines as illustrated in Figure 2. There are 3 transfer nodes 1 , 2 , 3 in 3 unidirectional bus lines. Every node capacity is 4. The travel time from the origin stop to change node is illustrated in Table 1 (if the line doesn't pass the node, the value is -1). Suppose the timetable is from 9:00~10:00. The value scope of the departure interval in double action 8 wait of 3 change nodes are specified respectively: $\alpha_1=0.2$, $\alpha_2=0.2$, $\alpha_3=0.6$.

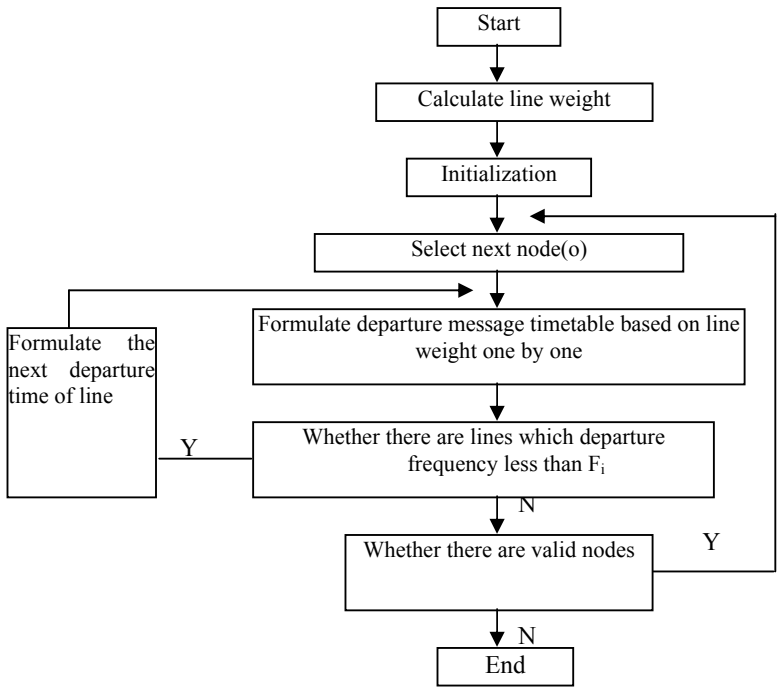

Figure.1 Flow process of basic solution

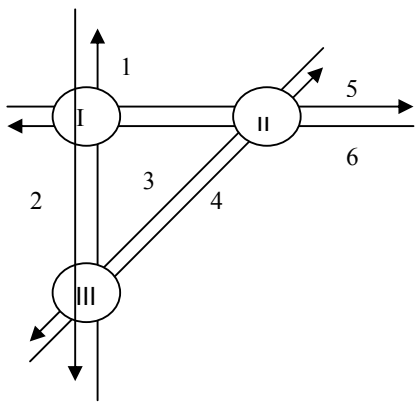

Fig.2 The basic network for example

Table.1 The traveling time of routes

Line	Node 1	Node 2	Node 3
1	16	-1	8
2	10	-1	16
3	-1	6	12
4	-1	8	22
5	7	15	-1
6	18	10	-1

Table.2 Structure of nodes

Node	Line number	μ_n	T_i/max	Corresponding line
1	4	4	18	6
2	4	4	15	5
3	4	4	22	4

Table.3 Data structure of bus

Line	$H_{\min i}$	$H_{\max i}$	Node	F_k
1	6	14	2	7
2	6	14	2	7
3	9	15	2	7
4	9	15	2	7
5	3	6	2	14
6	6	15	2	7

Step1: Calculate line wait. The wait of line 3 and line 4 are β_3, β_4 . $\beta_3 = \beta_4 = 0.231$. Calculate other line wait: $\beta_1 = \beta_2 = \beta_6 = 6/9 = 0.154$; $\beta_5 = 0.077$.

Step 2: Initialization. Nodes structure is illustrated in Table 2. Line data structure is illustrated in Table 3.All nodes are valid nodes.

Step 3: The wait of node 3 is largest, so node 3 is selected.

Step 4: $Y_{3t} = C_3 = 4$ .So the lines through 3 nodes are all selected. The wait factor of lines 3 and 4 are equal and largest. Based on the principle of the travel time from start stop to 3 node size down, the fourth node is selected. The earliest time is set for node 3. At this node, synchronous transfer is based on the condition: max (6 , 6 , 9 , 9) ≤d≤min(14 , 14 , 15 , 15), d = 9. At node 3, continuous meet time is formulated.

The travel time of line 4 from start stop to node 3 is largest, so buses start out as soon as possible in line 4. According to line 4 timetable, the departure timetable of 1, 2 , 3 is formulated. The timetable of node 3 is described in Table 4 and the arrival time of node 3 is illustrated in Table 5.

Table 4 Starting time of buses at node□

Line 1	9:00 9:14 9:23 9:32 9:41 9:50 9:59
Line 2	9:06 9:15 9:24 9:33 9:42 9:51 10:00
Line 3	9:02 9:11 9:20 9:29 9:38 9:47 9:56
Line 4	9:00 9:09 9:18 9:27 9:36 9:45 9:54

Table 5 Arrival time of buses at node③

Line 1	9:08 9:22 9:31 9:40 9:49 9:58 10:07
Line 2	9:22 9:31 9:40 9:49 9:58 10:07 10:16
Line 3	9:22 9:31 9:40 9:49 9:58 10:7 10:16
Line 4	9:22 9:31 9:40 9:49 9:58 10:7 10:16

From the tables we can see: line 2, line 3 and line 4 have three encounters every time at node 3. The first, second, third, fourth, fifth, sixth bus of line 2, 3, 4 encounters the second, third, fourth, fifth, sixth and seventh bus of line 1 at node 3. In given time slice, the number of encounters is 39, the number of encounter points is 7.

Step 5：The departure amount of line 2 is a little one. We may formulate the timetable for line 2 according to line 2 departure time in order to make the two lines have a synchronous transfer at node2 again.

The departure interval of line 2 is [6, 14] , so the other departure time for line 1 is 9:00。

Step 6：If other valid nodes exist, go to step 3. The wait factors of nodes 1 and 2 are equal. In addition, the number of vehicles arriving synchronously is equal to the line amount through nodes. However the wait factor of node 2 is larger so the node 2 is selected.

Step 7：As far as node 2 is concerned $Y_{2t} = C_2 = 4$. The departure timetable of line 3, 4 is determined. Calculate arrive time to determine line departure times. Departure time of line 6 is 6 times. Departure time of line 5 is 5 times.

Step 8：The departure time of line 6 is a little one. The departure time in line 5 is little 8. We can determine the departure time based on generating route departure times. Similarity, we can get other stops' timetables.

The result is as follows: the number of encounters is 15 in 1 set time at node 1; the number of encounter points is 14；the number of encounters is 37 in 1 set time at node 2；the number of encounter points is 7；the number of encounters is 39 in 1 set time at node 3；the number of encounter points is7；According to above departure times, we can get the total number of encounters in network as 91，the total number of encounter points is 28. The objective function value is 52.3511. The total wait time of the area is 52.3511. At last, result is obtained. The departure time of lines is in table 6.

Table.6 Starting time of routes

Line	Departure time						
1	9:00	9:14	9:23	9:32	9:41	9:50	9:59
2	9:06	9:15	9:24	9:33	9:42	9:51	10:00
3	9:02	9:11	9:20	9:29	9:38	9:47	9:56
4	9:00	9:09	9:18	9:27	9:36	9:45	9:54
5	9:02	9:05	9:11	9:14	9:20	9:23	9:29
6	9:00	9:07	9:16	9:25	9:34	9:43	9:52
Meeting time	9:22	9:31	9:40	9:49	9:58	10:07	

7. Conclusion

The node and line's wait of public transportation network are analyzed in detail in this article. The waiting factor is defined and the wait computational method is given in this paper. Based on this, the regional network with the greatest total wait time was taken as the study sample and the corresponding mathematical model was established. Using the heuristic algorithm to carry on the solution to the model, the following was obtained: This model can be effective in determining simultaneous arrivals in the network to reduce the public transportation's total wait time, thus enabling the passenger who needs to transfer lines to be able to do so in the shortest standby period possible. Further study on effect of departure frequency change on dispatch is needed. The regional bus dispatching prioritization model is established on the condition that the passenger flow is stable. Timely varied information on state of the road and emergency unpredictability inevitably change passenger flow quantity. We suppose the operational time of buses is constant. However, the operational time of buses is stochastic because of factors such as traffic signals, the state of road, pilot psychological factors and so on. It is necessary to probe bus dispatch optimization effected by random factor in uncertain environments.

REFERENCES

Ceder, A., Golany, B., Tal, O. Creating bus timetables with maximal Synchronization [J]. Transportation Research Part A 35(2001): 913-928.

Guan,J.F.,Yang,H.,Wirasinghe,S.C.,2003. Simmultaneous optimization of transit line configuration and passenger line assignment. Transportation Research Part B 40(10), 885-902.

Maged Dessouk, Randolph HallAli NowrooziKaren Mourikas. Bus disPatching at timed transfer transit stations using bus tracking [J]. Transportation Research Part C 7(1999): 187-208.

Murray, A. T., 2003. A coverage model for improving public transit system accessibility and expanding access. Annals of Operations Research 123, 143-156.

Pape, U., Reinecke, E., Reinecke, Y., 1992. Entwurf and implementierung eines linienplanungssystems fr den busverkehr im pnv unter einer objektorientierten grafischen entwicklungsumgebung . G ruppendiplomarbeit.

Shi Qin, Qin Yun-mei, Huang Zhi-peng. Maximal Synchronous Transfer Model of Bus Regional Dispatching. China Journal of Highway and Transport.Nov.2007 Vol.20, No.6: 90-94.

Teng Jing, Yang Xiaoguang. A Study on Bus Coordination Dispatching Pattern for Transit Transfer Centers, Urban Transport of China, Sep.2006 Vol.4 No.5: 19-25.

Valerie Guihaire, Jin-Kao Hao, 2008. Transportation network design and scheduling :A global review. Transportation Research Part A .42(2008)1251-1273

Voss, S., 1992. Network design formulation in schedule synchronization. In : Desrochers, Rousseau (Eds.), Computer-Aided Transit Scheduling.Springer, Berlin, pp.137-152.

Yang Xiaoguang, Zhou Xuemei , Zang Hua. A Study on Deadheading in Minimum Time of Public Transfer Under the Condition of ITS [J].Systems Engineering.2003, 21(2):56-59.

Yu, B., Yang, Z., Cheng, C., Liu, C., 2005. Optimizing bus transit network with parallel ant colony algorithm. In:Proceeding of the Eastern Asia Society for Transportation Studies,Vol.5,pp.374-389.

Zhao, F., Gan, A., 2003. Optimization of transit network to minimize transfers.Tech.Rep.BD015-02, Florida Department of Transportation. Center for Transportation Research, Florida International University.

Zhao, F., Ubaka, I., 2004. Transit network optimization-minimizing transfers and optimizing route directness. Journal of Public Transportation 7(1), 67-82.

Zhao, F., Zeng, X., 2006. Simulated annealing-genetic algorithm for transit network optimization. Journal of Computing in Civil Engineering 20(1), 57-68.

Study on the Method of 'Inverse Four-Step' Regulatory Transportation Planning

Jin Wang[1] , Xiaoguang Yang[1], Xianyao Zhao[2]

[1]Institute of Transportation Engineering, Tongji University.
PH:086-0-13916984597;email:wj7040@163.com
[2]Institute of Civil Engineering, Huazhong University of Science and Technology.
PH:086-0-13886065283;email:xyz0802@163.com

ABSTRACT

Good transportation planning is the key to solving urban transportation problems. There are some technologies which need to be utilized in present transportation planning practices. How to get effective feedback from transportation planning to land use planning? How to quantitatively consider the impact of traffic on the future environment? How to forecast the future transportation demands correctly when the urban environment is developing rapidly? Under these considerations, we proposed a reverse regulatory transportation planning method. With this method, we can determine a range of land regulatory indexes for traffic zones after we have set the traffic state on future road network and have calculated the regulatory generation trips of transportation zones. In this paper, the basic idea and related technologies of reverse regulatory transportation planning method have been studied preliminarily.

Key words: transportation planning, traffic demand forecast, traffic environment, land use, TOD

1 Introduction

Traffic planning theory appears relatively late in China, and it's almost the copy of other countries'. Of which, the most often used set of theories is 'traditional traffic planning mode', which originated from western countries at a mature stage of the urbanization process. The core of the traditional mode is 'four-step traffic demand forecasting'. Traditional traffic planning is a process from demand to supply, the major aim of traffic demand forecasting is to supply the traffic demand of the planning year, to adjust (even supplement) the planning road network, and to propose a series of corresponding strategies. In other words, traditional traffic planning method goes from discovering problems to solving them. It ignores the idea that planning should control and adjust the demand reasonably. The objectivity has made it urgent for us to find a set of traffic planning theories, which can suit our own national conditions at present and for a long period in the future (for example, 30-50 years) when urbanization process goes from early stage of rapid development to a comparatively mature developmental stage. This paper is just the initial exploration of that.

The most important factors that affect urban traffic are land use and traffic development policies. Urban traffic and urban land use acts upon and influences each other: if urban traffic leads urban land use, the interaction between them will be positive; but if urban land use leads urban traffic, the relationship will become negative. The essence of the traditional traffic planning theory is exactly in

accordance with the latter. In our country, the urbanization is in the early stage of rapid development now, disorder development of urban land and rapid expansion of cities have resulted in uncertainty of space structure and of function layout, which limits the application of the traditional traffic planning theory. Thus, we should actively doubt the adaptability of traditional traffic planning theory in our present stage. This paper has put forward a new set of traffic planning theories based on the idea of 'traffic control urban planning'. Its core is 'inverse four-step' traffic planning mode. Its main aim is to identify land use characteristics, to develop intensity and construction sequence of traffic zones in planning years, to propose the matching traffic development policies, etc.

2 Aims and Significance of Study

'Inverse four-step' traffic control urban planning theory is a challenge and a inversion to traditional 'four-step' mode (John et al. 1999). It's totally a brand new exploration to present urban traffic planning theory with an ultimate goal of building a city development form that is harmonious, sustainable and human-oriented. If there's some new progress in this research, it will influence current urban traffic planning theory directly, together with establishing practical urban traffic planning. Some planning ideas and technique means can also be applied to guiding practice and to the establishment of practical urban traffic planning, thus, the research in this paper is very important to improve current planning theory, to solve problems of traffic jams, and to build a harmonious city of sustainable development.

Based on urban master planning, the aim of traditional urban traffic planning is to supply urban traffic demand to improve and optimize urban traffic conditions. Traditional 'four-step' traffic demand forecasting consists of trip generation, trip distribution, mode split and traffic assignment. With all of these, basic data collection and traffic investigation are the basis. However, there exists many problems in practical application of traditional 'four-step' traffic demand forecasting and planning technique (Edward, 1996).

First of all, urban scale is expanding rapidly; economic development zones and residential districts are dilating to suburban areas; urban population is also increasing substantially. Now, the urbanization process in our country has been in the rapid development stage, and 'city blasting' will be inevitable. Urban expansion has been experienced by developed countries is an evident characteristic of our current urban construction, and is supposed to be the necessity to develop social economy quickly. Urban expansion is in some extent inevitable, and finally increases the difficulty of controlling and forecasting urban land use in the future (Polzon 1996).

Second, at rapid urbanization stage, it's likely that each function of the city may be changed or adjusted, including configuration of urban land use and intensity of urban land exploitation. In addition, according with rapid development of urban infrastructure and with improvement of social economy, there will be much uncertainty in the modes that inhabitants attend urban activities. Therefore, at this stage of urban development, it's impossible to forecast future urban traffic demand truly with the traditional 'four-step' mode.

Third, urban branch roads have an important effect on traffic assignment, but the establishment of urban traffic planning often doesn't consider them, mainly for two reasons. On the one hand, urban master planning itself doesn't refer to urban

roads. On the other hand, there is no integrated urban control detailed planning to depend on. No consideration of urban branch roads results in the reduction in capacity of urban road network, hence, link flows gained from traffic assignment are always higher than their practical values.

3 Specific Steps of Inverse 'Four-step' Traffic Control Urban Planning

On the basis of analyzing and applying current traffic planning theory and traffic analysis software, this paper puts forward a new idea named 'traffic control urban planning'. The ultimate aim is to account for the severe conflicts between traffic demand and traffic supply resulting from disorder, urban expansion and high development intensity of urban land.

3.1 Basic Procedure

Through inversing traditional 'four-step' model based on some mature theory and developed traffic analysis software, we can obtain production and attraction flow firstly and the land use indexes of traffic zone secondly.

Basic procedure for traditional 'four-step' model is as (Miller 1998): trip generation--trip distribution--mode split--traffic assignment, finally, we get each link flow of the planning road network. But 'inverse four-step' model is completely opposite to that: first, assume the possible most link flows of planning road network, get OD distribution flows between each couple traffic zones based on OD inversion technique; then transform OD matrix to PA matrix; third, carry out traffic mode split on the basis of current trip characteristics and future economic conditions; at last, get residential trip generation and identify some land use control indexes of future traffic zones such as construction land area, parking sets, branch road density, plot ratio, construction density, etc (Sadek, et al. 2002). Planning technical line is as figure 1.

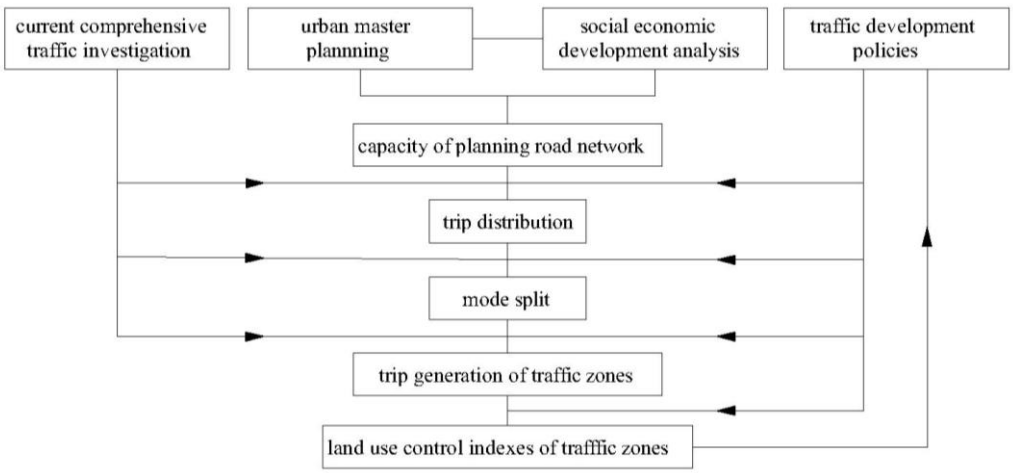

Fig. 1 **basic line of 'inverse four-step' traffic control urban planning**

3.2 Capacity of Planning Road Network

Capacity of urban planning road network is an important index to carry out and evaluate traffic planning. Provided capacity of road network, we could analyze the balance between traffic supply and traffic demand, identify urban development scale, establish planning road network, and propose sustainable traffic development strategies.

Capacity of road network depicts the capacity to contain urban traffic. Ideal capacity of road network refers to the most volume that only relates to road grade, road segment length, capacity and LOS (level of service) of adjacent intersections, and LOS of road segment. Of which, length of road segment should be longer than the biggest queuing length between the adjacent intersections. Capacity and LOS of intersections are identified on the grade and LOS of road segments. The capacity V of urban road network could be calculated by formula 1:

$$V = \sum_{i=1}^{n} C_i I_i N_i \alpha_i \beta_i \gamma_i \quad (\text{veh} \cdot \text{km/h}) \qquad (1)$$

Of which,

C_i --each lane's ideal capacity of grade i road (veh/h);

I_i --lane length of grade i road (km);

N_i --lane numbers of grade i road;

α_i --intersection's reduction coefficient of grade i road;

β_i --average saturation of grade i road;

γ_i --integrated reduction coefficient of grade i road;

i --grade of road.

Capacity of road network suggested by this paper is the ideal value under ideal conditions. As the form of road network and the road grade in future will not differ much from the planning alternative, the ideal capacity based on them is relatively exact.

3.3 Calculate OD Distribution Matrix of Traffic Zones

Given the capacity of urban planning road network, we could get the most trip demand of traffic zones through OD inversion technique (Gur, 1983), and finally get land use control indexes of each traffic zone through inversing current trip generation model. OD inversion technique is generated while the theory and model of traffic planning are relatively mature. At the same time, the application of electric computer, especially of simulation software to traffic planning makes OD inversion technique possible. All kinds of software have basically the same OD inversion principle and manipulation process, we don't introduce them one by one here.

3.4 Calculate controlling indexes of land use for traffic zones

Some controlling indexes presented in this paper such as plot ratio, construction density and branch road density are identified on a relative design code. In practical application, we should also take specific conditions such as urban scale, urban characteristics, land use layout, etc. into account. We should also calibrate certain factors through traffic investigation.

4 Testing in practice for the met hod

In Qianjiang in Hubei province, the urban traffic planning based on 'inverse four-step' traffic control urban planning theory and method has achieved agreement and applause of each expert attending the evaluation conference. At last, six exhibits of Qianjiang urban traffic planning are listed as figure 2 to figure 5, they're successively: capacity of urban planning road network, desire lines of traffic zones, trip production and trip distribution of traffic zones, and average control construction density of traffic zones.

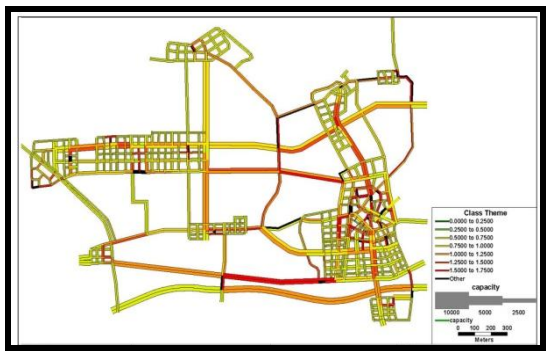

Figure 2 capacity of planning road network

Figure 3 desire lines of traffic zones

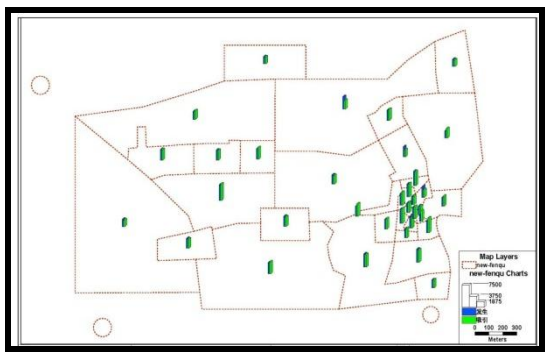

Figure 4 trip production and trip distribution of traffic zones (pcu)

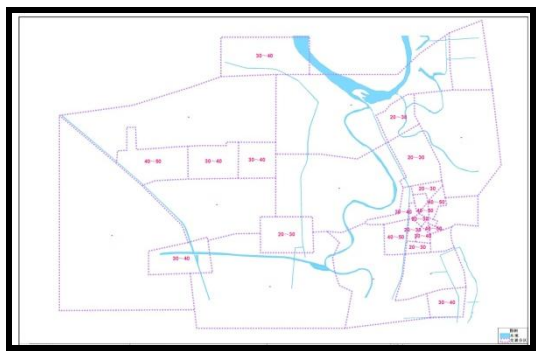

Figure 5 average control construction density of traffic zones (%)

Acknowledgements

This research reported in this paper has been supported by the National Natural Science Foundation of China (No. 70631002）

Reference s:

Edward A (1996). Mierzejewski. An assessment of uncertainty and bias: recommended modification to the urban transportation planning process[D].Florida (US): University of south Florida.

Gur, Y. J. (1983). Estimating trip tables from traffic counts: Comparative evaluation of available techniques. Transp. Res. Rec. 944, Transportation Research Board, Washington, D.C., 113–117.

John S. Miller(1999), Michael J. Demetsky. Reversing direction of transportation planning process [J]. Journal of transportation engineering, 1999， May: 231～237.

Miller, J. S. (1998). Reversing the direction of the transportation planning process: Measuring transportation infrastructure constraints on land use with historical data, PhD dissertation, School of Engineering and Applied Science, University of Virginia, Charlottesville, Va.

Polzon, S. (1996). Prescribing the future, not predicting the future: Are we moving beyond the need for travel demand modeling? Urban Transp. Monitor, 10(23), 3–5, 16.

Sadek, Adel W.; Porter, Andrea; Mark, Charles(2002). Deriving land use limits from infrastructure capacity: An artificial neural network approach. Proceedings of

the International Conference on Applications of Advanced Technologies in Transportation Engineering, p 844-851, 2002.

Robust Optimization Approach for Transportation Network Design under Demand Uncertainty

Yafeng Yin[1] and Yingyan Lou[2]

[1]Department of Civil and Coastal Engineering, University of Florida, Gainesville, FL 32611-6580. PH: 352-392-9537 Ext 1455; FAX: 352-392-3394; Email: yafeng@ce.ufl.edu

[2]Department of Civil and Coastal Engineering, University of Florida, Gainesville, FL 32611-6580. PH: 352-392-9537 Ext 1541; FAX: 352-392-3394; Email: yingyan@ufl.edu

ABSTRACT

This paper reviews our recent developments on applying a robust optimization approach to transportation network design problems where future travel demands are uncertain and traffic flows on the underlying network are in user equilibrium. We assume that the travel demands belong to an uncertainty set instead of having them follow some probability distributions and then design the network against the worst-case scenario realized in the set. The problems are formulated as mathematical programs with complementarity constraints, which are efficiently solvable by a cutting-plane scheme. Numerical examples are provided to demonstrate that the designs from the robust optimization approach perform more stably and guard better against worst-case scenarios than those from traditional deterministic approach.

INTRODUCTION

Network design problem (NDP) for transportation networks has been extensively studied in the literature. The problem is to determine a plan for modifying a road network (e.g., adding new roads and increasing the capacities of the existing ones) in order to minimize the total system travel cost or to optimize another performance measure subject to a given budget. In the literature, NDP has been formulated as a bi-level optimization problem or, equivalently, mathematical program with equilibrium constraints (MPEC), where users' responses in travel choices are captured by the lower-level user equilibrium (UE) problem or equilibrium constraints in form of a variational inequality. The formulation is thus nonlinear and non-convex, making it difficult to solve exactly. For an overview on NDP, see, e.g., Magnanti and Wong (1984) and Yang and Bell (1998).

NDP can be classified into two general categories depending on how additional capacities are represented, either as continuous or discrete variables. In the literature, many have considered continuous NDP or CNDP because the problem is more computationally tractable. However, an additional capacity is always stated in the unit of one lane in practice, thereby suggesting that discrete NDP or DNDP is more practical. On the other hand, the presence of the integer variables makes DNDP more difficult to solve because the gradient-based

approaches are not applicable. In the literature, algorithms for DNDP are primarily limited to, e.g., branch and bound (e.g., LeBlanc, 1975; Poorzahedy and Turnquist, 1982) and meta-heuristics such as genetic algorithms (e.g., Xiong and Schneider, 1992; Jeon et al., 2006). In addition, Gao et al. (2005) propose a decomposition technique and Zhang et al. (2009) present an active-set algorithm.

Previous studies on NDP typically assume that travel demands (or demand functions) are deterministic and known exactly. However, travel demands are intrinsically or epistemically uncertain. More specifically, the uncertainty could be attributed to contingent future developments in the socioeconomic system or prediction errors from travel demand modeling (e.g., Zhao and Kockelman, 2002) etc. A small number of recent studies account for such a demand uncertainty to obtain a network design that either 1) maximizes a reliability measure (e.g., Chootinan et al., 2005; Sumalee et al., 2006); or 2) maximizes system performance while satisfying a reliability-based chance constraint (e.g., Chen et al., 2007; Stathopoulos and Dimitriou, 2007); or 3) maximizes expected system performance or capacity (e.g., Waller and Zilliaskopoulos 2001; Sun and Turnquist, 2007); or 4) achieves a mean-variance tradeoff of the system performance (e.g., Chen et al., 2003; Yin et al., 2005). In general, those models can be viewed as a stochastic MPEC (e.g., Patriksson and Wynter, 1999), and they all require knowing the probability distribution associated with the travel demand for each origin-destination (O-D) pair, a type of information very difficult to obtain in practice.

In another stream of recent research, some (e.g., Yin and Lawphongpanich, 2007; Yin et al., 2008; Yin et al., 2009 and Lou et al., 2009) apply the notion of robust optimization (e.g., Ben-Tal and Nemirovski, 2002; Bertismas and Sim, 2003) to proactively consider demand uncertainty in network design. The approach differs from the above stochastic MPEC approach in the following aspects: 1) it is assumed that future travel demands belong to an uncertainty set instead of having them follow some probability distributions. Available information on future demand from transportation planning practice can be efficiently utilized to specify the uncertainty set; 2) the approach is flexible in representing the risk-taking behaviors of decision makers and controlling the conservatism of the resulting network design, and 3) the approach is amenable to an effective and efficient solution algorithm that has the potential for solving large network design problems. The purpose of this paper is to review those new developments because we believe that the robust optimization approach is general and can be applied to many other decision-making problems in transportation planning and management.

NETWORK DESIGN PROBLEM UNDER DEMAND UNCERTAINTY

To introduce our robust optimization approach to NDP under demand uncertainty, let N and A denote the sets of nodes and links in a transportation network. Instead of using probability distributions to model demand uncertainty,

we assume that future travel demands belong to an uncertainty set denoted as D As discussed in the next section, all available information on future travel demands should be used to specify D, but the key is to avoid being overly conservative with the belief that nature is neither an ally nor an enemy, but somewhere in between. At the same time, the construction of the uncertainty set should ensure that the resulting robust optimization model is computationally tractable.

For a given demand vector $d \in D$, $V(d)$ denotes the associated set of all feasible flow distributions and can be mathematically expressed as follows:

$$V(d) = \left\{ v \mid v = \sum_w x^w, \Delta x^w = E^w d_w, x^w \geq 0, \forall w \in W \right\},$$

where x^w is the vector of link flows associated with O-D pair w, v is the vector of total or aggregated link flows, and Δ is the node-link incidence matrix associated with the network. To specify the origins and destinations of link flows, E^w is a vector in $R^{|N|}$ with two nonzero components: one has a value of 1 in the component corresponding to the origin node of O-D pair w and the other has a value of -1 in the component for the destination. For each link $(i, j) \in A$, $t_{ij}(v_{ij}, y_{ij})$ denotes the travel cost (time) as a function of link flow v_{ij} and the expansion amount y_{ij} Below, $t(v, c)$ denotes a vector whose components consist of individual link travel costs, $t_{ij}(v_{ij}, y_{ij})$.

With an uncertainty set of future demands for the traffic network, the robust optimization approach is to design the network against the worst-case scenario realized in the set. More specifically, we attempt to find a capacity expansion plan that minimizes the maximum system travel time realized within the set. Without loss of generality, constructing new links can be treated as adding capacities to existing links with zero capacity. Using the above notation of robust optimization, a robust continuous network design model or RCND can be formulated as the following min-max program:

RCND

$$\min_{y} \max_{d,x,v,z,\pi} \sum_{ij \in A} t_{ij}(v_{ij}, y_{ij}) \cdot v_{ij}$$

s.t.
$$x_{ij}^w \cdot \left(t_{ij}(v_{ij}, y_{ij}) + \pi_i^w - \pi_j^w \right) = 0 \qquad \forall (i, j) \in A, w \in W \qquad (1)$$

$$t_{ij}(v_{ij}, y_{ij}) + \pi_i^w - \pi_j^w \geq 0 \qquad \forall (i, j) \in A, w \in W \qquad (2)$$

$$v \in V(d) \qquad (3)$$

$$d \in D \qquad (4)$$

$$\sum_{ij \in A} h_{ij}(y_{ij}) \leq B \qquad (5)$$

$$0 \leq y_{ij} \leq y_{ij}^{\max} \qquad \forall (i, j) \in A \qquad (6)$$

The objective of RCND is to minimize the maximum system travel cost realized from the uncertainty set of future demands. The decision variables of the outer problem (the minimization) compose a capacity expansion plan and those of the inner problem (the maximization) are the worst-case demand scenario and the associated UE flow distributions. Constraints (1)-(3) ensure that, for a given network design y and a demand vector d, the feasible flow distribution satisfies

UE conditions where variable π_i^w is the potential of node *i* for O-D pair *w*. Constraint (4) requires future demands to be realized from the uncertainty set and constraint (5) guarantees that the total cost of the expansion plan does not exceed *B*, the budget, where $h_{ij}(y_{ij})$ is the construction cost for link (i, j). Finally, constraint (6) ensures that the amount of capacity expansion for each link is nonnegative and less than its maximum. In the above, y_{ij} is a continuous scalar.

A robust discrete network design model, or RDND can be similarly formulated. Note that discrete capacity expansion (in the unit of one lane) can be always represented in binary digits. Let y_{ij}^k be a 0-1 variable in the k^{th} bit of the binary number corresponding to the capacity expansion of link $(i, j) \in A$. Let *K* be the number of bits (determined from the maximum possible number of lanes added), then the number of additional lanes is $\sum_{k=1}^{K} 2^{k-1} y_{ij}^k$, an integer between zero and $2^K - 1$. For example, if the number of additional lanes on link (i, j) is 3, *K*=2 and $y_{ij}^1 = y_{ij}^2 = 1$, leading to $\sum_{k=1}^{2} 2^{k-1} y_{ij}^k = 3$. y_{ij}^k can be treated as a continuous variable with two additional conditions $y_{ij}^k(1 - y_{ij}^k) = 0$ and $0 \le y_{ij}^k \le 1$. In the RDND formulation, y_{ij} represents a vector in R^K whose element is y_{ij}^k. RDND can be written as follows:

RDND

$$\min_{y} \max_{d,x,v,z,\pi} \sum_{ij \in A} t_{ij}(v_{ij}, y_{ij}) \cdot v_{ij}$$

s.t. (1)-(5)

$$y_{ij}^k(1 - y_{ij}^k) = 0 \qquad \forall (i, j) \in A, k \in \{1,2,..., K\} \qquad (7)$$

$$0 \le y_{ij}^k \le 1 \qquad \forall (i, j) \in A, k \in \{1,2,..., K\} \qquad (8)$$

With a simple transformation, it is easy to see that both CDND and RDND are MPEC or more precisely mathematical programs with complementarity constraints (MPCC), a class of optimization problems very difficult to solve for mainly two reasons. One is the fact that MPCC violates the Magasarian-Fromovitz constraint qualification and the other is the non-convexity of its feasible region (e.g., Scheel and Scholtes, 2000). Compounding to this difficulty is the fact that the problems have an infinite or astronomical number of constraints and decision variables.

UNCERTAINTY SET OF FUTURE DEMANDS

The above two robust models are worst-case oriented, but bounded by an uncertainty set. It is thus critical to specify an appropriate set to avoid being overly conservative and allow the flexibility in controlling the level of conservatism for designing the network expansion plans. Below we discuss three uncertainty sets that may be meaningful in confining uncertain travel demands. No underlying probability distributions of travel demands are assumed to be known, although such knowledge may be of use to obtain a reasonable uncertainty set.

Polyhedron. An example of a polyhedral uncertainty set is a box set (e.g., Soyster, 1973). Mathematically, $D = \{d \mid d_w^{\min} \le d_w \le d_w^{\max}, \forall w \in W\}$, where $d_w^{\min}$

and $d_w^{\max}$ represent the minimum and maximum travel demands for O-D pair *w*, respectively. The interval may be the confidence interval of an estimated demand obtained through a survey or by using an O-D estimation model. Although easy to specify, the box set may lead to a decision too conservative to be of interest. Additional information should be used to further confine the uncertainty. For example, $\sum_{w \in O_i} d_w \le Q_i^{\max}$, where O_i is the set of O-D pairs whose origin is node *i* and $Q_i^{\max}$ is the upper bound for the total number of trips generated from node *i*. The upper bound can be viewed as a variable to control the degree of uncertainty and may be determined via a trip generation model considering car ownership and population etc.

Ellipsoid. In its most familiar form, an ellipsoidal uncertainty set can be represented as $D = \{d \mid \sum_w \frac{(d_w - d_w^0)^2}{r_w^2} \le \theta^2\}$, where d_w^0 and r_w are the nominal demand and possible variation for O-D pair *w* and θ is a subjective value representing the decision maker's attitude toward risk. Given $d_w^{\min}$ and $d_w^{\max}$, one set of parameters for the above ellipsoid is $d_w^0 = \frac{1}{2}(d_w^{\min} + d_w^{\max})$ and $r_w = \frac{1}{2}(d_w^{\max} - d_w^{\min})$. When $\theta = 0$, *D* with the above parameters reduces to the singleton $\{d^0\}$, where d^0 is a vector of d_w^0. On the other hand, *D* becomes the largest volume ellipsoid inside and the smallest volume ellipsoid inscribing the box defined above when $\theta = 1$ and $\sqrt{m}$ respectively. In general, larger θ means the decision maker is more risk averse (Ben-Tal and Nemirovski, 2002).

Discrete. The set is similar in principle to Bertismas and Sim (2003). It is assumed that future demand of each O-D pair can be one of several values whose probabilities of occurrence, however, are unknown. These possible demand values are often identified with the alternative forecasts of socioeconomic and land-use developments by metropolitan planning organizations. To mathematically describe this set, let $d_w^s, s = 1,2,...,S_w$ denote the demand for O-D pair *w* under scenario *s*, where d_w^1 represents the nominal demand and z_w^s is a binary variable that indicates whether scenario *s* is realized for O-D pair *w*. Then, $\sum_{s=1}^{S_w} z_w^s = 1$ ensures that only one demand scenario will be realized for each O-D pair. In addition, we assume that there is an "uncertainty budget" Γ that allows demands for at most Γ O-D pairs to deviate from their nominal values simultaneously, i.e., $\sum_w \sum_{s=2}^{S_w} z_w^s \le \Gamma$. In words, Γ is a parameter for controlling the degree of conservatism and describing decision makers' attitudes toward risk. Then, the demand uncertainty set can be described as follows: $D = \left\{ d \middle| d_w = \sum_{s=1}^{S_w} z_w^s d_w^s,\ \sum_{s=1}^{S_w} z_w^s = 1,\ \sum_w \sum_{s=2}^{S_w} z_w^s \le \Gamma, z_w^s \in \{0,1\} \right\}$.

Combining the above uncertainty sets with two robust formulations yields different models, which can be solved by a cutting-plane algorithm presented in the next section. The choice of the uncertainty set should depend on the level of available information, i.e., planners' knowledge about future travel demands.

More importantly, it should ensure that the resulting robust counterpart is computationally tractable. For example, the discrete set in combination with RDND leads to an optimization model that is effectively and efficiently solvable (Lou et al., 2009).

CUTTING-PLANE SOLUTION SCHEME

The section presents a cutting-plane scheme for solving both RCND and RDND. The scheme solve a sequence of relaxed RCND or RDND with respect to a subset $\widetilde{D} \subset D$ that contains a smaller number of demand vectors and then solve another problem to generate demand vectors "as needed" to enlarge $\widetilde{D}$ and make it approximate *D* better.

In the following, we present the algorithm using the RDND formulation as an example. The relaxed RDND problem or R-RDND can be written as follows:

R-RDND

$$\min_{x,y,v,\pi,\xi} \xi$$

$$\text{s.t.} \quad \sum_{ij\in A} t_{ij}(v_{ij}^d, y_{ij}) \cdot v_{ij}^d \le \xi \qquad \forall d \in \widetilde{D} = \left\{d^1, \cdots d^n\right\}$$

$$x_{ij}^{w,d}\left(t_{ij}(v_{ij}^d, y_{ij}^k) + \pi_i^{w,d} - \pi_j^{w,d}\right) = 0 \qquad \forall (i,j) \in A, w \in W, d \in \widetilde{D}$$

$$t_{ij}(v_{ij}^d, y_{ij}) + \pi_i^{w,d} - \pi_j^{w,d} \ge 0 \qquad \forall (i,j) \in A, w \in W, d \in \widetilde{D}$$

$$v^d \in V(d) \qquad \forall d \in \widetilde{D} = \left\{d^1, \cdots d^n\right\}$$

(5), (7) and (8)

In the above, the superscript $(\bullet)^d$ denotes variables associated with a particular demand vector $d \in \widetilde{D}$. Let $(\hat{y}, \hat{\xi})$ be a global optimal to R-RDND. (To simplify our presentation, we ignore other components of the solution vector.) Note that $(\hat{y}, \hat{\xi})$ also solves the original RDND if, with the network design $\hat{y}$, the total system travel cost of the UE flow associated with every demand scenario in *D* is no greater than $\hat{\xi}$. Mathematically, this can be verified by solving the following worst-case demand problem or WCD:

WCD

$$\max_{d,x,v,z,\pi} \sum_{ij\in A} t_{ij}(v_{ij}, \hat{y}_{ij}) \cdot v_{ij}$$

$$\text{s.t.} \quad x_{ij}^w\left(t_{ij}(v_{ij}, \hat{y}_{ij}) + \pi_i^w - \pi_j^w\right) = 0 \qquad \forall (i,j) \in A, w \in W$$

$$t_{ij}(v_{ij}, \hat{y}_{ij}) + \pi_i^w - \pi_j^w \ge 0 \qquad \forall (i,j) \in A, w \in W$$

(3)-(4)

If the optimal objective value of WCD is no greater than $\hat{\xi}$, then $\hat{y}$ is optimal to RDND. Otherwise, an improved solution may be obtained by solving R-RDND with an expanded demand set $\widetilde{D} \cup \left\{\hat{d}\right\}$, where $\hat{d}$ solves the above WCD.

Both R-RDND and WCD are MPCC and require specialized solution algorithms to solve them, such as the manifold suboptimization algorithm by Lawphongpanich and Yin (2008) and the active-set algorithm by Zhang et al. (2009). Below we outline the cutting-plane solution procedure:

Step 0: Select a demand vector $d^1 \in D$. Set $n = 1$ and $\widetilde{D} = \{d^1\}$.

Step 1: Solve R-RDND with a subset $\widetilde{D}$. Let $(\hat{y}^n, \hat{\xi}^n)$ denote the resulting optimal solution.

Step 2: Solve WCD with capacity expansion plan $\hat{y}^n$. Let d_n denote the resulting optimal solution and $\hat{v}^n$ its corresponding UE flow.

Step 3: If $t(\hat{v}^n, \hat{y}^n)^T \hat{v}^n \le \hat{\xi}^n$, stop and $\hat{y}^n$ is an optimal capacity expansion vector. Otherwise, set $\widetilde{D} = \widetilde{D} \cup \{d_n\}$, $n = n + 1$ and go to Step 1.

The convergence proof of the above procedure can be found in Yin and Lawphongpanich (2007) and Lou et al. (2009).

NUMERICAL EXAMPLES

This section reports results from solving RDND with a discrete uncertainty set for two networks from the literature, Sioux Falls (e.g., LeBlanc et al., 1975) and Hull (e.g., Florian et al., 1987). The former consists of 76 links, 24 nodes and 528 O-D pairs while the latter comprises 741 links, 524 nodes and 142 O-D pairs. In the numerical examples, there are three possible demand scenarios for each O-D pair: nominal, low and high. The nominal demand is the original demand. The low and high scenarios are the nominal demand multiplied by uniform random numbers between [0.5, 1] and [1, 1.5], respectively. In both networks, all links are candidates for expanding capacity up to three additional lanes. Other details of the numerical examples can be found in Lou et al. (2009). The results reported as follows are from our GAMS implementation on a Dell Optiplex 755 computer with 3.16 GHz Intel Core2Duo CPU and 3.25GB of RAM.

Table 1 summarizes the computational efficiency for both Sioux Falls and Hull. In these examples, the cost budget *B* is 25 for Sioux Falls and 60 for Hull while the uncertainty budget Γ is 10 and 5 respectively. The computational CPU time is 392.05 and 474.11 seconds respectively, in which solving R-RDND consumes the majority of the resource. The elapsed time reported in the table includes the time for input and output. For Sioux Falls, it takes 7 iterations of the cutting-plane procedure while for Hull, it only takes 3 outer iterations, but requiring a bit more CPU time to solve two larger size sub-problems.

Table 1 Computation Efficiency

	Number of Iterations	Elapsed Time (mm:ss)	CPU Time (sec)	WCD (sec)	R-RDND (sec)
Sioux Falls	7	12:55	392.05	23.88	368.17
Hull	3	8:57	474.11	99.18	374.93

Figure 1 displays the amount of CPU time required to solve the RDND problem for Sioux Falls with the uncertainty budget Γ varying from 0 to 50. In general, it takes more outer iterations to solve the problem when the uncertainty budget is larger. But in all numerical experiments we conducted for Sioux Falls, the CPU time is less than 15 minutes. For Hull, it is less than 8 minutes with the uncertainty budget Γ up to 10. The experiments demonstrate that the algorithm is quite efficient and has the potential for solving larger

network design problems.

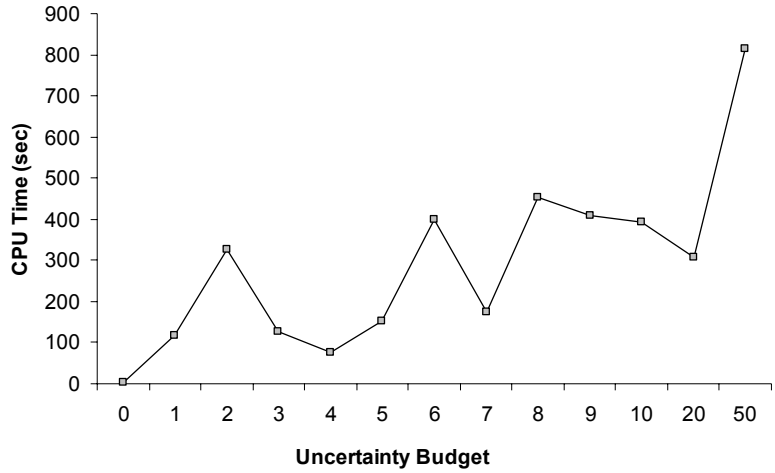

Figure 1 CPU time versus uncertainty budget

Table 2 reports the resulting robust and nominal expansion plans of the two examples illustrated in Table 1. The latter is obtained by solving RDND with $\Gamma=0$, i.e., a deterministic discrete network design problem with the nominal demand. It can be seen that although approximately 50%-60% of the investments in both plans are the same, the other differs in either the selection of link segment for expansion or the magnitude of capacity expansion.

Table 2 Comparison of Robust and Nominal Plans

Sioux Falls			Hull		
Link	Robust Plan	Nominal Plan	Link	Robust Plan	Nominal Plan
(6,8)	3	3	(1,207)	0	1
(8,6)	3	3	(5,406)	3	3
(10,16)	3	3	(8,215)	0	1
(11,14)	3	3	(10,241)	1	1
(13,24)	2	3	(11,272)	3	3
(14,11)	3	3	(270, 271)	0	1
(15,10)	0	1	(272,279,)	3	3
(16,10)	3	3	(280,281)	1	0
(22,23)	1	0	(282,283)	3	3
(23,22)	3	0	(406,412)	3	3
(24,13)	1	3	(412,410)	3	1
Total Cost	25	25	Total Cost	60	60

To compare the robust and nominal plans, we conducted three sets of Monte Carlo simulations. It is assumed that each of the low, nominal and high demand scenarios for each OD pair has a probability of 1/3, 1/3 and 1/3 to occur (discrete uniform distribution) in the first, 1/6, 1/6 and 2/3 ("pessimistically" asymmetric distribution) in the second and 2/3, 1/6 and 1/6 ("optimistically" asymmetric distribution) in the third simulation. In each simulation, 500 travel demand vectors were generated and for each of them, two UE distributions, one with robust plan and the other with nominal plan were obtained. The average, maximum and standard deviation of the total travel costs associated with the UE

distributions are computed and reported in Table 3. It can be seen that the robust plan for Sioux Falls reduces average, maximum and standard deviation of system travel costs by 2.5%, 3.0% and 6.3% respectively in the first, 3.2%, 3.8% and 6.7% in the second, and 2.1%, 1.8% and 2.3% in the third simulation. The reductions for Hull are 3.2%, 6.9% and 22.4% in the first, 4.3%, 6.5% and 16.9% in the second and 2.4%, 5.2% and 24.9% in the third simulation. The *t* and *F* tests show that the reductions are all statistically significant. The simulations confirm that the robust plans may lead to less volatile performances.

Table 3 Performances of Robust and Nominal Plans in Simulation

Simulation	Measures	Sioux Falls		Hull	
		Robust Plan	Nominal Plan	Robust Plan	Nominal Plan
Demands with Discrete Uniform Distribution	Average Travel Cost	7010.37	7183.42	40975.41	42290.13
	Maximum Travel Cost	7750.12	7985.76	55342.57	59175.90
	Std of Travel Costs	238.88	253.98	4112.58	5033.45
Demands with Pessimistically Asymmetric Distribution	Average Travel Cost	9880.67	10197.84	53870.98	56183.15
	Maximum Travel Cost	10899.70	11311.07	65196.74	69413.66
	Std of Travel Costs	332.23	354.55	5072.04	5929.25
Demands with Optimistically Asymmetric Distribution	Average Travel Cost	4987.23	5093.17	31518.91	32266.28
	Maximum Travel Cost	5467.39	5567.47	42384.06	44602.33
	Std of Travel Costs	155.78	159.40	2787.25	3481.39

Figure 2 and 3 compare the nominal (or the plan with $\Gamma = 0$) and robust plans with the uncertainty budget Γ varying from 0 to 50 for Sioux Falls and from 0 to 10 for Hull respectively under the discrete uniform distribution of future demands. There are three curves in both figures for relative percent difference in the mean, maximum and standard deviations of system travel costs (the performance resulting from the nominal plan minus the one from the robust plan divided by the latter). In general, as the uncertainty budget Γ increases, standard deviation associated with the robust plan becomes smaller, i.e., the total travel cost associated with the robust plan is less volatile. When the budget Γ is large enough, e.g., $\Gamma \geq 5$, the reduction in the maximum and average travel cost is pretty stable, approximately 2% and 2% respectively for Sioux Fall and 3% and 6% respectively for Hull. Note that when the budget Γ is very small, e.g., $\Gamma = 1$ or 2, the robust and nominal plans are either the same (for Hull), or have similar performance (For Sioux Falls, the reduction in average and maximum travel time is negative when $\Gamma = 1$ as shown in Figure 3, which, however, is statistically insignificant).

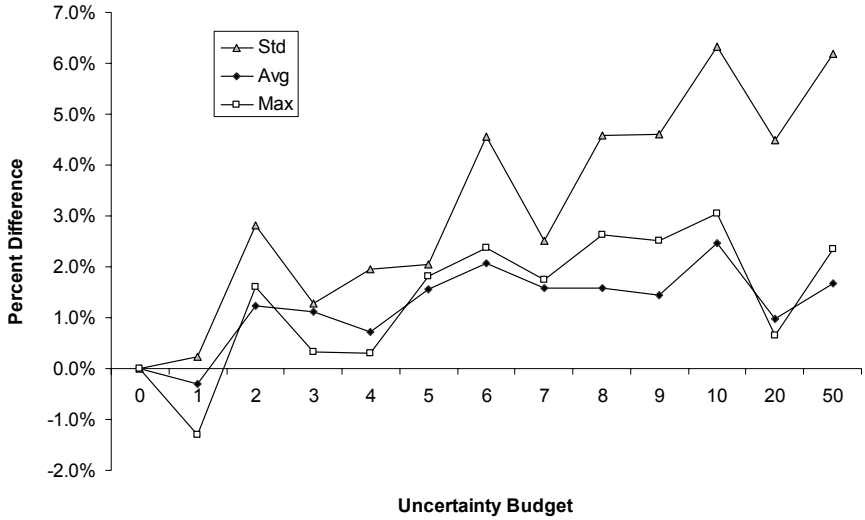

Figure 2 Comparison of the nominal and robust plans for Sioux Falls

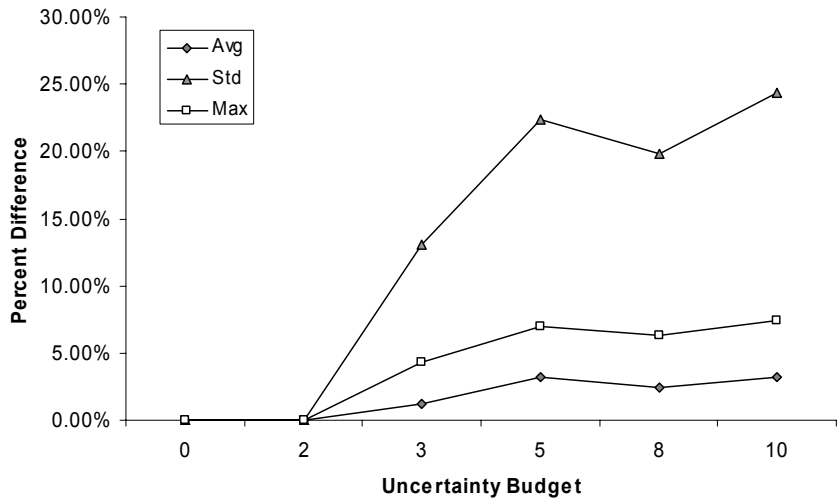

Figure 3 Comparison of the nominal and robust plans for Hull

CONCLUDING REMARKS

In this paper, we review a robust optimization approach for network design problem under demand uncertainty. Although the travel demand for each O-D pair is uncertain, this approach assumes that the vector of O-D travel demands realized for the network must belong to an uncertainty set. The network is then designed against the worst-case scenario realized in the set and the problems are then formulated as MPCC, which can be solved by the proposed iterative cutting-plane scheme. Numerical results from the Sioux Falls and Hull networks empirically demonstrate that the algorithm is effective in practice and has the potential to solve realistic network design problems. Moreover, the results from these two networks indicate that capacity expansion plans from our robust formulations are less volatile and perform better against worst-case demand

scenarios. Because many problems in transportation planning and management (e.g., congestion pricing and evacuation planning) share similar structure as network design, the proposed robust optimization framework can be applied to aid those decision-makings.

REFERENCES

Ben-Tal, A. and Nemirovski, A. (2002) "Robust optimization - methodology and applications." *Mathematical Programming Series B*, 92, 453-380.

Bertismas, D. and Sim, M. (2003) "Robust discrete optimization and network flows." *Mathematical Programming*, 98, 49-71.

Chen, A., Kim, J., Zhou, Z. and Chootinan, P. (2007) "An alpha reliable network design problem." *Transportation Research Record,* 2029, 49-57.

Chen, A., Subprasom, K. and Ji, Z. (2003) "Mean-variance model for the Build-Operate-Transfer scheme under demand uncertainty." *Transportation Research Record*, 1857, pp.93-101.

Chootinan, P., Wong, S.C. and Chen, A. (2005) "A Reliability-based network design problem." *Journal of Advanced Transportation*, 39, 247-270.

Florian M., Guelat J., and Spiess H., (1987) "An efficient implementation of the PARTAN variant of the linear approximation method for the network equilibrium problem." *Networks*, 17, 319-339.

Gao, Z., Wu, J. and Sun, H. (2005) "Solution algorithm for the bi-level discrete network design problem." *Transportation Research*, 39B, 479-495.

Jeon, K., Lee, J., Ukkusuri, S. and Waller, S. T. (2006) "Selectorecombinative genetic algorithm to relax computational complexity of discrete network design problem." *Transportation Research Record,* No.1964, 91-103

Lawphongpanich, S. and Yin, Y. (2008) "Solving Pareto-improving congestion pricing for general road networks." *Transportation Research*, Part C (under review).

LeBlanc, L.J. (1975) "An algorithm for the discrete network design problem." *Transportation Science,* 9, 183-199.

LeBlanc L.J., Morlok E.K., and Pierskalla W.P., (1975) "An efficient approach to solving the road network equilibrium traffic assignment problem." *Transport Research,* 9, 309-318.

Lou, Y., Yin, Y. and Lawphongpanich, S. (2009) "A robust approach for discrete network design under demand uncertainty." *Transportation Research Record (accepted)*.

Magnanti, T.L. and Wong, R.T. (1984) "Network design and transportation planning: models and algorithms." *Transportation Science*, 18, 1-55.

Patriksson, M. and Wynter, L. (1999) "Stochastic Mathematical Programs with Equilibrium Constraints." *Operations Research Letters*, Vol.25, No.4, 159-167.

Poorzahedy H. and Turnquist M.A. (1982) "Approximate Algorithms for the discrete network design problem." *Transportation Research*, 16B, 44-45.

Scheel, H., Scholtes, S., (2000) "Mathematical programs with complementarity

constraints: stationarity, optimality, and sensitivity." *Mathematics of Operations Research*, 25, 1-22.

Soyster, A.L. (1973) "Convex programming with set-inclusive constraints and applications to inexact linear programming." *Operations Research*, 1154-1157.

Stathopoulos, A. and Dimitriou, L. (2007) "A continuous network design problem with reliability constraints: genetic stochastic system design approach." *Transportation Research Board Annual Meeting 2007*, Paper #07-2074.

Sumalee, A., Watling, D.P. and Nakayama, S. (2006) "Reliable network design problem: the case with uncertain demand and total travel time reliability." *Transportation Research Record*, 1964, 81-90.

Sun, Y. and Turnquist, M.A. (2007) "Investment in transportation network capacity under uncertainty: simulated annealing approach." *Transportation Research Record*, 2039, 67-74.

Waller, S.T. and Ziliaskopoulos, A.K. (2001) "Stochastic dynamic network design problem." *Transportation Research Record*, 1771, 106-113.

Xiong, Y. and Schneider, J. B. (1992) "Transportation network design using a cumulative genetic algorithm and neural network." *Transportation Research Record,* No.1364, 37-44

Yang, H. and Bell, M.G.H. (1998) "Models and algorithms for road network design: a review and some new development." *Transportation Review*, 18, 257-278.

Yin, Y. and Lawphongpanich, S. (2007) "A robust approach to continuous network designs with demand uncertainty." *Transportation and Traffic Theory 2007*, Allsop, R.E., Bell, M.G.H., Heydecker, B.G. (Eds.), Elsevier, London, England, 110-126.

Yin, Y., Lawphongpanich, S. and Lou, Y. (2008). "Estimating investment requirement for maintaining and improving highway systems." *Transportation Research*, 16C, 199-211.

Yin, Y., Madanat, S.M. and Lu, X.Y. (2005) "Robust improvement schemes for road networks under demand uncertainty." *Transportation Research Board Annual Meeting 2005,* Paper # 05-1724.

Yin, Y., Madanat, S.M. and Lu, X.Y. (2009) "Robust improvement schemes for road networks under demand uncertainty." *European Journal of Operational Research* (in press).

Zhang, L., Laphongpanich, S. and Yin, Y. (2009) "An active-set algorithm for discrete network design problems." *Proceedings of 18th International Symposium of Transportation and Traffic Theory* (in press).

Zhao, Y. and Kockelman, K. (2002) "The propagation of uncertainty through travel demand models: an exploratory analysis." *Annals of Regional Science*, 36, 145-163.

ANALYSIS ON STANDARDS USED IN TRAFFIC IMPACT STUDY

LEI Lei[1],CAO Jing[2],YANG Xiaokuan[3]

[1]Transportation Research Center, Beijing University of Technology, Beijing, China. Tel: (8610) 6739-1678; Email:yuwenleilei@126.com
[2]Transportation Research Center, Beijing University of Technology, Beijing, China. Tel: (8610) 6739-1678; Fax: (8610) 6739-2991; Email: caojing@bjut.edu.cn
[3]Professor, Transportation Research Center, Beijing University of Technology, Beijing, China. Tel: (8610) 6739-1678; Fax: (8610) 6739-2991; Email: xiaokuan@hotmail.com

ABSTRACT

Since traffic impact study (TIS) of projects has been carried out in Beijing for more than ten years, a series of noticeable results have been achieved. However, there are still some unsolved problems in TIS. For example, there is a lack of quantitative analysis of traffic organization and public transportation. The objective of this paper is to attempt to develop standards of traffic impact study to assist the government in developing an appropriate evaluation criterion for assessing transportation related projects. A total of four evaluation indicators have been selected. The four evaluation indicators include: variation of v/c ratio, complexity of conflict, index of transit capacity and satisfactory degree of the public to projects. These indicators have been defined and modeled in quantitative format and the results can be applied in the evaluation process.

Key Words: Traffic Impact; Evaluation and Analysis; Quantitative Analysis

1. INTRODUCTION

Many traffic impact studies (TIS) of projects have been conducted since 1995 in Beijing. They have played a positive role in coordinating the relationship between city development and traffic infrastructure, relieving the conflicts between traffic supply and demand, and improving the traffic performance of highways (Pei et al. 2004). However, based on the experience in Beijing and other provinces, unified standards are not applied in TIS. The study on some important factors such as traffic organization, v/c ratio of intersections and public transit, has been limited in qualitative analysis. There is a lack of research of quantitative analysis on standard of traffic impact studies resulting in an inaccuracy of the conclusions in assessments.

On the basis of analysis of related influential factors in traffic impact studies and comprehensive investigations in Beijing, a total of four evaluation indicators have been proposed in this paper. The four evaluation indicators include: variation of v/c ratio, complexity of conflict, index of transit capacity and the degree of public satisfaction with projects. In order to identify the importance and acceptable degrees of each indicator in traffic impact studies, appropriate evaluation methods and

standards have been decided by modeling and quantifying these indicators. As a result, the conclusion of research can be beneficially applied in the evaluation process.

2.V/C RATIO AND SERVICE LEVEL OF SIGNALIZED INTERSECTION

Volume to capacity ratio (or v/c ratio) of section has always been used to evaluate the effect of traffic caused by projects (BJUT et al. 2008). As we all know, the change of v/c of intersections has played an important role in affecting the operation of the road network. Therefore, the variation of v/c ratio is used to reflect the traffic impact the projects bring to the neighborhood areas.

2.1 DEFINITION AND CALCULATION

Variation of v/c ratio in fact reflects the intensity of change of traffic volume produced by projects on intersections located near the affected areas. Its mathematical expression is as follows:

$$P = \frac{L_f - L_p}{M_{LOSi}} \qquad (1)$$

Where: P—variation of v/c ratio;

M_{LOSi}—allowable maximum range of variation of v/c ratio under given level of service i,

L_f—v/c ratio of intersection after implementation of projects;

L_p—v/c ratio of intersection at present.

2.2 EVALUATION STANDARD

The acceptable change of v/c ratio and LOS of network in different areas is not the same, so there are differences in allowable v/c ratio among different intersections. Therefore, the relative agencies can decide whether the projects are accepted or rejected, unlike traditional ways of evaluating traffic projects in which average approach is applied. In this study, the so-called “one-item denies all” approach is proposed. This approach attempts to demonstrate that if one and only one item (for example v/c ratio) is not acceptable for evaluation, this whole project will be rejected. As is known, there are three types of conclusions when conducting traffic impact studies for any transportation-related project. They are: accepting, needing improvement, and rejecting.

Table 1 Variation of v/c Ratio When Level of Service Changes

When LOS A→B	Accepting	Needing Improvement	Rejecting
Variation of v/c Ratio	≤0.4	0.4-0.9	＞0.9
Average speed（km/h）	≥50	45-50	＜45
When LOS B→C	Accepting	Needing Improvement	Rejecting
Variation of v/c ratio	≤0.5	0.5-0.9	＞0.9
Average speed（km/h）	≥40	35-40	＜35
When LOS C→D	Accepting	Needing Improvement	Rejecting
Variation of v/c ratio	≤0.5	0.5-0.9	＞0.9
Average speed（km/h）	≤30	25-30	＜25
When LOS D→E	Accepting	Needing Improvement	Rejecting
Variation of v/c ratio	≤0.6	0.6-0.9	＞0.9
Average speed（km/h）	≤20	15-20	＜15

As for variable P, it is determined that when the LOS has skipped more than two grades (such as A→C,B→D) the project is to be rejected. If the LOS has skipped less than two grades（such as A→B, B→C）then the above Table 1 can be used as evaluation criteria in terms of traffic intensity.

3. TRAFFIC ORGANIZATION

A lot of references have been involved in the traffic organization. Based on analysis of the distribution of traffic flow, location of access, as well as various conflicts, the traffic organization has been evaluated in the previous studies (Wang et al. 2007). However, these analyses were qualitative and more indicators about traffic organization were involved in evaluation making it difficult to evaluate appropriately. Hence, quantitative indicators have been brought forward to simplify the evaluation process on traffic organization.

3.1 DESCRIPTION OF INDICATOR

Traffic organization plays an important role in traffic impact evaluation on projects. Reasonable traffic organization can make existing road networks work well, eliminate traffic congestion and potential dangers, and keep trips safe and convenient. In order to improve the evaluation process in terms of traffic organization, a parameter called “complexity of conflict” is proposed in this study as a quantitative indicator of the evaluation on traffic organization.

3.2 DEFINITION AND CALCULATION

Complexity of conflict represents intensity and the degree of conflicts among any traffic movements as a result of the projects. This indicator is used to evaluate levels of traffic organization on the basis of number of conflicts within an affected area. Its mathematical equation can be expressed as follows:

$$C = K(1+\lambda_1\delta_1)(1+\lambda_2\delta_2)\sum\sqrt{\frac{N_1+N_2}{2}}C_i \quad (2)$$

Where: C—complexity of conflict;

K—distance punishment factor, which reflects the impact of distance from access of project to the nearest intersection and its values are shown in Table 2;

C_i—the degree of conflict intensity (n=1,2,…9), the value is in Figure 1;

$_1$—vehicle-bicycle conflict factor. The value is 0.5 for residential areas, commercial areas, and public buildings, while the value is 0.2 for others.

$_1$—0-1 variables. The value is 0 when there is no vehicle-bicycle conflict or 1 otherwise;

$_2$—emergency traffic impact index, of which the value is 0.2;

$_2$—0-1 variables. The value is 0 when evacuation corridor is set and 1 otherwise;

N_1—the number of lanes of conflicting flow 1;

N_2—the number of lanes of conflicting flow 2.

3.3 INTRODUCTION AND CALCULATION OF PARAMETERS

(1) Distance punishment factor K

This factor is used to reflect how distance from access connected with projects to the nearest intersection impacts traffic organization. The further the distance, the greater the impact, and vice versa (BMICPD et al. 2004). The value of the punishment factor is different regarding different ranges of distance and is shown in Table 2.

Table 2 Punishment Factor

Distance from intersection(m)	≥150	50-150	≤50
K	1	1.25	1.5

(2) Conflict intensity C_i

This factor is vital in evaluating traffic organization and reflects different kinds of traffic conflict generated directly by various traffic organizations. The greater the value of C_i, the heavier the traffic conflict is. The value of C_i is shown in Figure 1.

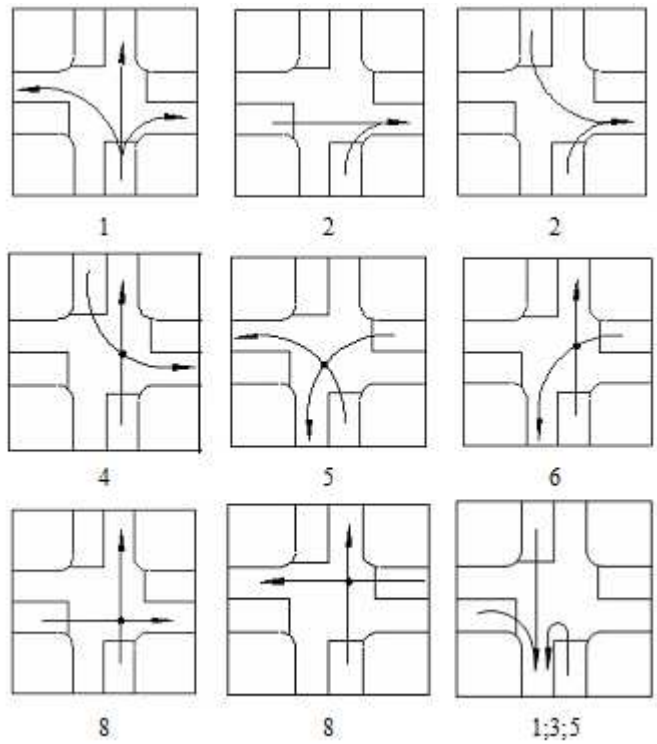

Figure 1 Complexity of Conflict in Different Cases

In figure 1, the last picture shows that when the number of lanes is 1, the conflict value is 5; when the number of lanes is 2, the conflict value is 3; when the number of lanes is 3, the conflict value is 1.

3.4 EVALUTION STANDARD

Based on the analysis of various traffic conflicts and the investigation of intersections, the evaluation criterion has been made in order to reduce conflicts and sustain safety. Finally, the evaluation conclusion for traffic organization is shown in Table 3.

Table 3 Complexity of Conflict

Indicator	Accepting	Needing Improvement	Rejecting
Complexity of Conflict	≤90	90~120	>120

4. PUBLIC TRANSIT

It's important to evaluate the impact of traffic caused by projects on public transit systems. Because of the many indicators involved in evaluation, it's difficult to obtain comprehensive data and the credibility of evaluation results seems rather low at present. In order to improve practicality of indicators, index of transit capacity has been selected to be an appropriate indicator in evaluation on public transit.

4.1 DESCRIPTION OF INDICATOR

The focus of the evaluation of impact on public transit systems is whether the demand for public transit trips generated by projects can be met. On one hand, the proportion of supply the nearest transit station to access offers to demand which is generated by projects should be considered. On the other hand, the service which is provided by public transit systems must also be considered. As the accessibility of transit stations is reduced, the probability of priority selection of station will be lower. This public transit indicator is provided on the basis of both considerations.

4.2 DEFINITION AND CALCULATION

Index of transit capacity is an indicator to demonstrate the ability of public transit to provide service to meet the travel demands generated by projects. The indicator allows the remaining capacity of public transit to measure the bus capacity and LOS. Accessibility adjustment is used to reflect the convenience of public transit, and there have been changes in capacity demand of public transit as accessibility is reduced. Its mathematical expression is as follows:

$$K_i = A \cdot Q_i = f(S_i) \cdot Q_i \tag{3}$$

Where: K_i—index of transit capacity in station i;

A—accessibility adjustment factor, is decided by the accessibility adjustment function $f(S_i)$. The value of it is shown in Table 4;

Q_i—The proportion of the remaining capacity to demand of public transit in station i ;

4.3 INTRODUCTION AND CALCULATION OF PARAMETERS

(1)Accessibility

The accessibility is obtained by function $f(S_i) = 0.15 \cdot \tanh(\frac{500 - S_i}{159.155}) + 0.85$, and the values are as shown in Table 4.

Table 4 Adjustment Factor of Accessibility

Accessibility (km)	0-200	200-300	300-400	400-500	500-600	600-700	700-800	800-1000
Adjustment Factor	0.998	0.988	0.960	0.896	0.804	0.740	0.712	0.702

(2) The proportion of the remaining capacity to demand of public transit

The remaining capacity can be gained by investigation of stations near the access of projects and public transit demand can be gained by trip prediction. The value is 1 when the capacity meets the demand and less than 1 otherwise.

4.4 EVALUATION STANDARD

Considering operation of public transit and actual need of evaluation, the results are divided into three conclusions according to the threshold as shown in Table 5.

Some of the thresholds should be adjusted in consistence with special cases in reality. The indicator is proposed to simplify the process of actual operation, considering the merits and demerits of other indicators comprehensively.

Table 5 The Value of Capacity Index of Transit

Indicator	Accepting	Needing Improvement	Rejecting
Capacity Index	≥1.2	1.2~1.0	<1.0

5 ENVIRONMENT INDICATOR

The indicator reflecting traffic impact on the environment is completely new in traffic impact studies. With more attention from government and public on living and working environments, the indicator reflects integrated effects of the surrounding environment and it definitely plays a more important role in the evaluation of planning projects. This indicator discussed in the paper is not the same as the environmental indicators which reflect the water pollution or air pollution. The indicator here is mainly put forward to describe the public's perception and feeling in regard to the external environment, as well as landscape created by projects. Therefore, the degree of public satisfaction with projects is brought forward to reflect traffic impact of related projects on the environment.

5.1 DESCRIPTION OF INDICATOR

According to the research of living environmental assessment, the criterion of livable city (You et al. 2008) is also available for environmental evaluation of traffic impact evaluation. Three factors, including safety, health and perception, are selected to assess environmental evaluation comprehensively in consistence with the demand of "livable city". Hence, the degree of public satisfaction with projects is proposed to integrate three factors above. This is a new indicator which reflects environmental effects caused by projects. It should be noted here that this indicator is different from those traditional environmental indicators.

5.2 DEFINITION AND CALCULATION

The degree of public satisfaction with projects is the degree of public satisfaction with environmental changes from safety, health and perception (or feeling). It reflects the influence on living and working environments when the projects are implemented.

$$E = \sum_{i=1}^{3} \alpha_i A_i \qquad (4)$$

Where: E —degree of public satisfaction with projects;

$_i$—the weight of factor i ;

A_1—safety satisfaction factor;

A_2—health satisfaction factor;

A_3—perception satisfaction factor,

5.3 DATA INVESTIGATION

The key of the environmental assessment is to gain the degree of public satisfaction with safety, health and perception of the projects. Therefore, the values of three factors are obtained through questionnaires. From the investigation results, the evaluation index of the degree of public satisfaction with projects can be obtained. In practical application, investigators need to collect as many samples as possible in order to increase the credibility of data.

5.4 EVALUATION STANDARD

Finally, the conclusions are divided into three results as shown in Table 6. In light of this fact, this indicator has occupied a smaller weight in traffic impact evaluation. It can be used as the reference indicator to assist with temporary decision making.

Table 6 Degree of Public Satisfaction with Projects

Indicator	Accepting	Needing Improvement	Rejecting
Satisfactory Degree	≥ 4	2-4	＜2

6 EVALUATION AND APPLICATION

On the basis of analysis of the indicators above, “Dual-degree evaluation method” is proposed to apply in the evaluation work. It means that variation of v/c ratio and complexity of conflict are used to be the criteria, and capacity index of transit and degree of public satisfaction with projects are used as reference indicators in evaluation. Specific operation is as follows: Variation of v/c ratio and complexity of conflict are kept as the previous and key indicators in evaluation. If both of them are accepted, the project will be permitted. If either of them is accepted, the project is to be improved. If neither of them is accepted, the project will be rejected. If both of them need to be improved, capacity index of transit and degree of public satisfaction with projects can be used as reference indicators to assist related agencies to work out an appropriate result for related projects.

7 CONCLUSION

On the basis of analysis of traffic demand and network structure, the flow distributions and travel mode distributions of traffic generated by related projects are obtained. Using the advanced experience of foreign countries (Guide for the Preparation of TIS 2002), a total of four indicators and corresponding evaluation methods are proposed to be applied in practice. These indicators are presented for practicality and reasonableness in the process of assessment, considering the merits and demerits of various indicators comprehensively. Variation of v/c ratio is proposed for the first time, which reflects the intensity of traffic flow on intersection. Complexity of conflict is proposed to do the quantitative analysis on conflicts of intersections, based on analyzing the factors and types of various conflicts affecting

the traffic organization. The environmental indicator of degree of public satisfaction with projects is also proposed as a reference indicator in traffic impact studies for the first time, as well. The theory proposed in the paper is the exploratory development, which requires a lot of data and cases to test and verify. It's necessary to do more investigations and collect much more available data to substantiate the validity of the evaluation standards set for these indicators. As a result, reliability and availability of the indicators and related parameters also need to be improved in evaluation.

BIBLIOGRAPHY

Beijing Municipal Institute of City Planning and Design (BMICPD), Beijing University of Civil Engineering and Architecture, and Beijing Traffic Management Bureau. (2004). Report of Traffic Impact Study, 2004.

Beijing University of Technology (BJUT), and Beijing HaiLuDa Engineering and Technology Limited Company. (2008). Report of Indicators and Standard Research on Traffic Impact Study of Projects in Beijing, 2008.

Guide for the Preparation of Traffic Impact Studies (TIS). State of California Department of Transportation(2002). http://www.dot.ca.gov/hq/traffops/developserv/operationalsystems/reports/tisguide.pdf (December 2002).

Pei, Y.L., and Wang, X.N. (2004). "Determining method of traffic impact range of project". Journal of Traffic and Transportation Engineering, 4(3):82-84, 2004.

Wang, X., Hong, K., and Li, L.L. (2007). "Design and research of traffic organization in traffic influence analysis". Shan Xi Architecture, 33(3):28-29, 2007.

You, Y., and Ming, L.B. (2008). "From 'livable city' to 'livable region'". Shanghai Urban Planning Review, (4):23-26, 2008.

Study on the Location Parking Index Based on Function Division of Parking Space

Li Lin-bo[1], Wang Man[2], Wu Bing[3]

[1,3]School of Transportation Engineering, Tongji University, 4800 CaoAn Road, Shanghai, 201804; PH (21)6958-3007; FAX (21) 6958-3712; Email: llinbo@tongji.edu.cn

[2] Ningbo Rapid transit Company, 668 LiYuan North Road, Ningbo city, Zhejiang province, 315000; PH:013957837152; Email: amanda_2007@yahoo.cn

Abstract: The method to determine the parking index of buildings is always based on the geographical position division and the building classification standard, which reflects the external parking demand characteristics of the building, but only considers the perspective of the geographical position and building and gets lop-sided. Therefore, the size of parking is difficult to determine for future needs with the change of the developing environment. This paper will revise the parking index model based on the ontological idea and function division of parking space with regard to its internal characteristic, in combination with the analysis of the parking location attribution, and increase the adaptability of the parking. At last, the paper will demonstrate that the new method used to determine the parking index is more comprehensive and objective when compared to the general method.

Keywords: parking index, the parking function, ontological idea, locational factor

0. Introduction

The parking problem is closely connected with the city plan, the city land-use and the structure of traffic infrastructures, which is important to ensure traffic safety, traffic free-flowing and the clean production environment (Wang Jing-xia, 1999). At the present time, the method used to determine the parking index is to adopt the investigation and statistical measure based on the geographical position partition and the construction classification standard, to a certain degree which reflects the external parking demand characteristic of the building, but has a potential hypothesis that the developing environment, which in fact always is in the process of dynamic changes, is consistent and stable. Therefore, the number of parking spaces resulting from the parking standard index is difficult to meet with the development of society and economy. In reality, we should make the parking size under the special environment condition in combination with the regional planning strategy. This paper should analyze the function of parking space in building and revise the parking standard index based on the ontological idea in combination with the consideration of location factors.

1. Analysis of the impact factors on parking demand

There are many impact factors on parking demand which include population scale, number of working position, vehicle volume and classification, parking management policy and so on from the view of the whole city planning. Also involved are the travel purpose, the parking price, parking utilization rate and turnover ratio, the form and intensity of land development, road capacity constraints and so on judging from the parking analysis of some building projects. However, it is

found that the main factors considered are from the external environment of the parking behavior. In fact, it is the internal slow variable that makes the decision for the parking demand.

Property of ontology is one kind of inside attribution of system, and the periphery environment can only be to be an object. If the system needs to increase its inner steady, the analysis must set off from the systematic property of ontology. (Guan Chu-du, 2000). However, current research almost unfolded surrounding the subjective and objective equilibrium theory. The property of subjective and objective equilibrium is a characteristic that the interaction of the systematic inner factors and the outside environmental factors make the subject and the object gain equal satisfaction. When creating a parking facilities plan, the traffic location factors surrounding the equilibrium of the parking demand and the traffic environment are always considered. The defects of the method lie in no discussion of the dominated effect exerted on the traffic demand by the inner factors of building. Once the outside environment changes, the parking facilities can't adapt to the changing needs. The only effective way is to improve the parking systematic stability using ontology theory if we want to make the parking facilities capable of withstanding the configuration of wide field environmental changes. For example, travel purpose and turnover rate of the parking space are the inherent characteristics of parking behavior. A different travel purpose often determines the parking time which is the key factor that decides the parking index of the building. It is more adaptive to determine the parking size based on these two factors. Therefore, in the study of parking index, we should focus on the internal slow variables while also considering the external environment.

2. Analysis of the parking function response for the parking demand

Different travel purposes will create different parking demands, and the parking demand diversity corresponding to the various parking spaces is the parking space function. In fact, even with a different building function in the same central business district, the function of parking spaces often is not consistent, mainly because the building function often determines different parking demand characteristics.

The different parking space function actually corresponds to different parking demand nature. According to the parking time, parking space function can be divided into long-time parking, medial-time parking and short-time parking, or be divided into internal and external service functions according to the service group. Generally speaking, commuter trips such as working and going to school have stable parking demand, and need long parking time and fixed parking place. The flexible travels for the purpose of business, catering and entertainment require a shorter parking time and involve careful parking space selection. Investigation of the parking characteristics of Gaoyang hotel and Yuehai hotel in Hongkou district of Shanghai (see fig.1 and fig.2) found that each period before late peak has a stable saturation, after late peak the parking saturation falls rapidly at the Gaoyang hotel. This status reflects the Gaoyang hotel parking place has a good operating factor in working hours but a low usage at night. Because the parking place services itself, there is a low parking saturation on holidays. On the contrary, at the Yuehai hotel, the parking saturation has the same change in the working days and holidays. In addition, the average parking time and peak parking time distribution also differs greatly in the

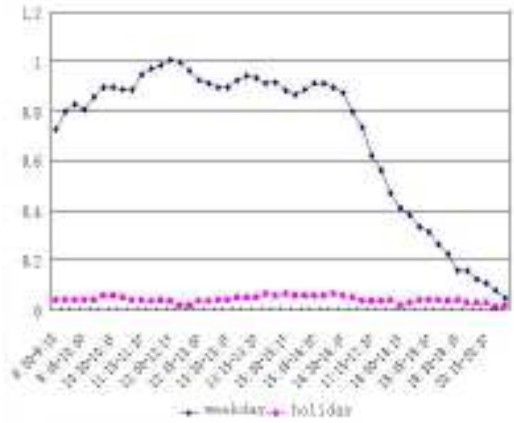

Fig.1 Parking saturation change status in Gaoyang hotel

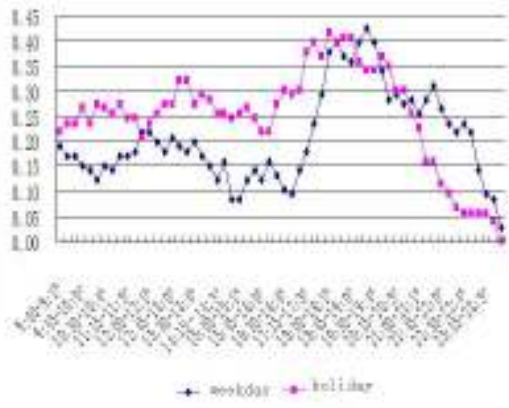

Fig.2 Parking saturation change status in Yuehai hotel

two parking places (see table 1). The survey found that the Gaoyang parking mainly services staff and foreign business personnel, and because travelers use the month card to pay for the parking fee and lightly consider the parking cost, the average parking time is longer. Yuehai hotel parking opens to the public, so parking demand is stable in the working days and holidays. Apparently, the different functions of parking space create the different usage. Therefore, if an analyis of the parking behavior with different demand characteristics from the parking space function division is performed, a better understanding of the response characteristics of different building parking demands will be achieved, thereby increasing the adaptability and stability in parking.

Table 1. Parking supply and demand status for Gaoyang hotel and Yuehai hotel

place	time	Number of the parking	Peak saturation	Average saturation	Turnover rate	Average parking time(minute)
Gaoyang hotel	Working day	136	1.01	0.70	2.32	239
	Holiday	136	0.07	0.04	0.26	235
Yuehai hotel	Working day	106	0.43	0.20	1.91	138
	Holiday	106	0.2	0.25	2.08	177

3. The influence of location condition on the parking demand

Location differences need to be considered because parking supply and demand relation is not only a project planning problem, but also a traffic resource allocation problem. Location becomes the compound concept of the trinity of position, transportation, and economics. We can think of it as the specific performance for the organic combination of natural geographic location and economic geographic location and traffic geographic location in space (Lu Hua-pu, 2006). Location factors and their different combinations form different location conditions also impacting the parking demand diversity.

From the analysis of the geographical location, parking demand diversity mainly

results from the difference of travel structure. The regional planning of urban areas creates different land use patterns which directly affect traffic structure. For example, central land use status requires public transport with a high capacity and the ability to require free traffic pattern conversely.

Traffic location can be considered from two aspects. One is traffic accessibility, which reflects the degree of convenience, the factor inducing motor vehicles into the parking places. Second is the bus service level, which reflects the ability of traffic sustainable development, the factor inhibiting parking behavior. Traffic accessibility and traffic area land-use clustering is proportional to the location potential, the ratio of the location potential between the ideal location and the study location. These reflect the advantage of the study location which also can be regarded as the effect value of traffic location on the travel.

The influence of the economic factor of location on the parking demand is mainly concentrated in the traveler. In a different area, the economic activity intensity diversity can also influence the parking demand: higher intensity, more travel times, more vehicles, more total parking demand. (Xiao Fei, 2009). On the other hand, whether the parking supply meets the parking demand also has influences on the development of regional economy.

4. Parking demand calculation based on the parking space function division

For parking demand at home and abroad, the calculation method has many major categories. One can be summarized as the parking demand and land-use analysis model with the parking production as the core, the other is the attracting travel model with the relationship between parking and vehicle travel as the core and the last is the multivariate regression analysis model based on the related analysis (Wu Tao, Yan Kefei, 2002). These methods are based basically on the subject and object equilibrium concept. This study will revise the parking index standard based on the analysis of parking space function division and location conditions to better reflect the building internal parking demands.

- The influence of the parking space function division on the parking index

First, the parking properties of the building should be identified as simple or public. Next, the parking space function needs be divided by referring the adjacent building with the same function, and determining the parking modifier based on the parking main function classification. Then, analyze the parking status quo and the policy guidance surrounding the parking, such as by parking sharing strategy to improve the overall efficiency of the parking. The parking space function correction coefficient is as follows:

$$\phi = \lambda \cdot \sum u_i d_i \qquad (1)$$

In equation: ϕ - parking space function correction coefficient; u_i - the modifier corresponding to different functions of parking space; d_i - share rate corresponding to different functions of parking space; λ - the modifier of the parking space sharing.

- The influence of the geographic location on the parking index

Both at home and abroad the location diversity in the static traffic aspects are mainly reflected in land use without consideration for the district function division. The regional diversity, historical background and structural diversity in different cities is different, so from the view of geographical factors, the determination of the

building parking index cannot be made according to the ring highway. Therefore, according to Wang Man (2009), this study would divide the city regions as urban center, urban edge, suburban area and suburban area edge to indentify the correction coefficient y_1 as table 2.

Table 2. Geographic location correction coefficient

Area / Correction coefficient	urban center	urban edge	suburban area	suburban area edge
y_1	1.0	1.0	1.1	1.2

- The influence of the economic location on the parking index

For the parking demand with the same nature, the land-use diversity would result in the demand difference. In CBD area, for example, there are three typical land-use patterns: the integration type, the hub type and the belt type center business district, others are mostly a combination of these three patterns. The different land use resulted in the different economic prosperity degree, which is reflected in the parking demand as parking demand characteristics. This study chooses the parking turnover as the representation of economic location in association with the comprehensive traffic survey data of Shanghai city (Wang Man, 2009). Therefore, the economic location correction coefficient can be represented:

$$y_2 = F_r \Big/ F_s \qquad (2)$$

In equation: F_r - the building parking turnover rate; F_s - the average turnover rate in city.

- The influence of the traffic location on the parking index

As indicated above, the influence of traffic location on the parking index is mainly embodied in two aspects: one is the traffic location potential and the other is the bus service level.

The influence of different traffic location potentials on parking demand is represented as the effect of location potential to travel which determines the concrete influence value. The traffic location potential means the ability to produce and attract travel, and is proportional to traffic accessibility and the traffic area land-use cluster (Wang Xiu-lin, et al. 2004). After calculating the inside accessibility and land-use cluster, we can get the traffic location correction coefficient as follow (Wang Man, et al. 2009):

$$y_3 = \left(\frac{K_r L_r}{K_s L_s}\right)^{\chi} \left(\frac{S_r}{S_s}\right)^{\delta} \qquad (3)$$

In equation： K_s - the standard average road grade; K_r - the reality average road grade; L_r - the reality road service lever ; L_s - the average road service lever; S_r - the reality cluster factor; S_s - the average cluster factor; χ - the elastic coefficient resulting from the contribution of traffic accessibility factors to the location potential growth; δ - the elastic coefficient of comprehensive cluster factors to the location potential growth.

The influence of public transportation on the parking lies in its ability to substitute cars. According to a survey, when the bus service level is high, 10 percent of people are willing to transfer from car to bus, with a higher service level, the proportion reaches 26%. With reference to the Hong Kong experience, it is suggested that the building of office, commercial and residential properties can decrease the parking supply 5% ~ 20% in a 500m range around the metro. It can greatly reduce the number of parking places in the central office building, while at the same time increasing the parking places of the rail transit site. The bus service level correction coefficient can be represented as follow:

$$y_4 = 1 - n_1 / n \qquad (4)$$

In equation: n_1 - the travel volume shifting from cars ; n - the total travel volume.

Through the analysis of the influence of the internal location factors on parking demand, we can obtain the method to identify the building parking demand under the consideration of the location conditions. The correction model can be expressed as:

$$P = \phi \cdot y_1 \cdot y_2 \cdot y_3 \cdot y_4 \cdot P_0 \qquad (5)$$

In equation: P - the building parking demand modifier; P_0 - the building parking demand by the standard parking index.

5. Case study

A building project with commercial and office integration located in Huaihai middle road in Luwan district of Shanghai, has technical parameters for the developing project as listed in the following table (see Table 3.)(Wu Bing, Li Lin-bo, Wang Man et al. 2009). According to the Shanghai Building Engineering Traffic Design and Parking (field) Set Standards, the building needs 385 parking places.

Table 3 . Basic technical parameter for the developing project

Total building area (m^2)	Hotel building area (m^2)	Office building area (m^2)	Hotel rooms (room)	Hotel apartments (room)	Villa guest rooms (room)
85,129	44,820	25,180	419	34	15

The analysis of the building attributes found that the parking place only opens to the internal personnel including stable office workers and flexible business flow into the building. But in fact, because of the uncertainty of business flow, in a certain level, it also owns the opening attributes of public parking.

The parking lot of the New Century building near the project, has the same function and attributes, so we thought that the new building would have the same parking demand properties as the New Century building. Through the investigation of the parking lot of the New Century building, we can get the parking number and parking time of different time periods (see fig.3 and fig.4).

After analyzing the peak time and parking time of the parking lot in the New Century building, the study defines 0~1.5 hours as short-time parking, 1.5~3 hours as middle-time parking and 3 hours as long-time parking. The investigation found that

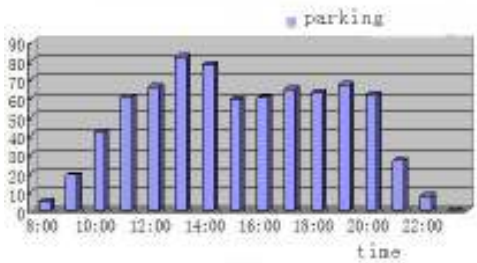

Fig.3 Parking time –vary figure in New century

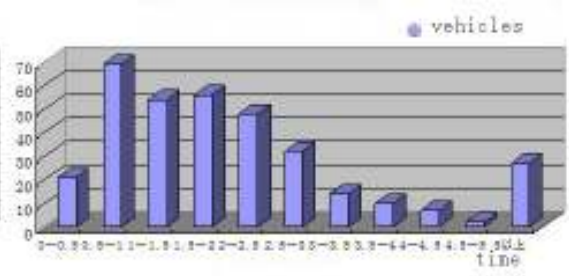

Fig.4 Parking time-distribution figure in New century

the average time is 52 minutes for the short-time parking, 135 minutes for the middle-time parking and 288 minutes for the long-time parking.

According to the Shanghai third traffic comprehensive survey data, the average parking time is 193 minutes in CBD and the corresponding parking space function is long-time parking, so we can get that $u_1 = 52/193 = 0.27$, $u_2 = 135/193 = 0.70$, $u_3 = 288/193 = 1.49$. According to the parking properties investigation in the area where the project is located, the share rate of different parking space function can take $d_1 = 15\%$,$d_2 = 50\%$,$d_3 = 35\%$,and get $\phi = 0.82$. At the same time, the parking peak in various parking lots is different in different time periods, so we can consider appropriate parking is shared and take λ for 0.9. Geographical location correction coefficient y_1 = 1. In the investigation case, the actual parking average turnover rate was 1.64, however the average turnover rate in the CBD was 2.35, so $y_2 = 0.763$. After the survey of the road grade level around the project and prediction, we can get K_r =1.778 , L_r =3.437 , L_s =3.520 , $K_s = 1.713$. This location has the fashion landmark, and through the analysis of the travel attraction to the eight business area, we can take s_r / s_s =1.1, and get $y_3 = 1.022$. The survey of the bus service level in this area found that 10 percent of travelers with motor vehicles were willing to shift to bus, therefore, y_4 can take 0.9. Now we can get the parking demand modifier as follows:

$$P = \phi y_1 y_2 y_3 y_4 P_0 = 0.82 \times 1.0 \times 0.763 \times 1.022 \times 0.9 \times 385 = 223$$

Comparing the modifier with the standard value, we found the parking volume in demand is decreased 162. In fact, the modifier is better to meet with the building parking demand with reference to the parking operation status quo in near buildings.

6. Conclusion

This study, aiming at the problems existing in the parking index standards, thought that the parking index based on the object and subject equilibrium theory cannot reasonably reflect the building's parking demand. To make the building parking scale meet the wide changes of the developing environment, we should adopt the concept of ontology to modify the parking standard index model based on the building parking space function division in combination with location condition. The

case study illustrates that the parking index based on the parking space function division and location conditions analysis can better reflect the building parking inherent demand, actively meet the wide changes of the developing environment, and provide a new train of thought to the development of the parking theory.

Reference:

Guan Chu-du. (2000). *Communication location Methodology and application*, Beijing: China communication Press.

Lu Hua-pu. (2006). *Theory and method in transportation planning*. Beijing: Tsinghua university press.

Wang Jing-xia. (1999). *Parking development strategy for urban in china*. Public Utilities, 5（13）:16~17.

Wu Bing, Li Lin-bo, Wang Man et al. (2009). *Traffic impact analysis for the 8th block recreational project in Luwan district*. Tongji University.

Wang Man ,Wu Bing ,Li Lin-bo. (2009). *Research on the quota of parking lots based on location condition, traffic information and safety*. 27(1): 44-47.

Wang Man. (2009). *Research on the supply of parking facilities in the city based on location condition*. Tongji University.

Wang Xiu-lin, Wang Chao, Liu Shu-hong, Wu Jia-you. (2004). *Study on parking demand forecasting model based on location and traffic allured*. Economic Geography. 24(6): 726-728.

Wu Tao, Yan Kefei. (2002). *The mechanism study on the parking demand management*. City Planning Review, 26(10): 85~88.

Xiao Fei. (2009). Parking in convergence zone of modern service industry. Tongji University.

Study on Traffic Impedance Based on Grey Theory

Wang Qiu-ping[1], Du Ye-fan[2], Wu Jin-pu[3]

[1]Professor, Institute of Civil Engineering, Xi'an University of Architecture & Technology, NO.13 Yanta Road, Xi'an, Shaanxi Province, ST: 710055; PH: 0086-(0)-1337 9254 751; email: wqp1168@sina.com

[2]Postgraduate Candidate, Institute of Civil Engineering, Xi'an University of Architecture & Technology, NO.13 Yanta Road, Xi'an, Shaanxi Province, ST: 710055; email: dyfduyefan@163.com

[3]Postgraduate Candidate, Institute of Civil Engineering, Xi'an University of Architecture & Technology, NO.13 Yanta Road, Xi'an, Shaanxi Province, ST: 710055; email:wjpwujinpu@163.com

ABSTRACT

Traffic impedance is an important parameter in the urban traffic network's study. It directly affects traffic flow path selection and flow assignment. Traffic impedance can be described by a traffic impedance function in the traffic flow assignment, so the accuracy of establishing a traffic impedance function immediately affects the study's performance on the traffic network equilibrium. In this paper, a traffic impedance function is established, which is based on a narrow-sense traffic impedance and grey system theory. In order to effectively determine this, the section between Lujia Village and Lijia Village in Xi'an is analyzed and the traffic impedance function of this section is fitted. Through a comparison with the survey data, it is shown that the analogue result is accurate. Because this section is located in the urban arterial street, the fitted traffic impedance function has a valuable reference to similar situations, especially the urban arterial street in Xi'an.

INTRODUCTION

Traffic impedance is an important parameter in the urban traffic network's study. It directly affects traffic flow path selection and flow assignment. Traffic impedance can be described by a traffic impedance function in the traffic flow assignment. The traffic impedance function refers to the relationship between travel time and traffic loading of road section and delay and loading of road intersection. (Shao Chun-fu 2006) Generalized traffic impedance includes many factors, such as travel time, traffic cost, traffic delay, comfort degree, security and convenience. After performing extensive studies and analysis, it can be concluded that travel time is a critical factor and that a narrower definition of traffic impedance is necessary. Traffic impedance refers to the required time when vehicles pass through the path. the traffic impedance function is the mathematical expression which quantifies traffic impedance.

In the urban traffic network equilibrium, traffic impedance function describes the relationship between traffic flow and travel time, and the relationship is usually

proportional. As the first step in the urban traffic network study, the accuracy of establishing a traffic impedance function immediately affects the study's performance on the traffic network equilibrium. At present, the most common section impedance function is function BPR in the traffic network equilibrium study. However, it is not suitable to use the BPR impedance function directly in an urban mixed traffic environment in China. On one hand, because the function is attained from an investigation of a statistical database of American suburban highways, it is only suitable for long-distance road networks. On the other hand, considering the special situation of urban mixed traffic networks in China, the section impedance function as well as the correlation parameters should be demarcated (Si Bing-feng and Zhong Ming 2008).

In view of the above, a traffic impedance function is established, which is based on a narrow-sense traffic impedance and grey system theory.

GREY SYSTEM AND GM(1, 1) MODEL

Grey system theory and modeling idea. Grey system prediction theory is a relatively new prediction theory developed in the early 1980s. It takes an uncertain system, which is "partial information known, partial information unknown", "small sample" and "poor information", as a research object. Then, through producing and developing the right "part" of the known information, the valuable information is extracted, thereby the correct description and effective monitor to the system operating behavior and evolved rule is realized (Liu Si-feng and Dang Yao-guo 2004).

Grey system searches variation regularity through mining and sorting original data, which is a method of using data to search for data on reality law. Based on least square method, GM(1, 1) model can fit the sequence pairs to be curved to the utmost extent, and achieve a corresponding function equation. Usually, even when a small amount of new data is given, the model can also simulate function precisely.

GM(1,1) model. GM(1,1) modeling and solution process are as follows (Liu Si-feng and Dang Yao-guo 2004):

Sequence operator treatment. Assuming the primitive sequence is:

$$X^{(0)} = (x^{(0)}(1), x^{(0)}(2), \cdots, x^{(0)}(n))$$

with: $x^{(0)}(k) \geq 0, \quad k = 1, 2, \cdots, n$

$X^{(0)}$'s 1-AGO sequence $X^{(1)}$:

$$X^{(1)} = (x^{(1)}(1), x^{(1)}(2), \cdots, x^{(1)}(n))$$

with: $x^{(1)}(k) = \sum_{i=1}^{k} x^{(0)}(i), \quad k = 1, 2, \cdots n$

Average of adjacent value in $X^{(1)}$ consist of sequence $Z^{(1)}$:

$$Z^{(1)} = (z^{(1)}(2), z^{(1)}(3), \cdots, z^{(1)}(n))$$

with: $z^{(1)}(k) = 0.5(x^{(1)}(k) + x^{(1)}(k-1)), \quad k = 2,3,\cdots n$

Model building and parameter solution. The basic form of building GM (1, 1) model is:

$$x^{(0)}(k) + az^{(1)}(k) = b$$

Then the least square estimation parameters column of GM(1,1) basic model is:

$$\hat{a} = [a,b]^T = (B^T B)^{-1} Y$$

with: $Y = \begin{bmatrix} x^{(0)}(2) \\ x^{(0)}(3) \\ \cdots \\ x^{(0)}(n) \end{bmatrix}, \quad B = \begin{bmatrix} -z^{(1)}(2) & 1 \\ -z^{(1)}(3) & 1 \\ \cdots & \cdots \\ -z^{(1)}(n) & 1 \end{bmatrix}$

By substitution of above parameters into the original model, GM (1,1) function is obtained:

$$\hat{x}^{(1)}(k+1) = \left(x^{(0)}(1) - b/a\right)e^{-ak} + b/a, \quad k = 1,2,\cdots,n$$

Then, by using the value which is obtained above with continuous subtraction reduction, the estimated value is attained:

$$\hat{x}^{(0)}(k+1) = \hat{x}^{(1)}(k+1) - \hat{x}^{(1)}(k); \quad k = 1,2,\cdots,n$$

GM(1, 1) model accuracy test. Substitute the value of sequence K into the GM(1,1) equation, the simulated value of original sequence is attained as well as the simulated error sequence ε:

$$\varepsilon(k) = x^{(0)}(k) - \hat{x}^{(0)}(k), \quad k = 2,3,\cdots,n$$

Its average relative error is:

$$\bar{\Delta} = \frac{1}{n-1}\sum_{k=2}^{n}\frac{|\varepsilon(k)|}{x^{(0)}(k)}, \quad k = 2,3,\cdots,n \tag{1}$$

Accuracy test level is shown in Table 1 (Liu Si-feng and Dang Yao-guo 2004).

Table 1. Accuracy test level.

precision rank	first order	second order	third order	fourth order
the critical value of relative error	0.01	0.05	0.10	0.20

Steps of fitting the road section impedance function with GM(1,1) model:

1) Take the investigated vehicle speed as original data sequence.

$$X^{(0)} = (x^{(0)}(1), x^{(0)}(2), x^{(0)}(3), \cdots, x^{(0)}(n))$$

2) Carry on operator processing to original data sequence.

Carry on 1-AGO operator processing to $X^{(0)}$ and obtain $X^{(1)}$, then $Z^{(1)}$ is attained with average of adjacent value in $X^{(1)}$.

3) Build GM(1,1) model, solve it and carry on subtraction reduction, then the time response function is shown as：

$$\hat{x}^{(0)}(k+1) = (1-e^{a})\left(x^{(0)}(1) - b/a\right)e^{-ak}; \quad k = 1, 2, \cdots, n$$

4) Check accuracy of the model according to the fitting value which is obtained from above.

5) When the distance is constant, according to the relationship between time and speed, the section impedance function which takes time as impedance is obtained.

EXAMPLE ANALYSIS

Background information. Based on the theory above, the traffic flow and vehicle speed in the section between Lujia Village and Lijia Village in Xi'an are analyzed, and the traffic impedance function of the section is obtained. In practice, the function is always estimated with five to eight data. Too many data will bring larger fitting errors and lower accuracy (Xie Chen-li and Xia Hong 2007). In view of the above, the author extracts eight data from even peak time and peak time respectively. The data obtained from field survey is shown in Table 2 and Table 3.

Table 2. Even peak time survey data.

the average minute traffic volume (pcu/min)	16	17	18	19	20	21	22	23
the average vehicle speed(m/s)	13.33	12.77	12.37	11.65	11.11	10.34	9.92	9.38

Table3. Peak time survey data.

the average minute traffic volume (pcu/min)	22	23	24	25	26	27	28	29
the average vehicle speed(m/s)	9.68	9.16	8.57	7.69	6.70	5.85	5.45	5.06

Establish traffic volume-vehicle speed function.

***Original data processing*.**

$$\text{Define:}\begin{cases} q_1 = k + 15 \\ q_2 = k + 21 \end{cases}$$

with: q_1——the average minute traffic volume in the even peak time;

q_2——the average minute traffic volume in the peak time;

k——sequencing time, $k \geq 1$;

***Establish traffic volume-vehicle speed function*.**

Based on the method stated in this paper, the fitting results are obtained as follows:

The traffic volume-vehicle speed function in the even peak time:

$$\hat{x}(q_1) = 13.60135527 \exp(-0.052752 \times (q_1 - 15)) \quad (2)$$

The traffic volume-vehicle speed function in the peak time:

$$\hat{x}(q_2) = 10.3459925 \exp(-0.10611 \times (q_2 - 21)) \quad (3)$$

Precision inspection. Simulate and restore the average vehicle's speed through using function (2) and (3), the results are shown in Table 4 and Table 5.

Table 4. Vehicle speed simulation value of even peak time.

the average minute traffic volume (pcu/min)	17	18	19	20	21	22	23
the average vehicle speed(m/s)	12.9025	12.2395	11.6106	11.0140	10.4480	9.9111	9.4019

Table 5. Vehicle speed simulation value of peak time.

the average minute traffic volume (pcu/min)	23	24	25	26	27	28	29
the average vehicle speed(m/s)	9.3044	8.3677	7.5253	6.7677	6.0863	5.4736	4.9225

According to function (1): $\overline{\Delta}_1 = 0.0067$; $\overline{\Delta}_2 = 0.0204$;

Compared with Table 1, the accuracy is the first order in the even peak time and the second order in the peak time. It is shown that the fitting is precise. The

comparison between prediction values and actual values is shown in Figure 1 and Figure 2.

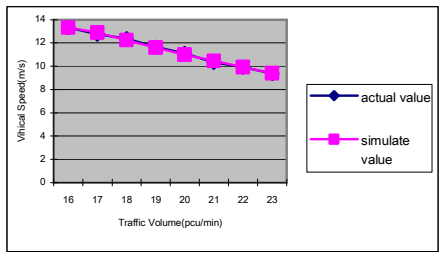

Figure 1. Chart of even peak time and actual value simulate comparison.

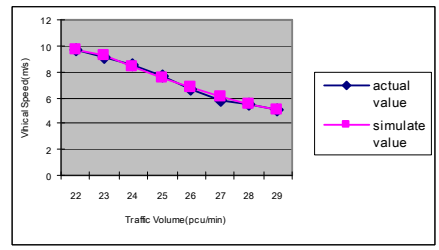

Figure 2. Chart of peak time simulate and actual value comparison.

Build road section impedance function. Assuming the road section length is *l* and time is taken as impedance, the section impedance function is:

$$t(q) = \frac{l}{\hat{x}(q)}$$

with：q = the average minute traffic volume (pcu/min)

$\hat{x}(q)$ = the section vehicle speed when the minute traffic volume is q (m/s)

t(q) = the time pass through section *l* when the minute traffic volume is q (s)

Then, the road section impedance function in the even peak time is:

$$t(q_1) = \frac{l}{\hat{x}(q_1)} = \frac{l}{13.60135527\exp(-0.052752\times(q_1-15))}$$

The road section impedance function in the peak time is:

$$t(q_2) = \frac{l}{\hat{x}(q_2)} = \frac{l}{\hat{x}(q_2) = 10.3459925\exp(-0.10611\times(q_2-21))}$$

CONCLUSION

The accuracy of road section impedance function is playing an important role on urban traffic network balanced research; it immediately affects validity of the research. Based on grey system theory, the author analyzed the section between Lujia Village and Lijia Village in Xi'an for example and fitted the traffic impedance function to this section. Through a comparison of the survey data, it is shown that the analogue result is accurate. Because this section is located in the urban arterial street, the fitted traffic impedance function has a valuable reference to the similar situation, especially the urban arterial street in Xi'an. During building model, several uncertain

factors were not considered, such as the drivers' psychological delay, weather conditions and curb parking. Thus, further research seems necessary.

ACKNOWLEDGEMENTS

Financial support was provided by Shaanxi Natural Science Foundation ($2007E_232$) and Shaanxi Provincial Department of Education (natural science research project (08JK334)).

REFERENCE

Liu Si-feng, Dang Yao-guo.(2004). "Grey Systems Theory and Applications". *Science Press*, Beijing.

Shao Chun-fu.(2006). "Traffic Planning". *China Railway Publishing House*, Beijing.

Si Bing-feng, Zhong Ming; GAO Zi-you.(2008). "A Link Resistance Function of Urban Mixed Traffic Network". *Journal of Transportation Systems Engineering and Information Technology*,8(1),68~71.

Xie Chen-li, Xia Hong.(2007). "Application of GM (1,1) gray model in trend prediction of the nuclear power plants". *Chinese Journal of Nuclear Science and Engineering*, 27(2),138~140.

The Attitude and Psychological Demand Related Determinants of Public Transport Use

WAN Xia[1], CHEN Jun[2] and WANG Wei[3]

[1] School of Transportation, Southeast University, Ph.D. Candidate, Nanjing 210096, P. R. China, PH: +86-13814176229, E-mail: xia_wan1983@163.com
[2] School of Transportation, Southeast University, Ph.D., Professor, Nanjing 210096, P. R. China, E-mail: chenjun@seu.edu.cn
[3]School of Transportation, Southeast University, Ph.D., Professor, Nanjing 210096, P. R. China, E-mail: wangwei@seu.edu.cn

ABSTRACT

This research aims at gaining a better understanding about how the travelers' attitude to public transport and psychological demands in travel affect the public transport use. Attitude and psychological demand questions are designed in the questionnaire and the survey data is obtained from the Huaibei in Anhui province. Besides descriptive statistics and cross-tabulation used in this study, the travelers' attitude and psychological demands are measured and a discrete mode choice model is built to analyze the related determinants of public transport use. The results suggest that although individual/household socio-demographics are still important, a clear relation is found among travelers' attitude, psychological demands and public transport use. Based on the results, advice is given for government and transportation planners to improve the competition of public transport.

1 INTRODUCTION

In order to design sustainable transportation systems, transportation planners must increase their understanding of the preference of individuals to choose their travel mode. And facilitating public transport use is considered one of the most effective policy options to moderate traffic congestion and environmental problems (Sinha, 2003). Thus, it is meaningful to study travelers' decision-making mechanics to gain some guidance for encouraging people to use public transport.

People's attitudes and psychological demands are generally acknowledged as important factors in travel mode choice, but little is known about this relationship in China. The researcher abroad is concerned about ways to encourage public transport use based on the analysis of habit, motivation and psychological demands of travelers (Satoshi, 2002; Benjamin, 2008). However, the present literature in China mainly focuses on the effect of individual/household socio-demographics (Liu, B.E. 2005; Shan X, 2007). With the survey data in Huaibei, Anhui province and a discrete choice model, this study provides some results about the attitudes and psychological demands influencing the public transport use in China.

2 DATA

The data source comes from the travel diary data of Huaibei in November,

2008. Random sampling and face-to-face interviews were applied in the survey. Apart from information on socio-demographic characteristics, 3150 respondents were asked some questions related with public transport to reflect their attitudes to public transport. They were asked to point out what is most important in travel with cited answers to explore the psychological demands of the respondents.

If the respondent used public transport in the survey day, we considered him to be a public transport user, regardless of whether he used another travel mode or not. Of the 3150 respondents, 708 were public transport users which accounts for 22.47 percent. The other 2442 respondents traveled by car, bicycle, motorcycle or on foot. Until 2008, Huaibei hadn't constructed mass rapid transit systems, therefore busing is the public transport referred to in this study.

3 ATTITUDE AND PUBLIC TRANSPORT USE

Four questions were asked in the survey to reflect the respondents' attitudes to transport mode as follows in Table 1:

Table1. The Questions Related the Attitudes towards the Transport Mode

Questions	Answers
1.Do you think public transport can moderate traffic congestion	1.Yes 2.No
2.Do you think wide use of cars is the primary cause of congestion	1.Yes 2.No
3.Do you think the use of public transport is convenient on travel	1.Yes 2.No
4.Would you adopt public transport as your travel mode if the public transport service is promoted in the future	1.Yes 3.No 2.Not sure

The effects of the attitude on travel mode choice are shown in Table 2. Crosstabs are used to decide whether the according variable's effect is significant.

Table2. Crosstab Analysis between Attitude and the Mode Choice

Attitudes question		Mode choice		Total	Pearson χ^2	Sig.
		Bus	Not bus			
Question 1	Answer Yes	23.1%	76.9%	100%	5.964	0.010
	Answer No	17.7%	82.3%	100%		
Question 2	Answer Yes	23.1%	76.9%	100%	0.562	0.367
	Answer No	21.8%	78.2%	100%		
Question 3	Answer Yes	25.5%	74.5%	100%	26.952	0.000
	Answer No	17.6%	82.4%	100%		
Question 4	Answer Yes	26.2%	73.8%	100%	84.135	0.000
	Answer Not sure	9.0%	91.0%	100%		
	Answer No	10.2%	89.8%	100%		

It is shown that the different feedback to question 1, 3 and 4 are significant at the level of $\alpha = 0.05$, according to the Pearson Chi-Square test. However, the different feedback to question 2 is not significant.

Table 2 shows that respondents who accept the point of view that the public transport can moderate traffic congestion are more likely to choose the bus system in their travel. Respondents who believe the use of public transport is convenient on their travel are also more likely to use the bus system. As seen from the results of

question 4, the bus users are prone to sequentially use public transport if the public transport service is promoted in the future. However, the individuals who don't use public transport in the survey present lack of confidence of public transport as compared to the actual bus users. Of the 708 bus user respondents, 1.8 percent chose not sure, and 8.3 percent chose won't use public transport. Conversely, 21.3 percent of respondents who don't use the bus in the survey stated they wouldn't use public transport in the future. The insignificance of the relation between feedback to question 2 and mode choice reflects that the attitude towards car usage is not an important factor in public transport use.

4 PSYCHOLOGICAL DEMAND AND PUBLIC TRANSPORT USE

In the survey, the respondent is requested to point out what is most important in his travel trips. He may choose two of the six options we provided, as follows: 1) quick arrival; 2) safe arrival; 3) comfortable travel; 4) travel convenience; 5) economical for travel; 6) expressing myself. The answer of every respondent reflects the psychological demands of him on his travel (see Table 3).

Table3. Crosstab Analysis between Psychological Demand and the Mode Choice

psychological demands		Mode choice		Total	Pearson χ^2	Sig.
		Bus user	Not bus			
quick arrival	choose	25.5%	74.5%	100%	9.846	0.002
	Not choose	20.6%	79.4%	100%		
safe arrival	choose	21.2%	78.8%	100%	12.465	0.000
	Not choose	28.0%	72.0%	100%		
comfortable travel	choose	8.4%	91.6%	100%	13.652	0.000
	Not choose	24.5%	75.5%	100%		
travel convenience	choose	21.3%	78.7%	100%	0.541	0.462
	Not choose	22.7%	77.3%	100%		
economical travel	choose	25.0%	75.0%	100%	7.626	0.006
	Not choose	20.8%	79.2%	100%		
self expression	choose	3.4%	96.6%	100%	4.022	0.045
	Not choose	22.2%	77.8%	100%		

As seen from Table 3, five kinds of psychological demands, including quick arrival, safe arrival, comfortable travel, economical travel and self expression, are significant at the level of $\alpha = 0.05$. The respondent requiring "quicker arrival" and "economical travel" is prone to use public transport, the difference between the decision to use or not use public transport is around 4 percent. While the respondents who chose "safe arrival", "comfortable travel" and "selfexpression" tend to not use public transport. Those who chose "comfortable travel" or "self expression" have more than a 16 percent possibility of not using public transport. The need for "travel convenience" is not a significant effective factor.

5. BINARY LOGISTIC REGRESSION MODEL

Model Structure. Since the outcome or response variable is binary when an individual chooses whether or not to use public transport, the binary regression

model is used to analyze the choice behavior. It was defined as y=0 (not use), or y=1 (use). In this research, there are several explanatory variables or predictors including socio-demographics, attitude to transport mode and psychological demand, which are denoted as x_1, …, x_n. Then the binary logistic regression is stated in terms of the probability that y=1 given x_1, …, x_n, as shown in the following expression:

$$p = \Pr(y = 1 \mid x) = (1 + \exp[-(\alpha + \sum_{k=1}^{n} \beta_k x_k)])^{-1} \quad (1)$$

Where p is the probability when y=1, α is the intercept parameter; β_k is the slope parameter of x_k. The odds of using public transport can be expressed as:

$$p/(1-p) = \exp(\alpha + \sum_{k=1}^{n} \beta_k x_k) \quad (2)$$

Explanatory variables. In our previous study (Wan X., 2008), the socio-demographics of respondents are significant influencing factors for mode choice, so they are selected as variables in the model. We employ a continuous latent variable to reflect the travelers' attitude towards public transport in the model. Based on the results in Table 2, the calculated method of latent variable is the score of question 1 plus questions 3 and 4. For questions 1 and 3, the respondent answering "yes" can get one score; for question 4, a "yes" choice can get two scores, and "not sure" deserves one score. For any question, if the answer is "no", the score is zero. The scope of the latent variable is form 0 to 4. The higher score the respondent attained, the more he advocates public transport. The six psychological demand options, except "travel convenience" are adopted as discrete variables in the model. The selected explanations along with their definitions are summarized in Table 4.

Table4. Explanatory Variables Used in the Model

	Variable	Description
Individual/household socio-demographics	Female	1, 0 otherwise
	Have driving license	1, 0 otherwise
	Have public bus commute ticket	1, 0 otherwise
	Higher education	1, 0 otherwise
	Age<30	1, 0 otherwise
	Aage>50	1, 0 otherwise
	One or more children under school age	1, 0 otherwise
	Household income >¥50,000	1, 0 otherwise
	One or more bicycles in household	1, 0 otherwise
	One or more motorcycles in household	1, 0 otherwise
	One or more private cars in household	1, 0 otherwise
	Company vehicle available	1, 0 otherwise

Attitude	the degree of advocating public transport	continuous variable
Psychological demand	quick arrival	1, 0 otherwise
	safe arrival	1, 0 otherwise
	comfortable travel	1, 0 otherwise
	economical travel	1, 0 otherwise
	self expression	1, 0 otherwise

Model Calibration and Discussion. By correlation matrix analysis, we removed the collinear variables, and eliminated the insignificant variables. Table 5 shows the final estimation results of the public transport use choice model. The binary logistic model without attitude and psychological demand variables is estimated as reference.

Table 5. Estimation Results of MODEL and MODEL Ref

Independent variables	MODEL			MODEL Ref		
	Parameter	Wald	Sig.	Parameter	Wald	Sig.
Constant	0.278	29.731	0.000	0.298	32.503	0.000
Female	0.269	10.930	0.002	0.378	11.125	0.000
Have driving license	-0.955	16.254	0.000	-1.565	17.144	0.000
Have bus commute ticket	1.334	13.126	0.000	1.364	18.536	0.000
Higher education	-0.430	16.250	0.000	-0.459	14.957	0.000
Age>50	0.631	3.123	0.063	0.752	2.908	0.082
Household	-0.410	5.782	0.020	-0.530	7.048	0.011
>1 bicycle in household	-0.504	14.002	0.000	-0.614	12.238	0.000
>1 motorcycle in household	-0.919	12.751	0.000	-1.193	14.933	0.000
>1 private car in household	-0.922	8.962	0.009	-1.021	7.324	0.010
Company vehicle	-1.365	13.257	0.000	-1.652	14.129	0.000
Attitude	0.232	20.631	0.000	/	/	/
Quick arrival	0.622	4.446	0.030	/	/	/
Safe arrival	-0.416	10.965	0.002	/	/	/
Comfortable travel	-0.932.	12.635	0.000	/	/	/
Economical travel	0.396	6.951	0.010	/	/	/
Self expression	-1.526	4.784	0.029	/	/	/
Hit rate	83.6%			77.1%		
Nagelkerke R^2	0.456			0.386		

The hit rate of mode with attitude and psychological demand variables is 83.6%, while the hit rate of reference mode is 77.1%. Based on the estimation result, some conclusions can be obtained.

Socio-demographics： Accordant with our previous study, females, elders, and those in possession of a bus commute ticket have a greater probability of using public transport; those with a higher income, higher education and with occupancy of

vehicles had a reduced possibility of bus use.

Attitude: The higher the score of attitude variable the traveler attained, the greater the possibility of him using public transport. It suggests that if somebody has the perception that public transport is friendly to the environment and has confidence in the quality of public transport services in the future, he is more likely to choose public transport instead of another mode. This suggests a need for the government and transportation planners to create a positive image of the public transport system in the future.

Psychological demand: Among six psychological demand options, quick arrival and economical travel have a significant positive effect on public transport use, which means travelers with stronger psychological demand for them will have a stronger tendency to choose the bus system. However, safe arrival, comfortable travel and self expression have significant negative effects on public transport use. Consequently, it could reflect the service quality of bus system in people's eyes. The bus system can provide quicker service for its mobility compared with on foot or bicycle usage, and provides lower cost service compared with using a car or taxi. In contrast, the bus system has disadvantages in regard to safety, comfort and status needs.

The difference of hit rate and Nagelkerke R^2 between two models demonstrates the effect of attitude and psychological demand on public transport use which indicates that these factors shouldn't be ignored in China.

6. CONCLUSION AND ADVICE

By descriptive statistics and logistic regression methods, this paper developed an empirical framework to examine the effect of the travelers' attitudes and psychological demands on travel mode choice. With the data of Huaibei travel dairy survey, the travelers' attitudes and psychological demands are successfully measured and proved to be effective for increasing the accuracy of the public transport use predicting model. For the mode including the attitude and psychological demand variables, the understanding of travel mode decision-making mechanics is improved.

Some useful advice can be drawn for government and transportation planners. Creating a positive image of public transport systems and widely propagandizing the public transport as an environmentally friendly transport mode could increase the possibility of travelers choosing public transport. Quick arrival and economical travel have been accepted as high grade characteristics for public transport, but the lack of ensured safety, comfort and self-expression on travel decrease the competition of public transport. These give some direction for improving the service of public transport in the future.

ACKNOWLEDEMENT

This research is supported by Major Program of National Natural Science Foundation of China (50738001), 863 Program(2008AA11Z201) and National Key Technology R&D Program (2006BAJ18B01).

REDRENCES

Benjamin Gardner (2008). "Modeling motivation and habit in stable travel mode contexts." *Journal of Transportation Research Part F*, pp.1-9.

Liu, B.E. (2005). "Development of a multinomial logit model for travel mode choice of resident." *Journal of Highway and Transportation Research*, pp. 116-119.

Satoshi Fujii (2002). "Application of attitude theory for improved predictive accuracy of stated preference methods in travel demand analysis" *Journal of Transportation Research Part A*, pp.389-402.

Shan X. (2007). "Research on urban bicycle transportation rational ridership and road resource allocation", *Doctoral dissertation*, Southeast University.

Sinha, K. C. (2003). "Sustainability and urban public transportation." *Journal of Transportation Engineering*, pp.331-341.

Wan X., Chen J, Wang W. (2008). "Travel characteristics and mode choice behavior of public transport", Proceedings of ICICTA2008, Vol.2, Changsha: 358-363.

A Study on the Matching of Urban Form and Traffic Pattern

Li Haifeng

College of Civil Aviation and Flight, Nanjing University of Aeronautics and Astronautics, P.O. Box 210016, Emperor Street 29, Baixia District, Nanjing; PH: +86(25)84893461; FAX: +86(25)84891289; email: seawind7510@163.com

ABSTRACT

Urban traffic is closely connected to urban planning and different urban forms have different traffic patterns. This paper studies the coupled relations among urban forms, rail traffic patterns, public transportation patterns, bicycle traffic patterns and pedestrian traffic patterns, and it may also serve as good reference to solving city traffic congestion.

1. URBAN FORM AND RAIL TRAFFIC

With the constant expansion of cities, various urban patterns have come into being, such as conglomeration, star patterns and ribbon patterns, etc. (Li Haifeng, 2006)

(1)URBAN FORM AND RAIL TRAFFIC

In the urban form of conglomeration, rail traffic lines fall into two types: diameter lines and ring lines, with the former linking satellite towns to the city, while the latter serving as the means by which the traffic in urban center is leaded and the passenger flows among satellite towns are conducted (Li Haifeng, 2006).

In a star-shaped city, rail traffic lines radiate from the city center. Conventional public transport serves as feeders for rail transit and connects peripheral passengers to the trunk line. The framework of a star-shaped city is the axial rail transit, with the urban periphery being interlaced with green space, forests, farmland, etc, and thus an eco-city development pattern is formed. Though experts point out that this is the ideal urban form, urban system planning of major Chinese cities has shifted from centralization to decentralization, such as ribbon patterns and twin cities, etc., in favor of the development of rail transit.

Rail traffic is environment-friendly.

Cluster city is ideal for leading urban concentric circle development, forming clusters of various functions and land nature on the outskirts of a city, separated by green belts, which is the practice of the well-known Finnish planner Saarinen's theory on organic decentralization planning. Each cluster is a functional aggregation and daily life and work can be carried out in the cluster. Highway or rail transit links different clusters (Bian Jingwei, 2006). In Nantong, Qinhuangdao and other Chinese cities it is proposed that clusters be connected by light rail's diameter lines.

(2)RAIL TRANSIT DEVELOPMENT PATTERN

1) Within the scope of city

Subway systems should be prioritized in urban centers, with light rail taken into consideration where passenger flow is small. In urban centers, with large populations, large traffic volume, and significantly concentrated passenger flow during rush hour, subways may be the only by means of rapid evacuation without crowding and congestion. On routes with small traffic flow it is more economical to build light rail, whose cost is only 1/5 to 1/3 of that of subway. The light rail layout of Changchun is arranged from the center to the outskirts of the city. In the United States, Boston's three green branch lines and Philadelphia's five light rails near City Hall are also good examples.

The use of trolleys should be properly developed. According to incomplete statistics, the return of the trolley is advocated in 350 cities around the globe. Rail and trolley bus use are flourishing in Germany, France, Belgium, Holland and other western European countries. Trolley is also considered an important vehicle in Eastern Europe, and Russia where there are 60,000 trolleys. In the United States, trolleys eliminated in the 1960s and 1970s, are desterilized. In some large and medium-sized Chinese cities a new air-condition trolley is being developed, such as Guangzhou, Beijing, Dalian, Shanghai and Hangzhou and so on.

2) Suburbs

Light rail and suburban railway should be developed in suburbs. Light rail and suburban railway are used to connect satellite towns to urban centers. The capacity of light rail is between those of subway and public trolley, which could be rated as medium capacity system. It is suitable for suburbs, sub-center, urban areas (small and medium-sized cities) and places where subways are not economical.

3) Metropolitan circle

Suburban railway should be developed in metropolitan circle. Suburban railway is used to manage high capacity passenger traffic between urban and suburbs, suburbs and suburbs, satellite towns, ribbon cities and metropolis circle. There should be feeders between suburban railway and city rail transit net, readily available to passengers.

Medium capacity monorail or rail traffic system could be applied to commuter lines linking suburbs of big cities, new towns, and residential areas to urban centers.

According to the analysis above, metropolitan circle's development model is MRT+LRT, suburban railway +MRT or guide rail. Trolley, LRT, MRT and MRT+LRT could be included in the city's development model. (Note: MRT-subway, LRT-light rail).

2. URBAN FORM AND REGULAR PUBLIC TRAFFIC PATTERN

The major urban form in China is conglomeration city, which may evolve into multi-center city, cluster city and ribbon city. Conventional public transportation serves as the main urban traffic mode, and express buses serve in the city's outskirts for commuters. Currently, China's national revenue is increasing and a family with an annual income of mere 50,000 Yuan can afford a car, which results in a steady

growth in the number of private cars, which occupy urban road system and pose a challenge to public transport. The typical urban expansion model has resulted from car increase, which consequently leads to sprawling urban area, and negatively impacts urban development. Public transport mode should be the main urban development pattern (Sui Dong et al., 2007).

Take Beijing for example. Beijing's affordable housing is gradually expanding to the outskirts of the city, with residents utilizing public transport to get around. Beijing planned several express bus lines, abbreviated as BRT, i.e. Bus Rapid Transit, which has the exclusive right of way, incorporating the rapidity of subway, light rail and the flexibility of buses. The typical BRT system is Curitiba BRT system in Brazil, which is composed of fast lines, interval lines and branch lines (Wei Yaping, 2003). Different kinds of lines represent different passenger flow and are distinguished by different colors. Different kinds of public traffic lines have different road way conditions. Beijing's BRT extends from city center to periphery, through which public traffic service is provided; traffic cost and the utilization of private cars are reduced for the owners of affordable housing who moved outside of city. On the contrary, Beijing's Tiantongyuan and Huilongguan have been developed on a large scale, but the traffic facilities have not kept pace and many residents have to opt for motor vehicle traffic.

There are five development patterns for BRT: as a transition of subway or light rail; becoming the main body of overall public traffic; as an extension of subway or light rail; a combination of subway and light rail; and stand alone BRT system.

3. URBAN FORM AND BICYCLE TRAFFIC PATTERN

(1) URBAN FORM AND BICYCLE TRAFFIC

The evolution of urban form can be divided into three stages, initial stage, intermediate stage and advanced stage. In initial stage, the city is rendered as concentric circles with a single center, with pedestrian and bicycle as the main traffic pattern. In intermediate stage of urban development, urban form turns into conglomeration and bicycles dominate in city traffic pattern, with public traffic taking a certain proportion. In advanced stage, urban form evolves to star shape, cluster and other urban form, where public traffic is the main body of city traffic patterns, and bicycle and car are complementary to it.

Most cities in China are in the form of concentric circles with a single center, for which, compared with ribbon and star shape cities, it is difficult to open up high speed and large capacity public traffic corridors. Within an area of 113 square kilometers occupied by concentric circles(R=6km), public traffic and bicycle traffic

are in rivalry, where bicycle traffic form enjoys an advantage (Chu Jinlong, 2007). Currently, urban form in China is evolving from conglomeration into star shape and multi-clusters. Traffic form is changing from bicycle-based traffic form to public traffic-based traffic form. With the expansion of city and the rapid growth of private cars, the rate of city residents utilizing motorized traffic increases year by year. As an example, the rate of residents in the urban district of Nanjing utilizing motorized traffic form was 32.71% in 2008, while the rate of those utilizing public traffic (including subway) is 21.56%. The residents' satisfaction rate is 42.4%. The rate of those residents utilizing bicycle traffic is nearly 50%. These, on one hand, indicate that city constructions are compact and commuting distance is short. On the other hand, these (statistics?) mean that public traffic development is stagnant. In Shenyang, residents 90% probability traffic time interval is [7,77] in 2005. 90% probability pedestrian traffic time interval is [5,50], 90% probability bicycle traffic time interval is [8,67]. 90% probability public traffic time interval is [18,107]. The average traffic time of residents by bicycle is 29 minutes in Shenyang. The upper limit of bicycle traffic time is up to 67 minutes, which exceeds rational traffic time interval of bicycle travel. These show that bicycle traffic patterns cannot meet the development of Shenyang City. Residents should choose other traffic patterns to reduce bicycle traffic (Li Haifeng et al., 2007).

(2) DEVELOPMENT PATTERN OF BICYCLE TRAFFIC

City land use in China is mixed, which makes pedestrian and bicycle traffic feasible. Mixed use of land function can reduce traffic distance, increase traffic efficiency, and reduce fuel consumption of vehicle, which will help to build a human-oriented traffic environment.

According to city land function layout, city railways, traffic main lines and natural barriers, the city can be divided into several bicycle traffic districts using ring lines and radial lines to form urban bicycle networks. According to bicycle traffic's time-space, bicycle traffic and pedestrian traffic should be advocated within the region. Efficient public traffic corridors should be built between regions.

In order to adapt to urban development, China should build a new traffic pattern which is different from Europe and the United States' Park and Ride system (Chen Jun, 2007), and which coordinates urban bicycle traffic with public traffic. Public traffic is the main body of this new urban traffic pattern with bicycle traffic as an

auxiliary, forming a perfect bicycle-public traffic transfer system. Land use functions are mixed in China's cluster cities. Business, leisure, entertainment, shopping, working and living are linked by bicycle traffic, which develops bicycle's advantage within short range and achieves seamless connection among bicycle, public traffic and rail traffic.

4. URBAN FORM AND PEDESTRIAN TRAFFIC PATTERN

(1) URBAN FORM AND PEDESTRIAN TRAFFIC

Pedestrian traffic, designed by J. H. Crawford, resembles six clover leaves. The population of the city is about 1,000,000 scattering in 100 communities, among which there are 18 smaller ones called practical areas away from the city center. These non-residential areas are reserved for different land uses.

There are three high-capacity subway lines in the city, each of which begins from a leaf, then runs through the city center and reaches the opposite leaf.

Satellite towns can be built on the basis of this six-leave-clover city form, with each taking the shape of a rough circle and holding one million residents. Fast light rail serves as the connection among them.

(2) THE DEVELOPMENT PATTERN OF CHINA'S PEDESTRIAN TRAFFIC

Some parts of cities can be rebuilt as walking areas in China. Public traffic acts as feeder around the periphery of walking areas. The Hunan road in Nanjing is the first commercial pedestrian street in China. On weekend nights, vehicle traffic is banned in the pedestrian sections with open space reserved for shopping and entertainment.. According to the situation in China, light rail, rail, and trolley can all be used as modes of transportation instead of high-capacity railways. Light rail is only applicable in cities with a population smaller than 500,000.

The method can be extended to other cities' commercial pedestrian street and old districts. The ancient Chinese road network layout is square, such as those left in Suzhou, Xi'an and other cities. These old districts maintain a moderate population, and can be divided into several small districts. Exclusive public traffic main lines and trolley can be used to transport passengers. Pedestrian traffic patterns within these districts can protect historical and cultural remains and give more open space to residents.

REFERENCES

Bian Jingwei(2006).Urban Space Development and Rail Transit. China Architecture and Building Press.

Chen Jun(2007).City Parking Facilities Planning and Information Adductive Technology. Southeast University Press.

Chu Jinlong(2007).Quantitative Analysis of Urban Space Pattern. Southeast University Press.

Li Haifeng(2006).Study on the Urban Form, Traffic Pattern and Resident Traffic Mode. Southeast University.

Li Haifeng, Wang Wei(2006).Study on the Rail Transit Network Configuration. Planners, Vol. 22, No. 5, pp. 85 – 88.

Li Haifeng, Wang Wei(2007).The Option Model of Traffic Mode Based On Neural Network. Journal of Highway and Transportation Research and Development, Vol. 24, No. 7, pp. 132 – 136.

Sui Dong, Li Haifeng, Wang Wei(2007). Proposing Diverse City Public Transit Mode. Planners,Vol.23, No. 8, pp.62 – 65.

Wei Yaping(2003).Urban Space Development Strategy. China Architecture and Building Press.

Study on Road Network Reserved Capacity on Different Levels of Service and Stochastic Conditions

Liu Zhengwei[1] and Cheng Lin[1]

[1]School of transportation, Southeast University, Nanjing 210096, China; PH 86-25-83795469; email: zw_liu0806@yahoo.com.cn

Abstract

The paper investigates the road network capacity under uncertainty. By showing the characteristics of route choice and considering the link travel time reliability on a certain level of service, we set a bi-level programming model and the road network capacity can be gained. Firstly we consider the single link of a route under uncertainty, and then extend it to the whole road network capacity on a certain service level. Using the model we can escape from calculating a huge amount of data which is used in the Monte-Carlo method. An example is calculated, and then the result shows the efficiency of the model.

Key words: road network capacity; bi-level programming; sensitivity analysis; user equilibrium

1. Introduction

In reality, the road network's normal functions are frequently affected by many factors, including natural factors (e.g., earthquake; flood; volcanic eruption; mud-rock flow; etc) and man-made factors (e.g., road maintenance; ramp closure; parking in the road; traffic accidents; terrorist activities; etc), which cause the uncertainty of the road network. Therefore, it is necessary to introduce the stochasticity into the design and evaluation of road networks. Traffic elements' capability and spatial layout determine the capability of road network. The capability of urban road network results from a single section's transportation capability extending to the whole network that means how many volumes the urban road network can accommodate on a certain service level (Cheng *et al*. 2004). The capability of urban road network reflects its ability to deal with transportation demand.

2. Problem analysis and road network capacity model

2.1 Notation

A road network is defined as a system, which can be represented mathematically as a graph G(N, A) with a set of nodes N and sections A. To make more sense of following sections, the notation shows as below:

$\boldsymbol{W}$ set of OD(origin-destination)

$\boldsymbol{R_{(i,j)}}$ set of routes from node i to j

$\boldsymbol{x_a}$ traffic volume of section a

$\boldsymbol{t_{a0}}$ free-flow travel time of section a

$\boldsymbol{T_a}$ actual travel time of section a

$\boldsymbol{T_{(i,j)r}}$ travel time of route r

$\boldsymbol{\delta_{ar}}$ 0-1 variable. If section a is a composition of route r, δ_{ar} equal to 1; otherwise, δ_{ar} equal to 0

$\boldsymbol{q_{(i,j)}}$ existing traffic volume from node i to j

$\boldsymbol{C_a}$ actual capacity of section a

$\overline{C_a}$ design capacity of section a

$f_{(i,j)r}$ traffic volume of route r
c_a broadly-defined traffic cost of section a
$c_{(i,j)r}$ broadly-defined travel cost of route r
$\pi_{(i,j)}$ minimum of broadly-defined travel cost from node i to j
μ multiplier of origin-destination matrix

2.2 Problem analysis

With the proportion of OD-matrix's construction unchanged, the capability of the network usually refers to the maximum volume it can accommodate on a certain service level. Customarily it could be represented by using reserved capacity, because once the OD-matrix's construction has been fixed, the capability of network can be depicted by the largest multiplier corresponding to the OD-matrix. Network elements' capability recession, the stochastic of road travel time, and the users' behavior in choosing routes are the important factors which affect road network capability (Cheng *et al*. 2005). The reliability of transportation network capability refers to the probability that it can accommodate the maximum volumes on certain service levels (Chen *et al.* 1999). A reliability study needs large amounts of historic data as well as many hypothesizes as it is a complex program.. Nevertheless if we change this question to the maximum volume that a road network can accommodate on certain service levels, the question transfers to the solution of the network capability's distribution. We can solve this question through using chance-constrained model (Charnes et al. 1963).

The following assumptions are proposed to be convenient to solve the problem:
(1) The network is in a state of equilibrium based on the traveler's experiences of the state of the network and his clear realization of the value of the broadly-defined travel cost. The network in a state of equilibrium can be depicted as: all the selected routes' travel cost is equal to the same value and no more than that of the routes not selected. Depict mathematically:

$$c_{(i,j)r} = \begin{cases} = \pi_{(i,j)}, & \text{if} \quad f_{(i,j)r} > 0; \\ \geq \pi_{(i,j)}, & \text{if} \quad f_{(i,j)r} = 0; \end{cases} \qquad \forall (i,j) \in W, \ \forall r \in R_{(i,j)} \tag{1}$$

(2) The intersections are in the ideal state (absolutely reliable).
(3) The variety of sections' traffic flows are independent.

2.2.1 Travel time and broadly-defined cost of section

The actual capacity of section C_a is a random variable. Simply, we assume that C_a satisfies uniform distribution: $[\theta_a \overline{C_a}, \overline{C_a}]$ $(0 \leq \theta_a < 1)$.

Based on the BRP function, T_a is a random variable subjected to the section's volume x_a and actual capacity C_a.

$$T_a(x_a, C_a) = t_{a0}\left[1 + \alpha\left(x_a / C_a\right)^{\beta}\right] \tag{2}$$

Where, α and β are the parameters of BRP function. So the expectation e_a and the variance σ_a^2 of the travel time of a section can be depicted as follows:

$$e_a = E\left(T_a\right) = t_{a0} + \alpha t_{a0} x_a^{\beta} E\left[\left(1/C_a\right)^{\beta}\right] = t_{a0} + \alpha t_{a0} x_a^{\beta} \frac{1 - \theta_a^{1-\beta}}{\overline{C_a}^{\beta}\left(1-\theta_a\right)\left(1-\beta\right)} \tag{3}$$

$$\sigma_a^2 = D(T_a) = \alpha^2 t_{a0}^2 x_a^{2\beta} D\left[(1/C_a)^\beta\right] = \alpha^2 t_{a0}^2 \frac{x_a^{2\beta}}{\overline{C_a}^{2\beta}} \left\{ \frac{1-\theta_a^{1-2\beta}}{(1-\theta_a)(1-2\beta)} - \left[\frac{1-\theta_a^{1-\beta}}{(1-\theta_a)(1-\beta)} \right]^2 \right\} \quad (4)$$

From Eq (3) and Eq (4), we know that x_a is in synchronous growth with e_a and σ_a^2. The broadly-defined travel cost of section a is defined as follows:

$$c_a = e_a, \quad \forall a \in A \quad (5)$$

2.2.2 Travel time and broadly-defined cost of route

Considering that intersections are in the ideal state, travel time of a route are only made up of travel times of the sections.

$$c_{(i,j)r} = T_{(i,j)r} = \sum_{a \in A} T_a \delta_{ar}, \quad \forall a \in A \quad (6)$$

From the CLT, this distribution satisfies the normal distribution as follows:

$$T_{(i,j)r} \sim N\left[E\left(T_{(i,j)r}\right), \sigma_{w(i,j)}^2 \right] \quad (7)$$

$$E\left(T_{(i,j)r}\right) = \sum_{a \in A} E(T_a)\delta_{ar} = \sum_{a \in A} \left[t_{a0} + \alpha t_{a0} x_a^\beta \frac{1-\theta_a^{1-\beta}}{\overline{C_a}^\beta (1-\theta_a)(1-\beta)} \right] \delta_{ar} \quad (8)$$

$$\sigma_{(i,j)r} = \sqrt{\sum_{a \in A} D(T_a)\delta_{ar}} = \sqrt{\sum_{a \in A} \alpha^2 t_{a0}^2 \frac{x_a^{2\beta}}{\overline{C_a}^{2\beta}} \left\{ \frac{1-\theta_a^{1-2\beta}}{(1-\theta_a)(1-2\beta)} - \left[\frac{1-\theta_a^{1-\beta}}{(1-\theta_a)(1-\beta)} \right]^2 \right\} \delta_{ar}} \quad (9)$$

Basically the mean and standard deviation of travel time of the route impact the user's decision and represent the important information of the network's travel time reliability.

2.2.3 Analysis of the user's selecting behaviors

Travel time of routes continues to change, and the road network is in equilibrium as probability. All conditions are shown as follows:

(1) The expectation of travel time $E(T_{(i,j)r})$ of the selected route r equals to $\pi_{(i,j)}$ (the minimum of all the travel time of the routes from node i to j). Eq (1) shows that mathematically.

(2) The reliability of travel time of the selected route satisfies the following requirement:

$$P\left(T_{(i,j)r} - \pi_{(i,j)} \le \varepsilon \pi_{(i,j)}\right) \ge \lambda_{(i,j)r} \quad \forall (i,j) \in W, \forall r \in R_{(i,j)} \quad (10)$$
$$0 < \varepsilon, \lambda_{(i,j)r} \le 1$$

Where ε is the parameter representing how much travel time can be longer than the expected minimum; $\lambda_{(i,j)r}$ represents the user's requirement of the reliability of the travel time.

With satisfying the Eq. (1), we transform the Eq. (10):

$$\begin{aligned} P\left(T_{(i,j)r} - \pi_{(i,j)} \le \varepsilon \pi_{(i,j)}\right) \ge \lambda_{(i,j)r} &<=> P\left(T_{(i,j)r} - E\left(T_{(i,j)r}\right) \le \varepsilon E\left(T_{(i,j)r}\right)\right) \ge \lambda_{(i,j)r} \\ &<=> P\left(\frac{T_{(i,j)r} - E\left(T_{(i,j)r}\right)}{\sigma_{(i,j)r}} \le \frac{\varepsilon E\left(T_{(i,j)r}\right)}{\sigma_{(i,j)r}} \right) \ge \lambda_{(i,j)r} \end{aligned} \quad (11)$$

It's easy to know that $\frac{T_{(i,j)r} - E\left(T_{(i,j)r}\right)}{\sigma_{(i,j)r}} \sim N(0,1)$, so the equation can be transformed to:

$$\frac{\varepsilon E\left(T_{wr}\right)}{\sigma_{wr}} \geq \phi^{-1}\left(\lambda_{wr}\right) \tag{12}$$

Plugging Eq (8) and Eq (9) to Eq (12), we can get:

$$\frac{\varepsilon \sum_{a \in A}\left[t_{a0} + \alpha t_{a0} x_a^{\beta} \frac{1-\theta_a^{1-\beta}}{\overline{C_a}^{\beta}(1-\theta_a)(1-\beta)}\right]\delta_{ar}}{\sqrt{\sum_{a \in A} \alpha^2 t_{a0}^2 \frac{x_a^{2\beta}}{\overline{C_a}^{2\beta}}\left\{\frac{1-\theta_a^{1-2\beta}}{(1-\theta_a)(1-2\beta)} - \left[\frac{1-\theta_a^{1-\beta}}{(1-\theta_a)(1-\beta)}\right]^2\right\}\delta_{ar}}} \geq \phi^{-1}\left(\lambda_{(i,j)r}\right) \tag{13}$$

2.2.4 The model of road network capacity based on uncertainty of the capacity of section

It's necessary to make the road network satisfy a certain service level when we indentify the capacity of it; and the service level can be respectively represented by different sections. To the respective users the degree of traffic jam must be an approximately acceptable level. We use the reliability of travel time of sections to represent the acceptable service level which is firstly proposed by Lo *et al* (Lo *et al*. 2000).

$$P\left(T_a \geq \varphi_a t_{a0}\right) \leq \gamma_a \tag{14}$$

Where φ_a represents crowding coefficient of section a and $\varphi_a \geq 1$; γ_a represents how much the probability of the travel time of section a exceeds the acceptable travel time, which reflects people's acceptable degree of section traffic crowding and $0 \leq \gamma_a \leq 1$. Different sections have different γ_a because people may obtain different acceptable crowding degrees. Using Eq. (2) we can transform Eq. (14) to:

$$P\left(C_a \leq \frac{x_a}{\left(\frac{\varphi_a - 1}{\alpha}\right)^{1/\beta}}\right) \leq \gamma_a <=> x_a \leq \left(\frac{\varphi_a - 1}{\alpha}\right)^{1/\beta} F_{C_a}^{-1}\left(\gamma_a\right) = \left(\frac{\varphi_a - 1}{\alpha}\right)^{1/\beta} \overline{C_a}\left[\theta_a + \gamma_a\left(1-\theta_a\right)\right] \tag{15}$$

Where $F_{Ca}^{-1}(.)$ is the inverse function of C_a distribution function.

Considering the reliability of travel time of section and the reliability of travel time of route we set up the bi-level programming model which meets the user equilibrium principle as below:

$$\text{(U)} \quad \begin{aligned} &\max \quad \mu \\ &s.t. \quad x_a\left(\mu q\right) \leq \left(\frac{\varphi_a - 1}{\alpha}\right)^{1/\beta} \overline{C_a}\left[\theta_a + \gamma_a\left(1-\theta_a\right)\right] \end{aligned} \tag{16}$$

Where $x_a(\mu q)$ meets user equilibrium assignment as below:

$$
\begin{aligned}
&\min \quad Z(x) = \sum_{a \in A} \int_0^{x_a} c_a(w)dw \\
&s.t. \quad \sum_{r \in R_{(i,j)}} f_{(i,j)r} = \mu q_{(i,j)}, \quad \forall (i,j) \in W \\
(L) \quad & f_{(i,j)r} \geq 0, \quad \forall (i,j) \in W, \forall r \in R_{(i,j)} \qquad (17) \\
& f_{(i,j)r}\left(\frac{\varepsilon E\left(T_{(i,j)r}\right)}{\sigma_{(i,j)r}} - \phi^{-1}\left(\lambda_{(i,j)r}\right)\right) \geq 0, \quad \forall (i,j) \in W, \forall r \in R_{(i,j)} \\
& x_a = \sum_{(i,j) \in W} \sum_{r \in R_{(i,j)}} f_{(i,j)r} \delta_{ar}, \quad \forall a \in A
\end{aligned}
$$

3. Solution algorithm

There are many methods to solve the bi-level programming problem, but in summary, there are four main categories (i.e. pole searching method, kuhn-tucker method, descent method and direct method) (Gao *et al*. 2000). This paper uses the descent method, pointing out how to get the lower variables' information about derivatives or differences of the upper variables. Because the upper problem has only one decision variable μ, we can regard it as a variable of the lower road network equilibrium problem. First, we choose a μ little enough, then continue changing it until an upper problem's restriction condition is violated by an equilibrium volume of section. The concrete algorithm is a sensitivity analysis method which can solve this problem efficiently. The special procedures are introduced as follows:

(1) Choose a much less multiplier of origin-destination matrix $\mu^{(n)}$, whose order is zero (n=0).

(2) With the defined $\mu^{(n)}$, we solve the lower road equilibrium problem and get the equilibrium volume of sections $x^{(n)}$.

(3) Using a sensitivity analysis method of road equilibrium problem we can get the descents of the section's volume about the multiplier of origin-destination matrix $\mu^{(n)}$.

(4) With the information of descents we can get a local linear approximation equation of the reliability restrictive Eq. (16), so we transform the upper problem to a linear planning problem. With solving the linear planning problem we can get a new multiplier of origin-destination matrix $\mu^{(n+1)}$.

(5) If $\forall a \in A, |\mu^{(n+1)} - \mu^{(n)}| \leq \varepsilon$, where ε is the predestinated error, stop the programming; or order $n = n+1$ and go back to procedure (2).

4. Illustrative example

As an example of the proposed model, a simple road network is considered (Fig. 1). In the road network there are nine nodes, eighteen sections and two pairs of OD {(1,9),(2,9)}. The two origin-destinations have two respective volumes: $q_{1,9}$= 600pcu/h, $q_{2,9}$= 400 pcu/h. The parameters in BRP function are α=0.15, β=4. We assume that C_a satisfies uniform distribution: $[\theta_a \overline{C_a}, \overline{C_a}]$ ($0 \leq \theta_a < 1$). Simply, we make the parameters

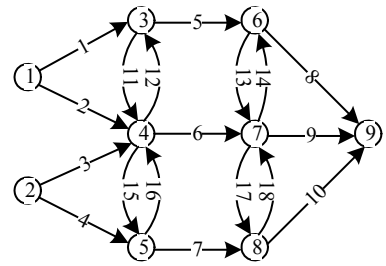

Fig.1 Road network for the illustrative example

of all the sections Θ_a=0.5, φ_a=1.2, ε=0.2. The information of capacities and free-flow travel time of the sections are presented in table 1.

Table 1 Design capacities and free-flow travel time of sections

No. of section	1	2	3	4	5	6	7	8	9
Free-flow travel time	15	15	15	15	10	10	10	15	15
Design capacity	1000	1000	1000	1000	1000	1000	1000	1000	1000
No. of section	10	11	12	13	14	15	16	17	18
Free-flow travel time	15	10	10	10	10	10	10	10	10
Design capacity	1000	1000	1000	1000	1000	1000	1000	1000	1000

On the same network condition we calculate it and find out the corresponding μ_{max} with setting up different $\lambda_{(i,j)r}$ and different γ_a (assume $\lambda_{(i,j)r}$ and γ_a of all the sections are same). The result is presented in table 2. The Fig. 2 illustrates it more clearly.

Table 2 Result

γ_a	μ_{max}	
	λ_1=0.9	λ_2=0.95
0.1	1.7	1.7
0.2	1.9	1.9
0.3	2.0	2.0
0.4	2.2	2.2
0.5	2.4	2.3
0.6	2.5	2.4
0.7	2.6	2.4

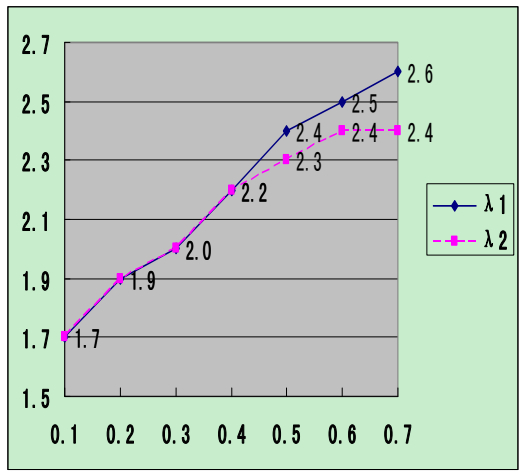

Fig. 2 The results comparison about λ_1 and λ_2

With Table 2 and Fig 2 it comes to the conclusion that the maximal multiplier of origin-destination matrix gets smaller along with $\lambda_{(i,j)r}$ getting bigger and γ_a getting smaller (i.e. the service level is improved), which means the capacity of the network decreases. The result illustrates that this model can efficiently give the information of the capacity of the road network on stochastic condition and a certain service level.

5. Conclusion

A bi-level programming model is set up to show the capacity of road network on different levels of service and stochastic conditions. This model introduces a method to solve the problem without a large amount of data which must be used in the Monte-Carlo method. The performance of the traffic flow in the model is deterministic user equilibrium, so it is used to long term capacity research. It also lays the foundation of further dynamic capacity research.

References

Charnes A, Cooper W (1963). Deterministic equivalents for optimizing and satisfying under chance constraints. *Operation Research*, 11, 18-39.

Cheng Lin, Li Qiang, Wang Jing-yuan, Wang Wei (2004). Urban road network

capacity reliability. *Journal of Southeast University* 20 (2), 235-239.

Cheng Lin, Wang Wei, Wang Jing-yuan, Shao Yun-hong, LU Ya-chen (2005). Urban road network capacity, traffic planning and traffic management. *Journal of Highway and Transportation Research and Development*, 22 (7), 118-122.

Chen A, Yang H, Lo H K, *et al* (1999). A capacity related reliability for transportation network. *Journal of Advanced Transportation*, 33 (2), 183-200.

Gao Zi-you, Song Yi-fan (2000). Urban Transportation Continuous Equilibrium Network Design Problem: Theory and Method. *Beijing: China Railway Press*.

Lo HK, Tung YK (2000). A chance constrained network capacity model. *Bell M GH, Cassir C,* ed. Reliability of transport network. *Hertfordshire: RSP Ltd*, 159-172.

Expansion and Validation of Beijing Household Interview Survey Data

XIAN Kai[1], LIU Zhili[2], ZHANG Dexin[3], DU Huabing[4]

[1] Beijing Transportation Research Center, No.9 Building, Beibinhe Road, Xuan Wu District, Beijing 100055, China; PH (86-10) 63372730; Email: xiank@bjtrc.org.cn
[2] MOE Key Laboratory for Urban Transportation Complex Systems Theory and Technology, School of Traffic and Transportation, Beijing Jiaotong University; Email: liuzhili@jtys.bjtu.edu.cn
[3] Beijing Transportation Research Center; Email: zhangdx@bjtrc.org.cn
[4] Beijing Transportation Research Center; Email: duhb@bjtrc.org.cn

ABSTRACT

In order to update the basic transport database and obtain an in-depth understanding of the travel demands and patterns in Beijing, a series of transport and traffic surveys have been undertaken by the government. The household interview survey (HIS) is the most important undertaking with sample size over 80,000 households. Because of complexity and limitation in various stages of the surveys, errors and under-reporting are inevitable. Therefore, results of sample data and sample expansion can not reflect the real travel characteristics. This paper introduces the data expansion and validation process of Beijing household interview survey data. Errors and under-reporting were eliminated by a series of processes, such as sample expansion, matrix estimation, independent data checking and comprehensive validation.

Keywords: *Household interview survey, Sample Expansion, Matrix Estimation, Comprehensive Validation*

INTRODUCTION

In 2005 and 2006, a series of transport and traffic surveys were undertaken by Beijing municipal government and the Household Interview Survey (HIS) is the most important undertaking with sample size over 80,000 households. However, it was expected that the sample size on some of the minority modes, trip purposes, and person types would still be low, therefore supplementary surveys on some specific modes and trips purpose were carried out together with a complete screenline traffic count. The sample size of each survey is as followed:

- Household Interview Survey: 81760 households (sample rate is 1.5%)
- Taxi Survey: 6529 taxis (sample rate is 9.8%)
- Metro Survey: All station boarding and alighting counts, and 62,097 questionnaires
- Special Generator Interview Survey:8500 travellers in 7 sites

- Floating population travel survey (Including hotel guest): 10,517 samples in 7 sites and 36 hotels.
- Screenline Traffic Count: 400 links on 9 screenlines

Each of these surveys was independently carried out, and thus they provide an opportunity for cross checking results among the different surveys as well as providing a basis for data consolidation.

GENERAL APPROACH

The Base Year 2005/06 travel database building process has taken into consideration of the types of travel and traffic data available while maximizing the advantages of HIS and other supplementary survey data sources in the data consolidation process.

In general the overall database building process is basically divided into the following four stages:

- Stage 1 – Carry out sample expansion for the different surveys including HIS, Taxi, Metro, Special Generators, and Floating population;
- Stage 2 – Build O/D matrices by modes for time periods of some of the surveys for matrix estimation purpose;
- Stage 3 – Consolidate and finalise O/D matrices by modes from various data sources; and
- Stage 4 – Update the HIS and other appropriate database based on the final O/D matrices by modes and time period

This paper mainly describes the HIS sample expansion and O/D matrix estimation process.

SAMPLE EXPANSION

Household interview survey collected information on household and personal profiles and most importantly the trip characteristics of each household member on the sample day. Sample expansion of household interview survey data was primarily undertaken by the following three criteria:

- Car Available (CA) and Non-Car Available (NCA) Household to ensure the number of cars and the distribution of CA households are correctly expanded and hence their travel characteristics are adequately accounted for in particular mode choice; and
- Permanent residents and Temporary Residents to ensure the population is correctly expanded and their travel behaviors are adequately accounted for in trip rate and mode choice; and
- Age Distribution to ensure the population by age groups is correctly expanded and thus the different travel behaviors of different age profiles are properly accounted for, such as students, workers and retired persons.

A stepwise expansion approach was undertaken. In brief, the car available households were first expanded to the number of cars by zone. This was then followed by expanding non-car available households based on the residual

households after discounting the car available households. Then population of car available households and non-car available households were expanded with the same factor as their households. After that, the expanded permanent residents and temporary residents were validated to their total control number separately. These expansion factors were applied to the HIS database and then age adjustment factors for each groups were calculated by the controlled and expanded age distribution. The last step was to apply the expansion factors to the trips data.

After HIS sample expansion, household, person and trip profile information were obtained, such as number of households by vehicle availability types, household size, proportions of workers and students, trip rate, mode choice, and trip purpose. The data was cross-examined among districts and zones to ensure that they are within reasonable range. The key output is a series of O/D matrices by modes and time periods.

O/D MATRIX ESTIMATION

O/D matrix estimation is a cross checking process based on the sample expansion results. The most important data for O/D matrix estimation is the prior O/D matrices and screenline traffic counts. Prior O/D matrices were consolidated from sample expansion results of HIS and the other supplementary surveys. Screenline traffic counts were compiled for O/D matrix estimation as these represent a separate and independent source of data from the HIS data. The types of screenline data were basically vehicle flows by mode and period (BTRC, 2007).

As metro is a separate system, the sample metro trips were expanded and validated at the same time, based on its boarding and alighting at each station by lines.

Definitions of modes and time periods in O/D matrix estimation process are shown in Table 1.

Table 1. Modes and time periods in O/D matrix estimation

Mode	Car, Motorcycle, Bus, Taxi, Coach, Bicycle
Time period	0:00-7:00, 7:00-9:00, 9:00-17:00, 17:00-19:00, 19:00-24:00

In this paper, the main feature of O/D matrix estimation process is the hierarchical approach. O/D trips between large areas were validated first. Then O/D trips in local area were validated. The study area was split into 21 sectors by screenlines (Figure 1).

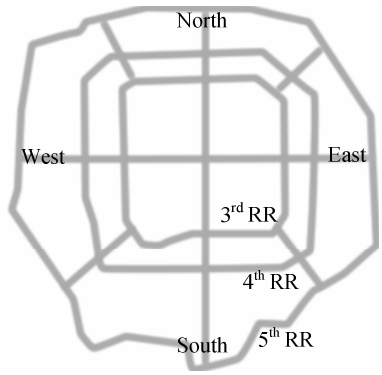

Figure 1. Screenlines and sectors

Different screenlines combinations were chosen to control the O/D movement between sectors. Four methods were considered and tested on different hierarchical approaches and path building methods (Table 2).

Table 2. Methods for O/D matrix estimation

Method	Screenline sequence for hierarchical estimation	Path Building
1	North/south→East/west→5th RR→4th RR→ 3rd RR→Radial	All or Nothing
2	(North/south+East/west)→ (5th RR +4th RR +3rd RR + Radial)	All or Nothing
3	(North/south+East/west+5th RR +4th RR +3rd RR + Radial)	All or Nothing
4	(North/south+East/west)→ (5th RR +4th RR +3rd RR + Radial)	Muti-path

Screenlines formed 20 sectors inside 5th ring road and 1 sector outside. O/D pairs between sectors were validated as they across the screenlines, while, intra-sector O/D movements were not validated during the matrix estimation process. Thus intra-sector O/D trips need to do additional validation. The intra-sector validation factor was calculated by the estimated and prior inter-sector trips. See Equation (1):

$$f_i^{Intra} = \frac{O_i^{est} + D_i^{est} - 2I_i^{est}}{O_i^{prior} + D_i^{prior} - 2I_i^{prior}} \quad i \in (1, 21) \tag{1}$$

Where:

f_i^{Intra} : intra-sector validation factor;

O_i^{est}, D_i^{est}, I_i^{est} : estimated trip ends and intra-sector trips of sector i;

O_i^{prior}, D_i^{prior}, I_i^{prior} : prior trip ends and intra-sector trips of sector i.

The O/D matrix estimation processes by modes by time periods were implemented using modeling software Cube ME. The input data includes prior O/D matrices, screenline traffic counts, highway network, and bus network. Each set of

data are given 'levels of confidence' or 'reliability' which conditions the influence of varying sources of data in the estimation. The estimation process is based on the Maximum Likelihood technique, coupled with an optimization procedure (CITILABS, 2004).

DATA CONSOLIDATION

After O/D matrix estimation, it is also necessary to use other independent sources of data for checking. Bus ridership, metro ridership, taxi ridership, car mileage, bus transfer per trip, and average trip distance were used for independent source of data checking. Differences were identified between the estimated results and the independent indicators. Then O/D matrix estimation approaches were chosen and improved.

The above O/D matrix estimation processes were done by trip modes and time periods. After completion of independent data checking, it is also necessary to check the integrated results of mode and time. The final overall daily person trips were consolidated from various data sources by summing across all mechanized modes (including bicycle) after O/D matrix estimation. The total person trip rates, modal split percentages, and trip length distribution were then referenced against historical patterns to ascertain whether they are consistent with socio-economic growth trends in terms of population and car fleet size as well as the expanding transport networks (BTRC, 2007).

The overall validation approaches were eventually selected in Table 3.

Table 3. Overall validation approaches

Mode	Approaches	
Car	O/D Estimation(Method 4) Independent data checking	Data Consolidation
Motorcycle	O/D Estimation(Method 4)	
Bus	O/D Estimation(Method 4) Independent data checking	
Metro	Sample expansion Independent data checking	
Taxi	O/D Estimation (Method 3) Independent data checking	
Coach	Sample expansion	
Bicycle	O/D Estimation(Method 3)	

DATABASE UPDATING

The final stage is to update the relevant database by time periods and modes based on the validated trip matrices. The purpose of this stage is to ascertain the resulting proportions of trips by trip purposes are in the right order, which has not been specifically dealt with in the expansion and validation process. If there appeared to be any unexpected results due to different levels of under-reporting by time

periods, some adjustments would be required based on previous results and references to other cities.

VALIDATION RESULTS

Comparing the validation results with sample data, we estimated that the overall under-reporting rate is 23%. According to other cities in China, the overall under-reporting rate is usually around 30% (GZTPRI, 2006; HKTD, 2003).

Key indicators before and after the validation process inside 6th ring road of Beijing were compared and shown in Table 4-5.

Table 4. Daily trips and trip rate

	Sample	Sample expansion	Validation Results
Trip Rate	2.16	2.16	2.64
Total trips (10000 trips)	30	2393	2920

Table 5. Daily mode share

Mode	Sample	Sample expansion	Validation Results
Car	28.2%	25.9%	29.8%
Taxi	2.4%	4.4%	7.6%
PT	27.7%	29.4%	29.8%
Coach	3.4%	3.1%	2.5%
Bicycle	38.3%	37.2%	30.3%
Total	100%	100%	100%

CONCLUSIONS

After a series of data fusion and validation process, such as sample expansion, O/D matrix estimation, independent data checking and integrated validation, under-reporting in HIS data had been eliminated. The consolidated data can reflect the current travel demands and patterns in Beijing; moreover the data played an important role in development of Beijing 2nd level transport model and supported some strategic transport planning or decision-making projects.

REFERENCES

Beijing Transportation Research Center (BTRC) (2007). *Beijing the 3rd comprehensive transport survey Main Report*. Beijing, China.

Beijing Transportation Research Center (BTRC) (2007). *Beijing the 3rd comprehensive transport survey Technical Report*. Beijing, China.

Beijing Transportation Research Center (BTRC) (2007). *Beijing the 3rd comprehensive transport survey Data validation Report*. Beijing, China.

CITILABS Inc. (2004), *Cube ME Manual.* CA, USA.

Guangzhou transport planning & Research institute (GZTPRI) (2006). *Guangzhou 2005 household interview survey report*. Guangzhou, China.

Hong Kong Transport Department (HKTD) (2003). *Travel Characteristics Survey 2002 Final Report*. Hong Kong.

Modeling logistics and Supply Chain with an Integrated Land Use Transport Model: PECAS

Ming Zhong[1], John Douglas Hunt[2], and John Edward Abraham[2]

[1]Dept. of Civil Engineering, University of New Brunswick, GD-128, Head Hall, 17 Dineen Dr., P.O. Box 4400, Fredericton, N.B., Canada E3B 5A3, Telephone: (506) 452-6324 Fax: (506) 453-3568, Email: ming@unb.ca

[2]Institute for Advanced Policy Research, University of Calgary, 2500 University Drive N.W., Calgary, Alberta, Canada T2N 1N4, Phone: (403) 220-8783, Fax: (403) 282-7026, Email: jdhunt@ucalgary.ca, jabraham@ucalgary.ca

Abstract

Decision-making regarding logistics and supply chain need to be based on freight transportation modeling, but most of transportation models only consider passenger travel demand. An integrated land use transport model is introduced here which addresses both freight and passenger demand modeling. The framework is called PECAS, which stands for Production, Exchange, Commodity Allocation System. PECAS consists of the following three modules: Activity Allocation (AA), Space Development (SD) and Transport Supply (TS) and is linked to an aspatial regional economic model. The focus of this paper is to illustrate the capability of its AA module in modeling logistics and supply chains, for which the major economic sectors are considered and the flows of all commodities, including goods, service, space, land and labor, are simultaneously determined from production zones to exchange zones to consumption zones. This paper gives a brief introduction to the framework and presents detailed methodologies used in determining the locations of activities and exchanges between them.

INTRODUCTION

PECAS stands for Production, Exchange and Consumption Allocation System. It is a recently-developed, generalized approach for simulating spatial economic systems. It is designed to provide a simulation of the land use component of land use transport interactive modeling systems.

PECAS is a spatial economic simulation system with a focus on transportation and land development planning. The PECAS framework draws from previous modeling experiences, especially MEPLAN (Echenique *et al.* 1990) and TRANUS (De la Barra *et al.* 1984), and provides significant improvements in theoretical basis and behavior representation (Hunt and Abraham 2005).

The PECAS modeling framework consists of the following three modules: activity allocation (AA), space development (SD), and transport supply (TS), and it is linked with an aspatial economic model. The AA module represents how activities locate within the space provided by developers and how these activities interact with each other at a given point in time. The SD module simulates the actions of developers in the provision of space (land and floorspace) where activities can locate, including the new development, demolition and re-development that occurs from one point in time to the next. The TS module uses its networks to establish congested network times and costs and associated interchange (dis)utilities that PECAS uses in its consideration of the interactions between land use zones. The aspatial economic module forecasts future economy status, which provides the area-wide scale of activities considered in the model. PECAS uses an aggregate, equilibrium spatial I/O modeling approach for allocating activities into different zones, but has a micro-simulation based space development sub-model.

The focus of this paper is to introduce the capability of PECAS AA module in determining supply/exchange chain at a given year. The AA module uses an aggregate, equilibrium structure with separate flows of exchanges (including goods, services, labour and space) going from production to consumption based on variable technical coefficients and market clearing with exchange prices. Flows of exchanges from production to exchange zones and from exchange zones to consumption are allocated using nested logit models according to exchange prices and transport disutilities. These flows are converted to transport demands that are loaded to networks in order to determine congested travel disutilities. Exchange prices determined for space inform the calculation of changes in space thereby simulating developer actions. The system is run for each year being simulated, with the travel disutilities and changes in space for one year influencing the flows of exchanges in the next year.

PECAS STRUCTURE

The "land use" part of PECAS has two component modules. One is the space development (SD) module, which represents the actions of developers in the provision of space (land and floorspace) where activities can locate, including the new development, demolition and re-development that occurs from one point in time to the next. The other is the activity allocation (AA) module, which represents how activities locate within the space provided by developers and how these activities interact with each other at a given point in time.

Treatment of Space

The area covered by PECAS is organized into a set of land use zones. Activities locate in these zones and interact between each other. Ideally these zones are the same as the transport zones used in the transport model being run with PECAS, or at least are aggregations of whole numbers of adjacent transport zones. The connectivity among the land use zones is then based on the representation provided by the TS module, where the multimodal transportation model uses its networks to establish congested network times and costs and associated interchange (dis)utilities that PECAS uses in its consideration of the interactions between land

use zones.

Treatment of Time

PECAS works through time in a series of discrete, fixed steps from one point in time to the next, with the AA module running first at each point in time and then the SD module considering the period from each point in time to the next. The steps can be of any fixed duration, but 1 year time steps are recommended since they allow an appropriately quick response of land developers in the SD module to the prices established in the AA module.

Figure 1 illustrates the interactions among the modules and with other models (aspatial economic model and transport model) when the above two modules are run as part of an integrated land use transport modeling system. Each year, the model-wide aggregate economic model runs to forecast future scale of each economic sector (such as agriculture, retail, heavy industry, and services). Then the AA module runs to allocate these economic activities into land use zones and determine the exchange flows between them. The flows are then loaded on the transport network and the TS module is used to calculate the congested travel times and disutilities. The TS module is normally run for each year (after the AA module completes its run for that year) or, if travel conditions are relatively stable, the transport model can be run less often to save computation time. The changes of economy determine the size of economic sectors (or activities) considered in the model and subsequent space demand. Each year, the AA module passes the price of each type of space to the SD module and the SD module simulates developers' actions based on the price signals received. As it can be seen in Figure 1, between any two successive years, changes in model-wide economy, activity location, and transport supply and disutility will be passed to the next year to influence how the whole economy is evolving. Such a process will continue until the end of the planning window.

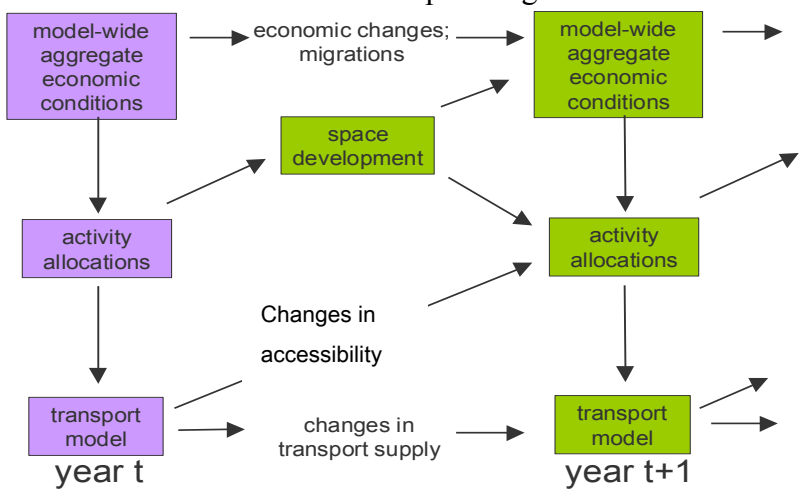

Figure 1 Interactions among modules simulating temporal dynamics

MODELING LOGISTICS AND SUPPLY CHAIN WITH ACTIVITY

on spatially-disaggregated forms of extended make and use input-output (I/O) tables, with variable technical coefficients and with households included – making the tables 'social accounting tables' rather than just input-output tables. Categories of activity

produce 'commodities' as indicated in the make table and consume these 'commodities' as indicated in the use table, where the 'commodities' include goods and services, labour and space (land and/or floorspace). The movement of these commodities from where they are produced (in zones) to where they are consumed (in zones) is the economic basis for travel and transport in the land use model. The travel conditions – distances, costs, times and associated (dis)utilities by mode – for the movement of these commodities determine how the transportation system influences the attractiveness of zones as locations for different activities.

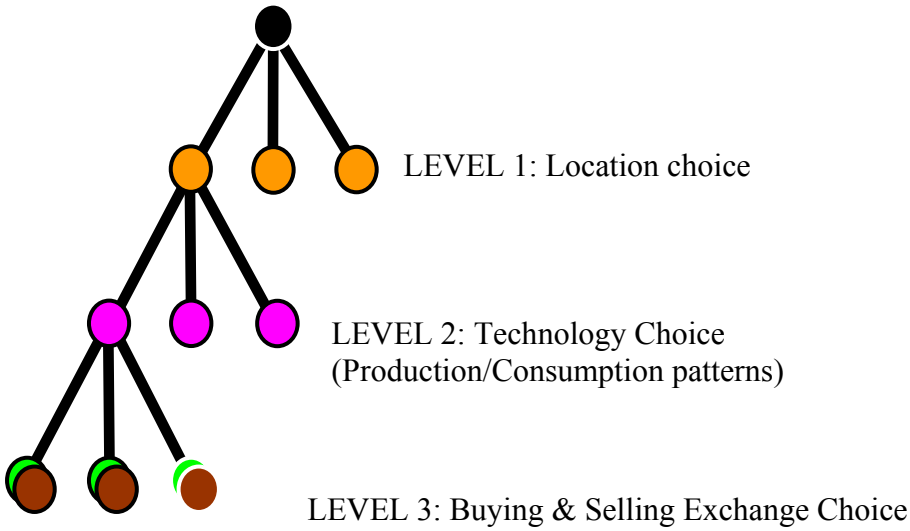

Figure 2 PECAS three-level logit choice model

The model-wide total quantity of production activity for each activity category is input to the AA module, which uses a three-level nested logit model to determine the exchange flows (or supply chains) of commodities considered, as shown in Figure 2. For each zone there are two 'lowest-level' logit allocation models (Level 3 in Figure 2) for each category of commodity considered in the model. The first is an allocation of the quantities purchased among various 'exchange locations' where they are sold to other activities. The second is an allocation of the quantities sold among the various exchange locations where they are bought by other activities. The utility of each alternative in these models is influenced by the price at the exchange location, and the characteristics of transporting the commodity to or from the exchange location. The composite utility values from these two 'lowest-level' logit models are called the 'buying utility' and the 'selling utility' for the commodity in the zone. They are used as the transportation-related inputs into the 'next-higher-level' logit allocation process for allocating the production and consumption of commodities by activities (Level 2 in Figure 2). It is the choice of which production technology to use, which in turn determines its commodity consumption pattern. The make and use technical coefficients indicating the rates at which activities produce and consume commodities are elastic, representing opportunities for substitution. From there, via the resulting utilities of production and consumption, they feed into the location utilities used at the 'highest-level' to allocate categories of industries and households to the land use zones (Level 1 in Figure 2).

The spatial allocation system with both buying and selling allocations gives

rise to exchanges from production to consumption locations in zones. The commodity flows or supply chains are being modeled as a process of moving goods or services from production to consumption zones through exchange zones. The exchange locations are location-specific markets for commodities, where sellers sell commodities to buyers. Prices are established at exchange locations so that the quantity bought equals the quantity sold – thus the spatial allocation procedure used in PECAS assumes a short-run market equilibrium in commodities.

The exchange zones simulate markets where the aggregate supply for each commodity (the sum of the selling allocations together with the quantity of imports, both of which are elastic with respect to exchange price), meets the aggregate demand for the commodity (the sum of the buying allocations together with the quantity of exports). The module solves for the equilibrium solution, adjusting the exchange prices in the exchange locations until all the markets clear, that is, where the total aggregate supply is equal to the total aggregate demand.

The AA module provides consistent activity allocations by activity category by zone, commodity flow quantities from production zone to consumption zone via exchange zone, imports and exports by exchange zone and exchange prices by commodity by exchange zone. It also provides the basis for assessing the changes in model-wide consumer surplus by production activity. In particular, the model-wide location composite utility for a given activity category is determined as follows:

$$CLU_a = (1/\lambda_a) \cdot \ln (\Sigma_{z \in Z} \exp (\lambda_a \cdot LU_{a,z})) \quad [1]$$

Where:

CLU_a = model-wide location composite utility for a unit of activity a.

λ_a = utility function dispersion parameter for allocation of activity a.

Changes in CLU_a for a given activity category can be used to calculate measures of the changes in consumer/producer surplus for different activity categories arising with the policy actions input to the model. These measures can help assess quality of life and business attractiveness for different household and industrial categories as represented.

CONCLUSIONS

This paper briefly introduces the PECAS framework with a focus on its AA module. The AA module is an aggregate I/O model, which allocates a forecasted future economy into zones based on a set of utility functions considering buying, selling, production/consumption, labor, space/land, and transport costs. This spatial I/O model (the AA module) produces, among other things, a landscape of prices by commodity, flow matrices by commodity and the locations of activities.

The theoretical base for the PECAS framework is described in detail in Hunt and Abraham (2005). Open software implementing the AA module has been developed in Java with many individuals and agencies' contributions.

PECAS or its components are being used in a number of practical modeling applications. A statewide model of Ohio is being developed using the full PECAS structure (PB Ohio *et al*, 1999). The Generation 2 modeling work in Oregon is using many of the elements of the PECAS activity allocation module as part of a larger system where various micro-simulation treatments are applied with the results of the activity allocation acting as inputs (Hunt, 2001). The full PECAS structure has been

used as the basis for a model specification for the Los Angeles Region, Baltimore, Montgomery and California State in the United States, City of Mumbai in India and the Province of Alberta, Canada (Zhong et al. 2007). A land use model for the Sacramento Region that is just starting to be developed is based in part on the PECAS activity allocation module (DKS et al. 2001). The intention is to use the full PECAS structure in the development of urban-level land use transport interaction models of both Edmonton and Calgary in Canada.

REFERENCES

De la Barra, T., Perez, B. and Vera, N. (1984). "TRANUS-J: Putting Large Models into Small Computers", *Environment and Planning*, 11B, 87-101.

DKS, Mark Bradley Research and Consulting, HBA Specto and Bowman, J.L. (2001). "Land Use and Transport Modeling Design Report". Prepared for Sacramento Area Council of Governments, Sacramento CA, USA.

Echenique, M.H., Flowerdew, A.D.J., Hunt, J.D., Mayo, T.R., Simmonds, D.C., and Skidmore, I.J. (1990). "The MEPLAN Models of Bilbao, Leeds and Dortmund", *Transport Reviews*, 10, pp. 309-322.

Hunt, J.D. (2001) "The 2nd generation Oregon statewide land use transport interaction model". Proceedings of the 7th International Conference on Computers in Urban Planning and Urban Management, Honolulu HI, USA, July 2001.

Hunt, J.D. and Abraham, J.E. (2005). "Design and implementation of PECAS: A generalized system for the allocation of economic production, exchange and consumption quantities". In: *Foundations of Integrated Land-Use and Transportation Models: Assumptions and New Conceptual Frameworks*, Lee Gosselin and Doherty editors, Elsevier (book chapter).

PB Ohio and Hunt Analytics (1999) "Ohio Statewide Travel Demand Model Final Report", PID 17803. Prepared for Ohio Department of Transportation Office of Technical Services, Columbus OH, USA.

Zhong, M., Hunt, J.D., and Abraham, J.E. (2007) "Design and Development of a Statewide Land Use Transport Model for Alberta", Journal of Transportation Systems Engineering and Information Technology, Vol. (7), No. 1, pp. 79-91.

Research on the Bicycle Capacity at Signalized Intersection Based on Fluid Diffusion Characteristics

Li Lilan[1], Zhang Yaping[2], Lan Xiang[2] Ye Ruimin[2] and Wang Yuping[2]

[1]School of Transportation Science and Engineering, Harbin Institute of Technology, Harbin, China; phone: 86-0451-86282117; fax: 86-0451-86283779; e-mail: lililan@hit.edu.cn.
[2]School of Transportation Science and Engineering, Harbin Institute of Technology, Harbin, China; e-mail: zxlt0905@163.com

ABSTRACT

Mixed traffic of bicycles and motor vehicles is a major characteristic of urban transportation in China, and has led to traffic accidents, serious congestion and capacity reduction on urban signalized intersections. Determining bicycle capacity on signalized intersections is not only the basis for intersection design and planning, but also for signal configuration and operation management. Motor vehicles are a major influence on bicycles crossing through an intersection. Based on an analysis of the fluid diffusion characteristics at signalized intersections, the paper established a fluid diffusion model on bicycle capacity. Comparative analysis of large data sets shows that the model provides good results.

Keywords: Bicycle, Capacity, Signalized intersection, Fluid diffusion

INTRODUCTION

Current research on bicycle flow characteristics in the world focus on adaptive signal timing for bicycles (Ananth P et al., 2007), bicyclist and motorist gap acceptance behavior in mixed-traffic (Taylor and H. Mahmassani, 1998), traffic signal clearance interval requirements for bicycle-automobile mixed traffic (Taylor, 1993), capacity (HCM2000, 2000), bicycle traffic arrival characteristics (Qu et al., 2004) and bicycle traffic geometry and timing design (Forester J., 1994; Sun et al., 2004).

When crossing an intersection, bicycle flow does not depend solely on independent decisions make by individual riders, but has fluid diffusion characteristics. When the bicycle flow in traffic is sparse, the fluid fluctuation is not obvious. When the bicycle flow comes up to a certain level, riders generally make decisions concerning their own speed and direction according to the available space, and fluctuations become very obvious.

From the perspective of an overall macro-observation, bicycle flow travels at the crossing, just like fluid, as long as where there is no "resistance". It "flows" forward, matching the "space occupy theory", which is the bicycle's fluid diffusion characteristic.

The bicycle's behavior at a signalized intersection show that bicycle flow stops at the parking line, gathering and forming in a queue during the red light; and when the green light is activated, the bicycle flow gathers speed to pass the stop line, the bicycle density lessens along with the continuing green-light time,.

In actual observation, we can find that right-turn vehicles, pedestrians and the expansion of the bicycle all have a great impact on bicycle intersection capacity.

THE BICYCLE FLUID DIFFUSION MODEL

Generally, when a bicycle is crossing through a signal, there are three states: waiting during a red-light; dissemination at the intersection during a green light; and changing into free flow gradually after crossing the intersection.

Its fluid diffusion model is described as shown in Figure 1 (Xiong and Qiu, 2005).

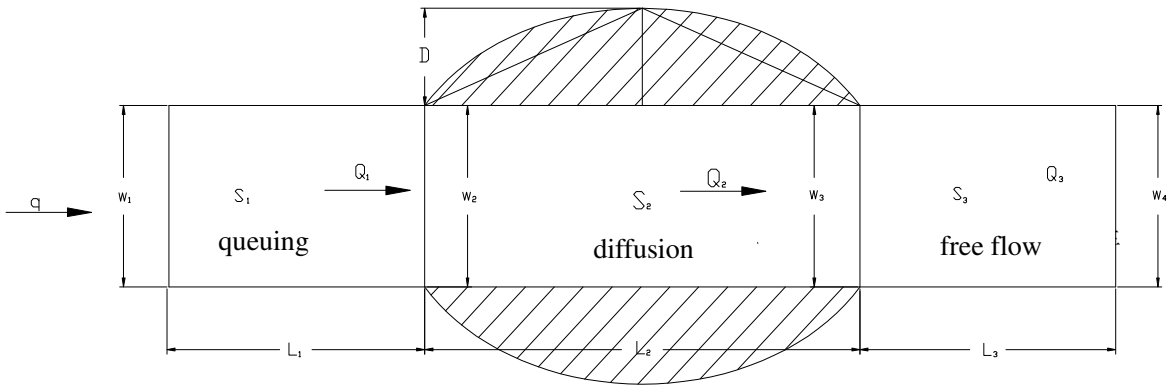

Fig.1 fluid diffusion model

Some definitions of concepts are given as follows: N is bicycle capacity in a signal cycle; q is bicycle average arrival rate of upper stream; G_e is signal green time; T is an average crossing time of bicycle; ρ_1 is queuing density; C is length of signal cycle; L_1 is length of the bicycle in a queue; L_2 is intersection width; L_3 is the length of the segment changing from bicycle diffusion flow to free flow; D is the maximum vector length of the bicycle's diffusion and distention at intersection; W_1 is the width of bicycle lane at the end of queuing length; W_2 is the width of bicycle lane at the parking line; W_3 is the width of the bicycle lane at the exit; W_4 is the borderline width of the bicycle lane while the bicycle flow changing from the aggregation flow to the freedom flow totally; S_1 is the area which is surrounded by the bicycles at the parking line; S_2 is the description of the bicycle running and diffusion at intersection. S_3 can contain aggregated compressing bicycle flow similar to S_1. After passing through S_3, the bicycles start to run in a state of free flow.

In a signal cycle, the single-lane flow rate N is as follow:

$$N = \int_T^{Ge} W_2 q dt + \int_T^{G_e} [\frac{(\rho_1 S_1 + W_1 qT)(W_3 + D)}{S_2} - W_2 q] e^{(-\frac{V(W_3+D)}{S_2} t)} dt \quad (1)$$

That is

$$N = W_2 q(G_e - T) + [\rho_1 S_1 + W_1 qT - \frac{W_2 qS_2}{V(W_3 + D)}][e^{\frac{V(W_3+D)}{S_2}G_e} - e^{\frac{V(W_3+D)}{S_2}T}] \quad (2)$$

Owing to

$$S_1 = W_1 * L_1 \quad (3)$$

$$S_2 = (W_2 + D) * L_2 \quad (4)$$

Taking into account the overwhelming majority intersection, W_1=W_2=W_3=W, the formula (2) can be simplified as:

$$N = q\{G_e - T + \rho_1(C - G_e)[e^{-1} - e^{-\frac{G_e}{T}}]\} \quad (5)$$

In a signal cycle, bicycle flow rate N raises along with the effective green time Ge. The less the T is, namely the speed passing through the intersection is greater, the greater the flow rate N is. This matches the real situation.

TRAFFIC SURVEY

This paper selects 4 signalized intersections in Harbin city to conduct the field survey. The intersections are as follows: intersection of XianFeng Road-XuanHuan Street (Intersection 1); intersection of HePing Road-XuanHuan Street (Intersection 2); intersection of HePing Road-ZhongShan Road (Intersection 3); intersection of HongQi Street -HuaiHe Road (Intersection 4). Survey results are shown in table 1 and figure 2.

Table 1 Signal timing at signalized intersection /s

Intersection1	Straight east-west	Left east-west	Straight north-South	Left north-South
	55	30	45	60
Intersection2	Straight + Left west	Straight + Left east	Straight north-South	Left north-South
	35	35	75	40
Intersection3	Straight east-west	Left east-west	Straight north-South	Left north-South
	45	30	45	20
Intersection4	Straight+ Left east-west		Left north-South	Straight north-South
	30		20	40

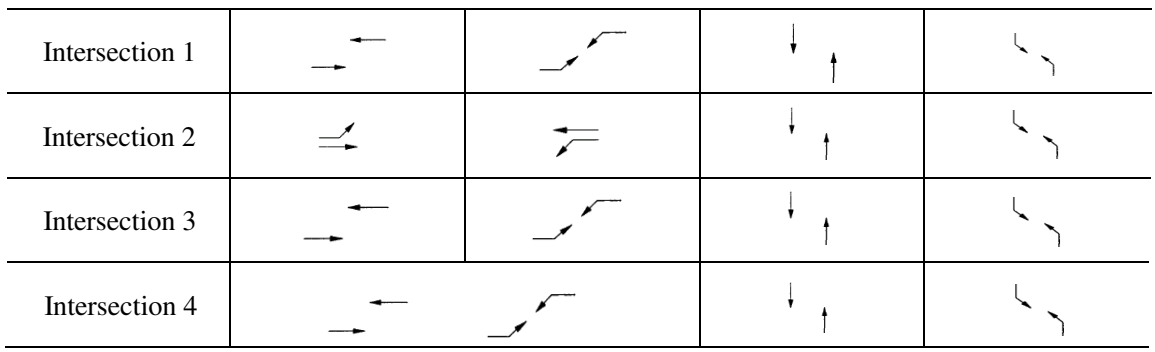

Figure 2 Phase distribution at signalized intersection

BICYCLE CAPACITY ANALYSIS AT SIGNALIZED INTERSECTION

Due to the function (5), bicycle capacity at Signalized intersection is as:

$$Cap = 3600 \cdot q\{\frac{G_e - T}{C} + \rho_1(1 - \frac{G_e}{C})[e^{-1} - e^{-\frac{G_e}{T}}]\} \quad (6)$$

The minimum safety headway time is 1.8s according to the experiments, so the maximum average arrival rate is 0.56 veh/s; generally, the density of bicycle in line in actual observation can reach 0.60veh/m^2, which is in basic accord with the investigation in document. In the four intersections investigated, the average running rate is 13.57km/h.

The width of signalized intersections is generally from 35m to 70m. The signal cycle gets its value in a certain range, getting the capacity as shown in table 2.

Table 2 A Part of Statistical Results of Evaluated Bicycle Capacity **veh· h^{-1}**

Signal time /s / Width (m)	*C*=120 *Ge*=40	*C*=130 *Ge*=50	*C*=140 *Ge*=45	*C*=140 *Ge*=50	*C*=150 *Ge*=50
35	207	333	197	278	231
40	193	314	183	262	216
45	181	297	172	247	204
50	170	282	162	234	193
55	160	268	154	222	183
60	150	255	146	211	174
65	140	242	138	201	166
70	130	229	131	191	158

Figure 3 shows that the relationship between the signalized intersection width and capacity. From the diagram, we find that there is a significantly linear relationship between the bicycle crossing width and capacity; while the crossing width increases, capacity decreases linearly.

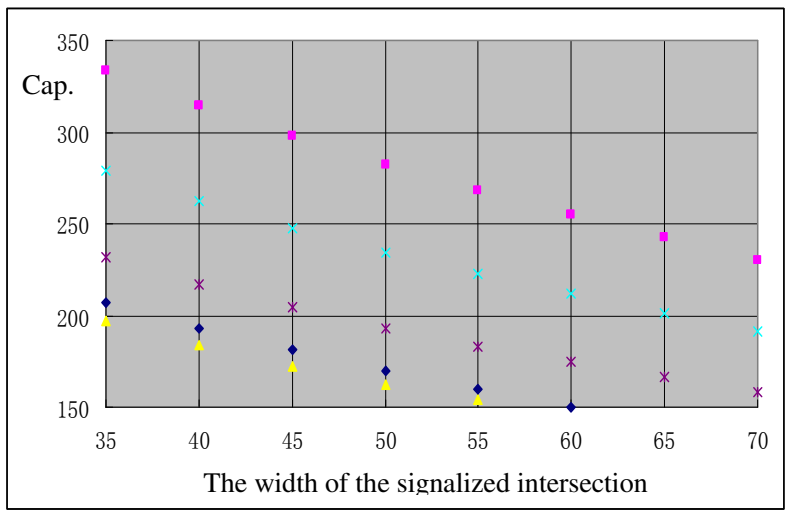

Figure3 Relationship between the width of a signalized intersection and capacity

BICYCLE FLUID DIFFUSION EFFECTS

A. Right turning and straight going vehicles in the same direction

The phenomenon of bicycle fluid diffusion in a signal control intersection has a great impact on straight and right turning vehicles, particularly right turning vehicles. Similarly, straight and right turning vehicles also produce a greater impact on the normal flow of bicycle traffic. This mutual influence constraints the performance of each, causing slow down for both bicycles and vehicles through the intersection.

B. Left turning vehicles in the opposite direction

For two-phase signal control intersections, when a green light starts, there is conflict between bicycle flow and left turning vehicles during the bicycle flow diffusion time. In this case, bicycles have a larger impact on the capacity of left turning vehicles.

BICYCLE FLUID DIFFUSION CORRECTION MODEL AND THE ACTUAL CAPACITY CALCULATION

Taking into account the actual operational modes according to analysis of 4.1 and 4.2, the maximum throughput *Cap'*/veh•h•lane can be calculated by reduced coefficient method:

$$Cap' = 3600 \cdot q \cdot f_{Rpb} \cdot f_{Lpb} \left\{ \frac{G_e - T}{C} + \rho_1 (1 - \frac{G_e}{C})[e^{-1} - e^{-\frac{G_e}{T}}] \right\} \tag{7}$$

$$f_{Rpb} = 1.0 - (1 - A_{Pbt})(1 - P_{RTA}) \tag{8}$$

$$f_{Lpb} = 1.0 - (1 - A_{Pbt})(1 - P_{LTA}) \tag{9}$$

Where f_{Rpb} is the impact factor of right turning vehicles in the same direction on the bicycle capacity; f_{Lpb} is the impact factor of left turning vehicles in the opposite direction of the bike capacity; $\mathrm{P_{RTA}}$ is adjustment factor of right turning phase for the protection, $0 < P_{\mathrm{RTA}} < 1$; P_{LTA} is adjustment factor of left turning phase for the protection, $0 < P_{\mathrm{LTA}} < 1$; A_{pbt} is adjustment factor of right and left turning vehicles when a bicycle is permitted to pass, $0 < A_{\mathrm{pbt}} < 1$.

Table 3 Different signal timing considering effects of vehicles **veh· h^{-1}**

Signal timing /s / Width (m)	*C*=120 *G*$_e$=40	*C*=130 *G*$_e$=50	*C*=140 *G*$_e$=45	*C*=140 *G*$_e$=50	*C*=150 *G*$_e$=50
35	307	328	315	325	323
40	293	319	305	316	314
45	277	308	292	306	304
50	260	296	279	294	293
55	243	283	264	282	281
60	224	269	248	268	267
65	206	254	232	254	253
70	188	328	315	325	323

Finally calculation results are based on a modified model that is the actual bicycle capacity in a signal control intersection, as shown in table 3. According to the value amended for some parameters for bicycles in the United States Capacity Manual, and combined with the actual situation in our country, the relevant parameter values are as follows: f_{Rpb}=0.87, f_{Lpb}=0.76.

CONCLUSIONS

Based on the fluid diffusion characteristics of bicycle and related theories, this paper establishes the fluid diffusion model of bicycle capacity at signalized intersections, demarcates the parameters, and analyzes the relationship between bicycle capacity with the signal cycle, green lights, and the bicycle arrival rate and so on. These factors impact development of theory and instruction for improving the signal timing and intersection channelization.

Mixed transportation is the main characteristic of most cities in China. How to determine the capacity of bicycles at intersection, to understand of the capacity characteristics of bicycles, the cooperative control of vehicles,, and to achieve the balance of development of non-motor vehicles and motor vehicles, is forever evolving. The actual survey indicates that effective time is wasted in waiting for right turn vehicles. It is meaningful for researchers to analyze the influence of the gap of turn right motor vehicles on the behavior of bicycle flow in depth, and how to coordinate control of motor vehicles to increase bicycle capacity at intersections.

REFERENCES

Transportation Research Board. (2000) Highway Capacity Manual 2000[DB/CD]. Special Report, *National Research Council*, Washington D.C.

D. Taylor and H. Mahmassani. (1998) Bicyclist and motorist gap acceptance behavior in mixed-traffic. *Transportation Research Board the 78th Annual Meeting. TRB*, National Research Council, Washington, D.C.

D. Taylor. (1993) Analysis of traffic signal clearance interval requirements for bicycle-automobile mixed traffic. *Transportation Research Records 1405, TRB, National Research Council*, Washington, D.C.

Forester J. (1994) Bicycle transportation. The MIT Press, London, England, 87-96.

Sun Mingzheng, Yang Xiaoguang. (2004) Machine-trip plane mixed traffic intersection design theory study. *Highway Traffic Technology*, Volume 21, No. 8: p23-28.

Qu Zhaowei, Zhou Jun, Wang Dianhai. (2004) Urban bike and pedestrian signals at intersections with the release of. *Highway traffic technology*, Volume 21, No. 8: 13-22.

Xiong Hui, Qiu Jiandong. (2005) Research of the capacity of bicycle on signalized intersections. *Journal of Beijing Institute of Technology*: 60-63

Analysis and Evaluation of Expressway Planning Schemes Based on Integrated Macro and Micro Simulation

LIANG Dui-dui[1], CHANG Yun-tao[2], Zhong-Ren Peng[3] and PANG Ying[4]

[1]School of Transportation Engineering, Tongji University; Room 334, School of Transportation Engineering, No.4800 Cao'an Road, Shanghai 201804, China; PH 13621856281; email: ddliang_03@163.com

[2]School of Transportation Engineering, Tongji University, Shanghai 201804, China; email: crchanghp@163.com

[3]Department of Urban and Regional Planning, University of Florida; P.O. Box 115706; Gainesville, FL 32611-5706, USA; PH 352-392-0997; FAX (352)392-3308; email: zpeng@dcp.ufl.edu

[4]School of Transportation Engineering, Tongji University, Shanghai 201804, China; email: selinajustpyy@126.com

ABSTRACT

Urban expressway plays an important role in the movement of goods, people, and services, and is essential for urban development and economic growth. Thus it is critical to plan it right in the first place, and to simulate the functions and evaluate the effectiveness of its planning scheme before implementation. We have developed an integrated macro and micro simulation method to evaluate the effectiveness of the planned expressway system. This paper summarizes the main contents of analysis and evaluation method in a case study. We found that the integrated macro and micro simulation method is very efficient and effective in analyzing and assessing the effectiveness of the planned expressway framework, and identifying the deficiency of the plan, which is unachievable by either macro and micro simulation alone. The method could be useful for other expressway planning, analysis and simulation.

1. INTRODUCTION

Urban expressway is the backbone of the urban transportation system, plays an important role in reducing traffic congestion, equilibrating road network traffic flow, separating fast traffic from slow traffic, and long-distance trips from short-distance ones *(Yang, et al., 2004)*. However, the investment for expressways is often large, which thus raises a higher demand for expressway planning. Any carelessness or deficiency of expressway schemes may lead to the congestion of local traffic in expressway systems, and even large-scale congestion in a transportation system. Thus it is critical to plan it right in the first place, simulate and evaluate the effectiveness of its planning scheme before implementation, which helps to identify the deficiency of the expressway plan and realize the planning objectives of expressway systems.

2. MAIN CONTENTS OF SIMULATION ANALYSIS AND EVALUATION

2.1 Overall layout of expressway systems

Based on the function requirements of urban expressway, analyze and assess:

1) Internal: Is the expressway trend consistent with the desire line of middle-long distance vehicle trips of internal city? Whether the expressway trend is compatible with urban spatial structure?

2) External: Does the layout of expressway systems help to evacuate external transportation and shield transit traffic quickly? Does the layout facilitate the smooth transition between internal and external transportation *(Miao, 1997)*?

2.2 Location of interchanges

The main content of analysis and evaluation regarding interchanges include their function orientation, configuration type selection, ramp combination and correlative noninterference setting. In addition, the effectiveness of the planned interchanges also needs to be simulated and evaluated to check whether they are beneficial to more orderly traffic *(Liu, 2000)*.

2.3 Setting of ramps

The analysis emphasis regarding ramp setting is the rational of their quantities and spaces, which is based on the fact that too many ramps and too small spaces will lead to traffic flows diverging, merging and weaving frequently, while too few ramps cannot provide enough flow for expressway mainlines *(Gao, 2006)*. In addition, the distances between on/off ramps and adjacent ground intersections as well as vehicle queues on ramps also need to be analyzed and assessed.

2.4 Traffic analysis of adjacent road networks

Does the capacity of on/off ramps match that of adjacent ground intersections? Is the structure of adjacent road networks reasonable? Are road functions of different types specific enough and meet the criteria? Are there frequent collisions between vehicles, non-motorized vehicles, and pedestrians, etc?

3. SIMULATION ANANLYSIS AND EVALUATION METHODS

Considering the complexity of analysis and evaluation of expressway planning schemes, this paper develops an integrated macro and micro simulation method. Two widely used traffic software TransCAD and VISSIM are applied. Figure1 shows the processes of the method.

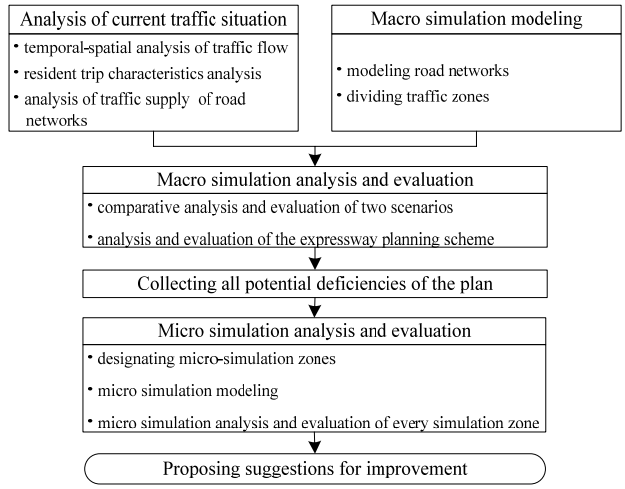

Figure1. Flow chart of analysis and evaluation of expressway planning schemes

3.1 Analysis of current traffic situation

Based on abundant basic data and urban comprehensive plans, conduct detailed analysis of current traffic situation through analyzing the temporal and spatial characteristics of traffic flow, trip characteristics, and the capacity and layout of the current road network in the study area.

3.2 Macro simulation modeling

The following two steps need to be taken to model road networks from a macroscopic perspective:

1) Modeling road networks: first specify required modeling parameters for every type of road (freeways, expressways, main trunk roads, secondary trunk roads and branches), then use TransCAD to establish macro-simulation models of road networks.

2) Dividing traffic zones: employ the common traffic zone division method to divide traffic zones or use the zones divided during transportation survey.

3.3 Macro simulation analysis and evaluation

In this stage we use TransCAD to analyze and assess the effectiveness of the planned expressway framework at the macroscopic level.

1) Comparative analysis and evaluation of two scenarios (without expressway system and with the planned expressway system): First, load the estimated OD distribution volumes of vehicles to the current road network and the network with the planned expressway framework respectively in TransCAD and carry out traffic assignment. Next assess the integral effectiveness of the expressway system through calculating and comparing a series of evaluation indicators including total travel time (veh·h), vehicle miles traveled (veh·km), the average speed of road networks (km/h), and so on.

2) Analysis and evaluation of the expressway planning scheme: Based on the macro-simulation results of the road network with the planned expressway

framework, make detailed analysis and evaluation of the planning scheme from different aspects as mentioned in the second part. Then collect all potential deficiencies of the expressway plan and determine all plots with these deficiencies to make a good preparation for the following in-depth micro simulation.

3.4 Micro simulation analysis and evaluation

Take the following three steps to simulate and evaluate whether the potential problems identified above will occur and how serious they would be in VISSIM.

1) Designating micro-simulation zones: Taking the plots with potential problems as the center, expand outward a certain distance (depending on the purpose of simulation) to designate micro-simulation zones.

2) Micro simulation modeling: For every simulation zone, build the micro simulation network and set up traffic flow characteristic parameters and traffic rules, where both traffic flow and route choice come from the macro-simulation results.

3) Micro simulation analysis and evaluation: Test and run every micro simulation model to assess whether the potential problems will happen and how serious they will be from qualitative and quantitative perspectives respectively.

3.5 Proposing suggestions for improvement

Combining the local conditions, put forward corresponding suggestions for improvement based on potential problems and their seriousness identified through integrating macro and micro simulation analysis and evaluation.

4. CASE STUDIES

We take the expressway planning scheme of Zhengzhou (Longhai Road and Shakou Road-Jingguang Road) as a case, to illustrate how to analyze and assess the effectiveness of expressway planning schemes in practice. The planning scheme is shown in Figure 2.

4.1 Preparing for simulation analysis and evaluation

1) Analysis of current traffic situation in downtown Zhengzhou

According to the transportation survey of Zhengzhou in 2007, the spatial distribution of traffic is quite unbalanced. It is mostly concentrated in the core region. The average trip rate of residents is 2.68 times/day; bicycle, electric bicycle and walking are still the main modes of residential travel; the vehicle trip accounts for 21.4% in total *(China Academy of Urban Planning & Design, 2007)*.

2) Macro simulation modeling of road networks

Taking the road network containing Shakou Road-Jingguang Road, Longhai Road and adjacent roads within 1~2 km along the planned expressway as the study area, we built macro-simulation network models with TransCAD. The central city of Zhengzhou is divided into 33 traffic zones (as shown in Figure 3).

3) Traffic demand forecasting in the planning year

By 2010, the average trip rate of residents will be 2.70 times/day; the total resident trip volume per day will approximately be 1134 times; the peak hour flow of vehicles will be 100 thousand pcu/h. The spatial distribution of vehicle trips in the

planning year is estimated and shown in Figure 3.

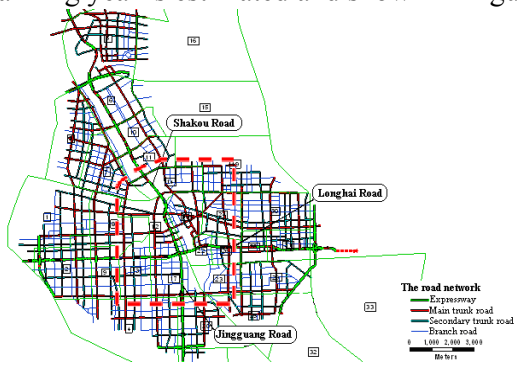

Figure 2. The expressway planning scheme of Zhengzhou

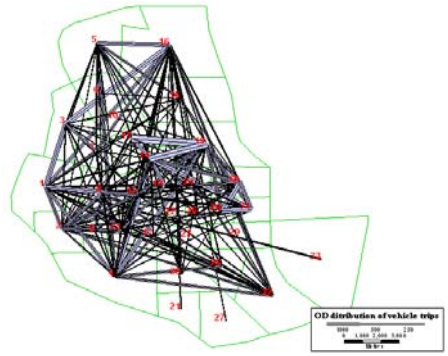

Figure 3. The OD distribution of vehicle trips in Zhengzhou in 2010

4.2 Macro simulation analysis and evaluation of the expressway system

Carry out macro simulation of two scenarios (without expressway system and with the planned expressway system) respectively in TransCAD and analyze the road network saturation in the core region (as shown in Figure 4 and Figure 5).

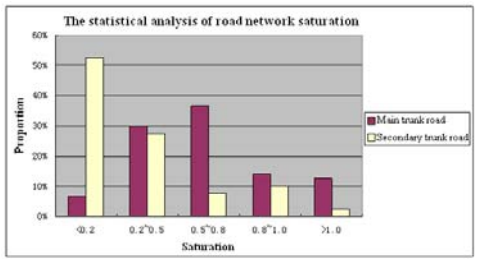

Figure 4. Analysis of saturation in the core region without expressway system

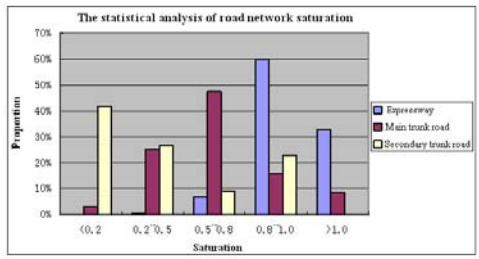

Figure 5. Analysis of saturation in the core region with the planned expressway

From Figure 4 and 5, we can see that a large amount of traffic transfers from adjacent ground roads to the planned expressway system, which results in a lot of traffic pressure to the expressway system, however, it decreases the traffic pressure of ground roads. At the core region, the saturation above 90% for expressway sections is higher than 0.8. The proportion of oversaturated sections of main and secondary trunk roads decreases from 13% and 3% to 8% and 0 respectively.

Furthermore, the comparison of the total travel time of two scenarios (Table 1) shows that the efficiency of the road network improves significantly. At the core region, the increase of vehicle miles traveled and the reduction of the total travel time implies that the vehicle speed improves in spite of increased traffic volume. This is also suggested by the average speed of the core region.

Table 1. The comparison of two scenarios

Scenarios \ Indicators	Total travel time of the road network (veh•h)	Total travel time in the core region (veh•h)	Vehicle miles traveled in the core region (veh•km)	Average speed in the core region (km/h)
Without expressway system	23584	4935	182488	29.3
With the planned expressway system	20709	4577	213685	41.5

4.3 Micro simulation analysis and evaluation of critical sites

Based on the plots with potential problems identified in the macro simulation, the study area is designated into 14 micro-simulation zones. We then applied VISSIM to carry out micro-simulation analysis and evaluation one by one. It is found that there are some potential deficiencies in the planning scheme. Take the 14th simulation zone as an example. The simulation results indicate that there are two potential problems in this area: (1) traffic on the off-ramp located in the western of Longhai Road-Weilai Road interweaves seriously with the ground traffic, which leads to long queues of off-ramp traffic with danger of extending to the expressway mainline (Figure 6). (2) On Longhai Road, the capacity of the ground road between Front Street and Dongming Road cannot satisfy the actual traffic demand, which causes heavy congestion on the ground road network (Figure 7).

Figure 6. The congestion of the off-ramp between Longhai Road-Weilai Road

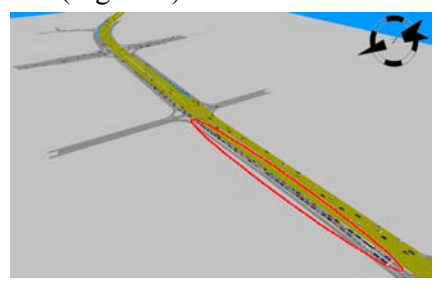

Figure 7. The congestion of the ground road between Front Street~Dongming Road

4.4 Corresponding suggestions for improvement of the planning scheme

Based on the simulation results, we can make specific suggestions for improvement. For the 14th simulation zone we suggest the following improvements: (1) According to the traffic turning characteristics of the off-ramp as well as the ground roads, adjust the intersection channeling scheme of the western approaches to meet the demand of traffic turning: increasing a left-turn lane and decreasing a straight lane. (2) Widen the ground road between Front Street and Dongming Road to add another lane to improve the capacity of the ground road.

5. CONCLUSIONS

The construction of urban expressways involves huge investments and has a profound influence on urban development and economic growth. Once implemented, it is very difficult to modify. Thus it is very crucial and necessary to evaluate the

effectiveness of its planning scheme before implementation. This paper summarized the main contents of simulation analysis and evaluation of expressway planning scheme and developed an integrated macro and micro simulation method, which was applied in an actual project of Zhengzhou. It was found that the integrated method is very efficient and effective in analyzing and assessing the effectiveness of the planned expressway framework, and identifying the deficiencies of the expressway plan, which is difficult to achieve only by macro or micro simulation. This method can shed a light on other similar expressway planning, analysis and evaluation.

REFERENCES

China Academy of Urban Planning & Design. (2007). *Transportation Development Planning of Zhengzhou*. Beijing.

Gao, J. (2006). "Study on the Key Problem of Planning and Design of Expressway in a Big City". *Southeast University Thesis*, Nanjing.

Liu, G. S. (2000). "Plan & Design of Urban Express Road System". *Urban Roads, Bridges & Flood Control*, Mar. 1: 1~6.

Miao, S. M. (1997). "Constructing the Planning Theory and Method of Urban Express Road System". *Urban Planning Forum*, No.5: 58~60.

Yang, X. G., Zhang, H. J., Wang, S. L. and Zhao, J. X. (2004). "Study on Transportation Connection Countermeasure of Shanghai Express Road System". *Urban Roads, Bridges & Flood Control*, May. 3: 9~12.

Evaluation of Traffic Impacts of Land Development Projects Based on Matter-element Analysis

PANG Ying [1], CHANG Yun-tao [2], PENG Zhong-ren [3], LIANG Dui-dui [4]

[1]School of Transportation Engineering, Tongji University; Room 334, School of Transportation Engineering, No.4800 Cao'an Road, Shanghai 201804, China; PH 15801942676; email: selinajustpyy@126.com

[2]Lecturer, School of Transportation Engineering, Tongji University; Room 572, School of Transportation Engineering, No.4800 Cao'an Road, Shanghai 201804, China; email: crchanghp@163.com

[3]Chair and professor, department of Urban and Regional Planning, University of Florida; 431-A Architecture Building; P.O. Box 115706; Gainesville, FL 32611-5706, USA; PH 352-392-0997; FAX (352)392-3308; email: zpeng@dcp.ufl.edu

[4]School of Transportation Engineering, Tongji University; Room 334, School of Transportation Engineering, No.4800 Cao'an Road, Shanghai 201804, China; email: ddliang_03@163.com

ABSTRACT

The assessment of the amount of traffic impact on land development projects is the basis of traffic impact analysis for decision making. This also provides theoretic support for the collection of traffic impact fees. Because the traffic impact analysis involves many factors that are difficult to quantify, we propose a traffic impact evaluation model for land development projects based on the matter-element analysis theory. Seven evaluation criteria are chosen to reflect the impact on the road segments, intersections, parking facilities, public transportation, traffic safety, pedestrian traffic, as well as the atmospheric environment. We further conduct a quantitative evaluation of air pollution using simulation software-VISSIM. A case study was carried out in Shanghai using the matter-element model proposed in the paper, and the impact of land development projects on the surrounding traffic network were quantified. We found that the matter-element evaluation model for traffic impact analysis could provide more objective and reasonable results.

1 INTRODUCTION

Traffic Impact Analysis (TIA) is a means of evaluating the influence on the surrounding road network for urban large-scale land development projects. The evaluation of traffic impacts, which is an important composition in traffic impact analysis, has recently become a core research problem. Currently, some mature evaluation methods, such as the analytic hierarchy process (AHP), the fuzzy comprehensive evaluation and the gray system evaluation have been widely used in the traffic impact analysis for different land development projects. However, there are great differences on methods chosen among different cities due to local traffic conditions and the research depth in traffic impact analysis. Most of the methods can only qualitatively determine the traffic impacts on traffic network, which cannot reflect the grade of traffic impacts definitely. Moreover, the selection of evaluation criteria often neglects the impacts on atmospheric environment. Both of them result in subjective bias during the evaluation process.

Matter-element analysis theory, established by a Chinese scholar-Prof. Caiwen, is a new interdisciplinary subject between mathematics and experimental science *(Cai, 1994)*. With the combination of qualitative and quantitative factors, the matter-element analysis method can quantify traffic impacts through the correlation degree analysis. The correlation degree analysis extends the evaluation value range from the conventional [0, 1] to the real axis $(-\infty, +\infty)$, which can highly increase the evaluation accuracy and influence the factors integrity.

Therefore, this paper introduces the matter-element analysis method into the evaluation of traffic impacts. Combined with a reasonable selection of evaluating criteria, we establish a traffic impact evaluation model based on matter-element analysis and quantitatively get the grade of traffic impacts for land development projects. The details are discussed in the following sections.

2 SELECTION OF EVALUATION CRITERIA

2.1 Road segments analysis

Considering the complex characteristics of urban traffic environments, we take the average load of main road segments in the study area I_1 *(Xiong, 2004)* as the evaluating criterion and its mathematical formula is as below:

$$I_1 = \sum_{i=1}^{n}\left(\left(\frac{Q_{sbi}}{C_i}\Big/\sum_{i=1}^{n}\frac{Q_{sbi}}{C_i}\right)\cdot I_{si}\right) \tag{1}$$

Where I_{si} is the impact factor of land development projects on road segments i, $I_{si} = \Delta Q_i / C_i$, ΔQ_i is the peak hour increased traffic volumes of road segments i in the planning year (pcu/h); C_i is the traffic capacity of road segments i (pcu/h); Q_{sbi} is background peak hour traffic volumes of road segments i in the planning year (pcu/h); n is the number of main road segments in the study area.

2.2 Road intersections analysis

For the road intersections, we take average traffic load of main intersections I_2 *(Li and Xu, 2008)* as the evaluating criterion and its mathematical formula is as follows:

$$I_2 = \sum_{i=1}^{n}\left(\left(\frac{1}{k_i}\sum_{j=1}^{k_i}\frac{Q_{cbij}}{C_{ij}}\Big/\sum_{i=1}^{n}\left(\frac{1}{k_i}\sum_{j=1}^{k_i}\frac{Q_{cbij}}{C_{ij}}\right)\right)\cdot I_{ci}\right) \tag{2}$$

Where I_{ci} is the impact factor of road intersections i, $I_{ci} = \sum_{j=1}^{k_i}\left(\left(Q_{cbij}/C_{ij}\Big/\sum_{j=1}^{k_i}Q_{cbij}/C_{ij}\right)\cdot I_{cij}\right)$, I_{cij} is the impact factor of the j^{th} entrance lane in i^{th} road intersection, $I_{cij} = \left(C_{ij} - Q_{cij}\right)/C_{ij}$, Q_{cij} is the peak hour traffic volumes of j^{th} entrance lane in i^{th} road intersections in the planning year, (pcu/h); Q_{cbij} is the background peak hour traffic volumes of j^{th} entrance lane in i^{th} road intersections in the planning year, (pcu/h); C_{ij} is the traffic capacity of j^{th} entrance lane in i^{th} road intersection, (pcu/h); k_i is the number of entrance lane in road intersection i; n is the number of road intersections.

2.3 Parking facilities analysis

In terms of parking facilities impact analysis, we select the parking facility load in the rush hour I_3 *(Xiong, 2004)* as the evaluating criterion and its mathematical formula is: $I_3 = D_3 / C_3$ (3)

Where D_3 is the peak hour parking demand in the planning year, (pcu/h); C_3 is the parking space numbers of land development projects.

2.4 Public transport facilities analysis

For the public transport facilities impact analysis, we take public transport load in the rush hour I_4 *(Xiong, 2004)* as the evaluating criterion and the formula is illustrated as follows: $I_4 = D_4 / C_4$ (4)

Where D_4 is the peak hour increased public transport demand in the planning year, (pcu/h); C_4 is the average passenger capacity hourly in one bus line.

2.5 Traffic safety analysis

For the sake of describing the influence quantitatively, we take the connection form between road and passageway of land development projects I_5 *(Shang, 2006)* as the evaluating criterion. The concrete quantification standards are as follows: (1) if the passageway is connected with branches, its value is 1; (2) if the passageway is connected with urban secondary main road directly, its value is 2; (3) if the passageway is connected with urban main road directly, its value is 3; (4) if the passageway is connected with urban expressway, its value is 4.

2.6 Pedestrian traffic analysis

In order to quantify the impacts on the pedestrian traffic, we select traffic load of pedestrian crossing I_6 *(Huo, 2007)* as the evaluating criterion and its formula is as follows: $I_6 = D_6 / C_6$ (5)

Where D_6 is the peak hour pedestrian crossing demand in the planning year, (pcu/h); C_6 is the service capability provided by pedestrian traffic facilities in the planning year, (pcu/h).

2.7 Atmospheric environment analysis

Attempting to quantify the influence on the atmospheric environment, we take the average air pollution degree I_7 as the evaluating criterion. Referring to the research achievements of Zhang Yi in Hunan University *(Zhang, 2006)* on the environment impact assessment of urban traffic network, we obtain the criterion value using the microscopic simulation software-VISSIM. We chose the emissions of CO, HC and NO_x in each of the road segments as the research objects, and then the sub-criterion $I_{7i}\,(i = 1, 2, 3)$ of basic criterion I_7 which reflects the total emissions of these three kinds of air pollutants is expressed as:

$$I_{7i} = 86400T \cdot Q_i \cdot \sum_{i=1}^{m} (L_i \cdot n_i) \quad (6)$$

Where I_{7i} is the total emissions for air pollutants i produced by all vehicle categories (mg); Q_i is the emissions factor for air pollutants i in urban traffic

network(mg/m/s), which is obtained by VISSIM simulation; L_i is the single lane length of road segments i; n_i is the total number of lane in road segments i; m is the number of road segments in traffic network; T is the length of control cycle. Through the respective computation of I_{7i} before or after the projects implementation in the planning year, we finally obtain the value of criterion $I_7 = \left(\frac{1}{3}\sum_{i=1}^{3} I_{7iafter} - \frac{1}{3}\sum_{i=1}^{3} I_{7ibefore} \right) \Big/ \frac{1}{3}\sum_{i=1}^{3} I_{7iafter}$.

3 ESTABLISHMENT OF MATTER-ELEMENT ANALYSIS MODEL

3.1 Determination of matter to evaluate

We take the urban road network system which is influenced by land development projects as matter N; $C_1, C_2, ..., C_n$ denotes the characteristics of traffic impacts and the corresponding value range is expressed as $X_1, X_2, ..., X_n$; then the matter to evaluate R can be represented as follows *(Cai, 1994)*:

$$R = \begin{bmatrix} N & C_1 & X_1 \\ & C_2 & X_2 \\ & \vdots & \vdots \\ & C_n & X_n \end{bmatrix} \tag{7}$$

3.2 Determination of classic field matter-element matrix

The classic field matter-element matrix R_j can be expressed as follows *(Wang, et al., 2007, Cai, 1994)*:

$$R_j = \left[N_j, C_i, X_{ji} \right] = \begin{bmatrix} N_j & C_1 & X_{j1} \\ & C_2 & X_{j2} \\ & \vdots & \vdots \\ & C_n & X_{jn} \end{bmatrix} = \begin{bmatrix} N_j & C_1 & \left[a_{j1}, b_{j1} \right] \\ & C_2 & \left[a_{j2}, b_{j2} \right] \\ & \vdots & \vdots \\ & C_n & \left[a_{jn}, b_{jn} \right] \end{bmatrix} \tag{8}$$

Where N_j denotes the j^{th} grade of the matter to evaluate. We call the value range $X_{ji} = \left[a_{ji}, b_{ji} \right]$ of characteristic C_i in grade j as the classic field.

3.3 Determination of controlled field matter-element matrix

The controlled field matter-element matrix R_p can be expressed as follows *(Cai, 1994)*:

$$R_p = \left[P, C_i, X_p \right] = \begin{bmatrix} P & C_1 & X_{p1} \\ & C_2 & X_{p2} \\ & \vdots & \vdots \\ & C_n & X_{pn} \end{bmatrix} = \begin{bmatrix} P & C_1 & \left[a_{p1}, b_{p1} \right] \\ & C_2 & \left[a_{p2}, b_{p2} \right] \\ & \vdots & \vdots \\ & C_n & \left[a_{pn}, b_{pn} \right] \end{bmatrix} \tag{9}$$

Where $P = \left[N_1, N_2, ..., N_n \right]$ denotes the whole of matter grade; X_{pi} denotes the value range of N to characteristic C_i, namely controlled field. The upper and lower limits of value range $\left[a_{pi}, b_{pi} \right]$ for characteristic C_i are the maximum and the minimum value of corresponding criteria.

3.4 Calculate the weight of each criterion

We determine the weight $\omega_i \left(i = 1, 2, ..., n\right)$ of characteristic C_i, where $\sum_{i=1}^{n} \omega_i = 1$; and determine the weight $\omega_{ik} \left(k = 1, 2, ..., n_i\right)$ of the sub-criteria C_{ik} on the base of basic criteria C_i, where $\sum_{k=1}^{n_i} \omega_{ik} = 1$. The weight ω_i and the sub-criteria weight ω_{ik} can be obtained through the Analytic Hierarchy Process (AHP) *(Lv, et al., 2003)*.

3.5 Compute correlation function

Correlation function measures how the value of matter-element at any point of the real axis is correlated to its value at some other point. Let d be the mold of $\left[a_{ji}, b_{ji}\right]$: $d = \left|X_{ji}\right| = \left|b_{ji} - a_{ji}\right|$; then the distance from point to interval is: $\rho\left(x_i, X_{ji}\right) = \left|x_i - \left(a_{ji} + b_{ji}\right)/2\right| - \left(b_{ji} - a_{ji}\right)/2$; and the correlation function can be defined as *(Cai, 1994)*:

$$K_j\left(x_i\right) = \begin{cases} -\rho\left(x_i, X_{ji}\right)/d & x_i \in X_{ji} \\ \rho\left(x_i, X_{ji}\right)/\left(\rho\left(x_i, X_{Pi}\right) - \rho\left(x_i, X_{ji}\right)\right) & x_i \notin X_{ji} \end{cases} \tag{10}$$

3.6 Determination of subjection degree

First of all, we carry on the first-stage evaluation to each of the characteristics and calculate the correlation of characteristic C_i with grade j : $K_{ij}\left(N\right) = \sum_{k=1}^{n_i} \omega_{ik} K_j\left(x_{ik}\right)$; then, we carry on the second-stage evaluation and calculate the correlation of N to grade j : $K_j\left(N\right) = \sum_{i=1}^{n} \omega_i K_{ij}\left(N\right)$. If $K_{j_0}\left(N\right) = \max K_j\left(N\right)$, we can conclude that matter to evaluate N belongs to grade j_0.

4 CASE STUDIES

We took a certain land development project-Debit Building in Shanghai as an example; used the model described above to explain the application of matter-element analysis theory in the evaluation of traffic impact. The original data are drawn from the reference *(Peng, et al., 2005)*.

4.1 Determination of matter to evaluate

According to the calculation method of criteria in the second part, combined with the current conditions of surrounding road network, we can obtain a matrix for matter to evaluate R as follows:

$$R = \begin{bmatrix} \textit{Traffic Impacts of Debit Building} & I_1 & 0.41 \\ & I_2 & 0.37 \\ & I_3 & 1.05 \\ & I_4 & 0.45 \\ & I_5 & 2.33 \\ & I_6 & 0.54 \\ & I_7 & 0.67 \end{bmatrix}$$

4.2 Determination of classic field and controlled field matter-element matrix

According to the method mentioned in 3.2, we can list the value range with respect to each evaluation criteria and obtain the following classic field

matter-element matrix:

$$R_1=\begin{bmatrix} \mathrm{I} & I_1 & [0.3,0.5] \\ & I_2 & [0.25,0.4] \\ & I_3 & [1.2,1.5] \\ & I_4 & [1.5,2] \\ & I_5 & [3.4,4] \\ & I_6 & [1,1.3] \\ & I_7 & [0.8,1] \end{bmatrix} \quad R_2=\begin{bmatrix} \mathrm{II} & I_1 & [0.2,0.3] \\ & I_2 & [0.15,0.25] \\ & I_3 & [1,1.2] \\ & I_4 & [1,1.5] \\ & I_5 & [2.8,3.4] \\ & I_6 & [0.7,1] \\ & I_7 & [0.5,0.8] \end{bmatrix} \quad R_3=\begin{bmatrix} \mathrm{III} & I_1 & [0.1,0.2] \\ & I_2 & [0.1,0.15] \\ & I_3 & [0.8,1] \\ & I_4 & [0.5,1] \\ & I_5 & [2.2,2.8] \\ & I_6 & [0.4,0.7] \\ & I_7 & [0.3,0.5] \end{bmatrix}$$

$$R_4=\begin{bmatrix} \mathrm{IV} & I_1 & [0.05,0.1] \\ & I_2 & [0.05,0.1] \\ & I_3 & [0.6,0.8] \\ & I_4 & [0.25,0.5] \\ & I_5 & [1.6,2.2] \\ & I_6 & [0.2,0.4] \\ & I_7 & [0.2,0.3] \end{bmatrix} \quad R_5=\begin{bmatrix} \mathrm{V} & I_1 & [0,0.05] \\ & I_2 & [0,0.05] \\ & I_3 & [0,0.6] \\ & I_4 & [0,0.25] \\ & I_5 & [1,1.6] \\ & I_6 & [0,0.2] \\ & I_7 & [0,0.2] \end{bmatrix}.$$

Meanwhile, we can also easily determine a controlled field matter-element matrix. For example, for the average load of road intersections I_2, its value range of controlled field is [0, 1].

4.3 Calculate the weight of each criterion

We then calculate the weight of the following seven criteria $I_1, I_2, I_3, I_4, I_5, I_6, I_7$ using Analytic Hierarchy Process (AHP). The results are as shown in Table 1.

Table1. Weight of Each Criterion Using AHP

Indices	I_1	I_2	I_3	I_4	I_5	I_6	I_7	ω_i	Consistency Check
I_1	1	1	1	2	6	5	7	0.251	
I_2	1	1	1	2	6	5	7	0.251	$\lambda_{max}=7.081$
I_3	1	1	1	2	5	4	6	0.232	$CI=0.013$
I_4	1/2	1/2	1/2	1	3	3	5	0.136	$RI=1.320$
I_5	1/6	1/6	1/5	1/3	1	1/2	2	0.043	
I_6	1/5	1/5	1/4	1/3	2	1	2	0.057	$CR=0.010$
I_7	1/7	1/7	1/6	1/5	1/2	1/2	1	0.031	

4.4 Compute correlation function

Firstly, we obtain correlation of criteria I_i to grade j- $K_j(x_i)$ for land development projects based on the method mentioned in 3.5 and the results are shown in Table 2.

Table2. Correlation of Each Criterion to Grade j

Indices	$K_j(x_i)$				
	I	II	III	IV	V
I_1	−0.45	−1.1	−2.1	−1.55	−1.44
I_2	0.2	−0.8	−0.88	−0.9	−0.91
I_3	−0.75	0.25	−0.5	−0.83	−0.9
I_4	−0.95	−0.92	−0.5	0.2	−0.8
I_5	−0.89	−0.78	0.22	−0.5	−0.85
I_6	−0.77	−0.53	0.47	−0.5	−0.71
I_7	−0.5	0.43	−0.57	−0.74	−0.78

We then calculate the correlation of land development projects to each grade, the results are shown as follows: $K_1(N)=-0.808$, $K_2(N)=-0.527$, $K_3(N)=-0.913$, $K_4(N)=-0.853$, $K_5(N)=-1.009$; where $K_{j_0}(N)=\max K_j(N)$, therefore, $j_0=2$.

Consequently, according to analysis results and the classification of traffic impacts, we can conclude that the traffic impacts of Debit building belong to grade II, namely, the land development projects have a great influence on the surrounding road network. We need to make some adjustments to the scale of land development

project and adopt the corresponding improvement measures to enhance the level of service. Meanwhile, we also need to collect appropriate traffic impact fees of this land development project.

5 CONCLUSIONS AND RECOMMENDATIONS

The evaluation of traffic impacts is an extremely complex process, which involves many factors that are difficult to quantify. Based on previous research, this paper makes an attempt to quantify criteria and establish the traffic impact evaluation model based on the matter-element analysis theory. The application indicates that the matter-element analysis method can quantitatively evaluate the grade of traffic impacts on land development projects, which effectively avoids subjective bias in conventional evaluations. Even though the matter-element analysis method enhances reliability and accuracy to a great extent on the evaluation of traffic impact, there is a high demand on reasonable selection and quantification of evaluation criteria, especially difficult quantitative ones like traffic safety and pedestrian traffic. Thus, further research is needed on selecting criteria that can make a comprehensive influence of urban land development projects on the surrounding road network.

REFERENCES

Cai, W. (1994). "Matter-element model and its application". *Literature Press of Science and Technology*, Beijing, 267~275.

Huo, J. F. (2007). "Study on traffic impact analysis of large-scale public building project in urban center". *Beijing Jiaotong University Thesis*, Beijing.

Li, Y., Xu, W. X. (2008). "Fuzzy evaluation on traffic impact degree of urban land development projects". *Highway*, 5(5): 104～109.

Lv, Y. B., Hu, T. J. and Lei, L. (2003). "System engineering". *Beijing Jiaotong University Press*, Beijing.

Peng, G. X., Chang, Y. T., Li, M., Lin, B. J. (2005). "Report of Debit Building traffic impact analysis (Final Version)". *Department of Traffic Engineering in Tongji University*.

Shang, Z. H. (2006). "Study on traffic impact degree of residential community". Chang'an University Thesis, Xi'an.

Wang, X. N., Sheng, H. F. and Meng, X. H. (2007). "Traffic impact evaluation model based on matter-element analysis". *Journal of highway and transportation research and development*, 24(3): 102～106.

Xiong, H. L. (2004). "Study of traffic impact degree for land development projects". *Southwest Jiaotong University Thesis*, Chengdu.

Zhang, Y. (2006). "Evaluation on environment effect of urban traffic network". *Hunan University Thesis*, Changsha.

Research on a model of public transportation network optimization based on the demand of citizen trips

Kang Yongzheng[1,2] Niu Xueqin [1,2] Liu Ruifen[1,2]

[1]School of traffic and transportation, Shijiazhuang Railway Institute, Shijiazhuang, Hebei, China, Post code 050043; PH (86) 311-87935516; FAX (86) 311-87935516; email: kyz1974@sina.com
[2]Traffic Safety and Control Lab of Hebei Province, Shijiazhuang, Hebei, China, Post code 050043; PH and FAX (86) 311-87935516; email: kyz1974@sina.com

ABSTRACT

Currently, public transportation systems in our cities generally have many problems, such as frequent transfer times, a low rate of stops overlap, causing a lot of wait time for passengers to catch buses. Undoubtedly these factors influence the citizens' choice of public transportation. These problems result from various reasons, such as irrational network and stops, low density of public transportation networks, and network density distributing not matching with citizen trips distributing. In public transportation systems, network is the basic of the function, so, optimizing the network is essential to improve the levels of the service of public transportation systems, improve the public transportation flow, and to establish the most economic and efficient method of transportation. Network optimization needs the support of related theories and technologies. Though some domestic research organizations have completed many helpful works and proposed many kinds of theories and methods of public transportation network optimization, most of the theories are not applied. Additionally, optimal methods lack of the support of corresponding theories. This paper studies the main factors influencing citizens' trips by analyzing public transportation network optimization. The primary goal of this is to build an optimal network model with minimal transfer times, and minimizing stops as the secondary goal. This model comprehensively reflects the design principle of the public transportation network and the limitations of various objective conditions. Through the qualification of stops, lines and network, we can decrease the number of the workable networks, and eliminate unnecessary calculation in the optimizing phase.

Key words: *public transportation network，optimization，model*

INTRODUCTION

Public transportation provides for much of the city public passenger volume; determining the level of public transport service, and influencing the effective operation management. The original distributions of city buses lines are mainly developed with the development of the city, and are usually designed based on some experiential methods of line planning (Chen Hongren et al.2001).. Among that, many

rational and feasible lines and some irrational aspect brought in by the limitations of the traditional planning methods both exist (Chang Yulin et al.2001). Thus, adjusting and perfecting public transportation networks according to the demand of citizen trips and directions as well as the changes in city development, is a important project of public transportation system planning, construction, and management (Hu Jianming et al.2001). By now, many experts have completed many helpful works, and proposed many kinds of theories and models of public transportation network optimization, but most of the theories are not applied, while the optimal methods lack the support of corresponding theories.

INVESTIGATION AND ANALYSIS OF CITIZENS' NEEDS FOR PUBLIC TRANSPORT

The ultimate aim of the public transportation network is to meet the citizens' trip needs as much as possible. In order to establish a rational optimization model of line networks, it is important to investigate and study the citizens' psychology and conduct, so as to determine the optimization objectives and restricting conditions of the model.

Citizens' needs for public transport are their expectations for public transport services. Recently, Shijiazhuang conducted a questionnaire on citizens' needs for public transport. 400 questionnaires were issued and 367 were returned, with a return rate of 91.8%.The survey found that: 34.47% of citizens wanting less transfers, followed by 25.31% wanting shorter travel time, 18.59% wanting shortest distance of travel, 12.44% wanting lower trip costs, and 6.19% for "other". Thus, the three main factors that affect citizens' needs for public transport are as follows: "number of transfers", "trip distance" and "travel time". A questionnaire conducted in Nanjing in 1999 showed similar results (Yang Xinmiao et al. 2000).

The number of transfers refers to the number of buses that a passenger needs to change during a single trip. It is one of the objectives of urban bus system planning to minimize the number of transfers (Fernadez et al. 1993). With the improvement of people's living standards, this requirement is increasing. Results from the survey concerning citizens' needs for public transport show: the number of bus transfers has the greatest impact on people's choice. If too many transfers are needed, travelers will give up buses and resort to more convenient transportation. In addition, in an operating system where public transport fares are unified, the increase of transfers also means an increase of costs (ZhaoFang et al. 2003).

Travel time is another major factor that affects citizens' bus travel. When travel time takes too long, people may choose other ways to travel.

Trip distance is another factor that affect citizens' bus travel. Trip distance usually includes two parts: distances in and out of buses. Distance out of buses refers to the distance that passengers need to walk. It includes the distance from the starting point to the get-on station, the distance of transferring and the distance from the get-off station to the destination (Wu Qiujin et al.2004;Yang Xinmiao et al.2000).

Obviously, the distance out of buses has a greater effect on citizens' bus travel. If this distance is too long, citizens may abandon the bus and choose other ways.

ESTABLISHMENT OF NETWORK OPTIMIZATION MODEL

In all the factors that affect citizens' needs for public transport, "the least number of transfers" is the most important one. So we put it as the primary goal of optimization. "The shortest travel time" is the second most important factor. But because it is related to the level of road traffic congestion and the start intervals, it is difficult to measure accurately. However, as the actual distances between sites are different, the storage of data becomes complex. Thus, we chose "the least number of stops" as the second goal of optimization. This will meet the requirement of the shortest route, be more in line with passengers' actual travel psychology and greatly simplify the computing and data storage.

The optimization of public transport networks has many characteristics, such as too many influencing factors, complex process and the unfixed passenger-flow distribution. So before we establish the model, we should summarize and simplify the actual situation. This article, based on the analysis and the optimization of the actual process, assumes that citizens' needs for public transport are fixed, considers citizens' needs for public transport, with a goal of the least number of sites that passengers have to go through, and finally establish the optimization model of public transport networks.

$$\begin{cases} \min Z = \alpha_1 \dfrac{\sum_{j=1}^{n}\sum_{i=1}^{n} TN_{ij} \cdot OD_{ij}}{\sum_{j=1}^{n}\sum_{i=1}^{n} OD_{ij}} + \alpha_2 \dfrac{\sum_{j=1}^{n}\sum_{i=1}^{n} N_{ij} \cdot OD_{ij}}{\delta \sum_{j=1}^{n}\sum_{i=1}^{n} OD_{ij}} \\ \text{s.t.} \quad 5\text{km} \le L \le 15\text{km} \\ \quad q_x \le 1.40 \\ \quad Q_k^{\min} \le Q_k \le Q_k^{\max} \\ \quad b_n \le 1.5 \\ \quad \rho_{\min} \le \rho \le \rho_{\max} \\ \quad T \le T_{\max} \end{cases}$$

In the formula, α_1, α_2 ——weight coefficient， $\alpha_1 > \alpha_2$;

n——number of nodes in bus network;

TN_{ij}——possibly the least times of transfersr from Note i to Note j in bus network;

OD_{ij}——traffic flow from Note i to Note j;

N_{ij}——possibly the fewest sites from Note i to Note j;

δ ——the reduction of sites equivalent to the addition of one transfer;

L——the length of a single line in public transport network；

q_x——non-linear coefficient；

Q_k——flow of cross-section of Line k；

$Q_k^{\max}$——the largest flow of cross-section of line k；

$Q_k^{\min}$——the smallest flow of cross-section of line k；

b_n——uneven coefficient of flow of cross-section；

ρ——density of Public transportation network；

T——largest time-consuming of one-way travel among 95% of citizens。

THE ANALYSIS OF THE MODEL AND RESTRICTING CONDITIONS

The above model comprehensively reflects the design principles of public transport networks and the constraint of various objective conditions. It excludes unreasonable alignments at the beginning of the road network. The constraints of line length and non-linear coefficient greatly reduce lines between points. The constraint of section traffic assures the smooth of lines and rationality of the network. In the collection formed by lines, the model adds constraints of public transport network density and the restriction of citizens' travel time with the deflection of a few networks that cannot satisfy the constraints. In this way, through all the constrictions of notes, lines and nets, the model reduces the number of lines and eliminates unnecessary calculations in the optimization stage.

In the model, the first constricting condition is length constriction of a single line. The length of a single line is related to the size of the city and urban citizens' average travel distance. A long line will increase the system's operating costs, while a short line is unfavorable to operation scheduling and will increase the number of transfers. According to the requirements of "Standards of Traffic Planning and Design of Urban Roads" and the actual situation in metropolis, the maximum is 15 km and the minimum is 5 km when the requirement of public transportation operation is taken into account.

The second constraint is a non-linear coefficient. The non-linear coefficient is the smaller the better, so passengers will arrive at the destination as soon as possible. For an average city, 1.15 ~ 1.20 is appropriate. For a single bus line, it is ideal to have it be less than 1.4.

The third restricting condition is the passenger-capacity of a single line. The maximum flow of a line section can be calculated as follows,

$$Q_k^{\max} = 60 C_x l_k X_{cr} / h_k$$

In the formula, C_x——passenger-capacity of different kinds of cars, generally, 72 people per single-compartment bus, 129 people per dual-hinge bus, 120 people per double-decked bus, and 26

people per medium-sized bus；

l_k ——fully loaded rate of line k, 0.85 in peak hour and 0.60in non-peak times；

X_{cr} ——influence coefficient caused by lines repetition, X is the largest coefficient that is repeated with a certain line；

$$X_{cr} = f(X_c) = \begin{cases} 1.00 & X_c = 0 \text{ or } 1 \\ 0.85 & X_c = 2 \text{ or } 3 \\ 0.70 & X_c \geq 4 \end{cases}$$

h_k ——intervals of bus start in peak hour。

Given the requirements of public transport operation, the flow of a section should be no less than the minimum flow.

The fourth restricting condition is the uneven coefficient of the volume of passenger traffic of a cross-section.

$$b_n = \max Q_s / \bar{Q}$$

In the formula, Q_s ——the volume of passenger traffic of Section S；

$\bar{Q}$ ——average volume of a line。

The fifth restricting condition is the density of the public transportation network. In the process of network optimization, it's size can not increase indefinitely, thereby there is an upper limit of the density of the network. $\rho_{\max}$ is a function related to the size of the city and the volume of passenger traffic.

The sixth restricting condition is citizens' trip time. $T \leq T_{\max}$ .The ceiling of 95% of urban citizens' largest one-way travel time will impact the selection of urban transport. Therefore, it should be considered as one of the constraints of the network optimization model.

CONCLUSIONS

This article is based on the study of the citizens' needs for public transport, through which, we can find the major factors affecting citizens' public transport, and finally build a network optimization model with the goal of the least number of transfers and the least number of bus sites. This model provides a theoretical basis for optimizing public transportation networks.

REFERENCES

Chen Hongren, Feng Shumin. (2001). "Optimization model of stratified public

transport network". Journal of Harbin Architectural University, 34(5): 113~115.

Chang Yulin, Hu Qizhou. (2005). "The linear model of urban public transportation network". China Journal of Highway, 18(1); 95~98.

Fernadez Rodrigo. (1993). "Expert System for the Preliminary Design and Location of High-capacity Bus stops". Traffic Engineering Control", 34(6): 533~539.

Hu Jianming. (2001). "Research of key theory and implementation technology of Intelligent public transport". Jilin University.

Wu Qiujin, Hartley J. (2004). "Using K-Shortest Paths Algorithms to Accommodate User Preference in the Optimization of Public Transport Travel " ASCE. The 8th International Conference on Applications of Advanced Technologies in Transportation Engineering, U.S: ASCE, 181~186.

Yang Xinmiao. (2000). "the research of key technologies of technical support system for the development of urban public transport". Nanjing: Southeast University.

ZhaoFang, AlbertGa. (2003). "Optimization of Transit Network To Minimize Transfers". Lehman Center for Transportation Research, 57~89.

Urban Transport Network Capacity Considering Level of Service

Lu Huapu[1] Yu Xinxin[1] Wang Haiwei[1,3] Bian Changzhi[1] Deng Ziyin[2]

[1]Institute of Transportation Engineering, Tsinghua University, Beijing, 100084; PH (86) 10-62772615; Fax (86) 10-62795339; email: weixx03@mails.tsinghua.edu.cn
[2]Department of Civil Engineering, Tsinghua University, Beijing, 100084; PH (86) 10-62770690; Fax (86) 10-62795339; email: snowrunfly@gmail.com
[3]Military Transportation College, Tianjin, 300171

ABSTRACT

This study deals with the problem of urban transport network capacity under a given level of service. After a thorough review of urban transport network capacity modeling and multiple objectivity programming, a multiple objectivity bi-level programming model is formulated, which considers that the network capacity analysis should link the level of service of a road network together. In an upper level program is a multiple objectivity model which includes: (i) the maximization of the network capacity; and (ii) the maximization of the level of service. And a logit-based stochastic traffic assignment model is adopted in the lower level model. Then the goal programming method is proposed. An example is given and numerical results show the algorithm is feasible for practical applications.

KEY WORDS

transport network capacity; level of service; multiple objectivity bi-level programming, O-D demand pattern

1. INTRODUCTION

Transport network capacity is very important to system planning and operation. But most previous researchers do not consider the level of service of network when computing the network capacity. Level of service, which significantly influences the network capacity, should capture the operating conditions of individual road segments or links in the network.

Transportation researchers and engineers have studied these issues during several decades. Buchanan proposed the concept of both network physical and even environmental capacity in their London case studies (Buchanan 1963; Smeed 1966). Iida proposed a heuristic method to determine the road network capacity based on a simple incremental assignment technique (Iida 1972). Yang formulated the problem for determining the maximum zonal trip generation as a bi-level programming problem (Yang and Bell 2000). And the multi-objective programming approach become popular in transport system research (Khorranshahgol and Steiner, 1988; Pearman et al. 1989; Gomes 1989; Won 1990; Azis 1990).

This study concerns the modeling of the transport network capacity under a

given level of service. A new definition of network capacity is proposed and a multiple objectivity bi-level programming formulation is formulated. Then an algorithm is proposed, and an illustrating example is analyzed. For the remainder, Section 2 formulates the multiple objectivity bi-level programming model. Section 3 is devoted to the algorithm and following with a numerical example in Section 4. Conclusions are offered in the last section.

2. FORMULATION

2.1 Definition of the transport network capacity

The transport network capacity is the maximum vehicle numbers that the network can support under given OD demand pattern and level of service.

2.2 Notations

A	link set
a	link index, $a \in A$
C_a	capacity of link a
x_a	flow on link a
RS	OD set
rs	OD pair index, $rs \in RS$
q_{rs}	OD demand between pair rs
f_{rs}	path flow on rs
k_{rs}	path between OD pair rs
$\delta_{a,k}^{rs}$	link-path incidence parameter; one if link a is on path k, zero otherwise
t_a	travel time on link a
G	network (N, A)
Q	multiplier for given OD demand pattern
$\beta(\cdot)$	the inverse cumulative distribution function for the standard Normal distribution
cl	the required degree of confidence
σ_a	the standard deviation of x_a/C_a

2.3 Level of service of network

The Highway Capacity Manual (TRB, 1980) states that for a single freeway section, a useful procedure in operational analysis should link the maximum service flow and the level of service of a road network together. The level of service should capture the operating conditions of individual road segments or links in the network. The higher x_a/C_a, the lower level of service of a road network, which make us define the level of service function of the network as follows:

$$\text{level of service function} = \left\{ \ln[\sum_a (\frac{x_a}{C_a}) + \beta(1-\text{cl})\sigma(\frac{x_a}{C_a}) \times n] \right\}^{-1} \qquad (1)$$

2.4 Multiple objectivity bi-level programming model

Here the multiple objectivity bi-level programming model is adopted. The lower-level problem is a SUE traffic assignment mode. The upper-level problem is the multiple objectivity programming model which includes: (i) the maximization of the network capacity; and (ii) the maximization of the level of service.

$$\max_{Q} \quad Q\sum q_{rs} \tag{2}$$

$$\max \quad \left\{ \ln[\sum_{a}(\frac{x_a}{C_a}) + \beta(1-cl)\sigma(\frac{x_a}{C_a}) \times n] \right\}^{-1} \tag{3}$$

$$st: \quad Q \geq 0 \tag{4}$$

$$\min \sum_{a}\int_{0}^{x_a} t_a(\omega)d(\omega) + \frac{1}{\alpha}\sum_{k} f_k^{rs}(\ln f_k^{rs} - 1) \tag{5}$$

$$s.t. \quad \sum_{k} f_k^{rs} = Qq_{rs} \quad \forall r,s \tag{6}$$

$$f_k^{rs} \geq 0 \quad \forall r,s \tag{7}$$

$$x_a = \sum_{r}\sum_{s}\sum_{k} f_k^{rs}\delta_{a,k}^{rs} \quad \forall a \tag{8}$$

3. SOLUTION ALGORITHM

Goal programming was developed by Charnes and Cooper in 1961 to resolve the multiple objectivity programming. The basic idea of goal programming is to make the objective function $f(x) = (f_1(x), f_2(x),..., f_m(x))^T$ near the target value $f^0 = (f_1^0, f_2^0,..., f_m^0)^T$,. This problem can be presented as the minimization of the deviation between $f(x)$ and f^0, which can be represented as

$$\min_{x \in X} d_p(f(x), f^0, \omega) \tag{9}$$

In our problem, we let $p = +\infty$, then the objective function is converted to

$$\min \quad t \tag{10}$$

$$s.t. \quad \omega_i(f_i(x) - f_i^0) \leq t, \ i = 1,2,..., m \tag{11}$$

$$x \in X, \ t \geq 0 \tag{12}$$

Following is the goal programming formulation.

$$\min \quad t \tag{13}$$

$$st: \omega_1(Q\sum q_{rs} - f_1^0) \le t \tag{14}$$

$$\omega_2(\left\{\ln[\sum_a(\frac{x_a}{C_a}) + \beta(1-cl)\sigma(\frac{x_a}{C_a})\times n]\right\}^{-1} - f_2^0) \le t \tag{15}$$

$$Q \ge 0 \tag{16}$$

$$\min \sum_a \int_0^{x_a} t_a(\omega)d(\omega) + \frac{1}{\alpha}\sum_k f_k^{rs}(\ln f_k^{rs} - 1) \tag{16}$$

$$\text{s.t.} \quad \sum_k f_k^{rs} = Qq_{rs} \quad \forall r,s \tag{18}$$

$$f_k^{rs} \ge 0 \qquad \forall r,s \tag{19}$$

$$x_a = \sum_r\sum_s\sum_k f_k^{rs}\delta_{a,k}^{rs} \quad \forall a \tag{20}$$

Using this model, we cannot compute the capacity of a network. If we want to obtain the optimal solution, the utility function of the road users should be given. Otherwise, we could only obtain the Pareto-optimal solution (Markowitz, 1959).

4. NUMERCIAL STUDYES

The test network is shown in Figure 1. Table 1 and Table 2 are the basic data.

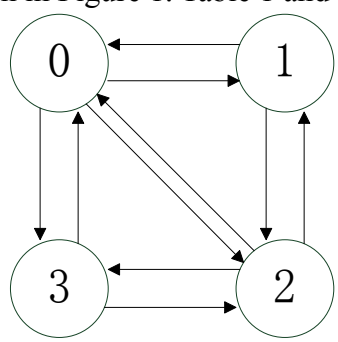

Figure 1.Test network for the proposed algorithm

Table 1.Basic OD matrix

OD zone	0	1	2	3	Production
0	6	5	6	7	24
1	4	5	7	3	19
2	3	6	4	3	16
3	4	5	7	2	18
Attraction	17	21	24	15	77

Table 2.Link character data of test network

Link	Start Node	End Node	AB Capacity	BA Capacity	AB free-flow	BA free-flow

					travel time	travel time
0	0	1	100	100	50	100
1	1	2	100	100	60	100
2	2	3	100	100	60	100
3	3	4	100	100	50	100
4	4	5	200	200	100	100

Table 3 shows the solution of test network.

Table 3 Pareto -optimal solutions

No.	ω_1	ω_2	f_1^0	f_2^0	Q	Capacity	LOS
1	1	53.48	60	0.4	0.882	67.914	0.548
2	1.2	143.82	60	0.4	0.980	75.460	0.529
3	1.44	72.16	80	0.4	1.110	85.470	0.509
4	1.73	280.82	80	0.4	1.230	94.710	0.491
5	2.07	70.55	100	0.35	1.353	104.181	0.473
6	2.49	346.98	100	0.35	1.488	114.599	0.455
7	2.99	208.61	120	0.35	1.637	126.059	0.437
8	3.58	971.28	120	0.35	1.801	138.665	0.419
9	4.3	536.11	140	0.3	1.981	152.531	0.401

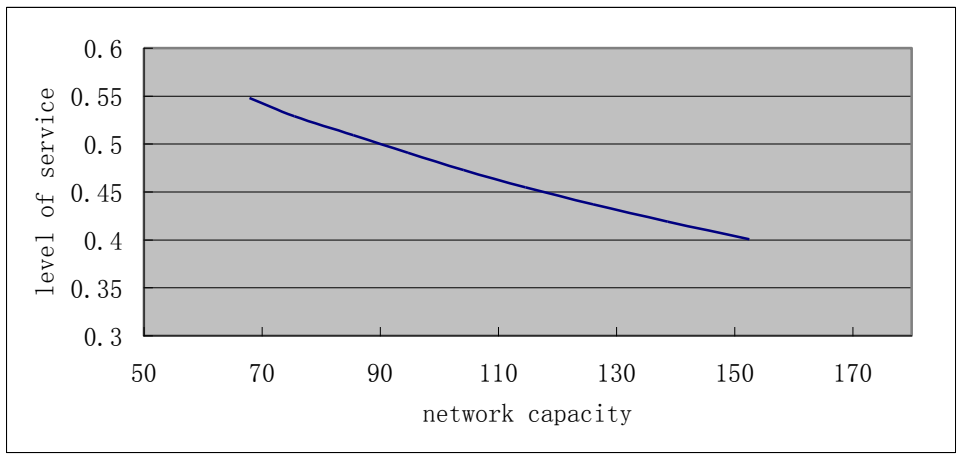

Figure 2 The relationship between capacity and level of service

According to numerical results, the relationship of the capacity and level of service is represented in Figure 2, which illustrates that the higher the network capacity, the lower level of service of a road network.

5 CONCLUSIONS

In this study, a multiple objectivity bi-level programming model is developed and an algorithm is proposed to analyze the transport network capacity considering the level of service. Numerical results show that the model and algorithm is effective. Moreover，this model can be extended to a case considering the elastic demand or

variable OD pattern.

ACKNOWLEDGEMENTS

This research is supported by National High-Tech Research and Development Program of China (863 Program) (Grant No.2007AA11Z202 and No.2007AA11Z233) and Beijing Science and Technology Commission Program (Grant No. D07020601400704).

REFERENCES

Asakura, Y., (1992). "Maximum capacity of road network constrained by user equilibrium conditions." Paper presented at the 24th Annual Conference of the UTSG.

Asakura, Y., Kashiwadani, M..(1993). "Estimation model of maximum road network capacity with parking constraints and its application." Infrastructure Planning Review 11, 129-136.

Buchanan, C., (1963). "Traffic in town." Report of the Steering Group and Working Group Appointed by the Minister of Transport London.

Iida, Y., (1972). "Methodology for maximum capacity of road network (in Japanese)." Transaction of Japan Society of Civil Engineers 205, 147-150.

Sheffi, Y., (1985). Urban Transportation Networks: Equilibrium Analysis with Mathematical Programming Methods. Prentice-Hall, Englewood Cliffs, NJ.

Smeed, R.I., (1966). "Road capacity of city centers." Traffic Engineering and Control 8, 455-458.

Yang, H., Bell, M.G.H., (1997). "Traffic restraint, road pricing and network equilibrium." Transportation Research 31B, 303-314.

Yang, H., Bell, M.G.H., Meng Q., (2000). "Modeling the capacity and level of service of urban transportation networks." Transportation Research 34B, 255-275

Hill M. (1973) "Planning for Multiple Objectives: An Approach to the Evaluation of Transportation Plans." Monograph No. 5, Regional Science Research Institute, Philadelphia. Pennsylvania.

Khorramshahgol R., Steiner H. M. (1988). "Resource analysis in project evaluation: a multi-criteria approach." Journal of the operations research society 39, 795-803.

H.M. Markowitz, (1959). Portfolio Selection: Efficient Diversification of Investments. Wiley, New Jersey.

THE BALANCE LINES OF INTERNATIONAL FREIGHT AND INCIDENTALS

Liu Xian[1]

[1]School of Economic Management of East China Jiaotong University, Eastern Shuanggang Street, Nanchang City, Jiangxi Province, RPC. , Post Code: 330013, Email: liuxian6401953@126.com

ABSTRACT

In cargo transportation between Europe and Asia, 'balance lines' in international freight and incidentals is a concept describing rational choices for shipping by freight over land or by ocean. Many factors cause warping in these balance lines, especially the lack of a comprehensive intercontinental rail cargo agreement. The balance lines of international freight and incidentals are thus relevant to a new comprehensive Eurasia railway cargo transportation convention. Taking balance lines into consideration could benefit trade between many countries. Although a long-term objective, the balance lines of international freight and incidentals should be pursued by European, Asian, and North African countries.

INTRODUCTION

Traditionally, there have been two main modes of cargo transportation between China and Europe: ocean shipping and land carriage. The trade and investment between EU and China is one of the most successful examples in international economic cooperation in the world. As economic cooperation increases between China and Europe it is important to select a reasonable cargo transportation mode. One important aspect of the selection is the comparison of cargo transportation costs.

BALANCE LINES OF INTERNATIONAL FREIGHT AND INCIDENTALS

Most cargo exported from China to Europe is conveyed by ship. However, the transportation process can be can be broken into three sections: first, shipping from inland depot to the Chinese port of embarkation (by train or truck transportation and sometimes by riverboat); second, by ocean-going vessel from China to a European port; and third, from the European port to the good's final destination. It is, therefore, not difficult to realize that the farther the freight is from the Chinese port, the more expensive the inland freight and incidentals are, and so too is the situation on the European leg of the journey. One can therefore appreciate the merits of international railway transportation.

Relative to every European location where freight is transported (especially at the inland locations) there are *balance lines* of international freight and incidentals. These lines are dynamic, they vary as the changing of ocean freight, port load and unload fees, international oil prices, exchange rates, premium, railway freight, cargo variety, canal tolls, storage and trans-shipment charges, what kind container is used (if a container is used), etc. For different locations where freight travels, the balance lines are different. For example, in China, transportation lines go roughly north-south.

If the freight locations are east of the north-south line, general freight and incidentals of ocean shipping and its parts are less costly since the routes are closer to the ports. If however, the freight locales and incidentals are west of the line, then the cost of general freight and incidentals using international railway transportation is less expensive (since the distance is that much closer to European destinations). If the freight locales are located on the north-south line, then the cost of shipping by sea or by rail is equal. The situation is the same for freight coming for importation of freight from Europe to China.

SELECTION OF CARGO TRANSPORTATION COURSES

Warping Phenomenon. In the course of arranging the cargo transportation from inland China locales to inland European locales, apart from common freight and incidentals, many other factors can influence the selection of a suitable transportation mode. These factors giving rise to a *warping* phenomenon in the selection of cargo transportation courses. For example, cargo checking and pick up procedures may vary in complexity, understanding bills of lading, language difficulties, force majeure situations, applicable insurance clauses, differing laws and importation regulations between countries, problems over the liquidity of transportation bills, the energy and motivation of shippers, importers and exporters accustomed to different procedures, etc. Even west of the balance lines of international freight and incidentals (where rail cargo is cheaper than ocean shipping) a lot of cargo exported from China is shipped by sea. The phenomenon is similar in how the courses of cargo transportations are chosen from inland Europe to inland China.

Warping aggravated by lack of comprehensive intercontinental rail agreement. There has been no integrated railway transportation convention in Eurasia for a long time. The reality is that since the 1950s, two agreements concerning intercontinental rail traffic have existed side by side, the "Agreement of International Railway Through Transport" (1951) and the "Convention Concerning International Carriage of Goods by Rail" (1975). China, Mongolia, Vietnam, North Korea, and many countries of the Commonwealth of the Independent States, etc., are parties to the Agreement. Those participating in the Convention include many European, North African, and Middle Eastern countries. These transportation agreements are essential for managing rail traffic through the rail systems of their member countries.

A comprehensive agreement bridging the Convention and the Agreement is important for the development of international trade between the signatories of the Convention and the Agreement. Currently, rail shipping from countries signed to the Agreement but not to the Convention (and vice-versa) involves time delays and additional expense. Way bills of countries signed to the Agreement are not recognized as law under countries signed to the Convention.

For example, cargo shipped from China to Western Europe by railway must first be transported to a border station in Eastern Europe. Acting as a shipping agent, the head of an Eastern European border station fills out a new *relative* way bill indicating the final destination for the cargo. It is necessary for the heads of border stations to continuously manage these transportation procedures as shipping agents, filling in Convention standard way bills for rail cargo arriving from Asian countries

signed to the Agreement. To complicate matters, some Eastern European countries have already retired or wish to retire from the Agreement and want to join the Convention exclusively.

Other uncertain factors impact shipping between Agreement and Convention signatories: the natural gas dispute between Russia and Ukraine, changes in the means of payment for freight and incidentals and the currency used in transaction, use of English in Agreement way bills, changes in customs declaration procedures, unenforced penalties for overdue shipping, etc. Railway cargo transportation across Eurasia thus faces many uncertain factors producing warping. Due to these difficulties, the choice to "give up on land, and go to the ocean" becomes the common practice in selecting transportation modes.

A COMPREHENISVE NEW EURASIAN RAILWAY CARGO TRANSPORTATION CONVENTION

A solution. In order to rationalize the railway cargo transportation sequence across Eurasia, and to develop reasonable competition between intercontinental railway cargo transportation and ocean shipping, a new comprehensive railway cargo transportation convention is needed that takes into account the balance lines of international freight and incidentals. The scope of the new convention could cover all of Eurasia, and even North Africa and the United Kingdom.

To merge and improve the two existing agreements, it will be necessary to summarize the historical experiences of operating the Convention and the Agreement while respecting sovereignties and desires of all countries fully. Earlier attempts to bridge the gap between the Convention and the Agreement, like the October 2003 Memorandum of Understanding and Cooperation on passenger and cargo transport in Yekaterinburg, Russia (Wanjian 2003), included limited temporary and local measures that were insufficient in altering the railway traffic situation across Eurasia.

Decreasing warping phenomenon. The signing of a new comprehensive Eurasia railway cargo transportation convention means that an integrated legal system managing Eurasian railway cargo transportation will need to be established. Once all countries will have common rules to follow, general transportation costs will decrease. The current warping phenomenon will be corrected and the *watershed function* of the balance lines of international freight and incidentals will come begin to improve trade over the whole. Shipping choices between China and Europe will become increasingly rational. In short, with a new agreement, there will be a new railway cargo transportation situation in Eurasia.

After the new convention becomes effective, not only would rail cargo shipping costs across Eurasia decrease, but other benefits could also be obtained: shortened transportation time, reduced load and unload frequency, increased arrival estimates, a lessened influence of inclement weather, improved speed of cargo loss investigations, etc. The serious phenomenon of "giving up on land, and going to the ocean" would be corrected. The more reasonable international division of labor and resource utilization could be realized. Meanwhile, shipping difficulties experienced with ocean shipping such as force majeure, pirates, and other troubles could be avoided altogether. To bring this mutually beneficial state of affairs into being depends on a new convention becoming effective.

The fair competition between international railway through goods traffic and ocean shipping will stimulate ocean shipping to improve its service quality further. The balance between the two transportation modes should be a balance at a higher level of service.

BENEFITS OF RATIONALIZED SHIPPING

Increased trade between East Asia and Europe. A new comprehensive Eurasian railway cargo transportation convention will make overland shipping more convenient. Cargo formerly shipped over ocean shipping might be transported by international railway through goods traffic after the new convention becomes effective. Some trade from Japan, Korea, Mongolia, Vietnam, China (including Taiwan and Hong Kong) will take shortcuts to reach parts of Europe. With a rationalized shipping system incorporating balance lines, local troubles impacting transportation networks such as warfare or piracy can be bypassed.

Increased traffic between Russia, Asian, and European countries. Russian railway transit traffic is endowed by the expanse of Russian lands spanning Europe and Asia, the vastest expanse of land in the world. Russia could obtain considerable income from railway traffic between East Asia and Europe. Currently, the density of Russia's railway network is far smaller than that of Chinese railway network, however, the benefit of a new comprehensive convention and rational shipping considering the balance lines of international freight and incidentals would benefit investment in an improved Russian railway network.

Many countries in Europe and Asia, that do not have Russia's obvious geographic advantage, could also obtain profits from more rationalized shipping decisions that improve everyone's situation. Central Asian and European countries (such as Kazakhstan and Poland) would also profit from improved and increased railway traffic, although the profits are different in degree.

OTHER BALANCE LINES

In choosing suitable transportation for shipping in the north-east region of China, there is another balance line for freight and incidentals. General freight and incidentals are equal relative to a specific destination, no matter which direction, when shipping cargo to Japan and other countries and regions either south through Dalian port or east through the lower reach channel of Tumen River (China owning the navigating right of the channel). The balance line of freight and incidentals could be taken as a watershed function to decide which way cheaper transportation way. As eastern ports in Russia and ports in North Korea are leased for Chinese cargo, these new shipping opportunities influence the balance lines of freight and incidentals in northeastern China. Furthermore, as global climate change warms the Arctic Ocean, a new commercial northeast passage may be realized. The balance lines of freight and incidentals produced by this new shipping option will be seen distinctly.

CONCLUSION

Although the heavy infrastructure of intercontinental rail traffic already exists (tracks, stations, communication apparatuses, warehouses, etc.) and is developed ceaselessly, the intercontinental legal environment remains deficient. This may be

remedied with a comprehensive new agreement for intercontinental rail cargo traffic. Work towards this goal does not require as much labor and investment of material and land resources. Strengthening mutual trust and cooperation between Eurasian countries energetically, can achieve a significant reward for all.

Although the achievement of rationalized balance lines needs time to develop, it is a realistic objective that deserves the participation of Eurasian countries (as well as North African countries and the U.K.). Because of the common interests of so many countries, improvements in Eurasian railway cargo transportation may become a reality, and not even in the remote future.

REFERENCES

"Agreement of International Railway Through Transport." (1951). http://www.fsou.com/html/text/iel/ >(Dec.6, 2005)

"Convention Concerning International Carriage of Goods by Rail." (1975). http://www.westsee.com/sw/law/ >(Nov.11, 2006)

Lu, D. (2005). "International Railway Through Goods Traffic Operating System Design and Realization." *Railway Transport and Economy* 27(11) 71-73.

The Standing Committee of the NPC. (1990). "The PRC Railway Law." http://www.people.com.cn/zixun >(Aug.28, 2007)

Wanjian, J. (2003). "China Railway Launches International Railway Through Goods Traffic and International Passageways Develops." *Railway Transport and Economy* 25(3) 4-7.

Traffic Management on an At-grade Signalized Intersection Connecting to Urban Expressway Ramps

Long Kejun[1] and Zheng Jianlong[1], Yang Xiaoguang[2], Zhou Zhigang[1]

[1] School of Traffic & Transportation Engineering, Changsha University of Science & Technology, Changsha Hunan Province, China; PH (86-731) 5258378; FAX (86-731) 5258375; email: lonkj@sohu.com

[2] School of Transportation Engineering, Tongji University, Shanghai, China; PH (86-021) 69589475; FAX (86-021) 69589475; email: yangxg@tongji.edu.cn

ABSTRACT

An elevated urban expressway connects to its frontage roads by on/off ramps. Under the expressway, frontage roads, two pairs of on/off ramp terminal and cross streets construct the complex at-grade intersection. One typical complex intersection under the Inner Ring Expressway in Shanghai was selected in this study. The main reason for congestion at this intersection is that traffic movements with different origin-destination (OD) weave within the section from the ramp terminal to the stop-line on the departure legs. To eliminate the weaving operation, lane function was reassigned, and signal timing was redesigned to a five-phase scheme. Simulation tool VISSIM 4.1 was applied to evaluate performance of the new intersection. Simulation results indicated that significant reduction of vehicle delay and queue length in the new scheme.

INTRODUCTION

In Shanghai, the urban expressways are elevated roads lying over their frontage roads, connecting to a frontage road by on- and off-ramps. Therefore, frontage roads, ramp terminal and street road constitute the special intersection type (see Fig. 1). Compared with standard street intersections, this intersection is more complex, due to the movements leaving or heading for the ramps within the intersection area. Also, this intersection is different from the Single Point Urban Interchange with frontage road (SPUI/F, see Fig. 2) in America, from the location and mode of connecting to intersecting street roads.

One problem in this intersection is an insufficient separation distance from the off-ramp terminal to downstream signalized intersection. This contributes to traffic conflicts and excessive congestion along the approach legs. A second problem is insufficient distance from the on-ramp terminal to the signalized intersection. This causes traffic conflicts along the departure legs. This paper focuses on this type of junctions and introduces improvements by optimizing traffic management and signal timing programs.

Professional research about this complicated intersection is not very rich. Intensive and relevant research has been conducted on single point urban

interchanges (SPUI) for 35 years in America. Messer et al. (1997) reported that the SPUI/F typically uses one actuated controller and operates with four basic phases: (1) crossroad left movements, (2) crossroad through movements, (3) frontage roads left-turn movements, and (4) frontage roads through movements. Jim C. Lee et al.. (2002) also compared the merits and adaptation of three-phase and four-phase. They proposed the signal interval calculating method and applied their findings to ten interchanges in the Phoenix, Arizona metropolitan area.

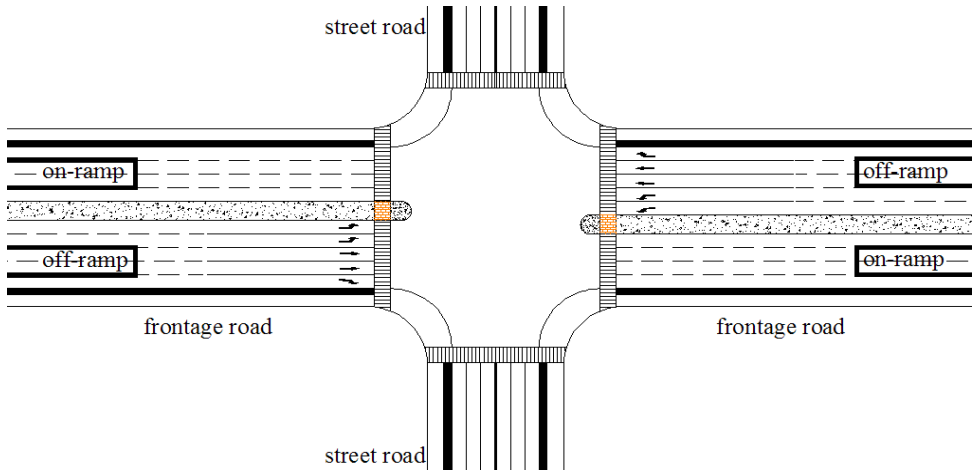

Fig. 1. Typical intersection connecting to expressway ramps.

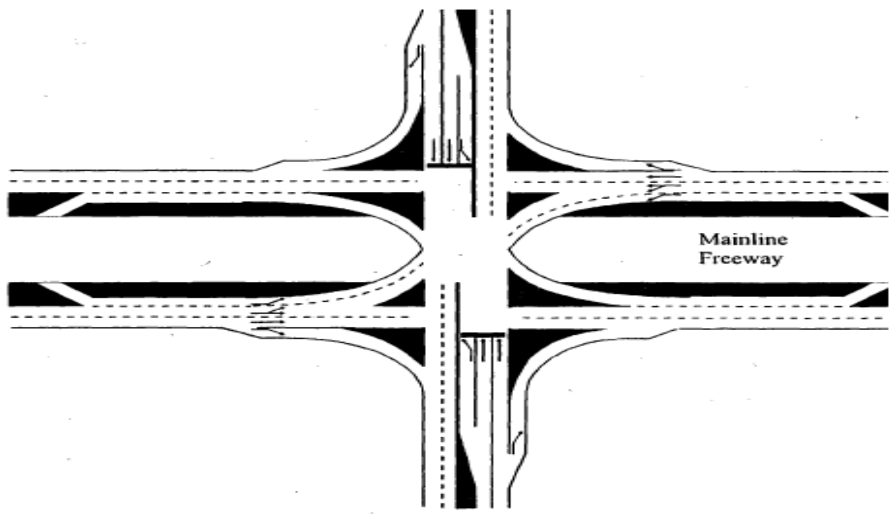

Fig. 2. Typical single point urban interchange with frontage road (From: Paul, Thomas [2]).

Recently, some researchers (Garber and Smith) found that SPUI is much easier to coordinate with an adjacent signalized intersection on the crossroad (relative to other diamond interchanges). Through coordination with other intersections, the systematic efficiency can be improved. Other research (Leisch et al., 1989) [4] studied the clearance interval and lost time at SPUI The SPUI's large size and lengthy travel paths require clearance intervals in excess of 8 to 9

seconds. They also observed that long clearance intervals create considerable lost time at the end of a phase, resulting in an SPUI capacity decrease. There are some American proposed guidelines for diamond interchange planning and design, The California Department of Transportation Division of Design (2001) proposed guidelines for single point interchange planning, design and operations. This guideline was applied in all states in America. Many researchers (Tian, 2004; Lindgren, 2004; Selinger; Messer, 1997; Engelbrecht, 2001) have applied a traffic simulator to evaluate the operational quality of diamond interchanges, including SPUI, SPUI/F, Tight Urban Diamond Interchange and standard diamond interchange.

Compared to SPUI, the type of more complex junction selected in this research is quite different from the diamonds with respect to geometric structure and traffic composition. So, this complex intersection requires special work.

The authors selected a typical Shanghai intersection as an example for research on the optimum traffic management and signal timing scheme. In the following sections, the existing condition of the intersection is introduced, improving alternatives are proposed, and simulation evaluation for the alternatives is conducted by VISSIM. Finally, a conclusion and recommendations are offered.

EXISTING CONDITIONS

The selected intersection is located in the Putuo District of Shanghai China. The frontage road of the Inner-Ring Expressway and Wuning arterial road are the intersecting roads. The existing intersection is a four-leg junction, with an intersecting angle of 70 degrees. The width of red-line of the expressway frontage road is fifty meters, The Wuning arterial is also fifty meters wide. On the northern and southern approach and departure legs, one pair of on/off ramp terminals connects to the elevated expressway. Distance from the ramp terminal to the junction stop-line is 60 to 105 meters.

Fig. 3. Existing geometric condition.

Function assignments for every approach are listed in Table 1. P.M. peak hour traffic volume in this junction was surveyed and listed in Table 1. The total volume is 9063 pcu/h, and the bus ratio is relatively high, especially on frontage roads. Signal timing is a three-phase scheme, and the circle length is 227 seconds. Left-turn movements on the northern/southern approaches are prohibited. They are accommodated by the U-turn and the adjacent intersection downstream.

Table 1 lists the theoretical value of saturation and delay at this intersection according to HCM2000. It shows that the degree of saturation on northern/southern approaches was only about 0.5. Delays on these two approaches were also small.. Field investigation indicated, however, that the junction was extremely saturated on every approach during peak hours. This significant inconsistency indicated that HCM2000 cannot analyze this junction correctly, because a large portion of delay was not generated on the approaches but on the departure legs. Therefore, our evaluation applied simulation tool VISSIM 4.1.

TABLE 1 Traffic volume during the Peak hour (P.M)

Approach	Direction	Number of lane	Volume (pcu)	Bus ratio	Saturation	Delay (s)
Northern	Left-turn	----	---	---		
	Through	4	1287	0.21	0.48	38.6
	Right-turn	2	998	0		
Southern	Left-turn	----	---	---		
	Through	4	1387	0.24	0.51	39.7
	Right-turn	1	788	0.12		
Eastern	Left-turn	2	605	0.25	0.54	45.7
	Through	3	882	0.1	0.94	100.3
	Right-turn	1	574	0.19		
Western	Left-turn	2	1173	0.08	1.05	118.0
	Through	3	943	0.06	1.01	117.6
	Right-turn	1	426	0		
sum			9063		Max: 1.05	Ave: 78.8

TABLE 2 Delay and queue length of the existing and improvement scheme

Approach	Movement direction	Delay (s)			Queue length (m)					
		Existing	Improvement scheme	Improvement effect (%)	Existing		Improvement scheme		Improvement effect (%)	
					Ave	max	Ave	max	Ave	max
N	Through	53.9	54.9	1.9	41.5	186	44	138	6.0	-25.8
	Average	53.9	54.8	1.7	41.5	186	44	138	6.0	-25.8
S	Through	128.9	54.5	-57.7	110	245	36.3	117	-67.0	-52.2
	Average	128.9	54.5	-57.7	110	245	36.3	117	-67.0	-52.2
E	Left-turn	66.1	42.1	-36.3	61	141	39	132	-36.1	-6.4
	Through	81.3	50.2	-38.3	66	153	42	137	-36.4	-10.5
	Average	75.7	47.2	-37.6	63.5	147	40.5	134.5	-36.2	-8.5
W	Left-turn	159.6	25.4	-84.1	257	418	40	104	-84.4	-75.1
	Through	129	49.7	-61.5	255	418	40	101	-84.3	-75.8
	Average	146.2	36.8	-74.8	256	418	40	102.5	-84.4	-75.5
Average of all		107.4	46.5	-56.7	117.8	249	39.8	122.3	-66.2	-50.9

Note: In the table heading, 'ave' denotes the average queue length of the movements, 'max' denotes the maximum queue length of the movements.

SIMULATION EVALUATING PRESENT PERFOMANCE

Results of the evaluation conducted by VISSIM 4.1 are listed in Table 2. Compared with table 1, the simulating results are clearly different from the theoretical results. From Table 2, the total average delay at this intersection was up to 107.4s, with the southern approach over 120s and western approach over 150s. Queue length was very long on every approach, especially on the western approach where the maximum length was longer than 410 meters. Very long

queues influenced the neighboring intersection and the expressway's mainline.

Through simulation and field investigation, we find the main reasons for congestion on this site include:

1) The distance from the ramp terminal to the intersection stop-line is too shor. The result is serious conflict between movements on the frontage road and the ramps and reduced passing efficiency.

2) Weaving operations on departure legs greatly degrade junction efficiency. For example, the northern departure leg, illustrated as Figure 4, has two weaving operations: (1) left turns from the western approach weave with right turns from the eastern approach and (2) movements with origins from the off-ramp and frontage road destination on the southern approach, weave with the origin frontage road and on-ramp destination.

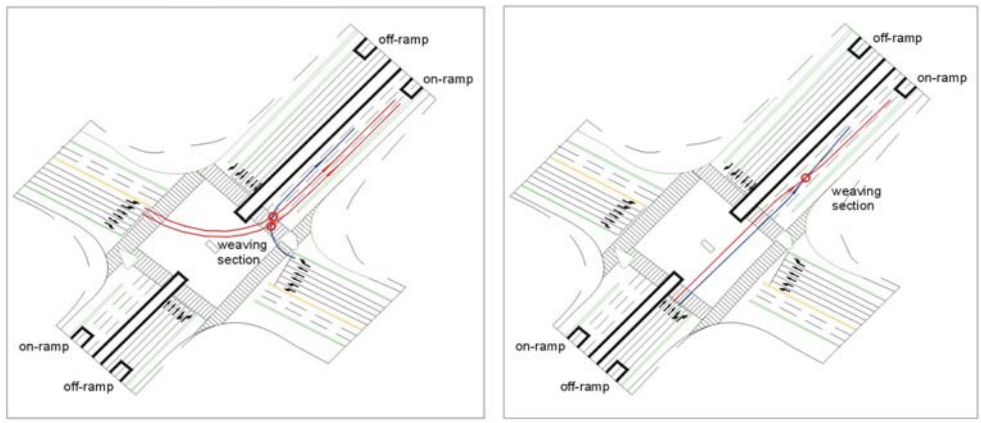

Fig. 4. Weaving operation on intersection departure legs.

3) The considerable volume of bicycle and pedestrian traffic, interweaved with right-turn vehicles, worsened operating conditions.

PROPOSED IMPROVEMENT SCHEME

Our findings above demonstrate that the main reasons for congestion at this junction are mainly from weaving operations on the approach and departure legs. Accordingly, we propose lane function assignment and signal timing measures to eliminate these weaving operations.

Lane function assignment

(1) On the northern approach: The bike lane was changed to a truck lane. There are six lanes on this approach. The lane next to the curb accommodates through movements of buses on the frontage road and vehicles from the off-ramp. The next two lanes are for right-turn movements from the off-ramp and frontage road. The next one is only for through frontage road movements heading for the on-ramp. The last two lanes are for through frontage road movements not entering onto the expressway through the on-ramp.

(2) On the southern approach: The bike lane is changed to a truck lane.

There are eight lanes. The lane next to the curb accommodates through bus only. The next three lanes are for right turns The next one is for through movements from the off ramp. The next is for through movements on the frontage road heading for the on ramp. Finally, the last two lanes are for through movements on the frontage road not entering the on-ramp.

Clear signs should be provided on the approaches to prevent drivers from selecting the wrong lane. The proposed sign layout is shown in Fig. 5.

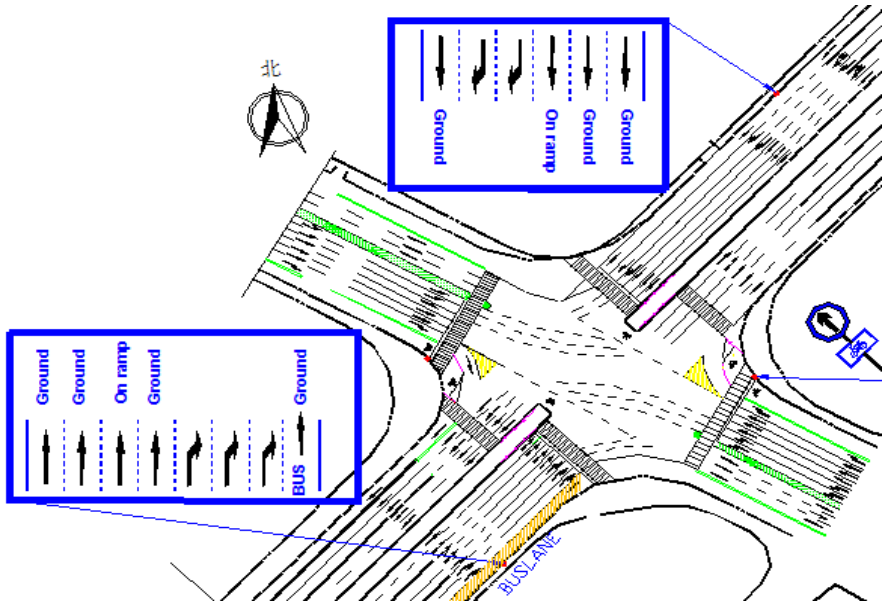

Fig. 5. Proposed traffic organization on northern approach.

Signal timing

A five-phase signal timing scheme was proposed, as shown in Table 3. Circle length is lessened to 150 seconds, in which:

Phase 1 is for a left turn on eastern/western approaches and right turn on the four approaches.

Phase 2 is for a left turn on a western approach, through movements on lane 4 of the southern approach and a right-turn of three approaches. Obviously, phase 2 is embedded between phase 1 and 3. Phase 2 has two advantages: (1) separating the through movements with different OD on the southern approach to eliminate the weaving operation and, (2) considering the imbalance of left-turn traffic volume between eastern and western approaches, shortening the green time of phase 1 and improving the efficiency of the whole intersection.

STUDY RESULTS

As pointed out above, the main bottleneck of this complex intersection is not the approach, but the departure legs. So the theoretic formula of Highway Capacity Manual 2000 was invalid for evaluation here. The proposed evaluation tool was simulation model VISSIM 4.1. Two simulation models were constructed for the present and the improving scenarios. Three performance measures —

delay and the average and maximum queue length — were selected for comparison. Simulation results are listed in Table 3.

TABLE 3 PROPOSED SIGNAL TIMING SCHEME

Phase	1	2	3	4	5
Vehicle movements					
Bicycle					
Pedestrian					
Green time (s)	40	28	34	20	15
Circle time (s)			150		

From Table 3, we can find that the proposed improvements result in significant efficiencies in delay and queue length:

On the northern approach, although the average queue length was slightly increased by 6.0 percent, the maximum length was reduced by 25.8 percent.

On the southern approach, delay of through movements was reduced by 57.7 percent. The maximum queue length was shortened to 117 meters not extending to the expressway mainline.

On the eastern approach, delay of left-turn and through movement was reduced by 36.3 to 38.3 percent.

On the western approach, delay was reduced by 61.5 to 84.1 percent and maximum queue length was shortened to 100 meters.

CONCLUSION

(1) The junction studied in this paper is more complex than the standard junction, due to the pairs of ramps on intersection legs.

(2) The main problem and traffic bottleneck in this intersection is located on the departure legs. Vehicles with different OD weave in the section from stop bar to on-ramp terminal and thus degrade the operating efficiency of the whole system.

(3) Appropriate lane function assignment was redesigned to eliminate the weaving operation.

(4) Signal timing was optimized as well. Movements with different OD were separated by special signal phase sequence. An embedded phase was applied.

(5) In this complex intersection, some traffic direction should be prohibited to simplify traffic composition. Here, the left-turn on northern/southern approaches was prohibited and replaced by through movement plus U-turn.

(6) Future work will be directed to signal coordination with the neighboring intersections.

ACKNOWLEDGMENTS

This research is supported by the National Natural Science Foundation of China (50608010) and Scientific Research Fund of Hunan Provincial Education Department (06B006).

REFERENCES

California Department of Transportation Division of Design (2001). "Single point interchange planning, design and operations guidelines," unpublished.

Dorothy, P. B. W. and Maleck, T. L (1997). *An evaluation of the Michigan urban diamond interchange with respect to the single-point urban interchange*, Michigan Department of Transportation, Traffic & Safety Division.

Engelbrecht, R. J., Venglar, S. P. and Zong, Z. T. (2001). "Research report on improving diamond interchange operations using advanced controller features," Texas Department of Transportation, Rep. FHWA/TX–02/4158-1.

Lee, J. C., Larwin, T. F. Jr., and Kidd, B. D. (2002). *Evaluation of operational efficiencies, cost and accident experience of four phase single point urban interchanges*. Arizona Department of Transportation, Rep. 501.

Leisch, J.P., Urbanik, T., and Oxley, J.P. (1989). "A comparison of two diamond interchange forms in urban areas." *ITE Journal,* Institute of Transportation Engineers, Washington, D.C., 21-27.

Lindgren, R.V. and Tantiyanugulchai, S. (2004) "Microscopic simulation at a diamond interchange." In *Proc. 83rd Annual Meeting of the Transportation Research Board*, Washington, D.C.

Messer, C.J., Bonneson, J.A., Anderson, S.D., and McFarland, W.F. (1991). *NCHRP report 345: Single-point urban interchange design and operations analysis*, Transportation Research Board, Washington, D.C.

Messer, C. J. and , Bonneson, J. A. (1997), "Capacity analysis of interchange ramp terminals", Texas A & M Research Foundation, Rep. NCHRP 3-47

Tian, Z. (2004). "Strategies for providing an integrated diamond interchange ramp-metering control system," Ph.D. dissertation, Office of Graduate Studies, Texas A&M University.

Selinger, M. J. and, Sharp, W. H., "Comparison of SPUI & TUDI interchange alternatives with computer simulation modeling," unpublished.

Wu, Z., Sun J., and Yang X. (2005)."Calibration of VISSIM for Shanghai Expressway Using Genetic Algorithm." In *Proc. Proceedings of the 2005 Winter Simulation Conference*, 2645-2648.

Yang, X. and Sun, M. (2003). "Research of Traffic Improvements on Wu-Ning Arterial-ZhongShan Arterial Intersection and Its Surrounding Network", Tongji University, China, Tech. Rep.

Pedestrian Simulation Research of Subway Station in Special Events

Guanghua ZHAO [1], guanghou ZHANG[2], yanyan CHEN[2], and ping WU[2]

[1]Beijing General Municipal Engineering Design & Research Institute, NO 32 XIzhimenbei Street Haidian district, Beijing China, 100082, email: g.h.zhao@bmedi.cn

[2] Transportation Research Center, Beijing University of Technology, NO 100 Ping Le Yuan Beijing China, 100124; email: guanghouzhang@emails.bjut.edu.cn

ABSTRACT

Special events are an important part of our daily life. During the special events, the relative subway station will involve a large number of pedestrians converging in a short amount of time. So, whether pedestrian organization of subway station is prepared well enough should be evaluated in advance. The involvement of pedestrian simulation can compare and evaluate the scenarios and thus be able to improve the service quality of traffic facilities. In this paper, a process on how to make an organization scenario with the help of pedestrian simulation tools is given following a brief overview of the pedestrian model research. Then the legion 2006 studio was used to test the pedestrian traffic organization plans of a typical subway station involved during the Olympic Games. At last, some improvement measures were given based on the simulation results.

KEYWORD: special events, pedestrian simulation, Legion

BACKGROUND

Special events are more and more common in our daily life. Because of a convergence of pedestrians in a short period of time and limited area, the pedestrians involved in special events are mostly encouraged to use public transport. During the 2008 Beijing Olympic Games, more than 60% of the audience selected public transportion. Gymnasiums are near the subway station, such as WUKESONG gymnasium. Whether the capacity of the facilities in the subway station is enough for the demand, whether the train timetable is suitable for such amounts of pedestrians, whether the temporary facility is required and how to set them are questions which should be solved in advance. But, due to the lack of historic demand and the unique character of each special event, the organization work is very complicated.

Simulation tools can play an important role in such issues. They are able to provide some numerical indication of different scenarios. Also, they can provide intuitive answers for the questions mentioned above.

This paper provides a process on how to make a decision with the help of simulation model. Firstly, a brief state-of-the-art overview of pedestrian model is presented. Then the pedestrian characteristics of subway stations during a special

event are analyzed based on amounts of survey. At last, a typical subway station which has important relevance to the Olympic Games is modeled with legion studio and advice for the pedestrian organization are given based on the simulation results.

PEDESTRIAN MODELING TECHNIQUES

This section presents an overview of pedestrian simulation models with a focus on the micro-models which are used to depict the detail pedestrian behaviors.

Cellular Automata Model (Burstedde et al. 2001) is an idealized model of physical systems, whose time and space are discrete and physical parameters can only be got from a limited set of values. Probability model will be built to decide whether the pedestrian will turn to other cells or just stay where he/she is.

Agent-based Models use an agent as their basic unit. An agent is a software entity that is "situated" in an environment, where it can sense happenings and act accordingly. Agents act autonomously and can communicate with each other. This unit represents human behavior quite well, in particular, our decision-making skills.

In addition to the above pedestrian models, there are also many pedestrian models have been studied and used, such as “Social Force Model”, “Mental Stress Model”, “Magnetic Force Model”, “Queuing Network Model” and “Discrete Choice Framework Model”.

A lot of simulation tools were developed based on the models mentioned above. The Rail Safety and Station Board (RSSB) listed the main simulation software which can be used to evaluate pedestrian organization (2003). Table 1 shows the software and its supplier.

Table 1. Main Software and Suppliers.

Software	Suppliers in brackets
Building EXODUS	Fire Safety Engineering Group
EGRESS	AEA Technology plc
Legion	Legion International Ltd.
MYRIAD	Crowd Dynamics
STEPS	Mott MacDonald

Among them, Legion studio is very professional software specializing in modeling crowd behavior. The core of Legion is Agent-based Model. It treats each person as a "virtual person" who senses their environment and makes decisions about where to move accordingly. Legion can be used in a lot of fields relevant to pedestrian such as new station designs, pre-feasibility assessment, and station refurbishment projects. So, in this paper, the Legion studio 2006 is used to build the simulation model of subway station.

PROCESS OF PEDESTRIAN SIMUALTION

After the confirming of the simulation tools, the process of the models building should be set too. Figure 1 shows the process of how to make a decision with the help of Legion.

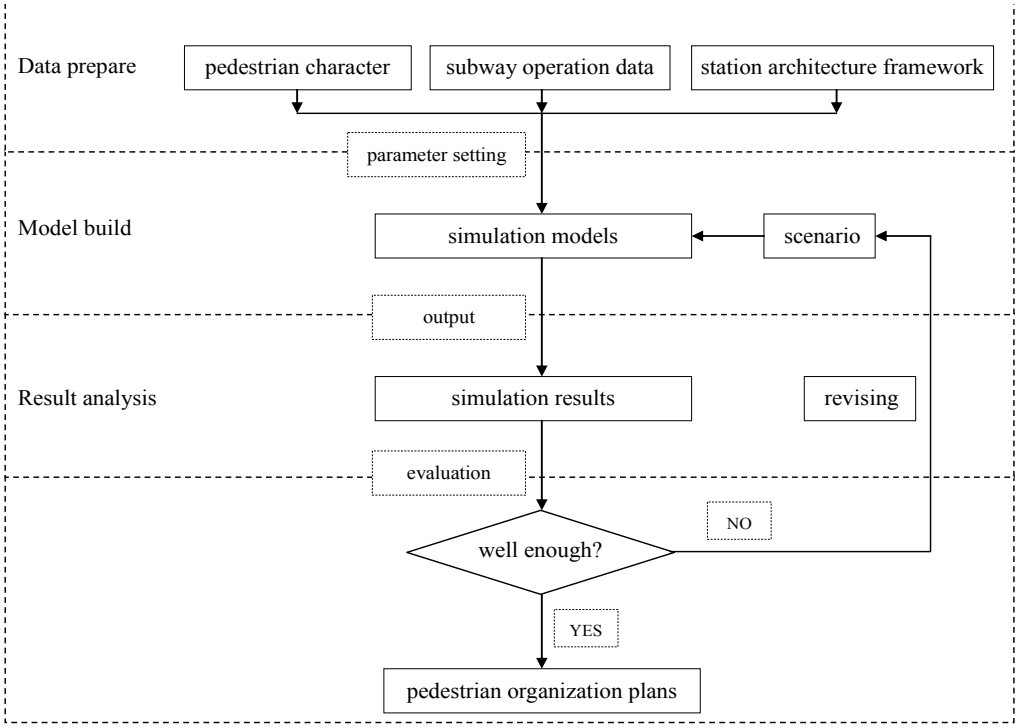

Figure 1. Main Survey Areas in Subway

Data Prepare

The data needs for simulation model can be divided into three types: pedestrian character data, subway operation data and the station architecture framework.

The pedestrian character data is the most complicated data and needs large amounts of input, such as the free speed and traffic flow relationship in pedestrian facilities, and the hobby of route-selecting. Lucky, these data can be obtained from historic data. The more survey and analyzing work done, the more accurate data one can get. Figure 2 shows the areas where the pedestrian character can be attained.

Entrance Passageway Stair AFC Concourse Platform

Figure 2.Main Survey Areas in Subway

Other data, such as pedestrian volume and the pedestrian constitute will be different from each other, because of the most special events are unique. But this

data can be obtained from the host of the special event.

Subway operation and station architecture framework data, such as the service time of ticket checking and the train timetable, can be obtained from the subway administers.

Models Build

Based on the preparing data and pedestrian organization scenario, the simulation model can be built appropriately.

Result Analysis

The simulation results should be analyzed to evaluate whether the pedestrian organization scenario is appropriate. The two main indications are density and evacuation time. Legion studio can output these indications freely. If the density is too high or the evacuation time is too long, the scenario should be revised and the simulation models should be built again.

TYPICAL STATION SIMULATUIION

Among 31 Olympic venues, the Workers Stadium (WS) is the most representative one. The WS is located in Workers Stadium North Road, Chaoyang District. It will host boxing, football games and other competitions. During the Olympic Games, subway lines 2 and 10 will take the main responsibility of evacuating the audience, especially subway line 2 which is closer to the Workers Stadium. Therefore, the DONGSISHITIAO station (DS station) of line 2 is chosen as an example of pedestrian simulation application.

Demand Forecast

The Workers Stadium can accommodate and audience of 65,700 people. According to Table 1, 40.7% of the audience will select subway and 18.3% of the audience will choose Line 2, so there are 12,034 people in all.

Table 2. Traffic Mode Split for Audience Evacuation

D / O	Line 2	Line 10	Bus	Special line	Other	Total
WS	18.3%	22.4%	8.30%	43%	8%	100%
Percent	40.70%	8.30%	43%	8%	100%	
Amount	12034	14709	5410	28291	5256	65700

Figure 3 shows the audience and daily volume of the DS station. Obviously, the sum of them is the total demand of the DS station during the evacuation time.

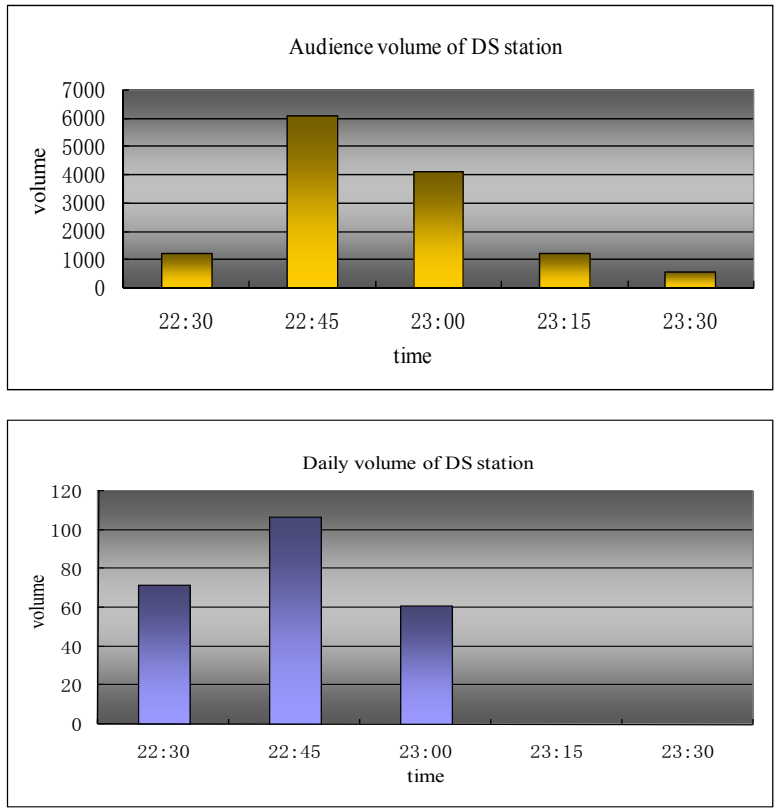

Figure 3. Audience and Daily Volume of the DS Station

Parameter Set

Table 3 shows the detail parameter setting during the model building.

Table 3. Detail Parameter Setting

Type	Detail	Parameter
Facility	Stair, escalator, exit, entrance, AFC	CAD
Constitute and volume	Commuter and audience	Figure 3
service	Ticket-checking	0 second for audience
Evaluation indications	Density and speed	LOS (HCM 2000)

Model Build

Figure 4 shows the layout of the DS station and the simulation model. As WS locates at the southeast of the DS station, most audience will choose Entrance C. So the initial scenario assumes that 80% of the audiences choose Entrance C and 20% of the audiences choose Entrance B.

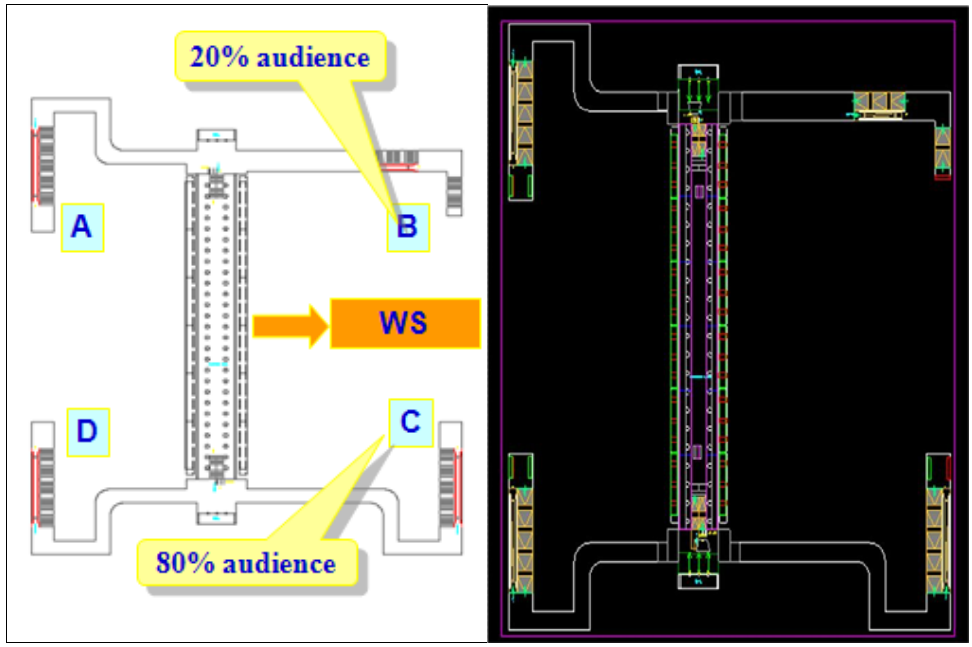

Figure 4. Layout of the DS Station and the Simulation Model

Result analysis

Figure 5 shows the average density of stair, passageway and platform. With the increase of volume in Entrance C, the density of the stair rises dramatically and is greater than 1 peds/m^2. The situation of passageway is much worse than the stair. The average density is above 2 peds/m^2. The LOS (level of service) of the passageway is E. The pedestrian will feel very uncomfortable here. The average density of the platform is below 0.4 peds/m^2 but it is partially because of the congestion of the stair. The pedestrian cannot reach the platform freely.

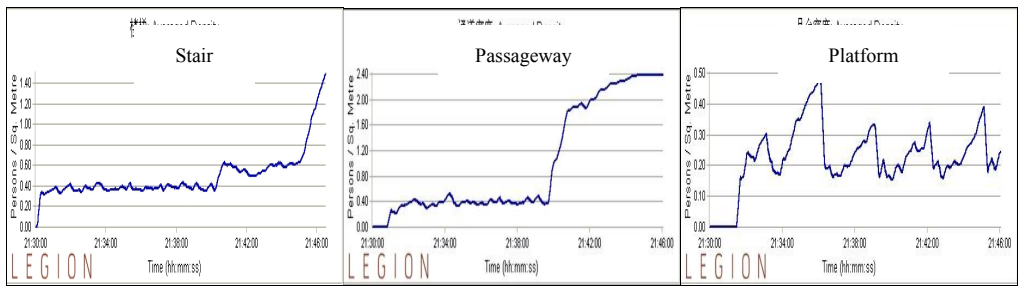

Figure 5. Average Density of Stair, Passageway and Platform

Based on the analysis of the simulation result, several problems of the initial scenario can be found:

- ✓ There are too many pedestrians at Entrance C during the peak time of the evacuation.
- ✓ There are only two ticket-checking channels between Entrance C and D.
- ✓ Commuter pedestrian has conflict with the audience and affect the efficiency of the evacuation.

Improve Measures

Most of the problems of the initial scenario can be solved with proper pedestrian organization. The following are the improvement measures:

- ✓ The stair between Entrance B and C are only used for descending pedestrians. Contrarily, the stair between Entrance A and D are only used for ascending pedestrian.
- ✓ Guiding the 40% of the audience to Entrance B to reduce the pressure of Entrance C.
- ✓ Setting waiting outside of the entrances to control the volume entering the station

Figure 6 shows the average density of the same places of the initial scenario. The improvement is very obvious. The average density of the stair raises is below 1 ped/m^2 which is LOS D. The change of passageway is the most obvious. The average density is lower than 0.5 peds/m^2. The LOS of the passageway is B. The pedestrian will not feel uncomfortable here. The average density of platform is still below 0.4 peds/ m^2. It is sure now that the timetable of the train is suitable.

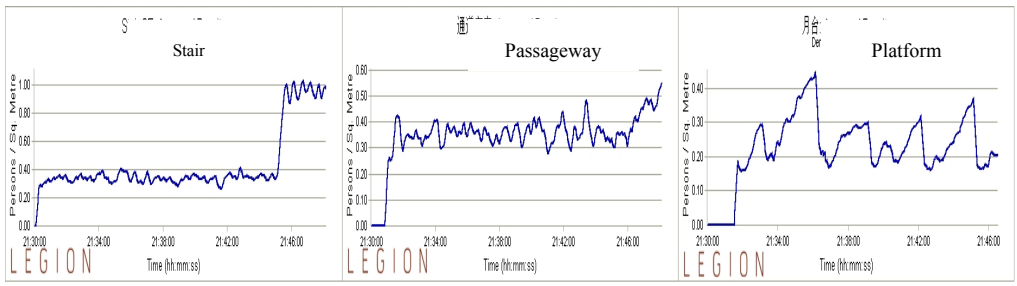

Figure 6. Average Density of Stair, Passageway and Platform

CONCLUSION

Special events are an important part of the society life. With involving a large number of pedestrians in a small area for a short period of time, most special events encourage the pedestrians to come by public transportion. The subway is the most suitable way. Therefore, the pedestrian organization for subway stations during special events is very important. Simulation can be used as an effective tool to support the decision making. But, however, the parameters should be set based on the characteristics of Chinese pedestrian. This paper built a simulation model of a typical subway station relevant with the Olympic Games. Based on the evaluation of the simulation results for the initial scenario, some improvement measures are provided. This process will be an example of pedestrian organization for subway stations during special events.

REFERENCES

Burstedde, C., Klauck,K. Schadschneider, A. and Zittartz, J. (2001). "Simulation of pedestrian dynamics using a two-dimensional cellular automaton", *Physica A: Statistical Mechanics and its Applications*, Volume 295, Issues 3-4, 15 June 2001, Pages 507-525.

Toshihiro Osaragii (2004)." Modeling of pedestrian Behavior and Its Applications to Spatial Evaluation", *Autonomous agents and Multi-agent Systems* 2004, 836-843.

Association of Signal-Controlled Method at Roundabout and Capacity

BAI Yu, XUE Kun and WANG Tao

Department of Road and Traffic Engineering, Tongji University, Shanghai,China.
PH (021) 69584674; FAX (021) 69584674-806; E-mail: rabbitby@263.net

ABSTRACT

Since the fact that the non-signal roundabout allows less flow rate, and with the increasing of roundabout flow rates, a series of problems have occurred in respect to traffic jams, rising accident rates, growth of traffic delays, increasing of saturation degrees, etc. Arrangement of signal control help to enhance the capacity at roundabout and security, but there exist a big difference for applicable conditions and traffic efficiencies under different signal control methods. The main concern of this text, on the foundation of Left-turn with Two-stop Control Method at Roundabout with consideration of the number of different entrance paths and on the basis of signal control theory and optimal method, is on the four control methods related with "Control of In-turn Discharge Clockwise at Signal-entrance Path", "Control of In-turn Discharge Clockwise at Signal-entrance Path + Interlace of Minor Flow", "Association Roundabout Control at Multi--entrance Path" and "Associated Roundabout Control at Multi--entrance Path + Left-turn Inductive Control". It is on such a basis that the methods analyzing the effect rule on capacity come from the signal period of time and space strategy parameters and radius of island under different signal control methods by applying approaches of numerical calculation and experimental traffic engineering. The research achievement will perfect the theory system for signal control roundabout and provide technical support for the reconstruction of uncontrolled roundabouts as well as selection of signal control methods for roundabouts, meaning significant application value.

INTRODUCTION

Uncontrolled roundabouts have unique features of less conflict points, no stopover and easy means of management, helping to effectively reduce vehicle delays and accident rates under a lower capacity. With increasing demand for island traffics, a series of problems occur for uncontrolled roundabouts, resulting in traffic jams, increased accident rates, more vehicle delays, a greater saturation, etc. From these, researchers from home and abroad have done so much in trying to find relative ways to improve. According to researchers of China, the idea of Control Method for Left-turn with Two-stops for effective signal control at roundabout is put forward, improving capacity of roundabout to the greatest extent. The same as the controlling method of other intersections, the control mode, phase and phase sequence of roundabout signals is quite necessary to be

decided according to practical situation. Applicable conditions and traffic efficiency vary under different control methods. It is on the basis of Control Method for Left-turn with Two-stops at Roundabout that a systematic traffic control method and relevant method for optimized controlling parameters is established as well as that research on the adaptability of all types of controlling methods are made in connection with the internal character of roundabouts and the operating features of such method.

RESEARCH REVIEW

It is divided into two directions of unsignal-controlled roundabouts and controlled roundabouts in the related domestic research. For the research of unsignal-controlled roundabouts, it mainly involves the study of traffic characteristics and its applicable conditions, capacity, delay, safety and geometrical design, etc. in which, for most cases, the capacity and delay of roundabout entrances under different conditions of entrances and loops is calculated by using gap-acceptance model (Yang 2004, Brilon 1997, Flannery 1998, Flannery 2000). Foreign researchers tend to connect safety with a geometric design of roundabouts made under the guidance of safety requirements for vehicles and pedestrians (Flannery 2001, Baranowski 2005, Douglas 2005). In the countries of the States, Australia and Britain, numbers of national regulations have been issued concerning roundabout designs, which have laid a foundation for the study of space related optimal design of signal-controlled roundabouts and evaluation of traffic efficiency.

The study on signal-controlled roundabouts started at a later time and according to designing guidance for roundabouts in the States and Australia, it qualitatively regulates that signal control could be implemented for certain entrances if necessary, stressing that it should be used with great care and should not be used for the purpose of a long-term solution to traffic jam. Baranowski (Baranowski 2005) made a study on the signal control method for roundabout pedestrians, exploring condition and safety of arranging signals for roundabout pedestrians. Akçelik made a study on the limit control of capacity at entrance of roundabouts (Akçelik 2005). We study the relevant research in our country in 1998, which was initially raised by researchers from the engineering department of Tongji University (Xue 2003, Wang 2007). They established basic principle and approach for left-turn with two-stop control at roundabouts and gave it a good study in the way of traffic laws, signal timing methods, applicable conditions, optimization control methods and efficiency evaluations. Mr. Ao Guchang (Ao 2003) put forward signal control method for roundabouts under conditions without straight flow.

Researches from home and abroad focus on the field of non-signal controlled roundabouts, with less time in the study of signal-controlled roundabouts. It needs further research in capacity of signal-controlled

roundabouts, condition of geometric topology, demand for mixed traffic flows and adaptability of signals at roundabouts.

INTRODUCTION TO SIGNAL CONTROL METHOD AT ROUNDABOUT

Control of In-turn Discharge Clockwise at Signal-entrance Path. In this control method, each entrance lane discharge In-turn of clockwise, see Figure 1.

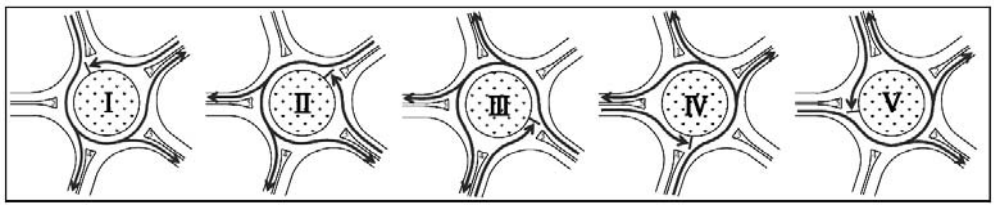

Figure 1. Phase sequence of control of in-turn discharge clockwise at signal-entrance path

This control method could be converted into a one-way closed intersection group (Figure 2). To take the five-fork intersection as an example, it could be regarded as an intersection group made of five intersections of A, B, C, D and E. To select datum point of coordination control, to set the Max delay as optimization target and to choose signal period, phase difference and queuing length as constraint condition, the optimization of other parameters will be carried out.

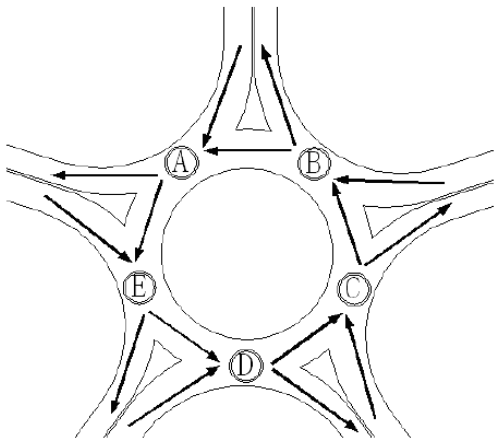

Figure 2. Schematic diagram for one-way closed intersection group of signal controlled intersections

Control of In-turn Discharge Clockwise at Signal-entrance Path + Interlace of Minor Flow. With consideration of order and efficiency of multi-fork roundabout, on the basis of Control of In-turn Discharge Clockwise at Signal-entrance Path, the interlace of secondary traffic flow is introduced (Figure 3), i.e. to treat a main flow and several secondary flows which have the least conflicts between each other as the same phase.

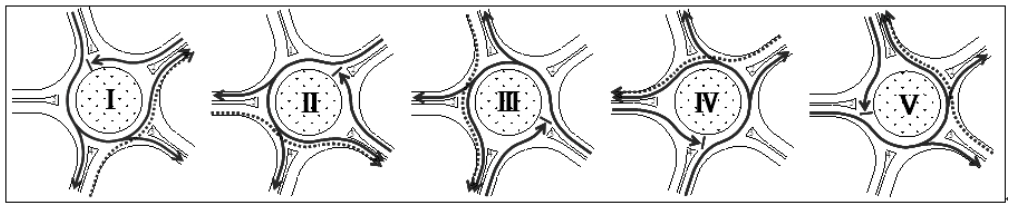

Figure 3. Schematic diagram for Control of In-turn Discharge Clockwise at Signal-entrance Path + the Interlace Phase of Minor Flow

Association Roundabout Control at Multi--entrance Path. Three phases are usually designed for three-fork roundabouts and twice is released within one period at each entrance (Figure 4). Two phases are usually designed for four-fork roundabouts (Figure 5). Twice is released within one period at each entrance of five-fork roundabouts, and release is made clockwise at entrance (Figure 6). Three phases are arranged at for six-fork roundabouts and release is made clockwise at entrance (Figure 7).

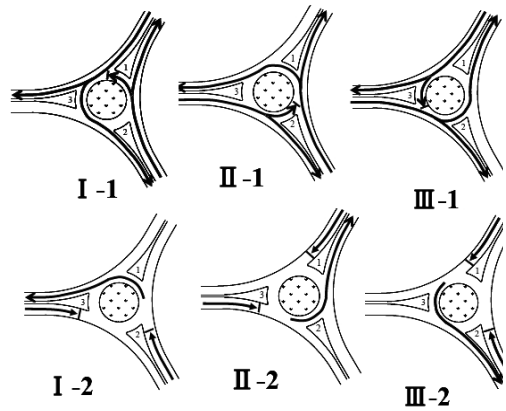

Figure 4. Schematic diagram for three-fork roundabout

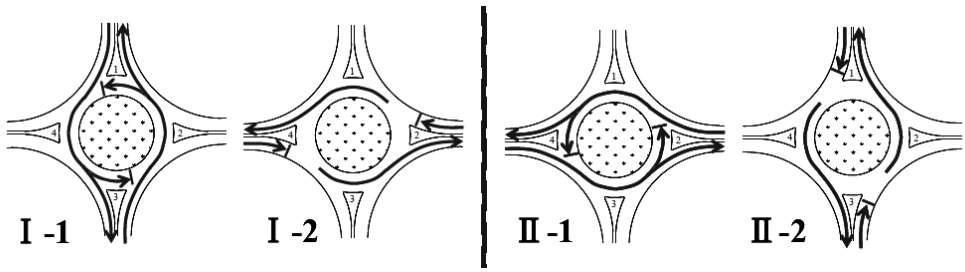

Figure 5. Schematic diagram for four-fork roundabout

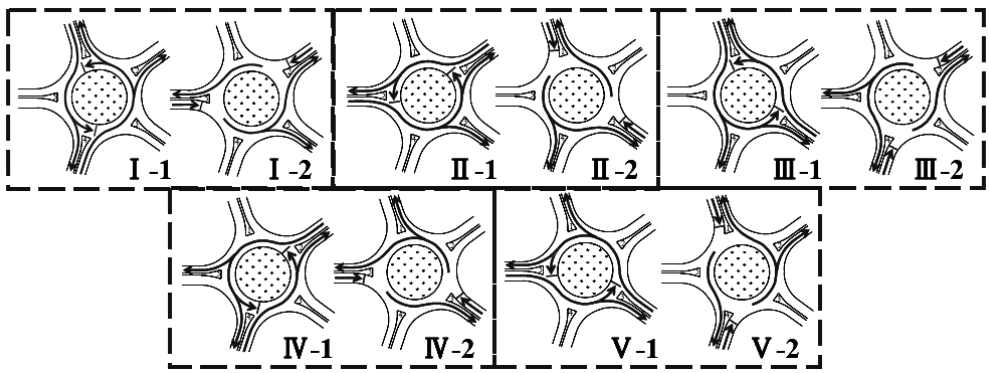

Figure 6. Schematic diagram for five-fork roundabout

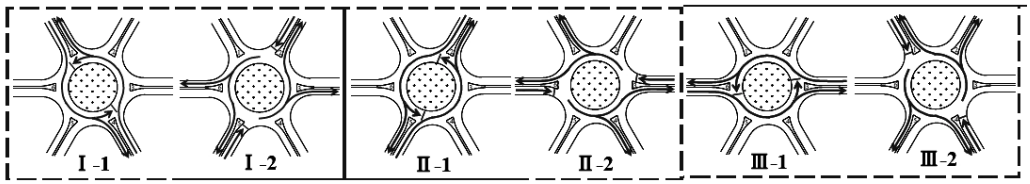

Figure 7. Schematic diagram for six-fork roundabout

Associated Roundabout Control at Multi-entrance Path includes, in two ways, the coordination of entrance signal and loop signal, and then the coordination with loop signal. The optimization model of timing parameters is established under the concept of equisaturation, but the space constraint of loop parking should be realized. When flow ratio between different entrance lanes in the same phase is unbalanced, or queuing vehicles inside the loop go beyond conflict point (or stop line) influencing the normal traffic, it is suggested to take coordination measures of delayed start-up, early disconnection or start-up and late disconnection for green signals of conflict flows.

Associated Roundabout Control at Multi--entrance Path + Left-turn Inductive Control. On the basis of control of association roundabout control at multi--entrance lane, for full utilization of left-turn green time, the arrangement of induction coil at partial positions of roundabout will help both to play function of left-turn capacity at intersection and to prevent occurrence of “deadlocking” to left-turn traffic flow on the loop. In the model of inductive flow, induction coil is arranged before the stop line of the left-turn lane at the entrance and during discharge of the left-turn phase at such entrance when the traffic volume passing the stop line of the entrance lane reach queuing capacity for the left-turn vehicle on the loop, the left-turn green light terminates. When the model of queuing induction is at the rear of the left-turn queuing space of loop, induction coil is arranged in advance at a proper distance, when the queuing position of the left-turn vehicle on the loop is approximately at the queuing capacity on the loop, the related left-turn green light at entrance terminates. (Figure 8, Figure 9)

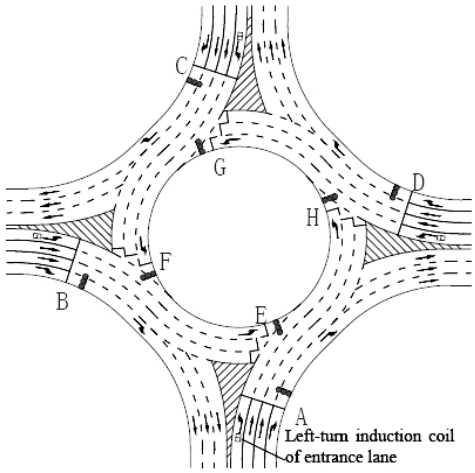

Figure 8. Flow induction control of entrance lane

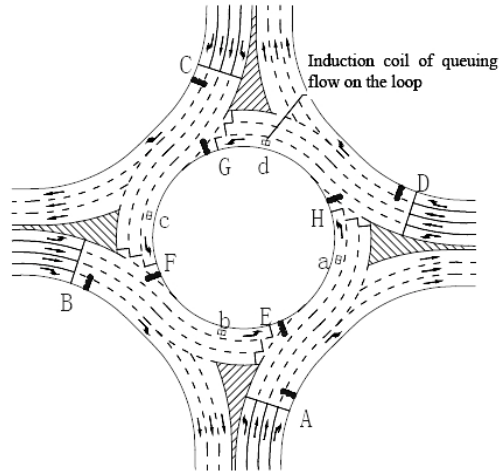

Figure 9. Control of queuing induction on the loop

CALCULATION METHOD FOR SIGNAL-CONTROLLED ROUNDABOUT CAPACITY

Capacity of straight traffic. In circumstances that the requirement for green intervals is met and after the straightforward vehicles go through the first stop line, no obstruction occurs on the loop helping to drive directly into exist lane through the roundabout. We can conclude that the capacity of the straightforward vehicles is the arithmetic product between saturation of straightforward lane and green ratio of signal phase, i.e.:

$$CAP_{iT}=3600\cdot n_{iT}\cdot S_{iT}\cdot \lambda_{iT}=3600\cdot n_{iT}\cdot S_{iT}\cdot (g_{eiT}/C) \quad (1)$$

In which, CAP_{iT} is the straightforward capacity (pcu/h) of No.i entrance, n_{iT} is the number of straightforward lanes at No.i entrance, S_{iT} is the saturation (pcu/s) of straightforward lanes at No.i entrance, λ_{iT} is the straightforward green ratio at No.i entrance, g_{eiT} is the effective straightforward green time (s) at No.i entrance, C is the signal period (s) at intersection.

Capacity of left-turn traffic. The left-turn capacity at signal-controlled roundabouts has a relationship with the way of signal control, at the same time, it is quite necessary to consider the constraint that loop capacity has on the left-turn vehicles for Associated Roundabout Control at Multi-entrance Path.

- Left-turn capacity at the first stop line.

The calculation method for left-turn capacity at the first stop line is similar to the straightforward case, which is equal to the arithmetic product between saturation of left-turn lanes and its green ratio of signal phase, i.e.:

$$CAP_{iL}^{a}=3600\cdot n_{iL}\cdot S_{iL}\cdot \lambda_{iL}=3600\cdot n_{iL}\cdot S_{iL}\cdot (g_{eiL}/C) \quad (2)$$

In which, CAP_{iL}^{a} is the left-turn capacity at the first stop line (pcu/h) of No.i entrance, n_{iL} is number of lanes for left-turn vehicles at No.i entrance, S_{iL} is the saturated flow (pcu/s) of left-turn lane at No.i entrance, λ_{iL} is the left-turn ratio

at No.*i* entrance and g_{eiL} is the effective left-turn green time (s) at No.*i* entrance. Others are the same as above.

- Consideration of restraints of loop capacity to left-turn vehicles.

In the case of symmetry timing, signal lights at the two relative entrances are the same. When the second stop line discharges, the first stop line will definitely cease to discharge. Hence, we can say that in this period, to certain entrances, the Max value of left-turn vehicles which are able to pass through the second stop line is the loop capacity corresponding to such entrance lane. In determining loop capacity, it is necessary to consider the number of lanes queuing on the loop and to guarantee that there will be no conflicts between left-turn tail position of this phase and left-turn head position of opposite phase when discharging.

To take crossing roundabouts as an example, the parking area is divided into two parts, in which the primary parking area is the partial loop way corresponding to the left-turn lane of entrance (Refer to Area 1 of Figure10) while the secondary parking area is the trapezoid space between the safety island of entrance lane and the central island (Refer to Area 2 of Figure10).

Capacity of left-turn vehicles on the loop corresponding to No.i entrance is as following:

$$CAP_{ihL}=\sum_{k=1}^{m}\left[\frac{\alpha_k \cdot R_k}{l_v}\right]+\sum_{k=m+1}^{n}\left[\frac{\beta_k \cdot R_k}{l_v}\right] \quad (3)$$

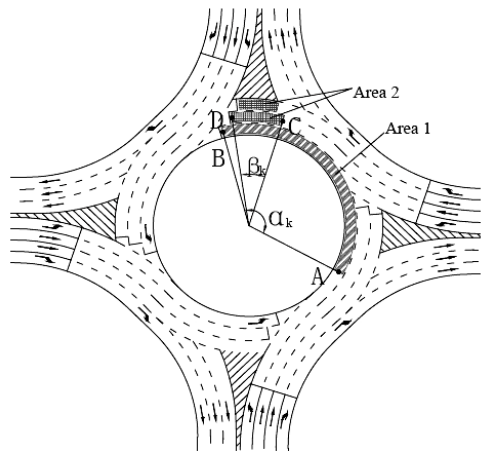

Figure 10. Schematic diagram of waiting area for left-turn vehicle on the loop.

In which, CAP_{ihL} is the capacity (pcu) of left-turn vehicle on the loop corresponding to No.*i* entrance, m is the number of loop way corresponding to left-turn lane of entrance, *n* is the total number of loop way (with exception of right-turn), α_k is the arc radian starting from the conflict point A corresponding to No.*k* loop way counting from inside to outside till the central point B of the second stop line, β_k is the arc radian starting from the conflict point C corresponding to No.*k* loop way counting from inside to outside till the central point D of the second stop line, R_k is radius corresponding to No.*k* loop way counting from inside to outside, l_v is the lane length (m) that a standard vehicle occupies while parking.

With consideration of left-turn capacities restricted by loop capacity:

$$CAP_{iL}{}^{b}=3600\cdot CAP_{ihL}/C \quad (4)$$

In which, $CAP_{iL}{}^{b}$ is the left-turn capacity at No.*i* entrance with consideration of loop capacity (pcu/h). Others are the same as above.

- Determination of left-turn capacity.

For the left-turn capacity of roundabouts under the control of association roundabout control at multi--entrance lane, it should be the lower value of left-turn capacity CAP_{iL}^{a} at the first stop line and left-turn capacity CAP_{iL}^{b} with consideration of capacity constraint on the loop, i.e.:

$$CAP_{iL}=min\{CAP_{iL}^{a}\ ,\ CAP_{iL}^{b}\} \qquad (5)$$

In which, CAP_{iL} is the left-turn capacity (pcu/h) at No.i entrance. Other items keep same as above.

INFLUENCE LAW ON CAPACITY BY TIME-SPACE PARAMETER

Besides the regular conditions of road way and traffics, main factors influencing capacity of signal-controlled roundabouts also include the number of roundabouts, radius of central island, signal period, interval of green time and so on (Wang 2007). The text puts emphasis on associability between radius of central island + signal period and capacity. Radius of central island influences the movement tracks of vehicles, left-turn capacity of the loop as well as on left-turn capacity of intersections. Signal period directly effects the capacity of a roundabout.

Capacity of associated roundabout control at Multi-entrance Path. For the purpose of indicating the influence on capacity by radius of central island and signal period under such control mode, it is necessary to assume that certain parameters are fixed values. Starting from the physical significance of parameters, it is assumed that when the roundabout is a cross orthogonal roundabout, number of entrance lanes, number of loop driveways and number of entrance lanes match. When saturation flow of through lane at entrance is 1650pcu/h and saturation flow of left-turn lane is 1550 pcu/h, they are symmetrically timed.

- Average capacity of straightforward signal lane at entrance CAP_T.

According to above calculation, the change law of average capacity of straightforward signal lane at entrance is as shown in Figure11 when changes with radius of central island and signal period. We get:

1. When radius of the central island R is given, the longer the signal period T is, the larger the CAP_T, similar to the ordinary signal-controlled intersections.

2. When signal period T is given, the larger the radius of the central island, the smaller the CAP_T.

3. When the radius of the central island is a groovy value, to choose the suitable signal period T and the Max value of CAP_T is 550~650 pcu/h.

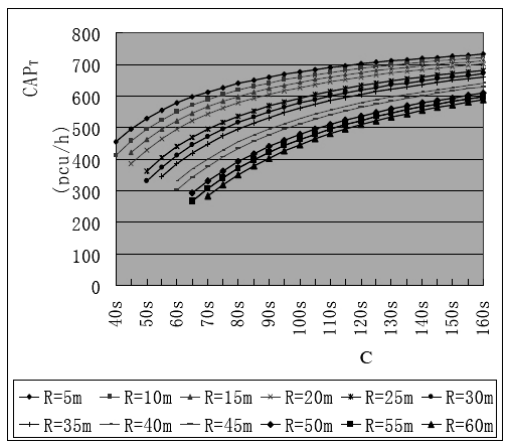

Figure 11. Capacity of straightforward signal lane

- Analysis on average capacity of left-turn signal lane at entrance CAP_L.

Considering capacity constraints of left-turn vehicles on the loop as well as the capacity at the first stop line, the change law of the capacity of the left-turn lane at entrance is as shown in Figure 12 when changes with radius of central island and signal period. We get:

1. When the radius of the central island, R, is given, CAP_L becomes larger in the first hand as the signal period, *T,* increases. When the capacity of left-turn vehicles at the first stop line within one period is larger than the capacity of left-turn vehicles on the loop, CAP_L becomes smaller with the increase of signal period, *T*.

2. When the capacity of left-turn vehicles at the first stop line within one period is smaller than the capacity of left-turn vehicles on the loop and signal period, *T,* is given, the smaller the radius, *R,* of central island is , the bigger the CAP_L is.

3. When the capacity of left-turn vehicles at the first stop line within one period is larger than the capacity of left-turn vehicles on the loop and the signal period, *T,* is given, the larger the radius, *R,* of the central island, the larger the CAP_L.

4. The smaller the radius, *R,* of the central island, the smaller the period length is when reaching the maximum value CAP_{Lmax} of capacity of the left-turn single lane.

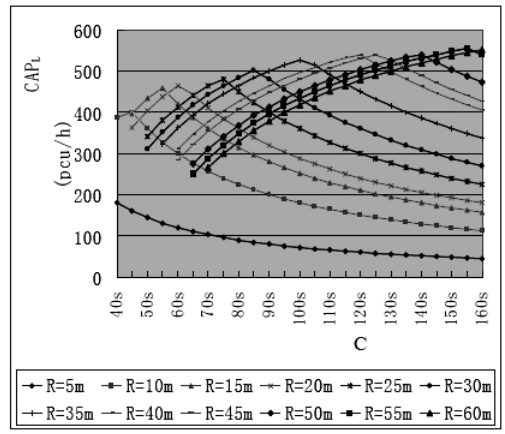

Figure 12. Capacity of left-turn single lane

5. For ordinary radius, *R,* of the central island and proper signal period, *T,* is chosen, the maximum value of CAP_L slightly increases when the radius becomes larger and the maximum value is around 450~550 pcu/h.

- Overall capacity of roundabout.

Change law of specific value of left-turn average capacity at intersections and straightforward single lanes develop when the radius of the central island and signal period change. From Figure 13, we get:

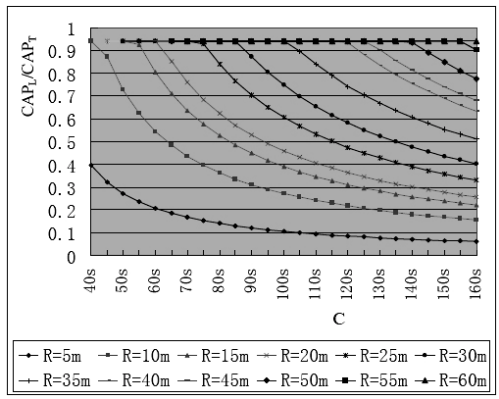

Figure 13. Specific value of capacity for left-turn and straightforward single lane

1. When the capacity of left-turn vehicles at the first stop line within one period is smaller than the capacity of left-turn vehicles on the loop, specific value of average capacity of left-turn and straightforward single lanes do not change with the period.

2. When the capacity of left-turn vehicles at the first stop line within one period is larger than the capacity of left-turn vehicles on the loop, the longer the signal period is at roundabout, the smaller the proportion of left-turn capacity is, which is more suitable to the traffic composition with higher proportion of straightforward traffics.

3. The larger the radius of the central island is, the more suitable is for traffic composition with higher proportion of left-turn traffics.

Change law of overall capacity at intersection (with exception of right turn) develops when the radius of the central island and signal period change. From Figure 14, we can find:

1. The main determinants for the maximum capacity which could be reached at signal-controlled roundabout are the number of entrance lanes and their relative loop number followed by the radius of the central island.

2. The larger the radius is, the more obvious it is for the increased signal period to enhance capacity.

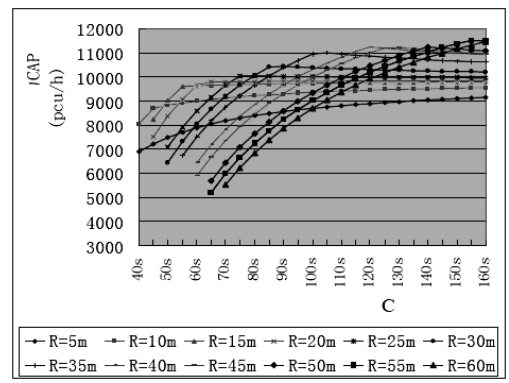

Figure 14. Overall capacity under condition of 3 left and 2 straight at each of entrance

3. The overall capacity is restricted by the left-turn capacity of loop way and when the radius is given, it will reach a higher point with the increase of period. Next, the increase of period influences less on the improvement of capacity, and even some of it will lead to a reduction of the overall capacity because of the larger proportion of the decreased left-turn capacity.

Capacity of control of in-turn discharge clockwise at single entrance lane. For roundabouts with in-turn discharge clockwise at a single entrance lane, when the radius of the central island reaches a certain value, the neighboring phases before and after will have a period of green overlapping time. Change law of overall capacity at intersection develops when radius of central island and signal period change. From Figure 15, we get:

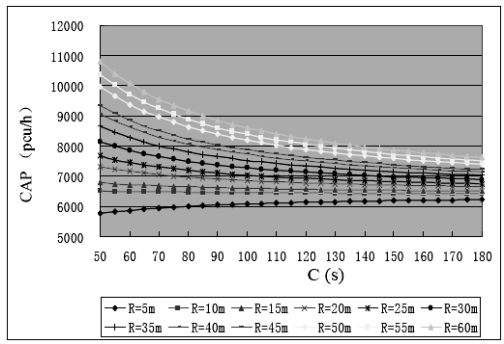

Figure 15. Capacity for discharge signal-controlled intersection at single entrance lane

1. For small-sized roundabouts (usually R<10m) with control of in-turn discharge clockwise at a single entrance lane, capacity slightly increases when the period becomes larger.

2. For small-sized roundabouts (usually R>10m) with control of in-turn discharge clockwise at a single entrance lane, because of existence of green overlapping, capacity decreases when the period becomes larger.

CONCLUSIONS

Arrangement of signal control at roundabouts will help greatly to improve capacity and safety, and applicable condition and traffic efficiency vary according to different ways of controlling. The research in this text intends to put forward four traffic control methods for motor vehicles at signal-controlled roundabouts, to establish models for straightforward and left-turn capacity of signal-controlled roundabouts as well as to analyze the law that signal period of time-space parameters and the radius of the central island influence the capacity of signal-controlled roundabouts under two ways of Control of Association Roundabout Control at Multi--entrance Path and Control of In-turn discharge clockwise at single entrance lane.

Studies have shown that the main determinants for the maximum capacity, which could be reached at signal-controlled roundabouts, are number of entrance lanes and its relative loop number followed by the radius of the central island. When the capacity of control of in-turn discharge clockwise at single entrance lane is adopted, capacity is smaller than that of control of association roundabout control at multi-entrance lane. In the case of a larger central island radius, it has superior adaptability for roundabout with a larger proportion of left-turn flow to that of associated roundabout control at multi-entrance lane. Meanwhile, because of constraints by left-turn waiting capacity on the loop, the capacity and period indicate a non-monotonic correlation, and capacity will be decreased if signal

period is greater than the best period. This research achievement will supply a theoretical foundation for the selection of a signal-controlled method.

ACKNOWLEDGMENTS

This work was supported by the National Natural Science Foundation of China (Project No.50708080) and the Specialized Research Fund for the Doctoral Program of Higher Education (SRFDP).

REFERENCES

Ao G. (2003). "*Theory and application of signalized roundabout crossings*". Journal of Tianjin Institute of Urban Construction, Vol. 9, no.3.

Akçelik R. (2005). "*Capacity and Performance Analysis of Roundabout Metering Signals*". TRB National Roundabout Conference，Vail，Colorado．

Brilon, W. (1997). "*Unsignalized Intersections in Germany - A State of the Art 1997. In Intersections without traffic signals*". Ed. Kyte, M. TRB, Portland.

Baranowski B. (2005). "*Pedestrian Crosswalk Signals at Roundabouts: Where are they Applicable?*". National Roundabout Conference. Transportation Research Board Federal Highway Administration, Vail, Colorado.

Baranowski B. (2005). "*Design Methods for Pedestrian Safety at Roundabout Entries and Exits: Crash Studies and Design Practices in Australia, France, Great Britain and the USA*". National Roundabout Conference, Transportation Research Board Federal Highway Administration, Vail, Colorado.

Douglas R. (2005). "*Estimating Roundabout Performance using Delay and Conflict Opportunity Crash Prediction*". National Roundabout Conference. Transportation Research Board Federal Highway Administration, Vail, Colorado.

Flannery A. (2000). "*A Delay Model For Single-lane Roundabouts In The United States*". TRB. Washingdon, D.C.

Flannery A. (1998). "*Safety, Delay and Capacity of Single Lane Roundabouts in the United States*". TRB. Washingdon, D.C.

Flannery A. (2001). "*Geometric Design and Safety Aspects of Roundabouts*". TRB .Washingdon, D.C.

Wang T. (2007). "*Space-time optimizing method of the signal control roundabout*". Master's Degree Thesis of Tongji University.

Xue K. (2003). "*Study of the Signal Control Theory of Cross Roundabout*". Master's Degree Thesis of Tongji University.

Yang X. (2004). "*A new traffic-signal control for modern roundabout: method and application*". IEEE Transactions on Intelligent Transportation Systems, Vol. 5, no.4, pp.282-287.

Case Study on the Computing Model of the Driving-into Rate of Service Area

Liying Mu[1*], Hongjun Cui[2] and Hongqi Hui[3]

[1]School of Economics and Management, Hebei University of Science and Technology, Shijiazhuang 050018, P.R. China; PH: 15130622321; email: molly1980@126.com

[2]School of Civil Engineering, Hebei University of Technology, Tianjin 300130, P.R. China; PH: 13114939326; email: cuihj1974@126.com

[3]School of Economics and Management, Hebei University of Science and Technology, Shijiazhuang 050018, P.R. China; PH: 13513312874; email: huihongqi@126.com

ABSTRACT

This paper establishes the relation model of driving-into rate and spacing of service areas. Based on the survey of Beijing-Shenyang expressway in Hebei province and the traffic data of service areas, this paper gets the relationship between spacing and driving-into rate of service areas, verifies that the driving time obeys the normal distribution using the Empirical Distribution Function of Probability and Statistics, then, establishes the Recursive Model of driving-into rate whose random variable is the driving time. The driving time is the function of spacing, so the relationship between spacing and driving-into rate is expressed by the formula. This model clarifies and quantifies the relationship between the driving-into rate and spacing by giving concrete form and makes up for the defects of the present methods. At the end, the two examples prove the applicability and advantage of new model.

KEYWORDS: expressway, service area, driving-into rate, model

INTRODUCTION

The driving-into rate (DR) of service area is the rate that the number of vehicles (NV) entering into the expressway service area (vehicles / day) accounts for the main line traffic volume of the highway (vehicles / day), which is the prerequisite for planning and designing service area district and directly determines the scale and operation of the service area (ITP 2004). The driving-into rate is affected by people's physiology and psychology, vehicle performance, traffic conditions, the spacing of service area and so on (Shaolan Guan et al.1995). Especially, the service area spacing which has great impacts on the driving-into rate (MCPRC 2004) can not be ignored. Nowadays, the recommended fixed value in Chinese existing norms can not reflect changes of the above-mentioned factors which are not applicable in some areas.

In addition, the current research about the driving-into rate does not explain the real relationship between service area spacing and the driving-into rate (**Huarong** Qin et al. 2005). For example, (Jinzhang Ji et al. 2006), in "Empirical Research on Computing Model of the Service Area Scale" the calculation model of the driving-into rate is $T = KA/3V$. T is the driving-into rate, A is average spacing of service area, and V is the average speed of different types of vehicles.

This model, having a simple linear relationship, has some defects. Firstly, K, determined by experience value, will make the driving-into rate deviate from the actual value. Secondly, the spacing which is different from a dozen or so *km* to

hundred *km* in a large region in actual is an average value in the formula. Thirdly, it is the most important that the driving-into rate is fixed when the spacing is made certain, but this is inconsistent with the actual.

Based on the current studies, combining with the investigation of Beijing-Shenyang Expressway Service Areas, we study the probability distribution of traffic time, find out the nature relationship between the driving-into rate and service area spacing, and establish the new model to calculate the driving-into rate. This model that rationally explains the relationship between the driving-into rate and service area spacing fetches up the disadvantages of current methods.

MODEL BUILDING ON THE RELATIONSHIP BETWEEN DRIVING-INTO RATE AND SERVICE AREA SPACING

Driving-into rate study of service areas of Beijing-Shenyang expressway

This investigation on five service areas of the Beijing-Shenyang expressway as the survey spots was made on June 2, 2007, containing infrastructure, traffic flow, the service areas, user information and so on. The data divided by driving time (DT) are classified into three kinds: trucks (T), large and medium-sized passenger cars (L) and small passenger cars(S). Firstly, we adapt the two types of data-----passenger cars (PC) and trucks. See Table 1:

Table 1. The Relationship Between Driving-into Rate and Driving Time

DT	NV		DT	NV		DT	NV		DT	NV	
	T	PC		T	PC		T	PC		T	PC
00:15	0	2	02:45	11	23	05:15	4	1	07:45	1	1
00:30	1	3	03:00	11	18	05:30	2	1	08:00	1	0
00:45	2	6	03:15	15	7	05:45	2	2	08:15	1	0
01:00	2	5	03:30	13	5	06:00	2	2	08:30	0	0
01:15	3	8	03:45	13	3	06:15	1	1	08:45	0	0
01:30	3	16	04:00	12	3	06:30	2	1	09:00	1	0
01:45	4	29	04:15	6	2	06:45	1	0	09:15	0	0
02:00	5	34	04:30	4	1	07:00	1	0	09:30	0	0
02:15	6	31	04:45	5	2	07:15	0	1	09:45	1	0
02:30	8	26	05:00	3	1	07:30	1	0	10:00	0	0
Total										148	219

The investigation shows that driving time has affection on the vehicle number. For better analysis, we take the data from Table 1 into legend (see Figure 1).

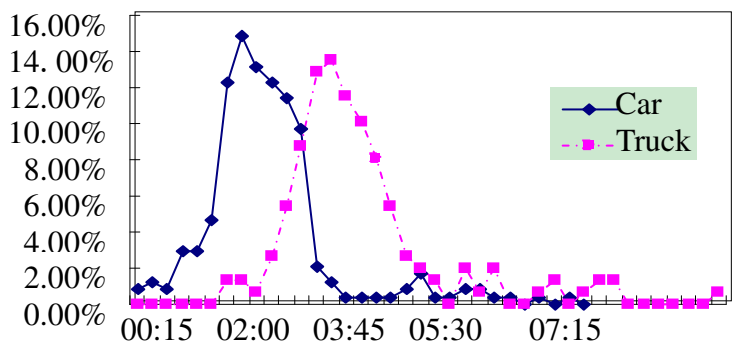

Figure 1. The Change of Vehicle Driving-into Rate Along the Driving Time

From the legend we know that there is the certain specific relationship between driving-into rate and driving time. The figure is similar to the graph of the normal distribution which has much good nature and is easy to conduct in-depth theoretical studies comparing with a common distribution. The following study will give actual form of the particular relationship.

Data Analysis

Analyzing the Figure 1, we suppose that the driving-into rate obeys the normal distribution $\xi - N(\mu,\sigma^2)$, hereinto, μ,σ are unknown parameters. χ^2 is satisfied with the Gaussian fitting test. The maximum likelihood estimator of $\hat{\mu}$ and $\hat{\sigma}$ represent μ and σ. According the Figure 1, the results are:

$$\hat{\mu} = \frac{1}{148}\sum_{i=1}^{148} x_i = \frac{31095}{148} = 210.1014,\quad \hat{\sigma} = \sqrt{\frac{1}{148}\sum_{i=1}^{148}(x_i - \bar{x})^2} = 94.10401.$$

Come to the conclusion that the χ^2 observation is $\chi^2 = 20.11141$. There are two unknowns that need to be estimated by the maximum likelihood estimates, so $l = 2$. When H_0 is true, χ^2 obeys $\chi^2(15-2-1)$. Since the significance level is $\alpha = 0.05$, the result is $\chi^2_{0.05}(13) = 22.362$. $\chi^2 = 20.11141 < 22.362$, so accept H_0; namely, the driving-into rate obeys the normal distribution means that driving time obeys the normal distribution under the condition that the significance level is $\alpha = 0.05$.

Similarly, for large and medium-sized passenger cars and small passenger cars, driving-into rate obeys the normal distribution under the condition that the significance level is $\alpha = 0.05$. After analyzing and calculating we gain:

The nonstop driving time of small passenger cars obeys $\xi - N(147.9918,\ 100.1667)$

The nonstop driving time of large and medium passenger cars obeys $\xi - N(148.9286,\ 69.5438)$

The nonstop driving time of trucks obeys $\xi - N(210.1014,\ 94.1014)$.

The above analysis shows that the driving time and driving-into rate basically obey the normal distribution. There is a fixed relationship between the driving time and driving-into rate that do not happen by chance. The reasons: firstly, the time of the vehicles can run before driving into the service area has great relationship with vehicle type and nature; secondly, physiological demand of drivers and passengers has some influence on the driving-into rate; thirdly, the road conditions also can affect the driving-into rate to some extent. Those reasons result in the fixed relationship between the driving time and driving-into rate. Building the calculating model for driving-into rate can provide a foundation for confirming the service area scale and spacing reasonably.

Model Derivation

Suppose: the traffic flow between origin r and destination s is T_{rs}, the distance from other service areas to origin r is L_i, there are n service areas between r and s. $(L_i / v - \mu)/\sigma = t_i$, μ is average value, v is vehicle driving speed, σ is variance, $\phi(t)$ is the function of Standard Normal Distribution.

Following:

The driving-into rate of the first service area is: $P_1 = \phi(t_1)$ (1)

The driving-into rate of the second service area is: $P_2 = (1-P_1)\phi(t_2) + P_1\phi(t_2 - t_1)$ (2)

Where: $P_1\phi(t_2 - t_1)$ is the probability that the vehicle drives into both the first and the second service area; $(1-P_1)\phi(t_2 - t_1)$ is the probability that the vehicle drives into the second but not into the first.

The driving-into rate of the third service area is:

$$P_3 = (1-P_1)(1-P_2)\phi(t_3) + (1-P_1)P_2\phi(t_3 - t_2) + (1-P_2)P_1\phi(t_3 - t_1) + P_1P_2\phi(t_3 - t_2) \quad (3)$$

Where: $(1-P_1)(1-P_2)\phi(t_3)$ is the probability that the vehicle draws into the third but not into the first and second; $(1-P_1)P_2\phi(t_3 - t_2)$, $(1-P_2)P_1\phi(t_3 - t_2)$ are the probability that the vehicle draws into both one or other in the middle and the third; $P_1 P_2 \phi(t_3 - t_2)$ is the probability that the vehicle drives into all service areas of the three.

To simplify the P_3:

$$P_3 = P_1(1-P_2)\phi(t_3 - t_1) + P_2\phi(t_3 - t_2) - P_1P_2\phi(t_3 - t_2) \quad (4)$$

Similarly, we can gain:

$$P_4 = P_1(1-P_2)(1-P_3)\phi(t_4 - t_1) + P_2(1-P_3)\phi(t_4 - t_2) + P_3(1-P_2)(1-P_1)\phi(t_4 - t_3) + (1-P_3)P_1P_2\phi(t_4) \quad (5)$$

$$P_5 = P_1(1-P_2)(1-P_3)(1-P_4)\phi(t_5 - t_1) + P_2(1-P_3)(1-P_4)\phi(t_5 - t_2) + P_3(1-P_4)(1-P_2)(1-P_1)\phi(t_5 - t_3) + P_4\phi(t_5 - t_4) + (1-P_1)(1-P_2)(1-P_3)(1-P_4)\phi(t_5) \quad (6)$$

Observing the structure of the formula P_i, we find the recursive formula, namely the driving-into rate of the N th service area is:

$$P_N = \sum_{i=1}^{N-1} P_i \prod_{j=i+1}^{N-1}(1-P_j)\phi(t_N - t_i) + \prod_{k=1}^{N-1}(1-P_k)\phi(t_N) \quad (7)$$

Analyzing the P_N: P_N has $N-i+1$ total factors, in the total factors of $\sum_{i=1}^{N-1} P_i \prod_{j=i+1}^{N-1}(1-P_j)\phi(t_N - t_i)$ the i th has $(N-i+1)$ multiple multiplication factors.

Between origin r and destination s the volume of a certain type of vehicles driving into various service areas is:

$$Q_N^{rs} = T_{rs} \cdot P_N^{rs} \quad (8)$$

Therefore, in highway design, as long as we predict the traffic distribution (OD Matrix) of the expressway service district, the total vehicle of each service area can be worked out by this formula, and then the driving-into rate of service area can be identified.

$$Q_N = \sum_r Q_N^{rs} = \sum_r T_{rs} \cdot P_N^{rs} \quad (9)$$

$$\alpha_N = \frac{Q_N}{A_N} = \frac{\sum_r T_{rs} \cdot P_N^{rs}}{A_N} \quad (10)$$

Where: Q_N is the volume of vehicles driving into the service area N; Q_N^{rs} is the volume of vehicles driving into the service area N between origin r and destination s; P_N^{rs} is the probability that vehicles drive into the service area N between origin r and destination s; α_N is the driving-into rate of the service area N; A_N is the main line traffic volume in the cross-section where the service area N locates.

MODEL ANALYSES

Model Application

Example 1: On the assumption that there are five service areas at a certain section of expressway, as shown: *R* is a city, *S* is another, 1, 2, 3, 4, 5 are separately on behalf of the five service areas. From R to 5, the distance between adjacent two points are 30 *km*, 80 *km*, 60 *km*, 50 *km*, and 40 *km*. There is a traffic flow from *R* to *S*; hereinto, there are 1000 small passenger cars, 500 large and middle passenger cars, and 800 trucks. Now calculate the volume of vehicle drawing into every service area. In reference to relevant information about the speed of a variety of cars, assume the average speeds of three kinds of vehicles are 110 *km/h*, 90 *km/h*, 70 *km/h*. The layout of the service area is shown in Figure 2:

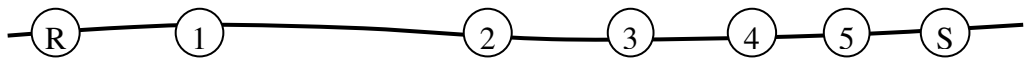

Figure 2. Arrangement of Service Facilities between R and S

Analysis: Via the above-mentioned proof we know that the vehicle driving-into rate obeys the normal distribution. The mean and variances of the vehicles in three types are: Small passenger car: $\mu = 147.9918$, $\sigma = 100.1667$, Large and middle passenger car: $\mu = 148.9286$, $\sigma = 69.54389$, Truck: $\mu = 210.1014$, $\sigma = 94.1014$.

Using formulas (7) and (8), we gain the vehicle driving-into rate in each service area and the volume of vehicle driving into the certain service area shown in Table 2.

Table 2. The Driving-into Number and Driving-into Rate of Service Area

Type	Probability	P_1	P_2	P_3	P_4	P_5	P_T
S	DR	9.44%	18.60%	25.27%	28.82%	29.38%	111.80%
	NV	94	186	256	288	294	1118
L	DR	3.18%	13.67%	27.04%	33.13%	31.57%	108.62%
	NV	16	68	135	166	158	543
T	DR	2.50%	10.81%	22.84%	29.78%	30.07%	96.00%
	NV	20	87	183	238	241	768

As Table 3 shows: $P_1, \cdots, P_5$ is the driving-into rate of service areas, P_T is total probability that vehicle drives into the service areas. It also contains the number of different kinds of vehicles that drive into the service areas. Following is the same.

Example 2: Change the spacing of the service areas, as shown: the distance from *R* to 1 is 30 *km*, the distances between 1 and 2, 2 and 3, 4 and 5, 5 and *S* are all 30 *km*; the distance between 3 and 4 is 100 *km*. Now calculate the volume of vehicle driving into every service area. Others are the same as example 1. The

layout of the service area is shown in Figure 3:

Figure 3. Arrangement of Service Facilities Between R and S After Changing the Distance

Analysis: The calculation process is the same as the example 1 and shown in Table 3.

Table 3. The Driving-into Number and Driving-into Rate After Changing the Distance

Type	Probability	P_1	P_2	P_3	P_4	P_5	P_T
S	DR	9.44%	12.20%	15.04%	30.06%	27.93%	94.68%
	VM	94	122	150	301	279	947
L	DR	3.18%	5.78%	9.77%	34.68%	30.55%	83.97%
	VM	16	29	49	178	153	425
T	DR	2.50%	4.54%	7.85%	28.23%	17.95%	71.06%
	VM	20	36	63	226	224	569

Result Analysis

The two examples show the changes of the driving-into rate of service areas in the condition that the spacing and number of service areas are changing. Table 3 shows that the distances between 1 and 2, 2 and 3, 4 and 5, 5 and *S* are the same, but the driving-into rate of each service area is different and is increasing with the increase of the distance from the origin.

A specific relationship exists between driving-into rate and travel distance of the vehicle. As Table 2 shows, in a certain travel distance, the driving-into rate of vehicle increases with the increase of the travel distance. The present methods which have the consistent driving-into rate following the consistent spacing have disadvantage, and ignore the influence of accumulated traveling distance of vehicles.

The driving-into rate is becoming steady with the accretion of the spacing. As Table 2 and Table 3 show, the driving-into rate reaches a steady value when the vehicle arrives at the fourth service area.

CONCLUSIONS

The driving-into rate is a decisive factor of the service area design. This paper studies the driving-into rate on support of substantial survey data in detail. Firstly, data is collated by the form of charts by which this paper analyzes the relationship of driving time and driving-into rate and verifies that the driving time obeys the normal distribution. Secondly, it is the emphasis that this paper deduces the recurrence formula of driving-into rate whose random variable is the driving time. This model clarifies and quantifies the relationship of the driving-into rate and spacing by giving concrete form, and makes up for the defects of the present methods. It is a breakthrough that the driving-into rate of each service area can be calculated in practical applications as long as the origin-destination trip matrix is obtained.

REFERENCE:

Huarong Qin (2005). “The service area function scheme founded on the demanding analyzing of the service objects” [D]: Master Degree Thesis. Xi’an: *Changàn University*

Institute of Traffic Planning (2004). "National Network Planning" [R].

Jinzhang Ji, Hao Chen (2006). "Case study on the calculation model of the service area scale". *Journal of Highway and Transportation Research and Development*, Issue 10, 171-173

Ministry of Communication of the People’s Republic of China (2004). " Highway Engineering Technical Standards"(JTGBOI-2003). *The People Traffic Press*.

Shaolan Guan (1995). "Highway Service District Building Scale". *Highway*, 7-11

Research on Dynamic Characteristics of Road Network in Snowy Conditions

Ren Xiaoqiang[1], Yang Longhai[2], Zhang Xiqiao[3] and Fan Dongxu[4]

[1]Changchun Municipal Engineering Design and Research Institute Xiantai street, Economic Development District, Changchun, Jilin Province, PRC, 130033, PH: +86 13904306610; email: rxqsir@vip.sina.com
[2]School of Transportation Science and Engineering, Harbin Institute of Technology, No. 202, Haihe River Road, Nangang District, Harbin, Heilongjiang Province, PRC, 150090, PH: +86 13936131585; email: yanglonghai@hit.edu.cn
[3]School of Transportation Science and Engineering, Harbin Institute of Technology, No. 202, Haihe River Road, Nangang District, Harbin, Heilongjiang Province, PRC, 150090, PH: +86 13258665713; email: zxq103@126.com
[4]School of Transportation Science and Engineering, Harbin Institute of Technology, No. 202, Haihe River Road, Nangang District, Harbin, Heilongjiang Province, PRC, 150090, PH: +86 13624617852; email: yyfdx_hit@126.com

ABSTRACT

The operational status of road networks in snowy conditions is quite different from that in general conditions, especially in the process of traffic assignment. Traffic assignment in snowy conditions of different snowfall degrees is studied in this paper, and the impedance function is modified by amending the three following parameters: time, speed and capacity.

In snowy conditions, speed is modified by considering the change of road surface friction coefficient. The minimum safe headway is taken into consideration in the modification of capacity, and the modification of time is obtained by simulation. Based on the new impedance function and equilibrium assignment model, the traffic in the road network are assigned in the snowy conditions of different snowfall degrees. An example was also cited to prove that the algorithm is feasible. By comparing the assignment results in the general conditions and snowy conditions of different snowfall degrees in the example, changes of characteristic indexes of road networks like average travel speed and traffic flow in all grade of roads are given. The changing trend of the indexes is also presented. At last, some suggestions are put forward on the value of reserve capacity to enhance the environmental adaptability of road networks in snowy conditions.

Key words snowy conditions, impedance function, traffic assignment, adaptability of road network

INTRODUCTION

In snowy conditions, traffic demand would not change obviously in a short time, but the operational status of road network changes. Since speed, time and capacity all change, the traffic volume assigned in the road network also changes. At present, the research abroad about urban roads in snowy conditions mainly concentrates on traffic signal timing and analysis of delay, such as the timing programs of SIGNAL85 and TRANSYT-7F(Bernardin et al., 1995) proposed by Bernardin and others. The domestic research mainly concentrates on the aspects of

traffic security management. There is currently little research on the dynamic characteristics of road networks in snowy conditions at home and abroad. In this paper, the process of the modification of speed, time, and capacity is given in snowy conditions of different snowfall degrees, and a new impedance function can be obtained based on the three modified parameters. It assigns traffic with the new impedance function, and then compares and analyzes the dynamic characteristics of road network by the traffic assignment results in general and the snowy conditions of the two snowfall degrees. A calculation example is showed in the second part. From the example, the theoretical results are tested and applied, and the changing range of road network indexes in snowy conditions can be obtained.

THEORETICAL ANALYSIS

In snowy conditions, the changes of operational characteristics of traffic flow and capacity of road sections are caused by the changes of road conditions. In the process of traffic assignment, the impedance of road sections affects people's route choice very much. Therefore, the three parameters of time, speed and capacity in snowy conditions are discussed and modified by establishing models. By combining the three modified parameters to set up the model, the new impedance function can be obtained.

The modification of speed in snowy conditions . The free-flow traveling time is achieved when the road section's saturation is very low and the vehicles run with free-flow speed. In this case, vehicles would not affect each other and run with the maximum speed. In this state, the running speed of vehicles could be considered to be mainly determined by the motive performance of vehicles and the road conditions.

When a car runs, adhesive conditions between the tires and ground surface must be satisfied, namely

$$p_t \le Z_\varphi \varphi \qquad (1)$$

Where Z_φ is the pressure between the driving wheel and the ground surface; φ is the adhesive coefficient between tires and ground surface.

From the formula, it can be known that the maximum value of traction force is $P_{t\max} = Z_\varphi \varphi$, at this time, vehicles get the maximum running speed, i.e. the free-flow speed. Under this state, there is:

$$Z_\varphi \varphi = Ggf + Ggi + C\rho AV^2 \qquad (2)$$

Where G is the car body weight; g is the acceleration of gravity; f the is rolling resistance; i is the road gradient; C is the car streamlined coefficient; ρ is the air density; A is the cars' windward area; V is the cars' running speed.

It can be known from vehicles structure:

$$Z_\varphi = Gg\left(d + h_g i\right)/L \qquad (3)$$

Where d is the distance from the car's center of gravity to driven shaft; h_g is the height of car center of gravity; L is the wheel base.

It can be known from formula (2) that the maximum speed that a vehicle can reach is determined by car weight and the adhesive coefficient between the tires and the ground surface. Under the snowy conditions, the adhesive coefficient

between the tires and the ground surface decreases, and the maximum traction force that a car can obtain decreases as well (Erwin R Boer1999; Daniel Isenberg, 2004). Meanwhile, the ratio of the free-flow speed in the two different conditions can be calculated from formula (2) and formula (3):

$$\frac{V_s}{V}=\left(\frac{\frac{d+h_g i}{L}\varphi_s - f_s - i}{\frac{d+h_g i}{L}\varphi - f - i}\right)^{1/2} \qquad (4)$$

Take the structural parameters of a certain type of HYUNDAI ELANTRA as an example. Its wheel base is 2.65m, the height of car's center of gravity is 0.4m and the distance from car's center of gravity to its moving shaft is 1.05m. In general conditions, the road adhesive coefficient $\varphi = 0.5$ and the rolling resistance $f = 0.02$. If no management measure is taken in snowy conditions of the two different snowfall degrees, the values of φ_s in different grades of roads are as the following table shows (Sandeep Datla and Satish Sharma 2007). Rolling resistance $f_s = 0.03$. In the design of urban roads, it is demanded to guarantee the minimum slope of road $i = 0.3\%$ in order to meet the requirements of water drainage. Substitute all the data into the formula (4), and then V_S / V is obtained in the two conditions (Lynette C. Goodwin and Mitretek Systems, Inc, 2002).

Table 1. The values of φ_s and V_S/V in snowy conditions

Road grade	φ_s		V_S/V (%)	
	Severe degree	Slight degree	Severe degree	Slight degree
Expressway	0.45	0.4	91.1	84.7
Main trunk road	0.4	0.35	84.7	77.7
Secondary trunk road	0.35	0.3	77.7	70.0
Branch road	0.3	0.2	70.0	51.4

The modification of capacity in snowy conditions . When traffic flow runs incessantly with the speed V and the vehicles keep the minimum longitudinal distance "safe headway" L, the number of passing vehicles reaches the maximum volume. Thus the ideal capacity is:

$$C = S/L = 1000V/L \text{ (pcu/h)} \qquad (5)$$

Where S is vehicle's driving distance per hour; L is safe space headway.

In the usual case, "safe space headway" includes the following four items:

he driving distance of vehicle in the driver's reaction time $L_1 = \frac{Vt}{3.6}$ (t=2.5s) ;,Vehicle's braking distance $L_2 = \frac{V^2}{254\varphi}$ (φ is the frictional factor between wheels and the ground surface), Vehicle's body length L_3 (generally take 5~10m), and Safe distance L_4 (generally take 3~5m).

Thereby, formula (5) can be rewritten as

$$C = \frac{1000V}{Vt/3.6 + V^2/254\varphi + L_3 + L_4} \quad (6)$$

It can be known from formula (6) that capacity can be regarded as a function between speed V and frictional coefficient φ. The higher the value of φ gets, the lower the value of braking distance L_2 will be. Thus, under the condition of the same speed, vehicles traveling with a higher value of φ can reduce the "safe space headway", so a higher value of capacity can be got. However, in the snowy conditions, the value of φ decreases significantly, which inevitably leads to the reduction of capacity.

When driving on the snowy roads, the driver had to keep a minimum distance from the car in front for the sake of safety. Therefore, study the relationship between headway L and speed V, select the frictional coefficient of the two kinds of ground surface and get the theoretical equation of the capacity in the two conditions:

$$C_s / C = \left(\frac{1000V_s}{V_s t/3.6 + V_s^2/254\varphi_s + L_3 + L_4} \right) / \left(\frac{1000V}{Vt/3.6 + V^2/254\varphi + L_3 + L_4} \right) \quad (7)$$

Judging from the above analysis, it can be seen that capacity reduces dramatically in snowy conditions and is greatly affected by the change of speed.

The modification of time in snowy conditions. Due to the change of capacity and the free-flow speed in snowy conditions, t_{0S} can't be expressed by L/V_S, it should accordingly be modified. Simulate the traffic operational characteristics in the typical road network in snowy conditions of the two different snowfall degrees by grey box theory. And then, according to the simulation results, deduce the linear functional relationship between the three modified parameters t_{0S}, L and V in different grades of roads. The mathematical models are as follows:

Table 2.The values of t_{0S} in snowy conditions

Grades of Road	$t_{0S} = f(L, V_S)$	
	Severe degree	Slight degree
Main trunk road	$t_{0S} = 1.084L/V_S$	$t_{0S} = 1.105L/V_S$
Secondary trunk road	$t_{0S} = 1.121L/V_S$	$t_{0S} = 1.162L/V_S$
Branch road	$t_{0S} = 1.176L/V_S$	$t_{0S} = 1.257L/V_S$

The impedance function in snowy conditions. Substitute the modified traveling time and speed as well as capacity into impedance function. Then, it is possible to obtain the impedance function in snowy conditions. Its expression is as follows:

$$t_s(q) = \eta t_{0S}\left[1 + \alpha(q/C_s)^{\beta}\right] \quad (8)$$

Where t_{0S} is the free-flow traveling time in snowy conditions; C_s is the capacity of road sections in snowy conditions; α, β are regression coefficients; η is the modified parameter of visibility in snowy condition.

The new impedance function in snowy conditions is simple and is easy to compute iteratively. What's more, the new impedance function can combine the computer technique Optional Input to establish the model. With the established model, traffic assignment in snowy condition would be realized.

ANALYSIS OF EXAMPLES

The sketch map of the road networks from the calculation example is shown in Figure 1; it is used to simulate the actual road network. The simulation of traffic demand is in the peak period. The road grade is divided into 3 parts: main trunk road, secondary trunk road, and branch road. The divisions of traffic zones and OD quantity are known. Based on the new impedance function after modification and stochastic user equilibrium, do traffic assignment in the road network of this calculation example in general and snowy conditions. Then the assignment results can be obtained in both conditions.

Compared with the traffic volume assigned in general conditions, it can be concluded that there are indeed changes when the traffic is assigned in snowy conditions. The related indexes of the assignment results are listed in Table 3 and 4.

It can be seen from Table 3 and Table 4, that when compared with general conditions, the trends of changes in both slight and severe snowfall conditions are the same, but the degree of changes in snowy conditions of severe snowfall is more strenuous. So, Table 3 is analyzed in that case. The value of $C \bullet L$ declines in snowy conditions. It means that the road service level decreases accordingly. Meanwhile, the average traveling speed in each grade of road slows down greatly, with 44.9% decline in main trunk roads, 49% decline in secondary trunk roads, and 57.6% decline in branch roads. The traffic volume in each grade of road doesn't follow the graded changing law, with 6.9% increase in main trunk roads, 1.2% increase in secondary trunk roads, but with 31.4% decrease in branch roads. The number of road sections reaching their saturation points appears to be in the increasing trend. The saturation degree in main and secondary trunk roads rises obviously, but it doesn't rise in branch roads. This is because the traffic volume in branch roads decreases as the branch road's capacity declines.

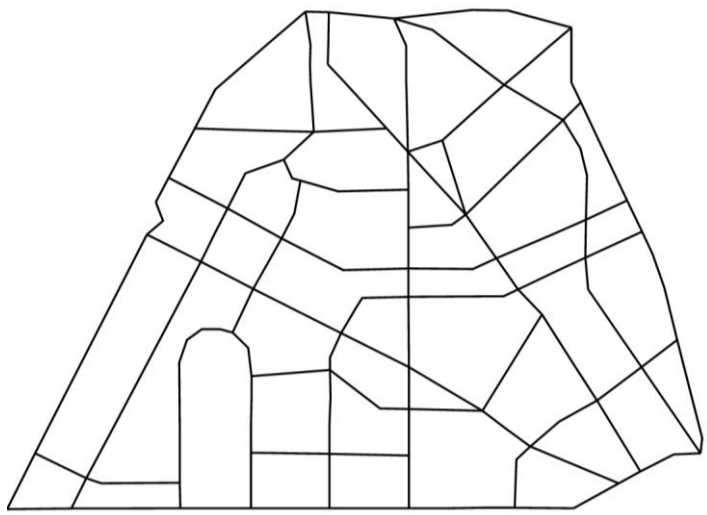

Figure1. The sketch map of the road network of the calculation example

Table 3. Indexes of assignment results in general conditions and slight

snowfall conditions

Road grade	C • L (puc • km/h)		The average traveling speed of road sections (km/h)		Traffic flow in each grade of roads (pcu/h)		The number of road sections reaching its saturation point	
	snowy	general	snowy	general	snowy	general	snowy	general
Main trunk road	41548	43936	12.1	16.7	311925	307995	44	38
Secondary trunk road	36982	39394	14.7	20.0	185374	184564	18	15
Branch road	9541	11165	10.5	17.2	33514	41014	7	7

Table 4. Indexes of assignment results in general conditions and severe snowfall conditions

Road grade	C • L (puc • km/h)		The average traveling speed of road sections (km/h)		Traffic flow in each grade of roads (pcu/h)		The number of road sections reaching its saturation point	
	snowy	general	snowy	general	snowy	general	snowy	general
Main trunk road	40502	43936	9.2	16.7	329368	307995	47	38
Secondary trunk road	34615	39394	10.2	20.0	186699	184564	21	15
Branch road	8351	11165	7.3	17.2	28135	41014	7	7

CONCLUSION

Judging from the theoretical analysis and the results of traffic assignment in the analysis of the calculation example in snowy conditions, it is concluded that the whole service level of the road network decreases. What's more, the average

traveling speed in each grade of roads also slows down, and it is in a way of decreasing by the order of branch roads, secondary trunk roads and main trunk roads. At the same time, the traffic flow also changes in each grade of road in the road network. It increases in both main and secondary trunk roads. The traffic flow has a great degree of increase in the main trunk roads but a sharp decrease in branch roads. In order to enhance the environmental adaptability of the road network, compared with the operational characteristics in general conditions, it is advised to reserve 10% capacity of the road network in main trunk roads and reserve 5% capacity in secondary trunk roads in snowy conditions. The values are obtained according to the analysis of the assignment results in the calculation examples. Thus doing, it can relieve the traffic pressure of the road network in special conditions, especially in snowy conditions, and it can also improve the environmental adaptability of the road network.

REFERENCES

Bernardin, Lochmueller and Associates, Inc. Anchorage (1995) Signal System Upgrade—Final report[M] .

Boer, Erwin R. (1999). "Car following from the driver's perspective"[J] . Transportation Research , (F2): 201-206.

Datla, Sandeep and Sharma, Satish. (2007). Impact of cold and snow on temporal and spatial variations of highway traffic volumes.

Eisenberg, Daniel. (2004). "Themixed effects of precipitation on traffic crashes"[J]. Accident Analysis and Prevention, (36): 637-647.

Goodwin, Lynette C. and Mitretek Systems, Inc (2002). Weather Impacts on Arterial Traffic Flow.

A Study on the Headway Distribution of the Xueyuan Roundabout

HAN Ping[1] and WANG Dian-hai[2]

[1]Transportation and traffic college, Jilin University, China; The School of Traffic and Transportation, Dalian Jiaotong University, China; P.C:116028; H.P:+86-13309846675; email: hp19720419@dl.cn
[2]Transportation and traffic college, Jilin University, China; P.C:130025; email: wangdianhai@sohu.com

ABSTRACT

The Cowan M3 distribution and its parameters are discussed based on four years of data observed from three approaches to the Xueyuan roundabout in Dalian to explore the suitability of the Cowan M3 distribution model. Already widely used around the world for capacity and performance analysis of roundabouts, the Cowan M3 distribution is explored to see if it correctly models the Xueyuan roundabout. By means of the goodness-of-fit test, it is concluded that the Cowan M3 distribution could be applied to the Xueyuan roundabout to analyze the headway of the traffic flow there. The minimum headway is between 0.38 seconds and 0.88 seconds, according to the observed data. As a result of vehicles experiencing free driving and a flow sharing priority, this 0.38s lower headway is observed and a higher proportion of free driving vehicles results when using the method of moments. There is a linear relationship between the proportion of free vehicles and the traffic volume. The results of this study are helpful in that they allow us to analyze the capacity and performance of the Xueyuan roundabout in Dalian.

Key words: roundabout, headway, the headway distribution, Cowan M3 distribution

INTRODUCTION

Headway is used to analyze traffic characteristics, capacity and performance for the roundabout. While analyzing the traffic characteristics, the distribution of the headway and of the special headway, the critical gap, can show information about vehicle arrival, vehicle lane changing, and how the traffic is moving. Also, when using the accept-gap theory in the capacity analysis of the roundabout, the distribution of the headway plays an important role. When analyzing performance, the distribution of the headway can be used to discuss delay. It is important to study how the traffic flow moves since a traffic jam affects roundabouts during peak volume times. This can hopefully have a positive

impact on roundabout operation and design.

A simple distribution, such as the negative exponential, has some disadvantages when trying to model the sharp peak and the long tail of the sample headway distribution. Instead, a composite distribution, like Cowan M3, is widely used for capacity and performance analysis of a roundabout like the Xueyuan. In this case, Cowan M3 is widely studied around the world.

The Cowan M3 distribution is the third of four distribution models (Cowan 1975). Akcelik, Hagring, and Troutbeck etc. researched the parameters of the Cowan M3 for an uncontrolled intersection and for roundabouts, and found that the τ parameter varied between 0.5 and 2.5s (Akcelik 1994, Hagring 1998). They also researched the relationship between the proportion of free vehicles (α) and the traffic flow ratio (q or τq), and found that there existed a linear or exponential relationship (Akcelik 1994, Tanyel and Yayla 2003). Hagring discussed the distributions for a simultaneous two-lane model, a superposed two-lane mode, and for a one-lane mode (Hagring 1998). Hagring also tested three methods for the estimation of parameters in the Cowan M3 distribution in a roundabout (Hagring 2002). Tanyel and Yayla discussed the parameters of the Cowan M3 distribution for Turkey and obtained a higher α because of the driver behavior experienced (Tanyel and Yayla 2003). In China, the Cowan M3 distribution, without being tested, was used to discuss the capacity of the roundabout in a recent year.

COWAN M3 DISTRIBUTION AND ANALYSIS METHODS

According to the studies of Cowan (1975), the Cowan M3 headway distribution model can be used in traffic engineering studies:

$$\text{Cowan M3:} \quad F(t) = \begin{cases} 0, t < 0 \\ 1 - \alpha e^{-\lambda(t-\tau)}, t \geq 0 \end{cases} \tag{1}$$

Where: λ is the decay constant
τ is the minimum headway between bunched vehicles
α the proportion of free vehicles.

The Cowan M3 distribution model is widely used in the capacity analysis of intersections without traffic signals. In this study, the Cowan M3 distribution and its parameters are applied to analyze the headway of traffic flow in the Xueyuan roundabout.

In order to determine the parameters of the Cowan M3 distribution, three different methods can be used: the method of moments, the maximum likelihood method, and the least squares method. Hagring stated that these methods normally provide reliable results and that they are quite easy to implement (Hagring 2002). Luttinen stated that the method of moments is an effective parameter estimation method and that it gives good results for α and λ, but that it should not be used to estimate τ (Luttinen 1999). Luttinen and Akcelik both stated that to choose a constant value for τ may be appropriate and that different τ values should be

determined for different traffic conditions (Luttinen 1999 and Akcelik 1994).

In this study, the method of moments is used in determining the parameters α and λ of the Cowan M3 distribution based on the observed τ. The following formula was used:

$$E(H) = \alpha(\tau + \frac{1}{\lambda}) \tag{2}$$

$$Var(H) = \frac{1}{\lambda^2} + (\tau + \frac{1}{\lambda})^2(\alpha - \alpha^2) \tag{3}$$

FIELD DATA COLLECTION

Field and Time. Data was collected for four years from the Xueyuan roundabout in Dalian, China. This intersection is one terminal of the Zhongshan road, the beginning of a highly technical district, and the unavoidable road to Lushun from the south (see Figure 1). As the highly technical and the Lushun districts continue to develop, the traffic flows of the three approaches of the Xueyuan roundabout is increasing every year. Traffic jams occur during peak traffic times more and more.

Observations are made by using video cameras positioned at a high building near the roundabout intersection where the view is adequate for observation. At least one hour of recordings are produced during the morning rush hour in May each year and the data is extracted from the recordings at the office.

Data Collection. At each intersection circle and approach, there are two or three lanes. In the study, the two or three lanes are treated as one lane. The headway is defined as the difference in time between when two vehicles in succession pass a common observed point through the same section of the roundabout, and which can provide an accessible opportunity. The time difference between two vehicles that arrived at the same time or almost at the same time is ignored since there is no opportunity and no gap between the vehicles. There were more than 500 pieces of data in each subset of each observed place.

From the data collected from the recordings and site observation, drivers did not pay attention to priority, so the phenomenon of sharing priority was also observed at the roundabout. Shared priority is the condition where the priority of the major-stream vehicles is not necessarily absolute and the minor-stream drivers accept relatively small gaps in the major stream to merge, causing major-stream drivers to have the need to decelerate or completely stop.

Figure1. The Xueyuan roundabout and observed place.

THE COWAN M3 DISTRIBUTION FOR THE XUEYUAN ROUNDABOUT

It is obvious that parameters of the Cowan M3 distribution are different in different regions due to local driver behavior. In this study, the parameters of the Cowan M3 distribution were investigated based on the observations made.

Minimum headway (τ). The minimum headway value has an important role in the validation of the Cowan M3 distribution. Studies have shown that headway values under 1.0 seconds are observed mostly between vehicles in different lanes on roads which have more than one lane.

Headway values are observed for major and minor streams and τ values are obtained by the data. From the data, the τ value can be chosen between 0.38 seconds and 0.88 seconds. The minimum headway value which was lower than 0.5 seconds was observed and the results can be seen in Table 1.

The λ parameter. The λ parameter can be defined as ‘‘the intensity of proportion of free vehicles on the traffic flow’’. In other words, the λ parameter shows the effect of the arrival of vehicles (Tanyel and Yayla 2003). The values of λ are obtained by using the method of moments. The results can be seen in Table 1.

Proportion of free vehicles (α). The proportion of free vehicles (α) is an important parameter that affects the structure of the Cowan M3 distribution. Thus, this parameter is strongly related to the τ parameter. The important decision to make is how to determine the proportion of free vehicles. In this study, the values of α were obtained by using only the method of moments instead of choosing the proportion of free vehicles. The results can be seen in Table 1. The values of α increase because the drivers travel freely and they do not care about shared priority.

Table 1. Parameters values according to the method of moments and observation.

Observed place	q(vps)	τ(s)	α	λ
XueYuan (circle1,06)	0.1542	0.75	0.8378	0.1424
XueYuan(circle2,06)	0.2112	0.88	0.8546	0.2133
XueYuan(circle3,06)	0.4668	0.58	0.754	0.4395
XueYuan(circle3,07)	0.4346	0.38	0.9061	0.1964
XueYuan (circle1,08)	0.471	0.58	0.657	0.4973
XueYuan(circle2,08)	0.5466	0.54	0.7863	0.5574
XueYuan(circle3,08)	0.591	0.46	0.7918	0.5889
XueYuan (approach 1 05)	0.4644	0.42	0.8218	0.2612
XueYuan (approach 2 05)	0.3122	0.75	0.7259	0.3707
XueYuan(approach 3 05)	0.4811	0.42	0.6743	0.4453
XueYuan (approach 1 06)	0.5167	0.46	0.5681	0.2880
XueYuan (approach 2 06)	0.3955	0.46	0.8029	0.2792
XueYuan(approach 3 06)	0.6133	0.5	0.6349	0.4338
XueYuan(approach 3 07)	0.6054	0.42	0.6529	0.4146
XueYuan (approach 1 08)	0.6883	0.42	0.6542	0.3257
XueYuan (approach 2 08)	0.4277	0.46	0.8174	0.3163
XueYuan(approach 3 08)	0.7056	0.46	0.6909	0.3991

Relationship between the proportion of free vehicles and volume. According to the studies of Troutbeck, Akcelik, and others, there is a linear relationship or an exponential relationship between the proportion of free vehicles (α) and the traffic flow ratio (q or τq) (Akcelik 1994, Tanyel and Yayla 2003). The regression analysis was done between α and τq for all data groups. The graphic can be seen in Figure 2. There was linear relationship. The equation obtained is given below:

For all the data: $$\alpha = 1.004 - 1.1328\tau q \quad (4)$$

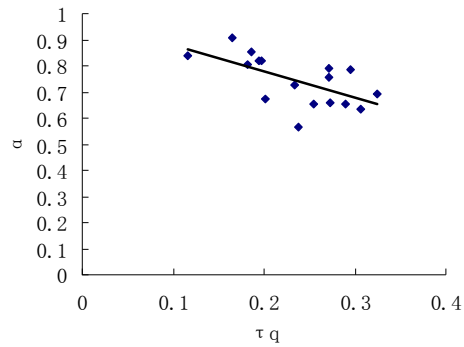

Figure 2. The relationship between α and τq.

Goodness-of-fit test. Once the parameters of the Cowan M3 distribution have been estimated, a goodness-of-fit test is needed to test whether the estimated distribution function is the distribution that has generated the sample.

*H*0: observed sample of headways from Cowan M3 (estimated distribution) (5)

Because the interest of this study is on the tail of the distribution, it is only necessary to test the null-hypothesis, Eq. (5) for $t > \tau$. In this study, χ^2 tests are used as well. The results show that all the subsets accept the null-hypothesis. Hence, the Cowan M3 distribution is fit for the headway distribution of the Xueyuan roundabout in Dalian. For example, the distribution of approach 1 in '06 was shown in Figure 3.

CONCLUSION

The Cowan M3 distribution model is found to be fit for the observed headways in the Xueyuan roundabout of Dalian. The result provides a basis to analyze the capacity and performance of the roundabout. The investigations on the parameters of the Cowan M3 distribution, the lower headway and the higher proportion of free vehicles, have shown that there is some difference between driver behavior in Dalian and driver behavior in other areas.

In order to achieve better results, a more detailed study on the parameters of the Cowan M3 distribution model, such as on the methods for parameter estimation, on the proportion of free vehicles, and on the relationship between the proportion and volume, should be conducted. The number of examples should be increased in order to gain a good result.

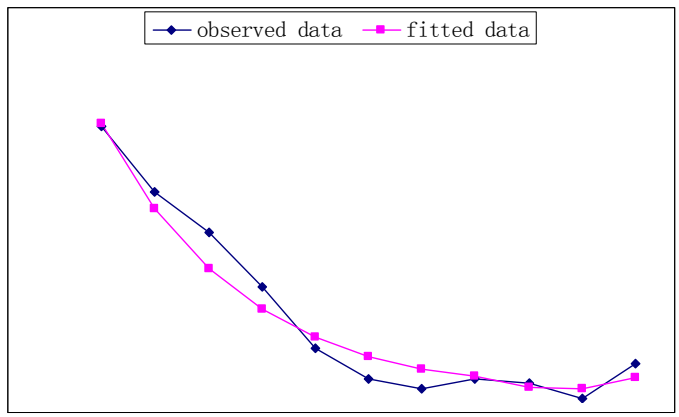

Figure 3. The observed data and M3 distribution.

REFERENCES

Cowan (1975). "Useful headway models". *Transportation Research* 9(6), 371–375.

AKÇELIK, R. and CHUNG, E. (1994). Calibration of the bunched exponential distribution of arrival headways. *Road and Transport Research* 3 (1), 42-59.

Hagring (1998). ‘‘A further generalisation of Tanners formula.’’ *Transportation Research Part B,* 32 ,423–429.

Serhan Tanyel, Nadir Yayla (2003). “A discussion on the parameters of Cowan M3 distribution for Turkey” *Transportation Research Part A*, 37, 129–143.

Hagring (2002).” Estimation of Parameters in Distribution of Headways in Roundabouts” *Journal of Transportation Engineering* vol 128, no.5 September 1,403-411.

Luttinen, R.T., (1999). “Properties of Cowan M3 headway distribution.” In: Transportation Research Board 1999 Annual Meeting Preprints. TRB, Washington DC, USA.

Troutbeck, Kako (1999). “Limited priority merge at unsignalized intersections” *Transportation Research Part A,* 33 ,291-304.

Study on Intersections with Median BRT Stations: Focused on Pedestrian Street-Crossing Characteristics*

ZHANG Ruhua[1], ZHU Xianyuan[2] and LEI Li[3]

[1]Ruhua Zhang, Transportation Research Center, Shandong University, Jinan250061, China; TEL (370) 893-9951; email: ruhua_zhang@163.com
[2]Xianyuan Zhu, Traffic Engineering Department of Shandong University, Jinan250061, China; TEL (358) 904-0174; email: kamen1984@163.com
[3]Lei Li, School of Energy and Power Engineering, Shandong University, Jinan 250061, China; email: leili@sdu.edu.cn

ABSTRACT

Median busways have caused many pedestrian crossing problems, especially when the bus station is placed beside an intersection. The Lishan Road station, which is set beside an intersection, is adopted as the case study for the analysis of pedestrian crossing characteristics. The pedestrian crossing characteristics found near the Lishan Road station are different from the characteristics seen at intersections without a busway in a number of ways. There is a larger pedestrian volume, the pedestrian arrival rate on the road sides obey the Negative Binomial Distribution, the passenger arrival rate in the middle of the road, influenced by the Bus Rapid Transit (BRT) operation, is impulsive and its cycle and peak value are not stable, the walking speed of pedestrians can be modeled by a normal distribution, and the walking speed on the crosswalk proximal to the BRT station is 7% higher than that of the distal. Since the setting up of BRT stations, the pedestrians' violation times has increased by 10-15%. The main reasons for this increase include the increase of pedestrian volume and the pedestrian desire to catch a bus causes the pedestrian to disregard any danger. The pedestrian crossing characteristics analysis in this paper can serve as a reference for signal-timing, policy making and the setting up of management facilities.

Key words: Median busway, pedestrian crossing, pedestrian crossing characteristics

FOREWORD

Research background. Median busway Bus Rapid Transit (BRT) systems should pay more attention to the issue of the street crossing of passengers, especially in the case of locating bus stations at intersections where passengers use crosswalks to cross the street. At intersections like these, traffic flow is intermixed with a large number of pedestrians and passengers. The trip purposes and routes of

pedestrians and passengers interweave and conflict because their behaviors have obvious differences. As bus passenger volume increases, the phenomenon of the interweaving and interference between pedestrians and passengers is becoming more acute, influencing an intersection's operation and also disturbing the implementation of the bus priority policy.

Currently, BRT systems are at their early stages in China, and there have been only a few studies on the issue of passengers crossing the street. Literatures (Gao Yangbing et al. 2005; Ma Wangjing 2007) have studied on the passengers street crossing facilities design and pedestrian phases combination design for median BRT station. However, these papers are only focused on a conceptive analysis and lack basic data. This study starts with the survey data, analyzes the pedestrian street-crossing characteristics, including walking speed, arrival regularity, and violation behavior, and provides data to aid in the design of passenger street-crossing facilities and signal optimization.

Study Object. The object of this study is the median BRT station which is located at the edge of an intersection and extended from the center of a crosswalk to form a "T" shaped region. This region is regarded as the research object. This study focuses on pedestrian street-crossing characteristics (as shown in Figure 1).

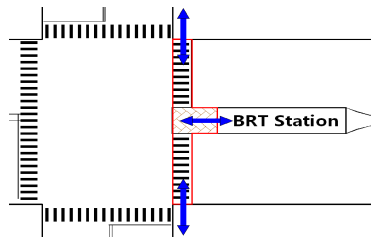

Figure1. Research object.

CROSSING PEDESTRIAN WALKING SPEED

The intersection of Lishan Road and Wenhuaxi Road is chosen as the study case. The equation for pedestrian street-crossing speed is as follows:

$$v_c = l_c / t_c$$

Where: v_c is the pedestrian street-crossing speed,
l_c is the length of the crosswalk, and
t_c is the time used to cross the street, excluding the delay in the street-crossing process.

Windows Movie Maker is used to collect t_c.

Pedestrian street-crossing speed. SPSS was used to analyze the pedestrian street-crossing speed and the statistical data is shown in Table 1. The street-crossing speed distribution histogram with a normal curve is shown in

Figure 2.

Table 1. Statistical Data of Pedestrian Walking Speed (Overall) (Unit: m/s).

Sample Size	Min. Value	Max. Value	Mean	Median	15th percentile	Standard Deviation	Variance
320	0.54	2.34	1.253	1.20	0.96	0.321	0.103

The fifteenth percentile is 0.96m/s, which is different from the 1.1m/s documented by HCM. The reasons for this include: (a) the main trip purpose is for purchasing because of a nearby Super Market and (b) the existence of the BRT station results in a severe interweaving of pedestrians and passengers, leading to a decrease in walking speed. By comparing the speed distribution histogram and the normal curve shown in Figure 2, we can see that the speed distribution is anisomerous. The peak value is found on the left. After transforming the survey data into a logarithmic model, and outputting the lognormal distribution Q-Q, we get Figure 3.

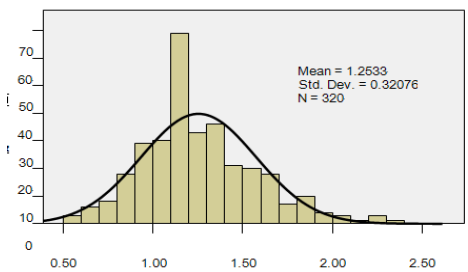

Figure2. Histogram of speed.

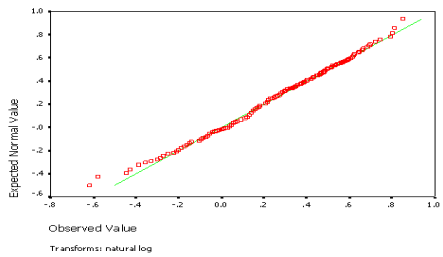

Figure3 . Normal Q-Q plot of speed.

According to Figure 3, the expected value and observed value anastomose very well. A goodness-of-fit test is performed on the converted speed using Kolmogorov-Smirnov. The outcome, shown in Table 2, shows the sample significance level to be greater than 0.05. As a result, it obeys a normal distribution and $\log X \sim N(1.253, 0.32)$.

Table 2. Kolmogorov-Smirnov test table for pedestrian speeds' logarithmic transformation.

Degree of freedom	Mean (m/s)	Standard deviation	Kolmogorov-Smirnov statistic value	Significance level
320	1.253	0.32	0.88	0.435

BRT stations' influence on walking speed. The BRT station on Lishan Road has an entrance on two sides. As a result, the passenger volume is different in each of the four crosswalks in that intersection. In order to study the BRT station's influence on pedestrian walking speed, the two crosswalks with the largest

difference in walking speed are chosen for a comparison: a) the northern crosswalk linking to the BRT station that has the largest passenger volume of the four crosswalks and b) the southern crosswalk farthest from the BRT station with a passenger volume small enough to assume that the pedestrian walking speed is not influenced by the passengers. The statistical results are shown in Table 3 below:

Table 3. Speed distributions of northern and southern crosswalk (Unit: m/s).

Location	Mean value	Standard deviation	Median	Min. Value	Max. Value	15th per-centile	Sample size
Northern crosswalk	1.22	0.31	1.16	0.54	2.34	0.93	179
Southern crosswalk	1.30	0.32	1.25	0.65	2.25	1.04	141

The average walking speed on the northern crosswalk is seven percent lower than that of the southern crosswalk. The fifteenth percentile speed on the southern crosswalk is 1.04m/s, which is almost the same as the speed stated in the HCM, 1.1m/s. Therefore, the BRT station has little influence on pedestrians using the southern crosswalk. However, the average pedestrian walking speed on the northern crosswalk is 1.22m/s and the fifteenth percentile speed is 0.93m/s, which is much lower than that of the southern crosswalk. Tables 5 and 6 show the speed distribution of the two crosswalks. The northern crosswalk walking speed is more discrete. There are two influencing factors leading to this phenomenon: a large pedestrian volume and the interweaving of and interference between pedestrians and passengers.

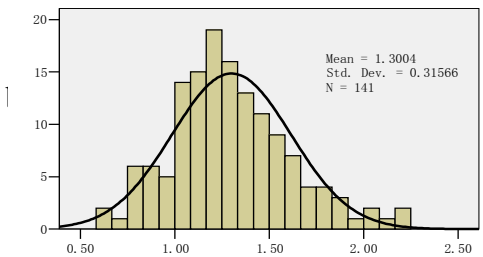

Figure 4. Histogram of speed. (Southern crosswalk)

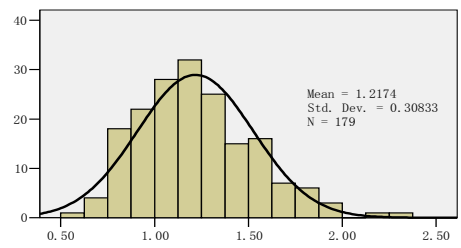

Figure 5. Histogram of speed. (Northern crosswalk)

Relationship between passenger volume and walking speed. According to the study above, the increase of passenger volume and interweaving of pedestrian flows are the two main factors influencing walking speed. However, different quantities of passenger volume have different levels of influence on walking speed. Consequently, this study chooses three time zones with different passenger volumes to analyze the influence level at different passenger volumes. The statistical results are shown in Table 4.

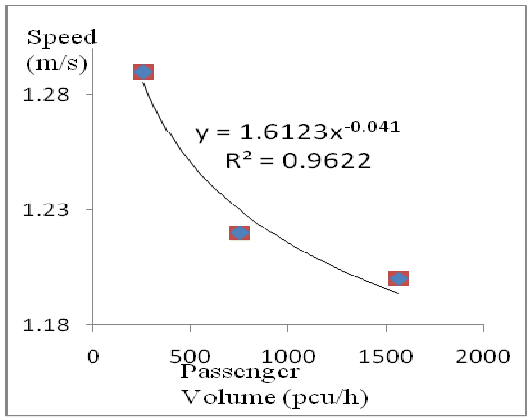

Figure 6. Relation between passenger volume and speed.

Table 4. Passenger Volumes' Influence on Walking Sp eed (Unit: m/s).

Time zone	Mean	Standard Deviation	Median	Min. Value	Max. Value	15th per-centile	Passenger Volume
1	1.29	0.29	1.22	0.68	2.34	0.94	256
2	1.22	0.33	1.20	0.67	2.21	0.92	750
3	1.20	0.35	1.15	0.54	1.94	0.92	1564

Passenger volume is closely related to walking speed. The walking speed decreases with the increase of passenger volume. The relationship between the two factors is not linear, but instead exponential. Due to the limited sample size, the speed for large passenger volumes could not be speculated.

Conclusion. Two conclusions are drawn from the above analysis: (a) the walking speed on the crosswalk which is linked to the BRT station is much lower than that of other crosswalks and (b) passenger volume is an important factor that influences the walking speed. Different sizes of passenger volume have different levels of influence on walking speed. The relationship between passenger volume and walking speed is exponential.

PASSENGER FLOW ARRIVAL REGULARITY

The arrival regularity is the basic rule of traffic movement, and provides support for the design of pedestrian traffic control systems. The arrival of pedestrians at a signalized intersection is random and is described by a discrete distribution of probability theory. The literature, specifically the work of Qu, Zhou, and Wang in 2004, has shown that the pedestrian arrival at intersections located near a business district obeys a negative binomial distribution. However, there have been few studies on the arrival regularity of BRT passengers alighting on a safety island.

General test. Select a non-holiday evening peak traffic time to collect data and use a sample interval of ten seconds. The survey data consists of two parts: (a) the number of pedestrians on the road-side (crossing street pedestrians and passengers included) and (b) the volume of passengers arriving at a safety island after getting off from a BRT, as shown in Figure 1. The statistical data is in Tables 5 and 6. After calculating the distribution model, apply it to the goodness-of-fit test. The goodness-of-fit test process is as follows:

(1) H0: Assume the arrival regularity obeys a negative binomial distribution.

(2) Set up the statistics: $x^2 = \sum \frac{(f_i - F_i)^2}{F_i}$;

(3) Test results: Look up the table, and then get the value of X^2_d. At the confidence level of 95%, accept the hypothesis H0 because the X^2 value of pedestrians on the roadside is less than X^2_d, and refuse the hypothesis H0 because the X^2 value of passenger flow on the median road is greater than X^2_d.

Table 5. Lishan Road & Wenhuaxi Road Intersection Arrival Rate Statistics.

Location	Avg.Volume (pcu/10s)	Variance	p		^{2}	^2_d	Sample Size
Road-side	4.367	7.748	0.56	5.64	10.52	16.9	360
Median-side	1.189	8.538	0.14	0.19	28.44	11.07	362

Therefore, the arrival regularity of pedestrians on the roadside obeys a negative binomial distribution, namely:

$$P(x) = C^{5.64-1}_{x+5.64-1} 0.56^{5.64} (1-0.56)^x, x = 0,1,2,\ldots 15$$

Where: x is the number of the arrival pedestrians.

The arrival regularity of passengers. From the last section, we can see that the arrival regularity of passengers on an average road is not in accordance with the negative binomial distribution, so this study selects other fitting methods.

The number and arrival law of passengers on an average road are jointly decided by the service frequency, rated capacity of BRT vehicles, and the number of passengers. Generally, the departing time interval of a successful BRT system abroad does not exceed one minute, assuming that the departing time interval is average and the arrival law of BRT passengers will show cyclically. However, the irregularity of vehicle arrival leads to uncertainties in passenger arrival because of the influence of intersection traffic lights and of the platform stopping time. Figure 8 shows the arrival rate of passengers at the observation periods and has a pulse and randomness in the cycle and peak. After analyzing the survey data, the sample data can be divided into two categories. The first category is one in which

no passengers arrive at the observed time, and the second is one in which passengers arrive at the observed time. Then, analyzing the second category, we get a pulse wave with a pulse width of four and a pulse amplitude of nine, based on the least square method (as shown in Figure 8).

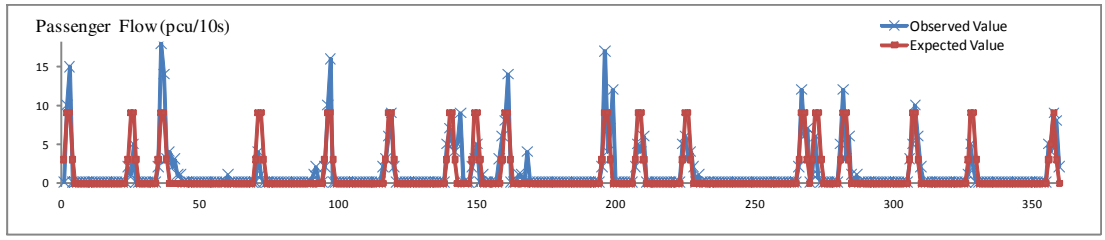

Figure 8. Passengers'arrival regularity.

Summary. First, the roadside pedestrian arrival conforms to the negative binomial distribution, but the median passenger arrival rule is obviously affected by the roadside passengers and does not conform to the negative binomial distribution. Second, the arrival of median passengers reflects a certain pulse character, but the pulsed-wave is not a perfect fit because of the high arrival of BRT vehicles with irregular coefficients.

VIOLATIONS

Generally speaking, the proportion of violations is about ten to fifteen percent higher after a BRT station is established. This data is shown in Table 6. The main reason for this increase in violations is that passengers become more concentrated, and the accumulation of passengers increases their sense of security. Subsequently, when the waiting time is more than what is acceptable to a pedestrian, that pedestrian will attempt to cross the crosswalk out of turn, and others will follow him or her. Passengers violate in order to catch BRT.

Table 6. Pedestrian Violations before and after BRT establishment.

Intersection	No BRT stations set (2007.11)	BRT stations set (2007.12)
Lishan- wenhuaxi	7.2%	19.9%
Lishan-jiefang	8.6%	12.5%
Lishan-heping	6.6%	10.9%

CONCLUSIONS AND OUTLOOK

When medium BRT stations are located at an intersection, the arrival regularity of pedestrians on roadsides conforms to a negative binomial distribution. Passenger arrival regularity is significantly different from the roadside design, and it is constrained by BRT vehicles and shows a certain degree of impulsiveness and randomness. The average pedestrian walking speed is 1.25

m/s and the fifteenth percentile walking speed is 0.96m/s, significantly different from the 1.1m/s stated in HCM. This is due to passenger interference. Considering the investigation time, the specific environment and that the sample size is limited, the data should not be used as a standard. However, it can serve as a reference for urban signal control at intersections in a mixed-traffic situation. From the above analysis, it can be concluded that the method proposed in this paper is feasible.

REFERENCES

Gao, Yangbing, Li, Xuhong and Yandong Zhu (2005). "Research on the Adaptability of Median Busway for Bus Rapid Transit." Urban transport of China. 3(1):9-14.

Ma, Wangjing (2007). "Research on bus signal priority control system for busway." Doctor Thesis.

Qu, Zhaowei, Zhou, Lijun and Haidian Wang (2004). "Bicycle and Pedestrians' Arrival and Departure Characteristics at Signalized Intersection." Journal of Highway and Transportation Research and Development. 21(8): 91-95.

The Analysis of Transportation Demand Generation Mechanisms of the Urban Agglomerations in China

Dong Zhi[1],Wu Bing[2] and Li Linbo[3]

[1,2,3]Key Laboratory of the Education Ministry of Road and Traffic Engineering, Tongji University. Shanghai 201804, China; email: 65dongzhi@tongji.edu.cn

ABSTRACT

The emergence and development of urban agglomerations is an inevitable trend of the rapid urbanization. Exploring the mechanism of transportation demand generation is the basis of transportation planning of urban agglomerations. Combined with the reality of urban agglomeration, the factors which impact the transportation demand generation in urban agglomerations are classified into the origin factors, promoting factors and inhibitory factors. This paper studies the transportation demand generation mechanism on both passenger transportation and freight transportation. The research findings identify the characteristics of the transportation demand generation of urban agglomeration in China.

1. Introduction to the Development of Chinese Urban Agglomeration

Due to the rapid development of urbanization, urban agglomerations emerge in the worldwide area. French geographer Jane • Gottman proposed the concept of Megalopolis in the year 1957 and a large number of domestic and foreign scholars devote to conduct related research afterwards. The first relevant monograph in China is "Chinese Urban Agglomeration" written by Yao Shimou. According to this monograph, urban agglomeration can be defined as a relatively complete city "aggregates", which is in specific geographical area with a considerable number of cities with different features and relied on the natural environmental conditions. Urban agglomeration usually has one or two super-or mega-cities as the core of the regional economy and contains modern transportation modes, accessible integrated transport network, as well as the highly-developed information network. (Yao Shimou, 1992)

Chinese urbanization process is speeding up and a group of urban agglomerations, represented as the Yangtze River Delta Urban Agglomeration, the Pearl River Delta Urban Agglomeration and the Beijing-Tianjin-Hebei Urban Agglomeration have formed. Urban agglomeration in the southeastern region of China, where the urbanization level is relatively high, is now in the stage of rapid development, while the central and western urban agglomerations are is continually forming and evolving.

2. Concept of Transportation Demand

In the monograph "Transportation Economics" written by Chen Yilong, transportation demand is defined as a kind of need with necessary capacity to pay in a

certain period of time on the movement of goods and passenger in social-economic living under a certain price level (Yilong Chen, Shao Zhenyi, 1999) .Transportation demand of urban agglomeration should be the need which is in favor of the economic and social development of urban agglomeration and the necessary displacement of people and goods. It is closely linked with all aspects of urban agglomeration development.

3. Analysis on Influencing Factors and Characteristics of Transportation Demand Generation of Chinese Urban Agglomeration

3.1 Classification of Transportation Demand of Urban Agglomeration

Transportation demand generation mechanisms of urban agglomerations aim at exploring the factors influencing transportation demand generation and the interactive process. Transportation demand of urban agglomeration is mainly divided into the passenger demand and freight demand, which have large differences in origination due to their different targets. Freight transportation demand can be divided into origin demand and induced demand. The generation of origin demand is the result of the uneven geographical distribution of natural resources which required by the social-economic activities in the urban agglomeration or among the urban agglomerations. Induced demand comes from the clear specialization of city functions and the separation of production and consumption in space. Passenger demand of urban agglomeration can be divided into the productive demand and consumed demand according to different travel purposes. Productive demand is related with the activities such as production, exchange and distribution, for example, the travel induced by various orders, sales, technical exchanges, and financial and labor activities in the urban agglomeration. Consumed demand makes consumption as the travel purposes, such as visiting relatives and friends, and taking holiday.

3.2 Analysis of the Factors Influenced the Transportation Demand Generation of Chinese Urban Agglomeration

3.2.1 Origin Factor

Origin factors, the primary power to generate transportation demand, come from the human instinct to survive and the difference in regional resource. First of all, the displacement of people and goods are born required. The resources and production to maintain human survival are distributed in various geographical regions in the urban agglomeration. No region can provide all the necessary resources; only through the transportation activities can the resources be obtained. Transportation activity is one of the human production and living activities.

Secondly, the uneven distribution of natural resources is objective geographical situation in China. 87% of Chinese proved coal concentrates in the Northern region; iron ore is mainly distributed in Hubei, Liaoning and Sichuan Province. (Peng Tang,2006) This uneven distribution of natural resources generates transportation demands in the urban agglomeration and among the urban agglomerations especially.

3.2.2Promoting Factor

(1) Specialization of urban development

The position of every city in the social productive activities in urban agglomeration is different. They resume different functions, and the core cities and their surrounding cities and towns can complement with each other on the functions. Goods, services, capital, information and commuting will form a close two-way contact. Specialized division of labor in society enhances the contact intensity within the urban agglomeration. With the continuous expansion of production scale, the economic collaborations and co-operations among the cities are strengthened, and a variety of economic entities have become more closely linked. The chance and frequency of movement of people and goods are increased, so that transportation demand is continuous generated and changed.

(2) Urban aggregation and diffusion

Urban aggregation refers to the flowing of socio-economic elements from non-city area to the city area or from the small and medium-sized cities to the core cities in the urban agglomeration. Urban diffusion is reflected in the impact caused by the urban development will influence adjacent area and the regional economic area and stimulate the economic and transportation development of adjacent area. In particular, the economic core city promotes the development of the entire urban agglomeration by technology diffusion, exportation of capital, industry diffusion and exemplary role through transportation services.

(3) Urban population movement

According to statistics, the cause of internal migration flows in urban agglomeration varied and the migrant workers take the larger proportion, this is because sustained and rapid economic growth of urban agglomeration attracts enormous scale migration of population. The scope of migrating is related to the level of economic development. From the sample from the census data can be seen that migrating population of Beijing-Tianjin-Hebei agglomeration, which the economical level is higher, possesses 73% of the whole population, while the proportion is 9% in Chengdu Plain agglomeration and the population is mainly migrating among the cities and towns in the urban agglomeration.

Because of the unique Chinese cultural traditions, thus there is difference in working, rest time, the period of holiday, and social organization structure and management practices. For instance, on the eve of annual Chinese Spring Festival, a large number of outside workers would return to their hometown to celebrate the Chinese New Year, so that enormous transportation demand is caused in the urban agglomerations. Influenced by the internal layout and related socio-economic factors, inter-city commuter flow in the urban agglomeration is constantly arising and growing. Some workers choose the way of life like migratory birds, such as some people in the Yangtze River Delta urban agglomeration choose to live in Jiangsu or Zhejiang Province but work in Shanghai.

(4) The improvement of residents' income level and consumption level

Urban agglomeration is the place where economic power and population gather and the as a gathering place and the improvement of income level and consumption level are more obvious than in other regions. According to the survey in the first half of the year 2008, average income level of Changsha, Zhuzhou and Xiangtan urban agglomeration is 27.3% higher than that of the entire Hunan Province. The overall consumption of central Plain Urban agglomeration is 85% more than that of the Henan Province. Purchasing ability is depended on the national income level, with the improvement of purchasing ability, the demand of required productive materials is increased and new integrated transportation demand is generated as well. The adjustment to consumption structure results in the increased demand in visiting relatives, resting, travelling and etc...

(5) Perfecting of transportation system of urban agglomeration

Perfecting of the transportation network can improve the accessibility and so that new demand is generated. In the same premise, the area which has better geographic location and more convenient transportation service would process more opportunities on external transportation links, thus the possibility of produced transportation demand is relatively high. The relevant developed urban agglomeration in China, such as the Yangtze River Delta urban agglomeration and the Pearl River Delta urban agglomeration, have a natural geographical advantage, diverse and convenient transport facilities, good port conditions which could promote international trade, resulting in a wider scope transportation demand.

3.2.3 Inhibitory Factor

(1) The shortage of transportation infrastructure of urban agglomeration

Transportation infrastructure is the basis of the economic development of urban agglomeration and the important conditions for the transportation demand generation. The shortage of transportation infrastructure and the incompletion of transportation structure would lead to the high transportation cost and reduction in transportation timeliness, thereby people's economic activities are confined to a small geographical space, and then people's transportation demand is inhibited.

(2)Rise in transportation charge and reduction in service quality

Changes in transportation charge would impact on the integrated transportation of urban agglomeration, especially the passenger demands. When the charge increase, some traveler would give up travelling so that these demand can not produced. The influence of the quality of transportation services is also large; travelers are expected to obtain good services. Low quality transportation services would fail to meet their expectations and requirements and they may reduce the demand, and therefore for this part of transportation demand is inhibited.

(3) Partition in regional administrative management

Regional transportation administration involves the administrative center, economic center and transportation center, etc. .

The non-cooperative phenomenon like local governments making their own decisions, duplicated construction and price competition are usually. Because of the partition of national transportation management system, regional transportation planning is decided by different transportation department, which has significant limitations. Partition in administrative regions blocks the horizontal movement of productive factors. Influencing factors on transportation demand generation of the urban agglomerations in China can be concluded in Figure1 below.

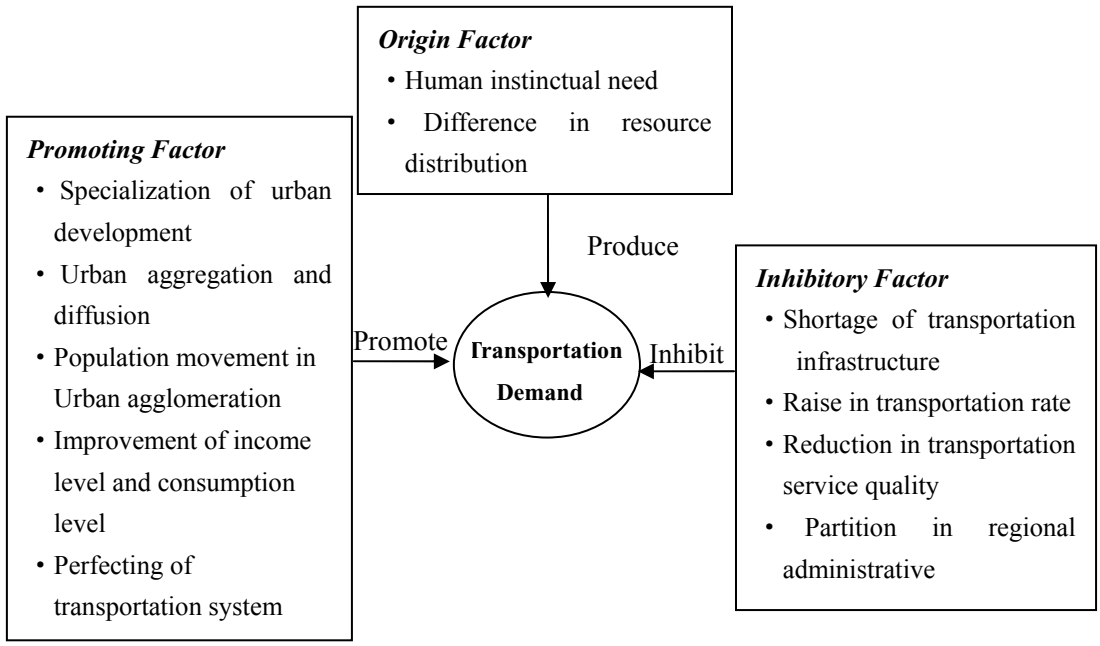

Figure1. Influencing Factors on Transportation Demand Generation of the Urban Agglomerations in China

3.3 Characteristics of transportation demand generation of urban agglomeration

The characteristics of urban agglomeration can be reflected in non-equilibrium in space and time, diversity and economic restrict.

3.3.1 Non-equilibrium in space and time

The transportation demands of urban agglomeration is uneven in space and time. From the perspective of space, uneven distribution of resources within urban agglomeration and urban specialized development introduce the regional difference in transportation demand generation. Take the Pearl River Delta urban agglomeration as an example, the distribution ratio of both freight transportation demands and passenger transportation demands of Guangzhou are head among all the cities, which are 35.66% and 27.65% respectively. The least distribution ratios of freight transportation demands and passenger transportation demands are appeared in Zhuhai(3.2%) and Huizhou(3.81%). From the perspective of time, cyclical individual movements, cyclical economic development and seasonal production and consumption lead to the transportation demand generation over time.

3.3.2 Economic constraints

When travelers have the expectation to move, the economic consideration and judge are inevitable. However, the considerations of different travelers are diverse, such as the length of time, the value of goods, the level of the transportation rate and etc. Competition of transportation markets in urban agglomeration and the adjustment to the transportation rate influences the freight demand. Therefore, under the economical restrict on transportation demands, the choice on transportation time and modes of different travelers is random, so that the transportation demand generation is fluctuated with the price.

3.3.3 Diversity of transportation demand generation

With continuously shortened inter-city distance time, there are different demands in the choice of travelling time, and modes according to different income levels, trip purposes and preferences. The requirements on the quality of transportation service are inevitable. These requirements are directly reflected in the choice made by travelers when they receive transportation services, and thus individual behavior has impact on the transportation demand generation.

4. Conclusion

Research on the transportation demand generation mechanism of urban agglomeration is the basis of transportation demand forecast of urban agglomeration. In this paper, transportation demand of Chinese urban agglomeration is investigated, and origin factor, promoting factor and inhibitory factor which influence the generation of transportation demand are proposed and discussed. The mechanism of transportation demand generation is further discussed and the characteristics of transportation demand generation is studied. It not only supplements the existing transportation demand theory, but also plays a vital role in configuring transportation modes, forming effective transportation capacity and improving integrated transport system of urban agglomeration.

REFERENCES

Jean.Gottman. (1961). “Megalopolis: the Urbanized Northeastern Seaboard of the United States” New York, the Twentieth Century Fund.

Zhu Zhao Hong, Yang Dongyuan, Wu Bing. (2007). “Transportation Planning of Urban Agglomeration”. Tongji University Press.

Yao Shimou. (1992). “Chinese Urban Agglomeration”. Chinese Science & Technology University Press.

Yilong Chen, Shao Zhenyi. (1999). “Transportation Economics”. People's Transportation Press.

Peng Tang. (2006). “The Characteristic and Influence of the Migrating People in Chengdu Plain Urban Agglomeration” Building of Sichuan Press.

Wang Qingyun. (2006). “The Theory and Practice of Transportation Development”. China Science&Technology Press.

Study on Residential Daily En-route Travel Choice Behavior with Traffic Information: Application of RP/SP Joint Survey and Disaggregate Model

ZHANG Yi[1], YUN Meiping[2], YANG Xiaoguang[3]

[1]Department of Traffic Engineering, College of Traffic and Transportation Engineering, Tongji University. No.4800 Cao'an Road, Shanghai, 201804; PH (Fax) (8621) 6958- 8994; email: darrenzhy@gmail.com

[2]Department of Traffic Engineering, College of Traffic and Transportation Engineering, Tongji University. No.4800 Cao'an Road, Shanghai, 201804; PH (Fax) (8621) 6958- 4674-803; email: yunmp@mail.tongji.edu.cn

[3]Department of Traffic Engineering, College of Traffic and Transportation Engineering, Tongji University. No.4800 Cao'an Road, Shanghai, 201804; PH (Fax) (8621) 6958- 9475; email: yxgits@vip.sina.com

ABSTRACT

En-route travel choice behavior is one of the primary travel behavior over residential daily trips. Providing traffic information will exert an impact on en-route travel choice behavior. Through comparative studies, the paper reveals that RP/SP joint survey and the disaggregate model are two suitable methods. On the basis of that, the paper develops a scheme for RP/SP joint survey and a Multinomial Logit (MNL) Model for modeling and analysis. The aim of the paper is to provide theoretical and practical support for the research of en-route travel choice behavior with traffic information in China.

KEYWORDS

En-route travel choice behavior; Traffic information; RP/SP joint survey; Disaggregate model

1. Background

The application of Intelligent Transportation Systems (ITS) has facilitated transportation system operations. As an important component of ITS, traffic information systems help travelers to enhance their travel reliability by providing effective traffic information. In recent years, traffic information service is developing in China and the travelers' behavior is changing accordingly. To research the characteristics and evolution mechanisms of the changes of travel behavior will help to make better use of traffic information service and enhance the efficiency of transportation systems.

The travel behavior of a trip could be considered as two parts, i.e., pre-trip

travel behavior and en-route travel behavior. En-route travel choice behavior is one of the primary travel behavior of residential daily trips. The en-route travel behavior of a single trip is mainly route choice. Considering a trip chain which links all trips in a day, the en-route travel behavior would be more complex than that of a single trip. The two most commonly accepted definitions of a trip chain are (Primerano et al. 2008): (1) a sequence of trip segments beginning at the "home" activity and continuing until the traveler returns "home" and, (2) a sequence of trip segments between a pair of anchor activities "home" and "work" or "school". Therefore the en-route travel behavior of a trip chain includes destination choice, travel mode choice, departure time choice, route choice, etc. Providing traffic information in a timely manner will make an impact on en-route travel choice behavior and bring changes to it. The data for the research is collected by specific surveys and the analysis is conducted based on appropriate models. Through comparative studies, the paper reveals that the RP/SP joint survey and the disaggregate model are two suitable methods. The paper further develops the survey scheme for a RP/SP joint survey and a Multinomial Logit (MNL) Model.

2. Research Progress in China

The research of traditional travel behavior has conducted for several decades. In recent years, the research on travel behavior with traffic information has been newly emerging. For example, Pei Yulong (2006) compared "the characteristics of trip and the regularity of information used before and after the information age, and concluded tendencies of trip development" (PEI et al.2006), Juan Zhicai (2008) discussed "the positive role and limitation of traffic information in order to provide correct cognition and reasonable thought of using traffic information for planning management department" (JUAN et al. 2008). At the same time, due to the limitation of data resources, analysis methods, etc., the overall progress of the research in China still appears to be macroscopic, with the general characteristics concluded as following:

(1) The survey data is insufficient as it's collected from household travel surveys but not specific surveys.

(2) The analysis methods needs to be updated from the current "four-stage" aggregate method to a disaggregate method so that the characteristics of individuals could be better revealed.

(3) The research findings stay at the descriptive level with less microscopic analysis.

Therefore, this study will focus to design a proper survey scheme for necessary data and apply appropriate models to analyze the data.

3. Application of RP/SP Joint Survey

3.1 RP Survey and SP Survey

The first stage of research on en-route travel behavior with traffic information is to conduct a survey for collecting necessary data. Generally, there're two kinds of surveys, the traditional Revealed Preference Survey, i.e., RP Survey and the emerging Stated Preference Survey, i.e., SP Survey.

In a RP survey, the data colleted is about the choices in real conditions of people's daily life. The parameter calibration of models based on such data is more reliable. On the contrary, a SP survey aims at revealing people's subjective preference in assumed conditions. Nowadays traffic information service is not widely used in China and the survey sample for a RP survey is not big enough for modeling. Therefore, a RP/SP joint survey is suggested in the research so as to combine the advantages of RP Survey and SP Survey and collect necessary data.

3.2 RP/SP Joint Survey

Compared to a RP survey or a SP survey, it's important to carry on the division and integration processes in a RP/SP joint survey. The division process is to divide the questionnaire into a RP part and a SP part. The integration process afterwards is to integrate different data from RP and SP survey so as to ensure its application in same models. The design of a RP/SP joint survey involves four steps: (1) determining variables, (2) classification of attributes, (3) determining attribute level and, (4) designing detailed survey scheme.

The main purpose of a RP survey part in a RP/SP joint survey is to collect personal attributes, including gender, age, occupation, income, travel mode, travel time, etc. These attributes are classified into different levels. In this study the age, occupation, income, travel mode are classified into five, six, six and seven levels respectively in the questionnaire.

The main purpose of a SP survey part is to collect data about characteristics of inhabitants' en-route travel behavior with traffic information. Assumed that inhabitants will receive sufficient en-route sufficient traffic information, the survey reveals their behavior including travel mode choice, departure time choice, route choice, etc.

To enhance the efficiency of SP surveys, it's recommended to optimize the questionnaire with mathematical method such as the Uniform Design Method (Guan 2004). At the same time the overall accuracy of collected data should be maintained. To better integrate RP and SP survey data, it's recommended to introduce scale parameter and anisotropic parameter and to obtain appropriate data for modeling (LIU et al. 2008).

4. Application of Disaggregate Model

4.1 Aggregate Model and Disaggregate Model

The models in common use are divided into aggregate model and disaggregate model. Survey data is collected from different traffic zones and processed with statistical methods, and then parameter calibration of an aggregate model could be obtained. But aggregate model doesn't represent choices of individual travelers well. Therefore it's not suitable for the research of en-route travel behavior with traffic information.

Disaggregate method is developed on the basis of Probability Theory. Compared to aggregate model, disaggregate model uses survey data directly without additional processing and is able to represent the choices of individual travelers. Therefore disaggregate model is more appropriate in travel behavior research, including departure time choice, pre-trip path choice, and en-route response to traffic information (Moshe et al. 2007).

4.2 Application of MNL Model

4.2.1 Construction of MNL Model

Logit Model is a binary choice disaggregate model used for prediction of the probability of occurrence of an event. It is a generalized linear model used for binomial regression. It makes use of several predictor variables that may be either numerical or categorical. Multinomial Logit Model, i.e., MNL Model is a kind of Logit Model in common use. MNL Model has a simple form and is easy to understand. The choice probability is between 0 and 1 and the sum of choice probability of all alternative parts is 1. Therefore MNL Model is suitable for research on en-route travel choice behavior with traffic information. The model is give by the following expression:

$$P_{in} = \frac{\exp U_{in}}{\sum_{i=1}^{j} \exp U_{in}}$$

where P_{in} is the choice probability of travel behavior i by traveler n, U_{in} is the utility of travel behavior i by traveler n, j is the number of different travel behavior, $0 < i \leqslant j$。

The linear model to determine U_{in} is give by the following expression:

$$U_{in} = \theta_0 + \theta' X_{in} = \theta_0 + \sum_{k=1}^{K} \theta_k X_{ik}$$

where U_{in} means the same as above, $X_{in} = [X_{in1}, X_{in1}, \cdots, X_{ink}, \cdots, X_{inK}]$ is

eigenvector of travel behavior i by traveler n, X_{ink} is the kth eigenvector of travel behavior i by traveler n, K is the number of eigenvectors, $\theta' = [\theta_1, \theta_2, \cdots \theta_k]$ is the undetermined vector parameter, θ_k is the kth parameter of characteristic variables.

4.2.2 Definition of Numbers of Travel Choice Behavior and Eigenvector

In research of en-route travel choice behavior with traffic information, travel choice behavior is defined as following: changing destination, changing route, changing travel mode, changing departure time of next trip and canceling next trip. Thus j equals 5. The eigenvector X is defined as personal attributes collected from the RP survey, including the following eight ones: gender, age, family size, occupation, income, trip purpose, travel mode and travel time. Thus K equals 8. With the data from a RP/SP Joint Survey and a MNL Model, the following analysis could be processed successfully.

5. Conclusion

With the development of traffic information service in China, it's necessary to research residential pre-trip and en-route travel behavior with traffic information. RP/SP joint survey and disaggregate model are two suitable methods. The RP/SP joint survey is a proper method to collect necessary data and the survey scheme should be carefully designed. The disaggregate models is another effective method for modeling in the research of travel behavior. Among disaggregate models, the MNL Model is proposed in the paper. The aim of the paper is to provide theoretical and practical support for travel choice behavior research and help make better use of traffic information service and enhance the efficiency of transportation system.

6. Acknowledgement

This research is supported by National Natural Science Foundation of China from project "Optimization and management of urban transport network (No. 70631002)" and project "Research on mechanism of route guidance utility (No.70501023)". The authors give acknowledgement to the above support.

References

David A. Hensher. (1994). "Stated preference analysis of travel choices: the state of practice." *Transportation*, 21(2): 107-133.

GUAN Hong-zhi. (2004). *Disaggregate model: a tool of traffic behavior analysis*, China Communications Press, Beijing.

JUAN Zhi-cai, and XIAN YU Jian-chuan.(2008). "Research on activity-travel

decision behavior with effect of traffic information." *China Journal of Highway and Transport*, 21(4): 97-102.

LIU Zhi-ming, DENG Wei and GUO Tang-yi. (2008). "Application of disaggregate model based on RP/SP survey to transportation planning." *Journal of Transportation Engineering and Information*, 6(3): 59-64.

Moshe Ben-Akiva, Jon Bottom, Song Gao, et al. (2007). "Towards disaggregate dynamic travel forecasting models." *Tsinghua Science and Technology*, 12(2): 115-130.

PEI Yulong, and MA Ji. (2006). "Survey and analysis of the information impact on urban trips." *Journal of Harbin Institute of Technology*, 38(2): 721-725.

Primerano F, Taylor MAP, Pitaksringkarn L, et al. (2008). "Defining and understanding trip chaining behaviour." *Transportation*, 35(1): 55-72.

A Particle Swarm Optimization Algorithm for Bilevel Programming Models in Urban Traffic Equilibrium Network Design

Hu Hui

Transportation and Economics Institute, Economics and Management School, East China Jiaotong University, P.O.Box, 330013, Nanchang; PH(086)-0791-7045027; email: hh24895@163.comm

ABSTRACT

A new algorithm is proposed to solve one usual model of bilevel programming models in urban transportation equilibrium network design. The upper model is solved by PSO and the lower model is solved by Frank-Wolfe, then iterations are continuously progressed between them so that the global optimum solution can be approximated. The algorithm is illustrated with an example and compared with other algorithms. Results demonstrate that the effectiveness of this algorithm, while iterations and extra computational burdens are not so heavy.

Key words: Equilibrium Network Design; Bilevel Programming Model; Frank-Wolfe; PSO Algorithm

INTRODUCTION

With a better understanding of urban transportation equilibrium network design problem, the bilevel programming model has been recognized as an ideal tool for transportation network design and a variety of bilevel models and solving algorithms have been developed. Gao Ziyou (2004), and Meng Qiang (2005) made a synthetic survey of its application in transportation network planning design and pointed out that the main difference among various bilevel programming models lied in constraints and upper/lower goal functions. Multiple combinations of different upper goal functions and different lower user behavior choice models make various bilevel models. Simultaneously, the solving algorithms of these models were summarized and non-numerical optimization algorithms are worth further investigations in Gao's studies. Meng attempted to give unified models and algorithms to solve bilevel programming model.

In this paper, a new algorithm based on PSO (Particle Swarm Optimization) is proposed to aim at solving a usual bilevel programming model in urban transportation equilibrium network design and it can provide reference for solving other bilevel programming models.

BILEVEL PROGRAM MODEL

One of bilevel programming models in transportation equilibrium network design is as below:Minimizing the sum of system impedance and investment in the whole

transportation network from the angle of system and decision-makers. Meeting user equilibrium principle criterion from the users' point of view. And these two rules can be expressed as the following bilevel model:

Upper model:

$$\min Z = \sum_{a \in A} t_a[f_a(y), y_a] f_a + \theta_a \sum_a G_a(y_a)$$

$$s.t. \quad y_a \geq 0, \forall a \in A$$

Lower Model:

$$\min Z \sum_{a \in A} \int_0^{x_a(y)} c_a(x, y) dx$$

$$s.t. \quad \sum_{k \in K} f_k^{ij} = q_{ij}, \forall i \in I, j \in J \qquad (1)$$

$$x_a = \sum_{ij} \sum_k f_k^{ij} \delta_{ak}^{ij}, \forall i \in I, j \in J, k \in K, a \in A \qquad (2)$$

$$f_k^{ij} \geq 0, \forall i \in I, j \in J, k \in K$$

The symbols in the above model are denoted as follows:

A: set of routes a in transportation network;

$t_a(f_a(y), y_a)$: impedance function of route a;

$G_a(y_a)$: investment function of route a,given an increased capacity y_a;

y_a: increased capacity of route a;

y: increased capacity of routes in network, they're decision variables in upper model;

θ_a: coefficient matching investment and system impedance.

K: path set from origin node i to destination node j in network;

I: origin nodes set;

J: destination nodes set;

q_{ij}: traffic demand between origin node i and destination node j;

c_a: transport cost in route a;

x_a: traffic flow volume of route a;

x: traffic flow volume of routes in network, they're decision variables in lower model;

f_k^{ij}: traffic flow volume of the path k in OD i-j pair.

δ_{ak}^{ij}: where δ_{ak}^{ij}=1 if route $a \in K_{ij}$, otherwise 0;

The constraint (1) represents the balance relationship among route traffic flow and OD demand; the constraint (2) reflects the associate linkage between route traffic flow and path traffic flow.

If one of solutions is provided (the increased vector of routes capacity) in upper model, it can be used in lower model then the lower model will become a standard user equilibrium assignment problem which can be solved using Frank-Wolfe algorithm, and the route traffic flow x will be got.

MAIN PROCEDURE OF PSO-BASED BILEVEL PROGRAMMING MODEL

It's challenging to solve the bilevel programming model, especially for the no-linear model which is a NP hard problem. The more the variables are in the model, the more difficult it is to search the global optimum solution. By analyzing and comparing various solving algorithms for known bilevel models, a new algorithm based on PSO and continuous iteration is proposed in this paper. The upper model can be solved by PSO and the lower level can be solved using Frank-Wolfe, then continuous iterations are progressed between upper model and lower model so that the optimum solution can be approximated.

PSO (Particle Swarm Optimization) is an intelligent random optimum algorithm developed by Kenndy and Eberhart who were enlightened from birds' seeking food. Although it has been used widely, PSO has its shortages, such as local minimum solutions, and convergence velocity slowing down at a later stage. So, many improved algorithms were proposed to avoid these shortcomings. One of them is based on random disturbance which can escape local optimum points and improve convergence performance.

Every solution is one of particles in searching space for optimum problems, and every particle has its adapting value (usually optimum function) which can be evaluated for the particle position. Particles in the population adjust their positions and velocities by pursuing two extreme numbers (one is the individual optimum solution Pbest, the other is the population optimum solution Gbest) in the iteration searching process. For bilevel model in urban transportation continuous equilibrium network design, the main procedures of algorithm based on PSO are as below:

Initialization Solution (increased routes' capacity). Position and velocity of Particles can be got according to population scale N, variable numbers. The random matrix is as followed:

$$\begin{bmatrix} y_{11} & y_{12} & \cdots & y_{1n} & v_{11} & v_{12} & \cdots & v_{1n} \\ y_{21} & y_{22} & \cdots & y_{2n} & v_{21} & v_{22} & \cdots & v_{2n} \\ \cdots & \cdots & \cdots & \cdots & \cdots & \cdots & \cdots & \\ y_{N1} & y_{N2} & \cdots & y_{Nn} & v_{N1} & v_{N2} & \cdots & v_{Nn} \end{bmatrix}$$

$\{y_{ij}, i = 1,2,\cdots N, j = 1,2,\cdots n\}$ denotes the position of particle i is j, in the model it's

the initial value of increased route capacity between $[R_{1j,}R_{2j}]$ ($R_{1j,}R_{2j}$ is the upper and lower limit for particle j) . v_{ij} is the corresponding velocity which can be a random number between $[v_{\min,}v_{\max}]$ or $[R_{1j}*u,R_{2j}*u]$(u is the coefficient between 0 and 1. And the current position (current solution) is set *Pi* for particle *i*, while *Pg* is set for the best position (best solution) in the initial population which can be obtained by comparing all particles goal value.

For all particles in the population, the following operations are executed:

① Positions and velocities are updated according to the following formula:

$$v_{ij}(t+1) = w*v_{ij} + c_1r_1(pbest_i(t) - y_{ij}(t)) + c_2r_2(Gbest_i(t) - y_{ij}(t))$$

$$y_{ij}(t+1) = y_{ij}(t) + v_{ij}(t+1)$$

w is a weighted coefficient, its value can be 0.1-0.9, or set a linear value between the maximum and minimum. The convergence performance can be got better if w is diminished by iteration. So, if maximum weighted coefficient and minimum weighted coefficient are set $w_{\max}, w_{\min}$ respectively and $iter, iterMax$ is the iterations and sum iterations for $iter, iterMax$, the calculation formula will be: $w = w_{\max} - iter \times \frac{(w_{\max} - w_{\min})}{iterM\,\mathrm{ax}}$.

c_1, c_2 is the learning factor, their value can be set 2; r_1, r_2 is a random number between 0 and 1.

②Solving the lower model: Using the particle i's position y_i (the solution of upper model) for lower model, the route flow volume x_i can be got by Frank-Wolfe which is a standard algorithm in traffic flow assignment.

③Using x_i , y_i in upper model, the adapting value can be got for particle i.

④If the adapting value of particle i is better than the individual optimum solution Pbest, the current position y_i will be updated while the lower model optimum solution will be x_i ; If the adapting value of particle i is better than the all particles'

best solutionGbest, then Pg is replaced by the current position y_i while the lower model best solution is x_i.

Decide whether the convergence criterion can be met. If met, the global solution is exported, the algorithm ends. Or, a random disturbance is initialized for optimum solutions so that optimum solution is updated, and return step (2) to continue.

CASE STUDY

To confirm the validity of the algorithm above mentioned, the example used in the Li Zongping's paper（2004） which confirmed his SA algorithm is selected for comparisons. The road network in the example is depicted as the figure 1:

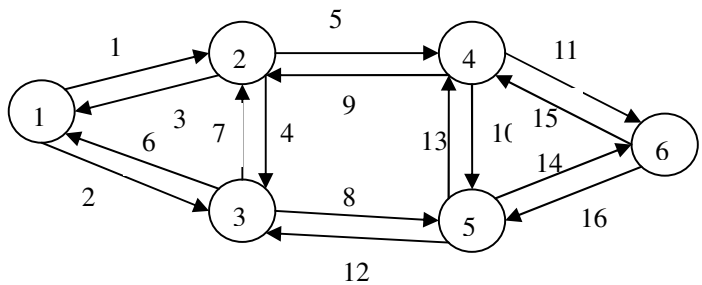

Figure 1. The Diagram of the Road Network

There're 2 OD pairs, 6 nodes, 16 routes. The OD demand is 10 between node 1 and node 6, while OD demand is 20 between node 6 and node 1. The impedance function is: $t(f_a, y_a) = A_a + B_a[x_a / (K_a + y_a)]^4$, the goal function is: $Z = \sum_a [t_a(x_a, y_a)x_a + \theta_a y_a]$, the parameters of routes are provided as the following table. The parameters of the algorithm are: population is 20, iteration is 40, learning factor c1,c2 is set 2, maximum weighted inertia value is 0.9, minimum weighted inertia value is 0.1. Concreted execution code is written in Matlab7.1 environment, the final result is given by comparing MNOS, EDO, simulation annealing algorithm as followed table 2.

Table 1 The Parameters of Road Impedance in Network

Route	A_a	B_a	K_a	θ_a
1	1	10	3	2
2	2	5	10	3
3	3	3	9	5
4	4	20	4	4

Table 2 Results Comparison of Different Algorithms

5	5	50	3	9
6	2	20	2	1
7	1	10	1	4
8	1	1	10	3
9	2	8	45	2
10	3	3	3	5
11	9	2	2	6
12	4	10	6	8
13	4	25	44	5
14	2	33	20	3
15	5	5	1	6
16	6	1	4.5	1

Route	MNOS	EDO	SA	PSO
y1				
y2	4.61	4.88		4.6175
y3	9.86	8.59	10.1740	9.8952
y4				
y5				
y6	7.71	7.48	5.7769	7.3707
y7		0.26		
y8	0.59	0.85		0.5931
y9				
y10				
y11				
y12				
y13				
y14	1.32	1.54		
y15	19.14	0.26		
y16	0.85	12.52	17.2786	20
Z	557.14	540.74	528.497	523.3811
N		12	24300	1160

Note: Z is the goal value of upper model function, N is the numbers using Frank-Wolfe solving flow assignment problem, the blank represents the increased capacity of route is zero. From the table 2, we can conclude that the PSO algorithm is better than other algorithms. Compared to SA, the iterations are less, while for EDO is not suitable for large scale transportation network although its' iteration is less.

CONCLUSIONS

A new algorithm based on PSO for a usual bilevel programming model is designed and the main procedures are developed in this paper. A study example is investigated. The calculation results are compared with other algorithms and the findings demonstrate the effectiveness of this algorithm.

ACKNOWLEDGEMENT

This research work has been funded by East China Jiaotong University Research, Project Num 08JG05.

REFERENCES

Gao Ziyou, Zhang Haozhi, Sun Huijun (2004). Bi-level Programming Models, Approaches and Applications in Urban Transportation Network Design Problems. *Journal of Transportation Systems Engineering and Information Technology.* 2004.4(1):35-44.

Lv Zhensu, Hou Zhirong (2004). *Particle swarm optimization with adaptive mutation*. Acta Electronica Sinica, 2004, 32(3): 416-420.

Li Zongping, Li Bing (2004). A Simulated Annealing Algorithm for Urban Transportation Continuous Equilibrium Network Design. *Systems Engineering*.V2004.2(22):87-91.

Meng Qiang, Li Dehong (2005). Transport Bilevel Programming Problems:Unified Models and Algorithms. *Journal of Transportation Systems Engineering and Information Technology.* 2005.5(4):120-140.

Zhao, Zhigang, Gu Xinyi, Li Taoshen (2007). Particle Swarm Optimization for Bilevel Programming Proble. *Systems Engineering Theroy & Practice*. 2007,8,(27):92-98.

Study on Interregional Transportation Infrastructure Integration Planning in China

LI Chaoyang[1] and ZHANG Yi[2]

[1]Department of Architecture, School of Naval Architecture, Ocean and Civil Engineering, Shanghai Jiao Tong University. No. 800 Dongchuan Road, Shanghai, 200240; PH (Fax) (8621) 6281- 3386; email: cyljjf@tom.com

[2]Department of Traffic Engineering, College of Traffic and Transportation Engineering, Tongji University. No.4800 Cao'an Road, Shanghai, 201804; PH (Fax) (8621) 6958- 8994; email: darrenzhy@gmail.com

ABSTRACT

Due to the lack of integrated planning of interregional transportation infrastructure, the development of interregional transportation system is restricted in China. Based on qualitative analysis and quantitative forecast, this paper analyzed general methods regarding demand forecast, organization planning and infrastructure integration of Interregional Transportation Infrastructure Integration Planning in China. Also this study applied the methods into practice in Suzhou City. The evaluation showed the methods were effective and applicable. This research provides theoretical and practical support for interregional transportation infrastructure integration planning.

KEYWORDS

Interregional transportation infrastructure; Integration planning; Qualitative analysis; Quantitative forecast; Urbanization

1. Introduction

Due to the lack of integrated planning of interregional transportation infrastructure, the development of interregional transportation systems is restricted (An 2003). This problem appeared in China with the rapid socio-economic development and has attracted nationwide attention. Many researchers have achieved fruitful research findings to address this problem. QUAN Yongshen, et al. (2007) emphasized on the development of regional transportation networks to solve the fundamental urban transportation problems. YANG Junyan, et al. (2007) indicated that the coordination of interregional transportation infrastructure was an important part of regional coordination of Yangtze River Delta. Li Jiawei, et al. (2008) developed a method to emphasize the integration of urban agglomeration transportation infrastructure.

Previous research findings indicated that the integration of interregional transportation infrastructure is of great importance not only for interregional transportation systems but also for socio-economic development in China. Currently, Interregional Transportation Infrastructure Integration Planning (ITIIP) is newly emerging throughout China. Based on qualitative analysis and quantitative forecast, this paper analyzed general methods of demand forecast, organization planning and infrastructure integration of ITIIP in China. Then this study applied the methods into practice in Suzhou City. The evaluation showed the methods were effective and applicable. This research provides theoretical and practical support for interregional transportation infrastructure integration planning.

2. Content of Integration Planning

The aim of ITIIP is to achieve integration at three levels: interregional transportation development strategies, organization patterns and infrastructures (Xi et al. 2007). As shown in Figure 1, the ITIIP includes several parts. Among them, interregional transportation demand forecast, interregional transportation organization planning and interregional transportation infrastructure integration planning will be discussed in this paper.

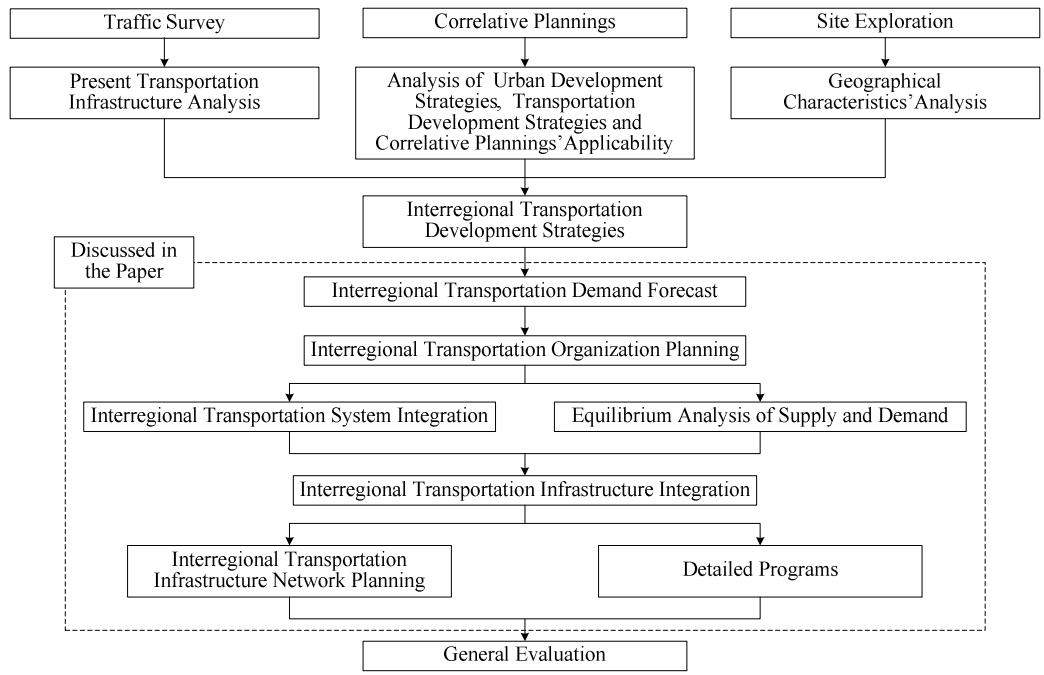

Figure 1. Flowchart of integration planning.

3. Demand Forecast, Organization Planning and Infrastructure Integration

3.1 Interregional Transportation Demand Forecast

3.1.1 Interregional Trip Generation Forecast

The ratio of interregional trip in daily trip is closely related to connection patterns of two districts. The patterns appear to be strong, intermediate or weak according to land-use, mobilization level, urbanization level, etc. When the land-use of each district is not mixed enough, it may result in a high ratio of interregional trips. When the land-use is properly mixed the ratio becomes reasonably low. As the mobilization and urbanization level is not high in China, the intermediate pattern is recommended for Chinese cities in the long run. Accordingly the ratio is about 50%. The model of interregional trip generation forecast is given by the following expression:

$$K_i = P_i \cdot F_i \cdot \alpha_i \varepsilon_i$$

where K_i is the interregional trip generation of District i on peak hour, P_i is the population of District i, F_i is the times of daily trip per capita of District i, α_i is the peak hour factor of District i, ε_i is the ratio of interregional trip generation in daily trip.

The population, times of daily trip per capita and peak hour factor could be obtained from correlative plannings such as Urban Master Planning and Comprehensive Transportation Planning. Then the interregional trip generation could be forecasted.

3.1.2 Interregional Travel Modal Split Forecast

At present, a large part of interregional trips in China are non-elastic and the options of travel mode are limited. Therefore existing methods for forecasting interregional travel modal split are not well applicable in integration planning. We recommend a forecasting method with a combination of qualitative analysis and quantitative forecast. Qualitative analysis is a macro-level method considering key factors including present travel modal split, development trends of urban layout and transportation system. Quantitative Forecast is a micro-level method based on the results of travel survey.

3.2 Interregional Transportation Organization Planning

Interregional transportation organization planning contains two parts: interregional transportation system integration planning and equilibrium analysis of supply and demand of interregional transportation infrastructure. The interregional transportation organization planning brings forward an ideal transportation organization pattern among districts to realize sustainable development of interregional transportation systems. As non-motorized traffic is still a primary composition of transportation systems in China, both motorized and non-motorized traffic should be taken into account in organization planning. The goal of equilibrium analysis of supply and demand is to examine whether the supply will

completely meet the demand and find out where the infrastructure supply is deficient. The equilibrium analysis should cover all modes of interregional transportation including non-motorized traffic, public transportation and so on.

3.3 Interregional Transportation Infrastructure Integration

The interregional transportation infrastructure integration contains two parts. The macro-level part is to determine the interregional transportation infrastructure network and the micro-level part is to put forward detailed programs. The macro-level part intends to establish overall scale and layout of interregional transportation infrastructure. The result of equilibrium analysis should be fully considered. The micro-level part puts forward programs to newly-construct or reconstruct infrastructure. The reconstruction programs contain route lines' optimization, widening alteration and key nodes' reconstruction. In addition, recommended and backup programs by stages should be included.

4. Practice in Suzhou City

The study area of an ITIIP in Suzhou City includes Gucheng District, Suzhou New District, Xiangcheng District, Wuzhong District, Suzhou Industrial Park, Changshu City and Wuxi City. The objective is to integrate interregional transportation infrastructure across the borders among these districts. The base year is 2006 and the targeting year is 2020. The strategy is to build a "New Suzhou Interregional Transportation System" in accordance with interregional transportation demand and socio-economic development. The interregional transportation demand in intermediate connection patterns in 2020 is forecasted and the O-D distribution is shown in Figure 2. The recommended interregional transportation organization is shown in Figure 3.

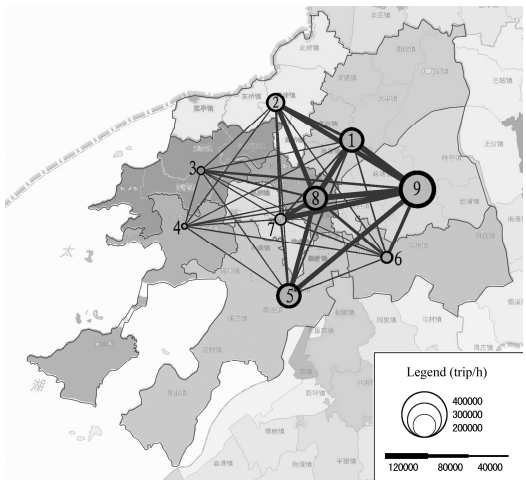

Figure 2. O-D distribution in intermediate connection pattern in 2020.

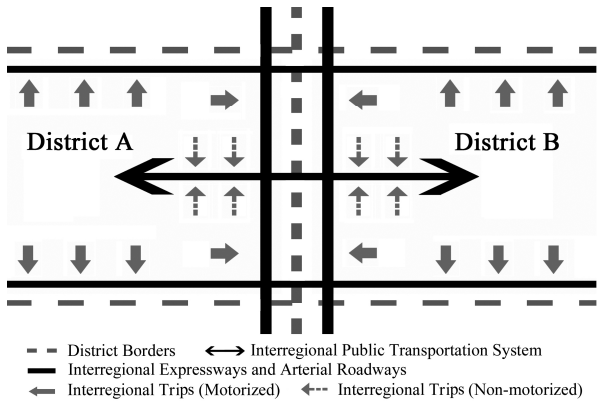

Figure 3. Recommended interregional transportation organization in 2020.

According to the equilibrium analysis of supply and demand, out of six borders, three borders' infrastructure supply will not meet the demand in 2020. The scale and layout of the infrastructure over these four borders need to be expanded. At the same time, the scale and layout of the infrastructure over other six borders need to be examined and optimized. The overall scale, layout and detailed improvement plans are listed in Table 1 and Table 2.

Table 1. Overall Scale of Interregional Transportation Infrastructure.

Borders	Railway	Rail Transit	Freeway	Urban Expressway	Arterial Road
Gucheng District-Suzhou New District	2	2	1	3	15
Gucheng District-Xiangcheng District	/	2	1	2	12
Suzhou New District-Xiangcheng District	2	1	3	5	8
Suzhou New District-Wuzhong District	/	1	1	3	23
Suzhou City-Wuxi City	3	1	4	2	3
Xiangcheng District-Changshu City	1	1	1	2	3

The general evaluation shows that the planning will raise the supply of interregional transportation infrastructure by 14.5% and improve the Level of Service (LOS) of interregional transportation systems by one grade. After the planning, the interregional transportation demand of 2020 will be well met, which will support the urbanization and socio-economic development of Suzhou City.

Table 2. Numbers of Detailed Programs.

Classification of Detailed Programs	New construction	Route lines' optimization	Widening alteration	Key nodes' reconstruction
Numbers of Detailed Programs	9	8	4	3

5. Conclusion

The integration planning includes demand forecast, transportation organization planning, transportation infrastructure integration, etc. By applying new methods, the interregional transportation demand could be well forecast. The processes of organization planning and infrastructure integration should be paid special attention to so as to adapt to the rapid development in China. A practical Integration Planning in Suzhou City provided valuable experience for further research. The practice also showed the Integration Planning would be helpful not only to interregional transportation system but also to socio-economic development in China.

References

An Xiaopeng. (2003). "The innovation on the supply system for the infrastructure of urban region in China." *Planners*, 19(7), 78-81.

Li Jiawei, Liu Binglian. (2008). "Study on the system paths for transportation infrastructure integrated development of urban agglomeration." *Logistics Technology*, 27(4), 5-7.

Quan Yongshen, Liu Ying, Chen Jinchuan. (2007). "Discussion on urban transportation issues & countermeasures." *Urban Transport of China*, 5(4), 5-9.

Xi Bao, Martin de Jong. (2007). "Infrastructure network integration and trans-regional governance - Harbin-Daqing-Qiqihar Industrial Corridor Case and Songhua River Water Crisis Case." *Journal of Public Management*, 4(4), 17-30.

Yang Junyan, Chen Wen. (2007). "Investigation of fatal issues in regional coordination of Yangtze River Delta." *City Planning Review*, 31(9), 17-23.

Repositioning of Empty Containers in the Transpacific Market: A Case Study

Yu Zhang[1], Cristiano Facanha[2]

1. Assistant Professor, Civil and Environmental Engineering, University of South Florida, 4202 E. Fowler Ave. ENB118, Tampa, FL 33620; PH (813) 974-5846, FAX (813) 974-2957; email: yuzhang@eng.usf.edu
2. Senior Associate, ICF International, 394 Pacific Avenue - 2nd Floor, San Francisco, CA 94111; PH (415) 677-7124; email: cfacanha@icfi.com

ABSTRACT

Although empty containers can be a great asset to a shipping company if they are strategically positioned, their transportation, handling, and storage represent considerable burdens that impact the company's profits. Trade imbalances between the U.S. and other regions of the world, especially Asian countries, have worsened the situation, and the intermodal coordination of empty containers has become a very challenging issue for shipping lines. The topic represents a very complex logistics problem with practical applications. The analysis focuses on one of the top seven shipping companies globally that is particularly strong on the transpacific trade market. The main goal was to model the operations of the company and introduce new strategies to reposition empty containers more efficiently. The concept of rail terminals should be implemented to provide economies of scale to reduce costs. Ports on the East Coast, which are currently not utilized to transport empty containers back to Asia, also played a role in the strategies considered in this study. The results indicated that the proposed repositioning plan would provide significant cost savings. Further sensitivity analysis is necessary for assessing the performance of the plan. Other complementary strategies, such as the use of a dedicated fleet of trucks to handle local transportation, could be introduced, and the cost-benefit should be compared for practical implications, as well as to improve the proposed model.

Key words: Logistics, Repositioning of Empty Containers, Shipping Line, Operational Strategy

BACKGROUND

One of the major trade problems that have arisen during the last few years, especially on the transpacific market, is the container imbalances between U.S. imports and exports. Their interference with the two-way operations has affected the finances of most shipping companies. The transportation, handling, and storage of empty containers have augmented carriers' overhead costs. The effects are even being felt in Asia, where the internal movement of containers has also suffered (Hanscom 1998). The economic growth in China has greatly contributed to this problem. During the last few years China has rapidly increased its exports to the U.S. (becoming the first source of U.S. imports), while their imports have increased at a slower pace.

An average of 250,000 containers is sent empty from North America back to Asia annually. Shipping costs related to the water portion of the trip are waived as ships have the extra capacity to carry the empty containers back to Asia. The capital

invested in this extra capacity (both in terms of containers and vessels) is not included in the previously mentioned repositioning costs. The latter are mostly composed of transportation (road and rail), handling (mainly at ports, but also at rail terminals) and inventory costs. The transpacific flow of empty containers is handled through four ocean terminals on the U.S. West Coast – Seattle, Portland, Oakland and Los Angeles.

An average container has a 10-year life span, so every year part of the container fleet is renovated while old containers are displaced. Most containers are purchased in China; therefore, new containers do not have to be repositioned. By the same token, displaced containers generally stay in North America in order to avoid repositioning costs.

CURRENT OPERATING PLAN

The selected shipping line goes through an annual "fleet sizing" exercise, which determines the containers that will be replaced and the number of new containers depending on demand forecasts. Containers can be of five different types: dry 20" and 40", which represent the fleet majority, as well as dry 40" (high-cube), dry 45" and reefer 40". On a weekly basis, a "container balancing analysis" is performed. Each location in the U.S. reports the number of containers available (supply of empty containers) and the number of containers needed (demand for empty containers). Because shippers need to book containers a few weeks prior to departure, demand for empty containers is known. This demand comes from both Asian and North American locations.

Based on transit time and rate matrices, each empty container is allocated to a point of demand. Priority is given to fulfill the demand of North American locations, as containers should be loaded as often as possible. Containers that cannot be allocated to North American loads are routed to a West Coast port (Seattle, Portland, Oakland or Los Angeles) based on the lowest cost on their way to Asia. As volumes do not change significantly from week to week, this procedure is not always used. Instead, the same pairs are usually selected, meaning that specific locations always supply empty containers to other specific locations.

In the process of repositioning empty containers, capacity constraints such as railroad equipment, railroad power, labor at ports and drayage equipment need to be considered. As full containers always have priority over empty containers, rail transit times are not always consistent (e.g., "empties" are left behind). Even though westbound vessels have extra capacity in terms of number of containers, there might be weight constraints due to the heavier nature of eastbound loads (e.g., metal scrap, garbage and other heavy goods).

Container Life Cycle

With respect to a container life cycle, it is first filled with exports from Asia, then travels by ship to the U.S. It is then sent from the arrival port in U.S. to a customer by a combination of truck and rail. Part of the empty containers will be repositioned within the U.S. to satisfy the demand of containers bound to Asia, while the remaining empty containers will need to be relocated back to Asia.

Baseline Costs

Based on the information provided by APL, baseline costs are estimated and shown in Table 1.

Table 1. Estimation of Baseline Costs.

Total feus repositioned to Asia	140,409
Total feus repositioned within U.S.	297,140
Trucking Costs	$74,567,838
Rail Costs	$73,051,908
Inventory Costs	$3,413,542
Handling Costs	$9,223,808
Terminal Costs	-
Total Cost	**$160,257,096**

LITERATURE REVIEW

A similar problem to the repositioning of empty containers is empty vehicle redistribution. Literature in that area can be traced back to 1970's. Assuming that decision-makers have complete information, Leddon and Wrathall (1967) developed deterministic models for railcar distribution. In the line of stochastic environments, various models have been developed, such as non-linear network programs (Jordan and Turnquist 1983, Beaujon and Turnquist 1991), multistage dynamic networks (Cheung and Powell, 1996), and logistic queuing network (Powell and Carvalho 1998). The other research direction pursued by researchers later is to develop control policies based on the traditional inventory control policies (s, Q) and (s, S). Literature fall into this category include a single-value threshold control policy (Du and Hall 1997), a pull-type decentralized control policy (Hall and Zhong 2002), and steady state repositioning policy (Köchel et al. 2003). Köchel et al. concluded from the literature that no closed-form solution of optimal empty container/vehicle reposition is available for the stochastic transportation service systems. Recently, Song (2005) studied a continuous-review two-depot service system and obtained an exact solution of the optimal vehicle redistribution policy by using uniformization technique and stochastic dynamic programming.

There is extensive literature in the repositioning of empty containers, called empty container allocation problem. Crainic et al. (1993a, 1993b) specifically considered the repositioning of empty containers in a stochastic environment as a mix integer program and extended it to a multi-commodity network flow model, which they solved with a Tabu search procedure. Nevertheless, their models charge a leasing cost as a fixed amount in one-off mode. Shen and Khoon (1995) then developed a decision support system to optimize container leasing decisions assuming that all demands, schedules and capacity were deterministic within the planning horizon. In their model, the leasing cost is charged according to the duration of the lease. In the line of stochastic environments, besides the models developed by Crainic (1993a, 1993b), others include a simulation model (Lia et al. 1995), a two-stage stochastic network model (Cheung and Powell 1996, Cheung and Chen 1998), a single commodity and multicommodity network model (Godfrey and Powell 2002a, 2002b, Topaloglu and Powell 2004). Lam et al. (2007) demonstrated the successful application of an approximate dynamic programming approach in deriving effective

operational strategies for the relocation of empty containers. Song (2007) found the optimal stationary policy of empty container repositioning in a periodic-review shuttle service system. Erera et al. (2007) developed a robust optimization framework using time-space networks. In their previous work (Erera et al. 2005), they also considered integrating repositioning with load assignment decisions.

Most of the models for empty container repositioning require a specified planning horizon (Crainic et al. 1993a, 1993b, Cheung and Powell 1996, Cheung and Chen 1998, Godfrey and Powell 2002a, 2002b, and Topaloglu and Powell 2004). Nevertheless, it was found that the length of planning horizon had a significant on the outcomes of those model; under a multi-modal circumstance, the longer the planning horizon, the more utilization of inexpensive and slow transportation modes. Traditional logistics solutions require tedious data collection effort, and the numerial optimization could be NP-hard to solve on some occasions (Daganzo 1999). In his monograph "Logistic System Analysis," Daganzo proposed an alternative approach for logistic system planning and analysis. With his method, "detailed data are replaced by concise summaries, and numerical methods are replaced by analytic models." He claimed that the analytic models can be solved accurately without various pieces of detailed information. This study intends to apply the methods for designing the strategies for repositioning empty containers in the continental U.S. Sensitivity analysis will also be conducted the responses of strategies to critical logistic parameters.

METHODOLOGY

Detailed data were provided for both eastbound loads (E_{ij}) and westbound loads (W_{ij}) between Asia and North America for 2002, divided in four quarters. Data were aggregated and included only major terminals (and not the first and last legs). Locations in Mexico and Canada were disregarded for simplification purposes. From this data, supply, demand, net supply, and net demand (of empty containers) in the U.S. were determined based on the above equations.

Three strategies are proposed: (1) introducing "terminals" into the shipping line's network. The investigation of current empty container management suggests that the introduction of "terminals" would increase efficiency and reduce overall cost. By adding terminals, road distance can be minimized by introducing more rail travel distances, which incur lower costs. Each terminal is assigned to an influence area that includes a fixed number of customers. Therefore, customers "belong" to a specific terminal. To simplify the modeling, terminals were assumed to handle the same number of containers. In this context, net supply refers to the difference between supply and demand at a given influence area if supply is higher than demand; net demand refers to the same difference should demand be higher than supply (net demand (ND) = - net supply (NS)). An influence area and its respective terminal belong to a region, which was chosen so that the demand and supply were slow-varying; (2) utilizing ports on East Coast. Empty containers are currently not sent back to Asia through the East Coast ports due to less frequent schedules and capacity constraints. However, we believe it is possible to reduce costs by utilizing such ports, especially for locations in the East Coast; and (3) utilizing a dedicated fleet of trucks.

Step 1: Preliminary Analysis

To account for stochastic variations in our network, the U.S. had to be divided into regions for which current supply and demand of containers were approximately uniform in each region.

Step 2: Optimization

The goal of this step was to develop a logistics cost function that could be minimized in terms of the number of terminals and the headways (decision variables). The cost function has a deterministic and a stochastic component and was divided into four levels:

- **Local Level**: This level concerns costs associated with the movement of containers from a terminal to customers in an influence area, and vice versa. It was assumed that road transportation is the only mode utilized in this level.
- **Regional Level**: This level deals with the movement of containers among terminals within the same region. It was assumed that only rail is utilized.
- **Inter-regional Level**: This level deals with the movement of containers between regions. It was assumed that the movement of containers between regions is done by rail.
- **National Level**: This includes the costs of transporting containers from terminals to seaports by rail.

Deterministic Component

a) Local Level

Local Level Parameters
c_t: Variable trucking cost ($/distance. container) $1/(mile.feu)
c_i: Inventory cost ($/time. container) $0.78/(day.feu)
s_t: Truck speed (distance/time) 1,200 miles/day
c_{ht}: Fixed trucking cost ($/container) $50/feu
– includes handling at customer and drop-off at terminal
D_L: Average local distance (miles)
A_R: Region area (miles^2)
N_R: Number of terminals in the region
MAX: Maximum between supply and demand (feu)

The local level involves the costs associated with the movement of containers between a terminal and its customers. Each terminal services one area of customers, which was approximated by a circle. A simplification could then be made for the average distance from a customer to its respective terminal. Assuming a uniform distribution of customers within an influence area, the average distance from each customer to the terminal was determined to be 2/3 times the radius of the area.

$$D_L = \frac{2}{3} \cdot (\text{Radius of area}) = \frac{2}{3}\sqrt{\frac{A_R}{N_R \cdot \pi}}$$

It has been assumed that handling costs are included in the fixed truck rate, as it was discovered that many costs are collected in contracts made for the outsourced modes of transportation. To model this level of the network, the supply and demand were paired so that the total number of round trips was the maximum of total supply and total demand for each area. It was also assumed that some of the customer

locations have simultaneous supply and demand. Thereby, we estimated that 10 percent of containers do not need to go through terminals.

Breakdown of Average Local Costs:

Transportation Cost = $c_t \cdot D_L \cdot 2 \cdot MAX \cdot 0.9$

Handling Cost = $c_{ht} \cdot MAX \cdot 0.9$

Inventory Cost = $\frac{c_i \cdot D_L}{s_t} \cdot MAX \cdot 0.9$

b) Regional Level

Regional Level Parameters
c_r: Variable rail cost with distance ($/distance. container) - 25 cents/(mile.feu)
c_{hr}: Fixed rail cost - handling ($/container) - $40/feu
c_{fr}: Fixed rail cost per dispatch ($/dispatch) - $200/dispatch
s_r: Rail speed (distance/time) - 600 miles/day
c_{fm}: Fixed cost of terminals ($/terminal) $\begin{cases} \$8000 & \text{for terminals at APL city} \\ \$80000 & \text{otherwise} \end{cases}$
c_m: Variable cost of terminal –renting ($/time.container) - 1 $/(day.feu)
D_R: Average distance between terminals in one region (distance) miles
δ_T: Terminal density, i.e. number of terminals in region/area of region (1/distance^2) 1/miles^2
H_R: Headway to transport containers among terminals (time) days
ND_R: Net demand in one area (feu)
NS_R: Net supply in one area (feu)

On the local level, containers in one area are transported from customers to a single terminal, which in turn fulfills the demand of containers within its influence area. The result will be either a net supply at the terminal (if supply > demand) or a net demand (demand > supply). The regional level cost involves the relocation of containers from terminals with net supply to terminals with net demand.

The distance between terminals in one region (D_R) was calculated based on the assumption that terminals were uniformly distributed. The constant k accounts for the fact that a rail line is never a straight line, and in this case took a value of 1.13 ($2/\sqrt{\pi}$).

$$D_R = k \cdot \delta_T^{-1/2} = k \cdot \sqrt{\frac{A_R}{N_R}}$$

Costs on the regional level were divided into transportation costs, handling costs, inventory costs and terminal costs. Transportation was only done by rail, and its costs have two components, c_{fr}, and c_r. The first one is related to the fixed cost per dispatch. The second one represents the portion that varies with distance. Note that the number of containers that have to be transported among terminals in one region is the net demand (the demand that cannot be satisfied by the supply) in the region, as containers will not be relocated unless they are needed somewhere. The handling cost involves the handling of each container from the rail storage area to the train on both origin and destination rail terminals. Last, inventory costs include both stationary and pipeline inventory. For the first one, it is assumed that, on average, containers spend

half headway at the origin rail terminal and half headway at the destination rail terminal.

$$\text{Transportation Cost} = c_{fr} \cdot \frac{1}{H_R} \cdot N_R + c_r \cdot D_R \cdot ND_R$$

$$\text{Handling Cost} = c_{hr} \cdot ND_R$$

$$\text{Inventory Cost} = c_i \cdot (H_R + \frac{D_R}{s_r}) \cdot ND_R$$

To compute the terminal costs, it was assumed that terminals were located at rail yards. As soon as containers become available at customer locations, they are shipped to the terminals, where they are stored until the next train dispatch. This assures that containers are always available at the terminals and enables economies of scale in dispatching a group of containers at once. It was assumed that each terminal serves the same number of containers, which was determined by the maximum between total supply and total demand in one region, divided by the number of terminals.

It was assumed that cities should receive priority as a terminal, and the cost there would be about $8,000 to rent a storage area. If the optimal number of terminals exceeded 56, the cost of opening a new terminal would then be $80,000. In addition, a rental cost was added. This was calculated by multiplying the rate per container times the maximum space needed by any given terminal.

$$\text{Terminal Cost} = c_{fm} \cdot N_R + c_m \cdot (\text{MAX} + 3\sigma) \cdot H_R$$

c) Inter-Regional Level

Inter-Regional Level Parameters
H_I: Headway to transport containers between regions (days)
D_I: Average inter-regional distance (miles)
L_E: Horizontal length of East region (miles)
L_W: Horizontal length of West region (miles)
ND_I: Net demand in one region (e.g., overall net demand in the East region) (feu)
NS_I: Net supply in one region (feu)

After containers are relocated among terminals within the same region, the net supply and net demand at the regional level are assessed for both the East and the West regions. It is intuitive that relocation at this level happens only if at least one region has an overall net demand. In this specific case, both East and West have overall net supply; therefore, this step was not necessary. However, this study is intended for more general cases, so the methodology for this step is as follows.

The average inter-regional distance was calculated by picturing a virtual regional terminal approximately in the middle of each of the two regions (Figure 1). As both regions – East and West – have the same vertical length, only the horizontal separation was taken into account.

$$D_I = \frac{L_E + L_W}{2}$$

Costs at the inter-regional level were divided into transportation, handling, and inventory costs, which have the same form described at the regional level. Therefore:

$$\text{Transportation Cost} = c_{fr} \cdot \frac{1}{H_I} + c_r \cdot D_I \cdot ND_I$$

$$\text{Handling Cost} = c_{hr} \cdot ND_I$$

$$\text{Inventory Cost} = c_i \cdot (H_I + \frac{D_I}{s_r}) \cdot ND_I$$

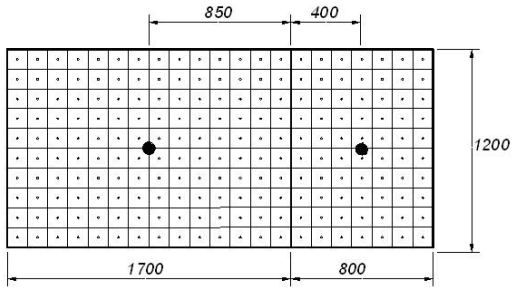

Figure 1. Average inter-regional distance.

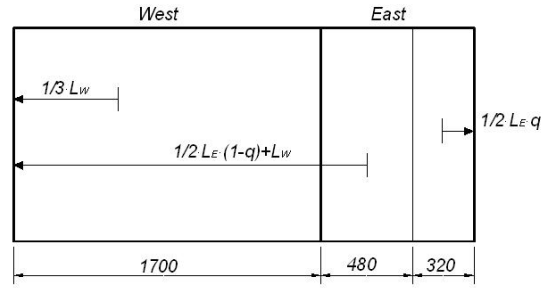

Figure 2. Average distances to ports.

d) National Level

National Level Parameters
D_{N1}: Average distance between terminals to the ports in the same region (miles)
D_{N2}: Average distance between terminals to the ports in the other region (miles)
H_{N1}: Headway to transport containers to terminals in the same region (days)
H_{N2}: Headway to transport containers to terminals in the other region (days)
$L1_R$: Horizontal length of same region (miles)
$L2_R$: Horizontal length of opposite region (miles)
V_R: Vertical length in one region (miles)
$SP1_R$: Supply that goes to ports in same region (feu)
$SP2_R$: Supply that goes to ports in opposite region (feu)

The national level is responsible for the relocation of remaining containers in the regions to the seaports on both West and East coasts after the regional net demand is fulfilled. There are additional capacity constraints on East coast ports due to fewer ship schedules bound for Asia. For simplification purposes, it is assumed that all ships provide the same proportion of their capacity to empty containers and also the same proportion at each port that they detour before they depart to Asia. From the analysis, ships at East ports can carry about 40 percent of the containers originating in East region; the remaining volume has to be transported to ports on the West Coast.

For the West region, due to the low density of containers in the Midwest, the average horizontal distance to the West Coast ports is one third of the region's horizontal length. After fulfilling the net demand of some of the terminals, the East region was divided into two subregions according to the capacity proportion. Containers in Subregion 1 were transported to East Coast ports with average horizontal distance equal to half of the subregion's horizontal length. Containers in Subregion2 were transported to West Coast ports, and the average distance was half of the subregion's horizontal length plus the horizontal-length of West region. There are four ports in each region. We assumed that the average vertical distance for each container to the ports is one eighth of the vertical length. Final numbers are presented in above Figure 2.

$$D_{N1} = L1_R \cdot q \cdot i + 1/8 \cdot V_R \qquad i = \begin{cases} 1/2 & for \quad east \quad region \\ 1/3 & for \quad west \quad region \end{cases}$$

where q is the proportion of containers transported to the ports in the same region.

$$D_{N2} = (1-q) \cdot (1-i).L1_R + L2_R + 1/8 \cdot V_R$$

For the containers transported to ports in the same region:

Transportation Cost 1 = $c_{fr} \cdot \frac{1}{H_{N1}} \cdot N_{N1} + c_r \cdot D_{N1} \cdot SP1_R$

Handling Cost 1 = $c_{hr} \cdot SP1_R$

Inventory Cost 1 = $c_i \cdot \left(\frac{H_{N1}}{2} + \frac{D_{N1}}{s_r} \right) \cdot SP1_R$

Note that the stationary inventory involves only half of the headway (inventory time at the port is not considered).

Similarly, for the containers transported to the ports in the other region:

Transportation Cost 2 = $c_{fr} \cdot \frac{1}{H_{N2}} \cdot N_{N2} + c_r \cdot D_{N2} \cdot SP2_R$

Handling Cost 2 = $c_{hr} \cdot SP2_R$

Inventory cost 2 = $c_i \cdot \left(\frac{H_{N2}}{2} + \frac{D_{N2}}{s_r} \right) \cdot SP2_R$

Stochastic Component

As the supply and demand for containers are not deterministic, stochastic variations were accounted for in this part. In the previous section, the expected number of containers was relocated within an area (local level), among areas in one region (regional level), and to the seaports (national level). This assured the whole country to be balanced. In other words, the net supply/net demand in all locations (e.g., seaports, terminals and customers) can be considered zero after the deterministic portion is solved.

Note that the deterministic component contains a term to account for the effect of demand and supply variance in the terminal renting cost, so this one is not included here. Thus, the stochastic component is concerned only with the relocation cost of containers among terminals.

The total container-distance traveled per terminal (p) was determined from a function formulated by Daganzo and Smilowitz (2003). The formula assumed that a region with an expected density of terminals (δ_R) had a net supply/net demand with zero mean and standard deviation σ, and N_R terminals.

$$p = \sigma \cdot \delta_R^{-1/2} \cdot f(N_R) = \sigma \cdot \delta_R^{-1/2} \cdot \left[0.43 + 0.02 \log_2 (N_R) \right]$$

The total cost has a similar form to that described in the regional level of the deterministic part. The number of containers in each terminal dispatch is $\sigma * H_R$, and it follows that:

Transportation Cost (regional) = $c_{fr} \cdot \frac{1}{H_R} \cdot N_R + c_r \cdot P_R \cdot N_R$

Handling Cost = $c_{hr} \cdot \sigma \cdot N_R$

Inventory Cost = $c_i.(H_R.\sigma + \frac{p_R}{s_r})$

The cost function included all costs in both deterministic and stochastic parts. Table 2 provides a summary of the cost function.

Table 2. Total Cost Function.

Deterministic Component	
• Local Level	$c_t \cdot D_L \cdot 2 \cdot MAX \cdot 0.9 + c_{ht} \cdot MAX \cdot 0.9 + \frac{c_i \cdot D_L}{s_t} \cdot MAX \cdot 0.9$
• Regional Level	$c_{fr} \cdot \frac{1}{H_R} \cdot N_R + c_r \cdot D_R \cdot ND_R + c_{hr} \cdot ND_R + c_i \cdot (H_R + \frac{D_R}{s_r}) \cdot ND_R$ $+ c_{fm} \cdot N_R + c_m \cdot (\mathrm{MAX} + 3\sigma) \cdot H_R$
• Inter-regional Level	$c_{fr} \cdot \frac{1}{H_I} + c_r \cdot D_I \cdot ND_I + c_{hr} \cdot ND_I + c_i \cdot (H_I + \frac{D_I}{s_r}) \cdot ND_I$
• National Level	$c_{fr} \cdot \frac{1}{H_{N1}} \cdot N_{N1} + c_r \cdot D_{N1} \cdot SP1_R + c_{hr} \cdot SP1_R + c_i \cdot \left(\frac{H_{N1}}{2} + \frac{D_{N1}}{s_r} \right) \cdot SP1_R$ $+ c_{fr} \cdot \frac{1}{H_{N2}} \cdot N_{N2} + c_r \cdot D_{N2} \cdot SP2_R + c_{hr} \cdot SP2_R + c_i \cdot \left(\frac{H_{N2}}{2} + \frac{D_{N2}}{s_r} \right) \cdot SP2_R$
Stochastic Component	$c_{fr} \cdot \frac{1}{H_R} \cdot N_R + c_r \cdot P_R \cdot N + c_{hr} \cdot \sigma \cdot N_R + c_i . (H_R . \sigma + \frac{p_R}{s_r})$

Constraints

The demand for empty containers in Asia did not have to be considered as a constraint. As empty containers are produced in Asia, they can be purchased there if it is more cost effective. Even though rail capacity can be an issue in practice, it was disregarded for simplification purposes. Port capacity was taken into account in order to prioritize the shipment of containers to different ports. We also assumed an infinite supply of trucks and of storage area at seaports and rail terminals. The number of terminals in the West region was constrained at 40, as it is the number of terminals served by the major rail companies.

Optimization Results

Regions were permitted to have different number of terminals and headways, so, in fact, there are two decision variables representing the number of terminals in each region and the three types of headways mentioned. The optimization model yielded the results shown in Table 3. Further analysis of such results is included in the Future Steps section.

Table 3. Optimization Results.

Optimization Results	East Region	West Region	Total
Total Cost	$58,098,500	$59,667,700	$117,766,200
Number of Terminals	53	40	93
Regional Headway (among terminals) (days)	5	4	
National Headway - to port in same region (days)	17	12	
National Headway - to port in opposite region (days)	11	-	

Step 3: Network Design

Step 2 provides the optimal number of terminals in both regions. Step 3 is responsible for choosing the location of such terminals, and determining their influence areas.

Actual Location of Terminals

Terminals for repositioning containers will be located at existing rail terminals, where yard space will be rented as needed. It was assumed that there would always be yard space available. From a list of rail terminals provided by the major rail companies, cities were ranked by the following factors (in order): (1) whether the shipping line currently has operations in such city (because there is an implicit penalty for opening a new facility), (2) number of rail routes that go through the city, and (3) number of rail companies that serve the city

The optimal number of terminals in the East, N_E*=53, matched up precisely with the number of leading cities on the ranked list. In the initial run of the optimization model output, number of terminals for the West region was 78. However, this value became unreasonable when compared to the number of existing rail terminals. A restriction was added to the model to reduce the number of terminals within the range of feasible rail terminals (Note: In the later section on sensitivity analysis, it can be seen that this restriction has a rather insignificant effect on the total costs.) The final result for the optimal value of terminals in the West was N_W*=40.

Determination of Influence Areas

Based on the actual location of terminals, it was assumed that each customer was allowed to send containers to its nearest terminal. The specific algorithm to assign influence areas to terminals assumed that demand was given by a function per square mile. Thus, we considered each 1x1 square mile to be a fictional customer with a demand for a certain amount of containers. The Voronoi Tesselation method was used to assign each fictitious customer to a terminal and thus determine the influence areas (Voronoi Tesselation 2003). Influence areas can be thought of as Voronoi regions, where all interior points are closer to the corresponding generator, or terminal, than to any other. Then, the Voronoi Tessellation is the set of Voronoi regions where no pairs of Voronoi regions have a common point. The distance is $d(z, z_i) = \|z - z_i\|$, where z is a terminal location coordinates and z_i is a 1 mile by 1 mile region representing a fictitious customer. Average distances were calculated from every $d(z,z_i)$.

Step 4: Cost Calculation

By determining the actual location of terminals, total logistics costs will be slightly different from the optimized costs. The same four levels considered will be evaluated in order to calculate the actual costs of the proposed strategies:

a) Local Level

Once the influence areas were determined, local level costs (from customers to terminals and vice-verse within an influence area) could be calculated.

For the purpose of determining the customer demand/supply density only, the 56 data points were regarded as terminals that handled containers in their own influence area. To allocate customers to terminals (to establish influence areas), it was determined that each customer was allowed to send containers to its nearest terminal. Assuming customers are uniformly located in each area and all the

customers within the same area are identical, the customer demand/supply density for each area could be obtained.

Based on this density function and on the location of terminals, the influence areas (e.g., total area, shape, and container average travel distance) could be determined through the same methodology. By combining the demand and supply of each customer within an influence area, the number of containers handled by the terminal was calculated. The local cost of transporting containers between customers and terminals was obtained as a function of the average travel distance and the volume of containers handled by a terminal.

b) Regional, Inter-regional and National Levels

Supply and demand values for each terminal were calculated by aggregating the supply and demand densities over each influence area. By regarding ports as terminals with net demand, balancing containers within the whole country was captured by a minimal cost network flow problem. The regional, inter-regional and national level costs were determined. In our specific case, inter-regional costs were not applicable as there were not any flows between both regions. Ports' demand was determined according to their capacity.

Cost Calculation Results

Based on the actual location of terminals and their respective influence areas, new costs were calculated. Table 4 compares such results with baseline and optimized costs, and it reflects that significant savings (19.07%) can still be realized by applying the proposed strategies. Additionally, the main differences between the actual and the optimized costs rely on rail costs. This is true, as rail distances are higher once the actual locations of terminals is determined, and terminals in the East region are forced to ship the remaining empty containers to the West Coast ports due to capacity constraints on the ports in the East Coast. Actual inventory costs are higher then optimized inventory costs as the maximum headway between the regional and the national was utilized to simplify the calculations. Both handling and inventory costs remain fairly constant, as they do not depend on the terminal locations.

Table 4. Cost Comparison.

Cost Item	Baseline	Optimization	Actual
Trucking Costs	$74,567,838	$42,284,200	$42,793,671
Rail Costs	$73,051,908	$45,277,987	$52,414,260
Inventory Costs	$3,413,542	$1,024,332	$5,185,021
Handling Costs	$9,223,808	$24,324,150	$24,324,150
Terminal Costs	$0	$4,825,590	$4,972,441
Total Costs	$160,257,096	$117,736,259	$129,689,443
% savings compared to baseline		26.53%	19.07%

FUTURE STEPS

The problem of repositioning empty containers has great depth. To get a more realistic view of the effects of our suggestions, the following further investigations should be considered. First, the optimization results from the previous section provided an optimal solution by minimizing total logistics costs based on several

parameters and constraints. To determine how robust the logistics cost function is to these parameters, constraints and strategies, sensitivity analyses should be performed. Second, based on the sensitivity analyses, the influence of strategies should be assessed. Third, it is important to assess the practical implications of implementing a terminal system to the reallocation of containers. These are difficult to model but are nonetheless significant. Fourth, more comprehensive research should be done on the costs of designing, implementing and operating a dedicated truck fleet for handling the local transportation. Finally, our model assumes that a rail terminal can use any headway. However, rail transportation is restricted to schedules. Synchronizing the reallocation of containers to involve the rail (and possibly port as well) schedules would provide a more practical idea of the entire system.

ACKNOWLEDGEMENT

The authors would like to thank Monica Menendez and Huifang Yin for their assistance on preliminary analysis for this study.

REFERENCES

Beaujon, G. J., and Turnquist, M. A. (1991). "A model for fleet sizing and vehicle allocation." *Transport Science,* 25, 19–45.

Cheung, R. K. M., and Chen, C. Y. (1998). "A two-stage stochastic network model and solution methods for the dynamic empty container allocation problem." *Transport Science,* 32(2),142–162.

Cheung R. K. M., and Powell, W. B. (1996). "An algorithm for multistage dynamic networks with random arc capacities, with an application to dynamic fleet management." *Operations Research* 44, 951–963.

Crainic, T. G., Gendreau, M., and Dejax, P. (1993). "Dynamic stochastic models for the allocation of empty containers." *Operations Research*, 41, 102–126.

Crainic, T. G, Gendreau, M., Soriano P., and Toulouse M. (1993b). "A tabu search procedure for multicommodity location/allocation with balancing requirements." *Ann Operations Research,* 41, 359–384.

Daganzo, C.F. (1999). *Logistics Systems Analysis. 3rd Edition*. Springer, Berlin.

Daganzo, C.F., and Smilowitz, K.R. (2003). *Bounds and Approximations for the Transportation Problem of Linear Programming and other Scalable Network Problems.* To be published.

Du, Y. F., and Hall, R. (1997). "Fleet sizing and empty equipment redistribution for center-terminal transportation networks." *Management Science,* 43, 145–157.

Erera, A. L., Morales, J. C., and Savelsbergh, M. W. P. (2005). "Global intermodal tank container management for the chemical industry." *Transportation Research, Part E*, 41, 551–566.

Erera, A.L., Savelsbergh, M., Uyar, E., 2007. Fixed routes with backup vehicles for stochastic vehicle routing problems with time constraints. Technical Report, The Supply Chain and Logistics Institute, School of Industrial and Systems Engineering, Georgia Institute of Technology.

Godfrey, G., and Powell, W. B. (2002a). "An adaptive dynamic programming algorithm for single-period fleet management problems I: Single period travel times." *Transportation Science*, 36, 21–39.

Godfrey, G., and Powell, W. B. (2002b). "An adaptive dynamic programming algorithm for single-period fleet management problems II: Multiperiod travel times." *Transportation Science*, 36, 40–54.

Hall, R. W., and Zhong, H. S. (2002). "Decentralized inventory control policies for equipment management in a many-to-many network." *Transport Research Part A,* 36, 849–865.

Hanscom, J. (1998). "Container imbalances – Worse to come.: *Seatrade Review*, 27(10), 27-29.

Jordan, W. C., and Turnquist, M. A. (1983). "A stochastic, dynamic network model for railroad car distribution." *Transport Science,* 17, 123–145.

Köchel, P., Kunze, S., and Niela¨nder, U. (2003). "Optimal control of a distributed service system with moving resources: Application to the fleet sizing and allocation problem." *International Journal of Production Economics,* 81–82, 443–459.

Lai, K. K., Lam, K. and Chan, W. K. (1995). "Shipping container logistics and allocation." *Journal of Operational Research Society*, 46, 687–697.

Leddon, C., and Wrathall, E. (1967). "Scheduling empty freight car fleets on the louisville and Nashville railroad." In *Second International Symposium on the Use of Cybernetics on the Railways*, October, 1–6, Montreal, Canada.

Powell, W. B., and Carvalho, T. A. (1998). "Dynamic control of logistics queuing networks for large-scale fleet management". *Transport Science,* 32, 90–109.

Shen, W.S. and Khoong, C.M. (1995). A DSS for empty container distribution planning. Decision Support System 15: 75–82.

Song, D. P. (2005). "Optimal threshold control of empty vehicle redistribution in two depot service systems." *IEEE Trans Automatic Control* 50, 87–90.

Song, D. P. (2007). "Characterizing optimal empty container reposition policy in periodic-review shuttle service systems", Journal of Operational Research Society, 58, 122-123.

Topaloglu, H., and Powell, W. B. (2006). "Dynamic programming approximations for stochastic, time-staged integer multi-commodity-flow problems." *Informs Journal on Computing,* 18(1), 31-42.

Voronoi Tessellation. (2003). http://www.csit.fsu.edu/~nguyen/Definition.html. Accessed multiple times on November 2003.

Further Development of the German Highway Capacity Manual (HBS2011)

Ning Wu, Ph.D.

Institute for Traffic Engineering, Ruhr-University Bochum, 44780 Bochum, Germany; phone: +49 234 3226557, fax: +49 234 3214151; e-mail: ning.wu@rub.de, http://homepage.rub.de/ning.wu

ABSTRACT

The first version of the German Highway Capacity Manual was published in 2001. Now, a new draft is prepared and it will be published in 2011 (HBS2011). For the new German Highway Capacity Manual, the major chapters are revised and some of them are totally rewritten.

In this paper, a short overview of the major developments in the new German Highway Capacity Manual is presented. Some new ideas and field dada under consideration are introduced. For example, according to the new measurements, the values of capacity for freeway segments are revised and for the on-, off-ramps, and weaving areas a totally new procedure is developed which considers the traffic flow conditions on the freeways and at on- and off-ramps simultaneously. Also for signalized and unsignalized intersections, the procedures are revised for taking account the new developments in the past 10 years.

INTRODUCTION

Germany has been involved in traffic engineering research since many decades. Initially, the more popular calculation procedures were mainly based on deterministic considerations. Publication of the U.S *Highway Capacity Manual* (HCM) in the 1950s spurred interest in the use of stochastic elements combined with empirical research in traffic engineering. Until 2001, the different calculation procedures used in German traffic engineering applications have never been concentrated into one guideline such as the HCM. Instead, these applications were incorporated in different highway design guidelines. A new era in the development of traffic engineering guidelines for German conditions began when the Federal Department of Transportation (DOT) commissioned the Ruhr-University in 1989 to develop a prototype for a German *Highway Capacity Manual* (HBS*)*. The first draft for this manual was finished in 1993 and was published a year later by Brilon, Grossman, and Blanke (Brilon et al. 1994).

The first edition of the *German Highway Capacity manual* (*Handbuch fuer die Bemessung von Strassenverkehrsanlagen*, HBS2001) was published in 2001 (FGSV, 2001). It was introduced by the German federal DOT as the methodological basis for capacity calculations and quality assessments. Similar to the US *Highway Capacity Manual* (HCM2000), HBS2001 is based on the concept of Level of Service. An overview on the current version of HBS2001 was given by BRILON (1998).

After its publication, HBS2001 has found wide applications. Because of the importance for the professionals in the practice, the German Road and Transportation Research Association (FGSV) decided to up-date this manual. Goals of the updating work are to revise the existing chapters and to complete the contents as good as possible. In comparison to the HBS2001, the methodologies for assessment should be given in more details in the new edition.

The Institute for Traffic Engineering at Ruhr-University has provided significant contributions to the development of the new HBS2011. In this paper the proposed major revisions in the new HBS2011 are introduced chapter by chapter.

TRAFFIC DEMAND AND CAPACITY (CHAPTER 2)

The chapter 2 of the HBS deals with the fundamental concept for dimensioning and traffic quality assessment procedures. The main topic of this chapter is to provide a procedure for determining the peak hour volume for dimensioning traffic facilities and computing capacities.

In the current HBS2001, the traffic volumes for dimensioning the different traffic facilities are not exactly defined. It is suggested to use the 30th hourly volume in the year as the dimensioning peak hour volume. However, it not clearly defined how this 30th hourly volume is estimated. Thus, a modification regarding this topic is needed.

In the proposed HBS2011, the 30th hourly volume in the year will continue to be used for dimensioning the peak hour volume. However, a functional relationship between the 30th hourly volume in the year and the considered peak hour volume will be given. The use of directional peak hour volumes or aggregated peak hour volumes is recommended depending on the specific traffic conditions. The procedure for estimating the proportion of peak hour volumes to annual average daily volume (ADV) is improved.

BASIC FREEWAY SECTIONS (CHAPTER 3)

In Germany, it still lacks a general speed limit on motorways or freeways. In addition, passing on the right lane is not allowed, and this rule is generally followed by drivers. As a result, the right lane is preferred for normal driving except when passing. This rule causes a lot of lane changing maneuvers. Furthermore, the speed limit for trucks is only 80 km/h. Those rules and characteristics together generate a special traffic flow and speed relationship on German freeways where a significant influence of volume on average speed occurs.

The current HBS2001 recommends the volume/capacity-ratio (v/c-ratio) to assess the quality of traffic flow on German freeways with two or three lanes each direction. The database based on the measurements from Ponzlet (1996). The database is now extended. In the proposed HBS2011, also the freeways with 4 lanes each direction will be incorporated.

The proposed capacity in HBS2011 for different freeway sections is illustrated in the Table 2. The Level of Service (LOS) is defined depending on the degree of saturation (Table 1).

Table 1 - LOS for freeways depending on the degree of saturation

LOS	Degree of Saturation at LOS (x_{LOS})
A	$\leq$ 0.30
B	$\leq$ 0.55
C	$\leq$ 0.75
D	$\leq$ 0,90[1)]
E	$\leq$ 1.00
F	–

[1)] 0.95 for sections with Variable Speed Limit

Table 2 - Capacity (veh/h) for freeways without speed limit

No. of lanes each direction	Grade	Long distance freeways			Metropolitan traffic freeways		
		Percent of trucks			Percent of trucks		
		0 %	10 %	20 %	0 %	10 %	20 %
2	≤ 2 %	3700	3600	3400	4000	3800	3600
	3 %	3600	3500	3300	3900	3700	3500
	4 %	3400	3300	3100	3700	3500	3300
	5 %	3100	3000	2800	3400	3200	3000
3	≤ 2 %	5400	5200	4900	5800	5500	5200
	3 %	5300	5100	4800	5700	5400	5100
	4 %	5000	4800	4500	5400	5100	4800
	5 %	4600	4400	4100	5000	4700	4400
4	≤ 2 %	7400	7100	6700	8000	7600	7100
	3 %	7200	6900	6500	7800	7400	6900
	4 %	6900	6600	6200	7500	7100	6600
	5 %	6300	6000	5600	6900	6500	6000

ENTRANCES AND EXITS (ON- AND OFF- RAMPS) AT FREEWAYS (CHAPTER 4)

The capacity and performance of entrances, weaving areas and exits has been studied by Westphal (1995). Although this investigation focused on urban freeways with speed limits of 80 or 100 km/h, Westphal's procedures are also recommended by the HBS2001 for all types of freeways. In the proposed HBS2011, a totally new procedure is introduced. The procedure is developed by Wu (2008). This procedure considers the major freeways, the on- and off-ramps and the weaving areas under consideration simultaneously. The capacity for exits is expressed by the following equation:

$$q_{a,LOS} = C_{a,LOS} \cdot \sqrt[a]{1 - \left(\frac{q_h}{C_{h,LOS}}\right)^a} \qquad (1)$$

with $q_{a,LOS}$ = maximum flow of the entrance, exit, or weaving area by a given LOS

$C_{h,LOS} = C_h \cdot x_{LOS}$

$C_{a,LOS} = C_a \cdot x_{LOS}$

C_h = capacity of the major freeway section

C_a = capacity of the road section at the entrance, exit, or weaving area

a = model parameter

x_{LOS} = degree of saturation for a given LOS (Table 1)

According to the equation (1), the LOS for the on-, off-ramps or the weaving areas can be defined depending on the traffic volume on the major freeway section and the entrance/exit. Figure 1 shows a picture depicting the equation (1) for a 1-lane entrance to a 3-lane freeway with C_h=5700 veh/h, C_a=1800 Veh/h, and a=1.9. Those

pictures are constructed for all types of entrances, exits, and weaving areas in the proposed HBS2011. The users can use those pictures directly for estimating traffic flow quality.

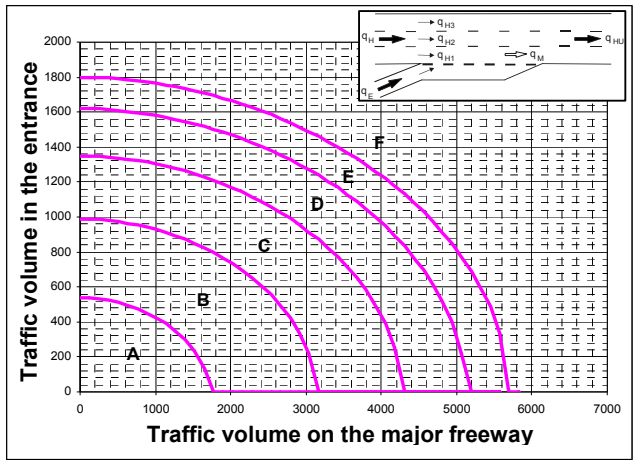

Figure 1 – An Example for the Definition of LOS (equation (1)) for a 1-lane entrance to a 3-lane freeway.

In order to ensure the downstream capacity, an extra-examination is needed for the downstream freeway section according to the Table 2 and Table 1.

TWO-LANE RURAL HIGHWAYS (CHAPTER 5)

The current procedure in the HBS2001 dealing with the capacity and traffic quality of 2-lane rural highways was introduced by Brilon and Weiser (1998, 2003). No significant changes are proposed for the new HBS2011.

SIGNALIZED INTERSECTIONS (CHAPTER 6)

This chapter will be totally revised, because some fundamental parameters and calculation procedures are not more up to date. In the new HBS2011, the chapter for signalized intersection will also be improved by avoiding overlapping with the German Guidelines for Traffic Signals (FGSV, 1992). The saturation flow rates will be recalibrated and the delay formula will be substituted by a new one which considers also the coordination and the traffic-actuated signal control. The details of this chapter are not discussed here because the revising work is still in process.

UNSIGNALIZED INTERSECTIONS (CHAPTER 7)

Calculation methods for unsignalized intersections have been developed cooperatively by American, Australian, and German researchers since many years. The new German version of the corresponding chapter tries to contribute some additional improvements in this area.

In the HBS2001 and HBS2011, the basic capacity will be calculated by Siegloch's formula. The critical gaps and follow-up times were estimated by comprehensive investigation in German (Brilon and Weinert, 2001). The problem of two-stage priorities was resolved like in the HCM2000.

Improvements that have not yet been included in the HCM2000 include:

- Impedance factors for rank 4 movements: The current HCM-solution is based on Grossmann's (1991) simulation results. Meanwhile, Wu (1998) has found a theoretical approach to that problem that enables a more precise estimation of impedance effects.

- The HCM2000 does not address the mixed and short lanes on traffic performance properly. In the HBS2000, the theoretical procedure developed by Wu (1997) is incorporated for minor approaches. In the new HBS2011, the procedure for the mixed and short lanes in major approaches is extended revised.
- Capacity calculations for roundabout entries are based on a calculation method described by Brilon, Bondzio, Wu (1997). This method is now recalibrated for taking into account the new developments in geometric design in the roundabout construction such as the mini-roundabouts, turbo-roundabouts etc.

According to those innovations, the unsignalized chapter of the HBS has a rather high standard regarding theoretical background.

URBAN ARTERIALS (CHAPTER 8)

In the current HBS2001, there is no procedure for assess the quality of traffic flow on urban arterials. In the proposed HBS2011, the procedure proposed by Baier et al. (2003) will be introduced. With this procedure, the traffic flow quality on the sections outside the influence of major intersections can be assessed.

PEDESTRIANS, BICYCLES, PUBLIC TRANSIT, AND PARKING (CHAPTER 9, 10, 11, AND 12)

Much emphasis in Germany is put on safe and comfortable operation of traffic for non-motorized road users and for public transit. In the current HBS2001, only the service quality for passengers inside the public transport vehicles (busses, trams) is considered. In the proposed HBS2011, the traffic flow of public transport vehicles on separate lanes and at (local) public transport stops are included. In this new procedure, also other road users such as taxis, cyclists, or HOV's are allowed to use the separated bus lane. The assessment of traffic flow for busses and trams mixed with the general traffic will be addressed in the other chapters. The procedures for capacity inside the public transport vehicles are excluded from the HBS2011. A separate guideline shall be developed for the public transport systems. A new chapter for bicycles is introduced in the proposed HBS2011. The existing chapters for pedestrians and parking systems are improved.

SUMMARIES

This paper illustrates the major contents of the future German HBS2011. It is intended to be published in the year 2011. Research projects are still underway for additional improvements. The new version of HBS that will be finished in the year 2011 will be comparable with the future HCM 2010 in many aspects.

The proposed paper shows the expertise of our institute in research on capacity and service quality analysis and the experience in developing highway capacity manuals in Germany and as a partner in the United States. Those expertise and experience can give the Chinese audience and institutes involving in research on capacity models and in developing capacity manuals useful knowledge and help them to speed up the developing process and avoid unnecessary errors and mistakes.

REFERENCES

Brilon, W., Wu, N. and Bondzio, L. (1997). "Unsignalized Intersections in Germany - A State of the Art 1997." *Proceedings of the Third International Symposium on Intersections without Traffic Signals*, Portland.

Brilon, W., Grossmann, M. and Blanke, H. (1994). "Verfahren fuer die Berechnung der Leistungsfaehigkeit und Qualitaet des Verkehrsablaufs auf Strassen (Methods for Capacity and Traffic Quality Estimation)." *Series Strassenbau und Strassenverkehrstechnik*, No. 669

Brilon, W. and Weiser, F. (1998). "Capacity and Speed-Flow-Relationships on Rural Two-Lane Highways in Germany." *Proceedings of the Third Internationla Symposium on Honghway Capacity- country Reports.* Copenhagen

Brilon, W. and Weinert, A. (2001). "Ermittlung aktueller Grenz- und Folgezeitlücken für Ausserortsknoten ohne Lichtsignalanlagen (Estimation of Critical Gaps and Follow-Up Time at Unsignalized Intersections)." *Forschung Straßenbau und Straßenverkehrstechnik*, Heft 828, Bundesminister für Verkehr

Brilon, W. (1998). "HBS - The future German Highway Capacity Manual." In: Rysgaard, R. (ed.) *Proceedings of the Third Internationla Symposium on Honghway Capacity- country Reports*. Copenhagen.

FGSV (2001). *Handbuch für die Bemessung von Straßenverkehrsanlagen* (HBS 2001, *German Highway Capacity Manual*). Forschungsgesellschaft für Straßen- und Verkehrswesen (Hrsg.), Nr. 299, FGSV Verlag GmbH.

FGSV (1992). *Richtlinien für Lichtsignalanlagen - Lichtzeichenanlagen für den Straßenverkehr (RiLSA, German Guidelines for Traffic Signals)*. Forschungsgesellschaft für Straßen- und Verkehrswesen (Hrsg.), Nr. 321.

TRB (2000). *Highway Capacity Manual* (HCM 2000). TRB, National Research Council, Washington, D.C.

Grossmann, M. (1991). "Methoden zur Berechnung von Leistungsfaehigkeit und Verkehrsqualitaet an Knotenpunkten ohne Lichtsignalanlagen. (Methods for Capacity and Traffic Quality Estimation)." Institute for Transportation and Traffic Engineering, Ruhr-University Bochum, No. 9

Baier, M.M. et al. (2003). "Verkehrsqualitaet auf Streckenabschnitten von Hauptverkehrsstrassen (Traffic Quality on Arterial Road Sections)." *Bericht der Bundesanstalt fuer Strassenwesen* V108. Bergisch Gladbach.

Ponzlet, M. (1996). *Auswirkungen von systematischen und umfeldbedingten Schwankungen des Geschwindigkeitsverhaltens und deren Beschreibung in Verkehrsflußmodellen (Influence of Environmental Conditions on Speeds)*. Institute for Transportation and Traffic Engineering, Ruhr-University Bochum, No. 16

Westphal, S. (1995). *Bemessung von Einfahrten an planfreien Knotenpunkten (Calculation of On- and Off-Ramps)*. Institute for Transportation and Traffic Engineering, Ruhr-University Bochum, No. 13

Wu, N. (1997). "Capacity of Shared-short Lanes at Unsignalized Intersections." *Proceedings of the Third International Symposium on Intersections without Traffic Signals*, Portland, Oregon,

Wu, N. (1998). "Impedance Effects for Streams of Higher Ranks at Unsignalized Intersections." *Proceedings of the 3rd International Symposium on Highway Capacity*

Wu, N. (2008). "A new Method for Estimating Traffic Quality of On-, Off-Ramps and Weaving Areas." *Unpublished manuscript.* Institute for Traffic Engineering, Ruhr University Bochum.

Operational Performance Evaluation of Different Exit Ramps on Florida's Freeways by Considering Number of Lane Change

Jian John Lu, P.E.[1]; Linjun Lu[2]; and Tangyi Guo[3]

[1]Professor, Dept. of Civil and Environmental Engineering, Univ. of South Florida, FL 33620. E-mail: lu@eng.uef.edu
[2]Graduate Research Assistant, Dept. of Civil and Environmental Engineering, Univ. of South Florida, FL 33620. Email: llu@mail.usf.edu
[3]Graduate Research Assistant, College of Transportation, Southeast University, Nanjing 210096, China. Email: transtorseu@hotmail.com

ABSTRACT

In the State of Florida, several types of exit ramps are used for traffic to exit our freeways, especially four typical types, which are single-lane exit ramp with a taper, single-lane exit ramp without a taper, two-lane exit ramp with an optional lane, and two-lane exit ramp without an optional lane. Drivers exiting freeways need to make decisions and execute maneuvers (i.e., lane change or lane merge) prior to the exit ramp in order to access cross roads at the interchanges. And different types of exit ramps lead to different driving maneuvers when exiting (fast-paced deceleration, lane changing, merging, unbalanced lane utilization), which also affects the operational performance on freeways. Bases on the facts, there are several issues and concerns that need to be addressed in selecting the most optimum types of freeway exit ramp(s) to use at a given interchange. This paper mainly focuses on different impacts of number of lane change by different types of ramp. A data collection of 24 sites were conducted to help set up a mathematical model, which could estimate the number of lane change by considering several possible independent variables. Results of the model could help choose optimal ramp type.

KEY WORDS

Operational performance; Exit ramp; Ramp type; Number of lane change.

BACKGROUND INFORMATION

There are several types of exit ramps used for traffic to exit freeways in the United States (i.e. Interstate and Turnpike Systems). Typically, four types of freeway exit ramps are most widely used in Florida, shown from Figure 1 to Figure 4. Drivers exiting freeways need to make decisions and execute maneuvers (i.e., lane change or lane merge) prior to the exit ramp in order to access cross roads at the interchanges. If the exit ramps are not sufficiently long, drivers must complete their driving maneuvers within a short distance, resulting in potentially unsafe driving actions (i.e., fast-paced deceleration, lane changing, merging, unbalanced lane utilization, etc.),

which will result in the development of shock-waves onto upstream traffic, etc. Considering these factors, there are several issues and concerns that need to be addressed in evaluating operational performance of each type of exit ramp and selecting the most optimum types of freeway exit ramp(s) to use at a given interchange.

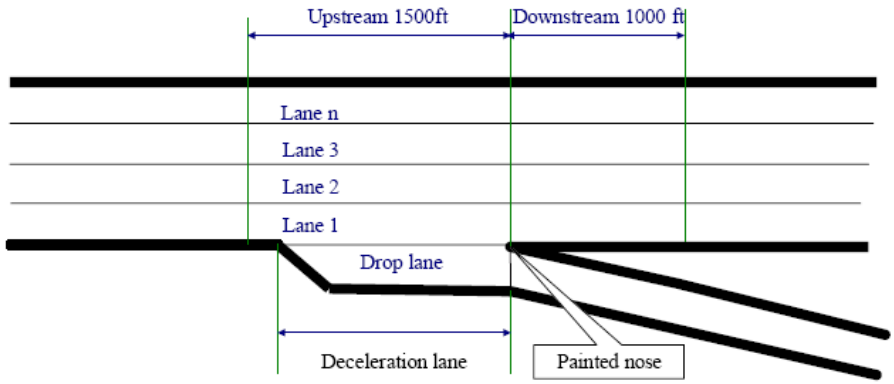

Figure 1. Type 1 exit ramp: single-lane exit ramp with a taper

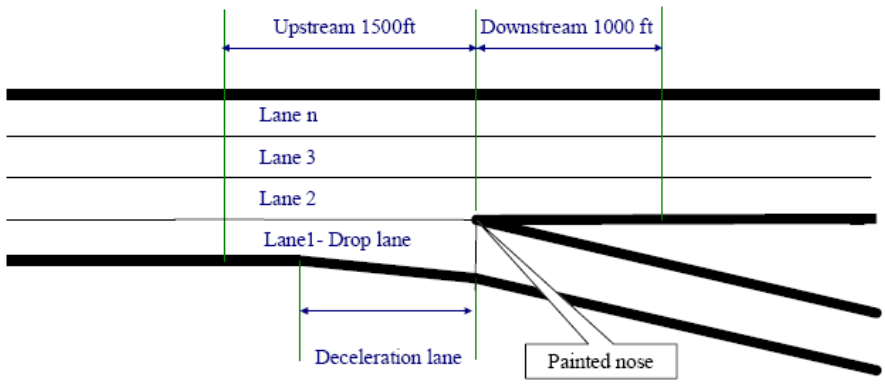

Figure 2. Type 2 exit ramp: Single-lane exit ramp without a taper

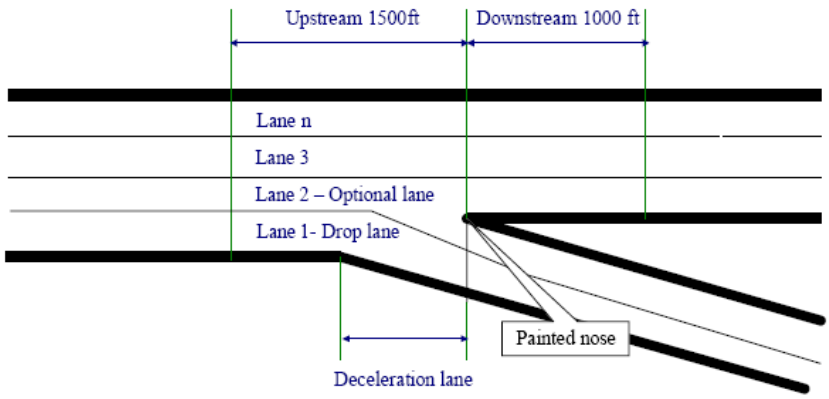

Figure 3. Type 3 exit ramp: Two-lane exit ramp with an optional lane

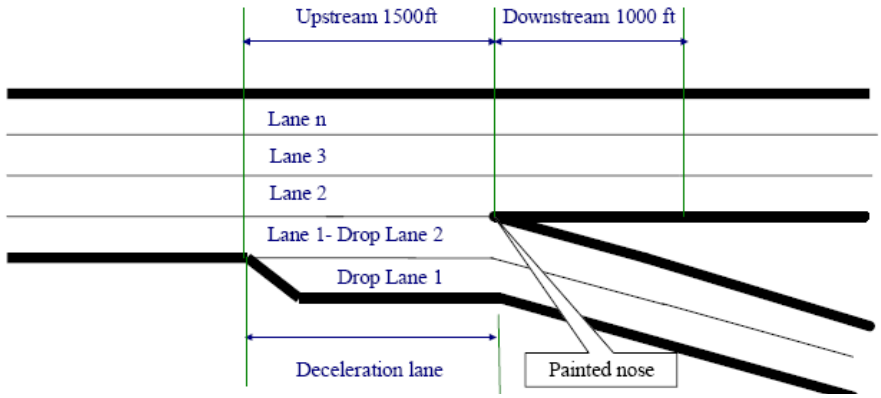

Figure 4. Type 4 exit ramp: Two-lane exit ramp without optional lane

Besides ramp type, some issues in the joint cross road of ramp can also affect safety problems, which include but are not limited to, control type of ramp terminal, downstream and upstream intersection, the distance between downstream intersection and ramp terminal, and the distance between upstream intersection and ramp terminal, shown in Figure 5. Inadequate distance for traffic to transit from the exit gore to the downstream or upstream intersection can cause complex weaving maneuver and additional rear end crash. Therefore, it is very important to present the minimal distance between these three intersections on cross road in order to prevent crashes on both exit ramp and cross road.

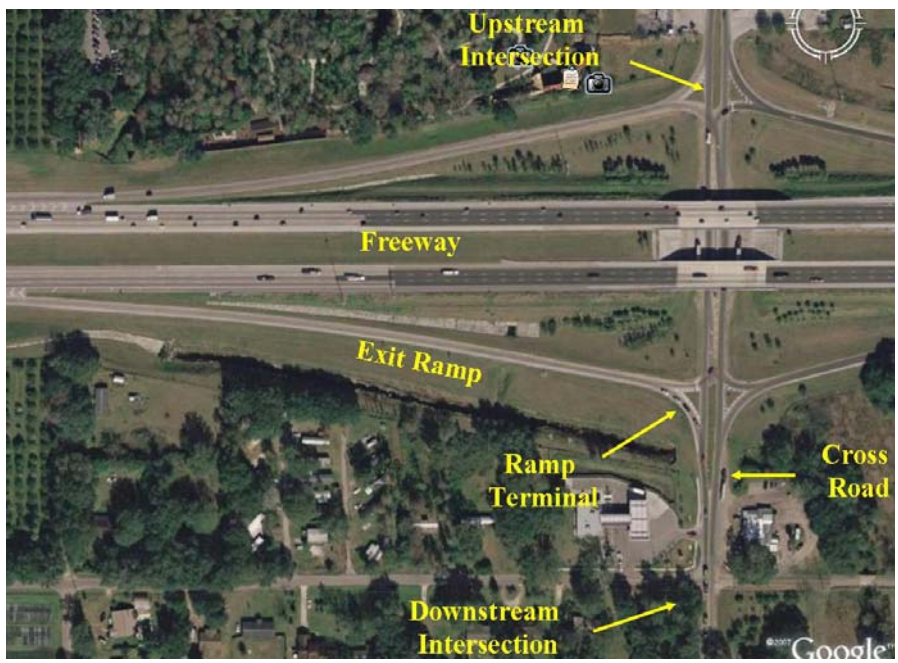

Figure 5. Exit ramp and joint cross road

All these issues have not been studied in the past and no clear guidelines,

either federal (AASHTO Green Book) or state, are currently not available in selecting exit ramp types. The Florida Department of Transportation (FDOT) in joint cooperative efforts with the local land use agencies set up a research project to determine the type of exit ramps that should be constructed at a given location considering the prevailing conditions applicable to traffic, roadway, and land-use developments.

The whole project contained three sections, freeway, ramp and cross road sections. This paper mainly focused on freeway section. Trying to find out the impacts of operational performance on freeway due to different types of ramp, and to help choose optimal ramp based on the performance.

METHODOLOGY AND DATA COLLECTION

The number of lane change on freeway is a very significant measure of effectiveness to evaluate the operational performance, which also affects safety. And number of lane change is the direct cause of potential crashes. The concept of number of lane change here refers to the changing lane maneuver that happens in the area of upstream section of painted nose (start point of exit ramp), which includes 1500 ft distance, see Figure 6. Vehicles exiting ramp need to change lane to the most right lane before entering ramp, if they are not at the right lane yet. Thus, the lane change happens from lane 1 to lane 4, lane 2 to lane 4, or lane 3 to lane 4. Lane change happening among lane 1 to lane3 will not be considered to be effective number here, because which is not the response of exit ramp. On the other hand, going through vehicles need to change to the through lane if they are on the most right lane before ramp. This is also effective number of lane change, because it is relational to ramp type.

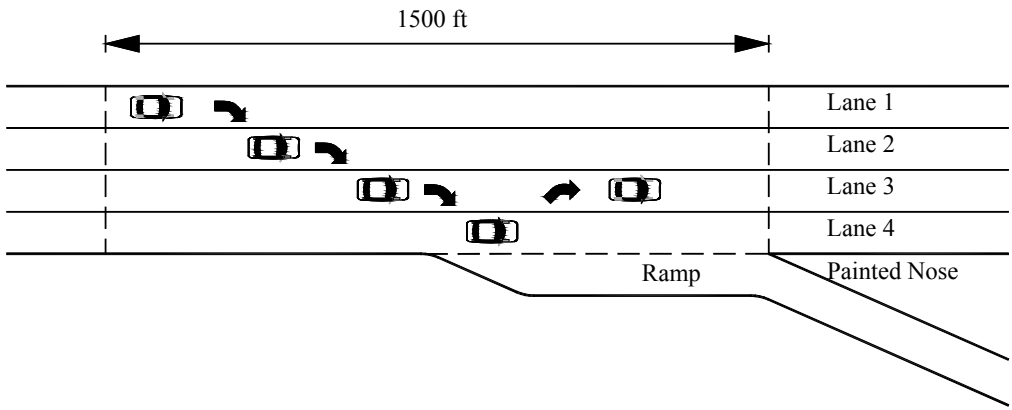

Figure 6. Number of Lane Change on Freeway

The exit ramp type is the first factor that has impacts on number of lane change. Because different types of ramps tell drivers different information and cause

different driving behavior. Besides it, other factors might also affect number of lane change. Volume on freeway is a reasonable factor because more vehicles on freeway, more vehicles exiting, and more probability of lane change. Volume on ramp has the same reason. Number of through lane on freeway also works, more lanes means more lane change. Another possible factor is operational speed on freeway, by the consideration that different speed provides diverse difficulty level of changing lane.

Data collection of totally 24 exit ramps was conducted to get all these data. Ramp type and number of through lane on freeway were known before observing. Volume on both freeway and ramp were captured by people counting in the field. The operational speed was detected in assistance of radar gun. And number of lane change was collected by setting up video cameras. All data are shown in Table 1.

Table 1. Demonstration of Lane Change

No.	Ramp Type	Number of Through Lane on Freeway	Freeway Volume (vph)	Ramp Volume (vph)	Operation Speed (mph)	Number of Lane Change
1	Ⅰ	2	1640	731	64.5	28
2	Ⅰ	3	1017	583	66.3	36
3	Ⅰ	3	2072	663	50.1	41
4	Ⅰ	3	2101	654	52.2	53
5	Ⅰ	3	2602	673	62.1	56
6	Ⅰ	4	3855	832	61.4	72
7	Ⅰ	3	3891	782	62.9	88
8	Ⅰ	2	2767	654	56.8	62
9	Ⅱ	2	5256	831	51.5	97
10	Ⅱ	3	5914	1418	48.7	214
11	Ⅱ	3	6756	966	53.8	188
12	Ⅱ	3	5139	954	62.9	176
13	Ⅲ	3	3821	1056	58.7	103
14	Ⅲ	3	3700	778	64.3	87
15	Ⅲ	3	4676	1123	53.0	164
16	Ⅲ	4	4425	1038	56.6	134
17	Ⅲ	4	6000	1852	60.2	166
18	Ⅲ	3	5157	1398	49.2	143
19	Ⅲ	3	6003	1211	60.8	158
20	Ⅲ	3	4524	845	45.6	120
21	Ⅲ	2	4519	1244	49.3	98
22	Ⅳ	3	4280	1214	49.9	143

23	Ⅳ	4	3028	784	64.5	119
24	Ⅳ	2	3933	547	55.9	117

A mathematical model was needed to be presented to evaluate and forecast the possible number of lane change based on all above data. An exponential model was selected, which fitted large number of dependent variables well. The format of the model is shown as following, including seven variables.

$$Y = \exp(a_0 + a_1X_1 + a_2X_2 + a_3X_3 + a_4X_4 + a_5X_5 + a_6X_6 + a_7X_7) \quad \text{Eq.1}$$

Where,

X_1 ——1 for ramp type II, 0 for others,
X_2 ——1 for ramp type III, 0 for others,
X_3 ——1 for ramp type IV, 0 for others,
X_4 —— Number of Through Lane on Freeway,
X_5 —— Freeway Volume (vph),
X_6 —— Ramp Volume (vph),
X_7 —— Operation Speed (mph) on Freeway, and
a_0 to a_7 —— Coefficients.

RESULTS AND CONCLUSIONS

Data of Table 1, including all variables in Equation 1 were analyzed by using mathematical software SPSS 16.0. Independent variables of ramp types are dummy variables, so ramp type I is chosen as the reference variable. In order to lower the errors, value of X_5 and X_6 were divided by 1000, and X_7 divided by 100. This made the absolute value of all variables at the same level. The distribution of error is supposed to be normal distribution, and the confidence coefficient is 95%.

Mathematical analysis showed that the absolute value of a_6 and a_7 were smaller than 0.001, which meant the ramp volume (a_6) and operation speed on freeway (a_7) had very little impacts on number of lane change (Y). Thus, variables X_6 and X_7 were eliminated to simplify Equation 1, see Equation 2.

$$Y = \exp(a_0 + a_1X_1 + a_2X_2 + a_3X_3 + a_4X_4 + a_5X_5/1000) \quad \text{Eq.2}$$

Where, all dependent and independent variables were same as Equation 1.

All coefficients in Equation 1 were calculated by non-linear regression process in SPSS, with fitting parameters, results see Equation 3 and Table 2 as followed:

$$Y = \exp(2.91 + 0.342X_1 + 0.304X_2 + 0.563X_3 + 0.139X_4 + 0.252X_5/1000) \quad \text{Eq.3}$$

Where, all dependent and independent variables were same as Equation 1.

Table 2.Mathematical Results of Equation 2

Variable	Coefficient	Std. Error	Standardized Coefficients Beta
Constant	2.910	0.195	
X_1	0.342	0.185	0.236
X_2	0.304	0.131	0.273
X_3	0.563	0.130	0.345
X_4	0.139	0.061	0.158
X_5	0.252	0.046	0.680

All Standardized Coefficients Beta showed the low fitting level of the model based on all field data. The reason might be the limited sample size of observation, as data of only 24 exit ramps were collected. And it is reasonable to believe that ramp volume would also affect the number of lane change. The number of lane change will increase with ramp volume increasing. And large sample size in the future might help find correlation ship between number of lane change and ramp volume. However, this model still demonstrated the relationships among number of lane change and all possible factors.

Compared to the coefficients of four exit ramp types, number of lane change of type I is the smallest, type IV is the largest, type II and type III are between them. If all other conditions are the same, such as volume speed and lanes, the possible number of lane change of exit ramp type I will be smaller than other three types, meaning the least probability of potential crashes. On the other hand, exit ramp IV has the highest probability of crashes. Exit ramp type II and type III are at the medium level, and type II are a little bit higher than type III. Also, the model indicates that the increasing of through lanes and volume on freeway will cause the increment of number of lane change.

All these conclusions suggest that, bases on the consideration of potential conflicts, one lane exit ramp is prior to two lane exit ramp. Ramp type I is prior to type II if one lane can provide enough capacity for ramp. Ramp type III is prior to type IV if ramp needs two or more lanes.

FUTURE RESEARCH

This research has provided statistical comparison of number of lane change among 4 types of exit ramps. The results and conclusions are benefit for the following research, which need to present quantified design guidelines of selecting optimal exit ramp under certain conditions including geometric and traffic characteristics. In addition, some design issues about the cross road should also be presented in the future.

ACKNOWLEDGEMENT

This research project was partly sponsored by the Florida Department of

Transportation. The FDOT is greatly appreciated for providing help on the information provided. The authors also would like to thank all the Graduate Research Assistants at the Department of Civil and Environmental Engineering of the University of South Florida for their assistance in field data collection and data reduction.

REFERENCE

Huaguo Zhou. (2005). "A Methodology to Evaluate the Effects of Access Control near Freeway Interchange Areas". Journal of Transportation, ASCE. Washington, D.C.

P. K. MUNJAL. (1971). "Propagation of On-ramp Density Perturbations on Unidirectional Two- and Three-Lane Freeways". Transportation Research. Washington, D.C.

J. Wu. (2007). "A detailed evaluation of ramp metering impacts on driver behavior". Transportation Research. Washington, D.C.

Hunter, M. (2001). "OPERATIONAL EVALUATION OF FREEWAY RAMP DESIGN". Transportation Research Record, No. 1751, Transportation Research Board, Washington, D.C.

Kwon, E. (2000). "MAXIMUM POSSIBLE WEAVING VOLUME FOR EFFECTIVE OPERATIONS OF RAMP-WEAVE AREAS: ONLINE ESTIMATION". Transportation Research Record, No. 1727, Transportation Research Board, Washington, D.C.

Newell, G F. (1999). "DELAYS CAUSED BY A QUEUE AT A FREEWAY EXIT RAMP". Transportation Research. Part B: Methodological, Vol. 33 No. 5. Washington, D.C.

McCartt, A T. (2004). "TYPES AND CHARACTERISTICS OF RAMP-RELATED MOTOR VEHICLE CRASHES ON URBAN INTERSTATE ROADWAYS IN NORTHERN VIRGINIA". Journal of Safety Research, Vol. 35 No. 1.

Strategic Transport Model of Beijing and Application to City Centre Transport Policies Evaluat ion

Rui Zhang[1, 2] and Haiyan Wu[2]

[1] PHD student, Beijing Jiaotong University, Beijing 100044 , China, PH (086) 10-5168 5072; FAX (086)10-6832 2547; email: zhangrui@bucea.edu.cn

[2] Beijing Institute of Civil Engineering and Architecture, China, No.1 Zhanlanguan Road, Xicheng District, Beijing 100044, China; email: jiaotong@bucea.edu.cn

ABSTRACT

The change in traffic policy affects the characteristics of traffic and the direction of sustainable development of a city to a great extent. As an international metropolis, Beijing shares the same kind of traffic problems with other cities of the developed world, in its pattern of traffic development, especially in the city centre. The paper first discusses the development of the strategic transport model of Beijing based on the tool of STM (Strategic Transport Model). Then the paper presents an analysis of traffic patterns in the city centre of Beijing, and the policies that can be used to improve travel in the area. The paper presents two scenarios: cordon charge and increase in parking fee policies. The model is used to compare each scenario with a base scenario of Do Nothing, thereby enabling the relative performance of different policy choices to be assessed. Lastly, the paper provides a relative comparison of the two scenarios using travel mode, trip starts, average speeds, etc., and analyzes the effect of each policy on the environment based on NOx emissions. The numerical study testified to the validity of the model.

BACKGROUND

With the rapid economic development in Beijing, travel demand is increasing continuously. There is growing concern about the impact of the private car on our towns and cities, in terms of congestion, atmospheric pollution and associated health concerns, severance and loss of amenity, and the implications for land use policy. To assist in making informed and appropriate transport policy decisions for the city, and assess urban transport policy impacts rapidly using limited data, a strategy transport model of Beijing based on STM (Strategic Transport Model) software of TRL was developed. This paper will describe the model and how it was used to assess the potential impacts of some transport policies on the city centre (within the second ring) of Beijing to verify the validity of the model.

MODELLING MECHANISMS

The STM is a multi-modal modeling framework. It currently uses a simplified, area-based, treatment of road congestion to avoid the necessity for a time-consuming assignment process.

The basic function of STM is to predict forecast trip matrices under policy

and planning scenario assumptions. From the predicted travel costs, measures of congestion and accessibility can be derived. Using speed and traffic flow information estimates of emission levels can also be developed.

The basic STM in Beijing was derived mainly from the basic model specifications. Basic STM incorporates four main elements in the development of travel demand forecasts:

- Trip generation
- Modal split
- Trip redistribution
- Congestion calculations

It's an equilibrium model in the sense that the basic processes are iterated until the starting costs and output costs are sufficiently coincident.

DEVELOPMENT OF THE STM FOR B EIJING

Trip generation model . Trip generation is based on trip rates and related populations. So, given trip rate (r) and corresponding population (pop) we can calculate the trip generation matrix. For home-based (HB) trip generation, suppose the zone number is n, time is t, trip purpose is p, population type is l. Then trip generation of i zone is $T_i, T_i = pop_{ipl} \times r_{ipl}$.

Car ownership model . We can also use a car ownership model to predict travel demand. There has been numerous research in the use of aggregate models to predict car ownership in China. However, research on the use of disaggregate models for trip generation is currently not available even though, there has been abundant research on the use of disaggregate models in developed countries (Gerard De Jong, James Fox, 2004).

In this paper we present an analysis of cross-sectional data on car ownership at the household level, gathered from the 2000 OD survey of Beijing. The relationship of GDP and car ownership is and income is inevitably a main factor that affects private car ownership. Other factors that should be considered are numbers of drivers licenses, distance between work place and home, annual registration fee, price of car and traffic conditions. The structure of the model is as shown in Figure 1.

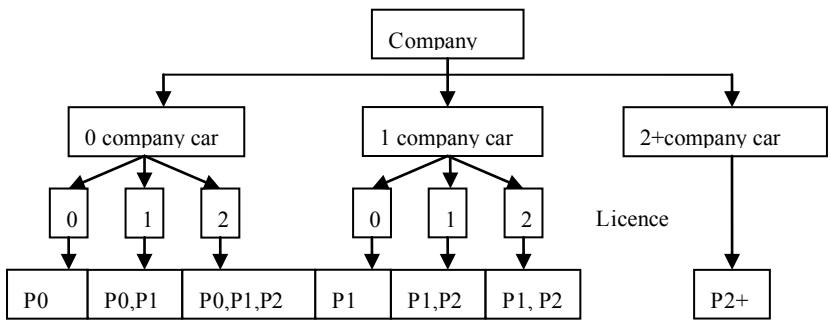

Figure 1. The structure of car ownership model

Generalized costs, calibration, modal split and redistribution . These processes fall within the iterative loop of the model. The modal shift and redistribution are driven by changes in generalized cost relative to the base. Generalized cost in STM is a combination of time and money costs (VOT). The time elements in the generalized costs include access, waiting, transferring and travel time. Money costs include internal and external costs. In this study, the traditional method (based on average income and working hours) is used to calculate VOT. The value of time is $\mathrm{VoT_j} = \alpha_{1j}\, t_j^{v} + \alpha_{2j}\, t_j^{ac} + \alpha_{3j}\, t_j^{wt} + \alpha_{4j}\, t_j^{tf}$, and the money cost is $\mathrm{Cost_j} = \mathrm{f_j} + \phi_j$.

Congestion modeling . STM does not perform an assignment calculation. A calculation is made outside of STM of the likely strategic routes between each zone pair. Each group of similar routes is converted into a zonal route. These routes are used for the purposes of estimating road speeds and journey times. STM road capacity restraint rests upon the assumption that the average traffic flow level in PCU-km within a zone is related to the average speed experienced by drivers moving within the zone according to a speed/flow curve (see Figure 2).

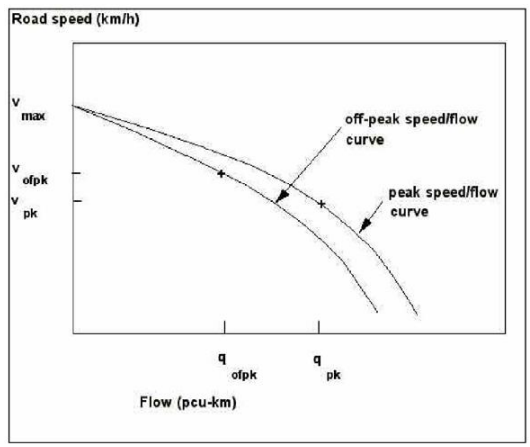

Figure 2. Speed/flow Curves (Marlow and Evans , 1978)

Several roads that represent the main network of Beijing had been surveyed. The calibration parameters of the speed/flow curve are shown in Table 1.

Tab le 1. Beijing Road Network Speed and Flow Values

Type	Max. Speed	Min. Speed	Max. Flow	Plat Flow	Road Grade(China)
1	120	25	1800	1500	Urban motorway
2	60	20	806	637	Urban artery road
3	50	18	560	410	Urban inferior artery road
4	120	50	1661	1275	Rural motorway
5	60	30	700	530	Rural first grade highway

6	50	20	460	310	Rural second grade highway

Elasticity of demand and model calibration. An elasticity of demand may be defined as: the proportional change in demand to the proportional change in the explanatory variable. The price elasticities, which were used in the STM, are as follows:

- Car trips with respect to fuel price
- Rail patronage (trips) with respect to rail fares
- Bus patronage (trips) with respect to bus fares

Basic STM uses the following elasticity values: Bus fares: -0.3, Car fuel: -0.15 and Rail fares: -0.4 (TRL Limited, 2005). For Beijing STM, a State Preference survey sheet has been designed using uniform design methods that include seven indictors (fuel price, fixed cost of commute trip, parking search time, time difference between PT and car, fare, crowding and punctuality), five levels of each indicator and ten cases. The elasticity difference of car fuel is very large from the basic STM one and the corresponding value is -0.36.

The modal split calculations used a model resembling an elasticity approach using "power law" terms. This redistributes total trips between each zone pair over the different modes in the base in accordance with the way in which generalized costs have changed from the base. The approach is incremental in the sense that it automatically reproduces the base market shares. Calibration is achieved by running the model and performing sensitivity tests for fuel price and public transport fares. The outputs demand responses for the study area as a whole are then compared with the upper elasticities. The modal split expression uses the same α coefficient, as seen in the following equation: $K_{mijpct} = \frac{k_{mijpct}(G_{mijpt}/(g_{mijpt}\cdot REI))^{-\alpha_{mpc}}}{\sum_n k_{nijpc}(G_{nijpt}/(g_{nijpt}\cdot REI))^{-\alpha_{npc}}}$ (Oldfield, 1993), where: K= proportion of trips; G= generalized cost; g= base generalized cost; k= base proportion of trips; REI = Real Earning Index relative to base year; α = elasticity calibration parameter;

The demand elasticity e_{fmpc} derived form upper equation is given by: $e_{fmpc} = -\alpha_{mpc}(1-\bar{k}_{mpc})\frac{\bar{f}_{mpc}}{\bar{g}_{mijpt}}$, where, $\bar{k}_{mpc}$, $\bar{f}_{mpc}$ and $\bar{g}_{mijpt}$ are proportions of trips, money cost and total generalized cost for mode m, purpose p, and car ownership c, respectively, and the bars denote that they are the base year values. These are origin-destination trip-weighted average value. Redistribution is based on changes in generalized costs from the base and changes in trip end factors.

EVALUATION OF CITY CENTER TRANSPORT POLICIES

Analysis of traffic in the city centre of Beijing. According to 2005 data, from traffic surveys of Beijing, the average number of person trips increased by 4%,

trips increased by 1.4 times, car trips increased from 5.02% to 23.24%, and the growth rate of private car is 27% (Beijing Government, 2005). All of these factors made the traffic in the city centre worse and lead to a series of unsustainable problems. The reasons for the worsening traffic can be due to the following three factors : 1) the areas of cultural relics are grouped in the city centre, thus limiting the adjustment and expansion of road infrastructure; 2) city construction and traffic development is not coordinated with each other; and 3) traffic is highly concentrated in the city centre and modal split is unreasonable because the quality of public transport makes it less competitive with the private car.

Policy analysis for city centre . Due to a lack of land resources and the strict restrictions imposed by cultural relic protection, from a sustainable standpoint, the road network in the city centre would be difficult to expand and modify. Thus, the main policy for the centre should be to stress public transport priority and to limit car traffic to some extent. From a strategic level, the following policies can be considered: public transport priority policy, parking policy and cordon charge policy

Scenario design. According to the policy analysis of the city centre, the following scenarios were considered in 2020:

- Do nothing;
- Charge cars for going in, out and through the second ring road (city centre boundary) at peak hour;
- Increase on-street parking fee by 100% and off-street parking fee by 30% in city centre;

Traffic policy evaluati on. Using the Beijing strategic transport model, the three scenarios were analyzed separately. To compare the effects of each policy, the cordon charge policy and the parking policy were compared with Do Nothing. We chose all regions and all purposes in a peak to compare the trip starts (person·km). The difference in traffic demand between the Do Nothing and the implementation of the cordon charge and increased parking fee policies were quite obvious. For the parking policy, average trip distance decreased by 0.188%, average speed increased by 0.028%. For the cordon charge policy, average trip distance decreased by 1.43%, average speed increased by 0.223%. The proportion of sustainable traffic modes like bus, rail, cycle and walk increased and the proportion of car travel decreased especially in the use of cordon charge policy. The whole traffic demand also decreased. Some of the results can be found in Figure 2.

Figure 3 shows the emission of NOx on the whole area of Beijing (The four middle zones consist of city centre). The darker the color, the higher the reduction in emissions. The analysis found that the cordon policy would be more effective in reducing emissions.

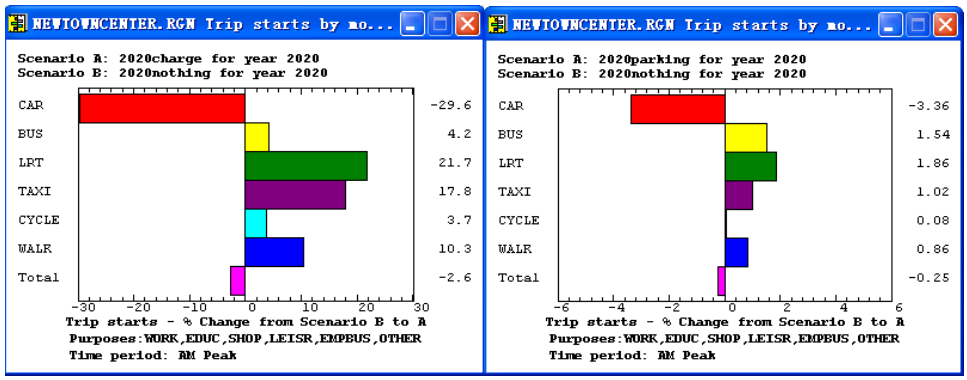

Figure 2. City centre trip starts ch ange by mode in 2020 by difference policy

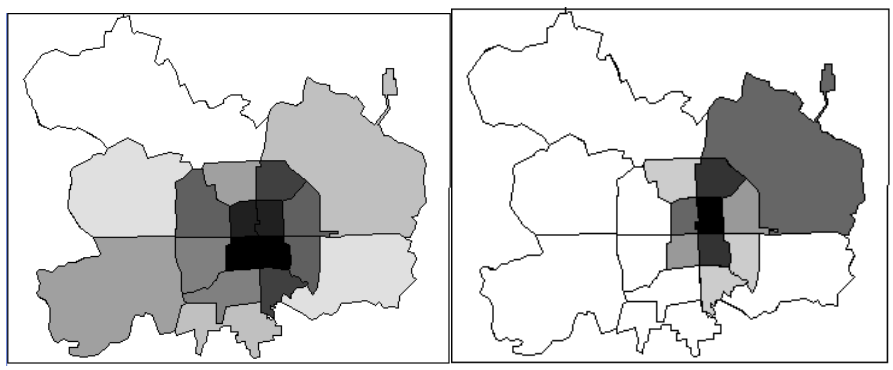

Figure 3. Emission NOx (g/hr) analysis (charge policy and parking policy)

CONCLUSION S

From the quantitative results of the Beijing strategic transport model and the qualitative analysis above, the two policies can be approved. The strategic transport model can solve the problem of inaccurate traffic forecast being caused by unsuitable policy and can be used as a computer tool for policy analysis and decision-making. The most important feature of the model is that different scenarios can be tested in a short time. The result of the model is not absolutely satisfactory right now, and there is still a need for further research in such areas as the size of the zones, the simplification degree of the road network, and in the use of elasticities of demand.

REFERENCES

Beijing Government. (2005). Transportation Developing Compendium of Beijing, Beijing Publishing House.

Gerard De Jong, James Fox, Andrew Daly, et al. (2004). “Comparison of car ownership models”. Transport Reviews, 24(4), 379-408.

Marlow M., Evans R. (1978). “Urban congestion survey 1976: traffic speeds in eight towns and five conurbations”. TRRL Supplementary Report, 438.

Oldfield R. H. (1993). “A strategic transport model for the London area”. TRL Research Report, 376.

TRL Limited. (2005). TRL Strategic Transport Model User Manual, 66, TRL Limited.

Real-time Monitoring System Architechure of Hazardous Goods Logistics Based on RFID

Minai He

Department of Transportation and Logistics Engineering， Shandong Jiaotong University， Jinan City， Shandong Province, China； PH(15853118170)； email:heminai@126.com

ABSTRACT

Hazardous goods logistics are very important to the national economy; this paper introduces a systems architecture of hazardous goods logistics management based on RFID, and it proposes a related model for operation and data flow. This architecture helps us to control the whole process of hazardous goods management, creating a visual transportation management system for hazardous goods based on Radio Frequency Identification (RFID). This system provides customers an advanced and scientific information management suite, and it reduces the rate of accidents during the transportation of hazardous goods.

Key words: Hazardous goods, Transportation, Identification, Visualization

1 SUMMARY of HAZARDOUS GOODS

According to the national standard *Classifying and Numbering of Hazardous Goods* (GB6944-86), hazardous goods are defined as those goods that are explosive, flammable, poisonous, perishable, or radioactive. These items require special preventive measures during transportation, handling, and storing, since they are extremely dangerous to people and the environment.

According to statistics, there are about 400 thousand tons of various hazardous goods produced every year in the world, and enormous numbers of fatalities occur during their storage and transportation. Once an accident occurs, serious outcomes are certain to follow. The chances of an accident happening during storage is usually smaller than that of transportation, since hazardous goods are usually stored far away from human living spaces. However, accidents that occur during the transportation of hazardous goods, including fires, explosions, leakage, poisoning, and pollution, do great harm to people, society, and the environment. Therefore, a greater focus on hazardous goods in transportation is needed. World governments have established many statutes and laws to ensure safety during the

transportation of hazardous goods and to standardize the logistical handling of such goods.

National and local governments have also become aware of the importance of developing of hazardous goods logistics. In 2001, the People's Republic of China passed new rules governing the transportation of hazardous goods. Local departments seriously sought to enforce requirements for three licenses and one surveillance. The three licenses include the capacity of company license, one showing the qualification of the personnel, and one verifying the technology of the vehicle. The surveillance is meant to ensure the supervision of the hazardous goods in loading and unloading, storage and transportation. Intended goals of this governance were to: ①re-censor those corporations transporting hazardous goods, ensuring that all practitioners were acting in accord with the capacity need; ② make sure that all practitioners were congnizant of their need to be qualified for transportation of the goods and to ensure that loading occurred with permission; ③ conduct across-the-board inspections regarding the technological capacity of vehicles transporting hazardous goods, with the ultimate goal of ensuring that all vehicles receive arterial technology.

However, the fact that more and more corporations and practitioners are transporting hazardous goods has still led to the destandardization of logistical operations and inadvisable management practices. We still see uneven levels in technology and logistical equipment, as well as uneven documentation levels. Accidents involving hazardous goods are still common. In addition, once accidents occur, their damage may be aggrevated by the fact that exact information about the goods cannot be immediately attained.

2 NECESSITY of BUILDING VISUAL LOGISTICS MANAGEMENT SYSTEM for HAZARDOUS GOODS

Road hazardous goods transportation is the term for the process of delivering hazardous goods by special-purpose vehicle. Road transportation, which plays an important role in hazardous goods transportation, is characterized by its numerous nodes, its ability to cover a wide area, its simple organization and flexibility, and so on. In order to ensure the safety of hazardous goods in transportation, China has established and utilized laws and regulations for road transportation, such as the "Regulations for Management of Road Hazardous Goods Transportation," "Transportation Rules of Hazardous Goods by Vehicles," "Vehicle Signs for Road Hazardous Goods Transportation," "Operation Regulation of Hazardous Goods Transportation," etc. These standards are the basis for a governing department, which should be strictly followed by corporations engaging in hazardous goods transportation. Considering the rapid development of the civil economy and rising number of hazardous goods in variety and quantity, the government cannot supervise

and control hazardous goods through traditional management methods.

Thanks to the development of certain computer technologies, the Internet, RFID, GPS and GIS can provide technical support for a Visual Logistics Management System for Hazardous Goods. Therefore, it is necessary to construct a uniform supervising plan for hazardous goods transportation and a visual logistics management system that can ensure the transmission of accurate, credible information in real-time, while preventing accidents from the start.

3 A SYSTEM ARCHITECTURE OF VISUAL HAZARDOUS GOODS LOGISTICS MANAGEMENT BASED on RFID

RFID is one kind of non-contact, automatic identification technology. Its basic principles are shown in Figure1.

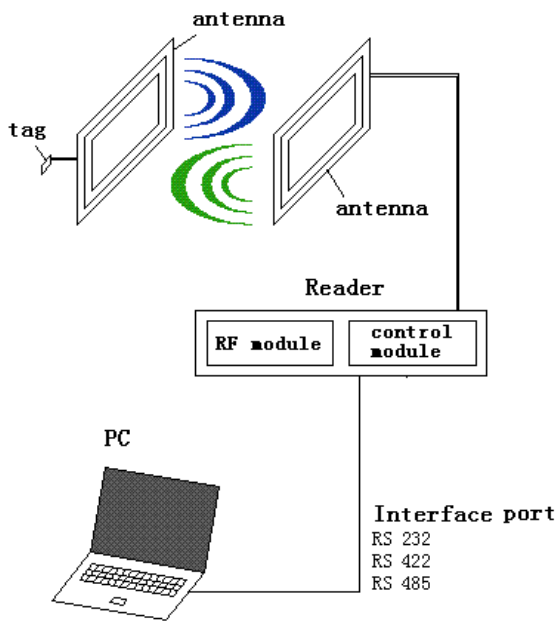

Figure 1.The basic principles of RFID

The RFID system is comprised of a reader, an electronic tag, and an antenna. The electronic tag carries information, used to store the related data and transportation information. The reader can generate radio waves through the antenna at a certain frequency. When the tag enters the broadcast area, it can broadcast the data from a tag, and data can also be written on the tag. At the same time, all data is updated by a management system. The topological structure of a visual logistics management system based on RFID is shown in figure 2.

Functions achieveable through the MIS include : ① monitoring and management of the logistical handling of hazardous goods; ②monitoring the inventory and status of the goods; ③ management and supervision of the technical

condition of vehicles transporting the goods; ④ supervision and control over the transportation route followed by vehicles, while also monitoring the position of the goods;⑤ monitoring the validity of customers receiving the goods; ⑥ the ability to create a centralized emergency response system ⑦ management of the dealers' qualifications.

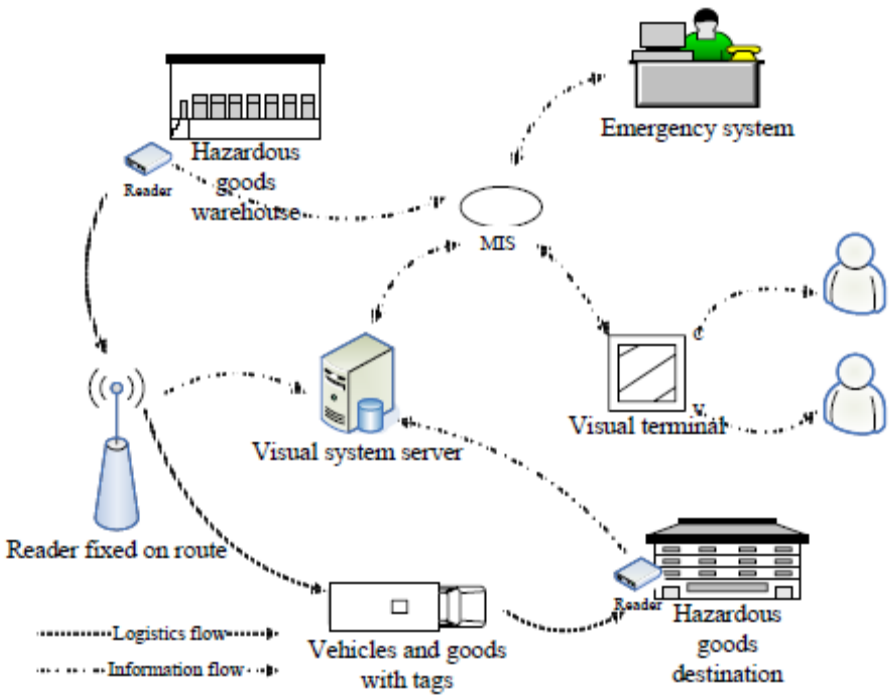

Figure 2.System Architecture of visual hazardous goods logistics management

The regional visual server system contains the perfect database for managing information such as the storage and handling processes of the hazardous goods, vehicle and route information, practitioner licenses, and emergency information. The visual device provides relevent goods information in real-time to the managers and customers.

4 OPERATIONS AND DATE FLOW OF VISUAL HAZARDOUS GOODS LOGISTICS MANAGEMENT SYSTEM BASED ON RFID

The visual hazardous goods logistics management system based on RFID enables automatic control of the whole process by identifying information stored on the tags. Its operations and data flow are shown in figure 3.

Hazardous goods should be delivered along a previously determined route. RFID readers are fixed at key points along the path, including the starting point, rest stop, and final destination point. When tagged vehicles arrive at a warehouse, the RFID reader reads the vehicle information. Every box of hazardous goods has a tag on it. After consignment at the warehouse, the PDA writes a transportation receipt

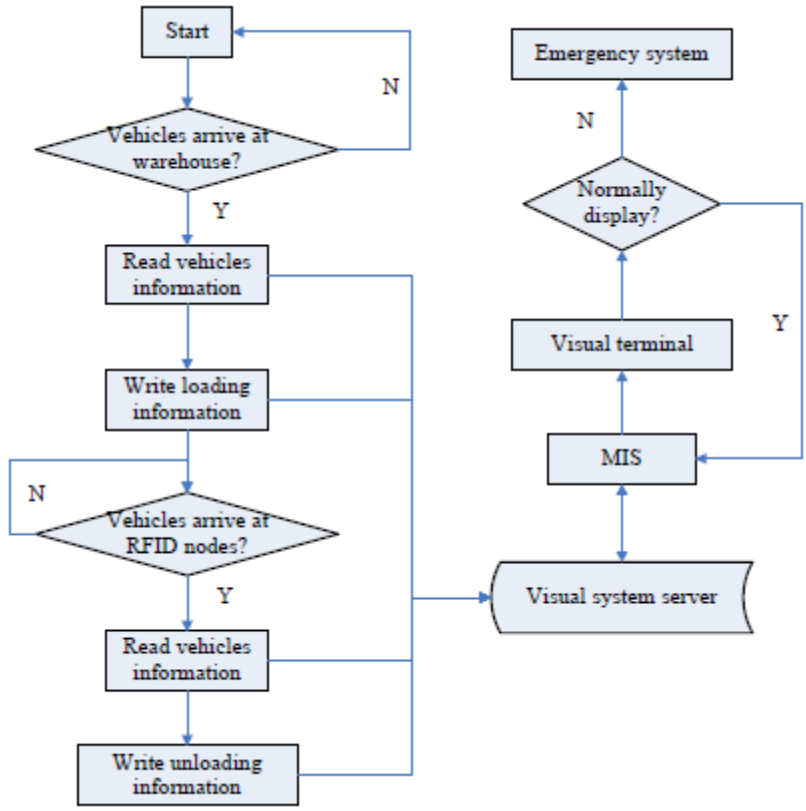

Figure 3 Operation and date flow of Hazard goods

onto the electronic tag, including the bill number, type, and serial number of hazardous goods; shipper and consignee information; normal route and so on. When vehicles and goods arrive at or depart from a rest stop or defined location, the RFID reader automatically reads the vehicle and goods information on the tags, stamping the arrival and departure times. It then sends that information to the regional visual system server, enabling system managers obtain the real time information. The visual terminal displays hazardous goods information to managers and customers. It could be the computer network terminal or portable data terminal, by which customers receive important information and control the hazardous goods. This ensures receipt of the information both visually and conveniently.

The route and condition of vehicles transporting goods is transmitted by a combination of gridding technologies, such as GIS and GPS. To keep the highways safe, 60km/h should be set as a reasonable maximum speed limit on ordinary highways, and the freeway should be limited to 80km/h. Twenty kilometers per hour should be the top speed during increment weather. The system would send a warning signal if it detects that the vehicle is exceeding the speed limit.

For some hazardous goods with special environmental requirements, like strict temperature or pressure control, related sensors are fixed on the vehicles to

detect real-time temperature or pressure, sending them to the visual system server. Once the temperature or pressure exceeds the limit, the system will immediately sound an alarm and take quick action to solve the problem.

When an accident occurs, an annunciator panel automatically sends an alarm to the visual system server, which immediately receives the accident location, vehicle information, and inventory of the hazardous goods. At the same time, an emergency response system is activated to organize responders and ensure minimum expense.

5 CONCLUSIONS

This paper presents a system architecture of visual hazardous goods logistics management. It also puts forth a model for operation and data flow. The system could supervise and control the hazardous goods logistics and state information, providing an interface for managers and customers. Development and application of the system is sure to transform the field of hazardous goods logistics, contributing to a safer society and healthy economy.

BIBLIOGRPHY

Li Jun, Zhang hongli, Liu Jianxin. "Vehicle visual scheduling system." *Journal of Traffic and Transportation Engineering*. 2004, (1).

Qiu Xiaoyong, Liu Kai, Feng Chun. "Exploring in development of RFID and modern logistics management." *Logistics Technology*. 2005, (2).

Dong Hongwei, Li Guohua, Cao Ronghui. "Design and development of Realtime Monitoring System for dangerous goods transport." *Railway Computer Application. 2008*, (2).

Chen Zixia. "Application of RFID and modern logistic." *Business Research*. 2003, (6)

Liu Kesheng, Dong Xuejie, Wu Liubing. "Application of Automatic Identification in Logistics Informationization." *Logistics Science and Technology*, 2003, (5).

Public Transport Incident Prediction Method By Road Traffic Delays

H. Z. Gao[1], Y. Han[2], L. L. Zang[3], C. Xu[4] and H. N. Wu[5]

[1] Business School, University of Shanghai for Science and Technology, P.O. Box 22, 516 Jungong Rd. Shanghai 200093, China, PH (86) 21- 5527 0592; FAX (86) 21-5527 0592; email: gao_hongzhen@163.com
[2]Business School, University of Shanghai for Science and Technology, P.O. Box 105, 516 Jungong Rd. Shanghai 200093, China, PH (86) 21- 5527 0592; FAX (86) 21-5527 0592; email: hanyin2000@sina.com
[3]Business School, University of Shanghai for Science and Technology, P.O. Box 105, 516 Jungong Rd. Shanghai 200093, China, PH (86) 21- 5527 0592; FAX (86) 21-5527 0592; email: zll0414@163.com

ABSTRACT

In order to reduce the running-time delay and improve the on-time arrival rate, this paper takes into consideration that most urban road networks are discrete traffic flows, combined with traffic signal control equipment and traffic flow collection device. We have used research on the public transport incident prediction model and algorithm by the road traffic delays in order to carry out an automatic prediction of the public transport incident delay making our public transportation more intelligent. This model could make a much better prediction and save much more time for dealing with the emergency, reducing the running delays and better meeting the passengers' demand for a shorter travel time.

INTRODUCTION

Compared with some developed countries, the level of public transportation service of some large and medium-sized cities in China is still relatively, mainly due to some aspects (Han, 2006): (1) Buses arriving and departing time is uncertain; (2) Informational services are nearly a blank; (3) Cannot get the information of whether or not public transportation incidences happen, there is no bus incident identification and coordination dispatching system; (4) Considering the incidents just based on the experience, there is no advanced scientific technology to ensure that we have made the right judgments, and the rapid response system dose not exist.

With the rapid development of intelligent transportation, minimization of the public transportation delay is a very important problem; bus delays have many causes, such as the road environment, traffic conditions, vehicle status, and queuing delay at signalized intersection, and so on. The four factors are interconnected, when any of the factors runs abnormally, a bus delay may happen. Therefore, in order to reduce the incidence of the delays, appropriate preventive and treatment measures should be adopted. The prediction of bus delays is based just on this principle.

PUBLIC TRANSPORT DELAYS AND FACTORS

Research shows that the public transport delay is related to lane occupancy, bus-running speed, and the queuing delay at signalized intersections. If lane occupancy becomes higher, the bus running speed becomes lower, the queue waiting time at signal intersection becomes longer, and the more bus delays will happen. Therefore, we can construct a bus delay prediction model from the three aspects.

Lane occupancy. Because of the complexity of traffic flow, the state of traffic operation in the road network varies with the time. Once traffic crowded incidents happen, the flow of the upper detector reduces; occupation rate increases; simultaneously downstream detector, the volume and occupation rate will decrease. Making judgments by the volume's or occupation rate's increase and reduction often do not reflect the substance of the process of crowding (Wang, 2005). In fact, because of the number of detected vehicles increases in unit time, the speed remains unchanged, and it will inevitably lead to the increase of the occupation rate. However, if the relative increment of volume is greater than the increment of the volume in the occupation rate, then it can judge that the traffic flow in this time is in a state of dissipation or it is in the state of crowded traffic.

In order to facilitate the discussion, we assume that the bus' length fixed L, detection coil width fixed d, according to occupation rate C's basic definition:

$$C=\frac{\sum_i (L+d)/v_i}{T}=\frac{L+d}{T}\sum_i \frac{1}{v_i}=(L+d)\frac{n}{T}\frac{1}{n}\sum_i \frac{1}{v_i}=(L+d)q\frac{1}{v}=(L+d)k \qquad (1)$$

Put formula (1) into traffic flow basic model:

$$q=k\bar{v}=\frac{C}{(L+d)}\bar{v} \qquad (2)$$

From type (2), we can see that when the speed is invariant, the traffic flow is proportional to occupation rate and their rate of change is the same, therefore, and can be:

(1) When the relative increment of flow is greater than the relative increment of occupation rate, the traffic tends to disperse;

(2) When the relative increment of flow is smaller than the relative increment of occupation rate, the traffic tends to crowd.

Public transport travel speed. Through the bus-car GPS system (Liu, 2008), we can get the real-time link travel speed $v_i(t)$, according to a large number of historical data we can get the minimum bus speed and stability bus flow, the threshold v, the crowded state discriminates is as follows:

(1) If $v_i(t)$ smaller than the established threshold v, then think section i

being crowded.

(2) If $v_i(t)$ greater than the established threshold v, then think section i unobstructed.

Queue delay at signal intersection. When it is a single lane, the capacity of intersection is limited; therefore, the queuing model belongs to a limited capacity system model, and the queue is a single row, so it is in accord with model M/M/1/N ^{j} /∞ (Han, 2003). Particularly, under steady-state conditions, the probability $P_{ij}^{(k)}(t)$ that there are k vehicles queuing at an intersection is unrelated with the moment.

The vehicles queued at a downstream intersection at section j during period i, to every vehicle, transfer probability is $\lambda_j(t)P_{ij}^{(0)}$, where $\lambda_j(t)$ is a vehicle arriving rate, $\lambda_j(t)$ is the vehicle arriving rate of entrance of section j at t moment which got from the detector, which means $\lambda_j(t)$ is a function related with t, take $\lambda_j(t)=\lambda_{ij}$;the maximum capacity of downstream intersection of section j in unit time is denoted by $\mu_j(t)$, let certain direction split g_{ij}, the effective service rate take $g_{ij}\mu_j(t)$,then suppose in any period i, the capacity in unit time is the same; so take $\mu_j(t)=\mu_j$, as one queuing vehicle bears off, the transfer probability is $g_{ij}\mu_j$.

List out the steady-state equation:

$$\begin{cases} g_{ij}\mu_j P_{ij}^{(1)} = \lambda_{ij}P_{ij}^{(0)} & \\ g_{ij}\mu_j P_{ij}^{(k+1)} + \lambda_{ij}P_{ij}^{(k-1)} = \left(\lambda_{ij}+g_{ij}\mu_j\right)P_{ij}^{(k)} & k \le N_j - 1 \\ \mu_j P_{ij}^{(N_j)} = \lambda_{ij}P_{ij}^{(N_j-1)} & \end{cases} \tag{3}$$

According to $\sum_{k=0}^{N_j} P_{ij}^{(k)} = 1$, let $\rho_{ij} = \dfrac{\lambda_{ij}}{g_{ij}\mu_j}$ then we can get

$$P_{ij}^{(k)} = \begin{cases} \dfrac{1}{N_j+1} & \rho_{ij}=1 \\ \dfrac{1-\rho_{ij}}{1-\rho_{ij}^{N_j+1}}\rho_{ij}^{k} & \rho_{ij}\neq 1 \end{cases} \qquad k=0,1,2,\cdots,N_j \tag{4}$$

Then queuing vehicle number at section *j* at i is

$$L_{ij}^{(q)} = \begin{cases} \dfrac{N_j(N_j-1)}{2(N_j+1)} & \rho_{ij}=1 \\ \dfrac{\rho_{ij}^2}{1-\rho_{ij}} - \dfrac{(N_j+\rho_{ij})\rho_{ij}^{N_j+1}}{1-\rho_{ij}^{N_j+1}} & \rho_{ij}\neq 1 \end{cases} \tag{5}$$

$$T_{ij}^{(q)} = \frac{L_{ij}^{(q)}}{\lambda_{ij}\left(1 - p_{ij}^{(N_j)}\right)} = \begin{cases} \dfrac{N_j - 1}{2\lambda_{ij}} & \rho_{ij} = 1 \\ \dfrac{\rho_{ij}}{\mu_j - \lambda_{ij}} - \dfrac{N_j p_{ij}^{(N_j)}}{\mu_j\left(1 - \rho_{ij}^{N_j}\right)} & \rho_{ij} \neq 1 \end{cases} \tag{6}$$

where, $P_{ij}^{(k)}(t)$ is the probability of the k queuing vehicles at intersection, N_j is capacity of section j, λ_{ij} is the vehicle average arrival rate of section j the during i period, g_{ij} is running direction split of the downstream intersection at section j during i period, u_j is the biggest capacity of the downstream intersection of section j in unit time, ρ_{ij} is traffic intensity.

When $T_{ij}^{(q)}$ becomes greater, the bus will be prone to have delays, rather than less prone to have delays.

MODEL CONSTRUCTION

According to the selected characteristic index, we construct the following model:

$$\min f = \alpha(\Delta q_{ij} - \Delta C_{ij}) + \beta(v_{ij}(t) - v) - \gamma T_{ij}^{(q)} \tag{7}$$

Where, $\alpha + \beta + \gamma = 1$, i is the time period (i=1, 2……n), j is section (i=1, 2……n), Δq_{ij} is relative increment of the flow in time i section j, ΔC_{ij} is relative increment of occupation rate in time i section j, $v_{ij}(t)$ is bus running speed in time i section j, v is the minimum speed under stable bus traffic flow, and $T_{ij}^{(q)}$ is queue delay at signal intersection in time i section j.

The greater f becomes, the greater the chance of delay. We can get the value of the threshold k based on historical data. When $f < k$, the delay incident will happen, when $f \geq$ k, the delays will not happen.

Before prediction, the test data should be calculated first, we get Δq_{ij} ΔC_{ij}, $T_{ij}^{(q)}$ and other data, then we can make the prediction. The prediction flowchart of the model is shown in Figure 1.

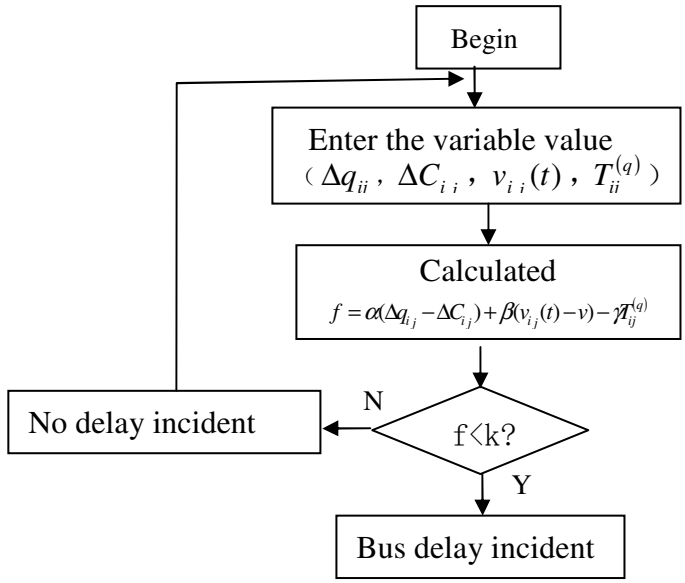

Fig.1 Bus delay incident prediction flowchart

MODEL SIMULATION

In order to survey the testing effect of the model, in the conditions that actual data is hard to collect, we often get the large number of incident and non-incident state test data by way of simulated methods (Wen, 2005). In this text, we choose a segment with three intersections and two bus stops (see Figure.2). Let $\Delta q_{ij} = \Delta C_{ij}, v_{ij}(t) = v$, Queue delay time $T_{ij}^{(q)}$=1(minute), $\alpha = \beta = 0.25$, $\gamma = 0.5$, so threshold $k = -0.5$. We input 100 groups of data, 60 of which are delay incident data, 40 of which are not delay incident data, to evaluate the model.

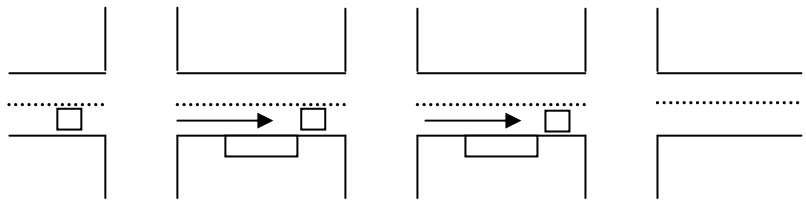

Figure 2 Traffic simulation map

Performance indexes usually used to evaluate incident detection algorithm are detection rate, false alarm rate and average detecting time. 100 groups' data are used to test the model. Calculate and output *f*. If $f < -0.5$, it is identified as the delay incident.

Test results are: detection rate is 96.3%, false alarm rate is 3.12%, and average detecting time is 40s.

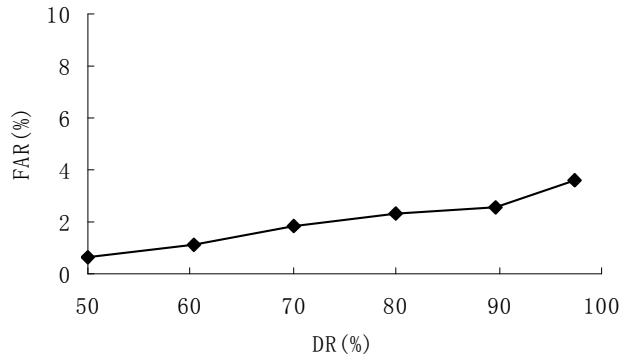

Figure 3 Relation between detection rate and false rate

Figure 3 shows the relation between detection rate and false rate, the results show that the model made a good prediction for the public transport delay incident. Through the test simulation, the model can effectively detect the occurrence of delays in public transport. Therefore, the prediction of the bus delay incidents can make a scheduling department to have advanced preparation to reduce bus delay time and shorten bus travel time.

CONCLUSION

A bus delay incident identification model was built on the testing data from annular induction coil, in-car GPS returns, and a vehicle random queuing model. Through test simulations, it can effectively identify the occurrence of bus delays in public transportation, the method and model has a great applicability.

Because public transportation incident forecasting is still in its infancy, if a model is to be applied to practice, further research needs to be done, for example, determining the parameter values such as α, β, γ and determining the average queue delay time.

ACKNOWLEDGEMENT

Shanghai Science and Technology Commission for major scientific and technological research projects (07DZ12061); Shanghai key subjects project（S30504; The major project of Shanghai Education Committee (07ZZ91); The Innovation Fund Project For Graduate Student of Shanghai (JWCXSL0802)

REFERENCES

Han Y., Z. S. Yang. “Design on intelligent real-time dispatching system of public transport network.” *The 2th International Conference on Traffic and Transportation Studies*, Guilin, 883-888. (2002)

Han Y. “Research on basic theories and implementation methods of public transportation intelligent dispatching system.” *Jilin University PhD thesis*. (2003).

Han Y. "Research on the theoretical model and method of the intelligent bus event identification and intelligent coordinate scheduling system." *The forefront engineering*, 3(1), 125-139. (2006).

Liu E. Q. "Study on the methods of traffic state identification for urban road basing on GPS data of services vehicles." *Jilin University master's degree thesis*. (2008).

Wang P. H. "Study on traffic emergence management system and some related theoretic question." *Tianjin University PhD thesis*. (2005).

Wen J. "Study on automatic detection algorithm for traffic incident using neural network based on rough set filtration." T*ianjin University master's degree thesis*. (2005).

Yang Z. S., Han Y. "Study on the method of basic data gathering and forecasting about public transport intelligent dispatching system". *The 2th Beijing International Exhibition and Seminar on Intelligent Transport Systems*, Beijing, 655-661. (2002).

S. B. Pattnaik, S. Mohan, and V. M. Tom. "Urban bus transit route network design using genetic algorithm." *Journal of Transportation Engineering*, 26(5), 368-375. (1998).

The Application of the Maximal Coverage and Partial Coverage Model in the Shelter Location Problem

Xiao-Qiang Ren[1], Juan Chen[2], Gao Guo[3] and Wen-Ping Cai[4]

[1]Engineer; Master; Changchun Municipal Engineering Design and Research Institute; PH (0431) 8996-5000; email: rxqsir@vip.sina.com
[2]Master candidate; School of Transportation Science and Engineering, Harbin Institute of Technology; PH (0451) 8233-9340; email:hitchenjuan@163.com
[3]Engineer; Changchun Municipal Engineering Design and Research Institute; PH (0431) 8996-5016
[4]PH (0431) 8469-5622; Changchun Municipal Government Center, the construction and management of investment projects

ABSTRACT

If there is a catastrophic event in a city, it is necessary to provide the suffering people with shelters to get a refuge. Based on the analysis on the city shelters planning principles, the covering area of the shelter should be big enough and should maximize the coverage level of the demand points. At the same time, it should consider the capacity of shelters, and this paper is aimed to modify the maximal covering location problem (MCLP), which based on the P-median model to get a capability limitative MCLP-P. The analysis of an example finds that the shelter layout has more applicability and also proves that the trimmed model is reasonable. Furthermore, it is expected to offer some reasonable evidences to build catastrophic facilities in the future.

1 INTRODUCTION

In the modern world, cities are more easily threatened by catastrophic events. If a serious natural disaster occurs in a city, especially an earthquake, it is impossible to evacuate all the residents to the suburban safe area. The aim is to build shelters to provide suffering people with safe places and prevent the harm of a secondary disaster. At the same time, it should ensure daily life, iatrical rescue and communication. In the preventable disaster system of the entire city, if emergency shelters can be planned and built, it will be a good measure in decreasing the casualty and economy losses of a fatal paroxysmal event, such as an earthquake, fire, flood, etc. The big earthquake of Wenchuan, in the southwest of China, brought serious disaster to the Chinese and revealed the importance of building shelters reduce the harm of a disaster.

2 PRINCIPLES OF SHELTERS LAYOUT

The main problem of a city shelter layout is: in a city, the density of the population is determined and evacuation routes are limited. Because of the shortage of funding and the restriction of the environment, few locations can be selected to be used as shelters (Huang et al., 2004).

2.1 Requirement for city shelter scale

There are two kinds of shelters (Su et al., 2004): permanent and temporary. A temporary shelter is a small, temporary facility that makes use of a sub-district park, small public square, etc, which, next to the residents' housing, averages 1~2m^2 for each person, totaling more than 1000m^2, and its service radius is 300~500m. A permanent shelter is a park, school, public square, playground, or stadium used for setting up tents and temporary buildings that can hold more than 1000 residents, averaging 2~3m^2 for each person, totaling not less than 15000m^2 with service radius is 500~2000m.

2.2 The confirmation of the shelter number and capacity

Before a shelters layout, it must take a risk analysis of the city to confirm the distribution of dangers, which is based on geographical factors, natural factors and the past years' statistics of the disaster dates (Zhou et al., 2007). Combining the economic level, it can confirm the shelter area of every person, at the same time, based on the incidence, it can confirm the appropriate region of the preliminary building shelter. Statistically, the location distribution within the region which can be used to build shelters, such as large gymnasium, park, school, church and so on. However, the population and its distribution in the city can confirm the number and the capacity of the rebuilt shelter.

3 ESTABLISHMENT OF THE SHELTER LAYOUT MODEL

Shelters belong to the public ministrant facility, so residents demands should considered to ensure the optimum shelter layout. At present, there are few mathematical models for city shelter layouts, so shelter layouts usually depend on the facility location problem (Yin, 2007). The facility location problem is ensuring one or more optimal facility locations with the optimum aims, such as the minimum distance, the lowest transportation cost, and the maximum market share (Sherali, 1991). Because of the particularity of shelters, this paper chooses the maximal covering model of partial coverage (MCLP-P) to make shelter layouts.

3.1 The maximal coverage and partial coverage model in the location problem

A basic assumption in almost all of the maximum covering location problem

(MCLP) formulated to date is that the demand points are assumed to be covered completely, if located within the critical distance of the facility and not covered at all outside of the critical distance, and rebuild P emergent facilities to cover most of the demand points within the stated critical distance (Orhan, 2004). Such an assumption is not always reasonable provided that the coverage does not change in a crisp way from "fully covered" to "not covered" at the critical distance. In some situations, it may not be possible to guarantee the full coverage of the demand points depending on the distance between the demand point and the facility site. The partial coverage, which is defined as a function of the distance of the demand point to the facility. We assume that the demand point can be fully covered within the minimum critical distance, partially covered up to a maximum critical distance, and not covered outside of the maximum critical distance.

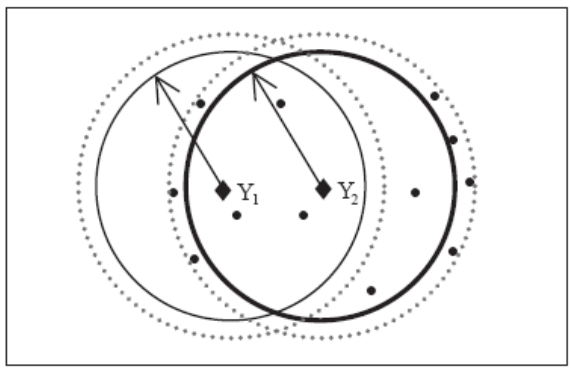

Fig 1 the maximal coverage and partial coverage.

Fig 1 depicts the partial coverage model to solve the location problem. Suppose that there are two potential facility locations and only one will be chosen. The solid line shows the radius of the full covered and the dotted line shows the partial covered. Within the full coverage range, location Y_1 can cover 6 demand points and Y_2 can cover 5 demand points. So, the MCLP will choose Y_1 as the optimal choice. If we employ the partial coverage idea, we may choose Y_2 instead of Y_1, because location Y_2 covers 5 demand points fully and an additional 7 demand points partially, but location Y_1 covers only 6 demand points fully.

3.2 The MCLP-P model

This MCLP-P model is based on the classical p-median model. However, the aim of this model is not the minimal critical distance but the maximal coverage of demand points. The model of the MCLP-P is as follows:

$$Z = Max \sum_{i \in I} \sum_{\notin M_i} C_{ij} x_{ij} \tag{1}$$

$$\text{s.t.} \quad \sum_{j \in J} y_j = P \tag{2}$$

$$x_{ij} \le y_j \qquad \forall i \in I, j \in M_i \tag{3}$$

$$\sum_{j \in M_i} x_{ij} \le 1 \qquad \forall i \in I \tag{4}$$

$$y_j \in \{0,1\} \qquad \forall j \in J \tag{5}$$

$$x_{ij} \in \{0,1\} \qquad \forall i \in I, j \in M_i \tag{6}$$

where I is the index set of all demand points, J is the index set of all potential facility sites, P is the number of facilities to be sited, M_i is the set of facility sites that can either fully or partially cover the demand point i, S is the maximal radius of full covered, T is the maximal radius of partial covered ($T > S$), D_{ij} is the travel distance between the facility j and the demand point i, C_{ij} is the level of coverage provided by the facility j to the demand point i.

$$C_{ij} = \begin{cases} 1 & D_{ij} \le S \\ f(D_{ij}) & S < D_{ij} \le T, (0 < f(D_{ij}) < 1) \\ 0 & \text{otherwise} \end{cases} \tag{7}$$

$$y_j = \begin{cases} 1 & \text{if a facility is sited at j} \\ 0 & \text{otherwise} \end{cases} \tag{8}$$

$$x_{ij} = \begin{cases} 1 & \text{if the demand point i is either partially or fully covered by a facility j} \\ 0 & \text{otherwise} \end{cases} \tag{9}$$

The objective function (1) maximizes the coverage level within the maximum critical distance T. Constraint (2) ensures that the total number of facilities sited equals P. Constraint (3) shows that if facility j is not sited, all x_{ij}'s associated with facility j will be forced to become 0. The constraints of type (4) require that the demand point will be covered by at most one of the facility locations sited. The constraint sets (5) and (6) impose binary restriction on the decision variables. In this paper, $C_{ij} = f(D_{ij})$, where $S < D_{ij} \le T$ and $0 < f(D_{ij}) < 1$. Based on the experience, we expect the function to be monotone decreasing with the increase in the distance between facility site and demand point and be zero at the distance T. $A = 5$

$$f(D_{ij}) = 1/(1 + e^{A(D_{ij} - (S+T)/2)}) \tag{10}$$

3.3 The trimmed MCLP-P model

When we have a shelter layout, the capacity of each shelter is limited if the population reaches to the upper limit. We can think that the shelter cannot offer refuge

service and the other people who need to be evacuated should be arranged to the nearest shelters. Therefore, it is better to build a location model with the capacity limitation when we have shelter layouts, so we can append restriction as follows: each shelter can only meet the refuge demand of a limited number of residents, limiting the capacity of each shelter. In this paper, we mainly consider the distance and the capacity between demand points and potential facilities. Based on the crucial degree to confirm the corresponding power coefficient, we apply different power coefficients to the objective function and calculate the maximal numerical value to confirm the final layout result. Suppose the capacity of the fixed shelter is V, the potential shelter's capacity is U, order $\omega_j = \begin{cases} 1 & U > V \\ 0 & U < V \end{cases}$, $\forall j \in J$, $W = r_1 C_{ij} + r_2 \omega_j$. Suppose the two power coefficients of distance and capacity are equal, namely: $r_1 = r_2$, so $W_1 = C_{ij} + \omega_j$. Hence, the objective function of the trimmed MCLP-P is:

$$Z = Max \sum_{i \in I} \sum_{j \in M_i} W_1 x_{ij} \tag{11}$$

4. ANALYSIS OF THE SHELTER LAYOUT

In this paper, we have a shelter layout with the standard of a fixed shelter. The fixed shelter is a place where refugees can live a long time; it needs to be big enough to provide the refugees sufficient space. In this paper, the population concentrative places are abstracted to a demand point, such as a residential area, marketplace, and recreation ground, etc.; the places that are suited to be a shelter are abstracted to a potential facility, such as a square, playground, and greenbelt. Based on the foregoing correlative requirement and experience, suppose S=1000m, T=1100m, V=6000, and the facility 1, 3, 6 is less than 6000, facility 2, 4, 5 is more than 6000, P=3. Based on the trimmed MCLP-P, Fig 2 depicts the shelters layout results.

Fig 2 shows that using different models can bring on different shelter layout results. The number of covered demand points is equal by using the capacity limitative MCLP and the no capacity limitative MCLP. Howver, the layout result by using the capacity limitative MCLP can accommodate more stricken residents. The number of covered demand points by using the capacity limitative MCLP-P is 1 fewer than by using the no capacity limitative MCLP-P, but the capacity of facility 2 is bigger than facility 1, which can accommodate more stricken residents and offer more refuge service. In addition, it can incarnate the function of shelters. Considering from the aspects of security and applicability, we choose the shelter layout result by using the capacity limitative MCLP-P. Therefore, it is necessary and important to consider the capacity of the shelter when we have a shelter layout, which can reduce the disaster loss and bring more value.

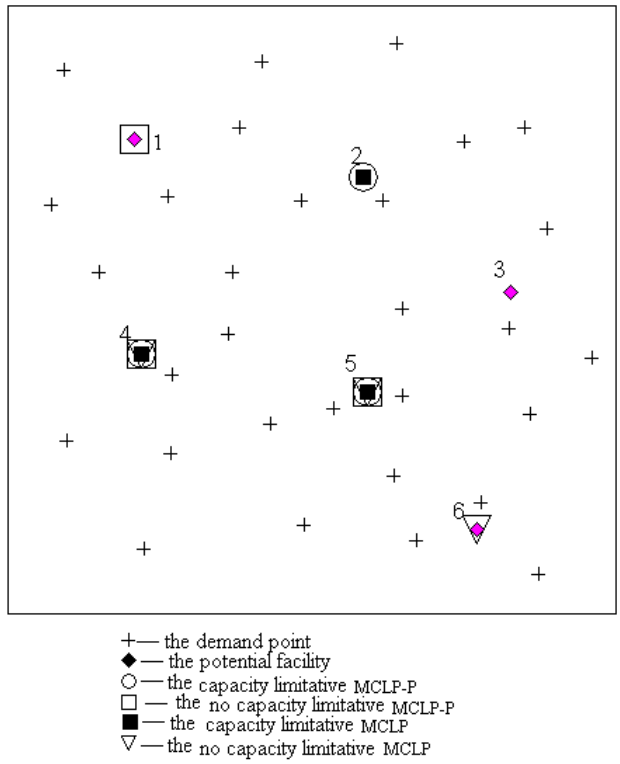

Fig 2 shelter layout results with different models

5 CONCLUSION

In this paper, we consider the capacity limit when we use the MCLP-P to plan a shelter layout and set up the capacity limitative MCLP-P. Through analyzing this example, we can see that the shelter layout results by using that model have more applicability, improving the value of shelters. But, in this paper, the trimmed MCLP-P only considers the capacity of the shelter and the distance between demand points and potential facilities, many other restrained factors are not involved, and they should also be ameliorated.

ACKNOWLEDGMENTS

This research is supported by National Natural Science Foundation of China (Project No. 70673016 and 70503008), and Heilongjiang Postdoctoral Science Foundation funded project (Project No.LBH-Q06060). This work was performed at the National Center of Technology, Policy and Management, Harbin China.

REFERENCES

Chung C. “Recent applications of the maximal covering location planning (MCLP.) model.” *Journal of Operational Research Society*; 37(8):735–46. (2006).

Huang he chao, Lin peng, and Lu zhao ming. “The application of p- median in the city

shelter layout." *Transaction of Applied Base and Engineering Science*. 62-66. (2004).

Orhan Karasakal, and Esra K. Karasakal. "A maximal covering location model in the presence of partial coverage." *Computers & Operations Research*. 31, 1515-1526. (2004).

Sherali HD, Kim S, Parrish EL. "Probabilistic partial set covering problem." *Naval Research Logistics*; 38:41–51. (1991).

Su, Y., and R. Liu. (2004) "The layout principle and essential of city earthquake shelter." Disaster. 19(1), 87-94.

Yin, D. (2007) "The applications of generalized maximal covering model in emergency facility location problem." Master Candidate Dissertation, Shandong University.

Zhou, X., M. Liu, and Y. Wang. (2007) "The research of emergent shelter optimization layout theoretic." Transaction of Safety and Environment .6, 118-121.

A Framework of The Traffic Organization Simulation System For Freeway Emergency Response

Shaowu Cheng [1], Xiaofei Ye [2], Shi An[3], and Tingting Yang[4]

[1]School of Transportation Science and Engineering, Harbin Institute of Technology Email: csw1968@163.com
[2] School of Transportation Science and Engineering, Harbin Institute of Technology Email: yexiaofei85@163.com
[3] School of Transportation Science and Engineering, Harbin Institute of Technology Email: anshi@hit.edu.cn
[4] School of Transportation Science and Engineering, Harbin Institute of Technology Email: ytt880808@163.com

ABSTRACT

To deliver emergency materials and evacuees to the destination within a limited amount of time, various traffic management and control measures must be employed to manage numerous traffic flows. A Freeway Emergency Traffic Organization Scenario (FETOS) is one of various combinations of traffic management and control measures. A framework of simulation system for the FETOS is presented in this paper. It consists of function modules of the simulation system, core models of the simulation system, and key technologies of implementing the simulation system. The simulation models include a freeway infrastructure model, a data model of the FETOS, a dynamic traffic flow model under the FETOS, FETOS simulation indexes, and their respective statistical models. Function modules include modules of modeling freeway networks, modules of modeling the FETOS, modules of system parameters configuration, module of simulation execution and control, module of visualizing simulation running process, module of generating and printing simulation reports, modules of open data interface, and modules of data backup and recovery. The key technologies of system implementation are also discussed.

INTRODUCTION

Emergency management can be divided into four periods (McLoughlin. D.1985): mitigation, response, relief and recovery. During the response period, a large number of people and materials need to be transported from one place to another (Henry X.Liu, Jeff X.Ban, Wenteng Ma, Pitu B. Mirchandani, 2006). In some cases, people and materials transportation must traverse multiple cities or provinces and freeway transportation is one of the main means of transportation (Henry X.Liu, Jeff X.Ban, Wenteng Ma, Pitu B. Mirchandani.2006). To ensure that the operation of emergency traffic flow on a freeway is efficient and orderly, effective traffic management and control measures must be taken. A FETOS can be

defined as one of various combinations of traffic management and control measures, and simulation is one of the main methods to optimize the FETOS. Through analyzing elements consisting of the FETOS and function requirement of a simulation system for the FETOS, a framework of simulation system for FETOS is presented in this paper.

FUNCTION MODULES OF THE SIMULATION SYSTEM FOR THE FETOS

Function modules of the simulation system for the FETOS consist of three parts: input module, simulation execution and control module, and simulation output module. Relationship among the modules is illustrated in Figure 1.

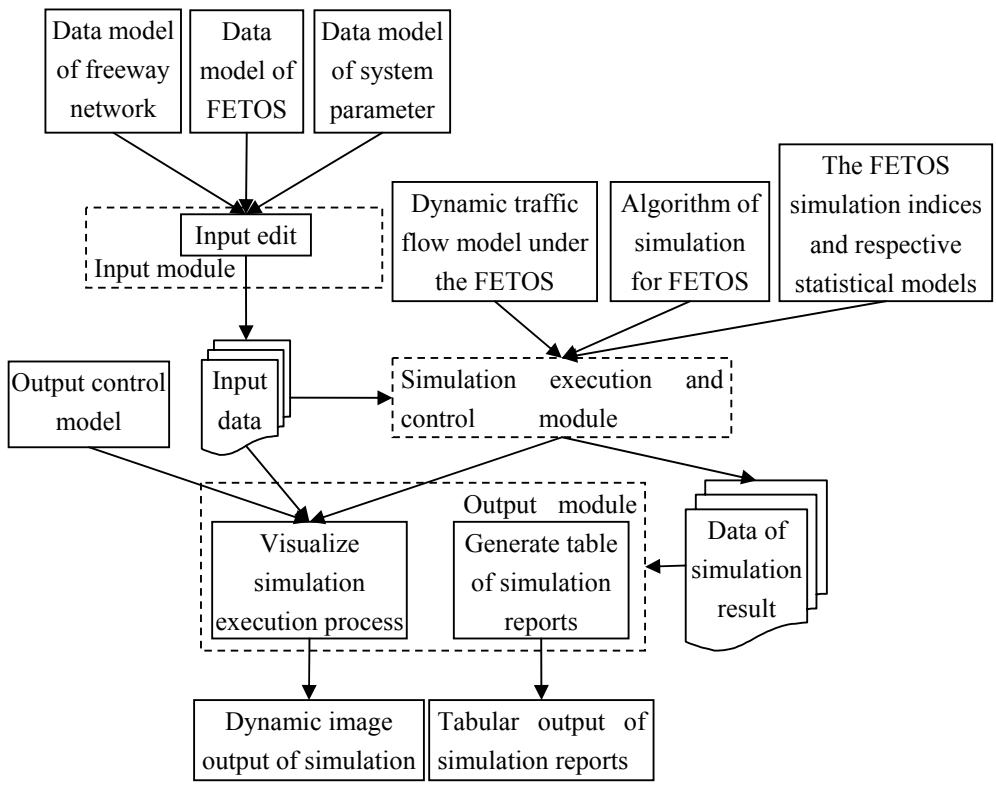

Figure 1. Relationship among modules of simulation system for the FETOS

Input module provides an interactive modeling environment for the simulation of the FETOS. Users can visually edit freeway networks, visually edit the FETOS, and visually configure system parameters, such as simulation running, controlling parameters, the vehicular operating parameters, etc. Models corresponding to the functions are a data model of freeway networks, a data model of the FETOS, and a data model of system parameters, respectively.

Simulation execution and control module, according to the FETOS data and system parameters (such as vehicular operation parameters, start and end time of

simulation, etc.) entered by a user executes the simulation algorithm generates vehicles, loads the vehicles into the freeway network, generates traffic flow data in accordance with dynamic traffic flow model under the FETOS, and logs files of the simulation execution and computes simulation indexes.

Output module submits both data of the simulation execution process and data of the simulation execution result produced by the simulation execution and control module to the user in two forms: dynamic images output of simulation execution process and tabular output of the simulation execution result.

THE CORE MODELS AND RESPECTIV FUNCTION MODULES

Core models of the simulation system for the FETOS include a data model of freeway networks, a data model of the FETOS, a dynamic traffic flow model under the FETOS, simulation indexes of the FETOS, and respective statistical models.

Data model of freeway networks and respective modeling module A data model of freeway networks abstracts the freeway network in the real world to describe the geometric characteristic of a freeway, location and properties of freeway infrastructures, and topological structures of a freeway network. During the simulation execution period, a data model of a freeway network function as a space reference frame of simulation execution, which describes boundary constraints of simulation execution, records and stores state information and statistical information of dynamic and static parameters, defining logic models and logical rules of driving vehicles (such as topological traces of vehicles travel) according to the geometric shape of the road, effective scope of the controller, and conflict rules at junctions. Quality of a data model of freeway networks has a direct impact on efficiency of simulation system execution. The entities that a data model of freeway networks describe includes segments of a freeway, functional lanes of a freeway, junctions between two freeways, ramps of freeways, and tollbooths, etc. A data model of freeway networks can be represented as relation tables corresponding to a module of modeling freeway networks, which is a component of the input module of the simulation system for the FETOS.

Data model of the FETOS and respective modeling module The function of the FETOS model describes organization and storage of data on the FETOS. A data model of the FETOS can be represented as relation tables. Data about the FETOS that users input to start a simulation execution is stored into the relation tables, which are built based on data model of the FETOS. A data model of the FETOS corresponds to the module of modeling the FETOS, which is also a component of the input module of simulation system for the FETOS. Through the module of modeling the FETOS, users can visually input data on the FETOS, such as ramp control data, control-flow control identification, etc.

The dynamic traffic flow model under the FETOS This is built based on the

Cellular Automaton (CA) (R. Jiang, Q. S. Wu.2003) to describe temporal and spatial evolution regularity of traffic flow under the FETOS. That is, the most important of core models of a simulation system for the FETOS. Although the Cellular Automaton model^0 is a kind of micro-model, efficiency of a CA model is better than a car-following model and the CA model avoids the "discrete-continuous-discrete" approximate process. Based on the shortcomings, analysis of the existing models for freeway traffic flow, the improvements of the NaSch model (K. Nagel and M. Schreckenberg.1992) for freeway traffic flow will be given in the future research, and multi-lane changing rules (M. M. Pedersen and P. T. Ruhoff.2002) for freeway traffic flow will be introduced to the coming model of freeway traffic flow. Further, the evolution rules of traffic flow, under various emergency traffic organization measures, will be developed, and, finally, a dynamic traffic flow model under the FETOS will be built.

Simulation indexes of the FETOS and respective statistical models Simulation indexes of the FETOS can be used to evaluate the FETOS. These indexes include traffic volume on all lanes and ramps, average speed of vehicles on the main lines, delay at tollbooths, average speed and average delay of vehicles, empty time of emergency traffic flow, freeway network load, freeway network reliability, ratio of emergency traffic flow and normal flow, and comprehensiveness and feasibility of emergency transport organizations plan. A number of important indexes, such as traffic volume, average speed, traffic density, average delay and emptying time, can be derived by calculating the road load. The road network reliability, such as flow through the above-mentioned indexes, can also be embodied in an intuitive visual display of the performance.

Output Control Model The compositions and functions of output control models are as follow. First, in dynamic presentations, the users intuitively feel the vehicles traveling on the freeway and changes the color and dynamic presentation at the network based on the types and speed of vehicles, dynamically displays the current means of transport organizational measures, the visual output of simulation results, the flow of segments nodes, and saturation distribution networks can observe a crowded bottleneck. Second, in output indexes, through the simulation process, in accordance with the above-mentioned statistical model, obtain statistical data, such as indexes that show the average speed and density of vehicles and other information.

KEY TECHNOLOGIES

User interface of the simulation system for the FETOS can be interactively implemented within the visual studio development environment. A data model of freeway networks and a data model of the FETOS can be interactively built in a relation database (such as MS SQL server, Oracle, and Sybase etc.). Off course, they also can be implemented by VC++ programming.

Dynamic traffic flow models under the FETOS and simulation algorithms can be implemented by VC++ programming. Visual C++ adopts an object-oriented programming idea and the mechanism that data packages and their operations are shaped into categories, objects and methods. Through derivatives, inheritance, overloading and other characteristics of VC, software can be reused and procedures for implementation can be automatically generated.

In order to visualize the process of simulation execution, component development technology is adopted to integrate arc objects with dynamic traffic flow models under the FETOS. Traffic states on a freeway network can be identified by colors (for example, red represents congestion state of traffic, and green represents fluent state of traffic). Traffic states on a freeway network can be obtained from dynamic traffic flow model under the FETOS.

CONCLUSION

This paper presents, through the analysis of the elements consisting of the FETOS and requirement of a simulation system for the FETOS, a framework of a simulation system for the FETOS and discusses function modules of the simulation system and correlation among modules, core models of the simulation system, and the key technologies of implementing the simulation system. The framework proposed has significance on guiding the development of a simulation system for the FETOS, which is our on-going work.

REFERENCES

McLoughlin, D. "A Framework for Integrated Emergency Management." *Public Administration Review*. 45:165-172. (1985).

Henry X.Liu, Jeff X.Ban, Wenteng Ma, Pitu B. Mirchandani. "Model Reference Adaptive Control Framework for Real Time Traffic Management under Emergency Evacuation." (2006)

W. Choi, H. Hamacher, S. "Tufecki Modeling of Building Evacuation Problems by Network Flows with Side Constraints." *European Journal of Operational Research*, 35(4):98~110. (1988).

R. Jiang, Q. S. Wu. "Cellular automata models for synchronized traffic flow." *J.Phys. A36,* 381~390 (2003).

K. Nagel and M. Schreckenberg. "A Cellular automaton model for freeway traffic." *J.Phys. I (France) 2*，2221~2229 (1992).

M. M. Pedersen and P. T. "Ruhoff. Entry ramps in the Nagel-Schreckenberg model." *Phys. Rev. E 65*，056706. (2002).

Application of Locating Technology in the Highway Emergency Response System

Hantao Zhao[1], Yunpeng Wang[2], Shiwu Li[3], Hongyan Mao[4]

[1]School of Vehicle Engineering, Harbin Institute of Technology. No.2, Wen Hua-xi Street, Weihai, Shandong.PH:0631-5687213; email:zht1919@163.com
[2]School of Traffic&Transportation, Jinlin University. No.5988, Renmin Street Changchun, Jilin.PH: 0431-85095086; email: wangyunpeng@jlu.edu.cn
[3]School of Traffic&Transportation, Jinlin University. No.5988, Renmin Street Changchun, Jilin.PH: 0431-85095086; email: lshiwu@163.com
[4]Library, Harbin Institute of Technology. No.2, Wen Hua-xi Street, Weihai, Shandong.PH:0631-5687498; email:mhy1222@163.com

ABSTRACT

The exact locating of emergency and rescue resources is not the only precondition for implementing rescue work, but also the input data for optimizing vehicle dispatching. In this paper, locating technology is applied to determine the location of emergencies in the highway emergency response system. According to the alarm information, such as road name, stake number and traveling direction, the algorithm of locating emergencies has been designed by the comprehensive use of the variable length subsection mode and the interpolation method. This study has been applied to the actual scheduling platform. The results show that the proposed algorithms achieve the precise position of emergencies and improve the performance of the emergency response system.

1 INTRODUCTION

Advanced algorithms can help to quickly and automatically detect incident. However, the status of national highway makes this manner difficult to be promoted. In general, when unexpected events happen on a highway, most of the information for assistance or alerts are derived from mobile phones, emergency telephones, traffic police and road patrol vehicles. Mobile phone alarms have obvious advantages. When emergency personnel have not yet arrived at the scene, command dispatching personnel can facilitate self-help or a police officer conducting an initial treatment. The biggest disadvantage of mobile phone alarms is difficulty determining the exact location of the incident, and more repeat alarms easily lead to police confusion. As an input parameter, the exact locating emergency is the precondition for implementing rescue work. So, it is necessary to research the exact locating of emergencies based on mobile phone alarms.

2 LOCATING TECHNOLOGY ANALYSIS

Traditional event locating is expressed by the relative positions (Gu Mingchen, 2005), which is more suitable for city streets. But for highways, the

marker positioned on both sides of the road is relatively simple and not easy to be confirmed. Some researchers have proposed to realize automatic locating by integrating the alarm telephone, electronic maps and GPS systems (Huang Tongyuan, 2003). Based on fuzzy information from alarm phones, patrol vehicles are dispatched to the scene of the accident. Then, according GPS coordinates, the feedback data can be displayed on the electronic map. Such locating means can precisely locate incident, but will inevitably lead to a lag time in making a decision because the site of the incident must be located after the patrol vehicles have rushed to the scene. Automatic Alarm System of America links private telephone companies and public service institutions together. China has not provided such a service of a private telephone company, but this will be the development trend of future locating systems.

Taking into account the specificity of the highway, alarm information can be described by a stake number. In this paper, the line used to calculate can be generated by using the variable length subsection mode on the highway, and then, in accordance with the alarm information of the road name, the stake number and the traveling direction, the interpolation method is used to calculate the exact location of incident.

3 KEY TECHNOLOGIES

3.1 Linear Reference Methods

The location of any unknown points can be determined by the distance and direction of known points on the linear characteristics, this method is known as Linear Reference Methods (LRM) (Li Qingquan, 2004). As an effective means for describing the location information of events, LRM has settled the expression of incident points in the transport network. Highway traffic incidents must occur or exist at a certain point or on a certain period in the road network. This phenomenon can be seen as one-dimensional, linear distribution rather than conventional two-dimensional, spatial distribution. To a single system with small amount of data, plane coordinates of the reference system are feasible for incident locating. But in the long run, highway GIS-T will be the integration of different types of traffic data; therefore, the conventional coordinate reference system is not suitable for the establishment of enterprise-level GIS-T. LRM can unify the integration interface of traffic information data and simplify the query method, which has been recognized as the best location reference method for traffic information systems.

Common LRM includes road stake number reference, road signs reference, node reference, and geodetic coordinate reference, as well as other extended ways. This article relates to the highway GIS-T, its line features decide that stake number reference is a more suitable method. Stake number is the main reference standard unit of highway measurement and is the locating method commonly used in transport industries, especially the road sector. Based on the stake number of a given point, such as the starting point of a route, the so-called “road-stake

number" reference method converts accident location and characteristics of road sections to the distance, in relation to the starting point, and determines the specific location. After recording the attribute information of incident location and confirming the LRM, the mapping for the information of unexpected events requires the use of virtual technology to determine the relative position of incident in the road entities, and an incident point diagram is finally generated in the electronic map automatically.

3.2 Linear Section Technology

Space geographical distribution of a highway has obvious linear features. Property information is collected by taking mileage piles, similar to a Linear Referencing System. In GIS, linear features are saved and managed with arc as the basic unit. All locations on the same arc have the same attributes. The multiplicity of highway attribute data determines that all the attributes are divided into multiple attribute sets in accordance with a certain standard and are set-up in a database separately. Each attribute set contains a number of characteristics of the highway. If the attribute data changes, the corresponding mileage of the attribute database changes. For highway data processing with these linear characteristics, GIS has provided three ways: isometric subsection method, variable length subsection method and dynamic segmentation method (Fu Zuoliang, 1994).

The variable length subsection method organizes data according to the start and finish of a variety of attribute changes in the road. The relative isometric subsection method, with small data redundancy, easy data updating and maintenance, is able to accurately reflect the real situation of all the relevant road attributes. For example, a pavement can be divided into several sections by both road types and road conditions. The variable length subsection mode can only deal with an attribute data set each time. The disadvantage is that the start and finish of the road sections require manual input, the same data will be duplicate saved when the road is delineated as different attributes of data sets and the various attribute data sets can not be integrated into spatial analysis and display.

4 ALGORITHM DESIGN

The initial incident information is obtained by alarm response staff. The contents of inquiry normally include sections, stake number, the directions of traffic, the availability of casualties, the impacted number of lanes, vehicle type, etc. Automatic locating of highway incidents just needs to consider the location-related alarm information.

The significant signs along the highway include toll stations, variable information boards, service area, and so on. The intervals between these signs are relatively distant, so they are unfit for describing the initial reference of incident location. Stake number is the unique identification information of highways, along the distribution-intensive, easy identified and reported. In addition, road names and directions of traffic could be accurately reported by police personnel. The

above-mentioned three elements constitute the input parameters of automatic locating.

The following steps are the design idea of the automatic locating incident algorithm:

(1) First, based on the stake number of highways, the line used to calculate a certain road section is constructed. The variable length subsection mode is used to divide this line into segmentations. At the same time, the data sets of stake number, road name, traffic direction and segmentation length are generated.

(2) Secondly, a mileage information table is built by the corresponding mileage of digital stake numbers. For vector stake numbers, a corresponding mileage value can be extracted by searching mileage information tables.

(3) Third, a MapObject point set is defined to store section name and traffic direction of alarm information. According to the contents of the object, the appropriate record of section attribute set is determined.

(4) Through cumulating the subsection length in the record, the current located section of stake number from alert information can be judged.

(5) The located section contains the stake numbers which are used for vectoring a highway. These discrete points can be seen as the start and finish of attribute changes; therefore, some more detailed subsections are automatically generated. The accumulation of these small subsections can judge the current located section of stake numbers from alert information. The start and finish coordinate of this current section is known and can be used to calculate the coordinate of the stake number by taking advantage of the interpolation method. Finally the point is located in an electronic map.

5 ANALYSIS OF TECHNOLOGY APPLICATION

(1) The line used to calculate

In order to clearly indicate the incident location, regional elements are used to store highway data in map scale 1:2000. Because of the obvious linear features of the highway, the locating algorithm needs to produce the line used to calculate which is connected by all vectors of stake numbers.

(2) Stake number description

The form of stake numbers is general described as “K*+***,” which needs to be converted to the specific numeral for program recognition. For example, if the stake number is “K2 +100,” then the mileage value is “2100m,” such data is necessary to calculate the location of the incident. For vectoring of stake number, the coordinates can be found by cumulating the subsection length. As for non-vectoring of stake number, the interpolation method is used to calculate the coordinates.

(3) Variable length subsection mode

The determination of incident location is the only target in this paper. The attributes of all sections include the code of section name, the code of traffic direction, the section length, as well as some fields automatically generated by the

attribute table. That is, we need only work with one attribute data set. The variable length subsection mode is selected to describe linear features. The selection of variable sections is based on linear features. The larger the arc curve is, the longer the section takes value.

For example, part of the attribute data sets of the Changji highway and Changyu highway is shown in Table 1. Field LENGTH is the section length, field CODE is the road code, field DIRECTION is the code of traffic directions, and other fields are automatically generated. Among them, 001 on behalf of Changji highway, 002 on behalf of Changyu highway, 0011 on behalf of the direction of Changchun to Jilin, and 0012 on behalf of the direction of Jilin to Changchun. Changyu highway is divided into four sections and Changji highway is divided into ten sections.

Table 1. Attribute data sets of Changji highway and Changyu highway

ID	FNODE_	TNODE_	LENGTH	CODE	DIRECTION	SHAPE
1	13	2	27027.77	002	0021	1
2	3	2	53174.97	002	0021	2
3	5	3	49604.38	002	0021	3
4	5	7	13713.09	002	0021	4
5	4	3	8431.051	002	0021	5
6	6	3	7931.204	001	0011	6
7	9	6	6130.557	001	0011	7
8	12	9	8100.018	001	0011	8
9	14	12	9875.148	001	0011	9
10	21	15	5170.029	001	0012	10

(4) Combination of variable length subsection and interpolation method

The variable length subsection method is used to describe the linear features of highway, and interpolation method is used to calculate coordinate values. If the division of sections is based on road linear, the distance between the start and finish of the section is not too short to adopt an interpolation method. As shown in Figure 1(a), if the coordinate of point E is solved by the coordinate of point A and point B, a large error will be produced through the interpolation method. This also explains why the section needs to be further divided. If the section is accumulated fully in accordance with the stake number, there is a larger calculation volume. As shown in Figure 1(b), before the interpolation between point C and point D, all the subsections require calculation. Therefore, the most suitable approach is the combination of these two variable length methods. As shown in Figure 1(c), in the first instance, the large section where the incident located should be calculated, then the subsections above this large section are cumulated, then the start and finish of the subsection where the incident located can be determined.

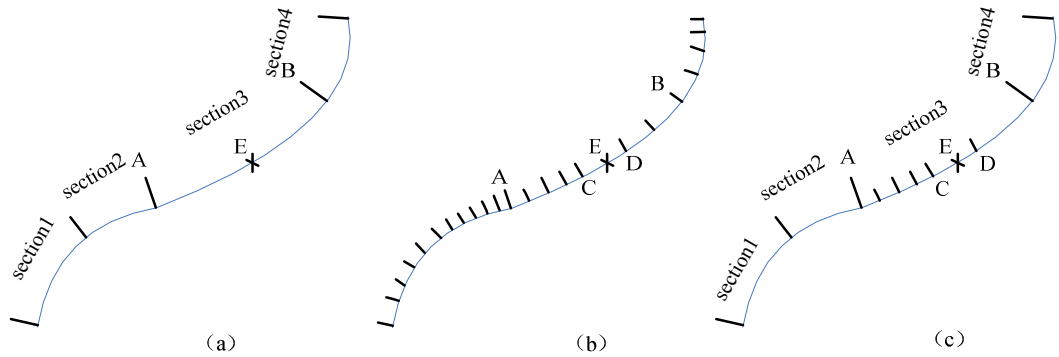

Figure 1. Variable length subsection for highway linear features.

5 CONCLUSIONS

The algorithm of locating emergency has been designed and the definition of the line used to calculate is put forward, which is produced by the variable length subsection mode. Based on the alarm information, the precise location of incident can be calculated by the interpolation method. This algorithm achieves accurate locating of incident on an electronic map after receiving a police alarm. However, the use of the variable length subsection mode needs to re-sub the road when the data is updated. The future research should concentrate on the dynamic segmentation method.

REFERENCES

Gu Mingchen "Study on the Critical Techniques of Road Traffic Safety Information System Based on GIS." *Master Degree thesis*, Changchun: Jilin University. (2005).

Huang Tongyuan. "Study on Superhighway Emergency and Security System." *Master Degree thesis,* Chongqing: Chongqing University. (2003).

Li Qingquan, Zuo Xiaoqing, Xie Zhiying. "Progress and Trend of Research on GIS-T Linear Data Model." *Geograpgy and Geo-information science*. Vol.20, No.3, 31-35. (2004).

Fu Zuoliang, Wang Liping, Xie Zhiying. "Reasearch and Realization of Dynamic segmentation technology." *Computer World,* No.4, 130-131. (1994).

Accident Prevention and Inducement Strategy in Highway Tunnel

Heng Ding[1], Xiao-yan Zheng[1], Wei-hua Zhang[1], Zhong-jie Zhao[2]

[1]School of Mechanical and Automotive Engineering, HeFei University of Technology, Hefei 230009, Tel: +86-551-2929107, Email: dh801101@163.com
[2] School of electronic and control engineering, Chang'an University, Xi-an 710064; email: zzj@chd.edu.cn

ABSTRACT

As the special section of a highway, the tunnel driving environment is poor. Accidents occurring in highway tunnel typically have the characteristics of high damage and difficult transaction. Taking the Xue Gong-Ling highway tunnel as the example, this paper discuses combining the advanced technique of intelligent transportation system (ITS) used in accident prevention and evacuation strategies of long highway tunnels, and solves the evacuation problem of drivers, passengers and vehicles when accidents or dangers occur. Under the state detection of traffic flow and environment in or out of the highway tunnel, a corresponding prevention scheme was executed for accident prevention. Once a single point accident or fire occurs in the highway tunnel, the threshold value h was stetted, waiting time T and minimum (diffuse time between fire and induced vehicle appropriative crossing, h) were compared, the Inducement Strategy was executed based on comparable results. Due to the long length of a highway tunnel, once there were both accidents happening in the same time, combined with the single point accident inducement strategy, a corresponding prevention scheme was executed according to different positions of accidents. Type and characteristics of accidents being considered, traffic can be evacuated rapidly through open or close induced vehicle appropriative crossing and people appropriative crossing. As a result, secondary accidents were avoided and the safety of driver and passengers can be ensured. Based on tunnel impact and a control development flat-form, the guiding strategy is simulated showing that this guiding strategy is a good way of controlling and inducing.

1. INTRODUCTION

As the highway workers have paid more and more attention on the environment, oil consumption, driving time and economic benefit, in many countries, especially in mountainous areas, more highway tunnels have been employed to conquer the landform limitation, optimize road linearity, and shorten traveling length. Therefore, characteristic accidents, such as a fire or a traffic accident, would be the ineluctable issue coming up with the tunnels. Related data show that the rate of fire or accident in tunnels is about 5 times per billion kilometers (Zhang Z D, 2003; Zhang H Y, 2003; Chen L D, 2003). Although the probability of fire and accident is very low, the after-effect is usually serious, especially in long highway tunnels (LU Mao-cheng, 2003). Therefore, an effective measure is the only way to keep the tunnels safe. The intractable issue to be solved now is to find a method that can play an important role

in preventing fires and accidents from occurring and can provide inducement information to drivers and passengers in time further avoiding secondary accidents.

2 SCHEME FOR ACCIDENT PREVENTION

It is well known that prevention is better than a cure. Not only accident management, but also prevention, should be provided in a perfect tunnel monitor control system. Preventatives can eliminate accidents during the germination phase and ensure the running safety of a tunnel. Therefore, the accident rate will fall, loss in calamities will decrease, the service life of the tunnel will be prolonged, and the road service level will be improved. Safety prevention includes two parts: outside and inside prevention (Chen J F, 2002).

2.1 Outside prevention

Some equipment, such as a video hard disk recorder, sensor, vehicle detector and video frequency monitor equipment, was set outside of the tunnel to avoid latent danger entering into the tunnel. All of the vehicles, which will enter into the tunnel, should be detected, and the system will distinguish whether or not there is latent trouble and give the corresponding directive. The judgment comes from the comprehensive analysis considering such factors as air cleanliness degree, fire, illuminative degree and video frequency data.

2.2 Inside prevention

Over-speed and overtaking vehicles are forbidden in tunnels and vehicles should drive in the given lines. By placing that equipment in the locale tunnel, monitoring systems acquire traffic flow information, including volume, temperature, brightness, etc. Data will be transmitted to a monitor center by a field control network then the monitor center would set out inducible information (Shen A Z, 2002). Relevant measures will be taken based on the degree of crowdedness in the tunnel.

(1) Speed-down adjustment

When micro-accidents occur, some vehicles will be blocked and an occasional crowd may appear in tunnel. In this instance, a tunnel can provide service as before with the help of inducement information shown on various message signs (VMS) given by the monitor center (NIU Yong-liang, 2006). The system indicates vehicles to slow down to the given speed limitation. If the traffic volume is too crowded, the monitor center can predict, according to data from the equipment set in the locale, the development trend of traffic flow and calculate the reasonable velocity and announce it.

(2) Closing line or lane temporarily

When there is serious jam in the tunnel caused by a small accident, the tunnel is still at the service-offering condition; however, the concentration of some harmful gases, such as CO, exceeds the regular provision. At this time, one line or lane should be closed until the harmful gas concentration decreases to a normal degree after ventilation for a period of time.

(3) Closing lane

If traffic is so crowded that, even though all ventilators work well, the

concentration of gases is still over the provision, or the converse wave caused by an accident happening in a downstream road, transmits into the tunnel, there will probably be a traffic jam or even an accident. Under this situation, we should close the whole lane or tunnel and induce vehicles to avoid the tunnel through vehicle appropriative crossing.

3. EVACUATION STRATEGY

However, even if the prevention monitor system works well, accidents in a tunnel cannot be completely avoided. Inducement projects will always play a very important role in the monitoring system. The system will enter the preparation phase when the scheme of an accident (including accident and fire in the paper) meets the condition for traffic inducement (including traffic accident, traffic jam, fire accident, lower air circumstance, abrupt power failure, ice and snow road surface, etc.) (JIANG Gui-yan, WEN, 2001; DAI Guo-ping, 2002; WANG Jin-guo, 2005). Manipulation interface of monitoring systems can give reference, but artificial confirmation will be necessary before entering the evacuation program. Some long and large highway tunnels are apt to have more accident spots, so it is probable that two or more accidents may happen at the same time (Pan Z, 2003). The evacuation scheme is often diverse enough for the different location and number of accidents.

3.1 Single point accident

According to Figure 1, provided that the accident or fire happens in the right lane, after confirmed by a manager, with the help of detecting system, alarm system and video monitor system, the position and the type of the accident can be estimated, and then the relevant control scheme will be executed (Ding Heng, 2008). Signals of control system forbid vehicles to enter both the left and right lanes. Closing the left lane prepares for inducing vehicles in the right lane going through vehicle appropriative crossing. Signals inside the left lane induce local vehicles driving continuously. At the same time, the system opens relative vehicle appropriative crossing, to induce the vehicles ahead of an accident point to turn left and pass through the inducement place, and finally avoid the tunnel by the left lane entrance. In this situation an obvious collision at the inducement place between induced vehicles and those had entered tunnel should be well disposed. In order not to affect regular performance of the latter passing through inducement place, the control scheme would give waiting time T and intercalate a threshold value h (value is advised 50s～60s) for induced vehicles. According to the compared result between T with $\min[(t-t_1), h]$, the system determines the entering time for induced vehicles(ZHAO Zhong-jie,2007).

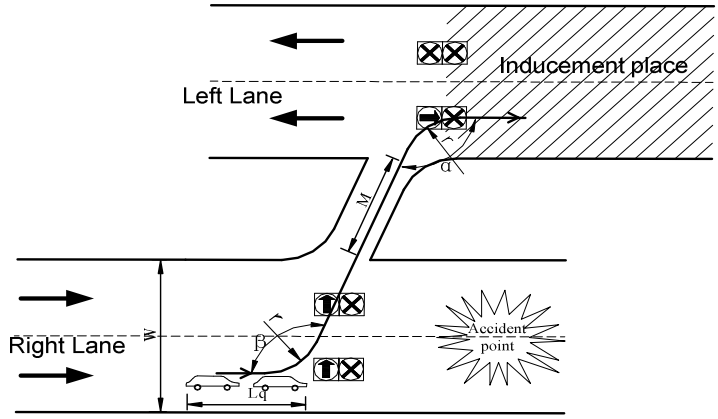

Fig. 1 Accident inducement.

Waiting time:

$$T = \frac{L - L_1 + d_1}{\overline{V}_a} - \left(\frac{M + \frac{W}{2\sin\beta}}{\overline{V}_v} + \frac{(\alpha+\beta)r + L_q}{\overline{V}_s} \right) + t_f + t_t + t_d \qquad (1)$$

L -the length of vehicle appropriative crossing (m);

d_1 -average vehicle length (m);

$\overline{V}_a$ -average velocity (m/s);

$\overline{V}_v$ -average velocity of vehicle running in vehicle appropriative crossing (m/s);

$\overline{V}_s$ -velocity of vehicle swerve (m/s);

t_f -response time (advice estimation time 1.5s+ response time 1.0s);

t_t -transmission time (s);

t_d -information dealing with time (s)。

In the formula (1), $d_1 \le 10$, d_1 can be ignored compared with L, t_t, t_d can be ignored too; t_f is about 2.5s, so formula (1) can be predigested as:

$$T = \frac{L - L_1}{\overline{V}_a} - \left(\frac{M + \frac{W}{2\sin\beta}}{\overline{V}_v} + \frac{r(\alpha+\beta) + L_q}{\overline{V}_s} \right) + 2.5 \qquad (2)$$

Compare result:

$$R = CMP\{T, \min[(t - t_1), h]\} \qquad (3)$$

R -result;

CMP -compare symbol;

t -the diffuse time between fire and induced vehicle appropriative crossing (normal traffic accident is $+\infty$.);

t_1-the shortest length of time driver can bear (advise 10～15s,fire accident, 0s for not fire accident.);

h-setting threshold value.

When the value of waiting time R is "<", those vehicles coming from the right lane are forbidden. After detecting all vehicles in the left lane heading away from inducement place, the system opens vehicle appropriative crossing and correlative pedestrian crossing, inducing blocked vehicles to get away. If R is ">", driveway indicator forbids vehicles in the inducement place in the left lane driving forward, and induces vehicles in the right lane to run away immediately. The left lane cannot work in a bi-directional way until all blocked vehicles in the right lane are evacuated; at the same time, the right lane is closed to undertake accident disposal and succor task. The traffic information "Frontage accident, please wait" is shown on the VMS at the entrance of the right lane.

3.2 Two-point accidents

It is more complex to induce vehicles when two-point accidents happen. Actually, the probability of a two-point accident is very low, but it cannot be eliminated, especially when the drivers may be scared by a previously occurring accident, which will probably result in a secondary one. The longer the tunnel is, the higher the rate of an accident happening. The evacuation strategy of a two-point accident in a long highway tunnel is significantly complex. Usually such accidents can be divided into two kinds: two accidents happening in the same lane and the two accidents happening in different lanes.

When two-point accidents happen in the same lane (Fig. 2), the system would forbid all vehicles from entering the tunnel, so vehicles ahead of the accident point avoid the tunnel through the first crossing ahead of the accident point. Before a driveway indicator sends out a signal to turn left, the control system uses formulas (2) and (3) to compare waiting time with threshold value separately. If R is "<", the system gives the waiting time induces vehicles to turn left and reach the other lane. When R is ">", waiting time will not be given and the system induces vehicles to run away from tunnel through vehicle appropriative crossing and inducement place directly. Cooperating with driveway indicator traffic signal does relevant manipulation, and VMS inside tunnel shows the relational information and the outside ones show waiting information.

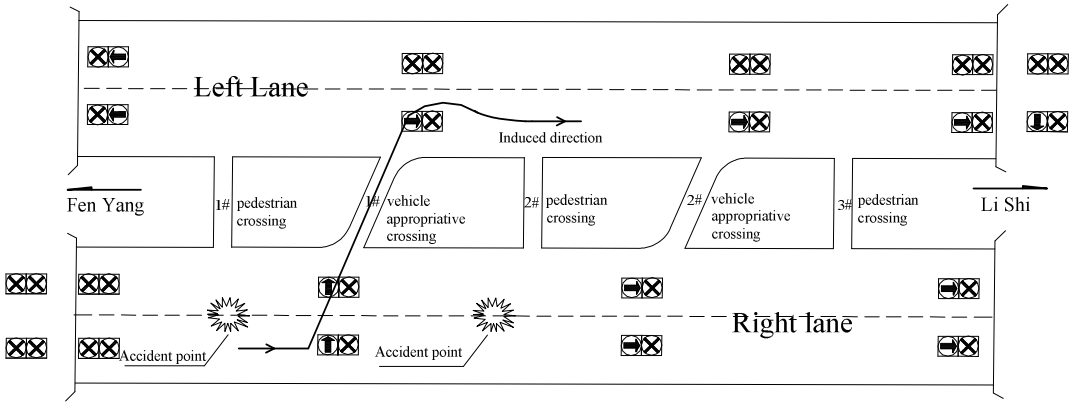

Fig. 2 Two-point accidents happen in the same lane.

When two-point accidents happen separately in different lanes, the first thing is to forbid all vehicles entering the tunnel too, then control system estimates whether or not the vehicles behind accident point can be induced. The rule is whether there is an accident point in the other lane in front of the crossing. If there is no accident point, crossing inducement is valid; otherwise, crossing cannot used for inducement. The situation of invalid crossing inducement in all traffic accidents is exceptive and the result is to close both lanes and induce drivers and passengers to abandon vehicles and run away.

If vehicles can be induced by crossing, the next step is to estimate the vehicles of both lanes, which may be induced by one or two vehicle appropriative crossing. There is no need to acquire the value of *R* when using one crossing inducing vehicles in two lanes (Fig. 3) because the shorter-length team has the priority to be induced. If vehicles need to be induced by two crossings (Fig. 4), the monitoring system should compare the threshold value separately and decides whether or not to give the waiting time, then shows information based on the value of *R*. Inside, VMS shows inducement information of current, the outside one shows running information inside the tunnel and provides estimative time and a displacing road to waiting vehicles.

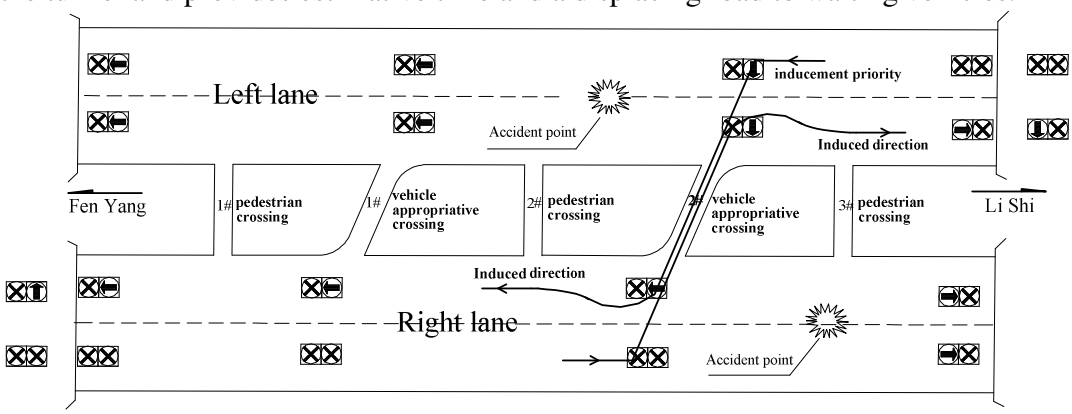

Figure 3 Inducement through the same vehicle appropriative crossing

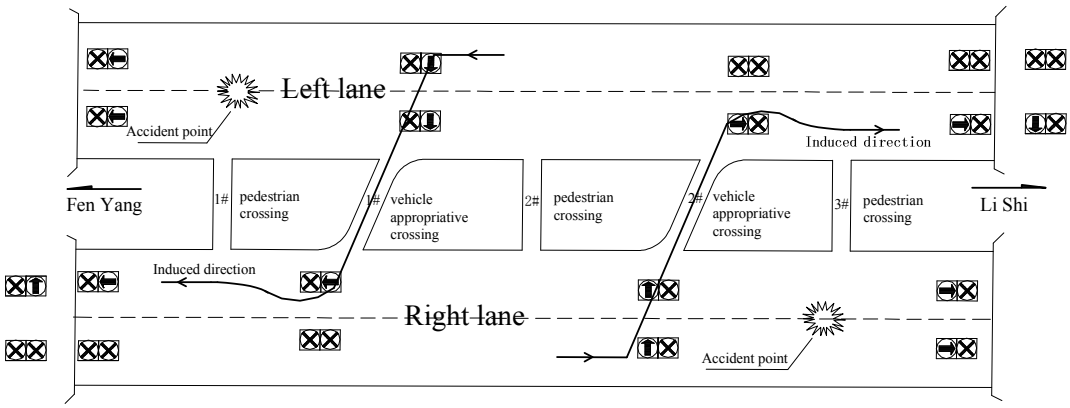

Figure 4 Inducement through different vehicle appropriative crossings.

By implementing evacuation and inducement strategies, control systems can be united with broadcast sub-systems, Route Guidance System, Vehicle Navigation System, etc., to ensure that passengers and drivers are induced safely and quickly, avoiding a secondary accident from occurring. When an inducement sub-system is executing its assignment, fire-fighting and alarm subsystems and an exigency succor sub-system must be started. After accidents are disposed, all of the correlative index should be checked, if the circumstances meet the need of normal exertion, both lines should resume.

4. CONCLUSION

(1) Practice tells us that the Scheme for Accident Prevention can reduce the accident rate about 83%.

(2) Aiming at accidents happening in different positions, using relevant and effective inducement strategies can shorten rescue time and increase rescue efficiency, consequently, ensuring the safety of drivers and passengers.

(3) The setting of threshold values reduces the difficult of establishment of rescue schemes and accelerates the rescuing procedure.

(4) Referring to the inducement strategy of this paper, control software has been developed and simulation control tests have been performed on the tunnel impact and control development flat-form. The results prove that an inducement scheme and the advice of waiting threshold values are feasible.

REFERENCES

Chen J F. "*Research about Traffic Inducement and Control in Tunnel.*" The paper of master's degree, Chang'an University, 1-3. (2002).

Chen L D, Wang J, Wu X Y. "*Research about highway tunnel fire prevention and control.*" UNDERGROUND SPACE, 23(1), 72-74. .(2003).

Ding Heng，Zhang Ya, Zhao Zhong-jie. "*Highway tunnel monitor system based on Controller Link network.* " Highway tunnel, 64(2), 47-49. (2008).

DAI Guo-ping, TIAN Pei-zhe, XIA Yong-xu. "*Ventilation scheme at fire in Er Lang Shan highway tunnel.*" Journal of Chang'an University: Natural Science

Edition, 22(6), 42-45. (2002).

JIANG Gui-yan, WEN Hui-min, YANG Zhao-sheng. "*Design of freeway automatic incident detection system and algorithm.*" Journal of Traffic and Transportation Engineering, 1(1), 77-81. (2001).

LU Mao-cheng, WANG Meng-shu, LIU Wei-ning. "*Study on the ventilation and disasters prevention for a two-direction road tunnel*." Journal of modern tunneling Technology, 40(5), 67-69. (2003).

NIU Yong-liang, Wang Jin-mei . "*Vehicle route algorithm of freight distribution.*" Journal of Traffic and Transportation Engineering, 6(2), 83-87. (2006).

Pan Z, Zhu K "*Highway Tunnel Fire Prevention.*" fire protection technique and production information, (2), 5-7. (2003).

Shen A Z. "*Guard Tunnel Traffic Accident- Discuss the Reason and Prevention Strategy about Frequent Accident in Tunnel.*". Journal of Zhejiang Police College Public Security Science Journal, 73(5), 45-47. (2002).

WANG Jin-guo, WANG Wei-Ya, TIAN Feng. "*Vehicle device system of intelligent guiding*." Journal of Traffic and Transportation Engineering, 5(2), 106-109. (2005).

Zhang Z D. "*Fire Accident Ventilation of Highway Tunne*l." Modern Tunneling Technology, 2(1), 34-49. (2003).

Zhang H Y. "*Man-made ingredient of highway tunnel safety.*" Highway, (10), 14-18. (2003).

ZHAO Zhong-jie, DING Heng, TIAN Mei. "*Strategy of dispersing disaster in highway tunnel.*" Journal of Chang'an University (Natural Science Edition), 27(1), 50-53. (2007).

LOCATING EMERGENCY RESPONSE FACILITIES FOR HAZARDOUS MATERIALS TRANSPORTATION WITH PROBABILISTIC RESPONSE TIME

Qingping Gao[1], Yu Luo[2], Qipeng Yan[1] and Yu Lin[3]

[1] College of Traffic and Transportation, Southwest Jiaotong University, Chengdu 610031, China; PH13880677360; email: gqp1977paper@163.com

[2] School of Computer Science & Engineering, University of Electronic Science and Technology of China, Chengdu 610054; PH13982097576; email: yuluo77@163.com

[3] Business School, Chengdu University of Technology, Chengdu 610059, China; PH13908210553; email: linyu-0000@163.com

ABSTRACT

This paper studies the emergency response facility location problem. It is assumed that the demand of a roadway segment is concentrated on its midpoint and the number of the emergency response facilities and candidate location sites are known. An optimization model considering the uncertain coverage probability and rescue effect for emergency response facility location and network design is developed. The objective is to maximize the total expected demand node covered, with the decisions being where to locate the response facilities and how to dispatch emergency response teams to demand nodes. A genetic algorithm is designed to solve the model, and the application of the model shows that the optimization model can improve the robustness of the emergency response facility location by considering coverage probability and rescue effect.

INTRODUCTION

It is one of the important problems in emergency management to locate emergency response facilities and design specialized emergency response networks. The quick arrival of specialized response teams at an accident site can expedite the emergency response process and increase the chances of avoiding or impeding the consequences of the accident. This facility location and network design problem has attracted significant research efforts resulting in some models being proposed to solve the problems. The existing models for locating response teams can be classified into four categories.

The first category model is the location set covering model (LSCM) whose aim is to minimize the number of facilities needed to cover all demand points or the expected response time of response teams (Konstantinos G. Zografos, Konstantinos N. Androutsopoulos, 2008). The second is the maximal covering location problem (MCLP), whose aim is to maximize population coverage subjected to limited response facilities and teams availability (Church R., C. ReVelle, 1974). The third is the maximal expected covering location problem (MEXCLP) with response team

availability and response time uncertainty (Ingolfsson A., S. Budge, E. Erku, 2008). A team that is responding to a call is unavailable to respond to a subsequent call. Response time is uncertain due to factors such as pre-travel delays, traffic congestion and weather (Daskin M. S., 1987). The fourth is the maximal arc-covering problem, involving locating facilities to maximize the total weighted arc length covered (Berman O., Verter V., Kara B.Y., 2007).

Once an accident occurs with the transportation of hazardous materials, the released hazardous materials can be harmful to the environment, property and human health. The undesirable consequences can be mitigated by the timely arrival of the response teams. Different response times lead to different emergency response effects and degrees of satisfaction.

In view of this, based on the assumption that the demand of a roadway segment is concentrated on its midpoint, an optimal model for locating emergency response facilities with stochastic response time is developed, where the uncertain emergency response effects, probabilistic coverage, population exposure, accident rate, equal workload constraints and response time constraints are considered. The objective is to maximize the total expected demand covered, with the decisions to be made being where to locate the emergency response facilities and how to dispatch emergency response facilities to demand nodes.

THE PROBLEM AND MATHEMATICAL FORMULATION

The roadway network can be transformed into a mathematical graph $G = (N, A)$, where every node represents the midpoint of a roadway segment while any arc denotes the connection between two successive midpoints. Assume that m is the number of demand nodes, n is the number of candidate locations, and q is the number of facilities to be located. Note that d_i denotes the population exposure in the accident, p_i denotes the accident rate, t_c denotes the threshold value of the maximum response time between any demand node and the corresponding response facility, and t_{ij} denotes the response time from candidate location j to demand node i with mean r_{ij} and standard deviation σ_{ij}. Let p_{ij} designate the probability that facility j covers demand node i, and let f_{ij} designate the emergency response effect and satisfaction degree. x_j is a binary variable that takes value 1 if a emergency response facility is located at node j and 0 otherwise, and y_{ij} is a binary variable that takes value 1 if demand node i is covered by the emergency response facility located at node j and 0 otherwise.

The mathematical formulation for the emergency response facility location problem can be expressed as follows:

$$\max \sum_{i=1}^{m} d_i p_i \sum_{j=1}^{n} p_{ij} f_{ij} y_{ij} \tag{1}$$

$$s.t. \quad \sum_{i=1}^{m} y_{ij} \le m x_j \tag{2}$$

$$\sum_{j=1}^{n} y_{ij} = 1 \tag{3}$$

$$\sum_{j=1}^{n} x_j \le q \tag{4}$$

$$\sum_{i=1}^{m} y_{ij} d_i p_i \le W \tag{5}$$

$$\sum_{j=1}^{n} y_{ij} r_{ij} \le t_c \tag{6}$$

$$x_j \in \{0,1\}, \quad j = 1,2,...,n \tag{7}$$

$$y_{ij} \in \{0,1\}, \quad i = 1,2,...m, \quad j = 1,2,...,n \tag{8}$$

Objective function (1) maximizes the total expected demand nodes covered. Constraint (2) implies that the demand at node i can be serviced by node j if only a response facility is located at node j and requires that at most m demand nodes can be serviced by node j. Constraint (3) implies that the demand of any node is covered by a single response facility. Constraint (4) requires that at most q candidate locations can be selected. Constraint (5) implies that the workload assigned to each response team should not exceed W, where $W = (1+\varepsilon)\sum_{i=1}^{m} d_i p_i \Big/ \sum_{j=1}^{n} x_j$. Constraint (6) implies that the maximum response time from a emergency response facility to a demand node should not exceed the threshold time t_c. Constraint (7) and Constraint (8) establish binary restrictions on the decision variables. As in MCLP, each response facility houses only one response team.

COVERAGE PROBABILITIES AND EMERGENCY RESPONSE EFFECTS

The facility location model presented in the previous section requires input values of the coverage probability p_{ij} and the emergency response effect f_{ij}. Response time includes pre-travel delay, including time spent on obtaining the address, time spent on deciding which team to dispatch, time to contact the response team crew, and time for the crew to reach the facility and start it, and travel time. Travel time is uncertain because of factors such as bad weather and traffic congestion. The model includes the parameter p_{ij}, the probability that facility j covers demand node i. Let t_{ij} denote the response time from candidate location j to demand node i with mean r_{ij}, standard deviation σ_{ij} and coefficient of variation $c_{ij} = \sigma_{ij} / \mu_{ij}$. The response time can be lognormally distributed, exponentially distributed, log-logistic distributed and gamma distributed.

If t_{ij} is lognormally distributed with the parameter a_{ij}, then

$$\mathrm{E}[\ln(t_{ij})] = \ln(r_{ij}) - 0.5\ln(1+ c_{ij}^2), \tag{9}$$

$$\mathrm{var}[\ln(t_{ij})] = \ln(1+c_{ij}^2), \tag{10}$$

$$p_{ij} = \Pr\{t_{ij} \le t_c\} = \Phi\left(\frac{\ln(t_c) - \ln(r_{ij}) + 0.5\ln(1+ c_{ij}^2)}{\sqrt{\ln(1+c_{ij}^2)}}\right). \tag{11}$$

where Φ is the cumulative standard normal distribution function and t_c is the coverage time threshold.

The uncertainty of emergency response effect and satisfaction degree can be expressed by a function f_{ij}. The usual function for emergency response effect can be expressed as follows:

$$f_{ij} = \begin{cases} 1 & t_{ij} < a_i \\ 1 - \left(\dfrac{t_{ij} - a_i}{b_i - a_i}\right)^k & a_i \le t_{ij} \le b_i \\ 0 & t_{ij} > b_i \end{cases}, \tag{12}$$

where a_i, b_i and k are constant parameters, t_{ij} is the response time from candidate location j to demand node i, and f_{ij} is the rescue effect of emergency response.

AN EXAMPLE

An example will show how the model presented in this paper can be used to optimize the emergency response facility location. The roadway network is shown in Figure 1, with 5 candidate emergency response facility sites and 5 demand nodes. The maximum number of emergency response facilities is 2, and the population exposure at node 1, 2, 3, 4 and 5 are 1000, 950, 800, 1080, 1900, respectively. Without loss of generality, we may assume $p_i = 1$ and $\varepsilon = 20\%$, and the values of $t_{ij}, \sigma_{ij}, t_c, p_{ij}$ and f_{ij} are shown in Table 1.

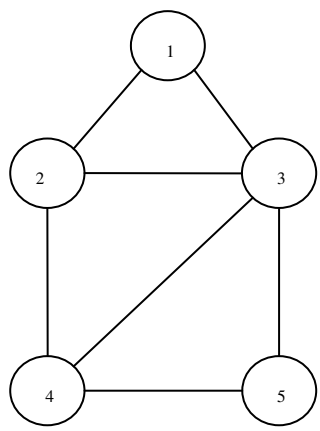

Figure 1. A simple network.

Table 1. The network parameters

Roadway Segments	t_{ij}	σ_{ij}	c_{ij}	t_c	p_{ij}	f_{ij}
1—2	530	10	0.019		0.841	0.717
1—3	515	30	0.058		0.801	0.747
2—3	535	5	0.009		0.841	0.709
2—4	510	30	0.059	540	0.842	0.757
3—4	535	10	0.019		0.694	0.712
3—5	500	5	0.010		1.000	0.766
4—5	520	10	0.019		0.976	0.710

The model of this example belongs to the class of NP-hard problems and can be solved using a genetic algorithm. If the workload constraint (5) is ignored, the optimal objective value is 5553.086 and the optimal solution is to locate response facilities at node 1 and node 5, to allocate demand node 1 and 2 to facility 1, and to allocate demand node 3, 4 and 5 to facility 5. If the workload constraint (5) is taken into account, the optimal objective value is 5418.196. The results show that the model can allocate relatively equal work loads to every response facility and avoid improper resource configuration by considering the equal workload constraint.

If the response time uncertainty is ignored, then the optimal objective value is 5730 and the optimal solution is to locate response facilities at node 2 and node 5, to allocate demand node 1, 2 and 4 to facility 2, and to allocate demand node 3 and 5 to facility 5. If the coverage probability and emergency response effect are considered, the optimal objective value is 4754.91 and the optimal solution is to locate response facilities at node 2 and node 5. We get optimal solution by considering not only the coverage probability but also the emergency response effect, which ensures robustness and effectiveness of this facility location model.

CONCLUSIONS

In this paper we investigated the response facility location problem. Based on the assumption that the demand of a roadway segment is concentrated on its midpoint, an optimal model for locating emergency response facilities with stochastic response time has been developed, where the uncertain emergency response effect and the probabilistic coverage are taken into account. The example result has shown that the model can allocate relatively equal workload to every response facility, ensure robustness and effectiveness of this facility location model.

REFERENCES

Konstantinos G. Zografos, Konstantinos N. Androutsopoulos. (2008). “A decision support system for integrated hazardous materials routing and emergency response decisions.” *Transportation Research Part C: Emerging Technologies*, 16(6), 684-703.

Church R., C. ReVelle. (1974). "The Maximal Covering Location Problem." *Regional Science Association*, 32, 101-120.

Ingolfsson A., S. Budge, E. Erku. (2008). "Optimal Ambulance Location with Random Delays and Travel Times." *Health Care Management Science*, 11(3), 262-274.

Daskin M. S. (1987). *Spatial Analysis and Location Allocation Models*, Van Nostrang Reinhold Company, New York.

Berman O., Verter V., Kara B.Y. (2007). "Designing emergency response networks for hazardous materials transportation." *Computers & Operations Research*, 34(5), 1374-1388.

Test and Analysis of Rail Break Emergency Treatment Device for Railway Switches

Xiangguo Li[1], Mingsheng Wang[2], Yunqing Zhang[3], Chao Ma[4] and Musong Li[5]

[1]School of Civil Engineering, Shijiazhaung Railway Institute, No.17 North 2nd-Ring East Road, Shijiazhuang, Hebei Province, China, 050043; PH(0311), 85281531; email: lixiangg2009@126.com
[2]School of Communication Engineering, Shijiazhaung Railway Institute, No.17 North 2nd-Ring East Road, Shijiazhuang, Hebei Province, China, 050043; PH(0311),87935276; email: wangmsh@sjzri.edu.cn
[3]School of Civil Engineering, Shijiazhaung Railway Institute, No.17 North 2nd-Ring East Road, Shijiazhuang, Hebei Province, China, 050043; PH(0311), 87935535; email: zyqlhb@163.com
[4]School of Civil Engineering, Shijiazhaung Railway Institute, No.17 North 2nd-Ring East Road, Shijiazhuang, Hebei Province, China, 050043; PH(0311),87936809; email: mach_74@163.com
[5]School of Civil Engineering, Shijiazhaung Railway Institute, No.17 North 2nd-Ring East Road, Shijiazhuang, Hebei Province, China, 050043; PH(0311), 87935555; email: lims106@126.com

ABSTRACT

The rail break emergency treatment device (RBETD) for railway switches has been developed to temporarily allow trains to pass through in case the stock rail of the railway switch cannot be replaced immediately after a break occurs. In order to test the soundness and reliability of its design so as to guarantee the safety of the running train, a field test was conducted with the emergency treatment device. The main components of the test include: the stress of the bottom edge of the common or frozen jointbar and the stress of the rail foot top at the center of the rail joint under different train speeds, the stresses of the vertical bearing plate of the device and the rail foot hook, the forces of the fastening screw, the transverse displacement of the rail head, and the sinking of the rail foot. Test results and subsequent calculations show that the emergency treatment device is safe as long as the train passes through at a speed less than 25 km/h with the help of the device.

INTRODUCTION

In the event that the stock rail of the railway switch cannot be replaced immediately after a rail breaks, Beijing Railway Bureau has designed an RBETD in order to guarantee the safety of the train while passing through at a limited speed (see Figure 1). In order to verify the reliability of the design and guarantee the safety of the running train, Shijiazhuang Railway Institute and Beijing Railway Bureau jointly

conducted a field test of the device at Handan Railway Station.

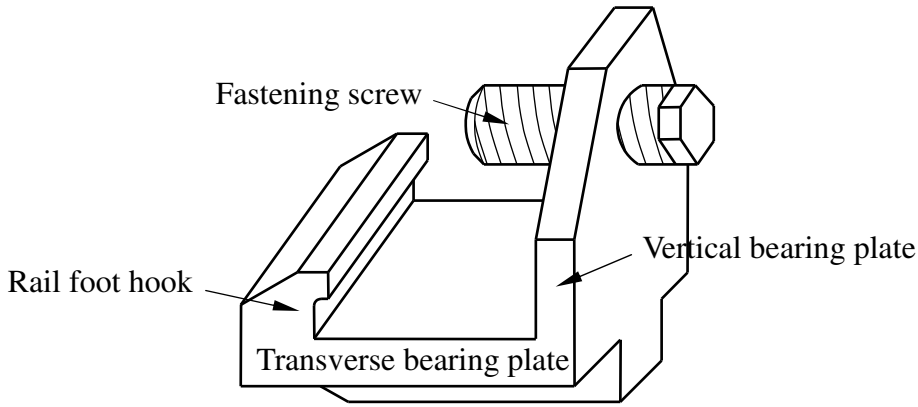

Figure 1. Rail break emergency treatment device

GENERAL DESCRIPTION OF THE TEST

Information on the railway line. The test was conducted on Track No.6 at Handan Railway Station (K431+650～K431+675 on Jing-Guang Railway). The segment lies in a curve with a 1000 m radius and 20 mm super-elevation of the outer rail. The track is constructed of 60 kg/m 25 m-long rail, 1760 pieces/km 69-type sleepers, and 300 mm-thick lime crushed stone ballast with good elasticity and no hardening. For test Section 1 (K431+650 of Jing-Guang Railway), the rail joint is 21 mm and close to the left sleeper's edge. For test section 2 (K431+675 of Jing-Guang Railway), the rail joint is 23 mm and is located at the middle of the span.

Operating conditions. The Dongfeng-7 dispatching locomotive was adopted in the test and the test speeds varied from 9.8 km/h to 44.0 km/h (measured by ground speed meter). It was tested 22 times, 16 times with common jointbar, and 6 times with frozen jointbar.

TEST PLAN DESIGN

Contents of test: (1) The stress of the bottom edge of the common or frozen jointbar and the stress of rail foot top at the center of the rail joint under different train speeds; (2) The stresses of the vertical bearing plate and rail foot hook, and force of the fastening screw of RBETD for railway switch; and (3) The transverse displacement of the railhead and the sinking of the rail foot, from which the dynamic change of track gauge and the dynamic joint stagger (horizontal and vertical) can be derived

Test method: Strain sensors were adopted for stress testing. Single-piece strain sensors were directly placed on appropriate positions on the structure and formed half-bridges with the corresponding temperature-compensation strain sensors (Cao, 2004; Wu, 1991). The stress was calibrated on the spot with the equal-strength beam.

The rail displacements were measured by leaf displacement meters, which adopted variable-sections but uniform-strength beamed copper leaf-springs as sensors. Strain sensors were symmetrically placed on both sides of the copper leaf to

form a half-bridge. A 1.5m-long steel rod with a diameter of 32 mm was driven into the subgrade to affix the displacement meter (Cao, 2004; Wu, 1991). The displacement sensor was affixed to the upper end of the rod and the displacement was measured with feeler gauge.

Arrangement of test points. Two sections were tested. Ten test points were arranged at Section 1, one point for the stress at the bottom edge of the common jointbar ($_A$), one point for the stress at the rail foot top ($_B$), one point for the stress of the vertical bearing plate of the emergency treatment device ($_C$), one point for the stress at the rail foot hook of the device ($_D$), one point for the inner force of the fastening screw of the device(P_G), and five points for rail displacement; Eight test points were arranged at Section 2, one point for the stress at the bottom edge of the common jointbar ($_A$), one point for the stress at the rail foot top ($_B$), one point for the stress of the vertical bearing plate of the emergency treatment device ($_C$), and five points for rail displacement.

Depending on the field test result in the case of a frozen jointbar, one test point was arranged at both Section 1 and 2 for the stress at the bottom edge of the frozen jointbar ($_A$). The arrangement of the Test Sections is shown in Figure 2.

Figure 2. Arrangement of test sections

Criterion for appraisal. Stress: less than the allowable stress for each part. Dynamic track gauge change: no more than (+8, -4) mm. Dynamic joint stagger: 3 mm.

TEST RESULTS AND ANALYSIS

Stress values. Table 1 shows the maximum stress values observed as the test train passed the test sections at different speeds. In Table 1, only the stresses with maximum absolute values are included, "-" for compressive stress and "+" for tensile stress. Test points No.1-16 are for the common jointbar, and points 17-22 are for the frozen jointbar. The test results show that:

(1) All stresses were less than the allowable value and had a sufficient margin of safety. The stress at the rail foot hook of the emergency treatment device was

especially far bellow the allowable value.

(2) There was no obvious relationship between the stress values and the speed of the test train, and the stress values were scattered to some extent. However, the stress values seem to be related to the position of the wheels and direction of the train, possibly due to the impact of the wheels on the rail joint. When the train was running in the same direction, the stress values increased with the train speed.

(3) Before the running test, the relation between the compressive force of the fastening screw (P_G) and the torque moment of the bolt (T) was determined through test: $T=KDP_G$, in which K is the torque coefficient ranging from 0.26～0.37 and adopted 0.30 practically in the test. The field test shows that a bolt torque moment of 400-500 N·m can meet the performance requirement.

Table 1. Maximum observed values of stress

No.	Speed ($km \cdot h^{-1}$)	Section 1					Section 2 (MPa)		
		$_A$(MPa)	$_C$(MPa)	$_B$(MPa)	$_D$(MPa)	P_G(kN)	$_A$	$_C$	$_B$
1	9.8	+188.78	-123.77	-58.19	+6.94	-45.79	+200.81	**-114.50**	-28.39
2	24.8	+150.84	-116.24	-45.84	+5.42	-43.01	+197.43	-109.28	-38.06
3	18.1	+198.30	**-127.30**	-60.71	+4.33	**-47.10**	+211.42	-105.79	-26.07
4	23.4	+146.29	-110.59	-38.10	+5.42	-40.92	+197.65	-107.10	-39.32
5	29.9	+198.95	-125.89	-56.10	+5.42	-46.58	+227.21	-105.57	-27.76
6	31.0	+159.29	-109.65	-39.14	+5.63	-40.57	+199.91	-106.45	-35.75
7	30.0	+206.97	-124.00	-58.82	+4.98	-45.88	+226.31	-103.18	-27.54
8	18.1	+145.86	-108.00	-38.94	+5.63	-39.96	+206.90	-104.92	**-41.63**
9	18.5	+189.42	-118.12	-53.38	+4.55	-43.70	+220.44	-99.70	-26.70
10	20.1	+143.69	-108.47	-40.19	+5.42	-40.13	+203.07	-101.44	-40.37
11	33.7	**+211.74**	-115.3	**-61.33**	+5.63	-42.66	+229.47	-100.13	-27.33
12	34.2	+166.88	-106.59	-36.63	+5.42	-39.44	+209.61	-105.14	-36.80
13	33.9	+210.00	-118.36	-59.03	+4.55	-43.79	**+235.78**	-100.13	-29.44
14	40.3	+166.01	-105.65	-36.42	+5.85	-39.09	+231.72	-101.44	-38.48
15	36.9	+207.94	-117.18	-58.82	+4.55	-43.36	+241.65	-99.70	-27.33
16	44.0	+172.30	-104.00	-37.68	**+7.59**	-38.48	+243.00	-107.32	-38.06
17	19.3	+230.16					+153.43		
18	19.5	+192.67					+179.83		
19	20.1	+234.06					+148.01		
20	34.5	+193.97					+184.34		
21	33.5	**+252.49**					+171.03		
22	33.8	+196.14					**+192.46**		

Test result analysis of the geometric shape and position. Table 2 shows the maximum observed values of the transverse displacement of the rail head, the sinking of the rail foot, the dynamic track gauge change, and the dynamic joint stagger. In Table 2 only the data with the maximum absolutes are included. For rail head transverse displacement, "+"indicates the displacement is toward the outside of

the rail, "-"indicates the displacement is toward the inside of the rail. For rail foot sinking; "+"indicates the displacement is downward; "-"indicates the displacement is upward. For track gauge change, "+"indicates the gauge is increased;"-"indicates the gauge is decreased. The test data shows that:

Table 2. Maximum observed values of displacement

Speed ($km \cdot h^{-1}$)	Section1 / Section2 (mm)					
	Transverse rail head displacement	Rail foot sinking	Gauge change		Joint stagger	
			increase	decrease	vertical	horizontal
9.8	+2.23/+1.82	+3.75/+3.78	+3.52/+2.98	-0.13/-0.60	1.07/1.02	1.18/0.54
24.8	+1.54/+1.77	+3.54/+4.05	+2.36/+2.85	-0.18/-0.25	1.13/1.52	1.38/0.76
18.1	**+2.47**/+1.54	+4.22/+3.84	**+3.94**/+2.54	-0.08/-0.46	1.43/1.01	1.42/0.72
23.4	+1.22/+1.76	+3.70/+4.28	+1.77/+2.80	**-0.86**/-0.34	1.91/1.45	1.31/0.84
29.9	+2.00/+1.62	+4.52/+4.23	+3.29/+2.83	-0.33/-1.01	1.92/0.35	0.95/1.33
31.0	+1.38/+1.80	+4.51/+4.18	+2.04/+3.25	-0.77/-0.62	1.51/**2.09**	1.39/1.05
30.0	+2.09/+1.67	+4.43/+4.05	+3.02/+2.93	-0.13/**-1.45**	1.81/1.45	1.11/1.11
18.1	+1.25/+1.89	+4.40/+4.26	+1.87/+2.60	-0.49/-0.50	1.63/1.59	1.33/0.88
18.5	+1.70/+1.71	+4.08/+3.93	+2.98/+2.84	-0.16/-0.35	1.23/1.12	1.00/1.01
20.1	+1.21/+1.93	+4.00/+4.37	+1.61/+2.60	-0.50/-0.58	1.46/1.71	**1.47**/0.87
33.7	+2.47/+1.61	+4.69/+4.25	+3.60/+2.81	-0.14/-0.38	1.89/1.30	1.33/1.10
34.2	+1.36/+1.92	+4.68/+4.36	+2.16/+3.57	-0.47/-0.46	1.77/2.00	1.30/1.12
33.9	+2.27/+1.67	+4.67/+4.20	+3.37/+2.76	-0.06/-0.50	1.65/1.32	1.23/1.26
40.3	+1.26/+2.87	+4.27/+4.26	+2.05/+4.38	-0.62/-0.52	**1.97**/1.91	1.39/**1.58**
36.9	+2.36/+1.63	**+4.79**/**+4.58**	+3.43/+2.71	-0.14/-0.40	1.83/1.11	1.23/1.02
44.0	+1.27/**+3.05**	+4.37/+4.35	+1.99/**+4.49**	-0.72/-0.33	1.77/1.84	1.34/1.41

(1) All the observed data in both sections were less than their allowable values. It should be noted that a few of the observed data were close to their allowable value.

(2) The observed data of the rail head transverse displacement, rail foot sinking, dynamic track gauge change, and joint stagger were not obviously influenced by the speed of the test train and were scattered to some extent, possibly due to the limited range of the speed change. As with the stress test, the running direction of the train had an effect on the observed data. With the same train speed, the data had greater values when the train was running southward rather than northward, possibly due to the impact of the wheels on the section of the rail joint. When the train was running in the same direction, the values of the observed data increased with the train speed.

Comparison between calculation result and observed data. The mid-span bending moment and vertical displacement of the jointbar were calculated with the railway engineering numerical calculation software, adopting the following parameters values: The elastic modulus of the rail and jonitbar E=2.1×10^5 MPa., the

inertia moment of 60 kg/m rail against the horizontal axis I_1=2879 cm^4(allowing for 6 mm vertical wear), the inertia moment of the common jointbar against the horizontal axis I_2=496.3 cm^4, the inertia moment of whole-section-frozen jointbar against the horizontal axis I_3=709.1 cm^4 and the elastic coefficient of the rail supporting point D=300 kN/cm (Goenraad, 2001; Gu, 2005, Hao, 2002).

The comparison between the calculation results and observed data shows that the calculated bending stress at the bottom edge of the jointbar is greater than the observed value while the calculated displacements are smaller than observed. However, both are less than their allowable values, which indicates that the bending strength of the jointbar is not fully utilzed due to the contact displacement between the rail and the jointbar.

CONCLUSIONS AND FUTURE RESEARCH

(1) The test analysis shows the train can temporarily pass through the broken section of rail at a speed under 25 km/h after the rail is strengthened with the railway switch RBETD combined with single-side jointbar. All the major safety indexes are below their allowable values, hence it is verified that the design and strengthening method of the device are reasonable, safe, and reliable.

(2) According to the test results, the maximum compressive force of the fastening screw is about 60 kN, hence the value of 66 kN adopted in the design is appropriate. The initial torque moment of 400-500 N·m of the fastening screw can meet the requirement to ensure the good performance of RBETD.

(3) The safe operation of RBETD can be assured with a common jointbar, hence a frozen jointbar is not necessary.

(4) The vehicle used in the test is the dispatching locomotive of Dongfeng-7 Model. It should be noted that in order to make a comprehensive appraisal of the running safety and railroad stability, the vertical and horizontal wheel-rail forces should be tested to obtain such important indexes as derail factor and wheel load decrement ratio.

ACKNOWLEDGEMENT

The Project Supported by the National Natural Science Foundation of China (No.50878134) and the Natural Science Foundation of Hebei Education Department (No. 2006142).

REFERENCES

Cao, L. Z. (2004). “Modern test techniques and devices”. *Publishing House of Beijing Space and Aeronautics University*.

Goenraad, E. (2001). “Modern railway track”. *MRT-Productions*.

Gu, A. J. (2005). “Railway track”. *Publishing company of China Railway*, 8-10.

Hao, Y. (2002). “Railway engineering”. *Publishing company of China Railway*, 3-11.

Wu, Z. Y. (1991). “Test techniques and test signal processing”. *Publishing House of Qinghua University*.

Capacity Reliability of Road Network under Adverse Weather Conditions Based on Fuzzy Theory

Zhang Xi-qiao[1,2], An Shi[2], Tang Yan-hong[1], Sheng Hong-fei[2]

[1] School of Management, Harbin Institute of Technology, Harbin 150090, China

[2] School of Transportation Science and Engineering, Harbin Institute of Technology, Harbin 150001, China

ABSTRACT： Under adverse weather conditions, both traffic system and physical environment have strong uncertainty and road network capacity is also changing and has strong fuzziness under dynamic situations. Based on analysis of the concept and meaning of road network capability, which has uncertain meaning, the capacity reliability of road network is taken as a fuzzy and random variable, therefore, fuzzy probability was applied to study it. The calculation and simulation method for reliability with random traffic flow and fuzzy road network capacity are discussed. The Bootstrap method based on experiential data was introduced to analyze reliability with fuzzy road network capacity. The area of fuzzy variable was given based on form and relative parameters in consideration of the practical requirements of traffic management.

Keywords: adverse weather, fuzzy theory, capacity reliability of road network

Reliability generally can be defined as the probability of completing the stipulated functions and tasks and it has extensive applications in computer system, correspondence and electric power engineering. However, research introducing the road network capacity reliability into the road network is still nearly a 10-year thing. Chen (Chen, 2000) set up a double-layer mathematical programming model of the capacity reliability, which can solve problems based on sensitivity analysis and Monte Carlo technique. Lo (2003) proposed PUE (probability user equilibrium) model to reflect the traveler's route choice behavior in stochastic road network and to calculate the road network capacity reliability. Bell (2000) took into account the difficulties of traffic data acquisition and made use of game theory to estimate the road network reliability. This paper will use fuzzy random theory to generate a city road network capacity reliability study.

1 Road network uncertainty analysis under adverse weather

The operation of a city transport system is affected by manifold factors under adverse weather and has a strong uncertainty. Urban transportation networks are closely related to traveler's activities, so it has more uncertainty. On the one hand, it is the fuzzy traffic change and there are some uncertainty factors to change the supply status of road network such as road status, visibility and traffic management situation and so on. On the other hand, the random change of traffic demand is affected by the travelers' path selections such as travel cost, personal preference, the status of road network, etc.

City road network capacity can be described with the fuzzy variables under adverse weather. The case or concept itself is described by fuzzy variables is ambiguous, whether an object is accord with vague concept is not clearly determined, but can only describe the possibility of the certain concept with the

subjection degree. Road network capacity is difficult but should not be simply divided into reliable or unreliable. Road network capacity is changing continuously and has strong ambiguity under dynamic situations.

Traffic demand can be described randomly under adverse weather. The randomness of cases or phenomena themselves is clear and the collection of random events demonstrates its clear extension.

The change of traffic demand has certain effects on the road network reliability which is the ability to adapt to the change of traffic demand. The change of traffic demand has fixed rules under adverse weather conditions and road network capacity has different reliability demands.

Road network reliability is a fuzzy random concept under manifold uncertainty. Generally, either the road network is in a normal situation or it is in an abnormal situation, and it does not have the transition situation in middle. But in fact road network has ambiguity, and it can also be regarded as the process from normal situation to abnormal situation. The control parameters of reliability which are in a limited state can be expressed with threshold cost. Therefore, it is statistically independent that the fuzzy random theory is used to study the change of road network capacity. The system will obtain new balance during this time.

2 The analysis of road network capacity reliability about fuzzy road network capacity of random traffic demand

For the fuzzy road network capacity $\tilde{C}$ and random traffic demand D,we can record fuzzy road network capacity as $\tilde{A} = \left\{ D \le \tilde{C} \right\}$; for any fixed threshold value, we can obtain interval $\tilde{C}_\lambda = [a_\lambda, b_\lambda]$. According to the concept of λ-cut set, we can think that any values are chosen about the posibility of the road network capacity is the same between a_λ and b_λ, when the threshold value of fuzzy road network capacity is λ, it is subjected to a uniform distribution of random variables between a_λ and b_λ. Therefore, the reliability problem of fuzzy road network can be converted into the probability problem of $\tilde{A}_\lambda = \left\{ D \le \tilde{C}_\lambda \right\}$. The probability of $\tilde{A}_\lambda = \left\{ D \le \tilde{C}_\lambda \right\}$ can be calculated with traditional reliability design theory.

Considering the above information, we can regard traffic demand and road network capacity as random variables to calculate the probability of the road network capacity reliability $\tilde{A}_\lambda = \left\{ D \le \tilde{C}_\lambda \right\}$,that is the following:

$$R_\lambda = P(\tilde{A}_\lambda) = P(D \le \tilde{C}_\lambda) \quad (1)$$

In the above formulas, $\tilde{C}_\lambda$—when the threshold value λ is given, the membership function $\mu_{\tilde{C}_\lambda}(C)$ of fuzzy road network capacity $\tilde{C}$ can determine the interval which is between a_λ and b_λ; and it can be determined according to the relation formula $\mu_{\tilde{C}_\lambda}(C) \ge \lambda$. Road network capacity in the above interval is subjected to the uniform distribution of random variables. R_λ—when the threshold value is λ, it is the probability of fuzzy road network capacity reliability. $P(D \le \tilde{C}_\lambda)$—when the threshold value is λ, when the fuzzy road network capacity is converted into random

road network capacity, random road network capacity outweighs the probability of random traffic demand.

When the general expression of the probability R_λ of λ-cut set of reliability of fuzzy road network capacity is obtained, the probability of fuzzy road network capacity reliability is the following:

$$R = P(D \le \tilde{C}) = \int_0^1 R_\lambda d\lambda = \int_0^1 P(D \le \tilde{C}_\lambda) d\lambda \qquad 2$$

In the above formula, $P(D \le \tilde{C})$ —it is the probability of fuzzy road network capacity reliability.

In formula 1, for any given threshold value λ, when we get the interval $\tilde{C}_\lambda$ of fuzzy road network capacity, the probability density function of road network capacity is the following:

$$f_{\tilde{C}_\lambda}(C) = \begin{cases} \dfrac{1}{b_\lambda - a_\lambda} & C \in [a_\lambda, b_\lambda] \\ 0 & other \end{cases} \qquad 3$$

Therefore, λ-cut-set probability of fuzzy road network capacity reliability is the following:

$$R_\lambda = P(D \le \tilde{C}_\lambda) = \int_{-\infty}^{+\infty} f(D)[\int_D^{+\infty} f_{\tilde{C}_\lambda}(C) dC] dD \qquad 4$$

In the above formula, $f(D)$ —the probability density function of traffic demand.

When fuzzy road network capacity $\tilde{C}$ is equal to threshold value λ, the interval which it belonged to obeys the random variable of uniform distribution, so we just consider the value between a_λ and b_λ when we calculate the integral value $\int_D^{+\infty} f_{\tilde{C}_\lambda}(C) dC$. Therefore, the value of traffic demand D is less than a_λ, traffic demand will not more than road network capacity, the integral value is 1; when the value of traffic demand D is more than b_λ, the traffic demand is always greater than the capacity of road network, the integral value is 0; the integral value is $(b_\lambda - D)/(b_\lambda - a_\lambda)$ when the value of traffic demand D is between a_λ and b_λ. From the above analysis, let us substitute formula 4 into the following:

$$R_\lambda = P(D \le \tilde{C}_\lambda) = \int_{a_\lambda}^{b_\lambda} \frac{1}{b_\lambda - a_\lambda} [\int_{-\infty}^{C} f(D) dD] dC = \int_{-\infty}^{a_\lambda} f(D) dD + \int_{a_\lambda}^{b_\lambda} \frac{b_\lambda - D}{b_\lambda - a_\lambda} f(D) dD$$

$$= \int_{-\infty}^{+\infty} f(D) \cdot \max[\min(\frac{b_\lambda - D}{b_\lambda - a_\lambda}, 1), 0] dD \qquad 5$$

where

$$\max[\min(\frac{b_\lambda - D}{b_\lambda - a_\lambda}, 1), 0] = \begin{cases} 1, & D \le a_\lambda \\ \dfrac{b_\lambda - D}{b_\lambda - a_\lambda}, & a_\lambda < D < b_\lambda \\ 0, & b_\lambda \le D \end{cases} \qquad 6$$

Formula 5 is used for the road network capacity reliability when the city road network is equal to the threshold value λ. Then, when the road network capacity reliability is equal to the threshold value λ, the integral value between 0 and 1 of the

reliability R_λ is the following:

$$R = P(D \le \tilde{C}) = \int_0^1 R_\lambda d\lambda = \int_0^1 P(D \le \tilde{C}_\lambda) d\lambda$$
$$= \int_0^1 \int_{-\infty}^{+\infty} f(D) \cdot \max[\min(\frac{b_\lambda - D}{b_\lambda - a_\lambda}, 1), 0] dD d\lambda \quad (7)$$

$P(D \le \tilde{C})$ is the probability of fuzzy road network capacity greater than or equal to the traffic demand D.

3 The way of Bootstrap about fuzzy random reliability analysis

When we analyze the reliability of fuzzy random road network capacity, we can use the λ-cut set concept of fuzzy collection and obtain the relation formula of fuzzy random road network capacity and analyze the fuzzy capacity reliability of road network through the ways discussed in the second section. Comparatively speaking , it is more measurable with the actual situation if we give an interval of fuzzy variables than if we use the direct form of its membership function and its parameters. When we analyze the fuzzy reliability, we can regard every interval as a λ-cut set of membership function of fuzzy variables. We can get the probability of fuzzy road network capacity reliability when experts give enough intervals (Dong , 2007).

Bootstrap is a simple and effective non-parametric statistical method which is proposed by Professor Efron in Stanford University in the United States (Efron, 1979). This method is widely used in engineering practices as it can make a statistical simulation on the basis of traditional mathematical statistics and create confident parameter intervals on the basis of small samples. Meanwhile, the method makes full use of information of sub-samples themselves so it does not need any assumptions for the overall distribution. Its basic principle is the following:

We assume there is a independent distribution sub-sample $X = (X_1, X_2, \cdots, X_n)$, which is from the unknown overall distribution R, but $\theta = \theta(R_n)$ is the unknown parameter of overall distribution. We suppose that R_n is the experience distribution drawn from sub-sample X, $\hat{\theta} = \hat{\theta}(R_n)$ is the estimation of θ. Estimation error is the following:

$$E_n = \hat{\theta}(R_n) - \theta(R) \quad (8)$$

According to the R_n,we can carry out sample by means of simulation, we assume that $X^* = (X_1^*, X_2^*, \cdots, X_n^*)$ is regeneration sample obtained from samples. Experience distribution R_n^* from X^* is the following:

$$E_n^* = \hat{\theta}(R_n^*) - \hat{\theta}(R_n) \quad (9)$$

According to the theory of Professor Efron, we can simulate E_n distribution by means of E_n^* distribution. E_n^* is self-assist statistics of E_n. When determining the parameters θ, we can make a close affinity between E_n^* and E_n

in formula 9, so we can get $\theta(R) \approx \hat{\theta}(R_n) - E_n^*$ and sample $\theta(R)$ of θ through single sampling X^* of R_n. From the above principle, we can get multiple $\theta(R)$ samples, therefore, we can get eigenvalue and its distribution of θ .

4 Analysis of Examples

It is inaccurate to express the road network capacity with defined data under adverse weather conditions. We suppose that "under adverse weather road network capacity of about 4304" is a fuzzy case $\tilde{C}$ where its membership function is expressed as a drop- ridge shaped distribution, as follows:

$$\mu(C) = \begin{cases} 1, & \text{当} C \le 4099 \\ \frac{1}{2} - \frac{1}{2}\sin\frac{\pi}{430}(C - 4304), & \text{当} 4099 \le C \le 4519 \\ 0, & \text{当} 4519 \le C \end{cases} \quad 10$$

Owing to the randomness of traffic demand (Yue, 2001), we can regard it as a random variable of normal distribution where its density function is the following:

$$D(x) = \frac{1}{200\sqrt{2\pi}} \exp(\frac{-(x-3857)^2}{80000}) \quad 11$$

We can calculate 10^4 according to the membership function of road network capacity. The result obtained is equal to $R = 0.9427848$ which is used as the theoretical value of city road network capacity reliability under adverse weather conditions. At this point, the road network capacity can satisfy the requirements of the traffic demand. We will get eight intervals according to these supposed eight different λ values and membership function of road network capacity and the concept of λ cut-set of fuzzy collation, meanwhile we can regard these λ value and its corresponding interval as a group of empirical data. We will estimate road network capacity reliability by means of different methods on the basis of eight different λ values and their corresponding intervals. After six repetitions, the results are shown in table 1:

Table 1 Count results of road network capacity reliability

serial number	λ value	R_n	Bootsprap method	
			average	95% confidence interval (M=1000)
1	0.1,0.2,0.3,0.4,0.5,0.6,0.8,0.9	0.945258	0.940503	[0.915349 , 0.965657]
2	0.05,0.1,0.3,0.4,0.55,0.60,0.75,0.95	0.945097	0.935551	[0.905865 , 0.965237]
3	0.05,0.15,0.25,0.4,0.5,0.8,0.85,0.9,	0.942266	0.940445	[0.915409 , 0.965482]
4	0.2,0.3,0.45,0.5,0.6,0.7,0.85,0.95	0.939388	0.932273	[0.905701 , 0.958844]
5	0.15,0.2,0.3,0.4,0.45,0.5,0.6,0.7	0.950494	0.948643	[0.935693 , 0.961593]
6	0.05,0.2,0.3,0.4,0.55,0.7,0.8,0.95	0.943177	0.942692	[0.905256 , 0.965038]

We see from table 1 that the Bootstrap method is obtained by means of the method of obtaining R_n. Even though it is aiming at self-assist sample $R_{w,l}$, its final result is closer to a theoretical value than R_n. Not only can it effectively reduce the fluctuation caused by interval change but it also can get the corresponding confidence interval according to different confidence limit. Meanwhile, it has certain practical significance.

5 Conclusion

Road network capacity reliability analyzes the city road network service capabilities from a macroscopic angle. The supply capacity of city road network and traffic demand is uncertain. We can regard traffic supply as the variable of fuzzy change and regard traffic demand as the variable of random change. Therefore, we can study road network capacity reliability by means of fuzzy random theory; that is, road network capacity reliability is regarded as a fuzzy random variable and to study the theoretical calculation method of random traffic flow of fuzzy road network capacity reliability analysis. The Bootstrap Method based on the experience data is introduced to analyze fuzzy road network capacity reliability. The fuzzy variable intervals obtained from empirical data become more affordable to the practical requirements of traffic management than its form of membership function and parameters.

REFERENCES

Bell, M G H. (2000). A game theory approach to measuring the performance reliability of transport networks. Transportation Research B. 34 (6): 533-546

Chen, A; Tatineni, M, Lee, D H; Yang H. (2000). The effect of route choice models on estimating network capacity reliability. Transportation Research Record, 1733: 493-513

Dong, Yuge; Wang, Ainan and Wu Chenglong.(2007). Application of Conventional Reliability Theory in Fuzzy Reliability Calculation. Transactions of the Chinese Society for Agricultural Machinery. 2007. 2(38): 142-145

Efron, B. (1979).Bootstrap methods. The Annuals of Statistics. 1979.7 (1): 1-26.

Lo, H K and Tung Y K. (2003). Network with degradable links: capacity analysis and design. Transportation Research B. 2003, 37: 345-313.

Liu, Gang and Qu Liang sheng.(2002). An Application of the Bootstrap Method in Machinery Fault Diagnosis. China Mechanical Engineering. 13(10):829-832

Yue, Li. (2001). A Combined Model for Time-dependent Trip Distribution and Traffic Assignment. 81th Annual Meeting of Transportation Research Board: 1-30

Real-Time Dispatching and Routing for Emergency Vehicles after Earthquake Disasters

Wen-Ping Cai[1] and Lei He[2] and Gao Guo[3]

[1] Changchun Construction Project Management Center, Changchun 130000, China; email: tianshi2554@163.com

[2]School of Science and Engineering on transportation, Harbin Institute of Technology, Heilongjiang Harbin 150090, China; tel: 13936643725; email: heleihit@163.com

[3] Changchun Municipal Engineering Design and Research Institute, Changchun 130000, China; email: helei297@sohu.com

ABSTRACT

The purpose of this paper is to build an effective mode for the dispatching and routing of emergency vehicles during disaster response. In this paper we consider the conditions of an earthquake disaster, for example, there are a large number of injuries which require medical treatment. The given conditions, including the injuries, casualties, roads, and traffic conditions, were utilized to dispatch and route emergency vehicles to the injured persons and then delivery them to the appropriate treatment center. In this paper, a real-time scheduling of the mathematical programming model is built for emergency vehicles to quickly select a reasonable route to save injured persons, and we utilize a case study to evaluate the performance of the proposed methodology. This is a highly effective mode for improving the emergency response capacity of the vehicle, improving rescue time and providing a theoretical basis and technical support for emergency rescue work.

1 INTRODUCTION

China is one of the most disaster-stricken countries in the world. An important element in post-disaster rescue is the emergency rescue of the injured persons. When an emergency situation arises, data including reports about injured persons, structural damage, road conditions, and traffic situations begin to flow to the Emergency Response Centers. ITS can monitor the real-time status of the roads and estimate the travel time of emergency vehicles. In the case of a major disaster, the discovery rate of casualties is extraordinary high. Therefore, an effective strategy for dispatching and routing is necessary for the decision makers involved in emergency rescue procedures.

There is limited research on the routing of vehicles in a disaster environment, although dynamic vehicle routing problems have been studied in the past. Afshin et al. (2003) provided an urban emergency transportation network to reduce loss of life based on the principles of minimized travel time and maximization of the capacity of rescue services. Yi and Kumar (2007) built a multi-stage model of network flow by

disassembling the rescue vehicle scheduling problem into the path of the vehicle structure and multi-item dispatching. Linet et al. (2004) discussed emergency material transportation scheduling in 2004, which describes dispatch orders for vehicles as consisting of sets of "broken" routes. Barbarosoglu and Arda (2004) proposed a two-stage multi-mode transport network model, and simulated the transport plan of relief materials. In such problems, a set of vehicles is routed over a particular timeline while new services are occurring in real time. To our knowledge, such a scenario has not been studied within a dynamic disaster environment.

2 POST-EARTHQUAKE ROAD CAPACITY

Road traffic capacity is influenced by many factors, such as lane width, lane number, and road surface conditions. The road capacity in disaster is impacted by the collapse of buildings along the street, displaced persons and vehicles, and the damage to the road itself. In the current study, the effects of damage to the road are not considered because urban roads have better seismic performance. The effects of the displaced persons by a stringent post-earthquake traffic management can also be ignored analogously.

Post-earthquake road capacity should be amended based on the actual road damage and the practical capacity in good condition, as shown in table 1. The value parameter denotes the increased travel time in different degrees of damage. The practical travel time is denoted by $t_{ij}(t)$ which is calculated by $\sum_n t_n^0(t) \cdot \xi_n$, where $t_n^0(t)$ is travel time in good condition.

Table 1. Value of ξ_n in different degrees of damage

Probability of buildings collapse	High	High	Low	Low
Probability of occupation road	High	Low	High	Low
The increase of travel time ξ_n	∞	2	1.7	1.0

3 MODEL DEVELOPMENT

In this paper, real-time information and the linked travel time estimates are used to calculate the dynamic shortest path. Mathematical programming models are used to find the best scenarios of emergency vehicle dispatching and routing. The final objective is to send the appropriate emergency vehicles to injured persons, and then deliver those persons to the appropriate hospitals. Thus, the problem can be divided into two parts: the vehicle dispatching problem and the vehicle routing problem.

3.1 VEHICLE DISPATCHING PROBLEM

The information on injured persons includes both their location and injury

classes. There are two injury classes: moderately injured and severely injured. The casualties are distributed randomly across the space affected; if a certain number are concentrated in a particular region, they then form clusters, which can be considered a small geographic region where a certain number of casualties are aggregated (Arun et al., 2009).

In the vehicle dispatching problem, an emergency vehicle is dispatched to an individual or cluster of casualties. Preference is given to the latter since it is more efficient to process groups than to serve individual casualties. This is the case since the emergency vehicle is likely to find some casualty for pickup within the cluster. If no clusters are present, the idle emergency vehicle is sent to the nearest high severity casualty.

3.2 VEHICLE ROUTING PROBLEM

Once injured persons have been picked up, the next task is to deliver them to appropriate hospitals. At each point, the dispatcher makes a dispatching decision for the emergency vehicles so that the system can use its resources with maximum efficiency. We assume at this point the travel time for each link is calculated and the shortest path for each pair of nodes is known based on the historical information.

While trying to minimize the total response time, the route and the destination of the emergency vehicles could change frequently. Too many and too frequent changes in the destination or route can be confusing and counter-productive. For example, before the reassignment vehicle 1 is assigned to an incident at node A, and vehicle 2 is assigned to an incident at node B. Under new demand conditions, if $t_{1,A} + t_{2,B} > t_{1,B} + t_{2,A}$, the result of reassignment could be that vehicle 1 is assigned to node B and vehicle 2 is assigned to node A. If the increase in travel time t_{1A} and t_{2B} are minor (for example less than 5%), $(t_{1,B} + t_{2,A}) - (t_{1,A} + t_{2,B})$ is a very small amount and perhaps less than the assignment before. This kind of route change should be avoided. The drivers should not change routes even if the destination is the same unless significant improvements could be achieved (Haghani et al., 2004).

3.3 MATHEMATICAL FORMULATION

The mathematical formulation for the real-time emergency vehicle dispatching problem minimizes the overall response time subject to vehicle availability and service constraints and is as follows:

$$\min a\sum_{i=1}^{N_v}\sum_{n=1}^{N}\sum_{j\in w^1,w^2} x_{ij}t_{ij}(t)\alpha_n + b\sum_{i=1}^{N_v}\sum_{n=1}^{N}\sum_{k\in w^2} x_{ik}t_{ik}(t)\alpha_n$$

S.T.

$$\sum_{j\in w^1,w^2} x_{ij} + \sum_{k=1}^{N_k} x_{ik} = 1 \quad \forall i \tag{1}$$

$$\sum_{j \in w^1, w^2} x_{ij} = 1 \qquad \forall i \in V^2 \tag{2}$$

$$\sum_{k=1}^{N_k} x_{ik} = 1 \qquad \forall i \in V^3 \tag{3}$$

$$\sum_{j=1}^{N_v} x_{ij} = 1 \qquad \forall j \in W^1, W^2 \tag{4}$$

$$\sum_{i=1}^{N_v} \sum_{n=1}^{N} \sum_{j \in w^1, w^2} x_{ij} t_{ij}(t) \le T_{j(t)} \tag{5}$$

$$-\left(\sum_{j \in w^1, w^2} x_{ij}^0 t_{ij}(t) - \sum_{j \in w^1, w^2} x_{ij} t_{ij}(t) - \varepsilon \right) \le M \cdot y_i \qquad \forall i \in V^2 \tag{6}$$

$$1 - \sum_{j \in w^1, w^2} x_{ij}^0 x_{ij} \le M \left(1 - y_i\right)$$

$$t_{ij}(t) = \sum_n t_n^0(t) \cdot \xi_n \tag{7}$$

Where:

i = The index of vehicles within No. i

N_v = The total number of emergency vehicles

j = The index of casualties within No. j

N_j = The total number of casualties

k =The index of hospitals within No. k

N_k = The total number of hospitals

N = The total number of paths

α_n = 1 if the a path was chosen; =0 otherwise

x_{io} = 1 if the a vehicle i is idle ; =0 otherwise

x_{ij} = 1 if the a vehicle i is dispatched to casualty j ; =0 otherwise

x_{ik} = 1 if the a vehicle i is dispatched to hospital k; =0 otherwise

$t_{ij}(t)$ = The travel time for vehicle i to arrive at casualties j while at time t

$t_{ik}(t)$ = The travel time for vehicle i to arrive at hospital k while at time t

$T_{j(t)}$ = The required response time for casualties j at time t

W^1 = The subset of casualties with moderately injured

W^2 = The subset of casualties with severely injured

V^1 = The subset of emergency vehicles with “idle” status

V^2 = The subset of emergency vehicles moving to casualties

V^3 = The subset of emergency vehicles moving to hospital

ξ_n = The increase of travel time of path n

$t_n^0(t)$ = The travel time in good condition of path n

a、b = The weight of two problems

The total travel time is the objective function of this formulation. The total travel time includes: the travel time to the casualties and the travel time to the hospitals. Constraint 1 states that every emergency vehicle must have a destination after assignment at time t. Constraint 2 ensures that emergency vehicles are dispatched to a destination. Constraint 3 states that the vehicles driving to hospitals can change their destination. Constraint 4 states that one vehicle must be dispatched to a casualty. Constraint 5 ensures that every casualty is treated justly. Constraint 6 is a mathematical expression of the reassignment conditions. Constraint 7 calculates practical travel time.

The model is solved by Flody's shortest path algorithm at every step during the dynamic solution process. The process is characterized by the concept that when faced with a new rescue request, the system recalculates the best path of each emergency vehicle and considers whether the reassignment conditions of real-time adjustments is satisfied, until a satisfactory solution is obtained.

4 CASE STUDY

In order to illustrate the advantages of the real-time vehicle scheduling model compared to the conventional scheduling model, the model is used in a road network which is abstracted from Changchun city, and compared with the conventional scheduling model. As shown in Figure 1, there are 26 nodes and 60 paths. Parameter values of the road travel times are shown in Table 2.

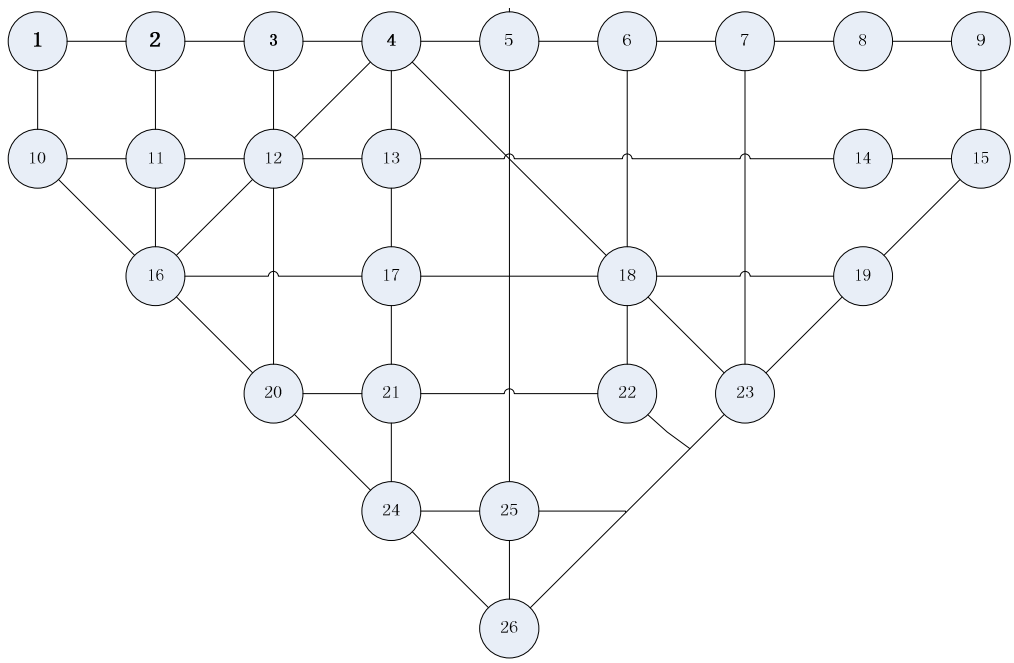

Figure 1. Emergency rescue network diagram

Table 2. Parameter values of the road travel time.

path	$t_n^0(t)\cdot\xi_n$	path	$t_n^0(t)\cdot\xi_n$	path	$t_n^0(t)\cdot\xi_n$	path	$t_n^0(t)\cdot\xi_n$	path	$t_n^0(t)\cdot\xi_n$	path	$t_n^0(t)\cdot\xi_n$
1	3.0	11	1.5	21	3.0	31	4.5	41	3.3	51	3.4
2	4.5	12	6.0	22	1.5	32	4.5	42	3.1	52	5.7
3	6.0	13	3.0	23	3.0	33	9.0	43	4.8	53	6.9
4	6.0	14	4.5	24	3.0	34	3.0	44	4.8	54	4.0
5	1.5	15	1.5	25	4.5	35	7.5	45	3.4	55	5.2
6	4.5	16	4.5	26	6.0	36	6.0	46	5.8	56	5.8
7	9.0	17	4.5	27	3.0	37	10.5	47	6.3	57	8.5
8	4.5	18	9.0	28	1.5	38	1.5	48	3.1	58	5.4
9	3.0	19	3.0	29	3.0	39	6.0	49	3.3	59	5.1
10	6.0	20	7.5	30	7.5	40	6.0	50	7.5	60	7.3

It is assumed that: hospitals are in nodes 11 and 23, there are two emergency vehicles at each hospital's location, relief demand generated by the system are A and B whose locations are nodes 17 and 24 with time interval 6 minutes. The required response times for A and B are 10 minutes and 9 minutes. The calculated results of the real-time model and are traditional model are shown in Table 3.

Table 3. Results of Emergency Vehicle Scheduling.

Scheduling strategy	Real-time	Traditional
Vehicle 1's mission and travel time	A, 11.7min	A, 11.7min
Vehicle 1's destination and travel time	Node 11, 11.7min	Node 11, 11.7min
Vehicle 2's mission and travel time	B, 14min	B, 14min
Vehicle 2's destination and travel time	Node 11, 6.3min	Node 23, 14min
Total travel time	43.7min	51.4min

As what can be seen from the results, response time of the real-time model is much less than the traditional scheduling model. This is because the real-time model ensures that emergency vehicles are always working efficiently. The model shows advantages in that when there is increased demand, the model can handle them in a more timely fashion and reduce response times.

5 CONCLUSION

This study concentrated on developing a dynamic dispatch strategy, by dividing the problem into two parts: the vehicle dispatching problem and the vehicle routing problem. An integer programming formulation was proposed for developing the real-time dispatching strategy. The formulation uses the shortest paths in as the routes for vehicles. A case study demonstrates that the real-time scheduling model,

compared with the traditional model, can significantly reduce the response times.

REFERENCES

Afshin, Mahmood, Hossein. (2003). "Obtaining the Emergency Transportation Network for Rescue and Relief Activities in Large Cities Based on the Life Loss Mitigation Criteria." *Earthquake Engineering.*, 231-240

Arun Jotshi, Qiang Gong, Rajan Batta. (2009). "Dispatching and routing of emergency vehicles in disaster mitigation using data fusion." *Socio-Economic Planning Sciences.,* 43,1-24

Barbarosoglu, Y Arda. (2004). "A Two-stage Stochastic Programming Framework for Transportation Planning in Disaster Response." *Journal of the Operational Research Society.,* 55,43-53

Haghani A, Tian Q, Hu H. (2004). "Simulation model for real-time emergency vehicle dispatching and routing." *Transportation Research Record.,* 1882,176-183

Linet Ozdamar, Ediz Ekinci, Beste Kucukyazici. (2004). "Emergency Logistics Planning in Natural Disasters." *Annals of Operations Research.,* 217-245

Yi W., Kumar A. (2007). "Ant Colony Optimization for Disaster Relief Operations." *Transportation Research.*, 43, 660-672

Establishment of Construction Safety Early-Warning System for Mountainous Freeways

Kaifeng Wang[1]， Xiedong Zhang[2], Xiaohuang Wang[3], Jianyi Yu[4], Sheng Yi[5]

[1]School of Transportation, Wuhan University of Technology, Wuhan, 430063, China, PH(13297988989);email: wangkaifeng@whut.edu.cn
[2]School of Transportation, Wuhan University of Technology, Wuhan, 430063, China, PH(18971022118);email:zhangxd@189.cn
[3]Hubei Hurongxi Expressway Construction Headquarter, Enshi, 445000, China, PH(15071720001);email:wangxiaohuang@163.com
[4]Hubei Hurongxi Expressway Construction Headquarter, Enshi, 445000, China, PH(13872736899);email:yujianyi@163.com
[5]Hubei Hurongxi Expressway Construction Headquarter, Enshi, 445000, China, PH(15071720008);email:yisheng@163.com

ABSTRACT

In recent years, with the rapid development of the national economy, frequent construction accidents on mountainous freeways result in a great loss of national property and become the focus of the nation's attention. It is urgent that we establish a construction safety early-warning system for freeways in mountainous regions in order to radically improve the situation of safety management. Major hazard identification and risk assessment is still lacking in the field. In order to solve this problem, a construction safety early-warning system for mountainous freeways was established. The targets, function, input and output of system were analyzed. The safety early-warning indicator system was made up of people, materials, environment, and management factors. The weights of factors were calculated by an analytic hierarchy process. The safety status grade was determined by a safety early-warning model. Results revealed that the safety early-warning system can reflect the safety status in freeway construction of mountainous regions objectively.

0 INTRODUCTION

Safety in mountainous freeways is needed for the sustained, healthy, stable development of the construction industry and essentially guarantees steady politics, stable society, and people living and working in peace and contentment. It is necessary to establish an early-warning system in freeway construction in mountainous regions for long-term and standard safety management. It helps to take corresponding measures quickly and efficiently to improve safety management in the event of accidents. The system monitors and controls the construction safety status. On one hand, it can take established management measures for restoration if accident

signs are recognized. On the other hand, it adopts corresponding emergency relief methods to reduce casualties and economic loss when accidents occur (Fan Hong 2005,Zhang Shilian 2006,Li Shirong 2004).

In foreign countries, the origin of economic early-warning methods was traced back to the Statistic General Assembly in Paris in the late 19th century. In the mid-30s of the 20th century, a diffusion index was applied. In the 50s, it came into practice. A synthetic index appeared in the 60s. Early-warning methods came to be mature in the 70s. Its theoretical research and application began in the mid-1980s. It has been used in everything from macroeconomics to corporation early-warnings, from qualitative analysis to combining qualitative and quantitative analysis, from point to status. But its development is far from mature. It belongs to the area of economic mutation (Wu Mingxia 2007, Zhu Jianjun 2007, Ren Hong 2005). In the field of freeway safety, early-warning system research is at a stand-still. Firstly, it is lacking advanced theory to support it. Secondly, it lacks the comprehensiveness, objectivity and dynamism needed to achieve full functionality of the early-warning system. Above all, applications of qualitative and quantitative analysis, forecasting methods and assessment means are insufficient (Choi H.H. 2004, Chua D. K. H. 2004,Sangoub Lee 2003,Osama Ahmed Jannadi 2003). Because of these problems, a safety early-warning system in freeway construction in mountainous regions was based on an unclear comprehensive assessment.

1 MODELING FRAME OF SAFETY EARLY-WARNING SYSTEM

1.1 Targets of system

The safety early-warning system in freeway construction in mountainous regions is used to determine whether the construction site is safe or not and take appropriate management measures. It can monitor, forecast and, warn various subsystems and adopt corresponding countermeasures.

1.2 Components, functions and input-output of system

The safety early-warning system is formed of three subsystems. The superior system is a database management system, and also is the input system. The mid-level system is comprised of a control system and also core processors including control system and convergence. The lower-level system is a generation subsystem consisting of graphics, conclusions, and recommendation output system.

The database management system is an integrated information system composed of entered qualitative and quantitative indicators. It contains all kinds of information which the mid-level system can order to call, query, add, delete and modify. The control system contacts the database management system with the generation subsystem, combining the functional requirement of subsystems according to the process of the safety early-warning system. It controls and manages subsystems. It also implements the man-machine dialogue interface and dynamic

management. The output system relates to the control system and generates corresponding graphics, conclusions and recommendations. The input of the safety system is the value of inspected indicators. The output is the warning degree.

Referencing the five-color warning system of the U.S. Department of Homeland Security as well as four-color warning of China's frame and guidance of contingency plans for public emergencies for relevant State Council departments and units, the system adopts three colors: red, yellow and blue. They correspond to three evaluation grades respectively. A red warning is adopted when safety status is poor. A yellow warning corresponds to general status. A blue level indicates a good status.

2 CONSTRUCTION OF SAFETY EARLY-WARNING SYSTEM MODEL

The safety system for freeway construction in mountainous regions is quite a complex, multi-level and nonlinear system. It has plenty of influencing factors, and many key factors cannot be carried out through quantitative analysis. A comprehensive assessment can solve qualitative factors and is appropriate for a multi-indicator and multi-layer system. Thus, the comprehensive assessment model of the safety early-warning system is established according to the characteristics of mountain freeways.

The construction safety status is divided into several grades. Evaluation grade set V is built:

$$V = \{v_1, v_2, \cdots, v_m\} \tag{1}$$

According to indicators in the system, bottom indicators are regarded as factors of safety comprehensive evaluation. Set U of evaluation factors is:

$$U = \{U_1, U_2, \cdots, U_n\} \tag{2}$$

Indicators' weight of various levels is determined according to a classification of evaluation factors and their importance to evaluated targets. Weight vector A is formed:

$$A = \{a_1, a_2, \cdots, a_n\} \tag{3}$$

The subjection degree of evaluation is determined using subjection function. Based on the model of comprehensive assessment, evaluation vector B is gained through determined weight vector A and relationship matrix R.

$$B = A \square R = (b_1, b_2, \cdots, b_n) \tag{4}$$

$$B = \sum_{j=1}^{n} b_j^2 \square j / \sum_{j=1}^{n} b_j^2 \tag{5}$$

The evaluation vector is changed to a single value though weighted mean., and eventually a safety grade is determined by comprehensive assessment.

3 CASE STUDY

Hubei Hurongxi Expressway is a major framework at home and an important part of the "six horizontal, five vertical and one ring" high grade highway network in Hubei province. It is also a fast-track of Shanghai-Chengdu's national highway from Yichang to Enshi connecting Chongqing, Chengdu and other major cities in the southwest. Hurongxi expressway is 320 kilometers long and the total investment is 204.5163 billion. It is divided into the Yichang-Enshi and Enshi-Lichuan projects. It was started on August 20, 2004. The project is expected to be completed in 2009.

Hurongxi expressway is located in a mountainous region of western Hubei province on Yunnan-Guizhou Plateau's northeast edge. Due to its special topography, complex technology, and difficult construction conditions, it is by far the largest investment, the most arduous project, the most complicated geologically, and the longest construction cycle expressway in Hubei province. The main line has four-lanes with the closed freeway building standard. The traffic speed is 80km/h.

Hurongxi expressway is currently one of the key high-risk projects in the country's transport infrastructure construction. It is also an important project of highway construction supervision. In order to ensure construction safety in production, the safety early-warning system of freeway construction in mountainous regions is built. A certain project is illustrated to evaluate the construction safety status using the early-warning system.

The construction safety status is divided into three grades. Corresponding evaluation grade set V is built:

$$V = \{v_1, v_2, \cdots, v_3\} = \{\text{safety grade, general safety grade, danger grade}\} \quad (6)$$

The indicators system is built based on basic principles of analytic hierarchy process as shown in Figure 1. The bottom twenty-four indicators are regarded as factors of safety comprehensive evaluation.

$$U = \{U_1, U_2, \cdots, U_{24}\} \quad (7)$$

According to features of mountain freeway construction and experts' advice, e each factor is compared to determine its relative importance and give corresponding value using 1-9 scale method created by Professor Satie. It constructs a judgment matrix of all levels. Then, it calculates weight vector and tests consistency. Due to limited space, only results are presented. Weight vector is given:

$$A=(0.1396062\quad 0.0504664\quad 0.0504664\quad 0.0504664\quad 0.0273645\quad 0.0532271$$
$$0.0170045\quad 0.0170045\quad 0.0108649\quad 0.1199108\quad 0.0951733\quad 0.0755389$$
$$0.0339422\quad 0.0339422\quad 0.0207853\quad 0.0478032\quad 0.0478032\quad 0.0203231$$
$$0.0110199\quad 0.0101616\quad 0.0340505\quad 0.0168001\quad 0.0118795\quad 0.0043959) \tag{8}$$

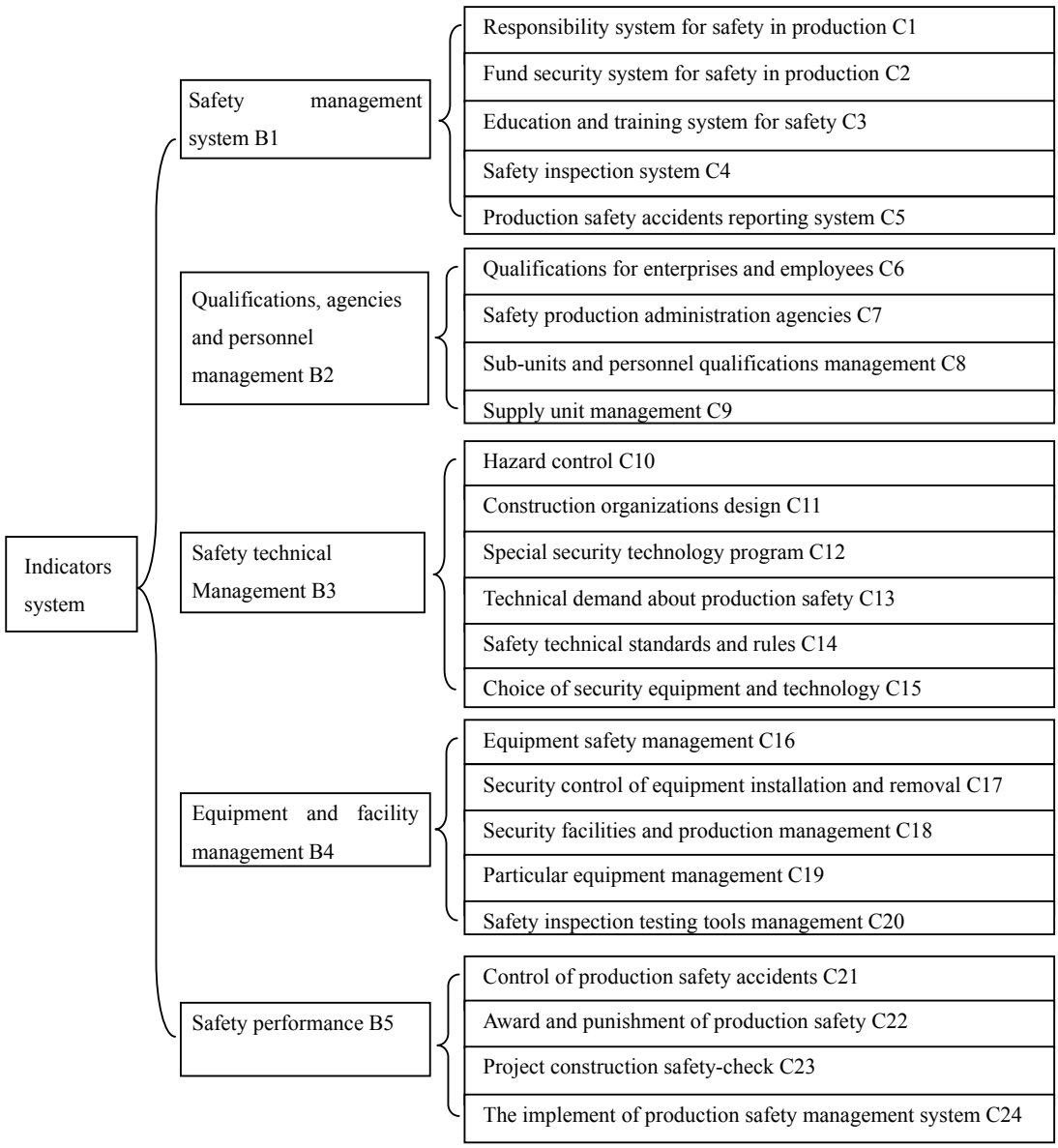

Figure 1: Indicators system of construction early-warning system of mountainous freeways

A score sheet is designed for each factor. Scores of factors are determined according to actual status in freeway construction of mountainous regions. Every factor is assumed to have x point. Subjection functions are built respectively:

$$\mu_{v1}(x)=\begin{cases} 0 & 0\le x<85 \\ \left(\dfrac{x-85}{10}\right)^2 & 85\le x\le 95 \\ 1 & 95<x\le 100 \end{cases} \tag{9}$$

$$\mu_{v2}(x)=\begin{cases} 0 & 0\le x<65 \\ \left(\dfrac{x-65}{10}\right)^2 & 65\le x<75 \\ 1 & 75\le x<85 \\ \left(\dfrac{95-x}{10}\right)^2 & 85\le x<95 \\ 0 & 95\le x\le 100 \end{cases} \tag{10}$$

$$\mu_{v3}(x)=\begin{cases} 1 & 0\le x<65 \\ \left(\dfrac{75-x}{10}\right)^2 & 65\le x\le 75 \\ 0 & 75<x\le 100 \end{cases} \tag{11}$$

Points are given by experts according to the score sheet. The subjection degree of evaluation is determined using the above subjection function. The relationship matrix R was also determined:

$$R=\begin{bmatrix} r_{11} & r_{12} & r_{13} \\ r_{21} & r_{22} & r_{23} \\ \vdots & \vdots & \vdots \\ r_{241} & r_{242} & r_{243} \end{bmatrix} \tag{12}$$

Based on the model of comprehensive assessment, B is determined through determined weight vector A and relationship matrix R .

$$B=A\circ R=(a_1,a_2,\cdots,a_m)\circ\begin{pmatrix} r_{11} & r_{12} & \cdots & r_{1n} \\ r_{21} & r_{22} & \cdots & r_{2n} \\ \vdots & \vdots & \cdots & \vdots \\ r_{m1} & r_{m2} & \cdots & r_{mn} \end{pmatrix}=(b_1,b_2,\cdots,b_n)=(0.172438,0.556829,0) \tag{13}$$

Using weighted mean, B is determined $B=1.91$ (14)

Thus, the freeway project is at the level of general safety. The results show that in order to raise the safety level, we need to establish and improve a responsibility system for production safety and strengthen hazard control. Because of the high risk

and many uncertain factors, it is difficult to evaluate the safety of a construction site accurately and objectively.

The system can understand and grasp overall construction site safety, find hidden causes of accidents and management shortcomings to establish early-warning system of construction safety. Also, it can improve the quality of information technology of safety management in freeway construction in mountainous regions.

4 CONCLUSION

It is urgent that we establish a safety early-warning system for mountainous freeways. Major hazard identification and risk assessment is still lacking in the field. A safety early-warning system for freeway construction in mountainous regions is established based on principles of comprehensive evaluation by studying factors of construction safety.

This system can reflect the safety status in freeway construction in mountainous regions objectively. Its interface is friendly for man-machine dialogue so as to provide the basis for construction safety evaluation and management decisions. Also, it can improve the quality of information technology of safety management for mountain freeways.

REFERENCES

Choi H.H.(2004). Risk Assessment Methodology for Underground Construction Projects[J]. Journal of Construction Engineering and Management, 130(2):258-272

Chua D. K. H.(2004). Incident Causation Model for Improving Feedback of Safety Knowledge. Journal of Construction Engineering and Management, 130(4):542-551

Fan Hong.(2005). Architectural Engineering Technology. Beijing: Chemical Industry Press.

Li Shirong.(2004).Safety Control in Construction Project. Beijing: China Architecture &Building Press.

Ren Hong.(2005).Safety Management in Construction Project. Beijing: China Architecture &Building Press.

Sangoub Lee.(2003).Predictive Tool for Estimating Accident Risk .Journal of Construction Engineering and Management, 128(4):452-457

Osama Ahmed Jannadi.(2003).Risk Assessment in Construction. Journal of Construction Engineering and Management, 129(5):492-500

Wu Mingxia.(2007).Construction Safety Management. Beijing: China Machine Press.

Zhang Shilian.(2006).Construction Safety Management. Beijing: China Architecture & Building Press.

Zhu Jianjun. (2007).Construction Safety engineering. Beijing: Chemical Industry Press.

A Study of Vehicle and Materials Depot Location Problems for Winter Road Maintenance

W.P. Cai[1], G. Liu[2], and W.S. Cao[3]

[1]Changchun Construction Project Management Center, No. 1031, Xiantai Street, Changchun, Jilin Province, PRC, PH:(86) 13904330707
[2]School of Transportation Science and Engineering, Harbin Institute of Technology, No. 202, Haihe Road, Nangang District, Harbin, Heilongjiang Province, PRC, 150090, PH:(86) 13766862168; email: hitliugang@gmail.com
[3]Changchun Construction Project Management Center, No. 1031, Xiantai Street, Changchun, Jilin Province, PRC, PH:(86) 13331677895

ABSTRACT

Salt spreading is a common practice in wintertime in many countries, and involves the spreading of salt on roads when ice or snow has made them slippery. The progress of optimization models of vehicle and materials depot locations can increase the efficiency or effectiveness of this practice, and also result in significant savings and reduced environmental and societal impacts. However, it is obvious that the depot location problem at the strategic level should be considered in conjunction with the vehicle routing problem at the operational level. As a result, this paper takes a Location-Routing Problem (LRP) based approach to the problems of depot location and vehicle routing with the purpose of aiding winter road maintenance planners. A two-stage TABU search algorithm is applied to solve the model.

INTRODUCTION

A chemical method is one of the winter road maintenance techniques used to clear roadways of snow and assumes a major role in winter road maintenance because of the effective performance and relatively low cost in comparison to alternatives. As highlighted by Perrier et al (2007), in recent years new technologies have been implemented in many agencies to help control the total costs associated with spreading materials, while also enhancing their effectiveness. However, the progress of optimization models of depot location not only increases the efficiency or effectiveness, but also results in significant savings, improved mobility, and reduced environmental and societal impacts. Unfortunately most agencies in China still rely in large part on decision rules dictated by field experience when making depot location decisions.

Perrier et al (2006) sorted the decision-making problems related to the materials spreading into strategic, tactical, operational, and real-time levels. Figure 1

shows the planning structure of winter road maintenance. The depot location problem is often solved by choosing a preset number of depots to open from a set of candidate sites based on some predefined strategic and operational objective. A number of different depot location models have been proposed in recent years. These models tend to take into account a large variety of characteristics of the problems arising in real-world applications (Muyldermans et al. 2002).

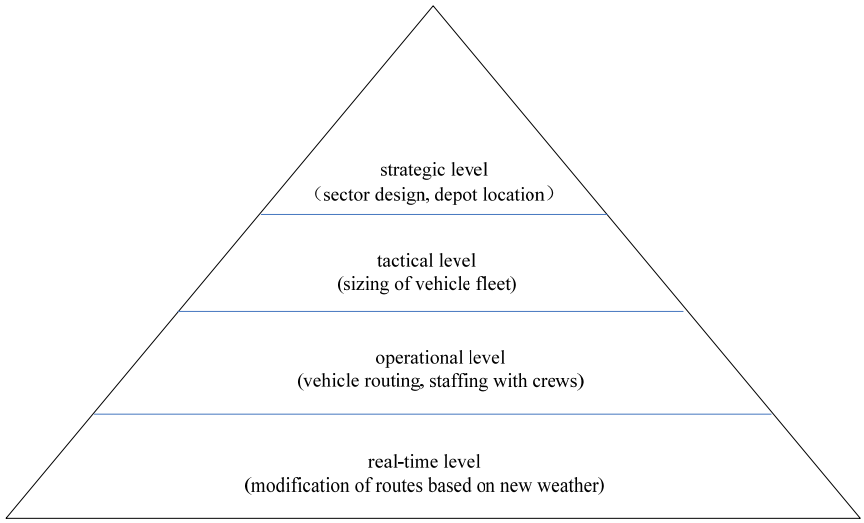

Figure 1. The planning structure of winter road maintenance

The vehicle routing problem requires that a set of routes is determined to optimize some performance criteria, such that all required road segments are serviced and all the operational constraints are satisfied. The proposed models for spreader routing generally assume a predetermined depot location and corresponding sector (Waddell B. 1994, Haghani A. 2002). Webb (1968) first pointed out that it is extremely undesirable to ignore the routing problem in the question of depot location. Some combined models for winter road maintenance have been proposed (Lotan et al 1996). However, there is not enough research that solves the combined problems of depot location and vehicle routing in an efficient manner. Most of the existing research on combined location routing problems assumes that the number of routes is equivalent to the number of vehicles.

The complexities involved in each of the problems of depot location and vehicle routing need careful analysis to determine the significant aspects of each problem in order to unify them in an integrated approach. In spite of the difficulty of the problem, recent developments of location-routing problems (LRP) in modeling and algorithms, and the increased performance of computers, all motivate the optimization models. As a result, this paper takes an LRP based approach to the integrated problems of depot location and vehicle routing with the purpose of aiding

winter road maintenance planners. The paper is organized as follows. In Section 1, a mathematical formulation of the problem is presented. Section 2 describes the solution methods. Computational experiments are performed in Section 3, and conclusions are given in the last section.

MATHEMATICAL FORMULATION

The Location-Routing Problem is proposed to optimize the location and quantity of depots, and solve the VRP at the same time. The problem of LRP for salt spreading operations is defined on a connected graph $G = (V, A)$. Before giving the mathematical formulation, we define some other notations:

V	The vertex set $\{v_1, \cdots v_k, v_{k+1}, \cdots, v_{k+n}\}$
A	The arc set $\{(v_i, v_j) : v_i, v_j \in V \text{ and } i \neq j\}$
V_t	The set of candidate depots $\{v_1, \cdots v_k\}$
V_c	The set of other vertex $\{v_{k+1}, \cdots, v_{k+n}\}$
k_i	The capacity of the depot
g_i	The fixed investment of establishing a depot
d_{ij}	The demand of arc (v_i, v_j)
C	The expense of unit demand
R	The set all routes which satisfy the demand of the arc
Q_c	The maximum capacity of the service vehicles;
m	The number of service vehicles;
H_i	The set of vehicle scheduling $\{S_{i1}, S_{i2} \cdots, S_{ih}\}$;
y_{ijs}	1 Only if arc (v_i, v_j) is assigned to S
	0 Otherwise
x_{ijr}	1 Only if the route r from the v_i to v_j
	0 Otherwise
u_{ri}	1 Only if v_i is the end point the route r
	0 Otherwise
o_i	1 Only if v_i is the depot location
	0 Otherwise

The formulation is then as follows:

Minimize

$$\sum_{i=0}^{n+k} \sum_{j=0}^{n+k} \sum_{b=1}^{m} d_{ij} x_{ijr} c + \sum_{i=1}^{k} o_i g_i \tag{1}$$

Subject to

$$\sum_{i=1}^{k} o_i k_i \geq \sum_{i=1}^{n+k} \sum_{j=1}^{n+k} d_{ij} \tag{2}$$

$$\sum_{i=1}^{k} o_i \leq P \tag{3}$$

$$\sum_{s \in H_i} y_{ijs} = 1, \quad (i = 1, \cdots, n) \tag{4}$$

$$\sum_{i=0}^{n+k} \sum_{j=0}^{n+k} x_{ijr} d_{ij} \leq Q_c, \ (r \in R_i) \tag{5}$$

$$\sum_{v_i \in S} \sum_{v_j \in S} x_{ijr} \leq |S| - 1, \ (b = 1, \cdots, m; S \subseteq V_t \cup V_c; |S| \geq 2) \tag{6}$$

$$\sum_{r \in R} u_{ri} - o_i \geq 0, \quad (i = 1, \cdots, k) \tag{7}$$

$$x_{ijr} \in \{0,1\}, \ (i = 0, \cdots, n+k; j = 0, \cdots, n+k; r \in R) \tag{8}$$

$$y_{ijs} \in \{0,1\}, \ (i = 0, \cdots, n+k; S \in H_i) \tag{9}$$

$$z_{ijr} \in \{0,1\}, \ (i = 0, \cdots, n+k; j = 0, \cdots, n+k; b = 1, \cdots, m) \tag{10}$$

$$o_i \in \{0,1\}, \ (i = 1, \cdots, k) \tag{11}$$

$$u_{ri} \in \{0,1\}, \ (\forall_r \in R; i = 1, \cdots, k) \tag{12}$$

The objective function (1) minimizes the total cost of the vehicle routing and depot location. Constraints (2) require that the capacity of all depots meet the materials requirement of all roads. Constraints (3) state that at most P materials depots are to be located. Constraints (4) require that every arc (v_i, v_j) is assigned to H_i. Constraints (5) state that the demand of every route is less than the capacity of the vehicle. Constraints (6) are the branch-eliminate constraints. Constraints (7) require that every depot has service vehicles. Constraints (8)-(12) require that the variables are integers.

HEURISTIC SOLUTION

Because of the complexity of the LRP, the problem is usually NP-hard. We apply the two-stage TABU search algorithm. Figure 2 describes the TABU-based algorithm.

(1) First, we establish the initial solution of the depot location. We randomly select a depot whose state is “open”.

(2) We apply two types of “moves” to construct the neighborhood of the current solution. One is the “exchange” move, and the other is the “increase” move. The “exchange” move is to open a depot and close a depot at the same time. The “increase” move is to increase the number of the depots.

(3) After every move at the stage of depot location, it is time to modify and search the optimal route.

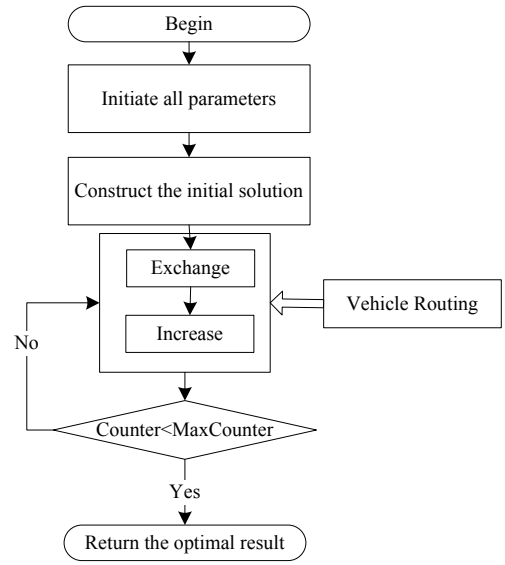

Figure 2. The description of the TABU-based algorithm

CASE STUDY

This section provides a case study to illustrate the models proposed in the previous sections. The test traffic network is the central part of the Changchun city which has been illustrated in Figure 3. Table 1 gives the parameters of the case.

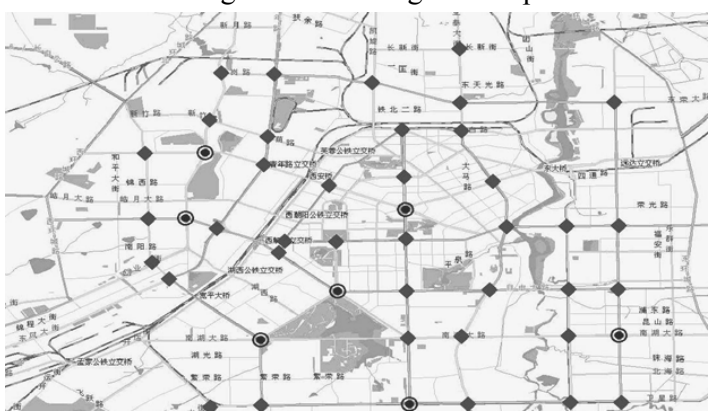

Figure 3. The test network

Table 2. The parameters of the case

Parameter(unit)	Value	Parameter(unit)	Value
road section(ind)	321	g_i (yuan)	10000
candidate depots(ind)	20	C (yuan/kilometer)	30
the number of spreader	13	Q_c (ton)	6

This paper compiles the algorithms program with the C++ language. The value of the parameters is as follows: $\alpha = 1, \beta = 1,\ \delta = 0.5, \eta = 1000$. The result is

shown in Table 3.

Table 3. Comparison of Results

Parameter	LRP	ARP
number of depots	7	8
the investment of depots	70000	80000
the cost of all routes	48563	46251
the total cost	118563	126251

CONCLUSION

The objective of this research was to develop a systematic optimization approach to integrate the winter road maintenance planning decisions for depot location and vehicle route design. The solution methodology achieves the objective of a more integrated and less sequential approach to the problems considered. Although there is much opportunity for further integrating the decisions studied in this research, the proposed methodology shows progress from the traditional sequential approach to winter road maintenance planning problems towards the eventual goal of a fully integrated approach. Since the solution methodology proposed in this research is heuristic solution based, there is no guarantee that an optimal or near optimal solution will be achieved.

REFERENCES

Haghani A, Qiao H. (2002). "Snow emergency vehicle routing with route continuity Constraints". *Transportation Research Record* 1783, 119-124.

Lotan T, Cattrysse D, Oudheusden V, Leuven KU. (1996). "Winter gritting in the province of Antwerp: a combined location and routing problem". *Belgian Journal of Operations Research, Statistics and Computer Science*, 36:141-57.

Muyldermans L., Cattrysse D., Van Oudheusden D., Lotan T.(2002). "Districting for salt spreading operations". *European Journal of Operational Research* 139, 521-532.

Perrier N., Langevin A., Campbell J.F.(2006). "A survey of models and algorithms for winter road maintenance Part I: system design for spreading and plowing". *Computers & Operations Research* 33, 209-238.

Perrier, N., Langevin, A., Campbell, J.F.,(2007). "A survey of models and algorithms for winter road maintenance Part III: vehicle routing and depot location for spreading". *Computers & Operations Research* 34, 211-257.

Waddell B. (1994). "Snow and ice control excellence with routing software". *Public Works* 125, 72-74.

Webb. M.H.T. (1968). "Cost functions in the location of depots for multiple delivery journeys". *Operational Research Quarterly* 19, 311-328.

Analysis of City Transportation Networks' Travel Ti me Reliability During Adverse Weather

Jian Wang[1], Guanglin Sun[2], and Xiaowei Hu[3]

[1]School of Transportation Science and Engineering, Harbin Institute of Technology, No. 202, Haihe River Road, Nangang District, Harbin, Heilongjiang Province, PRC, 150090, PH:(86) 13030092006; email: wang_jian@hit.edu.cn
[2]School of Transportation Science and Engineering, Harbin Institute of Technology, No. 202, Haihe River Road, Nangang District, Harbin, Heilongjiang Province, PRC, 150090, PH:(86) 15145014721; email: mumulinhit@tom.com
[3]School of Transportation Science and Engineering, Harbin Institute of Technology, No. 202, Haihe River Road, Nangang District, Harbin, Heilongjiang Province, PRC, 150090, PH:(86) 13936646128; email: hxwhit@163.com

ABSTRACT

Recently, meteorological disasters have had an expansive and complicated influence on city transportation networks. The reliability of travel time during adverse weather has gradually become the primary consideration before making travel decisions. Through the analysis of the impact of adverse weather on the transportation network, we adopt a disaster degree system to quantifiably describe the impact of weather on the transportation network. By combining the road network travel time reliability model and algorithm, we obtain the route travel time reliability and road network travel time reliability during adverse weather. Finally, we verify the effectiveness of this model through the calculation and analysis of an example.

1 INTRODUCTION

The transportation network is easily influenced by meteorological disasters. The problem of how to keep a transportation network working normally and functioning becomes important during adverse weather conditions. Travel time reliability is a typical index which can signify the uncertainty of the network and is a means to test random transportation network behaviors during adverse weather.

Travel time reliability is generally defined as an arrival possibility for travelers between a given origin and destination on time (Asakura, 1996). In Bell's (1997) paper, travel time reliability change was analyzed by sensitivity analysis to estimate travel time fluctuation with traffic demand changing. Hiroshi Wakabayashi (2000) built the framework of travel time reliability arithmetic during rain and snowy weather, which was applied to expressway networks. Stephen Clark et al (2005) analyzed transportation network travel time reliability with stochastic user demand. Until now, the majority of reliability research has been for normal transportation networks, so it is important to analyze transportation network travel time reliability

during adverse weather.

2 DYNAMICS OF EFFECTS ON TRANSPORTATION NETWORK TRAVEL TIME DURING ADVERSE WEATHER

In this paper, adverse weather is defined as rain, fog, snow, or dust storm disasters. The influence of adverse weather on a transportation network is similar to other disasters which have different effects in different terrains, different traffic facilities, etc.

The disaster degree system is used to denote how severely adverse weather affects transportation networks in cities. Adverse weather influences drivers' sight distance, friction on roads, and drivers' mental and emotional states. If these were to signify the degree, they create some difficulty in determining results. Two quantifiable factors were chosen: the number of traffic accidents (or traffic delays) and direct economic loss.

The calculation method of disaster degrees adopts a logarithm function to denote disaster (Feng Li-hua, 2000), which is:

$$\xi = \lg(DE) + \phi \tag{1}$$

Where ξ is degree; D is traffic accident numbers (or traffic delay); E is direct economic loss; ϕ is constant. The state of the transportation network is classified by four precautionary grades based on the disaster degree. The logarithm function is used to confirm the grade of emergency status:

$$N = a' \ln(\theta T) + b \tag{2}$$

Where N is precaution grade; θ is a possibility of degree to the mean ($\theta = \left| [\xi(t) - \bar{\xi}] / \bar{\xi} * 100\% \right|$, where ξ is degree; $\bar{\xi}$ is mean of degree); T is last time of disaster; a' and b are undetermined parameters. The range of N can be divided into four intervals according to the past data from the weather department:

(1) The fourth precaution grade. The degree reported by the meteorological department is minimal. The control mode of the transportation network is to release information and remind travelers to drive safely and slow down.

(2) The third precaution grade. When adverse weather occurs, the traffic information system must tell travelers suggested travel time and route by putting out information continuously. Relevant departments should prepare to manage the running of traffic on site.

(3) The second precaution grade. Alerting travelers to adjust their routes to avoid delay. The accident-prone locations should be supervised by traffic

management personnel.

(4) The first precaution grade. Remind travelers to avoid driving in these conditions. Begin emergency planning.

The effects of adverse weather on transportation networks is a stochastic process, which can be treated thusly: divide the last time of adverse weather effect into many periods of adverse weather, and each period has a mean of degree. We can determine the course of adverse weather effects.

3 PRESENTATIONS OF CAPABILITY AND FLOW FOR TRANSPORTATION NETWORK DURING ADVERSE WEATHER

Using the capability to describe a transportation network under adverse weather, the vector of every path in network is a state. That is $\tilde{c} = \{c_1, c_2, \cdots c_A\}$, so:

$$c_a(t) = \bar{c}_a - \delta_a(t) \tag{3}$$

Where c_a is real capacity of path a under adverse weather; $\bar{c}_a$ is capacity of path a in normal state; $\delta_a(t)$ is index function of emergence rank N:

$$\delta_a(t) = ce^N + d \tag{4}$$

Where c and d are undetermined parameters. So the network volume is:

$$x_w^k = \bar{x}_w - \frac{\lambda}{n} \sum_{a \in q, \not\in w} \delta_a^k \tag{5}$$

Where $\bar{x}_w$ is mean volume on route w(OD) under fine weather; δ_a^k is variable quantity of path a's capacity under adverse weather; λ is a constant; n is path number on route w(OD), so δ_a^k is:

$$\delta_a^k = h(\theta T)^{a'} + d \tag{6}$$

The possibility distribution of degree to the mean can be known by formula derivation, to get the possibility p_{at} of the real capacity c_a. Supposing c_{a0} is max capacity of path a under adverse weather, therefore:

$$p\{c_a = c_{at}\} = p_{at} \quad t = 0,1,\cdots,T_a - 1 \tag{7}$$

$$p_{at} \geq 0, \forall t \quad , 0 \leq c_{at} \leq c_{a0}, \quad t = 0,1,\cdots,T_a - 1 \tag{8}$$

The mean of whole path capacity change is $\bar{\delta}_a^k$ ($\bar{\delta}_a^k = \frac{\lambda}{n} \sum_{a \in q, \not\in w} \delta_a^k$) among route w on t period, and its possibility is p_{wt}.

4 THE TRAVEL TIME RELIABILITY OF TRANSPORTATION NETWORKS DURING ADVERSE WEATHER

4.1 Route travel time reliability

A transportation network is described by the real capacity $\overline{c}$, and the flow also describes the state of transportation network. The vector of actual capacity in all paths is called system state, which is $s=\{x_1,x_2,\cdots x_A\}$. Once traffic distribution mode (*TA*) is confirmed, the system state is known as:

$$s=\mathrm{TA}(\overline{c},x) \tag{9}$$

Travel time is the time superposition of every path chosen by travelers. Given that $\tilde{c}_0$ is ideal capacity of network under adverse weather; $\overline{x}_w$ is volume of w among OD in precaution stage; $\overline{x}$ is the vector of mean flow among OD:

$$\overline{x}=(\overline{x}_W, w\in W) \tag{10}$$

Supposing $t_{wq}(\tilde{c}_0,\overline{x})$ is the shortest travel time on route q among w(OD) under adverse weather; $t_{wq}(\overline{c},x)$ is actual travel time on route q among w(OD) in given state. So the route travel time reliability is defined as a ratio between $t_{Wq}(\overline{c},x)$ and $t_{Wq}(\tilde{c}_0,\overline{x})$ in acceptable level τ_{wq}, which is as follows:

$$R_{Wq}(\tilde{c},x)=P\left[t_{Wq}(\overline{c},x)/t_{Wq}(\tilde{c}_0,\overline{x})\le\tau_{Wq}\right] \tag{11}$$

Where τ_{wq} is a level of route with flow and weather effects fluctuating.

4.2 Transport network travel time reliability

The route travel time is the mean of a path's travel time, assuming city transportation network distribution is under user optimization control. So the mean of travel time on route w among OD is:

$$\overline{t}_W=\sum_{q\in P_W}\left[\left(x_{Wq}t_{Wq}\right)/x_W\right] \tag{12}$$

Since it is a problem to enumerate routes, it can be simplified. Supposing the possibility of choice of route q is p_{Wq}, and the travel time on path a is t_a, and γ_{waq} is 0 or 1(it's 1 if path a were chosen, or 0). According to equivalence substitution of the traveler route choice model, the travel time on w among OD is:

$$\overline{t}_W=\sum_{q\in P_W}\left[\left(x_{Wq}t_{Wq}\right)/x_W\right]=p_{Wq}\left(\sum_{q\in P}t_a\gamma_{waq}\right) \tag{13}$$

The transportation network's travel time reliability is defined as a weighted average of each OD, based on OD travel time reliability. That is as follows:

$$R_S(\tilde{c},x)=\sum\left[\overline{t}_W(\overline{c},x)R_W(\overline{c},x)\right]/\sum_{w\in W}\overline{t}_W(\tilde{c},x) \tag{14}$$

Adopt approximation algorithm to solve the route travel time reliability.

5 NUMERICAL ANALYSIS

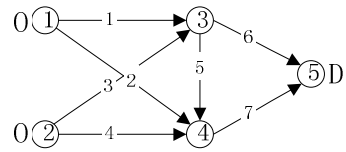

Figure 1. Test road network

The transportation network in Figure 1 has 5 joints and 7 paths, 2 OD s, and six routes. Assuming every path volume is changing with adverse weather on the third precaution stage, and the path's actual volume is x_k on k period, its possibility is p_{ak} shown in Table 1.

Table 1. Actual capacity and possibility of path under adverse weather

Path 1		Path 2		Path 3		Path 4		Path 5		Path 6		Path 7	
$\tilde{c}_{1k}$	p_{1k}	$\tilde{c}_{2k}$	p_{2k}	$\tilde{c}_{3k}$	p_{3k}	$\tilde{c}_{4k}$	p_{4k}	$\tilde{c}_{5k}$	p_{5k}	$\tilde{c}_{6k}$	p_{6k}	$\tilde{c}_{7k}$	p_{7k}
23	0.80	18	0.75	20	0.75	16	0.80	20	0.70	22	0.75	23	0.85
18	0.15	14	0.15	16	0.20	12	0.10	15	0.20	18	0.15	19	0.10
13	0.05	10	0.10	12	0.05	8	0.10	12	0.10	12	0.10	14	0.05

In the traveler route choice model (logit-model), suppose drivers choose route $q_3(2 \to 7)$ among OD $(1 \to 5)$. Select 20 transport network states in the third precaution stage, and show the volume x_k and possibility p_{ak} in Table2.

Assuming the acceptable level τ_{wq} of travel time is 0.6, so acceptable volume of route q_3 is 29, and acceptable volume of path 2 is 12, and path 7 is 15. Therefore the travel time reliability of route q_3 is as shown in Figure 2.

Table 2. Traffic flow and possibility of route q_3 in third precaution stage

Network state		Possibility	cumulative probability
State	Path 2	Path 7		
1	20	15	0.432	0.432
2	12	24	0.098	0.530
3	18	20	0.080	0.610
4	15	14	0.065	0.675

5	11	18	0.060	0.735
6	14	13	0.050	0.785
7	11	15	0.030	0.815
8	13	15	0.025	0.840
9	10	19	0.018	0.858
10	15	16	0.015	0.873
11	10	16	0.010	0.883
12	13	10	0.009	0.892
13	9	17	0.008	0.900
14	15	9	0.008	0.908
15	8	16	0.008	0.916
16	14	9	0.006	0.922
17	8	10	0.006	0.928
18	13	8	0.006	0.934
19	6	17	0.006	0.940
20	15	7	0.005	0.945

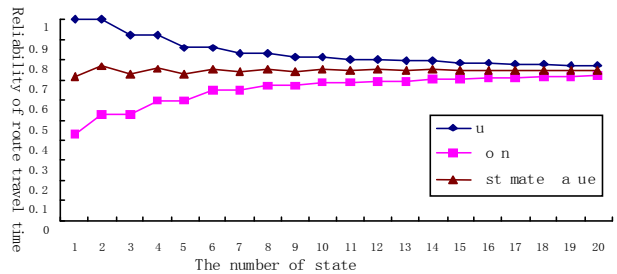

Figure 2. Estimated travel time reliability of route 3 in the third precaution step

Table 2 shows the travel time reliability estimated value of route q_3 in the third precaution stage. Given the acceptable volume of travelers, the estimated value of route travel time reliability quickly tends to be convergent with the number of network states increasing from Figure 2. The whole transportation network's reliability must be known according to each route's travel time reliability on one precaution stage, which is will allow the traffic department to improve the structure of the transportation network and guide travelers to choose the optimal route.

6 CONCLUSIONS

In this paper, the route and transportation network reliability are analyzed during adverse weather. Based on a system of weather degrees, the emergency transportation network is divided into four precaution grades, which will be helpful to traffic organization and management officials. However, because of fluctuations in adverse weather, the data collected here are not universally applicable, and the effects of adverse weather on the transportation network needs further study.

ACKNOWLEDGEMENTS

This research is supported by National Natural Science Foundation of China (Project No. 70673016 and 70503008), and Heilongjiang Postdoctoral Science Foundation funded project (Project No.LBH-Q06060). This work was performed at the National Center of Technology, Policy and Management, Harbin China.

REFERENCES

Asakura Y. (1996). "Reliability measures of an origin and destination pair in a deteriorated road network with variable flows." Proceeding of the 4th Meeting of the EURO Working Group on Transportation.

Bell M G H, Lida Y. (1997). "Transportation network analysis." John Wiley and Sons: 179-192.

Feng Li-hua. (2000). "Development in research of disaster grade." Journal of Catastrophology. 15(3): 72-77. (in Chinese)

Stephen Clark, David Watling. (2005). "Modeling network travel time reliability under stochastic demand." Transportation Research B. 39: 119-140.

Wakabayshi H. (2000). Snowfall weather forecast and expressway network reliability assessment. Bell M G H, Cassir C, ed. Reliability of Transport Networks, Hertfordshire: 103~118.

A Study of Transit Evacuation Route Planning Based on Time-Expanded Network

D.L. Zhang[1], J. X. Cui[2] and G. Liu[3]

[1] Highway Administration of Heilongjiang Province, Harbin; PH (86) 13945677151; FAX (86)451-86412866; email: hitliugang@live.cn

[2] School of management, Harbin Institute of Technology, Harbin; PH (86) 451-86412866; FAX (86) 451-86412866; email: daqing8210@126.com

[3] School of Transportation science and engineering, Harbin Institute of Technology, Harbin; PH (86) 451- 86412866; FAX (86)451-86412866; email: hitliugang@gmail.com

ABSTRACT

This research focuses on identifying optimal evacuation routing plans in public transit networks during various extreme events in urban road networks. The public transit evacuation system is modeled by a time-expanded network, based on a dynamic network flow model, and aims to minimize the total evacuation clearance time. This model transforms the public transit evacuation scheduling problem into a mixed-integer linear program (MILP). Also, a heuristic TABU-based search algorithm is used to find a high-quality solution in a reasonable amount of time. Finally, a case study is conducted using the central road network of Changchun city in China. Many numerical experiments are implemented in CPLEX 9.0 and the results show that time-expanded networks can effectively represent transit evacuation dynamics and the heuristic TABU-based algorithm can make an appropriate trade-off between solving efficiency and accuracy.

INTRODUCTION

In general, emergency evacuation of urban areas has gained prominent attention from both practitioners and researchers in the last three decades in the world (Wolshon et al. 2005, An et al. 2008, Liu et al. 2006). Among available modes of transportation, the use of public transit in evacuation situations is not well studied or understood (Liu and Hu. 2008). The use of public transit during evacuation is more crucial and should be well studied in some developing countries such as in China, as the population of transit-dependent citizens is very large. In addition to people without vehicles, the indigent, the elderly, the infirm and tourists also rely on the public transit system for evacuation. Accordingly, the purpose of this study is to make the existing transit system viable in emergency situations by developing a

practical "Public Transit Routing Plan" to deliver evacuees from the danger zone to safe destinations.

TIME-EXPANDED NETWORK OF PUBLIC TRANSIT EVACUATION

Here, we use a time-space network structure to present the schematic of the transit network. Let $G=(V,E)$ be the undirected graph of the city, where V and E stand for the set of nodes and the set of arcs, respectively. The set V is decomposed as $V=I\cup I^{'}\cup N$, where $I=\{s_1,s_2,...,s_n\}$ is the set of stations, $I^{'}=\{sh_1,sh_2,...,sh_l\}$ is the set of shelters, and N is the set of intersections.

Accordingly, the graph G is transformed into the time-expanded network $G^*=(V^*,E^*)$, where $V^*=I^*\cup I^{'}\cup S^*$ denotes the node set and E^* denotes the arc set. The network G^*, which is illustrated in Figure 1, consists of $T+1$ layers, and each layer represents a time period. The time-space network contains three types of nodes: *StatNodes*(I^*), *ShelterNodes* ($I^{'}$), and *SinkNodes* (S^*). The StatNodes are the set of station nodes with two attributes: location and time. The location of the stations is defined based on the existing transit system. Time is partitioned into equal-length time intervals (*intertime*). Let the time period set be defined as $\Re=\{0,1,2,...,T\}$. Nodes of the set I^* correspond to the copies of each station nodes $i\in I$ in each time period $\alpha\in\Re$; in other words, the *StatNodes* corresponds to the set $I\times\Re$. An element of this set is denoted by i_α, where $i\in I$ and $\alpha\in\Re$.

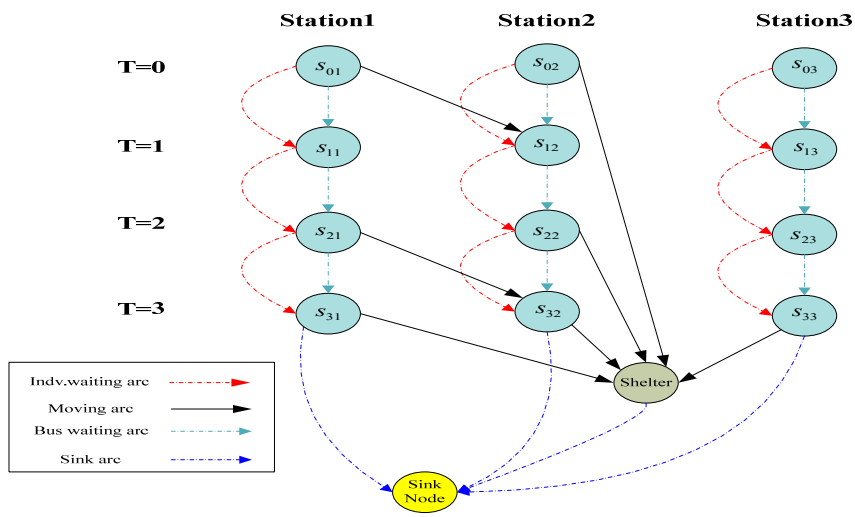

Figure 1.Topographical of a network.

The *ShelterNodes* set corresponds to the set of shelter nodes in which evacuees are accommodated temporarily. An artificial *SinkNode* is introduced, and its supply is set to the total demand on nodes in *StatNodes*.

The set E^* of arcs is decomposed into 4 subsets: movement arcs (M), individual waiting arcs (W_p), transit vehicle waiting arcs (W_b), and sink arcs (S).

The arcs in the set of movement arcs emanate from nodes in the *StatNodes* and enter nodes in *StatNodes* or *ShelterNodes*. To model a possible arc from station i at time period α to station j, we create an arc from node i_α to node j_β, where $\beta = \alpha + r_{i_a j} / \text{int}\, ertime$ and $r_{i_a j}$ is the travel time between station i and station j at time α. The movement arc between any pair of nodes is selected out of *k*-dissimilar paths between nodes. The capacity of movement arcs is equal to the capacity of transit vehicles, and their cost is equal to the time required to traverse the path.

The set of individual waiting arcs (W_p) includes the arcs from node i_α to node $i_{\alpha+1}$. Individuals at station i who are not picked up by any transit vehicle at time period α will move to the subsequent copy of station i at the next time period ($\alpha+1$) using the individual waiting arc. The individual waiting arcs have unlimited capacity and they can flow an infinite number of individuals from one time period to the next time period. Also, we introduce transit vehicle waiting arcs (W_B) from node i_α to node $i_{\alpha+1}$. Unlike individual waiting arcs, the transit vehicle waiting arcs are constrained in volume, and their capacity is limited to the vehicle capacity. The traverse time on both types of waiting arcs is equal to the length of the time interval (*intertime*).

The arcs in the set of sink arcs (S) emanate from the last copy of stations (i_T) in *StatNodes* and *ShelterNodes* and enter the *SinkNode*. The sink arcs between nodes in *StatNodes* and the *SinkNode* are unconstrained, and their traverse time is set to a big number to discourage the individuals to move to the *SinkNode*. The sink arcs between the shelter nodes and the *SinkNode* are also unconstrained in capacity; their traverse time, however, is set to be zero.

PUBLIC TRANSIT EVACUATION ROUTE PLANNING MODEL

Here the network flow formulation is used along with side constraints to formulate the public transit evacuation problem:

$$\min \sum_{(i,j)\in E^*} t_{ij} x_{ij} \tag{1}$$

$$\sum_{\{j:(i,j)\in E^*\}} x_{ij} - \sum_{\{j:(j,i)\in E^*\}} x_{ji} = \begin{cases} \delta_i & i \in I^* \\ 0 & i \in I' \\ -\sum_{n=1}^{|I^*|} \delta_n & i = s^* \end{cases} \tag{2}$$

$$x_{ij} - u y_{ij} \le 0 \qquad (i,j) \in M \tag{3}$$

$$\sum_{\{i:(i,j)\in M\}} \sum_{j\in I'} y_{ij} = \omega \tag{4}$$

$$\sum_{\{j:(i,j)\in\{M\cup W_B\}\}} y_{ij} - \sum_{\{j:(j,i)\in\{M\cup W_B\}\}} y_{ji} = b_i \tag{5}$$

$$-x_{ij} + u y_{ij} - M z_{il} \le 0; (i,j) \in M; (i,l) \in W_p \tag{6}$$

$$x_{il} - M(1 - z_{il}) \le 0; (i,l) \in W_p \quad (7)$$

$$y_{ij} \in \{0,1\}; (i,j) \in M \quad (8)$$

$$z_{il} \in \{0,1\}\ ; (i,l) \in W_p \quad (9)$$

$$x_{ij} x_{il} \ge 0;\ (i,j) \in E^*; (i,l) \in W_p \quad (10)$$

Where, I^* = *StatNodes*; I' = *ShelterNodes*; s^* =*SinkNodes*; M =set of movement arcs; W_p =set of waiting arcs for individuals; W_B =set of waiting arcs for transit vehicles; S = set of sink arcs; $E^* = \{M \cup W_P \cup W_B \cup S\}$; ω =total number of available transit vehicles; U =capacity of a transit vehicle; δ_i =supply at node $i \in I^*$; b_i =number of transit vehicles that start their trip from node $i \in I^*$; x_{ij} = flow of evacuees on movement arcs from node $i \in I^*$ to node $j \in \{I^* \cup I'\}$; x_{il} = flow of evacuees on individual waiting arcs from node $i \in I^*$ to its subsequent copy (node $l \in I^*$); y_{ij} = a binary variable related to the movement arcs that takes the value 1 if there is a flow of evacuees from node $i \in I^*$ to node $j \in \{I^* \cup I'\}$ and takes the value 0 otherwise; z_{il} = a binary variable related to the individual waiting arcs that takes the value 1 if there is flow of residents from node $i \in I^*$ to its subsequent copy (node $l \in I^*$) and takes the value 0 otherwise.

The objective function (1) aims to minimize the total system travel time as well as the waiting time. Constraint set (2) is comprised of 3 sets of constraints. Each set provides the standard flow conservation constraints for the nodes in *StatNodes*, s*helterNodes* and *SinkNodes*. Constraint set (3) determines the transit vehicle capacity constraint. These constraints guarantee that, at any time, transit vehicles cannot move more individuals than their capacity. These constraints also connect the binary variables y_{ij} to their corresponding x_{ij} variables. Constraint set (4) limits the total number of transit vehicles to the number of available transit vehicles. Constraint set (5) indicates that, for a given time period, the total number of vehicles that leave a station deducted from the number of vehicles that enter the same station is equal to the number of vehicles that start their trip from that station at that time period. Constraint sets (6) and (7) ensure a vehicle does not leave a station with positive residual capacity while there are individuals waiting at the station. Constraint sets (8) and (9) are the binary constraints, and the constraint set (10) is the non-negativity constraint.

TABU-BASED SOLVING ALGORITHM

The large amount of decision variables and constraints in the model suggests the application of an approximate solution approach. The TABU search algorithm is currently one of the most effective local search algorithms designed to find a near-optimal solution to many optimization problems that contain numerous permutations and combinations.

As shown in Figure 2, the TABU search algorithm is implemented for a fixed number of iterations (*MaxCounter*). At any iteration, the parameters are initialized

and a random construction procedure is used to build an initial feasible solution. Then, the 2-exchange search mechanism starts with this initial solution and iteratively identifies the most appropriate neighbor to move. Next, in order to diversify the search, the 3-exchange search mechanism is performed. The TABU mechanism allows neighbor S' to be selected (bad move) even if it is not a better solution compared to S. By operating this way, the search mechanism explores the solution space beyond the local optimal. Finally, the algorithm terminates by reporting the best found solution over all iterations (S^*).

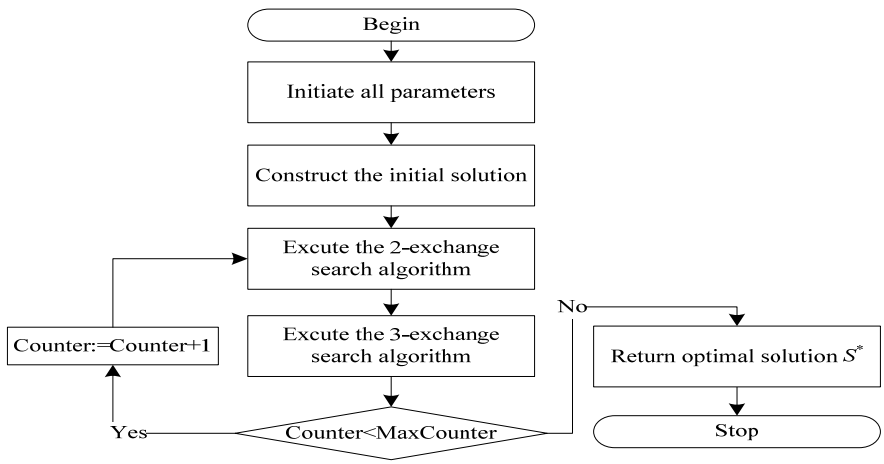

Figure 2.The description of the TABU-based algorithm.

CASE STUDY OF CBD IN CHANGCHUN CITY

This section provides a case study to illustrate the modeling techniques discussed in the previous sections. The test traffic network is the central part of the urban area in Changchun city, China, which has been illustrated in Figure 3. Regarding the transit system, there are 20 stations (represented by the *star* symbol).

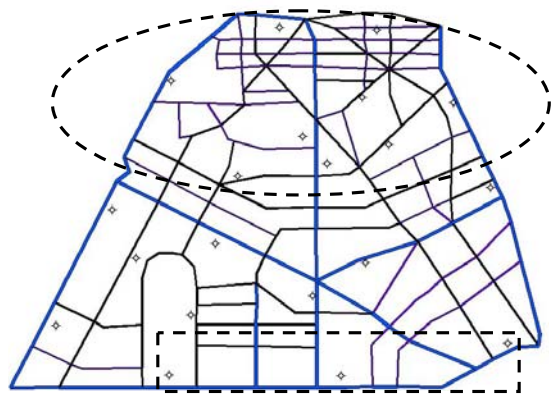

Figure 3. Sample line art illustration.

A hypothetical event is developed to test the public transit evacuation modeling strategy. Here, the evacuation area involves the metropolitan area with a radius of 3

miles around the incident location (enclosed by dotted ellipse in Fig.3) and 3 end points of the network (enclosed by dotted rectangle in Fig.3), which are sufficiently far from the incident location, to be considered shelter locations.

CPLEX 9.0 is used to get the exact solution and TABU-based algorithm is used to get an approximate solution. We introduce 3 measures of effectiveness for evaluation purposes: the computational time, the evacuation time (ET) and the evacuees' gap (EG). The evacuation time is the time that the last transit vehicle reaches the safe location. The evacuees' gap is calculated as $(P_{\%saved} - A_{\%saved})$ $/ P_{\%saved} \times 100$, where $A_{\%saved}$ is the actual percentage of evacuees who are evacuated safely from the incident location. Given the number of available transit vehicles (ω), the value $P_{\%saved} = (\omega \times U) / \ number\ of\ evacuees$, is the percentage of evacuees who are planned to be saved.

A comparison of computational performance on 4 sub-problems is illustrated in Table 1 for a 1-hour evacuation operation horizon.

Regarding the computational time, the average CPU time of the heuristic TABU search is significantly lower than that of CPLEX. Also, based on the comparison of *ET* and *EG* between the CPLEX and TABU search, we can conclude that the evacuation time derived from the heuristic TABU search is very close to that of the CPLEX. In addition, for a given evacuation time, the evacuees' gap reached by the heuristic TABU search is comparable with the evacuees' gap derived from CPLEX. It should be noted that, for no-notice evacuation modeling, the developed model shall be solved efficiently to get the solution quickly after the incident occurrence by TABU heuristic search algorithm which can make a good trade-off between the computational efficiency and solution accuracy.

Table 1. CPLEX vs. TABU search algorithm for 1-hour evacuation horizon.

Problem		CPLEX9.0			TABU		
Transit Dept. (%)	Num.of Bus	Time Elapsed (s)	ET (min)	EG (%)	Time Elapsed (s)	ET (min)	EG (%)
5	3	5009	10	0.00	7	12	0.00
5	5	5009	34	0.00	28	30	5.28
10	6	5023	10	0.00	11	12	0.00
10	20	5024	63	2.60	305	62	4.40
15	6	136	4	0.00	4	4	0.00
15	23	5023	56	0.05	147	53	2.16
20	15	5021	16	0.11	26	16	1.11
20	31	5009	55	0.05	176	57	2.21

CONCLUSION

The primary objective of this research is to improve the service level for transit dependent citizens in emergency situations. Based on the existing transit system, we developed a public transit routing plan (PTRP) model for an urban area to move residents from the danger zone to the safe location. The main assumption underlying

the model is that the locations of station points and shelters are known a *priori*. The problem follows the structure of the network flow problem with additional side constraints. A mixed integer linear programming formulation is used to model the problem. The no-notice characteristics of the emergency situation necessitate a solution approach that generates the solution in a short amount of time. We proposed a heuristic TABU search algorithm that demands significantly smaller computational effort compared to CPLEX to generate comparable results.

REFERENCES

An, S., Cui, J.X. and Wang, J. (2008). "An International Review of Road Emergency Transport and Evacuation ." *Journal of Transportation Systems Engineering and Information Technology*, 8(6), 38-45.

Liu, H.X., Ban, J.X., Ma, W.T. and Mirchandani, P.B.(2006). "Model reference adaptive control framework for real time traffic management under emergency evacuation." *Proc., 85th Annual Meeting*, Transportation Research Board, Washington, D.C.

Liu, X.M. and Hu, H.(2008). "Research status and prospect of emergency transportation evacuation". *Journal of Traffic and Transportation Engineering*, 8(3), 108-115

Wolshon, B., Urbina, E., Levitan, M., and Wilmot, C. (2005). "Review of policies and practices for hurricane evacuation II: Traffic operations, management, and control." *Nat. Hazards Rev.*, 6(3), 143-161.

Integrated Arterial Signal and Access Control Strategy under Non-Notice Emergency Evacuation: Modeling and Simulation-Based Analysis

Heng Wei[1], Harikishan Perugu[2], Qingyi Ai[3], and Xiaokuan Yang[4]

[1]Art-Engines Laboratory, 792 Rhodes Hall, Department of Civil & Environmental Engineering, University of Cincinnati, Cincinnati, Ohio 45221-0071, USA;. Tel: 513-556-3781; Fax: 513-556-2599; Email: heng.wei@uc.edu
[2]OKI Regional Council of Governments, 720 East Pete Rose Way, Suite 420, Cincinnati, Ohio 45202, USA; Tel: 513-619-7682; Email: hperugu@oki.org
[3]Art-Engines Laboratory, 735 ERC, Department of Civil and Environmental Engineering, University of Cincinnati, Cincinnati, Ohio 45221, USA; Tel: (513) 708-8928; E-mail: aiqi@email.uc.edu
[4]Transportation Research Center, Beijing University of Technology, Beijing 100022, China; Tel: 10-67391509; Email: xiaokuan@bjut.edu.cn

ABSTRACT

To better understand the traffic management and control needs under urban emergency evacuation situation caused by a non-notice disaster, two zones and three evacuation routes are in general identified to simplify the evacuation network planning. Two zones are referred to harm zone and buffer zone. Three types of evacuation routes are identified as: *harm-zone evacuee path* – the shortest path for evacuees from the target to evacuee-loading sites within the harm zone serviced by evacuation vehicles; *harm-zone vehicular path* – the shortest path for evacuation vehicles and on-road regular traffic within the harm zone to harm zone exits; and *buffer-zone vehicular path* – the shortest routes from harm zone exits to target shelters or outside of the buffer zone. However, a challenge rises in dealing with the mixed traffic of evacuation and regular vehicular flows in the buffer zone when modeling the *buffer-zone vehicular path*. In this study, the **I**ntegrated **A**rterial **S**ignal and **A**ccess **C**ontrol (IASAC) system is proposed with attempt to provide an alternative solution to buffer-zone traffic control. In the IASAC, SCOOT and BOTTLENECK systems and algorithms are coordinated together for traffic control along major corridors within the buffer zones. The algorithm embedded within the IASAC system is capable of predicting time-dependent demands of an urban corridors and coordinating signal control, and mid-block access metering control. A PARAMICS simulation-based test bed is designed for evaluating the IASAC system. A case study of two scenarios with and without IASAC control shows the potential benefit of the IASAC.

ITRODUCTION

When an unexpected disaster in an urban area like human-caused or terrorist-induced emergencies occurs without advance notice, the concentration of

population at the harm zone and the surge for evacuation can quickly congest existing transportation networks (Sbayti et al. 2006; Wolshon et al. 2005). Special traffic control plans are therefore necessary for specific evacuation routes (Alshih et al. 2003). A network "redesign" problem due to specific control requirements for evacuation has been emerged. The existing network "redesign" problem is actually confined to contra-flow problem due to lane traffic flow reversibility.

Our research (Yang et al. 2006; Wei et al. 2006; Wei et al. 2008) disclosed a broader scope of such a "redesign" problem and the emergency evacuation backbone network (E^2 Backbone Network) is proposed to provide an effective "platform" on the basis of which relationships between a harm zone, buffer zone, potential shelters, evacuation routing and travel behaviors, evacuation communication, and deployment of intelligent transportation security and management systems could be dealt with in a coordinated manner in the evacuation planning. Figure 1 shows an example of physical harm zones, buffer zones, and shelters, which are connected by the E^2 Backbone Network. The E^2 Backbone Network consists of major roadway arteries constituting the shortest routes among all potential targets and shelters.

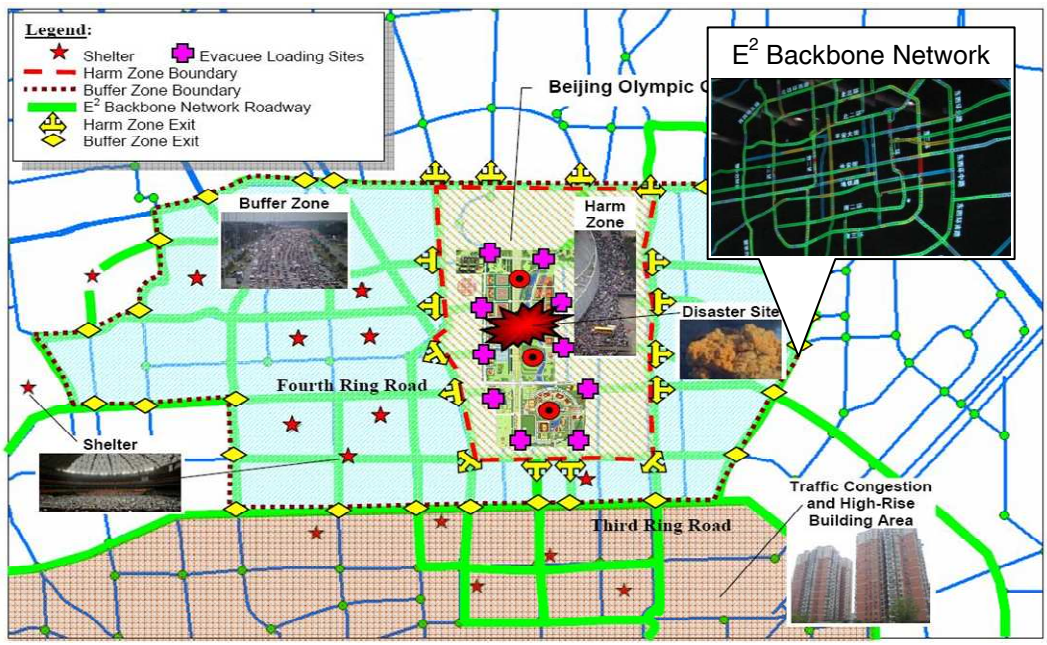

Figure 1. Exemplary Key Components of the E^2 Backbone Network.

On the basis of configuration of the E^2 Backbone Network, the network problem transforms to the optimization of the routes from the harm-zone exists to destinations, namely, specified shelters or boundary of the buffer zone. The calculation of such an optimum route bases the roadways over the E^2 Backbone Network while small local streets and other minor roadways will not be considered as the evacuation routes. In this way, the calculation becomes simpler

than traditional network routing optimization calculations that consider all the roadway segments over the network.

BUFFER-ZONE TRAFFIC CONTROL PLANNING OBJECTIVE MODEL

Arterial priority traffic control plan is considered to the buffer-zone routes; for example, SCOOT and BOTTLENECK systems and their algorithms could be used and coordinated together for traffic control along major corridors within the buffer zones (Perugu et al. 2007), which is termed as the **I**ntegrated **A**rterial **S**ignal and **A**ccess **C**ontrol (IASAC) system. The algorithm embedded within the IASAC system is capable of predicting time-dependent demands of an urban corridors and coordinating signal control, and mid-block access metering control. The IASAC algorithm can be adopted as an alternative solution to controlling the evacuation traffic of the buffer-zone routes (which are usually major urban corridors over the E^2 Backbone Network), and other traffic from crossing roadways and mid-block accesses. Top priority will be given to the flows on the evacuation routes while minimizing the delays of flows at crossing roadways and mid-block accesses. The algorithm keeps comparing the actual state and predicted traffic states at each designated time slice while the inputs are updated frequently. Assuming that a whole concerned corridor is divided into "*M*" segments, i.e., *i = 1 to M,* and destination segment is denoted by *j*. The number of time slice intervals are "*N*", i.e., *k = t to t+N.* The buffer-zone traffic control planning objective model is recommended as the following.

Objective: $Min.\ U_{br}(i) = \sum_{k=1}^{N}\sum_{i=1}^{M}\{TM(i,k)Q(i,k) + ERD(i,k) + MRD(i,k)\}$ (1)

s.t.: $ERD_i(k) = Min\{(q_i(k)G_i(k)\Delta T), (q_{i-1}(k)\Delta T + \lambda_i(k-1))\}$ (2)

$MRD_i(k) = 0.5T[\tau_i(k) + \tau_i(k+1)] = 0.5T[2\tau_i(k) + Q_i(k) - X_i(k)]$ (3)

Where,
- U_{br}(i, k) = Delay utility of ith segment;
- $TM(i, k)$ = Travel time on ith segment during kth time interval;
- $ERD(i, k)$ = Signal delay on main line at downstream intersection of ith segment during k*th* time interval;
- $MRD(i, k)$ = Signal delay at crossing road at the downstream intersection of ith segment during k*th* time interval;
- $q_i(k)$ = Approaching traffic flow at downstream intersection of ith segment during k*th* time interval;;
- K = discharge headway time during kth time interval;
- $G_i(k)$ = g/c (traffic signal green time to cycle length) ratio for downstream intersection of ith segment= $q_i(k)/(q_i(k)+q_{i'}(k))$;
- $q_i(k)$ = traffic demand of crossing street at downstream intersection of ith segment;
- T = Length of time interval;
- λ_i = queue length

$$\lambda_i(k+1) = \lambda_i(k) + \Delta T[(1-\beta_i)Q_i(k-K_{ij}) + q_i(k) - q_{i+1}(k)]$$

$_i$= turning ration at downstream intersection of ith segment;
$_i(k)$ = queue volume of crossing street at downstream intersection of ith segment;
$X_i(k)$ = Outflow rate of crossing street at downstream intersection of ith segment;

BUFFER-ZONE EVACUATION ROUTE TRAFFIC CONTROL

Concerning mixed regular and evacuation traffic existing in the roadways in the buffer zone, control along an evacuation route, is performed by selecting one of a set of patterns previously generated by the SCOOT signal optimization program. The objective of this module is to control both traffic flows on the roadways and traffic coming from the access points adjoining the corridor. The BOTTLENECK algorithm, used to be a coordinative ramp metering algorithm, is used for coordinated access meters for controlling conflict of the access traffic with the evacuation traffic.

The SCOOT model is based on the use of "cyclic flow profiles (CFP)." A CFP is a measure of the average one-way flow of vehicles past any chosen point on the road during each part of the cycle time of the upstream signal. The average flows in each part of the cycle can be taken over many cycle times and updated every 4 seconds. This CFP records can be easily generated using vehicle sensor data. With CFP central control unit can estimate how many vehicles will reach the downstream signals when they are red-hence both the size of the queue, and how long it will take to clear the intersection, and corresponding alterations in the signal timings are predicted. A SCOOT-prepared control plan is selected to match most closely the predicted traffic pattern in each section during the upcoming control period (Robertson et al. 1991).

BOTTLENECK algorithm is *coordinative* as well as *competitive* metering, in which two metering rates are computed for each access based on either local traffic conditions or system conditions; and the restrictive one is chosen. The bottlenecks can be identified on network using two types of criteria. The first is the capacity criterion to checks if the occupancy of a section exceeds a pre-determined occupancy threshold. The second is the vehicle storage criterion for identifying bottleneck sections. If a bottleneck is identified, the corresponding section is marked as a bottleneck section. A reduction of traffic demand from upstream accesses in the next control step is then needed to reduce its congestion. At this moment, the amount of demand reduction can be calculated for each bottleneck section (Chu et al. 2004).

The integrated algorithm consists of different steps for corridor control. Initially, all traffic variables are synthesized from raw data. A pre-defined "diversion policy" is established. Based on the diversion policy, a diversion

volume is assumed. For actual traffic volumes on mainline and alternate routes "Cyclic Flow Profiles" from SCOOT algorithm is used. Utilizing these volumes, access meter rates are estimated. Access meter volumes are estimated using the occupancy criterion in BOTTLENECK algorithm. For its capability of identifying bottleneck position on a particular section on the corridor, the algorithm can be also used for non recurrent congestion due to incidents. Based on the objective function, the diversion volumes are recalculated and they are compared. If the algorithm control comes out from inner loop, then the cycle lengths and metering rates are computed. Actually, this function establishes cycle length, offsets, and splits for a set of signal controllers along a section of arterial roadway. As the time control step is furthered, actual traffic variables are re-estimated from sensor data, and iterations are continued (Chang et al. 1993).

The core of implementing the integrated corridor control is the algorithm embedded within the central computer system that operates the corridor control system. Figure 2 shows the flowchart of steps for implementing the algorithm.

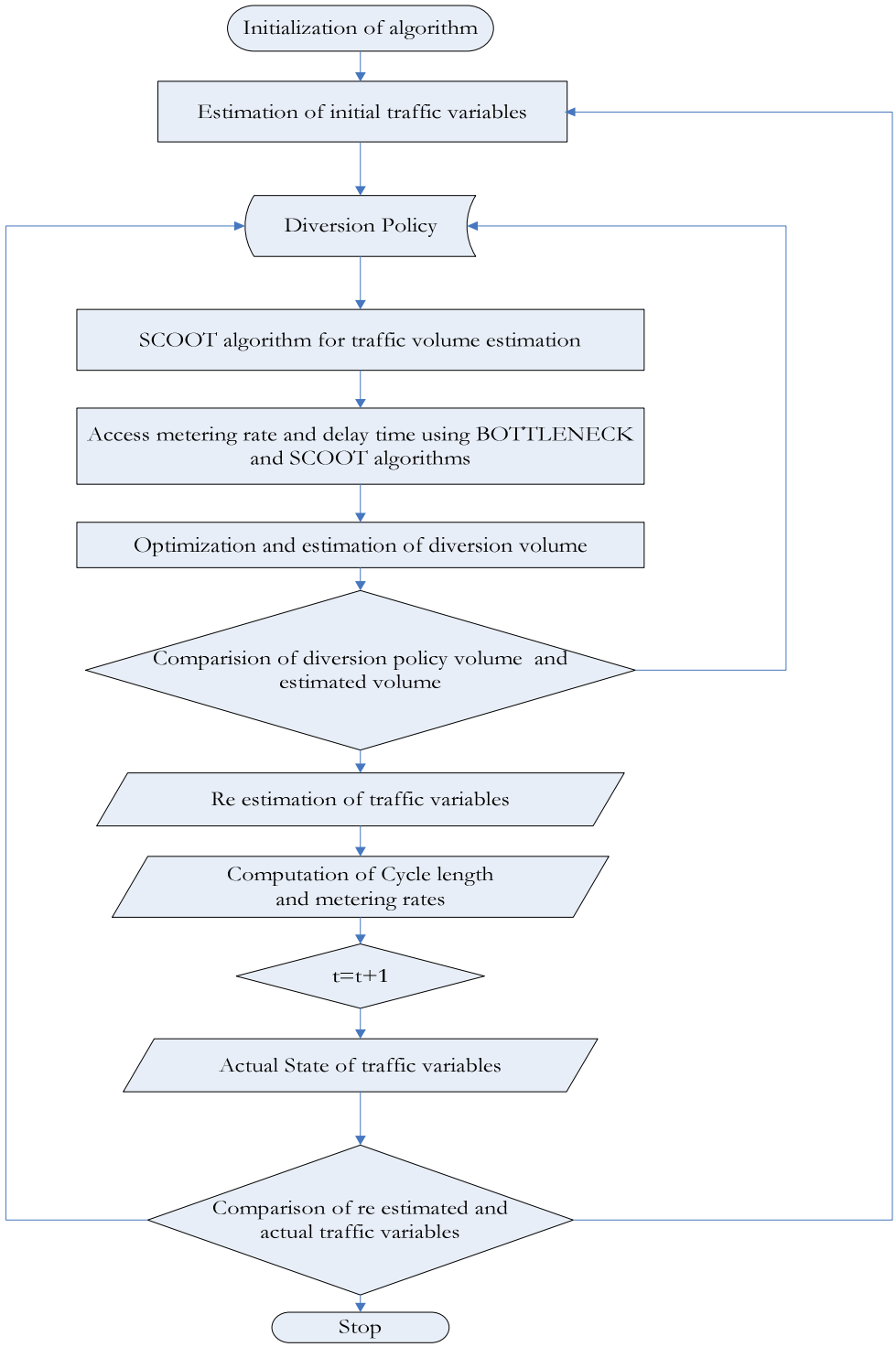

Figure 2. Flowchart of IASAC Algorithm.

The IASAC algorithm is developed to carry out major functions of the system that utilizes the interoperability of the traffic responsive signal strategy and access metering controls. The algorithm keeps comparing the actual state and predicted traffic states at each designated time slice while the inputs are updated frequently. Assuming that the total corridor is divided into "*M*" segments, i.e., *I* =

1 to M, and destination segment is denoted by *j*. The number of time slice intervals are "*N*", i.e., *k = t to t+N*.

KEY SUBMODELS INVOLVED IN THE IASAC SYSTEM

Corridor Traffic Demand Model

Using the discrete choice model (Chang et al. 1993; Reiss et al 1991), the traffic demand on the corridor is described as the following

$$Q(i, j) = \Theta_1 + \Theta_2 TM\ (i, j) + \Theta_3 \lambda_i + \varepsilon_1 \quad (4)$$

$$D(i, j) = \Theta_2 TPR\ (i, j) + \varepsilon_2 \quad (5)$$

Where: $Q(i, j)$ = the traffic demand between origin segment i and destination segment j on mainline;

$D(i, j)$ = the traffic demand between origin segment i and destination segment j on alternate route;

$TM\ (i, j)$ = expected travel time on streets for origin i to destination j;

$TPR\ (i, j)$ = expected travel time on parallel streets for origin i to destination j.

$\Theta_1, \Theta_2, \Theta_3$ are parameters;

ε_1, ε_2 error factors to capture unobserved factors.

Estimating Traffic Flow on Main Arterials

Traffic flow on the segment *i* of main arterial depends on the actual traffic demand that should be traveled on main line from *i* to *j* and the traffic joining from access points. Let us suppose there is an access point in every segment on mainline. Because of the traffic from access meters, there exists a significant time delay between the demand change at one segment and subsequent effects on downstream segments. The flow on main line is represented as below (Papageorgiou 1980).

$$Q_i(k) = \sum_{i=0}^{j} B_{ij}(k - K_{ij} + 1) X_i(k - K_{ij} + 1) \quad (6)$$

Where, K_{ij} = constant travel time in terms of number of intervals (k) from i to j;

B_{ij} = the traffic flow should be traveling from segment *i* to destination j or farther which includes diverted flow from arrival intersection as well as existing flow;

$X_i\ (k)$ = the access metering rate.

As the access points also have exiting flows, for true prediction of traffic flow on main line should include their effect. Using same theory and assumptions of Papageorgiou (1980), the exiting flow from mainline is given by the equation:

$$E_j\ (k) = \sum_{i=0}^{j} X_i(k - K_{ij} + 1)[B_{ij}(k - K_{ij} + 1) - B_{ij+1}(k - K_{ij} + 1)] \quad (7)$$

Then the actual demand on the mainline is given by expression

$$Q_i(k) = \sum_{i=0}^{j} \{B_{ij}(k - K_{ij} + 1) X_i(k - K_{ij} + 1)\} - E_{ij}(k) = \sum_{i=0}^{j} B_{ij+1}(k - K_{ij} + 1) X_i(k - K_{ij} + 1) \quad (8)$$

Estimating Access Metering Rate

To find the access metering rate, the queue volumes of each access should be known. Based on queue length, the queue volume is used as input variable to find the access metering rate. Each of access is assigned with weightage factor and all the access meters are coordinated and based on Bottleneck algorithm (PATH 2001). The access metering rate is given as:

$$X_i(k) = \tau_i(k-1) - \sum_{i=0}^{j} \left(Q_i(k - K_{ij} + 1)(\frac{WF_i(k)}{\sum WF_i(k)} \right) \quad (9)$$

Where, τ_i (k) is queue volume at i^{th} access meter; and $WF_i(k)$ is the weightage factor for i^{th} access meter.

For better access of the vehicles from surrounding land use to main arterial the gap of green times between intersection and access meter should be less than the travel time required for i^{th} section on main line. So, the access meter should satisfy following relation (PATH 2001).

$$TM_i(k) - \quad _i(k) > 0; \forall i \in M, k \in N \quad (10)$$

Where, κ is the discharge headway in terms of time interval k; τ_i (k) is queue volume at i^{th} access meter; and $TM_i(k)$ is travel time for i th segment on main line.

Signal Delay

To design the algorithm better, it is assumed each signalized intersection consisted by only one segment. And intersection should be located at the end of the segment in which the traffic flows comes from the access points, cross-streets and upstream sections. As this model is based on SCOOT algorithm for traffic responsive signal control, the under lying Platoon dispersion model (Hunt et al. 1982) is used to estimate the signal delay on mainline. This delay includes offset found earlier to facilitate the flows from access points.

$$SDM_i(k) = Min\{(q_i(k)G_i(k)\Delta T), (q_{i-1}(k)\Delta T + \kappa \hat{L}_i(k-1))\} \quad (11)$$

Where, $SDM_i(k)$ = signal delay on main line;

$q_i(k)$ = approaching traffic flow at intersection i and interval k in the direction of mainline;

κ = the discharge headway in terms of time interval k;

$G_i(k)$ = g/c ratio for i th intersection,= $q_i(k)/(q_i(k) + q_{i'}(k))$;

$q_{i'}(k)$ = traffic demand of crossing street;

T = the sample time interval of time horizon; and

λ_i = the queue length.

Queue length in the above expression depends on the turning ration at that particular intersection, which can be found using historical origin- destination studies. Thus, given by the expression

$$\lambda_i(k+1) = \lambda_i(k) + \Delta T[(1-\beta_i)Q_i(k-K_{ij}) + q_i(k) - q_{i+1}(k)] \quad (12)$$

Where, $_i$ is turning ratio. Similarly to find signal delay on parallel route same expression can be used.

$$SDPR_i = Min\{(d_i(k)G_i(k)\Delta T), (d_{i-1}(k)\Delta T + \lambda_i(k-1)\} \quad (13)$$

And queue length at intersections on parallel route is given by following equation

$$\lambda_i(k+1) = \lambda_i(k) + \Delta T[(1-\beta_i)D_i(k-K_{ij}) + d_i(k) - d_{i+1}(k)] \quad (14)$$

Access Meter Delay

If metering rate is $X_i(k)$ at access meter I, then average queue length can be approximated by taking average of queue lengths at k and $k+1$ intervals (Chang et al. 1993).

$$AMD_i(k) = 0.5T[\tau_i(k) + \tau_i(k+1)] = 0.5T[2\tau_i(k) + Q_i(k) - X_i(k) \quad (15)$$

SIMULATION-BASED EVALUATION OF IASAC SYSTEM

Building Simulation Environment for Case Study

The Colerain Avenue, Cincinnati, Ohio is selected as the case study site, which is a congested corridor connecting major residential areas with commercial areas and consists of numerous driveways and parkways. The microscopic simulation software is used as a simulation environment for building the test bed. Using the Modeller tool embedded within PARAMICS, a new network can be created through entering node, link, zone data and Origin/Destination demand matrices (Quadstone 2005). Then traffic is assigned using different assignment techniques, simulation runs are carried out to get results. Among all tools in PARAMICS suite, the *Programmers*' Application Programming Interface (API) is most valuable as it enables users to customize the simulation. The customization of functionality can be achieved through "plug-ins" (Jacob et al. 2005). The PARAMICS simulation program calls different functions for vehicle release, position update for vehicles, or to interface with other programs or data at every time step. These functions used for decision control, retrieving information or carry-on the simulation. Using API, these functions can be modified, replaced or added using any high level languages like C, C++ (Doshi et al. 2006).

Embedding IASAC Algorithms into Simulation System

In this study the intersections are coordinated with SCOOT signal control

system on mainline and alternate routes. The Split Optimization component in the algorithm minimizes the maximum degree of saturation on links at a node. The cycle length optimization component attempts to adjust the cycle time to maintain 90% link saturation at each node by changing the cycle length in 4 seconds increment. The algorithm is to find out the degree of saturation for each lane served by each phase. The cycle length optimization component decides to extend or shorten the green time for each phase based on degree of saturation. Initially it is necessary to know initial green time for each phase for each intersection, lane groups in each phase and corresponding detector numbers. This information can be stored in data structures during the *api_setup ( )* function call. the *net_post_action ( )* function is called at every time step during simulation, so that it is possible to check if the current phase is about to end within 5 seconds or if the last cycle length optimization was done before 300 seconds (Doshi et al. 2006). For access control, the Bottleneck algorithm requires two overriding PARAMICS API functions (which replaces existing ramp metering functions). The first one is *void api_setup (void)*, which is to read the data from input files. The second function is *net action (),* which is actual control logic of the algorithm and carried out at each ramp control cycle (PATH 2001).

Validation of the IASAC System Model

A 2.4 mile stretch of the Colerain Avenue in Cincinnati, from Blue Rock Road intersection and Poole Road intersection (see Figure 3), was found to be a good section to test the proposed control methodology. Actually there are 18 driveways on each side of the mainline in addition to 6 signalized intersections. For validation of the IASAC System Model the driveways traffic flow is controlled by limiting them to 6 access metering points. Figure 3 shows the Colerain Avenue with one possible alternate route. Blue Rock Road intersection and Poole Road intersection are traffic bifurcation points.

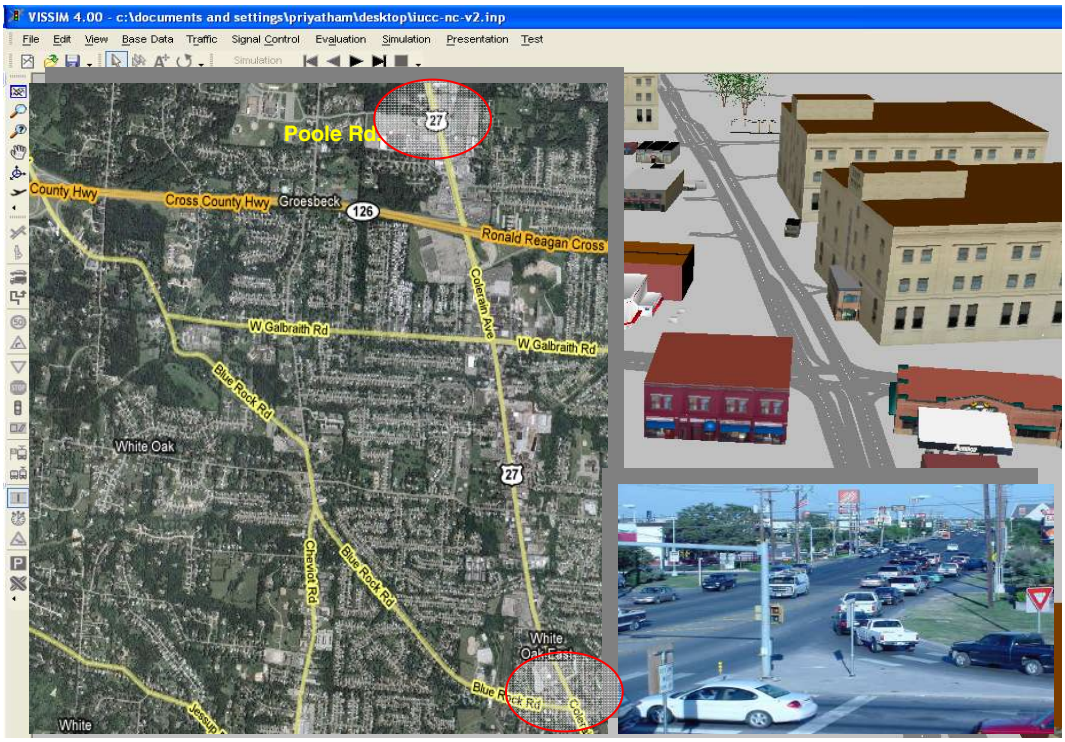

Figure 3. Colerain Avenue Corridor Network for Case Study.

All access meters are coordinated and each of them assigned equal weightage factor. The main line is divided into 10 segments and alternate route is divided into 4 segments. Each of segments contains an access point or a signalized intersection, u/s and d/s detectors, and a far downstream detector located at the end of the section. The access point is also provided with a detector, which will provide information about traffic entering the main line from the access point. The IASAC algorithm "plug-in" will receive the input data like speed, volume or occupancy, as well as the current metering rate from detectors. This algorithm also tries to find the best metering rates and green timings under different traffic and congestion scenarios. In this simulation the traffic volumes at access points are considered to be at least 150 vehicles/hr. The signal settings, access metering rates and optimum diversion rates are achieved by implementing the required code in the *Programmer* by using *call back functions* and *set functions* for the signal (Quadstone 2005).

Comparison of Two Scenarios with and without IASAC Control

In this simulation model, the input control variables are occupancies at the intersections and access points, signal green timings and current metering rates. Using these variables the algorithm can estimate demand on the main line, alternate route and access points. In order to evaluate the feasibility of the approach, the results obtained from the IASAC algorithm implementation have been compared with the results obtained from the base scenario – without control. As the objective is to assess the overall effectiveness of the control measures, the

mean travel time, vehicle miles traveled and mean speed between an origin/destination pair (Blue Rock Road intersection (zone 1) and Poole road (zone 2) , were used for evaluation. Table 1 provides the results obtained from the simulation of the proposed approach and base case.

Table 1. Comparison of Scenarios with and Without IASAC Control in Case Study

Parameter	Without IASAC CONTROL		IASAC CONTROL	
	North Bound	South Bound	North Bound	South Bound
Mean travel time in *sec* *(improvement %)*	850.1	1163.7	382.8 *(55 %)*	384.0 *(67%)*
Vehicle miles traveled in 1 hr *(improvement %)*	1548.1	1796.9	2385.1 *(54%)*	2745.2 *(53%)*
Mean speed in *mph* *(improvement %)*	14.9	10.9	33.1 *(122%)*	33.0 *(202%)*

From these results it is evident that the mean travel time in both directions on the corridor is drastically improved due to implementation of the IASAC control strategy. The increase in Vehicle Miles Traveled suggests that the corridor is more accessible to the vehicles. Improved average speed results shows that the recurrent congestion on the corridor is relieved. This case shows that the IASAC traffic control strategy performs much better than no control. When more detailed network information is provided using input control variables, the reliability of the system can be further increased.

CONCLUSION

This research proposes a framework for integrating arterial and access controls for evacuation routes in buffer zones. The application of IASAC traffic control strategy was examined for the arterial or express/collector traffic corridor using traffic simulation software PARAMICS. The results from the simulation analysis showed that it is very effective alternative to carrying out control plan for mixed regular and evacuating traffic. Using Application Programming Interface the algorithm has been developed and it is very adaptable to the field in the ITS framework. This research was sponsored through the University of Cincinnati Research Council's Interdisciplinary research Grants. The authors also express gratitude to Transportation Research Center at Beijing University of Technology, China for exchanging research ideas. The results and ideas presented in the paper represent the authors' point of views only.

ACKNOWLEDGEMENT

This research was sponsored through the University of Cincinnati Research Council's Interdisciplinary research Grants. The authors also express gratitude to Transportation Research Center at Beijing University of Technology,

China for exchanging research ideas. The results and ideas presented in the paper represent the authors' point of views only.

REFERENCES

Alsnih, R., and Stopher, P.R. (2003). "A Review of the Procedures Associated with Devising Emergency Evacuation Plans." CD-ROM, *82nd Annual Meeting of the Transportation Research Board.*

Chu, L., Liu, X.H., Recker, W., and Zhang, H.M. (2004). "Performance evaluation of adaptive ramp metering algorithms using microscopic traffic simulation model. *Journal of Transportation Engineering* Vol.130, No. 3, pp. 330-338.

Chang, G.L., Ho, P.K. Wei, C.H. (1993). "A dynamic system-optimum control model for commuting traffic corridors." *Transportation Research Part C: Emerging Technologies*, Vol. 1, No.1, pp. 3-22.

Doshi, H., Goel. S., and Ozbay, K. (2006). "EZ-Paramics-an object oriented programming Approach to Code API using PARAMICS Programmer." http://www.eden.rutgers.edu/~hpdoshi/EZParamics-Final.doc (6/10/2006).

Hunt, P.B., Robertson, D.I., Bretherton, R.D. (1982). "The SCOOT on-line traffic signal optimization technique (Glasgow)." *Traffic Engineering & Control*, Volume 23, Issue 4, 1982, Pages 190-192.

Jacob, C., and Abdulhai, B. (2005). "Integrated traffic corridor control using machine learning." *Proceedings of IEEE conference on Systems, Man and Cybernetics*, Vol.4, pp.3460-3465.

Perugu, H., Wei, H., and Nagaraju, C. K. (2007). "Heuristic System Model and Algorithms for Integrated Urban Corridor Traffic Control System with Access Management Measures," CD-ROM, *86th Transportation Research Board Annual Meeting*.

Papageorgiou, M. (1980). "A new approach to time of day control based on a dynamic freeway control model." *Transportation Research B*, Vol. 14, pp 349-360.

PATH (2001). *Evaluation of on-ramp control algorithms*. California PATH research report, UCB-ITS-2001-36. http://www.path.berkeley.edu/PATH/Publications/PDF/PRR/2001/PRR-2001-36.pdf>(January 5, 2006).

Quadstone Limited (2005). *Paramics Modeller V.5.1 Users Guide*.

Robertson, D. I., and Bretherton, R. D. (1991). "Optimizing networks of traffic signals in real time: The SCOOT method." *IEEE Transactions on Vehicular Technology*, Vol.40, No.1, 1991, pp.11-15.

Reiss, R. A., Gartner, N. H. and Cohen, S. L. (1991). "Dynamic control and traffic performance in a freeway corridor: a simulation study." *Transportation Research Part A*, Vol. 25A, No.5, pp 267-276.

Roess, R. P., Prassas, E.S., and McShane, W.R. (2004). *Traffic Engineering*. Pearson Prentice Hall Inc., New Jersey.

Sbayti, H., and Mahmassani, H.S. (2006). "Optimal Scheduling of Evacuation Operations." CD-ROM, *85th Transportation Research Board Annual Meeting*.

Wolshon, B., Hamilton, E. U., Levitan, M., and Wilmot, C. (2005). "Review of Policies and Practices for Hurricane Evacuation. II: Traffic Operations, Management, and Control." *Natural Hazards Review*, Vol. 6, 2005, pp. 143-161.

Wei, H., Q. Li, and Yang, X.K. (2006). "Emergency Evacuation Planning System Integrated with GIS-Based Traffic Simulation Models." CD-ROM, *Proceedings of the 2006 IEEE Intelligent Transportation Systems Conference*, Toronto, Canada, September 17-20, 2006.

Wei, H., Zeng, Q.A., Hu, H., Wang, X.H., and Kukreti, A.R. (2008). "Integrated Urban Evacuation Planning Framework for Responding to Human-Caused Disasters over Surface Transportation Network." *Journal of Transportation Research Record.* No. 2041, pp. 29-37.

Yang, X.K., Wei, H., et al. (2006). "Requirements for Urban Traffic Evacuation Modeling," White Paper for Research Project "Simulation-based Critical Technologies for Olympics Traffic Emergency Evacuation Plans," Beijing University of Technology Transportation Research Center, Beijing, China.

Impacts of the Modernization of Global Navigation Satellite Systems on Intelligent Transport Systems

Xin Shi[1]

[1]Centre of Transport Studies, Department of Civil and Environmental Engineering, Imperial College London, SW7 2AZ, London, UK; e-mail: xin.shi03@imperial.ac.uk; Tel: +44-(0)20-75946055

ABSTRACT

The development of Intelligent Transport Systems (ITS) is a key enabling technology to prevent traffic accidents, enable road charging, and reduce congestion. However, the deployment ITS is limited by positioning and wireless communication technologies. Global Navigation Satellite Systems (GNSS) can provide positioning and timing services globally but requires good visibility of navigation satellites that is difficult in urban area where ITS systems were deployed. Currently, only the Global Positioning System (GPS) operates at an accuracy of about 10 m. Advanced GNSS provides more navigation satellites and signals improving the visibility and positioning accuracy to sub-metre even centimetre level in real-time. Additional integrity information will be described for safety-critical applications. Potential improvements of current and new ITS applications enabled by the modernization of GNSS are presented in this paper. In addition, Precise Point Positioning (PPP) using only one GNSS receiver and wireless communication network is much more cost-effective as it removes the need of reference receivers and relative positioning used in current applications. The advantages of using PPP technology in ITS will be demonstrated in this paper.

INTRODUCTION

Intelligent Transport Systems (ITS) improve transport safety, reduce congestion and reduce air pollution.. In figure 1, the services shown in rounded rectangles and objectives shown in ellipses of ITS are summarized. *Emergency vehicle management* involves locating the accidents and informing the nearest and enough available emergency vehicle. For example, the European Community has planned to fully roll out a system named eCall (the pan-European in-vehicle emergency call) by 2010 (COM, 2007). This system could save up to 2,500 lives every year and reduce the corresponding congestion (COM, 2007). However, eCall has been rejected by the UK and some other countries because of the concern of high costs comparing with the benefits. *Advanced Vehicle Control and Safety Systems* (AVCSS) can increase safety by avoiding intersection collisions. The Cooperative Safety Systems (CSS) warns drivers when other vehicles are approaching at an intersection or when a driver should apply braking. Such warnings could be generated on-board and transmitted directly from one vehicle to another (VV), and/or generated by fixed monitoring systems and transmitted to the vehicle from a roadside sensor (R-V). Such systems have been demonstrated successfully, but their deployment is hindered by the need for different stakeholders; drivers, the government and –private industry to cooperate.. In addition, AVCSS can also

provide lane departure warning to prevent a vehicle drifting out of its lane and blind spot warning to assist drivers in changing lanes. However, these services require high accuracy of positioning in real-time that is not guaranteed by current GPS or any other positioning technique in urban area with existing GPS technology. Due to cost, the deployment of such systems is likely several years away (POSTnote, 2009).

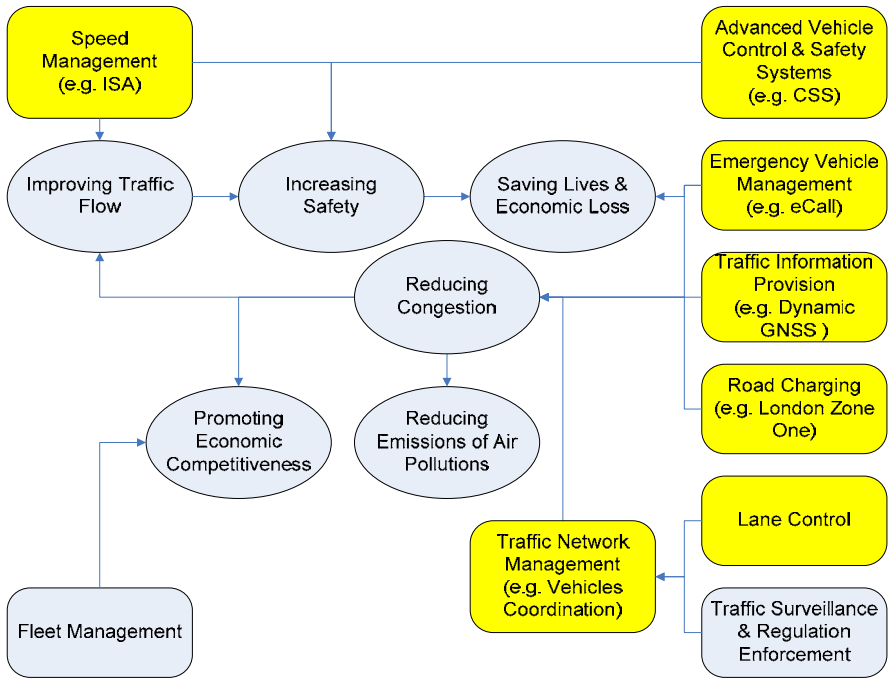

Figure 1. ITS Services and Objectives.

Speed Management applications such as Intelligent Speed Adaptation (ISA) and Adaptive Cruise Control (ACC) can improve traffic flow and increase safety by assisting drivers to stay within the designated speed limits. Many GPS devices, (e.g. TomTom), already provide warnings when the speed limit is exceeded. To exclude the drivers' influences, ISA may also be achieved by automatic intervention to slow down the vehicle. Recent research suggested that fatal accidents may be reduced by 42% if all vehicles were fitted with automatic governed ISA (ISA-UK, 2008). However, public acceptance of ISA is uncertain and no public traffic policies involving ISA was published. In addition, identifying the prevailing speed limit for ISA is also difficult. Unlike ISA, ACC does not vary the speed based on the digital speed map but on the separation from the vehicle in front. *Traffic Information Systems*, provide pre-journey and en-route traveller information, and route guidance, An *Traffic network management* collects and analyzes the vehicle coordinates in real-time. Based on the results, this management system can reduce congestion by controlling traffic signals and other methods. Again, the timing and accuracy of the collected vehicle coordinates and the costs of the system are key issues that must be addressed for the system to be useful.

The technologies required for ITS are near real-time on-board positioning and wireless communications. Among different positioning techniques, the satellite

positioning and navigation systems have obvious advantages such as the global coverage, no limitation of the network capacity, relatively high accuracy, real-time positioning, small size of on-board device and no roadside infrastructure required. However, the current limitations of GNSS systems highly limit the current and future ITS services highlighted in figure 1. This paper concentrates on the benefits of ITS from the modernization of GNSS consuming the wireless communication network is available that is usually the case in urban and rural area globally.

THE MODERNIZATION OF GNSS

GNSS including American GPS, Russian GLONASS, European GALILEO and Chinese BeiDou II has drawn huge interests and investments over the past ten years. Currently, only NAVSTAR GPS is operational with providing global coverage. The advancement of GPS technologies and infrastructures continues in improvement. In 2010 a new civil navigation signal is expected be available and the undifferenced code-phase based stand-alone positioning (using only one receiver) will be able to provide 3D accuracy at 2m (2σ). The carrier-phase based double-differenced (DD) real-time kinematic (RTK) positioning (using at least two receivers) 3D accuracy is 3cm (2σ) and the 3D accuracy of post-processed static positioning is 5mm (2σ). GALILEO is expected to reach its full operational capacity (FOC) around 2013 (EC, 2008). In this paper, only the free services including the Open Service (OS) provided by GALILEO and the modernized Standard Positioning Service (SPS) provided by GPS are considered.

PRECISE POINT POSITIONING (PPP)

PPP provides sub-metre level accuracy using only one receiver. Compared with conventional DD RTK positioning techniques, PPP does not reference stations. However, errors mitigated by 'differencing' in differential algorithms need to be properly modelled and estimated. Conventional PPP requires several tens of minutes (static mode) to hours (kinematic mode) to converge to a positioning accuracy at the decimetre to centimetre level. This research builds on GNSS modernization to achieve RTK PPP that has the advantages of global coverage, cost-effectiveness, high accuracy at decimetre level and improved availability.

TRIPLE-FREQUENCY RTK PPP

Conventional PPP is based on processing dual-frequency navigation signals. This paper developed RTK PPP based on processing triple-frequency code-phase and carrier-phase navigation signal observables. The satellite clock and orbit errors are eliminated by using precise products provided by International GPS Service (IGS) (IGS, 2009). The ionosphere delay is cancelled by linearly combining the observations based on the nature of this error (Kaplan, 2006). The troposphere delay is modelled following Hofmann-Wellenhof (1997) theory. The cycle slips and multipath are detected and corrected with methods suggested in Leick (2004) and Sauer (2003). Therefore, the triple-frequency observation equations applied in this research are given by:

$$\begin{cases} PR^s_{r,IF,GS}(L_1) = 0.5(PR^s_r(L_1) + \Phi^s_r(L_1) \\ PR^s_{r,IF,GS}(L_2) = 0.5(PR^s_r(L_2) + \Phi^s_r(L_2) \\ PR^s_{r,IF,GS}(L_3) = 0.5(PR^s_r(L_3) + \Phi^s_r(L_3) \\ \Phi^s_{r,IF,12} = \dfrac{f_1^2}{f_1^2 - f_2^2}\Phi^s_{r,f1} - \dfrac{f_2^2}{f_1^2 - f_2^2}\Phi^s_{r,f2} \\ \Phi^s_{r,IF,13} = \dfrac{f_1^2}{f_1^2 - f_3^2}\Phi^s_{r,f1} - \dfrac{f_3^2}{f_1^2 - f_3^2}\Phi^s_{r,f3} \end{cases} \quad (1)$$

where $PR^s_r(L_i)$ and $\Phi^s_r(L_i)$ are the measured code phase pseudo-range and the calculated carrier phase pseudo-range on carrier L_i respectively. For n satellites, there are $5n$ equations used to estimate $5+3n$ unknown variables. The unknown variable are the 3D receiver position coordinates, the receiver clock offset, the wet troposphere delay, and three real-value ambiguity in carrier phase for each satellite. Simulated GALILEO observations and corresponding IGS satellite orbit and clock corrections were generated by the GALILEO System Simulation Facility (GSSF) and used to test this model.

RESULTS

To simulate the urban environment, a high level of multipath is added onto the simulated GALILEO signals. The dual-frequency PPP using E1-E5b observations and the triple-frequency PPP observing six satellites were implemented. For both cases, the convergence performance are recorded and compared in Figure 2.

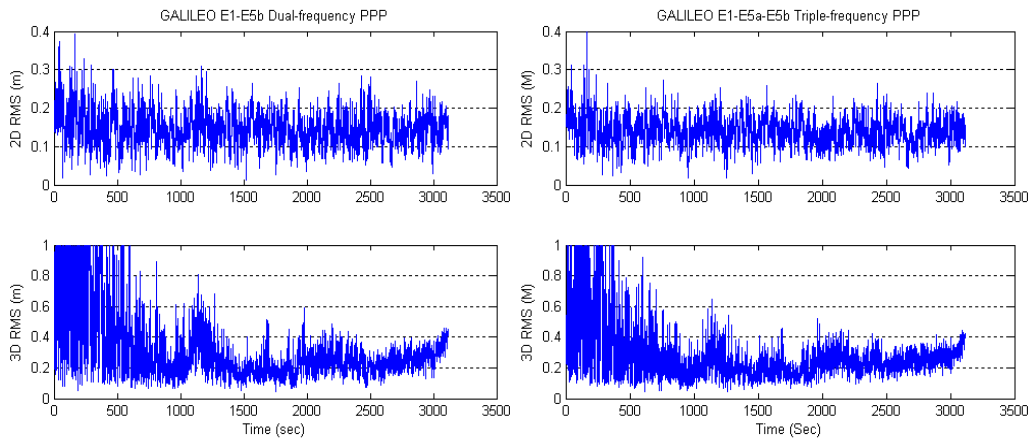

Figure 2. E1-E5b Dual-frequency and Triple-frequency PPP Observing Six Satellites.

As seen in Figure 1, there is almost no difference between these two processes, using all available observables may not lead to any improvements in PPP. In addition, the 2D RMS immediately converged to 40 cm precision. This performance is good enough to enable many 2D position required ITS services in real time. However, it did not converge to better precision due to the relatively high residual error bias mainly the multipath bias ranging from -40 cm to +40 cm. For services requiring 3D positioning, a very long initial waiting time of less than an

hour was inevitable. However, by checking the residual, satellites with relatively higher noise level can be identified and removed from the constellation. After removing the two noisiest satellites, the PPP performance is shown in Figure 3.

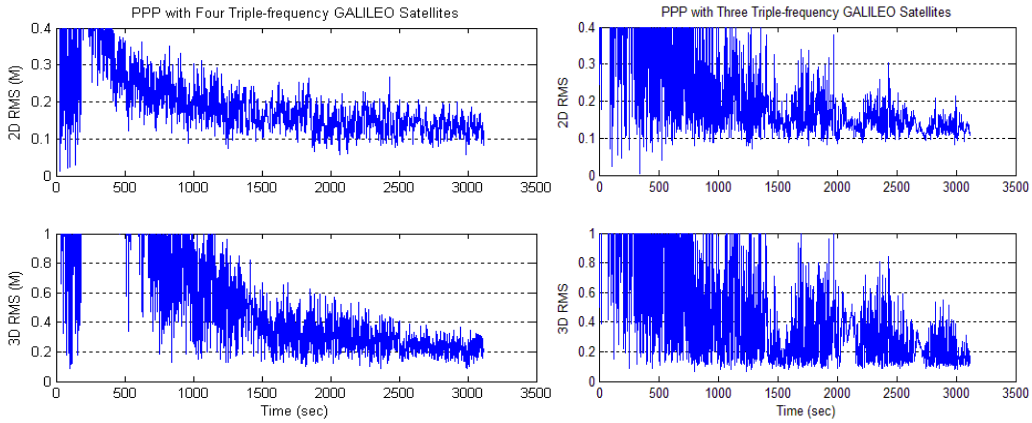

Figure 3. Triple-frequency PPP Observing Four or Three GALILEO Satellites.

By observing four satellites with relatively lower noise levels, both 2D and 3D RMS converged slower to sub-metre level than using observations from all six visible satellites and the 3D RMS initial waiting time was reduced to within 2500 seconds. If only three satellites with the lowest noise were observed, the PPP processing converged more slowly then observing four satellites. The 2D RMS and 3D RMS converged to 20 cm and 40 cm precisions with about 3000 seconds. The position convergence is determined by not only the residual error level but also the satellite geometry, using the smallest number of satellites with the lowest noise level does not guarantee the shortest convergence time of PPP.

CONCLUSION

This paper reviewed the main technical GNSS technology including positioning accuracy, GNSS availability. GNSS technology advancements were summarized and free GNSS services were evaluated to be used in ITS applications. With these free GNSS navigation signals, RTK PPP algorithms were developed and tested with simulated triple-frequency GALILEO signals in urban area. The results have shown acceptable real-time on-board processed positioning results with sub-metre level accuracy within an acceptable time for 2D applications. This new PPP algorithm has improved the GNSS availability by reducing the number of necessary visible satellites from four to three.

The developed triple-frequency PPP has shown many advantages that can benefit ITS application. First, it was designed to use free navigation information and only one GNSS receiver without the need of building the expensive reference station network. The deployment costs can be greatly reduced benefitting emergency vehicle management systems and other ITS applications. The global coverage of PPP and elimination of required fixed reference stations also greatly benefit emergency systems like eCall.

Second, the new PPP achieved 2D RMS positioning accuracy better than 040 cm immediately and 3D RMS sub-metre accuracy with about 10 minutes waiting

time. This high 2D accuracy can enable AVCSS such as lane departure warning and CSS. However, the waiting time for 3D precise positioning is still too long. As the positioning accuracy has been improved, the speed estimations have also become more accurate benefitting the speed Management applications such Intelligent Speed Adaptation (ISA) and Adaptive Cruise Control (ACC). In addition, better than the current road charging systems based on cameras, PPP can enable more detailed and reasonable charging policies such as multi-entry charges or even travelling route charging eliminating the need for additional costly roadside infrastructure to detect vehicles. Obviously, real-time accurate vehicle positions can improve the performance of Traffic Information Provision and Traffic network management.

Third, the developed PPP algorithm has proved to successfully cope with the higher level of navigation signal noise and smaller number of visible satellites due to high buildings and narrow roads in urban area then rural area and remote area. This is important because most of the ITS applications are utilized densely populated areas

The next step of this research may be strictly identifying the requirements of the ITS applications including the accuracy, integrity, and availability of the sensors. The integrity algorithms of PPP will be developed and the waiting time of PPP convergence will be further reduced by examining and eliminating the residual errors in GNSS observables.

REFERENCE

COM (2007), Towards Europe-wide Safer, Cleaner and Efficient Mobility: The First Intelligent Car Report, COMMUNICATION FROM THE COMMISSION TO THE EUROPEAN PARLIAMENT, THE COUNCIL, THE EUROPEAN ECONOMIC AND SOCIAL COMMITTEE AND THE COMMITTEE OF THE REGIONS, Brussels, 17/09/2007, 541 final.

EC (2008), European Parliament and the Council (EC), regulation No. 683/2008.

ESA (2005), European Space Agency, accessed online at www.esa.int/esaNA/SEMTHVXEM4E_galileo_0.html.

Hoffmann-Wellenhof, B., J. Collins, and Lichtehegger, H. (1997), *GPS Theory and Practice*, Springer-Verlag, New York.

IGS (2009), accessed online at igscb.jpl.nasa.gov/pub/product.

ISA-UK (2008), Intelligent Speed Adaptation Final Report, DfT, 2008.

Kaplan, D. Elliott and Hegarty, J. Christopher (2006), *Understanding GPS Principles and Applications*, 2nd edition, Artech House Inc..

Leick, A. (2004), *GPS Satellite Surveying*, 3rd ed., John Wiley & Sons Inc., New York.

McDonald K. D. (2002), The Modernization of GPS: Plans, New Capabilities and the Future relationship to Galileo, Journal of Global Positioning System, Vol. 1, No. 1:1-17, 2002.

POSTnote (2009), Intelligent Transport Systems, Parliamentary Office of Science and Technology UK January 2009, Number 322.

Sauer K. (2003), *Integrated High Precision Kinematic Positioning Using GPS and EGNOS Observations*, PhD thesis, Dept. of Civil and Environmental Engineering, Imperial College London, UK.

CAR-FOLLOWING CRITERIA AT A SIGNALIZED INTERSECTION IN BEIJING

Q. YU[1], J. LIU[2], J. RONG[3]

[1]Associate Professor, Key Lab of Transportation Engineering Beijing University of Technology, Beijing，100124, China. Email：yuquan@bjut.edu.cn

[2]Doctorate Candidate, Key Lab of Transportation Engineering, Beijing University of Technology, Beijing，100124, China. Email：ljg2006@emails.bjut.edu.cn

[3]Professor, Key Lab of Transportation Engineering, Beijing University of Technology, Beijing，100124, China

ABSTRACT

It is commonly agreed upon that car-following only takes place when the separation between two vehicles is within some threshold value. This threshold has been studied but most of the work focuses on highway or motorway traffic and does not consider car-following in intersection areas. This paper studies the car-following threshold criteria in a signalized intersection area. The close-range photogrammetry system is built to collect and analyze traffic data at a signalized intersection in Beijing. The speed difference analysis method and K means the cluster method is employed to distinguish the car-following status and to obtain the critical headway and spacing for car-following. The results show that the critical headway of car-following at the signalized intersection is three seconds and the critical spacing is 20 meters. The main contributions of the paper are the close-range photogrammetry system developed for data collection, and the speed difference analysis or judging the car-following status at a signalized intersection.

Keywords: car-following; signalized intersection; headway

INTRODUCTION

Micro traffic flows play an important role in the analysis of existing traffic facilities needing modification and also in the design of new facilities. It is of great importance to make sure that these traffic flows are able to reflect real traffic situations accurately. One important sub-process in micro traffic flows consists of the modeling of car-following behavior. Car-following phenomenon is concerned with the relationship between driver-vehicle systems and inter-vehicular dynamics in a single stream of traffic.

A traffic flow theory book (Daniel 1975) stated that car-following starts when spacing between the leading vehicle and the following one is less than 100m or 125m. The HCM 1994 (TRB 1994) defined that car-following criterion on highways is 5 seconds. The HCM 2000 (TRB 2000) defined car following criterion

on two-lane highways is 3 seconds. Paker (Paker 1996) used 5-second headway to research car-following behavior of heavy goods vehicles on a motorway. Weidman (Widedmann 1992) studied that car-following occurs when vehicle spacing is less than 150m. All these studies focused exclusively on highway or motorway traffic.

For the car-following data collection, Chandler, Herman and Montroll (Chandler 1958) used wire-linked vehicles. Ozak i(Ozaki 1993) collected data by using video taken from the 32th floor of a city office building. Treiterer and Myers (1974) used a helicopter as a tool to observe a platoon of 70 vehicles. Hoogendoorn (Saskia 2005) took pictures of freeway A2 in Utrecht from a helicopter. One of the main advantages of these last approaches was that the observation did not disturb normal traffic flow.

Headway and vehicle spacing are important to calculate the capacity of a signalized intersection and signal timing plan. It is obvious that at a signalized intersection, the traffic flow is restricted. But headway and vehicle spacing are not determined. One reason is that the past work foundation is located on a highway or motorway segment. Another reason may be that the traffic flow in a signalized intersection is complex and observation is difficult. This paper aims to research the car-following criterion in a signalized intersection.

DATA COLLECTION PROCESS

Unlike the helicopter observation method that is typically expensive, a close-range photogrammetry method is used in this study. Close-range photogrammetry technique is an old method, but is seldom used in traffic observation. It is easy to implement, and it is a low-cost method. It also does not require specialized training (ARIAS 2002). The method uses a common video tape recorder to obtain data and reference points (coordinates origin point), and analysis software to analyze the collected data. This paper does not intend to interpret the close-range photogrammetry method and its history. The important thing to be introduced here is the data collection system and field work used in this study.

FIELD WORK

The video data collection site is a signalized intersection named Jiang Zhaikou in Dongcheng District of Beijing City. The intersecting streets at the intersection are An-Dingmen Avenue and He Pingli North Street. The north-south An-Dingmen Avenue is the arterial.

The traffic signal control mode at this intersection is fixed time, three phase operation.

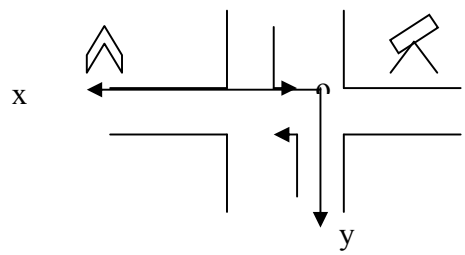

Figure 1 The ground reference system of the intersection named Jian Zhaikou

The date of video collection was April 16, 2006. The weather was fine. Video recording time was from 16:00 pm to17:00 pm. The video tape recorder was installed on the 11th floor of a neighboring residential building. The building is located at the north leg of the arterial. The coordinates of the observation system are calibrated by using tapeline measure and laser range finder. The reference frame is shown in the Figure 1. The X-axis is the stop line of the north approach. The origin point of the observation system lies in the base of a pole standing on the separated strap between the automobile lane and non-automobile lane. The area of the intersection which the video tape recorder shoots is 53m * 40 m. The left turn lane is the inner lane.

The recorded video film is fed into the computer and the dedicated analysis software is used to extract data from the video. The following information of each vehicle can be directly provided (at 0.02s intervals)——(1) x-y coordinates of the vehicle; and (2) speed of the vehicle (m/s). After filtering out data with pedestrian and bicycle interruptions, 200 pairs of vehicles were selected for the car-following analysis.

CAR-FOLLOWING DATA ANALYSIS AT A SIGNALIZED INTERSECTION

Whether a vehicle is in a car-following mode is determined in this study based on the difference of the speeds between the leading car and the following car in the traffic stream. Generally speaking, if the speed of the leading vehicle is less than the desired speed of the following vehicle, the follower is in car-following mode. However the desired speed of a vehicle cannot be determined by observation of the oscillation process and the chaos phenomenon of the vehicles (Widedmann 1992, Yu 2007). During the continuous acceleration and deceleration process of the vehicle, it may reach the desired speed, but only momentarily. Therefore, it is impracticable to judge whether a vehicle is in car-following mode based on the vehicle speed with respect to the desired speed. The speed difference between the leader and the follower can reflect the response of the follower to the leader and reveal whether the follower is in car-following mode.

For a leader-follower pair, the speed of the leading car may be greater or less than that of the following car, so the speed difference may be positive or negative. With the coordinates for both vehicles collected from the data acquisition system described earlier, the spacing between the vehicles can be determined using Equation 1.

$$s_{lf,t}=\sqrt{\left(x_{l,t}-x_{f,t}\right)^2+\left(y_{l,t}-y_{f,t}\right)^2} \quad (1)$$

Where， $s_{lf,t}$ = vehicle spacing between the leading vehicle and the following vehicle

at time t; $x_{l,t}, y_{l,t}$ = coordinates of the leading vehicle at time t; $x_{f,t}, y_{f,t}$ = coordinates of the following vehicle at time t; The speed difference can be determined using Equation 2.

$$v_{lf,t} = v_{l,t} - v_{f,t} \quad (2)$$

Where, $v_{lf,t}$ = speed difference between the leading vehicle and the following vehicle at time t; $v_{l,t}$ = speed of leading vehicle at time t; $v_{f,t}$ = speed of following vehicle

The headway between the vehicles can be estimated using Equation 3.

$$h_{lf,y} \approx s_{lf,t} / v_{f,t} \quad (3)$$

$h_{lf,y}$ = headway between the leading vehicle and the following vehicle at the location of y axle.

Table 1 Vehicle spacing of through vehicles

Particular leader-follower pair sample	No. of data points for sample pair	Minimum spacing (m)	Maximum spacing (m)	Mean spacing (m)	Std.Deviation
Sample1	461	5.98	13.74	9.3899	2.03958
Sample2	361	8.77	20.55	14.2250	3.24984
……	……	……	……	……	……
Sample 14	351	7.84	21.88	16.4822	3.77541
Sample 15	289	13.85	22.47	17.4573	2.06810

Table 1 shows part of the data collected. Sample i means particular leader vehicle i-follower vehicle i+1 pair sample. Analysis software shows 0.01s step results of through vehicle data points. Trajectories are recorded of 34 through vehicles during one cycle. These 34 vehicles all ran through the intersection. All 10154 data point records of vehicle spacing are collected.

At time t with equations one through three, we get headway, spacing and the speed difference of leader-follower pairs. A graph of scattered points of speed difference and headway is shown in Figure 2. Because it is not clear to see the order, we choose a display mode named Sun-Flower in SPSS software. It is shown in Figure 3.

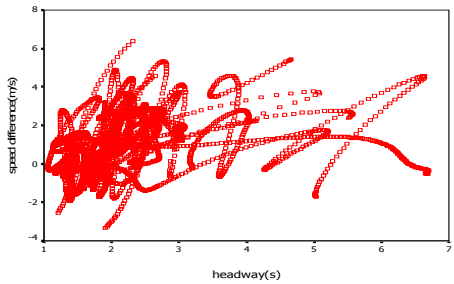

Figure 2. scattered points of speed

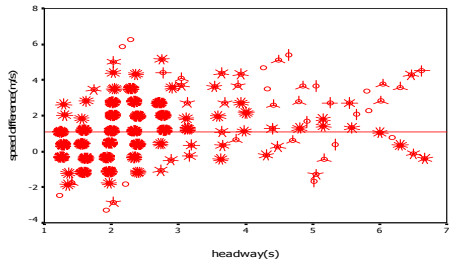

Figure 3. the sun-flower graph of scattered points.

It is clear that most points aggregate between 1s to 3s headway whether the speed difference is positive or negative. In the area with headways exceeding 3s, the points scatter. It is evident there is a critical point at 3s. K means the cluster method is used to analyze the headway data. Valid sample sizes are 31125 headway data, the value is 3s. Table 2 is the ANOVA analysis result. The table shows that the cluster effect is good. The graph of speed difference and spacing shows it is good as well. It is shown in Figure 4. Also does the graph of sun-flower display mode in Figure 5.

Table 2 the ANOVA table of the headway

	Cluster		Error		F	Sig.
	Mean Square	df	Mean Square	df		
Headway	14054.355	2	.258	31122	54403.419	.000

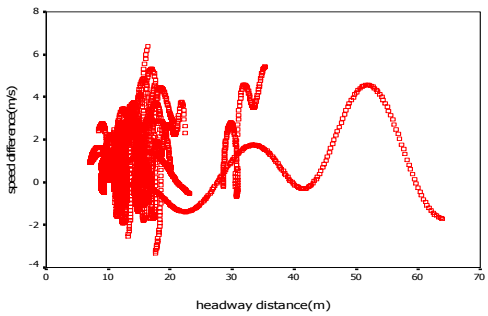

Figure 4 speed and vehicle spacing

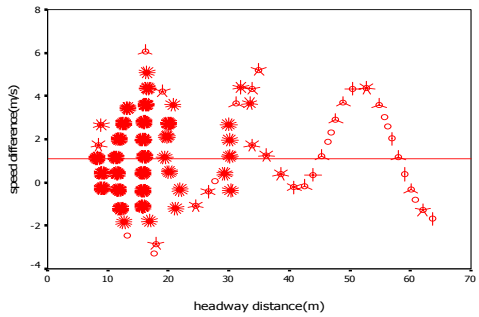

Figure 5 the sun-flower graph of scattered points

The vehicle spacing is from 10m to 30m so that the critical vehicle spacing is 20m. K means cluster method is used to analyze the vehicle spacing data. Valid sample sizes are 37482. We choose the second class vehicle spacing as the car following headway criteria at the signalized intersection, the value is 20m. Table 3 is the ANOVA analysis result. The table shows that cluster effect is good.

CONCLUSION

The car-following phenomenon has been observed in highway, expressway or motorway road segments in particular. This paper studies the car-following in a signalized intersection by the low-cost close-range photogrammetry method. By

speed difference analysis, the critical headway of 3s and the vehicle spacing of 20m are identified. With 3s headways, the saturation flow rate of through lanes in the signalized intersection is 3600/3=1200 vehicles. This paper does not intend to touch the car-following models, but introduces a feasible observation method to observe vehicles in a signalized intersection, and gives out the critical headway and vehicle spacing when there is car-following at the signalized intersection. This study should be beneficial to capacity and timing plans as well as signalized intersection safety.

Table 3 the ANOVA table of the vehicle spacing

	Cluster		Error		F	Sig.
	Mean Square	df	Mean Square	df		
Vehicle spacing	967068.701	2	13.936	37479	69394.061	.000

REFERENCES

ARIAS P, VÁZQUEZ S, LORENZO H, REGO T (2002), Photogrammetric survey in traditional rural constructions in Galicia (Spain). XVIII International Symposium of CIPA. Potsdam (Germany). September, 18-21: 188-195

Chandler, Herman and Montroll (1958), Traffic dynamics: studies in car following, Operations Research 6,165-184

Daniel L Gerlough, Mathew J Huber (1975), Traffic Flow Theory, TRB Special Report 165, Washington D.C

Ozaki (1993), Reaction and anticipation in the car following behavior, Proceedings of the 13th International Symposium on Traffic and Transportation Theory: 349-366

Paker M T (1996), The effect of heavy goods vehicles and following behavior on capacity at motorway roadwork sites. "Traffic Engineering Control."37(9):524-531.

Saskia Ossen, MSc, Serge P. Hoogendoorn (2005), car-following behavior analysis from microscopic trajectory data, Transportation Research Board Annual Meeting

Special Report 209 (1994, 2000), Highway Capacity Manual. Transportation Research Board, National Research Council, Washington, D.C

Treitrer and Myers (1974), The hysteresis phenomenon in traffic flow, Proceedings of the 6th Symposium on Transportation and Traffic Theory: 13-38

Wiedemann, R, et al (1992), Microscopic Traffic Simulation / The Simulation System-Mission. University of Karl-sruhe

YU Quan (2007), chaos research of vehicle spacing in signalized intersection, International Conference on Transportation Engineering, July, Vol.3: 2488-2493

Study of Drivers' EEGs and Application in Intellige nt Transportation Systems

Junqiang Peng[1] and Pingdong Wu[2]

[1]School of Mechanical and Electronic Engineering, Tianjin Polytechnic University, Box 300160, City, Tianjin; PH (+86)022-24528333; Email: junqiangpeng@tom.com
[2]School of Mechanical and Vehicular Engineering, Beijing Institute of Technology, Box 100081, City, Beijing, Email: wupindon@bit.edu.cn

ABSTRACT

A driver is a principal part of traffic, and a driver's state is related to traffic safety, such as in the case of a driver's dangerous emotional state, fatigued state, or drunken state. According to scientists' study, an Electroencephalogram (EEG) can reflect his different states more accurately. In the modern Intelligent Transportation Systems which consists of the network and information, if the driver's EEG information could be gathered in real-time, and the transportation system could be adjusted to this, then the driver could be alerted or measures could be taken by the car's safety equipment which is designed according to the drivers' EEG information. Compared to the traditional transportation system, this kind of system which uses the drivers' EEG information can greatly reduce traffic accidents.

By using the car simulation driving instrument and the EEG measuring instrument, the EEG measuring experiment was developed. The experiments of fatigued driving, drunken driving, and driving while emotionally unstable were designed, and drivers' EEG signals were measured when they were in normal, fatigued, drunken, excited, tense, and sad states. FFT and Wavelet Analysis signal processing methods were used to extract the characteristics of the EEG signals.

The EEG characteristics of the fatigues state were found by these methods, and the drunken state's characteristics were distinct, and the excited, tense and sad states' were also found. The EEG characteristics of drivers in different states can reflect drivers' state in real-time, so they can be applied to the Intelligent Transportation Systems.

INTRODUCTION

The rapid development of modern traffic has brought us convenience, but it also has given us a serious problem: traffic safety. If you search on the internet for traffic-related deaths, you would find that there were 50,000 to 60,000 deaths due to traffic accidents every year. How to reduce the number is a problem faced by many countries.

Now, the Intelligent Transportation Systems (Westin et al. 1999; Lu Huapu et al. 2003) mainly utilizes the information about the road and car, but of the factors related to traffic accidents, the driver is the most important. (Wang Yanzhong et al.

2007) If the state of the driver could be gathered and taken to the center of the Intelligent Transportation Systems, the traffic information would be full-scale and more exact.

According to research, the EEG, which is the signal recorded from people's scalps, can reflect information about the people accurately. Therefore, in this paper, the EEG of the driver was studied. First, the experiment system in this research is given, second, the experiment process is explained, next are the experiment results and the analysis of them, the last are the conclusions.

1 EXPERIMENT SYSTEM

Fatigued, drunken, excited, tense and sad: these five states are the most dangerous factors which may influence driving. While in these states,, the driver may make some mistakes in driving, so in this paper, the EEG characters of drivers in these five dangerous states were studied.

The experiment system includes the car simulation driving system, the dangerous state inducement system, the EEG measurement instrument, and the data analysis system (see Figure 1).

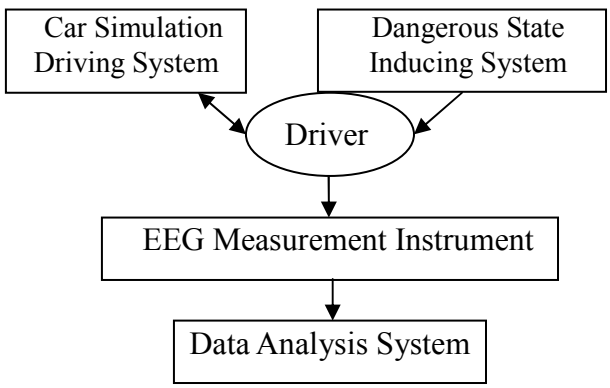

Figure 1. Frame of Experiment System.

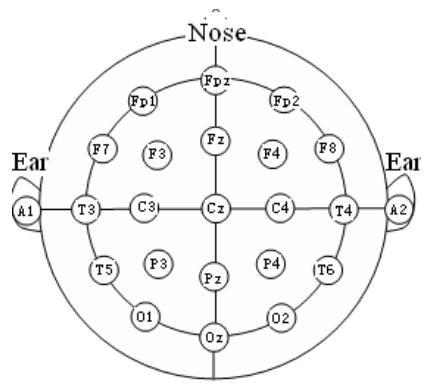

Figure 2: Location of Electrodes.

The car simulation driving system was chosen from the car driving school's teaching system. It is composed of a car cabin and a scene simulation system which can simulate many kinds of different scenes. The dangerous state inducing system can induce the experiment subject into the five kinds of dangerous states. The EEG measurement was chosen from the Japan Photoelectricity Company, type is EEG1100, which has one hundred and ninety two channels, and is one of the most advanced EEG measurement systems available.

2 EXPERIMENT PROCESS

To cover each of the five kinds of dangerous states, the experiments mainly were made of three parts: driving while fatigued, driving while drunk, and driving while excited, tense or sad .

Experiment subjects included graduate students, in good health, between 22 and 30 years of age.

Location of electrode: the electrodes were placed according to a 10-20 system standard which is the international standard. The referenced electrodes were A1 and A2 which were located on the ear. The EEG signals were recorded from the electrodes F3 and F4, C3 and C4, P3 and P4, O1 and O2, T3 and T4, which corresponded to the prefrontal area, frontal area, parietal area, occipital area and temporal area respectively (see Figure 2).

2.1 Experiment of fatigued driving

The experiment process was showed by figure 3.

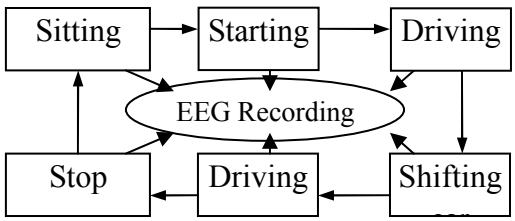

Figure 3. Experiment of Car Driving

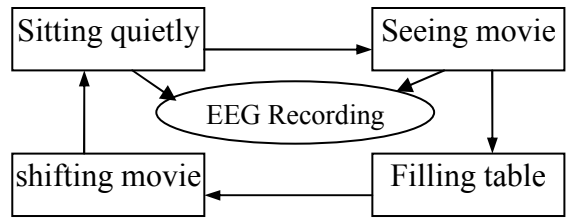

Figure 4. Experiment of Inducing Emotion

The high-speed road scene was chosen, the other cars and passengers were in normal mode, and the experiment was done five times following the process in figure 3 for every experimenter. At the same time, the subject's EEG was recorded by the EEG1100.

For the sake of contrast, first the subject drove in the normal state, and then drove the car following the experiment process, when he was in a fatigued state.

Five subjects participated in this experiment

2.2 Experiment of drunken driving

Experiment process: the subjects drank together, then they drove in the car simulation driving system. At the same time, their EEG was recorded. This experiment had some damage to the subjects' bodies, so only four experimenters participated in it.

2.3 Experiment of driving in a dangerous emotional state

This experiment's key point was the inducing of a dangerous emotion state: excited, tense, and sad. Now there are mainly three kinds of methods, such as picture inducement, movie inducement, and scene inducement. The movie inducement was chosen, for this method can arouse more obvious emotions, and the operation was simpler.

Before the experiment, many movie excerpts were compared, from them, the movie section which could induce the subjects' emotions more obviously was

selected. The process was as shown in Figure 4, first, sitting quietly for two minutes (the aim was recording the normal EEG as reference EEG), second, play the movie section (the aim was inducing the experimenter's emotion), third, the subject filled in the table of self-evaluating emotion (aim was to estimate the degree of the emotion). The emotion was divided into five degrees: zero (never), one (a little). two (normal), three (more), four (much).

In this experiment, twelve subjects participated.

3 RESULTS AND ANALYSIS

In the experiment, of all the EEG data from all the channels, the EEG of the frontal area is the most representative, so in this paper, the entire EEG signal was coming from the channel F3. More than four subjects had done the experiments, and the results in this paper were the same for every subject, so the entire EEG signal came from one representative subject.

The condition of the EEG signal used in this paper was as follows:

Time: 6 seconds. Sampling frequency: 500Hz. Number of data: 3000. In the figure, the x-coordinates were time, and unit was second(s). The y-coordinates were value of EEG signal, and unit was microvolt (μ v).

3.1 EEG characteristicss of fatigued driving

The EEGs of normal driving and fatigued driving were are shown in Figures 5 and 6.

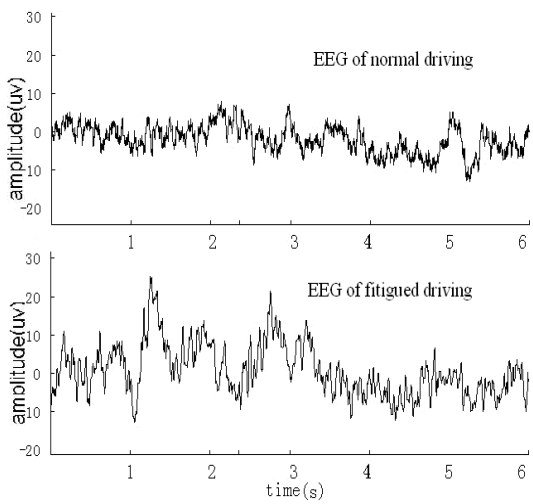

Figure 5. EEG of Normal Driving Fatigued Driving

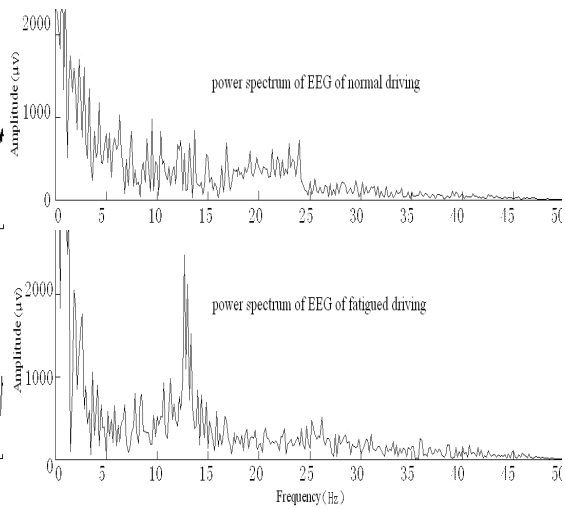

Figure 6. Power Spectrum of of Normal and Fatigued Driving

From Figures 5 and 6, we find that the energy of EEG when the subject was fatigued mainly focused in α-wave, of which the frequency was 10 to 13Hz, and the β-wave reduced much more, of which the frequency was 18 to 22Hz.

By using the method of power spectrum analysis, the characters of fatigued

driving can be obtained (Lin Chinteng et al. 2004). Because the EEG signal was non-linear and the value of correlation dimension was correlative closely to the complicated degree of the EEG signal (Jinghua et al. 1988), we found that when the subject was fatigued, the correlation was smaller than that of normal driving. The reason was that when people are fatigued, their ability to process thoughts is reduced. The value of correlation dimension can also be one EEG characteristic of fatigued driving.

3.2 EEG characteristics of drunken driving

Due to the degree of drunkenness, the EEG of drunken subjects appeared as different shapes and characters. EEG signals are shown in Figure 7.

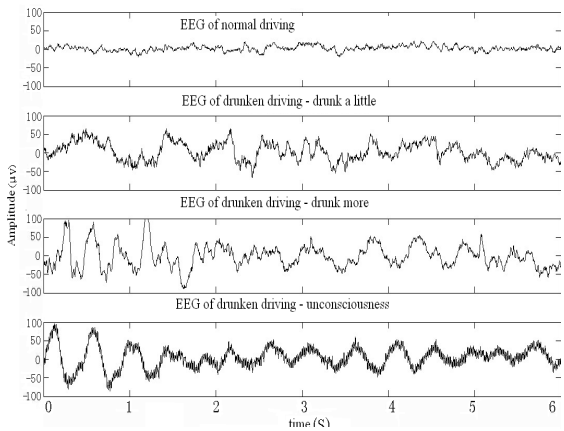

Figure 7. EEG of Drunken Driving

From Figure 7, we find that the EEG signal of drunken driving was different from that of normal driving. When the experimenter had drunk a little, when he was more excited and clear, the value of EEG signal increased much more, both in the low-frequency and high-frequency. But along with the increment of drunkenness, information on the subjects's brain received would decrease, and the random action of the nerve cells in brain would increase. From Figure 7 we find that the δ-wave, of which the frequency was 1 to 2 Hz, can be one EEG characteristic of drunken driving. Two methods of power spectrum analysis and wavelet analysis both can exstract the EEG characteristic. In this paper, the db6 wavelet was used to decompose the EEG signal into 6 parts, the sixth part ca6 represented the δ-wave , which power was as Table 1.

Table 1. Power of ca6 wave of Subjects

experimenter	Normal s	Drank a little	Drank more	Unconscious
1	4.01	12.91	17.70	18.52
2	3.06	13.92	18.73	20.50
3	3.95	15.89	18.65	19.55
4	4.96	13.90	19.66	22.57
mean	3.99	14.16	18.69	20.29

As seen in Table 1, the power of δ -wave of drunken driving was greater than that of normal driving, and along with the increment of drunkenness, the power of δ -wave was even greater. So the power of δ -wave can be taken as one EEG characteristics of drunken driving.

3.3 EEG characteristics of driving in a dangerous emotional state

The EEG signal of one subject in an excited state is shown in Figure 8 and that of the subject in tense and sad state is shown in Figure 9.

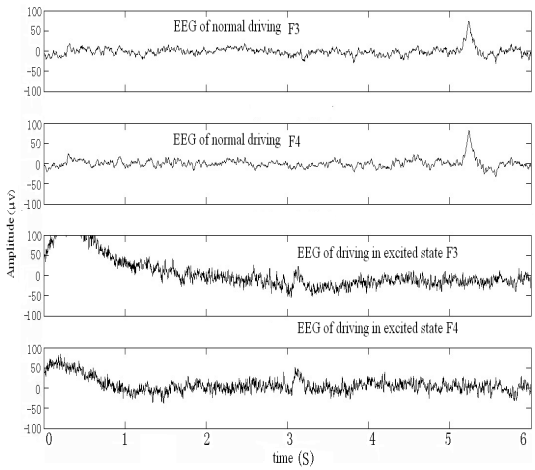

Figure 8. EEG of Normal Driving and Driving in Excited State

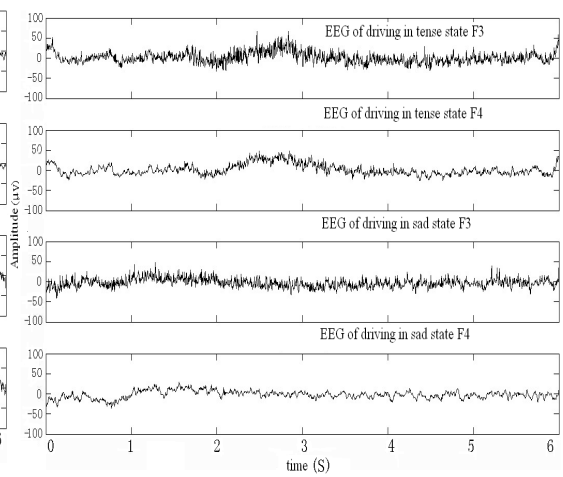

Figure 9. EEG of Driving in Tense and Sad State

As shown in Figure 8, when the subject was in the excited state, both the value and frequency of the EEG signal increased, among that, the β -wave increased more noticeably. As shown in Figure 9, when the subject was in a tense or sad state, the value of the EEG signal from the left frontal area was greater than that from right frontal area.

Table 2 shows the power of β -wave from channel F3 (left frontal area) and F4 (right frontal area), the computing method was wavelet analysis.

Table 2. Power of β-wave in Normal, Excited, Tense and Sad

Experimenter	normal		excited		tense		sad	
	F3	F4	F3	F4	F3	F4	F3	F4
1	1.32	1.83	4.73	4.82	4.37	1.52	4.52	1.29
2	1.35	1.58	4.55	4.49	4.94	1.68	4.82	1.33
4	1.76	1.96	4.86	4.77	5.03	1.49	5.22	1.27
5	1.52	1.63	4.53	4.49	4.51	1.28	4.57	0.91
6	1.55	1.79	4.39	4.22	4.84	1.61	4.76	1.35
7	1.46	1.20	5.02	4.81	4.63	1.42	4.35	1.47
8	1.08	1.13	5.28	5.03	4.99	1.55	5.18	1.58
9	1.21	1.19	4.88	5.02	4.85	1.38	4.66	1.22
10	1.93	1.77	4.97	4.84	5.27	1.79	5.05	1.32
11	1.89	1.46	5.22	5.28	5.33	1.68	4.66	1.59
12	1.90	2.08	4.47	4.38	5.82	2.11	4.83	1.37
mean	1.54	1.60	4.81	4.74	4.96	1.59	4.78	1.34

As shown in Table 2, when the subject was in an excited state, the power of the β-wave was greater than that of when the subject was in normal state. But when the subject was in tense or sad state, the power of β-wave showed asymmetry between the left and right frontal area, and the power of β-wave from the left frontal area was greater than that from right frontal area. So the power of β-wave can be taken as one EEG signal characteristics of driving in dangerous emotional state (Musha et al. 1997; Coan et al. 2003).

CONCLUSION

In this paper, the EEG characteristics of drivers in five dangerous states, fatigued, drunken, excited, tense and sad, were studied. Several EEG characteristics which can reflect the driver's state were discovered.

The research is limited to the lab now, and the experiment results need to be verified by more experiments and more subjects. For the application of EEG information of drivers in ITS, many problems need to be researched, such as how to measure a driver's EEG without influencing the driving, as well as how to abstract and recognize the EEG characteristics in real-time.

Along with the more research on the relation of EEGs to driving and traffic, the ITS will need more useful EEGs of drivers to optimize the traffic network.

REFERENCES

Chin-Teng Lin. (2004). "Assessment of Driver's Driving Performance and Alertness

Using EEG-based Fuzzy Neural Networks." 2004 IEEE International Conference on Systems, Man and Cybernetics. 2004:4034-4040.

Jong Min Lee. (2000). "Characterizing EEG during Mental Activity using Non-linear Measures: the More Concentration, the Higher Correlation Dimension." Proceedings of the 22"d Annual EMBS International Conference, July 23-28, 2000: 342-344, Chicago IL.

James A. Coan, John J.B. Allen. (2003). "The State and Trait Nature of Frontal EEG Asymmetry in Emotion." University of Arizona, 29 June 2003, USA.1113-1117.

Kazuhiko Takahashi. (2004). "Remarks on Emotion Recognition from Bio-Potential Signals." 2nd International Conference on Autonomous Robots and Agents December 13-15, 2004: 118-122, Palmerston North, New Zealand

Musha T. (1997). "Feature extraction from EEGs associated with emotions." Artificial Life and Robotics, 1997,1(1):15-19.

Weiling Xu, Jingxia Huang, Minfen Shen. (2004). "Extracting Time-Varying Rhythms of EEG Signal Based on Wavelet Packet Decomposition." Journal of Data Acquisition & Processing. 2004.19(1) (in Chines)

Short-term Forecasting of Uncertain Traffic States

Zhihua Xiong[1], Zhisheng Yao[2] and Chunfu Shao[3]

[1] MOE Key Laboratory for Urban Transportation Complex Systems Theory and Technology, Beijing Jiaotong University, Beijing, ST 100044; PH (86-010)-51687147; email: zh_xiong@163.com
[2] Beijing Municipal Institute of City Planning and Design, Beijing, ST 100045; email: yzhisheng@126.com.
[3] MOE Key Laboratory for Urban Transportation Complex Systems Theory and Technology, Beijing Jiaotong University, Beijing, ST 100044; email: cfshao@bjtu.edu.cn.

ABSTRACT

Short-term traffic flow forecasting is considered to be the core of intelligent transportation systems and the advanced technical support including traffic information service, traffic control, and guidance. Previous traffic information is on current or predicted traffic states, which are still deterministic and difficult to show with the uncertainty of the road network. Therefore, the analysis of reliability of short-term forecasting is proposed to deal with the uncertainty of traffic.

The reliability of short-term forecasting is described as a range of forecast values which show the deviation between forecast value and the measure. A state space model is used in this paper and the Monte Carlo method is performed to deal with uncertainty, where a random sample of traffic flow within a probability distribution is generated until at a steady state. Results show that the proposed model can reduce the disturbances between the forecast and actual traffic.

INTRODUCTION

Even though intelligent transportation systems are developing quickly all over the world, there is no comprehensive theory to support the intelligent transportation system (ITS) which affects the development of ITS technologies and the efficiency of travel. Based on modern information, communication, networking, and computer technologies combined with the conventional traffic flow theory, a comprehensive theory can be obtained which is suitable for ITS. Short-term traffic forecasting determines the traffic state in the next time window, based on the current time window or previous time windows and is a theory-supported practice in the field of traffic information service, traffic guidance, traffic management and relaxing traffic congestion.

Earlier attempts to obtain short-term traffic states primarily depended on linear models, such as historical trends, time series, and the Kalman filtering

approach. Next, wavelet and fractal theory emerged which are used to handle complex and nonlinear optimization problems. Forecast models based on artificial intelligence, such as neural networks evolved rapidly and a combination of two or more methods was created. Various approaches have been developed to forecast traffic states, but they usually obtain only a single future value rather than a range. However, transportation networks are disrupted by natural or man-made disasters or more commonly by routine events, such as congestion, collisions, and road maintenance. The uncertainty of travel exists due to these unexpected things. Traffic states at a given location may vary from day to day and a single value is difficult to show with certainty.

Therefore, a range of forecast values is proposed to show the comprehensiveness of the forecast model in dealing with such uncertainty. The Monte Carlo method is joined with the forecast model to deal with both the day-to-day recurrent traffic patterns and the real-time fluctuation, while the state space model is performed iteratively to obtain the range of forecast values and show the variability of the road network. The proposed model can generate traffic forecast values with reasonable accuracy.

SHORT TERM FORECAST BADED ON STATE SPACE MODEL

The state space model by R.E. Kalman is widely used in the field of traffic flow forecast. The forecast value can be obtained by the recursive relation of system state x_n and transfer equators between x_n and the observed y_n. It is expressed as:

$$x_n = F_n x_{n-1} + G_n v_n$$

$$y_n = H_n x_n + w_n$$

where x_n is the k dimension system state vector of n period of time and unable to be observed directly; u_n is r dimension system input vector of n period of time; v_n is system noise of n period of time and a zero mean white noise source with m dimension variance matrix Q_n, $Q_n = E(v_n v_n^T)$; y_n is j dimension observation vector; w_n is observed noise and a zero mean white noise source with j dimension variance matrix R_n, $R_n = E(w_n w_n^T)$; F_n, T_n, G_n and H_n are $k \times k, k \times r, k \times m, j \times k$ dimension coefficient matrix, state transfer matrix, input coefficient matrix, noise transfer matrix and observed matrix respectively.

The relationship between any period of time and previous p periods of time exists in time series $\{x_t\}$ made of observed sample $x_1, x_2, \ldots, x_N$ and can be

described by the state space model. The Kalman filtering algorithm is an efficient way to solve the state space model based on the linear minimum variance estimation theory. See references (Brockwell and Davis, 2001; Deng, 2005; Yao, 2007) for a complete description.

The algorithm can be shown as follows: (1) Identify initial coefficient matrix, initial system state x_0 and variance matrix V_0. Because the statistical distribution of system states are difficult to gain in practice, an autoregressive parameters estimation of the AR model which is made of observed samples is used to get these initial values by the Yule-Walker estimation and AIC criterion. For details see attached reference (Digalakis , Rohlicek and Ostendorf, 1993; Sun, Chen and Liu,2002). (2) Perform recursive relation of system state as previously mentioned. (3) Revise system state according to observed vector filter. (4) Determine convergence and output; otherwise, return to step 2.

UNCERTAINTY OF SHORT TERM FORECAST

The deviation of actual versus forecast values exists because of numerous factors, primarily imperfect data, model errors, and road network variability. With the development of traffic science and technology, automatic acquirement devices set on the roads have improved constantly, which makes it possible to perform short-term traffic flow analysis and forecasting accurately. Various models are dedicated to reducing error. However, the uncertainty of the road network is seldom considered in the process of performance and the forecast values are unable to show the comprehensiveness of the model in dealing with such uncertainty. Previous attempts to perform short-term forecasts make sure to fit the actual value. But the forecast value is not consistent with the actual value, no matter how accurate the model or perfect the data are. Therefore, reliability of forecast is proposed to show the ability of the model to deal with uncertainty, which is defined as the forecast value within the given range under uncertainty.

The day-to-day variations in travel demand and supply are disrupted by many sources ranging from daily fluctuation to unexpected events. If the variation can be assumed, the performance of the road network under uncertainty can be easily determined. Traffic volumes obey normal distribution which was demonstrated by Bell and Iida (1997) according to numerous detective data. The reliability is the probability of traffic volume not exceeding its capacity. The relation between its mean and variance is recommended (Yamada, Yoshimura and Mori, 2003):

$$\sigma = h_1 \times \mu^{h_2}$$

where $h_1 = 0.360, h_2 = 0.821$ is parameter respectively, μ, σ is mean and variance of

any link traffic volume.

RELIABILITY OF FORECAST

The MC method is usually used in reliability analysis. When multiple trials are performed, the range of measure value can be obtained by its probability distribution. To give an accurate range to show the reliability of forecasts, 95 percent traffic volume is recommended. It can be considered as the tolerance range not allowing to be exceeded and showing the probability that traffic volume may be within the range is 95 percent. That is to say, the traffic volume can only exceed the range once in twenty times.

The algorithm to determine the forecast reliability is as follows:

Step 0: Initialization. Set n=1.

Step 1: Establish short-term forecast model. The state space model is proposed as before.

Step 2: Perform state space model. A value that used to be the forecast value can be obtained which is only an initial value in the process of reliability analysis.

Step 3: Generate the stochastic variable. Traffic volume is assumed to be at normal distribution. Its variance can be obtained according to the analysis of uncertainty. A forecast value is made of the initial and the stochastic term.

Step 4: If $n < n_{\max}, n = n + 1$ go to Step 1.

Step 5: Obtain the upper and lower value of the forecast range, which is 95 percent of the statistics after many experiments.

ILLUSTRATION

To illustrate the reliability of forecast, we used traffic volume data from an expressway form 09/01/2007 to 09/11/2007, where time interval is 2 minutes. Data is divided into two parts, one from 09/01/2007 to 09/10/2007 to establish a forecasting model, the rest to fit the outputs of the forecasting model.

There is a time interval on the x axis which represents the whole day (24 hours) and traffic volume is shown on the y axis. The outcome of the state space model is shown in Figure 1(a). Mean absolute percentage errors (MAPE) of the model are shown in Figure 1(b). We can see that MAPE are high, especially in the first half of the x-axis when there were fewer vehicles because it was late at night.

The difference between a measured value of performing MC 500 times and the value of 1000 times is shown in Figure 2. The formula of measure value can be expressed as:

$$Transition = \begin{cases} 0, if \quad Lower < True < Upper \\ \min(abs(Upper - True), abs(True - Lower)), \quad other \end{cases}$$

$$Measure \quad value = \frac{Transition}{Ture} \times 100\%$$

where Upper and Lower is 95 percent traffic volume from MC trials and True is the actual value.

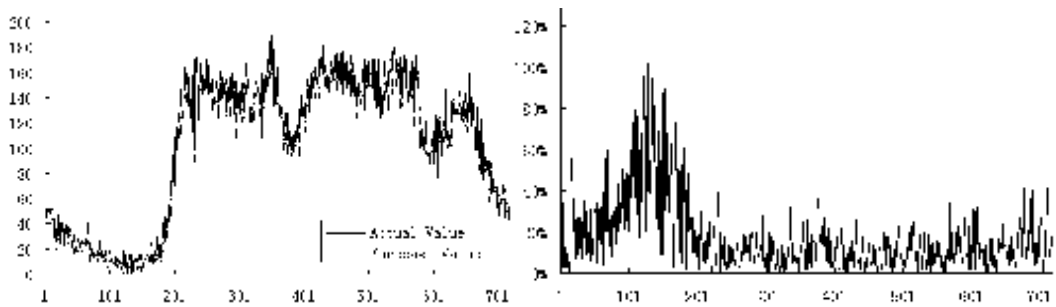

(a) (b)

Figure 1. Forecast value of state space model

Monte Carlo circulating frequencies (500 and 1000) can influence the accuracy of the forecast. It shows that the range was closer to actual values with the number of MC trials increasing.

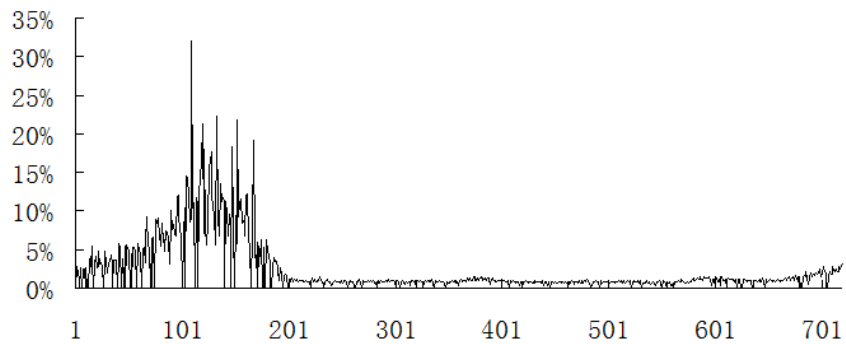

Figure 2. The effect of circulation frequency

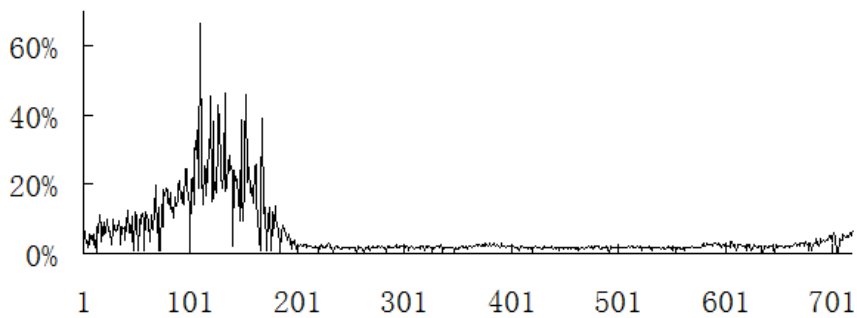

Figure 3. The effect of two methods

Figure 3 reflects the measure value of two methods. One is the MC method and the other is the traditional state space model. The MC approach performs better than traditional one, especially in the early time of day. Therefore, the proposed way to give an accurate range of forecast values may be more accurate than the traditional models and can show the capacity of the model dealing with uncertainty.

CONCLUSION

Short-term traffic state forecasting is one of the most critical aspects in ITS. Traditional methods seldom take the uncertainty of the road network into consideration. An accurate range of forecast values can be obtained by the MC method to show the uncertainty of the road network. The proposed approach performs better than the traditional one. More research is needed to verify the reliability of short-term forecasts.

ACKNOWLEDGMENTS

This research is sponsored by the National Nature Science Foundation of the People's Republic of china (No. 50578009), 973 Program (No. 2006CB705500).

REFERENCES

Bell M. G. H. and Iida Y. (1997). "Transportation network Analysis". John Wiley & Sons, New York.

Brockwell Peter J., Davis Richard A. (2001). "Time series: Theory and methods", Academic Press, 2rd edition, 314-386.

Deng Z. L. (2005). "Optimal Estimation Theory with Applications——Modeling, Filtering and Information Fusion Estimation", the Press of Harbin Institute of Technology, Harbin.

Digalakis V., Rohlicek J. R., Ostendorf M. (1993). "ML Estimation of a Stochastic Linear System with the EM Algorithm and Its Application to Speech Recognition". *IEEE Transactions on Speech and Audio Processing,* 1(4):431-442.

Sun Da-fei， Chen Zhi-guo, Liu Wen-ju.(2002)." Discussion of M aximum Likelihood Parameter Estimation Based on EM Algorithm". *Journal of Henan University(Natural Science)* ,32(4):35-41.

Yamada T ., Yoshimura Y., Mori K. (2003). "Road Network Reliability Analysis Using Vehicle Routing And Scheduling Procedure". *Proceedings of the 3rd International Conference on City Logistics,* Madeira, Portugal.

Yao Z.S. (2007) "Research on Theories and Methods of Short-term Traffic Flow Forecasting of Road Network Based on Real-time Data", Beijing Jiaotong University.

Dynamic Model of Transit Signal Priority on Colored Time Petri Net

Ciyun Lin[1], Zhaosheng Yang[1], and Bowen Gong[1]

[1] Department of Traffic and Transportation, Jilin University, Changchun, Jilin, China, ST 130022; PH (+86) 0431-85095767; FAX (+86) 0431-85095767; email: linciyun@email.jlu.edu, yangzs@jlu.edu.cn, gongbowen1982@gmail.com

ABSTRACT

A dynamic coordination strategy model of the transit signal priority and traffic signal control cooperative system is created by using Colored Time Petri Nets (CTPNs). To extend the coordination from isolated intersections to the arterial network of intersections, a multi-level and multi-group computer supported cooperative system is described based on CTPNs. Then inter-intersection and cross-intersection coordination strategy for busses and vehicles was proposed to model transit signal priority in urban networks.

INTRODUCTION

Traffic management systems address the problem of reducing congestion, vehicle delay time, fuel consumption, and pollution. The most common technique to regulate and manage urban traffic areas and surface street networks is traffic signal control (Dotoli and Fanti 2006). Traffic signal control plays a central role in modern urban traffic management (Dotoli et al. 2003).

Public transit, with the advantages of large capacity, reduced road occupancy, low fuel consumption and so forth, is considered to be one of the most effective ways to solve urban transportation problems (Han and Liu 2008). Transit signal priority (TSP) is a direct way to improve public transit service levels and attract residents to use public transit.

In traffic control systems, general vehicle signal control and transit signal priority control share resources, resource conflicts, a tendency to deadlock and overflow, and require well-planned synchronization and scheduling. They are controlled to achieve satisfactory performance which includes reduced travel time for transit customers, improved schedule adherence and side-street traffic, and the smooth flow of traffic. (Dotoli et al. 2006). Therefore, it is of practical importance to develop, verify and, validate simple, yet powerful models that help to design and improve the safety and efficiency of traffic signal control systems. Petri nets have been proven to be a powerful modeling tool for various kinds of discrete event systems (Chung and Huang 2007). Compared with other analytical and simulation methods, Petri nets have the following advantages (Dos Santos Soares and Vrancken 2007; Wang et al. 1999):

1) Petri nets can easily express concurrency, competition, and synchronization activities among traffic, TSP and traffic control

2) Petri net modeling allows easy changes to be made to the network configuration, the traffic signal control logic, timing and coordination, and the assumptions on intersection physical layout, vehicle flow rate, turning movement,

pedestrian movement, etc.

3) Petri net models are mathematically defined, which makes it possible to verify that the control logic enforces all required, ensuring that capacities are not exceeded and that gridlock will not occur as a result of the logic and timing.

In this paper, a dynamic coordination strategy model of the transit signal priority and traffic signal control cooperative system is created by using Colored Time Petri Nets (CTPNs). To extend the coordination from isolated intersections to arterial networks of intersections, a multi-level and multi-group computer supported cooperative system is described based on CTPNs. Compared to isolated intersections, it not only provides coordination strategy and priority plan for inter-intersection relations, but also coordination priority strategy and signal plan for cross-intersection relations.

THE DESCRIPTION OF THE BASIC COLORED TIME PETRI NET

A CTPN is defined as a bipartite directed graph represented by $CTPN = (\sum, P, T, A, N, C_o, G, E, R, I)$. Where $\sum$ is a finite set of non-empty types, called color sets; P is finite a set of places; T is finite a set of transitions; A is a finite set of arcs, such that $P \bigcap T = P \bigcap A = A \bigcap T\varnothing$; N is a node function. It is defined as $N : A \to (P \times T \bigcup T \times P)$; C_o is a color function that associates with each element in $P \bigcup T \neq \varnothing$ a set of colors in the set of possible colors Cl. C_o maps each place $p_i \in P$ to the set of possible token color $C_o(p_i) = \{a_{i,1}, a_{i,2}, \cdots, a_{i,ui}\} \subseteq Cl$, where $u_i = |C_o(p_i)|$ is the number of possible colors of tokens in p_i. Analogously, C_o maps each transition $t_i \in T$ to the set of possible occurrence colors $C_o(t_j) = \{b_{j,1}, b_{j,2}, \cdots, b_{j,uj}\} \subseteq Cl$ with $u_j = |C_o(t_j)|$. $G : T \to$ is a T guard function and $E : A \to$ is an arc expression function. R is the set of time values $R = (r_i / p_i \in P)$; I is an initialization function (Tian et al. 2003) . The detailed description of $CTPN$ can be seen in (Hrúz and Zhou 2007).

MODELING TRAFFIC SIGNAL CONTROL WITH TSP BASED ON CTPN

Urban Traffic Networks

In urban traffic networks, signalized intersections, links, vehicles and traffic signal lights whose signal plan is controlled by a traffic signal control system are the fundamental components. In CTPN model, a place $p_i \in P$ denotes a resource, corresponding to link cells and intersection cells. Five types of links are considered:

1) input links $L_i \in L_{in}$, which vehicles input to the traffic signal control network

2) intermediate links $L_i \in L_{\text{int}}$ which join two successive signalized intersection

3) output links $L_i \in L_{out}$, which vehicles exit the traffic signal control network

4) signalized intersection $I_i \in I_{sig}$

5) un-signalized intersection $I_i \in I_{unsig}$

In addition, transitions from T are timed transitions and model the flow of

vehicles into the system between consecutive cells. Five types of transitions are considered (Dotoli et al. 2004):

1) input transitions $t_{o,i} \in T_I$, modeling the arrival of a vehicle in a link from the outside of the considered intersection

2) output transitions $t_{i,o} \in T_O$, modeling the departure of a vehicle from a link to the outside of the considered intersection

3) flow transitions $t_j \in T_F$, modeling the flow of vehicles between two consecutive link cells

4) intersection transitions $t_j \in T_C$, modeling vehicles entering or leaving a cross section. The intersection transitions that model a vehicle entering the crossing sections are regulated by a multi-phase traffic signal or transit signal priority plan

5) lane changing transitions $t_j \in T_L$, modeling vehicles that change lanes in the road

The value of FT_j assigned to each $t_j \in T_O \cup T_F \cup T_C$ is equal to the average time interval in which a vehicle passes from a cell to the subsequent one or occupies an intersection cell. This depends on the average vehicle speed in the considered traffic scenario.

A colored token in a place represents a vehicle. The color of each token is the routing assigned to each vehicle indicating the different paths that a vehicle can follow starting from a particular position. For instance, a priority bus has a different color than a general vehicle. Their paths across the intersection also have different respective colors.

Matrices $Pre(p_i,t_j)$ and $Post(p_i,t_j)$ are determined by physical layout of the intersection, traffic organization, and signal phase numbers at intersection.

Inter-intersection Coordination Strategy for Busses and Vehicles

Transit signal priority is taken into account to achieve efficient performance. But this does not mean that transit signal priority is allowed to provoke perturbations in the normal traffic signal plan without any consideration. It makes sense to optimize the performance indices of the overall traffic, for instance, shortening and equalizing the queues at the intersections. The aim of inter-intersection coordination strategy is to coordinate busses and vehicles reasonably to share and use the limited resources of signal time and intersection space. We use a controllable time-sharing strategy to coordinate bus and vehicle signals (Ni et al. 2001).

The basic idea is that if bus traffic or vehicle traffic wants to obtain or occupy the signal resource and intersection's place resource, it must have a public token. The number who can obtain the token is defined as a focus point which can use the resource at a specified time without interruption unless it abandons the token voluntarily. The token's application and availability are determined by a coordination chair. If the token is in effect, insert into the FIFO application queue. If the token runs out of time and the queue is not empty, the token turns to queue lead

and lets the lead member occupy the resource. The coordination strategy process is demonstrated in Figure 1.

The problem of managing a transit signal priority request in inter-intersection relations is solved by a simple control algorithm described as follows (Di Febbraro et al. 2004):

Step 1: let T_{ask} be the instant at which a bus requests for signal priority and T_{arr} the time the bus is expected to arrive at the intersection.

Step 2: if at T_{arr}, the signal phase for the direction of priority comes from is expected to be green, then there will be no need for intervention. Exit the algorithm.

Step 3: if the red signal is expected, the local controller has to decide (Lin 2007)

Step 3.1 Green Extension: extending the current green time until the bus crosses the intersection

Step 3.2 Early Green: anticipating the next green time, shortening the current red one accordingly

Step 3.3 Phase Insertion: bus forward direction inserting a phase which can be used for bus and vehicle

Step 3.4 Actuated Bus Phase: inserting a phase which can only be used for the bus

Step 3.5 Phase Rotation: changing the signal phase sequence accordingly

Step 3.6 Phase Skipping: jumping a signal phase, and switching to implement the phase so that the bus can cross the intersection

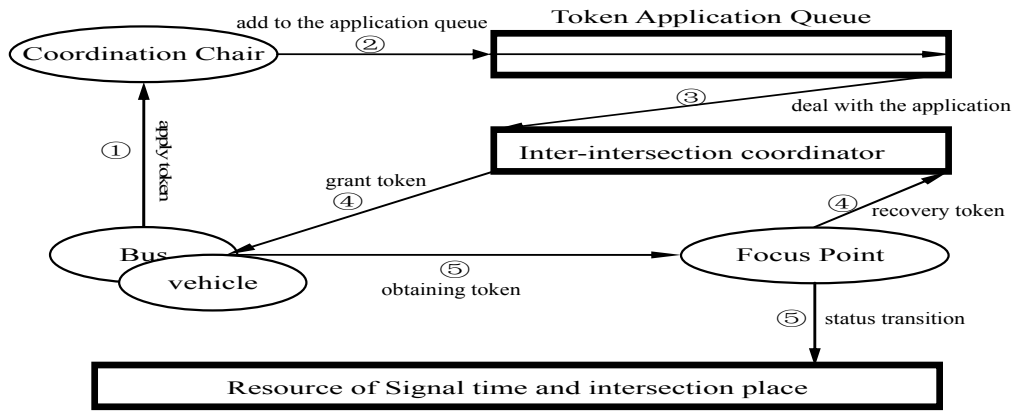

Figure 1. Processing of inter-intersection coordination strategy.

Note that above strategies are subject to (Long 2008):

$$\min d_p = \sum_{i=1}^{n}\sum_{j=1}^{m_i}(d_{ij}Q_{ij}^{V}P_V + d_{ij}Q_{ij}^{B}P_B) / \sum_{i=1}^{n}\sum_{j=1}^{m_i}(Q_{ij}^{V}P_V + Q_{ij}^{B}P_B)$$

$$S.T.\begin{cases}\sum_{i=1}^{n} g_i + L = C \\ C_{\min} \le C \le C_{\max}\end{cases} \tag{1}$$

Where d_p is the average delay per passenger; d_{ij} is the average delay per vehicle at approach j and phases i; Q_{ij}^V Q_{ij}^B are the traffic volume of general vehicles and bus respectively at approach j and phase i; P_V, P_B are the average passengers loaded on vehicle and bus respectively. n is the phase number of intersection, m_i is the number of approach during phase i; g_i is green time for phase i, L is the loss time, C is the cycle time, $C_{\min}$ and $C_{\max}$ is the minimum and maximum value of cycle time.

Cross-intersection Coordination Strategy for Bus and Vehicle

We now address cross-intersection coordination strategy of controlling traffic in an urban transportation network so as to increase the performances of public transit. The main objective is to minimize the travel time from the bus origin station to the destination, in order to maximize the efficiency of the bus. The basic idea is that the supervisor divides the task into several sub-tasks, and delegates the sub-tasks to different local controllers. The local controller uses inter-section coordination strategy for cooperation, optimization of the signal plan, and implementation of priority requests. The role of supervisor is to coordinate the work flow of sub-tasks, control resource access, and resolve conflicts. The procedure is described as follows:

Step 1: when a priority vehicle requests, at T, for signal priority, it communicates its location, direction and schedule to the supervisor; then, the supervisor deliberates, through knowledge of the traffic conditions over each arc of the arterial and bus status at T.

Step 2: the supervisor asks the corresponding priority controller to solve the priority control problem, providing guidance on whether or not to provide signal priority and decide when (the time instant) and how (priority strategy) to provide priority for the bus.

Step 3: each local controller solves the local problem described and determines its own optimal timing plan due to the minimize cost function:

$$\min R = (\sum_{i=1}^{n} D_i^{SP} - \sum_{i=1}^{n} D_i^{Int}) / \sum_{i=1}^{n} D_{Int} < \delta \tag{2}$$

Where R is delay ratio, D_i^{SP} and D_i^{Int} is i^{th} intersection's total vehicle delay with and without bus signal priority respectively, δ is a constant defined by traffic control manager.

Step 4: the supervisor computes the real travel time T_{bus} on the basis of the traffic conditions and the traffic signal timing plans determined in Step 3. If $T_{bus} > T_{plan}$, then go to Step 2. Otherwise, go to Step 5.

Step 5: among all the possible priority strategies, the supervisor chooses the best priority strategy. Then it communicates to the responding local controller and the priority bus.

SIMULATION

For the purpose of analysis, a simple simulation of an urban traffic network is used to verify the model. The traffic network consists of four signalized intersections. For simplification, all signalized intersections have four basic phase transition and

six priority phase strategies which are described above.

The TCPN model is implemented and simulated by CPN Tools. CPN Tools are tools for editing, simulating, and analyzing Colored Petri Nets (CPN Group 2007). Figure 2 shows a snapshot of a CTPN model of this paper in CPN Tools. In order to compare model performance of this paper, the priority logic is simulated in PARAMICS V6 which is a famous microcosmic simulator in traffic engineering.

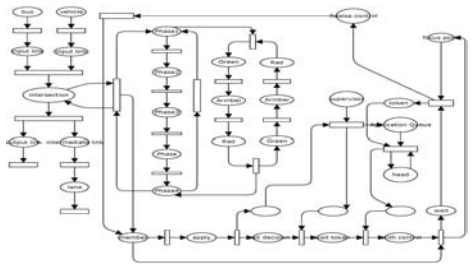

Figure 2. A snapshot of the CTPN model in CPN Tools

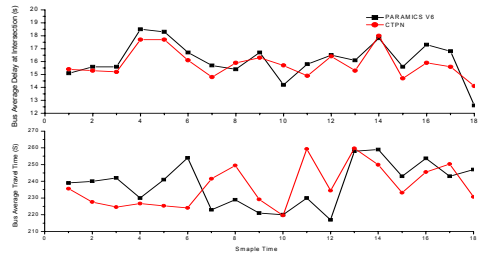

Figure 3. Bus average travel time, delay at intersection in CTPN and PARAMICS

In summary, the simulation results are similar to the PARAMICS results. Figure 3 shows the bus's average travel time and signal delay at the intersection in CTPN and PARAMICS V6.

CONCLUSION

This paper describes the processing of transit signal priority control in urban traffic networks based on CTPN models. A coordination model of the multi-level and multi-group system using CTPN is proposed, which worked when using inter-intersection and cross-intersection cooperation. CTPN was applied to four successive signalized intersections of simulated urban traffic networks. Finally, the CTPN model's performance was compared with the simulation of PARAMICS V6. Briefly, we can conclude that the traffic signal control system with transit signal priority can be implemented by the CTPN model and perform successfully..

ACKNOWLEDGEMENT

The authors wish to thank the National High-tech R&D (863 Program) with the grant No. 2007AA12Z242 and 2007AA11Z218.

REFERENCES

Chung, T., and Huang, Y. "Design of a supervisor for traffic light systems." *11th International Conference on Knowledge-Based and Intelligent Information and Engineering Systems, KES 2007, and 17th Italian Workshop on Neural Networks, WIRN 2007*, Heidelberg, D-69121, Germany, 704-711.

CPN Group, U. O. A. D. (2007). "CPN TOOLS--Computer Tool for Coloured Petri Nets.".

Di Febbraro, A., Giglio, D., and Sacco, N. (2004). "Urban traffic control structure based on hybrid petri nets." *IEEE Transactions on Intelligent Transportation*

Systems, 5(4), 224-237.

Dos Santos Soares, M., and Vrancken, J. "Scenario analysis of a network of traffic signals designed with Petri nets." *13th International Conference on Urban Transport and the Environment in the 21st Century, URBAN TRANSPORT 2007*, Southampton, SO40 7AA, United Kingdom, 289-297.

Dotoli, M., Fanti, M. P., and Meloni, C. "Real time optimization of traffic signal control: Application to coordinated intersections." *System Security and Assurance*, 3288-3295.

Dotoli, M., Fanti, M. P., and Meloni, C. "Coordination and real time optimization of signal timing plans for urban traffic control." *Conference Proceeding - 2004 IEEE International Conference on Networking, Sensing and Control*, Piscataway, United States, 1069-1074.

Dotoli, M., Fanti, M. P., and Meloni, C. (2006). "A signal timing plan formulation for urban traffic control." *Control Engineering Practice*, 14(11), 1297-1311.

Dotoli, M., and Fanti, M. P. (2006). "An urban traffic network model via coloured timed Petri nets." *Control Engineering Practice*, 14(10), 1213-1229.

Han, Q., and Liu, Z. "Research on real-time control strategy of intersections in ITS based on bus priority." *7th World Congress on Intelligent Control and Automation, WCICA'08*, Piscataway, NJ 08855-1331, United States, 7653-7656.

Hrúz, B., and Zhou, M. C. (2007). *Modeling and Control of Discrete-event Dynamic Systems: with Petri Nets and Other Tools*, Springer, London.

Lin, C. (2007). "Study on Bus Signal Priority System Design and Implementation," , Jilin University.

Long, K. "Bus priority signal control at isolated intersection." *International Conference on Intelligent Computation Technology and Automation, ICICTA 2008*, Piscataway, NJ 08855-1331, United States, 234-237.

Ni, X., Li, R., and Zheng, Q. (2001). "Modeling of Coordination Policy Based on Coloured Petri Nets." *Journal of Xi an Jiaotong University*, 35(10), 1004-1007.

Tian, F., Li, R., and Zhang, J. (2003). "Modeling and Performance Evaluation of Collaborative Works Based on Timed Colored Petri Net." *Journal of Xi an Jiaotong University*, 37(06), 560-564.

Wang, J., Jin, C., and Deng, Y. "Performance analysis of traffic networks based on Stochastic Timed Petri Net models." *Proceedings of the 1999 5th IEEE International Conference on Engineering of Complex Computer Systems (ICECCS'99)*, Piscataway, NJ, USA, 77-85.

Bus Location Display System Based on GPRS

Song Gao[1], Ling-yong Zhang[2], and Lei Zhong[3]

[1]School of Transportation and Vehicle Engineering, Shandong University of Technology, 12 Zhangzhou Rd. Zibo,China,P.O. Box 255049, PH (86)533-2786028; FAX (86) 533-2786837; email: gs6510@163.com
[2]School of Transportation and Vehicle Engineering, Shandong University of Technology, 12 Zhangzhou Rd. Zibo,China,P.O.Box 255049, PH (86)533-2786028; FAX (86) 533-2786837; email: zhanglingyong3@163.com
[3]School of Transportation and Vehicle Engineering, Shandong University of Technology, 12 Zhangzhou Rd. Zibo, China, P.O.Box 255049, PH (86)533-2786028; FAX (86) 533-2786837;email: zhonglei10086@163.com

ABSTRACT

We introduce a systematic design plan for an urban bus location display system based on GPRS. It adopts special APN transmissions as a GPRS communication project. The system consists of four modules: bus wireless terminals, bus-location display terminals, bus company data center, and GPRS network. In this paper, the development of the database and data processing key algorithm of the bus data center are introduced, and the development of wireless terminals as well as communication protocols between the bus data center and the wireless terminals are presented. An innovative data-sending algorithm of bus location information based on the bus's sequence is presented. Tests show that this system can display the location of the nearest bus in each bus station which indicates how far the closest bus is from this site. This system can be used as a subsystem for a bus scheduling system.

INTRODUCTION

With the rapid development of ITS and popularization of new technology in China, the bus location display system is used more and more as an important component of ITS (*Tang Xin-zhou, 2006*), especially for the bus transportation systems in small and medium-sized cities. As a result of low road network density and long time interval between regular buses, it is necessary that the bus location display system provides the location of the nearest bus to the station.

Owing to the bus's constant movement, wireless communication technology is the key to creating the bus location display system. GPRS (General Packet Radio Service) is a kind of data service for wireless data transmission based on GSM. It can provide continuous and timely information service, which makes the spatial data from the bus unit packed to send and receive (*Zhang, 2006*). GPRS wireless networks provided by Mobile Company covers every city, so it is a better choice to use GPRS as a communication link of the displaying system.

SYSTEM ARCHITECTURE AND PRINCIPLES

The system functions are as follows: displaying the location of the nearest bus in each bus station, which indicates that how far the most recent bus is from the site. If necessary, voice prompts can be addd according to the condition. It can be used as a subsystem of a bus scheduling system.

System Architecture. The overall structure of the system is shown in Figure 1.

The system consists of four modules: bus wireless terminals, bus-location displaying terminals of bus station plates, bus company data center, and GPRS Network (APN private network) (*Motorola Engineering Institute, 2005*). Current bus location information is sent to the data center by the bus wireless terminal through the GPRS network, processed by the data center, and sent to the bus-location displaying terminals of bus station through the GPRS network. Bus wireless terminals and bus-location displaying terminals of bus stations are called wireless terminals.

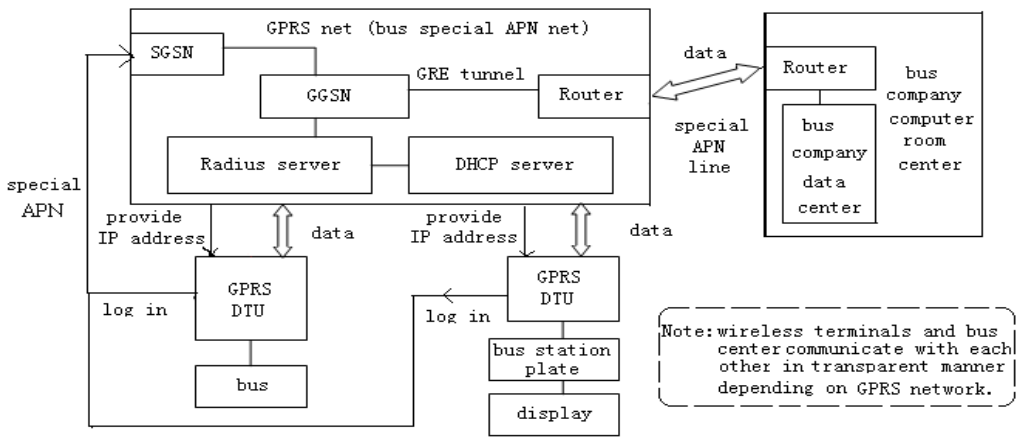

Figure 1. Overall block diagram of the system

GPRS is a kind of advanced mobile data communication. It has some special advantages compared to other data communication, for example: it has wide coverage, high transfer rate, short accessing time, it is always on, and charged by data flow. A vehicle monitoring system has frequent data flow in small amounts and requests rapid responses. Therefore GPRS is very suitable for data transmission for the vehicle monitoring system.

GPRS Communication Project. APN (Access Point Name) is a kind of wireless DDN service provided by China Mobile Company for GPRS users. APN consists of public the APN and special APNs. The consumers, who do not apply for special APN, only log onto the public APN by common SIM card. They log on the CMNET or CMWAP domain, and receive IP address 10.xxx.xxx.xxx. However, they cannot transmit data each other.

When one has applied for a special APN, he will obtain the accounts of the special APN from Mobile Company and a domain on GGSN (Gateway GPRS Support Node) nodes. Special SIM cards, for the service, are bound in this domain. When the consumers logs in, GGSN needs to check the accounts for the SIM card. If they are all right, a designated IP address would be allocated to SIM card. They can transmit data each other. One cannot call a special APN using public SIM card.

In this system, the special APN is adopted. The bus company would apply for a special APN which only could be used for the bus company, and is linked to the GPRS network of Mobile Company by the special APN line. The mobile company provides a private IP address for the bus center which is connected by special cable to the GGSN equipment of GPRS network. Wireless terminals would use the accounts of the special bus APN to log onto the GPRS net and obtain an IP address. In this way, the bus data center communicates with wireless terminals in the GPRS network.

Wireless terminals would make use of unified GPRS SIM card of Mobile Company, and the information is registered by the bus data center in order to identify them.

System Principles. Depending on GPRS networks, the wireless terminals and the bus center are linked in a wireless local area network, which has no distinction from wired LAN. They transmit data with each other relying on Socket and TCP/UDP technology.

The bus data center operates as the monitoring server (TCP/UDP) in the system, which establishes TCP connections with all wireless terminals. The center collects location information from all buses depending on their TCP program, and classifies the data to insert into the database, then processes the data by a data processing algorithm. At last the system sends the results to the terminals of bus stations which display the nearest bus location information.

Before bus departure, each wireless terminal is initialized, and the wireless terminal's information such as IP address is inserted into the data center's database. After departute, the bus location information from the same bus route is put into the same data table. Bus location information data sheets are associated with station data sheets through the station ID number. Bus location information of the same bus route is sorted according to its current location with station ID in each route table. The driver will press the arrival button when the bus has arrived at a station, so we can know the bus's location. Every time bus stops at a station, the bus terminal will send information to the data center, and the data center sorts the bus information by location or running sequence. The location information is displayed by LED in the bus stations.

In order to use this network effectively, Mobile Company does not require the GPRS to be on always. If there is no GPRS data exchange for some time, users will drop out of the GPRS network. The re-dial-up will bring additional data traffic,

which will have an impact on the real-time transmission. So "heartbeat packet technology" is carried out in the system, which sends a number of bytes of data to the GPRS network from time to time to ensure that it is always on (*Liu, 2006*).

BUS DATA CENTER DEVELOPMENT

Database Design of Bus Data Center. The database of the bus company data center includes two static data tables: bus route station name table (see Table 1) and bus route vehicle table (see Table 2), two dynamic tables: bus location collection table (see Table 3) and bus location station table (see Table 4). The contents of static data tables will not be changed until the amount of vehicles and station terminals are changed.

In order to facilitate the realization of the system, the system sorts the bus station terminal of each route by ascending serial number (see Figure 2). Because the bus is traveling in two ways, the serial numbers of bus station in diffirent directions are sorted together. In Figure 2, except the starting and terminal station, the intermediate stations are in pairs. Although they have the same station name in Figure 2, due to the different direction, the bus station terminal and SIM card number are different.

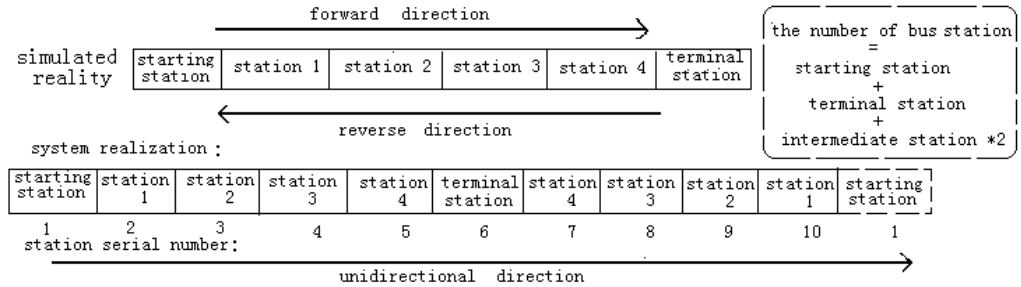

Figure 2. Compositor method of bus station

The abbreviations of database fields are shown in Table 5.

Table 1. Bus Route Station Name.

BR	SS	TS	AS	S1	SS1	S2	SS2	S3	SS3	S4	SS4	S5	SS5
2	A	C	4	A	13X	B	13X	C	13X	B	13X	A	13X

Table 2. Bus Route Vehicle.

BR	AB	BI1	SB1	BI2	SB2	BI3	SB3	BI4	SB4	BI5	SB5
2	5	XX	13X	XX	13X	XX	13X	XX	13X	XX	13X

Table 3. Bus Location Collection.

Running Sequence	BR	SB	CSN	BTIP	Time	WU
1	2	13X	1	10.X.X.X	9H30M	N
2	2	13X	3	10.X.X.X	9H31M	Y
3	2	13X	5	10.X.X.X	9H30M	Y

Table 4. Bus Location Station.

BR	SN	SS	STIP	MSRBS	Time	WSS
2	1	13X	10.X.X.X	2	9H31M	N
2	2	13X	10.X.X.X	3	9H31M	Y

When the system is working, the number of records remains unchanged in Table 3 and in Table 4, and the contents of the first three fields are also invariable, but the contents of other fields may be updated at any moment.

Table 5. Field Abbreviations.

Field abbreviation	Signification
AB	amount of buses
AS	amount of station
BI(X)	identification number of bus X
BR	bus route
BTIP	IP address of bus wireless terminal
CSN	current station number
MSRBS	how many stations the recent bus is from current station
SB(X)	SIM number of bus X
SN	station number
SS	starting station name
S(X)	station X name
SS(X)	SIM number of station X
STIP	IP address of station wireless terminal
TS	terminal station name
WSS	whether has been sent to the wireless terminal of station
WU	whether the information has been updated in the bus-location-station table

Data Processing key Algorithm of Bus Data Center. Considering the requirements of real-time, economics, and technical feasibility, it is not advisable to transmit the location information of each bus to the correlative wireless terminals of the bus station.

Since buses run in an orderly sequence, all buses of each route can be ordered in running sequence and be stored by records (see Table 3). Depending on Table 3, the system only sends the current bus location to the "empty" station terminal between two buses, as shown in Figure 3. A bus "parked" at a certain station, means the bus is stopping at the station, or has been driven out of the station, but has not yet reached the next station.

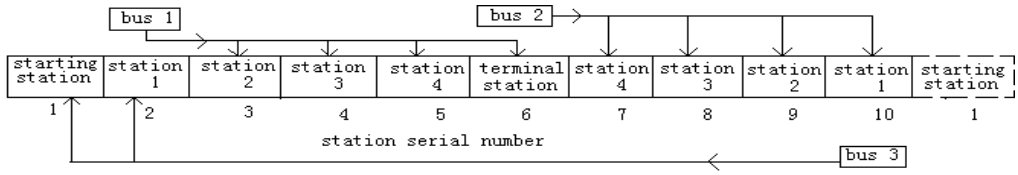

Figure 3. Sending algorithm of bus location information

The driver presses the button of arrival when bus arrives at a station. The bus terminal stores all the correlated information of each station terminal in memory orderly, so we can know the location of the bus by checking the button signal. After collecting the arriving signal, the bus terminal will send the current location to the bus company data centers.

DEVELOPMENT OF WIRELESS TERMINAL AND COMMUNICATION PROTOCOL

Development of Wireless Terminal. **The** wireless terminal controls the GPRS module with an 8 or 16 bit microcontroller via AT commands to achieve SOCKET communication (*Wang, 2006*), and outputs to an LED display module through parallel ports. The communication steps are introduced as follows (Siemens MC55 GPRS modules).

- Log on GPRS network by the special APN of the bus system.

  AT^SICS=0, conType, GPRS0<CR>

  AT^SICS=0, apn, "special APN"<CR>

- Establish SOCKET connections. Connect IP address XXX.XXX.XXX.XXX and port number PORT-S of bus data center server.

  AT^SISS=1, srvType, socket<CR>

  AT^SISS=1, conId, 0<CR>

  AT^SISS=1, address,"socktcp://XXX.XXX.XXX.XXX:PORT-S"<CR>

- Open TCP connection, and gain IP addresses 10.XXX.XXX.XXX and local port number PORT-C.

  AT^SISO=1<CR>

  AT^SICI=0<CR>

  ^ SICI: 0, 2, 1,"10.XXX.XXX.XXX"

  AT^SISO? <CR>

  ^SISO:1,..,"10.XXX.XXX.XXX:PORT-C","XXX.XXX.XXX.XXX:PORT-S"

Read *n* bytes of data; *n* is not more than 1500.

AT^SISR=1, *n*<CR>

Write *m* bytes of data; *m* is not more than 1500.

AT^SISW=1, *m*<CR>

<*m* bytes of data><CTRL+Z><CR>

Design of Communication Protocols between Bus Data Center and Wireless Terminal. Communication protocols between the bus data center and wireless terminal are divided into three kinds of data types: IP address and port number of wireless terminals are sent to the data center, wireless terminal of sends its location information to the data center, and the information from the data center is sent to the wireless terminal of the station. The protocols are shown in Figure 4.

1. protocol that IP address and port number of wireless terminals are sent to the data center.

beginning character					end character	
@	identification(bus/stop)	SIM NO.	IP address	port number	time	%

2. protocol that wireless terminal of bus sends its location information to the data center.

beginning character					end character	
$	bus SIM NO.	bus route number	current location	IP address	time	&

3. protocol that information data center has processed is sended to the wireless terminal of station plate.

beginning character					end character
#	stop SIM NO.	bus route number	the recent bus location	time	*

Figure 4. Communication protocols

CONCLUSION

Tests show that the plan for the urban bus location display system based on GPRS is correct. The bus wireless terminals, bus location displaying terminals, bus company data center, and GPRS Network can run stably. The key algorithm of data processing and the communication protocols between the data center and the wireless terminal is efficient.

The bus location displaying system can display the location of the nearest bus in each bus station which indicates that how far the closest bus is from this site. GPRS is a kind of wireless communication with a high data transfer rate, low error rate, low cost, and is free from the impact of bad weather.

REFERENCES

Liu Li, Deng Zhi-liang (2006). "Remote Fault Diagnosis System for Paver Based on Technology of GPRS." *Microcomputer Information*, 22(12-1):181-183.

Motorola Engineering Institute (2005). *GPRS Network Technology*. China Publishing House of Electronics Industry.

Tang Xin-zhou (2006). "The Application of CDMA&GPRS in the Urban Bus Station Name Displaying System." *Advanced Display*, (64):27-30.

Wang Jun, Hu Ping, Shi Tao, Jin Jing (2006). "The Implementation of Vehicle Monitor and Control System Based on GIS/GPS/GPRS." *Microcomputer*

Information, 22(9-2):290-292.

Zhang Jia-long, Zhao Jun-san, Rao Zhi-wen. (2006). "Logistics and Vehicle Monito--ring System Based on GPS/GIS/GPRS." *Geomatics&Spatial Information Technology*, 29(5):72-75.

Short-Term Traffic Flow Prediction Based on EMD and Artificial Neural Network

Xianglong Luo[1], Guohong Niu[2], Qianjiao Wu[3]

[1]School of Information Engineering, Chang'an University & School of Electronic and Information Engineering, Xi'an Jiaotong University, Central Section of the South 2nd Ring Road, Xi'an, 710064, China; PH(86)029-82334956; FAX(86)029-82334357; email: xlluo@chd.edu.cn.

[2]Xi'an Municipal Engineering Design & Research Institute, No.28,Zhuque Road, Xi'an,710068,China; PH(86)029-88421567; email: newgirl8074@yahoo.com.

[3]School of Information Engineering, Chang'an University, Central Section of the South 2nd Ring Road, Xi'an; PH(86)029-82334956; email: qjwu@chd.edu.cn.

ABSTRACT

An approach to short-term traffic flow prediction based on empirical mode decomposition (EMD) and artificial neural network (ANN) is proposed. The traffic flow is decomposed into different modes by EMD, and these different modes are predicted by appropriate ANNs. The predictive traffic flow is obtained by adding up all predictive values. This method is used to predict traffic flow with the actual measurement data. The results show that the proposed method has high predictive accuracy, and is more successful than the outcome of directly using ANN prediction.

INTRODUCTION

Traffic flow forecast has been a popular research topic in the field of intelligent transportation systems (ITS). Real-time and accurate traffic flow forecast is the premise and key of traffic control(Gao et al.2008; Liu et al.2004). Short-term traffic flow prediction analyzes traffic data and predicts the future traffic status within minutes, so that appropriate and timely traffic control measures are taken to provide real-time and effective road information for travelers. Dynamic path induction is used successfully to save travel time, ease road congestion, reduce pollution, and save energy (Gao et al.2008). Therefore, the traffic flow forecast is the premise of real-time control, and also is the theoretical basis of intelligent transportation systems.

In the 1960s, people began to use prediction models of other fields for short-term traffic flow forecasting, and a variety of prediction models and methods were developed. Generally speaking, there are four types of forecasting methods: based on traditional statistical theory approach, based on ANN approach, based on non-linear theory methods, and methods based on emerging new technologies (Gao et al.2008; Liu et al.2004). But the transport system is a giant time-variable, non-linear, uncertain, and complex system. Therefore, the prediction accuracy of

existing models have not achieved satisfactory results, and their accuracy and real-time usability need be improved.

In this paper, an approach to short-term traffic flow prediction based on empirical mode decomposition (EMD) and artificial neural network (ANN) is proposed. This method is used to predict traffic flow with actual measurement data. The results show that the proposed method has high predictive accuracy, and is more successful than the outcome of directly using ANN prediction.

EMD AND ANN TRAFFIC FLOW PREDICTION MEODEL

EMD is a new method to deal with non-linear and non-stationary signals. Non-stationary signals can be broken down into a number of intrinsic mode functions (IMF) by different scale level fluctuations or trends with EMD. Each component contains a different composition of the signal from high to low frequencies, and the EMD method is an adaptive decomposition based on the inherent characteristics of the signal itself (Huang N E et al.1998; 2003; Xuan et al.2008). The traffic flow is a typical non-stationary signal, therefore if it is decomposed by EMD, each component can better reflect the nature of the traffic flow and potential trends.

EMD algorithm. IMF is an innovative concept proposed by Huang (1998) in empirical mode decomposition, which is defined as a function that satisfies the following conditions: in the entire data set, the number of extrema and the number of zero crossings must either be equal or differ at most by one, at any point, the mean value of the envelope defined by the local maxima and the envelope defined by the local minima is zero. Then the sifting process is:

(1) For a given signal $x(t)$, construct its upper envelope and lower envelope by connecting all local maxima and local minima with cubic spline functions, respectively.

(2) Compute the envelope's mean $m(t)$ and extract the detail $h(t) = x(t) - m(t)$. Regard $h(t)$ as new $x(t)$ and repeat the operation above until $h(t)$ satisfies the IMF conditions, then obtain the first order IMF $c(t) = h(t)$.

(3) Let the residual $r(t) = x(t) - c(t)$ be a new signal, repeat (1), (2) and (3), obtain the other orders' IMFs.

Finally, we can obtain

$$x(t) = \sum_{j=1}^{n} c_j(t) + r_n(t)$$

Then, the signal $x(t)$ is decomposed into n intrinsic modes and a residue $r_n(t)$.

ANN model. The ANN model is a parallel processing technique inspired by the desire to emulate human learning activity. The back propagation (BP) network is the most commonly used learning algorithm and the initial connection weights of the nodes change during the training process to minimize the overall network errors (Kuang et al.2004; Xiang et al.2006). By dividing the nodes into different groups, an ANN model generally consists of an input layer, one or several hidden layers, and an output layer, each of which includes several nodes. In this paper, the number of hidden layers is one. The input vector is n measured traffic data of k moment ago $(x_{k-1}, x_{k-2}, \cdots, x_{k-n})$, the output is the predictive traffic flow value of k moment, and transfer functions and the nodes number of hidden layers are choose according to the different IMFs.

EMD and ANN traffic flow prediction model. At first, the signal of traffic flow is decomposed to obtain a number of IMFs and a residue. The random interference component is removed, and each IMF and residue is predicted by the appropriate artificial neural networks. Finally, the traffic flow is obtained by adding up all predictive values.

The specific algorithm is as follows:

Step 1: Carry out the traffic flow decomposition with EMD

Step 2: Analyze the IMFs, and remove the random interference

Step 3: Normalize all useful components of the traffic flow

Step 4: Establish different neural network models to predict the useful components

Step 5: Anti-normalize all predictive outcomes

Step 6: All anti-normalized data are accumulated to obtain the result of traffic flow prediction

Evaluation index. In order to evaluate the performance of the proposed method, following four indicators are selected as the basis for evaluation in this paper [8].

(1) Mean Absolute Error

$$MAE = \frac{1}{N}\sum_{t=1}^{N}\left|y_t - \hat{y}_t\right|$$

(2) Mean Square Error

$$MSE = \frac{1}{N}\sqrt{\sum_{t=1}^{N}\left|y_t - \hat{y}_t\right|^2}$$

(3) Mean Absolute Percent Error

$$MAPE = \frac{1}{N}\sum_{t=1}^{N}\left|\frac{y_t - \hat{y}_t}{y_t}\right|$$

(4) Mean Square Percent Error

$$MSPE = \frac{1}{N}\sqrt{\sum_{t=1}^{N}\left|\frac{y_t - \hat{y}_t}{y_t}\right|^2}$$

TRAFFIC FLOW PREDICTION WITH EMD AND ANN

To assess the performance of the proposed method, a measurement data of 30 second traffic flow with 660 points is used as the test data, the first 510 data are used as training samples of ANN, the last 150 data are used as test samples. The waveform is shown in Figure 1.

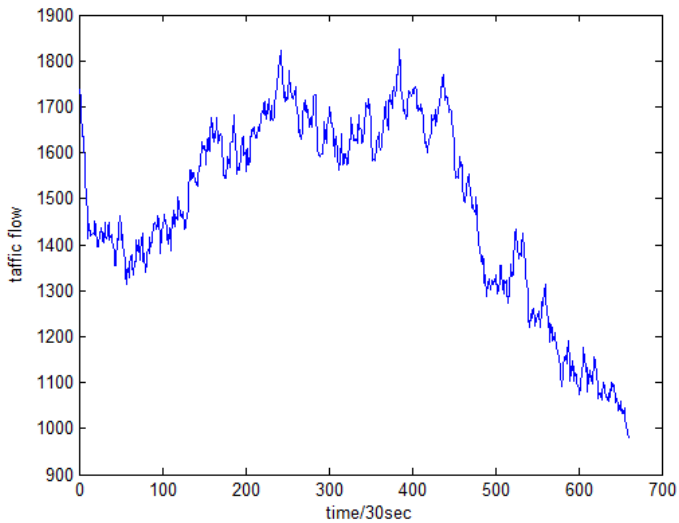

Figure 1. 30 second traffic flow data

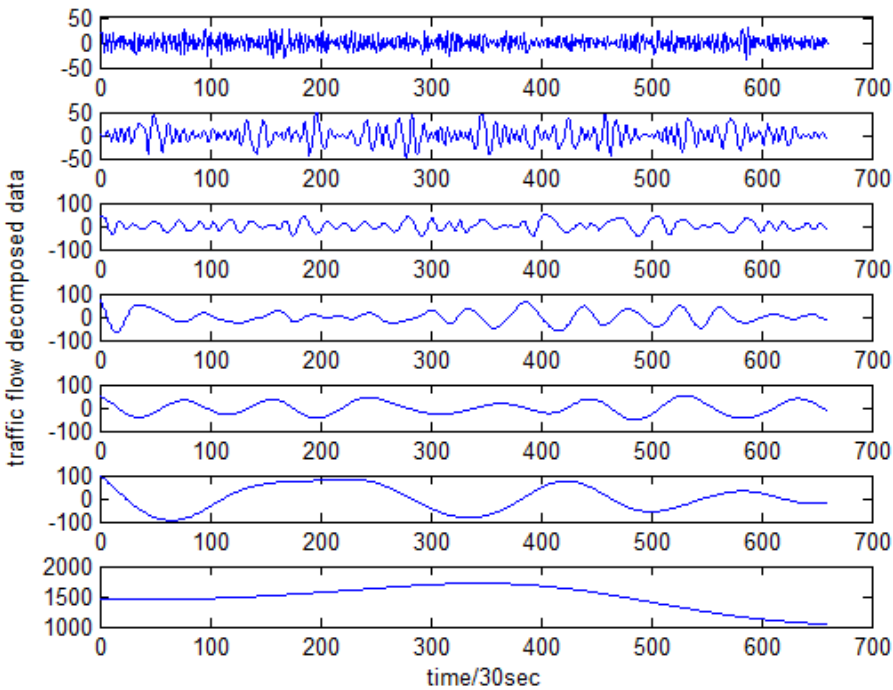

Figure 2. Traffic flow decomposition with EMD

According to the EDM algorithm, the traffic flow data is decomposed, and the result is shown in Figure 2. The traffic flow data is decomposed into 6 IMFs and 1 residue. In Figure 2, from top to bottom, the waveforms are IMF1 to IMF6 respectively, and the last is residue. Through the EMD, fluctuations of various components of traffic flow data are reduced. We can see that the first IMF is mainly random interference, so IMF1 is removed directly as random noise, while the other 5 IMFs and residue are predicted using different ANN models. All the predictive value of ANN models is accumulated, and the ultimate predictive value of traffic flow can be obtained. The result is shown in Figure 3.

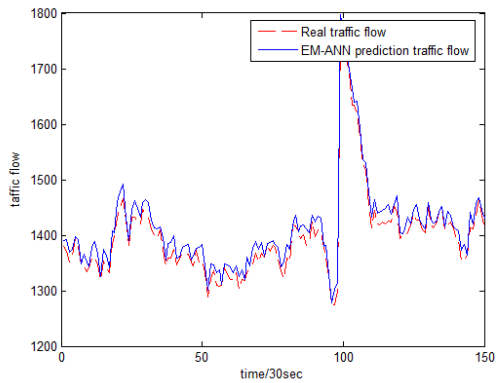

Figure 3. The forecast and the actual value with EMD-ANN

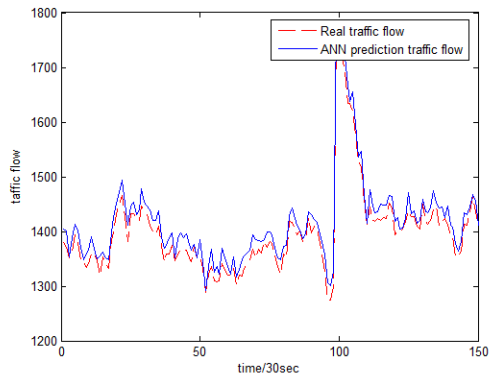

Figure 4. The forecast and the actual value with ANN

Table 1. Performance index of EMD-ANN and ANN

Performance Index / Prediction Method	MAE	MSE	MAPE	MSP
ANN	21.8906	6.287	0.0531	0.0346
EMD-ANN	12.3267	3.1530	0.0336	0.0121

In order to illustrate the superiority of the EMD-ANN method, the traffic flow is predicted directly using ANN. The result is shown in Figure 4. The prediction error of the EMD-ANN and ANN method is shown in Table 1. From Table 1, we can see that the EMD-ANN method has higher predictive accuracy than the ANN method.

CONCLUSION

In this paper, the method on the short-term traffic flow prediction is studied using EMD and ANN models. The traffic flow is decomposed into different IMFs and one residue by EMD. The random interference IMF is removed directly, and the useful IMFs and residue are predicted by appropriate ANN models. The traffic flow

is obtained by adding up all predictive values. This method is used to predict traffic flow with actual measurement data. The results show that the proposed method has high predictive accuracy which is higher than the accuracy of directly using the ANN model. The predictive method based on EMD and ANN is an effective prediction method of short-term traffic flow.

REFERENCES

Gao Hui, Zhao Jianyu, Jia Lei(2008). "Summary of Short-time Traffic Flow Forecasting Methods." *J. Journal of University of JiNan (Sic & Tech)*, 22(1), 88-94.

Liu Jing, Guan Wei(2004). "A Summary of Traffic Flow Forecasting Methods."*J. Journal of Highway and Transportation Research and Development*, 21(3), 82-85.

Huang N E, Shen Z, Long S R, etc.(1998). "The Empirical Mode Decomposition and the Hilbert Spectrum for Non-linear and Non-stationary Time Series analysis." *J. Proceedings of the Royal Society of London Series A*, 454, 903-995.

Huang N E，Wu M L，Qu W L，Shen S R(2003). "Applications of Hilbert-Huang Transform to Non-Stationary Financial Time Series Analysis."*J. Applied Stochastic Models in Business and Industry*, 19(3), 245-268.

Xuan ZhaoYan, Yang Gongxun(2008). "Application of EMD in the Atmosphere Time Series Prediction."*J. Acta Automatica Sinica*, 34(1), 97-101.

Kuang Aiwu, Huang Zhongxiang(2004). "Short-term Traffic Flow Prediction based on RBF Neural Network."*J. Systems Engineering*, 22(2), 63-65.

Xiang Hongyan, Zhu Shunying(2006)."Optimal Time Interval and Lookback Interval of Short-term Traffic Flow Prediction under Free Traffic Condition."*J. Journal of Wuhan University of Technology (Transportation Science & Engineering)*, 30(8), 626-628.

Huang Darong, Song Jun, etc.(2006). "Forecasting Model of Traffic Flow based on ARMA and Wavelet Transform."*J.Computer Engineering and Application*, 36, 191-224.

The Research of Signal Phase Sequences Based on the Conglomeration of Pedestrians and Bicycles

LIU Jin-guang[1], YU Quan[2], RONG Jian[3], and LIU Xiao-ming[4]

[1]Doctor candidate, Key Lab of transportation Engineering Beijing University of Technology, Beijing, 100124, China .Email: ljg2006@emails.bjut.edu.cn
[2]Associate Professor, Key Lab of transportation Engineering Beijing University of Technology, Beijing, 100124, China. Email: yuquan@bjut.edu.cn
[3]Professor, Key Lab of transportation Engineering Beijing University of Technology, Beijing, 100124, China
[4]Professor, Key Lab of transportation Engineering Beijing University of Technology, Beijing, 100124, China

ABSTRACT

The design of phase sequence is very important to signal control timing. The research embodied in this paper presents a new method of designing the phase sequence of the signal control, based on the conglomeration of pedestrians and bicycles in our country. Firstly，we present a new definition of the conglomeration of pedestrians and bicycles at the first phase after analyzing the two phases of the releasing characteristics of the signalized intersection.

Next, we present a new method which is based on suppositional grids to describe the conglomeration. Then, we present a new method to optimize the phase sequence based on the time-space resource usage of the intersection. In order to optimize the phase sequence quantitatively, we found the model of conflict timing between the conglomeration and the vehicles. As for estimating the optimal phase sequence, we used the model of conflict timing.

Finally, the application of this method is illustrated with the signalized intersection of Pingleyuan in Beijing. Under the simulation, the method gives an optimized result.

1. INTRODUCTION

Mixed traffic phenomena are one of the most remarkable characteristics in Chinese cities, which can cause traffic congestion and accidents in urban intersections. The optimization of the phase sequence of the signal control is the basis for the signal timing optimization. In view of the mixed traffic phenomena in China, this paper presents a new definition of the conglomeration of pedestrians and bicycles, and it presents a new method to optimize the phase sequence based on the time-space resource usage of the intersection. By optimizing the signal timing, we can cut down on traffic congestion and accidents at intersections.

There is some past research on signal phase sequences. In the HCM 2000

example, the vehicles were considered to be the main object for optimizing the phase sequence, while pedestrians and bicycles were seen as the affection coefficient for the saturation flow of the vehicles (HCM, 2000). In the "Manual of Traffic Signal Design", optimization advice is presented for the left and right turning phase without considering the pedestrians and bicycles (James H.Kell, 1991). Shladover proposed a method for the bicyclist phase, creating the signal phases by synchronizing the traffic signal with video images (Shladover, 2009).

In China, Yang Xiaoguang presented the combination phases for pedestrians, bicycles and vehicles (Yang, 2003). Wang Dianhai suggested setting the left turn bicycle phase and end bicycle phase and pedestrian phase ahead of time (Wang, 2004). Xu Liangjie proposed the method of dynamic ordinal samples cluster algorithms to optimize the phase sequence (Xu, 2005). Generally, these researchers mainly focus on the vehicle or consider the pedestrians and bicycles separately to optimize the phase sequence. This paper will present a new method to calculate the phase sequence based on the conglomeration of pedestrians and bicycles.

2. CONGLOMERATION OF PEDESTRIANS AND BICYCLES

Before giving the definition of the pedestrians and bicycles conglomeration, it is necessary to analyze the releasing characteristic in the green time of the signalized intersection. Then we will present a new method which is based on the suppositional grids to describe the conglomeration.

2.1 The releasing characteristic in the green

In China, there are many pedestrians and bicycles crossing intersections. Because of the red light of the controller, there are often a lot of pedestrians and bicycles assembled at the stop line. When the green light shows, the assembled pedestrians and bicycles begin to enter the crosswalk together (Figure 1). After the assembled pedestrians and bicycles all enter the crosswalk, the remaining pedestrians and the bicycles will enter the crosswalk randomly (Figure 2).

Based on the method of video analysis, we analyzed the releasing characteristic quantitatively and found the results shown in Figure 3, the time-space curve of the pedestrians and bicycles. One curve stands for a pedestrian or a bicycle. The x-coordinate stands for the green time, and the Y-coordinate stands for the displacement of the pedestrian or a bicycle. From the figure we can see that, in the first 8 seconds, the curves are very dense, it shows that the pedestrians and bicycles are clustered densely. After the 8th second, the curves are sparse, it shows that the pedestrians and bicycles are spread out. We can consider the first 8 seconds as the first phase of the releasing time, and the green time after the 8th second is considered the second phase.

Figure 1. the conglomeration mode.

Figure 2: the individual mode.

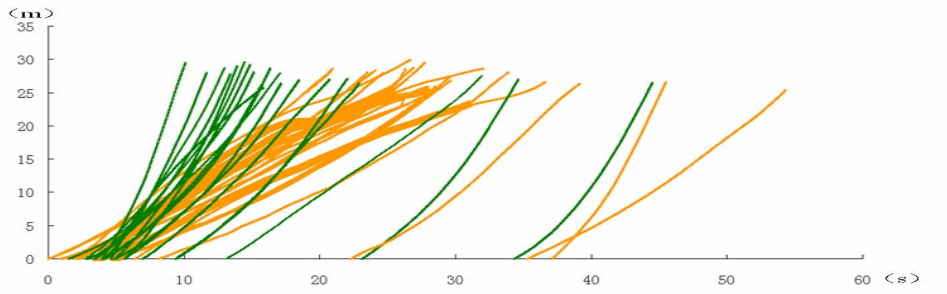

Figure 3. Time-space curve of the pedestrians and bicycles in one cycle

From these results, we can determine the definition of the conglomeration of pedestrians and bicycles: In the first phase of the releasing time, the pedestrians and the bicycles enter the crosswalk densely like a pack, and then they keep the shape of a pack to get through the crosswalk. This is considered to be the conglomeration of pedestrians and bicycles. The conglomeration of pedestrians and bicycles is the most distinct characteristic of the releasing process.

2.1 THE METHOD OF SUPPOSITIONAL GRIDS

In order to describe the conglomeration of pedestrians and bicycles, based on the occupation space of the pedestrians and bicycles and the crosswalk criterion, we present a method of suppositional grids to calculate the occupation, and the detailed method is described below.

In the HCM 2000 example, the space of the pedestrians walking in the crosswalk is $0.3\,m^2/P$. When the establishment of the road was evaluated, the space of the pedestrians walking in the crosswalk is $0.75\,m^2/P$ (HCM, 2000). In China, the research of the space of the pedestrians walking in the crosswalk is $0.35\text{-}1.2\,m^2/P$, the space of the bicycles in the crosswalk is $2.0\text{-}4.0\,m^2/B$ (REN, 2003).

In the crosswalk criterion (GB5768-1999) of China (GB5768-1999), the width of one zebra crossing is 0.45m, and the length of one zebra crossing is at least 3.0m which can be added 1.0m as one grade. The spacing of the two zebra crossings is 0.60m.

By way of calculating the occupation of the conglomeration of pedestrians and bicycles, we consider the pedestrians and bicycles as one unit, and the space of this unit is $0.3\text{-}4.0\,m^2/unit$.

In view of the research of the space of the pedestrians and bicycles and the

crosswalk criterion (GB5768-1999), we present the method of suppositional grids to divide the crosswalk. The width of the suppositional grid is 1.0m, and the length of the suppositional grid is 1.05m. Figure 4 shows the division of the crosswalk.

Based on the definition of suppositional grids, we can determine the size of the conglomeration of the pedestrians and bicycles. If the spacing of the projection area of the unit is less than one suppositional grid, and the quantity is more than two suppositional grids, the number of the suppositional grids is the quantity of the conglomeration of pedestrians and bicycles.

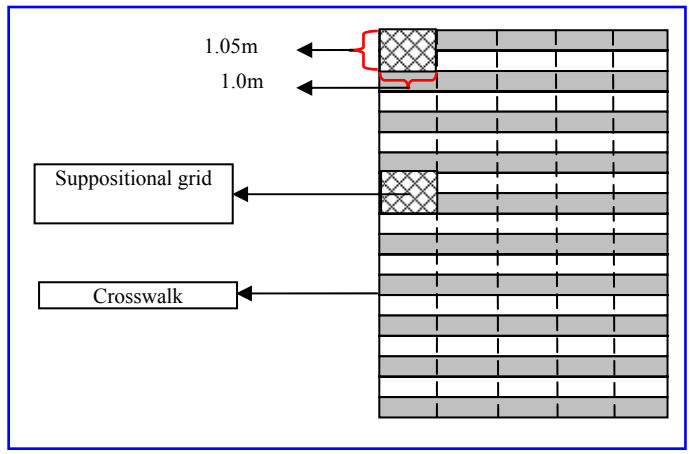

Figure 4. the suppositional grids of the crosswalk

3. THE METHOD OF THE PHASE SEQUENCE DESIGN

This paper presents a new method to optimize the phase sequence based on the time-space resource usage of intersections.

We should reduce the conflict time of the conflict area to improve the efficiency of the signalized intersection. First, we must find the conflict timing model between the conglomeration and the vehicles. As we know, the conflicting area between the conglomeration and the vehicles is on the crosswalk of the intersection. This is shown in Figure 5, while the area Q is the conflicting area. Based on the method of the suppositional grids, we can find the conflict timing model that is shown on the formula (1). After we calculate the conflict timing between the conglomeration and the vehicles, we can optimize the phase sequence from adjusting the starting timing of the conglomeration and the vehicles, and determine the optimal phase sequences.

$$t=L/V+x(Q/Y) \qquad (1)$$

Where T—conflict time, L—the length of the conflicting area, V—the reduced velocity of the conglomeration, X—the time interval of the consecutive conglomeration, Q—the length of the “suppositional grids” of the conglomeration occupying, and Y—the transverse amount of the “suppositional grids”.

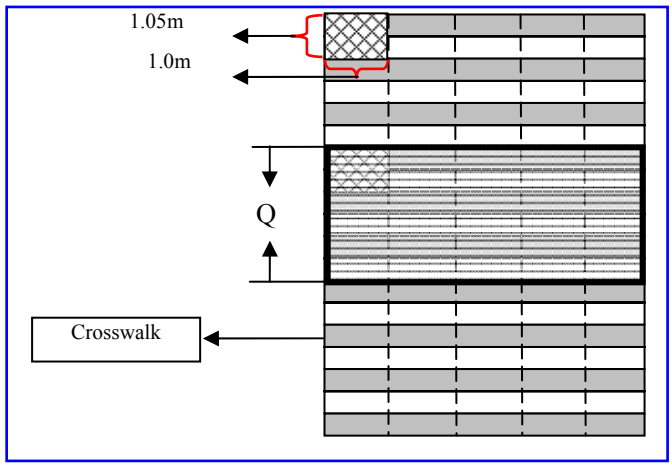

Figure 5. the conflicting area between the conglomeration and the vehicles

After determining the phase sequence through the method of the conflict timing model, we should choose a value to estimate the phase sequence. This paper chooses the time utilizing ratio of no-conflict to estimate the phase sequence. We can see that an intersection contains two kinds of resources:the space resource and the time resource. We found the model of the time utilizing ratio of no-conflict based on the time-space resource usage of the intersection.

The definition of the time utilizing ratio of no-conflict is a ratio between the no-conflict green timing and the whole green time in one signal cycle. It can estimate the intersection's efficiency, which is shown in the formula (2).

$$U = \frac{T - \sum_{i=1,j=1}^{n} (t_{(i,j)} - \bar{t}_{(i,j)})}{T} \qquad (2)$$

Where U—the time utilizing ratio of no conflicting, T—the whole green time of one cycle, n—the number of the conflicting area, $t_{(i,j)}$—the conflicting timing of the conflicting area, the letter "i" stands for the number of the vehicle flow, the letter "j" stands for the number of the crosswalk, and $\bar{t}_{(i,j)}$—the lead or lag time of the different phase sequences.

So from the model of the conflict timing we can determine the different phase sequences, and from the model of the time utilizing ratio of no-conflict we can estimate the phase sequences quantitatively. The optimization of the signal phase sequence is the first step to optimize the signal timing, and the time utilizing ratio of no-conflict is a very important estimation to optimize the signal timing following other values such as delay of the intersection, capacity of the interaction, and so on.

4. CASE STUDY

The application of this method is illustrated with the signalized intersection of Beijing Pingleyuan. The signalized intersection of Beijing Pingleyuan is a four-phase intersection. We chose the method of video analysis to investigate the intersection of

Beijing Pingleyuan. From the method of this paper, we calculated the conflicting time of the four import lanes with two directions applying the formula (1). The result is shown in Table 1.

Table. 1 the conflicting time of the intersection of Beijing Pingleyuan

Crosswalk	East		West		South		North	
Direction	N-S	S-N	N-S	S-N	E-W	W-E	E-W	W-E
Conflicting time（s）	5	6	6	7	3	4	3	5

If we want to reduce the conflicting time, we should adjust the signal phase sequence. From Table 1, we can see that, the scope of the adjustment of the east crosswalk and the west crosswalk is 5s-7s. The scope of the adjustment of the south crosswalk and the north crosswalk is 3s-5. We propose several strategies to adjust the signal phase sequence in Table 2, and we calculate the time utilizing ratio of no-conflict for every strategy to estimate the results by applying the formula (2). We used the simulation method to evaluate the strategies and determine the total delay of the intersection. From Table 2, we can see that the optimal signal phase sequence is number 4, and its time utilizing ratio of no-conflict is 1.0, but the total delay is 400.6s. This optimal strategy can produce a degree of order in the intersection, but the delay time could be better.

Table 2. four strategies and the time utilizing ratio of no conflicting

Design number	1		2		3		4	
Direction	N-S	S-N	N-S	S-N	E-W	W-E	E-W	W-E
Sequence adjust(s)	5	3	5	4	6	4	7	5
Time utilizing ratio of no-conflict	0.83		0.91		0.96		1.0	
Total delay(s)	509.2		328.0		366.6		400.6	

5. CONCLUSION

This paper presents a new method to analyze the phase sequence of signal controls based on the conglomeration of pedestrians and bicycles. We present a new definition of the conglomeration of pedestrians and bicycles after analysis of the signalized intersection. We present a new method to optimize the phase sequence based on the time-space resource usage of the intersection. The optimization of the signal phase sequence is a important step to optimize the signal timing. We will research the signal timing optimization of the intersection in the future study.

REFERENCES

James H.Kell, Jris J. Fullerton (1991). Manual of Traffic Signal Design. Institute of Transportation Engineers: 28-39

Jing Chunguang,WangDianha (2004). Analysis and dealing method to conflict of

mixed traffic at typical intersection . China civil engineering journal. 37(6):97-99

REN Fu-tian, LIU Xiao-ming, and RONG Jian (2003). Traffic Engineering. Beijing: People's Publishing of traffic：66-78

Research Institute of Highway; the Ministry of Communication (1999). GB5768-1999《road traffic sign》. China publishing company of the criterion：18

Shladover Steven，Kim ZuWhan，Cao Meng (2009). Bicyclist Intersection Crossing Times: Quantitative Measurements Relative to Signal Phase. 2009 TRB Annual Meeting, Washington DC

Transportation Research Board (2000). Highway Capacity Manual. Washington，D.C：National research council：16

XU Liang-jie (2005). The research on the optimal control to the single-control intersection. Southeast University：15-25

Yang Xiao-guang (2003). Urban traffic design manual. People's Publishing of traffic：70-90

Effects of Lane Changing in Heterogeneous Traffic Flow

Fa Zhang [1, 2] and Qiao-xia Zhao [3]

[1]Management School, Xi'an Jiaotong University, P.O. Box 710049, No. 28, Xian-ning West Road, Xi'an, China; PH86-29-84790831; email: richter2000@163.com

[2]Engineering School, Air Force Engineering University, P.O. Box 710038, Xi'an, China;

[3]Telecom School, Air Force Engineering University, P.O. Box 710077, No. 1, Feng-hao Road, Xi'an, China; PH86-29-84798644; email: zhaoqx2000@sohu.com

ABSTRACT

The effects of lane changing on the characteristics of traffic flow have not been investigated sufficiently. In this paper, we use a driving model based on finite-state-machine to investigate the effects of lane changing on macroscopic characteristics of traffic flow. In homogenous traffic, the effects of lane changing are not significant. However, in heterogeneous traffic composed of vehicles with different maximum speed, the flux in the low to middle density increase if lane changing is permitted. Furthermore, in heterogeneous traffic where vehicles only have difference in normal acceleration, lane changing can't increase the flux significantly. In conclusion, the effects of lane changing on traffic are tightly related to both the difference of vehicles and the density of traffic.

INTRODUCTION

Lane changing is one of the basic maneuvers in multi-lane traffic. However, the effects of lane changing on the characteristics of traffic flow have not been studied sufficiently. A few lane changing models have been proposed (Gipps 1986). Yang noted that there are two types of lane changing, named discretionary lane changing (DLC) and mandatory lane changing (MLC) (Yang 1998). Hidas pointed out the phenomenon of the forcing gap in lane changing (Hidas 2005). Kim found that the relationship of speed-flux in merging sections are different from that of the basic section because of the high frequency of lane changing (Kim, Son et al. 2002). Tanaka reported that there are high flux and low flux states if lane changing is permitted on two-lane roads (Tanaka, Nagatani et al. 2008). The effects of lane changing on the capacity of the highway are not clear. Coifman found that the capacity decreased because of lane changing (Coifman, Krishnamurthy et al. 2003). However, Jia found that the effects of lane changing are different in homogenous and heterogeneous traffic (Jia, Jiang et al. 2005; Jia, Li et al. 2006).

In this paper, we use a finite-state-machine (FSM) framework to model the driving behavior. Then we study the characteristics of homogenous and

heterogeneous traffic flow using microscopic simulation. Finally, the effects of lane changing are summarized.

FSM FRAMEWORK OF DRIVING

Driving is a complex process; it can be described with a finite state machine (FSM), as shown in Figure 1. The FSM has five states: staying in current lane (KCL), DLC intention, MLC intention, forcing gap (FG) and performing lane changing (PLC). At the beginning, we set the machine in the KCL state. MLC and DLC are different in the process of intention generating and disappearing. The MLC intention should persist till lane changing is finished. The DLC intention should only persist for certain duration and then disappear. If the vehicle is in the KCL state, and special conditions are satisfied, the machine switches into the state DLC Intention (DLCI) or MLC Intention (MLCI). In the MLCI state, once the safety condition is satisfied, the machine switches into the state PLC. If the safety condition has not been satisfied after a pre-determined length of time, the machine switches into the FG state. In the state DLCI, the driver checks the safety condition for a certain duration, if the condition is satisfied, the machine switches into PLC, otherwise the driver's intention of lane changing disappears and the machine switches into KCL. This model has been validated and can reproduce the characteristics of traffic flow.

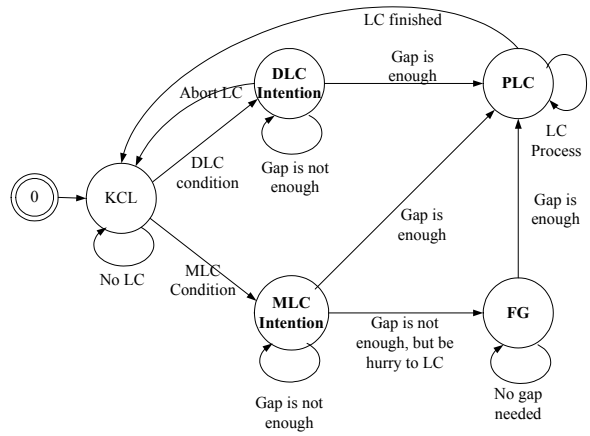

Figure 1. The Finite state machine of driving.

A decision tree is employed to model the longitudinal movement of vehicles (Zhang, Li et al. 2005). The traffic is classified into several states according to the lead gap and the difference of velocity between subject and its leader. Based on the traffic state, driver selects a basic maneuver from accelerating, decelerating or cruise. Once a basic maneuver is selected, the accelerate/decelerate rate will be calculated. The normal acceleration is smaller in high speed than in low speed

(Bham and Benekohal 2004), the two acceleration are a_1 and a_2.

EFFECTS OF LANE CHANGING IN HOMOGENOUS TRAFFIC

We investigate the effects of lane changing in homogenous traffic. Set the length of a two-lane road $L = 2000m$. There is only one type of vehicle on the road. Set $a_1 = 1.11, a_2 = 0.37$. In scenario LC, lane changing is permitted, $p = 0.5$. In scenario NLC, lane changing is not permitted, $p = 0$.

Initially, vehicles are located on the two lanes in a random manner. For density $5 < \rho < 130$ veh/km, with increment 5, we make 20 replications of simulation for each setting. In each test, we collect flux data and count the number of lane changes in steady state ($t \in [1000,1300)$). Then we calculate the mean of flux and lane changing rate in each density.

The relationship of flux-density in the two scenarios is depicted in Figure 2(a). The relationship of LC rate-density in scenario LC is shown in Figure 2(b). LC rate is defined as the ratio of number of lane changes in a unit time to the total number of vehicles. Counter intuitively, the flux-density curves have no significant difference in these two scenarios, though lane changes do occur in scenario LC.

The possible explanation is that flux reached its peak near the density $\rho = 40$. The gap between adjacent vehicles is large, there is almost no need to change lanes, as shown in Figure 2(b). Because lane changing seldom occurs at this density, the effect of lane changing is not significant. In density $40 \le \rho \le 80$, lane changing occurs frequently.

The gap between vehicles is small, lane changes do improve the speed of the subject vehicle, but at the same time, the followers in target lanes are hindered. The average speed does not increase, and the flux does not increase. Overall, flux does not increase even if lane changing is permitted in homogenous traffic.

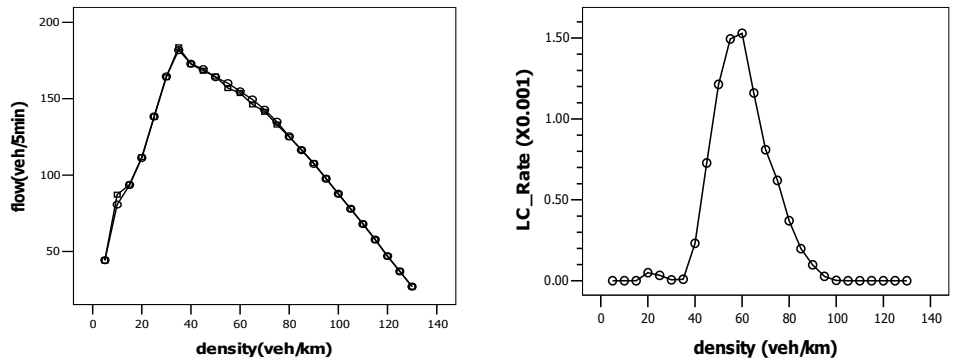

(a) Flux-density in two scenarios (b) LC Rate-density in LC

Figure 2. Characteristics of homogenous traffic flow.

EFFECTS OF LANE CHANGING IN DUAL-SPEED MIXED TRAFFIC

Here we study the effects of lane changing in the mixed traffic where there are two vehicles, and the only different is maximum speed. The maximum speed of the fast vehicle is $v_{\max} = 30m/s$, and slow vehicle is $v_{\max} = 10m/s$. Set the mix ratio of slow vehicles $f = 0.05$.

The flux-density relationship in two scenarios is depicted in Figure 3(a). The LC rate-density relationship in scenario LC is depicted in Figure 3(b). The flux in scenario LC is significant great than in scenario NLC when density is lower than the critical density. It implies that lane changing has effects if vehicles' max speeds are different, especially in the low and middle density.

The possible explanation is that in low density, the fast vehicle is hindered by the slow vehicle and generates intention to change lanes. The safety condition for lane changing is easily satisfied because the gap is large, so lane changing occurs frequently. After lane changing, the fast vehicle can increase its speed and slow vehicles are not affected.

The flux of mixed traffic increases because of lane changing in low density. In high density, the average speed is low, the fast vehicle and the slow vehicle have no distinction in their speed, lane changing seldom occurs, and the effect of lane changing is not obvious. These results imply that the difference of vehicle speed is important to the effects of lane changing.

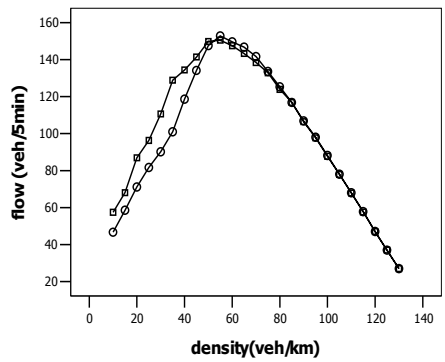

(a) Flux-density in two scenarios

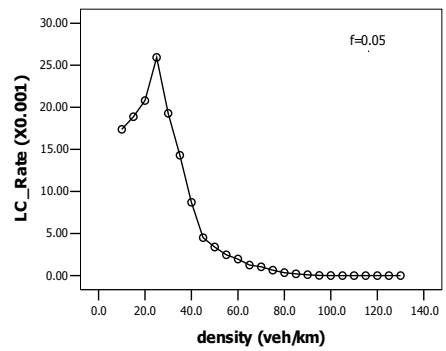

(b) LC Rate-density in LC

Figure 3. Characteristics of heterogeneous traffic with different max speed.

EFFECTS OF LANE CHANGING IN DUAL-ACCELERATION MIXED TRAFFIC

In this section we study the effects of lane changing in the mixed traffic where vehicles have different acceleration parameters. For type I, set

$a_1 = 1.3$, $a_2 = 1.0$, and type II $a_1 = 0.6$, $a_2 = 0.3$. The maximum speed of all vehicles is $v_{\max} = 30 m/s$. Set the mix ratio of type II vehicles $f = 0.05$ or 0.2 respectively. Initially all the vehicles are distributed on the two-lane road in a random manner. Make 20 replications for each density. Results are shown in Figure 4.

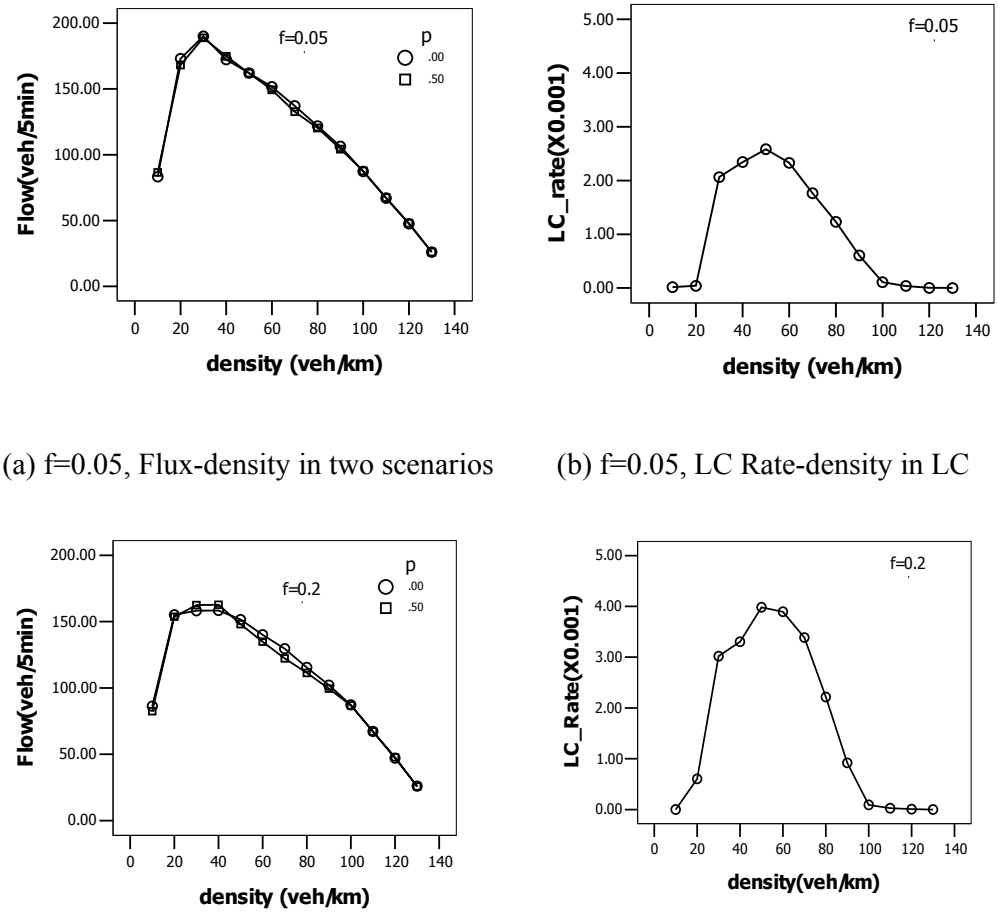

(a) f=0.05, Flux-density in two scenarios (b) f=0.05, LC Rate-density in LC

(c) f=0.2, Flux-density in two scenarios (d) f=0.2, LC Rate-density in scenario

Figure 4. Flux-density and LC rate-density in Dual-acceleration mixed traffic.

Figure 4(a) shows the flux-density curves when the mix ratio of low acceleration vehicles is small (f=0.05), and (b) is the LC rate-density curve in a scenario LC when f=0.05. Figure 4(c) and (d) are for mix ratio f=0.2. As shown in (a) and (c), lane changing has no obvious effect on the flux, even when the mix ratio of the low acceleration vehicle is 0.2. These results may be explained by the relationship of LC rate-density. The LC rate is very small, only several in a thousand, even though it will rise up when the mix ratio rises. These results indicate that lane changing has no significant effects on the characteristics of mixed traffic composed of vehicles with different acceleration rates.

CONCLUSION

The effects of lane changing on traffic have been unclear until now. In this paper we use a finite-state-machine to model driving on a multi-lane road. We investigate the effects of lane changing on the characteristics of traffic flow in several situations with microscopic simulation. In homogenous traffic, we find that lane changing behavior has no significant effects on flux. However, in the mixed traffic composed of fast vehicles and slow vehicles, the flux is greater than those in the scenario without lane changing. The effect is more obvious in low and middle density traffic than in high density.

Furthermore, in the mixed traffic composed of vehicles with differences in their normal acceleration, lane changing has no significant effects on flux. Based on these simulation results, the following conclusion may be made: the effects of lane changing on traffic are complicated, and closely relate to both the differences of the vehicles and the density range of traffic flow.

REFERENCES

Bham, G. H. and R. F. Benekohal (2004). "A high fidelity traffic simulation model based on cellular automata and car-following concepts." *Transportation Research Part C* 12: 1-32.

Coifman, B., S. Krishnamurthy, et al. (2003). Lane-change maneuvers consuming freeway capacity. *5th International Conference on Traffic and Granular Flow*, Delft, Netherlands.

Gipps, P. G. (1986). "A model for the structure of lane-changing decisions." *Transportation Research Part B* 20: 107-120.

Hidas, P. (2005). "Modelling vehicle interactions in microscopic simulation of merging and weaving." *Transportation Research Part C* 13(1): 37-62.

Jia, B., R. Jiang, et al. (2005). "Honk effect in the two-lane cellular automaton model for traffic flow." *Physica A* 348: 544-552.

Jia, B., X.-G. Li, et al. (2006). "A realistic two-lane cellular automata traffic model considering aggressive lane-changing behavior of fast vehicle." *Physica A* 367: 479-486.

Kim, S., Y. Son, et al. (2002). "Behaviors and characteristics of traffic flow within the influence zone of freeway merge area in Korea". *3rd International Conference on Traffic and Transportation Studies*, Korea.

Tanaka, K., T. Nagatani, et al. (2008). "Fundamental diagram in traffic flow of mixed vehicles on multi-lane highway." *Physica A* 387(5): 5583-5596.

Yang, Q. (1998). "A simulation laboratory fore evaluation of dynamic traffic management systems", *Massachusetts Institute of Technology.*

Zhang, F., J. Li, et al. (2005). "Single-Lane Traffic Simulation with Multi-Agent System". *The 8th IEEE Conference on Intelligent Transportation Systems*, Vienna, Austria.

Detecting the Type of Multi-fractality in Traffic Time Series

J. Yu [1], D. Liu[2], P. Shang [3], Z. Wang[1], J. Guan[1]

[1]Beijing STONG Intelligent Transportation System Integration Co., LTD, Mailbox 8192, Beijing 100081, P.R. China; PH +86-010-62132676-8805; FAX +86-010-62124578; email: yujianling2004@163.com
[2]Department of Mathematics, Linyi Normal University, Shandong Province 276005, P.R. China; email: liudehua0306@163.com
[3]Department of Mathematics, School of Science, Beijing Jiaotong University, Beijing 100044, P.R. China; email: pjshang@bjtu.edu.cn

ABSTRACT

In general, two types of multi-fractality can be identified in time series. One type connects with a broad probability density function for the values of the time series, while the other connects with different long-range correlations of the small and large fluctuations. Recent analyses of traffic time series indicate that it exhibits multi-fractal properties. But which type of multi-fractality does it exhibit?

In this paper, multi-fractal detrended fluctuation analysis (MF-DFA) is used to study traffic speed fluctuations. Collected data shows that the speed time series, observed by microwave detector system on the outer side of the North Second Ring Road over a period of about 60 days, has strong multi-fractal properties. By comparing the fluctuation function of MF-DFA results for the original series to those for shuffled series, we find that the type of multi-fractality in traffic speed time series is consistent with long range correlations of the small and large fluctuations. In addition, by comparing the generalized Hurst exponent and multi-fractal spectrum of the original time series with those of the corresponding shuffled series, the results show that the multi-fractal properties of shuffled time series are stronger than those of the original time series, and both distribution multi-fractality and correlation multi-fractality are present in the speed time series.

INTRODUCTION

The investigation of the temporal fluctuations in traffic time series has recently revealed its potential for providing information related to prediction (Shang P., Li X., 2005; Safanov L.A. et al, 2002). In the study of seemingly complex phenomena such as traffic time series, fractal analysis techniques, developed to draw qualitative and quantitative information from the data, have been applied to the study of a variety of irregular non-stationary time series and have been found to be very useful for detecting deep dynamical features. These methods are mainly useful to detect the presence of long-range power law correlations that have been found to exist in a variety of systems (Shang P., Li X., 2005). Safanov et al (Safanov L.A. et al, 2002) showed that fractal behavior

in traffic time series could be due to delays in human reaction. Shang and Li (Shang P., Li X., 2005) showed that fractal and chaotic characteristics exist in the traffic system.

The traffic speed time series is studied using a fairly robust and powerful technique called multifractal detrended fluctuation analysis (MF-DFA) (Kantelhardt et al, 2002). This method provides a systematic means to identify and quantify the long-range correlation among data sets obtained from diverse settings (Kantelhardt J.W. et al, 2001; Yu C.X. et al, 2003; Seely A.J.E., Macklem P.T., 2004; Vjushin D. et al 2001; Ivanova K. and Ausloos M., 1999). One reason to employ the MF-DFA method is that it avoids spurious detection of correlations that are artifacts of non-stationarity in the time series.

The focus of this paper is on the intriguing multi-fractal properties of the traffic time series. In general, two different types of multi-fractality can be identified in time series: multi-fractlity due to a broad probability density function for the values of the time series and multi-fractality due to different long-range (time) correlation of the small and large fluctuations.

The paper is organized as follows. Section 2 describes the acquisition of traffic data. Section 3 provides the multi-fractal detrended fluctuation analysis of traffic time series. In Section 4, we show the comparison of the results of MF-DFA analysis for the original time series to the results for shuffled time series. We then detect the type of multi-fractality in the traffic time series. The conclusions are summarized in Section 5.

DATA DESCRIPTION

The basic data used in this paper was collected by microwave detector system in Beijing on the outer side of the North Second Ring Road over a period of about 60 days. The system provided data on volume and time occupancy of certain sections, so we indirectly obtained the average speed of the section during the collection period of two minutes through the vehicle length parameter set by the microwave detector.

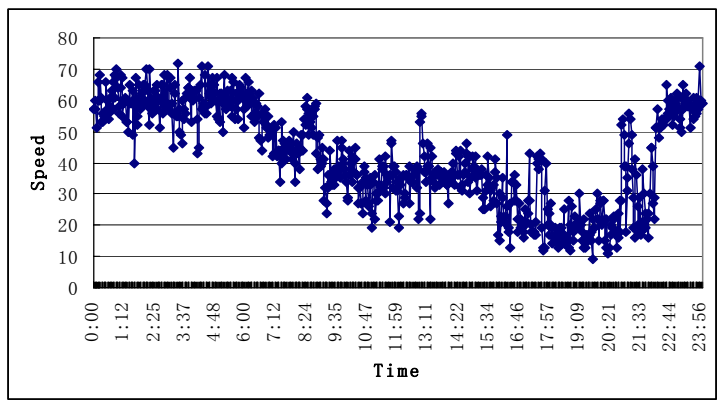

Figure 1. Time versus speed.

Figure 1 shows the time series plot of the speed data with the two-minute

sampling period, observed one day at one section on the outer side of the North Second Ring Road. A visual inspection of the speed series reveals significant variations in speed, but this is not enough to say anything regarding the existence of multi-fractality. Hence, additional tools are necessary to identify the possible presence multi-fractality.

MULTIFRACTAL DETRENDED FLUCTUATION ANALYSIS

Description of the Method. Traffic time series often present clear irregular dynamics, characterized by exchange of high frequency fluctuations that lend themselves to multi-fractal analysis evidencing the presence of different scaling behaviors for different intensities of fluctuations. Furthermore, the signal may appear non-stationary.

MF-DFA is a useful tool to characterize multi-fractality in non-stationary data. Traffic time series often exhibit non-stationary characters. So MF-DFA is used to analyze the multi-fractality of traffic time series. To illustrate the MF-DFA method, we consider the speed time series x_k, $k=1,2,...,N$.

First, estimate the signal profile:

$$Y(i)=\sum_{k=1}^{i}[x_k-\langle x\rangle],\quad i=1,...,N,\quad \text{here}\quad \langle x\rangle=\frac{1}{N}\sum_{k=1}^{N}x_k$$

Next, divide the profile $Y(i)$ into N_s=int(N/s) disjoint segments of equal length s. For each segment v, $v=1,2,...,N_s$ the local trend is to be calculated by least-squares fitting the polynomial of order m, to the data, and then obtain the qth-order fluctuation function:

$$F_q(s)\equiv\left\{\frac{1}{2N_s}\sum_{v=1}^{2N_S}\left[F^2(s,v)\right]^{q/2}\right\}^{1/q}$$

We are interested in how the generalized q dependent fluctuation functions $F_q(s)$ depend on the time scale s for different values of q. Determine the scaling behavior of the fluctuation function by analyzing log-log plots $F_q(s)$ versus for each value of q. If the time series x_k are long-range power-law correlated, $F_q(s)$ increases, for large value of s, as power-law:

$$F_q(s)\sim s^{h(q)}\quad (h(q)\text{ is the generalized Hurst exponent})$$

By knowing the spectrum of the generalized Hurst exponent, we can calculate the multi-fractal scaling exponent $\tau(q)$ using the following relation:

$$\tau(q)=q\,\tau(q)-1.$$

For various purposes, such as the description of the structure of the traffic time series over a certain period or the short-term prediction, it is helpful to be able to know the relationship between $f(\alpha)$ and $\tau(q)$. It can be easily obtained from a Legendre transformation (Peitgen H.O., Jurgens H., Saupe D., 1992).

Analysis of Multifractality. The MF-DFA fluctuation functions $F_q(s)$

are shown versus s in log-log plots in Figure 2. The different symbols correspond to the different values of the exponent q in the generalized averaging procedure q=-4.0,-2.0,-0.2,0.2,2.0,4.0. On a large scale, we observe the power-law scaling behavior.

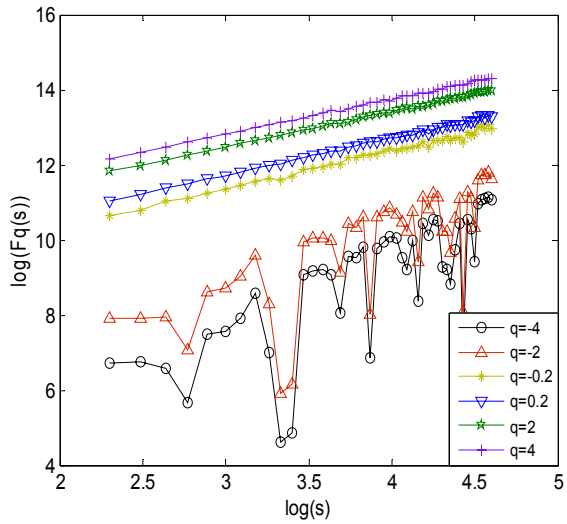

Figure 2. Graph of log(Fq(s)) versus log(s).

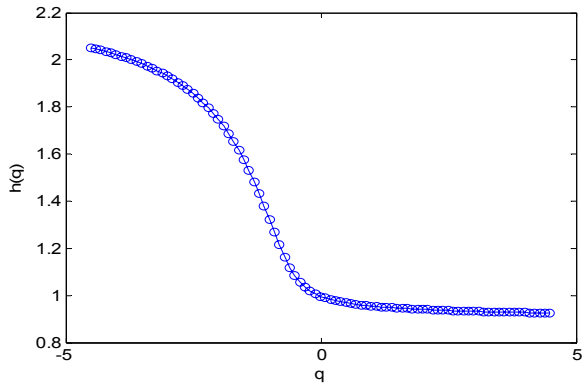

Figure 3. Graph of h(q) versus q.

Figure 3 shows the q dependence of the generalized Hurst exponent h(q) determined by fits in the regime 10<s<200, as shown for MF-DFA1. It can be seen that the exponent h(q) depends on q, and that h(q) decreases with increasing q.

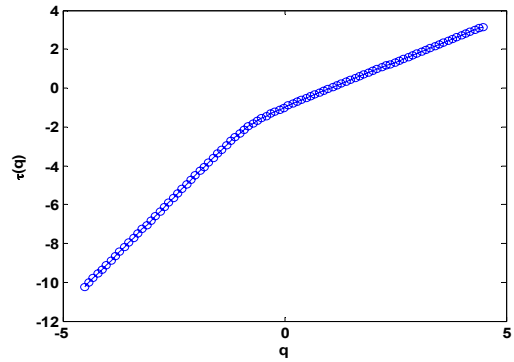

Figure 4. Graph of τ(q) versus q.

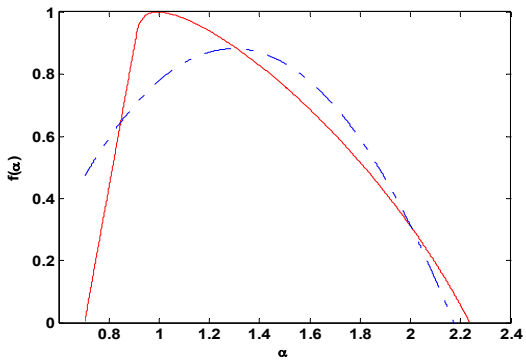

Figure 5. Graph of f(α) versus α.

Figures 4 and 5 show the corresponding exponents $\tau(q)=q\,\tau(q)-1$ and the corresponding $f(\alpha)$ singularity spectrum calculated from $h(q)$. We can see that the $\tau(q)$ curve clearly departs from a straight line (i.e. the q dependence of $\tau(q)$ is nonlinear). Furthermore, the spectrum $f(\alpha)$ displays the commonly observed bell shape. Thus, we conclude the speed time series has a behavior of multi-fractality.

The same method is used to analyze the shuffled time series. The results show that the $\tau_{shuf}(q)$ curve clearly departs from a straight line. The multi-fractal behavior of the speed time series cannot be removed by shuffling the original series. Comparing the spectrum for original series to those for shuffled series, it indicates that the shuffled series show stronger multi-fracrality than the original series.

Distinguishing the Two Types of Multifractality. As mentioned in the introduction, two different types of multi-fractality are prevalent in time series. The easy way to distinguish between them is to analyze the corresponding randomly shuffled series.

The shuffled series from correlation multi-fractals will exhibit simple random behavior. For distribution multi-fractals, on the contrary, the original $h(q)$ dependence is not changed. In order to directly determine the magnitude of the distribution multi-fractality, which is due to the broad probability density function, we compare the fluctuation function for the original series, $F_q(s)$, with

the corresponding shuffled series, $F_q^{shuf}(s)$. We consider the ratio $F_q(s)/F_q^{shuf}(s)$.

The scaling behavior of the ratio is:

$$F_q(s)\Big/F_q^{shuf}(s) \sim s^{h(q)-h_{shuf}(q)} = s^{h_{cor}(q)}.$$

If only distribution multi-fractality is present, $h(q)=h_{shuf}(q)$ depends on q. Deviation of $h_{cor}(q)=h(q)-h_{shuf}(q)$ from zero indicate the presence of correlations, and q dependence of $h_{cor}(q)$ indicates correlation multi-fractality. If only correlation multi-fractality is present, $h_{shuf}(q)$=0.5. If both distribution multi-fractality and correlation multifractality are present, both $h_{shuf}(q)$ and $h_{cor}(q)$ depend on q.

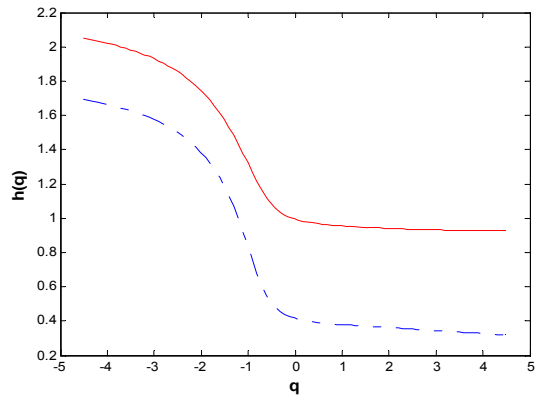

Figure 6. Graphs of h(q) versus q.

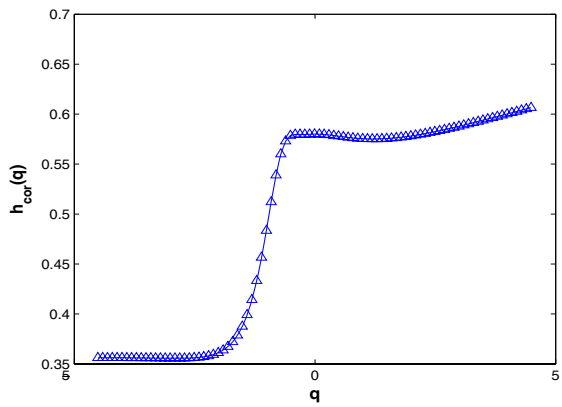

Figure 7. Graph of hcor(q) versus q.

The dependence of and $h(q)$ $h_{shuf}(q)$ are shown in Fig. 6. The solid line is the graph of $h(q)$ versus q and the dotted line is $h_{shuf}(q)$ versus q. The value of $h_{shuf}(q)$ decreases with increasing q. This suggests that the multi-fractality of speed time series is due to a broad probability distribution. Fig. 7 shows the q dependence on the slopes $h_{cor}(q)$. We can see that deviations of $h_{cor}(q)$ from zero indicate the presence of correlations, and q dependence of $h_{cor}(q)$ indicates correlation multi-fractality. From the data in Figures 6 and 7, we can conclude that both distribution multi-fractality and correlation multi-fractality are present in the speed time series.

CONCLUSION

The analysis presented in this paper shows that the MF-DFA method can reliably determine the multi-fractal scaling behavior of speed time series. In comparing the MF-DFA results for original series to those for shuffled series, we determine that the multi-fractality of the speed time series is mainly due to a broad probability density function, and that the multi-fractality of the shuffled series is stronger than that of the original series. These results may aid the application of multi-fractality in traffic flow theory. They also have signifigance for traffic time series theoretical modeling, short forecasting and the creation of control strategic plans.

ACKNOWLEDGEMENTS

This work is supported by a grant from the National High-tech Research and Development Program of China (863 Program) (NO.2007AA11Z212 and NO.2007AA11Z220).

REFERENCES

Ivanova, K., and Ausloos M. (1999). "Application of Detrended Fluctuation Analysis (DFA) method for describing cloud breaking." *Physica A,* 274:349-354.

Kantelhardt, J.W., Zschiegner, S.A., Bunde, E.K., Havlin, S., Bunnde, A., Stanley, H. E. (2002). "Multi-fractal detrended fluctuation analysis of nonstationary time series." *Physica A ,* 316:87-114.

Kantelhardt, J.W., Koscielny-Bunde, E., Rego, H. A., Havlin, S., Bunde, A. (2001). "Detecting long range correlations with detrended fluctuation analysis." *Physica A ,* 295:441-454.

Peitgen, H.O., Jurgens, H., Saupe, D. (1992). *Chaos and Fractals.* Springer-Verlag, New York.

Pengjian, Shang, Xuewei, Li, Santi, and Kamae (2006). "Nonlinear analysis of traffic time series at different temporal scales." *Physics Letters A;* 357, 314-318.

Safanov, L.A. et al (2002). "Delay-induced chaos with multi-fractal attractor in a traffic flow model." *Europhys Lett* , 57:51.

Seely, A.J.E., Macklem, P.T. (2004). "Complex systems and the technology of variability analysis." *Critical Care*, 8:367-384.

Shang, P., Li, X. (2005). "Chaotic analysis of traffic time series." *Chaos, Solitons and Fractals.* 25:121-128.

Vjushin, D., Govindan, R.B., Monetti, R.A., Havlin, S., Bunde, A. (2001). "Scaling analysis of trends using DFA." *Physica A*; 302:234-243.

Yu, C.X., Gilmore, M., Peebles, W.A. and Rhodes, T.L. (2003). "Structure function analysis of long-range correlations in plasma turbulence." *Physics Of Plasmas*, 10:2772-2779.

Link Average Speed of Traffic Flow Estimation Method Based on Floating Car

W. Zhu[1], A. Chang[2], G. Jiang[3], W. Zhang[4]

School of Prospecting and Surveying, Changchun Institute of Technology and College of Transportation, Jilin University, P.O. Box 130022, Changchun; PH: (384) 417-7881; email: zwg86@163.com
[2]College of Transportation, Jilin University, P.O. Box 130022, Changchun; PH: (389) 489-8035; email: changande1234@163.com
[3]College of Transportation, Jilin University, P.O. Box 130022, Changchun; PH: (318) 509-5505; email: jianggy@jlu.edu.cn
[4]College of Transportation, Jilin University, P.O. Box 130022, Changchun; PH: (357) 876-8721; email: zw.sunny@yahoo.com.cn

ABSTRACT

In floating car data collection, the link average speed of floating cars is exported as link average speed of traffic flow. This results in low quality traffic information being shared with the public. This paper investigates the quantitative relationship between link average speed of floating cars and link average speed of traffic flow considering the traffic conditions, and verifies the research with simulated data based on a part road network in Changchun. The results show that the link average speed of floating cars can not be used instead of the link average speed of traffic flow, and that the link average speed of traffic flow can be estimated accurately using the method described in this paper.

INTRODUCTION

Link average speed is regarded as an effective traffic parameter for measuring the degree of traffic congestion. Floating car data collection has become one of the main means for collecting link average speed (Jiang G., 2004).

In typical case, a single vehicle type (taxi, bus, logistics vehicle etc.) is selected as the floating car in order to reduce system costs (Turner S.M., 1998). However, the structure of vehicle type in traffic flow is very complex, and the running characteristics of different types on road are distinctive. Therefore, the Link Average Speed of Floating Cars (LASFC) cannot usually be substituted for the Link Average Speed of Traffic Flow (LASTF).

Currently, research on floating car-based traffic information collection technology focuses on traffic data estimation methods based on individual floating car, and the average traffic data of floating cars is directly exported to users (Quiroga, C.A., 1997, Young-Ji, B., 2005 and Dong, J., 2006). The relationship between traffic data for floating cars and traffic flow is infrequently discussed.

In this paper, we present a method, verified with simulated data, for estimating the LASTF based on floating car data, through analyzing the relationship between LASFC and LASTF.

MEAN VALUE OF LASTF ESTIMATION

Generally, the characteristics of the traffic environment (road facilities, regulation measures, driving behaviors etc.) are consistent in a given area. Therefore, the mean value of LASTF can be expressed as a function of the mean value of LASFC.

Road grade is one of the main factors affecting the functional relationship between the mean value of LASTF and LASFC. In addition, the functional relationships are affected by the traffic conditions. For instance, the gap between the mean value of LASTF and LASFC is very small in that vehicles run with no interference among each other when the link is clear. The gap is very small, too, during congestion, when vehicles run in a queue. However, the gap is relatively large and vehicles run without order when the link's traffic condition is neither clear nor fully congested.

In this paper, the LASFC is used as the evaluation index for identifying link traffic conditions. The LASTF can be expressed as follows:

$$V_T = \begin{cases} f_1(V_F) & V_F \le V_1 \\ f_2(V_F) & V_1 < V_F \le V_2 \\ \vdots & \vdots \\ f_n(V_F) & V_{n-1} \le V_F \end{cases}$$

Where V_T is the LASTF, V_F is the LASFC, f_i is the function between the mean value of LASTF and LASFC for speed interval i, n is the quantity of speed intervals and V_i is the upper boundary for speed interval i.

INTERVAL OF LASTF ESTIMATION

The interval of LASTF cannot be calculated by this equation. The transmission error and fitting error of function are the main factors involved in estimating the interval of LASTF from LASFC (Fei Y., 2005).

The transmission of error from LASFC to LASTF by the pervious equation originates from the transmission of standard deviation from LASFC to LASTF on the basis of error theories (Sha D., 2003). The standard deviation of LASTF can be expressed as follows:

$$SV_T = \left| \frac{\partial f(V_F)}{\partial V_F} \right| \cdot SV_F$$

Where SV_T is the standard deviation of LASTF, SV_F is the standard deviation of LASFC and f is the function between the mean value of LASTF and LASFC.

The statistic of t-distribution structured by the sample mean value and standard deviation of LASTF can be expressed as follows:

$$\frac{V_T - \lambda}{SV_T/\sqrt{N}} \sim t(N-1)$$

Where λ is the population mean value of LASTF and N is the sample size of floating car.

The fitting error of function approximately obeys normal distribution. If α is the given confidence level and ε is the limit of fitting error with α for sample data, the interval of LASTF can be expressed as follows:

$$\left[V_T - \frac{SV_T}{\sqrt{N}} t_{\alpha/2}(N-1) - \varepsilon,\ V_T + \frac{SV_T}{\sqrt{N}} t_{\alpha/2}(N-1) + \varepsilon\right]$$

VALIDATIONS AND ANALYSIS

Traffic volume, travel time and signal timing parameters were collected by the authors at South Lake Street in Changchun, China, on Aug 18, 2008. Figure 1 shows the surveying route and sections.

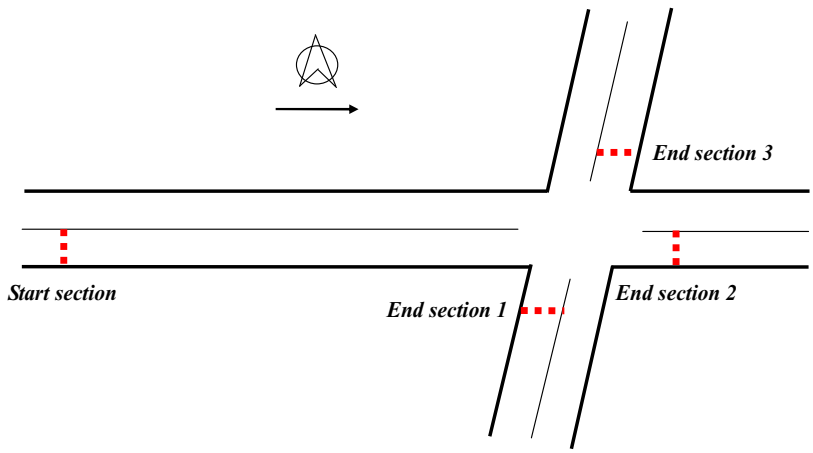

Figure 1. Route and sections of data collection.

The mean value of the average speed (LASFC and LASTF) was calculated at five-minute intervals from 04:00:00 to 08:00:00 a.m. for five successive working days. Measurements were taken using VISSIM 4.20 calibrated by measured data. In addition, two setting plans of control signals were designed. First, control signals were working full-time from 04:00:00 to 08:00:00 (designated the complete control plan). Second, control signals were working from 04:00:00 to 05:00:00 and closed from 05:00:00 to 08:00:00 (called the partial control plan).

Figures 2 and 3 show the fitting effects between the mean value of LASFC and LASTF for the complete control plan and partial control plan, respectively.

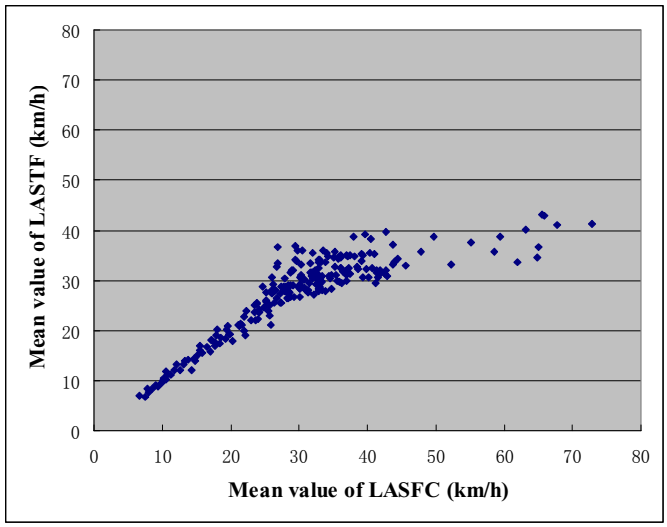

Figure 2. Fitting effect between the mean value of LASFC and LASTF for complete control plan.

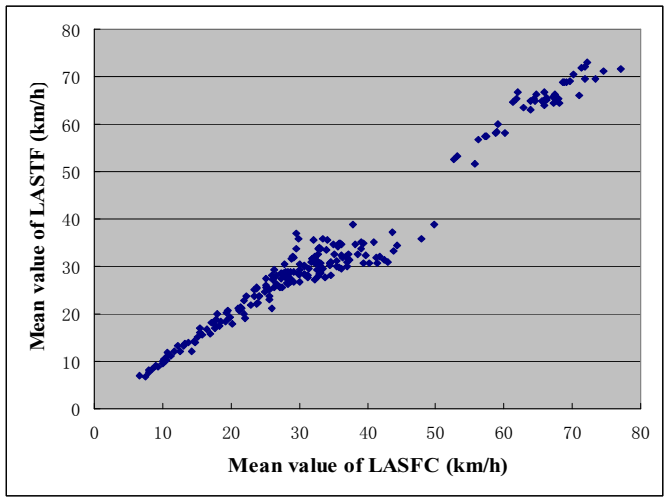

Figure 3. Fitting effect between the mean value of LASFC and LASTF for partial control plan.

Figures 2 and 3 show that the mean value of LASFC can be divided into three speed intervals: ≤25km/h, 25-50km/h and ≥50km/h. Tables 1 and 2 show the fitting results between the mean value of LASFC and LASTF for the complete control plan and partial control plan, respectively.

Table 1. Fitting results between the mean value of LASFC and LASTF for complete control plan.

Speed intervals	Functions	Correlation coefficients	Mean values of fitting error	Standard deviations of fitting error
≤25 km/h	y = 1.001x - 0.025	0.9789	0.8065	0.7756
25-50 km/h	y = 0.377x + 18.48	0.6052	2.1425	1.6000
≥50 km/h	y = 0.374x + 14.72	0.6033	2.3434	1.3195

Table 2. Fitting results between the mean value of LASFC and LASTF for partial control plan.

Speed intervals	Functions	Correlation coefficients	Mean values of fitting error	Standard deviations of fitting error
≤25 km/h	y = 0.982x + 0.225	0.9817	0.7876	0.6970
25-50 km/h	y = 0.432x + 16.26	0.6842	1.8460	1.5245
≥50 km/h	y = 0.853x + 8.884	0.9288	1.4942	1.1367

CONCLISION

In most cases, the LASFC cannot be equal to LASTF because sample sizes are much smaller than the total numbers of vehicles. The quantitative relationships between LASTF and LASFC are mainly affected by traffic conditions and setting plans of control signals. Consequently, the LASTF can be estimated from LASFC through the functions determined in advance.

RECOMMENDATIONS FOR FUTURE RESEARCH

The influencing factors on the quantitative relationship between LASTF and LASFC should be researched continuously using measured data, so that the functions determined are more accurate.

ACKNOWLEDGEMENT

This paper is financed by National High-tech R&D (863) Program of China (2007AA11Z245 and 2007AA12Z242) and the Doctoral Subject Research Fund of Higher Education of China (20070183129).

REFERENCES

Dong, Junyu. (2006). “Study on Link Speed Estimation in Urban Arteries Based on GPS Equipped Floating Vehicle,” *Chongqing University*, Chongqing,

China.

Fei, Yetai. (2005). "Error Theory and Data Processing," *China Machine Press*, Beijing, China.

Jiang Guiyan. (2004). "Technologies and Applications of the Identification of Road Traffic Conditions," *China Communications Press*, Beijing, China.

Quiroga, C.A. (1997). "An Integrated GPS-GIS Methodology for Performing Travel Time Studies," *Louisiana State University*.

Sha, Dingguo. (2003). "Errors Analysis and Measurement Uncertainty Evaluation," *China Metrology Publishing House*, Beijing, China.

Turner S.M., Eisele W.L., Benz R.J. et al. (1998). "Travel Time Data Collection Handbook," *FHWA-PL-98-035, Texas Transportation Institute*.

Young-Ji, Byon. (2005). "GPS-GIS Integrated System for Travel Time Surveys," *University of Toronto*.

A "Reality Vision" Navigation Technique based on Sequence Geo-referenced Image Databases

HU Qingwu[12], Liu Shoujun[2] and Mao Kai[2]

[1]School of Remote Sensing and Information Engineering, Wuhan University, No.129, Luoyu Road, P.R. China,430079;PH (86) 27-68778546; FAX (86) 27-68778546; email: qwhu@263.net
[2]Wuhan Leador Co., Ltd, Wuhan, P.R. China, 430074; PH (86) 27-87492808; FAX (86) 27-68778035; email: lsj@leador.com.cn

ABSTRACT

Mobile storage techniques have gained rapid development together alongside 3D technology, thus making mobile terminal integrated vision navigation possible. A vision vehicle navigation system can be a useful component of intelligent transportation systems, helping people to quickly find their destinations through realistic visual navigation guidance. In this paper, we propose a "reality vision" navigation system based upon a sequence geo-referenced image database. First, a sequence geo-referenced image collection technique with a land-based mobile mapping system is described. The sequence image database and index algorithm with spatial grid is designed to obtain fast query response with an image selection algorithm. Second, the road link model with sequence image database and a related navigation mode is presented as a way to realize reality vision navigation. Finally, we describe a prototype that is supported by Windows Mobile and can run with PDA、PND. The prototype can support an image database of a whole Wuhan city with data volume above 2GB and still achieve reality vision navigation.

INTRODUCTION

Due to the increasing public demand for spatial information services and location-based services, more and more navigation and LBS systems are being built. Navigation is a complex human activity (Burnett, Smith & May 2001) that has become a very popular research area. Researchers are especially interested in developing transportation systems that help drivers find their way in real or electronic worlds. The use of car navigation systems and personal navigation devices (PNDs) has spread rapidly, and all kinds of navigation systems come standard with new vehicles.. Many navigation systems use 2D maps to represent real-world objects, but they are unable to provide users with significant information

about the objects, such as their colors, shapes or materials. Features and navigational landmarks are not easily available in these systems, even though they can be very useful navigational tools. According to Coors et. al (2004), people recognize landmarks and find routes in the cities easier by using 3D vision models than using a symbolic 2D map which makes 3D visualization more relevant for navigation. Furthermore, the high visual correspondence between objects on a 3D map and real world objects increases the 3D map's navigational value.(Coors et. al., 2006). Thus the 3D vision personal or vehicle navigation systems have become a hotspot both in research fields and in practical areas.

Different applications involving 3D representations of real or virtual environments have been developed with the purpose of improving user navigation. Fukatsu S. et. al.(1998) introduced the simultaneous overlaying of global bird's-eye views as well as local views of the world. To aid the user in finding landmarks Elvins T. et. al.(1998) created miniature virtual worlds called Worldlets that act as 3D thumbnails. Sharkawi et. al (2008) proposed a 3D navigation system for virtual reality based on the 3D game engine for indoor or outdoor environment navigation applications. LI Yuan et. al (2008) presented a 3D indoor navigation framework of combining BIM with 3D GIS to provide 3D indoor navigation service for the emergency response. C. S. Wang et. al (2008) also successfully developed a 3D virtual navigation system for campuses, museums or art galleries. Chen (2008) discusses a multi-sensor-based 3D mobile navigation system and its application on telecommunication and social networking services. Although the 3D navigation has seen much development and various applications, it still some limitations. First of all, the 3D model represents a virtual scene which is very different from the real environment. The visual correspondence between 3D models and real-world objects still exists. Secondly, to generate the 3D map from satellite images and other 3D maps is time-consuming. Three-dimensional navigation cannot be widely used for the construction of another 3D map. Finally, the 3D map has demanding system memory and storage requirements.

In the following pages, we propose a reality vision navigation system based on a sequence geo-referenced image database. The geo-referenced images are taken as a 3D map, which produces a realistic representation of the scene. Thus, the images reduce the difference between the map and real world, helping people locate the landmark. The related data production and organization technique are discussed. An image navigation algorithm is presented to realize reality vision navigation. A reality image navigation prototype supported by windows mobile is developed.

RELATED WORKS

Image-based methods are a new approach to solving navigation problems. Instead of building a metric, or 3D, model of the environment, these methods work

directly within the sensor space, or image. The environment is represented as a topological graph, in which each node contains an image taken at some spot in the workspace. Typical image navigation techniques are adopted for Simultaneous Localization and Mapping, or SLAM. Visual SLAM systems using both monocular and stereo imaging to reconstruct 3D models of the environment have been studied in depth (A. J. Davison et. al, 2007). D. G. Lowe et. al (2004) and J. Tardif et. al (2008) present systems that use monocular vision and structure from motion techniques in order to provide a real-time estimate of the trajectory followed by a robot. Another typical image navigation application is that of unmanned aerial vehicles (UAVs). Researchers conduct image matching between a real-time imaging system and the image database for UAV navigation (Bruno Sinopoli et. al, 2001). Fiala (2005) provided an initial framework for immersive environments, in which the environment could be defined by a set of panoramas captured by catadioptric cameras, and the panoramas were defined as cubes. Sampling the plenoptic function from a single point and storing it in a cubic format is an idea used often in computer graphics. Fiala chose this idea for his framework because it would allow for the creation of new interpolated panoramas for 4 of the 6 sides used the image warping results of Seitz and Dyer (1996). Derek Bradley et. al (2008) presented an image navigation system based on real environments and using panoramas. This process has achieved actual applications for personal indoor navigation.

The current image navigation techniques focus on computer vision applications such as the SLAM and UAV systems. Images like monocular images or the panoramas have many advantages over 2D or 3D maps when seeking to achieve realistic representation. They can obviously be used for the vehicle navigation and personal navigation. Below we discuss the possibility of image navigation techniques vehicles and for personal navigation applications. These can be useful components of intelligent transportation systems, helping people to quickly locate their destinations through realistic visual guidance.

DATA COLLECTION OF IMAGE NAVIGATION

The land-based mobile mapping system integrates geodetic quality GPS, digital stereo cameras and inertial navigation system (INS) or dead reckon system (DR) that are mounted on a vehicle (Li D R et al, 2007). The system records highly accurate dual frequency GPS data and captures sequence images along the road in motion. Eight cameras are used in the mobile mapping system to form stereo images. GPS/INS/DR provides the orientation parameters for the stereo image models. It proves to be the most rapid, convenient, accurate and economic tool for collecting and updating geo-information data when used with sequence geo-referenced images, which can be used as the data source of image navigation (see Figure 1).

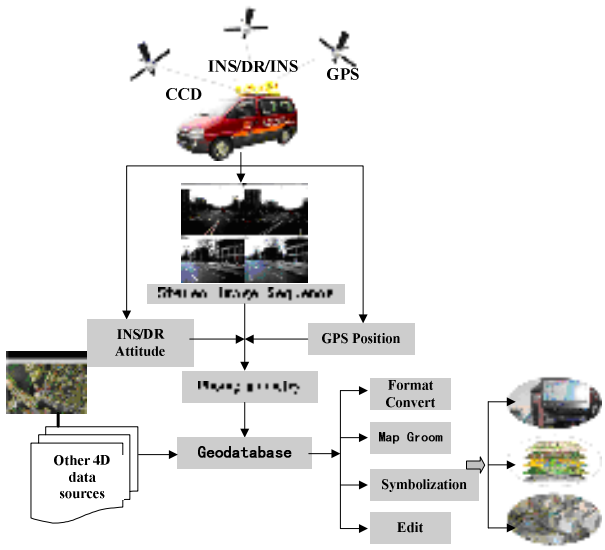

Figure 1 A land-based mobile mapping system for data collection

A land-based mobile mapping system is a close range photogrammetry system of direct geo referenced images. It closely simulates the perspective of human eyes and can collect a 360° sequence of street-view stereo image pairs at speeds over 100km/h. It can export vector maps, attribute data, and place digital measurable images in sequence. With the orientation data from DGPS/INS/DR, it can realize absolute position accuracy up to 0.5m and achieve a relative measurement at the centimeter level. The sequence geo-referenced image also records environmental information, such as transportation restrictions, POIs, and road networks to such a realistic degree that it can be used for navigation (see Figure 2).

Figure 2 Geo-referenced image databases for navigation

Geo-referenced images from a land-based mobile mapping system can overcome the probe error with manual labor, and it can reduce the time required to generate 3D maps. Consider, for example, street views of the real world. Compared to virtual 3D maps 2D maps, geo-referenced images can help people more easily

recognize a scene to locate an address or route. With a land-based mobile mapping system, we can obtain image navigation database directly from field work, thus making realistic 3D navigation possible.

IMAGE NAVIGATION MODEL

The geo-referenced images should integrate with 2D maps in order to support the path finding algorithm. Figure 3 represents the architecture of the image navigation system.

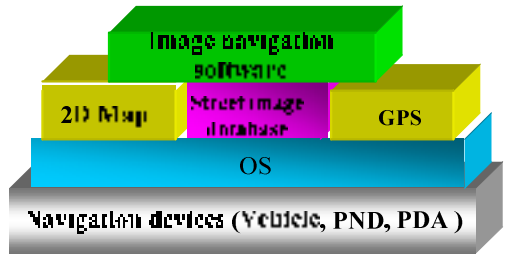

Figure 3 Architecture of the image navigation system

Street images are taken as a new data source combined with a 2D map. GPS matching with 2D map with the route can query the nearest reality image from the database to guide the user. The image navigation system should be run on common navigation devices such as a vehicle navigator, PND, PDA or smart phone. Thus the organization of the geo-referenced images becomes a key technique for the navigation system. Another question is the large volume of the image database. Usually, four to eight CCD sensors are installed on the land-based mobile mapping system. The data collection of street images can be defined as distance trigger of 8～20 meter or time trigger of 0.5～1. 0 second. One image has a volume size of 1.4 ～2. 0MB. A city about 200km^2 is about 1 TB volume and there are about 1,000,000 image files. The unique GPS time target is adopted to index the geo-referenced images (see Figure 4).

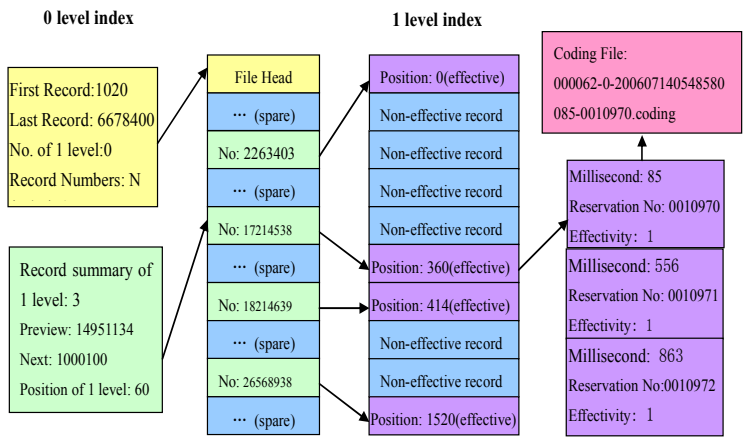

Figure 4 Geo-referenced image index model

For the street image index model, a position index of GPS time is built into the orientation. Then a time coding of each image is generated with two level indexes. 0 level records year to second. 1 level records milliseconds of each 0 level index item and its reservation information, such as the sensor ID. Each image will generate a one time coding file once it is captured. With the spatial position, it can query the image exposure time from the spatial index file. Then it can restore image files with image time stamp and find the image with the coding file.

Another key technique of the geo-referenced image database is the large data volume and number of files, especially for the navigator devices such as PND or PDA. Firstly, an image section algorithm is designed to reduce the data volume of geo-referenced images. The images are selected based on the road network, and POIs for the user will take care of the POIs. Only road intersections need detailed information. Images along the road link will be sampled at an interval of about every 50 meters (see Figure 5). Then a batch image compression process is used convert the image resolution from 1600×1200 to 256×256--a normal image size used to reduce data volume in portable screen devices.

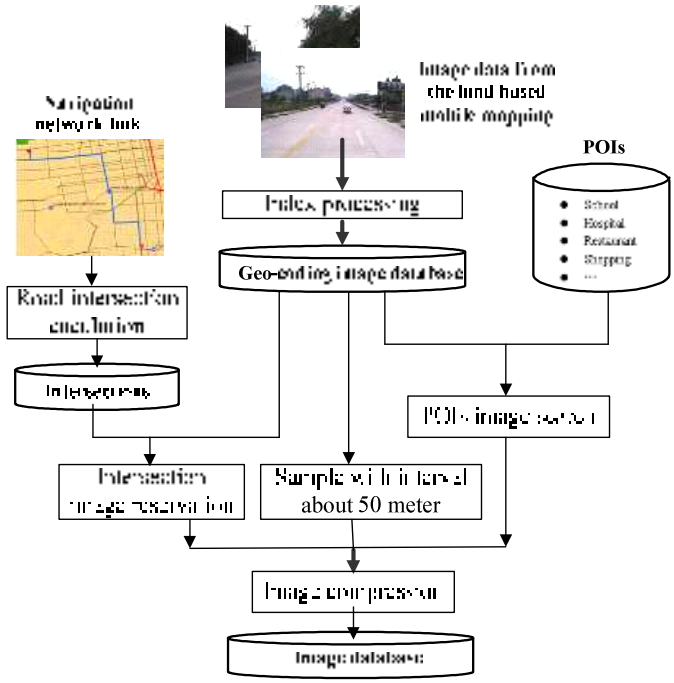

Figure 5 Image section algorithms for image navigation system

After the image selection, the image data volume of the 200km^2 city will be reduced from 2TB to 2GB, thus allowing it to be stored on the PND or PDA. 2GB images still have more than 100,000 files. In order to manage, query and store so many image files on the portable devices, a big image file is designed to store all the images in one file. Then the image file is connected with an image index target and

position as well as a network link ID. Each query therefore assigns each location or address an image index target. The index target will find the address of the image data in the big file. Comparing the query from the image folder with multiple image files, the big image file can avoid the search response time of operation systems, especially in a real-time application environment.

IMAGE NAVIGATION MODE

Geo-referenced images base navigation emphasis the reality experience for users during navigation. Geo-referenced images are taken as the main guide in navigation software. The 2D map serves as the eagle-eye for finding location addresses and routes. We designed two image navigation modes in the image navigation software. The first image navigation mode is the single image guidance mode (see Figure 6).

Figure 6 Single image navigation mode

Single image navigation mode uses the image as guidance, and the GPS position can be addressed on the geo-referenced image. The user can browse the left and right image of the current position. With the geo-referenced images and real scene, the user can still locate the address in case the GPS fails. The single image navigation mode is part of the personal navigation application. is suite of the personal navigation.

Another image navigation mode is the composite mode with images and a 2D map. This mode has the advantages of both 2D map navigation and single image navigation. The 2D map can show the current the GPS position alongside the planned path, allowing directions to be shown during navigation. The geo-referenced image can make it easier for the driver to locate the destination or landmark. (see Figure 7).

Figure 7 Composite navigation mode with image and 2D Map

Users can switch between composite navigation mode and single image navigation mode while *en route*. The routing plan can be done with the composite navigation mode. Before reaching the destination, the user can use the composite mode to obtain the general effect of the whole route plan. When nearing the destination, the single image navigation mode can be useful for finding the exact location of the destination. By comparison, GPS has a position error about 20 meters, especially in densely developed environments.

REALITY IMAGE NAVIGATION PROTYPE

We designed a reality vision navigation prototype of Wuhan city in order to verify the image navigation technique. With 3 sets of land-based mobile mapping systems, it only takes 2 months to collect the image navigation database with more than 3TB and 300,000 POIs. After creation of the image index and image selection, only about 3GB remain in the database for the final navigation system. We developed an image navigation mode in Windows Mobile 5.0 that can run with PDA、PND, allowing the image query response of the whole city to remain at less than 0.2s (Dopod , Windows mobile 5.0, 128M memory, 8G flash disk).

Table 1. Image query response of Wuhan city

	Data volume (GB)	Image number	Query response (s)
Hankou district	1.25	135058	0.13
Hanyang district	0.92	92325	0.08
Wuchang district	1.13	121347	0.11
Total city	3.30	348730	0.17

As Table 1 shows, the prototype can support the image database of a whole Wuhan city with data volume above 3GB and still reach reality vision navigation. The query response of the image based navigation averages about 0.17s. Figure 6 and Figure 7 show the navigation prototype of Wuhan city.

CONCLUSIONS

3D navigation is the future trend of vehicle navigation and personal navigation technologies. Sequence images captured along the road best resemble the habit of human vision and memory. It is unique in its ability to represent the real world. Geo-referenced images bypass the symbol representation errors occurring in map systems, and they incorporate more spatial semantics and non-spatial semantics than 2D maps and virtual 3D maps. Land-based mobile mapping systems provide a speedy tool for collecting and updating the image database necessary for the image-based navigation. With the spatial grid index algorithms of large volume geo-referenced images, portable devices can obtain fast access to the image database and destination addresses. This will be a new approach in 3D environment navigation. With the development of wireless communication, web service techniques, and intelligent vision, geo-referenced image navigation will become a new trend in the navigation systems. It will push the navigation system applications used in intelligent transportation and emergency response application. Some further research work will focus on supporting seamless access to geo-referenced images of different cities.

ACKNOWLEDGEMENTS

The research work is supported by the Electronic Industry Development Fund of China. (Grand NO: [2004]479) The author would like to thank Leador Co., Ltd to provide the prototype system and geo-referenced images data of the whole Wuhan city for research work.

REFERENCES

Burnett G., Smith D. and May A. (2001). “Supporting the Navigation Task: Characteristics of Good Landmarks,” in M.A. Hanson (ed.), *Contemporary Ergonomics*, Taylor &Francis, London, pp. 441-446.

Coors, V., C. Kray, K. Laakso, and C. Elting. (2004). “Presenting route instructions on mobile devices.” *Geo-Visualization*, 2004.

Coors, V., J. Haist, and T. Reitz. (2006), "A web 3D service for Navigation Applications." 1st International Workshop on 3D Geo information 2006. Kuala Lumpur, Malaysia.

Elvins T., Nadeau, D., Schul, R., Kirsh, D. (1998). "Worldlets: 3D Thumbnails for 3D Browsing.*'Proceedings on CHI 98* , ACM Press, 163-170.

Fukatsu S., Kitamura Y., Masaki T., Kishino F. (1998)."Intuitive Control of Bird's Eye Overview Images for Navigation in an Enormous Virtual Environment." *Proceedings of the 1998 ACM Symposium on Virtual Reality Software and Technology*, 67-76.

K.H. Sharkawi, M.U. Ujang and A. Abdul-Rahman. (2008)."3D navigation system for virtual reality based on 3D game engine." *The International Archives of Photogrammetry, Remote Sens Spat Inf Sci*, 2008, Vol.XXXVII, Part B4, 513-518.

LI Yuan, HE Zizhang. (2008). "3D Indoor Navigation: a Framework of Combining BIM with 3D GIS." 44th ISOCARP Congress 2008.

Ching-Sheng Wang, Yu-Hung Su and Ching-Yang Hong. (2008)."A 3D virtual navigation system integrating user positioning and pre-download mechanism." *Proceedings of the World Academy of Science Engineering and Technology*. v. 30: 172-176.

Chen Yuwei. (2008). *Multi-sensors Based 3D Mobile Navigation and Its Application on Telecommunication Services and Social Networking.*

A. J. Davison, I. Reid, N. Molton, and O. Stasse. (2007). "Mono SLAM: Real-time single camera SLAM." *IEEE Transactions on Pattern Analysis and Machine Intelligence*, 29(6): 1–16, June 2007.

D. G. Lowe. (2004). "Distinctive image features from scale-invariant key points." *International Journal of Computer Vision*, 60(2): 91–110, November 2004.

J. Tardif, Y. Pavalidis, and K. Daniilidis. (2008). "Monocular visual odometry in urban environments using an Omni directional camera." International Conference on Intelligent Robots and Systems, 2008.

Bruno Sinopoli, Mario Micheli, Gianluca Donatoy, T. John Koo. (2001). "Vision Based Navigation for an Unmanned Aerial Vehicle." *Proc. of the IEEE International Conference on Robotics and Automation (ICRA 2001)*, Seoul, Korea, May 2001.

M. Fiala. (2005). "Immersive panoramic imagery." *Canadian Conference on Computer and Robot Vision*, 2005.

S. M. Seitz and C. R. Dyer. "View morphing." *Computer Graphics, 30* (Annual Conference Series): 21–30, 1996.

Derek Bradley, Alan Brunton, Mark Fiala, Gerhard Roth. (2005). "Image-based Navigation in Real Environments Using Panoramas." IEEE International

Workshop on Haptic Audio Visual Environments and their Applications Ottawa, Ontario, Canada, 1-2 October 2005.

Li D R, HU Q W. (2007). *Digital Measurable Image Based Geo-spatial Information Service* (in Chinese). Geo Inf Sci J Wuhan Univ, 2007, 32(5): 377-380.

Signal Timing and Coordination –An Art of Engineer ing

Z. Tian[1]

Abstract

The scientific and engineering aspect of signal timing and coordination is reflected by sophisticated optimization algorithms, computer software, and roadway infrastructure to support servicing traffic flows. On the other hand, implementing a coordinated signal timing plan in the field often involves fine tuning of a plan in order to achieve the best performance. Such a field implementation and fine tune task provides a stage for the traffic engineers to demonstrate their intellectual and artistic skills of manipulating signal timing using the advanced traffic signal controller features. Therefore, traffic engineers often describe signal timing as a form of engineering art. This paper addresses such an artistic aspect of signal timing by illustrating various signal timing tricks applied on different cases. Specifically, the cases to be discussed include: left-turn phasing sequence, pedestrian handling, dealing with long arterials, and strategies for controlling closely-spaced signals. Applying the tricks and tips illustrated in this paper can provide quick fixes to some common operational problems without the need of significant capital investment. Finally, the paper also touches some basic issues related to traffic flow and roadway characteristics in China, and how the signal timing principles may be adapted to China's urban arterials.

Keywords: Signal Timing, Coordination, Art of Engineering, Traffic Flow

Introduction

Technology advancement over the last decade has significantly changed how modern traffic signal control systems operate. As one of the major components of Intelligent Transportation Systems (ITS), traffic signal control systems have adopted many such advanced technologies. Advancements of vehicle detection technology include development of video-detection systems to replace traditional inductive loops (Bonneson 1998; Tian et al. 2002; Tian and Abbas 2007). Advancements of detection technology also involve development of more efficient lane-by-lane detection schemes (Smaglik et al. 2005; Tian and Urbanik 2006; Wu and Tian 2007). Improvements in communication technologies allow fast signal timing exchange between a central computer and local controllers. Advanced computing technologies result in significant enhancements on signal controller features and functions, including more powerful processors and more sophisticated signal control algorithms for better handling of special service requests, such as bus priority, emergency vehicle preemption and transition.

Traffic engineers and scholars often describe traffic signal coordination as a form of art, resembling watching a ballet while observing traffic flows with well synchronized traffic lights. Because many factors cannot be explicitly considered and modeled, implementing the

[1] Zong Z. Tian, Associate Professor, Dept. of Civil and Environmental Engineering, University of Nevada, Reno, MS 258, Reno, NV 89557; zongt@unr.edu

best signal timing plan often involves fine tuning in the field, reflecting an engineer's artistic judgment and skillful mind trained by many years of experience and education. Such a field implementation and fine tune task provides a stage for the traffic engineers to demonstrate their intellectual and artistic skills of manipulating signal timing using advanced traffic signal controller features.

The primary objective of this paper is to address the artistic aspect of signal timing by illustrating various signal timing tricks applied in different case studies. The illustrated cases well reflect the author's many years of experience working in both the academic and practical fields. While the strategies proved to be effective in further improving signal timing solutions from traditional optimization models, they are not yet been explicitly modeled due to the nature and complexity of modeling them in scientific manners. However, with the advance of integrated approach to addressing engineering and scientific issues, these problems could be better modeled in the future. It is the author's intention to raise wide awareness of the signal timing field and to attract more scholars into this fascinating interdisciplinary field.

The Art of Signal Timing

Left-turn Phasing Sequence

One of the critical elements for signal coordination is the left-turn phasing sequence. It has been well recognized that the lead-lag phasing sequence can significantly improve progression bandwidth. In a recent study by Tian et al. (2008), the effectiveness of lead-lag phasing was given quantitative evaluations by developing a computer program that was able to randomly generate many network cases and to provide maximal bandwidth solutions. One of the major findings from the research (see Figure 1) was that lead-lag phasing can significantly benefit maximizing bandwidth over other phasing sequences, e.g., more than 70% of the cases.

While phasing sequence has generally been given more attention when dealing with coordination, it also affects operations at individual intersections. One of the phenomenons is the short-lane issue (Tian and Wu 2007; Zhang and Tong 2008). For example, a left-turn pocket is a commonly seen short-lane case, where queue blockage to the pocket section can reduce capacity and affect signal coordination. Depending on the proportion of left-turn and through traffic volumes, the sequence of leading or lagging the left-turn phase can make a significant difference in traffic operations. As can be seen in Figure 2, the figure on the left side shows the left-turn pocket is blocked by a through vehicle (typical when through traffic volume is higher than the left-turn traffic), while the figure on the right side shows the left-turn pocket is blocked by a left-turn vehicle (typical when the left-turn volume is higher than the through traffic). For the case shown in the left-side figure, lagging the left-turn phase is more effective because it would allow the left-turn vehicles getting to the stop line before the left-turn phase turns on. For the case shown in the right-side of the figure, leading the left-turn phase is then more effective because it would allow the through vehicles getting to the stop line before the through phase turns on. Signal-timing software generally does not take such short-lane case into consideration; however, some recent studies have attempted to address the short-lane issue using probability theories (Tian and Wu, 2006; Zhang and Tong 2008).

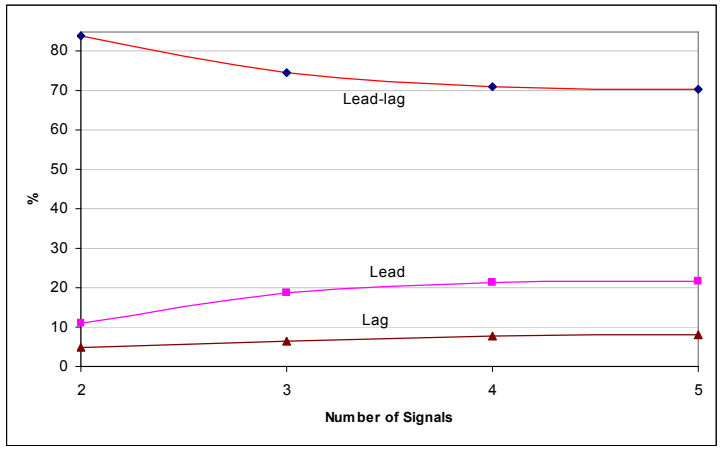

Figure 1 Percentage of Cases of Using Different Phasing Sequence for Maximizing Progression Bandwidth

Figure 2 Effect of Short Left-turn Lane and Phasing Sequence

Pedestrian Issues

As a major non-vehicular traffic mode, pedestrian crossing can affect signal operations and coordination in several ways. For signal operations and coordination, pedestrian timing needs to be programmed in traffic signal controllers, where the effect varies depending on the selection of pedestrian timing alternatives. Although practicing traffic engineers realize the importance of considering pedestrian timing, most signal timing optimization methodologies either completely ignore or give little consideration to pedestrian timing. Signal timing solutions derived from optimization methodologies without consideration of pedestrian timing generally cannot be implemented directly into traffic signal controllers. Because conflicting objectives generally exist between serving pedestrians and vehicular traffic, strategies for minimizing pedestrian impacts have been sought. Pedestrian crossing impact is best illustrated by the case of pedestrians crossing an arterial, where the time needed for pedestrians to cross is usually much longer than the time needed for vehicular traffic. The discussions next illustrate two common cases dealing with pedestrian handling in signal timing and coordination.

Pedestrian Timing Under Split Phasing

When split phasing is used for the cross street due to geometry and traffic flow patterns, pedestrian crossing has the most significant impact due to accommodation of two pedestrian splits for crossing both sides of the street. In a study by Tian et al. (2001), strategies were developed to provide a dynamic protected-permitted display, where a protected display is used when there is no pedestrian crossing in a cycle, while a permitted display is used when there are pedestrian crossings in a cycle. Such strategies are aimed at minimizing the pedestrian impact when split phasing is used. Figure 3 shows the phasing diagram for the side street under various pedestrian crossing scenarios. Using such a phasing scheme, only one pedestrian time split is needed for the side street, thus significant time savings could be

achieved compared to conventional ways of handling pedestrian timing.

Coordination Issues

In a study by Tian et al. (2000), two alternative treatments on pedestrian timings were addressed: timing based on pedestrian minimums where the required pedestrian crossing times were accommodated in the signal phase splits, and timing based on vehicle minimums where the phase splits were determined only based on vehicle demand. Various effects of the two pedestrian treatment alternatives were demonstrated through a case study. Various timing strategies were identified to minimize the negative effect while timing based on pedestrian minimums. These timing strategies included the appropriate setting of offsets, the effective use of side-street phasing, and the use of maximum recall. It was found that although timing based on vehicle minimums can generally result in a shorter system cycle length, timing based on pedestrian minimums can normally achieve the same operational efficiency. The most significant advantage of timing based on pedestrian minimums was that the signal system will always remain in coordination. The only drawback of timing based on pedestrian minimums is the likely use of longer cycle length. It was recommended that timing based on pedestrian minimum technique should be applied when longer cycle length was required for the system, and medium to high level pedestrian crossing activities exist.

Figure 4 illustrates how stops can be reduced by using the maximum recall feature in the signal controllers. The figure on the left shows that a max recall was applied at intersection #1, while the figure on the right shows no max recall was applied. Both cases resulted in the same vehicle delay, but by using max recall, the number of stops was reduced.

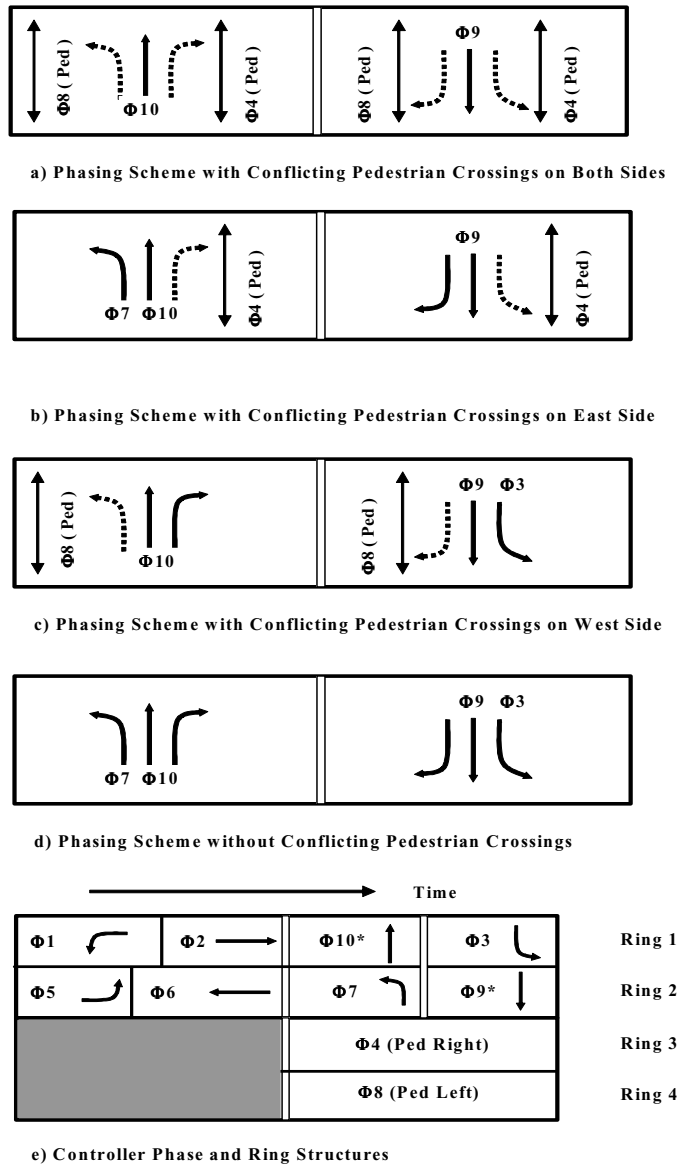

Figure 3 Strategies for Minimizing Pedestrian Impacts Under Split Phasing

Long Arterials

When a signal system has a large number signals (e.g., more than 10 signals), it is often difficult to achieve a good system bandwidth by using general signal-timing software packages, such as PASSER II, TRANSYT 7-F, and Synchro. In fact, attempting to achieve a total system progression band having low bandwidth efficiency may not be an efficient approach to developing signal-timing plans. In a study by Tian et al. (2007), a new approach to application of bandwidth-oriented signal timing was proposed based on a system partition technique. The proposed approach was to divide a large arterial signal system into sub-systems with 3 to 5 signals in each subsystem. Each subsystem was optimized to achieve the maximum bandwidth efficiency. A one-directional system progression bandwidth, normally the peak-flow direction was then formed by appropriately adjusting the offsets between each subsystem. Figure 5 illustrates a signal timing timing solution using the system partition technique. Such a signal timing solution would provide maximum progression for the peak

direction while still maintaining partial progression for the off-peak direction, where vehicles can at least go through each subsystem without having to stop.

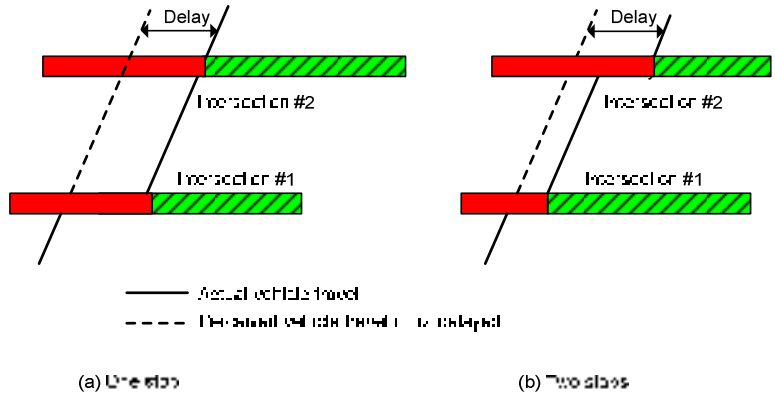

Figure 4 Use of Max Recall to Minimize Stops

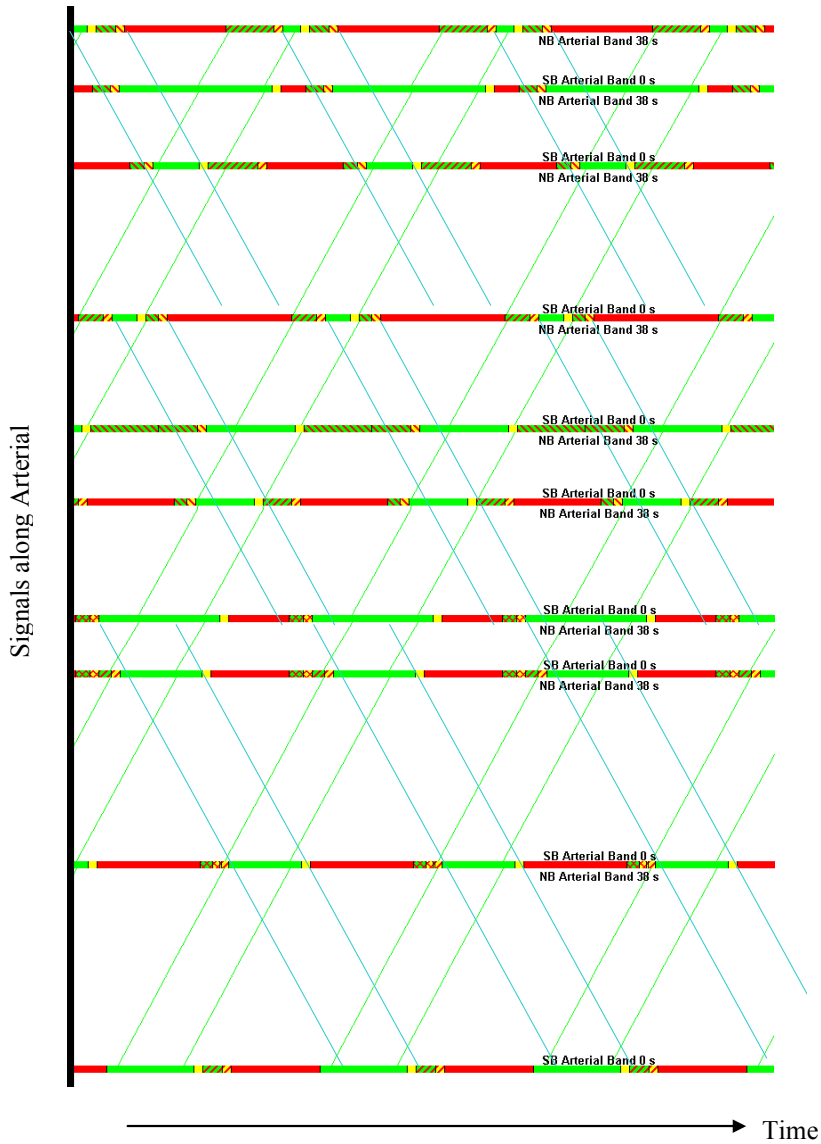

Figure 5 Partition Technique for Long Arterials

Concluding Remarks

This paper provided discussions on the artistic aspect of traffic signal timing and coordination. Through demonstration of various tricks for operating traffic signals, it indicated that many such cases have not been addressed by scientific and engineering models and algorithms. Rather, these signal timing techniques are mainly representations of the special skills of experienced traffic engineers, which reflect many years of field experience and manipulation of advanced traffic signal controller features. However, it is the author's intention to use such cases to draw interests from a broad range of scholars into addressing signal timing issues. Finally, the cases illustrated were mainly based on U.S. practice and traffic flow characteristics. The traffic conditions in China are quite different; therefore, adapting such strategies into China's urban arterials must take into consideration of its special traffic flow and signal system characteristics. For example, the pedestrian volume in

China is much higher than the U.S. Most urban arterials in China have low access control, where vehicles do not generally maintain a good platoon structure. The typical long peak period with high traffic demand also tend to make the actuated operation less effective.

References

Bonneson, J. A. (1998). "Probabilistic speed-estimation measurement errors through video images", Journal of Transportation Engineering, Vol. 124, No. 6, 611-613.

Messer, C.J., Whitson, R.H., Dudek, C.L., and Romano, E.J. (1973). "A variable sequence multiphase progression optimization program", Highway Research Record 445, 24-33.

Smaglik, E.J., Bullock, D.M. and Urbanik, T. (2005). "Evaluation of lane-by-lane vehicle detection for actuated controllers serving multilane approaches", Transportation Research Record No. 1925, 123-133.

Tian, Z., and Urbanik (2000). "Pedestrian timing treatment on coordinated signal systems", In: Proceedings of the 2nd International Conference on Traffic and Transportation Studies, ASCE, Beijing, China, 533-540.

Tian, Z. and Urbanik, T. (2006). "Green extension and traffic detection schemes at signalized intersections", Transportation Research Record 1978, 16-24.

Tian, Z. and Abbas, M. (2007). "Models for quantitative assessments of video detection system impacts on signalized intersection operations", Transportation Research Record (in press).

Tian, Z., Urbanik, T. and Gibby, R. (2007). "Application of diamond interchange control strategies at closely-spaced intersections", Transportation Research Record (in press).

Tian, Z., Mangal, V., and H. Liu (2008). "The effectiveness of lead/lag phasing on signal coordination", Presented at the 87th Transportation Research Board Annual Meeting.

Wu, N. and Tian, Z. (2007). "Modeling the lane-by-lane vehicle detection scheme at actuated traffic signals", Submitted to Transportation Science. Under Revision after 1st round Review.

Zhang, Y.L. and J. T. (2008). "Modeling Left-turn Blockage and Capacity at Signalized Intersection with Short Left-Turn Bay", Presented at the 87th Transportation Research Board Annual Meeting.

Highway traffic parameters estimation by using cell dwell time

H. Wang[1], Y. Han[2], Z. Liang[3]

[1]School of Transportation Science and Engineering, Harbin Institute of Technology, Harbin, China; email: hitwh@hit.edu.cn
[2]School of Transportation Science and Engineering, Harbin Institute of Technology, Harbin, China; email: hanyanquan521@163.com
[3]School of Transportation Science and Engineering, Harbin Institute of Technology, Harbin, China; email: liangzhongyan66@163.com

ABSTRACT

This paper investigates the method of collecting real-time traffic information using the cell dwell time (CDT) theory. In this novel technique, mobile phones are used as a tools to collect traffic information. The mobile phone network has extensive probes and can acquire exact information in any condition. Research suggests CDT is associated with traffic condition: high CDT values usually indicate high traffic congestion, low CDT indicates good traffic conditions. This paper illuminates the theory of using CDT to collect traffic information, and presents the traffic parameters estimate model. The vehicle routes between two cells can be confirmed by map matching technique. Based on the relationship of vehicle velocity, density and traffic volume, the traffic volume can be estimated. Using CDT theory, the researchers were able to obtain the average velocity of vehicles on the road. The results showed encouraging performance in traffic condition estimation and traffic parameters estimation.

INTRODUCTION

In general, there are two alternatives for collecting traffic information: fixed sensors or mobile sensors. The loop detectors, an example of fixed sensors, tend to be installed on major roads. They have significant maintenance requirements. Although fixed sensors allow the use of video and camera for collecting traffic parameters, those instruments do not work well in adverse weather. Using mobile phones as a traffic probe is a novel technique in collecting traffic information. The network of mobile phones presents extensive probes that can acquire exact information in any condition. The advantages of mobile phones as traffic probes include:

1) There is an abundance of probes to collect information. Every vehicle with a mobile phone can be a probe.
2) Using mobile phones as traffic probes makes it possible to monitor the whole road network over all time periods without additional equipment.

Using mobile phones as a traffic probe basically relies on two technologies: the network and the handset. The handset technology relies on additional technology in the handset, such as a GPS receiver. The network

method uses data already being used in the mobile phone system. Approaches that rely on additional technology in the handset have the potential to produce more accurate data. However, the trade-off is additional communication costs. The network solution is less accurate and more cost effective than the handset-based method.

In 1995, the US Federal Communications Commission launched enhanced 911 (e911) emergency services. It proposed that the operators must be able to locate the phones within 50 m 67% of the time, and/or 150 m 95% of the time by using the handset based solution. In addition, the network-based method has to provide the location within 100 m 67% of the time and/or 300 m 95% of the time[1].

Using cell dwell time (CDT) for traffic information collection and estimation, as presented in this paper, is one of the network-based technologies. The CDT was proposed by Wasan and Ratchata. In Bangkok's field experiment, they used the software installed in the handset to analyze traffic conditions. Their results showed that the CDT method is a relatively accurate and real-time solution to collecting traffic congestion information.

The mobile phone network is composed of a myriad of base stations. A mobile phone will chose the closest base station to transfer signals, so it switches from one cell to another cell as the user moves. The time that the phone remains registered in one cell is called cell dwell time (CDT). Research determined that CDT was associated with the traffic condition: high CDT values usually indicate high traffic congestion, and low CDT means good traffic condition, indicating free-flowing traffic.

TRAFFIC PARAMETERS ESTIMATION

Data collection

In the described method, every vehicle with a mobile phone becomes a traffic probe. The cellular network used by mobile phones is composed of myriad cells, with a base station at the center of each cell. When a mobile phone moves into a cell, it obtains a cord or ID to distinguish it from others. As the mobile phone moves to the edge of the cell, the signal diminishes until the phone transfers to the nearest cell with stronger signal. These ID cords are recorded by the network operator as the mobile phone is switched on. The transfer information of a phone between cells can then be collected anonymously and easily, and can be obtained from the original record of the network operator.

The collected CDT data should be classified first. There might be some noise data, which should be wiped off by the classification method. According to the coverage size of the cell, the range of CDT is established, as shown in Table 1. A CDT is treated as a noise data if it is larger than the maximum value in the Table.

Table 1. The range of CDT.

Cell size (meters)	CDTs (seconds)
0~300	0~500
300~500	0~700
>500	0~900

In the case of traffic congestion, the CDTs might overrun the normal data. The first step of data processing is smoothing the data via table 1. The next step involves calculating the average value of CDT. The average value *($\bar{c}$)* is calculated from the averaging of the sample n values:

$$\bar{c} = \frac{\sum_{i=1}^{i=n} c_i}{n}$$

Traffic parameters estimation

Consider a highway between towns that is covered by several mobile phone cellular base stations. Neglecting the influence of pedestrians for simplicity, let *i=1,2,3,,M* be the set of M cells. Let r^i denote the road stretch that is covered under cell *i*. Moreover, assume the following:

a) l_i the length of the stretch r^i

b) m^i the number of vehicles in r^i

c) n^i the number of mobile phones in r^i

d) c_p^i the CDT of the mobile phone *p* in r^i

e) $\overline{v_c^i}$ the average velocity of vehicles in r^i

f) v_p^i the velocity of mobile phone *p* in r^i

Assume that all recorded CDTs denote the cell dwell times of mobile phones in vehicles. Then:

$$v_p^i = \frac{l_i}{c_p^i}$$

according to the definition of space mean speed,

$$\overline{v_c^i} = \frac{1}{\frac{1}{n^i}\sum_{p=1}^{p=n^i}\frac{1}{v_p^i}}$$

In cases where there may be more than one phone in a specific vehicle, some

researchers decided to choose one phone, disregarding the others. In the paper, let λ represent the average number of mobile phones in a vehicle. λ is variable in different areas and can be confirmed by traffic surveys. The total number of mobile phones can be detected, so the number of vehicles can be calculated by:

$$m^i = n^i \times \lambda$$

Next, estimate the density and the flow of vehicles in r^i. Let k^i and q^i be the density and traffic volume, respectively. These values are defined as:

$$k^i = \frac{m^i}{l_i}$$

$$q^i = \overline{v_c^i} \times k^i$$

The traffic volume q^i is computed indirectly based on the traffic engineering theory.

SIMULATION AND RESULTS

For the sake of simplicity, the experiment was implemented in the following conditions:

1） The road is a highway between cities, with no bicycles or pedestrians.

2） It was covered by 11 cells. The coverage size of each cell was 500 meters.

The experiment was executed by vissim. Vissim is a microscopic, behavior-based multi-purpose traffic simulation program. The CDT data were noted by several time detecting buttons. The record data were analyzed by using the formula.

Figure 1 shows the measured velocity and true velocity. The velocity relative error is shown in Figure 2. The estimated traffic volume is shown in Figure 3. Figure 4 shows the relative error of detected traffic volume.

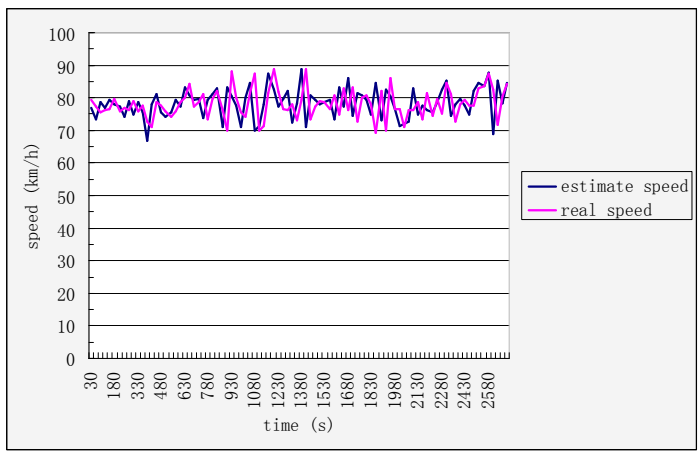

Figure 1. Estimated velocity vs. true velocity.

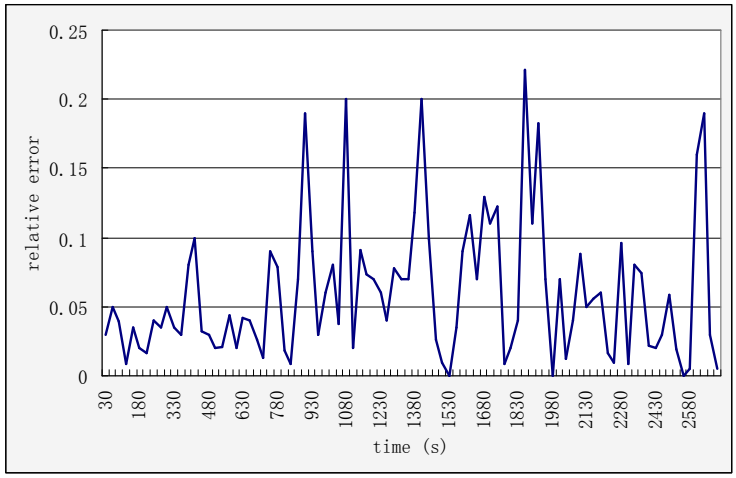

Figure 2. Relative error of estimated velocity.

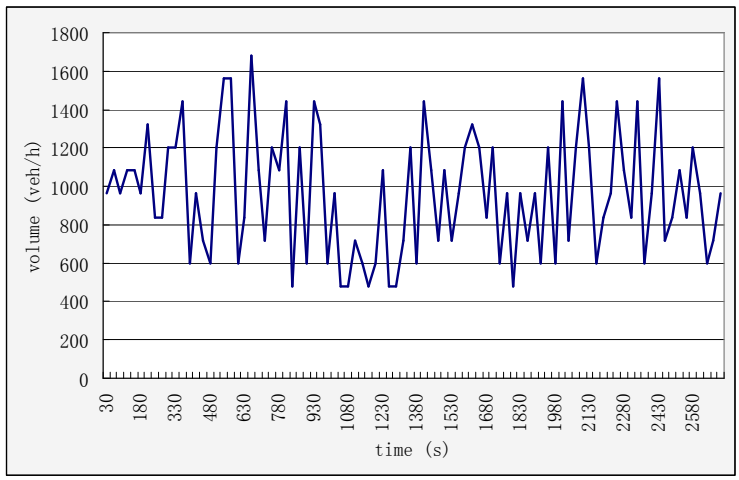

Figure 3. Estimated traffic volume.

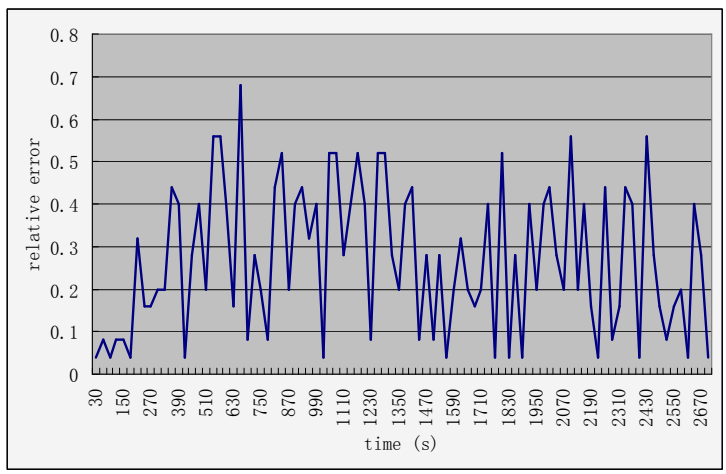

Figure 4. Relative error of detected traffic volume.

The experiment results show that the maximum relative error between the true vehicle speed and the estimated speed is about 22%, and over 90% relative error was below 10%. So the estimation of velocity is quite good. But

the detected traffic volume is not as satisfactory. Some relative error exceeds 65%. About 65% of the estimate volume error is below 30%. We ascribe the error to unpredictable driving behavior and complicated road conditions. In actuality, the volume we estimated is the traffic flow rate, which can be higher or lower than the actual traffic volume.

CONCLUSION

This paper investigates the collection of traffic information and estimation of traffic parameters using CDT. The experiment results show that using mobile phones to collect traffic information and estimate traffic parameters is a potentially useful method. The estimation of traffic parameters by using the information collected shows that adequate data is available. This technique may become another traffic probe application in the future.

Further research work will focus on the following:

1) Improving the parameter estimate modals.
2) Considering the impact of mobile phones that are not on the vehicles.
3) Investigating the road networks in the city. Junctions and traffic signal control systems will make estimation much more complicated.
4) Improving the experiment method and the simulation model.

REFERENCES

Bolla, R., Davoli, F. (2000). "Road traffic estimation from location tracking data in the mobile cellular network." *Wireless Communications and Networking Conference*, 2000. WCNC. 2000, IEEE.

Geoff, R. (2006). "Mobile phones as traffic probes: Practices, prospects and issues." *Transport Reviews*, vol. 26, no. 3, 2006.

Hellinga, B., Fu, L., Takada, H. (2003). "Obtaning Traveller Information Via Mobile Phone Location Referencing-Challenges and Opportunities." *2003 Annual Conference of the Transportation Association of Canada*.

Pattara-atikom, W., Peachavanish, R. *Estimating Road Traffic Congestion from Cell Dwell Time using Neural Network.* IEEE.

Pattara-atikom, W., Peachavanish, R., Luckana, R. (2007). "Estimating Road Traffic Congestion using Cell Dwell Time with Simple Threshold and Fuzzy Logic Techniques." *Intelligent Transportation Systems Conference*, 2007. IEEE.

Yim, Y. (2003). "The State of Cellular Phone Probes." *California PATH Research Report*, UCB-ITS-PRR-2003-25.

Real-time Optimization Model of Intelligent Public Transport Network and Its Algorithm

S. Bao[1], Y. Han[2], L. Wang[3]

[1]Business school, University of Shanghai for Science and Technology, P.O. Box 105, 516 Jungong Rd. Shanghai 200093, China, PH (86) 21- 5527 0592; FAX (86) 21-5527 0592; email: baoshengjie1987@hotmail.com
[2]Business school, University of Shanghai for Science and Technology P.O. Box 105, 516 Jungong Rd. Shanghai 200093, China, PH (86) 21- 5527 0592; FAX (86) 21-5527 0592; email: hanyin2000@sina.com
[3]Business school, University of Shanghai for Science and Technology, P.O. Box 105, 516 Jungong Rd. Shanghai 200093, China, PH (86) 21- 5527 0592; FAX (86) 21-5527 0592; email: li.goreldreremhap@yahoo.com.cn

ABSTRACT

Intelligent Transportation Systems—Public Transport (ITS—PT) make use of advanced techniques to obtain real-time public transport information to dispatch buses. ITS—PT is a new style of public transport dispatching, and it is an important step toward the realization of moderation management. This paper discusses the two dimensions of optimization of public transport networks, also called initial network optimization and real-time network optimization, and establishes the mathematical models to advance the optimization algorithm. The results achieve the goal of managing an urban public transportation system scientifically and modernly.

INTRODUCTION

With society's development, advanced science and technology are being applied to all trades and professions, offering a strong means of quick transmission, making information available for sharing and improving management. The public transport intelligent real-time dispatching system is intended integrate advanced techniques such as information technology, date communication, electron control, global positioning system information (GPS) and computer networks into the system (Moazzem et al.2000). It is wide ranging, real-time, accurate and highly efficient. This paper discusses the design of an intelligent real-time dispatching system for public transport networks, and studies the real-time dispatching control models and their solutions. The main purposes of real-time dispatching are the elimination of buses' actual running status from the schedule, selecting and assigning buses in real-time, use of other dispatching modes (vehicle frequency, etc.), and design for systems of Public Transport Network Optimization (PTNO) and Advanced Traveler Information Service (ATIS) at the same time.

In PTNO, the model is built using multi-objective programming (called initial network optimization). The model is built with the main target being the shortest pathway, so that the passenger flow obtains operating routes to arrive at destinations on time using real-time dispatching (called real-time network optimization).

In ATIS, the share of the data is furnished on Intelligent Cards (IC) and GPS, on Geographic Information System (GIS) and GPS, and on urban traffic management systems and public transport management systems. The

information can be provided to trip makers at home, work, wayside stops or on-board vehicles. With links to automatic vehicle location, traveler information systems specifically for transit are beginning to provide real-time information such as arrival times, departure times and delays. Travelers can access a variety of information, including transit routes, schedules, park-and-ride lot locations, weather and other information. The passenger flow en-route can obtain the public transport information by variable information plates and "Bus Route Guidance System (BRGS)" terminals oat the bus stops in the same time. Finally, it is proven that the real-time network optimization is rational, that the real-time dispatching system is advanced, and the information service system is timely and accurate. The application of the system also proves that it can offer a benefit for passengers and can attract more travelers to use public transit vehicles.

FOREWORD

Foreign research in public transport network optimization design starts very early. L. Bailiang et al established non-linear 0-1 plan model (Adamsli et al.1998), which considers passenger flow travel time and network fund investment as the expense objective functions. Y. Xinmiao, W. Wei et al proposed a fuzzy neural network forecasting model for public transport line passenger flow (Eberlin X.J et al.1998), etc. These models ushered in a brand-new research mentality for public transport network optimization in our country.

This paper proposes an optimization network model for public transport networks and basic ideas for network optimization, and it will be the foundation of future intelligent dispatching. According to the characteristics of modern urban development and urban transport development, the paper creatively proposes a new non-linear double-deck optimization model.

BASIC IDEA FOR AN IMPROVED PSO

The improved PSO algorithm uses a double-deck model implementing line network optimization. It first considers maximizing through passengers on the shortest path, and next considers minimizing the total travel time of through passengers in maximal through passenger volume groups (B.L.Lin et al.1999; Yang XinMiao 2000).

The model seeks the shortest path for a nonstop passenger volume group. It searches the shortest path in each pair of start and end points. Note the optimal path is not always a line between each pair of points, because line must not only satisfy the objective function of the model but must also satisfy all constraint conditions. Its searching process is as follows: First, it searches for the shortest path of a pair of points, then locates the second shortest path of this pair, the third shortest path, and so on. But the searching process is not unlimited; otherwise the result will be too large. Another constraint condition must be added, sorting according to the through passenger volume from in large to small consequence.

Second level of the model minimizes the average travel time of through passengers. Here “through passenger” refers to the maximal through passenger volume group found in the first level. Formula (1) Calculates the average shipping time of the line, which has the maximal through passenger volume. If it

is the minimal volume compared with other groups, it becomes the resulting line for this pair of start and end points. If it is greater than the average shipping time of through passengers in the shortest path, then it gets rid of it and continues searching. Formula (2): checking the second maximal through passenger volume, if the average shipping time is less than the shipping time in the shortest path, then it will be used. Otherwise, the result will be the through passenger volume of the shortest path.

Initial network optimization. The public transport network is adjusted and optimized so as to adopt real-time network optimization and real-time dispatching control (Adamsli et al.1998). This paper presents the algorithm for one-by-one searching and optimization.

Idea of solving problems. Formula (1) Decides the first route numbers with shortest pathways between a pair of nodes. It finishes the passenger flows OD matrix, defines numbers of OD nodes for traffic networks that can support buses, and runs the program that looks for the shortest pathway. Formula (2): To deduce traffic zones, the passengers are distributed over every node (on the basis of the averaging principle) in the same traffic zone. Formula (3) determines the second route numbers, which are, according to the OD matrix during investing passenger flows, traffic zones of OD nodes. OD passengers of all traffic zones are ordered from large to small until all routes have been arranged. Formula (4) searches surplus sections of many passenger flows to add third route numbers. In search for min $(D_{ij}+A)/Q_{ij}$, D_{ij} is the distance from node i to node j, Q_{ij} is the passenger flow from i to j, A is coefficient.

Mathematical model. The object functions the minimum of passengers' average distances, nonstop rate and daily average maximum full-loaded rate:

$$\min(L) = \frac{\sum_{i=1}^{n}\sum_{j=1}^{n} L_{ij} Q_{ij}}{\sum_{i=1}^{m}\sum_{j=1}^{m} D_{ij}} \qquad (1)$$

$$\max(\beta) = \frac{\sum_{i=1}^{n}\sum_{j=1}^{n} K_{ij}\delta_{ij}}{\sum_{i=1}^{m}\sum_{j=1}^{m} D_{ij}} \qquad (2)$$

$$\max(\gamma) = \frac{\sum_{k=1}^{N}\sum_{i=1}^{n}\sum_{j=1}^{n} q_{ijk} L_{ijk}}{\sum_{k=1}^{B}\sum_{i=1}^{n}\sum_{j=1}^{n} q_{oijk} L_{ijk}} \qquad (3)$$

The constraints are as follows:

$\delta_{ij}=1(i\neq j)$ or $\delta_{ij}=0$ (i=j), $R_{ij}\leqslant 1.41$, $O_{ij}\leqslant 1.3$, $T_{st}\leqslant 8.44$(min),

Where L is the average distance of passengers, N are the numbers of public transport routes, m are the numbers of traffic zones, n are node numbers of highway networks that can operate buses, K_{ij} are nonstop passengers from starting point i to destination j, L_{ij} are the distances from node i to node j, D_{ij} are

the OD from zone I to zone j, Q_{ij} are passenger numbers daily from node i to node j, δ_{ij} is the coefficient, R_{ij} is curve coefficient of the route, K_{ij} are various coefficients of the section of a highway, T_{ij} are the average walk times of the all passengers, q_{ijk} are actual passengers from node I to node j in k route, q_{oijk} are full loaded from node I to node j in k route. R_{ij} is the winding coefficient, O_{ij} is the variable coefficient, T_{st} are average walk times.

Algorithm application. Table 1 shows results before and after optimization in Tangshan City in China.

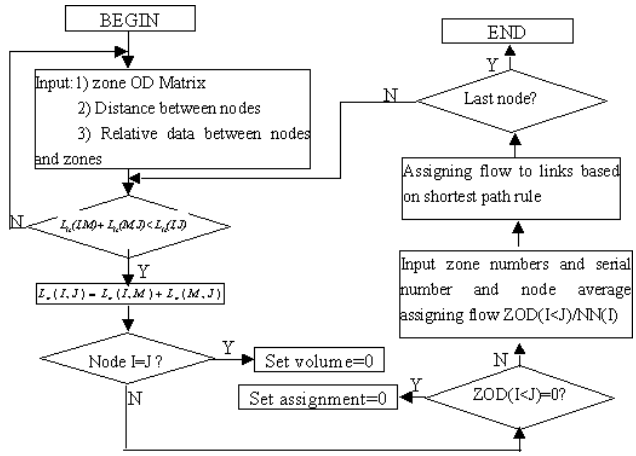

Figure 1. Diagram of flow distribution.

Table 1. Comparison of figures before and after public transit routine adjustment.

Plan	Before	Adjusted
Nonstop rate/%	40.84	43.62
Average walk time/min	7.68	6.58
Average distance/km	4.57	4.46
Average waiting time/min	9.3	6.2
Density of routine/km.km^{-2}	1.18	1.73
Routine multiplicity factor	2	1.48
Daily average full loaded rate/%	30.18	34.64
Mileage usage rate/%	98.05	98.90

Second level model. The objective function of the second level is to minimize the total riding time of all through passengers. The constraint condition is the same as with the first model; this model is proposed in domestic and foreign routes for the first time: distance between nodes is used to perform the modification:

$$\sum_{i=1}^{n}\sum_{j=1}^{n}\sum_{s=i+1}^{j-1}\left[Q_{ij}(d_s+u_s)\alpha\right]$$

The equation represents the time expense on the stops, when passengers on the vehicle must wait for other passengers getting on or getting off the vehicle. Where Q_{ij}, D_{ij} is the same mean with above formula: V_{ij} is running speed from i to j (km/h); K_{ij} is the speed correctional factor from i *to* j (different speeds when passing school, shopping center and normal running speed). Normally the value is 1. The real speed correctional factor can use experiential value in different running environments according to real investigating results; d_s is the number of passengers who got off at stop S; u_s is the number of passengers who got on at the stop S.

$$\min f(x_{ijs}) = \frac{\sum_{i=1}^{n}\sum_{j=1}^{n} Q_{ij}\frac{D_{ij}}{V_{ij}K_{ij}} + \sum_{i=1}^{n}\sum_{j=1}^{n}\sum_{s=i+1}^{j-1} Q_{ij}(d_s + u_s)\alpha}{\sum_{i=1}^{n}\sum_{j=1}^{n} Q_{ij}} \tag{4}$$

All through passenger riding times are the sum of running time between nodes and dwell time on stops, because public transport vehicles must decelerate and accelerate when starting and stopping, which must consume time, here the speed correct factor is α factor (for several vehicle doors, each passenger's getting on or off time).

Steps for improving the PSO algorithm. First plans for the first public transport line are as follows: (1) Determine all the start points and end points, establish the distance matrix between nodes and through passenger matrix between nodes. If all constraints are satisfied, search for the shortest path between each pair of start end point and calculate through passenger capacity shipping on the shortest path. (2) Search the shortest path group. Search the second, third, fourth and fifth shortest path groups according to the condition that the path length is not more than 5% more than the shortest path length, and calculate the through passenger volume of the searched path. In the same way, later path searches must satisfy all the constraints. (3) Sort the shortest path groups according to passenger capacity in large to small consequence. Judge these five groups to determine whether there are groups whose passenger volumes are less than the shortest path's, if there are, get rid of them, and sort the groups again. In this kind of situation, through passenger volume of the shortest path could be possibly placed in any position. (4) Calculate the average passenger shipping time in the through passenger group. Seek the line whose through passenger volume is more than that of the shortest path, and average through passenger shipping time is less than that of the shortest path. If a line is found, then it is the result. Otherwise, continue until a line is found (maybe it is the shortest path in the shortest path group). (5) After determining a public transport line for each pair of start and end points, sort all these lines according to through passenger volume from large to small, then take the first 20 lines as the first candidate group of lines. Determine the first optimized public transport line in these 20 lines according sequence of artery, branch and temporary lines. Plan the second public transportation line. Because there is a public transport line in the public transport network, before planning the second line, get rid of through passenger capacity shipping through the first public transport line from the through passenger flow matrix. Then repeat the steps of planning the first line. Pay attention to the constraint of the line overlapping factor. Build other

public transportation lines in turn, until the next line is lower than the lowest line-building standard. According to this method of determining a public transport optimization network, each line moves towards basically conforming to the passenger origin direction, and can guarantee the least transfer time of the entire service area. Using the proposed public transport network optimization method, a brand-new public transportation network may be established; it is undoubtedly reasonable for a new city. For an existing city, which has a relative scale of public transport networks, it is unreasonable to ignore the existing system. Because it takes a long time for people to get familiar with the public transport line, large-scale changes in public transport lines c can bring great inconvenience to resident trips; it would be contrary to the goal of network optimization. To give a better solution to this problem, this article proposes adjusting the existing public transport network, combining the produced optimization network and existing network infrastructure. The adjustment principle is as follows: keep the reasonable lines in the existing network, perform lengthening, reduction and partial re-routing to the partial lines, discard the unreasonable lines, and propose additional lines.

EXAMPLE ANALYSIS

Changchun's public transport network layout has some difference with the resident trips requirement. Including: 1) 13% traveling passengers' walking time amounts to 8 ~ 14 minutes; 2) the urban public transport line overlapping factor reaches as high as 1.8, including 16 lines' non-overlap sections of 0 ~ 2km; 3) the passenger average travel time is very long: 60% are higher than 45 minutes, 48% are higher than 50 minutes, and transfer time is high. Through passenger volume in 30 lines amounts to 410,048, combined with Changchun's present road network, consisting of 36 arteries managed by Changchun's public transport corporation. We adjusted our planning result by adding, keeping, discarding and changing processing. In the new network, 40% of passengers need not transfer. Thus, Changchun's public transport network optimization process is totally completed.

CONCLUSION

This paper put forward a public transportation network optimization model based on the mathematical planning method. In particular, it proposed the second level model for the first time in the world, and I believe it will be a good reference for research in public transport network optimization. This paper improves the PSO algorithm and applies it in actual optimization, thus proving its practical application value. This paper proposed the idea of average allocation of passenger capacity in traffic plots to nodes based on the passenger flow volume investigation. Thus, network design and line arrangement will be more reasonable. The algorithm's reliability and computational precision will be very high because of allocating passenger flow volume in traffic plots to corresponding nodes and lines, and full constraint designing. Line overlapping factors in the optimized network have measured up to reasonable technology requirements. While keeping unchanged the public transport line's total length, discarding the excessively overlapping parts in routes and adding blank route resident trips that are needed urgently, the passenger through rate can achieve levels above 40%.

ACKNOWLEDGEMENT

This research work is partially supported by the Shanghai Key Subjects Project (S30504); Shanghai Science and Technology Commission of Major Scientific and Technological Research Projects (07DZ12061) and the Major Project of Shanghai Education Committee (07ZZ91).

REFERENCES

Adamsli, A., and Turnau, A. (1998). "Simulation Support Tool for Real-time Dispatching Control in Public Transport." *Transportation Research*, 10(32), 73-87.

Bailiang, L., et al. (1999). "Public transport network optimization model based on minimization trip expense." C*hinese Road Journal*, 12(1), 79-83.

de Palma, A., and Lindsey, R. (2007). "Optimal Timetable for Public Transportation." *Transportation Research Part B*, 35(3), 789-813.

Eberlin, X.J., Wilson, N.H.M., and Barnhart, C. (1998). "The Real-time Deadheading Problem in Transit Operations Control." *Transportation Research*, 21(32),77-100.

Hossain, M., and Hasan, M.Z. (2000). "Simulation of Bus Operation under Mixed Traffic Conditions." *Proceedings of ICTTS'2000*, (13)2, 441~453.

Lin, B.L., Yang, F.S., and Li, P. (1999). "Designing Optimal Bus Network for Minimizing Trip Times of Passenger Flows." *China Journal of Highway and Transport,* 14(5), 79-83.

Spasovic, L.N., and Schonfeld, P.M. (2003). "Method for Optimizing Transit Service Coverage." *Transportation Research Record*, 14(2), 28-39.

Takashi, N. (2005). "Chaos and dynamical transition of a single vehicle induced by traffic light and speedup." *Physica A*, 34(8), 561-571.

XinMiao, Y., et al. (2000). "Public transport line's passenger flow fuzzy neural network forecasting model." *Highway Traffic Science and Technology*, 17(4), 38-4.

Yin, H., Weibin, L., and XiaoFeng, L. (1999). "Urban public transport line adjustment optimization PSO algorithm." *Chinese Road Journal*, 12(3), 100-104.

Zhigang, L., Jinsheng, S. (2007). "Double –deck programming model of district public transport timetable and vehicle dispatching." *System Engineering Theory and Practice*, 23(11), 153-141.

Frequency Optimization Model for a Public Traffic Scheduling System

C. Xu[1], F. Wu[2], Y. Han[3], H. Gao[4], Y. Zhang[1], Z. Li[1]

[1]School of Traffic and Transportation, Lanzhou Jiaotong University, P.O. Box 405, 88 Anningxi Rd. Lanzhou 730070, China, PH (86) 931- 4939 156; FAX (86) 931-4939 156; email: piano_2009@126.com
[2]School of Traffic and Transportation, Lanzhou Jiaotong University, P.O. Box 405, 88 Anningxi Rd. Lanzhou 730070, China, PH (86) 931- 4939 156; FAX (86) 931-4939 156; email: wufang@mail.lzjtu.cn
[3]School of Urban Construction and Environmental Engineering, University of Shanghai for Science and Technology, P.O. Box 105, 516 Jungong Rd. Shanghai 200093, China, PH (86) 21- 5527 0592; FAX (86) 21-5527 0592; email: hanyin2000@126.com

ABSTRACT

With the pace of social and economic development, the focus of public traffic scheduling is gradually changing from the previous pure emphasis on the economic benefits of public traffic enterprises to improving their service level. This paper presents an optimization scheduling model for a non-equivalent coordinated public transport network, which is based on the target of maximizing passenger benefit under the guidance of the basic idea while meeting the objective function, that of minimizing the total cost of passenger and public traffic operators. The research used an algorithm-hybrid of Genetic-simulated annealing (GA-SA) to optimize the frequency of public traffic scheduling, while using public traffic survey data of Shanghai to verify the model. The results indicate that the optimal model has strong practicability.

INTRODUCTION

As the society and economy rapidly develop, the policy of "people oriented public transport harmony" is advanced, and the government is focused on the level public transport service (Haghani et al. 2002). Little attention is paid to the public transport enterprise cost, however. Under the precondition of certain traffic route and vehicle choice, shortening passengers' trip time as much as possible is becoming one of the important criteria for evaluating the performance of a timetable plan (Huisman et.al 2006).

This paper studied a public transport network scheduling model based on non-equivalent real-time precedence coordinate optimization, which can be described as the target of minimizing passengers' transfer time, in a certain period and district, in coordination with the public transport lines (Cheng Li 2002).

PROBLEM DESCRIBED AND MODEL BUILT

In order to maximize social benefits, the objective function of the frequency optimization model is to minimize total cost of passengers and public traffic operators. The objective function is composed of four parts: (1) Passengers' total cost for waiting; (2) Passengers' total cost for riding; (3) Passengers' total cost for transfer; (4) public transport operator's total variable cost. Suppose that the general symbol: i, j is line (i, j =1, 2,...), s, t is station (s, t =1, 2,...) and u, v is vehicle (u, v =1, 2, ...).

Passengers' total cost for waiting. Passengers' total cost of waiting for

the bus is the accumulation of every passenger's waiting cost in the station; it can be expressed by the time and the value, which is the product of waiting time and unit waiting cost.

Suppose the arrival rate at which passengers arrive at station k is a constant. r_s is the arrival rate at which they randomly arrive at the station(person/minute), $d_{i,u}^s$ is the time at which bus u arrives at station s in line i, $d_{i,u-1}^s$ is the time when bus u-1 arrives at station s in line i. The number of waiting passengers is:

$$T_{w1}: T_{w1} = r_s(d_{i,u}^s - d_{i,u-1}^s) \quad (1)$$

Every passenger's average waiting time T_{w2} is:

$$T_{W2} = 0.5(d_{i,u}^s - d_{i,u-1}^s) \quad (2)$$

Passengers' waiting time in station s T_{wait} is:

$$T_{wait} = T_{w1}T_{w2} = 0.5r_s(d_{i,u}^s - d_{i,u-1}^s)(d_{i,u}^s - d_{i,u-1}^s) \quad (3)$$

Passengers' total cost for riding. Passengers' total cost for riding is composed of: (1) time it takes to carry passengers from station s-1 to s; (2) the waiting time for people who do not get off the bus.

(1) Suppose the number of passengers who were carried by bus u on line i from station s is $P_{i,u}^s$, and from station s-1 is $P_{i,u}^{s-1}$. The time that bus u is on line i from station s is $f_{i,u}^s$, from station s-1 is $f_{i,u}^{s-1}$. So the time it took to carry the passengers from s-1 to s is:

$$T_{i1} = (d_{i,u}^s - f_{i,u}^{s-1})P_{i,u}^{s-1} \quad (4)$$

(2) Suppose average time for a passenger unit to get on and off the bus is $\overline{ud}$ (minute/person, based on actual vehicle conditions). The rate that passengers get off the bus is q_s%. Because parts of the passenger unit get off the bus, every passenger who is on the bus must wait. Suppose the wait time is:

$$T_{\text{down}}: T_{down} = \overline{ud}P_{i,u}^{s-1}q_s \quad (5)$$

Because parts of passenger unit get on the bus, every passenger who is on the bus must wait. Suppose the wait time is:

$$T_{\text{up}}: \quad T_{\text{up}} = \overline{ud}r_s(d_{i,u}^s - f_{i,u-1}^s)P_{i,u}^{s-1}(1-q_s) \quad (6)$$

The waiting time for a passenger who does not get off the bus is T_{i2}:

$$T_{i2} = \begin{cases} T_{\text{up}} + T_{\text{down}} & \text{Suppose it is only one door to get on and off} \\ \max(T_{\text{up}}) \ T_{\text{down}} & \text{Supose there is one door to get on ,and the other to get off} \end{cases} \quad (7)$$

The time the passenger spends on the bus is T_{wait}:

$$T_{\text{wait}} = T_{i1} + T_{i2} \quad (8)$$

The cost passengers spend for transfer. The cost passengers spend for transfer is related to the transfer rate from line i to line j. Suppose the rate is $\omega_{i,j}^s$(%), $0 < \omega_{i,j}^s < q_s < 1$, $\delta_{i,j}^{s,t}$ where 0-1 is variable. "0" is representative, since it is impossible to transfer between two stations; otherwise, the result would be "1". So, the transfer time T_{transfer} is:

$$T_{transfer} = (f_{j,v}^{t} - d_{i,u}^{s}) P_{i,u}^{s-1} \omega_{i,j}^{s} \delta_{i,j}^{s,t} \quad (9)$$

Operator's cost. If we use time to denote operator's cost, it is the time $T_{\text{operation}}$ that the bus takes to run from the last station to this station:

$$T_{\text{operation}} = d_{i,u}^{s} - f_{i,u}^{s-1} \quad (10)$$

A public transport network optimization scheduling model. This model is based on non-equivalent real-time precedence coordination. Objective function:

Min

$$\left\{ \beta_1 \left[\frac{c_1}{2} \sum_i \sum_s \sum_u r_s (d_{i,u}^{s} - a_{i,u-1}^{s})^2 + c_2 \sum_i \sum_s \sum_u \{ (d_{i,u}^{s} - f_{i,u}^{s-1}) P_{i,u}^{s-1} + \overline{ud} T_{i2} \} + c_3 \sum_i \sum_j \sum_s \sum_t \sum_u \sum_v \delta_{i,j}^{s,t} (f_{j,v}^{t} - d_{i,u}^{s}) P_{i,u}^{s-1} \omega_{i,j}^{s} \right] \right.$$

$$\left. + \beta_2 \sum_i \sum_s \sum_u c_{i,u} (d_{i,u}^{s} - d_{i,u}^{s-1}) \right\} \quad (11)$$

Subject to:

$$s_i^{\min} \le f_{i,u}^{s} - d_{i,u}^{s} \le s_i^{\max} \qquad \forall i, s \quad (12)$$

$$s_j^{\min} \le f_{j,v}^{t} - d_{j,v}^{t} \le s_j^{\max} \qquad \forall j, t \quad (13)$$

$$f_{j,v}^{t} - d_{i,u}^{s} + M(1 - \delta_{i,j}^{s,t}) \ge 0 \qquad \forall i, j, s, t, u, v, j \ne i \quad (14)$$

$$\sum_t \delta_{i,j}^{s,t} = 1 \qquad \forall i, j, s, t, j \ne i \quad (15)$$

$$(f_{j.v}^{t} - d_{i,u}^{s}) \delta_{i,j}^{s,t} \le T \qquad \forall i, j, s, t, u, v, j \ne i \quad (16)$$

$$d_{i,u}^{s} - d_{i,u-1}^{s} \le h_i^{\max} \qquad \forall i, s, u \quad (17)$$

$$d_{j,v}^{t} - d_{j,v-1}^{t} \le h_j^{\max} \qquad \forall j, t, v \quad (18)$$

$$\frac{Q_{s.\max}}{N_s \times CAP} \le L_{\max} \quad (19)$$

$$\frac{Q_{s,\max}}{N_s \times CAP} \ge L_{\min} \quad (20)$$

β_1 is the weight factor of passengers' cost, according to passenger flow volume. β_2 is the weight factor of the public transport operator's cost. c_1 is the conversion factor that converts passengers' waiting time to trip cost (RMB /person minute): $c_1 = [1 + \alpha h_i] c_{\text{average}}$

As waiting time increases, c_1 increases. It is variable: α is passengers' complaint factor, $c_{average}$ is passengers' unit time value, c_2 is the conversion factor to convert passengers' riding time to trip cost (RMB / person minute). c_3 is the conversion factor that converts passengers' transfer time to trip cost (RMB /person minute). $c_{i,u}$ is the conversion factor that converts bus u running time on line i to operating cost (RMB/minute).

$h_{\text{i}}^{\max}$ and $h_{\text{j}}^{\max}$ are the maximum frequency on line i, j; $S_{\text{i}}^{\max}$ and $S_{\text{i}}^{\min}$ are the maximum and minimum stopping time on line i. $S_{\text{j}}^{\max}$ and $S_{\text{j}}^{\min}$ are the maximum and minimum stopping time on line j. t is the maximum transfer time (minutes), M is an arbitrarily large value, $L_{\max}$ and $L_{\min}$ are maximum load factors of lines i

and *j*.

From the model, we can see that the objective function is the frequency of every line in the network and 0-1 variable $\delta_{i,j}^{s,t}$ of the transfer station. $a_{i,u}^{s}$, $d_{i,u}^{s}$ and $\delta_{i,j}^{s,t}$ are variable, r_s, q, c_1, c_2, c_3, $c_{i,u}$ and $\overline{ud}$ can be obtained through research, and T and M are calibration factors.

OPTIMIZATION FREQUENCY BASED ON GA-SA ALGORITHM

Mixed GA-SA algorithm. GA-SA algorithm is an optimization algorithm that combines a genetic algorithm and simulated annealing algorithm. GA makes optimization come true through a group genetic operation, which is based on the idea of "survival of the fittest" (Kliewer et.al 2006). The local search ability of GA is poor. But it has the advantage in integral searches; SA has a strong ability in local searches, but it cannot make the search process go into a most hopeful area. We combine the two algorithms to optimize the search process and enhance search ability and efficiency under whole and part meaning. The model in this paper is a multiple objective nonlinear programming model. It is suitable for using the mixed GA-SA algorithm (Huisman et.al 2005).

Frequency optimization model on mixed GA-SA algorithm. Based on the mixed GA-SA algorithm, the steps of how to solve frequency are as follows:

Step 1: Input the number of lines in the public transport network and the number of 0-1 variables $\delta_{i,j}^{k,l}$ between every transfer station. At the same time, arrange every line and $\delta_{i,j}^{k,l}$ to ensure the arrangement of every variable in chromosome. Initialize parameters, including the range of frequency, population size N across probability R_c and mutating probability R_m, initial temperature S_0, genetic generation number i and threshold δ.

Step 2: Convert frequency to a binary string, and in accordance with population size and chromosome arrangement, produce N random chromosomes that are subject to frequency. They constitute the initial population. Every chromosome stands for a possible solution.

Step 3: Compute every chromosome's fit value $f(X_i)$ in number I generation, average fit value $\bar{f}_I$ and $|\bar{f}_I - \bar{f}_{I-1}|$, estimate if it is subject to $|\bar{f}_I - \bar{f}_{I-1}| < \delta$. If it is, go to Step 10. If it does not, go to Step 4.

Step 4: Compute every chromosome's chosen probability R_i, and accumulation probability λ_k.

Step 5: Get an evenly distributed random number ξ between 0 and 1. If $\xi \le \lambda_1$, choose the first chromosome to copy. If $\lambda_{k-1} < \xi \le \lambda_k$, choose the number ξ chromosome. Repeat this step N times and produce the next generation.

Step 6: Produce N evenly distributed random numbers ξ_1, ξ_2, …, ξ_k, …, ξ_N between 0 and 1 in turn. If $\xi_k < R_c$, let the chromosome X_k serve as the father chromosome and come into the crossing father chromosome population.

Step 7: Choose two chromosomes (p_1, p_2) randomly from the father population, choose a point randomly, and then cross two chromosomes. They produce son generation c_1, c_2. Compute fit value $f(c_i)$ of c_1, c_2. Start SA

algorithm. If $f(c_i) > f(p_i)$, let p_i stand for c_i. If not, accept c_i at the probability $\exp\{(f(c_i) - f(p_i))/T\}$. Leave the son chromosome and remove this father chromosome from the father population. Repeat this step until every father chromosome has been operated.

Step 8: Produce N evenly distributed random numbers ξ_1, ξ_2, …, ξ_k, …, ξ_N between 0 and 1 in turn. If $\xi_k < R_m$, let X_k mutate. Operation of SA is similar with Step (7).

Step 9: Lower temperature $T = T_0 \times a^K$, a is a constant between 0 and 1, K is the number of iterations.

Step 10: Let $I = I+1$, go back to Step 1.

Step 11: Stop computation. Output the son chromosomes that minimize the objective function.

EXAMPLE

Using the model above, passenger flow surveys and operating data of the No.59 and No.842 buses in Shanghai (the two lines cross in Wujiaochang), the average waiting, riding and transfer time value are respectively: the public transport passenger's unit time value is per-capital GDP per hour. It is 16095/(365×24)=1.84 RMB / hour·person =0.03 RMB / minute·person. The bus running speed is 20 km/h. The maximum transfer time is 15 minutes. Frequency change from 5 to 15, but it is a multiple of 0.5. The chosen optimization time period is 6:30 to 7:30. Passenger's average time of getting on and off is 4 seconds/ person; β_1=0.7, β_2=0.3. The Maximum number of iterations I=300. The threshold δ =1. Population size N=200. Initial temperature S_0=5000. Cross probability S_c=0.95. Mutation probability S_c=0.005.

The results are: the frequency of No.59 bus is 6.0 minutes, and No.842 bus is 7.0 minutes. The minimum objective function f^* = 6928.55 RMB. Passengers' total waiting cost is 754.36. Passengers' total riding cost is 3657.14 and total transfer cost is 1049.15 RMB, public transport enterprise's total variable cost is 1467.85 RMB. Through investigation and analysis of the basic related information for No.59, we can see passenger flow volume of the No.59 bus in a whole day. (Figure 1).

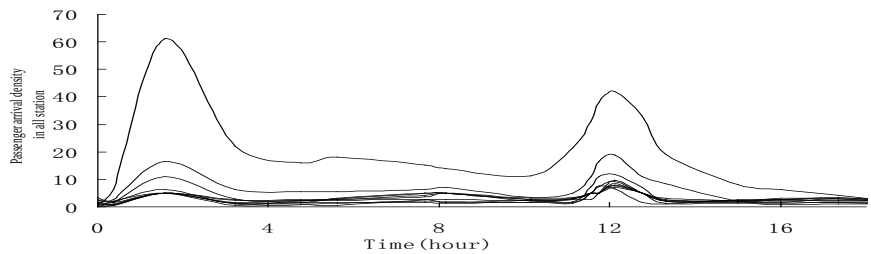

Figure 1. Passenger flow volume of No. 59 bus in one whole day.

The frequency distribution of No.59 bus in a whole day comes from the GA-SA Algorithm. (See Figure 2)

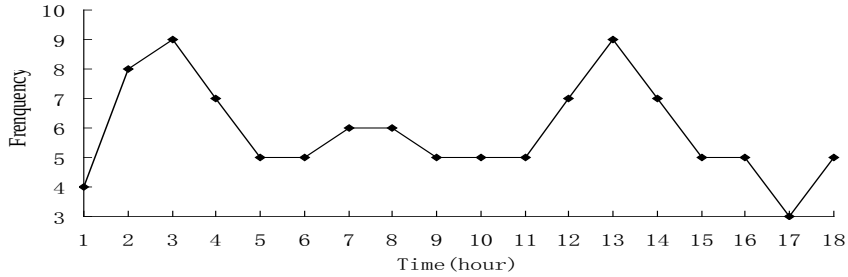

Figure 2. Frequency in a whole day by mixed GA.

From Figure 2, we can see that the result from the GA-SA algorithm conforms to the actual passenger flow distribution (Figure 1). Frequency also gets two rush hours. It corresponds with the morning and night rush hours. The result reflects passengers' benefit and shows that the model reflects fact. At the same time, it proves the GA-SA algorithm has a higher efficiency. It is feasible. The No.842 bus gets the same result.

CONCLUSION

The quality of public transport operation can directly affect enterprise's appearance and economic benefit. Improving operation has been a constant theme. This paper builds an optimization scheduling model of a non-equivalent coordinated public transport network which is focused on improving the public transport service level. This model, which has been verified with actual data, can support the decision-making in improving public transport operating management.

ACKNOWLEDGEMENTS

This research work is partially supported by Shanghai Key Subjects Project (S30504), Shanghai Science and Technology Commission of Major Scientific and Technological Research Projects (07DZ12061), and the Major Project of Shanghai Education Committee (07ZZ91).

REFERENCES

Haghani A., Banihashemi M. (2002). "Heuristic approaches for solving large-scale bus transit vehicle scheduling problem with route time constraints." *Transportation Research*, 36(2), 309-333.

Huisman, D., Freling, R., and Wagelmans, A. (2005). "Multiple-Depot Integrated Vehicle and Crew Scheduling." *Transportation Science*, 39(4), 491-495.

Huisman, D. and Wagelmans, A. (2006). "A Solution Approach for Dynamic Vehicle and Crew Scheduling." *European Journal of Operational Research,* 172(2), 453–471.

Kliewer, N., Mellouli, T., and Suhl, L. (2006). "A time-space network based exact optimization model for multi-depot bus scheduling." *European Journal of Operational Research*, 175(3), 1616–1627.

Li, C. (2002). "Iterative approximation of fixed points for strongly pseudocontractive mappings." *Sichuan University (Natural Science Edition)*, 38(2), 820-23.

Liu, Z., Shen, J. (2007). "Double–deck programming model of district public transport timetable and vehicle dispatching." *System Engineering Theory and Practice*, 23(11), 153-141.

Ren, C., Zhang, H., Fan, Y. (2005). "The Application of Mixed GA-SA Algorithm in intelligent public transport scheduling system." *System Simulation Journal,* 26(2), 2075-2081.

Takashi, N. (2005). "Chaos and dynamical transition of a single vehicle induced by traffic light and speedup." *Physica A*, 348(2), 561-571.

Zhao, X., Duan, Y., Zhang, W., and Gao, M. (2002). "Bus Scheduling Optimizing Model." *Lanzhou Higher Industrial Specialist College Journal,* 9(7), 60-65.

Mixed Traffic Micro-simulation of Urban Branch Roads

B. Liu[1,2], X. Lv [1,2], W. Li [1,2], Q. Li[1,2] , X. Wang[3]

[1]School of Traffic and Transportation, Shijiazhuang Railway Institute, Shijiazhuang, Hebei, China, Post code 050043; PH (86) 311-87935516; FAX (86) 311-87935516; email: tom667788@163.com
[2]Traffic Safety and Control Lab of Hebei Province, Shijiazhuang, Hebei, China, Post code 050043; PH and FAX (86) 311-87935516; email: tom667788@163.com
[3]School of Transportation Science & Engineering, Harbin Institute of Technology, Harbin, Heilongjiang, China, Post code 150090; PH (86) 451-81778812; FAX (86) 451-86283779; email: wxn1974@hit.edu.cn

ABSTRACT

At present, traffic micro-simulation studies are mostly based on the following model and lane changing model, which are the fundamental models. What make them distinct are their different forms and parameters. Although these methods can simulate the foreign traffic system fairly well, they can not precisely simulate the mixed traffic of Chinese urban branch roads. This study, which focuses on the unique situation of Chinese motorized vehicles and non-motorized vehicles advancing in a mixed way on the urban branch roads, puts forward a new model that can be applied to motorized and non-motorized vehicles. It is an advanced model for mixed traffic on urban branch roads.

Take motorized vehicles for example; it will no longer be limited to fundamental forms, such as free driving, following driving or lane changing driving and so on, but will always be in an advanced state. There is no rigid lane dividing principle when the vehicle is advancing. Its lateral location, speed and other factors depend on the comprehensive traffic circumstance around it. In theory, there are numberless possibilities and choices.

The principles of the non-motorized vehicles model resemble the motorized vehicles model. When the model was built, we used the crossing bridge of north Jianshe street in Shijiazhuang for testing and verification. It turned out that this method can make an accurate micro-simulation of mixed traffic on Chinese urban branch roads. In this way, it filled the blank left by the imported software.

INTRODUCTION

At present, the microscopic traffic simulation technology developed abroad is more sophisticated, but it is mainly based on the two basic models: car following and lane changing. Chinese microscopic traffic simulation software is mainly imported from abroad, and the related study has been carried out at Harbin Institute of Technology, Tongji University and Beijing Jiaotong University.

But there is no good solution to the microscopic simulation problem of mixed traffic. The phenomenon of the mixed traffic on urban branch roads in China is studied in this paper, breaking traditional ideas based on the car following and lane changing model and putting forward an advanced model applied to the mixed traffic of urban branch roads in China whose lanes are not divided. The results of research can simulate and analyze the phenomenon of mixed traffic on urban branch roads in China, and the theoretical and practical value is important.

RESEARCH AND ANALYSIS AT HOME AND ABROAD

The research on microscopic traffic simulation software started earlier abroad, and the technology has become more sophisticated, but the operation of the software is mainly based on the car following and the lane changing models (Hoogendoorn et al., 2001). The car following model can generally be divided into the following categories: stimulus- response model, safe spacing model, physiological-psychological model, fuzzy reasoning model and cellular automaton model. The lane changing model mainly includes the model based on demand generation and the model based on behavior threshold. In recent years, many scholars, such as Willmann, Kumamoto et al (Wardrop J.G et al., 1994) devoted themselves heart and soul to the related research.

The microscopic traffic simulation software used in China are mainly imported from abroad, and the related study has been carried out at Harbin Institute of Technology, Tongji University, Beijing Jiaotong University. For example, study includes the advanced car following model based on dynamic, which is put forward by HanZhi, the car following propounded by RongJian based on variable following time and stochastic factors, and XuLunhai's nonlinear model based on lagging time. However, this research is all about the improvement of the car following model and the lane changing model, not involving the problem of mixed traffic on urban branch roads in China whose driveways are not divided.

MAIN RESEARCH CONTENTS

This paper aims at the special urban phenomenon of mixed traffic in China, and it is based on the safe distance model of the car following model. The speed and angle of the vehicle is controlled by timely estimating the speed of the non-motorized vehicles ahead, and also the size and location of the interstitial provided for overtaking. Thus, the phenomenon of motor vehicles interfering with non-motorized vehicles can be achieved on the condition that there is no driveway division. In this case there is no specific concept of driveway. Vehicles keep on searching for n interstitial, which can be used to accelerate in the non-motorized vehicles, and the speed and angle is controlled according to the interstitials. The traditional car following and lane changing models are no longer observed by the vehicles' running, which observe the improved running model based on the characteristics of the two models. The

research mainly contains the following basic contents.

θ numerical is introduced in the safe distance model of the car following model. After a great deal of actual investigation and study, θ is the angle between the direction of the vehicle' speed and the direction of the path. The following speed and angle of the vehicle are expressed by the changing of the angle. Motor vehicles adjust their speed and angle according to the movement of all the non-motorized vehicles ahead (the speed of each vehicle, whether there is space or not, the angle between the gap and current vehicle, etc) when the distance between the non-motorized vehicles ahead and the vehicles behind is longer than the safety distance of collision criticality. The model is the mould model with a safe distance if θ numerical is 0 degrees; the maximum of θ numerical is 45 degrees when considering actual traffic and the behavior of the driver. The characteristics of the vehicle are described objectively and accurately as θ numerical and change back and forth from 0 degrees to its maximum.

The improved model is based on the safe distance model by analyzing the behavior of the driver under the mixed traffic conditions of China. Its formula is:

$$v_n(t+T)=\min\left\{\begin{array}{l}\dfrac{v_n(t)}{\cos\theta}+2.5\dfrac{a_nT}{1-\sin\theta}\left[1-\dfrac{v_n(t)}{V_n}\right]\left[0.025+\dfrac{v_n(t)}{V_n}\right], \\ b_n\cos\theta+\sqrt{\left[b_n^2\cos^2\theta T^2-2b_n\cos\theta\left[x_{n-1}(t)-S_{n-1}-x_n(t)-v_n(t)\right]-b_n\cos\theta v_{n-1}^2(t)/\hat{b}\right]}\end{array}\right\} \quad (1)$$

The mean is following:

a_n is the maximum acceleration that the driver of vehicle N will make.

b_n is the maximum deceleration that the driver of vehicle N will make.

S_{n-1} is the utility of vehicles N-1, equal to body length and parking space.

$\hat{b}$ is the maximum reducing speed that is perceived by the driver of vehicle N and which takes the driver of vehicle N-1.

θ is the angle between the direction of vehicle speed and the direction of the path, which ranges from 0 degrees to 45 degrees.

There are two items in the right of this formula. The first item is composed of the expected speed limit, the angle and the acceleration. Traffic flow is under the free state if this item plays an important role in most of the vehicles. Vehicles are free or under the condition of car following when θ equals 0 degrees and the vehicles' running observes the improved mixed running model according to the characteristics of the two models, and if there exist changes of the angle. The second item is composed of the expected limit of the angle, and the distance and reduced speed. Traffic flow is under crowded conditions if this item plays an important role with most of the vehicles. Vehicles are under the condition of car following driving when θ equals 0 degree and the vehicles' running observes the improved mixed running model according to the characteristics of the two models when there exist changes of

the angle. The progress of the vehicle is a process of changing its speed and angle. These change constantly according to the circumstance ahead of the vehicle.

INSTANCE ANALYSIS

To compare the safety spacing original model and the advanced integration model, we used the 6m-wide one-way section of road near the overpass in the Jianshe north street in Shijiazhuang as an example. Through field observation, a vehicle weaves its way through the flow of non-motorized generally at the speed of about 40km/h. We simulate the situation separately, using the traditional safety spacing model and the integrated forward model proposed in this paper, and the data of the result is shown in Figures 1, 2 and Table 1. According to the analysis of running time of vehicles and the trajectory, the result indicates that the situation of mixed traffic in which the driveway is not divided, existing in the urban branch roads in China, can not be simulated by the original and classic models based on car following and lane changing, and illustrates the applicability to the situation of the model presented in this paper.

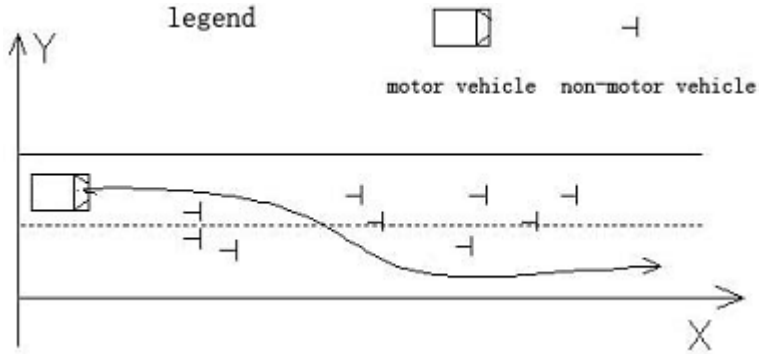

Figure 1. Trajectory by original model.

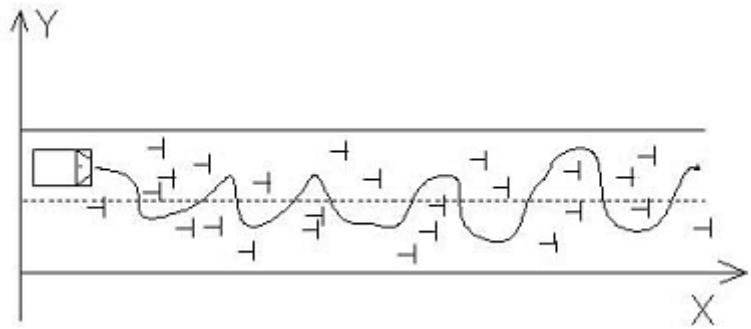

Figure 2. Trajectory by advanced model.

Coordinate values of the running trajectory from 1 to 10s is shown in table 1:

Table 1. Coordinate values of the running and trajectory (unit: m).

time（unit：s）	x in original	y in original	x in advanced	y in advanced
1	0	4.2	0	4.2
2	11.1	3.8	11.1	4.0
3	22.2	3.5	22.2	2.9
4	39.6	2.9	38.9	3.0
5	55	2.4	42.7	2.9
6	66.1	1.9	62.1	2.5
7	77.2	1.5	74.3	3.2
8	88.3	1.4	83.8	5.2
9	99.4	1.8	97.7	2.4
10	110.5	2.2	109.6	4.8

CONCLUSION

Targeting the situation of mixed traffic in Chinese urban roads whose driveways are not definitely divided, the motorized vehicle integration forward model is put forward in this research. It is based on the original and classic models of car following and lane changing. In the condition that the vehicle has no clear state of car following and lane changing, the forward speed and angle change in real time with the change of the front non-motorized vehicle speed, the gap between the vehicle and the angle of the current vehicle. Using the data from the vicinity of the overpass in the Jianshe north street in Shijiazhuang to demonstrate it, the study indicates that the situation can not be simulated by the microscopic traffic simulation software (such as Vissim, Synchro, etc). We have developed a separate simulation system based on the car following and lane changing models and the integrated forward model, and found that there is serious distortion in the simulation of the mixed traffic in the Chinese urban road whose driveway is not divided when using the classic microscopic traffic simulation models. The situation can be simulated precisely by the model put forward in this paper, however.

ACKNOWLEDGEMENT

This research was supported by Young Scientist Project of Natural Science Foundation of China (NSFC), “The method of reducing emission of air

pollutants from urban public transportation based on the behavior analysis.” （Grant No：70803007), Traffic Safety and Control Lab of Hebei Province opening issue Fund, “Three-Dimensional Visual plan and design system of Urban Mass Transit.” (Grant No：211001), Startup Foundation for Advanced Talents of Shijiazhuang Railway Institute（Grant No：8110053）and Special Foundation for Post-graduate Research of Shijiazhuang Railway Institute. Thanks for co-operation of Shijiazhuang Traffic Management Bureau.

REFERENCES

Hoogendoorn, S.P. (2001). “State-of-art of Vehicular Traffic Flow Modelling,” Proeeedings of the Institution of Meehanical Engineers, Part l: *Journal of Systems and Control Engineering*, 215(4):283-303.

Pei, Y., and Zhang, Y. (2004). Simulation of road traffic system, Bei Jing.

Wardrop, J.G., and Charlesworth, G. (1954). “A Method of Estimating Speed and Flow of Traffic from a Moving Vehicle,” Proceedings Of the Institute of Civil Engineers, Part2, 3:158-171.

Wilson, R.E.(2001). "An analysis of Gipps’s car following model of highway traffic." *Proceedings of the International Joint Conference on Pattern Recognition*. Coronado: 878~886.

Track Access Technology of Traffic Accident Vehicles Based on Video

B. Liu [1,2], X. Wang[1,2], W. Li[1,2], X. Wang[3]

[1]School of Traffic and ransportation, Shijiazhuang Railway Institute, Shijiazhuang Hebei, China, Post code 050043; PH (86) 311-87935516; FAX (86) 311-87935516; email: tom667788@163.com
[2]Traffic Safety and Control Lab of Hebei Province, Shijiazhuang, Hebei, China, post code 050043; PH and FAX (86) 311-87935516; email: tom667788@163.com
[3]School of Transportation Science and Engineering, Harbin Institute of Technology Harbin, Heilongjiang, China, Post code 150090; PH (86) 451-81778812; FAX (86) 451-86283779; email: wxn1974@hit.edu.cn

ABSTRACT

Traffic accident parameter determination is one of the most important topics in the traffic engineering domain. As a rule, parameter determination methods are all based on the brake marks, thrown objects etc. The results are often inaccurate due to the uncertainties of the road surface friction coefficient, the collision model and the geometric center of vehicles. In 2008, this study team proposed relying on large-scale construction of video surveillance equipment in China. A Gaussian mixture model is adopted to carry on background extraction and parameters such as vehicle movement path, real-time speed etc. were extracted from the video with Kalman Filter and obtained good results. Based on the research in 2008, this paper proposes that the background method of difference be used to replace the Gauss mixed model in the background extraction, and that a Kalman filtering track algorithm based on the fuzzy match be used to replace the traditional Kalman filtering track algorithm in the path track aspect. Through the theory, the example and the analysis, the newly proposed method is more effective.

INTRODUCTION

As a rule, parameter determination methods are all based on the brake marks, thrown objects etc. The results are often inaccurate due to the uncertainties of the road surface friction coefficient, the collision model and the geometric center of the vehicles. In 2008, this study team proposed relying on the recent large-scale deployment of video surveillance equipment in China. The Gaussian mixture model is adopted to carry out background extraction. Extracting parameters such as vehicle movement path, real-time speed etc. from the video fwas conducted using Kalman Filter, and it obtained good results. Based on the research in 2008, this paper proposes that the background method of difference be used to replace the Gauss mixed model in background extraction and that a Kalman filtering track algorithm based on the fuzzy match be used to replace the traditional Kalman filtering track algorithm in the path

track aspect. Through the theory, the example and the analysis, the newly proposed method is more effective.

ACTUALITY RESEARCH

Researchers have used processing by video technology in road traffic since the 1970s (M.Onoe, 1976). After the '90s, numerous countries invested massive funds to support research in this field. Massive work in lining up examination, transportation condition monitors, accident examination and other aspects has been done by numerous scholars on behalf of Hoose, Wan, Mieha, Poulos, Lu et al (P.G. Miehalo Poulos, 1993) (P.G. Michalo Poulos, 1992) (L. CyPers, 1990). For example, the Singapore EMAS system's vehicle examination system and the automatic accident examination system are all based on video detection technology. Mainland China started late in traffic flow research by use of video.

In 1998, The first domestic "video automatic observation system of vehicles running red lights" was developed by Beijing Zhonglian Tongda Technological Progress Limited Company. Soon after, massive work was done by Tan Tieniu, Liu Zhonghua, Liu Bo, Chen Zhaoxue and other scholars in the video examination of vehicles. In 2008, the Shijiazhuang Railway Institute proposed that traffic accident vehicles' paths could be extracted from the video footage, quantifying the parameter extracted from the video as the authority for judicature cognizance; it obtained good results. While the traditional Gauss mixed model and the Kalman filtering model are used in the study, its precision waits for further improvements.

THE MAIN RESEARCH

The goal of this study is to extract a car's track in a traffic accident, focusing on the precise trajectory caused by the specific target vehicle (people). This study contains basic elements as follows:

Background separation. For a specific traffic accident, the effective area should be separated from the vehicles and pedestrians in the video. The present paper uses the selective background renewal model. Its formula is as follows:

$$B_{i,j}^{t+1} = \begin{cases} (1-a)B_{i,j}^{t} + aI_{i,j}^{t}, if DB_{i,j} = 0 \\ B_{i,j}^{t}, otherwise \end{cases}, 0 \le a \le 1 \quad (1)$$

Where, $B_{i,j}^{t}$ is the pixel value of i line ,j row of background images at time t, $I_{i,j}^{t}$ is the pixel value of i line ,j row of input images at time t, a is the turnover rate.

Vehicle track identification. As shown in Figure 1, the vehicle track is detected in conventional traffic video detection technology, usually using black and white image analysis. The difference between the various parts of moving objects can not be carried out in this method. So it can't be ensured that the moving objects would be tracked precisely under different circumstances such as vehicles turning or sideslipping. As shown in Figure 2, if feature points as shown are selected to logo vehicle trajectory, the method of this paper ensures that the moving objects would be tracked precisely under several circumstances such as vehicles turning or sideslipping. In object tracking, the Kalman Filter model is proposed to deal with the vehicles turning, sideslipping, etc in this study. The method used in this paper is tailing after special point by improved Kalman Filter.

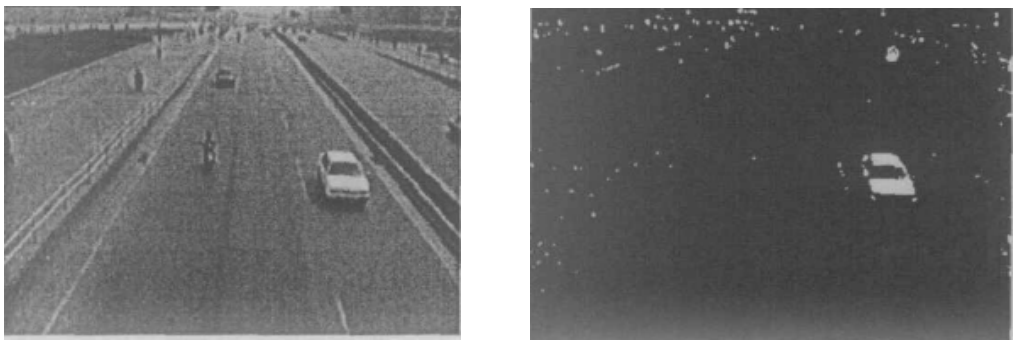

Figure 1. Classical video method of vehicle track determination.

Figure 2. Proposed method of vehicle track determination.

In the Kalman filter, the system model may be used to forecast the goal. When it carries on the forecast track of the object, we first need to establish a system mode model that suits the movement of the object track. Considering the vehicle path changes a lot in a traffic accident, and the space of time is small between the neighboring frames in a video sequence, we make following improvement to the Kalman filtering model:

$$p_t = \begin{bmatrix} p_x(t-1) + \left(p_x(t-1) - p_x(t-2)\right) \\ p_y(t-1) + \left(p_y(t-1) - p_y(t-2)\right) \end{bmatrix} = \begin{bmatrix} 2p_x(t-1) - p_x(t-2) \\ 2p_y(t-1) - p_y(t-2) \end{bmatrix} \quad (2)$$

Where, p_t is the center of mass position of movement object at time t, p_x is the x axis position component of the movement object center, p_y is the y axis position component of the movement object center.

Coordinate change. The coordinate changes between image plane and road plan. The vehicle's trajectory, which the video observed, will be restored to the road track of the vehicle. First, the corresponding equation is established relying on the correspondence relationship between the two-plane and the three-dimensional in photography space. After calibrating out the equation parameter, according to each image plane coordinate, we can determine its ground coordinates. The principle is shown in Figure 3. In Figure 3, S is the center of photography, A is any point on the ground, a is the projection point of A on the image plane. X, Y, Z are the three-dimensional coordinates. X, Y can be calculated by Equation (3).

$$\left.\begin{aligned} X &= \frac{a_1 x + a_2 y + a_3}{a_4 x + a_5 y + 1} \\ Y &= \frac{a_6 x + a_7 y + a_8}{a_4 x + a_5 y + 1} \end{aligned}\right\} \tag{3}$$

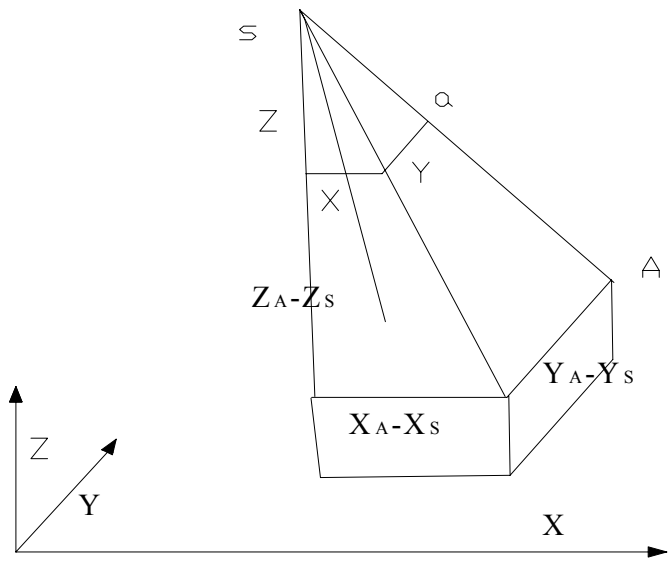

Figure 3. Three-dimensional coordinates.

CASE ANALYSIS

In this program, accident data is treated as a reference. The course of the accident is shown in Figure 2. The comparison result has been shown in Table 1. As shown in Table 1, this article's resulting algorithm examination is best in practice.

Table 1. Method comparison for traffic accident parameter identification.

Identification parameter	Brake marks method	Traditional video method	Proposed examination method	This article result algorithm examination
Velocity in collision (km/h)	42.3~63.4	43.7	45.6-47.8	46.2-26.9
Track length (m)	2.8	4.3	5.6	5.6
Efficiency of track length identification (%)	100	78	95	98

CONCLUSION

Compared with the traditional video detection of tire marks and thrown objects, the video examination data originates more directly, and as a result is more reliable. In 2008, this group proposed the vehicle's path parameter could be extracted from a traffic accident video. We have made improvement through nearly half a year of research into the background renewal algorithm and the vehicle path track algorithm. Looking from the example analysis result, the precision is further enhanced.

ACKNOWLEDGEMENT

This research was supported by the Young Scientist Project of Natural Science Foundation of China(NSFC), "The method of reducing emission of air pollutants from urban public transportation based on the behavior analysis" （Grant No:70803007）, Traffic Safety and Control Lab of Hebei Province Opening Issue Fund , "Three-Dimensional Visual Plan and Design System of Urban Mass Transit" （Grant No：211001）, Startup Foundation for Advanced Talents of Shijiazhuang Railway Institute（Grant No：8110053）and Special Foundation for Post-graduate Research of Shijiazhuang Railway Institute. Thanks for the co-operation of Shijiazhuang Traffic Management Bureau.

REFERENCES

A.Lipton, H.Fujiyoshi, R.S.Patil.Moving (1998). "target detection and classification from realtime video[C]."In Proceedings of the 1998 Workshop on Applications of Computer Vision, 1076-1081.

Bohang, L., and Yulong, P. (2007)."Lane-changing Based on Video." *Journal of Harbin University of Science and Technology*. 12 (3):7-11.

L.CyPers, F.Lemaire, P.Vervenneetal(1990). "CCATS: the image Proeessing-based traffic senso ." *Traffic Engineering and Control,* 31(6):371~378

Onoe, M., and Ohba, K. (1976). "Disital Image Analysis of Traffic Flow." *Proceedings of the International Joint Conference on Pattern Recognition. Coronado*: 803~804.

Pei Yulong, Xu Huizhi,(2006). "The control Mechanism of Lane Changing in Jam Condition [C]."The 6th World Congress on Intelligent Control and Automation.Dalian China,8655~8658.

P.G. MiehaloPoulos, R.D.Jaeobson, C.A. Andersonetal (1993). "Automatic ineident detection through video image Proeessing. " Traffic Engineering and Control, 34(2):66~75

P.G. MichaloPoulos, R.D.Jaeobson, C.A.Anderson et al (1992). "Field dePloyment of AUTOSCOPE in the FAST-TRAC ATMS/ATIS programme."Traffic Engineering and Control, 33(9):475~483

Wang Y. G., Pei Y. L., Zhao Y. D. (2008). "Vibration-Based Damage Detection With Structural Modal Characteristics." *Baltic Journal of Road and Bridge Engineering*, 3 (1): 21~28.

Wan, C.L., and Diekinson, K.W. (1989). "Road traffic monitoring using image processing a survey of systems, techniques and applications [C]." Symposium of the IFAC Conferenee on Control, ComPuters, Communications in TransPortation. Paris,France, 27~34.

Y.J.Lu,and X.Yuan (1992). "Color image analysis for vehicle speed measurement[J]." Canadian Joumal of Civil Engineering,20(2):228~235

Jung, Y., Ho, Y. (2000). "Multiple object tracking under occlusion conditions[J]."Visual Communication and Image Processing,1011-1021.

Collision Avoidance among Multiple Ship Agents

M. Pan[1], F. Yan[2], L. Zhao[1], M. Inaishi[3]

[1]Navigation College, Dalian Maritime University, 1 Linghai Road, Dalian, 116026; FAX(86)411-84723609;email:pan_my@hotmail.com, sabrinadmu@hotmail.com
[2]Information Science and Technology College, Dalian Maritime University, 1 Linghai Road, Dalian, 116026; email: yan_feiyang@163.com
[3]Department of Marine Electronics and Mechanical Engineering, Tokyo University of Marine Science and Technology, 2-1-6 Etchujima, Koto-ku, Tokyo, 135-8533; FAX (+81) 3-5245-7383; email: inaishi@kaiyodai.ac.jp

ABSTRACT

According to the characters of marine navigation, this paper extends the concept of the velocity obstacle and develops a reactive approach to collision avoidance among multiple ship agents. By selecting a reasonable velocity within free parts of its maneuvering space that aren't covered by the union of velocity obstacles of all other ship agents, a ship agent can navigate safely without collision. Simulation experiments show that our approach is able to navigate multiple ship agents with smooth and natural paths to avoid collision, and can be applied to multi-agent based marine traffic simulation systems.

INTRODUCTION

A simulation-based marine traffic flow analysis is widely used for safety assessment and maritime construction planning such as channel traffic control, port design, and water lane establishment. Simulation models are continuously upgraded with the advent of new computer technologies. The modeling of multi-agent and group behavior to simulate complex marine traffic flow has been gaining increasing attention (Inaishi, 2006). In this area, the motion planning of ship agents is a central problem. In previous works，we have studied how ship agents autonomously make their navigation plans, select routes and avoid collision with static obstacles in the environment (Pan, 2008). This paper further focuses on the collision avoidance among multiple moving ship agents and proposes a velocity obstacle-based approach.

The velocity obstacle concept (Fiorini, 1998) is a generally applicable, well-defined and simple technique that has been widely used for safe navigation among moving obstacles in robotics and virtual environments. This paper extends the concept to deal with encounters among multiple ships and develops a reactive collision avoidance model that agrees with marine navigation conventions to the outmost extent. In our approach, all ships navigate independently without explicit communication with each other. This is a simple and natural formulation that is applicable and easy to implement.

SHIP COLLISION AVOIDANCE

DCPA (Distance at Closest Point of Approach) and TCPA (Time to Closest Point of Approach) are two important concepts for ship collision avoidance, and they can be calculated easily according to the velocity triangle (see Figure 1).

$$DCPA = \sqrt{|V_{AB}|^2 - \left(\frac{V_{AB} \cdot (V_A - V_B)}{|V_A - V_B|}\right)^2} \qquad (1)$$

$$TCPA = \frac{V_{AB} \cdot (V_A - V_B)}{|V_A - V_B|^2} \qquad (2)$$

Many assessment models based on DCPA and TCPA have been proposed for evaluating the degree of collision risk and deciding appropriate avoidance action times (Imazu, 1983; Hasegawa, 1987). The collision avoidance action is generally decided based on the encounter situation between two ships according to the international convention for preventing ship collisions at sea (Zhao, 1994). For example, a collision avoidance pattern can be defined as follows (see Figure 2). If the target ship comes from (a) area, a right turn maneuver is needed; if the target ship comes from (b) area, a left turn plus speed reduction is safer than a sharp right turn; if the target ship comes from (c) and (d) areas, the ship maintains its route.

However, the international convention and the above collision avoidance pattern only solve the problem of an encounter between two ships. In a traditional marine traffic simulation system, encounter between more than two ships have to be divided into a series of encounters between two ships, with the most urgent encounter treated first. Obviously, the simple integration of encounters between two ships is difficult to reach from the complex interactions among all ships with a natural and realistic result.

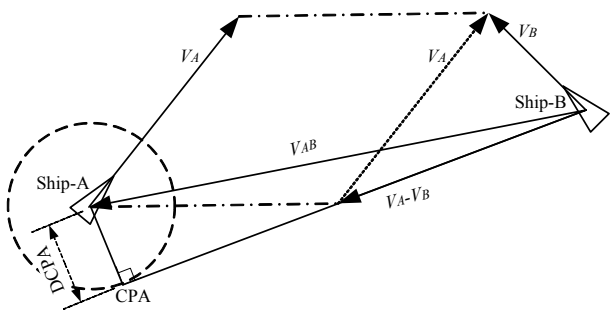

Figure 1. Velocity triangle.

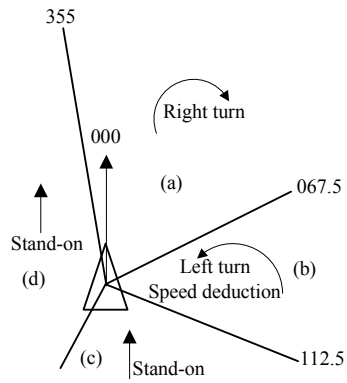

Figure 2. Collision avoidance action.

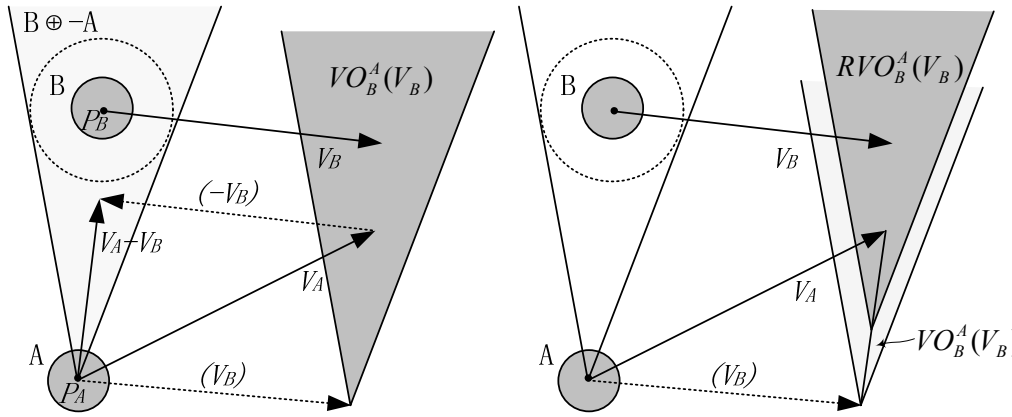

(a) Velocity obstacle **(b) Reciprocal velocity obstacle**

Figure 3. Velocity obstacle and reciprocal velocity obstacle (Jur, 2008).

VELOCITY OBSTACLE

Velocity obstacle is a simple and applicable approach for addressing motion planning in dynamic environments such as robot manipulators avoiding moving obstacles. The velocity obstacle can be geometrically defined as follows (see Figure 3(a) (Fiorini, 1998; Jur, 2008). Let $\lambda(P,V)$ denote the ray starting at P and heading in the direction of V, $-A$ denote the object A reflected in its reference point. If the ray starting at P_A and heading in the direction of the relative velocity of A and B (which is $V_A - V_B$) intersects the Minkowski sum of B and $-A$ (which is $B \oplus -A$) centered at P_B, velocity V_A is in the velocity obstacle of B.

Hence, the velocity obstacle of B to A is defined as follows:

$$VO_B^A(V_B) = \{V_A \mid \lambda(P_A, V_A - V_B) \cap B \oplus -A \neq 0\}. \quad (3)$$

As Figure 3(a) shows, the velocity obstacle is a cone with its apex at V_B. If $V_A \in VO_A^B(V_B)$, A and B will collide at some point in time. If V_A is outside the velocity obstacle of B, the objects will remain clear of each other. By choosing a velocity that lies outside any of the velocity obstacles induced by the moving obstacles and is most directed toward the destination, the robot (or other agent) will safely navigate among moving obstacles toward its destination.

Reciprocal velocity obstacle is an extension of velocity obstacle (Jur, 2008). In order to overcome the undesirable oscillatory motion that could be caused by the original concept of velocity obstacle, the reciprocal velocity obstacle translates its apex to $(V_A + V_B)/2$ instead of V_B (see Figure 3(b)). By preventing an old velocity from being re-chosen immediately in next planning cycle and requiring the choice of the closest velocity outside the other agent's reciprocal velocity obstacle, this guarantees oscillation-free navigation.

COLLISION AVOIDANCE AMONG MULTIPLE SHIP AGENTS

Velocity obstacle for ships. In the original concept of velocity obstacle, $B \oplus -A$ is the critical space that prevents object A from colliding with B (if

the ray of $V_A - V_B$ is tangent with $B \oplus -A$, object A will pass B with the minimal safe distance, radius of A). This definition of minimal safe passing distance is feasible and works well in the robot world. However, it is unsuitable for ships, which need larger and anisotropic passing distances to avoid collisions, due to their poor maneuverability and longilineal shape.

For navigating ships, ship domain is an important concept for assessing the avoidance of collisions. It is a buffer area around the ship that mariners want to keep clean and shut all other objects out of. Figure 4 shows a commonly used definition of ship domain and its frontier model. Obviously, using ship domain instead of the Minkowski sum of two objects to define the velocity obstacle is more feasible for marine navigation. So, this paper extends the velocity obstacle for ship collision avoidance (denoted by SVO) as follows (see Figure 5):

To simplify computation, the elliptical boundary of ship domain is replaced by its bounding box. Let D_A and D_B denote the ship domain of ship A and ship B, $-D_A$ denote ship domain of ship A reflected in its reference point, and the $conv(D_B \cup (-D))$ denote the convex hull of the union of D_B and $-D_A$. Then, the velocity obstacle of ship-B to ship-A is defined as follows:

$$SVO_B^A(V_B) = \{V_A \mid \lambda(P_A, V_A - V_B) \cap conv(D_B \cup (-D_A)) \neq 0\} \quad (4)$$

According to the navigation convention, for a pair of encountering ships, there is one obligation ship and one stand-on ship. The obligation ship has a duty to take collision avoidance maneuvers, and the stand-on ship has right to maintain its direction. So in order to enable unilateral action that guarantees both ships can keep each other out of their own ship domains, $conv(D_B \cup (-D_A))$ instead of $-D_A$ is used to define $SVO_B^A(V_B)$. Furthermore, the extension of reciprocal velocity obstacle proposed to overcome the undesirable oscillatory motion fails for such a case because it requires both objects to take avoidance action. In fact, because the stand-on ship maintains its velocity, the apex of $SVO_B^A(V_B)$ stays at the same position in next cycle which is also the reason why reciprocal velocity obstacle can protect against oscillatory motion. For example, Ship B is the obligation ship

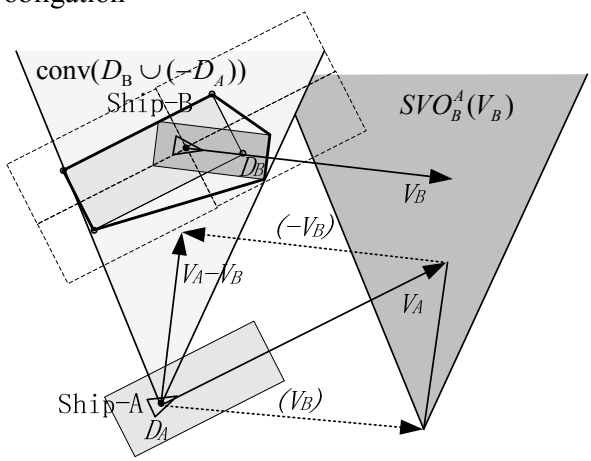

Figure 4. Ship domain.

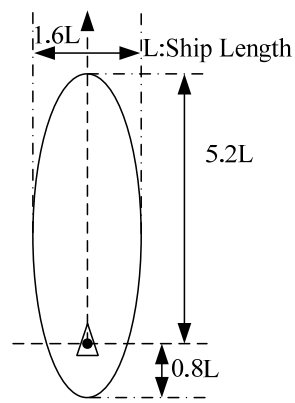

Figure 5. Velocity obstacle for ships.

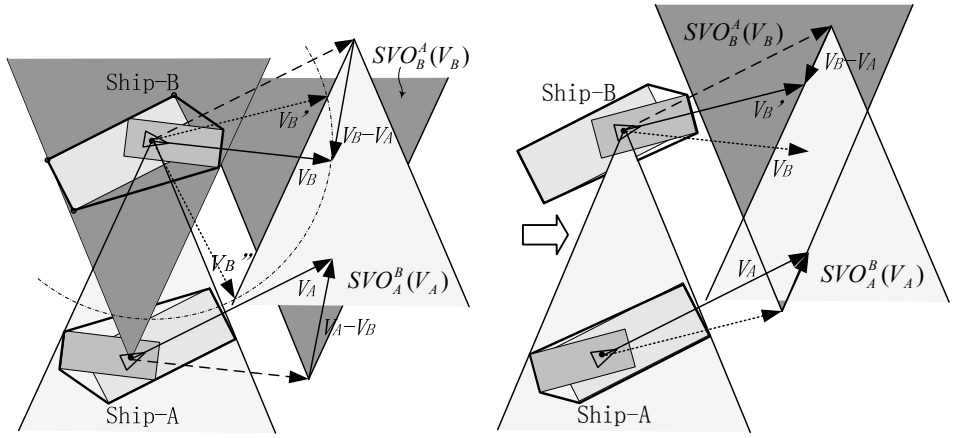

(a) Ship B should take a left turn. **(b) After Ship B takes left turn.**

Figure 6. Collision avoidance between a pair of ships.

and alters its velocity to V_B' so that it is outside the $SVO_B^A(V_A)$ and avoids collision with Ship A (see Figure 6 (a)). In the new situation, as the old velocity V_B is still inside the new $SVO_B^A(V_A)$ (see Figure 6 (b)), it cannot be chosen again as the new velocity for next cycle. Thus, oscillation between two velocities of V_B and V_B' can naturally be prevented. Although, due to the directional characteristics of ship domain, the $conv(D_B \cup (-D_A)$ is unable to always keep the same shape as $B \oplus -A$. If the new velocity V_B' is chosen close to $SVO_B^A(V_B)$, the old velocity V_B is still unable to escape out of the new $SVO_B^A(V_B)$. Figure 6(a) also shows why a left turn (V_B') is more feasible than a right turn (V_B'') when the target ship is coming from area (b) described in Figure 2.

Navigation of Multiple Ship Agents. Although the *SVO* is defined based on collision avoidance between two ships, its advantage lies in its ability to simply solve the problem of collision avoidance among multiple ships. It has been utilized to make decisions for ship agents to avoid collision with other moving ships in our multi-agent based marine traffic simulation system.

In the simulation system, ship agents are modeled to repeat a sense-decide-act cycle, perceiving the surrounding environment through a sensor to identify obstacles, making decisions to produce a steering order in the form of a velocity vector and executing the steering order by an effecter constructed according to TK model and PD controller of the ship (Pan, 2008). As subjected to these maneuverability and dynamic constraints, the admissible new velocities given the current velocity of a ship agent are restricted in limited set, called maneuver space. According to marine navigation conventions, the maneuver space can be defined as follows (Nagasawa, 1992). In geometry, it is a sector with apex at ship agent's center (see Figure 7).

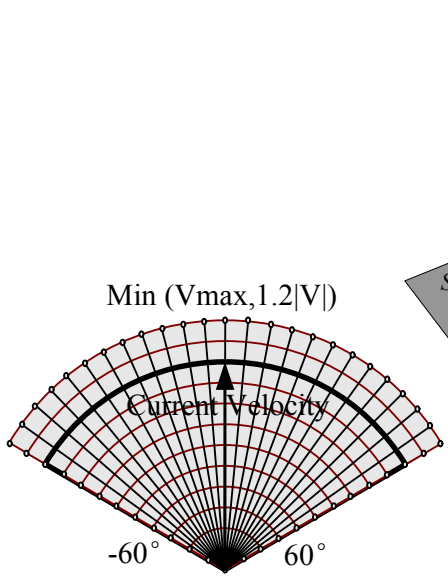

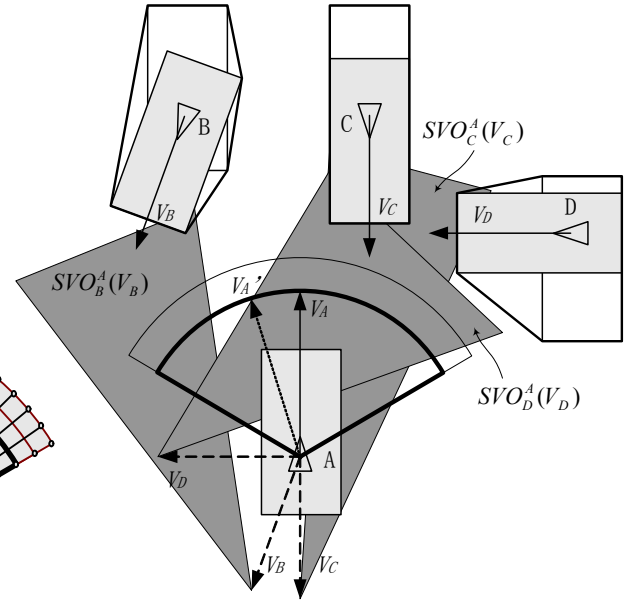

Figure 7. Maneuver space. **Figure 8. Collision avoidance among ship agents.**

$$MSpace(V) = \{V' | \frac{V' \cdot V}{|V||V'|} < \cos 60^o, |V'| < Min(V_{\max}, 1.2|V|)\} \quad (5)$$

When other ship agents appear in the sensing region of a ship agent, the union of all SVOs generated by the other ship agents is computed. To navigate without colliding with the others, the ship agent should choose a velocity within the free parts of its maneuver space that aren't covered by the union of SVOs (see Figure 8). In order to simplify the velocity selection computation, the maneuver space is quickly scanned to find a prefect new velocity that lies outside all the unions of SVOs and is closest to the current velocity. Differences between current velocity and the velocities within the left side of the maneuver space are multiplied by a factor of 1.5 to ensure the customary avoidance action of a right turn.

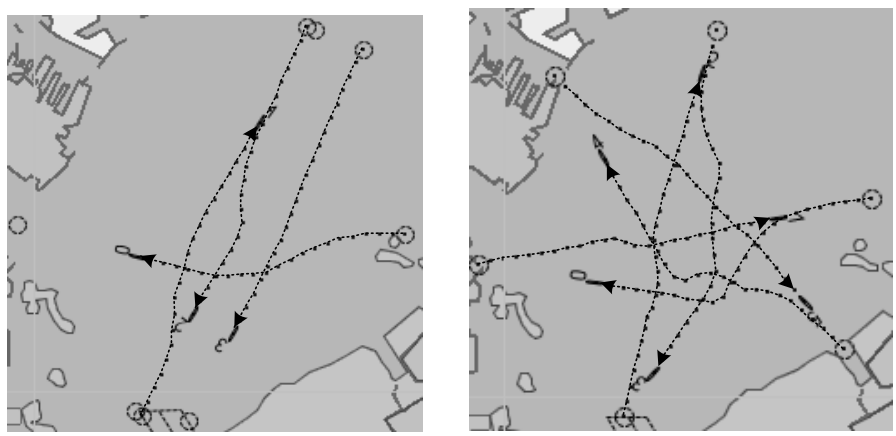

Figure 9. Example of simulation result (screenshots).

EXPERIMENT

Simulations have been conducted to investigate the effectiveness of the collision avoidance model. Figure 9 shows two example scenarios of complex encounters. All ship agents are modeled with equal size and maneuverability. The results show that the collision avoidance model navigated all ship agents safely without collisions and generated smooth and reasonable courses for the ship agents.

CONCLUSION

In this paper, we have extended the concept of velocity obstacle based on the characteristics of marine navigation and developed a reactive collision avoidance model that deals with collision avoidance among multiple ships. The model has been applied in a multi-agent based marine traffic simulation system and was shown to compute smooth and natural paths for ship agents in a dynamic environment. Because all ships navigate independently without explicit communication with each other, the model is a simple and natural formulation that is relevant and easy to implement.

REFERENCES

Fiorini, P. and Shiller, Z. (1998). "Motion planning in dynamic environments using velocity obstacles." *Int. Journal of Robotics Research*, 17(7), 760–772.

Hasegawa, K., Kouzuki, A. (1987). "Automatic collision avoidance system for ships using fuzzy control." The Kansai Society of Naval Architects, 205, 1-10.

Imazu, H. (1983). "The determination of collision avoidance action." Japan Institute of Navigation, 70, 31-37.

Inaishi, M., Kondo, H., Kondo, M., and Kawaguchi, A. (2006). "Marine traffic simulation using ship agent clusters: northbound traffic in Tokyo bay." Japan Institute of Navigation, 115, 11-16.

Jur, van den Berg, Lin, M., Manocha, D. (2008). "Reciprocal velocity obstacles for real-time multi-agent navigation." ICRA 2008, 1928-1935.

Nagasawa, A., Hara, K., Inoue, K., and Kose, K. (1992). "The subjective difficulties of the situation of collision avoidance." Japan Institute of Navigation, 86, 137-144.

Pan, M. Y., Inaishi, M., and Kawaguchi, A. (2008). "Ship cluster behavior model with strategic and tactical obstacle avoidance." Japan Institute of Navigation, 119, 43-49.

Zhao, J., Tan, M., Price, W.G., and Wilson, P.A. (1994). "DCPA simulation model for automatic collision avoidance decision making systems using fuzzy sets." OCEANS 94, 2, 244-249.

Traffic Signal Control Optimization of Urban Arterials Based on a Method of Main Intersection Control Strategies

B. Liu[1,2], X. Yan[1,2], J. Wu[1,2], L. Li[3], X. Wang[4]

[1]School of Traffic and Transportation, Shijiazhuang Railway Institute, Shijiazhuang, Hebei, China, 050043; PH (86) 311-87935516; FAX (86) 311-87935516; email: tom667788@163.com
[2]Traffic Safety and Control Lab of Hebei Province, Shijiazhuang, Hebei, China, 050043; PH and FAX (86) 311-87935516; email: tom667788@163.com
[3]Shijiazhuang Urban Planning & Design Insititute, Shijiazhuang, Hebei, China, 050043; PH and FAX (86) 311-88627800; email: tom667788@163.com
[4]School of Transportation Science and Engineering, Harbin Institute of Technology, Harbin, Heilongjiang, China, Post code 150090; PH (86) 451-81778812; FAX (86) 451-86283779; email: wxn1974@hit.edu.cn

ABSTRACT

Traffic signals on urban arterials operate in coordinated systems to provide smooth progression of major traffic movements. In recent decades, continued efforts have been made to research and develop coordinated traffic signal control strategies. As a result, many models, either off-line or on-line, have been developed. Despite the availability of customary models, all of them have been designed by coordinating all intersections at the same time, and there are many problems. For example, the individual intersection spacing may not be ideal, eventually leading to poor coordination.

An improved method is put forward in this paper to replace the classical method: the method of main intersection control strategies. The intersections on urban arterials that need to be coordinated are divided into two levels: the main intersection and the participation intersection. First, the intersections that are more important and appropriate to coordinate are selected as the main intersections. Then, the basic computing can be performed on the main intersections. The effect of coordination is better than the results from calculating all intersections directly. The rest of the intersections can be brought into the coordinated system through many other ways so as to minimize the impact on the system. Compared with the classic method, this method of main intersection control strategies optimizes the effectiveness of coordination, reduces the traffic delay and deals with the intersections step-by-step. In practical engineering, compared with the classical method, it has been proven that the new method can reduce the delay by about 10-20 percent. It has great value in practical application.

INTRODUCTION

Traffic signals on urban arterials operate in coordinated systems to provide for smooth progression of major traffic movements. In recent decades, continued efforts have been made to research and develop coordinated traffic signal control strategies. Despite the availability of customary models, all of them have been designed by coordinating all intersections at the same time. This causes many problems. For example, the individual intersection spacing may not be ideal, eventually leading to poor coordination. This paper presents an improved method to replace the classical method: the method of main intersection control strategies. Compared with the classical method, this method optimizes the effectiveness of coordination and reduces the traffic delay by dealing with the intersections step-by-step. In practical engineering, compared with the classical method, it has been proven that the new method can reduce traffic delays by about 10-20 percent or so and that it has great value in practical application.

ACTUALITY RESEARCH

Many experts have made in-depth studies about the timing design of traffic control systems by the numeric method. In China, Yang Peikun (L. Bohang, 2007) expounded the mechanism for the theory model of the ideal equidistant intersection in "Traffic Management and Control." Lu Huapu (J. Liye, 1996) brought forward the theory model, which was oriented toward the minimum delay of vehicles in two-way arterial travel. Yet his theory is based on the vehicles arriving at a uniform speed. Zou Chengwei and Li Zhihai conducted traffic control design at Harbin Hongqi Street. Abroad, national standards in America and Germany are all based on the numeric method. Some scholars (Van Aerde, Mohamadreza Farzaneh and Hesham Rakha) researched how to demarcate the classic models more accurately (Hesham Rakha, 2005). Despite the availability of customary models, all of them have been designed by coordinating intersections all at once, leading to many problems.

THEORY OF THE COMPOSITE NUMERIC METHOD

The composite numeric method has broken the basic pattern, of parallel computation with all intersections, of the traditional numeric method. Intersections are divided into two types: the main intersections and the participation intersections. First, according to different volumes or locations, select the more important and appropriate coordinating intersections to be the main intersections. Because of selection, most often, the coordination effects would be better than those that were calculated directly by the numeric method. Next, bring the rest into the traffic control system. We could adopt various ways to optimize the intersections brought in before, such as half-cycle, phase order, etc.

As shown in Figure 1, one should select four intersections, which are marked with yellow, to be the main intersections, then make fundamental calculations on these chosen ones by the numeric method. Then one would bring other intersections, which are marked with blue into the coordination with the main intersections and adopt methods of traffic signal optimization. Of course, this solution is the most applicable for the cases of alternating big and small intersections on urban arterials.

SELECTION OF MAIN INTERSECTIONS

The composite numeric method is used for the coordination of controlling main roads; the first problem deals with selecting the intersections that are the main intersections. We can take the selection through the following steps:

Determine the number of main intersections. Calculate the cycle C_i separately for each intersection and determine the total cycle C. Determine the ideal spacing L_{per} according to C and system speed V. Based on the basic concept that the ideal spacing is fluctuating in the vicinity of $VC/2$, calculate to the ideal spacing fluctuation range of main intersections, which equals $L_{per}\pm100$ meters in general. According to the system total length L and ideal spacing fluctuation range, determine the largest and smallest number of main intersections:

$$n_{\max} = l \Big/ (l_{per} - 100) + 1 \quad (1)$$

$$n_{\min} = l \Big/ (l_{per} + 100) + 1 \quad (2)$$

Where: $n_{\max}$ - Largest possible number of main intersections

$n_{\min}$ - Smallest possible number of main intersections

L- System total length

L_{per} -Ideal spacing fluctuation range

Determine the groups of main intersections. Set the number of all the intersections that need coordination as m, select n of them as the main intersections. There are C_m^n cases, and all the possible cases are:

$$k = \sum_{i=n_{\min}}^{n_{\max}} c_m^n \quad (3)$$

Where, k = Total number of possible options for main intersections;

i = Number of possible main intersections;

C_m^i = Total number of possible options for main intersections when the number of main intersections i is determined; and,

$n_{\min}$ and $n_{\max}$ are the same meaning with (1) (2) in 4.1.

Determine the specific main intersection groups. For each group, the total distance between the actual intersections and the ideal intersection will be calculated:

$$l_z = \sum_{i=1}^{m} l_i \qquad (l_i = \left| D_i - d_j \right|) \quad (4)$$

Where l_i is the distance between the number i actual intersection with the number i ideal intersection.

We use the traffic evaluation index W to ultimately determine the options for main intersection groups. The formula for W is:

$$W = 0.37Q - 0.63L \quad (5)$$

Where, W = Index of traffic evaluation;
Q = Traffic volume through main control intersection;
L = Distance between the actual intersection and the ideal intersection.

We can select the smallest values W of a group as the main intersections. That is, select the group as far as possible that has larger traffic volume and the smallest distance between the actual intersections and the ideal intersection.

INCORPORATE THE PARTICIPANT INTERSECTIONS

After the selection of main intersections, we face the problem of how to coordinate main intersections with the rest of the intersections. Other optimal methods in traffic control can be used, such as semi-cycle, phase adjustments, and so on:

Semi-cycle method. For some intersections with smaller traffic volume, the practical need for cycle time is close to half of the system cycle time. Therefore, we can set half of the system cycle time as signal cycle time for these intersections. That is the semi-cycle method.

Adjustment of the phase order method. In other words, two straight traffic volumes of the urban arterials are on different phases. This method can significantly reduce the loss of time, making the traffic operation achieve the best effect.

Set up hardware facilities. Hardware set up on the participant intersections can be taken into consideration. Essentially, this reduces the impact of pedestrians and vehicles from branch roads to vehicles on the urban arterials.

Figure 1. The main intersection and the participation intersection.

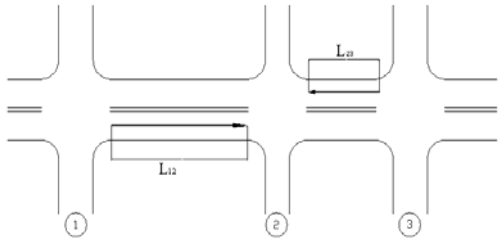

Figure 2. The distance between main intersection and the participation intersection.

CASE ANALYSIS

On November 18, 2007, we tested ten intersections along Yuhua Road in Shijiazhuang. As shown in Table 1, after the using the numeric method, the result of calculation for offset is very good. As shown in Table 2, the classic numeric method made the control system delay drop from 61.3V/S to 40.2V/S, while the composite numeric method made it reduce to 25.3 V/S, an obvious optimal effect.

Table 1. Calculated offset of main intersections.

Intersection	A	B	C	D
Ideal signal No	①	②	③	④
Signal location	right	left	left	left
Proportion of green time λ(%)	31.8	47.2	56.3	39.6
Loss of green time (%)	4.1	4.1	2.3	0.25
Proportion of green time of efficiency (%)	27.7	43.1	54	39.35
Difference of green time (%)	84.1	26.4	71.85	30.2
Relative green time (s)	135	42	115	48

Table 2. Data of delay of simulation in three conditions.

Instance	Delay of investigation	Delay of classical algorithm	Delay of of main intersections control strategies
Number	61.3	40.2	25.3

CONCLUSIONS

The numeric method is the basic method for urban arterial traffic control, and is also the most widely used method at present. We improved on the numeric method, on the premise of not increasing input parameters to the system. The example verified that the method can reduce traffic delays on urban arterials, and has more obvious effects on coordination.

ACKNOWLEDGEMENTS

This research was supported by Young Scientist Project of Natural Science Foundation of China (NSFC), "The method of reducing emission of air pollutants from urban public transportation based on the behavior analysis" (Grant No：70803007）, Traffic Safety and Control Lab of Hebei Province opening issue Fund, "Three-Dimensional Visual plan and design system of Urban Mass Transit"（Grant No：211001）and Startup Foundation for Advanced Talents of Shijiazhuang Railway Institute（Grant No：8110053）. Thanks for co-operation of Shijiazhuang Traffic Management Bureau.

REFERENCES

Bohang, L., Yulong, P. (2007). "Optimization and Improvement of Offset Model Based on Minimal Delay for Coordinated Traffic Signal Control." Proceedings of 2007 International Conference on Construction & Real Estate Management: *576-580.*

Liye, J., Bingjun, C., Diao, F., Fengtao, W. (1996). "Urban Traffic Optimal Decision-making Alignment-control Algorithm and Software Design." *Computer Study*. (2):20~22.

Rakha, H. (2005). "Macroscopic Modeling of Traffic Dispersion:" I*ssues and Proposed Solutions Transportation Research Board 84th.* 0855.05-09.

Yulong, P., Bohang, L. (2007). "Offset optimal model for urban main road." *Journal of Central South University*. 38(supp1):1023-1027.

An Interval-Varying Floating Car Data Clustering Approach Based on Self-Organizing Maps

Q. Li[1], J. Cao[2], Y. Yue[3]

[1]Transportation Research Center, State Key Lab of Information Engineering in Surveying, Mapping and Remote Sensing, Wuhan University; P.O. Box C307; 129 Luoyu Road, Wuhan, Hubei, China, 430079; TEL: (86-27)-68778035; email: qqli@whu.edu.cn

[2]Transportation Research Center, State Key Lab of Information Engineering in Surveying, Mapping and Remote Sensing, Wuhan University; P.O. Box C307; 129 Luoyu Road, Wuhan, Hubei, China, 430079; TEL: (86)-15926300335; email: longrning@gmail.com

[3]Transportation Research Center, State Key Lab of Information Engineering in Surveying, Mapping and Remote Sensing, Wuhan University; P.O. Box C307; 129 Luoyu Road, Wuhan, Hubei, China, 430079; TEL: (86-27)-68778035; email: yueyang@whu.edu.cn

ABSTRACT

Floating car data (FCD) are characterized by high dimensions and large data size with complex spatiotemporal relationships. This paper proposes a time interval-varying scheme for FCD dimensional reduction for clustering analysis, which can capture the main fluctuation closer to the original data. A self-organizing map is used as the clustering algorithm. Some interesting and hidden relationships between links can be found in the clustering results. The method proposed in this paper proved acceptable for FCD clustering, which is useful for road correlation analysis of the urban road network.

INTRODUCTION

A floating car equipped with a Global Position System (GPS) unit can be considered a moving geo-sensor with the ability to collect vehicle speed data. The data acquired by floating car is often used to indicate the traffic conditions of corresponding links. In order to understand road network traffic conditions, clustering is an often-used method that reveals the hidden spatiotemporal relationships that are of great value for many applications, such as traffic prediction. However, floating car data (FCD) are characterized by high dimensions and large data size with complex spatiotemporal relationships.

Focusing on the fluctuation of link average speed at different time intervals on a road network, this paper proposes a novel approach for road link traffic clustering based on a Self-Organizing Map (SOM) using a varying interval scheme for FCD dimension reduction.

RELATED WORKS

The most widely used clustering algorithms are K-means, c-means (CM) and fuzzy c-means (FCM) (Lee et al., 2006; Guo and Jiang, 2007). K-means clustering is sensitive to the initialization of clusters and data noises or outliers. CM and FCM algorithm may converge to create local solutions that are significantly inferior to the desirable global optimum (Selim and Ismail, 1984; Pollard, 1982). In order to find the global optimum, clustering methods using Genetic Algorithms (GA) have been proposed (Murthy and Chowdhury, 1996; Jones and Beltramo, 1991), which are usually computationally expensive. These methods are not feasible for large amounts of FCD with non-exhaustive enumeration and high dimensionality. SOM with excellent data mining capability and easy visualization is a potentially powerful clustering tool to solute these problems. It has been adopted in many fields, such as pattern recognition, data classification and image analysis (Oja and Kaski, 1999). In the field of traffic data analysis, there are some studies that aim to group the traffic flow time series from loop detectors and use equal-width schemes to prepare the input components of the SOM (Cheng et al., 2006a, 2006b, 2008).

If it can be considered a dimension in different time space, a floating car record attached to a link can be regarded as a point with high-dimension during a certain epoch (for example, 1440-dimention of a day at one-minute intervals). Thus, dimension reduction of FCD is critical and significant before conducting clustering. Major dimension-reduction methods include: Principal Component Analysis (PCA) (Cheng et al., 2006), Discrete Fourier Transformation (DFT) and wavelet decomposition (Qiao et al., 2003; Liu et al., 2008). A simple but rather useful technique for data dimension reduction is aggregation approximation (Keogh and Pazzani, 2000). Traditional traffic data aggregation schemes are based on equal-width methods, typically with 5 or 15-minute intervals, which may not be optimal for traffic changes that vary significantly throughout a day (Zheng and McDonald, 2006, 2007; Turner et al., 2000).

PROPOSED METHODOLOGY

The determination of the varying intervals is a Dynamic Programming (DP) problem. Using Sum Squared Error (SSE) as the error metric and given a sequence of source traffic data X of length N, finding the optimal aggregation intervals $\{[s_1,e_1],[s_2,e_2],\ldots,[s_M,e_M]\}$, $1 \leqslant i \leqslant M$, essentially minimizes the total: $SSE = \sum_{i=1}^{M}\sum_{j=si}^{ei}(x_j - y_i)^2$, where $y_i = \frac{1}{ei - si + 1}\sum_{j=si}^{ei} x_j$, $SSE(si, ei) = \sum_{j=si}^{ei}(x_j - y_i)^2$ is the i^{th} interval error, M is the number of aggregation intervals. The minimum total SSE indicates the least loss of traffic original information.

There exists an efficient algorithm to solve this kind of optimization problem. The algorithm based on DP with quality guarantees has been implemented in these studies (Jagadish et al., 1998, 2001). The crucial equation underlying the DP is:

$$SSE^*(i,k) = \min_{1 \le j < i}\{SSE^*(j,k-1) + SSE([j+1,i])\}$$

Where SSE*(i, k) is the minimum SSE for the data sub-vector X[1, i] aggregated at most k intervals and SSE([j+1, i])=SSE(j+1, i) is the SSE for the data sub-vector X[j+1, i] aggregated to one interval with the average of AVG([j+1, i]). Using iterative calculation, the solution for k intervals can then be reduced to the case of k-1 intervals by considering all possible left boundaries of the rightmost k^{th} intervals. Starting from SSE*(1,1), which is known, SSE*(N, M) can be found by calculating SSE*(i, k) for all $1 \le i \le N$ and $1 \le k \le M$ in increasing order of k, and for any fixed k, in increasing order of i.

An example of error comparison of the FCD aggregation scheme generated using the DP algorithm and equal-width scheme is shown in Figure 1. The error metric is Root Mean Square Errors (RMSE), which here is defined by:

$$RMSE = \sqrt{\frac{SSE}{N}}$$

As SSE is minimized in the optimal scheme, the RMSE is also the smallest. It is obvious that the varying aggregation intervals can catch the primary changes of the traffic feature, rather than reducing the dimension only.

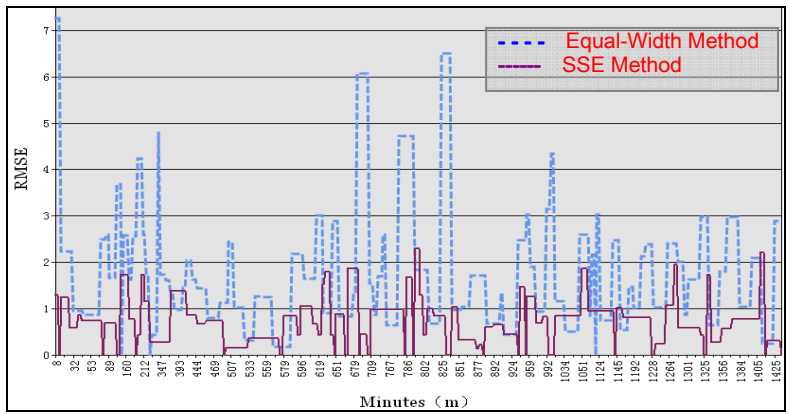

Figure 1. The RMSE of the equal-width method and the SSE method for the average link speed measurement.

SOM is a well-developed non-supervised neural network technique for data clustering with easy visualization. Details of SOM can refer to Oja et al. (1999). The size of the map usually reflects the number of clusters, depending on the amount of input samples. According to the empirical value, [10, 9] is used in this study. In order to interpret the results and find the clusters easily and exactly, a labeled map is used. Each link is considered a single label. During the training of the map, it can automatically assign labels to the nodes of a trained SOM. The closer labels are assigned to a particular cluster, and the farther ones are assigned to a different cluster. Moreover, several visualization methods of SOM are used in order to make the clusters or sub-clusters easily understood and interpreted.

CASE STUDY

The study used the FCD acquired from over 1000 of Nanchang's taxis

from July 14 to July 20 2008, including longitude, latitude, point speed and direction angle. The data were low-frequency and continuously transmitted. The study area included 77 links in the city central, as shown in Figure 2.

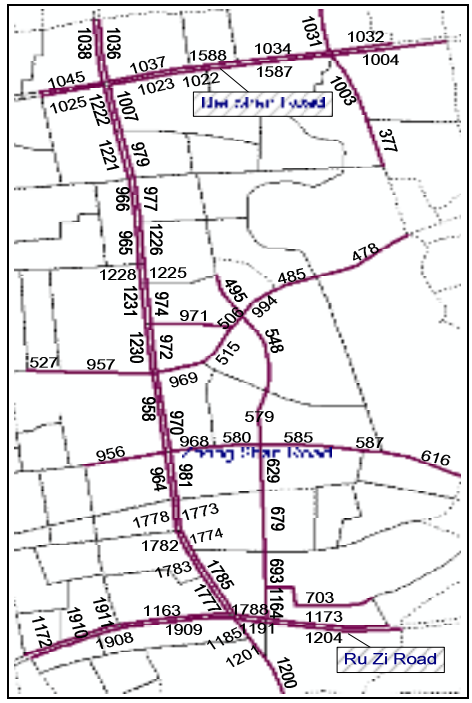

Figure 2. The study road links.

Using the proposed method, the FCD on the road links were divided into 96 optimal varying intervals for each day. The data that fell in the same interval were averaged as the link speed of that interval. Thus, the whole week average speed of each selected link was a vector with 672 dimensions. Thus, attributes of the studied links for a whole week were structured with a 77*672 matrix, which is the input of the SOM. The rows indicated the main links and the columns indicated the varying intervals that were the components of the samples. The resulting labeled map and the better visualization methods allowed us to better distinguish several obvious clusters and some sub-clusters.

The clustering results are shown in Figure 3. Some links are clustered in one group but some groups only have one link; these groups are the sub-clusters. Every lattice can be considered as one sub-cluster, and the sub-clusters can define the clusters according to the cluster boundaries' segmentation (see Figure 3(a) Clusters A, B, C for examples).

By comparing the clusters and the physical road network, some interesting relations between links in the same group can be easily found. For example, the links in the same sub-clusters are usually spatially close to each other or in the parallel direction, like Group 3 and link 1587 and link 1588 in group 4, or adjacent to intersections along the same street, like Group 1, or intersect at intersections, like Group 2. Table 1 illustrates some typical sub-clusters, and the positions of these links in the network can be shown obviously in Figure 2. The super-clusters can expose some hidden relationships between the links that are not connected with each other spatially. For example, link 1204 and link 1173 in Ru

Zi Road and link 1034 and link 1587 in Die Shan Road are far from each other (Figure 2), but they are in the same super-cluster A with similar speed levels (Figure 3(b)).

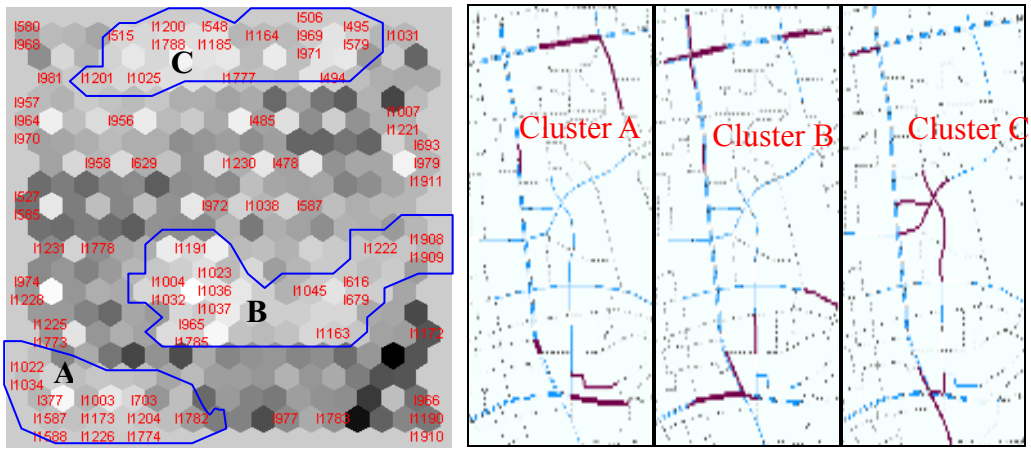

Figure 3. (a) is the clustering results, (b) Cluster A, B, C for an example.

Table 1. Some sub-clusters.

Sub-cluster	Link	Sub-cluster	Link
Group 1	l1908, l1909	Group 3	l1004, l1032
Group 2	l1023, l1036, l1037	Group 4	L377, l1587, l1588

CONCLUSION AND THE FURTHER RESEARCH

The method proposed in this paper proved acceptable for FCD clustering, which is useful for analyzing the fluctuation and the hidden relationships of FCD in the road network. Specifically, the varying aggregation level scheme fits for the dimensional reduction and feature extraction of the high-dimensional and large-size traffic data. The favorable features of SOM make it a potentially powerful tool for traffic data.

However, in order to indicate spatial distribution of the link traffic state (average speed) in the urban road network, the spatial attribute of road links (geometric shape, location, topological attributes etc.) should not be ignored. Therefore, our further research will consider these issues and use larger volume FCD.

REFERENCES

Cheng, Y. D., Hu, J. M., Zhang, Y., and Li, X. (2006). "Traffic Data Analysis Using Kernel PCA and Self-Organizing Map." *Intelligent Vehicles Symposium*, 472-477.

Cheng, Y. D., Zhang, Y., Hu, J. M., and Yao, D. Y. (2006). "Pattern Discovering of Regional Traffic Status with Self-Organizing Maps." *Proc. of the IEEE 2006 Intelligent Transportation Systems Conf.*, Toronto, Canada, 647-652.

Cheng, Y. D., Zhang, Y., and Hu, J. M. (2008). "Multi-Dimensional Traffic Flow Time Series Analysis with Self-Organizing Maps." *Tsinghua Science and*

Technology, 13(4), 220-228.

Guo, H. F., and Jiang, G. Y. (2007). "FCM Algorithm for Identifying Urban Road Traffic Condition with Loop Sensor Data." *Proc. of the 2007 IEEE International Conf. on Mechatronics and Automation*, Harbin, China, 3413-3417.

Jagadish, H.V., Koudas, N., Muthukrishnan, S., Poosala, V., Sevcik, K., and Suel, T. (1998). "Optimal Histograms with Quality Guarantees." *Proc. of the 24th VLDB Conf.*, New York, USA, 1998，275-286.

Jagadish, H.V., Jin, H., Ooi, B.C., and Tan, K.L. (2001). "Global Optimization of Histograms." *SIGMOD Record*, 30 (2), 223–234.

Jones, D. R., and Beltramo, M. A.(1991). "Solving Partitioning Problems with Genetic Algorithms." *Proc. of 4th International Conf. on Genetic Algorithms*, 442-449.

Keogh, E. J., and Pazzani, M. J. (2000). "A Simple Dimensionality Reduction Technique for Fast Similarity Search in Large Time Series Databases." *In 4th Pacific-Asia Conf. on Knowledge Discovery and Data Mining*, 122-133.

Lee, S. H., Lee, B. W., and Yang, Y. K. (2006). "Estimation of Link Speed Using Pattern Classification of GPS Probe Car Data." *LNCS* 3981, 495 – 504.

Liu, M. H., Yu, L., and Yuan, Z. Z. (2003). "Improved Aggregation Levels of ITS Data via Wavelet Decomposition and Fast Fourier Transform Algorithm." *Proc. of 2003 IEEE Intelligent Transportation Systems.* 2, 1780-1785.

Murthy, C. A., and Chowdhury, N. (1996). "In Search of Optimal Clusters using Genetic Algorithms." *Pattern Recognition Letters*, 17(8), 825-832(8).

Qiao, F. X., Wang, X., and Yu, L. (2003). "Optimizing Aggregation Level for Intelligent Transportation System Data Based on Wavelet Decomposition." *Journal of the Transportation Research Board*, 10-20.

Oja, E., and Kaski, S. (Eds) (1999). *Kohonen Maps*. New York, Elsevier.

Pollard, D. (1982). "A Central Limit Theorem for k-Means Algorithm." *Annals of Probability*, 10(2), 919-926.

Selim, S. Z., and Ismail, M. A. (1984). "K-means Type Algorithms: A Generalised Convergence Theorem and Characterization of Local Optimality." *IEEE Transactions on Pattern Analysis and Machine Intelligence*, 6(1), 81-87.

Turner, S. M., Eisele, W. L., Gajewski, B. J., Albert, L. P., and Benz, R. J. (2000). "Intelligent Transportation System Data Archiving: Statistical Techniques for Determining Optimal Aggregation Widths for Inductive Loop Detector Speed Data." *Journal of the Transportation Research Board* 1719, 85-93.

Zheng, P. J., and McDonald, M. (2006). "An Algorithm for High-Dimensional Traffic Data Clustering." *FSKD 2006, LNAI* 4223, 59-68.

Zheng, P. J., and McDonald, M. (2007). "Optimal Traffic Data Archive Scheme." *IET Intelligent Transport Systems and Services*, 1(2), 144-149.

A Route-based Model for Determining Interconnection of Isolated Traffic Signals

W. Ma[1], Y. Liu[2], X. Yang[3]

[1]Tongji University, Key Laboratory of Road and Traffic Engineering of the Ministry of Education, Shanghai 201804, China; email: awanjing@tongji.edu.cn
[2]Department of Civil Engineering, the University of Maryland, College Park, MD 20742; troybest@umd.edu
[3]Tongji University, Key Laboratory of Road and Traffic Engineering of the Ministry of Education, Shanghai 201804, China; email: angxg@tongji.edu.cn

ABSTRACT

Interconnection desirability testing between adjacent intersections is critical to analyzing traffic conditions and deciding whether the two isolated traffic signals should be interconnected. This paper reports the development of a route-based Interconnection Desirability Index model to evaluate the need to interconnect signalized intersections. In the first part, the shortcomings of existing traditional Interconnection desirability index model (link-based model) were analyzed. In the second part, a route-based model was built, considering not only the distance between intersections but also the signal phase plan and route volume composition. Finally, a case study, including two real intersections, is presented. The performance of traditional link-based models and the proposed route-based model were compared. Synchro and VISSIM were used to optimize and evaluate the isolated and coordinated signal timings. The results show that the proposed route-based model has the ability to describe the real relationship of adjacent intersections and find the most critical route for signal coordination. Moreover, the route-based model is more sensitive than link-based models under high interconnection desirability conditions.

INTRODUCTION

Modern traffic signal control strategy to reduce vehicle delay and fuel consumption has been enhanced by readjusting signal timing plans, installing control equipment and providing interconnection (Cohen. S. L, 1983; Wagner, 1980; Suhbier and Byrne, 1979). Even though few publications exist addressing when to interconnect a series of isolated signalized intersection, interconnection has been recognized as a viable traffic control improvement alternative. (Wagner, 1980; Yagoda, 1973; E. Chang, 1985) Many other researchers have found that a number of factors are important in determining the need for interconnection including geographic relationship, volume levels and traffic flow characteristics.

One of popular model used and indexed by the Traffic Control System Handbook (2005) was the coordination desirability index model developed by

Chang and Messer. It is described as (we call it the link-based model):

$$I = \left(\frac{0.5}{1+t}\right) * \left(\frac{q_{\max}}{q_T}\right) - (N-2) \quad (1)$$

Where t is link travel time in minutes, $q_{\max}$ is straight-through flow from upstream intersection (VPH), q_T is the sum of traffic flow at the downstream approach from the right turn, left turn, and through movements of the upstream signals, divided by the number of arrival links at the upstream intersection. N is the number of arrival lanes feeding into the entering link of the downstream intersection.

The inputting flow characteristics of a total link are considered in the model. However, one of the critical issues of signal coordination is that the route flow characteristics, rather than link flow characteristics, decide the benefit of interconnection of two isolated intersections. Moreover, the impact of a signal phase plan was not considered in the link-based model. Hence, this research will focus on fulfilling the following the two critical tasks.

ROUTE-BASED MODEL

Intersections should be interconnected only if the arrival flow rates of any movement downstream can be guided into compact platoons through an effective traffic signal timing plan. In order to capture the real desirability of interconnection, route volume characteristics and signal plan were considered in the proposed model (route-based model).

MODEL ASSUMPTIONS

To yield a tractable solution for the proposed formulations with realistic constraints, this study has employed the following assumptions:

Assumption 1: Data of every route.

The turn ratio at the downstream intersection of a movement of upstream intersection is needed in the model.

Assumption 2: signal phase plan

The signal phase design of intersections is input of the proposed model. Only the phase schema, including phase sequence and phase number, is needed.

NOTATION

To facilitate the presentation, all definitions and notations used hereafter are summarized:

- $\delta_{m,p}^{i}$ is the turn ratio of movement m at phase p of intersection *i*. $\delta_{m,p}^{i}$ = 1 if the movement m is not permitted at phase p.
- q_m^i is total volume of movement m at intersection *i.*
- p_i is the index of signal phase at intersection *i*.
- P_I is the number of phases of intersection *i.*
- A^N is the total number of lanes of downstream approach.

- $\lambda_{m,n}^{i,i+1}$ is the flow ratio of movement m of intersection *i* to movement n of intersection *i*+1.
- $R_{m,n}^{i,i+1}$ is the route composed by movement m of intersection *i* and movement n of intersection *i*+1.
- M_i is the number of movement of intersection *i*.
- The intersection i+1 represents the nearest neighbor to intersection *i*.

MODEL FORMULATION

The volume of movement in phase *p* of intersection *i* feeding movement *n* of intersection *i*+1, $q_{p,n}^{i,i+1}$:

$$q_{p_i,n}^{i,i+1} = \sum_{m=1}^{M_i} q_m^i \delta_{m,p}^i \lambda_{m,n}^{i,i+1} \qquad \forall i, m, p_i \qquad (2)$$

Maximum phase flow from intersection *i* to intersection *i*+1 feeding movement n of intersection *i*+1, $q_{\max,n}^{i,i+1}$:

$$q_{\max,n}^{i,i+1} = \max(q_{p_i,n}^{i,i+1}, \qquad \forall p = 1,2.....P_i) \quad (3)$$

The degree of arrival flow imbalance of movement *n* at downstream intersection *i*+1 ($IM_n^{i,i+1}$) is given by the ratio between the maximum phase traffic volume feeding from the upstream intersection *i* and the sum of traffic volume of all the phases coming from the upstream intersection. It can be stated as:

$$IM_n^{i,i+1} = \frac{q_{\max,n}^{i,i+1}}{\sum_{p_i=1}^{P_I} {}_{p,n}^{i,i+1} / P_I} \qquad \forall i, p_i \qquad (4)$$

$IM_n^{i,i+1}$ is the maximum degree of arrival flow imbalance of movement *n* of intersection *i*+1. Equation (5) indicates that the route composed by the movement corresponding to $q_{\max,n}^{i,i+1}$ of intersection *i* and movement n of intersection *i*+1 is one of the critical routes between the two intersections.

The interconnection desirability of the route decided by Equations (4) and (5) can be calculated by the Equation (6) based on the structure link-based mode:

$$IR_n^{i,i+1} = \left(\frac{0.5}{1+t}\right) * \left(IM_n^{i,i+1}\right) - (N-2) \qquad \forall i, n \qquad (5)$$

The maximum interconnection desirability of routes is adopted as the interconnection desirability of the intersections:

$$I_{keyRoute}^{ij} = \max(IR_n^{i,i+1}) \qquad \forall i, n \qquad (6)$$

The interconnection desirability of two intersections is equal to the largest index interconnection desirability of routes between two intersections.

SIMULATION AND EVALUATION

Comparing link-based and route-based index

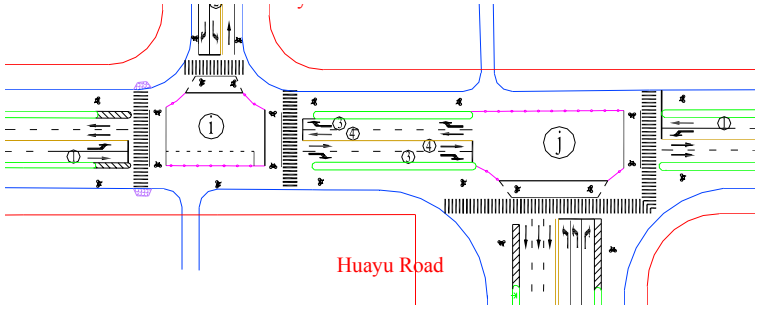

Figure 1. The geometry of the two intersections.

The two adjacent intersections in Ma'anshan City shown in Figure 1 were selected as a case to analyze the proposed model. The net distance between the two "T" type intersections is 50 meters (intersection *i* and intersection *j*). The traffic volume and turn ratio of related movements were calculated based on traffic survey data and shown in Table 1.

Table 1. Traffic volume of the two intersections

		i-j		j-i	
		Through (1)	Left (2)	Through (1)	Left (2)
Traffic volume		552	342	590	268
Turn ratio	Through	0.89	0.30	0.71	0.37
	Right	0.11	0.70	0.27	0.63

Let $R(im\text{-}jn)$ represent the interconnection desirability index of routes composed by movement m of intersection i and movement n of intersection j calculated by the proposed route-based model. Let $L(i\text{-}j)$ represent the interconnection desirability index from intersection i to intersection j calculated by link-based model. Based on the traffic survey data, the difference of route-based model and link-based model are shown in Figure 2.

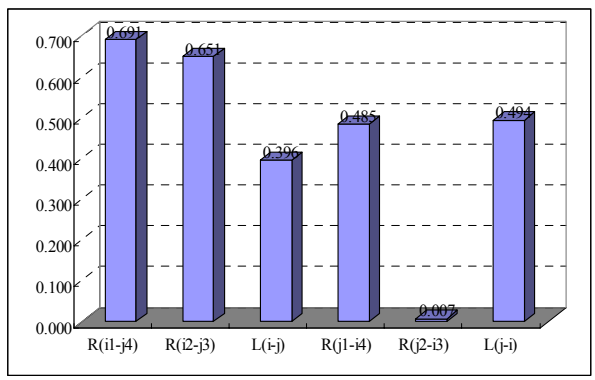

Figure 2. Differences of link-based model and route-based model.

Different routes have different interconnection desirability indices, and the index may larger or smaller than the results of the link-based model. this means that the link-based model does not reflect the real desirability of movements between the two intersections because the signal coordination should be

calculated based on routes. Moreover, the link-based model cannot identify the critical route that should be considered first in signal coordination. The critical route is *R*(i1-j4) based on the model (5) according to Figure 2. VISSIM was used to evaluate the efficiency of different signal plans and the results are shown in Figure 3.

Figure 3 indicates that signal coordination can create benefits for the given two intersections compared with no coordination scenario. The average delay of the intersection is various with the coordinated routes. The coordinated signal plan for route *R*(i1-j4) with the highest interconnection desirability index gets more benefit than other routes. The relationship between delay and interconnection desirability index with the change of difference of cycle arrivals under isolated conditions is show in Figure 4.

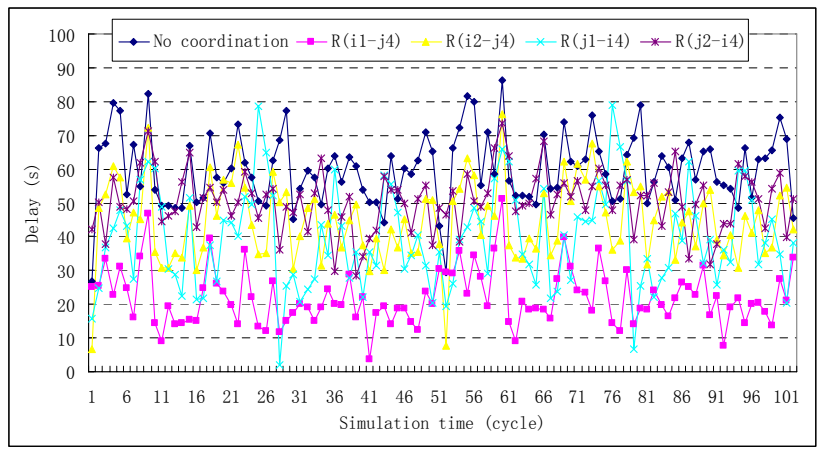

Figure 3. Impacts of different route on signal plans.

Figure 4 describes the relationship between average vehicle delay and interconnection desirability index under isolated condition. The average vehicle delay increases with the increase of the interconnection desirability index calculated by both link-based and route-based models. The gap of interconnection desirability index calculated by the models also increases with the increase of the interconnection desirability index. This means that the route-based model is more sensitive than the link-based model under high interconnection desirability.

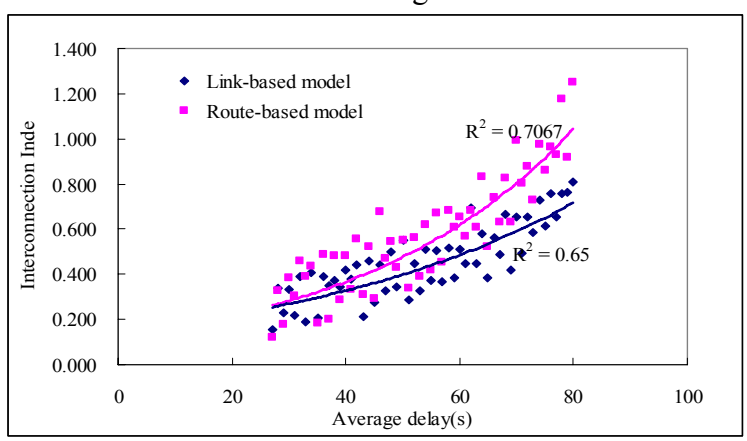

Figure 4. Relationship between delay and Interconnection desirability index.

CONCLUSION

This paper illustrates a route-based interconnection desirability index model that evaluates the need to interconnect signalized intersections. The proposed route-based model is capable of capturing the impact of signal phase plans and route volume characteristics, and produces detailed output information including the interconnection desirability index of every route and critical route between two intersections. The results of VISSIM simulation show that the proposed route-based model has the ability to describe the real relationship of adjunct intersections and find the most critical route for signal coordination. Moreover, the route-based model is more sensitive than the link-based model under high interconnection desirability.

Note that this paper has presented preliminary evaluation and sensitivity analysis results for the proposed model through a case study. More extensive tests or evaluations will be essential to assess the effectiveness of the proposed model under various traffic flow patterns and intersections.

ACKNOWLEDGEMENTS

The research is funded by projects of the National Natural Science Foundation of China (No: 70631002, 50808142), Shanghai Urban Construction and Communications Project (No: Construction Science 2008-2). The research is also supported by Program for Young Excellent Talent in Tongji University.

REFERENCES

Brabardonis, A., and May, A.O. (1984). “Computer Aoolications in Management," Traffic Sianal paper presented at -54th Annual ITE Meeting. San Francisco.

Chang, E.C. (1985). “How to Decide the Interconnection of Isolated Traffic Signals.” Proc*eedings of the Winter Simulation Conference.*

Cohen, S.L. (1983). “Concurrent Use of the MAXBAND and TRANSYT Signal Timing Programs for Arterial Sional Optimization.” *Transportation Research Record*, 906: 81-84.

Federal Highway Administration (2005). *Traffic Control Systems Handbook.* FHWA-HOP-06-006.

Suhbier, J.H., and Byrne, W.D. (1979). “Analytical Procedures for Urban Transportation Energy Conservation: Summary of Findings and Methodology Final Report - Volume I.” Cambridge Systematics. U.S. DOE.

Wagner, F.A. (1980). “Alternatives for Reducing Transportation Energy Consumption.”

Wagner, F.A. (1980). “Overview of the Impacts and Costs of Traffic Control Systems Improvements," Federal Highway Administration, U.S. DOT.

Yagoda, H.N., Principle, E.H., Vick, C.E., and Leonard, B. (1973). “Subdivision of Signal Systems into Control Areas," *Traffic Engineering*, 43(12).

Optimal Setting of the VMS's Future Range Based on the Characteristics of Driving Speed

T. Wang[1] and J. Chen[2]

[1]Transportation College, Southeast University, Nanjing, 210096; Jingqin Highway Management Office, Qin Huangdao City, Hebei Province, 066001; PH: 1-372-299-9880, 0311-83992188; email: wt_duzidengdai@sohu.com
[2]Transportation College, Southeast University, Nanjing, 210096; PH: 13913945222, 025-83795645; FAX: 025-83795645; email: chenjun@seu.edu.cn

ABSTRACT

This paper defines what VMS was and what the VMS's future range was, and points out the deficiency of the VMS's future range in China. The paper focuses on three themes: the VMS information reading, decision making and operating, main parameters that could affect the threshold scope of the VMS's future range and were reasonably analyzed in turn by the author. An optimal model for the VMS's future range is presented here, and some optimal quantitative methods to every concrete parameter are also introduced and constructed. Finally, some inherent relations between the characteristics of the vehicles' driving speed and the threshold scope of VMS's future range are studied through a discussion of the upper and the lower limit range of VMS's future range, and we discuss some important and useful conclusions to guide the VMS's project in the future.

INTRODUCTION

VMS is not only an information issue method, but also a kind of transportation control strategy. In the 1990s, with ITS technology development, there were more and more applications and some related research into VMS's use for highway or city expressway management (Li, X. 2008).

VMS's future range is the distances between VMS and the main road diversion points, or between VMS and alternative interchanges. Its establishment, whether it is reasonable or not, will relate to the VMS's effect (Abbas, M.M., et al., 1999). This article has taken VMS as a study object, thoroughly discussing the upper and lower threshold scope of VMS's future range, and elaborating on the intrinsic relations between the VMS's future range and the variation characteristics of vehicle speed in the road.

THE ESTABLISHMENT OF THE VMS'S FUTURE RANGE OPTIMAL MODEL

The driver's memory has a certain time limit for retaining VMS information. If the VMS's future range is too long, the VMS information will become fuzzy in his memory, so the driver can't judge how to change driving behavior. This can also produce a sense of distrust of VMS's information. If the VMS's future range is too short, the VMS is no better than the dummy (Jeffrey M. Henderson., 2004). Therefore, there is great significance for constructing a scientific and reasonable optimal model to calculate and study.

THE MAJOR INFLUENCING FACTORS AND ESTABLISHING CORRESPONDING MODEL FOR VMS'S FUTURE RANGE

The reaction of the driver to VMS information may divide into three stages: reading VSM information, judging and making a decision, and operation. The effect process of the VMS to the driver's behavior influence is as shown in Figure 1 (Che, G., et al 2006):

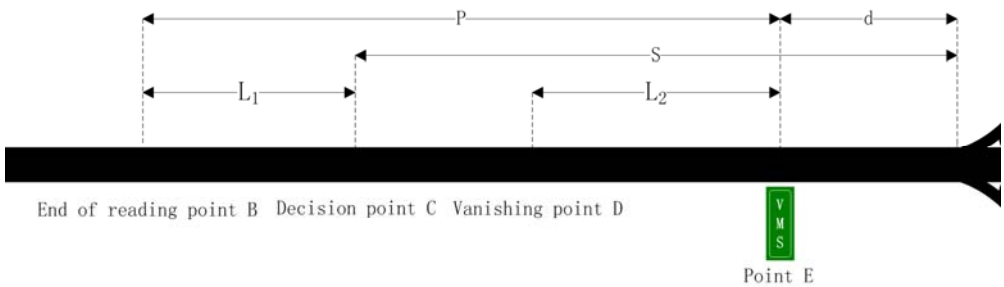

Figure 1. The influence of VMS on the driver's behavior decisions.

From Figure 1, we can determine an inequality:

$$d \geq S + L_1 - L_2$$

According to the memory material, people divide time, which maintains in the human brain, into three parts: the instantaneous memory, which does not surpass 1 or 2 seconds, the short-term memory, which does not surpass 1 or 2 minutes, and the long-term memory which surpasses 1 or 2 minutes (Zhidao Baidu, 2007). After the driver passes over Point D, VMS information rests on the driver's mind in the short-term memory. In the short-term memory, the driver should be able to arrive or pass over the road diversion point; otherwise, the VMS information will become fuzzy in his mind. Therefore, the distance L, which the driver has passed in the driver's short-term memory distance, should be less than the sum of VMS's future range d and disappeared distance L_2, so we can get the upper limit range of

d: $d + L_2 \leq L$

In summary, the value range of VMS's future range is defined as:

$$S + L_1 - L_2 \leq d \leq L - L_2$$

CALCULATING PARAMETERS OF THE VMS'S FUTURE RANGE OPTIMAL MODEL

From the above passage, the threshold value of VMS's future range d closely relates with four model parameters, which are L, L_1, L_2 and S. Its calculating formula is:

$$L = \frac{V_2 \times t}{3.6}$$

In this formula: V_2 is defined as a running speed (km/h), t is defined as the short-term memory time (s).

The decision distance L_1 is the distance that the vehicle passes in the time from when the driver will judge and decide to operate until the brake has an effect. Truly, it starts when the driver reads over the VMS information. The driver needs at least 0.4s conscious reaction time before he begins to brake, and 0.3s time to

produce the brake effect (Wei Wang, W., Guo, X. 2000). The total time comes to t_1=0.7s. The distance covered by the vehicle in this time is:

$$L_1 = \frac{V_1 \times t_1}{3.6}$$

In this formula: t_1 is defined as the total time(s) of sensory and braking reaction; V_1 is defined as a normal speed (km/h) on the road.

The disappeared distance L_2 (as shown in Figure 2) relates to four model parameters: H, b, e and ∂.

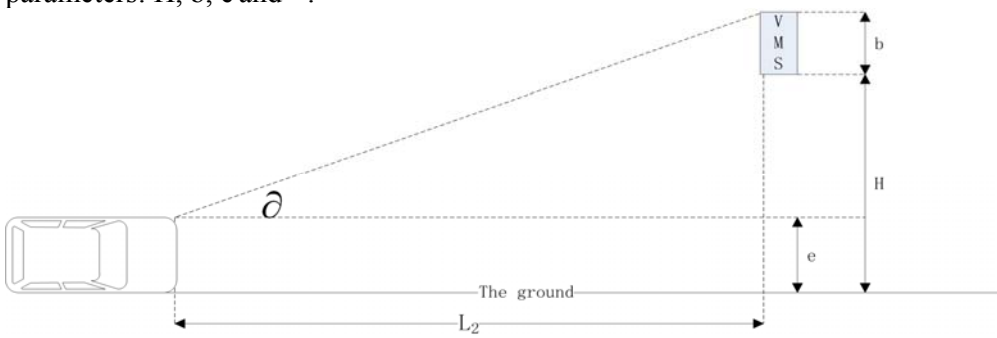

Figure 2. Calculating disappeared distance L_2.

Therefore, the disappeared distance L_2 can be calculated as follows:

$$L_2 = \frac{H + b - e}{\tan \partial}.$$

In this formula: e is defined as the driver's eye height (m), H is defined as the height from the VMS's bottom to the ground (m), b is defined as the VMS's width (m), ∂ is defined as the angle between the sight disappearing point and the VMS.

In the action distance S, the driver must be able to complete the total behavior according to the VMS information (i.e. change lanes, make deceleration, and change direction). The braking quality of the automobile mainly manifests on the braking distance. The braking distance's formula is (Yang, S. 2004):

$$S_1 = \frac{V_1^2 - V_2^2}{254\ (f + i + \phi)}.$$

In this formula: V_1 is defined as the speed（km/h) when the driver just read over VMS information, φ is defined as a road adhesion coefficient, i is defined as road longitudinal slope, f is defined as rolling resistance coefficient.

The process of changing traffic lanes is more complex, and it relates with the traffic flow density and running speed as well as the road condition (Chiu, Y. 2001). When calculating the braking distance, we should analyze it from the worst situation: in the changing traffic lane, the longest distance should occur when the automobile passes the vehicle in an adjacent lane and moves into that lane. The process in which the automobile overtakes another one as shown in Figure 3:

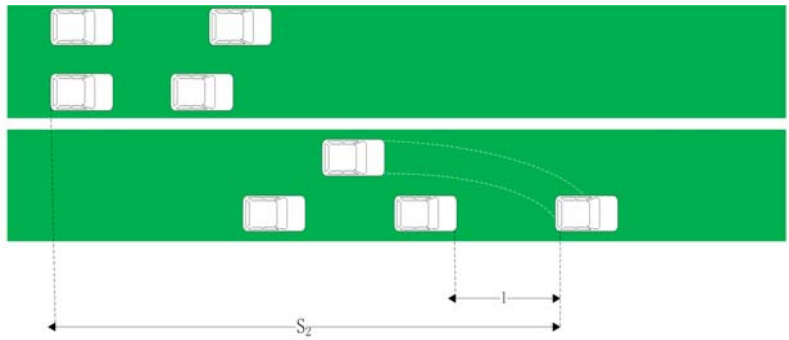

Figure 3. The process in which the automobile overtakes another one.

$$S_2 = \frac{V_1 \times l}{V_1 - V_3}$$

In this formula: S_2 is defined as passing distance (m), V_3 is defined as the speed of the passed automobile (km/h), l is defined as the minimum safe driving distance (m).

$$S = S_1 + S_2$$

In summary, the calculating formula for the value range of the VMS's future range d is as follows:

$$\frac{V_1 \times l}{V_1 - V_3} + \frac{V_1^2 - V_2^2}{254\ (f + i + \phi)} + \frac{V_1 \times t_1}{3.6} - \frac{b + 4.3}{\tan \partial} \le d \le \frac{V_2 \times t}{3.6} - \frac{b + 4.3}{\tan \partial}$$

EXAMPLE CALCULATION AND ANALYSIS

This article takes the most common overhang VMS as an example and calculates the threshold value scope of the VMS's future range. In the condition of traffic flow patency, the running speed V_2 is 0.5 the running speed V_1 after the driver adopts deceleration and changes lane when he reads over VMS information in front of him (Zhu, S. 2007). Because the velocity difference between the speed of the overtaking vehicle and the speed of the overtaken vehicle is generally in 20~30 km/h on the road (Erkin., 2004),

$$V_3 = V_1 - 25\,(\text{km/h})$$

Practice states that the driving safety distance is roughly equal to the driving speed. When the driving speed is 100km/h, the driving safety distance is about 100 meters (Admin., 2008). Deducting from this, the driving safety distance is approximately equal to the value of V_1. f relates to road surface type, tire structure and driving velocity etc. It is generally determined by experiments (Yang, S. 2004). f is 0.015 in this example. Φ mainly depends on roughness, moisture, muddiness of the road surface, the tire's pattern and pressure, driving speed and load etc. (Yang, S. 2004). In this passage, Φ is 0.6. The width b of the overhang VMS in the road is 1.94m. α is 7^o for the overhang VMS. e= 1.2m; H=5.5(m); i=3%; t=120s.

Leading the parameter value into the formula, we can obtain the overhanging VMS's future range d in the road:

$$\frac{V_1^2}{25} + \frac{V_1^2 - 0.25 V_1^2}{254 \times 0.645} + \frac{V_1 \times 0.7}{3.6} - \frac{1.94 + 4.3}{\tan 7^o} \le d \le \frac{0.5 V_1 \times 120}{3.6} - \frac{1.94 + 4.3}{\tan 7^o}$$

That is： $0.045 V_1^2 + 0.194 V_1 - 50.82 \le d \le 16.67 V_1 - 50.82$

From this calculation, we may conclude some variations between the threshold value scope of VMS's future range d and driving speed as follows:

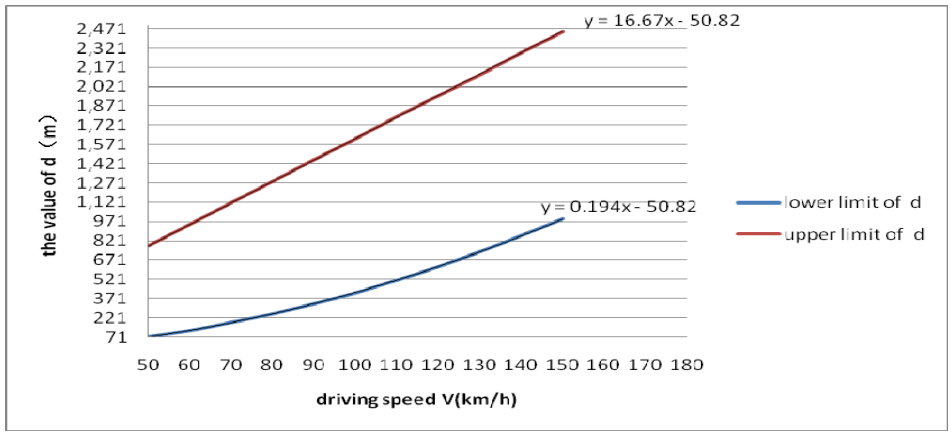

Figure 4. The variation between the threshold scope of d and driving speed.

From Figure 4, we can see that the variation characteristics of the driving speed are important aspects reflecting the traffic flows' characteristics. From these, we may reach the following conclusions:

The upper limit value tendency of VMS's future range d increases quickly, and the lower limit value tendency increases a little slower. When the driving speed is approximately 183 km/h, the upper and lower limit value tendencies increase equally. Along with the speed increasing, the increasing tendency of the lower limit value will surpass the increasing tendency of the lower limit value.

On the different kinds of roads (expressway, first class highway, the second class highway, the third class highway etc.) speed decreases gradually. Therefore, the threshold value choice scope of d also gets smaller and smaller, and the value of d is correspondingly shrinks.

CONCLUSIONS

From the above study, we can draw some useful conclusions:

When the other conditions are the same and the traffic flow density doesn't surpass the critical density, the average driving speed reduces along with the traffic flow density increase (He, H., Guan, W. 2006). For a much bigger traffic flow density, VMS's future range d is slightly smaller.

When there are many kinds of vehicles mixed (e.g. automobiles, buses and trucks mixed), the mutual interference leads the average driving speed to decrease, so VMS's future range d should select the smaller option.

On some roads that have good conditions, the average driving speed is much higher, the threshold value choice scope of VMS's future range d is a little bigger and the value of d is correspondingly a little bigger.

In summary, the setting of VMS's future range, whether it is reasonable or not, will affect the efficacy of the VMS. This article has conducted research into the threshold value scope of VMS's future range on the road, and elaborated some inherent relationships between VMS's future range and the driving speed, so this research has certain reference values.

ACKNOWLEDGEMENT

This research is supported by National Key Technologies R&D Program (2006BAJ18B01).

REFERENCES

Abbas, M.M., et al. (1999). "Optimizing VMS's Locations on Freeways Using Genetic Algorithms." TRB Annual Meeting.

Admin. (2008). "Guide Book for Safety driving in the Expressway." http://www.xz110.gov.cn/Article/JFTS/200808/2661.html.

Baidu, Z. (2007). "Uncovering the enigma of Memory" http://zhidao.baidu.com/question/38698607.html?si=4.

Che, G., Shi, J., and Sui, L. (2006). "Current Situation Initial Analysis of VMS [D]." *Road Traffic and Safety*. Vol.6,no.8.

Chiu, Y. (2001). "Determining Optimal Locations for Variable Message Signs Under Stochastic Incident Scenarios," Transportation Research Board, 80th Annual Meeting, January 7-11, Washington, D.C.

Erkin (2004). "When we march to the passageway of the expressway, why we need to avoid overtaking." http://glj.xjjt.gov.cn:10000/Article.asp?id=590.

He, H., Guan, W. (2006). "Evaluation of the Effects of Variable Message Signs at Urban Traffic Network." Institute of System Engineering, Traffic and Transportation School of Beijing Jiao Tong University.

Henderson, J.M. (2004). "A Planning Model for Optimizing Locations of Changeable Message Signs." A thesis presented to the University of Waterloo in fulfillment of the thesis requirement for the degree of Master. Waterloo, Ontario, Canada.

Li, X. (2008). *The research of Variable Message Signs' (VMS) location selection [D]*. Beijing Jiao Tong University Transportation Institute, Beijing.

Wang, W., Guo, X. (2000). *Transportation Engineering [M]*. Southeast University Press, Nan Jin.

Yang, S. (2004). *Road Survey and Design [M]*. China Communications Press, Beijing.

Zhu, S. (2007). *Design and Research of the Traffic Variable Message Sign [D]*. Beijing University of Technology, Beijing.

Urban Road Travel Speed Estimation Based on Low Sampling Floating Car Data

Y. Yue [1], H.X Zou [2], Q.Q Li[1]

[1]Transportation Research Center, State Key Lab of Information Engineering in Surveying, Mapping and Remote Sensing, Wuhan University; P.O. Box C307; 129 Luoyu Road, Wuhan, Hubei, China, 430079; PH: (86-27)-68778035; email: {yueyang, qqli }@whu.edu.cn

[2]Transportation Research Center, State Key Lab of Information Engineering in Surveying, Mapping and Remote Sensing & School of Remote Sensing and Information Engineering, Wuhan University; P.O. Box C307; 129 Luoyu Road, Wuhan, Hubei, China, 430079; PH: 13995605305; email: zhxtc830429@163.com

ABSTRACT

Using traffic data collected by floating car is a feasible way to determine road network traffic conditions. But conventional travel speed estimation from high sampling floating car data (FCD) is not applicable in practice. In this paper we propose a method for estimating road travel speed from low sampling FCD based on a trajectory-based approach, which also takes intersections into consideration. The experiment demonstrates that this approach can achieve a trade-off between low sampling FCD and higher estimation accuracy, and can be further used for traffic state analysis and short-term prediction.

INTRODUCTION

Traffic parameter estimation is important for real-time traffic management, short-term prediction and long-term transport planning. Using floating cars (taxis or buses), equipped with GPS to collect traffic data and extract traffic information is a feasible way to reflect traffic conditions of the whole road network, a system that has been widely used in recent years (Kerner et al., 2005; Chen et al., 2007; Weng et al.,2007). Conventional travel speed estimation methods based on high sampling floating car data (FCD) are not applicable in practice, however. The aim of our study is to propose a trajectory-based road travel speed estimation method using low sampling FCD.

In this paper, we chose an urban road as our study area. The rest of this paper is organized as follows: Section 2 reviews some related work. Section 3 describes our proposed road travel speed estimation method. Section 4 illustrates a case study and experimental result. The final section concludes with discussions on future directions.

RELATED WORK

Ideally, if there are enough floating cars running in the road network and data are transmitted under high frequency (sample interval <10s), the average of their instantaneous velocities can be used to represent the approximate road travel speed (Weng et al., 2007). However, more advanced methods have been used to get higher accuracy, such as statistic theory, which can describe the relationship among road travel speed, time period and other related factors (such as lanes and road class) by analyzing GPS instantaneous velocity over a certain time period (Rohini, 2002; Quiroga and Bullock, 1998; Zhang, H.S. et al., 2007). Another solution is to calculate average speed of two consecutive GPS signals and use the average speed as road travel speed (Kerner et al., 2005; Chen et al., 2007).

By far, most studies are based on high sampling FCD. But in practice, many FCD collection systems use low frequency sample technology (interval >30s). Chen et al. (2007) attempted to estimate traffic states using fewer GPS signals; however, other vehicle trajectory information is used in their study. Moreover, these works are essentially constrained to freeways, and do not consider the effect of intersections.

ROAD TRAVEL SPEED ESTIMATION METHOD FROM LOW SAMPLING FCD

This section describes precise map-matching and extraction of vehicle trajectory. The detailed method can refer to Brakatsoulas et al. (2005) and Zhang et al. (2007). In this section, we describe the proposed road travel speed estimation method based on the identified trajectory.

Related definition. The Digital Road Map (DRM) has many short links that do not cross any intersection, and their travel speeds are smoother than those of long links with intersections. Previous studies (Lao et al., 2007) have found that intersections could affect road travel speed. Therefore, in this study we artificially divide a road link into two parts: Smooth Part (SP) and Intersection Part (IP) (see Figure 1).

Here, DRM links between signalized intersections or primary zebra crossing are treated as SP. The length of IP is determined by a threshold, which is determined by road class and historical queue length. We also define two adjacent road links as Road A and Road B, represented as R_A and R_B. Meanwhile, two consecutive GPS signals are defined as G_j (x_j, y_j, T_j) and G_{j+1} (x_{j+1}, y_{j+1}, T_{j+1}), respectively, where (x, y) is the matched GPS coordinate and T is the corresponding time stamp.

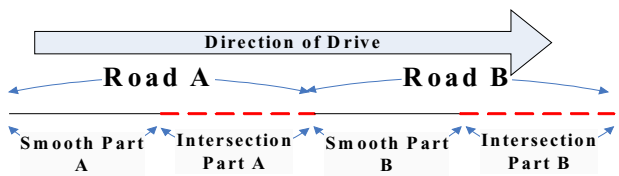

Figure 1. Road model.

The situation of low sampling FCD may cause two consecutive GPS signals that are not located in the same part of road, so we identify the distribution of two consecutive GPS signals as six types, based on their relation with R_A, R_B , SP and IP (see Figure 2).

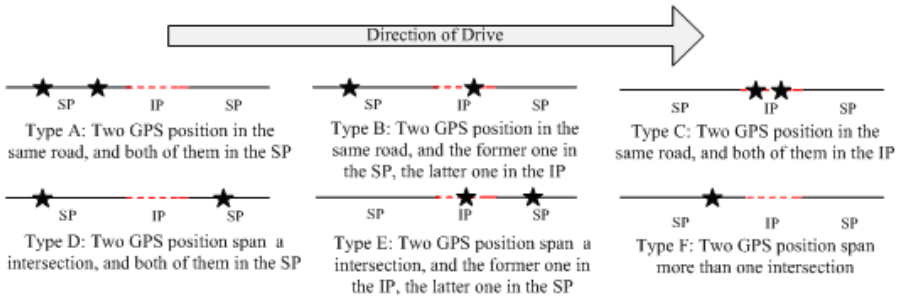

Figure 2. Distribution of Two Consecutive GPS Signals.

Proposed road travel speed estimation method from low sampling FCD. Since types B, C and F are less meaningful in terms of intersection travel speed estimation, only type A, D and E are discussed in this study. The proposed method is described as follows:

Step 1: Extract all trajectories passing through R_A or R_B, and identify useful GPS signal pairs according to Figure 2.

Step 2: Calculate SP's travel speed of R_A and R_B. First, GPS signal pairs belonging to type A are selected, and their average speed can be used as road travel speed:

$$V_{ave}^{A} = \frac{\Delta d}{\Delta T} = \frac{d_{j+1} - d_j}{T_{j+1} - T_j}$$

Where V_{ave}^{A} is the average speed from G_j to G_{j+1}, d_j and d_{j+1} are distance from the start point of R_A to G_j and G_{j+1}, separately, Δd is the distance from G_j to G_{j+1} and ΔT is the time interval from G_j to G_{j+1}.

SP's travel speed can then be calculated as a proportion of the distance from G_j to G_{j+1} and road length, which is described as:

$$TS_{SP}^{A} = (\sum_{i=1}^{n} V_A^i \times \alpha_A^i) / \sum_{i=1}^{n} \alpha_A^i$$

Where TS_{SP}^{A} is travel speed of R_A's SP, V_A^i is the distributed velocity contribution of R_A given by GPS signal pair i and α_A^i is the proportion of distance from G_j to G_{j+1} and road length.

Travel speed of R_B's SP can also be calculated as above, set as TS_{SP}^{B}. If there is no type A in some period, then use the average of instantaneous velocities in the SP as the approximate travel speed of SP.

Step 3: Calculate travel speed of R_A's IP, which will use TS_{SP}^{A} and TS_{SP}^{B}. First, GPS signal pairs belonging to Type D or Type E are selected. A GPS signal pair belonging to Type D can be used to calculate travel speed as:

$$\frac{L_A}{V_{\text{intersection}}} + \frac{L_B}{TS_B} = T_{j+1} - T_j$$

Where $V_{\text{intersection}}$ is the travel speed of R_A's IP from a GPS signal pair, L_A is the distance from G_j to the end point of R_A, and L_B is the distance from the start point of R_B to G_{j+1}.

A GPS signal pair belonging to type E can be used to calculate travel speed as:

$$\frac{L_A}{TS_A} + \frac{L_{\text{intersection}}}{V_{\text{intersection}}} + \frac{L_B}{TS_B} = T_{j+1} - T_j$$

Travel speed of R_A's IP can be calculated by the average of $V_{\text{intersection}}$, set as $TS_{\text{intersection}}^{A}$.

After the above three steps, travel speed of R_A can be calculated as:

$$TS_A = \frac{L_{TotalA}}{\frac{L_{\text{intersection}}}{TS_{\text{intersection}}^{A}} + \frac{L_{TotalA} - L_{\text{intersection}}}{TS_{SP}^{A}}}$$

Where L_{TotalA} is the length of R_A.

CASE STUDY

In this study, an arterial road between Square intersection and DingGong intersection in downtown area of Nanchang, a medium-sized Chinese city, was selected as our study road (Figure3.) The study road consists of 4 DRM links, and the length is about 867.4m.

Experiment data was obtained from a calling-taxi service system from 14th June, 2008 to 20th, June, 2008. On-board GPS are equipped on 1,245 taxis, which cover about 90% roads of this city. Each GPS signal includes vehicle information about unique ID, position, time stamp, heading direction and instantaneous velocity.

According to our statistics, a taxi returns 1200 to 2400 GPS signals every day (about a return of GPS signal during 50s). Figure 4 shows a vehicle's trajectory during 24 hours after map-matching and trajectory identification.

Three periods (6:00-7:00 (non-peak), 8:00-9:00 (morning peak), and 18:00-19:00 (evening peak)) were selected as our experiment periods, and the time interval was set at five minutes. In order to evaluate our proposed method, two other methods were selected for comparison purpose: (1) use the average of GPS instantaneous velocity as road travel speed; (2) calculate road travel speed based on trajectory, but do not consider the impact of intersections.

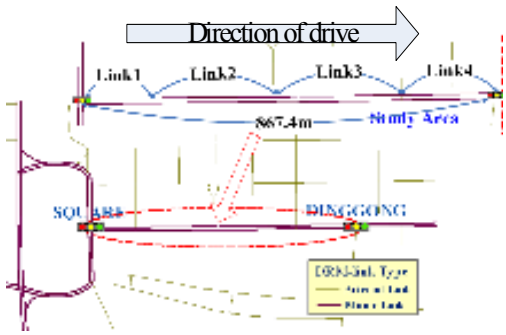

Figure 3. Study Area.

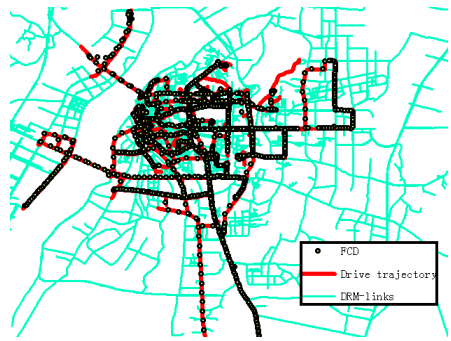

Figure 4. A Vehicle's trajectory during 24 hours.

Experiment results show that Method (1) depends on sample size, and that the accuracy of estimation cannot be reliable when sample size is low. Comparing this with Method (2), our method has no obvious superiority in smooth periods: both of them have a similar and better accuracy. But in congested periods, our method (Method (3)) decreases the impact of intersections and can achieve a better accuracy all the same, as illustrated in Figure 5. Table 1 shows the estimation accuracy in detail.

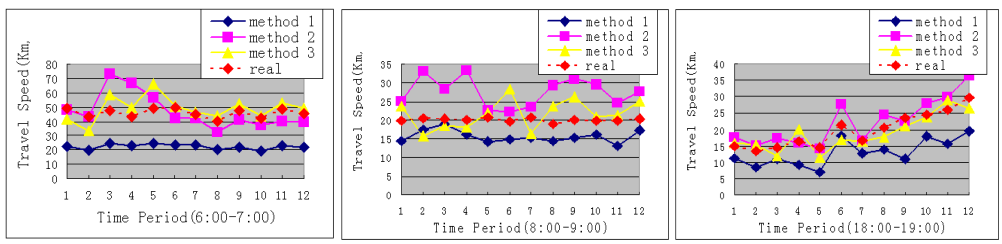

Figure 5. Experiment results.

Table1. Accuracy comparison (ARE=Average Relative Error (%); MRE= Maximum Relative Error (%); SE=Standard Error (km/h)).

	Time period								
	6:00-7:00			8:00-9:00			18:00-19:00		
Method	ARE	MRE	SE	ARE	MRE	SE	ARE	MRE	SE
(1)	23.9	27.0	25.1	4.4	6.6	4.9	6.7	12.6	7.6
(2)	8.5	25.5	11.9	7.4	13.3	8.7	2.8	6.8	3.6
(3)	6.1	16.9	7.9	3.8	8.7	4.6	2.4	4.6	2.9

CONCLUSION

This paper proposes a novel method for estimating road travel speed based on low sampling FCD and considering the impact of intersections. The method can serve as the basis for traffic state analysis and short-term traffic prediction. The experiment demonstrates that this approach can provide the basis for traffic state analysis and short-term prediction research.

For further work, we will improve the speed of map-matching and trajectory identification methods, extend this method to road networks and further develop the method to satisfy real-time requirements.

REFERENCES

Brakatsoulas, S., Pfoser, D., Salas, R., and Wenk, C. (2005). "On Map-Matching Vehicle Tracking Data." *Proc. of the 31st VLDB Conference*, Trondheim, Norway.

Chen, Y.K., Gao, L.L., Li, Z.P., and Liu, Y.C. (2007). "A New Method for Urban Traffic State Estimation Based On Vehicle Tracking Algorithm." *Proc. of IEEE Intelligent Transportation Systems Conference*, 1197-1100.

Kerner, B.S., Demir, C., Herrtwich, R.G., Klenov, S.L., Rehborn, H., Aleksic, M., and Haug, A. (2005). "Traffic State Detection with Floating Car Data in Road Networks." *Proc. of the 8th International IEEE Conference on Intelligent Transportation Systems*, 700-705.

Lao, Y.T., Yang X.G., Wu, Z. (2007). "Quantification of Congestion in Signalized Intersection Based on Loop Detector Data." *Proc. of the 2007 IEEE Intelligent Transportation Systems Conference*, 904-909.

Quiroga, C.A., and Bullock, D. (1998). "Travel Time Studies with Global Positioning and Geographic Information Systems: an Integrated Methodology." *Transportation Research Part C*. 6, 101-127.

Rohini, B. (2002). "Predicting Speeds on Urban Streets Using Real-time GPS Data." *Masters Abstracts International*. 41-04.

Weng. J.C., Rong, J., Yu, Q., and Ren, F.T. (2007). "Optimization on Estimation Algorithms of Travel Speed Based on the Real-time Floating Car Data." *Journal of Beijing University of Technology*. 33(5), 456-464.

Zhang, H.S., Zhang, Y., Wen, H.M., and Hu, D.C. (2007). "Estimation Approaches of Average Link Travel Time Using GPS Data." *Journal of Jilin University (Engineering and Technology Edition)*, 37(3), 533-537.

Zhang, W., Xu, J.M., and Lin, M.F. (2007). "Map Matching Algorithm of Large Scale Probe Vehicle Data". *Journal of Transportation Systems Engineering and Information Technology*. 7(2), 39-45.

Experimental Study on Sound Countermeasures against Driver Fatigue

R. Fang[1], X. Zhao[2], K. Mao[3], J. Ron[4], X. Liu[5]

[1]Beijing Key Lab of Traffic Engineering, Beijing University of Technology, Beijing 100124, China; PH: (86)67395426; email: frx.007@163.com
[2]Beijing Key Lab of Traffic Engineering, Beijing University of Technology, Beijing 100124, China; PH: (86)67390918; FAX: (86) 67390918; email: zhaoxiaohua@bjut.edu.cn
[3]Beijing Key Lab of Traffic Engineering, Beijing University of Technology, Beijing 100124, China; PH: (86)67390918;email: maokejun@emails.bjut.edu.cn
[4]Beijing Key Lab of Traffic Engineering, Beijing University of Technology, Beijing 100124, China; PH: (86)67392082; FAX: (86) 67392082; email: jrong@bjut.edu.cn
[5]Beijing Key Lab of Traffic Engineering, Beijing University of Technology, Beijing 100124, China; PH: (86)67391458; FAX: (86) 67391458; email: liuxm@bjut.edu.cn

ABSTRACT

Driver fatigue is one of the main causes of fatal accidents. The development of countermeasures against driver fatigue has been an urgent issue. This paper focuses on in experiments that, in the virtual driving environment, based on the formation mechanism of driver fatigue, caught the driver fatigue state of subjects, used sound as an environmental stimulus to intervene, and applied experimental data to analyze effects of different types of sound stimuli on driver fatigue. Four factors and three levels of orthogonal design were carried out in the experiment, according to eye movement and physiological indicators before and after different types of sound stimuli to identify the extent of driver fatigue. We then selected the most effective sound combination to combat fatigue. The result showed that sonic intensity and stimulation time were the most significant factors to fighting driver fatigue, and frequency and stimulating interval were weak factors.

INTRODUCTION

Driver fatigue is a behavior in which psychological and physiological functions decline. Efficiency and performance are impaired by long and monotonous continuous driving. (Lingcong, Z., Zhengguo, W., 2003). According to China's Ministry of Transportation and Communications, road accidents caused by driver fatigue both in absolute numbers and proportion is the highest, and is believed to account for 10–25% of all vehicle accidents. It can be seen that driver fatigue is a significant cause of traffic accidents. In response to this serious problem, it is very necessary to monitor fatigue and take effective countermeasures against driver fatigue to prevent road accidents.

To date, many countries have begun sound ergonomics research, and

have indicted that sound stimulus can reduce fatigue (Landstrom, U., Englund, K., 1999). Yukie Hirata found that when fatigue emerged, drivers stimulated with music could improve alertness, and avoid drowsiness (2001). However, very little evidence exists on how the sound affects driver fatigue. Research has generally suggested the possibility of using sound stimulus as a countermeasure against driver fatigue, but no further study has been done on the effect of the different factors of sound. The research described in this paper used orthogonal experimental methodology, conducted a driving simulation experiment, collected physiological data of drivers to analyze the different types of sound on the effects of reducing diver fatigue, then identified the most effective sound stimulus to use as a countermeasure against driver fatigue. This could play an important role in reducing driver fatigue and improving road safety.

EXPERIMENTAL SYSTEM

The driver physiological information collection experiment was carried out in a car driving simulator. The experiment used a virtual driving scene and real car cockpit, as in Fig. 1. P80 (Dinges and Grace, 1998) was used to monitor the state of fatigue. At the same time, 16 channel electroencephalogram (EEG) data was recorded.

Figure 1. Virtue driving scene.

Environment. In order to reach fatigue state as soon as possible, the road scene is monotonous, straight two-lane two-way road, without any indicatory signs. The driver was asked to drive at the right side of the center line, and followed the front car with stable speed of 50 km/h. The laboratory temperature was 20-23℃ and soft lighting was set at 5 Lux.

Participants: To exclude individual differences, all participants were males, aged around 25 years old, with more than two years' driving experience, good health and normal hearing and without any sleep–related disease. Before the experiment, all participants were requested to have adequate rest and do nothing provocative for 72 hours prior to the measurements.

Variables. In the recent years researchers have investigated different types of fatigue monitor indicators. However, PERCLOS (Wierwille, Ellsworth, Wreggit, Fairbanks, and Kim, 1994) and EEG (Eoh, Chung, and Kim, 2005; Lal, 2003) were found to be superior compared to other detection techniques and were both promising neurophysiologic indicators of driver fatigue. During this study we could obtain P70 (the proportion of time within one-minute blocks that the

eyelid covers 70% of the pupil) and P80 from the eye tracker. Four frequency components could be obtained from EEG recordings: delta (δ) (±0 to 4 Hz), theta (θ) (4–8 Hz), alpha (α) (8–13 Hz) and beta (β) (13–20 Hz).

METHOD

Orthogonal experimental design is an experimental design method used to examine many levels of many factors; this method is an efficient, rapid and economic method of experimental design (Xue, L., 2005). The main purpose was to balance the different types of sound stimuli, collect various physiological indicators and analyze effects of each factor on reducing driver fatigue.

Validation of factors and levels. By actual measurement, the noise of vehicle simulator was at 60 dB or so. This experiment simulated the actual driving state, and given that the long period of time driving above 85 dB in the noise environment would lead to hearing impairment, 60 dB, 70 dB, 80 dB were selected as the levels of sonic intensity; Research has shown that alert sounds should meet the requirement of high-frequency, so 1050 Hz，5800 Hz, 10750 Hz were selected as levels of sonic frequency. Three different stimulating times weretested in this study, and were between 3-7s; stimulating intervals varied between 10-60s. Table 1 shows the different factors and levels of sound.

Table 1. factor-level table.

	factors			
levels	A（dB）	B（Hz）	C（s）	D（s）
1	60	1050	3	10
2	70	5800	5	30
3	80	10750	7	60

A= sonic intensity; B= sonic frequency; C= Stimulating time; D=Stimulating interval

Design of test scheme. From the analysis above we can conclude that this was a four-factor and three-level experiment, so the orthogonal table $L_9（3^4）$ was the most appropriate.

Procedure.

Step 1: Before the experiment, subjects were ensured to be in full understanding of the experimental process, and randomly sampled the sequence of sound stimuli.

Step 2: The subject entered the laboratory, and experimental personnel placed EEG electrodes and adjusted eye-movement equipment, which required around 30 minutes per subject.

Step 3: The subject entered the driving simulator, and experimental personnel adjusted the relative position of each section of the virtual instrument and connected the feedback machine to the subject.

Step 4: We recorded physiological signals of subject in the natural, quiet state for five minutes.

Step 5: Testing began. Experimental personnel operated the data acquisition software, stimulated the subject with relevant types of sound when

the driving time was up to 30 minutes, then finished experiment after 10 minutes of sound stimulus.

Validation of fatigue indicators. Current studies both at home and abroad found that P80 provided a good indication of fatigue, which could truly represent fatigue and be the best way to evaluate fatigue (Kang Huawu, 2008). By combing the method of subjective evaluation and external evaluation during the driving, we found that P80 showed an increasing slope as the driver became fatigued. Hence, the paper took P80 as one of the fatigue indicators.

EEG is the golden standard for driving fatigue. The current study investigated EEG activity in separate frequency bands: delta, theta, alpha and beta, and four different algorithms: (i) (θ + α)/β, algorithm, (ii) α/β, algorithm, (iii) (θ+ α)/ (α + β), and algorithm (iv) θ/β. A greater increase of ratios was found for algorithm (i) (θ+ α)/ β at the end of the monotonous driving session, compared to the separate frequency bands and other three algorithms (Budi, Thomas, Jap, and Sara, 2007; Lal, 2007). By fitting the curve of P80 and the curve of absolute and relative EEG indicators, this paper obtained the same conclusion with the aforementioned research that algorithm (θ+ α)/ β showed regular change and had the same trend with P80.

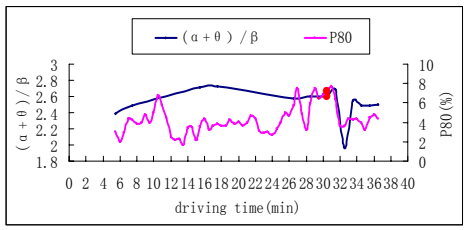

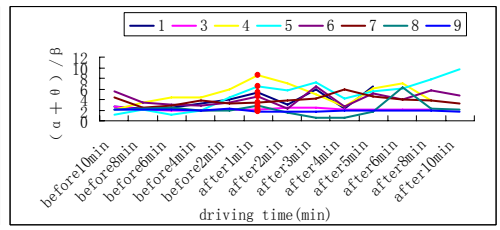

Figure 2. Trend graph of indicators. **Figure 3. changing law of（α+θ）/β.**

Figure. 2 and 3 showed that P80 and（α+θ）/β increased with the driving time. After the sound stimulus decreased with different degrees, this demonstrated that sound stimulus can reduce driver fatigue, but after a period of driving this downward trend was not obvious.

RESULT ANALYSIS

Identification of orthogonal experiment indicators. The EEG data of each sample after stimuli of nine types of sound were divided into one section every other minute. Eye movement signals were divided into one section every 30 seconds, then the average calculated regressing P80 and (α+θ)/β from the first point to the first minimum point after stimulus with the least square method.

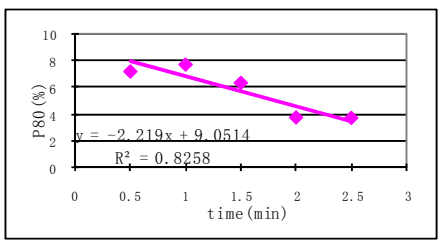

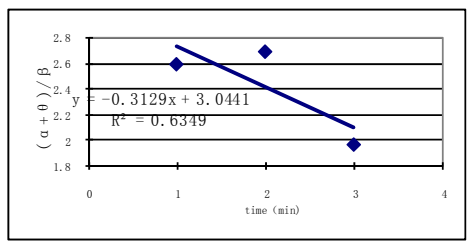

Figure 4. linear regression.

Figure 4 shows the example of regression processing of one type of sound stimulus; others were the same. The slope of regression equation demonstrated the recovery extent of driver fatigue. The slope of the regression equation was chosen as an indicator of the orthogonal experiment, and it was a "larger the better" experiment: the greater the slope was, the lower driving fatigue would be.

Variance analysis. SPSS generated $L_9(3^4)$orthogonal table by parameter settings. The slope of the linear regression equation was added to the table to set up data sets. The results of variance analysis are shown in Tables 2-5.

Table 2 shows that factors A ($p<0.05$), C ($p<0.05$) and D ($p<0.05$) had significant influence on experimental results, while factor B ($p>0.05$) had no significant influence. The important order of the factors that affected the P80 was A, C, D and B in turn.

Table 2. Tests of Between-Subjects Effects of P80.

Source	Type Ⅲ Sum of Squares	df	Mean Square	F	P
Corrected Model	303.195[a]	8	37.899		
Intercept	.309	1	.309	5.910	0.008
A	150.450	2	75.225	.048	0.831
B	20.420	2	10.210	11.730	0.003
C	91.552	2	45.776	1.592	0.256
D	83.733	2	41.866	7.138	0.014
Error	57.717	9	6.413	6.528	.018
Total	502.332	18			
Corrected Total	360.912	17			

a. R Squared=.840(Adjusted R Squared=.698)

Table 3. Single-factor statistic table of P80.

Factor \ Statistic		Mean	Std. Error	95% Confidence interval	
				Lower bound	Upper bound
A	1	7.50	3.429	-.256	15.257
	2	-6.8	1.034	-9.179	-4.502
	3	-1.3	1.034	-3.68	.996
B	1	-.793	1.034	-3.131	1.546
	2	-1.3	1.653	-5.009	2.469
	3	1.381	1.653	-2.357	5.120
C	1	-2.7	1.034	-5.028	-.351
	2	3.44	1.655	-.295	7.182
	3	-1.4	1.653	-5.174	2.303
D	1	-4.5	1.034	-6.823	-2.146
	2	2.35	1.653	-1.390	6.088
	3	1.45	1.653	-2.284	5.193

Table 3 shows the different levels of various factors on average. By visual analysis from the results, the intensity sequence of various factors and levels on results were: $A_2>A_3>A_1$, $B_1>B_2>B_3$, $C_1>C_3>C_2$, $D_1>D_3>D_2$.

Table 4. Tests of Between-Subject Effects of (α + θ)/β.

Source	Type Ⅲ Sum of Squares	d f	Mean Square	F	P
Corrected Model	12.991[a]	8	1.624	5.286	.011
Intercept	.513	1	.513	1.67	.229
A	5.364	2	2.682	8.732	.041
B	2.859	2	1.430	4.654	.007
C	5.632	2	2.816	9.167	.927
D	.047	2	.024	.077	
Error	2.765	9	.307		
Total	22.766	18			
Corrected Total	15.755	17			

[a]. R Squared=.825(Adjusted R Squared=.669)

Table 4 shows that factors C ($p<0.05$), A ($p<0.05$), B ($p<0.05$) had significant influence on experiment results, while factor D ($p>0.05$) had no significant influence. The important order of the factors that affected the （α＋θ）/β was C, A, B and D in turn.

Table 5 shows the different levels of various factors on average. By visual analysis from the results, the intensity sequence of various factors and levels on result were: $A_2>A_3>A_1$， $B_1>B_3>B_2$, $C_1>C_3>C_2$, $D_1>D_3>D_2$.

Table 5. Single-factor statistic table of （α＋θ）/β.

Factor \ Statistic		Mean	Std. Error	95% Confidence interval	
				Lower bound	Upper bound
A	1	.703	.750	-.995	2.40
	2	-1.4	.226	-1.906	-.882
	3	-.19	.226	-.698	.326
B	1	-.61	.226	-1.127	-.103
	2	.339	.362	-.479	1.158
	3	-.60	.362	-1.420	.217
C	1	-1.4	.226	-1.920	-.896
	2	.317	.362	-.501	1.135
	3	.214	.362	-.604	1.032
D	1	-.34	.226	-.857	.167
	2	-.21	.362	-1.028	.609
	3	-.32	.362	-1.141	.495

Variance Analysis concluded the important order of factors of sound stimulus on driver fatigue indicators:

P80: A>C>D>B

(α＋θ)/β: C>A>B>D

Combined with p value size of variance analysis, we comprehensively considered P80 as a primary indicator that should gave first priority. We finally ascertained the important order of four factors: A>C>B>D. By comprehensive balance analyzing，the optimum sound stimulus conditions are: $A_2 B_1 C_1 D_1$, that is, sonic intensity was 70 dB, sonic frequency was 1050 Hz, stimulating time was 3s, and stimulating interval was 10s.

CONCLUSIONS

The paper is based on variations of P80 and (α +θ)/β. By orthogonal experimental design, statistically analyzed experiment data, we concluded the best combination of sound stimulus to ease fatigue. This will provide new thoughts on reducing driver fatigue and lay a foundation for driver fatigue countermeasures based on audio, optical and vibration signals. However, because of limitations of time and experimental equipment, the paper only made a preliminary investigation into sound countermeasures, so a set of systematic theoretical systems has not formatted.

Future studies will focus on recordings from distinct groups of drivers rather than individuals, simultaneously integrate psychology, physiology, behavioral science and other disciplines to optimize the experiment program, and develop a comprehensive set of sound countermeasure systems.

ACKNOWLEDGEMENTS

The research was supported by the 2008 Scientific and Technological Innovation Platform-Study on Driving Error Mechanism and Countermeasures (JJ 004011200803). We would like to thank the drivers and laboratory technician for their participation.

REFERENCES

Budi Thomas Jap, B.T., Lal, S., Fischer, P., and Bekiaris, E. (2007). *Using EEG Spectral Components to Assess Algorithms for Detecting Fatigue.* Expert Systems with Applications.

Cardillo, Carlos. (2007). *Quantitative EEG Changes under Continuous Wakefulness and with Fatigue Countermeasures: Implications for Sustaining Aviator Performance.* Schmorrow, D.D., Reeves, L.M. (Eds.): Augmented Cognition, HCII 2007, LNAI 4565, pp. 13–22.

Dinges, D.F., Mallis, M., Maislin, G., and Powell, J.W. (1998). “Final report: Evaluation of techniques for ocular measurement as an index of fatigue and as the basis for alertness management.” (No. DOT HS 808 762). National Highway Traffic Safety Administration.

Eoh, H. J., Chung, M.K., and Kim, S.H. (2005). *Electroencephalographic Study of Drowsiness in Simulated Driving with Sleep Deprivation.* International Journal of Industrial Ergonomics, 35(4), 307–320.

Hirata, Y. "A Study of the Effective Way to Release Scent to Maintain Alertness." JSAE Review. 2001, (22):331~336.

Kanghua, W. (2008). *Driver fatigue detection system design based on PERCLOS*. Zhejiang University.

King, L.M. (2006). "Early Driver Fatigue Detection from Electroencephalography Signals Using Artificial Neural Networks." *Proceedings of the 28th IEEE EMBS Annual International Conference.* New York City, USA, Aug 30-Sept 3.

Lala, S. (2003). "Development of an algorithm for an EEG-based driver fatigue countermeasure." *Journal of Safety Research*. (34) 321– 328.

Lingcong, Z., Zhengguo, W. (2003). "Research Review of Vehicle Driver Fatigue." Human Working Efficiency. (9).

U. Landstrom, U., Englund, K., Nordstro M, B., and Ae stro M, A. (1999). **"**Sound exposure as a measure against driver drowsiness." National Institute for Working Life, 42(7), 927-937.

Wierwille, W. W., Ellsworth, L. A., Wreggit, S. S., Fairbanks, R. J., and Kim, C. L. (1994). "Research on vehicle-based driver status/performance monitoring: development, validation, and refinement of algorithms for detection of driver drowsiness." National Highway Traffic Safety Administration Final Report: DOT HS 808 247.

Zhenxue, L. *Experiment Design and Data Process*. Chemical Industry Press，2005, 62-74.

The Evaluation of Level of Service for Expressway in Operating Stage

Li Hong-ping[1] and Pei Yu-long[1]

[1] School of Transportation Science and Engineering, Harbin Institute of Technology, P.O. Box 2525, 202 Haihe Road, Nangang District, Harbin, 150090, China; PH (86) 451- 86282117; FAX (86) 451-86282832; email: lihongping1995@gmail.com

ABSTRACT

Because expressway construction has recently progressed rapidly in China, traffic management needs more efficiency. So we urgently need to study the expressway system's level of service (LOS) evaluation methods. In the planning, design, and operating stages, our aims in evaluating LOS and the data to be used were different, and we have accordingly adopted different evaluation methods for each stage. This paper investigates the LOS evaluation method in the operating stage, evolving a model to estimate travel speed based on the dual loop detectors that were developed, to verify the precision of the model. We have proved that it is feasible to replace the data of the section with that of lane 2 for analysis. Taking the travel speed index as a service measure, we developed a quantitative method for evaluating expressway LOS, and we developed procedures for operating quality analysis. We also successfully applied this method to an example.

INTRODUCTION

Constructing an expressway system is one of the most effective methods for optimizing a road network to alleviate traffic congestion in big cities. And expressway systems are playing a very important role in metropolitan transportation. The expressway system in Peking, for example, includes 4 ring roads and 15 radial roads. Its total length is about 380 kilometers, which is about 8% of the total length of the road network, but it will be taking on 50% of the vehicle traffic volume in the future. When more and more expressway systems are completed and put into use, the traffic management on expressways will have to become more efficient. The level of service is an important index to measure the operating quality of the road transportation system. Presently, the same method is applied to evaluate the level of service (LOS) of each kind of facility in the planning, design and operating stages in the widely used Highway Capacity Manual (HCM) (TRB,2000). LOS procedures in HCM vary little with the data in different stages. For an expressway, the goal and the data for an LOS evaluation in the operating stage are quite different from that of the planning and design stages, and different evaluation methods shall be developed for each respective stage in the process.

MODEL OF ESTIMATING TRAVEL SPEED BASED ON DUAL LOOP DETECTORS

Travel speed (TS) numerically equals to the ratio of mileage to travel time (TT). So travel speed forecasting and travel time forecasting are the same in essence, and the difference lies in the application. Whereas managers tend to use travel speed, users prefer travel time (Christopher, 2006). Travel speed or travel time forecasting is one of the key problems in ITS researches, and both present difficulties. According to the data used, forecasting methods can be divided into two types: those based on moving detectors (in-vehicle instruments), and those based on fixed detectors (such as loop detectors). Those methods based on fixed detectors have no recognized solutions (Jiang, 2004).

Spot speed obtained from dual loop detectors on an expressway mainline can be adopted to forecast travel speed. In the model shown on Figure1, l_i is the distance between detector *i* and the upstream detector, between the start detector and the start profile, or between the end detector and the end profile, km; L_i is the length of the forecasting section using the average spot speed obtained from detector *i*, km; L is the length of the whole section, km; $\bar{v}_{ti}$ is the average spot speed at detector *i*, km/h.

Equations (1) to (6) have been developed to estimate travel speed:

$$\bar{v}_{si} = \bar{v}_{ti} - \sigma_{ti}^2 / \bar{v}_{ti} \tag{1}$$

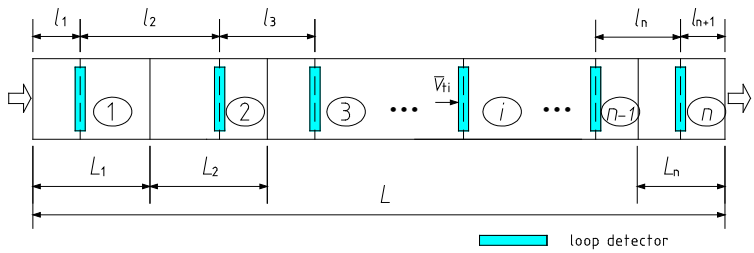

Figure 1. Travel speed forecasting model based on dual loop detectors.

$$L_i = \begin{cases} l_1 + l_2 \ / 2, & i = 1 \\ (l_i + l_{i+1}) / 2, & i = 2,3,\cdots \mathrm{n}-1 \\ l_n / 2 + l_{n+1}, & i = n \end{cases} \tag{2}$$

$$L = \sum_{i=1}^{n} L_i \tag{3}$$

$$TT = \sum_{i=1}^{n} t_i \tag{4}$$

$$t_i = L_i / \bar{v}_{si} \tag{5}$$

$$TS = L / TT \tag{6}$$

where $\bar{v}_{si}$ is the average space speed in section *i*, km/h; σ_{ti}^2 is variance of

average spot speed; *TT* is travel time, h; *TS* is travel speed, km/h.

LOS EVALUATION METHOD BASED ON TRAVEL SPEED INDEX

Expressway LOS Criteria Based on Travel Speed Index

Free flow travel speed (FFTS) is the travel speed of vehicles passing through a section in a free flow state. It is defined as the weighted mean value of the theoretical free flow speed of the components of the section, which includes a basic segment of the expressway, a diverging area, a merging area and a weaving area. The weight is the ratio of the length of each component to that of the section.

The expressway is divided into three components: the expressway's basic segment; its diverge and merge areas; and its weaving area (TRB, 2000).

(1) The diverge area is the distance extending from the physical diverge point to 450 m upstream, and merge area is the distance extending from the physical merge point to 450 m downstream.

(2) The weaving area is from a point at the merge gore where the right edge of the freeway shoulder lane and the left edge of the merging lane(s) are 0.6 m apart to a point at the diverge gore where the two edges are 3.7 m apart.

(3) The basic segment is outside the influence area of diverging, merging and weaving movements.

The theoretical free flow speed can be drawn from a fitted Greenshield model because of the direct correlation between the theoretical and measured free flow speeds (Sasaki, 1994; Li, 2007). The travel speed index (TSI) is defined as the ratio of actual travel speed to free flow travel speed. As a service measure, TSI indicates the extent the expected speed (FFTS) achieved. The expressway LOS criteria has been developed according to widely adopted 5-level categories (Su, 2000). They are: excellent, good, medium, bad, and worst . (Table 1). The traffic state in the 5 levels can be described respectively as free, smooth, steady, crowded and congested.

Table 1. Expressway LOS Criteria.

LOS	Ⅰ	Ⅱ	Ⅲ	Ⅳ	Ⅴ
TSI	≥0.90	[0.8,0.9)	[0.7,0.8)	[0.5,0.7)	＜0.5
Traffic state	free	smooth	steady	crowded	congested

Expressway LOS Procedures for Operating Analysis

Supposing the analysis period is divided into *i* intervals (usually 5 minutes), and the expressway LOS procedure is as follows:

(1) Calculating FFTS;

(2) Calculating TS in each interval, and labeled as TS_1、$TS_2 \cdots TS_i$;

(3) Calculating TSI in each interval and determining LOS, which is labeled as $SLOS_1$、$SLOS_2 \cdots SLOS_i$;

(4) Processing the evaluating result according to the users to facilitate understanding and communication.

MODEL VERIFICATION AND CASE STUDIES

Data Sets and Outcomes

The data includes two parts. The traffic flow data for developing the model is obtained from dual loop detectors on a section of the Yanan elevated expressway in Shanghai (Figure 2). And the measured travel speed for verifying the model is investigated by a car-following method (see Table 2). The travel time during a peak hour and a nonpeak hour is 530s and 372s respectively and the corresponding travel speed is 47.7km/h and 67.9km/h (the analysis process is omitted).

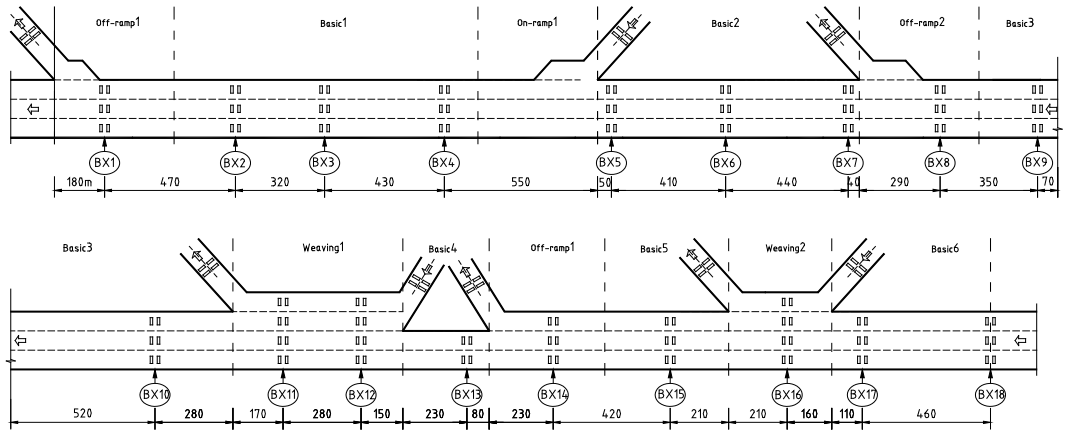

Figure 2. Road conditions and sites of loop detectors for travel speed analysis.

Table 2. Investigated Data of Travel Speed.

Period of Time	Time to Enter	Time to Leave	*TT*/s	*TS*/ (km·h^{-1})
Peak hour	8:03:28	8:11:43	495	51.1
Nonpeak hour	22:04:06	22:10:36	390	64.8

Note: L=7.02km.

Error of Travel Speed Forecasting.

The forecasted value of travel speed during a peak hour is less than that in a nonpeak hour (see Table 3), which mainly results from the instability of the traffic flow, and this instability cannot be reflected in the spot speed drawn from the detectors. The relative error in a peak hour forecast is -6.7%, greater than that in that of a nonpeak hour, but it meets our need for an operating analysis.

Table 3. Error Analysis for Travel Speed Forecasting.

Data	Profile Average		Lane 2	
Time Period	Peak Hour	Nonpeak Hour	Peak Hour	Nonpeak Hour
Measured TS / ($km \cdot h^{-1}$)	51.1	64.8	51.1	64.8
Forecasted TS /	47.7	67.9	45.5	68.2
Absolute Error/	-3.4	3.1	-5.6	3.4
Relative Error /%	-6.7	4.8	-11.0	5.2

Feasibility of Replacing Data of the Whole Profile by That of Lane 2.

In equation (5), the average spot speed can be the average of all lanes or one lane. Generally speaking, the margin of error would be lessened if the average of all lanes is included, but doing so also greatly increases the amount of data processing necessary, especially for real time analysis and information release. Therefore, we have used the average spot speed of one lane to estimate space mean speed. The lane is the one in which traffic flow characteristics are closest to that of the whole profile, and for a 3-lane profile, this turns out to be lane 2, the middle lane. (Li, 2007).

Space mean speed is estimated based on the average spot speed of the profile and lane 2 respectively (see Table 4). Relative errors are less than 10% except for 4 values in which they can be as much as 24.8%. As a whole, the relative errors in a peak hour are greater than those in a nonpeak hour.

Table 4. Space Mean Speed of the Profile Compared with That of the Lane2.

Detector No.	Section Type	Peak Hour				Nonpeak Hour			
		Profile $\bar{v}_{si}$ / ($km \cdot h^{-1}$)	Lane 2 $\bar{v}_{si}$ / ($km \cdot h^{-1}$)	Absolute Error/ ($km \cdot h^{-1}$)	Relative Error/%	Profile $\bar{v}_{si}$ / ($km \cdot h^{-1}$)	Lane 2 $\bar{v}_{si}$ / ($km \cdot h^{-1}$)	Absolute Error/ ($km \cdot h^{-1}$)	Relative Error/%
		①	②	③	④	⑤	⑥	⑦	⑧
BX1	Off-ramp	61.04	61.56	-0.52	0.8	71.75	74.62	-2.87	4.0
BX2	Basic	71.76	74.62	-2.86	4.0	76.37	76.84	-0.47	0.6
BX3	Basic	62.83	67.07	-4.24	6.7	64.95	66.68	-1.73	2.7
BX4	Basic	60.13	61.79	-1.66	2.8	69.73	66.62	3.11	4.5
BX5	Basic	75.52	77.62	-2.10	2.8	80.02	81.30	-1.28	1.6
BX6	Basic	79.11	84.66	-5.55	7.0	82.86	86.91	-4.05	4.9
BX7	Basic	70.06	78.32	-8.26	11.8	74.32	78.48	-4.16	5.6
BX8	Off-ramp	60.06	62.55	-2.49	4.1	66.70	66.32	0.38	0.6
BX9	Basic	68.80	63.26	5.54	8.1	73.25	68.90	4.35	5.9
BX10	Basic	62.73	60.84	1.89	3.0	69.90	67.37	2.53	3.6
BX11	Weaving	56.77	56.20	0.57	1.0	66.23	65.31	0.92	1.4
BX12	Weaving	53.59	51.28	2.31	4.3	63.16	61.32	1.84	2.9
BX13	Basic	39.16	39.66	-0.50	1.3	54.74	52.48	2.26	4.1
BX14	Off-ramp	29.86	22.45	7.41	24.8	55.47	54.20	1.27	2.3

BX15	Basic	19.69	19.51	0.18	0.9	71.92	81.76	-9.84	13.7
BX16	Weaving	21.51	16.86	4.65	21.6	56.22	57.27	-1.05	1.9
BX17	Basic	38.96	41.23	-2.27	5.8	61.56	62.36	-0.80	1.3
BX18	Basic	72.08	74.61	-2.53	3.5	66.48	72.57	-6.09	9.2

Note: Conversion equations in the table: ③=①-②; ④=｜③｜/①; ⑦=⑤-⑥; ⑧=｜⑦｜/⑤.

The travel speed estimate is based on the data of the profile as a whole and lane 2 respectively (see Table 3). The errors using the data from lane 2 are greater but not as much as those using the data of the whole profile. It is feasible to replace the data of the whole profile by that of lane 2 for LOS analysis, for which the data processing work can be greatly cut down in the Advanced Traveler Information System (ATIS) application.

LOS Analysis.

The level of services on the expressway from the respective time periods of 8:00 to 9:00 and 22:00 to 23:00 have been analyzed. The Greenshield model of each profile has been developed to calculate theoretical free flow speed, on which free flow travel speed is rendered as 82.5km/h (with the calculating process omitted). The values of service measure in each interval and the results of our LOS evaluation are listed in Table 5.

Table 5. Example of System LOS Analysis at Operating Stage.

	Peak Hour					Nonpeak Hour			
End Time	*TT*/h	*TS*/ (km·h^{-1})	*TSI*	*SLOS*	End Time	*TT*/h	*TS*/ (km·h^{-1})	*TSI*	*SLOS*
8:05	0.151	46.4	0.562	IV	22:05	0.102	69.0	0.836	II
8:10	0.148	47.6	0.577	IV	22:10	0.102	68.7	0.833	II
8:15	0.164	42.7	0.518	IV	22:15	0.104	67.3	0.816	II
8:20	0.171	41.0	0.497	V	22:20	0.103	68.3	0.828	II
8:25	0.186	37.8	0.458	V	22:25	0.103	68.2	0.827	II
8:30	0.193	36.5	0.442	V	22:30	0.103	68.0	0.824	II
8:35	0.180	39.0	0.473	V	22:35	0.100	70.0	0.848	II
8:40	0.178	39.4	0.478	V	22:40	0.100	70.4	0.853	II
8:45	0.165	42.6	0.516	IV	22:45	0.098	71.9	0.872	II
8:50	0.154	45.7	0.554	IV	22:50	0.097	72.4	0.878	II
8:55	0.164	42.9	0.520	IV	22:55	0.096	73.2	0.887	II
9:00	0.167	42.1	0.510	IV	23:00	0.095	73.8	0.895	II
	SLOS= IV*n*V(10-*n*)= IV6V4*						*SLOS*=II		

Note: The number of the intervals (*i*) is converted into 10 here, that is n and (10-n) are the proportions of the intervals with LOS IV and LOSV to the total intervals.

CONCLUSIONS

A real-time analysis and release of LOS is becoming indispensable in

expressway system management as managers cry for more effective evaluation methods. The expressway LOS procedures developed in this paper are based both on the user's perception of LOS levels and on the current situation of traffic management facilities which can directly bring it into effect. It should be pointed out that for a 2-lane or 4-lane expressway, this information must be analyzed using the method proposed in the paper to determine which lane's data can most closely represent that of the overall profile.

ACKNOWLEDGMENT

This research was supported by Specialized Research Fund for the Doctoral Program of Higher Education (200802131012, 200802131013).

REFERENCES

Christopher, R. B. (2006). "Travel time and congestion modeling." http://www.romdas.com/technical/tec-cong.htm>(Aug. 28, 2006).

Jiang, G.-Y. (2004). *Techniques of Discrimination of Road Traffic State and Its Application*. Peking: China Communication Press.

Li, H.-P., Pei, Y.-L., and Yang, ZH.-L. (2007). Factors influencing free flow speed on expressway. Journal of Jilin University., 37(4), 772-776.

Sasaki, T. and Iida, Y. (1994). *Traffic Engineering*. Peking: China Communication Press.

Su, W.-H. (2000). "Study on the theory and method of multiple objective comprehensive evaluation," Ph.D. dissertation, Xiamen Univ., Xiamen.

Transportation Research Board. (2000). *Highway Capacity Manual,* Washington, D.C.

Vehicle Detection from Videos Containing Complex Background Based on Bayesian Statistical Modeling

Li Ying-hong [1] Liu Ya-li [2] Pang Yi-gui[2] Yin Yi-xin [1]

[1]School of Information and Engineering, University of Science and Technology Beijing, Beijing 100080; PH: 010-88802226; email: lyh427@ncut.edu.cn
[2]Laboratory of Intelligent transportation System, North China University of Technology, Beijing 100144; email:liu.yali11@163.com

ABSTRACT

This paper proposes a novel method for the detection and segmentation of vehicles from video traffic surveillance. A Bayesian decision rule is derived for background and foreground classification based on the statistics of a principle feature. The kernel density function is used to represent feature statistics. Considering that background pixel variation has strong spatial and temporal correlations, the pixels of the video's background have been divided into two types of static or dynamic pixels which are described by different principal features. Foreground objects are extracted by fusing the detection results from both stationary and motional points. Gradual and sudden background changes, are addressed with different learning strategies proposed in this paper. Our experiments on traffic surveillance have shown promising results in extracting vehicles from their complex backgrounds.

INTRODUCTION

In real-time video surveillance and motion analysis applications, the primary task is to detect moving objects from video sequences efficiently. Frame difference including background subtraction and inter-frame difference is the common method utilized for this task. The need to construct efficient background models in real-time that adapt to the environment's changes can lead to an empty or tailing appearance in the image of inter-frame differences . This is because the camera's shooting speed usually does not match the foreground objects' speed. These two points limit the frame difference method in target detection. Recently, several other detecting methods suitable for a complex environment have been proposed (such as a method based on pixel filtering and an adaptive background modeling method). Among them, the adaptive mixture Gaussian model (MOG) is one of the most successful methods for its simple structure and low computational cost. But by only depending on the learning rate to adapt to background changes, the MOG faces trade-off problems. With its slow learning rates and convergence, it produces a wide model that has difficulty detecting a sudden change in the background. If the model adapts too quickly, slowly moving foreground pixels will be absorbed into the background model, resulting in a high false negative rate. Recently, some researchers have presented more improved mixture Gaussian models [Lee, D-S. (2004), Arandjelov, C. R. (2005), Chen, Z., Chen, X., Hong, H. (2007), Ma, Y., Zhu, W., etc. (2007), Chen, Z., Zhou, R., etc. (2007)], but the results still have not been satisfactory. In order to improve the robustness of the surveillance system, this paper proposes a novel method to extract foreground objects from a real-time complex video under the Bayesian decision framework. The proposed method can deal with the problems

both of gradual and sudden background changes in the detection of foreground objects and has detected vehicles effectively amid complex environments in our experiments.

THE METHOD OF MOVING FOREGROUND OBJECTS DETECTION BASED ON THE BAYESIAN DECISION RULE

The method of vehicle detection based on the Bayesian decision rule is composed of the following parts. During initial classification, pixels are classified simply by frame difference at first. In principal feature selection, different feature vectors are constructed to represent the statistical properties of the pixels according to their spectral, spatial, and temporal features. Employing classification under the Bayesian framework, from the statistical distribution of feature vectors we get background and foreground classification. In updating parameters, we update the background model and the feature vectors of the pixels.

Initial classification and feature vector selection

First of all, each pixel of the current frame is classified through the background subtraction initially. In this way, the pixel is classified as the background point if the pixel gray value is less than the threshold, otherwise it is classified as a changing point. Secondly, if the changing point pixel changes between frames then it is marked as a dynamic point, otherwise it is marked as static point. Considering that background variation at neighboring pixels has strong spatial and temporal correlations, the changed points are divided into two types of static or dynamic pixels so that they can be described by their appropriate principle features respectively. The principle features of the background at each pixel may provide enough information for foreground and background classification. For a static pixel, the stable and most significant features are its color, so the feature vector is represented by $v_t = [r_t, g_t, b_t]^T$. For dynamic pixels associated with non-stationary objects, color change occurrences $v_t = [r_t, g_t, b_t, \Delta r_t, \Delta g_t, \Delta b_t]^T$ are used as their dynamic features, where $\Delta r_t = r_t - r_{t-1}, \Delta g_t = g_t - g_{t-1}, \Delta b_t = b_t - b_{t-1}$.

But the adaptive mixture Gaussian model mentioned in section 1 only uses a color vector to represent the background features; it doesn't take into account the background variation's strong correlation in neighboring pixels. In addition, backgrounds having fast variations are not easily or accurately modeled with just a few Gaussians, so that model may fail to provide effective detection.

Baytesian models

This paper proposes a Bayesian framework **(**Liyuan Li, Weimin Huang, Irene Yu-Hua Gu, Qi Tian (2004)**),** which incorporates different types of features for modeling complex backgrounds. For a stable real-time outdoor surveillance system, background pixels are subject to Gaussian distribution, while the background models can be represented by significant vectors from a principal features analysis. According to the probability distribution of eigenvector, the pixels will be classified as foreground or background under the Bayesian framework. This method is described as follows.

Let $s = (x, y)$ be the position of an image pixel, $I = (s, t)$ be the input image

at time t, and v_t be a feature vector extracted from an image sequence at the point s and time t. Using the Bayesian decision rule, a posterior probability of v_t from the background b or foreground f is

$$P(B|v_t,s)=\frac{P(v_t|B,s)P(B|s)}{P(v_t|s)}, \qquad B=b \text{ or } f \qquad (1)$$

Using the Bayesian decision rule, a pixel is classified as background according to its feature vector observed at time t.

$$P(b|v_t,s)>P(f|v_t,s) \qquad (2)$$

Otherwise, it is classified as foreground.

Note that the feature vectors at the pixel s comes either from background or foreground objects, it follows

$$P(v_t|s)=P(v_t|b,s)P(b|s)+P(v_t|f,s)P(f|s) \qquad (3)$$

Substituting (1) and (3) into (2), then the Bayesian decision rule becomes

$$2P(v_t|b,s)P(b|s)>P(v_t|s) \qquad (4)$$

Therefore, if the prior probability and conditional probability $P(v_t|b,s)$, $P(b|s)$and $P(v_t|s)$ at pixel s are known in advance, the pixel can be classified as background or foreground according to the Bayesian decision rule.

The statistic characteristics of the feature vector

Generally, the prior probability and conditional probability $P(v_t|b,s)$, $P(b|s)$and $P(v_t|s)$ are unknown. A type of non-parameter kernel density function is used in this paper to estimate them.

According to the principle that background pixels are subject to Gaussian distribution and mainly located in the neighborhood of the mean, from a histogram distribution of the background, the feature vectors should be highly concentrated in a small region. But when moving objects cross the space, feature vectors can spread widely in the feature space. So some small significant feature vectors can be selected to represent the background effectively.

Let V_i be the quantized feature vectors (Liyuan Li, Weimin Huang, Irene Yu-Hua Gu, Qi Tian (2002)) which are stored according to a descending order (Liyuan Li, Weimin Huang, Irene Yu-Hua Gu, Karianto Leman, Qi Tian (2003)) of $P(v_t^i|b,s)$ for each pixel (i.e. $P(v_t^i|b,s)\geq P(v_t^{i+1}|b,s)$). Then for a proper selection of features, there should be two percentage values T_1, T_2 (i.e. T_1=80%～90%, T_2=10%～20%) and a small integer N_1 which are satisfied with the following conditions:

$$\sum_{i=1}^{N_1(v)}P(v_t^i|b,s)>T_1 \quad \text{and} \quad \sum_{i=1}^{N_1(v)}P_s(v_i|f)<T_2 \qquad (5)$$

where N_1 is a small number of the principal feature vectors at pixel $s(x,y)$. It is important to cut down the computation and storage efficiently for this method's practical application.

Under the Bayesian framework, the following information should be formed for each pixel:

(1) Construct the feature vector set which can represent the background effectively. $v_t^i = [a_1^i, \cdots a_n^i]^T$, where $i = 1, \cdots, N_2$ （$N_2 > N_1$）, the feature vectors are selected differently for static and dynamic points: there are $v_t = [r_t, g_t, b_t]^T$ or $v_t = [r_t, g_t, b_t, \Delta r_t, \Delta g_t, \Delta b_t]^T$ separately.

(2) Established a table of statistics for the principle feature including the prior probability and conditional probability, such as $p_v^{t,i} = P(v_t^i | s)$ and $p_{vb}^{t,i} = P(v_t^i | b, s)$.

ALGORITHM DESCRIPTION

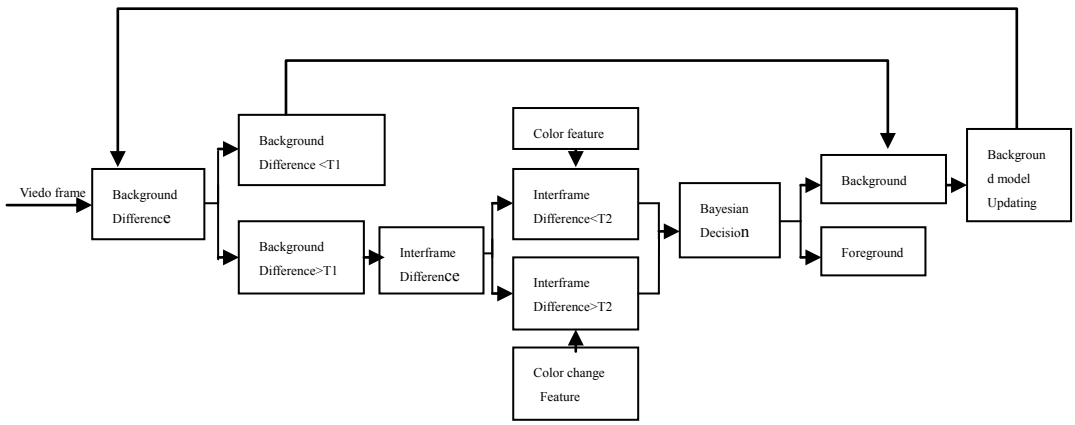

Figure1. Block diagram of the algorithm.

Arithmetic flow

Step 1: Initialize the probability of background pixels, and construct feature vectors set by learning.

Step 2: Classify each pixel by background subtraction $F_{bd}(s,t)$ and inter-frame difference $F_{td}(s,t)$. Meanwhile construct different feature vectors for static or dynamic pixels.

Step 3: Calculate the probability $P(b|s)$, $P(v_t|s)$ and $P(v_t|b,s)$ for all the stationary points and dynamic points as follows:

$$\begin{aligned} P(b|s) &= p_b^{s,t} \\ P(v_t|s) &= \sum_{i \in H(v_t)} k_i (v_i - v_t) \\ P(v_t|b,s) &= \sum_{i \in H(v_t)} k_i^b (v_i - v_t) \end{aligned} \qquad (7)$$

Suppose $v_t^{s,i}$ is the i th feature vector in the feature vector set at pixel $s(x,y)$, $H(v_t)$ is the matched feature set, where $H(v_t) = \{ i : \forall i \in \{1, \cdots N_2\}, |v_t - v_t^{s,i}| < \varepsilon \}$. The kernel function $k_i(v_i - v_t) = p_v^{s,t,i}$ and $k_i^b(v_i - v_t) = p_{vb}^{s,t,i}$, where $P(v_t|s)$ and $P(v_t|b,s)$ are probability kernel estimation functions. In this paper, the non-parameter kernel function (i.e. histogram) is to be adopted in the probability estimation.

Step 4: Decide if the pixel $s(x,y)$ is satisfied with the Bayesian rule

$2P(v_t|b,s)P(b|s) > P(v_t|s)$, and if it will be classified as background, let $s(x,y)$=0. Otherwise pixel $s(x,y)$ will be classified as foreground, in which case let $s(x,y)$=1.

Step 5: Utilize a morphological operation to remove the noise point.

Step 6: Update the probability tables and the background models.

Background and parameter updating

Probability Table Updating

$$p_b^{s,t+1,i} = (1-\alpha)p_b^{s,t,i} + \alpha M_b^{s,t,i},$$
$$p_v^{s,t+1,i} = (1-\alpha)p_v^{s,t,i} + \alpha M_v^{s,t,i},$$
$$p_{vb}^{s,t+1,i} = (1-\alpha)p_{vb}^{s,t,i} + \alpha(M_b^{s,t,i} \wedge M_v^{s,t,i}) \quad (8)$$

Where α is the learning rate, $\alpha \in [0,1]$, v_t is the feature vector at pixel $s(x,y)$. $M_v^{s,t,i}=1$ if v_t^i matches with v_t, otherwise $M_v^{s,t,i}=0$. If v_t doesn't match any vector in the feature vector set, the last vector in the feature vector set is replaced by a new feature vector, whose values are:

$$p_v^{s,t+1,N_2} = \alpha, \quad p_{vb}^{s,t+1,N_2} = \alpha, \quad v_t^{N_2} = v_t \quad (9)$$

Meanwhile, $M_b^{s,t}=1$ if the $s(x,y)$ is classified as the background by the Bayesian rule at last, otherwise $M_b^{s,t}=0$.

On the other hand, if $P(f|s)\sum_{i=1}^{N_1} P(v_t^i|f,s) > T$ (i.e. $\sum_{i=1}^{N_1} p_{vb}^{s,t,i} \cdot \left(1-\sum_{i=1}^{N_1} p_v^{s,t,i}\right) > T$ where $T \approx 90\%$), it shows that the background has sudden variations and the new features are becoming dominated immediately, the probability needs to be updated as follows

$$p_v^{s,t+1,i} = 1 - p_v^{s,t,i}$$
$$p_{vb}^{s,t+1,i} = \frac{\left(p_v^{s,t,i} - p_b^{s,t} \cdot p_{vb}^{s,t,i}\right)}{p_b^{s,t+1}} \quad (10)$$

where $i \in [1, N_1]$, $p_b^{s,t} = \sum_{i=1}^{N_1} p_v^{s,t,i}$, $p_b^{s,t+1} = \sum_{i=1}^{N_1} p_v^{s,t+1,i}$

Background Models Updating

Background subtraction has been used in the initial classification of pixels mentioned in section 2.1. To achieve this, an accurate and adaptive background is needed. So the background model should be updated in real-time.

If the background changes slowly, the background is updated as

$$B_c(s,t+1) = (1-\beta)B_c(s,t) + \beta I_c(s,t) \qquad \alpha_1 \in [0,1] \quad (11)$$

If the background changes suddenly to ($P(f|s)\sum_{i=1}^{N_1} P(v_t^i|f,s) > T$), the background is updated as $B_c(s,t+1) = I_c(s,t)$ (12)

Where, β is the updating rate of the background, $B_c(s,t)$ is the color value of pixel $s(x,y)$ in the reference background, and $I_c(s,t)$ is the color value at pixel $s(x,y)$ in the current frame.

EXAMPLES AND ANALYSIS

In order to verify the robustness and efficiency of this method, many real-time traffic surveillance videos each of whose size is 720 by 576 were tested on the VC++6.0 platform. In the experiments, the main parameters were initialized as $p_v^0 = 0$, $p_b^0 = 0$, $p_{vb}^0 = 0$. In terms of storage and computation, the number of the feature vector $v_t = [r_t, g_t, b_t]^T$ **was** set to 32, whereas the feature vector $v_t = [r_t, g_t, b_t, \Delta r_t, \Delta g_t, \Delta b_t]^T$ was set to 16. The two probability tables of every pixel of each frame can be calculated according its respective histogram. One is for stationary points and the other is for the dynamic points. The feature vectors were stored according to the descending order of $P(v_t|b,s)$. The learning rate was α. If it had been too small, the system would have been too slow to respond to the sudden background changes. In the experiment, we set the learning rate range from 0.005 to 0.01. β is the update rate of the background and ε is the match threshold. In the experiments α, β and ε are set to 0.02, 0.5, and 0.05 separately.

The following two figures show the results with different methods of foreground object detection. In Figure 2, employing mixture Gaussian models, the first column is raw video frame: 15, 46, and 110. The second column shows the background models corresponding to the first column generated by GMM. The third column is the detected foreground object. From the frame 15 to 46, the flasher is used to make the light change slightly. In frame 110, when the white car comes into the view of the camera, the light changes suddenly because of the strong light reflection. Seen from row 3, all the pixels change suddenly due to light reflection. These background pixels can be mistaken for the foreground. Thus the foreground object can't be extracted effectively from the image.

Figure 3 employs the method proposed in this paper, showing the achieved result of our proposed algorithm. The raw video frame is the same as that used in Figure 2. The first column is raw video frame: 15, 46, and 110. The second column shows the background models corresponding to the first column, but generated by the Bayesian framework both in gradual and sudden changes in their respective environments. The test indicates that the principal features are effective in representing the characteristics of their background.

The experiments were repeated under complex environments where they detected the vehicles effectively.

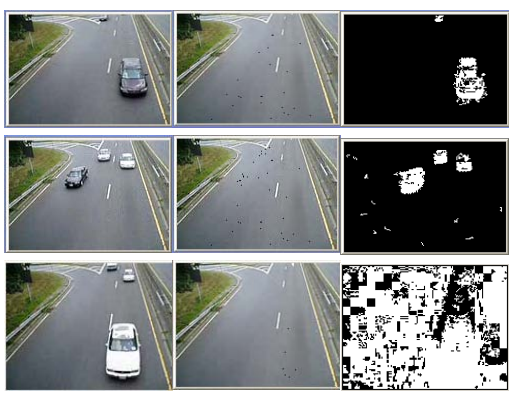

Figure2. Moving Object Detection Based on Mixture Gaussian Models.

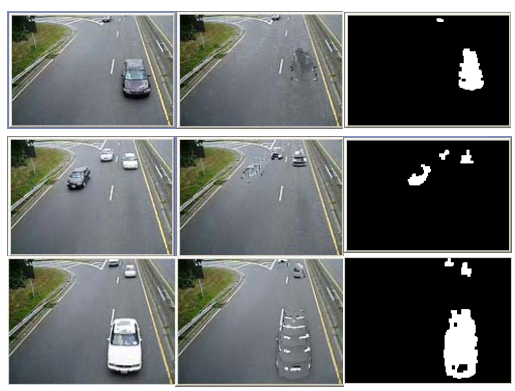

Figure3.Moving Object Detection Based on Bayesian Statistical Models.

CONCLUSIONS

In detecting foreground objects from complex environments, this paper proposed a novel statistical method for background modeling based on Bayesian decision theory. In the proposed method, different feature vectors are selected to represent the static and dynamic background pixels. From the statistics of their principal features, foreground objects are detected under a Bayesian framework. The experiments on vehicle detection were repeated with a variety of environments, and our research indicates that the proposed method using different features to model different parts of a vehicle's background is more effective than just using one type. The experimental results demonstrated a significantly improved performance in detecting foreground objects amid a complex background.

ACKNOWLEDGEMENTS

This paper was partly funded by the Scientific Research Common Program of the Beijing Municipal Commission of Education (KM200910009001) and PHR(IHLB)

REFERENCES

Arandjelov, C. R. (2005). "Incremental learning of temporally-coherent Gaussian mixture models" [A]. In: *Proceedings of British Machine Vision Conference* [C], Oxford, UK, 2005: 759-768.

Chen, Z., Chen, X., and Hong, H. (2007). "Moving Object Detection Based on Improved Mixture Gaussian Models" [J], *Journal of Image and Graphics*, 2007, 12(9):1586-1589.

Chen, Z., Zhou, R.， etc. (2007). "Simulation of an Improved Gaussian Mixture Model for Background Subtraction" [J]. *Computer Simulation*, 2007, 24 (11):190-192.

Liyuan Li , Weimin Huang , Irene Y. H. Gu , Qi Tian. (2002). "Foreground Object Detection in Changing Background Based on Color Co-Occurrence Statistics," *Proceedings of the Sixth IEEE Workshop on Applications of Computer Vision*, p.269, December 03-04, 2002

Liyuan Li ,Weimin Huang ,Irene Yu-Hua Gu ,Karianto Leman, Qi Tian. (2003). "Principal color representation for tracking persons." *IEEE Transactions on Volume*:*1*, pp.1007-1012, vol.1. Digital Object Identifier:10.1109/ICS MC.2003.1243946

Liyuan Li ,Weimin Huang ,Irene Yu-Hua Gu ,Qi Tian. (2004). "Statistical modeling of complex backgrounds for foreground object detection" .*Image Processing, IEEE Transactions on Volume 13*, Issue 11, Nov. 2004 pp. 1459 - 1472 Digital Object Identifier 10.1109/TIP.2004.836169

Lee, D-S. (2004). "On line Adaptive Gaussian Mixture Learning for Video Applications" [C]// *Statistical Methods in Video Processing*, LNCS3247.2004, 3247: 105-116.

Ma, Y., Zhu, W., etc. (2007). "Improved moving objects detection method based on Gaussian mixture model" [J], *Computer Applications*, 2007， 27(10): 2544-2548

An Improved Ant Colony Algorithm for the Shortest Path Problem in Time-Dependent Networks

Gao Hui [1], Liu Yongqiang [2], Chang Qing [3], and Xiong Huagang [4]

[1] DFH Satellite Information Technology Co.,Ltd,Beijing 100081;PH (010)68118008 ext.923;email:ghcc@263.net
[2]School of Electronics and Information Engineering, Beijing University of Aeronautics and Astronautics, Beijing 100191, China; PH (010)82317800; email:yongqiangliu@sina.com
[3]School of Electronics and Information Engineering, Beijing University of Aeronautics and Astronautics, Beijing 100191, China; PH (010)82317800; email:changq@263.net
[4]School of Electronics and Information Engineering, Beijing University of Aeronautics and Astronautics, Beijing 100191, China; PH (010)82317800

ABSTRACT

Research of the shortest path problem in time-dependent networks has important practical value. An improved pheromone update strategy is demonstrated here. Using this strategy, the residual pheromone of each path can accurately reflect the change of weighted value for each path. An improved ant colony algorithm for the shortest path problem in time-dependent networks based on our improved strategy is also presented here. The results of this experiment show that the improved algorithm has a greater probability to achieve an optimal solution, and the convergence rate of the algorithm is greater than that of a traditional ant colony algorithm.

INTRODUCTION

The shortest path algorithm plays an important role in many fields, such as communications systems and intelligent transportation systems. A large number of methods and algorithms to solve the shortest path problem have been proposed in many existing literatures, but most of them focus on a network with fixed weights, without taking into account time varying weights.

R W Hall (1986) firstly pointed out that the traditional shortest path algorithm cannot be used with time varying weight. The shortest path problem of some dynamic networks cannot be solved unless strict conditions of consistency have been established. A dynamic network model solved by the improved Dijkstra algorithm has been proposed by Tan Guozhen and Gao Wen (2002), but it has a high time complexity. A genetic algorithm has been adopted to solve the shortest path problem of dynamic networks by Liu Jianqiang and Liu Fenlin (2004), but this approach can easily lead to a premature convergence, and to a local optimal solution. A feedback

neural-network model has been used by He Hong, Zhu Daming and Ma Shaohan (2004), but it requires that the weight matrix must be symmetric and the link travel-time function must be continued and bounded. The traditional ant colony algorithm is used in time-dependent networks by Chen Lichao, Liu Jia and Lv Yanan (2007), but the pheromone update strategy cannot reflect changes in the weighted value of each side, so the efficiency of path choosing results is low.

This paper presents a pheromone update strategy of an ant colony algorithm applied to time-dependent networks, so that the residual pheromone of each path can accurately reflect its respective change of weighted value. An improved ant colony algorithm for the shortest path problem in time-dependent networks based on the improved strategy is presented below. This algorithm can be applied to both discrete and continuous networks effectively, and results not only in a fast convergence, but also greatly enhances the probability of finding a global optimal solution.

TIME-DEPENDENT MODEL

Model Description

Generally, dynamic networks are presented as (V, A, T), where $V = (v_1, v_2, ..., v_n)$ is a finite point set, A is the limited side set, and $A \in VxV$; $T = \{g_{i,j}(t) \mid (v_i, v_j) \in A, t \in [t_0, t_m]\}$ is the function of each edge (v_i, v_j), with the time extent $[t_0, t_m] \in R$. With $g_{i,j}(t)$ as a non-negative real number, this represents the time passed between joint v_i and v_j at the moment t; $t_0 \le t \le t_m, \forall t \in [t_0, t_m], t + g_{i,j}(t) \in [t_0, t_m]$.

The Shortest Path Model of Dynamic Networks

The model is described as:

$$\min \sum_{i=1}^{n-1} T_{v'_i, v'_{i+1}} \tag{1}$$

$$T_{v'_k, v'_{k+1}} = g_{v'_k, v'_{k+1}} \left(\sum_{i=1}^{k-1} T_{v'_i, v'_{i+1}} + t_s \right) \tag{2}$$

$$(v'_1, v'_2), ..., (v'_{n-1}, v'_n) \in A \tag{3}$$

$$v'_i \in V, i = 1, 2, ...n \tag{4}$$

$$0 < k < n, k \in N \tag{5}$$

With v'_0 as the starting point, v'_n as the ending point, and t_s as the departure time. The above equation (2) represents the time passed from the joint v'_k to v'_{k+1} by the path $(v'_1, v'_2, \ldots, v'_n)$ when starting off at the moment t_s. The constrained condition is (3) and (4) makes sure that the

path $(v'_1, v'_2, \ldots, v'_n)$ among the networks is connected, without any points of breakage.

THE INNOVATION STRATEGY OF A COLONY ALGORITHM

The Selection Strategy Between Adjacent Cities

The basic ant colony algorithm compares the taboo table with the other *n*-1 cities when an ant transfers from city *i* to *j*, computing the transfer probability of each city, which requires more expenditures of time.

In practical applications, ants must crawl in a network with a topology relationship. Ants cannot choose any city from all the cities in the non-taboo table, but only chooses a city with a direct path between them, and so must choose from the joints which have a path (v_i, v_j) between them. So, we only need to compute these cities' transfer probabilities, and, as a result, the calculation of the basic ant colony algorithm is greatly reduced, and our computing speed is greatly increased.

The Dynamic Pheromone Updates Strategy

There are two main points in the ant colony algorithm: one is the transfer probability computing strategy, the other is the pheromone updating strategy. The calculation of ants' transition probability also depends on the amount of pheromones we can detect. Thus in the ant colony algorithm, the pheromone update strategy is very important, since it determines the convergence speed of the algorithm.

In the basic ant colony algorithm, the pheromone update strategy can make sure that the corresponding pheromone concentrates in alignment with the path the ants chose, according to the edge weights that are unchanged after the ants accomplish a traversal.

In a time-dependent network, the edge weights are the functions of time, changing as the time changes. So a traditional pheromone update strategy cannot accurately reflect the corresponding pheromone alignment with the ants' choice of paths. Although this ant colony algorithm has a certain adaptability, and it can still lead to an optimal solution after several traversals, there is no doubt that it requires greatly increased computation time to do so.

Here we give a pheromone update strategy for an ant colony algorithm using a time-dependent network, so that we can accurately reflect the dynamic situation of the edge weights as well as the optimal solution of the chosen path.

$$\tau_{ij}(t+1) = \left[\ (1-\rho)\tau_{ij}(t) + \rho\Delta\tau_{ij} \ \right] * \lambda_{ij} \tag{6}$$

$$\lambda_{ij} = g_{ij}^{old} / g_{ij}^{new} \tag{7}$$

$$\Delta\tau_{ij} = \sum_{k=1}^{m} \Delta\tau_{ij}^{k} \tag{8}$$

$$\Delta\tau_{ij}^{k}=\begin{cases}\dfrac{Q}{L_k}, & \text{when ant k pass through the path ij}\\ & \text{between the time of t and t+1;}\\ 0, & \text{otherwise;}\end{cases} \tag{9}$$

g_{ij}^{old} and g_{ij}^{new} mean the time consuming on the road *(i,j)* before and after the update respectively.

Using this pheromone update strategy, the pheromone generated on each path after each traversal does not only reflect the optimal solution of the chosen path, but also the dynamic situation of the edge weights accurately.

The Optimal Individual Crossing Strategy

The basic ant colony algorithm leads both to the convergent solution and the local optimal one. In order to avoid such a situation, we combine the ant colony algorithm with a genetic algorithm. We first put the solution after each traversal together in the initial species, and then scanned the parents to see which ones had the same gene, and then chose the optimal gene among the gene pairs from the descendents which generated a single-point crossover in order to carry out their single-point crossovers.

This approach does not generate an unfeasible solution or enable a cross-operation with direction at the same time; not only can it speed up the convergence to a global optimal solution, but also helps avoid the local optimal solution to some extent.

The Steps of the Improved Ant Colony Algorithm

According to the improved strategy above, we propose the ant colony algorithm TDNACO, applying it to a time-dependent network. The details of this algorithm follows:

(1). At the beginning, every pheromone of the paths should be initialized by the following formula:

$$\tau_{ij}(0)=c \qquad (c \text{ is a constant}) \tag{10}$$

Set the iteration number at the same time;

(2). Put M ants on the initial node S;

(3). Calculate the transfer probability by the following formula:

$$p_{ij}^{k}(t)=\begin{cases}\dfrac{\left[\tau_{ij}(t)\right]^{\alpha}\left[\eta_{ij}\right]^{\beta}}{\sum_{l\in allow_k}\left[\tau_{il}(t)\right]^{\alpha}\left[\eta_{il}\right]^{\beta}}, & j\in allow_k\\ 0, & else\end{cases} \tag{11}$$

Where $tabu_k(k=1,2,...,m)$ means the cities that ant *k* has passed; $allow_k$ means the discrepancy between $tabu_k$ and the nodes connected with node *i* ; where $\eta_{ij}=g_{ij}(t)^{-1}$, $g_{ij}(t)$ is the time consumed on the path (v_i,v_j) when starting off at the moment *t*; then α, β shows how the pheromone and the inspiration information influence the ant's decision-making.

(4). If node *j* is not the destination node, then return to step 2, for a continued search; if *j* is the destination node, then ant *k* finds a path from the jumping-off point S to the destination, then identify the path and the time consumed as L_k.

(5). When all the M ants finish the searching task, there are M paths saved, and then the global update pheromone of each side is:

$$\tau_{ij}(t+1)=\left[\ (1-\rho)\tau_{ij}(t)+\rho\Delta\tau_{ij}\ \right]*\lambda_{ij} \tag{12}$$

$$\lambda_{ij}=g_{ij}^{old}/g_{ij}^{new} \tag{13}$$

g_{ij}^{old} and g_{ij}^{new} mean the time consumed on the path *(i,j)* before and after the update respectively.

$$\Delta\tau_{ij}=\sum_{k=1}^{m}\Delta\tau_{ij}^{k}, \tag{14}$$

$$\Delta\tau_{ij}^{k}=\begin{cases}\dfrac{Q}{L_k}, & \text{when ant k pass through the path ij}\\ & \text{between the time of t and t+1;}\\ 0, & \text{otherwise;}\end{cases} \tag{15}$$

ρ means the extent of the fading of the pheromone, $0<\rho<1$. $\Delta\tau_{ij}$ is the pheromone increment belonging to the path *ij*. *Q* is a constant, L_k is the length of the time consumed on the path from the starting point to the destination that ant *k* has passed.

(6). The M solutions need to be calculated as hybridized with each other; if the time consumed on the path is less than the result after hybridization, then the new path should replace the old one, and the pheromone should be updated for every corresponding path.

(7). Get the local optimal solution from the M solutions above according to the formula 16:

$$L_{k_{min}} = \min(L_k), (k = 1, ..., m) \quad (16)$$

(8) The minimal optimal solution from all the local solutions is the global optimal solution until now:

$$L_{min} = \min(L_{k_{min(l)}})(l = 1, 2, ..., \text{the current number of iterations}) \quad (17)$$

(9) If the number of iterations still does not reach the set number, then exit the procedure; otherwise add the number of iterations with one, then go to step 2.

THE SIMULATION RESULTS

To verify the algorithm, we needed to set up a topology network including 40 cities, and then calculate the edge weights with the TDNACO algorithm and the ACO algorithm. To simulate the actual situation of the change of the edge weights in the dynamic network, we needed to establish an independent thread, and then modified the weights randomly at a certain range every fixed time. The simulation results show that using the algorithm TDNACO makes it easier and faster to get the optimal solution than using the algorithm ACO with the same number of iterations. The simulation results are shown in Table 1.

Table 1. Simulation Results.

	TDNACO	ACO
Number of cities	40	40
Initial number of ants	8	8
Number of iterations	160	160
A	2	2
B	2	2
P	0.3	0.3
Q	1	1
Changing frequency of weights (ms)	5	5
Probability of optimal solution (%)	100	91
Average time of getting the solution (ms)	59.06	99.74

CONCLUSIONS

The research into the shortest path problem in time-dependent networks has increased practical value here, using an improved pheromone update strategy. Under this strategy, the residual pheromone of each path can accurately reflect the change of weighted value of each, as well as the optimal choice of the shortest path. Based on this improved strategy, an improved ant colony algorithm for the shortest path problem in time-dependent networks has also been presented here. The simulation results show that the algorithm TDNACO offers an easier and faster process to get the optimal solution than does the algorithm ACO with the same number of

iterations.

ACKNOWLEDGEMENT

This work was funded by the National Science Foundation of China (60879024, 60872062).

REFERENCES

Chen, L., Liu, J., and Yanan, L. (2007). "An Ant Colony Algorithm with Crossover Operators for the Shortest Path Problem in Dynamic Networks." *J. Computer Engineering & Science*, 2007, 29(5):81-82.

Dorigo M., Caro, G. D., and Gambardella, L. M. (1999). "Ant Algorithms for Discrete Optimization." *J. Artificial Life*, 1999, 5 (2):137-172.

Hall, R. W. (1986). "The Fastest Path through a Network with Random Time-Dependent Travel Time." *J. Transportation Science*, 1986, 20 (3):182-188.

He Hong, Zhu Daming, and Ma Shaohan (2004). "A New Algorithm for the Shortest Path Compution by Neural Networks on Time-Dependent Networks." *J. Journal of Fudan University (Natural Science)*, 2004, 43 (5):714-716.

Liu, J., and Liu, F. (2004). "The Optimum Route Algorithm for Dynamic Network Based on Genetic Algorithms." *J. Journal of Information Engineering University*, 2004, 5 (3):14-18.

Tan Guozhen and Gao Wen (2002). "Shortest Path Algorithm in Time-Dependent Networks." *J. Chinese Journal of Computers*, 2002 ,25 (2) :165-172.

Intelligent Emergency Traffic Evacuation Spatial Decision Support System for Urban Disasters

Zhichong Zou[1] and Yaowu Wang[2]

[1] Research Institute of System Engineering, School of Management, Harbin Institute of Technology, P.O. Box: 1423, Harbin City, Fayuan Street No. 13, PH: +86-451-86402180, Email: zouzhichong@sina.com
[2] Research Institute of System Engineering, School of Management, Harbin Institute of Technology, P.O. Box: 1423, Harbin City, Fayuan Street No. 13, PH: +86-451-86402180, Email: ywwanghit@vip.163.com

ABSTRACT

Extreme emergencies, whether caused by man or natural disasters, increasingly threaten urban life. Emergency traffic evacuation management is a complex procedure that includes routing evacuees, identifying exits, and designing traffic control. The evacuation routing models are vital to the evacuation planning problem. Real-time traffic evacuation management has become an increasingly attractive research topic, as a result of the rapid development and wide-spread deployment of a large number of applications for traffic data collection, processing, and dissemination.

In this paper we extend our existing work on developing Intelligent Emergency Traffic Evacuation System (IETES) as a spatial decision support system based on Exploratory Spatial Data Analysis (ESDA) technology for urban disaster environment traffic control. The IETES has been enhanced with the Dynamic Traffic Assignment (DTA) model and Real-time Evacuation Algorithm (REA) to solve emergency traffic resource distribution and dynamic existing problems. ESDA performs spatial traffic data mining and data analysis functions from urban Geographic Information System (GIS) databases to set up relation links between dynamic traffic flows and varying disaster environment, which could improve DTA and REA efficiencies. An inference engine designed on rules and cases could make IETES capable of thinking, learning, and decision supporting.

1. INTRODUCTION

Dynamic traffic assignment (DTA) models traditionally require a deterministically known time-dependent origin-destination (OD) demand matrix. However, traffic demand is rarely known in advance with certainty. At any given point in time, information is available on past and current demand levels (if a good monitoring system is in place), but future demands can, at best, only be probabilistically forecasted. However, notwithstanding this uncertainty, decisions need to be made on investment alternatives, traffic management, and control.

This paper focuses on the control of dynamic traffic systems through the development and real-time adaptations of the optimal routes for vehicles, when the OD demand is uncertain. Often, a single value for OD demand is employed for network analysis. However, if the goal of a particular DTA application is to develop route guidance and a certain demand level was used to develop an a priori path set, it

is unclear what action should be taken when predicted demand is not realized (Peeta and Ziliaskopoulos, 2002). It becomes necessary to design approaches that account for demand uncertainty and develop more comprehensive solutions that are less likely to fail under these extreme events and potentially reduce the variance of costs. The linkage between dynamic traffic flows and the environment is uncertain. How to discover the linkage for potential demand in uncertain and various extreme surroundings, the spatial decision support system with ESDA techniques maybe a possible solution.

2. DYNAMIC TRAFFIC ASSIGNMENT MODEL

The basic relationships of the cell transmission model that describe the propagation of traffic flow can be found in Daganzo (1994, 1995). The DTA model developed based on these relationships can be found in Ziliashopoulos (2000) and it is presented next for completeness. Table 1 summarizes the notations used in this model.

Table 1. Notation in Deterministic Model

SYMBOL	DESCRIPTION
k	Density
C	The set of cells: diverging cells(C_D), Merging cells(C_M), source cells(C_R) and sink cells(C_S)
T	The set of discrete time intervals
x_i^t	Number of vehicles in cell i at time interval t
N_i^t	The maximum number of vehicles in cell t at time interval t
y_{ij}^t	The number of vehicles moving from cell i to cell j at time interval t
E	The set of cell connectors: ordinary cell connectors(E_O), merging cell connectors(E_M), diverging cell connectors (E_D), source cell connectors(E_R), and sink cell connectors(E_S)
Q_i^t	The maximum number of vehicles that can flow into or out of cell i during time interval t
δ_i^t	The ratio v/w for each cell and time interval
$\Gamma(i)$	The set of successor cells to i
$\Gamma^{-1}(i)$	The set of predecessor or cell to cell i
d_i^t	The demand (inflow) at cell i in time interval t

$$\text{Minimize} \quad \sum_{\forall t \in T} \sum_{\forall i \in C/C_s} x_i^t \tag{1}$$

$$\text{Subject to:} \quad x_i^t - x_i^{t-1} - \sum_{k \in \Gamma^{-1}(i)} y_{ki}^{t-1} + \sum_{k \in \Gamma^{-1}(i)} y_{ij}^{t-1} = 0 \qquad \forall i \in C \setminus \{C_R, C_S\}, \forall t \in T, \tag{2}$$

$$y_{ij}^t - x_i^t \le 0, \quad y_{ij}^t \le Q_i^t, \quad y_{ij}^t \le \delta_j^t x_j^t \le \delta_j^t N_j^t \quad \forall (i,j) \cup E_O \quad \forall t \in T, \tag{3}$$

$$y_{ij}^t - x_i^t \le 0, \quad y_{ij}^t \le Q_i^t, \quad \forall (i,j) \quad E_S, \forall t \in T, \tag{4}$$

$$y_{ij}^t \le Q_j^i, \quad y_{ij}^t + \delta_j^t x_j^t \le \delta_j^t N_j^t \quad \forall (i,j) \quad E_D, \forall t \in T, \tag{5}$$

$$\sum_{\forall j \in \Gamma(i)} y_{ij}^t - x_i^t \le 0, \quad \sum_{\forall j \in \Gamma(i)} y_{ij}^t \le Q_i^t \quad \forall i \in C_D, \quad t \in T, \tag{6}$$

$$y_{ij}^t - x_i^t \le 0, \quad y_{ij}^t \le Q_i^t \quad \forall (i,j) \quad E_M, \forall t \in T, \tag{7}$$

$$\sum_{\forall i \in \Gamma^{-1}(i)} y_{ij}^t \le Q_i^t, \quad \sum_{\forall i \in \Gamma^{-1}(i)} y_{ij}^t + \delta_j^t x_j^t \le \delta_i^t N_j^t \quad \forall j \in C_M, \forall t \in T, \tag{8}$$

$$x_i^t - x_i^{t-1} + y_{ij}^{t-1} = d_i^{t-1}, \quad j \in T(i) \quad \forall i \in C_R, \forall t \in T, = x_i^0 \quad \forall i \in C, \tag{9}$$

$$y_{ij}^0 \quad \forall (i,j) \in E, \tag{10}$$

$$x_i^t \ge 0 \quad \forall i \in C, \forall t \in T, \tag{11}$$

$$y_{ij}^t \geq 0 \quad \forall (i,j) \in E, \forall t \in T, \tag{12}$$

Note that the boundary conditions consist of the states of the sink and source cells and the initial value x_i^0 of all cells $i \in C$, The sink cells are set to have infinite capacities ($N_i^t = \infty \quad \forall i \in C_S, \forall t \in T$) and allow infinite input flows ($Q_i^t = \infty \forall i \in C_S, \forall t \in T$). Thus, their occupancies are not constrained. The input flow to a sink cell will be determined by the state and characteristics of its predecessor cell. The source cells have infinite capacity ($N_i^t = \infty \forall i \in C_R, \forall t \in T$) but finite output flow. The basic relationship of the source cells is as follows:

$$x_i^t = x_i^{t-1} + d_i^{t-1} - y_{ij}^{t-1}, \quad j \in \Gamma(i) \forall t \in T,$$

Where d_i^t is the demand (inflow) at cell i in time interval t. The initial values x_i^0 can be set to initial traffic conditions in the network at the beginning of the time period of interest. In the following section, we relax the assumption of determinism d_i^t and instead we treat it as a random variable with known probability distribution. In general, for both planning and operational applications, it is unclear what action should be taken or what the cost is, when the forecasted demand is not realized.

It becomes necessary, therefore, to develop a systematic way of accounting for uncertain demand and to develop a more comprehensive solution, which is more likely to withstand extreme events. One such possibility is to run the deterministic model with a large number of randomly generated demand patterns, and to infer some rules and principles from results. Such an approach has been proposed by Peeta and Zhou (1999) to produce comprehensive DTA solutions. The only drawback with this approach appears to be the computational requirements of a single DTA run and the enormous amount of scenarios that need to be run to produce meaningful results and inferences.

3. EXPLORATORY SPATIAL DATA ANALYSIS MODEL

Data mining, or knowledge discovery in a database, is a technique of analyzing data to discover previously unknown information. The goal is to reveal regularities and relationships that are not easily found. This is accomplished through an analysis of the patterns that form in the data. Various algorithms have been developed to perform this analysis. Spatial data mining differs from regular data mining in conjunction with the differences between non-spatial data and spatial data. The attributes of a spatial objects stored in database may be affected by the attributes of neighbor objects. In addition, spatial location, and implicit information about the location of objects, may be the exact information extracted by spatial data mining.

Many spatial data mining methods are used for knowledge discovery from the GIS database. Compared with other methods, Exploratory Spatial Data Analysis (ESDA) technology is more suitable for IETES. ESDA technology matured from computational geography. Essential to ESDA is a kind of “data drive” analysis method. It put emphasis on spatial relations and differences of data. Null hypothesis is ESDA technology’s application condition. ESDA technology includes spatial weight matrix, variation chat, and spatial relation analysis technology. They are introduced as the following:

The definition of spatial weight matrix is the key difference between spatial

statistics and traditional statistics. That is also the foundation of utilizing ESDA. The goal of establishing a spatial weight matrix is to definite spatial objects' adjacent relationships. The formula of spatial weight matrix is as:

$$\mathbf{W} = \begin{bmatrix} W_{11} & W_{12} & \cdots & W_{1n} \\ W_{21} & W_{22} & \cdots & W_{2n} \\ \cdots & \cdots & \cdots & \cdots \\ W_{m1} & W_{m2} & \cdots & W_{mn} \end{bmatrix} \tag{13}$$

Adjacent rule of above matrix (where i=1, 2, …, n; j = 1, 2, …, m):

$$W_{ij} = \begin{cases} 1 & \text{Position of } i \text{ is adjacent to that of } j; \\ 0 & \text{Position of } i \text{ is not adjacent to that of } j. \end{cases} \tag{14}$$

If we define distance "d" between two objects is the adjacent range, the rule will be:

$$W_{ij}(d) = \begin{cases} 1 & \text{Distance of } i \text{ and } j \le \mathrm{d}; \\ 0 & \text{Distance of } i \text{ and } j > \mathrm{d}. \end{cases} \tag{15}$$

Two rules mentioned above can be used together and separately. If two objects are not at adjacent physical position, but they are related closely, usually we regard they are neighbors. The spatial weight matrix is a prejudgment of spatial objects' relations.

Variation chat reflects the relations and changing trend of spatial data. Connotative knowledge can be discovered through variation chats. Theory variation chat, experimental variation chat, and cloud variation chat are often used in spatial data mining. Theory variation chat is presented as:

$$\gamma(h) = \frac{1}{2} E\left[\left(Z(x) - Z(x') \right)^2 \right] \tag{16}$$

x is an observation position, and x' is the other adjacent observation position. Further more $h = x' - x$ means the distance between the pair of observation position x and x'. Function $Z(x)$ is the value of target point Z at position x. So the theory variation $r(h)$ describes position relations of point Z at distance h.

To discover spatial objects' distribution mode, spatial relation analysis technology is be used. It includes Moran Iand Geary C statistics. Those are all core concepts of ESDA technology.

Moran I model has the definition of:

$$I(d) = \frac{\sum_{i}^{n} \sum_{j \neq i}^{n} w_{ij} (x_i - \bar{x})(x_j - \bar{x})}{S^2 \sum_{i}^{n} \sum_{j \neq i}^{n} w_{ij}} \tag{17}$$

Here $S^2 = \frac{1}{n} \sum_{i}^{n} (x_i - \bar{x})^2$, x_i means target observe value at position i. $\bar{x} = \frac{1}{n} \sum_{i=1}^{n} x_i$; w_{ij} is the spatial weight value.

The Moran I model can be used to measure spatial relativity to discover differences and relationships of observation. When observation values are adjacent within some distance "d", Moran I is prominent and positive. When they are not adjacent, it is negative. When the observation values distribute at random, Moran I is null.

Geary C model always included positive distribution in asymmetry. The model is as follows:

$$C(d) = \frac{(n-1)\sum_{i}^{n}\sum_{j}^{n} w_{ij}(z_i - z_j)^2}{2nS^2\sum_{i}^{n}\sum_{j}^{n} w_{ij}} = \frac{(n-1)}{2n^2}\sum_{i}^{n} C_1(d) \tag{18}$$

Assume Geary C statistics are the model average value. When there is no spatial correlation that value is 1. Low and prominent value (0, 1) indicates positive spatial correlation. High and Prominent value (>1) indicates negative spatial correlation (Cliff A D 1981).

4. IETES ESDA PROCEDURE

The goal of knowledge discovery is to find out hidden information from a mass of problems to help urban planning. Connotative knowledge can be discovered from a GIS database by ESDA technology. The general process of knowledge discovery by ESDA in data manager module is running like a loop (Fig. 1), which is called an Artificial Intelligence Learning Loop.

The loop is composed of three steps. The first step is called "needed connotative knowledge confirmation" based on null hypothesis. It determines whether we could find out useful information from raw data, and what kind of information could be discovered. It is the only constraint to stop the loop. IETES provides an interface program for users' interference.

The second step is the process of data mining is combined in two consecutive parts, discovery scope definition and ESDA performance. Discovery scope definition could be executed by GIS database filter with running general attribute mining programs. It aims at providing a definite spatial data mining scope matched with a problem description for ESDA. Within a definite scope and given environment, the ESDA program could perform spatial data mining process in a GIS database for knowledge discovery.

The last step of the loop is verifying results. Knowledge discovered by ESDA engine is unilateral and lacking in experience accumulation, so it is too rough to solve problems. According to planners' experiences and stored knowledge in the knowledge base, the raw results should be verified. New knowledge brings new understanding of those problems. The learning loop needs another run for further discovery. The loop would meet its end until the problems are solved or no more new discoveries could be found. Usually the loop would be stopped after several cycles according to the complexity of the problems.

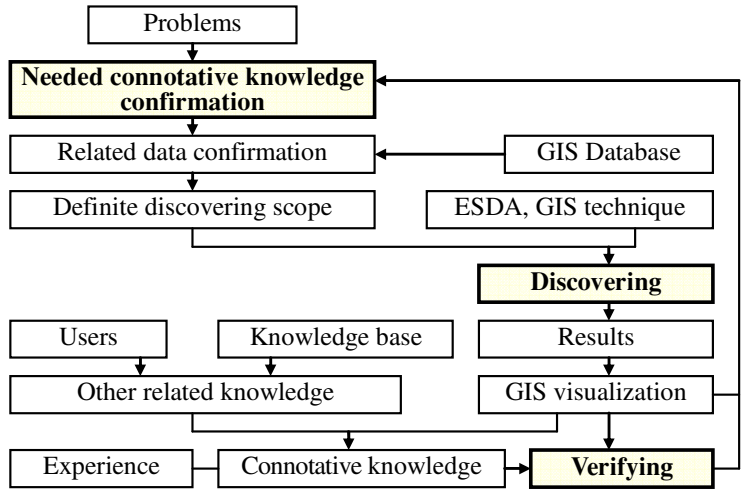

Figure 1. Framework of discovering knowledge from GIS database

There are two kinds of inference modes of IETES. One is based on rules and the other is based on cases. Inference based on rules indicates the action of deriving logical conclusions from regulations known or assumed to be true. The general idea of inference based on rules is setting up communications between the GIS database and knowledge base. Usually rules inference and cases inference (structure analysis and case models) work together for decision supporting and knowledge expression. A working mechanism of inference based on rules and cases is shown in Figure 2.

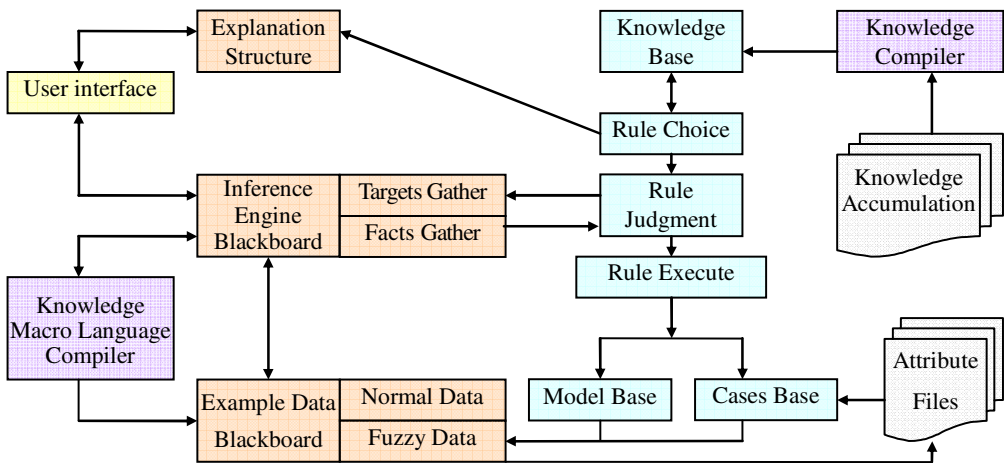

Figure 2. Working Mechanism of Inference Based on Rules and Cases in IETES

6. CONCLUSION

A combination of DTA and ESDA provides a reliable approach to solve temporal-spatial related problems for emergency traffic control. We developed an intelligent system, IETES, to perform an automatic procedure for emergency decision supporting. Real-time traffic flows' temporal-spatial relations could be discovered from the GIS database by the ESDA module in IETES. Such a relation makes it possible for the DTA module to fulfill traffic resource distribution for emergency use. Inference engines based on cases and rules endow IETES with the

capability of thinking like humans. As an intelligent system, IETES could "learn" from cases and "remember" by accumulating discovered knowledge.

REFERENCES

Daganzo, C.F., (1994). "The cell transmission model: a simple dynamic representation of highway traffic consistent with the hydrodynamictheory." Transportation Research 28B (4), 269–287.

Daganzo, C.F., (1995). "The cell transmission model, part II: network traffic". Transportation Research 29B (2), 79–93.

Peeta, S., Ziliaskopoulos, A., (2002). "Fundamentals of dynamic traffic assignment: the past, the present and the future." Networks and Spatial Economics 1:2, 201–230.

Peeta, S., Zhou, C., (1999). "Robustness of the off-line a priori stochastic dynamic traffic assignment solution for on-line operations". Transportation Research 7C (5), 281–303.

Ziliaskopoulos, A.K., (2000). "A linear programming model for the single destination system optimum dynamic traffic assignment problem". Transportation Science 34, 1–12.

Estimation of Original-Destination Matrices for Public Traffic Passenger Flow

Zhang Jian[1], Li Wenquan[2] and Zhao Jinhuan[3]

[1]School of Transportation, Southeast University, No.2 Sipailou, Nanjing 210096, P. R. China; email: jianadamzhang@gmail.com
[2]School of Transportation, Southeast University, No.2 Sipailou, Nanjing 210096, P. R. China; PH: +86-25-83795647, email: wenqli@seu.edu.cn
[3]School of Transportation, Southeast University, No.2 Sipailou, Nanjing 210096, P. R. China; email: zhaojinhuan2003@163.com

ABSTRACT

In this paper, the estimation of origin-destination (OD) matrices for public traffic passenger flow is given. As the basis of transit scheduling, more accurate OD matrices mean more scientific operations and more rational utilization of staff and vehicles. In order to improve the estimation precision, characteristics of a passenger's trip, land use around bus stops, and transferring function are considered. Kolmogorov-Smirnov (K-S) Test method is adopted to analyze the trip stops. The result shows that it follows a Poisson distribution. According to passengers boarding and alighting, the OD estimation based on the trip's character is present. Attracting coefficient and weight are employed to estimate the OD matrices based on the land use around the stops. The stop significant coefficient, which relates to the route number of stations as starting, ending and midway, is also proposed to estimate the OD matrices based on transferring function. Analytic hierarchy process (AHP) is used to combine these three factors, and the last OD matrices are gained. Real data are applied to test the estimation methodology. Good agreement between predicted and observed matrices is found, and the results prove that the method is feasible to heighten accuracy.

INTRODUCTION

Large scale direct sampling of passenger OD is costly and it is prone to biases and errors. The estimate of OD matrix is an essential source of traffic demand information for most transit planning processes, and for the management and control of the transit system. A good deal of models and methods have been researched for the estimation of OD matrices in road networks, but to our knowledge, not many papers on the problem of transit passenger OD estimation had been presented in literature. Notable examples include the paper by Lam et al. (2003), who investigated the transit passenger OD estimation problem in congested transit networks where updated passenger counts and outdated OD matrices are available. Li and Cassidy (2007) presented an algorithm to generate estimates based upon passenger boarding and alighting counts at each stop along a route. In the statistical approach, Cascetta and Nguyen (1988) presented a broad review of statistical estimation procedures for the OD matrix, including maximum likelihood and Bayesian estimation. Wong and

Tong (1998) presented a maximum entropy estimator.

However, all the above studies had not considered using the land around bus stops and transferring function, even though both are important. The flow's character is analyzed by K-S Test method. AHP is introduced to combine the above three factors and to obtain the last OD matrices estimation. The scope of this paper is eminently practical, and this paper is organized as follows. In Section 2, on the basis of the surveyed data, the trip's character was drawn. Some useful concepts and notations are proposed. Section 3 describes the estimation formulation. A case study is provided in Section 4 and the conclusions are given in Section 5 together with suggestions for further studies.

PREPARATIONS

Distribution of trip. The survey route is 212 Road in Changzhou. It has fourteen stops. Taking one trip as an example (as shown in **Table 1**), it is analyzed by the single sample Kolmogorov-Smirnov test (K-S test), and the results are shown in **Table 2**.

Table 1. Statistics for passengers and stops

Stop	1	2	3	4	5	6	7	8	9	10	11	12	13	14
Counts	6	8	13	16	14	10	4	8	5	2	3	3	2	1

It is well known that the traveler's distance is similar to following a normal distribution. It means that most of the travel time between origin and destination are concentrated in an area. Passengers, who travel by bus, get off the bus at one stop at the biggest probability, after having traveled a certain number of stops.

Table 2. K-S test result

		Data
Sample Size		95
Parameters of Poisson Distribution	Average	5.4842
Difference	Absolute Value	0.093
	Positive	0.093
	Negative	-0.070
Test Statistics		0.903
P Value		0.389

From **Table 2**, the value of P is 0.389, which is far larger than 0.05, and so it is accepted that the stops of trip follows a Poisson distribution.

Land use around stops. It is well known that different land uses correspond to different trip products and attractions. We quantitated the land use around stops by using boarding and alighting counts. As is eminently practical, there are seven classes of land use: living space, public facilities (including office administration, health, education, etc.), commercial space, industrial space, external traffic (railway stations, bus stations, etc.), streets and squares (parking, etc.), and others (Dou, 2006). Moreover, in urban public transit, work or school passengers are the majority, so attracting coefficients of living and industrial space are defined as one (as shown in

Table 3). Different routes have different attracting coefficients of any class, but the method of quantification is not change.

Table 3. Attracting coefficients of every land use

id	1	2	3	4	5	6	7
Land Use	Living	Public Facilities	Commercial Space	Industrial Space	External Traffic	Streets, Squares	Others
Coefficients	1.0	0.7	1.1	1.0	1.2	0.8	0.6

Transferring function. Generally, the more routes at a stop, the bigger possibility of transferring at the stop, and the more passengers attracted. It also means that, the larger scale of the stop, the more passengers.

FORMULATION

Maximum entropy (ME) method is adopted, for it is the best among the methods such as generalized least square method, maximum likelihood method, and information minimizing method (Chen et al., 2003; Liu et al., 2007). Suppose we have OD matrices along a route with *n* stops. Let $O(i)$ be the number of passengers boarding at the stop i. $X_1(i,j)$ is denoted as the OD matrix based on characters of passenger flow. The simultaneous probability of OD traffic flow is W, as follows, $W(X_1(i,j)) = X_1(i,j) * X_1(1,2)^{x_1(1,2)} * X_1(1,3)^{x_1(1,3)} \cdots * X_1(n-1,n)^{x_1(n-1,n)} / \prod_{i,j} X_1(i,j)!$, where $x_1(i,j)$ was surveyed. Because $\max W(X_1(i,j))$ equals to $\max \ln W(X_1(i,j))$, applying the Stirling's Formula: ln X!=XlnX-X, we get the mathematical model as follows,

$$\begin{cases} \max \ln W(X_1(i,j)) = -\sum_i \sum_j (X_1(i,j) \ln X_1(i,j) / x_1(i,j) - X_1(i,j)) \\ s.t. \quad \sum_i \sum_j X_1(i,j) P_k(i,j) = V_k, k = 1,2,...,2(n-1) \\ V_k = \sum_{j=i+1}^{n} X_1(i,j), k = 1,2,...,n-1 \\ V_k = \sum_{i=1}^{j-1} X_1(i,j), k = n, n+1,...,2(n-1) \end{cases},$$

and $P_k(i,j)$ is the coefficient correspond to V_k. Applying the method of Lagrangian Multipliers, we obtain the maximum entropy estimate of $X_1(i,j)$ as

$X_1(i,j) = x_1(i,j)\prod_k (\lambda^k)^{p_k(i,j)}$, where $\lambda^k = \exp(-\mu^k)$, μ^k is the Lagrangian operator.

$$V_k = \sum_i \sum_j [x_1(i,j)\prod_k (\lambda^k)^{p_k(i,j)}]P_k(i,j)$$

We adopt the solution presented by Liu (2007), because of the solution's simpleness and accuracy. For stop j, let S_{jl} be the land area of l ($l = 1,2,...,7$), and let X_l be the attracting coefficients. The attracting weight of stop j (Z_j) could be calculated. Let $X_2(i,j)$ be the OD matrix based on the land use around stops. $X_2(i,j) = O(i)Z_j / \sum_{i+1}^{m} Z_j = O(i)\sum_l S_{jl}X_l / \sum_{i+1}^{m}\sum_l S_{jl}X_l$, where $O(i) = \sum_{j=i+1}^{n} X_1(i,j)$. It is assumed that there are n_{1j} midway routes, n_{2j} starting routes, and n_{3j} ending routes at stop j. And the weight of j stop scale is defined as $T_j = n_{1j} + \lambda_1 n_{2j} + \lambda_2 n_{3j}$. λ_1, λ_2 are respectively given the coefficient as starting and ending stop).Let $X_3(i,j)$ be the OD matrix based on transferring function.

$$X_3(i,j) = O(i)T_j / \sum_{i+1}^{m} T_j = O(i)(n_{1j} + \lambda_1 n_{2j} + \lambda_2 n_{3j}) / \sum_{i+1}^{m}(n_{1j} + \lambda_1 n_{2j} + \lambda_2 n_{3j})$$

How to get a feasible OD matrix integrating the three factors? AHP is adopted. The last OD matrix is $X(i,j) = \eta_1 X_1(i,j) + \eta_2 X_2(i,j) + \eta_3 X_3(i,j)$.

By investigation from relevant experts, we give the three factors' impact coefficients, as follow:

$$A_1 = \begin{pmatrix} 1 & 3 & 3 \\ 1/3 & 1 & 1 \\ 1/3 & 1 & 1 \end{pmatrix}; A_2 = \begin{pmatrix} 1 & 2 & 7/3 \\ 1/2 & 1 & 8/5 \\ 3/7 & 5/8 & 1 \end{pmatrix}$$

Table 4. Combination coefficients

Characters of Passenger Flow η_1	Land Use Around Stops η_2	Transferring Function η_3
0.5570	0.2430	0.200

Consistency of the above two matrices' is tested by AHP, and the combination coefficients are shown in Table 4. In order to check the effectiveness of estimation,

ER is introduced (Eq. 10), and its value is between zero and one. The smaller theER's value, the better fit between estimation and measure. $x(i, j)$ is the measured number of passenger who board at stop i for stop j.

$$ER = \sqrt{\sum_i \sum_j (x(i,j) - X(i,j))^2} \,/\, (\sqrt{\sum_i \sum_j x^2(i,j)} + \sqrt{\sum_i \sum_j X^2(i,j)})$$

NUMERICAL EXAMPLE

Take 20 Road of Changzhou as an example (Chen Xuewu, 2008), one trip (start from 7:30 a.m., down direction) was surveyed. The data of 21 stops' boarding and alighting counts are shown in **Table 5**, and the results are shown in **Table 6**.

Table 5. Original data

Stop	1	2	3	4	…	18	19	20	21
Boarding	33	51	22	17	…	2	1	0	0
Alighting	0	2	1	3	…	9	7	12	25
Attractive weight(km^2)	0.648	0.792	0.723	0.651	…	0.567	0.617	0.691	0.523
midway	0	19	1	23	…	2	2	1	0
starting	11	0	0	0	…	0	0	0	5
ending	11	0	0	0	…	0	0	0	5

Table 6. Estimate OD matrix

OD	2	3	4	5	6	…	17	18	19	20	21	Boarding
1	2	1	2	4	2	…	6	1	1	0	3	33
2	0	0	1	1	1	…	5	1	0	4	1	51
3	0	0	0	0	2	…	1	5	1	1	0	22
4	0	0	0	0	1	…	4	4	1	0	2	17
5	0	0	0	0	0	…	1	3	1	1	1	14
…	…	…	…	…	…	…	…	…	…	…	…	…
16	0	0	0	0	0	…	0	1	2	2	0	5
17	0	0	0	0	0	…	0	0	1	1	1	3
18	0	0	0	0	0	…	0	0	0	0	2	2
19	0	0	0	0	0	…	0	0	0	1	0	1
20	0	0	0	0	0	…	0	0	0	0	0	0
Alighting	2	1	3	5	6	…	39	15	7	12	25	294

Estimate OD matrix and survey OD matrix (as shown in **Table 7**) are compared and the error comparison is calculated (as shown in **Table 8**).

Table 7. Survey OD matrix

OD	2	3	4	5	6	…	17	18	19	20	21	Boarding
1	2	1	2	3	2	…	6	1	1	0	3	32
2	0	0	2	1	1	…	7	1	0	4	1	48
3	0	0	0	0	2	…	1	5	1	1	0	22
4	0	0	0	0	1	…	4	4	1	0	2	16
5	0	0	0	0	0	…	3	3	1	1	1	14
…	…	…	…	…	…	…	…	…	…	…	…	…
16	0	0	0	0	0	…	0	1	2	2	0	5
17	0	0	0	0	0	…	0	0	1	1	0	2
18	0	0	0	0	0	…	0	0	0	0	2	2
19	0	0	0	0	0	…	0	0	0	1	0	1
20	0	0	0	0	0	…	0	0	0	0	1	1
Alighting	2	1	4	4	6	…	38	18	12	12	24	301

Table 8. Error comparison of estimate and survey

	Characters of Passenger Flow	Land Use Around Stops	Transferring Function	Combination
ER (%)	18.32	28.17	39.65	9.24

CONCLUSIONS

In this paper, three factors are considered separately in advance, and then are integrated by AHP. A real example shows that the combination has a better result. It proves that the proposed method could indeed improve the estimation accuracy. However, some parameters are required to be investigated by the expert. The researchers will have a further study on the scientific decision of parameters' value.

ACKNOWLEDGMENTS

The work is supported by the National High Technology Research and Development Program of China (No.2007AA11Z210) and the National Key Technology Research and Development Program (No.2006BAJ18B03).

REFERENCES

Cascetta, E., Nguyen, S. (1988). "A unified framework for estimating or updating origin/destination matrices from traffic counts." *Transportation Research B*, 437–455.

Chen Xuwu (2008). "Optimization of the public transportation network in Changzhou city." *Guide to optimization technology of public transit network*

Chen Senfa, Zhou Zhenguo, Yu Donghua (2003). "Theory and applications of dynamic OD matrix estimation algorithm." *Journal of Southeast University(Natural Science Edition)*, 33(1), 106-110.

Dou Qingfeng (2006). "Prediction Research about Public Transit Passenger Volume of Urban in Chongqing City." *.Xi'an University of Architecture*, 8, 22-24.

Liu Cui, Chen Hongren (2007). "Study on OD Matrix Estimation of Transit

Passenger Flows." *Urban Transport of China*, 5(4), 81-84.

S. C. Wong, C. O. Tong (1998). "Estimation of Time-dependent Origin-Destination Matrices for Transit Networks." *Transportation Research 32*(1), 35-48.

William H. K. Lam, Z. X. Wu, K. S. Chan (2003). "Estimation of Transit Origin–Destination Matrices from Passenger Counts Using a Frequency-Based Approach." *Journal of Mathematical Modelling and Algorithms*, 2, 329-348.

Yuwei Li, Michael J. Cassidy (2007). "A generalized and efficient algorithm for estimating transit route ODs from passenger counts". *Transportation Research B* 41, 114–125.

New Methods for Research in Multi-Agent Traffic Signal Control

Wu Qian-jiao[1]and Lan Rong[2]

[1] School of Information Engineering, Chang'an University, Central Section of the South 2nd Ring Road, Xi'an,710064,China; PH(86)029-82334956; FAX(86)029-82334357;mail:qjwu@chd.edu.cn
[2]School of Economics and Finance, Xi'an Jiaotong University, Xian 710064, China;email:wu_lan@mail.xjtu.edu.cn

ABSTRCT

Urban traffic control is a large and complex system. When traffic congestion occurs it generally cannot be resolved by the workings of a single intersection. Using a multi-agent system to set up a traffic control framework, we can simulate different control strategies. We have defined different kinds of traffic-control-agent classes while researching the interactions and dynamic adapting mechanism among agents. Utilizing self-organization and sliding window skills, we have designed an effective congestion control mechanism. In simulating the traffic environment, we obtained a valuable experimental result.

INTRODUCTION

The goals of an intersection's traffic signal include maximum traffic capacity, a shorter average delay, shorter length of waiting in queue, and so on (He et al, 2002, Wang et al, 2006,Wen et al, 2001). When traffic congestion occurrs, it generally cannot be resolved by the workings of a single intersection. A systemized approach is necessary, in order to analyze and describe a traffic system and then work out ways to control an ongoing traffic problem. To do so, we need to use a better research method than the class idea. As a result of the development of computing technologies, artificial evaluation systems based on multi-agents have proven to be an effective choice to analyze and control complex traffic systems (Zheng et al, 2006).

In this paper, both traffic control architecture and the coordination mechanism are determined by the agents. Using this framework, an intersection is defined as an intersection agent, and the road section is described as a road segment agent. Therefore, different kinds of agents and the relationship among them have mapped a complex traffic network. Under normal traffic conditions, the relationship between agents is light, but when an abnormal situation appears to affect one agent, it may either be resolved by itself or it may need the help of other, connected agents. Depending on the specifics of each incident and its effects, we have set up a self-organizing system to adjust to and address the problem.

THE TRAFFIC AGENT MODEL

First, some definitions follow in order to make this process clear.

Definition 1: Under ideal conditions, the speed of a vehicle is the constant v_0 while passing through the intersection, its passing time is t0, and t0 is decided by

$T0=S/V_0$

And *s* is the distance through the intersection, as shown in Figure 1.

This indicates that no delays exist when the vehicle passes through the intersection.

If a vehicle slows-down from v_0 to v_i while passing through an intersection, the vehicle's delay time is t_d, which is decided by formula (1); if there is a traffic queue, the vehicle's waiting time is t_w while waiting at the red light.

$$t_d = \begin{cases} 0 \quad ; \ v = v_0 \\ 2*((v_0+v_i)/(v_0-v_i))*(s/v_0) \quad ; \ a = (|v_i - v_0|)/t \quad is \quad cons\tan t \\ 2*(v_0+v_i)/(v_0-v_i)*(s/v_0)+(n*(d_s+d_v)+s)/v_0+t_w \quad ; \end{cases} \tag{1}$$

Where n is number of waiting vehicles in the queue, d_s is their inter-vehicle distance, and d_v is the standard length of each vehicle.

Definition 2: The length of a waiting queue q(t) is decided by the formulation (2)。

$$q(t+\Delta t) = \begin{cases} q(t)+u_a(\Delta t)*\Delta t - v_a(\Delta t)*\Delta t \quad , green \quad time \\ q(t)+u_a(\Delta t)*\Delta t \quad , red \quad time \end{cases} \tag{2}$$

Where $u_a(t)$ denotes a vehicle's speed of arrival at the intersection, $v_a(t)$ denotes a speed of departure from the intersection, and q (t) denotes the number of vehicles stopped until the time t.

An intersection and its lanes can be tracked so as to reflect their ability to respond to the traffic's status at given times and their ability to buffer conditions for a given vehicle. The length of a vehicle queue in an intersection is related to the speed of a vehicle's arrival, the speed of a vehicle's departure, and its previous status, but is not related to its future status.

Definiton 3: The first-in first-out server (FIFOS) is the vehicle which first arrives at the intersection and will first leave the intersection. Overtaking other vehicles and jumping the queue are not allowed.

Definition 4: (FIBS) is the first-in back server, this denotes a vehicle that arrives later but is first served.

One intersection-agent adopts the fuzzy control strategy. The longest queue and the maximum quantity of arrival vehicles in a lane are input parameters of the intersection, while the traffic signal phasing and signal timing scheme are determined by a fuzzy controller (He et al, 2002, Wang et al, 2006,Wen et al, 2001) in order to reduce the vehicles' mean delay time.

Intersection agent. Fuzzy control is one of the most effective methods to realize the control of an intersection signal (Liu and Wang, 2004, Ehlert and Rothkrantz, 2001). The intersection agent can make use of a fuzzy strategy to

model intelligence. Intersection agents need to control the intersection signal and to coordinate with other agents. Therefore, we have designed a two-fuzzy intelligent traffic control system of isolated intersections. A block diagram of an intersection agent is shown below, in Figure 1.

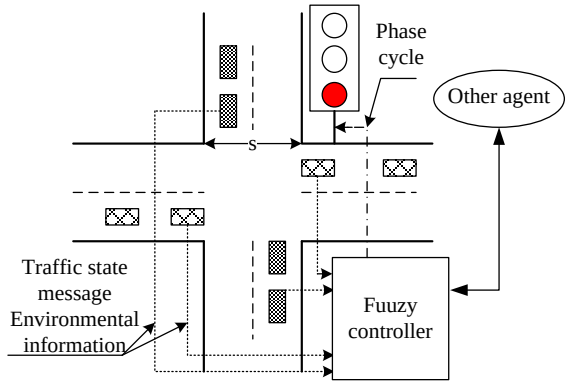

Figure 1. Block diagram of intersection agent.

The road segment agent. The goal of the road segment agent is to adjust the flow according to the traffic's status. It realizes this aim through restricting speed instruction. The speed is restricted by forecasts and statistical attributes of the flow and is then communicated via output to traffic speed signals. When the road agent receives another agent's request message to increase or reduce output speed, it can modify the traffic speed signal intelligently. A diagram of the Road section agent is shown below in Figure 2.

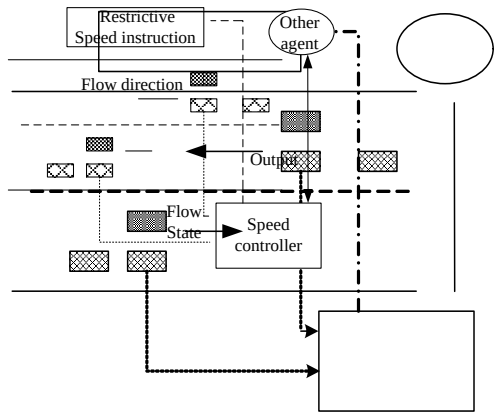

Figure 2. Road segment agent.

AREA TRAFFIC COORDINATION CONTROL

An area traffic network consists of a group of basic agent units. According to the statement above, the basic unit of an agent is divided into an intersection agent and a road segment agent. A intersection agent controls the traffic signal, including the phase, cycle and split, and the status information from that agent is communicated to the neighborhood agents. The road segment agent adjusts the speed and time occupancy rate of the vehicles, the status information of the agent notifies its neighborhood agents. The neighborhoods of an intersection agent are directly interconnected road segment agents, but when two intersections are very

close, we ignore the connection road and consider the neighborhood as being the next intersection.

Coordination process. Traffic flow queue length increases when the intersection's congestion is beginning to emerge. After some signal cycles, the intersection's congestion will become more serious if its status has not changed. At this moment, the agent needs to seek help from its neighborhoods, and multiple agents start to coordinate. When its neighborhood agents get a message requesting help, they take a series of steps to reduce the vehicle flow into the congested intersection. These steps include reducing the vehicle speed for an upstream road agent or improving the vehicle speed for a downstream agent, in order either to decrease green time or cycle for the upstream intersection agent or to increase green time or cycle for the downstream agent. Road segment agents take the FIBS to restrict speed, and intersection agents use the FIFO to improve capacity.

The size of a coordination domain and the number of agents needed to be enjoined are decided by the congestion level. Since the traffic parameters are time-varying, therefore, this multi-agent coordination is self-organizing.

A neural network based on unsupervised learning is self-adaptive to adjust the network by learned form samples, and the network can adapt to the new input samples. A self-organizing feature map can discern analogous input vectors from learning, and the neighborhood analogous inputs have the same answer.

Figure 3 shows the neural network model of a multi-agent self-organizing feature map in an area traffic control system.

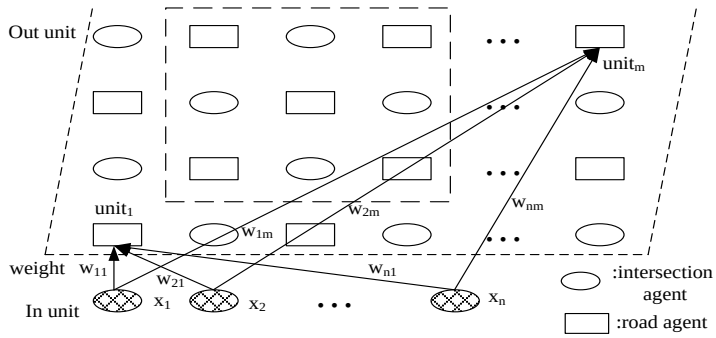

Figure 3. Self-organizing Feature Map Model.

Learning algorithm. The status parameters of a intersection agent represent the input vector of the control system, where X denotes input vector, $X=[x_1,x_2,\ldots,x_n]^T$, output unit is arranged on a 2-d grid, and W is the defined weight vector of the i^{th} output unit, $W=[w_{1i},w_{2i},\ldots,w_{ni}]^T$, (i=1,2, …,m);

The winner unit is decided by

$$q(x) = \min_{\forall i} \|x - w_i\| \tag{3}$$

Where q(x) points to the winner unit of its input x, it represents x and its neighborhood to emerge from an abnormal traffic state, according to the severity level of the incident we determine the neighborhood N_q (k), and to modify the

weight as formulation (4).

$$w_i(k+1) = w_i(k) + \eta_{qi}(k)[x(k) - w_i(k)] \tag{4}$$

Where focal functions $\eta_{qi}(k)$ are defined by

$$\eta_{qi}(k) = \begin{cases} \mu(k), i \in N_q(k), o < \mu(k) < 1 \\ 0, i \notin N_q(k) \end{cases} \tag{5}$$

Learning efficiency function $\mu(k)$ decreases with time.

Learning as traffic proceeds modifies the weight efficiency according to the facts, as vehicles resume a normal traffic state.

Improved algorithm. 1) In using the above method, the workload increases with an increase in the number of agents, with a position for a sliding window, and where l is size of the window, the input vector is written

$$x \in \{x1, x2, \cdots xi, \cdots\}, X = [x_i, x_{i+1}, \cdots, x_{i+l}]\text{，} \quad \text{i=0，1，2，…；}$$

2) The learning efficiency can be improved by designing a learning strategy. The status and action of the agent is used to grasp all the estimated results of status-action to decide which action to take next. Therefore, Q-learning [4] is a good idea with a higher convergence speed.

Interaction protocol. Protocol mainly includes message format and communication interaction processes.

The message is composed of an ID, the time, type of help, and level. ID shows the agent's physical position, and the time includes the incident's start time and end time, type of help and level describes the degree of severity and type of help sought.

Communication processes use a "handshake" idea. Firstly, the agent puts out a call for help, the neighborhood agents get the help message to adjust the program at their individual position, and they send a response. The process is repeated until normal traffic status reappears. If the neighborhood agent cannot help, it broadcasts the help message to its neighbors, and then repeats the above processes.

SIMULATION EXPERIMENT

In order to verify the view of multi-agent coordination, we set up an area of traffic coordination simulation architecture that included a 4x3 and 8x6 intersection using C^{++} language. Assuming the length of the road segment is 1 km, each intersection has 2 lanes, and its 4-phase max of cycle time equals 120s, the vehicle speed in each section is 30 km/s, and the simulation results compare to the fixed cycle, as shown in Table 1 and Table 2.

Table 1. Simulation results by 4x3.

	Intersection average value in area		
	Queue q(t)	Delay td(s)	Leave vehicle
Agent excellent	14	120	17
Agent bad	17	135	14
Fixed cycle	17	138	14

Table 2. Simulation results by 8x6.

	Intersection average value in area		
	Queue q(t)	Delay td(s)	Leave vehicle
Agent excellent	12	118	15
Agent bad	15	131	13
Fixed cycle	18	140	12

We compared Table 1 and Table 2, to discover the more effective process with the greater number of agents and area size of traffic coordination under a heavy congestion situation. Our simulation results found that agent coordination is frequently necessary when traffic congestion and multi-agent coordination control can relieve congestion effectively, but when the traffic is normal, traffic agents are related lightly and there is no obvious difference between using a multi-agent coordination system and a fixed cycle control model.

CONCLUSION AND FUTURE RESEARCH

In this paper, the intersection agent and the road segment agent are separately defined while the feature and function of different agents are more specifically described. We designed a traffic coordination model and simulation plan based on multi-agent coordination by means of a message system allowing agents to request and receive help. When traffic incidents emerge, the multi-agent coordination is available to respond. A position sliding window algorithm can reduce the computing scale. Further efforts can be pursued to improve the features of each agent and the specific coordination mechanisms of agents' actions.

REFERENCES

He Ning, Yang Tao, Li Chaoyang, Qian Linbo (2002). "Positive Research and Application of Signal Intersection Traffic Delay and Queue Length". *Journal Of Highway And Transportation Research And Development*, Beijing, 119 (15), 106-109.

Wang Yanna, Zhou Zili, Wang Xinwei, (2006). "Traffic Signals Control in Multi-Phase Cross Based on Fuzzy Control." *Computer Engineering*. 32(2), 229-231.

Wen Huiying, Yin Hongbin, Xu Jianmin (2001). "A Method of Fuzzy Traffic Control of Signalized Intersection". *Journal of South China University of Technology (Natural Science Edition),* 29 (12),22-25

Zeng Jianqin, Liu Kun, Wang Guocheng, Fang Tingjian (2006). "Mass approach to traffic simulation." *Journal Of the University Of Science And Technology Of China* . 36(2), 193-197.

Ma Shoufeng, Li Ying. (2003). "Agent-based traffic coordination control method for two adjacent intersections". *Journal of Systems Engineering*.

Liu Xiaomin, Wang Feiyue. (2004). "Study of Intersection Traffic Flow Control On the Basis of Agents" *Journal of System Simulation*

Ehlert., P.A.M., and Rothkrantz L.J.M. (2001) "*Microscopic traffic simulation with reactive driving agents," Intelligent Transportation Systems Proceedings*, Oakland, CA: IEEE.

Jee-Hyong Lee, Hyung Lee-Kwang. (1999). "Distributed and Cooperative Fuzzy, Controllers for Traffic Intersections Group.*" IEEE Transactions on System, Man and Cybernetics:* 263-271.

Hong Wei, Mu Xuan-qin, Wang Yong, Qin Zhong-yuan, Zhang Li-hao (2001). "A Cooperative Fuzzy Control Method for Traffic Lights". *Journal of System Simulation,* 13 (5), 551-554.

An AHP-based Performance Evaluation Model of Transportation Control System: The Experience from West Liaohe Rd., Dalian

Ding Jianmei[1] and Wang Changhong[2]

[1] School of Mechatronics Engineering, Harbin Institute of Technology, 91 West Dazhi Street, Harbin 150001, China, PH (86) 451- 8628 2485; FAX (86) 451-8628 2485; email: djm801@126.com
[2] School of Astronautic, Harbin Institute of Technology, 91 West Dazhi Street, Harbin 150001, China, PH (86) 451- 8641 6066; FAX (86) 451-8641 6066; email: cwang@hit.edu.cn

ABSTRACT

Vehicle delay, stopping times, queuing length and API are selected as the evaluation vectors and a comprehensive AHP evaluation model is proposed to assess the constructed signal control method. Typical arterials are chosen to conduct the simulation tests by VISSUM, including Beixin Str. for passenger transport arterial, West Liaohe Rd. for freight transport arterial and Xuefu Rd. for mixed transport arterial. Comparison is done between the normal signal control method and the proposed one. The simulation result shows that the proposed signal method can decrease the vehicle delay and improve the average velocity significantly.

LITERRATURE REVIEW

City road traffic signal control systems are widely used in foreign countries so that the basic theories and algorithms have reached a mature state, which formed the offline systems TRANSYT represented and the adaptive systems SCOOT and SCATS represented. Either from the engineers' points of view or from the administrator's points of view, the evaluations of the systems' effect are important to discriminate test means, which are also the essential references for optimizing signal control parameters, and adjusting and perfecting the system.

Hunt et al. (1982) applied the analytical hierarchy process to study the assessment of the traffic control systems and analyzed the effectiveness of the indicators based on SCOOT. Chard and Lines (1987) systematically introduced the traditional traffic control evaluation model and methods. Papageorgiou proposed the evaluation indicators system of Rout Traffic Control Strategy for Real-time and chose a typical southern city of Paris as the case to verify its efficiency.

Aiming at serving the entire users, the assessment of coordinated signal control system is very important for controlling the size of facilities, saving investment and developing an appropriate traffic control measures at an acceptable

level in order to maximize the benefits of system and guide planning and designing a balanced system. For example, Shanghai successfully developed the Chinese-made adaptive signal control system, SUATS, based on the introduced SCATS system. However, fewer of these studies consider the complex issues existing in the motor vehicle itself, thus the effect of their controls should be studied further. This paper studied the - evaluation system, and proposed a single-criterion AHP model.

SINGLE-CRITERION AHP MODEL

Indicators Selection: Various factors on level of service of signalized intersections can be reflected relating delays, such as saturation rate, velocity ratio, the number of stops etc., Since delay is a main causation of additional fuel consumption and air pollution, this article selects vehicle delay, queue length, number of stops, and the Air Pollution Index (API) as indicators.

Mitigating vehicle delay, (s/veh) is always the traveler's request as to travel on a comfortable road network with less congestion and more rational traffic controls. Number of stops is defined as the ratio of actual journey time and the ideal (the free flow). The average queue length (veh) reflects the traffic operation conditions at intersection; API simplified several monitored air pollutant concentrations into a single conceptual-form index. The values of the first three indicators are obtained through the empirical formula projections. Table 1 gives the threshold criterion.

Table 1. Critical Value for Evaluation Indexes

Traffic conditions	Vehicle delay (s)	Queue length (m)	Number of stops	Air Pollution Index API
I	≤30	≤10	(0, 0.3]	(0, 50]
II	(30, 50]	(10, 25]	(0.3, 0.5]	(50, 80]
III	(50, 70]	(25, 40]	(0.5, 0.7]	(80, 90]
IV	(70, 90]	(40, 60]	(0.7, 0.9]	(90, 120]
V	>90	>60	>0.9	>120

Status Matrix Construction: Because of the significant differences between delays and queue lengths on the value and dimension, and avoiding the impact of dimension and value of the variables to ensure that the property variables in the analysis are equal, Standardized Processing of the attribute data should be taken before calculating of property variable distances. According to the characteristics of delay, queue length, journey time index and API, adapting Negative type is in Figure 1.

Considering that traffic artery makes up of some series form of intersection, finite element analysis is used for reference, traffic trunk is dispersed into intersections, and the whole traffic management effect is gathered at each intersection synthetically afterwards.

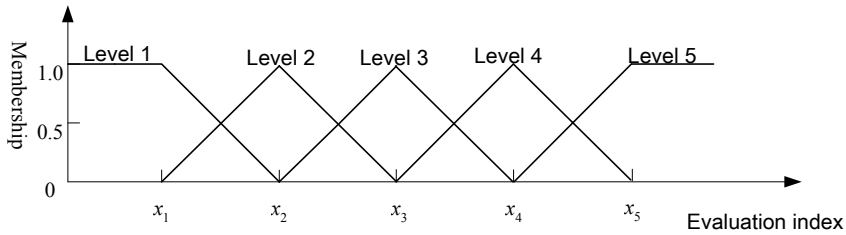

Figure 1. Membership function of grading index

Status matrix evaluates intersections separately, the degree of membership of the evaluation objects (intersection) and alternative sets of elements (five indicators) are determined then. Setting that the i artery, the j intersection and the l direction's evaluation is u_{ijl}, the degree of membership of evaluation object subjecting to the k index is r_{ijlk} (i=1,2…,m; j=1,2,……,n; k=1,2,……,4), then the status matrix of the intersection can be showed as:

$$R_{ijl} = \begin{bmatrix} r_{il11} & r_{il12} & \cdots & r_{il14} \\ r_{il21} & r_{il22} & \cdots & r_{il24} \\ \cdots & \cdots & \cdots & \cdots \\ r_{i\ln 1} & r_{i\ln 2} & \cdots & r_{i\ln 4} \end{bmatrix} \quad i = 1,2,\cdots,m \quad s = 4 \tag{1}$$

AHP Based Evaluation Model: In some intersections, setting the weight of the four traffic flow direction is w'_l ($l \in [1,4]$),the evaluation matrix of that intersection's traffic status can be showed in the augmented matrix in Equation (2):

$$R_{ij} = \begin{bmatrix} R_{ij1} & R_{ij2} & R_{ij3} & R_{ij4} \\ 0 & 0 & 0 & 0 \\ 0 & 0 & 0 & 0 \\ 0 & 0 & 0 & 0 \end{bmatrix} \cdot \begin{bmatrix} w'_1 & 0 & 0 & 0 \\ w'_2 & 0 & 0 & 0 \\ w'_3 & 0 & 0 & 0 \\ w'_4 & 0 & 0 & 0 \end{bmatrix} \tag{2}$$

Set the weight distribution vector of the j intersection in the i artery satisfies w''_j , then the overall traffic conditions of the i artery can be showed as the matrix R_i, according with:

$$R_i = \begin{bmatrix} R_{i1_{grade1}} & R_{i2_{grade1}} & R_{i3_{grade1}} & R_{i4_{grade1}} \\ R_{i1_{grade2}} & R_{i2_{grade2}} & R_{i3_{grade2}} & R_{i4_{grade2}} \\ R_{i1_{grade3}} & R_{i2_{grade3}} & R_{i3_{grade3}} & R_{i4_{grade3}} \\ R_{i1_{grade4}} & R_{i2_{grade4}} & R_{i3_{grade4}} & R_{i4_{grade4}} \\ R_{i1_{grade5}} & R_{i2_{grade5}} & R_{i3_{grade5}} & R_{i4_{grade5}} \end{bmatrix} \tag{3}$$

Let the weight vector of the four evaluation index w_m , then the evaluation

model of the traffic management effect in the *i* artery can be vectored further:

$$R_i = \begin{bmatrix} R_{i1_{grade1}} & R_{i2_{grade1}} & R_{i3_{grade1}} & R_{i4_{grade1}} \\ R_{i1_{grade2}} & R_{i2_{grade2}} & R_{i3_{grade2}} & R_{i4_{grade2}} \\ R_{i1_{grade3}} & R_{i2_{grade3}} & R_{i3_{grade3}} & R_{i4_{grade3}} \\ R_{i1_{grade4}} & R_{i2_{grade4}} & R_{i3_{grade4}} & R_{i4_{grade4}} \\ R_{i1_{grade5}} & R_{i2_{grade5}} & R_{i3_{grade5}} & R_{i4_{grade5}} \end{bmatrix}^T \cdot \begin{bmatrix} w_1 & w_2 & w_3 & w_4 \\ 0 & 0 & 0 & 0 \\ 0 & 0 & 0 & 0 \\ 0 & 0 & 0 & 0 \\ 0 & 0 & 0 & 0 \end{bmatrix} \tag{4}$$

Then further simplify the formula:

$$R_i = \left[\sum_{\tau=1}^{5} R_{i1_{grade\tau}} \cdot w_1 \ \sum_{\tau=1}^{5} R_{i2_{grade\tau}} \cdot w_2 \ \sum_{\tau=1}^{5} R_{i3_{grade\tau}} \cdot w_3 \ \sum_{\tau=1}^{5} R_{i4_{grade\tau}} \cdot w_4 \right] \tag{5}$$

Let λ represents Confidence level and if there is an undetermined object R_i, then ascribing R_i to the mode which has the shortest distance with it. In general, the criterion of confidence level is divided by the positive sequence, that is, stronger is much better, and the strong should occupy quite large proportion. In this paper, the confidence level is limited within 50%;at the same time, the management level is not under the secondary level.

$$k_0 = \min\left\{ \sum_{k=1}^{4} \sum_{\tau=1}^{4} R_{ik_{grade\tau}} \cdot w_k \geq \lambda, \ 1 \leq k \leq 4 \right\} \tag{6}$$

APPLICATION CASE

Simulation Experiment: West Liaohe Rd. in Golden Port Zone of DaLian is one of the important channels linking the main city of Dalian and Xiao yaowan Development Zone, the proportion of large vehicles is 14%, in which large trucks account for 10%. So the vehicle type of large trucks is chosen as a typical representative of the freight main road and VISSIM software was used to carry out the traffic simulation.

AHP method was used to determine the weight of the four intersections in West Liaohe Rd. According to many years studies, practical experiences, the references of the characteristics of intersections and traffic flow and other factors, 18 experts from Harbin and Dalian, who have been long engaged in the traffic design and management to fix the score of the intersections, then constructed judgement matrix to solve the maximum eigenvalue, so the weight can be determined, and the corresponding consistency check can be carried out.

There was a significant difference between the running states of traffic flow controlled by different conditions. In this paper, the first grade indexes (delay, queue length, number of stops and the Air Pollution Index API) were done for Single-level Sequencing by entropy weight method, using the Matlab to write simple calculation procedure, then analyzing the weight vector of first grade indexes under the optimize control scheme and conventional control program. The results are listed in Table 2.

Table 2. Intersection Weight of West Liaohexi Rd.

Intersection	I_1	I_2	I_3	I_4	w'_i
I_1	1	1/2	4/5	2/3	0.174
I_2	2	1	8/5	6/7	0.313
I_3	5/4	5/8	1	5/7	0.209
I_4	3/2	7/6	7/5	1	0.304

$\lambda_{\max}$=4.0189, *CI*=0.0063, *RI*=0.9, *CR*=0.007, pass the consistency check

$$\left[w_{Delay} \quad w_{Ququing} \quad w_{StopppingtimeS} \quad w_{API}\right]=\left[0.2748 \quad 0.2836 \quad 0.2001 \quad 0.2416\right]$$

$$\left[\overline{w}_{Delay} \quad \overline{w}_{Ququing} \quad \overline{w}_{StopppingtimeS} \quad \overline{w}_{API}\right]=\left[0.2761 \quad 0.2712 \quad 0.2001 \quad 0.2527\right]$$

Characteristics of the intersection and volume are the main considerations to determine the weight of different traffic flows in an intersection, and hierarchy general ranking is the ultimate referenced. The four direction of traffic flow cover from east to west, left of west to east, straight of south to north as well as left of south to north. The corresponding weights are (0.35, 0.15, 0.35, 0.15) for West Liaohe Rd &West Huanghe Rd, (0.2, 0.25, 0.15, 0.4) for West Liaohe Rd and Jinma Rd, (0.2, 0.35, 0.2, 0.25) for West Liaohe Rd and Liaoning St, and (0.15, 0.4, 0.25, 0.2) for West Liaohe Rd & Dongbei Da St.

Evaluation of Control Effect: According to the actual situation in each intersection, taking the weight vector w''_i in different directions of the West Liaohe Rd, the weight vector of the four intersections w'_i and the weight of single index w as consideration, data were integrated layer by layer, as Table 3.

Table 3. Weight of Traffic Flow Direction for West Liaohe Rd.

ID	Intersection	Optimized project	Normal project
1	W. Liaohe Rd. &W. Huanghe Rd.	$R_1=\begin{bmatrix}0.7900 & 0 & 0.8525 & 0.1260\\ 0.2100 & 0.1717 & 0.1475 & 0.3360\\ 0 & 0.6071 & 0 & 0.4860\\ 0 & 0.2213 & 0 & 0.0520\\ 0 & 0 & 0 & 0\end{bmatrix}$	$R'_1=\begin{bmatrix}0.7925 & 0 & 0.9000 & 0.1435\\ 0.2075 & 0 & 0.1000 & 0.2065\\ 0 & 0.7913 & 0 & 0.5265\\ 0 & 0.2087 & 0 & 0.1235\\ 0 & 0 & 0 & 0\end{bmatrix}$
2	W. Liaohe Rd. & Jinma Rd.	$R_2=\begin{bmatrix}1.0000 & 0 & 1.0000 & 0.6613\\ 0 & 0.4317 & 0 & 0.3387\\ 0 & 0.5458 & 0 & 0\\ 0 & 0.0225 & 0 & 0\\ 0 & 0 & 0 & 0\end{bmatrix}$	$R'_2=\begin{bmatrix}1.0000 & 0 & 1.0000 & 0.2159\\ 0 & 0.0133 & 0 & 0.7146\\ 0 & 0.7767 & 0 & 0.0695\\ 0 & 0.2100 & 0 & 0\\ 0 & 0 & 0 & 0\end{bmatrix}$
3	West Liaohe Rd. & Liaoning Str.	$R_3=\begin{bmatrix}1.0000 & 0.2233 & 1.0000 & 0.6850\\ 0 & 0.5450 & 0 & 0.3150\\ 0 & 0.2317 & 0 & 0\\ 0 & 0 & 0 & 0\\ 0 & 0 & 0 & 0\end{bmatrix}$	$R'_3=\begin{bmatrix}0.9930 & 0.2383 & 0.9825 & 0.5432\\ 0.0070 & 0.3117 & 0.0175 & 0.3288\\ 0 & 0.4337 & 0 & 0.1280\\ 0 & 0.0163 & 0 & 00\\ 0 & 0 & 0 & 0\end{bmatrix}$

4	West Liaohe Rd. &Great Northeast Str.	$R_4=\begin{bmatrix}0.5375 & 0.0133 & 0.5625 & 0.1960\\ 0.0625 & 0.5433 & 0.0375 & 0.1540\\ 0.0980 & 0.4433 & 0 & 0.2383\\ 0.3020 & 0 & 0.4000 & 0.1250\\ 0 & 0 & 0 & 0.2867\end{bmatrix}$	$R'_4=\begin{bmatrix}0.5100 & 0.0917 & 0.6000 & 0.2260\\ 0.0900 & 0.5017 & 0 & 0.1240\\ 0.2960 & 0.4067 & 0.0800 & 0.2267\\ 0.1040 & 0 & 0.3200 & 0.3353\\ 0 & 0 & 0 & 0.0880\end{bmatrix}$
Control Evaluation	Status matrix	$R=\begin{bmatrix}0.8229 & 0.0507 & 0.8413 & 0.4317\\ 0.0555 & 0.4441 & 0.0371 & 0.2771\\ 0.0298 & 0.4597 & 0 & 0.1570\\ 0.0918 & 0.0455 & 0.1216 & 0.0470\\ 0 & 0 & 0 & 0.0872\end{bmatrix}$	$R'=\begin{bmatrix}0.8135 & 0.0777 & 0.8573 & 0.2748\\ 0.0649 & 0.2218 & 0.0211 & 0.3660\\ 0.0900 & 0.5951 & 0.0243 & 0.2090\\ 0.0316 & 0.1054 & 0.0973 & 0.1234\\ 0 & 0 & 0 & 0.0268\end{bmatrix}$
	Evaluation vector	$R_{Per}=[0.5132 \quad 0.2156 \quad 0.1765 \quad 0.0738 \quad 0.0211]'$	$R'_{Per}=[0.4867 \quad 0.1748 \quad 0.2439 \quad 0.08800 \quad 0.0068]'$

Taking 70% as the confidence level, the optimize system get the secondary level of control, while the conventional control program is at the three-tier level. It indicates that the proposed trunk signal control scheme is effective. Similarly applying the single-criteria composite AHP model to evaluate the signal control effect of Xuefu Road and Beixin Street, the results verify the effectiveness of the proposed control program of this article.

CONCLUSION

As a multi-factor, multi-variable, multi-level complex system, urban road traffic system of traffic control technology develops extremely rapidly. Neural Network Control, Fuzzy Control and other intelligent control technology are gradually applied to the trunk road traffic control system. In this system, the differences of the objective things show similar characteristics that are hard to judge, so it is difficult to introduce absolute, fixed standards.

Based on the above research results, this paper selected vehicle delay, queue length, number of stops and API as evaluation index vectors and proposed the single-criteria compound AHP model to assess city trunk roads signal control effect, which solved the evaluation of multi-variables, discrete data. Use West Liaohe Rd. as a simulation object, results show that applying the allocation proposed in this paper can effectively reduce vehicle delay and improve the efficiency of vehicle travel at different traffic composition conditions.

ACKNOWLEDGEMENT

This research work is partially supported by National Key Technology R&D Program of China under granted number 2006BAJ18B03-05.

REFERENCES

Chard B M, Lines C J. (1987). “TRANSYT: the latest developments”. *Traffic Engineering and Control*, 28(4), 387-390

Dion, F., Hellinga, B., (2002). "A rule-based real-time traffic responsive signal control system with transit priority: application to an isolated intersection". *Transportation Research Part B: Methodological*, 36(4), 325-343

Hunt,P. B. Robertson,D. I. Bretherson R. D.. (1982). "The Scoot on-line traffic signal optimization technique". *Traffic Engineering and Control*, 23(4), 190-192

Michael D.M. (2005). "Use of Performance measures for surface transportation in different institutional and cultural contexts: the case of Australia, Japan and New Zealand". *Transportation Research Record*, 1924, 163-174

Pei Y. L., Wang Y. G., (2006). "A real-time optimization algorithm with evolving fuzzy wavelet neural network for passenger flow prediction in dynamic transit scheduling". *DCDIS Series A*, 13(c), 666-670

Rakha, H.; Farzaneh, M., (2006). "Issues and solutions to macroscopic traffic dispersion modeling". *Journal of Transportation Engineering,* 132(7), 555-564

Wang, Y. G.; Pei, Y. L.; Zhao, Y. D. (2008). "Vibration-based damage detection with structural modal characteristics". *The Baltic Journal of Road and Bridge Engineering*, 3(1), 21-28

An Optimized Signal Control Method for a Freight Arterial Transport System

Wang Changhong[1], Ding Jianmei[2]

[1] School of Astronautic, Harbin Institute of Technology, 91 West Dazhi Street, Harbin 150001, China, PH (86) 451- 8641 6066; FAX (86) 451-8641 6066; email: cwang@hit.edu.cn

[2] School of Mechatronics Engineering, Harbin Institute of Technology, 91 West Dazhi Street, Harbin 150001, China, PH (86) 451- 8628 2485; FAX (86) 451-8628 2485; email: djm801@126.com

ABSTRACT

Complexity is an obvious feature of the components of traffic in our country. The vehicles' operating speed declines because of complex vehicle composition, differences in vehicles' mechanical properties, and the different saturations of traffic flow on trunk freight roads. This paper argues that there are traffic delays which are influenced by the three aspects. We analyze the mutative regularity of traffic control parameters on a freight-traffic road and research applicable methods for traffic control on freight-traffic trunk roads which include the discussion of the timing of yellow lights, signal cycles and offset optimization. VVISSIM is applied to verify the optimized methods.

INTRODUCTION

Domestic scholars have made many efforts to improve methods for traffic control in complex traffic components (Zhao L et al. 2008), however most of these have been proposed to optimize a single intersection. The optimization of controlling traffic signals on trunk traffic has been seldom studied previously, especially in sections and intersections with high proportions of trucks, where traffic flow is significantly affected by them. And conventional approaches can't adapt to this situation (Luo X. et al. 2000).

ANALYSIS OF DELAYS ON FREIGHT-TRUNK ROAD

Influences of vehicle component on delays. The differences among vehicles impacts their operating speed on city roads, and because of the existence of intersections and traffic lights, traffic delays can differ according to traffic flows.

The velocity distribution of a single vehicle fits Normal Distribution if its slowest and fastest speeds are v_1, v_2 respectively. In the axis of time, the vehicle starts at t_0 travels at the speed of v_1 and arrives at $t_0 + l/v_1$; if the vehicle starts in the speed of v_2, it will arrive at $t_0 + l/v_2$, so the time cost should be $[t_0 + l/v_2, t_0 + l/v_1]$.

At a green light, if the flow rate is not saturated, the time range of a vehicle's arrival at the next intersection is reckoned according to the lowest speed of the last vehicle and the fastest speed of the first vehicle. If the first vehicle leaves the intersection at t_1 and the last one leaves at t_2, then the vehicles will arrive at the next intersection during $[t_1 + l/v_2, t_2 + l/v_1]$.

The number of vehicles waiting at the next intersection is shown as the

following :

$$m_i = \begin{cases} m_{i-1} + q_i - s_i, & m_{i-1} + q_i - s_i > 0 \\ 0, & m_{i-1} + q_i - s_i \le 0 \, or \quad redtime \end{cases} \tag{1}$$

where m_i is the number of vehicles waiting in the ith period of time, and m_{i-1} is the number of vehicles waiting in the $i-1$th period of time, q_i is the number of arriving vehicles in the ith period of time, and s_i is the rate of vehicles leaving at the ith period of time, which are all at the following intersection.

The delays in the vehicle team are shown as:

$$D = \sum_{i=1}^{p} t_i m_i \tag{2}$$

where m_i is the number of stopping vehicles at the ith period of time, t_i is the value of the ith period of time, and D is the delay of the vehicle team.

The upper and lower limit of D can be reckoned as follows: the upper limit and lower limit occur when the head vehicle arrives at the next intersection at the highest speed and the last vehicle arrives at the next intersection at the lowest speed, and there are no vehicles left in the rear.

Influence of different vehicles' mechanical properties on delays. Delays are mainly due to the intersections of an urban artery, and the intersections of urban arteries are usually signalized intersections. The queue waiting time and dispersing time in signalized intersections constitute a major component of traffic delays. Assuming that the traffic flow arrives into an intersection at a uniform speed, and the traffic waits only because of a red light, the traffic flow passes through the intersection at a faster speed in effective green time and the queue dissipates gradually. Because of a light's restrictions, vehicles passing through the intersection usually have status such as equable motion, deceleration, stopping, acceleration, and resumed equable motion, as shown in Figure 1.

The deceleration time, stopping time and acceleration time are respectively t_a, t_b, t_c. After converting the process of deceleration and acceleration, the blocking time of the head vehicle is the red light time, and then the process of the car passing through the intersection is deceleration, stopping and acceleration, as shown in Figure 2.

In an ideal state, all vehicles have the same maneuvering performance. The blocking time of the head vehicle, the arriving flow rate and the saturation flow rate are respectively r, q, s. The delay can be shown as follows:

$$d = 0.5r \cdot H = 0.5q \cdot s \cdot r^2 / (s - q) \tag{3}$$

If there is a vehicle which experiences bad maneuvering performance in the traffic platoon, the delays of the entire traffic flow will change, as shown in Figure 3.

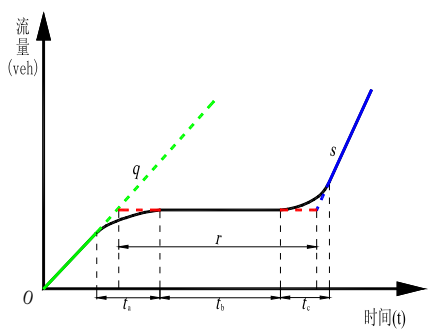

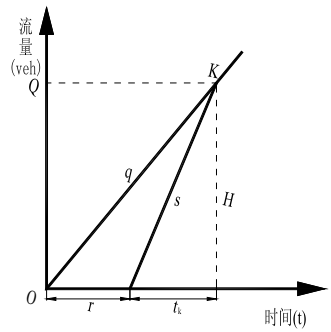

Figure 1. Actual vehicle's delay model. Figure 2. Delay model at ideal condition.

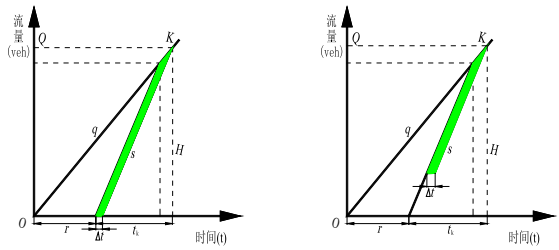

a) b)

Figure 3. Effects of a vehicle's capability difference in the delay model.

When the head vehicle experiences bad maneuvering performance, because of its longer starting time, the blocking time of the entire traffic flow will increase, as shown in Figure 3a. Use Δt to express the difference value of the starting time between bad maneuvering vehicles and normal vehicles. And the delay of the traffic is:

$$d_1 = 0.5(r + \Delta t) \cdot H_1 = d + 0.5(2r \cdot \Delta t + \Delta t^2) \cdot q \cdot s / (s - q) \tag{4}$$

If the vehicle in the middle of the traffic has bad maneuvering performance, that will increase the starting time of the subsequent vehicles, as shown in Figure 3b, then, the delay of the traffic is:

$$d_2 = d + 0.5q \cdot s \cdot \Delta t^2 / (s - q) + r \cdot q \cdot s \cdot \Delta t / (s - q) - s \cdot \Delta t \cdot \overline{h}_t \tag{5}$$

where $\overline{h}_t$ is the average headway if vehicles have the same maneuvering performance .

Influence of different saturation on delays. In a low saturation environment, the effects of each vehicle on other vehicles are minimal, and the relationship between traffic composition and traffic delay is weak. In a high saturation environment, the available space within which to freely travel is minimal, headway is limited within an invariable level, and the vehicles cannot choose freely where to go. In this situation, the difference between composition and delay is minimal. In a general saturation environment, the effect between vehicles is augmented simultaneously by headway changes at any moment, increases in lateral interference, and the rising effect between different roadways. Different vehicle proportions, especially those of larger vehicles, directly result in different saturation rates.

Denoting $s^{'}$ for our expression, the traffic delay is:

$$d^{'} = 0.5q \cdot s^{'} \cdot r^2 /(s^{'} - q) \tag{6}$$

At the same time, if the mobility of the vehicle differs from this, then according to the mobility of vehicle, the actual traffic delay in different locations can be showed as follows:

$$d_1^{'} = d^{'} + 0.5(2r \cdot \Delta t + \Delta t^2) \cdot q \cdot s^{'} /(s^{'} - q) \tag{7}$$

$$d_2^{'} = d^{'} + 0.5q \cdot s^{'} \cdot \Delta t^2 /(s^{'} - q) + r \cdot q \cdot s^{'} \cdot \Delta t /(s^{'} - q) - s^{'} \cdot \Delta t \cdot \overline{h}_t \tag{8}$$

SIGNAL CONTROL OPTIMIZATION

Yellow-light time. The "Traffic Engineering Manual" completed by ITE confirms the model of yellow-light time (y) and red-light time (r) (Institute of Transportation Engineer 1999)：

$$y + r = \delta_0 + \frac{v}{2a + G} + \frac{W + L_v}{v_{ip}} \tag{9}$$

where, δ_0 is reaction time (s), v is the vehicle speed in an import road (m/s), a is minus speed in import (m/s2), G is the import gradient, denoting in %, if declivity, then being negative, W is the intersection width (m), and the distance from the stop line to the conflict trajectory intersection L_v is the vehicle length (m), v_{ip} is the speed in the passing intersection (m/s).

In a freight artery, due to the decrease of a and v_{ip} in our formula (9), then the value of $y + r$ increases, and conflict flow in a non-freight artery can be divided absolutely within 3s yellow light time. Moreover in a freight artery, after researching the simulation of Synchro software and making practical observations, the following result is obtained：When the yellow light time's interval is 4-5s, the conflict flow can realize separation, and this interval can be mostly determined according to the intersection's size. For an intersection within 30 meters, the interval is 4s; for the other, it is 4-5s; for a freight artery, the recommended yellow-light time is 4s, and the red-light time is 1s.

Signal cycle. The best cycle time can yield a transportation benefit index at the maximum level in signal intersections (Wang J. G.. et al. 2000). The Webster method is the most classic, where the optimized cycle length is mostly reckoned from the lost time and the sum of flow ratio in the critical lane group; thus the flow ratio in the critical lane group is relative to the saturation ratio (Wang Y. G.. et al. 2008).

In the ideal situation, the best cycle time can be calculated by the Webster method:

$$c_0 = \frac{1.5 \times \sum (t_l + l / v + t_a - y) + 5}{1 - \sum \max(q_i / s_i)} \tag{10}$$

where c_0 is the best cycle time (s), t_l is the start-up lost time (s), y is the yellow-light time (s), v is the average driving speed (m/s), l is the distance from the stop line to the conflict dot (m), and t_a is the braking time (s).

In this paper, when we determine the optimum cycle time, the delay is the

benefit index with which to deduce cycle time, and the signal cycle of the freight roads intersection is:

$$\min(D) = \min[0.5q \cdot s' \cdot r^2 / (s' - q)] \quad (11)$$

Formula (11) shows that the value of the saturation flow rate is essential to obtain the optimal solution, and it is affected by large vehicles' correction coefficient which is closely related with the PCE. We observed traffic flow characteristics during our investigations of West Liaohe Road, Dalian City, and the straight lanes' vehicles discount coefficient and the left turn and right turn conversion coefficient are shown in Table 1 and Table 2, which are used to calculate the optimum cycle times.

Table 1. PCE of a straight lane.

Vehicle type	straight lanes vehicles discount coefficient
Small vehicle	1
Middle-sized vehicle	1.294
Large vehicle	1.775

Table 2. PCE of left-turning and right-turning lanes

lane	vehicles discount coefficient		
	small vehicle	Middle-sized vehicle	large vehicle
Left-turn	1	1.380	1.867
Right-turn	1	1.430	2.019

In formula (10), the saturation flow rate of a single freight road is shown, where as travel speed decreases, start time and braking time per cycle increase. Compared with a non-freight road, traffic demand in all directions of the intersection changes little (reduced to about 8-13%). This makes the optimum cycle time larger.

According to the survey data on the freight road, if the head and the tail end of traffic are large vehicles in an entrance driveway, the green time loss is 2.1s, yellow terminal loss is 0.2s, and the start time losses are 2.1s + 0.2 s = 2.3s; its traveling speed is 5.6 ~ 8.3 m/s, the average speed v value is 7.0 m/s, and the large vehicle braking time is 1.5s, while the optimum cycle time of the freight road is calculated below as:

$$c_0 = \frac{1.5 \times \sum (l/7 - 0.2) + 5}{1 - \sum \max(q_i / (1800 \times f_{hv} \times \prod f_i))} \quad (12)$$

where $\prod f_i$ is the product of a vehicle's modification coefficient excepting a large vehicle's.

After calculation, the optimum cycle time of a freight road is longer than that of a non-freight road by 12~31%.

Phase offset. This means that the offset time between two adjacent intersections start or end with the green light. In order to enable vehicles to pass more intersections with signal coordination control systems, phase offset must fit with their travel time, so the phase offset is a key parameter in reckoning signal coordination control systems (Lu K. et al. 2008).

Phase offset mainly depends on the distance between intersections and their

average travel speed. A vehicle's average speed on a freight road is lower than on a non-freight road, so the phase offset increases, and the increasing ratio is the reciprocal of the ratio of the two average speeds, which is calculated as follows:

$$O_v = (v_c / v_v) \times O_c \tag{13}$$

Where O_v is the phase offset in a large vehicle environment (s), v_v is the average travel speed with a large vehicle (km/h), v_c is the average travel speed in a smaller vehicle environment (km/h), and O_c is the phase difference in a smaller vehicle environment (s).

CASE ANALYSIS

West Liaohe Road (6 lanes of two-way traffic) at the Dalian Golden Port is an important channel. Its proportion of large cars is as much as 14%, and one of the large trucks on this road accounted for 10%, which is a typical percentage on the freight corridors. Table 3 shows our simulation result.

Table 3. Comparative Analysis Simulation Result

Intersection name	Direction	Flow (pcu/h)	Ordinary			Optimize		
			Delay (s)	Queue (m)	Stops (times)	Delay (s)	Queue (m)	Stops (times)
West Liaohe and West Huanghe	M. St.	1107	40.1	41.0	0.34	35.7	35.0	0.35
	M. L.	233	34.1	41.0	0.33	44.7	34.5	0.37
	S. St.	424	10.8	47.5	0.12	10.7	49.0	0.12
	S. L.	268	29.6	47.0	0.31	28.6	48.5	0.31
West Liaohe and Jingma road	M. St.	856	21.4	48.5	0.16	14.8	28.5	0.16
	M. L.	403	20.0	47.0	0.15	16.6	26.5	0.15
	S. St.	515	23.3	45.0	0.20	23.3	43.0	0.19
	S. L.	206	15.1	39.5	0.16	15.0	38.0	0.16
West Liaohe and Liaoning Street	M. St.	195	17.6	22.0	0.26	17.2	20.5	0.24
	M. L.	292	29.7	16.5	0.31	25.8	18.0	0.27
	S. St.	756	30.7	41.0	0.24	29.5	33.0	0.24
	S. L.	189	18.0	40.5	0.15	18.1	32.5	0.18
West Liaohe and Northeast Street	M. St.	1337	11.7	22.5	0.23	15.5	25.0	0.28
	M. L.	59	75.2	22.5	0.86	85.1	24.5	0.90
	S. St.	427	37.2	39.0	0.30	35.0	40.0	0.33
	S. L.	399	19.3	38.0	0.22	21.4	39.5	0.24
Average			27.48	37.281	0.289	27.31	33.500	0.281

Note: M. equals to main, St. equals to Straight, L. equals to Left, S. equals to Secondary

The major road intersections that cross West Liaohe Road are the Yellow River West Road, the Jinma Road, the Liaoning Road and Northeast Street. Separately for the two-way lanes 6, 8, 4, and 6, the intersection spacing is 739, 1038,

and 317 meters, respectively. Using VISSIM software to simulate the optimization method of this paper, the conventional method was considered separately.

In using this simulation analysis, compared with conventional traffic signal control, the most optimized control method can reduce vehicle delay, queue length and number of stops, so it can effectively improve the efficiency of the vehicle form.

CONCLUSION

We analyzed the impact of vehicles' composition and maneuverability on delays on a freight road, by investigating and analyzing road saturation and vehicle speed. We demarcated the PCE value of different functions of the freight lane, given the recommended value of yellow light time in traffic signal control for a freight artery. We deduced the calculation formula of the best cycle time and phase offset for an actual freight artery, using the Liaohe West Road in the Dalian Economic Development Zone as an example. Using VISSIM in the simulation and analysis with both optimized and conventional methods, we verified the effectiveness of the optimized method proposed in this paper.

ACKNOWLEDGEMENTS

This research work was partially supported by the National Basic Research Program of China under the Grant number 2006CB705505. The authors also wish to thank the editors and reviewers of *ICCTP* 2009 for their assistance during this project.

REFERENCES

Institute of Transportation Engineers. (1999). "Traffic engineering handbook". Washington DC: ITE.

Lu, K. and Xu, J. M. (2008) "Offset model for arterial road coordinate control and its optimization method". *China Journal of Highway and Transport,* 21(1), 83-88.

Luo X., Du J. Y., and Chen Y. W. (2000). "Analyses on multi-traffic flow s characteristics" *Journal of Southwest Jiaotong University*, 35(3), 297-300.

Pei Y. L. and Wang Y. G., (2006). "A real-time optimization algorithm with evolving fuzzy wavelet neural network for passenger flow prediction in dynamic transit scheduling". *DCDIS Series A*, 13(c), 666-670.

Wang J. G., Chu S. X., and Yu Q. (2005). "Split coordination optimization model of arterial coordination control system", *Journal of Transportation Engineering and Information*, 3(2), 13-18.

Wang, Y. G.., Pei, Y. L., and Zhao, Y. D. (2008). "Vibration-based damage detection with structural modal characteristics". *The Baltic Journal of Road and Bridge Engineering*, 3(1), 21-28.

Zhao L., Shao C. Q., and Rong J. (2008). "Analysis of traffic composition affecting saturation flow at signalized intersection". *Highway Engineering*, 33(4), 88-91.

A reserve capacity model of optimal traffic lane allocating

ZHANG Peng[1, 2], LI Wen-quan[1]

[1]School of Transportation, Southeast University, Nanjing 210096, China; email: zhangpeng547@126.com
[2]School of Automobile and Traffic Engineering, Jiangsu University, Zhenjiang 212013, China

ABSTRACT

In urban transportation networks, road flows may be unbalanced because of the difference of traffic demand in space (e. g. on/off duty). Aiming to make full use of the existing road resource and alleviate transportation congestion, a reserve capacity model of optimal lane allocating is proposed. The lane numbers in both directions of two-way roads and signal timing parameters of intersections are optimized to make the traffic distribution more balanced in lanes, so as to make the network accommodate more traffic demand. A bilevel programming model is proposed: the lower-level problem represents a network equilibrium model; the upper-level problem is to allocate lanes and optimize signal timing to maximize reserve capacity of road networks, taking account of drivers' route choice behavior. A numerical example is presented to illustrate the application of the model.

1. INTRODUCTION

In urban transportation networks, road flows may be unbalanced because of the difference of traffic demand in space (e. g. on/off duty). Generally, variable lanes approach is used to deal with that. However, the result may be counterproductive; that is, although it could help to alleviate local traffic congestion, it may lead the entire urban road traffic conditions to deteriorate, if the variable lanes program is based on only one or a number of roads (ZHAI Zhong-min, 2004). Aiming to make full use of the existing road resource and reduce transportation congestion, a reserve capacity model of optimal lane allocating is studied from the system point of view in this paper.

Webster and Cobbe (1966) brought up the concept of reserve capacity of a simple signal-controlled intersection. Wong and Yang (1997) extended the concept of reserve capacity to a general signal controlled road network, a bilevel programming model was set up, and presented a heuristic to solve the problem(Wong et al. 1997). But parameters optimized are green splits only. Ceylan and Bell(2004), Suh-Wen Chiou (2007) studied on reserve capacity of coordinated fixed-time signalized road network respectively (Ceylan et al. 2004, Chiou Suh-Wen 2007). Besides green splits, offsets and the common cycle time are also considered. However, the improvement of reserve capacity is very limited just simply by setting traffic signals.

Ziyou and Yifan (2002) combined the problem of reserve capacity of signalized road networks with that of the continuous equilibrium network design

(Gao Z Y et al. 2002). An integrated method has been presented to maximize the possible increase in travel demands of the road network while the minimization of investment in link capacity expansions is pursued with respect to the green splits at individual junctions. Tong and Ziyou (2004) combined the problem of reserve capacity with the discrete network design (Zhao Tong et al. 2004). The reserve capacity of road network is maximized by setting traffic signals at individual intersections and constructing new roads. Zhao tong (2006) suggested an approach of adding new roads to maximize the traffic capacity of the network to satisfy the increasing urban traffic demand, while still keeping that traffic demands within the environment constraint (Zhao tong et al. 2006). However, the parameters optimized on signal timing are green splits only in these studies, and the delay formulae are of simple BPR-like forms.

In fact, apart from the approaches of expansion or construction to existing road networks, the variable lanes control is also an effective measure to alleviate traffic congestion. Moreover, the investment is small and effect is fast (ZHAI Zhong-min, 2004). Reallocating of lanes not only changes the capacity of junctions, but also changes signal control delay of vehicles, which will affect drivers' route choice behavior. Therefore, it is necessary to make decisions from the system perspective, using systems analysis methods. A bilevel programming model is proposed in this paper: the lower-level problem represents a network equilibrium model; the upper-level problem is to allocate lanes and optimize signal timing to maximize reserve capacity of road networks, taking account of drivers' route choice behavior. The path impedance is composed of driving time and delay time at junctions.

This paper has been organized as follows. In the next section, some basic notions are defined. The capacity model of signal-controlled road network and its solution algorithm are presented in section 3 and 4. In section 5, a numerical example is given. Finally, conclusions are drawn in section 6.

2. BASIC NOTATION

The notations used in this paper are given as follows:

O: the set of all origin nodes; D: the set of all destination nodes; r: an origin node, $r \in O$; s: a destination node, $s \in D$; A: the set of links in the network; R: the set of signal-controlled intersections in the network; $n_{i\text{-}j}$: lane number of the link i-j from junction i to adjacent junction j(i-$j \in A$), $\boldsymbol{n}$ is a vector of lane numbers of all links; $\lambda_{i\text{-}j}$: green split of the link i-j from junction i to adjacent junction j(i-$j \in A$), $\boldsymbol{\lambda}$ is a vector of all green splits; C_j: cycle time of signal-controlled intersection j, $\boldsymbol{C}$ is a vector of all cycle times; L_j: total lost time per cycle of signal-controlled intersection j; K: the set of paths from original node r to destination node s; $\mathbf{q}$: the current O-D matrix; μ: the O-D matrix multiplier(suppose all demand multipliers between each O-D pair are the same); h_k^{rs} :flow on path k from original node r to destination node s; $f_{i\text{-}j}(\mu, \boldsymbol{C}, \boldsymbol{\lambda}, \boldsymbol{n})$: flow on link i-$j \in A$， it is a function of upper-level decision

variables μ, $\boldsymbol{C}$, $\boldsymbol{\lambda}$, $\boldsymbol{n}$; $\delta_{i-j,k}^{rs}$: takes a value of 1 if link *i-j* is on path *k* from origin node *r* to destination node *s*, and 0 otherwise; t_{i-j}: total journey time (or cost) function on link $i\text{-}j \in A$; $c_{i\text{-}j}(\lambda_{i\text{-}j}, n_{i\text{-}j})$: capacity of signal-controlled link *i-j* ($j \in R$.).

3. FORMULATION OF THE PROBLEM

Suppose that the lane numbers in both directions of all two-way roads are adjustable. The total lane number of a two-way road is fixed:

$$n_{i\text{-}j} + n_{j\text{-}i} = \mathrm{n_{ij}} \tag{1}$$

where $n_{i\text{-}j}$, $n_{j\text{-}i}$ are of positive integer, $\mathrm{n_{ij}}$ is sum of lane numbers in both directions ($i\text{-}j$, $j\text{-}i \in A$) of a two-way road.

In order to ensure that queues and delays at network intersections under equilibrium conditions be accepted by network users, flows on any signal-controlled links must be constrained so as not to exceed a prescribed maximum acceptable value, i.e., capacity constraints are given as follows:

$$f_{i\text{-}j}(\mu, \boldsymbol{C}, \boldsymbol{\lambda}, \boldsymbol{n}) \le x_{i\text{-}j} \cdot c_{i\text{-}j}(\lambda_{i\text{-}j}, n_{i\text{-}j}) \quad j \in R, \quad i\text{-}j \in A \tag{2}$$

where $x_{i\text{-}j}$ is the maximum acceptable degree of saturation for link $i\text{-}j (j \in R)$. Furthermore, the signal timing variables at signal-controlled intersections should satisfy some linear constraints which include cycle time, minimum and maximum green times. Signal timing variable constraints are given as follows:

$$C_{min} \le C_j \le C_{max} \quad j \in R \tag{3}$$

$$\lambda_{min} \le \lambda_{i\text{-}j} \le \lambda_{max} \quad j \in R \tag{4}$$

where C_{min} is minimum cycle time, C_{max} is maximum cycle time; λ_{min} is minimum green split, λ_{max} is maximum green split. Green split and lost time must satisfy the following relationship:

$$\sum_{n=1}^{N_j} \lambda_{nj} + L_j / C_j = 1 \qquad j \in R \tag{5}$$

where N_j is the number of phases of signalized intersection j, λ_{nj} is the green split of the phase n.

Therefore, the upper-level model has the following form:

$$\text{Max} \quad \mu \tag{6}$$

$$s.t. \quad n_{i\text{-}j} + n_{j\text{-}i} = \mathrm{n_{ij}} \quad i\text{-}j \in A, j\text{-}i \in A \text{且} n_{i\text{-}j}, n_{j\text{-}i} \text{ are of positive integer} \tag{7}$$

$$f_{i\text{-}j}(\mu, \boldsymbol{C}, \boldsymbol{\lambda}, \boldsymbol{n}) \le x_{i\text{-}j} \cdot c_{i\text{-}j}(\lambda_{i\text{-}j}, n_{i\text{-}j}) \quad j \in R, \quad i\text{-}j \in A \tag{8}$$

$$C_{min} \le C_j \le C_{max} \quad j \in R \tag{9}$$

$$\lambda_{min} \le \lambda_{i\text{-}j} \le \lambda_{max} \quad j \in R \tag{10}$$

$$\sum_{n=1}^{N_j} \lambda_{nj} + L_j / C_j = 1 \qquad j \in R \tag{11}$$

where $f_{i\text{-}j}(\mu, \boldsymbol{C}, \boldsymbol{\lambda}, \boldsymbol{n})$ is obtained by solving the following network equilibrium problem:

$$\min \quad \sum_{i-j \in A} \int_0^{f_{i-j}(\mu, C, \lambda, n)} t_{i-j} dx \tag{12}$$

$$s.t. \quad \sum_{k \in K} h_k^{rs} = \mu \cdot q_{rs} \qquad \forall r \in O, s \in D \tag{13}$$

$$f_{i-j} = \sum_{r\in O}\sum_{s\in D}\sum_{k\in K} h_k^{rs}\cdot\delta_{i-j,k}^{rs} \qquad \forall i-j\in A \tag{14}$$

$$h_k^{rs} \geq 0 \qquad \forall r\in O, s\in D, k\in K \tag{15}$$

where t_{i-j} is composed of the link driving time (for example, BPR-like form) and intersection delay. The average signal control delay per vehicle for a given link (i-j) entering a signal-controlled intersection is recommended by HCM2000 (initial queue delay is not included):

$$d = \frac{0.5C(1-\lambda)}{1-[\min(1,x)\lambda]} + 900T\left[(x-1)+\sqrt{(x-1)^2+\frac{8kIx}{cT}}\right] \tag{16}$$

For a detailed description, see HCM(2000).

Once n_{i-j}=0, and then c_{i-j}=0, t_{i-j}=∞. In this case, the two-way road is turned into a one-way road, and its direction is from j to i.

4. SOLUTION ALGORITHEM

In order to solve the problem we must evaluate the changes in equilibrium link flows caused by the changes in signal timing variable, O-D demand multiplier and lane numbers under the condition that all constraint conditions are not being violated. It is difficult to evaluate the changes in equilibrium link flows directly because of the implicit, nonlinear function form of equilibrium link flows. A good idea is to use the linear function to approximate the nonlinear function of $f_{i-j}(\mu, \boldsymbol{C}, \boldsymbol{\lambda}, \boldsymbol{n})$. Therefore, we must calculate the derivative of the link flows, with respect to signal timing variable($\boldsymbol{C}$ and $\boldsymbol{\lambda}$), O-D demand multiplier(μ) and lane numbers($\boldsymbol{n}$) (Wong and Yang 1997). But the lane numbers($\boldsymbol{n}$) are of positive integer, the difference of equilibrium link flows respect to $\boldsymbol{n}$ can be adopted as approximation of the derivative(Yi-fan and Zi-you,1998).

Let μ^*, $\boldsymbol{C}^*$, $\boldsymbol{\lambda}^*$, $\boldsymbol{n}^*$denote an initial solution to O-D demand multiplier, cycle time, green split and lane numbers respectively, and let $f_{i-j}(\mu^*, \boldsymbol{C}^*, \boldsymbol{\lambda}^*, \boldsymbol{n}^*)$ denote the corresponding equilibrium link flows, which are solved from lower-level problem.

$$\begin{aligned} f_{i-j}(\mu,C,\lambda,n) \approx f_{i-j}(u^*,C^*,\lambda^*,n^*) &+ \sum_{i-j\in A}\left[\frac{\partial f_{i-j}(\mu^*,C^*,\lambda^*,n^*)}{\partial\mu}\right](\mu-\mu^*) + \sum_{j\in R}\left[\frac{\partial f_{i-j}(\mu^*,C^*,\lambda^*,n^*)}{\partial C_j}\right](C_j-C_j^*) \\ &+ \sum_{i-j\in A,j\in R}\left[\frac{\partial f_{i-j}(\mu^*,C^*,\lambda^*,n^*)}{\partial\lambda_{i-j}}\right](\lambda_{i-j}-\lambda_{i-j}^*) + \sum_{i-j\in A}\left[\frac{\Delta f_{i-j}(\mu,C,\lambda,n)}{\Delta n_{i-j}}\right](n_{i-j}-n_{i-j}^*) \end{aligned} \tag{17}$$

When substituting (17) into the upper-level problem, the upper-level problem becomes an inter-nonlinear programming problem with the variable μ, $\boldsymbol{C}$, $\boldsymbol{\lambda}$ and $\boldsymbol{n}$. This inter-nonlinear programming problem can be solved by the well-known branch and bound method (Gupta and Ravindran, 1985), thus one can get a new improved point (μ, $\boldsymbol{C}$, $\boldsymbol{\lambda}$, $\boldsymbol{n}$) from which a new inter-nonlinear programming problem is again generated and again solved by the same method, and so on. Therefore, the method is in fact a sequence of linear approximations to the original bilevel problem.

5. A NUMERICAL EXAMPLE

The example network is shown in Fig. 1 This problem has three O-D pairs(1-4, 5-6 and 6-5), eleven links (arrows denote the directions of links, the figures next to links are driving times of free flows, and the unit is second) and six nodes, of which nodes **2** and **3** are of signal-controlled intersections(two-phase). There is only one lane on each link, and the saturated flow for all lanes is 1800 pcu/h. The link driving time is expressed as follow:

$$t_{i-j}^{1} = t_{i-j}^{0}\left[1.0 + 0.4\left(f_{i-j} \Big/ c_{i-j}\right)^{4}\right]$$

The average signal control delay per vehicle are expressed as formula(16), where only the signal-controlled links (j is 2 or 3) have signal control delay, T=0.25，k=0.4，I=1.

The current O-D: q_{56}=1000pcu/h, q_{65}=300pcu/h, q_{14}=500pcu/h; the current signal timing: C_2=60s, C_3=120s, L_2=L_3=10s, $\lambda_{5\text{-}2}$=$\lambda_{6\text{-}2}$=0.5, $\lambda_{5\text{-}3}$=$\lambda_{6\text{-}3}$=0.5; we can get the current distribution of traffic flow: $f_{1\text{-}2}$= $f_{2\text{-}3}$= $f_{3\text{-}4}$= 500 pcu/h，$f_{5\text{-}3}$= $f_{3\text{-}6}$=840 pcu/h，$f_{5\text{-}2}$= $f_{2\text{-}6}$=160 pcu/h，$f_{6\text{-}3}$= $f_{3\text{-}5}$=300 pcu/h. It can be seen that link 5-3 is congested, but other links are unoccupied. The reason is the difference of traffic demand in space (q_{56}> q_{65}) and the difference of traffic impedance between links ($t_{5\text{-}2}$> $t_{5\text{-}3}$). Then we use the model proposed by this paper to optimize lane numbers in both directions of two-way roads and signal timing parameters, the object is to maximize reserve capacity of the road network.

At the process of iterative calculation, the lost time of signalized intersections (2 and 3)is 10s. The lower and upper bounds of the green splits are 0.05 and 0.95 respectively. The lower and upper bounds of the cycle times are 20s and 180s respectively. The maximum degree of saturation for all signal-controlled links take the same value of x =0.85. Convergence criterion δ=0.005, initial points are: μ=1, C_2=60, C_3=120, $\lambda_{5\text{-}2}$=$\lambda_{6\text{-}2}$=0.5, $\lambda_{5\text{-}3}$=$\lambda_{6\text{-}3}$=0.5.

After optimized calculation, we get lanes' reallocation: $n_{5\text{-}2}$=2, $n_{2\text{-}6}$=2, as shown in Figure 2; the optimized signal timing: C_2=99s, C_3=180s, $\lambda_{5\text{-}2}$=0.3730, $\lambda_{5\text{-}3}$=$\lambda_{6\text{-}3}$=0.3197; the maximized O-D matrix multiplier μ=1.630. The maximized O-D demands between different O-D pairs are: q_{56}=1630pcu/h, q_{65}=489pcu/h, q_{14}=815pcu/h, and the distribution of traffic flow are: $f_{1\text{-}2}$= $f_{2\text{-}3}$= $f_{3\text{-}4}$= 815 pcu/h, $f_{5\text{-}3}$= $f_{3\text{-}6}$=489 pcu/h, $f_{5\text{-}2}$= $f_{2\text{-}6}$=1141 pcu/h, $f_{6\text{-}3}$= $f_{3\text{-}5}$ = 489pcu/h. It can be seen that the traffic flows on each links are more even, the road resources have been fully utilized.

It is worth mentioning that, if we increase the lanes of congested path 5-3-6($n_{5\text{-}3}$=2，$n_{3\text{-}6}$=2) in accordance with the common sense, the traffic pressure on this path can be alleviated, but the maximized O-D matrix multiplier μ=1.445<1.630. Readers can check on their own. The reason is that the impedance difference between two parallel paths (5-3-6 and 5-2-6) is further increased, so the traffic flows on each links are more uneven, road resources are not fully utilized.

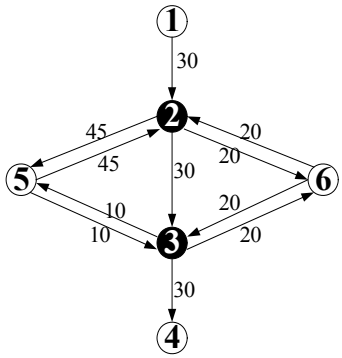

Fig. 1. Example network.

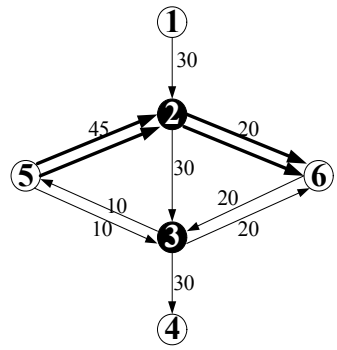

Fig. 2. Improved network.

6. CONCLUSION

A bilevel programming model of reserve capacity based on variable lanes is proposed in this paper. From the above discussion we can conclude that the traffic flows on each links are more even and the road resources can be fully utilized after the lane numbers and signal timing are optimized by this model, thus the reserve capacity of road network can be increased as much as possible.

ACKNOWLEDGEMENT

This work is supported by a national project from Ministry of Science and Technology, P. R. China #2006BAJ18B00.

REFERENCES

Chiou Suh-Wen (2007). "Reserve capacity of signal-controlled road network". *Applied Mathematics and Computation*,190, 1602-1611.

Gao Z Y, Song Y F.(2002). "A reserve capacity model of optimal signal control with user-equilibrium route choice".*Transportation Research*, 36B, 313-323.

Halim Ceylan, Michael G. H. Bell(2004). "Reserve Capacity for a Road Network Under Optimized Fixed Time Traffic Signal Control". *Intelligent Transportation Systems*, 8,87–99.

O. K. Gupta and A. Ravindran(1985). "Branch and bound experiments in convex nonlinear inter programming". *Management Science*, 31, 1533-1546.

Song Yi-fan, Gao Zi-you(1998). "A Heuristic Solution Algorithm for the Continuous Equilibrium Network Design Problem". *JOURNAL OF NORTHERN J IAOTONG UNIVERSITY*, 22(6), 19-24.

TRB. Highway Capacity Manual 2000. *National Research Council, Washington D.C., USA*, chapter 16.

Webster, F. V. and Cobbe, B. M. (1966). "Traffic signal." *Road Research Technical Puper No. 56*, HMSO, London.

Wong, S.C., Yang, H.(1997). "Reserve capacity of a signal-controlled road network". *Transportation Research B 31*, 397-402.

Zhai Zhong-min(2004). Optimization on Traffic Organization. China

Communications Press, Beijing, China, 10-12.

Zhao Tong, Gao Zi-you(2004). "A Reserve Capacity Model of Optimal Signal Controlwith the Urban Transport Discrete Network Design Problem". *Systems Engineering-theory and Practice*, 8, 118-123.

Zhao Tong, Gao Zi-you(2006). "The combined problem of the comprehensive discrete network design under environment restraints and optimal signal controls". *China Civil Engineering Journal*, 39(2), 102-106.

Side Road Traffic Considered in Transit Signal Priority Control

Jia Xu[1] and Hangfei Lin[2]

[1]School of Transportation Engineering, Tongji University, No.4800, Cao'an Road, Shanghai, China, PH (086) 021-69584683; email: karensmail@126.com
[2] School of Transportation Engineering, Tongji University, No.4800, Cao'an Road, Shanghai, China; PH (086) 021-69584683; email: linhangfei@126.com

ABSTRACT

To overcome the shortcomings in existing control mechanisms and adapt to domestic transit operation conditions such as high frequency and overlapped bus routes, many researchers work on various optimization methods. In fact, the effectiveness of priority control varies with side road traffic demand. If a side road is less congested, priority control has less of an impact, whereas otherwise the impact increases accordingly. There is still a lack of effective means by which to solve this problem.

Based on former studies, this paper analyzes how priority control impacts side road traffic, optimizes key parameter settings like minimum green time and maximum green time, and adopts conditional priority as well as appropriate compensation strategies. It is hoped that this transit signal priority system can alleviate excessive changes in side road traffic.

BACKGROUND

The study of Transit Signal Priority (TSP) started 40 years ago. In theory, TSP can raise bus speeds and increase the attractiveness of the transit system; it can also reduce transit operation expenses and improve efficiency. However much research and prior experiments have showed that the benefits of TSP change with traffic demands on side roads. Lee (2006) indicated that TSP increased side road delay by 14.17%; Ma (2006) found that exclusive priority control increased the vehicle delay of a non-priority phase from 29.8s/veh to 35.2s/veh.

Therefore this paper considers side road traffic endurance and optimized control logic such as the key parameter setup in the logic, the judgment criteria of granting priority, and the adoption of certain compensation strategies. We aim to create a control system that can realize transit priority control objectives and reduce the impact of side road traffic at the same time.

BASIC TSP CONTROL LOGIC

The basic control logic of TSP is shown in Figure 1. Key technologies include bus detection and location, short-period travel time forecast, TSP control logic and their combination.

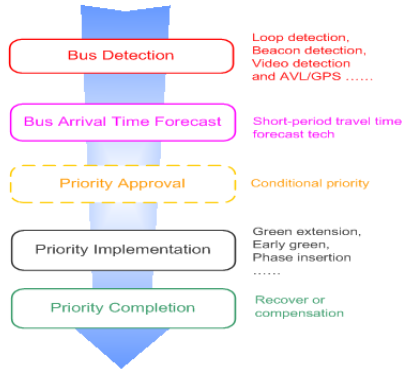

Figure 1. Basic control logic and key instruments of TSP.

This basic control logic focuses more on the provision of effective and exact priority for buses. It is less concerned with other traffic conditions in the network, especially side road traffic.

STUDY OF CONTROL PARAMETERS

TSP control uses **maximal green time** to determine the maximal green extension extent for priority requests and uses **minimal green time** to guarantee necessary travel time in the non-priority phase. Basic control uses an experienced calculation method. Lee (2006) used 25% of the whole cycle as a green extension in trials. Furth (2000) used an early green strategy in the experiment, where minimal green time is 6s of the non-priority phase. However, it is difficult to obtain an ideal and unified effect when these methods are applied to varying side road traffic conditions.

Consideration of side road traffic

TSP impacts side road traffic in the following ways:

- In peak hours, the green extension of the priority phase will cause an accumulation of queuing vehicles on a side road and those vehicles cannot be released in one cycle time. Then second stops may occur and vehicles can even spill over into the upstream intersection.
- In peak hours, the early green of the priority phase will occupy non-priority green time and many vehicles cannot pass through in the reduced green time (or minimal green time), so second stops and overspills occur.
- Frequent bus arrivals request TSP frequently. This can cause increased delays, second stops and even congestion that spreads to the whole network.
- If the local intersection is a part of whole coordinated system, TSP may break up or disrupt its coordination.
- Bicycle and pedestrian safety should be considered, but most basic control has already taken them into account, so this paper did not focus on them.

Concisely speaking, TSP will reduce the pass-through time of side road traffic and require more capacity to accommodate these queuing and arriving

vehicles. However, with ordinarily designed approaches, it is not always possible to widen the approach or add another lane, so the capacity of the existing approach can remain unchangeable. Conversely it will require minimal green time in the non-priority phase in order to limit the extent of TSP.

A prerequisite of this paper is that approach design and signal planning is matched to its actual conditions before the TSP application and the capacity of the approach is not changed.

Minimal green time

Minimal green time is related to an early green strategy. We know that traditional minimal green time takes into account the factors below:

- Safety: drivers need minimal green time to respond to signal changes.
- Basic pass-through demand: each phase should allow a certain number of vehicles through to reduce the average wait for a queue.
- Pedestrian: pedestrians need enough time to cross the intersection safely.

However, when the TSP is applied to an intersection, the minimal green time of a side road should satisfy more serious conditions during peak hours. When an early green is adopted, the back of the queue (Q) should be shorter than what this lane can accommodate (L).

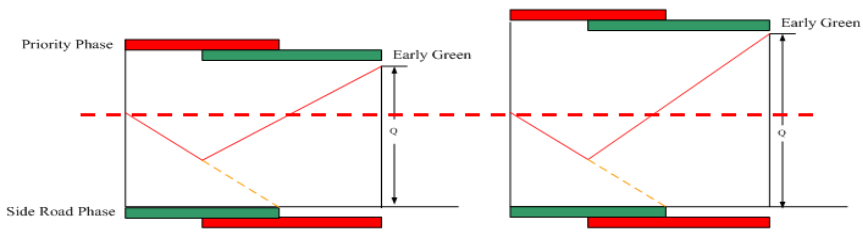

a) Side road arrival rate is low b) Side road arrival rate is high

Figure 4. Queue increase during Early Green.

According to HCM2000, the average back-of-queue characteristics at signalized intersections are

$$Q=Q_1+Q_2 \tag{1}$$

where

Q = maximum distance in vehicles over which the queue extends from the stop line during an average signal cycle (veh),

Q_1 = first-term queued vehicles (veh)

$$Q_1 = PF_2 \frac{\frac{v_L C}{3600}\left(1-\frac{g}{c}\right)}{1-[\min(1.0, X_L)\frac{g}{c}]} \tag{2}$$

where

PF_2 = adjustment factor for effects of progression,

v_L = lane group flow rate per lane (veh/h),
C = cycle length (s),
g = effective green time (s), and
X_L = ratio of flow rate to capacity (v_L/c_L ratio).

And,

Q_2 = second-term queued vehicles (veh).

$$Q_2 = 0.25 c_L T[(X_L - 1) + \sqrt{(X_L - 1)^2 + \frac{8 k_B X_L}{c_L T} + \frac{16 k_B Q_{bl}}{(c_L T)^2}}] \quad (3)$$

where

c_L = lane group capacity per lane (veh/h);
T = length of analysis period (h);
X_L = v_L/c_L ratio;
k_B = second-term adjustment factor related to early arrivals;
Q_{bL} = initial queue at the start of the analysis period (veh) ; and
C = cycle length (s)..

In the early green strategy, $Q_{bl} = Q_1(g' = g - t_b, C' = C - t_b)$ (t_b = early-start green time) because $Q_2 = Q_2$ (g', v_L), $Q_1 = Q_1$ (g', v_L), and $Q = Q1 + Q2 \leq L$
So minimal g' (minimal green time for the side road phase) is the function of L and v_L. It relates to parameters in the control logic with side road traffic and road conditions.

Maximal green time

Maximal green time is related to the green extension strategy. The maximal green time of the priority phase equals the maximal red phase of the non-priority phase. When a green extension is adopted, the queue remains after the completion of a whole cycle if the side road arrival rate is high and feeds into the initial queue in the next cycle (Figure 5). If the side road capacity has been determined, limits on maximal green time can insure that the back-of-queue will be shorter than the length of the lane.

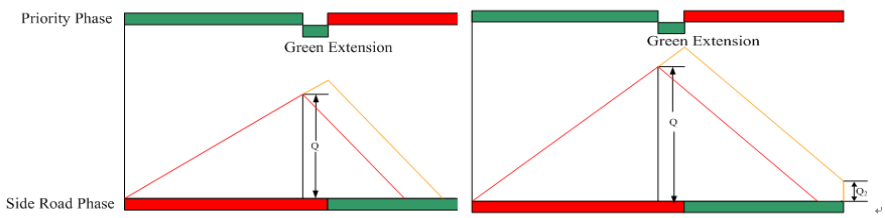

a) Side road arrival rate is low b) Side road arrival rate is high

Figure 5. Queue increase of Green Extension.

In a green extension strategy, $Q_{bl} = v_L t_a$ (t_a = extended green time), because

$Q_1(C'=C+t_a, v_L)+Q_2(v_L) \leq L$ so [t_a +g (the green time of the priority phase)] makes the maximal green time for the priority phase and is a function of L and v_L too. It ties the parameter of the control logic with the side road traffic and road conditions.

COMPENSATION STRATEGIES

Studies show that mainline benefits compared to side road drawbacks (measured in total hours per year) reveal a ratio of almost 9 to 1. Where a non-priority phase is curtailed due to a priority call, compensation can be afforded in two ways: the first is to compensate for the loss in exactly the next phase or to spread it over a period of time by simply increasing the normal green setting for the non-priority phase appropriately. However, compensation for time lost should be immediate and non-optimum normal maximums could lead to inefficient operation whenever the bus priority system is out of action (Muthuswamy, 2007).

In this paper, the compensation strategy is used as a standard function of TSP just after the priority phase (figure 6).

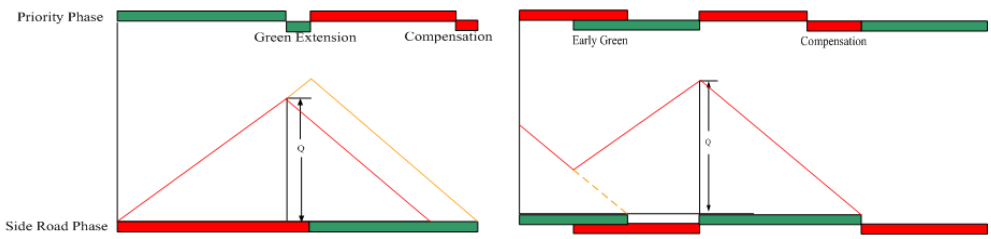

a) Green extension b) Early green

Figure 6. TSP with compensation.

In the green extension strategy, side roads can be compensated for lost time in TSP in the same cycle; in the early green strategy, side roads can be compensated in the next cycle. But if this time TSP is utilized again, it is the controller's task to determine whether or not to give compensation or TSP, balancing between the benefits of this side road's condition or the needs of buses (in a forecasted delay). This is the most effective compensation for side road traffic loss with the least impact on priority control continuity. In this way, intervals between requesting buses are required to be longer than at least one cycle and are easily met in most situations.

CONDITIONAL PRIORITY

The frequency of priority requests is important because an intersection may need some time to recover, i.e., to clear queues that have accumulated or to return to a background cycle to allow adequate traffic progress. If interruptions occur too frequently, the intersection may not get a chance to recover. By using conditional priority, the frequency of these interruptions will be responsively reduced.

Conditional priority systems can also be tailored to minimize their impact on

critical intersections by varying the "reliability" criterion from intersection to intersection. By using a looser criterion at the busiest intersections, the likelihood of interruption at those intersections goes down. Of course, accordingly, the likelihood of interruption at the succeeding intersections will go up. But by the same token, using a tighter criterion at one or two intersections upstream of a critical intersection will lessen priority requests at that critical intersection.

To evaluate the effects of conditional priority control in simulation, VISSIM and its VAP interface have been used to design and write the control logic (for the model setup, see Xu 2008). According to transit operation requirements, three reliability criteria are added to reduce TSP call frequency. Results are listed in Table 1.

Table 1. Summary of simulation result.

Criterions	Operation results	Side road impact compared to exclusive TSP
1 Transit speed	Average speed was 25.3km/h	Delay reduced by 15%
2 Schedule adherence	Performance improved by 22%	Delay reduced by 18%
3 Headway fluctuation	Headway variation contained in 15% (C1)	Delay reduced by 12%

*C1= coefficient of headway variation

CONCLUSION

This paper analyzed how priority control impacts side road traffic and ways to optimize key parameter settings like minimum green time and maximum green time. We also adopted conditional priority as well as appropriate compensation strategies. It is hoped that this transit signal priority system can adapt well to and alleviate excessive changes in side road traffic.

REFERENCES

Furth, P.G., and Muller, T.H.J. (2000). "Conditional Bus Priority at Signalized Intersections: Better Service Quality with Less Traffic Disruption". *TRB 2000 Annual Meeting CD-ROM,* Washington D.C.

Jia Xu, Chen, X., Wang, Y., and Yang, C. (2008). "The Study and Simulation of Detector Setup in Transit Signal Priority". *Presentation and publication at the 13th International Conference Proceedings of Hong Kong Society for Transportation Studies,* Hongkong, China

Lee, J. (2006). "TSP-Advance: An Advanced Transit Signal Priority System development and evaluation". *TRB 2006 Annual Meeting CD-ROM, 06-1339*, Washington D.C.

Satyanarayana Muthuswamy, P.E. "Evaluation of Transit Signal Priority and Optimal Signal Timing Plans on Transit and Traffic Operation". *TRB 2007 Annual*

Meeting CD-ROM, 07-1780, Washington D.C.

Skabardonis, A. (2000). "Control Strategies for Transit Priority." *TRB 2000 Annual Meeting CD-ROM*, National Research Council, Washington.DC.

Vasudevan, M., and Chang, G. (2001). "Design Framework for Integrating Real-Time Bus Priority Control with Robust Arterial Signal Progression." *TRB 2001 Annual Meeting CD-ROM*, *01-2474,* Washington, DC.

Vasudevan, M. (2005). "Robust optimization model for bus priority control under arterial progression". Ph.D. Thesis, University of Maryland

Wanjing Ma (2007). "Development and Evaluation of a Coordinated and Conditional Bus Priority Approach." *TRB 2007 Annual Meeting CD-ROM, 07-1154,* Washington D.C.

Short-term Traffic Flow Prediction with ACD and Particle Filter

G. Y. Zhang[1, 2] , Q. Zhao[1], Z.W. Luo[1], H.Wei[3]

[1]Shanghai Super Star Industrial Development Co., Ltd (Fu Dan University Post-Doctoral Station), 11th Floor, Shanghai Science & Technology Tower, No.285, Jian Guo Road West, Shanghai, P.R.C, PH (86-21)-64452140; FAX (86-21) 64452125; email: zhaoqiang1@gmail.com
[2]Shanghai Finance University, Shanghai, 201209;email: zhanggy@shfc.edu.cn
[3]Fudan University, Shanghai, 200433; email: weihui@fudan.edu.cn

ABSTRACT

Urban road traffic is a non-linear, non-stationary, and uncertain process; its uncertainty increases rapidly when making short-term (five minute-long) traffic flow prediction. The state-of-the-art in traffic flow prediction is reviewed here, including Time-Series, Artificial Neural Network, Ada-Boost, and Support Vector Machine based algorithms. A novel prediction method is proposed for short-term (five minute-long) traffic flow prediction. The time interval between vehicles is treated as a stochastic variable and described with the Marked Point Process in the ARCH (autoregressive conditional heteroskedasticity) framework. Different point processes may generate a corresponding ACD (autoregressive conditional duration) model for the prediction of time intervals between vehicles in the traffic's flow. A particle filter is applied with measured vehicle speed data for traffic flow speed and density prediction. We apply this algorithm to the Traffic Guidance System of the Cross-River Tunnel, Lujiazui, Pudong, Shanghai. Nine congestion levels are proposed and the prediction error for short time (five minute-long) is within three levels.

INTRODUCTION

Traffic prediction (Lingras Pawan, 1999) uses a dynamically retrieved traffic data series to predict future traffic status. In general, the basic parameters include traffic flow density, average speed, and the road occupancy ratio. Predictions can be divided into long-term and short-term types. Long term refers to intervals including thirty minutes, one hour, one day or longer. Short-term refers to short intervals such as five minutes, normally no longer than fifteen minutes.

Since the traffic flow is a real time, non-linear, high-dimension, and unstable stochastic process, the shorter sample intervals display more stochastic and unstable characteristics. It is related to the past traffic flow status of a current road segment and the up/down flow of an investigation point. In addition, the weather, traffic accidents, and environmental factors also impact the traffic flow process.

The real-time data analysis based on short-term traffic flow prediction is one of the important foundations for traffic information, traffic diversion, and control. A major body of work has been previously done in this area.

The main traffic prediction methodologies (Lingras Pawan, 2000; Ye Zhirui, 2003; Sun HY, 2003; Weng XX, 2006; Turochy R.E. 2004; Chen SY, 2006; Attoor Sanju Nair, 2006) include linear system theories, knowledge based intelligence models, a non-linear system theory, a combined model based method, and a traffic simulation-based approach.

The models yield different types of performance in terms of accuracy, time, response, and compatibility. Linear system prediction is precise and easy to operate, but it cannot match the accuracy and dynamic response requirements for a complicated road network. A knowledge-based intelligence model has strong data fitting ability; it can provide good prediction when a traffic accident occurs by utilizing required data input. Its shortcoming is the complication of an algorithm, parameter choice, and applicability. A non-linear system responds to non-linear characteristics of traffic flow systems. It affords a high level of accuracy but it requires complicated calculations. Its theory foundation still requires further research. The combined model-based prediction method may well combine the strengths of each model, which requires further investigation in determining the consistency among different models. An unsuitable combination may lead to big variations. In addition, its application requires complicated calculation, which is not suitable for a large-scale traffic system.

This paper proposes a novel five-minute-based traffic flow prediction method: with the Vehicle Detector (VD) under the road surface to measure the stochastic process of the vehicle passing interval, under the ARCH framework, we use the marked point process to describe the process. Different point processes present different ACD models which can be used for the vehicle passing interval description. The practical filter used for an unstable dynamics system can be applied to the prediction of average speed and traffic density with the statistical data from the VD. This algorithm has been used for the sample analysis of a traffic diversion project in the cross-river tunnel at Lujiazui, Pudong, Shanghai.

ACD MODEL

The ACD Model (Engle R.F.,1994) is created for the analysis of an event whose last period is based on the passed samples. It can convert the time interval among the events to a temporal points system. Different points processes may have different ACD models, the most simple one being the Poisson process.

Defining the interval as: $x_i=t_i-t_{i-1}$, t_i is the ith event occurence time, Ψ_i is the conditional expectation of the ith interval:

$$E(x_i \mid x_{i-1}, x_{i-2}, \cdots, x_1) = \psi(x_i \mid x_{i-1}, x_{i-2}, \cdots, x_1; \theta) \equiv \psi_i$$

The key point of this model is the hypothesis that the existing relationship is determined by the information of a history-based conditional expectation function, in addition, x_i and Ψ_i is independent on random variables with the same distribution, where the interval x_i has the following relationship with Ψ_i :

$$x_i = \psi_i \varepsilon_i$$

where $\varepsilon_i \sim i.i.d$ is an independent temporal series with specific distribution. Its density is $P(\theta, \phi)$, where θ, ϕ are estimated parameters. The ACD model has one simple form where the conditional expected value is only based on its historical intervals. This may be presented in the following functions:

$$\psi_i = \omega + \sum_{j=0}^{p} \alpha_j x_{i-j} + \sum_{i=0}^{q} \beta_j \psi_{i-j}, \quad i = 1,2,\cdots$$

Where, $\omega > 0$, $\alpha = (\alpha_1, \alpha_2, \cdots, \alpha_p) \geqslant 0$, $\beta = (\beta_1, \beta_2, \cdots, \beta_q) \geqslant 0$, $\gamma = \alpha + \beta < 1$, the stability of the random process is guaranteed. In addition, $x_0 = \Psi_0 = 0$, p and q are the delayed orders of the model. The ith interval's conditional aspect is determined by its delayed p conditional expectation and q historical intervals.

Here, we apply the simple but successful EACD (1,1) model to describe the vehicle detection intervals, E present for the ε_i exponential distribution.

$$\psi_i = \omega + \alpha x_{i-1} + \beta \psi_{i-1}, \quad \alpha, \beta \geq 0, \omega > 0, i = 1,2,\cdots$$

The parameters estimation of the EACD model uses the following function:

$$L(\theta) = -\sum_{i=1}^{N(T)} (\log(\psi_i) + \frac{x_i}{\psi_i})$$

PARTICLE FILTER

The basic synthesis of the Particle Filter (Doucet, 1998) is achieved by using a randomly sampled series and a sample weight to calculate the posteriori probability distribution. By making the suggested density distribution match the a priori density distribution, the series applies particle filtering steps, as shown in the following equations (m=1,2,⋯M):

Generated Particle: $x_k^{(m)} \sim p(x_k \mid x_{k-1})$

Calculated Weight: $w_k^{*(m)} = w_{k-1}^{*(m)} p(z_k \mid x_k^{(m)})$

$$\text{Weight Normalization:}\quad w_k^{(m)} = \frac{w_k^{*(m)}}{\sum_{m=1}^{M} w_k^{*(m)}}$$

$$\text{Estimation:}\quad E(g(x_k \mid z_{1:k})) = \sum_{m=1}^{M} g(x_k^{(m)}) w_k^{(m)}$$

Since the series weight-based method has the problems of weight depravation and particle exhaust, a re-sampling method may solve these two problems, by replicating the particles relative to the weight and by taking the random samples:

$$\left\{ \tilde{x}_k^{(m)}, \frac{1}{M} \right\}_{m=1}^{M} \sim \left\{ x_k^{(m)}, w_k^{(m)} \right\}_{m=1}^{M}$$

Where, x_k is the sample of a status vector at time k, then z_k is the measured vector at time k.

SHORT-TERM TRAFFIC FLOW PREDICTION

In the traffic guidance project at the Lujiazui Cross-river tunnel, Pudong, Shanghai, the 49683 recorded event intervals of 6:00-20:00 during 16/02/2009-20/02/2009. These are analyzed below; precisely 500 points are presented in Figure 1.

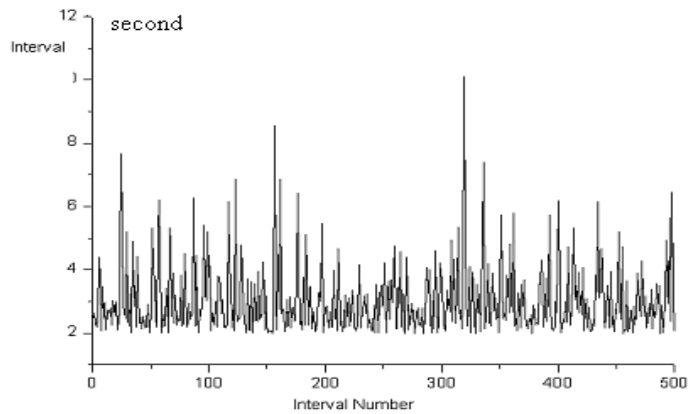

Figure 1. Vehicle Intervals.

The BHHH algorithm in the GAUSS system is used for EACD (1,1) parameters estimation, while the model may be written as: $\Psi_i = 0.126 + 0032 x_{i-1} + 0.932\ \Psi_i$, its validation is shown in Figure 2.

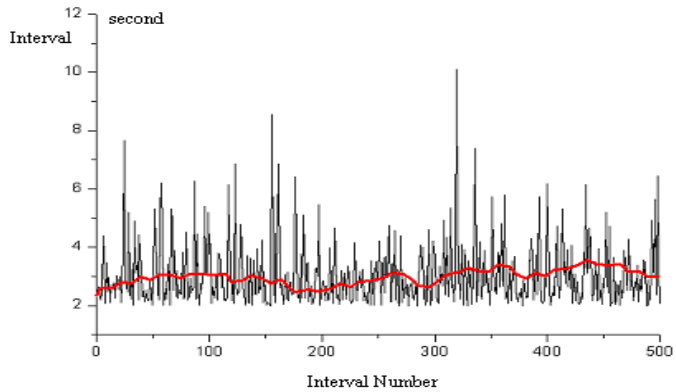

Figure 2. EACD (1,1) Model Fitting Result.

This model well describes the vehicle detection intervals, where the mean value is 3.5, five minutes are used as a traffic flow calculation unit. The short-term traffic prediction is the calculation for the intervals based on the EACD (1,1) model, where its status equation is:

$$x_i = \psi_i \varepsilon_i = (\omega + \alpha x_{i-1} + \beta \psi_{i-1})\varepsilon_i = (0.126 + 0.032 x_{i-1} + 0.932 \psi_{i-1})\varepsilon_i \,,$$

$$\varepsilon_i \sim Exp(1,1) \qquad 1)$$

Since it is the prediction of five-minute-based events in the future, without recorded data for validation, here the status value has a zero mean white noise which is used as the recorded value: $z_i = x_i + \mu_i$

Equation (1) is an non-linear status model which can only be well predicted with a PF method. Based on the algorithms presented in section 3, the result time series is $\{x_i/(x_1+x_2+\cdots+x_N) \leqslant 600\}$, where N is the predicted five-minute short-term traffic flow.

Figure 3 presents the recorded five-minute traffic flow data fit with the predicted value (the dot line is the recorded value):

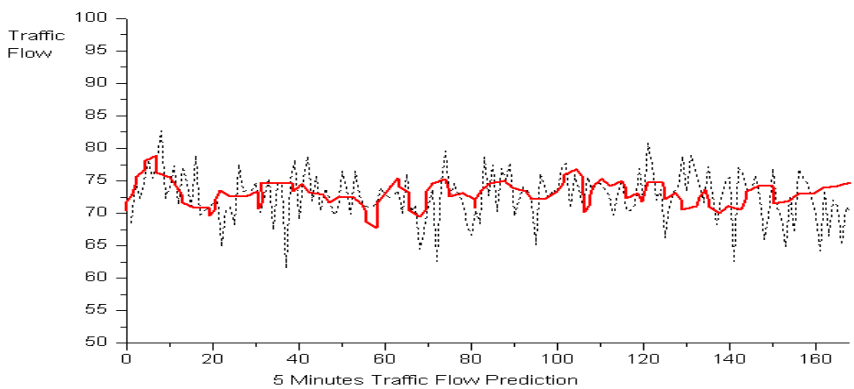

Figure 3. The prediction by particle filter.

The resulting well fitted recorded data may divide the road congestion to nine grades, where the five- minute traffic flow prediction error is within three grades, and may be used as the output of a guidance system.

CONCLUSION AND FUTURE WORK

This paper proposes the ACD model and PF combined approach for a short-term (five-minute) traffic flow prediction algorithm that was validated by using it with a city traffic guidance project. The desired effect was achieved.

Future research may be based on the choice between different ACD models for better description and prediction of traffic flow.

REFERENCES

Chen S.Y., Wang, W. (2006). "Traffic volume forecasting based on wavelet transform and neural networks" [C]. *3rd International Symposium on Neural Networks*. Chengdu, China, 2006. Heidelberg, Germany :Springer Verlag, 2006:1-7.

Doucet A. and Godsill S. (1998). "On sequential Monte Carlo sampling methods for Bayesian filtering" [R]. Cambridge: University of Cambridge, 1998:1-36

Engle, R.F. and Russell, J.R. (1994). "Forecasting Transaction Rates: the Autoregressive Conditional Duration Model." *NEBR Working Paper* 4966.

Nair, A.S., Liu, J., Rilett, L., Gupta, S. (2006). "Non-linear analysis of traffic flow" [C]. *IEEE Conference on Intelligent Transportation Systems*. Oakland, CA, USA:IEEE.

Pawan, L., Satish, S. C., and Gopalakrishnan, S.. (1999). "Short-term traffic volume forecasts: existing and future research" [C]. *Canadian Society for Civil Engineering-1999 Annual Conference.* Montreal ,Canada: Canadian Society for Civil Engineering,1999:429-438.

Pawan, L., Satish, S. C., Osborne, P. ,Iftekhar, K. (2000). "Traffic volume time-series analysis according to the type of road used" [J]. *Computer-Aided Civil and Infrastructure Engineering,* 2000, 15(5):365-373.

Sun, H.Y., Liu, H.X., Xiao, H., et al. (2003). "Use of local linear regression model for short-term traffic forecasting" [J]. *Transportation Research Record* 1783, 2003:143 — 150.

Turochy, R. E. and Pierce, B. D. (2004). "Relating short-term traffic forecasting to current system state using non-parametric regression" [C]. *7th International IEEE Conference on Intelligent Transportation Systems.* Washington D.C., USA, 2004. Piscataway, USA:IEEE,2004:239-244.

Weng, X.X. and Du, G.L. (2006). "Hybrid Elman neural network model for short-term traffic prediction"[C]. *8th IASTED International Conference on Control and Applications*. Montreal, Canada, 2006.Anaheim, CA,

USA :ACTA Press Anaheim,2006:281-284.

Ye Zhirui, Zhang Yunlong, and Middleton, D. R.(2003). “Unscented Kalman filter method for speed estimation using single loop detector data” [J]. *Transportation Research Record* 1968, 2006:117-125.

ALINEA-Based Urban Expressway On-ramp Local Metering Strategy

Fei Zheng[1],Yuchuan Du[2] and Lijun Sun[3]

[1]Ph.D.Candidate, Room 306, School of transportation Engineering, Tongji University, 4800 Caoan Road, Shanghai 201804, China; PH (86) 13918225569; FAX (86) 021-69588634; email: zftj9@hotmail.com

[2]Ph.D, Associate Professor, Room 306, School of transportation Engineering, Tongji University, 4800 Caoan Road, Shanghai 201804, China; FAX (86) 021-69588634; email: duyuchuantj@126.com

[3]Ph.D, Professor, Room 306, School of transportation Engineering, Tongji University, 4800 Caoan Road, Shanghai 201804, China; FAX (86) 021-69588634; email: ljsun@tongji.edu.cn

ABSTRACT

In response to on-ramp queue length and control-threshold restriction, an ALINEA-based local traffic-responsive metering strategy controls the Wuyi on-ramp in the Shanghai urban expressway network. The ALINEA parameter study results, integrating data analysis, determined the ALINEA parameter's values. The analysis of a local ramp's traffic-responsive metering mechanism fixes on its control-threshold parameters. The Wuyi on-ramp data analysis determines the control-threshold parameters and builds the Wuyi on-ramp control-threshold table. The queue-length subsection restriction model was built according to the analysis of an ALINEAR classic queue model given the Wuyi on-ramp's physical characteristics. The control-threshold and ALINEA algorithm and the queue length subsection restriction model constitute the Wuyi on-ramp local traffic-responsive metering strategy. The off-line simulation results show that this ramp metering strategy can not only even out the ramp volume's pulse characteristics but can also increase the mainline speed and relieve the mainline downstream congestion.

INTRODUCTION

Ramp metering, when properly applied, is a valuable tool for efficient traffic management on freeways and freeway networks (Emmanouil Smaragdis et al., 2004). Based on the results of several field implementations in European countries (M .Papageorgiou et al.,1991 and 1997), the ALINEA ramp-metering control strategy, proposed by Papageorgiou in the 1990s, has been shown to be a remarkably simple, highly efficient and easily implemented ramp metering application (Xu Yang et al., 2002). Simulation-based evaluation studies on a number of adaptive ramp-metering environments showed the competitive performance of ALINEA compared to other coordinated ramp metering systems (H.M.Zhang et al., 2001). Because of the high performance of this algorithm, ALINEA is an excellent tool when embedded into a coordinated ramp control or integrated control system (Xu Yang et al., 2002).

To ease the mainstream congestion caused by an urban expressway on-ramp pulse traffic stream and to mitigate the effects on the surface street caused by the

queue length at the on-ramp, it is necessary to undertake further study of the urban expressway on-ramp control strategy. The city's (internal) expressway on-ramp metering strategies may benefit from highway ramp control strategies and the experiences of other countries in reducing their urban expressway traffic congestion so as to improve the efficiency of our road networks. But the highway and the urban expressway have important differences, both in facility structures and in transport modes. So the Shanghai urban expressway on-ramp local-metering strategy cannot simply use the ALINEA algorithm but we here propose a control threshold and an extension of the queue length model to cooperate with the ALINEA algorithm. Simulation results and our analysis are presented in Section 4.

THE ALINEA STRATEGY

The ALINEA algorithm, a local feedback ramp metering strategy, attempts to maximize the mainline throughput by maintaining a desired occupancy on the downstream mainline freeway. The ALINEA strategy makes use of real-time traffic measurements in the vicinity of a freeway ramp, in order to calculate suitable ramp metering flows. It's activated at each time interval T. The metering rate, at the end of each running period T, is calculated based on the following formula:

$$r(k) = r(k-1) + K_R \times [O_{dir} - O_{out}(k-1)] \qquad (1)$$

Where r(k) is the ramp flow (in veh/h) to be implemented during the new period, k; O_{dir} is the desired occupancy (in %, typically, it is set equal to or slightly less than the critical occupancy) of the downstream detector station; then O_{out}(k-1) is the last measured downstream occupancy (in %), and K_R (in veh/h) is a regulator parameter.

The ALINEA algorithm has three parameters to be calibrated: the desired occupancy of the downstream detector station, the update cycle of each metering rate T, and a constant regulator K_R. The following is a summary of parameter settings used in previous research and implementations (Papageorgiou et al., 1990, 1991, and 1997; Xu Yang et al., 2002).

1. The desired occupancy can be equal to or close to the occupancy value at capacity, which can be found in the volume-occupancy diagram. Various values ranging from 0.18 to 0.31 have been found in previous applications.

2. Control results have been found to be insensitive for a wide range of values of the regulator KR, used for adjusting the constant disturbances of the feedback control. In real-world experiments, the algorithm has been determined to perform well for KR=70.

3. A wide range of values for the update cycle of the ramp-metering rate have been used: from 40 seconds to 5 minutes.

The ramp flow r(k) resulting from (1) is truncated if it exceeds a range [$MinR^T_{ramp}$, $MaxR^T_{ramp}$], where $MinR^T_{ramp}$ is the minimum admissible ramp flow and $MaxR^T_{ramp}$ is the ramp's flow capacity. This application of ramp metering may lead to the formation of an on-ramp queue. If it appears likely that the queue length exceeds a certain limit, such as that which interferes with the surface street traffic, ramp

metering is temporarily disengaged to allow a decrease of the ramp queue (Emmanouil Smaragdis et al., 2004). The ramp flow is truncated based on the following formula:

$$Max[d(k-1)-\frac{L_{\max}-l(k)}{T}, MinR_{ramp}^{T}] \le r(k) \le Min[d(k-1)+\frac{l(k)}{T}, MaxR_{ramp}^{T}] \quad (2)$$

Where d(k-1) is the ramp flow demand during the last period, k-1; L_{max} is the ramp maximum admissible queue length, and l(k) is the queue length at the beginning of the period k.

CONTROL THRESHOLD

The purpose of this study lies in the practical metering application of the Wuyi on-ramp in the Shanghai urban expressway network. The Wuyi on-ramp metering strategy cannot simply transplant the ALINEA strategy, which is successful in freeway ramp metering, but expands the ALINEA strategy according to the differences between the freeway and the urban (internal) expressway.

The differences between the freeway and the urban expressway may be classified as follows:

1) The mainline traffic flow and the ramp demand of urban expressways are clearly more than that of a freeway, especially the peak time ramp and mainline demand. Because the distances between the neighboring ramps of an urban expressway are much shorter than that of a freeway, the mainline traffic status of an urban expressway is more easily affected by its ramp flow.

2) The average trip distance on the Shanghai urban expressway network is less than five km, whereas drivers commonly use the freeway for long-distance travel. So the urban expressway users are more sensitive than the freeway users to the queue time. Though the urban expressway ramp length is shorter than the freeway's, the average ramp demand of an urban expressway is much higher.

Recent applications of ALINEA revealed a number of issues and needs that are not sufficiently covered by ALINEA or other available local ramp metering strategies (Emmanouil Smaragdis et al., 2004), including:

1) Use of upstream (rather than downstream) measurements.

2) Use of flow-based (rather than occupancy-based) set values and measurements.

The mainline traffic situation can be divided into three types: smooth traffic, traffic congestion and traffic jam. Therefore, the urban expressway ramp metering strategy may be divided into three types of control modes: no control, ramp metering and ramp closure. The control conditions, which decide the ramp status to be changed, constitute a control threshold table.

CONTROL CONDITIONS

No-control to ramp-metering

During the no-control status, ramp flow cannot commonly change the mainline status from free to congested. When the sum of the mainline upstream volume and the same time ramp flow exceeds a certain limit, such as the mainline

downstream capacity, the mainline traffic status can be changed to congested status. This control condition may be concluded from the following formula:

$$\begin{cases} q_{upstream} + q_{ramp} \geq CQ^{T}_{downstream} \\ o_{downstream} \geq O^{on}_{downstream} \end{cases} \quad \text{(no-control to ramp-metering)} \quad (3)$$

Where $q_{upstream}$ is the mainline upstream volume during the period T; q_{ramp} is the ramp flow at the same period T; $o_{downstream}$ is the real-time detecting occupancy of the downstream mainline; $CQ^{T}_{downstream}$ is the mainline downstream maximal admissible volume in the period T; and $O^{on}_{downstream}$ is the mainline downstream critical occupancy.

Ramp-metering to ramp-closure

When ramp-metering cannot ease the mainline downstream congestion and ramp flow may lead mainline traffic status to become worse, the on-ramp should be closed. For this control condition, the downstream mainline traffic situation is traffic congestion and the upstream mainline traffic demand is the main reason for downstream traffic congestion. The downstream mainline traffic congestion has affected the upstream mainline traffic. The ramp-metering to ramp-closure condition reads

$$\begin{cases} q_{downstream} \leq Q^{close}_{downstream}, o_{downstream} \geq O^{close}_{downstream} \\ s_{upstream} \leq S^{close}_{upstream} \end{cases} \quad \text{(ramp-metering to ramp-closure)} \quad (4)$$

Where $q_{downstream}$ is the downstream mainline volume during the period T; $o_{downstream}$ is the real-time detecting occupancy of the downstream mainline; and $s_{upstream}$ is the real-time detecting speed of the upstream mainline. For the ramp-metering to ramp-closure condition, $Q^{close}_{downstream}$ is the critical traffic volume of the downstream mainline during the period T, and $O^{close}_{downstream}$ is the critical traffic occupancy of the downstream mainline, and $S^{close}_{upstream}$ is the critical speed of the upstream mainline. These critical factors may be found through the traffic data analysis.

Ramp-metering to no-control

After the ramp is operating under metering status for some time, the downstream mainline traffic eases up again. If the ramp flow and the upstream demand meet certain conditions, the ramp status may change into no-control again. This control condition can be concluded by the following formula:

$$\begin{cases} q_{ramp} + q_{upstream} < CQ^{T}_{downstream}, o_{downstream} < O^{on}_{downstream} \\ s_{upstream} > S^{open}_{upstream} \\ t \geq N_{open} T \end{cases} \quad \text{(ramp-metering to no-control)} \quad (5)$$

Where t is the real-time detecting time; $S^{open}_{upstream}$ is the critical speed from the ramp-metering status to the no-control status; N_{open} is the minimum update cycle number when the ramp is at the ramp-metering status; and other factors are the same

with the formula (3) and (4).

Ramp-closure to ramp-metering

After the ramp is closed, the mainline traffic situation becomes increasingly better. Until the upstream speed and the downstream volume exceed these critical values and several update cycles have passed, the ramp may be changed into metering status again. This condition can be read:

$$\begin{cases} q_{downstream} > Q^{close}_{downstream}, o_{downstream} < O^{close-on}_{downstream} \\ s_{upstream} > S^{close}_{upstream} \\ t \geq N_{on} T \end{cases} \quad \text{(ramp-closure to ramp-metering)} \qquad (6)$$

Where $O^{close\text{-}on}_{downstream}$ is the critical occupancy of the downstream mainline, then N_{on} is the minimum update cycle number for the ramp-closure to ramp-metering control condition. Other factors are the same as in formula (3), (4), and (5).

Control Threshold Table

Through the analysis of the detecting data related to the Wuyi on-ramp metering strategy, from July 25, 2007 to July 31, 2007, these critical values were fixed and placed on the control threshold table of the Wuyi on-ramp metering strategy.

Table1. Control threshold about Wuyi on-ramp.

Control Condition	$o_{downstream}$	$q_{downstream}$	$s_{upstream}$	$q_{ramp}+q_{upstream}$	Time
No-control to ramp-metering					
Ramp-metering to ramp-closure	>30%	/	/	≥80pcu/**min**	/
	>45%	<30pcu/min	<20km/h		/
Ramp-metering to no-control	<30%	/	>40km/h	<80pcu/min	T≥5min
Ramp-closure to ramp-metering	<40%	>30pcu/min	>20km/h		T≥3min

QUEUE LENGTH SUBSECTION RESTRICTION MODEL

The ALINEA classical queue restriction model has proven to be efficient for freeway ramp metering. While the ramp demand of an urban expressway is heavier than that of a freeway, and the ramp queue space of an urban expressway is shorter than a freeway's, a more sensitive queue restriction model should be proposed.

Both $MinR^{T}_{ramp}$ and $MaxR^{T}_{ramp}$ are used in the freeway ramp metering strategies with experienced values (Xiao-peng Zhou, 2006)), so the new extreme values for the urban expressway ramp queue control models should be fixed, based on the following formulas:

$$CQ^{T}_{upstream} + MinR^{T}_{ramp} \xrightarrow[\infty]{} CQ^{T}_{downstream} \qquad (7)$$

$$AQ^{T}_{upstream} + MaxR^{T}_{ramp} \xrightarrow[\infty]{} CQ^{T}_{downstream} \qquad (8)$$

where $CQ^{T}_{upstream}$ is the upstream mainline capacity; $CQ^{T}_{downstream}$ is the downstream mainline capacity; and $AQ^{T}_{upstream}$ is the upstream mainline peak period

average volume in one period T. Based on the analysis of the traffic data related to the Wuyi ramp, $MinR^{T}_{ramp}$= 4veh/T and $MaxR^{T}_{ramp}$=24veh/T。

The urban expressway ramp is divided into an inclined part and a horizontal part. Queuing vehicles expect to wait at the horizontal part from a secure point of view. The queue length of the Wuyi on-ramp's horizontal part is L_{hor} and L_{hor}=36veh, and the queue length of the Wuyi on-ramp is L_{end} and L_{end}=92veh. A separate part of the ramp's horizontal part is designated the expected queue section, and the entire horizontal part and a part of the inclined ramp constitute the maximal queue section.

So the queue length subsection restriction model reads:

$$Max[d(k\text{-}1)-\frac{L-l(k)}{T}, MinR^{T}_{ramp}] \le r(k) \le Min[d(k\text{-}1)+\frac{l(k)}{T}, MaxR^{T}_{ramp}] \qquad (9)$$

If l(k)<20veh, then L= L_{exp};

If 20veh=<l(k)<36veh, then L= L_{hor};

If 36veh=<l(k)<64veh, then L= L_{max};

If 64veh=<l(k), then L=L_{end}。

Where L_{exp} is the expected queue section and L_{exp}=20veh; L_{max} is the maximal queue section and L_{max}=64veh. Other factors are the same as in Formula (2).

As compared to Formula (2), the advantage of this queue restriction mode is its great sensitivity. When l(k) is short, L is short too. So the L's sensitivity to the change of l(k) is improved. The lower boundary of r(k) increases with the increase of l(k). When l(k) exceeds a certain limit, L is changed and L's sensitivity to l(k) decreases. So the lower boundary of r(k) can't be a sustained increase. The queue length subsection restriction model makes the r(k) lower boundary increase more smoothly.

SIMULATION AND ANALYSIS

This on-ramp metering strategy was tested in a simulation environment which was coded by VB. The utilized parameter values were K_R＝70 veh/h, O_{dir}＝30 %, and T=60 sec.

Impact on the downstream mainline traffic

Table 2. Speed and traffic volume compare of main line.

RAMP STATUS	SPEED OF DOWNSTREAM MAINLIEN			VOLUME OF DOWNSTREAM MAINLINE		
	MAXIMUM (km/h)	MINIMUM (km/h)	AVERAGE (km/h)	MAXIMUM (veh/min)	MINIMUM (veh/min)	AVERAGE (veh/min)
NO CONTROL	66.70	12.30	26.13	72	30	59.36
METERING	60.88	20.89	44.06	77	21	55.89

The following is our analysis of the results of Table 2.

1) Speed in the downstream mainline increases palpably under the ramp metering. The statistics of a seven day period shows that as against no control, with this method, the average speed of downstream mainline increases by

17.93 km/h.

2) The average volume of the downstream mainline is 55.89 veh/min, which is close to the no-control average volume.

Though the average volume of the mainline is slightly less than the no-control average volume, the average mainline speed is much more than the no-control speed. Results from the simulation show that this ramp metering strategy can improve downstream mainline traffic conditions as compared to no control.

Impact on the Wuyi on-ramp

Table3. Impact on the Wuyi on-ramp.

MAXIMUM QUEUE LENGTH (PCU)	AVERAGE QUEUE LENGTH （PCU）	METERING TIME（MIN）
48	3.2	332

From Table 3, although ramp metering improves the mainline traffic conditions, the Wuyi on-ramp traffic flow is also affected. The maximum queue length over seven days is 48 pcu, which does not go beyond the L_{max}. The average metering time is 332 minutes and the average queue length is 3.2 pcu. So the queue length subsection restriction model keeps the queue length at an expected length and avoids interference with surface street traffic.

CONCLUSION

In this paper, an extension of the feedback local ramp metering strategy ALINEA for urban expressways was proposed, allowing the urban expressway ramp to have three control models, including no control, ramp metering, and ramp closure. The ramp control model was changed according to the comparison of the control threshold and the real-time detecting traffic data. During the ramp-metering cycles, the queue length subsection constraint model was proposed to avoid the ramp queue length exceeding the ramp's capacity for queue length. So this local metering strategy for an urban expressway may be constituted with three parts: a ramp-model control threshold, an ALINEA algorithm and the queue length subsection constraint model. The off-line simulation results show that the ramp metering strategy can both increase the main line speed and relieve the urban expressway main line downstream congestion. This queue length subsection constraint model also avoids an on-ramp queue's interference with surface street traffic.

ACKNOWLEDGEMENT

This work was supported by a grant from the National Science & Technology Pillar Program (No.: 2006BAG01A02)

REFFERENCES

Chu, L., Liu, X., Reocker W., and Zhang, H.M. (2002). "Performance Evaluating of Adaptive Ramp Metering Algorithm", submitted to *Journal of Transportation Engineering*

Lianyu, Chu and Xu Yang. (2003). "Optimization of the ALINEA ramp metering control using genetic algorithm with micro-simulation". *Transportation Research Board 82nd Annual Meeting*, Washington, DC.

Papageorgiou, M ., Blosseville, J-M., and Salem, H.H. (1990). "Modeling and Real-time Control of Traffic Flow on the Southern Part of Boulavard Peripherique in Paris;" *Coordinated On-ramp Metering, Transportation Research* vol.24A, no.5, pp.361-370

Papageorgiou, M., Salem, H.H., and Blosseville, J-M. (1991). "ALINEA: a local feedback control law for on-ramp metering", *Transportation Research Record*, vol.1320, pp.58-64

Papageorgiou, M., Salem, H.H., and Middleham F. (1997). "ALINEA Local Ramp Metering: Summary of Field Results," *Transportation Research Record*, vol. 1603, pp.90-98.

Smaragdis, E., Papageorgiou, M., and Kosmatopoulos, E. (2004). "A flow-maximizing adaptive local ramp metering strategy "， Transportation Research Part B: Methodological, Volume 38, Issue 3, March 2004, Pages 251-270

Xu Yang and Lianyu Chu. (2002). "GA-based Parameter Optimization for the ALINEA Ramp Metering Control". *The IEEE 5th International Conference on Intelligent Transportation Systems*, Singapore.pp.627-632

Xiao-peng Zhou. (2006). "Research on Urban Expressway on-ramp Control". Tongji University

Zhang, H-J. (2005). "Study on Coordinated Responsive on-Ramp Metering Methodology for Urban Freeway". Tongji University.

Zhang, H.M., Kim, T., Nie, X., Jin, W., Chu, L., and Recker, W. (2001). "Evaluation of On-Ramp Control Algorithm", *California PATH Research Report*, UCB-ITS-PRR-2001-36, University of California,Berkeley

An Active Parking Guidance Information System Based on Dynamic Agent Negotiation

WANG Longfei[1], CHEN Hong[1] and LI Yang[1]
[1] Department of Traffic Engineering, School of Highway, Chang'an University, Xi'an PH (86)29-82334886; Email: choseoner002@gmail.com (WANG Longfei); hongchen.good@gmail.com (CHEN Hong); dorothy06@gmail.com (LI Yang);

Abstract

In order to solve the parking problems in the metropolises, a new approach integrating active pattern for parking guidance information system including parking lots, cars, parking information service center and traffic management center is proposed. Active parking mode can avoid some inherent problems, such as low guidance obedience rate, low information resources utilization rate, as well as low overall system performance. Through implementing the self-interested negotiation among the functional entities of parking guidance system, an overall balance of interests can be achieved. Through using the intelligence, adaptability and collaboration of agents, the active parking guidance system can automatically execute park searching, parking price negotiation, parking space booking and parking routes negotiation and guidance.

Key words: Multi-agent System; Parking Mode; Active Parking Guidance; Negotiation Framework;

1. Introduction

During the fast-development of urban cites, the number of vehicles increase rapidly so that the parking demand is much greater than supply in metropolises. Thus the parking problem is serious than ever before. Currently, the Parking Guidance Information System (PGIS) is employed as a main technical measurement to solve the parking problem. The PGIS collects all the available parking information, and later releases all the processed information to the drivers with parking demand through various ways (radio, VMS, Web, telephone, short message). A typical architecture of existing PGIS is shown in Figure 1.

However, this general information-based guidance pattern can be defined as "passive parking guidance", which does not consider the activity, individual requirements, as well as the vital interests of the drivers and can't effectively solve the interests' conflicts problem between the whole traffic system and drivers, resulting in low parking obedience rate and weak collaboration performance.

This paper intends to apply the concept "activity" to establish an active parking guidance pattern which emphasizes the collaboration, interaction and negotiation between the PGIS and the drivers. It aims at providing a better connection for the two and thus maximizing the overall benefits of the PGIS and the parking

guidance service quality. Another contribution of our work is to establish the framework for the theoretical system of active parking negotiation.

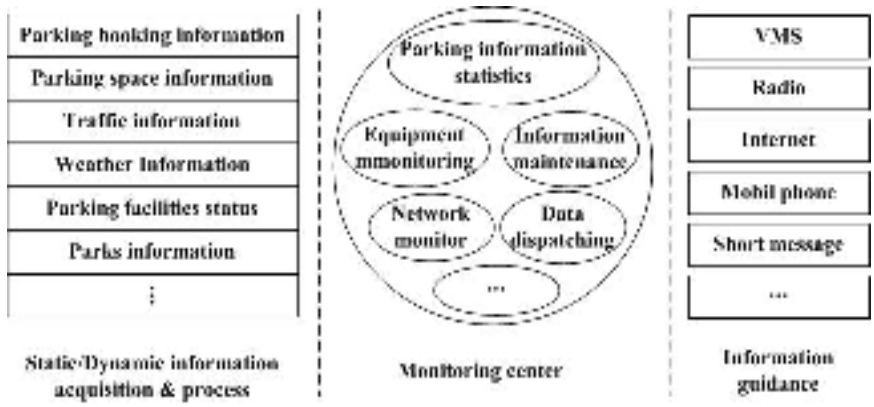

Fig. 1. A typical PGIS architecture

2. Limitations of traditional passive parking guidance

With the objective of the optimization of overall system, passive parking guidance pays more attention on the collection, processing, transmission, distribution of meta-information by parking and traffic, and treats the travelers as passive recipients in the whole parking-decision-making process, so this pattern neglects the activities, personal interests and individual needs of the travelers as active individuals.

Static parking routes guidance rarely considers traffic congestions. Even though dynamic parking routes guidance take into account the dynamic traffic assignment, due to the neglect of the travelers' personal interests, it cannot effectively solve the benefit conflicts (system optimum or individual optimum) between parking guidance system and the individual travelers, thus resulting in low parking obedience rate, weak comprehensive and collaboration performance.

To simplify these issues and data processing, the traditional passive parking guidance system adopts a number of idealistic assumptions conditions (travelers' behaviors are predictable or travelers all comply with the guidance information) to develop the traffic model and design of optimization algorithms (Chen O J W, 1998); however it is difficult to overcome the inherent shortcomings.

The processing of guidance information overly depends on statistical methods, fuzzy theory and mathematical programming model, which seldom takes into account the travelers' interests of. Even more, the characteristics of non-linear, dynamic time-varying and high distribution in the large-scale urban transportation system can also cause a rigid mechanism in passive parking guidance system.

3. Active parking guidance

3.1 Active traffic guidance

Active traffic guidance first appeared in the study of coordination between the urban traffic control system (UTCS) and urban traffic flow guidance system (UTFGS)

(Fisk C S, 1984). Traffic managers developed the control and guidance strategies for the transport network from the point of view of the entire system optimum, which conflicts with the individual traveler optimum. Therefore, in order to improve overall network performance, researchers began to study the coordination strategies between traffic managers and travelers while focusing on travelers by coordinating UTCS and UTFGS (Chen O J W, 1998), which is the initial active guidance mode with the participation of travelers.

However, such primitive coordination is based on the assumptions that travelers' behaviors are predictable or travelers all comply with the guidance information. Thus the methodologies, such as the evolutionary game theory, bounded rationality, artificial psychological and artificial emotion to study driver's response to the guidance information are applied. While the estimated traveler's demand is often inconsistent with the real situation and the travelers still accepted the information passively.

So, actually this primitive coordination is not an exact equitable negotiation between system managers and travelers' respective objectives. When the objectives of system and travelers are inconsistent, or even opposite, it is very difficult to achieve a valid coordination.

3.2 Active traffic guidance

Parking guidance system and the travelers are two different entities with different benefits seeking. They have a "competitive benefits" relationship in parking facilities, road resources, and time and space resources. The mode of coordination and cooperation in existing traffic systems cannot effectively solve the conflicts. Parking guidance system and the travelers need to start a negotiation based on their respective interests such that:

(1) Simultaneously improve user acceptance while enhancing net-work performance.

(2) Achieve an efficient reallocation of network capacity over time and space without seriously violating any individual user's preferences.

(3) Not to seriously affect the other parties and maximize their own interests.

Here, negotiation is also a kind of coordination, but put more emphasis on participants' activities in the coordination process, as well as the satisfaction of participants' interests. Therefore, the active parking negotiation between the parking guidance system and travelers needs deep negotiation, and can clearly demonstrate the self-interest of in the process of interaction, cooperation, thus conform to the real transport environment.

Negotiation theory has played an important role in intelligent UTCS and UTFGS. Negotiation will be the major activities in building the active parking guidance system. By using multi-agent technology for modeling traffic control systems, traffic management and decision-making can be easily implemented in the

form of interactive negotiation.

In recent years, new technologies, such as Vehicle Information Communication Systems (VICS), GPS, GIS, wireless communication, and mobile computing have gradually been applied into parking service systems. Agent technologies have the great potentials in solving the problems in the dynamic distributed and complex traffic environment (Hernandez, J. Z., 2002, Choy, M. C., 2003, Chen, B., 2008) and can be integrated with the new technologies mentioned before to provide a good solution and to establish the negotiation network and automation mechanism for the active parking guidance system with highly interactive and dynamic behaviors (Chou, S., 2008). The active agent-based parking negotiation network system architecture is shown in Figure 2.

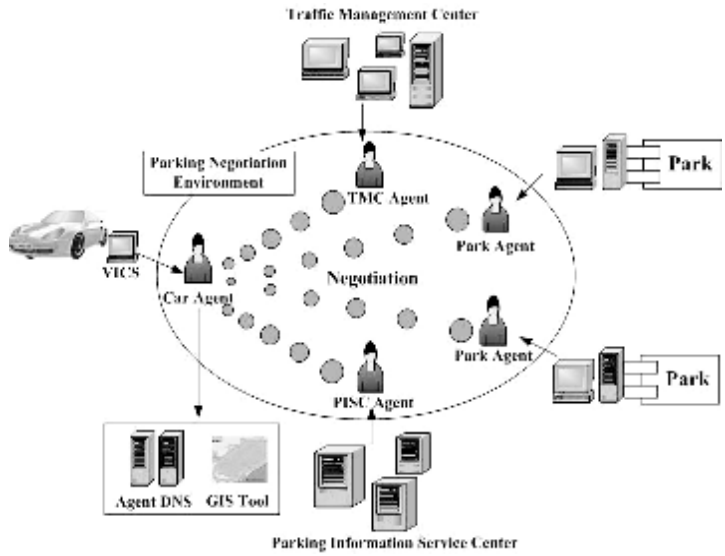

Fig. 2. Active parking negotiation network system

4. Negotiation framework system for active parking guidance

4.1 Negotiation activities under active parking guidance

Analyzing the negotiation demand of parking guidance system entities, including motor vehicles (Traveler), car parks, parking information service centers, traffic management centers, is the first step for designing the active parking guidance system. In order to study the internal parking guidance negotiation mechanism, parking system entities functions, behavioral characteristics, interactive mode, the characteristics of information, should be emphasized. The proposed active interaction among the functional entities is shown in figure 3.

4.2 Negotiation framework theory under active parking guidance

(1) Negotiation participants combining method

The determination of negotiation participants combining is the first step to ensure the effective negotiation functions. Before establishing all kinds of specific

negotiations, the challenge is to design a highly efficient, dynamic and flexible combination method for all the participants based on the participants' characteristics and negotiation environment.

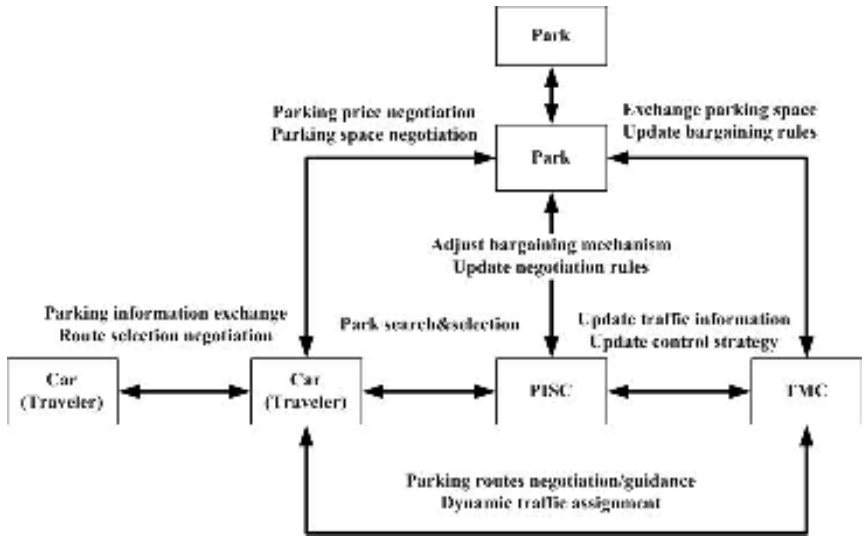

Fig. 3. Active interaction of the functional entities in PGIS

(2) Negotiation issue selection

Under different negotiation environment and information status, the selection of negotiation issue should base on the analysis of the characteristics and its impact on the overall parking guidance service standards, and specific negotiation activities.

(3) Negotiation primitive language design

Based on the characteristics of parking negotiation participants, contents and structure of interactive issues, interactive mode, specific scenes, and the specific information requirements of the participants, negotiation primitive language should be designed easily for the participant to clarify their intention.

(4) Negotiation protocol design

Effective negotiation protocol can improve the parking guidance efficiency, fulfill the requirements of real-time multi-point negotiation, speed up the flow of guidance information, reduce negotiation conflict, and finally ensure the efficient, safe and stable negotiation. To design the simple and efficient negotiation protocol, it should consider the characteristics and combining manner of all the negotiation participants, and the negotiation issue under specific negotiation activity.

(5) Negotiation strategies set design

Building of active parking negotiation strategies set requires a comprehensive analysis of the various possible negotiation combinations of participants and negotiation issue selection of active parking guidance under different specific negotiation environment and negotiation protocol.

(6) Negotiation decision-making model

Based on the negotiation combinations, characteristics of negotiation issue and the inherent complexity of parking guidance system, the design of negotiation utility computing model and evaluation model should include self-interest of participants (maximize their own interests), timeliness and non-precision in the processing of data, and to exactly express the true interests of participants.

5. Conclusion

Active parking guidance is an advanced method compared with traditional passive parking guidance. The concept of "Active" can avoid some inherent problems, such as low guidance obedience rate, low information resources utilization rate, as well as low overall system performance. The negotiation theory and method for active parking guidance proposed in this paper provides a theoretical support and a scientific basis for the active mode of parking guidance. Through realizing the self-interested negotiation among the motor vehicles (traveler), car parks, parking information service centers, traffic management centers, an overall balance of interests can be achieved. Intellectualization is the development direction for the parking guidance system. Integrating the "Active mode" with parking guidance system provides an absolutely new idea for the design and implementation of "intelligent" PGIS, and as well offers a targeted solution for the existing inherent problems in the PGIS.

6. Acknowledgement

This study is funded by the "China's Eleventh Five-year Plan"—"Engineering technology of Urban parking facilities (2006BAJ18B06)".

References

Fisk, C. S. (1984) "Game theory and transportation systems modeling." *Transportation Research,* 18B, 310-313.

Chen, O. J. (1998). "Game-theoretic formulations of interaction between dynamic traffic control and dynamic traffic assignment." *Transportation Research,* 179-188.

Choy, M. C. (2003). "Cooperative, hybrid agent architecture for real-time traffic signal control." *IEEE Transactions on Systems, Man and Cybernetics Part A: Systems and Humans*, 33 (5), 597–607.

Chou, S. (2008). "Dynamic parking negotiation and guidance using an Agent-based platform." *Expert Systems with Applications*, 805 – 817.

Chen, B. (2008). "Integrating mobile agent technology with multi-agent systems for distributed traffic detection and management systems." *Transportation Research Part C*, unpublished.

Hernandez, J. Z. (2002). "Multi-agent architectures for intelligent traffic management systems," *Transportation Research Part C*, 10 (5–6), 473–506.

Research on vehicle information extraction from high-resolution satellite images

Sun Qi[1], Liang Yanping[1] , Tan Qulin[2] and Zhang Sulan[1]

[1]MOE Key Laboratory for Transportation Complex Systems Theory and Technology, School of Traffic and Transportation, Beijing Jiaotong University, 100044, Beijing; PH (86)10-51687138; Fax (86)10-51688344; email: ypliang@bjtu.edu.cn;
[2] School of Civil Engineering, Beijing Jiaotong University, 100044, Beijing

ABSTRACT

A series of sensors on the pavements being used for traffic flow data detection have some disadvantages. With recent advances in high-resolution commercial remote sensing systems, detecting traffic flow data from remote sensing images over large regions is an attractive option in traffic information collection technology. The main goal of this research is exploring vehicle information from high-resolution satellite remote sensing images. A new method for vehicle detection based on object-oriented image analysis is developed and applied in this paper. Analyzing high-resolution satellite image characteristics, object-oriented segmentation is implemented here in order to generate image objects. Then feature space is created by extracting features of these objects, to be used for vehicle detection, classification, and traffic flow information analysis. Our experimental results as described and assessed here show how this method is effective. Our research provides a means of traffic flow information collection in ITS as compared to traditional approaches.

INTRODUCTION

Many studies reveal that advanced traffic data collection and traffic information extraction are a foundation for intelligent traffic guidance or reasonable traffic flow distribution in ITS. Since the 1970s, various technologies have been developed to explore traffic flow information from sensor data (Shi Zhongke, Cao Li, 2007). Recently more vehicle information has been extracted from traffic images using a ground-based video imaging system. However, due to the limited coverage of this method, we can't use it to access a wide range of traffic information at the scene. We expect to collect more valuable traffic data from a more distant perspective. With the development of commercial satellite remote sensing technology, we can use ideal image data to exploit traffic information for a global and detailed analysis (Eikvil, L., et al., 2008). The traffic data collection from satellite images has the potential to be a meaningful supplement for ground traffic monitoring systems in ITS.

The main goal of this research is to extract vehicle information from a high-resolution satellite image. This paper introduces a new method for vehicle detection based on object-oriented image analysis. By analysis of image characteristics, object-oriented segmentation is implemented to generate image objects, and the features of these image objects are extracted to build feature space, to be used for vehicle detection and classification, and furthermore for traffic information analysis. Lastly, the experiment is assessed, and the method for vehicle extraction proved to be valid.

METHODOLOGY OF OBJECT-ORIENTED IMAGE INTERPRETATION

Usually we use the naked eye to identify feature categories from images, and so-called visual interpretation. In this process, our eyes discern color, texture, shape and other characteristics of images. The higher the spatial resolution is, the more features we can analyze in detail, and the higher the accuracy of our classification will be. Yet most computer image analysis is based on pixels. A pixel's features, such as graying and texture, are analyzed, and the feature's differences are used to discriminate between categories of features in determining classification. For higher-resolution imagery, the differences increase not only among objectives but also in the internal parts of the objectives (Markham B L, et al., 1981). So pixel-based image analysis, applied in a high-resolution image, is very sensitive to noise and can lead to error classification.

Thus, to improve accuracy in classification, an image analysis unit becomes a homogeneity image unit (so-called image object), which is obtained by taking into account shape, texture and other characteristics. We can describe object-oriented image analysis to detect and classify vehicles from satellite remote sensing images as follows:

(1) Multi-segmentation under certain criteria creates image objects to build a hierarchical image object network;

(2) Extract image objects features to constitute feature space for classification;

(3) Execute classification algorithms to identify image objects in feature space.

VEHICLE INFORMATION EXTRACTION FROM A SATELLITE IMAGE

Segmentation

Image segmentation, the key step in image processing, is used to subdivide the entire image into regions to extract a target of interest. This paper takes multi-segmentation algorithm twice (see Figure 1), using bottom-up region merging technology from the pixel level to the entire image at different scales. Firstly, segment at large scale and create image object level-1 for road region identification, as this region is valid for traffic information extraction. Secondly, further segment at a small scale in the road region, which is identified on level-1 (see section 3.3). The second segmentation results, in the image object on level-2, are prepared for vehicle classification. Finally, the object network is constructed, affording the advantage that the object knows its neighborhood, its super-object and its sub-object (User Guide eCognition, 2007).

Figure 1. Multi-scale segmentation.

Segmentation criteria

The successful design of segmentation requires better criteria, including:

(1) Setting image layer weights w_L. It is necessary to expand differences among the objectives by increasing important layer weights (Jensen, J.R, 2005).

(2) Setting scale parameter. This depends on the classification task or the size of the objectives. For example, setting a larger scale can merge larger-difference image objects for road classification.

(3) Setting Composition of Homogeneity Criteria. A homogeneity Criterion is used as a synonym for minimized heterogeneity. Internally, three criteria are considered: color, compactness and smoothness. The relationship between them is shown in formula (1). Adjusting weights can create objects under different criteria. For example, adding color weight allows spectral-heterogeneity to the image so objects can emerge for the classification of bright vehicles, while a dark vehicle is distinguished by adding shape weight.

Multi-segmentation can be described using the following formula. Two image objects which have a lower difference f than a certain threshold T (determined by the scale parameter), can merge. So we adjust the w_{color} scale parameter, w_{color} and $w_{compact}$ to change the segmentation criteria (Ursula C Benz, etc. 2004).

$$\begin{aligned} f &= w_{color}h_{color} + (1-w_{color})h_{shape} \\ &= w_{color}h_{color} + (1-w_{color})[w_{compact}h_{compact} + (1-w_{compact})h_{smooth}] \le T \end{aligned} \quad (1)$$

The best segmentation criterion is not uniform because of its condition influence. To choose the best one, we have to compare segmentation results under different criteria.

Image objects

The primary segmentation produces objects with coarse heterogeneity on a large scale. We can identify some objects as part of the road because they are similar to it. After the road is identified, (see section 3.3), new information is generated to be used for the next segmentation. The second segmentation limited within the road region generates objects with more precise criteria for vehicle classification. In this way, the pixel level, the image object levels and the entire image compose a hierarchical object network.

Feature extraction

Features of the image object include color, shape and so on. In the hierarchical object network, the image object of each level corresponds to a feature vector, which constitutes the feature space (Guan Yuanxiu, 2008).

Depending on the demands of the road and the vehicle classification, both the Object Feature and the Class-Related Feature are extracted. The Object Feature is used to evaluate an image object itself as well as its location in the hierarchy object network. For example, using a "Mean" can identify both bright vehicles and road markings because of their more obvious mean range in good lighting conditions, while using a shape feature in the form of an external rectangular "Length", or by specifying the "Length/Width" feature, we can extract other artificial objects. Class-related features, constructed by referring to a classified image object (either in a vertical or neighbor relationship), can be used to classify the unclassified image objects. For example, using the above-mentioned Object Feature can easily classify part of the road surface but not all of it. In the rest of the region, the border and the road markings embedded in the road surface can be classified by class-related features. For example we can use the feature of "relative border to classified objects" in order to classify the border and the road markings with a value more than 0.5 or even close to 1.

Classification

Classification is the process by which we link image objects with a class hierarchy. Using a certain classification algorithm, we can classify each image object to a specific category (or unclassified), which is executed according to the difference of features in section 3.2.

For high-resolution remote sensing images, it is difficult to classify image objects as a particular type that only depends upon a single feature. Fuzzy classification is a powerful soft classifier that uses a membership function to replace its feature value with a membership value for a certain category (between 0-1 fuzzy values) (Benz, 2004). If the value is in the required range, the image object will likely belong to a certain defined class, and if it is out of range, it will of course not belong to that class. Considering different objectives to extract, here are two fuzzy classification algorithms, the Conditions Combination for bright vehicle classification and the Nearest Neighbor algorithm for dark vehicles.

Regional restriction for vehicle information extraction

Selecting "Ratio" and "Length/Width" features to identify the road region, the process is described as follows:

$$if\,[Ratio(object) \in RLR]\ AND\ [Length/width(object) \in RL/W],\ then\ land\ cover(object) = road \tag{2}$$

RLR, RL/W are allowed the "Ratio" and "Length/Width" ranges of the image objects of the road.

Formula 3 can classify part of the road's objects but not all the real-world road objects. In the rest of the unclassified objects, some objects can be classified further. This process can be described as follows:

$$if\,[rel.border\ to\ Road\ Region \in RB],\ then\ unclassified(object) = road \tag{3}$$

Using the "relative border to" feature, RB is limited within the range of another road region, such as its boundary or road marking.

Bright vehicle classification

On a small scale, bright vehicles contrast sharply with road objects, considering their spectral characteristics. So after extracting its features, a bright vehicle can be detected further with features, such as "Mean," "Area" and "Length/Width." So on the basis of the description above, the following process should be added:

$$\begin{aligned} &if\,[Length(road\ object) \in VL]\ AND\,[Width(road\ object) \in VW] \\ &AND\,[Length/Width(road\ object) \in VL/W],\ then\ road(object) = vehicle \end{aligned} \tag{4}$$

VL, VW and VL/W are used to limit the range of image objects' $Length$, $Width$, $Length/Width$.

Dark vehicle classification

With its low contrast, a dark vehicle can be identified by various features. The color and texture of a dark vehicle are not obvious and internal gray value is heterogeneous. If we use the Conditions Combination described in section *Bright vehicle classification*, it will result in error classification. Thus, we take advantage of the nearest neighbor algorithm to classify a dark vehicle in the feature space. First, we select a feature and edit the "Nearest Neighbor" membership function, and the slope of that function determines the membership value of its image objects. The image objects,

closer to the samples, are probably identified as being in a certain class, and then classified according to the category of the nearest sample.

EXPERIMENT AND DISCUSSION

Figure 4 shows a high-resolution image with a scene of a road link in a certain city. Orthorectified image data (after radiometric correction and orthorectification) was selected from QuickBird, including four spectral bands (red, green, blue and Near IR), and a panchromatic band. The spectral bands with 61cm (2ft) or 70m (2.3ft) resolution are suitable for texture analysis, and the panchromatic band with 2.44m (8ft) or 2.80 (9.2ft) resolution is fit for spectrum analysis (Digitalglobe Inc, 2009). We cut out part of the image as a study area, and combined layers of R, G, B bands to form a true color image after its histogram equalization (see Figure 2).

Figure 2. True color image after histogram.

Segmentation at large scale

We set the band layer weights to R: G: B: NIR: Pan = 1:1:1:0:1. The high-resolution image, especially the true color image, is more distinguishable （Jensen, J.R , 2005; Dai Changda, et al., 2004).

The segmentation results were analyzed to determine which parameters of criteria afford better results under these conditions (see Figure 3). Segmentation at a small scale, such as 100 or 300, yields a complicated result which is difficult to classify the road region. Segmentation at a 600 scale generates image objects, and some of them are similar or close to road objects, which are useful for classification. So we can set the scale parameter to 600, set the shape as 0.1, and the compactness as 0.5 respectively.

Figure 3. Segmentation at a 600 scale,Classification using Object Feature and Class-related Feature.

After the primary image segmentation, object features such as "Ratio" (the ratio of a green band layer) and "Length/Width" were extracted, so we could identify part of the road. The class-related feature such as "Relative Border to" was extracted for further road object classification. If the feature value was more than 0.4, the boundaries and the road markings within the road region were classified as a road category. We repeated this classification process twice, and then got the result.

Segmentation at small scale

In the road region, we executed a second image segmentation on a small scale. We could choose the best scale value by comparing all the segmentation results with different scale values and different heterogeneity values. It is important for bright vehicle identification to increase the color weight. However, an appropriate shape

parameter often improves the quality of the identification. We discovered that the best criteria settings are where scale, shape and compactness are respectively set at 80, more than 0.3, and 0.5, and the result can be seen in Figure 4.

Figure 4. Segmentation under certain criteria.

Vehicle information extraction

Bright vehicles with obvious mean and shape features contrast sharply with other image objects, which are marked with black pixels (see Figure 5). This image was obtained by applying the Conditions Combination classification algorithm.

Figure 5. Bright vehicles classification

Dark vehicles requiring more features for identification can be classified using the Nearest Neighbor classification in the feature space. As shown in the Nearest Neighbor membership functions (see Figure 6), the length membership function is wider than others, which implies that length is not the most important feature for dark vehicle classification. In Figure 6, the dark vehicles are marked in blue.

Figure 6. Nearest Neighbor membership functions and dark vehicle

Assessment

More tests were implemented, and a nearly 10% error ratio exists by comparing the automatic extraction with visual interception. The error-classification mainly occurs in the shadow region.

CONCLUSION

This study focused on vehicle information extraction from high-resolution satellite images by using object-oriented image analysis. Different features were used to extract bright vehicles and dark vehicles separately and acceptably accurate classification was obtained. However, there are still some error classifications, and the shadows of vehicles and buildings are the main reason. Thus, it will be necessary in the future to eliminate shadows in the pre-processing of satellite images. In addition, we extracted vehicle information from satellite images of a one-way street and did not include a two-way street. So both shadows and two-way traffic flow will be taken into account in further research.

ACKNOWLEDGEMENT

This study was supported by the National Natural Science Foundation of China (40801121)

REFERENCES

Benz, U.C., Hofmann, P., Willhauck, G., Lingenfelder, I., and Heynen, M. (2004). "Multi-resolution, object-oriented fuzzy analysis of remote sensing data for GIS-ready information". *ISPRS Journal of Photogrammetry & Remote Sensing*, 58, 239–258.

Dai Changda, Jiang Xiaoguang, Tanglingli (2004). *Remote sensing image application processing and analysis*, Tsinghua Press, Beijing.

Digitalglobe Inc (2009). *QuickBird Orthorectified Satellite Imagery Guide*, http://www.digitalglobe.com/index.php/48/Products?product_id=7.

Eikvil, L., Aurdal, L., and Koren H. (2008), "Classification-based vehicle detection in high-resolution satellite images". *ISPRS Journal of Photogrammetry & Remote Sensing*, doi:10.1016/j.isprsjprs.

Guan Yuanxiu, Cheng Xiaoyang (2008). *Guide for high-resolution satellite images processing*, Science Press, Beijing.

Jensen, J.R. (2005). *Introductory Digital Image Processing: A Remote Sensing Perspective*, China Machine Press, Beijing.

Markham B. L. and Townshend J. R. G. (1981). "Landcover classification accuracy as a function of sensor spatial resolution". *Proc 15th international symposium of remote sensing of environment,* Ann Arbor. 1075.

Shi Zhongke, Cao Li (2007). *Traffic image Detection and Analysis*, Science Press, Beijing.

User Guide eCognition (2007). Website: http://www.definiens.com.

Map Matching Algorithm of a Center Terminal Based on the Road Network Topological Structure

Yang Zhaosheng[1] and Wang Zhijian[2]

[1]Yang Zhaosheng, Department of Traffic and Transportation, JiLin University, Changchun, Jilin; email: yangzs@mail.jlu.edu.cn
[2]Wang Zhijian, Department of Traffic and Transportation, JiLin University, Changchun, Jilin; email: wzjian0722@163.com

ABSTRACT

Using a traffic guidance system, we studied the map-matching algorithms of a center terminal to monitor the probe vehicle real time and obtain vehicle traffic information when driving. Realizing that the GPS information period is too long in the center terminal, we are introducing the idea of partitioning the road network into grids and are proposing a map-matching algorithm. Our process is suited to a complicated road section in a big city, based on the road network's topological structure. The results of our simulation of real driving data show that this map-matching algorithm affords higher accuracy and can better solve the matching problem for complex road networks in cities.

INTRODUCTION

The development and maturity of GPS technology provides a powerful method of identifying vehicle's accurate positioning in real time。In intelligent transportation systems, the exploitation and application of vehicle navigation and monitoring systems are achieved gradually. Probe vehicle technology is a new kind of traffic information collecting technology It collects vehicle GPS data at a large scale and monitors the city's traffic condition. Creating a map-matching algorithm of a center terminal is the core problem of the probe vehicle technology. A map-matching algorithm of a center terminal has the following negative characteristics: the GPS data scale is big (about 14,000 vehicles), the adjacent GPS of the same vehicle signal period is too long (20s-60s), and relevant information between GPS points is poor. In this paper, we designed a map-matching algorithm of a center terminal based on the road network's topological structure, verified with the vehicle GPS data of Guang Zhou City. The results show that the map matching algorithm has a high level of precision and efficiency, which can meet the needs of Guang Zhou City's high-capacity.

GPS DATA ANALYSIS AND PROCESSING

The quality of GPS data is the basis of the map matching. GPS data is often lost or inaccurate in urban canyon environments where GPS signals are often blocked by high-rise buildings (Mohammed et al. 2007). For the data to be uploaded to the center terminal, we must first process the data. We put the abnormal GPS data into different categories and put forward corresponding methods of treatment. Abnormal data is mainly divided into static drifting data, incorrect data, and dynamic drifting data, as follows.

Static drifting data

If the vehicle drives at low-speed or stops, GPS data will be static drifting data. For a random drifting of GPS positioning errors, it makes the system give the vehicle positioning information at the current actual location for the center of a circular area with a random jitter. The method by which we can judge the drifting data is described as follows:

If the vehicle's speed is less than 2m/s, we can calculate the distance between the current point to pre-positioning points (for which the design admits 3). If the distance between these is less than the normal GPS positioning error upper limit, that indicates that the current vehicles are either driving at low-speed or stopping. Now the corresponding matching points of the current points should be the true location of the vehicle, (instead of being just the current positioning of the follow-up matching point). This should be the case until the vehicle speed is higher than 2m/s.

GPS signal interruptions and inaccuracies

GPS receivers can display some abnormal conditions, such as: continuously unchanging GPS information; lack of GPS information; or a vehicle's sudden increase in speed that is very high (more than 35m/s) and so on. The abnormal data are directly removed.

Dynamic drifting data

Since GPS signals are often blocked by high-rise buildings, it can render the distance of two adjacent GPS points as higher than a certain threshold. We consider the GPS data to be dynamic drifting data. The dynamic drifting data are directly removed too.

MAP-MATCHING ALGORITHMS

Fixing The Candidate Road Segment

The first step is to obtain the candidate road segment of map-matching. If we acquire the GPS positioning data, we can draw the candidate road segment from the digital map database by its error region. This way, we can reduce the number of candidate road segments and the computing time of map-matching. The selection of a candidate road segment should reduce its computational volume, conserve memory, and ensure the algorithm in real-time. We select the candidate road segment twice in order to reduce its computational complexity.

First Selection of the Candidate Road Segment

We introduced the idea of partitioning the road network into grids, in which the recorded road segment intersects with the grid or is contained in the grid. To increase the efficiency of this searching process, all grids are stored according to serial number order. After acquisition of the GPS data, we find the GPS location grid by half seeking. Since the GPS point may be in the border of the grid, we first select a 3 S * 3 S grid area in which nine grids link up together and we can obtain the road segment information that these grids store at the same time. The example in Table 1 follows. When the GPS is in grid 6, the sifted area finally includes the grids 1, 2, 3, 5, 6, 7, 9, 10 and ll (FU Mingjie et al. 2005).

Table 1. 3 S *3 S grids area.

1	2	3	4
5	6	7	8
9	10	11	12
13	14	15	16

We fix the candidate road segment by two different forms which are determined by the quality of the GPS data.

(1) When it contains the GPS initial matching points or when the last GPS data is removed as abnormal, we can fix the grid number which the GPS point is in and extract the candidate road segment which is stored in the grids at the same time.

(2) When the last GPS point can be matched as normal, we use the road network topology to determine the candidate road segment of the current GPS point. When the center terminal gathers GPS data of the same vehicle in a period interval, the vehicle may drive over some road sections. We need to do the depth searching for the two ends of the matching road in the road network. The algorithm begins with the two end points of departure, using a heuristic search for the information of adjacent points in a certain region. We then fix the candidate road segment which has topological connectivity to the matching road (Zhang et al. 2007). We control the heuristic searching number of adjacent points to control the scale of the region, which determines the number of candidate road segments. The example in Figure 1 follows.

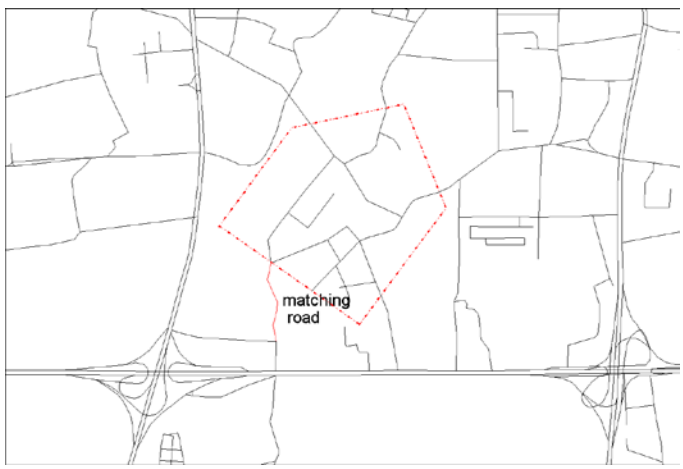

Figure 1. Candidate Road Segments by Heuristic Search.

The Secondary Selection of the Candidate Road Segment

We carry out the secondary selection of a candidate road segment based on previous accumulated experience.The rules are as follows:

(1) If the angle between the direction of a moving vehicle and the direction of a road exceeds the acceptable threshold, we regard the road as not appropriate for the candidate road segment.

(2) If the distance between GPS points and the candidate road segment exceeds the acceptable threshold, we regard the road as not appropriate for the

candidate road segment.

(3) We do perpendicularity projection from the GPS point to the candidate road segment. If the projection entirely matches the road, we regard the road as the candidate road segment. If the projection does not match the road (matching up to the road's extended line), we do not regard it as the candidate road segment.

(4) In the background database of the navigation electronic map, we confine the direction of traffic flow for each road. We select the candidate road segment by judging the vehicle direction according to the permitted direction of the road.

Elevation-Assisted Map-Matching Algorithm

Algorithm rules: when there is only one candidate road, we can directly match it. If the candidate road segments are more than one road, we cannot directly match them, since this requires the adoption of road network topology relations and GPS information to calculate matching degrees. In the map-matching algorithm, we calculate the degree of map matching, using three parameters: the angle between the direction of a moving vehicle, the direction of a road, its distance, and its elevation.

$$f(d,\theta,z) = w_d \bar{d} + w_\theta \bar{\theta} + a\bar{z}$$

Function $f(d,\theta,z)$ consists of the matching degrees of candidate road segments. w_d, w_θ and a represents respectively the weights of the angle, distance, and elevation of matching degrees, satisfying the formula $w_d + w_\theta = 1$ and a has a value of 0 or 1. When the vehicle is near a viaduct, a has a value of 1, otherwise a has a value of 0. When the vehicle is near an intersection, w_d has a value of 0.4 and w_θ has a value of 0.6, otherwise w_d has a value of 0.6 and w_θ has a value of 0.4.

$$\bar{d}_i = \frac{1/d_i}{\sum_{i=1}^{n} 1/d_i}, \quad \bar{\theta}_i = \frac{1/\theta_i}{\sum_{i=1}^{n} 1/\theta_i}, \quad \bar{z}_i = \frac{1/z_i}{\sum_{i=1}^{n} 1/z_i}$$

In the formula: n represents the number of the candidate road segment; d_i and θ_i represent the distance and angle of the candidate road segment in which the road segment is marked i. Normally, d_i and θ_i cannot be valued as 0. If d_i or θ_i equal 0, we define them with a very small value, where $\bar{d}_i$ and $\bar{\theta}_i$ represent the nuisance value of the distance and angle of the candidate road segment (Christopher et al.2000).

The matching process is as follows: first, we calculate all the matching degrees of candidate road segments. Second, we select the maximal matching degree f_m and the secondary maximal matching degree f_n. Third, we calculate the formula $f_m - f_n > f_{th1}$ (f_{th2} is introduced to distinguish the road segment which has close matching degrees and a value of 0.2) and $f_m > f_{th2}$ (f_{th2} is the credible matching degree with a value of 0.8).

Delay Map Matching

When the matching degree cannot satisfy the matching requirements, we do

not match the GPS at once and save the longitude and latitude of the GPS point and acquire the next GPS's point information. We then match the next GPS point. We repeat the above process until one GPS point can be matched. We match the GPS point using the topology between the GPS point whose point we did not match and the point we can match. If the GPS point still cannot be matched, we consider building the shortest path between the GPS point which we cannot match. The driver is able to choose the shortest path to the next point by empirical experience. The delay map-matching process is shown next in Figure 2.

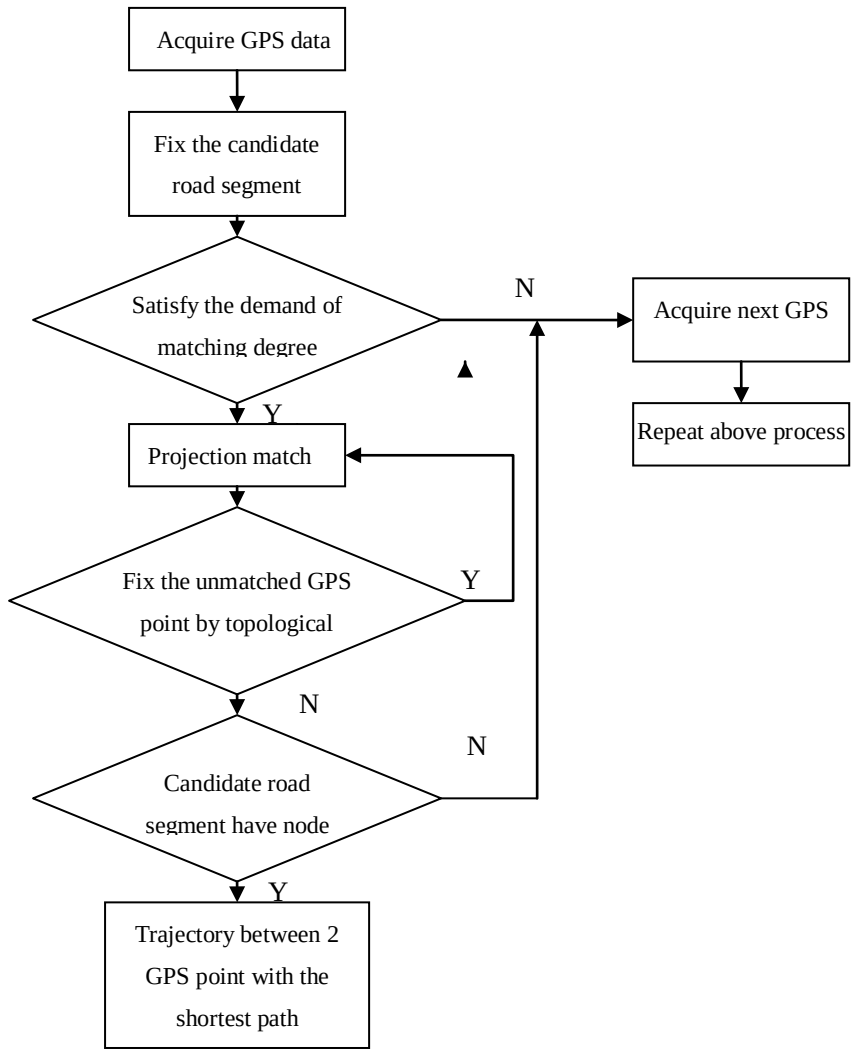

Figure 2. Delay map matching process.

Map-Matching Algorithm Process

The map-matching algorithm process is as follows:

(1) Acquire the GPS data information when time is T;

(2) Judge whether the GPS data is available or not. If the data is not available, go to 12;

(3) Judge whether the vehicle is moving at low speed or stops or not. If it is moving slowly, go to 12;

(4) Judge whether the GPS data is dynamic drifting data or not. If it is, go to

12;

(5) Judge whether the last GPS data is normal or not. If it is abnormal, go to 6, otherwise go to 7;

(6) Make sure the number of the grid where the GPS data is in, draw the road segment information and fix the candidate road segment. Go to 8;

(7) Fix the candidate road segment through heuristic searching and go to 8;

(8) If we do not get a candidate road segment, go to 9; If we get one candidate road segment, g to 10; If we get more than one candidate road segment, go to 11;

(9) Put the GPS point as the real position, go to 12;

(10) Carry out the projection match and acquire the latitude and longitude, go to 12;

(11) Calculate the matching degree of the candidate road segment. Judge whether the matching degree meets the necessary requirements or not. If the matching degree meets the requirements, go to 12. Otherwise, go to delay matching;

(12) Acquire the next set of GPS information.

ALGORITHM VALIDATION

We validated the algorithm using GPS data and a navigation electronic map for Guang Zhou. For the map matching of its center terminal, we analyzed the topology between the candidate road segments of adjacent GPS points for the same vehicle. We extracted the GPS data of one probe vehicle from the traffic information center and carried out map matching, using the algorithm we created. The effect in Figure 3 displays the drawing of our map matching when the vehicle is around the viaduct.

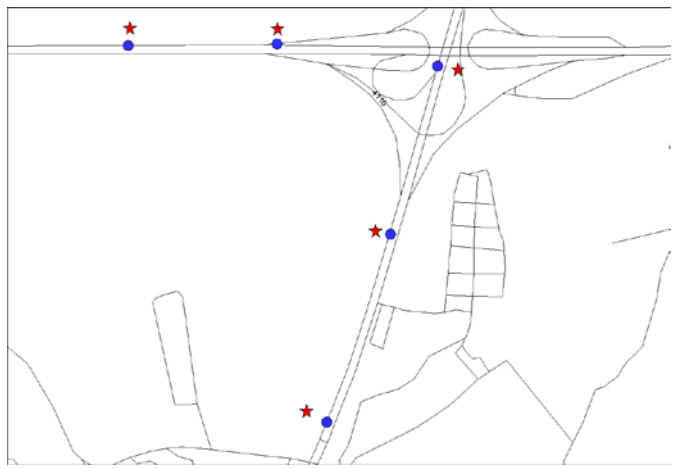

Figure 3. Map matching around viaduct.

CONCLUSION

The need for a map matching algorithm of the center terminal is the core problem of probe vehicle technology. In this paper, we created the complete map-matching algorithm of a center terminal based on the road network topology, which

is validated by the GPS data of a probe vehicle in Guang Zhou City. Our result shows that the algorithm can effectively fulfill the map matching of 14,000 cars equipped with GPS in real time with higher accuracy, to better solve the matching problem when the vehicle is in a complex road network and near a viaduct.

REFERENCES

Fu Mingyin and Li Jie. (2005). **"**A Quick Map Matching Algorithm for Vehicle Navigation Systems," *Transactions of Beijing Institute of Technology*. Vol 25, No.3, 226-229.

Quddus, M. A. (2007). "Current map-matching algorithms for transport applications: State-of-the art and future research directions," Transportation *Research Part C* 15 (2007), 312–328.

White, C. E., Bernstein D., and Kornhauser, A.L. (2000). "Some map matching algorithms for personal navigation assistants." *Transportation Research Part C* 8 (2000), 91-108.

Zhang Wei, Xu Jianmin, and Liu Mianfeng. (2007). **"**Map Matching Algorithm of Large Scale Probe Vehicle Data." *Journal of Transportation Systems Engineering and Information Technology*. Vol 7, No.2, 40-45.

An Improved A* Algorithm for the Intelligent Transportation System

Li Yan[1] and Gao Yang[2]

[1]School of Information Engineering, Chang'An University, No. 126, Yanta Road, Xi'an, P.R. China, 710064, PH (86)29-84749299; FAX (86)29-84749299; email: xaliyan72@163.com
[2]Xi'an Surveying and Mapping Institute, No 1, Yanta Road, Xi'an, P.R. China, 710054; PH (86)29-84749207; FAX (86)29-84749029; email: xagpsgy@163.com

ABSTRACT

In an intelligent transportation system (ITS), route planning is very important for vehicle navigation. It is necessary to optimize the algorithm of route planning to meet the real time requirement of the system. Based on the analysis of the temporal complicacy and spatial complicacy of the A* algorithm, this paper proposes a modified A* algorithm which can run much more efficiently compared to the original A* algorithm. First, this paper adopts the data structure of a binary heap, not a linear array, to implement the operation of its priority queue and to successfully improve the efficiency of searching the minimum cost node. Secondly, according to the special spatial distribution feature of the road network, a search mechanism to restrict the search district is introduced here, which can greatly reduce the search data volume of the algorithm. Finally, this paper makes tests in a real road network in Xi'an. The tests also prove that the modified algorithm is workable and time-saving.

INTRODUCTION

The intelligent transportation system (ITS) is thought of as the best method with which to solve the problem of traffic congestion all over the world. Route planning is an important basic function of the system, and is also a popular area of research in this field.

The core of route planning is the search for the shortest route (Wang, 2007), and nearly twenty kinds of shortest route search algorithms have been discussed and are widely used at present. According to their search mechanisms, these algorithms can be divided into three kinds: breadth-first search, depth-first search and heuristic search (Lu, 2001).

Among these, the A* algorithm adopting the best-priority search mechanism is a relatively advanced heuristic algorithm, and it is highly effective in searching for the shortest route in a road network. However, because the route planning function is used frequently in the system and the computational complexity of its algorithm is high, it is necessary to further optimize the A* algorithm to meet the real time requirements of a practical system.

A*ALGORITHM (Zhao, 1999; Xia et al., 2001)

A distinct feature of the A* algorithm is to use a heuristic estimate function of cost. Cost can be distance, time, fees, etc. The estimated function of cost from current node i to the goal node can be defined as follows:

$$f'(i)=g(i)+h'(i)$$

In the above equation, $g(i)$ is the real cost from the start node to the current node i. $h'(i)$ is the estimated minimum cost from current node i to the goal node, and $f'(i)$ is the estimated minimum cost from start node to the goal node through node i.

The basic principle of the A* algorithm is: when meeting with a new node in the search course, calculate the minimum cost from the node to the goal node through the estimate function, and then continue to search from the minimum estimate-cost node. In a word, the aim of the A* algorithm is to minimize $f'(i)$.

In the A* algorithm, two lists are used to record operated nodes. *Openlist* stores the nodes that have been generated but not extended (and generates all successor nodes), and *Closelist* stores the nodes that have been generated and extended. At every step of the A* algorithm, extend the best node whose estimate-cost is the smallest in all generated nodes of *Openlist*, then move it to *Closelist* where its successor in put in *Openlist*. After checking every generated node to determine whether it has appeared, which ensures the node will be recorded only once in one of two lists, estimate its cost. Repeat the above process until the goal node is generated. In this way, the solution route can be obtained.

AN IMPROVED A* ALGORITHM

Using binary heap as a priority queue

The core step of the A* algorithm is to find the minimum cost node *BEST* in *Openlist*. This is a process of cycle comparison. If the nodes to be compared are stored in disorder, all nodes must be scanned one by one to find which one represents the minimum cost. With a large volume of data, this will undoubtedly become a bottleneck restricting the speed of calculation.

To solve this problem, the most effective way is to arrange these nodes in the order of their estimated cost and to construct a priority queue in an ascending order of estimated cost. Therefore the qualified node can be easily found out in every cycle and the efficiency of the algorithm will be greatly increased. As distinct from general algorithms using a linear array, this paper adopts a binary heap as the data structure of the priority queue.

Williams put forward the method of HEAPSORT in 1964, in which the heap, a specific data structure, is introduced. (Tang et al., 2000) Heap is defined as the following: if and only if a sequence of n elements $\{k_1, k_2, \ldots, k_n\}$ satisfies the following formula, it is called a heap.

$$\begin{cases} k_i \le k_{2i} \\ k_i \le k_{2i+1} \end{cases} \text{ or } \begin{cases} k_i \ge k_{2i} \\ k_i \ge k_{2i+1} \end{cases} \qquad \left(i = 1,2,...,\left\lfloor \frac{n}{2} \right\rfloor \right)$$

The binary heap can be considered to be a full binary-tree, which shows that the values of all non-leaf nodes are not larger (or not less) than the values of their left and right child nodes. So the element on the top of the heap (or the root of the full binary-tree) must be the minimum value (or maximum value) of n elements in the heap.

In this paper, the binary heap is used as an efficient data structure in the priority queue, which includes three main operations:

① Sift (h): Adjust the disorder sequence h to become a binary heap. First, put the minimum value on the top of the heap, and then from the top of the heap, put nodes on suitable sites by comparing the values of their left and right child nodes. This process of adjustment from heap top to bottom is called "Sift".

② Insert (x,h): Insert element x into heap h and cull the Sift to adjust h to become a binary heap. First add x into the bottom layer of the heap, then traverse the route from the node of the new leaf to the top to find a suitable site in which to put the new element.

③ Min (h): Find the minimum element of h and delete it in h, then adjust h to become the binary heap by using Sift(h). Its operation time is mainly spent on the adjustment of the binary heap.

Because the original A* algorithm adopts a linear array as the data structure of its priority queue, it is necessary to traverse all nodes in *Openlist* in every manipulation. Its time complexity is about $O(N^2)$. But the algorithm using the binary heap structure only needs traverse nodes from the top of the heap to the current node in the binary heap and its time complexity is about $O(E\lg N)$. Therefore it saves time and increases the efficiency of the algorithm.

RESTRICTING SEARCH DISTRICT

The shortest route algorithm derived from computer science only considers the topology feature of a net but neglects the spatial distribution feature of a road network, which means the search lacks specific direction and gets a shortest route tree in which the start node is the root and the goal node lies on the leaf. In the course of creating this route tree, there are still a lot of redundant calculations. This is mainly attributed to the unrestricted search district of the algorithm.

The node coordinate of the road network is of real significance, and it denotes the actual location of the node in mapped space. In the course of the route search, if the start node and goal node are given, the spatial distribution of the shortest route can be determined approximately. To determine whether a node should be involved in the search process one should consider the spatial relations among the node, the start node and the goal node. From the perspective of probability, the

shortest route is most likely composed of the nodes within the area around the line segment between the start node and the goal node.

As figure 1 shows, *A* is the rectangle formed by spread of the start node *s* and the goal node *e* and the search for the shortest route is limited in *A*.

In the process of searching for the route, determine the spatial relationship between node *n* and district *A* when meeting the node *n*.

Case 1: if *n* is in *A*, it means the node *n* can be the composition of the shortest route.

Case 2: If *n* is not in *A*, it means the node *n* cannot be the composition of the shortest route.

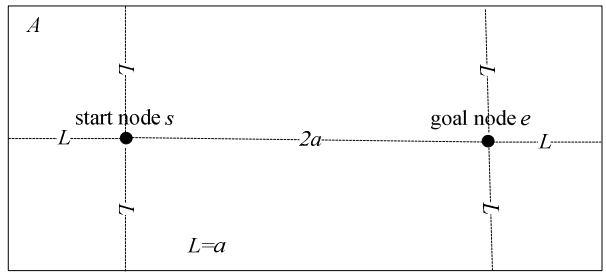

Figure 1. Restricted search district.

Restricting the search district can reduce the search space of the shortest route and raise the algorithm's efficiency. But because this method is incomplete, it needs to be further improved. After all the nodes in the restricted search district are operational, if the route cannot be obtained, the search district should be expanded properly.

The principle of optimizing the algorithm by restricting the search district operates as follows: in the process of searching for the route, analyze the spatial distribution relation among the nodes that can constitute the last search result, the start node, and the goal node, and sift the nodes that have almost no likelihood of forming the shortest route. Therefore, the search space and computation can be reduced and the algorithm can be optimized.

IMPLEMENTATION OF THE IMPROVED ALGORITHM

Use *Openlist* to store the nodes which have been generated but not extended and adopt the binary heap as the data structure of *Openlist*. Use *Closelist* to store the nodes that have been generated and extended. Take *s* as the start node of the search and take *e* as the goal node. Let *A* be the restricted search district formed from *s* and *e*. The cost of *s* is *g(s)*=0 and the costs of other nodes = ∞. Besides, in order to save the solution route, add a backward pointer in the data structure of the node. The search steps of the improved A* algorithm are as follows:

① Empty *Openlist* and *Closelist*.

② Insert (*s*,*Openlist*): put *s* in the binary heap *Openlist*.

③ If *Openlist*=*NULL*, turn to step ⑥.

④ *BEST* =Min*(Openlist)*: find the minimum estimate-cost node *BEST* ; move *BEST* to *Closelist* and judge whether *BEST* is the goal node *e*. If yes, it is successful and then turn to step ⑦, otherwise, extend *BEST* and produce the successor nodes according to the topology of the road network. Then judge every successor node *n*, if $n \in A$, operate *n* as follows:

a) Calculate the cost of node *n*: *g*(*n*)=cost of *BEST*＋cost from *BEST* to *n*.

b) If there is a node *m* same with node *n* in *Openlist* and cost $g(n) < g(m)$, then $g(m) = g(n)$ and turn the backward pointer of *m* to *BEST*.

c) If there is a node *m* that is the same as node *n* in *Closelist* and the cost $g(n) < g(m)$, then $g(m) = g(n)$. Turn the behind pointer of *m* to *BEST*, then delete *m* in *Closelist* and Insert (*m,Openlist*).

d) If *n* doesn't appear either in *Openlist* or in *Closelist*, turn the backward pointer of *n* to *BEST*, and calculate $f'(n)=g(n)+h'(n)$ and then Insert (*n, Openlist*).

⑤ Return to step ③.

⑥ Expand *A* and judge whether *A* exceeds the map space of the road network. If yes, that means failure, which means there is no route between start node *s* and goal node *e*. Otherwise, turn to step ①.

⑦ Track back from *BEST* node, which means to traverse all nodes from the backward pointer of *BEST* to the start node, and then get the solution route.

PERFORMANCE EVALUATION

In order to verify the performance of the proposed algorithm, a simulation program for searching for the shortest route based on this algorithm was designed with Embedded Visual C++ 4.0 and a series of related tests were performed on an embedded platform whose frequency was 200MHz and whose memory was 64MB with the operating system of Windows CE 4.0. We carried out 10 long-distance route search tests in the actual road network of Xi'an city, which contains 2709 nodes and 3769 arcs as Figure 2 shows, and the results are shown in Table 1. Table 1 lists the performance comparison of three kinds of algorithms: the original A* algorithm, the A* algorithm using a binary heap and the A* algorithm based on the binary heap and the restricted search district. In the table, N_1, N_2 and N_3 respectively denote the total numbers of operated nodes of three kinds of algorithms, and T_1, T_2 and T_3 respectively denote their run-time. The unit of run-time is second.

Table 1. Performance comparison of three kinds of algorithms..

	1	**2**	**3**	**4**	**5**	**6**	**7**	**8**	**9**	**10**
$\mathbf{N_1}$	2122	2046	1983	2055	2187	1789	2012	1645	2178	1965
$\mathbf{T_1}$	13	12	12	12	13	11	12	11	13	11
$\mathbf{N_2}$	2122	2046	1983	2055	2187	1789	2012	1645	2178	1865
$\mathbf{T_2}$	10	10	9	10	11	9	10	9	10	9
$\mathbf{N_3}$	1024	1014	1045	1023	1111	945	1035	1344	1687	1003

T_3	4	4	4	4	5	3	4	7	8	3

The test results can be summarized as follows:

(1) The mechanism of adopting the binary heap as a data structure for a priority queue can reduce the search for the minimum cost node, and therefore reduce the run-time of the algorithm.

(2) If the start node and the goal node are located in the center region of the map, the mechanism of restricting the search district can reduce the number of operated nodes, and then greatly improve the efficiency of the algorithm. However, if the start node and the goal node are both located in the border region of the map, the algorithm's efficiency may be relatively lower (as the results of the 8th test and the 9th test show), because the first restricted search region doesn't completely contain all the nodes of the solution route.

(3) In most cases, the improved A* algorithm has better overall performance than the original A* algorithm.

Figure 2. The road network of Xiàn city.

CONCLUSION

In order to meet real time requirements of route planning in ITS, this paper presents a novel improved A* algorithm which adopts the binary heap as the data structure for the priority queue. Using this method improves the efficiency of searching for the minimum cost node and restricts the search district to reduce the search space. Tests have shown that the improved algorithm is workable and time-saving.

REFERENCES

Lu Feng. (2001). "Shortest Path Algorithms:Taxonomy and Advance in Research", *Acta Geodaetica Et Cartographic Sinica*. 30 (3).August 2001. 269-275

Tang Wenwu, Shi Xiao-dong, and Zhu Da-ku. (2000). "The Calculation of the Shortest Path Using Modified Dijkstra Algorithm in GIS". *Journal of Image and Graphic.* Vol.5 (A), No.12. Dec.2000.1 019-1023

Wang Yuanbiao. (2007). "Efficient Implementation to Dijkstra Arithmetic in ITS." *Computer Engineering*. Vol.33 No.6 March 2007.256-261.

Xia Bing and Pao Yuan-lu. (2001). "Research on Shortest Path of Vector Map". *Microcomputer Development*. (2001). (5).30-32.

Zhao Yilin. (1999). *Vehicle Location and Navigation System*. Publishing House of Electronics Industry. (1999). 4 .117-123.

Study of the Parking Guidance Reliability of Urban Parking Variable Message Signs

Li Dongping[1], Yan Kefei,[2] and Cui Xiaotian[3]

[1] School of Transportation Engineering, Tongji University, Shanghai, China, 201804, PH (86)-1590-186-2739, E-mail: ldong_p@yahoo.com.cn
[2] School of Transportation Engineering, Tongji University, Shanghai, China, 200092, PH (86)-21-69583709, E-mail: tjykf@hotmail.com
[3] School of Transportation Engineering, Tongji University, Shanghai, China, 201804; Shenzhen Urban Transport Planning Center, Shenzhen, China, 518034; PH (86)-1361-289-5019, E-mail: cxt@sutpc.com

ABSTRACT

Reliability is a key factor in ensuring the benefits of urban parking message signs. First, this paper seeks to define the reliability of parking guidance provided by urban parking variable message signs (VMS). By analyzing drivers' parking choices under guidance and in optional parking lots, our reliability model has been formulated. Then, the influence factors of guiding reliability are studied, and the results show that the locations of VMS, the changing of parking spaces, and parking flow are the most important factors affecting the reliability of guidance. We find that the parking guidance VMS product affords the greatest benefits within certain conditions of parking supply and demand. Finally, to improve guidance reliability, this paper proposes several suggestions to optimize the configuration of the parking VMS, which could help to systematically improve the effectiveness of urban parking VMS.

INTRODUCTION

With the development and application of information, the urban Parking Guidance Information System (PGIS) has become the most important method used to reduce the parking problem. The primary way to promulgate parking guidance information is via the Variable Message Sign (VMS) (Wardman, 1997, Chatterjee, 2002). The existing research demonstrates that parking flow can be guided best through optimizing the numbers and locations of VMS (Yan Kefei, 2006; Li Dongping, 2007). It also shows how optimal display can redistribute parking flow to minimize driving distance or queue length (Thompson, 2001, Chen Jun, 2006, Mei Zhenyu, 2008). In the process, VMS not only reflects the operating conditions of parking lots, but also forecasts available parking spaces. However, there are contrary conditions between the display information in VMS and the actual usable spaces in the parking lot (Chen Qun, 2007). This last issue constitutes the reliability problem in parking guidance. With less reliability, drivers' acceptance of the VMS is lessened, which ultimately impacts the efficacy of the PGIS. Reliability is often used to

evaluate the travel time and network capacity (Noland, 1998, Clark, 2005), and Lam (2003) uses reliability as a basis for evaluating parking time. This paper defines the reliability of parking guidance, using VMS, and analyzes its influencing factors, then puts forward a method to optimize the benefits of parking VMS.

FOUNDATION OF RESEARCH

Definition of the reliability of parking guidance

Drivers choose parking lots, using parking guidance information, and then they arrive at parking lots under two conditions: usable space and unusable space. This paper's definition of parking guidance reliability includes: the destination, the location of parking lots and their guidance information, the drivers' choice of parking lots, the timing of drivers' arrival at parking lots, and the ratio of parking flow with usable spaces, and the total parking flow. The following can be denoted as ψ:

$$\psi = Q_m / Q \quad (1)$$

Where, ψ is the guiding parking reliability of VMS; where ψ is greater, the reliability is better. Q_m is the parking flow in chosen parking lots with parking guidance information. Q is the total parking flow.

Basic assumptions

The research is based on some assumptions, including:

(1) All drivers passing the message signs observe the displayed information and believe them to be correct.

(2) Drivers decide on a parking choice once they see the message signs, and once they have made a decision, they do not change their minds. After they arrive at parking lots, drivers wait for spaces if there is no availability of spaces, and the service rule is first come,first served.

(3) All drivers in the parking zone can see the parking guidance information, so that all can be guided by it.

(4) All vehicles in the chosen parking lots drive along a common route and do not make a detour or drive the wrong way, and road traffic conditions are otherwise normal.

(5) The display variety cycle ΔT is longer than the maximum driving time t_m from the deciding node to the parking lot.

PARKING GUIDANCE RELIABILITY

Parking choice model

Drivers always choose parking lots to minimize disutility (van der Waerden, 2003), and the parking choice model is given as the following:

$$P_{ijk} = \frac{l^{kj} \cdot \exp(-\theta U_{ijk})}{\sum_{k=1}^{K} l^{kj} \cdot \exp(-\theta U_{ijk})}, \quad (i = 1, \cdots, I; j = 1, \cdots, J; k = 1, \cdots, K) \qquad (2)$$

$$U_{ijk} = \alpha_m t_m^{ik} + \alpha_w t_w^{kj} + \alpha_f f^k / t_f \qquad (3)$$

Where, P_{ijk} is the probability of selecting parking lot k from deciding node i to destination j. And U_{ijk} is the utility for drivers from deciding node i to destination j, in choosing parking lot k. And t_m^{ik} is the driving time from deciding node i to parking lot k, which can be calculated from the VMS to the parking lot. And t_w^{kj} is the walking time form parking lot k to destination j; f^k is the fee at parking lot k, and t_f is the value of time. $\alpha_m, \alpha_w, \alpha_f$ are the relative importance weighting coefficients. θ is the scale parameter. I, J, K are the sets of the deciding nodes, drivers' destinations and the parking lots. Available parking lots are defined as those for which the walking time from parking lot k to destination j is in the range of a maximum acceptable walking time T_w. And l^{kj} denotes the efficiency of parking lots:

$$l^{kj} = \begin{cases} 1, & t_w^{kj} \le T_w \\ 0, & t_w^{kj} > T_w \end{cases} \qquad (4)$$

With the parking guidance information, when VMS displays that parking lot k is full, the parking lot is not available, so the available variable of the VMS display δ^{ik} is adopted to revise the parking choice utility (Thompson, 1998):

$$P_{ijk}(o) = \frac{\delta^{ik} l^{kj} \exp(-\theta U_{ijk})}{\sum_{k=1}^{K} [\delta^{ik} l^{kj} \exp(-\theta U_{ijk})]} \qquad (5)$$

Where, $P_{ijk}(o)$ is the probability of selecting parking lot j form deciding node i with destination k using the parking VMS. δ^{ik} is the Boolean variable:

$$\delta^{ik} = \begin{cases} 1, & \text{if message sign i displays parking lot k available} \\ 0, & \text{other} \end{cases} \qquad (6)$$

When all the effective parking lots displayed on the VMS are "Full," all the vehicles may queue to park. Here, parking choice behavior is consistent with behavior absent parking guidance information.

Amount of parking flow

First, the amount of parking flow in parking lot k is deduced, given the driving time delay from the deciding node with VMS i to parking lot k. When time is t, the vehicle from the deciding node i has to reach the parking lot k at $t + t_m^{ik}$, so we can assume that $\Delta T > \max\{t_m^{ik}\}$. Thus, the arrival parking flow is $r^k(t)$ between the variety cycle $\Delta T = T^{N+1} - T^N$ as shown in the following:

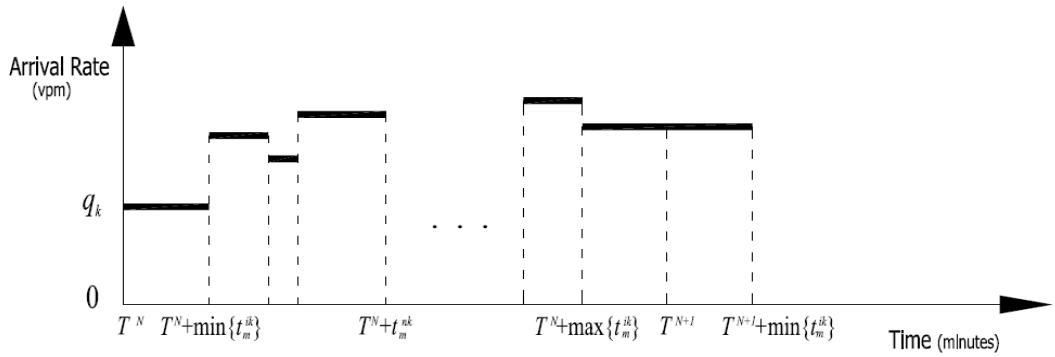

Figure 1. Arrival parking flow between $T^N \sim T^{N+1}$ in parking lot k.

At time T^N, each message sign changes the display in VMS. In the time $T^N \sim T^N + \min\{t_m^{ik}\}$, the arrival rate at parking lot k is influenced by the last variety cycle of redistributed parking. From the time $T^N + \min\{t_m^{ik}\}$, the arrival rate is dually affected by the last and the parking is redistributed with parking guidance information, till time $T^N + \max\{t_m^{ik}\}$. And from $T^N + \max\{t_m^{ik}\}$ to $T^{N+1} + \min\{t_m^{ik}\}$, the arrival rate at parking lot k is only affected by this parking guidance information. Sequencing t_m^{ik} from lesser to greater, the arrival rate at parking lot k is affected by parking flow from each of the deciding nodes, one by one, in this variety cycle. So, the arrival rate at parking lot k ($r_k(t)$) in time $T^N \sim T^{N+1}$ can be deduced as following:

$$r_k(t) = \begin{cases} \sum_{i=1}^{I}\sum_{j=1}^{J} q_{ij}^{N-1} P_{ijk}^{N-1} & t \in (T^N \sim T^N + \min\{t_m^{ik}\}) \\ \sum_{i=x+1}^{I}\sum_{j=1}^{J} q_{ij}^{N-1} P_{ijk}^{N-1} + \sum_{i=1}^{x}\sum_{j=1}^{J} q_{ij}^{N} P_{ijk}^{N} & t \in (T^N + t_m^{xk} \sim T^N + t_m^{(x+1)k}) \\ \sum_{i=1}^{I}\sum_{j=1}^{J} q_{ij}^{N} P_{ijk}^{N} & t \in (T^N + \max\{t_m^{ik}\} \sim T^{N+1}) \end{cases} \quad (7)$$

Where, $x = 1,2,\cdots,I$, and t_m^{xk} is sequenced t_m^{ik} from lesser to greater, $\min\{t_m^{ik}\} = t_m^{1k} \le t_m^{2k} \le \cdots \le t_m^{Ik} = \max\{t_m^{ik}\}$. So, in a variety cycle of VMS, the number of the arrival rate might be $I+1$. And q_{ij}^N is the parking flow rate from the deciding node i to destination j in the variety cycle N.

The amount of arriving parking flow at parking lot k is ($R_k(t)$) from T^N to $T^N + t$ can be calculated as

$$R_k(t) = \int_{T^N}^{T^N+t} r_k(t)dt \quad (8)$$

Secondly, the departure rate from parking lot k is $d_k(t)$, the departure amount of the parking flow from parking lot k is ($D_k(t)$) from T^N to $T^N + t$ can be calculated as:

$$D_k(t) = \int_{T^N}^{T^N+t} d_k(t)dt \quad (9)$$

Lastly, the amount of the parking flow of parking lot k ($S_k(t)$) from T^N to $T^N + t$ is the amount of arriving vehicles $R_k(t)$ less the amount of departing vehicles $D_k(t)$:

$$S_k(t) = R_k(t) - D_k(t) \quad (10)$$

This time, the number of total parked vehicles in parking lot k ($Q_k^N(t)$) is:

$$Q_k^N(t) = Q_k^N(0) + S_k(t) \quad (11)$$

Where, $Q_k^N(0)$ is the number of parked vehicles at the beginning of variety cycle T^N.

Parking guidance reliability model

Due to the variety cycle of VMS and PGIS, this paper measures the parking reliability guidance of a one time cycle from T^N to T^{N+1}.

According to Formula (11), the availability of spaces in parking lot k at $T^N + t$ is as follows:

$$V_k(t) = C_k - Q_k^N(t) \quad (12)$$

Where, $V_k(t)$ is the number of vacant spaces. When $V_k(t) > 0$, there are vacant spaces, achieving parking reliability; and when $V_k(t) \le 0$, there are no vacant spaces, lacking parking reliability. This is denoted as $\psi_k(t)$:

$$\psi_k(t) = \begin{cases} 1, & V_k(t) > 0 \\ 0, & V_k(t) \le 0 \end{cases} \quad (13)$$

According to Formula (7), there might be $I+1$ arrival rates at parking lot k in $T^N \sim T^{N+1}$. The parking flow achieves parking reliability at parking lot k in $T^N \sim T^{N+1}$ which is calculated:

$$Q_m(k) = \int_{T^N}^{T^{N+1}} r_k(t)\psi_k(t)dt \quad (14)$$

In the parking guidance zone, the parking guidance reliability in the variety cycle $T^N \sim T^{N+1}$ of VMS can be shown as follows:

$$\psi = \frac{\sum_k Q_m(k)}{Q} \quad (15)$$

Combining Formula (2) ~ (15), parking guidance reliability in variety cycle $T^N \sim T^{N+1}$ of VMS can be calculated, which can optimize the configuration of VMS and PGIS.

According to Formula (12) ~ (14), as the number of vacant spaces decreases, especially when the parking supply can't meet the demand, the system's parking guidance reliability decreases. To depict more precisely the guiding benefits of parking VMS, the relative parking guidance reliability is adopted as follows: the relative parking reliability with and without VMS ϕ is denoted as follows:

$$\phi = \frac{\psi - \varphi}{\psi} \qquad (16)$$

Where ϕ is the relative parking guidance reliability of parking VMS, ϕ is larger when the benefit of parking guidance is higher, whereas φ is the parking reliability without parking guidance information. As contrasted with ψ, the calculation of φ adopts parking choice model Formula (3) which does not need to be revised with Formula (4).

Model algorithm

The key to solving the above model is to construct the connections between the models. After gradually solving the models, the parameters can be calculated, and their reliability can be obtained. The calculation flow chart is as follows:

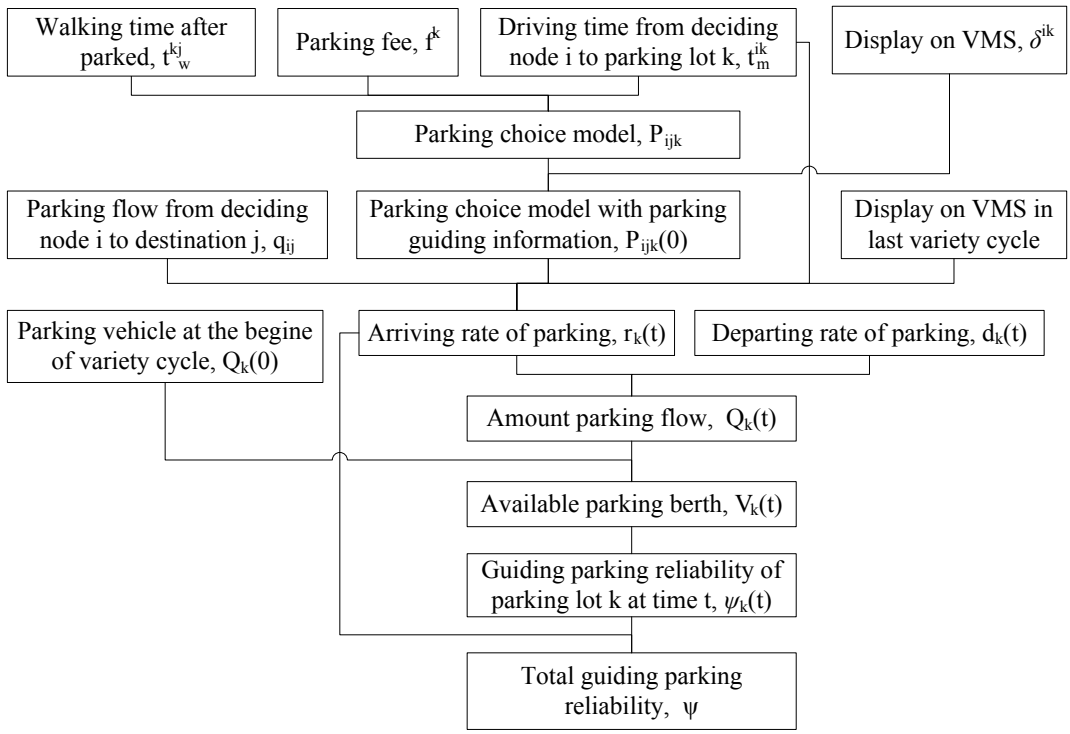

Figure 2. Calculation flow chart of parking guidance reliability.

From Figure 2, the key influence factors in parking guidance reliability are the driving time from deciding node i to parking lot k (t^{ik}_m), the display information on VMS (δ^{ik}), the parking flow (q_{ij}), and the departure rate ($d_k(t)$).

NUMERICAL EXAMPLE

The paper uses a simple numerical example network to explain how to calculate parking guidance reliability and to determine the effect of influencing

factors. The numerical example network is shown in Figure 3. Where, S is the deciding node, the location of VMS is A, and B are the parking lots, which are all in walking distance limitation $1^{AD}=1^{BD}=1$. D is the destination. The values of basic variables and parameters are as follows: $t_m^{SA}=5\min$, $t_m^{SB}=3\min$, $t_w^{AD}=2\min$, $t_w^{BD}=3\min$, $f^A=f^B=\$1$, $t_f=4\$/h$, $\alpha_m=1$, $\alpha_w=0.7$, $\alpha_f=0.05$, $\theta=1$, $\Delta T=T^{N+1}-T^N=10\min$, $C_A=50$, $C_B=100$.

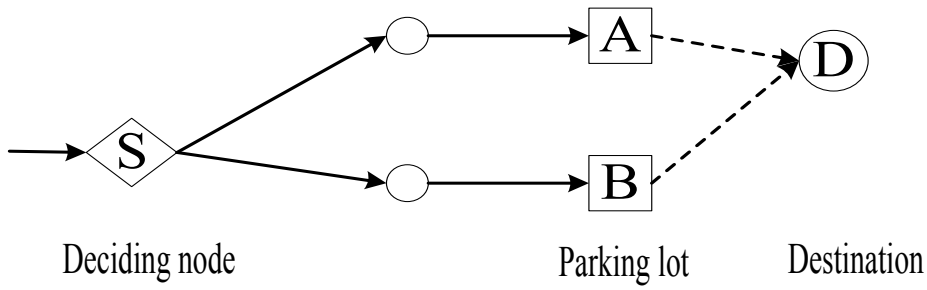

Figure 3. Numerical example network.

The parking arrival rate in the last variety cycle is assumed to contrast as ($q_{N-1}=6veh/\min$), and the availability of each parking lot in VMS is usable. To explain the effect of the influencing factors, the reliability under different conditions of parking supply and demand, and the display of VMS are calculated in Table 1.

Table 1. Parking reliabilities under different conditions.

Q(0)	q_N VMS	1	2	3	4	5	6	7	8	9	10
		Parking reliabilities									
$Q_A^N(0)=40$	(1,1)	1	1	1	1	1	1	1	0.924	0.841	0.783
	(1,0)	1	1	1	0.853	0.752	0.696	0.661	0.636	0.618	0.604
$Q_B^N(0)=80$	(0,1)	1	1	1	1	1	0.840	0.705	0.624	0.570	0.532
	NO	1	1	1	1	1	1	1	0.924	0.841	0.783
$Q_A^N(0)=20$	(1,1)	1	1	1	1	1	0.851	0.725	0.666	0.620	0.575
	(1,0)	1	1	1	1	1	1	1	0.944	0.884	0.839
$Q_B^N(0)=90$	(0,1)	1	1	1	0.920	0.610	0.507	0.410	0.348	0.307	0.277
	NO	1	1	1	1	1	0.851	0.725	0.666	0.620	0.575

Annotate: (1,1) means that parking lot A and B are available. (1,0) means that parking lot A is available and B isn't available, and (0,1) is the inverse. "NO" means that there is no VMS.

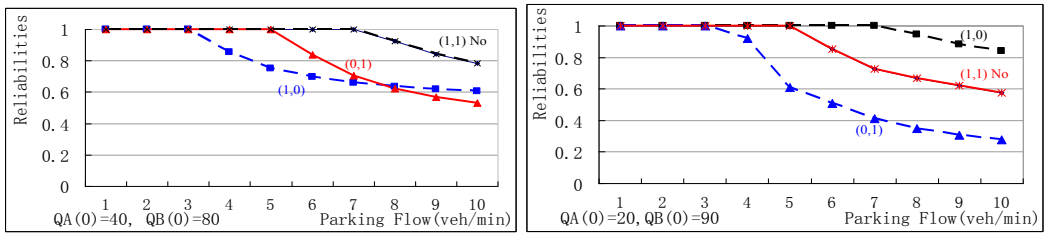

Figure 4. Chart of parking reliability under different conditions.

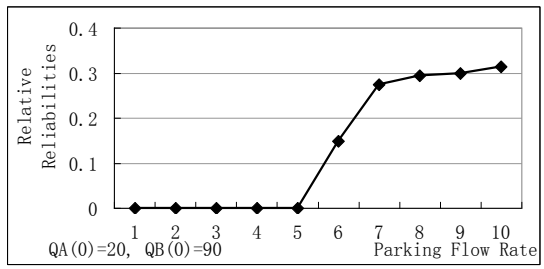

Figure 5. Relative guiding parking reliability under different parking supply and demand.

From the numerical example, we can reach the following conclusions:

(1) The key factors affecting the parking guidance reliability of VMS are the variety of parking spaces (parking vehicle arrival rate and departure rate) and the display conditions of VMS. When there is no optimization of the VMS display, its reliability may be lower than where there is no VMS, which shows that poor parking guidance information leads to poor results.

(2) When the parking supply is much greater than the parking demand, the parking guidance benefits are minimized. When the parking supply is less than or equal to the demand and the use of parking lots are unequal, the parking guidance benefits are maximized.

CONCLUSIONS

This paper analyzed drivers' parking choice behavior using the parking guidance of VMS, for which we studied the parking arrival flow rate. The parking guidance reliability model shows that driving time, VMS display, parking arrival rate and vehicle departure rate are key factors in parking reliability. The best guidance benefit was produced when the use of parking lots were unequal and VMS was optimized. This research can lead to a maximum benefit in the use of parking VMS.

ACKNOWLED GEMENT

The research is supported by the National High-tech Research Development Program of China (863 Program) (2008AA11Z201).

REFERENCES

Chatterjee, K., Hounsell N.B., Firmin P.E., et al. (2002). "Driver response to variable message sign information in London." Transportation Research Part C, 10(2), 149-169.

Chen Jun, Zhou Zhiyong, Wang Wei. (2006). "Urban parking pre-dispatch methods with non-opposite information appearance." China Journal of Highway and Transport, 19(4): 103-108.

Chen Qun, Yan Kefei, Wang Rentao, et al. (2007). "Parking Space Information Prediction Based on Phrase Construction and Elman Neural Network." Journal of Tongji University (Natural Science), 35(5):607-611.

Clark, S. and Watling, D. (2005). "Modeling network travel time reliability under stochastic demand." Transportation Research Part B, 39(2):119-140.

Lain, W. H. K., Tam, M. L., Iida, Y., and Bell, M. G. H. (2003). "Reliability assessment on searching time for parking in urban areas." The Network Reliability of Transport. Oxford: Elsevier: 61-78.

Li Dongping. (2007). Research on the optimal combination technology of the urban parking of the urban guidance parking message signs. Nanjing: Southeast University, School of Transportation.

Mei Zhenyu, Xiang Yiqiang, Chen Jun, et al. (2008). "Parking guidance information configuration model based on optimized combination method." Journal of Zhejiang University (Engineering Science), 42(1):139-144.

Noland, R.B., Small, K.A., and Koskenoja, P.M., et al. (1998). "Simulating travel reliability." Regional Science and Urban Economics, 28(5):535-564.

Thompson, R.G., Kunimichi Takada, and Kobayakawa S. (2001). "Optimization of parking guidance and information systems display configurations." Transportation Research Part C, 9 (1):69-85.

Thompson, R.G., and Richardson, A.J.. (1998). "A Parking Search Model." Transportation Research Part A, 32(3):159-170.

van der Waerden, P., Borgers A., and Timmermans, H. (2003). "Travelers Micro-Behavior at Parking Lots: A Model of Parking Choice Behavior." The 82nd Annual Meeting of the Transportation Research Board: 1–18.

Wardman, M., Bonsall, P.W., and Shires, J.D. (1997). "Driver response to variable message signs: A stated preference investigation." Transportation Research Part C, 5(6):389-405.

Yan Kefei, Chen Qun, Wen Ya, et al. (2006). "Location of sign boards in a parking guidance information system (PGIS) based on genetic algorithm." China Civil Engineering Journal, 39(7):104-109.

Study on Signal Timing Methods of Optimizing Urban Transportation Network Efficiency

Xianmin Song[1], Dianhai Wang[2] , and Ying Peng[3]

[1]Lecturer, College of Transportation, Jilin University, Changchun, 130022, P.R. China. Phone; 86-0431-85095857. E-mail:songxianmin0708@yahoo.com.cn
[2]Professor, College of Transportation, Jilin University, Changchun, 130022, P.R. China. Phone; 86-0431-85095857. E-mail: E-mail: wangdianhai@sohu.com
[3]Assistant, Shandong Transport Vocational College, Jinan, 250000.P.R. China. Phone; 86-0536-8781841,pengying530@126.com

ABSTRACT

The disequilibrium between traffic supply and demand leads to unbalanced traffic flow in urban transportation networks. By analyzing the mutual influence between the traveler route selection and signal timing, a bi-level program model is proposed in order to optimize transportation network efficiency. In light of the similarity between the game theory and the bi-level program, some simple changes are made for the purpose of simplifying the computation of the problem. Finally, a practical network is designed to validate the bi-level program model. Results indicate that the model can improve road network efficiency and decrease vehicle delays.

INTRODUCTION

Traditional signal timing design is carried out in a given traffic flow mode and does not consider the mutual influence between traffic flow and signal timing. So Allsop (1974) suggested that traffic control and path selection must be considered to analyze the impact which signal timing has on the traffic flow distribution pattern. The derivatives of this include the balanced signal control problem. Smith (1979) proved that Webster's saturation control strategies and traffic assignments are not the optimal control strategies. Bentley and Lambe (1980) proposed user-optimal piecewise linear objective function as the signal timing standard. Chen (1989) considered the issue as a Bi-level mathematical programming problem, the upper part reflecting the traffic signal control manager or the control objectives (such as minimum delay), and the lower part describing the behavior of user-optimal path selection. Chen applied this model to a large network with a heuristic algorithm successfully in Chicago. Smith (1990) studied the combination of dynamic traffic assignment with the conditions of a progressive introduction of the dynamic concept. Owen Jianwen Chen and Moshe E. Ben-Akiva (1998) placed dynamic traffic control and dynamic traffic assignment in combination as traffic managers in a traveller's non-cooperative game.

Domestic research about balance network traffic signal control started a little late, but the principle can be summarized with the following aspects: (1) Summary of research results from abroad; (2) improvement of road resistance function; (3) improvement of the distribution of the lower balance model; (4) development of the research model algorithm.

MODEL FOUNDATION

Basic Theory

The internal mechanism of traffic control aims are shown in Figure 1. The decision-making process consists of two levels and two policy-makers: traffic managers and travelers. Comprehensive consideration of the interactions among these groups should be made before the scientific and systematic ultimate decision in order to achieve system optimization. The problem is a typical bi-level planning and decision-making problem, so the bi-level programming model is described as an ideal tool to solve the problem. The upper planning presents the problem that when the section flow is *y*, solving the optimal signal control variable, this plan reflects the driver's considerations of path selection behavior at traffic control. The lower planning at the signal control presents variables for *x* with the equilibrium assignment problem, and the plan reflects the driver's considerations of traffic control parameters in the selection of a path. In this way, the bi-level programming model can describe the traffic control strategy based on the balance of networks toward the goal of an optimal system.

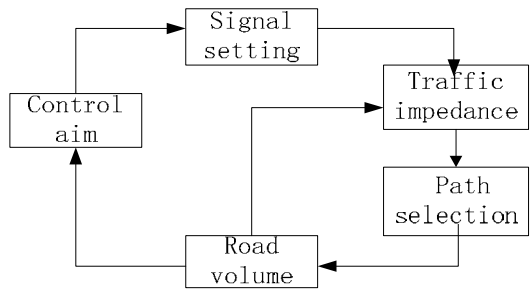

Figure 1. Traffic control aim inter-mechanism.

Basic Model

Upper Programming

Confirmation of the objective function is made by selecting an appropriate indicator to describe which network is running. On the single road sections as shown in Figure 2, the flow-speed relationship diagram under the assumption of the Greenhill rule is in a non-crowded region, while the flow is increased and the speed is reduced until the road reaches maximum capacity. In a crowded region, the flow and speed are decreased. Traffic managers expect to maximize the number of vehicles through the road in per unit time, while the driver would expect to maintain a high speed in order to reduce the travel time. So we consider the maximum product of flow and speed as the objective function to describe the network traffic flow's optimal state.

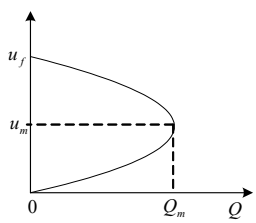

Figure 2. U-Q in Greenshields.

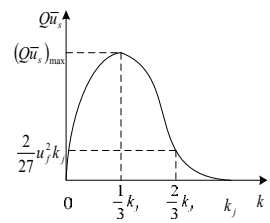

Figure 2. $Q\bar{u}_s - k$ in Greenshields

Taking the Linear relationship of velocity and density as $\overline{u}_s = u_f\left(1-k/k_j\right)$ which is rendered by Greenshields as an example, in order to get the maximum product of volume and velocity, we map the graph of $Q\overline{u}_s - k$ as shown in Figure 3, $\frac{1}{3}k_j$ and k_j are the extreme point, $\frac{1}{3}k_j$ is the maximum point , k_j is the minimum point, and $\frac{2}{3}k_j$ is inflection point. Using this as an analogy for a traffic network, according the sum of all the volumes of each turn in the maximum network, the aim-function of which is built on the upper programming model, we can describe the control object of the traffic managers.

To sum up, the upper programming model can be expressed as follows:

$$\begin{aligned} \max F &= \sum_i\sum_j\sum_h q_{ijh}u_{ijh} = \sum_i\sum_j\sum_h q_{ijh}\frac{l_{ij}}{t_{ijh}} = \sum_i\sum_j\sum_h q_{ijh}\frac{l_{ij}}{r_{ijh}+d_{ijh}} = \sum_i\sum_j\sum_h F(q_{ijh},g_{ijh}) \\ s.t. \quad & q_{ijh}\left(g_{ijh}\right) \le X_{ijh}^{\max}C_{ijh}\left(g_{ijh}\right) \\ & g_{ijh}^{\min} \le g_{ijh} \le g_{ijh}^{\max} \\ & c_j^{\min} - L_j \le \sum_{i\in I_j}\sum_{h\in H_{ij}} g_{ijh} \le c_j^{\max} - L \end{aligned} \tag{1}$$

Where q_{ijh} is the turning volume from the intersection i after intersection j to intersection h; u_{ijh} the travel speed of turning (i,j,h); l_{ij} is the distance between intersection i and intersection j. And $t_{ijh}(\cdot)$ is the impedance function of turning (i,j,h), where $t_{ijh}(\cdot) = r_{ij}(\cdot) + d_{ijh}(\cdot)$; $r_{ij}(\cdot)$ is the running time, if the node i and j are non-adjacent, then $r_{ij}(\cdot) = \infty$; $d_{ijh}(\cdot)$ is the delay time of turning (i,j,h) at the signal intersection j. And $X_{ijh}^{\max}$ is the maximum allowable saturation of the phase whose turning is (i,j,h); and C_{ijh} is the capacity of the lane whose turning is (i,j,h); where $g_{ijh}^{\min}$ and $g_{ijh}^{\max}$ are the minimum and maximum effective green times of the phase whose turning is (i,j,h); $c_j^{\min}$ and $c_j^{\max}$ is the shortest and longest cycle time at the intersection j; then L_j is the total loss time at intersection j.

Lower Programming

If it is assumed that travelers have determined their own path choice behavior using the UE principle according to control measures that have been developed as well as the road network traffic conditions, then the lower problem can be denoted in the transformation formula of Beckmann. Considering the impact of intersection delay on calculating the resistance of the road and the selection of a route as well as

the distinctness of delay at various turnings, we can transform the transformation formula of Beckmann into the following model (2):

Where： q_{ij} is the volumes of link (i,j); h_k^{rs} is the volumes of route k between r and s; f_{rs} is the volumes between r and s; $\delta_{ij,k}^{rs}$ is the relationship of route/link, if link (i,j) is on the route k which connecting the OD, then $\delta_{ij,k}^{rs}=1$, or else $\delta_{ij,k}^{rs}=0$.

$$\begin{aligned}
&\min\ Z=\sum_i\sum_j\int_0^{q_{ij}} r_{ij}(\mu)d_\mu+\sum_i\sum_j\sum_h\int_0^{q_{ijh}} d_{ijh}\left(u,g_{ijh}\right)d_u\\
&s.t.\qquad \sum_k h_k^{rs}=f_{rs}\\
&\qquad q_{ijh}=\sum_r\sum_s\sum_k h_k^{rs}\delta_{ijh,k}^{rs}\\
&\qquad q_{ij}=\sum_i\sum_j\sum_h q_{ijh}\\
&\qquad h_k^{rs}\ge 0
\end{aligned}\tag{2}$$

Math Expression

Via an analysis of the upper programming and lower programming model above, we integrate upper programming and lower programming into a model. Then the bi-level programming model based on the efficiency of the road network optimal signal control problem can be shown as formula (3):

$$\begin{aligned}
&U3:\\
&\max F=\sum_i\sum_j\sum_h q_{ijh}u_{ijh}=\sum_i\sum_j\sum_h F(q_{ijh},g_{ijh})\\
&s.t.\qquad q_{ijh}\left(g_{ijh}\right)\le X_{ijh}^{\max}C_{ijh}\left(g_{ijh}\right)\\
&\qquad g_{ijh}^{\min}\le g_{ijh}\le g_{ijh}^{\max}\\
&\qquad c_j^{\min}-L_j\le\sum_{i\in I_j}\sum_{h\in H_{ij}} g_{ijh}\le c_j^{\max}-L_j\\
&L3:\\
&\min Z=\sum_i\sum_j\int_0^{q_{ij}} r_{ij}(\mu)d_\mu+\sum_i\sum_j\sum_h\int_0^{q_{ijh}} d_{ijh}\left(u,g_{ijh}\right)d_u\\
&s.t\qquad \sum_k h_k^{rs}=f_{rs}\\
&\qquad q_{ijh}=\sum_r\sum_s\sum_k h_k^{rs}\delta_{ijh,k}^{rs}\\
&\qquad q_{ij}=\sum_i\sum_j\sum_h q_{ijh}\\
&\qquad h_k^{rs}\ge 0
\end{aligned}\tag{3}$$

Thus, $q_{ijh}\left(g_{ijh}\right)$ is determined by lower programming. By inference, the optimal conditions of model (3) are equal to the math expressions which Beckmann used to describe the Wardrop equilibrium state. Model (3) is a strictly convex programming problem, which has the only optimal solution concerned with route volumes.

Model Improvement

Generally speaking, solving the bi-level programming problem is very

complex, which is one of the reasons is the bi-level programming problem is an NP-hard problem. The non-convex aspect of the bi-level programming problem also shows that even if a double-layer solution can be found, usually the optimal solution is only a partial rather than a globally optimal solution. To improve on this, we take both bi-level programming and game theory with the same basic features into account, by using some approaches of game theory to describe the traffic signal control problem based on the operational efficiency of the road network, in order to simplify the model solution.

According to game theory, if we consider that the upper and lower decision-makers control their decision-making variables respectively and independently, then the bi-level programming problem can be showed as:

$$
\begin{aligned}
&U4: \\
&\max F = \sum_i \sum_j \sum_h q_{ijh} u_{ijh} = \sum_i \sum_j \sum_h F(q_{ijh}, g_{ijh}) \\
&s.t. \qquad g_{ijh}^{\min} \le g_{ijh} \le g_{ijh}^{\max} \\
&c_j^{\min} - L_j \le \sum_{i \in I_j} \sum_{h \in H_{ij}} g_{ijh} \le c_j^{\max} - L_j \\
&L4: \\
&\min Z = \sum_i \sum_j \int_0^{q_{ij}} r_{ij}(\mu) d_\mu + \sum_i \sum_j \sum_h \int_0^{q_{ijh}} d_{ijh}(u, g_{ijh}) d_u \\
&s.t \qquad \sum_k h_k^{rs} = f_{rs} \\
&q_{ijh} = \sum_r \sum_s \sum_k h_k^{rs} \delta_{ijh,k}^{rs} \\
&q_{ij} = \sum_i \sum_j \sum_h q_{ijh} \\
&h_k^{rs} \ge 0
\end{aligned}
\qquad (4)
$$

In upper programming U4, the link volumes $(\cdots, q_{ij}, \cdots)$ and the turning volumes $(\cdots, q_{ijh}, \cdots)$ are determined by the lower programming L4. Therefore, in model (4), the lower decision variable q_{ijh} is no longer a function of the upper decision variables g_{ijh}.

Example Design and Result Analysis

As the road network shows in Figure 4, we assign 1,3,7, 9 as the occurence and attraction points of traffic, and the trip volumes between OD pairs are shown in Table 1.

Table 1. Initial values among OD.

O	1	3	7	9
1				380
3			360	
7		380		
9	390			

In the network, 4-5-6 is a two-way, four-lane main road, where the designated speed is 50km/h. The others are secondary roads, which are also bi-directional four-lane roads, where the designated speed is 40km/h. The practical capacity of sections is 1350 veh/h. The distance between the intersection (m) as shown in Figure 4, the Free travel time of the links of the various sections in the transportation network, as shown in Figure 5.

There are five signal control intersections in network transportation, thus intersections 5 use four phases, with the phase settings shown in Figure 6, where the minimum and maximum effective green time of each phase is 17s, 12s, 17s, 12s and 45s, 40s, 45s , 40s. The intersection 2,4,6,8 uses three-phase phase settings as shown in Figure 7, where the minimum and maximum effective green times of each phase are 17s, 12s, 12s and 60s, 50s, 50s. Assuming that each phase of the green light loss time is 3s, all right-turn traffic volume is unrestricted by the red light, so the saturation flow rates of straight and left turn intersection imports are 1600veh/h and 1400veh/h.

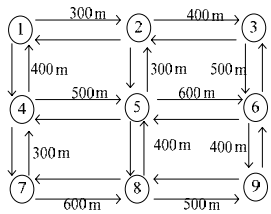

Figure 4. Distances among links in the example

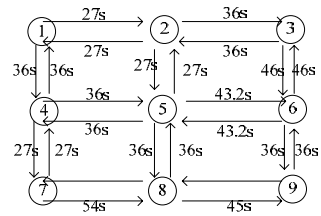

Figure 5. Free travel time of links.

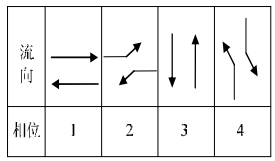

Figure 6. Phase of No.5 intersection

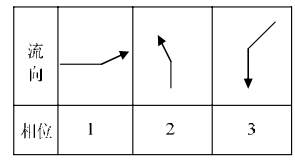

Figure 7. Phase of other intersections

The initial signal timing parameters of each phase in the signal control intersection are shown in Table 2.

Table 2 Initial green time of phases

Phase / Intersection	1	2	3	4
2	18	18	35	
4	31	20	20	
5	29	20	29	20
6	15	15	41	
8	27	22	22	

In this paper, By using a simulated annealing algorithm, the robust climbing law of Jane icosahedrons and model (4), volumes of each route through the iteration are gained, as shown in Table 3.

Table 3. Traffic volumes of links.

Section Point	1	2	3	4	5	6	7	8	9
1	0	898	0	833	0	0	0	0	0
2	863	0	920	0	695	0	0	0	0
3	0	834	0	0	0	692	0	0	0
4	898	0	0	0	708	0	860	0	0
5	0	746	0	716	0	592	0	634	0
6	0	0	665	0	689	0	0	0	726
7	0	0	0	907	0	0	0	673	0
8	0	0	0	0	595	0	671	0	767
9	0	0	0	0	0	797	0	726	0

Through our calculations, the initial solution of the corresponding objective function value is 96,625, and the total delay of all vehicles within the transportation network is 733,640. According to modes built for this paper, the optimal solution corresponding to the objective function value is 99,076, and the total delay of all vehicles in the transportation network is 636,680. That is, through the optimization of this algorithm, the total delay of vehicles in this network decreases by 13.22%.

CONCLUSIONS

According to the balanced distribution of network traffic flow, this paper proposed bi-level programming models which can reach network optimal efficiency. At last, we designed a practical network to validate the bi-level program model based on network efficiency optimization. The results indicate that the model can improve road network efficiency and decrease vehicle delays.

ACKNOWLEDGEMENT

The research was supported financially by program 973 (2006CB705505) and program 863 (2007AA11Z209).

REFERENCES

Allsop, R E. “Some Possibilities for Using Traffic Control to Influence Trip Distribution and Route Choice.” *Transportation and Traffic Theory, Sixth International Symposium on Transportation and Traffic Theory*, D J Buckley, Ed., New York: Elsevier, 1974, 345-375.

Ben-Ayed O and Blair C E. “Computational Difficulties of Bi-level Linear Programming.” *Operations Research*, 1990, 38(1): 556-559.

Ge Ying-en Yang Peikun. “A Review of Combined Route Choice intersection Control Problems” [J]. *Journal of Highway and Transportation Research and*

Development, 1998,15(2):33-37.

Liu Can-qi. "Traffic Equilibrium Assignment Model Special for Urban Road Network" [J]. *Journal of Highway and Transportation Research and Development*, 2003, 20(6):97-100.

Meneguzzer C. "An equilibrium route choice model with explicit treatment of the effect of intersections" [J]. *Transportation Research*, 1995, 29B: 329-356.

Meng Qiang; Li De-hong. "Transport Bilevel Programming Problems: Unified Models and Algorithms" [J]. *Communication and Transportation Systems Engineering and Information*, 2005,5(4):120-140.

Yuan Zhen-Zhou. "A Study on Link Travel Time Functions for Dynamic Traffic Assignment" [J]. *Communication and Transportation Systems Engineering and Information*, 2002,2(2):54-58

Zhou Xi-Zhao. "Advance in Research on Integration of Real-time Adaptive Traffic Control and Dynamic Traffic Assignment" [J]. *Journal of Shanghai Maritime University*, 2002，23(3):32-38.

The Prediction of Urban Bus Travel Time

Li Rui[1] and Li Wenquan[2]

[1]PH.D Student, School of Transportation, Southeast University, No.2 Sipailou, Nanjing 210096, P. R. China; Tel:15895985925; Email: lirui84517@163.com
[2]PH.D Professor, School of Transportation, Southeast University, No.2 Sipailou, Nanjing 210096, P. R. China; TEL: +86-25-83795647, email: wenqli@seu.edu.cn

ABSTRACT

First of all, according to the studying and analysis of the existing travel time prediction model, the idea for prediction is acquired based on the analysis of the surveyed travel time data. The improved prediction model should focus on the benefits of the existing model as much as possible. Besides that, the improved model should choose different parameters for travel time prediction. The thesis gives the improved travel time prediction model in order to improve the existing model according to the ideas for travel time prediction. At last, according to the test for the improved model, the thesis can find that the improved travel time prediction model has a higher forecast accuracy and practicality.

INTRODUCTION

With China's rapid socio-economic development, transportation systems have quite an effect on the appearance of a new socio-economic development's "bottlenecks", showing serious congestion in big cities. In this regard, China has already made the development of urban public transport a priority, improving the proportion of residents' travel in order to alleviate the stress which urban bus traffic has faced. Although China has already offered to "give priority to the development of urban public transport" as a transport policy for more than ten years, the effect is not obvious. A lot of cities' public transport has undergone slow development or even serious recession. Taking Nanjing as an example, public transportation's contribution rate to all means of transport in the town in 2005 is 22.6%. However, in 2006 only 18.61 percent of residents in Nanjing's main city chose public transit for their trip. China's major cities' public transport is in an annual decline in the proportion of travel, which is mainly due to the low level of public transport service and the public transit punctuality rate. Therefore, the ability to facilitate economic and efficient access to public transport vehicles at urban road travel time in our country has become a constrained quasi-urban bus departure and arrival points of improved bottlenecks.

In recent years, domestic and foreign scholars have carried out a series of research on the travel time prediction of urban public transport, made some research results. The freeway travel time prediction model(Nam Do H et al. 1996) which takes into account random queuing theory and the number of vehicles on roads and so on had been set up; the signal control section of the vehicle on the distribution of travel times based on macro-delay Model(Rauphail et al. 1995)had

been predicted; a method which can predict travel time easily and efficiently(Zhang et al. 2003) had been proposed in 2003; travel time prediction of the basic formula(Yang et al. 1999,2004) based on Kalman filtering theory and Markov queuing model theory had been set up from 1999 to 2004; travel time prediction algorithm(Wen et al. 2006) based on gray correlation analysis of real-time has been studied in 2006.

Based on the analysis of domestic and foreign research results in the field of city public transport travel times forecasting, this thesis sets up an easy and accurate travel time prediction to improve the model, followed by the detailed description of the model. At last, a precision test to this model is given.

URBAN BUS TRAVEL TIME SURVEYS AND ANALYSIS

The paper investigates urban bus travel time of the No.3, No.47, No.52, and No.114 buses between Nanjing Xuanwu Lake Park and Shanxi Road. The survey time is 9:00am-12:00am from August 15, 2008 to August 29, 2008. The travel time investigation takes into account the different times of business days and holidays.

A 15 day survey data collation (10 minutes per vehicle travel times for an average of measured values) is shown below. As can be seen from Figure 1: the public transport travel time curve is obviously divided into two parts; the upper part of the curve contains bus travel times of the measured value during holidays, and the lower part of the curve contains measured values of bus trip time during a normal working day, indicating that sections holidays investigate bus travel times higher than the general working public transport travel times, which investigate the nature of sections of the zone.

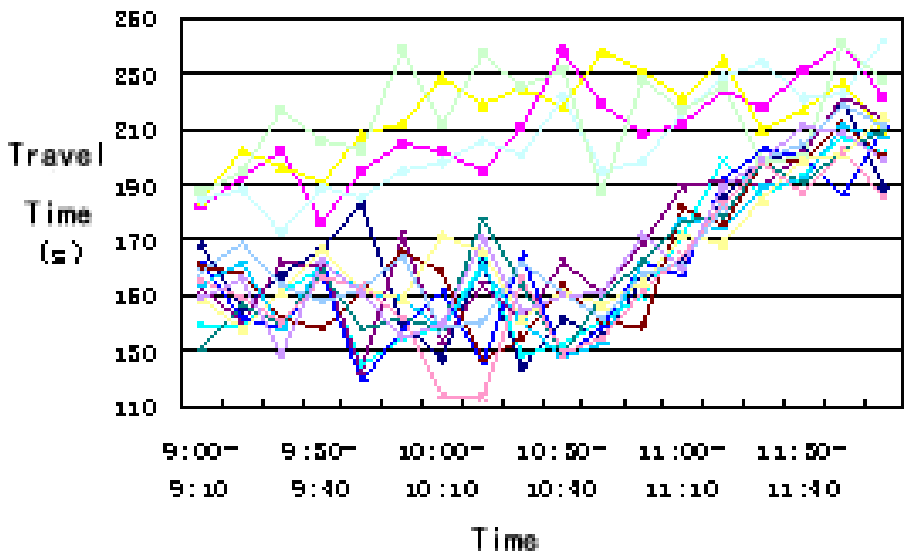

Figure1. Bus travel time (measured)

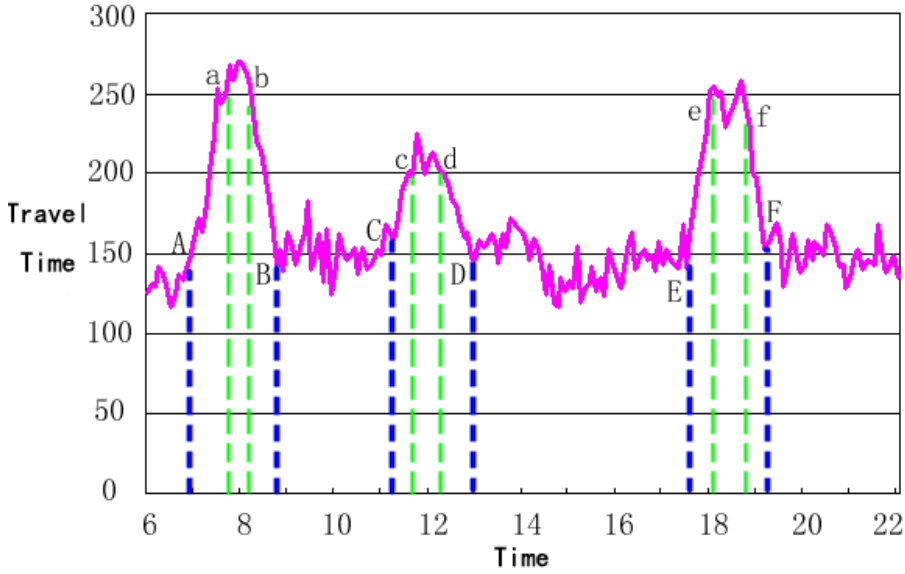

Figure 2. Bus travel time calibration stage (one day)

Figure 2 shows the Nanjing bus tours through a whole day.

According to the observation of the whole day of Nanjing city bus travel time, we can see that the travel time can be divided into peak hours and peace hours. Bus travel time is very stable at these times, but travel time is less stable when travel time is converting between peak hours and peace hours. Therefore, the travel time curve will be divided into the phases of stable changes in travel time and phases of dramatic changes in travel time. The stability of link travel time is shown, including changes in phase a-b, B-C, c-d, D-E, e-f. The link travel time phases of dramatic changes are also shown, including A-a, b-B, C-c, d-D, E-e, f-F.

MODEL

Taking into account the existing vehicle travel time prediction model, there are many inadequacies. This paper establishes a travel time prediction model based on the characteristic of urban buses and can reflect the different travel times throughout the whole day. In the paper, the prediction model will be divided into two separate parts for prediction. The first part of prediction uses the simple moving average method for prediction of travel time, and the result of the prediction reflects the approximate range of travel times. The second part of the trend prediction uses the moving average method for prediction of travel time, but this part of the process of predicting travel time mainly reflects the recent trend. Then it uses the weighted average of the result of the two parts, the integration value of prediction for different prediction periods, and its prediction model prediction value of the various parts of the share of different weights. Specific model is as follows:

$$\hat{z}_{(t)} = \omega_1 \hat{z}_{1(t)} + \omega_2 \hat{z}_{2(t)} \qquad (1)$$

$$\omega_1 + \omega_2 = 1 \qquad (2)$$

$\hat{z}_{1(t)}$ and $\hat{z}_{2(t)}$, respectively, for the first part and second part of the travel time prediction value, ω_1 and ω_2, respectively, on behalf of its weights.

$$\hat{z}_{1(t)} = \frac{z_{(t-1)} + z_{(t-2)} + \cdots + z_{(t-N)}}{N}, \quad t \geq N \qquad (3)$$

i for the first one of $z_{(i)}$ period of travel time measured data, N is the number of measured data.

Travel time prediction value of the second part of the trend of $\hat{z}_{2(t)}$ using the moving-average method of travel time changes in the process of prediction, the second part of $\hat{z}_{2(t)}$ is determined mainly by the first $M_{2(t)}^{(1)}$ moving average and the second moving average $M_{2(t)}^{(2)}$ consisting of the calculation formula:

$$\hat{z}_{2(t+T)} = a_{(t)} + b_{(t)}T, \quad T = 1 \qquad (4)$$

$$\begin{cases} a_{(t)} = 2M_{2(t)}^{(1)} - M_{2(t)}^{(2)} \\ b_{(t)} = \dfrac{2}{N-1}(M_{2(t)}^{(1)} - M_{2(t)}^{(2)}) \end{cases} \qquad (5)$$

$$M_{2(t)}^{(1)} = \frac{z_{(t)} + z_{(t-1)} + \cdots + z_{(t-N+1)}}{N}, \quad t \geq N \qquad (6)$$

$$M_{2(t)}^{(2)} = \frac{M_{2(t)}^{(1)} + M_{2(t-1)}^{(1)} + \cdots + M_{2(t-N+1)}^{(1)}}{N}, \quad t \geq N \qquad (7)$$

$a_{(t)}$ is the intercept; $b_{(t)}$ is the slope; $M_{2(t)}^{(1)}$ and $M_{2(t)}^{(2)}$, respectively, are the prediction processes of the second part of the first period of a moving average t and the second moving average.

Determination of model parameters is divided into the moving average value N and the determination of the weight values. The travel time prediction model for the first part of the number of moving average can take a large number; for the city bus lines. It can take an hour or a period of time, namely time to research their trip, so that the average journey time will be more precise. The travel time prediction model for the second part of the number of moving average can take a small number. In general, it can choose 10 minutes before the forecast period. The prediction model in the first part of the forecast model and the second part of the forecast model regarding the choice of weights, in general obey the

following principles: the stability of travel time to predict changes in stage, the first part of the right to a significant predictive value in the second part of the forecast weight value; in dramatic changes to the travel time prediction stage, the second part of the right to a significant predictive value of the predictive value in the first part of the weight. The prediction model of the right to re-value the main section of the projected range of the actual situation, the forecast interval, creates the need for public transport travel times above a certain understanding of the situation. In this paper, the "test method" determines the prediction model in the first part of predictive value and predictive value of the second part of the weight value. Weights are based on the value of options, primarily on the basis of predicted travel time $\hat{z}_{(t)}$ and the degree of measured values of the fitting.

MODEL TEXT

Because public transport travel times to improve the model contain four kinds of situations (working travel time dramatic changes in phase, changes in phase stability as well as dramatic changes in holiday travel time, and stability of phase change stage), so the test process model separately carries out inspection of the above four kinds of circumstances. Test time parameter selection is in the following Table 1:

Table1 Observed time

	Business Day, Dramatic phase	Business Day, stable phase	Holiday, Dramatic phase	Holiday, stable phase
Time	August 28, 11:20-11:30	August 28, 9:40-9:50	August 24, 9:50-10:00	August 24, 11:10-11:20

Because of space limitations, this only highlights the dramatic changes in working stages of the travel time on public transport travel time of the inspection process.

Use of survey data as a prediction model to improve prediction data source calculation model process is divided into Part I, Part II, and weight to calculate the three parts:

According to the first part of the model to improve the prediction formula, the second part of the formula of working travel time prediction phase of dramatic changes in the data source are calculated, respectively, to have been dramatic changes in travel time working stage. The second part of the first part of the predictive value is as follows:

Table 2 Prediction of travel time prediction model part Ⅰ on August 28

Time	$\hat{z}_{1(t)}$(s)	Time	$\hat{z}_{1(t)}$(s)
11:20-11:21	185.6	11:25-11:26	189.7
11:21-11:22	186.4	11:26-11:27	190.5
11:22-11:23	187.2	11:27-11:28	191.3
11:23-11:24	188.0	11:28-11:29	192.2
11:24-11:25	188.9	11:29-11:30	193.0

Table 3 Prediction of travel time prediction model part Ⅱ on August 28

Time	$\hat{z}_{2(t)}$ (s)	Time	$\hat{z}_{2(t)}$ (s)
11:20-11:21	200.7	11:25-11:26	183.6
11:21-11:22	197.0	11:26-11:27	189.1
11:22-11:23	193.7	11:27-11:28	194.8
11:23-11:24	188.5	11:28-11:29	201.9
11:24-11:25	182.7	11:29-11:30	211.9

Because of dramatic changes in phase, travel time prediction values of the second part of the prediction results for the impact are higher, so the second part of prediction values corresponding to the weight value should be greater than the first part of the corresponding weights. Mining test value method of weights to choose eventually determines the working phase of dramatic changes in travel time on public transport travel times the weight of the value of ω_1, ω_2, respectively, 0.3 and 0.7.

The above three parts organizing the process of prediction have been dramatic changes in travel time working phase bus travel times as follows:

Table 4 Prediction of travel time prediction model on August 28

Time	Prediction result(s)	Time	Prediction result(s)
11:20-11:21	196.2	11:25-11:26	185.4
11:21-11:22	193.8	11:26-11:27	189.5
11:22-11:23	191.8	11:27-11:28	193.8
11:23-11:24	188.4	11:28-11:29	199.0
11:24-11:25	184.6	11:29-11:30	206.2

For public transport travel times to improve the prediction model of evaluation, this thesis compares the simple moving average method and the trend of moving average method, as well as comparing measured data to determine its prediction accuracy.

Table 5 Bus travel times and the comparison between several models

Real Time (s)	Improved Model			Simple Moving Average Method			Trend Moving Average Method		
	Predict Time (s)	Absolute Error	Relative Error (%)	Predict Time (s)	Absolute Error	Relative Error (%)	Predict Time (s)	Absolute Error	Relative Error (%)
193	196.2	3.2	1.7	185.6	7.4	3.8	200.7	7.7	4.0
186	188.4	2.4	1.3	188	2.0	1.1	188.5	2.5	1.3
185	184.6	0.4	0.2	188.9	3.9	2.1	182.7	2.3	1.2
186	189.5	3.5	1.9	190.5	4.5	2.4	189.1	3.1	1.7
207	206.2	0.8	0.4	193	14	6.8	211.9	4.9	2.4

From the other three kinds of situation prediction results, the prediction model to improve prediction results are generally better than the above two

methods.

CONCLUSIONS

This paper investigates Nanjing bus travel time and outlines its rules. Then, the paper offers the ideas of the urban bus travel time prediction model. At last, the travel time prediction model is offered According to the test, the improved model offered in this paper can predict the urban bus travel times more precisely than the other method; therefore, it should be promoted widely.

ACKNOWLEDGMENTS

The work is supported by the National High Technology Research and Development Program of China (No.2007AA11Z210) and the National Key Technology Research and Development Program (No.2006BAJ18B03).

REFERENCES

Nagui M Rouphail, Navaneet Dutt(1995). “Estimation travel time distributions for signalized links”model development and potential ITS application Proceedings of the 1995 Annual Meeting of ITS America.

Nam Do H.and Drew Donald R(1996).Method for Estimation Freeway Travel Time in Real Time from Flow Measurements[J].Journal of Transportation Engineering,1996:185-191.

Xiaoyan Zhang, John A Rice(2003). Short-term time travelprediction[J]. Transportation Research Part C :187-210.

Wen Huiying, Xu Jianmin, Fu Hui(2006). Estimation Algorithm with Kalman Filtering for Road Travel Time Based on Grey Relation Analysis [J]. Journal of South China University of Technology(Natural Science Edition),34（9）:66-69.

Yang Zhihong, Yang Zhaosheng, Yu Dexin, Chenlin(2004). Travel time prediction method based on Malcov queuing model [J]. Journal of Jilin University of Technology(Natural Science Edition), 34（4）:671-674

Zhu Zhong, Yang Zhaosheng (2006). A Real time Travel Time Estimation Model Based on the Kalman Filtering Theory for Traffic Flow Guidance System [J]. SYSTEMS ENGINEERING-THEORY & PRACTICE, 9:74-78.

A New Cellular Automaton Traffic Flow Model for an Off-Ramp Junction of a Chinese Urban Expressway

Ci Yusheng[1, 2], Wu Lina[3], Pei Yulong[1] and Ling Xianzhang[2]

[1]School of Transportation Science and Engineering, Harbin Institute of Technology, Harbin 150090, China; PH (86) 451- 8628 2832; email: crest8168@126.com
[2]Postdoctoral Station of Civil Engineering, Harbin Institute of Technology, Harbin 150090, China; PH (86) 451- 8628 2117; email: ciyusheng1999@126.com
[3]The Department of Automobile, Heilongjiang Institute of Technology, Harbin 150050, China; PH (86) 451- 8802 8723; email: wlncys2006@126.com

ABSTRACT

A numerical simulation model was applied to study the characteristics of an off-ramp junction's traffic flow, based on analyzing the traffic flow of a Chinese urban expressway. In the course of this study, we constructed lane-changing rules with which to analyze special traffic flow characteristics. This construct was based on influences such as traffic volume parameters; the mainline rate; acceleration and deceleration values; and the length of the deceleration lane. Finally, we developed a new cellular automaton simulation model for the off-ramp junction of a Chinese urban expressway. Additionally, we analyzed the mainline traffic volume rate with different operation speeds, off-ramp junctions with different deceleration lane lengths, and the tendency chart of the mainline flow with different inflow probabilities. The results showed significant disturbance occurring between the outflow rates, mainline flow, and the operation speeds of mainline vehicles. By contrast, our new cellular automaton model was an efficient tool in the study of traffic flow from off-ramp junctions

INTRODUCTION

Traffic behavior for a single vehicle can't be represented in macroscopic models of traffic wave and gap-acceptance theory. However, as a microscopic and discrete model, the cellular automaton model focuses on the individual vehicle's kinestate of traffic flow. Furthermore, its updating rules can be changed easily, so this model can be suited to different traffic flow simulations as well as actual road and traffic conditions.

The NS model (1992) was put forward by Nagel and Schreckenberg, which proposed a one-dimensional stochastic cellular automaton model describing traffic flow on a highway. Lighthill and Whitham (1995) first brought forward hydro-dynamic theory and developed a simple continuum model, and later researchers applied this theory to study road ramp areas' traffic flow characteristics. Banks (1990) reported that queues first form in the median lane at a location well in

advance of the on-ramp. Cassidy and Bertini (1999) reported that bottlenecks activated some distances downstream of on-ramps, which could be explained by lane-changing behavior. Helbing, Dietrich, and While (1999) as well as Dong Li-yun (2002) used cellular automata doing traffic flow simulation experiments. Cassidy, Shadi, and John (2002) studied the freeway traffic near an off-ramp, where the ramp's queues were confined to the right-most exit lane, and where non-exiting drivers reduced their speeds upon seeing these queues. They found that this diminished flows in all lanes, and that the lengths of these exit queues negatively correlated with the discharge flows in the freeway segment's adjacent lanes. Robert, Bertini, and Cassidy (2002) used surveying data to study queue discharge features at a freeway bottleneck downstream from a merge.

Here, a two-dimensional cellular automaton model was used to simulate the traffic flow for an off-ramp junction of a Chinese urban expressway, which was based on special lane-changing rules. So, traffic flow characteristics for the off-ramp junction was studied with different acceleration lengths, levels of mainline traffic volume, and off-flow rates.

THE TRAFFIC FLOW SIMULATION MODEL

The Mathematical model with simplified representation. In the deceleration lane at off-ramp junctions, the traffic conflict is actually the vehicles' lane changing problems within a too-limited space. That's to say, shoulder lane vehicles change lanes from the deceleration lane to the ramp, and then travel along the off-ramp. Thus, as simplified in Figure 1, we just consider the shoulder lane of the mainline. Briefly, the upstream and downstream sections of the off-ramp junctions are marked by U and D, and the ramp section for R. In this paper, the length of deceleration is L_w and vehicles diverge in this limited length following corresponding lane-changing conditions. Otherwise, vehicles' update their status within the rules of the single lane NS model beyond the speed-down area.

Lane-changing behaviors include mandatory lane-changing, so they meet very simple lane-changing conditions. Each time step can be subdivided into two sub-steps in the two-lane model by the procedure of updating the location. In the first sub-step, parallel lane-changing is done by way of the lane-changing condition being satisfied. In the second sub-step, vehicles update locations under the rule of the single-lane NS model. The Imperative operation is applied to deal with the lane-changing of the ramp traffic's flow, so that all vehicles meeting the above-mentioned lane-changing principle transfer to the deceleration lane at road section L_w.

Simulation parameter selection. The length of a cell just equaled 1/7 of the average space headway, which was 1 meter for a cell. In other words, seven continuous cells had the same states and contained one vehicle. The length of a cell

was one of the key parameters in the simulation model.

Vehicles in an off-ramp junction were always influenced by off-flow from the mainline, whose operation speed always lowered the design speed, and the maximum speed approximately equaled the free flow speed. Therefore, the maximum speed in this simulation model was 90 km/h. In other words, the maximum speed of the cellular automaton v_{max} equaled 25L/s, where the range of speed was between 0 and v_{max}.

In this simulation model, the values of the maximum acceleration and deceleration $\pm a_{max}$ equaled $\pm$7m/s^2. This means that the maximum acceleration and deceleration values of the cellular automaton equaled ± 7 L/s^2, where the range of acceleration and deceleration was between -a_{ma} and a_{max}.

We selected a time step of 0.5 seconds, in this paper, given the actual traffic flow situation and its values for vehicle speed and acceleration. If the updating time step was longer, both acceleration and deceleration would change rapidly.

In order to guarantee the stability of the traffic flow simulation and to achieve a good effect from the special research expressway segment, a closed expressway system was selected for the boundary conditions of the NS model.

In this model, the simulation system was an unblocked expressway system with both sources and exports. Vehicles were generated in the mainline from the left boundary of the mainline, and they weren't subject to investigation outside the research area.

Simulation operation rules. At time t, if $v_n(t) \leqslant gap_n(t)$, the vehicle accelerated, so that:

$$a_n(t) = \begin{cases} gap_n(t) - v_n(t), & gap_n(t) - v_n(t) < 7 \\ 7, & gap_n(t) - v_n(t) \geqslant 7 \\ 0, & v_n(t) = v_{\max} \end{cases} \quad (1)$$

Where $v_n(t)$ was the speed of a self-vehicle at the time t; $a_n(t)$ was the acceleration of the self-vehicle between time t and t+1; and $gap_n(t)$ was the interval between the self-vehicle's head and the front vehicle's tail at time t, so that: $gap_n(t) = x_{n-1}(t) - x_n(t) - 7$.

At time t, if $v_n(t) > gap_n(t)$, the vehicle decelerated, so that:

$$a_n(t) = \begin{cases} gap_n(t) - v_n(t), & v_n(t) - gap_n(t) < 7 \\ -7, & v_n(t) - gap_n(t) \geqslant 7 \end{cases} \quad (2)$$

At time t, the acceleration of a present vehicle was known, and the deceleration we supposed for the front vehicle was the maximum deceleration -7 L/s^2, so at that at the time of t+1:

If $v_n(t+1) \leqslant gap_n(t+1)$, then acceleration for the present vehicle was still $a_n(t)$;

If $v_n(t+1) > gap_n(t+1)$, then $a_n(t) = a_n(t) - 1 \geqslant -7$, and didn't compute $v_n(t+1)$ and $gap_n(t+1)$ until $v_n(t+1) \leqslant gap_n(t+1)$. The $a_n(t)$ at the moment was the modified actual acceleration for the present vehicle at the time of *t*.

In the condition of probability of P_b, vehicles made adjustments such that adjustment rules would still reduce the speed, where the deceleration incrementation was $\triangle a \in [-7, 0]$. Additionally, the adjustment deceleration plus $\triangle a$ advanced to a maximum deceleration.

Cells would update continuously according to the speeds available from that lead time.

$$v_n(t+1) = v_n(t) + a_n(t)/2 \text{ , } x_n(t+1) = x_n(t) + v_n(t+1)/2 \tag{3}$$

where $x_n(t)$ was the location of the present vehicle at the time of *t*.

We assumed the location $x_0(t)$ was the target vehicle A, and the front and rear vehicles in the left or right lane locations were $x_{n\text{-}1}(t)$ and $x_n(t)$, respectively. If the target vehicle satisfied the following conditions:

$$\begin{cases} x_{n-1}(t) - x_0(t) - 7 \geqslant 0 \\ x_0(t) - x_n(t) - 7 \geqslant 0 \end{cases} \tag{4}$$

where $x_0(t)$ was the location of the vehicle in the acceleration lane at the time of *t,* then $x_{n\text{-}1}(t)$ was the location of the front vehicle at the time of *t.*

SIMULATION SYSTEM DEVELOPMENT

The procedure for traffic flow simulation of cellular automata contained five steps: network setting; initial state setting; cells' speed and location updating; simulation image generation; and traffic flow analysis.

Vehicle generation model. We first needed to satisfy demand for adequate actual traffic flow input. That was the vehicle generation model. At the time of the simulation, vehicles were continually generated at the left boundary cross-sections of the mainline. This reflected the randomness of system initialization, with both the vehicles themselves and their arriving time.

The generation model was divided into two parts: the vehicles' random generation and the initially produced status. First, a constant *P* was set belonging to [0, 1], and generated a random number according to weibrnd (0.8, 2.6, 10000, 1). Finally, comparing the two values and judging the front n cells, if the all n cells were full, a vehicle would be generated with a speed assigned in the range of [0, V_{max}].

Status updating model. Because of the different characteristics of operation speeds for different design speeds, the values for maximum speed and deceleration were set, and also for lane-changing and random probabilities. Utilizing the updating time step setting, the speed, deceleration and location updating for every cell were set.

In this paper, cells in the mainline and the deceleration lane had different maximum speeds, and according to different ramp areas, vehicles in different lanes had different lane-changing directions and probabilities.

The simulation image model. The output for simulation results was shown in both image and numerical value, so that the simulation image model could also help us judge our rationale for the simulation model, either way.

Because of the simulation updating time step, the simulation image dealt with noncontinuity, and the system yielded a critical image for every time interval, so we could realize the process of vehicles moving forward.

Traffic operation analysis model. The traffic operation analysis model was set for calculating the traffic flow rate, speed, and density after every time interval. So in this paper, we analyzed traffic flow variabilities for upstream, downstream, and off-ramp flows, as well as for the densities and speeds of both passing lanes and mainline lanes.

SIMULATION RESULTS

Before doing simulation experiments, several parameters had to be set, such as the length of the ramp junctions, the updating time step, the vehicles' generation rate, their lane-changing rate, their maximum acceleration and deceleration, their maximum speed, etc.

The actual inputs were as follows

a) The length of the ramp junctions were between 330 and 680 meters, i.e., the length of the passing lanes were between 50 to 400 meters;

b) The design speeds for the mainline were 60, 80 and 100km/h, which means that the maximum speeds for cells in the mainline and ramp were [19,22,25] and [11,14,20] L/s;

c) The maximum acceleration was 7 L/s^2;

d) The probability for vehicle generation and lane-changing belonged to [0,1];

e) The random changing probability was 0.2; and

f) The updating time step was 0.5 s, where the simulation time was 1800 s.

After doing several experiments, we developed an actual traffic flow rate diagram for different speeds, where the vehicle generation rate is 0.3, the lane-changing rate for the mainline is 0.2, the lane-changing rate for deceleration lane is 1, and the length of the ramp junction is 500 m.

Additionally, we constructed an actual traffic flow rate diagram for the different lengths of the deceleration lanes, which is based on the probability for the vehicle generation rate and lane-changing rate, which are 0.2. From the diagram, the length of the deceleration lane has an obvious affect on its capacity for off-ramp junctions.

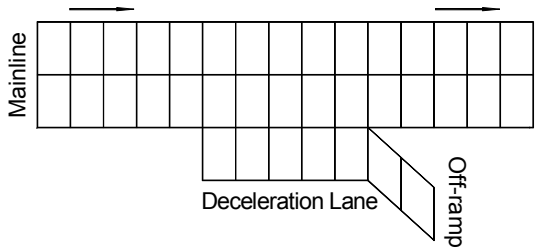

Figure 1. A celluar frame for off-ramp junction.

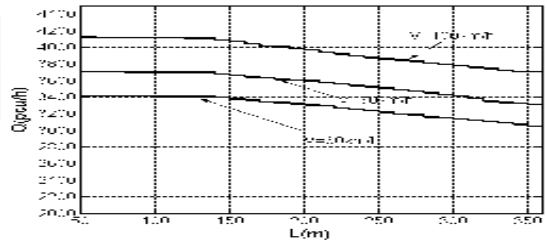

Figure 2. Traffic flow simulation results for off-ramp junctions.

In this paper, the outflow volume for the mainline is shown by the number of vehicles through a cross section of mainline downstream, and marked Q_o. Figure 4 is the relationship between generation probability and out-flow probability where the maximum speed for the mainline is $V_{\max} = 22$ and the ramp is $V_{\max} = 14$.

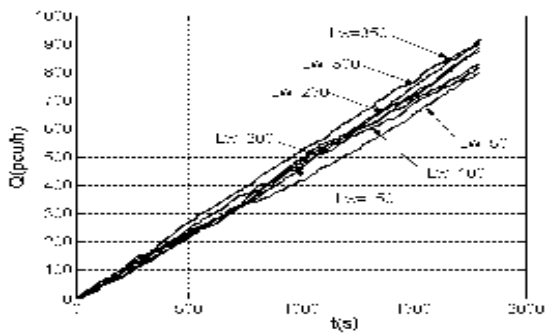

Figure 3. The influence with different lengths of deceleration lane.

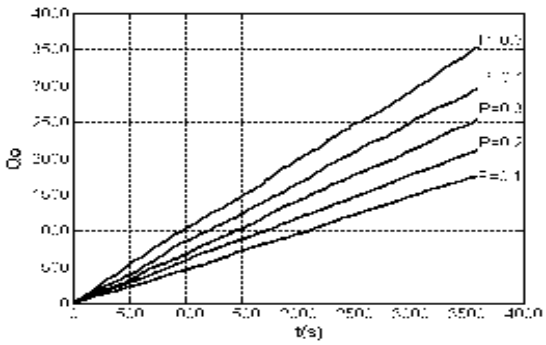

Figure 4. The flow tendency chart of mainline downstream.

The data demonstrates that with the increasing of inflow rate *P*, as well as the increasing of flow on both the ramp and the mainline, the ramp outflow gradually increases because of lane-changing over time. The mainline inflow rate increases when the volume of vehicles on mainline lanes is not heavy ($P \leqslant 0.3$), but when the vehicles' volume on the mainline lanes are very heavy, as more and more vehicles of the ramp change lanes, the downstream traffic on the mainline makes it more difficult to proceed, so the inflow gradually decreases, and when $P = 0.9$, the outflow falls to only about 200 veh/h, which is almost traffic jam condition.

CONCLUSIONS

A new cellular automaton simulation model was set up for an off-ramp junction in a Chinese urban expressway; it can be used to analyze traffic flow, level of service, etc. The simulation results showed that there was a significant disturbance between the outflow rates and the mainline flow, as well as in the operation speeds of

mainline vehicles. Our research showed that our new cellular automaton model was an efficient tool in the study of traffic flow for off-ramp junctions.

ACKNOWLEDGEMENTS

We would like to thank the Fund of Transportation Science and Technology at HIT, the Heilongjiang Institute of Technology (Y08010), the Specialized Research Fund for the Doctoral Program of Higher Education (200802131013), and the National Natural Science Foundation of China (50778056), for providing the financial support that made this study possible.

REFERENCES

Banks J H. "Flow processes at a freeway bottleneck" [J]. *Transportation Research. Record*, 1990, 1287: 20-28.

Bertini R L., and Cassidy M J. "Some observed queue discharge features at a freeway bottleneck downstream of a merge" [J]. *Transportation Research Part A*, 2002, 36:683-*697*.

Cassidy M J, and Bertini R L. "Some traffic features of freeway bottlenecks" [J]. *Transportation Research Part B*, 1999, 32: 49-59.

Cassidy M J, Shadi, B., Anani, J., and Haigwood, M. "Study of freeway traffic near an off-ramp" [J]. *Transportation Research Part A*, 2002, 36: 563-572.

Wolf, D. E. "Cellular automata for traffic simulations" [J]. *Physica A*, 1999, 263: 438-451.

Dong Li-Yun, Xue Yu, Dai Shi-qiang. "One-dimensional cellular automation model of traffic *flow* based on car-following idea" [J]. *Applied Mathematics and Mechanics*, 2002, 123(4): 363-370.

Helbing D, and Schrechenberg M. "Cellular automata simulating experimental properties of traffic flow" [J]. *Phys Rev E*, 1999, 59(3):R2505-R2508.

Lighthill M J and Whitham G B. "A theory of traffic flow on long crowded roads" [J]. *Proc. Roy. Soc*, 1955, A229: 317-345.

Nagel K, Schrechenberg M. "A cellular automaton model for freeway traffic" [J]. *J Phys I France*, 1992, 2: 2221-2229.

Whle, J, Neubert, L, Esser, J, and Schrechenberg. M. "A cellular automaton traffic flow model *for* online simulation of traffic" [J]. *Parallel Computing*, 2001, 27:719-735.

A Manual Calibration Method for Simulation of A Freeway Weaving Section

Dai Jingguo[1], Sun Jian[2], and Li Keping[3]

[1] Master Candidate, Department of Transportation Engineering,
TongJi University, Shanghai; email address: linnydai@gmail.com
[2] Assistant Professor, Department of Transportation Engineering,
TongJi University, Shanghai; email address: sunjian@126.com
[3] Professor, Department of Transportation Engineering,
TongJi University, Shanghai; email address: keping_li@vip.163.com

ABSTRACT:

This paper presents a procedure for constructing and calibrating a detailed model of a freeway weaving section using VISSIM5.0. This is applied to the Wuning on-ramp in the Inner Ring Elevated Roads of Shanghai. This test site provides several challenges for microscopic modeling: the contact between the road surface and the freeway, traffic characteristic of a weaving section, and the influence of the next off-ramp fifty meters away. A qualitative set of goals was established for the calibration. These were met with relatively few modifications to VISSIM's driver behavior parameters. A manual methodology calibration using Latin orthogonal square experiment for weaving section is presented in this paper. The actual data obtained by loop-detectors is used to demonstrate the feasibility, application, and benefits of the proposed methodology.

INTRODUCTION:

It has long been recognized that simulation modeling is a very useful tool for the design of improvements to urban freeway systems. However, there is something wrong with the simulation model. This is because the parameters used to describe driver behavior and vehicle performance characteristics are immeasurable. Engineers often use default values for parameters such as car-following sensitivity and gap acceptance because it can be difficult to obtain accurate estimates for these parameters. The procedure by which the parameters of the model are adjusted so that the simulated response agrees with the measured field conditions is what is known as model calibration.

Field data used as input for the model was compiled from two separate sources: loop-detectors on the on-ramps and mainline, and a manual survey of on-ramps and mainline using cameras. The model construction procedure consists of: 1) combination of weaving section and flat signal intersection, 2)identification of important geometric features, 3) collection and processing of traffic data, 4) analysis of the mainline and onramp data to identify the reason of bottleneck, and finally

5)VISSIM coding. Calibration and validation was then made based on collected data.

This work is part of a larger project that has as its central goal the design and implementation of an improved on-ramp control system for Shanghai Urban Elevated Roads. As is described above, the Wuning on-ramp is a typical test site, and presents three complicating features. Although this paper is based on a single test-case, practitioners wishing to use microsimulation to study unidirectional freeways may find many of the details on how certain features were implemented and how problems related to incomplete data were overcome to be useful.

THE VISSIM MODEL DEVELOPMENT

Overview of the program

VISSIM5.0 is the microscopic traffic simulator that was used to create the detailed model of the Wuning on-ramp. Its traffic model is based on the work of R.Wiedemann, The behavioral model for the driver involves a classification of reactions in response to the perceived relative speed and distance with respect to the preceding vehicle.

Coding of the network geometry

The site and time period chosen for the simulation study is the Wuning on-ramp in the Inner Ring Elevated Roads of Shanghai including the close flat signal intersection, between 4:30 pm and 5:30 pm (Figure 1). This is a single point on the Freeway system which can reflect the traffic condition in its entirety. It sustains heavy congestion during the afternoon peak. The site is equipped with a complete set of loop-detectors which helps us collect traffic data. Simulation models require a detailed and complete description of the layout of the site in order to produce a realistic output.

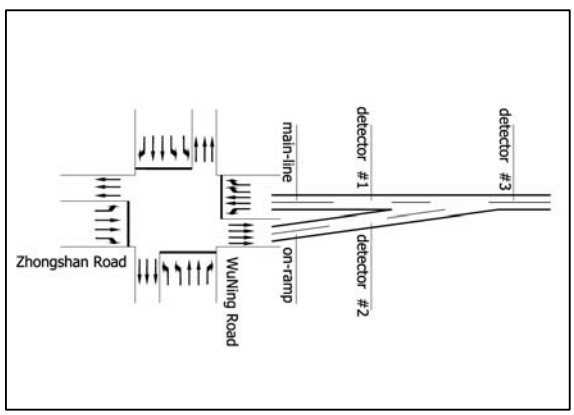

Figure 1: Test Site for Simulation

The relevant features of the test site were marked with the scaled aerial CAD-graphs including both freeway and surface road obtained from Government. Links and link connectors were then traced on this background image in VISSIM. In addition to the freeway geometry, coding of the supply side of the model also entailed the placement of the control hardware elements:

loop-detectors and signal heads including the flat intersection.

Coding of traffic demands

The traffic demand in this paper is to use aggregate vehicle sources, and to direct traffic using turning percentages. The data of flat intersection is collected by manual investigation, and that on the freeway is given by loop-detectors. The vehicle population presented in this paper is categorized into vehicles types. A single type gathers vehicles that share common vehicle performance attributes.

THE VISSIM MODEL CALIBRATION

Pre-checking

The purpose of pre-checking model is investigating whether the traffic characteristics in the model are in accordance to the actual situation. In this paper, it can be observed mainly through the three control points to control the model data credibility: the main line before the weaving section, the onramp before the section and then end of section. The positions of three control points are corresponding to the actual detector-loops. The elements of pre-checking are given in **Table 1**.

Table 1. List of Pre-checking elements

Num	Characteristic Description	Accomplish or not
1	Both main-line and onramp vehicles have deceleration behavior	Yes
2	Vehicles entering into the weaving section have obviously acceleration phenomenon.	Yes
3	At peak hours, the vehicle speed on main line and ramp is closed to the measured data obtained from the loop-detectors.	Yes

Minimum simulation number

According to experience, the minimum simulation number is 6 times in the beginning. Different random number seeds are selected to run the test model 6 times. Accounting to the actual needs of simulation objects, the desired confidence interval is ± 10%. Initial simulation results are given in **Table 2**.

Table 2. Minimum Stimulation Number

Random seeds		5	15	25	35	45	55	Standard deviation	t-Distribution	N	confidence interval	Desired the largest confidence interval
VI FLO	1	1279	1284	1232	1180	1206	1218	41.18	2.5705818	6	86.44	103.02

	2	636	706	712	702	708	720	30.66	2.5705818	6	64.36	70.73
	3	1907	1996	1921	1855	1904	1941	46.62	2.5705818	6	97.84	159.72
	1	21.6	21.4	21.5	21.5	21.4	21.6	0.09	2.5705818	6	0.19	1.79
SPEED	2	30.6	31.3	31.2	31.1	31.4	31.1	0.28	2.5705818	6	0.58	2.59
	3	61.2	70.9	72.4	72.9	69.8	68.8	4.27	2.5705818	6	8.97	9.79

*ps：In this t- distribution, confidence is 95%, and freedom is 5。

It can be seen that in the data above three points meets the demand when the desired confidence interval is twice the standard deviation. It is appropriate that 6 times is the selected number of the smallest simulation.

CHANGEABLE MODEL PARAMETERS

Drivers might behave differently on weaving section. Thus, the parameters described in this section apply equally to all vehicle types, but were adjusted for each link type. Link types are analogous to vehicle types. The driver behavior parameters that were changed from their default values to define each link type are described in Table 3.

Table 3. Classification Parameters

Parameters	CC0（m）	CC1（s）	CC2（m）	DLCD（m）	MDCB（m/s^2）
Level 1	1.00	0.5	3	50	-2
Level 2	2.00	1.0	5	100	-3
Level 3	3.00	1.5	7	150	-4
Level 4	4.00	2.0	9	200	-5

CC0: Standstill distance **CC1**: Headway time **CC2**: Following' variation

DLCD：Desired Lane Change **MDCB**：Maximum deceleration for cooperative barking

SIMULATION EXPERIMENT

This paper uses a Latin orthogonal square experiment to calibrate the driver behavior parameters. According to the parameter selection, it use $L_{16}(4^5)$ orthogonal table to experiment. The experiment is repeated 6 times with each parameter group, taking the average of test data as a result. First of all, detected flow gaining from detector #2 is selected for calibration targets. The experimental results are given in **Table 4**:

Table 4. Initial Calibration

	CC0（m）	CC1（s）	CC2（m）	DLCD（m）	MDCB（m/s^2）	Traffic capacity
1	4	2	9	200	-2	420
2	4	0.5	7	100	-5	560
3	3	1.5	7	150	-2	449
4	4	1	3	150	-4	559

5	2	2	7	50	-4	279
6	1	2	5	150	-5	276
7	1	0.5	3	50	-2	679
8	2	0.5	9	150	-3	663
9	2	1.5	3	200	-5	341
10	4	1.5	5	50	-3	341
11	3	1	9	50	-5	334
12	1	1	7	200	-3	593
13	1	1.5	9	100	-4	332
14	3	0.5	5	200	-4	660
15	3	2	3	100	-3	352
16	2	1	5	100	-2	642
Ⅰ	1880	2562	1931	1633	2190	
Ⅱ	1925	2128	1919	1886	1949	
Ⅲ	1795	1463	1881	1947	1830	
Ⅳ	1880	1327	1749	2014	1511	
Range	130	1235	182	381	679	

Based on the above analysis data, the following judgment is developed：

- The results of test 8,14,16 are better than others
- Based on range analysis, parameter changes on the results of the impact from strong to weak are as follows:CC1>MDCB>DLCD>CC2>CC0.

According to the experiment above, new parameter combinations are generated with the three groups for speed calibration. In the same measure, 6 times simulation is experimented, and a T test is the Statistical method of this experiment. The combinations and experiment results are given in **Table 5**.

Table 5. Simulation Results with T test

NO.	CC0（m）	CC1（s）	CC2（m）	DLCD（m）	MDCB(m/s²)	Traffic capacity	T-test （<2.015?）
1	2.00	0.50	9.00	150.00	-3.00	663	1.668
2	1.00	0.50	9.00	50.00	-3.00	643	-0.723
3	1.50	0.50	9.00	100.00	-3.00	662	1.234
4	3.00	0.50	5.00	200.00	-4.00	660	0.995
5	3.00	0.50	7.00	150.00	-4.00	642	-0.518
6	3.00	0.50	9.00	100.00	-4.00	551	-7.485
7	2.00	1.00	5.00	100.00	-2.00	642	-0.614
8	1.00	1.00	5.00	100.00	-2.00	680	4.250
9	1.50	1.00	5.00	100.00	-2.00	665	1.927
10	2.00	1.00	7.00	150.00	-2.00	501	-11.947

CALIBRATION TAGET

Three possible combinations (No.2,5,7) are selected by the experiment above. Simulation speed and flow is collected by using these parameters, then compared to the measured value (half hour). The results are given in **Table 6**.

Table 6. Verification Value

Group		Detector #1		Detector #2		Detector #3	
		Flow	Speed	Flow	Speed	Flow	Speed
Desired value		1200	23.8	600	5.5	1800	41.7
2	simulation	1207	21.5	603	5.6	1809	49.7
	deviation	0.56%	9.80%	0.56%	1.82%	0.50%	19.26%
5	simulation	1207	21	603	6	1802	50
	deviation	0.56%	10.29%	0.50%	1.82%	0.11%	20.42%
7	simulation	1207	21	603	6	1805	45
	deviation	0.56%	9.80%	0.56%	2.12%	0.25%	8.71%

The final selection of driver behavior parameters is group 7 as shown in **Table 6**. This parameter set is the most parsimonious among those sets that also met the calibration goals. Through the Latin orthogonal square experiment, the analyst can calibrate the driver behavior parameters of a simulation model.

SUMMARY AND CONCLUSIONS

This document has outlined a complete methodology for constructing and calibrating a simulation model of a unidirectional freeway with on-ramp control. The procedure included gathering and processing of field data from the database, microscopic simulation with VISSIM, and calibration of simulation model with a Latin orthogonal square experiment. Deficiencies in the field data were dealt with by assembling a composite typical day using data from several different days. A successful calibration of the VISSIM model was carried out based on the comprehension of driver behavior. In conclusion, this study has shown that the VISSIM simulation environment is well-suited for freeway studies involving complex flat interactions. With few and well reasoned modifications to its driver behavior parameters, the simulation model is capable of reproducing the field-measured response on the on-ramps and mixed-flow lanes.

Research will now continue using the calibrated VISSIM model to investigate a wide variety of ramp control strategies for the Inner Ring Elevated Roads of Shanghai during the peak period. Ramp control strategies will include local and system-wide alternatives. Caltrans will consider implementing improved ramp control strategies based on their assessment of the predicted results.

ACKNOWLEDGEMENTS: National High Technology Research and Development Program("863"Program) of China (Item No.:2007AA11Z245) and Tongji University Youth Action Plan for Cultivating Talents (Item No.:2007KJ027)

BIBLIOGRAPHY

Balakrishna Ramachandran and Constantinos Antoniou. “Calibration of Microscopic Traffic Simulation Models: Methods and Application.” National Technical University of Athens. TRB 2007 Annual Meeting.

Gomes, Gabriel and Adolf May. "A Microsimulation Model of a Congested Freeway using VISSIM", Department of Mechanical Engineering, U.C. Berkeley, 2004 Conference of the Transportation Research Board in Washington D.C.)

Cassidy, M. and J. Han. "Validation and Evaluation of Freeway Simulation Models.” Final Report FHWA/CA/Purdue-RR-95-1.FHWA, U.S. Department of Transportation, 1995.

Cheu, R., W. Recker, and S. Ritchie. "Calibration of INTRAS for simulation of 30-second loop detector output.” Transportation Research Record No. 1457. TRB, National Research Council, Washington, D.C., 1994. 208-215.

Hall, F., L. Bloomberg, N.M. Rouphail , B. Eads, and A.D. May. "Validation Results for Four Models of Oversaturated Freeway Facilities.” Transportation Research Record 1710, TRB, National Research Council, Washington, D.C., 2000,

PTV. "Vissim User Manual - V.5.00”. Karlsruhe.

EFFICIENT LINK TRAVEL TIME ESTIMATION FOR SIGNALIZED LINK BY SMALL SIZE PROBE REPORTS*

LI Qiang[1], MIWA Tomio[2], MORIKAWA Taka[3]

[1] Graduate School at Shenzhen, Tsinghua University; Tel: +86-755-26036129, Fax: +86-755-26036005, Email: liqiang@sz.tsinghua.edu.cn
[2] Department of Civil Engineering, Nagoya University, Tel: +81-52-789-3565, Email: miwa@civil.nagoya-u.ac.jp
[3] Graduate School of Environmental Studies, Nagoya University, Tel: +81-52-789-3564, Email: morikawa@civil.nagoya-u.ac.jp

ABSTRACT

For probe vehicle system, there are only few travel time data (sample) available for real-time link travel time estimation due to limited number of probe vehicles. However, the population of link travel time (travel times of all vehicles) has large variance. In this circumstance, it is difficult to reliably estimate the population mean by the sample mean directly. In this paper, the population is redefined by the link travel times of such vehicles which have through movements at upstream and downstream intersections. However, there are still two groups of vehicles (without delay and with delay) with significantly different travel time. The relationship between the three variables (two means of the groups and the portion of the first group) is analyzed and an estimation method based on the relationship is proposed. The comparison between the new and the conventional method shows that the proposed method can provide more precise estimation result.

Keywords: probe vehicle, sample size, signalized link, travel time estimation

1 INTRODUCTION

For probe-based real-time link travel time estimation, the population of link travel time is defined by link travel times of all vehicles traveling a link during a time interval. And the sample is the travel time data from probe vehicles (PVs) on the link in the time interval. The cost and the capacity of the communication between PVs and the operation center impose the restrictions on the number of PVs. Hence the

* Supported by National Natural Science Foundation of China (ID:50808108)

number of PVs in the road network is limited and the sample size is very small. For a typical signalized link which has four-way intersections on both ends, there are nine distinct subpopulations associated with each combination of access and departure movements (left turning, right turning and through). These subpopulations have different travel time characteristics. Further more, the population also can be divided by intersection delay (some vehicles will experience the intersection delay at downstream intersection of the link, while the others will depart without intersection delay) and the two subpopulations also have significant different travel time. Therefore, the population has large variance and is seriously non-normal.

Various approaches have been developed to estimate the adequate number of PVs (e.g., Chen and Chien, 2000; Cheu et al., 2002; Hellinga and Fu, 1999; Quiroga and Bullock, 1998; Srinivasan and Jovanis, 1996). In these studies, sample mean is directly used to estimate the population mean. If the sample size is very small (less than 5) while the population has large variance and is seriously non-normal, it is difficult to reliably estimate the population mean by the sample mean directly. However, for probe-based estimation, it is still expected that a reliable estimation can be obtained by a small-size sample. Therefore, it is necessary to develop a new estimation method for probe-based estimation and it is the primary objective of this paper.

This paper is consisted by four sections. The next section describes the properties of link travel time which are useful for probe-based link travel time estimation. And then, the proposed estimation method is introduced and is compared with conventional estimation method. Finally, conclusions are drawn.

2 PRELIMINARY ANALYSIS FOR LINK TRAVEL TIME

In a previous study by the authors (Li et al., 2008), the properties of link travel time are discussed and some conclusions that are useful for probe-based link travel time estimation are made.

A corridor that consists of four links (link 2 ~ link 5) and the adjacent links are simulated for 3 hours using VISSIM – a microscopic traffic simulation software developed by PTV AG (http://www.english.ptv.de/). Figure 1 shows the road network (Traffic in Japan keeps left), origin zones (1~12), signal scheme and turning rate. Vehicles are generated at each origin zone with Poisson distribution. The imaginary time period is morning. The base vehicle input of each zone and the temporal variation are set as Table 1. Each intersection is controlled by a two-phase fixed-time

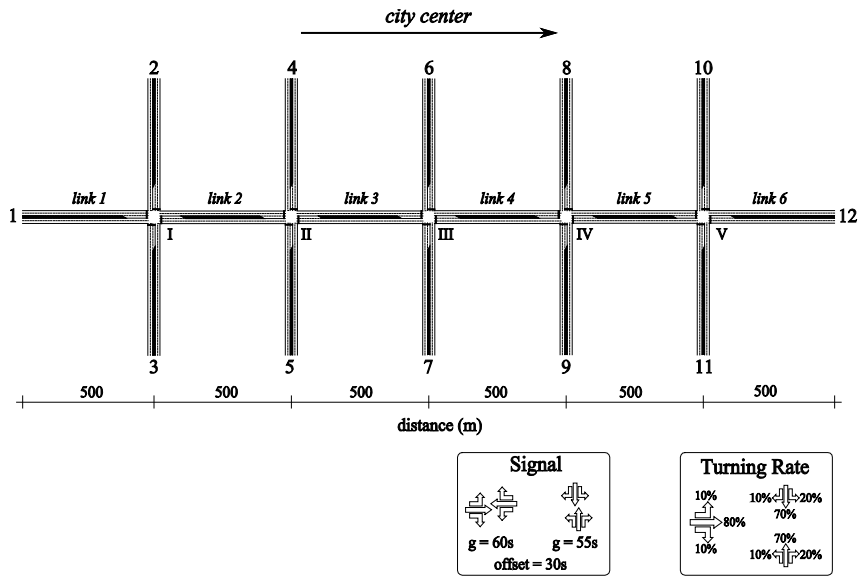

Figure 1. Simulation Network (adapted from Li et al., 2008)

Table 1. Vehicle Inputs

Base Vehicle Inputs (Veh/h)		Temporal Variation	
Origin Zone	Vehicle Inputs	Time (s)	Proportion of Base Vehicle Inputs
1	1000	0 ~ 900	0.1
2~11	800	900 ~ 1800	0.2
12	500	1800 ~ 2700	0.5
		2700 ~ 3600	1
		3600 ~ 4500	1.2
		4500 ~ 6300	1.5
		6300 ~ 7200	1
		7200 ~ 8100	0.8
		8100 ~ 10800	0.5

signal with a cycle length of 140 s. The offset time of two consequent intersections is 30 s. The imaginary network is a corridor towards city center. Hence the turning movements towards city center are emphasized in turning rate setting.

For each link in the corridor, we are only interested in the travel times reported by the vehicles which have through movements at upstream and downstream intersections (abbreviated as TT). The link travel times and the flow (only through movement at upstream) are aggregated by signal cycle. Figure 2 shows the aggregation result of mean link travel time and flow for link 5. The figure also shows the individual travel time reports from the vehicles with TT (×) and the temporal variation of vehicle inputs (dot line).

The aggregation results are discussed in two stages divided by the traffic

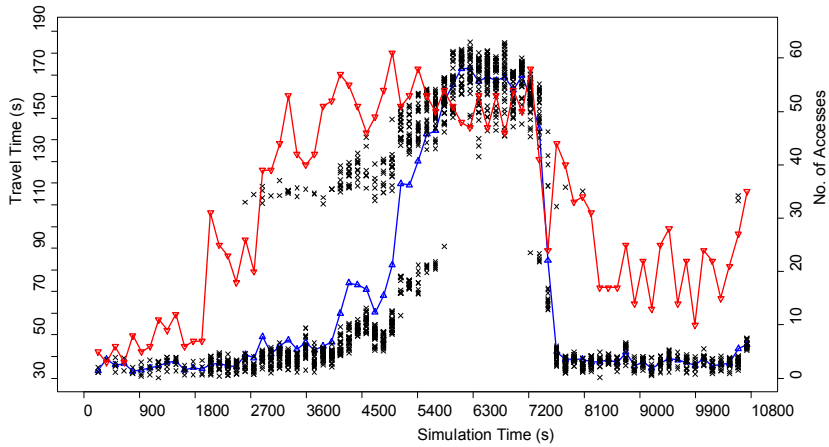

conditions at upstream intersection.

During undersaturated conditions, all vehicles that access a link in a signal cycle at upstream can depart the link in a signal cycle at downstream. The travel times of such vehicles will be small and similar. Consequently, mean link travel time will be stable at a relatively low level over time (time period 0 s ~ 3600 s in Figure 2).

Under saturated/oversaturated conditions, the arrival distribution is close to uniform over green time and the queue length at downstream intersection increases over time. Then mean travel time also increases over time (time period 3600 s ~ 7200 s in Figure 2). As shown in Figure 2, in this stage, travel times can be divided into two groups: one without delay (Group 1) and the other with delay (Group 2). Further, as mean travel time increases, the average travel time of the two groups (μ_1 and μ_2) increase and the proportion of Group 1 (p) decreases. That is, μ_1, μ_2 and p have some relationship.

3 PROPOSED ESTIMATION METHOD

For arterial road, the subpopulation with TT is usually dominant in the nine subpopulations and the mean travel time of vehicles with TT can represent the traffic condition of the link in an interval. Thus, the population is redefined as the link travel times of all vehicles with TT during a time interval in this paper.

3.1 Relationship between μ_1, μ_2 and p

Under saturated/oversaturated conditions, there will be some vehicles queued

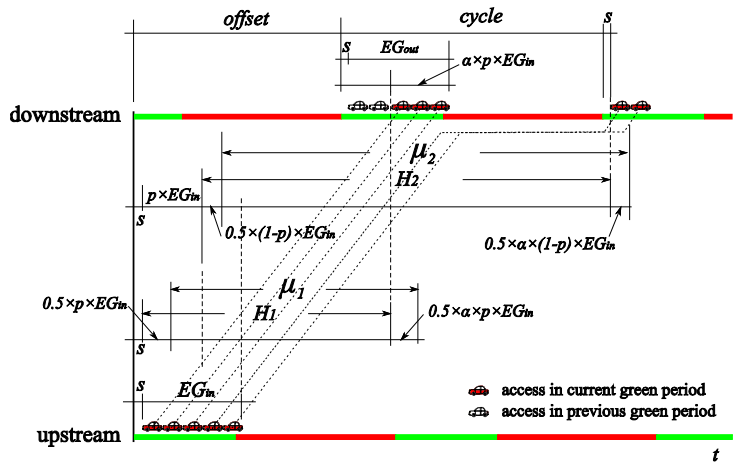

Figure 3. Vehicles that Access a Link in a Green Period

at downstream and thus the vehicles that access a link in same signal cycle will not be able to depart the link in the same signal cycle and some vehicles will experience the intersection delay. Then, under uniform assumption which is reasonable during saturated/oversaturated conditions, the access time and departure time of these vehicles can be illustrated as Figure 3. This figure is a time-space diagram and color bars at upstream and downstream intersection present the green and red periods of traffic signal. The vehicles with TL/TR (through access movement and left/right departure movement) access the link together with the vehicles with TT and will queue in left/right turning lanes at downstream intersection. That is, the length of the queue of vehicles with TT at downstream will become shorter than the length at upstream. The parameter α in the figure reflects the reduction of the length and is dependent on the turning rate at downstream intersection. The notation in the figure is described in the next paragraphs.

The relationship between μ_1, μ_2 and p can be obtained from Figure 3 and Eq. 1 and 2 show the relationship. Eq. 3 shows the formulation for calculating mean travel time and Eq. 4 shows that the difference between μ_1 and μ_2 is independent from p.

$$1 \quad \frac{H_1 \quad 0.5 \quad (1 \quad) \quad p \quad EG_{in}}{offset \quad EG_{out} \quad p \quad EG_{in} \quad 0.5 \quad (1 \quad) \quad p \quad EG_{in}} \qquad (1)$$

$$offset \quad EG_{out} \quad 0.5 \quad (1 \quad) \quad p \quad EG_{in}$$

$$_2 \quad \underline{H_2} \quad 0.5 \quad (1 \quad) \quad (1 \quad p) \quad EG_{in}$$
$$\underline{offset \quad cycle \quad p \quad EG_{in}} \quad 0.5 \quad (1 \quad) \quad (1 \quad p) \quad EG_{in} \tag{2}$$
$$offset \quad cycle \quad 0.5 \quad (1 \quad) \quad EG_{in} \quad 0.5 \quad (1 \quad) \quad p \quad EG_{in}$$

$$p \quad _1 \quad (1 \quad p) \quad _2 \tag{3}$$

$$_2 \quad _1 \quad cycle \quad 0.5 \quad (1 \quad) \quad EG_{in} \quad EG_{out} \tag{4}$$

where

p the proportion of Group 1
H_1, H_2 travel time of head in Group 1 and Group2
$_1, \ _2,$ mean of Group1, Group 2 and all
$cycle, offset$ signal length and signal offset between upstream and downstream instersection
EG_{in}, EG_{out} effective green time of upstream and downstream intersection for through movement
reduction rate of length of vehicles with TT between downstream and upstream

3.2 Procedure of Proposed Estimation Method

Under saturated/oversaturated conditions, since the two groups have relatively small variances, μ_1 and μ_2 can be estimated by small size sample reliably. Obviously, estimating μ_1 (or μ_2) and then obtaining μ_2 (or μ_1) and p by the relationship and finally calculating mean travel time by μ_1, μ_2 and p is a possible method to estimate mean travel time, which is the proposed method of this paper.

The pseudocode for the proposed estimation method is the following.

```
1   divide sample x to two groups x1 and x2
2   if size(x1) > size(x2)
3         x2 = x2 – diff_μ1_μ2
4         estimating μ1 by mean(x1, x2)
5         calculating μ2 and p
6         if p>95% p=1
7         calculating μ
8   else
9         x1 = x1 + diff_μ1_μ2
10        estimating μ2 by mean(x1, x2)
11        calculating μ1 and p
12        if p<5% p=0
13        calculating μ
```

As shown in Figure 2, link travel time becomes one group when undersaturated conditions at upstream intersection and when the queue length at downstream is relatively long (see 6300 s ~ 7200 s in the figure). The primary target of the proposed method is the population with two groups. The accuracy of the

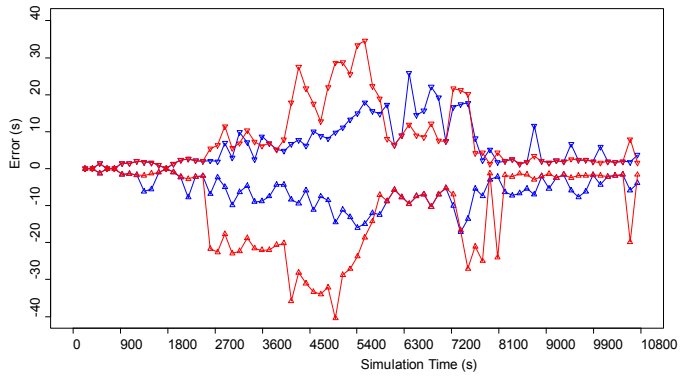

proposed method declines when the population has only one group. However, the modification of p in step 6 and step 12 can improve the accuracy of the proposed method when the population has one group.

3.3 Comparison with Conventional Methods

The travel time reports in each signal cycle on link 5 from the simulation described in section 2 is treated as a population. Then, the estimation results by the proposed method and the conventional method, in which the sample is directly used to estimate, are compared at three levels of sample size n = 3, 5.

For each sample size, 1000 times of sampling are performed. Figure 4 illustrates 0.05 quantile and 0.95 quantile of the estimation errors by these two methods of three sample size levels. As shown in the figure, for almost every signal cycle, the proposed method can provide more precise result, especially when the link travel time has two groups (3600 s ~ 6000 s). For 6300 s ~ 7200 s, the performance of the proposed method is lower than the conventional method. However, in this period, the mean is relatively large and thus the large error is not so critical.

4 CONCLUSIONS

A new link travel time estimation method is proposed in this paper. The comparison between the new and the conventional method, in which the population mean is directly estimated by sample mean, shows that the proposed method can provide more precise estimation results, especially when the distribution of the travel time has two groups.

In the proposed method, it is assumed that (1) the traffic signals are constant and known; (2) the vehicles with TT account for a considerable part of the total nine movement pattern; and (3) the parameter α which is relevant to turning rate is constant and known. For real arterial link, if the majority of the vehicles get across the link with TT, there is a method that can estimate the signal time and turning rate. The proposed method can be used to estimate the mean travel time with small sample size. However, it is necessary to conduct a field test to verify the proposed method.

REFERENCES

Chen, M. and Chien, S. I. J. (2000). Determining the number of probe vehicles for freeway travel time estimation by microscopic simulation. Transportation Research Record, No.1719. TRB, National Research Council, Washington, D.C., pp. 61-68.

Cheu, R. L., Xie, C. and Lee, D. H. (2002). Probe vehicle population and sample size for arterial speed estimation. Computer-Aided Civil and Infrastructure Engineering, Vol. 17, pp. 53-60.

Hellinga, B. and Fu, L. (1999). Assessing expected accuracy of probe vehicle travel time reports. Journal of Transportation Engineering, Vol. 125, No. 6, pp. 524-530.

Li, Q., Miwa, T. and Morikawa, T. (2008). Preliminary analysis on link travel time for probe-based estimation method by microscopic simulation. International Journal of ITS Research, Vol.6, No.1, pp.21-27.

Quiroga, C. A. and Bullock, D. (1998). Determination of sample sizes for travel time studies. ITE Journal, Vol. 68, No. 8, pp. 92-98.

Srinivasan, K. and Jovanis, P. (1996). Determination of the number of probe vehicles required for reliable travel time measurement in an urban network. Transportation Research Record, No.1537, TRB, National Research Council, Washington, D.C., pp. 15-22.

Phase and Timing Optimization at Actuated-coordinated Signal Control Intersection

Mao Chengyuan[1] and Pei Yulong[2]

[1] School of Transportation Science and Engineering, Harbin Institute of Technology, P.O. Box 2525, 202 Haihe Rd., Harbin 150090; PH (86) 451- 8628 2116; email: maozhang1982@126.com

[2] School of Transportation Science and Engineering, Harbin Institute of Technology, P.O. Box 2526, 202 Haihe Rd.. Harbin 150090; PH (86) 451- 8628 2832; FAX (86) 451-8628 2832; email: yulongp@263.net

ABSTRACT

Ordinarily, an actuated-coordinated signal control intersection has a fixed phase whose order is settled. Each phase has a minimum and maximum green time to fit the traffic's randomicity and fluctuation. But if the traffic of some phases fluctuate remarkably and if there is little or no traffic comes in certain cycles or periods, the intersection runs the same phase number and order and sets the minimum green time accordingly. This would render the green time as obsolete and increase traffic delays in other phases. This paper considers the influence on drivers as caused by changing phase, optimizes the phase number and order of actuated-coordinated signal control intersection based on fuzzy control theory. It uses the intersection of Daxin Street and North Fourteen Street in Harbin as an example, simulates the intersection's traffic signal control with Vissim, and estimates the result thus validating the optimized method's availability and usability.

INTRODUCTION

In recent years road mileage, number of vehicles and drivers has been on the rise. As a result there has been an increasing demand for infrastructure to allow smooth traffic flows. Traffic jams and accidents occur frequently and many studies search for effective measures to solve existing traffic problems based on traffic control theory. Today, the actuated-coordinated signal control technique is well-developed in some developed countries (Chen et al. 2007), but it is in its primary stages in our country, and its application rate is poor. Compared to pre-timed signal control, the actuated-coordinated signal control is more adaptable to traffic's randomicity and nondeterminacy, and it could improve traffic capacity at intersections, reduce delays, and parking numbers. Much of the research conducted in this area applies fixed phase number and order at signal intersections, but this method is not the best timing scheme at some intersections with traffic changing obviously (Gao et al. 2003).

TRAFFIC DETECTING METHOD AT INTERSECTION

Consider the typical crossroads. The detectors' setting is shown in Figure1. There are four inlets in each direction, and each inlet has left turning, straight, and right turning driveway. Each driveway has two detectors; namely the upper detector and the stop-line

detector. The detectors check the incoming and outgoing traffic volume, and the information acquired could include cars' running speed, capacity, saturation flow rate, and headtime in green time (Wang et al. 2008).

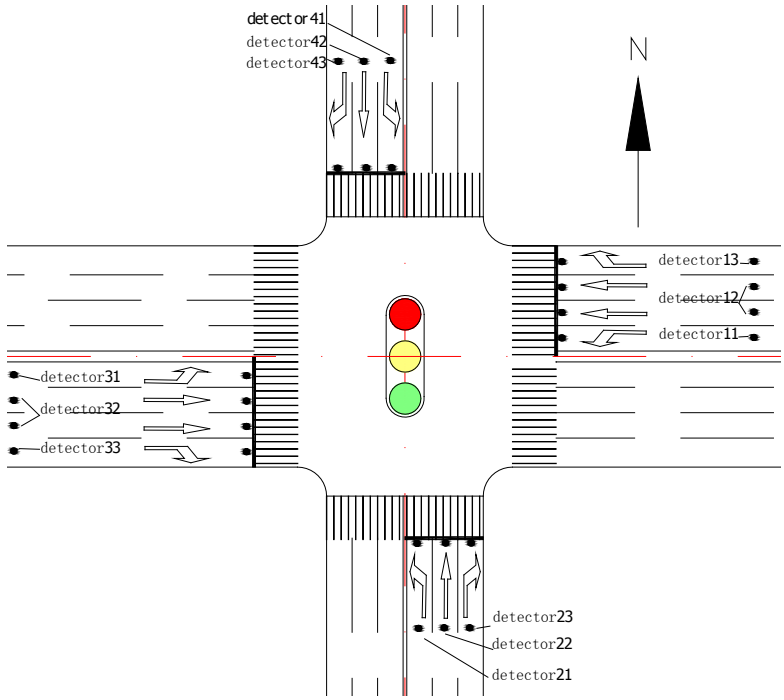

Figure 1. Detectors setting at actuated-coordinated signal control intersection

The traffic quantity data received from upper detectors set at left turning, straight, and right turning driveway of each direction are named as follows: Q_{IEL}, Q_{IES}, Q_{IER}, Q_{ISL}, Q_{ISS}, Q_{ISR}, Q_{IWL}, Q_{IWS}, Q_{IWR}, Q_{INL}, Q_{INS}, Q_{INR}.

The traffic quantity information received from stop-line detectors set at left turning, straight, and right turning driveway of each direction are named as follows: Q_{OEL}, Q_{OES}, Q_{OER}, Q_{OSL}, Q_{OSS}, Q_{OSR}, Q_{OWL}, Q_{OWS}, Q_{OWR}, Q_{ONL}, Q_{ONS}, Q_{ONR}.

Setting l is the distance between upper detector and stop-line detector, Q_{max} is the maximum number of detected vehicles at this driveway, h is the minimum headway, then $Q_{max}=l/h$ (Peng et al. 2001).

In order to acquire more information of flow direction at intersect detectors could be set at each outlet to judge the flow direction, and this would provide traffic information for the next intersection (Peng et al. 2001).

OPTIMIZING PHASE AND TIMING

The main parameters of conventional actuated-coordinated signal controls are: initial green time G_{min}, unit extended green time G_0 and maximum green time G_{max}. In the optimized method G_{max} is not a main parameter any more. The particular flow of optimized control method is shown in Figure 2 and the steps are as follows:

① G_{min} is calculated according to the distance between the stop line to the farthest conflict point which the car needs to pass in the green phase, and the speed of the car passing the intersection. The G_{min} should be long enough to ensure the first car could pass the

intersection. Set G_{min} to a certain phase.

②When G_{min} counts down to 0, search phases which have vehicles waiting.

③Judge phases if there are cars waiting over time in these phases. If so, then compare the former green phase's weight of right-to-pass with other phases according to overtime waiting, choose the phase with largest weight, and give the pass right to this phase; If the phase with largest right-to-pass weight is the former green phase, then extend the green time according to the queue length; if the phase with largest right-to-pass weight is not the former green phase, then give this phase G_{min}.

④Turn to step ②.

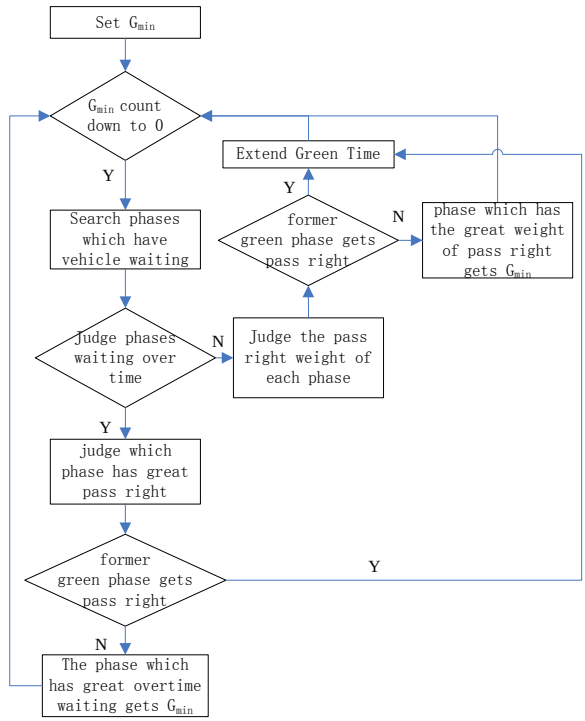

Figure 2. Flow chart of optimized actuated-coordinated signal control method

Estimate the phase which has the largest pass right, according to the waiting overtime or queue length. We now need to consider the yellow time coming after changing phase to clear cars left on the stop line (Wang 2008), and we also need to pay attention to the great influence on driver behavior caused by changing phase.

When the right-to-pass according to overtime waiting has been estimated, the main comparison factor is waiting time between the former green phase and other phases which has vehicles waiting. In fact, we just need to compare the waiting time between the former green phase and the phase which has the longest waiting time. Unlike the common actuated-coordinated signal control method, the driver cannot judge the next green phase by his general driving knowledge and needs to pay attention to the lights changing randomly, and this would cause a delay when vehicle start. We call the delay T_e in this paper. If T_{ot} is the former green phase's waiting-overtime while getting right-to-pass, G_{omin} is the former green phase's G_{min}; T_c is the time clearing cars left the stop line; T_{tmax} is the maximum overtime waiting of other phase's vehicle. The rules of right-to-pass are as follows:

①If T_{ot}-G_{omin}+T_c+T_e<T_{tmax}, then change the green phase and the phase which has the

greatest weight of right-to-pass gets green light.

②If T_{ot}-$G_{o\min}$+T_c+T_e≥$T_{l\max}$, then the former green phase still keeps the green light, and sets an extend green time.

If there is no vehicle waiting overtime, judge the right-to-pass based on the vehicle's queue length. We only need to compare the weight of right-to-pass between the former green phase and the phase which has the longest queue length. By using the data derived from the upper detectors and stop-line detectors, we can set parameters as the in queue number of i phase's cars Q_i, the cars' average speed V_i, the average headway h_i The time for cars of i phase in queue passing the intersection is calculated as T_i=$Q_i h_i$/V_i. If T_{ol} is the time for cars of former green phase in queue pass the intersection, the maximum T_i is T_{lmax}, T_{lmax} =max{T_i}, then the judging rules of right-to-pass are as follows:

①If T_{ol}-$G_{o\min}$+T_c+T_e<$T_{l\max}$, then change the green phase. The phase which has the greatest weight of right-to-pass gets green light.

②If T_{ol}-$G_{o\min}$+T_c+T_e≥$T_{l\max}$, then the former green phase still keeps the green light. Set an extended green time according to vehicle queue length of former green phase.

If the traffic volume is low and all detectors get no signals of incoming cars, set all lights to yellow flashing signal in order to warn drivers.

The differences between common and optimized actuated-coordinated signal control method are as follows:

①No limit to $G_{\max}$. If the vehicles in one phase come in continually and other phases do not witness vehicles for long periods, then this phase keeps green lights till other phases have vehicle waiting.

②$G_{\min}$ setting. The $G_{\min}$ calculation of common actuated-coordinated signal control method is based on traffic in each direction and thelost time phase. But with the optimized method, the $G_{\min}$ only provides a time to make sure the first car in the traffic flow could pass intersection. $G_{\min}$'s influence factors are then car's speed and the distance between stop line and the farthest conflict point.

③No fixed phase number and order. Signal cycle means a period of time between one main phase and the green light phase. With the optimized actuated-coordinated signal control method, the cycle could have two phases or more. If cars come symmetrically at intersection, the cycle usually has four phases. The phase's order is not fixed in a single form like east-west straight→east-west left→north-south straight→north-south left, but applies the method of instantaneously judging a phase's right-to-pass.

④The method of instantaneously judging phase's right-to-pass could reduce the green time of phases in which there are no incoming vehicles. However, the drivers have to observe the signal changes, and this would cause driver fatigue. In order to reduce delays caused by drivers judging the lights changing randomly, we could set a yellow light after the red light to provide a next green phase information to drivers.

CASE STUDY

Consider for example, the intersection of Daxin Street (east-west direction) and Northfourteen Street (north-south direction) in Harbin. Traffic flow in each direction and flow of intersection which occured between 7am and 8am on April 5th, 2006 is shown in **Table 1**.

Each inlet of this intersection has a right-turn lane, so the right turning vehicles have little influence on other cars, and there is no necessity to set a right turning phase.

The cars' starting to lose time on east-west straight, east-west left, north-south straight, north-south left is 2.7s, 4.1s, 3.0s and 3.8s; the average speed of vehicles is 25km/h; the average headway is 6m; the delay caused by drivers' judgment is 1s. According to the former conditions, $G_{\min}$ calculated is 8s, 10s, 7s and 8s (ignore the influence of pedestrians and non-motorized vehicles).

Table 1: Each Direction Traffic Flow on Daxin Street and North Fourteen Street Intersection

Inlet direction	East			South			West			North		
Flow direction	Left	Straight	Right	Left	Straight	Right	Left	Straight	Right	Left	Straight	Right
Average traffic	85	565	86	167	143	56	56	504	66	79	154	25
Minimum traffic	68	452	72	80	116	40	32	308	28	56	96	12
Maximum traffic	104	704	108	236	160	68	76	624	84	120	220	36
Saturation traffic	1621	3243	1621	1044	1044	1044	1653	3306	1653	1174	1174	1174

By simulating and analyzing with Vissim, a comparison is drawn of conventional and optimized actuated-coordinated signal control and is shown in **Table 2**.

Table 2: Comparison Result of Conventional and Optmized Actuated-coordinated Signal Control

Items	Conventional method(s)	Optimized method(s)	Effect(%)
Delays	12.4	10.7	13.7
Stops	0.54	0.43	20.4

According to the delay shown in **Table 2**, if we ignore pedestrians and non-motorized vehicle and contrast the optimized method with the conventional, the optimized method we could reduce the delay by 1.7s delay and 0.11 stops. This would mean an overall reduction of about about 13.7% and 20.4%. This gives good reason to believe that the optimized method could improve the intersection's passing efficiency remarkably.

CONCLUSION

①The method of instantaneously judging a phase's right to pass is considered from the angle of reducing the green time of phases which have few or no incoming vehicles .By simulating and analyzing with Vissim, the optimized method has some practicability.

②When contrasted with the conventional actuated-coordinated signal control, the optimized method gives a new concept, namely overtime waiting, and increases the phase order's flexibility. However, the phase order of this method would change the drivers' conventional thinking, and cause driver tension.

③This optimized method is still in the theoretical step, and ignores the influence of pedestrians and non-motorized vehicle. We need combine this method with practice in order to research further.

REFERENCES

Chen F. K., Wu Z. (2007) "Study on actuated signal controlled intersection based on Vissim." *Science paper Online*, http://www.paper.edu.cn (Apr. 5, 2007)

Gao H. J., Li L. X., Chen L. (2003) "Changeable phases signal control of traffic intersection." *Journal of traffic and transportation engineering*, 3(3), 79-83.

Peng G., Wang H., Yang X. G. (2001). "Traffic signal phasing under the condition of route guidance system." *China Journal of Highway and Transport*, 14(4), 85-88

Peng G. X., Zhang Y. (2001). "Study of the way of setting ripple changes." *China Journal of Highway and Transport*, 14(9), 59-62

Wang, Y. G.; Pei, Y. L., Zhao, Y. D. (2008). "Vibration-based damage detection with structural modal characteristics." *The Baltic Journal of Road and Bridge Engineering*, 3(1), 21-28

Wang X. T. (2008) "Research on phase optimization of traffic signals setting for junctions." *Communications Standardization*, 1, 140-144

Wang J. Y., Wang W., Hu M. W. "Study on Method for Pedestrian Signal Timing at intersections." *6th International Conference of Transportation Professionals*, 2006, Dalian, 669-674

Signal Intersection Optimal Control Model of Small Region Based on Traffic Equilibrium Theory

LIU Wei[1, 2], JIAO Hai-xian[2], and GONG Wei-yong[2]

[1]College of Traffic and Transportation, Southwest Jiao tong University, P.O. Box 610031, Chengdu, Sichuan, China; email:neway119@qq.com
[2]College of Traffic and Transportation, Chongqing Jiao tong University, P.O. Box 400074, Chongqing, China.

ABSTRACT

When traffic volume is distributed proportionally on a road network, it can relieve the traffic congestion of partial road nodes and make full use of road capacity. This article sets up an equilibrium model for regional signal coordination control according to the origin and destination demand between road nodes in small regions. This model is set up using the traffic equilibrium principle and dynamic traffic assignment theory. By coordinating the split of the signal between the intersections in the region, this model adjusts the turning volume at road intersections, distributes the traffic flow proportionally on the road network, avoids the vehicles crowding at some road intersection, effectively promotes road network efficiency, reduces delay in the road intersection, and alleviates traffic congestion. The model applies the traffic flow equilibrium theory to the region coordination control, makes the traffic flow in accordance with the optimization pattern movement, and realizes the traffic flow distribution proportionally.

INTRODUCTION

The urban road network is divided into many sub-networks by the urban expressway, and the optimization control of the intersections to each sub-network is the base of whole road network optimization coordination and control. It is an important means of improving efficiency in the whole network. Through coordination and optimization control the traffic congestion caused by the control of intersections can be reduced, distribution of the traffic flow on the road network can be balanced, and traffic flow can, as a result, run in a more efficient and orderly manner.

The region's traffic optimization control is one of the important areas for traffic control research and application. Since Webster proposed the simple point control timing method, the research of intersection optimization control has been one of the key research areas. Hong (Hong et al. 2001) used the genetic algorithm to establish the road intersection dynamic optimization control model. Chiou (Suh-Wen Chiou

2005) used the Wardrop theory as the basis and established a bi-level planning model to optimize the control of traffic networks. X.-H.Yu, (X.-H.Yu et al. 2006) used the stochastic process to establish the discrete time of network auto-adapted optimization control model. Chiou (Suh-Wen Chiou 2008) built a network balance control method on the basis of considering the user route choice. At present, the road intersection control delay computation has many kinds of models, The main choices include the model computation method (Gao Yang-bin, 2004) and the simulation analytic method (Zhuang Yan,2006). The difficulty of signal control and assignment of traffic flow at intersections does not allow for the impedance of intersections to be reflected easily. Brian (Brian et al. 1999) proposed a road intersection dynamic delay model based on the SCATS system, but did not solve the problem that transportation plan and the signal intersection control delay parameter coordinated each other. The dynamic traffic assignment combines with the intersection turning delay and uses the green ratio as variable, obtains the parameters of signal control through the balanced traffic assignment，realizes the region's road intersection balanced control.

SMALL REGION SIGNAL CONTROL OPTIMIZATION GOAL AND RESTRAINT ANALYSIS

The arterial road coordination control is mainly aimed at minimizing traffic flow direction vehicles.and ,as far as possible getting through the intersection in the green bands if cars run according to the design speed. This can reduce the signal control delay and interference to the main direction of the traffic flow.

The small region traffic control distributes traffic flow on the road network reasonably based on systematic perspective; it combines traffic control signal design with traffic flow equilibrium theory, enables the path to obtain the full use, and avoids the individual road intersection crowding which in turn causes traffic congestion in the region.

TARGET ANALYSIS OF SMALL AREA BALANCED TRAFFIC CONTROL

The small region balanced traffic control aims to minimize the total travel time on the road network. Each route of OD (Origin-Destination) pair's which has been used by cars has the same travel time and impedance according to the traffic equilibrium theory. The model considers the dynamic traffic assignment and the green ratio design of intersection turning directions together. The signals of each direction at intersection adjusts the balanced distribution of traffic flow on the road network, and then reaches the state of the intersection optimum control and small area traffic flow balanced distribution.

IMPEDANCE RESTRAINT OF SMALL AREA BALANCED CONTROL

The time impedance of vehicles on road network is composed of two parts The first one is the time impedance caused by vehicles travelling on the road section. The other is the impedance which is produced by the vehicle traveling on the road intersection. The road section travel time impedance research has many achievements. The mature impedance function has the BPR function and its function equation is: $t_a = t_{a,0}[1+\alpha(v_a/c_a)^{\beta}]$, of which t_a is road section impedance of link a, $t_{a,0}$ is free travel time of link a, v_a is traffic volume of link a, c_a is capability of link a, α, β is impedance parameter. They are calibrated by the traffic flow investigation data.

Traffic impedance which is produced in the road intersection is mainly the time delay while the vehicle gets through the intersection. Currently there are many methods used to compute the signal intersection's delay computation including the sample investigation computational method, the HCM (Highway Capacity Manual) computation method, the Webster delay computation method, and the Australian ARRB method (Zhang, 2002). The result of above computed models is vehicles' average delay which enter the road intersection. However, the intersection balanced control needs each turning direction time impedance to carry on the computation.

The road intersection impedance computation model is referred to in **Figure 1**.

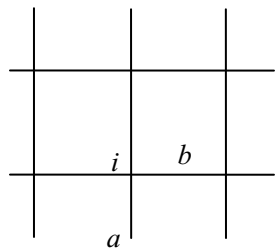

Figure 1. Node traffic turning impedance computation model

The road network model（N，A）like Figure 1 demonstrates that N is the set of nodes in the network and A is the set of links in the network. Road intersection $i, i \in N$ is a road intersection in the small control area, path *a*, *b* connected by road intersection *i*, the turning impedance from link *a* to link *b* is calculated by the ARRB model which has been improved as follows:

$$t_{a,b}(x_{a,b}) = T \cdot (1-\theta_{a,b})^2 / 2(1-x_{a,b}/c_{a,b}) + n_0 \cdot x_{a,b}/c_{a,b} \qquad (1)$$

$x_{a,b}$ —traffic volume from link a to link b, $a \neq b$,a,b belongs to A which is the set of links of small area road network.

T —signal cycle of the intersection i. T is constant

$\theta_{a,b}$ —green ratio from link a to link b in road intersection i.

$c_{a,b}$ — lane capacity from link a to link b, $c_{a,b} = \frac{3600}{T} \cdot \frac{\theta_{a,b} \cdot T - t_s}{t_0}$, t_s is green time lost , t_0 is the average headway when the vehicles continuously pass the stop line, t_s, t_0 is constant.

n_0 — the number of overflow vehicles in the intersection which entrance lane from link a to link b.

OPTIMAL CONTROL MODEL OF TRAFFIC FLOW BALANCED DISTRIBUTION

Assume that the driver should be able to choose an optimal route and cause total traffic cost to be the smallest, its mathematical programming question is the UE model. According to the shown in figure 1, the optimum balanced control model would be as follows:

$$\min Z = \sum_i \sum_b \sum_{a(a \neq b)} \int_0^{x_{a,b}} t_{a,b}\left(x_{a,b}\right) dx + \sum_b \int_0^{x_b} t_b(x_b) dx \qquad (2)$$

$$s.t. \quad \sum_k f_k^{rs} = q_{rs} \quad \forall r, s$$

$$f_k^{rs} \geq 0 \ \forall k, r, s$$

$$x_b = \sum_{rs} \sum_k f_k^{rs} \delta_{b,k}^{rs} \ \forall a$$

$$x_{a,b} = \sum_{rs} \sum_k \sum_{a \neq b} f_k^{rs} \delta_{b,k}^{rs} \delta_{a,k}^{rs}$$

$$0 \leq \theta_{a,b} \leq 1, \quad a,b \in A, \quad i \in N$$

In the model, $q_{r,s}$ —the OD traffic flow from node r to node s in the small area;

$f_k^{r,s}$ —the traffic volume belongs to OD pair r –s, which gets through route k.

$\delta_{a,k}^{rs}$ —state variable, if route k from node r to node s gets through link *a*, its value is 1, otherwise is 0.

Other variables' meaning is the same as above. $x_{a,b}, \theta_{a,b}$ is variable of the model to be solved . The green ratio of each turning direction and each link's traffic volume under balanced control can get by solving the model.

THE ALGORITHM OF THE MODEL

The method of small area traffic balanced control realizes the traffic flow

distribution proportionally on the network by adjusting the green ratio of each turning direction at the intersection. It reduces the total travel time to a minimum which cars in the network expend. The traffic flow reaches optimal state. The solution method of equation (2) is as follows:

Step 1: Initialization: according to $t_{a,b} = t_{a,b}(0)$, $t_b = t_b(0)$ $\forall a,b,a \neq b$, implement all or nothing assignment, obtain each link and intersection traffic volume x_b^1, $x_{a,b}^1$, $\forall a,b,a \neq b$,set n=1.

Step 2: Renew each link and intersection impedance: $t_b^n = t_b(x_b^1)$, $t_{a,b}^n = t_{a,b}(x_{a,b}^1)$, $\forall a,b,a \neq b$.

Step 3: Seek for the next iterative direction: According to $\{t_b^n, \forall b\}$, $\{t_{a,b}^n, \forall a,b,a \neq b\}$ Implement all or nothing traffic assignment, obtain a group of additional traffic volume $\{y_b^n, \forall b\}$, $\{y_{a,b}^n, \forall a,b,a \neq b\}$.

Step 4: Determine the iteration distance : Calculate λ_b, $\lambda_{a,b}$ by dichotomy following

$\sum (y_b^n - x_b^n) t_b(x_b^n + \lambda_b(y_b^n - x_b^n)) = 0$, $\sum (y_{a,b}^n - x_{a,b}^n) t_{a,b}(x_{a,b}^n + \lambda_{a,b}(y_{a,b}^n - x_{a,b}^n)) = 0$.

Step 5: Determine the new iterative beginning: $x_b^{n+1} = x_b^n + \lambda_b(y_b^n - x_b^n)$, $x_{a,b}^{n+1} = x_{a,b}^n + \lambda(y_{a,b}^n - x_{a,b}^n)$.

Step 6: Astringent examination criteria: If

$$\sqrt{\sum_b (x_b^{n+1} - x_b^n)^2} \Big/ \sum_b x_a^n < \varepsilon, \quad \sqrt{\sum_b \sum_{a,a \neq b} (x_{a,b}^{n+1} - x_{a,b}^n)^2} \Big/ \sum_b \sum_{a,a \neq b} x_{a,b}^n < \varepsilon_1 \text{（}\varepsilon, \varepsilon_1\text{）},$$

stop calculation, otherwise set n=n+1, and return to the second step.

APPLICABLE CONDITION AND SCOPE OF THE MODEL

Balanced Control model of regional intersections is based on small areas which are divided by primary roads. Each small area is an optimal balanced control unit. The input datum of the balanced control model need intelligent transportation system collect and supply. The control parameters which the balanced control model had figured out require coactions with intelligent information guidance system to guide the traffic flow distribution proportionally in accordance with the model expectation. Then, traffic flow realizes well-proportioned distribution in the control areas. The coordination and optimization between control areas can use arterial road line control method, reach optimal arterial route and intersection coordination operation, achieve the concordant control condition of each control unit, and the entire traffic network optimization.

CONCLUSION

The small area intersection balanced control model uses the traffic equilibrium theory to calculate the intersection signal parameters and distribute the traffic flow. It utilizes the green ratio as model variable, integrates the dynamic traffic assignment, distributes the traffic flow proportionally in the road network, and improves the travel condition in the road network while avoiding some excessively congested intersections. The model calculates the control parameters by using intersection turning impedance. This may make traffic plan and traffic management more coordinated and can alleviate traffic congestion more efficiently. But the traffic impedance model of intersection control needs further study. The balanced control model needs the intelligent guidance information system to help drivers plan the route correctly.

REFERENCES:

Brian Wolshon, William C. Taylor. (1999). "Analysis of intersection delay under real-time adaptive signal." Transportation Research Part C. 7,53-72

GAO Yang-bin. (2004). "Models for the traffic delay of signal intersection. Technology and Economy in Areas of Communications." 26 (6),49-51

Hong K.Lo,Elbert Chang.(2001), Yiu Cho Chan. "Dynamic network traffic control." Transportation Research Part A, 35,721-744.

Suh-Wen Chiou. (2005)." Joint optimization for area traffic control and network flow." Computers and Operations Research, 32,2821–2841

Suh-Wen Chiou.(2008). "An efficient algorithm for optimal design of area traffic control with network flows." Applied Mathematical Modeling (in press), doi:10.1016/j.apm. 2008.08.009

X.-H. Yu, W.W. Recker . (2006). "Stochastic adaptive control model for traffic signal systems." Transportation Research Part C 14, 263-282

ZHANG Qi-sheng, ZHANG Ya-ping.(2002)."Section 7:The Capacity of intersection." *Highway capacity analysis*, China Communications Press, Beijin, 7.3.

ZHUANG Yan ,ZENG Wen-jia. (2006). "Study of traffic delay model at signalized intersection." Journal of Shen Zhen University Science and Engineering.23 (4), 309-313

A Novel Real-time Road Shape Describing and Parameter Obtaining Method

Meng Wu[1]， Yang Gao[1,2]and Peng He[1]

[1]Xi'an Surveying and Mapping Institute, No.1, Yanta Road, Xi'an, P.R. China, 710054; email:wumeng19nudt@163.com
[2]College of Geology, Engineering, and Geometrics, Chang'An University, No. 126, Yanta Road, Xi'an, P.R. China, 710054.

ABSTRACT

This paper presents a novel method of road shape describing, in which the real time sequence road images are shot by cameras fixed on Autonomous Navigation Vehicles (ANV) placed on a structured road. Through the pre-processing of real time images, the road lines in images are extracted in real time. Further, a parameterized road shape describing method is also proposed. All parameters' meanings are indicated and the real time parameter calculating problem is settled. The experiment results present that accuracy of real time parameter obtaining is above 99.1%. This method will provide basic data sustainment for research on Initiative Safety Technology (IST) of ANV which require real time road information, such as Vehicle Deviation Warning System, etc.

INTRODUCTION

An increasing amount of attention has been paid in recent years to the research on vehicle Initiative Safety Technology. Presently, there are a great many new technologies on IST like: Lane Deviation Warning System, Anti-drowsiness System, Speed Recognition Systems, Tire Pressure Monitoring System, and Vehicle Distance Control System (E.D.Dickmanns,1992.). In comparioson to Passive Safety Technology, the research significance of IST lies in preventing accidents and reducing casualties.

Vehicle and the road are the two core objects inevitable to study in IST. Relationship between vehicle and road is the basis and premise for the study of other technologies. Among those new technologies, road line shape description and position relationship between lines and vehicle are the foundational investigations. It is well known that the road line detection technique is mature and there are also some road line shape describing models(E.D.Dickmanns,1986.), however, rare existing methods can model simply and calculate description parameters accurately in real-time.

In this paper, we address the problem of real-time road shape describing and parameter obtaining. Based on modeling of some coordinates and preprocessing of images, a fully automated real-time road shape describing and parameter obtaining method is proposed. Researches in this paper are all based on prototype HONGQI Autonomous Land Vehicle (**Figure1**). The main vision sensor is a video camera mounted on the top left corner of the windshield.

Figure.1. HONGQI prototype

COORDINATE SYSTEM TRANSFORMATION

In this paper，we define the coordinate system as follows: the vehicle coordinate system $V_{(x_V, y_V, z_V)}$， the camera coordinate system $C_{(x_C, y_C, z_C)}$， the image coordinate system $I_{(x_I, y_I)}$ and the image-in-memory coordinate system $B_{(c,r)}$ (N. Apostolo,2003.). Firstly, we use

$$C = {}^{C}_{V}R(V - {}^{V}_{C}T) \tag{1}$$

to illustrate the rotation and translation transforms from the vehicle coordinate system to the camera coordinate system. The listing angle ψ, pitching angle θ and the rotating angle φ are used to define the rotation transformation. Order of rotation transformation is defined as:

$${}^{C}_{V}R = R_Y(\psi)R_X(\theta)R_Z(\varphi) \tag{2}$$

The pin-hole model for camera imaging is also utilized here：

$$x_I = f\frac{x_c}{z_c}, \quad y_I = f\frac{y_c}{z_c} \tag{3}$$

Lastly, transformation from image coordinate system to image-in-memory coordinate system is described as:

$$B = \begin{bmatrix} N_r & 0 \\ 0 & N_c \end{bmatrix}\begin{bmatrix} x_I \\ y_I \end{bmatrix} + {}^{B}_{I}T \tag{4}$$

N_r and N_c denote numbers of rows and columns of pixels corresponding to length in unit in image coordinate system respectively.

IMAGE PREPROCESSING

After construction of coordinate systems, it is necessary to follow some image preprocessing steps for aiming of obtaining road lines in image frame(Zhencheng Hu,2004):

Step 1: Choose region of interesting (ROI) in the image shot by the camera. As in **Figure 3** and **Figure 4**, the image size is 1024*256.

Step 2: Make use of the Sobel operator to do edge detection in the image.

Step 3: Automatically set the gray thresh to get binary image. Even on conditions of different illumination, threshold which is set via taking some fixed percent of the highest pixel value among the whole image can be easily chosen by equalizing bar graph.

Step 4: Use Hough transform to extract two brightest points which represent two sides of the road, as in **Figure 2** and **Figure 3**. By means of looking over continuous points in image space which are corresponding to peak values in Hough transform, the start and end points of two straight lines are obtained. **Figure 3** lines out two straight road lines extracted from original image by making use of start and end points' coordinates.

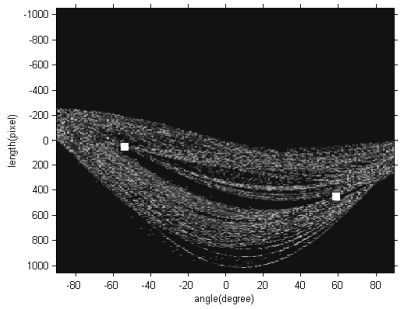

Figure.2.(left) Hough transforming
Figure.3.(right) Detected road lines and their start, end points

Step 5: Calculate the vanishing point according to start and end points' coordinates and draw the two road lines, as in Figure 4.

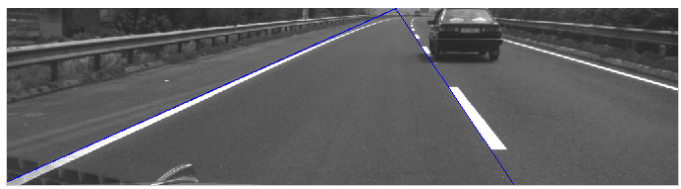

Figure.4. Extracted two road lines

ROAD SHAPE DESCRIPTION IN IMAGE

To describe road line shape, line model building is necessary. Given camera parameters $\varphi = 0$, $\theta = \pi/2$, $\psi = \pi/2$, ${}^{V}_{C}T = (0,0,-h)$, coordinates in image-in-memory frame ${}^{B}_{I}T = (0,0)$,utilizing (1)~(4) to calculate point coordinates from (x,y,z) in vehicle frame to (r,c) in image-in-memory frame, we have relations

$$r = \frac{z+h}{r_f x}, \quad c = \frac{y}{c_f x}.$$

Given $\varphi = 0, \theta = \frac{\pi}{2} - \theta_0, \psi = \frac{\pi}{2} - \psi_0$, we have

$$r = \frac{-x\theta_0 + y\psi_0\theta_0 + z + h}{r_f(x - y\psi_0 + z\theta_0 + h\theta_0)}, \quad c = \frac{x\psi_0 + y}{c_f(x - y\psi_0 + z\theta_0 + h\theta_0)}. \tag{5}$$

$c_f = \frac{1}{N_c f}$ and $r_f = \frac{1}{N_r f}$ are ratios of focal length f to length and width of a pixel respectively. On condition of only considering the level curvature diversion of highway, the road curve in the tangent plane can be presented as

$$\kappa(l) = 2c_{h2} + 6c_{h3}l$$

When the curvature is small, after twice integrals, we obtain the description form of the road curve in the vehicle frame as

$$\begin{aligned} x_V(l) &= l \\ y_V(l) &= c_{h0} + c_{h1}l + c_{h2}l^2 + c_{h3}l^3 \\ z_V(l) &= 0 \end{aligned} \tag{6}$$

From the equations in fore-mentioned camera modeling, when φ = 0, θ = 0, ψ = 0, we may take out the parameter *l* and we have

$$c = \frac{c_{h0}r_f}{c_f h}r + \frac{c_{h1}}{c_f} + \frac{c_{h2}h}{c_f r_f}\frac{1}{r} + \frac{c_{h3}h^2}{c_f r_f^{\,2}}\frac{1}{r^2} \tag{7}$$

when road shape is straight or a curve, viz. $c_{h3} = 0$, (7) in simpler form is

$$c = \frac{c_{h0}r_f}{c_f h}r + \frac{c_{h1}}{c_f} + \frac{c_{h2}h}{c_f r_f}\frac{1}{r}$$

Put equation (6) into (5) and eliminate parameter *l*, then we have

$$c = \frac{c_{h0}r_f - c_{h1}r_f h\theta_0}{c_f h(1 - c_{h1}\psi_0)}(r + \frac{\theta_0}{r_f}) + \frac{c_{h1} + \psi_0}{c_f(1 - c_{h1}\psi_0)}$$

We can finally unify 2D road parameter depiction when parameters are in different conditions as

$$\begin{aligned} c_r &= (p_2 - p_1)(r - p_0) + p_3 + p_4\frac{1}{(r - p_0)} + p_5\frac{1}{(r - p_0)^2} \\ c_l &= (p_2 + p_1)(r - p_0) + p_3 + p_4\frac{1}{(r - p_0)} + p_5\frac{1}{(r - p_0)^2} \end{aligned} \tag{8}$$

so left and right side road curves are expressed as (8).

RELATIONS BETWEEN ROAD SHAPE AND PARAMETERS

Equation (8) above defines the road shape model, but the physical meaning of those parameters in (8) are unknown. Assuming the initial values of (8) as $p_0 = -128$, $p_1 = 1.20$, $p_2 = 0$, $p_3 = 128$, $p_4 = 0$, and $p_5 = 0$, we can see the actual meaning of these parameters through displacing their values.

From **Figure 5a** to **Figure 5f**, the light lines denote the road when the parameters are equal to the initial values, in contrast, the dark lines denote the road when the value of some parameter has changed. **Figure 5a** shows the vanishing point becoming farther with the sole displacement $p_0 = -98$; **Figure 5b** shows the road width becoming narrower with the sole displacement $p_1 = 1.0$; **Figure 5c** shows the road deflects from the original location with the sole displacement $p_2 = -0.3$; **Figure 5d** shows the road departure in horizontal direction with the sole displacement $p_3 = 100$; **Figure 5e** shows the road turning left with the sole displacement $p_4 = 120$; **Figure5f** shows the road turning right with the sole displacement $p_5 = 400$.

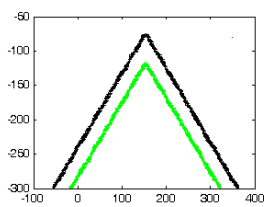

a

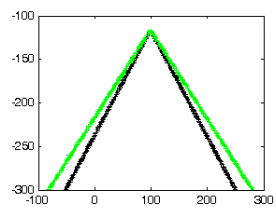

b

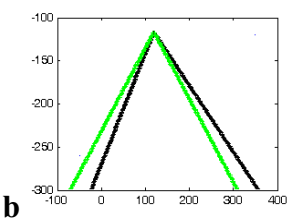

c

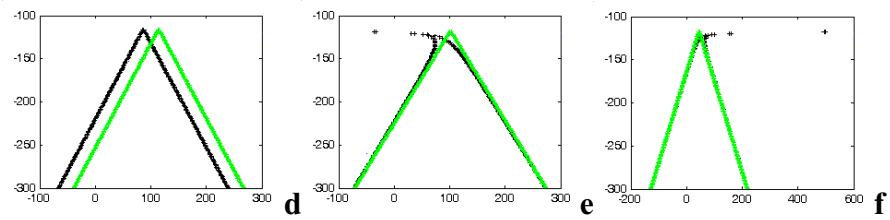

Figure. 5a-5f .The actual meaning of the road parameters

OBTAINING OF ROAD PARAMETERS FROM IMAGE SEQUENCE

From the physical meaning of parameters in equation (8), when (8) describes a straight road, it can be simplified as

$$\begin{cases} c_r = (p_2 - p_1)(r - p_0) + p_3 \\ c_l = (p_2 + p_1)(r - p_0) + p_3 \end{cases} \tag{9}$$

Compared with a general using straight line equation

$$y = k(x - x_0) + b$$

It is obvious that we can obtain the road parameters in (9) in image frame directly or indirectly from detected lines by Hough transform. p_0 is the position of vanishing point, so we can take cross point of two road lines as its value. p_3 can be calculated utilizing known start and end points of left or right line at will, it controls the road's horizontal displacement. p_2 and p_1 can be gained through calculating $p_2 - p_1$ and $p_2 + p_1$ from the slope of left and right lines，where p_2 controls angle offset, p_1 controls road width.

So that p_0，p_1，p_2，p_3 values can be obtained from sequential images. In **Figure 6**, calculating results of p_0，p_1，p_2，p_3 from continuous 2560 frames images are shown. Through the analysis of comparing with 2560 road images and the calculating results, the angle offset of only 23 frames present positive and negative pulsate of the same absolute value and further more, the pulsate do not influence the calculation results of other parameters. As in left-down figure of **Figure 6**, parameters obtaining accuracy in real-time is above 99.1%. Experiments illustrate that parameters of exact road shape information can be gained in real time by making using of road shape description model viz. equation (8) and this simple and convenient calculating method.

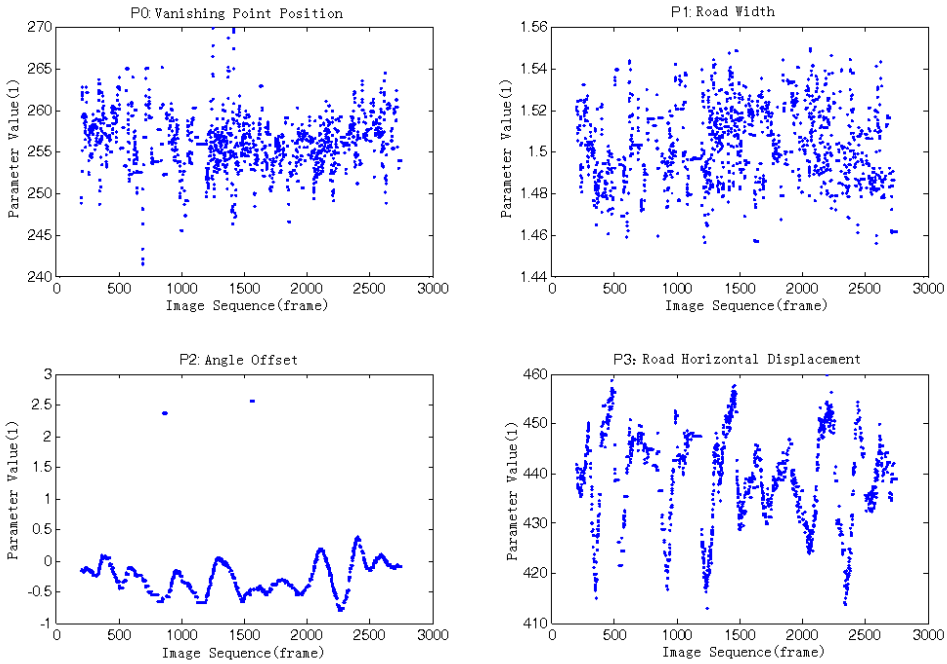

Figure.6. Obtaining road parameters from sequential images

CONCLUSION

Using the projection modeling and image preprocessing, we propose a novel road shape describing model. Through the research on relationships between road line shapes and parameters in the model, the representation and meanings of the road parameters in image frame are gained. Finally, a novel method of road shape describing and calculating parameters in real time are presented. Experiments illustrate that the validity of the method is well established. This simple way of modeling is accompanied by an excellent performance----accuracy of better than 99.1% and can be applied to engineer practice. This research will be followed by further study on the application of parameters calculation method in real time when road lines are of large curvature.

REFERENCES

E.D. Dickmanns (1986). "A curvature-based scheme for improving road vehicle guidance by computer vision." SPIE Conference on Mobile Robots, vol.727, pp.161-168, Oct.. J.

E D.Dickmanns(1992), "Recursive 3D road and relative ego-state recognition." *IEEE Trans. On Pattern Analysis and Machine Intelligence,*NO.14, pp199-213.

N. Apostolo (2003). "Robust vision based lane tracking using multiple cues and particleltering." In Proc.IEEE Intelligent Vehicles Symposium.

Zhencheng Hu(2004). "Solution of camera registration problem via 3d-2d parameterized model matching for on-road navigation." International Journal of Image and Graphics, Vol. 4, No. 1 1C1.

Adaptive Control Method of Multi-phase Intersection Based on Traffic Status Identification

Yang Wenchen[1], He Zhaocheng[2], and Chen Ningning[3]

[1]Yang Wenchen, Graduate, Intelligent Transportation Research Centre, Sun Yat-sen University, Guangzhou 510275, China; email:ywc_678100@163.com
[2]He Zhaocheng, Associate professor, Intelligent Transportation Research Centre, Sun Yat-sen University, Guangzhou 510275; China
[3]Chen Ningning, Doctoral Candidate, Intelligent Transportation Research Centre; Sun Yat-sen University; Guangzhou 510275; China

ABSTRACT

Adaptive signal control methods have the ability to improve operations at isolated intersections. However, most of these experiences mainly focus on one specific traffic status, so other traffic characteristics are not fully considered. In this paper, the traffic status of an isolated intersection is identified using a two-dimensional fundamental diagram divided into four levels. An adaptive traffic signal control method based on traffic status identification is proposed. Different signal control performance indexes (PIs) are chosen in different traffic levels. Appropriate evaluation parameters are selected for the PIs according to real-time traffic characteristics. An enumeration algorithm is put forward to solve the optimized model of PIs. Then, a signalized intersection in Shenzhen city is studied through theoretical calculation and simulation evaluation via a microscopic traffic simulation software, Paramics. The results indicate that the signal strategy derived from the proposed method is more effective than the original F. Webster method strategy, because the proposed PIs outperform those of F. Webster on all four traffic levels.

Keywords: Adaptive signal control; Traffic status identification; Signal timing; Traffic simulation.

1 INTRODUCTION

The F. Webster signal timing method developed by F. Webster and B. Cobber has been adopted in traditional fixed-time intersection management. This method takes under-saturated traffic flow into account, and selects delay as performance index (PI) (Webster & Cobbe, 1966). But the timing strategy derived from this method does not perform well in high traffic flow. Time loss increases as the result of insufficient cycle time, which is caused by static cycle time and split assignment (Quan, 1989). Akcelik and Kimber's researches have clearly modified the F. Webster method by revising evaluation parameter models (delay, stop times, capacity) and PI. They studied the parameter models in circumstances of high-saturation and over-saturation (Kimber, 1976; Akcelik, 1980, 1981). But the PI in the Akcelik method is still mainly determined by delay. This proves to be a weakness in a busy traffic status, because the capacity is the most important factor in PI for the intersection in an over-saturated status.

The real-time, traffic-responsive, multi-object signal optimization methods have

evidently demonstrated the ability to reduce the stops while delaying and improve capacity at isolated signalized intersections (Bullock, 2000; Yu, 2004). To meet real-time traffic demands, these methods make evaluation parameter coefficients adapt to the change of traffic flow. These methods mainly include two types. One typically has single fixed PI, decided by the delay, stops or capacity (Hong, 2004). The PI is decided by fixed control object, but traffic flow characteristics at intersections are not entirely considered. The other type proposed respectively by Denos and Li is based on traffic status identification. In their research, the traffic status is identified by saturation, and is divided into high saturation and low saturation (Denos, 1964; Li, 2006). These methods provide two different PI models to high saturation and low saturation respectively. However, two levels cannot explicitly consider the lower and over-saturated flow, and evaluation parameters are mostly based on F. Webster method, but the delay and stop index value cannot reflect how the actual traffic performs when the traffic flow at intersections increases.

Identifying different traffic status from different traffic parameters is to discuss in this paper. The recent progress of research in traffic flow theory indicates that traffic states distribute in two-dimension areas rather than lie exactly on the curve in the fundamental diagram, which is specifically the *y*-*O* diagram (total traffic flow rate of intersection; average time occupancy of intersection) in this paper (Kerner, 1996, 2002). In the light of that, this paper identifies the traffic status of isolated intersections into four levels with the combination of *y* and *O*.

This paper differs from the earlier work of Bullock, Hong, and Denos. Based on two-dimensional identification, a multi-object adaptive signal timing method is proposed, which selects different PI and appreciates evaluation parameters according to different real-time traffic status. The optimal control strategy of the proposed adaptive method is searched by the enumeration algorithm. Finally, to validate the rationality and effectiveness of the proposed method, a case study of the signalized intersection in Shenzhen is carried out, and simulation evaluation is done via Paramics.

This paper is organized as follows. Four traffic levels of intersection status, the proposed adaptive method and the solution of enumeration algorithm are described in Section 2. Section 3 presents the calculation of evaluation parameters in Shenzhen intersection. Section 4 shows traffic simulation and the comparison of control effects.

2 ADAPTIVE MODEL BASED ON TRAFFIC STATUS IDENTIFICATION

2.1 Traffic status

The *y*-*O* diagram in **Figure 1(a)** shows the distribution of traffic data at Hongli-Xinzhou intersection of Shenzhen during a month (March 1st, 2008 to March 31st, 2008). From the diagram, four distinct patterns can be identified: the linear Area I with low traffic flow rate, the linear Area II with high flow rate, the nonlinear Area III and the plateau Area IV.

The *y*-*O* diagram can be simplified as shown in **Figure 1(b)**, and four levels of traffic status are identified accordingly. In figure 1-b, O_s stands for the time occupancy of key lane in phase *i*, corresponding to saturated flow. When *O* is over O_s, the intersection is surely over-saturated and the traffic status is labeled as congestion. Otherwise, the under-saturated status is identified to three traffic levels by y_1 and y_2. Thus, the traffic status at intersection is

divided into four different levels: free, smooth, busy and congested. y_1 and y_2 are determined by the actual characteristics of signalized intersection. Taking Hongli-Xinzhou intersection as an example, the advised experimental y_1 is 0.6 and y_2 is 0.72.

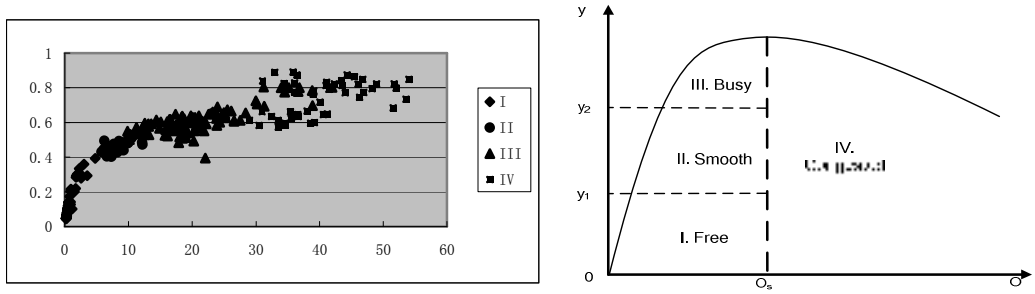

(a) The O and y distribution **(b) The changing trend of O and y**

Figure 1. The principle of traffic status identification

2.2 The signal timing optimization model

Adaptive signal timing is decided by maximizing the PI, which lies on the control objective. In this paper, considering safety, economic and management demands at isolated intersection, promising control objects are proposed for different levels. The adaptive signal control objectives in four traffic levels are shown in **Table 1**.

Table 1. The control objectives of four traffic levels

Traffic level	Traffic characteristics	Management objectives
Free	Free flow	Safety & Delay minimum
Smooth	Uniform arrival	Comfort maximum
Busy	Markedly increasing	Economic benefits maximum
Congested	Forced-flow	Management efficiency maximum

First, in free level, drivers expect to pass intersections without stopping, but traffic safety is as important as delay minimization. Therefore the minimum constraints of cycle and green time are brought in to guarantee traffic safety. Second, according to the smooth and comfortable control aim at a smooth level, the objective function is to obtain a control strategy with the minimum of delay and stop times. Third, in the busy level, inadequate capacity will produce long queues and spillbacks in the high flow rate phases. So the capacity of each phase should be considered in the objective function to ensure adequate capacity. Fourth, delay and stop times are always high for every phase in the congested level. The best way to improve management efficiency in congested level is to increase the capacity of each phase. The capacity should then, be the most important factor in the objective function.

Previous researches have clearly verified the following points. First, PI is decided by delay, stops rate or capacity models (Nagui, 1999). Second, steady-state delay and stop rate model in F. Webster method have better performance if intersection saturation is under 0.6. Third, delay model in HCM2000 and Steady-state stop rate model in Akcelik method are more suitable for the traffic flow between low and high saturation. Fourth, when saturation is high, Transient Function delay and stop rate model, considering high-saturated and over-saturated traffic status, could make up for the lacks of the models above (Li, 2004;

HCM2000, 2000).

Based on the analysis of the control objectives in **Table 1** and the analysis of evaluation parameter discussed above, the objective functions (PI), weight coefficients and constraints for these four levels are shown in **Table 2** (Pitu, 2001; Akcelik, 1980; Li, 2006).

Table 2. The objective functions, weigh coefficients and constraints

Level	Objective function	Weight coefficients	Constraints
Free	$\min f(C,g_i)=\sum_{i=1}^{n} D^W \Big/ \sum_{i=1}^{n} q_i$	None	$C_{\min} \le C \le C_{\max}$ $g_i^{\min} \le g_i \le g_i^{\max}$
Smooth	$\min f(C,g_i)=\sum_{i=1}^{n}(k_i^1 D_i^H + k_i^2 H_i^W)$	$k_i^1 = 2Y \cdot \sqrt[7]{S_i}$ $k_i^2 = \sqrt[7]{S_i} \cdot \frac{1-Y}{0.9}$	$C_{\min} \le C \le C_{\max}$ $g_i^{\min} \le g_i \le g_i^{\max}$
Busy	$\min f(C,g_i)=\sum_{i=1}^{n}(\frac{k_i^1 D_i^H + k_i^2 H_i^A}{k_i^3 Q_i})$	$k_i^1 = 2(1-Y)$ $k_i^2 = 1.1 \cdot (1-Y)C/n$ $k_i^3 = 2Y(\frac{3600}{C})$	$C_{\min} \le C \le C_{\max}$ $g_i^{\min} \le g_i \le g_i^{\max}$ $x_i < 0.9$
Congested	$\min f(C,g_i)=-\alpha \sum_{i=1}^{n} Q_i \Big/ \sum_{i=1}^{n} D_i^T$	α : Adjustment coefficient. Generally: α =1000	$C_{\min} \le C \le C_{\max}$ $g_i^{\min} \le g_i \le g_i^{\max}$ $x_i < 0.95$

The meanings of parameters in **Table 2** are as follows:

i: Phase i.

l_i: Loss time of phase i;

g_i: Effective green time;

Q_i: Capacity of phase i;

D_i^W: F. Webster total delay;

D_i^T: HCM2000 total delay;

D_i^H: Transient total delay;

H_i^W: F. Webster total stops;

H_i^A: Akcelick total stops;

k_i^1 : Weight coefficient of delay;

k_i^2 : Weight coefficient of stops;

k_i^3 : Weight coefficient of capacity;

$g_i^{\min}$: Smallest effective green time;

$g_i^{\max}$: Largest effective green time;

$C_{\min}$: Smallest cycle time;

$C_{\max}$: Largest cycle time.

The detailed description of the delay and stop rate models is presented in Li's research (Li, 2004) and the coefficient modeling principle is studied in Xu's research (Xu, 2005). Note that drivers enhance the patience in higher traffic flow. The timing thresholds of high saturation level could be larger.

2.3 The solution of adaptive timing models

In the adaptive signal timing models above, y_i, q_i and l_i are known variables, and C and g_i are unknown variables. Based on an equal saturation assignment of effective green time, leaving just one variable C, the proposed signal timing models are solved and the best signal timing strategies are found by the algorithm shown in **Figure 2**.

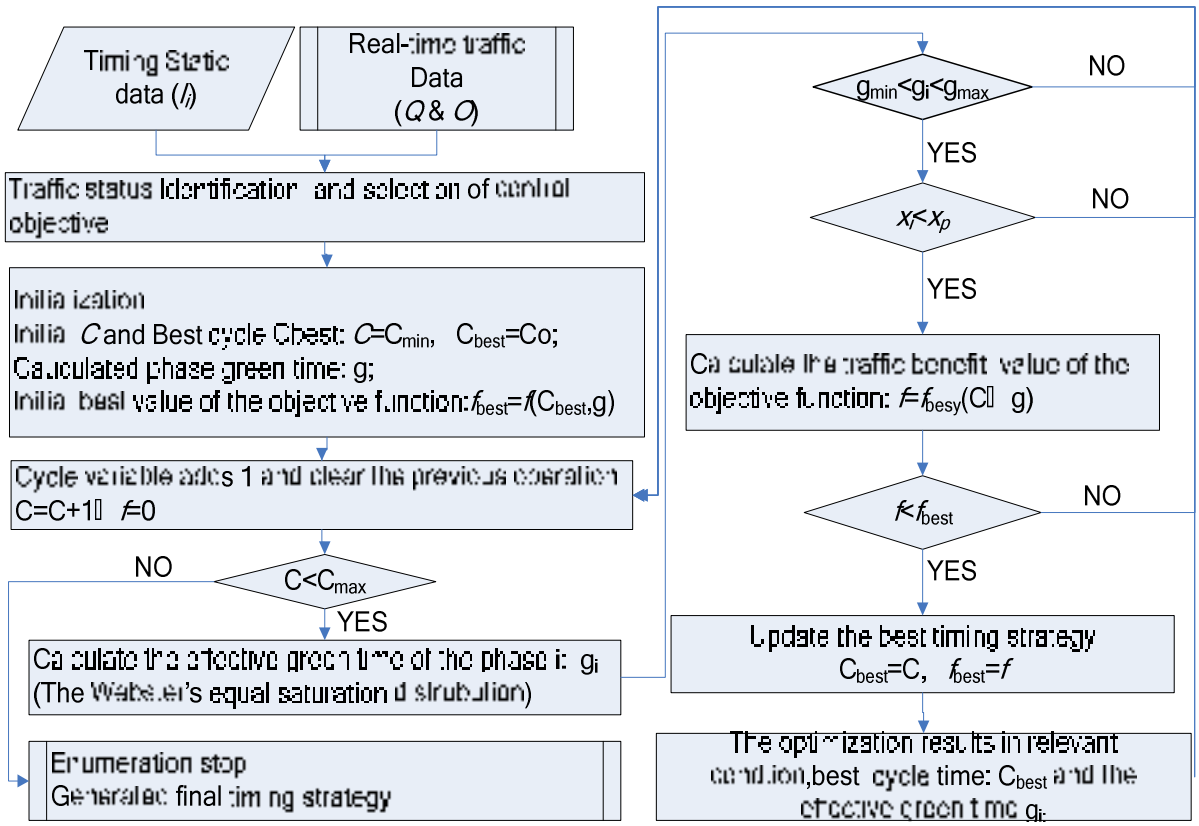

Figure 2. The adaptive timing optimization flow based on enumeration algorithm

Considering that the constraints of cycle time and effective green time are presented and the searching area is not large in these models, this paper solves the optimization model by the enumeration algorithm in order to enhance accuracy. The enumeration algorithm enumerates every integral value of C in its finite solution set and gets the best solution through comparing the calculated objective value.

3 CASE STUDY

Hongli-Xinzhou intersection in Shenzhen is a typical urban isolated signal control intersection (**Figure 3**). The eastbound, southbound, westbound and northbound entries are widened and the intersection is under four-phase signal control (the right-turn vehicles are not under the signal control). The data of phase, containing flow and the average traffic volume in four different levels are shown in **Table 3**. In **Table 3**, NS means northbound straight, NL means northbound left turn.

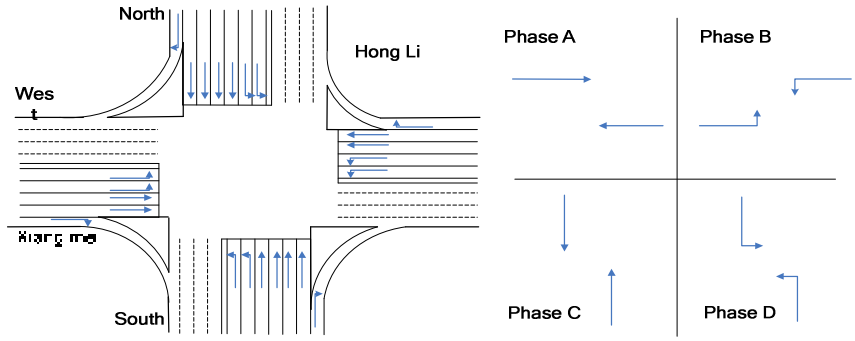

Figure 3. Traffic flow distribution and phase-graph

Table 3: Traffic data of Hongli-Xinzhou **intersection**

Phase name	A	B	C	D
Containing flow	ES,NS	EL,WL	NS,SS	NL,SL
Free flow volume: q	126,76	52,64	271,325	28,120
Smooth flow volume: q	475,365	287,250	847,1142	144,406
Busy flow volume: q	604,494	404,317	1107,1389	236,530
Congested flow volume: q	822,642	513,384	1619,1764	252,529
Phase saturated flow volume: S*	6600,6600	3100,3100	6600,6600	3100,3100

*The straight saturated flow volume is 1650 while the left-turn saturated flow volume is 1550.

Based on the experiential values researched by Guo (Guo, 2008) and the traffic characteristics of HongLi-Xinzhou intersection, signal timing constraints and thresholds of traffic status identification are shown in **Table 4**.

Table 4. Constraint limits and timing thresholds in four levels

Traffic level	l_i(s)	y_i	O_i	x_p	g_{min}(s)	g_{max}(s)	C_{min}(s)	C_{max}(s)
Free	4	[0,0.5]	[0,0.5]	0.90	10	30	30	90
Smooth	5	(0.5,0.72]	[0,0.5]	0.90	10	40	40	120
Busy	6	(0.72,0.9]	[0,0.5]	0.90	15	60	40	160
Congested	6	(0.9,1]	(0.5,1]	0.95	15	80	40	250

In order to evaluate the adaptive signal timing performance, this paper compares the adaptive signal timing proposed with F. Webster timing, which is widely used in isolated signal control. The calculated evaluation parameters contain the cycle time(C), the average delay (d), the average stops time (h), the intersection capacity (Q) and the phase effective green time (g_1-g_4).The statistical results are shown in **Table 5**.

Table 5. Performance comparison between adaptive timing and Webster timing

Level	Timing	C(s)	d(s)	h	Q(veh/h)	g_1(s)	g_2(s)	g_3(s)	g_4(s)
Free	Adaptive	63	20.71	0.743	3702	10	10	15	12
	F. Webster	63	20.71	0.743	3702	10	10	15	12

Smooth	Adaptive	105	44.49	0.845	3946	13	18	30	24
	F. Webster	88	47.63	0.871	3751	10	15	24	19
Busy	Adaptive	190	69.40	0.862	4351	29	38	60	39
	F. Webster	152	67.37	0.887	4199	22	29	47	30
Congested	Adaptive	241	87.46	0.88	4494	37	49	80	51
	F. Webster	247	90.14	0.88	4486	39	51	80	53

The calculation results in **Table 5** indicate that compared with F. Webster timing method, the adaptive timing decreases the delay and stops rate and increases the capacity in high saturation level. Especially at a busy level, the decrease of stops and the increase of road capacity are obtained with sacrificing some delay and this is consistent with the management objectives. In free level, as the traffic flow rate is low, the adaptive timing and F. Webster timing are the same.

4 Simulation Experiments

Traffic simulation is an effective way to analyze the effects of signal timing. Paramics is a microscopic traffic simulation software developed by QuadStone in UK. Signalized intersections could be well modeled and simulated via Paramics (Quadstone, 2003). This paper models Hongli-Xiangmei signalized intersection via Paramics's Modeller module. The signalized model of Paramics simulation is shown in figure 4, and considering the traffic flow characteristics and safety demands at signalized intersection, simulation parameter settings are as follows. Driver reaction time is 1.5s, target headway is 2.5s, the queue gap distance is 10m, the queuing speed is 7.2kph, the simulation seed is from one to ten and heavy vehicles weight is 3.0 (Wang, 2000).

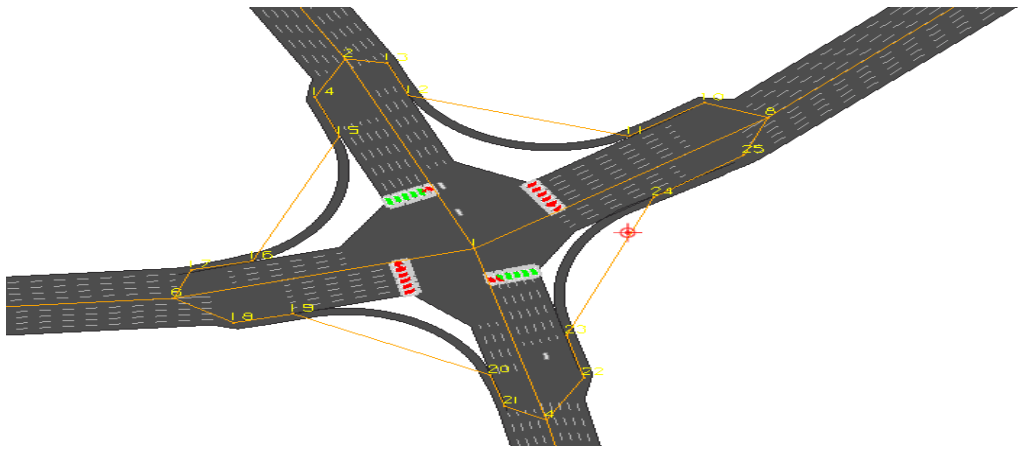

Figure 4. Paramics simulation model of HongLi-Xiangmei intersection

For each level, F. Webster signal timing and optimized adaptive signal timing, generated by optimized timing program, are set in Paramics's Modeller signalized unit. Then, to simulate real-life traffic arrival, different simulation seeds are selected for every time simulation. As a result, the 10 simulations for each timing strategy are carried out respectively in Paramics' Modeller module. Considering the actual valuation demands for isolated signalized intersection, the evaluation parameters extracting from Paramics' Analyzer module include the average delay (d), the average stops time (h), the average queue length

(N), the average OD flow volume (q) and the average speed (V). The statistical results are shown in **Table 6**.

Table 6. Performance comparison based on Paramics modeling and simulation

Level	Timing	d (s)	h (s)	V (km/h)	N (Veh/s)	q (Veh/h)
Free	Adaptive	17.73	17.56	15.93	0.33	256
	F. Webster	17.73	17.56	15.93	0.33	256
Smooth	Adaptive	34.61	13.51	9.99	1.79	1230
	F. Webster	39.82	13.05	8.84	2.06	1222
Busy	Adaptive	63.13	12.69	6.53	3.64	1433
	F. Webster	58.63	13.70	6.47	3.56	1349
Congested	Adaptive	58.60	14.30	4.99	3.56	1433
	F. Webster	82.50	12.60	6.50	4.80	1368

In **Table 6**, for four levels, the adaptive method makes majority evaluation parameters better by giving up one parameter, while the F. Webster method makes most parameters worse. The evaluation parameter comparisons under four different levels are shown in **Figure 5**. The analysis results of adaptive method are listed as follows: (i) In smooth level, the delay and queue length reduce by 13%, the larger capacity and speed are increased slightly, while the stops time nearly stay stable. (ii) In busy level, the capacity increases by 6.2%, delay decreases by 8% and stops drop by 7%, which is consistent with control objectives. Queue length and speed almost remain steady. (iii) In congested level, the delay sharply decreases by 28%, the queue length greatly declines by 25% and the capacity increases by 4.8%, but stop time rise and speed falls correspondingly. (iv) In free level, the control effects of two methods are the same because of the same timing caused by low flow rate.

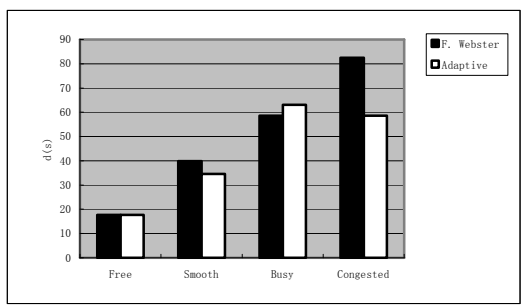

(a) The delay comparison of four levels

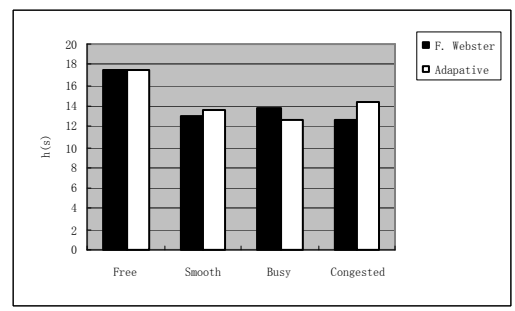

(b) The stops comparison of four levels

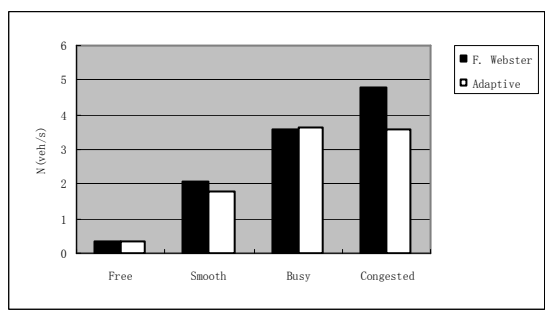

(c) The queue comparison of four levels

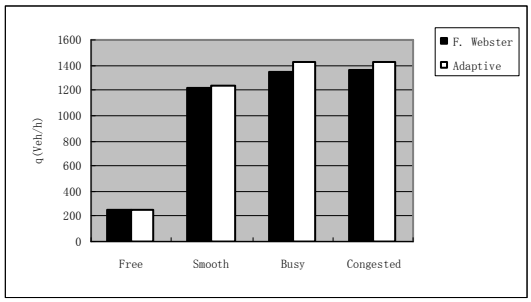

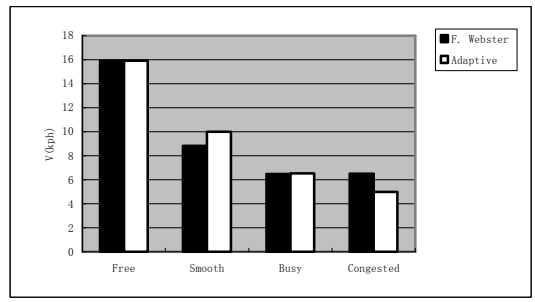

(d) The OD comparison of four levels **(e) The speed comparison of four levels**

Figure 5. The evaluation parameters changes between two timings

However, in busy level, there is a defect that delay increase is considerably larger for capacity increase. But this situation does not take place in congested level. That is because phase delay constraint is considered in PI model in congested level. Therefore, when priority is given to heavy phase flows at busy level, the delay of remaining flows rises greatly and leads to the delay of signalized intersection increases.

5 CONCLUSION

An adaptive signal timing optimization method of isolated intersections is proposed, which is based on traffic status identification with the combination of flow rate and time occupancy. Different control objects and appropriate evaluation parameters are chosen for four different traffic levels according to the characteristics of traffic flow. An enumeration algorithm is used to find out the optimal strategy. To compare the proposed adaptive signal control method with F. Webster method, a typical intersection in Shenzhen is taken as a case study and simulated via Paramics. The calculation and simulation results show the following conclusions. (i) The signal control objectives of the four levels can be achieved in simulation, and the proposed adaptive method based on traffic status identification contributes to the traffic management at busy signalized intersections. (ii) To avoid magnifying the effects of heavy phase flow, delay constraint should be taken into account in busy and congested level. (iii) In low flow rate level, the results of adaptive method is the same as those of F. Webster method, so PI model and constraints need further research.

REFERENCES

Akcelik, R. (1981). "Traffic signals: capacity and timing analysis. " *ARR,* NO. 123.

Akcelik, R. (1980). "Time-dependent Expressions for Delay, Stop Rate and Queue Length at Traffic Signals." *Internal Report AIR,* 367–1.481-508

Bullock, D. and Urbanik, T. (2000). "Traffic Signal Systems addressing diverse technologies and complex user needs." *Transportation in the New Millennium,* Transportation Research Board.

Guo, W. Q. (2008). "Research on Optimization Methods of Signal Timing Parameters for Traffic-Actuated Control." Master degree thesis, Sun Yat-Sen University, Guangzhou, China.

Hong, L. (2004). "Traffic adaptive control for oversaturated isolated intersections: Model development and simulation testing." *Journal of Transportation Engineering,* 130(5):

594-601.

Kerner, B. S. (2002). “Synchronized Flow as a New Traffic Phase and Related Problems for Traffic Flow Modeling.” *Mathematical and Computer Modelling,* 35:

Li, X. N. (2006). “Study on Adaptive Control Method of a Single Intersection.” Master degree thesis, Dalian University of Technology, Dalian, China.

Li, H. Q. (2004). “Study on the Optimization Methods of Signal Timing Parameters of Urban Traffic Control.” Master degree thesis, Jilin University, Jilin, China.

Manual, H. C. (2000). "HCM 2000." Washington, DC: Transportation Research Board.

Mirchandani, P. and Head, L. (2001). “A real-time traffic signal control system: architecture, algorithms, and analysis.” *Transportation Research Part C,* 9(6): 415-432.

Quadstone. (2003). “Paramics 4.2 User Manual.” Quadstone Ltd, Edinburgh, Scotland.

Quan, Y. S. (1989). “Urban Traffic Control.” *The People Traffic Press,* Beijing: 71-97.

Rouphail, N., Tarko, A., and Li, J. (1999). “Traffic Flow at Signalized Intersections.” *79th TRB Annual meeting.* Washington, DC: Transportation Research Board.

Webster, F.V., and Cobbe, B.M. (1966). “Traffic Signals.” *Technical Paper 56,* Road Research Laboratory, London.

Wang, W. and Guo, X. C. (2000). “Traffic Engineering.” *Southeast University Press,* Nanjing: 114-153.

Xu, X. Q. and Huang, W. (2005). “Multiphase signal real-time controlling model of isolated intersection and its algorithm.” *Control Theory & Applications.* 22(3): 413-422.

A Collaborative Software Framework Design in Supporting GLITS I-75 Integrated Freeway & Arterial Operation Project

Ken Yang[1]

[1]Iteris Inc., 1120 East Long Lake Road, Suite 222, Troy, MI 48085 USA; PH (248) 740-8720 X 202; FAX (248) 740-8701; email: kyang@iteris.com

ABSTRACT

This paper summarizes the software design within the GLITS (Great Lakes ITS) I-75 Freeway and Arterial Integration project. The GLITS I-75 Project was a pilot project of the Integrated Corridor Management (ICM) aimed at coordinating freeway and arterial operations to quickly release freeway bottlenecks by optimizing the parallel arterial road's capability to accommodate traffic diversion from the freeway. This software framework links two different types of traffic management systems (freeway and arterial) and smoothly integrates corresponding functions together, minimizing the changes of their existing architectures. The paper will include the following aspects: 1) Functions requested to coordinate the freeway and arterial operations within GLITS I-75 Project; 2) Existing software architecture analysis for both freeway management and arterial management; 3) Concept of the collaborative software framework; and 4) GLITS I-75 Project software design summary.

INTRODUCTION

According to the previous study, 70% of freeway congestion is caused either by traffic bottlenecks (40%), by incidents (25%), or by special events (5%) (1). It is obvious that the existing freeway management system could not eliminate congestion alone without considering the potential impact of freeway traffic diversion on the parallel arterial roads. Here comes the concept of the Coordinated Freeway / Arterial (CFA) Operations, which is intended to optimize the corridor level freeway /arterial operations for many purposes, such as (1)(2)

- Traffic Incident Management;
- Work Zone Management;
- Planned Special Events Management, and
- Day-To-Day or Recurring Operations.

As a pilot CFA type project, the GLITS I-75 Project is focusing on the integration of freeway/arterial "Traffic Incident Management" and "Planned Special Events Management" functions. The goal of the project is to verify whether or not there could be certain carefully pre-defined signal timing plans that could be arranged along the arterial roads to better divert nearby congested freeway traffic and relieve the freeway congestion rapidly.

One of the core issues of the GLITS I-75 Project's design work is to develop an "expert system" to coordinate the existing freeway and arterial traffic operations in dealing with various freeway lane restriction scenarios. At the real world, there are two different types of ATMS software systems are running at the region, one is the MITSC's (Michigan ITS Center) freeway management system, and one is the RCOC TOC's (Road Commission for Oakland County Traffic Operation Center) arterial management system. The challenge of this design work is how to build an add-on software system, which will cross the boundary of two existing ATMS

software systems, and will smoothly integrate their relating functions together but minimize affecting the existing operations.

To achieve this, a collaborative software framework is proposed. This paper will be organized in the following manner. First, a summary of the CFA function requests within the GLITS I-75 Project. Second, the existing software architecture analysis for both freeway management and arterial management is presented. The concept of the collaborative software framework is discussed. Finally, the GLITS I-75 Project software design is summarized.

CONCEPT OF THE GLITS I-75 PROJECT

Before the concept of CFA, the freeway and the arterial management systems are working separately most of the time, even though, they maybe share certain information and device controls. The coordinated traffic signal controlling on the arterial roads majorly focuses on the coordination of arterial intersections without considering its impact on the nearby freeway traffic. The major concept of the CFA is to involve the "corridor" plan to target the integrated freeway/arterial corridor performance. It is based on the assumption that there would be certain carefully designed signal timing plans that could be pre-determined along the arterial roads; Once the nearby freeway suffers traffic congestion because of the traffic demand highly exceeds the capacity, the different corridor operational strategies will be triggered depending on the different combinations of the freeway and arterial traffic patterns, with a series of pre-determined operations such as DMS message displaying, diversion sign igniting, as well as special arterial signal timing plan activation (1)

Scope of the GLITS I-75 Project

Oakland County, Michigan, is one of the most affluent counties in the United States. It is located in southeast Michigan about 20 miles north of Detroit. The GLITS I-75 Project is scoped along 6 miles of the interstate I-75 corridor within the Oakland County, from Square Lake Road to Lapeer Road, including the Opdyke Road, a short portion of Lapeer Road, and crossing roads at interchange areas (e.g., M-59, Square Lake Road and University Drive). (Please refer to Figure 1). The I-75 freeway has 4 lanes in each direction within the GLITS I-75 Project area. Opdyke Road runs parallel to I-75 for the length of the project and has two lanes in each direction with an additional center turning lane. The project will include only the northbound (NB) direction of travel, with four interchanges in project vicinity. In addition, as shown in Figure 1, there is a sports stadium within the project area (Palace of Auburn Hills), which means there would be periodical sports or entertainment related special events occurring within the project corridor area.

Along the GLITS I-75 corridor, MDOT houses the extensive freeway traffic control system via MITSC. MITSC's freeway ITS components within the project region include CCTVs, detector stations and a CMS. On the other hand, RCOC is in charge of arterial traffic signal operations within Oakland County (with 650 SCATS equipped intersections and more than 600 fixed timing intersections). There are 18 SCATS intersections that cover the project defined major arterial road – Opdyke Road – along the GLITS I-75 corridor. As the advanced adaptive signal system, SCATS can support various levels of signal timing implementations that could either be pre-programmed, or could work in dynamic mode, where the signal timing plans are automatically adjusted by the SCATS system itself.

New Software Framework Required by the GLITS I-75 Project

Based on the existing MITSC and RCOC TOC software systems, the GLITS I-75 Project will include certain software enhancement for integrating freeway and arterial control functions on the GLITS I-75 corridor. The software framework of the GLITS I-75 is expected to be capable of "closely" merging the two existing ATMS (Advanced Traffic Management System) software systems, which shall be featured at least as the followings:

- The software framework shall take the maximum advantage of the existing two ATMS software systems with minimum changes of their existing operations.
- The software framework shall support smoothly data exchange / integration between the existing two ATMS software systems.
- The software framework shall coordinate related functions between the two ATMS software systems to fulfill the goal of the integrated freeway / arterial operations
- The software framework shall support integrated GLITS I-75 corridor traffic information access capability for other agencies (authorized users), as well as the general public.

CONCEPT OF THE COLLABORATIVE SOFTWARE FRAMEWORK

As we know, most of the current enterprise computing environments are featured as "Distributed Computing", which majorly based on the "client/server" model. This is also the common solution of ITS ATMS software systems, such as the existing ATMS software systems running at the MITSC and the RCOC TOC.

The concept of the "collaborative" software framework is initially coming from the intension of migrating / upgrading of the existing enterprise-wide software system. The basic idea is very simple, in order to make numerous software functions/components (including existing and new) to work coordinately and effectively, this type of the software framework should at least have the following features:

- Effective data sharing / exchanging mechanism;
- Supporting "Loosely-coupled" software structure;
- Supporting abundant data exchanging patterns;
- Standardizing communication and data exchanging protocols, and
- Scalable and flexible architecture for easy deployment and later maintenance.

Eventually, the "collaborative software framework" is particularly useful when building a software system upon previously existing software system; and it will stand for maximizing the software integration and minimizing adaption cost at the same time.

GLITS I-75 PROJECT SOFTWARE FRAMEWORK

Existing TMC Software Framework within GLITS I-75 Project

The existing ATMS software framework at both MITSC and RCOC TOC subscribes to a traditional "client/server" model, which normally relies on the "Request/Response" data operation approach for data retrieval, with a central database server and distributed clients.

The MITSC houses the freeway traffic control system for the region. The MITSC already provides extensive surveillance and motorist information functions along the freeway part of the

GLITS I-75 corridor. The existing MITSC ATMS software already provides most of the surveillance and management functions for freeway operations, such as device operations (CCTV cameras, CMS signs), traffic status monitoring, incident / special event management, as well as ATIS information distribution. Figure 2 illustrates the existing MITSC system software framework.

On the other hand, Road Commission for Oakland County (RCOC) is in charge of arterial traffic signal operations within Oakland County. At the RCOC TOC, besides SCATS signal control system, the existing RCOC's ATMS software system provides similar functions as those provided by the MITSC software but for arterial management. **Figure 3** illustrates the TIMS software architecture in the RCOC TOC. Most importantly, the RCOC TOC's ATMS system maintains several external interfaces that tie the RCOC TOC with external agencies. One of the most important interfaces is the link between the RCOC TOC and the MITSC. It enables the RCOC and MITSC to exchange real-time traffic information and share a certain level of device (CCTV) control.

Add-on Function Needs in the GLITS I-75 Software System

In details, for purposes of the integrated freeway/arterial operations, the following software enhancements are needed within the GLITS I-75 Project:

- New software interfaces need to be developed, such as
  - The interface that ties the MITSC software system with the SCATS "Event Manager" – the SCATS application is used the adjust signal timing plan.
  - The interface that retrieves new SCATS information.
- New software components that could smoothly merge the MITSC ATMS software system and the RCOC TOC ATMS software system together, providing on demand data exchange capability.
  - Freeway and arterial MOE (Measure of Effectiveness) data exchanging between MTISC and RCOC TOC.
  - Device status and alarm data exchanging between MITSC and RCOC TOC.
  - Automatic notification function to the RCOC traffic engineers for any activation/deactivation of special arterial signal timing plans.
- New software applications that provide data archiving / processing capability, such as
  - Data archiving capability for both freeway and arterial (SCATS) data;
  - Data mining and fusion capability of diversion detection and tracking in supporting of the semi-automatic operation mode, and
  - Rule-based response plan decision support capability.
- New web interface for presenting the integrated traffic information of both freeway and arterial roads.

The GLITS I-75 Project's Software Framework

The attached **Figure 4** gives the diagram of the GLIST I-75 software framework. As we can see, this software framework is build based on the existing MITSC and RCOC ATMS software system, with the following "collaborative" features:

- It smoothly bridged two existing ATMS software systems.
- It included build-in on-demand data sharing services.

- It added the additional required functionality, such as the data archiving/fusing functions, and decision support functions.

In details, the followings software components played the core role in this software framework to make it works collaboratively.

- "Data Exchanger" – The "Data Exchanger" manages the data sharing functionality at the both systems. In work with the lower-level "Message Server" component, it is in charge of processing and publishing new traffic data at each system.
- "Message Server" – The "Message Server" component acts as a low-level data buffer layer between the MDOT system and the RCOC system in supporting of the "Publish and Subscribe" data sharing mechanism. In corresponding with the "Data Exchanger" component, any data updating on one side could be rapidly reflected on the other side.
- "GLITS Data Fusion Application" – The "GLITS Data Fusion Application" is a server-side application that is in charge of archiving and fusing data from both freeway (MITSC) and arterial (RCOC TOC) systems to generate
  - Corridor level congestion report;
  - Diversion opportunity identification, alerts, and tracking information, and
  - Diversion condition monitoring
- "Diversion Alert Application" – The "Diversion Alert Application" is a thin, front-end application that displays diversion alert information and response plans for the operator's decision support purpose.
- "GLITS Corridor Web Site" – "GLITS Corridor Web Site" is at dedicated web site to present the integrated corridor traffic information to the external authorized agencies and general public.

The major benefits of this "collaborative" software framework are:

- Maximum leveraging of existing software architecture;
- Flexibility of adjustment;
- Message-base mechanism that adds stability of the software system and loosens the tight connection with a database, and
- Minimal new software development efforts.

SUMMARY

This paper presents the "collaborative" software framework design in supporting GLITS I-75 Integrated Freeway and Arterial Operation Project. This software framework links two different types of traffic management systems (freeway and arterial) and smoothly integrates corresponding functions together, minimizing the changes of their existing architectures.

ACKNOWLEDGEMENTS

The Authors would like to thank the Road Commission for Oakland County Traffic Operation Center (RCOC TOC) and the FAST-TRAC project in their support of this paper.

REFERENCE

Federal Highway Administration. "Operations Story: About Us." (Washington, DC, August 2005) http://www.ops.fhwa.dot.gov/aboutus/opstory.htm.

Coordinated Freeway and Arterial Operations Handbook. FHWA-HRT-06-095, USDOT, May, 2006.

Figure 1 Scope of the GLITS I-75 Project

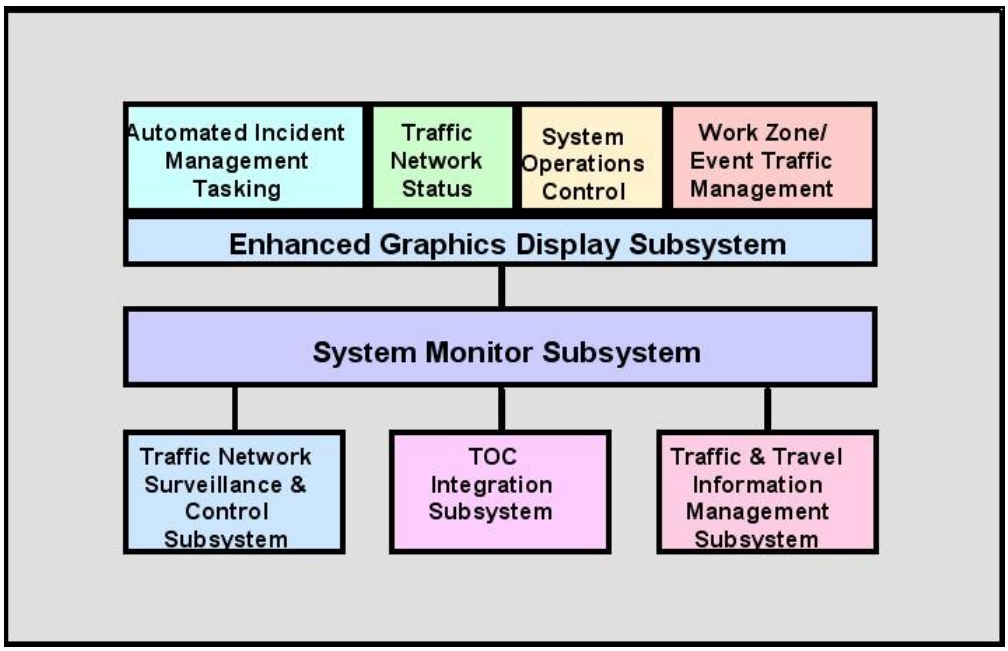

Figure 2 MITSC Freeway Operation ATMS Software System

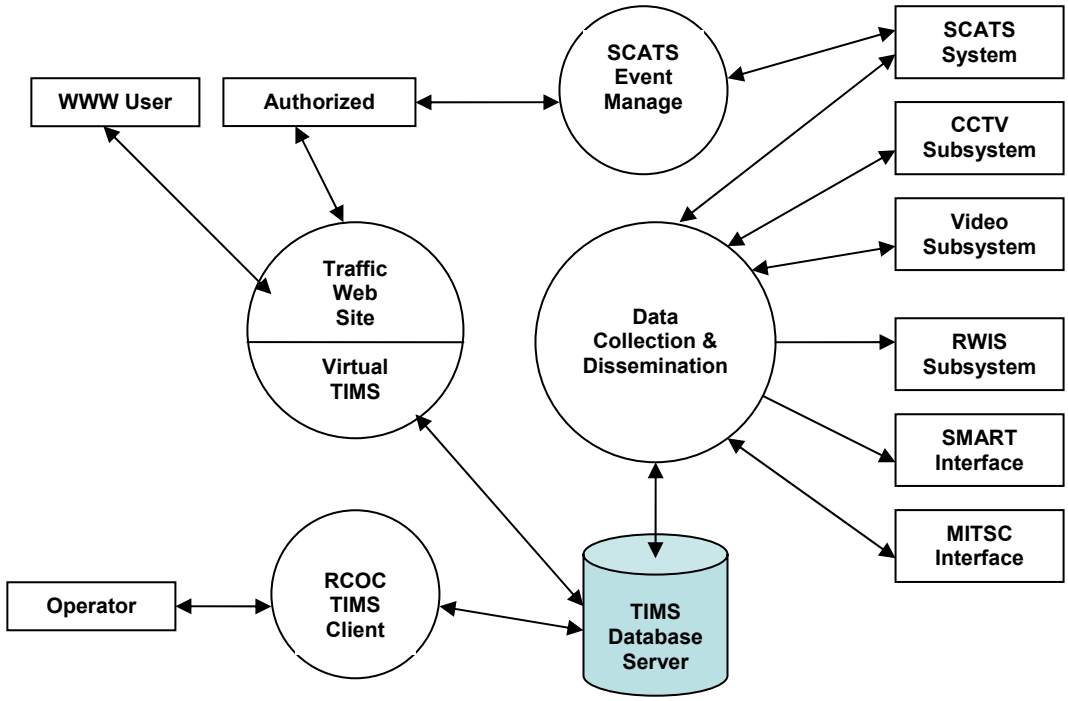

Figure 3 RCOC TOC Arterial Management ATMS Software System

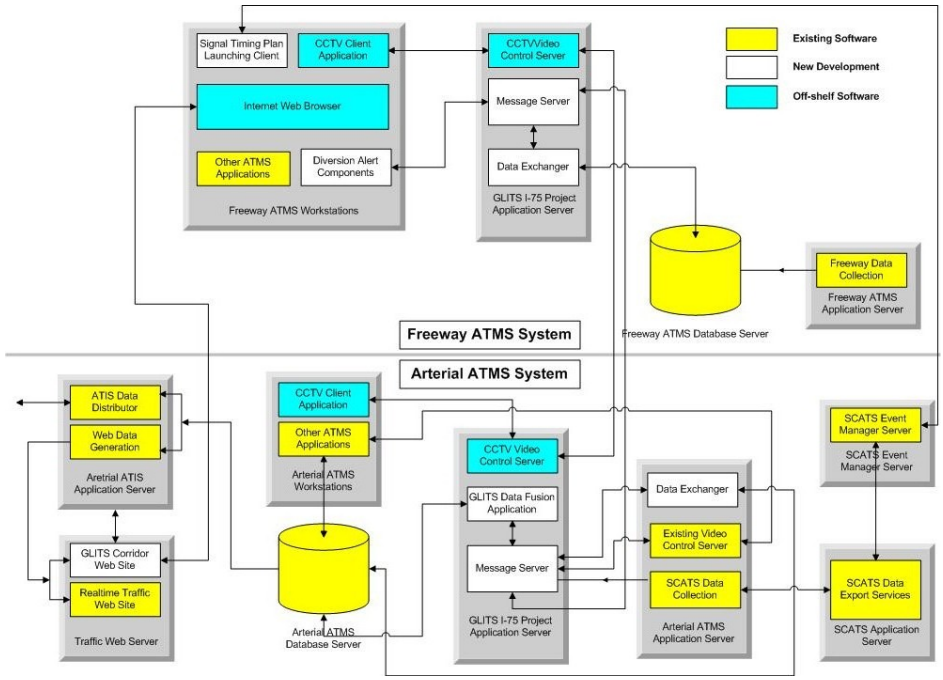

Figure 4 "Collaborative" GLITS I-75 Software Framework

Investment and Finance for the Intelligent Transportation System in China

Mingquan Wang[1], Yali Zhao[2], Dongyuan Yang[3], Xiaofa Shi[4], and Ying Hui[5]

[1]PhD Student, School of Transportation Engineering (STE), Tongji University, Shanghai 200092, China; E-mail:MingquanChina@gmail.com
[2,5]Doctor of STE, Tongji University
[3]Vice-president of Tongji University, Professor of STE,Tongji University
[4]Associate Professor of STE, Tongji University
*This Study was supported by the projects of the National Natural Science Foundation of China, with grant No.50738004;
*This Study was supported by the projects of the National High-Tech.Research Plan of China, with grant No. 2007AA11Z245.

ABSTRACT

Based on the development of Chinese Intelligent Integrate Transportation Systems, this paper shows the problems found in the process of the investment and finance of urban Intelligent Integrate Transportation Systems, especially when the problem faces the planning and Decision-Making process. In addition, this paper introduces some good examples that happened in the U.S. and other developed countries, besides the experience of success and failure in the construction of the highways in our country, and the expectations of finding a suitable way to develop our country, based on the last experiences. Afterwards, this paper shows the way to settle the problem of how to tighten the cooperation of the reform and administration, public and private investment departments. The major findings and lessons from this application are discussed, together with conclusions and Observations regarding further potentials and refinements.

INTRODUCTION

ITS (Intelligent Transportation System) is not a new word for us, especially in the big city. Nowadays, when the cities (Urbanization) of China have become bigger and bigger (Metropolitan Overspread), the Chinese Government faces the current situation, such as irrational economic structure, severe land wastage, intensive land-use-pattern, huge energy consumption, and so forth. These issues make the transport and logistics fee high, and the further deterioration of the living environment, as well as a large number of traffic emissions and sound pollution. The transportation time and fee for an ordinal people (Population Explosion) becomes high, and the traffic and transportation issue is no longer a construction problem but a control and management transportation systems issue.

Nowadays, the analysis for the economical benefit of transportation is difficult because of its public attribution. However, when it comes to the ITS, the city has come to a crucial period speeding up the construction of ITS. Therefore, we must face the investment and finance process, like it happened some years ago when we started to improve our national highway system.

DEVELOPMENT OF ITS

Intelligent Transportation System is a set of advanced information technology, data communication technique, electronic control technology and computer processing technology effectively applied to the management of transportation systems, people, vehicles and road close cooperation and harmony. Therefore, ITS plays a role in creating a framework of large, all-round, real-time, accurate and efficient transport management systems. Nowadays, in the 21st century, when United States, Europe, Japan and other countries and regions, are widely using ITS technology in an integrated transport system to improve traffic information, intelligence has become a modern transport development orientation.

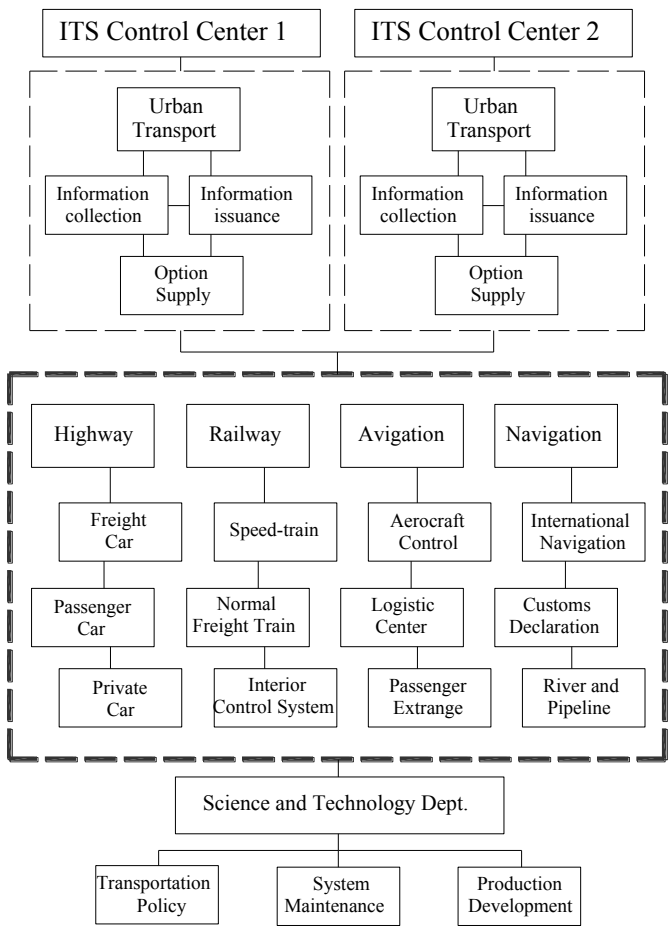

Figure 1. Framework for ITS Control Center .

Intelligent Transportation Systems uses widely information and communication technology to improve traffic management and operation of the system, providing a better way for the majority of those who travel, in order to integrate a variety of modes of transport, and improving the overall efficiency of transport.

Europe, the United States and Japan's experience shows us the ITS characteristics: 1) Developed rapidly. The progress of product research and development is rapid, from design to production to market, the cycle is becoming shorter and shorter; 2) Applications of integrated high-tech. The core technology called real-time traffic forecasting applies advanced detection, communications, remote sensing and computer technology into integrated transport systems, on behalf of the newest traffic technology; 3) Unprecedented huge scale. The scale and investment is huge. The U.S. Ministry of Transportation invests 1 billion dollars each year in research and development of highways and advanced intelligent traffic management systems.

DILEMMA OF ITS DEVELOPMENT IN CHINA

The urban infrastructure includes roads, bridges, rail transportation, public transport, water, electricity, coal, afforestation, environment, public health and other municipal and public infrastructures. As public goods, ITS infrastructure, like others, is basic, huge, public sharing, and should be planned in advance.

In China, the project policy is formed like a plan made by the government. As a result, the State Government and its development have both the obligation to have the right management, which needs to be planned in a more careful and flexible way to make a more relaxed investment policy. Therefore, the normal process is followed by Strategic Plan, Long-term plan, Middle-term Plan, Short-term Plan, and Dynamic Plan. In different levels of the investment policy making and planning, the participants and tasks are different, so as it is the development methods and support systems.

In other facets, technically speaking, although ITS has been developed rapidly in foreign countries, it has its problems and difficulties in China: ①ITS exceeds the start-up phase to development phase, but far from maturity phase; ② ITS is still focusing in information and communication technology; the real Intelligent Transport is also little; ③Lack of theoretical research, results are not mature enough and the application is not wide enough; ④Standardization should also be improved.

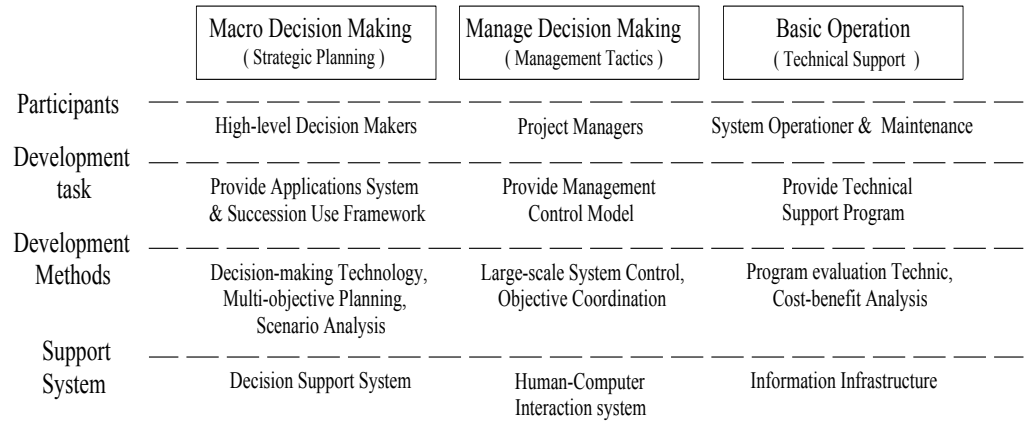

Figure 2. Investment Decision -Making Level Task in China .

Consequently, the process of the development of the ITS is a long way for us, and this puzzle is the investment step; it does not matter that the problem is a policy making or a technical one, despite that, we should do some research about this in order to know more about the dilemma.

FOREIGN INVESTMENT AND FINACING SYSTEM

Even though the ITS requires a huge investment, the recovery period is long, and even in some projects, funds cannot be recovered at all. Therefore, all countries with ITS on the financial arrangements use a number of policies and provision of the relevant budget to support their projects.. Take the United States, Japan and Sweden for example, they have been targeted for specific budget of the ITS.

Country -Scale-Budget Investment :

The Netherlands take the ITS development plan into the whole country Transport Policy. The Sweden put the transport policy making power & responsibilities to the Ministry of Communications. It follows Swedish National Road Administration (SNRA) and Swedish Road Information & Traffic Management Department (SRITMD) to coordinate government activities related to ITS units. SNRA annually deals with about 1.05 billion Swiss Currency (about 132,500,000 U.S dollars) ITS-related budget. SNRA as well, cooperates with local governments to improve local traffic signal control systems, plans to improve 3500 signal control cross, and conforms these crosses' information into a sharing network. The scheme will last for about 10 years, and the annual investment will be 130,400,000 Swiss Currency.

Private -capital -Budget Investment :

Investment and financing for ITS projects are similar to other transport facilities projects; they are constrained by the national capital shortage dilemma. As a consequence, the country encourages private investments in a participatory way to

build ITS facilities. To encourage private investments, government should relief taxes threshold and strengthening the legal system. In Japan and USA, the budget makes the scale of the ITS investments, and the capital can come from the company which is interesting in these projects, and the ownership of the ITS facilities can rely on the one who invests in them.

Government subsidies, business income tax reliefs, civil construction of national recognition, can be means to enhance the credibility of the participating units, and other ways of making access to private capital. At the same time, an integrated ITS program evaluation system should also be surfaced.

MIXED-METHOD INVESTMENT AND FINANCE IN CHINA

Reference to Chinese highway construction and operation mode, a government funded construction and commissioning should be an operated corporate mode, besides private enterprises operating modes if there is no fund construction budget. The great mode improves Chinese infrastructure development and promotes security of Chinese economic development. Therefore, based on ITS systems and development projects, it is a good way to use a different method of finance, access to sufficient funds to encourage community involvement and promote the development.

In order to achieve ways to link with each other, exchange data with each other and get co-operation, the Government has to intervene in private investment, avoiding the attention and the profit, in order to draw a clear relationship between rights and obligations. ITS plans on the construction, government and non-governmental cooperation in the specific way of relevant experience at China and abroad can generally be summarized as Table 1 shows.

Table 1. Mixed Investment and Finance Mode .
(I: Investment; C: Construction; B: Build; O: Operate; T: Transfer; R: Rehabilitate)

Mode	I-C-O Body	Ownership
BOT	Non-governmental Organization	Government.
BTO	Government-entrust Non-governmental investors	Government ownership first, then operation right.
ROT	Non-governmental organizations, Expanded and operate the leasing facilities	Government.
OT	Government Investment and constructed first, Non-governmental operate then	Government.
BOO	Non-governmental organizations	Non-governmental organizations
BOOT	Non-governmental organizations, operate itself then.	Government
BT + OT	One Non-governmental investors first, another operate then	Government ownership first, then operation right.

Government funding or private investment participation should be in line with Chinese financial law regulations and policies. Regarding of support for the ITS industry, we should also put forward specific regulations and policies for the entrance of government and non-governmental capital to prepare the way to long-term steady source of funds for ITS, through establishing a legal basis.

ITS construction costs are often very large; they have a very long recovery period, and the project may last for many years. The operating profit is also high, besides the Department's own profits, it may also include government subsidy, business Incentive such as tax relief. Through the participation of the country and the private capital, we should also enhance the credibility of the participating units to encourage their active participation.

However, grant awards and incentives should be strictly assessed and the adoption of a system should be regulated by the application of specific conditions and targets in order to avoid controversy or create unfairness.

CONCLUSION

ITS covers a wide range of promotion, in addition to the technical requirements to ensure the standardization of data can be exchanged with each other, the device can be linked with each other, the facilities can be operated by each other, the administrative unit for communication and coordination mechanisms, and even re-organization for the business mode can be done. As a whole, regulations and policies must be appropriate to distinguish, with a clear division of powers and responsibilities vested in the transport management policy and strategy formulation implementation to improve the efficiency of the ITS.

The Chinese Government clears the various powers and responsibilities between departments, but to achieve a complete and efficient ITS, it is bound to bring a lot of need for the integration of administrative functions. Investment conflicts various sub-systems, one department conflicts others, the government conflicts enterprises, so the program may face many difficulties and contradictions, when the apparent different government and private capital investors are put together. As a result, there is an urgent need to establish appropriate laws and regulations to establish coordination across the industry, providing industry responsible for the jurisdiction of each other and opening up the problems to solve them, otherwise, the building of Intelligent Transportation Systems will be delayed.

BIBLIOGRAPHY

Alison Conway. (2004). “Potential Application of ITS Technologies to Improve Commercial Vehicle Operations, Enforcement, and Monitoring.” Journal, Transportation Research Board.

Chandler Duncan. (2004). "The Industry Cluster as a Planning Construct for Freight ITS." Journal, Transportation Research Board.

Huang Bin. (2002). "Research on investment and financing model for the Urban Rail Transit project." Journal, Urban Subway Research, Beijing, pp. 14-17.

Joseph M. Sussman. (2004). "ITS: What We Know Now That We Wish We Knew Then: A Retrospective On the ITS 1992 Strategic Plan." Journal, Transportation Research Board, pp. 18-23.

Kuo-Ann Chiao and Manny Insignares. (2004). "NYMTC ITS Integration Strategy: Mainstream ITS into the Transportation Planning Process." Journal, Transportation Research Board.

Sun Ning. (2002). "Research on urban railway construction investment and financing model". Journal, China Subway, Beijing, pp. 57-66.

Science Institute of Ministry of Communication. (2001). China Intelligent Transportation System Architecture General Report , Report, Beijing.

WHITE PAPER. (2003). "European transport policy for 2010: time to decide." Report, European Commission, Europe.

Advanced Traveler Information Impact on Truck Route Choice

Xiao Qin, Ph.D., PE[1], Junhee Han, Ph.D.[2], Bruce X. Wang, Ph.D.

1. Department of Civil and Environmental Engineering, South Dakota State University, Brookings, SD 57007, email: qinxiao@hotmail.com
2. Department of Mathematical Science, University of Arkansas, 315 SCEN Building, Fayetteville, Arkansas 72701, email: jhan@uark.edu
3. Department of Civil Engineering, Texas A&M University, College Station, TX 77843, email: bwang@civil.tamu.edu

Abstract

Traffic congestion was inevitable because of the reduced capacity caused by the construction zone activities. In rural or suburban areas, highway network is not as permeable as urban areas, thus making advance traveler information more critical. The study investigated truck drivers' route choice behavior under the Advanced Traveler Information System (ATIS) using before and after traffic count collected at a number of locations in and around a suburban work zone in Wisconsin, USA. Variable message signs were used to inform approaching motorists of existing delays ahead by publishing real-time delay messages and divert trucks to alternative routes when congested. After including variables such as total traffic, truck percentage and time of day, delay information, however, is no longer statistically significant in the Multinomial Logit Models (MNL). The findings suggest that motorists may rely more on their own perception of congestion or upcoming congestion than the delay messages. The results help to understand the heavy vehicle driver behavior and develop more efficient and effective work zone management strategies.

Key Words: Truck Route Choice; Traveler Information; Multinomial Logit Model (MNL).

Introduction

Moving people and goods efficiently and safely on the nation's highways continues to challenge transportation researchers and practitioners with better solutions. Among all the factors accounting for delay and safety, work zones are constantly listed as one of the top public concerns. In order to mitigate work zone congestion by diverting traffic to alternative routes to an appropriate level without compromising their pavement and safety conditions, an in-depth understanding of heavy vehicles route choice behavior is indispensible. Work zones are usually congested because of the lower operating speed and reduced capacity. Work zones are also the places where many conflicts are taking places: conflicts between safety and mobility, conflicts between construction schedule and travel demand, conflicts between road users and workers, and conflicts between enforcement and driver compliance. Conflicts, on

the other hand, create opportunities for applying innovative technologies to ease the pain of traveling through and around work zones. Among these, intelligent transportation systems (ITS) technologies involving the use of electronics, computers, and communications equipment to collect, process, and analyze information are appealing solutions that make the work zone travel safer and more efficient. One of the ITS applications is the Advanced Traveler Information Systems (ATIS).

ATIS is beneficial in terms of providing drivers information ahead that may assist them in taking appropriate actions. Previous research shows that motorists' route choices can be affected by the provision of real-time traveler information (Abdel-Aty and Abdalla, 2004, Liu and Mahmassani, 2000). However, it is driver's decision that finally determines the actual surface traffic distribution and travel time. Substantial studies reveal that the process of individual decision-making is complicated, depending on the alternative route availability, route preference, value of time, traveler information reliability, driver's gender, age and other socio-economical factors (Abdel-Aty and Abdalla, 2004, Khattak, et al. 1993A, Khattak, et al. 1993B, Jou, et al. 2004, Benson 1996, Polydoropoulou et al. 1996, Lotan 1997).

Traveler information has proved to be an effective means to mitigating congestion in urban areas (Levinson and Huo, 2003, Chu et al. 2005, Lee and Kim 2006). Minnesota researchers developed a route choice model for predicting how drivers respond to the information provided by Variable Message Signs (VMSs) and whether drivers will divert to avoid incidents (Levinson and Huo, 2003). Empirical traffic and occupancy data were collected from loop detectors on both freeway mainline and ramps, as well as the messages on VMSs and a detailed incident log. The outcome of the weighted probit-based model showed that the diversion rate was significantly impacted by factors such as: alternative exit availability, nature of incident, time period, type of message, and the interaction between alternative exit availability and type of message. In Southern California, two separate studies evaluated the effectiveness of Advanced Work zone Information System (AWIS) and its resulting traffic diversion and safety impacts (Chu et al. 2005, Lee and Kim 2006). Using the detector data, Chu et al. observed the decrease in the maximum mainline delay and further suggested that AWIS improved safety by smoothing traffic flow (Chu et al. 2005).

Equally important, the congestion issues caused by work zones or incident circumstances in rural environment were studied and real-time information systems implemented were evaluated (Horowitz et al. 2003, Tudor et al. 2003). The influence of VMS on alternative route selection for rural Wisconsin freeways was examined through the Travel Information Prediction System (TIPS) (Horowitz et al. 2003). TIPS provided drivers with real-time travel time information through a collection of PCMSs. Each sign had two message frames publishing the distance to the end of the work zone and estimated travel time, along with three alternative routes. The impact was determined by traffic volume variations before and after the implementation of TIPS. The study reported little changes in alternative route selection far upstream of the work zone but a 7-10 percent increase in near upstream of the work zone. One of the weaknesses of the study is that it did not distinguish truck drivers from passenger car drivers. It is known that truck percentage is normally higher in rural or suburban areas than in the urban freeway system. Hence,

a work zone located on a freight corridor should be planned with extra cautions to avoid any negative impacts caused by excessive heavy vehicles.

The objective of the study was to investigate truck driver behavior under the effect of ATIS through their route choice decision-making process in a congested state along a suburban interstate highway. Using MNL models, a number of route choice decision-making contributing factors as well as their magnitude of influence were studied. It was assumed that truck drivers would take one of the two alternative routes (one designated detour and one without being signed as a detour) to avoid unreasonable delay and congestion on the interstate highway. The results help to understand the heavy vehicle driver behavior and develop more efficient and effective work zone management strategies.

Work Zone Description

Work zones unfortunately create bottlenecks on the Interstate highways which normally carry large volume of commercial vehicles. The congestion issue may become even more poignant on rural Interstate highways where the road network is not as permeable as urban freeway system. Extra concerns such as the diverted truck impact on alternative routes and their communities are valid and necessary. To fully investigate the route choice issues directly connected to the drivers especially truck drivers, the study location selection is the key. The premise is that the location has to have comparative alternative routes. In other words, the alternates should be attractive to drivers who are willing to consider diversion if delayed. Although no work zone is perfectly designed to fit the laboratory condition, the work zone I-39/90 crossing of the Rock River has many desirable features for observing routes choice activities.

Wisconsin Department of Transportation (WisDOT) performed $1.8 million bridge repair project on I-39/90 over the Rock River in northern Rock County, near Edgerton, where traffic was reduced to one lane in each direction. This segment of I-39/90 is a 4-lane divided roadway carrying over 54,000 vehicles per day with considerable amount of truck traffic of over 15,000 per day, about 28% of total traffic. During the rehabilitation, the northbound bridge was closed, and traffic was reduced to one lane in each direction and routed to the southbound side of the roadway by a median crossover (the capacity was reduced to half, which inevitable creates significant congestion).

Figure 1 shows that WisDOT provided an alternative route allowing drivers to divert from the freeway to avoid excessive delay. The designated alternative route, called alternative 1 in the study, includes US 14 and US 51, which are both two-lane undivided highways. Northbound drivers can take an exit ramp to US 14 and return back to I-39/90 via entrance ramp from US 51. Another alternate, called alterative 2 in the study, winds through Milton on the east side of I-39/90 including part of STH 26 and STH 59. Alternative 1 and 2 have approximate travel times of 21 minutes (13.4 miles) and 26 minutes (16.9 miles) respectively during normal conditions, as compared to 11 minutes (12.2 miles) on the mainline. Highway facilitates on both routes can accommodate heavy trucks but alternative 2 crosses two business districts: Milton and the east side of Janesville. More business activities happen on the east

Figure 1. Work zone and alternative routes.

side of I-39/90 compared to the west side. Another concern is safety for having large truck and high traffic volume appearance near school zones located on STH 26 and STH 59. Therefore alternative 2 was intentionally not signed as a detour but local commuters knew the alternatives. In short, alternative 1 carries less traffic and has much lower v/c ratio than alternative 2.

Data Collection and Processing

A total of eight data collection points were selected on three routes in and around the work zone: two detectors were on the mainline (No.5 0506 and No.6 0512 Sensors); two were on the off-ramps leading to the alternative routes (No.7 0601 and No.8 5623 off ramps), two were on the on-ramps returning to the mainline from the alternates

(No.1 5630 and No.2 5625 on ramps), and two were on the alternative routes (No.3 0602 and No.4 0604 Sensors). All detectors collected volume, speed, occupancy and vehicle classification. The data were time stamped and aggregated on 15-minute intervals. The detector locations are listed as follows and their approximate locations are depicted in Figure 1.

Data collection started one week before the construction and continued throughout the entire work zone period as listed in Table 2. Besides the traffic data, published delay time which was recorded or logged by the ATIS system was also recorded. The data used in the study include total traffic volume approaching work zone (T), truck percentage (PT), approaching traffic operating speed (S), day of week (DOW), time of day (TOD), and delay time on the message board (D).

Table 1. Work Zone Schedule.

Schedule	Dates	Traffic Control Description
I	Before May 6 (Sun)	Before the work zone, no traffic control
II	May 15 (Tue) ~ May 22 (Tue)	Work zone with traffic control, real-time delay system in operation

Work Zone Delay Time

A real-time traveler information system was operated through a contracted vendor. The delay time was defined as the difference between the estimated travel time based on real-time traffic data and the travel time under free-flow condition in the approaching area. Remote traffic microwave sensors (RTMSs) continuously collected speed data and reported to the master controller. The algorithm in the master controller calculated the instantaneous travel time based on the collected speed data from which the delay time was derived as the difference between the congestion and free-flow conditions. The approaching area was divided into several segments by the sensors. For each segment, the travel time was calculated by dividing the distance between two sensor locations with the average speed of the sensors. The total travel time before entering work zone was the sum of all the travel times in individual segments. The delay time is expressed in the following equation:

$$D = \sum_{i=1}^{n} \frac{l_i}{(v_i + v_{i-1})/2} - \sum_{i=1}^{n} l_i / v_f \qquad (1)$$

Where:
D – Delay time
l_i – Length of segment i
v_f – Free flow speed
v_i – Speed in ith segment
v_{i-1} – Speed in (i –1)th segment

Relative Difference (RD) of Traffic Volume

Data collected during schedule I without traffic control and work zone activities were

considered as baseline data. The difference of traffic volumes on each route between schedules I and II for each time interval (15 minutes) was used to explain the driver's decision on choosing different routes. Because traffic varies during different time of day, the difference was normalized by the baseline (traffic volume from schedule I) to standardize the scale along with the time line, called relative difference (RD).

$$RD = \frac{V_{Schedule\ II} - V_{Schedule\ I}}{V_{Schedule\ I}} \quad (2)$$

Where V is the observed traffic volume during 15-minute time period

RD was transformed to a value between 0 and 1 that is appropriate for a logistic model. The value of the response variable reveals the driver preference to choosing one of the routes, for example, if alternative 1 has a value of one, it means that in the same 15-minute interval, largest change (increase traffic) was observed on this route compared to normal conditions. It indirectly measures that more drivers prefer alternative 1 to others. For example, in Figure 2 we can easily observe that truck drivers prefer to take the alternative routes over the main route on Friday if the approaching traffic volume is above the average volume of the day. Furthermore, if so they prefer alternative route 1 to alternative route 2.

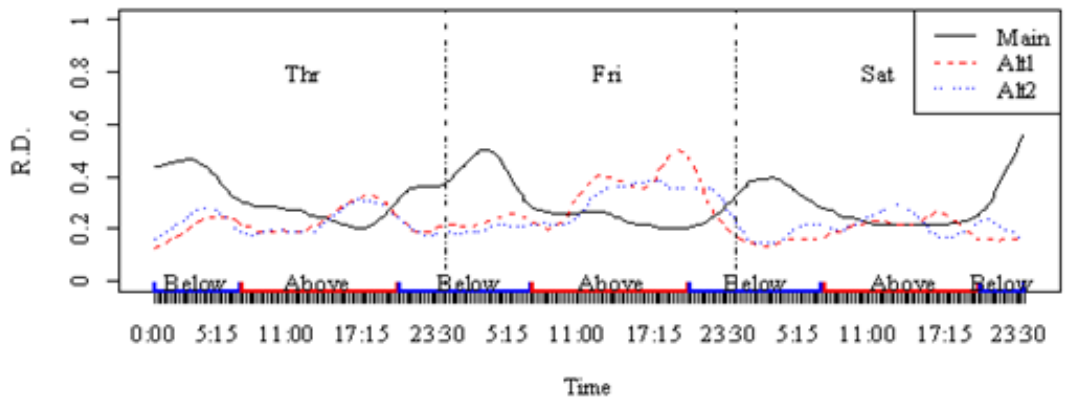

Figure 2. RD between Schedule I and II*.

* . "Above" represents the times of a day when traffic volume is *above* the average and "Below" for the opposite.

Despite the prearranged periodical trips to inspect the conditions of detectors and recover any incidents during data collection, some data were still lost due to such reasons as low or dead battery, damaged hoses, and detector memory overflow.
The most complete and comparative dataset includes only Thursday and Friday. Table 2 shows the summary statistics for the variables. All the statistics were calculated based on 15-minute interval data. To be more homogenous, data were split by average daily traffic volume. There were some variations in the total approaching traffic.

Table 2. Variable Summary Statistics (15-minute).

Variable	Schedule		I		II	
	Time of Day (TOD)		Above*	Below*	Above	Below
Day of Week (DOW)	Thu		57	39	53	43
	Fri		57	39	70	26
Total (T)	Thu	Mean	797.44	297.9	816.76	331.64
		S.D.	122.46	162.91	119.78	144.55
		Range	[566, 1070]	[105, 620]	[597, 1117]	[157, 585]
	Fri	Mean	789.6	277.66	764.75	292.31
		S.D.	66.98	155.29	37.26	154.76
		Range	[685, 935]	[148, 701]	[712, 828]	[133, 675]
Truck (PT)	Thu	Mean	0.31	0.41	0.32	0.41
		S.D.	0.03	0.08	0.04	0.07
		Range	[0.25, 0.38]	[0.30, 0.58]	[0.25, 0.39]	[0.29, 0.52]
	Fri	Mean	0.3	0.41	0.31	0.42
		S.D.	0.02	0.07	0.02	0.06
		Range	[0.27, 0.34]	[0.30, 0.52]	[0.26, 0.34]	[0.30, 0.53]
Speed (S: mph)	Thu	Mean	64.06	61.42	64.85	61.27
		S.D.	1.53	3.4	1.11	3.52
		Range	[59.33, 67.58]	[53.67, 66.42]	[62.58, 67.50]	[55.00, 66.75]
	Fri	Mean	65.08	61.36	65.63	60.96
		S.D.	1.23	2.74	1.06	3.16
		Range	[63.17, 67.67]	[56.50, 66.17]	[63.25, 67.83]	[54.83, 65.92]
Delay (D: min)	Thu	Mean	No Construction		18.2	11.89
		S.D.			9.66	1.14
		Range			[9.00, 39.30]	[10.50, 13.60]
	Fri	Mean	No Construction		9.21	12.39
		S.D.			0.89	1.59
		Range			[8.00, 10.50]	[9.50, 15.50]

Truck Driver Route Choice Models

Truckers' route choice decisions are heavily affected by their traveling environment in addition to individual preferences. The environmental factors can be approximately categorized into:

1) Perceivable information: drivers' perception of traffic congestion that can be described as real-time traffic conditions such as traffic volume, truck percentage, operating speed;
2) Temporal information: drivers' trip purposes that can be replaced by such factors such time of day, day of week; and
3) Advisory information: posted delay time on the PCMSs.

In this study, the placement of the delay message was 8 miles away from the

work zone activity area. It was possible that the back of the queue had not reached the message sign by the time drivers read the delay message. Hence, the delay information was an advisory message. It either conformed to drivers' observation, reinforcing their decisions of taking detours, or conflicted with what drivers have seen, dividing drivers' into two groups: the group of compliance and the group of ignorance.

To construct route choice models using before and after traffic data, a multinomial logistic (MNL) model was designed to examine the factors that were significantly associated with the diversion. First, some notations are defined at 15-minute intervals:

p_{i1}= the probability that truckers at ith 15-minute prefers to choosing alternative 1.
p_{i2}= the probability that truckers at ith 15-minute prefers to choosing alternative 2.
p_{i3}= the probability that truckers at ith 15-minute prefers to choosing mainline.

Let $\boldsymbol{X}$i be a vector of explanatory variables for the characteristics of traveling environment at each 15-minute interval.

$$\log\left(\frac{p_{i1}}{p_{i3}}\right) = {}_1\mathbf{X}_i \tag{3}$$

$$\log\left(\frac{p_{i2}}{p_{i3}}\right) = {}_2\mathbf{X}_i \tag{4}$$

$$\log\left(\frac{p_{i1}}{p_{i2}}\right) = \log\left(\frac{p_{i1}}{p_{i3}}\right) - \log\left(\frac{p_{i2}}{p_{i3}}\right) = ({}_1 - {}_2)\mathbf{X}_i = {}_3\mathbf{X}_i \tag{5}$$

Where ${}_3 = {}_1 - {}_2$
Therefore:

$$p_{i1} = \frac{e^{{}_1\mathbf{X}_i}}{1 + e^{{}_1\mathbf{X}_i} + e^{{}_2\mathbf{X}_i}} \tag{6}$$

$$p_{i2} = \frac{e^{{}_2\mathbf{X}_i}}{1 + e^{{}_1\mathbf{X}_i} + e^{{}_2\mathbf{X}_i}} \tag{7}$$

$$p_{i3} = \frac{1}{1 + e^{{}_1\mathbf{X}_i} + e^{{}_2\mathbf{X}_i}} \tag{8}$$

Where

$\mathbf{X}$ – vector of predictor variables
– vector of coefficients.

Analysis and Discussion

Driver's decision-making is a complicated process which is in no way decided by a single factor such as delay time. Especially when delay message conflicts with driver's observation, the faith in the accuracy and reliability of the delay information dominates driver's route choice. By incrementally adding other variables to the

model, we can have a better understanding of how the factors as well as their interactions work together. Some variables are notably correlated in the model such as delay time, total traffic, truck ratio, and time of day. When two variables are highly correlated, only one of them remains in the model. To simplify the model, only two-way interaction is considered.

A set of models were tested with different variables of interest that help to understand and quantify the odds of truckers to choose alternative routes instead of mainline. The univariate models test the statistical significance of each variable in affecting driver's route choice independently. The significant variables then constitute multivariate models to improve the model performance. Examining the p-values from the MNL models in Table 3, we see that almost all the variables are statistically significant except for the one containing speed variable. One plausible explanation is that speed is highly correlated with total traffic and truck percentage. The addition of speed variable to the model with total traffic and traffic percentage does not gain extra benefit in the goodness-of-fit.

Table 3 MNL Route-choice Models.

Model	AIC	Deviance	Test Stats.*	p-value*	Significance
Null	13677	13673	-	-	-
DOW	13599	13587	86	0	Yes
TOD	13513	13505	168	0	Yes
PT	13431	13423	250	0	Yes
T	13362	13354	319	0	Yes
S	13470	13462	211	0	Yes
D	13645	13637	36	0	Yes
T+PT	13333	13321	33	0	Yes
T+PT+S	13335	13319	2	0.37	No
T+PT+TOD	13319	13303	18	0	Yes
T+PT+TOD+DOW	13290	13266	37	0	Yes

* Tests and p-values are based on the likelihood ratios using the differences of deviances which are known to follow the Chi-square distributions with corresponding degrees of freedom.

With a three-category outcome (three routes) there are implicitly two equations. For each variable, the first coefficient is for the first equation that estimates the preference of choosing alternative 1, and the second coefficient is for the second equation that estimates the preference of choosing alternative 2. The coefficients in the MNL models are directly related to the odd ratios that quantify the change of the odds with the increase of 1-unit in the variable. Note that the estimated coefficients are in a format of natural logarithm and the odds ratio can be obtained by exponentiating them. A few important observations can be made from the estimates of the parameters listed in Table 4. First, neither alternative route is favored compared to the mainline if no other factors are considered. Second, temporal variables such as day of week or time of day are consistent in affecting truckers' route choice decision in which the mainline is still preferred over the alternative routes. Third, traffic conditions influence truckers in such a way that more approaching traffic (a stronger indicator of possible congestion) encourages truckers to take alternates though the preference of one over the other is marginal.

Finally, higher truck percentage leads to more reluctance to take the detour. It may be caused by the concerns from truck drivers about the pavement or traffic conditions on alternative routes.

Table 4 MNL Model Parameter Estimates.

Models	Route	Intercept	Thu.	DayTime (Below)	PT	T	S	D
Null	Alt1	-0.086						
	Alt2	-0.180						
D	Alt1	0.238	-0.523					
	Alt2	-0.013	-0.395					
TOD	Alt1	1.490		-4.830				
	Alt2	1.350		-4.720				
PT	Alt1	0.278			-0.765			
	Alt2	0.101			-0.559			
T	Alt1	-1.100				0.002		
	Alt2	-0.950				0.001		
S	Alt1	-7.980					0.122	
	Alt2	-7.310					0.111	
D	Alt1	-0.192						0.014
	Alt2	-0.255						0.010
DOW+TOD	Alt1	-0.860	-0.358	0.353	-1.060	0.002		
	Alt2	-1.320	-0.228	0.611	-1.020	0.002		
DOW+TOD+PT+T	Alt1	-0.860	-0.358	0.353	-1.060	0.002		
	Alt2	-1.320	-0.228	0.611	-1.020	0.002		

The last model is recommended as the best one for predicting heavy vehicle route choices because of the smallest AIC value. Its explicit model specification for Alt 1 is Equation 9 and the model for Alt 2 can be obtained by replacing all s in the model with the coefficients in Alt 2. Most of the coefficient estimates in this model are fairly similar to other models except that the delay time is no longer included. The delay information becomes statistically insignificant after the model includes other variables; it is plausible that the delay information is correlated with other perceivable traffic variables.

$$log\left(\frac{p_{i1}}{p_{i3}}\right) = \quad _0 + \quad _1 \cdot T_i + \quad _2 \cdot PT_i + \quad _3 \cdot TOD_i + \quad _4 \cdot DOW_i \qquad (9)$$

Conclusions and Future Recommendations

The study investigated the truck driver route choice decisions under the effect of ATIS implemented in a work zone on I-39/90, a major truck corridor connecting Chicago, IL, Madison, WI, and Twin Cities, MN. During the construction, the northbound was closed, and traffic was reduced to one lane in each direction and switched to the southbound side of the roadway via a median crossover. Traffic congestion was

inevitable because of the reduced capacity. To mitigate the congestion, two alternative routes have been planned, one with detour signage and the other without. In addition, to facilitate drivers' route choice decision-making, real-time delay message system was implemented.

The preliminary analysis shows that during the congestion, delay time message had statistically significant impact on truck drivers' decision-making in taking alternative routes if it was tested alone. An extensive model comparison was followed. In particular, we have found through the study that heavy vehicle driver's route choice decision was affected by 1) time of the day, a strong trip purpose indicator; 2) total approaching traffic to the work zone, a perceivable signal for congestion or upcoming congestion; and 3) truck percentage. High truck percentage discourages truckers themselves to take detours. The plausible reason may be due to the extra concerns from truck drivers of the pavement or traffic conditions on alternative routes. The study provides crucial information for traffic engineers whose objective is to alleviate mainline congestion by diverting traffic to alternative routes whose capacity is underutilized to an appropriate level without compromising the alternative highway pavement conditions as well as its traffic safety by the surge of truck traffic. By understanding the limitation of ATIS, the trucker route choice behavior as well as the similarities and dissimilarities between truckers and car drivers, a congestion mitigation plan can be designed more effectively and efficiently.

A discrete choice study is suggested in future research where every truck driver will be tracked in regard to their route choice decisions. The results can also be verified through a stated preference type of survey. The disaggregate level research may reveal other factors in motorist's route choice behavior and provide more definitive conclusions.

References

Abdel-Aty, M. and Abdalla, P.E.F. (2004). Modeling drivers diversion from normal routes under ATIS using generalized estimating equations and binomial probit link function, *Transportation* 31 (3), pp 327-348.

Benson, P.G. (1996). Motorist attributes about content of variable message sign, Transportation Research Record 1550, pp 48-57.

Chu, L.Y., Kim, H.K., Chung, Y., and Recker, W. (2005). Evaluation of Effectiveness of Automated Workzone Information Systems. *Journal of the Transportation Research Board, 1911*, pp 73-81.

Horowitz, A. J., Weisser, I. and Notbohm, T. (2003). Diversion from a Rural Work Zone Owing to a Traffic-Responsive Variable Message Signage System. *Transportation Research Record 1824*, pp 23-28.

Jou, R.C., Lam, S.H., Weng, M.C. and Chen, C.C. (2004). Real time traffic information and ITS impacts on route switching behavior of expressway drivers, *Journal of Advanced Transportation* 38 (2), pp 187-223.

Khattak, A., Koppelman, F., and Schofer, J. (1993). Stated preference for investigating commuters' diversion propensity, *Transportation* 20 (2), pp 107-127.

Khattak, A., Schofer, J., and Koppelman, F. (1993). Commuters' enroute diversion and return decisions: Analysis and implications for advanced traveler information systems, *Transportation Research Part A* 27, pp 101-111.

Polydoropoulou, A., Ben-Akiva, M., Khattak, A., and Lauprete, G. (1996). Modeling Revealed and Stated En-Route Travel Response to Advanced Traveler Information Systems. *Transportation Research Record* 1537, pp 38-45.

Lee, E.B., and Kim, C.M. (2006). Automated Work Zone Information System (AWIS) on Urban Freeway Rehabilitation: California Implementation. In *Transportation Research Record: Journal of the Transportation Research Board, No. 1948*, pp 77-85.

Levinson, D. and Huo, H. (2003). Effectiveness of Variable Message Signs. In *Transportation Research Board: 2003 Annual Meeting CD-ROM*, Paper No. 03-0128, TRB, National Research Council, Washington, D.C.

Liu, Y. H. and Mahmassani, H.S. (2000). Global maximum likelihood estimation procedure for multinomial probit (MNP) model parameters, *Transportation Part B* 34, pp 419-449.

Lotan, T. (1997). Effects of Familiarity on Route Choice Behavior in the Presence of Information. *Transportation Research C* 5, pp 225-243.

Tudor, L. H., Meadors, A. and Plant, R. (2003), Deployment of Smart Work Zone Technology in Arkansas. *Transportation Research Record 1824*, pp 3-14.

Identifying Alternative Routes with Integration of ITS into Traffic-Diversion Strategies

Heng Wei[1], Yinhai Wang[2], Abi Mogharabi[3], and Qingyan (Ken) Yang[4]

[1]Art-Engines Laboratory, 792 Rhodes Hall, Department of Civil & Environmental Engineering, University of Cincinnati, Cincinnati, Ohio 45221-0071, USA;. PH: (513) 556-3781; FAX: (513) 556-2599; email: heng.wei@uc.edu

[2] Department of Civil & Environmental Engineering, University of Washington 121 More Hall, Box 352700, Seattle, WA 98195-2700, USA; PH: (206) 616-2696; FAX: (206) 543-5965; email: yinhai@u.washington.edu

[3] Iteris, Inc., 1515 1700 Carnegie Avenue, Santa Ana, CA 92705, USA; PH: (949) 270-9400; FAX: (949) 270-9401; email: axm@iteris.com

[4] Iteris Inc., 1120 East Long Lake Road, Suite 222, Tory, MI 48085 USA; PH (248) 740-8720 X 202; FAX (248) 740-8701; email: kyang@iteris.com

ABSTRACT

Traffic diversion and emergency traffic management strategies call for integration of not only advanced information colleting/disseminating devices such as Changeable Message Sign (CMS), video-detection and loop detection, and control system, but also appropriate roadside signing route guidance systems. Well signage-equipped alternate routes could play a vital role in supporting the congestion alleviation and incident management, especially in a mixed roadway network consisting of freeways, arterials, and local streets. While many researchers claimed the importance of dynamic routes for en route drivers, geographical, geometric and environmental conditions and the category of a specific roadway may objectively define its role as a "permanent" alternate route to certain freeways or major traffic generators/attractors. This raises several issues in identifying such "permanent" alternate routes and integrating a signing route guidance system into the implementation of local intelligent transportation systems. This paper attempts to develop a methodology to identify the "permanent" alternate routes for traffic diversion strategies, and to prioritize Intelligent Transportation Systems (ITS) element candidate locations in the concerned network. A scenario of incident management and operation is demonstrated to discuss how a "permanent" alternate route guidance system could be identified and integrated with ITS, using a mixed network near Los Angeles International Airport as an example. Finally, types of diagrammatic alternate route signs are addressed with design samples.

INTRODUCTION

Utilizing real-time traffic situation and route guidance advisory information to divert traffic from heavily loaded roadways to lightly loaded roadways has been long identified as one of potential solutions to alleviating urban traffic congestions. A Mixed roadway network consisting of freeways, arterials and other local streets is commonly located in an urban area. Terrible congestion frequently happens on freeways while some arterials or other local streets are lightly loaded. In Southern

California's mixed roadway networks, for instance, drivers are frequently trapped in severely congested freeways due to myopic decision making while possible alternate routes in local streets are not heavily loaded. Such a flow distribution underutilizes the overall network's capacity. Integrated with advanced traffic information/management systems (ATIS/ATMS), route guidance, and driver information systems may be employed to improve the network efficiency via disseminating alternate routes information (Papageogiou et al. 2003). In this way, relative traffic equilibrium over the roadway network is expected to be reached. However, the implementation of ATIS technologies in real life, especially of the real-time route guidance information into a real roadway network, is currently limited (Abdel-Aty et al. 2004). In addition to the computational effort needed for validated algorithms, difficulties in making consistent interactions between information and drivers' routing diversion behavior and a lack of route signing guidance systems are limiting the efficiency of ATIS.

An investigation (Wardman et al. 1997) discloses too wide a range of variables in estimating the proportion of drivers following en route real-time information via changeable message signs (CMS) to divert routes, namely, 5 to 80%. Clearly this range is hardly convincible to support the use of CMS for fine tuning the pattern of demand. A key weakness is the CMS' inability to display messages that are consistent with driver diversion response attitudes in the relevant roadway network (Peeta et al. 2001).

In the analysis of operation concept (Iteris 2003; 2004) with intelligent transportation systems (ITS), an alternate route guidance system is envisioned to play the role of supporting the implementation and operations of ATIS/ATMS. It requires integration of advanced information colleting/disseminating devices such as CMS, video-detection or loop detection, and control system. Ideally a genuine control strategy can optimize the network traffic conditions to avoid traffic congestion on alternate routes due to drivers' overreaction (Abdel-Aty et al. 2004). For the sake of fiscal constraints, however, it is not feasible to install surveillance detectors over all roadways in the entire network. The authors' practical design experience and literature review indicate that an appropriately designed static signing or trailblazer guidance system has proven cost-effective in supporting the implementation of ATIS/ATMS. To a specific trip attractor (e.g., airport, employment center), there usually are several alternate routes in existence. To determine such "permanent" alternate routes, important or vulnerable links or nodes of the roadway network should be identified at first. Vulnerability should explicitly account for the availability of alternate routes' excess capacity and travel time (Iteris 2001). For non-crossed freeways (e.g., freeways 1-210, SR-710, and SR-110 within the City of Pasadena roadway network), arterials and local streets could be used as connectors between freeways while continued guidance signs are needed along the routes.

This paper attempts to build up a methodology to identify important or vulnerable locations from the standpoint of its "importance to the network", and to prioritize ITS element candidate locations in the network. This approach was derived from our participated ITS deployment projects (Iteris 2001; 2003; 2004) most of which were conducted in Southern California areas. The paper then

discusses how a "permanent" route signing guidance system could be determined and integrated with ATIS/ATMS, which is presented with a scenario of incident management and operation in a mixed network near Los Angeles International Airport. Finally, the paper addresses the issue in building up a route guidance system with the use of special features of local streets (e.g., one-way) as a connector between freeways. A typical example of such connectors linking I-210, SR 101 and SR 710 in Southern California area is exhibited in the discussion. Several types of alternate route guidance signs are briefly discussed based on the authors' practical experience and literature review.

TRAFFIC DIVERTION ROUTES IN A MIXED ROADWAY NETWORK

Prioritizing Corridors and Key Locations for ITS Elements

A number of cities' roadway networks in Southern California are mixed with freeways, arterial corridors, and other local streets with severe traffic congestion problems. Inglewood, for example, a city located in the South Bay region of Southern California on the southern tip of the Los Angeles city limits, has 200 miles of streets, about 140 signalized intersections surrounded by two major freeways, I-405 and I-105, as shown in **Figure 1**. The City is a regional transportation hub and attracts traffic from numerous venues including the Great Western Forum, Hollywood Park Race Track, Hollywood Park Casino, Los Angeles International Airport (LAX), and two major Medical hospitals – Centinela Hospital Medical Center and Daniel Freeman Memorial Hospital. Due to its important location in the urban flow of Greater Los Angeles, Inglewood is faced with the "big city" challenges of traffic congestion, pollution, and special event managements. Inglewood has always experienced very high daily traffic levels on freeways and major arterials.

To solve these problems caused by heavy traffic, ITS solutions have been recommended for the traffic congestion alleviation and incident management in this area. As part of the ITS strategies, a route guidance system along pre-determined (or "permanent") alternate routes is viewed as a key element to support the implementation of the City's ATIS/ATMS. Effective alternate routes are expected to bear some throughput from multi-regional cut-through traffic heading to various traffic generators/attractors such as LAX, the traffic impacted by freeway incident along freeways I-405/I-105 and the vicinity of the freeway interchanges in that area. To determine alternate routes, key locations (links and nodes) that are important to the network need to be identified and prioritized for ITS elements deployment (Iteris 2001). In the meantime, most of such important links/nodes are viewed as vulnerable links/nodes (Murray-Tuite et al. 2004). A location's "importance to the network" can be evaluated with the following aspects (Iteris 2001; 2003; 2004):

- High Accident History;
- Critical Signal Timing to Coordination;
- Key Point to Routing – cameras and/or detectors placed in the vicinity of other field elements of the signal system, such as changeable message signs and traffic signals, can be used for an overview of their operation.
- High Frequency of Queuing;
- Special Traffic Generators;

- Intersections with Poor Level of Service;
- High Volume; and
- Proximity to Traffic Generator.

Practical experiences in network operational assessments ((Iteris 2001; 2003; 2004; Wei 2000) revealed that above features are usually used to evaluate criticality of a location with respect to its functional importance to the network. In other words, those nodes possessing those features mostly stay at worse level of service or bear heavier traffic. Thus, they are usually evaluated as critical nodes. It is therefore assumed that results from evaluations of those critical nodes can be used to represent the critical performance status of the entire network, provided that no sufficient ITS field elements cover the entire network of investigation.

Selection criteria proposed in the study combined all above analyzed aspects and the various agency needs and requirements in order to develop one uniform ranking system. **Table 1** presents the proposed quantitative criteria to initially prioritize ITS field surveillance locations by using the following equation (Iteris 2001):

$$P_j = \sum_{i=1}^{6} k \times f_i \times w_i$$

Where, P_j = priority ranking of detector type j; k = detector type factor; f_i = feature weight for criteria i; and w_i = importance weight assigned to criteria i.

Table 1. Criteria to Prioritize Field Elements Locations and Their Weights.

i	Criteria	Range	Feature Weight (*f*)	Important Weight (*w*)	Detection Type Factor *k*	
					Video Detection (*j*=1)	Data Detection (*j*=2)
1	Average number of accidents per year over a 5 year period	> 20	4	5	1	0
		10 ~ 20	3			
		5 ~ 0	2			
		< 5	1			
2	Intersection Level off Service (LOS)	F	4	4	1	1
		E	3			
		D	2			
		C, B, or A	1			
3	Average Daily Traffic Volume (ADT)	> 60,000	4	3	1	1
		45,000 ~ 60,000	3			
		30,000 ~ 45,000	2			
		< 30,000	1			
4	Proximity to Freeway On-ramp	Adjacent	4	2	1	1
		Not adjacent	0			
5	Proximity to Traffic Generator	Adjacent	4	1	1	1
		Not adjacent	0			
6	Type of Traffic Control	No CCS (TBC)	0	2	1	1
		TOD CCS	2			
		ATC	4			

Source: Iteris, Inc. Preliminary CCTV and System Detection Master Plan for South Bay ITS Project. October 26, 2001 (Iteris 2001)

- No CCS (TBC) = no Central Control System (Time Based Control)
- TOD CCS = Time of Day Control (TODC) using computerized Traffic Control
- ATC = Adaptive Traffic Control (ATD) with Traffic Responsive Plan Selection
- Operating characteristics of intersections are often described by use of the concept of level of service (LOS). LOS is a qualitative description of an intersection's performance based on traffic

delays. An intersection's LOS could range from A representing free-flow conditions, to F jammed conditions.

- Average Daily Traffic represents the average total number of passenger vehicles, trucks and busses that pass an intersection in a 24-hour period.

After the locations of detection elements are initialized, selected intersections are ranked based on the corridor rankings in which they are located. The corridors are ranked in principal, major and minor priority corridors. Usually freeways providing regional and interstate services, principal arterials providing regional access, and end-to-end traffic signal controlled corridors crossing multi-jurisdictions are ranked the top, or called principal priority corridors. Major arterials with intermediate capacity roadways providing local access to major commercial and industrial parcels and some regional access are ranked the second, or termed major priority corridors. Collectors with intermediate capacity roadways providing access between local streets and the arterial streets as well as local streets are ranked the third, or termed minor priority corridors. Critical locations are divided into principle important location, major important location and minor important location, depending on their improvement priority determined by following the above analysis procedure and method. **Figure 1** illustrates an example of such a classification and identifications in the City of Inglewood roadway network, Southern California.

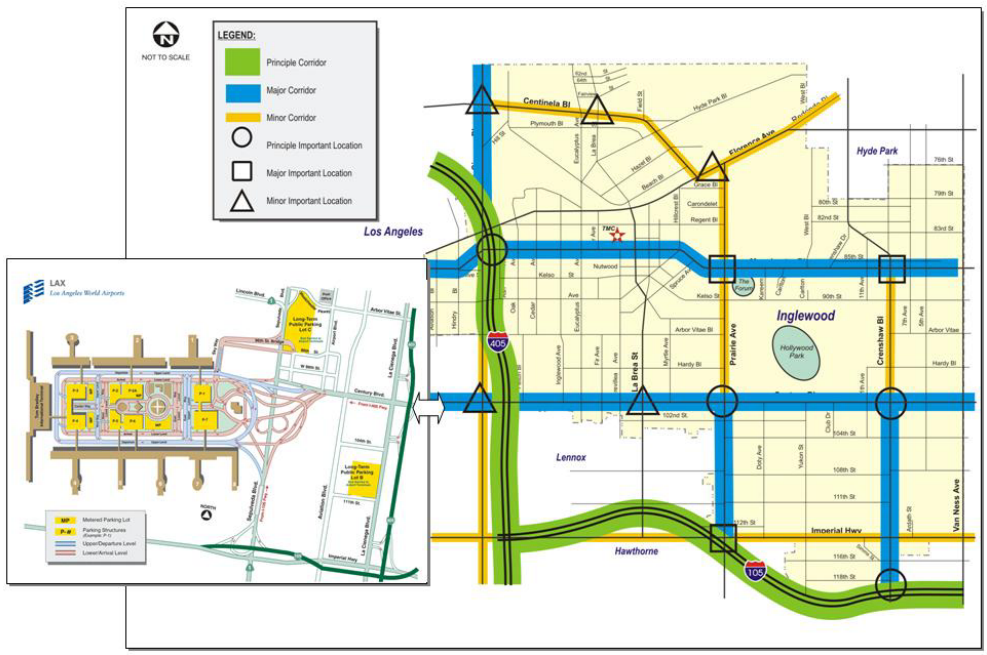

Figure 1. Priority Arterial Corridors Example Surrounding California LAX An Incident Management Scenario using Alternate Routes.

Upon compiling the rankings, an initial cutoff was established to identify those intersections that warrant deployment of ITS elements (e.g., CCTV cameras, video/data detector, signal controller upgrade, CMS and static directional signs) under immediate- and ultimate-term, depending on the discussions among related

city traffic engineers and planner as well as projects consultants (which is beyond the paper's focus and will not be discussed in details).

As a result of comprehensive analysis using the above method, priority corridors and important locations are identified, as shown in **Figure 1**. A high-level strategy for deployment of ITS elements are suggested and presented by an area ITS plan, as illustrated in **Figure 2**. Traffic analysis using Synchro indicates that most segments of the identified alternate routes (represented by dot line in **Figure 2**) for traffic leading to LAX are currently operating at the level of service C, meaning that those routes have capacity to accommodate diverted traffic from freeways I-405/I-105 as an incident or congestion occurs. When an incident happens on a priority corridor, ATMS could be implemented to divert traffic trapped in congestion to other alternate routes. Static roadside directional signs and limited number of CMS or Trailblazer Signs (TBS) to be installed along those routes constitute a signing route guidance system. The following scenario attempts to present how the signing route guidance system supports the implementation of ATIS/ATMS with incident management. **Figure 3** illustrates the concept of operations with an example of operating scenarios, which are envisioned to operate in a three-step fashion:

1. Traffic detection technology collecting traffic flow data from system detectors and calculates volume, occupancy and speed on a real-time basis.
2. Incident detection algorithms that interpret changes in certain traffic-flow parameters for determining the presence of capacity-reducing incidents.
3. Information dissemination and divert traffic via route guidance system and alternative signal control strategies.

Traffic Detection: There is an assumption that the system detectors installed on priority corridors are continuously measuring and collecting traffic flow data, as shown in **Figure 3**. Traffic flow data measured by loop detectors consist of 30-second counts of both volume and occupancy measured 24hr/day for each travel lane. Volume and Occupancy data is used to derive traffic flow speeds. A front-end-processor (FEP) and controller keeps transmitting field traffic flow data into a data processing server in which the traffic-detection system resides, as shown in **Figure 4**. In the meantime, operators in the TMC are monitoring the traffic flow via Closed Circuit Television (CCTV) cameras installed along the corridors as well as the Geographical Information System (GIS) map interface module imbedded in ATMS. Detector data containing such anomalies as missing values and unreasonably high or low values will be filtered to ensure "smoothed" data for data aggregation. The level of data aggregation must be therefore treated specifically concerning the cyclic nature of traffic at signal-controlled junctions along arterials, or simply by a certain period of time (e.g., aggregation by minute). Data measured in the format of volume and occupancy as well as speed is received by the incident detection subsystem through data acquisition on a certain time interval, as shown in **Figure 4**.

Incident Detection: An automatic incident detection algorithm embedded in ATMS automatically detects incoming traffic volume and occupancy as well as the derived speed from the traffic detection subsystem. If variables at a particular detector and its downstream detector have abnormal or over-threshold changes, depending on the type of incident detection algorithm that is being used, a potential incident somewhere between the upstream detector and the downstream detector

may be inferred.

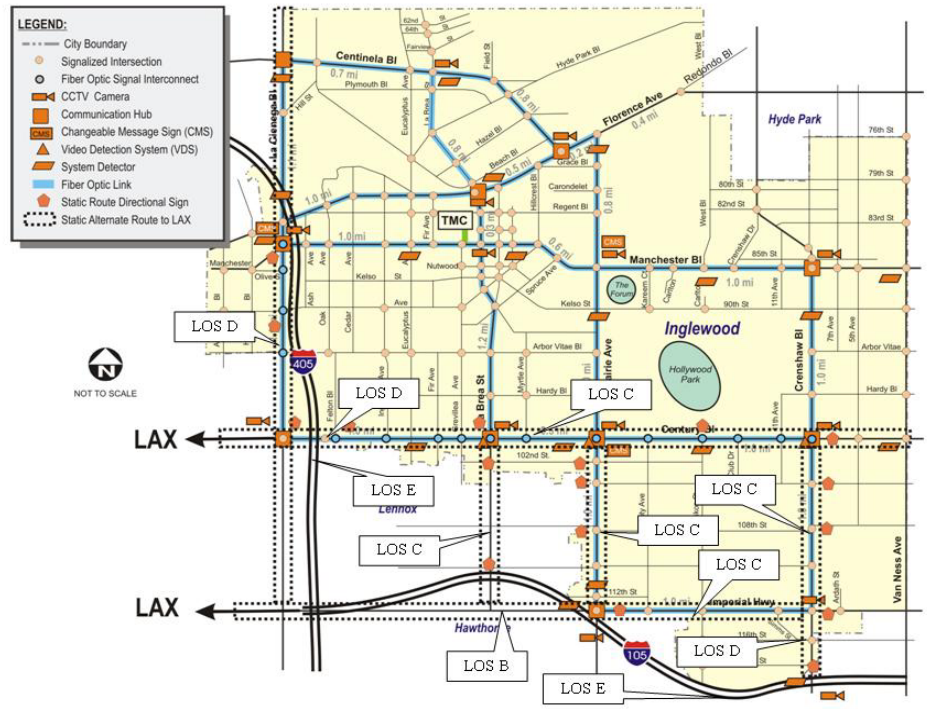

Figure 2. Proposed Alternate Routes to LAX and ITS Elements.

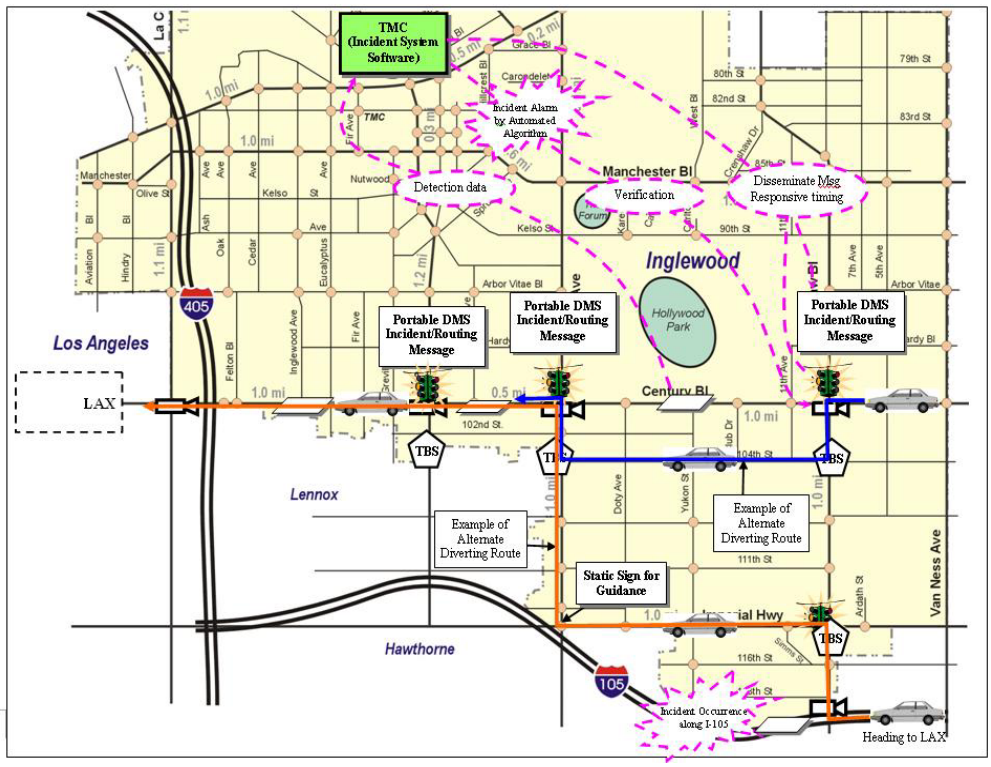

Figure 3. Operational Scenario of Route Guidance with ATIS/ATMS.

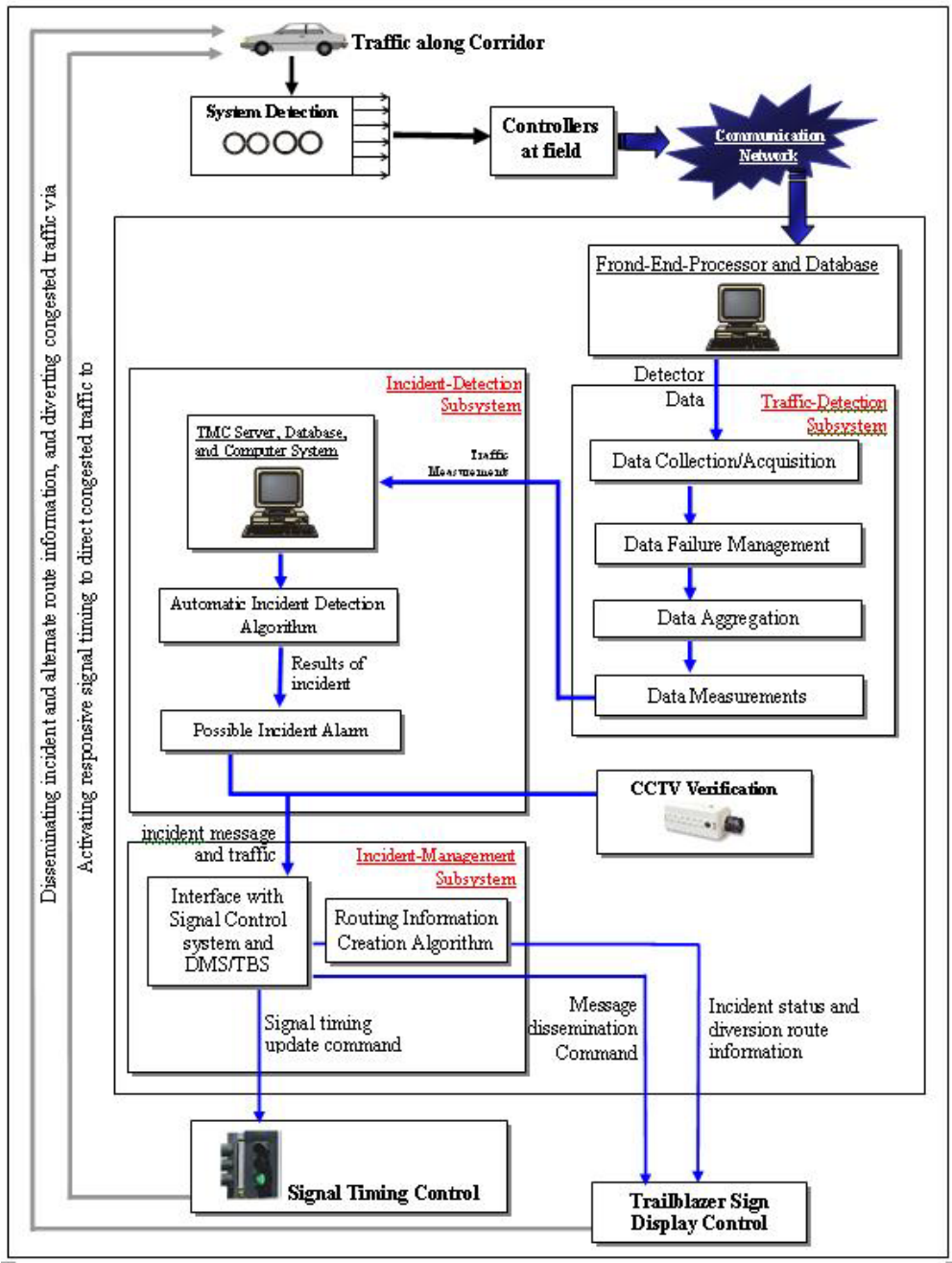

Figure 4. Concept of Operations for the Incident Management Scenario.

For example, as shown in **Figure 3**, the identified incident location is on the segment of Century Boulevard between Prairie Avenue and Crenshaw Boulevard. The videowall and/or workstations in TMC will display a message box with a flashing alarm incident message. In the meantime, the incident location is also highlighted or flashed onto the GIS-based map. The operator could then click on an incident icon on the map to display details about the traffic flow in the vicinity of the

incident. The operator then remotely controls the CCTV cameras at both Century/Crenshaw and Century/Prairie to verify the incident (**Figures 3** and **4**).

Divert Traffic via Route Guidance System and Signal Control Strategy: If an incident is verified, incident notification messages will be automatically sent to CMS and trailblazer signs (TBS) on the arterials in the vicinity of the incident location. The same alerts will also be displayed to traffic operators in the TMC. The messages displayed may guide drivers around the incident location to use other alternate routes.

The TBS and other roadside static directional signs will indicate the guidance information for detour, as shown in **Figure 4**. To make efficient use of the alternate routes and quickly disperse the accumulated traffic, signal control timing plans in the vicinity of the incident location will be adjusted on a real-time basis to accommodate the diverting traffic demand.

Similarly, traffic heading to LAX on I-105 could use an alternate route on a major or minor corridor to avoid incident related congestion occurring on that freeway. An example of this alternate routing from the freeway is shown in **Figure 4**. A TBS and a static directional sign will help guide the drivers the alternate route to LAX. A CCTV camera installed near the I-105 ramps along Crenshaw will allow the operators in TMC monitor traffic status near the I-105 and Crenshaw Boulevard.

DIAGRAMMATIC SIGNS FOR ALTERNATE ROUTE GUIDANCE

Trailblazer signs (TBS) and diagrammatic signs are recommended based on a number of studies on effectiveness of various roadside static signs (Zwahlen et al. 2003; Spencer et al. 2004). Diagrammatic signs have been proven very effective but quite costly, especially for multiple-lane streets connecting to freeway ramps, or exclusive turning lanes (Zwahlen et al. 2003). Zwahlen et al's study (2003) indicates that ground mounted diagrammatic signs on multi-lane arterials in advance of highway interchanges do provide useful navigational information, including the correct lane to enter the desired entrance ramp. Most evaluators felt that two right shoulder mounted diagrammatic signs, placed ½ mile (800 m) and ¼ mile (400 m) in advance of the interchange, are recommended. Hanscom (1971) reported, via a before-and-after study, successful applications of the diagrammatic signs on locations where "erratic maneuvers" frequently occur. Erratic maneuvers include weaving, hesitations, stop, and backup behaviors.

Several types of diagrammatic signs are recommended and introduced in the paper: freeway and arterial connector guidance, route information system (RIS) guidance, alternate route mileage information sign, and dynamic alternate route guidance signs. Typical examples of those diagrammatic signs are illustrated in **Table 2** and described below. Additionally, Carolina DOT's permanent static trailblazers (NCDOT 2001) of Hurricane Evaluation Route and incident alternate route on I-95 could be referred to a new design of traffic diversion alternate signs and location determination.

Route Information System Guidance (RIS) Sign: the development of the RIS stemmed from the need to show not only the usual information but also to give graphic representations of network-based route system (e.g., ring roads of a road network) (Vialis Traffic & Mobility 2004). The RIS indicates a tailback by means of

light points that may appear in a static or dynamic road sign. The example in **Table 2** shows a dynamic sign provides route direction information about the loop roads and shows congestion situation graphically. The system can inform through traffic of any congestion on the through route and also show any alternate routes. A detour route on this board can be shown if a severe congestion happens or a road is closed.

Table 2. Examples of Diagrammatic Signs for Alternate Route Guidance.

Route Information System Guidance Sign	
	Showing the usual information and give graphic representations of network-based route system (e.g., ring roads or a section of the road network) (Photo courtesy of Vialis)
Alternate Route Travel Time/Mileage Guidance Sign	
	Presenting travel time and/or mileage information to each egress that connects to other major routes or corridors (Photo courtesy of Vialis)
Dynamic Alternate Route Guidance Sign	
	Assisting the management of traffic for special planned or emergency events (Photo courtesy of the Minnesota DOT)

Source: Vialis Traffic & Mobility 2004; FHWA 2003

Alternate Route Travel Time/Mileage Information Sign: this sign is typically used for a principle corridor to present travel time and/or mileage information to each egress that connects to other major routes or corridors. **Table 2** shows an example of real-time route information (Vialis Traffic & Mobility 2004).

Dynamic Alternate Route Guidance Sign: it is used to manage traffic for special planned or emergency events. It is essential that the diverted traffic encounter an equal or higher level of service on the alternate route compared with the mainline. Alternate route plan deployment typically requires significant law enforcement resources for alternate route traffic management and operations surveillance. Technology applications of dynamic alternate route guidance signs could reduce field personnel requirements. **Table 2** shows a dynamic trailblazer sign. During the program planning phase, stakeholders managing planned special events at permanent venues should evaluate the need for installing these devices along commonly used alternate routes serving the event venue (FHWA 2003).

CONCLUSIONS

The study presented in this paper discloses the functional and operational importance of a signing alternate route guidance system for traffic diversion strategies in a mixed roadway network. The most significant contribution of the study is the newly proposed concept of merging roadside signing route guidance systems into ATIS/ATMS planning and implementation in a mixed network. This paper presents a practical method to identify locations that are important to the network and to determine alternate routes to specific freeways and large traffic generators/attractors via an analysis of incident management scenario. The paper addresses signing route guidance system connecting non-crossed freeways in a mixed roadway network utilizing local streets. Finally, the authors attempt to summarize types of alternate route guidance signs with illustration of design examples. They are expected to provide necessary alternate route guidance infrastructures for enhancing ITS functionality. It is believed to be an important topic that has not been drawn intensive attention in past. Further research will focus on a system design of a specific alternate route guidance system for a typical freeway in an urban area, and conduct a microscopic simulation study to evaluate the operation and benefits of the alternate routes with ITS technology alternatives.

ACKNOWLEDGEMENTS

Special thanks go to Ramin Massoumi, George Hattrup and Raymond Lee of Iteris for their contributions to several referred reports from which examples of the case study were adapted. This paper represents the authors' views only.

REFERENCES

Abdel-Aty, M and Abdalla, M. F. (2004). "Modeling Repeated Multinomial Route Choice under ATIS Using Generalized Estimating Equations with Polytomous Logit Function." CD-ROM, Pre-Print of the 83th Transportation Research Board Annual Meeting.

Federal Highway Administration (FHWA) (2003). "Managing Travel for Planned Special Events." FHWA Report No.: FHWA-OP-04-010, 2003.

Hanscom F.R. (1971). "Evaluation of Diagrammatic Signing at Capital Beltway Exit No. 1." Report to the Virginia Highway Research Council, September 1971.

Helmut T. Zwahlen, H. T., Russ, A., Roth, J.M., and Schnell, T. (2003). "Evaluation of the Effectiveness of Ground Mounted Diagrammatic Advance Guide Signs for Freeway Entrance Ramps." CD-ROM, Pre-Print of the 82nd Transportation Research Board Annual Meeting.

Iteris, Inc. (2001). Preliminary CCTV and System Detection Master Plan for South Bay ITS Project, October 26, 2001

Iteris, Inc. (2003). Concept of Operations for City of Inglewood ITS Design – Appendix for City of Inglewood Preliminary ITS Design, March 2003.

Iteris, Inc. (2004). SR 710 Mitigation Project - SR 110 To SR 210 Connector / Marengo Avenue Interchange Emphasis Directional Signing Report. Federal Aid Project RABA 01-5064(026), February 2004.

Mark E. Spencer, M.E., and West, J. (2004). "San Jose's Parking Guidance System." CD-ROM, Pre-Print of the 83rd Transportation Research Board Annual Meeting

Murray-Tuite, P. M., and Mahmassani, H.S. (2004). "A Methodology for the Determination of Vulnerable Links in a Transportation Network." CD-ROM, Pre-Print of the 83th Transportation Research Board Annual Meeting.

North Carolina Department of Transportation (NCDOT) (2001). "Hurricane Floyd – Lesson Learned."April 2001.

Papageorgiou, M., Diankaki, C., Dinopoulou, V., Kotsialos, A., and Wang, Y.B. (2003). "Review of Road Traffic Control Strategies." Proceedings of the IEEE, Vol. 91, No. 12, pp. 2043 – 2067.

Peeta, S., and Gedela, S. (2001). "Real-Time Variable Message Signs Based Route Guidance Consistent with Driver Behavior." CD-ROM, Pre-print of Paper the 80th Transportation Research Board Annual Meeting.

Vialis Traffic & Mobility (2004). Route Information System (RIS), http://www.vialis.nl/engels_verkeer/index.htm> (November 2004).

Wardman, M., Bonsall, P.W., and Shires, J.D. (1997). "Driver Response to Variable Message Signs: A Stated Preference Investigation." Transportation Research Part C. Vol. 5, No. 6, 1997, pp. 389-405

Wei, H. (2000). HCM-Based Freeway Operational Analysis for FSOA Project (Draft). Draft Project Report prepared by TranSmart Technologies, Inc. for Parsons Transportation Group, September 2000.

An EEG Predictor of Driving Fatigue

Xie Xiaoli, Liu Xiaoming, Hu Jiangbi, Cao Xintao and Wang Weili

Transportation Research Center, Beijing University of Technology, No. 100 Ping Le Yuan, Beijing, 100022; email: xxl@emails.bjut.edu.cn

ABSTRACT

Driving fatigue is one of the main causes of traffic accidents. Many researchers believe that electroencephalography (EEG) is an accurate and promising method to detect driving fatigue. Based on the theories of biocybernetics, this article developed an EEG-based driving fatigue prediction indicator, and the process of calculating it was detailed. After indoor-experimental verification, it was found that the indicator has a good linear correlation with spirit response speed. The results have implications for predicting driving fatigue and are helpful for future development of driving fatigue countermeasures.

INTRODUCTION

Driving fatigue is no doubt harmful to traffic safety. While fatigue-related accidents are not a big part in all road traffic accidents, they are much more serious than the others. Therefore, it is necessary to take a series of countermeasures to avoid driving fatigue accidents.

At present, there are three main categories of countermeasures: behavioral countermeasures, technological countermeasures, and regulatory countermeasures. Behavioral countermeasures have little effect and few lasting restorative benefits; regulatory countermeasures are inflexible and their enforcement is costly and difficult; technological countermeasures' validity remains to be seen (Hartley 2004). In these three categories of countermeasures, research is focused on technological countermeasures, because they have some characteristics such as real-time and accuracy, which can make the countermeasures more effective to reduce fatigue-related accidents. In technological countermeasures, many researchers believe that electroencephalogram (EEG) can reflect the state changes of driving fatigue accurately and can be used as a predictor.

However, EEGs are only digital signals. These signals have no meaning themselves. They must be analyzed, and then quantitative indicators, which can represent the individual's mental state, can be determined. In past studies, researchers used EEGs as general engineering signals, and always extracted indicators based on signal spectral analysis. Compared with the indicators associated with slow-wave increase or slow-wave frequency increase used in conventional visual analysis of the EEG, these indicators are just a more precise expression form, and the effect does not exceed the effect of visual EEG analysis. Budi Thomas Jap investigated 8 EEG power spectrum indicators commonly researched in previous studies in a driving

simulator and found that the relationship between these indicators and the degree of driving fatigue are not entirely consistent with other research (Jap 2009). Therefore, these indicators are not precise predictors of driving fatigue, and their reliability has not been proven.

Since EEG signals are biomedical signals, in order to reflect the status of driving fatigue more accurately, more and more researchers are introducing the methods that are more suitable when analyzing biomedical signals. Peng (2007) introduced non-linear theory and believed that the correlation dimension indicator can reflect the characteristics of EEG when the driver is fatigued. Peng (2008) also proposed a new method to process EEG signals, which combined the Hilbert-Huang Transform method and approximate entropy method. He proved that the calculated values of that method can help distinguish the EEG between sitting quietly and driving between normal state and fatigue state. However, these indicators are rather cumbersome to calculate, so it is difficult to apply it in practice.

In order to get fatigue information from EEG signals, from the point of ergonomics, this paper introduces biocybernetic theories to process EEG by multiphase information analysis and develops a new driving fatigue indicator.

EXPERIMENTAL PROGRAMS

Experimental protocol

In the real world, it is dangerous for drivers to take part in driving fatigue experiments. In addition, the EEG recording system has poor anti-jamming ability, so the requirements on collecting environmental factors are higher, and it is difficult to control the factors in the real environment (Lal and Craig 2001). Therefore, as the basis for follow-up study, this article used simulation experiments. In the future, the effectiveness of the indicators can be verified using a driving simulator or in a real road environment.

Driving is a task composed of mental work and manual work. The volume of manual work is equal to the volume of general administrative work, while the volume of mental work is larger. Therefore, driving is a kind of sensory nerve task; driving fatigue is almost mental fatigue. Hence, mental fatigue research methods can be introduced into the study of driving fatigue. In the study of mental fatigue, the medical model of mental fatigue is very difficult to set up because there are many factors that may affect it. Therefore, sleep deprivation is commonly used to set up the medical model of mental fatigue. This is because: firstly, the negative effects of sleep deprivation on the human body are similar to the effects of mental fatigue, such as the level of operation is reduced and alertness is decreased; secondly, the controllability of sleep deprivation is larger, namely, the deprived time can be shorter or longer; thirdly, sleep deprivation is safe and does not harm human physiological and psychological functions. Consequently, although the negative statuses of human physiological and psychological functions affected by mental fatigue are not equal to which affected by sleep deprivation, the latter is accepted as a special case of the former (Xue et al. 2006).

Accordingly, this paper used the sleep deprivation method. The experiment started at 3:00 p.m. and at the beginning of the experiment all the participants had

been awake at least 19 hours. The fatigue arising from this situation is considered driving fatigue.

Independent indicators

The main purpose of this paper is to verify whether the developed EEG indicator can predict the degree of driving fatigue. Because fatigue cannot be directly measured, it is necessary to introduce some indicators as independent indicators to quantify the extent of driving fatigue. These factors are recognized in a large scope and easy to control. Through analyzing the relationship between these independent indicators and the developed EEG indicator, the effectiveness of the EEG indicator can be determined. However, many studies have overlooked the importance of independent indicators, and usually determine the extent of driving fatigue arbitrarily. In this way, their experimental results are unreliable. In this study, two independent indicators were used.

Subjective evaluation indicator

Most driving fatigue studies used the subjective evaluation method. This article asked the subjects to fill out self-reported fatigue level questionnaires (see Table 1) according to their own subjective feelings. Zhao (1992) had presented the questionnaire design principles and quantified methods. The quantified values were called subjective fatigue degree (SFD).

Table 1. Self-reported fatigue level questionnaire.

State / Level	Very alert	Alert	Not sure	Fatigue	Very fatigue
3 2 1					
-1 -2 -3					

Compared with other methods, subjective evaluation methods are simple to conduct and can save resources, but lacks objectivity. In order to ensure the reliability of scientific research, this kind of indicator should not be used alone, and some objective indicators need to be taken into account (Lal and Craig 2001).

PVT indicator

Psychomotor vigilance task (PVT) is a widely used standard test for the spirit response speed, which has better objectivity and reliability with mental fatigue (National Highway Traffic Safety Administration 1998). For driving fatigue measurement, PVT is suitable. Since the main requirement of driving task is response fast, and PVT is based on reaction time. Therefore, in the study of driving fatigue, it is appropriate to use the PVT result as an independent indicator.

According to the principle of PVT, the paper programmed the test using Stim2 software of Neuroscan. The task for the participants is to respond using a button when visual signals are shown in the middle of a black 17-inch LCD screen. The signal was yellow circle with a radius of 4 centimeters, and the emergence was random from 2 to 10 seconds. Participants were asked to use their right hand

(left-handed person left hand), and when the signal appears, press the mouse button as soon as possible. After the signal disappeared, the software will record the reaction time automatically. The task lasted 10 minutes. The length of the test and the data statistical method are various, but, once they are specified, PVT scores can be compared between different experiments.

The paper deleted the beginning three and the ending two data from every task result to remove the effect of adaptation. Then the average reaction time of the original 1 minute and the last 1 minute was calculated to present participants' mental status before and after PVT. As an independent indicator, it was named as vigilance reaction time (VRT).

EEG indicator

The NeuroScan 36 channel EEG recording system was used to record the EEG, whose Ag/AgCl electrode cap is easy to wear. Thirty-two EEG channels were recorded following the International 10-20 Montage system and referenced to right ears and sampled at 1000 Hz covering the major areas of the brain.

This article introduced biocybernetics theories to obtain fatigue information from EEG signals and developed a new indicator. The theoretical bases of the new indicator are as follows.

a. The human brain can be perceived as a control system, and EEG indicators are variables that change with time and space, which can describe its activities. Therefore, in the analysis of EEG, the laws and models that have been expounded in physical, mechanical, and other systems can be used. It will be helpful for understanding the nature of brain activities and patterns.
b. According to bio-medical theories, when the brain is fatigued, the power spectrum value of EEG alpha band will increase, while the information transmission and coordination between the two cerebral hemispheres will decrease (Feng 1986). In cybernetics theories, the amplitude-frequency and phase-frequency characteristics of the system transfer function, as well as the coherence function, can reflect the information transmission and coordination capability of the system.
c. During the process of driving, the entire brain takes part in the task. Because the temporal lobe is easily affected by outside sounds, such as human voice and car audio, the EEG signals from the frontal lobe, parietal lobe, and occipital lobe of the brain are taken into account.

Based on the theoretical analysis above, this article developed an indicator, named driving fatigue level (DFL), to measure the degree of driving fatigue. The calculation program is as follows.

a. Scan4.3 software was used to transfer the recording reference to linked ears and then remove the vertical ocular artifacts from original EEG data.
b. To the corresponding lobar, the signal from the left lead x_k is as input, and the signal from the right y_k is as output. Calculate the Fourier transform of x_k and y_k, recorded as X_f and Y_f.
c. Calculate the self-power spectrum of x_k, recorded as G_{xf}, and the cross-power spectrum of x_k and y_k, recorded as G_{xyf}.

Where, N is the number of signal sampling point, "*" indicates complex

conjugate.

d. Calculate amplitude-frequency and phase-frequency characteristic of transfer function between x_k and y_k.

if $X = \frac{G_{xyf}}{G_{xf}}$, then amplitude-frequency characteristic $|H_{xyf}| = |X|$, and

phase-frequency characteristic $\theta_{xyf} = \tan^{-1}\frac{\mathrm{Im}(X)}{\mathrm{Re}(X)}$

e. Calculate coherence function γ^2_{xyf} between x_k and y_k.

f. According to the self-power spectrum of the left lead signal from corresponding lobar, find alpha-wave dominant frequency (shown in Figure 1).

g. Obtain values at the point of alpha-wave dominant frequency, and calculate DFL.

$$G_{xf} = \frac{1}{N}|X_f|^2 = \frac{1}{N}X_f{}^* X_f \quad f = 0,1,\cdot\cdot,N-1 \qquad G_{xyf} = \frac{1}{N}X_f{}^* Y_f \quad f = 0,1,\cdot\cdot,N-1$$

$$\gamma^2_{xyf} = \frac{|G_{xyf}|^2}{G_{xf}G_{yf}} \quad f = 0,1,\cdot\cdot,N-1 \qquad DFL = \frac{1}{3}\sum_{lobar}\frac{\sqrt{G_{xf}}}{|H_{xyf}|\times\log_e|\theta_{xyf}|\times\gamma^2_{xyf}}$$

Experimental procedure

Nine young male participants who were licensed drivers were recruited in the study. The average age was 25. The participants first wore the EEG electrode cap, and then filled in the self-reported fatigue level questionnaire. Thirdly, they were asked to do a PVT test, and at the same time the EEG was recorded. After PVT, they were asked to fill in the self-reported fatigue level questionnaire again.

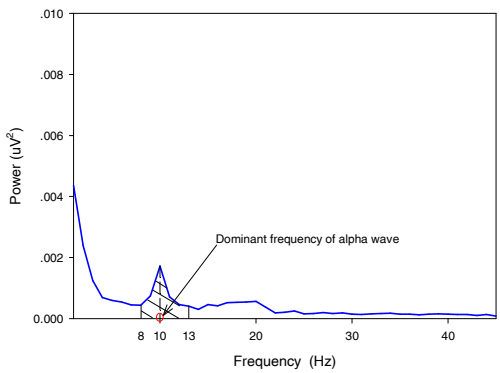

Figure 1. Alpha-wave dominant frequency calculation diagram.

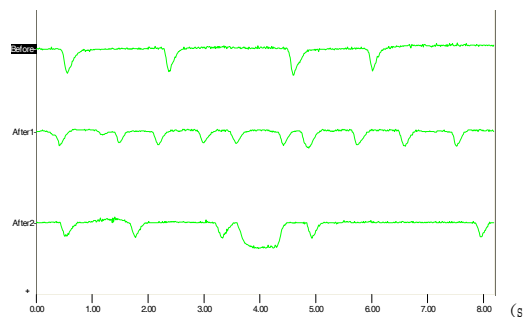

Figure 2. Example of vertical EOG before and after PVT test.

DATA ANALYSIS

Participants completed a PVT test under sleep deprivation. Their status was similar to the status under driving fatigue. Although the test time was only 10 minutes, it was enough to affect the mental state. This can be seen from the participants' vertical electrooculogram (EOG). As it was shown in Figure 2, there were three 8-second examples about the vertical EOG before and after the PVT. The EEG recording system collects EEG as well as EOG. EOG are electrical eye movement records from which we can see the movement of the eyelid. The movement of the

eyelid can reflect the level of fatigue to some extent (National Highway Traffic Safety Administration1998). As can be seen from Figure 2, at the beginning of PVT test, the blinks were fast, large-range, and independent. At the end of the test, the blinks became smaller in amplitude, faster in frequency, and continuous. Some participants' blinks became longer in time, as shown in Figure 2 After2.

Therefore, this article compared the EEG indicator with independent indicators before and after the PVT test (shown in Figure 3). It can be seen from the chart that:

a. all participants SFD were increased, which means that the PVT test can affect their mental state and make them feel fatigue;
b. except for the 2nd and the 3rd participants, VRT and DFL was also increased with SFD; and
c. VRT and DFL had same change trend.

The Pearson correlation test was made between the growth of SFD, VRT, and DFL. Table 2 shows the results.

As shown in Table 2, DFL growth and VRT growth had little correlation with SFD, which means that the estimation about fatigue made by their own are not accurate. Even the estimation can be quantified, but it is still difficult to meet the requirements of data analysis. From Table 2, the positive correlation between DFL growth and VRT growth was high. Then a linear regression analysis was made between them, as it was shown in Figure 4.

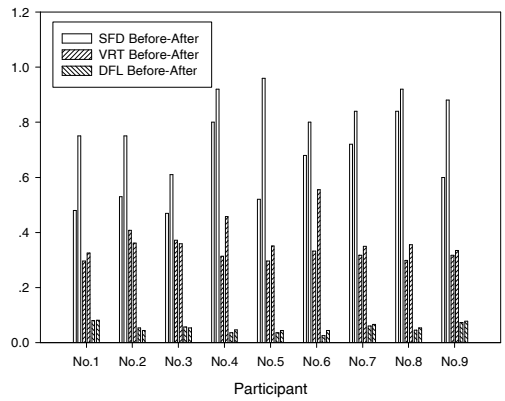

Figure 3. Changes of SPD, VRT, and DFL before and after every test.

Table 2. Pearson correlation matrix of SFD growth, VRT growth, and DFL growth.

	SFD growth	VRT growth	DFL growth
SFD growth	1.000		
VRT growth	-0.288	1.000	
DFL growth	-0.219	0.915	1.000

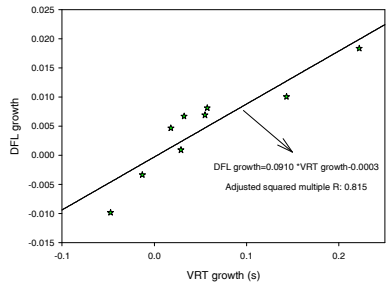

Figure 4. Linear regression results between DFL growth and VRT.

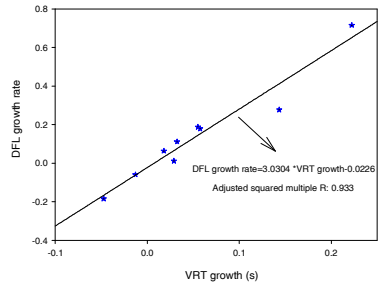

Figure 5. Linear regression results between DFL growth rate and VRT growth.

DFL growth was divided by the DFL before PVT test, and then the DFL growth rate was calculated. It removed individual impact on DFL. Figure 5 shows the results of linear regression between DFL growth rate and VRT growth.

CONCLUSION

PVT reaction time reflects the operational efficiency from eye to hand. Compared to the subjective methods or biochemical methods, it is more reliable and more acceptable to evaluate fatigue by operating performance (Zhu 2003). In this paper, there is a fine positive correlation between the growth rate of the EEG indicator and PVT growth, which means that the DFL growth rate can accurately reflect changes in operating performance. If this EEG indicator can be verified in the real driving environment, it could be used as a real-time driving fatigue monitoring instrument and applied to the field of fatigue countermeasures.

FUTURE WORK

This paper applied a sleep deprivation method to induce mental fatigue. After all, the mechanism of sleep is not the same as the driving fatigue mechanism, so, the findings of this paper required verification in the real world.

The purpose of driving fatigue research is to determine the threshold of fatigue and to judge a driver's fatigue level. If the driver was judged fatigue by the threshold, then he or she is not safe to drive. It is a feasible method to determine the threshold by the relationship between DFL growth rate and driver reaction time, and it is worth continued research.

REFERENCES

Jap, B. T., Lal, S., Fischer, P., and Bekiaris, E. (2009). "Using EEG spectral components to assess algorithms for detecting fatigue." *J. Exper Systems with Applications*, 36: 2352-2359.

Cao, X., Miao, D., Liu, L. (2006). "Methods of evaluation of mental fatigue." *J.Journal of Forth Military Medical University*, 27(4):382-384.

Feng, Q. (1986). "The principle and application of computer analysis about ECG and EEG [M]." Science Press.

Hartley, L. R., Rothengatter, T. (Editor), and Huguenin, R. D. (Editor). (2004). "Fatigue and driving, traffic, and transport Psychology[M]." Elsevier Ltd.

Li, H. (2005). "Based on the comprehensive integration of driving fatigue identification [D]." Central South University master's thesis, 54-55.

National Highway Traffic Safety Administration. (1998). "Evaluation of Techniques for ocular measurement as an index of fatigue and the basis for alertness management." DOT HS 808 762[R]. U.S. Department of Transportation, 28-30.

Peng, J., Wu, P., and Yin, G. (2007). "Exploring the characters of electroencephalogram for fatigued drivers." *J. Transactions of Beijing Institute of Technology*. 7:585-589.

Peng, J., Wu, P., Yin, G., Chen, Z., and Ma, S. (2008). "Application of combining Hilbert-Huang transform with approximate entropy in EEG signal analyzing of fatigued driving." *J. of Highway and Transportation Research and Development*. 6:126-129.

Saroj K.L. Lal and Ashley Craig. (2001). "Electroencephalography activity associated with driver fatigue: implications for a fatigue countermeasure device." *J. of Psychophysiology*, 15(3):183-189.

Zhao, C., He, C. (1992). "A preliminary study of long-distance coach drivers fatigue." *J. Psychological Science*, 1.

Zhu, Z. (2003). "Engineering psychology tutorial [M]." People's Education Press.

Calculation Method for Braking Torque of Self-excited Retarder

YANG Xiaojun[1],HE Ren[2], and SHEN Haijun[3]

[1]Jiangsu Province Key Laboratory of Automotive Engineering, Jiangsu University, Zhenjiang, Xuefu Road 301; PH (86)0511-88780721-2958, (86)13405586165; email: xjyang2008@126.com.
[2]Jiangsu Province Key Laboratory of Automotive Engineering, Jiangsu University, Zhenjiang, Xuefu Road 301; PH (86)0511-88791872, (86)13951282383; email: heren1962@163.com.
[3]Jiangsu Province Key Laboratory of Automotive Engineering, Jiangsu University, Zhenjiang, Xuefu Road 301; PH (86)0511-88791872, (86)15896381345; email: haijunrunner@yahoo.com.cn.

ABSTRACT

The total braking torque(T) of a self-excited retarder is mainly made up of both the electromagnetic torque(T_g) of its power generation unit and the braking torque(T_e) of its eddy current brake. Calculation formulae for T_g and T_e were derived from the structure parameters respectively on the basic of the Magnetic Flux method and the Electromagnetic Theory. After verification by experiment, the total braking torque calculated theoretically was basically consistent with the experimental result for a 500Nm self-excited retarder. This would lay a theoretical foundation for further study on the relation between braking torque and structural parameters and optimizing the design for a self-excited retarder.

INTRODUCTION

Self-excited retarder is a kind of electromagnetic brake which integrates a power generation unit and an eddy current brake. When a vehicle brakes or decelerates, the power generation unit makes use of vehicle's movement inertia as initial power and transforms vehicle's kinetic energy into electrical energy which further powers the eddy current brake to achieve the purpose of brake or deceleration. So a self-excited retarder does not require vehicle batteries to provide excitation current and is free from the additional energy loss. At same time, it avoids bringing negative impact to other vehicle's electronic equipment. The total braking torque(T) of a self-excited retarder is mainly made up of both the electromagnetic torque(T_g) of its power generation unit and the braking torque(T_e) of its eddy current brake, i.e. $T=T_g+T_e$.

THE ELECTROMAGNETIC TORQUE(T_g)

The power generation unit, a rare-earth permanent magnet synchronous generator with radial structure, is usually divided into two parts: one is the stator (i.e. magnetic pole and armature winding) fixed on transmission body, another is the rotor(i.e. permanent magnet) connected to the vehicle's drive shaft by flange. Both the virtual displacement and the Maxwell tensor are two basic methods to caculate the electromagnetic torque(T_g) of a permanent magnetic machine. However, the former employs that one large number subtracts from another similar and this directly leads to reduction of T_g's effective bits. And the later is more sensitive to the density of finite element mesh and its accuracy depends on the selected integral path and the mesh quality[TANG Renyuan, 1997]. The Magnetic Flux method introduced in this paper is unsignificantly sensitive to the density of finite element mesh and is just determined by the magnetic flux within a pole space and less affected by the partial error.

The internal phasor diagram of a permanent magnet synchronous generator is shown in Figure1.

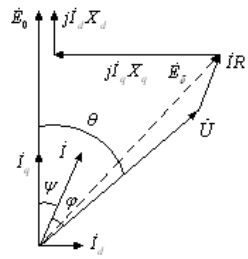

Figure 1: The internal phasor diagram of a permanent magnet synchronous generator.

The relation between variables described by Figure1 can be rewritten as the following equation(1):

$$\begin{cases} U\cos\theta = E_0 - I_d X_d - IR\cos(\theta-\varphi) \\ U\sin\theta = I_q X_q - IR\sin(\theta-\varphi)\psi \end{cases} \tag{1}$$

where, θ: power angle which is positive when $\dot{E}_0$ advances $\dot{U}$ in phase, φ: power factor angle which is positive when $\dot{I}$ advances $\dot{U}$ in phase, ψ: internal power factor angle which is positive when $\dot{E}_0$ advances $\dot{I}$ in phase, $\dot{E}_0$: no-load electromotive force, $\dot{U}$: armature terminal voltage, $\dot{I}$: armature winding current of each phase, R: armature winding resistance of each phase, X_d :direct-axis synchronous reactance, X_q: cross-axis synchronous reactance, I_d and I_q are the direct-axis armature current and the cross-axis armature current respectively, and $I_d = I\sin(\theta-\varphi)$, $I_q = I\cos(\theta-\varphi)$.

If disregarding the voltage of armature winding resistance, the inductive electromotive force $\dot{E}_\delta$ (i.e. air-gap EMF) of each phase approximately equals to armature terminal voltage $\dot{U}$. Thus, the equation(1) can be simplified as:

$$\begin{cases} E_\delta \cos\theta = E_0 - I_d X_d \\ E_\delta \sin\theta = I_q X_q \end{cases} \quad (2)$$

Projecting I_d and I_q onto $\dot{E}_\delta$, the electromagnetic power P_{em} of air-gap can be obtained:

$$P_{em} = mE_\delta I\cos\varphi \quad = mE_\delta(I_q\cos\theta + I_d\sin\theta) \quad (3)$$

where, m : phase-number of a permanent magnet generator. Air-gap EMF E_δ can be caculated by the following[TANG Renyuan, 1997; LIN Rongwen, 2004]:

$$E_\delta = \sqrt{2}\pi f \Phi_{1N} N_1 K_{dp} K_\Phi \quad (4)$$

where, $f = pn/60$: frequency of output voltage, p: the number of pair-poles, n: rotator speed, Φ_{1N}: fundamental air-gap flux when a permanent magnet generator is loaded, N_1 : number of series-wound armature winding for each phase, K_{dp}=$K_{d1}K_{p1}K_{sk1}$: winding factor. Thereinto, K_{d1} is armature winding distribution factor, K_{p1} is armature winding short-distance factor, K_{sk1} is flume factor.

According to the relation between torque and power, i.e. $P = wT$, the electromagnetic torque can be obtained.

$$T_g = \frac{P_{em}}{w} = \frac{mE_\delta}{w}(I_q\cos\theta + I_d\sin\theta) \quad (5)$$

where, $w = 2\pi n/60$ which is mechanical angular velocity of a permanent magnet generator. From the equations(4), (5):

$$T_g = \frac{mp}{\sqrt{2}}\Phi_{1N} N_1 K_{dp} K_\Phi (I_q\cos\theta + I_d\sin\theta) \quad (6)$$

If Φ_{1N} and θ can be caculated accurately, the electromagnetic torque(T_g) of the power generation unit can be obtained. Caculating Φ_{1N} and θ can be recured to magnetic vector potential A on the stator's inside surface and two-dimensional finite element analysis. First, node's magnetic vector potential A within a period, which is caculated by the finite element analysis, is sampled to be discrete sequence. Second, the discrete sequence is taken the Fourier Transform. Hence, the node's magnetic vector potential A can be described as[J.M Arinescu, 1988; LI Kaicheng, 2000; LIN Rongwen, 2004]:

$$A(x) = \frac{a_0}{2} + \sum_{k=1}^{\infty}[a_k\cos\frac{k\pi}{l} + b_k\sin(\frac{k\pi}{l})] \quad (7)$$

where, l: arc-length of half period(each pole).

In equation(7), a_1 is half of q-axis component of each-pole magnetic flux within armature unit-length, b_1 is half of d-axis component of each-pole magnetic flux within armature unit-length. Therefore, synthetic magnetic flux of each pole is:

$$\Phi_{1N} = 2L_{ef}\sqrt{a_1^2 + b_1^2} \tag{8}$$

where, L_{ef} : armature calculation-length.

Power angle can be expressed as:

$$\theta = arctg\frac{a_1}{b_1} \tag{9}$$

From equations(6), (8) and (9), the electromagnetic torque(T_g) can be caculated accurately.

THE BRAKING TORQUE(T_e)

The structure of an eddy current brake is usually divided into two parts: one is the rotor(i.e. rotary drum) connected with drive shaft by flange, another is the stator(i.e. pole and excitation coil) fixed on transmission body. The air-gap between the primary and the secondary is from 1mm to 1.5mm. Rotary drum is made of iron with good magnetoconductivity and low remanence ratio, such as electrical pure iron, low-carbon steel or alloy steel etc. Its outerside surface usually is founded with cooling fin so as to dissipate heat in time.

Magnetic field generated by excitation current forms a closed-loop in magnetic pole, air-gap and rotary drum, shown as Figure 2. Rotating drum cuts magnetic line and

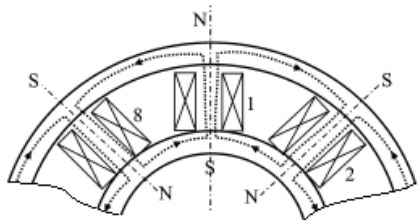

Figure 2: Distribution of magnetic pole and magnetic line.

produces eddy current in its inside surface. Because of skin-effect, eddy current mainly distributes within a thin layer of drum's inside surface and behaves as decaying exponential $e^{-\sqrt{w\mu\sigma z/2}}$ with the deepening of penetration depth. The equivalent penetration depth Δh is usually employed in engineering calculation and the amplitude of eddy current in the point of Δh reduces e times compared with that of inside surface[HE Ren, 2006], i.e. $e^{-\sqrt{w\mu\sigma\Delta h/2}} = e^{-1}$. Thus Δh can be obtained.

$$\Delta h = \sqrt{\frac{2}{w\mu\sigma}} = \sqrt{\frac{2\rho}{w\mu}} \tag{10}$$

where, σ : drum conductivity, ρ : drum resistivity and $\rho = 1/\sigma$, $\mu = \mu_r\mu_0$: drum magnetic permeability, μ_r : relative magnetic permeability, μ_0 : vacuum magnetic permeability, w: angular velocity of magnetic field and $w=2\pi N_p n/60$, N_p: the

number of pair-poles, n: the rotor speed.

In order to facilitate the analysis of braking power for the eddy current brake, the following assumptions are made: (1)The magnetic flux generated by excitation current just distributes within magnetic poles and disregards the flux leakage. (2)The relative magnetic permeability of magnetic material is a constant. (3)Ignore the mutual interaction between magnetic poles. (4)Magnetic line vertically penetrates the inside surface of drum. (5)Arc region, which is the area of drum's inside surface opposite the magnetic pole, is approximately regarded as a rectangle. This arc region can be equivalent to numerous linear conductors and all of them parallel drum-axes as shown as Figure 3.

When drum rotates, linear conductors vertically cut magnetic line with the speed $v=Dw$. According to the law of electromagnetic induction, electromotive force ε generated on linear conductor is

$$\varepsilon = Bvb = BDwb \tag{11}$$

where, D: inner radius of drum, b: length of magnetic pole along drum-axis, B: air-gap magnetic flux density.

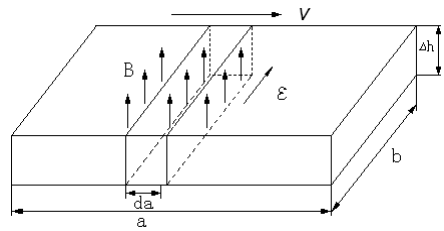

Figure 3: Schematic diagram of calculation model.

Resistance, current and power of linear conductor respectively is :

$$dR = \rho \frac{b}{\Delta h \cdot da} \tag{12}$$

$$di_e = \frac{\varepsilon}{dR} = \frac{BDw\Delta h}{\rho} da \tag{13}$$

$$dp = \frac{\varepsilon^2}{dR} = \frac{B^2 D^2 b w^2 \Delta h}{\rho} da \tag{14}$$

From equation(14), the braking power of each excitation coil can be obtained:

$$p = \int_0^a dp = \frac{B^2 D^2 w^2 S_{极}}{\rho} \Delta h \tag{15}$$

Hence, the total braking power of eddy current brake is:

$$P = \frac{2N_p B^2 D^2 w^2 S_{极}}{\rho} \Delta h \tag{16}$$

where, $S_{极} = a \times b$: pole area, a : the length of magnetic pole along rotor's circumference. Air-gap magnetic flux density B is the interactional result of the excitation current and the eddy current. Likewise, the magnetomotive force is also the interactional result of the excition curren and the eddy current. Therefore, the following equation holds[SUN Weimin, 2005]:

$$\Phi_m^{'} = \Phi_m - \Phi_e \tag{17}$$

where, Φ'_m : air-gap magnetomotive force, $\Phi_m = N_2 I$: magnetomotive force generated by excitation current, I: the excitation current, N_2 : the number of excitation coil, $\Phi_e = eI_e$: magnetomotive force generated by eddy curren, $e = \pi^2 \mu_0 \Delta h^2 / (3\rho^2)$: eddy current loss coefficient, I_e : the eddy current of the whole arc region[ZHAO Kaihua, 1985; SUN Weimin, 2005], and from equation(13)

$$I_e = \int_0^a di_e = \frac{BDaw\Delta h}{\rho} \tag{18}$$

Thus, magnetic flux of the arc region can be described as:

$$\theta = BS_{极} = \frac{\Phi_m - \Phi_e}{R_m} \tag{19}$$

The total reluctance R_m of magnetic circuit is[ZHAO Kaihua, 1985; SUN Weimin, 2005]:

$$R_m = 2R_{m0} + R_{m1} + 2R_{m2} + R_{m3} \approx R_{m0} = \frac{2L_0}{\mu_0 S_{极}} \tag{20}$$

where, R_{m0} : air-gap reluctance, R_{m1} : drum reluctance of a pole pitch, R_{m2} : magnetic yoke reluctance, R_{m3} : core reluctance L_0 : air-gap length.

From equation (19) and (20)

$$B = \frac{\mu_0 \rho N_2 I}{2\rho L_0 + \mu_0 Daew\Delta h} \tag{21}$$

Thus, from equation(16), (21) and $P = Tw$, the braking torque of the eddy current brake can be obtained:

$$T_e = \frac{2\mu_0^2 N_p N_2^{\ 2} D^2 w S_{极} \rho \Delta h I^2}{(2\rho L_0 + \mu_0 Daew\Delta h)^2} \tag{22}$$

THEORETICAL CACULATION AND EXPERIMENTAL RESULT

The power generation unit parameters of a 500Nm self-excited retarder are that

the number of pair-poles p=12, the number of armature winding for each phase N=8, the phase-number m=3, the rotor's outer diameter D_1=248mm, the stator's inner diameter D_2=249.5mm, the stator's outer diameter D_3=302mm, the length of air-gap δ=1.5mm. And the mechanical parameters of the eddy current brake are that the number of pair-poles N_p=6, the pole area $S = 36mm \times 48mm$, the drum inner diameter D_4=360mm, the drum outer diameter D_5=386mm, the length of air-gap L_0=1mm.

Theoretical curve of braking torque and that of experiment is shown as Fig.4. The total braking torque of theoretical calculation is basically consistent to the experimental result when drive shaft speed is lower than 1750r/min. But the difference between them tends to rise with the increase of drive shaft speed from 1750r/min. One of the main reasons for this phenomenon is that some factors which affect the braking torque, such as magnetic flux leakage, hysteresis loss and magnetic saturation etc, are not taken into account in order to simplify the derivation.

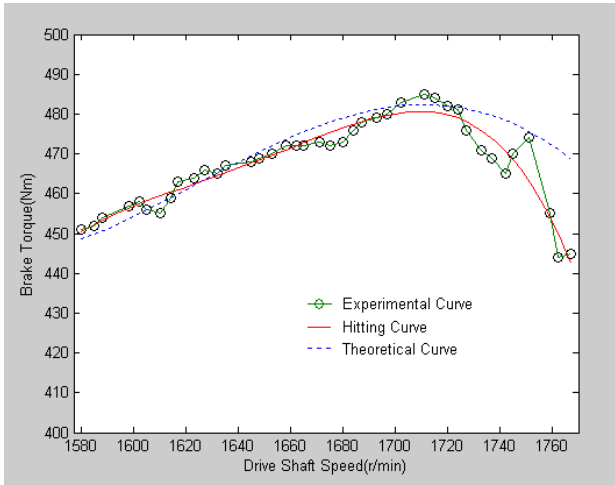

Figure 4: Braking torque curve.

CONCLUSION

The purpose of this study is to derive caculation formulae for the total braking torque from the structure parameters of a self-excited retarder. When the drive shaft speed is lower than 1750r/min, the relation between the total braking torque and the structure parameters can be precisely discribed by these formulae. So they can be taken as a reference in the design of the self-excited retarder. But further studies will be expected so as to perfect these formulae when the drive shaft speed is higher than 1750r/min.

REFERENCES

HE Ren, YI Fengyan (2006). "Evaluation method of performance characteristic of eddy current retarder[J]." *China Journal of Highway and Transport*. 19(5): 114-118.

J.M Arinescu, N.Marinescu (1988). "Numerical computation of torque in permanent magnet motors by maxwell stress and energy method[J]." *IEEE Trans On Magnetics*. 24(1): 463- 466.

LI Kaicheng, ZHANG Jianmei (2000). "Using flux method to calculate magnetic torque of permanent magnet synchronous machine[J]." *Micrimotors.Servo Technique.* 33(3): 14-15.

LIN Rongwen, JIANG Hui (2004). "Calculation of electromagnetic torque for rare earth permanent magnet synchronous motor by using FEM[J]." *Micromotors*. 37(5): 21-23.

SUN Weimin, ZHANG Yueming (2005). "A new calculation method of brake torque for eddy current retarder[J]." *Modern Machinery*. (4): 21-29.

TANG Renyuan (1997). "Modern permanent magnet machines-theory and design[M]." Beijing: *China Machine Press*.

ZHAO Kaihua, CHEN Ximou (1985). "Electromagnetics[M]." Beijing:*Higher Education Press*.

Fuzzy Control of AMT Clutch Engagement during the Vehicle Start ing

Liu Wen-guang[1] and He Ren[2]

[1]Key Laboratory of Automotive Engineering, Jiangsu University, Zhenjiang; PH (0511) 88780271-2958; email: liuzhangwang2000@163.com
[2]Key Laboratory of Automotive Engineering, Jiangsu University, Zhenjiang; PH (0511) 88780271-2958; email: heren@ujs.edu.cn

ABSTRACT

Clutch engagement process of automatic mechanical transmission is investigated during the process of starting the vehicle. The kinetics of clutch engagement is analyzed and the dynamical equation was deduced. Clutch engagement speed is changed by body load and road condition. A method of correcting the driving intention is proposed to adopt quality of vehicle conversion coefficient. The more fuzzy input parameters arouse the more control rules and increase computational load of ECU; the method of double fuzzy controller is brought forward to control speed of clutch engagement. Simulation of the model is carried out in Matlab/Simulink. Results show that fuzzy control rules with quality of vehicle conversion coefficient can effectively improve clutch engagement process.

INTRODUCTION

In the development process of automatic mechanical transmission (AMT), the key issue is to control clutch engagement[Wang Yuncheng, 2000]. Automatic mechanical transmission removes the clutch pedal and controls clutch disengagement or engagement by ECU. The clutch control rules directly affect the vehicle starting and the service life of the clutch[Qi Zhanning, 2001]. During the process of starting a vehicle a basic requirement is that the process be smooth and without interference. A clutch engagement process is affected by the load, degree of slope, engine's rotation speed, gearshift and non-linear dynamic characteristics of the clutch, time-delay characteristics of the clutch engagement, external disturbance, and time-varying factors. It is difficult to control the clutch engagement for these very reasons. All across the world, scholars have conducted research and put forward various control methods[Lei Yulong, 2000]. However, these control methods involve complicated operations or their validity and robustness falls short of need. It is also difficult to guarantee real-time capability.

Road conditions and load differ each time a commercial vehicle starts up. In order to improve a vehicle's capacity to adapt to varied load and road conditions, clutch engagement speed is modified to use the parameters of vehicle load and degree of slope. At present, the throttle opening and the throttle opening rate of change are the input parameters of the controller, but the method that the vehicle load

and the varied road environment correct the clutch engagement has not been put forward. In this paper, the quality of vehicle conversion coefficient is a parameter to correct the driving intention to improve the clutch engagement. As more input parameters increase computational load, the double fuzzy controller is brought forward. This method of using the double fuzzy controller to control clutch engagement speed decreases the vehicle jerk and the friction..

QUALITY OF VEHICLE CONVERSION COEFFICIENT ζ

When the vehicle is started, incorrect clutch engagement speed arouses vehicle jerk or increases the friction work. Quality of vehicle conversion coefficient ζ is brought forward to correct the driving intention which is the output of the fuzzy controller.

Premising quality of vehicle without load is m. Road resistance reflects the road condition when the vehicle starts. Road resistance F_φ is:

$$F_\varphi = F_f + F_i = fmg\cos\alpha + mg\sin\alpha \qquad (1)$$

Where, F_f is rolling resistance. F_i is slope resistance. f is rolling resistance coefficient. α is an angle of slope.

When α is less, $\cos\alpha \approx 1$, $\sin\alpha \approx tg\alpha = i$.

Where, i is an angle of slope.

$$F_\varphi = mgf + mgi = mg(f + i) \qquad (2)$$

When the vehicle starts, vehicle speed is low thus air resistance is ignored.

Premising quality of vehicle with load is m_1, road resistance is:

$$F_\varphi = m_1gf + m_1gi = m_1g(f + i) \qquad (3)$$

Conversion quality of vehicle m' is the ratio of road resistance and rolling resistance with load. The formula is:

$$m'gf = m_1g(f + i)$$

$$m' = \frac{f + i}{f} m_1 \qquad (4)$$

Quality of vehicle conversion coefficient ζ is the ratio of conversion quality of vehicle m' and quality of vehicle without load m. The formula is:

$$\zeta = \frac{m'}{m} = \frac{f+i}{f} m_l \Big/ m \qquad (5)$$

DYNAMIC ANALYSIS OF THE CL UTCH

The role of the clutch is power transmission during the vehicle starting and the clutch engagement process is shown in Figure 1 [He Zhongbo, 2002; Liu Haiou, 2005].

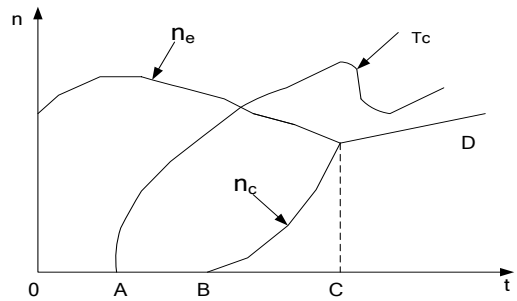

Figure 1. Clutch engagement Process.

From 0 to A, this stage eliminates the clutch idle stroke, so there is non-torque transmission. The clutch should engage as quickly as possible in this stage.

From A to B, friction is generated between the clutch master disc and the clutch slave disc. Transmission torque cannot overcome resistance torque, so the vehicle remains stationary. Considering the friction work, the clutch should engage as quickly as possible.

From B to C, the vehicle starts up because transmission torque from the clutch master disc to the clutch slaver disc can overcome resistance torque. The vehicle jerk is caused in this stage. In order to achieve smooth start-up of the vehicle, this stage should be a slowly bonding one.

Beyond C, clutch engagement speed has little effect on the friction work and the vehicle jerk because speed of the clutch slave disc has accorded with the speed of the clutch master disc. The clutch engagement should be completed quickly.

The clutch engagement dynamic model of the mathematical expression is[Luigi Glielmo, 2000; Zhao Yongsheng, 2006]:

$$J_e \dot{\omega}_e = T_e - c_e \omega_e - T_c \qquad (6)$$

$$J_v \dot{\omega}_v = T_c - c_v \omega_v - T_f \qquad (7)$$

Where the subscripts ‘e’ and ‘c’ are used for the engine and the clutch, respectively, ω_e is crankshaft angular speed (also called angular speeds of the engine)， J_e is the

moments of inertia for the engine, T_e is engine torque, c_e is damping coefficient at the engine, T_c is torque transmitted by the clutch, J_v is equivalent moment of vehicle inertia (it takes into account the presence of the clutch, the mainshaft, the powertrain and the vehicle), which will also depend on the gear ratio, ω_c is clutch disc angular speed, c_v is corresponding friction coefficient and T_f is equivalent load torque. Equation (6) models the rotation of the crankshaft, whereas (7) models the rotation of the so called clutch disk. The remaining part of the powertrain transmission system is simply modeled through the equivalent vehicle inertia J_v, and load torque T_f.

During the clutch engagement process, the dynamic characteristic of the diaphragm spring that the relationship between the load on the big end and the deformation on the small end is[Xi Gang, 2000]:

$$F_1 = \frac{\pi E\delta \ln(R/r)}{6(1-\upsilon^2)(R_1-r_1)^2}(\lambda_{11b} - k_{R1}\lambda_2)\times[(h - k_{r_1}\lambda_{11b} + k_1 k_{R_1}\lambda_2)\times (h - 0.5k_{r_1}\lambda_{11b} + 0.5k_1 k_{R_1}\lambda_2) + \delta^2] \quad (8)$$

Where R is outside radius of the diaphragm spring, r is inside radius of the diaphragm spring, E is elastic modulus, υ is poission ratio, h is inner cone higher, δ is plate thickness, R_1 is outer bearing radius, r_1 is inner bearing radius, λ_{11b} is the deformation of the big end, k_{R_1} is the ratio of the arm of force, $k_{R_1} = (R_1 - r_1)/(R_1 - r_F)$, r_F is deformation of the small end, k_{r_1} is the ratio of the arm of force, $k_{r_1} = (R - r)/(R_1 - r_1)$.

Generally the transmission torque of the dry clutch T_c is decided by the force, friction area and friction coefficient, which can be expressed as a function of the normal force applied to the clutch disk as follows:

$$T_c = z\mu F_1 R_{f,eq} \quad (9)$$

FUZZY C ONTROL OF THE CLUTCH ENGAGEMENT SPEED

Clutch engagement process is a nonlinear process. The open throttle and the road conditions embody the requirements for the vehicle start-up. The throttle opening and the throttle opening rate of change reflect the driving intention. In order to fully reflect the conditions of start-up, quality of vehicle conversion coefficient is a corrected factor to amend the driving intention which is the output of the fuzzy controller. The speciality of the fuzzy controller is the logic inference, and this simulates abstract thinking and results in a good convergence and robust capability.

With regard to the fuzzy controller, the throttle opening and the throttle opening rate of change are the subjective factors of the input parameters. The speed difference between the clutch master disc and the clutch slave disc and the speed of the clutch slave disc are objective factors of the input parameters. The speed of the clutch slave disc reflects the vehicle jerk. The speed difference between the clutch master disc and the clutch slave disc reflects the friction at work during the clutch engagement process. The fuzzy controller which possesses the two subjective factors entirely reflects the driving intention and controls the clutch engagement better. More input parameters in the single fuzzy controller cause more fuzzy rules and lead to more computational load of the single-chip. The input parameters of a single fuzzy controller have been disassembled to double fuzzy controllers. The method decreases the rules of each fuzzy controller and operator load of ECU and improves real-time capability.

It is shown that a large throttle opening leads to rapid start-up and a slower throttle opening to a slow run. The throttle opening and the opening rate of change are the input parameters of the first fuzzy controller. Controller's output reflects the driving intention.

Another fuzzy controller's input parameters have the driving intention which is been corrected by the quality of vehicle conversion coefficient, the speed of the clutch slave disc, and the speed difference between the clutch master disc and the clutch slave disc. The output is the clutch engagement speed. The clutch engagement speed has related with the vehicle jerk. In general[Qi Zhanning, 2001], the upper limit of the jerk is $10m/s^3$.

The linguistic sets of the throttle opening α are defined as[Wang Yuncheng, 2000]:

VS: Very Small, S: Small, M: Medium, B: Big, VB: Very Big.

The linguistic sets of the throttle opening rate of change $\dot{\alpha}$ are defined as:

NB: Negative Big, NM: Negative Medium, NS: Negative Small, ZO: Zero, PS: Positive Small, PM: Positive Medium, PB: Positive Big.

The linguistic sets of the driving intention I are defined as:

VS: Very Small, S: Small, M: Medium, MB: Medium Big, B: Big.

All of the speed of the clutch slave disc n_c, the speed difference between the

clutch master disc and the clutch slave disc Δn and the clutch engagement speed e have the same linguistic sets. These sets are defined as:

VS: Very Small, S: Small, LS: Little Small, M Medium, LB: Little Big, B: Big, VB: Very Big.

The normal Gauss function is adaptable to every variable membership function. The normal Gauss function reflects the change characteristic of the input parameters[Jiang Fachao, 2005]. A series of fuzzy rules are built according to the driving experience. The fuzzy inference rules of the driving intention are shown in Table 1.

Table 1 . The inference rules in t he driving intention fuzzy controller .

I	$\dot{\alpha}$						
	NB	NM	NS	ZO	PS	PM	PB
α VS	VS	VS	S	S	S	M	MB
S	VS	VS	S	S	M	MB	MB
M	VS	S	M	M	M	MB	B
MB	VS	S	M	M	MB	B	B
B	VS	S	M	MB	B	B	B

The correct value to the driving intention ω is that the quality of vehicle conversion coefficient ζ amends the value of driving intention from the first fuzzy controller. The formula is :

$$\omega = \lambda \cdot \mathrm{I} / \zeta \qquad (10)$$

Where, λ is coefficient.

Another fuzzy controller's input parameters are the correct value to the driving intention, the speed of the clutch slave disc and the speed difference between the clutch master disc and the clutch slave disc. The fuzzy rules are:

if ω=VS and n_c=VS and Δn=VS then e=VS

if ω=VS and n_c=VS and Δn=S then e=VS

⋮

The fuzzy algorithm of the clutch engagement adopts product way. The different input parameters operate the different output. The diagram of fuzzy control system is shown in Figure 2.

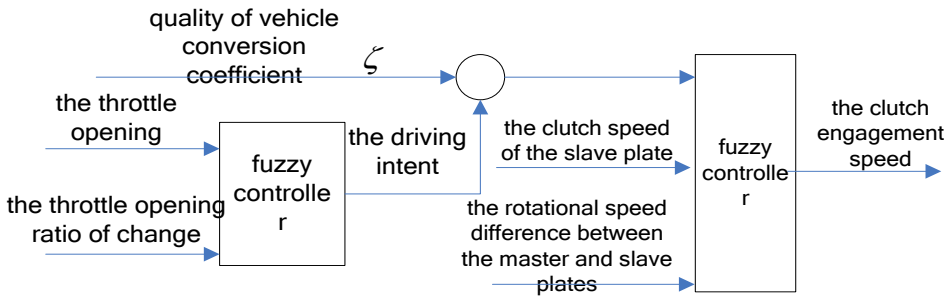

Figure 2. Diagram of fuzzy control system .

PID CONTROL OF THE CLUTCH ENGAGEM ENT PROCESS

Because the arithmetic power of ECU is limited and more fuzzy control rules increase operator load of ECU, the PID control method is adopted in this paper.

PID control method making use of proportion, integral, and differential calculates the system error to control the object. Proportional coefficient k_p rapidly takes response system change to output and effectively overcomes the effect of disturbance. The differential coefficient k_D reduces the steady-state error by correcting the accumulated error after the system stabilizes. The integral factor k_I reduces the overtop time and accelerates the system's response speed.. PID controller's equation is:

$$u_k = u_{k-1} + \Delta u_k \qquad (11)$$

$$\Delta u_k = k_p(e_k - e_{k-2}) + k_I e_k + k_D(e_k - 2e_{k-1} + e_{k-2}) \qquad (12)$$

where: $e_k = y_k - p_{k+1}$

RESULT OF SYSTEM SIMULATION

When the vehicle starts up on the upward slope, the system simulation based on all above control algorithms is conducted. The results of system simulation are shown in Figure 3. and Figure 4.

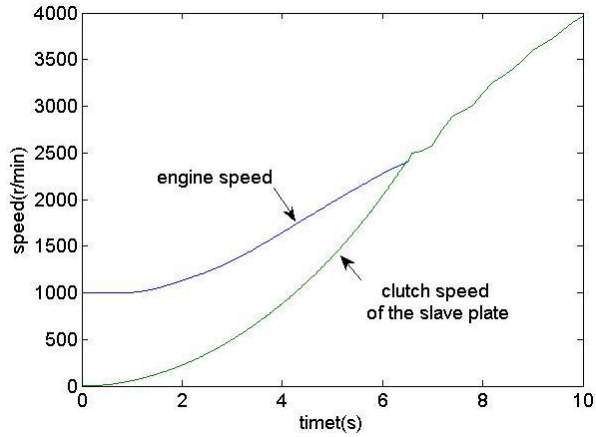

Figure 3. Clutch engagement without the vehicle mass conversion coefficient.

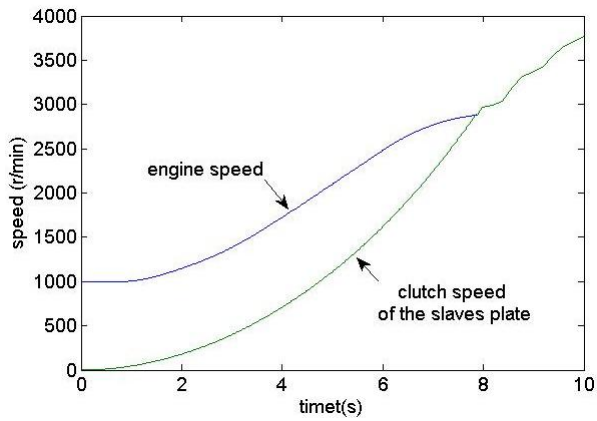

Figure 4. Clutc h engagement with the vehicle mass conversion coefficient .

Figure 3 shows the clutch engagement process without quality of vehicle conversion coefficient. The ECU does not correct the engagement speed in accordance with external condition changes and this causes a great jerk. Figure 4 shows the clutch engagement process with quality of vehicle conversion coefficient. The clutch engagement speed is confirmed by the subjective factors and the external condition. The driver's driving intention are thus fulfilled.

CONCLUSION

Quality of vehicle conversion coefficient reflects the load of the vehicle and the road conditions, which corrects the output parameter of the fuzzy controller. The fuzzy control method is adopted to control the clutch engagement speed. A larger number of input parameters in the single fuzzy controller cause the multiple number of fuzzy rules. The more rules lead to an increase in computation. The method used in this paper can decrease the number of fuzzy rules. The speed of the clutch slave disc is one of the input parameters of fuzzy controller. The result of simulation is good and meets the start-up demand of the vehicle and improves overall comfort.

RE FERENCES

He Zhongbo, Li Gouzhang, Zhang Peilin, Rao Jinsong, and Xi Junqiang. (2002). "Experimental study of clutch half joint in the starting process." Issues in Journal of Ordnance Engineering College, 14(2), 43-47.

Jiang Fachao,Chen Quanshi, and Cao Zhengqing (2005). "Optimal control of automated mechanical transmission clutches." Issues in Tsinghua Univ (Sci &Tech), 45(2), 242-245.

Lei Yulong, Niu Mingkui, and Ge Anlin. (2000). "A Research on Starting Control Strategy of Vehicle with AMT." Seoul 2000 FISITA World Automotive Congress. 1-4

Liu Haiou，Chen Huiyan，Ding Huarong, and He Zhongbo.(2005). "Adaptive clutch engaging process control for automatic mechanical transmission." Issues in Journal of Beijing Institue of Technology,14(2), 170-174

Luigi Glielmo, Francesco Vasca. (2000). "Engagement Control for Automotive Dry Clutch." Issues in Proceedings of the American Control Conference Chicago, Illinois, 1016-1017

Qi Zhanning, Chen Quanshi, and Ge Anlin. (2001). "Fuzzy Control of the AMT Vehicle's Starting Process Based on Genetic Algorithm." Issues in Chinese Journal of Mechanical Engineering, 31(7), 8-11.

Wang Yuncheng, Shi Guobiao, Wang Wangyu and Yu Haitao. (2000). "Fuzzy Control of Clutch in Automated Mechanical Transmission System during Starting a Vehicle." Issues in Transactions of the Chinese Society for Agricultural Machinery, 31(6), 32-35.

Xi Gang, Zhang Jianwu, and Chen Li.(2000) "Nonlinear Control of Membrane Spring Clutch." Issues in Chinese Journal of Mechanical Engineering, 36(9), 98-102

Yongsheng Zhao, Liping Chen, and Yunqing Zhang. (2006). "Enhanced Fuzzy Slideing Mode Controller for Automated Clutch of AMT Vehicle [J]."SAE Pape, 2006-01-1488

Ration effect on rheological and combustion properties of coal -oil--water slurry

Zhang Qiang[1,2], Tian Ying[1,3], and Tian Da-feng[3]

[1] College of Mechanical Engineering, Liaoning Technical University, Fuxin, 123000, China.
[2]State Key Laboratory of Structural Analysis for Industrial Equipment, Dalian University of Technology, Dalian 116023, P.R.China.
[3] Fuxin Miming Company, Fuxin,123000, China.

ABSTRACT

This paper selects a suitable dispersant and emulsifier to prepare an oil base coal-oil-water slurry of Fuxin coal and Datong coal, studies a three-phase (oil, water, coal) ratio to the influence of rheological properties, and discussed combustion characteristics. The test result indicated: At 35% oil in the oil base coal-oil-water slurry belongs to Herschel-Bulkley fluid; at 30% oil belong to bulge plastic fluid. In other words the lower the oil content the higher the C/W proportion and viscosity. The coal-oil-water slurry caloric value drops along with the W/O proportion rise and W/C proportion drop. Under the identical shear rate, the apparent viscosity of Fuxin coal is bigger than the Datong coal. Under the same mass concentration, the combustion ash of Fuxin coal is lower than the Datong coal. Coal-oil-water slurry is thus found to have good combustibility and combustion efficiency and it is an industrial fuel prospect.

INTRODUCTION

The water-coal-slurry mixture which is composed of few chemical additives (approximately 0.5%-1%), 60%-70% powdered coal, and 30%-40% (Yu. et al. 2006) water is an ideal substitution fuel with low pollution, high efficiency, and is a strong fluid fuel. (YU et al.2003, ZOU et al.2006) The coal type, the chemical property, the grain shape and the grain-size distribution, the chemical additive composition, the pulping craft, the temperature and some factors which thick liquid density and affect the rheological properties..This article mainly studies 3 raw materials' (coal, oil, water) ratio to rheological properties and flammable influence by oil base water-coal-slurry (GU et al.1996, A TESO K G et al.2002, GUO et al.2005).

EXPERIMENT

Raw material and instrument

Fuxin coal（coal granularity <331μm is in proportion of 100%，coal granularity <31μm is in proportion of 53.88%，coal granularity <2μm is in proportion of 3.56%, M=5. 14，A=12. 20，V=29. 28，FC=53. 38). The ash is 5.09%; the calorific value is 31.48MJ/kg；Datong coal (coal granularity <331μm is in

proportion of 100%, coal granularity <31μm is in proportion of 59.78%, coal granularity <2μm is in proportion of 4.98%, M=2. 43, A=7. 13, V=34. 20, FC=56. 24). The ash is 10.2%, the calorific value is 33.28MJ/kg、0 diesel oil, chemical additive (alkyl phenyl polyethyleneoxide ether). 510 Fourier infrared spectroscopes, NXS-11 rotational viscosimeter, GR3500 oxygen bomb type calorimeter instrument.

Experimental Technique

The chemical additive is added to the diesel oil and take water to make oil base water. The Fuxin coal (Datong coal) is then placed under high speed agitation thus preparing the Fuxin coal (Datong coal) oil base water-coal-slurry.

1) According to proportion of coal: Water=1: 1, changes the oil content respectively is 30%, 35%, 40%, carries on the viscosity test to the Fuxin coal (the Datong coal) , make the rheological property curve.

2) Oil 40% invariable, the change internal phase coal and water proportion respectively is 3:2,2:3,1:4, carries on the viscosity test to them, make the rheological propertyless curve.

3) To prepares six kind of oil base water-coal-slurry by step 1 carry on the calorific value and combustion test,

4) To prepares six kind of oil base water-coal-slurry by step 2 carry on the calorific value and combustion test,

EXPERIMENTAL RESULTS

Influence three -phase ratio rheological property

Oil affects

The oil base water-coal-slurry of Fuxin coal (Datong coal) the viscosity and the shear rate relations see Figure 1 (Figure 2), From Figure 1, 2 we can see water-coal-slurry big change along with oil content change. the yield stress increases,along with the oil content reduction, the oil base water-coal-slurry transfers to pseudo-plastic fluid, when the oil content is 30%, two kind of oil base water-coal-slurry transforms into the bulge bingham fluid, then the yield stress increases rapidly, because COWS is the key of coal grain suitable stable three-dimensional structure. This kind of hydromass will certainly to have a high viscosity and static stability. The hydromass the rheological propertyless had along with the oil quality percentage drop, the hydromass present submits -pseudo-plastic, when the oil content drops more, causes the hydromass viscosity to increase and forms the bulge bingham fluid.

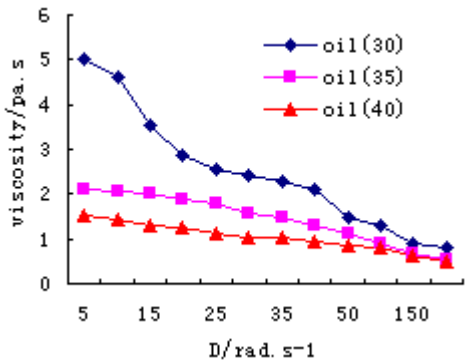

Figure 1. Viscosity curve at C_F /different oil .

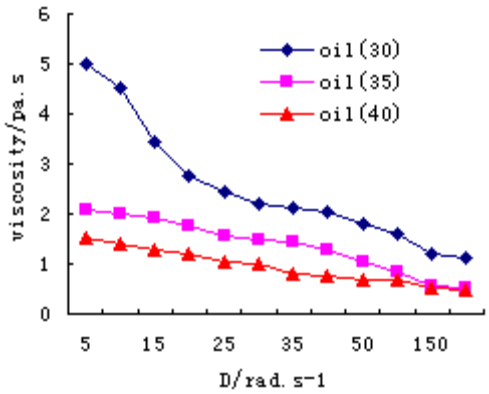

Figure 2. Viscosity curve at C_D /different oil .

Coal-water scale effect

From Figure 3, 4 we can know, the performance viscosity is increasing along with coal water proportion increase, the coal water proportion is higher, increases scope to be bigger. The water-oil -slurry is the typical pseudo-plastic fluid, the coal-oil -slurry is the typical bingham fluid, but oil- water-coal -slurry is pseudo-plastic fluid, the yield stress is reduces, then tends to be stable along with coal water proportion enlargement, the system deviates the plastic flow pattern to become submits - pseudo-plastic fluid.

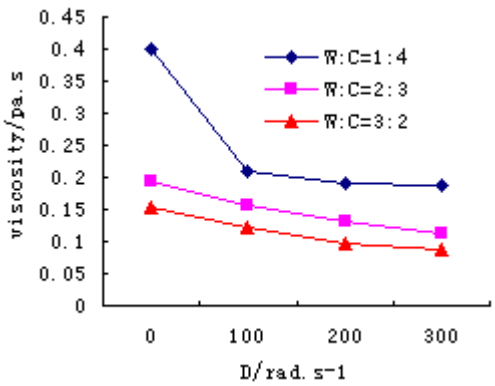

Figure 3. Viscosity curve at C_F/W

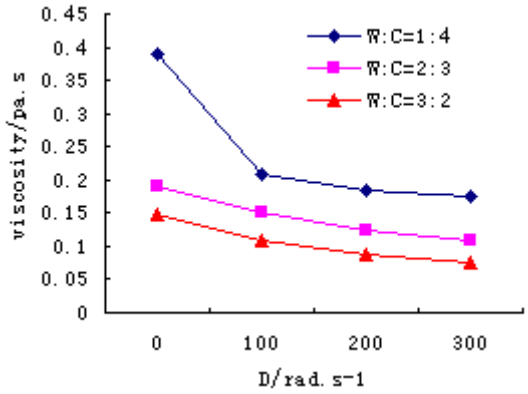

Figure 4. Viscosity curve at C_D/W

Influence flammable of three -phase ratio

Oil-water ratio effect

From Figure 5 we can see, when the coal content maintains is invariable, system calorific value reduces along with incompatible ratio increase, because the oil low heat value is bigger than water, the oil quality score influence system calorific value drops; But identical incompatible ratio, the Datong coal preparation calorific value is oil-water –slurry bigger than Fuxin coal preparation, because Datong coal low heat value is bigger than Fuxin coal.

Coal water scale effect

We can see from Figure 6 , when the oil content is invariable, system calorific value increases along with water coal ratio increase, because coal low heat value is bigger than water, the Datong coal-slurry calorific value is bigger than Fuxin coal-slurry. From Figure 5, 6 we know: the coal and the oil relative quantity were mainly the combustion calorific value, the water has not affected nearly to the system calorific value, two kind of anthrax calorific value were difference, the Datong coal calorific value is bigger than Fuxin coal under the identical condition, because the Datong coal low heat value is higher than Fuxin coal.

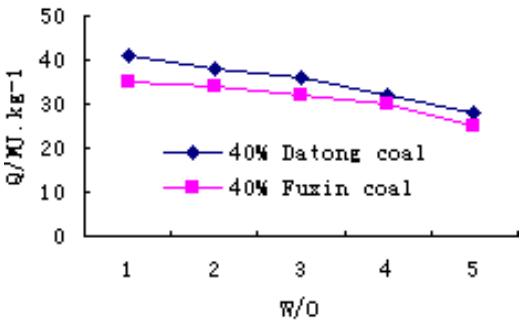

Figure 5. Heat curve at O/W

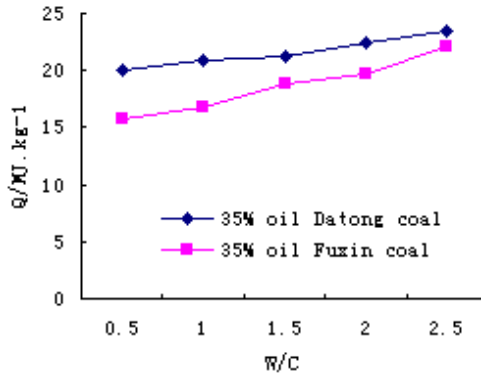

Figure 6. Heat curve at C/W

Coal ash affects

From Figure 7, 8 : Under on the same scale and quality fuel burning condition, the Datong coal ash is bigger than Fuxin coal, It is related with the preparation coal itself ash content ,It is not related with the temperature and the oil-water proportion .

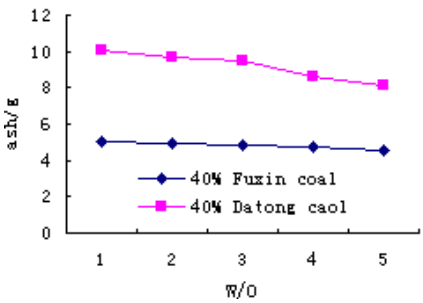

Figure 7. Gradation cur ve at O/W

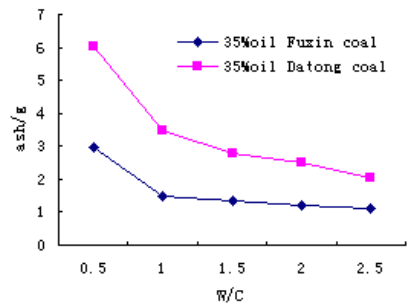

Figure 8. Gradation curve at C/W

CONCLUSIONS

1) The coal-oil-water slurry caloric value drops along with the W/O proportion rise and W/C proportion drop, the herschel-bulkley fluid change to bulge plastic fluid.

2) Under the identical shear rate, the apparent viscosity of Fuxin coal is bigger than the Datong coal; under the same mass concentration, the combustion ash of Fuxin coal is lower than the Datong coal.

REFERENCES

A TESO K G, BO YLU F, S IRKEC IA A, and D INCER H. “The effect of coal properties on the viscosity of coal-water slurries.”[J]. Fuel, 2002, 819~823

GU YDW, CRAW FORDRJ, and MA INWAR ING D E. “The wetting behavior of several organic liquids in water on coal surfaces.” [J].Fuel,1996,75(2): 238~242（in Chinese）.

GUO Yang-hong , WANG Wei-zhou , and ZHANG Dong-liang .”Effect of three-phase ratio on rheological and combustion properties of coal-oil-water slurry.” [J]JOURNAL OF XI AN UNIVERSITY OF SCIENCE AND TECHNOLOGY2005.24（5）：517~520（in Chinese）

YUCHIWei, L I B ao-qing, and L IW en. “Effect of pore structure on the properties of coal water slurry.” [J]. Journal of Fuel Chemistry and Technology, 2006, 34 (1): 529~535（in Chinese）.

YUCH IWei, L I Bao-qing, and L IW. “Effect of mcerals on the properties of coal water slurry.” [J]. Journal of Fuel Chemistry and Technology, 2003, 31 (5) : 415~419. （in Chinese）

YUCHIWei, LI Bao-qing, and L IW en. “Study on the properties of coal water slurry prepared with different coal ranks.” [J].Journal of Fuel Chemistry and Technology, 2005, 33 (2) : 156~160.

ZOU Li-zhuang, ZHU Shu-quan, and WANG Xiao-ling. “Study on the interaction between different CWS dispersants and coal:Ⅺ Interface properties of dispersant2modified coal particles and its effect on the properties of CWS.” [J]. Journal of Fuel Chemistry and Technology, 2006,34(2) :160~165.（in Chinese）

ZHU Shu-quan and ZHAN Long. “Study of slurry ability of the Chinese coal.”[J] . Journal of China coal society,1998, 23(2):198~201. （in Chinese）

YUCHIWei, LI Bao-qing, and L IW en. “Study on the properties of coal water slurry prepared with different coal ranks.” [J].Journal of Fuel Chemistry and Technology, 2005, 33 (2) : 156~160.

Research on the 25kW FCPS's Temperature Controlling Simulation

Hou Xianjun[1], Gui Wengang[2], Jin Xue[3], and Pan Mu[4]

[1]School of Automobile Engineering, Wuhan University of Technology, Campus Box 32, Wuhan 430070,China; PH:027-87850553; FAX:027-87658437; email:houxj@whut.edu.cn
[2]School of Automobile Engineering, Wuhan University of Technology, Campus Box 32, Wuhan 430070, China; PH:027-87850553; FAX:027-87658437; email:guiwengang@163.com
[3]School of Automobile Engineering, Wuhan University of Technology, Campus Box 32, Wuhan 430070, China; PH:027-87850553; FAX:027-87658437; email:jinxue19841007@126.com
[4]Stake Key Laboratory of Advanced Technology for Materials Synthesis and Processing, Wuhan University of Technology, Campus Box 32, Wuhan 430070, China; PH: 027-87651837; FAX: 027-87879468; email:panmu@whut.edu.cn

ABSTRACT

A simulation model about the temperature controlling system of 25kW fuel cell power system(FCPS) which was analyzed by MATLAB/SIMULINK was built. This generates a control variable by the fuzzy control method to drive the radiator fan operating at different speeds in experiment, in order to make the FCPS work in optimal temperature state, and is stabilized at 63℃. This verifies the accuracy of the simulation analysis.

INTRODUCTION

As a green energy technology, the fuel cell technology is dominant in energy saving and environmental since it uses renewable energy-Hydrogen and realizes zero-emission. The proton exchange membrane fuel cell (PEMFC) is the most widely used of all existing fuel cell technologies. But the efficiency of fuel cell is about 50%, which means output power equals to heat dissipation. Thus the heat dissipation of PEMFC power system is very huge and is about 2-3 times that of an internal combustion engine exhaust heat. Due to the temperature sensitivity of the proton exchange membrane, the performance of fuel cell is badly affected by temperature. In low temperatures, the polarizations of fuel cells are increased and ohm impedance is bigger, which makes causes deterioration in performance. When the temperature rises, it will reduce ohm impedance, reduce polarization, and improve the speed of electrochemical reaction as well as the rate of proton transferrance in the membrane. This will result in better performance. When the

temperature is too high, the membrane activity reduces，and the performance level falls once again(Li Zhonghua 2007). At the same time, to make sure the temperature of fuel cell is well distributed, the temperature difference of the coolant's inlet and outlet should be no more than 10℃, the optimum being 5℃. Because of the low temperature of heat dissipation of fuel cell, the cooling system is in high demand (Hu Yunyu 200). Recently, there has been much research conducted in the area of fuel cell system models and control methods. For example, Geyer H K and Ahluwalia R K have invented a computer simulation tool, GC, which can be used for designing and analyzing the fuel cell system model. But there are only a few dynamic models of fuel cell system(Geyer H K 1998); Wohr M and Amphlett J C have researched on dynamic response of temperature (Wohr M 1998, Amphlett J C 1996); Pathapati P R has presented an integrated dynamic model of fuel cell system, whose model takes the transformation of fuel cell temperature, fluid influx of channel, and the influence of double-layer charge into account, and is realized in SIMULINK (Pathapati P R 2005). The control methods of fuel cell include traditional control, predictive control, fuzzy contro,l and neural network control .

25KW FCPS TEMPERATURE CONTROLLING MODEL

System structure model

The object of FCPS temperature control is the working temperature of the fuel cell stack. The executing mechanism includes water pump, radiator, fan, etc and water is the medium. The working principle is cooling water takes heat from fuel cell by cooling water pump, then transits through the water tank, and exchanges heat with air by fan in order to control the temperature of the stack. In this paper, owing to the huge dissipation heat of FCPS, two radiators are used, and each has its own fan. The cooling water pump is held working at a certain rotating speed keeping the water flux constant. The speed of the fan is adjusted to control the wind flux to finally control the temperature. The structure of FCPS temperature controlling system refers to **Figure 1**. The simulation model of FCPS temperature controlling system refers to **Figure 2**. It includes a fuel cell stack submodel, radiator submodel, water tank, and conduit submodel as well as a control unit submodel.

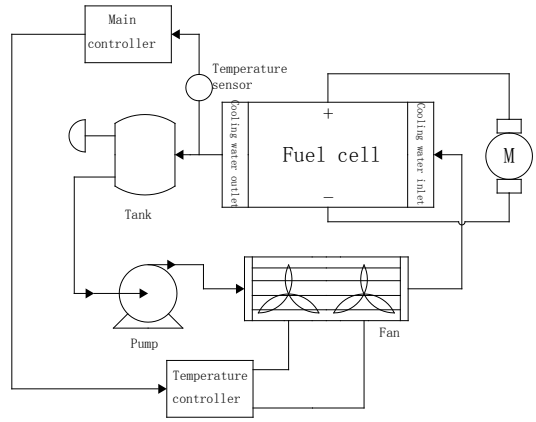

Figure 1. Structure of FCPS temperature controlling system.

The simulation model of FCPS temperature controlling system is based on the following parameters (see **Table 1**).

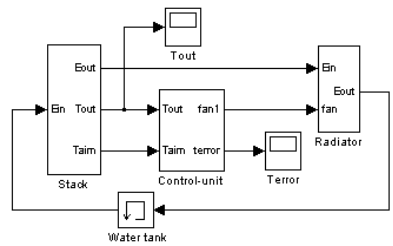

Figure 2. Simulation model of FCPS temperature controlling system.

Table 1. Parameters of PCPS temperature controlling system's simulation model.

Net output power of stack (kW)	Radiator length× width× thickness （mm×mm×mm）	Radiator pipe size length× width （mm×mm）	Cooling area of radiator （m^2）	Rated current of fan （A）
25	570×380×26	26×2	8.58	25
Rated voltage of fan （V）	Flux of water pump （L/min）	Ambient air temperature （℃）	Ambient water temperature （℃）	Total volume of cooling water (L)
12	170	25	20	25

Approaches of heat loss

The working principle of fuel cell stack is to convert the chemical energy of fuel (hydrogen) and oxidant (oxygen or air) to electricity directly by electrochemistry reaction, consume reactant, discharge outcome and release heat. The chemical reaction is:

$$H_2 + \frac{1}{2}O_2 \xrightarrow{Ele+Heat} H_2O$$

Fuel cell has three ways of discharging waste heat △Q: eradiation of fuel cell, water vaporization dissipation inside fuel cell, and discharging by circulating water. Reactant gas of fuel cell will bring in and take away some heat, but it can be ignored due to the slight difference between inlet and outlet temperature and the small heat capacity of gas. Analysis has shown that the waste heat of fuel cell is mainly taken away by water circulation $\triangle Q_{cool}$, occupying 90% of the gross. Eradiation and vaporization heat dissipation share little(Yan Fuwu 2005). To put the margin of heat dissipation in the design, the model could be simplified as: $\triangle Q=\triangle Q_{cool}$.

Stack model

According to the above analysis, we know that the heat dissipation and the electricity of stack export as 50% severally, the waste heat is taken away by circulation water only. So through a set of experiment data, we get a current (A) - power (W) curve of 25kW FCPS (see **Figure 3**). We then build a Look-up Table model in MATLAB/SIMULINK. After importing a time-current signal we can get a time-power signal, which is equivalent to time-heating power signal, namely an export E_{out} of the stack model. We can conclude the target working temperature based on the time-current data. Hold the rotating speed of water pump and the quality of cooling fluid at a constant. Control outlet temperature to 50℃ when current is under 110A, control outlet temperature to 58℃ when it is between 110-130A and control outlet temperature to 63℃ when it is over 130A. In this way it can reduce another export T_{aim} of the stack model. The stack model is shown in **Figure 4**.

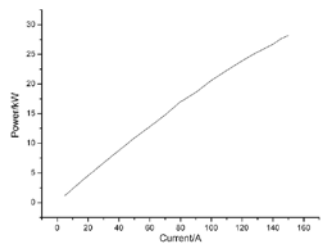

Figure 3. The Current-Power curve of 25kW FCPS.

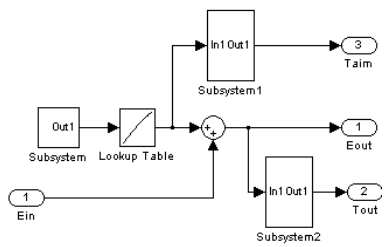

Figure 4. Stack model.

Radiator model

The heat taken away by the cooling system Q_{cool} is dissipated through the radiator, which means that $Q_{rad} = Q_{cool}$. Pump should have enough displacement and pressure in order to provide enough cooling water. At the same time, ensure enough air passes through the radiator to take the heat away when cooling water passes through the radiator. This can be computed as: $Q_{cool} = C_a \cdot \rho_a \cdot V_a \cdot \triangle t_a$.

Here C_a is specific heat of air, ρ_a is air density, V_a is flux of cooling air entering the radiator and equals the product of wind speed and positive area of radiator. In other words the fan should provide enough air. $\triangle t_a$ stands for the temperature difference between atmosphere and the one passed through the radiator, $\triangle t_a = T_{air,\ out} - T_{atm}$.

At the same time, heat dissipation of radiator is in direct proportion to air flux and temperature difference. That is: $Q_{rad} = K_{rad} A_{rad} (T_{rad} - T_{air})$.

Here K_{rad} is the heat transfer coefficient of the radiator; A_{rad} is the heat dissipation area of radiator; T_{rad} is the average temperature of cooling water in the radiator and is expressed by the arithmetic mean of inlet temperature $T_{rad,\ in}$ and outlet temperature $T_{rad,\ out}$. T_{air} is average temperature of cooling air and is expressed by arithmetic mean of ambient temperature T_{atm} and outlet temperature of cooling air $T_{air,\ out}$ (Yang Liansheng 1981). During the process of building the radiator model, we set the cooling water flux as fixed value. It means that the cooling water pump runs at a constant rotating speed. **Figure 5** shows the radiator model.

Tank and conduit model

Some heat is taken away by tank and conduits, so there is a certain temperature difference between the cooling water inlet and outlet. Cooling water flowing in the conduit also brings transmission delay. According to the law of thermodynamics we can build a simple tank and conduit model. But the heat taking away by the tank and conduit is limited, affects the whole model very little, so the model can be simplified (Gu Jing 2007). THeSpecific model is shown in **Figure 6**.

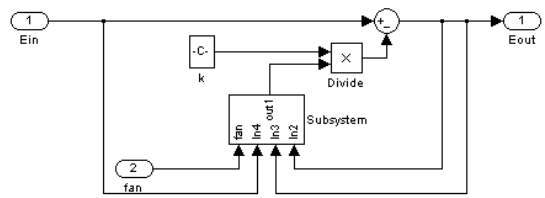

Figure 5. Radiator model.

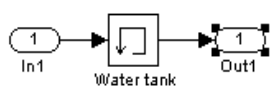

Figure 6. Tank and conduit model.

Control unit model

For the FCPS temperature control, the mathematical model and control parameters are not easy to determine accurately, but we can use fuzzy inference control. **Figure 7** shows the chart of control unit principle.

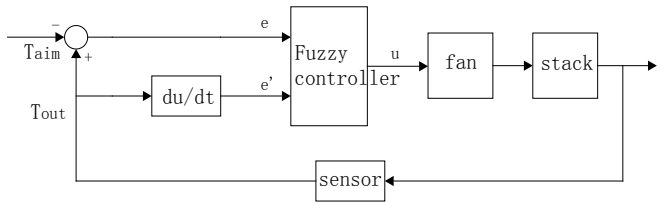

Figure 7. The chart of control unit principle.

In **Figure 7**, e expresses the difference between outlet temperature and target temperature. e' expresses the gradient change of outlet temperature.

The FCPS's temperature control is set according to experience. The experience -control method not only wastes resources but also cannot gain a high level of control. The FCPS fuzzy temperature control system built in this paper is based on multivariate fuzzy inference theory and FCPS experiment data. It can build wind speed (or fan rotating speed), basic rule, and control experience repository. We just need to modify the control algorithm of the module and verify the validity of the control algorithm by simulation. The model takes the target temperature and actual export temperature as input value. After dealing with input value, it produces an error signal and changes the rate of control objective separately. The model exports opening signal of cooling fan (in this simplified model, wind speed is exported) after fuzzy control calculation. Export signal Terror is the error of actual temperature and target temperature, just for observation. The control unit model refers to **Figure 8**.

SIMULATION ANALYSIS AND EXPERIMENTAL VERIFICATION

The paper gives a time-current signal as is shown in **Figure 9**. Dash dot line in **Figure 10** is target temperature controlled curve according to a Time-Current curve. Import a time-current signal to stack model, then simulate in SIMULINK and we get a simulation temperature curve shown as the solid line in **Figure 10**. Take the fan rotating speed which was gained in simulation model for reference to do experiment, and we can gain the experiment temperature curve. This is shown as the broken line in **Figure 10**.

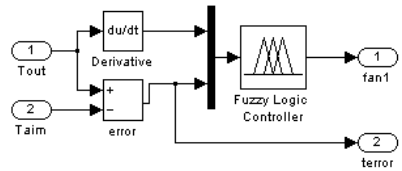

Figure 8. Control unit model.

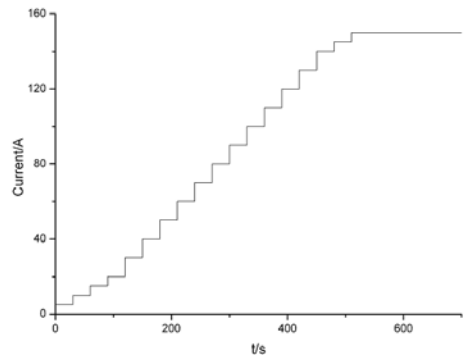

Figure 9. FCPS Time-Current signal.

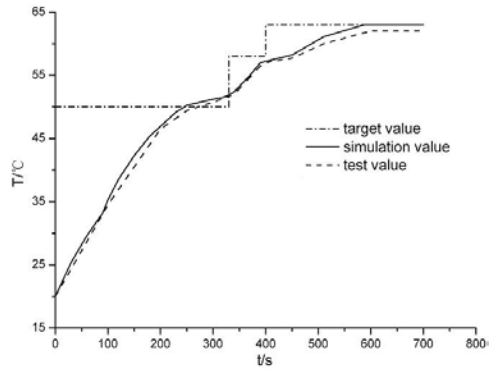

Figure 10. Target value, simulation value, test value's temperature curve.

From **Figure 10** we can see that, in simulation analysis, the temperature of the stack is low when the fuel cell starts working, so we do not control the fan. With the electrochemical reaction of fuel cell, temperature goes up. When the current works on 80A(270s), we start to control the fan and control stack temperature at 50℃. When the current is between 100~130A(330~450s) we control temperature at 58℃. When current has stopped transmitting 130A(450s), we keep the fan speed at maximum, and finally hold the temperature at a steady 63℃. In the experiment, the temperature is controlled and balanced at the three phases of target temperature and finally stabilized at 62℃. By comparing the temperature curve which was controlled by the experiment with that of simulation, we find that the model temperature is consistent on the whole with the experiment-controlled temperature curve. There are

some differences, the main reason being that temperature has a huge inertia and lag, and is greatly affected by ambient temperature.

CONCLUSION

The paper establishes simulation model of FCPS temperature controlling system. It includes fuel cell stack submodel, radiator submodel, water tank & conduit submodel as well as control unit submodel. It also simulates and analyzes 25kW FCPS's temperature controlled under the multivariate fuzzy inference theory by MATLAB/SIMULINK, and uses the results for experiment controlling. Finally we find that the experiment temperature curve is consistent with the simulation temperature curve on the general trend, and finally stabilizes at 62℃. It verified the validity of the control algorithm. The simulation analysis can provide reference for experiment research, reduce experiment task, and will play an important role in the design of FCPS.

REFERENCE

Amphlett J C, Mann R F (1996). "*A model predicting transient responses of proton exchange membrane fuel cell.*" Journal of Power Sources, (61),183- 191.

Geyer H K, Ahluwalia R K (1998). "*GC tool for fuel cell system design and analysis: user Documentation*." Argonne National Labs, Report No. ANL -989.

Gu Jing, Lu Languang, Ouyang Minggao （2007）."*Thermal management subsystem model and temperature control for fuel cells*,". Journal of Tsinghua University(Science and Technology), Vol. 47 (11) :2036 - 2039. (in Chinese)

Hu Yunyu, Zhang Yuancai (2006) "*Thermal and water Management method of proton exchange Fuel Cell Engine for Vehicle*." Shanghai Auto,(4) :3-5. (in Chinese)

Li Zhonghua, Du Chuanjin, Hou Xianjun (2007) "*Thermal management for proton exchange membrane fuel cells*.".East China Electric Power, Vol. 35 (2):19 -22. (in Chinese)

Pathapati P R, Xue X, Tang J (2005). "*A new dynamic model for predicting transient phenomena in a PEM fuel cell system*." Renewable Energy, (30) : 1 - 22.

Wohr M, Bolw I K (1998). "*Dynamic modeling and simulation of a polymer membrane fuel cell including mass transport limitation*." International Journal of Hydrogen Energy, 23(3) :213 - 221.

Yan Fuwu, Li Xiaoyi, Xiao Helin(2005). "*Calculation and Finite Element Analysis on Water-Heat Management System For Fuel Cell Engine*." Automobile Technology & Material, (1):3 - 6. (in Chinese)

Yang Liansheng. (1981) "*Internal combustion engine design*." China Agriculture Mechanical Press, 437 - 445. (in Chinese)

Study on Energy Consumption by Land Cargo Transportation

Huang Shunquan[1], Yu Siqin[2], and Liu Zhongmin[3]

[1]Shanghai Maritime University, 1550 Pudong Avenue, Shanghai China, ST 200135; PH (86-21)28842865; FAX (86-21)58606090; email: sqhuang@163.com
[2]Shanghai Maritime University, 1550 Pudong Avenue, Shanghai China, ST 200135; PH (86-21)68553541; FAX (86-21)68553541; email: ysq@shmtu.edu.cn
[3]Shanghai Maritime University, 1550 Pudong Avenue, Shanghai China, ST 200135; PH (86-21)58855200-4201; FAX (86-21) 68553541; email: jmx@shmtu.edu.cn

ABSTRACT

As a key component of the Tertiary Sector, transportation consumes more and more energy and its consumption, which grows more rapidly as time goes by, takes up more than half of those consumed by the tertiary sector. Over half of which are being consumed by transportation by land, making it a giant consumer of energy. However, no dedicated research has been made so far on energy consumption by land cargo transportation as a primary problem and no specific data collection system on energy consumption by the sector has been worked out in the nation.

This paper builds a multivariable linear regression model, taking into consideration energy consumption by land cargo transportation and its underlying causes, and taking statistics by land cargo transportation enterprises as samples. Through analysis, the paper finds out what the most important causes are and to what extent the influence can be, discovering the key issue and most difficult part in energy saving and consumption reducing.

Transportation, as an essential contributor to rapid economic growth, is highly and closely related to economic development, and its output has been taking an increasingly larger share in the nation's gross national product, for it is a very important sector in our country's national economic system. (Energy Information Administration 2006) In addition, it is also essential to modern transportation system and logistics system, playing a major role in our nation's transportation system. Since road transportation vehicles are the largest energy consumers among motor vehicles, improving energy consumption efficiency and saving energy have great role to play in China's energy safety, environmental protection and the sustainable development of economy and society (Samaras et al.1999).

As energy is relatively scarce and non-renewable, energy saving and improving energy utilization efficiency becomes an important principle in energy consumption (Schipper et al.1993). According to the 11th Five-year Plan, China's energy consumption per unit GDP shall decrease by 20 percent at the end of the period, which makes studies on energy consumption a tough task in monitoring energy consumption (Environmental data compendium 1995). Since the methods and means that have been used to collect information concerning energy consumption in road transportation can not be applied to analyzing energy consumption by current land cargo transportation, reliable data can not be collected cost-efficiently, making it impossible for enterprise to collect information and control energy consumption in a scientific way. As a result, how to solve above-mentioned problem becomes the most

important and most difficult task in finding solutions to energy saving in China. This paper thinks analyzing and conducting research on energy consumption by land cargo transportation and establishing a scientific, simple and practicable data collecting model on energy consumption is essential to coming up with a solution to energy saving and consumption reduction for cargo transportation by land.

ESTABLISHMENT OF MODELS

Since there are few approaches by which people can get information on energy consumption by road transport industry or road transport enterprises, statistics collected are incomplete and it's also very difficult to obtain complete data. Thus relevant indicators are not available, including those on turnover and transport capacity by cargo vehicles and passenger vehicles using different fuels, making the analysis more difficult. This paper discusses road transport vehicle's energy consumption structure, influencing factors and its extents by establishing a regression model with statistics collected on 79 vehicles from a road cargo transport enterprise. This enterprise is a large-scale port logistics company in Shanghai, which has a strong representation in the field of container road transport in China.

RESEARCH APPROACHES

This paper adopts the approach of stepwise regression analysis with SPSS software. In statistics, stepwise regression includes regression models in which the choice of predictive variables is carried out by an automatic procedure. The specific approach is to introduce variables one by one until no significant variables can be selected or removed by the regression equation. The introduction of a variable or removed a variable from the regression equation is a step of stepwise regression. Every step must be tested to ensure that each time the regression equation contains only significant variables before the introduction of a new variable. Usually, this takes the form of a sequence of F-tests (He Xiaoqun 1998).

MODEL OF TOTAL OIL CONSUMPTION BY VEHICLES

With SPSS software, this paper makes a detailed stepwise regression analysis of total oil consumption (y_1) and its seven key influencing factors, including mileage (x_1), the number of goods carried (x_2), cargo weight (x_3), loaded one-way trip mileage (x_4), carrying rate (x_5), whole-trip kilometers utilization rate (x_6) and the age of vehicles. Through a series of tests and optimization, a multivariable linear regression model for total oil consumption and its seven key influencing factors can be found:

$$y_1 = -3.566 + 0.331x_1 + 0.807x_3 + 0.031x_4 - 0.513x_6 + u$$

MODEL OF OIL CONSUMPTION PER 50 KILOMETERS BY VEHICLES

With SPSS software, this paper also makes a detailed stepwise regression analysis of total oil consumption per 50 kilometers (y_2) and its seven key influencing factors, including mileage (x_1), the number of goods carried (x_2), cargo weight (x_3), loaded one-way trip mileage (x_4), carrying rate (x_5), whole-trip

kilometers utilization rate (x_6) and the age of vehicles. Through a series of tests and optimization, a multivariable linear regression model for total oil consumption per 50 kilometers and its seven key influencing factors can be written as follows:

$$y_2 = 34.452 + 0.115x_3 - 0.086x_5 + u$$

ANALYSIS OF INFLUENCING FACTORS

As we can see from the models, the most important factors that pose great influence on total oil consumption by road cargo transport vehicles are mileage, cargo weight, mileage of loaded one-way trip, and kilometers utilization rate. According to the parameters' signs in these models, we find that the coefficient signs for kilometers utilization rate are negative, indicating that the higher the kilometer utilization rate, the lower the oil consumption, thus the higher oil utilization rate. Likewise, the higher the kilometers utilization rate, the higher the loaded mileage in proportion to the whole trip, and the lower the deadhead mileage in proportion to the whole trip, the more efficiently the energy is utilized. Therefore, raising kilometers utilization rate is one of the most important methods to save energy and reduce fuel consumption for vehicles. Of course, there are many approaches by which to raise kilometers utilization rate. For example, the enterprises can cooperate to exchange information on cargos available and offer stowage service. Besides, it is advisable the government and agencies build logistics information systems or platforms, enhancing allocation of freight cars and information exchange between enterprises.

From the coefficient signs of three other independent variables, we can see that vehicle mileages, cargo weight and loaded one-way mileage are in proportional to vehicle's total energy consumptions. The longer the distance covered, the more energy the vehicle consumes; and more weight requires more power, thus requires more energy. In addition, the longer the loaded mileage, the more energy the vehicle consumes. Of course, there are many factors that have influences on vehicle's energy consumption. For example, when the vehicle ages, the vehicle's performance lowers and the engine's condition decreases because of friction. Surely, the vehicle's technological standard is also important. As a result, those vehicles that are out of date, low-efficient and consumes much energy should be replaced by vehicles that are highly efficient and energy-saving due to the use of high technology. Then by using vehicles that involve advanced energy-saving technologies, energy utilization rate can be increased, thus reducing energy consumption.

ANALYSIS OF THE EXTENT OF INFLUENCE

The Extent of Influence the Factors have on the Vehicle's Total Energy Consumption

To make an analysis of the extent of influence these influential factors have on vehicle's total energy consumption, we have to standardize the data and establish a regression model, acting on these standardized data. Thus a model can be obtained:

$$y_1' = (3.56E-013) + 0.976x_1' + 0.105x_3' + 0.048x_4' - 0.113x_6' + u$$

Here in this model, y_1'、x_1'、x_3'、x_4'、x_6' stand for the standardized indicators of total vehicle energy consumption (y_1), mileage (x_1), cargo weight

(x_3), loaded one-way trip mileage (x_4), and whole-trip kilometers utilization rate (x_6).

According to the structure of the regression model, we can see that, among the four influencing factors---mileage, cargo weight, loaded single-trip mileage, and kilometers utilization rate, kilometers utilization rate changes in the opposite direction as the vehicle's total oil consumption does, that is to say, it is inversely proportional to fuel consumption. Nevertheless, mileage, cargo weight and loaded single-trip mileage change in the same direction as the vehicle's fuel consumption does, that is to say, they are in proportional to fuel consumption.

If other variables remain unchanged, fuel consumption will decrease by 0.113 units when kilometers utilization rate increases by 1 unit. Likewise, fuel consumption will increase by 0.976 units when mileage increases by 1 unit, and fuel consumption will increase by 0.1105 units when cargo weight increases by 1 unit. When loaded single-trip mileage increases by 1 unit, fuel consumption will increase by 0.048 units. Therefore, it is the mileage that has most influence on fuel consumption, and kilometers utilization rate ranks only second. Influences that mileage, cargo weight, loaded single-trip mileage, and kilometers utilization rate have on vehicle's total energy consumption are illustrated in Figure 1.

Changes of the influentia l factors	Of mileage on total energy consumption	Of cargo weight on total energy consumption	Of loaded single-trip mileage on total energy consumption	Of kilometers utilization rate on total energy consumption
1.00	0.976	0.105	0.048	-0.113
2.00	1.952	0.21	0.096	-0.226
3.00	2.928	0.315	0.144	-0.339
4.00	3.904	0.42	0.192	-0.452
5.00	4.88	0.525	0.24	-0.565
6.00	5.856	0.63	0.288	-0.678
7.00	6.832	0.735	0.336	-0.791
8.00	7.808	0.84	0.384	-0.904
9.00	8.784	0.945	0.432	-1.017
10.00	9.76	1.05	0.48	-1.13
11.00	10.736	1.155	0.528	-1.243
12.00	11.712	1.26	0.576	-1.356
13.00	12.688	1.365	0.624	-1.469
14.00	13.664	1.47	0.672	-1.582
15.00	14.64	1.575	0.72	-1.695

Figure 1 . Influences all factors have on total energy consumption (in unit) .

As we can see, mileage has the greatest influence on energy consumption. So we should take routes that are in good condition to improve kilometers utilization rate when the transportation distance is long. Thus fuel utilization rate can be improved and energy consumption can be minimized.

The Extent of Influence Key Factors have on the Vehicle's Total Energy Consumptio n per 50 kilometer s

Making analysis of the effects on energy consumption, we can get another model:

$$y'_2 = (3.84E-011) + 0.280x'_3 - 0.353x'_5 + u$$

Here y'_2、x'_3、x'_5 are respective standardized indicators of total fuel consumption per 50 kilometers, cargo weight, and whole-trip vehicles kilometers utilization rate.

As we can see from the structure of the regression model, vehicle's kilometers utilization rate changes in the opposite direction as total fuel consumption per 50 kilometers does, that is to say, the rate is inversely proportional to the total fuel consumption. Besides, cargo weight changes in the same direction as the total fuel consumption does, i.e. it is proportional to the fuel consumption.

The rest of the variables remaining unchanged, if kilometers utilization rate increases by one unit, the total fuel consumption per 50 kilometers will decrease by 0.353 units. Likewise, if cargo weight increases by 1 unit, the total fuel consumption per 50 kilometers will increase by 0.280 units. So kilometers utilization rate has the greatest impact on fuel consumption per 50 kilometers. Influences that cargo weight and whole-trip kilometers utilization rate have on fuel consumption per 50 kilometers are as in Figure 2 .

Changes of influential factors	Of cargo weight on fuel consumption per 50 kilometers (in unit)	Of kilometers utilization rate on fuel consumption per 50 kilometers (in unit)
1.00	0.280	−0.353
2.00	0.56	−0.706
3.00	0.84	−1.059
4.00	1.12	−1.412
5.00	1.4	−1.765
6.00	1.68	−2.118
7.00	1.96	−2.471
8.00	2.24	−2.824
9.00	2.52	−3.177
10.00	2.8	−3.53
11.00	3.08	−3.883
12.00	3.36	−4.236
13.00	3.64	−4.589
14.00	3.92	−4.942
15.00	4.2	−5.295

Figure 2 . Extent of influence factors have on fuel consumption p er 50 kilometers (in unit) .

In order to conduct a more detailed analysis, we collected data on some

vehicles at random that are loaded on both trips. Analysis shows that a vehicle may consume some 30 liters of fuel per 50 kilometers if it is partly loaded on both trips (to and from), and some 37 liters of fuel if it is fully loaded. Analysis also shows that the longer the distance that the vehicle covers when fully loaded, the lower the fuel consumption per 50 kilometers, justifying the conclusion that the higher the kilometers utilization rate, the lower the energy consumption. Since the vehicle has to consume some 30 liters of oil when it is on the trip back unloaded, it may consume 57 liters of oil if it is fully loaded, much higher than what the vehicle consumes when it is fully loaded on its trip back. As a result, to increase fuel utilization rate, it is important to load the vehicle reasonably and improve its kilometers utilization rate.

Speaking of the influences cargo weight has on unit fuel consumption, we should make sure that the vehicles are fully loaded but not overloaded. Because of fierce competition, road transport enterprises often overload their vehicles to reduce cost, raising turnover. But actually, overloaded vehicles often consume more unit fuel, raising cost and decreasing the profit. So it is advisable that the vehicles be reasonably loaded not overloaded. Only in this way can we maximize fuel utilization rate.

CONCLUSIONS

With the analysis of models, it is safe to say that road cargo transport enterprises should take kilometers utilization rate, mileage, and cargo weight etc into consideration when taking measures to save energy. Of them, the first two factors are the ones that have the greatest influences, and kilometers utilization rate changes in the opposite direction as total fuel consumption and unit consumption do, that is to say, improving kilometers utilization rate can help save energy, reduce energy consumption and increase energy consumption rate. However, the last three factors change in the same direction as energy consumption does, that is to say, energy consumption can be decreased by lowering the three factors. It should be added that vehicle's technological level has great impact on the vehicle's fuel consumption level, and to improve the vehicle's technological level means to improve oil saving-related technologies and vehicle operation-related technologies. That is to say, new style high-tech vehicles should be used to replace high energy-consumption vehicles and the ones that are worn, and research on energy-saving technology shall be conducted to improve the vehicle's overall energy utilization rate. In addition, driver's experience is very useful to energy saving. However, the two problems exist in most cargo transport enterprises, making it necessary to take a comprehensive consideration. Experienced drivers can have obvious impact on energy saving if these vehicles are of high-tech and the operation is free of human interference.

ACKNOWLEDGMENT S

This research was supported by Shanghai Maritime University Leading Academic Discipline Project. Project Number: XR0101.

REFERENCES

Energy Information Administration. "Annual Energy Outlook 2006 with Projections to 2030.":http://www.eia.doe.gov/oiaf/aeo/pdf/overview.pdf.

Environmental data compendium 1995.Paris(France):Organization for Economic Cooperation and Development(OECD),1995.

He Xiaoqun. “Methods and Applications of Modern Statistical Analysis.” China Renmin University Press, 1998.

Samaras, Z.,Zachariadis, T., Babajimopoulos, A., Hassel, D., Weber, F-J, Sonnborn, K-S et al. “Study on transport-related parameters of the European road vehicle stock. In: Final Report to the European Commission.” Study Contract No.B98-B27040-SIN 6516-ETU.Thessaloniki.(Greece): Aristole University Mechanical Engineering Department.1999.

Schipper, L.,Figueroa, M.J.,Price, L.,Espey, M. “Mind the gap:the vicious circle of measuring automobile fuel use.”EnergyPolicy1993,21(12):1173-90.

Case study: Analysis of CO_2 emissions caused by Customers transportation in Shanghai and Shenzhen IKEA

Zhao Yali[1] and Yang Dongyuan[2]

[1] Key Laboratory of Road and Traffic Engineering of the Ministry of Education, TongJi University, Room 202 of 75#, 600, Yingkou Road, Shanghai, China, 200433; PH: 13311984129; email: ally1009@yahoo.com;
[2] Key Laboratory of Road and Traffic Engineering of the Ministry of Education,TongJi University; email: yangdyk@yahoo.com.cn

ABSTRACT

Transportation is one of the areas where increasing levels of CO_2 emission have been the hardest to curb. The Chinese government has a clear policy for sustainable transportation development. However, the question of how to transfer policies into viable actions is very important. This paper discusses this issue from a business aspect. A sustainable policy is strategically important for business to survive and develop in China. Firstly, this paper gives an overview of the national sustainable transportation policy and its impact on business. Secondly, Shanghai IKEA is used as a case study and the transport characteristics of its customers are analyzed. CO_2 emissions for different modes are also calculated. Finally, based on the analysis, some reasonable suggestions are put forward keeping IKEA's business in mind.

BACKGROUND: SUSTAINABLE TRANSPORTATION POLICY , LOW-CARBON ECONOMY IN CHINA AND **IKEA 'S EFFORTS TO** REDUCE CO2 EMISSIONS

"China's Sustainable Development Strategy Report in 2009", which has just been published by the Chinese Academy of Sciences in March 2009, identified the strategic objective to develop a Low-carbon economy in China. The aim is to reduce CO_2 Emissions per GDP will be reduced by 50 percent before the year 2020. The report indicated that Energy-saving and CO_2 reduction could be important sources of competitive strength for companies. (Chinese Academy of Sciences, 2009)

Transportation is one of the areas where the trends of increased CO_2 emissions have been the hardest to curb. This is due to the existing policies for reductions accepted around the world (WWF, IKEA, 2008). In its sustainable transportation policy China specifies public transportation priority, transport demand management, and energy sustainability as required expectations. Also, sustainability is not just the responsibility of the government. All of the members of society should take responsibility. It concerns everybody and every enterprise could contribute for

it.

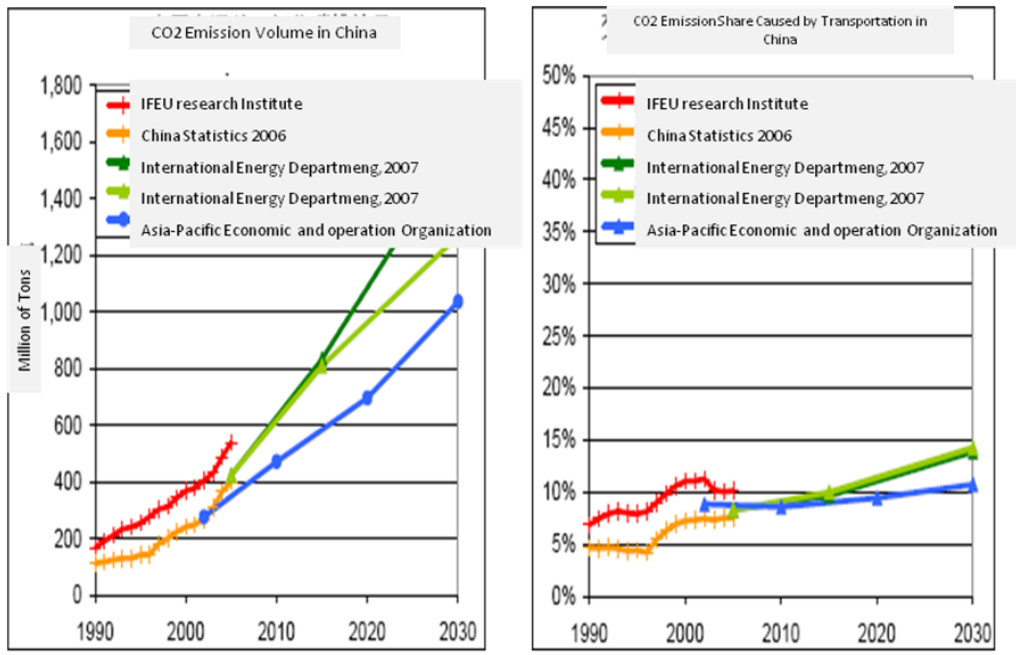

Figure1 . CO2 Volume and Transportation Share in China .

Two of the world's leading organizations are working closely to promote the responsible and sustainable use of natural resources. WWF, the global conservation organization, and IKEA, the home furnishings company, co-operate in the areas of responsible forestry, better cotton production, and climate change. The climate change projects explore ways in which joint efforts can contribute to reducing emissions of the greenhouse gas Carbon Dioxide (CO2). WWF and IKEA have decided to work together in the following areas:

- Energy efficiency and increased use of renewable energy at IKEA's suppliers leading to reduced energy use and reduced emissions of CO2 while simultaneously reducing the total supply cost.
- Sustainable transportation for customers which will result in reduced emissions of CO2.

The climate change projects have been propelled in China, Poland, Sweden and the UK.

CUSTOMERS SURVEY CONDUCTED IN SHANGHAI IKEA AND SHENZHEN IKEA AND DATA ANALYSIS

In order to gather information about CO2 emissions from customers who came to and from IKEA, an interview was conducted in early 2009. These interviews were conducted simultaneously on January 13, 16, 17, 18, and 19 in Shanghai and Shenzhen. The survey was planned and implemented by WWF, IKEA, and Tongji University. 375 effective samples in Shenzhen and 368 samples in Shanghai were

recorded.

CUSTOMER DISTRIBUTION IN THE CITY

In Shanghai, almost 50% customers came from Minhang District, Xuhui District, and Pudong District. We can see from Figure 2 that Shanghai IKEA is located at the very center of Shanghai City, which in turn is surrounded by buildings. It mostly attracts customers living near the store.

In Shenzhen, almost 74% customers hail from Nanshan and Futian Districts. We can see from Figure 3 that Shenzhen IKEA is located in Nanshan District. This store also attracts customers from surrounding areas.

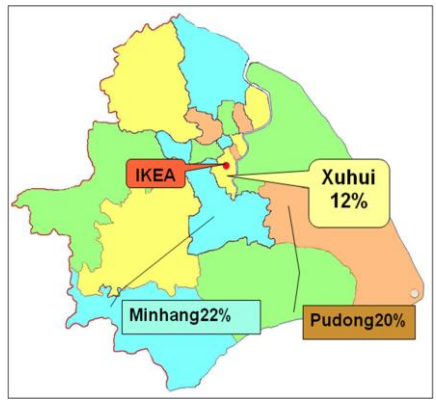

Figure 2. Shanghai IKEA and its high customer areas.

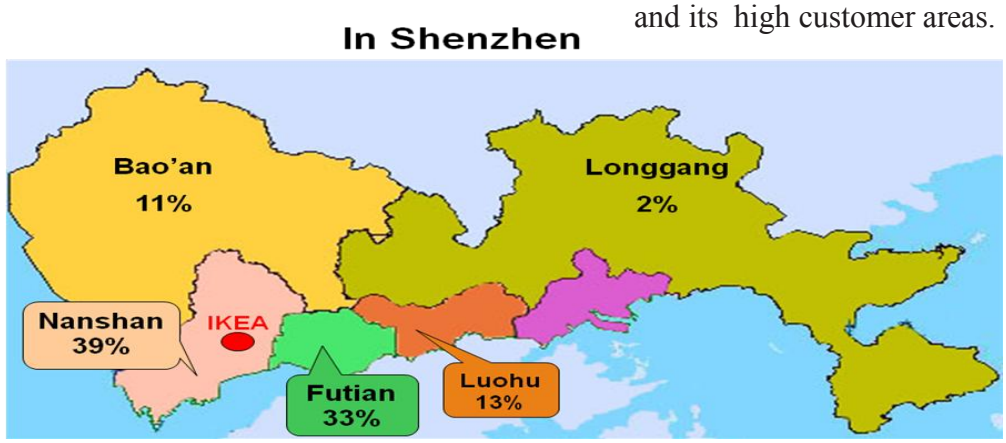

Figure 3. Shenzhen IKEA and its high customer areas .

MODE SPLIT OF CUSTOMER'S TRANSPORTATION

From the survey we get a clear information of mode share of bus, metro, private car, and taxi. Table 1 displays this information.

Table 1 . Mode Share of Ike Customers .

Mode share	Bus and metro	Private car	Taxi	Others
Shanghai	73%	12%	8%	7%
Shenzhen	50%	38%	8%	4%

Data shows a clear difference in level-of-service of transit in Shanghai and Shenzhen.

Figure 4. Location of Shenzhen IKEA Shanghai IKEA .

Shenzhen IKEA is surrounded by the freeway and is clearly convenient for car users. Shanghai IKEA is also located near Ring Road in Shanghai City. It is again easily accessible by car. There are also two metro lines which cross at this location. With the improvement in Shanghai's metro system, the metro is taking on a larger share of the transit pie. This is why we see an obvious difference between the modes of transit in Shanghai and Shenzhen.

ESTIMATING CO2 EMISSIONS BY CUSTOMERS

Usually we have two methods to calculate CO2 emission, fuel-based and distance-based. In the fuel-based methodology, fuel consumption is multiplied by the CO2 emission factor for each fuel type. This emission factor is relevant to the fuel's heat content, the fraction of carbon in the fuel that is oxidized, and the carbon content coefficient. In the distance-based method, CO2 emissions can be calculated by using distance based emission factors. In this method, the data we need may include vehicle mileage, freight ton-kilometers (or miles), passenger kilometers (or miles), etc.

For IKEA case study we used the distance-based method. Sampling data is amplified by the actual number on the survey day. We give a universal CO2 Emission factor for different transport modes.

Table 2 . CO2 Emission Factor based on Transport Mode (g/km) .

Mode	Bus	Metro	Motorcycle	Car	Bicycle	Taxi	Electronic bicycle
factor	19.74	61	220	506	0	168.67	0

Referred to 《Revised 1996 IPCC Guidelines for National Greenhouse Gas Inventories: Reference Manual》

Based on the above factors, we get the results of Customers CO2 emissions. Shanghai IKEA emitted 275T CO2 on the survey days with 73000 customers. Shenzhen IKEA emitted 230T CO2 with 41000 customers. Therefore the average CO2 per customer in Shanghai and Shenzhen IKEA is 3767g and 5610g.

FACTORS AFFECTING CUSTOMERS CO2 EMISSION

Clearly the transport mode structure and trip distance are two main factors that affect CO2 emission. It mostly depends on level-of-service of facility and location. (Jean-Pierre Nicolas, 2009)

The average transit share of the central city in Shanghai (inside Out Ring Road) is 33.1% This includes bus, metro, and taxi. (Shanghai Urban Comprehensive Transportation Planning institute, 2008). For IKEA Shanghai the number is 73%. Because IKEA is established in large cities in China, motorization transportation is a principal part of customers' transportation. We can therefore compare transit share in motorized transportation with IKEA. In Shanghai, the average number is 65%. It means IKEA Shanghai is promoting sustainable customer transportation. In Shenzhen, the average is 44.3%. For Shenzhen IKEA the average number is 50%. Here we can see that the mode share of IKEA customers is different from the whole mode structure in the city. See table 3.

Table 3 . Mode Structure Comparison .

share	Shanghai IKEA	Average[1] in Shanghai	Shenzhen IKEA	Average[1] in Shenzhen
Transit[2]	87%	65%	60%	55%
Car	13%	35%	40%	45%

[1] Average mode share in motorized transportation in the central city

[2] Including bus, metro and taxi

In conclusion it can be said that Shanghai IKEA is promoting a sustainable transportation structure. The Shenzhen IKEA, is still promoting a relatively average number.

The location of any particular Ikea also plays a big role. Today, it is difficult for IKEA to get a large piece of land in an urban center.. It is expensive and unavailable. Hence most of IKEA's new locations in China are situated outside the central city and are accessible by car.

In the survey, we also examined the tendency of customers to shift to public transport in the peak period and on weekends. 41% of car users in Shanghai would like to shift during such periods. 29% of car users in ShenZhen would like to make the same shift.. 68% of taxi users in Shanghai would like to change to bus or metro. 64% of taxi users in Shenzhen would like to change. The data also reveals that lifestyle habits will also affect the mode structure and in turn affect CO2 emissions.

MEANINGFUL LOCATION DECISION S FOR IKEA

If reducing CO2 emission per customer is the only objective in location

decisions for IKEA, achieving the objective will be relatively simple. IKEA is dedicated to environment protection but also hopes to attract more customers and increase volume of sales.

According to our analysis, IKEA is more attracted to nearby districts. First, it should not be isolated from the city and this will prevent the business from losing customers because of a longer commute. Second, the stores should be in or near compact commercial areas. Admittedly it is difficult to find core commercial areas, but sub-centers or new districts of cities are equally good choices.

High transit accessibility is thus a key factor for CO2 emission reduction. But car accessibility is also very important. IKEA's service area is identified as regional. It always takes metropolis or capital cities in China as location. These cities have a powerful economical influence on regional areas. Long distance trips will also depend on car transportation. Both car accessibility and transit accessibility must be considered while deciding on a location.

REFERENCES

Chinese Academy of Sciences, "China's Sustainable Development Strategy Report in 2009.", 2009.3;

Jean-Pierre Nicolas and Damien David. "Passenger transport and CO2 emissions: What does the French transport survey tell us?" Atmospheric Environment, 43 (2009) 1015 – 1020

Revised 1996 IPCC Guidelines for National Greenhouse Gas Inventories: Reference Manual, 1996

Shanghai Urban Comprehensive Transportation Planning institute, Shanghai Comprehensive transportation annual report [R], 2008

WWF(World Wild Foundation). "IKEA, Approaching the urban transportation challenge in the 21st century[R]." 2008;

Effect of Electro-mechanical Coupling on Dynamic Performance of Crankshaft of ISG HEV

J. Zhou[1], F. Sun[2], X. Hu[1], and X. Cheng[1]

[1]National Engineering Lab for Electric Vehicle, Department of Mechanical and Vehicular Engineering, Beijing Institute of Technology, Beijing, China, PC100081; PH 15911017000; email: fayever_828@163.com

[2]National Engineering Lab for Electric Vehicle, Headmaster's Office, Beijing Institute of Technology, Beijing, China, PC100081; email: sunfch@bit.edu.cn

ABSTRACT

Based on dynamic simulation and finite element analysis, this paper studies the effect of electro-mechanical coupling on the dynamic characteristics of a crankshaft used in ISG HEV. First, a dynamic model of an electro-mechanical coupling shaft system including flexible crankshaft is built. Then a qualitative analysis of the dynamic property of crankshaft was performed, when the ISG motor worked at assistant pushing mode and power generating mode and when the ISG motor has not coupled to the crankshaft of the engine. It is found that there was no obvious difference on torsional vibration performance of the electromechanical coupling shaft system. But the bending stress of the crankshaft changed a lot, when the flywheel was superseded by the ISG rotor. The results are useful for designing the electromechanical coupling shaft system of a hybrid electric vehicle.

INTRODUCTION

Compared to traditional internal combustion engine vehicles, a hybrid electric vehicle has less fuel consumption and reduces greatly poisonous emissions. Considering the cost and the easy implementation of mass production, Integrated Starter/Generator Mild Hybrid Vehicle (ISG-MHV) has a growing market popularity (Chan, C.C., 2002, Yue, D.P., 2005, Zhou, L.B., 1999). In order to analyze some dynamic problems of the hybrid system electro-mechanical coupling shafting formed from the rigid connection between the ISG motor and the crankshaft, we employed the finite element analysis and multi-body dynamics combined method to analyze the change of stress distribution law and torsional vibration performance for the hybrid system shafting with ISG motor instead of flywheel. This is significant and instrumental for the transformation from conventional vehicles to hybrid electric vehicles.

1 TO BUILD THE FLEXIBLE MULTI-BODY DYNAMIC MODEL.

Finite element analysis not only offers the finite element model to the multi-body dynamic analysis, but also services the crankshaft stress analysis. At the same time, the flexible multi-body dynamic simulation can compute the stimulus for

the hybrid shafting during a cycle and provide the load for analyzing the stress concentration.

1.1 The finite element model for the crankshaft.

For an ISG hybrid electric vehicle, the crankshaft, main bearings, linkage mechanism, pistons and ISG motor make up the hybrid dynamic electro-mechanical coupling shafting. Since the crankshaft has a great influence on the shafting dynamic characteristics, the elastic deformation during running of the crankshaft has to be considered in the computation analysis. Therefore, a finite element model of the crankshaft has been built to generate a modal neutral file, including the crankshaft material, node, element and modal information through the modal comprehensive analysis.

1.2 The models for rigid parts.

Given the inertia force from the high-speed parts, such as the linkage mechanism and pistons, directly and greatly affecting the dynamic performance of the hybrid dynamic shafting, the mass and the design mass should be consistent. The centroid, mass and moment of inertia are required for the multi-body dynamic analysis (Hao, Z.Y., 2005). We thus accurately established 3-dimensional solid models for the pistons, linkage mechanism, belt wheel and simplified ISG rotor. With this, we obtain the corresponding dynamic parameters that were inputted into the simulation software to achieve the rigid model for the hybrid electro-mechanical coupling shafting.

1.3 To apply constraints and forces.

In multi-body dynamic analysis, the practical motion relationship between two parts is generally simplified to the idealized constraint. For example, the constraints between the piston and piston pin, piston and connecting rod small end, and connecting rod big end and crank pin are simplified as hinge constraints. The constraint between piston and cylinder wall is viewed as sliding. We ignored the elastic deformation of all the above mentioned parts and the temperature influence on the torsional-vibration-damper. The torsional-vibration-damper is used for controlling the torsional vibration of the crankshaft system and connecting the belt wheel and the crankshaft by computable stiffness and damping. The support to the crankshaft from main bearings is very important to the system dynamic analysis. The linear spring model, nonlinear spring model and hydrodynamic model are used to stimulate the main bearing's dynamic features (Zissimos, P. M.,2001). In this paper, the hydrodynamic model provided by ADAMS was selected (MSC). The multi-body dynamic model stimulus for the electro-mechanical coupling shafting consists of the cylinder pressure, the force moment on the crankshaft output end from ISG motor, and the power consumed by accessories. To analyze ISG motor's influence on the dangerous stress distribution of crankshaft, the assistance mode and the generation mode with the maximum torque for ISG motor at a constant speed were analyzed. This assumed as given the ISG hybrid electric vehicle control algorithm, while the

in-cylinder pressure curve was measured and the power consumed by accessories was computed and applied to the belt wheel. The multi-body dynamic analysis model of electro-mechanical coupling shafting used to analyze the system dynamic response under steady conditions is shown in Fig.1.

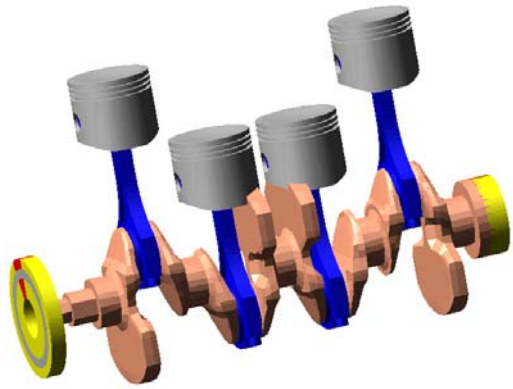

Figure 1. Dynamic analysis model of electro-mechanical coupling.

2 RESULTS AND ANALYSIS.

2.1 Dynamic analysis for the electro-mechanical coupling shafting.

Under the assistance mode and the generation mode with the maximum moment from ISG motor on a constant speed, the hybrid dynamic electro-mechanical coupling shafting was simulated through flexible multi-body dynamic analysis. The simulation result was in comparison with crankshaft-flywheel system, called flywheel mode before transformation to hybrid electric system. The results indicate that there is a similarity for the vertical stimulus on crank pins under the three above mentioned modes. Namely, the force on the crank pin at the second cylinder is minimum; the first near to the belt wheel and the third are larger; the fourth close to the ISG motor is maximum. Therefore, we merely analyzed the dangerous stress on the crank pin at the fourth cylinder. The comparison of the vertical force on the crank pin at cylinder four under the three modes during two cycles of engine is shown in Fig.2. The amplified one is Fig.3.

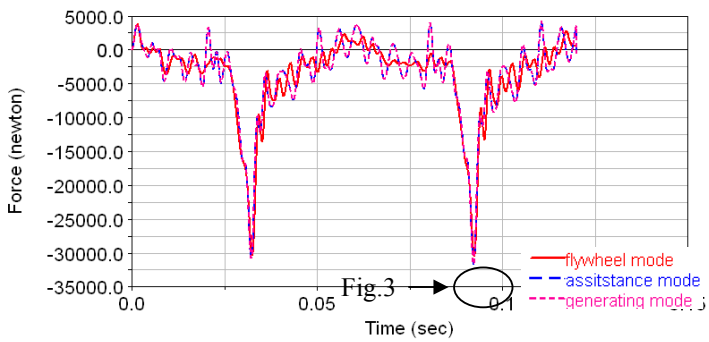

Figure 2. The comparison of the vertical force on the crank pin at the four the cylinder under the three modes.

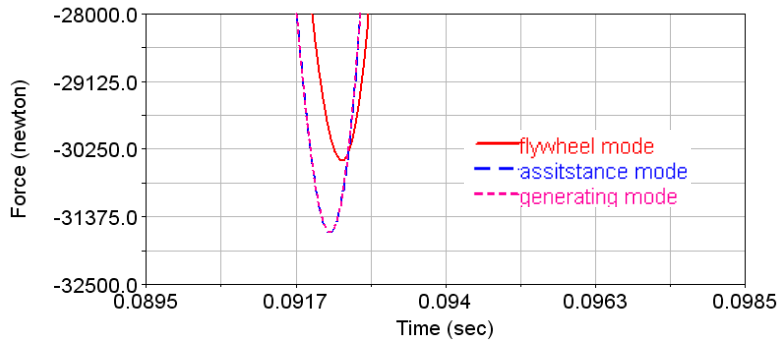

Figure 3. The amplification of Figure 2.

From Fig. 2, we can see that since the rotator mass and moment of inertia for ISG motor are smaller than the flywheel, the vertical force on the crank pin increases. As shown in Fig. 3, in generation mode the maximum force is 31640N, which is 1210N more than 30430N in the flywheel mode. The result illustrates that ISG motor has a great influence on the crankshaft in terms of the force condition. To more clearly explain the dangerous stress change of the crankshaft after connecting rigidly the ISG motor to the output end of the crankshaft, it is necessary to analyze the crankshaft's stress distribution.

2.2 Stress analysis for the crankshaft.

From this analysis, we see that the force on the crank pin at the fourth cylinder is maximum. We thus built a 1/4 model of a single crank to implement the stress analysis. Considering that the connecting rod big end applies force on the crank pin through the bearing, according to the empirical methods and the distribution law of the pressure of the finite-width oil film, we ignored the effect from the peak pressure mutation at the oil hole. We also assumed that the force boundary condition was that the load was distributed as a quadratic parabola along the connecting rod axial direction and as a cosine within 120-degree range of the circumferential direction. It is shown in Fig. 4 (Yin, J.M., 1997). The force was applied in the form of the function and assigned to all the valid nodes when computing.

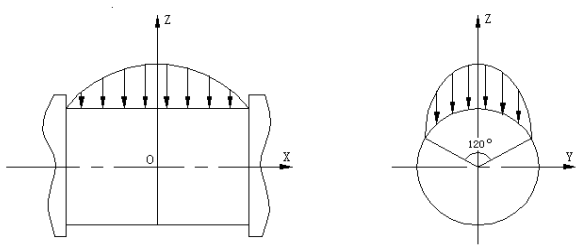

Figure 4. The pressure distribution of connecting rod journal.

Figs.5 and 6 are the stress distribution of the crank, when the vertical force on the crank pin is maximum under generation mode and flywheel mode respectively. From the stress nephogram, we clearly know that the forced dangerous points focus

on the lower part of the transition fillet between the main journal and the crank arm and on the topper part of the transition fillet between the connecting rod journal and the crank arm. The two crank stress distributions are basically similar, but the maximum stress value for the generation mode is 219.39MPa. This is much higher than that of the flywheel mode, 182.7MPa. According to the stress analysis, the fracture of the crankshaft is mainly due to the two transition fillets of the maximum dangerous stress, so the bending fatigue calculation at the transition fillets must ensure the satisfaction of the design requirement. Given the calculating formula of the fatigue safety coefficient provided by Yang (1980), we obtain a coefficient value of 1.09 after connecting rigidly ISG motor to the crankshaft output end. This exceeds the allowable range, 1.3-1.8. Therefore, the crankshaft could not meet the bending fatigue strength just with an electro-mechanical coupling transformation. The result shows that the connecting rigidly of the ISG motor rotator to the crankshaft output end without any transformation causes the change of the crankshaft structural strength. In order to meet the design requirement, the hybrid electro-mechanical coupling shafting should be redesigned and the materials should be reselected. In addition, the processing technology should be improved and the checking work should be implemented periodically to adapt to the different strength requirements between hybrid electric vehicles and conventional cars.

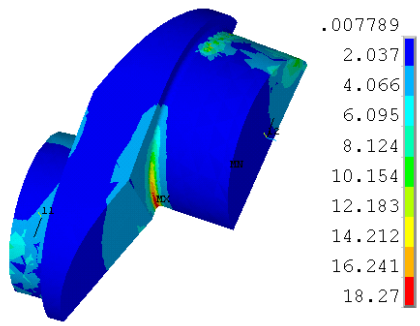

Figure 5. Stress nephogram when the vertical force on the crank pin is maximum in flywheel mode.

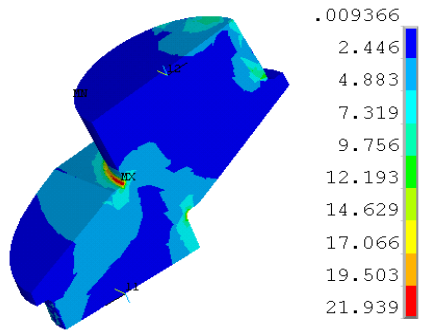

Figure 6. Stress nephogram when the vertical force on the crank pin is maximum in generation mode.

2.3 Torsional vibration analysis of the electro-mechanical coupling shafting.

A tangential force and a normal force whose size and direction are changing over time are imposed on each crank when running, so the torsional and the bending deformations of the crankshaft vary periodically. Connecting rigidly the ISG motor rotator to the crankshaft output end also has the same effect. As any elastic system with inertial mass, the electro-mechanical coupling shafting will form bending and torsional vibrations. In this paper, only the torsional vibration of the shafting is considered, because the bending rigidity is relatively large and the corresponding natural frequency is relatively high. This causes the possibility of bending resonance within the engine's working rotational speed range to be extremely small and negligible. To perform a torsional vibration analysis of a crankshaft based on the Hafner-Maass method, the inertia of each crankshaft throw about the crankshaft axis should be reduced to a physical equivalent torsional vibration train system. The natural frequencies for the conventional crankshaft system and the electro-mechanical coupling shafting after the hybrid dynamic transformation are shown in Table 1.

Table 1. The torsional vibration natural frequency of crankshaft system and electromechanical coupling shaft system.

Order(m)	Crankshaft System(Hz)	Electromechanical Coupling Shaft System(Hz)
1	703.91	1332.53
2	1917.69	2494.33
3	2877.50	3306.72
4	3439.51	6797.40
5	8397.52	8397.52
6	16285.17	16285.18

The speed range of the engine we researched is 800—3800r/m, that is to say the fundamental frequency is 13.3—63.3Hz. Our calculations shows that the harmonic orders of driving torque corresponding to the first order torsional vibration natural frequency of the two system are both above 11. The amplitude of driving torque declines with the rising of the harmonic order. The driving torque is always very small when the harmonic order is above 12 and will not induce obvious vibration (Liang, J., 1989). We know from Table1 that the torsional vibration natural frequency increased, when the rotor of ISG rigidly connected to the crankshaft. The corresponding harmonic order of driving torque is higher than 12 and avoids the resonance appearance at the working speed of engine. Therefore, the transformation of the crankshaft is safe and feasible on torsional vibration performance.

CONCLUSION

In this paper, the dangerous stress and torsional vibration characteristics of an electromechanical coupling shaft system used in ISG_HEV were analyzed, based on

multi-body dynamics and finite element method. The results show that because inertia and mass of rotor are lower than the flywheel, the contacting force between con rod and crank pin increased. For this reason, the rotor of ISG connected rigidly to the output terminal of crankshaft increased the dangerous stress of the crankshaft. On the selected engine, the crankshaft which was transformed to adapt to the HEV cannot meet the requirements of bending fatigue strength. Consequently we suggest that the crankshaft should be adjusted and checked again. Furthermore, the torsional vibration natural frequency of the crankshaft system changed after installing the ISG, but the resonance will not appear at the working speed of the engine. That is why the transformation of hybrid is safe and feasible in torsional vibration analysis. Generally, the transformation from IC engine automobile to HEV is easiest to realize, but the crankshaft system should be adjusted to meet the requirement of HEV.

REFERENCES

Chan, C. C., Sun, F.C., and Zhu, J. G. (2002). *Modern electric vehicles*. Beijing Institute of Technology Press, Beijing:.

Hao, Z. Y., Duan, X. B., Song, B. A., and Yue, D. P. (2005)."Dynamic simulation of crankshaft system for automotive diesel engine."

Liang, J., and Huo, Q. Z. (1989). *The vibration of internal combustion engine* (in Chinese). Tianjin University Press, Tianjin, 124-125.

MSC.http://www.mscsoftware.com/.

Yang, L. S. (1980). *Internal combustion engine design* (in Chinese). Chinese Agricultural Machinery Press, Beijing, 211-213.

Yin, J.M., Wang, D.H., and Yuan, Y.N. (1997). "Study on crankshaft strength of X6135 engine using 3-D FEM." *Chinese Internal Combustion Engine Engineering,* (2), 71-77.

Yue, D. P.(2005). "Study on electro-mechanical coupling dynamics of hybrid shafts system of mild HEV." Tianjin University.

Zhou, L. B. (1999). "Internal combustion engine." *China Machine Press*. *Society for Agricultural Machinery*, 36(7), 4-7.

Zissimos, P. M. (2001). "A crankshaft system model for structural dynamic analysis of internal combustion engines." *Computer and Structure*, (79), 2009-2027.

Forecast the Automobile Population Based on Scenario Analys es

Yuee Gao[1], Yanjiang Lou[2], Chao Wang[3]

[1]China Communication and Transportation Association, Beijing, 100000; xicheng District Street of South-Yuetan 26; PH (86) 010-68596749; FAX (86) 010-68596229; email: ly08@sina.com
[2]Audit Office of Heilongjiang Province, Harbin, 150001; West Dazhi Street 106; PH (86) 0451-82528017; email: louyanjiangsj @163.com
[3] The 5th Engineering Co., Ltd. of China Railway 11th Bureau Group, Chongqing, Sha Pingba District Street of Xinqiao xincun71, PH (86) 023-89065265; FAX (86) 023-89065253; email: jiaotongwangchao@sina.com

ABSTRACT

Saving resources, protecting the environment and adopting sustainable development policy will be the objective requirements of highway transportation development in the future. The development of a long-term forecast the automobile population in a critical element to making long-term development plans for the China's highway transportation as well as the policies of environmental protection and energy conservation. Based on the analysis of China's economy, the forecast considers the factors of growth rates of economy, population, and automobile inventory and correlates the distributions of per capita GDP in different regions. The forecast uses methods of trends extrapolation, elasticity coefficient modeling, and inventory scenario comparison and calculates transportation future workload. From these analyses, the forecasted result is that by 2030, the automobile population is estimated to be 230-250 million, which is 1.7-1.9 times that of 2020, and 4.6 times that of 2010.

KEYWORDS: scenario analysis, automobile inventory, forecast

INTRODUCTION

Scientific and accurate forecasts of China's future automobile populations is an important basis for reasonable predicting of our nation's highway transportation and the long-term or short-term development plans of automobile industry in addition to the related policy concerning to environmental protection and energy resources (Chen, 2005).

Potential sources of uncertainty include numerous factors that could contribute to increase of automobile ownership. Although prior research has been conducted in predicting automobile populations have been conducted in China and worldwide, few the complexity of the transportation system and the diversity the related influential factors required by the transportation suggest multiple forecasting methods be used.

The metaphase and long-term forecast of the automobile population with consideration of scenario analysis tally more properly with the reality of China. The result of this study can be used as a guide for making reasonable projects of automobile production and highway transportation, adjusting production and demand and making decisions.

ANALYSIS ON FORCASTING METHODS OF AUTOMOBILE QUANTITY

The current forecasting methods of automobile populations can be generally divided into four categories: (1) time order, that is, the method of forecasting the future state with the previous materials; (2) is the regression forecasting method to find out the relationship between the forecasting variable and its related variables according to the historical materials at hand, so as to forecast the future state; (3) the judgment analysis method, which draws upon experiences and comprehensive analysis of similar states; (4) nerve network forecasting method, which employs of artificial intelligence technology with auto-organization and self-adoption features(Zhou et al., 2001).

Many variables influence the forecasting automobile populations, including, but not limited to, regional economic development, environmental quality, the increase of disposal income, policies, natural condition, highway conditions, the density of road nets and the changes in other industries related to the automobiles. All these factors constitute a quite complicated forecasting problem. So considering the above analysis, this paper describes a metaphase and long-term forecast of China's automobile population using the methods of trends extrapolation, elasticity coefficient, trend comparisons between domestic and worldwide populations, and calculation of transportation workload.

2 THE FORECAST OF AUTOMOBILE QUANTITY

2.1 Method of trends extrapolation

Using historical rates of increases in automobile population, trends were identified to to predict future tendencies of automobile quantity The increasing speed of future automobile quantity will be set up according to three schemes (Development Research Center of the State Council, 2004); the forecasting results of the 3 schemes are presented in Table 1.

Table 1. Automobile Forecast with Trend Extrapolation Method.

item	Period								
	2004-2010			2011-2020			2021-2030		
Volume growth rate (%)	11	12	13	9	10	11	6	6.5	7
Vehicle Population (10^4)	5039	5317	5609	11929	13792	15926	21363	25890	31328

2.2 The analysis method of elastic coefficient s

Since the increases of automobile populations is highly correlated stages of economic development, and possesses its own phase feature, the method of elasticity coefficients was used adopted to predict China's future automobile populations. The elastic coefficient targets in different historic stages are represented in Table 2(Ma et al., 2007).

Table 2. Elastic ity Coefficient of Automobile Development at Different Historical Periods .

Stage	Period	Growth Rate of GDP (%)	Growth rate of Maintain Volume (%)	Elastic Coefficient
five years	1980-1985	10.71	12.49	1.17
	1985-1990	7.87	11.42	1.45
	1990-1995	12.00	13.53	1.13
	1995-2000	8.27	9.12	1.10
	2000-2003	8.36	13.99	1.67
ten years	1980-1990	9.28	11.95	1.29
	1990-2000	10.12	11.30	1.12
other stage	2000-2003	8.36	13.99	1.67
	1980-2003	9.52	11.93	1.25
	1995-2003	8.31	10.92	1.31

Using this method, the period for the most rapid increase in population is expected to be 2005-2010The calculation results of automobile quantity in 2010, 2020 and 2030 are represented in Table 3.

Table 3. Automobile Forecast Using E lasticity Coefficient Method .

Indicator	Period								
	2004-2010			2011-2020			2021-2030		
Growth rate of GDP (%)	8	8	8	7	7	7	6	6	6
Elasticity coefficient	1.4	1.5	1.6	1.3	1.4	1.5	1.1	1.2	1.3
Growth rate of Maintain volume(%)	11.2	12	12.8	9.1	9.8	10.5	6.6	7.2	7.8
Maintain volume of automobile(10^4)	5094	5317	5549	12170	13543	15062	23059	27144	31920

2.3 The method of scenario analogy between domestic and abroad .

2.3.1 The analysis of foreign countries scene

The onset and rate of industrialization vary among countries and depend on varying economic conditions, including changes of interest rate. Consequently, the automobile populations of different countries per thousand capita GDP vary over time.. Using literature search, several countries were chosen that had similar economic development as China's reference system. The Table 4 shows the distribution on vehicles possessed by one thousand people and average GDP in

different countries.

Table 4 . Vehicle Ownership per T housand Capita GDP by Country .

Categories of per Capita GDP	Country	Per Capita GDP / (dollars)	Vehicle Ownership per Thousand (1000 Vehicle)
1000-3000 dollars	Malaysia	1170	51.90
	Brazil	2190	74.70
3000-5000 dollars	Brazil	3700	87.34
	Malaysia	3890	126.60
	Japan	4940	250.96
5000-10000 dollars	South Korea	5770	48.40
	South Korea	8910	292.4
Over 10000 dollars	South Korea	10240	133.50
	Japan	10440	323.39

2.3.2 Forecasting of the amount of automobile in different periods of China.

Using the previous forecasts (comparison with foreign automobile populations), China's future traffic policy, the current China vehicle population in various regions, (China Automotive Technology & Research Center, 2001-2004, National Bureau of Statistics of China, 2006), forecasts of future automobile populations were calculated for 2010, 2010, and 2030 and shown respectively in Tables 5 through 7.

Table 5. List of per capita GDP, population and automobile ownership in 2010 .

Income Distribution (dollars)	Population /10^4	per Capita GDP / Dollars	Vehicle Ownership per Thousand People / (veh/1000 pp)	Automobile Pop. forecast (veh)
＜1000 dollars	35164	746	5	1758200
1000-3000 dollars	72647	1676	30	21794100
3000-5000 dollars	16977	3850	70	11883900
5000-10000 dollars	8943	7090	180	16097400
≥10000 dollars	914	10479	200	1828000
Average	134645	2125	40	53858000

Table 6. List of per capita GDP, population and automobile ownership in 2020 .

Income Distribution (dollars)	Population /10^4	per Capita GDP / Dollars	Vehicle Ownership per Thousand People / (veh/1000 pp)	Automobile Pop. forecast (veh)
＜1000 dollars	2960	795	5	148000
1000-3000 dollars	80817	1974	50	40408500
3000-5000 dollars	29709	3769	80	23767200
5000-10000 dollars	23070	6883	200	46140000
≥10000 dollars	9531	13882	250	23827500
Average	146087	3867	100	146087000

Table 7. List of per capita GDP, population and automobile ownership in 2030 .

Income Distribution (dollars)	Population /10^4	per Capita GDP / Dollars	Vehicle Ownership per Thousand People / (veh/1000 pp)	Automobile Pop. forecast (veh)
1000-3000 dollars	39133	2262	50	19566500
3000-5000 dollars	49463	4037	100	49463000
5000-10000 dollars	38129	6786	180	68632200
≥10000 dollars	28366	16386	400	113464000
Average	155091	6524	180	279163800

The result of the international scene analogy predicts the prospect of China automobile market. China's automobile quantity increase from 53 million to 54 million cars in 2010; and from 130 to 150 - hundred million by 2020. By 2030, the vehicle population is predicted to be between 250 and 280 million.

2.4 The method of transportation workload calculation

The transportation load which the automobile transportation considers the composition of transportation system to calculate the automobile quantities. The average finished workload of highway passengers and goods transportation of China's whole society in 1980-2004 is shown in Figure 1. With the increased proportion increasing of the minibus, the average workload of the whole society's passenger buses tends to decrease. With the change of truck's structure and the increase of loaded Lorries, the workload of Lorries tends to rise. From this analysis, the rapid increase of cars is expected to continue into the future. With the constant increase of large size bus, mini cars and the decreasing proportion of medium cars, the transportation workload of each car will continuously increase. Predictable result of the whole society's automobile quantity in 2010, 2020, and 2030 is shown in Table 8.

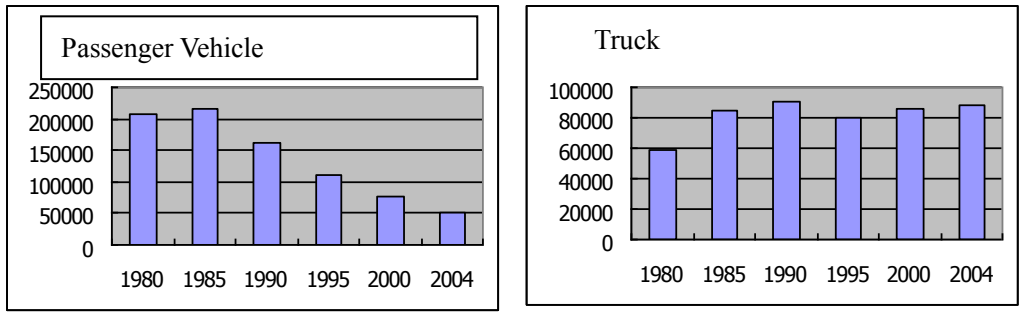

Figure 1. Workload Completed by Passenger vehicle and Truck s (1980-2004).

Table 8. Automobile Inventory in 2010, 2020 and 2030 .

Year	Passenger vehicle /[(10^8·passenger)·km]	Truck /[(10^8·t)·km]	Passenger Vehicle /[(passenger·km)·veh $^{-1}$]	Truck /[(t·km)·veh $^{-1}$]	'Automobile Population /10^4veh
2010	14300	11000	35000	80000	5461
			30000	70000	6338
2020	25000	16000	25000	90000	11778
			20000	80000	14500
2030	30000	22000	12000	100000	27200
			10000	90000	32444

According to transportation workload forecast China's automobile quantity in 2010, 2020, 2030 will separately up to 54 to 64 Million, 120 to 150 million, and 247 to 330 million, respectively.

3 THE ANALYSIS OF FORECASTING RESULT

The future China's automobile population depends on the rate of increase of of economic development and energy supply. The China's automobile population predictions for years 2010, 2020 and 2030 were developed through the use of the following methods: this forecasting result, the method of trends extrapolation, elastic coefficient, scenario analogy between domestic and international, and transporation workload conribution analysis.. Table 9 summaries the results of thes different forecasting methods.

Table 9. Automobile forecast results with different methods .

method	2010 /10^4 veh	2020 /10^8 veh	2030 /10^8 veh
trends extrapolation	5000-5600	1.2-1.6	2.1-3.1
elastic coefficient	5000-5600	1.2-1.5	2.3-3.2
scene analogy	5300-5400	1.3-1.5	2.5-2.8
transportation workload	5400-6400	1.2-1.5	2.7-3.3

CONCLUSION

In the coming 20 or 30 years, the China's automobile quantity will increase at a rapid rate. The forecasting result of automobile quantity shows that, by the year 2030, it will reach 230 million to 250 million, which is 1.7 times as much as the automobile quantity of 2020 and 4.6 times of 2010. The large extent of increase could provide additional pressures to the land and energy resources and the environmental quality.

The restriction of resources and the protection of the environmental are two subjects that must be considered in the development of China's highway transportation future. Such consideration would warrant the use of scientific development concepts in order to conserve resources, to protect environment, and to adopt sustainable development policy.

ACKNOWLEDGMENT

This research was supported by the Research Fund for National "863"Project (Grant, No. 2005AA516051)

REFERENCES

Chen Qingtai. (2005). China's Automobile Society - the Prospect and Policy Questions. Peking: China Development Press, 24-52.

China Automotive Technology & Research Center. (2001-2004). "The Annual Development Report on World Auto Industry."

Development Research Center of the State Council. (2004). "The Growth and External Environment of China's Auto Industry."

MA Yan-li, GAO Yue-e. (2007). "Forecast of Automobile Population in China." Journal of Highway and Transportation Research and Development. 24(1): 121-125.

National Bureau of Statistics of China. (2006). Statistical Yearbook of Chinese City in 2005. Peking: China Statistics Press.

Zhou Qian, Yang Dongyuan. (2001). "Multi-relative Factor Forecast of Vehicle Population by Neural Network." Journal of Highway and Transportation Research and Development, 18(6): 71-74.

The research of control strategy of permanent magnet synchronous motor for Hybrid electric vehicles

Wu Hong Xing[1]，Shi Jian Fei[2]，Ji Heng[1]，Zhao Guo Ping[1]

[1] Department of Environmental Engineering, Harbin Institute of Technology, Harbin, Heilongjiang 150001, China; TEL: 086-45186413611; Fax: 086-45186403003; Email: whx0422@sina.com

[2] Department of Electrical Engineering, Heilongjiang August First Land Reclamation University Daqing, Heilongjiang 163000, China; TEL: 086-45186413611; Fax: 086-45186403003; Email:sjfjs1226@yahoo.com.cn

ABSTRACT

Electric vehicles require high reliability, relatively wide torque and speed ranges and a high-power volume ratio. At present, induction motors, permanent magnet synchronous motors and switched reluctance motors have been successfully applied to hybrid vehicles; but there are still many deficiencies. Permanent magnet synchronous motors are widely used in the drive of electric vehicles because of their efficiency, high power density and high-torque characteristics. In the paper a mathematical model for vector control algorithms, control methods, and control strategies for use by hybrid electric vehicle will be developed. Meanwhile, an analysis of control system mechanisms, design software, and hardware based on DSP-based control will also be undertaken. An application of vector-driven direct torque control will be examined. The experimental results proved that the system has good performance.

Keywords: permanent magnet synchronous motor, electric vehicle, energy feedback

1. ITRODUCTION

Hybrid electric vehicles (HEV) and fuel cell vehicles (FCEV) have become hot spots for R&D (Guo Wei et al. 1999). Permanent-magnet synchronous motors are widely used in electric vehicles because of their relatively high efficiency, high power density, high torque unit current, and wide-speed operation. Additionally their performance closely emulates the driving performance of traditional motor vehicles (Chu C.L et al. 2001). In this paper, based on mathematical modeling of permanent magnet synchronous motors, a vector control algorithm for permanent magnet synchronous motors to maximize torque/current control of permanent magnet synchronous motor used for hybrid electric vehicles will be presented. The goal is to maximize torque control per unit current output. This is a major current control strategy optimization for permanent magnet synchronous motors. When a permanent magnet synchronous motor operates with maximum torque/current control, it lets the motor accelerate with maximum electromagnetic torque (At this point the motor voltage and current

limits are reached), which makes the engine start quickly. In addition, starter/generator system's efficiency can improve because of the minimum of inverter output current.

2. BASIC MATHEMATICAL MODEL OF PERMANENT MAGNET SYNCHRONOUS MOTOR

Vector control is actually the control of current vector phase and amplitude of the motor's stator. When excitation flux of the permanent magnet and direct-axis and cross-axis inductance are determined, the motor torque is dependent on the stator's current space vector i_s, and the size and phase of i_s is dependent on i_d and i_q, that is to say, it can control the motor torque by controlling i_d and i_q. A certain degree of speed and torque correspond to a particular theoretical values of i_d and i_q, i_d^* and i_q^*. By controlling these two currents the actual values of i_d and i_q can be brought closer to the theoretical values i_d^* and i_q^*. The tighter vector control enables more precise control of the motor's torque and speed. (Kim Junha et al. 2002)

Because the actual feed current for the armature windings of the motor is three-phase AC current with values i_u, i_v and i_w there are three current control values, i^*_u, i^*_v and i^*_w, that the system can command. The theoretical values i_u^*, i^*_v and i^*_w are derived from the following conversion($e^{j\theta}$ transformation) and are based on i^*_d and i^*_q:

$$\begin{bmatrix} i_U^* \\ i_V^* \\ i_W^* \end{bmatrix} = \sqrt{\frac{2}{3}} \begin{bmatrix} \cos\theta & -\sin\theta \\ \cos\left(\theta - \frac{2\pi}{3}\right) & -\sin\left(\theta - \frac{2\pi}{3}\right) \\ \cos\left(\theta + \frac{2\pi}{3}\right) & -\sin\left(\theta + \frac{2\pi}{3}\right) \end{bmatrix} \begin{bmatrix} i_d^* \\ i_q^* \end{bmatrix} \tag{1}$$

Using the current control loop, the actual three-phase currents to the motor, i_U, i_V and i_W can be made consistent with the given theoretical values, thus realizing the control of motor's torque. (Cikanek et al. 2002)

3. THE CONTROL STRATEGY OF PERMANENT MAGNET SYNCHRONOUS MOTOR USED FOR ELECTRIC VEHICLE

Maximum torque/current control, also known as the maximum torque control of unit current output, is a major current control strategy used for permanent magnet synchronous motors. When permanent magnet synchronous motors adopt maximum torque/current control, the motors accelerate with the maximum electromagnetic torque deliverable within the motor voltage and current limits. This high torque makes the engine start quickly. In addition, starter/generator system efficiency can be improved because of the minimization of inverter output current. Next, we will do the specific analysis for the maximum torque/current control. (W. Xia et al. 1998)

When operating at the maximum torque/current control a motor's current vector should meet the following conditions:

$$\begin{cases} \dfrac{\partial (T_{em} / i_s)}{\partial i_d} = 0 \\ \dfrac{\partial (T_{em} / i_s)}{\partial i_q} = 0 \end{cases} \tag{2}$$

We can get the relationship between the electromagnetic torque, cross-axis, and direct-axis current components:

$$T_{em}^* = \sqrt{i_d^* (1 - i_d^*)^3} \tag{3}$$

$$T_{em}^* = \frac{i_d^*}{2}[1 + \sqrt{1 + 4i_q^{*2}}] \tag{4}$$

Stator's current component i_d^* and i_q^* can be expressed as:

$$\begin{cases} i_d^* = f_1(T_{em}^*) \\ i_q^* = f_2(T_{em}^*) \end{cases} \tag{5}$$

For any given torque, it can obtain the two weights of the smallest current which that can be used as current control command while achieving the maximum torque motor/current control. The current control curves found in Figure 1 are derived from Eq. (5).

The control operation of PMSM is closely related to the inverter system and the motor's performance is generally restricted by the inverter. The most obvious limitation is the extremum with the virtual value of phase voltage of the motor $U_{\lim}$, and the extremum of the virtual value of phase current $I_{\lim}$. Both are restricted by the inverter's DC side voltage and the maximum inverter output current. On the system's d-q axis the limit of voltage is $u_{\lim} = \sqrt{3}U_{\lim}$ and the limit of current is $i_{\lim} = \sqrt{3}I_{\lim}$.

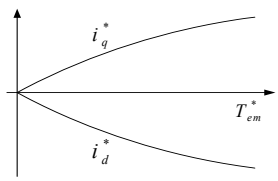

Fig.1 Curve of i_d^*、i_q^*

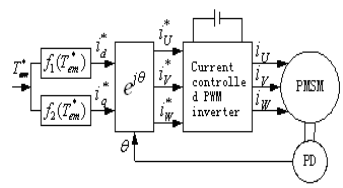

Fig.2 Control system of maximum rate of torque/current

Figure 2 is the system diagram of torque control link in the largest torque/current control. When the motor runs at high speed, the resistance is far less than the reactor, you can ignore the resistance of the voltage's drop, there is:

$$u = \sqrt{u_d^2 + u_q^2} = \sqrt{(X_q i_q)^2 + (X_d i_d + e_0)^2} \tag{6}$$

Where, X_d and X_q are the direct-axis reactance and cross-axis reactance of the motor, and e_0 is the no-load back-EMF. $e_0 = \omega\psi_f = \sqrt{3}E_0$
Using $u_{\lim}$ in place of u, Eq. 7 can be obtained:

$$(L_q i_q)^2 + (L_d I_d + \psi_f)^2 = (u_{\lim} / \omega)^2 \tag{7}$$

The equation above is the equation of a current limit circle. When the motor is running, the stator's current space vector can not only exceed the motor's voltage limit ellipse, but also the current limit circle. Motor's maximum torque/current track and the current limit circle intersect at point A, as shown in Figure 3:

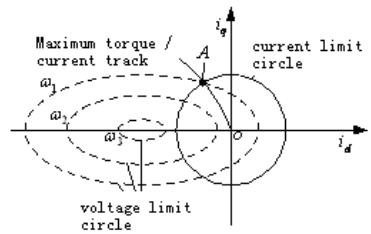

Fig.3 Vector graph of stator's current

The speed which corresponds to the voltage limit ellipse that goes through point A is ω_1. In OA paragraph of the maximum torque/current trajectory, the motor can run in the constant torque corresponding to the points of this trajectory, and the speed corresponds to the voltage limit circle which through this point is the turn-speed under this torque. Then, point A corresponds to the turning speed when the output torque of the motor is greatest. Turn-speed can be obtained through the following formula:

When $L_d \neq L_q$, (Salient-pole permanent magnet synchronous motor)

$$\Omega = \frac{u_{\lim}}{p\sqrt{(L_q i_{\lim})^2 + \psi_f^2 + \dfrac{(L_d + L_q)C^2 + 8\psi_f L_d C}{16(L_d - L_q)}}} \tag{8}$$

In the equation $C = -\psi_f + \sqrt{\psi_f^2 + 8(L_d - L_q)^2 i_{\lim}}$

When $L_d = L_q$, (Surface permanent magnet synchronous motor)

$$\Omega = \frac{u_{\lim}}{p\sqrt{(L_q i_{\lim})^2 + \psi_f^2}} \tag{9}$$

From Figure 3 we can see, when the motor runs at constant torque, the greater the torque value is, the lower the turn-speed is. Because voltage and current can not exceed their limits when the motor is running, so the torque corresponded to the point A is the maximum output torque of the motor. When maximum torque/current control is used and the current of the motor reaches its limit (corresponding to the maximum torque/current limit and current limit circle's node A), the cross-axis and direct-axis currents of the motor can be obtained from the following formula:

$$\begin{cases} i_d = \dfrac{-\psi_f + \sqrt{\psi_f^2 + 8(L_d - L_q)^2 i_{\lim}^2}}{4(L_d - L_q)} \\ i_q = \sqrt{i_{\lim}^2 - i_d^2} \end{cases} \tag{10}$$

While the electromagnetic torque is:

$$T_{em} = \frac{(4\psi_f + C)\sqrt{4\psi_f C + C^2}}{16(L_q - L_d)} \tag{11}$$

The current vector for the starter/generator at constant torque control can be found from Eq. (10). The starter/generator will provide acceleration with the maximum electromagnetic torque at a given speed when the current vector value follows along the maximum torque/current trajectory presented previously.

4. THE MANUFACTURE OF THE DRIVING SYSTEM OF PERMANENT MAGNET SYNCHRONOUS MOTOR

With a driving control system composed of DSP as the core a block diagram of the control circuit is shown in Figure 4. The motor's three-phase windings are controlled by a three-phase bridge circuit composed of IGBT modules made with EXB841integrated circuits.

DSP is composed of TI TMS320LF2407. Six way comparison units are used as the drive signals for the three-phase IGBT bridges. The signals will go to the EXB841 drive unit after they are processed; the capture unit 3 receive the pulse signal from the sensor which can control the phase; the mouth of analog-digital conversion unit 2, 3, 4 receive the signal from the current sensor of stator windings, the mouth 10 receives the sign from the current sensor of the axial coil.

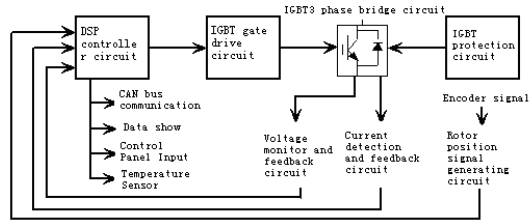

Fig.4 The controller's circuit diagram of permanent magnet synchronous motor

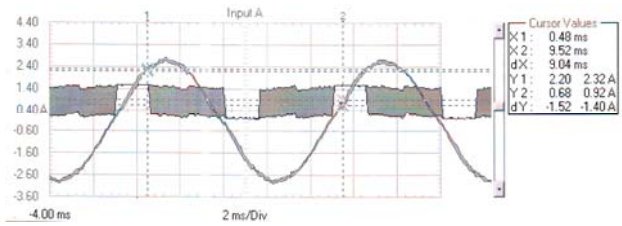

Fig.5 SPWM wave and phase's current wave of the PM synchronous motor driver

5. EXPERIMENT AND CONCLUSION

For the design of a motor control system, bench tests and functional tests can not only shorten the hybrid vehicle test cycle, reduce the risk and cost of R&D, but also guide further research for the system. This section researches the functional test of the permanent magnet synchronous motor system.

Figure 6 is the three-dimensional map of speed-torque-efficiency in electrical state; Figure 7 is the shadow map of peed-torque-efficiency in electrical state.

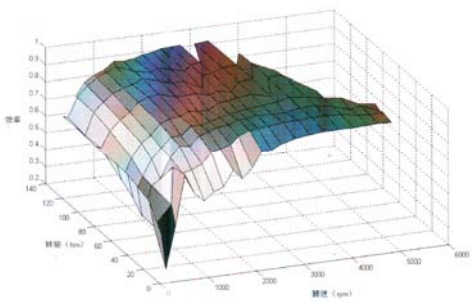

Fig.6 Three dimensional graphics of motor Speed - torque - efficiency in driving

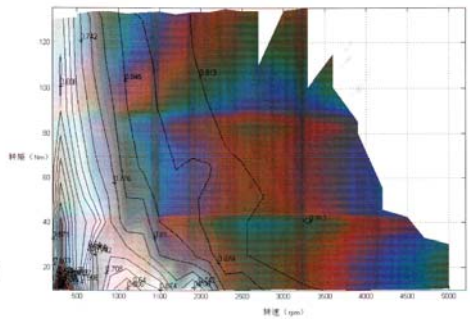

Fig.7 Dot band chart of motor speed - torque - efficiency in driving

From the comparison of experimental and theoretical efficiency, we can see that theoretical efficiency increases with the torque. In the calculation of theoretical efficiency additional wastage and mechanical wastage have been ignored as well as the effects that rising temperatures bring to electrical resistance of the motor. These simplifications will result in an increase in the value of theoretical efficiency at large torques. At low motor currents the measurements by the laboratory equipment will lead to higher relative error. Thus, the actual experimental efficiency at lower torques will be closer to theoretical efficiency and closer to experimental efficiency at higher torques.

ACKNOWLEDGMENT

The project described in this paper has been supported by Development Program for Outstanding Young Teachers in Harbin Institute of Technology, 2007 and Natural Scientific Research Innovation Foundation in Harbin Institute of Technology, 2008.53 NO. FEQQ18400009...

REFERENCES

Guo Wei, Ma Zhiyuan. (1999).Torque Given Control of Switched Reluctance Motor Drive Suitable for Electric Vehicle. EVS16, Proceeding CD.

Chu C.L., Tsai, M.C., Chen H.Y. (2001).Torque control of brushless DC motors applied to electric vehicles. Electric Machines and Drives Conference. IEMDC 2001. IEEE International , 2001.

Kim Junha, Nam Kwanghee.(2002). Dual inverter control strategy for high speed operation of EV induction motors. Proceedings of the 2002 28th Annual Conference of the IEEE Industrial Electronics Society, Sevilla, Spain.

W. Xia, Philip.(1998). Chin. A Specially Designed EV PM Motor Drive. Energy Management and Power Delivery, 1998. Proceedings of EMPD '98. 1998 International Conference on , Volume: 2 , 1998: 718 ~722 vol.2

Cikanek, S.R, Bailey K.E.(2002) Regenerative braking system for a hybrid electric vehicle. Proceedings of the American Control Conference 2002.

Monitoring Model for Three -Way Catalyst Converter Efficiency Based on Exotherm

PENG Xiaohong [1] and QIU Zhaowen [2]

[1]Department of Automobile, Shaanxi College of Communication Technology, Xi'an 710021, Shaanxi, China; PH (86) 029-86405046; email: xiaohongpengcau@163.com

[2]School of Automobile, Chang'an University, Xi'an 710064, Shaanxi, China; PH (86) 029-82334425; email: qzw@chd.edu.cn

ABSTRACT

This paper analyzes the mass-transfer and diathermancy of the three-way catalytic converter (TWCC). Applying mass-conservation and energy-conservation for gas and solid, the paper establishes a TWCC inner equation and makes the model dimensionless. The numerical models between the conversion efficiency and outlet-inlet gas temperature difference of TWCC working at a stable condition are derived. Lastly, the verified experiment is processed and the reasons for the errors are explained. The results show that the models are useful.

INTRODUCTION

Today every new gasoline car is equipped with a three-way catalytic converter (TWCC) in combination with a fuel control system to reduce the pollutant in the exhaust from the gasoline engine. On-board fault diagnosis (OBD) for TWCC is necessary under new emission legislation. The OBD system can monitor the catalyst performance and the engine operation. The monitoring methods and technologies for three-way catalyst converter (TWCC) efficiency are core techniques of the OBD system. The main methodologies currently assess catalyst performance indirectly by existing sensors.

Exhaust emission limits imposed on HC suggest that a catalyst assessment system based on a sensor monitoring this pollutant is more desirable, although a CO or NOx sensor is also a possibility. Presently, HC sensors are under development, but they are not yet commercially available. Therefore, until the necessary technological progress is made, a compromise technical solution must be found for the design of low-cost monitoring systems based on existing sensor technology.

Two alternative technologies are now under development (Botsaris and Sparis, 2000). The first approach, adopted by many auto manufacturers, uses existing oxygen sensors. With the oxygen sensor approach, an additional oxygen sensor is installed after the catalyst to evaluate the catalyst performance by comparing its signal with the normal oxygen sensor placed before the catalyst. Another approach using oxygen sensors for catalyst efficiency monitoring is temperature sensors known as thermocouples. The approach has not yet been introduced in car production. Because the reactions occurring in the catalytic converter are strongly exothermic,

the measurement of the exhaust gas temperature difference of the catalytic converter out-inlet offers valuable information regarding its efficiency. So the second approach is also called the exotherm method (Tsinoglou and Koltsakia, 2002).

Temperature sensor technology is quite advanced, so it is used widely in the avigation and automobile fields. Compared with the oxygen or HC sensor, the temperature sensor has the advantage of quick response, dependability and lower cost. Presently, the high temperature sensor can meet the demands of auto-exhaust emission measurement. So the exotherm method is one direction for study on OBD monitoring of TWCC.

However, OBD monitoring studies use temperature sensors mainly to centralize experimentation and to utilize some experiential or qualitative evaluation strategy. From the standpoint of hydrodynamics and multiphase catalytic exotherm, this paper probes the relation of the catalytic thermal quantitied index, i.e., catalytic outlet-inlet temperature difference, and TWCC efficiency, and establishes a quantitative control model.

ANALYSIS FOR TWCC TRANSFER -MASS AND TRANSFER -HEAT

Inside the TWCC, there are not only catalytic reactions in the gas phase and solid phase, but also complicated transfer-heat phenomena. The vehicle emission is produced in engine flow via the paths of a TWCC' carrier, where CO, HC and Nox react in the catalyst process. Simultaneously, the pollutants exchange the heat with the TWCC carrier, which includes the process of intricate chemical and physical reaction. The pollutants transfer heat and mass by convection. Heat is exchanged between the emission in the pathes and the carrier. The mass is transferred between the pollutants in the pathes and the exhaust emission is absorbed in the catalyst surface because of the concentration difference. The emission absorbed in the catalytic surface reacts differently than in phase catalysis, which would come into being in an exothermic reaction. The temperature grad in the TWCC brings transferring heat in solid phase, and the heat flows to the ambient through the shell of TWCC.

TRANSFER -HEAT AND TRANSFER -MASS MODELS FOR TWCC

Currently, most TWCCs used in vehicles are a type of beehive ceramic. So in this paper the object is this type TWCC. As the catalyst converter is beehive, the carrier of TWCC is folded with thin pathes. When the exhaust gas rushes into the carrier, in fact, the exhaust gas rushes into the pathes. Therefore, in order to establish the transfer-heat and transfer-mass models of TWCC, firstly, the models for the single path are set up.

TWCC Transfer -mass Models of Gas Phase and Solid Phase.

$$\varepsilon \frac{\partial C_{g,i}}{\partial t} + \frac{\rho_p v_p}{\rho_g} \frac{\partial C_{g,i}}{\partial x} = k_{f,i} \cdot S(C_{s,i} - C_{g,i}) \quad (1)$$

$$S_{cat} R_i(\overline{C}_s, T_s) = \frac{\rho_g}{M_g} k_{f,i} \cdot S(C_{g,i} - C_{s,i}) \quad (2)$$

Where ε is void of monolith; $C_{g,i}$ is gas state concentration of species "i", mole fraction; ρ is gas density, kg/m^3; v is gas velocity, m/s; $k_{f,i}$ is mass transfer coefficient of species "i", cm/s; S isgeometric surface area p.u.reactor volume, cm^2/cm^3; $R_i(\overline{C}_s, T_s)$ is specific reaction rate for species "i", mol/(Pt·cm^2·s); and T_S is wall temperature, K.

TWCC Transfer -heat Models of Gas Phase and Solid Phase.

The TWCC carrier transfer-heat model of the gas phase is the following equation:

$$\varepsilon \rho_g \frac{\partial T_g}{\partial t} + \rho_p v_p \frac{\partial T_g}{\partial x} = h_x \frac{S}{C_{p,g}} (T_s - T_g) \quad (3)$$

Where T_g is gas temperature, K; h_x is the heat transfer coefficient in the direction of x axle, J/(cm^2·s·K).

The TWCC carrier transfer-heat model of solid phase is established based on the single pathes model.

So The TWCC carrier transfer-heat model of solid phase is:

$$(1-\varepsilon)\rho_s C^M_{p,s} \frac{\partial T_s}{\partial t} = (1-\varepsilon)\left[\lambda_{s,x} \frac{\partial^2 T_s}{\partial x^2} + \lambda_{s,y} \frac{\partial^2 T_s}{\partial y^2} + \lambda_{s,z} \frac{\partial^2 T_s}{\partial z^2}\right] + h_x S(T_g - T_s) + S_{cat} \sum_{i=1}^{n} (-\Delta H)_i R_i(\overline{C}_s, T_s) \quad (4)$$

Where $C^M_{p,s}$ is the specific heat of the wall, J / (kg·K); λ_s is thermal conductivity of solid, J/(cm^2·s·K); $(-\Delta H)_i$ is the heat of combustion of species "i",J/mol.

DIMENSIONLESS TO TWCC TRANSFER -HEAT AND TRANSFER -MASS MODELS

Predigestion of the Models. Considering that the rate of chemical reaction is far faster than the rate of thermal response, the time to respond gas phase can be

ignored, i.e. $\frac{\partial T_g}{\partial t} = \frac{\partial C_{g,k}}{\partial t} = 0$.

Then the equation (1) and (3) can be predigested to the following two equations:

$$\frac{\rho_p v_p}{\rho_g}\frac{\partial C_{g,k}}{\partial x} = k_{f,k}\cdot S(C_{s,k} - C_{g,k}) \quad (5)$$

$$\rho_p v_p \frac{\partial T_g}{\partial x} = h_x \frac{S}{C_{p,g}}(T_s - T_g) \quad (6)$$

Because the TWCC's carrier is symmetrical along the axis, its coefficients of heat exchange in the direction of the y and z axes are the same. Then, $\lambda_{s,y} = \lambda_{s,z}$, the equation (4) can be predigested to:

$$(1-\varepsilon)\rho_s C_{p,s}^{M}\frac{\partial T_s}{\partial t} = (1-\varepsilon)\left[\lambda_{s,x}\frac{\partial^2 T_s}{\partial x^2} + 2\lambda_{s,y}\frac{\partial^2 T_s}{\partial y^2}\right] + h_x S(T_g - T_s) + S_{cat}\sum_{i=1}^{n}(-\Delta H)_i R_i(\overline{C}_s, T_s) \quad (7)$$

Dimensionless to TWCC Transfer -heat and Transfer -mass Models.

$$\overline{v}\cdot\frac{\partial \overline{C}_{g,k}}{\partial x} = \frac{Sh\overline{D}_k}{\overline{R}_h^2}(\overline{C}_{s,k} - \overline{C}_{g,k}) \quad (8)$$

$$\overline{S}_{cat}\overline{R}_k(\overline{C}_s, T_s) = \frac{Sh\overline{D}_k\varepsilon}{\overline{R}_h^2 D_a}C_{g,co}^{in}\overline{\rho}_g(\overline{C}_{g,k} - \overline{C}_{s,k}) \quad (9)$$

$$\frac{\partial \overline{T}_g}{\partial \overline{x}} = \frac{Nu\varepsilon}{Pr\,Re\,\overline{R}_h}\overline{T}_g^{0.832}(\overline{T}_s - \overline{T}_g) \quad (10)$$

$$\frac{1}{Pr\,Re}(\overline{\lambda}_{s,x}\overline{R}_h\frac{\partial^2 \overline{T}_s}{\partial \overline{x}^2} + 2\overline{\lambda}_{s,y}\frac{\partial^2 \overline{T}_s}{\partial \overline{y}^2}) + \frac{Nu\cdot\varepsilon\overline{T}_g^{0.832}(\overline{T}_g - \overline{T}_s)}{Pr\,Re\,\overline{R}_h(1-\varepsilon)} + \frac{\overline{S}_{cat}HeDa}{(1-\varepsilon)}\sum_{i=1}^{n}(-\Delta\overline{H})_i\overline{R}_i(\overline{C}_s, T_s) = 0 \quad (11)$$

TEMPERATURE MONITORING MODEL FOR CONVERSION EFFICIENCY OF TWCC

The average conversion efficiency of TWCC is defined as follows:

$$\eta = \frac{\sum_{i=1}^{n}(-\Delta H)_i C_{g,i}^{in}\eta_{i,\ ave}}{\sum_{i=1}^{n}(-\Delta H)_i C_{g,i}^{in}}\times 100\% \Rightarrow \sum_{i=1}^{n}(-\Delta H)_i C_{g,i}^{in}\eta_{i,\ ave} = \eta\cdot\sum_{i=1}^{n}(-\Delta H)_i C_{g,i}^{in} \quad (12)$$

The following model can be deduced with the above control models, which is the Temperature Monitoring Model for Conversion Efficiency of the TWCC:

$$\eta = \frac{\sum_{i=1}^{N} C_i M_i \cdot \sum_{i=1}^{N} C_i \rho_i c_{pi}}{\sum_{i=1}^{N} \rho_i C_i \cdot \sum_{i=1}^{n} (-\Delta H)_i C_{g,i}^{in}} \Delta T_{ave} \qquad (13)$$

The equation (13) indicates that the catalyst temperature difference is related to its efficiency, when the inlet-gas concentration is stable. So, in that case, catalyst efficiency or age can be evaluated by measuring catalytic outlet-inlet temperature difference.

VERIFYING EXPERIMENT FOR THE MODELS AND ERROR ANALYSIS

A TWCC in good condition is used in the verifying experiment on the engine bench, when the engine is in stable condition. The thermocouple sensors are used to measure temperatures in the TWCC inlet and outlet. At the same time, the concentrations of the inlet and outlet gas are gained from an AVL five-gas instrument. Combining with the different of the inlet-outlet exhaust temperature, this paper applies the above Temperature Monitoring Model to compute the conversion efficiency of the TWCC and, then, compares it with the measured result.

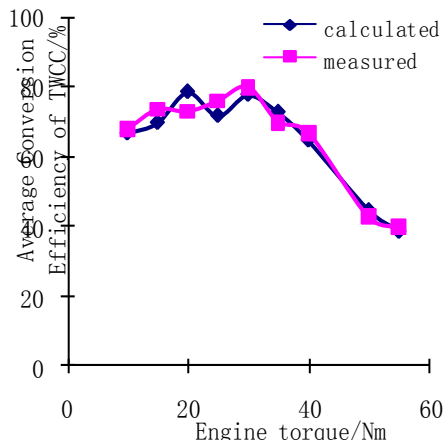

Figure 1. Comparison with average conversion efficiency of a TWCC at different engine torque .

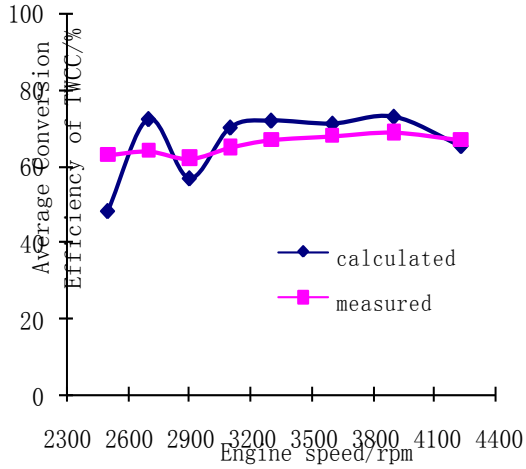

Figure 2. Comparison with average conversion efficiency of a TWCC at different engine speed .

It is shown in Figures 1 and 2 that the results of verifiying experiment and calculating with the model are consistent on the whole. The average error is 8.68%. Three reasons for the error were identified: First, the error is brought on by connatural error of the measuring devices. When measuring, the two devices cannot be absolutely synchronous. The temperature should be read at the same time when sampling, but it is difficult to finish. The temperature sensor's reliability and human error can be potential trouble. Second, the hypothesis of the model can be imperfect, which must make some error compared to the experiment result. Third, the selection of parameters in models can be problematic, because those parameters can vary from

the exhaust gas temperature and pressure.

CONCLUSION

The phenomena of transfer-mass and transfer-heat in theTWCC are discussed. From the standpoint of hydrodynamics transfer-heat and multiphase catalytic exotherm, according to gas phase and solid phase mass conservation and energy conservation within TWCC, the paper develops transfer-mass and transfer-heat conservation models for a monolithic catalytic converter and offers controlling equations to develop the monitoring model.

By making the equations dimensionless, the TWCC monolithic monitoring model is developed and the application of the monitoring models is analyzed. The analysis indicates that catalyst efficiency or age can be evaluated by measuring catalytic outlet-inlet temperature difference. Lastly, the verifying experiment is processed. It shows that the results of a verifiying experiment and calculating with the model are consistent on the whole. So, the model developed is useful for monitoring TWCC on board.

REFERENCES

Ali Akcayol, M. (Oct., 2005). "Artificial neural network based modeling of heated catalytic converter performance." Applied Thermal Engineering, 25(14/15), 2341-2350.

Botsaris, P. N., and Sparis, P D. Ambient temperature influence on catalytic outlet-inlet temperature difference, Proc. Instn Mech. Engrs Part D, Journal of Automobile Engineering, Vol214, 2000:95.

Fisher, G. B., Theis, J. R., Casarella, M. V., and Mahan, S. T. (1993). The role of ceria in automobile exhaust catalysis and OBDII catalyst monitoring, SAE Paper #931403.

Hepburn, J. S., and Gandhi, H.S. (1992). "The relationship between catalyst hydrocarbon conversion efficiency and oxygen storage capacity," SAE Paper 920831.

Sparis, P. D., and Botsaris, P. N. (1994). "Three-way catalyst assessment via inlet-outlet temperature measurements: A preliminary report," SAE paper 942055.

Sparis, P. D., and Botsaris, P. N. (1995). "Measurements of three-way catalyst performance under a stepwise constant idle speed schedule, SAE paper 952400.

Theis, J. R., Labarge, W. J., and Fisher, G.. B. (1993). "The effects of catalyst volume and ceria content on the emission performance and oxygen storage capacity of automobile catalysts, SAE Paper 932666.

Theis, J. R. (1994). "Catalytic converter diagnosis using the catalyst exotherm." SAE paper 942058.

Tsinoglou, D. N, and Koltsakia, G. C. (2002). "Potential of thermal methods for catalyst on-board diagnosis." Proc. Instn Mech. Engrs, Part D, Journal of Automobile Engineering, 216, 566.

Study on Burner Type Diesel Particulate Filter System Using Compressed Air from Turbocharger

X. Li[1], X. Zi[2], F. Yan[1], G. Yao[2], and J. Suo[2]

[1]School of Automotive Engineering, Wuhan University of Technology, Wuhan 430070, P.R. China
[2]Department of Automotive Engineering, Tianjin Transportation Institute, Tianjin 300161, P.R. China

ABSTRACT

Progress in diesel engine and filtration materials have made it easier to apply a burner type diesel particulate filter (DPF) in emission control. A full-flow burner type regeneration system is developed to remove diesel particulate matter (PM) deposited in DPF. Auxiliary air from a turbocharger is used to assist the ignition of burner and complete the combustion. Seeking the optimal parameters in terms of spray angle, injection pressure and spray position, a computational fluid dynamics (CFD) model is constructed and validated. Simulation with this CFD model identifies the main impact factor. A bench experiment is used to investigate characteristic of this regeneration system. The results show that exhaust temperature can be enhanced to 300 ℃ in 100 s by the burner, when the engine works at 0 N·m. The exhaust can be heated up to 500 ℃ when the burner and DOC (diesel oxidation catalyst) work together. The burner system can regenerate DPF efficiently in a wide operating range combining with fuel additive.

INTRODUCTION

Diesel engines have been recognized as one of the most efficient power sources for transportation machinery, since the air pollution and energy problems have become increasingly severe. However, their particle emission is still a big problem, although much progress has been made in the past twenty years. For compliance with tightening emission regulations, diesel particulate filters (DPF) are widely acknowledged in particle emission control.

The great difficulty in DPF application is its regeneration, since the soot collected in a filter has to be burnt off periodically to prevent clogging of the filter and passive influence on the engine. Usually the required temperature-level of this combustion is above 500 ℃. Even this range may be lowered to 300℃. By means of catalyst, either coatings or fuel-borne, the regeneration can not be fulfilled in all operating conditions yet. So many active regeneration technologies, such as electrical heating, microwave heating and infrared heating, have been studied (He, et al, 2007; Tim, 2007; Tan, et al, 2005).

Compared with other technologies, regeneration by burner has higher energy

efficiency and is easier to control (Paul, et al, 2002; Zi, et al, 2008). There are two kinds of burner DPF systems: one is by-pass and the other is full-flow. In the by-pass system, the exhaust will not pass through the burner and DPF in the regeneration process. In this way, the combustion in the burner will not be affected by the exhaust. But the location of the burner in the exhaust system becomes a serious problem, because of its volume and cost. So full-flow burner is preferable in commercial applications. However, in a full-flow DPF system, the exhaust will pass through the burner in the regeneration process, which brings about the difficulty of combustion. In this paper, a full-flow burner using compressed air from a turbocharger is designed to reduce system cost and complexity. Compared with traditional design processes, the computational method is not limited by economic or technical constraints. So a CFD model is constructed in the full-flow burner design to determine the optimal parameters. According to the simulation results, a full-flow burner DPF after-treatment system is set up for experimental investigation of thermal response.

DPF REGENERATION SYSTEM

Figure 1 shows a schematic of the burner-type DPF regeneration system designed in this work. Engine exhaust gas passes through the wall-flow filter during the filtration period. A full-flow burner, DOC and DPF are arranged in turn in the exhaust tailpipe. Because the power of the burner mainly depends on the limited air supplied from a turbocharger, so a diesel fuel injector is located on upstream DOC aiming at enhancing exhaust temperature by HC's oxidation process. In addition, Fuel additive (Fe based fuel borne catalyst) is used to extend the regeneration area in the engine MAP and prolong regeneration intervals. In the regeneration process, the exhaust will be heated initially by the burner. When exhaust temperature at the DOC inlet reaches 300 ℃, diesel fuel is sprayed upstream DOC and the exhaust will be heated further to the regeneration temperature.

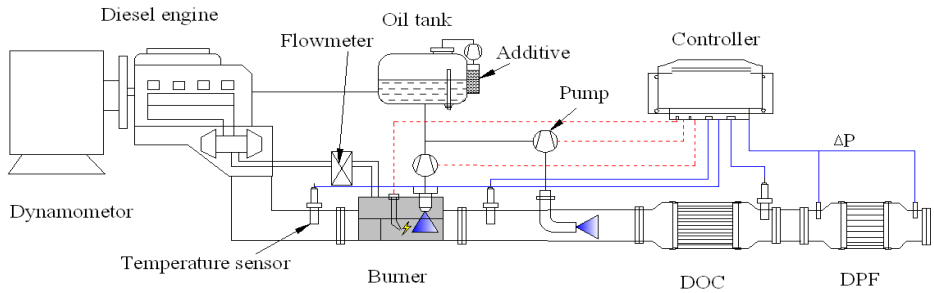

Figure 1. Schematic of DPF regeneration system .

BURNER CONFIGURATION AND OPTIMIZATION

Full-flow burn er configuration. A full-flow burner used in this paper is shown in Figure 2. The combustion chamber is "submersed" in the engine exhaust. This permits exhaust to circulate around the outside of the combustion chamber. In

this manner, the combusted fuel heat, as well as radiant heat emitted from the combustion chamber wall, is transferred to the exhaust. This limits heat loss during the combustion process.

The burner is fired with diesel. A schematic of the air distribution system in the burner is shown in Figure 3. The atomized fuel is provided by a swirl nozzle at the center of the first combustion chamber. Six small holes surrounding the nozzle let compressed primary air enter into the combustion chamber. A pair of electrodes operable to ignite fuel is located near the nozzle. The fuel is atomized and ignited in the first combustion chamber before entering the secondary combustion chamber. And it is completely burned in the secondary combustion chamber assisted by six swirl generator surrounding the expand chamber, through which the secondary air supply will flow to secure a homogeneous turbulent flow of the combustion air.

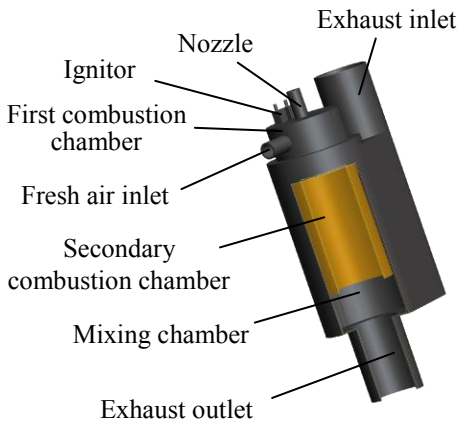

Figure 2. Layout of the burner .

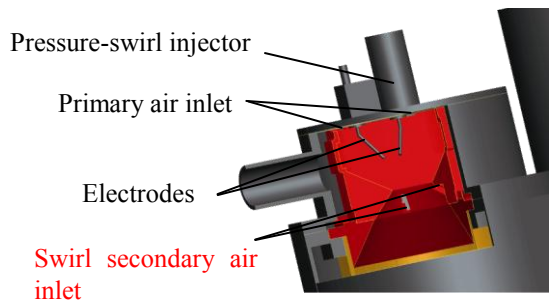

Figure 3. Schematic of air distribution system in burner .

CFD model and validation. Simplified assumptions introduced to the model are the following: First, the exhaust inlet and outlet are not modeled. Under this assumption, the mixture of engine exhaust and combustion air will not be considered. This leads to a lower number of mesh cells, better computational stability and minimization of computational time. Second, the combustion air inlet duct is not modeled. This simplification assumes that the combustion air flow will not be affected severely. Thus, only the combustion chamber is modeled. The surface of computational mesh is displayed in Figure 4. Tetrahedral mesh elements are applied. The proportion between primary and secondary air is 2:3. The length of the first combustion room is 40 mm, and its diameter is 72 mm. The length of the second combustion room is 195 mm, and its diameter is 94 mm. The entire mesh consists of about 71,953 cells. A pressure-swirl atomizer fuel spray model, probability density function (PDF) combustion model and RNG k-ε turbulent flow model are used in the simulation (Chiara, et al, 2007; Marek, et al, 2007).

Validation of the model is based on the mean temperature of the combustion chamber outlet. A SOFIM 8140.27S diesel engine was used in this project. The

details of the engine specification are listed in Table 3. Boundary conditions were set up as follows:

– inlet velocity for primary/secondary combustion air,

$v_1=v_2=15$ m/s, $T_{air}=300$ K

– outlet pressure at the combustion outlet,

$P_{out}=25$ kPa

– constant wall temperature of outer housing of combustion chamber,

$T_{wall}=500$ K

– constant mass flow for diesel fuel supply,

$Q_{fuel}=1$ kg/h, $T_{fuel}=300$ K

Figure 5 shows the results of the simulation and experiment. Experimental results are in good agreement with the CFD model.

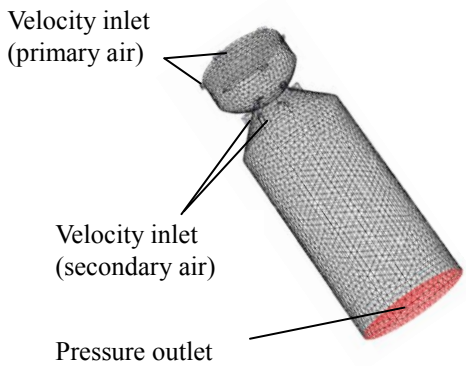

Figure 4. Computational mesh

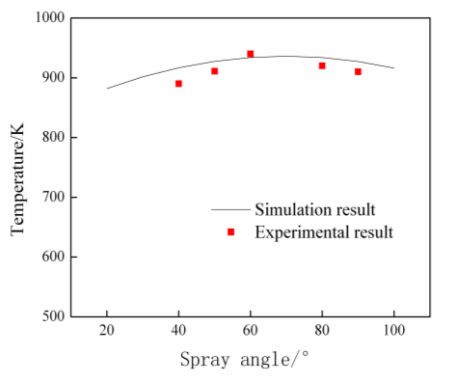

Figure 5. Comparison of experimental and simulati on results .

Configuration optimization . The main factors, which affect the combustion process, include spray position, spray angle and injection pressure. To determine the optimal parameters, an orthogonal experiment design is adapted. Due to the shape of the combustion chamber, interaction between the main factors must be considered. Table 1 shows the factors used in the experiment and Table 2 illustrates the simulation results. Injection position 1, 2 means the distance between the spray point and the center of the first combustion chamber is 0 mm, 10 mm.

Table 1. Factors and levels in the CFD experiment .

level	factor		
	Injection position （A）	Spray angle/° （B）	Spray pressure/MPa （C）
1	1	40	0.6
2	2	60	0.8

Table 2. CFD Orthogonal experiment a nd result .

Experiment number	factor						average outlet temperature /K
	A	B	A×B	C	A×C	B×C	
1	1	1	1	1	1	1	921
2	1	1	1	2	2	2	915
3	1	2	2	1	1	2	942
4	1	2	2	2	2	1	940
5	2	1	2	1	2	1	874
6	2	1	2	2	1	2	902
7	2	2	1	1	2	2	960
8	2	2	1	2	1	1	989
M1(average of level.1)	929.50	903.00	946.25	924.25	938.50	931.00	
M2(average of level.2)	931.25	957.75	914.5.0	936.50	922.25	929.75	
R（Maximum difference）	1.75	54.75	31.75	12.25	16.25	1.25	

The performance of the burner mainly depends on air-fuel atomization and mixture formation. When the injection position moves toward the secondary combustion chamber, the decrease of primary air utilization will lead to lower mixture velocity of fuel and air. In the same way, the increase of the spray angle will bring about the better mixture of fuel and air. But a too large spray angle will enhance spray wall-impingement. The range analysis shows that the spray angle is the most important factor influencing combustion performance. The optimal scheme is $A_2B_2C_2$.

ANALYSIS OF REGENERATION SYSTEM CHARACTERISTICS

Experimental apparatus. As shown in Figure 1, three K-type thermocouples are arranged before burner DOC and DPF respectively. Pressure gage is located across DPF, which is made of Silicon Carbide and not catalyzed. The DPF is 178 mm in diameter and 152mm in length. The specifications of SOFIM 8140.27S diesel engine and other experimental apparatus can be seen in Tables 3 and 4.

Table 3. SOFIM engine specification .

Engine configuration	Turbocharged direct injection
Cylinder Configuration	Inline 4
Displacement/L	2.499
Compression Ratio	18.3∶1
Maximum Torque/（N·m/r/min）	225/2000

Table 4. Equipment and instruments .

Name	Type
Dynamometor	CW160
Data collector	2700
Pressure gage	ZHP118

Characteristic s of engine exhaust. In order to analyze the characteristics of the regeneration system, engine exhaust temperature and intake pressure are

investigated first. Figure 6 shows the change of exhaust temperature with engine speed and torque. From the graph it can be seen that most of the exhaust temperature is lower than 200 ℃ when the load of the engine is low. Figure 7 shows the change of intake pressure with engine speed and torque. It is clear that when the engine operates at low speed and load, the intake pressure is very low. This means little fresh air can be supplied by the turbocharger.

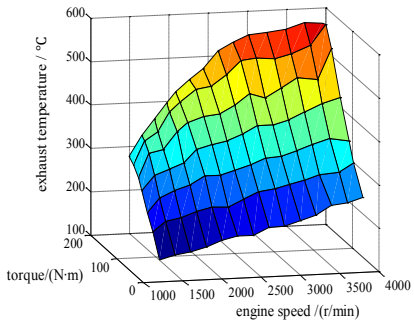

Figure 6. Change of exhaust temperature with engine speed and torque .

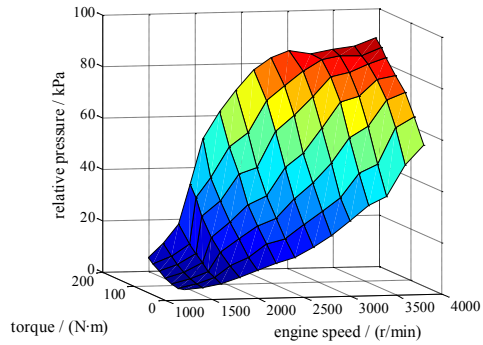

Figure 7. Change of intake pressure with engine speed and torque .

Figure 8 shows the change of exhaust temperature, backpressure and intake pressure with engine speed, when the engine works at 100% load. The DPF loading condition is 6g/L.

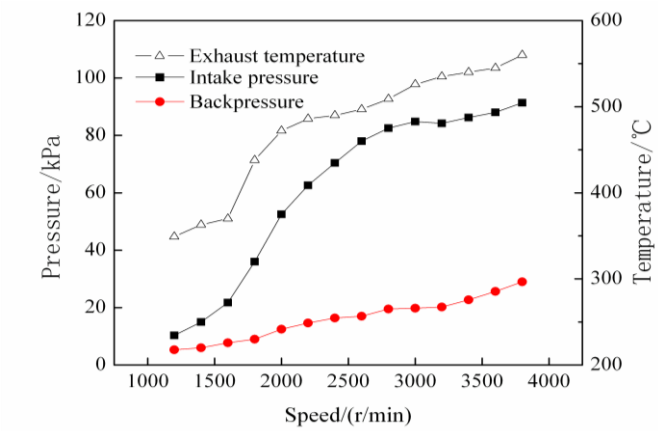

Figure 8. Effect of engine speed at 100% load on exhaust temperature, intake pressure and bac kpressure.

It is clear that exhaust temperature, backpressure and intake pressure increase with the engine speed. This is mainly caused by the increase of exhaust velocity. Although the backpressure and intake pressure both increase with the engine speed, the intake pressure increases more quickly because of the characteristic of turbocharger. The maximum difference between the backpressure and intake pressure reaches 65 kPa. Bigger pressure difference means more fresh air can be obtained

from the turbocharger. And when the engine works at high speed, exhaust temperature is high too. Both of these two conditions are helpful for DPF regeneration. But at low speed and low load operating condition of engine, regeneration is difficult due to the low exhaust temperature and low pressure difference between the turbocharger and exhaust pipe. So it is important to study the characteristic of the regeneration system as the engine operates at low speed and load.

Thermal response of the burner DPF system. The performance of burner DPF system at 0 N·m is shown in Figure 9. The fuel consumption of the burner and DOC is 1.0 kg/h, 1.5 kg/h respectively. It can be seen that performance of the burner at low engine speed is better and the temperature has been enhanced from 124 ℃ to 326 ℃ by the burner. Although temperature at the burner outlet increases with engine speed, the velocity of exhaust flow through the burner increases simultaneously. This means more exhaust will be heated up at the same time. So the difference of burner outlet temperature before and after burner working (△T) decreases as engine speed increases. The space velocity plays an important role in the application of DOC during the heating process. The geometry dimension of DOC used in Figure 9 is Φ120 mm×220 mm. Data in Figure 9 illustrate that DOC outlet temperature has been heated up from 178 ℃ to 500 ℃ at 2400 r/min. But when engine speed reaches 3200 r/min, temperature at DOC outlet is only enhanced to 413 ℃. The main explanation may be the higher space velocity. So a bigger DOC is applied in the experiment below.

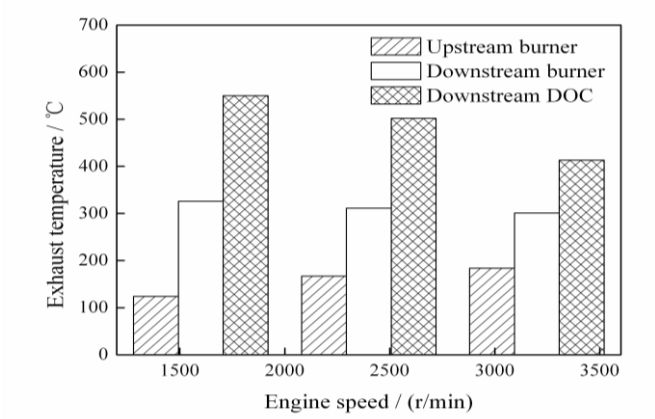

Figure 9. Performance of regeneration system at different speed .

Figure 10 shows the comparison before and after the scheme was optimized at 3200 r/min, 0 N·m. Introducing bigger DOC is effective for heating up to a temperature of 500 ℃. The geometry dimension of DOC used in Figure 10 is Φ150 mm×220 mm.

Regeneration characteristics in engine condition of 2800 r/min, 40 N·m are shown in Figure 11. The exhaust has been heated up to 300 ℃ in 100 s by the

burner and heated up to 500 ℃ further by the after-treatment system in 300 s. In the prophase of the heating process, temperature downstream from the burner increases much faster. But when fuel is injected before DOC, the speed of temperature increase begins to slow down. This may be caused by the increase of backpressure due to higher exhaust temperature, which brings about an unfavorable influence on air supply from the turbocharger. With a fuel additive, when the exhaust temperature arrives at approximate 480 ℃, the backpressure begins to decrease and regeneration occurs.

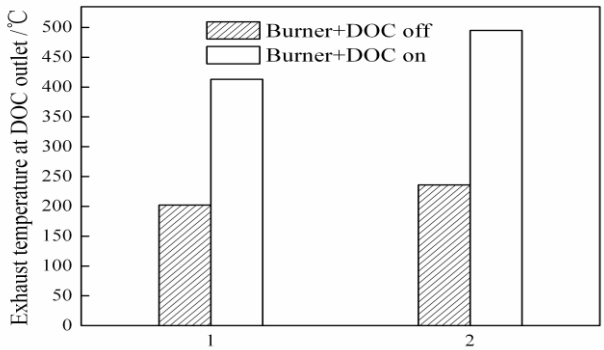

1. Before optimized 2. After optimized

Figure 10. Comparison before and afte r optim ization.

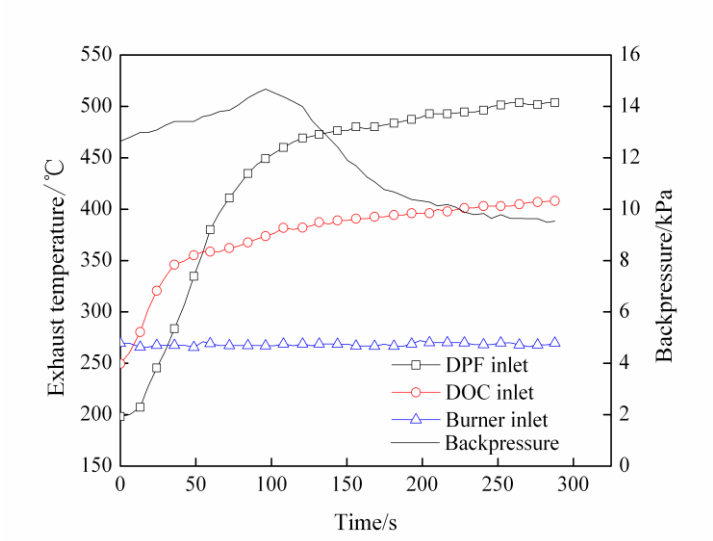

Figure 11. Regeneration characteristics in engine condition of 2800 r/min, 40 N·m.

CONCLUSION

A full-flow burner DPF system is designed to remove particulate matter from a diesel engine and the thermal response of this after-treatment has been investigated.

1) Result from the three dimensional simulation shows that: Spray angle is the most important factor which influences the burner performance after the main burner configuration is decided.

2) It is feasible to use compressed air from the turbocharger for DPF regeneration. The exhaust can be heated up to 300 ℃ at 0 N·m in 100 s when the full-flow burner works alone.

3) The burner DPF system, which can be divided into two steps in the heating process, can effectively enhance the exhaust temperature to 500 ℃ in a wide operation range.

4) The optimization of DOC space velocity and use of fuel additive are propitious for the application of the full-flow burner DPF system.

REFERENCE S

Chiara, G., Alessandro, P., and Leonardo, T. (2007), "Numerical and experimental investigation of a mild combustion burner." Combustion and Flame, 151: 649-664.

He, H., Weng, D., and Zi, X. Y. (2007), "Diesel emission control technologies: a review ." Environmental Science, 28(6):1169-1177.

Marek, S., and Pavel, Petr, S. (2007). "Computational support in experimental burner design optimization ." Applied Thermal Engineering, 27:2727-2731.

Paul, Z., Clive, T., Dave, P., et al (2002). "Development of a full-flow burner DPF system for heavy duty diesel engines." SAE Paper 2002-01-2787.

Tan, P. Q., Hu, Z. Y., Lou, D. M., et al (2005). "A review of regeneration technology for diesel particulate filters." Vehicle Engine, 159(5):6-9.

Tim, J. (2007), "Diesel emission control overview." AVECC 2007 International Metropolitan Vehicle Pollution Control Seminar, Beijing, 79-89.

Zi, X.Y., Wang,C., Yao, G.T., et al (2008). "Study on working pattern recognition for regeneration system of diesel particulate filter". Vehicle Engine, 174(2): 83-86.

RUNOFF POLLUTANTS CO NTROL BY ASPHALT PER MEABLE PAVEMENT

Xiaoguang Xie[1], Yongpeng Xu[2], Long Wang[3]

[1]Associate Professor, School of Transportation Science & Engineering, Harbin Institute of Technology, Harbin, Heilongjiang, PH 0451-86282120, FAX 0451-86283779, Email: xxg75@126.com
[2]Associate Professor, School of Municipal and Environmental Engineering, Harbin Institute of Technology, Harbin, Heilongjiang, PH 0451-86282060, FAX 0451-86282330, Email: xuyongpeng123@163.com
[3]Associate Professor, School of Transportation Science & Engineering, Harbin Institute of Technology, Harbin, Heilongjiang, China, PH 0451-86282120, FAX 0451-86283779, Email: hitlongwang@sina.com

ABSTRACT

Asphalt permeable pavement (APP) is a passive structural low impact development material and component of green infrastructure for rainfall-runoff control. Multifunctional engineered APP can fulfill requirements as a load-transmitting surface while serving as a more environmentally conscious infrastructure material that functions to restore the in situ hydrology, reduce runoff, filter, and treat infiltrating runoff, reduce thermal pollution and temperature, also provide the load-carrying capacity of conventional pavement. Based on the determination of main value indices for runoff pollutants, the efficiency of controlling runoff pollutants has been studied from materials and structures of permeable pavement in this paper, then put forward to the keys of material and structure design for permeable pavement, which will provide techniques for designing ecotypic permeable pavement. All the results indicate high particle separation and the removal rate of chemistry oxygen demand can be achieved with APP. The effectiveness of APP for particle and COD removal also requires that these particle deposits are managed on a periodic basis through practices such as pavement cleaning.

INTRODUCTION

Conventional pavements are the most common examples of impervious surfaces in the urban environment and in part cause a significant modification of the local hydrologic cycle (Kuang 2007). Expansive impervious areas have a significant impact on reductions in groundwater recharge, the depletion of soil moisture, and the corresponding increase in runoff, also reduction evaporation and evapotranspiration, known as heat island effects (Sansalone et al. 2004). With respect to the problems caused by impervious pavements, asphalt permeable pavement functions as a passive

unit operation and process for storm water quality and quantity control through infiltration, evaporation, filtration, absorption and reaction mechanisms. Permeable pavement reduces runoff, flooding, and treatment requirements; act as a sorbent filter that reduces the pollutant loads of phosphorus and nutrients to the environment; and reduces pavement and water temperatures. It also increases infiltration back to the soil to provide groundwater recharge to enhance future water supplies (Sansalone et al., 2008). But there is little study on runoff pollutant control by asphalt permeable pavement, especially in China. So this study focuses on the efficiency of controlling runoff pollutant by materials and structures of asphalt permeable pavement which is very significant to purify underground water and make full use of rainfall.

METHOD

Indices of Runoff Pollutants

Studies indicated that runoff pollutants included suspended solids (SS), chemical oxygen demand (COD), phosphorus and nutrients, and the levels of Zn, Cu, Cd, Pb, Cr, Ni and so on (Park 2004; Li 2005), in which SS and COD are the main pollutants, which mainly come from tire abrasive granules, pavement material abrasive granules, leak of transportation goods and other granules relative to transportation. So the main runoff pollutant indices are determined as COD and SS.

Chemical Oxyge n Demand

Under the fixed condition, the consuming quantity of oxidant in dealing with water samples with strong oxidant is named by chemical oxygen demand, ab. COD (O_2，mg/L), which reflects the contaminated degree of reductive substances in the water sample.

Suspended Solid

Solid in the water can be divided into soluble solid and suspended solid, ab. SS(mg/L). The percentage of removal rate of SS indicates the degree of removal rate of solid granules in the water.

Water Sample

Water samples come from two kinds, one is highway runoff collected at the drainage in the rain; the other is prepared in the lab according to the components and quantities of runoff pollutants.

Compaction

In the paper, self-designed vibrating compaction method is adopted. Through test study on optimum vibrating techniques, vibration parameters are determined as follows: vibration frequency(30Hz), low swing (0.957mm), vibration force (7kn)、vibration time(2.5minutes). Specimen dimension: ϕ150mm×100mm. For cement permeable pavement materials, in order to avoid cement mortar staying on top or bottom during the compaction, the uniformity tests have been done under different vibrating times, then the optimum vibrating time is determined as 1min.

STRUCTURE OF PERMEAB LE PAVEMENT

Permeable pavements have been more and more widely applied in the USA, Europe, Australia and Japan in the last two decades. Especially in Japan, infiltration facilities including permeable pavements were introduced and progressively implemented during the 1980s. When rainfall infiltration was first implemented, its primary objective was to reduce runoff volume. With the enhanced recognition of water quality benefits, as well as the Japanese desire to maintain closeness with nature in an urban setting, however, permeable pavement philosophy has shifted more towards groundwater cultivation than runoff reduction since the 1990s. Until now typical permeable pavements have been formed in Japan. Permeable pavement has seldom been studied in China for its durability. But from the view of alleviating heat island effects, supplying groundwater, reducing runoff and so on, permeable pavements have more advantages, so this kind of permeable pavement should be designed at the roads of squares, resident sections, parking lots and some places in which load bearing is lower and traffic volume is smaller. The structure of permeable pavement in this paper is as follow Figure1.

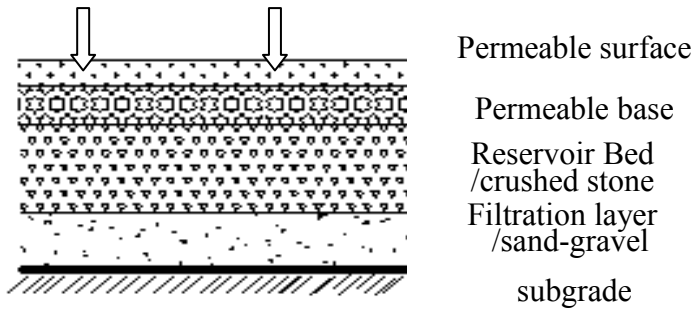

Figure1. Structure of permeable pavement.

TEST

Materials Composition

In order to distinguish the degree of removal rate of pollutants in different asphalt mixtures, continuous gradation and gap gradation of asphalt permeable mixture are adopted in the permeable pavement surface. While cement stabilized aggregate is adopted in the permeable base. Single seize as 13.2mm is applied to aggregate layer and 4.75mm is applied to sand-gravel bed course. The gradations are tabulated in Table1.

The optimum asphalt-aggregate ratio of permeable asphalt mixture is determined according to Marshall test，which is respectively as 2.8% for continuous gradation and 3.0% for gap gradation. The coarse skeleton of cement stabilized aggregates is shown in Table1, where air voids are filled by 15% of cement mortar, composed by w/c (0.36) and water reducer（0.6%）. Above materials are compacted

by vibrating techniques (seen as compaction).

Table1. Gradations of different layers .

gradation	Air void /%	seize/mm cumulative passing percentage/%											
		26.5	19.0	16.0	13.2	9.5	4.75	2.36	1.18	0.6	0.3	0.15	0075
continuous gradation of HMA	26.2	100	72	60.2	48.5	34.7	15.6	9.1	7.7	5.8	3.6	1.6	0
Gap gradation of HMA	20.2	100	100	100	50	50	25	25	13	13	5	5	5
Cement stabilized aggregate	21.8	100	89.7	80.8	61.7	29.3	0	0	0	0	0	0	0

Efficiency in Removal Pollutants of Structure Layer s

The values of COD and SS are measured for original water samples and through the structures' sample, accordingly, the removal rates of COD and SS are calculated, detail results are as follow Figure2.

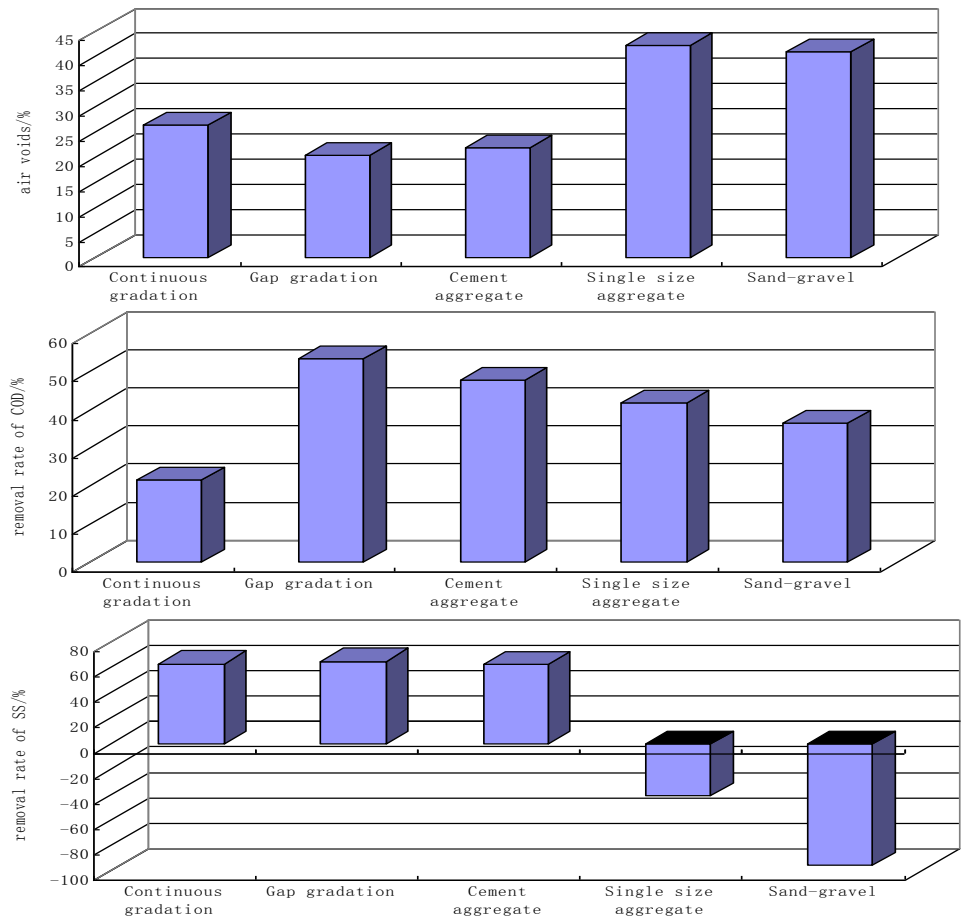

Figure2. Main technique value s of materials.

Some conclusion could be derived from Figure2,

① For permeable surface and base, the removal rates of COD are accreting from 21.74% to 47.83% with the decrease of voids from 26.2% to 21.8%, while the removal rates of SS are equal（62.82%~62.04%）, which mainly due to the COD depending on the filtration and absorption of porosity, so pore characteristics is critical to determine the functions of permeable pavement, which is less relation to the component material. Thus, pore characteristics are the key to design the permeable pavement.

② For loose reservoir bed and filtration layer, the air voids of crushed stone and sand-gravel are similar, so the removal rates of COD are equivalent, ranging from36%~42%. But value of SS is increasing evidently compared with water sample, that is, the removal rate of SS is negative. The reason is that materials of loose reservoir bed and filtration layer are dirty, including sand and mud and so on, which lead to sand and mud flowing with water sample when water pass through the structure layers.

③ Although the air voids of continuous and gap gradation are similar, the removal rates of COD are quite different. With the decrease of air voids, the removal rates of COD could improve to 2.47 times, from 21.74% to 53.62%, while the removal rates of SS are equivalent(62.82%~64.77%) and has similar trend with COD, little different is minor range. So the removal rate of COD is intimately relative to pore characteristics.

Efficiency in Removal Pollutants of Structure Combinations

There are two kinds of combination of structure layers, one is Permeable surface+ permeable base, the other is Reservoir bed+ Filtration layer. Calculating the removal rates of COD and SS, detail results are tabulated in Table2.

Table2. The removal rate of pollutant through diffe rent layers combination .

Structure layer	material	COD		SS	
		value（mg/L）	Removal rate /%	value（mg/L）	Removal rate /%
Permeable surface+ base	Continuous HMA+ Cement stabilized	101.7	43.48	2567.6	35.81
	Gap HMA+ Cement stabilized aggregate	79.9	55.62	2418.8	39.53
bed+ Filtration layer	Single size aggregate+sand-gravel	96.8	46.20	8328.4	-108.21
bed+ Filtration layer	Single size aggregate+sand-gravel+ fiber	63.5	64.72	1980.2	50.49

① From Table2, the removal rate of COD of structure combination is not the cumulated by the removal rate of individual structure layers. The removal effect of

structure combination is determined by the removal effect of individual structure and structure combining mode. The removal effect of COD mainly depends on the filtration, block and absorption of pore structure. While different layers may have similar pore characteristics, then the removal rates have similar values, so the removal rate of COD through structure combination is equivalent to the structure layer having higher removal rate of COD.

② Materials of different structure layers should be designed according to the functions of individual layers. That is, if the removal effect of COD is supposed on surface layer, the relationship between pore characteristics and the removal rate of asphalt mixtures should be studied further, then instructing the material design of permeable asphalt mixture according to pore structure.

③ The removal rate of SS for structure combination is lower than the removal rate of individual structure layers. The reason is that as the height of structure is increasing, the content of minor gravels is also increasing, while these gravels could flow with water sample, which makes the value of SS accreting. Also, fiber can make decisive function to retain the suspended solid.

CONCLUSION

- Although the materials of different Structure layers are quite different in the permeable pavement, they all have certain removal effects on COD, which indicates that the organic pollutants stayed in the pore structure of permeable pavement through filtration, absorption and block the function of purifying the water.
- Mixtures of permeable surface and base have been wrapped by binder and have better space network structure, which make suspended solids to stay in the inner pore structure, then exhibiting better removal rate of SS. While dirty aggregates exist in the loose reservoir bed and filtration layer，suspended solids increase when water sample flows through the structure layers, then the removal rate of SS is negative.
- The removal rate of COD of structure combination is not cumulated by the removal rate of individual structure layers, and is equivalent to the structure layer having higher removal rate of COD. The removal effect of structure combination is determined by the removal effect of individual structure and structure combining mode. While the removal rate of SS of structure combination is lower than the removal rate of individual structure layers.
- Permeable pavement structures have better removal effect of organic pollutants in the runoff, but increase the content of suspended solids. For the organic pollutants having heavier influence on water than suspended solids, it can be derived that permeable pavement has the efficiency on control runoff pollutants and fiber can be used in the subbed course to filtrate the suspended solids to purify the groundwater.

- It is just a beginning to study permeable pavement from control runoff pollutants. In order to apply the permeable pavements widely, the mechanism of pore structure controlling runoff pollutants should be researched deeply, which will benefit to carry out material and structure design definitely.

REFERENCE

Kuang, X., Kim, J.Y., and Gnecco, L. (2007). "Particle Separation and Hydrologic Control by Cementitious Permeable Pavement." Journal of the Transportation Research Board, 111-117

Li, Yingxia; Lau, Sim-Lin; Kayhanian, Masoud; Stenstrom, Michael K(2005). "Particle size distribution in highway runoff." Journal of Environmental Engineering, 131(9):1267-1276

Park, S. B., and Tia, M. (2004). "An experimental study on the water-purification properties of the porous concrete." Cement and Concrete Research, (34):177-184

Sansalone, J., Teng, Z. (2004). "In Situ Partial Exfiltration of Rainfall Runoff. I: Quality and Quantity Attenuation." Journal of Environmental Engineering, 990-1007

Sansalone, J., Kuang, X., Ranieri, V. (2008). "Permeable Pavement as a Hydraulic and Filtration Interface for Urban Drainage." Journal of irrigation and drainage engineering, 666-674

Research on Numerical Simulation of Pollutant Dispersion at Expressway Toll Plazas Based on Multi-influencing Factors

Z. Qi[1], J. He[1], X. Li [1], C. Zhao[1], and X. Bao[1]

[1]Transportation College, Southeast University, Si pai lou 2, Nanjing, China, 210096; PH (86)025-83790839; email: qzg_21202120@163.com

ABSTRACT

Currently, expressway toll stations in China generally use loading-based toll collection. Because vehicles spend long time either stationary or accelerating/decelerating in low gears, air quality is particularly susceptible to the accumulation of vehicle-emitted pollutants at toll plazas. In this work three-dimensional computational fluid dynamics (CFD) simulations were carried out to analyze the pollutant concentration distribution in the vicinity of tollbooths. Several influencing factors including wind velocity, wind direction and topography of toll plazas were considered. A simulation instance of the Wuzhuang toll plaza in Hefei-Nanjing expressway was performed. The simulation results show that the increase in wind speed facilitates the pollutant dispersion. There is higher concentration of pollutant as the angle between the direction of wind and traffic becomes larger. The existence of retaining walls impedes the pollutant dispersion. However, the slope of retaining walls has little influence on the variation of pollutant concentration.

INTRODUCTION

Automotive exhaust is the major source of air pollution at toll plazas. At the present time, expressway toll stations in China generally use loading-based toll collection. Vehicles spend a long time either stationary or accelerating/decelerating in low gears passing through the toll plaza, leading to relatively greater concentrations of pollutants in exhaust emissions than is the case at cruising speeds. The health of tollbooth workers is affected due to the proximity of the pollutant source. Therefore, it is significant to determine how these pollutants distribute at toll plazas and if, modifying some parameters, the pollution in the vicinity of tollbooths can be decreased.

Several field measurements of pollutant concentrations at toll plazas have been conducted in the past (Diab et al., 2005; Tsai et al., 2004). However, a limitation of direct field measurements is that all possible influencing factors are simultaneously operative and it is difficult to distinguish between those that are and are not significant. These factors include, among others, wind speed, wind direction, topology, traffic density, and they are all intertwined. Wind tunnel experiments and

numerical simulations provide an opportunity to examine the effects of various factors individually or in combination.

Recently, numerical simulations of pollutant dispersion without the need of complex experimental setups have been more frequent. Researchers have proposed two-dimensional and three-dimensional CFD models to simulate pollutant dispersion in street canyons. The results showed favorable agreement with the wind tunnel experimental results (Chang and Meroney, 2001; Sagrado et al., 2002; Chan et al., 2002). Compared to field measurements and wind tunnel experiments, numerical simulations are relatively inexpensive and more effective. Consequently, numerical simulation has become a powerful research tool. However, little is known about numerical simulations on pollutant dispersion at toll plazas. This paper presents three-dimensional numerical simulations on pollutant dispersion at toll plazas with the CFD code FLUENT 6.3. Flow and pollutant concentration are calculated based on the standard k-ε turbulence model. Effects of wind speed, wind direction and slope of retaining walls on pollutant dispersion near tollbooths are studied.

DESCRIPTION OF NUMERICAL SIMULATIONS

2.1 Toll plaza dimension .

As Fig. 1 shows, a simplified toll station with seven tollbooths was designed according to General Specification of Freeway Traffic Engineering and Roadside Facilities. In accordance with the toll station, three CFD models considering different influencing factors were built as shown in Fig. 2. The widths of outside traffic lanes, general traffic lanes and shoulders are 4.0 m, 3.2 m and 0.75 m respectively. The total width of the toll plaza is 44 m. The toll canopy is 6 m above the ground. The dimensions of toll islands and tollbooths are $60\times2.2\times0.2$ m^3 and $2.5\times1.5\times2.4$ m^3 respectively.

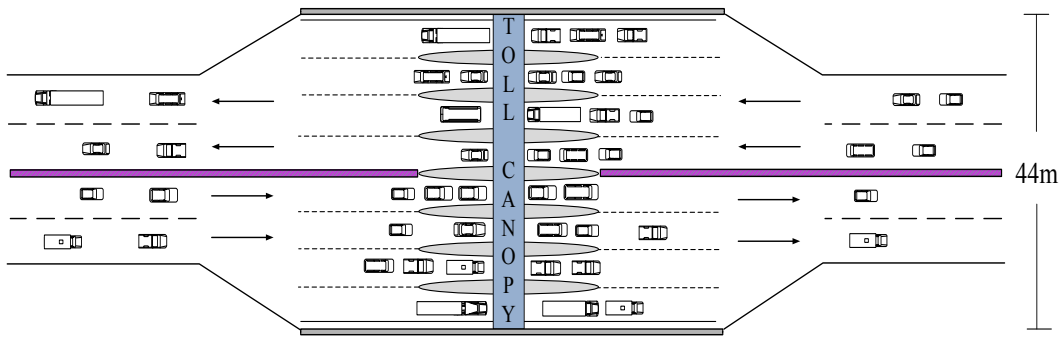

Figure 1. Schematic diagram of the toll station model.

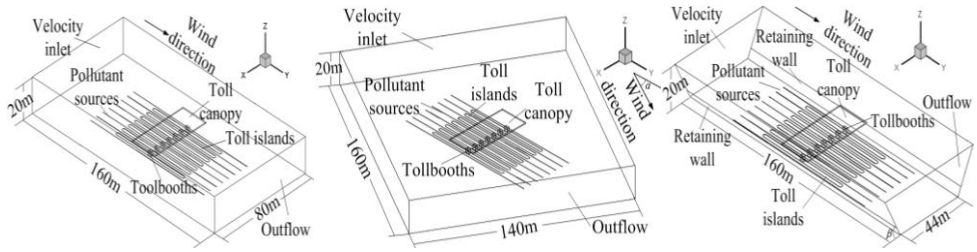

(a) (b) (c)

Figure 2. Illustrations of the computational domains considering the effects of (a) wind speed, (b) wind direction, and (c) slope of the retaining walls on pollutant dispersion.

From Fig. 2 we can see that the Y axis is parallel to the direction of traffic. α is the angle between the wind direction and the Y axis, as shown in Fig. 2(b). It should be noted that there are retaining walls on both sides of some toll stations due to topographic conditions and β means the slope of retaining walls, as shown in Fig. 2(c).

2.2 Simulation scheme .

In this study, we conducted three-dimensional CFD simulations to analyze the effects of wind speed, wind direction and slope of retaining walls on pollutant dispersion with FLUENT. This code has been widely used in simulations of pollutant dispersion in urban environments, especially in street canyons, with favorable results (Nazridoust and Ahmadi, 2006; Sabatino et al., 2007). In this paper, we designed a simulation scheme with nine cases to study the effects of different influencing factors on pollutant dispersion, as shown in Table 1. In case 1~3, wind speed is variable with the fixed wind direction and without retaining walls. In case 4~6, wind direction changes with the same wind speed and no retaining walls exist. As for case 7~9, wind speed and direction are both invariable with different slopes of the retaining walls.

Table 1. Simulation scheme with nine cases

	1	2	3	4	5	6	7	8	9
Wind speed at 20 m height/(m/s)	10	6	3	10	10	10	10	10	10
α/°	0	0	0	30	45	60	0	0	0
β/°	-	-	-	-	-	-	30	45	60

2.3 Boundary conditions .

In this paper, we chose CO as the representative pollutant to analyze the pollutant dispersion around tollbooths. The pollutant source was modeled as eight lines placed in the middle of each traffic lane with dimensions of 100×0.2 m^2 (Chan et al., 2002). We calculated the pollutant source strength, according to the investigation data of the Chayuan Toll Station (Chen et al. 2007), was 1.89×10^{-4} kg/s. The Chayuan Toll Station is located on the Chongqing-Guizhou highway with eight lanes and the

average traffic volume is 8000 vehicles per day. Velocity inlet boundary condition was used for the inlet wind flow. Thus, in all cases, incoming wind velocity had an atmospheric boundary layer profile $u = u_{z_0} \times (z / z_0)^{1/7}$. For the outlets at the end and lateral sides of the domain, an outflow boundary condition was assumed. All other solid surfaces of the domain (surfaces of tollbooths, toll canopy and retaining walls) were defined as walls with no slip velocity boundary condition. The line sources of CO were treated as mass flow inlets.

RESULTS AND DISCUSSIONS

Flow velocity and CO concentrations at the 1.5m height plane (tollbooth workers breathing height) were calculated. We also compared CO concentration on three observation lines: the center line of the computational domain perpendicular to the X axis (y=0 m) and the other two lines before (y=-5 m) and after (y=5 m) it. Because the flow velocity distribution is similar, only three representative contours of velocity magnitude are given in Fig. 3.

3.1 Effect of wind speed .

As shown in Fig. 3(a), wind speed approximately presents zonal distribution and decreases gradually along the positive direction of the Y axis. Wind speed decreases significantly in the areas behind the tollbooths which obstruct the airflow. The CO concentrations under different wind speeds were simulated, according to the case 1~3, and the results are shown in Table 2. Comparing the CO concentrations under three wind speed conditions, the maximum values all appear on the line behind the tollbooths (y=5 m). As wind speed increases, the maximum value of the CO concentration (68 mg/m^3, 50 mg/m^3 and 38 mg/m^3) reduces. This demonstrates that larger wind speed facilitates the pollutant dispersion and that pollutant accumulates behind the tollbooths. Chen et al. conducted field measurements of the CO concentration at Chayuan Toll Station in June and July, 2003. As shown in Table 3, the mean CO concentration outside the tollbooths is 10.865 mg/m^3. The results of measurements and simulations above are close. This demonstrates that the simulation results are reliable and further simulations can be carried out.

3.2 Effect of wind direction .

The CO concentrations under different wind directions were calculated according to case 4~6 and the results are summarized in Table 4. As shown in Table 4, when α increases, the range of the CO concentration extends. Additionally, the area of great CO concentration diverts from behind the tollbooths to the spaces among the tollbooths. This demonstrates that wind direction has a considerable influence on pollutant dispersion. Therefore, we can conclude that a smaller angle between the direction of wind and traffic better facilitates the pollutant dispersion in the vicinity of tollbooths.

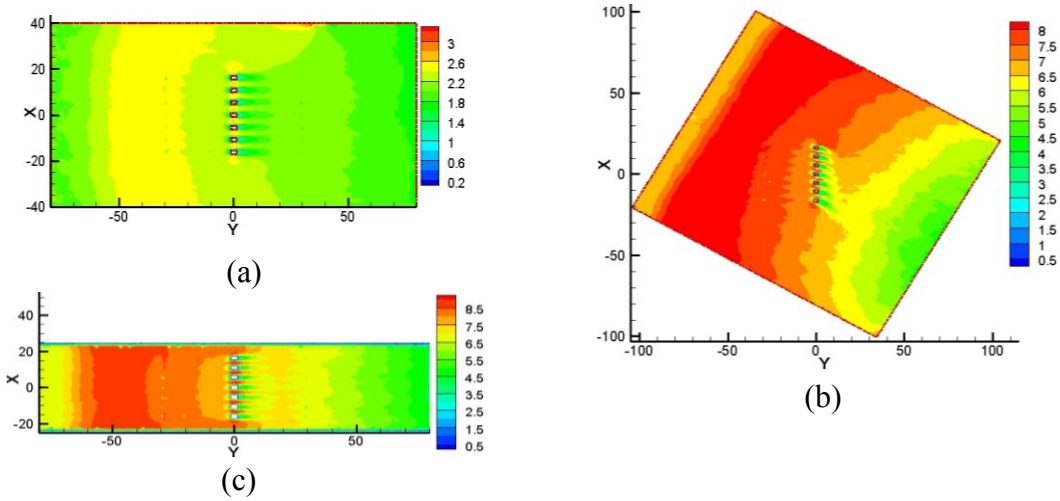

Figure 3. Flow velocity at the 1.5 height plane when (a) wind speeds of 3m/s, (b) α is 30° and (c) β is 30° , respectively.

Table 2. Range of CO concentrations under different wind speeds (mg/m ^{3})

Wind speed (m/s)	3	6	10
y=-5	0~28	0~18	0~14
y=0	0~22	0~15	0~12
y=5	0~68	0~50	0~38

Table 3. Statistics on the CO concentration (mg/m ^{3}).

Samp le number	mean concentration outside the tollbooths	standard deviation
12	10.865	3.305

3.3 Effect of the slope of retaining wall .

The CO dispersion of different slopes of retaining walls were simulated according to case 7~9. The results are also shown in Table 4. Table 4 shows that the ranges of the CO concentrations and the maximum values under three conditions are close. As a result, we can conclude that there is little influence on the pollutant dispersion when the slope of retaining walls changes.

Table 4 . Range of CO concentrations under different wind directions and slopes of retaining walls (mg/m ^{3}).

α/°	30	45	60	β/°	30	45	60
y=-5	0~30	0~160	0~600	y=-5	0~58	0~38	0~40
y=0	0~60	0~850	0~3800	y=0	0~158	0~106	0~110
y=5	0~325	0~525	0~750	y=5	0~140	0~102	0~155

A SIMULATION INSTANCE

The selected toll station is located on the Hefei-Nanjing expressway with 22 toll lanes, 48 km west from Nanjing. The retaining walls are 5 m high and their slope is 60° , because the ground is higher on both sides of the toll plaza. The distance between the retaining walls is about 120 m. The toll canopy is about 120 m long, 20 m

wide and 1m thick.

Two three-dimensional CFD models were established, according to the actual size of the Wuzhuang Toll Station, to study the effects of retaining walls on the pollutant dispersion. The computational domains have the approximate dimensions of 180 m × 160 m × 30 m. Based on the investigation data in September, 2006, the daily average traffic volume of the Wuzhuang Toll Station is 13860 vehicles per day. We again chose CO as the representative pollutant and the emission source strength is 3.21×10^{-4} kg/s. In this study, CO concentrations in the vicinity of tollbooths were calculated and the simulation results are shown in Table 5.

Table 5 . Range of CO concentrations with and without retaining walls (mg/m ^{3}).

with retaining walls	without retaining walls
0~24	0~12

As shown in Table 5, it is obvious that the average CO concentration is lower when no retaining walls exist. Therefore, the toll station should be located on flat and open land where pollutants dissipate easily.

CONCLUSIONS

Effects of wind speed, wind direction and slope of retaining walls on pollutant dispersion were studied using the CFD code FLUENT and some conclusions were obtained as follows.

Higher wind speed and smaller angle between the direction of wind and traffic better facilitates the pollutant dispersion in the vicinity of tollbooths. The existence of the retaining walls does not facilitate the pollutant dispersion. The slope of the retaining walls has little influence on the variation of the pollutant concentration. It is noted that there are some points where the concentration is much higher than others. This is because turbulence in the vicinity of the tollbooths leads to the accumulation of the pollutant.

Because of lack of the comprehensive field measured data, we paid more attention to the qualitative analysis of the simulation results. Future research can examine the effects of traffic density and toll collection mode on pollutant dispersion. In this paper, the simulation results of pollutant dispersion at the toll plaza with FLUENT are reasonable. As a result, the application of FLUENT to the CFD simulations on pollutant dispersion at toll plazas has good future prospects.

ACKNOWLEDGEMENTS

The authors would like to thank Southeast University for its financial support (project “Southeast excellent young staff foundation 2008-2011”).

REFERENCES

Chan, T. L., Dong, G., Leung, C. W., Cheung, C. S., and Hung, W. T. (2002). Validation of a two-dimensional pollutant dispersion model in an isolated street canyon.” Atmospheric Environment, 36, 861-872.

Chang, C.H., and Meroney, R. N. (2001). "Numerical and physical modeling of bluff body flow and dispersion in urban street canyons." Journal of Wind Engineering and Industrial Aerodynamics, 89, 1325-1334.

Chen, K. J., Chen, K. L., Zhang, L. J., and Leng, G. Y. (2007). "Characteristics and influencing factors of air pollution in and out of the highway toll gates."Environmental Science, 28, 1847-1853.

Diab, R. D., Foster, S. J., Francois, K., Martincigh, B. S., and Salter, L. F. (2005)."Carbon monoxide levels at a toll plaza near Durban, South Africa."Environmental Chemistry Letters, 3, 91-84.

Nazridoust, K., and Ahmadi, G. (2006). "Airflow and pollutant transport in street canyons." Journal of Wind Engineering and Industrial Aerodynamics, 94, 491-522.

Sabatino, S. D., Buccolieri, R., Pulvirenti, B., and Britter, R. (2007). "Simulations of pollutant dispersion within idealised urban-type geometries with CFD and integral models." Atmospheric Environment, 41, 8316-8329.

Sagrado, A. P. G., van Beeck, J., Rambaud, P., and Olivari, D. (2002). "Numerical and experimental modelling of pollutant dispersion in a street canyon." Journal of Wind Engineering and Industrial Aerodynamics, 90, 321-339.

Tsai, P. J., Shih, T. S., Chen, H. L., Lee, W. J., Lai, C.H., and Liou, S. H. (2004). "Assessing and predicting the exposures of polycyclic aromatic hydrocarbons(PAHs) and their carcinogenic potencies from vehicle engine exhausts to highway toll station workers." Atmospheric Environment, 38, 333-343.

Several Questions of Highway Influence Assessment on Dongting Lake Ecosystem in China

Liu Su[1], Zhang Yaping[1,2] and Xu Zhuokui[1]

[1]School of Transportation Engineering, Changsha University of Science and Technology, P.O. Box 410076, PH (+86)13055161279; email: liusuyx@126.com
[2]School of Transportation Science and Engineering, Harbin Institute of Technology, P.O. Box 150090, PH (+86) 15846598208; email: zxlt0905@163.com

ABSTRACT

A large number of research documents and on-the-spot investigation of Dongting Lake in China show that urban action and water conservancy action of highway and separate-approach action of highway affecting migrant bird's habitat are the main actions of influence by highway on Dongting Lake ecosystem. The assessment index system of influence by highway on Dongting Lake ecosystem is set up. The index system consists of classification of highway, urban action of highway and water conservancy action of highway. Some factors of sensitive area on which urban action act by highway and election of the monitoring areas with 3S technology, and it's technique of assessment, the technique of area analysis on which water conservancy action act by highway are studied. Monitoring areas on which water conservancy action act by highway are divided out. The above items are the basis of monitor and assessment about influence by highway on Dongting Lake ecosystem with 3S Techniques.

Keywords: Dongting Lake ecosystem, 3S techniques, Assessment index, Urban action of highway, Water conservancy action of highway.

INSTRUCTION

It is shown that there is a great influence on the ecological environment about highway construction. The wetland is the most important to the ecological landscape and biodiversity on our planet, and one of the ecological environments on which human society develops (Daniel J. et al. 1998). Wetlands provide water resource and a mass of food and materials of our production. At the same time, wetlands play an important role in the following aspects: maintaining resources of biodiversity and rare species (Kevin J. et al. 2003), to keep from and delay flood, conservation storage fights drought, maintaining water and soil, reducing environment pollution, providing travel resources, and maintaining balance of ecology of the earth.

The Dongting Lake is one of the six wetlands in China. Since the 20th century, people had enclosed lakes and built up fields on a large scale. Hundreds of dykes formed, which are not of uniform size. The wetland of Dongting Lake is incoherent. Area of the lakes reduced seriously. Dongting Lake's flood regulating and storing, navigation, biodiversity, ecological environment were endangered seriously. Nowadays, water resource is being polluted by use of agriculture fertilizer; industry

and sanitary sewage, medicinal liquid for prevent infection of blood fluke. So it is necessary to protecting wetland resources in Dongting Lake.

There are 303 kinds of birds live in Dongting Lake area, its quantity reaches1.5 millions. There are 37 habitats that over ten thousand of birds gathered in each habitat. 119 kinds of fishes live in the lakes. Dongting Lake is the main producing area of black carp, grass carp, silver carp and bighead in China. This area is also the main habitat for Chinese sturgeon, white sturgeon, neomeris phocaenoides and white-flag dolphin. Dongting Lake wetlands is the most important habitat of migratory bird in midstream and downstream basin of the Changjiang River, its migratory birds has various in style, quantity heavy, intensive degree high characteristic. Now, the environment of these bird's habitats is endangered by change of ecology caused by change of water level, economic actions of people, killing the wild animal illegally by local people, the silt depositing and pollution, and the water level reducing by the famous Three Gorges Engineering.

As we all known, highway construction is the founder of economic development of Donting Lake area. But highway construction and operation will bring disadvantage to Dongting Lake ecosystem. For assessment of influence by highway on Dongting Lake ecosystem, we should take something into account: enclosing lakes and building up fields over a long time, industry and sanitary sewage, use of medicinal liquid to prevent from infection of blood fluke and unreasonable use of biodiversity resources of wetland. Based on that Dongting Lake ecosystem is protected very well, the highway construction in this area is good, which is the historical responsibility of the work for highway construction in Dongting Lake area.

For assessment of influence by highway on Dongting Lake ecosystem, we should answer the following questions firstly: 1. What are the main factors of highway that influences Dongting Lake ecosystem? 2. How to build the assessment index system of influence by highway on Dongting Lake ecosystem? 3. How to develop the technology and methods of assessment of influence by highway on Dongting Lake ecosystem based on 3S Techniques?

MAIN CAUSES IN INFLUENCE BY HIGHWAY ON DONGTING LAKE ECOSYSTEM

A large number of research documents and on-the-spot investigation of Dongting Lake tell us (Mao Wenyong 2003; Dai Mingxin 2004; Li Rendong et al.2004; Dong Xiaolin 2003): the long-term silt depositting, enclosing lakes and building up fields over a long time are the main factors which shrank the water area of Dongting Lake; enclosing lakes and building up fields, hunting excessively, industry and sanitary sewage, fertilizer and medicine liquid for prevent infection of schistosome are the main factors lead to threaten the biodiversity of Dongting Lake ecosystem; industry and sanitary sewage, fertilizer and medicinal liquid to prevent from infection of blood fluke are also main factors which lead to polluted the quality of Dongting Lakes water. So, when we assess the influence by highway on Dongting

Lake ecosystem, the factors described above should be taken into account.

A. Influence by highway urban action on Dongting Lake ecosystem

Under the influence of highway, urban areas will extent and rural area will become towns or urban, which is the highway urban action (Zhao Kang 2003).

Some scholars carried researches about change of land use in this area between 1979 and 1999 based on 3S technology (GPS, RS and GIS). According their result, construction area increased obviously in past twenty years, amount to 15467hm^2. From 1990 to 2000, there are 5520hm^2 farmlands changed to construction area, among which: 54.83% turned to urban; 32.18% turned to industry and communication area; 13% turned to residential area for farmers. From the situation described above, we can know how seriously the highway urban action influenced the ecosystem of Dongting Lake (Li Rendong et al. 2004).

According to the dot-axis pattern of the government's development plan of urban of Dongting Lake area, the emphases of construction and planning are East-belt, Middle-belt and Southwest-belt of this area. The axis of East-belt consists of part of Jingguang Railway, Jingzhu Expressway, G107 National Highway, Xiang River, and the east lakeshore of East Dongting Lake. The axis of Southwest-belt consists of part of Shichang railway, Changchang expressway, G319 National Highway, and the section Changde-Linli-Zhanggongmiao of G207 National Highway. The axis of Middle-belt consists of the four branches of Ouci River, the canal of Nanmao, the watercourse of Songli and Muping Lake, and the main highway connecting Yiyang city, Yuanjiang City, Maocaojie, Nan County, Huarong County and Shishou City in Hubei province. So, the long-term urban action in this area should be taken into account seriously when we do our research.

Because of urban action induced by highway, some indirect long-term disbennifit to the Dongting Lake ecosystem exists: wetlands were occupied by the construction of town; wetlands were polluted by garbage and sewage produced by the action of people in the town; wetlands were changed to use for other intent by people, which will lead to disbennifit to biodiversity.

B. Influence by highway water conservancy action on Dongting Lake ecosyste m

The area of Dongting Lake is the important comprehensive agricultural commodity production base of China. The agriculture economy is high developed. In this area, flood disaster often occurred. Since 1949, water conservancies have been built extensively. Highways in the area do great contribution to the water conservancy, fighting floods, and economic development. Highways and other constructions of communication should be worked together with water conservancies, which will do good to the conservation of Dongting Lake ecosystem. In general, the highway in this area should be constructed with good water conservancy action:

1) The integration of highways and dykes. The people, farmland and people's economic activity centralized in dykes, whose area amounted to 72.3% of all area of Dongting Lake area. The renovation of these dykes is the important work to the

water conservancy of the area of Dongting Lake. Nowadays, the total amount of dykes is 227. It is 226 that ten thousand mu of dykes of the above are counted. It has very great potentiality on integration of highways and dykes. The integration can provide the communication of each dyke, at the same time, can reduce area of wetlands and farmlands occupied by highway construction. When flood occurred, the highway based on the dyke will play an important role in fighting flood.

2) The coordination of highways with irrigation and water conservancy facilities. The renovation project of Dongting Lake, which has been carrying through, has adjusted the old layout of irrigation facilities seriously (Lu Xinhai et al. 2002). This change properly diminished the function of older bridges and culverts, which made older highway don't work together with water conservancies, even disuse these constructions. So the work of reconstruction and construction is very difficult. Besides provide communication functions, the coordination of highways with irrigation and water conservancy facilities can satisfy the needs of farmlands irrigation and fighting flood, and also benefit the conservation of Dongting Lake ecosystem.

The degree of integration of highways and dykes, the degree of coordination of highways with irrigation and water conservancy facilities, produce indirect long-term influence on the ecosystem of Dongting Lake area.

C. Influence by separate **-approach action of highway on migratory birds'** habitats in Dongting Lake wetlands

Highways break the wetland into pieces; the animals living in certain area can not court and get food in more wide area (Richard et al. 2000). Split up in kind will occur if long-term separation to one specie last, which is disadvantageous to the biodiversity. The construction of highways extends the area of people's activity, which endanger the nature and the conservation of some rare resources. The influence described above is the so-called separate-approach effect of highway.

In the area of Dongting Lake, people had enclosed lakes and built up fields over a long time, which produced many dykes. These dykes were not of uniform size. In term of the length and scope of the area, the influence by separate-approach action of dyke is more serious than that of highway. So the latter is less serious on the ecosystem of Dongting Lake wetlands. But, it is proved that the construction, car lights and noise of highway do have influences on the migratory birds' habitats (Rien Reijnen et al. 1995), which is different with the change of geographical environment. In general, the influence by construction and operation of highway on migratory birds' habitats should be researched seriously.

MAIN INDEXES IN ASSESSMENT OF INFLUENCE BY HIGHWAY CONSTRUCTION ON DONGTING WETLANDS ECOSYSTEM

The assessment indexes of influence by Highway on Dongting Lake ecosystem should be the quantization indexes, should reflect the region characteristic and change of ecosystem influnced by every influence factor. As far as the choice of

the indexes, we should take the main influence factors by highway on Dongting Lake ecosystem into account seriously. The indexes should be lay particular emphasis on to some extent.

A. Index of highway classification

According to the highway engineering technological standard (JTG B01-2003) published by department of communication of PR. China, and the reality of that there are a lot of rural highway in Dongting Lake area, the index of class of highways is classified as follows: expressway, 1st class highway, 2nd class highway, 3rd class highway, 4th class highway and rural highway.

B. Index of highway urban action

The index of highway urban action consists of land-use index and society-economy index.

1) Land-use index

Land-use index consists of agriculture-land index, construction-land index and unused-land index.

Agriculture-land index includes such indexes as farmland, garden plot, woodland, grassland and other.

Construction-land index includes such indexes as urban, town, rural residential area, communication, water conservancy, self-existent industry and land for special use

Unused-land index includes such indexes as unused land that it is unused and other than land for agriculture and construction, other land that is water area other than water area for agriculture and construction. Unused land index includes such indexes as desolate land, marsh, sandlot and naked-land; other land includes index includes such indexes as river, reedy area and shoal.

We use the change value of these indexes and the rate of change of these indexes to reflect the influence degree of highway urban action directly:

If $A_j^{t_1}$, $A_j^{t_2}$ represent the area of land of kind j in class i at time t_1 and t_2, so we can get $\Delta A_{ij}^{t_1-t_2}$,the corresponding area changed of land of kind j in class i (a class includes some kinds) , and $\alpha_{ij}^{t_1-t_2}$,the corresponding rate of change:

$$\Delta A_{ij}^{t_1-t_2} = A_{ij}^{t_2} - A_{ij}^{t_1} \qquad \alpha_{ij}^{t_1-t_2} = \Delta A_{ij}^{t_1-t_2} / A_{ij}^{t_1}$$

So as for class i: $\sum_{j=1}^{n} A_{ij}^{t_1}$, $\sum_{j=1}^{n} A_{ij}^{t_2}$ are the area of time t_1 and t_2, then $\Delta A_{ij}^{t_1-t_2}$, the corresponding area changed, and $\alpha_{ij}^{t_1-t_2}$, the corresponding rate of change, could be calculated:

$$\Delta A_i^{t_1-t_2} = \sum_{j=1}^{n} A_{ij}^{t_2} - \sum_{j=1}^{n} A_{ij}^{t_1} \qquad \alpha_i^{t_1-t_2} = \Delta A_i^{t_1-t_2} / \sum_{j=1}^{n} A_{ij}^{t_1}$$

2) Society-economy index

Society-economy index consists of agriculture population in town,

non-agriculture population in town, general production value of agriculture, general production value of industry and production value of foodstuff.

We use the change value of these indexes and the rate of change of these indexes to reflect the influence degree of highway urbanization indirectly.

So, as for the society-economy index of class j in the period between t_1 and t_2, we have:

$$\Delta B_j^{t_1-t_2} = B_j^{t_2} - B_j^{t_1} \qquad \beta_j^{t_1-t_2} = \frac{\Delta B_j^{t_1-t_2}}{B_j^{t_1}}$$

In the formula: $B_j^{t_2}$, $B_j^{t_1}$ are society-economy index of class j at t_1 and t_2; $\Delta B_j^{t_1-t_2}$ is the value changed of the index; $\beta_j^{t_1-t_2}$ is the change rate of the index.

C. Index of highway water conservancy action

1) Index of integration of highways and dykes

This index is the quotient of two number of one certain highway: length of integration of highway and dykes and the general length of this highway:

$$\phi = (\sum_{j=1}^{n} l_{ij}) / L_i$$

where ϕ represents the index of integration of highways and dykes; l_{ij} is the length of integration of highway--i and dyke—j; L_i is the general length of highway—i.

2) Index of coordination of highway bridges and culverts

This index is the quotient of two number of one certain highway: one number is the number of coordination of highway bridges and culverts with irrigation and water conservancy facilities n_i ; another number is the general number of highway bridges and culverts N_i, $K_i=n_i/N_i$, in which K_i is the index of coordination of highway bridges and culverts.

THE AREA MONITORED WITH 3S TECHNOLOGY FOR INFLUENCE OF URBAN ACTION OF HIGHWAY, AND THE METHODS OF MONITORING AND ASSESSMENT

A. Analysis of sensitive area influenced by urban action of highway in Dongting Lake

There are 208 towns and cities in the area of Dongting Lake, about 140 towns and cities, among which 69.3%, are along the classified highway in this area. These towns and cities are the start, end or important station of highway, they are also important points of economic development, and of course they are sensitive areas influenced seriously by urban action of highway.

To expressway, the area easily influenced by urban action of highway is the one in which there are junctions of interchange, or entrance to way and way out.

To other class highway, because of their character of open and intersection at grade, sensitive areas can be easily influenced by urban action of highway distribute widely.

Development of industry promotes the urbanization in Dongting Lake area.

Highway construction is the founder of industry and urbanization, and after the construction of highways, the area along these highways would be industrialized and urbanized rapidly.

The determination of sensitive area is not only decided by the actuality of influence by urban action of highway in Dongting Lake wetlands ecosystem, but also the future of influence, so the long-term plan of town and city construction in Dongting Lake area should be taken into account.

In addition, the degree of influence of highway urban action on Dongting Lake wetlands ecosystem is in correlation to the highway location relative to Dongting Lake wetlands.

After establish of PR. China in 1949, 15 farms owned by the government had been built. These farms are located in center area of Dongting Lake area and the area between north Dongting Lake and Jing River, which are wetland easily destroyed. And each farm was connected by various class highways and roads, so these farms have become various scale towns and cities. The influence by these towns and cities on Dongting Lake wetland ecosystem should be taken into account seriously, and these areas should be classified as sensitive area influenced by highway urban action.

The influence of urban action of rural roads is little relatively, but it is widely and largely in amount. Along the roads, there are a lot of farmer's houses and some other constructions distributed widely, for which we can not set up city infrastructures. So the influence of road's urban action should be considered as a whole.

B. The choice of area to be monitored for influence of urban action on Dongting Lake wetlan ds ecosystem

To technology, the indexes of influence by highway urban action on Dongting Lake wetlands ecosystem have some statistical characters. So some sample areas, part of all sensitive areas influenced by urban action of highway, could be monitored, and after statistical computing, from the data of these samples we can get the index of influence by urban action of highway statistically.

To economy, because of high price of high resolving power satellite images, and high expense of on-the-spot investigation, we choose some proper sample areas equably to represent all sensitive areas influenced by urban action of highway, which is depend on amount of the funds of research. And in these sample areas, the areas of urbanization really occurred is selected for monitoring area based on 3S technology.

After thinking of causes described above, we select Lixian County, Jingshi Town, Anxiang County, Nanxiang County, Huarong County, Qianlianghu farm, Baoheti Town, Hanshou County, Haozigang Town, Xihu farm, Maocaojie Town, Yuanjiang City, Fengnan Town, Xiangying County, Quyuan farm, Lujiao Town, Datong farm and Junshan District, Yueyang City, all 18 sensitive areas influenced by urban action of highway, as the monitoring areas (see Figure 1).

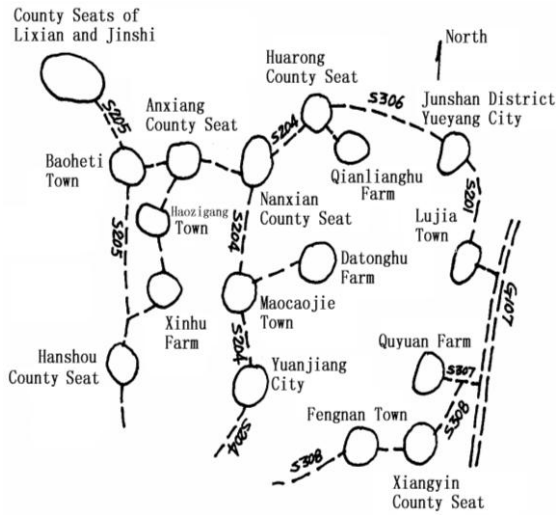

Figure 1. Areas monitored based on 3S technology for highway water conservancy action

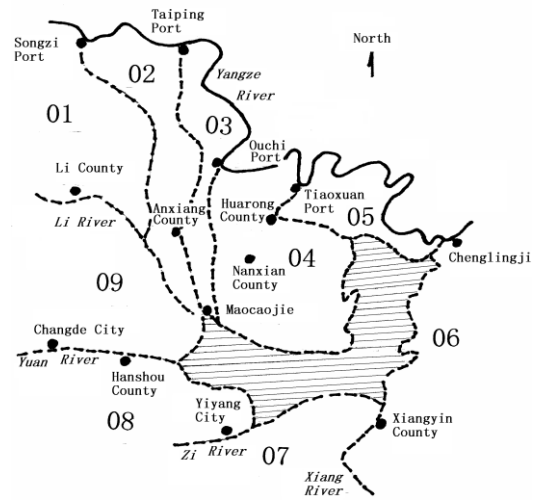

Figure 2. Areas monitored based on 3S technology for highway urban action

C. Methods of monit oring and assessment of influence of urban action of highway on Dongting Lake ecosystem

The monitoring and assessment may be based on multi time interval and multi-band TM satellite images and ERDAS processing. Detail methods and technologies include: technology of urban area classify based on remote image; grading of urban area and fixing on right for each grade; analysis of spatial-temporal character of urban land-use change; analysis of correlation between spatial-temporal character of urban land-use change and each index of society-economy; research on policies and technologies for control the influence of urban action of highway, which is for the conservation of wetlands; analysis and computing for mathematical statistic model of influence by urban action of highway on Dongting Lake wetlands ecosystem.

THE AREA MONITORED BASED ON 3S TECHNOLOGY FOR INFLUENCE BY WATER CONSERVANCY ACTION OF HIGHWAY, AND THE METHODS OF MONITORING AND ASSESSMENT

A. Separation of monitoring wetlands area influenced by water co nservancy action of highway in Dongting Lake area

The water conservancy construction is focused on the flood protection and drain waterlogged farmlands and farms irrigation in dyke. There are close relationships between Integration of highways and dykes and coordination of highways with water conservancy facilities. The analysis on water conservancy action of highway should take wider spatial area and two indexes of water conservancy action into account, which will benefit to macro-hold integration of highways and dykes and coordination of highways with water conservancy facilities under the highway-line running rationally.

Along the center lines of watercourses of rivers mentioned above, the whole monitoring area is separated into nine parts, each part is the basic unit in monitoring and analysis of influence by water conservancy action of highway on Dongting Lake ecosystem. In analysis, intra-unit and between-unit, the present situation and the trend of degree of integration of highways and dykes and coordination of highways with water conservancy facilities will be analyzed (see Figure 2).

B. Methods of area analysis on influence by water conservancy action of highway in Dongting Lake area

The methods of area analysis on influence by water conservancy action of highway in Dongting Lake area are based on 3S technology. The location of highways, dykes and water conservancies facilities is relatively stable, the area analysis on influence by water conservancy facilities of highway should use GIS as the platform. Up-to-date digital topography map reflecting the actuality of water conservancy action of highway and the data from on-the-spot investigation or remote images should be collected, the former is principal and the latter is secondary, as the data source of expert system for area analysis on influence by water conservancy action of highway on Dongting Lakes wetlands ecosystem. Aided by the expert's analytical system, in large area we can analyze and assess the integration of highways and dykes and the coordination of highways with irrigation and water conservancy facilities, we can also do spatial analysis on some correlative problem, which can support technologically the future highway's planning and reconstruction of existing highways. The aim of analysis is to take full advantage of highway's communication function, as well as to protect the Dongting Lake wetlands ecosystem.

CONCLUSION S

This paper focused on several problems of assessment on influence by highway on Dongting Lake ecosystem:

1) The main factors of influence by highway construction on Dongting Lake wetland ectope are: urban action of highway, water conservancy action of highway and highway's separate-approach action on migratory birds' habitats ecosystem.

2) The index system for assessment on influence by highway. The choice of index should emphasize on some certain causes.

3) According the analysis of monitoring area of urban action of highway, and to take the technology and economy into account, 18 areas of town or city are selected as monitoring area for assessment of influence by urban action of highway on Dongting Lake ecosystem. The main technology of monitoring and assessment will be based on 3S technology.

4) Based on multi time interval and multi-band TM satellite images and procession of ERDAS, the monitoring, analysis and assessment of influence by urban action of highway may be carried on.

5) Along center line of Yangtze River's four watercourses, Xiang River, Zi

River, Yuan River and Li River, the whole monitoring area for assessment on influence by water conservancy action of highway is separated into nine parts; each part is the basic unit of monitoring and analysis.

6) Area analysis on influence by water conservancy action of highway should be based on 3S technology, and ArcGIS could be the platform of integration of data source. The analysis area should be a large area, and then the integration of highways and dykes and the coordination of highways with irrigation and water conservancy facilities should be spatial analyzed with relational geography.

ACKNOWLEDGMENT

This work was supported in part by project of Scientific Department of Hunan Province, China under Grant 04SK3012.

REFERENCES

Dai Mingxin. Handbook of Highway environmental protection. (2004). Beijing. China communications Press: 34-48

Daniel J. Smith, Larry D. Harris, Frank J. Mazzotti. (1998). Highway-Wildlife Relationships (Development of a decision-based wildlife underpass road project prioritization model on GIS with statewide application). University of Florida: 6-8

Dong Xiaolin. (2003). Evaluation of Environment After project of Highway Construction. Beijing. China communications Press: 54-76

Kevin J. Gutzwillera, Wylie C. Barrow. (2003).Bird communities, roads and development: prospects and constraints of applying empirical models. Biological Conservation 113: 239–243

Li Rendong,Zhuang Dafang,Hu Wenyan. (2004). Analysis of the Land Use Changes Based on Remote Sensing and GIS: a Case Study of the Dongting Lake Area. Transaction of the CSAE, 1: 303-306

Lu Xinhai, Zhanglou. (2002). The Analysis of the Relationship Between Wetland Road Construction and Cropland Irrigation Work Optimization of Capital Construction, 2: 41-43

Mao Wenyong. (2003). An Introduction to Assessment of Influence on ecosystem (Recension). Beijing. China Environmental Science Press: 274-283

Richard T.T. Forman, Robert D. Deblinger. (2000). the Ecological Road-Effect Zone of a Massachusetts (U.S.A) Suburban Highway. Conservation Biology, volume 14, No.1: 36-46

Rien Reijnen, Ruud Foppen, Cajo Ter Braak, Johan Thissen. (1995). The Effects of car traffic on breeding bird populations in woodland. III. Reduction of Density in Relation to the Proximity of Main Roads. Journal of Applied Ecology. volume 32: 187-202

Zhao Kang. (2003) Influence of Highway construction and Protection to Resource of Wetland. Highway, 2: 87-89

Research on Urban Intersection Vehicle Emission Reduction Based on Microcosmic Simulation

Y. Wang[1], D. Guo[1], S. Li*[1], C. Zheng[1,] W. E[1], Y. Chen[1] and X. Lu[1]

[1]Traffic Environment Laboratory, Traffic & Transportation School of Jilin University, Jilin Changchun, Tel:043184049946. *Corresponding author, S. Li Shiwu; E-mail: shiwu@jlu.edu.cn

ABSTRACT

This research uses a Gongnong square intersection as a research object and TSIS for vehicle emission simulation. We obtain the input parameters, including road structure and traffic flows, through a field survey of Gongnong square,. Then taking emission as the main indicator and traffic delay as a second indicator, we use CORSIM modules of TSIS to simulate traffic operation. Two modified interchange projects are presented to judge whether reducing the vehicle emission and improving the traffic flow can be achieved simultaneously. This research offers a foundation for further road network analysis and research on emission reduction.

1. PREFACE

Signalized road intersections always are the crucial points with traffic-related pollutant concentrations, because levels often prove to be very high (Horowitz,1982). Interchanges are increasingly used to replace a variety of types of intersections and, thus, to improve traffic flow management and safety level. Transportation officials may also consider improvements in air quality and reductions in emissions, as they attempt to maximize interchange benefits (Witkowski,1988).

A model appears to be an important forecasting tool to reproduce traffic behavior along each link connected to the intersection. The application of TSIS is needed for this study (Wang, 2008). Once data, such as topographic and geometrical features of the road, vehicular flows, and lights intersection settings, have been provided; parameters such as the queue maximum length, the number of vehicles stopped, and the mean delay can be evaluated. Thus, different driving kinematics (acceleration, cruise, deceleration, idle) affecting vehicles approaching to or departing from the intersection are computed. In turn, these are the basic inputs for the emission model to estimate pollutant modal emissions along each link. Based on these data, we can project delay time and emission in different situations.

2. MODEL INTRODUCTION AND APPLICATION

TSIS-CORSIM is a microscopic traffic simulation software package for signal systems, freeway systems, or combined signal and freeway systems (Mctrans, 2007). The model, based on a simplified box model applied to the intersection area,

results from a comparison with respect to two of the most currently used intersection models. Starting from the queue and modal emissions algorithms both are implemented in the TSIS model.

2.1. Simulation procedure

The intersection model has been developed according to the scheme described in Figure 1. Vehicle queue parameters and emissions estimation finally result from a model built in a cascade fashion by a queue algorithm and a modal emission model. If the data including traffic light settings, traffic flows, intersection geometry and morphlogy, and car fleet composition are input, all the other models can be used to estimate a vehicle queue and total emissions at the intersection.

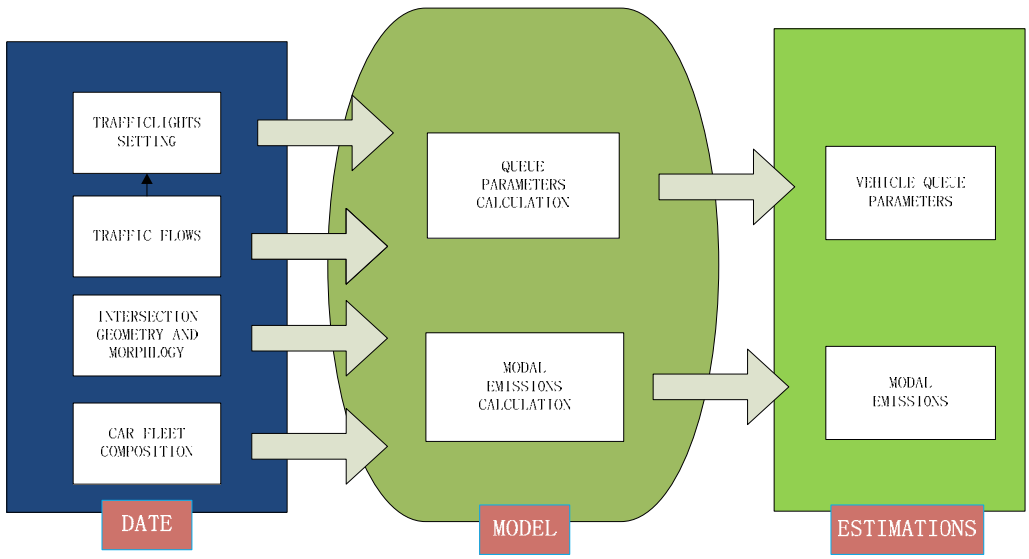

Figure 1. Simulation procedure of the intersection modeling for the estimation of delay time and emissions.

2.2. Queue and emission models

As showed in Figure 1, the first step is aimed at the investigation of traffic light settings, traffic flows, intersection geometry and morphlogy, and car fleet composition. The second step is to simulate queue parameters and emissions for estimating the delay time and emissions.

Once data such as vehicle flows, traffic lights setting and intersection geometry and morphology have been input, parameters such as the queue maximum length, the number of vehicles stopped and the mean delay per vehicle during an entire signal cycle can be calculated.

Emissions during the acceleration, cruise, deceleration and idle modes are estimated by means of the corsim module. Once car fleet compositon has been provided, the instantaneous emission rate of each car can be seen in the simulation and the total emissions of a district can be calculated.

3. SITE DESCRIPTION AND TRAFFIC SURVEY

Analysis of the intersections in Changchun city indicates that more serious traffic jams appear in Gongnong square, Xinmin square, Zhanqian square, Renmin square and other road intersections. However, only the Gongnong square intersection is a five-way plane intersection. This can be regarded as a T-shaped intersection and a cross intersection in this analytical process. As one of the most important intersections in Changchun city, both traffic and emissions have been locally collected by the intersection area.

First, we gathered field data on traffic light settings, intersection geometry and morphlogy, and then surveyed the vehicle flows, car fleet composition and turn ratios.

3.1. Site description

Gongnong square is a five-way plane intersection, and vehicle flow is heavy. It can be driven south on Renmin street, east on Nanhu road, west on Nanhu road and on Gongnong street in four directions from Renmin street. It can be driven north on Renmin street, west on Nanhu road, south on Renmin street and Gongnong street four directions from the east on Nanhu road.

At the same time, the left-turn vehicle flow from the north on Renmin street and the left-turn vehicle flow from the east and west from Nanhu road both need to drive through the flow. This creates transportation confusion at peak periods throughout the intersection, when vehicles are packed in like sardines. The vehicles from the north on Renmin street and the east from Nanhu road always need to wait for two or more signal cycles when driving through the intersection. This condition has a serious impact on the smooth operation of the entire intersection. Figure 2 is an overview of Gongnong square intersection.

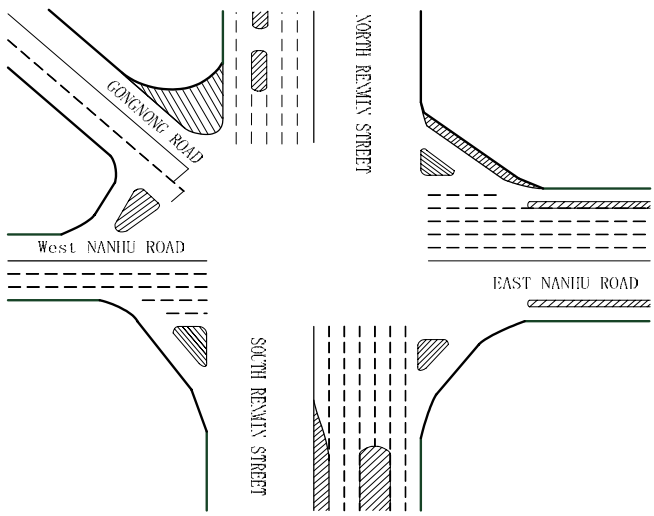

Figure 2. Overview of Gongnong square intersection.

3.2 Traffic survey

In order to simulate the situation of the Gongnong square intersection, beside inputting the geometry and morphology, we also need to investigate the vehicle flow, car fleet composition, and turn ratios of each inlet. Considering that the periods of time will have great influence on vehicle flow and emissions, we select the weekday morning and evening pea. Survey results can be used for simulating the discharge conditions and delay time in peak hour. The traffic survey result is shown in Tables 2 and 3.

Table 2. Gongnong square intersection's vehicle flows and car fleet composition in morning and evening peak period.

Inlet Name	Total vehicle flows（veh/h）	Bus（veh/h）	Truck percent (Barring bus)
North Renmin Road	1828	146	1%
North Renmin Road	1937	116	2%
East Nanhu Road	1572	66	1%
West Nanhu Road	720	48	1%
Gongnong Road	662	22	1%

Table 3. Gongnong square intersection's turn ratios of each inlet in workday's morning and evening peak period.

Inlet Name	Turn Ratio (%)				
	North Renmin Road	Sourth Renmin Road	East Nanhu Road	West Nanhu Road	Gongnong Road
North Renmin Road		65.75	25.82	7.77	0.66
North Renmin Road	55.66		20.75	0.98	22.61
East Nanhu Road	22.14	16.79		29.90	31.17
West Nanhu Road	31.95	10.83	54.72		2.5
Gongnong Road	⊗	92.75	⊗	7.25	

4. ANALYZING MODELLING RESULTS

The aim of this paper is to optimize emissions. At the same time, since delay time is a complementary indicator, we want to verify whether improvements also achieve optimization in delay time. Finally, we examine the effect of different projects on vehicle emissions by comparing data simulation before and after the project was implemented.

Interchanges can be a feasible alternative to reduce vehicular emissions and make intersections more environment-friendly. We select incomplete interchange and cloverleaf interchange as two hypothetical cases. In order to simplify the introduction, using project A represents an incomplete interchange and project B represents a cloverleaf interchange. Project A changes the north-south direction of Renmin Street to an incomplete interchange. Project B is a modified cloverleaf interchange. For better channelization, we took Gongnong road into the entire project. After simulating three projects, we compared the delay time and emissions.

4.1. Comparision of delay time

Table 4 indicates that project B accounts for the least queuing delay compared to the original project. Absence of traffic signal control and of traffic in different directions through a loop ramp simultaneously reduces the queuing delay and control delay time by as much as 99.39%. Project A also has a very good improvement compared with the original project. The north-south direction of vehicles on Renmin street, separated from the other three roads and lacking a traffic signal, eliminates traffic flow interference and also reduces queuing delay.. At the same time, control delay of project A shows a great improvement.

Table 4. Comparision of delay time in the three projects.

Delay categories		Control delay （sec/veh）	Queuing delay （sec/veh）
Original project		1837.1	1943.8
Project A	Incomplete interchange	1245	1277.1
	Reduction percent	－32.23%	－34.30%
Project B	Cloverleaf interchange	18.4	11.8
	Reduction percent	－99.00%	－99.39%

4.2 Comparison of emission

As shown in Table 5, there are significant reductions from the change from intersection to interchange. Project A had 18.01% reductions in total exhaust compared with 24.51% reduction in project B. For the three emissions, project B performs better than project A by 3%-13%. For aggregate emissions, project B is

lower than project A by 6%.

These findings indicate that project B is the better option for achieving significant reductions in emissions and corresponding reductions in delay time. They demonstrate that changing the intersection can reduce total emissions and make traffic run more smoothly.

Table 5. Comparision of vehicle emissions in the three projects.

Project	CO(g/h)	NOx(g/h)	HC(g/h)	Aggregate(g/h)
Original project	3568.766	405.202	223.343	4197.311
Project A	2910.422	360.0255	171.0645	3441.512
	－18.45%	－11.15%	－23.41%	－18.01%
Project B	2654.730	372.381	141.375	3168.486
	－25.61%	－08.10%	－36.70%	－24.51%

5.CONCLUSION

A hypothetical case study has offered a method for evaluating the user benefits from highway improvements. Our research compared two interchange projects and an intersection in terms of the delay and vehicle emissions for a workday's morning and evening peak periods. The results indicate that the interchange generates delay and total vehicle emissions reductions.

The model presented in this paper has been implemented into a geographic information system focused on the Gongnong square intersection, with the aim of managing atmospheric pollution due to urban traffic. It was found that the cloverleaf interchange performed better than the existing intersection control in reducing vehicular emissions. The project's positive environmental impacts include:

(1) Travel time benefits, including control delay and queuing delay from the interchange and highway as well as improved crossing capacity at th Gongnong square intersection.

(2) Improved air quality due to a reduction of idling and stop-and-go traffic situations.

6. ACKNOWLEDGEMENTS

This work is financially supported by the National Natural Science Foundation of China (Grant No.50678072) and the National Key Technology R&D Program (No.2006BAJ18B02).

REFERENCES

Horowitz, J. L. (1982) *Air quality for urban transportation planning*. MIT Press, Cambridge, Mass.

McTrans Center (2007). "Traffic software integrated system-corridor simulation."

University of Florida,<http://mctrans.ce.ufl.edu/featured/TSIS/>(October 24, 2007).

Sun, F. (2008). *Research on the method of reducing emissions on the urban intersection based on microcosmic simulation*, Master's degree thesis of Jilin University. Chang chun, 6:18-32.

Wang Y. (2008). “Signal timing optimization simulation on urban road intersection based on vehicle emissions. ” 2008 International Conference of Chinese Logistics and Transportation Professionals, 4762-4767.

Witkowski, J. M.. (1988).”Benefit analysis for urban grade separated interchanges.” *Journal of Transportation Engineering*, ASCE, 114(1), 93-109.

The Method of Determining Traffic Impact Range of Developing Project Based on Threshold Value

ZHOU Chao[1], WANG Xiaoning[2] and DENG Shuanglong[2]

[1]China Highway Engineering Consulting Group Company Ltd, P.C. 100000, PH 13091711424, email: nn2k@163.com
[2]School of Transportation Science and Engineering, Harbin Institute of Technology, P.C. 150090, PH 15046118683, email: wxn1974@hit.edu.cn

ABSTRACT

It is important to determine the scope of the traffic impact on the traffic impact analysis scientifically and rationally. This paper studies the method of determining threshold value of traffic impact range. It is reasonable that the decreasing of service level of signal intersection surrounding projects by one grade is regarded as the threshold value. The method of application is introduced by taking the example of Harbin International Exhibition and Sports Center developmental project. The result shows the method of determining the threshold value of traffic impact range is rational, simple and effective.

CLOUD MODEL

Deduced from the theory of cooperative, this method considers approximately the traffic impacts to the surrounding road sections which are induced by project practice as the poison gas discharged into air, which is composed of many subsystems (Soumya et al. 1993; Wang et al. 2001). In this kind of open and steady-going system, all subsystems are distributed in the whole impact range as circles, which diffuse under the impact of project practice in a turbulence field of turbulence distributing equably in all directions. The impact of project practice is associated with its type and intensity and is positively related to the intensity (e.g. the larger-scale commercial projects possess a much heavier traffic impact to the surrounding road networks than the projects of researching and developing of new science and tech). The impact received by the road sections and intersections in the impact range is equal to the impact induced by the local subsystem. The impact reaching the distance of x off the project entity can be computed in the following equation, in which the average value $\overline{C}$, of the impact degree C, can explain the impact induced by the project entity at some distance.

$$C(x) = \frac{\xi Q}{4\sqrt{\pi x^2}} \quad (1)$$

In the equation above, ξ represents the outer-oriented diffusion ratio of the traffic impact, the value of which is related to the type and intensity of the project,

$\xi \in$（0，1）. Q represents the unit impact to the surrounding road network. By supposing C_d as the ultimate impact and $\overline{C} = C_d = \xi Q / 4\sqrt{\pi} x_d^2$, we can acquire the maximum distance that the project impact can reach under the condition of ultimate impact as follows:

$$x_d = \beta \sqrt[3]{\frac{\xi P a}{4\sqrt{\pi} C_d}} \tag{2}$$

By utilizing the equation above, we can determine the maximum range of the different impacts induced by the project practice. In this equation, β can be adjusted to 1, 0.3, 0.05, and so on. The C_d can be determined by trial balance. Also, with some available software of transportation planning, such as TRIPS, we can determine C_d by analyzing the difference of traffic state in the surrounding road network before and after the project practice simply by choosing the apt traffic volume and the level of service. The determination of constant a in the equation is also related to the type and intensity of the project, $a \in (0.15，1)$.

This method can be applicable for every project of different type, scale and intensity, and for TIA of long term and short term. However, because the C_d in the equation is different in different projects, the results may have some errors. Also, the model is too complicated to adopt in real tasks.

EXPERIENTIAL METHOD

Each of the following items should be considered in a TIA once it happens:

①The traffic volume of the surrounding roads has effects on the in and out traffic volume of the project.

②At the planned entrances, the surrounding roads do not have left-turn lanes.

③At the entrances and exits, the stadium does not meet demand.

④The entrance lanes in the drawing plan are too close to the other entrances or intersections.

⑤The project is for special use or restricted by some conditions in detailed planning.

For the developing and utilizing of some local lands, the impact range of some districts is composed of all roads and intersections, where the induced traffic volume exceeds the capacity during peak hours by 5%, and places where the characteristics of traffic vary.

As the methods above mostly refer to the American experience, further research has not been carried out to see whether they can be adopted well in our

country or not. The impact range is mostly determined by the location, features and type of the project.

THE DETERMINATION OF THE THRESHOLD VALUE

The Concept of Threshold

The threshold value is introduced here to explain when we should take the surrounding roads or intersections into consideration for the traffic impact range, according to how much they are affected by the project practice.

The Basic Principles of Determining the Threshold Value

①The combination of qualitative analysis and quantitative analysis. Because the types and scales of projects vary greatly, in addition to the different locations and different states of the surrounding road networks, it is easy to make the problem much more complicated when simply the quantitative analysis is done. This requests us to use qualitative analysis for some special problems, to which quantitative analysis is not applicable (Huang et al. 1999).

②The combination of universality and particularity. In the determination process of the threshold value, the more complicated and more special parts which surround the project entity should be isolated to be determined by qualitative analysis; while in ordinary situations, the determination should be made by the following methods.

The Classification of the Proposed Projects

According to the practical state of our country, projects are classified into three kinds (Zhang et al. 2001):

①projects with a particularly sensitive location

②special projects

③common projects

Because the first two belong to special cases, the determination of the impact range for them should be considered from the state of the project location and the self characteristics of the project; while the third one belongs to common cases. This paper focuses mainly on the third case.

Methods of Determining the Threshold Value

In practical cases, the threshold value is used to determine whether the surrounding parts of the project entity should be considered in the traffic impact range under some specific traffic impact. However, theoretically, the essence of threshold value is the new traffic demand resulted from the project practice, while the new induced traffic demand may lower the service level of the surrounding traffic establishment, or even the service level of the whole road network. The impact to the surrounding roads resulting from the induced traffic volume can be concluded into three kinds: the surrounding signalized intersections, entrance and exit of the project entity and the surrounding road sections. When determining the

impact range, it is unreasonable to simply lay the impact resulting from the project on the entrance and exit. As we know, the intersections play a more important role in traffic improvements, simply because they are the bottle-necks of the whole road networks. So, this paper takes the surrounding signalized intersections as research objects. We find that it is reasonable to take the service level decreasing by one grade as the threshold value.

THE DETERMINATION OF THE IMPACT RANGE

According to the former discussion, the threshold value is determined by the service level of signalized intersections decreasing by one grade. So, the parts which achieve the threshold value will be included in the impact range. That is to say, we should compute the service levels of the surrounding signalized intersections before and after the project practice first, and then determine the impact range by linking the intersections at which the service level decreases by one grade as the boundary of the impact range.

Classification of Service Level

Service level is defined as a kind of quality criteria to measure the condition of traffic flow and the feeling of drivers and passengers. The mean stop delay of each vehicle in the standard analysis period of 15 minutes is used to represent the service level of signalized intersections. The criteria of service level are listed in Table 1.

Calculation of Delay of Intersections

This paper uses the method from the American Road Capacity Manuscript to calculate the delay of intersections. In every group of lanes, average delay of each vehicle is computed by formula (3), while the average delay of the induction section and the whole intersection can be computed by formula (4) and (5) respectively.

$$d = 0.38C\frac{(1-g/C)^2}{[1-(g/C)(X)]} + 173X^2\left[(X-1)+\sqrt{(X-1)^2+16X/c}\right] \tag{3}$$

In this formula, d represents the average delay of each vehicle in each group of lanes, *s/veh*; C represents the cycle time of the signal, *s*; g/C represents the ratio of each group of lanes; X represents the saturation of each group of lanes. C represents the capacity of each group.

$$d_A = \sum_i d_i v_i / \sum_i v_i \tag{4}$$

d_A - delay of induction section A, s/veh; d_i - delay of group i in induction section A, s/veh;

v_i - Correction flow of group i.

Furthermore, average the delay of each induction section; we can achieve the average delay of the whole intersection:

$$d_J = \sum_A d_A v_A / \sum_A v_A \quad (5)$$

d_J – average delay of each vehicle in this intersection, s/veh;

v_A - Correction flow of induction section A, veh/h.

The level of service for the intersection can be determined by referring to Table 1 according to the average delay of the intersection acquired above.

Table 1. Level of Service Standard of Signal Intersection

Level of Service	Average Delay (s)	Level of Service	Average Delay (s)
A	≤5.0	D	25.1～40.0
B	5.1～15.0	E	40.1～60.0
C	15.1～25.0	F	>60.0

NUMERICAL STUDIES

Taking the TIA of the Harbin International Exhibition and Sports Center (IESC) as an example, we use the methods introduced above to determine the impact range. In order to determine the level of service for the intersections, we assume:

①In the completion year of the project, the signal timing of intersections does not vary. Data is from the investigation (Harbin Transportation Planning and Research Agency et al. 2002) in 2002.11.17-2002.11.20 by authors.

②In the completion year of the project, the asymmetry coefficient of the two directions of roads is 0.5. At each intersection, the ratios of left-turn, right-turn and straight-proceed are the same as the data of investigation in 2002.

③In the completion year of the project, the function of each lane is the same in 2002.

According to Formula (3), (4) and (5), the average delay at the intersections near the IESC before and after its completion is calculated. Also, we listed the level of service in Table 2.

Table 2. Vehicle Average Delay and Level of Intersection Service of Intersection of Project Build Former and After

No.	Name of Intersections	Former Average Delay	Later Average Delay	Former Level of Service	Later level of Service
1	Hongqi Street—Huaihe Road	19.3	25.2	C	D
2	Nanzhi Road—Huaihe Road	9.7	11.5	B	B

3 Huanghe Road—Huashan Road	6.3	13.7	B	B
4 Huanghe Road—Songshan Road	9.8	16.3	B	C
5 Changjiang Road—Huashan Road	15.6	26.4	C	D
6 Changjiang Road—Songshan Road	17.0	24.8	C	C
7 Songshan Road—Minjiang Road	6.9	15.7	B	C
8 Hongqi Street—Minjiang Road	20.0	24.6	C	C
9 Hanshui Road—Huashan Road	7.9	13.2	B	B
10 HanshuiRoad—Songshan Road	13.0	23.1	B	C
11 Hongqi Street—Hanshui Road	14.9	25.0	B	C

Table 2 shows that the levels of service of Intersections 1, 5, 10, 11 decrease by one grade, so, according to the former discussion, these intersections should be included in the impact range; and by linking these intersections along the roads they belong to, we can determine the impact range, which is encircled by the linking of HuaiHe Road、HuaShan Road、HanShui Road and NanZhi Road.

CONCLUSION

Based on the review and analysis of the traditional methodologies to determine the traffic impact range, this study develops the concept of the threshold value for determining impact range and the way to calculate the threshold value. The threshold value presented in this paper is defined as one lower degree of level of service for intersections which surround the proposed project. Then, the traffic impact range is determined by connecting the intersections which meet the demand of the threshold value. In order to illustrate this methodology, a case study based on Harbin International Exhibition and Sport Center project is introduced. The main conclusion of this study is the fact that this new method based on the threshold value is reasonable, and it is more convenient and less complicated than traditional ones. Also, it is a practical method that can be widely used in China.

REFERENCES

Soumya S Dey, Jon Fricker D (1993). A Proposed Three-Step Process For Traffic Impact Analysis In Indiana [J]. ITE Journal 63,7: 19–24.

Wang Li (2001). Determining the Cloudy Model of Traffic Impact Analysis [J]. China Journal of Highway and Transport, 14,1: 100–102.

Huang Zhaoyi, Huang Xian, Yan Kefei (1999). Research on Method: The Traffic Impact Borderline of Traffic Impact Analysis [A]. The Academic Committee Proceeding of China City Traffic Planning, Geological Press.

Zhang Zidong (2001). Study on the Threshold Value of City Traffic Impact Analysis [D]. The Master's Degree Paper of Beijing University of Technology.

Harbin Transportation Planning and Research Agency (2002). Report of Study on Harbin Transportation Planning. Traffic Management and Traffic Planning of Harbin International Exhibition and Sport Center.

The Transportation Planners Council of The Institute of Transportation Engineers (1988). A Summary of A Proposed Recommended Practice: Traffic Access and Impact Studies For Site Development [J]. ITE Journal: 17–24.

Calculation Method on Traffic Noise Pollution of Interchange Based on Geometric Alignment

WANG Xiaoning[1], TONG Jingjing[2] and DENG Ke[1]

[1]School of Transportation Science and Engineering, Harbin Institute of Technology, P.C. 150090, PH 15046118683, email: wxn1974@hit.edu.cn
[2]LLA(Shanghai) Consultancy Limited, Rm.708, Tongji United Plaza C，No.1388, Siping Road, Shanghai, P.C. 200092, FAX (0086) 21-33626390, PH 15121108051, email: jingjingt163@163.com

ABSTRACT

In order to study the calculation method of interchange noise pollution, the traffic noise is connected with the length of the ramp according to the feature of traveling with variable speed on the ramp. The thesis chooses the equivalent sonic level as the assessment index, defines the concept and discusses the calculation method of relative equivalent sonic energy according to the definition of equivalent sonic level; it also establishes the functional relationship between relative equivalent energy and the length of the ramps. The calculation formula of interchange equivalent sound level is deduced through the integral operation of the ramp length. Take Heda interchange in Heilongjiang province for example. The result shows that this method can calculate the noise pollution in the variable motion sections on the ramp as well as the noise pollution according to the interchange geometric alignment design conditions.

INTRODUCTION

As important nodes of highway and urban road network, interchanges have particularly serious noise pollution problems (Wang 2005; Wang 2005; Zhang 2005; Zhang 2005). Because of the various forms and complex structures, the geometric design condition will affect the driving noise intensity directly. The key point of interchange's noise calculation, compared with noise calculation of road sections, is the calculation method on variable motion sections (American Association of State Highway and Transportation Officials et al. 2001). According to the principle of vehicle radiation noise accumulated gradually with travel distance, this paper defines notion of relative equivalent sonic energy at first, secondly on the basis of summarizing and generalizing the research of the relationship between noise level and speed home and abroad, provides the fitting relationship between relative equivalent sonic energy and vehicle speed, and then establishes the conic relationship between relative equivalent sonic energy and the length of ramps according to the functional relationship between vehicle speed

and the length of ramps. Finally through the integral operation, the relative equivalent sonic energy per vehicle when accelerated traveling on the ramp is given and the calculation method of interchange noise is proposed based on the definition of equivalent sound level and noise superposition formula (Wang 2007).

CONCEPT AND CALCULATIO N METHOD OF RELATIVELY EQUIVALENT SONIC ENERGY

According to the definition of sound level, the value at point *j'* is:

$$L_{P\,j'} = 20\lg\frac{P_{j'}}{P_0} = 10\lg\frac{P_{j'}^2}{P_0^2} \qquad (1)$$

Where $L_{Pj'}$ is the sound level of point j', dB;

$P_{j'}$ is the sound pressure of point j', Pa;

P_0 is the standard sound pressure, taking the hearing threshold sound pressure （2×10^{-5}Pa）.

According to formula (1), it gets:

$$10^{0.1L_{Pj'}} = \frac{P_{j'}^2}{P_0^2} \qquad (2)$$

This paper chooses the equivalent sound level to calculate noise pollution, which is defined as follows:

$$L_{eq} = 10\lg\frac{1}{T}\int_0^T 10^{0.1L_{P\,j'}}\,dt \qquad (3)$$

Where T——The noise measurement time;

$L_{Pj'}$—— The sound level of point j',dB.

According to formula (2) and (3), it defines u as relative equivalent sonic energy at point *j'*. So U representes the total of that between [0，T]. According to formula (4), the relative equivalent sonic energy at point *j'* can be obtained if its sound level is known.

$$u = \frac{P_{j'}^2}{P_0^2} = 10^{0.1L_{Pj'}} \qquad (4)$$

THE FITTING RELATIONSHIP BETWEEN RELATIVE EQUIVALENT SONIC ENERGY AND VEHICLE SPEED

This paper divides vehicles into five types, namely motorcycle, light-duty vehicle, medium-duty, heavy-duty and oversize vehicle. Based on some researches, this paper calculates sound level at the situation of V=10、20、30、40、50、60、70、80、90 and 100km/h. Then through analyzing the mean value of sound level at the same speed, this paper gets the sound level at that point and the relationship between sound level and vehicle speed by fitting (see Table 1).

Table 1. The Relationship Between Noise Level and Vehicle Speed

Vehicle Type	The Relationship Between Sound Level and Vehicle Speed
Light-Duty Vehicle	$L_1 = 8.93L_n(V) + 35.35$
Medium-Duty Vehicle	$L_2 = 12.89L(V) + 26.52$
Heavy-Duty Vehicle	$L_3 = 9.33L_n(V) + 42.03$
Oversize Vehicle	$L_4 = 6.54L_n(V) + 60.09$
Motorcycle	$L_5 = 7.09L_n(V) + 49.41$

According to formula (4), the relative equivalent sonic energy u, when the vehicle is at a certain speed, can be calculated. And Table 2 is the result of fitting u and V by quadratic polynomial.

Table 2 The Relationship Between Relative Equivalent Sonic Energy and Vehicle Speed

Vehicle Type	The Relationship Between Relative Equivalent Sonic Energy and Vehicle Speed
Light-Duty Vehicle	$u_1 = 7589.6V^2 - 273184V + 4E+06$
Medium-Duty Vehicle	$u_2 = 100746V^2 - 6E+06V + 8E+07$
Heavy-Duty Vehicle	$u_3 = 46174V^2 - 1E+06V + 2E+07$
Oversize Vehicle	$u_4 = 288873V^2 - 1E+07V + 2E+08$
Motorcycle	$u_5 = 43587V^2 - 2E+06V + 4E+07$

THE FUNCTIONAL RELATIONSHIP BETWEEN SPEED AND RAMP LENGTH OF VARIABLE MOTION SECTION

When driving on interchange ramps, the changes in speed are very complex, because both uniform motion and variable motion exist. Generally, the speed changing process on the ramp can be divided into four situations, namely the process with one deceleration and one acceleration, the process with one deceleration only, the process with one acceleration only and the process with more than one deceleration and acceleration. According to the above situations, this paper establishes the function between vehicle speed and the length of the ramp in variable motion sections. Researches show that though the ramps' alignment composition is different, the vehicle speeds the ramps can support are different, the expressions of relationship between speed and ramp length are different, the forms are the same, which can be expressed by formula (5):

$$V = el^2 + fl + g \qquad (5)$$

Where V is vehicle speed driving on the ramp, km/h;

L is the ramp length of driving, m;

e、f、g is coefficients.

The calibration of coefficients e、f、g in formula (5) refers to reference (El-Aassar et al. 2006).

THE RELATIVE EQUIVALENT SONIC ENERGY OF VARIABLE MOTION SECTION

From Table 2, the relationship between relative equivalent sonic energy per vehicle of type i and speed can be represented by formula (6).

$$u_i = \alpha V^2 + \beta V + \chi \quad (6)$$

When taking formula (5) into formula (6), it gets:

$$u_i = M_1 l^4 + M_2 l^3 + M_3 l^2 + M_4 l + C_2 \quad (7)$$

The coefficients of M1、M2、M3、M4 and C2 in formula (7) refer to reference.

When driving on ramps, the relative equivalent sonic energy is accumulated gradually with the driving length on ramps. So using the knowledge of advanced mathematics, the total relative equivalent sonic energy per vehicle when driving from point a to point b on a ramp is:

$$U = \int_a^b f_l(l)\,dl \quad (8)$$

Taking formula (7) into formula (8) and making definite integral, it gets the relative equivalent sonic energy of variable motion section:

$$U = \left[\frac{M_1}{5} l^5 + \frac{M_2}{4} l^4 + \frac{M_3}{3} l^3 + \frac{M_4}{2} l^2 + C_2 l \right]_a^b \quad (9)$$

THE RELATIVE EQUIVALENT SONIC ENERGY OF UNIFORM MOTION SECTION

According to the velocity V of uniform motion, the corresponding sound level can be obtained based on Table 1. Also the relative equivalent sonic energy u of uniform motion section can be deduced based on formula (4). Furthermore, the total relative equivalent sonic energy *U'* accumulated in the uniform motion section will be deduced by multiplying the driving ramp length by u.

THE EQUIVALENT SOUND LEVEL OF RAMP S

The relative equivalent sonic energy accumulated at the left-turn ramp is equal to the sum of the relative equivalent sonic energy accumulated in the variable motion section U and the uniform motion section *U'*. Take the left-turn ramp for example, hypothesize that there are n_1 left-turn ramps at a intersection, and the traffic volume of No.k_1 ramp with No.i vehicle is A_{zdk1i}, so the equivalent sound level of left-turn ramp is 10 times the logarithm of all relative equivalent sonic energy.

$$L_{zz} = 10 \lg \sum_{k_1=1}^{n_1} \sum_{i=1}^{5} A_{zdk_1 i} [U + U'] \quad (10)$$

Where L_{zz} is the total equivalent sound level of all left-turn ramp, dB;

k_1 is the number of left-turn ramp;

n_1 is the total number of left-turn ramp;

A_{zdk1i} is the traffic volume of no.k_1 ramp with no.i vehicle, pcu/h

U is the relative equivalent sonic energy of variable motion section;

U' is the relative equivalent sonic energy of uniform motion section.

NUMERICAL STUDI ES

Take Heda interchange located at the crossing of Yibao highway and Heda highway for example. According to the method in segment 3, the fitting relationship between velocity and length at the variable motion section of every ramp is shown as follows (see Table 3).

Table 3 The Fitting Relationship Between Velocity and Length at Variable Motion Section of Heda Interchange Ramp

Title	The Stake Number	The Fitting Relationship
Ramp A	k0+000~k0+731.19	$V=2E\text{-}04l^2\text{-}0.1547l+84.929$
Ramp F	k1+80~ k1+331.114	$V=\text{-}3E\text{-}05l^2+0.1403l\text{-}48.37$
Ramp G	k0+000~ k0+290	$V=\text{-}2E\text{-}05l^2\text{-}0.047l+84.99$
	k0+510~k0+650	$V=\text{-}3E\text{-}05l^2+0.0932l+29.257$
Ramp B	k0+000~ k0+260	$V=\text{-}0.0024l^2+0.0572l+67.241$
	k0+460~k0+786.11	$V=0.0007l^2\text{-}0.7879l+272.36$
Ramp C	k0+380~ k0+450	$V=\text{-}0.0001l^2\text{-}0.037l+117.46$
	k0+740~k0+820	$V=\text{-}3E\text{-}05l^2+0.1018l+13.468$
Ramp D	k0+353.39~k0+563.39	$V=\text{-}4E\text{-}05l^2+0.1197l+31.348$
Ramp E	k0+550~k0+760	$V=\text{-}4E\text{-}05l^2+0.1368l+5.6962$
Ramp H	k0+600~k0+811.817	$V=\text{-}4E\text{-}05l^2+0.1411l\text{-}1.2509$

According to the designed traffic flow of Heda interchange and the data in Table2 and Table 3, the equivalent sound level of every ramp about Heda interchange in scheme 1 can be calculated (see Table 4).

CONCLUSION

According to the features of ramp variable motion sections, the thesis defines notion of relative equivalent sonic energy, derives the relationship between the relative equivalent sonic energy and the length of ramp by fitting, then deduces the calculation formula of interchange equivalent sound level through the integral operation of ramp length, and finally purposes the noise calculation methods of the left-turn ramp as well as the right-turn ramp. The Numerical Studies show that this method can evaluate the influence of interchange geometric alignment to the ramp noise. If the geometric design condition of a interchange and its traffic value are known, the noise pollution can be calculated.

Table 4 The Equivalent Sound Level Summaries of Heda

Interchange

	Title	The Equivalent Sound Level（DB）
The Left-Turn Ramp	Ramp A	113.97
	Ramp F	118.81
	Ramp G	118.27
	Ramp B	120.23
The Right-Turn Ramp	Ramp C	115.88
	Ramp D	112.01
	Ramp E	107.01
	Ramp H	106.51

REFERENCES

Ahmed El-Aassar (2006). Modeling of atmospheric refraction effects on traffic noise propagation.

American Association of State Highway and Transportation Officials (2001). A Policy on Geometric Design of Highways and Streets [Z]. AASHTO, Washington, D.C, 748~754.

Wang Wentuan and Shi Jinghua (2005). The Variation Low and Influence of Traffic Noise About Interchange. Journal of Safety and Environment, 5(3):41~44.

Wang Xiaoning (2007). Study on Analysis and Evaluation of Road Traffic Pollution About Interchange. Harbin Institute of Technology.

Wang Yi (2005). Talking About Interchanges' Construction and Reconstruction From the Angle of Protecting Sonic Environment. Journal of Environment and Landscape Architecture, 7(1):23~25.

Zhang Anting and Zhuang Yiting (2005). The Noise Pollution and Preventing of Overpass and Interchange. Research of Environmental Sciences, 18(6):120~122.

Zhang Yimei, Chen Dongguang and Zhao Xianyao (2005). The Query and Countermeasure of Constructing Large-scaly Interchange at CBD. Journal of Huazhong University of Science and Technology(Urban Science Edition), 22(2):39~41.

The Study on Design Method of Vehicle Intake Silencer Based on Three-Dimension/One-Dimension Models Coupling

J. Li[1] and Q. Guan[2]

[1]Traffic College, Northeast Forestry University, He Xing Road 26#, Harbin City, 150040. PH: 13624614575; email:lijk_01@tom.com.
[2]Traffic College, Northeast Forestry University; Harbin City, 150040.

ABSTRACT

Stricter noise legislation makes it increasingly important to utilize the intake silencer on automobiles. Analysis of research on automobile intake silencers identifies its main problems for domestic engines. This research applies a reliable test platform and theories, as well as acoustics analysis software and hydrodynamics,,to propose a new method of designing an intake silencer. The purpose is to control air intake noises effectively and to reduce overall vehicle noise. A 1-Dimension (1-D) model for a certain gasoline engine and 3-Dimension(3-D) model for a Helmholtz intake resonator were set up with GT-POWER and STAR-CD software respectively, to form a combined model for both engine and silencer. A 1-D/3-D coupling model was developed. It reduced overall engine noise by 4.2dB. Simulation results compared favorably with test results, verifying the rationale for the design of the silencer.

INTRODUCTION

Engine intake noises have become an important automobile noise source. To improve NHV quality, it is most effective to use a properly structured intake muffler. It should reduce vehicle noises while leaving the interior engine structure and automotive power performance basically unchanged.

Domestic automobile manufacturers have not yet achieved a design that satisfactorily reduces intake noises and adapts to newer regulatory demands. Relevant research methods are somewhat backward. Therefore, improving the standards of intake muffler design is very significant (Pang, 2006).

USING SOUND INTENSITY FOR NOISE MEASUREMENT AND NOISE SOURCE IDENTIFICATION

To measure sound intensity, two microphones must be placed at an appropriate distance. They are often assembled into a microphone sound intensity probe. The use frequency of a sound intensity probe is closely related to the small interval distance, so there is no need to consider the phase difference problem between the sound and vibration velocity signal (Mo, 2002).

Through testing and analysis of the sound intensity spectrum, we found the

noise:

(1) of an internal combustion engine increase with its speed.

(2) near the engine inlet are larger than others and the intake noise frequency mainly focuses on 100 ~ 1231Hz.

SETTING UP THE MODEL OF INTAKE RESONATOR

Identification for intake system noises frequency

Acoustic radiation on the engine surface can be measured by an automotive chassis dynamometer. Through frequency analysis, the time-domain signal of the intake noises measured are transferred by Fast Fourier Transform(FFT), as shown in Figure 1.

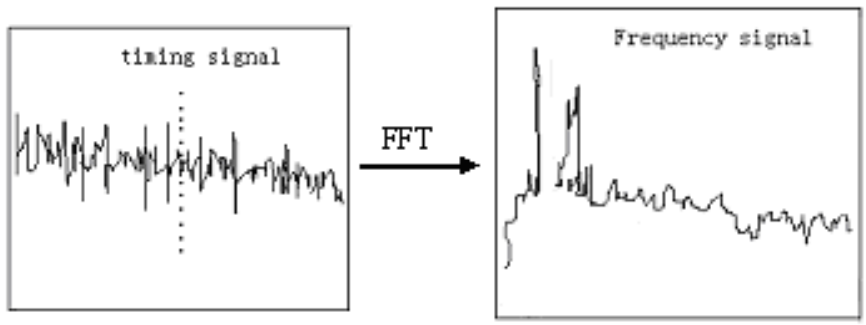

Figure 1. Signal for time-domain , frequency-domain in intake system noise.

The study found that the noise spectrum at low frequencies had three obvious peaks in the engine intake manifold. The center frequency is respectively 120,210 and 270Hz, via formulas (1) and (2). We can see that certain frequency noises can be reduced in the intake process by designing a reasonable resonant. The above three peaks of low-frequency band noises can be mainly eliminated through the muffler.

Considering the installation location and anechoic frequency of the resonator in the engine, the resonator structure size was derived, as shown in Table 1.

Table 1. Resonator size.

number	1	2	3
V/L	2.45	0.87	0.41
S/mm^2	298	317	308
L/mm	21	16	19

Setting up the intake resonator model grid

To verify whether the designed resonator can meet the noise reduction expectation without affecting vehicle performance, a 1-D/3-D coupled simulation between resonator and engine was set up and installed between the air filter and inlet pipe.

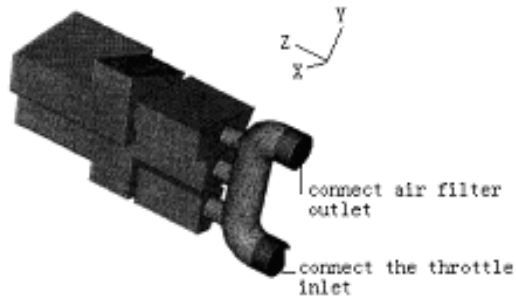

Figure 2. Three dimensional computational grid of resonator.

The calculation border region of the selected resonator 3-D model is as follows: The inlet air side is at the outlet of the filter. The outlet air side is at the inlet of the throttle valve. We take a 3-D resonator CAD model to the grid generator to divide the computational grid. A total 66008 units and 86900 nodes were generated. From Figure 2, the model can better reflect the actual geometric structure of the resonator.

Calculation model

The mathematical model of the resonator internal flow field is mainly composed of the mass conservation equation, momentum and energy conservation equations, state equation and thermodynamic relation, and formula k-ω equation as follows:

(1) Turbulent kinetic energy k

$$\frac{\partial}{\partial t}(\rho k)+\frac{\partial}{\partial x}\{\rho\mu_j k-[\mu+\frac{\mu t}{\sigma k}]\frac{\partial k}{\partial x_j}=\mu(P+P_B)-\rho\varepsilon-\frac{2}{3}[\mu_t\frac{\partial \mu i}{\partial xi}+\rho k]\frac{\partial \mu i}{\partial xi}+\mu_t P_{NL}\ (1)$$

σ_k for the turbulent Prandtl number, P_{NL} for the nonlinear term.

(2) Turbulent and kinetic energy dissipation rate ε

$$\frac{\partial}{\partial t}(\rho\varepsilon)+\frac{\partial}{\partial xj}\{\rho\mu_j\varepsilon-[\mu+\frac{\mu_t}{\sigma_\varepsilon}]\frac{\partial}{\partial x_j}\}=C_{\varepsilon 1}\frac{\varepsilon}{k}\{\mu_t P-\frac{2}{3}[\mu_t\frac{\partial \mu i}{\partial xi}+\rho k]\frac{\partial ui}{\partial xi}+$$

$$C_{\varepsilon 3}\frac{\varepsilon}{k}\mu_t P_B-C_{\varepsilon 2}\rho\frac{\varepsilon^2}{k}+C_{\varepsilon 4}\rho\varepsilon\frac{\partial ui}{\partial xi}+C_{\varepsilon 1}\frac{\varepsilon}{k}\mu_t P_{NL}\qquad(2)$$

$C_{\varepsilon 1}$、$C_{\varepsilon 2}$、$C_{\varepsilon 3}$、$C_{\varepsilon 4}$ for constants of the model, shown in Table 2 and the turbulent viscosity $\mu_t=\rho C_\mu\frac{k^2}{\varepsilon}, C_\mu$ for experience constant $C_u = 0.09$.

Table 2. The standard turbulence model constants.

σ_k	σ_ε	σ_h	σ_m	$C_{\varepsilon 1}$
1.0	1.22	0.9	0.9	1.44
$C_{\varepsilon 2}$	$C_{\varepsilon 3}$	$C_{\varepsilon 4}$	k	
1.92	1.44	-0.33	0.419	

Algorithm and boundary conditions

Using pressure implicit with splitting of the operators (PISO) algorithm, resonator boundary conditions are as follows: import and export are both setting the speed import. The initial value is zero, when calculating. STAR-CD will automatically read the GT-POWER's calculation results and then obtain the flow rate value of imports. Turbulent density is 0.02 and the length is 0.003m. Take the gas as ideal gas, and the wall temperature for a fixed temperature which can meet the ideal gas state equation.

GASOLINE ENGINE AND EXHAUST MUFFLER MODELING

Gasoline engine model

We set up a gasoline engine model and selected a reasonable combustion model. Based on the first law of thermodynamics, its mathematical description is:

$$\frac{d(m_c \mu')}{d\alpha} = -p_c \frac{dV}{d\alpha} + \frac{dQ_F}{d\alpha} - \Sigma \frac{dQ_W}{d\alpha} - h_{BB} \frac{d_{mBB}}{d\alpha} \tag{3}$$

m_c for gas quality in cylinder,p_c for gas pressure , u' for internal gas energy, α for the crank angle,$-p_c \frac{dV}{d\alpha}$ for the work by cylinder, $\frac{dQ_F}{d\alpha}$ for fuel generation heat quantum, $\Sigma \frac{dQ_W}{d\alpha}$ for piston wall loss heat, $h_{BB} \frac{d_{mBB}}{d\alpha}$ for the enthalpy value.

Using the engine combustion model provided by GT-POWER, the combustion room is divided into two regions, according to the combustion exothermic rule Weber function:

$$\frac{dx}{d\alpha} = \frac{\alpha}{\Delta\alpha_c}(m+1) y^m e^{-ay(m+1)} \tag{4}$$

Where $dx = dQ/Q, y = (a - a_0)/\Delta a_c$,Q for the total heat released by combustion, a_c for the start angle, m for the shape factor, and $\Delta\alpha_c$ for the combustion duration. A friction model is set up following Chen-Flynn. At resonator module, setting the resonator CFD control model, the volume V=3.5L, fluid convergence diffrence sets to zero, the engine pre-cycle number for 5. After the model is completed, we loadedthe required noise sensors, set the frequency octave with a

range of 100 ~ 4 000Hz.

Exhaust muffler model

Using the muffler module inner GT-POWER, an exhaust muffler model was set up (Song, 2005).The pipe length of import and export is 0.1m, the diameter set atr 0.0486m, the expansion cavity length for 0.2823m, perforated pipe aperture at 4mm, perforation rate 20%, the perforated plate is partition, and hole diameter is 5mm. Then, using GT-POWER and STAR-CD coupling technology, the gasoline engine model, resonator, and exhaust muffler were organically combined. This constitutes the resonator-gasoline engine simulation platform, as shown in Figure 3.

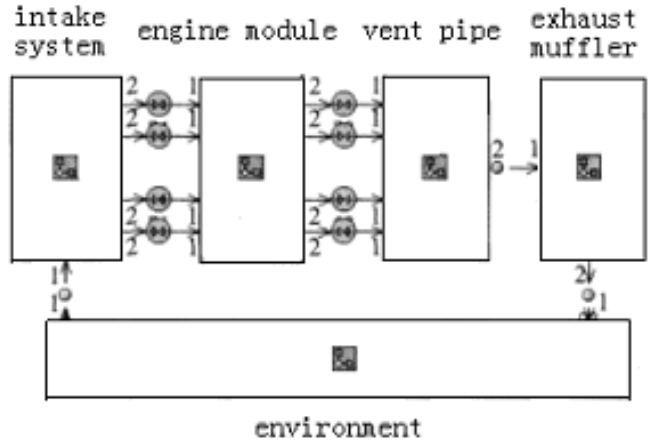

Figure 3. Resonator-gasoline engine simulation platform.

ANALYSIS OF RESULTS

Performance analysis of resonator

When the acoustic frequency f = 120Hz and the acoustic wave incident frequency is equal to the structure frequency of resonant, a strong resonance occurred in the cavity. Then, we used insertion loss to evaluate the dispersed voice performance of the resonator.

Figure 4 shows the calculation results of insertion loss to the engine intake manifold, when installing a resonator at the different stable conditions.

As can be seen, the noise of the intake system has been significantly inhibited at the resonant frequency point. Because only three resonator cavities are in the resonator, the frequency of noise production is concentrated at about 120, 210, and 270Hz. The max value of insertion loss can reach 10dB. Where resonant cavity characteristics occurred, the reduction noise effect is clear in the narrow band. The others are almost not. The increase of insertion loss means that the radiation noise becomes small.

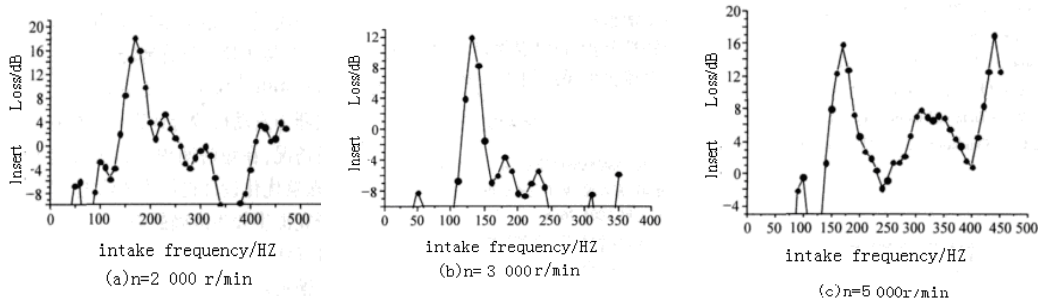

Figure 4. The insertion loss of resonator at different rotating speeds.

The impact of the resonator on engine performance

Against the experimental data of engine out-characteristics, the model sets the engine operating parameters and the initial boundary value conditions for nine work conditions. They respectively correspond to the full load conditions under the rev 1500 rpm, 2000 rpm, 2500 rpm, 3000 rpm, 4000 rpm, 4500 rpm, 5000 rpm and 5500 rpm. This allows for evaluation of the accuracy of the cycle model set up by the whole engine.

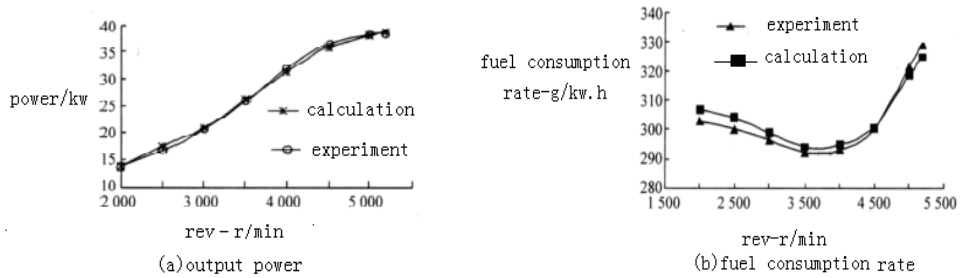

Figure 5. Data comparison between the calculated value & experimental value.

Figure 5 shows that engine output power has significant decline under rev 4000~4500 rpm, while others decreased slightly. The overall output power changed little (Zhang, 2004).

EXPERIMENTAL STUDY

Model validation

To verify the validity, Figures 5(a) and 5(b) respectively express the comparison results between calculated value and experimental measurement data on engine output power and fuel consumption rate. The results have a minor deviation at some condition point, but the deviation is not more than 4% in the majority of conditions. Therefore, the results are deemed to be acceptable (Heinrich, 2005).

The out-vehicle noise experiments

In accordance with the requirements of the noise regulations, an out-vehicle noise experiments were carried out. The results are expressed in Table 3. The experiment field was in highway maintenance center in the open air.

Table. 3. Experimental results of the out-vehicle acceleration noises Unit: dB(A).

Structure	The out-vehicle acceleration noise measurement				Average
Original vehicle	Left side	78.5	77.8	77.9	78.0
	Right side	74.9	75.1	74.8	74.9
Bettement vehicle	Left side	73.6	73.8	74.2	73.8
	Right side	71.3	72.4	73.6	72.6

The results show that the vehicle acceleration noise has been reduced from 78dB (A) to 73.8 dB(A) after the installation of the resonator.

CONCLUSION

The study has shown that an intake resonator can effectively reduce engine intake noises and at some frequencies can reduce them significantly. The full vehicle noise decline can be as large as 4.2dB(A) without distinct changes in engine power. Through the coupling calculation between the resonator and engine, the 3-D flow fields can be simulated within the resonator, thereby obtaining much accurate air flow data in a short time. This provides an important basis for optimal design of the resonator and more accurate ways for the general simulation study of gasoline. This creates the conditions for further study of airflow regeneration noises.

REFERENCES

Heinrich, C.,. and Scharrer, O. F. (Jan. 6, 2005). “Investigation of a 22 step valve train and its influence on combustion by means of coupled CFD simulation.” SAE Paper.

Mo,Q.Y,.An, J.,, and Li, W. (2002). “Using sound intensity measurement to measure mechanical noise and identify noise source.” *Journal of Northwest Forestry University*, (01).

Pang, J.,,et al. .(2006). *Automotive Noise and Vibration*. Beijing Institute of Technology Press, Beijing.

Song, Y., Ge, Y., and Zhang, H. (2005). “Automobile exhaust muffler design study.” *Vehicles and power technologies*, (02).

Zhang, W., and Liu, G., et al..(2004). “A new type of muffler design and test research.” *Journal of Harbin Engineering University*, (05).

Study on Traffic Noise Characteristics of large grade Interchange

WANG Dejun[1], WANG Xiaoning[1] and Luo Lianghao[1,2]

[1]School of Transportation Science and Engineering, Harbin Institute of Technology, P.C. 150090, PH 13604513232, email: wxn1974@hit.edu.cn
[2]Report of Study on Harbin Transportation Planning, P.C. 150000, PH 13804585533, email: nn2k@163.com

ABSTRACT

Because of the analysis of interchange traffic noise pollution is not systematic and deep enough in transport project environmental impact appraising, this paper analyzes large-scaly interchange's characteristics from perspective of occupation, capacity, driving speeds, the turning radius of ramps and vehicle operation conditions, and analyzes the impact factors of large-scaly interchange traffic noise from perspective of vehicle density, velocity, vehicle types, driving cycles, pavement material, slopes, distances and obstacles. At last this paper presents that large-scaly interchange has the characteristics of different traffic noise influence due to different location and the scale of interchanges, relative slight single vehicle noise, needing consideration of acceleration and deceleration noise and complexities of noise source, etc.

INTRODUCTION

The large-scaly interchange, the significant nodes of highway and urban road network, plays an important part in improving intersections' capacity, solving the problem of traffic congestion and guaranteeing traffic unimpeded (Qiao et al. 2001). While at the same time, the large-scaly interchange noise is one of the main source of environmental pollution, and its evaluation and management is one of the main tasks in the transport project environmental impact appraising. However at practical operation, because of the not systematic and deep enough analysis of the interchange noise features, the quality of environmental impact appraising is influenced (Duan 2000). So in order to provide reference for interchange noise impact appraising, this paper analyzes interchange properties, noise influence factures and its characteristics systematically on the basis of summarizing and generalizing the relative researches.

THE DEFINITION OF LARGE -SCALY INTERCHANGE

The large-scaly interchange in this paper has large area occupation and serious environmental pollution, and it is the crossing by too or more road at different plane, and connected by ramps (Wu et al. 2002). Interchanges can be classed into highway interchanges and

urban road interchanges, the functions, main components and design methods of which are basically the same. But because they are affected by topography, ground objects and toll mode, the two types of interchange are different at the land using, design indexes and environmental pollution characteristics.

THE PROPERTIES OF LARGE -SCALY INTERCHANGE

1 Large Area Occupation

The interchange scale needs to be determined at feasibility research stage and preliminary design stage. Generally speaking, the area occupied by interchange usually is large (see Table 1).

Table 1 Land Occupation of Domestic Interchanges Constructed in Recent Years

Title of Interchange	Occupation (m^2)	Region	Built-Up Year
Gonghexinlu Interchange	200,000	Shanghai	2005
Daxinglu Interchange	50,000	Xi'an	2006
Tingjiao Interchange	70,000	Nansha	2006
Shuangqiaomen Interchange	345,000	Nanjing	2004

2 Great Capacity

According to traffic survey data statistics, a straight lane capacity in plane intersection is 1800~2000 pcuh/h, a turning lane is 1700 pcu/h, and roundabout intersection is over 3000pcu/h. The total capacity of an interchange is 10000~15000pcu/h, which is 6~8 times greater than that of a plane intersection.

3 High Driving Velocity

Because of signal control and other interferences when passing a plane intersection, the delay time is so long and the vehicle velocity is slow. The interchange not only realizes every traffic flows' spatial separation, but also eliminates some interferences including signal control, so its vehicle velocity is improved and the delay time is reduced. The traffic investigation shows that the vehicle velocity is 16~20km/h on the road with plane intersection while the straight velocity is 60~70km/h and turning velocity is 30~50km/h on the road with interchange.

4 Small Turning Radium of Ramps

Ramp is the connection road which is connected by two intersect roads and turning vehicles can driving on it. Because of the limitations of the connected road and using land, the ramp radius is smaller than that of the main line and connected road (see Table 2 and Table 3).

Table 2 The Minimum Circular Curve Radius of Ramps

Vehicle Velocity of Ramp(km/h)		80	60	50	40	35	30
The minimum circular curve radius(m)	General Value	280	150	100	60	40	30
	Limit Value	230	120	80	45	35	25

Table 3 The Main Line Design Velocity of Intersection

The Main Line Design Velocity(km/h)		120	100	80	60	40
The Minimum Horizontal Curve Radius(m)	General Value	2000	1500	1100	500	250
	Limit Value	1500	1000	700	350	150

5 The Complex Driving Conditions

On a free interchange, the velocity of turning vehicles on ramp, which come from main line I to main line II, is slower than that on the main line. So the process of driving from main line I to a ramp and then to main line II is a variable motion, which can be divided into five stages: distributary's driving, reduction's driving, uniform (or variable) driving, acceleration's driving and confluence's driving. On toll collection interchanges all the turning vehicles will stop at the toll station. So there is reduction's driving stage when arriving the toll station and acceleration's driving stage when leaving it.

6 The Serious Traffic Noise Pollution

The large-scaly interchange has serious traffic noise due to its great capacity, high velocity and complex driving conditions, etc. Zhang Anting monitored and evaluated the noise pollution of Yayuan interchange in Shenzhen (see Table 4) (Zhang et al. 2005). According to "Standard of environmental noise of urban area" (GB3096-93), which specified the standard of 70 dB in the day and 55dB at night, the noise pollution of Yayuan interchange is serious, especially at night.

Table 4 The Vertical 24 Hour Equivalent Sound Level of Yayuan Interchange

Monitoring Point	The Vertical Dimension From Bridge Surface /m	The Horizontal Distance From Bridge Surface /m	L_d/Db	L_n/dB
Floor 5 of Yayuan Hotel	3	18	70.8	66.6
Floor 6 of Police Bureau	9	15	69.9	64.8
Floor 10 of Police Bureau	21	15	69.7	64.6
Floor 16 of Police Bureau	39	15	70.5	65.9

THE INFLUENCE FACTURES OF LARGE -SCALY INTERCHANGE NOISE

The large-scaly interchange noise is produced mainly by vehicle's driving system and the friction between tire and road surface.

And the noise produced by vibration of structures is also an important component. The main factors that affect the interchange noise are:

(1) Traffic Flow Density

According to some researches the noise level will increase about 3dB when traffic flow density increases 1 time. So the traffic flow density is the key factor and interchange capacity is the direct acting factor.

(2) Velocity

The regression formula of the mean radiation noise level per vehicle type L_{wi} and velocity is shown as follows based on "Specifications for Environmental Impact Assessment of Highways" (Chang 2001).

Heavy-duty Vehicles: $L_{w,L} = 77.2 + 0.18v_L$ (1)

Medium-duty Vehicles: $L_{w,m} = 62.6 + 0.32v_m$ (2)

Light-duty Vehicles: $L_{w,s} = 59.3 + 0.23v_s$ (3)

Where i is the type of vehicle.

(3) Vehicle Type and Driving Cycle

The vehicle noise of uniform motion is related to engine noise, driving transmission system noise and vehicle structure. The noise approximate scope when the velocity is 30km/h refers to "Specifications for Environmental Impact Assessment of Highways". In general condition, the noise of variable motion is much serious than that of uniform motion.

(4) Pavement Material

The noise of tire is related to pavement material and pavement texture. Its correction value is shown as follows (see Table 5).

Table 5 Correction Value of the Pavement

The Pavement	$\Delta L_{pavement}$ (dB)
Asphalt Concrete Pavement	0
Cement Concrete Pavement	1~2

The experimental result shows that the pavement material affects tire noise much of light-duty vehicles. On the rigid pavement, its strength is proportional to velocity, and when the velocity is over 80km/h, the tire noise plays a dominant role.

(5) Longitudinal Slope

When driving on a slope, dynamic noise is proportional to longitudinal slope. The correction value is shown as follows.

Heavy-duty Vehicles: $\Delta L_{ls} = 98\beta$ (dB) (4)

Medium-duty Vehicles: $\Delta L_{ls} = 73\beta$ (dB) (5)

Light-duty Vehicles: $\Delta L_{ls} = 50\beta$ (dB) (6)

Where β is road longitudinal slope, %.

(6) Distance

Distance has significant attenuation of noise. Researches show that the sound level reduces 3 dB when distance increases 1 time (Chang, 2001)

(7) Obstacle

The obstacle's noise attenuation is an important factor. The most typical obstacle is noise barrier, which is usually installed near buildings where influents to people's life and study. In addition, houses and greenbelts also have additional attenuation to propagation of noise. The general rural houses are much dispersive and its additional attenuation value refers to the relevant references. The forest belts' noise attenuation is much difference due to its wood breed, planting method, density and seasonal variation. Usually its value is estimated as follows.

$$\Delta L = k \cdot b \tag{7}$$

Where k is the mean attenuation coefficient of forest belt, taking 0.12 ~ 0.18 Db;

b is the width of forest belt passing by noise, m.

THE NOISE PROPERTIES OF LARGE -SCALY INTERCHANGE

1 The Different Noise Influence with Different Location

The interchange's location affects its pollution directly. When the highway interchange is far from urban area with low building density, the noise influence is little. While the urban interchange is at high density place, so the traffic noise affects people's life and study directly (Wang 2007).

2 The Different Noise Influence with Different Scale

Generally speaking, because of large-scaly interchange's many connecting sections, ramps, lanes and great capacity, its noise is more severe and the influence range is extensive.

3 Relative Slight Noise of Single Vehicle

Because of the spatial division of conflict flows in interchange, the traffic flow is continuous which has the characteristics of great capacity, little energy consumption, less tire and mechanical wear and so on. So the noise of single vehicle is relative slight.

4 The Noise of Acceleration Motion and Reduction Motion Needs To Be Considered

When driving from the main line, vehicles decelerates into a ramp. And after a uniform motion, the vehicle accelerate leaves the ramp and into a connection road. The condition is opposite when driving into ramps. So acceleration reduction motion noise is important in interchange.

5 The Complex Noise Source

The trunk road noise source can be considered as a limited

discontinuous line-source, and the noise maximum value is at the point of 10～15m from road surface. However, the interchange noise source is not linear. When monitoring at nearby location, the noise source can be considered as a discontinuous line-source composed by every point-source. When the monitoring point is higher, the noise of other roads (including interchange branches) will be greater until the interchange can be considered as an area-source.

6 The Prominent Noise of Connecting Section

The design velocity of interchange main line and ramp are different. If the difference is great, the noise of braking at the connecting section will be greater. And the vibration of bumping at bridge-head as well as ear-piercing noise is also the part of influence.

CONCLUSION

On the basis of summarizing and generalizing the relative interchange traffic noise, this paper definite the interchange from the angle of transport project environmental impact appraising, and analyzes the properties of interchange as well as the main factors that affect traffic noise. At last this paper presents the noise characteristics of large-scaly interchange from the perspective of different traffic noise influence due to different location and the scale of interchanges, relative slight single vehicle noise, needing consideration of acceleration and deceleration noise and complexities of noise source, etc.

REFERENCES

Chang Yulin (2001). Study on Source Environment Analysis and Prediction Technique of Urban Traffic System [D]. Southeast University, Nanjing, 27-35.

Duan Yonghui (2000). Thinking About Improvement and Development of Environmental Impact Assessment [J]. Environmental Protection Science, 26(4):40-43.

Qiao Xiang and Lin Huiru (2001). Highway Interchange Planning and Design Practice [M]. Chain Communications Press, Beijing, 7-18.

Wang Xiaoning (2007). Study on Analysis and Evaluation of Road Traffic Pollution About Interchange. Harbin Institute of Technology.

Wu Guoxiong, Li Fang (2002). Interchange Design Exemplification [M]. Chain Communications Press, Beijing, 1-6.

Zhang Anting and Zhuang Yiting (2005). The Noise Pollution and Preventing of Overpass and Interchange. Research of Environmental Sciences, 18(6):120~122.

Effect of Density Variation of Coarse Aggregate on Asphalt Mixture Properties

GE Zhe-sheng[1] and XU Ke[2]

[1]South China University of Technology Road Research Institute, China; email: zsge@scut.edu.cn
[2]Guangdong Changda Highway Engineering Limited, China; email: drxuke@gmail.com

ABSTRACT

There are very few research achievements about the effect of aggregate density variation on the properties of asphalt mixture. In this paper, it was studied by testing in the laboratory at the same gradation and the same asphalt aggregate ratio. The results showed that, as aggregate gradation, water absorption, asphalt aggregate ratio remain unchanged, the coarse aggregate density increases, percentage of voids decrease accordingly. When the density increases by 0.2 g/cm^3, percentage of voids reduces by 1%, and the voids in mineral aggregate of the mixture changes little, and the mixture's capacity to prevent deformation at the high temperature decreases accordingly, but the density variation changes very little about the water stability and anti-cracking at low temperature. Considering the percentage of voids changing range of the asphalt mixture, it is suggested that during the production process, the density of the same batch of the coarse aggregate can only float within the range of ± 0.1kg/cm^3.The result of this research can be taken as a useful reference as modifying and revising the related technical specifications of the asphalt pavement.

FOREWORDS

Asphalt mixture gradation variation, temperature variation, compaction variability have been very much concerned by both domestic and oversea scholars, and have drawn attention of numerous professional road technicians. But there are very few researches about the mixture properties by the density variation of aggregate. In Asphalt Pavement Construction Technical Specification (JTG F40-2004), the requirements about aggregate density on the highway with asphalt surface are as follows the min of the relative density of the surface layer is 2.60, the min of the relative density of the fine aggregate is 2.50; the min of the relative density of the other layers of coarse, fine aggregate is 2.50. However, there isn't any specification requirement about the density variation range of the same batch. During the usual construction, in the same stone processing plant, the relative density of the limestone floats from 2.60 to 2.80.

This paper intends to focus on the research of the impact on the volume index and the pavement properties of the mixture caused by the density variation of the coarse aggregate, which was tested in the laboratory at the same gradation and the same asphalt aggregate ratio.

TESTING MATERIALS

Asphalt. Using the SBS modified asphalt, Table 1 shows its technical indicators.

Table 1. Specifications of Asphalt.

Test item		Test results
Penetration 25℃,100g , 5s，0.1mm		56.3
Penetration Index PI		0.33
Ductility 5℃,5cm/min ,cm		35.6
Softening point $T_{R\&B}$（℃）		88.6
Flashing point（℃）		294
Solubility（%）		99.8
Storage stability: 163℃，48hrs，Minus of penetration℃		0.3
Elastic recovery 25℃，%		95.0
Dynamic viscosity (Pa·s)	135℃	2.05
	165℃	0.52
Rotating thin film heating test (RTFOT) Residues (163℃,85min)	Change of Quality (%)	-0.09
	Ductility 5℃,5cm/min,cm	30.5
	Penetration ratio (%)	84.0

Aggregate. During the construction process of the middle layer AC-20C of the highway, 4 kinds of coarse aggregate with the 4 different densities from the mixing plant were chosen. Table 2 shows the test results of the key technical index of these 4 kinds of materials. Table 3 and table 4 show the test results of the technical index of the fine aggregate and slag.

Table 2. Specifications of Coarse Aggregate.

Test item	Coarse Aggregate 1	Coarse Aggregate 2	Coarse Aggregate 3	Coarse Aggregate 4
Crushing value (%)	20.4	15.6	13.2	13.5
Los Angeles abrasion value (%)	18.0	13.8	12.5	13.4
Apparent relative density	2.623	2.688	2.748	2.823
Bulk relative density	2.588	2.653	2.713	2.784
Water absorption (%)	0.52	0.49	0.47	0.50
Adhesion with SBS(Level)	5	4	4	5
Particle content of the needle plate (%)	7.5	5.5	4.7	6.3
Washing Method <0.075mm Particle content (%)	0.2	0.4	0.6	0.2
Soft stone content (%)	0	0.2	0.5	0.2

Table 3. Specifications of Fine Aggregate.

Test item	Test results
Apparent relative density	2.744
Washing Method <0.075 Particle content (%)	14.1
Sand equivalent (%)	72.9

Table 4. Specifications Slag.

Test item	Test results
Apparent relative density (t/m^3)	2.685
Water content	0.12
Plasticity index	2.1
Appearance	No aggregate caking

Mixture gradation and asphalt aggregate ratio. Table 5 is the gradation of AC-20C type of mixture. The asphalt aggregate ratio is confirmed to be 4.4%.

Table 5. AC-20C Asphalt Mixture Gradation.

Gradation	Sieve the quality of the adoption of the following percentage /% (Square hole sieve, mm)												
	31.5	26.5	19	16	13.2	9.5	4.75	2.36	1.18	0.6	0.3	0.15	0.075
Upper Limit	100	100	100	92	80	72	56	44	33	24	17	13	7
Lower Limit	100	100	90	78	62	50	26	16	12	8	5	4	3
Target Gradation	100	100	94.1	84.0	78.3	59.6	36.1	30.4	24.5	18.5	13.1	9.5	5.4

VOLUME INDEX OF THE MIXTURE

4 kinds of mixture with the same kind of asphalt of SBS modified asphalt, the same gradation of AC-20C, the same asphalt aggregate ratio of 4.4% were created, but four different kinds of limestone with the different density. The test results about their volume index from table 6 show that,

a) As the aggregate gradation, water absorption, and asphalt aggregate ratio remain the same, the density of coarse aggregate increases, and percentage of voids decreases accordingly; density increases by 0.2 g/cm^3, percentage of voids reduces by 1%;

b) Because the aggregate gradation is the same, the voids in mineral aggregate (VMA) Changes little;

c) The stability of the mixture decreases with the increasing of the density, the flow value increases accordingly, and the capability to prevent deformation becomes weaker and weaker.

Table 6. Mixture Volume Index.

Coarse aggregate type	Apparent relative density /g/cm^3	Bulk relative density /g/cm^3	Water absorption /%	Percentage of voids /%	VMA /%	Stability /kN	Flow value /0.1mm
Aggregate 1	2.623	2.588	0.52	4.2	13.1	14.30	15.40
Aggregate 2	2.688	2.653	0.49	3.9	13.1	12.28	18.70
Aggregate 3	2.748	2.713	0.47	3.6	13.0	11.10	29.50
Aggregate 4	2.823	2.784	0.50	3.2	12.9	9.53	35.10

PROPERTIES OF THE MIXTURE

First of all, those four kinds of mixture in table 6 were tested through high-temperature rutting test about the high temperature performance. Table 7 gives out the related result. Table 7 shows that at the same asphalt aggregate ratio, same gradation, anti-deformation became weaker and weaker at the high temperature while the density increases.

Table 7. Mixture Rutting Test Results.

Coarse Aggregate Type	Rutting Test Dynamic Stability /（times/mm）			Average /（times/mm）
	1	2	3	
Aggregate 1	6425	6387	6345	6386
Aggregate 2	6130	6209	6108	6149
Aggregate 3	5812	5789	5634	5745
Aggregate 4	5138	4987	5156	5094

Secondly, those four kinds of mixture in table 6 were tested through the Marshall immersion test about their water stability. Table 8 gives out the test results. From the table, the difference of the residue stability of these four mixtures is very small. All are more than 90%.

Table 8. Mixture Marshall Immersion Test Results.

Coarse Aggregate Type	Asphalt aggregate ratio /%	Percentage of voids /%	60℃,1h Stability /kN	60℃,48h Stability /kN	Residual stability /%
Aggregate 1	4.4	4.2	14.30	12.90	90.2
Aggregate 2	4.4	3.9	12.28	11.19	91.1
Aggregate 3	4.4	3.6	11.10	10.08	90.8
Aggregate 4	4.4	3.2	9.53	8.70	91.3

Finally, those four kinds of mixture in table 6 were tested through the

low-temperature -10℃ bending test about their anti-cracking at the low-temperature. Table 9 gives out the test results. From the table, the flexural strength, flexural modulus and tensile strain changed very little, which means the anti-cracking of the mixture at the low temperature is equivalent.

Table 9. Mixture at Low Temperature Bending Test Results.

Coarse Aggregate Type	Asphalt aggregate ratio /%	Porosity /%	Flexural strength /MPa	Modulus /MPa	Tensile strain /uε
Aggregate 1	4.4	4.2	7.76	2896	2678
Aggregate 2	4.4	3.9	7.27	2197	3308
Aggregate 3	4.4	3.6	7.84	2530	3098
Aggregate 4	4.4	3.2	8.08	2851	2835

CONCLUSION

The effect on the volume index and the pavement properties of the mixture caused by the density variation of the coarse aggregate was studied, which was tested in the laboratory at the same gradation and the same asphalt aggregate ratio. The results show, as mineral aggregate gradation, water absorption, asphalt aggregate ratio remain unchanged, the coarse aggregate density increases, percentage of voids decrease accordingly. When density increases by 0.2 g/cm^3, percentage of voids reduces by 1%, and the voids in mineral aggregate of the mixture changes little. Mixture's capacity to prevent deformation at the high temperature decreases accordingly, but the density variation changes very little about the water stability and anti-cracking at low temperature. Considering the percentage of voids changing range of the asphalt mixture, it is suggested that during the production process, the density of the same batch of the coarse aggregate can only float within the range of ± 0.1kg/cm^3.

REFERENCES

Ministry of Transport of the People's Republic of China (2004), Asphalt Pavement Construction Technical Specification, Beijing.

Study of an image-based gradation measurement techniques of the asphalt mixture

Z. Y. Sun[1], C.F. Wang[2] and A. M. Sha[2]

[1] College of Information Engineering, Chang'an University, Xi'an, China, 710064
[2] Key Laboratory for Special Area Highway Engineering of Ministry of Education, Chang'an University, Xi'an, China, 710064

ABSTRACT

Gradation is one of the key factors affecting various performances of asphalt pavement. Current gradation testing methods, extracting-sieving method and burning-sieving method, have many disadvantages since some important properties of the aggregate particles may not be obtained due to the lack of an objective way of quantifying critical aggregate properties. This paper uses the digital image processing techniques to carry out a series of image processing operations to the side images of the asphalt mixture specimen girder, and calculates the passing rates of aggregate particles with different sizes according to the geometrical characteristics of each aggregate particle after segmentation of the aggregate particles. Furthermore, it draws the gradation curve according to the passing rates. The paper also carries out an error analysis to the measured data. The result shows that the method based on image processing is worth being promoted in practice.

KEYWORDS: asphalt mixture, gradation, aggregate, digital image, boundary rectangle, fitting ellipse

INTRODUCTION

Asphalt pavement is the main type of highway pavements in China (Zhang 2003). How to assure the quality of the building material of the asphalt pavement is important. Gradation is the mineral composition of the asphalt mixture. The traditional asphalt mixture gradation testing methods, extracting-sieving method and burning-sieving method, have weaknesses such as complicated operation, time consuming, and low data accuracy. Also, the experimental data seriously depends on the operator.

The main properties of aggregate particles studied using digital image processing techniques are size, shape (Maerz 2004, Pan and Tutumluer 2005), and angularity (Shu et al 2006). Besides, someone gives 3D description of the aggregate particles based on the image processing techniques (Corriveau et al 2005, Barrot et al 2006). Some of the studies use the Fourier analysis method (Wettimuny and

Penumadu 2004), and the others use the wavelet analysis method (Shin and Hryciw 2004). The properties of asphalt mixture are mainly gradation (Abdullah and Obaidat 1998), air voids (Arambula et al 2007), and the automatic test system (Sun et al 2005).

The data precision obtained from the recent study is not high enough and the study of the gradation of aggregate particles in the asphalt mixture using digital image processing techniques is still limited. This paper uses the image acquisition device at relatively low expense to obtain the images and applies the digital image processing techniques to achieve the automatic measurement of the aggregate gradation in the asphalt mixture to obtain the better data precision.

ASPHALT MIXTURE DIGITAL IMAGE ACQUISITION

The asphalt mixture specimen is cut into girders and the side images are acquired by using a fixed line scan camera. The image acquisition hardware is sketched in Figure 1.

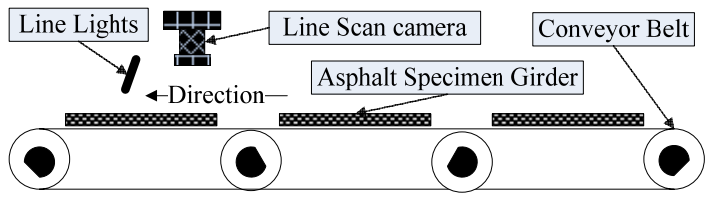

Figure 1. Sketch map of image acquisition hardware

The physical length of the acquired image is 10cm, which is equal to 2048 in pixel. One of the gray-scale images acquired and its histogram are shown in Figure2.

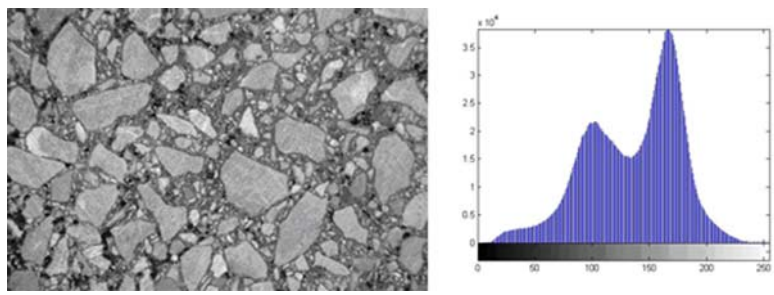

Figure 2. Gray-scale image and its histogram

DIGITAL IMAGE PROCESSING TECHNIQUES OF ASPHALT MIXTURE

The paper adopts the digital image processing techniques to carry out a series of processing and analysis to the acquired asphalt mixture image, and gets the area and volumetric percentage of the aggregate particles with different particle sizes.

Asphalt Mixture Image Preprocessing Techniques

One of the most common problems encountered during image is poor contrast resulted from the illuminating environment. It can often be improved by amplitude rescaling of each pixel. This method modifies the gray-scale value of each pixel dot by dot to modify the dynamic scope of gray-scale in the image. It can expand or compress the gray-scale scope, or compress in some dynamic area whereas expand in another area. The gray-scale image after contrast manipulation and its histogram are shown in Figure 3.

This paper uses median filtering processing to the asphalt mixture images to clean the salt and pepper noises (Gonzalez, 2002). In median filtering, the neighbors must be set, and the output value of the pixel in question equals to the median of the neighbors. The shape of the neighbors determines the geometric space and the size of the neighbors determines the number of values that the median comes from. This paper selects 3*3 neighbors to carry out median filtering operation because the 2*2 neighbors can not clean the noise well whereas the 5*5 neighbors can result in blur of the particle edge. The image after median filtering processing is shown in Figure 4.

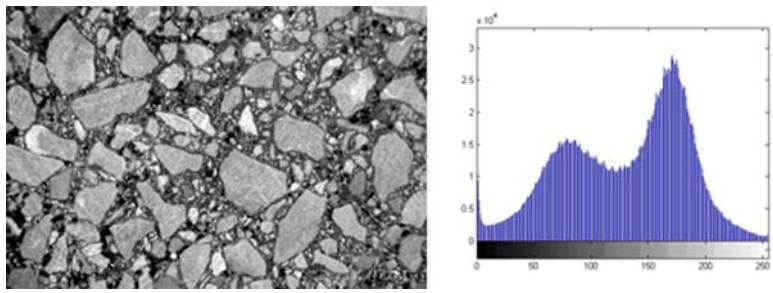

Figure 3. Gray-scale image after contrast manipulation and its histogram

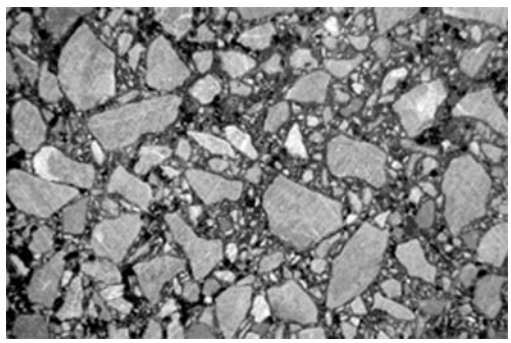

Figure 4. Median filter image (3*3 neighbors)

Binary asphalt mixture image processing

There are many methods to obtain binary image from gray-scale image among

which the gray-scale based method is usually used. This paper uses an adaptive threshold method to obtain the binary image. The binary images obtained are shown in Figure 5. There are some conglutinations of the particles, thus, morphological operations (Gonzalez, 2002) need to be carried out after getting the binary image of the asphalt mixture. First, the erosion operation is carried out to separate the particles. Then, the close operation to fill the holes which are caused by the noise points in the particles, and then uses the dilation operation to restore the particle size. The binary image after the morphological operations is shown in Figure 6.

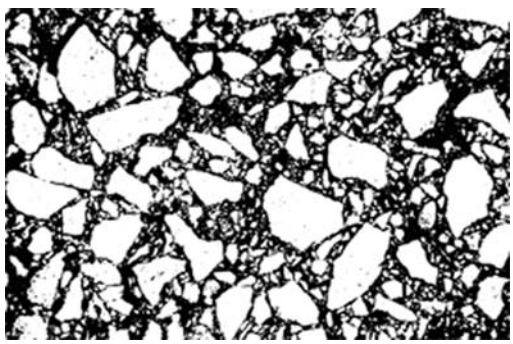

Figure 5. Binary image

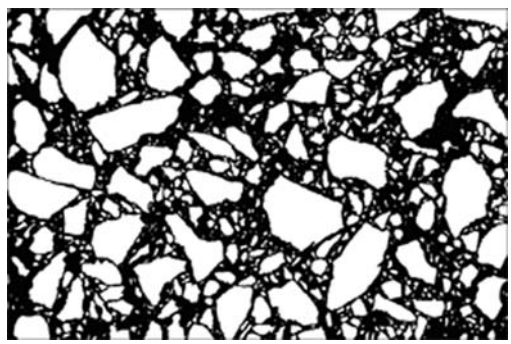

Figure 6. After morphological operations

Asphalt mixture image segmentation

There are many kinds of image segmentation methods. It can be generally divided into region based, edge based and the combination of the two. After getting the binary images of the asphalt mixture, there are at least two methods to obtain the edge images. One is through the image calculating, the other is the edge tracing method. Image calculating method needs to carry on the erosion operation and then subtract from the original binary image, which is more complicated. This paper carries on edge tracing on the binary image directly and obtains the edge image.

Particle analysis

The particle analysis can be carried on by both the binary image and the edge image. This paper carries on particle analysis based on the binary image and draws the label of each particle in the asphalt mixture image (Figure 7). It extracts characteristics such as area, boundary rectangle, fitting ellipse of each particle and save the data into a Microsoft Excel file.

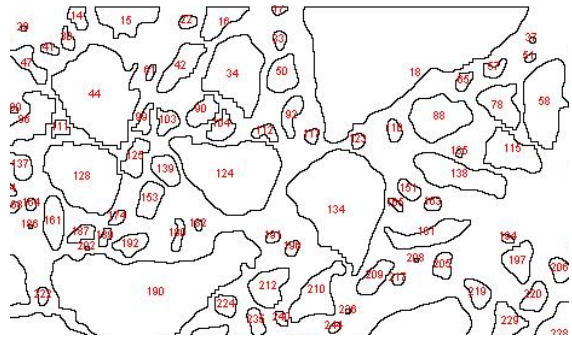

Figure 7. Part of the labeled image

DATA ANALYSIS AND ERROR ANALYSIS

In order to simulate the sieving process accurately, this paper extracts characteristics such as the area and minimum edge rectangle of each aggregate particle, and then calculates the area of the particles, the volume of the restored ball according to the sieve size and the short edge of the boundary rectangle separately to get the passing rate of the aggregate particles with different particle sizes, and further draws the gradation curve.

Data analysis

This paper calculates the passing rate with two different methods. AC-13-area presents the passing rate calculated by area of the aggregate particles; AC-13-volume presents the passing rate calculated by volume of the restored ball and the volume is calculated by using: $v = 4\pi (A/\pi)^{3/2}/3$, where v is the volume of the restored ball and A is the area of the particle.

25 images of the AC-13 gradation asphalt mixture are processed in this paper and the average passing rate of each control sieve (Table1) is obtained. From Figure 8, it can be seen that the measured data is smaller than the designed values.

Table 1. Average passing rate of AC-13 gradation asphalt mixture

Sieve size (mm)	Passing rate (%)		
	AC-13-design	AC-13-area	AC-13-volume
0.075	4	0	0
0.15	9	0.0463877	0.0010796
0.3	15	0.4330286	0.0194674
0.6	24	2.3584637	0.20614
1.18	38	8.926129	1.237419
2.36	55	21.2791	4.7327562

4.75	77	42.469925	18.38467
9.5	93.5	68.684775	52.520292
13.2	95	95.714447	87.732932
16	100	100	100

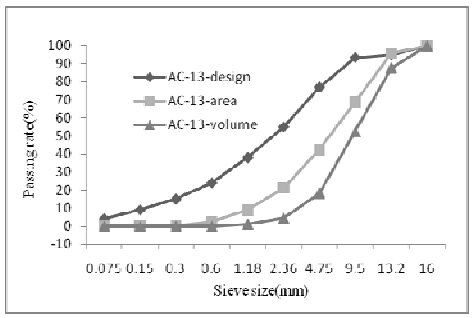

Figure 8. Comparison of gradation curve of AC-13 gradation asphalt mixture

Further, this paper calculates the coarse aggregate and fine aggregate separately to find the factor affecting the measured result. According to the highway criterion, the aggregate particles are divided into coarse aggregate and fine aggregate. The coarse aggregate includes aggregates with particle size larger than 2.36mm, and the others are fine aggregate. The gradation curve for the fine aggregate drawn according to the passing rates is shown in Figure 9. The gradation curve for the coarse aggregate drawn according to the coarse aggregate passing rates is shown in Figure 10.

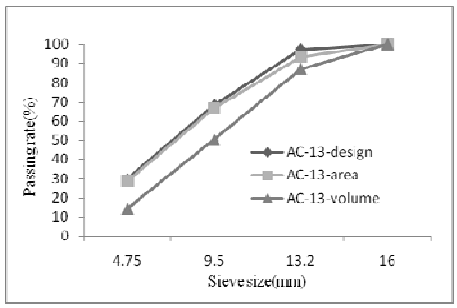

Figure 9. Comparison of gradation curve of coarse aggregate

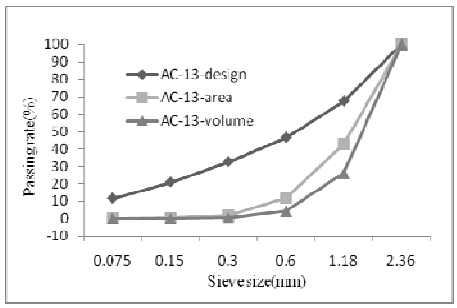

Figure 10. Comparison of gradation curve of fine aggregate

Error analysis

For the measurement of the coarse aggregate whose particle size is greater than 2.36mm in the AC-13 gradation asphalt mixture, the passing rate calculated according to the particle area is not significantly different than the design gradation and its gradation curve is almost the same as the design gradation curve (Figure 9).

The gradation of the fine aggregate in the AC-13 asphalt mixture is smaller than the design value (Figure 10) because of the cohesion of the small particles and the excessive erosion operations during the binary image morphological processing. Beside, the image resolution and the illuminating environment where the images were acquired are also the factors affecting the recognizing and extraction of the fine aggregate particles.

The result calculated according to the volume of restored ball is smaller than the design value since the images being processed are 2D images of the asphalt mixture and only one section plane of the asphalt mixture girder is processed.

CONCLUSION

There are many test methods for the size and shape properties of single aggregate particles and the gradation of mineral aggregate mixture using the image processing techniques. However, the study of the gradation of the aggregate particles in the asphalt mixture has not been well studied. This paper uses the digital image processing techniques and obtains relatively good results.

There are difference between the designed the gradation and the measured gradation, this paper considers the coarse aggregate and fine aggregate separately and gets the results that the fine aggregate particles can not reflect the true condition of the asphalt mixture and result in errors.

However, the image-based aggregate gradation measurement of asphalt mixture could greatly improve the measuring speed and data accuracy after error compensation, thus can be taken as an effective substitution of present test methods. In the future work, image resolution will be increased and new image processing techniques will be employed to improve the measurement precision of the fine aggregate particles.

REFERENCE

Abdullah, W.S., and Obaidat, M.T. (1998). “Influence of aggregate type and gradation on voids of asphalt concrete pavements”. *Journal of Material in Civil Engineering*, 76-85

Arambula, E., Masad, E., and Martin, A.E. (2007). “Influence of air void distribution on the moisture susceptibility of asphalt mixes”. *Journal of Material in Civil Engineering*, 655-664

Barrot, D., Jr, P.G., Mandayam, S., and Sukumaran, B. (2006). “Synthesis of sand particles from 3D shape descriptors using topographic reconstruction techniques”. In Proceedings of GeoCongress 2006: Geotechnical Engineering in the Information Technology Age, ASCE, Atlanta, Georgia

Corriveau, J., Barrot, D., Mandayam, S., and Sukumaran, B. (2005). “3-D shape

descriptors for geomaterial aggregates using multiple projective representations". In Proceedings of the Sessions of the Geo-Frontiers 2005 Congress: Site Characterization and Modeling, ASCE, Austin, Tex, 1-15

Gonzalez, R.C., and Woods, R.E. 2002. "Digital image processing". 2ed Edition. Publishing House of Electronics Industry, Beijing

Maerz, N.H. (2004). "Technical and computational aspects of the measurement of aggregate shape by digital image analysis". *Journal of Computing in Civil Engineering*, 10-18

Pan, T.Y., and Tutumluer, E. (2005). "Imaging based evaluation of coarse aggregate size and shape properties affecting pavement performance". *Advances in Pavement Engineering*, ASCE, Austin, Tex, 1-15

Peng, Y., Sun, L.J, Wang, Y.Q., Shi Y.J. (2007). "Application of digital image processing in evaluating homogeneity of asphalt mixture". *Journal of Jilin University (Engineering and Technology Edition)*, 37(2), 334-337

Shin, S.C., Hryciw, R.D. (2004). "Wavelet analysis of soil mass images for particle size determination". *Journal of Computing in Civil Engineerin*g, 19-27

Shu, X., Huang, B., Chen, X., and Robison, L. (2006). "Effect of coarse aggregate angularity on rutting performance of HMA pavement". Pavement Mechanics and Performance, Shanghai, China, 6-8 June 2006. ASCE, 126-133

Sun, Z.Y., Wang, C.F, Sha, A.M. (2005). "Research on automatic measurement system of the asphalt mixture". In Proceedings of the Seventh International Conference on Electronic Measurement & Instruments, Beijing, 5-253-5-259

Wettimuny, R., and Penumadu, D. (2004). "Application of Fourier analysis to digital imaging for particle shape analysis". *Journal of Computer in Civil Engineering*, 2-9

Zhang, X.N, Li, Z., Yu J.M. (2002). "Evaluating the volumetric properties of asphalt mixtures with digital image processing technique". *Journal of South China University of Technology (Natural Science)*, 30(11), 113-118

Zhang D.L(2003). "Asphalt pavement construction manual". China Communications Press, Beijing, China

Analysis of Thermal Stress Response in Asphalt Overlay

Xu Wensheng[1], Tian Wei[2*] and Luo Hui[3]

[1]School of Civil Engineering and Mechanics, Huazhong University of Science & Technology; Hubei Key Laboratory of Control Structure; Wuhan Huazhong Keda Civil Engineering Inspection Center, 430074, Wuhan, Hubei, China; email: italy-wolf@163.com

[2]Wuhan Harbour Engineering Design & Research Institute; Key Laboratory of Bridge & Tunnel Technology of the Ministry of Communications, 430074, Wuhan, Hubei, China; email: mimikid_jj@163.com

[3]School of Civil Engineering and Mechanics, Huazhong University of Science & Technology, 430074,Wuhan, Hubei, China; email: autumn_luoh@163.com

ABSTRACT

The thermal stress response in asphalt overlay under different cooling conditions was analyzed considering thermal-viscoelasticity of asphalt mixture. The influence of cooling speed, initial temperature, cooling range, pavement thickness and base modulus on temperature stress were represented. The results indicate that, the cumulated thermal stress in asphalt overlay is small at high temperature; initial temperature and cooling speed distinctly affect thermal stress in asphalt overlay; reflective cracks occur in thinner asphalt overlay more easily, while top-down cracks happen in thicker asphalt overlay more easily; and too large base modulus is unsuitable to controlling thermal crack in asphalt overlay.

KEY WORDS

road engineering; asphalt overlay; thermal-viscoelasticity; thermal stress

INTRODUCTION

Thermal cracks seriously shorten service period of asphalt pavements in seasonal frost regions and permafrost regions. Wang (Wang and Zhu, 2004) studied thermal stress condition of asphalt concrete under low temperature. On the basis of the theory of thermal elastic mechanics, the accumulated thermal stress of an one -dimension asphalt concrete bar was computed in consideration of asphalt mixture's modulus changing with decreasing temperature; Li (Li et al., 2006) analyzed thermal cracks based on the fracture mechanic theory; Yang (Yang and Liu, 2006) did thermal-structural analysis of asphalt pavements. The influence of temperature-dependent material properties, such as asphalt mixture stiffness, has been taken into account. Zheng (Zheng, 2001) and Tian (Tian et al., 2002) carried out the thermal stress test of asphalt concrete beam by the thermal stress restrained sample tester (TSRST). Qian (Qian et al., 2003) studied thermal stress in asphalt overlay based on thermal-viscoelasticity theory by using the finite element method,

but the effects of cooling condition and pavement structure parameters were not analyzed, thus their conclusion could not be applied directly to asphalt pavement design. This paper simulated thermal stress response in asphalt overlay under various cooling conditions based on thermal-viscoelasticity theory by using the commercial finite element software ANSYS. A parametric study is also done to isolate the effect of various factors on thermal stress response, aiming at the understanding of the mechanism of thermal cracking in asphalt pavements.

THERMAL-VISCOELASTICITY

Asphalt mixture is thermal-viscoelastic under normal environmental temperature. The relaxation is usually defined by the Generalized Maxwell model (Zheng et al., 2003; Zheng et al., 2004; Qian et al., 2006). For the Generalized Maxwell consisting of of N sets of Maxwell models, the relaxation modulus E is defined by Eq. 1 below:

$$E(t) = \sum_{1}^{N} E_i e^{-t/\tau_i} \tag{1}$$

Where, $\tau_i = \eta_i / E_i$ is the relaxation time of the ith Maxwell element.

Actually, the relaxation modulus and creep compliance both vary with time and temperature, independently. Usually, high temperature would accelerate its creeping or relaxing process. The relaxation occurred during a long time under a lower temperature could take place in a shorter time under a higher temperature. This is called the correspondence principle. And correspondence principle could be described as (Zheng, 2001):

$$E(T,t) = E(T_0, t/\alpha_T), \tag{2}$$

Where, T_0 is the reference temperature, α_T is the shift factor.

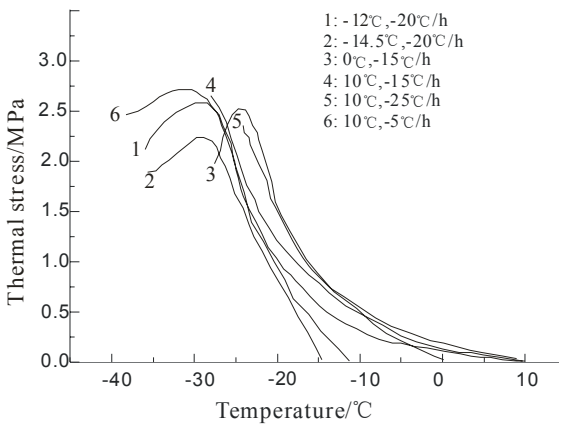

Fig. 1 Test results of TSRST

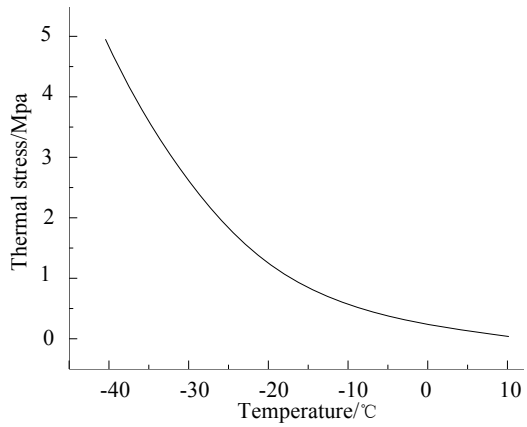

Fig. 2 FEM numerical result of TSTST

VALIDATION OF THE SIMULATION BASED ON THERMAL-VISCOELASTICITY

Zheng (Zheng et al., 2004) chose seven initial temperatures for the thermal stress restrained sample test which are spaced 5 ºC apart, and the lowest initial temperature is -20 ºC. The cooling rate is -5 ºC/h, -10 ºC/h, -15 ºC/h and -20 ºC/h, respectively. The results are shown as Fig. 1.

The numerical simulation of the TSRST was carried out to validate the application of thermal-viscoelastic theory for calculating thermal stress in asphalt mixture. The TSRST sample was discretized in Solid185 which is a type of element in ANSYS. The parameters of the asphalt mixute are shown in Tab. 1 and Tab. 2.

Tab.1 Parameters of the Maxwell model

E_1/MPa	659.9	τ_1/s	4 315 000	E_4/MPa	432	τ_4/s	145 100
E_2/MPa	10 410	τ_2/s	32.12	E_5/MPa	4 148	τ_5/s	191.6
E_3/MPa	2 535	τ_3/s	986.4	E_6/MPa	1 613	τ_6/s	7 570

Tab.2 Values of α_T at different temperatures

Temperature/℃	-20	-15	-10	-5	0	5	10	15
α_T	0.0117	0.0546	0.2402	1	3.953	14.87	53.36	183.3

One case of the test of TSRST was chosen to be simulated. Its initial temperature is 10 ºC, and the cooling rate is -5 ºC/h. In the simulation, the thermal shrinkage coefficient is approximately considered as constant during the cooling process . And the numerical result is shown as Fig. 2.

Fig. 2 shows that the numerical result is almost consistent with the test results (shown in Fig. 1) before temperature falling to -30 ºC. The thermal-viscoelasticity numerical model could reveal the stress relaxation of asphalt concrete accurately.

NUMERICAL MODEL FOR THE ANALYSIS OF THERMAL STRESS IN ASPHALT PAVEMENTS

Basic assumptions

Some assumptions of material characteristics and asphalt pavement structures are made as below:

a) The asphalt overlay is thermal-viscoelastic, the materials of other layers are all homogeneously isotropic and elastic;

b) The gravity of asphalt pavements is ignored;

c) The lateral sides of the pavements are horizontally restrained, and the top surface of overlay is free in all degrees, and the subgrade bottom is fixed.

Parameters of simulated asphalt pavements

Since different pavement structures lead to different thermal stress responses, it's necessary to analyze the effect of various structures. For the simulations below, the parameters are the same as those listed in Tab. 3, except for additional

explanations.

Tab.3 Numerical parameters of asphalt pavement

Layer No.	Layer name	Thickness (mm)	Young's modulus(MPa)	Poisson's ratio	Thermal shrinkage coefficient
1	Asphalt overlay	70	—	0.3	2E-5
2	Base	150	1500	0.25	1E-5
3	Sub-base	150	600	0.35	1.5E-5
4	Subgrade	1000	40	0.35	50E-5

Temperature field of asphalt pavements

The one-dimensional model was chosen to represent the temperature field in asphalt pavements under cooling conditions, which is listed as Eq. 3:

$$T(t,z) = T_0 + \Delta T_m \frac{t}{t_m} \exp(-z / z_0), \tag{3}$$

Where, z is the depth of asphalt pavement, ΔT_m is temperature cooling range, t_m is cooling time, and z_0 is the depth constant which usually varies from 0.2 m to 0.3 m.

THE ANALYSIS OF THERMAL STRESS IN ASPHALT OVERLAY

Asphalt mixture is typically a thermal-viscoelastic material in service environment. Thus, the thermal stress in asphalt overlay must be influenced by temperature load which could be characterized by initial temperature, cooling rate and cooling range. Furthermore, the performance of asphalt pavements is essentially related to the overlay's and base's thicknesses and moduli. It's necessary to analyze thermal stress response of various structures under different temperature loads.

The effect of base state on thermal stress response was studied. Two models were created: the base is intact in model 1, but cracked in model 2. The initial temperature was 5 ºC, the cooling range was 30 ºC, and the cooling rate was 10 ºC/h. The results are shown as Tab. 4.

Tab.4 Thermal stress of the two different models

Model No.	Thermal stress at overlay bottom(MPa)	Thermal stress at overlay surface(MPa)
1	4.77	8.39
2	9.168 822	9.087 229

It is shown in Tab. 4 that tensile thermal stresses at both bottom and surface of asphalt overlay of model 2 are more disadvantageous than that of model 1. So

model 2 was chosen to accomplish the parametric study below.

Influence of initial temperatures

In this simulation work, the initial temperatures were -5 ºC, 0 ºC, 5 ºC, 10 ºC, respectively. The cooling range was 40 ºC, and the cooling rate was -10 ºC/h. The results are shown in Fig. 3 and Fig. 4.

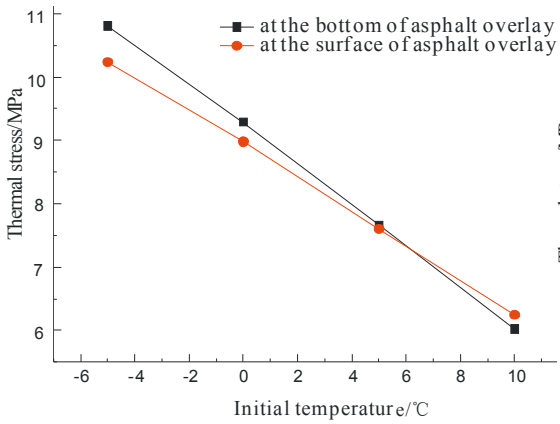

Fig. 3 Influence of initial temperature

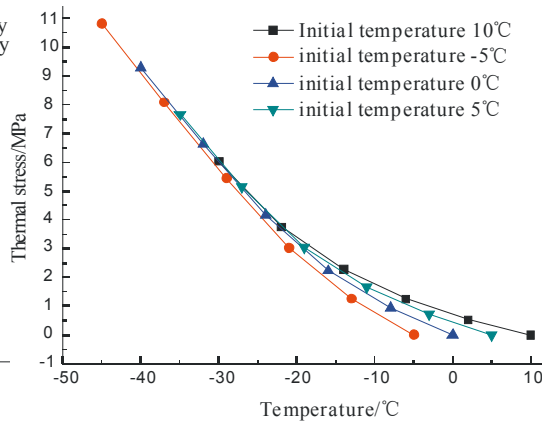

Fig. 4 Thermal stress-temperature curve of various initial temperatures

It can be seen from Fig. 3 that the thermal stress increases with the falling of initial temperature. This is to say, to the same cooling range and cooling rate, the lower initial temperature, the greater the thermal stress. Furthermore, for high initial temperature, after cooling, the thermal stress at asphalt overlay surface is smaller than that at overlay bottom. For low initial temperature, the thermal stress at overlay surface is greater than that at overlay bottom. Thermal stress at bottom is more susceptive to initial temperature.

Fig. 4 presents thermal stress-temperature curves of various initial temperatures. The lower initial temperature is, the steeper the curve. This is to say, though cooling range is small, thermal stress could still be great, if initial temperature is low enough. At low temperature section of Fig. 6 (≤-20 ºC), the curves are almost the same, which indicates that it behaves more like elasticity than like viscoelasticity when temperature is lower than -20 ºC for asphalt concrete.

Influence of cooling range

In this simulation, the initial temperature was -5 ºC, the cooling rate was -10 ºC/h, and the cooling range varied from 10 ºC to 40 ºC at the interval of 10 ºC. The numerical results are shown in Fig. 5.

Fig. 5 shows that the greater cooling range is, the higher thermal stress at overlay surface and bottom. The increase of thermal stress is not linear but accelerative to cooling range, which was caused by the viscoelastic characteristic.

Influence of cooling rate

To study the influence of cooling rate on thermal stress in asphalt overlay, the parametric study of cooling rate was done. The cooling range was 30 ºC, and the initial temperature was 5 ºC. The cooling rate was -5 ºC/h, -10 ºC/h, -15 ºC/h and -20 ºC/h, respectively. The results are shown in Fig. 6 and Fig. 7.

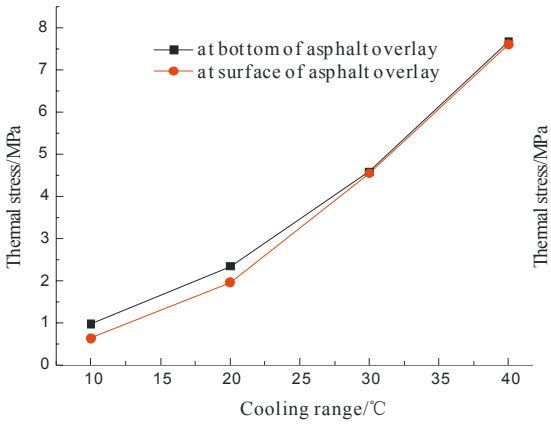

Fig. 5 Influence of cooling range

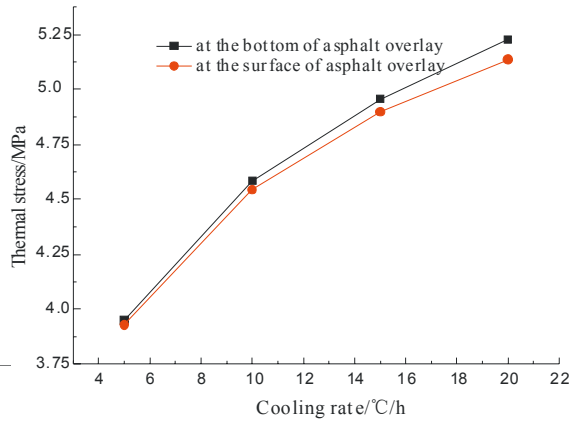

Fig.6 Influence of cooling rate

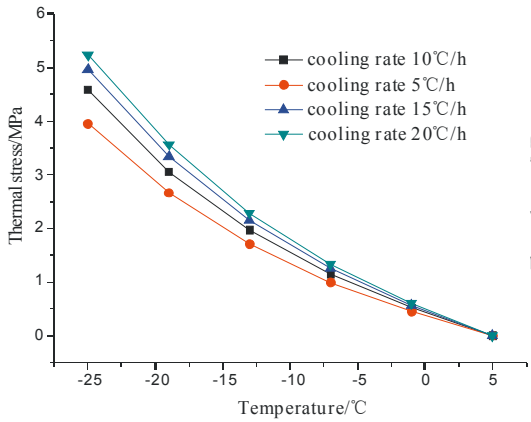

Fig. 7 Thermal stress-temperature curve of different cooling rates

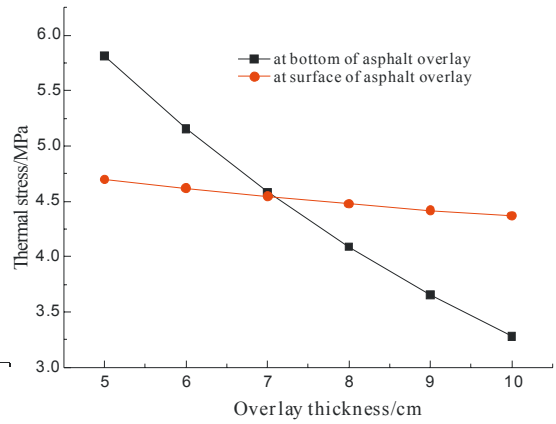

Fig. 8 Influence of asphalt overlay thickness

It can be seen from Fig. 6 that thermal stress increases as cooling rate increases . Furthermore, the stress at the bottom of asphalt overlay increases more quickly than that at the surface, which indicates that thermal stress at the bottom of asphalt overlay is more susceptive.

Fig. 7 is temperature-thermal stress curves of various cooling rates. It shows that the greater cooling rate, the steeper curve is. In ultra disadvantageous cooling load, for example, the raid of cold snap, great thermal tensile stress would occur in asphalt overlay.

Influence of overlay thickness

Aimed at secondary road, such pavement structures whose overlay thickness varies form 5 cm to 10 cm at the interval of 1 cm were simulated. In the numerical

analysis, the cooling range was 30 ºC, the cooling rate was -5 ºC/h, and the initial temperature was 5 ºC. The results are shown in Fig. 8.

Fig. 8 shows that thermal stresses both at surface and bottom of asphalt overlay fall with the increase of overlay thickness. This is to say, greater thickness of asphalt overlay leads to smaller thermal stress under the same temperature loads. But, with the increasing of overlay thickness, the thermal stress at overlay surface falls slowly, while that at bottom falls rapidly. This indicates that the stress at the bottom is dominant for cracking when overlay thickness is greater than 7 cm, since in this situation the stress at bottom is higher than that at surface. When overlay thickness is smaller than 7cm, the stress at surface controls the cracking of asphalt overlay. Therefore, reflective cracks appear easily in thinner asphalt overlay , while cracks tend to start from the surface for thicker asphalt overlay.

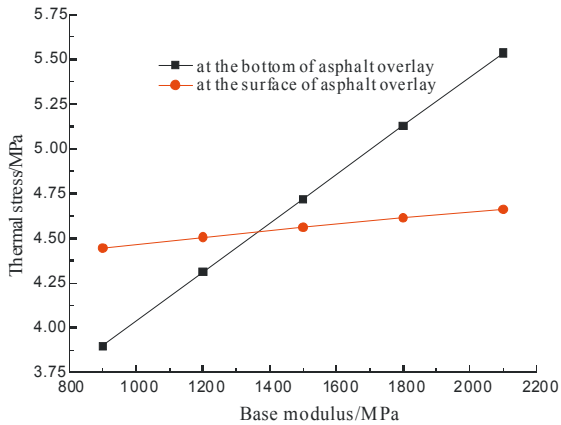

Fig. 9 Influence of base modulus

Influence of base modulus

Base modulus is a key index of pavement design, so the parametric study about base modulus was done. The cooling range was 30 ºC, the cooling rate was -5 ºC/h, and the initial temperature was 5 ºC. Base modulus was 900 MPa, 1200 MPa, 1500 MPa, 1800 MPa and 2100 MPa, respectively. The results are shown in Fig. 9.

It is shown in Fig. 9 that thermal stress increases with the increase of base modulus, especially that at overlay bottom. Bases whose modulus is not very stiff may limit thermal stresses, leading to better control of thermal crack in asphalt pavements. The modulus between 1200 MPa to 1500 MPa is recommended, taken the bearing ability of wheel loads into account.

CONCLUSIONS

A three-dimension finite element model of asphalt pavements was created based on thermal-viscoelasticity theory. The thermal stress in asphalt overlay was analyzed, and the parametric studies were done to isolate the influence of different factors, such as cooling rate, cooling range, initial temperature, base modulus and overlay thickness. Some conclusions were draw from the numerical work.

a) The thermal stress accumulated in asphalt concrete is not considerable until the temperature is lower than -5 ºC;

b) Initial temperature and cooling rate affect thermal stress in asphalt overlay. The lower initial temperature is, the greater thermal stress. The slower cooling rate is, the smaller thermal stress;

c) Reflective cracks occur more easily in thinner asphalt overlay , while top-down cracks occur more easily in thicker asphalt overlay;

d) Bases whose modulus is not very stiff may limit thermal stress induced in asphalt overlay, leading to better control of thermal cracking in asphalt pavements.

REFERENCES:

Li C.L., Li C.X., Chen G.Y. (2006). "Fracture Mechanic Analysis of Temperature Stress of Semi-rigid Base Asphalt Pavement." *Journal of Highway and Transportation Research and Development,* 23(10), 33-36.

Qian G.P., Guo Z.Y., Zheng J.L. (2003). "Calculation for Thermal Stresses of Asphalt Pavement under Environmental Conditions Based on Thermal-viscoelasticity Theory." *Journal of Tongji University*, 31(2), 150-155.

Qian G.P., Zheng J.L., Zhou Z.G. (2006). "Incremental Thermal-viscoelastic Constitutive Relation of Asphalt Mixtures." *Chinese Journal of Applied Mechanics*, 23(3), 338-345.

Tian X.G., Ying R.H., Zheng J.L. (2002). "Tests on Thermal Stress in Asphalt Cement Sample and Its Numerical Simulation." *China Civil Engineering Journal*, 35(2), 25-30.

Wang J.C., Zhu X.R. (2006). "New Evaluation of Temperature Stress in Asphalt Concrete Pavements under Low Temperature." *Highway*, 2, 60-64.

Yang X.L., Liu B.Y. (2006). "Coupled-field Finite Element Analysis of Thermal Stress in Asphalt Pavement." 23(11), 1-5.

Zheng J.L. (2001). "Study on The Thermo-viscoelastic Characteristics of Asphalt Pavements' Thermal Cracking." Ph.D. Dissertation. Xi'an: Chang'an University.

Zheng J.L., Zhou Z.G., Zhang Q.S. (2003). "Theory and method of crack resistance design for asphalt pavement." China Communications Press, Beijing.

Zheng J.L., Tian X.G., Ying R.H. (2004). "A Laboratory Research on the Thermo-viscoelastic Constitutive Model of Bituminous Mixtures." *Journal of Changsha University of Science and Technology (Natural Science)*, 1(1), 1-7.

Effect by Different Factors on Ductility of Evaporated Residue of Modified Emulsion Asphalt

FU Zhipeng[1,2], LIU Zhanliang[3] and JING Lin[1]

[1]Key Laboratory for Special Area Highway Engineering of Ministry of Education, Chang'an University, Xi′ an 710064, China; PH: (086)15809268165; email: fuzhipeng2008@126.com
[2]The First Highway Survey and Design Institute of China CO.LTD, Xi′ an 710075, China
[3]Department of Transportation, Shijiazhuang Institute of Railway Technology, Shijiazhuang 050041, China; PH: (086)15027739515; email: lzldjh@126.com

Abstract: Ductility is an important property of evaporated residue of modified emulsion asphalt. Ductility of the modified asphalt will change after treated by emulsification. In order to analyze the influence of different factors on the ductility of the evaporated residue of modified emulsion asphalt, ductility values of the residue are measured with different emulsifiers, solution PH values and stabilizers. Furthermore, mechanism of the coefficients that may lead to behavior changes of the ductility is analyzed. The test results show that the ductility of the evaporated residue of modified emulsion asphalt is sensitive to different emulsifiers, solution PH values and stabilizers. Ductility of the modified asphalt will have great loss after treated by emulsification. Ductility of the evaporated residue will present different behavior with different emulsifiers and modified asphalt; it will increase as the solution PH value increased; ductility loss of the residue caused by the organic stabilizer is larger than the inorganic salt stabilizer; behavior changes of the ductility loss are different from the content change of the two kinds of stabilizers.

Key word: *pavement engineering; modified emulsion asphalt; evaporated residue; ductility; effect factors*

1 Introduction

Modified emulsion asphalt has many advantages, such as normal temperature construction, low cost and low pollution. It is widely used in road construction and maintenance (Chenhui et al. 2007). The modified emulsion asphalt is mainly composed by the modified asphalt and water. While the oil-water mixed system is unstable systems, its storage is not easily. In engineering, modifications are often made to improve its stability, such as adding the emulsifier and stabilizer, or changing the solution PH value (Mingjian et al. 2008; Yu 2007).

The ductility is an important index of evaporated residue of modified emulsion asphalt. It will directly affect the pavement performance of the modified emulsion asphalt. Ductility of the evaporate residue will change by the admixture added. In order to analyze the ductility change law of the evaporated residue of the modified emulsion asphalt, the effect of the emulsifier, stabilizer and the solution PH value are analyzed in this research, and some suggestions on the processing modified emulsion

asphalt are provided.

2 Materials and Methods

2.1 Performance indexes of modified asphalt

Three types of modified asphalt are used in test and their basic performance indexes are shown in the Table.1.

Table.1 Basic indexes of the three type modified asphalts

Serial name	Type of the asphalt	Ductility(5℃)	Penetration(25℃)	Softening point
A1	SBS modified SHELL asphalt	53.7	71.8	63.4
A2	SBS modified SK asphalt	71	94.1	65.7
A3	SBR modified SK asphalt	147	103.3	47.2

2.2 Preparation of evaporated residue of modified emulsion asphalt

Firstly, the admixtures, such as the emulsifier and stabilizer, are added into the water to form emulsion. Then the emulsion is heated up to about 75～80℃ until the emulsion becomes transparent. Meanwhile, the modified asphalt is heated up to 175～180℃. Subsequently, the hot modified asphalt is slowly added into the transparent emulsion and the high speed shearer is used to stir for 45 minutes, then the emulsion asphalt is formed when the emulsion is cooled and the foam disappeared. In the end, the evaporated residue of modified emulsion asphalt would be made through heating the modified emulsion asphalt directly.

3 Effect of emulsifier

3.1 Emulsion mechanism

Water repels oil, so the emulsion composed of asphalt and water will present layer phenomenon. The emulsifier as a surfactant can make the asphalt particles homogeneous dispersion in solution. The emulsion mechanism is as follow.

(1) For the emulsifier molecular has a hydrophilic (water-attracting) group and a hydrophobic (oil-attracting) group, the emulsifier has adsorbability. This structure not only can decrease the interfacial tension between the asphalt and water but also has the function to connect the asphalt and the water.

(2)When the emulsifier is added, the molecules of the emulsifier will be soon absorbed on the surface of asphalt particles and the hydrophobic group will insert the asphalt particle to form interfacial film which can make the asphalt particles keep discrete state in the collision.

(3)The interface film between the asphalt particle and water can form a double electric layers structure, in which the inner layer is arranged densely and very solidity, but the outer layer will exists a sliding film between the water and the colloidal particle. Sliding surface exist the potential difference which will keep the asphalt particles separation in repulsion, so the stability of the emulsion is improved.

In brief, the emulsifier can improve emulsion stability through decreasing interface tension, stabilizing interface film and increasing the mutual exclusion force of the interface charges.

3.2 Results and Analysis

In this test, two type emulsifiers (cationic emulsifier E1 and E2) are used. One cationic emulsifier, E1, is added to the modified asphalt A1 and A2； another cationic emulsifier E2 is added to the modified asphalt A2 and A3. Various kinds of emulsifier is analyzed, including 0.6%，0.8%，1.0%，1.2%，1.4% and 1.6%. The oil-water ratio is 50:50. Results of ductility of the evaporated residue with different emulsifier contents are shown in Figure.1.

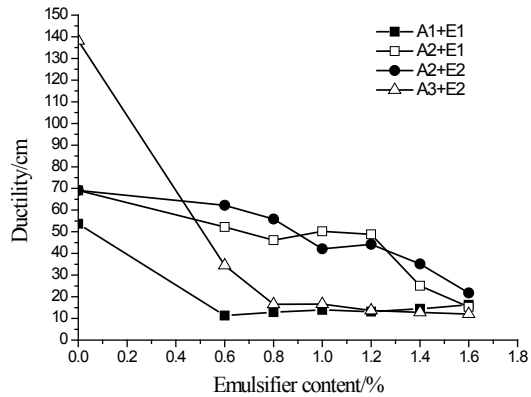

Figure.1 Ductility change curve of asphalt with different emulsifier

Analytical results showed as follows.

(1) When the emulsifier E1 is added, ductility of the evaporated residue of modified emulsion asphalt A1 and A2 will reduce in different degree. When content range of the emulsifier E1 is 0.6%～1.4%, the ductility of the modified asphalt A1 will slowly increase with the growth of the emulsifier E1 content, but the ductility of the modified asphalt A2 will decrease at first, then increase and arrive a certain peak, last decrease rapidly.

(2) When the emulsifier E2 is added, ductility of the evaporated residue of modified emulsion asphalt A2 and A3 will also decreased. When content range of the emulsifier E2 is 0.6%～1.4%, ductility of the modified A2 and A3 will slowly decreased with the growth of the emulsifier E2 content. For different emulsifiers, such as the emulsifier E1 and E2, evaporated residue of the modified asphalt A2 has different change laws of the ductility.

(3)When the different modified asphalts and emulsifiers are mixed, ductility of the evaporated residue will present different behaviors as the emulsifier content changed, some will always keep reducing and some will present ductility recovery. However, for the particular modified asphalt and emulsifier, the behavior of the ductility is fixed.

(4) The cause for ductility loss of the modified asphalt is that asphalt particles are encapsulated by interface film of the emulsifier. The different emulsifiers have different volatile performance. When emulsion loses water, the asphalt particles combine again. Some interface film of the emulsifier still exists in the asphalt, like a wall to separate the asphalt particles to combine indeed, so ductility properties will reduce when the emulsifier is added.

4 Effect of the stabilizer

4.1 Stabilization mechanism

(1)When inorganic salt stabilizer is added into emulsion, the ions of the inorganic salt stabilizer can not only improve the thickness of the double electric layers around the asphalt particles but also enhance the potential difference and repulsive force among the asphalt particles. So, inorganic salt stabilizer can improve the stability of the emulsion.

(2)According to Stokes theory, when organic stabilizer is added into the emulsion, viscosity of the continuous phase is increased, density difference between water and colloidal particle is reduced. At the same time, the thickness of interfacial film is increased. Thus, organic can improve the stability of the emulsion.

4.2 Results and Analysis

In engineering, the calcium chloride (CaCl2) is often used as the inorganic salt stabilizer and the polyvinyl alcohol (PVA) is often used as the organic stabilizer (Jinjing et al. 2008). In this test, the modified asphalt A2 and the water are mixed to form the emulsion, in which the oil-water ratio is 20:80. Emulsifier E1 is added with a fixed content of 0.8%, the different contents of the calcium chloride and PVA is added in emulsion to analyze the effect of the stabilizer on ductility of evaporated residue. Several different contents of the stabilizer is analyzed, including 0.1%, 0.2%, 0.4%, 0.6%, 0.8% and 1.0%. The curves of the ductility of evaporated residue with different stabilizer contents is shown in Figure.2

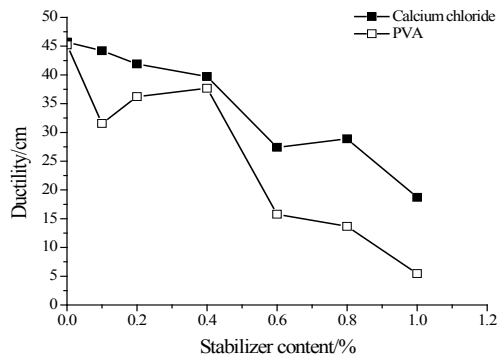

Figure.2 Ductility change curve of evaporated residue by different stabilizer

The results are shown as follows.

(1)When the stabilizer content range is 0.0%～1.0%, the ductility loss of evaporated residue will increase based on the growth of stabilizer content, but the behaviors of the evaporated reside of the modified emulsion asphalt A2 are different for the two stabilizers. Final ductility loss caused by organic stabilizer is larger than inorganic stabilizer.

(2)For inorganic salt stabilizer, ionic charge can enhance the interface film thickness and make it even firmer. When emulsion loses water, the buffer function of interface film in the modified asphalt will increase with increasing the content of the inorganic salt stabilizer, so ductility of the evaporated residue will always present downward trend with the inorganic salt stabilizer content improved.

(3) For organic stabilizer, as content of the organic stabilizer is enhanced, ductility of the evaporated residue will decrease at first, then increase and arrive at a certain peak, finally, decrease sharply. When emulsion loses water, PVA particles are dispersed in the modified asphalt; when PVA particles play a role of buffer function, ductility of the evaporated residue will decrease; when the PVA particles play an

interconnect action, the ductility will increase.

5 Effect of solution PH value

5.1 Effect mechanism of PH value

A suitable PH value of the solution may not only enhance the activity of emulsifier but improve the emulsion stability, because the PH value can affect the ionization state of the emulsifier and improve the potential difference as well (Jingyi et al. 2007). In summary, acid or neutral solution is fit for the cationic emulsifier; alkaline solution is fit for the anionic emulsifier. Now, people in engineering mainly take the cationic emulsifier.

5.2 Results and Analysis

In this test, cationic emulsifier E1 and E2 are separately added into modified A2; emulsifier contents both are 0.8%; water-oil ratio both is 80:20. In order to analyze the influence of PH value taken on ductility, the hydrochloric acid solution with 35% concentration is added into the emulsion to regulate the solution PH value. Ductility of the evaporated residue with different PH value is measured. The test results are shown in the Figure.3

The test results show that the solution PH value has great influence on the ductility of the evaporated residue. The ductility of the evaporated residue will increase as the solution PH value enhanced. Recent research demonstrates that the stability of emulsion asphalt will decrease with the growth of solution PH value. As solution is improved, interface film around the asphalt particles will become thinner and its buffer function will become thinner, so ductility of the evaporated residue will become larger as the growth of the PH value.

6 Conclusions

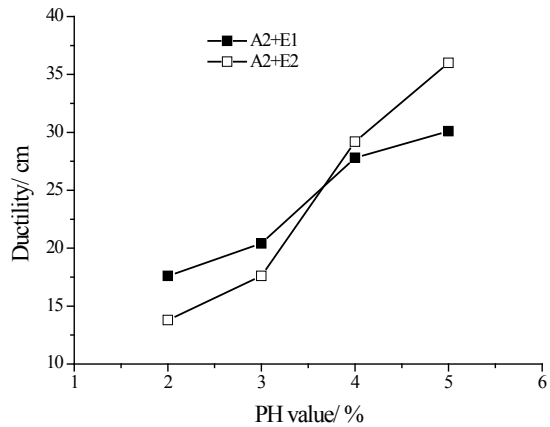

Figure.3 Ductility change curve of the evaporated by different PH values

(1) The emulsifier will decrease the ductility of the evaporated residue of modified emulsion asphalt. For the same modified asphalt, different emulsifiers can lead to different ductility loss. In engineering, various emulsifiers need contrast test to measure the emulsion stability and the ductility loss of the evaporated residue. Then, suitable emulsifier is determined through tradeoff between ductility and stability.

(2) Both of inorganic salt stabilizer and organic stabilizer can lead the ductility loss of the evaporated residue. Organic stabilizer can lead more ductility loss than inorganic salt stabilizer. In practical engineering, we need to strictly select stabilizer and control addition quantity of stabilizer.

Reference

FENG Chenhui, Li Jiang, Zhao Dejun(2007).“Study of initial strength evaluation method of emulsified asphalt mixture.” *Petroleum Asphalt*, 21(6), 41-45

LI Mingjian, JIANG Wei, ZHENG Tao, XIAO Jingjing(2008).“Study on Influence of Stabilizer on Storage Stability of Modified Asphalt Emulsion.” *Communications Standardization*, 2008(7), 143-145

MA Yu(2007),“Studies on Performance and Storage Stability of Modified Asphalt Emulsion.” *Journal of Chongqing Jiaotong University*, 26(5), 77-79

XIAO Jingjing, ZHENG Nanxiang, SONG Zheyu(2008).“Study on Effect of Emulsifier on Modified Emulsified Asphalt and Its Mechanism.” *Journal of Zhengzhou University: Eng Sci*, 29(3), 5-9

ZHANG Jingyi, GAO Shumei, He Zonghua(2007).“The performance effect of chemical modification to emulsified SBR modified emulsified asphalt.” *Petroleum Asphalt*, 21(3), 24-27

Analysis of Elastic Slab on Non-Uniform Support Foundation Using A Weighted-Residual Method

Zhu Luo[1, 2] **and Zhi Fu**[2]

[1]School of Transportation, Southeast University, Nanjing 210096, China; PH (86)-139-1146-3195; Fax (86)-10-6207-9556; email: z.luo@rioh.cn
[2] Research Institute of Highway Ministry of Communications, Beijing 100088, China PH (86)-137-0109-4958; Fax (86)-10-6207-9556; email: z.fu@rioh.cn

ABSTRACT

Based on the assumption of Kirchhoff thin plate, we derive the constitutive equations and the boundary conditions on all four edges for variable Winkler foundations to solve the problem of Cement Concrete Pavement (CCP) supported by a non-uniform foundation. The constitutive equation is a fourth-order differential equation with variable coefficients that has no known analytical solution. A Weighted-Residual Method (WRM) is developed to solve the problem approximately. In our WRM numerical tests, a mixed-type trial function, i.e., the biharmonic function, and a weight function based on the least-square method are selected to eliminate residual errors. Results show that, compared to the finite element method, the WRM computational method produces a relative error of only 3.2%, which satisfies the error requirement of general engineering applications. The novel WRM developed in this paper appears to be a good approximation method in solving the problem of CCP supported by non-uniform foundations.

INTRODUCTION

The theory of CCP design assumes a uniform distribution of foundation under the pavement. It is therefore difficult to apply the theory directly to deal with local differential settlements which occur commonly in the highway construction practices. Taking the mountainous expressway that crosses many cut-to-fill locations in south China as an example, it developed 7.9 percents broken slab ratio in 11km pavements after opening to traffics in the early two years (Luo Zhu, 2003). This paper focuses on the mechanical model of non-uniform foundation by establishing a new calculation method.

THE GOVRENING EQUATION AND BOUNDARY CONDITIONS

Like all elastic plates, the design of slab on non-uniform support is special case of the problem of solving the governing differential equation with certain boundary conditions. In the case of non-uniform support, the assumption of Kirchhoff thin plate first published in 1850 still holds (Timoshenko 1959).

Based on this assumption, the geometric equations, physical equations,

deformation compatibility equations (Qu et al. 2000), and the governing differential equation on non-uniform foundation can be derived as follows:

$$D\nabla^2\nabla^2 w(x,y) + k(x,y)w(x,y) = q(x,y) \qquad (1)$$

where ∇^2 is Laplacian Operator, $\nabla^2 = \frac{\partial^2}{\partial x^2} + \frac{\partial^2}{\partial y^2}$; $W(x,y)$ is deflection function; $q(x,y)$ is external loads distributing function; $k(x,y)$ is foundation distributing function; D is bending rigidity of plate, $D = \frac{Eh^3}{12(1-\mu^2)}$, which E, μ, h refers to Elastic Modulus, Poisson's Ratio and slab thickness respectively.

The four free-edge boundary conditions of plates are given as follow:

(1) The moments on edges of the plate are equal to zero, that is M_x=0, M_y=0.

(2) The total transverse shearing force is also equal to zero, that is $Q_x + \frac{\partial M_{xy}}{\partial y} = 0$, $Q_y + \frac{\partial M_{xy}}{\partial x} = 0$.

THE BASIC PRINCIPLE OF WRM

For the differential equation derived from non-uniform support is a Variable Coefficient Fourth-order Differential Equation, it is hard to find an analytical solution method. The WRM, an effective method in solving differential equation approximately, is introduced herein to tackle this difficult problem in this paper.

The basic idea of this method is presented below (Qiu 1991). For example, the governing differential equation for a certain problem is

$$P_m(u) = f_0 \qquad \text{in domain } \Omega \qquad (2)$$

The boundary equation is

$$Q_t(u) = f_t \qquad \text{at boundary } \Gamma_t \ (t = 1,2,\cdots, m) \qquad (3)$$

where P_m is m orders partial differential operator, Q_t is $t-1$ orders boundary normal differential operator, ft（t=0, 1,…, m）is coordinate functions, the boundary of Ω domain is given as

$$\Gamma = \bigcup_{t=1}^{m} \Gamma_t \qquad (4)$$

First, let the trial function $\bar{u}$ as

$$\bar{u} = \sum_{i=1}^{n} c_i \phi_i \qquad (5)$$

where $\{\phi_i\}$ is the base of trial function, c_i is parameter to be determined.

Substituting the trial function in equation (5) into the governing equation (2) and boundary equation (3), the domain residual error and boundary residual error can be computed with equations (6) and (7) respectively.

$$R_I(\tilde{u}) = P_m(\tilde{u}) - f_0 \qquad (6)$$

$$R_t(\tilde{u}) = Q_t(\tilde{u}) - f_t \qquad (t=1,2,\ldots,m) \qquad (7)$$

Various methods can be used to eliminate the residual error. We multiply the domain weight function with the domain residual error and the boundary weight function with the boundary residual error. Then, the unified equation for eliminating the residual error becomes:

$$\int_\Omega R_I(\tilde{u}) W_{Ij} d\Omega + \sum_{t=1}^{m} \int_{\Gamma_t} R_t(\tilde{u}) W_{tj} d\Gamma = 0 \qquad (j = 1,2,\cdots, n) \qquad (8)$$

This unified equation includes a series of equations, which has n unknown parameters. We can solve this system of equations and substitute the c_i solutions back into the trial function equation (5). This gives the approximate solution to the original problem.

THE SELECTION OF TRIAL FUNCITON

It is important to select a trial function which has significant influence on the precision in lower-order calculation. There is no universal technique in the selection of a good trial function. Engineering judgment and familiarity with particular problem domains are often relied upon for such selection process.

The more information we know about the problem, the more easily we are able to select a good trial function. If the selected trial function is close to the true analytical solution, the WRM can benefit from fast convergence and computational efficiency. If the selected trial function contains all the characters of the true analytical solution, the WRM may even produce the exact solution.

There are three types of trial functions. If the assumed that the trial function is just a solution to the boundary equations that is called a “boundary-type” trial function compared to the “domain-type” trial function. If the assumed trial function is neither a solution to the governing equation nor one to the boundary equation, it is usually called as a “mixed-type” trial function.

The principle for selecting a trial function is that the linear combination of the function base should approach the true exact solution. It means that the function base

must be a perfect sequence and linearly independent to each other.

THE SELECTION OF WEIGHT FUNCITON

Various kinds of weight functions, based on different methods including Least Square Method, Collocation Method, Sub-domain Method, Galerkin Method, and Moment Method can be used to eliminate the residual error. Theoretically, different types of weight functions can be chosen that can result in different levels of solution precision and computational complexity (Miltiades Elliotis et al. 2007). In this paper, we select the Least Square Method and its basic principle is discussed below. In order to minimize the integral of the squared domain residual error, we apply the extreme condition of functional theory:

$$I(C_j) = \int_v R^2 dv \qquad (9)$$

$$\frac{\partial I}{\partial C_j} = 0 \qquad (10)$$

Then, the equation for eliminating the residual error is obtained:

$$\int_v R \frac{\partial R}{\partial C_j} dv = 0 \qquad (j = 1,2,\cdots,n) \qquad (11)$$

Equation (11) is then used to determine the parameters $C_j (j = 1,2,\cdots,n)$.

ANALYSIS OF A NUMERICAL EXAMPLE

As shown in Figure 1, a square cement concrete slab with four free edges is arranged at the cut-to-fill location of a road section. The side length of the slab is 4m and the thickness is 0.25m. The Elastic Modulus and Poisson's Ratio of the concrete is 3.5×10^4MPa and 0.15 respectively.

The shadowed areas of the figure represent vehicle footprints which are rectangular for convenient comparison with the finite element method. The individual footprint area is 400cm^2 with the pressure of q_0=0.625MPa (Deng et al. 2001). The distribution of Winkler foundation is exponential along the X-axis as shown in formula (12).

$$k = 97.98\exp(0.1014x) \qquad (12)$$

where k is foundation reaction modulus (MPa/m), and x is abscissa.

It is difficult to find a trial function that meets the requirement of both the governing equation and boundary equation. So a mixed-type trial function is chosen. Since the biharmonic function is effective in solving plastic slab problem (Xu et al. 1980), the following biharmonic trial function is used in calculation

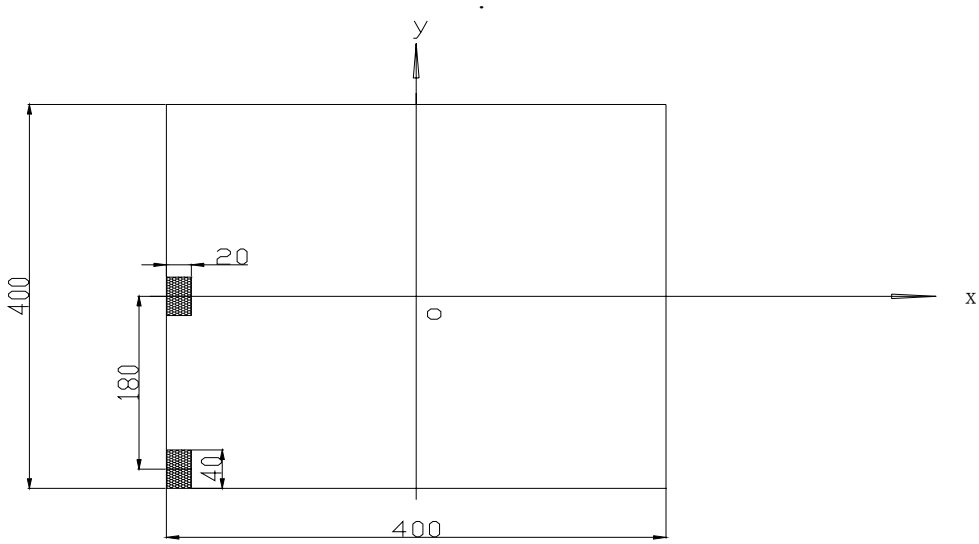

Figure 1. The layout of a plate (unit: cm)

$$\overline{w}=\sum_{i=1}^{\infty}\begin{bmatrix}\sin\alpha_{i1}x(c_{i1}e^{\alpha_{i1}y}+c_{i2}e^{-\alpha_{i1}y}+c_{i3}ye^{\alpha_{i1}y}+c_{i4}ye^{-\alpha_{i1}y})+\\ \cos\alpha_{i1}x(c_{i5}e^{\alpha_{i1}y}+c_{i6}e^{-\alpha_{i1}y}+c_{i7}ye^{\alpha_{i1}y}+c_{i8}ye^{-\alpha_{i1}y})+\\ \sin\alpha_{i2}y(c_{i9}e^{\alpha_{i2}x}+c_{i10}e^{-\alpha_{i2}x}+c_{i11}xe^{\alpha_{i2}x}+c_{i12}xe^{-\alpha_{i2}x})+\\ \cos\alpha_{i2}y(c_{i13}e^{\alpha_{i2}x}+c_{i14}e^{-\alpha_{i2}x}+c_{i15}xe^{\alpha_{i2}x}+c_{i16}xe^{-\alpha_{i2}x})\end{bmatrix} \quad (13)$$

where, $\alpha_{i1}=i\pi/l_x$, $\alpha_{i2}=i\pi/l_y$, l_x and l_y refer to slab length and width.

The trial function (13) fits the biharmonic equation $\nabla^4\varphi=0$, so it can effectively reduce the domain residual error and computational complexity (He 2006). For easier explanation, we used only the first order of the trial function to illustrate the numerical example.

A weight function based on the Least Square Method is selected (Xu et al.1997). Let i=1 in formula (13) and then put it into formula (8), the unified equation for eliminating the residual error can be derived as

$$AC=b \quad (14)$$

where A is a matrix of 16×16, C is the coefficient vector to be determined, b is the load vector.

Solving equation (14), we find the values *C:*

$$\mathrm{C}=\frac{q_0\times10^{-4}}{D}[4,21,-3,-4,2,40,-10,0,25,55,-7,-1,-8,-65,0,-2]^{\mathrm{T}} \quad (15)$$

where q_0 is the footprint pressure, D is the bending rigidity of the slab.

Substituting all parameters into equation (13), we obtained the approximate deflection function.

Extreme value analysis indicates that the maximum deflection is 0.6314 *mm*, and the maximum deflection calculated by finite element method is 0.6521 *mm*. The relative error is only 3.2% which satisfies the error requirement in engineering applications. The numerical example above demonstrates that the WRM has a necessary accuracy in solving the problem of CCP supported by non-uniform foundations.

CONCULSIONS

Based on the assumption of Kirchhoff thin plate, we derived the constitutive equations and the boundary conditions on all four edges using variable Winkler foundation model to solve the problem of CCP supported by non-uniform foundations. The governing constitutive equation is a fourth-order differential equation with variable coefficients, which has no known analytical solution. The WRM is selected to solve the equations owning to its straightforward underlying principles, convenient implementation, efficient calculation, and great precision. A numerical example shows that the relative error is only 3.2%, when WRM is compared with finite element calculation, which satisfies engineering requirement. WRM is therefore demonstrated to be a novel computational approximation method.

REFERENCES

Deng, X., and Huang, X. (2001). *Principle and design method of pavement*. China Communication Press.

Luo, Z.. (2003). *Mechanical analysis of Cement Concrete Pavements supported by uneven foundation*. Research Institute of Highway Ministry of Communications, P.R.C.

Elliotis, M., Georgiou, G., and Xenophontos, C. (2007). "The singular function boundary integral method for biharmonic problems with crack singularities." *Engineering Analysis with Boundary Elements*, 31(3), 209-215

Qiu, J. (1991). *The theory and application of weighted residuals method*. China Astronautic Publishing House.

Qu, Q., Zhang, Q., Ji, Q., and Liang X. (2000). *Elastic plate theory*. China Communication Press.

Timoshenko, S. P. and Woinowsky-Krieger, S. (1959). *Theory of plates and shells*, McGraw-Hill.

He, X. (2006). "The nonlinear behaviors of a symmetric isotropic laminate in a mixed boundary condition subject to an arbitrary thermal field coupled with mechanical loading." *Journal of Computational and Nonlinear Dynamics*,

1(2), 168-177

Xu, C., Chen, X., and Zheng, R. (1997). *New computational mechanics, the theory, techniques and application of weighted residuals method*. Tongji University press.

Xu, W., and Chen, Q. (1980). *Least Square Method boundary collocation method in solving plane problem*. China civil engineering society, 13(2).

Plastic Behavior for Compaction Pile with Hole Expanded by Blasting or Tamping Techniques

Li Xiaowei[1], Zhao Junhai[2], Wei Xueying[3], Xiao Haibing[4], MaQing[5]

[1]Ph.D., School of Civil Engineering, Chang'an University, Chang'an Road 161, P.O. Box 197, Xi'an, P.R. China, Zip: 710061; or School of Civil Engineering, Panzhihua University; PH (86) 029-82337238; email: lilixxxwwwr@126.com
[2]Professor, Ph.D., School of Civil Engineering, Chang'an University, Chang'an Road 161, P.O. Box 197, Xi'an, P.R. China, Zip: 710061; email: zhaojh@chd.edu.cn
[3]Assistant Professor, Ph.D., School of Civil Engineering, Chang'an University, Chang'an Road 161, P.O. Box 197, Xi'an, P.R. China, Zip: 710061; email: weixy@chd.edu.cn
[4]M.S., School of Civil Engineering, Chang'an University, Chang'an Road 161, P.O. Box 197, Xi'an, P.R. China, Zip: 710061; email: mailangwan@163.com
[5]M.S., School of Civil Engineering, Chang'an University, Chang'an Road 161, P.O. Box 197, Xi'an, P.R. China, Zip: 710061; email: maqing20032003@yahoo.com.cn

ABSTRACT

This paper presents a new method to predict the plastic radius of compaction pile with hole expanded by blasting or tamping techniques. The new formulae are obtained based on Yu's unified strength theory. The strength difference in tension and compression and intermediate principal stress effect on the material strength are considered, and, hence, the obtained formulae can be used for a wide range of materials. The plastic zone of soil during hole-forming by blasting and tamping techniques can be predicted based on the derived formulae in this study. The effects of the blasting and tamping process on the adjacent piles can be reasonably assessed, and the weight of hammer and tamping times can then be determined. Previous results obtained based on Tresca, Mises, and Mohr-coulomb criterion are all special cases of the results derived in this paper.

Keywords: Highway engineering, Unified strength theory, foundation, compaction pile, hole-forming, tamping techniques

INTRODUCTION

Compaction pile is one of the most effective techniques for roadbed foundation in Loess Plateau of North China. As well known, dry loess has better capacities and can sustain nearly vertical slopes, being perennially under-saturated. However, when locally saturated, it disaggregates instantaneously and loses its capacity. The consequence of this process will result in foundation collapse. The technique of compaction can eliminate the collapsibility of roadbed and improve its bearing capacity. There are basically two steps in the construction of compaction pile. (1) Make a hole with pressing in steel sleeve, vibrating sunken tube, or explosive

expansion to evacuate the soil. (2) Fill in and tamp the soil or lime-soil repeatedly until the hole is filled.

Original soil layer above pile top is a minimum of 1 meter in the process of hole-forming of compaction pile (GB50007, 1990). According to the Chinese codes, the pile spacing can be determined by the average compaction coefficient of soil among piles and the pile diameter. Usually the compaction coefficient should not be less than 0.93, and the spacing is estimated in the range of 2.0-2.5 times of pile diameter. However, the provisions from Chinese codes (GB50202, 2002 and JGJ79, 2003) are only associated with the physics nature of soil density, while regardless of the mechanics feature of that. The previously obtained formulae for estimating the plastic zone and deformation are mainly based on the Mohr-Coulomb strength criteria. The effect of intermediate principal stress on the material strength cannot be included in the model and, therefore, usually cannot accurately predict the plastic zone and deformation.

In this paper, plastic analysis of compaction pile with hole-forming by explosive expansion or tamping technique is investigated, and the formulae to predict the plastic zone obtained in this paper is based on the unified strength theory. The strength difference in tension and compression and intermediate principal stress effect on the material strength are considered, and, hence, the obtained formulae can be used for a wide range of materials. The effects of blasting and tamping process on the adjacent piles can thus be reasonably assessed, and the weight of hammer and tamping times can then be determined. Previous results obtained based on Tresca, Mises, and Mohr-coulomb criterion are all special cases of the results derived in this paper.

UNIFIED STRENGTH THEORY

Based on twin shear strength theory, Yu M.H. (Yu M.H., 1994, 1998, 2004) developed the unified strength theory. The theory takes the effect of σ_2 into consideration and uses a unified mechanical model to describe the features of different materials. Its mathematical expression is simple and given as follows:

$$F = \sigma_1 - \frac{\alpha}{1+b}(b\sigma_2 + \sigma_3) = \sigma_t \qquad \sigma_2 \le \frac{\sigma_1 + \alpha\sigma_3}{1+\alpha} \tag{1a}$$

$$F = \frac{1}{1+b}(\sigma_1 + b\sigma_2) - \alpha\sigma_3 = \sigma_t \qquad \sigma_2 \ge \frac{\sigma_1 + \alpha\sigma_3}{1+\alpha} \tag{1b}$$

$$\alpha = \sigma_t / \sigma_c \quad , b = \frac{(1+\alpha)\tau_s - \sigma_s}{\sigma_s - \tau_s} = \frac{(1+\alpha) - B}{B-1}, \qquad B = \frac{\sigma_S}{\tau_S}$$

where α is tension-compression resistance ratio, i.e., σ_s versus σ_c, and generally less than 0.5 for rock and soil, and b is parameter for the influence of intermediate principal shear stress.

In Geotechnical Engineering, the former equations are generally expressed by cohesion force (shear strength) c_0 and internal fractional angle φ. The parameters in formulae (1a, 1b) can be substituted by the parameters of c_0, φ as follows:

$$\alpha = \frac{(1-\sin\varphi)}{(1+\sin\varphi)}, \sigma_t = \frac{2c_0\cos\varphi}{1+\sin\varphi}, \tau_s = c_0, B = \frac{2\cos\varphi}{1+\sin\varphi}, \quad b = \frac{2(1-\cos\varphi)}{2\cos\varphi-(1+\sin\varphi)}$$

PLASTIC ZONE OF SOIL MEDIA AROUND A PILE WITH HOLE FORMED BY EXPLOSION TECHNIQUE

Analysis of soil media around a pile with hole expanded by blasting technique. The following assumptions are made in this study:

(1) It is coupled charge mode. The cross-section of blast-hole spaces is circular. Considering the dynamic compressive response time of soil is much longer than that of explosion, linear blasting cartridge along its axis line is assumed to detonate at the same time, neglecting the influence of variation of soil lateral pressure along the pile on the effect of blasting compression.

(2) The problem is treated as plain strain problem according to the characteristics of the problem. In the process of piling construction in which holes are formed by explosion technique, soil layer with a 1- to 2-m thickness is required above the soil media. The layer is generally evacuated until explosion expanded piling is tamped. Soil is compacted latterly through explosion expanded action among piling, which is settled at appropriate pile spacing. Therefore, this paper assumes that the soil media around a hole is a problem of plain strain in the process of pore-forming by explosion expansion technique. Polar coordinate is taken and the positive direction directs outward along radial (see Figure 1). Soil media around a hole is assumed as a cylinder with a thick wall. At a point far away from the center, both radial stress and tangential stress are equal to original soil stress.

When

$$r \to \infty$$

Static earth pressure is given by:

$$p_2 = k_0 \gamma z$$

The pressure p_2 is assumed as linear distribution along the depth direction *h*; r_0 is the radius of the borehole; r_a is the radius of the expanded hole by explosion; and r_b is the radius of plastic zone induced by the explosion process.

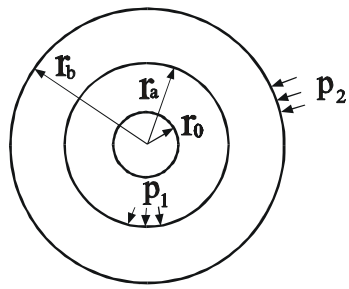

Figure 1. Schematic diagram of a hole formed by blasting technique.

A formula is obtained from literature (Lin, Hu W., and Peng G., 2003) as follows:

$$r_a^2 = r_b^2 - \left(r_b^2 - r_0^2\right)\left(\frac{4p_1 r_0^{1.5}}{\rho_m D^2 r_b^{1.5}} + 1\right)^{-0.25} \tag{2}$$

where ρ_m is the initial compaction density of soil, and p_1 is the initial stress on the wall of blast hole.

Given by:

$$R_a = \frac{r_a}{r_0}, R_b = \frac{r_b}{r_0}$$

Formula (2) can be expressed as:

$$R_a^2 = R_b^2 - \left(R_b^2 - 1\right)\left(\frac{4p_1}{\rho_m D^2 R_b^{1.5}} + 1\right)^{-0.25} \tag{3}$$

The formula reflects the expansion rule of blast hole, when soil medium is subjected to the action of blast. Formulae (2, 3) indicate that the radius of expansion of an expanded hole is related to the radius of plastic region, initial stress of explosion, radius of blast hole, medium density, and longitudinal wave speed.

Radius of plastic region. When explosive is fully coupled, initial pressure of the wall of blast hole can be predicted as:

$$p_1 = \frac{\rho_0 D \rho_e D_e^2}{2\left(\rho_0 D + \rho_e D_e\right)} \tag{4}$$

where ρ_e is explosive density, D_e is the blast speed, ρ_0 is the initial density of soil medium, and D is the longitudinal wave speed.

When $r = r_b$ (see Figure 2), the radial stress component in elastic region for circular hole is:

$$\sigma_{rb} = -p_1 R_b^{-1.5} \tag{5}$$

According to the theory of elastic mechanics, the stresses in soil media around a pile can be obtained as:

$$\sigma_r = -\frac{r_a^2\left(p_1 - p_2\right)}{r^2} - p_2, \quad \sigma_\theta = \frac{r_a^2\left(p_1 - p_2\right)}{r^2} - p_2, \quad \sigma_z = \nu\left(\sigma_r + \sigma_\theta\right)$$

In plastic region, due to $\nu \to 0.5$, the following relationship can be obtained:

$$\sigma_z = \frac{\left(\sigma_r + \sigma_\theta\right)}{2}$$

Owing to $\sigma_1 \geq \sigma_2 \geq \sigma_3$, the relationship among stresses are given as follows (Zhao, Zhang, and Liao, et al., 2000):

$$\sigma_1 = \sigma_\theta = \frac{r_a^2(p_1 - p_2)}{r^2} - p_2 \tag{6}$$

$$\sigma_2 = \sigma_z = \frac{(\sigma_r + \sigma_\theta)}{2} \tag{7}$$

$$\sigma_3 = \sigma_r = -\frac{r_a^2(p_1 - p_2)}{r^2} - p_2 \tag{8}$$

The equilibrium equation is obtained from plastic mechanics and given as follows (Wang, Xiong, and Huang, 1982):

$$\frac{d\sigma_r}{dr} - \frac{\sigma_r - \sigma_\theta}{r} = 0 \tag{9}$$

Substitute formulae (6, 7, and 8) into formula (1) of unified strength theory, and the following formulae are obtained:

$$\sigma_\theta = \frac{2(1+b)\sigma_t}{2(1+b)-b\alpha} + \frac{\alpha(2+b)\sigma_r}{2(1+b)-b\alpha}$$

$$\sigma_r - \sigma_\theta = \frac{2(1+b)(1-a)\sigma_r}{2+2b-b\alpha} - \frac{2(1+b)\sigma_t}{2+2b-b\alpha} \tag{10}$$

Substitute formula (10) into (7), considering boundary conditions:

$$r = r_a, \sigma_r = -p_1$$

Integrate formula (9), and the radial stress can be obtained:

$$\sigma_r = -\left(p_1 + \frac{\sigma_t}{1-\alpha}\right)\left(\frac{r}{r_a}\right)^{\frac{2(1+b)(\alpha-1)}{2(1+b)-b\alpha}} + \left(\frac{\sigma_t}{1-\alpha}\right) \tag{11}$$

When $r = r_b$, the radial stress of outer boundary in plastic region is equal to that of inner boundary in elastic region.

Using:

$$\nabla = \frac{2(1+b)(\alpha-1)}{2(1+b)-b\alpha}, \quad \zeta = \frac{\sigma_t}{1-\alpha}, \quad R = \frac{r}{r_a}$$

According to formula (10), the following formula can be obtained:

$$\sigma_{rb} = -(p_1 + \zeta)(R_b)^\nabla + \zeta \tag{12}$$

Substitute formula (12) into formula (5), and the following equation is obtained:

$$-p_1 R_b^{-1.5} = -(p_1 + \zeta)(R_b)^\nabla + \zeta$$

The above formula, which is the unified solution of plastic radius of soil media, can be expressed as follows:

$$-p_1 R_b^{-1.5} + (p_1 + \zeta)(R_b)^{\nabla} - \zeta = 0$$

Expression ∇, ζ based on c_0, φ, and leading to:

$$\nabla = \frac{-2}{1+\cot\varphi}, \quad \nabla + 2 = \frac{2}{1+\tan\varphi}, \quad \zeta = c_0 \cot\varphi \tag{13}$$

$$-p_1 R_b^{-1.5} + (p_1 + c_0 \cot\varphi)(R_b)^{\frac{-2}{1+\cot\varphi}} - c_0 \cot\varphi = 0 \tag{14}$$

where p_1 is determined by formula (4). The plastic boundary scale radius of soil media among piles with holes expanded by blasting technique, R_b, is obtained by substituting p_1 into formula (14). Substitute R_b into formula (3), and post-expansion scale radius of soil media R_a is determined. The relationship between initial stresses of pre-blasting and plastic scale radius is predicted by formula (14) using a varying internal cohesion force and fractional angle. The relationships between p_1 and R_b are plotted in Figure 2 (a) and (b), respectively. It can be found that the required initial blast stress p_1 increases with the increasing cohesion force and fraction angle if the radius R_b is the same.

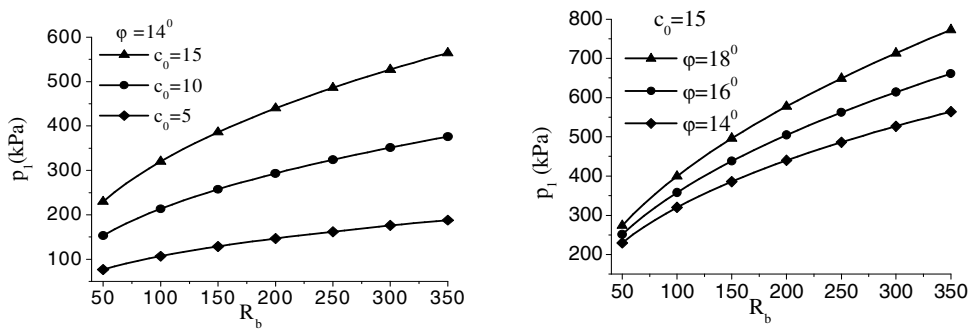

(a) **(b)**

Figure 2. Relationship between p_1 and R_b.

STRESS ANALYSIS OF SOIL MEDIA AROUND PILE SUBJECTED TO TAMPING

Plastic analysis of soil media around pile subjected to tamping. It is proven from engineering practice that the initial hole diameter has generally no change through the process of filling and tamping. Here we assume that the deformation of soil media around a pile is very small, and the soil media can be treated as homogeneous materials and a semi-infinite body.

Thus, the geostatic stresses in perpendicular directions are the same as that in horizontal plane. Polar coordinate is used for stresses analysis (see Figure 3). Soil media around a hole is assumed as a cylinder with a thick wall. At an infinite point,

both radial stress and tangential stress are equal to original soil stress. When $r \to \infty$,

equations (6)-(8) can be obtained based on the theory of elasticity.

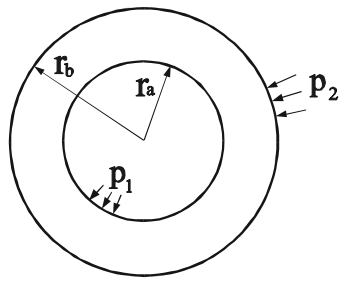

Figure 3. Schematic diagram of tamping

When $r = r_b$, solve formulae (8, 11), leading to:

$$-\left(\frac{r_a}{r_b}\right)^2 (p_1 - p_2) = -\left(p_1 + \frac{\sigma_t}{1-\alpha}\right)\left(\frac{r_b}{r_a}\right)^{\frac{2(1+b)(\alpha-1)}{2(1+b)-b\alpha}} + \frac{\sigma_t}{1-\alpha} + p_2 \quad (14)$$

According to formula (13), the above formula can be expressed as follows:

$$(p_2 + \zeta)R_b{}^2 - (p_1 + \zeta)R_b{}^{\nabla+2} + (p_1 - p_2) = 0 \quad (15)$$

$$p_2\left(R_b{}^2 - 1\right) + p_1\left(1 - R_b{}^{\nabla+2}\right) + \zeta\left(R_b{}^2 - R_b{}^{\nabla+2}\right) = 0 \quad (16)$$

When formulae (15, 16) are expressed by notation φ, c_0, formula for plastic radius of soil media around a pile forming by tamping is given as follows:

$$(p_2 + c_0\cot\varphi)R_b{}^2 - (p_1 + c_0\cot\varphi)R_b{}^{\frac{2}{1+\tan\varphi}} + (p_1 - p_2) = 0$$

$$p_2\left(R_b{}^2 - 1\right) + p_1\left(1 - R_b{}^{\frac{2}{1+\tan\varphi}}\right) + c_0\cot\varphi\left(R_b{}^2 - R_b{}^{\frac{2}{1+\tan\varphi}}\right) = 0 \quad (17)$$

Application of the formula for plastic radius of soil media around a pile forming by tamping.

(1) When $\alpha = 0, \sigma_t = 0$, formula (14) can be expressed as follows, which is suitable for granular soil (Han, and Huang, 1999):

$$p_2 R_b^2 - p_1 R_b + p_1 - p_2 = 0 \quad (18)$$

Solve the former formula, and lead to:

$$R_b = 1, \quad \text{or} \quad R_b{}' = \frac{p_1 - p_2}{p_2}$$

(2) When $\alpha = 0$, formula (24) can be rewritten as follows, which is applicable for ideal elasto-plastic model (Han, and Huang,1999).

$$(p_2 + \sigma_t)R_b^2 - (p_1 + \sigma_t)R_b + p_1 - p_2 = 0 \quad (19)$$

Solve the former formula, and lead to:

$$R_b = 1, \text{or} \quad R_b' = \frac{p_1 - p_2}{p_2 + \sigma_t}$$

CONCLUSIONS

In this paper, a newly developed unified strength theory is used to carry out the plastic analysis of compaction pile. The unified strength theory includes the strength difference in tension and compression and intermediate principal stress effect on the material strength. Hence, the obtained formula to predict the plastic zone and deformation can be applicable for a wide range of soil material. Previous results obtained based on Tresca and Mohr-Coulomb criterion are all special cases of the results derived in this study. The obtained formula can be applicable to estimate the influences on the adjacent pile in the process of forming a new hole with the blasting or tamping method. The weight of hammer and tamping times can then be reasonably determined based on the results.

ACKNOWLEGEMENT

This research investigation is funded by the Nature Science Foundation of Shaanxi province of China under Grant SJ08E$_2$04 and the Foundation from State Key Lab of Western Architecture & Technology under Grant 08KF01. These financial supports are gratefully acknowledged.

BIBLIOGRAPHY

GB50007. (1990). *Code for design of building foundation*, China Architecture & Building Press, Beijing.

GB50202. (2002). *Code for acceptance of construction quality of building foundation*, China Architecture & Building Press, Beijing.

JGJ79. (2003). *Technical code for ground treatment of buildings*, China Architecture &Building Press, Beijing.

Han X.L., Huang Y. (1999). "Analysis on the stress of the soil around the hole in hole-formation with lime soil compaction pile." *Xi'an Univ. of Arch & Tech*, 3(31): 256-259

Lin D.N., Hu W., Peng G. (2003). "Analysis on blasting extrusion characteristic of soil and rock." *Chinese Journal of Rock Mechanics and Engineering*, 22(11), 1767-1770.

Yu M.H. (1994). "Unified strength theory for geomaterials and its applications." *Chinese Journal of Geotechnical Engineering*, 16(2), 1-10.

Yu M.H. (1998). "Chapter 7: Unified strength theory." *Twin shear strength theory and its application*, Science Press, Beijing. 249-288.

Yu M.H. (2004). "Chapter 7: Unified strength theory." *Unified strength theory and its applications*, Springer, Berlin. 129-174.

Wang R., Xiong Z.H., Huang W.B. (1982). "Chapter 7: Problems about axial and spherical symmetry." *Foundation for plastic mechanics*. Science Press,

Beijing, 112-136.
Zhao J.H., Zhang Y.Q., Liao H.J. et al. (2000). "Unified limit solution of thick wall cylinder and thick wall spherical shell with Unified strength theory." *Chinese Journal of Applied Mechanics*, 3(17), 157-161.

Bridge Damage Assessment by Dynamic Response in Time Domain

Jianqing Bu[1], Zhanyou Yan[2] and Xiangguo Li[3]

[1]School of Civil Engineering, Shijiazhaung Railway Institute, No.17 North 2nd-Ring East Road, Shijiazhuang, Hebei Province, China, 050043; PH(0311),87936227; email: bujq@sjzri.edu.cn

[2]School of Civil Engineering, Shijiazhaung Railway Institute, No.17 North 2nd-Ring East Road, Shijiazhuang, Hebei Province, China, 050043; PH(0311), 87935217; email: yanzhanyou@163.com

[3]School of Civil Engineering, Shijiazhaung Railway Institute, No.17 North 2nd-Ring East Road, Shijiazhuang, Hebei Province, China, 050043; PH(0311), 87936636; email: lixg@sjzri.edu.cn

ABSTRACT

This paper presents the bridge damage identification from the dynamic response induced by the vehicle moving on a simply supported bridge deck modeled as a finite element model based on the sensitivity analysis. The moving vehicle is modeled as a two-degree-of-freedom system comprising of five parameters. The damage indices are defined by the bend stiffness reduction of the bridge element. Starting with the zero damage indices vector, the identification can be realized based on the least-squares method and the regularization technique from measured bridge responses measurement. Measurement noise and road surface roughness are considered in the numerical simulations. Simulation studies indicate that the identified results are acceptable and the proposed method is feasible.

INTRODUCTION

Damage detection of the structural system has been a research-active topic in the last several decades. Specially integrated with structural health monitoring technique, damage identification online is becoming more and more important and practical for large projects in civil engineering. Li and Haldar (2004) proposed a novel system identification procedure for nondestructive damage evaluation of structures from dynamic responses. It is a finite-element-based time domain linear system identification technique and capable of identifying structural properties at the elemental level. Majumder and Manohar (2003) presented the time domain approach for damage detection with vibration data as well. In addition, Banan and Hjelmstad (1994) proposed two algorithms for estimating member constitutive properties of a finite-element model with known geometry and topology from measured displacements under a static loading. Yang et al. (2004) extracted the fundamental bridge frequency from the dynamic response time history of a vehicle passing over

the bridge.

This paper presents the bridge damage identification from the dynamic responses of a simply supported bridge modeled as a finite element model based on the sensitivity analysis. The moving vehicle is modeled as a two-degree-of-freedom system comprising of five parameters. The damage indices are defined by the bend stiffness reduction of the bridge element. Starting with the intact bridge system, the identification can be realized based on the least-squares method and the regularization technique from the measured bridge responses. Effects from different response types, locations, noise levels, and road surface roughness are included in the study.

THEORY ON BRIDGE PARAMETERS IDENTIFICATION

Five-parameter vehicle model. The five-parameter vehicle model of the two-degrees-of-freedom system shown in Figure 1 comprises of five components: an upper mass (m_{v1}) of the bogie, a lower mass (m_{v2}) of the axle connected to a damper (c_v), a spring (k_{v1}), and another spring (k_{v2}) to represent the stiffness of the tire. The equations of motion of the masses m_{v1} and m_{v2} are respectively:

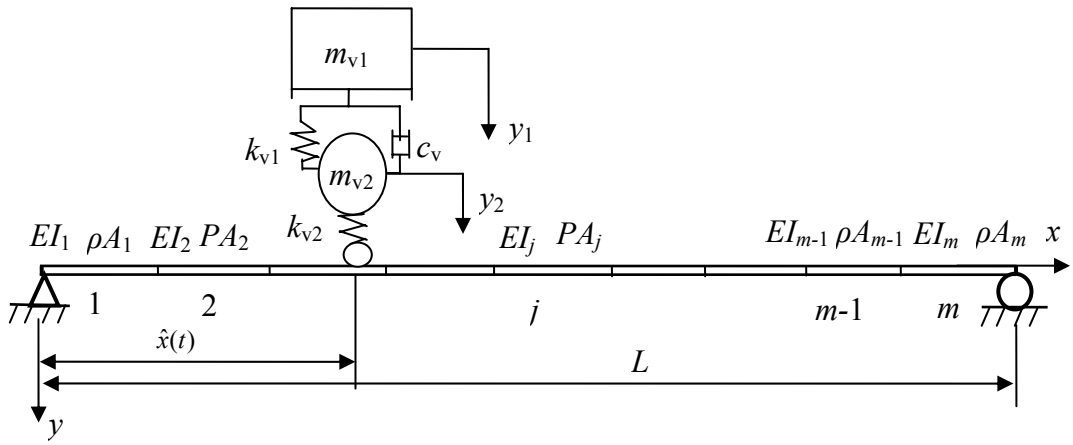

Figure 1. Vehicle-bridge system.

$$m_{v1}\ddot{y}_1 + c_v(\dot{y}_1 - \dot{y}_w) + k_{v1}(y_1 - y_2) = 0 \quad (1)$$

$$m_{v2}\ddot{y}_w - c_v(\dot{y}_1 - \dot{y}_2) - k_{v1}(y_1 - y_2) + k_{v2}\left[y_w - (w(\hat{x}(t)) + r(\hat{x}(t))\right] = 0 \quad (2)$$

and the interaction force (P_{int}) between the vehicle and the bridge can be expressed as:

$$P_{\text{int}} = (m_{v1} + m_{v2})g + k_{v2}[y_2 - (w(x(t) + r(\hat{x}(t))] \quad (3)$$

where $r(\hat{x}(t))$ (Honda et al., 1982) is the roughness of the surface at the interaction point between the vehicle and the bridge.

Equation of Motion for the Vehicle-Bridge System. The elemental mass

and stiffness matrices are obtained using the Hermitian cubic interpolation shape functions. The simply supported beam structure is discretized into *m* Euler beam elements. The equation of motion for the bridge can be written as:

$$M_{\mathrm{b}}\ddot{R} + C_{\mathrm{b}}\dot{R} + K_{\mathrm{b}}R = H_{\mathrm{c}}P_{\mathrm{int}} \tag{4}$$

where $M_{\mathrm{b}}, C_{\mathrm{b}}$ and K_{b} are the mass, damping, and stiffness matrices of the bridge respectively. $\ddot{R}, \dot{R}$ and R are the nodal acceleration, velocity, and displacement vectors of the bridge respectively, and $H_{\mathrm{c}}P_{\mathrm{int}}$ is the equivalent nodal load vector from the bridge-vehicle interaction force. H_{c} is a $N \times 1$ matrix with zero entries except at the DOFs (degrees-of-freedom) corresponding to the nodal displacements of the beam elements on which the load is acting, and N is the number of DOFs of the bridge after considering the boundary condition.

The Rayleigh damping is used to model the structural damping here. The damping matrix can be presented as a linear combination of the mass and stiffness matrices, such as:

$$C_{\mathrm{b}} = \alpha_1 M_{\mathrm{b}} + \alpha_2 K_{\mathrm{b}} \tag{5}$$

in which α_1 and α_2 are two Rayley damping coefficients, determined generally by two adjacent modal damping ratios and its corresponding natural frequencies in radian.

Based on Equation (3), combining Equations (1) ,(2) and (4), we have:

$$\begin{bmatrix} M_b & H_c^T m_{v1} & H_c^T m_{v2} \\ 0 & m_{v1} & 0 \\ 0 & 0 & m_{v2} \end{bmatrix} \begin{Bmatrix} \ddot{R} \\ \ddot{y}_1 \\ \ddot{y}_2 \end{Bmatrix} + \begin{bmatrix} C_b & 0 & 0 \\ 0 & c_v & -c_v \\ 0 & -c_v & c_v \end{bmatrix} \begin{Bmatrix} \dot{R} \\ \dot{y}_1 \\ \dot{y}_2 \end{Bmatrix} + \begin{bmatrix} K_b & 0 & 0 \\ 0 & k_{v1} & -k_{v1} \\ -k_{v2}H_c & -k_{v1} & k_{v1}+k_{v2} \end{bmatrix} \begin{Bmatrix} R \\ y_1 \\ y_2 \end{Bmatrix} = \begin{Bmatrix} H_c^T(m_{v1}+m_{v2})g \\ 0 \\ k_{v2}r(\hat{x}(t)) \end{Bmatrix} \tag{6}$$

To find the time response of the beam and the vehicle from Equation (6), a step-by-step solution can be obtained using the Newmark method.

Once the nodal responses of the bridge are obtained, the vertical deflection, velocity, acceleration, and strain responses of the bridge at position *x* and time *t* can then be expressed as the following :

$$w(x,t) = H(x)\,R(t), \quad \dot{w}(x,t) = H(x)\,\dot{R}(t), \quad \ddot{w}(x,t) = H(x)\,\ddot{R}(t) \tag{7}$$

$$\varepsilon(x,t) = -z\frac{\partial^2 w(x,t)}{\partial x^2} = -z\frac{\partial^2 H(x)\,R(t)}{\partial x^2} \tag{8}$$

where $H(x)$ is a $1 \times N$ vector with zero entries except at the degrees-of-freedom

corresponding to the nodal displacements of the *j*-th beam element on which the point *x* is located.

Sensitivity analysis of bridge responses respect to damage indices. The damage indices (α_s^j) is defined to represent the reduction of the elemental bend stiffness of the bridge. The physical parameters become:

$$(EI)_d^j = (EI)_0^j(1+\alpha_s^j) \qquad (-1 \le \alpha_s^j \le 0,\ j = 1, 2, \cdots, m) \tag{9}$$

where $(EI)_0^j$ are the parameters of the intact bridge, and $(EI)_d^j$ are the parameters of the damaged bridge. The *j*-th elemental bend stiffness can be found in Figure 1.

Taking the first derivative of Equation (6) with respect to the damage indices (α_s^j) of the bridge, $j = 1, 2, \cdots, m$, we have:

$$\overline{M}\ddot{S}_{(\alpha_s^j)} + \overline{C}\dot{S}_{(\alpha_s^j)} + \overline{K}S_{(\alpha_s^j)} = \overline{P}_{(\alpha_s^j)} \tag{10}$$

where:

$$\overline{M} = \begin{bmatrix} M_{\mathrm{b}} & H_{\mathrm{c}}^T m_{\mathrm{v1}} & H_{\mathrm{c}}^T m_{\mathrm{v2}} \\ 0 & m_{\mathrm{v1}} & 0 \\ 0 & 0 & m_{\mathrm{v2}} \end{bmatrix}, \overline{C} = \begin{bmatrix} C_{\mathrm{b}} & 0 & 0 \\ 0 & c_{\mathrm{v}} & -c_{\mathrm{v}} \\ 0 & -c_{\mathrm{v}} & c_{\mathrm{v}} \end{bmatrix}, \overline{K} = \begin{bmatrix} K_{\mathrm{b}} & 0 & 0 \\ 0 & k_{\mathrm{v1}} & -k_{\mathrm{v1}} \\ -k_{\mathrm{v2}}H_{\mathrm{c}} & -k_{\mathrm{v1}} & k_{\mathrm{v1}}+k_{\mathrm{v2}} \end{bmatrix},$$

$$\ddot{S}_{(\alpha_s^j)} = \begin{bmatrix} \frac{\partial \ddot{R}_1}{\partial(\alpha_s^j)} & \frac{\partial \ddot{R}_2}{\partial(\alpha_s^j)} & \cdots & \frac{\partial \ddot{R}_N}{\partial(\alpha_s^j)} & \frac{\partial \ddot{y}_1}{\partial(\alpha_s^j)} & \frac{\partial \ddot{y}_2}{\partial(\alpha_s^j)} \end{bmatrix}^{\mathrm{T}},\ \dot{S}_{(\alpha_s^j)} \text{ and } S_{(\alpha_s^j)} \text{ are similar}$$

with $\ddot{S}_{(\alpha_s^j)}$, and $\overline{P}_{(\alpha_s^j)} = \begin{bmatrix} -\frac{\partial K_b}{\partial(\alpha_s^j)}R - \alpha_2 \frac{\partial K_b}{\partial(\alpha_s^j)} & 0 & 0 \end{bmatrix}^{\mathrm{T}}$.

The mass, damping, and stiffness matrices in the above equations are time varying. The sensitivity matrices in Equation (10) can be obtained by Newmark method similarly.

The sensitivity time history vertical deflection, velocity, acceleration, and strain responses of the bridge at position *x* and time *t* can then be obtained based on the bridge nodal response sensitivity derived from Equation (10).

IDENTIFICATION OF BRIDGE PARAMETERS

Formulation. The case when a vehicle moves across the bridge deck from left to right at a constant speed is studied. The measured bridge response in time domain will be used to identify the bridge element damage indices. Below we try to make use of *v* and *S* to express bridge response (deflection, velocity, acceleration, or strain) measurement and its sensitivity with respect to the bridge damage indices.

v_m denotes the measured bridge response.

Assuming initial zero values to the damage indices vector to be $p_0 = \{\alpha_s^1, \alpha_s^2, \cdots, \alpha_s^m\}^{\mathrm{T}} = \mathbf{0}$, the corresponding response (v_0) and sensitivity matrix ($\overline{S}_0$) can be solved from Equations (5) and (10). The difference between the measured and calculated bridge responses can be obtained by the following formulation.

$$\Delta v_r = v_m - v_r, \; r=0, 1, 2,\ldots \tag{11}$$

The difference vector Δp_r can be solved from the following equation.

$$\overline{S}_r \Delta p_r = \Delta v_r, \; r=0, 1, 2,\ldots \tag{12}$$

where $\overline{S}_r$ is a $N_{\mathrm{t}} \times m$ matrix. N_{t} is the number of sampled data points and r is the number of iterations.

The bridge responses sensitivity matrix with respect to the bridge damage indices for a one-degree-of-freedom system and a two-degrees-of-freedom system, respectively, can be formulated same form as:

$$\overline{S}_r = \begin{bmatrix} \dfrac{\partial v_r(1)}{\partial(\alpha_s^1)_r} & \dfrac{\partial v_r(1)}{\partial(\alpha_s^2)_r} & \cdots & \dfrac{\partial v_r(1)}{\partial(\alpha_s^m)_r} \\ \dfrac{\partial v_r(2)}{\partial(\alpha_s^1)_r} & \dfrac{\partial v_r(2)}{\partial(\alpha_s^2)_r} & \cdots & \dfrac{\partial v_r(2)}{\partial p(\alpha_s^m)_r} \\ \vdots & \vdots & \cdots & \vdots \\ \dfrac{\partial v_r(N_t)}{\partial(\alpha_s^1)_r} & \dfrac{\partial v_r(N_t)}{\partial(\alpha_s^2)_r} & \cdots & \dfrac{\partial v_r(N_t)}{\partial(\alpha_s^m)_r} \end{bmatrix} \tag{13}$$

where $\ddot{y}_r$ are the acceleration responses of the bridge vehicle in r-th iteration step, and $(\alpha_s^j)_r$ is the j-th bridge element damage indices corresponding r-th iteration step.

With the updated damage indices vector $p_{r+1} = p_r + \Delta p_r$ (r=0, 1, 2,…) in the next iteration, the response (v_{r+1}) and sensitivity ($\overline{S}_{r+1}$) can be calculated again. The above process is repeated until the identified damage indices increment of the successive iterations is smaller than a pre-defined tolerance level, namely defined as

following form:

$$\left\|\Delta p_r\right\| < Tolerance \tag{14}$$

where ||•|| is the norm of the matrix, and the tolerance is taken equal to 1.0×10^{-6} in the following numerical simulations.

The absolute error in the identified results is calculated as $AE = \sum_{j=1}^{m} \left\| \left(\alpha_S^j\right)_{true} - \left(\alpha_S^j\right)_{identified} \right\|$, where ||•|| is the norm of the vector. The formulation for identification from measured velocity or displacement responses of the bridge can be similarly derived.

Regularization. The set of damage indices difference Δp_r obtained from Equation (12) using a straight-forward least-squares solution would be unbound. A regularization technique (Law et al., 2001) can be used to solve the ill-posed problem in the form of minimizing the function.

$$J(\Delta p_r, \lambda) = \left\|\overline{S}_r \Delta p_r - \Delta v_r\right\|^2 + \lambda\left\|\Delta p_r\right\|^2 \tag{15}$$

where λ is the non-negative regularization parameter corresponding to the optimal results. The *L*-curve method (Hansen, 1992) is employed to determine the optimal regularization parameter. Optimizing Equation (11) is equivalent to the solution with the following damped least-squares method.

$$\Delta p_r = (\overline{S}_r^{\,T}\overline{S}_r + \lambda I)^{-1}\overline{S}_r^{\,T}\Delta v_r \tag{16}$$

where I is the identity matrix. Singular value decomposition is used in the pseudo-inverse calculation in this paper.

SIMULATION STUDY

In the numerical simulation studies, the parameters of the vehicle-bridge system are defined as following. Parameters of the simply supported bridge: for the single-span bridge: L=30m, EI=2.5×10^{10} Nm^2, ρA=6.0×10^3 kg/m and ξ=0.02 for all modes; Parameters of vehicle: for the five-parameter vehicle: m_{v1}=3.6×10^3 kg, c_v=1.0×10^3 Ns/m, k_{v1}=6.0×10^5 N/m, m_{v2}=0.4×10^3 kg, k_{v2}=8.5×10^5 N/m.

The simply supported bridge is discretized into ten Euler Bernoulli beam elements. The speed of the vehicle is 20 m/s and the sampling frequency is 200 Hz, the number of sampled data points N_t is 300. Road surface roughness of class A to D according reference is included in the following numerical simulations.

White noise is added to the calculated acceleration responses of the system to simulate the polluted measurements.

$$v_m = v_{\text{calculated}} + E_P \times N_{\text{oise}} \times \sigma(v_{\text{calculated}}) \tag{17}$$

where v_m is simulated measured acceleration responses, $v_{\text{calculated}}$ is calculated acceleration responses, E_P is noise level, N_{oise} is the standard normal distribution vector with zero mean value and unit standard deviation, and $\sigma(v_{\text{calculated}})$ is the standard deviation of the calculated acceleration responses.

Effect of Different Road Class. Here we make use of noise-free strain responses at *L*/3 of the bridge span to identify bridge damage indices for different road classes (from A to D). The 4th bridge element is assumed to be damaged, $\alpha_s^7 = 10\%$, and the other elements are intact. The identified results are listed in Table 1.

Table1. Identified damage indices (%) with different road surface roughness.

Element No.	Road surface roughness of the bridge			
	Class *A*	Class *B*	Class *C*	Class *D*
1	0.00	0.08	0.16	0.17
2	0.00	-0.06	-0.08	-0.10
3	0.00	0.04	0.07	0.08
4	-10.00	-9.95	-9.92	-9.91
5	0.00	0.04	0.08	0.09
6	0.00	-0.04	-0.08	-0.09
7	0.00	-0.01	-0.07	-0.08
8	0.00	-0.07	0.10	-0.10
9	0.00	0.07	0.11	0.11
10	0.00	0.13	-0.19	-0.21
AE (%)	0.00	0.55	1.01	1.11
Iteration times	36	40	38	38

From Table 1, we can obtain following observations. All the identified results are accepted, the identified accuracy decrease with Road class, and the road surface roughness may affect the vehicle-bridge system similar to random noise. The worst results correspond with the Road class D; its absolute error (*AE*) is 1.11%. However, the iteration times are almost not affected by road surface roughness. This indicates that the proposed method is practical and efficient. Because the surface of the bridge is relatively good in general, so the road surface roughness is taken as class C below.

Effect of measured station and different types responses. In this case, we assume $\alpha_s^2 = \alpha_s^9 = 5\%$, $\alpha_s^4 = 10\%$ and the other elements damage indices are zeros. The noise-free vertical displacement, velocity, acceleration, and strain responses at

L/4, *L*/2 and *L3*/4 of the bridge span identify bridge damage indices, respectively. Table 2 gives the identified results.

Table 2. Identified damage indices (%) from different response measurements.

Element No.	Vertical displacement			Vertical acceleration			Strain		
	L/4	*L*/2	3*L*/4	*L*/4	*L*/2	3*L*/4	*L*/4	*L*/2	3*L*/4
1	0.07	0.00	-0.08	-0.03	0.00	0.00	0.07	0.00	-0.08
2	-4.96	-5.00	-4.99	-4.99	-5.00	-5.00	-4.96	-5.00	-4.99
3	-0.08	0.00	0.01	0.02	0.00	0.00	-0.08	0.00	0.01
4	-0.05	0.00	-0.02	-0.01	0.00	0.00	-0.05	0.00	-0.02
5	-9.97	10.00	-9.98	-9.99	-10.00	-10.00	-9.97	10.00	-9.98
6	-0.05	0.00	-0.01	-0.01	0.00	0.00	-0.05	0.00	-0.01
7	0.02	0.00	-0.01	0.00	0.00	0.00	0.02	0.00	-0.01
8	-0.07	0.00	-0.03	-0.07	0.00	0.00	-0.07	0.00	-0.03
9	-4.97	-5.00	-4.98	-4.98	-5.00	-5.00	-4.97	-5.00	-4.98
10	0.10	0.00	-0.07	0.14	0.00	0.00	0.10	0.00	-0.07
AE (%)	0.54	0.00	0.28	0.32	0.00	0.00	0.54	0.00	0.28
Iteration times	26	48	35	52	47	54	24	51	34

We can infer from Table 2 that the measured station locations clearly affected identified results, the middle span responses give better results, and response types cause different effects on the identified results. When the measured station is not in the middle span, vertical acceleration responses give the best results, vertical velocity responses give the worst results, and the results from vertical displacement and strain responses are same. The acceleration and strain responses are easily obtained accurately in actual testing, this point proves that this method can be used to solve practice problems.

Table 3. Identified damage indices (%) with different noise level.

Element No.	Noise level（%）					
	0		5		10	
	Strain	Acceleration	Strain	Acceleration	Strain	Acceleration
1	-5.00	-5.00	-5.11	-4.90	-5.33	4.76
2	0.00	0.00	-0.16	-0.15	-0.35	0.29
3	0.00	0.00	-0.08	0.09	-0.13	-0.15
4	-10.00	-10.00	-10.30	-10.19	-10.63	-10.48
5	-15.00	-15.00	-15.46	-15.37	-15.80	-14.26
6	-15.00	-15.00	-15.45	-14.62	-15.85	-15.68
7	-10.00	-10.00	-10.20	-10.19	-10.50	-9.56
8	0.00	0.00	-0.11	-0.08	-0.13	0.12
9	0.00	0.00	-0.16	0.12	-0.35	-0.29
10	-5.00	-5.00	-5.13	-5.08	-5.38	-5.30
AE (%)	0.00	0.00	2.05	1.66	4.25	3.60

Iteration times	50	45	51	45	53	46

Effect of different noise level. We assume six elements to be damaged, $\alpha_s^1 = \alpha_s^{10} = 5\%, \alpha_s^4 = \alpha_s^7 = 10\%, \alpha_s^5 = \alpha_s^6 = 15\%$ and the other elements to not be damaged. The identified results in Table 3 are obtained from vertical acceleration and strain responses at the middle span with noise level 0, 5% and 10%.

We can see clearly from Table 3 that the identified absolute errors increases with noise level, iteration times slightly vary with noise level, and the vertical acceleration responses give better results than strain responses.

CONCLUSIONS

From the simulation studies we can conclude the following:

(1) The identification is not very sensitive to the measured noise and the road surface roughness affect the identified results similarly with random noise.

(2) The identified damage indices results from different types of responses of the bridge at different measured stations all are accepted. The measured locations and response types all affect the identified results. We suggest that vertical acceleration and strain responses at middle span should be adopted in the practice.

ACKNOWLEDGEMENT

The Project Supported by NNSF of China (No.50878134) and Natural Science Foundation of Hebei Province (No. E2006000394).

REFERENCES

Banan, M. R. and Hjelmstad, K. D. (1994). "Parameter estimation of structures from statistic response. I. Numerical simulation studies". *J. Struct. Engrn.*, ASCE, Vol.120 (11), 3259-3283.

Hansen, P.C. (1992). "Analysis of discrete ill-posed problems by means of the L-curve". *SIAM Review*, Vol.34 (4), 561-580.

Honda H., Kajikawa Y. and Kobori T. (1982). Spectra of road surface roughness on bridges [J]. *J. Struct. Divis.* 108(ST9), 1956-1966.

Law, S.S., Chan, T.H.T., Zhu, X.Q. and Zeng, Q. H. (2001). "Regularization in moving force identification". *J. Engrg. Mech.*, ASCE, 127(2), 136-148.

Li, X. L. and Haldar, A. (2004). "Element level system identification with unknown input with Rayleigh damping". *J. Engrg. Mech.*, Vol.130 (8), 877-885.

Majumder, L. and Manohar, C. S. (2003). "A time-domain approach for damage detection in beam structures using beam vibration data with a moving oscillator as an excitation source". *J. sound and vib.*, Vol.268 (4), 699-716.

Yang,Y. B., Lin, C. W. and Yau, J. D. (2004). "Extracting bridge frequencies from the dynamic response of a passing vehicle". *J. sound and vib.*, Vol.272, 471-493.

Viscoelastic Mechanical Properties of Crumb Rubber Modified Asphalt Mixture

WANG Lan[1], CHANG Chun-qing[2], XING Yong-ming[3]

[1]College of Civil Engineering, Inner Mongolia University of Technology, P.O. Box 010051, Huhhot, China; PH(86)0471-6577274; FAX(86)0471- 6575700; email: Wanglan661018@163.com

[2]College of Civil Engineering, Inner Mongolia University of Technology, P.O. Box 010051,Huhhot,China; PH(86)0471-6576543; FAX(86)0471-6575700; email: iamccq@126.com

[3]College of Science, Inner Mongolia University of Technology, P.O. Box 010051, Huhhot, China; PH(86)0471-6576556; FAX(86)0471-6576556; email:xymjs@yahoo.cn

ABSTRACT

Crumb rubber modified asphalt (CRMA) mixture is a typical viscoelastic material. The pavement made from CRMA mixture has anti-skid surfaces and the pavement is good in reducing the traffic noise. Moreover, building the road with CRMA mixture is important in controlling the pollution cased by a large amount of discarded tires. In order to study the rheological characteristics of CRMA mixture, a series static creep testes for the material has been performed at -15℃、0℃、15℃、30℃ and 45℃ respectively. The experimental results indicate that the Burgers model is good in simulating the viscoelastic characteristics of CRMA mixtures. Viscoelastic parameters and time dependence of creep stiffness modulus can be obtained from the simulation of the experimental data. The result shows that creep stiffness modulus decreases rapidly at the initial stage of loading, then the rate of change decreases, and finally creep stiffness modulus approaches to a stable value at the end of loading.

Keywords: crumb rubber modified asphalt mixture; viscoelasticity; creep; creep stiffness modulus；Burgers model

1. Introduction

CRMA is prepared by adding crumb rubber powder into asphalt. The application of crumb rubber particles can improve the mechanical properties of asphalt at low temperatures and improve the durability of the pavement. Moreover, consuming discarded tires in making CRMA benefits the effect of controlling the pollution caused by the large number of discarded tires and has reduced the cost of building roads (Palit, 2004).

As a typical viscoelastic material, an asphalt mixture has creep and

relaxation properties (Judith, 2006; Jincheng, 2007; Naisheng, 2007). The uniaxial static compression creep tests of Open-Graded Friction Courses (OGFC) CRMA mixture of 20% porosity were carried out on a UTM-25 material testing machine. The rheological and viscoelastic characteristics of CRMA were obtained from the results of the tests.

2. Creep test of crumb rubber modified asphalt mixture

OGFC-13 was adopted in the tests. CRMA material was obtained from Tianjin, and the aggregate was basalt. The specimens of 20% porosity were used in the following experiments. The specimens were prepared by a rolling compaction machine. Both diameter and height of the test specimens were 100 mm. In order to observe the viscoelastic behavior of CRMA mixture in a large range of temperatures, the experiments were carried out at -15℃、0℃、15℃、30℃ and 45℃ respectively. Because of the temperature sensitive deformation of the material, different stresses were selected as 0.5 Mpa at -15℃ and 0℃; and 0.1 Mpa at 15℃、30℃、and 45℃. Control testes were performed at each temperature. In order to reach the uniform temperature, the specimens were conditioned for four hours in the environment chamber before each test. The specimens were first preloaded with 1% of testing load for three minutes. Then loading and unloading were carried out during specified time periods. The sample deformation was measured by strain transducer (as shown fig.1). The experimental data was collected at every twenty seconds. The creep test curve is shown in fig.2. The time period of each creep test was 60 min.

3. Analysis of the experimental results

(1) The viscoelastic constitutive model of CRMA mixture

Fig.1 Loading in creep test

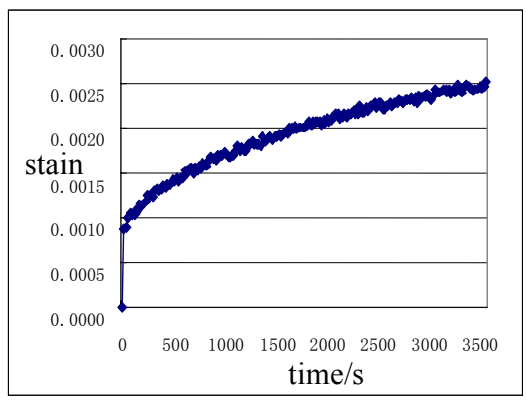

Fig.2 curve of creep test

Based on the experimental data, the Burgers model has been demonstrated appropriate in representing viscoelastic characteristics of CRMA mixture. The total deformations defined by this model are elastic deformation、viscoelastic reheology deformation and viscoelastic deformation. The constitutive equation is shown as follow:

$$\sigma + p_1\sigma + p_1\ddot{\sigma} = q_1\dot{\varepsilon} + q_2\ddot{\varepsilon}$$

Where $$p_1 = (\eta_1 E_1 + \eta_1 E_2 + \eta_2 E_1)/E_1 E_2$$

$$p_2 = \eta_1\eta_2 / E_1 E_2$$

$$q_1 = \eta_1$$

$$q_2 = \eta_1\eta_2 / E_2$$

The constitutive equation of Burgers model is expressed by viscoelastic parameters

$$E_1E_2\sigma + (\eta_1E_1 + \eta_1E_2 + \eta_2E_1)\dot{\sigma} + \eta_1\eta_2\ddot{\sigma} = E_1E_2\eta_1\dot{\varepsilon} + E_1\eta_1\eta_2\ddot{\varepsilon}$$

Substitute $\sigma = \nabla(t)\sigma_0$ in the constitutive equation and perform Laplace transform, we have

$$\sigma_0/s + p_1\sigma_0 + p_2 s\sigma_0 = q_1 s\bar{\varepsilon}(s) + q_2 s^2\bar{\varepsilon}(s)$$

Solve the above equation, we have

$$\bar{\varepsilon}(t) = \sigma_0\left[\frac{1}{s^2(q_1 + q_2 s)} + \frac{p_1}{s(q_1 + q_2 s)} + \frac{p_2}{q_1 + q_2 s}\right] \quad (1)$$

Replace the creep strain by reversion of Laplace transform, we have

$$\varepsilon(t) = \sigma_0\left[\frac{p_1q_1 - q_2}{q_1^2} + \frac{t}{q_1} + (\frac{p_2}{q_2} - \frac{p_1q_1 - q_2}{q_1^2})e^{-\lambda t}\right] \quad (2)$$

where $\lambda = q_1/q_2$.

If equation (2) is expressed in viscoelastic parameters

$$\varepsilon(t) = \sigma_0\left[\frac{E_1 + E_2}{E_1E_2} + \frac{t}{\eta_1} + \frac{1}{E_2}e^{-\lambda t}\right]$$

where $\lambda = E_2/\eta_2$.

(2) Parametric fitting of rheological data

Fitting of creep test results was carried out in determining coefficients in the Burgers model (Reibo, 2004; Xuejun, 2004). The instantaneous elastic strain ε_0

can be obtained from the recorded data. So the elastic modulus of spring is

$$E_1 = \sigma_0 / \varepsilon_0$$

Eliminate the instantaneous elastic strain from the model, the remaining strain is

$$\varepsilon(t) = \sigma_0 \left\{ \frac{1}{E_1} + \frac{t}{\eta_1} + \frac{1}{E_2}\left[1 - e^{-E_2 t/\eta_2}\right] \right\}$$

$$\delta(t) = \varepsilon(t) - \varepsilon_0 = \sigma_0 \left\{ \frac{t}{\eta_1} + \frac{1}{E_2}\left[1 - e^{-E_2 t/\eta_2}\right] \right\}$$

When time approaches infinite, the equation becomes

$$\delta(t)_{t\to\infty} = \sigma_0 \left\{ \frac{t}{\eta_1} + \frac{1}{E_2} \right\}$$

So we can get viscosity coefficient η_1 by measuring the slope of the last section in the strain / time curve

$$\eta_1 = \sigma_0 / \tan\theta$$

Set $t = 0$ in equation (1) and $\delta(t)_{t\to\infty} = \sigma_0 / E_2$, the elastic modulus of spring in delay element becomes

$$E_2 = \sigma_0 / \delta(t)_{t\to\infty 2}$$

In order to get the viscosity coefficient of dashpot in **the** delay element, convert equation (1) into

$$-\delta(t) + \frac{\sigma_0}{E_2} + \frac{\sigma_0 t}{\eta_1} = \frac{e^{-E_2 t/\eta_2} \cdot \sigma_0}{E_2}$$

Take logarithm at both sides

$$\log\left\{ -\delta(t) + \frac{\sigma_0}{E_2} + \frac{\sigma_0 t}{\eta_1} \right\} = \log\frac{\sigma_0}{E_2} - \frac{E_2 t}{\eta_2}\log e$$

and denote the slope of the function above as γ， we have

$$\tan\gamma = -\frac{E_2}{\eta_2}\log e$$

Therefore

$$\frac{\eta_2}{E_1} = -\log e / \tan\gamma \qquad \eta_2 = -\frac{0.4343}{\tan\gamma} E_2$$

All viscoelastic parameters of the Burgers model are represented in Table 1

Table.1 Fitting parameters of the viscoelastic model

E1	η1	E2	η2
1200	2388231	1100	211075

Experimental data can be fitted by the viscoelastic parameters in table 1 (Fig.3). Good agreement between the Burgers fitting curve and the experimental data has been observed.

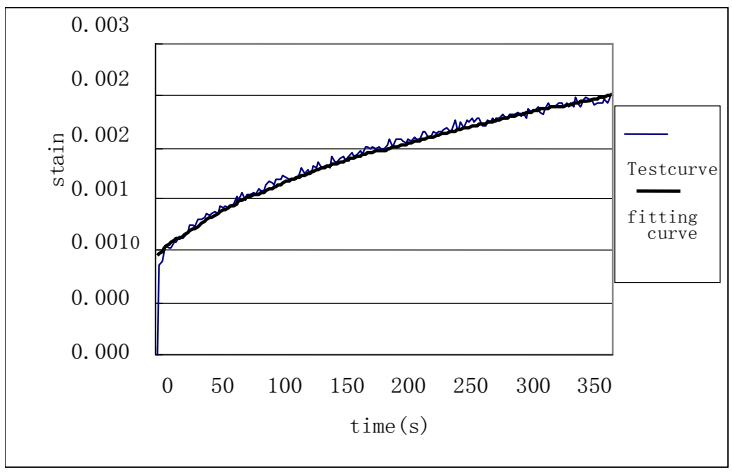

Fig.3 Fitting curve of creep test date

(3) Creep stiffness modulus

The time dependence of creep stiffness modulus of CRMA mixture has been observed at different temperatures in the creep tests (Fig 4). It is noticed that time

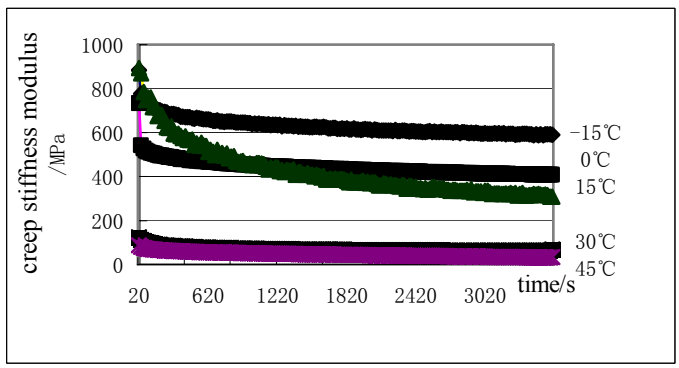

Fig.4 Time dependence of creep stiffness modulus of crumb rubber modified asphalt mixture

dependence of creep stiffness modulus is similar at different temperatures. Creep stiffness modulus decays rapidly at the initial phase of loading, then the decay rate

slows down and finally the creep stiffness modulus approaches to a stable value at a preset temperature. The final stable value of creep stiffness modulus is lower at higher temperatures.

4. Conclusion

(1) The creep behavior of CRMA mixture has been studied by static compression creep test. A good agreement between the simulation curve of the Burgers model and the experimental curve has been observed. Burgers model therefore has been proven adequate to describe the viscoelastic characteristics of CRMA mixture.

(2) The creep stiffness modulus decays rapidly at the early stage of loading, then the decay rate slows down and finally the creep stiffness modulus of CRMA approaches to a stable value at different temperatures. The smaller creep stiffness moduli are observed at high temperatures.

(3) The viscoelastic parameters of CRMA mixture from the static creep test provide good working references for the design of crumb rubber modified asphalt pavement.

References

Jianlong Zheng, Song tao Lu, Xiaoge Tian. The Viscoelastic Parameters of Asphalt Mixture and Application [J]. Journal of Zhengzhou University,2004,25（4）: 8~11.

Judith C. Wang, S.M.ASCE and Xiangwu Zeng, M.ASCE。Influence of Temperature and Pressure on the Dynamic Properties of Rubber-Modified Asphalt Concrete [J]. Joural of Materials in Civil Engineering © ASCE / January/Feberuary2006 / 125:0899-1561.

Jincheng Hou. Viscoelastic Study of Fiber Modified Asphalt Concrete [D].Dalian: Master thesis of Daliann Maritime university.2007:40 ～45.

Palit S. K, Sudhakar Reddy, K, Pandey, B. B. Laboratory Evaluation of Crumb rubber modified asphalt mixtureMixes[J]. Joural of Materials in Civil Engineering© ASCE / January/Feberuary2004 / 45**:** 0899-1561.

Reibo Ren, Yiqiu Tan, Daihui Zhong. Viscoelastic **T**heoretical Analysis of Asphalt Pavement [J]. Sichuan Building Science And Research,2004,30(1):76～79.

Xuejun Ding,Chang Li. Stress of Pavement Structure Under Horizontal Loads [J]. Chinese Journal of Geotechnical Engineering,2004,24(4) :428.

Viscoelastic Analysis of Asphalt Pavement Using a Regularized Interconversion Technique between Creep and Relaxation

Yaoting Zhu[1], Lu Sun[2], Kesi You[1]

[1]Transportation College, Southeast University, 2 Sipailou, Nanjing, 210096, China; PH (+86) 25-83792619; email: zhuyt@yahoo.cn

[2]Associate Professor, Department of Civil Engineering, Pangborn Hall, Catholic University of America, 620 Michigan Ave., N.E., Washington D. C. 20064; PH (202)319-6671; Fax: (202)319-6677; email: sunl@cua.edu

ABSTRACT

This study illustrates a regularized method in the viscoelastic analysis of asphalt pavement based on time-domain creep tests. The method is capable of overcoming the ill-posedness of interconversion between creep compliance and relaxation modulus by solving a Volterra integral equation of second kind with regularization. The discrete data of relaxation modulus is calculated by the regularized method and fitted to the generalized Maxwell model. After the viscoelastic parameters of asphalt mixtures are obtained, the nonlinear finite element model of pavement is developed and the computed results indicate that the viscoelastic mechanical responses of pavement are greatly affected by temperature and loading time. The results of this study are expected to be utilized to predict and validate the distress of asphalt pavement in the design and maintenance periods.

Keywords: Asphalt mixtures; Viscoelasticity; Creep tests; Regularization methods; Finite element method.

INTRODUCTION

Asphalt mixtures are typical composite materials which are composed of graded aggregates, asphalt binders, and air voids. The mechanical behavior of asphalt mixtures is complex, and exhibits nonlinearity with correlation to time, frequency and temperature. However, many design methods still employ linear elastic theories to calculate the pavement responses. In order to analyze the responses of pavement structure more realistically, the nonlinear constitutive law of asphalt mixtures is usually expressed by viscoelastic models (Huang 1993, Sun and Luo 2008).

To formulate the characteristic functions of viscoelastic materials, creep compliance and relaxation modulus are usually employed. The two functions which are usually obtained by corresponding tests are related by a convolution (Tschoegl 1989). Once the source function (the function from which one converts) is given, the target function (the function to which one converts) can be predicted by an interconversion method. In generally, it is difficult to implement a constant-strain

relaxation test on stiff asphalt mixtures, while a constant-stress creep test is much easier. Therefore in order to obtain the viscoelastic parameters of asphalt mixtures, it is necessary to firstly carry out creep tests and then to convert creep compliance to relaxation modulus.

The objective of this paper are (1) to present a regularized method for solving the ill-posed problem of interconversion between creep compliance and relaxation modulus; (2) to fit the calculated relaxation modulus to a generalized Maxwell model; (3) to illustrate the viscoelastic mechanical response of asphalt pavement with respect to different temperatures and loading time by finite element method.

NUMERICAL CALCULATION OF THE RELAXATION MODULUS

There are various methods for acquiring discrete relaxation modulus from creep data. Because of the relationship between creep compliance and relaxation modulus, the direct methods must require the solution of a Volterra integral equation of first kind, which is an ill-posed problem (Hopkins and Hamming 1957). In this section, we convert the Volterra integral equation to a second kind by the mathematical differential and discrete relaxation modulus is determined by solving the Volterra integral equation of second kind with regularization.

In the time domain, the general constitutive equation of linear viscoelasticity can be stated by the Boltzmann superposition integrals

$$\sigma(t) = \int_0^t E(t-\tau)\dot{\varepsilon}(\tau)d\tau\,, \tag{1}$$

$$\varepsilon(t) = \int_0^t D(t-\tau)\dot{\sigma}(\tau)d\tau\,, \tag{2}$$

where $\sigma(t)$ and $\varepsilon(t)$ are stress and strain functions, respectively; $E(t)$ and $D(t)$ are relaxation modulus and creep compliance, respectively; t is time. *Eqs.* (1) and (2) indicate that the stress (or strain) at the present time t under an arbitrary strain (or stress) history follows a linear superposition of all strains (or stress) applied at previous time τ.

Applying the Laplace transform and the inversion of Laplace transform to *Eqs*. (1) and (2), we obtain

$$t = \int_0^t E(t-\tau)D(\tau)d\tau\,, \tag{3}$$

$$t = \int_0^t D(t-\tau)E(\tau)d\tau\,, \tag{4}$$

Eqs. (3) and (4) are the Volterra integral equation of first kind.

Differentiating *Eqs.* (3) and (4) with time t, we find

$$1 = E(0)D(t) + \int_0^t \frac{\partial E(t-\tau)}{\partial t} D(\tau)d\tau\,, \tag{5}$$

$$1 = D(0)E(t) + \int_0^t \frac{\partial D(t-\tau)}{\partial t} E(\tau)d\tau\,. \tag{6}$$

Eqs. (5) and (6) are Volterra integral equations of the second kind which are well-posed. For the given discrete creep data $D(t)$, we can use *Eq*. (6) to compute discrete values of $E(t)$. It can be seen from *Eq*. (6) that the derivative of $D(t)$ should first be given. As we known, it is still an ill-posed problem to determine the derivative of $D(t)$. In this paper, we use a method to compute the numerical differentiation of $D(t)$ to overcome the ill-posedness, which is under the frame of Tikhonov regularization.

Discrete values of $D(t)$ obtained from experiment, are given at a discrete set of points $0 = t_1 < t_2 < \cdots < t_n$. We can approximate $D(t)$ by a cubic spline function $D_*(t)$ defined as follows (Wang et al. 2002):

(1) $D_*(t_i+) = D_*(t_i-)$, $D_*'(t_i+) = D_*'(t_i-)$, $D_*''(t_i+) = D_*''(t_i-)$;

where $D_*(t_i \pm)$ denotes the right and left limit of $D_*(t)$ at point t_i, $i = 2,3,\cdots,n-1$.

(2) $D_*''(t_1) = D_*''(t_n) = 0$;

(3) at point t_i, $i = 2,3,\cdots,n-1$, the third order derivative of $D_*(t)$ satisfies

$$D_*'''(t_i+) - D_*'''(t_i-) = \frac{1}{\alpha}\frac{t_{i+1} - t_{i-1}}{2}(D(t_i) - D_*(t_i)), \tag{7}$$

where α is the regularization parameter.

The above method is effective and well-posed in the numerical differential of general function, especially discontinuous function. For keeping the numerical integral method simple and stable, the compound trapezoidal formula of Newton-Cotes methods for integration *Eq*. (6) is used in this paper, namely

$$1 = D(0)E(t_i) + \frac{1}{2}(t_2 - t_1)\frac{\partial D(t_i - t_1)}{\partial t}E(t_1) + \frac{1}{2}\sum_{j=2}^{i-1}(t_{j+1} - t_{j-1})\frac{\partial D(t_i - t_j)}{\partial t}E(t_j) + \frac{1}{2}(t_i - t_{i-1})\frac{\partial D(t_i - t_i)}{\partial t}E(t_i). \tag{8}$$

LABORTORY CREEP TESTS AND RELAXATION MODULUS OF ASPHALT MIXTURES

Static creep is the simplest response of viscoelstic behavior and it is easy to be carried out in the laboratory. Static compressive creep tests are conducted to obtain material parameters of a linear viscoelastic constitutive model. The tests are generally implemented under static loading and isothermal conditions, and creep deflection is measured by linear variable differential transformer (LVDT).

The asphalt mixtures used in this study are a 13*mm* AC surface mixture. The coarse aggregates of mixtures were crushed limestone and the SBS polymer-modified asphalt cement was used as the asphalt binder. The stress level was 0.1 MPa, and three test temperatures were used: 0℃, 20℃ and 30℃. The data of creep compliance and calculated relaxation modulus at 20℃ are shown in Figure 1. As quasi-elastic method is usually used to provide an approximation for the

characteristic of asphalt mixtures, the result of $E(t)$ compared with $1/D(t)$ is shown in Figure 2. It is found that the quasi-elastic method cannot exactly describe the entire time-history behavior of asphalt mixtures, especially for long times.

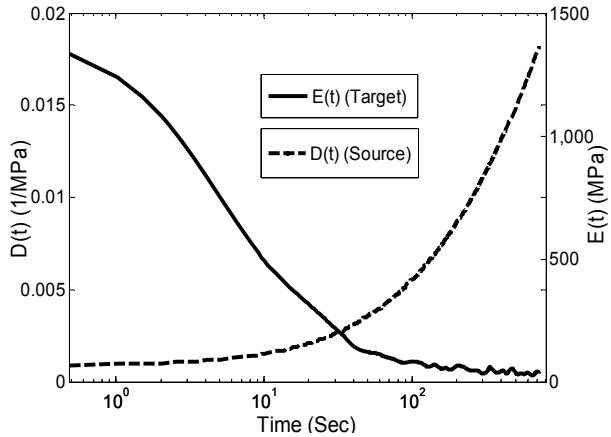

Figure 1. Creep Compliance *D(t)* and Calculated *E(t)*

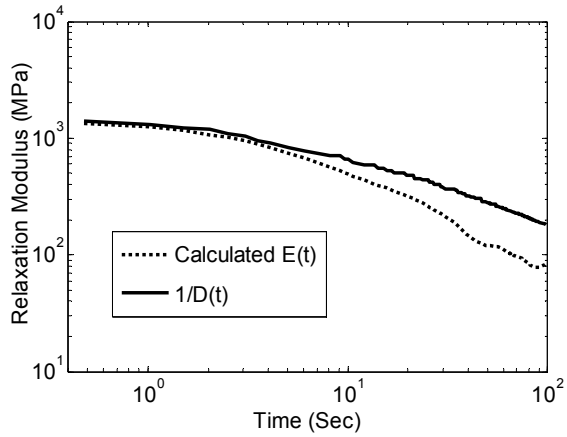

Figure 2. Calculated *E(t)* Compared With Reciprocal of *D(t)*

To formulate the physical model of relaxation modulus, the generalized Maxwell model is widely employed to express the viscoelastic characteristics of asphalt concrete. The model consists of n Maxwell elements connected in parallel and the relaxation modulus is given by a Prony series,

$$E(t) = E_n + \sum_{i=1}^{n-1} E_i e^{-E_i t/\eta_i} \qquad \text{and} \qquad \rho_i = \frac{\eta_i}{E_i} \tag{9}$$

where E_n, E_i, η_i and ρ_i are equilibrium modulus, spring modulus, dashpot viscosity and relaxation time, respectively.

The parameters of Prony series can be determined by solving a system of linear algebraic equation, such as collocation and linear least-squares methods (Park and Scharpery 1999). However, the relaxation times and sampling points are selected arbitrarily, the spring modulus may generate negative results which have no physical meaning. The other method for determining the parameters is the solution of

constrained nonlinear least squares (Mun et al. 2007). In this study, the second method is chosen and implemented by using MATLAB software. The discrete relaxation modulus is fitted to Prony-series as shown in Figure 3.

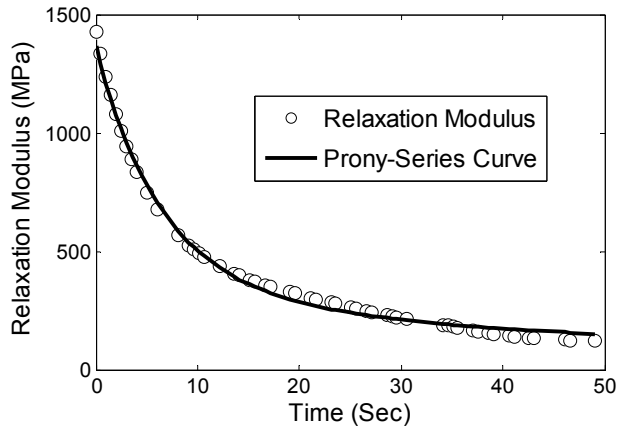

Figure 3. Prony-Series Fit to the Calculated Relaxation Spectra

VISCOELASTIC ANALYSIS OF PAVEMENT STRUCTURE

The finite-element method is well-suited for pavement analyses, especially for complex situation, such as different types of load, pressure, material nonlinearity and dynamic analysis. In this study, 3-D pavement model of dual tire is developed. To indicate the configuration of tire and pavement surface contact, the dual circular area is replaced by a rectangular area (Huang 1993), and the 3-D finite-element model is a quarter of geometric dimension by symmetrical principle.

The viscoelastic model of asphalt concrete is introduced into the finite element analysis of pavement structure. The base layer, subbase layer and subgrade layer are assumed linear elastic, the viscoelastic parameters of AC layer are given by the above sections. The nonlinear results of the analyses are summarized in Figure 4. In the figure, four different parameters are compared, namely, deflection of pavement surface, pressure strain of top subgrade, stress at bottom AC layer and tension stress at bottom base layer. It is observed that the deflection of surface pavement and pressure strain of top subgrade increase with time and temperature. Stress at bottom AC layer and tension stress at bottom base layer decrease with time, while they increase with temperature.

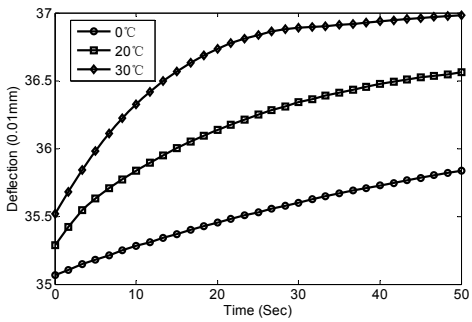

(a) Deflection of Surface Pavement

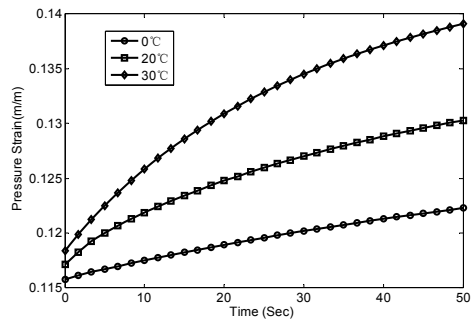

(b) Pressure Strain of Top Subgrade

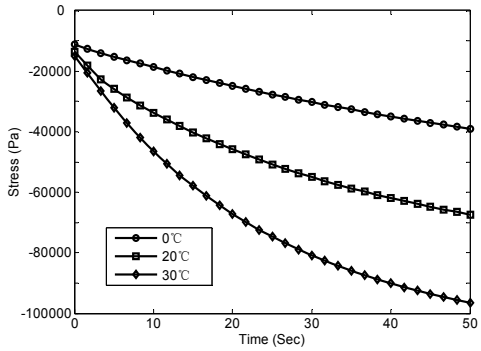

(c) Stress of Bottom AC Layer

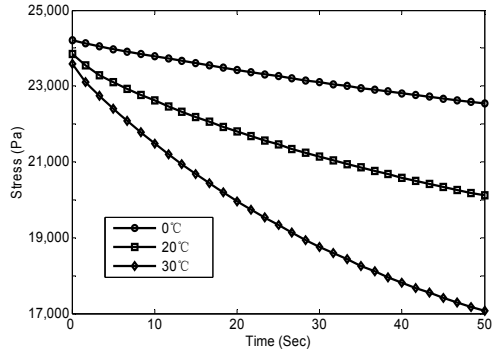

(d) Tension Stress of Bottom Base Layer

Figure 4. Viscoelastic Responses of Asphalt Pavement

CONCLUSION

Nonlinear analysis based on viscoelastic model for calculating mechanical response of asphalt pavement is presented in this paper. The method of acquiring relaxation spectra is effective to overcome the ill-posed nature of integral equation by equation transformation and a regularized method. The viscoelastic response of pavement suggested that all mechanical parameters were greatly sensitive to the temperature and loading time. The calculated results can be utilized to predict and validate the distress of asphalt pavement in the design and maintenance periods.

REFERENCES

Hopkins I. L. and Hamming R. W. (1957). "On creep and relaxation." *J. Appl. Phys.*, 28(8), 906-909.

Huang Y. H. (1993). *Pavement Analysis and Design*, Prentice Hall, New Jersey.

Mun Sungho, Chehab G. R., Kim Y. R. (2007). "Determination of time-domain viscoelastic functions using optimized interconversion techniques." *Road Mater. Pavement*, 8(2), 351-365.

Park S. W. and Schapery R. A. (1999). "Methods of interconversion between linear viscoelastic material functions. Part I—a numerical method based on Prony series." *Int. J. Solids Struct.*, 36, 1653-1675.

Sun Lu, Luo F. Q. (2008). "Transient wave propagation in multilayered viscoelastic media: theory, numerical computation, and validation." *J. Appl. Mech.*, ASME, 75(3), 031007 (15 pages).

Tschoegl N. W. (1989). *The Phenomenological Theory of Linear Viscoelastic Behaviour*, Springer-Verlag, Berlin.

Wang Y. B., Jia X. Z., Cheng J. (2002). "A numerical differentiation method and its application to reconstruction of discontinuity." *Inverse Probl.*, 18(6), 1461-1476.

Performance of Pavement Plate Reinforced with Modified Unsaturated Polyester Fiberglass Reinforced Plastic

XU wei[1], LI Guang-yuan[2], CEN Guo-ping[3]

[1]Instructor，Airport Construction Department，Engineering Institute， Air Force Engineering University, Xi'an, P.O. Box 710038, PH (86) 029-84787705; FAX (86) 029-84787704; Email: kgywx_xuwei@126.com

[2]Ph.D, Associate Professor, Airport Construction Department，Engineering Institute，Air Force Engineering University, Xi'an, P.O. Box 710038, PH (86) 029-84787705; FAX (86) 029-84787704; Email: guangyuanli@163.com

[3]Ph.D, Professor, Airport Construction Department，Engineering Institute， Air Force Engineering University, Xi'an, P.O. Box 710038, PH (86) 029-84787731; FAX (86) 029-84787731; Email: cenguoping@163.com

Abstract: In order to study material performance of modified unsaturated polyester Fiberglass Reinforced Plastic (FRP) pavement plate and its application in rapid crater repairing on airfield pavement, experiments were conducted to test its flexural and direct tension strengths; and the loading-vehicle was used to simulate one type of airplane to run on the repaired pavement with the FRP plate hundreds of times. It was discovered that the optimal mesh size of fiberglass in FRP plate was 120; the flexural tension strength of the plate could reach 240MPa; the direct tension strength of that could reach 200MPa; and the direct tension elastic modulus of that is larger than 15GPa. These data indicated that the toughness and the performance to resist flexural tension damage of the reinforced material were better. The results indicate that the damage to FRP plate was mainly induced at joints between the plate and subgrade. The flexural deflection not more than 5cm could be served as a standard to judge whether the repaired pavement could be used continuously.

Keywords: *Airfield engineering, Assembly pavement plate, Fiberglass Reinforced Plastic (FRP), Crater repairing; Toughness; Flexural tension strength; Flexural deflection*

Introduction

Assembly pavement plate, originated from World War II, was often made of armor plate with hole, aluminum plate and Fiberglass Reinforced Plastic (FRP) plate. It was often put to use as the assembly material in rapid crater repair after one airfield was attacked. It has the merit of light weight, being convenient of storage, being convenient to put together, and being able to be used directly after completion of construction. The Engineering Research & Development Center (ERDC) of USA has successfully studied the folded FRP pavement plate for practical application. This study aimed at one kind of pavement plate reinforced with modified unsaturated polyester fiberglass reinforced plastic. The experiments on material performance and simulated loading were carried out to analyze its characteristics and use demand.

1 Experiment on Material Performance

The tested pavement plate with a height of 1cm was pressed with fiberglass

having different fineness and modified unsaturated polyester.

The results of related study indicate that the carrying capacity of repaired pavement structure (Fig.1) depends on the height of backfill subgrade, compaction ratio and elastic modulus of the materials. The vertical cumulative plastic deformation of pavement structure will be induced by repeated loading of airplanes, which will cause out of joint between pavement and understructure and the flexural deformation of pavement plate. If the toughness and the tension resisting capacity of pavement are not sufficient, the fracture from below to top will happen.

According to the deformation characteristics induced by loading of assembly pavement plate, flexural modulus, flexural strength, tension modulus, tension strength and Poisson's ratio of four kinds of FRP plate with fiberglass having different fineness were tested.

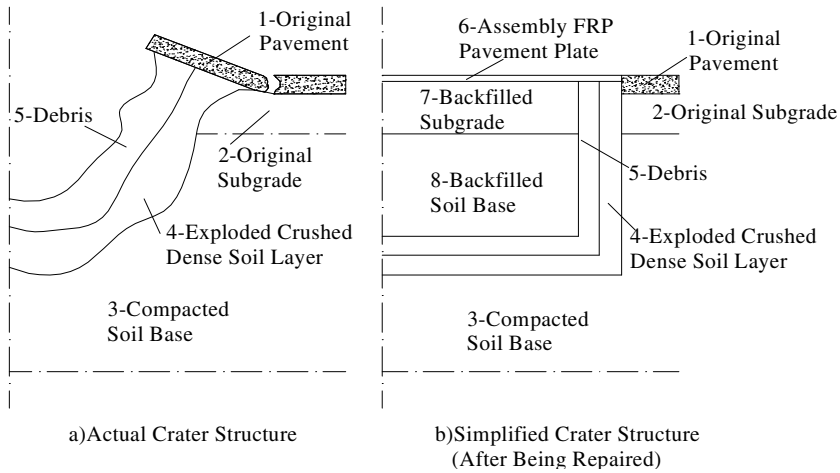

Fig.1 Airfield pavement structure before and after crater being repaired

1.1 Specimen Molding

According to Specification of Testing Method about Flexural Property of Fiber reinforced material (GB3356-1999), flexural tension specimens were fabricated with the length of 150mm, width of 12.5mm, and height of 10mm; direct tension specimens were fabricated with the length of 230mm, width of 25mm, and height of 10mm. To avoid stress concentration in the holding part for direct tension specimens, the hard aluminum sheet having the length of 50mm and width of 25mm was used as tension strengthening sheep. The hard aluminum sheet was then stuck in the two terminals with omnipotent glue as the tension strengthening sheet before experiments.

1.2 Experiment Method

1.2.1 Flexural Tension Property Experiment

The flexural loading experiment was executed in the trisection point with the testing machine of MTS-810. The initial loading is 10N; loading speed is 2mm per minute. Data was collected automatically by computer to draw loading versus deflection (*P* versus *f*) curve (Fig.2).

The flexural elastic modulus E_f is:

$$E_f = \frac{\Delta P \cdot L^3}{4b \cdot h^3 \cdot \Delta f} = K_f \cdot \frac{L^3}{4b \cdot h^3} \tag{1}$$

Where, P is the loading increment in the initial straight line part of P versus f curve; f is the deflection of the midpoint in the specimen; L is the space between fulcrums on the specimen, whose value was taken as 136mm; b is the width of specimen; h is the height of specimen; K_f is the gradient in the initial straight line part of P versus f curve.

The flexural elastic strength σ_f is:

$$\sigma_f = \frac{3P_f \cdot L}{2b \cdot h^2} \tag{2}$$

Where, P_f is the maximum loading when the specimen was broken in the flexural tension experiment.

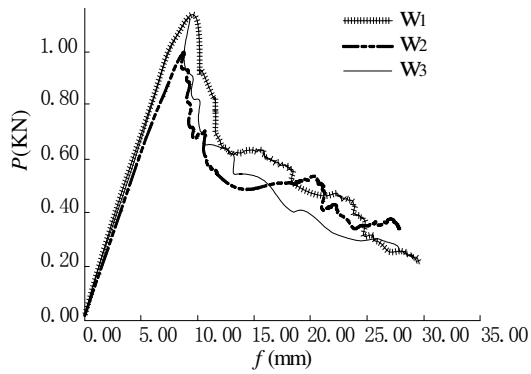

Fig.2 *P-f* curve (120 order fiberglass)

1.2.2. Direct Tension Property Experiment

To accurately obtain the values of direct tension modulus E_t and Poison's ratio μ, two strain gages were separately stuck in the middle of the specimen along the axial direction and transverse direction. The strains in these directions were ε_{z1} and ε_{h1}. To eliminate eccentricity influence, two other strain gages were also stuck on the reverse side of the specimens. The two strains were ε_{z2} and ε_{h2}. The specimen was clipped by a clamp of the tension testing machine in the experiment. The loading is 0.5KN per level. The strain reading was recorded to draw the curve of σ versus ε_z, and ε_h versus ε_z curves (such as Fig.3 and Fig.4).

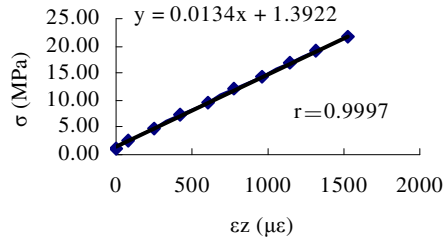

Fig.3 σ-ε_z curve (120 order fiberglass)

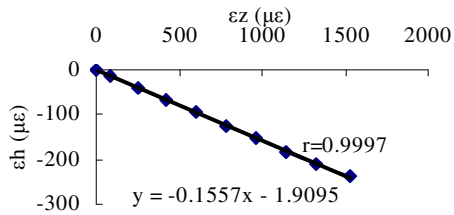

Fig.4 ε_h-ε_z curve (120 order fiberglass)

The direct tension modulus is:

$$E_t = \frac{\Delta P}{b \cdot h \Delta \ \varepsilon_z} \tag{3}$$

In equation (3), $\Delta\varepsilon_z$ is the strain increment in axial direction.

The Poisson's ratio is:

$$\mu = -\frac{\varepsilon_h}{\varepsilon_z} \tag{4}$$

where, $\varepsilon_h = \frac{(\varepsilon_{h1} + \varepsilon_{h2})}{2}$, $\varepsilon_z = \frac{(\varepsilon_{z1} + \varepsilon_{z2})}{2}$。

The direct tension strength is

$$\sigma_t = \frac{P_b}{b \cdot h} \tag{5}$$

In equation (5), P_b is the maximum loading when the specimen was broken in the direct tension experiment.

1.3 Analysis on Experiment Results

1. The maximum value of flexural tension strength and flexural tension modulus are from the fiberglass pavement plate with the fineness of 120 order. The values were respectively 244.06MPa and 13284.63MPa. The results indicate that the flexural property of FRP pavement plate was affected by the fineness of fiberglass and the optimum fineness request of fiberglass existed.

2. The direct tension property of FRP pavement plate with the fineness of 120 order was better (201.59MPa, 15.73MPa) in the experiment.

3. The results of flexural tension experiments and direct tension experiments can be used in the data computing and analysis. The result of finite element simulating indicates FRP pavement was mainly affected by flexural tension stress on the bottom between the loading points and direct tension stress between during the loading circle induced by airplane. The computed stress value was about 20MPa to 30MPa, which were far below the actually obtained flexural and tension strengths.

4. The actually obtained flexural and tension property of FRP pavement plate was better than the similar materials used abroad.

Tab.1 Experiment Results of Material Property of FRP pavement plate

Serial Number	Fineness of Fiberglass (order)	Flexural Tension Strength $_f$（MPa）	Flexural Tension Modulus E_f（MPa）	Direct Tension Strength $_t$（MPa）	Direct Tension Modulus Et（GPa）	Possion Ratio μ
1	80	212.61	9258.16	160.40	10.97	0.17
2	120	244.06	13284.63	201.59	15.73	0.16
3	150	203.80	11624.07	197.84	13.53	0.15
4	200	210.79	10772.96	180.34	16.53	0.14

Tab.2 Proper Index of FRP Pavement Plate Abroad

Serial Number	Name of Index	Value of Index
1	Flexural Tension Strength(MPa)	198.55
2	Direct Tension Strength(MPa)	117.2
3	Direct Tension Modulus(GPa)	10.34

2 Simulating Experiment

Using the original cement concrete pavement with a thickness of 30cm, the simulated crater with the diameter 4m and the maximum depth 1.4m was dug. Subgrade was backfilled with the disintegrated slag in excavation to the distance of 70cm from pavement surface and not compacted. Graded gravel was backfilled on the disintegrated slag layer, whose maximum particle size is 40mm and virtual pavement depth is 5cm. The graded gravel layer was compacted 8 times with 8 ton compactor and then leveled manually. Because the compactor is too light, the compact ratio can not reach the desired level. The case machine was used to compact for second round. Finally the surface was leveled with a plate vibratory compactor. Cement mixing chip was paved on the graded gravel lever and the FRP pavement plate with the fiber of 120 order was placed on it.

The loading experiments were executed with a special loading simulating the moving airplane tire, whose pressure is 1.8MPa and the single tire load is 1500kg, to simulate the passing of airplane on the pavement. The passing speed is controlled between 5 to 10km/h. Because the subgrade of repaired pavement structure is flexible , the plastic deformation can be observed after only some passing times. The out of joint of FRP plate is very obvious but it is not removed. After 160 passing

times, the FRP plate was removed, the maximum deformation of the subgrade can be observed as 5.2cm. The subgrade was not damaged, and the FRP plate was paved again. After 244 passing times, the deformation of the subgrade can be observed as 6 cm, and the area around the tested points had upheaval. The rutting was then backfilled with the chip of maximum size 10mm, and compacted by a plate ram. After compaction, the FRP was paved, continuing to pass 434 times. The FRP plate was not broken during the entire testing period. But after more than 400 passing times, the FRP plate was observed with some extent of plastic deformation. It was discovered that the damage of FRP plate was mainly induced by out of joint between plate and subgrade, or tension damage from bottom to top on the plate.

3 Conclusions

It is important and meaningful to have the rapid runway repair with the assembly pavement plate. This paper presented an analysis of the characteristics and using request of modified unsaturated polyester fiberglass reinforced plastic pavement plate. The results indicate that the toughness of FRP plate and tension resisting capacity can carry some times passing of simulated airplane loading although the plastic deformation of subgrade is big during the experiments. The experimental results are consistent with the simulation results. Considering the smoothness request of pavement, the deformation of plate not exceeding 5cm was suggested as the control standard of repaired airport pavement.

Bibliography

Bull JW, Woodford CH. 1995. “The numerical analysis and modeling of repaired runways following chemical explosive crater formation”. In: Bull JW, editor. Numerical analysis and modeling of composite materials. Glasgow: Blackie, p28-51.

LI Jin-jun, Huang Mao-song. 2006. “Analysis of Plastic Deformation of Soft Clay Foundation under Traffic Loading”. China Journal of Highway and Transport. 19(1): p1-5 (in Chinese)

Park JM, Lee J, Park TW. 1996. “Improved interfacial shear strength and durability of single carbon fiber reinforced isotopic polypropylene composites, using water-dispersible graft copolymer as a coupling agent”. Polymer Composites, p375-403.

Park JM, Kim JW, Goda K. 2000. “A new method of evaluating the interfacial properties of composites by means of the gradual multi-fiber fragment test”. Composites Science and Technology, 60(3):p439-450.

Study on Permanent Deformation Characteristics of Asphalt Pavement Based on Discrete Element Method

J. Z. Pei[1] and M. F. Chang[2]

[1]Key Laboratory for Special Area Highway Engineering of Ministry of Education, School of Highway, Chang'an University, South 2nd Ring Road, Xi'an, 710064, Shaanxi, China; PH (86) 13891921101; FAX (86) 029-87818191; email: jianzhongpei@163.com

[2]Key Laboratory for Special Area Highway Engineering of Ministry of Education, School of Highway, Chang'an University, South 2nd Ring Road, Xi'an, 710064, Shaanxi, China; PH (86) 15829387533; email: mfchang99@126.com

ABSTRACT

In this paper, the microscopic mechanism of rutting formation is studied by the Discrete Element Method (DEM). The particles in discontinuous asphalt mixtures are discretized into circular rigid particles by DEM, then the initial model is created in accordance with the actual pavement. The displacement vector changes of particles under loading and the process of rutting formation are presented in this paper. The asphalt pavement model has been built to simulate the material properties of asphalt pavement by the PFC2D software. At the same time, the displacement vector changes in each layer have been analyzed under loading. In addition, the mechanisms of permanent deformation have been studied and the rutting formation process of asphalt pavement has been simulated. The results show that the Discrete Element Method used to study permanent deformation characteristics of asphalt pavement is reasonable and feasible.

KEY WORDS

Discrete Element Method (DEM) model, asphalt pavement, permanent deformation, microscopic characteristics

INTRODUCTION

The permanent deformation (i.e. rutting) of asphalt pavement is one of the most important forms of early damage in highway. Influencing factor diversity in high temperature characteristics and complexity in rutting formation are caused due to the inherent viscoelastic characteristics of asphalt mixture, and then permanent deformation has become a prevailing problem. Many countries and relevant associations began to pay attention to permanent deformation as early as in 1962. It is undeniable that permanent deformation is still one of the important study areas for mechanical properties of asphalt pavement.

In recent years, great achievements in understanding permanent deformation mechanisms have been made by asphalt pavement researchers. Novak, M. of the University of Florida studied the tire contact stresses and their effects on instability

rutting of asphalt mixture pavements based on three-dimensional finite element analysis (Novak, M. 2003). Brown, E. R. of Auburn University evaluated the rutting of the 2000 National Center for Asphalt Technology (NCAT) Test Track and compared laboratory rutting tests and field performance(Brown, E.R. 2004). Topal, A. and Sengoz, B. studied the relation between fine aggregate angularity and the resistance to rutting of hot-mix asphalt(Topal, A. 2005). Drakos, C. A. of University of Florida identified the differences between stress states under the Asphalt Pavement Analyzer (APA) loading device (hose) and stress states under radial truck tires, and interpreted rutting mechanisms(Drakos, C. A. 2006). Lee, S. J. of Clemson University studied the application of crumb rubber modifier (CRM) in asphalt mixtures to improve the properties of binder by reducing the binder's inherent temperature susceptibility and obtained a better rutting resistant hot mix asphalt (Lee, S. J. 2008).

The Particle Flow Code (PFC) software based on the Discrete Element Method can be used to study the microscopic characteristics of asphalt mixture. Discrete Element Method whose theoretical basis is Newton's second law was put forward by Cundall in 1971. The calculation method is relaxation iteration for mechanical parameters (such as force and displacement) in each step and the iteration process was iterated until the system reaches equilibrium. You Z.P. had used DEM for asphalt mixtures: Development of a Micromechanical Modeling Approach to Predict Asphalt Mixture Stiffness Using Discrete Element Method (You, Z. 2003), Discrete Element Modeling to Predict the Modulus of Asphalt Concrete Mixtures (You, Z. 2004), and Micromechanical Modeling Approach to Predict Compressive Dynamic Moduli of Asphalt Mixture Using the Distinct Element Method (You, Z. 2006). Furthermore, Rothenburg, L. studied the micromechanical model of asphalt concrete in connection with pavement rutting problems in permanent deformation of asphalt pavement (Rothenburg, L. 1992).

PARALLEL BOND MODEL OF DISCRETE ELEMENT METHOD (DEM)

Circles (two-dimension) or spheres (three-dimension) are used to represent the simulated particles in DEM. The parallel bond model which can transmit both forces and moments between particles describes the constitutive behavior of a finite-sized piece of cementious material deposited between two balls. A parallel bond is defined by the following five parameters: normal and shear stiffness, $\bar{k}^n$ and $\bar{k}^s$; normal and shear strength, $\bar{\sigma}_c$ and $\bar{\tau}_c$; and bond radius, $\bar{R}$. The total force and moment associated with the parallel bond are denoted by $\bar{F}_i$ and $\bar{M}_3$, with the convention that this force and moment represent the action of the bond on particle B of Figure 1(Itasca Consulting Group, Inc. 2004).

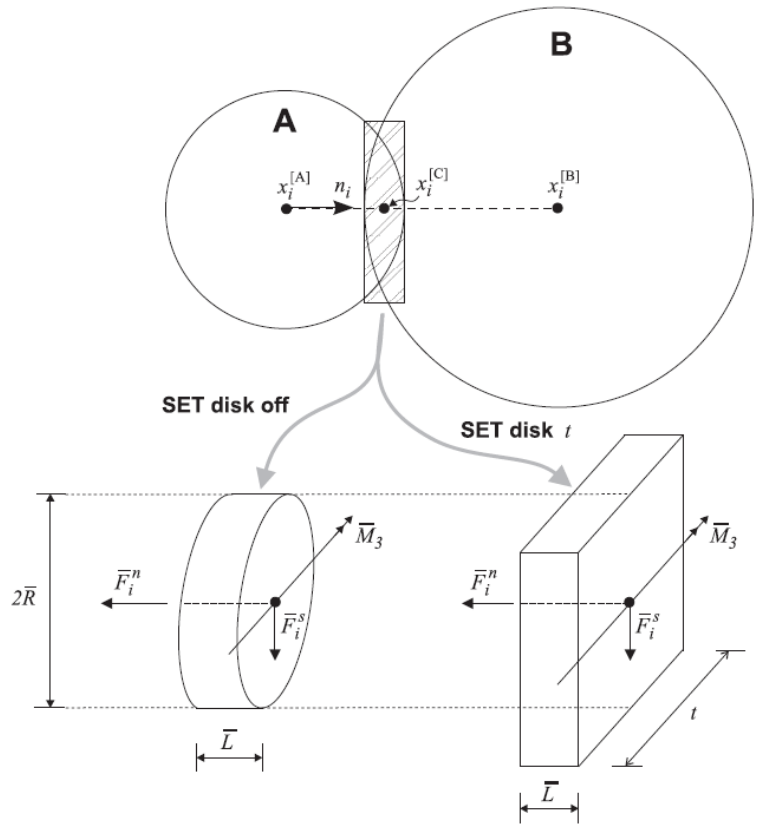

Figure 1. Parallel bond depicted as a finite-sized piece of cementious material

The force vector can be resolved into normal and shear components with respect to the contact plane as

$$\overline{F}_i = \overline{F}_i^n + \overline{F}_i^s$$

Where, $\overline{F}_i^n$ and $\overline{F}_i^s$ denote the normal and shear component vectors, respectively. The area of the bond cross-section is given by:

$$A = \begin{cases} \pi \overline{R}^2 & \text{(SET disk off)} \\ 2\overline{R}t & \text{(SET disk } t\text{)} \end{cases}$$

Where, $\overline{R}$ is the radius of the bond cross-section; SET disk off denotes that the bond cross-section is circular approximately; SET disk t denotes that the bond cross-section is rectangular approximately.

ASPHALT PAVEMENT MODEL

According to the structure of asphalt pavement, five structure layers are employed in the model (Figure 2 (a)). The voids of upper surface course is 4%, and the thickness in each structure layer is 5cm, 7cm, 8cm, 35cm and 20cm from top to bottom, respectively. Parallel bond model is employed for the 20cm asphalt concrete surface course to simulate the viscoelastic interaction between binder and aggregates; Base course thickness is 35cm using contact bond model. The reason is that

materials in this layer are mainly granular materials and the contacts between particles can be regarded as point contacts; Sub-base course thickness is 20cm using contact bond model as well.The particle contacts in this layer are also point contacts.

Table 1. Parallel bond model parameters of pavement materials

Parameters	Particle radius (mm)	Density (kg/m^3)	Normal stiffness (Pa/m)	Shear stiffness (Pa/m)	Normal strength (Pa)	Shear strength (Pa)
Upper surface course	2.5~5	2400	1×10^7	1×10^7	1×10^{10}	1×10^{10}
Intermediate surface course	5~8	2500	1×10^8	1×10^8	1×10^9	1×10^9
Lower surface course	7~9	2600	1×10^9	1×10^9	1×10^8	1×10^8

Table 2. Contact bond model parameters of base course and sub-base course materials

Parameters	Particle radius (mm)	Density (kg/m^3)	Normal strength (Pa)	Shear strength (Pa)
Base course	8	2300	1×10^7	1×10^7
Sub-base course	9	1800	1×10^7	1×10^7

The contact forces between particles in the model can be traced by PFC2D after generating the model meeting voids requirement, which is shown in Figure 2 (b). The types of contact forces include compression and tension, the size of lines denotes the magnitude of the contact forces, i.e. the thicker lines represent larger contact forces. The model is run by PFC2D to reach equilibrium state before applying loading to it. The range of mean contact force is from 5.899e+002N to 5.899e+002N. Consequently, the mean contact force keeps constant. The range of mean unbalanced force is from 4.580e-003N to 8.021e+002N, then the final mean unbalanced force is close to zero. The results of mean contact force and mean unbalanced force indicate that the system reaches the equilibrium state.

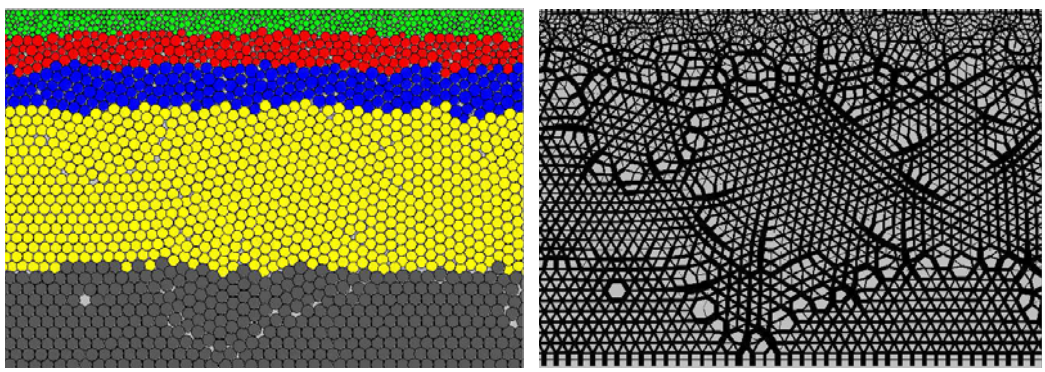

(a) Asphalt pavement model **(b) Contact force vector between particles**

Figure 2. Asphalt pavement model and contact force vector between particles

RESULT AND DISCUSSION

Five balls connected together represent one tire in loading model. The space between two tires is 10.65cm (i.e. half of the diameter of the equivalent circle) and the loading model is shown in Figure 3(a). The pavement structure produces deformation after loading. Then, the magnitude of pavement permanent deformation is obtained by tracing the vertical displacement of particles contacting between upper surface course and tires. The model after loading is shown in Figure 3 (b).

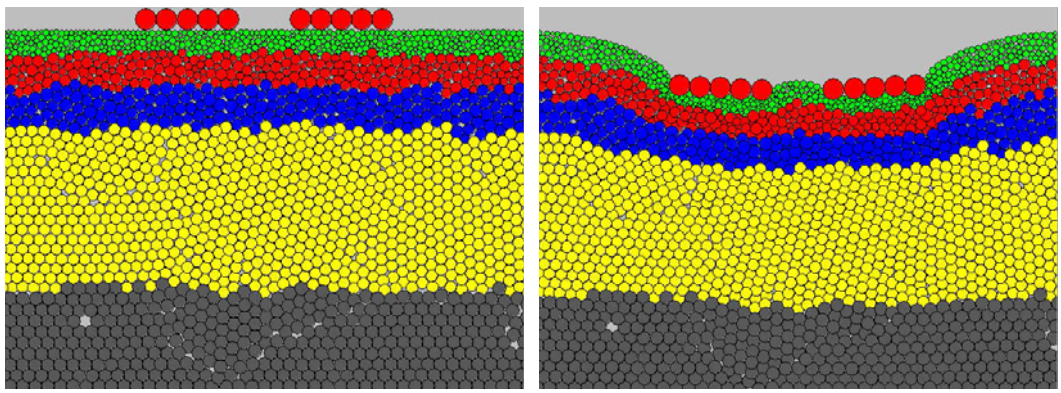

(a) Loading model **(b) The model after loading**

Figure 3. The models before and after loading

In the process of simulating rutting formation by PFC2D, particles' vertical displacements are traced at seven positions in each layer, which are external edge of left wheel mark, center of left wheel mark, internal edge of left wheel mark, middle of two wheel marks, internal edge of right wheel mark, center of right wheel mark and external edge of right wheel mark, respectively. The vertical displacement curves at seven positions in each layer are shown in Figure 4. The shape of three displacement curves of the surface course is "W" approximately, i.e. rutting depth at wheel marks is larger than that at the middle of two wheel marks, which are consistent with rutting of actual pavement. Due to the fact that rutting caused by two wheels are basically the same, the particle vertical displacements under the left wheel mark are selected to show rutting depth change in each layer (Figure 5). The figure shows that rutting depths at internal, external edges and center of left wheel mark are the same basically, and the change trend of rutting depth curves is consistent. However, the curve at the middle of two wheel marks is different from other curves. Rutting depth in initial stage is less than that at other three positions, then the second half curve tends to be consistent with other curves gradually. The reason is mainly that vehicle loadings at the middle of two tires are less than those at the wheel marks along traffic direction and the vertical displacements under loading are small. Furthermore, the vertical displacements in each structure layer decrease as the structure layer depth increase gradually, which makes the curves' change trend to be the same basically.

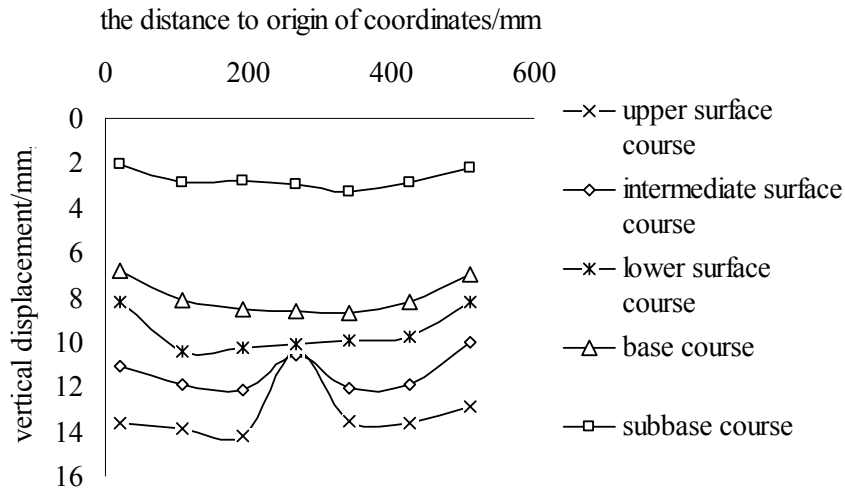

Figure 4. Vertical displacement curves at seven positions of each course

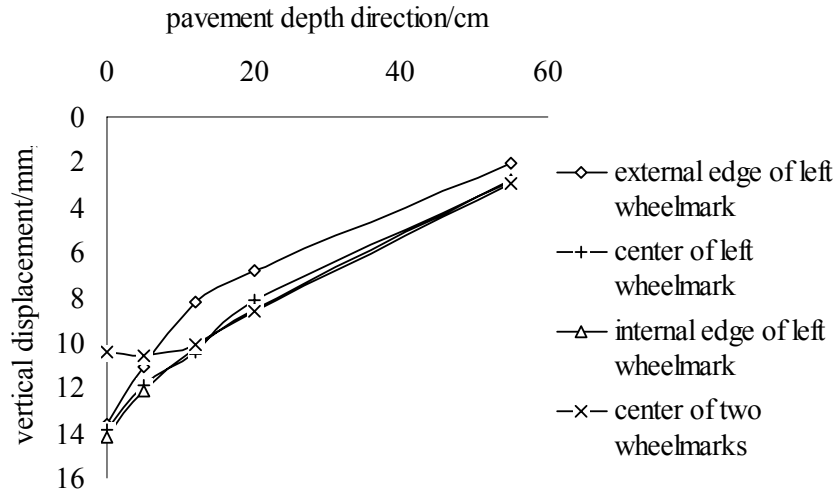

Figure 5. Displacement curves along pavement depth direction

Particles' displacement vectors of the model are described in Figure 6, and the vectors density indicates the degree of displacement change. The arrows in the figure indicate the movement direction of particles and the length of the arrows indicates the magnitude of particle displacements. The longer arrows represent larger displacements. The shape of the rutting profile is "W" approximately, which is similar to the curve shapes in Figure 4. Additionally, particles' displacement vectors contacting with tires are closest and the displacement is barely produced between particles far from tires position. Because the maximum loading is applied to particles contacting with tires, and the loading applied to particles decreases along depth direction gradually, producing smaller vertical displacement correspondingly.

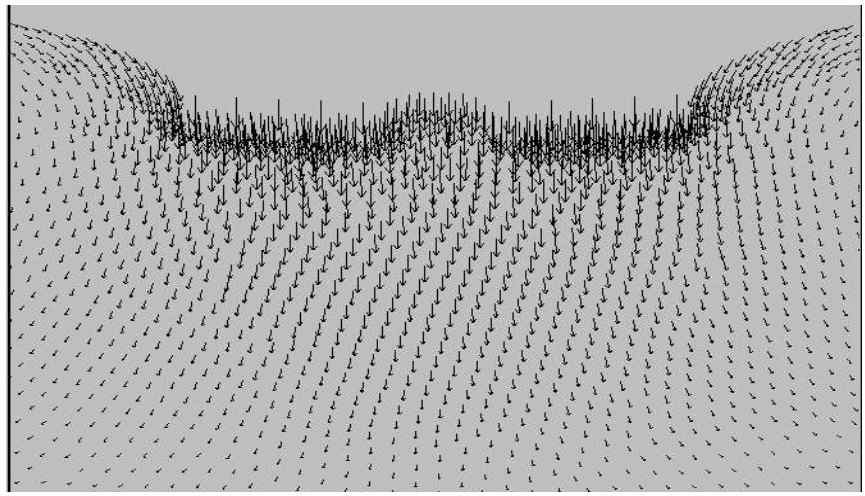

Figure 6. Particles displacement vector after loading

CONCLUSION

According to the results of the numerical simulation, the traced displacement changing curves with time steps and displacement vectors of particles contacting with tires and comparing the rutting depths of each structure layer, the conclusions are as follows:

(1) The rutting changing curves based on DEM are consistent with actual rutting results, which shows that Discrete Element Method used to study the microscopic characteristics of asphalt mixture is feasible.

(2) Figure 6 shows that particles' displacement vectors are similar to the movement of aggregate particles under repeated loading in actual pavement.

(3) The microscopic mechanical response of surface course structure established based on parallel bond under loading can be used to explain permanent deformation to a certain extent.

The above conclusions prove that simulating the structure composed of granular and binder materials by DEM is reasonable. However, the mechanical response of asphalt mixture is complicated under many factors' comprehensive action. Consequently, it is necessary to select reasonable parameters to simulate viscoelastic properties of asphalt mixture using the parallel bond model. Though the method can be employed to simulate rutting formation process, deviations still exist. On the one hand, circles representing particles in PFC2D are different from three-dimensional shapes of aggregates used in asphalt pavement. On the other hand, the model parameters are different from actual pavement parameters.

ACKNOWLEDGMENTS

We wish to express our thanks to National Natural Science Foundation of China (Grant No. 50608006), Natural Science Foundation of Shaanxi Province (Grant No. 2007$E_2$23) and Support Program for New Century Excellent Talents from Ministry of Education of China (Grant No. NCET-07-0120).

REFERENCES

Brown, E. R., Prowell, B., and Cooley, A. (2004). **"**Evaluation of rutting performance on the 2000 NCAT test track." *Asphalt Paving Technology*: *Association of Asphalt Paving Technologists-Proceedings of the Technical Sessions, Asphalt Paving Technology 2004,* 73, 287-336.

Drakos, C. A., Roque, R., Birgisson, B., and Novak, M. (2006). **"**Identificationof a physical model to evaluate rutting performance of asphalt mixtures." *ASTM Special Technical Publication*, *Performance Tests for Hot Mix Asphalt (HMA) Including Fundamental and Empirical Procedures,* n1469, 156-176.

Itasca Consulting Group, Inc. (2004). Particle Flow Code in 2-Dimensions: Theory and Background [CP]. *Version 3.1*. *Itasca Consulting Group, Inc*., 22–23.

Lee, S. J., Akisetty, C. K., and Amirkhanian, S. N. (2008). **"**The effect of crumb rubber modifier (CRM) on the performance properties of rubberized binders in HMA pavements." *Construction and Building Materials,* 22(7), 1368-1376.

Novak, M., Birgisson, B., and Roque, R. (2003). **"**Tire Contact Stresses and Their Effects on Instability Rutting of Asphalt Mixture Pavements: Three-Dimensional Finite Element Analysis." *Transportation Research Record,* n1853, 150-156.

Rothenburg, L., Bogobowicz, A., and Hass, R. (1992). "Micromechanical Modelling of Asphalt Concrete in Connection with Pavement Rutting Problems." *7th International Conference on Asphalt Pavements,* 230-245.

Topal, A., and Sengoz, B. (2005). **"**Determination of fine aggregate angularity in relation with the resistance to rutting of hot-mix asphalt." *Construction and Building Materials,* 19(2), 155-163.

You, Z. (2003). "Development of a Micromechanical Modeling Approach to Predict Asphalt Mixture Stiffness Using Discrete Element Method." University of Illinois at Urbana-Champaign, published by UMI, a Bell & Howell Information Company, Ann Arbor, MI.

You, Z., and Buttlar, W. G. (2004). "Discrete Element Modeling to Predict the Modulus of Asphalt Concrete Mixtures." *Journal of Materials in Civil Engineering,* ASCE, 16(2), 140-146.

You, Z., and Buttlar, W. G. (2006). "Micromechanical Modeling Approach to Predict Compressive Dynamic Moduli of Asphalt Mixture Using the Distinct Element Method." *Transportation Research Record: Journal of the Transportation Research Board, National Research Council,* Washington, D.C., 73-83.

Mechanism of Rutting Formation in Long and Steep Climbing Sections of Asphalt Pavement

J. Z. Pei[1], Y. Chen[2] and M. F. Chang[3]

[1]Key Laboratory for Special Area Highway Engineering of Ministry of Education, School of Highway, Chang'an University, South 2nd Ring Road, Xi'an, 710064, Shaanxi, China; PH (86) 13891921101; FAX (86) 029-87818191; email: jianzhongpei@163.com

[2]Key Laboratory for Special Area Highway Engineering of Ministry of Education, School of Highway, Chang'an University, South 2nd Ring Road, Xi'an, 710064, Shaanxi, China; PH (86) 13759917123; email: nianqinen_023@yahoo.com

[3]Key Laboratory for Special Area Highway Engineering of Ministry of Education, School of Highway, Chang'an University, South 2nd Ring Road, Xi'an, 710064, Shaanxi, China; PH (86) 15829387533; email: mfchang99@126.com

ABSTRACT

Road condition surveys show that the long and steep climbing section of asphalt pavement is one of the regions with the most significant rutting that seriously affects the road performance. And rutting is more serious for steeper longitudinal slope. In this paper, the changing rule of shear stress and its distribution characteristics in pavement are analyzed on conditions of different longitudinal slope and different horizontal attachment coefficients by a finite element method. The results show that the maximum shear stress is less subjected to the component of gravity when the longitudinal gradient changes. Due to the existence of longitudinal gradient, the changes of the adhesion between tires and road affect the shear stress significantly. The peak maximum shear stress gradually moves to the surface with increasing the horizontal force coefficient. The research results presents guides on how to prevent and control distresses for asphalt pavements on a long and steep slope. .

KEY WORDS

Long and steep climbing section, asphalt pavement, rutting, slope, adhesive coefficient, maximum shear stress

INTRODUCTION

With construction and development of freeways in mountainous areas in recent years, the “long” and “steep” slope has been inevitably faced in road design. Higher rutting resistance is demanded for asphalt pavement in mountain freeways. Road condition surveys have shown that rutting is most likely to occur in the climbing sections of mountainous freeways . The degree of rutting, particularly in the longer section of the larger and climbing slope, is far greater than that in flat sections., Therefore the road destruction of these sections starts earlier. This is the most

prevalent form of early destruction in mountain asphalt pavement. Mechanics analysis indicates that the major reason of the severe rutting is mainly due to the shear resistance of asphalt mixture that is insufficient at high temperature. Therefore it leads to shear slip. Shear stress is of great importance to control rutting.

Highway researchers are very interested in shear strength, which is an important index of pavement mechanical properties. Norman, W. M. carried out a systematic study from the shear resistance stability of pavement under static load conditions. He considered the internal force distribution in tires and the horizontal shear stress under braking and accelerating (Norman, W. M. 1951). In order to study the stress distribution in roads, Subbaraju, B. H. buried sensors into the specimens and imposed loading to test and analyze the shear stress simultaneously, and gave the specific mechanics formula(Subbaraju, B. H. 1965). Edward, S. B. gave the stress state for roads when the pavement is subjected simultaneously horizontal shear stress and vertical shear stress. He pointed out that horizontal shear stress must be taken into account in road design. Shear stress arising from road increases greatly under combined vertical and horizontal force , bringing down the road stability (Edward, S. B. 1965). In China, the corresponding studies are mainly as follows: Professor Dai, J. L. of Chang'an University developed DLG-A road material shear apparatus and studied the shear resistance properties for the material between pavement layers with the shear apparatus. Professor Sun, L. J. of Tongji University researched the shear resistance properties for asphalt mixture by uniaxial penetration test and unconfined compression test. Three-dimensional finite element analysis was used to demonstrate the feasibility of the method in his research (Sun, L. J. 2005).

The above studies show the importance of shear strength in pavement mechanics research. However, the long and steep slope sections have never been taken as a special topic. In addition, the influence of shear stress changes on pavement structure, which are caused by gradient, slope length and speed change in the process of climbing, has never been studied. In this study, finite element simulation is carried out and the influences of different gradients, horizontal force coefficients, temperature and loading on shear stress in long and steep slope pavement are analyzed.

FINITE ELEMENT MODEL FOR CLIMBING SECTIONS

Vehicle movement is mainly formed by the external transmission force that depends on the contact between tires and pavement.. When vehicles move uniformly and in a straight line on a horizontal road, it is important to overcome the rolling resistance from the ground and the air resistance. The vehicles must also overcome the gravity force component along the ramp as well in the climbing process. Additionally, it is important to overcome the acceleration resistance when the vehicles speed up (Wang, B. G. 1992). The gravity force component along the ramp and the air resistance are not considered for studying the mechanical properties of climbing sections. The driving resistance i.e. the force paralleling to the driving

direction in climbing is as follows:

$$F_R = F_f + F_i$$

Where, F_R is the driving resistance; F_f is the rolling resistance, $F_f = Gf\cos\alpha \approx Gf$;

F_i is the gravity force component along the ramp, $F_i = fG\sin\alpha \approx fG\alpha$.

In order to simulate the mechanical state of pavement in climbing sections, different horizontal loadings are applied to the tires positions in a finite element model for different longitudinal slopes and horizontal force coefficients according to the above equation.

PAVEMENT STRUCTURE MODEL AND MATERIAL PARAMETERS

Pavement material parameters. In order to reflect the mechanical properties of long and steep climbing slope, three typical pavement structures as presented in Table 1 are selected for this study (Sun, L. J. 2005):

Table 1. Three typical pavement structures and material parameters

Structure type	Jinan-Qingdao Freeway		Beijing-Tianjin-Tanggu Freeway		Capital Airport Freeway	
	Thickness /cm	Modulus /MPa	Thickness /cm	Modulus /MPa	Thickness /cm	Modulus /MPa
Upper surface course	4	1200 (350)	4	1300 (350)	4	1200 (350)
Intermediate surface course	5	1000 (500)	6	1100 (500)	6	1000 (500)
Lower surface course	6	700	8	700	13	700
Base course	34	1500	18	1500	20	1500
Subbase course	18	550	31	1500	30	550
Soil matrix	200	35	200	35	200	35

（Note: the moduli in parentheses are at high temperature）

Loading. Loading is simplified to be circular and uniform distribution loading in traditional pavement stress analysis. But this simulation approach will mutate at loading circumference, which makes theoretical values of some stress components at surface circumference approach infinity and cause singular point problems under uni-directional horizontal force, then leading to the difference between theoretical values and measured values. A large number of references indicate that the shape of the tires acting on pavement is roughly rectangular (Shen, J.N. 2001). Based on the relevant surveyed data, the rectangular loading is used in this paper whose area is 18cm * 20cm. The distance between the middle of the two tires is 30cm. The standard axle load is 100kN and pressure is 0.7MPa.

RESULT AND DISCUSSION

Influence of horizontal force coefficient on pavement structure. The changes of maximum shear stress σ_{max} and maximum shear strain ε_{max} beneath the wheel center are shown in Figure 1 and Figure 2, which include three pavement structures with horizontal force coefficients being 0.1, 0.3 and 0.5, respectively. σ_{max} and ε_{max} in the figures increase with increasing the horizontal force coefficient beneath the wheel center and the curve is nonlinear. Furthermore, σ_{max}/f and ε_{max}/f increase when the horizontal force coefficient f increases. For general pavement, there is always a certain horizontal force which is not of large influence on pavement maximum shear stress and maximum shear strain; For the long and steep slope sections, speeding up before climbing and slowing down during the course of climbing for vehicles especially the driving at low speed of overloading and heavy-load vehicles, will produce greater horizontal force coefficient which brings about significant influence on σ_{max} and ε_{max} of the pavement. Therefore, the maximum shear stress for design should be considered additionally for long and steep slope special sections (near the grade change point).

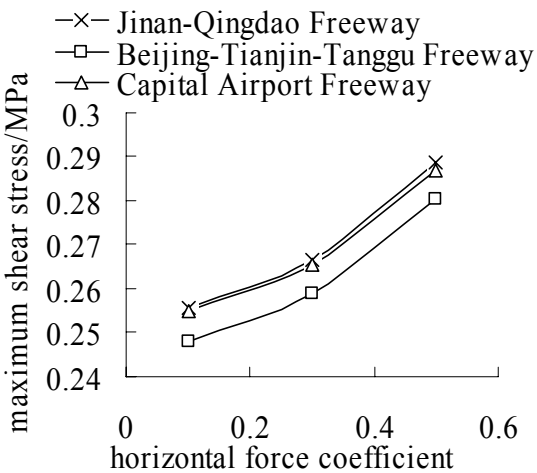

Figure 1. The relation between horizontal force coefficient and σ_{max}

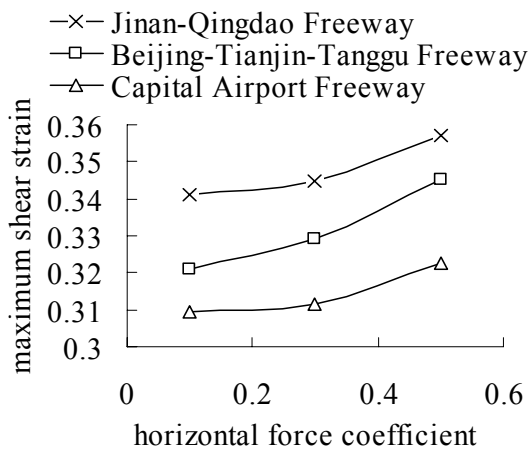

Figure 2. The relation between horizontal force coefficient and ε_{max}

Influence of road longitudinal slope on pavement structure. The influence of road longitudinal slope on pavement structure mainly lies in the force component along the ramp during the course of climbing for vehicles. Maximum shear stress and maximum shear strain below the wheel center are shown in Figure 3 and Figure 4, which include three pavement structures with longitudinal slope

gradients being 1%, 3% and 5% respectively. The relation between σ_{max}, ε_{max} and the gradient is linear in Figure 3 and Figure 4. Without considering other factors, the influence of gradient increase on pavement maximum shear stress and maximum shear strain is small. . Consequently, the influence on the mechanical properties of the integral pavement structure is small. However, when the slope increases, the vehicle speed decreases and the pavement attachment coefficient increases. Combined with the overloading and high temperature effect, it leads to more significant pavement distresses on the long and steep longitudinal slope. Gradient is a key factor for the structural design of long and steep pavement.

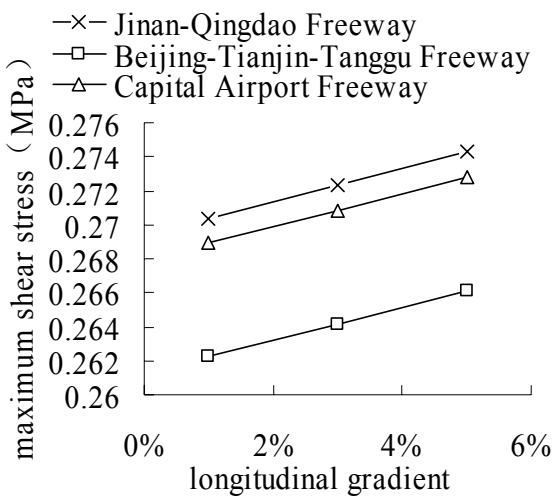

Figure 3. The relation between longitudinal gradient and σ_{max}

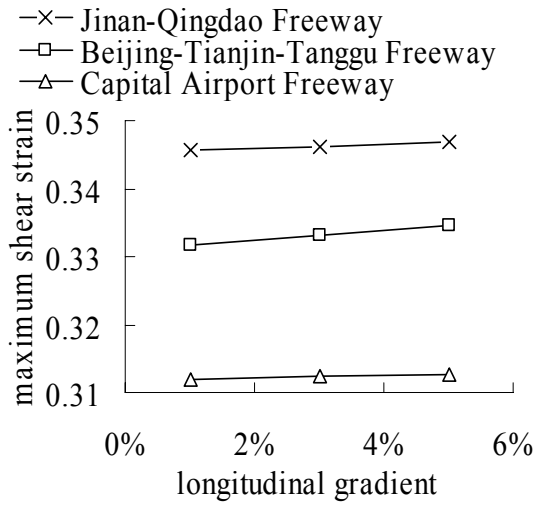

Figure 4. The relation between longitudinal gradient and ε_{max}

Influence of environmental temperature and overloading on pavement structure of long and steep slope. The stress and strain for the three pavement structures under high temperature and room temperature are calculated for the evaluation of the influence of environmental temperature and overloading. The results are shown in Table 2. At the same time, σ_{max} and ε_{max} are calculated for the three pavement structures when the overloading ratio is 30%, 60% and 90% respectively. The results are shown in Table 3. It can be seen that the influence of environmental temperature on asphalt pavement is most significant. Asphalt mixture's strength drops significantly as temperature increases because of the temperature sensitivity of asphalt mixture. The results in Table 2 show that σ_{max} increases by 10.3%, 9.18% and 9.52%, respectively, and the corresponding ε_{max} increases by 218.2%, 225.4% and 253.1% for the three pavement structures. The

shear strain increases significantly; the influence of overloading on pavement structure is also significant. Shear stress and shear strain increase with the overloading rate in the same proportion as well.

Table 2. σ_{max} and ε_{max} for the three pavement structures under different temperatures

Temperature state	Jinan-Qingdao Freeway		Beijing-Tianjin-Tanggu Freeway		Capital Airport Freeway	
	σ_{max} /MPa	ε_{max}	σ_{max} /MPa	ε_{max}	σ_{max} /MPa	ε_{max}
Normal temperature	0.267	0.345	0.259	0.329	0.265	0.311
High temperature	0.295	1.097	0.282	1.070	0.291	1.099

Table 3. σ_{max} and ε_{max} for the three pavement structures under different overloading rates

Overloading rate	Jinan-Qingdao Freeway		Beijing-Tianjin-Tanggu Freeway		Capital Airport Freeway	
	σ_{max} /MPa	ε_{max}	σ_{max} /MPa	ε_{max}	σ_{max} /MPa	ε_{max}
0%	0.267	0.345	0.259	0.329	0.265	0.311
30%	0.347	0.448	0.336	0.428	0.346	0.405
60%	0.427	0.551	0.414	0.526	0.425	0.498
90%	0.507	0.655	0.492	0.625	0.504	0.592

Influence of pavement structure thickness. Three typical pavement structures including Jinan-Qingdao freeway, Beijing-Tianjin-Tanggu freeway and the Capital Airport freeway are chosen for this study. The three asphalt pavements have semi-rigid base course and the main differences are the thickness of the urface course. The specific thickness is as follows: Surface course structure of Jinan-Qingdao freeway is "4cm +5cm +6cm"; Surface course structure of Capital Airport freeway is "4cm +6cm +8cm"; Surface course structure of Beijing-Tianjin-Tanggu freeway is "4cm +6cm +13cm". The analysis indicates that the shear stress decreases as the surface course thickness increases, but the shear strain has not decreased accordingly. τ_{max} in Beijing-Tianjin-Tanggu freeway is between that in Jinan-Qingdao freeway and Capital Airport freeway under a variety of factors. ε_{max} in Beijing-Tianjin-Tanggu freeway is lower than that in the other two pavement structures; The relation between the horizontal force coefficient and maximum shear

strain in Beijing-Tianjin-Tanggu freeway is relatively weak as shown in Figure 2. Therefore, the influence of pavement thickness on the long and steep longitudinal slope is significant. Based on the analysis in this research, the pavement structure combination of "4cm +6cm +8cm" is recommended by the authors.

Discussion to key structure course. Generally speaking, the upper surface course is mainly a function course for drainage and noise reduction in pavement structure design. The intermediate surface course is mainly as structure course for bearing vehicles loading. The lower surface course is mainly for resisting fatigue bending and tensile stress (Zhang, D. L. 2003). This paper focuses on horizontal force's increase in long and steep slope pavement caused by low speed of vehicles. The maximum shear strain for the three pavement structures along the pavement depth distribution is analyzed as shown in Figure 5, Figure 6 and Figure 7. The shape of maximum shear strain with pavement depth from the figures is close to an "M". Two maximum shear strains appear at about 4cm and 10cm, which are at the interface between the upper surface course and the intermediate surface course, and between the intermediate surface course and the lower surface course. Thereby, the interfaces of each surface course should be treated specially in the long and steep slope pavement design. Furthermore, the surface deformation intensifies with the horizontal force coefficient's increase and the maximum shear strain location tends move to the surface. The distribution of $\varepsilon_{\max}$ along the pavement depth under high temperature is shown in Figure 8. It can be concluded that the maximum shear strain transfers from the interfaces between each course to the upper surface course as temperature increases . The maximum shear strain calculated in this paper under high temperature is at a distance of 3cm from the surface.

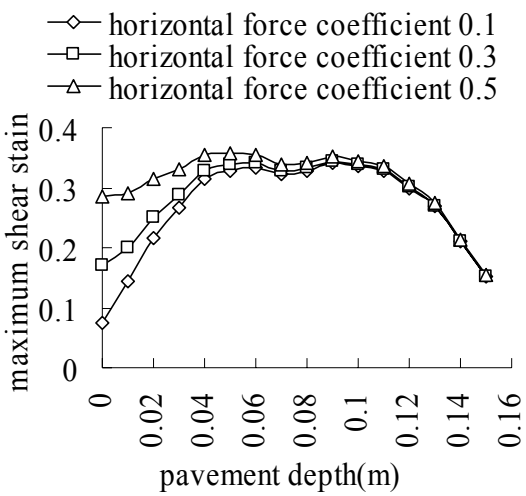

Figure 5. Distribution changes of $\varepsilon_{\max}$ in Jinan-Qingdao freeway along pavement depth

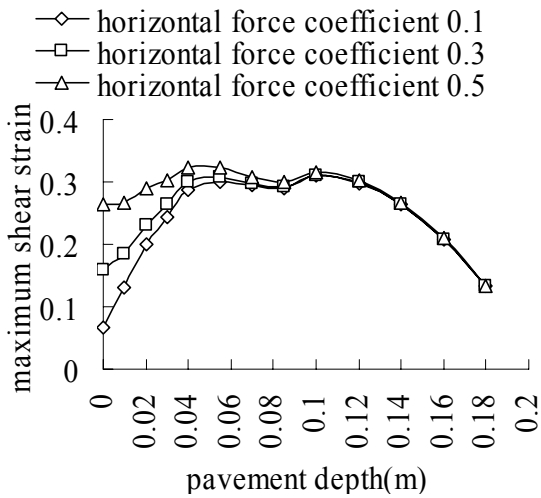

Figure 6. Distribution changes of $\varepsilon_{\max}$ in Capital Airport freeway along pavement depth

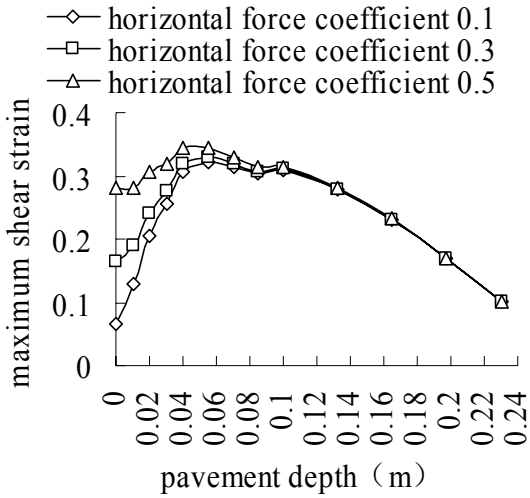

Figure 7. Distribution changes of ε_{max} in Beijing-Tianjin-Tanggu freeway along pavement depth

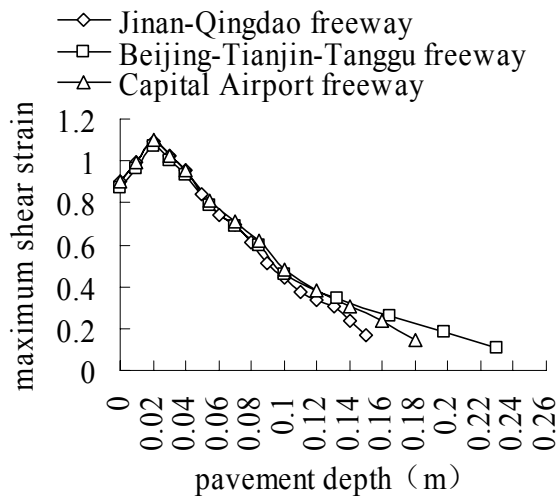

Figure 8. Distribution changes of ε_{max} under high temperature along pavement depth

CONCLUSIONS

The conclusions are as follows:

(1) The key factor of the difference between long and steep slope and flat slope is horizontal adhesive force between tires and pavement caused by longitudinal slope. The maximum shear stress of pavement increases, then the maximum shear stress of pavement and the peak shear strain locations move to the surface gradually as the horizontal adhesive coefficient increases. The maximum shear stress is less affected by gravity component on the pavement caused by longitudinal gradient changes.

(2) Considering the horizontal force, the pavement structure combination of "4cm +6cm +8cm" is recommended in this research and is more favorable for long and steep sections through calculating three different thickness combinations of surface courses.

(3) It is discovered that the maximum shear strain is at the joints of each surface course and its locations move to the surface under higher temperature in summer. Based on the calculation results in this research, the maximum shear strain is at the middle and lower part of the surface course

ACKNOWLEDGMENTS

We would like to thank National Natural Science Foundation of China

(50608006), Natural Science Foundation of Shaanxi Province (2007$E_2$23) and New Century Excellent Talents Plan of Ministry of Education (NCET-07-0120).

REFERENCES

Edward, S. B. (1965). "Shear Load on Pavement." ASTM.

Norman, W. M. (1951). "A Rational Approach to the Design of Bituminous Paving Mixture." ASTM.

Shen, J. N. (2001). "Road performance of Asphalt and Asphalt Mixture." Beijing: *China Communications Press*.

Subbaraju, B. H. (1965). "Model Study of Stress in Asphalt Pavemnet." ASTM, 1965 Edward S. Barber, Shear Load on Pavement, ASTM.

Sun, L. J. (2005). "Structural Behavior Study for Asphalt Pavements." Beijing: *China Communications Press*.

Wang, B. G., and Deng, X. J. (1992). "Pavement Mechanics Mumerical Calculation." Beijing: *China Communications Press*.

Zhang, D. L. (2003). "Asphalt Pavement Engineering Manual." Beijing: *China Communications Press*.

Study on Safety Stability of Excavating Shallow Depth Neighborhood Tunnel in Traversing Construction

LI Yun-peng[1], HAN Chang-ling[2], AI Chuan-zhi[1]

[1]School of Mechanical and Electrical Engineering, China University of Petroleum, Beijing, 102249, China, liyp996@163.com
[2]First Highway Survey and Design Institute of China, Xi'an Shaaxi 710075, China, hanchngl@163.com

ABSTRACT

In order to study the safety stability of shallow tunnels under unsymmetrical pressure and traversing existing roads, a 3D numerical model of considering real surface elevation changes was established for a different construction scheme in a different range according to the Changshao neighborhood tunnel engineering on the Xi-kang Expressway. The construction process of traversing the S102 road was simulated in the entrances' range. The deformation law, the stress distribution, the deformation characteristics of middle wall and lining supporting structure, and the settlement law of existing highway surface were obtained for range of the shallow covering excavation and shallow hiding excavation. The safety evaluations on the engineering construction of traversing the existing highway were made. The analyzed results had positive effects on the successful construction of the Changshao neighborhood tunnel.

INTRODUCTION

China is a mountainous nation. The land is about 75% mountainous region or hills. The mountain area in the west is more than 90%. The medium or short tunnels and bridges adapt to the characteristics of the mountainous area and are in the highest proportion in the highway construction of mountainous regions. For example, the bridge-tunnel on the Shi-Tai speedway is 60.1% of total length; that on the Xi-Han Freeway is 76%; that on the Xi-Kang Freeway is about 68%; that on the An-Chuan Freeway is 77.8%; that on the Ya-Xi Freeway is 54.5%, etc. By strengthening the environmental awareness and improving the construction technology, double parallel mountain tunnels and small spacing tunnels increase considerably. Many scientific workers have made a lot of researching results in neighborhood tunnel design and construction technology, such as the dynamic elastic-plastic numerical simulation of construction process for the neighborhood tunnel on the Beijing-Fuzhou Expressway (Jin X, 2003), the visco-elastic-plastic finite element analysis on the stability of close

double tunnel excavation and support (Zhang Y., 1999), the three-dimensional numerical simulation of the tunnel traversing building foundation engineering (Li J.,2005), the numerical simulation study on the interaction and environmental geotechnical problems of tunnels for fold shield tunneling (Wang M.,2002), the detailing mechanical analysis on the construction process of shallow small spacing tunnels in soft rock by using the finite element method (Liu H., 2003), and so on (Qu X., 2002, Li Y., 2006). However, with the shallow tunnel with bias pressure having complex topography and geology environment, the construction conditions and the excavation methods of tunnels are usually different, and the interaction mechanism between the surrounding rock and the structure of tunnels is still not fully known and understood. Thus, the entire construction process of the tunnel entry of traversing the S102 highway is simulated by using the three-dimensional numerical method based on neighborhood tunnel engineering at Changshao. The deformation laws of rock around neighborhood tunnels and the deformation characteristics of middle wall and lining supporting structure as well as the settlement laws of highway road surface are given. Also, the security of traversing construction is evaluated, and the important reference information for neighborhood tunnel engineering is obtained.

ENGINEERING SUMMARY AND NUMERICAL MODEL

The Changshao Tunnel (18 bidding) is located at 10 km to Zhen-An county town in Shaanxi province. The entry and export segments of tunnels traverse the S102 highway. The geological plan and section of tunnels are shown in Figure 1 and Figure 2. The surrounding rock of the left and right tunnels at the entry is strong weathering phyllite with joint development and poor stability. Tunnel entrances belong to over-shallow burying tunnels. The bidding segment of the left line is LK108 + 780 ~ LK108 + 845. The construction is divided into three segments, and the lengths of each segment excavation are respectively 15 m, 30 m, and 20 m. The overlying layer in LK108 + 780 ~ LK108 + 825, burying deep in 4 m-6 m, is filling soil and loose. The construction ways all adopt covering excavation. Support uses composite lining structure. The entrance of the right line tunnel is the shallow tunnel with bias pressure, which is located in RK108 + 760 ~ RK108 + 845. The engineering segment of traversing provincial highway S102 is located in RK108 + 755.76 ~ RK108 + 806, and its burying depth is about 4 m. Also the segment RK108 + 806 ~ RK108 + 845 is a shallow bias pressure tunnel. The tunnel spacing between the left and right lines at the entrance segment is about 11.1 m. The remaining core soil method is adopted for right line excavation.

According to the geochemical condition of the Changshao Tunnel, a 3D simulating model is set up as shown in Figure 3. The upper boundary of the model is on the surface of the mountain. The elevation of the lower boundary is 446 m. The ranges of horizontal boundaries are x [200 m, 440 m], and y [150m, 390 m]. The

coordinates of starting points are respectively 303.84 m, 293.71 m, and 519 m for the left line and 283.12 m, 279.80 m, and 519 m for the right line. Those of ending points are respectively 440 m, 311.4 4 m, and 519 m for the left line and (440 m, 287.28 m, and 519 m) for the right line. The number order of construction steps is given in Figure 3. The number of mesh elements is about 43.1 million, and the computational mechanical parameters are listed in Table 1.

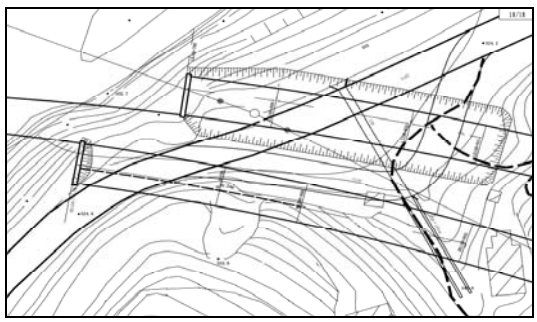

Figure 1. Geological plan of tunnels.

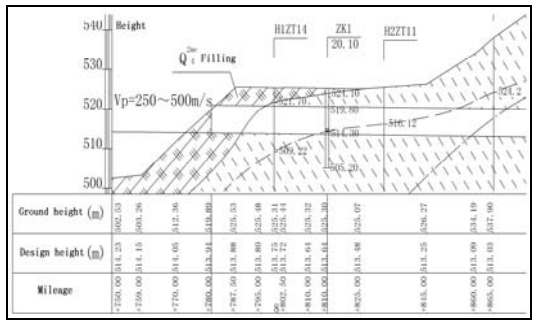

Figure 2. Geological section of tunnels.

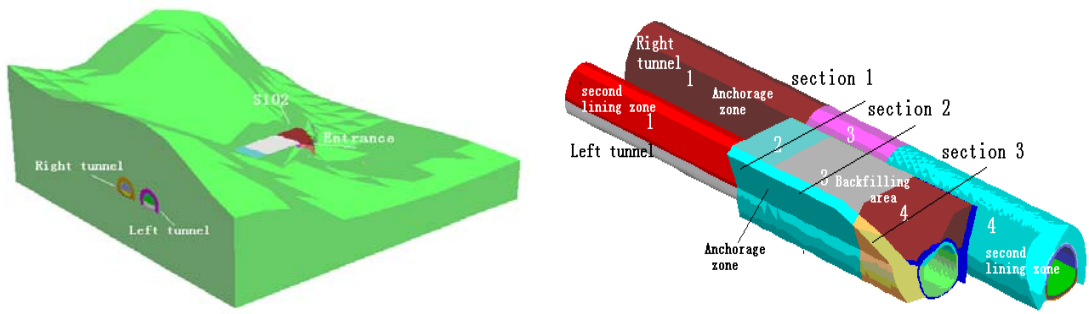

Figure 3. 3D numerical model.

Table 1. Mechanical Parameters of Calculating Model.

Material	C(MPa)	φ(^{0})	μ	E(GPa)	γ (KN/m^3)
Steel centering+ C25(28mm thick)	2.8	63	0.17	32.625	29
Steel centering+ C25(45mm thick)	2.7	60	0.18	30.877	28
Reinforced concrete(C25,60mm thick)	2.3	54	0.2	41.223	25
Over-tremie pipe zone	0.18	39	0.35	1.533	19.6
Surrounding rock of V classification	0.15	27	0.38	1.5	19.5

RESULTS OF NUMERICAL SIMULATION

According to engineering, the construction process is divided into three states. First, construct the secondary segment of the left line about 15 m; next, construct the third segment of the left line and the third segment of the right line about 30 m.

Finally, construct the fourth segment of the left line about 20 m, and construct the fourth segment of the right line about 57.6 m.

The stress distribution laws under the above three states are shown in Figure 4. From Figure 4 analysis, the maximum tensile stress under state 1 is less than 0.4 MPa; the maximum compressive stress is less than 3.0 MPa; and the surrounding rock does not have obvious bias pressure phenomenon. The maximum tensile stress under state 2 is less than 0.5 MPa; the maximum compressive stress is less than 5.0 MPa; and the surrounding rock has obvious bias pressure phenomenon. The maximum tensile stress under state 3 is less than 0.6 MPa; the maximum compressive stress is less than 5.0 MPa; and the surrounding rock has obvious bias pressure phenomenon.

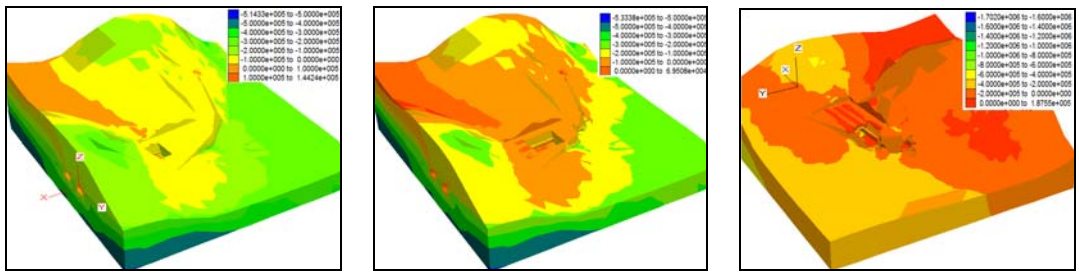

(a) state 1 **(b) state 2** **(c) state 3**

Figure 4. Stress distribution under three kinds of states.

From Figure 5 analysis, the horizontal deformation caused by excavation under state 1 is symmetric in the deforming trend, and the deformation of surrounding rock at two sides of the tunnel is convergent. The deformations at the side wall of tunnels are symmetric in the area of excavating influence, and their magnitudes vary between $-1 \times 10^{-3} \sim 1 \times 10^{-3}$. The deformation under state 2 is similar to that under state 1, but the side wall deformation of the left tunnel becomes symmetrical, and two side deformation of the right tunnel is asymmetrical due to right tunnel excavation. Also, the whole tunnel including the middle wall has the moving trend toward the left tunnel. The horizontal deformation of two side rock around excavation area caused by excavation under state 3 obviously has the displacement trend along the same direction, and other deformation laws are similar to that under state 2.

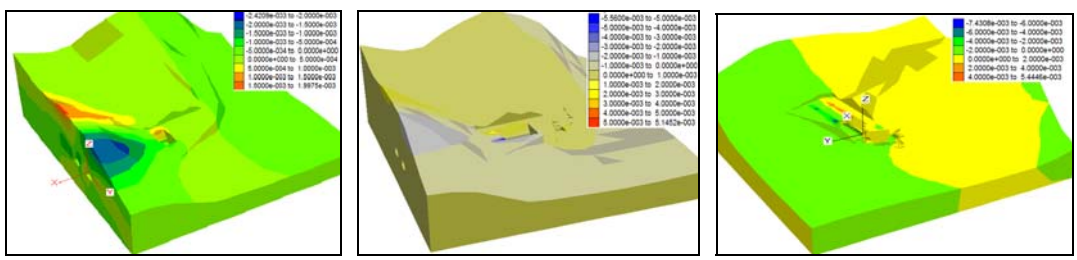

(a) state 1 **(b) state 2** **(c) state 3**

Figure 5. Horizontal deformation laws under three kinds of states.

The peripheral rock of the left and right tunnels in section 3 (LK108 + 780) is basically in tensile state along single direction from Figure 6, especially on the left side and vault of the left tunnel. The distribution laws of minimum principal stresses of peripheral rock around two tunnels are the same. There is a shear zone of maximum shear stress at the intersection between the right tunnel surface and the bias pressure mountain. In addition, the zone is through the middle wall and the right side springing of the left tunnel. The other shear zones are also formed from the left spandrel to the right springing of each tunnel, but shear stress values are all less than 1 MPa. The tensile state along single direction of the left and right tunnels in section 2 (LK108 + 806) appears only at the left and right spandrels and springing. The obvious bias pressure zone occurs at the top of the right tunnel. The middle wall also undergoes the obvious bias pressure action. The maximum shear stress in section 2 appears at the spandrels and springing of two tunnels, but the magnitudes are all less than 1 MPa. Section 1 (LK108 + 837) is located at the junction of deep and shallow burying change. The mountain bias pressure of the right side of the right tunnel is also low. The stress distribution law in the section is smoother than section 2, and bias pressure of the tunnel is relatively small. The maximum shear stress also appears at spandrels and springing.

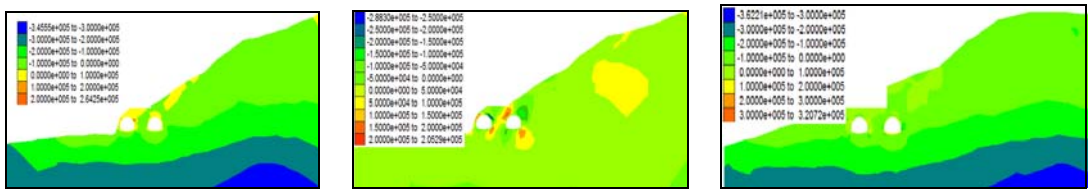

(a) σ_1 **in section 3** **(b)** τ_{max} **in section 3** **(c)** σ_1 **in section 2**

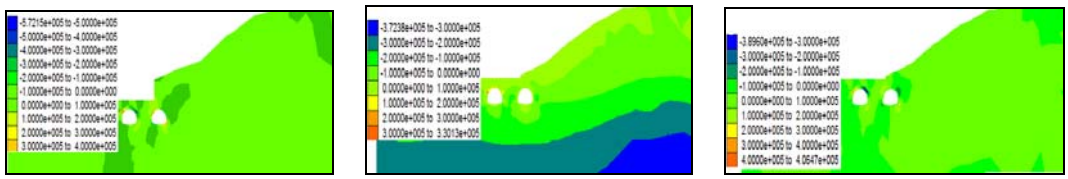

(d) τ_{max} **in section 2** **(e)** σ_1 **in section 1** **(f)** τ_{max} **in section 1**

Figure 6. Stress distributions in three typical sections.

From the analysis of Figure 7, the vault area of lining structure of the left and right tunnels in section 3 is moved toward the left side, and the maximum offset on the right is 6 ~ 8 times of that on the left. Even though the right tunnel floor areas have upward displacement, the lining deformation of the left and right tunnels is basically downward displacement, and the deformation of the right line is more than that of the left line. The two tunnel lining structures are both asymmetric. The lining

deformation on the top right side of the right and left tunnels is greater. Thus, the section of the lining structure becomes narrow and irregular deformation occurs. The lining deformation laws at section 2 and section 1 are similar to those at the section 3.

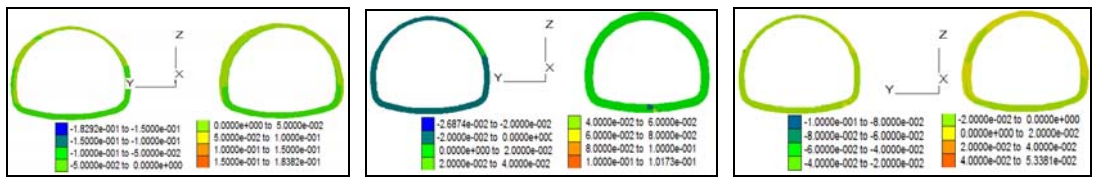

(1) section 3 (2) section 2 (3) section 1

Figure 7. Lining structure deformation in three sections.

CONCLUSION

(1) For the shallow and bias pressure tunnels, the maximal displacements appear at the deep burying area of the right tunnel and the shallow burying area of the left line, and the displacements within the middle wall are greater than the other parts around tunnels. The vertical deformation on the tunnel top in deep burying region is greater than that in shallow burying region, and that in backfilling area is greater than that in the shallow area of the right tunnel. The middle wall has a moving trend toward the left side, and that in deep burying region is obviously greater than in shallow region.

(2) During the construction, the plastic areas mainly appear in deep burying area and the middle wall, and the area magnitude is greater only in the gully region of the right tunnel. Also, the area extends to the surface so during the construction of the right line, the region should be focused.

(3) The lining structure in the tunnel entry segment is basically in a one-directional tensile stress state, but maximum tensile stress values are smaller and will not affect the stability of the lining structure. Except for the lining floor areas in the tunnel entrance region, the lining deformation is basically downward displacement. The lining deformation in shallow burying area is irregular and has a moving trend toward the left side. Therefore, the suggestion is presented that the bias pressure and shallow burying neighborhood tunnels that support and lining structure should adopt asymmetric geometric form to be more effective for the stability of tunnels.

REFERENCES

Jin Xiaoguang, Liu Wei, Cheng Shaohua (2003), "Numerical simulation of construct procedure in little distances highway tunnel, Proceedings of symposium on

highway tunnel." China Communications Press, P118-124.

Li Jin-jun WANG Xian-chun , ZHUANG Ji-dong , HUANG Mao-song (2005), "3 - D Numerical Simulating Study on Excavation of Shallow Burying Tunnel Through the Building Foundation." Chinese Journal of Underground Space and Engineering, 1 (1), 78-82.

Li Yunpeng, Wang Zhiyin,Han Changling, et al. (2006), "Simulating Study on Construction Process of Tunnels with Small Spacing for Different Surrounding Rock Classification." Rock and Soil Mechanics, 27 (1), 11-16.

Liu Hongzhou (2003), "Study on the application of construct design technology in little distances double tunnel." Proceedings of symposium on highway tunnel, China Communications Press, P125-130.

Qu Xue bing, SHU Hong wei (2002), "Construction simulation of underground excavation about super2shallow2burial tunnel." Building Science Research of Sichuan, 28 (4) 51-53.

Wang Mingnian, Li Zhiye, Liu Zhicheng, Zhang Chengmang (2002), "A mechanical research on shallow buried three-hole parallel nearby tunnel construction." Railway Construction Technology, NO.4, P11-14.

Zhang Yujun, Zhu Weishen,Yang Jialin (1999). "Plane visco-elasto-plastic FEM calculation for the stability of the excavation and lining structure of a nearby double tunnel." Chinese Journal of Rock Mechanics and engineering, 18 (Sup), P855-859.

New Concrete Improving Performance of Airfield Pavement

Guangyuan Li[1] and Wei Xu[1, 2]

[1]Engineering Institute, Air force Engineering University, Xi'an 710038; PH (029) 84787705; FAX (029) 84787705; email:guangyuanli@163.com
[2]School of Highway, Chang'an University, Xi'an 710038; PH (029) 84787705; FAX (029) 84787705; email:wuxixuwei@163.com

ABSTRACT

In order to study the feasibility of new types of concrete in airfield pavement, the long-term performance of steel fiber concrete, polypropylene fiber concrete and latex concrete were evaluated by testing in parallel their flexural modulus, anti friction and anti filter performance, and their fatigue and anti freezing performance. The results show that latex concrete has low flexural module and is useful to reduce inner stress of pavement slab. However, the latex concrete has poor anti freeze performance and is therefore only applicable in non-freezing districts. Steel fiber concrete and polypropylene fiber concrete have excellent anti-fatigue and anti-freeze performance; therefore, they can improve the airfield pavement life.

INTRODUCTION

Airfield pavements differ from other types of pavements in that higher surface strength and durability are required. Dry-hard concrete was used usually in airport construction. In recent years, new kinds of concrete also come in use in architecture, hydraulic projects and road engineering. However, the application of these concrete has been little on airport due to the harsh field environment of airport and higher strength and durability requirements such as adaptability to environment, stress fatigue and surface performance. This article presents the results of the experiment evaluating the flexural tension modulus, wearing resistance, impermeability, frost resistance, and fatigue strength of plain concrete, steel fiber concrete and polypropylene concrete.

EXPERIMENT MATERIALS

The materials according to specifications were used in this experiment. The materials include Portland cement of 42.5Mpa, 20mm-40mm and 5mm-20mm crashed stone, sand of 2.9 fineness modulus, air-entraining and water-reducing additive of FSW-7 made in Xian, and the sheer-type steel fiber made in Jiangshu, China. The ratio between length and diameter is 50 for the steel fiber. Latex with the acrylate modifier of No. 2438 was adopted. Polypropylene fiber was adopted produced in Haichuan, China. The tests were conducted according to the Test Method of Cement and Concrete for Highway Engineering (JTG E30-2005).

FLEXURAL TENSION MODULUS

The flexural tension modulus of concrete was studied first. The mixing proportion of the concrete was shown in Table 1.

Table 1. Mixing proportion of concrete.

Water (kg)	Cement (kg)	Sand (kg)	Big stone (kg)	Little stone (kg)	Steel fiber (kg)	Latex (kg)	Polypropylene （g）	28days Flexural tension strength
6.57	15.5	33.67	16.7	25	0	0		4.6 MPa
6.57	15.5	33.67	16.7	25	3.18	0		5.5MPa
6.57	15.5	33.67	16.7	25	3.18	0.775		4.78MPa
6.515	15.5	33.67	16.7	25	3.18	1.55		4.37MPa
6.57	15.5	33.67	16.7	25	0	0	34	4.78MPa

Flexural tension moduli are given as follow:

Species of specimen	Polymer cement ratio	Flexural tension modulus
Plain concrete	0	3.500×10^{4} MPa
Steel fiber concrete	0	4.100×10^{4} MPa
Steel fiber latex concrete	0.25	2.797×10^{4} MPa
Steel fiber latex concrete	0.5	2.468×10^{4} MPa
Polypropylene fiber concrete	0	3.400×10^{4} MPa

According to the results of experiment, the flexural tension modulus of latex concrete decreased more significantly than the steel fiber concrete and the plain concrete. The flexural tension modulus continuously decreased with increase of latex content, which proved that the deformation resistance capability of steel fiber latex concrete was better. Flexural tension strength decrease was not obviously.

WEARING-RESISTANCE EXPERIMENTS

This part studied the wearing-resistance performance of steel fiber latex concrete, polypropylene concrete and plain concrete.

The abrasion loss of plain concrete is 1.8kg per square meter, and the abrasion loss of polypropylene concrete is 1.76kg per square meter. The average abrasion loss of steel fiber concrete is 2.45kg per square meter which is more than others. One reason for this higher loss is due to the poke-action induced by contacting between abrading wheel and steel fiber that leads to large bulks flaking off. Another reason for this is the existing of latex that could lead to the softening of concrete. The results of this experiment, therefore, do not represent the wearing-resistance; hence more reliable evaluating method was needed.

IMPERMEABILITY EXPERIMENTS

The experimental results show that there is no permeability observed when each sample was prepared at the mixing proportion of 5.0MPa. This phenomenon indicates that the impermeability performance is ideal of all the concrete above.

FROST-RESISTANCE EXPERIMENTS

Results of experiments. The mixing proportion shown in Table 1 was adopted in frost-resistance experiments. The fasten-frost method was used. The steel fiber concrete and polypropylene fiber concrete out-performed others after 300 cycles. These samples were shown in Figure.1.

Figure 1. Steel fiber concrete and polypropylene fiber concrete after the freeze-thaw test.

Analysis of results. The frost-resistance performance of concrete can be improved by adding steel fiber and polypropylene fiber. The improvement relates to the chemical ingredient of organic fiber and shape of the fiber. The latex concrete with low modulus and the good deformation resistance capability, showed worse frost-resistance performance. For the mixes using latex and steel together, the frost-resistance performance was not improved significantly.

The water consumption per unit of concrete must be controlled strictly in addition to controlling the water- cement ratio of for all tests to improve the frost-resistance of concrete. The water consumption should less than 150kg per stere.

FATIGUE EXPERIMENTS

Mixing proportion. The mixing proportion of plain concrete, steel fiber concrete and polypropylene concrete are given in Table 1.

Making method of specimen. The specimen for flexural fatigue test was made using a cubic-shaped mould with the dimension of 150mm×150mm×550mm. The specimen

of flexural fatigue experiments were divided into three groups: the plain concrete was marked as the A group, the polypropylene concrete was marked as the B group, and the steel fiber concrete was marked as the C group. The specimen was taken out from mould after 24 hours. Fatigue experiments started after 90 days of standard maintenance. The specimen was taken out from maintenance room 7 days before experiments start.

Method of fatigue experiments

(1) The quatre girder with a span of 450 mm was used in the flexural fatigue test. At least 3 specimens were tested for each mix. The flexural strength of each specimen and average flexural strength was calculated as the parameters of the fatigue tests. The results of flexural strength with static loading were shown as Table.2

Table 2. Results of average flexural tension tests using static loading.

Group	A	B	C
Flexural tension strength (MPa)	5.23	5.58	6.53

(2) The stress level of fatigue loading was defined as the ratio of actual loading stress to flexural tension strength under static loading, which are taken as 0.9, 0.85, 0.80 and 0.75.

(3) The minimum loading in fatigue experiments was used as 10 percent of maximum loading. The eigenvalue of fatigue cycle in experiment was taken as $\rho =$ 0.1.

$$\rho = P_{\min} / P_{\max} \tag{1}$$

(4) The fatigue test involves firstly a 100N load put on girder repeatedly to eliminate the error. When the machine and instrument ran normally, the fatigue experiment started. The loading used a sine wave and the frequency was 10Hz.

(5) The experimental data were analyzed statistically. The fatigue experiments result is rather disperse. The disperse data was eliminated from the regression for the fatigue equation.

Fatigue experiments result. The experiment result of concrete flexural tension strength was shown in Table 3. The experiment result shows a linearity relationship in single logarithm coordinate (see Figure 2.)

Analysis on fatigue experiments. The intercept and slope of fatigue equation of polypropylene fiber concrete and steel fiber concrete are higher than those of the plain concrete. The difference in intercept is bigger than that of the slope, which

indicates that adding of fiber not only improves the flexural fatigue performance but also decrease the stress sensitivity of concrete. The fatigue life of polypropylene fiber concrete and steel fiber concrete is longer than that of the steel fiber concrete for all stress levels. The improvement in steel fiber concrete is more than that in polypropylene fiber concrete. The reason for this is that the adding of polypropylene fiber and steel fiber not only improve the flexural tension strength but also increase the tenacity which involves partial plasticity destroying instead of the complete brittleness destroying.

Table 3. Experiment results of concrete flexural tension strength.

Number	Stress ratio	Times of fatigue experiments	Fatigue equation
A	0.90	95	$y = -0.0647\lg N_t + 1.0307$ $R = 0.9954$
	0.85	676	
	0.80	4396	
	0.75	18696	
B	0.90	364	$y = -0.0732\lg N_t + 1.0904$ $R = 0.9961$
	0.85	2326	
	0.80	8763	
	0.75	43478	
C	0.90	1415	$y = -0.0805\lg N_t + 1.1535$ $R = 0.9864$
	0.85	7244	
	0.80	18391	
	0.75	114637	

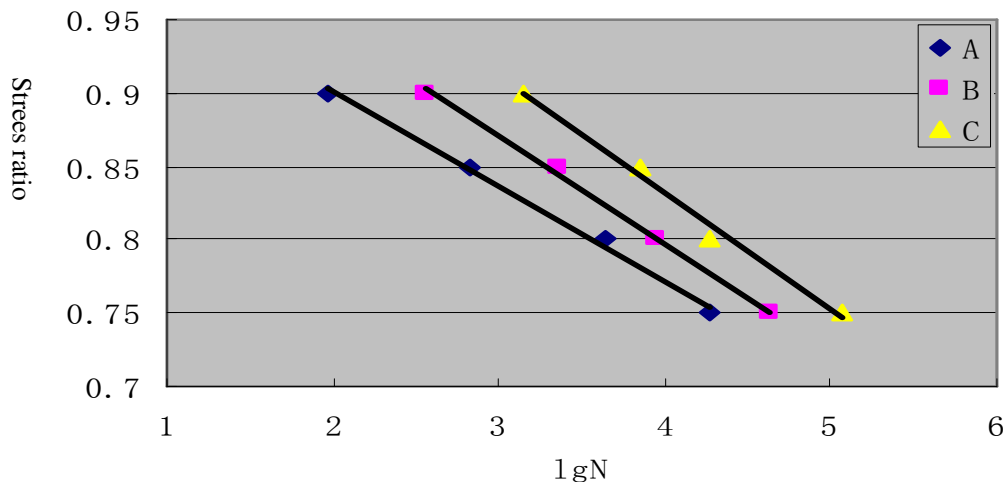

Figure 2. Fatigue logarithm curve.

CONCLUSIONS

According to experiment results, the wearing-resistance performance of polypropylene fiber concrete and steel fiber concrete is superior for airport use.

The dry-hard concrete and dry-hard steel fiber concrete are suitable for cold region use. The polypropylene fiber concrete can be used if the proper gas content can be ensured. However, the steel latex concrete, polypropylene latex content and polymer concrete is not proper for cold region use. The polymer concrete without any kinds of fiber should be forbidden for cold region use..

The fatigue life of polypropylene fiber concrete and steel fiber concrete is superior to that of the plain concrete, which shows that the fiber not only improves the flexural fatigue life of concrete but also prolongs the life of pavements.

BIBLIOGRAPHY

China Communication Administration. (2005). "*Test Method of cement and concrete for highway engineering*." *(JTG E30-2005)*.

Liang, L. (2002). *Polymer concrete*, China communication press.

Luo, L., Huang, P., and Wang B. (2002). "Mechanical performance of polymer cement slurry." *Chang'an University Journal* , 22(3).

Luo, L., Zhong, M., and Huang, C. (2004). *Steel fiber enhanced polymer concrete bridge surface pavement*, South China University of Technology Press.

Wang, Z. (1994). *Test study and engineering application of steel fiber concrete in airfield*, Guangdong science and technology press.

Zhang, X., and Jiang, Z. (2002). "Study on impact-proof and abrasion-proof concrete in runway." *Journal of Nanjing University of Aeronautics & Astronautics.*

Zhao, G., Pen, S., and Huang, C. (1999). *Steel fiber concrete structure*, China Architecture and Building Press.

Constitutive Relationship of Asphalt Mixture for Finite Element Method

Shaopeng WU[1] Hong WANG[2] Yao YAO[3]

[1]Professor. Key Laboratory of Silicate Materials Science and Engineering, Wuhan University of Technology, Wuhan 430070, China; PH (86) 027-87162595; FAX (86) 027-87162595; email: wusp@whut.edu.cn

[2]Ph.D Candidate. Key Laboratory of Silicate Materials Science and Engineering, Wuhan University of Technology, Wuhan 430070, China; PH (86) 027-87162595; FAX (86) 027-87162595; email: wanghong@whut.edu.cn

[3]Undergraduate. College of Chemistry and Molecular Sciences, Wuhan University, Wuhan 430072, China; PH (86) 0-13476054355; email: emmakudo1988@yahoo.com.cn

ABSTRACT

Asphalt mixture, an important part of roadway construction, is a type of typical viscoelastic materials. Temperature, speed and time of applied load etc. have obvious effects on asphalt mixture's mechanical property. It is necessary to research the material's constitutive relationship. Especially, there is an increasing need for the use of numerical methods in road design. In this study, several basic viscoelastic theories-small strain theory, Burgers model and Generalized Maxwell model are introduced. It is worth mentioning that some methods are illustrated about how to apply experimental data to finite element software. Ultimately, the study is aimed at providing numerical simulation that attempts to increase the prediction accuracy of stress in asphaltic pavement for more reliable pavement design.

KEY WORDS: Asphalt Mixture, Constitutive Relationship, Finite Element

1. INSTRUCTION

Asphalt mixture becomes brittle at low temperatures and soft at high temperatures. This change due to temperature is called ‘‘temperature susceptibility”, which is the main reason for the distresses of the asphalt pavement (Al Hadidy, A.I. et al, 2009). The special viscoelastic material-asphalt mixture should be studied effectively before the distresses' mechanisms are predicted and the corresponding measure is developed. Some research has been done about the testing methods of the asphalt mixture. However, it is still difficult on how to obtain the viscous and elastic parameters from the testing information and to simulate the viscoelastic mixture and its mechanical property using the analysis software.

This study will focus on two aspects: 1)to introduce the asphalt mixture's viscoelasticity theory; 2)to apply the special performance to the analysis

software-ANSYS. All those are studied on the assumption that the asphalt mixture is isotropic and viscoelastic. Ultimately, the paper is aimed at providing numerical simulation to increase the prediction accuracy of stress in asphaltic pavement design.

2. SMALL STRAIN VISCOELASTICITY

A type of material is viscoelastic if its stress response consists of elastic parts and viscous parts(ANSYS, 2006; Mulungye, R.M. et al, 2007; Wang, J.Y. et al, 2008). Upon application of a load, the elastic response is instantaneous while the viscous part occurs over time. Asphalt mixture is this type of material. Generally, the stress function of the viscoelastic material is given in an integral form. Within the context of small strain theory, the constitutive equation for an isotropic viscoelastic material can be written as:

$$\sigma = \int_0^t 2G(t-\tau)\frac{de}{d\tau}d\tau + I\int_0^t K(t-\tau)\frac{d\Delta}{d\tau}d\tau \qquad (1)$$

Where σ is the Cauchy stress; e is the deviatoric part of the strain; Δ is the volumetric part of the strain; $G(t)$ is the shear relaxation kernel function; $K(t)$ is the bulk relaxation kernel function; t is the current time; τ is the past time; and I is the unit tensor. The kernel functions are assumed to satisfy a linear viscoelastic model of a generalized Maxwell model. For a majority of simulations, the kernel functions are represented in terms of Prony series, which assumes that:

$$G(t) = G_\infty + \sum_{i=1}^{n_G} G_i e^{(-\frac{t}{\tau_i^G})} \;;\; K(t) = K_\infty + \sum_{i=1}^{n_G} K_i e^{(-\frac{t}{\tau_i^K})} \;; \alpha_i^G = \frac{G_i}{G_0} \;;\; \alpha_i^K = \frac{K_i}{K_0} \qquad (2)$$

Where G_∞ and G_i are shear elastic moduli; K_∞ and K_i are bulk elastic moduli;

and G_0 and G_0 are the transient moduli.

$$G(t) = G_\infty + G_0\sum_{i=1}^{n_G}\alpha_i e^{(-\frac{t}{\tau_i})} \;;\quad K(t) = K_\infty + K_0\sum_{i=1}^{n_K}\alpha_i e^{(-\frac{t}{\tau_i})} \qquad (3)$$

Where: τ_i^G and τ_i^K are the relaxation times for each component.

3. CREEP PROPERTY OF ASPHALT MIXTURE

3.1 Constitutive model of creep property

Creep of asphalt pavement could cause rutting at high temperatures. The Burgers model can describe the deformation of the asphalt mixture effectively, especially on the course of loading by equation (4).

The change of deformation or strain of the asphalt mixture with time can be shown by creep test under dead load. The least-squares procedure is used for

establishing the viscoelastic model. Consequently the trend of the elasticity E_i and the viscosity η_i with time and temperature is brought forward.

$$\varepsilon(t)=\sigma_0\left[\frac{1}{E_1}+\frac{1}{\eta_1}t+\frac{1}{E_2}(1-e^{-\frac{E_2}{\eta_2}t})\right] \tag{4}$$

Where $\varepsilon(t)$ is the total stress; E_1 and E_2 are the elastic parameters; η_1 and η_2 are the viscous parameters; and σ_0 is the dead load. Especially, the creep stiffness modulus is the important parameter by equation (5):

$$S(t)=\frac{\sigma_0}{\varepsilon(t)}=\frac{1}{\left[\frac{1}{E_1}+\frac{1}{\eta_1}t+\frac{1}{E_2}(1-e^{-\frac{E_2}{\eta_2}t})\right]} \tag{5}$$

3.2 Application of creep model in the Finite Element

The numerical simulation has become more and more necessary now because the physical test is complicated and costly. As a result, it is very important to predict the asphalt mixture's mechanical property using modeling techniques.

In the study, the Burgers model is transferred to the Prony series(Chen, J.Y. et al, 2007). For example, equation (5) is transferred to equation (3) using the least-squares method. And a_i and t_i are obtained ultimately.

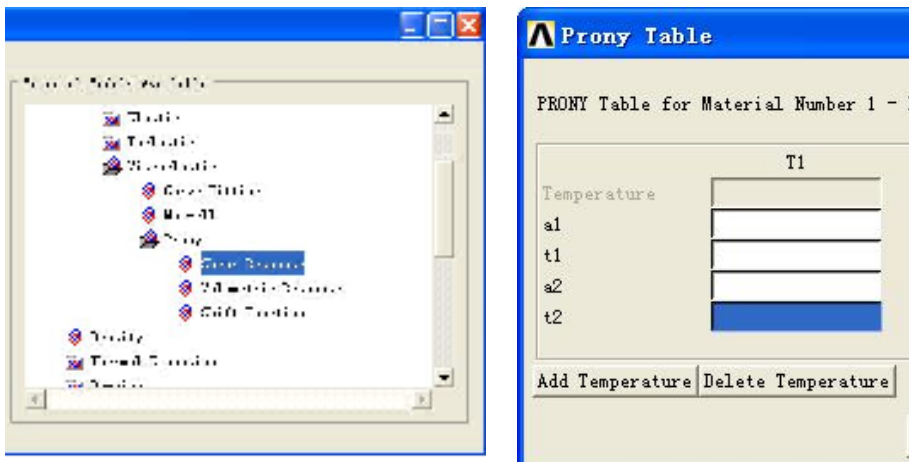

Figure 1. The inputting dialog box of the prony series

Where $\mu(t)$ is the mixture's Poisson's ratio. Figure 1 shows how to input the corresponding parameters in ANSYS about the Burger model. For the asphalt

mixture: $G_\infty = 0$. Especially, $G(t) = \dfrac{S(t)}{2(1+\mu(t))}$.

4. RELAXATION PROPERTY OF ASPHALT MIXTURE

4.1 Constitutive model of relaxation property

Asphalt mixture is easy to become relaxed at low temperatures, which will cause the cracking of asphalt pavements. However, the stress relaxation of the asphalt mixture will have to be considered when the environmental temperature is too low or the relaxation capability of the mixture is insufficient (Sheng, J.A., 2001; Liu, L.X., 2006).

The Generalized Maxwell model is used for the relaxation simulation of the mixture. When the load σ is applied, the total strain ε is the addition of the elastic strain ε_1 and the viscous strain ε_2, which is shown by equation (6):

$$\varepsilon = \varepsilon_1 + \varepsilon_2 \tag{6}$$

The Generalized Maxwell model consists of the Umpty parallel Maxwell models. The corresponding relaxation modulus is expressed by equation (7):

$$G(t) = \sum_{i=1}^{n} \frac{\sigma_i}{\varepsilon_0} = \sum_{i=1}^{n} E_i e^{-t/\tau_i} \tag{7}$$

Where $G(t)$ is the relaxation modulus; σ_i is the i th stress of the Maxwell model; $\tau_i = \rho_i$, which is the i th relaxation time of Maxwell model. The least-squares procedure is used for establishing the Generalized Maxwell model.

4.2 Application of relaxation model in the Finite Element

There are two methods which are used for inputting the Generalized Maxwell model in finite element analysis. One method that the Generalized model is transferred to the Prony series is the same as that for the Burgers model. Another method to input the Generalized model in ANSYS software directly needs 10 steps (ANSYS, 2006).

Figure 2 indicates the inputting dialog box of the 10-steps Generalized model. 95 constants (C1-C95) can be defined by Figure 2. The commonly constants to input include C46、C50、C51-C60、C61-C70. Where: C46 is the summation of all Maxwell model's E_i, $\sum_{1}^{n} E_i$; C50 is the number of Maxwell elements (10 max) used

to approximate the shear modulus relaxation; C51-60 are $E_i / C46$ of every Maxwell model element, as a result; $\sum_{1}^{n} E_i / C46 = 1$ and C61-C70 are η_i / E_i of the generalized model. However, the volume relaxation modulus is used rarely.

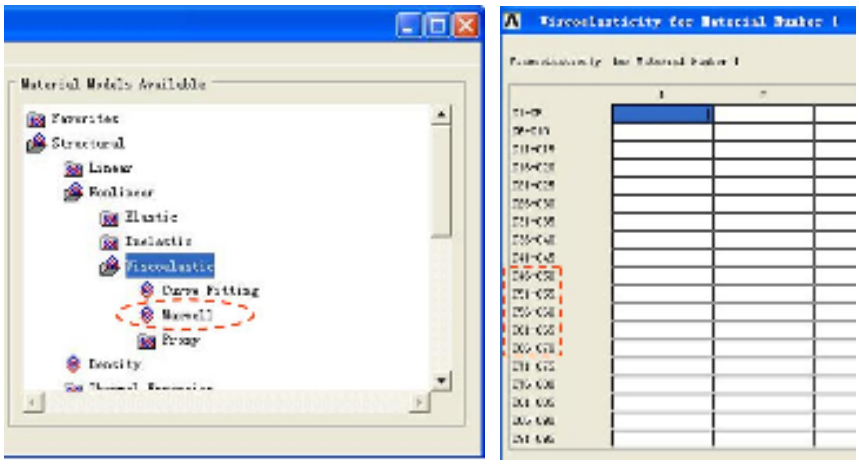

Figure 2. The inputting dialog box of the 10-steps Generalized model

5. AN EXAMPLE ABOUT THE VISCOELASTIC MATERIALS CRE EP

In the study an example is introduced about comparing the asphalt mixture's creep data to simulating model by ANSYS software. The uniaxial creep test is the common method to study the rheologic model of the asphalt mixture. The dense-graded asphalt mixture AC-13 was used in the test. The specimens were cylindrical . The height was 100mm and the diameter was 100mm too. And the universal testing machine (UTM) was used for this purpose. In the study the uniaxial dead-load compression creep test was conducted by applying a constant load equal to 0.1MPa, with a 3600-s loading. The environmental temperature was 40℃. In order to compare the experimental data to the finite element simulation result, Solid185 element with viscoelasticity, an eight-node element, and three degrees of freedom was used for modeling the above specimen. In order to model the actual creep test, the 3D model's boundary conditions are considered as the following: 1) The bottom nodes were fully constrained; 2)the 0.1MPa - load were applied at the top nodes.

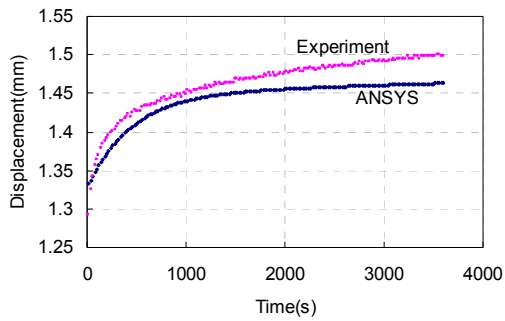

Figure 3. The creep curved drawing of asphalt mixture

Combining the foregoing theory, the corresponding parameters were shown in table

1. Figure 3 indicated that the correlation coefficient between the experiment and the finite element had achieved 94%.

Table 1. Properties of the elastic and viscoelastic material

Burgers model	Prony Series	Command stream of asphalt mixture's properties
$E_1 = 7.561$ $E_2 = 66.988$ $\eta_1 = 2036000.038$ $\eta_2 = 30113.296$ $\mu = 0.250$	$G_1 = 3.0245$ $a_1 = 0.1017$ $a_2 = 0.8983$ $\tau_1 = 403.8767$ $\tau_2 = 299706.7263$	Mp, ex, 1,7.561 !initial modulus Mp, prxy, 1, 0.25 !Poisson's ratio Tb, prony, 1,1,2,shear !Prony series Tbtemp, 45 !temperature Tbdata,,0.1017,403.8767,0.8983,2.997E5

6. CONCLUSION

[1] How to choose an appropriate model plays an important role in the viscoelastic materials' analysis. Burgers model can describe the creep of the viscoelastic material, however, the Generalized Maxwell model does the relaxation test better.

[2] More and more accurate numerical simulation has been requested by engineers for asphalt pavement designs. In the study the application of viscoelastic models in the Finite Element is introduced, which can be proved to be effective by the examples about the creep test's simulation.

REFERENCE

Al Hadidy, A.I., Tan, Y.Q. (2009). "Mechanistic approach for polypropylene-modified flexible pavements." *Mater. Des.*, 30, 1133-1140.

ANSYS(2006). *ANSYS Theory Manual.* USA..

Chen, J.Y., Zhou, C.H. et al(2007). "Data processing and viscoelastic computation for creep test of asphalt mixture." *Journal of Southeast University*, 37(6), 1091-1095. (in Chinese)

Liu, L.X. (2006). *Principle of viscoelastic mechanical and material science about asphalt mixture*. China communications press. Beijing. (in Chinese)

Mulungye, R.M., Owende, P.M.O. et al(2007). "Finite element modeling of flexible pavements on soft soil subgrades." *Mater. Des.*, 28, 739-756.

Sheng, J.A (2001). *Asphalt and asphalt mixtures' service performance* . China communications press, Beijing. (in Chinese)

Wang, J.Y, Zhang, Z.Q. et al(2008). "Using material curve fitting of ANSYS to model viscoelastic material." *Sciencepaper Online*. (in Chinese)

LIMIT VALUE OF RAILWAY BRIDGE FOR TRAFFIC SAFETY

ZHOU Zhihui[1] ,QIN Wenxiao[2] ,ZHANG Jun[2] and ZENG Qingyuan[2]

[1]Postdoctoral Work Station of Traffic and Transportation Engineering, School of Civil Engineering and Architecture, Central South University, Changsha 410075, Hunan Province, China; Tel: +86-731-2656645; email: zzhyy@mail.csu.edu.cn
[2]School of Civil Engineering and Architecture, Central South University, Changsha 410075,Hunan Province,China;Tel:+86-731-2656645;email: wenzh@mail.csu.edu.cn

Abstract: The safety of running trains on five bridges where the lateral vibration amplitudes surpass the limit values given by relative code is analyzed. The results suggest that the existing limit values of bridge lateral vibration amplitude for traffic safety are too conservative. A new method for establishing the limit value of bridge lateral vibration amplitude for traffic safety is proposed on the basis of the theory of energy random analysis for train derailment. The detailed steps of the method include the presentation of the condition for derailment prevention, the determination of the critical system of beam and pier for derailment prevention, and the calculations of the limit value of bridge lateral vibration amplitude of the system of beam and pier for traffic safety. The recommended limit value of lateral vibration amplitude for traffic safety for the 32 m-long T-shape pre-stressed concrete bridge is determined as L/4000.

Key words: limit value, derailment, traffic safety, railway bridge, vibration amplitude

1 Introduction

With the launch of the railway speed-up campaign in the China, lateral vibration amplitudes of part bridges has surpassed the limit value given by the Code for Rating Existing Railway Bridges and train speed has to be restricted under some value. While some bridges on the Jingtong line have been used for 30 years with lateral vibration amplitudes surpassing corresponding limit values, the trains have never derailed. Therefore whether the limit values given by the existing code are too conservative needs to be studied, and it is valuable to establish proper limit values with which the safety of running trains on bridges can be reflected properly.

In the Soviet Union, based on the operation criteria for the vehicle, the limit values of the basic natural period for bridges were established. The limit values of lateral vibration amplitude of typical beams for traffic safety were determined according to the control criteria of Q/P $\leqslant$0.8 (Gu, P.2000). The ordinary values of lateral vibration amplitude and lateral basic natural frequency of piers were put forward (Cao, X.Q., Wu, D.J., and Luo,W.W. 1998). The limit values of lateral

rigidity for light piers were determined according to the control criteria of Q/P ≤ 1.0(Li, Y.S.2005). There exist two fundamental problems in these methods. 1) Derailment cannot be judged well by means of the control criteria of Q/P ≤1.0(or 0.8)(Zhai,W.M. 2002). 2) The limit values of the system of beam and pier for traffic safety have not been presented. In this paper, the safety of running trains on five bridges with lateral vibration amplitudes surpassing limit values is analyzed. A new method for establishing the limit values of bridge lateral vibration amplitude for traffic safety is proposed, and the limit value of the lateral vibration amplitude of the 32 m-long T-shape pre-stressed concrete bridge for traffic safety is determined.

2 Analysis of Safety of Running Train on Bridge with Lateral Vibration Amplitudes Surpassing Limit Values

Based on the theory of energy random analysis for train derailment (Zeng, Q.Y., Xiang, J., and Luo,P. 2004), the safety of running trains on five bridges where the lateral vibration amplitudes surpasses the limit values given by existing code is calculated. The calculated results (Table 1) parallel the fact that derailment has not occurred on these bridges for many years. The results also prove that existing limit values for traffic safety are too conservative.

Table 1. Calculated results on safety of running train on five bridges

Bridge name	Train speed /(km·h^{-1})	A_{max1} /mm	A_{max2} /mm	Limit value /mm	Calculated results
Yanconggou bridge	50	8.46	8.51	3.52	No derailment
Donggou bridge	60	9.60	10.20	2.67	No derailment
Wuhu Yangze bridge	80	3.46	4.06	3.56	No derailment
Yinhe bridge	80	—	3.11	2.29	No derailment
Xinzhen Bridge	80	—	7.41	3.56	No derailment

Note: A_{max1} stands for maximal measured lateral vibration amplitude and A_{max2} stands for maximal calculated lateral vibration amplitude.

3 Method for Establishing Limit Value of Bridge Lateral Vibration Amplitude for Traffic Safety

3.1 Condition of Derailment Prevention

The theory of random energy analysis for train derailment was put forward (Zeng, Q.Y., Xiang, J., and Luo,P. 2004). The energy increment criterion for derailment evaluation is used to judge whether a train derails, which is expressed as Eqs. (1) and (2).

$\Delta\sigma_{cr} \geq \Delta\sigma_{pr}$ no derailment (1)

$\Delta\sigma_{cr} < \Delta\sigma_{pr}$ derailment (2)

Input energy increment of the train-bridge (track) system $\Delta\sigma_{pr}$ is obtained

from field measurements and the work increment done by resistant forces of the system is determined by theoretic calculation. There exists a small error in both the field measurements and the theoretic calculation. Accounting for the effect of the above error, a conservative means is adopted as follows. Assuming that the calculated value $\Delta\sigma_{cr}$ is larger than its true value by 10% and the measured value $\Delta\sigma_{pr}$ is likely to be less than its true value by 10%, the condition of derailment prevention with safety coefficient K (K=1.23) can be obtained by Eq. (3).

$$\Delta\sigma_{cr} \geq K\Delta\sigma_{pr} \tag{3}$$

3.2 Determination of critical system of beam and pier for derailment prevention

The calculation model for the spatial vibration of the train-beam-pier system is established and the safety of running trains on the system of beam and pier is calculated with the theory for train derailment. The system of beam and pier with different lateral rigidity consists of given beams and different piers with different lateral rigidity. With the height of the pier becoming larger step by step, the lateral rigidity of the pier decreases and the ability of the system of beam and pier for resisting derailment also decreases. When the lateral rigidity of piers decreases to a certain value, Eq. (3) cannot be satisfied. Eq. (3) can be satisfied with the lateral rigidity of pier used in the previous step. So the system of beam and pier used in the previous step is the critical system of beam and pier for derailment prevention.

3.3 Determination of limit value of lateral vibration amplitude for traffic safety for system of beam and pier

The smoothness and comfort of running trains on the critical system of beam and pier are calculated. If the indexes of smoothness and comfort satisfy the criteria for qualification, the critical system of beam and pier is the one with minimal lateral rigidity that can ensure the safety, smoothness, and comfort of the running train. If the indexes of smoothness and comfort cannot satisfy the criteria for qualification, the height of the piers needs to be lowered. The smoothness and comfort of running train on the new system of beam and pier are calculated sequentially, until the lateral rigidity of the pier that can ensure smoothness and comfort of the train is found. The system of beam and pier is just the one with minimal lateral rigidity that can ensure the safety, smoothness, and comfort of the running train. According to the calculated results of vibration response for the train-bridge system, the lateral vibration amplitude of the beam for the system of beam and pier with minimal lateral rigidity can be determined as limit value of bridge lateral vibration amplitude for traffic safety.

4 Limit Value of Lateral Vibration Amplitude for Traffic Safety for 32 long T-shape Prestressed Concrete Bridge

4.1 Calculation model and Calculation cases

Spot test and theoretical calculation both verify that vibration responses of the train-bridge system with the formation of full empty wagons C62 are larger than those with other train formations. Accordingly, the train with formation of full empty wagons C62 has the maximum probability of derailment (Xiang, J.,Kong F.B., and Zeng, Q.Y.2007). A train formed with 29 freight wagons C62 hauled by a locomotive DF4 is determined as the calculation model of the freight train for the analysis of the safety, smoothness, and comfort of running trains. Furthermore, a train formed with 14 passenger cars hauled by a locomotive SS8 is determined as the calculation model of passenger trains. The maximal calculation speeds for freight train and passenger train are chosen as 80 km/h and 180 km/h respectively. To reflect the lateral rigidity of multi-span simple supported bridge, a seven-span simple supported bridge (32 m-long T-shape pre-stressed concrete beam and pier with standard design No: 2019) is chosen as the bridge calculation model.

4.2 Determination of critical system of beam and pier for derailment prevention

The theory of energy random analysis for train derailment is used to calculate the safety of running trains on 32 m long T-shape pre-stressed concrete bridges. The height of the pier increases from 8.1 m to 23.1 m, 1 m for each step. Part results are listed in Table 2 and Table 3. According to the calculated results, when the height of the pier is less than 22.1 m, freight and passenger trains will not derail on the system of 32 m-long beam and pier. When the height of the pier is equal to 23.1 m and the speed of freight train is equal to 80 km/h, the condition of derailment prevention Eq. (3) cannot be satisfied. So the height of pier 22.1 m is determined as the critical pier height for the 32 m-long T-shape prestressed concrete bridge. The system of 32m-long beam and pier with height of 22.1m is the critical system of beam and pier for derailment prevention.

Table 2 Calculated results on safety of running freight train

Condition of bridge pier	*Train speed/(km·h^{-1})*	$\Delta\sigma_c/(cm\cdot s^{-2})$	$K\Delta\sigma_p/(cm\cdot s^{-2})$	*Whether Eq(3) is satisfied*
Bridge pier	80	61	45.0	Satisfaction
is not	70	36	25.7	Satisfaction
considered	60	32	20.9	Satisfaction
Height of	80	56	45.0	Satisfaction
bridge pier	70	32	25.7	Satisfaction
is 22.1m	60	28	20.9	Satisfaction
Height of	80	33	45.0	No satisfaction
bridge pier	70	30	25.7	Satisfaction
is 23.1m	60	29	20.9	Satisfaction

Table 3 Calculated results on safety of running passenger train

Condition of bridge pier	*Train speed/(km·h^{-1})*	$\Delta\sigma_c$ */(cm·s^{-2})*	$K\Delta\sigma_p$ */(cm·s^{-2})*	*Whether Eq(3) is satisfied*
Bridge pier is not considered	180	19	8.0	Satisfaction
	170	24	12.2	Satisfaction
	160	17	6.6	Satisfaction
Height of bridge pier is 23.1m	180	20	8.0	Satisfaction
	170	19	12.2	Satisfaction
	160	24	6.6	Satisfaction

4.3 Determination of limit value of lateral vibration amplitude of system of beam and pier for traffic safety

The vibration responses of the train-bridge system in normal conditions are calculated for the critical system of beam and pier for derailment prevention. The calculated results are listed in Table 4. When the speed of the freight train does not exceed 80 km/h, the Sperling index of locomotive is less than 3.45 and the Sperling index of vehicles is less than 4.25. They both satisfy the criteria for qualification of freight train. When the speed of the passenger train does not exceed 180 km/h, the Sperling index of locomotive is less than 3.45and the Sperling index of vehicles is less than 3.0. They both satisfy the criteria for qualification of freight train. Therefore, the smoothness and comfort of running trains can be ensured on the critical system of 32 m-long beam and pier for derailment prevention.

Table 4 Calculated results on smoothness and comfort of running train

Train type	*Train speed /(km·h^{-1})*	*Sperling index of locomotive*		*Sperling index of vehicle*		A_{max} */mm*
		Vertical	Lateral	Vertical	Lateral	
Freight train	80	2.96	3.37	3.89	4.22	8.04
	70	2.85	3.28	3.75	4.18	7.23
	60	2.78	3.13	3.62	4.13	5.86
Passenger train	180	3.04	3.28	2.87	2.91	3.11
	150	2.96	3.24	2.75	2.84	2.86
	120	2.87	3.15	2.66	2.70	2.73

Note: A_{max} stands for maximal calculated lateral vibration amplitude.

When the height of the pier is equal to 22.1 m, corresponding system of 32m-long beam and pier is called the system of beam and pier with minimal lateral rigidity, it can ensure the safety, smoothness, and comfort of running trains. The lateral vibration amplitude of the system of 32m-long beam and pier with minimal

lateral rigidity is equal to 8.04 mm. When bridge lateral rigidity is larger than the minimal lateral rigidity and the bridge lateral vibration amplitude is less than 8.04 mm, the safety, smoothness, and comfort of running trains can be ensured. When the bridge lateral rigidity is less than the minimal lateral rigidity and the bridge lateral vibration amplitude is larger than 8.04 mm, the safety, smoothness, and comfort of running train cannot be ensured So 8.04 mm (L/3980, L is the span length of beam, and its unit is mm) can be determined as the limit value of lateral amplitude for traffic safety of 32 m-long T-shape pre-stressed concrete bridges. Finally, L/4000 is determined as the recommended limit value of lateral amplitude for traffic safety of 32 m-long T-shape pre-stressed concrete bridges. The recommended limit value (L/4000) is larger than the limit value (L/9000) given by existing code.

5 Conclusions

1) The safety of running trains on five bridges where the lateral vibration amplitudes surpass the limit values given by relative code is analyzed. The calculated results prove that the existing limit values of bridge lateral vibration amplitude for traffic safety are too conservative.

2) A new method for establishing the limit value of bridge lateral vibration amplitude for traffic safety is proposed. The recommended limit values of lateral vibration amplitude for traffic safety of the 32 m-long T-shape pre-stressed concrete bridge on speed-raised lines are determined as L/4000.

Acknowledgements

This paper is sponsored by National Basic Research Program of China (2007CB714706), National Natural Science Foundations of China (No50678176), Foundations of Railway Bureau in China (2009G029-D), and Postdoctoral Science Foundation of Central South University.

References

Cao, X.Q., Wu, D.J., and Luo,W.W. (1998). Report on the specification for inspecting railway bridge Rrigidity, Shanghai Railway University, Shanghai.

Gu, P.(2000). “Determination of allowable lateral amplitudes of railway steel bridges based on derailment factor of freight vehicle”. Journal of the China Railway Society, 22(supple),87-91.

Li, Y.S. (2005). Theory and experiment study on lateral vibration of railway bridge piers. Beijing Jiaotong University, Beijing.

Zeng, Q.Y., and Guo, X.R. (1999). Theory of analysis of vibration of the train-bridge time-varying system and its application, China Railway Press, Beijing.

Zeng, Q.Y., Xiang, J., and Luo,P. (2004). “The mechanical mechanism of derailment and the theory of derailment prevention”. Journal of Railway Science and Engineering,1(1),19-31.

Zhai,W.M. (2002). Vehicle-track coupling dynamics. China Railway Press, Beijing.

Finite element analysis on shear-lag effect in curved continuous box girder with corrugated steel webs

Hu Zhaotong [1] and Chen Xi [2]

[1]Chang'an University, College of highway, P.O.Box 710064, Xi'an, China. PH (029)82334831, Fax (029) 82334831, E-mail: hzt@gl.chd.edu.cn

[2]Sichuan Guangnan Express Highway Co.Ltd, P.O.Box 637000, Nanchong, China.

ABSTRACT The box-girder with corrugated steel webs is a new type of steel-concrete structure in China. Corrugated steel webs are used to replace the concrete webs of the traditional box girder. In this paper, the program of ANSYS is used to build the finite element model of a curved continuous box girder with corrugated steel webs. changing tendency, the rule of distribution, and characters of shear-lag effect are analyzed by comparison with the changing radius of curvature, width-span ratio, distance of webs, eccentric load, etc… ,which can influence the shear-lag effect of curved continuous box girder with corrugated steel webs. Finally, the effective distribution width of the box girder is analyzed. It is proven that curvature radius, width span ratio, and eccentric load are important influence factors and the suggestions on diminishing the shear-lag effect in the design of curved continuous box girder with corrugated steel webs are made.

KEY WORDS corrugated steel webs, curved continuous box-girder, shear-lag effect, finite element analysis

INTRODUCTION

Corrugated steel webs are used to replace the concrete webs of box-girder. It is a new combinatorial structure using external pre-stressing force technology. The strong shear capacity of corrugated steel webs and the advantages of the high compressive strength of concrete are fully used. The internal forces in the structure are reasonable, and can be consistent with the demand of light-weight bridge structures compared to ordinary concrete box-girder bridges. In recent years, the application of corrugated steel webs to curved box-girder bridges is gaining more and more attention. For the curved continuous box-girder, considering the shear-lag effect would bring the coupling effect of bending, twisting, and shear-lag, which increases the complexity of calculation and analysis. The box girder in the longitudinal bending loads, due to shear lag-effect, will cause the width of wing plate to be reduced. There is still a lack of a reasonable calculation method for the effective distribution width of box-girders in the current bridge design specification in China.

In this paper, the calculation models of curved continuous box-girders with corrugated steel webs are built by finite element method. The shear lag-effect of curved continuous box -girders with corrugated steel webs is analyzed. Changing tendency, the rule of distribution, and characters of shear-lag effect are analyzed by comparison with changing radius of curvature, width-span ratio, distance of webs, eccentric load, cross-section type of box girder, etc…

FINITE ELEMENT MODEL

In this paper, the large-scale common program of ANSYS is used to calculate the bridge as space structures. Due to the difference of the force characteristics and thickness of members, the box-girder with corrugated steel webs uses the two different types of modules to simulate the box-girder structure. Three-dimensional solid element SOLID65 is used to build the model of the

roof and bottom plate. The thickness of webs is very thin, thus the plate elements are used to simulate. The roof, bottom plate, and corrugated steel webs of connections use sharing nodes. This article does not consider the action of external pre-stressed reinforcement; in the model, the pre-stressed reinforcement unit is not set up.

The calculation model is the three-span uniform section of the curved continuous box-girder with corrugated steel webs. There are 77937 model units, of which 14,876 are plate elements and 63,061 are three dimension solid elements, as shown in Figure 1.

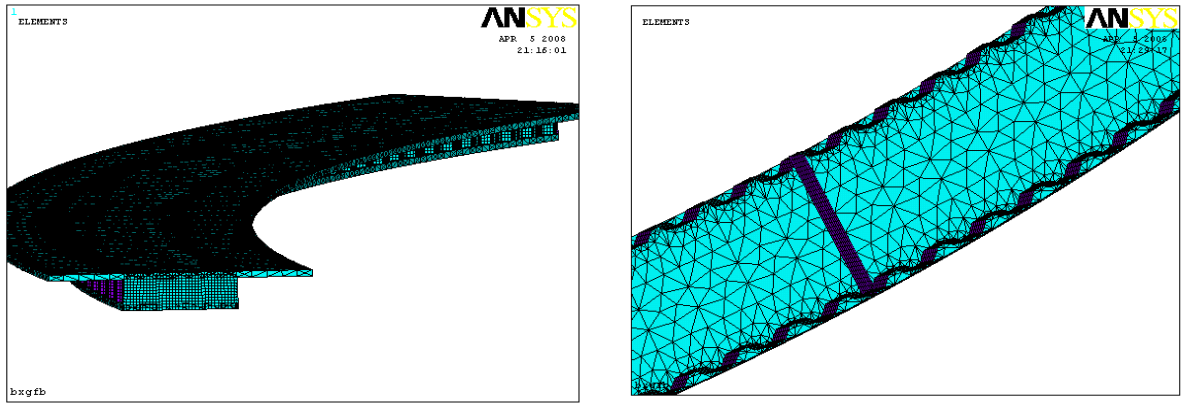

Figure.1. Finite element model of curved continuous box-girder with corrugated steel webs

In this paper, comparison is made withthe model tests of a 40m span pre-stressed simply supported box girder with corrugated steel webs on the Nanning to Baise expressway (Cheng Delin 2007); model scale ratio of 1:4 and uses the same boundary conditions of practical bridge. Compared with the finite element calculations and experimental measured values, the relative difference is less than 5%. It is proven that the finite element model can ensure the calculation accuracy of the box-girder with corrugated steel webs and the actual situation of the bridge is simulated accurately. Therefore, the finite element analysis model is correct and the calculation results are reliable.

ANALYSIS SHEAR-LAG EFFECT OF CURVED CONTINUOUS BOX GIRDER WITH CORRUGATED STEEL WEBS

1. Formula of shear-lag coefficient

Classic shear-lag coefficient is defined as:

λ＝the normal stress obtained by considering shear-lag effect / the normal stress obtained by elementary beam theory (1)

The normal stress is obtained by elementary beam theory, i.e. the average normal stress

$$\sigma_d = \frac{\int_0^b \sigma dy}{b_c} \qquad (2)$$

2. The influence of curvature radius on the shear-lag effect

The shear-lag coefficients of different curvature radius of curved continuous box-girder bridge under the load is calculated. The radius of curve R is chosen by four cases: 50m, 75m, 150m, and 300m and the calculation results are as follows:

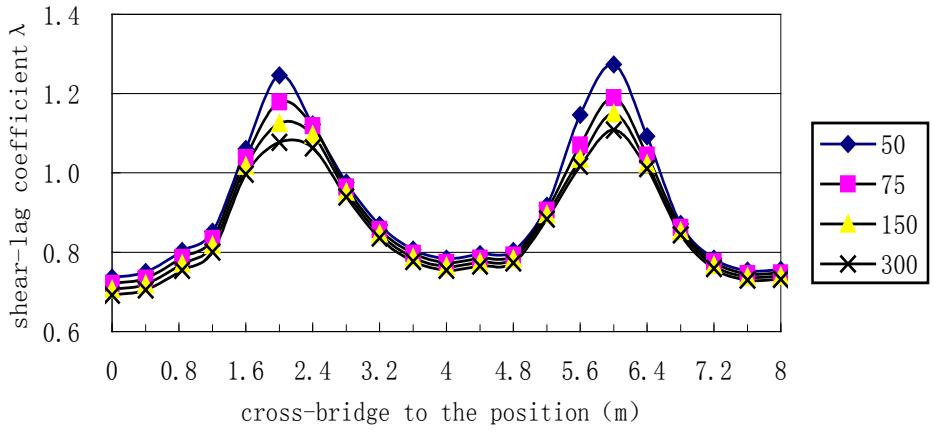

Figure. 2. The transverse distribution of the shear-lag coefficient for different curvature radius along the cross-section of box-girder

As shown in figure 2, as the curvature radius decreases, the shear-lag coefficient of the curved continuous box-girder increases. The shear-lag coefficients differs from outside to inside of the box-girder, it is larger on the outside.

3. The influence of width-span ratio of box-girder on the shear-lag effect

Set the calculation span L = 20m, and the width-span ratio of the box girder B / L as 0.1,0.2,0.3,0.4, and 0.5 with the width B of the roof slab of box girder as 2m, 4m, 6m, 8m, and 10m respectively. The bottom width changes along with the roof at a fixed rate. Under the load, the biggest shear-lag coefficients of the roofs of the box-girder along with the change of width-span ratio are computed separately.

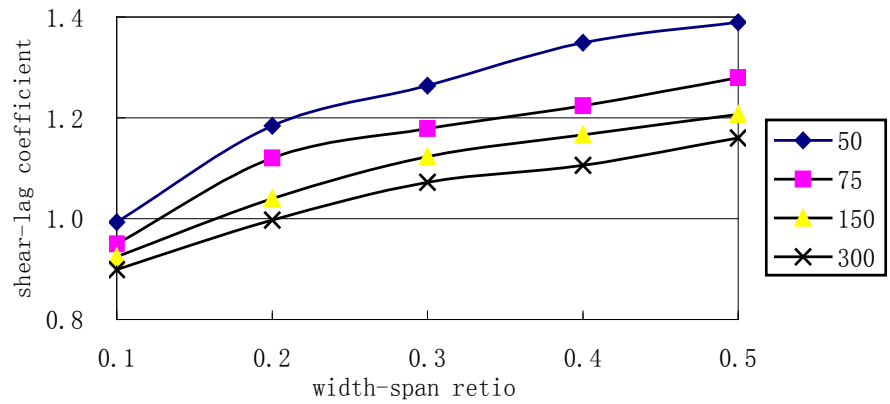

Figure.3. The transverse distribute of the shear-lag coefficient for different wide-span ratios along the cross-section of box girder

We can see from Figure 3, along with the increasing width-span ratio, the shear-lag coefficient λ increases. The curvature radius is smaller; the shear-lag coefficient λ increases quicker. If the curvature radius is 50m, when the width-span ratio B/L from 0.1 to 0.5, the shear-lag coefficient λ at the cross-section of mid-span will increase 39.9% at most.

4. The influence of spacing of box-girder webs on the shear-lag effect

With a certain width of the roof of box-girder, the method that reduces the distance between the webs to obtain the narrow bottom slab is used frequently, but the computed result show (see

Figure 4)that the too-small web spacing will cause the shear-lag coefficient of box-girder to increase.

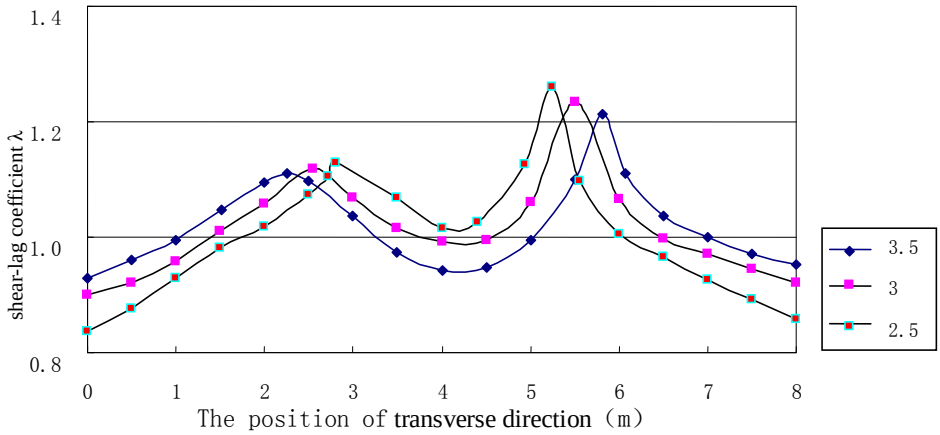

Figure.4. The transverse distribution of the shear-lag coefficient for different web spacing along the cross-section of box-girder

5. The influence of eccentric load on the shear-lag effect

As a result of the curvature existence, each section of the curved box-girder is under a combined stress condition due to the action of the bent, cut, and torque (Xu Yanqiu et al. 2003). As compared with the concrete web of box-girder, although the corrugated steel web of box-girders has many superiorities, its torsional stiffness is smaller than that of the concrete girder. At the same time, because the corrugated steel web is thin in comparison with the top and bottom concrete slab, its in-plane flexural rigidity is slight, enabling the crosswise frame function for limited the section distortion to decrease. In addition, the longitudinal rigidity of the corrugated steel web is very small. Thus, under the eccentric load, the warping normal stress produced by constraint torsion and distortion will rise to a higher level. Obviously, this could be disadvantageous to the stress condition of box-girder with corrugated steel webs.

As Figure 5 shows, the distribution of the shear-lag coefficient of box-girders with corrugated steel webs are non-uniform, extremely under the eccentric loads. The eccentric load side has a very high peak value, so certain amounts of cross diaphragms are needed to strengthen the lateral stiffness and the anti-distortion rigidity.

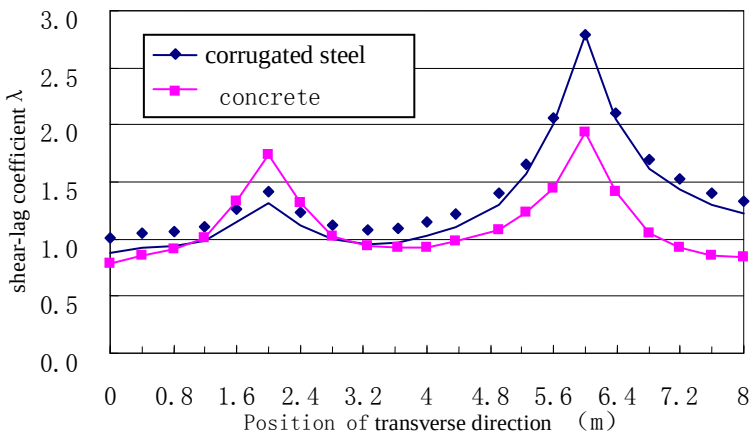

Figure.5. The transverse distribution of the shear-lag coefficient of the section of mid-span under

the eccentric loads

THE EFFECTIVE DISTRIBUTION WIDTH OF CURVED BOX-GIRDER WITH CORRUGATED STEEL WEBS

1. The formula for calculating the effective distribution width

The mathematical expression for the effective distribution width of box girder is as follows (Fan Lichu 1996):

$$b_c = \frac{\int_0^b \sigma dy}{\sigma_{\max}} \qquad (3)$$

In the formula: b_c— effective distribution width of flange, b — actual width of flange,

y— coordinate along cross-section width direction.

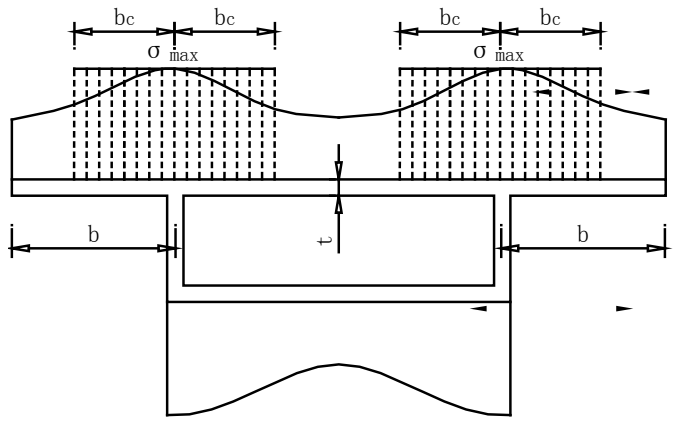

Figure.6. Effective distribution width of box-girder

The ratio of effective width to actual width is defined as the effective width coefficient. The effective width coefficient is used to weigh the effective distribution width.

2. The computation of the effective distribution width for the curve box girder

The effective distribution width of the concrete box girder and box girder with corrugated steel webs were calculated in this article. The results demonstrate that the effective width of the box girder with corrugated steel webs is smaller than the concrete box girder in the same section and the same horizontal position of the roof slab, as shown in figure 7. It illustrates that the effective width of box-girders with corrugated steel webs is narrower, which sets a higher requirement for the concrete pressive strength of box-girders with corrugated steel webs.

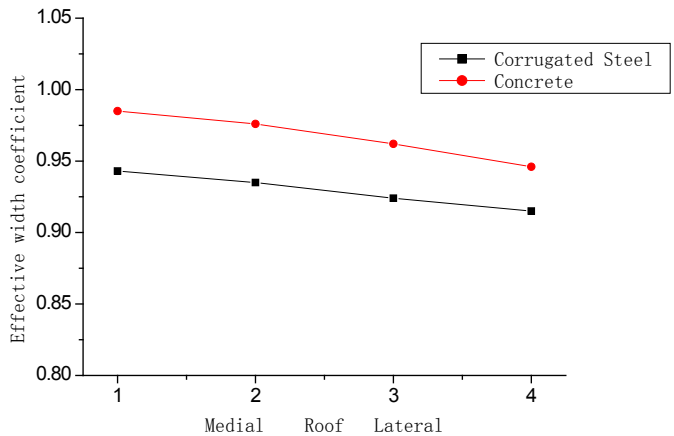

Figure.7. The effective width coefficient of the box-girders

CONCLUSION

(1) FEM analysis showed that the parameters, curvature radius, width-span ratio, and load eccentricity, etc…, would obviously influence the shear-lag effect of the curved continuous box-girder with corrugated steel webs. The curvature radius and eccentric loading are among the significant influence factors. Therefore, we should take it more seriously in engineering practice.

(2) The effective distribution width of the curved continuous box-girder with corrugated steel webs is narrower than that of the concrete box girder due to the shear-lag effect, so there are higher requirements for the concrete pressive strength for the roof slab and bottom slab of the box-girder with corrugated steel webs.

REFERENES

[1] Cheng Delin. (2007). "Bending performance of pre-stressed steel-concrete box Beam of corrugated steel webs [D]." Xi'an. Chang'an University,

[2] Xu Yanqiu, Xu Kebin, Wang Li. (2003). "Analysis of thin-walled curved-box beam using 3D FEM [J]." *China civil engineering journal*, 58-62.

[3] Fan Lichu. "Bridge Engineering". *(Fist volumes)*[M]. (1996). Second edition. Beijing: China Communications Press.

[4] Hu Zhaotong, Liu Yunxin, Cai Jianming. (2005). "A study on shear lag effect for continuously curved RC box-girders [J]." *Highway*, 19-21.

Nonlinear Analysis of Time-dependent Effect for Reinforced Concrete Thin-wall Box Girders Exposed to Fire

ZHANG Gang[1], HE Shuan-hai[2], WANG Ling-bo[3]

[1]Key Laboratory of Old Bridge Detection and Reinforcement Technique in Traffic Industry, Chang'an university, P.O. Box, 651,Xi'an, The Middle of The 2th Ring Road; PH(029)82334870;FAX(029)82334872; email: zhangg_2004@126.com
[2]Key Laboratory of Old Bridge Detection and Reinforcement Technique in Traffic Industry, Chang'an university, P.O. Box,651,Xi'an,The Middle of The 2th Ring Road; PH(029)82334871; FAX(029)82334871; email:keji_1@chd.edu.cn
[3]Key Laboratory of Old Bridge Detection and Reinforcement Technique in Traffic Industry, Chang'an university, P.O.Box, 651,Xi'an,The Middle of The 2th Ring Road; PH(029)82334870; FAX(029)82334872; email:Nancywlb1984@163.com

Abstract

Aimed for fire-resistant performance for reinforced concrete thin-wall box girders, the energy equation and compound boundaries conditions were created. Analyses were performed to study the time-dependent laws of deflection for reinforced concrete thin-wall box girders exposed to fire. The results indicate that the vertical-deformation ability of reinforced concrete thin-wall box girders effectively increases with the increment of concrete cover thickness. The vertical-deformation presents a nonlinear increasing trend with the increment of extending-fire time.

Subject heading

thin-wall box girders; deformation; nonlinear analysis; extending-fire time

Introduction

The reinforced concrete thin-wall box girder is a wide application. However, its structure wall is thin. Temperature inside the walls changes when high temperatures penetrate the thin wall with extension of fire time, thus fire-resistant performance is relatively weak (Zhang et al 2007). High temperature performance tests about new grade steel (Yu et al 2005), as well as concrete-filled steel tube (Han et al 2002) were performed by some famous scholars. Fire-resistant performance for columns (Lu et al 2006; Haksever et al 1981) including T-shaped cross sections (Wu et al 2007) were studied. Different fire procedures for reinforced concrete cross-sections exposed to fire (Daniel et al 2007) and test methods (Yu et al 2005) were put forward. Presented fire-resistant studies were commonly based on reinforced concrete solid members. Research on hollow, open, and thin-wall members was relatively scarce. Analysis for the deformation of reinforced concrete thin-wall box girders exposed to fire was necessary. A series of parameters, including thermal performance and material performance of steel and concrete, were presented. Some factors, including cover thickness and extending-fire time, contributing to deformation of reinforced concrete thin-wall box girders were studied.

Heat attack model

Heat conduction between concrete and crystal water (Daniel et al 2007) is considered, the energy equation can be expressed as follows:

$$Q(t)+\frac{\partial\left(k(t)\partial T(t)\right)}{\partial x^2}+\frac{\partial\left(k(t)\partial T(t)\right)}{\partial y^2}+\frac{\partial\left(k(t)\partial T(t)\right)}{\partial z^2}=\rho(t)c(t)\frac{\partial T(t)}{\partial t}+\frac{\partial L_w(t)}{\partial t} \quad (1)$$

Where $H(t)$ is the enthalpy, t is the time, $k(t)$ is the coefficient of heat conduction, $Q(t)$ is the heat quantity, $\theta(t)$ is the temperature, $\rho(t)$ is the density, $c(t)$ is the specific heat, and $L_w(t)$ is the latent heat function.

The compound boundaries conditions can be expressed as follows:

$$q=m_1\beta(T_{sur}-T_{air})^n+m_2 v\delta(\alpha e_{fire}T_{fire}^4-e_{sur}T_{sur}^4) \quad (2)$$

Where q is the heat flux, β is the heat convection coefficient, T_{sur} is the surface temperature of concrete, T_{air} is the air temperature, T_{fire} is the fire temperature, v is the radiation view factor, δ is the Stefan-Boltzmann constant, α is the absorptivity of surface, e_{fire} is the emissivity of the flame associated with fire, e_{sur} is surface emissivity of concrete, and m_1 and m_2 are partial factors.

Materials properties

According to the references (Lu et al 2006;Wu et al 2003), thermal performance of concrete, including thermal conduction and specific heat and density, is listed in Table 1.

Table 1.Thermal Performance of Concrete

Temperature	Thermal conduction	Specific heat	Density
20 ℃	1.6 W/(m·℃)	850 J/(kg·℃)	2489 kg/m^3
200 ℃	1.5 W/(m·℃)	939 J/(kg·℃)	2388 kg/m^3
400 ℃	1.3 W/(m·℃)	1038 J/(kg·℃)	2276 kg/m^3
600 ℃	1.2 W/(m·℃)	1136 J/(kg·℃)	2164 kg/m^3
800 ℃	1.0 W/(m·℃)	1235 J/(kg·℃)	2052 kg/m^3
1000 ℃	0.9 W/(m·℃)	1334 J/(kg·℃)	1940 kg/m^3

According to the references (Cai et al 2003;Lu et al 2006;Wu et al 2003), thermal performance of steel, including thermal conduction, specific heat, and density, is listed in Table 2.

Table 2.Thermal Performance of Steel

Temperature	Thermal conduction	Specific heat	Density
20 ℃	53 W/(m·℃)	612 J/(kg·℃)	7800 kg/m^3
200 ℃	50 W/(m·℃)	612 J/(kg·℃)	7800 kg/m^3
400 ℃	44 W/(m·℃)	612 J/(kg·℃)	7800 kg/m^3
600 ℃	34 W/(m·℃)	612 J/(kg·℃)	7800 kg/m^3
800 ℃	24 W/(m·℃)	612 J/(kg·℃)	7800 kg/m^3
1000 ℃	24 W/(m·℃)	612 J/(kg·℃)	7800 kg/m^3

According to the reference (Cai et al 2003), mechanics performance of concrete, including the ratio of Poisson, reduction coefficient of strength, and elastic modulus, are listed in Table 3.

Table 3.Mechanics Performance of Concrete

Temperature	Ratio of Poisson	Reduction coefficient of strength	Reduction coefficient of elastic modulus
20 ℃	0.15	1.000	1.000
200 ℃	0.15	1.000	0.700
400 ℃	0.15	1.000	0.540
600 ℃	0.15	0.584	0.370
700 ℃	0.15	0.388	0.300
800 ℃	0.15	0.192	0.280

According to the references (Cai et al 2003, Lu et al 2006), mechanics performance of concrete, including the coefficient of heat expansion, reduction coefficient of yield strength, and elastic modulus is listed in Table 4.

Tab.2 Mechanics Performance of Steel

Temperature	Coefficient of heat expansion	Reduction coefficient of yield strength	Reduction coefficient of elastic modulus
20 ℃	12.0×10^{-6}	1.000	1.000
200 ℃	13.6×10^{-6}	1.000	0.902
400 ℃	15.2×10^{-6}	0.674	0.763
600 ℃	16.8×10^{-6}	0.346	0.388
700 ℃	17.6×10^{-6}	0.182	0.200

Fire model

The standard fire curve (International Standard ISO384.1975) is expressed as follows:

$$T_{air}(t)=345\log_{10}(8t+1)+T_0 \quad (3)$$

Where T_0 is the initial temperature and $T_{air}(t)$ is the even air temperature after t minutes.

The simply supported beam exposed to ISO 834 fire is given (see Figure 1), even loads are applied on the upper plate whose value q=20kN/m^2, the span distance L=16m.

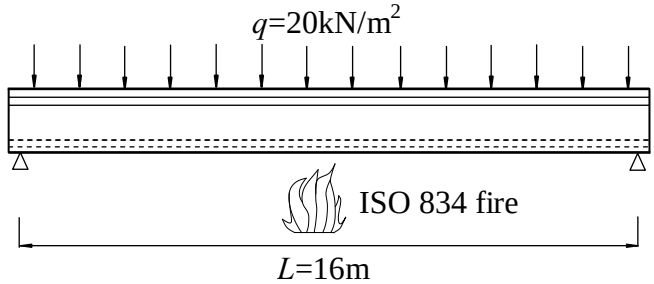

Figure 1. Model beam exposed to fire

The cross-section configurations of the simply supported beam, including section dimension and steel, are given (see in Figure 2.). The diameter of steel Φ=28mm, C represents cover thickness of concrete.

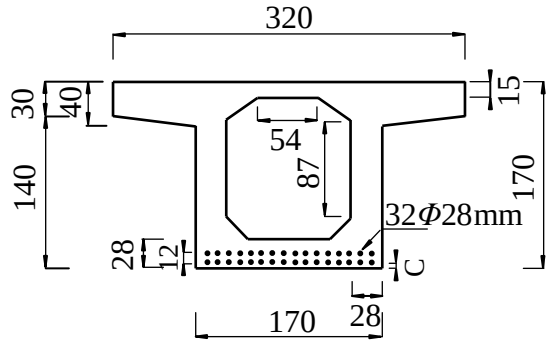

Figure 2. Cross-section configuration.(Dimension in cm)

Heat quantity is applied outside of the box section (except the upper plate) as a temperature-rise curve form of ISO 834 (see Figure 3.). The upper plate is exposed to the ambient temperature, which its value is 20℃.

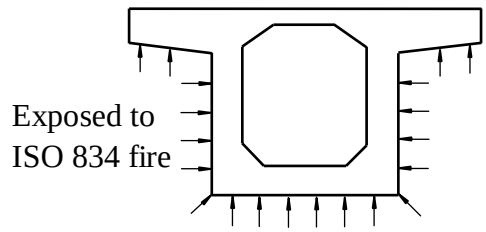

Figure 3. Fire field model for cross section

Some design parameters, including cover thickness, yield strength, and compressive strength, at room temperature for the model beam are listed in Table 5.

Table 5. Design parameters of model beam exposed to fire

Load cases	Cover thickness	Yield strength at room temperature	Compressive strength at room temperature
SSB1	3.0 cm	400 MPa	32 MPa
SSB2	4.0 cm	400 MPa	32 MPa
SSB3	5.0 cm	400 MPa	32 MPa

Case study

Time-dependent curves with deflection in the span centre for reinforced concrete thin-wall box girders with variations of cover thickness are presented (see Figure 4). Analysis results indicate: deflection hardly produces a variation within 20 minutes, deflection in the span centre modeled a type of parabola that is decreasing after 20 minutes.

As showed in Figure 4，under the condition of cover thickness equaling 3 cm，deflection in the span centre is 90 mm when the fire time is equal to 100 minutes, deflection in the span centre is 140 mm when the fire time is equal to 150 minutes, and deflection in the span centre is 220 mm when fire time is equal to 200 minutes.

Under the condition of cover thickness equaling 4cm，deflection in the span centre is 70 mm when the fire time is equal to 100 minutes, deflection in the span centre is 120 mm when the fire time is equal to 150 minutes, and deflection in the span centre is 170 mm when fire time is equal to 200 minutes.

Under the condition of cover thickness equaling 3cm，deflection in the span centre is 60 mm when the fire time is equal to 100 minutes, deflection in the span centre is 100 mm when the fire time is equal to 150 minutes, and deflection in the span centre is 150 mm when the fire time is equal to 200 minutes.

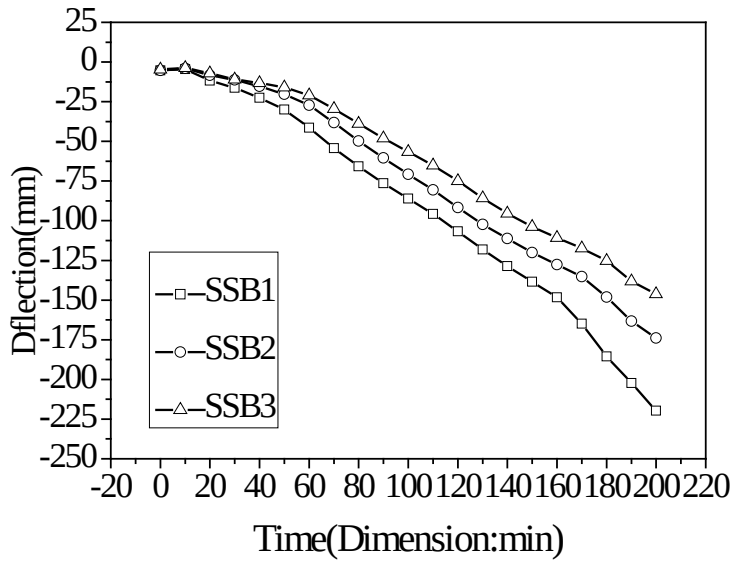

Fig.4 Time-dependent curves with variation of cover thickness

Conclusions

The concrete cover thickness and extending-fire time were considered in order to study the time-dependent laws of deflection for reinforced concrete thin-wall box girders subjected to fire. The study indicates that deflection in the span centre shows a nonlinear decreasing trend during the whole fire time. Meanwhile, variation tendency for deflection in the span centre shows a decreasing trend with the increment of cover thickness. Therefore, fire resistance can be promoted by the step of increment of concrete cover thickness.

References

Cai Y., and Huang D.Y., and Xiong X.Y.(2003). “Material behaviors and mechanical model of pre-stressed concrete structure at high temperature.” *J.Building Science Research Si Chuan*. 29(4),82-84.

Daniel,D.C., and Antonio,R.M.(2007). “Nonlinear analysis of reinforced concrete cross-sections exposed to fire.” *J. Fire Safety*, 42(2),139-149.

Haksever, A., and Anderberg, Y. “Comparison between measured and computed structural response of some reinforced concrete columns in fire.” *J. Fire Safety*,1981,26(4):293-299.

Han, L.H., and Yang, H., and Huo, J.S.(2002). “Residual strength of concrete filled

steel tubular columns with rectangular sections after exposure to standard fire." *Engineering Mechanics*, 19(5),78-86.

International Standard ISO384.(1975). *ISO-834 Fire resistance test-elements of building construction*, Geneva.

Lu, Z.D., and Yu, J.T., and Xu Z.H.(2006). "Nonlinear analysis of steel reinforced concrete columns under fire." *J. Tongji University*,34(11):1445-1450.

Wu B.，and Xu Y.(2007). "Fire resistance of reinforced concrete columns of T-shaped cross section. " *J. Civil Engineering*,40(3)：30-34.

Wu B. (2003). *Mechanics performance of reinforced concrete structure exposed to fire*, Bei Jing.

Yu, Z.W., and Wang, Z.Q., Shi, Z.F.(2005). "Experimental research on material properties of new Ⅲ grade steel bars after fire." *J. Building Structures,* 26(2)：112-116.

Zhang, G., and He, S.H., and Song, Y.F. (2007). "Safety mode for evaluation hydration heat temperature damage on concrete box bridge." *J. Safety and Environment*, 7(4),143-147.

Construction Control of Cable-stayed Bridges Based on ANN and GA Hybrid Algorithm

Zeying Yang[1*] , Haiming Yi[1], Jianbo Qu[2], Junjie Song[3], Xuefu Li[4]

[1*]School of Civil and Hydraulic Engineering, Shandong University, Jinan, 250061, China; email: yangbridge2003@yahoo.com.cn
[2]Highway Bureau of Shandong Province. Jinan 250014, China
[3]Highway Bureau of Weifang Municipality Weifang 261000, China
[4]Highway Bureau of Weicheng urban area in Weifang Municipality, Weifang, 261021, China

ABSTRACT

This paper presents a new method of using ANN (Artificial Neural Networks) to control cable-stayed bridges at deferent erection stages during construction: predicting height mark deviation of main beams of cable-stayed bridges during construction given influencing factors (temperature at the moment of measurement, depth of stretched cross-section of main beams, depth of discussed cross-section of main beams, distance between the stretched cross-sections of main beams and axle wire of pylons, and distance between the discussed cross-sections of main beams and axle wire of pylons). A hybrid algorithm (G-Prop) that combines a genetic algorithm (GA) and back-propagation (BP) is used to train ANN with a single hidden layer. The case study shows that ANN based on GA and BP is a powerful instrument for predicting height mark deviation of main beams of cable-stayed bridges during construction and for construction control of cable-stayed bridges.

1 INTRODUCTION

It is a fact that control of endogen force and deformation of cable-stayed bridges at deferent erection stages during construction is very important for the cable-stayed bridges' safety and durability. But how to control them into permitted ranges is still a big challenge for bridge engineers.

Because of self-anchored cable systems, the cantilever method has been widely used for the main girder erection of cable-stayed bridges (Pao-Hsii Wang et al. 2004). The cantilever method is considered to be the natural and logical solution for constructing cable-stayed bridges of large span, where new girder segments are installed and then supported by new cable stays in each erection stage and the construction process keeps going stage-by-stage until the bridge is completed. Since no auxiliary supports are needed for constructing the bridge girder in the cantilever method, a lot of construction cost and time can be saved. There are two basic alternates to the cantilever method. One is named the single cantilever method and the other is the double cantilever method. In the former, the side span girders of the

bridge are erected on auxiliary piers and afterwards the stiffening girder in main span is erected by one-sided free cantilevering until the span centre or the anchor pier on the far end is reached. In the latter, the bridge girder is erected from both sides of the tower towards the anchor piers and the main span centre by double-sided free cantilevering (M. Virlogeux 1991).

For the cantilever method, only through adjusting the height mark of the formwork erection of every girder segment, can the shape of main girders be controlled successfully. In order to adjust the height mark of the formwork erection of every girder segment, the height mark deviation of the main beam should be predicted ahead of time.

It has been recognized that there are many influencing factors of the height mark deviation of main girders. Furthermore, the relationship between them is too complex to be represented by explicit mathematical functions. This paper presents a new method of using ANN (Artificial Neural Networks) to solve the problem: predicting the height mark deviation of the main beam given influencing factors, which aims to provide bridge engineers with an useful approach.

2 ANN BASED ON GA AND BP

2.1 Back-Propagation ANN

In this paper, a three-layer feed forward neural network, which is shown in Fig.1, is established to map the nonlinear relationship between influencing factors and the height mark deviation of the main beam. According to literature (Anbang Gu and Yongshui Zhang. 2005), the input layer of the network consists of six neurons: temperature at the moment of measurement, depth of the stretched cross-section of main beam, depth of the discussed cross-section of main beam, distance between the stretched cross-sections of main beam and axle wire of the pylon, and distance between the discussed cross-sections of main beam and axle wire of the pylon. They are the vectors $X: x_1, x_2, x_3, \cdots, x_6$ respectively. The number of neurons in the output layer is one, which corresponds to the number of outputs: the height mark deviation of main beam, which is the vector y.

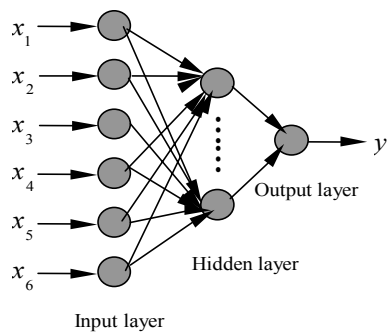

Figure 1. Architecture of back-propagation neural network.

2.2 Hybrid Algorithm Based on GA and BP

Even as BP methods are successfully used in many fields, due to its leaning ability, it does encounter certain difficulties in practice (P.A., Castillo et al. 2000): Convergence tends to be extremely slow and very dependent on the initial weights; convergence to the global optimum is not guaranteed, and learning constants and hidden layer size must be guessed heuristically or through systematic tests. Evolutionary neural networks are a more efficient way of searching, but still, they search over a subset of all possible parameters. The hybrid approach of GA and BP to train ANN makes use of the advantages of both algorithms: the ability of the GA to find a solution close to the global optimum and the ability of the BP to tune a solution and reach the nearest local minimum by means of local search from the solution found by the GA.

GA is used to modify the initial weights only, while BP is used to train from those weights. This makes a clean division between global and local search. The hidden layer size is searched for through the application of some new GA operators: substitution, addition, and elimination. These operators are developed to perform incremental (adding hidden neurons) or decremental (pruning hidden neurons) learning. For detail, refer to (P.A., Castillo et al. 2000). This paper used MATLAB to develop the calculating program.

3 APPLICATION, RESULTS AND EVALUATION

The objective of this study is to investigate the feasibility of using neural networks to predict the height mark of main girders of cable-stayed bridges during construction given the chief influencing factors. In order to use neural networks, a reliable comprehensive dataset is needed for training and testing the networks. Dataset used in this paper come from the construction process of an actual cable-stayed bridge over the Yellow River, which was completed last year. This bridge is a pre-stressed concrete cable-stayed bridge of 3 pylons and twin cable planes with spans arranged as (42 + 42 + 300 + 300 + 42 + 42) m. The cantilever method was used to construct it. The elevation view of the main span of this cable-stayed bridge is shown in Fig.2.

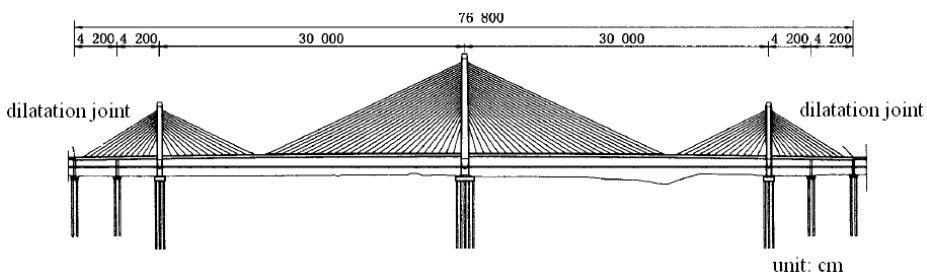

Figure 2. The elevation view of the main span.

According to the construction procedure, the patterns in the dataset were divided into two sets. The first set (obtained by measuring in the anterior construction procedures) is used for training the network. The second set (obtained by measuring in the posterior construction procedures) was used for testing the trained network. The overall procedure of this study is shown in Fig.3.

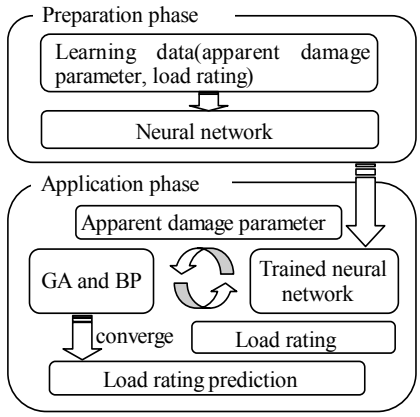

Figure 3. Load rating prediction procedure. There is a preparation phase and an application phase.

In the preparation phase, first the neural network was trained using training data. Error comparison is demonstrated in Fig. 4. Fig.4 shows that, for training data, the error between the prediction and actual values is dramatically less than the error between results obtained from the conventional computing method and actual values.

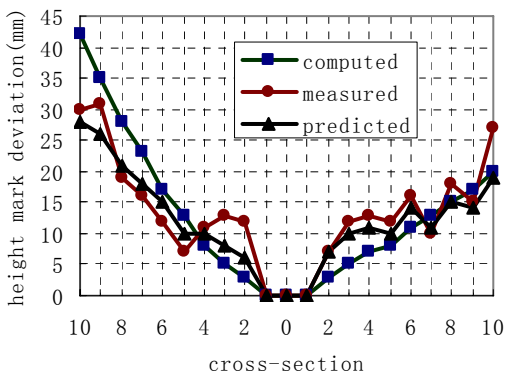

Figure 4. Comparison of relative error for training data.

In the application phase, after the neural network was trained using the training data, it was applied to test data. Error comparison is demonstrated in Fig. 5. Fig.5 shows that, for testing data, the error between the prediction and actual values is also dramatically less than the error between results obtained from the conventional computing method and actual values.

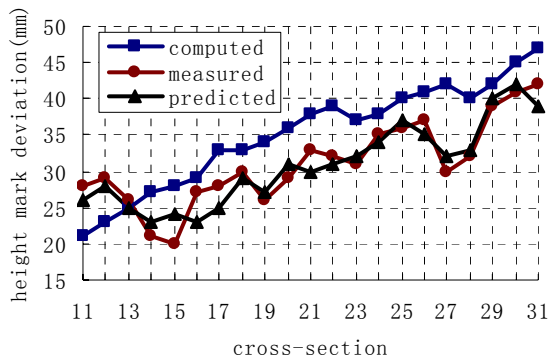

Figure 5.Comparison of relative error for testing data.

The real power of the network is demonstrated in Fig.4 and Fig.5, which show very good agreement between the predicted and actual values for both the training and testing data. The ANN trained by the hybrid algorithm of GA and BP obtains a much higher degree of generalization and can be used in practice.

4 CONCLUSION

In this study a neural network was designed and trained for predicting the height mark deviation of the main girder of cable-stayed bridges. This neural network had been used to control the construction of an actual cable-stayed bridge over the Yellow River. The cable-stayed bridge over the Yellow River has been utilized for two years safely, which demonstrates that ANN based on GA and BP can be used in the construction control of cable-stayed bridges.

ACKNOWLEDGEMENTS

This work was supported by the National Natural Science Foundation of China (50708056), and the Shandong Encouraging Fund for Excellent Scientists (2007BS04025).

REFERENCES

Anbang Gu, Yongshui Zhang., *Cheking and controlling of bridge during construction*. China mechanic press, Beijing, china, 2005.

M. Virlogeux, Erection of cable-stayed bridges, *Proceedings of the Conference of Cable-stayed Bridges-recent developments and their future*, Yokohama, Japan , 1991, pp. 329–346.

P.A., Castillo, J., Merelo, A. Prieto, V. Rivas, G. Romero., G-Prop: Global optimization of multiplayer perceptrons. *Neurocomputing* , Vol. 35, No. 5, 2000, pp. 149-163.

Pao-Hsii Wang, Tzu-Yang Tang, Hou-Nong Zheng, Analysis of cable-stayed bridges during construction by cantilever methods, *Computers and Structures* , Vol. 82, No. 3, 2004, pp. 329–346.

Experimental Investigation of the First Precast Bi-pre-stressing Simple Girder Concrete Bridge

Minjuan Zhou[1] and Nan Wang[2]

[1] Shijiazhuang Institute of Railway Technology, Shijiazhuang, Hebei Province; PH (311) 88621091; FAX (311) 88621073; email: zzrsb888@126.com

[2] Shijiazhuang Institute of Railway Technology, Shijiazhuang, Hebei Province; PH (311) 88621562; FAX (311) 88621073; email: wn31875062@163.com

ABSTRACT

The experimental investigation of the first precast bi-pre-stressing simple girder concrete bridge in China, the Da-Tun Bridge, is presented. The structure and fabrication of the bridge, especially the post-tensioning reinforcement setup of the upper end of the girder, are introduced. In addition, the details of the comprehensive tests on the Da-Tun Bridge, including pre-stressing loss measurement and analysis, static tests, and live loading tests, are also presented. The corresponding major building technologies are tested and improved after the experiments. Finally, the load carrying capacity of the girder and the operating performance of the Da-Tun Bridge are evaluated. Some issues arose in this bi-pre-stressing practice and a possible solution is presented as well.

KEY WORDS

Da-Tun bridge; precast bi-pre-stressing; experimental Investigation

INTRODUCTION

Beam reinforcement using compressed steel bars to make the upper end of the concrete beam under pre-tensioning force in addition to the conventional pre-stressing concrete technique was invented by Dr. H. Reiffenstuhl and applied to the construction of the Alm Bridge in Austria. In Poland, Dr. S. Drewnowski tested many beams with post-compressed reinforcement and presented a new type of anchorage system. This construction method is called the Bi-Pre-stressing System (Ye et al, 1990, Cormack, 1990, Barker and Puckett, 1997) in Japan and some bridges were built by this method recently. The traditional pre-stressed concrete systems could be grouped into pre-tensioning and post-tensioning systems. In the 1960s, with the development of higher strength steel, better attachment hardware, better construction techniques, and simplified design methods, the use of post-tensioning to reinforce structures became popular worldwide. The Bi-pre-stressing System is developed on the base of conventional post-tensioning concrete technology. It further strengthens the system by applying pre-tension force to the upper end of the concrete beam via embedded pre-compressed reinforcing steel bars. In China, the bi-pre-stressing system and corresponding technologies

have been studied since the 1990s. In this paper, the experimental investigation of the first precast, bi-pre-stressing simple girder concrete bridge in China, the Da-Tun Bridge, is presented.

BRIEF INTRODUCTION OF THE THEORY

Bi-pre-stressing system: upper end setup of the girder. Concrete is strong in compression and weak in tension. For the working girder in a bridge, its upper end is under compressive force while the lower end is under tensile force. The conventional "Pre-stressed concrete" is concrete that is pre-compressed by stressing the reinforcement in the lower end before loads are applied. Since the tensile force in the lower end under loads will be counteracted by this pre-stressed compressive force, the pre-stressing technology greatly increases the concrete's ability to resist tensile forces without excessive cracking. There are two types of pre-stressing systems: pre-tensioning and post-tensioning systems. Pre-tensioning systems are methods in which the strands are tensioned before the concrete is placed (PCI Design Handbook, Chen et al 1999). This method is generally used for mass production of pre-tensioned members. Post-tensioning systems are methods in which the tendons are tensioned after concrete has reached a specified strength. This technique is often used in projects with very large elements. The main advantage of post-tensioning is its ability to post-tension both precast and cast-in-place members (Chen et al 1999). Similarly, in this study, to further counteract the compressive force in the upper end when it is under loads, we can pre-compress the high-strength steel bars in the prepared duct with a jack and fix them later with an anchorage bolt. Therefore, after the jack is removed, the high-strength steel bars will cause the upper side of the concrete to be under tensile force. Together with the conventional post-tensioning technology applied in the lower end of the girder, the girder is further strengthened. One type of the upper end setup for the bi-pre-stressing system is illustrated in Figure 1.

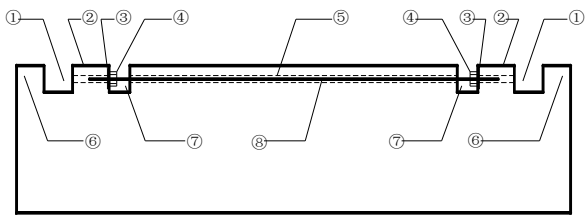

Figure 1. A type of upper end setup in the bi-pre-stress girder.

①jack slot,②anchorage bearing,③pad ,④archer bolt,⑤prepared duct,⑥jack counteract bearing ,⑦anchorage slot,⑧pre-compressed steel bar

The reason of girder thickness can be reduced without loss of equivalent load-carrying capacity. Suppose the girder cross section is rectangular, neglecting the weakening caused by the prepared duct, then under working load, as

illustrated in Figure 2, the stresses in the cross section should be subject to

$$\sigma_{hs} = \frac{N_y - N_y^{'}}{A} - \frac{N_y e_y + N_y^{'} e_y^{'}}{I} y_s + \frac{M}{I} y_s \le [\sigma_{ha}] \tag{1}$$

$$\sigma_{hx} = \frac{N_y - N_y^{'}}{A} + \frac{N_y e_y + N_y^{'} e_y^{'}}{I} y_x - \frac{M}{I} y_x \ge 0 \tag{2}$$

Where σ_{hs} and σ_{hx} are stress at the top and the bottom end of the cross section respectively, N_y and $N_y^{'}$ are the pre-stress caused by the strand at the bottom and pre-stress caused by the steel bar on the top respectively, e_y and $e_y^{'}$ are the distances of the N_y and $N_y^{'}$ to the central axis of the cross section, y_s and y_x are the distances of the top and bottom to the central axis of the cross section, M is the deflection moment of the cross section caused by the load, $[\sigma_{ha}]$ is the design stress, I is the inertia moment of the cross section, and $A = bh$ is the cross section area of the girder. Set $\sigma_{hx} = 0$, $y_x = kh$.

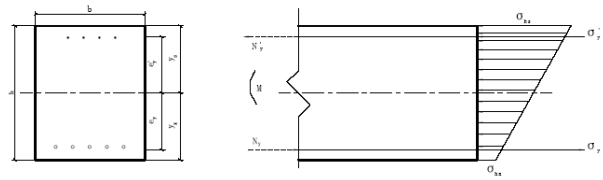

Figure 2. Stress analysis of the cross section in the girder.

Then solve Eq.(1) and Eq.(2), we have

$$\sigma_{hs} = \frac{N_y - N_y^{'}}{kbh} \tag{3}$$

For the conventional pre-stressed concrete girder, $N_y^{'} \equiv 0$. Suppose the width of the girder *b* is fixed, then σ_{hs} will increase when the thickness of the girder *h* decreases, When *h* is too small, $\sigma_{hs} > [\sigma_{ha}]$, the girder has failed. However, for the bi-pre-stressing girder, $N_y^{'} \neq 0$, when *h* decreases, by adjusting N_y and $N_y^{'}$, we still can keep $\sigma_{hs} \le [\sigma_{ha}]$. Therefore, in a bi-pre-stressing system, the thickness of the girder can be further reduced.

INTRODUCTION OF THE DA-TUN BRIDGE

The first precast, bi-pre-stressing simple girder concrete bridge in China, the Da-Tun Bridge, was constructed between 2000-2001, in LuanPing County, HeBei Province, China, over the Maoniu River. The total span of the bridge is 125m. The box girder span length is 40m, girder height is 1.35m and it employs the bi-pre-stressing setup as shown in Figure 1. The cross section of the box girder and corresponding steel bar layout is shown in Figure 3.

Figure 3 shows the Cross section of the box girder and corresponding steel bars layout, all sizes marked out in the figure are in mm.① #1-#6 pre-compressed steel bar, from left to fight, $\phi 32mm$,②pre-tensioned strand, $7 \times (7 \times \phi 5mm)$,③

pre-tensioned strand, $9\times(7\times\phi 5mm)$,④pre-tensioned strand, $9\times(7\times\phi 5mm)$,⑤ pre-tensioned strand, $12\times(7\times\phi 5mm)$ .Figure4 shows the field view of the cross section of the box girder.

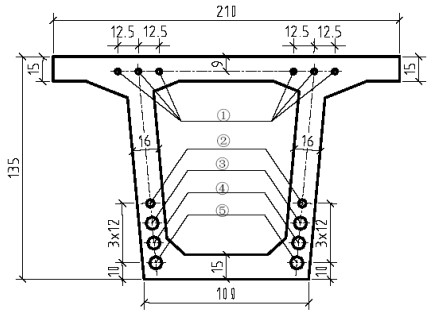

Figure 3. Cross section of box girder.

Figure 4. Cross section of the box girder

EXPERIMENTS

Pre-stress loss experiments. The key of the bi-pre-stress technique is how to control or reduce the pre-stress loss in the upper end of the girder. The major pre-stress loss in the Da-Tun Bridge construction included loss due to concrete shrinkage, loss due to elastic shortening, loss due to creeping of concrete, loss due to relaxation of pre-stressing steel bars, and loss due to friction. In order to achieve the equivalent pre-stress effect, pre-stress loss experiments are designed and performed. The experimental setup is shown in Figure 5.

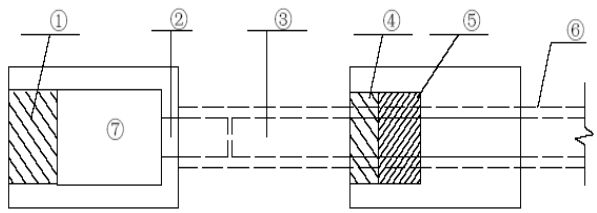

Figure 5. Pre-stress loss experiment setup.

①load Sensor #1,②retractable spear,③pre-compressed steel bar ,④load Sensor #2,⑤anchor bolt,⑥prepared duct, ⑦hydraulic jack

First, The load sensor #1 (BLR-1, 100T, Shanghai MB Automation Instrumentation Co.,Ltd, Shanghai, China) is used to measure the input pressure generated by the hydraulic jack (MJD100-300, Shanghai Liliang Hydraulic Co., Ltd, Shanghai, China). Then we fix the anchor bolt as shown in Figure 6 and remove the

hydraulic jack (MJD100-300, Shanghai Liliang Hydraulic Co., Ltd, Shanghai, China). Next, from the load sensor #2 (BLR-1, 100T, Shanghai MB Automation Instrumentation Co., Ltd, Shanghai, China), we can read the residual pressure of the steel bars. The difference between the readings of the two load sensors is believed to be the pre-stress loss at the exposed end of the reinforcing steel bar in the experiment.

The corresponding field view of the pre-stress loss experiment is shown in Figure 6.

Figure 6. Pre-stress loss experiment field view

For a girder later making up the Da-Tun Bridge, the pre-stress loss experiment is executed on the 6 reinforcing steel bars in the upper end, as marked out in Figure 3. The results are shown in Table 1. The input pressure is read from the load sensor #1 as shown in Figure 5 and the output pressure is read from the load sensor #2 as shown in Figure 5 after 24 hours.

Table 1. Pre-stress loss experiment result

Number of the reinforcing steel bar	Input pressure (*kN*)	Output pressure after 24 hours (*kN*)	Loss (*kN*)	Loss ratio %
1#	589.9	441.8	148.1	25.1
	627.8	517.1	110.7	17.6
2#	605.4	525.9	79.4	13.1
	559.6	452.6	107.0	19.1
3#	568.5	415.2	153.3	27.0
	582.0	483.3	98.7	17.0
4#	589.9	480.8	109.1	18.5
	535.0	471.9	63.1	11.8
5#	617.2	432.1	185.1	30.0
	596.6	419.7	176.9	29.6
6#	586.7	527.0	59.7	10.2
	592.0	438.3	153.7	26.0
Average	587.6	467.1	120.4	20.4

As shown in Table 1, the pre-stress loss ratio shows a maximum of 30%, a minimum of 10.2%, and an average loss of 20.4%, while the design pre-stress loss ratio is <15%. In order to meet the design loss, we examined the procedures and made some revisions:

1)Make the thread groove finer for the anchor bolt and try to further fasten the anchor bolt.

2)Reduce the length of the exposed ends of the reinforcing steel bars, to reduce the pre-stress loss due to flexion of the exposed end.

3)Compress the two ends of the reinforcing bars simultaneously, slowly, and smoothly.

After the revision, in repeated tests and corrections on multiple girders, the pre-stress loss could be lowered to below 15%.

Girder load capacity experiments. The static load capacity experiments scene is shown in Figure 7.

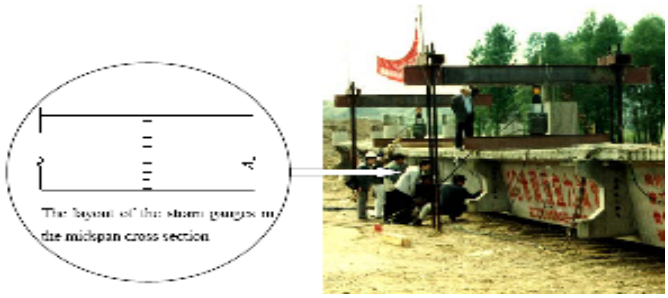

Figure 7. Going-on static load experiment of a single girder.

We apply load to the girder at two locations at the same time and at each location the basic setup of the supporting setup is shown in Figure 8.

Figure 8. Static load experiment setup.

The supporting setup is anchored underground, as shown in Figure 8, counteracted by the hydraulic jack (MJD300-300, Shanghai Liliang Hydraulic Co., Ltd, Shanghai,, China), which is now used to apply load to the steel beam laid on the girder and therefore equivalently. A line load is applied to the girder at this location. Load is applied to the girder in three rounds, each including 7 steps from 0kN to 368kN. Strain gauges (XT-5, Xingtai Electronic Equipment Factory, China) are attached on the surface of both sides of the tested girder, 4 cross sections, and on each sections 9 locations from the bottom end to the top end of the girder, as pointed out in Figure 8, totaling 36 measurement points, so for both sides, totaling 72 points. Some typical results are shown in Figure 9 and Figure 10. In Figure 9, the plane section hypothesis is tested on the mid-span cross section of the girder. On the mid-span cross section, the strain-load relation is approximately linear and the deflection is regarded as elastic, which means the plane section hypothesis fits.

For the hypothesis evaluation of the girder mid-span section under various loads, the x-axis stands for the height of the strain gauge location from the bottom of the girder and the y-axis stands for the strain under various loads.

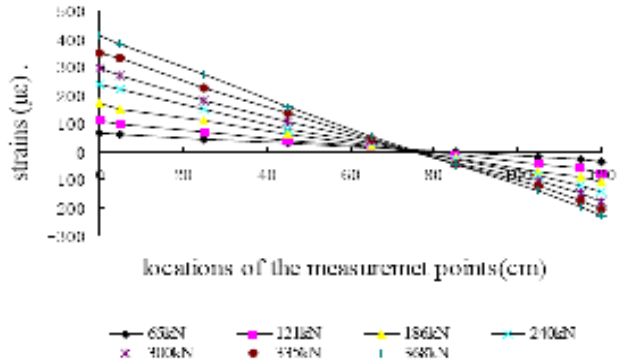

Figure 9. The plane section.

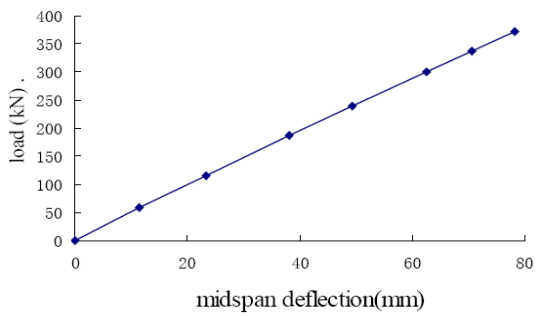

Figure 10. The load-deflection relation curve in the mid-span cross section of the girder.

Eventually, the Da-Tun Bridge was constructed with 3x5 matrix of the girders we studied before. The overview of the bridge was already shown in Figure 5.

We tested the static load property of the bridge, as shown in Figure 11, in a similar way to the girder experiments. The bridge cross section also agrees to the plane section hypothesis, indicating the bridge is working in an elastic way. The curve of the deflection - load is nearly linear. The approximate deflection-span ratio is 1/1826, meeting the requirement of the design ratio, which is <1/600. It also shows sufficient emergency capacity.

Figure 11. Static load experiment of the Da-Tun Bridge.

We also did some experiments to test the dynamic deflection and oscillation response of the bridge. A heavy truck is asked to move over the bridge at a velocity of 10*km/h* to 60*km/h* and along middle of the bridge width. The maximal dynamic deflection turns out to fall between 1.26-1.46mm and the maximal shock factor in the experiments is 1.039. When the truck's velocity is 40*km/h*, though the design shock factor is 1.0375, the difference between the design and measured maximal shock factor is less than 0.1% , therefore the shock factor is regards as acceptable. A typical test curve is shown in Figure 12. It is believed that because the higher measured shock factor is partly due to the fact that the actual rigidity of the bridge is higher. We also tested the oscillation property of the bridge by driving a heavy truck onto the bridge, then over a temporary bump (deliberately laid there), and breaking quickly after the truck passed over the bump. In the repeated experiments, the maximal oscillation amplitude is 1.479mm. Oscillation is the first order transverse deflection oscillation mode, with frequency = 2.403Hz and damping constant = 0.025. A typical test curve is shown in Figure 13.

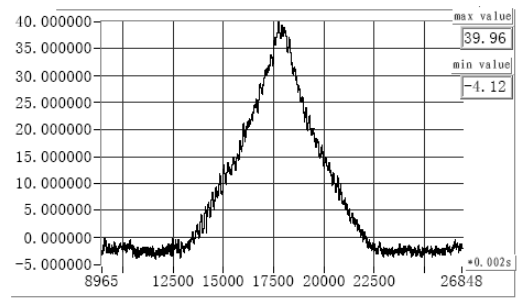

Figure 12. Typical working bridge test curve when the truck velocity is 40km/h. X-axis, y-axis stands for time and deflection amplitude respectively.

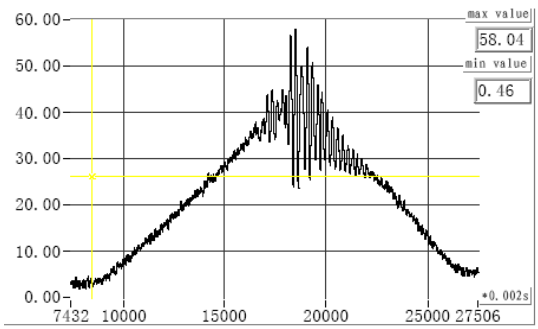

Figure 13. Typical working bridge shock test curve. X-axis, y-axis stands for time and deflection amplitude respectively.

All experiments in this section follow the Code of "Design of reinforced concrete and pre-stressed concrete highway bridges and culverts, JTJ023-85" of Chinese Ministry of Communications and the code of "Standard Methods for Testing of Concrete Structures, GB 50152-92" of the Chinese Ministry of Construction. (Chinese Ministry of Communications 1985, Chinese Ministry of Construction 1992).

CONCLUSIONS

The bi-pre-stressing technique is promising in China, especially for long span, large-scale, precast bridge construction, such as overpass bridges, flying bridges, and fly-over crossing bridges in the districts where the highway traffic is heavy or the river network is intensive. The comprehensive experiments on the Da-Tun Bridge shows that, 1) The construction technology presented in the paper is feasible, 2) the elastic property of the bi-pre-stressing simple girder bridge is satisfactory and the emergency capacity is sufficient, and 3) the problems of the anchorage system and pre-stress loss could yet be improved.

ACKNOWLEDGMENT

This work is part of the Nine-Five scientific project (No.95050203) of "Study on the bi-pre-stressing bridge", supported by Chinese Ministry of Communications.

REFERENCES

Ye, Jian-shu, Fu, Guan-hua, Ma, Yue-feng, An, Lin, Yang, Yi-wen, Chen, Xiao-qiang (1990), "Anchorage of post-compressed steel bar in Bi-prestressed concrete beams", *Journal of Highway and Transportation Research and Development*, 17(3), 21-24.

Cormack, G.(1990), "Advances In Concrete Construction - Materials And Techniques", *New Zealand Engineering*, 45(7), 8-9.

Barker, R. M., and Puckett, J.A. (1997),*Design of Highway Bridges*, John Wiley and Sons, Inc,.

PCI Design Handbook – *Precast and Prestressed Concrete*, 3rd ed., Prestressed Concrete Institute, Chicago, IL.

Chen, Wai-Fah, Duan Lian Ed (1999). *Bridge Engineering Handbook*, 1St ed., CRC Press, Boca Raton Florida.

Don Ariyawardena, Nihal; Ghali, Amin (2002), "Design of precast prestressed concrete members using external prestressing", *PCI Journal*,47(6), 108-109.

Nasvik, Joe (2003), "Post-tensioned concrete comes of age: while traditional reinforced concrete construction hasn't changed much in the past four decades, post-tensioned design and construction methods have become simpler", *Concrete Construction*, 1(2),35-48.

Walley, F. (1996), "Prestressing", Proceedings of the Institution of Civil Engineers, *Structures and Buildings,* 116(3-4), 390-403.

Chinese Ministry of Communications (1985), "*Design of reinforced concrete and prestressed concrete highway bridges and culverts*", JTJ023-85, Chinese Ministry of Communications.

Chinese Ministry of Construction (1992), "*Standard Methods for Testing of Concrete Structures*", GB 50152-92, Chinese Ministry of Construction.

Study on Long-Term Behavior and Ultimate Strength of CFST Columns

Xianyan Zhou[1], Guohui Cao[2], Ran He[2] Xiangrong Liu[2]

[1]School of Civil, Architectural and Mechanics, Central South University of Forestry and Technology, Changsha, 410004, China, e-mail: zxy560805@163.com
[2] School of Civil Engineering, Hunan City University, Yiyang，413000, China, e-mail: cgfcivil@163.com

ABSTRACT

Long-term tests (864 days) were conducted on three types of columns, including plain concrete (PC) columns, reinforced concrete (RC) columns and concrete-filled steel tube (CFST) columns. The shrinkage and creep performance and the ultimate strength of the columns were tested and analyzed. The results show that the shrinkage strain of RC columns is about 87.6% of that of PC columns, the shrinkage strain of the CFST columns is about 34.8% of that of PC columns, and that the effect of expansion agent on shrinkage strain is about 2% for the PC columns. It was also found that the smaller the loading age, the greater the creep coefficient. Reinforcement can significantly reduce the creep deformation of PC columns. The creep coefficient of steel pipe surface is larger than that of inner concrete for CFST columns, leading to a longer life due to the creep of inner concrete to achieve stability. The loading age and the reinforcement have great impact on extreme compressive strain and ultimate strength. The hoop effect of RC columns is obvious. Loading rate influences the stress redistribution of CFST columns. The stress redistribution effect is relatively small for columns with loading course. However, the effect on the ultimate strength is very small for columns with or without loading courses. The difference of two is only 2.4%.

INTRODUCTION

Concrete-filled steel tube (CFST) members as axial compression members or eccentric compression members have been used widely in actual projects. The creep performance is one concerned problem in the actual project applications (Zhong 2003, Wang and Han 2000). The shrinkage and creep problems of CFST are more complex than plain concrete since CFST is a composite structure composed of steel pipe and core concrete. The curing of core concrete in steel pipe is different from that of common concrete (Yao et al. 2007). During the creep process of CFST members, stress redistributes in the steel pipe and concrete, leading to a three dimensional stress state for the steel pipe and concretes. The stress redistribution caused by creep is even

more complex (Han et al, 1999).

Furlong discovered that creep had great effect on the mechanical properties of CFST through the experimental studies (Furlong 1968). This is the earliest research report on creep properties of CFST members. Afterwards, many domestic scholars have studied the creep of CFST members and led to some research results. Tan et al. carried on the long-term load experiment for the CFST compression members (Tan and Qi 1987). Wang and Han carried on the thorough analysis to the axial compressive CFST structures (Wang and Han 2000, Han et al. 2007)Han et al. studied the ultimate strength and deformation properties of axial compressive square CFST columns under long-term load (120d) (Han et al. 2001). A more than 2 year's experimental studies was conducted by Yao et al. based on the Mao Caojie bridge in which Yao studied the shrinkage and creep performance of the CFS^T (Wang and Han 2000). In this paper, long-term tests (864 days) were conducted on three types of columns, including plain concrete (PC), reinforced concrete (RC) and CFST columns. The shrinkage and creep performance, and the ultimate strength were tested and analyzed.

SPECIMEN DESIGN

Thirteen circular short column specimens were manufactured, including PC column, RC column, and CFST columns. Specimens are 150mm in diameter, 600mm in height. Loading age, loading stress, with/without reinforcement and mixing expansion agent of specimens were considered. Eight specimens were studied for the long-term load experiment, and 5 specimens were used as shrinkage contrast specimens. The basic parameters of specimens are given in Table 1. The concrete strength grade is C50; and the mixing amount of expansion agent is 6%. The reinforcement ratio of RC column is 1.49%; and the inner strain gauges of concrete for long-term tests were placed in 1#, 4#, 11#, and 13# specimens. The mechanical properties of concrete are given in Table 2, and themechanical properties of steel bars can be found in Table 3.

SHRINKAGE DEFORMATION

Shrinkage was tested on the 3#, 6#, 9#, 13# specimens that were cured for 7d. The longest observation time is 871 days. The range pole was installed in specimens' surface symmetrical position (test distance is about 280 mm). Shrinkage deformation of concrete was measured using dial gauge. Concrete strain gauges were pre-embedded in the 13# specimen (CFST columns) to test the shrinkage deformation of core concrete. All of tests were conducted at the ambient temperature and humidity. The actual temperature ranged from -1.2 to 39.4°C, and the actual environment humidity ranged from 37 to 87%.

Table 1. Basic parameters of specimens

Group	No. of specimen	Whether reinforced	Loading age/d	Time/ d	Initial load stress /MPa	Whether add expansion agent	Ultimate Load /kN
I	1#	PC	14	864	11.60	no	790
	2#		28	850	11.60	no	842
	*3#		Contrast specimen start to test at 7d			no	797
II	4#	RC	14	864	11.60	no	980
	5#		28	850	11.60	no	1058
	*6#		Contrast specimen start to test at 7d			no	900
III	7#	PC	7	846	10.50	no	592
	8#					yes	784
	*9#		Contrast specimen start to test at 7d			yes	842
IV	10#	CFST	7	846	10.50	no	1110
	11#					yes	1137
	*12#		Contrast specimen start to test at 7d			no	1118
	*13#					yes	1113

* contrast specimens.

Table 2. Mechanical properties of concrete

Age/ d	Common concrete		CFST concrete		
	Cubic compressive strength /MPa	Elastic modulus /GPa	Cubic compressive strength (add expansion agent)/MPa	Cubic compressive strength (no expansion agent)/MPa	Elastic modulus (add expansion agent)/GPa
7	43.6	/	46.2	39.4	/
14	47.9	43.0	52.6	45.6	47.4
28	54.0	43.6	57.0	50.0	48.9
90	/	46.1	/	/	/
196	/	46.4	/	/	/
393	69.8	47.7	69.0	63.9	/
896	72.4	49.2	71.2	69.5	49.5

Table 3. Mechanical properties of steel

Content	Diameter or thickness /mm	Yield strength /MPa	Tensile strength /MPa	Elastic modulus /GPa	Elongation after fracture /%
steel bar	8.20	548.2	594.3	195	6.2
steel pipe	0.80	222.8	258.7	205	8.4

Figure 1 shows the shrinkage strain comparison curve of the 3# and 6# columns, and Figure 2 gives the shrinkage strain comparison curve for the 9# and 13# columns. The following conclusions were obtained based on the measured results:

(1) From Figure 1, the shrinkage strain of the RC column (6#) is about 87.6% of that of the PC column (3#). The RC column and the PC column however show the same change tendency in shrinkage strain. The shrinkage strain development of earlier period was rather quick. For the PC column, shrinkage completed in 1 month, 2 months, 3 months, 6 months, and 1 year were 53.1%, 70.7%, 79.7%, 90.6%, 97.5% of the total shrinkage, respectively.

(2) From Figure 2, the shrinkage strain of the CFST column (13#) is about 34.8% of that of PC column (9#). The curing of core concrete in steel pipe is different from that of common concrete, causing the small shrinkage deformation for core concrete of the CFST. Shrinkage deformation of both columns develops quickly in earlier curing period, which contributes to the long time stability.

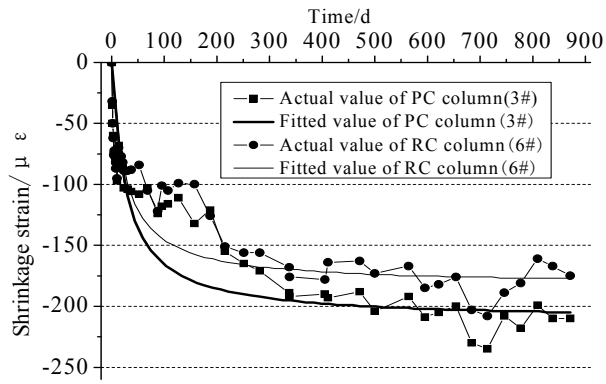

Figure 1. Shrinkage strain comparison of 3# and 6# columns

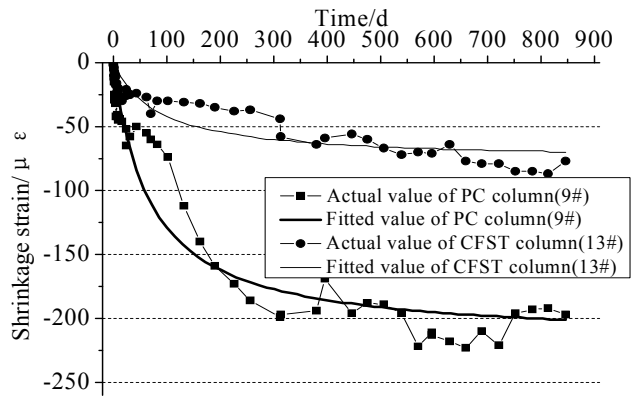

Figure 2. Shrinkage strain comparison of 9# and 13# columns

(3) Contrasting shrinkage strain curve of the 3# specimen to that of the

9# specimen shows that shrinkage strain development in earlier stage would be relatively slow for PC column (9#) using mixed expansion agent, which achieved stability for a longer time. The effect of expansion agent on shrinkage strain is about 2% for PC columns.

CREEP DEFORMATION

Creep deformation. Long-term tests (864 days) conducted on the three types of columns using creep loading device are shown in Figure 3. The loading age, loading stress, with/without reinforcement or mixing expansion agent were considered.

Figure 3. Loading device for creep test

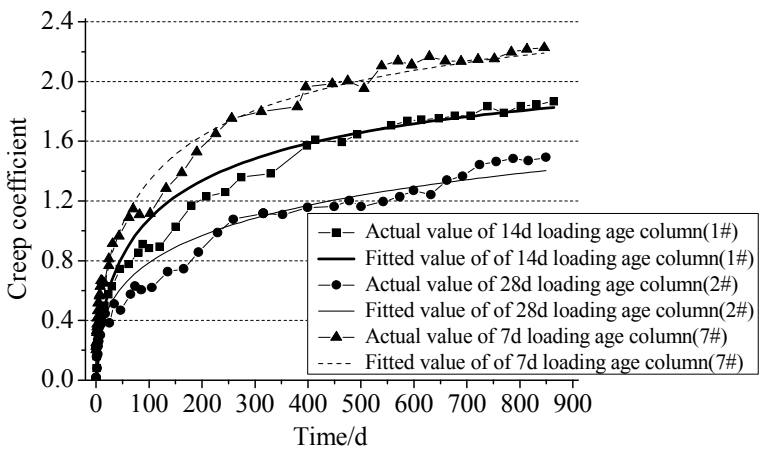

Figure 4. Effect of loading age on creep coefficient

Figure 4 shows that the creep curve of PC column has the same change tendency at different loading ages. the creep development in earlier period is fast, and the development in later period is relatively slow. The younger the loading age is, the greater the creep will be. Creep coefficient of the specimen loaded on the 7 day (7#) increased about 20.0% compared to that of the 14-d

loading age (1#). Creep coefficient of the 7-d specimen (7#) increased about 56.2% compared to that of the 28-d specimen (1#).

Figure 5 shows that reinforcement can significantly reduce the creep deformation of concrete columns. Creep curve of RC columns and PC columns have the same change tendency. The creep development in earlier period is quick, while the creep development in later period is relatively slow. Creep coefficient of the 14-day RC column (4#) is about 35.2% less than that of PC column (1#). Creep coefficient of the 28-day RC column (5#) is about 24.2% less than that of PC column (2#).

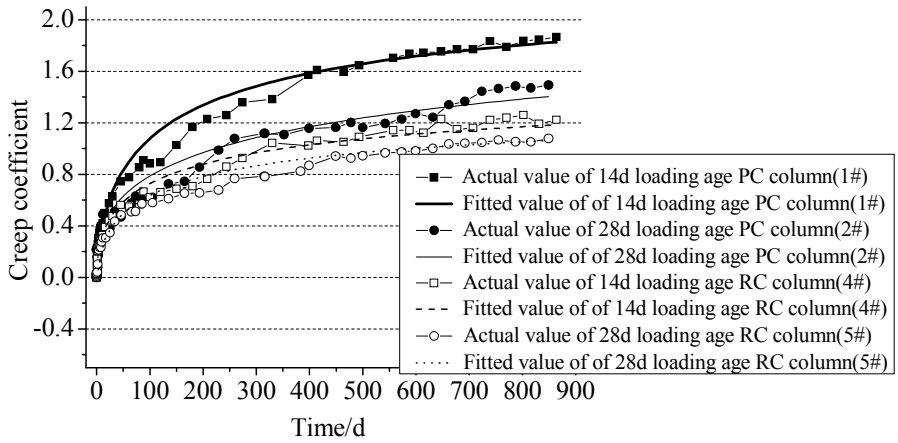

Figure 5. Effect of reinforcement on creep coefficient

Creep analysis. Based on the actual creep coefficient, the fitting curve obtained according to the expression proposed by Branson et al. (Zhou and Chen 1994) and the comparison to two kinds of common creep coefficient model, including ACI-209R-92 mode (ACI 1992) and CEB-FIP(MC90) mode (CEB-FIP 1990), are shown in Figure 6 and Figure 7.

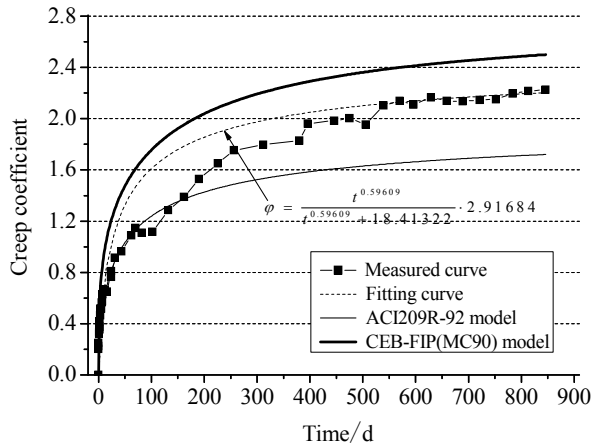

Figure 6. Creep coefficient comparison of 7d loading age

(1)Figure 6 shows that the 7-d loading PC column (7#) holds load for 846 days, and that the creep coefficient calculated using the ACI209R-92 model is 21.9% less than fitted value. The creep coefficient calculated using the CEB-FIP (MC90) model is 13.4% higher than the fitted value. Therefore, creep coefficient can be more accurately predicted according to CEB-FIP (MC90) model.

(2)Figure 7 shows that the 28-d PC column (2#) holds load for 850 days, and that the creep coefficient calculated using the ACI209R-92 model is 2.0% less than the fitted value. The creep coefficient calculated using the CEB-FIP (MC90) model is 30.1% higher than the fitted value. Therefore, creep coefficient can be more accurately predicted according to the ACI209R-92 model.

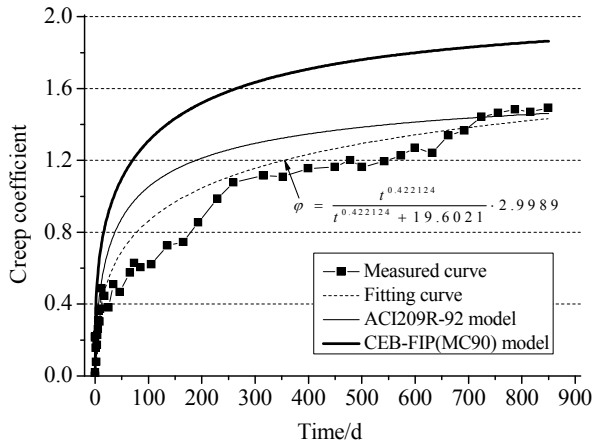

Figure 7. Creep coefficient comparison of 28-d loading age

ULTIMATE STRENGTH EXPERIMENT

Test results. When unloaded after a 2-year testing period, the longitudinal pressure strain was measured, and the destruction shape of specimens as shown in Figure 8. Test results are shown in Table 1. The destruction characteristic of the specimens is as follows:

(1) For PC columns, the longitudinal crack appeared on both the bottom and the top of the specimens, which later on shifted to the middle. It was the shearing failure that caused the loss of supporting capacity for the specimens.

(2) For RC columns, when load level reaches the supporting capacity, bulging deformation was observed at the middle of specimen. Both the bottom and the top of specimen crushed. It was the steel bar compressive buckling that caused the loss of supporting capacity for the specimens.

Figure 8. Destruction shape of specimens

(3) For CFST columns, when load level reaches the supporting capacity, bulging deformation was observed at the middle of steel pipe. It was the steel pipe compressive buckling that caused specimen losing supporting capacity.

Test result analysis. Load-strain relation of columns with and without mixing expansion agent is shown in Figure 9. The figure shows that the ultimate strength of PC column (8#) with expansion agent was 32.4% higher that that of PC column (7#). Under the same load condition, the outside strain of CFST column without loading course (12#) was about -11.9%~52.0% larger than that of CFST column with loading course (11#). The deviation is small at the initial period, while that near destruction is big. The stress redistribution effect is relatively small for the column with loading course (11#). However, the effect of loading course on the ultimate strength is very small, and the difference is only 2.4%.

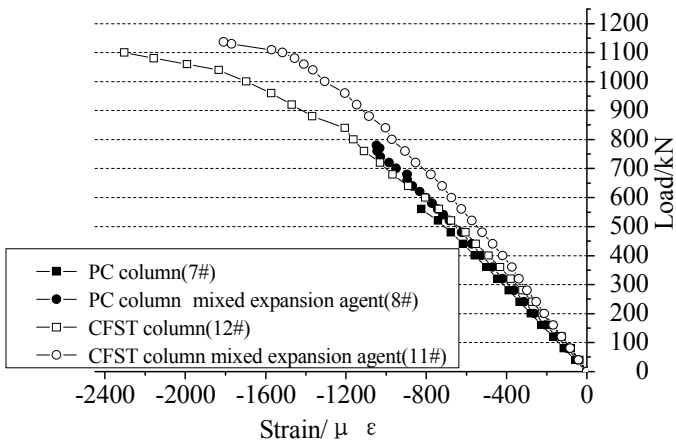

Figure 9. Load-strain relation of columns with/without expansion agent

CONCLUSIONS

Based on the results of the long-term and ultimate strength experiments, the following conclusions can be drawn:

(1) The shrinkage strain of RC columns is about 87.6% of that of PC columns; the shrinkage strain of the CFST columns is about 34.8% of that of PC columns; the effect of expansion agent on shrinkage strain is about 2% for PC columns.

(2) The smaller the loading age is, the greater the creep coefficient will be. Reinforcement can significantly reduce the creep deformation of concrete columns. The creep coefficient of steel pipe surface is larger than that of inner concrete for CFST column. Owing to the creep of the inner concrete, long-term stability can be achieved.

(3) The creep coefficient can be more accurately predicted using the CEB-FIP (MC90) model for the 7-d PC columns; the creep coefficient is more accurate according to the ACI209R-92 model for the 28-d PC columns.

(4) The loading age and the reinforcement have great impact on extreme compressive strain and ultimate strength. The hoop effect of RC columns is obvious. Loading course influence the stress redistribution of CFST columns. The stress redistribution effect is relatively small for column with loading course. However, loading course has little the effect on the ultimate strength, the difference of ultimate strength with loading course and without loading course is only 2.4%.

REFERENCES

ACI Committee 209(1992). Prediction of creep, shrinkage, and temperature effects in concrete structures(ACI 209R-92). America Concrete Institute. Farmingtion Hills, Mich.

CEB-FIP Model Code for Concrete Structures(1990). Comite Euro International du Beton/Federation International de la Precon-strainte. Paris.

FURLONG, R.W. Design of Steel-encased Concrete Beam-columns[J]. Journal of Structural Division, 1968, 94(1): 267-281.

Han, B., Wang, Y.F. (1999). Study on Creep of Concrete-filled steel tube Members Under Axial Loading. Journal of the China Railway Society, 21(6): 87-90.

Han, L.H., Tao, Z., Liu, W., et al(2001). Effects of Long-term Loads on the Strength of Concrete-filled Steel Box Columns. China Journal of Highway and Transport, 14(3): 57-66.

Tan, S.J.,and Qi, J.L. (1987). Study on the Creep Influence on the Strength of Concrete-filled steel tube Members Under Long-term Compressing Loads.

Journal of Harbin Architectural and Civil Engineering Institute, 38(2): 10-24.

Wang, Y.F., and Han, B. (2000). Creep Analysis of axially Compressed Concrete-filled steel tube Members. China Journal of Highway and Transport, 13(2): 57-60.

Yao, H.X., Cheng, Z.Q., Li, Y. (2007). Experimental Study on Shrinkage and Creep Behavior of Concrete-filled steel tube[J]. Journal of China & Foreign Highway, 27(6): 133-136.

Zhong, S.T. (2003). Concrete-filled Steel Tubular Structures. Beijing: Tsinghua University Press.

Zhou, L., and Chen, Y.C. (1994). Creep and shrinkage. Beijing: China Railway Press.

Observation and theoretical analysis of the temperature field on the cross section of concrete filled steel tubes arch bridge rib

Sun Hang[1], Sheng Hongfei[1], Li Yan[2] and Li jianglong[1]

[1]School of Transportation Science and Engineering, Harbin Institute of Technology, No. 202, Haihe River Road, Nangang District, Harbin, Heilongjiang Province, PRC, 150090, PH:(86) 13936130776; email: brigde_hit@126.com
[2]School of Civil Engineering, Harbin Institute of Technology, No. 202, Haihe River Road, Nangang District, Harbin, Heilongjiang Province, PRC, 150090

ABSTRACT

The author has carried on an outdoor long-term temperature field observation experiment of a full-scale concrete component which is used in the Mudanjiang Bridge in Yilan, which is a half-through arch bridge with concrete-filled steel tubes, for nearly three years. Through the test, we obtain the disciplinarian of the temperature field on the cross section of the ribs, which is due to the solar radiation, the atmosphere temperature, and natural reasons. Using the heat transfer theory principle and finite element method, the paper proposed a computational method for the arch rib section's temperature field of concrete filled steel tubular arch bridges. The paper provides the basis and the reference for the construction of this kind of bridge, which built is in an area where the temperature difference is large. The study also provides reference for the determination of temperature effect in the construction and design standard of concrete filled steel tubes arch bridges, which will be established in the future.

Keywords:*concrete filled steel tubes;arch bridge; temperature field; solar radiation*

1 INTRODUCTION

Massive domestic and foreign research papers related to temperature characteristics and the temperature field of bridges were researched on reinforced concrete bridges, pre-stressed concrete bridges, and steel bridges. Moreover, most bridge cross sections are the box section and many countries' standards of bridges also have the corresponding stipulation. Just a few papers research on the temperature characteristics and temperature field of steel-concrete composite girder bridge. In the research field on temperature characteristics and arch rib temperature of concrete filled steel tubes arch bridges, only professor Chen Baochun, from Fuzhou University, had tested the temperature field of a concrete filled steel tubular member from when it was cast to hardening for nearly a month. The diameter of the steel tubular is 0.55 meter. Professor Chen Baochun introduced the influence of the hydration heat of concrete and the ambient temperature with emphasis and he established the corresponding finite difference procedure (Chen Baochun et al. 2000). In the temperature characteristic research of concrete filled steel tubes arch bridges in his paper, he arranged very few measuring points and supposed that

the arch rib section's temperature field had axial symmetry. Because the component stands in the outdoor visor place throughout the entire test process and the different regions have different climatic conditions, the analysis cannot reflect the real temperature field on the cross section of the ribs, which was under the combined action of the solar radiation and the ambient temperature (Xu aiming et al. 1993).

This paper takes the test results of the arch rib section's temperature field of the concrete filled steel tubular arch bridge built in Yilan as the foundation and proposes a computational method for the arch rib section's temperature field of concrete filled steel tubular arch bridges by using heat transfer theory principle and finite element method. The paper provides the basis and the reference for the construction of this kind of bridge, which is built in areas of large temperature difference. The study also provides a reference for the determination of temperature effect in the construction and design standard of concrete filled steel tubes arch bridges, which will be established in the future.

2 SIMPLE INTRODUCTION ABOUT THE EXPERIMENT

In order to determine the section's temperature distribution characteristics and rules of the concrete filled steel tubular component, we have carried out a outdoor long-term temperature field observation experiment of a full scale concrete component which is used in the Mudanjiang Bridge in Yilan, which is a half-through arch bridge with concrete-filled steel tubes, between 1998 to 2000. The data acquisition time interval was 3 hours and the test contents are as follow:

1) Determination of the time change regulation of the ambient temperature and the component's temperature in the season with the greatest date temperature difference;
2) Determination of the ambient temperature and component's temperature in the most bumper year temperature difference season;
3) Component's temperature field and the surrounding environment of the component's surface.

The detailed dimension of the cross section of arch rib component and the measuring point's position are show in figure 1. The units are centimeters in the chart. The digit 1~10 are the temperature measuring points. 4 points are arranged in the steel tube surface. 5 points are arranged in the core concrete. 1 point is arranged in the side toward the sun . All of the measuring points are arranged in equal intervals and symmetrical pattern.

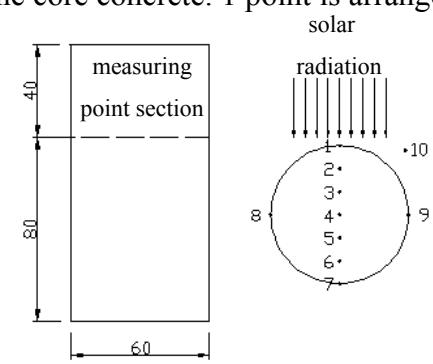

Figure 1. Component measuring points

3 THE RESULT ANALYSIS

This article uses the mean value of the measured data of the same spot position on two components as the data of experimental analysis and the statistical analysis software to analyze and compute the test data.

3.1 Influence of daily temperature difference

The measured typical curves of each moment of the arch rib section's temperature field of the concrete filled steel tubular arch bridge in the hot summer are shown in Figure 2 and for the cold winter in figure 3.

Through the analysis and comparison of massive data measured in the summer high temperature and winter low temperature conditions, we can draw the following conclusions:

1) The change of temperature in the core concrete is obviously lagging relative to the steel tube surface.
2) In one day, temperature change of the sun-facing side's surface is large, but the shady surface's and the core concrete's change is small.

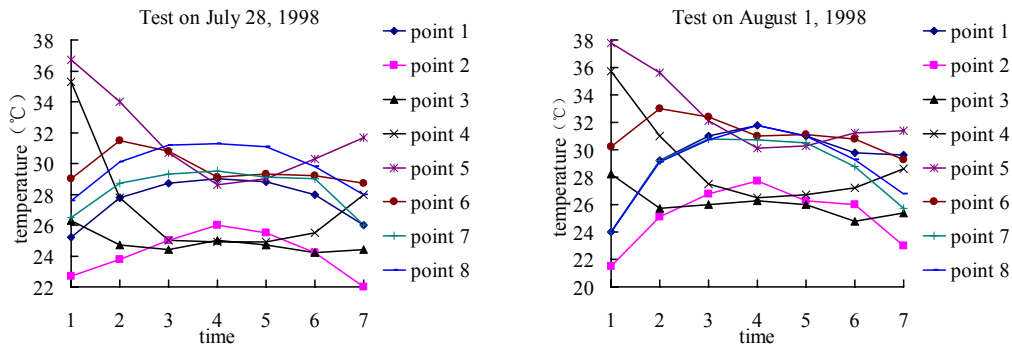

Figure 2. component section actual temperature field tested in summer

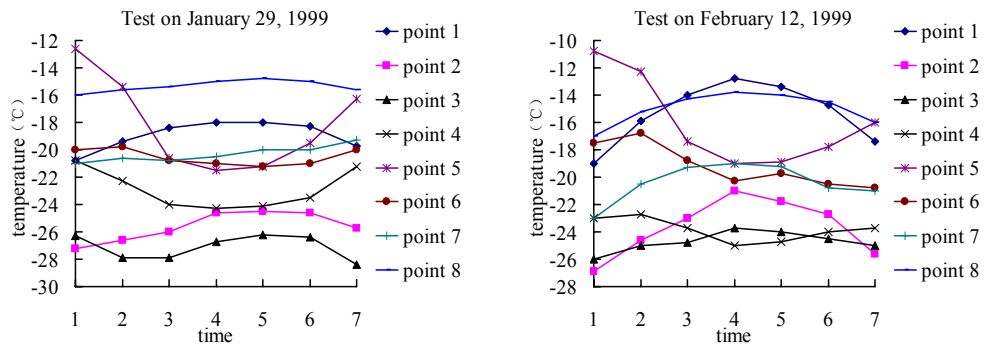

Figure 3. component section actual temperature field tested in winter

3.2 Influence of year temperature difference

The Harbin area has continental climate, the four seasons are distinct and temperature difference between the summer and winter is large. The steel tube surface temperature is deeply affected by factors such as ambient temperature and solar radiation. But the core concrete is less affected than the steel tube. The maximum disadvantageous ambient temperature and the component temperature obtained in the summer and the winter, which has great influence to the long-term temperature difference, are shown in Table 1. We can see from Table 1 that the section average temperature of the concrete filled steel tubular is higher than the free air temperature in summer and lower in winter.

Table 1. The highest, the lowest temperature actual value in a year of component different position

Project	Position				
	Ambient temperature	Steel tubular in sun side	Steel tubular in shady side	Core concrete	Atmospheric temperature
The highest temperature in summer(℃)	34.3	39.6	30.7	33.3	30.5
The lowest temperature in summer(℃)	-28.7	-28.1	-27.6	-25.8	-24.2

4 THEORETICAL ANALYSIS AND CALCULATION OF ARCH RIB SECTION'S TEMPERATURE FIELD OF CONCRETE FILLED STEEL TUBULAR ARCH BRIDGE

The section's temperature field of concrete filled steel tubular arch bridges is a transient three-dimensional temperature field. As the simplified computation, the hypothesis is as follows:

1) The concrete filled steel tubular arch bridge is a homogeneous and isotropic continuum.
2) The arch rib is a tall and slender structure. We suppose the structure temperature field along the arch rib axial direction is uniform and the interface of the arch rib and the pier is the heat insulation boundary. In other words, there is no heat conduction along the arch axis direction. The arch rib section's temperature field of the concrete filled steel tubular arch bridge is simplified to the plane problem of the arch rib section :

$$T=f(x,y,t) \tag{1}$$

3) The concrete and steel tubular have good contact and the temperature and heat flow on the contact face is continuous, which is the completely contacting boundary condition (Fourth kind of boundary condition) .

Based on above hypotheses and the Fourier heat conduction theory, we can determine the no inner heat source two-dimensional transient heat conduction equation:

$$\frac{\partial T}{\partial t}=\frac{k}{\rho c_p}\left(\frac{\partial^2 T}{\partial x^2}+\frac{\partial^2 T}{\partial y^2}\right) \tag{2}$$

In the formula: $T[°C]$——transient state temperature of the object;

$t[s]$——time of the process；

$k[w/(m\cdot°c)]$——the coefficient of heat conductivity of material, which is a constant;

$\rho[kg/m^3]$——density of material, which is a constant;

$C_p[J/(kg\cdot°c)]$——the specific heat at constant pressure of material, which is a constant;

$x, y[m]$——Decca rectangular coordinates.

We determine the initial condition by the reference, unifying the actual situation of Harbin area, and the actual result. Before the sun rising, the temperature remains constant for several hours. The temperature of the internal place of the component approaches the exterior temperature (the temperature gradient is 0). Therefore this article uses the temperature mean value of every point in 5 o'clock as the initial uniform temperature to compute the summer sunshine's influence. Likewise, we consider 15 o'clock as the initial time to compute the winter cold night divergent radiation and use the temperature mean value of every point in 15 o'clock as the initial uniform temperature.

The boundary conditions of the arch rib section's temperature field of the concrete filled steel tubular arch bridge divide into two parts, which are the sun side and the shady side. According to the principle that "the quantity of heat on the boundary surface does not extinguish" and by using the weighted residual method, we can deduce the basic equation using the finite element method of the no inner heat source two-dimensional transient temperature field (Qu zhaojun et al. 2000).

$$\iint_D [k(\frac{\partial W_l}{\partial x}\cdot\frac{\partial T}{\partial x}+\frac{\partial W_l}{\partial y}\cdot\frac{\partial T}{\partial y})+\rho c_p W_t\frac{\partial T}{\partial t}]dxdy-\oint_\Gamma kW_l\frac{\partial T}{\partial n}ds=0\ (l=1,2,...,n) \quad (3)$$

In the formula: D——the Definition Domain of the temperature field;

T——undetermined parameter;

W_l——weighted coefficient;

Other symbols are the same as the previous formula.

We have established a calculating program with the finite element method in the foundation of formula (3), which also considers the characteristics of the arch rib section's temperature field of the concrete filled steel tubular arch bridge we have researched. The element shape of the program is the triangle (figure 4) and this element can be use to solve the two-dimensional stable state, the transient state, and the axial symmetry questions.

We choose the structure's temperature field to confirm the computational accuracy of the procedure, which is at the most disadvantageous time in the high temperature summer: 11o'clock and 14 o'clock. The calculated results and actual value comparisons are show in Fig. 5.

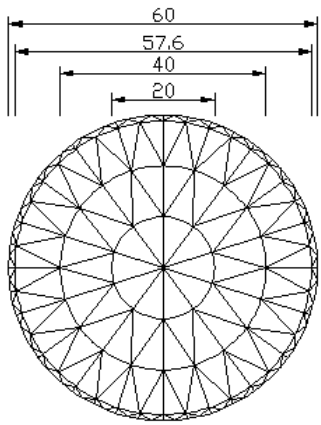

Figure 4. finite element unit division of calculation model

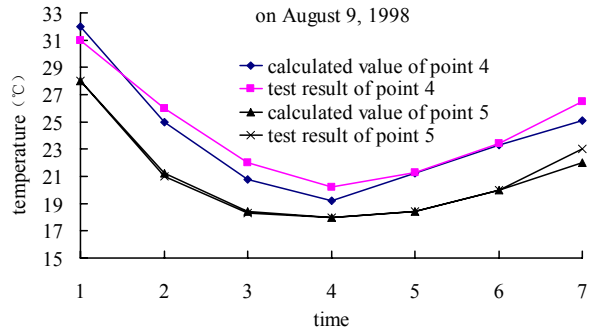

Figure 5. Temperature field actual value and calculated value of the component

5 CONCLUSION

This study has shown that the distribution of the section's temperature field of the concrete filled steel tubular members are as follow:

1) The change laws of the steel tube surface temperature and ambient temperature are basically synchronous. But the change of temperature in the core concrete is obviously lagging.
2) The temperature on the sun side of the concrete filled steel tubular members is far higher than the ambient temperature. The biggest differential value may achieve 10℃.
3) The change range of section's temperature field of concrete filled steel tubular members is far greater than that of the ambient temperature field.

REFERENCES

Chen baochun. (2000). "Analysis of thermal difference magnitude in thermal lnner force calculation of CFST arch bridge." China journal of highway and transport. Xi an. China. Feb.12, 54-58

Xu aiming,Chen baochun. (1993). "Value Analysis of CFST Arch Bridge s Temperature Stress." Journal of fuzhou university(natural sciences edition). Fuzhou. China. Mar(3), 17-20

Kong xiangqian. (1998). "Application of finite element method in heat transfer (The third edition)." Scientific Press. China. 45-47

Qu zhaojun. (1982). "Principle of using finite element method to solve temperature stress." Bridge Construction, wuhan. China. 23-25

Zhu bofan. (1989). "temperature stress and temperature control of Mass concrete."

Chinese Electricity Press. Beijing. China. 88-102

Influencing Factor Analyses of Section Types on Vehicle-bridge Interaction of Concrete Box Girder with Corrugated Steel Webs

Baodong Liu[1], Pengfei Li and Lingxiang Xue

[1]School of Civil Engineering, Beijing Jiaotong University, Beijing 100044, China, email: baodongliu@vip.sina.com

ABSTRACT

Along with the further study on concrete box girder bridges with corrugated steel webs, its dynamical characteristics, including vehicle-bridge vibration response, received much concern. Section types of concrete box girder bridges with corrugated steel webs have a great influence on its dynamic performance. Two parallel boxes double cells and single box double cells are common in practical applications. By constructing the finite element models of girders with these section types, the natural vibration characteristics are obtained and compared**.** The vehicle-bridge coupling response is discussed while vehicles are on different lanes and at different speeds. The comparison shows that the torsional rigidity and integrity of the two parallel boxes double cells girder is weaker than the single box double cells girder. The change of deflection at mid-span is linear when the number of vehicles increase, and the vehicle-bridge vibration response is more remarkable when the excited frequency is close to the bridge's first natural frequency.

Keywords: Box girder with corrugated steel webs, Vehicle-bridge coupling vibration, Section types, Natural vibration characteristics

INTRODUCTION

The concrete box girder with corrugated steel webs is a new structure, which is formed with concrete roof and floor, external and internal prestressed reinforcement, and corrugated steel webs. The concept of the concrete box girder with corrugated steel webs was put forward by French engineers in 1975. The Connac Bridge, the first concrete box girder with corrugated steel webs, was built in France in 1986. So far, there are many of this of type bridge in European countries and Japan (Song et al, 2002). In China, the development is relatively slow and only five bridges with this kind of girder have been built. Since the first concrete box-girder bridge with corrugated steel webs was built, the performance study of this kind of bridge has caused the close concern of many scholars. There have been a considerable amount of research work about the working performance under the static bending and shear forces (Liu et al, 2008; Khalid Y A et al, 2004), but the research about the dynamic performance is still very scarce (Chen et al, 2007). The dynamic performance of the structure is the foundation of dynamical response. The dynamic performances of different section types are compared by the finite element method. Based on the principles of the modal synthesis method, a comprehensive model is set up to simulate the dynamic responses of the vehicle-bridge system while the vehicle is passing the

concrete box girder with corrugated steel webs. The dynamic responses with one or more vehicles, different vehicle parameters, and different vehicle speeds are considered respectively.

THE MODEL OF VEHICLE-BRIDGE

The vehicle-bridge coupling system is very complex. In order to reduce the degrees of freedom, the modal synthesis method is chosen to obtain the dynamic response of the concrete box girder with corrugated steel webs. Only limited numbers of modes should be considered. The natural vibration characteristics of the girder can be calculated using the finite element method. The limited numbers of modes can be decided considering the vertical mode participation mass. As to the simplified model of the vehicle, the three-axle vehicle can be simplified to body, spring suspension device, axle, and tire. Vehicle vibration is mainly summarized as vertical vibration, longitudinal rocking vibration, and transverse rocking vibration of car body and vertical vibration and longitudinal rocking vibration of wheelset. Figure 1 is three-axle vehicle model (Xue Lingxiang, 2008).

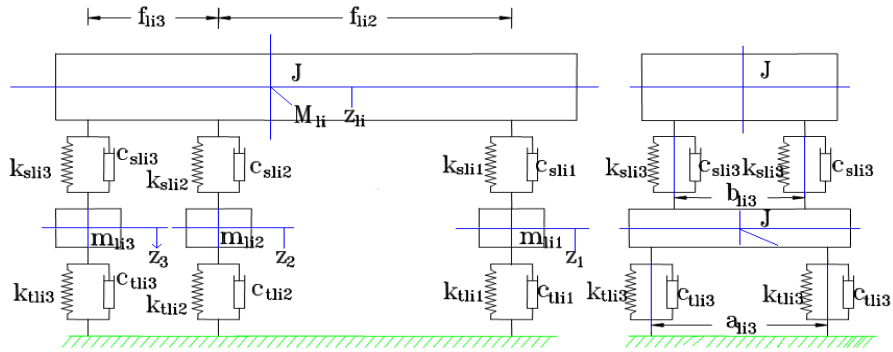

Figure 1. Three-axle vehicle model

Assuming the wheels and the bridge deck have the same displacement, the vehicle and bridge can be combined as a united dynamical system. The vibration time can be separated to many time intervals△t, the dynamic equilibrium equation can be built at the beginning and end of each time interval. The dynamic responses of the vehicle and the girder in every moment are calculated by the Newmark-β step-by-step integration method (Wang and Xu, 2000).

NATURAL VIBRATION CHARACTERISTICS

A real concrete box girder with corrugated steel webs in Qinghai province is taken as the research object. The section types are single box double cells and two parallel boxes double cells. The strength of the corrugated steel is Q345 and the thickness is 12mm. The concrete grade is C50. The specific sizes are shown from Figure 2 to Figures 4.

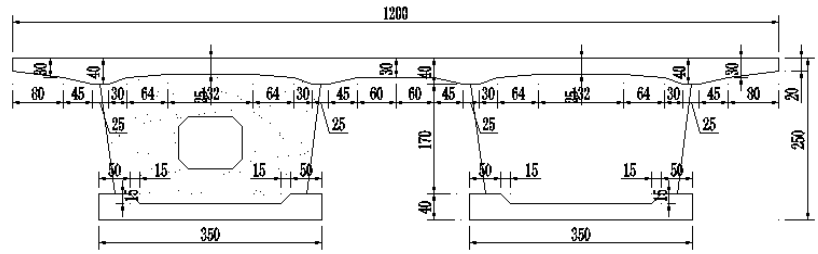

Figure 2. Section size of two parallel boxes double cells girder

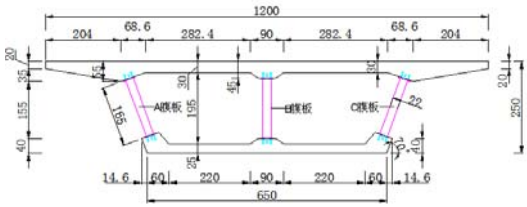

Figure 3. Section size of single box double cells girder

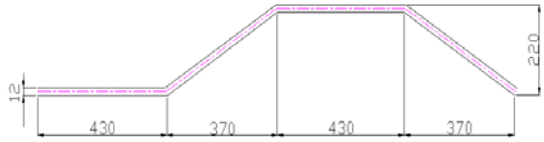

Figure 4. Size of corrugated steel webs

The models of the box girder with corrugated steel webs are built by the finite element analysis program MIDAS. The span length is 49.92m. The concrete roof and floor use the solid element and the corrugated steel webs use the plate element.

The first twenty order modes of each box girder are calculated and compared. The vertical mode participation mass of the first twenty modes is almost ninety percent for both models. The natural vibration characteristics are the basis of the structure's dynamic response, so the natural vibration characteristics of box girders with different section types are compared in the Table 1.

Table 1. Comparison of the first four order modal shapes and frequencies

mode	single box double cells（Hz）	two parallel boxes double cells（Hz）
First	First-order vertical bending(2.765)	First-order vertical bending(3.343)
Second	Horizontal vibration(6.602)	Torsional vibration(6.513)
Third	Second-order vertical bending(6.782)	Second-order vertical bending(8.616)
Fourth	Torsional vibration(7.244)	Horizontal vibration(8.880)

Table 1 shows that the natural vibration characteristics are greatly different between the single box double cells girder and the two parallel boxes double cells girder. Although the first order modal shapes are similar, the frequency of the single box double cells girder is 82.7 percent that of the two parallel boxes double cells girder. So the vertical rigidity of the two parallel boxes double cells girder is larger. The torsional vibration of the two parallel boxes double cells girder appear in second-order mode while the torsional vibration of the single box double cells girder appear in fourth-order mode. The torsional frequency of the two parallel boxes double cells girder is 88.8 percent that of the single box double cells girder. So the torsional rigidity of the two parallel boxes double cells girder is small and the integrity of the girder is weaker.

COMPARISON OF VEHICLE-BRIDGE COUPLING VIBRATION

The three-axis vehicle, whose total weight is 325kN, is used to simulate the dynamical responses of the vehicle-bridge system. The front axle's weight is 65kN, and both medial axle and rear axle's weight is 130kN. The specific parameters are shown in Table 2.

Table 2 Vehicle parameters

axle	axle weight（kN）	pendulum spring stiffness (kN/m)	pendulum spring Damping（kN/m/s）	tire stiffness（kN/m/s）	tire damping (kN/m/s)
front axle	65	500	10	1000	4
medial and rear axle	130	1200	16	2300	16

The dynamic responses of box girders with different section types are calculated while the vehicle is passing the bridge. The effect on dynamic responses of bridges are discussed when vehicles are on different lanes and with different speeds.

(1)The mid-span's time-deflection curves for one vehicle passing the outside lane of the girder at 50km/h are shown in Figure 5.

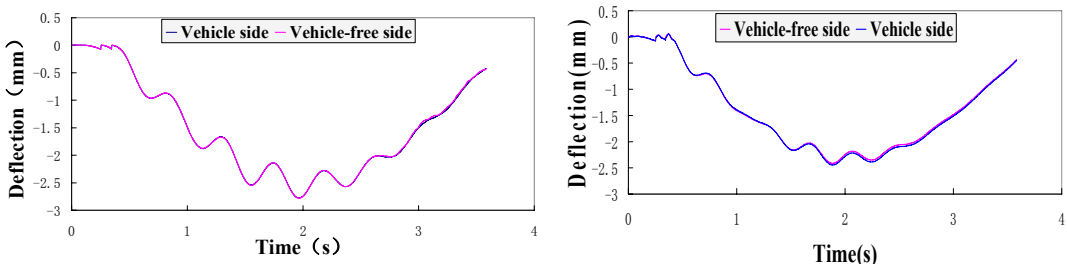

(a) Single box double cells **(b) Two parallel boxes double cells**

Figure 5. Mid-span time-deflection curve when one vehicle passing outside lane

According to Figure 5, the mid-span responses of both lanes are very similar for the single box double cells box girder. So the partial vehicle load has little influence on single box double cells box girder. For the girder with two parallel boxes double cells, the mid-span deflection of the vehicle side is slightly larger than the vehicle-free side, which shows that the partial vehicle load has some influence on it. Compared with the whole bridge's weight, the weight of vehicle body is so small that the effect of the influence is not remarkable. The vertical deflection of the single box double cells girder is a little bigger than that of the two parallel boxes double cells girder, which is because its vertical rigidity is comparatively small.

(2)The mid-span's time-deflection curves for two vehicles passing the girder in parallel at 50km/h are shown in Figure 6.

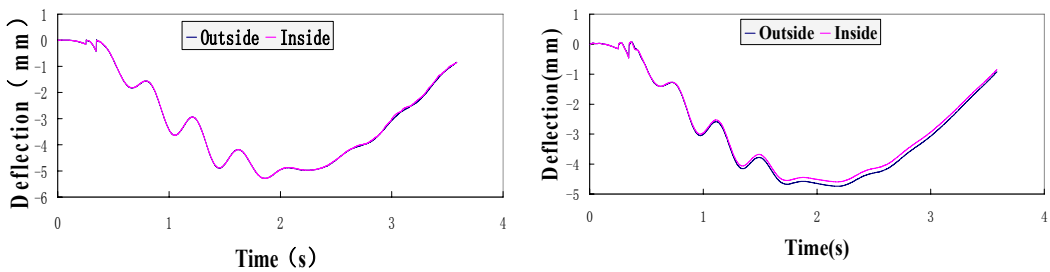

(a) Single box double cells **(b) Two parallel boxes double cells**

Figure 6. Mid-span time-deflection curve when two vehicles passing in parallel

According to the Figure 6, the mid-span deflections of both lanes are very similar for the single box double cells box girder. For the two parallel boxes double

cells girder, the mid-span deflection of the outside lane is somewhat larger than the inside lane. The participation of the torsional vibration mode is the main reason for this difference. The torsional rigidity of the two parallel boxes double cells girder is small and the integrity of the girder is weak. The deflection while two vehicles are passing the bridge is about twice that of one vehicle, which means that the bridge's response is linear under this loading.

（3）The mid-span's time-deflection curves for two vehicles passing the girder in opposite directions at 50km/h are shown in Figure 7.

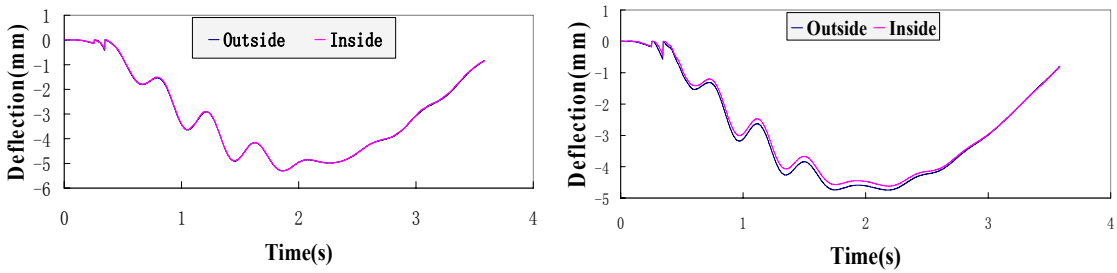

(a) Single box double cells **(b) Two parallel boxes double cells**

Figure 7. Mid-span time-deflection curve when two vehicles passing in opposite

According to the Figure 7, the vehicle-bridge vibration response of two vehicles passing the bridge in opposite directions is the same with that in parallel due to structural symmetry.

(4) In order to compare the vibration response of the girder when the vehicles are passing the bridge at different speeds. The deflections of the mid-span are calculated while the vehicles are at different positions. The mid-span's position-deflection curves for one vehicle passing the bridge at 50km/h and 100 km/h are shown in Figure 8.

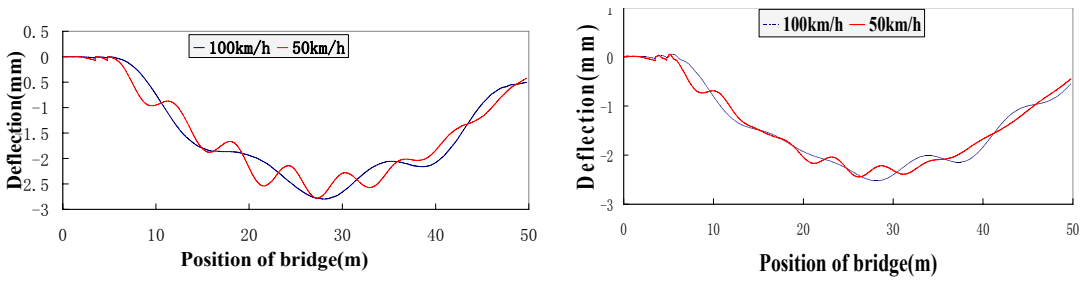

(a) Single box double cells **(b) Two parallel boxes double cells**

Figure 8. Mid-span position-deflection curve when one vehicle passing the bridge at different speed

According to the Figures 8, the average of dynamic deflection at 50km/h is similar with that at 100km/h, but the deflection disturbance is more significant than that at 100km/h. Time between the vehicle's front axle and rear axle through the same point can be taken as a cycle. When the vehicle's speed is 50km/h, the excited frequency is about 2.894Hz, which is close to the single box double cells girder's first natural frequency (about 2.765Hz), so its dynamic response is more remarkable. The more the excited frequency is closer to the bridge's first natural frequency, the more remarkable the bridge's dynamic response.

CONCLUSIONS

The natural vibration characteristics of different section types are obtained and their dynamic characteristics are compared. The vehicle-bridge dynamic interaction system model is set up and composition is programmed to get the vehicle-bridge's dynamic response while vehicles are passing the bridge.

The following conclusions have been drawn from the above analysis:

(1) The torsional rigidity and integrity of the two parallel boxes double cells girder are weaker, so the mid-span deflections of different lanes are not coincidental.

(2) The vertical deflection of the single box double cells girder is a little larger, due to its vertical rigidity being comparatively small. The change of bridge's deflection is linear with the number of vehicles increased.

(3) The more the excited frequency is closer to the bridge's first natural frequency, the more remarkable the bridge's dynamic response.

ACKNOWLEDGEMENT

The research of this project is partly supported by the Ministry of Communications Science and Technology Project (200431822315).

REFERENCES

Song Jianyong, Wang Tong, and Zhang Shuren. (2002). "*Extramrporeal Prestressed Concrete Composite Bridge with Corrugated Steel Webs"* [J]. Northeastern Highway, 25 (1):38-40.

Liu Bao-dong, Chen Haibo, and Ren Hongwei. (2008). "*Improvement Study of the Dynamic Characteristics for Concrete Box-Girder with Corrugated Steel Webs"*[J]. China Railway Science, 29(3):29-33.

Khalid Y A, Chan C L, and Sahari B B. (2004). *"Bending Behaviors of Corrugated Web Beams"* [J]. Journal of Materials Processing Technology, 150 (3):242-254.

Chen Haibo, Liu Baodong, and Ren Hongwei.(2007). "*Research on Dynamic Characteristic of Concrete Box-girder with Corrugated Steel Webs"*[J]. Journal of Highway and Transportation Research and Development, 24 (2): 80-83

Xue Lingxiang. (2008). "*Studies on Coupling Vibration of Highway Vehicle-bridge System under the influence of Creep*"[D]. Beijing, Beijing Jiaotong University.

Wang Yuan-feng, Xu Shi-jie. (2000). "*Study on Dynamic Interaction of Highway-bridge with Vehicles*"[J]. China Journal of Highway and Transport, 13(4):37-41.

Model Test Study of System Transformation for Jiangdong Bridge

Ruili Shen[1], Dongchun Qi[2], Maolin Tang[3], and Yong Yan[4]

[1]Ruili Shen, Pro., School of Civil Engineering, Southwest Jiaotong University, Chengdu 610031. China, E-mail: rlshen@163.com

[2] Dongchun Qi, Dr. Student, School of Civil Engineering, Southwest Jiaotong University, Chengdu 610031, China, E-mail:qidongchun@163.com

[3] Maolin Tang, Associate Pro., School of Civil Engineering, Southwest Jiaotong University, Chengdu 610031, China. E-mail: tmllpl@126.com

[4] Yong Yan, Dr. Student, School of Civil Engineering, Southwest Jiaotong University, Chengdu 610031, China. E-mail: mryan5@163.com

Abstract : Jiangdong Bridge in Hangzhou is a spatial cable, self-anchored suspension bridge. In order to research structural system transformation through a model test, a total bridge test model has been designed according to geometric scaled ratio of 1:16 and force scaled ratio of 1:4. During the test, five pairs of temporary hangers were first tensioned to make the main cables form spatial space curves. Then the permanent hangers were tensioned symmetrically step by step from bridge tower to mid-span. Temporary hangers were dismantled gradually when their role was substituted by permanent hangers. Based on the control requirement, the force of the intermediate temporary hangers needed to be adjusted several times. The control target of hanger tension was according to unstressed length of the hangers in calculations. However, in practical experiments, the final target was hanger tensile force reaching the calculated value after the hanger was installed. The tests indicate that both control results are consistent. In this paper, the test scheme of system transformation, test process and results of test research are emphatically introduced.

Keywords : self-anchored suspension bridge; total bridge model test; structural system transformation; spatial cable; unstressed length of hanger

1 Introduction

The main bridge of Jiangdong Bridge in Hangzhou is a three-span single-column pylon, spatial cable plane, separate steel box and single-span suspended self-anchored suspension structure with a span arrangement of (83+260+83)m. The stiffening girder was designed as a separated twin-box girder connected by the box section beam. The width of the stiffening girder is 47m. The horizontal ratio of rise to span of main cables is 22/260, the largest ratio in the world. The structural form of the Jiangdong Bridge is similar to the Yongjong Bridge in Korea. But the

Yongjong Bridge is a highway and railway suspension bridge which adopts the steel truss stiffening girder. Compared with the Jiangdong Bridge, the height and rigidity of the stiffening girder is relatively large, and the bridge width is relatively narrow (Ochsendorf, J.A. 1999). For the Jiangdong Bridge, it is necessary to find the reasonable sequence of hanger installation, verify pre-displacement and pushing process of saddles by model experiments. These test conclusions can help to guide construction control and construction process of real bridge.

2 Test model design

Considering the requirements of structural parameters, model materials, fabrication technology and laboratory conditions, the geometric scaled ratio of the model was 1:16, and the force scaled ratio was 1:4. Full length of the model was 26.625m. In the model design, the geometric relation between the main cable and the stiffening girder should strictly satisfy the similarity ratio requirement. The test model was composed of double main cables, 26 pairs of hanger, steel box, horizontal connection box, anchoring beams at the end, pylons, saddles, temporary piers and test system. Figure 1 shows the general view of the test model. In this paper, the symbol "LS" expresses a temporary hanger and "S" expresses a permanent hanger.

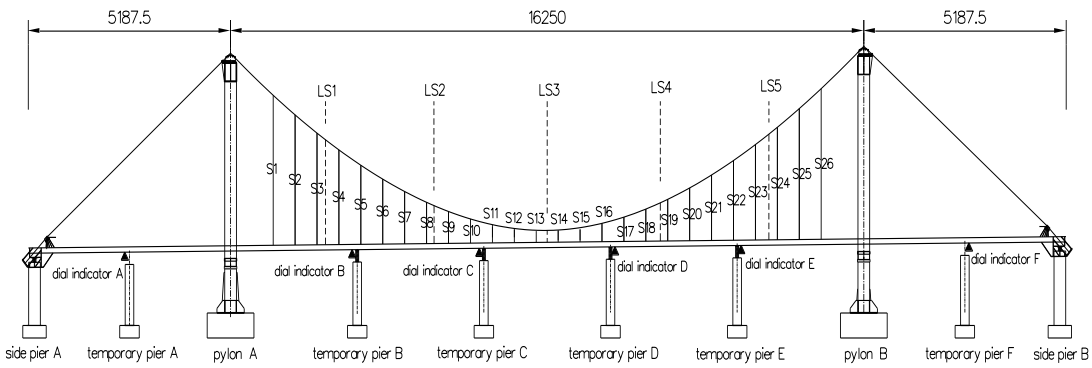

Figure 1. General view of the test model (unit: mm) .

The test model was designed according to the relations of deformation and force similar to actual bridge. Due to material constraints, it is currently impossible for all parameters to meet law of similarity. Based on the structure mechanical properties, the main parameters should satisfy the law of similarity (Yao, Z. 1996). Table 1 lists the similarity relations of main parameters.

Table 1. Similarity relations of main design parameters

Parameter	Similarity law	Similarity coefficient (real bridge/model)
Cross-sectional area	$A_m = mn^2 AE/E_m$	1024
Bending moment of inertia	$I_m = mn^4 IE/E_m$	262144
Torsion moment of inertia	$J_m = mn^4 JG/G_m$	262144
Mass moment of inertia	$I_{\rho,m} = mn^4 I_{\rho,\rho}$	262144
Concentrated load	$P_m = mn^2 P$	1024
Distributed load	$W_m = mnW$	64
Linear displacement	$Y_m = nY$	16
Angular displacement	$\phi_m = \phi$	1
Axial force	$N_m = mn^2 N$	1024
Moment	$M_m = mn^3 M$	16384
Support reaction	$R_m = mn^2 R$	1024

Note: m expresses the force reduced scaled ratio, n expresses the geometric reduced scaled ratio. Parameters with subscript m are design parameters of the test model.

3 Model test research of structure system transformation

The system transformation for self-anchored suspension bridges refers to transferring the weight of the stiffening girders to the main cables and pylons by means of a certain hanger tension procedure, implementing the stiffening girder separation from the construction brackets. Theoretically speaking, the erection process of hangers is similar to that of stay cables. The methods, such as jacking up the stiffening girder, jacking up the saddles, preloading the main cables and directly tensioning the hangers, can be adopted. For long-span, self-anchored suspension bridges, especially for the single-span suspended structures, because the pre-offsetting of main saddles is large, the elevation difference is also large at the main cable erecting stage compared with the configuration at the finished bridge state. The main cables of the Jiangdong Bridge form three-dimensional curves, and before the main cable spatial curves form, many hangers can't be installed. Therefore, the feasible method of the hanger installation scheme is tensioning hangers directly.

For the directly tensioning method of self-anchored suspension bridges, the method of calculation is the stress-free state method. Based on the unstressed length of hangers, determine hanger tension and structure internal force (H.-K. Kim 2002). Because force measurement precision is higher than that of length measurement in model tests, we stretch hangers according to hanger tension rather than the unstressed length of the hangers. For elastic structures, both have a corresponding relationship each other. The situation is reverse in field construction, so the control

idea is the length control mainly, and force checks as servant.

This experiment has carried out three test schemes. As space is limited, we introduce the recommended scheme and omit the other two schemes in this paper. The recommended scheme is the planned demolishing of the temporary pier of side span before system transformation, and appropriately adjusting the order of hanger tensioning to improve installation angle of hangers.

3.1 Principle of determining system transformation scheme

The system transformation of the Jiangdong Bridge is necessary to satisfy the following requirements.

(1) Force and alignment of structure members meet the design requirements during the system transformation.
(2) Dip angle of the line connecting the cable band center and anchoring point should not exceed the permissible angle value range of steel pipes in the longitudinal and lateral directions. The designed value is 4 degrees, and the practical dip angle should be less than the allowable value.
(3) The safety coefficient of the permanent hanger tensile force can't be too low during system transformation. Hanger tension should be controlled under 230t in a real bridge and the corresponding value in the test model is under 2246N.
(4) Considering some factors such as temporary hanger anchorage, cable band installation and temporary hanger tension control. The maximum tension of temporary hangers is less than 120t in real bridges and the force should be controlled below 1171N during the test.
(5) The allowable displacement of the pylon top should be controlled below 6mm during system transformation of the model bridge.
(6) The stiffening girder stress can't exceed the allowable value during system transformation.

3.2 Description of the test

In this experiment, five pairs of temporary hangers were first tensioned step by step. The purpose of this action was to stretch the main cables to form spatial curves, which had little difference with the final alignment, and be helpful to installing the permanent hangers. Installation direction of the permanent hangers was from the bridge towers symmetrically to the center of the main span. Temporary hangers could be removed gradually when their role was substituted by permanent hangers. The temporary hangers at mid-span needed to be relaxed several times when the tensile forces had exceeded the normal value. Once the towers' longitudinal offset reached a certain value, pushing of the saddles should be executed. The frontal test found that the tension of each temporary hanger especially the middle ones would increasingly deviate from theoretical value, which led to the tensile forces of all permanent hangers deviating greatly from their theoretical values later in the

construction period. It was key to guarantee the permanent hanger tension reached a reasonable target value under the completed bridge stage by ensuring the temporary hanger forces were up to the design value in each working condition. Therefore, the tension of all temporary hangers should be adjusted to the calculated value after five pairs of temporary hangers had been anchored.

The calculated results showed that the problem, the traverse angle of S9/18 being more than 4 degrees when installing, could be solved by adjusting temporary hanger tensile forces; however there were still ten hangers whose installation angle exceeded by 2 degree. In the range of 1/4 span~3/8 span, the calculated angle difference of cable bands before and after hangers were installed was slightly large. In addition, due to the influence of LS2/4, the initial tension of S8/19 was extremely small and S8 appeared the situation of work in the later stages after anchored, that it was difficult to ensure construction quality.

In order to solve the above problem, a proposal scheme was put forward. The main idea of this approach was now that the installation angle of ten pairs of hangers was more than 2 degrees and transverse angle variation of the hangers in 1/4~3/8 span was large. The problem could be solved in the two pairs of hangers' installation, thus thoroughly solving the problem of the other hangers' installation? After repeated calculations (the finite element analysis software is Bridge Nonlinear analysis system BNLAS (Tang, M. 2003) developed by Southwest Jiaotong University), it was found that by adjusting the installation procedure of several permanent hangers it could greatly improve the transverse angle difference of hangers between the hangers' erection stage and finished stage, that is to say, after installing S6/21, measures were taken to install S9/18 in advance. In this case, the angle difference variation of the hangers which had not been installed was rather small; cable clamps were not influenced by subsequent process and could fix ahead of time. It was very favorable for quickening engineering schedule and improving construction quality. The sequence and control parameters of the recommended system transformation scheme are presented in Table 2.

Table 2. Sequence and control parameters of the recommended scheme .

Step	Operation content
1	Installing LS1 with 158.6N and LS5 with 155.7N
2	Pushing saddles toward mid-span by 0.02m at first time
3	Installing LS2 with 496.2N and LS4 with 480.9N
4	Pushing saddles toward mid-span by 0.017m at second time
5	Installing LS3 with 746.6N
6	Pushing saddles toward mid-span by 0.007m at third time
7	Adjusting all temporary hangers to the design value
8	Installing S1 with 401.5N and S26 with 410.2N
9	Installing S2 with 523.1N and S25 with 540.1N
10	Decreasing LS3 tensile force to 586N
11	Installing S3 with 488.3N and S24 with 500.4N; demolishing LS1/5
12	Installing S4 with 601.1N and S23 with 623.4N
13	Decreasing LS3 tensile force to 804.2N
14	Installing S5 with 488.9N and S22 with 517.4N
15	Installing S6 with 457.9N and S21 with 506.6N
16	Increasing LS2 tension to 892.7N and LS4 tension to 859.7N
17	Installing S9 with 867.6N and S18 with 1084.4N
18	Installing S10 with 1646.2N and S17 with 1699.4N
19	Pushing saddles toward mid-span by 0.007m at fourth time
20	Demolishing LS2/4
21	Installing S7 with 801.3N and S20 with 802.6N
22	Installing S8 with 559.5N and S19 with 555.5N
23	Installing S11 with 2192.6N and S16 with 2210.7N
24	Installing S12 with 1882.8N and S15 with 1883.9N
25	Pushing saddles toward mid-span by 0.006m at fifth time
26	Installing S13 with 1026.2N and S14 with 1021.1N
27	Pushing saddle toward mid-span by 0.0022m at fifth time
28	Demolishing all temporary hangers and temporary supports
29	Adjusting all hangers tension
30	Applying secondary dead load

3.3 Partial experimental results

As shown in Figure 2, the variation rule of hanger tension is described as follows: for a certain hanger, the anchoring force was relatively great. The tensile force decreased rapidly when installing a pair of hangers nearby. Moreover, the variation of the hanger tension tended to stability after a pair of hangers nearby it had been anchored.

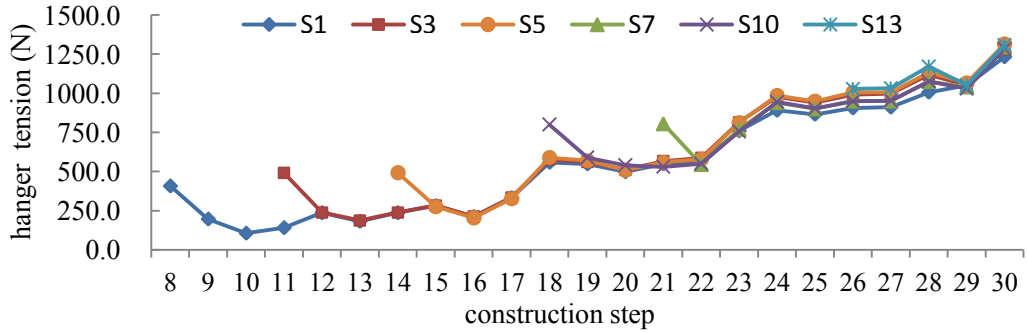

Figure 2. Tension of hangers in the construction process.

Figure 3 shows the experimental curves of support reaction of temporary piers. From the diagram it may be seen that support reactions gradually decreased with the construction progress, which suggested the weight of stiffening girder had transferred to the main cables from temporal piers by installing hangers. In later stages, the bearings on the two temporary piers near to pylons had no contact with the stiffening girder, but the ones close to mid-span bore a little pressure and the temporary piers could be safely demolished in order to complete system transformation.

Figure 4 shows the measured deflection curve of the stiffening girder during system transformation. We can see that the stiffening girder had almost no vertical displacement before the stiffening girder broke away from the bearings on temporary piers. However, once disengaging occurs, the vertical displacement changed obviously, thus the deflection at mid-section in the middle span was about 2.5cm under secondary loads.

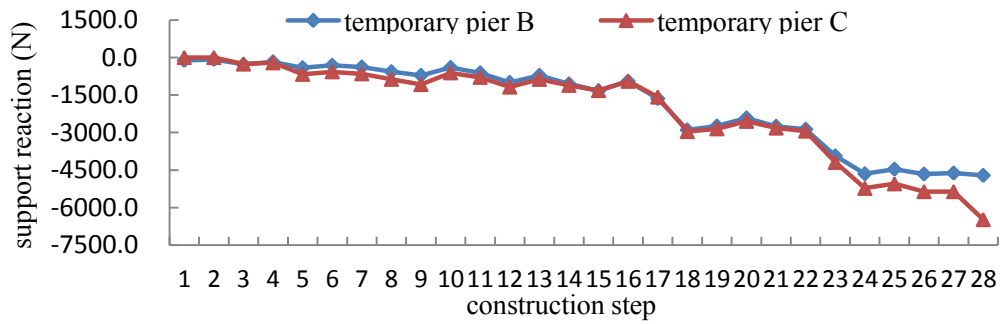

Figure 3. Support reaction of temporary piers in the construction process.

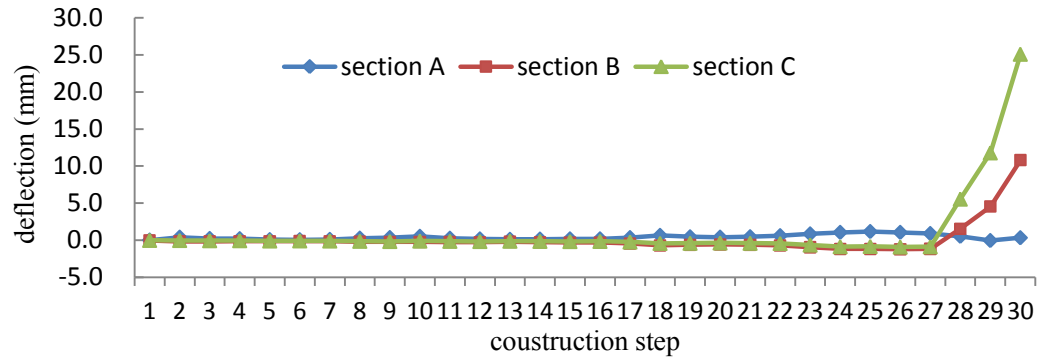

Figure 4. Deflection of stiffening girder in the construction process .

Figure 5 shows the envelope diagram of the transverse angle difference of hangers in the construction process compared with the finished bridge state. It can be seen that transverse angle difference of hangers was less than 2 degrees except that of LS9/18 and LS10/17 which were close to 4 degrees.

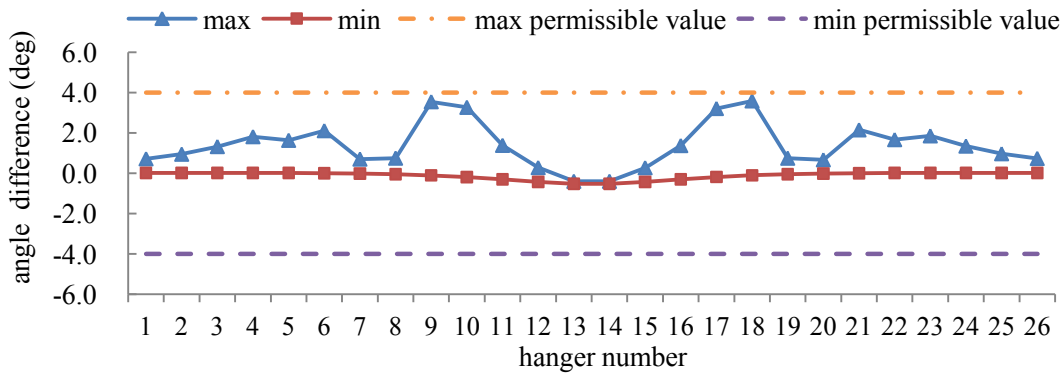

Figure 5. Envelope diagram of transverse angle difference of hangers .

4 Concluding remarks

Through the above research, the main conclusions are drawn as follows:

(1) The measured values of hanger tension and main cable configuration were identical to the calculated results satisfactorily. It shows that the calculation method ensures enough precision in cable force control and linear control, and can completely reflect the force state of the actual structure despite the width of the stiffening girder reaching to 3m.

(2) System transformation of the spatial cable self-anchored suspension bridge was implemented under the conditions of ensuring every temporary hanger tension at each step and reasonable tension sequence. The tensile forces of all hangers had almost attained the target value when all hangers were installed. Only individual hanger had the needed adjusting in fine. The alignment of the main cables and the stiffening girder was smooth.

(3) Once the stiffening girder was separated the from construction brackets, elevation variation of the stiffening girder was significant if the tensile force of every hanger increased or decreased a certain value on the whole. Individual adjustment of a certain hanger would have an obvious effect on the force of hangers nearby and play limit action for improvement of the stiffening girder alignment. According to this result, if the distribution of hanger tension is uneven, individual hanger tension can be adjusted. When the alignment can't achieve the demand, hanger tension needs to be adjusted one by one in order to make all the hangers increase or decrease by a certain value.

(4) In the model test, the problem of excessive installation angle of several hangers was solved successfully by adjusting the tension sequence of the hangers. In practical construction, after preliminary stretching S9/18, S10/17 was stretched, then tensile forces of the above four hangers were adjusted to achieve the design values simultaneously.

(5) The measured deformation of main cables and stiffening girder was in fair agreement with the calculated value. These indicated that main cable configuration and pre-displacement of saddle, etc. coincided with practical situation.

References

H.-K. Kim, M.-J. Lee, S.-P. Chang. (2002) "Non-linear shape-finding analysis of a self-anchored suspension bridge." Engineering Structures , 24, 1547-1559.

Ochsendorf, J.A., Billington, D.P. (1999). "Self-anchored suspension bridges." Bridge Engineering, 4(3), 151–157.

Tang, M. (2003). Geometric Nonlinear Analysis of Long-Span Suspension Bridge and Its Software Development. Doctoral Thesis, Southwest Jiaotong University.

Yao, Z., Liu, Z. (1996). Structure Test, Shanghai: Tongji University Press.

Experimental Study on Performance of the Bridge Deck Pavement of SF-PFSC

TIAN Wenling[1,2], WANG Xiaowei[1,2], GAO Shuling[1,2], ZHOU Mingjie[1,2], ZHAO Xiaoyan [1,2], ZHANG Erlong[2]

[1]College of Civil Engineering, Hebei University of Technology, Tianjin300401, China; PH (86-22) 6043-5988; email: wltian@henbut.edu.cn

[2]Civil Engineering Technology Research Center of Hebei Province, Tianjin300401, China

ABSTRACT

To improve the mechanical properties and durability of bridge deck pavement, four types of concrete are involved in this study, that is Plant concrete(PC), steel fibers reinforced concrete(SFC), steel fibers and polypropylene fibers reinforced concrete(SF-PFSC) and SF-PFSC with air-entraining agent (SF-PFSC+). The experimental researches on mechanical properties, impermeability and frost resistance of above four types concrete were done. The experimental results show that, comparing with other concrete with the same fibre volume ratio, , SF-PFSC, in which the steel fabre was partial replaced with polypropylene fibers, presents better flexural strength, flexural toughness and good durability, impermeability and frost resistance. By adding air-entraining agent, SF-PFSC+ shows not only excellent mechanical properties but also better impermeability and frost resistance. therefore, the SF-PFSC and SF-PFSC+ are suitable in the bridge deck pavement and can prolong the service life of bridge deck.

KEY WORDS: steel fibers(SF), polypropylene fibers(PFS), Concrete, mechanical properties, durability

INTRODUCTION

Presently most of the built and being built bridge deck pavements are the asphalt concrete. There are various premature damages of asphalt pavements on deck effected by environment and vehicals. these deterioration would have influence on performance and lifetime of bridge. The steel fibers reinforced concrete (SFC) applied to the deck pavement can improve the mechanical properties and toughness. The research results show that multi fibers reinforced concrete can make up the insufficiency of single fiber and improve obviously mechanical properties and durability of concrete. In this study, the mechanical properties and durability of the concretes which are the SF, the steel-fibers and the polypropylene fibers reinforced concrete (SF-PFSC) and the SF-PFSC with air-entraining agent (SF-PFSC+) were concerned with, and the influence on SF-PFSC durability by adding air-entraining

agent were also researched.

EXPERIMENT DESIGN

Based on the researches done by Dun F.Q.,and Zhang E. L (Dun 2008; Zhang 2008), While the volume ratio of SF and PFS are 0.5~0.7% respectively, SF-PFSC presents better mechanical properties and durability, more volume ratio of fibre can affect the concrete workability. In this study, the volume ratio of steel fibre is 0.7% and PFS is 0.5% in SF-PFSC. The volume ratio of SF is 1.2% in SFC. the content of air-entraining agent is 0.03% of amount of cement in SF-PFSC+. concrete proportion of specimen were shown in Table 1.

Table 1. concrete proportion of specimens

Type	Cement	Water	Sand	Coarse Aggregate	Expansion Agent	Water Reducing Agent	SF	PFS	Air-entraining Agent
PC	419	155	806	986	25	10	0	0	0
SFC	475	175	806	986	25	10	93.6	0	0
SF-PFSC	475	175	806	986	25	10	54.6	4.6	0
SF-PFSC+	475	175	806	986	25	10	54.6	4.6	0.143

The tests of concrete workability, mechanical properties, impermeability and frost resistance were done according to the *Experiment Method of the Steel Fibers Reinforced Concrete (CECS 13:89,1996)*.The specimen is 100 mm cube for compressive strength, there are three specimens for each group. The specimen for flexural strength and toughness is beam which the dimension is 100mm*100mm*400mm, three specimens for each group. The specimen for impermeability is truncated cone with the size 175mm*185mm*150mm, there are six specimens for each group. Approach to frost resistance is rapid freeze/thaw cycle, and measuring the compressive strength and flexural toughness after freezing and thawing..

Table 2. Experimental Results of mechanical properties.

Specimen	Slump (cm)	Compressive Strength (MPa)	Flexural Strength (MPa)	Flexural Toughness Index		
				I_5	I_{10}	I_{30}
PC	16	51.1	5.26	5.24	6.12	6.12
SFC	10	45.0	6.48	6.88	9.16	11.54
SF-PFSC	17	38.2	4.45	5.40	11.68	33.70

DISCUSSION OF EXPERIMENT RESULTS

Concrete workability. The slump of fresh concrete are shown in Table 2. The results show that PC workability is the better than that of other concrete, adding fibers can decrease the slump. The slump of SF-PFSC increases 40% than that of

SFC and can meet the requirement of flowability. It is concluded that when the total volume ratio of fibers is same, the replacement of partial SF with PFS is advantageous to improve SFC working performance.

Compressive strength The specimen curing age is 28-day and 100-day. The experimental results of compressive strength are shown in Table 2 and Table 4, respectively. From Table 2, The results show that the SFC and SF-PFSC 28-day compressive strength are slightly lower than that of PC. The SF-PFSC 28-day compressive strength is slightly higher than that of SF.

However, from the results showed in Table 4, when the curing age of concrete is 100d, the SF and SF-PFSC compressive strength are higher than that of PC.

Flexural strength The specimen curing age is 28d. The experimental results of 28-day flexural strength are shown in Table 2. The fibers could improve the PC flexural strength; the SF-PFSC flexural strength is the biggest of all the specimens, which increases 23.7% than that of PC. When the fibers ratio is the same, the SF-PFSC flexural strength is slightly higher than that of SFC.

Flexural toughness. Flexural toughness is expressed by the toughness index according to ASTM C1018 (Ashour, 1993). This method regards 3δ, 5.5δ and 15.5δas specified deflections(shown in Figure 1),here,δ is the deflection in accordance to the initial cracking,. The flexural toughness indexes(I_5, I_{10}, I_{30})are calculated by equation (1)~(3):

$$I_5 = \frac{A_1 + A_2}{A_1} \qquad (1)$$

$$I_{10} = \frac{A_1 + A_2 + A_3}{A_1} \qquad (2)$$

$$I_{30} = \frac{A_1 + A_2 + A_3 + A_4}{A_1} \qquad (3)$$

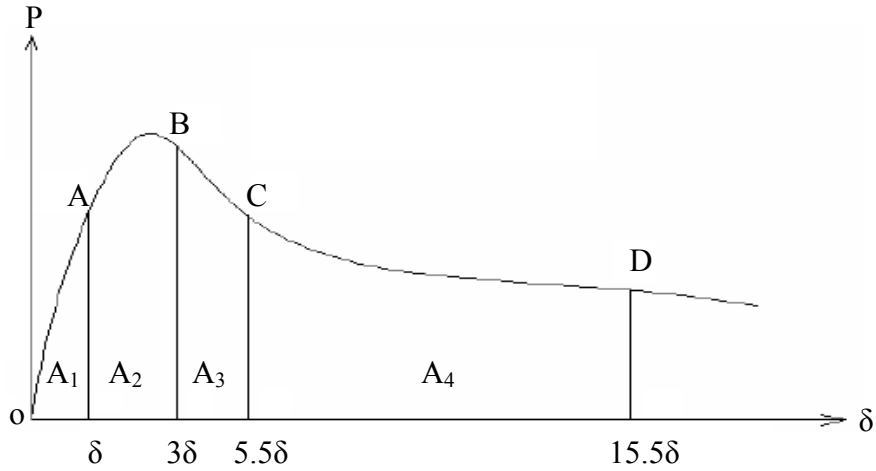

Figure 1. Toughness index of ASTM C1080.

The flexural toughness experimental results are shown in Table 2, and the Load-deflection response is shown in Figure 2.,From the toughenss test results, it can be seen that the flexural toughness indexes of SFC and SF-PFSC are bigger than

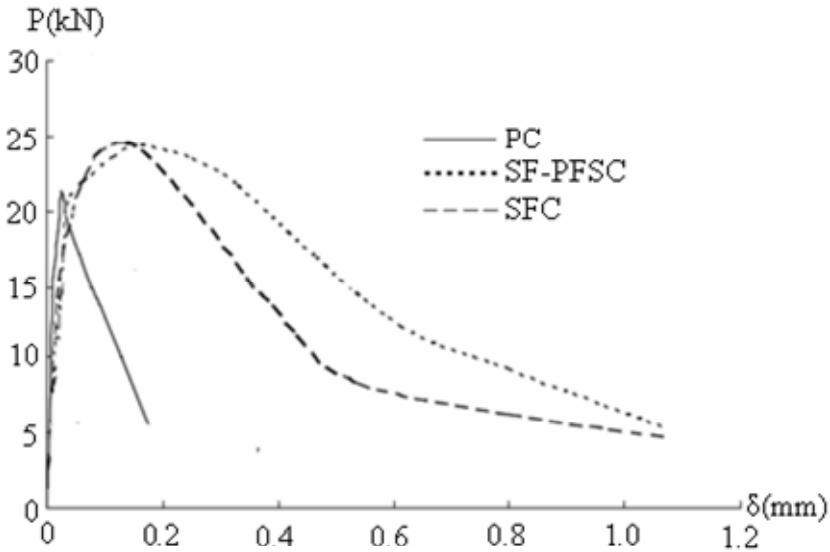

Figure 2. P-δ response of concrete

those of PC; I_{10} and I_{30} of SF-PFSC are the biggest of all, which respectively increase 113% and 479% than those of PC. Comparing the P-δ curves, the SF-PFSC descending stage is slowest, I_{10} is up to11.68, a growth of 122% on I_5, andI_{30} increases 172% than I_{10} as well. SF-PFSC presents better ductility of post peak. When the fibers total volume ratio is same, the partial replacement of SF with PFS can improve SFC flexural toughness.

Experimental results of impermeability. three PC specimens were

seepaged when the pressure is 2.0 MPa,. For SF, SF-PFSC and SF-PFSC+, there were no seepaged specimens untill seepage pressure reached 3.0 MPa and seepage depths were measured. The experimental results are shown in Table 3.

Table 3. Experimental Results of Impermeability.

Specimen	Load Time (h)	Seepage Pressure (MPa)	Average seepaged Depth (mm)
PC	64	2.0	permeable
SFC	224	3.0	53
SF-PFSC	224	3.0	37
SF-PFSC+	224	3.0	31

From the test results, the impermeability of fibers reinforced concrete is better than that of PC. Comparing the average seepage depths of SFC and SF-PFSC, it is can find that the seepaged depths of SF-PFSC is 70% that of SFC, the impermeability of SF-PFSC is better than that of SFC when the seepage pressure is same. Because the fibers of different sizes and properties are distributed to be An openwork fabric or structure in the cement matrix, the fibers spacing is decreased, and superimposed and strengthening effect of various interface layers is created in three dimensions. The pore structure of concrete is optimized, the size and open air of pore is decreased, it would cause the decrease of water permeate (Sun D.S., 2004, Wang H.X., 2004). It is concluded that the replacement of partial SF with PFS is advantageous to improve impermeability of SFC, when the fibers total volume ratio is same. The average seepage depth of SF-PFSC+ is 84% of SF-PFSC. It can be seen that adding air-entraining agent can improve impermeability of SF-PFSC.

Experimental results of frost resistance. After 150 times of freezing/ thawing cycles, weight loss of specimen began to increase obviously, the various spalling damages occurred on the specimen surface finished, and then the mechanical properties and flexural toughness tests were done. . The curing age of the specimen is 100-day. The test results are shown in Table 4. The frost index are present by AFT/BFT.

the Frost index of the peak load and compressive strength of SF-PFSC are lower than those of SFC after the freezing and thawing test, the decrease ratios of flexural toughness indexes of SF-PFSC are near to those of SFC. It is concluded that the replacement of partial SF with PFS can improve frost resistance of SFC when the fibers total volume ratio is same. The decrease ratios of SF-PFSC+ peak load and compressive strength are 24% and 70% of PC respectively, 45% and 85% of SF-PFSC respectively. The decrease ratios of SF-PFSC+ peak load and compressive strength are 24% and 70% of PC respectively, 45% and 85% of SF-PFSC

respectively. The decrease ratios of I_5 and I_{10} for SF-PFSC+ are 3.6%, 5.9% (As shown in Table 4), they are near to those of SF-PFSC and SFC. I_{30} of SF-PFSC+ is the biggest, the decrease ratio of it is 4.1%, and it is lower than those of SF-PFSC and SFC. It can be draw a conclusion that adding air-entraining agent can improve frost resistance of SF-PFSC.

CONCLUSION

Through the analysis of test results, we may draw the following conclusions.

(1)The replacement of partial SF with PFS can improve workability, mechanical properties, impermeability and frost resistance of SFC when the total volume ratio is same.

(2)Adding air-entraining agent can improve impermeability and frost resistance of SF-PFSC. SF-PFSC+ shows not only excellent mechanical properties but also better impermeability and frost resistance..

ACKNOWLEDGEMENT

The authors are grateful for the support of sustentation fund of scientific research key project of Hebei Provincial Communications Department (No.Y-060225).

Specimen		Peak load (kN)	Compressive Strength (MPa)	Flexural Toughness Index		
				I_5	I_{10}	I_{30}
PC	BFT	19.7	51.4	5.32	7.10	7.10
	AFT	17.8	43.4	4.98	6.50	6.50
	AFT/BFT	9.6%	18.4%	6.4%	8.5%	8.5%
SFC	BFT	22.2	56.2	6.24	13.88	34.52
	AFT	20.4	46.6	6.11	14.30	33.70
	AFT/BFT	8.1%	17.1%	2.1%	5%	5%
SF-PFSC	BFT	21.6	58.4	6.05	12.59	36.40
	AFT	20.5	49.5	5.85	11.86	34.55
	AFT/BFT	5.1%	15.2%	3.3%	5.8%	5.1%
SF-PFSC＋	BFT	21.8	51.9	5.98	13.65	36.20
	AFT	21.3	45.2	5.76	12.84	34.71
	AFT/BFT	2.3%	12.9%	3.6%	5.9%	4.1%

REFERENCES

Ashour, Samir A and Wafa, Faisal F. (1993). “Flexural behavior of high-strength fiber reinforced concrete beams.”*ACI Structural Journal,* 90(3), 279-287.

CECS 13:89. (1996). *Experiment Method of the Steel Fibers Reinforced Concrete*. China Plan Press, Beijing.

Dun F.Q. (2008) “*The research on the application of HFRC in the bridge deck pavement*.” Hebei University of Technology, Tianjin.

Sun D.S. and Deng M. (2005). "Study on durability of the fiber and hybrid fiber reinforced expansion concrete." *Industrial Construction,* 35(04), 69-71.

Wang H.X., Chen Y.Z., Ding Q. J., Hu S.G. (2004). "The effection of hybrid fibers on the mechanical properties and impermeability of high-performance concrete." *China Concrete and Cement* Product, 1, 38-40.

Zhang E. L. (2008). "*Experiment study on mechanical properties and durability of complex fiber concrete*." Hebei University of Technology, Tianjin.

Study on Experiment of Concrete Mixed with II Degree Flyash under the Corrosion of Freeze Thawing

Lihua Lu[1,2], Sili Chen[2], Xiating Feng[1], and Haixia Sun[2]

[1,2]Associate Professor; Ph.D. candidate of Northeastern University, Shenyang,; School of Architecture and Civil Engineering, Shenyang University of Technology, 110178, China; email: llh_wxy@yahoo.com.cn, PH (138) 98845691

[2]Professor, Ph. D, School of Architecture and Civil Engineering, Shenyang University of Technology, 110178; PH (131) 09862737; email: 362902422@qq.com,

[1]Professor, Ph.D., College of Resources and Civil Engineering, Northeastern University, 110001; PH (138) 08671436; email: xtfeng@whrsm.ac.cn;

[2]Associate Professor, Ph.D. candidate; School of Architecture and Civil Engineering, Shenyang University of Technology, 110178; PH (024)25496533; email: sunhx99@126.com

ABSTRACT

As an industrial waste, fly ash has been widely used in bulk and low strength concrete. Bridges have to endure numerous freeze-thaw cycles and the erosion of air pollution when exposed to air. Therefore, the durability investigation of fly ash concrete bridge in the extremely cold area is necessary. In this paper, the concrete (designated as C50 fly ash concrete) was prepared by mixing II degree fly ash with water, cement, and water reducing agent. The water-cement ratio was selected by contrast analyses of several samples. The strength of C50 fly ash concrete was tested after 150 freeze-thaw cycles and corrosion in Na_2SO_4 and HCl solutions of different concentrations, respectively. The strength declination was achieved, which is similar to the ordinary concrete. As the erosion liquid concentration increased, its influence on strength of concrete also increased. The conclusions of this paper provide important reference data for the design and application of fly ash concrete in cold regions.

INTRODUCTION

In the extremely cold regions, bridges exposed to air are frequently subjected to acid rain, corrosive gas or liquid, and the impact of freeze-thaw cycles. These adverse environments severely affect the durability of the bridges; therefore a lot of bridges in the far north of China have to be reinforced before they meet the designed life span.（Pu 1994) In the extremely cold areas, the complete or partial loss of bearing capacity of the concrete under the impact of corrosive freeze-thaw cycle is one of the main factors that shortens the life of bridges. Therefore, to improve the durability of concrete in cold areas is one main method to improve the durability of concrete bridges in the extremely cold areas.（Tang 2007) Although the research on enhancing the quality of the concrete through Ⅰ degree fly ash has a wide range of applications,

Ⅰ degree fly ash accounts for only a small part of the ash in the plants. The higher prices also hindered its effective utilization. In contrast, II degree fly ash, with a larger output, can be mixed into the concrete to produce high quality concrete. Therefore, it is an effective way for the cement concrete industry and the environment to achieve sustainable development.（Wu 2004)

In this paper, II degree fly ash mixed with super-plasticizer was used to prepare the fly ash concrete. Meanwhile, the rule of strength variation of different-volume fly ash concrete was also explored using repeated freeze-thaw circles under the corrosion of Na_2SO_4 and HCl solutions. These results will provide an important reference for the durability design and application of fly ash concrete in cold regions.

MATERIALS PREPARATION AND TEST METHODS

Materials Preparation. Materials were prepared following the steps below:

(1) Cement: ordinary Portland cement 52.5 made in Benxi, Liaoning;

(2) Fly Ash: II degree fly ash, made by Shenhai Thermoelectricity Plant in Shenyang Liaoning, particle fineness modulus 17.5;

(3) Aggregate: a) fine aggregate: sand, well graded; b) coarse aggregate: limestone gravel, graded good (maximum diameter 25mm);

(4) Water: general water, pH value of 7.2;

(5) Admixture: super-plasticizer made in Shenyang;

Ratio and samples. Newly mixed concrete with II degree fly ash at the contents of 10%, 18% and 25% and 1% super-plasticizer were used to produce 100 × 100 × 100mm cubic specimens using the standard test casting. In the standard conservation room, the specimens was conserved for one day, demodulused, numbered, and then continued to be conserved in conservation-boxes. After 28 days, they were placed in the indoor environment at 20-25 ^{o}C. The strength values after 7d, 14d, 28d, 60d, 90d and 120d were measured using 6 individual specimens as shown in Table 1. The representative value of the strength was obtained by removing the maximum and the minimum values and averaging the strength value of the four specimens.

30 groups of allocated proportion and strength tests were carried out according to “A Practical Handbook for the Concrete Mix” and “Concrete Standards and Engineering Applications”（Li 2007, Leng and Zhang 2005). 7 representative groups of the allocated proportion data were listed in Table 2 with the unit as kgm^{-3}.

Concrete freeze-thaw cycle test. In order to stimulate the real building corrosive conditions in nature, the strength variation of concretes with water-cement ratio of 0.38, sand rate of 29%, and content of II degree fly ash at 0%, 10%, 18%, 25% were

subjected to freeze-thaw cycle tests. In detail, the concrete samples were frozen first and then treated by Na_2SO_4 or HCl solutions. The two-step procedure was repeated 150 times. The concentrations of the Na_2SO_4 solution were 0.05, 0.1, and 0.5 $molL^{-1}$, respectively. The pH value of the HCl solutions was 3, 4, and 5, respectively. Figure 1 shows the strength variation curves of the concretes after 150 freeze-thaw cycles using Na_2SO_4 (left) and HCl (right) as the corrosion solutions.

Table 1. Average compressive strength of concrete

Age Period	0%	10%	18%	25%
3 d	35.78	32.20	29.58	22.27
7 d	42.17	40.70	37.72	30.76
14 d	51.64	49.68	45.53	37.45
28 d	55.36	54.42	52.48	49.20
60 d	59.28	59.82	61.82	55.50
90 d	61.52	62.76	62.40	61.92
120 d	63.69	66.18	66.68	67.20

Table 2. Experimental allocated proportion and actual compressive strength

Number	Cement	Fly ash	Sand	Stone	Water	water reducer
1	462.5	154.2	334.8	1209.3	166.5	4.625
2	397.1	132.9	468.6	1115.7	166.5	3.971
3	365.1	121.7	361.7	1306.6	166.5	3.651
4	347.1	115.6	366.7	1324.7	166.5	3.471
5	462.5	154.2	258.7	1286.8	166.5	4.625
6	478.4	159.4	255.3	1297.0	166.5	4.784
7	365.1	121.7	460.3	1206.1	166.5	3.651

TEST RESULT AND ANALYSIS

Affect of ash fly quantity on concrete strength. All experimental results showed that under standard conservation conditions, the compressive strength of the concrete mixed with 25% fly ash increased slowly and doesn't meet the desired standard of the concrete C50. After 90 days, the compressive strength of concrete mixed with 10%, 18% and 25% II degree fly ash became equal to that of concrete C50 as shown in table 1. This means that the compressive strength of the fly ash concrete increased continually from the 28^{th} to the 120^{th} day; whereas the strength of the control non-fly ash concrete increased relative slowly. After 120 days, the strength of the fly ash concrete was close to or higher than that of the ordinary concrete, suggesting that the dense surface of the II degree fly ash particles slowed down the early development of

the strength. At the early stages, the internal energy of fly ash was not released; and the strength of the concrete was dominated by the hydrates in the cement. Therefore the reaction rate was relatively slow which resulted in lower strength in the early stages. SiO_2 and Al_2O_3 from fly ash and cement can hydrate $Ca(OH)_2$; then $Ca(OH)_2$ covers the surface of fly ash and generates calcium silicate and calcium acuminate. Due to the hydrolyzed layer between $Ca(OH)_2$ thin film and fly ash surface, Ca^{2+} gives a reaction with living tissue of fly ash and product gathers in layers. If the hydrolyzed layers aren't filled with products, the strength doesn't increase more. With the products filling in the hydrolyzed layers, fly ash and products form firm connection and lead to increased concrete strength, impermeability and abrasion resistance. This is the main reason for the lower early strength and the high mature strength（Hansson and Strunge 1985）.

Affect of freeze-thaw cycle on concrete strength. Figures 1 and 2 show that the compressive strength of II degree fly ash concrete and C50 concrete both decreased obviously after the freeze-thaw cycle test using Na_2SO_4 corrosion.（Liu and Ning 2005). With the increase of the Na_2SO_4 concentration, the fly ash II concrete strength decreased. In addition, the strength of the II degree fly ash concrete decreased more obviously than that of the ordinary concrete after treated with the same Na_2SO_4 solution; and the strength decreased more obviously with the increasing of the II degree fly ash content. The reason for this is that the effect of fly ash quantity on liquor concentration is insensitive and that the acid fastness fly ash is better than common concrete. The appropriate amount of fly ash makes the inside of concrete hydrate continually; and the products fill in the interval of concrete. The concrete become gas-tight and dense; consequently, the strength of concrete continues to grow. The change strengthens the chemical resistance, infiltration and frost resistance and improves the durability of concrete.

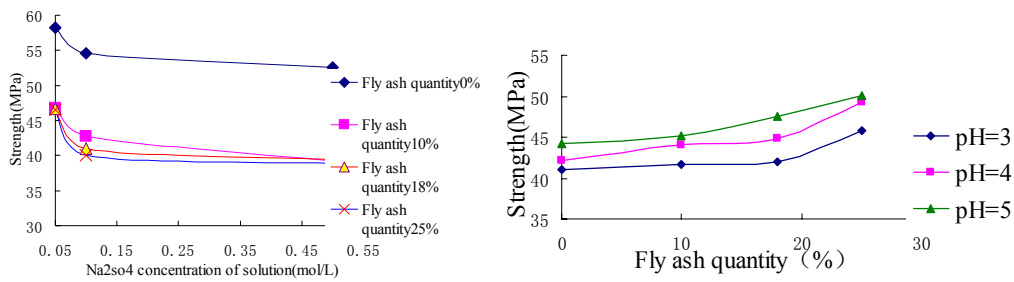

Figure 1. Strength variation curves of fly ash concrete taking Na_2SO_4 (left) and HCl (right) as the corrosion solution after 300 freeze-thaw cycles

Figure 2. The destruction process of concrete containing 18% quantity fly ash after 150 freeze-thaw cycles

CONCLUSIONS

In this paper, II degree fly ash was used instead of cement to produce the fly ash concrete. The reasonable usage of fly ash in concrete will save large amount of cement therefore lower the construction cost. Besides, the successful usage of the fly ash will provide valuable data for the production of other kinds of high quality concrete to satisfy the social and engineering requirements.

Four conclusions are drawn as follows based on the experimental study:

(1) The compressive strength of II degree fly ash concrete increased relatively slowly in its earlier period of conservation, and its strength did not meet the standard of C50 after 28 days. However, with extension of conservation time from the 28th day to the 120th day, its strength increased continually due to the interaction between the active components in the concrete. Finally the strength meets the standard of C50 after 120 days. This result suggests that the concrete contains reasonable amounts of fly ash II and super plasticizer can satisfy the strength standard of C50.

(2) The freeze-thaw cycle experiment showed that both SO_4^{2-} and H^+ ions had negative impact on the strength of the II degree fly ash concrete. Although the strength of both the ordinary and the fly ash II concrete decreased with the increasing of the ion concentration, , the decrease extent of the II degree fly ash was lower, suggesting the action of II degree fly ash in improving the concrete strength and corrosive abilities.

(3) Based on strength change from freeze-thawing tests of fly ash concrete at different fly ash quantities, once the II degree fly ash concrete became corroded and frozen, its strength could not match the strength standard of the ordinary concrete, suggesting that the II degree fly ash concrete be unsuitable for winter use. However, in conditions of non-freezing, the II degree fly ash can be used as an ingredient for high strength concrete with prolonged service life.

REFERENCES

Hansson, C. M. Strunge, H. Markussen, J. B. and Forlund, T. (1985). "The Effect of Cement Type on the Diffusion of chloride." *Nordic Concrete Research*, 470-80.

Leng, F., and Zhang, R. (2005). *Standard Specification for Concrete and Application,* Beijing, China Building Materials Industry Press

Liu, Y., and Ning, B. (2005). *Corrosion environment mechanism arcims of concrete*. Coal Mine Security, 36(4), 37-38

Li, Y. (2007). "Test about the better quality High grade concrete mix with fly ash." Railway Investigation and Surveying.

Pu, X. xincheng. (1994). "High strength concrete and base slag concrete." *Concrete.* (3), 9-18

Tang, J. (2007). *Study on the application of fly ash concrete ratio*.

Wang, S., Zhang, J., and Tang, H. (2007). "Study on High Performance concrete ratio design and its Property test." *Fujian Building Materials,* v(03).

Wu, J., (2004). *Study on High strength and property and more impurities concrete*. Congqing University.

Experimental Research on the Shear Strength Deterioration between the Freezing and Thawing Surface of Melting Soil Slope in Seasonal Frozen Regions

Cheng Yong-chun[1], Ge Qi[2] and He Yan[3]

[1]Department of Road and Railway Engineering, Jilin University, 5988, Renmin ST, Changchun, China; PH (+86) 431-85095446; FAX (+86)431-85095446
[2] Department of Road and Railway Engineering, Jilin University, 5988, Renmin ST, Changchun, China; PH (+86) 13604335801; email:jddaoqiao@163.com
[3] Department of Road and Railway Engineering, Jilin University, 5988, Renmin ST, Changchun, China; PH (+86) 15948366646

ABSTRACT

In seasonal frozen areas, shallow landslide hazards usually occur in soil slopes, which pose a serious threat to road safety. The factor leading to the soil slope failure is the shear strength reduction of the soil in the zone between the freezing and thawing surface. In this research, model experiments of freeze-thaw soil interface with different aggregate materials are designed by alternating the freeze-thaw cycling time and the water content of soil. Subsequently, the relationship between the shear strength and freeze-thaw cycling time is obtained. Finally a shear strength deterioration modal of the soil surface is proposed. The major parameters and influence factors of melting soil slope failure are related to the earth stress and slope geometry, so based on the fully understanding of the shear strength, the research result could not only present guidance to locate the landslide position, but also offer advices for slope design and stability analysis in seasonal frozen regions.

Key words: road engineering; deterioration model; freezing and thawing surface; shear strength; seasonal frozen regions

INTRODUCTION

Slope instability damages, earthquakes and volcanoes are three major global geological disasters. In seasonal frozen regions, because of water moving through the soil, as well as soil gravity, shallow landslide hazards in soil slopes usually occur in spring thawing period, which pose a serious threat to the safe operation of highways (Sally, 2008). The research of the impact of freeze-thaw (F-T) cycles on soil shear strength has not only a certain effect in accelerating the movement of frozen soil (Liu, 2006), but also a practical significance in engineering design, construction and management in cold regions (Chen, 2003).

After a few F-T circles, the soil structure changes, the frost water enlarges the soil voids, and reduces shear strength of the soils (Xu, 2006). At the same time, water in the F-T soil layer moves out and gathers above the F-T layer. This forms an interlayer between the soil, and the shear strength of the interlayer decrease

substantially, which results in the increase in the probability of a slide. It is believed that when the soil is melting, sliding will go along the freezing-thawing surface, which is parallel to the slope surface (Chen, 2008). Soil slope sliding depends largely on the soil shear strength indicator (Sean, 2001). When the slope angle keeps unchanged, as the slope thawing depth increases, the downslide force from the gravity of the thawed soil will increase. The normal part of the gravity of the upper thawed soil can offer certain compressive stress, but the increase rate is less than the increase rate of downslide part of the gravity .When the shear strength along the shear surface τ_f loses to some degrees, the safety factor of the slope will reduce, therefore the research on the deterioration of shear strength along the boundary surface of the freezing and thawing zones can serve as the starting point for slope stability analysis by means of the mechanical model.

Because of the difficulty in modeling a freezing - thawing interface, the present literatures have only presented the limited research on the shear strength of the entire zone of the melted soils. There is no research that has addressed the shear strength variation on freezing - thawing surface and shear strength parameter changes in the critical state, as well as the analysis of shear strength deterioration in the freeze-thaw cyclic condition. It is necessary to setup a reasonable experiment method for predicting and analyzing the ultimate shear strength of the freezing-thawing surface.

Experiment on shear strength of freeze-thawing surface

The basic principles and methods of the experiment

In order to analyze the shear strength deterioration on sliding surface under the circumstances of different freezing - thawing circles and water contents, when there is relative movement inside the soil mass, a direct shear testing plan is designed as follows.

Freezing point of salt water is lower than the common water, so in this research we use different water to model the supper and lower parts of the sample and get freezing-thawing surface at $-3°C$. We obtain a shear strength curve of the freezing and thawing surface, and then simulate the actual situation of the freeze and thaw effect on the shear strength of the freezing - thawing surface.

(1) The correction coefficient

In this experiment we adopt EDJ-Ⅰ strain-controlled direct shear equipment.

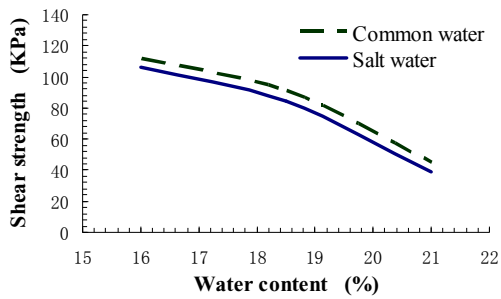

Figure1. Shear strength comparison with different water content between samples made by salt and water, respectively

Because of the use of salt water, taking into account the difference of salt water and common water, in this text we put forward the correction coefficient of the two materials.

$$\tau_S = \eta \cdot \tau_W \quad (1)$$

In which η is the correction coefficient of shear strength, τ_S is shear strength of the salt water sample, and τ_W is the shear strength of the common water sample.

In this text we take the correction factor as 0.946, with which to correct the shear strength value of the test samples (see Figure.1).

(2) The basic parameters of the soil

We alter the moisture content based on the optimum moisture content of the slope soil. We used a mould to make a soil sample with the diameter of 61.8mm and height of 20mm. We made 15 samples at every water content level. Then we get the shear strength through the curve. With the same method, we change the F-T times and compare the shear strength deteriorations.

The basic index is listed, such as natural water content, the largest dry density and the optimum moisture content (See Table 1).

Table1. The basic parameters of the soil

	Natural water content	Largest dry density	Optimum moisture content
Values	3.2%	1.68g/cm^3	21%

Analysis of the results

We compared the experimental results of the samples which experienced the F-T circles and the samples which did not, and we analyzed the levels of the shear strength deterioration under different water contents and F-T circle time.

From the failure mode of different samples, we know when the freezing-thawing surface slides, the upper part and lower part failed with the increasing strain. We can see ice crystal structure on the lower freezing surface. In addition, we observed that the readings of the direct shear machine often move back and forth. From the failure mode we can judge that when the freezing-thawing surface was subjected to shearing, the slippage occurred on the freezing-thawing surface, because the friction coefficient on the surface is less than the soil itself. That is why the shear strength of the freezing - thawing surface is lower than those of common samples.

The shear strength of the samples with the same water content is presented as follows (see Figure 2).

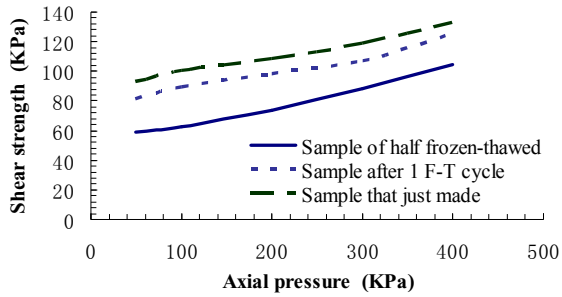

Figure 2. Comparison of the shear strength of the tested samples

Samples in group 1 are not frosted, in group 2 are after one time F-T circle, and in group 3 are in the semi-frozen state. We can conclude that the shear strength on freezing - thawing surface is obviously less than the other two conditions. Under the same normal stress，the shear strength of group 2 is just 74.4% of the shear strength of group 1.

The shear strength of the tested samples which are just separately made, through an F-T circle, and in the semi-frozen state are compared (see Figure 3). We can draw a conclusion that the shear strength on the freezing-thawing surface with different water contents are less than that on the surface of just-made samples and samples through F-T circles, the former is about 76.2% of the latter. As the water content increases, the decline is more obviously observed. As for the test samples with water content of 21%, the shear strength is 61.6% of the samples with water content of 16%.

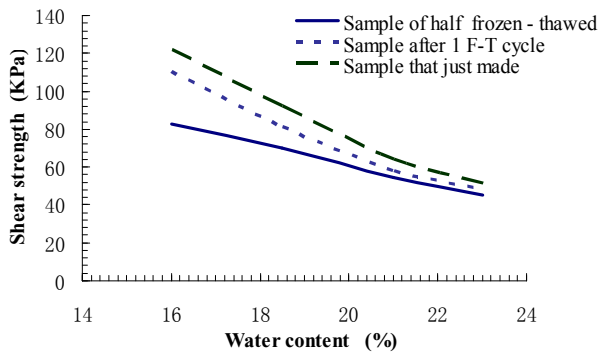

Figure3. Comparison of the shear stress strength at different water contents

The effect of water content on shear strength under the same normal pressure is compared in Figure 4.

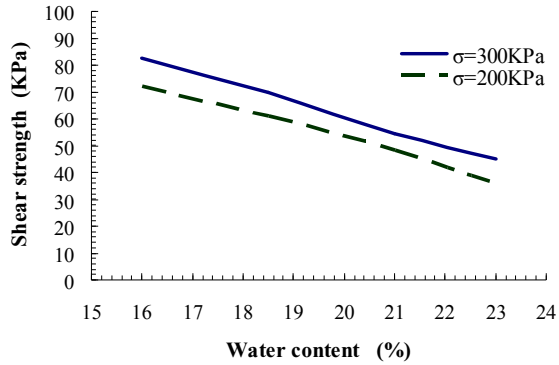

Figure4. The variation of shear strength of the interface with different water contents

We can find that with the increase of water content, the shear strength of the freezing-thawing surface decreases obviously. As the water content increases from 16% to 21%, the shear strength of the freezing-thawing surface has a decline of 32.6%. It illustrates that water in the soil plays an important role in the progressive slide, and water content reduction is the key to prevent slide. As the axial pressure increases from 200kPa to 300kPa, the shear strength of the freezing-thawing surface increases by 12.7%.

F-T shear strength deterioration model based on the test results

Considering the effects of F-T cycles on the shear strength of the freezing –thawing surface, we separately make samples with different types of water (salt water and common water). After the F-T cycles, they are directly sheared under the state of the half zone frozen. We analyzed the deterioration of the shear strength after the F-T circles (see Figure 5). The experiment data shows that the shear strength decreases with the increases in water content and the F-T circle times. With the same water content, the shear strength of the sample which went through 5 times F-T circles is 70.3% of the former shear strength.

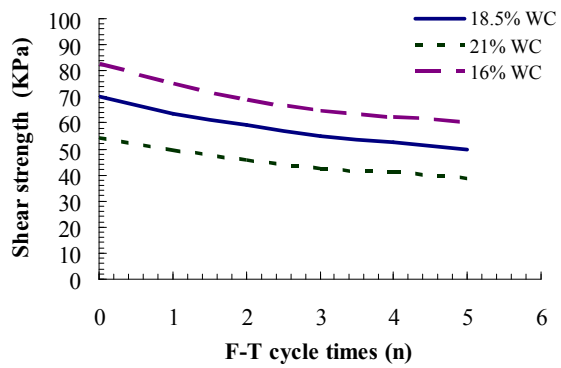

Figure 5. The shear stress strength of the interface under different F-T cycle times

In order to analyze the effect of F-T times on the shear strength, we propose the F-T deterioration model based on the test results. we take

$$\beta_n = \frac{\tau_n}{\tau_0} \qquad (2)$$

In which β_n is the deterioration coefficient, τ_n is the F-T shear strength after n times F-T cycles and τ_0 is the initial F-T shear strength.

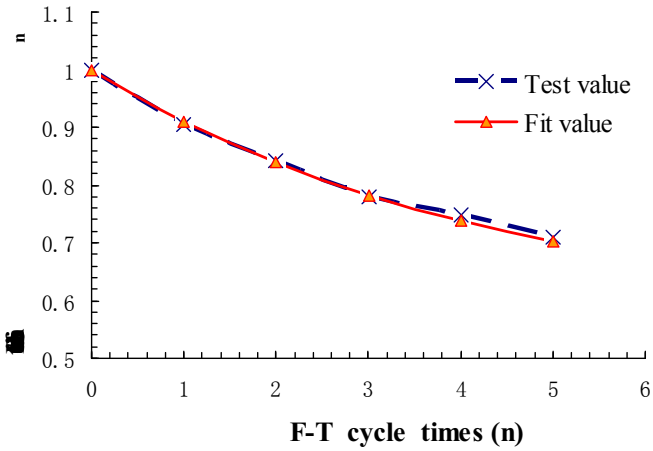

Figure 6. Curve fitting of the F-T deterioration model and experimental values

From equation (2), we got the curve of β_n and n through the experiment, which was presented in Figure 6), then had the curve fitting, and got the F-T deterioration model:

$$\beta_n = 0.47e^{-0.234n} + 0.57 \qquad (3)$$

In which, n is F-T circle times. The F-T deterioration model is based on the experiment results, and could present guidelines for analysis of soil slope stability in seasonal frozen regions.

CONCLUSION

1. In the paper, a testing method is discussed and applied a test method to locate freezing - thawing surface using the trait salt water which has low freezing point. The direct shear tests are conducted on the freezing - thawing surface for the soil samples are subjected to different F-T cycle times. The results show that the shear strength of the freezing - thawing surface decreases with the F-T circle times increased.
2. The water content is the main factor that affects the shear strength, as the water content varies from 16% to 21%, the shear strength decreases by 39.9%.
3. In the paper, curve fitting is employed to establish the shear strength deterioration model on the freezing-thawing surface. The model truly reflects the shear strength

deterioration of the inner freezing-thawing surface when the soil slope is melting.
4. The shear strength deterioration along the freezing-thawing surface that the research brought forward can provide guidance for future analysis of soil slope stability in seasonal frozen regions.

REFERENCES

Chen, Bo (2008). "The analysis on freeze-thaw collapsing mechanism and stability of soil cutting slope." *Heilongjiang Transportation Technology*, 2: 65 - 66.

Chen, Zu-yu (2003). "Stability analysis of soil slope–principle · method · program." *China irrigation work and water electricity publication company*, Beijing.

Liu, Hong-jun, Wang Pi-xiang (2006). "Stability analysis of loss of stability caused by freeze and melt of earthen side slopes of highways." *Journal of Harbin Institute of Technology*, Vol.38 (15): 764 - 766.

Shoop (2008). "Mechanical behavior modeling of thaw-weakened soil." *Cold Regions Science and Technology*, 52:191 - 206.

Fitzsimons (2001). "Direct shear tests of materials from a cold glacier: implications for landform development." *Quaternary International*, 86:129 – 137.

Xu, Shan-shan, Gao Wei (2006). "Analysis of the stability of the soil cutting side slope freeze-thaw and sliding of highway in cold area." *Low Temperature Construction Technology*, 2: 10 - 12.

Design and Construction of Overlay with Mechanical Joint Element on Used Concrete Pavement

ZHOU Mingjie [1,2], ZHAO Xiaoyan [2], TIAN Wenling [2],
WANG Xiaowei [2], XU Xinwei [2]

[1] School of Civil Engineering, Tianjin University, Tianjin, No.92 Weijin Road Nankai District; PH (86) 22-60435983; FAX (86) 22-60435940; email: zhoumingjie922@163.com,
[2] Civil Engineering Institute, Hebei University of Technology (Civil Engineering Technology Research Center of Hebei), Tianjin, PH (86) 22-60435588; FAX (86) 22-60435528; email: zhaoxiaoyan@henbut.edu.cn

ABSTRACT

Reinforcing the bonding of the young concrete overlay and the old concrete with mechanical joint element (MJE) is an effective measure to repair the used concrete pavement. Splitting tests of the young and old concrete samples with MJE were carried out and the simulation results using the finite element method to assess mending effects by MJE under wheel load were analyzed. The design method and construction method to repair the used concrete pavement with reasonable MJE ratio is proposed. Example calculation results indicate that the repaired pavement with MJE presents good performance under the comprehensive fatigue stress of load and temperature in design period.

Key words: used concrete pavement; mechanical joint element; interface; design method; construction method

INTRODUCTION

At present, the repaving design of old concrete pavement is still in research stage in China. The lightly damaged old concrete can be used as the lower structure layer of the repaired roads. This measure makes use of waste to reduce environment pollution. Large quantity of base material and the expense of machinery and manpower to break the old concrete can be saved (Feng, X. D. 2007). But the bonding between the young and old concrete usually presents bad performance. Young and old concrete will crack easily at their joints under the wheel load. A design and construction method of overlay with MJE on used concrete pavement is proposed in this article. The performance of the used concrete can be improved greatly and the social and economic efficiency is considerable.

In the US, the anchor bolt was once used on the edge of the highway and the bridge pavement to prevent the edge rolling-up; in Switzerland, there was the application example of mechanical joint in the bridge, but in other countries the standard and the criterion were not formed yet. The design and construction method of repaving with MJE is put forward by use of research results about the young and old concrete with MJE of our team (Zhao, X.Y. 2004 and Xu, X.W. 2006). Performance under the fatigue stresses of wheel load and temperature of the repaired road with MJE is discussed.

DISCUSSIONS ON TEST AND NUMERICAL SIMULATING RESULTS

Splitting test specimens were described in reference (Zhao, X. Y. 2004). Specimen making and split test are indicated in Figure 1. The strength grades of the young and old concrete were C40 and C35 respectively. Splitting strength of the young and old concrete combining specimen with MJE embedded with epoxy resin mortar and the combining specimen without MJE were 2.43MPa and 1.95MPa respectively (Zhao, X. Y. 2009). The result indicates that the MJE can improve the combined performance of young and old concrete significantly. The models of the finite element analysis were described as reference (Xu, X.W. 2006). Results of numerical simulations of the repaving road slab with MJE ratio of 0% and 0.35% is indicated in reference (Xu, X.W. 2006).

Pre-cracking, the displacement in y direction of the model of 0.35% MJE ratio is approximately equal to that without MJE. Post-cracking, the shear stresses in x and y direction of the model with 0.35% MJE ratio are less than those of the model without MJE, which indicates that MJE can control the development of shearing stress and inhibit the development of crack in the young and old concrete interface effectively when the MJE ratio reaches 0.35%.

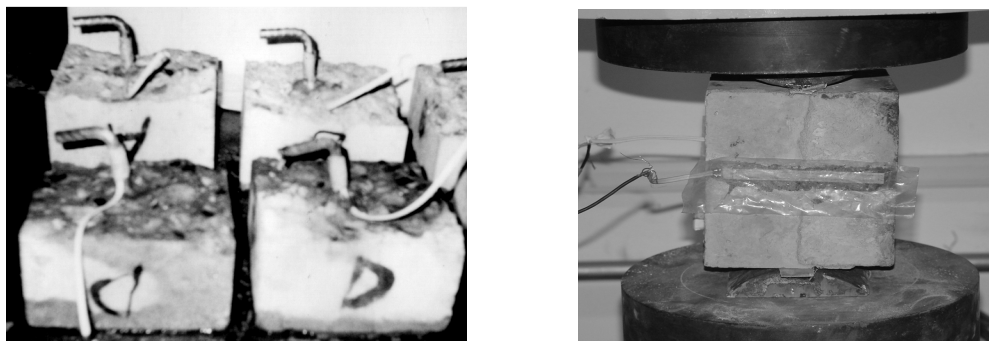

Figure 1. Specimens making and split test

DESIGN METHOD OF OVERLAY WITH MJE ON USED CONCRETE PAVEMENT

Specifications of Cement Concrete Pavement Design for Highway (Zhongjiao Highway Plan Design Institute, 2002) specified that the stress of the overlay and the old concrete slab is calculated according to the combined double slab when the combined overlay structure on used concrete pavement is designed. Thickness, flexural tensile strength, standard value of modulus and equivalent rebound modulus of base of old concrete slab are determined by measured values mentioned in section 8.4. The thickness of overlay is determined by the stress of the old concrete slab that meets the requirement of equation (3.0.3). The clauses and equations mentioned in this section are quoted from reference (Zhongjiao Highway Plan Design Institute, 2002).

Only the stress of the old concrete slab is calculated in this method, the stress state of the young and old concrete interface isn't considered. Considering that the interface will possibly be destroyed before the old concrete slab, it's necessary to validate the bonding performance. The design method that considered temperature fatigue stress of the young concrete overlay and the interface between the young and old concrete slab is discussed by the following example.

The surface course of a constructed highway in natural zoning for highway

Ⅱ is ordinary concrete, the board is 5m long, the longitudinal joint is the rabbet with tension bars. Traffic investigation indicated: standard axle load date function number of times is 3800 present and the highway is open to traffic for 10 years. Investigation evaluation showed that grading standard of pavement damage and load transfer capacity of the joint is good. The combined concrete pavement is planed to repair the concrete road.

Original concrete surface course is 0.3m thick, 1/3 thickness of slab is planed to be broken, and the residual old concrete slab is 0.20m thick. 0.12m thick young concrete layer is planed to be repaved on the old concrete slab. The original base is cement stabilized grain (cement content 5%) with a thickness of 0.18m. The cushion is the 0.15m thick low dose soil stabilized with inorganic binding materials. Design reference period of highway is 30 years. The safety class is I (first class). Wheel path lateral distribution coefficient in critical loading position is 0.22. The annual average rate of traffic growth is 5%. The accumulated standard load acting number on lane in design reference period calculated according to equation A.2.2 is 1009×10^4, so the road belongs to heavy traffic classes. (The letters' meanings in the equation is referred to <Specifications of Cement Concrete Pavement Design for Highway>. And so are the letters in the following equations.)

$$N_e = \frac{N_s\left[(1+g_r)^t-1\right]\times 365}{g_r}\eta = \frac{3800\times\left[(1+0.05)^{20}-1\right]\times 365}{0.05}\times 0.22 = 1009\times10^4$$

The standard value of flexural tensile strength of surface plain concrete is 5.0MPa. The standard value of modulus is 31GPa correspondingly. Rebound modulus of subgrade is assumed as 30MPa. Rebound modulus of the cushion and the cement stabilized grain base is 600MPa and 1300MPa respectively. The splitting strengths of the old concrete and the combine concrete of young and old concrete are 2.40MPa and 2.43MPa according to the test results. The standard values of their flexural tensile strengths are 4.13MPa and 4.15MPa correspondingly. The standard value of modulus of the old concrete is 27GPa. The equivalent rebound modulus of base top surface (Et) is calculated as 165MPa.

Traditional design of combining overlay with used concrete pavement. According to the appendix C, the stresses on critical loading position of the upper (σ_{ps1}) and lower concrete slab (σ_{ps2}) due to standard axle load are calculated as 0.27MPa and 0.66MPa. Correspondingly, the fatigue stresses on critical loading position are 0.67MPa (σ_{pr1}) and 1.63MPa (σ_{pr_2}) calculated according to equation B.1.2.

$$\sigma_{pr} = k_r k_f k_c \sigma_{ps} \qquad \text{(B.1.2)}$$

The maximum temperature gradient is taken as 88C/m according to natural zoning for highway. The thermal stress coefficient (B_x) is taken as 0.69 according to Fig.B.2.2. The maximum thermal curling stress of the lower slab of the combining concrete pavement (σ_{tm2}) is calculated as the following.

$$\xi_2 = 1.77 - 0.271\ln\left(\frac{h_{01}}{h_{02}}\frac{E_{c1}}{E_{c2}} + 18\frac{E_{c1}}{E_{c2}} - 2\frac{h_{01}}{h_{02}}\right)$$

$$= 1.77 - 0.27\ln\left(\frac{0.12}{0.2}\times\frac{31000}{27000}+18\times\frac{31000}{27000}-2\times\frac{0.12}{0.2}\right)$$
$$= 0.96$$
$$B_{x2} = \xi_2 B_x = 0.96\times 0.69 = 0.66$$
$$\sigma_{tm2} = \frac{\alpha_c E_{c2}(h_{01}+h_{02})T}{2} B_{x2}$$
$$= \frac{1\times 10^{-5}\times 27000\times(0.12+0.2)\times 88}{2}\times 0.66$$
$$= 2.51\text{MPa}$$

k_t is the thermal fatigue stress coefficient of ordinary concrete surface; σ_{tr} is the thermal fatigue stress at the critical loading position. They are calculated as 0.581 and 1.46MPa according to equation B.2.3 and B.2.1.

$$k_t = \frac{f_r}{\sigma_{tm}}[a(\frac{\sigma_{tm}}{f_r})^c - b] \qquad \text{(B.2.3)}$$

$$\sigma_{tr} = k_t \sigma_{tm} \qquad \text{(B.2.1)}$$

The safety class of the highway is First. The target reliability is 95%. The relative deflection level class is low, so reliability coefficient γ_r is determined as 1.33.

$$\gamma_r\left(\sigma_{pr}+\sigma_{tr}\right) = 1.33\times(1.63+1.46) = 4.11MPa < f_r = 4.13MPa$$

So the assumed thickness 0.12m of the concrete overlay can bear fatigue stress acting of wheel load and temperature in design reference period fully.

Calculating the temperature fatigue stress of the young concrete and the interface. The temperature fatigue stress is calculated according to two methods. The first method is taking the repaving as a separate type overlay; the other is taking the repaving as a new concrete monolayer. The higher value will be chosen to combine with the load fatigue stress.

If the temperature fatigue stress is calculated according to a separate type overlay, the maximum thermal curling stress of the upper slab of the separate type overlay (σ_{tm1}) is calculated as 1.23MPa according to equation C.2.2. Thermal fatigue stress coefficient of young concrete overlay (k_t) and thermal fatigue stress on critical loading position (σ_{tr}) are calculated as 0.360 and 0.44MPa according to equation B.2.3 and B.2.1. Thermal fatigue stress coefficient (k_t) and thermal fatigue stress on critical loading position (σ_{tr}) of the interface are calculated as 0.421 and 0.52MPa according to equations B.2.3 and B.2.1.

If the temperature fatigue stress is calculated according to the new concrete monolayer, the maximum thermal curling stress of the upper slab of the separate type overlay (σ_{tm}) is calculated as 1.13MPa according to equation B.2.2. Thermal fatigue stress coefficient (k_t) and thermal fatigue stress on critical loading position (σ_{tr}) of the upper slab are calculated as 0.33 and 0.37MPa according to equations B.2.3

and B.2.1. The thermal fatigue stress coefficient (k_t) and thermal fatigue stress on critical loading position (σ_{tr}) of the interface between young and old concrete are calculated as 0.393 and 0.44MPa according to equations B.2.3 and B.2.1.

$$\sigma_{tm} = \frac{\alpha_c E_c h T_g}{2} B_x \qquad \text{(B.2.2)}$$

The temperature fatigue stress of the young concrete overlay and the interface is taken as 0.44MPa and 0.52MPa individually to combine with relative load fatigue stress. So the stresses of the young concrete overlay and the interface between young and old concrete slab are:

$$\gamma_r\left(\sigma_{pr}+\sigma_{tr}\right)=1.33\times\left(0.67+0.44\right)=1.48MPa<f_r=5MPa$$

$$\gamma_r\left(\sigma_{pr}+\sigma_{tr}\right)=1.33\times\left(0.67+0.52\right)=1.58MPa<f_r=4.15MPa$$

The results indicate that the young concrete overlay and the interface of the young and old concrete with MJE can completely bear fatigue stress acting of wheel load and temperature in design reference period.

CONSTRUCTION OF OVERLAY WITH MJE ON USED CONCRETE PAVEMENT

Removing the old damaged concrete. The damaged concrete should be removed completely before the construction of combining repaving. Rap on the road surface with a steel stick or drag a piece of steel chain to detect the damaged concrete is a simple and reliable method. A shrill ring indicates the concrete is fine. The damaged concrete should be removed by light pick; the removing depth should not exceed one third thickness of the old surface.

Embedment of MJE. The second step is to drill on the remainder old concrete with percussion drilling of diameter 22mm. The holes with the depth of 50mm are arranged as cinquefoil pattern. The space between each other is 400mm, and the MJE rate is 0.35%. The surface of the old concrete and the hole should be cleaned by blasting or by high pressure water-jet. The old concrete should be waterlogged for 24h to be soaked completely, which could avoid insufficient hydration of young concrete. Then, the water on the old concrete surface and in the holes should be eliminated; the MJE should be embedded in the hole with epoxy resin mortar containing 10%U-type expansive agent. Then the embedded MJE should be cured for 24h.

Construction and maintenance of young concrete. Clean out the leftover residues from the old concrete surface with compressed air. Paving young concrete immediately after the interface bonding mortar layer is brushed on the old concrete surface. The grade of young concrete should be one grade higher than that of old concrete. Road Portland cement or ordinary Portland cement with less caloric and less shrinkage should be chosen as possible. Dual maintenances of sprinkling and film cover should be taken as possible. High quality curing agent with water retaining rate higher than 90% should be sprayed on the young concrete surface. The curing film should be placed when water film formed. Sand should be put on the curing film on joints uniformly to avoid the film being blown away. To prevent the young concrete cracking because of high temperature in the hydrated process water should be sprayed on the film. Curing time should not be less than 14d. In addition,

the raw materials, mixture ratio, technology of mixing and transportation as well as the construction and curing method should also conform to the specification of <Technical Specification For Construction Of Highway Cement Concrete Pavements> (Highway Scientific Institute, 2003) and <Technical Specifications of Cement Concrete Pavements Maintenance of Highway> (Ministry of communications of PRC, 2001).

CONCLUSIONS

The splitting test results indicate that MJE can improve the combine performance of the young and old concrete significantly. The MJE ratio of 0.35% is determined by finite element analysis. Based on the traditional design method of concrete pavement, performance of the young and old concrete road slab and their interface with MJE was discussed. Results indicated that the young and old concrete slab and their interface with MJE proved to have good performance under the fatigue stress of wheel load and temperature in design reference period. Construction scheme of this repairing method include pretreatment of the old concrete, MJE embedding and maintenance of young concrete.

ACKNOWLEDGEMENT

The authors are grateful for the support of sustentation fund of scientific research key project of HeBei Province department of communications (No. Y-060139).

REFERENCES

Feng, X. D. and Jianming,Y.(2007). "Design and Construction of Asphalt Concrete Paved on Old Cement Concrete Road Surface." *Zhejiang Buildings*, 24(2), 35-37.

Highway Scientific Institute, Ministry of communications of PRC. (2003). Technical Specification for Construction of Highway Cement Concrete Pavements JTG F30-2003, People communications press, Beijing, 6-89.

Ministry of communications of PRC. (2001). Technical Specifications of Cement Concrete Pavements Maintenance of Highway JTJ 073.1-2001, People communications press, Beijing, 38-50.

Xu, X. W. (2006) The Interlayer Performance of Young and Old Concrete Linked by Reinforced Bar, Hebei University of Technology, Tianjin**,** 41-43.

Zhao, X. Y. (2004) Study On Combination Capability Of Young And Old Concrete With Mechanical Joint Element, Hebei University of Technology, Tianjin, 11-19.

Zhao, X. Y. and Tian, W. L (2009). "Study on Combining Performance of Young and Old Concrete with Mechanical Joint Element", *Key Engineering Materials.* 400-402, 537-542.

Zhongjiao Highway Plan Design Institute. (2002). Specifications of Cement Concrete Pavement Design for Highway JTG D40-2002 People communications press, Beijing, 31-46.

RESILIENT MODULUS OF THE GRADED AGGREGATE MATERIAL UNDER LONG-TERM DYNAMIC REPEAT LOAD

Long Wang[1], Xiaoguang Xie[2], and Bin Xu[3]

[1] Associate Professor, School of Transportation Science & Engineering, Harbin Institute of Technology, Harbin, Heilongjiang, China, PH 0451-86282120, FAX 0451-86283779, Email: hitlongwang@sina.com
[2] Associate Professor, School of Transportation Science & Engineering, Harbin Institute of Technology, Harbin, Heilongjiang, PH 0451-86282120, FAX 0451-86283779, Email: xxg75@126.com
[3] Engineer, Ying Kou Transportation Bureau, Ying Kou, Liaoning 115000, China PH 013703976465, Email: ykbhgl@126.com

ABSTRACT

In order to investigate the modulus growing rule of graded aggregate materials under long-term vehicle loads and confirm the long-term using characteristics of graded aggregate base asphalt pavement, the resilient modulus of graded aggregate specimen has been studied under the long-term condition of different confined stresses and dynamic stresses by using middle-type dynamic triaxial instrument. Test results showed that graded aggregate material's modulus are growing with increasing dynamic load repeating time and are confined by asymptote when dynamic load level is constant. The modulus curve can be regressed by logarithm or power equation, but it is more reasonable to adapt hyperbola model. Graded aggregate materials modulus is stabilized under long-term dynamic repeat load. It is not the traffic load accumulation causing pavement fatigue crack, but the softening of graded aggregate materials' modulus under asymmetrical traffic load.

INTRODUCTION

For granular materials, the degrees of deformation and the changes of resilient modulus are relevant to repetition frequency of load. However, there is less research on dynamic triaxial instrument test of graded aggregate material under long-term dynamic repeat load, there is no clear relationship between resilient modulus and long-term dynamic load repeat times, and the dominant damage of graded aggregate base asphalt pavement can not be predicted. So it is necessary to study the growing rules and impacting factors of the resilient modulus of graded aggregate material under long-term dynamic repeat load, which will set up the foundation for predicting the long-term characteristics of graded aggregate base asphalt pavement.

TEST EQUIPMENT AND METHODS

The middle-type dynamic triaxial instrument was adopted to study the resilient modulus of graded aggregate materials under long-term dynamic load. The specimen diameter is 20cm, height is 50cm.Graded aggregate materials used in the experiments are crushed by limestone and gradation is dense-framework type, the specimens are mold with vibration method (Wang 2005). Definite load control conditions simulating the physical and stress state of highway surface (Wang 2006), three kinds of confining pressure are used in test respectively, 50KPa, 100KPa and 150KPa, each confining pressure adopting three kinds of dynamic stresses to cover the critical state. Each specimen is experimented by vibrating 10,000 times with half-sine wave and loading time for 0.2s, unloading time for1.8s, cycling time for 2s.

THE RESILIENT MODULUS OF GRADED AGGREGATE MATERIAL UNDER LONG-TERM DYNAMIC LOAD

The design parameters of graded aggregate materials are calculated by the dynamic triaxial test in the provisions of dynamic load cycles, the dynamic cyclic loading frequency provided by literature is 200 times, fewer cycles in other civil engineering related industry (SL237 1999), with the aim of dynamic cyclic loading activity can not destroy the structure of the sample, which is appropriate corresponding to the actual state of static load or without greater plastic deformation. In fact, graded aggregate materials in pavement will receive millions or tens of millions times vehicle load. Standardized method to determine the parameters of the provisions specifications might not be reasonable to explore long-term using characteristics of graded aggregate base bitumen pavement for the modulus calculation results must be consistent with the structure state and stress state of the specimen.

The Relationship between Resilient Modulus and Dynamic Load Times

Figure 1 is the relation of modulus and dynamic load times of the dense-framework structure specimen in the conditions of the three confining pressure, nine dynamic stress and dynamic load for 10,000 times. As we can see from the figure, besides the curve which σ3 is equal to 50kPa and dynamic stress level is 1.15, the other curves of modulus are all growth trend. In the early stages of load (N <2000 times) the modulus increased rapidly in all three confining pressure, the growth rates are ΔM_{early}(100kPa) = 7.2%, and ΔM_{early} (150kPa) = 12.9%; when load times got into the medium-term (N = 2000-8000), modulus of growth slowed down, and they are ΔM_{middle} (100kPa) = 1.1%, ΔM_{middle} (150kPa) = 1.6 %; to the latter load times (N = 8000-10000), modulus is almost not increased, maintained at a stable state, the growth rates of the later modulus are ΔM_{later}(100kPa) = 0.2%, ΔM_{later}(150kPa) = 0.4%.

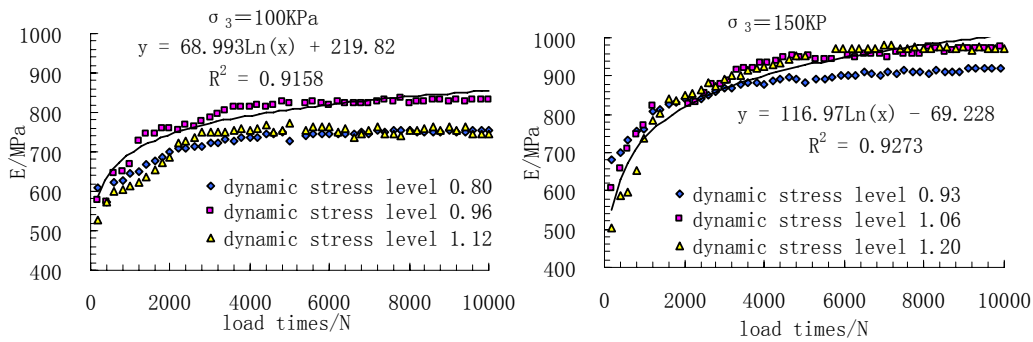

Figure1. The relation between load times and resilient modulus of longtime.

Under a number of dynamic load conditions, the resilient modulus of graded aggregate materials are always in a "hardening state", and there is no "softening state" after peak, the phenomenon shows that under vehicle loading, the resilient modulus of graded aggregate base is growing; when it grows to a certain extent level, it will become stable, that is the modulus growth confined by asymptote. Under the three confining pressures, the average growth rates of modulus are respectively 38%, 35% and 63%. The modulus growth rate is basically same under the same confining pressure and different dynamic stress level. When the dynamic stress ratio exceeds the certain limit (such as σ3 = 50kPa, dynamic stress level = 1.15), the structure of graded aggregate material rapidly destroys and modulus will attenuate in a straight line. Under normal state, the modulus curve can be regressed by logarithm or power equation, results are in figure 1.

The regression curve can be approximately expressed by resilient modulus changing rule with load frequency of graded aggregate material, but the regression curve modulus increase along with the number of load times, it can not express the characteristics that there is a limit (asymptote) when the resilient modulus of graded aggregate material increases with the number of load times. So we can divide integral into subsection based on the different modulus increasing rate, it is the early stage when loading times N ≦ 2000, this period is a rapid growth stage, it can be regressed by logarithm or power equation.

$$E = aN^b \qquad N \leqq 2000 \qquad (1)$$

When the number of loading times N ≧ 2000 times, the hyperbola model is adopted in order to accurately express how asymptote constrains the modulus growth.

$$E = \frac{N}{a + bN} \qquad N \geqq 2000 \qquad (2)$$

After simplification, it gets:

Table1. The asymptote regression equation in section of resilient modulus.

dynamic stress kPa	σ_3 kPa	dynamic stress level	regression equation	R^2	asymptote equation	using condition
269	50	0.69	E_1=203.6 $N^{0.1284}$	0.96	$E_{max}=588.2$	N<2000
			$E_2=\frac{N}{0.3488+0.0017N}$	0.93		N>2000
359	50	0.92	E_1=262.62 $N^{0.0932}$	0.97	$E_{max}=625.0$	N<2000
			$E_2=\frac{N}{0.4666+0.0016N}$	0.95		N>2000
449	50	1.15	E=-1.769 N + 540.08	0.96		state of destroying
449	100	0.80	E_1=391.62 $N^{0.0732}$	0.76	$E_{max}=769.2$	N<2000
			$E_2=\frac{N}{0.2704+0.0013N}$	0.98		N>2000
539	100	0.96	E_1=258.87 $N^{0.1421}$	0.91	$E_{max}=833.3$	N<2000
			$E_2=\frac{N}{0.2871+0.0012N}$	0.95		N>2000
628	100	1.12	E_1=300.92 $N^{0.1055}$	0.97	$E_{max}=769.2$	N<2000
			$E_2=\frac{N}{0.3461+0.0013N}$	0.82		N>2000
628	150	0.93	E_1=392.58 $N^{0.0995}$	0.96	$E_{max}=909.1$	N<2000
			$E_2=\frac{N}{0.2383+0.0011N}$	0.97		N>2000
718	150	1.06	E_1=295.16 $N^{0.1371}$	0.97	$E_{max}=1000.0$	N<2000
			$E_2=\frac{N}{0.3224+0.0010N}$	0.91		N>2000
808	150	1.20	E_1=131.17 $N^{0.2478}$	0.93	$E_{max}=1000.0$	N<2000
			$E_2=\frac{N}{0.3690+0.0010N}$	0.98		N>2000

$$\frac{1}{E} = a\frac{1}{N} + b \qquad (3)$$

Where, a and b are regression coefficients and with a more specific meaning: a=1/E when $N \rightarrow 0$, 1/a is initial resilient modulus; b is the reciprocal of resilient modulus as the N $\rightarrow \infty$, which 1/b is the largest resilient modulus (*Emax)* of graded aggregate material. The reciprocal of Resilient modulus (1/E) is linear relationship to reciprocal of load times (1/N), the regression equations are summarized in Table 1.

The Influence on Resilient Modulus of Graded Aggregate Material by Dynamic Stress Levels

In a confining pressure, the destruction state of the sample is defined as 4% plastic strain when dynamic stress repeats 10000 times and this stress is defined as the critical damage dynamic stress σ_{dcr}. The ratio of dynamic stress of test and critical damage stress is defined as dynamic stress level, and its value reflects the intensity level of the graded aggregate materials to receive dynamic load. Under long-term dynamic load and the same stress level, resilient modulus of graded aggregate material increases and keeps steady towards the end, but with different levels of dynamic stress, resilient modulus sometimes increases and sometimes decreases. The relation of dynamic stress level and resilient modulus of graded aggregate material is shown in figure 2. When the dynamic stress level is low (σ_d / σ_{dcr}<1), resilient modulus of graded aggregate material increases with the dynamic stress level increasing; when the dynamic stress level is high (σ_d/σ_{dcr}> 1), the resilient modulus decreases with the dynamic stress level increasing. The peak of resilient modulus appears near σ_d /σ_{dcr}=1, and 4% plastic deformation as the definition of critical stress is appropriate. It is validated by the resilient modulus changing rule.

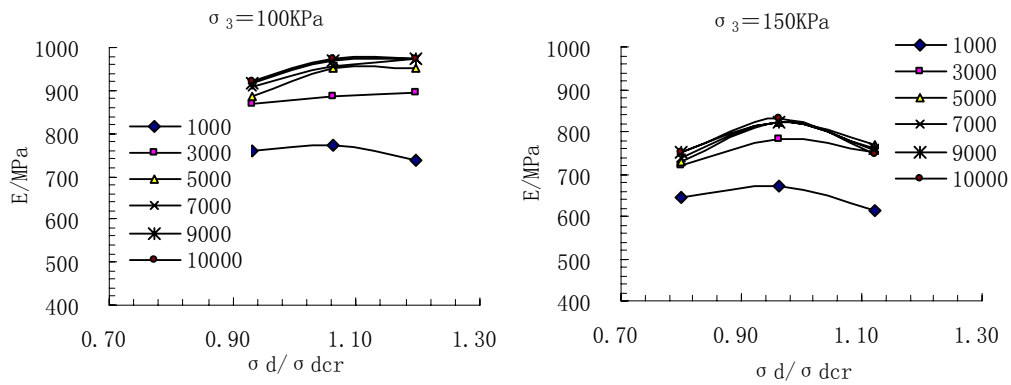

Figure2. The relation between dynamic stress level and resilient modulus.

Under long-term vehicle load, modulus reduction of graded aggregate base will in general lead to asphalt surface fatigue cracking, but experimental results in Figure 2 show that resilient modulus grows with the dynamic load times increasing

and keeps stabilized in the end at the same dynamic stress level.

It is illustrated that increasing the number load times can not lead to fatigue cracking on the same stress level; the more the number of loads, the smaller the possibility of fatigue cracking. In fact, the fatigue cracking of some graded aggregate base bitumen pavement is an objective reality; the reason is that the traffic wheel load intensity is in homogeneity. When the level of dynamic stress is $\sigma_d / \sigma_{dcr} > 1$ from Figure 2, the resilient modulus of graded aggregate material is decreasing, resulting in "softening strength", which leads to larger the tensile stress of asphalt bottom layer, appearing fatigue cracking. The statistical analysis of Literature (Hang 2005) shows that load spectrum level of vehicle load axle is uneven in China, the ratio of axle load exceeds 61% -71%. The literature (Hu 2005) tire pressure measurement showed that the grounding pressure of heavy vehicles is the tire pressure 0.9 ~ 1.7 times, the greatest pressure of touching the ground is the tire pressure 1.5 ~ 3.5 times, which illuminate that it is not the traffic load accumulation leading to pavement fatigue crack, but the modulus soften of graded aggregate materials under asymmetrical traffic load.

CONCLUSION

The main conclusions are as follow:

（1）The resilient modulus of graded aggregate materials are growing with dynamic load repeated time increasing and are confined by asymptote when dynamic load level is constant.

（2）The modulus curve can be regressed by logarithm or power equation， it is more reasonable to adopt hyperbola model.

（3）It is not the traffic load accumulation leading to graded aggregate base bitumen surface layer fatigue crack, but the graded aggregate material's "modulus soften" under asymmetrical traffic load.

REFERENCES

Wang, L. (2005). "Study on compacting standard of the soil-aggregate mixture." Journal of Harbin Institute of Technology, 37(1): 229-232.

Wang, L. (2006). "Study of intensity and deformation of Granular Materials on Vibration Compaction." Harbin Institute of Technology, PH.D dissertation, 45-47.

Ministry of Hydraulics (1999). Test Methods of Soils for Hydraulic Engineering (SL237-1999).China Communication Press.

Hang, W., Li, X., and He, J. (2005). "Overloading Vehicles Axle-loads Survey and Analysis." Journal of Highway and Transportation Research and Development, 22(8):146-149.

Hu, X, and Sun, L. (2005). "Measuring Tire Ground Pressure Distribution of Heavy Vehicle." Journal of TongJi University (Natural Science), 33(11): 1443-1448.

Prediction of the Soft Roadbed Deformation Based on a Creep Damage Model

Y. L. Wang[1,2] and Y. Wang[3]

[1]Key Laboratory of Geotechnical and Underground Engineering of Ministry of Education, Tongji University, Shanghai 200092, P.R. China; PH(086) 21-65982553; FAX(086) 21-65982553;email: wyldhh@126.com

[2]Department of Geotechnical Engineering, Tongji University, Shanghai 200092, P.R. China; PH(086) 21-65982553; FAX(086) 21-65982553; email: wyldhh@126.com

[3]Institute of Rock and Soil Mechanics, Chinese Academy of Science, State Key Laboratory and Geotechnical Engineering, Wuhan, Hubei 430070, P.R. China; PH(086) 27-87199775; email: wang831yong@163.com

ABSTRACT

It is important to predict roadbed settlement occurred during construction and post-construction periods for highway projects built on the soft ground. A creep damage mechanical model is constructed on basis of the rheological and structural properties of soft soil to predict the deformation of the roadbed. Deformation of the roadbed and variation of the pore water pressure during the different construction periods are analyzed. The settlement of post-construction is predicted in a case study. Calculation results are compared with the traditional model and the creep damage model. It is shown that the creep damage model can better describe the soft roadbed deformation in preloading and post-construction periods. Calculation results from the creep damage model show that creep and structural effects can not be ignored in soft roadbed deformation prediction.

KEY WORDS: Highway; Soft roadbed deformation; Foundation reinforcement

INTRODUCTION

With the rapid development of national highway network, experiences have been accumulated in highway roadbed treatment. However, problems such as pavement cracking and bridge slab staggering arise exist in some highways built on soft soil foundation shortly after being open to traffic.These problems mainly caused by the settlement or differential settlement of the roadbed, which can lead to a significant economic loss (Wang et al. 2005). Inadequate deformation forecast of subgrade construction of soft soil and inadequate understanding of the soft soil characteristics are main factors of the problem. Soft soils have the salient rheological property besides the ordinary characteristics of consolidation. Soft soil creep in the whole process of deformation leads to the accumulation of deformation during a long period after construction. Besides, the natural soft soil also has different levels of structural characteristics (Leroueil 1990). The additional deformation caused by structural rearranging after structural damage of soft soil. Since the disturbance of

soft soil in the course of foundation treatment changes structural properties of the original foundation, it is different between the undisturbed soil and the actual disturbed soil after reinforcement in physical mechanical index. These are the key reasons why the deformation calculated by using traditional methods is not accurate enough. In this paper, a creep damage mechanical model is proposed to describe the integrative action of structural and rheological characteristics of soft soil. Calculations of roadbed deformation and pore pressure development are carried out by using the finite element method.

CREEP DAMAGE MODEL OF SOFT SOIL

The mechanical characteristics of soft soil, such as elasticity, plasticity and viscosity,are very complex. It can be regarded as a kind of elastic viscoplastic body. Total strain increment is composed of instantaneous linear elastic strain, viscoelastic strain and viscoplastic strain. Sun (Sun et al, 2006) proposed a modified viscoelastic-viscoplastic creep model. The viscoelastic-viscoplastic flexibility matrix can be expressed as:

$$\left[C_{vep}\right]=\left[C_{ep}\right]+\frac{[A]}{E_1}(1-e^{-\frac{E_1}{\eta_1}dt})+dt\frac{1}{\eta_2}\left\langle \Phi(\frac{F}{F_0})\right\rangle \tag{1}$$

The model parameters can be determined by creep tests of soft soil (Zhao et al. 1996).

In order to describe the structural damage process of soft soil, it can be simplified as a process that the undamaged modulus attenuates gradually. So the effect from structural property of soft soil is considered as an attenuation factor added to the soft soil creep model. The structural damage variable can be expressed as:

$$\omega=1-\omega_0-e^{-D(\varepsilon_p'-\varepsilon_p^{\,0})} \tag{2}$$

Where $\varepsilon_p' = \int_0^t \dot{\varepsilon}_p' dt$ is cumulative plastic strain; $\varepsilon_p^{\,0}$ is the initial plastic strain; ω_0 is the initial damage factor; D is the model parameter reflecting structure damage speed. Damage variable includes the structural damage evolution rule, which can be obtained by fitting undisturbed and remolded soil compress curves (Sun et al. 1999). The formula of total strain increment is:

$$\{d\varepsilon\}=\left[C_{Dvep}\right]\{d\sigma'\} \tag{3}$$

Where $\left[C_{Dvep}\right]$ is the creep damage flexibility matrix. The soft soil creep damage model described in Eq.(3) can characterize the soft soil creep deformation and damage of the structural deformation with the finite element program.

EXAMPLE FOR DEFORMATION PREDICTION OF THE HIGHWAY SOFT

ROADBED

Overview of the highway soft roadbed reinforcement section. Surcharge preloading technique in combination with sand pad and dewatering plastic sheet is adopted to improve the soft roadbed. From top to bottom of the foundation layers are as follows: ①the surface soil is gray with the thickness of 0.5~1.0m, containing a few bricks and plant roots,mainly is silty clay; ②The liquid-and-plastic muddy clay layer is grey, saturated with the thickness of 10~12m, which is highly compressible and the main layer for treatment; ③the alluvial layer is sub-clay with the thickness of 14~18m, which is plastic and compressible. Reinforcing schemes are as follows: A sand pad with 60cm thick, inserted with two layers of mesh-based compound geo-textile fiber,is constructed on the top of the ground. The dewatering plastic sheets of type SPB–1, with the width of 100mm, thickness of 4.6 mm and length of 13m, are driven through the muddy layer. They are arranged in a quincunx layout with the spacing of 1.2m. An embankment, which is 4.18m high, 32m wide and with a grade ratio 1:1.5, is constructed on the top of the sand pad. The construction work is finished within 160 days. The loading can be considered as 4 steps (0.8 m, 1.2 m, 1.2 m and 0.98 m) in calculation. Each loading step lasts for 40 days including 25 days of loading and 15 days of interval.

The finite element model and calculated parameters. The creep damage model proposed above is used to predict deformation of the soft roadbed based on Biot's consolidation theory. In order to simplify the calculation, the plane finite element method can be used when the band drain is equivalent to sand drain. The actual sand drain foundation is replaced by sand wall foundation according to the principle of constant consolidation effects.

The equivalent diameter formula from band drain to sand drain proposed by Hansbo (1979) is as follows:

$$d = a\frac{2(w+t)}{\pi} \tag{4}$$

Where d is equivalent diameter; a is conversion coefficient (generally assigned 0.6~ 0.9); w is width of band drain; t is thickness of band drain.

According to the actual condition, the equivalent diameter of the band drain can be assigned 60mm. The radius of daub area is assigned 150mm. The permeability coefficient of soft soil needs to be revised when sand wall foundation replaces the sand drain foundation. The revising formula can be expressed as follows (Zhao et al. 1998):

$$\begin{cases} k_{rx} = D_x k_x \\ k_{rz} = D_z k_z \end{cases} \tag{5}$$

Where k_{rx} and k_{rz} are horizontal and vertical permeability coefficients of sand wall

after adjustment respectively, k_x and k_z are horizontal and vertical permeability coefficients of the original foundation; D_x and D_z are horizontal and vertical adjustment coefficients. In this paper, D_x and D_z are assigned 0.913 and 2.168 respectively. The sand wall span is adjusted as 4.0m. The course to install band drains may cause large disturbances on the soft soil.It may destroy the structure of the original foundation soil. The in-situ test formula of the scale of turbulence proposed by Wang et al. (2005) is as follows:

$$SD = \frac{S_u - S_u^*}{S_u} \times 100\% \tag{6}$$

Where S_u and S_u^* are peak vane shear strengths of the soil before and after installing band drains respectively.

Contrastive analysis has been done by the in-situ vane shear test before and after the installation of band drains in this study. The average disturbance degree of the foundation is about 31%. It shows that the effect on soil structure in the process of foundation reinforcement cannot be neglected. So the initial damage factor of the forecast analysis model in the finite element calculation is assumed to be 0.31. The poisson ratio of each layer is assigned 0.32, and parameter d_p of the mucky clay layer is assigned 0.25 in the calculation. Table1 lists the calculation results.

Table 1. Calculation Parameters of the soil layers

Soil Layer		Sand Mat	Mud	Clay
Horizontal coefficient of permeability	k_{rx} (10^{-5}cm/s)	100	0.323	1.49
Vertical coefficient of permeability	k_{rz} (10^{-5}cm/s)	100	0.246	1.28
Elasticity modulus parameter	K_G	100	15	60
Elasticity modulus parameter	n	0.65	0.9	0.8
Viscoelastic modulus parameter	E_1 (MPa)	7.8	1.6	3.9
Viscoelastic modulus parameter	n_1	1.0	1.06	0.71
Double yield surface model parameter	M_1	1.8	0.76	1.32
Double yield surface model parameter	M_2	1.7	0.62	1.25
Double yield surface model parameter	h	100	42.6	51
Double yield surface model parameter	t	10	7.9	8.6
Double yield surface model parameter	a	0.3	0.18	0.26
Viscoelastic coefficient of viscosity	η_1 (10^5kPa/d)	0	0.287	1.77
Viscoplastic coefficient of viscosity	η_2 (10^5kPa/d)	1000	0.23	2.56
Damage parameter	D		2.2	

RESULTS AND DISCUSSION

Excess pore water pressure forecast during construction period. The constructing load is simplified to a linear loading process. Variation curves of excess pore water pressure along the vertical and horizontal direction of the foundation are shown in Figure1. As is shown in Figure1(a), the pore water pressure decreases rapidly and primary consolidation deformation is completed quickly due to the

effects of band drains around the foundation reinforcement areas under different load. But the primary consolidation settlement of bottom layer after construction is one of the most important reasons for excessive post-construction settlement of the profound soft roadbed reinforced by preloading technique. Extending preloading period can effectively relieve the embankment settlement. As is shown in Figure1(b), the excess pore water pressure around the sand wall is zero. The soil between two sand walls is less than outer embankment, which weakens gradually near to far from the embankment under different load. It indicates that band drains play an important role in accelerating dissipation of the excess pore water pressure and the most deformation of soft soil layer during the construction. It also causes less post-construction settlement.

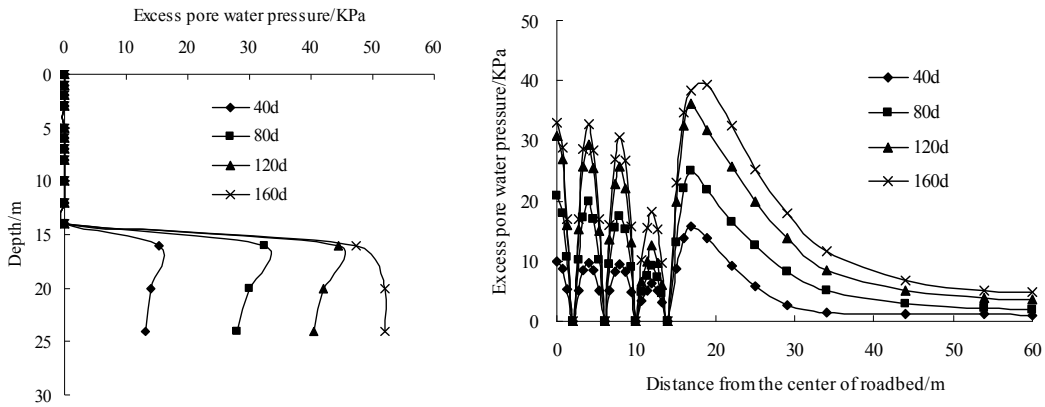

(a) Vertical direction (b) Horizontal direction

Figure1. Variation curves of excess pore water pressure of the roadbed

Comparative analysis of different models. Three different models**,** the common modified Cambridge model**,** the creep model and the creep damage model ,are used to predict the deformation of foundation in this paper. The results of foundation settlement and pore water pressure are showed in Figure2. From Figure2(a), the maximum deformation is calculated with the creep damage model. The second deformation is calculated with general soft soil creep model without considering the additional deformation generated from the structural damage of soft soil. The minimum deformation is calculated with the modified Cambridge model usually used for soft soils with the finite element method. The key reason for which is that the modified Cambridge model can not describe secondary consolidation settlement or structural damage of the soil. From Figure2(b), structural damage and creep of soft soil will influence the pore water pressure. the calculated pore pressure is relatively larger, and the soil deformation is affected by the pore water pressure.

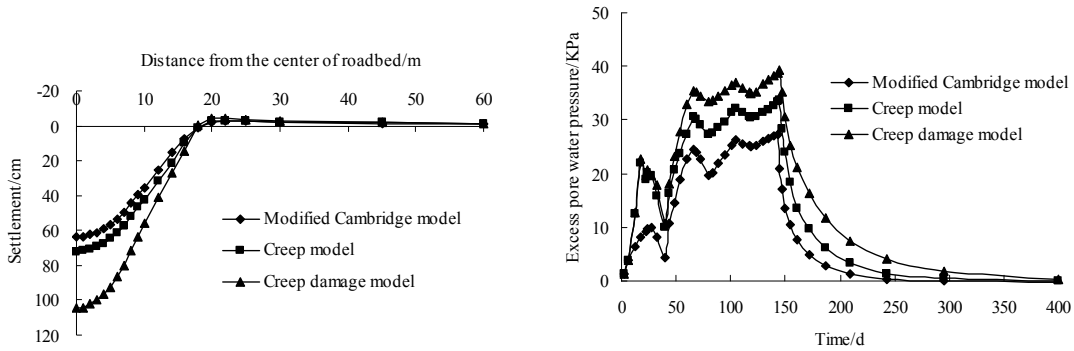

(a) Settlement (b) Excess pore water pressure

Figure 2. Settlement and excess pore water pressure with different models

Prediction of post-construction settlement. Above-mentioned models are used to predict the roadbed deformation during and after the construction periods. The calculated values contrasted with on-site monitoring data are shown in Figure3. Figure3 indicates that there is little difference of the deformation in the preloading construction period between the calculated and the measured with the modified Cambridge model because the primary consolidation settlement of soft soils is basically completed. But the error is a bit large in post-construction periods because the additional deformation aroused from the creep and structural damage of soft soils can not be considered in the traditional model. Predictive results calculated with the creep damage model proposed in this paper agree better with the measured values during and after the construction periods. The creep damage model can quantitativly reflect the influence due to the damage based on band drains and rheology of soft soils. The creep deformation and the additional deformation caused by structural damage of soft soil exist in the whole process of consolidation, which lead to the larger settlement after construction of the roadbed. It also illustrates that the creep damage model can reasonably describe the intrinsic property of soft soil.

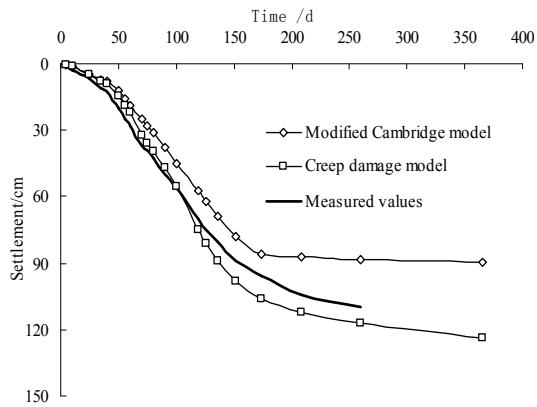

Figure 3. Predictive results with different models

CONCLUSION

A creep damage model is proposed to predict the deformation and variation of pore

water pressure in a highway roadbed reinforced with the preloading technique. The model is analyzed based on the finite element method. The major results are as follows: (1) The creep damage model, considering the structural damage and creep, can reasonably describe the deformation characteristics of soft soil, and effectively predict the settlement of roadbed during construction period and post-construction period. (2) The creep deformation and the additional deformation caused by structural damage of soft soil exist in the whole process of consolidation. The structural damage and creep will influence the development of pore water pressure and the pore water pressure will also influence the deformation of soft soil. (3) The primary consolidation settlement of bottom layer after construction is one of the most important reasons for excessive post-construction settlement of the deep soft roadbed with preloading technique. Therefore, determination of the reasonable reinforcement depth and preloading time are the two keys to reduce post-construction settlement of the highway on soft soil foundation.

REFERENCES

Hansbo, S. (1979), "Consolidation of Clay with Special Reference to the Influence of Vertical Sand Drains." *Proc*. *SGI*, (18).

Leroueil, S., and Vaughan, P. R. (1990). "The General and Congruent Effects of Structure in Natural Soil and Weak Rock." *Geotechnique*, 40(3), 467-488.

Sun, H., and Zhao, X. H. (1999). "An analysis of elastoplastic anisotropic damage on soft soil." *Rock and Soil Mechanics*, 20(3), 7-12.

Sun, J. Z., and Wang, Y. (2006). "Analysis of deformation of soft ground considering damage and creep." *Journal of Wuhan university of technology*, 28(4), 75-78.

Wang, Y. Q., and Hong, B. N. (2005). "Analysis of settlement estimation method and error of soft soil base in expressway." *Transportation Science & Technology,* 210(3), 6-9.

Wang, J., Gao, Y. F., and Gao, H.Z. (2005). "Quantitative Analysis of Foundation Treatment Disturbance of Structured Soft Clay Ground." *Rock and Soil Mechanics*, 26(5), 789-794.

Zhao, W. B., and Shi, J. Y. (1996). *Rheology and consolidation of soft soil,* Hohai university press, Nanjing, China.

Zhao, W. B., Chen, Y. H., and Gong, Y. P. (1998). "A methodology for modeling sand-drain ground in plain strain analysis." *Journal of Hydraulic Engineering,* (6), 35-39.

Research on Relationship between Fine Aggregate Angularity and Asphalt Mixture's Anti-Shear Ability

[1]Zhou Chang-jun, Feng De-cheng, Zuo Wen-xin, Quan Lei

[1]School of Transportation Science and Engineering, Harbin Institute of Technology, Haihe Street, Nangang District, Harbin; Phone:86+451+13766830235; email: zhouchangjun.hit@163.com

ABSTRACT

To compare fine aggregate angularity (FAA) of three different fine aggregates including a crushed sand, chips and a natural sand, two methods, i.e. modified Uncompacted Void Content Test and modified Sand Flow Test were carried out. Results indicate that crushed sand's FAA is similar to chips' and both of them are better than natural sand's. The modified Sand Flow Test is recommended. Under normal temperature, the static Triaxial Shear Strength Tests were carried out for SMA-13s and AC-13s, which are different in fine aggregate. These mixtures were made by standardized compaction or gyratory compaction method. It is discovered that that there is a direct correlation between FAA and mixture's anti-shear ability.

KEYWORDS: fine aggregate angularity, asphalt mixture, triaxial shear strength test, anti-shear ability

1 INTRODUCTION

FAA, reflecting fine aggregate' s shape, texture and roughness, has direct influences on the interlocking between aggregates and on the cohesion between aggregates and asphalt, which fundamentally affects asphalt mixture's anti-shear ability. In this article, tests, i.e. modified Uncompacted Void Content Test and modified Sand Flow Test were carried out to estimate FAA of a crushed sand, chips and a natural sand. And static Triaxial Shear Strength Tests under normal temperature were also tried out to compare anti-shear abilities among the three mixtures called crushed stone mixture, chips mixture and natural sand mixture, which contain different fine aggregate respectively. A relationship between FAA and asphalt mixture's anti-shear ability was established.

2 FINE AGGREGATE ANGULARITY

Presently there are mainly two methods to evaluate fine aggregate roughness and angularity including the Uncompacted Void Content (UVC) Test (Figure 1) originated from AASHTO 33 (SHRP) and the Sand Flow Test originated from AFNOR NF P l8-564/1981 from France (Figure 2). Both tests are adopted in China and are numbered T0344—2005 and T0345—2000 respectively in Test Methods of Aggregate for Highway Engineering.

In the SUPERPAVE design system uncompacted void content acts as one of identity characters of fine aggregates, which is commonly thought to be a paramount role when designing HMA with super performance. With regulating FAA, designers

hope to make HMA great internal friction and great anti-shear ability to resist rutting (Brian Prowell et al 2005). This article utilizes the FAA apparatus to get FAA of raw materials and single-size aggregates. Greater UVC means relatively greater internal friction angel, smaller content of spherical particles and rougher texture. It is hard to get an accurate bulk density in T 0344—2005 since experience plays an important role in results. So we adopted apparent density (ignoring open void). This would only magnify UVC, not changing the ranking of those aggregates' UVC.

Figure 1. Uncompacted Void Content Test Apparatus

Figure 2. Sand Flow Test Apparatus

Sand Flow reflects surface texture and roughness of fine aggregates. It has effects on the stability and plastic deformation of asphalt mixture. The Test regulates the same mass of aggregate to get the same bulk (Shen Jinan, etc, 2005). Instead of this approach, we just filled up the cylinder with aggregates and made the surface even. This simplifies the operation without sacrificing precision of the test.

UVCs and sand flow of the aggregates were obtained (Table 1 and Table 2).

Table 1. Results of Modified Uncompacted Void Content Test

Fine Aggregate	Uncompacted Void Content(%)		
	Crushed Sand	Chips	Natural Sand
Raw Material	42.3	42.8	38.9
1.18~2.36mm Aggregate	47.8	48.6	44.2

Table 2. Results of Modified Sand Flow Test

	Raw Material			1.18~2.36mm Aggregate			2.36~4.75mm Aggregate					
Funnel Aperture	18mm			16mm			18mm			18mm		
Fine Aggregate	CS	C	NS	CS	C	NS	CS	C	NS	CS	C	NS
Sand Flow/s	18.2	14.4	15.4	24.5	24.3	23.0	17.5	17.6	16.8	24.8	25.4	23.7

Note: CS, C, NS represent crushed sand, chips and natural sand, respectively.

Since gradations are different, UVC and sand flow could not give a clear ranking of FAA among raw materials of the three fine aggregates. Results of single size aggregate, 1.18~2.36mm for example, from the two methods could effectively show the ranking: FAA of chips and FAA of crushed sand are better than FAA of natural sand, while the former two are similar to each other. The reasons can be given like these: (1) Natural sand, weathered in billions of years, has slick shape and no crushed surfaces. All of these factors bring up good workability but poor FAA. (2) Chips, the scrap from stone pits, are weak parts of rocks and have crushed surfaces. Besides, chips own many elongated flaky particles. The FAA of chips is supposed to be good. (3) Crushed stones contain no soft or weathered rocks, and have more crushed surfaces and less elongated flaky stone pits than chips. All of these lead to good FAA. The results reflect the difference among these three fine aggregates, which reveals that it is proper to modify test methods of FAA.

Compared to the UVC test, sand flow test is easier to operate. As a result, it is a recommended method to evaluate FAA in China. However this method needs to be modified as mentioned before. We suggest the modified sand flow test as an alternative for evaluating FAA.

3 RELATIONSHIP BETWEEN FINE AGGREGATE ANGULARITY AND STONE MATRIX ASPHALT'S ANTI-SHEAR ABILITY

Asphalt mixtures, no matter from Marshall mix design procedure or other similar ones, although owning sufficient stability, could not prevent pavements from early damage. Empirical design procedures could neither describe actual state of pavement such as shear stability, nor pavement performance (Norman W. Mcleod, 1951). V. A. Endersby (1949) originally brought forward how to make asphalt concrete specimens for triaxial test and how to do the test. V. R. Smith (1949) elaborated the state of shear forces in pavement by virtue of elasticity theory, proposed a failure standard for mixture, and defined specific anti-shear abilities for mixture under varied loads with a nomogram. Edward S. Barber (1965) presented stress state of pavement when bearing horizontal shear forces and vertical forces at one time. In that situation, shear stress in pavement would increase evidently. Thus he declared that horizontal shear forces are indispensable in pavement design. W. S. Housel (1936), R. G. Hennes & C. C. Wang (1965) used triaxial test data to explain mixture performance from the point of mechanics respectively.

The stress state of a triaxial test is similar to the triaxial stress state of asphalt pavement, and can evaluate the material's mechanical parameters. Based on the Mohr-Coulumb Principle, we obtained the anti-shear parameters of asphalt mixture i.e. cohesion (c) and internal friction angel (φ), and explored the effects of FAA on c and φ. It is well known that temperature impacts on anti-shear strength of asphalt mixture. Temperature affects c significantly while affects φ little. FAA mainly affects φ. Thus triaxial tests under normal temperature can evaluate internal friction angels,

which reflect the variety among FAA of the three fine aggregates.

Basic parameters of fine aggregates and asphalt are shown in table 3 and table 4 respectively. An SMA-13 gradation is adopted for mixtures shown in Table 5. The three kinds of mixture shared an asphalt aggregate ratio, which was the optimal asphalt aggregate ratio of chips mixture. Triaxial test results are show in table 6.

Table 3. Parameters of fine aggregate

Items	Crushed Stone Value (%)	Apparent Density (g/cm^3)	Accumulated Density (g/cm^3)
Crushed Stone	18	2.720	1.62
Chips	25	2.689	1.53
Natural Sand	19	2.593	/

Table 4. Basic parameters of asphalt

Items	Temperature（℃）				PI_{lgPen}	T_{800}	$T_{1,2}$
	35	25	15	5			
Penetration（0.1mm）	118	86	44	6	-0.280	51.1	-16.6
Softening Point（℃）				47.3			
Ductility under 15℃（cm）				60.2			

Table 5. Gradation of SMA-13

Mass Percentages under Following Sieves(mm)（%）									
16	13.2	9.5	4.75	2.36	1.18	0.6	0.3	0.15	0.075
100	95	62	23	18	16	14.5	13	12	10.5

Table 6. Summary of SMA's Anti-Shear Strength Parameters

Forming Method	Asphalt Aggregate Ratio (%)	Parameters	Crushed Stone	Chips	Natural Sand
Standardized Compaction	5.8	c（kPa）	389.89	494.01	418.51
		φ（°）	59.02	50.83	48.83
Gyrating Compaction	5.8	c（kPa）	484.41	611.98	595.61
		φ（°）	33.07	32.61	31.36

Under the two methods, crushed stone mixture has biggest φ, natural sand mixture has smallest φ. This illuminates that fine FAA is good for interlocking among gravels, which enhances asphalt mixture's stability when bearing loads. Although chips and crushed stone have similar FAA, chips contain more elongated flaky particles which tends to break because of local stress concentration on these particles' tops. Natural sand, slick, dusty and without crushed surfaces, could not interlock well with each other and could not bond well with asphalt. And these will lead to aggregates dislocation under shear loads.

Since crushed stones are cleaner and have more crushed surfaces than chips, they can absorb more asphalt than chips. The asphalt content is optimal asphalt

content of chips mixture. Thus, with this asphalt content, asphalt membrane could not be formed thick enough in crushed stone mixture. That's why its *c* is relatively small. Without crushed surfaces, natural sand mixture has relatively small *c* too.

4 RELATIONSHIP BETWEEN FINE AGGREGATE ANGULARITY AND ASPHALT CONCRETE'S ANTI-SHEAR ABILITY

In asphalt concrete, the suspended dense structure, is different from stone matrix asphalt, dense framework structure. It is necessary to check the effects of FAA on asphalt concrete structure. So specimens of AC-13 was formed and tested too. The gradation and triaxial test results are listed in table 7 and table 8 respectively.

Table 7. Gradation of AC-13

Mass Percentages under Following Sieves(mm)（%）									
16	13.2	9.5	4.75	2.36	1.18	0.6	0.3	0.15	0.075
100	97	78	41	28	18	14	10	7	5.2

Table 8. Summary of AC's Anti-Shear Strength Parameters

Forming Mothod	Asphalt Aggregate Ratio/%	Parameters	Crushed Stone	Chips	Natural Sand
Standardized Compaction	4.3	*c*（kPa）	523.93	764.13	600.25
		φ（°）	59.77	53.84	55.89
Gyrating Compaction	4.2	*c*（kPa）	373.74	488.49	729.83
		φ（°）	54.98	49.25	35.92

Comparing data in table 6 with data in table 8, the conclusion can be made like this: regardless of standardized compaction or gyrating compaction, the effects of fine aggregate angularity on asphalt concrete is very similar to the effects of fine aggregate angularity on stone matrix asphalt.

5 CONCLUSIONS

In this article, FAA of a crushed stone, chips and a natural sand were obtained by virtue of two methods, i.e. modified Uncompacted Void Content Test and modified Sand Flow Test. Triaxial tests of SMA-13s and AC-13s specimens were also carried out. Through those tests, conclusions are summarized as following:

(1) Two methods, i.e. modified Uncompacted Void Content Test and modified Sand Flow Test are effective and feasible. Modified sand flow test is recommended to evaluate fine aggregate angularity because of its simplicity .

(2) FAA of crushed stone is similar to FAA of chips. Both of them are better than FAA of natural sand.

(3) Crushed stone mixture's internal friction is biggest, chips mixture's is smaller and natural sand mixture's is smallest. This result verifies the validity of the two modified FAA methods.

(4) Good FAA offers asphalt mixture relatively large internal friction angle , making interlocking among aggregates well, which ensures aggregates hard

to dislocate when taking loads, and then improves mixture's anti-shear ability. To be more precise, there is a direct correlation between FAA and mixture's anti-shear ability.

REFERENCES

Brian Prowell, Jingna Zhang and E. Raybrown (2005). "Aggregate Properties and the Performance of Superpave-Designed Hot Mix Asphalt." Transportation Research Board—National Research Council. Transportation Research Board. Washington, D.C., 2005. 500 Fifth Street, NW Washington, DC 20001, Transportation Research Board Business Office

Edward S. Barber. (1965) "Shear Load on Pavement". A.S.T.M 5th conference

Norman W. Mcleod. (1951) "A Rational Approach to the Design of Bituminous Paving Mixture". A.S.T.M

Shen Jinan, Li Fupu, etc, (2005) JTG E42—2005, *Test Methods of Aggregate for Highway Engineering*[S], Beijing, China.

V.A.Endersby. (1949) "The History and Theory of Triaxial Testing and Preparation of Realistic Test Specimens". A.S.T.M., San Francisco, October,1949

V.R. Smith. (1949) "Triaxial Stability Method for Flexible Pavements Design, Proceedings of Association of Asphalt Paving Technologists", Vol.18, February,14 and 15, 1949:20~35

William L. Helwitt, (1965) "Continuation of Study on the Theoretical Design of Fexible Pavement Based on Shear Strength". A. S .T.M 5th conference, 1965:75~78

W.S.Housel. (1936) "Internal Stability of Granular Materials, Proceedings" A. S.T. M. volume 26, part II, 1936:61~63

Application of High Performance Concrete Mixed with Steel Slag Powder in Concrete Pavements

Yunfeng Li[1], Fanying Kong[1] and Rongqiang Du[1]

[1]College of Civil Engineering and Architecture, Shandong University of Science and Technology, Qingdao, 266510, China; email: hhliyunfeng@126.com

ABSTRACT

Steel slag is a solid waste discharged in large quantities by the iron and steel industry in China. The recycling of steel slag will inevitably become an important measure for the environment protection and therefore will be of great social and economical significance. Used in combination with Super-plasticizer admixture, steel slag powder can lead to economical high performance concrete for highway pavements with enhanced durability and reduced cement content. The properties of steel slag cement and concrete with different types of steel slag and different dosage of admixtures are studied in this paper. The effectiveness of using steel slag powder for suppressing Alkali Aggregate Reaction is also analyzed. The results show that properties and durability of concrete can be greatly improved steel slag powder.

INTRODUCTION

Steel slag is a solid waste discharged in large quantities by the iron and steel industry in China. The recycling of steel slag will inevitably become an important measure for the environment protection and therefore can lead to great social significance (Sun et al. 2007). The manufacturing of Portland cement is a highly energy-intensive process. One of the most significant activities stressed by the engineers and scientists related to concrete industry aims at a high percentage of replacement of clinker in cement with secondary raw materials, with the possibility of improvement of cement characteristics and durability of concrete. Via these approached, the consumption of natural raw materials, thermal and electric energy, together with the reduction of CO_2 emissions can be decreased. One less energy intensive materials being sought are industrial by-products that are easily available, require little or no pyro-processing and have inherent or latent cementitious properties. Such industrial by-products are commonly called as supplementary cementitious materials or mineral additives. Mineral additives are usually available in large quantities that can be used to replace Portland cement in concrete (Muhammad and Emmanuel 2007). These include fly ash, steel slag, blast-furnace slag, silica fume, natural pozzolans, rice-husk ash, and metakaolin.

Steel slag includes a certain scale mineral such as C_2S and C_3S, and can be

applied in cement and concrete as mineral admixtures (Zhu et al. 2005). When super fine steel slag powder is mixed into concrete as an active admixture, concrete properties will be improved greatly so as to produce high performance concrete. The hydration heat can be effectively decreased; resistance to abrasion and durability and the workability and mechanical properties of the concrete can all be enhanced. When compound mineral admixtures with steel slag powder and blast-furnace slag powder are mixed into concrete, the performance of concrete can be improved further due to the synergistic effect and activation of each other (Liu and Yang 2006, Sun and Huang 2006). Therefore, the mineral admixture will be a perfect component of green concrete and its utilization will be a valuable resource for recycling.

MECHANICAL PROPERTIES OF HPC WITH STEEL SLAG POWDER

Materials. Chemical composition and properties of steel slag powder and blast furnace slag are listed in Table 1. The 42.5R Portland cement was used in concrete, and the blast furnace slag (S95) was also used as a partial replaced material in the cement and concrete.

Table 1. Chemical composition and properties of materials.

Admixture	Constituent (wt %)						Property		
	SO_3	SiO_2	CaO	MgO	P_2O_5	fCaO	Specific surface area (m^2/kg)	Density (g/cm^3)	Fluidity ratio (%)
Steel slag	0.47	18.28	39.69	9.37	1.26	1.98	387	3.46	103
Blast furnace slag	2.78	32.10	39.26	9.27	0.023	0.12	382	2.94	102

Mix Proportions. The concrete specimens were prepared with two types of mineral admixtures, steel slag powder and blast furnace slag powder. The concrete specimens prepared with mineral admixture are summarized in Table 2.

Compressive strength of steel slag concrete. The compressive strength of concrete specimens were determined after the 3, 7, 28 days of curing, respectively. The variation of compressive strength of steel slag concrete was shown in Figure.1. As expected, the compressive strength increased with age in all the concrete specimens. The results showed compressive strength of concrete with only steel slag decreased with the mixed content; the compressive strength was lower than that of blast furnace slag concrete. However, increase in compressive strength of concrete with steel slag was higher than that with blast furnace slag between 7 days age and 28

days age. The compressive strength of concrete with compound mineral admixture (mix code 6) had the highest value.

Table 2. Mix proportion of steel slag concrete

Mix code	Cement content (kg/m^3)	Steel slag content (kg/m^3)	Blast furnace slag content (kg/m^3)	Water content (kg/m^3)	Sand content (kg/m^3)	Stone content (kg/m^3)
0	476.0			212.5	551	1228
1	428.4	47.6		212.5	551	1228
2	380.8	95.2		212.5	551	1228
3	333.2	142.8		212.5	551	1228
4	285.6	190.4		212.5	551	1228
5	333.2		142.8	212.5	551	1228
6	333.2	47.6	95.2	212.5	551	1228
7	333.2	71.4	71.4	212.5	551	1228
8	333.2	95.2	47.6	212.5	551	1228

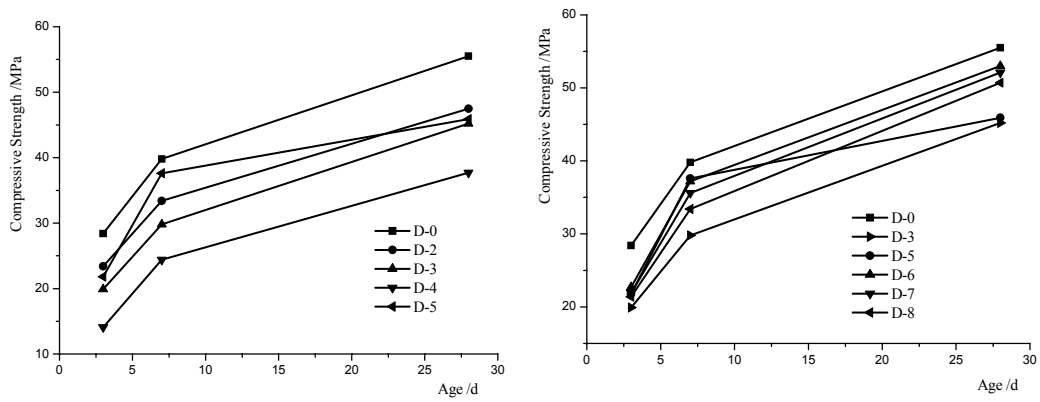

Figure 1. Compressive strength of concrete with mineral admixture

Flexural strength. The flexural strength of concrete with steel slag and blast furnace slag were also determined after the 3, 7, 28 days of curing. The variation of flexural strength of steel slag concrete was shown in Figure 2. Test results showed that flexural strength of steel slag concrete tended to increase fast compare to compressive strength at later age. When steel slag content was 10 percent of the total cement, the flexural strength was higher than that of the plain concrete at 28 days age. The flexural strength of concrete with compound mineral admixture showed the improvement due to the synergistic effect. The highest value was measured in concrete with steel slag powder to blast furnace slag ratio of 2.0.

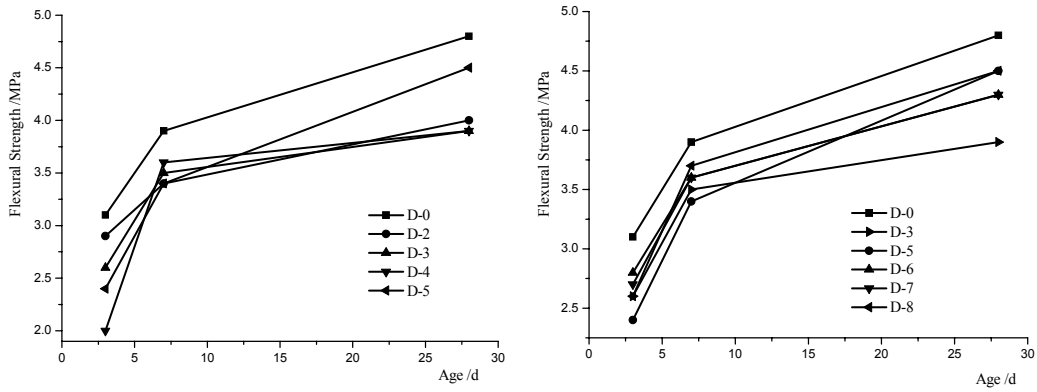

Figure 2. Flexural strength of concrete with mineral admixture

According to the test results, compressive and flexural strength of concrete with steel slag powder tend to decrease while the content of steel slag increases. Properties of concrete will be greatly enhanced when compound mineral admixture with steel slag powder and blast furnace slag is mixed into concrete. Steel slag and blast furnace slag show the synergistic effect and mutual activation in concrete. On the other hand, steel slag concrete has lower strength at early age; therefore, steel slag should be used to control hydration process so that high strength and high performance concrete can be obtained.

EFFECTIVENESS OF STEEL SLAG POWDER ON SUPPRESSING ALKALI AGGREGATE REACTION

ASTM C441 tests. ASTM C 441 uses Pyrex glass aggregate in mortars to accelerate the testing and provides reliable results. Mix proportion of AAR tests with Pyrex aggregate are listed in Table 3.

Table 3. Mix proportion of AAR test with Pyrex aggregate

Code	Cement (g)	Steel slag (g)	Blast furnace Slag (g)	Aggregate (g)	Water （g）	Fluidity (mm)	Curing temperature(℃)
1	400	0	0	900	166.5	103	40
2	300	100.0	0	900	181.2	112	40
3	300	0	100.0	900	182.4	111	40
4	300	33.3	66.7	900	184.3	113	40
5	300	50.0	50.0	900	179.7	110	40
6	300	66.7	33.3	900	178.7	107	40
7	320	80.0	0	900	183.3	114	40
8	280	120.0	0	900	182.5	107	40

The inhibition effect of steel slag powder and blast furnace slag on the AAR

expansion was shown in Figure 3.

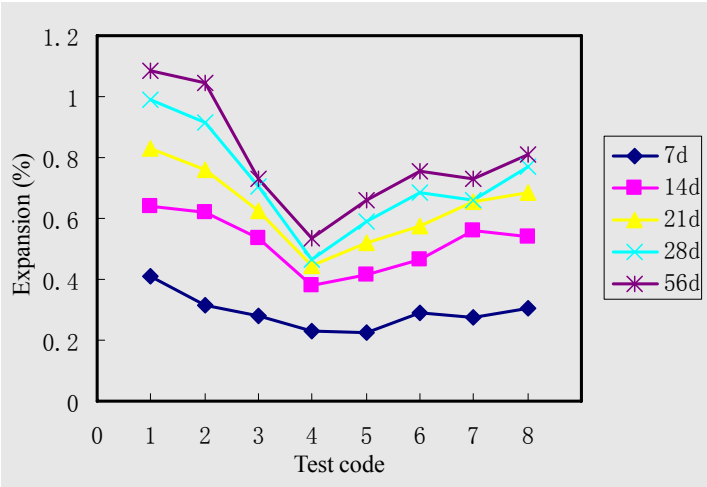

Figure 3. AAR expansion from ASTM C441 tests

It is seen from Figure 4 that the AAR expansion might be effectively inhibited by the addition of mineral powders, and the best result was achieved when steel slag powder and blast furnace slag were added (Code 4). The 56-day expansion of the mortar bar was decreased to about 50% of the expansion of the controlled specimens.

Accelerated tests. When actual aggregate was tested, a suitable method could be used to assessing the effectiveness of steel slag powder on suppressing AAR expansion with the temperature was higher and the alkali solution was more concentrated. The specimens were cured in the solution of 1mol/l NaOH at 80°C. Mix proportion of AAR tests with actual fine aggregate are listed in Table 4.

Table 4. Mix proportion of AAR test with fine aggregate

Code	Cement (g)	Steel slag (g)	Blast furnace Slag (g)	Aggregate (g)	Water （g）	Fluidity (mm)	Curing temperature(℃)
1	400	0	0	900	158	110	80
2	300	100.0	0	900	160	112	80
3	300	0	100.0	900	167	108	80
4	300	33.3	66.7	900	169	118	80
5	300	50.0	50.0	900	160	119	80
6	300	66.7	33.3	900	160	115	80

The inhibition effect of steel slag powder and blast furnace slag on the AAR was shown in Figure 4.

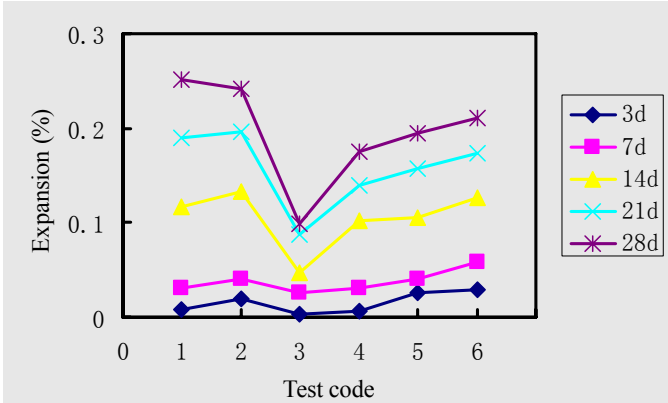

Figure 4. AAR expansion from accelerated tests

It is seen from Figure 5 that the AAR expansion with fine aggregate might be effectively inhibited by the addition of mineral powders, and the best result was achieved when blast furnace slag were added (Code 3). The 28-day expansion of the mortar bar was decreased to about 40% of the expansion of the controlled specimens.

CONCLUSIONS

The high performance concrete can be produced using mineral admixtures - steel slag powder and blast furnace slag. The recycling of steel slag can bring enormous economic benefit and environmental benefit.

Compressive and flexural strength of concrete with steel slag powder tend to decrease as the content of steel slag increases. Properties of concrete will be greatly enhanced when compound mineral admixture of steel slag powder and blast furnace slag is mixed into concrete. Steel slag and blast furnace slag show synergistic effect and mutual activation in concrete. On the other hand, steel slag concrete has lower strength at early ages; therefore, steel slag can be used to control the hydration process so that high strength and high performance concrete can be obtained.

The effectiveness of steel slag powder on suppressing AAR expansion was assessed using the method of ASTM C441 and the accelerated test method. Results show that mineral admixtures with steel slag powder as partial replacement for Portland cement in concrete is an effective means for controlling expansion due to AAR. At most a 50% decrease in expansion rate of mortar bars can be achieved. According to the research, properties and durability of concrete can be greatly improved using mineral admixtures such as steel slag powder.

ACKNOWLEDGEMENTS

The authors would like to acknowledge the Science and Technology Program of

Qingdao (08-2-1-18-nsh) and Shandong Provincial Education Department (J07YA15) for financial support of the project.

REFERENCES

Liu, T. C. and Yang, H. M. (2006). "Ultrafine steel slag and latest advance in blending materials of high performance concrete." *Metal Mine,* 41(9), 8-13

Muhammad, I. A. K. and Emmanuel, R. (2007). "Effect of mineral additives on some of durability parameters of concrete." *Proceeding of International Conference on Advances in Cement Based Materials and Applications in Civil Infrastructure*, Lahore-Pakistan, 289-299.

Sun, J. Y. and Huang, C. H. (2004). "Influence of slag and steel slag composite on properties of high content slag concrete." *New Building Materials*, 20(7), 13-15.

Sun, S. S., Zhu, G. L., Zhang, Y. (2007). "Application Technology of Iron and Steel Slag in China." *China Waste Steel*.

Zhu, H., Ding, Q. J. and Peng, Y. Z. (2005). "Effect of Super-fine Steel Slag Powder on Mechanical Properties of Concrete." *Journal of Wuhan University of Technology*, 27(1), 40-43.

Mechanical Characteristics of Reinforced Gravity Oblique High U-shaped Abutment

Qin Li-hui and Liu Gui-wei

School of Transportation Science and Engineering, Harbin Institute of Technology, P.O. Box 2531, Harbin 150090, China; PH (86) 451 - 8628 2121; FAX (86) 451-8628 2121; email: qinlh1977@163.com

ABSTRACT

Gravity abutment is a kind of commonly used understructure of highway bridges. It depends on its gravity to balance outside load and maintain stability. For some reason, many diseases appear on the gravity abutment in engineering practice. It is indicated by investigation that disciplinary disease appears on gravity when the height and width increase. It will extend rapidly once cracks appear and then construction in service is affected significantly. Therefore, it is urgent and necessary to investigate the reinforcement method of gravity abutment. According to resemble rule, the test project of the oblique U-shaped high abutment is designed. The message is recorded and analyzed in detail about the stress and displacement of the abutment model forced by outside load. The mechanical characteristics are achieved before and after reinforcement, for a different reinforcement project in the abutment process, under the action of solid force and outside load.

INTRODUCTION

In recent years, freeway construction has developed rapidly with large investment in highway construction in China. For special geographical conditions, it is necessary to traverse mountains or railways through the use of bridges, in which high gravity abutments covers higher proportions. On some gravity abutments cracks will appear with different grades on their front or side walls when their height exceeds eight meters or width exceeds fifteen meters. However, the high and wide abutment's disciplinary disease has not been the only problem of design or construction (Yang, 2002). In this paper, a resemble simulation test was implemented and stress and displacement of the gravity oblique high U-shaped abutment was investigated during a soil filling course. Angle-smoothening (Liu, 1998) and the carbon fibre reinforcement method (Li, 2003; Huang, 2005) were used and an improvement effect was achieved under the press of soil.

TESTING PROJECT OF GRAVITY OBLIQUE U-SHAPED ABUTMENT

Introduction of Bridge. The bridge at 46.15km of the Ji-Wu highway located in Shulan city has a U-shaped concrete gravity oblique abutment. Its length is 52.86m, design span is 2×16m, and oblique angle is sixty degrees. The width of this bridge is 14m plus 2×2m sidewalk. The structure of the main beam is a pre-stressed concrete simple beam and the infrastructure is an enlarged basement. However, cracks occurred at the abutment's body and side walls not long after its coming into service and vertical cracks were much more serious. It was been run-through and the

width of the cracks were very big as shown in Figure 1.

Model's Size and Material. According to the resemble rule of the abutment model test (Xu, 1995), the scale of the test model was determined to be ten to one. The height was one meter, the length of the front wall was two meters, oblique angle was sixty degrees, and the inner slope was three to one. Experimental materials included C15 chip stone concrete and 325 silicate cement. The ratio of the mixture of concrete was 1: 3.35: 5.50 (cement: sand: stone) and the ratio of water and cement was 0.52. Inside the abutment was adopted simulated sand soil and the ratio was 3:1:0.3(soil: sand: stone). Two models were constructed as shown in Figure 2. One was an U-shaped abutment with an oblique angle of sixty degrees and the other was constructed by angle-smoothening.

Figure 1. Vertical crack of abutment

Figure 2. Abutment model

Testing Instrument and Observed Location. Displacement and strain are recorded by a centesimal apparatus and static strain gauge, individually, loading by weighing sensor in steps.

The centesimal apparatuses were located in the top, middle, and bottom of the front wall's central section and the long side wall's tail, as shown in Figure 3.

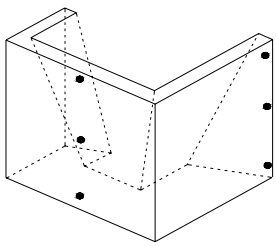

Figure 3. Location of displacement observation

Strain patches were located at the tail of the long side wall and the top, two-third of the way, and the middle of the intersection between front wall, long, and short side walls, just as Figure 4 presented.

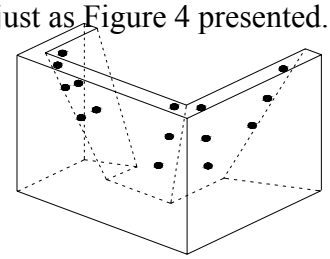

Figure 4. Location of strain observation

Loading Procedure. Loading level was set to be two tons. It was necessary to upload by level and unload after cracks appeared. The abutment model was held still for five to ten minutes after each uploading and then data was recorded. After the last uploading, ten to thirty minutes was needed to hold it still.

TESTING DATA ANALYSIS

General Oblique U-shaped Abutment. Height-directional displacement along the bridge of the general oblique U-shaped abutment front wall's middle part can be seen in Figure 5. Figure 6 presents the height-directional displacement through the bridge of long side wall's tail.

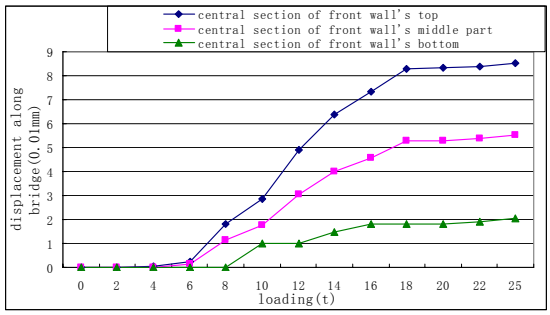

Figure 5. Displacement of front wall's central section of general abutment

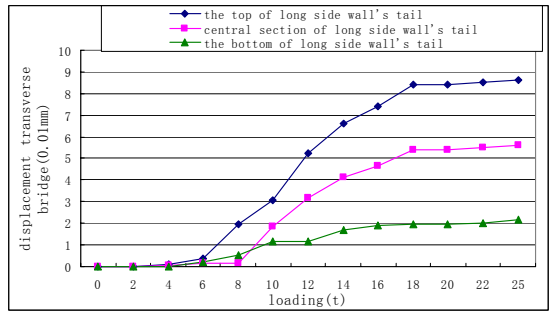

Figure 6. Displacement of long side wall's tail of general abutment

Recorded experimental data proved that displacement increased with the augment of load. When the load reached twenty-five tons, the maximum displacement along the bridge at the middle part of the front wall was 0.076mm and appeared at the top of the front wall. The maximum displacement through the bridge at the long side wall's tail was 0.086mm and appeared at the top of the long side wall's tail.

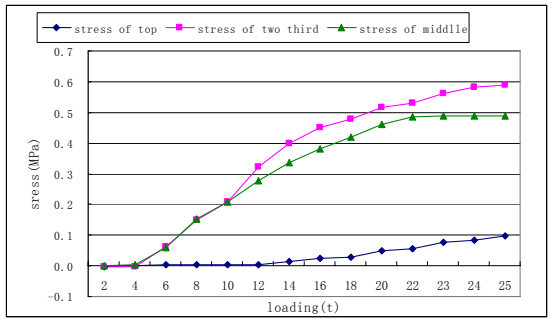

Figure 7.Stress of general abutment

The elastic modulus of C15 chip stone concrete equaled to 4.2×10^3 MPa. Stress was analyzed by recording strain data from multiple elastic moduli. The testing result showed that stress increased with the augmentation of load. When the load reached twenty-five tons, the maximum stress of the intersection between the front wall and long side wall was 0.588 MPa and it appeared at a location two-third of the way to the bottom, as shown in Figure 7.

Angle-smoothening Ablique U-shaped Abutment. Height-directional displacement along the bridge of the angle-smoothening oblique U-shaped abutment's front wall's middle part can be seen in Figure 8. Figure 9 gave the height-directional displacement through the bridge of long side wall's tail.

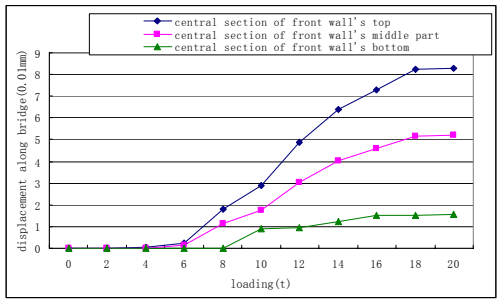

Figure 8. Displacement of front wall's central section of angle-smoothening abutment

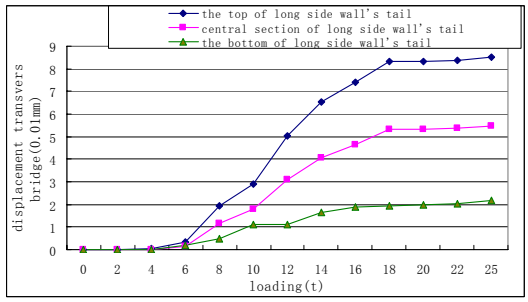

Figure 9. Displacement of long side wall's tail of angle-smoothening abutment

Test results show that displacement along the bridge increased with the augmentation of uploading. When the load reached twenty-five tons, the maximum displacement along the bridge at the middle part of front wall was 0.077mm, appearing at the top of the front wall. The maximal displacement through the bridge at the long side wall's tail was 0.085mm and appeared at the top of the long side wall's tail.

It also showed that stress increased with the augmentation of uploading. When the load reached twenty-five tons, the maximum stress of the intersection between the front and long side wall was 0.319 MPa and it appeared at a location two-third of the way to the bottom, as shown in Figure 10.

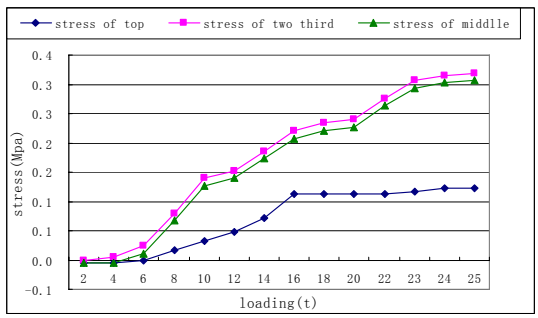

Figure 10.Stress of angle-smoothening abutment

Stress decreased greatly after the angle-smoothening reinforcement method was used. However, displacement showed little difference.

Carbon Fibre Reinforced Oblique U-shaped Abutment. The general abutment model was affixed with two rings of carbon fibre and the width of the carbon fibre was five meters. The first bar was affixed at the top of the abutment and the second's location was two-third of the way to the bottom. The angle-smoothening abutment model was affixed with only one ring of carbon fibre located at the top of the abutment.

This part was to analyze the model with one affixed ring of carbon fibre and the model with two affixed rings of carbon fibre. Displacement data along and through the bridge was listed in Table 1. It can be seen that the displacement was very small for carbon fibre. When the load reached 60 tons, vertical cracks appeared and the maximum displacement along bridge was 0.074mm and its location was the

top of the front wall's central section. The maximum displacement through bridge was 0.039mm and the location was the top of long side wall's tail.

Table 1. Displacement of abutment affixed one ring of carbon fibre unit: mm

load	displacement along bridge at central section of front wall			displacement throughbridge at the tail of long side wall		
	top	middle	bottom	top	middle	bottom
20t	0.005	0.003	0	0.007	0.005	0.003
30t	0.014	0.004	0	0.011	0.007	0.004
40t	0.029	0.019	0	0.025	0.017	0.007
50t	0.063	0.041	-0.01	0.027	0.021	0.010
60t	0.074	0.052	-0.02	0.039	0.026	0.017

Displacement data along and through the bridge of this model was listed in Table 2. Maximum displacement along the bridge was 0.018mm and its location was the top of the front wall's central section. The maximum displacement through the bridge was 0.033mm and the location was the top of the long side wall's tail. The displacement of the two rings of carbon fibre reinforced model was less than that of the one ring of carbon fibre reinforced model. Therefore, it can be concluded that the effect of carbon fibre reinforcement is better than the angle-smoothening method to decrease displacement. The effect of two rings of carbon fibre was better than that of one ring.

Table 2. Displacement of abutment affixed two rings of carbon fibre unit: mm

load	displacement along bridge at central section of front wall			displacement transverse bridge at the tail of long side wall		
	top	middle	bottom	top	middle	bottom
20t	0.007	0.004	-0.005	0.006	0.004	0
30t	0.011	0.007	-0.005	0.007	0.004	0
40t	0.015	0.01	-0.006	0.009	-0.005	0
50t	0.017	0.011	-0.01	0.032	0.006	0
60t	0.018	0.012	-0.01	0.033	0.025	-0.01

For stress data analysis, it mainly covered two issues: the model with one affixed ring of carbon fibre and model with two affixed rings of carbon fibre.

Stress data of this model was listed in Table 3 and the maximum stress was 0.764MPa when loads reached 60 tons with two-third of the way to the bottom as the location.

Table 3. Strain and stress of abutment model affixed one ring of carbon fibre

load	strain (με)			stress (MPa)		
	top	two third	middle	top	two third	middle
20t	-6.67	44.76	-4.76	-0.003	0.188	-0.020
30t	28.57	94.76	23.81	0.120	0.398	0.100
40t	65.71	115.24	40.95	0.276	0.484	0.172

50t	57.14	162.86	66.67	0.240	0.684	0.280
60t	16.19	181.9	121.43	0.068	0.764	0.510

Stress data of this model was listed in Table 4. We can see that the maximal stress was 0.463Mpa when the load reached 60 tons and the location was two-third of the way to the bottom. Different from one ring of carbon fibre, stress decreased markedly.

Table 4. Strain and stress of abutment model affixed two rings of carbon fibre

load	strain (με)			stress (MPa)		
	top	two third	middle	top	two third	middle
20t	-0.95	0.95	-0.95	0.000	0.004	-0.004
30t	5.71	53.33	-0.95	0.024	0.224	-0.004
40t	15.24	89.52	44.76	0.064	0.376	0.188
50t	15.24	94.76	71.43	0.064	0.398	0.300
60t	15.24	110.29	107.62	0.064	0.463	0.452

CONCLUSION

For the gravity oblique high u-shaped abutment, conclusions can be drawn as follows by investigation.

(1) Displacement and stress increases with the augment of load. The maximum displacement along the bridge appears at the top of the front wall's middle part and the maximum displacement through the bridge appears at the top of the long side wall's tail. The maximum stress appears at the location of two-third of the way to the bottom of the intersection between the front wall and long side wall.

(2) The maximum displacement along the bridge is 0.076mm for the general abutment, it is 0.077mm for the angle-smoothening abutment, and it is 0.074mm and 0.018mm for the abutments with one and two affixed ring(s) of carbon fibre, respectively.

(3) The maximum displacement through the bridge is 0.086mm for the general abutment, it is 0.085mm for the angle-smoothening abutment, and it is 0.039mm and 0.033mm for the abutments with one and two affixed ring(s) of carbon fibre, respectively.

(4) The maximum stress is 0.588 MPa for the general abutment, it is 0.319 MPa for the angle-smoothening abutment, and it is 0.764MPa and 0.463Mpa for the abutments with one and two affixed ring(s) of carbon fibre, respectively.

(5) Good effects can be obtained using the angle-smoothening and carbon fibre reinforcement method.

(6) The effect of two rings of carbon fiber reinforcement is better than that of one ring to decrease both the abutment's displacement and stress.

REFERENCE

Huang, Y. (2005). "Carbon fibre strengthening technology for bridges." *Technology*

of Highway and Transport. (1), 79-83

Li, H. F., and Xiong, X. G. (2003). "Application of carbon fiber reinforcement plastics to reinforcing bridge." *Highway*. (2), 103-107.

Liu H. S., and Song Z. F. (1998). "Reforcement of U-shaped abutment." *Highway*. (8), 13-14.

Xu, T. (1995). "Resembling method and its application." *China Machine Press*, Beijing.

Yang, Z., and Zhang, W. L. (2002). "Crack Repair for patch stone concrete abutment." *Highway*. (6), 106-107.

Application of Thermal Stress Controlling in Construction of Large Bridge Cushion Cap

XU Wei[1], ZOU Jianwen[1], REN Huixing[2]

1. Department of Building Engineering, Tongji University, Shanghai 200092, China;
2. CCCC Second Highway Engineering Co. Ltd, Xian710065, China.
PH (086) 021- 65985998;email:zoujianwen7866@yahoo.com.cn

Abstract: With respect to the construction of large bridge cushion cap concrete without poured joint in deep water, thermal stress during concrete hardening is destructive to durability. In this paper, a concrete thermal stress physical formula represented by the deformation component and variable temperature component is given based on the analysis of temperature stress influence. The calculation parameters of the main cushion cap with dimension of 113.75 m long, 48.1 m wide, and 13.3m high are determined. Comparison is made between the monitoring value and calculated results, which are obtained by simulation analysis of thermal stress variation during concrete hardening. The analysis shows that rational controlling temperature standard, cooling with cold water pipes, and curing in time play an important role in cracks protection. The dangerous age and the location where cracks could occur are given. These could provide valuable a reference for the design and construction of the other similar projects.

Keywords: *Bridge Cushion Cap; Construction ; Thermal Stress; Calculation; Durability ； Detect test*

1. Introduction

The crack caused by the temperature stress of concrete has a great impact on concrete's durability, which has drawn wide attention in engineering. In construction, because of the heat of hydration produced in the process of hydration of concrete, at the early stage, the inside temperature of concrete goes up so quickly that concrete expands out of shape. The concrete's elastic modular is small, consequently, the stress caused by expansion distortion controlled is small too. With the gradual dropping of temperature, concrete creates contraction distortion while its elastic modular increases. The controlled distortion caused by the dropping of temperature produces compressing stress inside the concrete and tensile stress on the surface.

If the surface tensile stress exceeds concrete's maximum tensile strength, cracks will appear on the surface of concrete（YUAN, 2002）. When the concrete's temperature drops gradually, the volume of concrete becomes smaller. Meanwhile concrete emerges with contraction distortion due to the carbonization and evaporation of extra moisture in the hardening process. However, limited by the condition of foundation and structural boundary, concrete cannot distort freely, thus temperature stress comes into being. When the two stresses pile up and exceed concrete's maximum tensile strength, shrinking cracks appear around the juncture of

concrete's base plate and inside（WANG, 1997; ZHU, 1999）.

Based on an oversize bridge cushion cap construction in deep water, this paper has adopted the finite element method to do some research into the change patterns of the heat stress field in the process of concretion of concrete's components and made comparison and analysis between calculated temperature stress and the temperature stress measured in practical construction. The conclusion may serve as a reference for similar projects.

2. Heat Stress Calculation Theory

Analysis of the concrete hardening process is based on the elastic deformation stage to judge temperature cracks appearance according to whether the tensile stresses exceed the tensile strength of concrete. With the assumption that linear expansibility is invariable when temperature varies with time, the strain component of each point in the elastic solid is given as:

$$\begin{aligned} &\varepsilon_x = \varepsilon_y = \varepsilon_z = \alpha T \\ &\gamma_{yz} = \gamma_{zx} = \gamma_{xy} = 0 \end{aligned} \qquad (1)$$

Where T is variable temperature in the elastic concrete; α is linear expansibility. The physical equation of heat elastic mechanics is:

$$\begin{aligned} \varepsilon_{\mathrm{x}} &= \frac{1}{E}\left(\sigma_x - \nu\sigma_y\right) + \alpha T \\ \varepsilon_{\mathrm{y}} &= \frac{1}{E}\left(\sigma_y - \nu\sigma_x\right) + \alpha T \\ \gamma_{xy} &= \frac{2(1+\nu)}{E}\tau_{xy} \end{aligned} \qquad (2)$$

The stress component is given from equation (2).

$$\begin{aligned} \sigma_{\mathrm{x}} &= \frac{E}{(1-\nu^2)}\left(\varepsilon_x + \nu\varepsilon_y\right) - \frac{E\alpha T}{1-\nu} \\ \sigma_{\mathrm{y}} &= \frac{E}{(1-\nu^2)}\left(\varepsilon_y + \nu\varepsilon_x\right) - \frac{E\alpha T}{1-\nu} \\ \tau_{xy} &= \frac{E}{2(1+\nu)}\gamma_{xy} \end{aligned} \qquad (3)$$

The theory with calculating the temperature stress field of concrete with the finite element method is that the strain increment of concrete is composed of elastic strain increment $\Delta\varepsilon_{\mathrm{n}}^{f}$, temperature strain increment $\Delta\varepsilon_{\mathrm{n}}^{T}$, authigenic volumetric deformation increment $\Delta\varepsilon_{\mathrm{n}}^{0}$, time deformation increment $\Delta\varepsilon_{\mathrm{n}}^{c}$, and shrinkage deformation increment $\Delta\varepsilon_{\mathrm{n}}^{\mathrm{s}}$（ZHU, 1999）. According to linear elastic theory, the

relationship of stress and strain under complex stress conditions can be defined as:

$$\Delta\sigma_{\mathrm{n}} = D_n\left(\Delta\varepsilon_n - \eta_n - \Delta\varepsilon_n^T - \Delta\varepsilon_n^0 - \Delta\varepsilon_{\mathrm{n}}^{\mathrm{s}}\right) \quad (4)$$

Where $\Delta\sigma_n$ is the stress increment matrix; $\Delta\varepsilon_n$, total strain increment; η_{n}, time deformation influence factor; and D_n, modified elastic matrix. From the balance equation of the finite element, the primary equation can be given as:

$$K\Delta\delta_n = \Delta P_n^T + \Delta P_n^C + \Delta P_n^0 \quad (5)$$

Where K is the stiffness matrix of structure; $\Delta\delta_n$, nodal displacement increment; ΔP_n^T, temperature load vector; ΔP_n^C, equivalent load vector yielding by creep, and ΔP_n^0, authigenic volumetric deformation load increment.

3. Analytic Model

The main cushion-cap is dumb-bell shaped with dimensions of 113.75m long, 48.1m wide, 13.324m high, and plane blocking 51.35×48.1m. A total of 42271m^3 C35 concrete is deposited.

（1）Elastic modular

Elastic modular E on different ages is calculated by formula (6) and the E is increasing with age is shown in Figure1.

$$E = 3.9\frac{t+0.885}{t+7.75} \quad (6)$$

（2）Compression strength

7d and 28d compression strength is R_7=31.8MPa and R_{28}=45.0MPa respectively.

（3）Adiabatic temperature rise

Heat of hydration of cement Bao-lei P.O 42.5 is 270J/g in 3 days and 292J/g in 7 days respectively. Taking θ_0=42.0℃ as the final adiabatic temperature rise, it is calculated by（7）at different ages and the result is shown in Figure2.

$$\theta = 42.0\frac{\mathrm{t}-0.682}{\mathrm{t}-0.325} \quad (\mathrm{t}\geqslant 1.2) \quad (7)$$

There, t—age, θ - adiabatic temperature rise at age t.

（4）Coefficient of temperature conductivity

The coefficient of heat conductivity λ can be computed as λ=11.02kJ/m.h.℃ according to the proportion of concrete so that the coefficient of temperature conductivity a=0.0048m^2/h can be obtained.

（5）Poisson ratio is 0.167 and linear expansion factor is taken as α=8.5×10^{-6}（1/℃）by the detection of results of the other cushion cap brought into effect already.

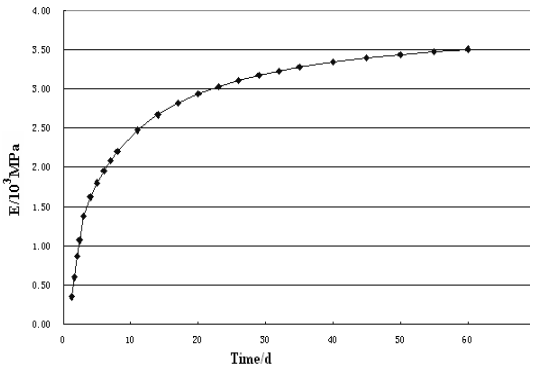

Fig.1. Variation of elastic modular

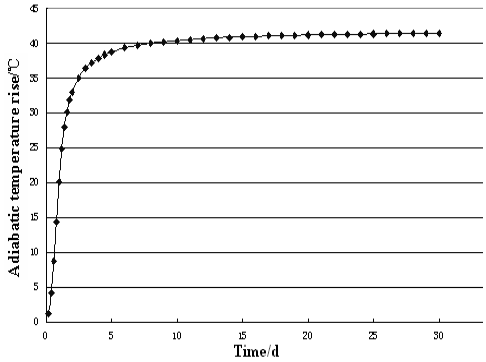

Fig.2. Adiabatic temperature rise

4. Calculated Result

The temperature field and stress field are treated in the same meshing and program adopting the three-dimensional finite element method. The influence of the cooling water pipe is considered and the concrete creep is calculated by the relaxation method（Code, 1987）.

（1）Characteristic number of stress

The characteristic number of stress shows larger tensile stress in the surface of the 2, 3, 4 layer. The largest inner tensile stress（3.08MPa）is found in the first layer in. Although the fourth layer in reaches the smallest tensile stress, it cannot be ignored due to yielding at an early age.

（2）Curve of stress variation

Figure 3 shows the curves of stress, change of stress point, and the curve of concrete tensile strength. Inner points are compressing stress in 4 days and tensile stress will come into being afterwards. The tensile stress increases quickly after the next layer of concrete being poured to reach the largest value in about 17 days. Surface points are almost tension in the beginning and reach the largest value in about 3-5days, then decrease gradually and become compression after 10 days.

Compared to the tension curve of concrete, surface tensile stress of every layer in 4 days is almost in proximity to the tensile strength of concrete, which the assurance coefficient is about 1.12～1.20 in 3 days. It is the danger period to develop cracks. Meanwhile the inner tensile stress of the first layer is approximately the same as the tensile strength of concrete at the age of 17～20 days but it is far lower than the tensile strength at the other ages.

Calculation results show that every layers' concrete tensile stress is less than tensile strength in the corresponding age, but the danger age during which the assurance coefficient is lower to quite a few cracks appear.

5. Detect Test Result

（1） Law of stress variation

Figure 4 shows the stress change of first layer concrete. $\sigma_{1.2}$, the stress point located on the distance of 57.5cm of lower surface, indicate that tensile stress is low in early ages and mostly compression stress later. $\sigma_{1.5}$ and $T_{1.5}$ represents inner stress

and temperature variation, respectively, located 40cm under top surface. It indicates that tensile stress appears immediately when the next layer of concrete is poured and it shows compression stress at an early age. The tensile stress enhances quickly reaching a maximum value of 3.52MPa , which is close to the tensile strength of concrete, and then reduces gradually. $\sigma_{1.8}$ represents the stress point near the steel suspension box-cofferdam that tensile and compression stress are all lower.

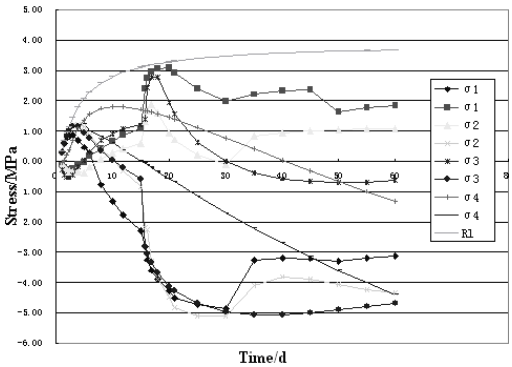

Fig.3. Inner and outer stress variation.

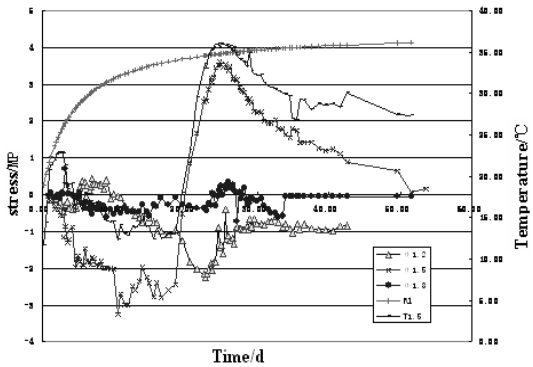

Fig.4.The first layer stress variation

Figure5 shows the second layer concrete stress variation. $\sigma_{2.5}$ and $\sigma_{2.6}$ represent the inner stress variation of the stress point located 40cm under the upper surface. $\sigma_{2.8}$ represents the stress point near the steel suspension box-cofferdam that tensile stress appears at an early age and compression stress mainly later.

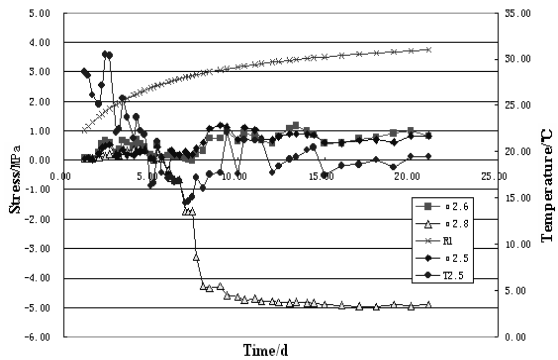

Fig.5. The second layer stress variation

（2）Characteristic number of stress

The tensile stress at the lower part and middle part of the cushion cap and side surface of the steel suspension box are not larger. There will be a big tensile stress in the first layer inner point near the top surface after upper concrete is poured; the tensile stress value is almost the concrete tensile strength.

6. Discussion

（1）According to the comparison of the monitoring result and calculation result, we know the calculation result corresponds to the monitoring result well. However, there exist errors between the two because the superficial point in the monitoring distance from the surface is more than 30cm.

（2）Interlamellar pouring intermission, water cooling time, local variation of

cooling pipe spacing, the difference between initial conditions and boundary conditions, the instability or inhomogeneity of concrete property, and more influence the monitoring result and calculation result.

（3）Thermal cracks can be avoided by strictly implementing temperature control standards and measures, paying attention to concrete prophase maintenance, and reduction of temperature difference between the upper and lower layer.

7. Conclusion

（1）The temperature control calculation provides the basis for temperature control in construction. The temperature monitoring plays an important role in testing the rationality and validity of temperature control standards, checking the safety condition of crack resistance, and holding temperature information timely.

（2）The temperature difference is large when the concrete pouring intermission is too long, 5～10 days later there will be large tensile stress in the sloping surface, which can causes the surface to crack. In addition, it is necessary to pay attention to the stress concentration caused by the wedge-shaped structure.

（3）The superficial tensile stress is larger in 4 days and cracks easily appear on the surface in this period. Active temperature control measures and an emergency plan should be taken.

（4）The monitoring result shows that the cooling water pipe is a very efficient method for temperature control in concrete. Shortening the concrete pouring intermission is beneficial to decreasing the temperature difference. Superficial thermal retardation and maintenance plays a very important role in preventing the surface cracking. The research provides scientific data and experience for temperature control of large cushion cap.

Acknowledgements

The research is supported by the 11th Five-Year Science-Technological Support Programs of the Ministry of Science and Technology of the People's Republic of China (Grant NO. 2006BAG04B05).

Reference

Code for design of dry dock (1987). Beijing: China communications press. (in Chinese)

WANG Tie-meng（1997）. Control cracking of engineering structure. Beijing: China architecture and building press, 5-16(in Chinese)

Y. Yuan, Z.L. Wan (2002). Prediction of cracking within early-age concrete due to thermal, drying and creep behavior. Cement and Concrete Research.32 (2002) 1053–1059

ZHU Bo-fang（1999）. Thermal stresses and temperature control of mass concrete. Beijing: China electric power press, 156-218 (in Chinese)

Impact of Gradation Types on Freeze-Thaw Performance of Asphalt Mixtures in Seasonal Frozen Region

Decheng Feng[1], Junyan Yi[1], Lei Wang[2], Dongsheng Wang[1]
[1]School of Transportation Science and Engineering, Harbin Institute of Technology, Harbin, 150090; email: hitjyyi@126.com
[2]Liaoning Province Highway Administration, Liaoning Shenyang, 110000; email: hitwanglei@sina.com

ABSTRACT

Asphalt pavement performance in seasonal frozen region is affected severely by the freeze-thaw cycles. Gradation has important effects on asphalt mixture's freeze-thaw durability. This paper presented the standard test methods of freeze-thaw cycles and analyzed the freeze-thaw durability of asphalt mixtures with different gradation. The test results showed that the freeze-thaw damage of asphalt mixtures goes through three stages. With the increase of freeze-thaw cycles, the splitting strength of mixtures decreased and the volume expanded gradually. The performance stabilized until the next rapid deterioration caused by the loss of interfacial adhesion between the asphalt and aggregate. The results also indicated that the mixtures with dense gradation had the best freeze-thaw stability than others, and the semi-open graded mixtures performed worst. The study results can be used in technical guideline for freeze-thaw durability of asphalt mixtures in seasonal frozen region.

Keywords: asphalt mixtures; freeze-thaw cycling; gradation; splitting strength; volume; interfacial adhesion

FOREWORDS

Asphalt mixture is a typical viscoelastic material. It's properties are affected by the temperature. In the seasonal frozen regions of China, the variation of water phase state due to changing temperature was the prime reason of asphalt mixture deterioration. There were researches on the freeze-thaw performance of asphalt mixture under the temperature cycles ranged from -20℃ to 20℃ (Pan et al. 2003, Hou et al. 2006), which mainly considered the temperature change within one year without consideration of the temperature range during years of asphalt pavement life cycle. Considering the combined impact of freeze-thaw cycling and traffic load on service life, the accumulative deterioration of asphalt mixtures would be severe.

Furthermore, the existing studies on the freeze-thaw performance of asphalt mixture mainly concerned the strength such as indirect tensile strength and fatigue life (Pan et al. 2003, Cao et al. 2004, Huang et al. 2005). There were only few studies on the variation of asphalt mixture samples' saturated weights (Hassan et al. 2002).

The objective of this paper was to characterize the asphalt mixture performance under freeze-thaw cycles using mechanical method and physical properties.

1 TEST METHODS AND MIXTURES CHARACTERIZATION

1.1 Introduction of test methods

The existing freeze-thaw stability test mainly considered the environmental effects within one year, which could be defined as "small cycles". And the range of temperature could be from -20℃ to 20℃. However, in the service life, the asphalt pavement would be also under the effects of high temperature along with low temperature. The temperature could range from -20℃ to 60℃ and should be included to analyze the asphalt pavement performance. In this experiment, three types of hot mix asphalt (HMA) mixtures were selected. For each type of HMA, three specimens were unconditioned, and the other specimens were water conditioned by vacuum saturation with distilled water for 15 minutes. Then for each of the three type of HMA mixtures, freeze-thaw cycles up to 8 cycles or to failure was conducted. Each cycle consisted of freezing for 8 h at -20℃ followed by soaking for 4 h at 60℃. Indirect tensile strengths were determined at 0, 2, 4, 6 and 8 cycles for conditioned specimens. Besides strength, the volume and weight were measured in the process of freeze-thaw cycles for every two cycles.

1.2 Materials

Crushed limestone aggregate was used in this experiment. Penetration grade 80-100 asphalt cement was used for AC and AM mixtures and rubber asphalt was used for OGFC mixtures. Properties of binders are shown in Table 1.

Asphalt mixtures for this experiment consisted of AC-16, AM-16 and OGFC-19. Mixtures design was performed according to Marshall Mixture Design Method. The final gradations are shown in Table 2.

All mixtures were added with hydrated lime to improve the ability of anti-stripping. The basic properties of the mixtures are shown in Table 3.

Table 1. Properties of Binders

Test	Ordinary Binder Properties	Rubber Asphalt Properties
Penetration at 25℃/0.1mm	93.7	62.3
Softening point /℃	45.9	63.6
Ductility at 15℃/cm, 5cm/min	>150	—
Retained penetration after RTFOT/%	60	61.1
Retained ductility at 15℃ after RTFOT/cm, 5cm/min	149	—
Viscosity at 180℃, Pa·s	—	2.31

Table 2. Mixtures Gradations

Sieve size (mm)	Percentage passing (%)		
	AC-16	AM-16	OGFC-19
19	100	100	100
16	95	97	95
13.2	84	78	80
9.5	70	63	57.5
4.75	48	36	20
2.36	34	22	15
1.18	25	15	12
0.6	18	10	9.5
0.3	13	7	7.5
0.15	10	4	5.5
0.075	6	3	4

Table 3. Mixtures properties

Mixtures	Properties	
	Percent air voids (%)	Asphalt content (%)
AC-16	6±1	5.2
AM-16	12±1	4.2
OGFC-19	18±1	5.2

2 RESULTS AND DISCUSSION

2.1 Impact of freeze-thaw cycles on mixture strength

The results of indirect tensile strength (ITS) and tensile strength ratio (TSR) for the three types of asphalt mixtures under different freeze-thaw cycles were shown in Figure 1.

It can be seen that the tensile strength of the three types of asphalt mixtures decreased with the increase of freeze-thaw cycles. In the first several cycles, the strength of mixtures have a sharp decrease, and then keep steady except AM mixtures. For AM mixtures with semi-open gradation, the strength kept reducing with the increase of the freeze-thaw cycles. Comparing with AC and OGFC mixtures, it could be concluded that there should been also a steady state of strength for AM mixtures in the next several cycles. The different strength decrease curve indicated the impact of gradation on the mixture performance in freeze-thaw cycles. The ITS of OGFC with skeleton-gap structure is smaller than AC and AM mixtures. The AC mixture with dense structure had best performance.

However, the change of TSR among the three mixtures gave different results. After 2 cycles, the TSR for OGFC reduced sharply to 60 percent for unconditioned specimens, and then gradually decreased until to 40 percent. As for AC mixture the values for the two similar states are 80 and 60 percent accordingly. However, for AM mixture, the decrease of strength does not have the steady state like the other two

mixtures. After the first cycle, the TSR of AM is higher than OGFC. After the last cycle, AM showed worst performance. Therefore the effect of gradation on asphalt mixture's freeze-thaw performance was important. Mixtures with dense structure and small air voids had the best performance.

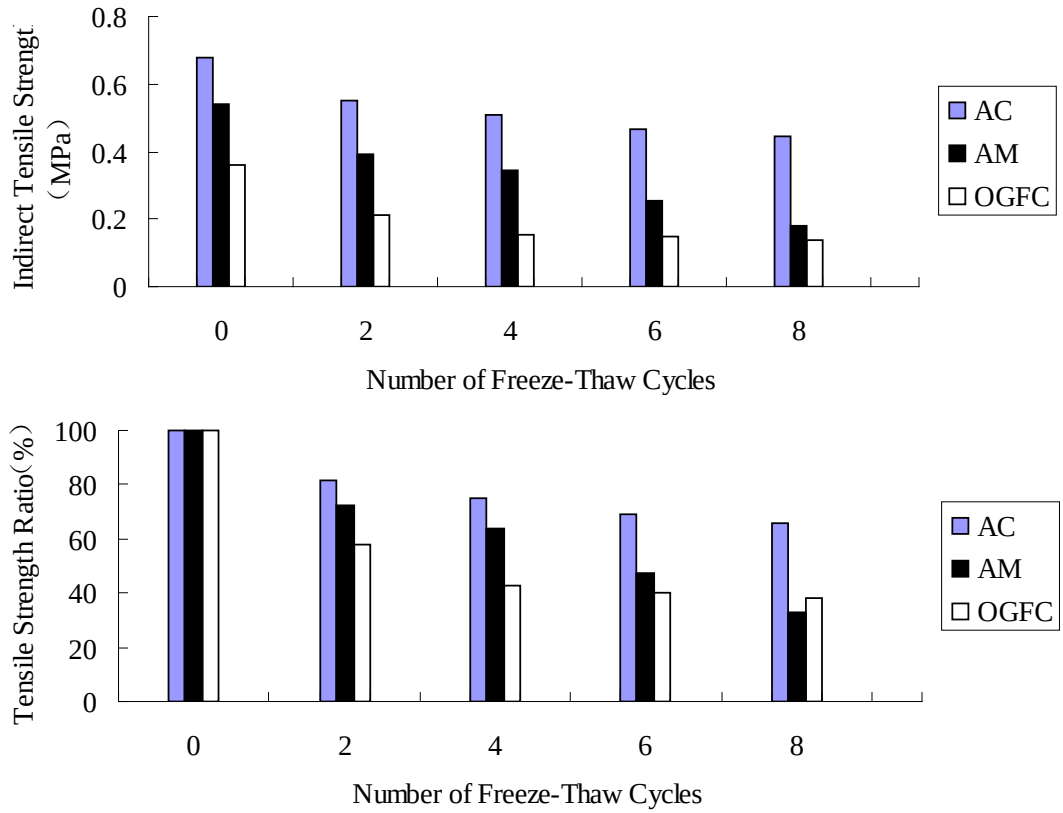

Figure 1. Impact of freeze-thaw cycles on ITS and TSR of three types of asphalt mixtures

Moreover, due to the interconnected air voids in OGFC mixture, the water could flow freely, which could reduce effect of water expansion at low temperature. Thus mixtures with middle percent air voids (from 8 to 13 percent) had the worst freeze-thaw performance, because the water entering into mixtures could not flow away freely.

The test results also indicated that the three types of asphalt mixtures performance decreased with the increase of freeze-thaw cycles. All the three curves had a relatively steady stage with the slope keep relatively smooth. However, the steady stage occurred after different cycles: for OGFC and AC mixtures, steady stage occurred after 4 cycles at which TSR was 60 percent for AC mixture and 40 percent for OGFC mixture. As for AM mixture, the steady stage occured when TSR was less than 30 percent. Considering the cumulative damage in the service period of pavement, it could be deduced that the three types asphalt mixtures would fail after more freeze-thaw cycles in service life due to the cumulative impact. In this research, surface raveling occurred in some specimens of OGFC and AC mixture in the last

several cycles which indicated the failure of interfacial adhesion between the asphalt binder and aggregate. As a conclusion, the deterioration of asphalt mixture under the impact of freeze-thaw cycles could be divided into three stages: strength decrease, performance stabilization and interfacial adhesion failure.

2.2 Impact of freeze-thaw cycles on physical properties of mixtures

Under freeze-thaw cycles, the physical properties of all specimens changed. The volume was obtained by measuring the height and diameter, while weight was obtained by weighing the dry mixture after splitting test. The variations of physical properties after freeze-thaw cycles are shown in Figures 2~5. It is noted that all specimens used to test the volume undergo 8 cycles.

The volume for all specimens increased during the first several cycles and then kept relatively steady. This could be explained by the viscoelastic properties of asphalt mixture. For viscoelastic material, the structure could have certain volume expansion to compensate the effect of water expansion. Therefore the mixture would have residual creep deformation due to expansive load. When the air void volume in specimens expanded to fit the expansion of water, the whole volume would not change too much. After this stage, the intrusion of water on the interface between asphalt and aggregate would be the main factor influencing the mixtures performance.

Figure 5 indicates the variation of weight for all mixtures under freeze-thaw cycling, which can be defined as weight loss rate Δm_m:

$$\Delta m_m = \frac{m_0 - m_n}{m_0} \times 100$$

where Δm_m = accumulated percentage of weight loss;

m_0 = initial sepcimen weight;

m_n =weight of undamaged particles in the specimen after n freeze-thaw cycles.

The line in Figure 5 was based on the average value. It could be seen that the weight loss rate increased sharply in the last cycles, which characterized the failure stage of the specimen. The weight loss rate developed differently for three types of asphalt mixtures. For AC mixture, the weight loss rate was small. However, for AM mixture, there was rapid weight loss during the last several cycles which agreed with the continuous decrease of strength. For OGFC mixture, although the weight loss rate was also large (>5%), the ITS remained to keep steady since the weight loss mainly appeared in the edge of specimens and did not cause the structure failure.

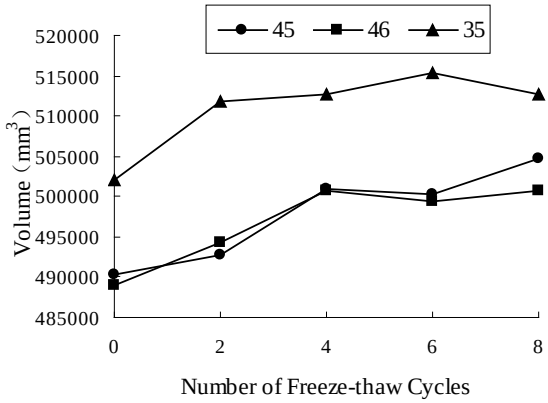

Figure 2. Volume change for AC

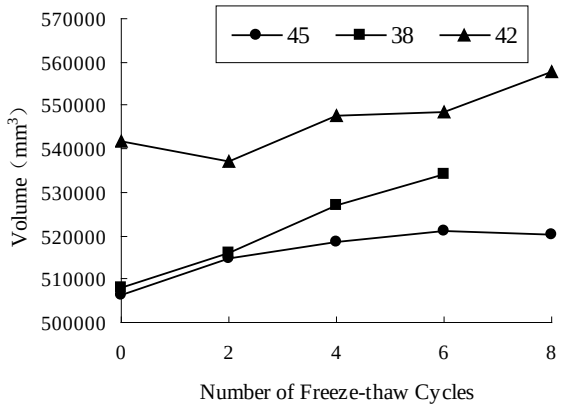

Figure 3. Volume change for AM

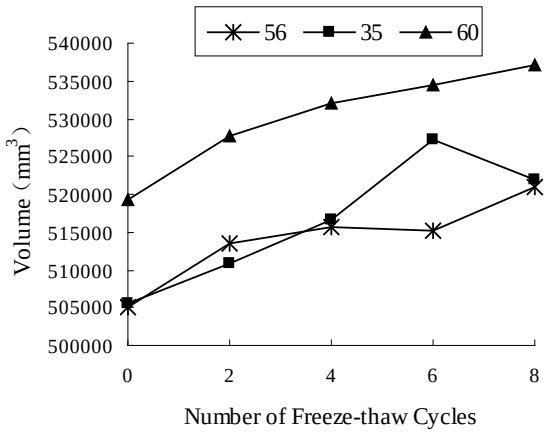

Figure 4. Volume change for OGFC

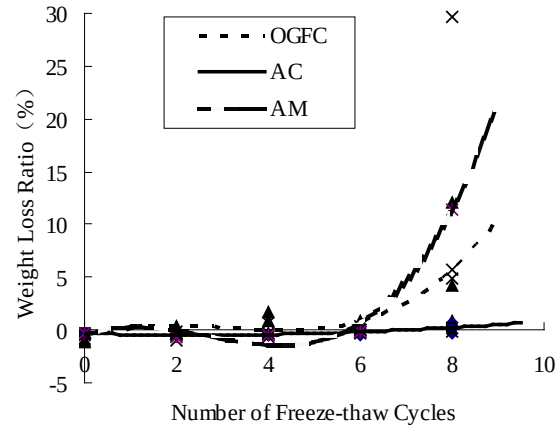

Figure 5. Weight change for all mixtures

3 CONCLUSIONS AND RECOMMENDATIONS

This study mainly focused on the freeze-thaw performance of three types of mixtures. The following conclusions were drawn:

(1) Gradation had important effect on the freeze-thaw performance of asphalt mixture. AC mixture had the best performance in the under freeze-thaw cycling, and AM mixture with the semi-opened gradation worst.

(2) The failure of asphalt mixture specimens in freeze-thaw cycles could be divided into three stages. For different mixtures, the TSR varies in terms of performance stability.

(3) With the increase of freeze-thaw cycles, the volume of mixtures increased, while weight loss rate decreased.

REFERENCES

Cao Xiao-yan, Chen Yong-xing, Bao Fu-tang (2004). “Research of freeze-resistance performance of asphalt mixtures”. *Journal of Heilongjiang institute of technology* 18(2):36-38.

Hassan Y., Abd EI Halim A.O., Razaqpur A.G., Bekheet W., Farha M.H (2002). “Effects of Runway Deicers on Pavement Materials and Mixes: Comparison with

Road Salt". *Journal of Transportation Engineering*, ASCE, Vol.128, No.4:385-391.
Hou Shu-guang, Wang Hong-chang, Huang Xiao-ming, Li Zhi-dong (2006). "Analysis of Freeze-thaw Fatigue Performance for Asphalt Mixture in Low Temperature Zone". *Journal of Highway and Transportation Research and Development* 23(4):7-10.
Pan Bao-feng, Wang Zhe-ren, Chen Jing-yun (2003). "Test and study of the alternate freezing and thawing capability of the bituminous mixture". *China Journal of Highway and Transport* 16(2):1-4.
Huang Shin-che, Raymond E.Robertson, Jan F.Branthavr, et al (2005). "Impact of Lime Modification of Asphalt and Freeze–Thaw Cycles on the Asphalt–Aggregate Interaction and Moisture Resistance to Moisture Damage". *Journal of Materials in Civil Engineering*, ASCE, Vol.17, No.6:711-718.

Study On Shear Properties for Adherence of New and Old Concrete and Its Practical Calculation

L. Li[1] and Z. L. Wang[2]
[1]School of Civil Engineering, Xihua University, Chengdu 610030,China, PH (028) 66383995; email: lili126@126.com
[2]School of Civil Engineering, Southwest Jiaotong University, Chengdu 610031,China

ABSTRACT

A full–range shear experiment of 6 groups with 18 specimens was carried out to investigate the effective adherence of new and old concrete in structure strengthening. The influence of various techniques to interface shear properties is examined. The experiment results show that the shear strength of the interface can be improved remarkably with bonded-in reinforcement. Based on the research results, the practical calculation formula was put forward which can take account of the influence of roughness, agent and bonded-in reinforcement. The formula was also validated by other experiments and can be used in the strengthening design for concrete structure.

INTRODUCTION

It is a common practice in the repair and strengthening the existing structure to add new concrete on the top of the old element of reinforcement concrete. The effective adherence of the interface is a key factor to assure new and old concrete bearing load together. It could usually be improved by enhancing shear capability of the interface. Many researchers (Gao, 2001; Guo, 2003; Han, 2003 and Yuan, 2001) focus their works mainly on the properties such as: tensile, direct shear, collapse model test or multi-axial stress. The factor of bonded-in reinforcement at the interface, widely used at present in strengthening engineering, is usually ignored. Shear experiment with Z-shape specimens are carried out in this paper. The factor of boned-in reinforcement at the interface between new and old concrete is taken into account as well as roughness, agent factors. Based on the research results, the practical calculation formula was put forward and validated by other experiments and can be used in the strengthening design for concrete structure.

SHEAR EXPERIMENT

Figure 1 shows a Z-shape specimen with dimension 300mm×100mm×350mm and load management. The dimension of interface between new and old concrete is

125mm×100mm. The strength grade of old concrete is C30 and of new concrete C40 with casting time space 4 months. All the 18 specimens are divided into 6 groups marked A, B, C, D, E, and F. Specimens in A, B, and C groups have only different face management and with no bonded-in reinforcement at interface. D and E groups have 4 ϕ 10 shear reinforcements at interface in each specimen with planting depth 5cm and 10cm respectively.

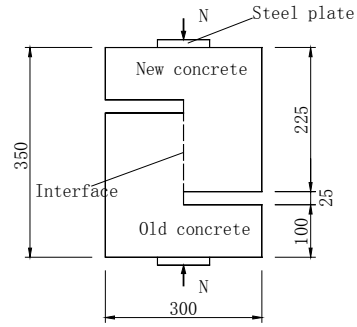

Figure 1. Z-shape specimen and load management(unit:mm)

EXPERIMENT RESULTS

Results of shear strength of concrete interface are shown in table 1. From the results of A, B, and C groups, the shear strength of B group with neat cement is the highest and the casting directly sample has the lowest strength. However, the strength of all specimens with three agents are smaller than that of F group, in which all specimen are casted at the same time for new and old concrete.

On the other hand, bonded-in reinforcement at interface could remarkably improve the shear strength of specimens in D and E groups by 8.77Mpa and 14.73MPa respectively.

Table 1. Results of shear strength of concrete interface

Specimen No.	Agent type	Interface Roughness /mm	Planting depth/cm	Broken load/kN	Shear strength /MPa	Average strength/ MPa
A-1	Casting directly	1.93	—	63.8	5.1	4.13
A-2		1.93	—	42.5	3.4	
A-3		2.03	—	48.8	3.9	
B-1	Neat cement	2.04	—	74.4	5.95	6.03
B-2		3.00	—	73.8	5.9	
B-3		2.38	—	78.1	6.25	
C-1	Merchandise agent	2.07	—	26.9	2.15	2.03
C-2		1.90	—	24.4	1.95	

C-3		1.86	—	25.0	2	
D-1	bonded-in	1.82	4～5	118.8	9.5	8.77
D-2	reinforcement	2.10	4～5	111.3	8.9	
D-3	ϕ 10	1.79	4～5	98.8	7.9	
E-1	bonded-in	1.97	9～10	168.8	13.5	14.73
E-2	reinforcement	2.23	9～10	197.5	15.8	
E-3	ϕ 10	2.15	9～10	186.3	14.9	
F-1	—	whole specimen	—	63.8	5.68	
F-2	—		—	42.5	5.92	5.73
F-3	—		—	48.8	5.60	

LOAD- STRAIN CURVE OF SPECIMENS

All the Load- strain curves for the specimens without bonded-in reinforcement are shown in Figure 2. Results from specimens with reinforcement are shown in Figure 3.

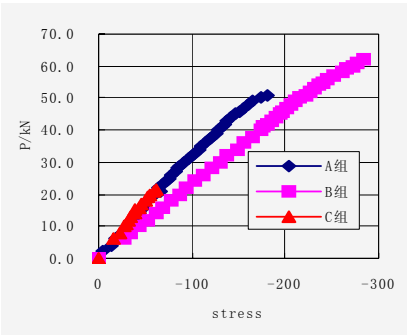

Figure 2. Load-strain curves of specimens without bonded-in reinforcement

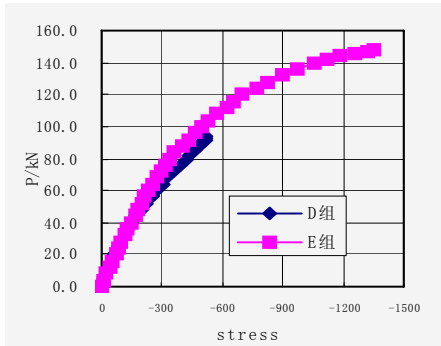

Figure 3. Load-strain curves of specimens with bonded-in reinforcement

The stress of the specimens in A, B, and C groups is smaller than 300 μ ε as shown in fig.2 and it increases linearly. It implies a brittle fracture failure mode. The stress of the specimens in D and E groups with bonded-in reinforcement are more than 600 μ ε even more than 1200 μ ε as shown in Figure 3 which can be considered as ductile fracture at the interface.

PRACTICAL FORMULA OF SHEAR STRENGTH

Based on the experiment, the shear capacity denoted by V_n of the interface could be decomposed into three parts (Equation 1). The first is cohesive force V_J, the second is friction force V_M caused by bonded-in reinforcement, and the third is V_D provided by bolt pin action of bonded-in reinforcement.

$$V_n = V_J + V_M + V_D \tag{1}$$

5.1 Practice formula for total shear strength of interface τ_J

From the experiment results, τ_J is related with concrete interface roughness, agent type and the cube compressive, which is denoted by Equation 2.

$$\tau_J = V_J / A_c = \zeta_1 \zeta_2 f_{cum} \tag{2}$$

Where, A_c is area of interface concrete, ζ_1 is roughness factor, ζ_2 is agent factor, f_{cum} is average compressive strength of new and concrete. ζ_1 could be fitted by experiment data. So Eq. (2) could be rewritten by

$$\tau_J = 0.06956\zeta_2 \cdot f_{cum} \tag{3}$$

5.2 Practice formula for friction shear strength τ_M provided by friction force

There are mainly three failure modes in the interface with bonded-in reinforcement: cone-bond compound failure, bond failure and reinforcement failure.

(1) Cone-bond compound failure

in this case, τ_M could be rewritten by

$$\tau_M = \frac{\mu \cdot F_G}{A_c} = \frac{\mu \rho_e f_t D^2}{d^2}\left(\frac{\tau_u}{f_t} - 1\right)\left(\frac{\tau_u}{f_t} + 1\right) + \frac{4\mu \rho_e D \tau_u}{d^2}\left(h_{ef} - \frac{D}{2}\left(\frac{\tau_u}{f_t} - 1\right)\right) \tag{4}$$

where f_t is tensile strength of concrete, ρ_e is steel ratio of bonded-in reinforcement of the interface, and d is the diameter of reinforcement.

(2) Bond compound failure

$$\tau_M = \frac{\mu \cdot F_G}{A_c} = \frac{4D\rho_e}{d^2} \cdot \mu h_{cf} \tau_u \tag{5}$$

(3) Cone-bond compound failure

$$\tau_M = \frac{\mu \cdot F_G}{A_c} = \mu \cdot \rho_e \cdot f_y \tag{6}$$

5.3 Shear strength τ_D caused by bolt pin action

Introduce the shear factor β caused by bolt pin action, τ_D could be written as

$$\tau_D = \beta \tau_M \tag{7}$$

Therefore, total shear strength of interface at different failure mode could be written by Eq. (8) (9) and (10)

(1) Cone-bond compound failure

$$\tau = 0.06956\zeta \cdot f_{cum} + \frac{\gamma\mu\rho_e f_t D^2}{d^2}(\frac{\tau_u}{f_t} - 1)(\frac{\tau_u}{f_t} + 1) + \frac{4\gamma\mu\rho_e D\tau_u}{d^2}\left(h_{ef} - \frac{D}{2}(\frac{\tau_u}{f_t} - 1)\right) \tag{8}$$

(2) Bond compound failure

$$\tau = 0.06956\zeta \cdot f_{cum} + \frac{4D\rho_e}{d^2} \cdot \gamma\mu h_{cf}\tau_u \tag{9}$$

(3) Cone-bond compound failure

$$\tau = 0.06956\zeta \cdot f_{cum} + \gamma \cdot \mu \cdot \rho_e \cdot f_y \tag{10}$$

Where ζ is agent influence factor. No agent $\zeta = 1$; only neat cement $\zeta = 1.5$. $\gamma = 1 + \beta$.

The formula is applicable only when the roughness is within 1.7mm and 3.0mm.

5.4 Formula validation

In Eq.(1), the first term V_J is the shear force of interface concrete in the case of no bonded-in reinforcement and the second and the third terms are the shear force provided by bonded-in reinforcement. The Comparison of calculation results by formula and experimental results are shown in tab.2

Table 2. Comparison of calculation results by formula and experimental results

Specimen No.	Concrete strength old/new /MPa	Interface Roughness/mm	Agent type	Planting depth/cm	τ_J /MPa	τ_G /MPa	τ /MPa	Test shear strength τ_0 /MPa	τ / τ_0
A	55/60	1.93	Casting directly	—	4.0	0	4.0	5.10	0.78
	55/60	1.93		-	4.0	0	4.0	3.40	1.18
	55/60	2.03		-	4.0	0	4.0	3.90	1.03
B	55/60	2.04	Neat cement	—	6.0	0	6.0	5.95	1.01
	55/60	3.00		-	6.0	0	6.0	5.90	1.02
	55/60	2.38		-	6.0	0	6.0	6.25	0.96

C	55/60	2.07	Mercha	-	2.0	0	2.0	2.15	0.93
	55/60	1.90	ndise	-	2.0	0	2.0	1.95	1.02
	55/60	1.86	agent	-	2.0	0	2.0	2.00	1.00
D	55/60	1.82	bonded -in	4～5	4.0	4.73	8.73	9.50	0.92
	55/60	2.10	einforcem ent	4～5	4.0	4.73	8.73	8.90	0.98
	55/60	1.79		4～5	4.0	4.73	8.73	7.90	1.11
E	55/60	1.97	bonded- in reinforc ement	9～10	4.0	10.6	14.6	13.50	1.08
	55/60	2.23		9～10	4.0	10.6	14.6	15.80	0.93
	55/60	2.15		9～10	4.0	10.6	14.6	14.90	0.98

From data shown in Tab.2, an average value of τ / τ_0 term $\bar{X} = 0.995$, the standard deviation $\sigma = 0.089$ and the coefficient of variation $\delta = 0.09$ could be obtained. This validates Eq. (1) proposed in the paper.

Eq.(1) could take fully account of different influence factors such as interface roughness, agent type, strength of new and old concrete and the planting depth of bonded-in reinforcement. Furthermore, the formula was also validated by other experiments and could be used in the strengthening design and calculation for concrete structure.

CONCLUSIONS

Based on the shear capacity experiments of new and old concrete with Z-shape specimens, the practical formula of shear strength of interface is proposed in this paper. Several conclusions could be drawn as following:

(1) The shear strength of interface, with roughness and agent pushing on old concrete surface, is smaller than that of whole specimen. In the specimens with agent pushing, neat cement is the most effective.

(2) With bonded-in reinforcement, the shear strength of interface could be increased remarkably, that could achieve level of the strength of whole specimen. And that strength quantity value is determined by planting depth, steel ration of bonded-in reinforcement, and compressive strength of concrete and epoxy resins.

(3) According to the experiment results, mechanics of shear failure at interface is analyzed. Practical formula for shear strength of interface calculation is put forward in the paper, which is applicable to the roughness within 1.7mm and 3.0mm. And the formula is also validated by experiment data.

ACKNOWLEDGEMENTS

This work was supported by Key Scientific Research Fund of Xihua University, and under grant number Z0820605.

REFERENCES

Gao, J.P., Pan, J.L., and Wang, Y.G. (2001). Effect of different bonding agents on bond strength between fresh concrete and hardened concrete. *Journal of Harbin University of C .E .& Architectur*. Vol. 34（5）：25-29

Guo J. J. (2003). Study on new and old concrete bonding mechanics after high temperature[D]. Dalian university of technology Ph.D thesis.

Han J. H., Zhao, G.F., and Zhang L. S. (2003). Experimental research on fracture properties of adherence for new to old concrete[J]. *China Civil Engineering Journal*. Vol. 36（6）：31-35

Wang Z.L., Lin, Y. J., and Qian, Y. J. (2005). Experimental Research on Shear Properties of New-to-Old Concrete Interface[J].*Journal of South-west Jiaotong University*. 47（4）

Yuan, Q., Liu, J. (2001). Study on Adhesive Strength of Young on Old Concrete[J]. *Journal of Building Structures*. 22(2):46-50

Research on Flame- Retardant Technique in Application of Asphalt Pavement in Highway Tunnel

JI Lun[1], TAN Yi-qiu[1], QI Guang-yuan[2] and CHEN Zheng-jin[3]

[1]School of Transportation Science and Engineering, Harbin Institute of Technology, 202 Haihe Road, Nangang District, Harbin 150090,P.R. China; TEL（86）15804509168, E-mail: jilun@hit.edu.cn;

[2]Heilongjiang Institute of Technology, Harbin 150050, P.R. China; TEL（86）13796086688, E-mail: m7gjb@126.com ;

[3]Zhe Jiang Provincal Transportation Engineering Construction Group, Hangzhou 310051, P.R. China; TEL（86）13262773151, E-mail: czj88998899@126.com.

ABSTRACT

Highway tunnels are mostly paved with asphalt concrete pavement. One of the components, asphalt is inflammable. And once it is ignited, large quantities of heat, smoke and poisonous gas are released and spread quickly, in tunnel fire, which will cause the difficulties of the escape and rescue seriously. This paper presents research on mineral-inorganic flame-retardant used in asphalt concrete pavement to avoid the huge damage caused by tunnel fires. The mechanism of flame retardancy was investigated systematically based on plenty of tests. Results indicated that the flame-retardant technique can slow the fire spreading and prolong the time of escape and rescue.

Foreword

Most highway tunnels were paved with asphalt concrete pavement because of its many advantages. However, serious tunnel fire incidents often occurred in many countries around the world, such as the famous tunnel fire disaster in Mont Blanc tunnel, and tunnel fire in Limao Mountain in Zhejiang Province of China. In both cases the asphalt concrete pavement was severely damaged and it caused serious economic losses. During the tunnel fire, temperature can reach 800℃ and higher in a short period. Although asphalt is difficult to burn in normal temperature, it can burn at high temperatures and release large quantities of smoke and toxic gases. Researchers at home and abroad have carried out some research about it. However, there is a lack of research about the heat, toxicity, smoke density and issues involving the escape and rescue conditions of security.

1 Research on the flame retardancy of mineral powders and aluminum hydroxide (ATH)

The so-called fire retardancy of material is the ability to postpone or terminate the combustion process under certain conditions. Flame Retardant Materials are designed to enhance the flame retardancy, and to ensure adequate time for fire-fighting or self-help.

1.1 Evaluation method of flame retardancy

Limit Oxygen Index (LOI) has been adopted as the index to evaluate the flame retardancy of materials by most international organizations, such as ISO04589, the United States ASTM2863, and Japan JISK7201. Besides, China developed a national standard "plastic combustion performance test method of oxygen index"

(GB/T2406-2006). LOI is defined as the minimum oxygen concentration in air of N_2 and O_2 to maintain burning. If the LOI is greater than 27%, the materials will be self-extinguishing.

1.2 Evaluation of the flame retardancy of Mineral powders

Mineral powders proportion in asphalt mixture is about 5%~10%, almost 1-1.5 times of asphalt. If mineral powders occur endothermic and dehydrated chemical reactions near asphalt, fire-retardancy of materials can be achieved through interruption of heat exchange.

Many tests were carried out for the study of flame-retardancy of mineral powders. AH-90 asphalt was used in the tests, and whose limiting oxygen index was 19.3%. The LOIs of several mineral powders are listed in Table 1. The ratio of powder to asphalt is 1:1 in these cases.

Tab.1 Limiting Oxygen Index (LOI) of mineral powders

mineral powders	DC	T	S	G	DA	Y
LOI (%)	24.3	27.0	25.1	23.9	25.0	23.0

It can be seen from Table 1 that T has a significant flame-retardancy performance. Two other mineral powders were tested in order to eliminate the dilution effect of powder on the asphalt. The results are listed in table 2.

Tab.2 Comparison of LOI for mineral powders

mineral powders	Content of mineral powders				
	70%	80%	100%	120%	150%
T	24.7	25.8	27.0	27.6	28.0
DA	24.9	25.0	25.0	25.2	25.1
Y	22.5	22.8	23	22.9	22.5
Assuming the role of the added value of dilution	4.4	4.6	4.7	4.8	4.5
Definite enhancement of T %	1.0	1.9	3.0	3.6	4.2

Flame-retardant performances of mineral powders are presented in Figure 1.

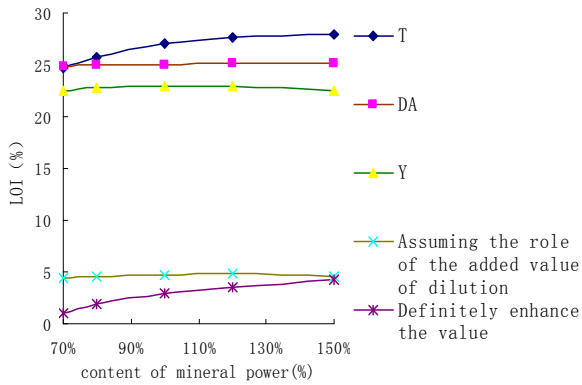

Fig.1 Flame retardancy analysis of mineral powders

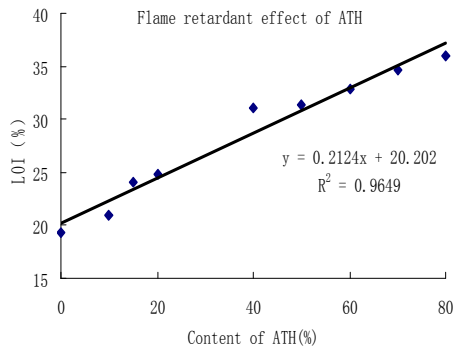

Fig.2 Flame retardant effect of ATH

Assuming DA and Y mineral powders are added as a dilution role, LOI of T was improved markedly as their contents increase. Usually the proportion of mineral powders to asphalt is about 1.3~1.4, it can be seen that the mineral powder has significant flame retardancy.

1.3 Evaluation of the flame retardancy of aluminum hydroxide (ATH)

LOI of mixture with different contents of ATH are shown in Figure 2.

Figure 2 indicates that there exists a linear increase relationship between LOI and ATH content. When the content is greater than about 32%, the LOI is more than 27% and reaches the standard of self-extinguishing.

1.4 Flame retardant system design and performance evaluation

In order to guarantee flame retardancy and smoke suppression performance, ATH content is determined as 20% of asphalt. Ratio of mineral powders to asphalt is 1:1 and filler-asphalt ratio is 1.2:1 (named A-T), less than the normal filler-asphalt ratio. LOI test results have shown although the synergistic effects between the two are not obvious, the self-extinguishing performance of material has been achieved fully.

2 Flame retardancy mechanism

Combustion and flame retardancy are a very complex process, involving a lot of influencing factors. Fundamentally speaking, flame retardancy of asphalt is to affect or interrupt some stages during the combustion process by either a physical or a chemical way. Flame-retardant technology can be divided into gas flame retardancy, condensed phase flame-retardancy and interruption of heat exchange. Ideal temperature of flame retardant material is 230~400C, considering the ignition scope of asphalt, control conditions of asphalt mixture construction and the safety of the fire.

Studies on the flame -retardant mechanism were carried out by Differential Scanning Calorimetry (DSC). Test conditions are as follows: 5mg Samples, room temperature as the initial test temperature, 5℃/min heating rate, 20ml/min nitrogen flow rate. Test and analysis results are shown in Figure 3.

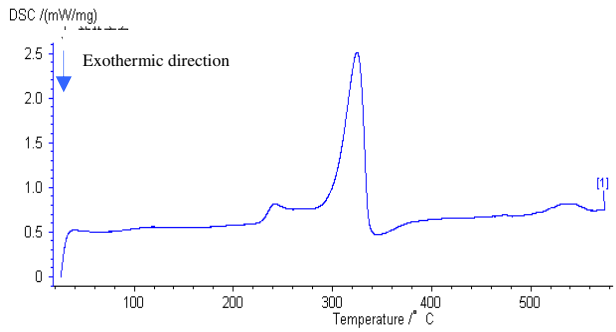

Fig.3 Curves of DSC

DSC data show there was a turning point at 220℃ and a peak of heat absorption at 300℃. Test results indicate that the sample heat absorption changes at this temperature and the material shows flame-retardant properties. The system has shown excellent flame retardancy at 300℃~340℃ because of obvious chemical or physical interaction.

3 Security Analysis of the System

To study the fire-retardant construction process, the use of stage and safety and environmental protection requirements under the conditions of fire, the following research and analysis were performed.

3.1 Security assurances of storage and processing - the flash point and ignition point tests

Flash point and ignition point are the indicator of construction security of asphalt mixture and they are measured by the Cleveland Open Cup (the COC). The test results indicated the flash point and the ignition point were 282℃ and 304℃ separately. When the temperature was up to 240℃, the bubbles spill from a asphalt specimen. The flash point and the ignition point can not be confirmed through experimentation methods. **Matrix asphalt, there will appear the phenomenon of water precipitation in the course of the experiment and it can be seen that the flame-retardant program will not affect the construction safety?.** At the same time, ATH shows bad temperature stability under the experimental conditions. In order to prevent fire retardant failures, the temperature of asphalt mixture must be controlled.

3.1 Comparison of 200℃ Volatile Components

Asphalt mixture construction **was under one certain temperature**?. It should be studied whether flame-retardant materials added into asphalt will volatile or make asphalt decomposed, resulting in environmental pollution, reducing the flame retardancy or harming health of workers, especially in the circumstances of ventilation adverse in tunnel. Based on these, headspace sampling-gas chromatography-mass spectrometry analysis method was adopted to compare volatile organic compounds under 200℃.

Agilent headspace sampling-gas chromatography-mass spectrometry analyzer was used in laboratory test, model Agilent 7964 headspace sampler, 6890N GC-5973N MSD?. Experimental conditions: Headspace, Vials heating temperature 200℃, heating time 30min, the sample temperature 200℃, transmission line temperature 200 ℃, injection time 1min. GC6890N-5973NMSD: GC injection port 220℃, do not split injection. HP5 30mΦ0.25mmΦ0.25mm capillary column, programmed temp erature, initial 35℃ (keep 10min) and then 15℃/min rise to 220 ℃ (keep 5min). MS monitors MSD: interface temperature 250℃, electron bombardment source EI, the quality of scanning range 15-300, NIST05 database search.

A-T test results are presented in Figure 4. The first peak in the figure is the air peak during the trial process. Test results have shown there is no release of organic matter except for water precipitation, resulting in the column loss and the safe system.

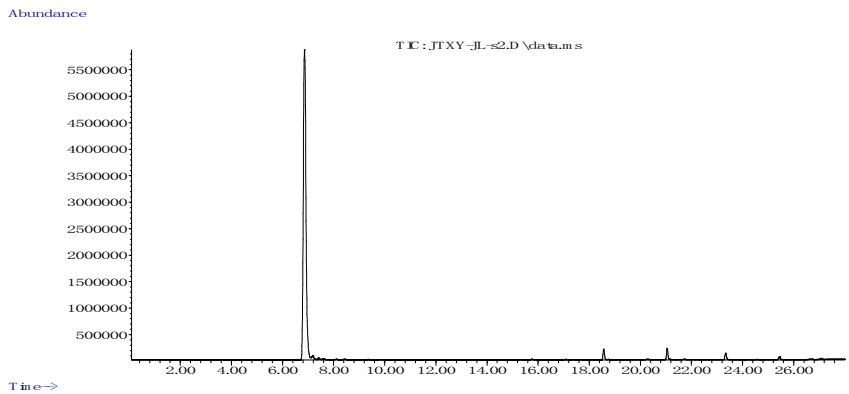

Fig.4 TIC of A-T flame-retardant asphalt

Figure 5 shows that there is release of three kinds of toxic organic compounds from the flame retardant asphalt, including 1,2-dichloroethane; 2-chloroethanol; and

three (2-chloroethyl) phosphate?.

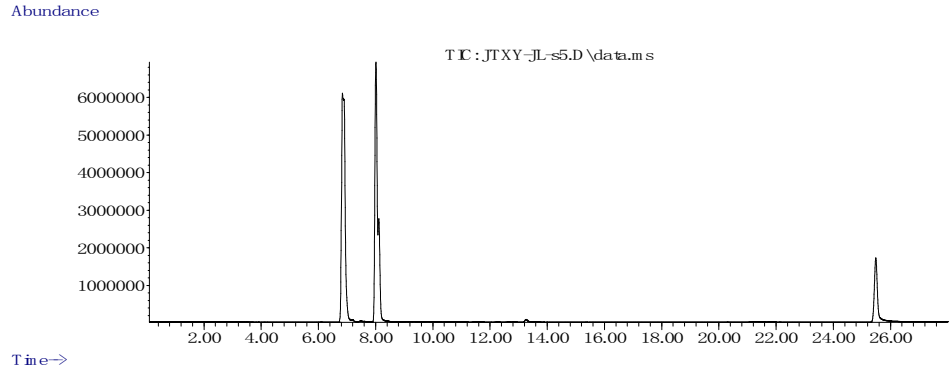

Fig.5 TIC of another one flame-retardant asphalt

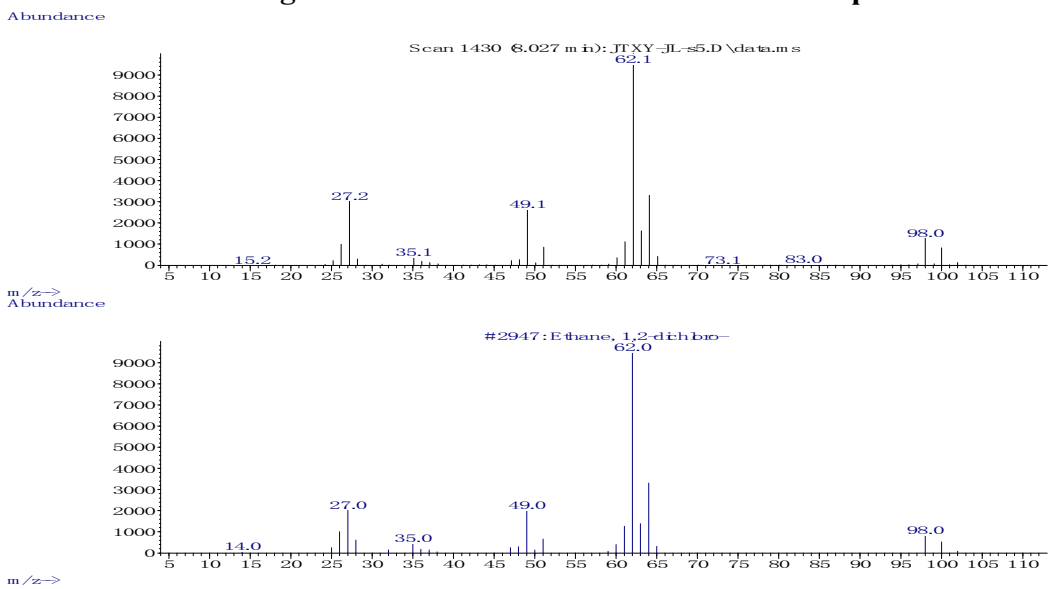

Fig.6 Index chart of 1，2-dichloroethane

3.2 Heat release and smoking characteristics

At present, cone calorimeter has been widely used to measure combustion characteristics of materials and evaluate their fire risks. The experimental environment and the actual fire are very similar and there was good correlation between experimental and model test results.

In general, when the fire developed to flashover, hot radiation flux of high temperature gas and flame are about 75kW/m^2. Therefore, the typical radiant flux Level of 25kW/m^2, 50kW/m^2 and 75kW/m^2 were selected. **In this test, 50kW/m^2, matrix asphalt and fire-retardant asphalt with 2.36mm and below the SMA-13 gradation value, 10.0% oil stone radio were used , with the British company FTT Cone Calorimeter (Cone Calorimeter).** The results are in Table 3.

Tab.3 Cone calorimeter radiation test results

Test indicators	Ignition time	exothermic rate (kW/m^2) Maxi-mum	exothermic rate (kW/m^2) average	Mass loss rate (%)	smoke generation rate (m^2 • m^2 • g^{-1})	exothermic rate (MJ/m^2 • g^{-1})	Specific extinction area SEA (m^2 •kg^{-1})
Matrix asphalt mixtures	114s	195.0	58.6	11.7	11.2	0.45	839.3
A-T mixtures	122s	85.4	36.0	9.8	3.0	0.3	292.3

Weight-loss curve?, heat release rate and smoking rate curve of the two asphalt mixture are shown in Figure 7 and Figure 8.

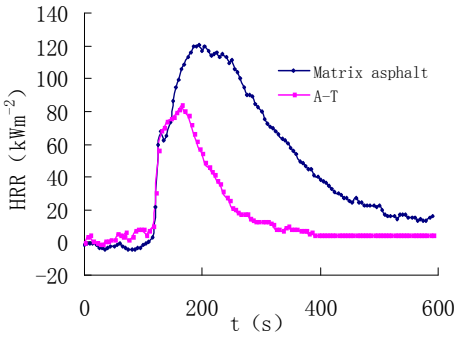

Fig.7 Heat release rate curves

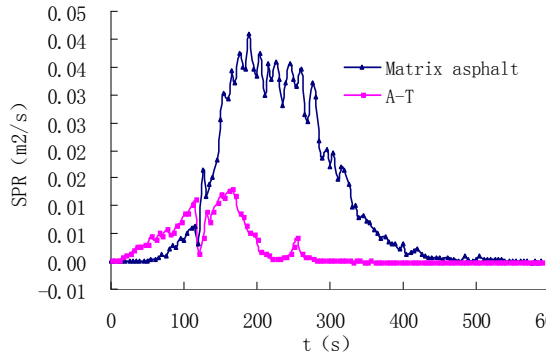

Fig.8 Smoking rate curves

Test results indicate:

(1) the ignition time are similar; in the radiation intensity, the flame retardant performance was not obvious.

(2) matrix asphalt heat released rate (HRR) larger, which suggestes much heat was releaseed per unit during burning. Matrix asphalt mixtures heat release research peak quickly, and may maintain a certain time at a higher level. The A-T system can effectively reduce the temperature of the fire scene. Heat release rate of matrix asphalt mixtures is almost 1.5 times of that of modified asphalts (A-M)，which reduces heat release capacity of asphalt and avoid the sudden increase of temperature in fires and thus save time for escape.

(3) Smoking rate of matrix asphalt is almost 3 times of A-T. The smoking rate curve indicates that the smoking rate of matrix asphalt is very large, almost 4~5 times of A-T, and the high smoking rates can be maintained for a period of time. From A-T Asphalt Mixture the smoking rate curve indicates that in the combustion process, it will have **certain hours?** to reduce the smoking rate; a small peak appeared at **200~300C, because the isolated membrane of flame retardant, which interrupted the heat exchange, was damaged, and caused heat and smoke release suddenly (similar to exothermic rate curve)?.**

(4) Specific extinction area of matrix asphalt is 2.87 times to? A-T. It can be seen that A-T greatly reduces the ability of asphalt smoking.

(5) A-T program is a safe flame-retardant program, and there is no toxic gas release in the construction.

4 Feasibility study of ATH taking place of mineral powders ?

Screening test, density test, hydrophilicity test, plasticity index test, and heat stability test were required in "Highway Engineering Test Aggregate of Order (JTG E42-2005)". The conventional indicators of T, ATH, and A-T were carried out and the test results are shown in Table 4:

Tab.4 Conventional performance of flame-retardant mineral powder, ATH and A-T

Pilot project	T	ATH	ATH：T =1：5

Density（g/cm^3）	2.63	2.38	2.58
Hydrophilic factor	0.8	1.2	0.9
Heat stability	There is no change in color	Heated to 200℃, there is a small amount of water vapor produced, cooled slightly pale yellow	Heated to 200℃ produced a small amount of water vapor, after cooling the color did not change significantly

It can be seen that the basic indicators of the mineral powders can meet performance requirements. As for the construction of asphalt mixture to control the temperature, the general does not exceed 195C, therefore, requested that the construction process should strictly be according to construction specifications to ensure that the flame-retardant material would not be lost? .

5 Asphalt mixture test comparision

With the middle value of SMA-13 gradation, asphalt mixture were made by SBS modified and ordinary mineral powder, T mineral powder and flame retardant mineral powder (ATH:T= 1:5) and matrix asphalt mixtures ?. The performances of different mixtures were compared under the best the amount of asphalt (optimal asphalt content?). The results are in Table 5.

Tab.5 Performance comparison of asphalt mixtures

Asphalt case	Water immersion residue stability（%）	Freeze-thaw splitting intensity ratio（%）	Dynamic stability（Times •mm^{-1}）	limiting flexural strain（μm）
SBS	84.0	88.4	4846	4721
T	82.7	83.8	1876	2892
A-T	80.8	81.8	1760	3120

The indicators of flame-retardant mineral are less than powder modified asphalt, but the indicators all meet the norms. The residual stability and freeze-thaw stability ratio of mixture with ATH or not reduced near 2%, dynamic stability index were equal, and the limit of bending tensile strain still improved. Therefore, ATH mixture did not adversely affect performance.

6 Conclusion

(1) Flame retardancy of asphalt can be achieved by adding A-T and the self-extinguishing performance can be satisfied.

(2) Differential Scanning Calorimetry (DSC) shows A-T fire-retardant system has multi-flame-retardant mechanism such as endothermic, coverage, and dilution.

(3) Flash point, ignition point and toxicity of materials meet requirements of environmental protection and construction safety.

(4) Heat release and smoking characteristics of A-M are proved better than matrix asphalt, which help ensure visibility of fire site and the conditions of escape and rescue.

(5) Road performance of A-T retardant system can meet the requirements of

specification.

(6) A-T retardant technology provided a powerful guarantee for the safe operation of traffic tunnels.

BIBLIOGRAPHY

A.G.Bendelius.Tunnel fire and life safety within the word road association.Tunnelling and Underground Space Technology, 2002, Vol.17 (2): 159 ~ 161.

Camino G. Combustion and Fire Retardant in Polymerie Materials.Polimeri, 1994,15 (2): 37-42.

CHEN Hui-qiang, CHEN Shi-Zhou, flame-retardant modified asphalt technology research. Technology of Highway and Transport Apr. 2003.

CHEN Ti-ching. "Gas chromatography and its analytical application." Chemical Industry Press (1987).

Chen Xin and so on.Cone Calorimeter stop at fire-retardant materials research applications, in 2005 Chinese Flame Retardant Society, 154-156.

CUI Yong-fang. "Practical organic spectral analysis." Chemical Industry Press (1994).

Haack A. Fire protection in traffic tunnels: General aspects and results of the EUREKA project [J]. Tunneling and Underground Space Technology, 1998,13 (4) :377-381.

Huang Zhi-yi. Investigation of Combustion Mechanism and Safety Experiments of Fire Processes in Long Tunnel with Asphalt Pavement. PhD thesis. Zhejiang University .2007.

J. Hietaniemi, R. Kallonenr, et.Burning Characteristics of Selected Substance: Production of Heat, Smoke and Chemicals Species.Fire Matter, 1999 (4):171-185.

JI Jing-wei, YANG Li-zhong, FAN Wei-cheng. External thermal radiation on the combustion properties of Materials Experimental study [J]. Combustion Science and Technology .2003, 9 (2):139-143.

Kalkanoglu Husnu M. Hal ogren free flame- retardant bitumen roofing composition. US Patent, 05437923. 1995.

Keith Attenborough. Prediction and measurement of the acoustical performance do pores road surface.Inter-Noise.1992 :223-228.

LDWascott. The Flame Retardant of Molybdenum Trioxide. J. Anal. Appl. Pyrolysis, 1985 (8): 163.

OU Yu-xiang, practical Flame Retardant Technology, Beijing Chemical Industry Press, 2005.

PAAtkinson.PJHaines, et.The mechanism of action of tin compounds as flame retardants and smoke suppressants for polyester thermosets.Polymer Degradatiaon and Stability, 2002, Vol.71 (3):351-360.

People's Republic of China National Standard "plastic combustion performance test method of oxygen index" (GB/T2406-2006),National Quality and Technical Supervision.

ShuiYu Lu, Ian Hamerton.Recent development in the chemistry of halogen free f lame retardant polymers.Progress in Polymer Science, 2002, Vol.27

(8):1661-1712.

SHU Zhong-jun, CHEN Qiang. Bamboo flooring with ordinary combustion properties of solid wood floor Cone Calorimeter Experimental Study [J] fire science .2007 (3):148-152.

T.Kunihik. Science of Flame Retardant for Polymer.J.of Polymer, 2000 (4):242-247

WJKennelly. Molybdateasa Component of Low Smoke, High Performance Plastics.Fire Safe, 2000 (12):73-80.

YANG Liang, GUO Zhong-yin. Highway tunnel road work environment survey and analysis. Road, 2004 (3):148-152.

YANG Qun, GUO Zhong-yin, LIN Xi-xiong. Research on Fire-Retarded Open-Graded Friction Course Used in Road Tunnel. OURNAL OF TONG JI UNIVERSITY (NATURAL SCIENCE).

YANG Yun, ZHANG Heping, ZHANG Jun, XU Liang, WANG Wei. Using Cone Calorimeter Study of Combustion Characteristics of plywood. [J] Combustion Science and Technology .2006 (2):159-163.

Fracture Mechanics Analysis of Cracking in Asphalt Pavement Widening

Jun-hui ZHANG[1], Jian-long ZHENG[2], and Bao-shan Huang[3]

[1]Ph.D., Postdoctoral researcher, School of Traffic and Transportation Engineering, Changsha University of Science & Technology, Changsha , Hunan, 410004,China; PH (0086) 731- 2309106; e-mail: zjhseu@163.com

[2]Prof., School of Traffic and Transportation Engineering, Changsha University of Science & Technology, Changsha , Hunan, 410004,China; PH (0086) 731-2309106; e-mail: zjl@csust.edu.cn

[3]Ph.D., P.E., Department of Civil and Environmental Engineering, University of Tennessee, Knoxville, TN 37996, U.S.A; Ph: (865)974-7713; e-mail: bhuang@utk.edu

ABSTRACT

In order to prevent or mitigate reflective cracking in road widening, which is always along the traveling direction up the joint of the new and existing bases resulting from their different properties, this study investigates the influence factors of crack propagation and the effect of geogird in widened asphalt pavements through extensive finite element analysis based on linear elastic fracture mechanics using the computer code ABAQUS. The results indicate that increasing surface hot-mix asphalt thickness and decreasing surface modulus could effectively mitigate the reflective cracking. The potential of reflective cracking propagation would be significantly reduced when the new and existing pavement bases have a uniform modulus. In addition, geosynthetics reinforcement could effectively reduce the degree of stress centralization and delay the reflective cracking of the widened asphalt pavements.

INTRODUCTION

For a road-widening project, the existing asphalt pavement surface is usually milled off and then a fresh asphalt mixture is paved across the new and existing bases. Because of the inherent differences between the new and existing bases, there is always a latent crack along the joint between them, which can propagate upwards under repeated traffic load and eventually result in reflective cracking in the asphalt surface along the traveling direction. This type of reflective cracking is the primary problem in HMA (hot mixture asphalt) pavement widening (Van Meurs A N G et al. 1999).

Several technologies have been identified to prevent or delay reflective cracking in in HMA pavements. These include: designing more crack-resistant asphalt mixtures (Barzin Mobasher et al. 1997), selecting alternative pavement structures, improving construction quality control, and applying crack insulating products such as geosynthetics reinforcement, etc… (Sam-Deok Cho et al. 2006). In addition, numerous studies can be found for the analysis of the crack growth process in asphalt pavement

(Birgisson B et al. 2002).

Nevertheless, little research can be found on the analysis of reflective crack propagation in widened asphalt pavements. Linear elastic fracture mechanics was employed to analyze various influence factors for the propagation of reflective cracking in widened asphalt pavements using the computer code ABAQUS (Hibbitt, Karlsson & Sorensen 2001) in this study. The effects of geosynthetic reinforcement in widened asphalt pavements were also investigated.

FINITE ELEMENT ANALYSIS

Finite element modeling

The HN Expressway starts from Shanghai, the biggest business center in China, to Nanjing, the capital of Jiangsu Province. It was widened in 2003. Figure 1 shows the latent crack between the new and existing bases. Under repeated traffic load, a reflective cracking of the asphalt surface along the traveling direction eventually appeared (Figure 2). In this project, a layer polypropylene geogrid under the surface was used and strided over the new and existing bases. The calculation model could be sketched as shown in Figure 3. Zero vertical deformation was assumed for the bottom of the subgrade. Similarly, zero horizontal displacement was assumed for the right and left boundaries of the base, subbase, and subgrade.

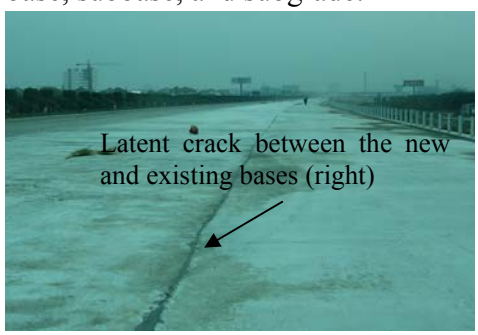

Figure. 1 Latent crack

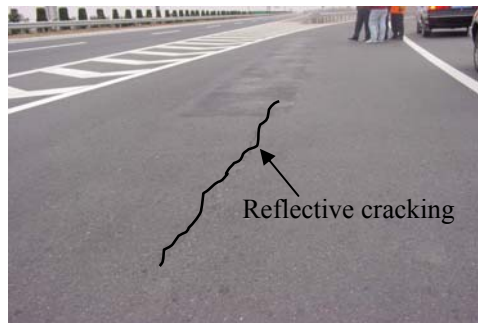

Figure. 2 Reflective cracking in road widening

To improve the finite element analysis (FEA) efficiency, plane strain conditions were assumed. The geogrid was simulated using two-node non-compression bar elements with linear elastic properties (T2D2). The pavement structure was described by elements with four-node bilinear displacement and reduced integration with hourglass control (CPE4R). Singularity at the crack tip was considered during the analysis.

Before fracture mechanics analysis, a *seam* that is a term in ABAQUS and used to define an edge must be created. It is originally closed but can open during an analysis. Its crack properties can be determined using contour integral analysis. Then, fracture mechanics analysis could be made using the software ABAQUS.

Under a relatively small deformation, the influences of interface behaviors between geosynthetics and pavement structure on the system performance are expected

to be less important (Han J and Gabr M A 2002). In this study, the interface was assumed to be fully bonded for simplicity. The keywords *Embedded Element* in ABAUQS was used to embed the geogrid elements to pavement elements in the numerical modeling.

Mode of traffic load

Because the design tire pressure is 0.7MPa in China, the applied load on the asphalt surface was 0.7MPa and the contact area was a square with sides of 30cm. Two load conditions, symmetrical load and unsymmetrical load, were selected (Figure 4). The "*y*" axle points to the depth of pavement. Assigning the surface thickness of HMA and the crack length as "*T*" and "*C*" respectively, four ratios of "*C/T*", 0.2, 0.4, 0.6, and 0.8, were considered during the finite element analysis.

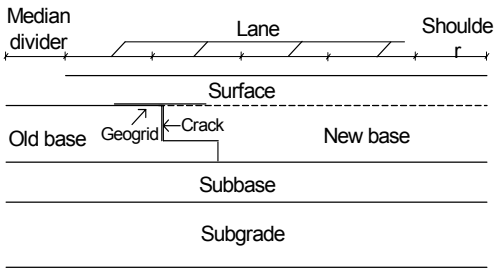

Figure. 3 Sketch of finite element model

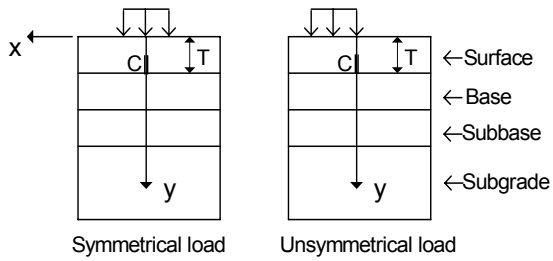

Figure. 4 Patterns of traffic load

CONSTITUTIVE MODELS AND MATERIAL PARAMETERS

Although asphalt mixtures exhibit visco-elastic and plastic characteristics, for pavement stress and strain analysis, linear elastic analysis generally provides quick and reasonable solutions. The materials were assumed to be linear elastic in the present analysis. Thus, two parameters, Youngs modulus and Poisson's ratio, were needed to adequately describe their mechanical properties.

For the reference model, the surface had a thickness of 18cm and a modulus of 1200MPa; the new and existing bases both had the same thickness of 40cm and the same modulus of 1500MPa; and the subbase was 20cm thick and had a modulus of 300MPa. In addition, a thickness of 400cm for the subgrade was selected according to several trial calculations. Its modulus was 40MPa. The Poisson's ratio of subgrade and other materials of pavement structure were 0.35 and 0.25, respectively.

The polypropylene geogrid had a tensile stiffness of 400kN/m. The tensile stiffness, *J*, is defined as the tensile force per unit width divided by the average strain in the geogrid. Three conditions: 1) Unreinforced, 2) a layer of gerogrid with *J*=400kN/m, and 3) a layer of gerogrid with *J*=1600kN/m, were considered during the FEA. The Poisson's ratio of geogrid was 0.18.

For a widening project, the modulus of the existing base is usually known. Thus, the influence of the new base on crack propagation could be obtained by changing the modulus ratios of the new and existing bases. Five modulus ratios, from 1 to 5, were

included. All of the calculation conditions described above are summarized in Table 1 and the values underlined are in the reference model.

Table. 1 FEA Plan

Variables	Value
Surface HMA modulus/MPa	1000, 1200, 1400, 1600, 1800
Surface HMA thickness/cm	14, 16, 18, 20
Modulus ratios (the new base/ the existing base)	1, 2, 3, 4, 5
Values of C/T (crack length/surface thickness)	0.2, 0.4, 0.6, 0.8
Geogrid	1)Unreinforced;2) J=400kN/m;3) J=1600kN/m

ANALYSIS OF INFLUENCE FACTORS CRACKING

Many factors, such as the thickness and modulus of the surface layer and stiffness of new and existing bases materials, could influence the reflective cracking in widened asphalt pavements. The following FEA focuses on the sensitivity of crack propagation to each of these factors. The stress intensity factors of K_1 and K_2, which are induced by tension and shear, were chosen to describe the crack-resistance of the widened asphalt pavements. When the calculated value of K_1 was negative, it was set to zero.

Influence of surface HMA modulus

Jun-hui ZHANG reported that K_1 is negative under symmetrical or unsymmetrical load (ZHANG Jun-hui 2006), which indicated that the widened pavement cracking was caused only by shear stress. Therefore, only the stress intensity factors of shear type K_2 was considered. Figure 5 presents the results of K_2 with different surface modulus under symmetrical and unsymmetrical load (right Y axis). It can be shown that K_2 increases as the surface modulus and the value of C/T increase. At the same time, the value of K_2 under the unsymmetrical load is significantly greater than the value under the symmetrical load. It can be concluded that unsymmetrical load conditions is more critical to the reflective cracking propagation in widened asphalt pavements.

Influence of surface HMA thickness

Figure 6 presents K_2 for the reference model under unsymmetrical load conditions with the variation of surface thickness. It can be seen that the increase of surface thickness can reduce K_2 more significantly when the C/T value is relatively low and K_2 increases more rapidly at the later state of crack growth. For example, when the surface thickness is 18cm, K_2 is 119.9kPa·m$^{1/2}$ and 209.2kPa·m$^{1/2}$ when C/T varies from 0.2 to 0.8, respectively. Therefore, the increase of surface thickness can delay reflective cracking in HMA pavement widening and this effect decreases gradually with the cracking propagation.

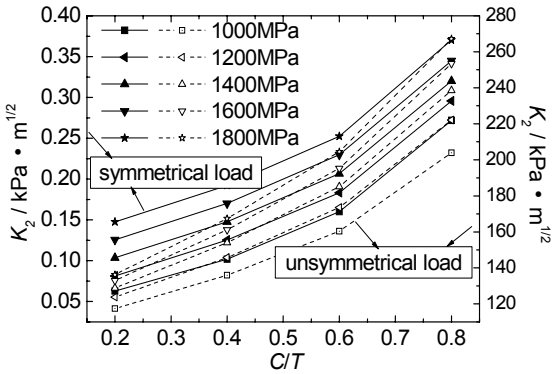

Figure. 5 Curves of K_2 with different surface modulus

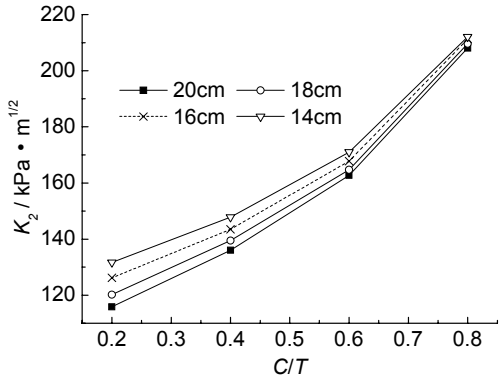

Figure. 6 Curves of K_2 with different surface thicknesses

Influence of base modulus

Because K_2 is caused by shear, the absolute value can describe the degree of stress concentration. As shown in Figure 7, the absolute value of K_2 decreases initially and then increases gradually with increasing modulus ratios under the symmetrical load (left Y axis). The minimum value of 0.1194kPa·m$^{1/2}$ is achieved when the modulus of the new pavement base is equal to that of the existing base.

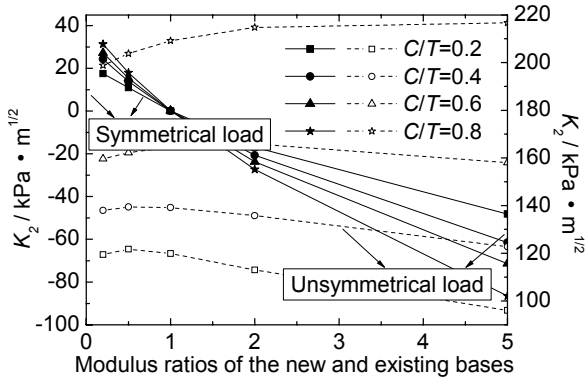

Figure. 7 Curves of K_2 with different modulus ratios of the new and existing bases

Studies suggested that the fracture intensity was about 400kPa·m$^{1/2}$~500kPa·m$^{1/2}$ (Miao-juan PENG et al. 1998), which is far greater than the maximum of K_2 216.7kPa·m$^{1/2}$ under the unsymmetrical load in this study. Although K_2 under the unsymmetrical load (right Y axis) is significantly greater than the ones under the symmetrical load, it is less sensitive to the variation of the modulus ratios, as shown in Figure 7. Since cracks propagate over the course of the pavement's service life and traffic load is a combination of both symmetrical and unsymmetrical loads, the selection of similar modulus between the new and existing pavement bases appear to be critical in preventing and/or mitigating the development of longitudinal reflective cracking in widened asphalt pavements. On the other hand, the similar modulus between the new and existing bases can reduce differential settlement (Jun-hui ZHANG 2006), which in turn will be beneficial to the crack-resistance of the widened asphalt pavement.

ANALYSIS OF EFFECT OF GEOGRID

Studies showed that the crack insulating effects of geosynthetics under the unsymmetrical and symmetrical loads in asphalt pavement widening were similar (Jun-hui ZHANG 2006). Only the effect of geogrid under the symmetrical load condition was evaluated in this study. Figure 8 presents the results of the tensile stress σ_x along the crack line with different crack lengths. It is shown that there is a tension stress (i.e. a positive value) near the upper asphalt surface when the crack length is less and there is a compressive stress near the upper asphalt surface when the crack length is larger (i.e. *C/T* is equal to 0.6). Although the crack tip is pressed this moment, the crack near the base bottom is open. Thus, the geogrid is also stretched to make the crack heal, which indicates the effects of delaying reflective cracking. These effects increase with increasing geogrid stiffness. In addition, no matter how long the crack is, the geogrid can reduce the degree of stress concentration at the crack tip all along.

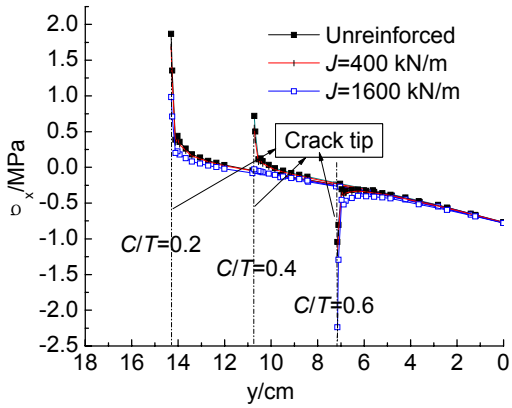

Figure. 8 Curves of σ_x with different crack length

DISCUSSION

In order to keep the modulus of the new and existing pavement bases close, the modulus of the existing base can be gained before widening in the field. Then, the mixture can be designed in the laboratory to make the modulus of the new and existing bases close.

To insert a geogrid layer between the surface and base cannot guarantee an effective prevention of reflective cracking because the risk that the debounding phenomena occur is very high. A prime coat should be sprayed above the base before geogrid construction. When it is dry, the geogrid can be laid across the joint between the new and existing bases. Then, a seal coat is paved, the stone spreader and asphalt distributor should be driven smoothly to avoid dragging the geogrid. Therefore, the link of the geogrid, base, and surface can be guaranteed this way.

CONCLUSIONS

1) The increase of the surface hot-mix asphalt modulus would enhance the reflective cracking propagation in widened asphalt pavements and should be avoided.

2) The increase of surface thickness could effectively reduce the potential for crack propagation in widened asphalt pavements.

3) Maintaining close (if not completely equal) values of modulus (stiffness) between the new and existing pavement bases is critical to reducing the potential for reflective

cracking propagation in widened asphalt pavements.

4) Finite element analysis indicated that the effects of geosynthetics in reducing the degree of stress concentration at the crack tip during crack propagation, which in turn, leads to improved cracking resistance of widened asphalt pavements.

ACKNOWLEDGMENTS

The effort of Xiao-ming Huang, the deputy dean of the Transportation School of Southeast University, in coordinating the project was highly appreciated.

REFERENCES

Barzin Mobasher, Michael S Mamlouk and How-Ming Lin. (1997). "Evaluation of Crack Propagation Properties of Asphalt Mixtures." *Journal of Transportation Engineering*, Vol.123(5):405-413.

Birgisson B, Soranakom C, Napier A L, and Roque R.(2002). "Numerical Simulation of the Cracking Behavior of Asphalt Mixtures." *Erol Tutumluer, Yacoub M. Najjar, and Eyad Masad(ed). Proceedings of Sessions of the 15th Engineering Mechanics Division Conference*, New York, 46-64.

Han J and Gabr M A.(2002). "Numerical Analysis of Geosynthetic-Reinforced and Pile-Supported Earth Platforms over Soft Soil." *J. Geotech. Geoenviron.Eng*, ASCE, Vol,128(5):44-53.

Hibbitt, Karlsson & Sorensen.(2001). "ABAQUS Analysis User′s Manual." USA: HKS.

Jun-hui ZHANG. (2006). "Research on deformation behavior and differential settlement limitation of expressway widening on soft soil foundation." *PhD. Dissertation*, Southeast University, Nanjing, Jiangsu. (in Chinese)

Miao-juan PENG, Deng-liang ZHANG, and Yong-xu XIA.(1998). "Computational Method and Its Application of Fracture Mechanics for the Asphalt Pavement on Semi Rigid Type Base Course." *China Journal of Highway and Transportation*, Vol, 11(2):30-38. (in Chinese)

Sam-Deok Cho, Dae-Young Lee, and Nam-Ho Kim.(2006). "Effect of the Crack Prevention of Asphalt Pavement using Geosynthetics." *Don J. DeGroot, Jason T. DeJong, J. David Frost, and Laurie G. Baise(ed). Proceedings of GeoCongress 2006.* Atlanta, Georgia, USA, 1-6.

Van Meurs A N G, Van Den Berg A, Venmans A A M, Van M A and Zwanenburg C.(1999). "Embankment widening with the gap-method." *Barends(ed). Geotechnical engineering for transportation infrastructure*, Rotterdam, 1133-1138.

Sensitivity Analysis of the Dynamical Parameters on Road Materials

Wei hai-bin,Liu han-bing,Zhang he-feng,Li chang-yu
Transportation College, Jilin University, Changchun, 130022, FAX (0431-85095446), Email: weihb@jlu.edu.cn

ABSTRACT

In this paper, on the basis of the dynamic tri-axial test achievements of road base materials, the elastic-plastic constitutive model is constructed with the finite element software of ABAQUS to design computing models and analyze the results of numerical simulations, the sensitivity of road base materials mechanics parameters influential factor is studied. The calculated curves of the dynamical deformation behavior of silty clay are agreement with the measured ones. The effect of parameters such as cyclic load's magnitude, confining pressure, cyclic stress ratio, frequency, the number of cyclic load, and load wave is compared. It is found that confining pressure is the primary influential factor to the sensitivity of dynamical parameters. At the same time, it shows that the Finite Element Method (FEM) is valid to analyze the characteristics of mechanical parameters.

Keyword：road materials；dynamical parameters；sensitivity；numerical simulation

1 Introduction

At the present, the results of soil dynamic parameters mainly obtained from field and laboratory experiments are not consistent with the objective values. Therefore it is necessary to analyze the sensitive degree of the dynamic parameters influence factor on sub-grade structure property changes. In this study, on the basis of numerical simulations and laboratory tests, we carried on the analysis of factors that influence the sub-grade stability, provided some reference for soil test personnel, and presented a useful approach for the research on dynamic constitutive model and more complicated influencing factors of soil.

2 Dynamic tri-axial test and model establishment

2.1 Dynamic tri-axial test

The test soil samples are obtained from middle liquid-limit silty clay in the soil field of the Changchun Weixing road. The basic physical mechanical parameters are in table 1.

Table 1 physical mechanics index of test silty clay

Density	Optimum moisture content	Liquid-limit	Plastic limit	Plasticity index	Cohesive force	Internal friction Angle
ρ/（g/cm^3）	ω/%	ω_L/%	ω_P/%	I_p	c/kPa	φ
1.96	21	34	22.4	11.6	47	34

In this test, the soil sample is the cylinder compaction molding specimen. The diameter is 70 mm and the height is 140 mm (as shown in Figure 1). The test instrument is the Japanese DTC-306 multiple-function electro-hydraulic servo

dynamic tri-axial apparatus. According to the criteria (Soil test Technical Manual2003), the criteria of failure is that the failure strain ε_d, which is the sum of elastic strain and plastic strain, rise to 5%.

2.2 Elasto-plastic constitutive model

The stress-strain relationship of soil is nonlinear. The deformation increment of roadbed material consists of elastic and plastic parts. Elastic increment satisfies Hooke's law (Qian jiahuan,Yinzongze1996), while the plastic ones satisfies the flow rule. Therefore it is suitable to conduct numerical analysis using an elasto-plastic constitutive model. It is shown as follow.

$$\{d\sigma\} = [D_{ep}]\{d\varepsilon\}; \quad (1)$$

$$\{d\varepsilon\} = \{d\varepsilon^e\} + \{d\varepsilon^p\}; \quad (2)$$

$$\text{Where, } [D_{ep}] = [D] - \frac{[D]\left\{\frac{\partial g(\sigma)}{\partial \sigma}\right\}\left\{\frac{\partial f(\sigma)}{\partial \sigma}\right\}^T [D]}{A + \left\{\frac{\partial f(\sigma)}{\partial \sigma}\right\}^T [D]\left\{\frac{\partial g(\sigma)}{\partial \sigma}\right\}} \quad (3)$$

$[D_{ep}]$—elasto-plastic stiffness matrix.

2.3 The establishment of three-dimensional finite element model

Establish the three-dimensional finite element model by ABAQUS software (as shown in figure 2). Define the material attribute of the soil: density is 1.96g/cm^3; young modulus is 18MPa; Poisson's ratio is 0.35; the permeability coefficient is $1.0e^{-7}$ mm/s; porosity is 0.3; internal friction Angle is 34°; expansion Angle is 0°; and consolidated un-drained. Because the internal friction Angle is 22° bigger, the Drucker-Prager model can not approach to the Mohr-Coulomb model very well, it uses the Mohr-Coulomb model. The type of the load exerted on the sample is the sine wave and the soil sample weight is also taken into consideration. The sine wave frequency is 1Hz, i.e. q(t) = 0.5q_d +.05q_d sin2 π t, the q (t) stands for dynamic axial load value of any moments-t. They are divided into 975 crunodes and 742 units.

Fig1. Test soil samples

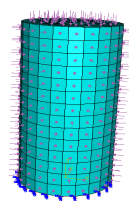

Fig2. Finite element model

Due to the beginning stage of experiment being unstable, the nonlinear static load stage of the test and data processing is flexible and inaccurate. It takes the

second loading point as the beginning of processing and analysis of data. Plastic deformation of each cycle begins to be accumulated from the second loading. Then compare the numerical value of the experiment with the numerical value of finite element modeling. This paper takes four groups of data and carries on the analysis and comparison (as shown in figure 3). It is obvious that the cumulative plastic deformation increases gradually along with the increase of the number of cycles. In each group of data of the experiment and simulation, the plastic deformation is consistent with the variation trend of the cycle index-n. The simulated value and the experimental value of the i time ($1 \le i < n$) cyclic plastic deformation are very close. Namely, each cycle of plastic deformation and accumulative plastic deformation fit very well.

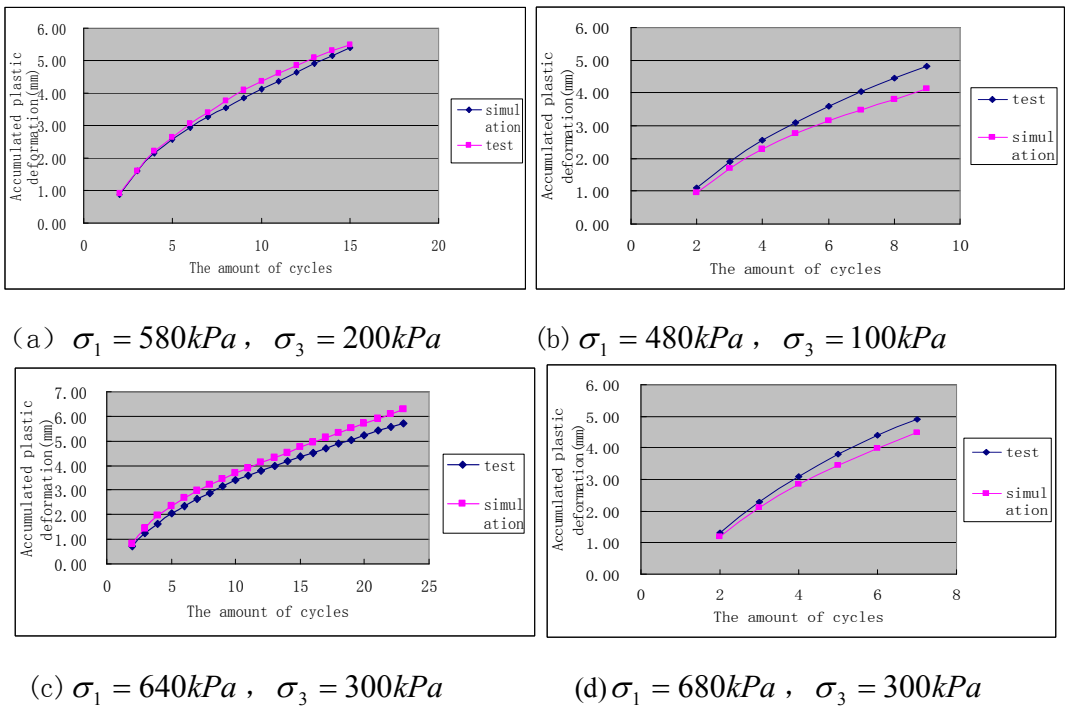

(a) $\sigma_1 = 580kPa$， $\sigma_3 = 200kPa$ (b) $\sigma_1 = 480kPa$， $\sigma_3 = 100kPa$

(c) $\sigma_1 = 640kPa$， $\sigma_3 = 300kPa$ (d) $\sigma_1 = 680kPa$， $\sigma_3 = 300kPa$

Fig3. The comparison between plastic deformation of simulation and experiment

Figure 4 is the deformation graph of the soil test piece under cyclic load. It causes certain residual deformation. There is certain contraction deformation on the upper piece and inflation deformation on the bottom.

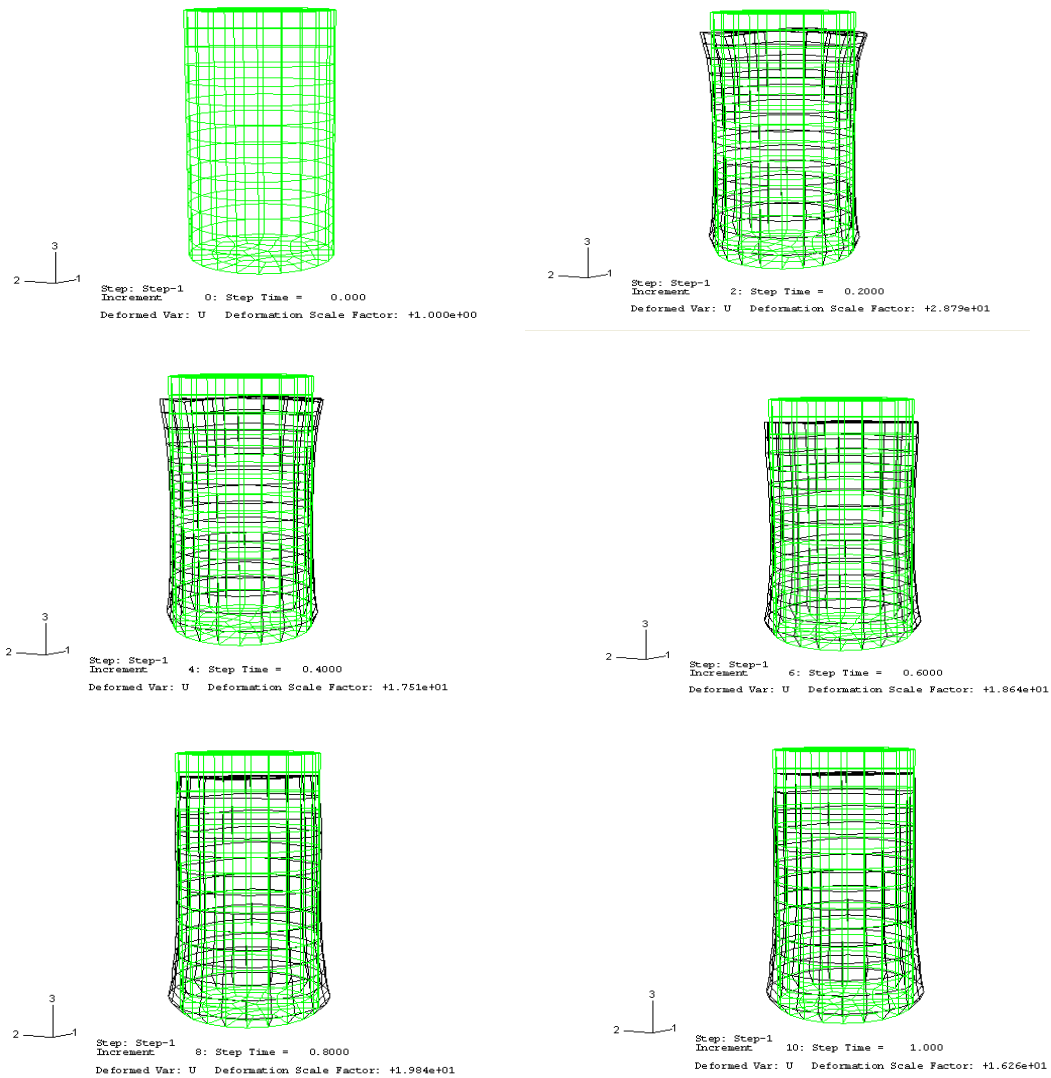

Fig4. The graph of deformation in one cycle

3. Results and discussions

The main influencing factors of soil plastic deformation are divided into two categories as external factors and internal factors. Numerical simulation methods are used to study the influencing factors of soil plastic deformation, which are the dynamic stress amplitudes, confining pressure (Simonesn E,Isacsson U.2001), frequency, loading waveform, and time of cyclic loading. Take the data of soil test ($\sigma_1 = 580kPa$， $\sigma_3 = 200kPa$), from which the simulation matches the experiment very well as the research object. Under the condition that other factors are invariable, analyze how each factor influences the soil plastic deformation through the change of one of the factors (Andersen K H,1980).

3.1 Stress amplitudes' influence on plastic deforma tion

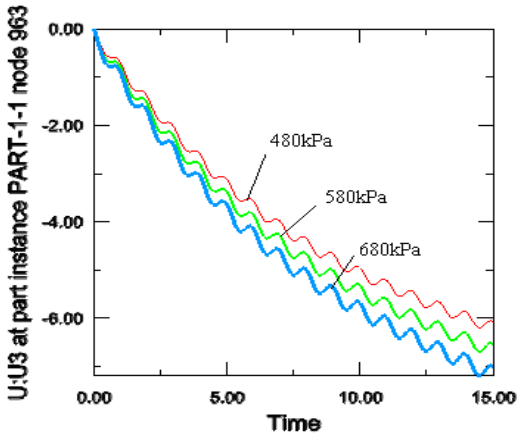

Fig5. Stress amplitude's influence

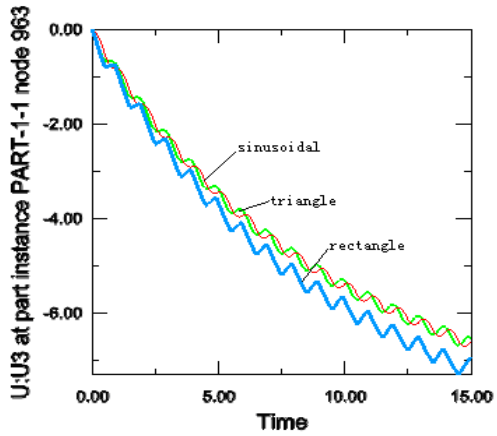

Fig6. waveform's influence

As shown in Figure 5, the accumulated plastic deformation increases gradually along with the increase of the stress amplitude. When the confining pressure is certain, the bigger the dynamic shearing stress that is exerted on the test sample, the bigger the plastic deformation. Through the analysis above, the increase of roadbed subsidence caused by traffic loading will follow = the increase of traffic volume and the carrying capacity of heavy-duty trucks. Roadbed subsidence caused by traffic loading will tend to be steadily increasing along with the passage of time and the time of traffic loading.

3.2 Different load waveforms' influence on plastic deformation

Figure 6 shows the characteristics of accumulated soil deformation. Under the action of the periodical load, it causes certain plastic deformation every time the cyclic load reaches the initial position. When the loading waveform is, respectively, a rectangle, a triangle, and a sinusoid, different waveforms have different effects on plastic deformation. The graph shows that the plastic deformation under the action of the rectangular wave is bigger than the one under the action of the sine wave and the one under the action of the triangle wave. The plastic deformations are very close under the action of triangle wave and sine wave. Thus, the plastic deformation under different waveforms depends on how long the maximum load has an effect on the soil sample.

3.3 Confining pressure influence plastic deformation

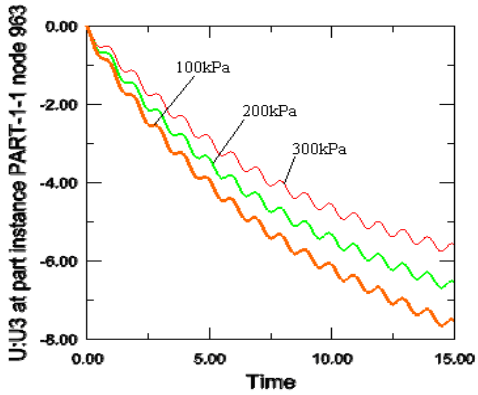

Fig7. Confining pressure influence

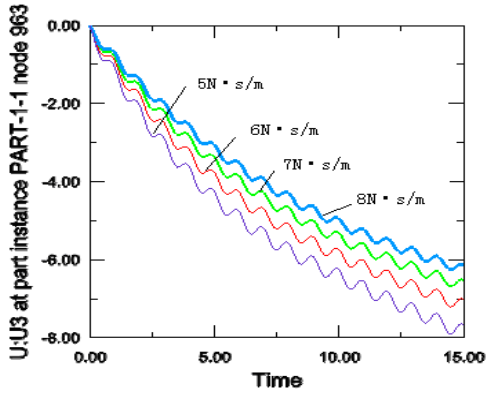

Fig8. Damping coefficient influence

From Figure 7 the relationship between displacement and time and the relationship between plastic deformation and cyclic times are shown. Plastic deformation increases gradually along with the growth of cyclic times. When the cyclic stress amplitude is certain, the greater the confining pressures, the slower the growth of the soil deformation.

3.4 Damping coefficient influence plastic deformation

Figure 8 shows that plastic deformation increases gradually along with the growth of cyclic times . When the cyclic stress amplitude is certain, the greater the damping coefficient, the slower the growth of the soil deformation.

3.5 Frequency's influence on plastic deformation

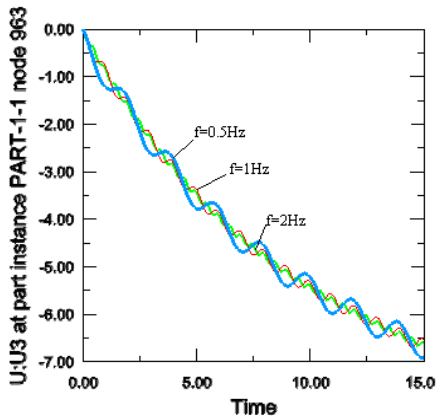

Fig9. Frequency's influence

As shown in Figure 9, the lower the frequency is, the bigger the amplitude of plastic deformation is; the higher the frequency, the smaller the amplitude of plastic deformation. The variation trend of the strain amplitude which works on the cumulative plastic deformation along with the change of frequency is the same. As frequency increases, the amplitude of plastic deformation decreases. At low frequency, the sample will be destroyed only under less cyclic weeks. Along with frequency increases, more cyclic weeks are needed to destroy the test sample.

4 Conclusions

1. It is convenient to achieve the optimum design of multi-factor experiment by the means of the ABAQUS. This provides a useful method for sensitivity analysis of rock mass mechanical parameters.

2. The research showed that the initial elastic modulus, damping coefficient, and load form have the greatest effects on plastic deformation of soil. The stress amplitude, confining pressure, frequency, number of cyclic, and the loading waveform has the least. We also found that the influence on the plastic deformation of the loading wave is dependent on the time length of the maximum load .

3. The results reflect the effect rule between the mechanical parameters of rock mass and sub-grade stability. It also provides a reference for engineering construction and feedback design.

Reference

Earth institute of water conservancy science council in Nanjing. Soil test Technical Manual [M].Beijing：Public traffic press，2003.157-175.

Andersen K H,et al.Cyclic and static laboratory tests on drammen clay. Journalof the Geotechnical Engineering Division, ASCE,106(5),1980,P499-529.

Simonesn E,Isacsson U.soil behavior during freezing and thawing using variable and confining pressure triaxial tests[J].Canadian geotechnical joumal,2001,38(4):863-875.

Qian jiahuan,Yinzongze.Soil Engineering Theory And Compute[M].Beijing. China WaterPower Press.1996

Dynamic Effects of Moving Vehicular Loads on Continuously Reinforced Concrete Pavements on Winkler Foundation

Shihua Liang[1], Xueqiang Yang[1], Tian Qi[2], Ganbin Liu[3]

[1]Institute of Geotechnical Engineering, Guangdong University of Technology, Guangdong, Guangzhou 510006, China, PH (86) 2031676577; email: shihua_L@126.com

[2]Construction Quality and Safety Testing Centre of Guangzhou Suijian, Guangdong, Guangzhou 510150, China

[3]Institute of Geotechnical Engineering, Ningbo University, Zhejiang, Ningbo, 315211, China

ABSTRACT

In this paper, the dynamic response of a moving load on continuously reinforced concrete pavement is analyzed. The pavement rested on Winkler viscoelastic foundation is treated as orthotropic thin slab with a width of b and infinite value in length. The triangular series and Fourier transformation are introduced to analyze the response, and the solution of vertical displacement under a rectangle harmonic moving load is derived. Numerical results were obtained using the inverse Fourier transformation which was used to analyze the influence of load velocity, damp coefficient of ground and reinforcement ratio on the vertical displacement. This work provides useful theoretic references for the design of continuously reinforced concrete pavement.

INTRODUCTION

The present design of rigidity pavements is based on the theory of thin plate on Winkler soil (Yoder et al. 1975). For the case of low speed vehicles the theory is satisfied. However, as the increase of the speed of vehicles, the consideration of the vehicular dynamic effect on the pavement becomes more important. The response of slab to special dynamic loads has been studied using different methods by Cheng (1987), Zheng (1989), Huang (1990), and Hou (2003). Sun (1996) studied the transient response of infinity plate on elastic soils. Kim and McCullough (2003) studied the dynamic response of infinity plate on Winkler foundation under moving load of mutative amplitude.

Continuously reinforced concrete pavements (CRCP) are always subjected to moving loads; it is therefore more meaningful to study the dynamic response of CRCP under the moving loads. In this paper, the pavement rested on a Winkler viscoelastic foundation is treated as an orthotropic thin slab with a width of b and an infinite value in length. The triangular series and Fourier transformation are used to

analyze the response. The solution of vertical displacement under a rectangle harmonic moving load is derived.

GOVERNING EQUATION

The pavement rested on a Winkler viscoelastic foundation is treated as orthotropic thin slab with a width of *b* and an infinite value in length. The dynamic response is considered as a three-dimensional problem in the Cartesian co-ordinates of (x_1, x_2, t) as given in Figure 1. The load is considered as a harmonic rectangular one with the amplitude of $q_0 e^{i\omega t}$, the length of $2a_1$, the width of $2b_1$, and the velocity of c along the x_1 axis. The vertical displacement of the plate is $W(x_1, x_2, t)$, and the soil is considered as a Winkler model. The following assumptions are introduced to solve the dynamic equation of the CRCP model: (1) the steel bar is perfectly bonded with the concrete. The plate is considered to be an orthotropic thin plate with small thickness. (2) the pavement is of infinity along the longitudinal side with a width of *b*. Only the steel bar along the longitudinal side is considered.

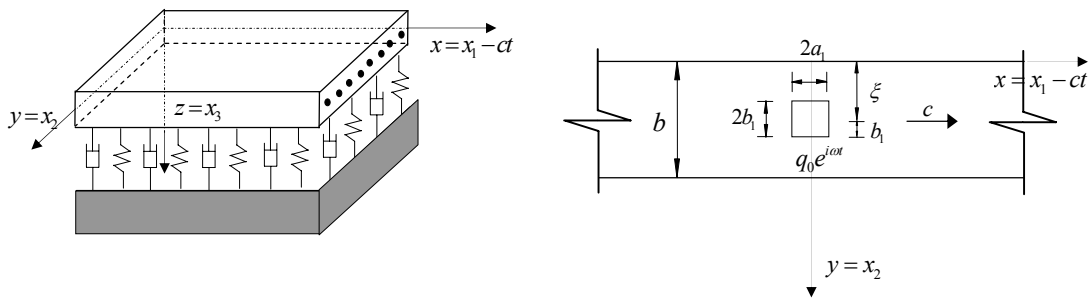

Figure 1. Calculating model.

The vertical displacement of the plate along *z* axis is $W(x_1, x_2, t)$. For the sake of simplifying the model of thin plate, the vertical strain of the plate is assumed to be small and negligible. The horizontal displacement of the plate is set as zero, and the strain caused by σ_z、τ_{xz}、τ_{zy} is also neglected. The equilibrium equations of the plate are given as:

$$\frac{\partial M_{x_1}}{\partial x_1} + \frac{\partial M_{x_1 x_2}}{\partial x_2} = \beta_{x_1} \tag{1a}$$

$$\frac{\partial M_{x_2}}{\partial x_2} + \frac{\partial M_{x_1 x_2}}{\partial x_1} = \beta_{x_2} \tag{1b}$$

$$\frac{\partial \beta_{x_1}}{\partial x_1}+\frac{\partial \beta_{x_2}}{\partial x_2}-F(x_1,x_2,t)-\rho_c h\frac{\partial W}{\partial t^2}=-q(x_1,x_2,t) \tag{1c}$$

in which M_{z_1}, M_{z_2}, $M_{z_1x_2}$ are the bending moment of the plate along the x_1, x_2 axis and the torsional moment along the x_1x_2 axis respectively; $q(x_1,x_2,t)$ is the load; $F(x_1,x_2,t)$ is the counterforce on the soil; $\rho_c h$ is the density of the plate of unite area; and *h* is the thickness of the plate.

The bending moment and the displacement of the plate satisfied the following equations:

$$M_{x_1}=-\left(D_{11}\frac{\partial^2 W}{\partial x_1^2}+D_{12}\frac{\partial^2 W}{\partial x_2^2}\right) \tag{2a}$$

$$M_{x_2}=-\left(D_{12}\frac{\partial^2 W}{\partial x_1^2}+D_{22}\frac{\partial^2 W}{\partial x_2^2}\right) \tag{2b}$$

$$M_{x_1x_2}=-2D_{66}\frac{\partial^2 W}{\partial x_1\partial x_2} \tag{2c}$$

in which D_{ij} is the rigidity of the plate, which can be expressed as:

$$D_{ij}=\int_{-h/2}^{h/2}C_{ij}z^2\mathrm{d}z \qquad (i,j=1,2,6) \tag{3}$$

in which $C_{11}=\frac{E_1}{1-\mu_1\mu_2}$, $C_{22}=\frac{E_2}{1-\mu_1\mu_2}$, $C_{12}=\frac{E_1\mu_2}{1-\mu_1\mu_2}$, $C_{66}=G_{12}$, $E_1\mu_2=E_2\mu_1$, E_1, E_2, μ_1, μ_2 are the moduli of the plate respectively; $E_1=E_fV_f+E_m(1-V_f)$, $E_2=\frac{E_fE_m}{E_mV_f+E_f(1-V_f)}$, $\mu_1=\mu_fV_f+\mu_m(1-V_f)$, $G_{12}=\frac{G_fG_m}{G_mV_f+G_f(1-V_f)}$, $G_f=\frac{E_f}{2(1+\mu_f)}$, $G_m=\frac{E_m}{2(1+\mu_m)}$, E_f, μ_f and E_m, μ_m are the Young's modulus and Poisson ratio of the steel bar and the concrete respectively.

The following equation can be derived from Equations (1) and (2):

$$D_{11}\frac{\partial^4 W}{\partial x_1^4}+2(D_{12}+2D_{66})\frac{\partial^4 W}{\partial x_1^2\partial x_2^2}+D_{22}\frac{\partial^4 W}{\partial x_2^4}+\rho_c h\frac{\partial^2 W}{\partial t^2}=q(x_1,x_2,t)-F(x_1,x_2,t) \tag{4}$$

The counterforce on the ground for the viscoelastic Winkler fou

ndation can be written as:

$$F(x_1,x_2,t)=K_L W(x_1,x_2,t)+\eta\frac{\partial W(x_1,x_2,t)}{\partial t} \tag{5}$$

in which K_L is the rigidity of the foundation and η is the damping coefficient.

DYNAMIC RESPONSE OF CRCP UNDER MOVING POINT LOAD

As the load moves at the velocity of c, the auxiliary spatial coordinate is introduced by letting $x=x_1-ct$， $y=x_2$. Then Eq. (4) and (5) reads:

$$\begin{aligned}&D_{11}\frac{\partial^4 W}{\partial x^4}+2(D_{12}+2D_{66})\frac{\partial^4 W}{\partial x^2\partial y^2}+D_{22}\frac{\partial^4 W}{\partial y^4}+\rho_c h\left(\frac{\partial^2 W}{\partial t^2}-2c\frac{\partial^2 W}{\partial t\partial x}+c^2\frac{\partial^2 W}{\partial x^2}\right)+\\&\eta\left(\frac{\partial W}{\partial t}-c\frac{\partial W}{\partial x}\right)+K_L W=q(x,y,t)\end{aligned} \tag{6}$$

The boundary of the pavement is assumed to be simply supported, therefore at $y=0,b$:

$$W(x,y,t)\big|_{y=0,b}=0\ ;\quad \left(D_{12}\frac{\partial^2 W}{\partial x^2}+D_{22}\frac{\partial^2 W}{\partial y^2}\right)\Big|_{y=0,b}=0 \tag{7}$$

The local harmonic load, a rectangular load, is introduced to simulate the vehicle load as shown in Fig. 1. By introducing $e^{i\omega t}$, the moving load can be expressed as:

$$q(x,y,t)=\begin{cases}q_0 e^{i\omega t} & \xi-b_1<y<\xi+b_1;\ -a_1<x<a_1\\ 0 & \text{elsewhere}\end{cases} \tag{8}$$

in which ω(rad/s) is the radius frequency; ξ is the distance between the load center and the boundary of the plate.

Adopting the approximate pattern of the displacement $W(x,y,t)$ and the load $q(x,y,t)$, and considering the simply supported boundary condition of the pavement, $W(x,y,t)$ and $q(x,y,t)$ can be expressed as:

$$W(x,y,t)=\sum_{m=1}^{\infty}X_m(x,t)\sin(\alpha_m y) \tag{9}$$

$$q(x,y,t)=\begin{cases}\sum_{m=1}^{\infty}q_m(x,t)\sin(\alpha_m y) & -a_1<x<a_1\\ 0 & \text{elsewhere}\end{cases} \tag{10}$$

in which $q_m(x,t)=\frac{4q_0}{b\alpha_m}\sin(\alpha_m\xi)\sin(\alpha_m b_1)$; $\alpha_m=\frac{m\pi}{b}$; b is the width of the pavement.

Substituting Eq. (9) and (10) into Eq. (6):

$$\begin{aligned} &D_{11}\frac{\partial^4 X_m}{\partial x^4}-2\alpha_m^2\left(D_{12}+2D_{66}\right)\frac{\partial^2 X_m}{\partial x^2}+\alpha_m^4 D_{22}X_m+\rho_c h\left(\frac{\partial^2 X_m}{\partial t^2}-2c\frac{\partial^2 X_m}{\partial t\partial x}+c^2\frac{\partial^2 X_m}{\partial x^2}\right)+\\ &\eta\left(\frac{\partial X_m}{\partial t}-c\frac{\partial X_m}{\partial x}\right)+K_L X_m=\begin{cases} q_m(x,t) & -a_1<x<a_1 \\ 0 & \text{elsewhere} \end{cases} \end{aligned} \tag{11}$$

Since the load is harmonic, the factor $e^{i\omega t}$ is neglected during the solving process. The Fourier transform is then introduced as:

$$\overline{f}(\beta)=\int_{-\infty}^{\infty} f(x)e^{i\beta x}\mathrm{d}x \tag{12a}$$

$$f(x)=\frac{1}{2\pi}\int_{-\infty}^{\infty}\overline{f}(\beta)e^{-i\beta x}\mathrm{d}\beta \tag{12b}$$

In the frequency domain, Eq. (11) then reads:

$$\overline{X}_m(\beta,\omega)=\frac{\overline{q}_m(\beta,\omega)}{\overline{\varphi}_m} \tag{13}$$

in which

$$\overline{\varphi}_m=D_{11}\beta^4+2\alpha_m^2\beta^2\left(D_{12}+2D_{66}\right)+D_{22}\alpha_m^4+\rho_c h\left(-\omega^2+2c\omega\beta-c^2\beta^2\right)+\eta(\mathrm{i}\omega-\mathrm{i}\beta c)+K_L$$

$$q_m(x,t)=\frac{8q_0}{b\alpha_m\beta}\sin(\alpha_m\xi)\sin(\alpha_m b_1)\sin(\beta a_1)$$

The following equation is obtained by applying inverse Fourier transformation to Eq. (13):

$$X_m(x,\omega)=\frac{1}{2\pi}\int_{-\infty}^{\infty}\frac{\overline{q}_m(\beta,\omega)}{\overline{\varphi}_m}e^{-i\beta x}\mathrm{d}\beta \tag{14}$$

Substituting Eq. (14) into Equations (9) and (2), the expression of the vertical displacement, bending moment and the torsional moment of the CRCP under moving load are obtained as follows:

$$W(x,y,t)=\frac{1}{2\pi}\sum_{m=1}^{\infty}\int_{-\infty}^{\infty}\frac{\overline{q}_m(\beta,\omega)}{\overline{\varphi}_m}e^{-i\beta x}\mathrm{d}\beta\cdot\sin(\alpha_m y)e^{i\omega t} \tag{15}$$

$$M_x=\frac{1}{2\pi}\sum_{m=1}^{\infty}\left[D_{11}\int_{-\infty}^{\infty}\frac{\overline{q}_m(\beta,\omega)}{\overline{\varphi}_m}\beta^2 e^{i\beta x}\mathrm{d}\beta+D_{12}\int_{-\infty}^{\infty}\frac{\overline{q}_m(\beta,\omega)}{\overline{\varphi}_m}\alpha_m^2 e^{i\beta x}\mathrm{d}\beta\right]\sin(\alpha_m y)e^{i\omega t} \tag{16}$$

$$M_x=\frac{1}{2\pi}\sum_{m=1}^{\infty}\left[D_{12}\int_{-\infty}^{\infty}\frac{\overline{q}_m(\beta,\omega)}{\overline{\varphi}_m}\beta^2 e^{i\beta x}\mathrm{d}\beta+D_{22}\int_{-\infty}^{\infty}\frac{\overline{q}_m(\beta,\omega)}{\overline{\varphi}_m}\alpha_m^2 e^{i\beta x}\mathrm{d}\beta\right]\sin(\alpha_m y)e^{i\omega t} \tag{17}$$

$$M_{xy} = -\frac{1}{\pi}\sum_{m=1}^{\infty} D_{66}\int_{-\infty}^{\infty} \frac{\bar{q}_m(\beta,\omega)}{\bar{\varphi}_m} \mathrm{i}\beta\alpha_m e^{\mathrm{i}\beta x}\mathrm{d}\beta\cos(\alpha_m y)e^{\mathrm{i}\omega t} \tag{18}$$

NUMERICAL RESULTS

A fast Fourier transformation is employed with a grid of 2048×2048 points over a range of $-16 < \beta, \gamma < 16$ to satisfy the precision of the calculation. The influence of load velocity, viscoelastic damping and reinforcement ratio on the vertical displacement is discussed and the results are given in Figures 2-4.

Table 1. Calculation parameter.

Modulus of Steel(E_f)	2×10^{11}Pa	Rigidity of ground(K_L)	138.6×10^{6}Pa
Poisson's ratio of Steel(μ_f)	0.28	Thickness of plate (h)	0.25m
Modulus of Steel concrete (E_m)	2.4×10^{9}Pa	Width of plate (b)	0.75m
Poisson's ratio of concrete (μ_m)	0.167	Width of load b_1	0.15m
Ratio of reinforcement (V_f)	0.008	Velocity and frequency	50m/s，10Hz
Damp coefficient of ground(η)	1.732×10^{6}Pa.s		

Considering the case of flexible pavements, the effect of the load velocity is shown in Figure 2. The maximum load velocity is $c = 200$m/s which is approaching the Rayleigh wave speed of the soil. Since the load is assumed to be moving at a constant velocity, the displacement of the soil is constant along the direction of the load, that is, the displacement response moves with the load.

Figure 2(a) gives the displacement varying with x at $y = b/2$ and Figure (2b) gives the displacement varying with y at $x = 0$. It can be seen that the displacement at the load center decreases with the increase of the load velocity which is given by Wang (2001). Due to the low velocity of the load, the displacement amplitude is symmetry to the axis $x = 0$; however as the load velocity increases，the displacement

becomes asymmetry. Since the plate is assumed to be simply supported along the width side, meaning that the displacement is zero at $y = 0$ and $y = b$, the maximum displacement occurs at the center of the load.

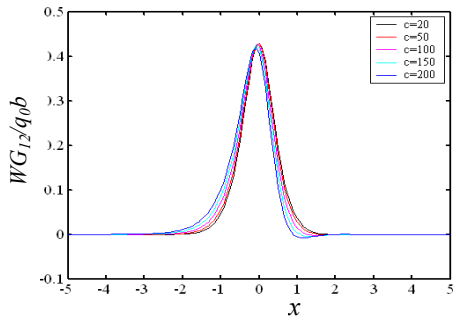

Fig.2(a) Curve of Vertical displacement along x axis with different speeds

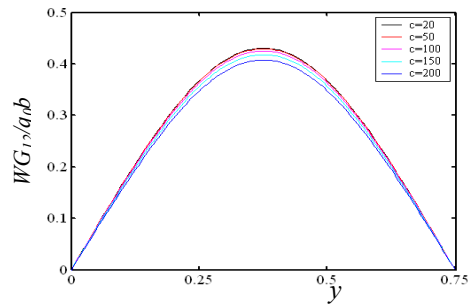

Fig.2(b) Curve of Vertical displacement along y axis with different speeds

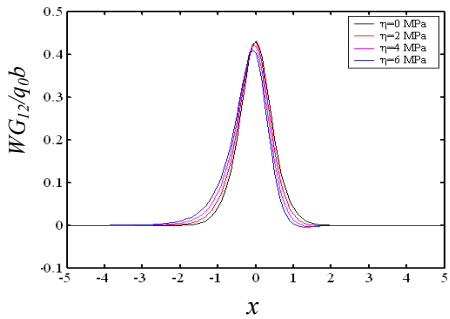

Fig.3(a) Curve of Vertical displacement along x axis with different damp coefficients

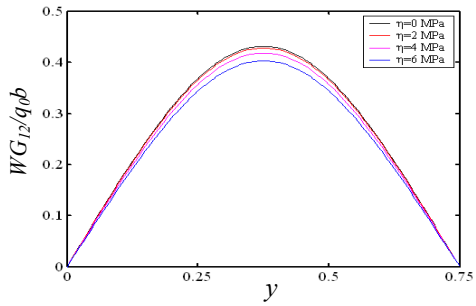

Fig.3(b) Curve of Vertical displacement along y axis with different damp coefficients

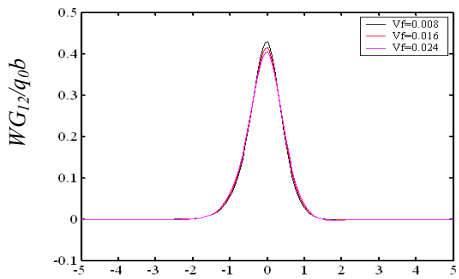

Fig.4(a) Curve of Vertical displacement along x axis with different ratios of reinforcement

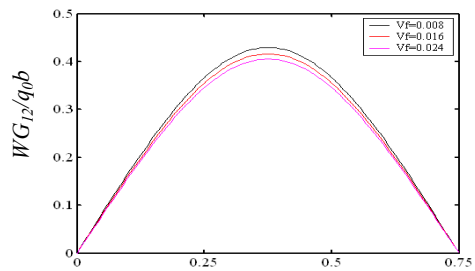

Fig.4(b) Curve of Vertical displacement along y axis with different ratios of reinforcement

Figure 3(a) gives the influence of the viscoelastic damping on the vertical displacement along x axis at $y = b/2$. Figure 3(b) gives the influence of the

viscoelastic damping on the vertical displacement along y axis at $x = 0$. It can be seen that the influence of the viscoelastic damping is similar to that of the load velocity. Figure 4 shows the effect of the reinforcement ratio on the displacement. The displacement response is symmetry to the center axis. The reinforcement ratio of the x axis only influences the displacement at the load center（a）; however the reinforcement ratio of the width side significantly influenced the displacement（b），and the displacement decreases as the reinforcement ratio increases.

CONCLUSION

The dynamic response of CRCP on viscoelastic soil under moving load is studied, and the influence of the parameters of the system is given through numerical analysis. It is shown that the vertical displacement of the CRCP decreases with the increase of the load velocity and is asymmetric at the center of the load. The influence of the viscoelastic damping is similar to that of the load velocity; the displacement of the pavement decreases as the reinforcement ratio increases.

REFERENCES

Yoder, E. J., and Witczak, M. W. (1975). *Principles of Pavement Design*. John Wiley & Sons, New York.

Cheng, X. (1987). "Dynamic response of plates on elastic foundation under moving load". *Journal of Applied Mathematics and Mechanics*, 8(4), 347-355.

Zheng, X., and Wang, S. (1989). "Dynamic analysis of simply supported rectangular plates on an elastic foundation under moving load". *ACTA AERONAUTIC ET ASTRONAUTICA SINICA,* 10(10), 557-560.

Huang, X., and Deng, X (1990). "The mechanical analysis of plate on viscoelastic winkle foundation under moving load". *Journal of Chongqing Jiaotong Institute,* 9(2), 45-51.

Hou, Y., Sun, S., and Guo, Z. (2003). "Dynamic Response sensitivity analysis of plate on elastic foundation subjected to moving point loads". *Journal of Tongji University*, 3(1), 31-35.

Sun, L., and Deng, X. (1996). "General theory for steady dynamic problem of infinite plate on an elastic foundation". *Journal of Acta Mechanic,* 28(6), 756-760.

Kim, S. and McCullough, B. F. (2003). "Dynamic response of plate on viscous Winkler foundation to moving loads of varying amplitude". *Engineering Structure*, 25, 1179-1188.

Wang, H., Hu, C., and Wang, B. (2001). "Responses of continuously reinforced concrete pavement under transient load". *Engineering Mechanics,* 18(5), 119-126.

Theoretical Analysis of Design Parameters on Semi-rigid Asphalt Pavement with Flexible Base

Ruibo Ren[1]， Hiwen Li[2], and Zheren Wang[3]

[1]Professor, School of civil engineering, Shandong Jianzhu University, China.rrbgq@sdjzu.edu.cn
[2]Assistant Researcher, Shandong Provincial Academy of Building Research, China.lihiwen@sina.com
[3]Professor, School of Communications Science and Engineering, Harbin Institute of Technology, China. wangzheren@sina.com

ABSTRACT

Reflective cracking is one of the main distresses for the cement/lime/flyash stabilized base in China. Although a flexible base can and has been utilized as a sandwich layer to reduce reflecting cracks from the stabilized base, the repetitive truck traffic load may cause higher tensile stress at the bottom of the asphalt surface course due to a large deformation from the flexible base. This high tensile stress may lead to fatigue cracking. To minimize the tensile stress at the bottom of the asphalt layer, and to establish optimum structure design parameters to reduce the maximum tensile stresses at the bottom of the asphalt surface course, a nonlinear, finite element technique was utilized to support the experimental pavement in the Tonghua Highway in the Jilin province. Based on the analyses, to minimize the tensile stress at the bottom of the asphalt layer, the value of the flexible base modulus should be more than 400MPa and that of semi-rigid, sub-base modulus should be more than 1500MPa, which can guide the design and construction of the semi-rigid asphalt pavement with a flexible base.

INTRODUCTION

Reflective cracking is a major and costly problem in China. It occurs in the top surface layers, above existing cracks in the lower, stabilized layer. This type of cracking can lead to premature deterioration of the pavement structure through the infiltration of moisture. A flexible base has been successfully utilized to reduce reflecting cracks from the cement/lime/flyash stabilized base (He 1997). A flexible base is placed between the asphalt surface and the cement/lime/flyash stabilized base (sandwich structure). However, higher tensile stress could be produced at the bottom of the asphalt surface course for structures with a flexible base as the sandwich layer. Therefore, because flexible base material can produce elasto-plastic deformation, under the repetitive actions of heavy vehicle loads, an asphalt surface course cannot meet the needs of fatigue resistance performance. This phenomenon has been demonstrated with dynamic triaxial tests (He 1997, Ling 1999). Since the elastic layered system theory is different from the actual state of pavement (Ren 2001), the finite element technique was utilized by characterizing a flexible base as nonlinear (elasto-plastic) material (Bathe 1976).

The nonlinear, finite element technique was utilized to support the experimental pavement in the Tonghua Highway in the Jilin province. Lessons learned from the finite element analyses and some design parameters, suggest pavements used in the Tonghua Highway are expected to be applicable to a wide range of pavement projects.

MATERIAL ELASTO-PLASTICITY AND YIELDING RULE

The characteristics of the elasto-plastic materials are that deformation will be irreversible and perpetual when unloaded, as shown in Fig. 1. When material is loaded, it is impossible to tell if it is nonlinear elastic or nonlinear elasto-plastic. However, when material is unloaded, the difference is obvious as nonlinear elastic and/or elastic material will return to the original location (refer to Fig. 1). As shown in Fig. 1, depending on different loading history, elasto-plastic material yielded permanent deformation (Xue 2005, Drucker 1952, Xia 1991). Based on the dynamic triaxial test results, the behavior of flexible base deformation can be characterized as elasto-plastic material. Thus, to simulate the field condition, the elasto-plastic finite element technique was utilized to describe the pavement behavior.

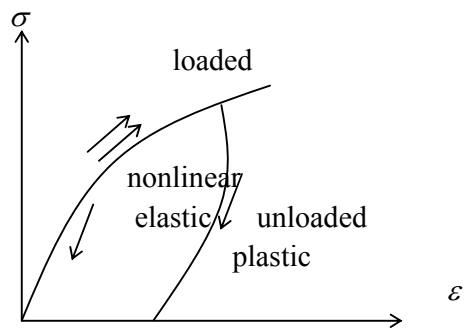

FIG.1. Nonlinear elastic and elasto-plastic.

This paper adopted linear Drucker-Prager yielding rule to describe the elasto-plastic behavior of flexible base. The linear Drucker-Prager yielding rule is very similar to that of Mohr-Coulomb, which is a modified yielding rule of VonMises (Drucker 1952, Xia 1991). The main difference of VonMises from linear Drucker-Prager and linear Mohr-Coulomb is that the yielding rule takes into account the influence of lateral pressure. According to reference (Xia 1991), linear Drucker-Prager yielding function is given as:

$$F = \sqrt{3}\alpha I_1 + \sqrt{3J_2} - \sigma_y = 0 \qquad (1)$$

where, I_1 is lateral pressure (in MPa); J_2 is the second stress invariable; σ_y is the yielding stress which relates to material's cohesion and internal frictional angle.

The yielding function of linear Mohr-Coulomb is shown in Eq. 2:

$$F = \frac{1}{2}(\sigma_3 - \sigma_1) + \frac{1}{2}(\sigma_3 + \sigma_1)\sin\phi - \cos\phi = 0 \qquad (2)$$

Where, ϕ is internal frictional angle; $\sigma_1, \sigma_2, \sigma_3$ are principal stresses. According to Equation 1, when the flexible base material was analyzed with the Drucker-Prager yielding rule by elasto-plastic finite element method, it should be determined if the yielding state is achieved or not. If achieved, it should be calculated with elasto-plastic theory; if not, it should be calculated with elastic theory.

The laboratory test results indicate that the cohesion of the flexible base material (grading macadam) is near 0 and the internal frictional angle ranges from 35^0 to 40^0. It has been observed that when there is a better construction quality control, the internal frictional angle can be increased to approximately 45^0 (He 1997). For this study, the internal frictional angle of 40^0 was selected.

SURFACE COURSE BOTTOM TENSILE STRESS ANALYSIS OF EXPERIMENTAL PAVEMENT IN TONGHUA HIGHWAY WITH NONLINEAR FINITE ELEMENT METHOD

Experimental Pavement in Tonghua Highway and Design Parameters

The typical structures with layer thickness and layer modulus of the experimental pavement sections in the Tonghua Highway are presented in Figure 2. A dual circular load with uniform pressure of 0.7MPa was adopted. The circular diameter is 21.3cm (CCCC Highway Consultants Co.,Ltd. 2006). Although the behaviors of an asphalt surface course and soil subgrade are all nonlinear, relative to a flexible base, they are insignificant. Therefore, all other materials, except for the flexible base, were treated as elastic materials.

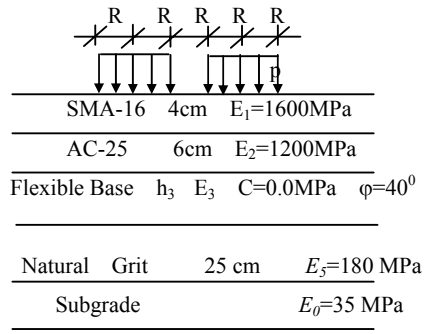

FIG.2. Experimental Pavement Structure of Tonghua Highway.

Since the load and geometric are symmetric, to simplify the analyses, a three- dimensional symmetric model was adopted. In addition, an eight-node spacial element was utilized in the analyses. Except subgrade Possion Ratio μ of 0.35, all other pavement layers have Possion Ratio μ of 0.25 (He 1997).

Analysis Results

To evaluate the impacts of the flexible base and semi-rigid subbase

modulus on the maximum tensile stress at the bottom of asphalt surface course, the thickness of the flexible base varied from 10, 12, to 15cm. Similarly, its moduli varied from 200, 300, 400, 500, 600, to 700MPa. The moduli of lime-flyash stabilized subbase in pavement structure in Figure 2 varied from 1000, 1500, 2000, 2500, to 3000MPa. The maximum tensile stresses at the bottom of AC-25, are presented in Figures 3, 4 and 5 respectively.

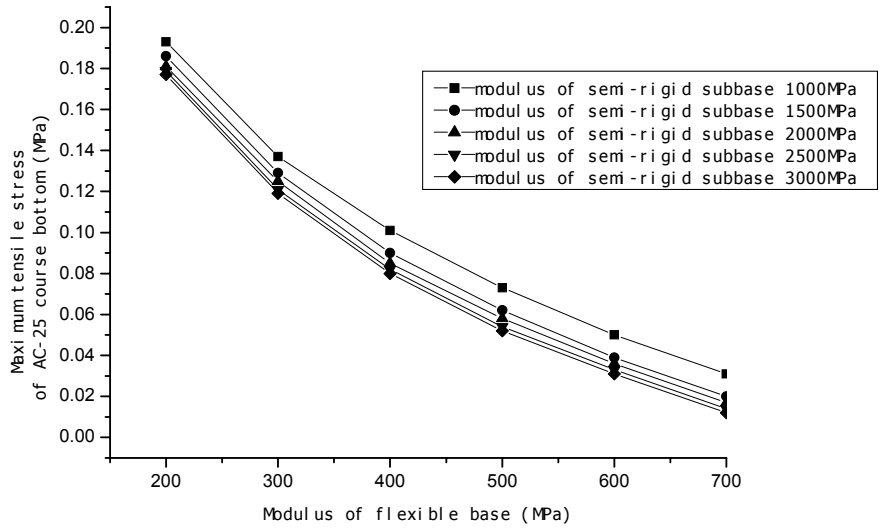

FIG.3. Maximum tensile stress at the bottom of AC-25 with varying flexible base modulus (h_3=10cm).

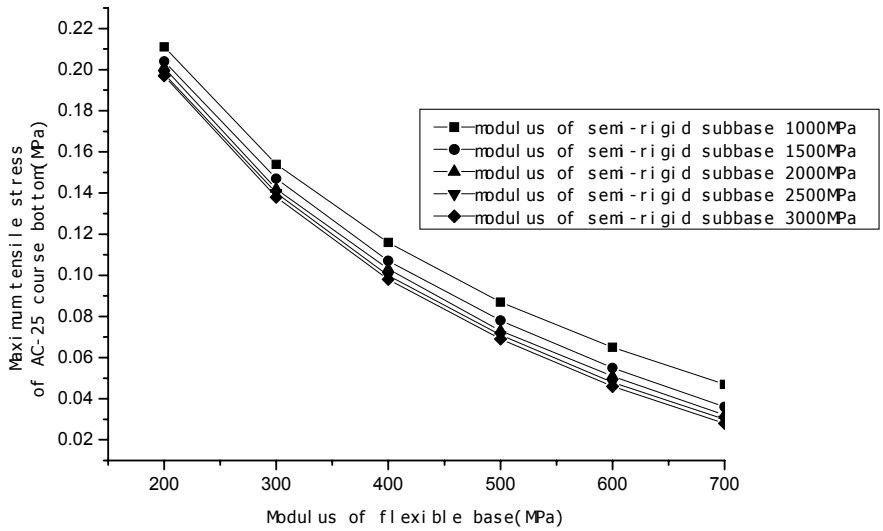

FIG.4. Maximum tensile stress at the bottom of AC-25 with varying flexible base modulus (h_3=12cm).

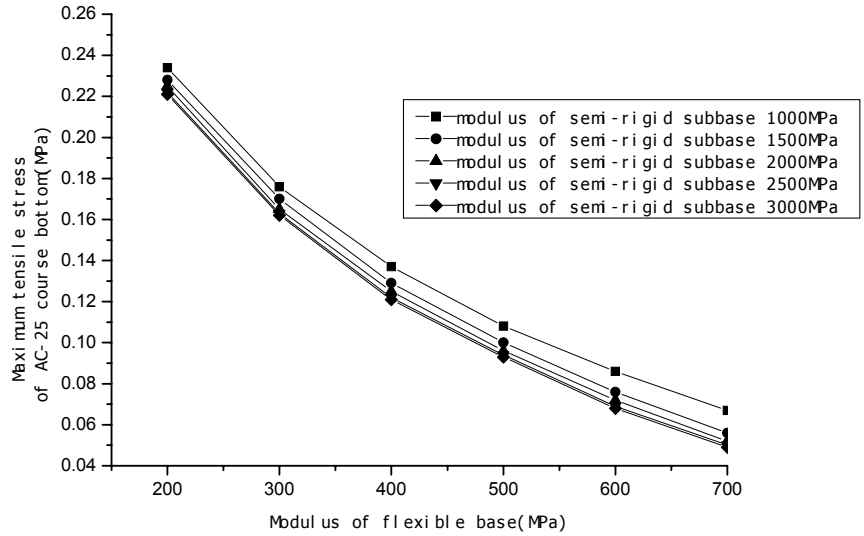

FIG.5. Maximum tensile stress at the bottom of AC-25 with varying flexible base modulus (h_3=15cm).

Figures 3, 4 and 5, indicate that the impacts of semi-rigid subbase modulus on the maximum tensile stresses at the bottom of the asphalt surface course vary insignificantly in pavement structures in Figure 1 when the modulus of flexible base is smaller. With the increasing of modulus of the flexible base, the impact of the semi-rigid subbase modulus becomes more significant. It was observed that when the modulus of the flexible base was higher than 400MPa, the varying slope of the maximum tensile stresses at the bottom of the asphalt surface course was less evident. When the modulus of semi-rigid subbase was lowered, the impact of the semi-rigid subbase modulus on the maximum tensile stresses at the bottom of the asphalt surface course was higher. When the modulus of the semi-rigid subbase was higher than 1500MPa, the varying of maximum tensile stresses at the bottom of the asphalt surface course was minimal. Thus, to reduce the maximum tensile stresses at the bottom of asphalt surface course, the modulus of flexible base should be more than 400MPa; the modulus of semi-rigid subbase should be more than 1500MPa.

CONCLUSIONS

Reflective cracking is a major concern for the cement/lime/flyash stabilized base in China. Although a flexible base can and has been utilized as a sandwich layer to reduce reflecting cracks from a stabilized base, higher tensile stress could be produced at the bottom of an asphalt surface course when subjected to a heavy truck traffic load, which may lead to fatigue cracking. In this study, the nonlinear, finite element technique was utilized to support the experimental pavement in the Tonghua Highway in the Jilin province. The main goal is to establish optimum structure design parameters to reduce the maximum

tensile stresses at the bottom of the asphalt surface course. Based on the analyses, the observations and conclusions are as follows:

(1) When the modulus of the flexible base was higher than 400MPa, evidence of the varying slope of maximum tensile stresses at the bottom of the asphalt surface course was lower.

(2) When the modulus of the semi-rigid subbase was higher than 1500MPa, the varying of maximum tensile stresses at the bottom of the asphalt surface course was very small.

(3) For the pavement structure in Figure 2, the optimal design parameters are that the modulus of the flexible base should be more than 400MPa. Similarly, the modulus of the semi-rigid subbase should be more than 1500MPa.

ACKNOWLEDGMENTS

Special thanks to Hai Luan, researcher of the Jilin Highway Survey and Design Institute, for providing the surveyed parameters of the Tonghua Highway.

REFERENCES

He, Z.Y. (1997). "Study on preventing semi-rigid asphalt pavement reflecting cracks and road performance." *Ph.D. dissertation of South-east university*:35-56.

Ling, T.Q., Wang, S.J., and Xu, Z. H. (1999). "Displacement and stress analysis of materials nonlinear performance." *China Journal Highway and Transport.* Vol.12(1):1-6.

Ren, R.B., Tan, Y.Q., Tan and Zhang, X.N.(2001). "Solution for solving asphalt pavement multilayered viscoelastic body surface deflection in the FWD dynamic case." *China Journal Highway and Transport.*Vol.14(2):9-12.

Bathe K J., and Wilson, E. L. (1976) "Numerical methods in finite element analysis." *Prentice-Hall,Inc.*/VA:31-82.

Shouyi, X. (2005). "Finite element method." *China Building Material Industry Press*./88-131.

Drucker, D.C. (1952). "A more fundamental approach to plastic stress strain relations" *Proc.1st U.S.Nat.Congr.Appl.Mech.* / VA 86-197.

Xia, Z.X. (1991). "Plastic mechanics." *China Tongji University Press./*77-132.

CCCC Highway Consultants Co.,Ltd.(2006). "Specification for Design of highway asphalt pavement." *China People Pommunication Press./*10-45.

Seismic Hybrid Simulation of a Multi-Span Bridge

Cai Xin-jiang[1] and Tian Shi-zhu[2]

[1]School of Civil Engineering, Harbin Institute of Technology, Harbin, 150090; PH (0451) 86282985-810; email: caixinjiang77@126.com
[2]School of Civil Engineering, Harbin Institute of Technology, P.O. Box 2549, Harbin, 150090; PH (0451) 86283185; FAX (0451) 86282074; email: tianshizhu@hit.edu.cn

ABSTRACT

A seismic hybrid simulation between four universities was introduced in this work using a platform named NetSLab. The platform is capable of transferring control and feedback signals among distributed laboratories or computers connected by the Internet. A multi-span bridge was loaded to simulate the responses corresponding to different earthquake hazard levels, in which two FRP retrofitted RC columns were tested physically, and the other three columns were simulated numerically. The results demonstrate that NetSLab has adequate for applications, and the bridge with retrofitted RC columns has adequate seismic behavior under earthquake excitation.

Keywords: hybrid simulation; NetSLab; multi-span bridge; columns; retrofitted

INTRODUCTION

In order to be able to execute testing of large scale specimens to give better insight of structures under earthquake excitation, the concept of hybrid simulation is developed. The prototype structure is divided into substructures, each of which can be tested or calculated at a different site; all substructures are conducted concurrently to form uniform testing. At present, some research efforts have been madeExamples include: NEES in USA connected several universities with high performance networks to explore the benefits of integrating laboratory resources (NEES, 2003; Stojadinovic *et al.*, 2006; Takahashi *et al.*, 2006) and ISEE in Taiwan area developed a testing platform named PNSE based on database approach and TCP/IP approach (Wang *et al.*, 2005). Furthermore, there are several plans such as ED-Net in Japan and KOCED in Korea (Park, *et al.*, 2003; Takashi *et al.*, 2005). In China, a networked testing platform, named NetSLab, has been developed, which solved the technologies of data transmission and collaborative control on the Internet. A series of simulations and tests were executed by the researcher (Fan *et al.*, 2009). A five-column bridge is chosen as the prototype structure in this paper for the demonstrative hybrid simulation.

PROTOTYPE BRIDGE AND SCALED SPECIMENS

The Russian river bridge, as shown in Figure 1, is selected as the prototype structure.

The superstructure is assumed to be a box section with a depth of 1.6m and width of 8m for a 2 lane highway bridge. There are two columns that serve as physical substructures, which consist of CFRP retrofitted RC columns at Harbin Institute of Technology laboratory (HIT Lab) and GFRP retrofitted RC columns at Hunan University laboratory (HNU Lab). The height scale of the two specimens is chosen to be 1/6 based on the available equipment and physical size of each laboratory. Table 1 gives a summary on the parameters of specimens of a multi-span bridge. Figure 2 shows the elevation view of the specimens C-5.

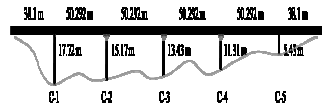

Figure 1. Schematic diagram of prototype bridge

Table 1. Parameters of specimens of multi-span bridge

Properties		C-1	C-2	C-3	C-4	C-5
Prototype structure	Height (m)	17.72	15.17	13.43	11.31	5.43
	Diameter (m)	2.1	2.1	2.1	1.8	1.8
Model structure	Height (m)	3	—	—	—	0.9
	Diameter (m)	0.35	—	—	—	0.3
Similarity coefficient	Height	1/6	1	1	1	1/6
	Displacement	1/6	1	1	1	1/6

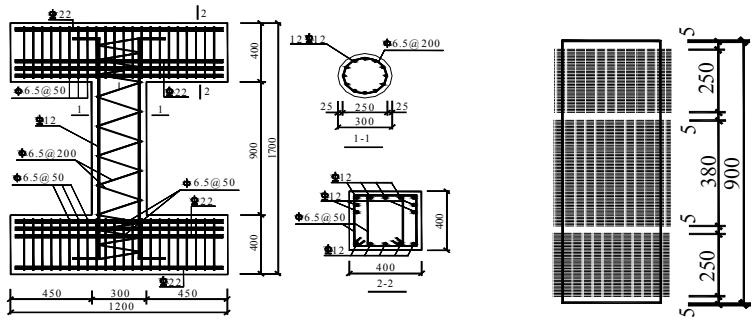

(a) Dimension and reinforcement **(b) Wrap form of CFRP**

Figure 2. Elevation view of specimens C-5

HYBRID SIMULATION METHOD BASED ON NETSLAB

Hybrid simulation is root in pseudo-dynamic testing, which integrates a physical model and a numerical model into a hybrid model. Based on the network, it integrates several single laboratories into a powerful and distinctive networked structural laboratory, which can enhance testing capability and share resources.

NetSLab (Networked Structural Laboratories)

NetSLab is a testing platform based on the concept of Client/Server that links several remotely distributed laboratories by Internet. The frame of NetSLab is

illustrated in Figure 3. Controller organizes the procedure, carries out the analysis, and controls the progress and data communication among all participants. There is only one Controller per testing for the current study. Testers carry out the detailed task for each step to create new results according to previous results. There may be multiple testers in one testing. The testers are further categorized into two types: Actual-Tester, who operates the equipment in each laboratory to generate actual results, and Virtual-Testers, who uses computation to provide analytical data. Remote-Viewer monitors the process and shares the results online without any interference of the test processing. Each component will communicate with NetSLab based on TCP/IP protocol (Xiao *et al.*, 2005; Wang *et al.*, 2007).

The control algorithm is shown in Figure 4. Based on the input information about the testing model, Controller first reads an earthquake record, then calculates the displacement and sends it to Actual-Tester for operating the actuator, and to Virtual-Tester if it is involved. After the actuator achieves the target displacement, Actual-Tester sends the measured restoring force to Controller. Meantime, the calculated restoring force based on selected numerical models by Virtual-Tester is also sent to Controller, and Controller then calculates the displacement for next step.

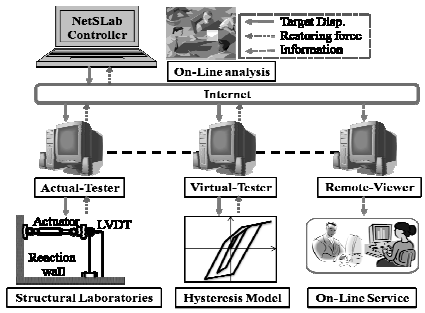

Figure 3. Frame of NetSLab

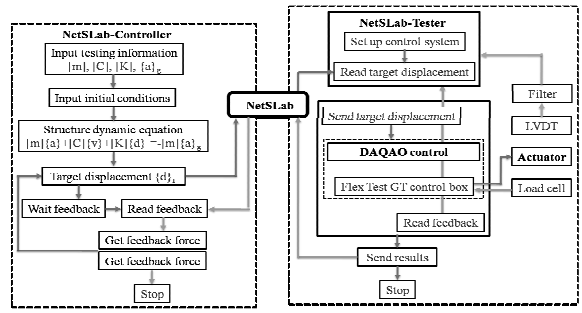

Figure 4. Control algorithm of NetSLab

Bridge testing framework

The hybrid simulation frame of a multi-span bridge is illustrated in Figure 5. The superstructure is assumed to have infinite stiffness and the mass is supported by five columns, then the bridge is modeled as SDOF system in longitudinal direction. The superstructure-to-column connection of C-1 and C-5 are rigid connections and the other three is a hinge connection. The columns C-1 and C-5 are designed as physical substructures and tested in HIT Lab (named PDT-C1) and HNU Lab (named PDT-C2), as shown in Figure 6 (b)(c). The columns C-2, C-3 and C-4 are designed as numerical substructures and are calculated in computers at University of Southern California, Tsinghua University and Hunan University.

(a) Testing frame of bridge **(b) PDT-C1 in HIT** **(c) PDT-C2 in HNU**

Figure 5. Hybrid simulation frame of multi-span bridge

Selection of earthquake excitation

The EL-Centro (S-N) wave, including the max peak ground accelerations from the 1940 Imperial Valley earthquake, is selected for the testing. The bridge is tested by subjecting to increasingly higher seismic demands which represent frequent level earthquakes, design level earthquake and the rare level earthquake. The time step is 0.02s and the step number is 300. The input information of earthquake ground motions is illustrated in Table 2.

Table 2. Input of EL-Centro earthquake ground motions

Seismic fortification intensity	Hazard levels	Scaling factor	Peak value
7° frequent	63%	0.206	0.07g
7° design	10%	0.647	0.22g
8° rare	2%~3%	1.176	0.4g

TESTING RESULTS AND ANALYSIS

The running interfaces of Controller and Actual-Tester are illustrated in Figure 6. It includes the input of acceleration record, displacement and time curve, hysteresis curve, schematic diagram of structure vibration and information in each testing step, et al. The smooth running of NetSLab is validated by the testing.

Figure 7 shows the hysteresis curve of the specimens. PDT-C1 is a RC short column retrofitted with CFRP to prevent brittle shearing damage. PDT-C2 is a RC column retrofitted with GFRP to prevent flexure or premature shear damage. From Figure 7, we can see the failure modes of PDT-C1 and PDT-C2 are all ductility bend failure in the testing. Before yielding, the hysteretic loop is long-narrow and shuttle-shape; the pinching phenomenon is very significant and the changing of stiffness is very limited. But after yielding, the displacement increases significantly and the restoring force changes from line to curve. Furthermore, the hysteretic loop becomes satiety and changes to S-shape. Pinching phenomenon and stiffness decrease very significantly, which proves that FRP has strong confining effects on core concrete.

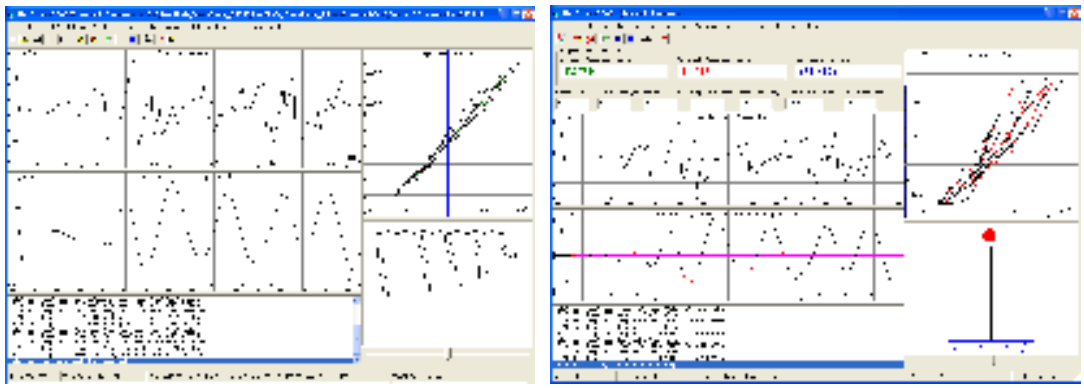

(a) NetSLab-Controller (b) NetSLab-Actual-Tester

Figure 6. Running interfaces of NetSLab (0.4g)

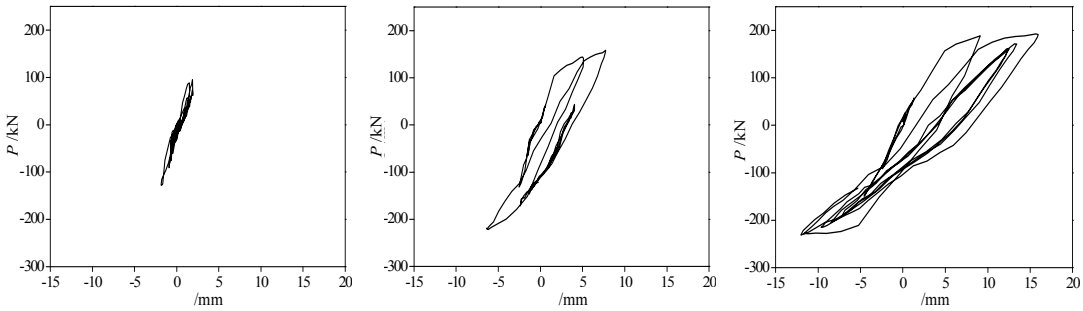

(a) PDT-C1 (0.07g) (b) PDT-C1 (0.22g) (c) PDT-C1 (0.4g)

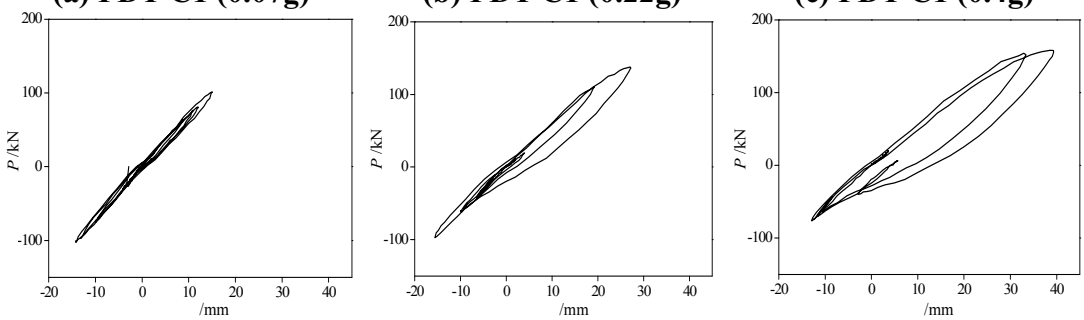

(d) PDT-C2 (0.07g) (e) PDT-C2 (0.22g) (f) PDT-C2 (0.4g)

Figure 7. Hysteresis curve of PDT-C1 and PDT-C2

CONCLUSIONS

Hybrid simulation is an experimentally based method for investigating the seismic response of a structure. An Internet-based platform, called NetSLab, has been utilized in this work for the execution of networked collaborative hybrid simulation among distributed structural laboratories. A multi-span bridge with five columns is chosen as the prototype structure to evaluate the performance of NetSLab. The physical substructures testing sites include the HIT Lab and HNU Lab, and the numerical substructures testing sites include Tsinghua. USC and HNU. The

successful application of hybrid simulation among four universities proves the feasibility of NetSLab. The efficient control and feedback of data is also validated by the testing, and the results also prove that the developed testing system NetSLab is adequate for bridges under earthquake excitation.

ACKNOWLEDGEMENT

Supported by NSFC under Grant No.50338020 and Grant No.90715036.

REFERENCES

Fan, Y.L., Guo, Y.R., Xiao, Y., and Cai, X.J. (2009). Seismic Response of a Multi-Span Bridge Based on Remote Testing Platform NetSLab. Key Engineering Materials, Vols. 400 - 402, pp. 743 - 748.

NEES, The MOST Experiment, July 30, 2003. Report of NEESgrid, USA, 2003. http://www.nees.org.

Park, D.U., Yun, C.B., Lee, J.W., Nagata, K., Watanabe, E. and Sugiura, K. (2003). On-Line Pseudo-dynamic Network Testing on Base-Isolated Bridge Using Internet and Wireless Internet. CD-ROM, In Proceedings of the 16th KKCNN Symposium on Civil Engineering, Korea, pp. 121-128.

Stojadinovic, B., Mosqueda, G. and Mahin, S.A. (2006). Event-Driven Control System for Geographically Distributed Hybrid Simulation. Journal of Structural Engineering, Vol. 132, No. 1, pp. 68 - 77.

Takahashi, Y. and Fenves, G.L. (2006). Software Framework for Distributed Experimental–computational Simulation of Structural Systems. Earthquake Engineering and Structural Dynamics, Vol. 35, No. 3, pp. 267 - 291.

Takashi, Y., Kazutoshi, N., Eiichi, W., et al. (2005). International Collaborative Pseudo-dynamic Testing Method for Continuous Elevated Bridges by Using Internet. Advances in Experimental Structural Engineering, ASCE, Vol. 18, No. 1, pp. 371 - 376.

Wang, D.P., Tian, S.Z. (2007). Remote Collaborative Pseudo-dynamic Testing System Based on Acquisition Board Control. Progress in Natural Science, Vol. 17, No. 12, pp. 1487 - 1493.

Wang, K.J., Lin, B.Z., Cheng, W.C., et al. (2005). A Platform for Networked Collaborative Structural Experiments. Advances in Experimental Structural Engineering, ASCE, Vol. 18, No. 1, pp. 433-440.

Xiao, Y., Hu, Q., Guo, Y.R., Zhu, P.S. and Yi, W.J. (2005). Network Platform for Remote Structural Testing and Shared Use of Laboratories. Progress in Natural Sciences, Vol. 15, No. 12, pp. 1135 - 1142.

Experimental Study on Behavior of Geotextile-Reinforced Soil

HU You-chang[1]， SONG Hai[1]and ZHAO Zheng-jun[1]

[1]School of Transportation, Wuhan University of Technology, Wuhan 430063, P.R.China; PH (86) 27-86551193; FAX (86) 27-86551193; email: huyouchang@163.com

ABSTRACT

In order to investigate the behavior of geosynthetic-reinforced soil (GRS), a series of laboratory experiments were conducted on GRS samples made up of granular soil and a nonwoven geotextile. The resilient deflection, resilient modulus, California Bearing Ratio (CBR) and unconfined compressive strength of the GRS mass were the parameters examined to evaluate the performance of the GRS samples. The focus of the tests was to determine the effects of the vertical spacing of the reinforcement and the relative compaction of the granular soil on the performance of the GRS mass. Based on the test results, it was concluded that the compressive strength of geotextile-reinforced soil increases significantly with the decrease in reinforcement spacing or with the increase in the degree of the relative compaction of fill. Furthermore, the well-compacted granular soil reinforced with closely spaced geotextile not only has a higher compressive strength compared to that with widely spaced reinforcement, but also exhibits both ductile and flexible failure mode making it a desirable composite material for the construction of supporting structures. In addition, it was found that the standard laboratory soil resilient modulus and CBR test methods are unsuitable for geotextile-reinforced soil because sliding occurs along the geotextile-soil interface under test loading due to the lack of adequate anchorage of the geotextile in the small sample.

INTRODUCTION

Geosynthetic-Reinforced Soil (GRS) is different from Mechanically Stabilized Earth (MSE) conventionally used in retaining structures (Barrent et al. 2007; Adams et al. 2007a). MSE structures rely on the use of widely spaced metallic or high strength geosynthetics as tie-backs or “quasi-tiebacks” and heavy concrete facial blocks or panels to stabilize the backfill. GRS structures on the other hand rely on the closely spaced geosynthetic reinforcements and the well compacted granular fill with minimal facial elements to create an inherently strong reinforced soil composite (Barrent et al. 2007). A GRS mass is internally stable, but a MSE mass is

not by itself stable. GRS is superior to MSE in resisting both static and dynamic loads (Barrent et al. 2007).

The high bearing capacity of GRS and the small deformation under service loads, led to the use of GRS structures as bridge abutments in recent years (Helwany et al. 2007). GRS bridge abutments are easier to construct and more economical than their conventional reinforced concrete abutments counterparts. The cost saving and ease of construction are - due to the much shorter construction period, lesser excavation, cheaper materials (geotextile and granular soil), and the elimination of piles even when constructed over a weak foundation (Lee et al. 2004). In addition, there is an improved transition from abutment to bridge, unlike the "bump" often experienced at the ends of a bridge resting on conventional concrete abutments. In United States of America, GRS bridge-supporting structures are, therefore, considered a significant advancement in developing technologies to rapidly construct bridges as part of the Federal Highway Administration's "Bridge of the Future" program (Adams et al. 2007a).

Lee and Wu (2004) reviewed some typical observations of several full-scale GRS abutment and pier models.. Adams et al. (2007b) carried out an experimental study on small models of GRS piers, and found that the performance of GRS structure was significantly affected by the reinforcement spacing, but was not affected by reinforcement strength within a working load of 200 kPa. Hu et al. (2008) conducted laboratory tests to investigate the deformation behavior of geogrid-reinforced silty sand. Numerical analysis of GRS structures were also proposed by some researchers, such as Helwany et al. (2007), Wu et al. (2006) and Hatami et al. (2006).

The widely accepted views on the reinforcement mechanism can be categorized as "membrane effect", "confinement effect" and "stress-spreading effect" (Sharma et al. 2009 and Bao 2004). Bao (2004) divided the reinforcement mechanism into "direct reinforcement effect" induced by soil-geosynthetic interaction， and "indirect reinforcement effect" resulting from the composite soil (quasi-rigid mass) formed by the reinforcement material and the adjacent thin soil layer. This idea serves as a guide to understanding GRS properties. However, the performance of GRS mass is mostly unclear until now.

In order to help understand the behavior of GRS mass subjected to vertical loading, the author carried out an experimental laboratory investigation using GRS samples maked up of a granular soil and a nonwoven geotextile reinforcement. Tests of resilient modulus, California Bearing Ratio (CBR) and unconfined compression were conducted on several GRS samples with varying reinforcement spacing/number of

reinforcement inclusions and relative degrees of compaction of the soil At the same time, the same tests were also conducted on a control sample of the granular soil without reinforcement for comparison.

MATERIALS USED FOR THE EXPERIMENTS

The soil used in all tests was a mixture of a crushed stone and clay with a maximum dry density of 21.3 kN/m^3 at the optimum water content of 7.08 %. The particle size distribution of the crushed stone is shown in Figure 1. The clay consists of grains smaller than 0.075 mm in diameter. The ratio of crushed stone to clay was 85:15 by mass. The reinforcement layers were a nonwoven geotextile with a unit mass of 174 g/m^2 and a tensile strength of 3.5 kN/m at 103.2 % tensile strain.

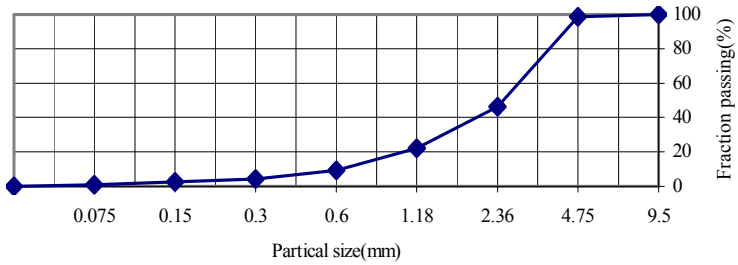

Figure 1. Particle size distribution of crushed stone

TEST SAMPLES AND REINFORCEMENT ARRANGEMENT

According to the Chinese standard test methods for highway engineering (Ministry of Transport of P.R. China 2007, 1994), all samples used in the study were cylindrical specimens made by compressing them in rigid molds. The CBR and resilient modulus test samples had a diameter of 15.2 cm and a height of 12 cm. The soil in the samples was respectively compacted to 92 %, 96 % or 100 % of the maximum dry density at the optimum water content of 7.08 %. The reinforcement arrangements are shown in Figure 2, where *n* is the number of reinforcement layers.

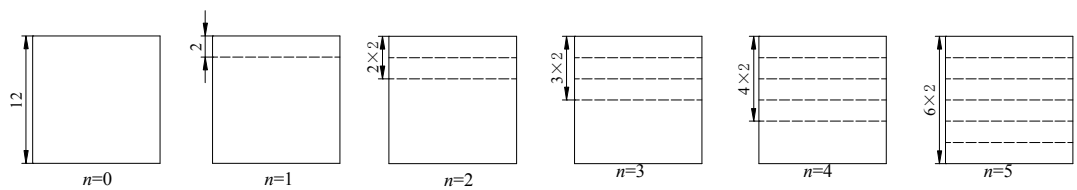

Figure 2. Reinforcement arrangement for CBR and resilient tests (size unit: cm)

For the unconfined compression (UC) tests, samples with a diameter and height of 15 cm were made at 96 % and 100 % relative compaction, at a water content of 7.08 %.

The reinforcement arrangements are shown in Figure 3.

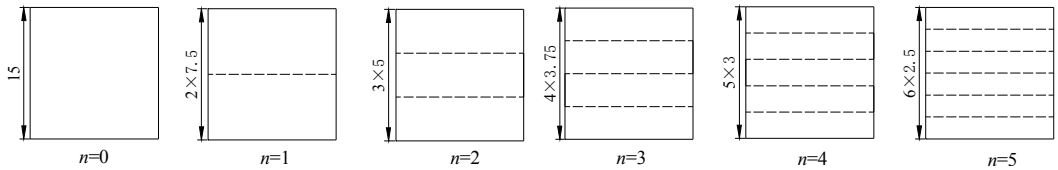

Figure 3. Reinforcement arrangement for UC tests (size unit: cm)

TEST PROCEDURE

All of the laboratory tests were conducted as per standard methods noted above. Figure 4 shows the experimental set-up. Testing load was applied at a constant rate of 1.2 mm/min through a rigid 5 cm circular plate for the CBR and resilient tests and through a 15 cm circular plate for the unconfined compression tests.

TEST RESULTS AND ANALYSIS

Resilient Modulus Tests: The resilient modulus test results are shown in Figure 5 to Figure 9where K is the relative compaction of soil, p is the pressure applied, l is the resilient deflection and E is the resilient modulus.

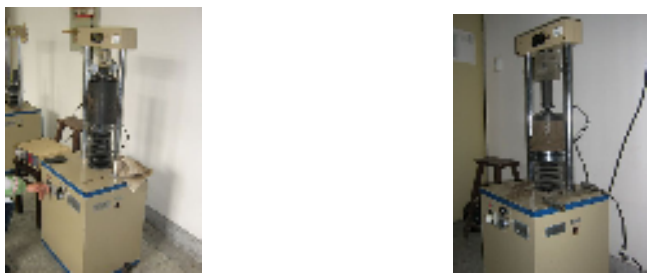

a) Resilient/CBR test b) Unconfined compression test

Figure 4. Experimental set-up

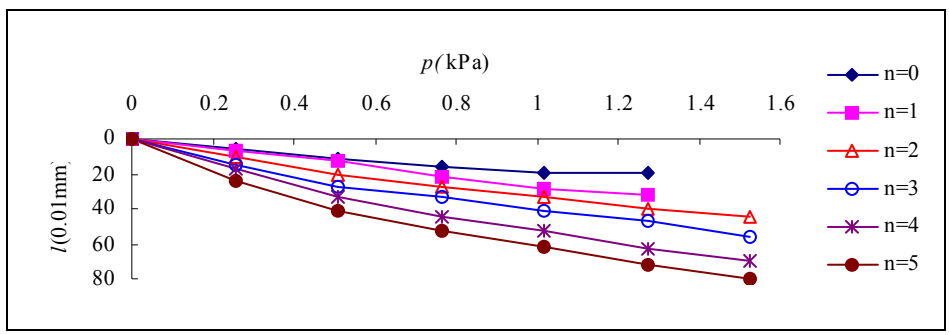

Figure 5. Pressure-resilient deflection curves at K=92 %

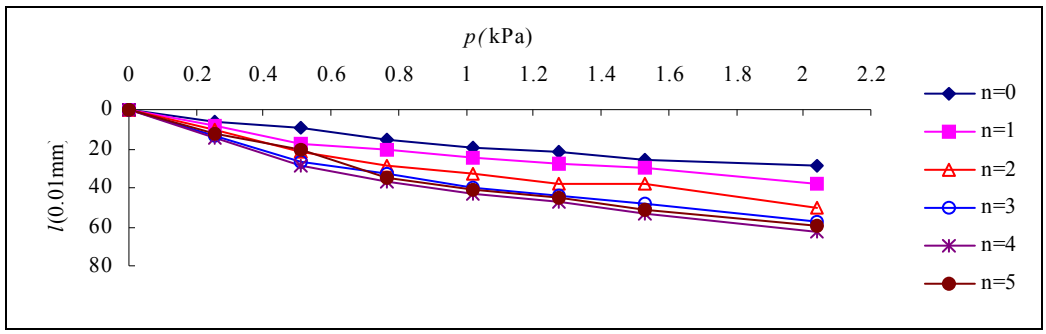

Figure 6. Pressure-resilient deflection curves at *K*=96 %

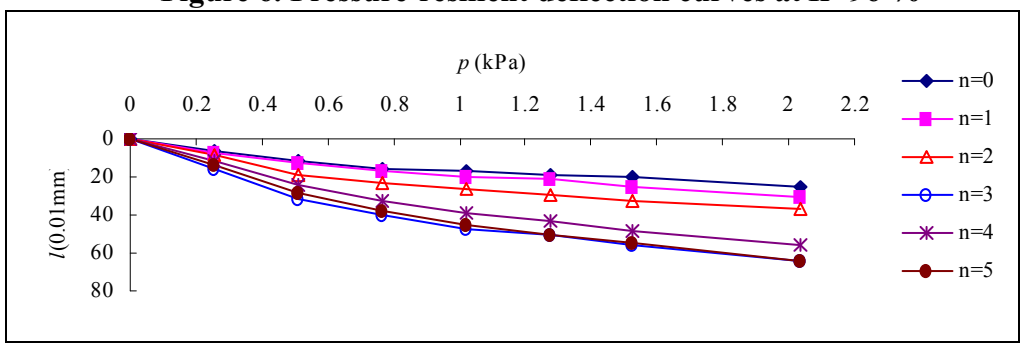

Figure 7. Pressure-resilient deflection curves at *K*=100 %

For a given pressure, the resilient deflection of the reinforced soil increases with n for a relative compaction (K) of 92% (see Figure 5). Similar trends are observed for K=96 % and K=100 % except for reinforcement inclusions exceeding 3 layers (see Figure 6 and Figure 7). The pressure-resilient deflection curves for samples with 3, 4 or 5 reinforcement layers (n =3 to 5) are very similar in magnitude and shape for K=96 % or K=100 %. Coinciding with the effect and trend of K or n on the resilient deflection noted above, the resilient modulus (E) decreases as n increases at K=92 %, or at $K \geqslant 96$ % for $n \leqslant 3$. For K=96 % or K=100 %, E has nearly the same magnitude for n equals to 3, 4 or 5 (see Figure 8).

The above test results imply that the geotextile inclusions reduce the stiffness of the reinforced soil making the soil softer. This outcome is due to the small size of the samples, in which the geotextile cannot be anchored strongly to avoid sliding along the geotextile-soil interface when the sample was centrally loaded during the resilient tests. In the actual GRS structures, such sliding cannot occur under working load (Adams et al. 2007a). Therefore, the standard laboratory method for evaluating resilient modulus prescribed in JTG E40-2007 is not suitable for geotextile-reinforced soil. For this reason, a test method using larger dimensional GRS mass and larger loading plate, such as the field plate load is suggested for geotextile-reinforced soil.

Figure 9 shows the relationship between the resilient modulus and the relative

compaction of the soil. For the soil without geotextile reinforcement, E varies directly with K, which agrees with a lot of experimental data previously presented. For the soil reinforced with 1 or 2 geotextile inclusions, E also increases with K, but the rate of increase from K=96 % to 100 % is greater than that from K=92 % to 96 %, indicating that the higher the degree of compaction, the more reinforcing benefit the GRS mass will experience.

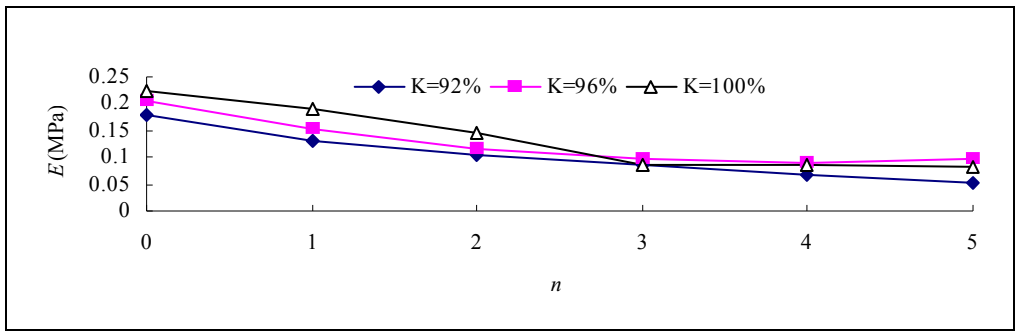

Figure 8. Relationship between resilient modulus and number of reinforcement layers

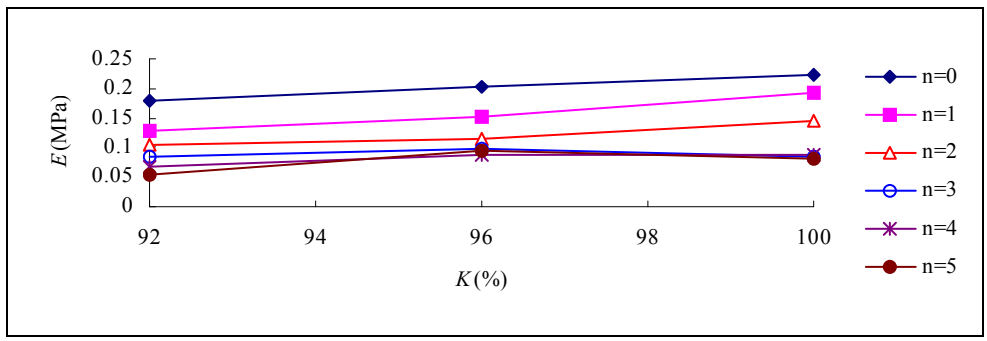

Figure 9 Relationship between resilient modulus and relative compaction of soil

It can be seen from Figure 8 and Figure 9 that the resilient modulus of the reinforced soil samples with n=3, 4 and 5 are approximately equal. This is because nearly no deformation took place in the lower half part of the sample under a lower level of stress due to the small loading plate diameter and lower pressure applied. Based on this observation, it can conclude that the geotextile reinforcement layers placed within the lower half of the sample results in almost no improvement to the properties of the reinforced soil.

CBR Tests: Similar to the resilient modulus, the CBR of the geotextile-reinforced soil is affected by K, and slightly by n. Generally, CBR increases with K, but fluctuates with n (see Figure 10) due to the same reason for the resilient modulus discussed above. Therefore the CBR test carried out in laboratory with a small sample is not a rational method for geotextile-reinforced soil.

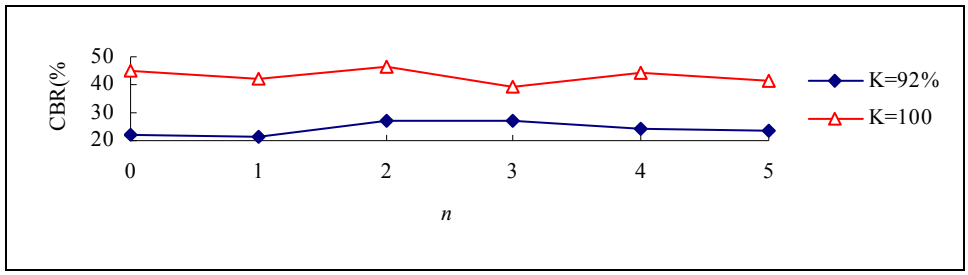

Figure 10. Relationship between CBR and number of reinforcement layers

Unconfined Compression Tests: The relationships between compressive stress and strain of the samples with and without geotextile reinforcement are presented in Figure 11 to Figure 14, where q is the compressive stress and ε is the vertical strain.

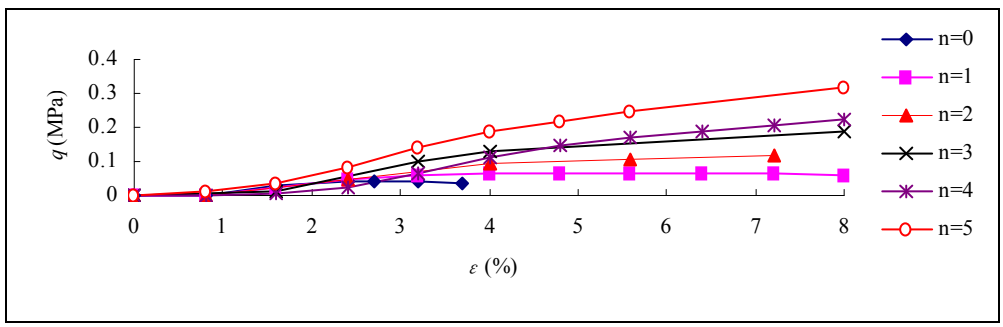

Figure 11. Compressive stress-strain curves while $\varepsilon \leqslant 8$ % at K=96 %

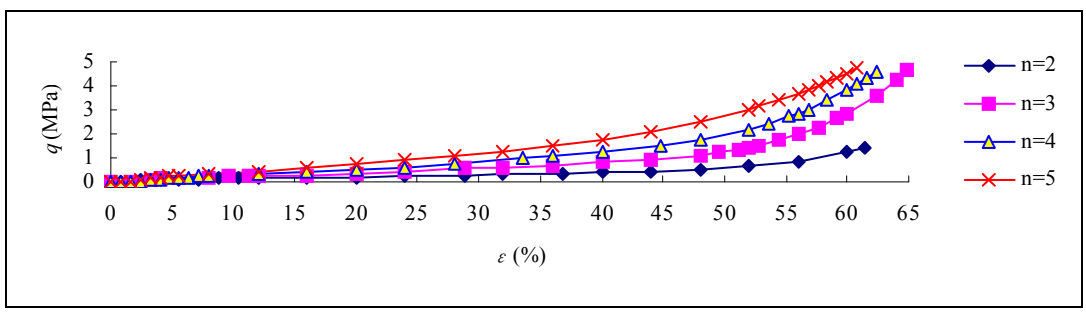

Figure 12. Compressive stress-strain curves at K=96 %

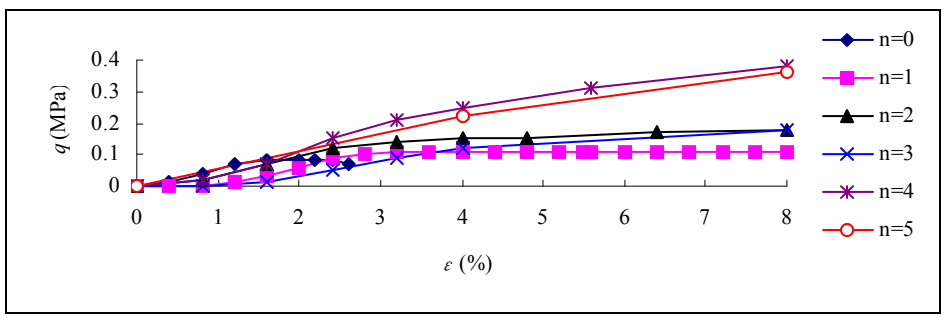

Figure 13. Compressive stress-strain curves while $\varepsilon \leqslant 8$ % at K=100 %

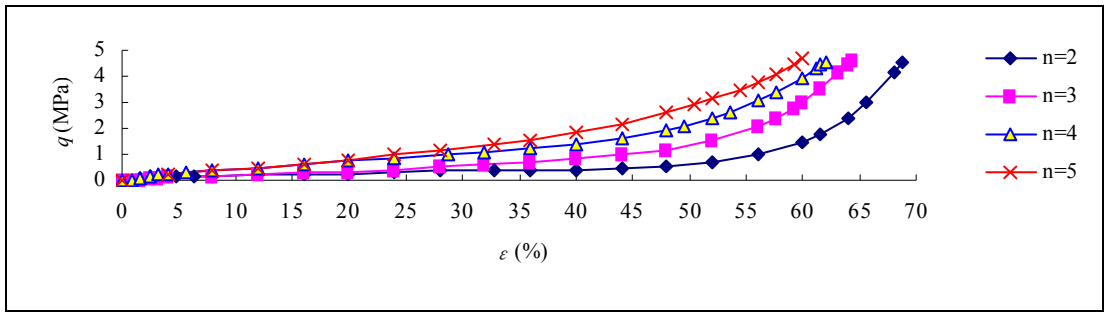

Figure 14. Compressive stress-strain curves at *K*=100 %

A summary of the results of the ultimate compressive strength, q_u, and the corresponding vertical strain, ε_u, for sample with varying reinforcement inclusions (n) are presented in Table 1. It should be noted that the values of q_u in Table 1 represent the maximum stress for the samples without and with one geotextile inclusion (n=0, 1), or the approximate compressive stress of the point of maximum curvature on q- ε curve for sample with more than one reinforcement inclusions (n= 2, 3, 4 or 5)-see Figure 12 and Figure 14.

Table 1. Ultimate compressive strength and the corresponding strain

n	*K*=96%		*K*=100%	
	ε_u (%)	q_u (MPa)	ε_u (%)	q_u (MPa)
0	2.4	0.04	1.6	0.08
1	5.6	0.06	3.6	0.11
2	56.7	0.80	61.0	1.60
3	56.5	2.06	55.0	1.96
4	52.0	2.20	51.0	2.25
5	50.3	2.81	48.7	2.73

As can be seen in Figure 11 to Figure14, the geotextile inclusions have a significant effect on compressive behavior of the reinforced soil when the compressive strain exceeds a critical value of about 4 % at *K*=96 % and 8% at *K*=100 % for the reinforced soil used in this study.

The important results are as follows:

1. The samples without reinforcement and with only one reinforcement layer placed at mid height demonstrated a fragile failure, and as a result these samples have a lower ultimate compressive strength occurring at a relative small strain (see Table. 1). This indicates that the granular soil reinforced with widely spaced geotextile is fragile and weak and therefore unsuitable for

retaining support structures.

2. On the contrary, the samples with 2-5 geotextile reinforcement layers (i.e. reinforcement spacing of 7.5-2.5 cm) exhibited a highly ductile and flexible behavior when subjected to vertical stress, even though the geotextile is very weak (ultimate tensile strength of 3.5 kN/m). The more closely the spacing of the geotextile reinforcements, the better performance of the reinforced soil. It was observed that even if the vertical strain exceeded 60%, except for some grains dropping from the vertical surface of the sample during loading (see Figure 15), samples with 3 or more geotextile reinforcement layers still maintained the form of a highly compacted mass. This experimental result agrees with recommendations proposed by Lee and Wu (2004) and observation presented by Adams (2007b). Therefore, GRS, well-compacted granular soil reinforced with closely spaced geosynthetic, is a desirable composite material for constructing supporting structures.

Figure 15. Picture of reinforced soil at the end of test

CONCLUSIONS

The following conclusions can be drawn from the test results of the investigation:

1. The standard laboratory soil resilient modulus and CBR test methods are unsuitable for geotextile-reinforced soil because the geotextile cannot be anchored strongly in the small sample to avoid sliding along the geotextile-soil interface under test loading.
2. The compressive strength of geotextile-reinforced soil increases significantlywith the decrease of reinforcement spacing and with the increase in the degree of relative compaction of the soil.
3. The well-compacted granular soil reinforced with closely spaced geotextile has a higher compressive strength and exhibits a ductile and flexible failure mode. This makes GRS a desirable composite material for the construction of

retaining support structures.

REFERENCES

Adams, M. T., Schlatter, W., and Stabile, T. (2007a). "Geosynthetic reinforced soil integrated abutments at the bowman road bridge in defiance county, ohio." *Geosynthetics in Reinforcement and Hydraulic Applications* (*GSP 165*), ASCE, Denver, Colorado, USA, 119-129.

Adams, M. T., Ketchart, K., and Wu, J. T. H. (2007b). "Mini pier experiments—geosynthetic reinforcement spacing and strength as related to performance." *Geosynthetics in Reinforcement and Hydraulic Applications* (*GSP 165*), ASCE, Denver, Colorado, USA, 98-106.

Bao, C. G. (2004). "Study on the interaction behavior of geosynthefics and soil in China." *Proc. of the 3rd Asian Regional Conference on Geosynthetics*, Seoul, Korea, 104-115.

Barrett, R. K., and Ruckman, A. C. (2007) "GRS – A new era in reinforced soil technology." *Geosynthetics in Reinforcement and Hydraulic Applications* (*GSP 165*), ASCE, Denver, Colorado, USA, 153-164.

Hatami, K., and Bathurst, R. J. (2006). "Numerical model for reinforced soil segmental walls under surcharge loading." *Journal of Geotechnical and Geoenvironmental Engineering*, ASCE, 132(6): 673-684.

Helwany, S. M. B.， Wu, J. T. H.， and Kitsabunnarat, A. (2007). "Simulating the behavior of GRS bridge abutments." *Journal of Geotechnical and Geoenvironmental Engineering*, ASCE, 133(10): 1299-1240.

Hu, Y. C., Deng, W., and Lin. H. Q., et al. (2008) "Experimental study on resilient modulus of soil reinforced by biaxial geogrid." *Rock and Soil Mechanics*, 29(3): 759-763.

Lee, K. Z. Z., and Wu, J. T. H. (2004). "A synthesis of case histories on GRS bridge supporting structures with flexible facing." *Geotextiles and Geomembranes*, 22(4): 181-204.

Ministry of Transport of P.R. China (1994). *JTJ 057-94: Test methods of materials stabilized with inorganic binders for highway engineering.* China Communications Press, Beijing.

Ministry of Transport of P.R. China (2007). *JTG E40-2007: Test methods of soils for highway engineering*. China Communications Press, Beijing.

Wu, J. T. H., Lee, K. Z. Z., and Pham, T. (2006). "Allowable bearing pressures of bridge sills on GRS abutments with flexible facing." *Journal of Geotechnical and Geoenvironmental Engineering*, ASCE, 132(7): 830-841.

Sharma, R., Chen, Q., and Abu-Farsakh, M. et al. (2009). "Analytical modeling of geogrid reinforced soil foundation." *Geotextiles and Geomembranes*, 27(1), 63-72.

Study on the Frost Resistance Test Method of Lime-fly ash Stabilized Material Base Course

Zhiguo Chen [1,2], Zheren Wang [2], Xiwei Wang [3], Yufeng Zhao [4]

[1]Jilin Provincial Communications Scientific Research Institute，Key Laboratory of Highway Construction & Maintenance Technology in Seasonally Frozen Soil Region, Jilin Changchun, 130012;
[2]School of Transportation Science and Engineering, Harbin Institute of Technology, Heilongjiang Harbin, 150090; Email: jcczg@vip.sina.com.
[3]Jilin Provincial Highway Administration;
[4]Highway Survey and Design Institute in Chang Chun;

ABSTRACT: Lime-fly ash stabilized material has been commonly used as base course in seasonal frozen region in China for its high strength and good water stability. But the frost damage happens both during the pavement construction and in service life. During the pavement construction, if the lime-fly ash base layer was exposed in winter, the surface of base course could be frozen resulting in severe deterioration. In this situation, it was not uncommon to remove the whole base course and repave it. However, it was not only a waste of money but also a waste of time. In service life, if the lime-fly ash base course was saturated, it could be severely damaged after several freeze-thaw cycles. Therefore, a study of the frost resistance ability of lime-fly ash material would have great significance. Based on the investigation of ten–year lowest temperature in seasonal frozen region in China and the actual in-service temperature of semi-rigid base, the frost resistance test method of lime-fly ash stabilized mixture was developed. The test was conducted on lime-fly ash mixtures with different mixing ratio. The frost resistance index was determined according to the retained strength ratio. The relationship between water absorption, density and frost resistance index was discussed as well.

Keywords: lime-fly ash, stabilized material, road base, frost resistance test method, frost resistance index.

In China, most of the expressway use lime-fly ash stabilized aggregate as base course due to it's high strength, good water stability and environment-friendliness. Table 1 shows the properties of lime-fly ash mixture.

Table 1. Properties of Lime-fly Ash Stabilized Crushed Stone

items	values
180d compressive strength（MPa）	5.8~7.5
180d tensile strength（MPa）	1.3~1.6
Compressive resilient modulus（MPa）	1300~1700

tensile resilient modulus（MPa）	4500~6000
coefficient of shrinkage（10^{-6}）	20~35
strain of drying shrinkage（10^{-6}）	350~750

However, in seasonal frozen region, the lime-fly ash stabilized material's performance could be severely impacted by low temperature and freeze-thaw cycles. The frost damage could happen both during the pavement construction and in service life. During the pavement construction, if the lime-fly ash base layer is exposed, the surface of base course could be frozen in winter, resulting in severe deterioration. In this situation, it is not uncommon to remove the whole base course and repave it. It is not only a waste of money but also a waste of time. In service life, if the lime-fly ash base course is saturated, it could be severely damaged after several freeze-thaw cycles. So in the design procedure of lime-fly ash stabilized aggregate base, the frost resistance index should be considered.

1. Test Parameter

Currently, there is no well-accepted frost resistance index and corresponding experiment method for lime-fly ash stabilized mixture. Some research has been done to solve this problem. However, as different test methods were used, the results can not be cross-checked with each other. It is necessary to establish a consistent frost resistance test methods and propose parameters to evaluate the frost resistance ability of lime-fly ash stabilized mixture.

1.1 Freezing-thawing temperature and time

Test temperature in frost resistance test method should be the same as the in-place temperature of lime-fly ash stabilized base course in winter. Based on investigation of experiment road, the temperature at top of the base course was from -15°C to -18°C, was and -13°C to -16°C at the bottom. The difference of temperature between pavement surface and the top of base course was 2°C to 3°C. Based on these data and the concrete freeze-thaw test method (freezing temperature is -20°C) in "Testing methods of concrete", freezing temperature of frost resistance test for lime-fly ash stabilized mixture was determined to be -18 ± 1°C. Because the specimen melts faster in water, thawing temperature was determined to be close to room temperature, 20±1°C, which also simulates realistic temperature in water.

The time required to freeze and thaw the samples was determined first. The cost, including the on-site laboratory's test equipments, were considered along with the realistic environment that the lime-fly ash stabilized base course experienced in winter. Only large-scale scientific research institutes and engineering laboratories are equipped with air-cooled refrigeration equipments. Many on-site laboratories could only use compact refrigeration equipment. Considering the effectiveness of freezing equipment and the number of samples frozen, it was determined to use nine test specimens, 16 hours of freezing and 8 hours of thawing time, resulting in 24 hours for one freeze-thaw cycle.

1.2 Curing Age and Freeze-thaw Cycles

1.2.1 Curing age

"Technical code for construction of highway roadbed" specifies that construction of lime-fly ash stabilized base should be suspended one and a half month before the first freezing period. The strength of lime-fly ash stabilized mixture is a function of curing temperature and age. Considering the actual and required curing temperature (20℃), 28 days curing age was selected to evaluate frost resistance property during pavement construction. To determine the suitable age for testing the in-service frost resistance, compressive strength test was conducted to study the relationship between strength and age of the mixture. The study results are shown in Figure 1. It could be seen that after 180 days, the increase of strength slowed down significantly. Therefore, 180 days was selected as the standard curing time.

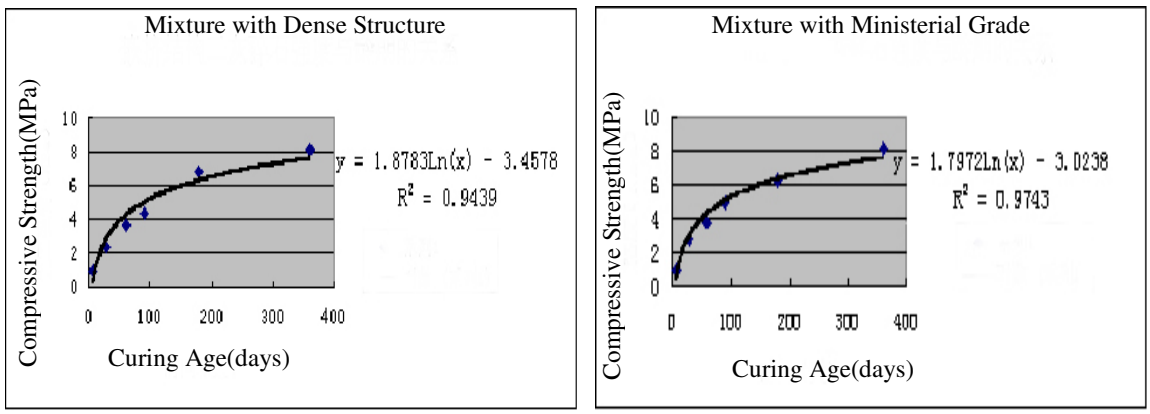

Figure 1 Relationship between Strength and Age of Lime-fly Ash Stabilized Mixture

1.2.2 freeze-thaw cycles

According to freeze-thaw cycle test results of lime-fly ash stabilized mixture specimens with 28 days curing age after 10 cycles, the strength and material loss after the first 5 cycles was not significant. However, after 10 cycles they became significant. Therefore, the retained strength after 5 freeze-thaw cycles was selected to evaluate frost resistance during construction. For 180 days curing age mixture, the retained strength after 10 freeze-thaw cycles was selected to evaluate frost resistance.

2. Test Method

Samples were prepared with optimum moisture content to obtain the maximum dry density. Cylinder samples with diameter of 150mm and height-diameter ratio of 1:1 were used in the test. Samples with 28 and 180 days curing time were used for 5 and 10 freeze-thaw cycles respectively.

Test procedures consist of the following steps:

(1) Before the end of curing time, samples were saturated for 24h at room temperature.

(2) Determine the dry weight. Measure the hight of the samples H_1 to an

accuracy of 0.1mm with a square caliper.

(3) The samples were divided into two groups with 9 samples each group. The first group of specimens were then compressed at a uniform rate with a speed of 1mm/min till failure. Record the maximum compressive load P(N).

(4) The second group was frozen for 16h±1h at -18℃±1℃ using constant temperature refrigerator(or kitchen refrigerator).

(5) The samples prepared by step (4) were weighed and the height, H2, was measured to an accuracy of 0.1mm with a square caliper. Then the specimens were placed into water at 20℃ for 8h±1h.

(6) The samples prepared by step (5) have experienced one freeze-thaw cycle. The weight was determined and steps (4) to (6) were repated.

(7)After 5 or 10 required freeze-thaw cycles the samples were saturated for 24h, the dry weights were determined and the heights of the samples were measured.

(8) Placed the samples on the elevating table of road materials strength tester, The specimens were then compressed at a consatnt rate with a speed of 1mm/min till failure. Recorded the maximum compressive load P(N).

(9)The unconfined compressive strength were calculated using equation (1)

$$Rc\ (R_{DC}) = P/A = 0.000057P \quad (1)$$

In this formula:

Rc, R_{DC}=Sample's unconfined compressive strength before or after freeze-thaw cycles, N;

P=Peak load, N;

A=Cross section area of sample, mm^2.

(10) Standard deviation, Cv, should not be more than 20%.

3. Frost Resistance Evaluation

Frost resistance is the capability of resisting freezing and thawing in the water-saturated state. During the construction period in spring and autumn and in-service in winter, the materials are subject to moisture and subsequently freezing and thawing at low temperature. The expansion of ice in pores generates tension and as the temperature increases, the pressure gradually disappears before the next freeze-thaw cycle. The internal pore water froze to cause frost heave. The pressure is related to the moisture content, freezing speed, and the structure of the pores. After repeated freeze-thaw cycles, cracks occur and freeze-thaw resistance of the material can be determined.

3.1 Frost resistance evaluation indicator

Lime-fly ash stabilized aggregate mixtures with different gradation were tested for 5 and 10 freeze-thaw cycles after 28 and 180 days, respectively. The mix design and aggregate gradation are shown in Table 2.

Table 2. The Mix Design and Gradation of Lime-fly Ash Stabilized Aggregate and Sand Gravel

Serial number	The proportion lime: flyash: macadam	Maximum particle diameter (mm)	Aggregate gradation (%)								
			37.5	31.5	19.0	9.5	4.75	2.36	1.18	0.6	0.075
1	7: 18: 75	37.5	100	90	60	30	5	0			
2	7: 18: 75	31.5		100	80	50	10	2	0		
3	6: 14: 80	31.5		100	68	34	21	14	10	8	5
4	6: 14: 80	31.5		100	95	46	24	18	13	10	3

Note: 5 and 6 is lime-fly ash stabilized sand gravel

Test results of lime-fly ash stabilized mixture are shown in Table 3 and Table 4 respectively.

Table 3.Test Results of Lime-fly Ash Stabilized Mixture after 28 Days and 5 and 10 Freeze-thaw Cycles

Serial number	The proportion lime: flyash: macadam	Strength (MPa) and C_V							
		28d		5 freeze-thaw cycles			10 freeze-thaw cycles		
		strength (MPa)	C_V (%)	strength (MPa)	C_V (%)	Retained percentate	strength (MPa)	C_V (%)	Retained percentage
1	7: 18: 75	2.3	8.7	1.125	15.5	0.528	0.201	0.597	0.087
2	7: 18: 75	2.4	8.4	1.070	4.1	0.446	0.387	0.496	0.161
3	6: 14: 80	2.4	10.0	1.325	18.8	0.552	0.256	0.602	0.107
4	6: 14: 80	2.8	9.0	1.136	25.4	0.406	0.337	0.519	0.120

Table 4.Test Results of Lime and Fly Ash Macadam after180-day Age and 10 Freeze-thaw Cycles

Serial number	The proportion lime: flyash: macadam	Strength (MPa) and C_V				Retained percentage BDR (%)
		180d		10 freeze-thaw cycles		
		strength (MPa)	C_V (%)	strength (MPa)	C_V (%)	
1	7: 18: 75	6.7	7.7	5.2	17.2	77.6
2	7: 18: 75	7.1	8.4	5.0	18.4	70.4
3	6: 14: 80	7.5	8.9	5.1	20.3	68.0
4	6: 14: 80	5.8	7.9	4.4	12.8	75.8

Frost resistance analysis of lime-fly ash stabilized mixture:

- Strength and mass loss of 28-day samples were significant after 5 freeze-thaw cycles. Therefore, the retained strength ratio after 5 freeze-thaw cycles could be used as frost resistance index.

$$BDR=R_{DC}/R_C \times 100\% \quad (2)$$

In Equation (2), BDR is freeze-thaw Retained strength percentage of semi-rigid material.

- For 180-day curing age samples, the retained strength ratio after 10 freeze-thaw cycles could be used as the indicator to evaluate frost resistance performance. Based on the test results shown in Table 3 and Table 4, the frost resistance index of lime-fly ash stabilized mixture are shown in Table 5.

Table 5. Frost Resistant Index of Lime-fly Ash Stabilized Mixture

Test conditions \ Freezing zone	Middle, light freezing zone
28-day age and 5 freeze-thaw cycles	≥ 40%
180-day age and 10 freeze-thaw cycles	≥ 65%

3.2 Relationship between frost resistance index or water absorption and the test cycles.

3.2.1 Relationship between frost resistance index and the number of freeze-thaw cycles.

Figure 2 shows the results of freeze-thaw test after 28 day curing age. The linear regression with a negative slope indicated that the mixture strength decreased with the development of the freeze-thaw damage resulting from the decrease of mixture density. After 5 freeze-thaw cycles, the frost resistance index was between 50% to 70%, which meant that the retained strength was 50% to 70% of the original strength before freeze-thaw test.

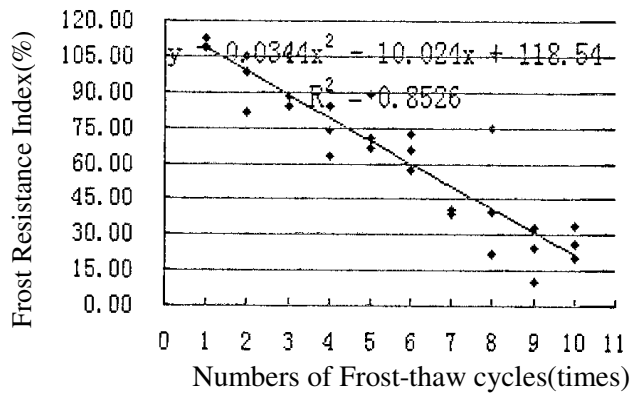

Figure.2 Plot of Frost Resistance Index versus Number of Freeze-thaw cycles

3.2.2 Relationship between water absorption and the number of freeze-thaw cycles

Figure 3 shows the relationship between water absorption and the number of freeze-thaw cycles. It can be seen that water absorption increased with the increase of the test cycles. It could be due to the increase of the internal voids and the decrease of the density, which caused the decrease of the strength. The curve also

showed that the water absorption increased significantly after 5 test cycles.

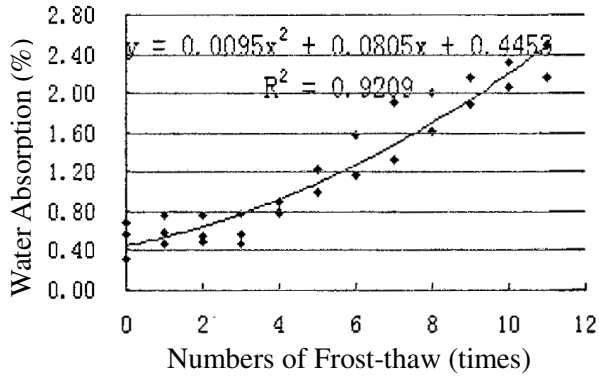

Figure 3. Water Absorption over Test Cycles

3.2.3 Relationship between water absorption and frost resistance coefficient

Figure 4 shows the relationship between frost resistance index and water absorption.

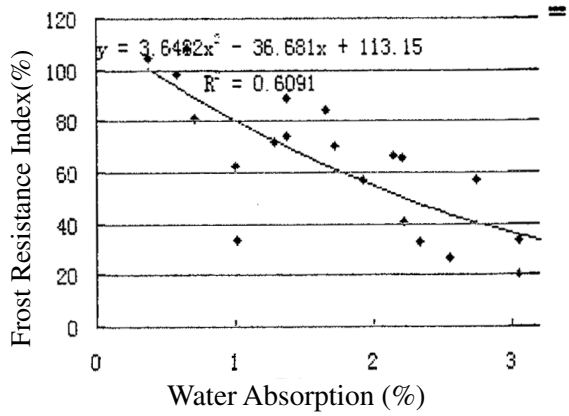

Fig.4 Frost Resistance Index versus Water Absorption

The frost resistance index decreased with the increase of water absorption. This indicated that the mixture's frost resistance capacity is affected by the specimen's density. The lower was the density, the lower was the capacity. The inflection points of relationship curve are located at 1.5% to 2% of water absorption and frost resistance index of 50% to 60%. These diagrams show that the water absorption is representative of the durability. Therefore water absorption is used as indicator to frost resistance design.

4. Analysis of Freeze-thaw Test on Semi-rigid Base

As can be seen from the test results, water absorption gradually increases after the freeze-thaw damage occurs. From the microscopic perspective, lime-flyash stabilized materials contain large pores, capillary pores and the gel pore, among which the free water contained in large pores dominates. When the temperature drops below freezing temperature, the gel and aggregate will contract and water will be frozen, which results in volume expansion. When the internal pores increase, water

absorption gradually increases and density gradually decreases.

The strength of lime-flyash stabilized materials mainly forms by the space grid structure, the gel and some fibrous or rod-like crystals. The induced stress which results from freezing, is similar to the damage mode under uniaxial compression load, as shown in figure 5(a). And the penetration pressure from thawing is similar to the damage mode under uniaxial tension load, as shown in figure 5(b).

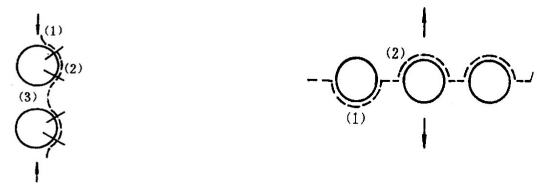

(a) (b)

Fig5. The Damage Mode of the Semi-rigid Material on the Effect of the Frost Thawing

With the increase of age, the pozzolanic reaction is further developed, which results in the structure mentioned above. Therefore, the strength and frost resistance of lime-flyash stabilized material continues to increase. For lime and fly ash stabilized mixture, frost resistance will be improved as the early strength increases.

5. Conclusions

This research established a freeze-thaw test method simulating the in-service condition of the lime-fly ash stabilized base course. Experiment was conducted using this method. By analyzing the test results, the frost resistance index was defined and adopted as an indicator of the mixture's frost resistance capacity. The relationship among water absorption, density and frost resistance index was discussed as well.

Reference

Zhang Dongqing, Liu Yanling. "The Construction Summarization of Lime-flyash Stabilized Macadam in ChangYu Express Highway". JiLin Provincial Communication Technology Supplement. 2002：50-52.

Lin Xiuxian. "Study on the Semi-rigid Base Asphalt Pavement". 1990，(4):1-9.

Zhou Xiaolong. "Vibration and Compaction Technology of Semi-rigid Mixture" Research Report[R].1992.

Sun Meili. "Component and Design Method of Lime-flyash Stabilized Macadam under Vibration and Roller Technology". Northeast highway[J].1998，21（2）30-32.

Yan Jiaji. "Road Building Material". [M]. BeiJing：China Communication Press, 2000.

Jiang Aifeng, Ren Huiqing. "Proportioning Design of Lime-flyash Stabilized Macadam". TongJi University Transaction. [J].1999，27（3）：309-313.

Jiang Zhenxiong. "Initial Discussion on Proportioning Design of Lime-flyash Stabilized Macadam".

Feng Decheng, Wang Caixia, Wu Sigang. “Study on Anti-Freezing Index of Semi-rigid Base” Research Report. [R].2003.

Computer-Aided Error Detection Of Horizontal And Vertical Alignment In Highway Construction

LIU Su[1], ZHANG Yaping[1,2], YU Lu[2]

[1]School of Transportation Engineering, Changsha University of Science and Technology, P.O. Box 410076, PH (+86)13055161279; email: liusuyx@126.com
[2]School of Transportation Science and Engineering, Harbin Institute of Technology, P.O. Box 150090, PH (+86) 15846598208; email: zxlt0905@163.com

ABSTRACT

In this paper, a computer-aided method is applied to the detection of horizontal and vertical alignment error during highway construction. The design criterion of highway centerline point corresponding to the detection point of highway midline is put forward. The step-swinging compression method is used to find the corresponding design centerline point. Based on this criterion and the step-swinging approach compression method, highway plane alignment deviation could be divided into transverse deviation and longitudinal deviation along the route. Both the encoding of the types of highway curve and the interval discrimination of the curve of plane alignment are discussed in the step-swinging approach compression method and computer aided calculation of highway plane alignment. Based on these studies, the computer-aided error detection of horizontal and vertical alignment in highway construction is established and used in the project Highway Survey and Design Software Development Integrated in Hunan Province China. Software examples and other examples provided in this paper show that this method is feasible.

Keywords: Road engineering, highway detection, horizontal and vertical alignment error during highway construction, the step-swinging approach compression method

INTRODUCTION

In recent years, relevant foreign literature has focused on existing selected flat vertical alignment optimizing fitting model, flat vertical alignment computer-aided calculation (CAD) (M.Easa, 1999), using GPS system for highway alignment detection (Thomas G. Davis., 1999), etc, for the research of highway alignment detection. It is difficult to find relevant research literature of highway alignment detection for domestic highways (Shao Weihan and Chris Rizos., 1999). The detection of horizontal and vertical alignment error during highway construction is not only important in highway alignment detection, but also important in highway construction quality detection. The usual practice is: detecting highway construction plane and elevation measurements; checking centerline milestones in accordance with the related linear design parameters of the highway plane and longitudinal alignment; calculating the deviation of plane and longitudinal alignment for each centerline milestone to calculate the standard deviation through the statistical

analysis, which then can be used as the precision index for measuring highway flat vertical line construction (WAN Wen-rui. 2002). The above detecting method of solving deviation of plane and longitudinal alignment can't solve the key problem of assessing the deviation of plane alignment (M.Easa , 1999).

THE PROCESS OF COMPUTER-AIDED HORIZONTAL AND VERTICAL ALIGNMENT ERROR DETECTION DURING HIGHWAY CONSTRUCTION

Computer-aided horizontal and vertical alignment error detection during highway construction can be carried out according to the following process:

(1) Detect the control point of the existing highway construction and control network to ensure that the control points of the plane and elevation measurement are accurate and reliable.

(2) Sample at the scene of highway pile-middle lofting $l_i^{'}$, get the coordinate of detection point of the highway midline (x_i, y_i, $H_i^{'}$, $l_i^{'}$).

(3) Search for the milestone (l_i) which has the shortest horizontal distance from the detection point of highway midline by the coordinates of the detection point of the highway midline (x_i, y_i, $H_i^{'}$, $l_i^{'}$) on the platform of detection software with the step-swinging approach compression method, and then calculate the design coordinates of horizontal and vertical alignment (X_i, Y_i, H_i, l_i).

(4) Calculate the horizontal deviation of the horizontal alignment (d_i), the azimuth angle of horizontal deviation (α_{di}), vertical deviation (Δl_i), the deviation between design line and completion line or construction line on the vertical section (ΔH_i). The formulae are as follows:

$$d_i = \sqrt{(x_i - X_i)^2 + (y_i - Y_i)^2}$$

$$\alpha_{d_i} = Arc\sin((x_i - X_i)/\sqrt{(x_i - X_i)^2 + (y_i - Y_i)^2})$$

$$\Delta l_i = l_i^{'} - l_i$$

$$\Delta H_i = H_i - H_i^{'} + \Delta h_i, \qquad i = 1,2,3,...,n$$

Where Δh_i is the difference of height between highway midline point and roadbed design elevation , which can be used to correct ΔH_i.

(5) Grant d_i, Δl_i, ΔH_i for deviation statistics according to the highway construction contract section, and ignore the affect of the errors of elevation control points and the three-dimensional detection to the construction deviation. Thus there may be a reflection of the centerline of highway contract tenders lofting plane and elevation accuracy of the standard deviation σ_j, σ_H:

$$\sigma_{dj} = \pm\frac{1}{\sqrt{N}}\sqrt{\sum_{i_0}^{i_n} d_i^{\,2}}\ ;\quad \sigma_{\Delta lj} = \pm\frac{1}{\sqrt{N}}\sqrt{\sum_{i_0}^{i_n} \Delta l_i^{\,2}}\ ;$$

$$\sigma_j = \pm\sqrt{\sigma_{dj}^{\,2} + \sigma_{\Delta lj}^{\,2}}\ ;\quad \sigma_{Hj} = \pm\frac{1}{\sqrt{N}}\sqrt{\sum_{i_0}^{i_n} \Delta H_i^{\,2}}\ ,\quad j = 1,2,3,...,N$$

Where i_0, i_n are from the middle initial contract tenders of the highway to termination points of the serial number of points in the section j.

(6) Count σ_j, σ_{Hj} of each contract section by weighted statistics using the length of the contract section during highway construction (D_j), and then get the accuracy of the road lofting plane and elevation of the whole highway midline (σ, σ_H):

$$\sigma = \pm\sqrt{(\sum_{j=1}^{N} D_j \sigma_j^{\,2}) / \sum_{j=1}^{N} D_j}\ ; \qquad \sigma_H = \pm\sqrt{(\sum_{j=1}^{N} D_j \sigma_{Hj}^{\,2}) / \sum_{j=1}^{N} D_j}$$

CONFIRMATION OF THE DESIGN MIDLINE POINT AND CORRELATIVE ALGORITHM

We can get the coordinates of the detection point of the highway midline (x_i, y_i, $H_i^{'}$, $l_i^{'}$), (i=1, 2,…, n) by detecting the on-scene samples. The corresponding coordinates of the highway design centerline point (X_i, Y_i, H_i, l_i) can be searched and confirmed by a certain algorithm on the three-dimensional coordinate software platform of highway horizontal and vertical alignment.

A. Determination criterion of design midline point

It appears easy to observe measurement error due to the impact of construction when the highway is completed or under construction. In addition, the actual design line of roads failed to fit the highway midline entirely. It comes to bias. Therefore, the sample testing from the scene by the middle of the highway coordinates (x_i, y_i, $H_i^{'}$, $l_i^{'}$), can not directly be obtained from the corresponding point of the centerline highway design route mark of mile l_i and (X_i, Y_i, H_i, l_i) coordinates, thus it is not possible to calculate the deviation of the centerline, as well as to inform (X_i, Y_i, H_i, l_i) the construction lofting precision.

As shown in Figure 1, the horizontal alignment deviations $\sqrt{d_i^{\,2} + \Delta l_i^{\,2}}$ can be decomposed into a line perpendicular direction of the deviation along the horizontal line d_i and the direction of vertical deviation Δl_i. From the $\sqrt{d_i^{\,2} + \Delta l_i^{\,2}}$, d_i and Δl_i constitute three differential right triangles, we can see the highway centerline and the corresponding point of the design of the highway centerline connection point d_i (horizontal deviation) in the middle lane highway design point of the middle line. Thus, d_i compares with the same road midline of the corresponding point and non-point design of the centerline of Highway Connection $d_i^{'}$, it makes:

$$d_i = \min$$

Therefore, d_i =min is a criterion for detect point of the centerline with the corresponding point of highway design. With highway centerline of highway design with the corresponding point midline point criterion, a theoretical basis is established when the design of the centerline on a highway mark of mile points plane coordinate and automatically searching.

Testing from the scene by the middle of Highway coordinate (x_i, y_i, H_i', l_i')

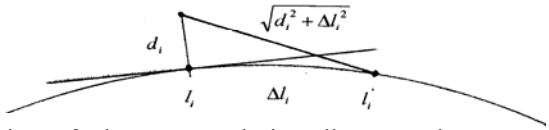

Point of the center design line on the highway (X_i, Y_i, H_i, l_i)

Figure1. Graphic of the deviation of highway's plane line

B. Principle of the step-swinging approach compression method

Swing by step approach compression method and the centerline of highway correspondence highway design midline point mark of mile plane coordinate and the principles are as follows:

A highway centerline of point $J_i(x_i, y_i)$, corresponds to the search mark of mile l highway design point of the centerline $Z_l(X_l, Y_l)$. (X_l, Y_l) can be calculated from the horizontal alignment obtained mark of mile l. Let searching mark of mile l be l_0, search for the pile step away from ΔS (> 0), and $l = l_0 + \Delta S$.

The horizontal alignment error can be calculated as follows:

$$d_{l_0-J_i} = \sqrt{(X_{l_0} - x_i)^2 + (Y_{l_0} - y_i)^2}\ ; d_{l-J_i} = \sqrt{(X_l - x_i)^2 + (Y_l - y_i)^2}$$

$$\Delta d = d_{l-J_i} - d_{l_0-J_i}$$

If $\Delta d = d_{l-J_i} - d_{l_0-J_i} < 0$ that $d_{l-J_i} < d_{l_0-J_i}$, assume that $l = l + \Delta S$. Continue to iterative approach, the cycle of $\Delta d = d_{(l+\Delta S)-J_i} - d_{l-J_i}$, till $d_{(l+\Delta S)-J_i} > d_{l-J_i}$, d_{l-J_i} and l as a second stage iterative cycle of the initial relative value;

Here, $l = l - 0.1\Delta S$ (step reduced to 0.1ΔS, and reverse search), $\Delta d = d_{(l-0.1\Delta S)-J_i} - d_{l-J_i}$

If $\Delta d = d_{(l-0.1\Delta S)-J_i} - d_{l-J_i} < 0$, suppose that $l = l - 0.1\Delta S$, Continue to iterative approach, the cycle of $\Delta d = d_{(l-0.1\Delta S)-J_i} - d_{l-J_i}$, until $d_{(l-0.1\Delta S)-J_i} > d_{l-J_i}$, d_{l-J_i} and l as the third stage iterative cycle of the initial relative value;

Let $l = l + 0.01\Delta S$ (step reduced to 0.01ΔS, and reverse search), and the steps are similar to the cycle of iterative calculation above.

Step-final stage of search for one millimeter, and with one more step on the opposite direction of the search, cycle iterative approach till $d_{(l\pm 0.001)-J_i} > d_{l-J_i}$, and d_{l-J_i} =min.

Let $d_i = d_{l-J_i}$, which is the distance between the highway centerline as the detection point $J_i(x_i, y_i)$ and point $Z_{li}(X_i, Y_i)$ highway design centerline of horizontal alignment error. Corresponding highway design centerline point mark of mile $l_i = l$, highway design plane coordinate $(X_i, Y_i) = Z_l(X_l, Y_l)$ centerline point. α_{di} can be obtained by coordinating reverse calculation.

EXAMPLES

This paper uses highway construction deviation of computer-aided detection method for calculating the highway construction of horizontal and vertical alignment error. The methods are feasible in two situations. One is algorithm-curve in a variety of types and another is various types of embankment design elevation of superelevation rotational pattern under all circumstances. Table 1, Table 2, and Table 3 took "Highway integrated setting software"--vertical and horizontal alignment deviation of relevant as an example.

Table 1 Instance of coordinate calculation of one freeway's circular curve with unsymmetrical connecting curve

JD_{10}	JD_{11}	JD_{12}		Main mark of milestone in the curve	X	Y
X=250220.00	X=250505.000	X=249797.647		Mark of milestone: k117+776.508	250349.691	494741.198
Y=495232.00	Y=494153.451	Y=493038.803		HY: k 118+27.735	250404.553	494496.184
R=1100	Ls1=251.227	P1=2.389	Q1=125.5	QZ: k 118+348.532	250404.019	494176.523
T1=607.920	Ls2=277.968	P2=2.925	Q2=138.9	YH: k 118+669.328	250311.599	493870.513
T2=620.046	E=102.717	D=57.178	L=1170.7	HZ: k 118+947.296	250172.771	493629.924
Line Rotation Angle: A (jd_{10}-jd_{11}-jd_{12})= 47°12'03" D_{10-11}=1115.568 D_{11-12}=1320.147						

Table 2 Instance of deviation of plane line

Milestone of Detection midline point	X Coordinates of points	Y Coordinates of points	X Coordinate design point	Y Coordinate design point	Horizontal deviation	Vertical deviation
K117+780	250350.494	494737.792	250350.584	494737.817	0.094	0.004
K117+840	250365.701	494679.702	250365.776	494679.721	0.077	0.053
K117+900	250380.140	494621.473	250380.151	494621.476	0.011	0.047
K117+960	250392.894	494562.837	250392.961	494562.851	0.069	0.058
K118+060	250408.689	494464.175	250408.720	494464.179	0.031	0.010
K118+460	250382.003	494067.201	250382.060	494067.187	0.058	0.097

Table 3 Instance of deviation of one freeway's vertical section line

Milestone of Detection centerline point	Elevation of centerline point	Design elevation of roadbed	Design elevation of centerline point	Revised Δh_i	ΔH_i
K100+020	98.945	98.94	98.94	0	-0.005
K100+040	98.854	98.87	98.87	0	0.016
K100+060	98.825	98.81	98.81	0	-0.015
K100+080	98.725	98.74	98.74	0	0.015
K100+100	98.656	98.67	98.67	0	0.014
K100+120	98.630	98.61	98.61	0	-0.02
Design Elevation of Roadbed: the elevation of edge of central belt; Superelevation Rotational Type : Rotating around central belt					

CONCLUSIONS

A. This paper proposes a criterion of centerline point design, that's d_i =min, and the step-swinging approach compression method in which the highway horizontal alignment deviation is divided into transverse deviation and longitudinal deviation along the route.

B. The vertical alignment deviation ΔH_i should be amended in highway construction automatic calculation according to the different types of roadbed design elevation, the super-elevation rotational pattern and stages.

C. The method of computer-aided error detection of horizontal and vertical alignment in highway construction based on the step-swinging approach compression and the criterion d_i =min was successfully adopted in the project Highway Survey and Design Software Development Integrated in Hunan Province China. Software examples and other examples provided in this paper show that this method is feasible.

REFERENCES

LIU Bo-ying, YAO Zu-kan. (2002) Engineer 's Handbook for Highway Design. Beijing. *China Communications Press*: 184-200.

M.Muthusubramanyam,M.ASCE.(2003) Graphical Solution for Vertical Curve Computation. *Journal of Surveying Engineering*,Vol.129 No.3:125-126.

M.Easa,Member,ASCE. (1999) Optimum Vertical Curves for Highway Profiles. *Journal of Surveying Engineering*,Vol.125 No.3: 147-157.

Shaowei Han and Chris Rizos. (1999) Road Slope Information from GPS-Derived Trajectory Data. *Journal of Surveying Engineering*,Vol.125 No.2:59-68.

Steve Y.W.Lam, M.ASCE, and Conrad H.W.Tang. (2003) Geometric Modeling Systems for Construction Surveying of Highway Tunnels. *Journal of Surveying Engineering*,Vol.129 No.4:146-150.

SUN Jia-si. (2001) Design Material for Highway 2 (Route survey). Beijing. *China Communications Press*: 221-273.

The Ministry of Communications. (1994) Design Specification for Highway Route(JTJ 001-94). Beijing. *China Communications Press*: 66-72.

Thomas G. Davis. (1999) Total Least-Spiral Curve Fitting. Journal of Surveying Engineering,Vol.125 No.4:159-176.

WAN Wen-rui. (2002) Technology for Highway's Geometry Linear Detection. Beijing. *China Communications Press*: 20-40.

An Estimate Method for Accuracy of Fitting Horizontal Alignment in Old-Highway Based on Fitting Normal Error

Liu Su[1], Zhang Yaping[1,2] and Feng Yuqin[2,3]

[1]School of Transportation Engineering, Changsha University of Science and Technology, Changsha, China; P.O. Box 410076, PH (+86) 13055161279; email: liusuyx@126.com
[2]School of Transportation Science and Engineering, Harbin Institute of Technology, P.O. Box 150090; email: zxlt0905@163.com
[3]Heilongjiang Institute of Technology, Harbin, China; P.O. Box 150090; e-mail: fengyuqin1998@163.com

ABSTRACT

After discussion about definition and constitution and properties of fitting normal error, one new method is put forward, that suggests the fitting normal error represents the error of fitting the horizontal alignment in old-highway. In addition, the accuracy indexes of fitting horizontal alignment in old-highway based on fitting normal error is established. The algorithms of swinging approach on compressible size step can be used to calculate the fitting normal error. From the way and basic norm of decision about fitting normal error' sign discussed, It is practicable that the quantity of fitting the horizontal alignment in old-highway is controlled by the accuracy index of fitting the horizontal alignment in field and interior work. Finally, an example of estimate for accuracy of fitting horizontal alignment in reform design of the State Highway G321 is offered.

Keywords: Fitting horizontal alignment in old-highway, Fitting normal error, Fitting accuracy, Algorithm of swinging approach on compressible size step

INTRODUCTION

It is very common to redesign and reform old-highways through measuring the horizontal and vertical section lines (Chen et al. 2005; Thomas et al.1999). They also need fitting. Furthermore, the vertical section lines are on the basic of the horizontal alignment. From redesigning and reform old-highway horizontal alignment angle, work of horizontal alignment has more load and higher level skill demand, which makes the horizontal alignment be the key of fitting the horizontal alignment in old-highway (Liu Su 2004). In recent decade years, researches on the horizontal alignment in old-highway, such as at home and abroad, are not much on the discussion about the fitting accuracy (Easa.1999; Muthusubramanyam.2003; Shao et al.1999; Steve Lam et al. 2003), but more about the algorithm of the computer auto fitting normal error (China Ministry of Communications 1999). There is a fitting error in the comparison between the fitting horizontal alignment function

and the original horizontal alignment in old-highway, caused by the effect of the measure error, crossing line point of intersection operational error and curve element configure error, which affects the quality of the fitting plan lines in old-highway (Survey Adjustment Group in School of Geodesy and Geomatics of Wuhan University 2003). So it's necessary to make a reach on the fitting normal error of the horizontal alignment and fitting accuracy in the old-highway reform plan and on the criterion of corresponding technology, too (He Yi 1998). The method of accuracy of fitting horizontal alignment in old-highway is discussed with the example of fitting the horizontal alignment in the redesigning and reform of the State Highway G321 based on the fitting accuracy of the horizontal alignment in this paper.

FITTING NORMAL ERROR OF PLANE LINE IN OLD-HIGHWAY

A. The definition of fitting normal error of the horizontal alignment in old-highway

According to an interval, which is from the end-point i-1th of horizontal curve to the end-point i^{th} of horizontal curve, it is divided into N parts. Supposed that the function of i^{th} section fitting the horizontal alignment of old-highway as follows:

$$F_i = \begin{pmatrix} x \\ y \end{pmatrix} = \begin{pmatrix} f_{xi}(l, R_i, Ls_{i1}, Ls_{i2}) \\ f_{yi}(l, R_i, Ls_{i1}, Ls_{i2}) \end{pmatrix} (i = 1,2,...,N) \quad (1)$$

Where, x and y are in the coordinates of one point on this horizontal alignment (including the straight line and horizontal curve), l is the mark of mile, R_i is the radius of curve, Ls_{i1} and Ls_{i2} are the length of the first and second transition curve respectively.

One section of plane of road is divided into two equal parts by a midline, in which number of points is n_1. Based on the control of the high grate plane, the coordinate of fitting reference point by measuring divided point will be calculated as follows:

$$(X_k, Y_k) \quad (k = 1,2,...n_i)$$

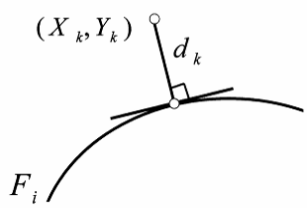

Figure 1 Diagrammatic sketch of fitting normal error

Seek the function of shortest distance to the fitting horizontal alignment in Fig.1:

$$d_k \quad (k = 1,2,..., n_i)$$

Where d_k is on the direction of the centerline normal of interpreter point to the fitting centerline, and d_k is regarded as the fitting normal error from point (X_k, Y_k) to the

curve (see Fig 1). The fitting normal error of the horizontal alignment d is the token of the fitting error.

B. **The structure and the property of the fitting normal error of the plane line in old-highway**

Supposed that the fitting normal error of the horizontal alignment d in old-highway is formed by sum of Δ_p, ε_1 and ε_2 where Δ_p represented the fitting error of the controlling point; ε_1 represented the fitting error of the crossing line, and ε_2 is the curve fitting error. Namely,

$$d = \Delta_p + \varepsilon_1 + \varepsilon_2 \tag{2}$$

Δ_p is caused by three factors, such as accident error, measuring error of old-highway constructing period, the error of equal divisions made in reform design period and the measuring error of the coordinate. ε_1 is the fitting system error, which is caused by the system warp for point of intersection of beeline threading . Where ε_2 is the fitting system error, caused by ΔR, ΔLs the stating system error of curve radius R and the length of transition curve.

The fitting criterion of the method of least square shall be satisfied in the fitting horizontal alignment in old-highway, as

$$\sum_{k=1}^{n_i} d_k^2 = \min \tag{3}$$

And the one fitting it is called unbiased fit, that is,

$$E(d) = E(\Delta_p) + E(\varepsilon_1) + E(\varepsilon_2) = 0 \tag{4}$$

Since Δ_p is an accident error, so it can be concluded that $E(\Delta_p) = 0$, that is $E(\varepsilon_1) + E(\varepsilon_2) = 0$ can be concluded from (4). If $\varepsilon_1 = \varepsilon_2 = 0$, the fitting horizontal alignment in old-highway will satisfy the fitting criterion of method of least square (3), which is an unbiased fit. On the contrary, if $\varepsilon_1 + \varepsilon_2 \neq 0$, then the fitting horizontal alignment in old-highway won't satisfy the criterion of method of least square, when it is a biased fit. As a result, Fig.2 shows the biasness and linearity of the straight segment and curve segment fit. The statistical properties of ration of the fitting normal error of the horizontal alignment in old-highway show the fitting quality of the horizontal alignment.

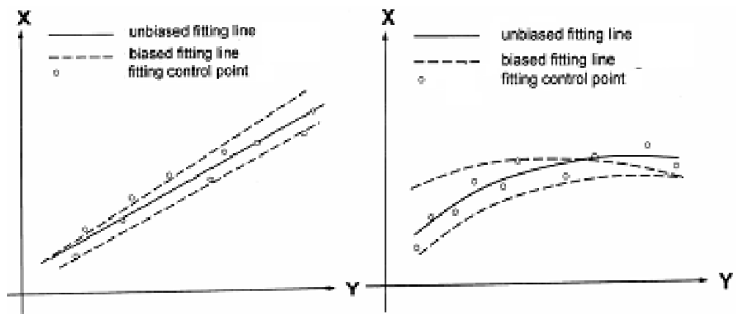

Figure 2 Diagrammatic sketch of fitting straight line and curve

The fitting normal error d is affected by the fitting accident error and the leading fitting system error.

Δ_p comes from the fitting field work, while ε_1 and ε_2 come from the fitting interior work. As usual, the fitting field works contents two major subjects. One is the fitting reference point conformed by the equal divided highway. Another is the measure of fitting reference point coordinate. In order to conform the equal divided highway error of the fitting, it is necessary to make reference point becomes the major point to decide the value of Δ_p, and it is based on premise that measuring error in the old-highway construct period and the measuring error of fitting control coordinate during the redesigning and reform period satisfy enough accuracy. There are two major works during interior work of fitting horizontal alignment, which are the threading point of intersection and state curve elements (curve radius, transition curve). ε_1 and ε_2 are the major errors which cause the biasness of the fitting normal error *d*. If Δ_p satisfies enough accuracy, the magnitudes and signs of ε_1 and ε_2 decide the magnitude and direction of d and it's systematic rather than random.

C. Arithmetic of *d* the fitting normal error of the horizontal alignment in old-highway

Arithmetic of computing *d* is the key to the arithmetic of the fitting index of horizontal alignment in old-highway. Considering constrains above, the paper put forward the algorithm of swinging approach on compressible size step is used to get solve:

Let (X_k, Y_k) $(k = 1,2,...,n_i)$ be the fitting reference point coordinate of the horizontal alignment in old-highway i^{th} section, corresponds to (x_l, y_l) coordinate of point in the midline in the fitting horizontal alignment function F_i of searching mark l. And point (x_l, y_l) can be obtained by calculating of the fitting horizontal alignment coordinate function (Liu Su 2004). If the original number of the searching mark l is l_0 and the searching length is the distance ΔS (>0), and $l = l_0 + \Delta S$, also, then there will be an error from fitting reference point (X_k, Y_k) to the midline point of the fitting function (x_{l_0}, y_{l_0}) and (x_l, y_l) as follows;

$$d_{l_0-k} = \sqrt{(x_{l_0} - X_k)^2 + (y_{l_0} - Y_k)^2} \; ; \; d_{l-k} = \sqrt{(x_l - X_k)^2 + (y_l - Y_k)^2}$$

And the difference of biasness likes this: $\Delta d = d_{l-k} - d_{l_0-k}$

If Δd <0, then $d_{l-k} < d_{l_0-k}$, and if $l = l + \Delta S$ and $\Delta d = d_{(l+\Delta S)-k} - d_{l-k}$ is kept iterative approach to calculate circularly, till $d_{(l+\Delta S)-k} > d_{l-k}$, d_{l-k} and l are taken as the second comparative original number of iterative circle calculate and $l = l - 0.1\Delta S$ is assumed (the length is reduced to $0.1\Delta S$ with reverse searching), $\Delta d = d_{(l-0.1\Delta S)-k} - d_{l-k}$ will be solved.

If Δd <0, $l = l - 0.1\Delta S$ and is kept iterative to

calculate $\Delta d = d_{(l-0.1\Delta S)-k} - d_{l-k}$ repeatedly, till $d_{(l-0.1\Delta S)-k} > d_{l-k}$, d_{l-k} and l are taken as the third comparative original number of iterative circle calculate and $l = l + 0.01\Delta S$ is assumed (the length is reduced to $0.1\Delta S$ with reverse searching), and the same steps continued……

The length of last part is 1mm, opposing to the last step and iterative circularly till $d_{(l\pm 0.001)-k} > d_{l-k}, d_{l-k} = \min$ will be obtained.

$d_k = d_{l-k}$ is taken as fitting normal error of horizontal alignment in old-highway , and it is caused by the departure of the fitting reference point (X_k, Y_k) ($k = 1,2,...,n_i$).The responding mile mark of the fitting horizontal alignment in old-highway is l, and the plane coordinate is (x_l, y_l) .

D.* Judgment of sign to fitting normal error *d

Since the increasing direction of fitting midline mark regarded as the progress direction, the distance which fitting reference point departure around the midline is the determinant benchmark of the sign of the normal error d. In order to facilitate judge the sign of fitting normal error, the right is positive, to the left is negative. To confirm the sign of d needs to calculate the coordinate azimuth angle α_d that from (x_l, y_l) , the respond fitting midline point to the fitting reference point, then compares it with the tangent azimuth angle of the fitting midline point (x_l, y_l) in this horizontal alignment segment. Table 1 shows the Correlate data about some normal errors of N42 fitting horizontal alignment in one partition of State Highway G321.

Table 1 Correlate data about some normal errors of N42 fitting horizontal alignment in one partition of State Highway G321

Channel mark	Tangent azimuth angle	Normal azimuth angle	Normal error
191676	323°48′	53°48′	-0.269
191696	323°46′	53°46′	-0.34
191716	323°38′	53°38′	-0.365
191736	322°05′	52°05′	-0.278
191756	318°46′	48°46′	-0.204
191776	316°07′	226°07′	0.081
191796	311°18′	221°18′	0.237
191816	307°10′	217°10′	0.233
191836	303°25′	213°25′	0.101

THE FITTING ACCURACY INDEX AND CONTROL OF THE HORIZONTAL ALIGNMENT IN OLD-HIGHWAY

According to the structure and quality of the fitting normal error of the horizontal alignment in old-highway, the accuracy index- mean-square deviation, which can show the affect degree of the accident error and system error, shall be taken to measure the fitting quality of the horizontal alignment.

Considered the maneuverability, the mean-square deviation shall be replaced

by formal approximation of estimative error in fitting as the fitting accuracy index of the horizontal alignment.

If d_k ($k = 1,2,...,n_i$), the fitting normal error of the plane line i is taken, there will be a fitting accuracy index of the plane line *i* as follows:

$$m_i = \sqrt{\sum_{k=1}^{n_i} d_k d_k \Big/ n_i} \quad (i = 1,2,...,N) \tag{5}$$

The fitting accuracy index of the horizontal alignment in old-highway like this:

$$m = \sqrt{(\sum_{k=1}^{n_1} d_k d_k + \sum_{k=1}^{n_2} d_k d_k + ... + \sum_{k=1}^{n_N} d_k d_k) \Big/ (n_1 + n_2 + ... + n_N)} = \sqrt{\sum_{i=1}^{N} n_i \cdot m_i^2 \Big/ \sum_{i=1}^{N} n_i} \tag{6}$$

THE EXAMLLE OF THE ACCURACY EVALUATION OF FITTING HORIZONTAL ALIGNMENT IN ONE SEGMENT OF G321

One project in one partition of State Highway G321 is a technology reform basing on the original second highway with whole length of 120 km. It is right to recover the horizontal alignment in old-highway, the 1st class plane control lead based on state coordinate system to equal divide the old-highway and measure the coordinate, because the horizontal alignment in old-highway is complex and the design data about the original line is not compete. So it is quite important to separating of the horizontal alignment in old-highway during threading point of intersection and using line software, such as AutoCAD. In order to get generalized results, the paper chooses total 67 partitions from K170+000 to K207+309.55 in the old partition, divided by interval, which is from the *i*-1th end-point of horizontal curve to the i^{th} end-point of horizontal curve. And the fitting accuracy of the horizontal alignment of every segment is obtained, on the base of the fitting normal error of 18000 calculated fitting reference points. As a result, Fig.3 is a chart of accuracy distribution of fitting horizontal alignment in one partition of every partition .If the fitting accuracy limited error is 0.500m,then the 24th, 27th, 33rd, 34th, 35th, 40th fitting accuracy of horizontal alignment are lower in the Chart, which is 0.748m; 1.273m; 1.987m; 1.061m; 1.797m; 0.743m.The fitting accuracy of the horizontal alignment in old-highway from K170+000 to K207+309.55 will be 0.190m, which will satisfy the fitting accuracy limited error after refitting the six horizontal alignment and correcting . Fig.4 is a chart of accuracy distribution of fitting horizontal alignment after correction.

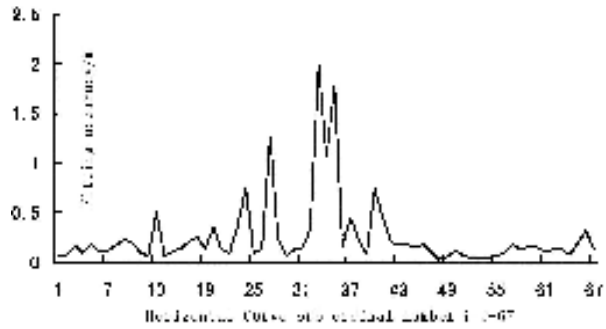

Figure 3 Chart of accuracy distribution of fitting plane linear in one partition of State Highway G321

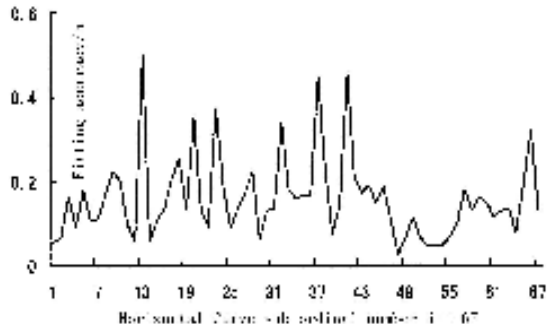

Figure 4 Chart of accuracy distribution of fitting plane linear after correction

CONCLUSIONS

The fitting error of horizontal alignment in old-highway can be signaled by the fitting normal error of horizontal alignment. Furthermore, the normal error is caused by three factors, such as accident error, measuring error of old-highway constructing period, the error of equal divisions made in reform design period and the measuring error of the coordinate formed, which are the result of the effect of accident error and system error. The fitting normal error of horizontal alignment in old-highway can be got from the computer, and algorithm of swinging approach on compressible size step. Finally, judgment of sign of fitting normal error can be got by comparing the fitting azimuthally angle and king pile tangent to confirm the deflection of the normal. Since increasing direction of fitting midline is mark of highway, turning to left is positive, while turning to right negative.

In addition, the accuracy index can be used to show the fitting quality of the pale lines in old-highway. According on the fact that the fitting accuracy index of the partition horizontal alignment can reflect the fitting quality of the horizontal alignment of partition in old-highway; the fitting accuracy index of the horizontal alignment in whole old-highway can reflect the fitting whole quality of the horizontal alignment in the old-highway basing on the fitting accuracy of the partition horizontal alignment

Furthermore, the fitting quality of the horizontal alignment in old-highway can be controlled in field and interior. The example of accuracy estimation of fitting horizontal alignment in one partition of State Highway G321 can prove that the estimated method of fitting accuracy of the horizontal alignment in old-highway, which bases on the normal error, works. The study about the limited error of the fitting horizontal alignment in old-highway and the related technology criterion still has a long way to go.

REFERENCES

Chen De-hua, MO Hai-ying. (2005). Discussion on Horizontal Alignment Fitting for Old Road Reconstruction, *Central South Highway Engineering*, 30(3): 97-102

China Ministry of Communications. (1999). Specification for Highway Reconnaissance Survey (JTJ 061-99). Beijing. *China Communications Press*, 67-89

He Yi. (1998). Research on Application of Rational Cubic Spline Curve in Highway Alignment Design, *China Journal of Highway and Transport*, 11(1): 47-53

Liu Su. (2004). Research of Automatic Calculation of Shortest Distance of Highway's Centre-Line from the Route's Control Point, Highway, (3):15-18

Liu Su. (2004). Research of the Computer-Aided Method of Survey Deviation Detection on Highway's Plane and Vertical Section Line, *Journal of Central South University (Science and Technology)*, 35(6): 1031-1034

M. Easa.(1999) Optimum Vertical Curves for Highway Profiles . Journal of Surveying Enjineering,Vol.125 No.3, ASCE: 147-157

M. Muthusubramanyam. (2003).Graphical Solution for Vertical Curve computation. *Journal of Surveying Engineering,*Vol.129 No.3, ASCE: 125-126

Shaowei Han and Chris Rizos. (1999) Road Slope Information from GPS-Derived Trajectory Data. *Journal of Surveying Engineering,*Vol.125, No.2, ASCE: 59-68

Steve Y.W.Lam and Conrad H.W.Tang. (2003). Geometric Modeling Systems for Construction Surveying of Highway Tunnels. *Journal of Surveying Engineering*,Vol.129, No.4, ASCE:146-150

Survey Adjustment Group in School of Geodesy and Geomatics of Wuhan University. (2003). The Basis of Error Theory and Survey Adjustment. *Wuhan University Press*, 55-58

Thomas G. Davis.(1999). Total Least-Spiral Curve Fitting. *Journal of Surveying Engineering*,Vol.125 No.4, ASCE:159-176

Effects of Layer Interface Conditions on Fatigue Behavior of Asphalt Pavements with Semi-rigid Bases

Zhao Yan-qing[1] Zhou Chang-hong[2] Tan Yi-qiu[3]

[1]Department of Transportation Engineering, Dalian University of Technology, #2 Linggong Road, Dalian 116024; PH (86) 411-84707761,email:Yanqing_zhao888@126.com

[2]Department of Transportation Engineering, Dalian University of Technology, #2 Linggong Road, Dalian 116024; PH (86) 411-84707761,email: zhow@yahoo.cn

[3]School of Transportation Science & Engineering, Harbin Institute of Technology, #92 Xidazhi Street, Harbin 150001, PH (86) 451-86412114, email: yiqiutan@163.com

Abstract: Effects of the layer interface condition on fatigue behavior of asphalt pavements with semi-rigid bases were evaluated in this study by means of viscoelastic three-dimensional finite element analyses. The Coulomb friction model was adopted to simulate the behavior of the layer interface. Effects of the position of the frictional interface, temperature, and friction coefficient were investigated. The results show that fatigue cracking is unlikely to occur in AC layers for a properly designed asphalt pavement with semi-rigid bases if all layer interfaces are fully bonded. A frictional interface can result in large horizontal tensile stress at the bottom of the AC layer that forms the interface. Depending on the position of the frictional interface, fatigue cracking may initiate at the bottom of HMA or at the bottom of an intermediate AC layer. With the increase of the Coulomb friction coefficient, the tensile stress at the bottom of the corresponding AC layer can be significantly reduced, especially at high temperatures.

Keywords: viscoelasticity; three-dimensional finite element method; Coulomb friction model; fatigue cracking; friction coefficient.

1. Introduction

Fatigue cracking has long been recognized as one of the major distress types of asphalt pavements. In China, semi-rigid materials (e.g., cement treated or lime-flyash treated aggregates) are widely used as base materials for asphalt pavements. Semi-rigid bases possess high elastic modulus values and provide a good load carrying capacity to the pavement structure. Thus, tensile stress and tensile strain at the bottom of the asphalt concrete (AC) layer can be efficiently reduced, which results in less fatigue cracking. However, severer fatigue cracking in AC layers is still observed in some asphalt pavements with semi-rigid bases. The reason for the occurrence of AC fatigue cracking could be that fatigue cracking first takes place in semi-rigid bases under repeated traffic loading, reducing the semi-rigid bases to materials like granular bases, which leads to large tensile stress and strain at the bottom of the AC layer and subsequently fatigue cracking in AC layers develops. Studies have shown interlayer conditions have significant influences on asphalt pavement responses (Romanoschi et al. 2001; AlHakim 2002). Filed experiences also suggest that poor interlayer conditions may play an important role in the fatigue cracking of asphalt pavements with semi-rigid bases. It is the purpose of this paper to investigate this issue by performing mechanistic analysis of relevant pavement responses. Traditionally, asphalt pavement responses are analyzed using linear-elastic layered theory, which may not be capable of reflecting the real behavior of asphalt pavements since asphalt concretes are typical viscoelastic materials. In this study, effects of interlayer conditions on the fatigue behavior of asphalt pavements are investigated by conducting three dimensional (3D) finite element (FE) analyses in which asphalt concretes are

modeled as viscoelastic materials.

2. Finite element model and material properties

A typical asphalt pavement with a semi-rigid base, as illustrated in Figure 1, was selected for analysis in this study. Asphalt concretes were treated as viscoelastic materials while the semi-rigid base, granular base, and subgrade were treated as linear elastic materials whose elastic moduli and Poisson's ratios are listed in Figure 1. According to Boltzmann superposition principle, a viscoelastic material has the following constitutive relationship:

$$\sigma(\xi) = \int_0^{\xi} E(\xi - \tau) \frac{\partial \varepsilon}{\partial \tau} d\tau \qquad (1)$$

where σ and ε are stress and strain respectively, E is the relaxation modulus of the viscoelastic material, τ is integral variable, and ξ is reduced time. The following relationship exists between reduced time ξ and physical time t:

$$\xi = \int_0^t \frac{dt}{\alpha_T} \qquad (2)$$

where α_T is time-temperature shift factor. Time-temperature shift factors reflect the effects of temperature on a material's mechanical properties. Once the time-temperature shift factors are known, the mechanical properties of asphalt mixtures at various temperatures can be determined from those at the reference temperature. As can be seen from equation 1, the relaxation modulus is the basic parameter to characterize the viscoelastic material's mechanical property. However, determination of the relaxation modulus directly from laboratory testing requires complex operations and expensive equipment and often involve large errors. In this study, the viscoelastic properties of asphalt mixtures were obtained by conducting complex modulus tests at various conditions and then converting the complex modulus results to relaxation moduli. Complex modulus tests of SMA13, Superpave20, and Superpave25 were performed at five temperatures (4, 15, 25, 40 and 50℃). At each temperature, complex moduli were determined at seven frequencies (25, 20, 10, 5, 1, 0.5 and 0.1Hz). Details about the complex modulus tests and results were documented elsewhere (Zhao et al. 2006). Interconversion from the complex modulus to the relaxation modulus is based on theoretical formulations presented by Schapery (Schapery et al. 1999). Details on the numerical analyses of Interconversion and results can be found elsewhere (Zhao et al. 2007). The resulting relaxation moduli are represented using the Prony series as follows:

$$E(t) = E_{\infty} + \sum_{m=1}^{M} E_m \exp(-t/\rho_m) \qquad (3)$$

where ρ_m is relaxation time, $\rho_m = \frac{\eta_m}{E_m}$; E_{∞} and E_m are spring moduli, and η_m is the viscosity of the dashpot. The parameters of the Prony series and time-temperature shift factors at a reference temperature of 25℃ for various asphalt mixtures are presented in Table 1 and Figure 2 respectively (Zhao et al. 2006, 2007).

SMA13	4.0cm	Viscoelastic	μ =0.3
Superpave20	6.0cm	Viscoelastic	μ =0.3
Superpave25	8.0cm	Viscoelastic	μ =0.3
Semi-rigid base	40.0cm	E= 2000 MPa	μ =0.25
Granular subbase	20.0cm	E = 250 MPa	μ =0.35
Subgrade	E= 60 MPa	μ =0.4	

Figure 1 Asphalt pavement structure

A dual-tire assembly with a center-to-center distance of 32cm was used in this study. Each tire has a contact area of 18.9 ×18.9cm^2. The intensity of the load is assumed to vary with time according to a haversine function as follows (Huang 1993):

$$L(t) = q\sin^2(\frac{\pi}{2} + \frac{\pi \times t}{d}) \qquad (4)$$

where d is the duration of load and q is the amplitude of load. In this study, a haversine load with a duration of 0.1s and a peak load of 0.7MPa was adopted to simulate the applied traffic loading. The commercial software ABAQUS was used to create a three-dimensional finite element model for the pavement, as shown in Figure 1, and relevant user subroutines were developed for analyses. Due to the double symmetry of geometry, boundary conditions, and load configuration about the x and y axes, only a quarter model was analyzed. The dimensions of the FE model were 3.0m×3.0m×5.0m in the X, Y and Z directions respectively. Eight-node linear brick elements with reduced integration were selected to discrete the model and the resultant mesh contains 24,098 elements and 26,208 nodes. In addition to the symmetric boundary conditions, roller support and fixed support were adopted on vertical boundaries and the bottom of the model, respectively. Such boundary conditions have been successfully used by Zaghloul et al. (1993) and Kuo et al. (1995).

Two interlayer condition models, the Coulomb friction model and elastic stick model, are commonly used in pavement analysis. Yoo et al. (2006) compared pavement responses calculated using the two models and measured field responses. The results did not show the superiority of one model over the other. Thus the Coulomb friction model was used in this study for its simplicity. The Coulomb friction model assumes no relative motion occurs between the surfaces defining the interface if shear stress is less than the critical stress, $\tau_{\max}$, which is proportional to the normal pressure at the interface as presented in equation 5:

$$\tau_{\max} = \mu p \qquad (5)$$

where p is the normal stress at the interface and μ is the friction coefficient. In this study, a wide array of friction coefficients ranging from 0.0 to 1.0 with an interval of 0.2 were used to evaluate the effects of different layer interface conditions.

Table 1 Prony series coefficients of relaxation moduli

Term	ρ_m (s)	E_m （MPa）		
		SMA13	Sup20	Sup25
1	0.000002	1768.87	2713.77	2131.19
2	0.00002	2857.03	3856.26	3162.95
3	0.0002	4086.33	4911.19	4218.94
4	0.002	4472.95	5000.64	4461.53
5	0.02	3302.65	3762.55	3350.93
6	0.2	1578.41	2034.68	1666.81
7	2	550.03	845.38	572.76
8	20	176.11	312.06	162.21
9	200	61.55	117.84	46.97
10	2000	24.32	48.47	15.71
11	20000	11.20	23.14	6.10
12	200000	3.25	7.16	2.95
13	2000000	9.34	20.02	0.51
	E_∞	45	50	10.4

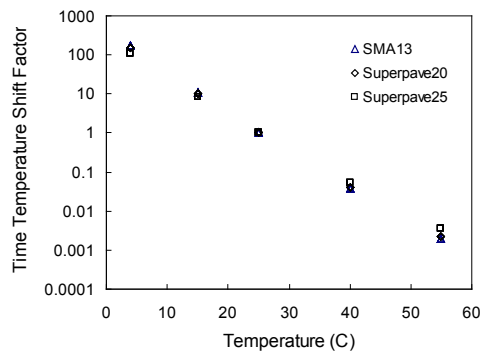

Figure 2 Time-temperature shift factors

3. Analysis results and discussion

Horizontal tensile stresses at the bottom of the AC layers, which are the critical responses for fatigue cracking in China's asphalt pavement design method, were calculated at three different temperatures (10, 25 and 40℃). At each temperature, analyses were performed for four different cases of layer interface conditions as shown below:

- Case 1: All layer interfaces were fully bonded.
- Case 2: The Coulomb friction model was adopted at the SMA13-Superpave20 interface and other interfaces were fully bonded.
- Case 3: The Coulomb friction model was adopted at the Superpave20-Superpave25 interface and other interfaces were fully bonded.

- Case 4: The Coulomb friction model was adopted at the Superpave25-base interface and other interfaces were fully bonded.

If the Coulomb friction model was used for a layer interface, responses were calculated at various friction coefficients (0.0, 0.2, 0.4, 0.6, 0.8 and 1.0). Results obtained from Case 1 formed the basis for comparisons. Figure 3 shows the variations of horizontal tensile stresses with loading time at the bottom of the Superpave25 layer for Case 1. Positive and negative values indicate tensile and compressive stresses respectively. To illustrate the effectiveness of the semi-rigid base in reducing fatigue cracking, results were obtained by replacing the semi-rigid base in Figure 1 with a granular base (E=300MPa), which can also be regarded as a severely cracked or deteriorated semi-rigid base, are also presented in Figure 3. The semi-rigid base and granular base are respectively labeled as 'SRB' and 'GB' in the figure.

As shown in Figure 3, except for the case of the semi-rigid base at 40℃, tensile stresses developed at the bottom of the Superpave25 layer during loading phase and the tensile stresses gradually changed to compressive stresses during unloading phase. This is due to the fact that the pavement deflects downwards during the loading phase and elastic layers (base, subbase, etc.) tend to rebound to its original shape instantaneously during the unloading phase, while AC layers rebound gradually due to their creep behavior, which causes compressive stress at the bottom of the AC layer (Wang et al. 2006). Figure 3 shows that peak tensile stress occurred before the 0.05s loading time at which peak load took place. Tensile stress is influenced by both the applied load and stress relaxation characteristics of asphalt mixtures. Once the effects of stress relaxation exceed those of the applied load, tensile stress starts to decline, which causes a peak tensile stress time prior to 0.05s. At higher temperatures, the effects of stress relaxation become more evident and thus peak tensile stress happens at an earlier loading time. For example, the peak tensile stress time for the case of the semi-rigid base at 10℃ was 0.0465s and it was advanced to 0.033s at 25℃.

As expected, the use of the semi-rigid base in asphalt pavement greatly reduced the potential of fatigue cracking in AC layers. Compared to asphalt pavement with the granular base, the maximum tensile stresses at the bottom of the Superpave25 layer were reduced by 69% and 91% at 10℃ and 25℃, respectively, when a semi-rigid base was used. The bottom of the Superpave25 layer was even subjected to horizontal compressive stress at 40℃ for the case of the semi-rigid base. The results indicate that for a properly designed asphalt pavement with semi-rigid bases, fatigue cracking is unlikely to occur at the AC layers if the semi-rigid bases are in good condition and all layer interfaces are fully bonded. Following analyses were performed only on the asphalt pavement with semi-rigid bases, as shown in Figure 1.

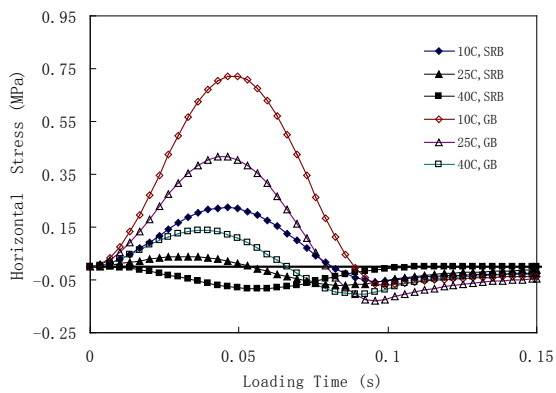

Figure 3. Tensile stresses at the bottom of Superpave25 layer (case 1)

Figures 4, 5, and 6 present the horizontal tensile stresses at the bottom of the Superpave25 layer for various interface condition cases and temperatures. Only the results calculated using a friction coefficient of 0.6 are presented in these figures. As shown in these figures, with the use of the friction condition at a layer interface, if the bottom of the Superpave25 layer was subjected to horizontal tensile stress during the loading phase, the horizontal stress gradually changed to compressive stress as time continued, similar to what happened in Case 1. The use of the friction condition at the SMA13-Superpave20 or Superpave20-Superpave25 interface did not adversely affect the tensile stress at the bottom of the Superpave25 layer. Compared to Case 1's results, the tensile stress at the bottom of the Superpave25 layer became less for Case 2's interlayer condition and Case 3's interlayer condition resulted in compressive stress during the loading phase. However, the use of the friction condition at the Superpave25-base interface significantly increased the tensile stress at the bottom of the Superpave25 layer. The tensile stresses increased by 1.9 and 6.1 times for Case 4 compared to Case 1's results at 10 and 25℃, respectively. At 40℃, the horizontal stress varied from compressive stress for Case 1 to tensile stress with a maximum value of 0.12MPa for Case 4.

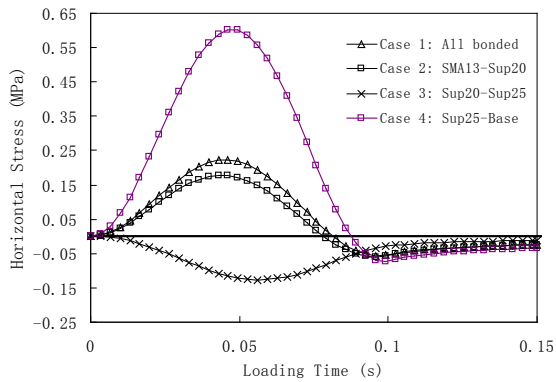

Figure 4. Horizontal stresses at the bottom of Superpave25 layer (10℃, μ=0.6)

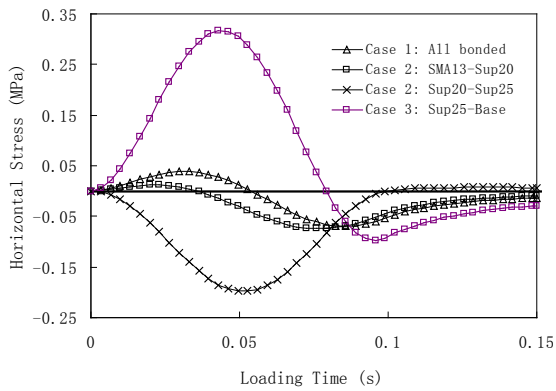

Figure 5. Horizontal stresses at the bottom of Superpave25 layer (25℃, μ=0.6)

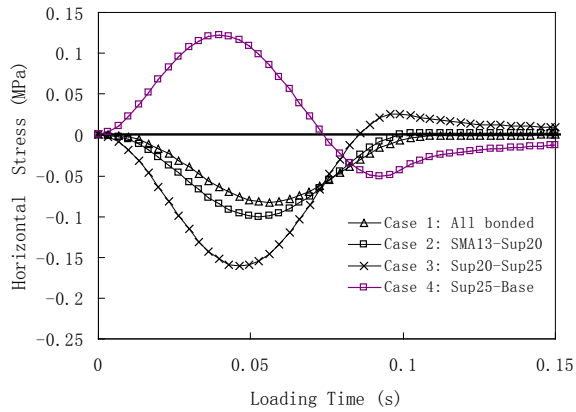

Figure 6. Horizontal stresses at the bottom of Superpave25 layer (40℃, μ =0.6)

Table 1 lists the maximum tensile stresses at the bottom of the Superpave25 layer obtained at various friction coefficients. For comparison purposes, the results from pavements with granular bases and Case 1's interlayer condition are also presented in the table. As shown in Table 1, the variations of the friction coefficient for Case 2 and Case 3's interlayer conditions had little influence on the maximum tensile stress while the maximum tensile stress decreased significantly as the friction coefficient increased for Case 4, especially at high temperatures. For example, the tensile stress decreased by 15.2% as the friction coefficient increased from 0.0 to 1.0 for Case 4 at 40℃. It can be observed from Table 1 that the maximum tensile stresses obtained from Case 4 were close to those obtained from pavements with granular bases and Case 1's interlayer condition. This observation indicates that fatigue cracking could develop at the bottom of HMA in asphalt pavements with semi-rigid bases if the AC-base interface is not fully bonded.

Table 1. Maximum horizontal tensile stress at the bottom of Superpave25 layer (MPa)

Interface Case	Temperature (℃)	Coulomb friction coefficient 0	0.2	0.4	0.6	0.8	1	Case1 (SRB)	Case1 (GB)
Case 2: SMA13-Sup20	10	0.1794	0.1790	0.1786	0.1782	0.1779	0.1775	0.2232	0.7229
	25	0.0121	0.0121	0.0120	0.0120	0.0120	0.0119	0.0384	0.4160
	40	0.0027*	0.0027*	0.0027*	0.0027*	0.0027*	0.0027*	C	0.1376
Case 3: Sup20-Sup25	10	C	C	C	C	C	C	0.2232	0.7229
	25	0.0071*	0.0071*	0.0071*	0.0071*	0.0071*	0.0071*	0.0384	0.4160
	40	0.0266*	0.0264*	0.0262*	0.0261*	0.0259*	0.0258*	C	0.1376
Case 4: Sup25-Base	10	0.6125	0.6091	0.6057	0.6024	0.5991	0.5959	0.2232	0.7229
	25	0.3283	0.3242	0.3201	0.3162	0.3124	0.3086	0.0384	0.4160
	40	0.1357	0.1310	0.1268	0.1227	0.1188	0.1151	C	0.1376

Note. C = compressive stress; *tensile stress occurs during unloading phase.

Although a friction model at the SMA13-Superpave20 or Superpave20-Superpave25

interface did not increase the tensile stress at the bottom of the Superpave25 layer, it had an adverse effect on the tensile stress at the bottom of the AC layer which formed the frictional interface, shown in Figures 7 and 8. Figures 7 and 8 respectively presents the horizontal stress at the bottom of the SMA13 layer for Case 2 and at the bottom of the Superpave20 layer for Case 3 with a friction coefficient of 0.6. For comparison purposes, results from Case 1 are also presented in the figures. For Case 1's interface condition, the bottom of the SMA13 or Superpave20 layer was subjected to compressive stress during the loading phase and the compressive stress changed to tensile stress with the inclusion of a friction model at the corresponding interface. The maximum tensile stress at the bottom of the Superpave20 layer reached 0.48, 0.24, and 0.11MPa at 10, 25 and 40℃, respectively. Such large tensile stresses were likely to initiate fatigue cracking at the bottom of the Supepave20 layer.

Tables 2 and 3 list the maximum tensile stresses calculated at different friction coefficients. As shown in these tables, the tensile stress at the bottom of an AC layer was somewhat influenced by the variation of the friction coefficient of the corresponding interface, especially at high temperatures. Analyses of other results indicated that variation of the friction coefficient at one interface had little influence on the tensile stress at the bottom of other AC layers.

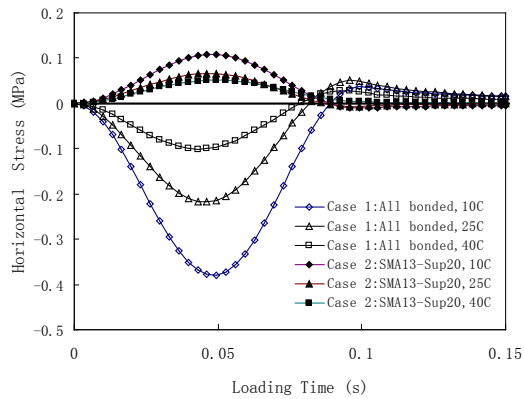

Figure 7. Horizontal stresses at the bottom of SMA13 layer (μ =0.6)

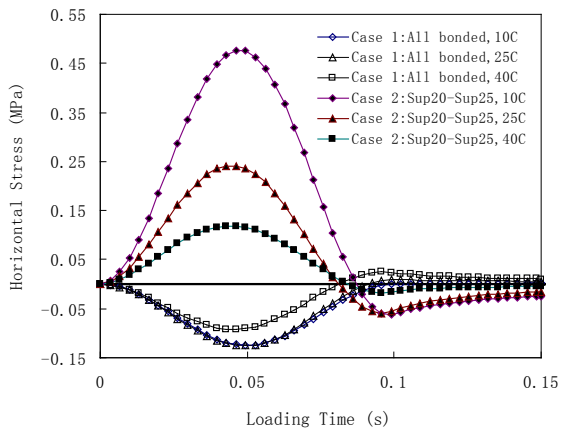

Figure 8. Horizontal stresses at the bottom of Superpave20 layer (μ =0.6)

Table 2. Maximum horizontal tensile stress at the bottom of SMA13 layer (Case 2, MPa)

Temperature	Coulomb friction coefficient						Case 1
(℃)	0	0.2	0.4	0.6	0.8	1	(SRB)
10	0.1093	0.1087	0.1080	0.1074	0.1067	0.1061	0.0371*
25	0.0692	0.0681	0.0670	0.0658	0.0646	0.0634	0.0512*
40	0.0609	0.0577	0.0545	0.0512	0.0480	0.0450	0.0285*

Note. *tensile stress occurs during unloading phase.

Table 3. Maximum horizontal tensile stress at the bottom of Superpvae20 layer (Case 3, MPa)

Temperature	Coulomb friction coefficient						Case 1
(℃)	0	0.2	0.4	0.6	0.8	1	(SRB)
10	0.4847	0.4821	0.4795	0.4770	0.4745	0.4720	0.0015*
25	0.2510	0.2477	0.2444	0.2412	0.2382	0.2353	0.0092*
40	0.1318	0.1272	0.1228	0.1187	0.1150	0.1113	0.0247*

Note. *tensile stress occurs during unloading phase.

4. Conclusions

Base on the results presented, the following conclusions can be drawn regarding the fatigue behavior of asphalt pavements with semi-rigid bases:

- Fatigue cracking is unlikely to occur in AC layers for a properly designed asphalt pavement with semi-rigid bases if the semi-rigid bases are in good condition and all layer interfaces are fully bonded.
- A frictional interface can result in large horizontal tensile stress at the bottom of the corresponding AC layer, and consequently fatigue cracking in the AC layer.
- Depending on the position of the frictional interface, fatigue cracking may initiate at the bottom of HMA or at the bottom of an intermediate AC layer.
- With the increase of the Coulomb friction coefficient, the tensile stress at the bottom of the corresponding AC layer could be significantly reduced, especially at high temperatures. However, the influence of the friction coefficient variation on tensile stress in other AC layers is negligible.

Acknowledgements

The financial supports provided by the National Science Foundation of China (No. 50778057) and Research Funding of Dalian University of Technology (No. 3015-893301) are greatly appreciated

Reference

1. AlHakim, B., (2002) The Importance of Good Bond between Bituminous Layers, Proceedings of 9th International Conference on Asphalt Pavements, Copenhagen, 2002.
2. Huang, H., (1993) Pavement Analysis and Design , Prentice Hall, Inc.

3. Kuo, M.C., Hall, K.T., and Darter, M., (1995) Three-dimensional finite element model for analysis of concrete pavement support, Transportation Research Record No. 1505, Washington, D.C., 119-127.
4. Romanoschi, S. A., and Metcalf, J. B. (2001) Characterization of asphalt concrete layer interfaces. Transportation Research Record No.1778, Washington D.C., 132-139.
5. Schapery, R.A., and Park, S.W., (1999) Methods of Interconversion Between Linear Viscoelastic Material Functions, Part I, Numerical Methods, International Journal Solids & Structures, Vol 39, No3, 1677-1699.
6. Wang, J., Birgisson, B., Roque, R., (2006) Effects of Viscoelastic Stress Redistribution on the Cracking Performance of Asphalt Pavements, Journal of the Association of Asphalt Paving Technologists, Vol 75, 637-675.
7. Yoo, P.J., Al-Qadi, I.L., Elseifi, M.A. and Janajreh, I., (2006) Flexible pavement responses to different loading amplitudes considering layer interface condition and lateral shear forces, The International Journal of Pavement Engineering, Vol. 7, No.1, 73-86.
8. Zaghloul, S.M., and White, T.D., (1993) Use of a three-dimensional, dynamic finite element program for analysis of asphalt pavement, Transportation Research Record No. 1388, Washington, D.C., 60-69.
9. Zhao, Y., Wu, J., Wen, J., (2006) Determination and Analysis of Dynamic Modulus of Asphalt Mixture and Its Master Curve, Highway, Vol8, 98~101.
10. Zhao, Y., Huang, D. and Pan, Y., (2007) Analysis of Viscoelastic Responses of Asphalt Pavements with Flexible Bases, Journal of Chinese Society of Civil Engineering, Vol40, No5, 96-99.

Damage Model Analysis of SBS Modified Asphalt Mixture

Ying Ronghua, Chen Xiao, Wu Ting and Zhang Zhiyong
(School of Traffic and Transportation Engineering, Changsha University of Science & Technology)

Abstract: The visco-elastic models and the damage models, which are coupled to the visco-elastic continuum damage model, are used for analyzing the uniaxial tension tests of the SBS modified asphalt mixture. The fatigue damage characteristics of the SBS modified asphalt mixture and damage effect have been considered in terms of energy and a fatigue damage model. The models and testing results correlate well with each other. The model can predict the fatigue life of the SBS modified asphalt mixture under different tensile strain levels.

Key words: modified asphalt mixture; tension tests; visco-elastic; damage factors; fatigue damage

Research in years suggests that asphalt mixture is a complex thermal rheological material. Its deformation is related to force state, temperature and loading rate. In practical engineering, the suitable temperature range of the asphalt pavement is -25 ~ 75℃. Therefore, it is necessary to understand the stress - strain relations of asphalt mixture at different temperatures. As asphalt pavement undertakes repeated external loading, it is also needed to recognize the fatigue properties of asphalt mixture. Currently, the main theoretical research model of asphalt mixture is the visco-elastic model, which can better reflect the strain rate effect of creep, relaxation and elastic modulus but can not explain the stress relaxation phenomenon. The damage constitutive model that reflects the reduction of effective area through the changing of damage parameters are able to reflect stress - strain curves in the whole process but not the strain-rate effect of material deformation. Previous asphalt mixture fatigue models are mostly regularity formula aimed at specific problems, which are applicable under certain conditions. However, its physical meaning is not clear.

In this study, uniaxial tensile tests of the equal strain rate loading control and strain control fatigue tests with triangular waveform on the SBS modified asphalt mixture are carried out with the electro-hydraulic servo test system of MTS810 at different temperatures. Then the two constitutive models are correlated with the data of uniaxial tensile test to establish a viscoelastic continuum damage constitutive model. According to the fatigue test interpreted with the energy principle, a fatigue damage model considering the tensile strain level is proposed . Because the damage effects of materials are taken into account, the model predictions match well with the experimental results and reflect the stress and strain levels in the SBS modified asphalt mixture.

1 Experimental study

1.1 Experimental materials

The SBS modified asphalt of AH-70 of Caltex is used in the test. The aggregate is a limestone and its mechanical properties are presented in Table 1,. The mineral powder is the limestone powder. The AC-13 gradation recommended in standards is adopted. It is shown in Table 2. The asphalt-aggregate ratio is 5% determined by the Marshall method.

Table 1 Test result of limestone

Crushing value/%	Sturdiness/%	Abrasion value/%	Compressive strength	Adhesion	Absorption/%
18.8	3.0	19.5	Grade 1	Grade 4	≤0.73

1.2 Specimen fabrication

Taking similar conditions between a lab compaction method and the field compaction method as a criterion, wheel-grind compaction is consistent with field condition and is therefore selected as the lab compaction method. After the SBS modified asphalt mixture is compacted using the wheel-grind compaction method, the sample is cut into trabecular specimens by a rock cutting machine. The specimen size is 45 mm × 45 mm × 250 mm (Lv, 2001). In order to eliminate the error in the preparation process, the specimens are processed repeatedly to meet the requirement that the ends of specimens of a total of 30 are horizontal.

Table2 Gradation composition

Gradation type	The percentage passing the following sieve pore/%									
	16.0	13.2	9.5	4.75	2.36	1.18	0.6	0.3	0.15	0.075
AC-13	100	97.5	79	58	44.5	32.5	24.0	17.0	12.0	6.0

1.3 Loading mode

In uniaxial tensile tests it is loaded at four temperatures -15, -5,5, and 15 ℃ under equal strain rate, and the loading rate is ε = 10-31 / s. Each specimen is loaded to the residual strength stage. Three specimens are tested at each temperature. In the uniaxial cyclic loading test, the triangular waveform loading is adopted for the tensile strain levels of 0.30%, 0.40% and 0.45% according to the strain control mode. The test temperature is -5℃, load rate $\dot{\varepsilon}$ = 10-31 / s, and the fatigue criterion is that the strength is decreased to 50% of the initial strength (JTG F40-2004). In order to eliminate the influence of eccentricity, specimens are preloaded at a small stress level and is recovered.

1.4 Testing system

The electro-hydraulic servo test system of MTS810 is used to carry out the experimental study. The load range of MTS810 is ±10 t (± represents tension and compression respectively), and it is automatic in the entire testing process through the computer control. In addition, MTS has a corollary temperature control system-the Tenny environment box with temperature control accuracy of ± 0.1 ℃.

1.5 Data acquisition and processing

Results of this study are acquired by the computer system which is the corollary equipment of MTS loading system with the interval time of 0.1s. Data are transmitted through electrical signals. Because of the effects of impedance and drifting, the collected data often fluctuate around the true values. So the Origin 6.0 filter (FFT) is used to filter collected data to attain the approximate real smooth curve (Figure 1). At higher temperatures, the deformation of SBS modified asphalt mixture is shown as an increasing curve, shown in Figure 1. The creep phenomenon of the material is obvious in Figure 1. At lower temperatures, the deformation of SBS modified asphalt mixture is shown as rising, linear and brittle until fracture of materials happens. It is also discovered that the failure strength decreases when the temperature increases.

Figure 2 shows the peak stress curve related to cycle number under different strains in the uniaxial cyclic loading tests. Shown in Figure 2, the peak stress also increases when the level of strain increases . The fatigue life varies with different strain levels.

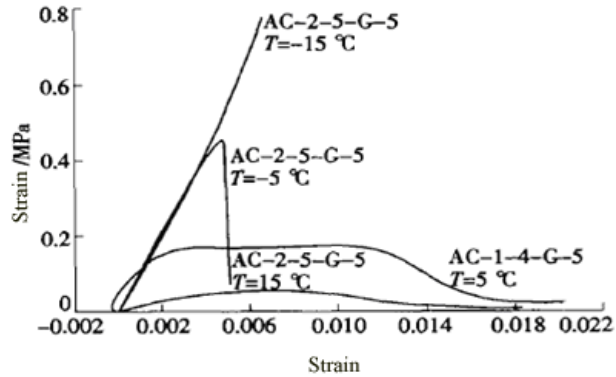

Figure1Stress-strain curves at different temperatures

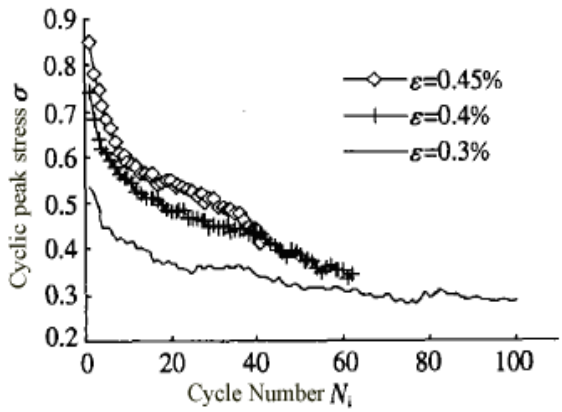

Figure2 Cyclic peak stress curves with cycle number changing

2 Establishment and Analysis of constitutive model

2.1 Establishment of viscoelastic damage constitutive model under uniaxial tension

2.1.1 Visco-elastic constitutive model of asphalt mixture

There are many constitutive models used to describe asphalt mixture by applying visco-elastic constitutive models, which include the Burgers, Kelvin, Maxwell and the generalized Maxwell models. The Maxwell model can be adopted to describe the main features of the viscoelastic creep and relaxation behavior of asphalt mixture. The Maxwell model reflects a viscoelastic fluid model. A large number of tests proved that asphalt mixture is a viscoelastic fluid material. Moreover, the Maxwell model is relatively simple. In this study the Maxwell model is selected to describe the viscoelastic behavior of SBS modified asphalt mixture. The constitutive equations of Maxwell model are as follows (Yang, 1992).

$$\sigma + \frac{\eta}{E}\dot{\sigma} = \eta\dot{\varepsilon} \tag{1}$$

By the Boltzmann superposition principle:

$$\sigma(t) = \varepsilon_0 G(t) + \int_0^t G(t-\xi)\frac{d\varepsilon(\xi)}{d\xi}d\xi \tag{2}$$

Where: G(t)-the relaxation function of the Maxwell model, G(t)=Eexp(-tE/η);when t=0, $\varepsilon_0 = 0$.

2.1.2 Determination of continuum damage factors

Compacted SBS modified asphalt mixture specimens have a lot of internal defects (voids, cracks and crushing). In essence, these micro-defects are discrete. As a simple approximation, in the continuum damage mechanics, all micro-defects are distributed. The impact to material caused by distributed micro-defects is expressed by one or several internal continuous field function of damage variables. The damage and fracture research results about rocks, cement concrete materials show that Weibull distribution is suitable for describing damage and fracture process of such materials, so the Weibull function will be used to describe the distribution of these defects (Yu and Feng, 1997).

$$\phi(\varepsilon) = \frac{m}{\alpha}(\varepsilon-\gamma)^{m-1}\exp\left[-\frac{(\varepsilon-\gamma)^m}{\alpha}\right] \tag{3}$$

While the damage factor D is determined by the number of defects, and $\frac{dD}{d\varepsilon} = \phi(\varepsilon)$, so

$$D = \int_\gamma^\varepsilon (x-\gamma)^{m-1}\exp\left[-\frac{(x-\gamma)^m}{\alpha}\right]dx = 1-\exp\left[-\frac{(\varepsilon-\gamma)^m}{\alpha}\right] \tag{4}$$

In this formula location parameter γ is equivalent to the damage threshold. Because there are voids when the asphalt mixture is shaped, it is considered that γ=0, and the damage value of asphalt mixture can be defined by Weibull function with two parameters: $D = 1-\exp\left(-\varepsilon^m/\alpha\right)$.

2.1.3 Visco-elastic continuum damage model

When specimens are subjected to tension, the deformation is always associated with defects. The viscoelastic damage constitutive model can be set up under the uniaxial tension (Yu and Qian, 1993).

$$\sigma(t) = (1-D)\left[\varepsilon_0 G(t) + \int_0^t G(t-\xi)\frac{d\varepsilon(\xi)}{d\xi}d\xi\right] = \exp\left[-\frac{\varepsilon(t)^m}{\alpha}\right]\left[\int_0^t E\exp\left[\frac{E(\xi-t)}{\eta}\right]\frac{d\varepsilon(\xi)}{d\xi}d\xi\right] \tag{5}$$

To the loading at equal strain rate, when $\frac{d\varepsilon(t)}{dt} = \varepsilon = \frac{\varepsilon(t)}{t}$:

$$\sigma(t) = \exp\left[-\frac{\varepsilon(t)^m}{\alpha}\right]\frac{\varepsilon(t)}{t}\eta\left[1-\exp\left[-\frac{Et}{\eta}\right]\right] \tag{6}$$

If $G'(t)$ is defined as a tensile modulus when the damage is considered in direct tension test, the tensile modulus is obtained by moving the strain to the left of the formula:

$$G'(t)=\frac{\sigma(t)}{\varepsilon(t)}=\exp\left[-\frac{\varepsilon(t)^m}{\alpha}\right]\frac{\eta}{t}\left[1-\exp\left[\frac{Et}{\eta}\right]\right] \tag{7}$$

From Formula 7, we can see that even if the damage of materials is not considered, its tensile modulus is also gradually decreasing. If using the reduction of original damage modulus as the damage value of the material, the viscous flow deformation in the material deformation used as a part of damage is included to the damage values of materials that are not used to reflect damage changes of the material.

2.1.4 Comparison of theoretical model predictions with test results

According to the time-temperature equivalence principle, a master curve of 15℃of tensile modulus is obtained by using Arrhenius shift factors to the tensile modulus of SBS modified asphalt mixture curves shown in Figure 1 at different temperatures. The displacement factor is:

$$\alpha_T=\exp\left[-\frac{\delta H}{R}\left[\frac{1}{T}-\frac{1}{T_0}\right]\right] \tag{8}$$

Where: δH is the activation energy of the material. For this material, δH =133938.5; R is the universal constant (8.314). T is temperature, and T_0 is the reference temperature, which are absolute temperatures.

Table3 The shift factor at different temperatures with the reference temperature of 15℃

Reference temperature/℃	-15	-5	5	15
The shift factor α_T	0.001497	0.015384	0.133702	1

Using fitting function DamageEvisco of the Nonlinear Curve Fitting in Origin6.0, as shown in Figure 3, each parameter of the visco-elastic damage model at 15℃ is obtained: m = 0.09604, α = 0.71774, η = 8548.89 MPa • s, E = 407.138 MPa, R2 = 0.977.

Comparing the tensile modulus curve at 15℃ with the original curve, Figure 3 shows that the results of theoretical calculations are well fitted with the experimental results. The consistency indicates relevance of the model for the tensile modulus.

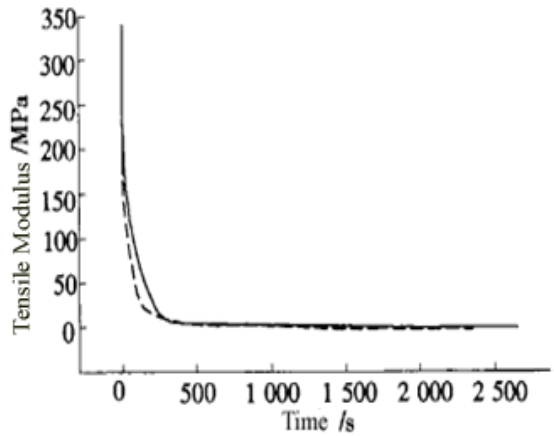

Figure3 the main curve of tensile modulus and the fitting curve of asphalt mixture at 15℃

2.2Establishment of fatigue damage model under uniaxial cyclic tension

It is necessary for asphalt pavement to withstand traffic loads and repeated variation of temperature in the long-term process. So it is more practically significant to do research on the fatigue characteristics of asphalt mixture. In the existing fatigue damage models, there is Chaboche model, Wang model, Lemaitre model and so on. In essence, a variety of models are just regular formula to the specific problem. They are applicable under certain conditions, but its physical meaning is not clear. The process of fatigue damage in fact is an irreversible process of energy consumption. Therefore, the plastic strain energy consumed in each cycle of the damage course (known as the cyclic hysteresis energy) can be adopted as the state parameter to define the damage function, so that the obtained damage model has clear physical significance. The energies dissipated in each strain cycle can be determined by the areas of the hysteretic loop of stress-strain curve. The energies consumed in each cycle of stress are the areas of hysteresis loop of this cycle, that is:

$$\Delta W_i = \int_0^T \sigma(t)\varepsilon(t)dt \qquad (9)$$

Where: T-a cycle period.

In the whole process of fatigue life, the accumulative dissipated energy is the sum of all hysteresis energy, that is:

$$W_F = \sum_l^{N_F} \Delta W_i \qquad (10)$$

Where: N_F is the fatigue life; W_F is the total energy consumption when achieving the fatigue failure.

In the previous energy model, the majority uses the cyclic hysteresis energy ΔW_i as a state parameter. The evolution of damage is manifested as the accumulation of cyclic hysteresis energy, and it is often assumed that the hysteresis energy ΔW_i in each cycle is constant. The test results show that the cyclic hysteresis energy under different strain levels changes with the cycle number Ni (shown in Figure 4), and it is related to the level of tensile strain that is the maximal tensile strain. The equation can be assumed:

$$\Delta W_i = aN_i^b \varepsilon^c \qquad (11)$$

Where: a, b, c-material parameters; N_i- the cycle number; ε- the level of tensile strain that is the maximal tensile strain.

The Formula11 is transformed into the logarithmic form to obtain a bivariate polynomial of first power, and the equation can be obtained by the regression of multivariate function:

$$\Delta W_i = 0.095 N_i^{-0.16891} \varepsilon^{0.97686} \qquad (12)$$

Where: N=201, R^2=0.885. The curves of the equation after regression are shown in Figure 4.

A large number of test studies have shown that the relationship between the total absorbed energy of SBS modified asphalt mixture and fatigue life at different strain levels satisfy the formula:

$$W_F = a_f N_F^{b_f} \qquad (13)$$

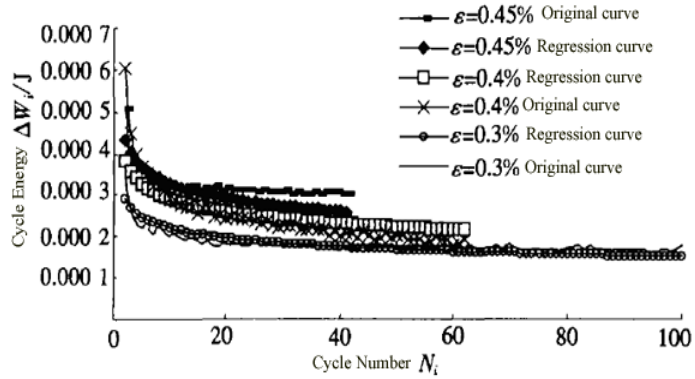

Figure4 The relationship between cycle energy and cycle number

Table4 Fatigue life of asphalt mixture under uniaxial tension and the accumulative dissipated energy

Tensile strain rate/%	Temperature/℃	Fatigue life/times	Accumulative dissipated energy
0.30	-5	42	0.013824
0.40	-5	62	0.016098
0.50	-5	100	0.018387

Through the regression of the data listed in Table 4, in which N = 3, R2= 0.9935, it is obtained:

$$W_F = 0.0043 N_F^{0.318} \tag{14}$$

From the viewpoint of energy, it can be defined that the damage in a cycle is equal to the ratio of the hysteresis cycle to the accumulative dissipated energy, that is:

$$D_i = \Delta W_i \Big/ W_F \tag{15}$$

The cumulative damage after cycling of N times is as follows:

$$D_N = \int D_i dN \tag{16}$$

The Formula (14) and formula (15) are substituted into the Formula (16):

$$D_N = \frac{a\varepsilon^c N^{b+1}}{a_f (1+b) N_F^{b_f}} = \frac{26.583\varepsilon^{0.977} N^{0.831}}{N_F^{0.318}} \tag{17}$$

Formula (17) is the energy expression of fatigue damage function D of the SBS modified asphalt mixtures under uniaxial tension considering both strain level and cycle number. When N = 0, D0 = 0; when N = NF, substitution of the strain level can be used to obtain the damage value related to the strain level. The test results are substituted into the formula to obtain the damage value of 1, which shows that the derivation formula is reasonable and correct. At the same time, prediction formula of the fatigue life related to the strain level can also be obtained through Formula (17).

3 Conclusion

1) The characteristics of the visco-elastic models and the damage models, which are coupled to visco-elastic continuum damage model, are analyzed by a large number uniaxial tension tests of SBS modified asphalt mixture. The model can reflect not only the strain-rate effect but also the stress relaxation phenomena. It also can obtain stress response at different temperatures based on

the Arrhenius shift factor.

2) Through the cyclic tensile test, the fatigue damage characteristics of the SBS modified asphalt mixture and damage effect have been considered in terms of energy and a fatigue damage model with the consideration of tensile strain level. The model can be used to predict the fatigue life under different tensile strain levels.

3) Damage value related to the strain level was obtained by using the fatigue damage model under uniaxial cyclic tension, which verifies that the theoretical value is consistent with the test results.

References:

JTG F40-2004.Technical Specifications for Construction of Highway Asphalt Pavements[S].

Lv Weimin (2001). Design Principle and Method of Asphalt Mixture[M]. Shanghai: Tongji University Press, 2001.

Yang Tingqing (1992). The Viscoelastic Mechanics[M]. Wuhan: Huazhong University of Science and Technology Press, 1992.

Yu Shouwen, Feng Xiqiao (1997). The Damage Mechanics[M]. Beijing: Tsinghua University Press, 1997.

Yu Tianqing, Qian Jicheng (1993). The Damage Theory and Application[M]. Beijing: Defense Industry Press, 1993.

Flutter Derivatives Identification of Aeroelastic Model of Hangzhou Bay Bridge

F.Y. Xu[1], X. L. Hu[2] and A. R. Chen[3]

[1]School of Civil & Hydraulic Engineering, Dalian University of Technology, Dalian, PH (86) 0411-84707995; email: fuyouxu@hotmail.com
[2]School of Transportation, Southeast University, Nanjing, (86) 025-83794100; email: aluntj@sina.com
[3]Department of Bridge Engineering, Tongji University, Shanghai, PH (86) 021-65975573; email: a.chen@mail.tongji.edu.cn

ABSTRACT

The method for identifying flutter derivatives of deck section model is popularized to full bridge aeroelastic model. The flutter derivatives of aeroelastic model of Hangzhou Bay Bridge are studied comprehensively using the stochastic subspace identification technique. The wind tunnel tests are conducted in smooth and turbulent flows with 3 attack angles and 5 yaw angles. The research results reveal that evident difference exists between section and aeroelastic model flutter derivatives. In turbulent flows, the flutter derivatives stabilities of aeroelastic model are more unsatisfactory. At the same reduced wind speed, with the alteration of attack angles and yaw angles, no monotonous laws for aeroelastic model flutter derivatives can be obviously observed.

INTRODUCTIONS

The bridge engineering is entering a new era characterized by construction of many cross-sea bridges. China has also initiated the along-the-Pacific highway project crossing Bohai Strait, Yangtze River, Hangzhou Bay, Pearl River and Qiongzhou Strait (Xiang, 2000). With the increase of bridge spans, the wind-resistant performances become more important, and the wind loads accompany the whole processes of construction and service. Flutter derivatives identification of bridge is one key aspect in the research of wind-resistant performance of large-span flexible bridges.

The methods for flutter derivatives identification of rigid section model are most studied and have the widest application. However, they can only reflect the bridge deck cross-sectional self-excited characteristics. Flutter derivatives of full-bridge aeroelastic model considering 3-D effect, multi-modal coupling effect as well as a variety of non-linear factors caused by the large added angle of attack, geometric non-linearity and so on. It can give a more reasonable and detailed explanation about the flutter mechanism of 3-D full-bridge structures. For identifying flutter derivatives of full-bridge model, one can measure the structural transfer function affected by aeroelastic characteristics, perform parametric optimal estimation using the least square method with a good applicability (Zasso, 1996). The stochastic subspace technique (Qin, 2004; Chen, 2006) can identify flutter derivatives directly based on signals acquired in turbulent flow field. Traditional identification of flutter derivatives study mainly concern the single orthogonal

direction to the span and consider this direction as the most dangerous state, while less study is undertaken concerning skew wind conditions. The flutter study of Hong Kong Tsing Ma Bridge section model under skew wind conditions shows that (Zhu, 2002): for different attack angles, critical flutter speed changes non-monotonically with yaw angle, and the minimum flutter critical wind speed often arises under skew wind conditions. The actual strong winds often deviate from the orthogonal direction to the span.

So far, no literatures have been found concerning flutter derivatives identification of full-bridge aeroelastic model under skew wind conditions in wind tunnel tests. The relevant investigations will be comprehensively performed in this study.

OVERVIEW OF THE WIND TUNNEL TEST OF HANGZHOU BAY BRIDGE

Hangzhou Bay Bridge is situated in coastal area of Zhejiang Province, where is frequently attacked by typhoons. This cable-stayed bridge has two diamond-shaped pylons and the main span is 448m. The wind resistance performance is essential throughout construction and service phases. The wind tunnel test for flutter derivatives identification of full-bridge aeroelastic model of the bridge was conducted, and the test cases include 2 flow fields (smooth and turbulent) with 3 attack angles(-3º,0º,+3º) and 5 yaw angles (0º,10º,20º, 30º,40º). The geometric scale of the full-bridge aeroelastic model is selected to be 1:100, and the aeroelastic model in wind tunnel is shown in Figure. 1.

Figure 1. Full bridge aeroelastic model of Hangzhou Bay Bridge.

DETERMINATION OF MODEL PARAMETERS

The relevant parameters of full bridge aeroelastic model are listed in Table 1, in which the deck section mode parameters are also provided. Parameters such as the first-order symmetric vertical bending frequency f_h and torsion frequency f_α, modal mass m_h, moment inertia I, and so on, obtained from the analysis of actual bridge design data, are also presented in Table 1. And the structure modal damping ratios ξ_h, ξ_α of the actual bridge are assumed to be 1%. It can be seen from Table 1:

For full-bridge aeroelastic model, some difference still exists between the actual and the expected goal values of f_h and f_α even after substantial adjustment tests. This is mainly due to the aeroelastic model involves lots of components and deviations of component's mass, mass distribution, stiffness, and boundary conditions from their ideal values. Frequency and damping ratios errors will affect the flutter critical wind speed, but not the specific values of flutter derivatives. Determination of mode mass of aeroelastic model is less convenient than section model.

Table 1. Design Parameters of Hangzhou Bay Bridge Models.

Parameters	Actual Bridge	Section model		Aeroelastic Model	
		Goal	Actual	Goal	Real
m_h (kg/m)	29740	6.069	6.07	2.974	2.974 Nominal
I (kg·m^2/m)	4313000	0.18	0.18	0.04313	0.0431 Nominal
f_h (Hz)	0.3685	3.083	3.07	3.685	3.520~3.525
f_α (Hz)	0.9513	7.959	7.93	9.513	9.862~9.88
$\varepsilon = f_\alpha / f_h$	2.58	2.58		2.80	
ξ_h (%)	1	0.50~0.62		0.65~0.78	
ξ_α (%)	1	0.52~0.65		0.70~0.78	

There exists obvious deviation of full-bridge aeroelastic model mode mass calculated by using coordinates expansion technique from expected values, and the main possible reasons may include: (1) the test scheme itself lacks in precision; (2) errors in calculation of actual bridge modal mass; (3) errors in the model fabrication. The modal mass of aeroelastic model was suggested to be directly calculated from the real bridge according to the geometric scale, and the reasonable explanation was presented (Xu, 2006). The vertical bending and torsion modal mass used in the flutter derivatives identification program of this paper, i.e., the nominal values in Table 1, are calculated from those of the real bridge.

FLUTTER DERIVATIVES IDENTIFICATION

Displacement micro sensors are employed at the mid-span of aeroelastic model to acquire signals of vertical, lateral and torsion displacements under conditions of different flow fields, attack angles, yaw angles and wind speeds. And displacement signals here are obtained through ambient excitation in the turbulent flow field and pulse excitation at the mid-span in the smooth flow field, respectively. Flutter derivatives identification through lateral displacement signals shows poor accuracy due to the relatively strong noise compared with the weak signals. In this paper, the stochastic subspace technique is used to identify 8 flutter derivatives, $H_1^* \sim H_4^*$ and $A_1^* \sim A_4^*$, which are related to vertical bending and torsion. Due to limited space, the specific identification method and process are not given here, but the detailed introduction can be found in other relevant literatures.

Section model and aeroelastic model in the smooth flow field. Flutter derivatives of section model, aeroelastic model as well as flat plate in smooth flow field with 0º attack angle are shown in Figure 2.

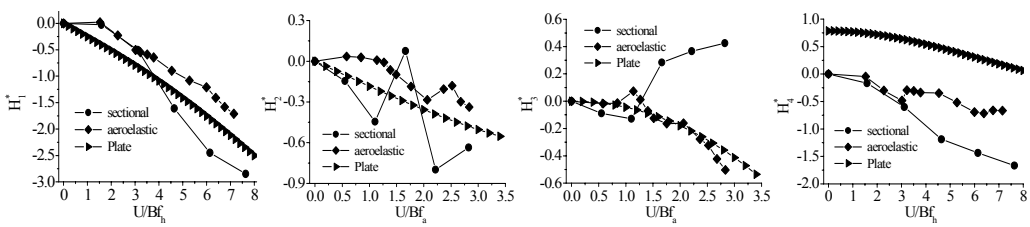

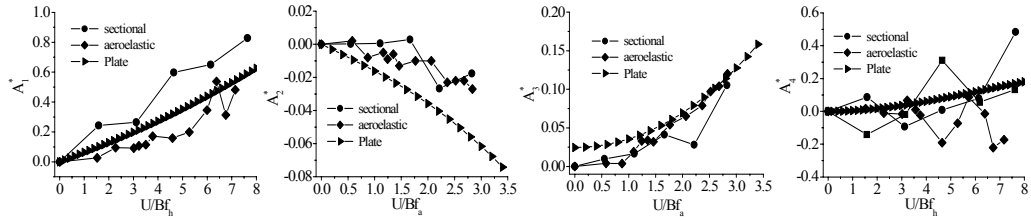

Figure 2. Flutter derivatives in smooth flow.

It can be observed as: (1) Between section and aeroelastic models, H_1^*, H_4^*, A_1^* and A_3^*, are in good agreement, and they have the similar trends to those of flat plate. (2) Monotonic relationship does not exist between section and aeroelastic models with reduced wind speed. (3) At higher reduced wind speed, the flutter derivatives identification accuracy of section and aeroelastic models is relatively poor.

Aeroelastic model in the smooth and turbulent flow field. Flutter derivatives of aeroelastic model in smooth and turbulent flow fields are shown in Figure 3. Small differences exist between identified frequencies with different wind speed at the same wind speed. Therefore the physical wind speed is adopted.

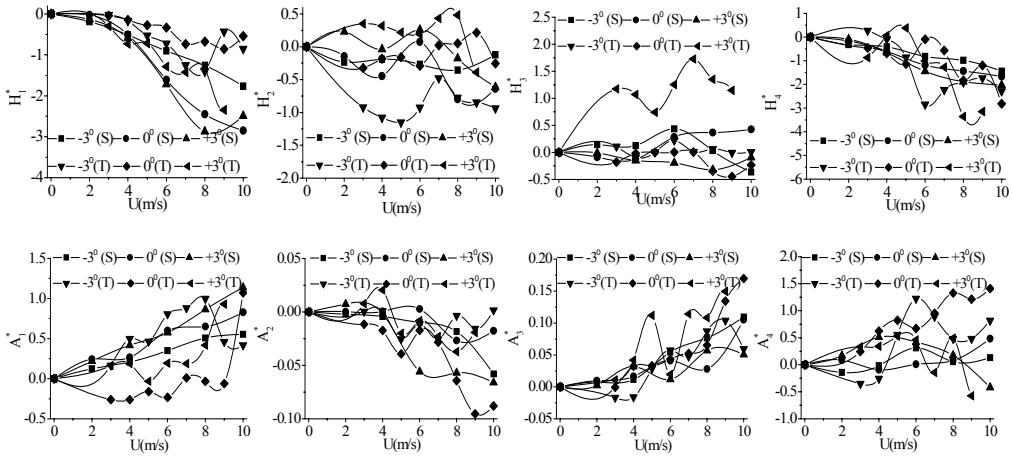

Figure 3. Aeroelastic model flutter derivatives.

From Figure 3, it can be observed as: (1) Flutter derivatives in turbulent flows have poor stability. The possible reason could be that the amplitude is relatively larger and the nonlinearity is more obvious under the condition of pulse excitation in smooth flow field. (2) Significant deviations exist under conditions of different flows and attack angles. Therefore from the perspective of improving flutter derivatives identification stability, the identification had better be undertaken in smooth flow field.

Aeroelastic model with skew winds. Due to the fixed wind direction in the tunnel, skew winds can only be realized by change of the angle between bridge model axis and flow direction. What should be noted is that all the parameters such as the deck width, the modal mass, etc. used to identify flutter derivatives under skew winds are taken as those under 0º yaw angle wind. Flutter derivates of with different yaw angles of

10º,20º,30º,40º are shown in Figure 4.

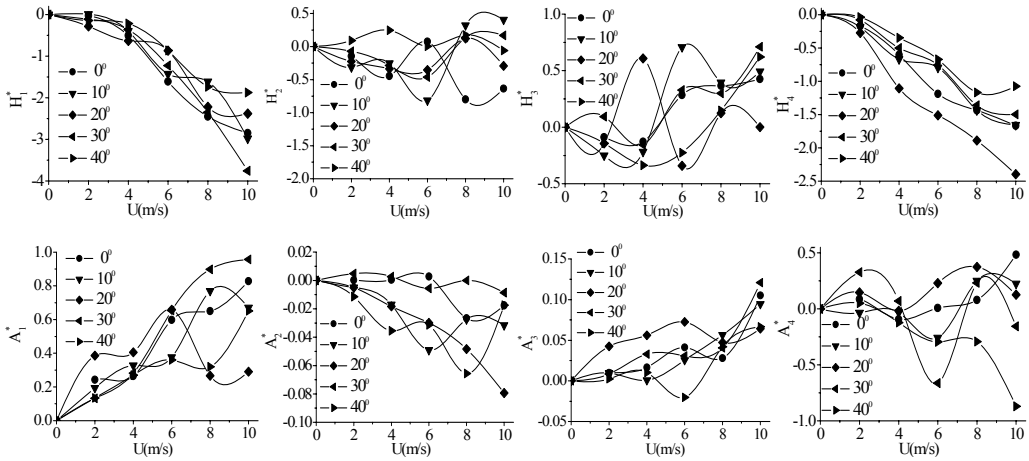

Figure 4. Aeroelastic model flutter derivatives with different yaw angles.

From Figure 4, it can be seen as follows:

(1) No obvious monotonic relation exists between flutter derivatives and yaw angles due to the involvement of complex vibration modes of pylons and cables.

(2) H_1^*, H_4^*, A_1^* and A_3^* have good trends at different yaw angles, and flutter derivatives of section and aeroelastic model with different wind attack angles have similar characteristics. This proves that the identification stability of flutter derivatives is related to their respective characteristics.

(3) Structural modal coupling may happen under different wind loads due to different wind yaw angles, i.e., significant differences exist among the state matrices.

(4) The flutter derivatives under orthogonal wind condition show more stability relatively than those under skew wind condition.

Analysis for stability of identification results.

(1) The deck of Hangzhou Bay Bridge has a streamlined cross-section, and vortex-induced vibrations occur within a very wide range of wind speeds in wind tunnel test, therefore the stability of flutter derivatives of section model is not quite satisfactory.

(2) Stability of flutter derivatives of aeroelastic model is less satisfactory than that of section model. The main reasons include existence of more modes participation in the vibration of aeroelastic model, different effective attack angles, internal modes phase differences, more unfixed modal coupling and more obvious non-linearity.

(3) Obvious difference appears between the flutter derivatives from smooth and turbulent flows, and the former one is more stable. This is mainly due to less modes participation in smooth flows and relatively pure signals for the pulse excitation way. While in turbulent flow field, more modes participation exists, especially those of cables, and the noise-to-signal ratio is relatively high, the identification is thus quite difficult.

(4) Multi-modes participation exists in the vibration of cable-stayed bridges, and it also has a higher degree of modal coupling than those of suspension bridges. It is easy

to understand that the accuracy and stability of flutter derivatives identification of full-bridge aeroelastic model of suspension bridges are more satisfactory, and this point can be verified through wind tunnel test.

(5) The generalized modal mass of the bridge system and the deck width are utilized in flutter derivatives identification of aeroelastic model. The identification results may vary greatly for various bridge types, span arrangement, tower and cable forms, even if the deck cross-section is the same.

(6) The noise, uncertainty of the test equipment system and multi-modes participation may lead to significant deviations of identification results from the theoretical ones, especially at high speed wind when the linear assumptions and small amplitudes can not be met.

CONCLUDING REMARKS

In smooth and turbulent flows, with 3 attack angles and 5 yaw angles, flutter derivatives of full-bridge aeroelastic model of Hangzhou Bay Bridge are identified by the stochastic subspace identification technique. For flutter derivatives, significant difference exists between section and aeroelastic model of Hangzhou Bay Bridge. There is no evident monotonic relationship between flutter derivatives and wind attack and yaw angles. Poor stability appears in flutter derivatives identification of aeroelastic model in turbulent flow field with skew winds. This is mainly due to strong asymmetry of the model and wind system under conditions of different attack and yaw angles. Due to the influence of multi-modal coupling, flutter derivatives of full-bridge aeroelastic model of Hangzhou Bay Bridge are not quite stable. For identification of flutter derivatives of full-bridge aeroelastic model under skew winds, more comprehensive and in-depth studies still need to be done.

REFERENCES

Chen, A. R., Xu. F.Y., Ma, R.J. (2006). "Identification of flutter derivatives of bridge decks using stochastic search technique." *Wind and Structure,*9(6), 441-455.

Qin, X. R., Gu. M. (2004). "Determination of flutter derivatives by covariance-driven stochastic subspace identification technique." *Wind and Structure,* 7(3), 173-186.

Xiang, H.F. (2000). "Prospect of world's bridge projects in 21st century." *China Civil Engineering Journal,* 33(3),1-6.

Xu, F.Y. (2006). "Identification of flutter derivatives and flutter analysis of bridges." *Tongji University*.

Zasso, C. S., Cigada, A., Negri, S. (1996). "Flutter derivatives identification through full bridge aeroelastic model transfer function analysis." *Journal of Wind Engineering and Industrial Aerodynamics*, 60(1-3), 17-33.

Zhu, L.D., Xu Y.L.(2002). "Tsing Ma Bridge deck under skew winds: flutter derivatives." *Journal of Wind Engineering and Industrial Aerodynamics,* 90(7), 807-837.

A Discontinuous Numerical Method for Asphalt Mixture

ZHOU Changhong[1], ZHAO Yanqing[1], and WANG Zheren[2]

[1]Department of Traffic and Transportation, Dalian University of Technology, Dalian, P. R. China; PH (+86)411-84707761; email: zhow@yahoo.cn
[2]School of Science and Engineering on Communication, Harbin Institute of Technology, Harbin, P. R. China; PH (+86)451-86282119

ABSTRACT

In order to simulate discontinuum mechanics of asphalt pavement, a new numerical scheme—*Meshfree Manifold Method* is deduced by integrating *Numerical Manifold Method* and *Mesh-free Method*. It is not only appropriate for contact computation but also can eliminate the limitation of regular mesh method. Meanwhile, two useful element models were provided, kernel principles linkage of asphalt mastic and searching for support nodes were discussed. An example was given to show its efficiency in simulating discontinuous deformation of asphalt mixture. This method is promising in solving fracture or large deformation problems.

INTRODUCTION

The commonly used methods to numerate discontinuous mechanics mainly include DEM *(Discrete Element Method)*, DDA (*Discontinuous Displacement Analysis*), and NMM (*Numerical Manifold Method*). Among these methods, DEM is the most successful to be applied for asphalt mixture, it is a mature method in solving the discontinuous problems and large deformation cases. However, because DEM tightly depends on combination of elastic or viscous components to reflect the contact state between particles, it hardly achieves stress distribution of asphalt mastic. This paper introduced NMM simulated the discontinuous deformation of asphalt mixture.

NMM was established by Shi Genhua (1991 and 1997) by using finite covering system in modern manifold, it takes advantage of finite element method , discontinuum kinematics , combines discontinuous and continuous deformation into a uniform mathematical expression. Lin(1995), Ohtsubo(1997) and Lu(2002) also made a great contribution to the development of NMM.

Asphalt mixture is filled with a lot of gaps, cracks, irregular aggregates, asphalt and other materials, so FEM-mesh-based NMM faces difficulties such as volume integration, displacement coordination between materials and mesh deformity caused by large deformation. However, *Meshfree/Meshless Method* (MFM) can provide a way to solve this problem. MFM was developed in 1970's, which mainly includes: SPH(*Smooth Particle Hydrodynamic Method*, Lucy, 1977),

RKPM (*Reproducing Kernel Particle Method*, Liu, 1995), DEM(*Diffuse Element Method*, Nayroles, 1992), EFGM(*the Element-free Galerkin Method*, Belytschko, 1994) and so on. EFG is suggested to be used for its symmetrical coefficient matrix and agreement with variational method.

In theory, *Meshfree Manifold Method* (MMM) is good at dealing with discontinuous problems of asphalt mixture, especially for large deformation, cracks, and material coupling calculation.

GENERALLY MANIFOLD COVERING SYSTEM

In *Numerical Manifold Method*, there are two mesh sets—physical mesh and mathematical mesh (Figure 1). Physical meshes are enclosed by objects' borders, cracks, blocks and the interface between different materials, which define the physical region of integration. Mathematical meshes are also named mathematical covers, which only define the precision of approximate solution. They can be any shapes but must cover the entire physical region.

Mathematical covers are divided by physical meshes into physical covers, and the overlap of physical covers is defined as the element of MANIFOLD. It is the basic unit of NMM and can be any shapes.

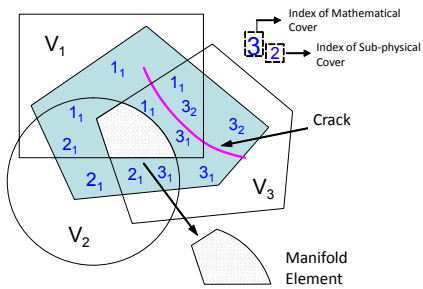

Figure 1. 2D Manifold covering system

VARIATION PRINCIPLE OF MINIMUM POTENTIAL ENERGY

Approximate displacement functions. If $(u_i(x,y,z), v_i(x,y,z), w_i(x,y,z))$ is the displacement function defined on Physical cover U_i, which can be expressed as a series forms as follow:

$$u_i = (u_i(x,y,z) \quad v_i(x,y,z) \quad w_i(x,y,z))^T = S \cdot D_i \tag{1}$$

Where, S is the basic series, D_i is the freedom degree of cover U_i.

Total displacement function. Assuming a point (x,y,z) is covered by q physical covers, the displacement function can be obtained by weighted mean of the q displacement approximation functions as follow,

$$\begin{Bmatrix} u(x,y,z) \\ v(x,y,z) \\ w(x,y,z) \end{Bmatrix} = \sum_{i=1}^{q} N_i(x,y,z) \begin{Bmatrix} u_i(x,y,z) \\ v_i(x,y,z) \\ w_i(x,y,z) \end{Bmatrix} = \sum_{i=1}^{q} N_i(x,y,z) \cdot S \cdot D_i = T \cdot D \tag{2}$$

Where, $N_i(x,y,z)$ is weight function of physical cover.

Global control equations. Assuming there are n physical covers in the

solution domain , according to the principle of minimum potential energy, we have the global control equations as follow,

$$\begin{bmatrix} K_{11} & K_{12} & K_{13} & \cdots & K_{1n} \\ K_{21} & K_{22} & K_{23} & \cdots & K_{2n} \\ K_{31} & K_{32} & K_{33} & \cdots & K_{3n} \\ \vdots & \vdots & \vdots & \ddots & \vdots \\ K_{n1} & K_{n2} & K_{n3} & \cdots & K_{nn} \end{bmatrix} \begin{Bmatrix} D_1 \\ D_2 \\ D_3 \\ \vdots \\ D_n \end{Bmatrix} = \begin{Bmatrix} F_1 \\ F_2 \\ F_3 \\ \vdots \\ F_n \end{Bmatrix} \tag{3}$$

Where K_{ii} is only determined by the material of physical cover U_i, and $K_{ij}\ (i \neq j)$ is the impact matrix of cover U_j on cover U_i.

COMBINATION WITH MESHLESS METHOD

Approximation scheme on compactly supported domain. In EFG, if n points lie in the neighborhood of evaluation point x, the weighted squared error norm of $u^h(x)$ in those points can be given by MLS (*Moving Least Squares*) as,

$$J = \sum_{i=1}^{n} w_i(x - x_i)\left[u^h(x) - u(x_i)\right]^2 = \sum_{i=1}^{n} w_i(x - x_i)\left[p^T(x_i)a_i(x) - u(x_i)\right]^2 \tag{4}$$

Where, $p^T(x) = \left[p_1(x) \quad p_2(x) \quad \cdots \quad p_m(x)\right]$ is m-times complete basis monomial, $a(x)$ is the coefficient vector, m is the number of basis monomial, and $w_i(x) = w(x - x_i)$ is the weight function of point x_i in point x.

Shape function of Meshfree Manifold Method. Let Eq. (4) obtain the minimum-style, shape function is gotten:

$$N(x) = p^T(x)A^{-1}(x)B(x) \tag{5}$$

Where $A(x) = \sum_{i=1}^{n} w_i(x)\,p(x_i)\,p^T(x_i)$, $B(x) = \left[w_1(x)\,p(x_1) \quad \cdots \quad w_n(x)\,p(x_n)\right]$

Then, substitute Eq. (5) into Eq. (2) and (3), we can obtain the equations of MMM scheme.

AVAILABLE ELEMENT MODELS

For MMM, two useful models are shown in Figure 2. In both models, edge nodes are placed at the mid of each edge, and face nodes and body node are all coincide with their centroid. Although 22-nodes model may be not so accurate, it can simplify the calculation and cut off more than 70% freedom degree.

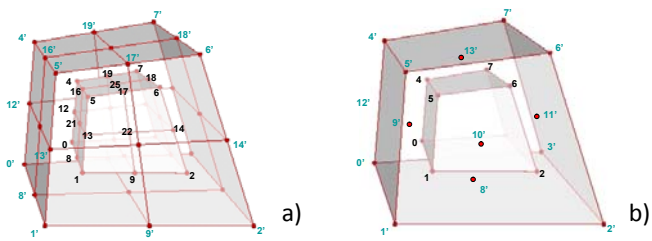

Figure 2. Element models: a)77-nodes model, b)22-nodes model

DEFINITION OF ASPHALT MIXTURE SOLUTION DOMAIN

Linkage of Asphalt mastic. Overlap between asphalt regions usually results in difficulties on numerical integration. While meshfree method can offer facilities for this integration (Figure 3a):

To define each node with two attributes: particle index and material index. All nodes on particle A (such as points *a*, *b*, *c*, *d* and *f*) have a particle id *A*, and all nodes on particle B (such as points *c*, *d*, *e*, *f*, *g* and *h*) have a particle id *B*. So node *c* and *d* have two particle ids, *A* and *B*. In the same way, a node locates in one material body has a single material id; otherwise, it will has more than two material ids. For example, node *b*, *d*, *e* and *g* have asphalt index; and node *a* and *h* have both index of stone and asphalt. Node *f* is an exception, which should be ignored in computation.

Searching for support nodes. If domain size (length, width and height(L_i), or sphere radius(r)) has been assigned, any node x_i who agrees with all the following three rules will be defined as the influence node of evaluation node x_I: a) $|x_I - x_i| \le L_i$ or $|x_I - x_i| \le r$; b) x_I and x_i have the same particle id a_k; c) x_I and x_i have the same material id m_s.

Background integration on asphalt mastic. Like meshfree method, since asphalt mastic connects with each other, integration must be calculated depending on background lattices (like Figure 3b). As shown in Figure 4, the global integration on asphalt region Ω can be translated into weighted summary of all lattice points like Gauss integral. The valid point will be determined by relative position of lattice point to the integration domain. Additionally, if lattices on borders are further refined in the same way, integral precision will increase obviously.

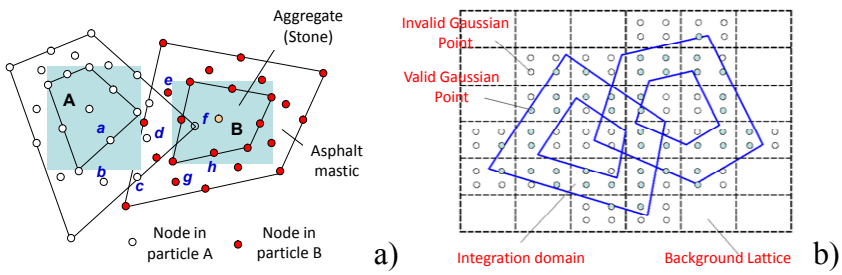

Figure 3. Likage and background integration for asphalt mastic

NUMERICAL EXAMPLES

In order to test the validity of MMM, a simple asphalt mixture model composed of 16 polyhedral particles was used to analyze the influence of aggregate-asphalt modulus ratio to stress distribution (Figure 4a). In this model, the diameters of particles subject to AC-16 gradation . For simplifying calculation, the model is only composed of two different sieve size particles(13.2~16mm, 11granules; 16~19mm, 5 granules). Bottom of the model is fixed, the side is free. A vertical pressure is loaded on the top, the strength varies linearly along with the time (p_{min}=0 at 0*sec*, and p_{max}=10N at 1.0*sec*). Aggregate modulus is assumed as 40Gpa and

Poisson's ratio is 0.25. For comparison, three different modulus of asphalt mastic are selected: i) Ea = 130Mpa; ii) Ea = 650Mpa; iii) Ea = 1300Mpa. Poisson's ratio is always 0.3.

The results are shown as Figure 4b) ~d) and Table1.

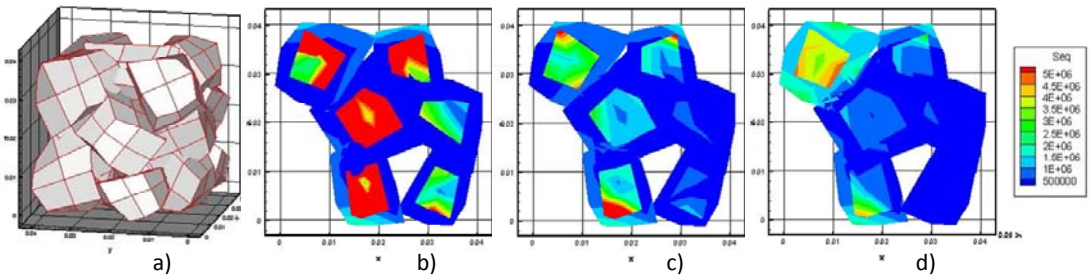

Figure 4. Numerical model (a) and contour of equivalent stress slice when t=0.1s (Ea: b-130Mpa, c-650Mpa, and d-1300Mpa).

As shown in Figure 4, the discontinuous features of asphalt mixture model lead to irregular distribution of inner stress, and it is obvious that stress is more concentrated on aggregate.

For No.3 particle (Table 1), if taking the mean equivalent stress ratio of two materials as evaluation index, the results show that: with the ratio increasing, stress in asphalt mastic increases slightly, while stress in aggregate decreases dramatically. This indicates that: the greater the modulus ratio is, the more stress the aggregate is concentrated on; smaller modulus ratio can help stress distributes more evenly. This conclusion is very useful in practice: in order to give full play to ultimate strength of aggregate and asphalt, we should keep the modulus ratio at a reasonable level to achieve stress coordination between aggregate and asphalt.

Table 1. Relation of Mean Stress And Modular Ratio for No.3 Granule

Aggregate-asphalt modulus ratio Es/Ea		40GPa /130MPa	40GPa /650MPa	40GPa /1300MPa
Equivalent stress of aggregate /MPa	Max	17.9151	3.8091	1.8774
	Min	0.3286	0.2720	0.2604
	Mean $\bar{\sigma}_s$	7.6104	1.5779	0.8231
Equivalent stress of asphalt mastic /MPa	Max	0.8664	1.6105	3.0732
	Min	0.0845	0.0477	0.0776
	Mean $\bar{\sigma}_a$	0.2766	0.3239	0.4002
Stress ratio $\bar{\sigma}_s / \bar{\sigma}_a$		27.51	4.87	2.06

Additionally, although reducing the aggregate-asphalt modulus ratio can make the inner stress distribution more uniform, while, average stress among different particles are definitely different (Figure 4b~d). So it can be discovered that re-distribution of stress is the integrated result caused by the strength (or stiffness) balance from particles inside and outside.

CONCLUSION

a) Based on the combination with *Numerical Manifold Method* and *Meshfree Method*, an efficient numerical method— *Meshfree Manifold Method* was deduced, which provides a good method to simulate discontinuous mechanics of asphalt mixture. And it is promising in simulating the process of crack or large deformation.

At the same time, numerical example given in this paper shows that:

b) The stress distribution of asphalt mixture is closely related to the modulus ratio of aggregate and asphalt mastic. The greater the modulus ratio is, the more stress the aggregate is concentrated on. Although reducing modules ratio can make stress distribution more balance inside the particles, unbalance between the particles.

c) In order to take advantage of ultimate strength of material, it is necessary to keep the mechanical status of aggregate and asphalt mastic harmony by adjusting modulus ratio.

REFERENCES

Belytschko, T., Lu, Y. Y., and Gu, L. (1994). "Element-free Galerkin Methods." *Int. J. Num. Methods Eng*, 37: 229-256.

Lin Jeen-shang (1995). "Continuous and discontinuous analysis using the manifold method." *Proc. of the 1st International Conference on Analysis of Discontinuous deformation*, Taipei.

Liu, W. K., Jun, S. L., Shaofau, A., et al(1995). "Reproducing kernel particle methods for structural dynamics." *Int. J. Num. Methods Eng*, 38,1655-1679.

Lu Ming (2002). "High-order manifold method with simplex integration." *Proc. of the 5th International Conference on Analysis of Discontinuous deformation*, Wuhan , China.

Lucy, L. B. (1977). "A numerical approach to the testing of the fission hypothesis." *The Astron Journal*, 8, 1013- 1024.

Nayroles, B., Touzot, G., and Villon, P. (1992). "Generalizing the finite element method: diffuse approximation and diffuse elements." *Computational Mechanics*, 10, 307-318.

Ohtsubo H, Suzuki K, Terada K, et al. (1997). "Utilization of finite covers in the manifold method for accuracy control." *Proc. of the 2nd International Conference on Analysis of Discontinuous Deformation*, Kyoto, 317-322.

Shi G. H. (1991). "Manifold method of material analysis." *Transaction of the 9th Army Conference on Apllied Mathematics and Computing*, Minneapolis, Minnesota, USA, 57-76.

Shi G. H. (1997). "Numerical Manifold Method." *Proc. of the 2nd international conference on analysis of discontinuous deformation*, Kyoto, Japan, 1-35.

A Safety Evaluation Method of Existing Flexible Suspension Bridge with Double Cable

Li-Xia Lin[1] Ya-Ping Wu[2] and Nan-Hong Ding[3]

[1]School of Civil Engineering, Lanzhou Jiaotong University, Lanzhou, 730070, P.R. China; email:linlixia@126.com
[2]School of Civil Engineering, Lanzhou Jiaotong University, Lanzhou, 730070, P.R. China; email:wypsw@163.com
[3]School of Civil Engineering, Lanzhou Jiaotong University, Lanzhou, 730070, P.R. China; email:nanhongd@126.com

ABSTRACT

The inspection and assessment are necessary because it can provide the necessary scientific foundation for the maintenance, rehabilitation and technical reconstruction of existing suspension bridges. Most stiffening girders of suspension bridges are steel truss girders or steel box girders. The safety evaluation of steel beams is to evaluate the ultimate state of the structure so as to avoid disastrous accidents during serving. In this paper, through field investigation of the defects and static and dynamic load tests of the bridge, combined with the finite element analysis, a safety evaluation method is developed and adopted to evaluate the load-carrying capacity of the Qingcheng suspension bridge. In the procedure the coefficient of considering load-carrying capacity and effect of fatigue and rust of the steel is adopted. The evaluation method of this paper can provide reference for safety evaluation and reinforcement construction of existing suspension bridges.

Introduction

At present, the main methods of evaluating the load-carrying capacity or the safety of the bridges are as follows: assessment based on appearance investigation, assessment based on calculation according to the design code, the load test, the assessment by expert system, and assessment based on theory of time-dependent reliability (Shi 2001). The Evaluation Method of Load-Carrying Capacity of the Highway Existing Bridge (on trial) had been enacted by the China Communications Ministry in 1988. However, it only applies to existing reinforced concrete bridge and pre-stressed concrete bridges. Currently, there isn't any code for safety evaluation of steel bridges in China (Lei, 2000). In addition, most of the assessments according to design code are inclined to be conservative and aren't accurate to reflect the mechanic behavior after the structure deteriorates. Currently, a more reasonable way is to combine the calculation results with the load test data to evaluate the load-carrying capacity of bridges. In this paper, with consideration of the characteristics of the fatigue and rusting of existing steel bridges and combining the static and dynamic load tests with the finite element analysis, the assessment of a suspension bridge with double flexible cable is carried out. This can be carried on

in two steps as follows: Carry load tests on the bridge, and then judge the possible damage according to the experimental results or determine load-carrying capacity and evaluate the safety of the bridge.

Field investigation of the defects and static and dynamic load tests of the bridge

Brief introduction of the bridge. The Qingcheng Bridge is over the Yellow River and is about three kilometers away from the Daxia reservoir in China. It has already been in use for 20 years. The structural form is a flexible suspension with a double cable (see Figure 1). The main span is 180m and the bridge approach on each side is composed of 4×16m simple supported bridges. The height of the reinforced concrete cable tower is 18.5m. The rise-span ratio is 1/12 and both the upper and lower cables are all steel wire rope composed of 6φ45mm. The diameter of the upper suspender is 25mm and of the lower one is 45mm. The stiffening girder is composed of longitudinal and transverse beams which are made of 16Mn I-steel.

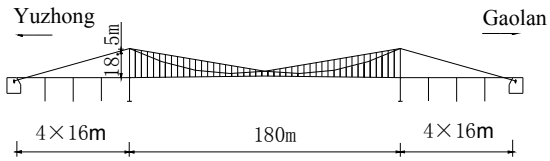

Figure 1. Sketch of Qingcheng Bridge (unit: m)

Field investigation of the defects. Some longitudinal and transverse beams of the stiffening girder have corrosion. A few clamps slipped along the cable. The suspenders do not bear the loads uniformly because some suspenders unload and others overload. The concrete protection course of the cable tower has some damage and stripping. The crack of the R.C. cable tower is serious, especially in the bottom parts. The width of some cracks even reaches 3.4mm. After years of service, the deck elevation has changed a lot with the following characteristics: The maximum settlement exists in the middle of the main span and the value is 1.054m, it reaches 0.58% of the span length. From the beginning to now the camber changed from 1m to 0, some place in the middle span even lower than the horizontal line.

Static and dynamic tests of bridge. Static tests are carried on by design load (a car weight 20t) and six loading conditions are considered (see Table 1). The distance from the center of the front wheel to that of the rear wheel is 4m; the front axle Load is 7t, and that of the rear is 13t. During the load test, the car is forward Gaolan. The control sections are edge of bearing (section I), l/8(section II), l/4(section III), 3l/8(section IV), middle span (section V), middle of 24# cross beam(section VI) and bottom of cable tower. Dynamic tests take a car weight 20t as a vibration source to measure the dynamic response and natural frequency and impact factor for further assessment.

COMPARISON OF RESULTS

Finite element analysis model. This part is about the three-dimensional finite element analysis of the suspension in which the program ANSYS is used. The

cable and suspender are simulated by the three-dimensional tension-only nonlinearity link element (link 10). The cable tower and the longitudinal and transverse beams of the stiffening girder are simulated by the three-dimensional beam element (beam 44). The deck is simulated by the shell element (shell63). The total bridge is divided into 6492 elements and 4550 nodes. It is considered that the nonlinearity effect is caused by large displacement with small stain, gravity stiffness and initial stress of cable.

Table 1. Loading conditions and control sections

Loading conditions	Distance from the rear axle to centre line of bridge span	Distance from the control section to centre line of bridge span
1	89m (the car is near Yuzhong)	89m (section I, near Yuzhong)
2	68 m (the car is near Gaolan)	68 m (section II, near Gaolan)
3	4 m (the car is near Yuzhong)	4 m (section III, near Yuzhong)
4	29 m (the car is near Yuzhong)	22 m (section IV, near Yuzhong)
5	1 m (the car is cross the centre line)	0m (section V)
6	6m (the car is near Gaolan)	6m(section VI, near Gaolan)

Table 2. Comparison of Results

Loading conditions	Item(stress /MPa or displacement/m)	Theory value	Test value	Checkin-g factor
1	Shear stress of the stiffening stringer on section I	27.5	20.8	0.756
2	Nomal stress of longitudinal beam bottom on section II	162.6	125.6	0.772
3	Nomal stress of longitudinal beam bottom on section III	169.6	130.6	0.770
4	Nomal stress of longitudinal beam top on section IV	26.9	19.2	0.738
5	Vertical displacement of longitudinal beam on section V	0.524	0.387	0.738
	Vertical displacement of the cable on section V	0.512	0.362	0.707
	The max normal stress on bottom section of cable tower	0.376	0.378	1.005
	Longitudinal displacement at top of cable tower	0.004	0.004	1.000
6	Normal stress in the bottom of the stiffening cross beam (24#) on section VI	58.9	46.5	0.790

Table 3. Frequency/Hz

Vertical vibration/ n	Vibration mode	Frequency of theoretical value	Frequency of test value
1	Vertical symmetric bending	0.3398	0.3549
2	Vertical Antisymmetric bending	0.4676	0.4867

Comparison of results calculated by finite element analysis and experimental data. Table 2 shows the theoretical value and the test value of the deflection (stain) of control sections in each loading condition. The checking factor, the ratio of experimental data to the theoretical value, is less than 1.0; so it can be concluded that the total rigidity of bridge superstructure is good and the bridge is working in a

normal state. The first two vertical vibration modes and frequencies are tested in the dynamic test (see Table 3). The experimental frequencies are all higher than theoretical values, which verifies that the rigidity of the bridge is good. Therefore, the suspension system is working in a normal state. However, the checking factor of stress on the bottom section of the cable tower is 1.005. Considering the results of gap observation and the longitudinal displacement of top cable tower, it can be concluded that the load-carrying capacity of the cable tower is lower because of the development of a crack. The checking factor is not enough to determine the load-carrying capacity of the bridge(Song, 2002). Therefore in the following parts of the paper, an expression for safety evaluation using the coefficient of load-carrying capacity andconsidering the fatigue and rust of steel is proposed and adopted to evaluate the load-carrying capacity of the Qingcheng Bridge.

EVALUATION OF LOAD-CARRYING CAPACITY

Currently, in China there isn't any code for load-carrying capacity evaluation of existing highway suspension or steel bridges. Some countries have a code on load-carrying capacity evaluation (BD21/01, Eurocode No.3). In report (Lichtenstein Consulting Engineers, Inc. 2001), it is proposed that the expression of load-carrying capacity should be

$$R.F = \frac{R_u - \gamma_D D}{\gamma_L L(1+\mu)} \tag{1}$$

Where $R.F$ is the coefficient of load-carrying capacity; R_u is the actual ultimate strength of section evaluated; γ_D is the factor for dead loads; γ_L is the factor for live loads; μ is the impact factor for live loads; D is the dead loads effect of section evaluated;L is the live loads effect of section evaluated. If $R.F \geq 1$, the load-carrying capacity can meet the requirement, otherwise, it can't.

During the evaluation, the rust effect can't be neglected because of the generally existing rust in steel bridges. Using the factors, γ_1 and γ_2 to modify the design value of the bending strength R, it yields $R_u = \gamma_1\gamma_2 \cdot R$

From Eq. (1) we have

$$R.F = \frac{\gamma_1\gamma_2 R - \gamma_D D}{\gamma_L L(1+\mu)} \tag{2}$$

Considering the bending resistance failure on normal section, R=310MPa, the information of dead loads is definite when testing the bridge, so γ_D=1.0. According to the code *JTG D60-2004*, γ_L= 1.4. From the experimental data, the impact factor μ=0.1. There is some rust in the longitudinal and transverse beams of the stiffening girder, but the loss ratio of section area is less than 5%,and the

mechanic performance has no conspicuous changes (Hui, 1992, Eung, and Ram, 2003); it can be seen that $\gamma_2 = 1.0$.

Currently, the study on the fatigue of highway steel bridges is relatively deficient. In the book (Pan, 1983), a method is proposed to calculate the fatigue reduction factor γ_1.

$$\gamma_1 = \frac{1}{(a\beta \pm b) - (a\beta \mp b)\rho} \qquad (3)$$

Where $a = \frac{R}{2\varepsilon_r K\sigma_\rho}$, $b = \frac{R}{2K\sigma_b}$

Where ε_r is the factor of underload causing the increase of fatigue strength due to underload; K is the coefficient of uniformity of fatigue strength; σ_b is the ultimate strength of material; ρ is the coefficient of cyclic and $\rho = \frac{\sigma_{\min}}{\sigma_{\max}}$; β is the coefficient of stress concentration, that is, $\beta = \frac{fatigue\ \ strength\ of\ \ basic\ \ material}{fatigue\ \ strength\ of\ \ conjunction\ \ material}$; σ_ρ is the fatigue strength corresponding to the number of cycles which can be got from the fatigue graphs (Pan, 1983,1999).

The basic material of the bridge-stiffening girder is 16Mn I-steel, adopting a high strength bolt as the conjunction. Therefore, ε_r=1.4, K=0.83, σ_b=520MPa, β=1.83. From the experimental data, ρ=-0.25. Through traffic volume investigation and record of stress history, it can be seen that the number of cycles is about 400,000 (bridge works 20 years). Consider the fatigue graphs of 16Mn I-steel. It can be seen that σ_ρ=365MPa. Recall from Eq.(3) and substitute the parameters by the values above, the value of the fatigue reduction factor γ_1 in the current state is equal to 0. 905.

From Eq.(2), it can be seen that the value $R.F$ of the longitudinal beams in the middle span bridge section is 1.313, and the value $R.F$ of the longitudinal beams in the $l/8$ section is 1.410. It can be concluded that the bridge in its current state still has the ability to serve under design load after considering the fatigue and rust of the deck system.

CONCLUSIONS

With consideration of the characteristics of the fatigue and rusting of existing steel bridges and combining the static and dynamic load tests with the finite element analysis, the assessment of a suspension bridge with double flexible cable is carried

out in this paper. Firstly, from load test data combined with the finite element analysis, it can be concluded that the cable tower should be strengthened due to the large horizontal displacement of the cable tower top; Due to the large settlement and light torsion of the deck the suspension system needs to be adjusted. Secondly, compare the experimental data with the theoretical value; it can be seen that the total rigidity of the bridge superstructure is good and the bridge is working in its normal state. Thirdly, the checking factors and the coefficient of load-carrying capacity of stiffening girder show that the stiffening girder can satisfy the requirements and need not be strengthened. The evaluation method of this paper can provide references for safety evaluation and reinforcement construction of existing suspension bridges.

ACKNOWLEDGEMENTS

This research was sponsored by the National Natural Science Foundation of China (grant no. 50678076).

REFERENCES

BD21/01, (2001). *The Assessment of Highway Bridges and Structures*, British Department of Transport, London.

Eung, H.C. and Ram C. (2003), "Corrosion Condition Evaluation at Muddy Creek Bridge", *J. of Performance of Constructed Facilities,*17(4),206-209.

Commission of the European Communities. (1997). *Eurocode No.3, Design of Steel Structures, Part 2. Steel Bridges*, Luxembourg.

Ministry of the Communications of the People's Republic of China. (2004). *General Code for Design of Highway Bridges and Culverts (JTG D60-2004)*. Beijing.

Hui Y.L. (1992), "Approach to Mechanical Behavior of Rusty Reinforcement", *Industrial Construction*, 10, 33-36.

Lei, J.Q. (2000), "Comments and Cures of Steel Bridge of Highway Bridge in the 20th Century in China", *Highway*, 1, 20-23.

Lichtenstein Consulting Engineers, Inc. (2001), "Manual for Condition Evaluation and Load Rating of Highway Bridges Using Load and Resistance Factor Philosophy", *Final Report Prepared for National Cooperative Highway Research program, Transportation Research Board, Rational Research Council.*

Ministry of the Communications of the People's Republic of China. (1988). *Method for Evaluation of Load-Carrying Capacity of Highway Existing Bridge (on trial)*,China Communication Press, Beijing.

Pan J.Y. (1983), *Study on Welded and Bolt-connected Bridge*, China Railway Publishing House, Beijing.

Pan J.Y. (1999), "Research and Innovation of Fatigue Design Theory for High Strength Bolt and Weld Steel Railway Bridges", *China Railway Science*, 20(2), 35-41.

Shi, M. (2001), *Study on Assessment of Load-carrying Capacity for Middle and*

Small Bridge, Ph.D. Dissertation, Tongji University, Shanghai.

Song, Y.F. (2002), *Load Test and Stuctural Assessment of Highway Bridges*, China Comuniation Press, Beijing.

Relation of Stability Coefficient to Design Parameters for Curved Continuous Rigid Frame Bridges with Long-span and High-pier

Wang Jun-li[1] and He Shuan-hai[2]

[1]Professor, Doctor. Key Laboratory of Old Bridge Detection and Reinforcement Technique in Traffic Industry, Chang'an University, Xi'an， 710064， China PH(086)02982334867. E-mail: wjl@gl.chd.edu.cn

[2]Professor, Doctor. Key Laboratory of Old Bridge Detection and Reinforcement Technique in Traffic Industry, Chang'an University, Xi'an， 710064， China PH(086)02982334871. E-mail: keji_1@chd.edu.cn

Abstract: Based on the nonlinear theory, through changing the design parameters, the stability of model curve rigid frame bridges with long-span during cantilever construction was analyzed; The results show that the central angle of the curve dominated the stability coefficient; The nonlinear stability coefficient of bridge is 35% of eigenvalue flexure. Data was collected for a large number of long-span rigid frame bridge which have been built. Through comparison and classifying, the results indicate that the types of piers and its design parameters (the central angle of curve , slenderness ratio of piers, and the main pier types, the number of tie-girder) are related to the stability coefficient. The simple and creditable formulas can be taken as reference in designs.

Introduction

Long-span curve bridges with high piers are continuous rigid frames in general, which are built by the method of sub-segmental cantilever construction. During the construction stage, the T- rigid frames suffer less constrain; their inter-force and deformation are very complex (He and Xiang, 2003). The gravity centers of each section of the curve's supper-structure are not in one line, so that the piers are under eccentric compression. Torque, rotation angle and lateral displacements of piers and beams were formed by gravity. These characteristics make major long-span curved bridge design and construction more complex than a straight bridge (Wang and He, 2005, 2006). In this paper, based on non-linear mechanics, through analysis the stability of long-span high-pier curved bridges, the relationship of stability and curved bridge design parameters was pointed out, which provided the basis for the large span continuous rigid frame bridge design, construction and monitoring.

Methods of non-linear analysis

To solve the non-1inear mechanics problems, the incremental method is usually used. The structure's critical loads are divided into several increments， each increment load corresponding to the deflection curve can be regarded as the linearity approximation. Such linear treatment can be quite accurate to the original non-linear course. When the structures bear a group of loads, we assume the loads grow in fixed proportion. The critical proportion determines the critical loads. We can determine the critical loads by the critical proportion.

The concrete constitutive uses formula(1):

$$\sigma = k_3 f_c \frac{A(\varepsilon/\varepsilon_0)+(D-1)(\varepsilon/\varepsilon_0)^2}{1+(A-2)(\varepsilon/\varepsilon_0)+D(\varepsilon/\varepsilon_0)^2} \quad (1)$$

Where k_3 =1,A=1.74,D=0.5, ε_0 =0.002, f_c is the axial compression strength of concrete.

Reinforced uses formula(2). $(\sigma_e, \varepsilon_e)$ is the elastic limit point.

$$0 \le \sigma_s \le \sigma_e \quad \varepsilon_s = \sigma_s / E_s ; \quad \sigma_s \ge \sigma_e , \quad \sigma_s = \sigma_e \qquad (2)$$

In the stability analysis, piers are compression members; reinforced bars and concrete are equivalent strain. Therefore, the stability calculations still use integral models, which is a isotropic hardening model with nonlinear constitutive relation.

Nonlinear stability analysis in cantilever construction stage

Taking Xu Shui river bridge in the Shan Xi province as the background, the curve central angle is 38° and the piers are 120m high. During cantilever construction, the loads composed by the weight and construction loads consider geometric and material non-linearity . Since the age of concrete is short, the material elastic modulus was reduced by 10%. The results are shown in table 1. Based on the calculation results, we can indicate that eigenvalue coefficients are the biggest; The stability coefficients which consider the large deformation are slightly reduced; The stability coefficients which only consider nonlinear material will be about 47**%** of the eigenvalue coefficient; In considering the combined large deformation and material nonlinearity, stability coefficients are reduced significantly, about 35**%** of the eigenvalue coefficients .

Table 1 Results of Stability Coefficient under Different Considering Factors

Linear elasticity	Geometric nonlinearity	Material nonlinearity	Dual nonlinearity
7.62	7.37	3.63	2.68

When considering material nonlinearity stability, the stability problem has been transformed for the solving of ultimate load. The carrying capacity of the structure is lost because of pressure and bending effects for piers. It is obvious that the continuous rigid frame bridges are the second type of instability. Material yield has become a major factor in controlling its ultimate bearing capacity.

Non-linear stability analysis for different central angles of curve in cantilever construction stage

The central angles of curve bridges are 0°、22.92°、28.65 °、38.2°、45.82°、57.30°、76.39°、114.59°, the height of the piers are 120m. Considering the weight and construction loads in the largest cantilever construction stage, combined with large deformation and material nonlinearity, the ultimate load coefficients of the T rigid-frames were calculated. They are shown in table 2. The relationship between central angles of the curve and the ultimate load coefficients are shown in Fig.1. The formula of the relationship between load coefficient P_{cr}/P and the curve central angle φ is formula(3)

$$P_{cr}/P = 5.37647 - 0.15255\varphi + 0.00348\varphi^2 - 4.57639\times10^{-5}\varphi^3 - 3.04149\times10^{-7}\varphi^4 \qquad (3)$$

Table 2 Nonlinear Stability Coefficient at Different Central Angle of Bridge

central angle(/°)	0	22.92	28.65	38.2	45.82	57.30	76.39	114.59
Nonlinear coefficients	5.38	3.23	2.99	2.67	2.45	2.25	1.89	1.26

It is obvious that the eigenvalue coefficients and non-linear coefficients at the construction stage are reduced with the larger central angle of the curve; the non-

linear coefficients decreased quickly. Therefore, the relevance between the non-linear coefficient and the central angle is greater.

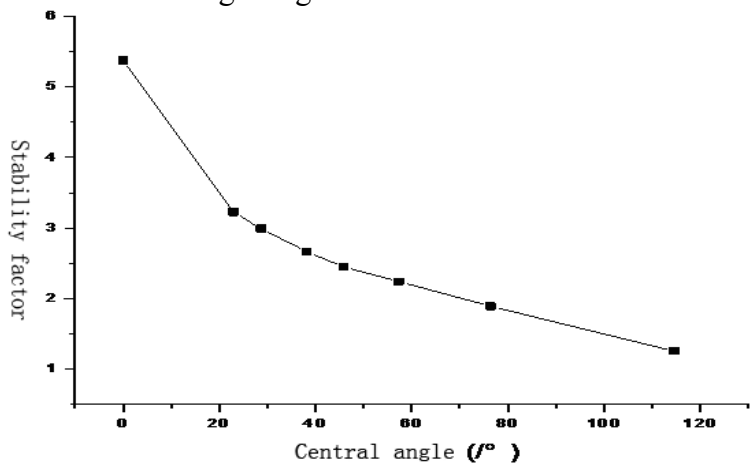

Fig.1 Relationship between nonlinear stability factors and central angles

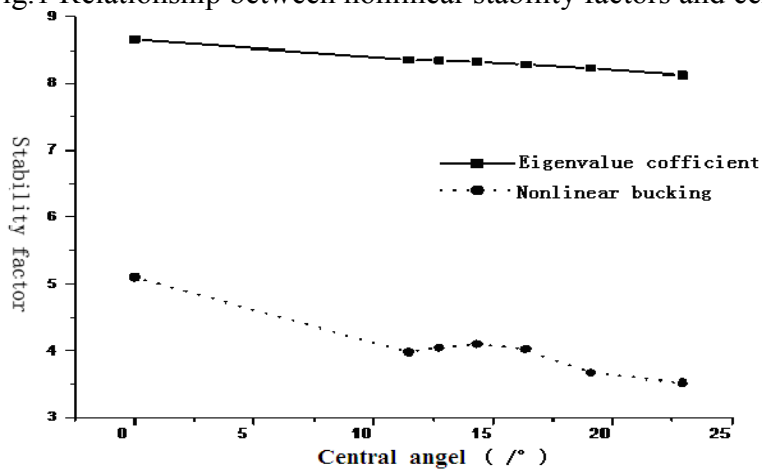

Fig.2 Relationship between stability factors and central angles

Slenderness ratios of bridge piers and their stability

Taking the Xu Shui river bridge in the Shan Xi province as the background, its design parameters were changed so that the central angles of the curves are 114.59°、76.39°、57.30°、45.84°、38.20°、28.65°、22.92°、0° and the slenderness ratios of the bridge piers are 33.15、37.30、41.44、45.59、49.73、53.87、58.02、62.17、66.31. This considers the self-weight and construction loads in the largest cantilever construction phase. When it considered the combination of large deformation and material nonlinearity, the T rigid-frame nonlinear stability coefficients were calculated. The relationship between slenderness ratio of the bridge piers, the curve central angle and the nonlinear stability coefficient is shown in the Fig.3.

Space of coupled double Thin-wall pier on stability

Drawn from the results in Fig 4 . As the double-limb space H is increased, the stability coefficients of main piers λ are increased. The relationship between H and λ can be fit for the formula (4).

$$\lambda = 8.88575 + 1.04663\,H + 0.02373\,H^2 - 0.00242\,H^3 \qquad (4)$$

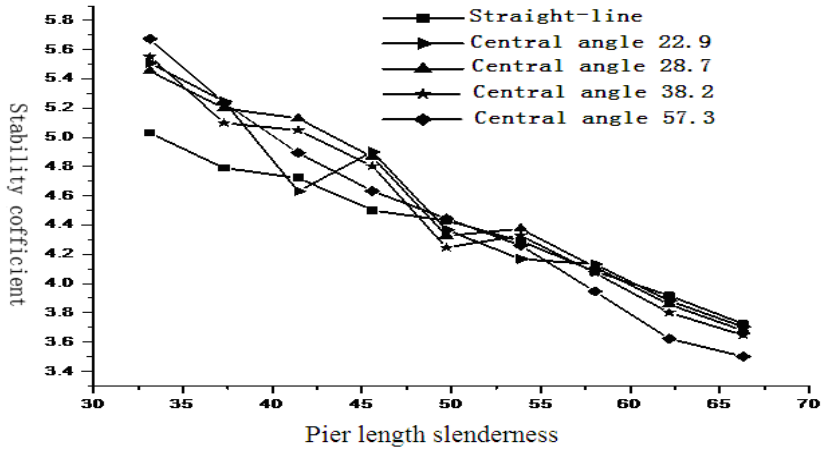

Fig.3 Relationship between slenderness ratio and nonlinear factors

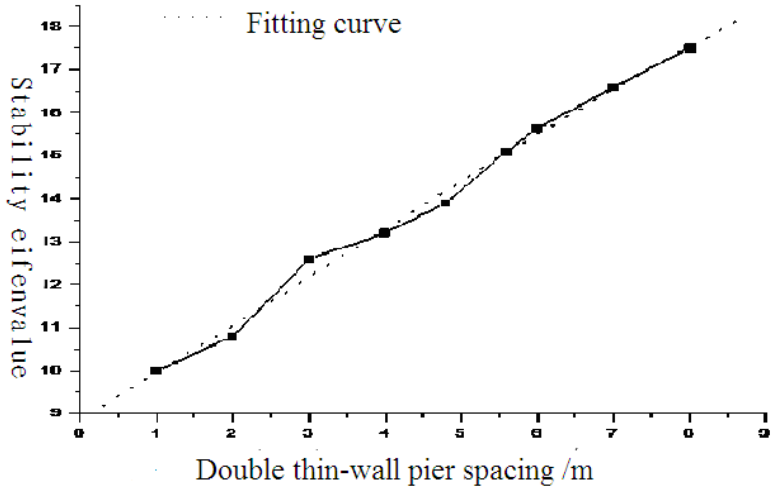

Fig.4 The space *H* and stability coefficient λ

By studying the design parameters and the stiffness of the thin wall on the structures, as well as their stability, through the optimize regression analysis of pier design parameters, we can get the conclusion as follows: With the decrease of the stiffness of the thin wall, the stability coefficient will be reduced; With the decrease of the space of the double-limb thin wall *H*, the stability coefficient λ will be reduced. As we can see, the stability of the bridge is also more sensitive to the space of double-limb piers.

Settings of tie beams on stability

The Long Tan river bridge has the highest piers of continuous rigid frame bridges in the domestic. The results are in table 3(a). In order to strengthen the rigidity of thin-wall hollow piers in longitudinal bridges, one tie beam was set every 60m. In view of this, tie beams increase the stability of the high-piers in longitudinal bridges. Through the spatial analysis, we could see that the first-order instability of the bridge is in transverse, and the stability factor was still large, so we could remove the tie beam when the bridge had been completed. During the construction, we could solve the stability problem by temporary support. To do that, we could not only solve the problem of excessive tensile stress of the tie beam, but also could reduce the

longitudinal stiffness of continuous rigid frame bridges, which is more conducive to the structure of the force.

Table 3(a) Stability Coefficient of Piers 178m High

Number of tie beam	0	1	2
Eigenvalue coefficients for cantilever construction	6.52	8.72	8.66
Eigenvalue coefficients for full-bridge	11.89	11.80	11.78
Nonlinear coefficients for cantilever construction	5.40	5.39	5.29
Nonlinear coefficients for full-bridge	5.32	5.39	5.34

For another long-span continuous rigid frame bridge, the height of the piers is 120m (spans are 110m+200m+110m). The nonlinear stability for thin wall piers is located at 0, 1, 2, 3, and 5 tie beams. The results are in table 3(b). The relationship between the stability factor and the number of tie beams is in Fig.5. As we can see, setting up a tie beam in the cantilever construction stage can improve the stability. However, additional tie beams will lead to the T-rigid frame stability factor being reduced with the increased number of tie beams. As we can see, setting up more tie beams is not favorable for the stability of the structure.

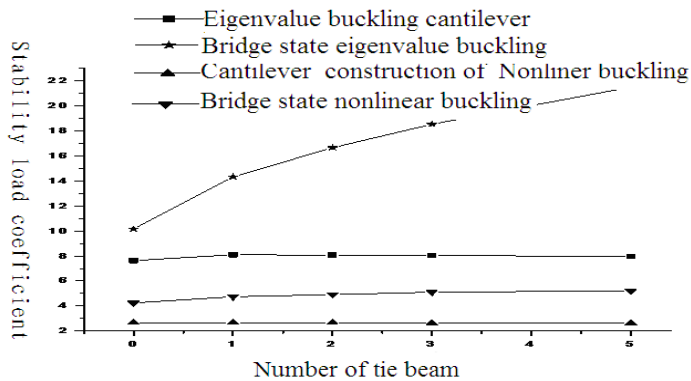

Fig.5 Stability coefficient λ and the number of tie beam

Table 3(b) Stability Coefficient of Piers 120m High

Number of tie beam	0	1	2	3	5
Eigenvalue coefficients for cantilever construction	7.62	8.10	8.06	8.03	7.97
Eigenvalue coefficients for full-bridge	10.15	14.32	16.65	18.53	21.50
Nonlinear coefficients for cantilever construction	2.67	2.68	2.67	2.65	2.63
Nonlinear coefficients for full-bridge	4.25	4.74	4.91	5.10	5.22

Piers setting of continuous rigid frame bridges

Based on the design of piers for dozens of typical high pier long-span continuous rigid frame bridges gathered in our country, through summing up and analyzing, we could see that there was certain regularity for span and the height of main piers, types of pier(double limb or single limb),cross section types(solid or hollow);While the span in above 160m, the main piers were set up for the hollow piers of the thin wall of one pair of limbs,their interval distance was mostly above 8m;While the span was smaller than 160m, the main piers were mostly set up for the solid thin wall with one pair of limbs,their interval was mostly under 8m;The heights of piers were 60～110m, one tie beam was set transversely; The heights were above 110m, 1 or 2 tie

beams were set up; The width of the piers in the transverse bridge was the same as the box beam. For the higher piers , their vertical width was greater ,which is a need of stability for the bridge.

Conclusion

Considering the large deformation and nonlinear material, the stability coefficient of high pier and long-span curve continuous rigid frame bridges is 35% of eigenvalue buckling. With the central angle increase, the stability coefficient will decrease rapidly, and the impact of the central angle is very prominent; There are certain regularities of design parameters and stability of large-span curved bridges. However, the span and pier height are dependent on the geomorphology and traffic requirements. Therefore, selecting the rational design type of the main pier is conducive to the structure internal force and structure stability; For small-span, we can select dual-limb solid thin-wall piers. Most spaces are at 8m below. But, as curved bridges, because of torsion, the thin-wall pier should not be too thin in the construction stage. While the span in above 160m, the distance between limbs is mostly above 8m. The stiffness of the piers was reduced with the increased height. When deformation need has been met, we can select thin-walled hollow single piers with bigger cross-sectional width to enhance the stability of the main piers; The heights of piers were 60～110m, one tie beam was set transversely; The heights were above 110m, 1 or 2 tie beams were set up, which is a need of stability for the bridge in construction and the full-bridge.

References

He Chang and Xiang Zhong-fu. (2003).“Nonlinear stability analysis of tall piers with incipient defect ”. J. Chongqing Jiaotong University,22(3):14-17

Wang Jun-li and He Shuan-hai.(2005)“Nonlinear stability and model test of reinforce concrete for high piers” J. Chang’an University 25(4):31-34

Wang Jun-li and He Shuan-hai.(2006).“ Nonlinear analysis of long-span curve rigid bridges with high piers during cantilever construction”. J.Traffic and Transportation Engineering, 6(2):30-34.

Matthew J.Moyer and Mervyn J.Kowalsky（2003）“Influence of Tension Strain on Buckling of Reinforcement in Concrete Columns”. J. Structural, 100(1):75-85

A Study on Spatial Correlation and Power Spectrum of Natural Wind at Xihoumen Bridge

LIU Ming，LIAO Haili，LI Mingshui, MA Cunming

Research Center for Wind Engineering, Southwest Jiaotong University, Chengdu, China, 610031, Email: rainmanok@gmail.com

Abstrat: In design of a long-span bridge, gust response of the bridge is very important and must be taken into account. The long-span structure has low natural frequency, small mass and extremely low inherent damping. The spatial correlation and spectrum of the wind in the low-frequency range affect the gust response However, there are very limited field data about spatial correlation of natural wind and wind spectrum. In the wind-resistance design, the decay factor is set to be 7, which affects the wind-resistance design of a long span bridge. Therefore, natural wind were measured at Xihoumen Bridge and the wind speed spectrum and spatial correlation are calculated. The results show that the spatial correlation of the natural wind is lower than that specified in the wind-resistance design specification of China in the low-frequency ranges. The most appropriate wind spectrum and decay factors fitting to the field measurements are recommended. This means that there is a possibility of being able to modify the design specification of long span bridge concerning gust response. The calculated results provide credible technical guide to construction of Xihoumen Bridge and ensure wind resistance safety.

Keyword: *Field measurement, Wind spectrum , Spatial correlation, Decay factor*

1.Introduction

With the emergence of high-strength materials and the development of design and construction technology, the development of long-span bridges has become more and more rapid. Because of large flexibility, relatively small mass and extremely low inherent damping, long-span suspension bridges are susceptible to vibrate caused by wind. Hence the effect of wind-induced responses has to be taken into account in the design of long-span suspension bridges. The power spectral density (PSD) and spatial correlation of wind-speed are important factors which affect the gust response of structures.

Xihoumen Bridge, located in the Xihoumen bay of ZhouShan City of China, is one of the longest span suspension bridges .It has a total length of 2713m including the main span of 1650m, and two side spans of 578m and 485m, respetively. The bridge is 36m wide with four traffic lanes, with a height clearance of 64.6m above water level. In order to investigate wind characteristics and to provide reliable field measurement data, anemometers were installed on the bridge deck 3.5m above the

deck and about 68m above the sea level. Field measurements at this bridge were conducted from October 2007 to March 2009.

These calculated results can provide credible technical guidance to construction of Xihoumen Bridge with ensured wind-resistance safety. The results can be used as references to the other bridges.

2. Field measurement

This paper presents full-scale data measured at the Xihoumen Bridge with focus on a power spectral density (PSD) and spatial correlation of wind-speed fluctuation, which are important factors of the wind-resistance design of a long-span bridge.

Four 3D anemometers are installed on the bridge deck (approximately 68m above sea level), The layout of anemometers at Xihoumen Bridge is shown in Fig1.Using data of any two anemometers, spatial correlation can be analyzed as a function of distance (T.Miyata et al., 2002). The average PSD quantities can be obtained using the data of the four anemometers.

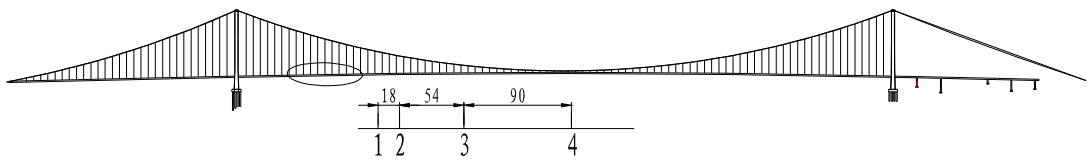

Fig1. Layout of anemometer at Xihoumen Bridge

3. Characteristics of wind

Fig. 2 and Fig.3 show the measured results of wind speed with four 3-D ultrasonic anemometers during a strong wind. As shown, the 10-min average wind speeds of the four anemometers are very similar. The 10-min mean wind speeds range from 1m/s to 19.4m/s. The longitudinal turbulent intensity (I_u) is from 0.04 to 0.25, and the longitudinal gust factor (G_u) is from 1.72 to 2.90. The average quantity of 10-min mean wind speed is 9.83m/s.

The mean values of I_u, I_v and I_w are 0.15, 0.114 and 0.05, respectively, and the ratio among them is I_u:I_v:I_w =1:0.75:0.35, which shows that the result from this field measurement is different from the recommended values by wind-resistance design specification of China. And the mean values of G_u,G_v and Gw are 2.32, 0.27 and 0.10, respectively.

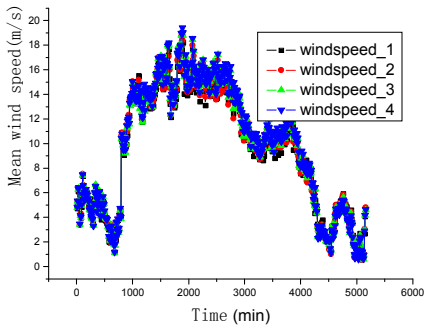

Fig2. 10-min average wind speed

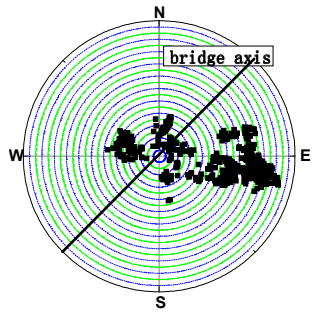

Fig3. 10-min average azimuth

2 Power spectral density

Power spectral density can describe the energy distribution of fluctuating wind velocity in frequency domain. Davenport has fitted some longitudinal wind velocity spectrum based on the field data measured in different regions and at different heights all over the world. Following that some researchers presented some empirical expressions based on Davenport's spectrum. Among many proposed spectra, the Kaimal spectrum and Panofsky spectrum have been recommended by wind-resistance design specification of China.

The field measured power spectral density of wind velocity was calculated using the Fast Fourier Transform technique (FFT) on transforming the turbulence velocity fluctuation time series data. Segment average and Hanning data windows were employed to smooth the spectrum. The parameters such as mean square value of longitudinal velocity fluctuation and longitudinal mean velocity are chosen to normalize the power spectral density and frequency.

Fitting the measured spectrum to theoretic spectrum (Pang, 2006), the following expressions can be used to describe the wind characteristics at Xihoumen Bridge during this strong wind:

Longitudinal wind spectrum: $$\frac{nS_u(n)}{\sigma_u^2} = \frac{6.79f}{(1+13.16f)^{5/3}} \quad (1)$$

Lateral wind spectrum: $$\frac{nS_u(n)}{\sigma_u^2} = \frac{4.18f}{(1+7.91f)^{5/3}} \quad (2)$$

Vertical wind spectrum: $$\frac{nS_w(n)}{\sigma_w^2} = \frac{0.38f}{(1+0.41f)^2} \quad (3)$$

Where S_u (n), S_v (n), S_w (n) are longitudinal, lateral and vertical power spectral density, respectively, n is the frequency; $f=nz/U$, and z is the height.

The comparison of longitudinal and vertical wind velocity spectrum with fitted spectrum has shown in Fig.4. It is shown that the fitted spectrum can describe the wind characteristics at Xihoumen Bridge very well.

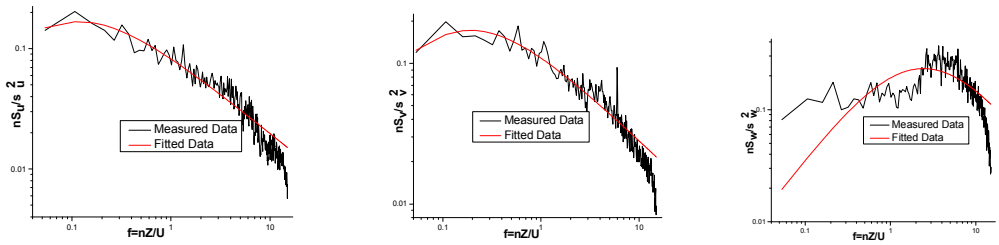

Fig4. Power spectrum of measured data at Xihoumen Bridge

3 Spatial correlation of winds

To determine the spatial correlation of wind, co-coherence of wind records are calculated, which is defined by the following equation (R. Toriumi et al., 2002):

$$Co-coherence=\frac{S_{uu}^{C}(,x1,x2,f)}{\sqrt{S_{uu}(x1,f)S_{uu}(x_2,f)}}=\exp(-k\frac{f\Delta y}{U}) \qquad (4)$$

Where $S_{uu}(x_1,f)$、$S_{uu}(x_2,f)$ is the spectrum of wind-speed fluctuation (u) at x_1 and x_2. $S^{C}_{uu}(x_1,x_2f)$ is the real part of cross-spectrum of u between x_1 and x_2, k is the decay factor, f is the frequency, $\Delta y=(|x_1-x_2|)$ is the transverse distance and U is the mean wind speed.

Co-coherence of data at Xihoumen Bridge calculated with Eq.(4) is shown in Fig.5. It is shown that no matter the distance is large or small, the coherence is unity when the frequency is zero. In addition, there is a tendency for the coherence to decrease with the increase of the distance between measurement points.

The decay factors are shown in Fig.8.and Table 1. It is seen that the decay factors range widely. While the distance is 18m, the decay factors are similar to the recommended values in wind-resistance design specification of China. Others are smaller than the recommended ones. There is a tendency for the decay factors to decrease with the increase of distance.

It also can be fund from Fig.6 that the decay factors have a weakly increasing trend with the increase of mean wind speed.

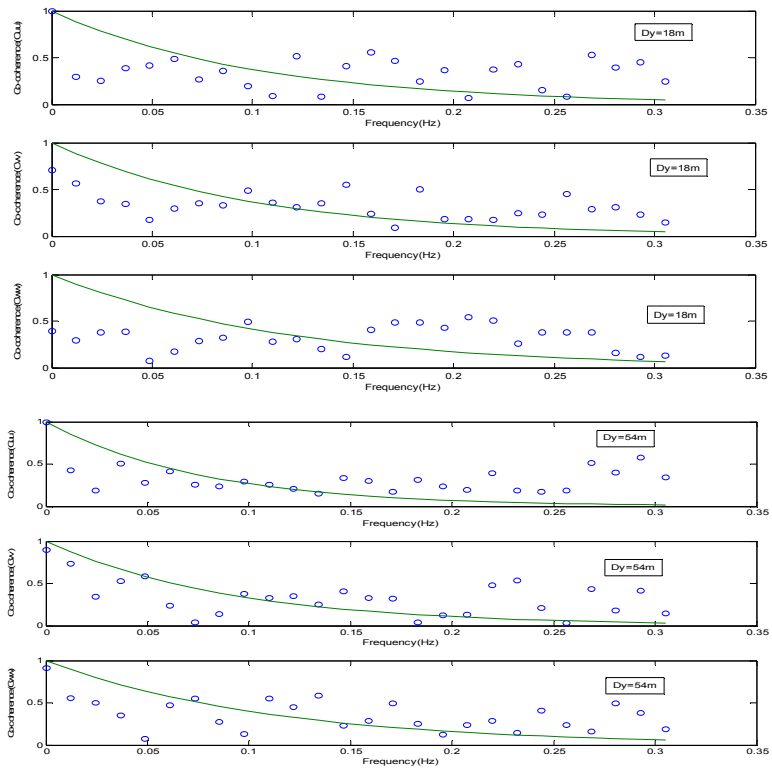

Fig.5 Co-coherence of measured wind data at Xihoumen Bridge

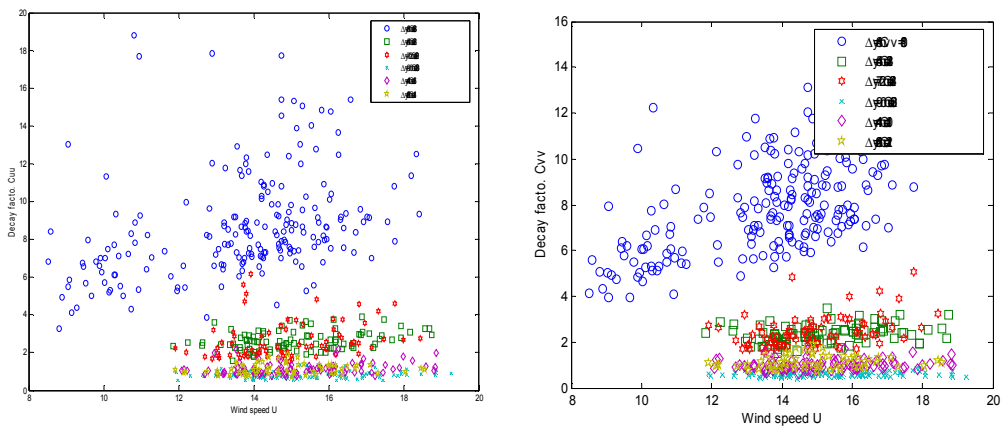

Fig.6 Decay factors at Xihoumen Bridge

Table 1. Decay factors at Xihoumen Bridge

Distance(m)	C_{uu}	C_{vv}	C_{ww}
18	8.68	8.01	9.19
54	2.63	2.34	2.85
72	2.69	2.46	2.56
90	0.84	0.62	1.21
144	1.16	1.01	1.23

162	1.14	1.12	1.16

4.Conclusions

This paper presents part of results from field measurements at the Xihoumen Bridge, Wind power spectral density and spatial correlation were analyzed and discussed. Some conclusions from this study are summarized as follows.

(1) Power spectral density were analyzed by fitting the PSD to Kaimal spectrum and Panofsky spectrum. The modified expressions can describe the wind characteristics at Xihoumen Bridge during this strong wind very well.

(2) It is seen that the decay factors range widely. While the distance is 18m, the decay factor is similar to the recommended values in wind-resistance design specification of China. But However other factors have lower values than the recommended ones. There is a tendency for the decay factors to decrease with the increase of the distance. The results show that the coherence is close to unity when the frequency is zero.

(3) These results come from the field data during only one strong wind. So a continuous and long-term field measurement should be carried out. More data should be collected to understand the general characteristics of natural wind at Xihoumen Bridge.

Acknowledgments

The research is supported by the National Science and Technology Support Key Project Plan under Grant No.2008BAG07B02, and the National Science Foundation of China under Grant No.50808148, which is gratefully acknowledged.

References

Pang Jia-bin.(2006). “Field Investigation and Wind Tunnel Simulation of Strong Wind Characteristics in Coastal and Mountainous Regions”, Ph.D Dissertation, School of Civil Engineering, The Tongji University, Shanghai,China,2006

R. Toriumi, H. Katsuchi, N. Furuya.(2000) “A study on spatial correlation of natural wind”, *Wind Engineering and Industrial Aerodynamics*, 87(2000),203-216

T. Miyata, H. Yamada, H.K atsuchi, M.K itagawa.(2002). “Full-scale measurement of Akashi-Kaikyo Bridge during typhoon”, *Wind Engineering and Industrial Aerodynamics*, 90(2002),1517-1527

Influence Factors Analysis of Buffeting Response of Self-anchored Cable-stayed Suspension Bridge

HUANG Haixin[1], ZHANG Ying[2] ,Liu Bo[1] and XU Fuyou[3]

[1]School of Civil Engineering, Hebei University of Technology, Tianjin 300401,PR China;PH./ FAX (86) 022- 85627187; email: hhxhebut@yahoo.com.cn
[2]Library, Hebei University of Technology, Tianjin 300401,PR China;PH./ FAX (86) 022- 85627187; email: hhx_zy@sina.com；
[3]Bridge Engingering institute，Dalian University of Technology, Dalian 116023, PR China;PH./ FAX (86) 0411- 84707995; email: xufuyou@hotmail.com

ABSTRACT

Self-anchored cable-stayed suspension Bridges ，as a new type of bridge is rarely investigated. Based on simulating turbulent wind fields, the effects of some factors such as geometrical nonlinearity, lateral aerodynamic memory effect, and fluctuating wind on main cables on buffeting response of the Dalian Harbor Sea-routine Bridge, a self-anchored cable-stayed suspension with 800m main span, are analyzed and the characteristics of buffeting response for the new type of bridge are summarized. It is worthy of concern in results that fluctuating winds on the cables causes the vibration of main cables and brings coupling vibration of the stiffing girder, which makes a greater effect on the girder of a self-anchored cable-stayed suspension bridge than those on the girder of a general suspension bridge.

Keywords: Self-anchored cable-stayed suspension bridge; Buffeting; wind field

1. INTRODUCTION

The 1360m long Dalian Harbor Sea-routine Bridge,as shown in Figure 1.,is a combined system bridge containing both self-anchored suspension bridges and cable-stayed bridges. It serves as a part of the Across Sea Highway of Dalian City in Northeast China and provides the vital linkage between the urban area and the economic development area. The bridge deck consists of a pre-stressed concrete box girder within the cable-stayed bridge and a steel box girder within the suspension bridge,which to a larger degree reduces investment and improves the mechanical properties of the structure. Moreover,the total 8 hangers were arranged at the connecting zone so as to improve the fatigue of the side hanger cables. Differing from traditional cable-stayed suspension bridges, the main cables of the Dalian Harbor Sea-routine Bridge are anchored at the ends of the stiffening girder,so it is

named as a self-anchored cable-stayed suspension bridge. As a result, the horizontal components of the main cables' force are transferred to the girder, which will reduce the stiffness of the girder due to P-Δ effects (Huang et al.,2007); The wind-reduced vibration of the new type of cable supported system will be more serious. The Dalian Harbor Sea-routine Bridge is located at the entrance of Dalian Bay. The bridge site is mainly affected by tropical cyclones, or typhoons, that generally occurre between May and August. Therefore, the aerodynamic behavior of the Dalian Harbor Sea-routine Bridge is of great concern, not only to the bridge itself, but also to the new type of combined system.

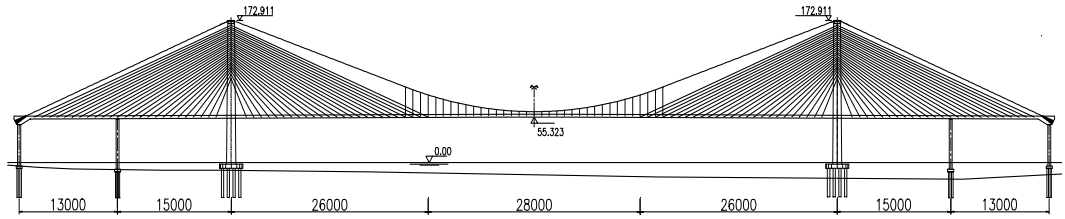

Figure 1. Layout of Dalian Harbor Sea-routine Bridge（unit: cm）.

In the current study, buffeting response of the Dalian Harbor Sea-routine Bridge is performed and the effects of some factors such as geometrical nonlinearity, lateral aerodynamic memory effect and fluctuating wind on main cables on buffeting response have been analyzed. Some characteristics regarding buffeting response and several suggestions being favorable to guide the anti-wind design of the new type of system are obtained.

2. SIMULATION OF WIND FLUCTUATIONS

The turbulent wind field is a random variable related to time and spatial position and it has been recognized that the along-wind turbulence “u” and vertical turbulence “w” can be considered as stationary Gaussian random processes with zero means. Therefore, they can be generated using the techniques for digital simulation of multidimensional random processes. According to a theory developed by Shinozuka, the sample of random process F(t) can be expressed as (Cao et al.,1998)

$$f_j(t) = \sum_{m=1}^{j} \sum_{l=1}^{N} \left| H_{jm}(w_{ml}) \right| \sqrt{2\Delta w} \cos[w_{ml} t + \theta_{jm}(w_{ml}) + \phi_{ml}], j = 1,2,\cdots,n \qquad (1)$$

Where N is the sum of sampling frequencies; $\Delta\omega = \omega_{up} / N$, ω_{up} is the maximum circular frequency(i.e.,when $\omega > \omega_{up}$, $S(\omega) = 0$); ϕ_{ml} is a random phase angle with indexes; $\theta_{jm}(w)$ is the argument of $H_{jm}(w)$; $H_{jm}(w_{ml})$ is a element of Cholesky decomposed matrix of cross spectral density matrix.

The Eqs.(1) is adopted to simulate the wind fields of the Dalian Harbor Sea-routine Bridge and some parameters related to the simulation are given, such as bridge deck elevation of 60m, terrain roughness length of 0.01m, mean wind velocity of 40m/s, the maximum circular frequency of 4πrad/s,time interval of 0.025s,the total 195 nodes along the girder and the tower as well as the main cables,10 min duration. The comparison between the simulated correlation function as well as power spectra at midspan and goal results are shown in Figure 2 and Figure 3 and it can be indicated that the simulated fluctuating wind velocities are available.

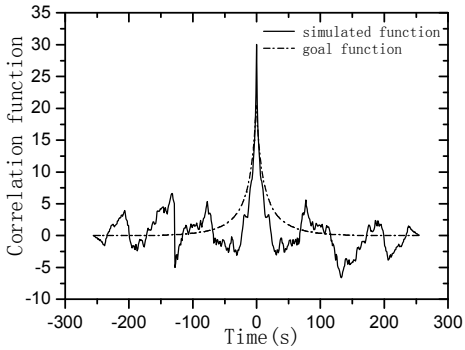

Figure 2. Horizontal fluctuating velocity correlation functions at mid-span.

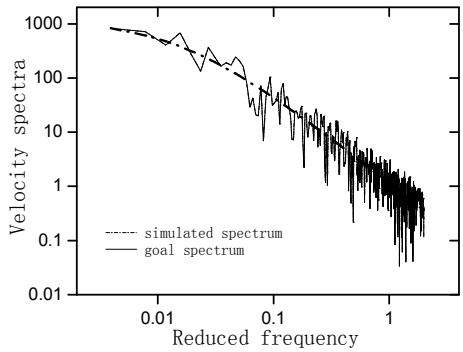

Figure 3. Horizontal fluctuating velocity power spectra at mid-span.

3. CALCULATION OF AERODYNAMIC FORCES

3.1. CALCULATION OF BUFFETING FORCES

A.G.Davenport gave the buffeting force expressions in the time domain based on quasi-steady theory(Chen et al.,2000), as follows

$$\left.\begin{aligned} D_b(x,t) &= \frac{1}{2}\rho U^2 B[2C_D(\alpha_s)\frac{u}{U}+C_D^{'}(\alpha_s)\frac{w}{U}] \\ L_b(x,t) &= -\frac{1}{2}\rho U^2 B\{2C_L(\alpha_s)\frac{u}{U}+[C_L^{'}(\alpha_s)+C_D(\alpha_s)]\frac{w}{U}\} \\ M_b(x,t) &= \frac{1}{2}\rho U^2 B^2[2C_M(\alpha_s)\frac{u}{U}+C_M^{'}(\alpha_s)\frac{w}{U}] \end{aligned}\right\} \quad (2)$$

Where u and w are horizontal and vertical fluctuating wind velocity,respectively; C_D, C_L and C_M are drag, lift and moment coefficients with mean static wind attack of α_s ,respectively,which can be obtained from wind tunnel test ; $C_D^{'}=dC_D/d\alpha$, $C_L^{'}=dC_L/d\alpha$ and $C_M^{'}=dC_M/d\alpha$.

Based on the above the simulated fluctuating wind velocity,the buffeting forces acting on the overall bridge can be obtained.

3.2. CALCULATION OF SELF-EXCITED FORCES

Scanlan put forward, firstly, the mathematical model of self-excited forces expressed with aerodynamic derivatives in the frequency domain based on the linear hypothesis(Xiang, 1994). This assumption, however, is not appropriate for long-span bridges, where nonlinearity due to either geometric or aeroelastic effects must be considered. As an alternative method, buffeting response of long-span bridges under wind turbulence can be analyzed in the time domain. An efficient calculating method involving impulse response functions of self-excited forces for long-span bridges developed by Y. K. Lin (Liu et al.,1996)) is adopted in this study.

4. INFLUENCE FACTORS ANALYSIS OF BUFFETING RESPONSE

4.1. INFLUENCE OF GEOMETRIC NONLINEARITY

It is well known that long span bridges should take geometric nonlinearity into account. The comparison, considering geometric nonlinearity or not, of vertical, lateral and torsional displacements at midspan of the girder are shown in Figure 4. It can be seen that the effects considering nonlinearity on the vertical displacements of buffeting response may be neglected, but on the lateral and torsional displacements the effects are considerable and all results are smaller than those only considering linearity. The reasons of which are that the P-Δ effects reduced the stiffness of the girder. For the cable supported bridges, however, the main members of the supporting loads are the main cables and hangers as well as the stays. The lateral displacements enlarged the axial forces of those members and therefore gave more contributions to the overall stiffness of the structure due to the effect of stress stiffening.

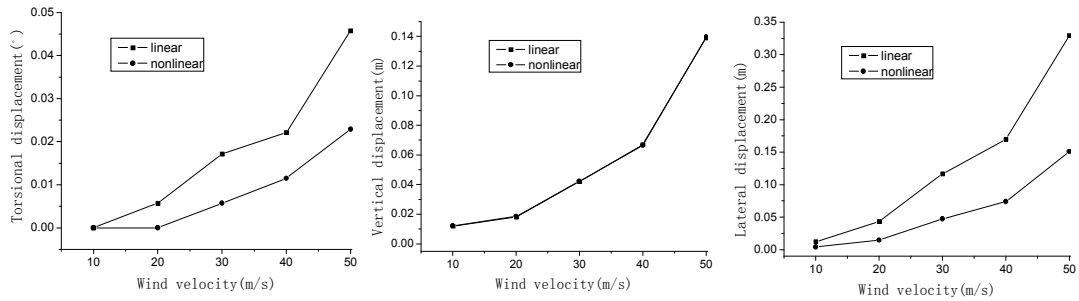

Figure 4. Comparison of displacements at midspan considering nonlinear factors or not.

4.2. INFLUENCE OF LATERAL AERODYNAMIC MEMORY EFFECT

The effects of lateral motion on sel-excited forces are in general not considered because aerodynamic derivatives related to the lateral freedom degree can not be obtained due to extensive use of a double freedom section model in wind tunnel tests so far, which will affect the precision of the buffeting response and accurate evaluation of structural fatigue life. Hence,the lateral aerodynamic derivatives

according to expression given by Y. K. Lin (1996) are used to analyze the buffeting response here. It can be observed from Figure 5 that lateral aerodynamic memory effect has little effect on vertical displacements, whereas influence on torsional displacements, especially on lateral displacements, has a considerable effect and the tendency becomes greater with the addition of wind velocity. So the long span self-anchored cable-stayed suspension bridge should consider the effects of lateral aerodynamic memory effect on the buffeting response.

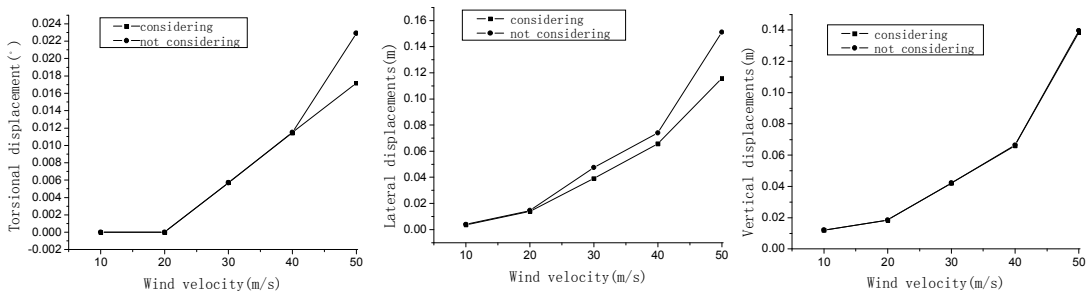

Figure 5. Comparison of displacements at midspan considering lateral aerodynamic memory effect or not.

4.3. INFLUENCE OF FLUCTUATING WIND ON MAIN CABLES

Buffeting response analysis of bridges donsn't generally take the influence of fluctuating wind on main cables into account. One of the reasons lies in the limitation of the method of simulating wind fields; the other is that some researchers think subjectively that the influence is but little, but the actual conditions have not been known clearly so far due to lack of specific materials. Based on the above simulated turbulent wind fields containing the main cables, the results of the buffeting response at midspan of the Dalian Harbor Sea-routine Bridge are shown in Figure 6.

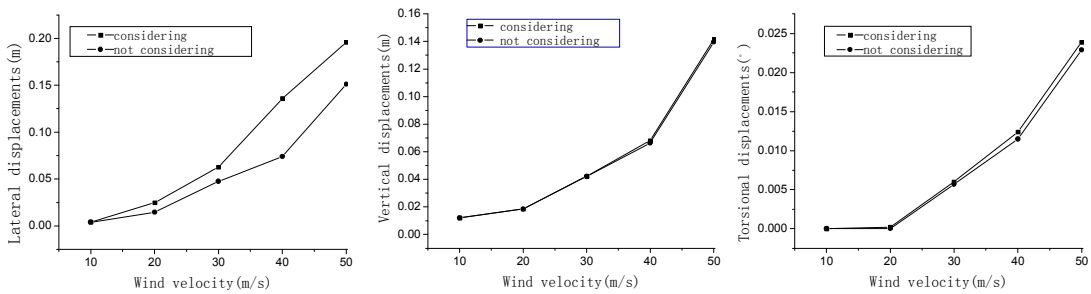

Figure 6. Comparison of displacements at midspan considering fluctuating wind on cables or not.

The fluctuating wind on the main cables makes a considerable effect on the lateral displacements of the girder at the midspan.Effects on torsional displacements can also not be ignored, which are different from those of Jiangyin Bridge,a long span suspension bridge with 1385m main span. The reasons for the greater effects lie in that, on the one hand, the cables of self-anchored cable-stayed suspension bridges are denser than those of suspension bridges, which results in greater fluctuating wind loads, and on the other hand the gravity stiffness is smaller because loads supported by the main cables are only a part of the overall loads of the bridge, which made the main cables liable to vibration under fluctuating wind loads and further enlarged the vibration of the girder due to the coupling effects between main cables and the girder. In other words, the main cables and the girder are connected through, not only hangers, but also anchor block at the ends of the girder. It is therefore worthy of concern the effects of fluctuating wind on the main cables on the girder of self-anchored cable-stayed suspension bridges.

5.CONCLUSIONS

The paper analyzes the buffeting response of self-anchored cable-stayed suspension bridges such as the Dalian Harbor Sea-routine Bridge. The theoretical analysis reveals that the effects of geometrical nonlinearity and lateral aerodynamic memory effect on the girder of the new type of cable supported bridge can not be ignored; the former reduces the lateral and torsional displacement of the girder at midspan and the tendency becomes more obvious with the addition of wind velocity whereas the latter reduces the torsional displacement and especially the lateral displacement at the same position. It is worthy of concern that the fluctuating wind on the main cables makes a greater effect on torsional displacement of the girder than those of general suspension bridges.

ACKNOWLEDGES

The research is supported by the Chinese National Natural Science Funds(N0.50708012).

REFERENCES

Cao,Y.H.,Xiang,H.F.,and Zhou,Y.(1998). “Simulation of stochastic wind field on long-span bridge”， *China Civil Engineering Journal,* 31(3):72-79.

Chen, X., Matsumoto, M., and Kareem. A.(2000). “Aerodynamic coupled effects on flutter and buffeting of bridges.” *Journal of Engineering Mechanics*, ASCE, 126(1):17-26.

Huang,H.X., Zhang,Z., and Shi,L.(2007). “Dynamic analysis of self-anchored cable-stayed suspension bridge.” *Journal of Dalian University of Technology*,47(4),557-562.

Liu,C.H.,Xiang,H.F.,and Gu,M.(1996). "3D Nonlinear Time--domain Buffeting Analysis for Long Span Bridges." *Journal of Tongji University* ,4(4):380-385.

Xiang, H.F. (1994). "Wind engineering mechanics and aerodynamics of long-span bridges." *Bulletin of National Science Foundation of China,*3,232-234.

Stiffness Reduction Factor of Reinforced Concrete Bridge Pier Considering Characters of Nonlinear

Pengfei Luo[1], Dongjian Shen[1], Haijie Mi[2],
Xiangya Kong[1], Jianxin Wang[3]

[1]College of Urban and Rural Construction, Agricultural University of Hebei, P.O. Box 071001, Baoding; email: luopengfei1234@yahoo.cn
[2]Shijiazhuang Branch of China United Telecommunications Corporation, P.O. Box 050000, Shijiazhuang; email: mihaijie1007@yahoo.com.cn
[3]519 Team of North China Geological Exploration Bureau, P.O. Box 071051, Baoding; email: wjxbg@sina.com

Abstract

The method of stiffness reduction had been adopted to consider nonelastic characteristics of reinforced concrete in concrete structure standard of the United States and Canada. Concrete structure design code of China also accepted the method of stiffness reduction as a supplementary way to solve the second-order effects problem when necessary. However, bridge code of China still uses amplified coefficient of eccentricity to consider nonlinear characteristics of reinforced concrete. In view of the absence of investigation in the stiffness reduction of reinforced concrete bridge pier, this paper adopts the numerical integral method to computerize simulation and analyze the regulation of the stiffness change for rectangular section reinforced concrete bridge pier under different axial compression ratio and different forces of horizontal earthquake action, which is verified according to the test result. As a result, a stiffness reduction factor is proposed to consider nonlinear characteristics of reinforced concrete bridge pier.

Keywords: Reinforced concrete bridge pier, numerical integral method, nonlinear characteristics, stiffness reduction factor

1. Preface

Reinforced concrete bridge pier represents characters of material and geometric nonlinearity under ultimate limit state. The material nonlinearity is affected mainly by nonlinear elastic constitutive relation of components material, components cracking and slippage of reinforced bar. The geometric nonlinearity displayed mainly at additional internal force and additional displacement caused by axial force acting on deflection components or vertical load acting on lateral displacement structure, which is second-order effects. The stiffness reduction method had been adopted to consider nonelastic characteristics of reinforced concrete in concrete structure standard of the United States and Canada. Concrete structure design code of China also accepted the stiffness reduction method as a supplementary way to solve the second-order effects when necessary. However, bridge code of China still uses the amplified coefficient of eccentricity to consider nonelastic characteristics of

reinforced concrete. In view of the absence of investigation in the stiffness reduction of reinforced concrete bridge pier, this adopts the numerical integral method to computerize simulation and analyze the stiffness change regulation. In particular, for rectangular section reinforced concrete bridge pier under different axial compression ratio and different forces of horizontal earthquake action in test model of literature [4], and it is verified by the test results. Finally, a stiffness reduction factor is proposed to take account of the above-mentioned two nonlinear characteristics of reinforced concrete bridge pier.

2. Analysis principle

The moment-curvature relation computer program is compiled by numerical integral method to computerize simulation the rectangular section member, which is analyzed under different axial compression ratio and different forces of horizontal earthquake action.

2.1. Basic assumptions of the program

To computerize simulation nonlinear full range analysis of rectangular section reinforced concrete bridge pier with biaxial bending and compression, the computer program is based on following assumptions:

1). The average strain accords with the assumption of plane section in the whole force analysis process.

2). The strength of concrete is neglected in tensile area, and the stress-strain relationship of concrete in compressive region references the kent-park model [5], as shown in Figure 1.

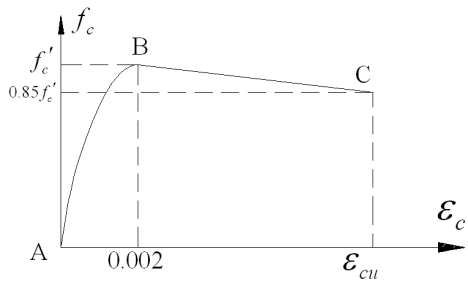

Figure 1. Stress-strain curve of concrete.

In Figure 1, the characteristics of the curve are as follows:

$$\sigma_c = \begin{cases} AB: f_c'[2\varepsilon_c / 0.002 - (\varepsilon_c / 0.002)^2], \\ \qquad (\varepsilon_c \le 0.002) \\ BC: f_c'[1 - 0.15(\varepsilon_c - 0.002)/(\varepsilon_{cu} - 0.002)], \\ \qquad (0.002 \le \varepsilon_c \le \varepsilon_{cu}) \end{cases} \quad (1)$$

Where, f_c' is the prism compressive strength of concrete, and ε_{cu} is the ultimate compression strain of concrete, which is 0.004255. Considering eccentrical compression and primary axial compression model have influence on descent segment, this adjusts the slope of the descent segment to be 0.15.

3). Stress-strain curve of longitudinal reinforcement is assumed to perfect plastic elastic material and takes the double broken line model shown in Figure 2.

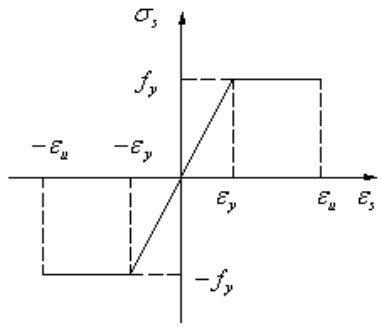

Figure 2. Stress-strain curve of reinforcing bar.

4). The spalling of cover concrete is not considered.

5). Dividing the section into numbers of small rectangle units and approximate thinking its resultant force located in the centroid of units.

6). Concrete shrinkage and creep effect in compressive region is ignored.

2.2. Programming principle

The moment-curvature relation of rectangular section reinforced concrete bridge pier with biaxial bending and compression is gotten by adding curvature step by step under axial force N and loading angle α. α is shown in Figure 3 and its positive direction is anticlockwise. The specific method is as follows:

1). Preliminary selection distance R and angle θ are shown in Figure 4. Thus, the distance between each reinforcing bar of the section and neutral axis, as well as the distance between each concrete elements centroid and neutral axis can be calculated from:

$$r_i = R - (x_i^{'} \cos\theta + y_i^{'} \sin\theta) \qquad (2)$$

Where x_i', y_i' are coordinates of point i.

2). To determine section initial curvature Φ_0.

Based on plane section assumption, concrete stress σ_{ci} of point i and reinforcing bar stress σ_{sj} of point j are obtained according to strain equation $\varepsilon_i = \Phi_0 r_i$ of point i and stress-strain relationship of concrete and reinforcing bar. Therefore, the section internal force N', $M_{\mathrm{x}}^{'}$ and $M_{\mathrm{y}}^{'}$ are gotten by the equilibrium condition of force.

3). Comparing obtained force N' with N, as well as the resistance loading angle β ($\beta = arctg(M_{\mathrm{x}}^{'} / M_{\mathrm{y}}^{'})$) with the given loading angle α to see whether they satisfy the requirement error. If they do not satisfy the above-mentioned two requirement error, then change the location parameter of neutral axis and the normal angle, and recalculate until they satisfy the requirement error. Therefore, M' is the corresponding

M value of the reinforced concrete bridge pier with biaxial bending and compression when the value of curvature Φ is given.

4). Adding curvature Φ in proportion, and repeating steps 1~3, seeking the corresponding value of M. Obtaining the value of Φ_u and M_u when the maximum compressive strain of the edge in compressive region arrives the instability strain of compression reinforcement.

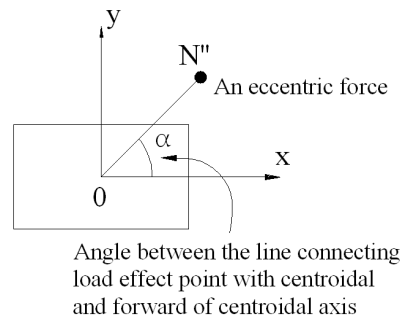

Figure 3. Definition of loading angle α .

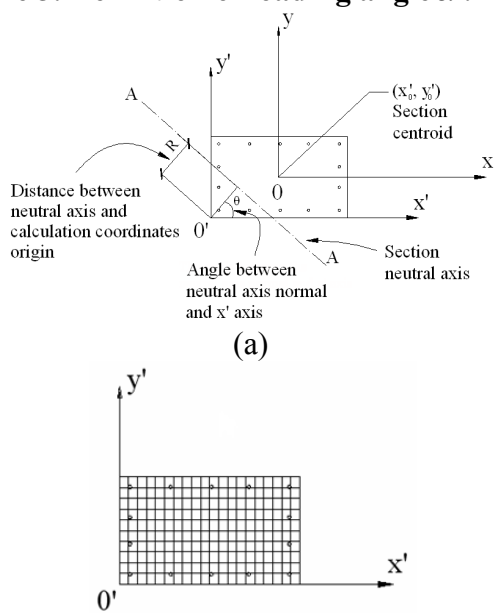

Figure 4. Calculated models.

3. Program verification

3.1. Verification of the moment-curvature relation

To verify the reliability of the computer program, the nonlinear program of the normal section bearing capacity of the rectangular section reinforced concrete bridge pier is applied to simulate and analyze the test model in the literature. The theoretical value and the test value are shown in Figure 5~8.

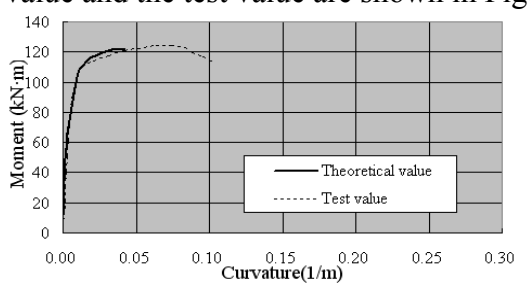

Figure 5. Moment-curvature relation of 1# bridge pier.

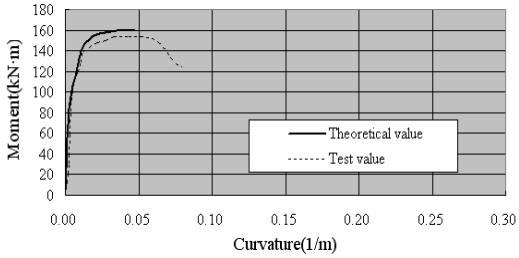

Figure 6. Moment-curvature relation of 2# bridge pier.

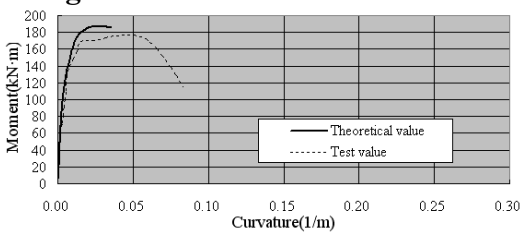

Figure 7. Moment-curvature relation of 3# bridge pier.

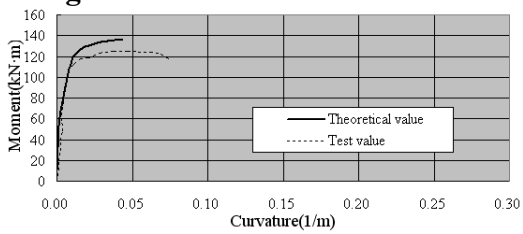

Figure 8. Moment-curvature relation of 4# bridge pier.

We can see that the theoretical value of the moment-curvature relation agree well with the test value of the moment-
curvature relation from Figure 5~8.

3.2. Verification of horizontal displacement of the theoretical value and the test value.

Based on the test model in the literature and taking 1# bridge pier for example. It can be divided into five equal portions along the height and its axial compression ratio is 0.1, then choosing eight degree of earthquake resistance protection seismic and the second kind of ground. Thus, the standard value of horizontal earthquake action is 20.97kN and the moment of each section is obtained. According to the moment-curvature relation computer program in this paper, the curvature of each section can be gotten by the moment of each section. Then the horizontal displacement of the top of the bridge pier is calculated from the curvature distribution along height of the bridge pier.

The moment considered second-order effects of each section are gotten on the basis of the horizontal displacement of the top of the bridge pier, so as to determine the curvature considered second-order effects of each section, then the final horizontal displacement of the top of the bridge pier as shown in Table 1 is calculated from the curvature distribution along the height of the bridge pier, which has considered the second-order effects.

Table1. Summary of results for horizontal displacement.

Speci-men	Axial Compressi-on Ratio	Calculated Value (mm)	Test Value (mm)	Percent Difference
1	0.1	7.69	7.58	+1.45%
2	0.175	19.85	17.73	+11.96%
3	0.25	52.22	57.86	-9.75%
4	0.125	29.45	23.58	+24.89%

We can obtain that the horizontal displacement of the theoretical coincides quite well with the horizontal displacement of the test.

4. The analysis procedures for determining the stiffness reduction factor of rectangular section reinforced concrete bridge pier

4.1. Calculation procedures

1). Determining the geometric parameters, sectional reinforcement and concrete strength of the example according with current standard.
2). Selecting different axial compression ratio of the example to calculate the moment-curvature relation.
3). Determining the force of horizontal earthquake action and dividing the example into five equal portions along the height.
4). Determining the horizontal displacement according to structural mechanics method and the moment of each section considered second-order effects.
5). Obtaining the curvature of each section according to the moment-curvature relation.
6). Obtaining the stiffness reduction factor on the basis of bending energy equivalent principle.

4.2. Calculation the stiffness reduction factor

The internal force of each elements and the displacement of each nodes are calculated from the moment-curvature relation. Figure 9 represents the final deformation of some the bridge pier segment, which has totally n nodes and is divided into $n-1$ elements. The average bending stiffness $(\overline{EI})_i$ of the i element is calculated from the moment of the element and the rotation angle of the element nodes. Supposing the average moment of the i element is $\overline{M_i}$, and the relative rotation of two ends of the element is $\Delta\varphi_i$ and the length of the element is Δs_i, then the average curvature can be written as:

$$\overline{k}_i = \frac{\Delta\varphi_i}{\Delta s_i} \qquad (3)$$

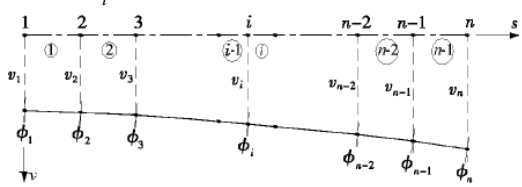

Figure 9. The final deformation of some bridge pier segment

By the moment-curvature relation, the average bending stiffness $(\overline{EI})_i$ of the i element can be written as: $(\overline{EI})_i = \dfrac{\overline{M_i}}{\overline{k_i}}$ (4)

The whole equivalent bending stiffness of the bridge pier segment can be calculated from the bending energy equivalent principle of the investigated bridge pier segment. Therefore, the equivalent bending stiffness reduction factor α_e is obtained.

Bending deformation energy of some bridge pier segment can be written as:

$$E_b = \frac{1}{2}\sum_{i=1}^{n}\overline{M}_i\Delta\varphi_i = \frac{1}{2}\sum_{i=1}^{n}(\overline{EI})_i\overline{k}_i^2\Delta s_i \quad (5)$$

Supposing the bending stiffness of some uniform-section elastic pole is $(EI)^*$, which has the same bending deformation energy with the original bridge pier segment in the same forming process condition. It can be written as follow:

$$E_b = \frac{1}{2}\sum_{i=1}^{n}(EI)^*\overline{k}_i^2\Delta s_i \quad (6)$$

$(EI)^*$ can be calculated from formula (5)~(6), then the equivalent bending stiffness reduction factor α_e can be shown as the following:

$$\alpha_e = \frac{(EI)^*}{EI} = \frac{\sum_{i=1}^{n}(\overline{EI})_i\overline{k}_i^2\Delta s_i}{EI\sum_{i=1}^{n}\overline{k}_i^2\Delta s_i} \quad (7)$$

5. Calculation examples analysis for determining the stiffness reduction factor of rectangular section reinforced concrete bridge pier

5.1. Basic parameters of the examples

The data of the test model in literature [4] is taken to use computer to computerize simulation under different axial compression ratio and different forces of horizontal earthquake action. The cubic compressive strength of concrete is 35.0 N/mm^2 and the elastic modulus of concrete is 40GPa. The main reinforcing bar is Φ10 of HRB335, whose yield strength is 375.0 N/mm^2 and elastic modulus is 200GPa. Other parameters are shown in Table 2.

Table2. Some parameters of the examples.

Specimen	Axial Compression Ratio	Bridge Pier Height (m)
1	0.1	3.0
2	0.175	3.3
3	0.25	3.6
4	0.125	3.9

5.2. Calculation results analysis for the example

Based on the formula (7), the stiffness reduction factors of rectangular section reinforced concrete bridge pier are finished into Table 3.

Table3. Stiffness reduction factors.

Specimen	Axial Compression Ratio	Stiffness Reduction Factor
1	0.1	0.39
2	0.175	0.35
3	0.25	0.24
4	0.125	0.28

6. Conclusion

Through theoretical analysis of the test results, we can obtain that the theoretical results agree well with the test results. The axial compression ratio has influence on stiffness reduction factor. The suggestion stiffness reduction factor of rectangular section reinforced concrete bridge pier is 0.3, which is an average value.

Bibliography

American Concrete Institute (ACI). (2008). *Building Code Requirements for Structural Concrete (ACI318-08) and Commentar*y, Michigan, U.S.A.

Canadian Standards Association (CSA). (2004). *Design of Concrete Structures (CSA-A23.3-04)*, Ontario, Canada.

Ministry of Communications of the People's Republic of China. (2004). *Code for Design of Highway Reinforced Concrete and Prestressed Concrete Bridges and Culverts (JTG D62-2004)*, Beijing, China(in Chinese).

Niu Songshan, Zheng Gang, Tang Guangwu, Lan Haiyan. (2005). "Experimental Research on Moment-Curvature Relation of Pier's Plastic Hinge Under Cyclic Loading.", *Technology of Highway and Transport*, 2005(5), 91~95(in Chinese).

R.Park and T.Paulay. (1975). "Chapter 2: Stress-strain relationships for concrete and steel and Chapter 6: Ultimate deformation and ductility of members with flexure" *Reinforced Concrete Structures*, John Wiley & Sons, New York, 2.1.3 and 6.6.1~6.63.

Liu Yi, Zhu zhanyou, Weiwei, Baishao Liang. (2007). "Discussion of the Stiffness Reduction Factor of Bent-columns.", *Journal of Chongqing University (Natural Science Edition)*, 30(4), 63(in Chinese)

This page intentionally left blank

A Fuzzy Neural Network Technique for Crack Assessment of RC Bridges

Zhijian Hu[1] and Zhaofang Hu[2]

1 Communication School, Wuhan University of Technology, No. 1040 Heping Avenue, Wuhan, 430063; PH (86)027-88611055; FAX(86)027-86551193; email: huzhijian2008@yahoo.com.cn

2 Communication Department of Jiangxi Province, Nanchang,330002; PH(86)0791-6243872; FAX(86)0791-6243872;email:zfanghu@jxjt.gov.cn

Abstract: As cracking is one of the leading and most critical types of deterioration for reinforced concrete (RC) bridges, how to properly assess cracking condition is of great importance for effective concrete bridge management. However the current assessment techniques are subjective, time-consuming, and rely mostly on human visual inspection. In order to improve the effectiveness of cracking condition assessment, a fuzzy neural network (FNN) system was developed in this study, as an alternative to traditional assessment methods. Based on the comprehensive analysis of RC bridge cracking，this paper also set up the assessment criteria for RC bridges for both flexural cracking and shear cracking, and gives the form of membership function for each criterion. Finally the system was verified using statistical crack samples of several RC bridges.

Keywords: RC bridges; Cracking Assessment; criteria; fuzzy-neural networks

1 Introduction

Cracking can be of various sizes and can occur anywhere on concrete surface, and may also lead to severe deterioration, such as rebar corrosion, to reinforced concrete (RC) bridges if they are wide and/or deep enough. Elzafraney (Elzafraney 2005)has analyzed microcracks quantitatively for RC bridge deck; the causes of transverse RC deck cracking have been summarized by classifying them into three categories and the effects of design factors were studied with a finite-element method(Hadidi 2005., Saadeghvaziri 2005). The influence factors of cracking, however, are too complicated to be analyzed precisely.

Furthermore, as cracking is one of the leading and most critical types of deterioration for RC bridges, how to properly assess cracking severity is of great importance for effective concrete bridge management. In order to evaluate cracking effectively, and due to the fact that the current assessment techniques are subjective, time-consuming, and rely mostly on human visual inspection, many studies have been conducted in this field. AbdelRazig and Chang(AbdelRazig and Chang 2000) constructed a model applying digital image processing and neural network techniques for constructed facilities surface quality assessment; condition state evaluation systems of concrete slabs and existing RC bridges were developed using neuro-fuzzy hybrid system, that considering cracking with the maximum crack width and crack condition(Kawamura 2003). In many cases cracking is only roughly considered as a kind of defect with no more attention being paid(Brito 1996, Zhao 2002).

Based on the comprehensive analysis of RC bridge cracking，in this study, the assessment criterion system of simple supported RC bridges was set up for both flexural cracking and shear cracking, and the membership functions were specified for each criterion. Next, the fuzzy-neural network system was developed to assess the crack condition of RC bridges. Finally the system was verified using statistical crack samples of several RC bridges.

2 Assessment criteria

Actually cracking on a RC beam surface can be classified under the following major categories: flexural cracking which is induced by flexural stresses; shear cracking which often occurs in the regions between a supported point of a beam (or slab) and its 1/4 span, induced by shear stresses; shrinkage cracking due to drying and thermal shrinkage; and the longitudinal horizontal cracking caused by reinforced bar corrosion. As for existing concrete bridges which have serviced for a certain period, the shrinkage due to drying and thermal has completed, and the shrinkage cracking could be ignored since they are always stable. The longitudinal horizontal cracking always means severe rebar corrosion and can be considered as a key factor in the analysis and assessment of rebar corrosion. So for in-service RC bridges attentions should be paid to flexural cracking and shear cracking when studying cracking.

The influence factors for condition state assessment of flexural cracking and shear cracking were sorted into two types: indirect and direct. The indirect factors include age, traffic volumes, the heaviest traffic load, environment, the structure type, concrete grade etc., while the direct factors are the cracking shape, space, location, degree of orientation, width, depth, length, and crack number. Of course it is impossible to consider all the factors to evaluate the cracking for RC bridges. So the assessment criteria must be extracted from all the factors before the assessment process goes on.

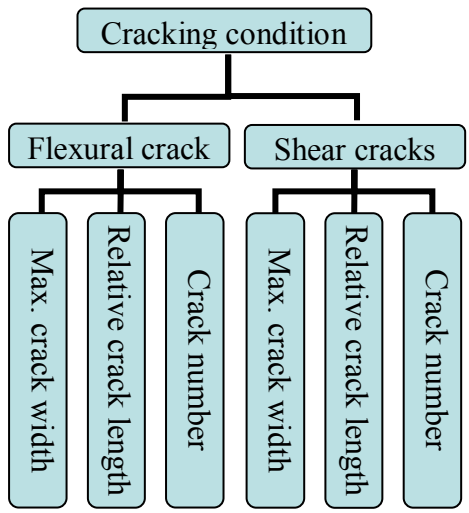

Fig. 1. The criteriA for cracking condition

Based on an overall analysis, Fig.1 presents the criteria for simple supported RC bridge cracking condition state assessment. Here the relative crack length is the ratio of the widest crack length to the beam height or of its vertical reflection height to the beam height for shear cracking. And in terms of these criteria the cracking condition

has 5 rates with larger number indicating more severe condition, as shown in Table 1.

Table 1 Definitions for crack condition states

Cracking condition	Definition
1 (Excellent)	No visible cracks
2 (Good)	The max. crack width is less than the acceptable value
3 (Moderate)	The max. crack width is larger than the acceptable value, but its relative length is small
4(Severe)	The max. crack width is larger than the acceptable value, and its relative length is medium
5(Dangerous)	The max. crack width is larger than the acceptable value, and its relative length is large

The final general assessment result for a simple supported RC bridge depends on the more severe cracking condition between the flexural cracking and the shear cracking.

3 Fuzzy neural network (FNN)

Here the neural network techniques were combined with fuzzy logical system to develop the FNN system in which membership functions and fuzzy rules were described with the neural network implicit language. Fig.2 indicates the topological configuration for a multi-layer FNN with application of the error back propagation (BP) method. Details about FNN could be found in references(Kawamura 2003, Zhao 2002).

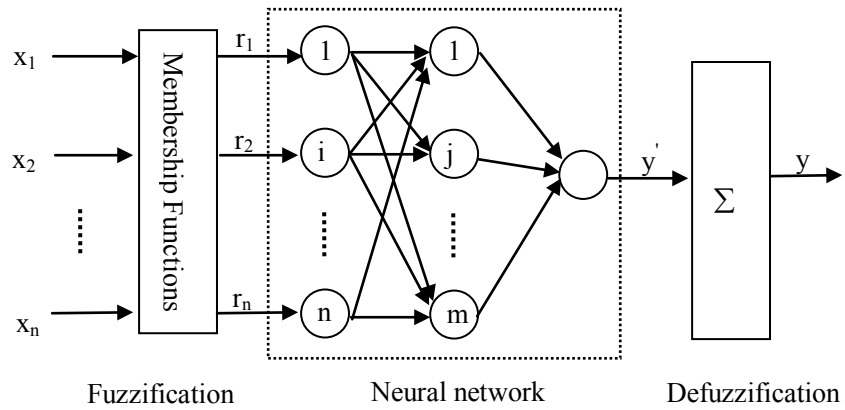

Fig.2. Configuration for the fuzzy-neural network

3.1 Fuzzification and defuzzification

With the pre-processing of inputs and the post-processing of outputs FNN is able to integrate fuz-zy concepts into the input-output system. For in-stance, if a variable space was divided into five independent subsets, named as A、B、C、D and E, respectively,

Then a n dimensional input vector X_n could be extended into a 5n dimensional vector, written as：

$$X_{5n}=\left[U_{A(x_1)}(x_1),U_{B(x_1)}(x_1),\cdots\cdots;U_{D(x_n)}(x_n),U_{E(x_n)}(x_n)\right]^T \qquad (1)$$

where $\left\{U_{A(x_i)}(x_i), U_{B(x_i)}(x_i), \cdots\cdots, U_{E(x_i)}(x_i) \mid (i=1,2,\cdots,n)\right\}$ are the grades of membership function of x_i corresponding to each fuzzy subsets..

And the centroid-average method was used to defuzzify the system outputs,, expressed as：

$$y = \sum_{k=1}^{M} (k \times y_k^{'}) / \sum_{k=1}^{M} y_k^{'} \qquad (2)$$

where y is the defuzzified output, M is the number of possible values for a certain variable, k is the value given to the variable and $y_k^{'}$ is the system output corresponding to k.

3.2 Membership function

The form of membership functions is crucial for fuzzy inference, but now its choice can only rely on experiences without any theoretical proof. For those qualitative problems such as cracking condition, the monodrome function is enough. While for those quantitative criteria such as the max. crack width, the monodrome function may be too simple and may also lead to wrong results since the cut-off points of data space cannot be defined properly. In the present study sigmoid functions were applied. A sigmoid function is given as:

$$F(X) = \left[1 + e^{-X}\right]^{-1} \qquad (3)$$

$$X = Wx + \theta \qquad (4)$$

where X is the weighted sum of input variables, W is the weight vector and θ is the threshold vector(Kawamura 2003a).

(1) Membership function for relative crack length

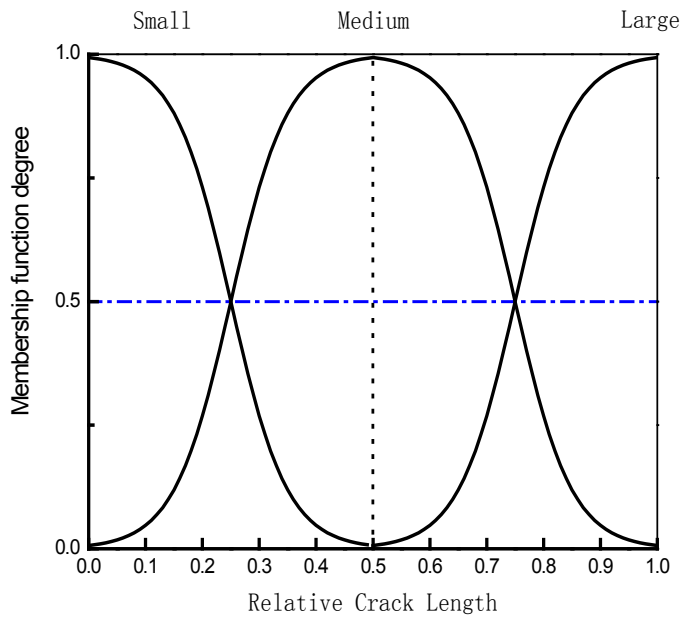

Fig.3. Membership function for relative crack length

The relative crack length is the ratio of the widest crack length to the beam height or of its vertical reflection height to the beam height for shear cracking. And its evaluation space was set with 3 fuzzy subset: Small, Medium and Large, as shown in Fig.3.

(2) Membership function for max. crack width

The max. crack width can be obtained easily., and its limited value was set to be 1mm. If the measured value is larger than 1 mm, it means this width belongs to the "huge" subset and its grade of membership function equals to that of 1mm. The membership function for the max. crack width was shown in Fig. 4.

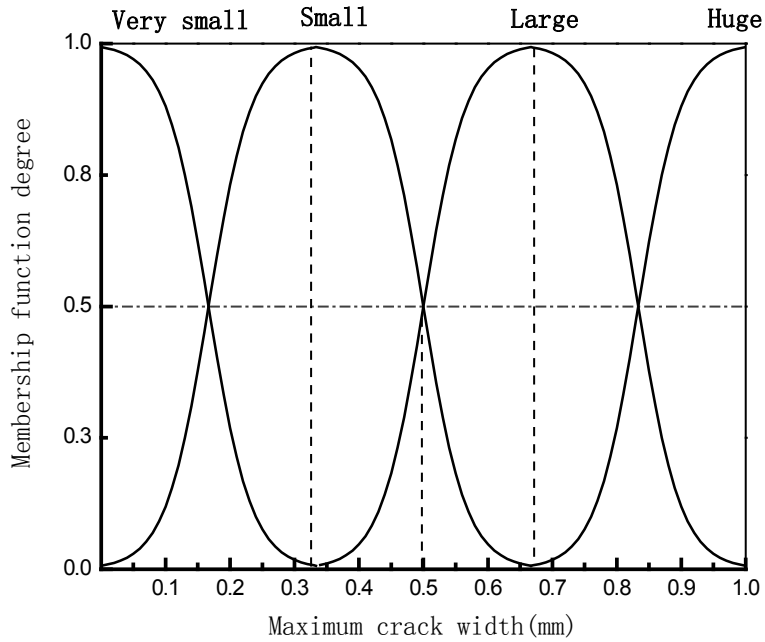

Fig.4. Membership function for max. crack width

(3) Membership function for crack number condition

Even located in the same region different cracks may bring different influences upon the structure due to their differences in length and width. So the influences of cracking length and width must be considered when the criterion, the number of crack, is evaluated. The following formula describes the cracking number condition with considering the cracking length and its width.

$$\text{points of crack number condition} = \sum_{i=1}^{3}\sum_{j=1}^{3}\omega_{ij}N_{ij} \qquad (5)$$

where N_{ij} is the number of crack in each interval designated in Table 2, and ω_{ij} are the corresponding weights which can be decided according to Table 2. "-" means in these cases the cracking is negligible. And the cracks whose widths are less than 0.05mm are omitted due to they are invisible and insignificant.

The maximum value for crack number condition points was set to be 15 since it means there were at least 10 wide and long cracks, which might not be achieved because the structure would have failed before it occurred. Fig.5 presents the form of membership function for crack number condition.

Table2 Weights for cracks

Width / Relative length	>0.3mm	0.15~0.3mm	<0.15mm
>0.8	1.5	1.2	—
0.3~0.8	1.3	1.0	0.7
<0.3	—	0.8	0.5

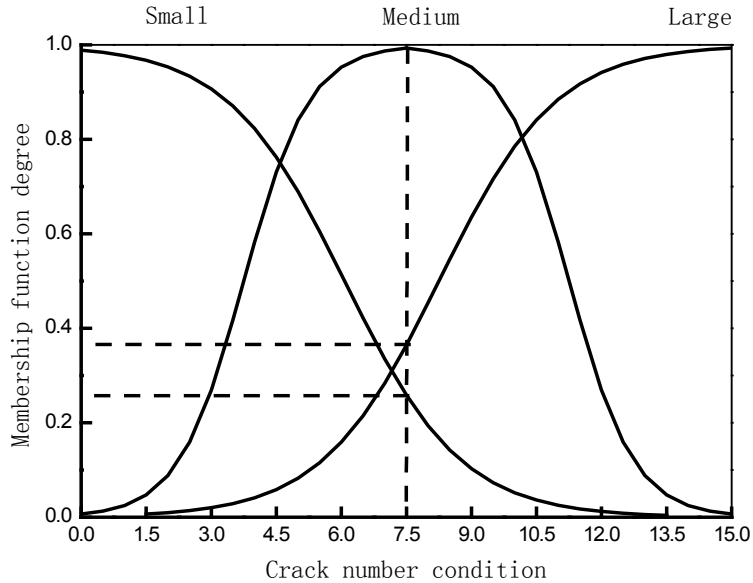

Fig.5. Membership function for crack number condition

(4) Machine learning for membership functions

The aforementioned initial forms of membership functions may not be effective enough to practical applications. Fortunately, however, they could be modified by altering the weights and the thresholds in the process of neural network machine learning. Fig.6 indicates the form alteration of the corresponding membership function with the weight and the threshold altered using machine learning.

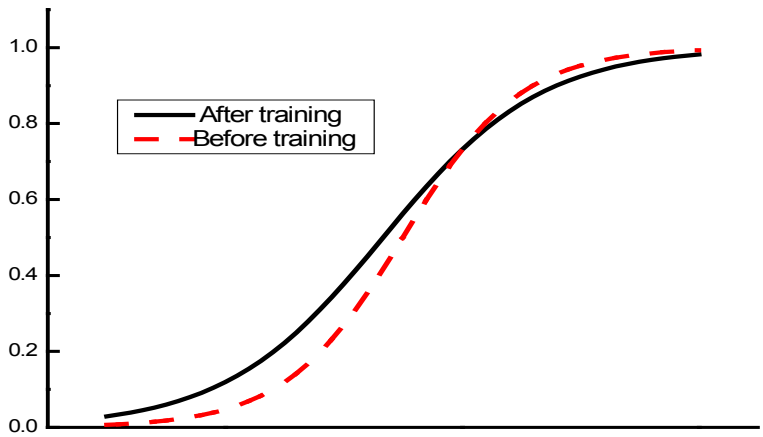

Fig.6. Machine learning for membership functions

4 Illustrative examples

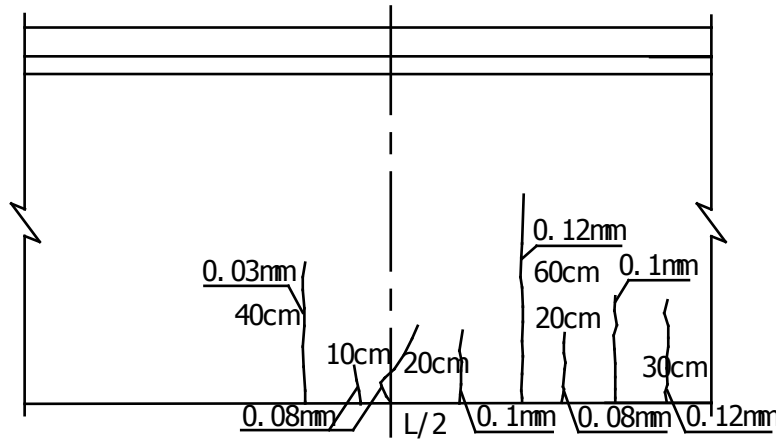

Fig.7. Flexural cracks on the central art of a T shape RC beam

Fig.7 indicates the flexural cracks on the central part of a T shape RC beam with the height of 110cm. With removing the cracks narrower than 0.05mm the input-output sample could be formed as: (0.54 0.12 4.4 1). After fuzzification the extended sample was given as: (0.000 0.985 0.015 0.802 0.198 0.000 0.000 0.506 0.459 0.036 1 0 0 0 0). By collecting data from 4 simple supported RC bridges in Jiangxi province, the People's Republic of China, 42 input-output pairs were obtained. In order to make FNN learn about the past enough to predict properly to the future, the 3-way cross validation was implemented in this study. 42 samples were randomly divided into 3 mutually exclusive subsets, namely, A, B and C, with each subset 14 samples. Each time, use one subset as the testing set and the other two as the training sets. And repeat 3 times.

Table 3 Comparison of FNN outputs with the target values with subset C being tested

Samples	Target values for dataset C	Outputs of FNN system for dataset C being tested
29	(1.0 0.0 0.0 0.0 0.0)	(0.9997 0.0002 0.0002 0.0000 0.0000)
30	(1.0 0.0 0.0 0.0 0.0)	(0.9996 0.0002 0.0002 0.0000 0.0000)
31	(1.0 0.0 0.0 0.0 0.0)	(0.9996 0.0002 0.0002 0.0000 0.0000)
32	(1.0 0.0 0.0 0.0 0.0)	(0.9996 0.0002 0.0002 0.0000 0.0000)
33	(1.0 0.0 0.0 0.0 0.0)	(0.9995 0.0002 0.0002 0.0000 0.0000)
34	(1.0 0.0 0.0 0.0 0.0)	(0.9997 0.0001 0.0001 0.0000 0.0000)
35	(0.0 0.5 0.5 0.0 0.0)	(0.0000 0.4381 0.4572 0.0000 0.1047)
36	(1.0 0.0 0.0 0.0 0.0)	(0.9997 0.0001 0.0001 0.0000 0.0000)
37	(1.0 0.0 0.0 0.0 0.0)	(0.9997 0.0001 0.0001 0.0000 0.0000)
38	(1.0 0.0 0.0 0.0 0.0)	(0.9996 0.0002 0.0002 0.0000 0.0000)
39	(1.0 0.0 0.0 0.0 0.0)	(0.9996 0.0002 0.0002 0.0000 0.0000)
40	(1.0 0.0 0.0 0.0 0.0)	(0.9996 0.0002 0.0002 0.0000 0.0000)
41	(0.0 0.5 0.5 0.0 0.0)	(0.0000 0.4226 0.4426 0.0000 0.1348)
42	(0.0 0.5 0.5 0.0 0.0)	(0.0001 0.4985 0.5001 0.0000 0.0014)

The final multi-layer FNN configuration was determined as 3-10-10-21-5-1 with the learning rate and the momentum factor both 0.25 and the acceptable error 0.01.

The simulation results of FNN were exhibited in Table 3, Figs. 8 and 9 with subset C, A and B being tested, respectively. As mentioned earlier, in the present study, the BP method was applied as a learning method, and the resubstitution method was applied to the system as a training method. Comparison of the system outputs in Table 3, Figs.8 and 9 with the target values reveals that the total agreement ratios are 78.5%, 85.7% and 100% for A, B and C being tested, respectively. In the case subset A being tested 3 outputs show totally deviation from the target values because of the lack of training samples whose target values are 4 to 5. While when B was tested two outputs deviate from the target values. If the testing sample No. 10 in subset B (its system output is 3.007 and its corresponding target value is 2~3) were not taken into consideration as a deviating sample, then the total agree ratio for this case could be 92.9%. Therefore, FNN system could achieve the expected agree ratio if the number of available samples with various cracking condition used for learning is enough.

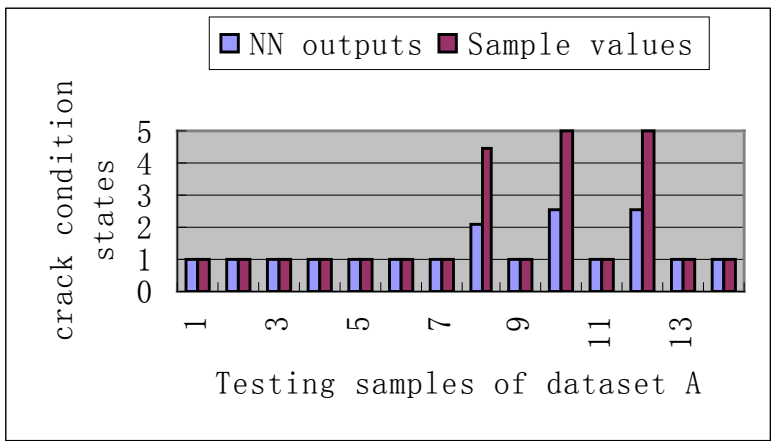

Fig.8. Comparison of the simulation results with the target values for dataset A being tested

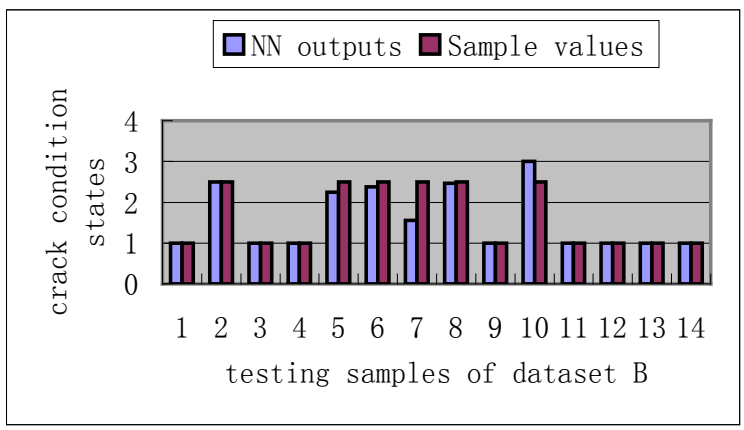

Fig.9. Comparison of the simulation results with the target values for dataset B being tested

5 Conclusion

Based on the comprehensive analysis of RC bridge cracking，in this study, the assessment criterion system of simple supported RC bridges was set up for both flexural cracking and shear cracking, and the membership functions were specified for each criterion. Then the fuzzy-neural network system, which is introduced into engineering applications as an alternative to traditional methods, was developed to assess the crack condition of RC bridges. Finally the system was verified using statistical crack samples of several RC bridges.

However, since the reliability of the system depends on the distribution of training samples used for learning, the performance of the FNN system should be improved by using a larger number of samples with various cracking conditions.

References

AbdelRazig Y.A. and Chang L.M. (2000). "Intelligent Model for Constructed Facilities Surface Assessment." *J. Construction Engineering and Management*, ASCE, 126(6), 422-432

Brito J.D. (1996). "An Expert System for Concrete Bridge Management." *Engineering Structures*, 19(7), 519-526

Elzafraney M (2005). "Quantitative Microstructural Investigation of Deteriorated Reinforced Concrete Bridge Deck." *J. Materials in Civil Engineering*, 17(2), 159-167

Hadidi R., Saadeghvaziri M.A.(2005). "Transverse Cracking of Concrete Bridge Decks: State-of-the-Art." *J. Bridge Engineering,* ASCE, 10(5), 503-510

Kawamura K.(2003a). "Condition State Evaluation of Existing Reinforced Concrete Bridges Using Neuro-Fuzzy Hybrid System." *Computers & Structures,* 81,.1931-1940

Kawamura K(2003b). "Performance Evaluation of Concrete Slabs of Existing Bridges Using Neural Networks." *Engineering Structures,* 25, 1455-1477

Saadeghvaziri M.A., Hadidi R.(2005). "Transverse Cracking of Concrete Bridge Decks: Effects of Design Factors." *J. Bridge Engineering*, ASCE, 10(5), 511-517

Zhao Z., Chen C.(2002). "A Fuzzy System for Concrete Bridge Damage Diagnosis." *Computers & Structures*, 81, 629-641

Experimental Research on the Combined-method of Vacuum Well-point Dewatering and Preloading

Yang Hai-xu[1] and Wang Hai-biao[2] and Dong Xi-bin[2] and Yin Jian-ming[1]
[1]School of Civil Engineering , Northeast Forestry University; Harbin ,China； Tel: (86)0451-89630732; Email: yhxcumt@163.com Harbin ,China；
[2]School of Engineering Technique, Northeast Forestry University. Harbin,China

ABSTRACT

In order to improve soft clay subsoil effectively in practice, the vacuum well-point dewatering and preloading method was used to test in Songhuajiang River flood land. Based on the field data observed in practice and effective stress theory of K.Terzaghi, the mechanism of improving soft ground by the vacuum well-point dewatering and preloading and the change of effective stress and effective reinforcement depth were studied. The experiment results showed that pore water pressure decreased quickly in sand drain but slowly in soil. Decrease of groundwater lever had great influence on preloading effectiveness .The effect of water closing was harmful to soil consolidation. With vacuum well-point dewatering and preloading, not only consolidation degree and speed increased but also the stability of side slope and the soil were improved. It is concluded that using vacuum well-point dewatering and preloading would speed up consolidation in the bank area of Songhuajiang River and similar areas.

Key words:
Vacuum well-point dewatering and preloading ； Effective stress；Pore water pressure；Effective reinforcement depth； Groundwater lever

In recent years more roads, bridges and structures were built in the bank area of Songhuajiang River. One tall building which has three basement stories was constructed in li-min development area located in Songhuajiang River north bank. The ground base is typical Songhuajiang flood land. The subgrade soil has large natural water-content, high compressibility, low bearing capacity, bad water permeability and high groundwater lever. In order to increase stability of ground base and consolidation degree of soil and improve shear strength of ground, It is effective to use vacuum well-point dewatering and preloading method to speed up consolidation and reduece erection time. Based on the observation of field test, the mechanism of improving soft ground by the vacuum well-point dewatering and preloading and the reinforcement effects were studied in this paper.

1 Introduction to construction method:

Physico-mechanical index of subgrade soil is shown in table 1.

There were two sets of light Vacuum Well Point established on both sides of testing soil at the same time withW-4 Mechanical Vacuum Pump configured. Arrangement of field test was shown in Fig 1.

Table 1 Physico-mechanical index of subgrade soil

Level number	name	lever depth /m	water content /%	void ratio e	plasticity index $/I_P$	liquidity index $/I_L$	modulus of compressibility /MP_a	permeability coefficient 10^{-6}/cm·s^{-1}
2	fine sand	3.5	26	0.76	—	—	11.05	9.57
3	grayish brown silty clay	3.6	30.8	0.88	12.3	0.967	5.28	1.45
4	grayish black muddy clay(containing fine sand)	7.6	38.5	1.12	13.6	1.574	3.08	4.90
5	grayish green fine sand(containing muddy)	4.2	40.2	1.31	14	1.59	3.11	5.28

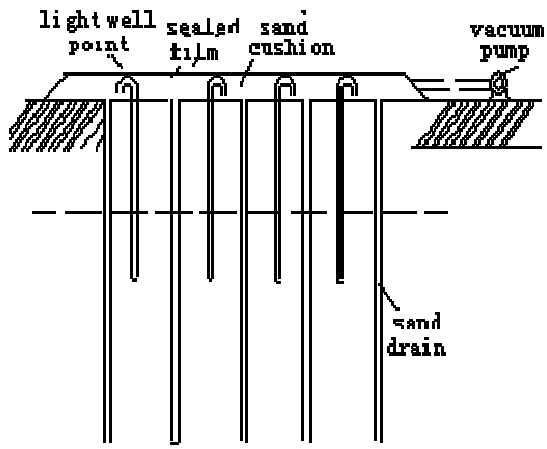

Fig. 1 Field test on soft clay ground well-point dewatering and preloading under combined-method of vacuum

The well point had a buried depth of 7m. Dewatering lasted for 90 days in an aimed and planned way. It was 0.3m sand cushion on the top of ground and a layer of 40mm earth work fabric as flowing layer with 5% slope. A bag of sand-well were strike to a depth of 12m. After well-point dewatering equipment buried, dewatering began. To cut off water source recharge from Songhuajiang River, a grouting isolated land was set on lateral side of dewatering area. Sealing system was consisted of double-layerPVC film . The vacuum degree increased at first 3 days and then decreased to reach a constant of 80 kPa since pumping. Because ofthe promissory construction conditions, the practical dewatering process was only carried out in 80d. In order to check the quality of reinforcing ground soil and pre-dominate the consolidation and settlement of each soil layer during strengthening, ground surface settlement, layered sedimentation, lateral displacement, pore water pressure and vacuum degree were monitored at the construction process. Base on the observation data of pore water pressure, vacuum-pumping and dewatering stopped when soil consolidation degree forereached 95%.

2 Mechanism analysis of foundation soil

The vacuum well-point dewatering and preloading technique is the combined-method of vacuum and dewatering preloading, which has drainage consolidation, dewatering and vacuum preloading function at the meantime pumping by vacuum device and decreasing groundwater lever by means of well-point dewatering equipment. In the loading, the pore water pressure depressed and effective stress increased while total stress is invariable. Based on the action of vacuum and dewatering preloading, the variation of pore water pressure and increase of effective stress have specific regular

pattern. Mechanism of improving ground by the combined two methods of vacuum dewatering and preloading was analyzed through the variation of effective stress and analysis of stress path.

2.1 **Stress path of the vacuum well-point dewatering and preloading technique**

The variation of effective stress of ground soil in the course of combined-preloading of vacuum dewatering and loading was analyzed with K.Terzaghi theory. The distribution of soil stress before vacuum pumping and dewatering were shown in Fig.2.

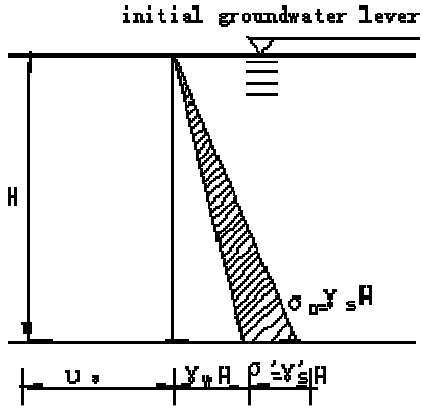

Fig.2 Distribution of effective stress before vacuum-pumping and dewatering

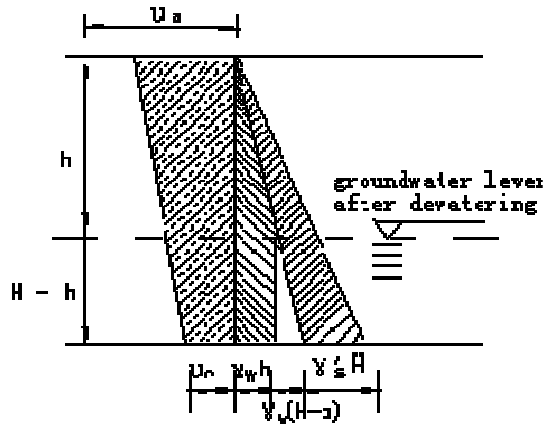

Fig.3 Distribution of effective stress after combined preloading

γ_s and γ_s' is the gravity density and flotation gravity density of ground soil respectively. $_w$ is the gravity density of water. Fig.2 showed that initial static pore water pressure $u_0 = \gamma_w z$ in which z is the depth of ground level calculated. Initial total stress of soil is $\sigma_0 = \gamma_s H$. In some position of soil the effective stress is σ', and gravity pressure of water is μ; each point in soil is subjected to atmospheric pressure μ_a before vacuum pumping and dewatering.

According to K.Terzaghi effective stress theory, the effective stress during reinforcement is equal to

$$\sigma' = \sigma_0 - \mu_0 + \mu_1 + \mu_2$$

μ_1 is suction pressure formed in pore space of soil when vacuum preloading; μ_2 is vacuum degree varied with depth. While stopping vacuum and dewatering preloading, soil body under groundwater lever is in over consolidation. Distribution of effective stress of soil after combined preloading was showen in Fig.3.

Static water pressure and effective stress of Z point after combined preloading were expressed as following equations:

$$\begin{cases} \begin{cases} u = 0 \ , & (z \le h); \\ \sigma' = \gamma_s{}' z + \mu_1 + \mu_2 = \gamma_s{}' z + \gamma_w z + \mu_2 = \gamma_s z + u_2, & (z \le h); \end{cases} \\ \begin{cases} u = \gamma_w (H - h), & (z > h); \\ \sigma' = \gamma_s{}' z + \mu_1 + \mu_2 = \gamma'_s z + \gamma_w h + u_2, & (z > h). \end{cases} \end{cases}$$

The varied process of effective stress can be analyzed by reinforced stress path for soil, shown in Fig.4. Any unit stress condition is K_0before reinforcing, and total stress path (TSP) is fixed. Effective stress path (ESP) is AB line ($\varepsilon_v = \varepsilon_h$) after combined preloading. Whereas in site some cracks parallel to borderline line in reinforced soil body can be observed, which is due to the whole soil body was subjected to isotropic consolidation pressure produced by vacuum and dewatering preloading and shrinkage of soil body occurred. So horizontal displacement was turned into inside when soil subsided, At the same time the maximum horizontal displacement occurred in surface of soil edge. Therefore, effective additional stress caused by vacuum and dewatering preloading made soil effective stress downward departure from K_0 line, then ESP line was AD line.

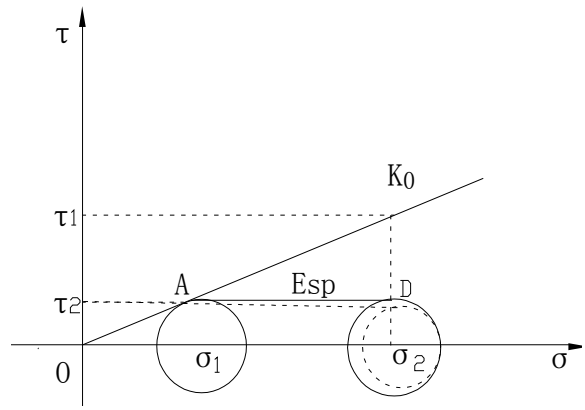

Fig.4 Stress path for soil in vacuum watering test area

2.2 **effective depth of vacuum and dewatering preloading**

Fig.5 and Fig.6 showed the actual observation records. After 5 days draining，the vacuum degree reached a constant of 80 kPa. Through practical monitoring, vacuum degree in 12m sack sand-drain degreased 25% because of resistance of sand drain, which verified that sand drain can transfer vacuum degree and draining. Vacuum degree had a quick attenuation under sand drain, and reinforced effect was non-ideal； Most settlement occurred in sand drain after draining. It could be concluded that effective depth was consistent with depth of sand drain.

Effective depth is reinforced by the combined two methods of vacuum dewatering and preloading Firstly, gas in sand cushion was drawn-off after the surface of foundation produced vacuum, and then atmospheric pressure in sand cushion and sand drain fall down one after the other. Differential pressure in soil and cushion and sand drain made soil body become consolidation. Onthe other hand, continuous air suction and drawing water of vacuum preloading made a descent on groundwater lever.

Otherwise, groundwater drained by well point brought on a sharp decline of original phreatic line again. Therefore, it is logical that vertical gravity stress in soil layer was changed; initial stability conditions and corresponding stress distribution were destroyed. Internal stress of soil had a new stabilization.

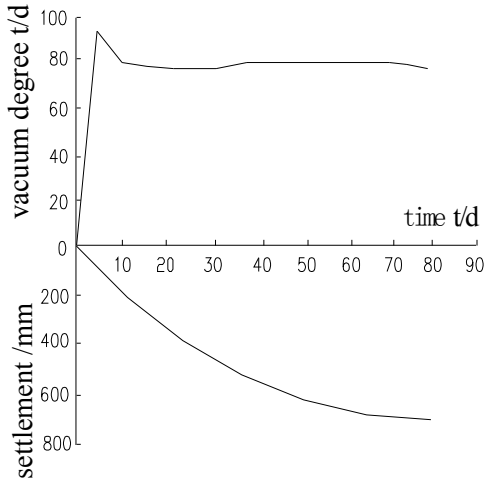

Fig 5 Curve of P-T-S (vacuum degree,settlememt,time)

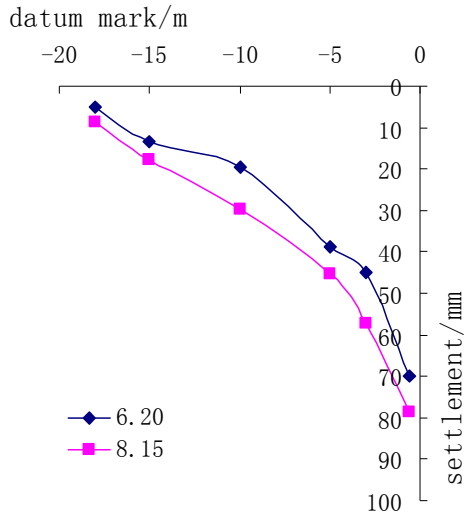

Fig.6 Curves of laminar settlement in reinforced area by vacuum dewatering

Sedimentation measured on June 20th could be acquired from curves of laminar settlement shown in Fig.6: the total settlement was 70 mm within 0~18 m, and the settlement was 18 mm approximately which was 26% of total sedimentation within 12~18m under sand drain based on the field observation record and other literatures, it is the vacuum preloading method that is useful to increase effective stress down depth in soil under sand drain, but reinforced effect was determined by dewatering preloading. Beyond sand drain strengthening action was inconspicuous for a sharp decent of vacuum degree under sand drain by combined-method of vacuum and dewatering preloading, Although reinforced effect was influenced by vacuum preloading, drainage consolidation caused by dewatering preloading was the definitive factor of reinforced effect. The influenced depth and reinforced effect produced by the combined two preloading methods were better than by single vacuum preloading obviously.

3 Groundwater lever

The groundwater lever had a great influence on reinforced effect of soil by preloading. Decreasing degree of groundwater is related with action intensity of sucking vacuum, property of foundation, supply of water source and well point equipment and so on.

During vacuum preloading, vacuum pressure on reinforced area reduced pore water pressure, so pore water in soil was absorbed by differential pressure and produced seepage to ground surface. If the pressure of sand drain was smaller than pressure of soil at the same depth, pore water could leak through liquid to sand drain. Two-way seepage of pore water led to a descent of groundwater lever. While pressure was balanced, the line of groundwater lever reached a stable level. In this research, groundwater lever was decreased by 1.5m measured by water level gauge after

vacuum pumping was carried for 20d, and subsequent descending speed was very slow. The groundwater level was fallen down continuously and quickly in the procedure of preloading of the combined-method for soil which had higher sand-carrying capacity; 25d later, descending level reduced by 7.3m. Descending groundwater level not only decreased static pressure and increased effective stress of soil, but also made fully use of top vacuum preloading.

The pore water pressure measured before testis directly proportional to the depth of soil. Descending speed of pore water pressure in sand drain was faster than in soil body during construction due to the permeability of sand drain is greater than soil body. All the transitive effect of vacuum pressure in soil body filled in pore water was non-ideal.

5 CONCLUSION

1) It is seen that the combined-method of vacuum and well point dewatering preloading is useful to strengthen soil and increase the consolidation speed and degree; besides, the combined two methods not only improved the stabilization of side slope and foundation, but also unlikely produced extrusion on around soil.

2) Several factors, such as climate conditions, groundwater level and surrounding influent stream, have great influences on the decreasing speed and degree of groundwater level, as well as reinforced effect. Therefore some steps should be modified to eliminate external detrimental factors to accelerate soil consolidation. It is effective to adopt the combined-method of vacuum and dewatering preloading to improve soft foundation. Anticipated effect could be reached in two and half months.

3) When vacuum degree reached 80 kP_a, the soil body generated inboard horizontal deformation. At the same time, cracks occurred around boundary apparently. It should be paid attention that a rather large lateral deformation will affect surround buildings.

Bibliography

Chaia J.C, Miurab N, Bergado D.T (2008). Preloading clayey deposit by acuum pressure with cap-drain:Analyses versus performance. *J.*Geotextiles and Geomembranes, 26 :220–230.

Qian J.H, Zhao W.B, cheung Y.K,et al (1992).The theory and Practice of Vacuum Preloading. Computers and Geotechnics, 13(2):103-118.

Chen H, .S.W.(1985).Numerical Analysis of Soft Foundation Vacuum Preloading. 5th.international conference on numerical methods in geomechanics .Nagoya ,April 1-5,1985:643-647.

Wang Z.W，Zai J.Z.(2004).Research on Comparative Tests of Reinforcement for Bridge-slope Subgrade by Vacuum Well-point Dewatering Combined with Equal Preload. *J. Rock Mechanics and Engineering*(chinese), 8(23):2579-2584.

Tran T. A , Mitachi T (2008). Equivalent plane strain modeling of vertical drains in soft ground under embankment combined with vacuum preloading . *J. Computers and Geotechnics*, 35:655-672.

Experimental Research and Damage Model of Square Concrete-Filled Steel Tube Subjected To Cyclic Loading

DU Xi-kai[1,2], WANG Tie-cheng[1], HE Hongming[2] ,YI Kai[3]

[1]School of Civil Engineering, Tianjin University, Tianjin 300072, China; PH(0312)7521862;email:duxk126@126.com
[2]Department of Civil Engineering, Hebei Agriculture University, Baoding, Hebei, 071001,China: PH(0312)7521862;email:duxk126@126.com
[3]College of Math and Computer Science Hebei University ,Baoding, Hebei, 071000,China: China: PH(0312)7521862;email:yikai@hbu.cn

ABSTRACT

Nine square concrete-filled steel tube (CFT) columns with different axial load level (0.165~0.517), slenderness ratio (10.82~32.88), and constraining factor (0.61 ~1.51) were tested under a constant axial load and cyclically varying lateral loads. The experimental results showed that the hysteresis curves of the test columns are plump in shape without significant pinch phenomenon, which means that the stiffness and strength of the columns deteriorated slowly and the columns have a good ability of energy dissipation. Based on the analysis of the experimental data, the expressions of maximum strength Q_u and ultimate deformation δ_u of square CFT column are proposed. Park damage index is employed for CFT columns seismic damage evaluation. According to the test data, the value of parameter β is determined.

INTRODUCTION

With the advantages of high load-bearing capacity, excellent seismic behavior, good fire-resistance and easy for construction, CFT is greatly used in bridge construction practice. CFT includes circular CFT and square CFT. In comparison, square CFT has higher flexural strength, simpler joint details and is easier for connection on site (Han,2004). Thus, researchers and engineers are paying more attention on square CFT structure and its seismic behavior. Studies by many researchers had shown that parameters such as axial load level, slenderness ratio, steel ratio and strengths of materials have different effects on the seismic behavior of the columns (Amit et al,2002). However, the research on this aspect is still insufficient and the conclusions made by the different researchers do not concur. On the other hand, the study of the accumulated damage model of square CFT is also insufficient. In this paper, nine square CFT columns were tested under combined constant axial load and cyclic lateral load in order to investigate the hysteresis behavior

of the columns. According to the analysis of experimental results, the damage accumulation model of the square concrete-filled steel tube based on the deformation and energy dissipation was established.

EXPERIMENTAL PROGRAM

Nine specimens were designed for the test. The dimensions and parameters of the test specimens are shown in Table 1. In table 1 B, t and L are the width of the cross-section of specimen, the thickness of steel tube and the length of specimen respectively. λ is the slenderness ratio of the specimen, which is defined by CECS159:2004. $\xi = f_y A_s / f_c A_c$ is the constraining factor of the column. Where A_s is the cross- section area of steel tube and A_c is the cross-section area of concrete. $n_0 = N/N_0$ is the axial load level of the specimen, where N is the applied axial load. $N_0 = A_c f_c + A_s f_y$ is the nominal axial load capacity of the specimen.

Table 1. Properties of Test Specimens.

specimen	$D \times t \times L$ /mm	f_y (*MPa*)	f_{cu} (*MPa*)	ξ	λ	n_0	N (*KN*)
RS-4L	250×4×530	265	29.2	0.61	11.19	0.182	501
RS-6M	250×6×530	317.6	29.2	1.12	10.82	0.331	1162
RS-10H	250×10×530	242.2	29.2	1.51	11.46	0.517	2000
RM-6L	250×6×1270	317.6	29.2	1.12	25.93	0.165	581
RM-10M	250×10×1270	242.2	29.2	1.51	27.47	0.381	1474
RM-4H	250×4×1270	265	29.2	0.61	26.81	0.491	1353
RT-10L	250×10×1520	242.2	29.2	1.51	32.88	0.190	737
RT-4M	250×4×1520	265	29.2	0.61	32.08	0.364	1002
RT-6H	250×6×1520	317.6	29.2	1.12	31.03	0.447	1569

Specimen design and construction. The square steel tubes were made from four sheets of steel plate by welding and the grade of steel plate was Chinese Standard Q235. The properties of steel plate were measured by conducting the test according to the Chinese Standard Metal Tension Test Method (GB/T228-87). The measured steel yield strength (f_y) was listed in table 1. The target grade of concrete used was Chinese standard C40. During the preparation of the specimens, three 150*mm* concrete cubes were cast and cured in condition similar to the specimens. The concrete cubes were tested according to the Chinese standard Test Method for the Mechanics Properties on Ordinary Concrete (GBJ81-85) and it was found that the concrete cubic compressive strength (f_{cu}) equaled 36.5 N/mm^2. The concrete compression strength (f_c=0.8 f_{cu}) was 29.2 N/mm^2.

Test set-up and load procedure. Figure. 1 shows the schematic of the test set-up. The axial load was applied with a 3,200 *kN* hydraulic jack on top of the specimen. The lateral load was applied with a hydraulic jack fixed to the reaction wall, and the maximum moving distance of the jack was 500 *mm*.

The axial load was applied and maintained constant until the failure of the specimen. According to the Chinese standard Specification of Testing Methods for Earth-

quake Resistant Building（JGJ101-96）, the lateral load was applied under load-displacement control condition. Before the yield of the specimen, the lateral load was controlled by load and applied step by step. Every one-third of the specimen lateral yield load was applied in one cycle at each of the lateral load level. After the specimen yielded, the lateral load was controlled by displacement. The integral multiple of the yield level lateral displacement was taken to control the applied lateral load and three cycles were imposed at each displacement level until the specimen lateral load resistance had deteriorated to 85% of the lateral load capacity.

TEST RESULT AND ANALYSIS

From the experimental observation, all the specimens had the same failure mode. The column stiffness had not deteriorated significantly from initial loading to yield of the compression flange of the steel tube. With the increase of lateral displacement, the bulge at the bottom of the steel tube compression flange took place, but was flatten when unloaded and during reverse loading, the flange at the opposite face begins to bulge. The location of the bulge of the steel tube was at 40~70mm above the bottom of the column. The lateral stiffness of the column began to decrease, but the lateral load was still increasing. The bulge grew with load cycling and increasing lateral displacement. The lateral load of the column began to decrease when the compression side of the web of the steel tube bulged. Several specimens cracked at the welded corner before it failed.

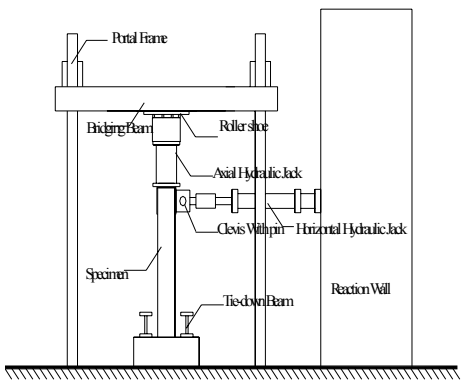

Figure.1 Schematic of the test

The lateral load-lateral displacement responses of some specimens are shown in Figure 2. These figure show that the hysteretic loop of the specimens are plump in shape and have no significant pinch phenomenon, which indicate that the

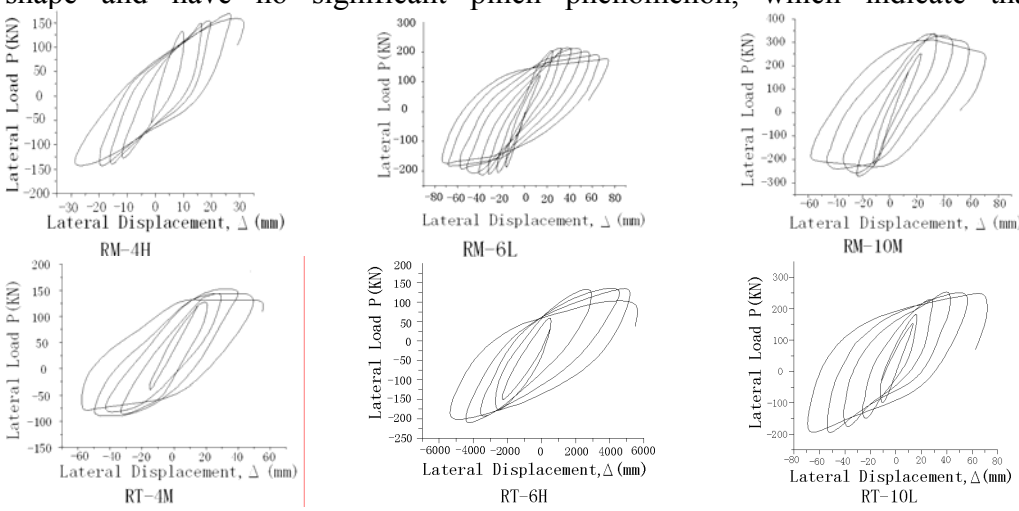

Fig.2. Lateral load-lateral displacement (P- Δ) response

square concrete-filled steel tube column has better hysteretic behavior and greater energy-dissipation characteristics.

The maximum horizontal strength Q_u and ultimate deformation δ_u of the specimens are listed in table 2.

Table 2. Test Result of the Specimens.

specimen	RS-4L	RS-6M	RS-10H	RM-6L	RM-10M	RM-4H	RT-10L	RT-4M	RT-6H
Q_u（KN）	398	566	737	210	290	151	215	120	166
δ_u(mm)	23.76	31.63	32.4	67.81	58.16	27.48	67.81	56.98	52.57

SEISMIC DAMAGE MODEL

Park model (Park et al,1985), accepted for most engineers in seismic engineeringfield is used for square CFT columns in this paper. Seismic structural damage is expressed by Park model as a linear combination of the damage caused by excessive deformation and that contributed by absorbed hysteretic energy. The damage index is given by

$$D = \frac{\delta_M}{\delta_U} + \beta \frac{\int dE}{Q_Y \delta_U} \tag{5}$$

In which δ_M is the maximum deformation under earthquake; δ_u is the ultimate deformation under monotonic loading; Q_y is the calculated yield strength; dE is incremental absorbed hysteretic energy; β is a non-negative parameter.

According to reference ZHANG-sumei(2005), the yield strength Q_y is given by

$$\boldsymbol{Q_y = (0.8 - 0.24 n_0) Q_u} \tag{6}$$

In which Q_u is the maximum strength of CFT column subjected to reversed loading. The following is proposed for evaluating Q_u based on the analysis of the experimental data

$$\boldsymbol{Q_u = (2.72 \lambda^{-0.2} - 8.33 \times 10^{-3} \lambda n_0^3) \frac{M_u}{L}} \tag{7}$$

Where M_u is the ultimate moment of square CFT column, which can be evaluated by CECS159:2004. L is the length of column.

Based on reference ZHANG-sumei (2005) and the analysis of the experimental data, the ultimate deformation under monotonic loading δ_u can be evaluated by following:

For $0 \le n_0 \le 0.5$

$$\boldsymbol{\delta_u = \left[\left(115 n_0^2 - 53.9 n_0\right) \lambda^{-0.75} - 2.08 \times 10^{-3} \lambda + 1.17\right] \frac{Q_y L^3}{EI} - \frac{0.15 Q_u}{K_d}} \tag{8}$$

Or for $0.5 \le n_0$

$$\delta_u = (1.8\lambda^{-0.75} - 5.21\times10^{-4}\lambda + 0.292)\frac{Q_y L^3}{EI} - \frac{0.15Q_u}{K_d} \quad (9)$$

In which the stiffness in the elastic stage, EI, is given by CECS159:2004; K_d is the stiffness of descending stage of lateral load verses lateral displacement curve，which can be expressed

$$K_d = \left[-0.1\left(\frac{\lambda}{50}\right)^{1.4} n_0^{0.4}\xi^{-0.3}\right]\frac{L^3}{3EI} \quad (10)$$

The evaluated yield strength Q_y and the ultimate deformation δ_u of the specimens are listed in table 3.

DETERMINATION OF β

The load-deformation curve for each test is integrated up to the failure point to get absorbed hysteretic energy E_h, which is listed in table 3. Then, at the point of failure, D=1.0, the corresponding value of β is evaluated by Eq 5. The β of all specimens is listed in table 3. The average of β, 0.03, is proposed for evaluating damage index of square CFT column. In fact, parameter β has a correlation with axial load level n_0, slenderness ratio λ and constraining factor ξ. Reasonable β expression will need more test data.

Table 3 . Evaluated Data of the Specimens

specimen	Q_Y（KN）	Q_u（KN）	δ_u(mm)	E_h（KN.mm）	β
RS-4L	276.96	366.19	27.12	107011.41	0.0087
RS-6M	449.49	623.74	37.90	19677.71	0.143
RS-10H	498.13	736.92	34.20	49005.11	0.0183
RM-6L	166.38	218.83	81.13	191552.21	0.0116
RM-10M	182.76	257.92	60.53	222137.51	0.002
RM-4H	85.90	125.94	40.06	36742.01	0.029
RT-10L	158.02	209.49	83.77	106814.58	0.024
RT-4M	73.03	102.48	60.50	72785.27	0.004
RT-6H	120.23	173.54	73.87	82931.62	0.031

CONCLUSION

Square CFT column has high lateral load bearing capacity and high lateral stiffness under combined lateral load and axial load. Even though the flange of the steel tube has bulged, the lateral load is still increasing and the stiffness has no significant deterioration.

The hysteretic curves of the specimens are plump in shapes, and have no significant pinch phenomenon, which indicate that square concrete-filled steel tube column has high energy dissipation capacity.

Based on the analysis of the experimental data, the expressions of maximum strength Q_u and ultimate deformation δ_u of CFT column are proposed.

Park damage index is employed for CFT columns seismic damage evaluating. According to the test data, the value of parameter β is determined.

REFERENCES

Amit H. Varma , James M. Ricles, Richard Sause and Le-Wu Lu(2002), "Seismic Behavior and Modeling of High-Strength Composite Concrete-Filled Steel Tube (CFT) Beam-Columns", Journal of Constructional Steel Reseach, 58 : 725-758.

CECS 159:2004, Technical specification for structures with concrete rectangular steel tube members, Chinese Planning Press, Beijing, China.

GB/T228-87(1987) ,Metal Tension Test Method , Chinese Planning Press, Beijing, China.

GBJ81-85(1985),Test Method for the Mechanics Properties on Ordinary Concrete , Chinese Planning Press, Beijing, China.

Han Lin-hai(2004), "Concrete-Filled Steel Tube –Theory And Practice", Science Press, Beijing, China.

JGJ101-96(1997), "Specification of Testing Methods for Earthquake Resistant Building", China Architecture And Building Press, Beijing, China.

Park Y J and Ang A H S.(1985),"mechanistic seismic damage model for reinforced concrete", ASCE, J of structural engineering, 111(4):722~739.

Zhang sumei and LIU jiepeng(2005) , "Hysteresis Behavior of biaxially loaded high strength Concrete-Filled square hollow Sections Beam-Columns", journal of building structure , Vol.26. No 3.june:9~17.

FUNCTION DESIGN OF CEMENT STABILIZED CRUSHED STONE DRAINAGE BASE

Lin Tian[1], Xiaoguang Xie[2], and Decheng Feng[3]

[1] Candidate of PhD, School of Transportation Science & Engineering, Harbin Institute of Technology, Harbin, Heilongjiang, PH 0451-86282120, FAX 0451-86283779, Email: TL0451@yahoo.com.cn
[2] Associate Professor, School of Transportation Science & Engineering, Harbin Institute of Technology, Harbin, Heilongjiang, PH 0451-86282120, FAX 0451-86283779, Email: xxg75@126.com
[3] Professor, School of Transportation Science & Engineering, Harbin Institute of Technology, Harbin, Heilongjiang, Email: fdcgxy@vip.sina.com

ABSTRACT

Based on analysis of the influence degrees of structure types at early damages of cement pavements in large-grade highways, combined structure type of cement stabilized crushed stone drainage base and semi-rigid base is proposed. Base on function analysis of drainage base, design principles and indices of the cement stabilized crushed stone mixture are determined. And then, the type of coarse framework, distributing of cement slurry, and the component of grading are determined according to new characters of material design method which including the optimum vibrating compaction techniques and the dynamic stress press-in test having confined pressure and the volume design method in grading components. Finally, the method for determining the reasonable consistency of cement stabilized crushed stone mixture is presented, which adopts porosity diversity and strength as evaluation criterion. The void-framework cement stabilized crushed stone mixture demanding drainage base function will be consequently designed.

INTRODUCTION

Cement concrete pavement has the advantages of high strength, good capacity of supporting and separating loads, heavier rigidity, better stability and durability, no rutting and less maintenance cost, so it has been extensively used in the high-grade highway in China, especially in the overload heavy-traffic pavements. However, the early damages also appear in concrete pavement, such as surface cracking, broken slab, deformation, blow-up and mud-pumping (Grogan 1994). By analysis, water is one of the most important factors (Hall 1994). The water goes into the surface of base through the cracks and turn into mud, with fine aggregate under heavy traffic loads, eroding the base and then bursting out from cracks, a phenomenon called mud-pumping. The phenomena of mud-pumping weaken the support at the edge and separates cement concrete pavement from the base, then

accelerates the destructive process of cement concrete pavement. Use of the cement stabilized crushed stone permeable base can weaken the water pressure, balance the load-carrying capability and avoid the damages on the pavement.

MIXTURE DESIGN INDICES ON THE FUNCTION ANALYSIS

Function Analysis

In order to relieve the cement concrete pavement damage, cement stabilized crushed stone base should have the following functions:

(1) Function of Drainage: Good function of drainage can relief the dynamic water pressure caused by heavy traffic with high-speed, which reliefs not only the washing and pumping of semi-rigid base, but also the empty and break of concrete slab.

(2) Good Function to Resist Permanent Deformation: In order to ensure the structural integrity and prevent concrete slab separating from base, cement stabilized crushed stone permeable base should have less residual deformation.

(3) Enough Strength: As the base, cement stabilized crushed stone should have enough strength to support traffic loading and give support to increase fatigue life of cement concrete pavement.

Design Indices

Besides using VV to reflect drainage ability and compressive strength to represent mechanical strength, permanent deformation is taken into account based on the function analysis. Specific mixture design indices are as follows:

(1) VV≥15%;

(2) 7d compressive strength≥3MPa;

(3) Cumulative permanent deformation under 25KN.

MIXTURE DESIGN CHARACTERS

Optimal Molding Techniques

Contrast tests between vibrating and static stress compaction indicate that vibrating compaction can obviously improve compressive strength and be close to rolling methods in site (Tian et al. 2006). Thus, by ensuring the uniformity of cement mortar and keeping the integrity of aggregates, vibrating compaction method is adopted in which optimum techniques are as follows: vibrating force 7KN, vibrating frequency 30Hz, amplitude of vibration 0.694mm, time of vibration 1min.

Dynamic Stress Press-in Test

The strength of stone mixture roots in the function of inner frictional angle, and lateral confinement σ_3 should be considered to evaluate the resistance deformation ability. Thus on the basis of classical C.B.R method, dynamic stress press-in test has been put forward, which bears dynamic semi-sine wave load using MTS machine with frequent 0.1 HZ and slot time 0.9 seconds by steps, each steps

having 100 times.

Volumetric Design Method

The volumetric design method (see Equation 1) is used to design the cement stabilized crushed stone (Zheng and Hu 2004).

$$q_c + q_f = 100$$
$$q_c \times (VCA_{DRC} - V_v) / (100 \times \rho_{f(s)c}) = q_f / \rho_{tf} \quad (1)$$

Where, q_c = weight percent of coarse aggregate, %;
q_f = weight percent of cement mortar, %;
VCR_{DRC} = impaction void volume of coarse aggregate, %;
VV = Volume of air voids, %;
$\rho_{f(s)c}$ = impaction density of coarse aggregate, g/cm^3;
ρ_{tf} = density of cement mortar， g/cm^3.

DESIGN STEPS

（1）design of coarse aggregate skeleton and cement mortar
（2）volumetric design of the mixture
（3）determination of the reasonable mixture consistency

DESIGN EXAMPLES

Raw Materials

Selected Aggregate is Jilin Province limestone (Table 1) and cement is ordinary Portland cement with cement mark 42.5, which meet the demand of specifications.

Table1. Sifting and Density Values of Coarse Aggregate.

seize /mm		31.5	26.5	19.0	16.0	13.2	9.5	4.75
Passing rate/%	1#	100	95.6	48.7	15.9	1.2	0.3	0.2
	2#	——	——	100	98	79.5	32	0.2
density g/cm^3			2.734	2.730	2.740	2.736	2.751	2.750

Design of Coarse Aggregate Skeleton

According to technical specifications of drainage base recommended in China and successful experiences abroad, five kinds of coarse aggregate skeletons are selected for experimentation using CBR test and dynamic test in order to determine the gradation of coarse aggregate skeleton with higher strength and smaller permanent deformation. Gradation 1 and gradation 2 are the medians in Technical Specifications, gradation 3 and 4 are trend of cement stabilized crushed stone derived from better experiment gradation. Gradation5 is the median of AASHTO NO.67 gradation value. Specific gradations are shown by Figure 1, and the test results are

summarized in Table 2.

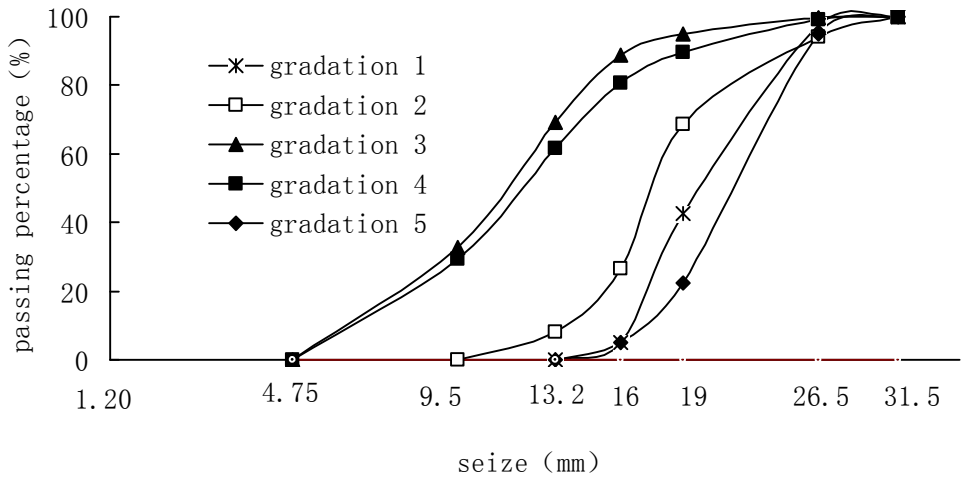

Figure1. Graduations of Coarse Aggregate Skeleton.

Table2. CBR and Cumulative Permanent Deformation of Coarse Aggregate Skeleton.

item \ number	1	2	3	4	5
impaction density (g/cm^3)	1.735	1.770	1.732	1.730	1.651
impaction void /%	36.7	35.5	36.9	36.7	40.0
CBR values/%	125.6	121.3	45.3	163	178.8
5kN permanent deformation /mm	0.80	0.59	1.34	0.78	1.15
10kN permanent deformation /mm	1.09	0.79	1.39	1.43	1.05
15kN permanent deformation /mm	1.47	1.45	1.62	1.60	1.21
20kN permanent deformation /mm	2.26	1.98	2.78	2.01	1.52
25kN permanent deformation /mm	2.95	2.34	3.58	2.18	2.46
cumulated permanent deformation /mm	8.56	7.15	10.72	8.00	7.39

CBR and the cumulative permanent deformation are regarded as the main values to evaluate the mechanical properties of the aggregate skeletons. CBR can reflect the ability to resist load, dynamic load test can reflect material's ability in resisting permanent deformation at different stage by the accumulated permanent deformation under different stress state stages. So it is used as the main index to evaluate the ability of resisting deformation. From Table 2, CBR and cumulative permanent deformation have the same assessment of outcomes. Higher the CBR

value, smaller the corresponding value of accumulated permanent deformation. Therefore, based on the data coming gained from two kinds of tests, frame 4 and 5 are determined as the optimum framework structures.

Design of Cement Mortar

Taking into account the characteristics of the northern cold regions, cement mortar is composed by ordinary Portland cement, sand, slag, water and water reducer. Cement mortar is designed with orthogonal method, in which water-cement ratio, the amount of sand, slag dosage, dosage of water reducer are considered. Each factor considers four levels using the corresponding L16 (4^5) orthogonal test table. Combination of specific tests and test results are shown in Table 3. By using a direct comparison of test data, the efficacy of factor analysis, variance analysis and so on, comprehensive considering standards of 7d, 28d compressive strength, flexural strength and mobility, number 5 is fixed on the best ratio of mortar as cement stabilized gravel mixture.

Table3. The Specific Test Combinations and Test Results.

Number	w/c	Sand (%)	Filler (%)	Water Reducer (%)	7d BS (MPa)	7d CS (MPa)	28d BS (MPa)	28d CS (MPa)	Fluidity (cm)
1	0.42	0	0	0	10.33	56.9	10.60	67.2	>25
2	0.42	10	10	0.3	9.35	64.8	10.93	67.2	23.9
3	0.42	20	20	0.6	9.55	51.6	10.51	64.1	16.9
4	0.42	30	30	0.9	6.60	25.1	7.82	33.9	22.3
5	0.45	0	10	0.6	10.47	59.1	10.81	70.2	>25
6	0.45	10	0	0.9	8.45	55.6	8.96	67.5	>25
7	0.45	20	30	0	7.60	38.7	8.68	43.4	16.0
8	0.45	30	20	0.3	9.25	45.1	9.89	57.3	15.9
9	0.48	0	20	0.9	9.48	56.8	10.44	62.2	23.6
10	0.48	10	30	0.6	7.82	49.6	8.72	62.1	14.1
11	0.48	20	0	0.3	6.85	46.6	7.71	59.1	>25
12	0.48	30	10	0	8.06	51.1	9.17	64.7	23.1
13	0.51	0	30	0.3	7.22	49.3	9.32	52.6	17.3
14	0.51	10	20	0	7.23	50.0	8.19	60.6	20.5
15	0.51	20	10	0.9	6.80	49.0	7.25	60.4	24.5
16	0.51	30	0	0.6	6.65	38.2	7.92	54.4	>25

NOTE：BS represents Bending Strength, CS represents Compressive Strength.

Designed to Determine the Volume of Mixture Gradation

Assuming that VV= 20%, using the method described above, the quantity of coarse aggregate skeleton is determined as 85% and cement mortar is 15%, in which

percent of the cement is 10.8%.The compressive strength of the mixture has reached 11.2 MPa, which is much higher than the strength requirements of base. In economic terms, the increase of cement dosage will bring substantial increase in cost. Comprehensively considering the strength of cement stabilized crushed stone and economic factors. And number 5 cement mortar is adjusted. The adjusted mass ratio is, water: cement: slag: water reducer = 0.45:1:0.93:0.01.

DETERMINATION OF REASONABLE CONSISTENCY

Evaluation Standards of Reasonable Consistency

Uniformity of air voids: The difference between upper and lower percentage of voids in a specimen should be less than 5% , which serves as the standard to evaluate the uniformity of voids. The method of measuring the voids is as follows: the cylindrical (Φ15×15cm) specimen is cut into two parts from the mi ddle, forming upper part and lower part. The air voids of each part are measured. Then the void difference (△VV) can be calculated by Eq.1-2. When △VV is positive number, it means the upper VV is larger than the lower part. The negative △VV means larger VV in the lower part. The smaller ｜△VV｜ means more equal void and good permeable performance.

$$\triangle VV = VV_{up} - VV_{down} \quad (2)$$

Strength: 7d unconfined compressive strength≥3MPa is the standard to evaluate the strength of the mixture.

Definite Method of Reasonable Consistency

Comparing different water-cement ratios with △VV and the strength (see Figure 2), the scope of water-cement ratio demanding the uniform voids and strength is determined. When water-cement ratio is ≤0.39, the △VV is <5% and when water-cement ratio is ›0.31, then 7d compressive strength is≥3MPa, so the water-cement ratio should be between 0.32 and 0.39. Considering strength, binding conditions and uniformity of void inside the sample specimen, the best water-cement ratio is determined as 0.36.

CONCLUSION

Based on the above analysis, conclusions are as follow:

(1) According to function requirements of drainage base, three design indices are determined for cement stabilized crushed stone mixture.
(2) Adopting the new methods of best vibrating compaction and dynamic stress press-in test, coarse aggregate skeleton type, cement mortar and graduation of cement mixture are determined.
(3) The method of determining optimum water-cement ratio is put forward.

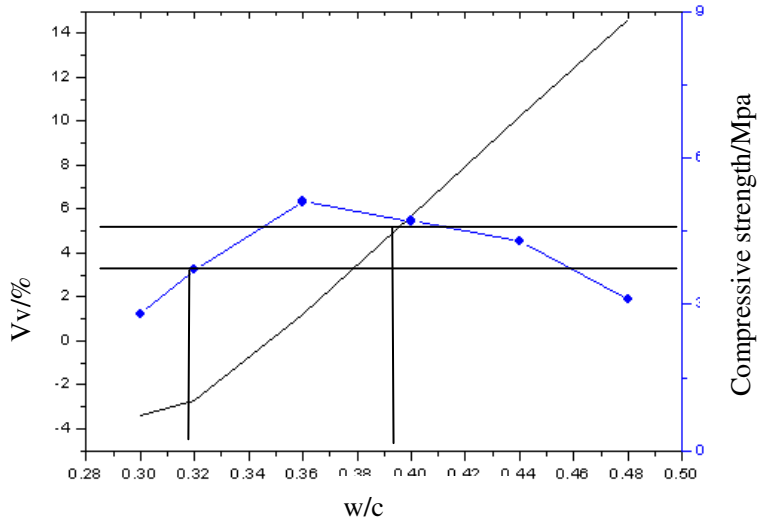

Figure 2. Relationship between Cement-Water Ratio and Strength.

REFERENCES

Grogan, W.P. (1994). "Evaluation of Drainage Base Course for Pavements. Infrastructure." New Materials and Methods of Repair Proceedings of the Materials Engineering Conference, 693-700

Hall, M. (1994). "Cement-stabilized Open-grade Base Strength Ttesting and Field Performance versus Cement Content." Transportation Research Record, 22-31

Tian Bo, Niu Kaimin, Tan Hua(2006). "Research on the mold method of permeable base." Highway, 150-154

Zheng, M. (2004). "Research on permeable base." Ph.D dissertation of Changan University, 38-41

Hu, Y. (2004). "Design Method for Permeable Base." Highways & Automotive Applications, 84-86

Heat Reflection Coating Design and Performance

FENG Decheng[1] and ZHANG Xin[2]

[1] School of Transportation and Engineering, Harbin Institute of Technology, Harbin, China; PH (+86) 0451-86282116; email: fdcgxy@vip.sina.com
[2] School of Transportation and Engineering, Harbin Institute of Technology, Harbin, China; PH (+86) 0451-86282116; email: zhangxinblack@gmail.com

ABSTRACT

The hot mix asphalt (HMA) pavements absorb heat from the sun causing increased temperature of the pavements and the cities as the albedo of the HMA surface is only 0.05-0.15. High temperature may incrase the potential of rutting and urban heat island (UHI). Decrease of the pavementsurface temperature can be achieved by using heat reflection coating. In this research, an easy construction and cheap heat reflection coating material is developed. Using the coating, the surface temperature is 11.4℃ lower than the common HMA surface. Other performance such as anti-skid, moisture resistance, adhesive force and rigidity are tested. The results show that the coating satisfies the requirements. The cost of the coating is much cheaper than the other heat reflection coating.

Key words: heat reflection coating, lower temperature effect, anti-skid experiment

Introduction

Hot mix asphalt pavement is commonly used to pave highway and city streets. In early period, a lot of damages such as cracking, rutting and moisture damage appear. Rutting is one of the major reasons to cause rehabilitation or reconstruction. The research done by Sheng (2001) showed that over 80% of the pavement reconstruction is caused by deep rutting.

High temperature increases the rutting potential. As we known, the HMA is a temperature sensitive material. At high temperatures, the anti-shear performance decrease. HMA pavements tend to be absorptive with an albedo of approximately 5-15% (Berzt, 1998). In summer, the pavement surface temperature is 15-25℃ higher than the air temperature.

Conventional method to solve the rutting is to improve the high-temperature performance by using high quality asphalt and aggregate or appropriate gap-graded aggregate gradation. All these are passive to accept the high temperature. At the same time, these high quality aggregate and asphalt increase the construction cost, thereby,

decrease the economical effectiveness of the roadway system. The gap-graded gradation is difficult for construction. Even taking these methods, the problem of rutting is still not fully solved.

Can we solve the problem more directly? One important reason that causes the high temperature of the pavements has been ignored – the low albedo of the HMA surface. For a surface under the sun with insulated underneath structure, the equilibrium surface temperature, T_s is obtained from

$$(1-\alpha)I = \varepsilon\sigma(T_s^4 - T_{sky}^4) + h_c(T_s - T_a)$$

α	solar-reflectivity or albedo of the surface
I	total solar radiation incident on the surface, W/m^2
ε	emissivity of the surface
σ	Stefan-Boltzmann constant, 5.6685×10-8 Wm^{-2}K^{-4}
T_s	equilibrium surface temperature, K
T_{sky}	the effective radiant sky temperature, K
h_c	convection coefficient, Wm^{-2}K^{-1}
T_a	air temperature, K

From the formula (Berzt, 1998), increase the albedo of the pavement surface, we can get lower T_s, which indicates a a lower temperature of HMA. The study done by Sheng (2001) showed the dynamic stability (DS) increase exponentially with the decrease of temperature. It proves that rutting can be controlled by increasing albedo.

There are some possible ways to increase the pavement surface albedo. One technique for light-colored pavement is to use white or light colored aggregate in an asphalt binder. Light colored aggregates that are suitable for asphalt include high silica gravel, quartz, white stone, white marble and some types of granite (Rosenfeld, 1995). But the cost is high if local source for such aggregates is not available. Another possible method to improve the albedo is using heat reflection coat. It is widely used in building roof and oil deposit. The heat reflection for pavements is developed by Japan. It can decrease the temperature about 10℃. But the cost is as high as \$40-53/m^2 (Kinouchi, 2001).

Another benefit of increasing the pavement albedo in cities is to mitigate urban heat island (UHI) effect. Summer urban heat islands with daytime average air temperature 2.5 higher than surrounding rural areas are found throughout the world (Akbari, 1990). The urban heat islands caused an increase of 1.5-3.0% in peak cooling demand for each 0.5℃ increment (Akbari, 1993). In big cities such as Chicago and L.A., asphalt pavement consumes more than 20% of the surface area. It is considered that dark pavements and the surface of the building is one of the major heat sources causing the urban heat island, as it absorbs more heat from the

sun. If we can decrease the pavement surface temperature, UHI in big cities can be mitigated effectively.

2. Coat design

According to conversation of energy and heat conduction, the surface temperature is lower when the albedo is higher. The objective of this study is to design a coat with high albedo without glaring for the consideration of driving safety. A pavement coating is developed to satisfy both high albedo and low brightness with innovative technology. The function of this technology is based on a thin paint coating on the surface of the conventional dark asphalt pavement, which gives relative high reflectivity for the near infrared region and low reflectivity for the visible range. This results in increased albedo while maintaining the dark colored pavement surface.

The coat is composed of basic resin materials, pigment, functional filler and auxiliary materials. The scattering rate is used to represent the albedo. The scattering rate m is obtained from: $m=n_p/n_r$

Where n_p is the refraction coefficient of pigment, n_r is the refraction coefficient of basic resin materials. The high m can be obtained by using pigment with high refraction coefficient and basic resin materials with low refraction coefficient. Usually the colophony is used as basic materials. However, considering its high cost and pollution to environment, the silane-acrylate emulsion can be used as basic materials.

The refraction coefficient is affected by the diameter of the particles. The smaller the particles are, the higher the refraction coefficient is. Therefore the small fine hollow glass pigments are chosen. The fine glass particles are included in the paint to add additional effects on reducing thermal conduction and heating of the coat. TiO_2 is used as the color pigment. Five different cases are provided to compare.

3 Test methods

3.1 Temperature reduction experiment

As an important property, the temperature reduction effect is tested. In this study, the indoor simulation solar radiation system (Liang, 2005) is taken to test the effect of the coating. The lamp-house is iodine-tungsten light which has similar spectrum with the sun. The radiation intensity is 788 W/m^2 and the radiation time is 7 hours. The temperature is tested by sensor fixed in the surface. To compare with the Japanese coating, five coating materials and the Japanese coating are painted on 30×30 cm specimens to test the effect of temperature reduction.

3.2 Anti-skid performance

After applying the paint coating, the pavement surface can be slippery and dangerous to drivers. The anti-skid performance must be tested. In this study, the BPN is used to evaluate the skid resistance of the painted surface. The paint coating surface is tested with and without water application. In this study, six surface coating materials including the five developed in this study and one Japanese coating were tested.

3.3 Coat performance

The coating materials should be adhesive to the pavement surface with the application of rains and wheels. The adhesive force, rigidity and water-endurance are tested.

3.3.1 Adhesive force

The adhesion between the coating and the underneath material (HMA) is the necessary condition to increase albedo. Van de Walls force and hydrogen bond provides main part of the adhesive force. It is an important index for the coating. In this research, the experiment follows the method GB/T9286-88.

3.3.2 Rigidity

Rigidity is an important index to evaluate the service life of the coating material. The rigidity is tested by pencil method. Different rigidity pencil is used to distinguish the rigidity of the coat. Use a pencil to draw on the paint coating. If it can write without groove, the rigidity of the coating material equals the rigidity of the pencil.

3.3.3 Water-endurance

Considering the actual condition, the coating can be easily eroded by rain. An experiment is designed to simulate such condition. The coating material is painted on a test board first, and 1/3 of the test board is put in 40℃ flowing water. The time for the coating material to be peeled off from the board surface is then recorded.

4 Results

4.1 Temperature reduction test

The temperature reduction test results are presented in Figure 1. From Figure 1, the surface temperature of specimens with coating are lower than the specimen without coating, which proves that using coating can decrease the temperature effectively. Different coating materials also showed different effect in temperature deduction. Case 1, 2, 3, 4, 5 decrease 3.6℃, 8.5℃, 9.8℃, 11.4℃ and 9.7℃ respectively. Case 4 is the most effective one in all tested groups, which lowers the temperature 11.4℃. The Japanese coat decrease 6.3℃ and is less effective than the

case 4 coating.

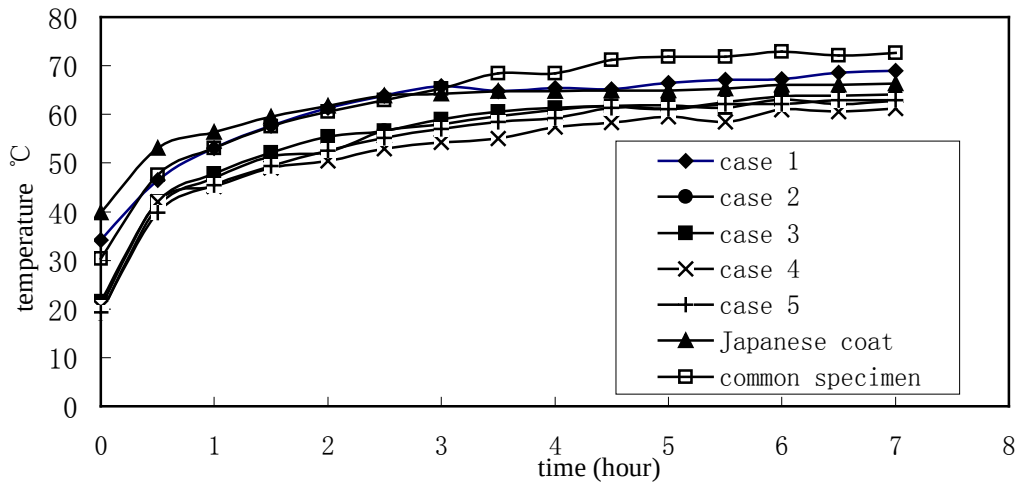

Figure 1 the results for lower temperature for different cases

4.2 Anti-skid performance

Following the method described above, the results are showed in table 1. From table 1, compared with the conventional HMA, the paint coating decreases the anti-skid performance largely. But most of them can still satisfy the minimum BPN requirement of 45. Case 5 does not satisfy the requirements. The Japanese coating has relative better anti-skid performance.

Table 1 the results for anti-skid performance

Specimens	Without water BPN	Water BPN
Without coat	84	64
Case 1	61.8	47.9
Case 2	71.1	51.4
Case 3	78.1	47.9
Case 4	64.4	49.9
Case 5	70.7	40
Japanese coat	69.4	51.6

4.3 Coating performance

The results of coating performance are showed in table 2. From the table 2, the different cases have similar adhesive, rigidity and water-endurance performance. It is because all the coats have the same basic resin materials. The coats developed have good adhesive and rigidity. Case 4 have the best water-endurance performance.

Table 2 the results for coat performance

Project	Case 1	Case 2	Case 3	Case 4	Case 5
Adhesive (%)	100	100	100	100	100
Rigidity	4H	4H	4H	4H	4H
Anti-water(h)	360	360	360	400	360

5 Cost and economical analysis

The Japanese coating chooses colophony or resin as the basic materials and fine hollow ceramic as functional pigments. The colophony is expensive which lead to the high cost of the coating material. In this study, silane-acrylate emulsion is chosen as the basic materials, which is cheap and no pollution to environment. Considering the construction technology and materials price, the cost of the coating is about $\$1/m^2$, which is much cheaper than the product provided by Japan.

Although the price is low, the working life of the coating developed is short. This is because the basic material is water-soluble. Compared with the colophony materials, the coating cannot be used for long time. According to field observation, the life of the coating is 2 months. Since the typical high temperature season is 1-2 months, such coating material can be applied to the highway and urban roads before the high temperature season every year.. When the season is over, the coating will break off. The overall economical value of such coatings is still higher than the Japanese coating with has longer working life (15 years) but much higher initial price. .

Conclusions

1) The heat reflection coating developed in this research can effectively reduce the pavement surface temperature. The surface with Case 4 coating is 11.4℃ lower than the reference specimen. Compared with the Japanese coating, the developed cases have better effect.

2) After applying the paint coating, the anti-skid performance decrease largely. But all cases except case 5 can satisfy the specification requirements.

3) Through the coating performance test, the coatings developed have similar adhesive force, rigidity and water-endurance performance.

4) The developed coating has better economy effect than the Japanese coating. The costing is much cheaper than the Japanese coat because the using silane-acrylate emulsion instead of colophony.

References

Akbari, H. (1993). “Monitoring peak power and cooling energy savings of shade tress and white surfaces in the Sacramento Municipal Utility District service

area: data analysis, simulation and results." Lawrence Berkley National Laboratory, Berkley, CA.

Akbari, H., Davis S. (1990). "Cooling our communities: A guidebook on tree planting and light-colored surfacing." US Environmental Protection Agency, Office of Policy Analysis, Climate Change Division.

Berzt, S., Akbari H. (1998). "Practical issues for using solar-reflective materials to mitigate urban heat island." Atmospheric Environment, 95-101.

Liang, Manjie (2005). "Asphalt pavement light thermal reaction mechanism and heat-reflection coating engineering research." Dissertation for master degree in engineering, Harbin Institute of Technology, 43-50.

Kinouchi, T., Yoshinaka T. (2001). "Development of cool pavement with dark colored high albedo coating." 11-16.

Rosenfeld, A., Akbari H. (1995) "Mitigation of urban heat islands: materials, utility programs, updates." Energy and Buildings, 255-265.

Sheng, Jinan. (2001). "Asphalt and hot mix asphalt performance." People transportation public, 338.

Research On Key Question Of Joint Of Large Span Pre-Stressed Box-Girder Concrete Continuous Rigid Frame Bridge With High Piers

Wang Guanghui[1] Wei Chenglong[2] Liu Xiaoyan[3]

1 Lecturer, The Department Of Civil Engineering & Architecture，Hunan Institute of Science & Technology, Xueyuan Road, Yueyang City, 414000; School of Civil Engineering & Architecture, Changsha, Changsha University Of Science & Technology, Chiling Road No.45 410076; PH (86) 730-8648810 ; email: wgh325@126.com

2 Professor, The Department Of Civil Engineering & Architecture，Hunan Institute of Science & Technology,Xueyuan Road, Yueyang City, 414000; PH (86) 730-8648810; email: weichl@csust.edu.cn

3 Professor, School of Civil Engineering & Architecture, Changsha,Changsha University Of Science & Technology, Chiling Road No.45 410076; PH (86) 731-5256066; email: Xiaoyanliu2003@126.com

ABSTRACT

In the construction of a Large Span Pre-stressed Box-girder Concrete Continuous Rigid Frame Bridge with High Piers, the joint plan of the bridge depends on the construction conditions and design status. In this study, several joint plans were analyzed using the nonlinear finite element method for finding an optimum joint plan. In the analysis, the space beam elements were used to simulate the piles, the piers and the beams, and the link element to simulate pre-stressed reinforcement. The technology of element life and death was used to simulate the construction process. The non-line effects associated with big distortion, concrete shrinkage, and creep were considered in the simulation. Aiming at the high temperature joint of the bridge, a new technique, namely ‘loading anti-jacking force’, was proposed based on the analysis of the impaction related to the high temperature joint of the structure. In addition, the formula of the anti-jacking force was given originally. This research demonstrated that the non-linear finite element method is effective in engineering practice. This research can provide references for the design, the construction, and the monitoring of similar bridges.

KEY WORDS: bridge engineering; continuous rigid frame bridge; nonlinear finite element method; joint plan; high-temperature joint; anti-jacking force

INTRODUCTION

Because of its light, low-cost, mature technology, adaptability , and other advantages, LPBCCRFBHP (the Large Span Pre-stressed Box-girder Concrete Continuous Rigid Frame Bridge with High Piers) is favored by many bridge builders, especially in the application on mountain highway construction. The

LPBCCRFBHPs commonly use cantilever concreting construction technique. There are two main problems involved in the design and construction of LPBCCRFBHP: the bending deflection of the box-girder is oversize and the box-girder cracks (Wu Xiaoguang et al. 2001). The cantilever concreting construction can be used to adjust the elevation of formwork erection, the pre-stressed effective means, etc., resulting in avoiding or reducing the occurrence of the above two issues in the box-girder segmental (Cai Sujun et al. 2007). Therefore, to fulfill the design requirements and to ensure the state of stress and beam-line, the joint construction section of the bridge is one of the key concerns. In the actual construction, the joint actual temperature is often higher than the design temperature because of the limitation of machine equipment, and the rushing of construction progress. Hence, , the joint construction programs need to be adjusted according to the actual conditions, especially the actual temperatures at joint sections.

In this study, the Yesan River Bridge, which is designed as a LPBCCRFBHP, was analyzed in order to choose an optimum plan of the tentative joint program. The Yesan River Bridge is a grand bridge in Yichang-Enshi expressway in the Hubei province of China, which is a part of the Shanghai-Chengdu National Highway. The superstructure of the main bridge is a three-span Pre-stressed concrete Continuous Rigid box-girder Frame Bridge (as shown in Figure 1). The No. 3, 4 piers of the main bridge were the thin-walled high piers, with heights of 120.0m and 86.5m respectively . Two side span folds and a central span fold were designed all over the bridge and the length of each fold was 2.0m.

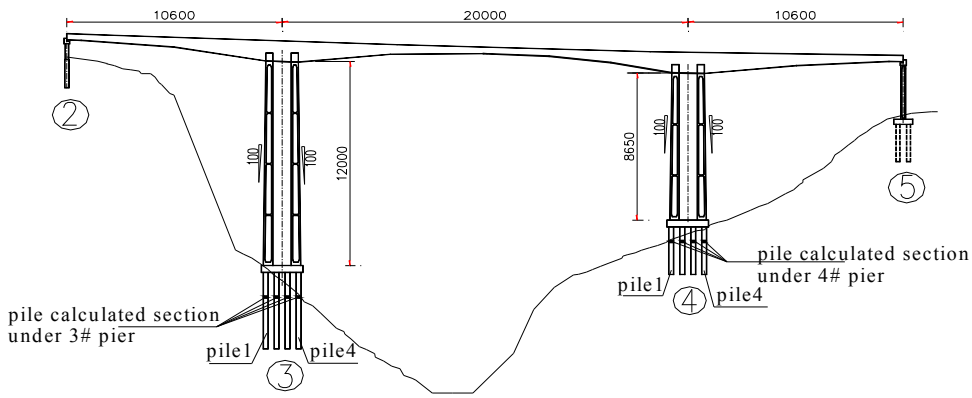

Figure 1. The sketch of the superstructure of the main Yesan River Bridge.

DICISION OF NEW JOINT SCHEME

THE JOINT SCHEME

The cantilever concreting construction was used in the Yesan River Bridge. The full-bridge joint order is both sides first, and then the middle. Because the 3 # T pier structure has completed the largest section of the cantilever construction, and 4 # T pier structure of the cantilever construction is a month later than 3 # T pier structure, there is enough time to destroy the center cradle of the pier 3# structure. According to the construction site, the following joint plans were put forward:

Plan one: Don't dismantle the cradle; the section of three folds all use the cradle to fold directly. Put pressure on the side span to adjust linear and the stress.

Plan two: As shown in Figure 2, after the 3# pier central span cradle is demolisted, the 3# pier side span folds. Then the 4# pier central span cradle transfers to 3# pier T structure to carry on the 4# pier side span fold. And pier 4# T structure of central span cradle will be back to joint section dismantling principal truss of the cradle, using the bottom of the cradle and the side form carrying on the central span joint construction.

Plan three: As shown in Figure 2, after removing the central span cradle of 3# bridge pier, we put the 3# bridge pier side span together, and then put the cradle of 4# bridge pier central span forward. The cradle truss of the 4# pier mid-span can be removed after the bottom-cradle, side die and inner die of 4# pier mid-span have been hanging at the largest cantilever segment of 3# T and 4# T piers mid-span. Then start to construct the joint paragraph of the 4# bridge pier side span and central span in turn.

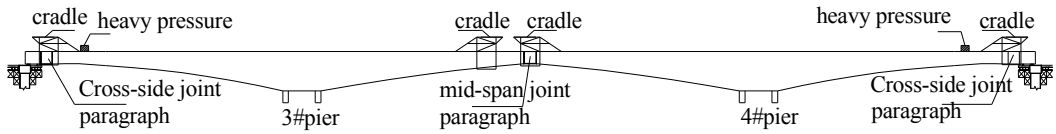

Figure 2. The schematic of the joint program.

In the simulation, non-linear space beam elements were used to simulate pile, pier and main beam, and member-units to simulate the pre-stressed reinforcements. The model of the structure's spatial analysis was established to analyze the designed joint program and the options above. The calculation model is shown in Figure 3.

Figure 3. The model of structures calculation anal ysis.

ANALYSIS OF THE RESULTS

The originally designed joint program and the three new options above were analyzed. The main beam deformation and the difference of stress after 1500 days after the completion of the bridge are shown in the Figure 4.

The results shown in Figure 4 demonstrate that there is only a small difference between the first program (side span's matching weights is 45 t) and the designed program about the bending deflection of each side span section. The largest bending deflection deviation in the central span is the lower 27 mm. The largest stress deviation of the section on edge is about 0.4 mpa, and that on the lower edge is about -0.3 mpa. The difference in the linear and forcement is so large that it can't be

adjusted in joint construction. For these, the first joint program is not feasible. The second program is coherent with the first program in the condition that the side span's matching weights is 45 t in the first program, but because of the cradle's removing around the joint paragraph of the central span, it will bring some security risk in the process of construction. In addition, the main truss of the cradle is removed after the side span of the pier. # The 4 T configuration gets joint in the second program; this will affect the process of the joint of the central span. In the third program, the process of the joint is in the condition that 4# T pier side span's matching weights is 55 t, the largest deviation of the linear and stress is respectively 4.6 mm and 0.05 mpa at last. After the joint of the main Yesan River Bridge, the side span's joint error of the pier # 3 T configuration, the side span's joint error of the pier # 4 T configuration, and central span's joint error are 11 mm, 8 mm, and 10 mm respectively. While the allowed maximum deviation of the linear is 20 mm in the process of the joint, these factors indicate the availability of the third joint program. Hence the third program was adopted in the construction of main Yesan River Bridge.

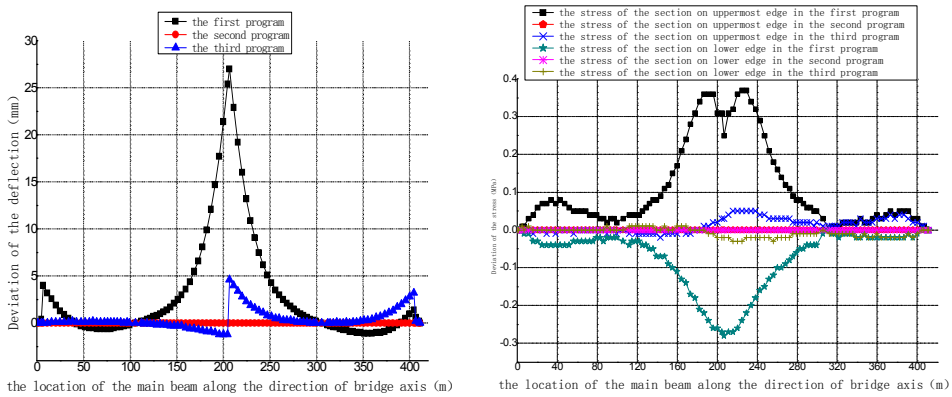

Figure 4. Comparison of the three new joint programs and the original designed joint program (deviation of the deflection = the deflection of the original designed joint program - the deflection in the first(second, third) program).

JOINT AT HIGH TEMPERATURE

THE DETERMINATION OF REASONABLE JOINT TIME AT HIGH TEMPERATURE

The pre-stressed concrete continuous rigid frame bridge is the multiple statically indeterminate structure. If the joint temperature is a little high, the new deposited concrete in the joint paragraph will shrink in the process of hardness with the dropping of the temperature, at the same time the deposited beam of the both ends of the colong kou will shrink with the dropping of the temperature. (Hu Wenxue et al. 2007) Hence, the cracks will appear between the joint paragraph and the deposited beam of both ends and the connectivity of the jointed beams can't be ensured. The dropping of the temperature will also induce a greater secondary inner force, which will superpose with the inner force produced by the shrinking of the concrete (Zhou

Guangwei et al. 2006). In addition, the dropping of the temperature will induce the shrinkage of high piers, especially for height-difference piers. Under the same dropping temperature condition, the difference of volume contraction is higher as the height difference of piers is higher. The effect of this reason is similar with non-uniform settlement of the foundation.

About the upstream of the Yesan River Bridge, the original design was to make the joint in 15+5℃. Due to the effect of the progress, the upstream of the Yesan River Bridge is scheduled to start the joint of the main span on August 2. In August, the air temperature around the Yesan River Bridge is about 19-37℃ (the lowest-highest temperature). Through the surveying, the average temperature of the box beam concrete was found to be higher than 19℃, as the observed temperature data shown in Table 1. As shown in Table 1, the lowest data of the main beam's average temperature was around 26℃ and appeared in the early morning in the range of 3 to 6 o'clock. At this period of time, the air temperature and beam body temperature didn't have large change, so we chose 5 pm to start the rigid lock work.

Table 1. The temperature from July 31 to August 1 about the Yesan River Bridge's right pieces atmosphere（℃）.

time	the maximum temperature of the box beam's concrete	The average temperature of the box beam's concrete	air temperature
31-Jul 06:00	26.58	26.24	19.3
31-Jul 08:00	27.23	26.28	20.3
31-Jul 10:00	28.2	26.37	29.7
31-Jul 11:30	29.86	26.5	32.8
31-Jul 13:30	37.12	27.17	36.6
31-Jul 15:00	43.66	27.85	37.1
31-Jul 17:00	50.16	28.47	35.9
31-Jul 19:00	41.59	27.53	28.6
31-Jul 21:00	35.11	26.71	24.3
1-Aug 00:00	29.27	26.55	19.6
1-Aug 03:00	27.82	26.32	18.9
1-Aug 05:00	26.38	26.19	19.0

THE EFFECT OF JOINT TO THE STRUCTURE AT HIGH TEMPERATURE

The average temperature of main beam concrete is -2.1℃ in cold weather through our observation, so from the 26℃ (when the central span get joint) to cold winter (about -2.1℃), the temperature's change is 28℃ on the dropping side. Such a change will cause a large affect to the removement of the bridge pier and inner force of the structure. In the simulation, two extreme beam temperatures (about -2℃ and 32℃) were used while the central span get joint is 26 ℃.

DISPLACEMENT OF HIGH PIERS

Based on the simulation for the joint process of the Yesan River Bridge under extreme beam temperatures, some conclusion could be drawn : the effect of different

joint temperatures is large due to the displacement of the pier-top and the vertical displacement of the middle of central span. If the central span get joint in designed temperature (15℃), when the structure as an integrity achieves the extremely high temperature or low temperature, the position displacement of the pier-top is roughly the same, but the deformation of the central position of the central span in the condition of dropping temperature is twice than the rising temperature. If the central span get joint at high temperatures (26℃), when the whole structure's temperature achieves the maximum temperature, the deflection and settlement of the pier-top are not very large, but when the whole structure's temperature achieves the minimum temperature (-2℃), the deflection of the pier-top can reach to 3.1 cm, the settlement of the pier-top is about 3 cm, too; besides, the absolute elevation of the central position dropped 7.2cm. It's worth to figure out that the settlements of the two high pier-tops are different to each other. There is additional stress in the structure due to the large deflection of the pier-top and the non-uniform settlement of the high pier-tops.

THE INTERNAL FORCE OF THE STRUCTURE

When the joint process of the Yesan River Bridge is at high temperatures and under the extreme beam temperatures, the simulation demonstrated that the force of high piers is slightly influenced by the beam temperature when the central span was jointed at different temperatures. When starting the joint in the same temperature, the effect of the temperature is large due to the structure's stress, especially to the stress of pile while the pile appeared prodigious tensile stress. For example, in the pile-bottom section of pile 1 of pier 4#, the tensile stress reach to 2.19 MPa, so is 1.20 MPa in the pile-bottom section of pile 2 of pier # 4's leg. Such a large tensile stress together with the live load will make the stress in the section of pile-bottom ascend the limitation of the concrete's stress and induce cracks.

COUNTERMEASURE OF THE JOINT WHILE TEMPERATURE IS HIGH

Some effective measure (Biao Wu 2006) was adopted when the joint temperature is high, for example, loading anti-jacking force. The effect of temperature and the shrinkage and creep of concrete on the linear and force of structure can be eliminated by loading anti-jacking force on 3# pier and 4# pier before the mid-span was jointed. Imposed anti-jacking force diagram is in Figure 5：

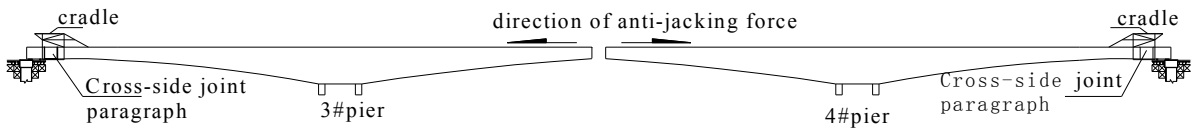

Figure 5. Impose anti-jacking force.

TO DETERMINE THE SIZE OF THE ANTI-JACKING FORCE

The purpose of the anti-jacking force is primarily to offset temperature and concrete shrinkage and creep of the linear structure and the impact of stress. The

anti-jacking force required to meet the following formula：

$$\{u\}_{F+\Delta T}^{\text{High temperature closure}} - \{u\}^{\text{Design temperature closure}} \le [\delta_u]$$
$$\{\sigma\}_{F+\Delta T}^{\text{High temperature closure}} - \{\sigma\}^{\text{Design temperature closure}} \le [\delta_\sigma] \quad \cdots\cdots(1)$$

where u is the horizontal displacement of the nodes of the main beam; σ is a structural stress; F, ΔT are the anti- jacking force and the temperature difference between the temperature of the high temperature joint and the design temperature joint; $[\delta_u]$, $[\delta_\sigma]$ are the given displacement and stress for the anti-jacking force optimized. According to the experience of monitoring and control many continuous rigid frame bridges, $\delta_u^{\max}$ check 0.005m, $\delta_\sigma^{\max}$ get 1.0MPa。

Through optimizing calculation, it must impose 26 t anti-jacking forces at the top of mid-span on 3# pier T structure in advance, and 28 t on 4 # pier. However, the anti- jacking force must be imposed symmetrically. 27 t anti-jacking force on the joint of the bridge in the central span was optimal to eliminate the adverse effects during high temperature joint. The deviations of the pier top are very close while the 27t anti-jacking force is imposed during the high temperature joint and the design temperature joint. The stresses at the bottom of the pile have a large difference up to 0.63 MPa, which is mainly caused by high-rise pier. However, it is still a degree of optimization that imposes 27 t anti-jacking force compared to not imposing any force during the high temperature joint.

LOADING ANTI-JACKING FORCE

Anti-jacking force was symmetrically imposed on the box beam of the lower reaches of the web on the axillary stems. For the Yesan River Bridge, a 27 t anti-jacking force was imposed on the web on the lower and upper reaches. Each jack on the lower reaches and the upper reaches are 13.5 t. Figure 6 shows a photograph while imposing the anti-jacking force.

Figure 6. Imposing anti-jacking force.

CONCLUSION

Based on the actual construction conditions of Yesan River Bridge, comparative analysis of four joint plans were conducted through a non-linear finite element method in this research. A new joint plan was nailed down and applied to joint the right pieces of the Yesan River Bridge.

Extreme temperatures of the continuous rigid frame bridge and a series of joint temperatures were considered in the simulation. The results demonstrate that the joint temperature has a great influence on the deviation of the pier-top and the vertical deviation of mid-span of central span section. If the central span is jointed under design temperature, the pier-top-change rate is roughly equal when the whole structure reaches an extreme high or an extreme low temperature, but the deformation that caused by temperature cooling is 2 times of that caused by temperature rising. Considering varied joint temperature of the mid-span, a high pier bridge stress is slightly affected by the joint temperature, whereas the force of main beam and the pile are highly affected by the joint temperature. Under a same joint temperature, the stress of the various key cross-section of the structure is greater impacted by temperature changes, and the pile is affected most.

Through loading anti-jacking force to joint continuous rigid frame bridge under high temperature conditions, the pier-top deviation and pier-top-pile cross-section of the tension can be greatly reduced to meet the design requirements; the value of anti-jacking force is identified by the deviation of the pier top and the force of the structure together.

ACKNOWLEDGEMENT

The authors gratefully acknowledge the support provided by Open-end Fund Of Key Laboratory Of Bridge And Tunnel Engineering Of Changsha University Of Science & Technology.

REFERENCES

Ma Bao lin.Large Span Continuous Rigid Frame Bridge With High Piers. Beijing: China Communication Press, 2001.

Zhang Jiyao, Wang Changjiang, Cantilever Concreting of Pre-stressed Concrete Continuous Girder Bridge. Beijing: China Communication Press, 2004

The Second Highway Survey and Design Institute. Shanghai-Chengdu national trunk highway Enshi in Hubei Yichang to Yesan rivers in two phases Bridge Design.2004

Cai Sujun, Zhang Xiedong, and so on Influence of the Different Girder Joint Scheme of Continuous Girder Bridge on Construction Control. Transportation Science & Technology, 2007, (5): 18 ~ 21

Wu Xiaoguang, Shao Xinpeng, Wan Zhenjiang Rigid Frame Bridge [M]. Beijing: China Communication Press, 2001.

Hu Wenxue, ZhongYong, Discussion About The problems of Non-design Joint Temperature Jiont Of The Continuous Rigid Frame Bridge. CENTRAL SOUTH HIGHWAY ENGINEERING 1998,29 (4): 27 ~ 28.

Zhou Guangwei; Chen Deliang; Liu Rong, Study on Rational of Determination Joining Temperature of PC Continuous Rigid Frame Bridge and Their

Resolutions. Journal of Changsha Communications University, 2006,22 (3): 15 ~ 19

Biao Wu.The Joint Section of Construction Push About Continuous Rigid Frame Bridge With Dwarf pier. Highway, 2004, (7): 165 ~ 167

Research on Structural Design of Interlocking Concrete Block Pavement for Rural Road

Ma Songlin[1], Hou Xiangshen[1] , Wu Dayong[1]

[1]School of Transportation Science and Engineering, Harbin Institute of Technology, Add.：202 Haihe Road, Nangang District, Harbin 150090, P.R. China; Tel.：86-451-86282120; Fax ： 86-451-86283779; E-mail: masonglin@hit.edu.cn

ABSTRACT

In China thousands of kilometers of rural roads need to be paved. In order to reduce the construction and maintenance costs, the interlocking concrete block pavement can be used in low traffic rural road. The structural design criteria of interlocking concrete block pavement with different types of base causes was researched. The results indicated that the design criteria is different for different base course. The methods of the criteria calculating and structure design were given.

KEYWORDS

Rural road; Interlocking concrete block pavement; structural design

INTRODUCTION

Interlocking concrete block pavement is a pavement which is aligned tightly with high strength concrete block and has property of integrity due to joint transferring shear force. Interlocking concrete block pavement is seldom used in driveway pavement in China at present. There are many merits of this kind of pavement such as strength and durability of structure, low construction costs and the convenience of maintenance, especially no need of heavy machine during construction of the pavement. These merits meet the requirement of rural road construction in China; therefore the study of interlocking block pavement in rural road construction was carried out.

FAILURE STYLES OF INTERLOCKING BLOCK CONCRETE PAVEMENT

There are 6 kinds of failure in interlocking concrete block pavement (B.Shackle, 1985). ① Loose and separation of blocks. Under vehicular load, there is a trend of separation in blocks. Especially in the condition of slope, due to the vibration of vehicles, blocks are slid along direction of slope and joints are separated in blocks at the top of slope so that interlocking of pavement is lost. The paver shape or laying pattern was selected to prevent the failure. ② Breaking or striping of block edge. Because paver is rotate under vehicular load, the breaking or striping of edge is easy to occur. To prevent this failure the block should be manufactured in chamfering edge of surface. ③ Break or abrasion of block. Two reasons can result in break of paver. One is cavity beneath of paver because the surface of base course is not even, another is low bending strength of paver. Controlling construction quality is to prevent the former and controlling manufacture quality of paver is to prevent the latter. Abrasion is due to insufficient rigid of aggregate in block or not suitable dosage or grade of cement. ④ Permanent deformation and sag of pavement. Permanent deformation and sag usually occur in pavement. The large permanent deformation not only deteriorates

service level of pavement, but also results in seeper. Water leak along the joints of blocks can destroy the bearing capacity of pavement structure. Therefore permanent deformation is adopted as the criterion of structural design occur because of insufficient compaction of base or sub-base can results in sag of pavement. ⑤Shear failure. Shear failure occur in pavement with unbounded base such as granular. The reasons of shear failure are low strength basement and high loading. ⑥ Fatigue cracking of base course. Fatigue damage will be happened in interlocking block pavement with semi-rigid base course under repetitive loading. This kind of damage is similar to asphalt pavement. Fatigue cracking of base is main factor in damage of base and destructing of pavement structure. Therefore bending stress at the bottom of base is used as criterion of structural design of interlocking block pavement with semi-rigid base course.

ANALYSIS OF STRUCTURAL DESIGN CRITERIA

According to the analysis of mentioned failure styles of interlocking block pavement, the former three kinds of failure are not related to structural design. For rural road the shear damage is hardly happened due to overloading vehicles. Therefore in structural design the exceeding permanent deformation and fatigue cracking of semi-rigid base must be controlled.

Interlocking block pavement is flexible pavement consisting rigid units. If base course is unbound granular, the permanent deformation will accumulate in pavement under repetitive vehicle loading. When the depth of permanent deformation rises to some value, the service capacity of pavement will be extremely influenced. Therefore the depth of tolerance permanent deformation in design period is adopted as structural design criterion of interlocking block pavement. Namely DR (depth of permanent deformation calculated) $\leq$ [DR] (tolerance permanent deformation)

The fatigue bending stress of base course usually adopts as criterion in the design of flexible pavement with semi-rigid base course in order to control cracking of base course. But cracking of base course of interlocking block pavement take place, the service capacity of the pavement is not destroyed. The fatigue life of the pavement should be divided into two stages. In former stage fatigue life is predicted through bending stress of semi-rigid base course. In latter stage fatigue life is predicted according to calculating tolerance permanent deformation through elastic modulus of cracked stabilized coarse aggregate base (equivalent modulus of compacted granular). The structural design of interlocking pavement should be separated into two stages. For interlocking block pavement with stabilized fine aggregate base, when cracking of base take place, the load carrying capacity of the pavement will decrease rapidly, the fatigue bending stress of base course is used as criterion of structural design only(Yao Zukang,2003).

CALCULATION OF STRUCTURAL DESIGN CRITERIA OF INTERLOCKING BLOCK PAVEMENT WITH SEMI-RIGID BASE COURSE

When a base course is stabilized coarse aggregate, the two stage design method should be used. In former stage fatigue life is decided by fatigue bending stress of base course bottom, whereas in latter stage fatigue life is determined by permanent deformation of a cracked stabilize coarse aggregate.

The formulation of tolerance bending stress of base course bottom in interlocking block pavement with semi-rigid base course is following:

$$[\sigma] = 3.0 \cdot \frac{\sigma_S}{K_d \cdot N_m^{0.1}} \quad (1)$$

Where

$[\sigma]$—tolerance bending stress of half rigid base bottom (Mpa);

σ_s—maximum strength of half rigid base (Mpa);

Nm—cumulative number of standard axle load;

Kd—coefficient of dynamic load ， Kd=1.05。

CALCULATION OF PERMANENT DEFORMATION OF INTERLOCKING BLOCK PAVEMENT WITH GRANULAR BASE

The formulation of permanent deformation of interlocking block pavement usually is achieved with regress analysis method according to results of site test.

In accordance with the research of relevant test in Tongji University, the formulation of permanent deformation of interlocking block pavement with granular base as follows (Sun Linjun,1996):

$$D_R = 1.9 \cdot C \cdot l \cdot e^{-11h} N_m^{0.265} \quad (2)$$

Where

h —thickness of block (cm);

l —deflection of pavement under vehicle loading once （mm）;

Nm—cumulative number of axle load related to l ;

C —when h=8，10，12cm，C=1.17，1.25，1.34 respectively。

Therefore structural design of interlocking block pavement with granular base is carried out with the formulation when cumulative number of standard axle load and tolerance permanent deformation are determined, deflection of pavement can be calculated through FEM of pavement simultaneously.

In order to analyze the relationship between the fatigue life of two stages, structural model of interlocking block pavement with different block thickness and different modulus of sub-grade are used to calculate the respective numbers of axle load of two stage fatigue life: Nm-σ(first stage) and Nm-l (second stage). The result of calculation is shown in **Figure 1**. it can be seen that the ratio of Nm-σ and （Nm-σ+Nm-l）is limited in minor range when base thickness is same although different block thickness and different modulus of sub-grade.

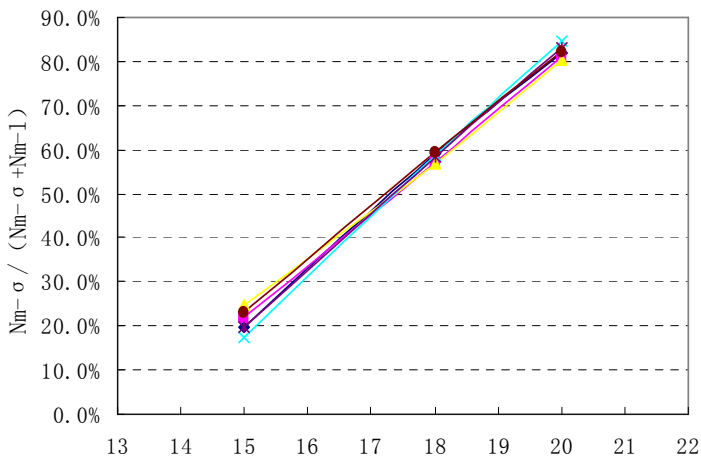

Figure 1. Relationship between base thickness and N_m- /（N_m- +N_m-$_l$）

In pavement structural design Nm-σ/（Nm-σ+Nm-l）in table 1 can be determined according to assumed base thickness.

Table 1. Ratio of N_m- /（N_m- +N_m-l）in structural design pavement

Thickness of base (cm)	15	16	17	18	19	20
N_m-σ/(N_m-σ+N_m-l）(%)	30	43	55	65	75	85

In structural design of interlocking block pavement the calculation of both stage must meet the requirement of design criteria, if the calculated permanent deformation in second stage is much less than tolerance permanent deformation, a new calculation should be carried out with reduced ratio of Nm-σ/(Nm-σ+Nm-l).

CONCLUSION

Through the analysis of failure styles of interlocking block pavement, the permanent deformation and fatigue cracking of semi-rigid base course were adopted as design criteria to control pavement failure for rural road. Where base is granular material, the depth of permanent deformation is used as criterion of structural design. Where base course is stabilized coarse aggregate, structural design is divided into two stages, in first stage the bending stress of semi-rigid base course is used as design criterion, whereas in second stage the permanent deformation of granular base course assumed to be same thickness with semi-rigid base course is used as design criterion.

REFERENCES

B.Shackle. (1985). “The Evaluation and Application of Mechanistic Design Procedure for Concrete Block Pavements.” Proceeding of the 3rd International Conference on Concrete Block Paving, 114~120,1985.

Sun Linjun. (1996) . “The Method of Structural Design of Interlocking Block Pavement for Road and Stock Yard of Port Area.” Journal of Tongji University, 24(1): 17~21,1996.

The Standard of the PRC.(1997).Technical Code of Road and Stock Yard Pavement for Port Area. China Communications Press,1997.

Yao Zukang. (2003). “The Comments for Present Criteria of Asphalt Pavement Design.” Highway. 2003 (2). 44~49,2003.

The Analysis of Dowel and Tie Bars Effects on Curling up in Concrete Pavement Slabs

Xinkai Li[1], Songlin Ma[1], Xiangshen Hou[1]

[1]School of Tranportation Science and Engineering, Harbin Institute of Technology, P.O. Box 150090, City, Harbin, P.R.China; PH (86) 451- 86282120; FAX (86) 451-86282116; email: lxkhit@126.com

ABSTRACT

The effects of dowels and tie bars on curling in concrete pavement slabs is still not clear in design. Therefore, a 3D finite element model (FEM) of the multi-slabs resting on elastic foundations is developed to investigate this effects, and the design plan of dowels and tie bars in FEM are determined according to cement concrete pavement design specification in China, and in FEM beam element is employed to simulate the dowels and tie bars. From the calculated results, the tie bars effects on slab curling is little, and dowels effects is very obvious at slab joints where the stress will increase and curling up will decrease, but for the whole slab the effects of dowels is not obvious.

INTRODUCTION

A concrete slab will tend to curl when it is subjected to a temperature gradient extending vertically through the slab thickness. The tendency to curl induces stresses in the pavement as the pavement is restrained by its weight, the interface between slab and foundation, and the dowels and tie bars from adjacent slabs. The thermally induced stress caused by such interaction can be a significant factor in contributing to early pavement cracking.

Therefore, over the years, the problem of curling stresses received attention from many researchers. From the Westergaard's solution in 1927 to now, many models were developed, especially the finite element models. Those researchers developed techniques for dealing with the problems of slab's self weight, partials contact, nonlinear temperature gradient, and the combined effect of thermal and traffic loads (B. Chubane et al. 1995; Brucea.S. 2002; E. Masad et al. 1996). However, the effects of dowels and tie bars on curling stresses didn't attract attentions of researchers and it is not very clear for the curling stress in jointed concrete pavement (Gergis W. et al. 2001; I.E. Harik et al. 1994).

In this article, 3D finite element modeling is used to examine the effects of dowel and tie bars on curling stresses in jointed concrete pavements. The basic feature in the model is a detailed modeling of dowel and tie bars. The dowel and tie bars using beam elements are embedded in concrete using solid brick elements. After a brief description of the features of the 3D FEM, the curling stress and displacement of multi-slabs with dowel and tie bars are compared with the results with no dowel and tie bars. Then the influence of dowels, tie bars is discussed. The role of dowel bars in activating magnitude of stresses and reducing magnitude

of displacement at joints due to uniform negative temperature differential is discussed and the effects of tie bars on slab curling is analyzed also.

THE FEM OF MULTI-SLABS CURLING

The Parameters in FEM

The multi-slabs resting on elastic foundation are modeled through finite element procedure ABAQUS and the sizes of each slab are 4m×4m×0.2m (length ×width ×height).The interface between slab and fo undation is very complicated and important to concrete pavement and in this FEM the interface is assumed to be frictionless (unbonded). The frictionless interface is simulated through contact elements which can well model the separation of slab and foundation as slab edge curling up. The values of parameters in FEM are listed in **Table 1**.

Table 1. The values of parameters in FEM

Parameters	Elastic Modulus （MPa）	Possion's ratio	Density (Kg/m^3)	Thermal conductivity （W/mK）	Coefficient of Thermal Expansion	Thickness of Slab (cm)
Slab	30000	0.15	2400	6	$5e^{-6}$	20
Foundation	400	0.30	2000	0	0	200
Parameters	Elastic Modulus （MPa）	Possion's ratio	Density (Kg/m^3)	Thermal conductivity （W/mK）	Coefficient of Thermal Expansion	Diameter X Spacing (mm)
Dowel bars	2e5	0.3	7830	10	$5e^{-6}$	28 X 300
Tie bars	2e5	0.3	7830	10	$5e^{-6}$	14 X 800

In FEM the temperature gradient is assumed to be linear along thickness of slab and the " negative gradient " is considered only because slab edge curling up is more often and serious to slab, especially in northeast of China. The term "negative gradient" is used when the temperature of the slab top is smaller than that of the slab bottom. The heat change between slab and foundation is ignored. The temperature differential is assumed to be -1.0℃/cm.

The 3D eight nodes continuum is employed in FEM. Through comparison of different element sizes, the number of elements of slab, 20×20×2 (length × width ×height), is selected. **Figure 1** presents the meshed model.

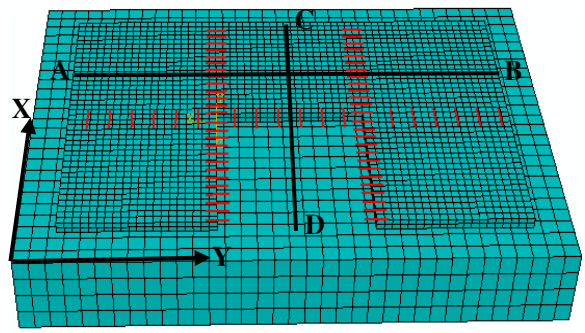

Figure 1. The Finite element model

Verification of FEM

If the self weight of slab is ignored, the close form solution of single slab curling up due to temperature gradient can be derived through slab geometrical relationship. The curling deflection can be calculated by following equation (1) (Masad E. et al. 1996; Yao Zukang 1981). Therefore, this case is selected to validate the FEM.

$$\delta = \frac{\alpha \Delta FL^2}{2h} \qquad (1)$$

Where: δ — The vertical displacement of arbitrary point in slab;

α — Coefficient of thermal expansion of concrete;

ΔF — Temperature gradient along slab thickness;

h — Slab Thickness

L — The distance from arbitrary point to slab center.

It can be known that the self weight of slab is closer to zero the results should be converge to results of Equation (1). In FEM changing the parameters of slab density can realize the self weight of slab to be close to zero. If the slab weight is assumed to be W, and when slab weight is from W to 0.001W in FEM, the calculated results are presented in **Figure 2**.

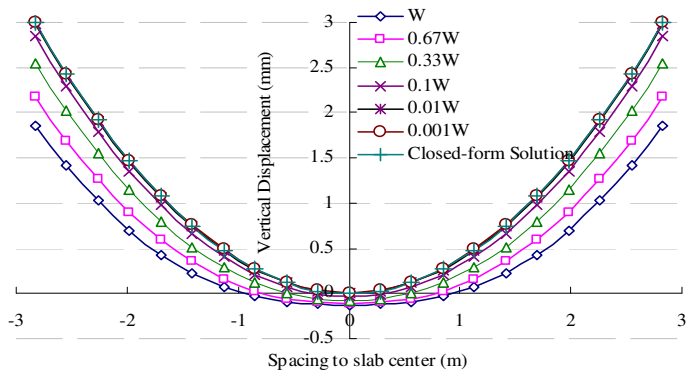

Figure 2. The vertical displacement as different slab self weights

In **Figure 2** with slab self weight decreasing the curling deflection increases. when the self weight is converge to zero the calculated results is very close to close-form solution by Equation (1).Through the comparison of FEM and Closed-form solutions this FEM can be used for calculating the responses of slab.

THE EFFECTS OF DOWEL AND TIE BARS ON SLAB CURLING

Figure 3(a) illustrates the deflection and maximum principal stress profiles that six concrete slabs take due to the application of negative linear gradients of −20 ℃.

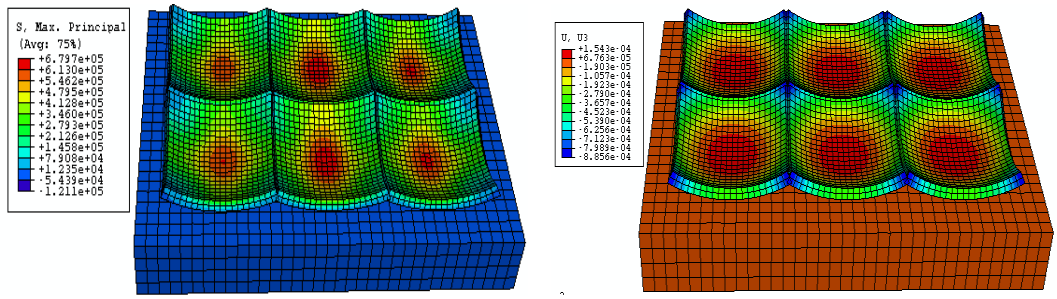

a)Maximum principal stress b）Vertical curling deflection

Figure 3. Deformed slab due to curling

In the case of negative temperature gradient, the slab will be supported over its middle portion while the joints and slab side-edges deflect upward. The stress and displacement along the slab longitudinal centerline AB in **Figure 1** are investigated to explain the effects of dowel bars. The stress and displacement along the slab transverse centerline CD in **Figure 1** are investigated to explain the effects of tie bars.

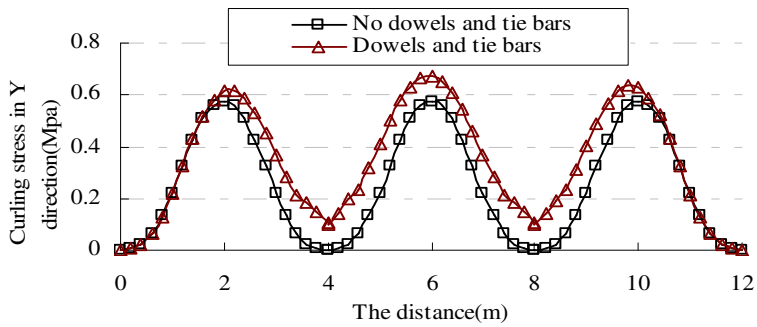

a) The vertical displacement

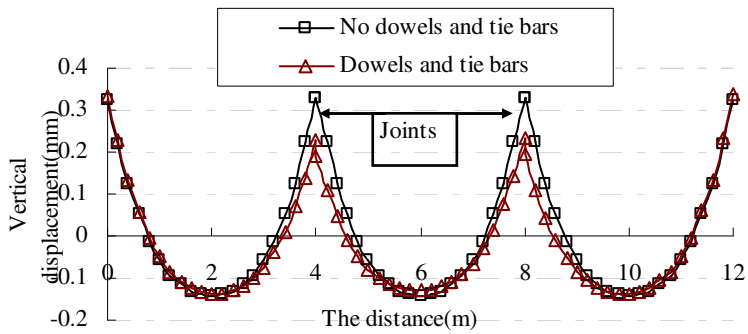

b) The stress in Y direction

Figure.4 The calculated results by FEM along line AB

The 3DFEM computed distributions of the stress in Y direction and vertical displacement along line AB are shown in **Figure 4**. From **Figure 4a)** the dowel bars contribute to reduce vertical displacement at joints, but the effects of dowel bars on whole slab curvature are not obvious. From **Figure 4b)** due to the contribution of dowel bars to restrain slab curling the curling stress at joints increases and the curling stress in whole slab increases also.

The transverse centerline CD in **Figure 1** crosses the longitudinal joints

including tie bars, therefore the line CD is selected to illustrate the effects of tie bars on curling. The 3DFEM computed distributions of stress in X direction and Vertical displacement along CD are shown in Figure 5. From Figure 5 it can be found that the effects of tie bars on slab curling is very little and can be ignored.

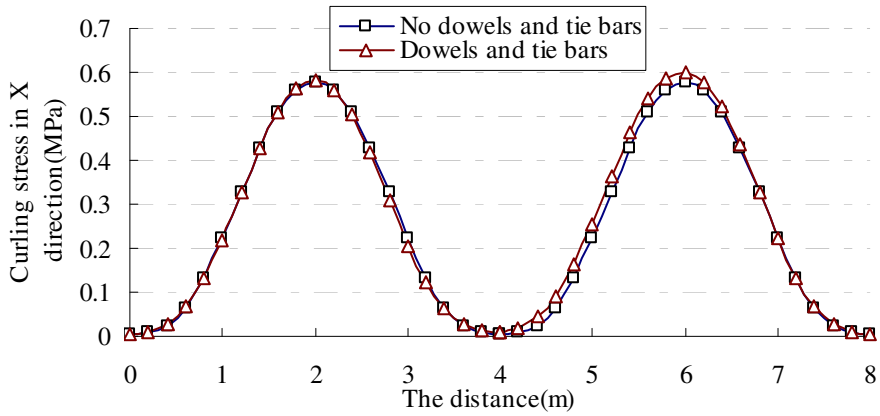

a) The vertical displacement

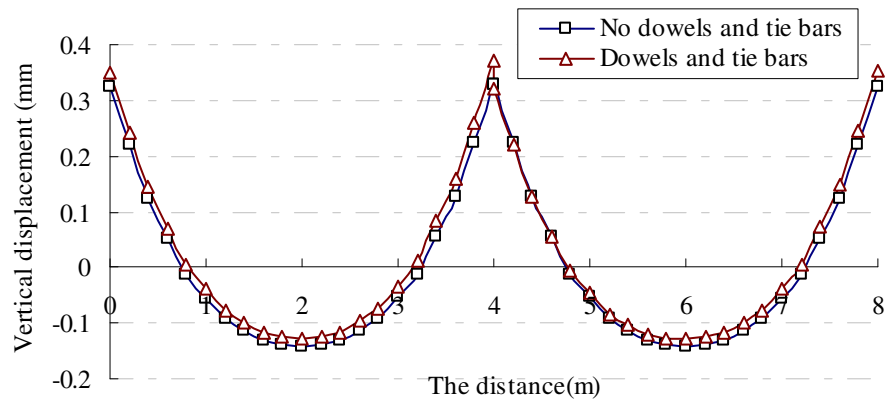

b) The stress in Y direction

Figure.4 The calculated results by FEM along line CD

CONCLUTIONS

A 3D finite element model is developed to investigate the effects of dowel and tie bars on curling in concrete pavement slab. After the 3DFE model is validated, the results of dowel and tie bars are compared with the results of no dowel and tie bars. From the comparison indicate that the effects of dowel bars on slab curling is obvious and dowel bars will restrain the curling deflection and increase the stress in whole slab, especially on joint, and the effects of tie bars is not obvious and can be ignored.

REFERENCES

B. Chubane and M. Tia (1995). "*Nonlinear temperature gradient effect on maximum warping stresses in rigid pavements.*" *Transportation Research Record*, 1370, 11–19.

Brucea.S. (2002). *Why slabs curl? PartI and PartII.*" *Cement and Concrete*

Research, March.

E. Masad, R. Taha, and B. Muhunthan.(1996). "*Finite-element analysis of temperature effects on plain-jointed concrete pavements." Journal of Transportation Engineering*, ASCE, 122(5), 388–398.

Gergis W. William S., N. Shoukry. (2001). "*3D Finite Element Analysis of Temperature-Induced Stresses in Dowel Jointed Concrete Pavements." The International Journal of Geomechanics*, vol.1(3), 291–307.

I.E. Harik, P. Jianping, H. Southgate, and D. Allen.(1994). *'Temperature effects on rigid pavements.' Journal of Transportation Engi neering,* ASCE, 120(1), 127–143.

Masad E., Taha R., Muhunthan B. (1996). *'Finite-element analysis of temperature effects on plain-jointed concrete pavements.' Journal of Transportation Engineering.*, ASCE, 122(5), 388~398.

YAO Zukang. (1981). *'The Curling Stress Analysis in Cement Concrete Pavement.' Journal of Tongji University,* 1981.03: 44~54.

Experimental Analysis of Interface Bond Performance of UTW

Yu-qiang Huang[1], De-cheng Feng[1], Xin-kai Li[1], and De-you Feng[1]

[1]School of Transportation Science and Engineering, Harbin Institute of Technology, Harbin 150090, China

ABSTRACT

The interface bond condition between the concrete panels and asphalt pavement influences the stress status of Ultra-Thin Whitetopping (UTW) slabs. Therefore, it's necessary to understand the performance of interface bonding between the thin concrete slabs and old asphalt pavement. Previous researches mostly used straight sniping experiment or wedge split experiment to evaluate the interface bond condition; however, those tests do not represent the actual bonding behavior between UTW slabs and asphalt pavement sufficiently. In this paper PCC-AC composite beams were designed and cast and were subjected to three point loading test. The Crack Mouth Opening Displacement (CMOD) curves and Mid-span deflection-Load curves were collected through the experiments of different bond conditions. By comparison of results obtained from testing beams with different interface conditions, it was proved that this test can be used to evaluate interface bonding conditions of UTW pavements.

Key words: UTW; interface bond.

INTRODUCTION AND BACKGROUND

Ultra-thin whitetopping (UTW) is a rehabilitation technique for distressed asphalt concrete (AC) pavement, usually consisting of constructing a thin layer of concrete slabs (50-100mm) on top of the AC pavement (Charles J. Churilla. 1998). In total, 313 projects comprising of almost one million square yards of UTW in 35 states were constructed through the end of 2002 in the United States (ACPA.2003). Good field performance records indicated that UTW can be an effective rehabilitation technique for deteriorated asphalt pavement.

Previous researches howed that interface bonding between the UTW slabs and the asphalt pavement played a major roles in affecting the UTW performances. Interface bonding reduces stresses in the concrete slabs significantly by making the two layers as a monolithic pavement system.(Sanford et al.1992). The service levels of UTW pavements are largely dependent on the existence and maintenance of sufficient interface bond strength between the concrete and asphalt layer (Chung-Lung Wu et al.2007).

Because of the much smaller size of UTW slabs, when the wheel load travels on one edge of the slab, the other side of the slab tends to move up, which would cause tensile stresses on the interface. In the meanwhile, the interface under the loads is under compression (Figure.1). Interface bond strength between the asphalt layer and UTW is one of the most important factor in affecting UTW pavement performance.

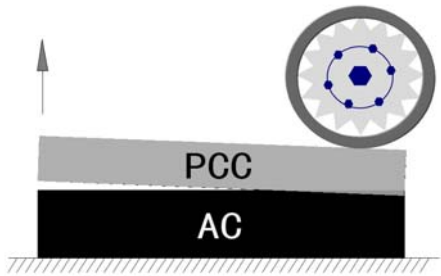

Figure.1. Performance of UTW with wheel load

EXPERIMENTAL PROGRAM

Many test methods have been used for evaluating interface bond strength, including straight pull experiment, straight snips experiment, three points bending resistance experiment, four points bending resistance experiment and wedge split experiment (SONG Yu. 2005).

In the straight pull experiment setup, specimens need to be perforated for fixing, which will result in strength reduction. As a result, asphalt concrete will be damaged easily at the perforated locations. Therefore, , straight pull experiment is not applicable for asphalt concrete specimen.

The principal theory of three point-bending resistance experiment and four-point bending resistance experiment is to simulate the layer structure of pavement. Load is placed at the center of the specimen and the interface movemenst caused by the deflection are then calculated. However, neither of two test methods can simulate the interface contact between UTW and asphalt realistically since the test result is mostly impacted by level friction. The same situation is also relevant to straight snips experiment.

In the wedge split experiment, a rectangular slot is cut at one side of the specimen along the interface. Loading is then applied at the rectangular slot to split the specimen in order to evaluate the resistance to shearing. However, the cracking behavior of interface contact is not the same as that of UTW.

In order to simulate the interface bonding behavior between UTW and asphalt pavement more realistically, a new test method was developed in this study. As presented in Figure 2, the test procedure include the following:

- Make PCC-AC composite beam in the size of 400×100×100mm
- Conduct three point bending resistance experiment
- Take the measurements and record of load, span centre deflection and cracking process of the PCC-AC composite beam
- Study cracking behavior under different interface bonding conditions.
- The distance between pivot and joint face is 150mm.

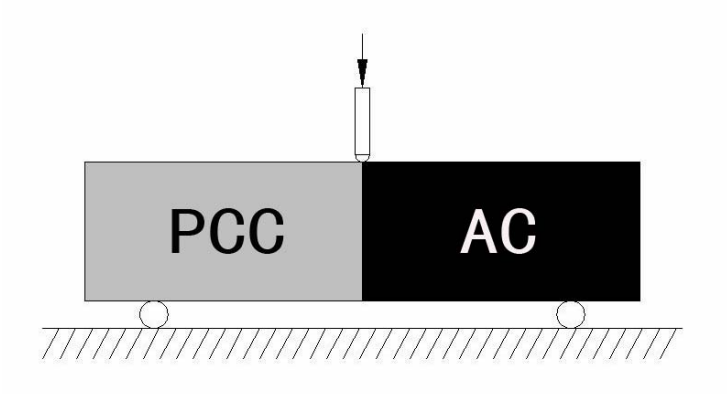

Figure.2. Graphic of PCC-AC composite beam test

MATERIAL

There are two gradations for asphalt mixture：AC-13I and AC-20I. No. 90 petroleum asphalt for pavement is used in this experiment. The performance of the asphalt mixture has been verified to meet specification requirements.

Typical mixing proportions for concrete were used for UTW. The water-cement ratio is 0.30, with a 28-day flexural strength 6.56Mpa, also meeting requirement.

INTERFACE TREATMENTS

The contact surface of asphalt layer was processed to create four different surface conditions to simulate interface bonding behaviors under different surface conditions (Table.1).

Table.1. Surface treatments

Surface treatments	Original	Tack coat with macadam	Milled	Notched
Fig				

EXPERIMENT PROCESS

The asphalt concrete specimens are cast in vibration compaction. It is concreted for 28 days before subjected to the three points loading experiment using a MTS machine. Before loading, the wire-type displacement transducer is attached to one side of the composite beam to measure the cracking course. (Figure.3)

Figure.3. Experiment process

EXPERIMENT RESULTS

Table.2. Experiment results

Surface treatments	Crack position	Cracking surface condition	Crack	cracking surface

Original	Bonding interface	smooth		
Tack coat with macadam	Bonding interface	smooth		
Milled	AC (close to interface)	rough		
Notched	AC (close to interface)	rough		

COMPARISONS OF THE AC-13I AND AC-20I SPECIMENS

As shown in Figure 4, for the original asphalt surface, the loads increase rapidly in both tests of AC-13I and AC-20I. The peak load values appear at the point where width of crack is about 1mm. After that, the values drop quickly. The specimens lost the ability to carry loads when the width of crack is about 4mm. The limiting load of AC-20I specimen is higher than that of AC-13I specimen because the average grain size of AC-20I is coarser and its surface pore is larger than AC-13I. As a result, more cement mortar entered the structure of AC-20I ,which resulted in enhanced interface bonding.

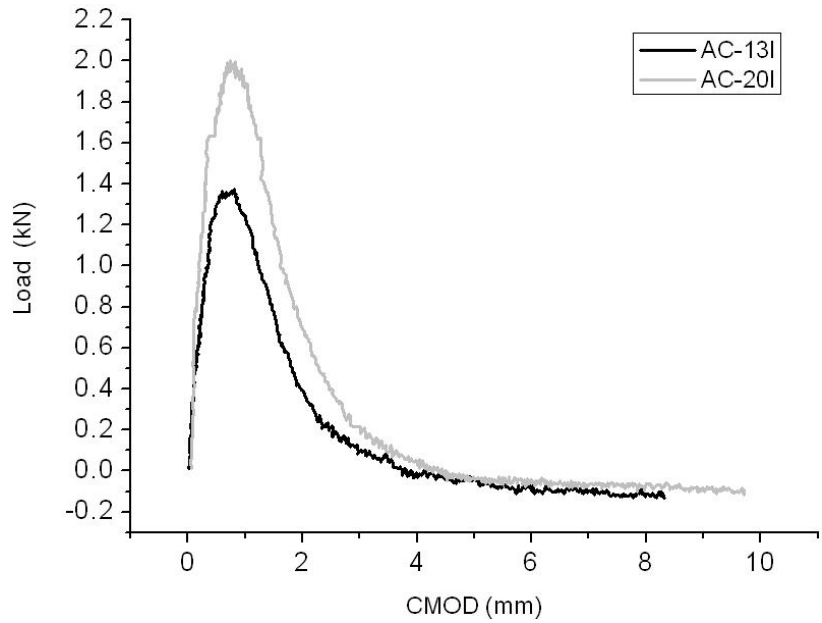

Figure.4. CMOD-Load curve of original surface

In the condition of tack coat with macadam (Figure.5), crack appears at the tack coat and the cracking surface is smooth. The concrete connect tightly with the macadam. The limiting load of AC-20I specimen is higher than AC-13I specimen, appears when the crack width is about 3.5mm. This is mainly caused by the rougher surface and larger surface pore of AC-20I . As a result, the bonding area of AC-20I is larger and lead to a stronger interface bonding.

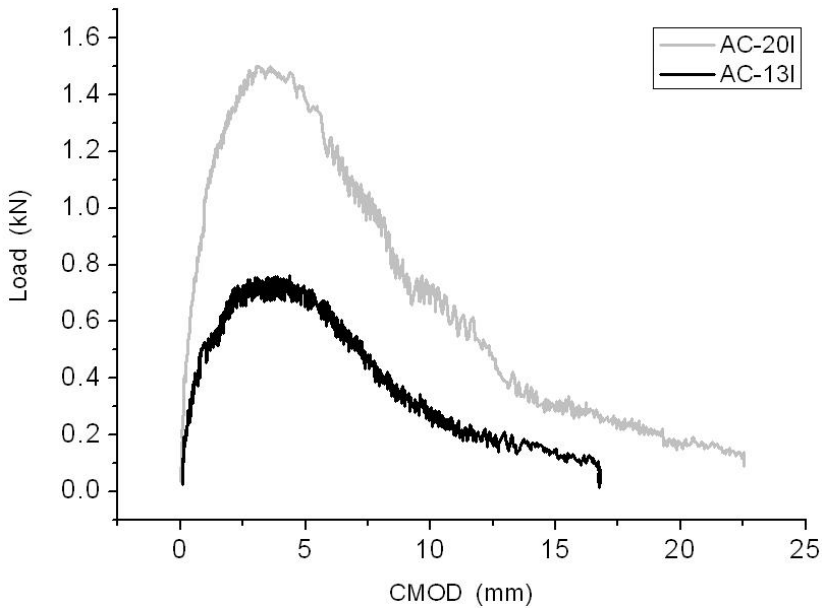

Figure.5. CMOD-Load curve of tack coat with macadam

CONTRAST BETWEEN DIFFERENT SURFACE TREATMENTS

In the condition of AC-20I specimen, CMOD-Load curve fig (Figure.6) and midspan deflection-Load curve fig(Figure.7) with different Surface disposes as follow:

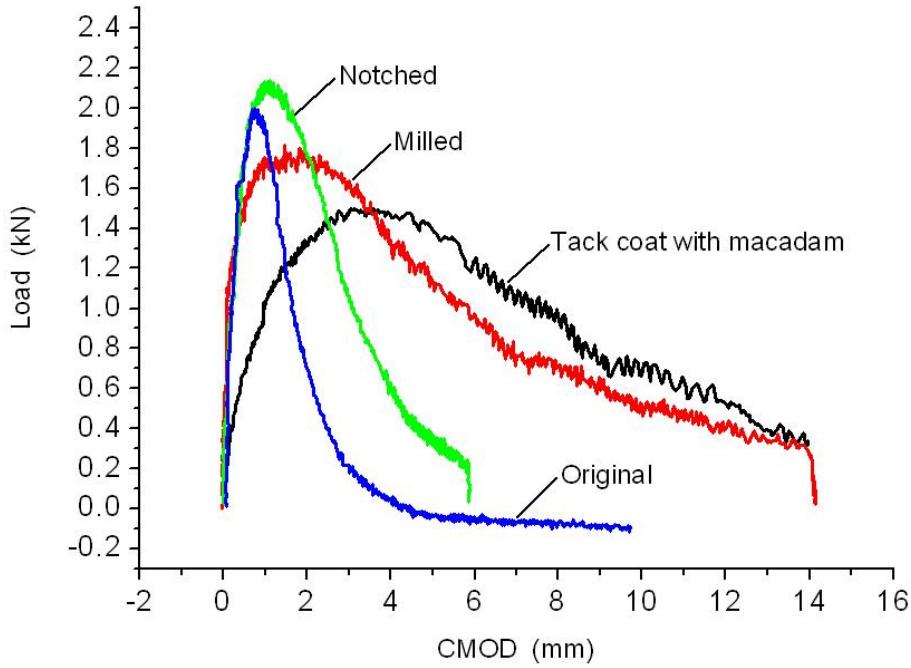

Figure.6. CMOD-Load curve

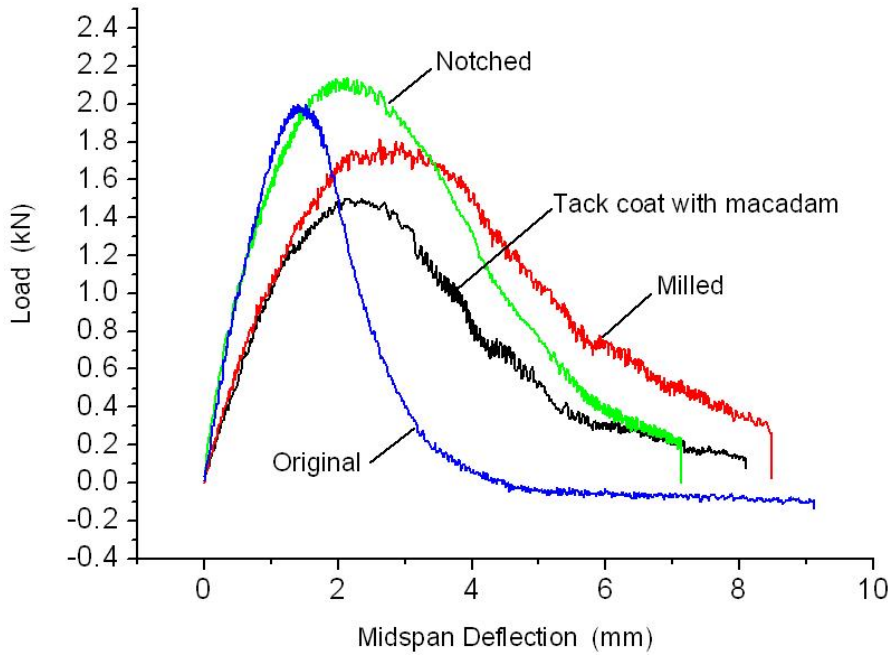

Figure.7. Midspan deflection-Load curve

Interface treatments increase the breaking energy of the specimen and reduce the break speed for the higher interface bonding strength. In the case of specimens with original interface, the load peak value appears very early and the break speed of interface is very fast. Interface contact conditions have a major effect on the stress condition of the pavement structure (JI XIAO-ping et al.2007).

For specimens with milled and notched surfaces, the failure occured in the asphalt concrete. Those crack curves represent the failure performance of asphalt concrete but not the interface. In these two cases, the bonding strength is higher than the tensile strength of asphalt mixture.

For specimens treated by tack coat with macadam failures occurred at the interface. Its interface failure speed is higher than those that with original surface. The interface bond strength depends on the strength of tack coat. When the bond strength of tack coat exceeds the tensile strength of asphalt mixture, the specimens will fail in the asphalt mixture.

CONCLUSIONS

Through comparisons of different tests for evaluating interface behavior, such as straight sniping or wedge split test, the three point composite beam test is designed. Different interfaces are considered for this experiment. Through the experimental analysis the following conclusions can be drawn.

1) Three point beam test is capable of evaluating the interface bond conditions through experiment results.

2) From test results observed, the bigger surface pore and roughness of AC will increase the bond area of interface of AC and PCC, which result in a stronger bonding.

3) Treating asphalt concrete surface with different modes can improve the interface bonding strength, especially the interface with milled and notched surfaces.

REFERRENCE

American Concrete Pavement Association (ACPA).(2003). “UTW Scores A Million.” *Concrete Pavement Research & Technology*

Charles J. Churilla. (1998). “Ultra-Thin Whitetopping” FHWA *Public Roads*. 62(2)

Chung-Lung Wu, Mang Tia , and Bouzid Choubane. (2007).“Forensic Investigation of Ultrathin Whitetopping Pavements in Florida,” *Journal of performance of constructed facilities © ASCE*

JI Xiao-ping, LI Bing, WANG Yu.(2007). “Influential analysis of dynamic performance of asphalt pavement under different interlayer touch condition,” *Technology & Economy in Areas of Communications*

Sanford P. LaHue and Robert J. Risser, Jr.(1992). “Ultra-thin concrete overlay supports truck loads.” Arlington Heights, IL

SONY Yu.(2005). “Research on the test and evaluation method of combinatition state between surface course and base course in asphalt pavement.” *Dissertation for the master degree in engineering*. Harbin Institute of Technology

The Analysis of the Correlation between International Roughness Index and Body Ride Comfort

Xiangshen Hou[1], Xuerong Liang[2], Songlin Ma[1], and Wanghua[1]

1 School Of Transportation Science and Engineering, Harbin Institute of Technology, Harbin,China;Tel.(0086)451-86282840;Fax(0086)451-86283779;Email:houxiangshen@126.com

2 Third Railway Survey and Design Institute Group Corporation, Tianjin,China;Tel.(0086)22-26178948;Fax(0086)22-26753108;Email:liangxuerong0825@163.com

ABSTRACT

It's generally accepted that there is good correlations between International Roughness Index (IRI) and body ride comfort. However, the study in this paper has discovered that the road displacement frequency power spectrum densities are not quite corresponding to the IRI. This paper establishes the body-vehicle vibration model of 3 degree of freedom as the model to calculates a_w as evaluation parameter, and analyze systemically the relationship between IRI and human body ride comfort. It has been concluded that the IRI can't reflect the differences of the road roughness and a_w is a better parameter of the ride comfort.

KEYWORDS

Body-vehicle Vibration Model, Road Evenness, IRI, Body Acceleration, PSD

FOREWORD

To convert the different road evenness indexes, the World Bank organized the international study group which included the experts of Brazil, England, U.S., France, and others in 1982. Through many researches and testing, the International Roughness Index (*IRI) was developed* to evaluate the road evenness level (Li, 2002).

The IRI adopts mathematics model to simulate quarter vehicle, running at the road profile with a velocity of 80km/h. IRI is the displacement accumulation of the vehicle suspension, and the effect of vibration frequency is not taken into account. However, body ride comfort is directly related to vibration frequency (Zhao, 2000).

For the description of the road evenness, GB7031-86 is adopted, and denotes the road evenness with road displacement dimensional frequency *PSD,* its detailed form is in Formula (1) (GB7031-86, 1986).

$$G_d(n) = G_d(n_0)\left(\frac{n}{n_0}\right)^{-w} \quad (1)$$

Where n is the dimensional frequency, namely the reciprocal of the wavelength, (number of the wave in one meter), m^{-1};

n_0 is reference dimensional frequency, $n_0 = 0.1 m^{-1}$;

$G_d(n_0)$ is the PSD of the road displacement under the reference dimensional frequency, namely road roughness coefficient, $m^2/m^{-1}=m^3$;

w is the waviness parameter, which decides the frequency structure of the PSD of the road; normally assumed to be 2. It means that the scope of PSD is uniform.

From analysis of real road profile of some road sections, it is observed that w isn't a constant. The value ranges from 1.6 to 2.4, with an average value of 2.0. Figure 1 shows the PSD of three real road profiles.

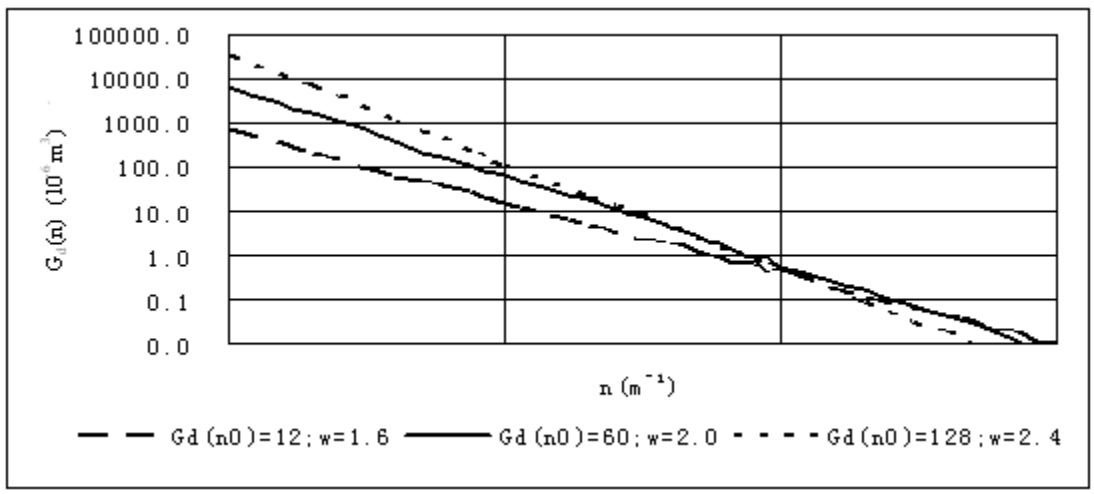

Figure 1. The relationship between PSD and n

The result in Figure 1 also shows that frequency characteristics of PSD is not constant.. IRI can't denote the ride comfort of the passenger.

EVALUATION OF THE HUMAN BODY RIDE COMFORT

Currently, the most popular evaluation standard for the human body vibration is ISO 2631-1:1997(E) ***ISO2631-1 Mechanical Vibration and Shock Evaluation of Human Exposure to Whole-Body Vibration-Part1: General Requirements*** which is issued I 1997. The standard presents a frequency response range between 0.5~80Hz, and within this frequency range the human body has different sensitivity degrees to different frequencies. To the vertical vibration, the frequency weighted function is close to the Formula (2).

$$w(f)=\begin{cases}0.5 & (0.5\le f\le 2)\\ \dfrac{f}{4} & (2<f\le 4)\\ 1 & (4<f\le 12.5)\\ \dfrac{12.5}{f} & (12.5<f\le 80)\end{cases} \tag{2}$$

Filtered through the frequency weighted function ($w(f)$), the real acceleration function $a(t)$ can be converted into frequency weighted acceleration function $a_w(t)$, which is related to human body ride comfort. In the whole time of vibration analysis, it can calculate the total effect of the vertical vibration to the human body according to the next formula:

$$a_w=\left[\frac{1}{T}\int_0^T a_w^2(t)dt\right]^{\frac{1}{2}} \tag{3}$$

In ***General Requirements*** a_w is the standard of comfort level of the passenger. The detailed standard values are shown in Table 1.

Table 1 correlation between a_w and the human subjective feelings

a_w (m/s^2)	human subjective feelings
<0.315	comfortable
0.315~0.63	A little uncomfortable
0.5~1.0	uncomfortable
0.8~1.6	quite uncomfortable
1.25~2.5	Very uncomfortable
>2.0	Most uncomfortable

BODY-VEHICLE VIBRATION MODEL OF 3 DOF

To compare a_w with IRI, the body-vehicle vibration system is predigested to a 3 DOF model (Tao, 2004).

Premises of the model

(1) the tire and the road are in full contact with no separation
(2) the roll and pitch t vibrations are small and were not considered; only the vertical vibration is calculated
(3) the stiffness of the suspension, the tire and the chair are linear; the damp of the suspension and the chair are also linear to the comparative velocity; the damp of the tire is small and was not considered
(4) the human body is at the top of the vehicle axle, and is fixed

(5) there are rigid joints between the vehicle and the suspension

According to the premises, the predigested vibration model is shown in Figure 2:

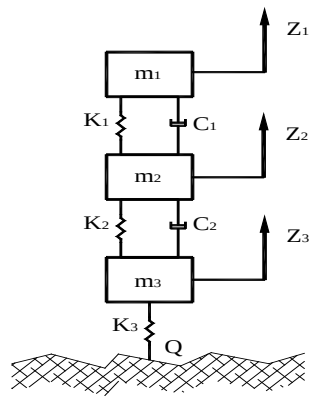

Figure 2.Human body-vehicle vibration model

c_1 is half of the damp of the chair (the vehicle is symmetrical between left and right, so the parameters of the model, such as m_1、 k_1 and c_1 is the half),

c_2 is the damp of the suspension, z_1 is the vertical displacement of the chair

z_2 is the displacement of the vehicle, z_3 is the displacement of the tyre

and Q is the road roughness.

Parameters of the Model

As presented by Pan Li, 2004, the following parameters of the human-chair system are used:

m_1=32.5kg; m_2=345kg; m_3=40kg; k_1=4950N/m; k_2=20000N/m; k_3=192000N/m; c_1=130N·s/m； c_2=1500N·s/m。

Establishment of the Vibration Differential Equation

The vibration differential equation of the model of 3 degree of freedom is:

$$\begin{cases} m_3 z_3'' + k_3(z_3 - Q) = c_2(z_2' - z_3') + k_2(z_2 - z_3) \\ m_2 z_2'' + c_2(z_2' - z_3') + k_2(z_2 - z_3) = c_3(z_1' - z_2') \\ \qquad + k_3(z_1 - z_2) \\ m_3 z_1'' + c_1(z_1' - z_2') + k_1(z_1 - z_2) = 0 \end{cases} \tag{4}$$

The road roughness Q is a discrete highness sequence ($[h_1, h_2, ...h_i...]$), so Equation (4) can be revolved with numerical method. First, it is necessary to reduce the derivative order of Equation (4). According to the definition of Formula (5), the Equation (4) can be converted to Equation (6):

$$\begin{aligned} u_1(t) &= z(t) = (z_1, z_2, z_3) \\ u_2(t) &= z'(t) = (z_1', z_2', z_3') \end{aligned} \tag{5}$$

$$u' = \frac{d}{dt}\begin{pmatrix} u_1 \\ u_2 \end{pmatrix} = \begin{pmatrix} 0 & I \\ -M^{-1} \otimes K & -M^{-1} \otimes C \end{pmatrix} \otimes \begin{pmatrix} u_1 \\ u_2 \end{pmatrix} + \begin{pmatrix} 0 \\ M^{-1} \otimes Q' \end{pmatrix} + \begin{pmatrix} 0 \\ M^{-1} \otimes Q \end{pmatrix} = \frac{d}{dt}(u_1, u_2) \tag{6}$$

This conversion increases the number of Equation (4), but it reduces the derivative order of Equation (4). With Runge-Kutta numerical method, the variable z_1、 z_2、 z_3 and z_1'、 z_2'、 z_3' can be resolved.

To solve for differential coefficient, the human body acceleration (a_{ti}), can be resolved from z_1'. The acceleration in frequency field can be available according to Flourier transform. Weighed in frequency field with the function $w(f)$ and transformed with Flourier contrary transform, frequency weighed acceleration sequence a_{wti} is available. Therefore, the human body total weighted root mean square acceleration is calculated as:

$$a_w = \left[\frac{1}{N} \sum_0^N a_{wti}^2) \right]^{\frac{1}{2}} \tag{7}$$

In the formula, the letter 'N' is the number of the disperse point in the stochastic sequence of the weighed acceleration.

COMPARISON AND ANALYSIS BETWEEN IRI AND HUMAN BODY ACCELERATION

Frequency parameter *w* decides frequency structure of PSD, and the human body ride comfort has different susceptivities for different frequency structures. In order to compare IRI and weighted root mean square acceleration, this paper separately calculates the values of IRI and a_w when the frequency parameters are either the same or different.

Frequency parameters are the same

The factors that affect human body ride comfort are vibration frequency and acceleration slope. When the frequencies are the same, the frequency structures of PSD are the same, there is one-to-one relationship between IRI and a_w.

Based on the real road profile, the results of IRI and a_w (when w=2), are shown in Table 2 and Figure 3.

Table 2 The value of IRI and a_w when w=2

$G_d(n_0)\times 10^{-6}\mathrm{m}^2/\mathrm{m}^{-1}$ $n_0=\mathrm{m}^{-1}$	*IRI* (m/km)	a_w ($\mathrm{m/s}^2$)
8	1.5	0.11
17	2.2	0.15
33	3.0	0.20
60	4.2	0.27
123	6.1	0.41
239	8.7	0.58

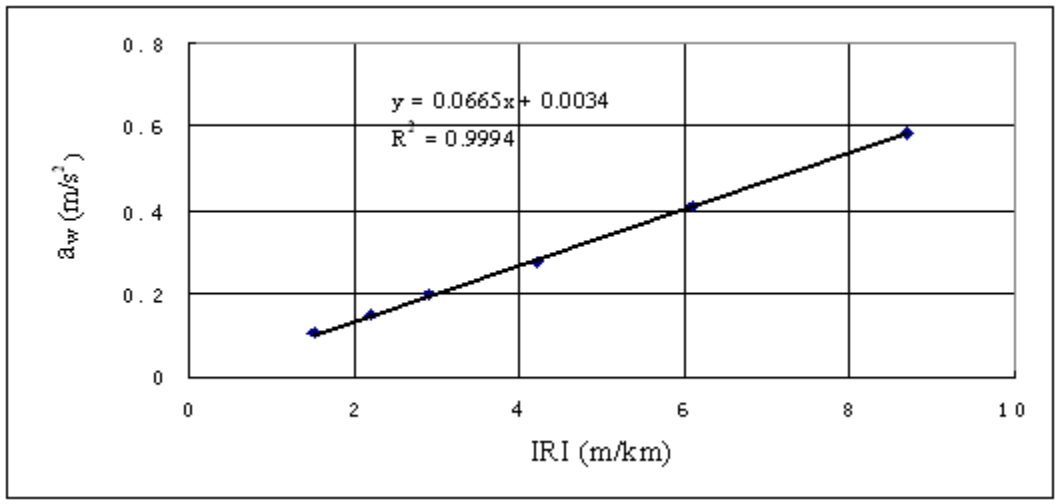

Figure 3. The relationship between a_w and IRI when w=2.

As shown in Figure 3, IRI and a_w have linear correlation when the frequency parameters are the same and the frequency structure is constant. In this case, IRI can reflect the human ride comfort.

Frequency parameters are not the same

The analysis of the real road profile shows that the frequency parameters are always different. When the frequency structures of the PSD are different, there isn't one-to-one relationship between IRI and a_w. For each IRI value, there can be some different a_w values. Choosing five different road sections with the same IRI (IRI=3.0) and five different frequency parameters (w=1.6，1.8，2.0，2.2 and 2.4), this paper calculates the five values of a_w. The results are shown in Table 3 and Figure 4.

Table 3 The different a_w with the same *IRI*

w	$G_d(n_0)\times 10^{-6}$	a_w

(f=1)	(m^2/m^{-1})	(m/s^2)
1.6	18	0.140
1.8	23	0.166
2.0	32	0.199
2.2	37	0.224
2.4	45	0.247

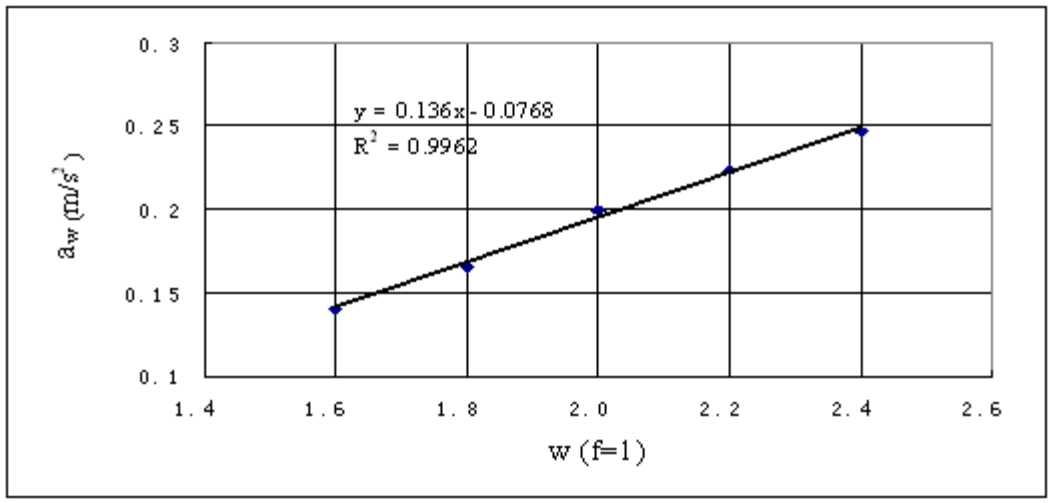

Figure 4. Relationship between a_w *and w* when IRI are same

From the results, there are different values of a_w to the same *IRI*. When the frequency parameters are different, IRI can not reflect the ride comfort of the passenger.

CONCLUSION

This paper establishes the human body-vehicle vibration model of 3 degree of freedom and vibration differential equations, calculates the *IRI* and human acceleration based on the *PSD* of the road, and analyzes the correlation of *IRI* and human acceleration. The results show that *IRI* can not reflect the ride comfort of the passengers because the frequency parameters are not the same.

REFERENCES

GB7031-86(1986).The Input Of Vehicle Vibration—The Express Method Of Pavement Roughness.Chinese Stangdard, 1986.

Li Taoling, Sun Lijun(2002). Simple Understand to the Concept of Road Roughness. Shang Hai Highway, 2002 (12):57~60

ISO2631-1(1997). Mechanical Vibration and Shock Evaluation of Human Exposure

to Whole-Body Vibration-Part1: General Requirements.1997:1~30

Pan Li(2004). The Modeling and Simulating of Vehicle based on People-Chair System. Master's degree dissertation of Zhejiang Institute of Technology.2004:8~70

Tao Xianghua, Huang Xiaoming(2004).Three-Mass Vehicle Model of People–Vehicle-Road Interaction. Transportation Engineering Transaction, 2004(3):11~15

Zhao Jihai, Wang Zheren, Guan Chaoli(2000). Measurement Analysis and Application of the Road Roughness. Publishing Company of Beijing Institute of Technology. 2000:17~20

The Application of Anti-rutting Agent on Improving the High-temperature Stability of Asphalt Pavement

Ping LI[1], Hui-Shan LI[1], Han-Qing LIU[1] and Yu QIAN[2]

[1]College of Civil Engineering, Lanzhou Univ. of Tech., No.287 Langongping Street, Lanzhou, ST 086-0931;PH (086) 0931-2755683;Fax (086) 0931-2976327; Email: liping@lut.cn
[2]Tianhong Communications Tech. Co., Ltd., No.14 Chang'an Street, Xi'an, ST 086-029; PH (086) 029-83273199; Email: Qianyu@126.com

ABSTRACT

In this study a new anti-rutting agent (ARK-1) was introduced to analyze effect on pavement performance of asphalt mixture. Taken three gradations of AC-13 mixture with ARK-1 and without ARK-1 as investigation objects, high-temperature and water stability as well as cracking resistance at low-temperature were measured respectively. The results of tests show that the ARK-1 is feasible to improve pavement performance of asphalt mixture and its influence on high-temperature stability of asphalt mixture is obviously superior to that on water stability and cracking resistance at low-temperature. A project example of Louding freeway between stations 35+450 and 36+450 was proved that the costs of pavement with the ARK-1 would be more economical than that of pavement with SBS-modified asphalt binder.

INTRODUCTION

Largely northwest regions of China belong to arid or semi-arid climate, where the air temperature in July and August is more than 30℃ usually, and surface temperature of asphalt pavement may be up to more than 50℃ due to absorbing energy more than releasing energy of conduct, convection and radiation. As a result, rutting will be rapidly occured and developed at high temperature under heavy truck traffics. Therefore it is necessary to effectively and economically improve high-temperature stability of asphalt mixture.

In recent years there are many researches to improve high-temperature performance of asphalt mixture, shown in previous work by the authors (Wu and Xu, 2005; Wang *et al*., 2007; Xiao *et al.*, 2007; Xu *et al.*, 2004). Many studies were uneconomical or ineffective, or difficult to construction technique. A new anti-rutting agent (ARK-1) mixed with asphalt mixture, was studyed in laboratory. In order to verify ARK-1 effect on rutting resistance, comparing studies between ARK-1 and SBS-modified asphalt binder were done in Luoding freeway which was constructed in July 2005.

MATERIALS AND EXPERIMENTAL METHODS

Asphalt Binder/Aggregate Tests

Asphalt binder used in this study was AH-90 produced by the Lanlian oil refinery. All of aggregates were crashed sandstone collected from a stone quarry at Anning area in Lanzhou city where sandstone has higher intensity and hardness for pavement construction. Mineral powder used in tests could be obtained after the sandstones were levigated.

Three gradations of AC-13 including upper limit, middle value and modified lower limit (hereinafter referred to "lower limit") were analyzed in this study and gradation compositions of mixture were listed in Table 1.

Table 1. Gradation compositions of mixture

Items	Mesh passing (%)									
Sieve size (mm)	16	13.2	9.5	4.75	2.36	1.18	0.6	0.3	0.15	0.075
Upper limit	100	100	85	68	50	38	28	20	15	8
Middle value	100	95	76	53	37	26	19	15	10	6
Lower limit	100	90	68	47	29	25	22	10	8	6

ARK-1 Tests

ARK-1 is a kind of black solid-state particles which contains more than 95 % fiber polymers and less than 5 % fillings. Its density is about 0.91 ~ 0.98 g/cm^3 and its size is about 2 ~ 4 mm by using sieving test and its melting index (MI) is more than 0.1 g/10mins to ensure enough melt flow rate at 190 ℃ and under 50kN load pressures during mixing procedure. Softening point of ARK-1 is between 150 ℃ and 170 ℃.

Controlling the homogeneity and storage of mixture with ARK-1 is much simpler than that of mixture with SBS or SBR. When mineral aggregates are heated up to 170 ~180℃, the amount of ARK-1 is directly entered into heated mineral aggregates and mixed continuously till all ARK-1 is completey melted in heated mineral aggregates. Compared with common asphalt mixture, ARK-1 mixture has the same method for controlling quality, storage and transportation except that the whole mixing procedure of ARK-1 mixture takes about four minutes longer than that of no ARK-1 mixture does.

Wheel Tracking Tests

The specimens were mixed in the optimal asphalt contents and compacted by the Plate Compactor. Demansion of specimen is 300×300×50mm (three specimens per parallel control test) with 0%, 0.3 %, 0.4 % and 0.5 % ARK-1 (weight ratio of ARK-1 to aggregate). Slab of the compactor may pass on 24 times to and fro and 9 kN load pressures during compacting. In this study wheel tracking instrument was made by Changsha Yaxing Digital-control Co., Ltd.. And all wheel tracking tests were conducted at 60 ℃ (0.5 ℃ accuracy) and 0.7 MPa (0.05 MPa accuracy) to measure Dynamic Stability(DS) and rutting depth.

Water Stability and Cracking Resistance Tests

MARSHALL-Immersion Test and Indirect Tension Test under freeze-thaw (AASHTO T283) in this study were carried out to evaluate water stability of asphalt

mixture with ARK-1. The residual stability, indirect tensile strength and test strength ratio (TSR) of asphalt mixture at 25℃ (0.5℃ accuracy) were measured to determine if different ARK-1 contents would be beneficial for water stability.

Cracking resistance of asphalt mixture at low-temperature was conducted to measure flexural-tensile strength, stiffness modulus and flexural-tensile strain under 50mm/min of loading rate by using bending experiment.

RESULTS AND DISCUSSION

Results of the Marshall Tests

Marshall Stability and Flow Value of three gradations of AC-13 varying with ARK-1 contents are presented in Figure 1. The Marshall stability is gradually increasing and the flow value is gradually reducing with the increasing ARK-1 contents. Based on chemical analysis, heated ARK-1 can formed to some silky plastic fibre, which can reinforce interactions and improve adhesion ability among asphalt binder, aggregate skeleton and mineral power. The Marshall stability is obviously increased when ARK-1 contents are more than 0.3%.

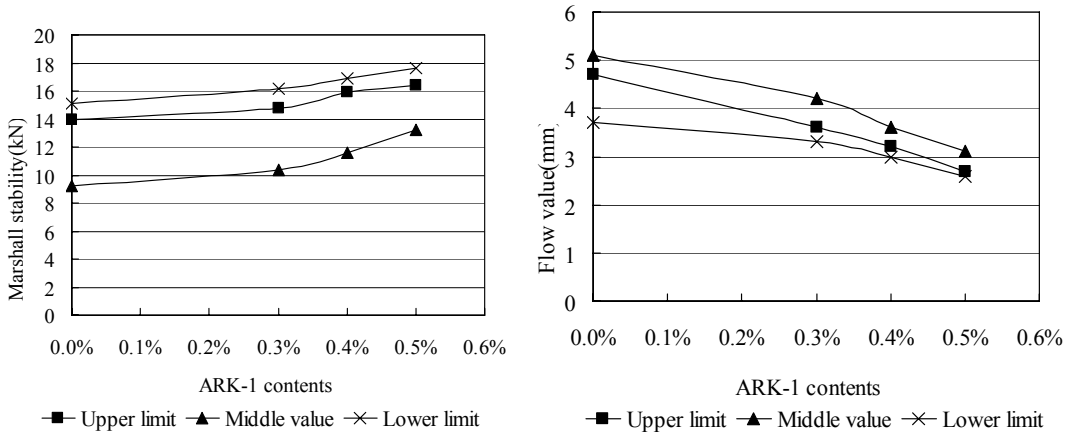

Figure 1. Results of the Marshall tests

Results of Wheel Tracking Test

Figure 2 shows Dynamic Stability and rutting depth of three gradations of AC-13 varying with ARK-1 contents. High-temperature stability of asphalt mixture with ARK-1 is obviously superior to that of asphalt mixture without ARK-1 because ARK-1 can improve elasticity of the asphalt mixture to resist permanent deformation. The results of Figure 2 that the rutting resistance of upper limit gradation is slightly better than that of the other two gradations are different from the results of Figure 1 that anti-deformation of lower limit gradation is better than that of the other two gradations. Sometimes it can be disucssed for us to absolutely rely on the results of the Marshall tests for evaluation the high-temperature stability of asphalt mixture. This opinion had been also given in previous work by the author (Sheng, 2001).

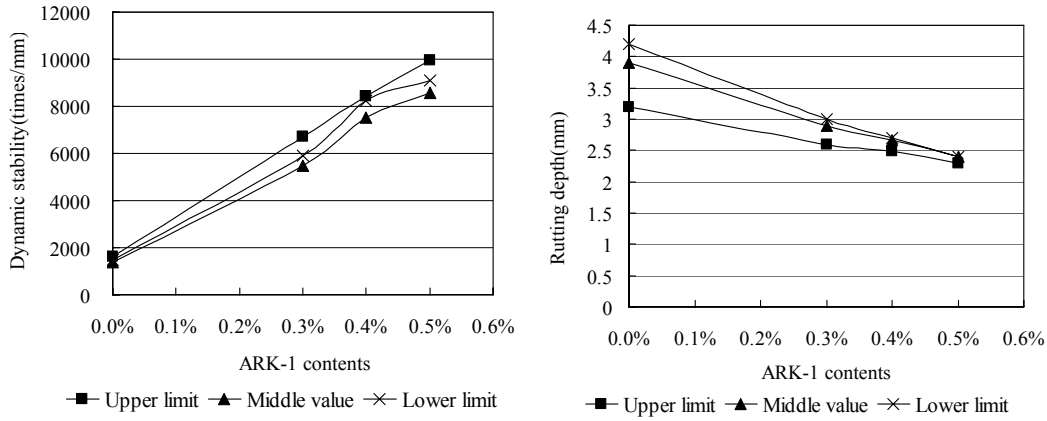

Figure 2. Results of the wheel tracking tests

Results of Water Stability and Cracking Resistance Tests

Marshall Immersion Test

Results of Marshall Immersion Test are presented in Table 2. Variation of residual stabilities of all samples with ARK-1 is no as obvious as that of Marshall Stability. Although residual stabilities of any samples with ARK-1 are gradually decreasing, immersed Marshall Stability of all samples with ARK-1 are higher than those of samples without ARK-1 if compared with the same type of gradations. So ARK-1 is beneficial to the improvement of water stability of asphalt mixture.

Table 2. Results of immersion Marshall tests

Types	ARK-1 contents (%)	Marshall stability(kN)	Immersed Marshall stability (kN)	Residual stability (%)
Upper limit	0.0	13.9	12.7	91.0
	0.3	14.8	13.4	91.0
	0.4	15.9	14.2	89.4
	0.5	16.4	14.7	89.8
Middle value	0.0	9.2	8.3	90.2
	0.3	10.4	9.3	89.8
	0.4	11.6	10.5	90.6
	0.5	13.2	12.0	90.8
Lower limit	0.0	15.1	14.2	93.8
	0.3	16.2	15.0	92.5
	0.4	16.9	15.5	91.6
	0.5	17.6	16.2	92.2

Results of Freeze-thaw Indirect Tension Test

Results of freeze-thaw Indirect Tension Test are shown in Table 3. Before and after suffered freeze-thaw process, indirect tensile strengths of all samples with ARK-1 are higher than those of samples with no ARK-1 and test strength ratios (TSR) of all samples exceed 80%. Ductility of samples with ARK-1 has been enhanced although TSR of samples with ARK-1 is reducing under the freeze-thaw condition.

Table 3. Results of freeze-thaw splitting tests

Types	Items ARK-1 contents(%)	Splitting tensile strength before freeze-thaw (MPa)	Splitting tensile strength after freez-thaw (MPa)	TSR (%)
Upper limit	0.0	0.564	0.544	96.5
	0.3	0.821	0.772	94.0
	0.4	0.942	0.864	91.7
	0.5	0.956	0.883	92.4
Middle value	0.0	0.645	0.631	97.8
	0.3	0.891	0.806	90.5
	0.4	0.945	0.872	92.3
	0.5	0.925	0.837	90.5
Lower limit	0.0	0.802	0.780	97.2
	0.3	1.103	1.006	91.2
	0.4	1.145	1.085	94.8
	0.5	1.212	1.091	90.0

Results of Bending Test

Results of bending test are shown in Table 4. Flexural-tensile strengths and strains of all samples with ARK-1 are higher than those of samples with no ARK-1 and stiffness modulus of samples with ARK-1 are slightly lower than those of samples with no ARK-1 except few samples. Cracking resistance of samples with ARK-1 has been improved but not so obviously as high-temperature stability of asphalt mixture. 0.4% ARK-1 combined with asphalt mixture is the more available and economical contents to improve cracking resistance of asphalt mixture.

Table 4. Results of bending tests

Types	ARK-1 contents(%)	Flexural-tensile strength (MPa)	Stiffness modulus (MPa)	Flexural-tensile strain (με)
Upper limit	0.0	10.5	6122	1715
	0.3	12.5	6288	1988
	0.4	12.9	5690	2267
	0.5	13.1	5768	2271
Middle value	0.0	11.3	6734	1678
	0.3	13.2	6995	1887
	0.4	13.2	6209	2126
	0.5	13.7	6356	2149
Lower limit	0.0	12.4	8068	1537
	0.3	13.4	7232	1853
	0.4	13.8	6497	2124
	0.5	13.7	6558	2092

FIELD TESTS AND APPLICATION

Luoding freeway in the east of Gansu province is from Ning county of Qingyang city to Shibali of Anding region. This route is 57.898km long and design speed is 80km/h and subgrade is 24.5m wide including four 3.75m carriage ways,

3.0m central strip, 2.5m hard shoulder and 0.75m soil shoulder. In the design of pavement central strip and hard shoulder have the same pavement structure with carriage ways as shown in Table 5.

Table 5. The scheme of pavement structure

Structure layer	Material	Thickness(cm)
Upper layer	AC-16	4
Mid-layer	AC-20	5
Lower layer	AC-25	6
Upper base	cement stabilized gravel (5.5% cement)	34
Lower base	cement stabilized gravel (4% cement)	20

Two test sites were chosen in the 16th section of contracts situated in Taiping village of Huining town at Baiyin area. One test site (referred to"No.1") between stations 35+450 and 35+950 was constructed with 0.5% ARK-1 asphalt/ aggregate mix at upper layer and 0.3% ARK-1 at mid-layer. The other test site (referred to "No.2") between stations 35+950 and 36+450 was constructed with 6% (weight to weight ratio) SBS-modified asphalt binder/aggregate mix at upper layer and 4% SBS-modified asphalt binder/aggregate mix at mid-layer. The costs between ARK-1 and SBS-modified asphalt in the two test sites were analyzed in Table 6. 1

Table 6. The cost analysis ofARK-1 and SBS in the two test sites

Test sites	Layer	Admixture contents	Material costs (RMB)	Total costs (RMB)
No.1	Upper layer	0.5% ARK-1	￥265,400	￥573,600
	Mid-layer	0.3% ARK-1	￥308,200	
No.2	Upper layer	6% SBS	￥344,000	￥643,400
	Mid-layer	4% SBS	￥299,400	

The costs of upper layer and mid-layer in No.1 road could save 11% as cheap as those of the two layers in No.2 road. Rutting problems had not been observed in the two test sites after four hot summer seasons.

ARK-1 has much more application on highway construction due to its convenient storage and transportation, simple construction technology as well as lower costs than SBS-modified asphalt binder. For example, asphalt pavement with 0.4% ARK-1 at upper layer had been used in the section of steep slope road from Lanzhou to Lintao city. Many national trunk highways in Qinghai province, such as 109, 214, 215 and 227 routes, had utilized ARK-1 to improve the high-temperature stability of asphalt pavement.

CONCLUSIONS

Based on the laboratory work conducted and the field tests in this research, the following conclusions and recommendations are drawn:

1. ARK-1 can reinforce interactions among asphalts, mineral aggregates and powders, and can enhance flexibility of mixture to resist permanent deformations of pavement. So it is feasible to ameliorate pavement performance of asphalt mixture.

According to the results of the laboratory work, the influence of ARK-1 on pavement performance at high-temperature is obviously superior to that of ARK-1 on pavement performance at low-temperature and water stability.

2. ARK-1 has the simpler construction technique because it can be directly added into mineral aggregates and no obvious segregation problem has been observed during mixing procedure. The methods of storage and transportation of mixture with ARK-1 are similar to those of common asphalt mixture so that it is unnecessary to increase special equipments for pavement construction.

3. ARK-1 is often employed at upper and middle layer of asphalt pavement and propositional weight ratio of ARK-1 to aggregates is between 0.3%~0.5%. Compared with SBS-modified asphalt binder, asphalt pavement with ARK-1 can be save more than 20% costs of pavement construction per kilometer. Therefore, ARK-1 will have more application on pavement engineering.

ACKNOWLEDGMENTS

This research was supported by the Fund of Natural Science of Gansu Province (project number: 0803RJZA011) and by the Dr. Fund of Lanzhou University of Technology (project number: Z42001). The authors would like to thank the 16th project department of Luoding freeway for their technical support of test site.

REFERENCES

Shi-sheng WU and Xi-juan XU. (2005). "A study on performances of asphalt mixtures intermingled with anti-rut agent PR PLASTS." *J. Highway.* 15(1), 156-159.

International Conference on Transportation Engineering (ICTE). (2007). *Effect of asphalt pavement layers on rutting development*, Hui Wang, Qi-sen Zhang, and Ji-qing Tan.

Fei-peng XIAO, Serji Amirkhanian, and Hsein Juang, C.(2007). "Rutting resistance of rubberized asphalt concrete pavements containing reclaimed asphalt pavement mixtures." *J. of Materials in Civil Engineering.,* ASCE, 19(6), 475-483.

Application of Advanced Technologies in Transportation Engineering(AATT). (2004). *Use of a premium SBS modified bitumen to combat severe rutting in asphalt pavement*, Shi-fa XU, Zhao-hui ZHOU, and Pei-zhong QIAN.

Jing-an SHENG. (2001). "Section 4: High-temperature stability performance of asphalt mixture" *Pavement performance of asphalt and asphalt mixture*, The people's Communications Press, Beijing, 4.308-4.314.

Shake Table Test on Seismic Response of Non-free Liquefiable Site

X. Z. Ling[1]; X. Gao[2]; L. Tang[3]; P. J. Xu[4] and L. Q. Wu[5]

[1] Centre of Subgrade and Defense Engineering, Harbin Institute of Technology, Harbin 150090, China; PH (86) 451-86283173; email: xianzhang_ling@263.net

[2] Centre of Subgrade and Defense Engineering, Harbin Institute of Technology, Harbin 150090, China; email: klgaoxia1984@163.com

[3] Centre of Subgrade and Defense Engineering, Harbin Institute of Technology, Harbin 150090, China; email: hit_tl@163.com

[4] Centre of Subgrade and Defense Engineering, Harbin Institute of Technology, Harbin 150090, China; email: pjxuhit@163.com

[5] School of Civil Engineering and Architecture, Zhejiang University of Science and Technology, Hangzhou 310023, P.R. China; PH (86) 571-85070518; email: wuliquan1966@163.com

ABSTRACT

The evaluation of seismic site response is particularly useful for geotechnical engineers involved in the design of foundations in liquefiable sites. The shake table test is aimed at observing and analyzing the site response under different effects of shaking frequency and intensity. The soil profile consisted of a clayey layer over liquefiable sand over clay. The shaking sequence applied to the model was a small scaled, small and large El Centro motion ($a_{max,\ base}\approx0.15g$, time interval 0.006 sec; $a_{max,\ base}\approx0.15g$, time interval 0.02 Sec; $a_{max,\ base}\approx0.50g$, time interval 0.02 Sec). The aim is to observe and analyze the site response under different shaking frequencies and intensities. The tests reproduced the macro-phenomena of soil liquefaction induced by earthquake. The excess pore water and peak accelerations under different shaking frequencies and intensities are discussed. The research has enhanced our current understanding on the mechanism of seismic soil-pile interaction during the development of liquefaction.

KEY WORDS

Liquefiable site, soil-pile-structure interaction, shaking frequency, shaking intensity, shake table test

INTRODUCTION

Geotechnical earthquake engineers have recognized the importance of the seismic induced soil response for the ground motion analysis and seismic design of many geotechnical installations, such as pile-supported bridges, tunnels, and buried pipelines. It is well known that loose, cohesion-less sands and silts below the water table develop high pore water pressures or liquefy during strong earthquake shaking. The high pore water pressures may lead to a significant degradation of strength and stiffness in soils, which in turn, results in increased soil deformation. Additionally, wave propagation theory stipulates that soil layers modify the characteristics of the input seismic waves while they are traveling though it (Kobayashi et al., 1986),

therefore influencing the acceleration record in soils. So seismic design of geotechnical installations in liquefiable ground is very different from that in non-liquefiable ground. It is very necessary to understand the seismic response of non-free liquefiable sites.

Some investigations of the seismic induced soil response have been reported (Trifunac, et al., 1996, Su, et al., 2006, Rayhani, et al., 2008) in terms of a different research method. This paper focuses on the shaking frequency and shaking intensity on seismic site response, based on shake table tests.

The shake table test is an effective approach for studying seismic site response. An advantage of the shake table test is that it facilitates performing a physical parameter study, and thus allows the observation of the effects of parameters such as duration, shake intensity, and soil properties. This paper focused on the seismic response of non-free liquefiable site based on shake table tests to make quantitative predictions of the prototype response. The prototype is the collapsed Shengli Bridge in the 1976 Tangshan earthquake. The dynamic properties of non-free liquefiable ground under three cases were obtained, namely the scaled El Centro excitation with peak accelerations of 0.15g and El Centro waves with peak accelerations of 0.15g and 0.50g. The experimental results can help to improve the understanding of seismic interaction of the pile group-soil-bridge structure and the nonlinear behaviour of the structures.

SHAKE TABLE TEST

The experimental model is schematically illustrated in Fig.1. The shake table model test was performed using the MTS shaking table facility at the state's key laboratory for Disaster Reduction in Civil Engineering, Tongji University, Shanghai, China.

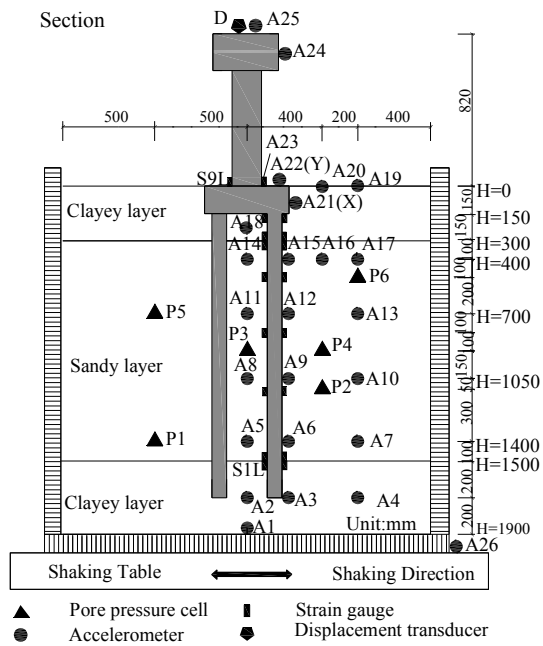

Fig.1 Side view of layout of instrumentation

The dimensions of the shaking table are 4m×4m, with maximum payload 25000kg. The laminar box is 2m long, 1.5m wide, and 2m high, developed by Wu (2004). The Shengli Bridge collapsed in the Tangshan Earthquake in 1976 is taken as the prototype for model simulation. The reduced scaling factor is 1:10. The model structure consists of a 2×2 pile group, pile cap, and column with a 360kg mass placed on it. They are prefabricated with micro concrete and galvanized iron wires. The pile-column is prefabricated with micro-concrete and the galvanized iron wires. The materials of the model ground used in this experiment are yellow sand and soft clay in Shanghai. The non-uniform coefficient is about 3.5. The average and maximum soil particle diameters are 0.35mm and 2mm, respectively.

The model was firstly subjected to white noise with a peak acceleration of 0.02g to find their natural periods of vibration. Then, it was shaken with a number of 1940 El Centro earthquakes conducted in series with sufficient time between shakes to allow for the dissipation of excess pore pressures. These earthquake motions were chosen because they contain different frequency content and shaking characteristics. The shaking sequence applied to the model was small and large El Centro motion (Case 1, $a_{max,\ base}\approx 0.15g$, time interval 0.006 sec; Case 2, $a_{max,\ base}\approx 0.15g$, time interval 0.02 Sec; Case 3, $a_{max,\ base}\approx 0.50g$, time interval 0.02 Sec). Comparison of the results from the three tests demonstrates the effects of shaking frequency and shaking intensity on seismic response of non-free liquefiable sites.

EXPERIMENTAL RESULTS AND ANALYSIS

Macroscopic Phenomena. Under the scaled 0.15g El Centro excitation, a little water appeared along the internal walls of the laminar box. Slight liquefaction occurred in the sandy layer. The column vibrated with very small amplitude. Under the 0.15g El Centro excitation, besides the same phenomena as the above, water appeared not only along the internal walls of the laminar box, but also around the pile cap.

Fig.2 Macro-phenomena under 0.50g El Centro excitation

Under the 0.50g El Centro wave, strong sand blasting, small sand hills, and water emitting occurred, with the whole sandy layer liquefied. The foundation settlement ranged from 3cm to 5cm, as seen in Fig.2-②, Fig.2-③ and Fig.2-⑥. Concrete peeling, bar bending, and tensile failures of the stirrups occurred at the bottom of the pier, shown in Fig.2-④. Some cracks appeared along the piles as shown in Fig.2-⑤. When the test finished, the whole foundation settlements ranged from 2cm to 5cm, seen in Fig.2-⑦.

Excess Pore pressure response. Fig.3 shows the input base motion for the three cases. Fig.4 shows the time histories of excess pore pressure at a depth of 0.70m for three cases, which shows a remarkable difference in response due to the shaking frequency and intensity. The excess pore pressure emerged at about 5.0 Sec in Case 1, much earlier than those in Cases 2 (about 12.0 Sec). The peak value, buildup rate, and dissipation rate in Case 1 is larger than in Case 2. It can be concluded that, the larger the shaking frequency, the less time it takes for the excess pore pressure to emerge, the larger the peak excess pressure, buildup rate and dissipation rate.

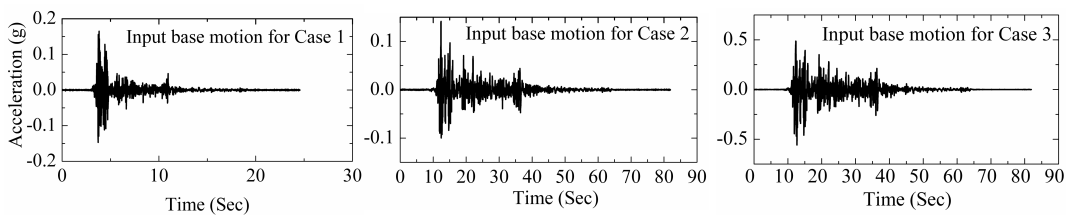

Fig.3 Input base motion for three cases

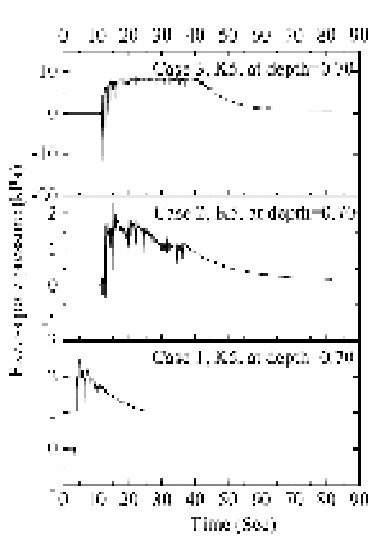

Fig.4 Time histories of excess pore pressure for K5

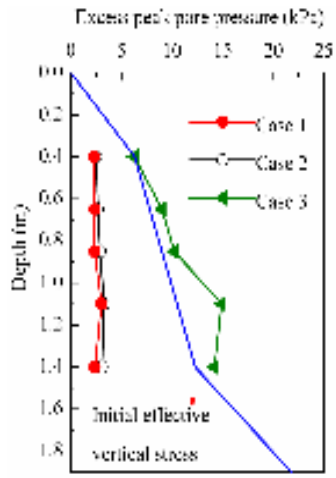

Fig.5 Variation of excess peak pore pressures with depth

It is seen from Fig.4 that the excess pore pressure emerged at almost the same time in Cases 2 and 3 (both at about 12.0 Sec). The peak excess pore pressure and dissipation rate in Case 3 are much larger than in Case 2. The excess peak pore pressure emerged later in Case 3 than in Case 2. It is observed that, the larger the shaking intensity, the larger the peak excess pore pressure and buildup rate, the later the peak excess pore pressure appears, and the slower the dissipation rate.

Fig.5 shows the variations of peak excess pore pressure with depth for three cases. It is clear that under large base input motion (case 3), the excess pore pressure near the ground surface of the sandy layer decreased after shaking. Large shear strain developed under low confinement and a slow dissipation process appear to be responsible for this phenomenon. Negative excess pore pressure developed in all three cases and in case 3 was the strongest, reaching values up to -15kPa. This may be the result of large shear strains with an un-drained dilative response of the liquefied soil. As indicated by the profiles of peak excess pore pressure in Fig.5, in which the solid line denotes the initial effective vertical stress of soil, the sand liquefied at all measured levels in Case 3, while the excess pore pressure ratios in Cases 1 and 2 are all less than 0.4. The excess pore pressure ratio is defined as the ratio between excess pore pressure and the initial effective vertical stress. It is obvious from Fig.5 that shaking frequency has little influence on the peak values of excess pore pressures; however, shaking intensity has the opposite effect.

Acceleration response. It is only when the earthquake is large enough to cause full liquefaction in the soil (case 3) that interesting observations can be made from the soil accelerations. The accelerations of soil between and around the piles were measured.

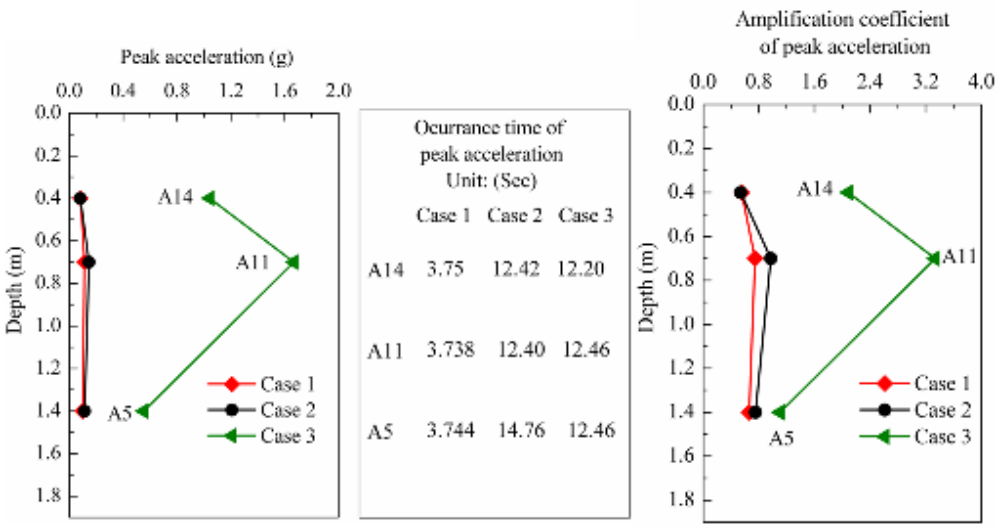

Fig.6 Variation of peak acceleration and amplification coefficient with depth for soil between the piles

Fig.6 shows the variation of peak acceleration and its amplification coefficient with the depth for sandy soil between piles. It was found that shaking frequency has little effect on the peak acceleration. Peak acceleration emerged later in Case 2 than that in Case 1. The shaking intensity has significant effect on peak acceleration. The acceleration records close to the sand surface decreased significantly due to the liquefaction process. Peak accelerations emerged at almost the same time when subjected to different shaking intensities.

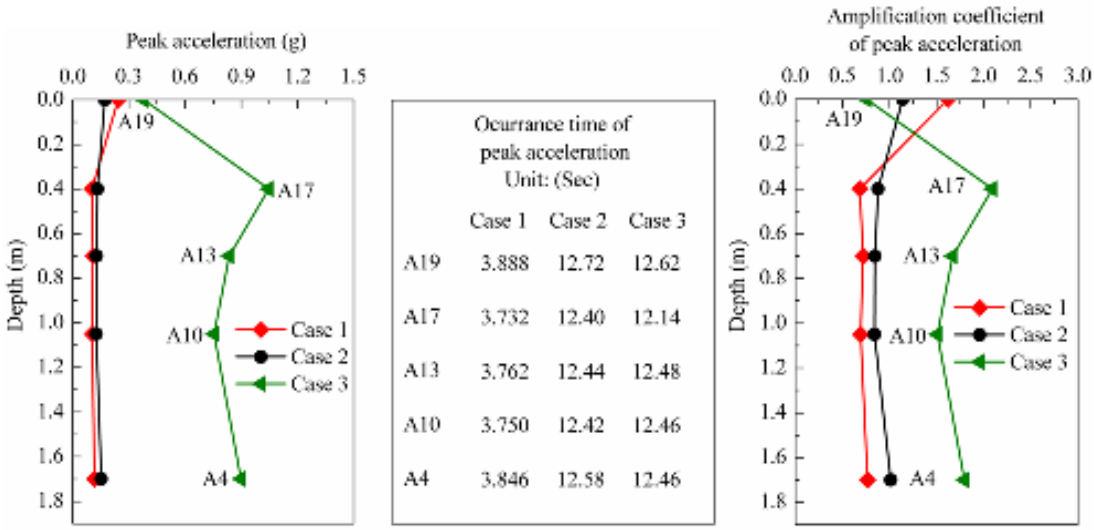

Fig.7 Variation of peak acceleration and amplification coefficient with depth for soil around the pile

As shown in Fig.7, the amplification coefficients of surface soil around the pile for Cases 1 and 2 are greater than 1.0, indicating the accelerations were amplified at the ground surface. Additionally, the acceleration at the surface was more strongly amplified under high shaking frequency. It is possible that the

introduction of piles leads to local densification and additional cyclic shear strains being mobilised in the vicinity of the piles. This would lead to dilative behaviour, which would manifest itself as an increase in accelerations. Slight de-amplification of the input motion at the surface in Case 3 is due to the onset of liquefaction. It is clear that shaking intensity has a significant effect on the variation of peak acceleration with depth, especially at the ground surface. The peak accelerations at the ground surface under different shaking intensities demonstrates the opposite variation trend. This phenomenon is partly due to the soil liquefaction.

Comparison of the results from Figs. 6 and 7 shows that a large difference occurs in the peak accelerations of soil between and around the piles. The peak accelerations of soil between the piles under the three cases have almost the same variation trends. However, under large input motion, the peak acceleration of soil around the soil takes the opposite variation trend, compared with other cases. Though soil liquefaction occurs, soil between the piles may be restricted by piles, resulting in the same trend of accelerations under the three cases. However, soil around the soil will laterally spread over underlying liquefied sand, leading to the difference in peak acceleration variations under different shaking intensities.

CONCLUSIONS

The study presents the macro-phenomena of the seismic disasters induced by earthquake. Under the 0.50g El Centro input excitation, concrete peeling, bar bending, and tensile failures of the stirrups occurred at the joints of the pier and the cap.

From the measured excess pore pressures, it is clear that, the greater the shaking frequency, the larger the peak excess pore pressure, buildup rate, and dissipation rate; the larger the shaking intensity, the larger the peak excess pore pressure and buildup rate. The slower the dissipation rate; negative excess pore pressure developed in all three cases, which may be the result of large shear strains with an un-drained dilative response of the liquefied soil.

The shaking frequency has little influence on soil accelerations between the piles and the shaking intensity has significant effect; accelerations of soil around the piles at the surface were more strongly amplified under high shaking frequency. Under large shaking intensity, the sand liquefies at all measured levels, with slight de-amplification of input motion at the surface due to the liquefaction process.

ACKNOWLEDGMENTS

The authors gratefully acknowledge the financial support provided by the National Natural Science Foundation of China under NSFC Contract No. 90815009, 50378031 and 50178027, and the Supported and Guidance Plan Found of Zhejiang province, China, under Contract No. 2008C23019. Special thanks are due to the state key laboratory for Disaster Reduction in Civil Engineering, Tongji University in China, and personal thanks go to professors Li-chu Fan and Zhao-ji Shi.

REFERENCES

Kobayashi H, Seo K., Midorikawa S. (1986). Estimated Strong Ground Motions in the Mexico City Earthquake. The Mexico Earthquakes 1985, Factors Involved and Lessons Learned. American Society of Civil Engineers, New York.

Rayhani, Mohammad H. T., Naggar, Hesham El. (2008). Physical and Numerical Modeling of Dynamic Soil-Structure Interaction. Geotechnical Earthquake and Engineering and Soil Dynamics IV Congress 2008, ASCE,1-11.

Su, D., Li, X. S. (2006). Effect of Shaking Intensity on Seismic Response of Single-pile Foundation in Liquefiable Soil. Ground Modification and Seismic Mitigation, ASCE, 379-386.

Trifunac, M. D., Todorovska, M. I. (1996). Nonlinear Soil Response-1994 Northridge, California, Earthquake. Journal of Geotechnical Engineering, 122, 9, 725-735.

Wu X.P., Sun L.M., Hu. S.D., Fan L.C. (2004). Develoment of Laminar Shear Box Used in Shaking Table Test. China Civil Engineering Journal, 37(11):67~72,84 (in Chinese).

Rut-resisting Capacity of the Whole Surface Course in Continuous Upgrade Under Heavy Loading

Guan Hongxin[1] and Zhang Qisen[2] and Xu Yang[3] and Zhou Libo[4]

[1]Associate Professor, School of Traffic and Transportation Engineering, Changsha University of Science & Technology, Wangjiali Road 960#, Changsha City, P.R.C, PH (086) 0731-5258575; Fax (086) 0731-5219375; Email: guanhxin@sina.com
[2]Professor, Changsha University of Science & Technology, Wangjiali Road 960#, Changsha City, P.R.C, PH (086) 0731-5219011; Fax (086) 0731-5219011; Email: 13808418373@hnmcc.com
[3]Senior Engineer, Hunan Traffic Design Institute, Wujialing Road, Changsha, P.R.C, Email: xyhnjt@163.com
[4]Student, School of Traffic and Transportation Engineering, Changsha University of Science & Technology, Wangjiali Road 960#, Changsha City, P.R.C, PH (086) 0731-5258575; Fax (086) 0731-5219375; Email:zlbily2002@yahoo.com.cn

Abstract: The causes for rut distress in 13km continuous upgrade section of Jingzhu freeway in China were studied with repeated wheel tracking tests. The test structures were SMA16+AC20+AC25 and FAC13+FAC20+FAC25 that were the same as sections investigated. The rut tests were developed under two kinds of test conditions to compare rut-resisting capacity. For test condition 1, wheel loading pressure was 0.7Mpa and wheel moving speed was 21 cycles/ minute; for test condition 2, wheel loading pressure was 1.1Mpa and wheel moving speed was 7 cycles/ minute. Dynamic stability (DS) results show that asphalt mixtures used in the two surface course structures all satisfied the limitations of Chinese specifications. Testing results also show that FAC13+FAC20+FAC25 surface course is stronger to resist rut than SMA16+AC20+AC25 surface course. DS values of the two surface course combinations under test condition 1 are larger than the DS controlling standard(DS0) for asphalt mixtures, but the values under test condition 2 both decrease greatly even to be less than that of DS0. The test results are consistent with the rut distress found in the 13km continuous upgrade section. Based on these results, the authors suggest that rut test for the whole asphalt surface course should be developed under a special testing condition for long continuous upgrade section and the special condition should be set in terms of field truck moving speed and loading weight.
Key words: *asphalt surface course, rut*-resisting capacity*, continuous upgrade*

Introduction

A long continuous upgrade section will be designed when the alignment of mountain highways is restricted to local terrains. One of the main characteristics of asphalt pavements in long continuous upgrade section is the low moving speed of vehicles, which prolongs the wheel loading duration on pavements. Korkila-Tanttu (2007) concentrated on how loading speed affects the permanent deformation (rutting) of unbound pavement layers; Paulo A. (1998) studied the effect of truck moving speed on rut depth of bituminous mixtures of steep upgrade section by means of field investigation and laboratory testing.

The other main characteristic is that relative deep permanent deformation will appear in about every surface layer under heavy loading. Wu Rui-Lin(2008) developed a total thickness rutting test to study the effect of aggregate quality and temperature on rut resistance of asphalt pavements. With the combination of laboratory rutting tests on the sample from a corresponding location of road shoulders, Wang Hui（2007）analyzed the influence of the high temperature stability of every asphalt surface layer on rut; Yang Jun（2007）studied the influence of middle surface layer on rutting resistance with a circular road tracking test(CRT) and Hamburg wheel tracking test(HW TT). The contribution of each pavement layer to surface rutting was studied to characterize the rutting mechanism in flexible pavements (Haider 2006, Lin Chih-Hsien 2005, Haddock John E. 2005).

In this paper, total depth sample rut tests are developed under low moving speed and heavy loading pressure corresponding to the field condition of truck moving speed and axial loading to study rut-resisting capacity of the whole surface course.

Rut distress

There is a typical case about rut developing in long continuous upgrade section. That is the 13 km asphalt pavements upgrade section in Jingzhu freeway in Guangdong province in China. Two different asphalt surface course structures were used successively in that section. After almost the same serving time, rut distress found in the two asphalt surface courses are quite different.

The initial pavement structure in the long continuous upgrade section is 4.5cm SMA-16 topper surface layer + 5.5cm AC-20 middle surface layer + 6cm AC-25 bottom surface layer + 36cm 6% cement stabilized crushed-rock base course + 20cm 6% cement stabilized crushed-rock subbase, which was constructed in April 2003.

Rut distress was investigated on the initial pavement structure in April 2005. The investigated results are shown in Table 1. After the investigation, the surface course layers whose rut depth was deeper than 20mm were maintained with FAC mixture. The maintaining method was to dig surface course layers and then reconstruct it again. The reconstructed surface course was 4.5cm FAC-13 topper surface layer + 5.5cm FAC-20 middle surface layer + 6cm FAC-25 bottom surface layer. Mixtures of the 3 layers all used modified bituminous. About 2 years later, rut distress was investigated again on the reconstructed pavement structure in January 2007. The results are also shown in Table 1.

The data in Table 1 show that rut resisting capacity of the reconstructed asphalt surface course is stronger than that of the initial asphalt surface course. In general, SMA is stronger to resist rut than FAC, and AC is weaker to resist rut than FAC. This indicates that rut resisting capacity of the whole asphalt surface course needs to be tested and evaluated when designing the asphalt mixtures.

Table 1 Rut Depth in Serious Section

No.	length (m)	wheel track	initial surface course, 2 years later		reconstructed surface course, about 2 years later		upgrade slope
			average rut depth (mm)	maximum rut depth (mm)	average rut depth (mm)	maximum rut depth (mm)	

1	60	left	43.5	63	5	7	3%
		right	64.5	67	6.5	10	
2	196	left	13.7	31	4.2	7	1%
		right	21.1	50	9.5	22	
3	313	left	26	46	8.5	10	2%
		right	40.4	60	15	12	

Reappearing tests

Laboratory rut tests for initial and reconstructed asphalt surface layers of the continuous upgrade section were developed with improved wheel tracking testor (Fig.1). The improved wheel tracking testor enables loading pressure to vary from 0.7 to 1.4Mpa, test wheel moving speed to vary from 7 to 56 back and forth/minute, and sample height to vary from 3 to 20cm. The raw materials used for rut tests were the same as those used in initial and reconstructed asphalt surface course materials. The gradations for each layer are shown in Table 2. The bituminous binder is AH-70 for AC20 and AC25, SBS modified AH-70 for SMA16, FAC13, FAC20 and FAC25. The Methyl Cellulose for SMA16 is VIATOP80 produced by German JRS Company.

Fig.1 wheel tracking testor

Table 2 Gradation of bituminous mixture for each surface course

	Percent passing (%)												
size(mm)	31.5	26.5	19	16	13.2	9.5	4.75	2.36	1.18	0.6	0.3	0.15	0.075
SMA16			100	95	75	55	25	20	16.4	14.0	12.3	11.1	10.2
AC20		100	97.8	85	77.3	63.7	44.9	31.6	24.5	17.4	11.7	8.8	6.3
AC25	100	99.1	82.1	71.8	62.6	53	41.9	32.3	22.5	17	8.3	6.9	5.3
FAC13				100	95.9	68.6	33.7	29.3	22.3	16.6	11.8	9.3	6.8
FAC20		100	96	86.8	72.4	56.2	30	15.9	13.3	10.7	8.18	6.7	5.32
FAC25	100	96	82.5	72.5	63	51	26	20	14.5	10.5	9	6.5	5

In order to find the reasons for rut distress, laboratory rut tests were made on each layer of initial surface course and reconstructed surface course. Laboratory rut tests were also developed on the whole initial surface course and the whole reconstructed surface course. Rut test samples are shown in Table 3.

Table 3 Rut Test Samples

No.	rut test sample	No.	rut test sample
1	5cmSMA16(modified bituminous)	4	5cmFAC13(modified bituminous)
2	5cmAC20	5	5cmFAC20(modified bituminous)
3	4.5cmSMA16+5.5cmAC20	6	4.5cmFAC13+5.5cmFAC20

+6cmAC25	+6cmFAC25

Three kinds of testing conditions were introduced into rut tests, which are shown in Table 4. The standard testing condition was set in terms of Chinese Specifications. The nonstandard testing condition 1 and 2 were set only for the whole surface course. The nonstandard testing condition 2 was set in terms of field investigation results from the 13km long continuous upgrade section in Jingzhu freeway. Traffic investigation results show that trucks averagely overload 60% of the standard loading weight and move at about one-third of design speed averagely.

Table 4 Testing Conditions

conditions	standard condition	nonstandard condition 1	nonstandard condition 2
temperature	60℃	60℃	60℃
loading press	0.7 Mpa	0.7 Mpa	1.1 Mpa
moving speed	42 cycles/minute	42 cycles /minute	14 cycles /minute
Sample thickness	5cm	16cm	16cm

Testing samples were shaped with a rut shaping instrument. The samples were all 300mm long and 300mm wide. Combined samples marked with No.3 and No.6 in Table 3 were shaped successively from the bottom layer to the top layer.

The results of laboratory rut tests were expressed as dynamic stability (DS).To verify the feasibility of repeated loading tests, parts of DS results of repeated loading tests were compared with the testing results from asphalt mixture design of initial or reconstructed asphalt surface layers. The comparison are shown in Table 5, which were all obtained under the standard testing condition.

Table 5 The Precision of Reappearance Tests

Sample	DS of reappearance tests(cycles/mm)	DS* (cycles/mm)	Error	DS controlling standard (times/mm)
5cmSMA16	14098	11800	19.5%	3000
5cmAC20	1716	2097	18.2%	1000
5cmFAC13	10612	8986	18.1%	2800
5cmFAC20	5843	4910	19%	2800

DS*: DS from mixture design of initial or reconstructed asphalt surface layers

The data in Table 5 indicate that DS values of the 4 mixtures are all larger than those of the DS controlling standards of China. But it only indicates that these mixtures can resist rut under design axial loading and design vehicle speed. Considering rut distress found in the field, rut-resisting capacity of these mixtures' combination still needs to be further compared .

Results and Discussion

Rut test results under nonstandard condition are shown in Figure 2. The initial structure is marked with SMA16 + AC20 + AC25, and the reconstructed structure is marked with FAC13 + FAC20 + FAC25 in Figure 2. From Figure 2, some results can be found as below:

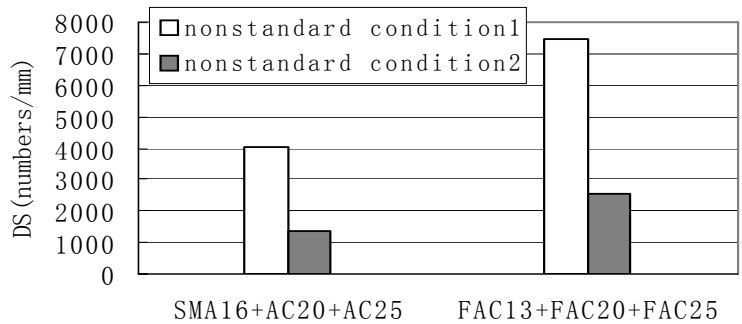

Fig. 2 DS of the whole surface course under nonstandard condition

(1)DS value of the whole initial surface course is about half of the whole reconstructed surface course. This indicates that rut-resisting capacity of FAC13+FAC20+FAC25 structure is greater than that of the SMA16+AC20+AC25 structure, which supports the investigated data in Table 1 very well. Because DS controlling standard for the whole surface course has not been set in China, it is hard to attribute the rut distress to designers.

(2)Although DS values of the two whole surface course structures under nonstandard condition 1 are all greater than 3000 cycles/mm, DS values under nonstandard condition 2 decrease greatly even to be less than the DS controlling standard for asphalt mixtures. This is the real cause for serious rut distress found in SMA16+AC20+AC25 structure.

Conclusions

In this paper, repeated loading tests have been developed with modified wheel tracking testor to compare rut-resisting capacity between SMA16+AC20+AC25 structure and FAC13+FAC20+FAC25 structure that had been used in the 13km continuous upgrade section successively. As mentioned above, some conclusions can be drawn as below:

(1)DS values of each layer of the asphalt mixtures all satisfy the corresponding DS controlling standards of China, but rut distress still happened. This indicates that only setting DS controlling standards for asphalt mixtures is unable to resist rut of surface course effectively.

(2)Rut resisting capability of the whole FAC13+FAC20+FAC25 structure is stronger than that of the whole SMA16+AC20+AC25 structure;

(3)Under 0.7 Mpa loading pressure and 21 cycles/ minute loading frequency, DS values of the whole surface course are larger than those of DS standards for asphalt mixtures. However, rut distress still happened. It indicates that this rut testing condition is not appropriate for the 13km continuous upgrade section asphalt surface course.

(4)Under 1.1 Mpa loading pressure and 7 cycles/ minute loading frequency, DS values of the whole surface course decrease greatly, even to be less than the DS controlling standard for asphalt mixtures, which induces rut distress directly.

(5)Test results are consistent with rut distress found in the 13km continuous upgrade section.

Based on these conclusions, the authors suggest:

(1)Rut test on the whole asphalt surface course under a special testing condition should be developed for long continuous upgrade sections. The special condition should be set in terms of field truck moving speed and loading weight.

(2)DS controlling standard of the whole asphalt surface course for long continuous upgrade section should be set

References:

Korkila-Tanttu, Lenna(2007). "Speed and reloading effects on pavement rutting", *Proceedings of the Institution of Civil Engineers: Geotechnical Engineering*, Vol 160(3), 123-127

Paulo A. A. Pereira, Jorge C. Pais, Jorge B. Sousa(1998). "Validation of SHRP A-698 Permanent Deformation Concepts for Different Truck Speeds", Fifth International Conference on Bearing Capacity of Roads and Airfields, Trondheim, Norway

Wang Hui, Zhang Qi-Sen, Tan Ji-Qing(2007). "Effect of asphalt pavement layers on rutting development", International Conference on Transportation Engineering, ICTE 2007, p 1915-1920

Wu Rui-Lin, Shi Li-Wan, Yu Hai-Yang, Ma Guang-Hua(2008). "Total thickness rutting research on key influencing factors of asphalt pavement". Journal of Wuhan University of Technology, Vol 30(1),58-61

Yang Jun, Cui Juan, Wan Jun, Shi Xiao(2007). "Strategy of improving rutting resistance based on contribution rate of different layers". Journal of Southeast University (Natural Science Edition), Vol 37(2),350-354

Haider, Syed Waqar, Chatti, Karim, Emin Kutay, M., Eason, James, Redelius, Per(2006). "Effect of design and site factors on structural rutting of flexible pavements in the LTPP SPS-1 experiment". Asphalt Paving Technology: Association of Asphalt Paving Technologists-Proceedings of the Technical Sessions, Vol 75,425-456

Lin Chih-Hsien, Chen Wei-Chyum(2005). "Developing a four-layer system rutting model in highway". Journal of the Chinese Institute of Engineers, Vol 28(2),371-374

Haddock John E., Hand Adam J.T., Fang Hongbing(2005), "White Thomas D. Determining layer contributions to rutting by surface profile analysis". Journal of Transportation Engineering, Vol 131(2),131-139

Integration of Fortran with ANSYS in Transient Thermal Simulation

Tao Zhang[1] and Yanlin Yu[2]

[1] School of Civil and Safety Engineering, Dalian Jiaotong University, Dalian, China; PH (086) 411- 84106242; email: Zhang_tao4567@163.com
[2] School of Civil and Safety Engineering, Dalian Jiaotong University, Dalian, China; PH (86) 411- 84106242; email: yyl66669999@sohu.com

ABSTRACT

Bridge structures are subjected to thermal effects due to interaction with environmental conditions or due to special effects. Interaction with air temperature and solar radiation leads to seasonal and daily temperature changes in the bridge. At the present there is a more and more popular trend in using ANSYS software to simulate and analyze the finite element models in order to design automation and customization in bridge design. The ability to create automatic design has been an important research and engineering topic. This paper presents an operational system for automating engineers that integrates the Fortran program with ANSYS through APDL (ANSYS Parametric Design Language) in the Transient Thermal Simulation in bridges. In addition, we use an example to validate the program.

INTRODUCTION

ANSYS is one of the most famous and general Finite Element Analysis Software in the world. It has very powerful calculation and analysis ability. It is advanced technology, which integrates computer technology and engineering analysis technology. Design automation and customization with finite element analysis as a simulation tool is becoming more and more desired. , It is very important in transient thermal simulation in bridges.

ANSYS includes several modules: structure, thermal, and so on. When we aim at the thermal of structure, ANSYS can deal with three basic problems: thermal convection, thermal conduction, and thermal radiation. But the ambient condition and the temperature field is very complicated, so we need to consider a great deal of meteorology data, solar radiation, and complicated boundary conditions. In the past we converted this data and input the information to ANSYS manually (Josef, Erwin and Franz, 2003). This procedure has been regarded as not only time-costly but also less cost-effective. So, The Second Development Based on the ANSYS is necessary. We take APDL as the secondary development for ANSYS. The Fortran program is developed to generate the thermal parameter according to the energy theory.

THE SECONDARY DEVELOPMENT

The ANSYS program offers powerful second development to accommodate automation and customization. That is APDL. While customization is limited in that

only simple inputs and message menus can be generated. Speed can be slow for complex operations on large models such as with a great deal of meteorology input data. With the help of the Fortran program, initial conditions and boundary conditions for transient thermal simulations are generated. The output data from Fortran can be saved in array files that are read by APDL. Through macro command, ANSYS starts to run. Using the named parameters in ANSYS as the interface and the APDL for model manipulation, the user can accomplish the desired transient FE analysis and temperature response within ANSYS. Figure 1 shows a flow chart of the secondary development to simulate the transient thermal field. Each step requires special attention to achieve the final objective of the analysis.

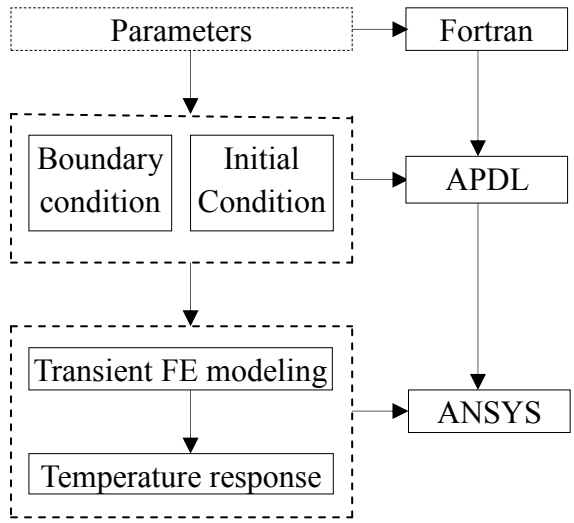

Figure 1. Procedure of the simulation.

Fortran program. The parameters to be considered in the transient thermal bridge design temperature are identified as belonging to the following groups (Tong, Tham and Lee, 2001):

Geometric: geometry of the cross section, bridge orientation

Material: thermal conductivity, density, specific heat, color

Geographical: altitude, latitude

Time: hour of the day, day of the year

Climatic: solar radiation, air temperature, wind speed

The first two parameters are internal factors related to bridge characteristics. The final three categories are external factors related to the environmental characteristics of the bridge location (Peng, Qiang, 2007).

After inputting thermal parameters, a Fortran program was used to evaluate the temperature conditions according to heat gain or loss by heat transfer for any specific situation (Figure 2).

APDL in thermal simulation. APDL stands for ANSYS Parametric Design Language, a scripting language that can be use to automate and customize common

tasks or even build your model in terms of parameters.

As with Fortran output arrays, the indices for initial temperatures and boundary temperatures are sequential integer numbers beginning with one. *DIM in APDL is used to define array parameters.

In transient thermal analysis, the uniform temperature is used during the first iteration of a solution to evaluate temperature-dependent material properties (Barr, Stanton and Eberhard, 2005). Initial conditions can be generated by TUNIF in APDL by assigning a uniform temperature to all nodes.

Thermal loads can be applied by SFL in APDL which generates boundary condition by specifying surface loads on the selected lines of area regions. For the bridge section, the line represents either edge of the section area elements. Thermal surface loads can be transferred from lines to elements with the SFTRAN or SBCTRAN commands.

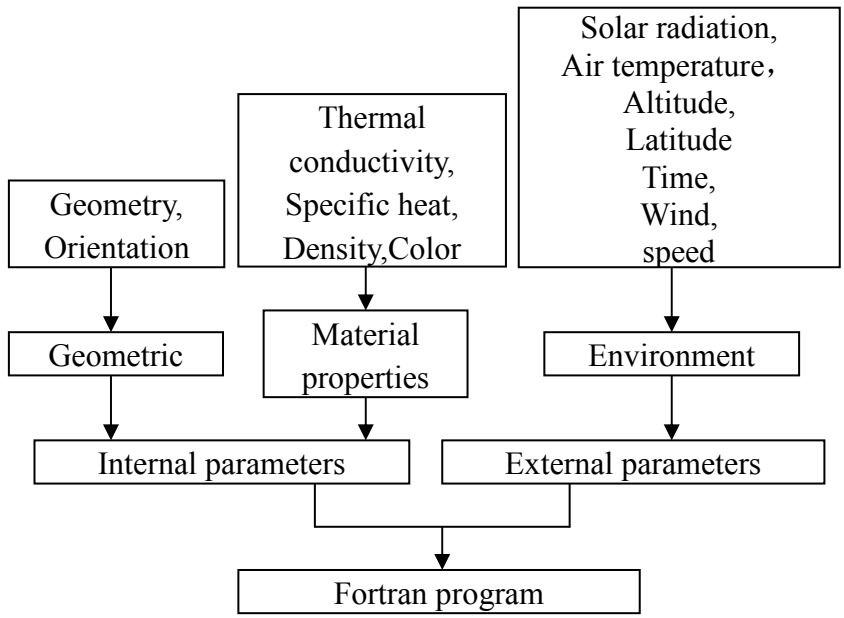

Figure 2. Parameters by Fortran program.

ANSYS. In the stage of pre-processing, we develop several works:

According to the requirements, one should take into account bridge structure dimension parameters such as length, width, section shape etc.

Material parameter. In our case, it is linear and isotropic; the density.

Element type.

FE model and meshing

Case study

Temperature variations with bridges can cause thermal stresses and deformations that are comparable in magnitude to stresses induced by vehicle loadings (Troy and Yoo,2003; Francis and Leslie,2001; Hui, Zi-shan and

Hong,2007). Thus, a bridge designer needs to calculate very detailed temperatures with thermal simulation, which often results in a large expenditure of time and effort (Song qing, Jin fei and Tongsheng, 2008; Fernando, Pedro,1993).

The temperature problem is caused by the thermal environment (Figure 3). Surface temperatures varying with the time result from numerous random inputs, namely, the surrounding air temperature, the solar energy, and convection caused by the wind vector. A computer Fortran program is developed to deal with this input data. Since times are continually changing, random and transient thermal parameters must also vary with these inputs. The final surface temperatures are computed according to the heat convection, thermal irradiation, and solar radiation.

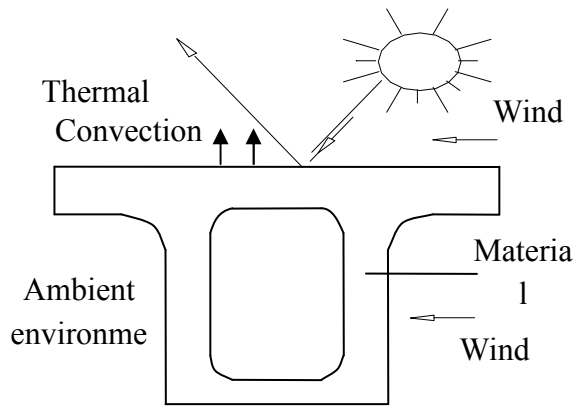

Figure 3. Temperature influence factors to concrete bridge.

In APDL, thermal parameter arrays outputted by Fortran program are defined as initial conditions and boundary conditions. As ANSYS batch file, key steps are provided below in APDL. The general structure of the batch file was to have a master file that initialized a few items such as simulation name, then called a series of scripts, followed by selected post-processing steps:

Initial conditions defined: variables initialized, options selected for later conditional checks

Geometry imported

Material model defined

Geometry meshed

Boundary conditions defined

Finite element model solved

In ANSYS post processing stage, we gain the thermal flux and the temperature field respectively. The simple way to observe the effect of the sunshine is thermal flux (Figure 4). Because the temperature of the inner is hotter than the outer, the thermal flux follows this direction. The temperature file shows the tendency that the surface temperature is higher than the bottom temperature (Figure

5). This is in agreement with theoretical analysis. After thermal analysis, the structural analysis is performed.

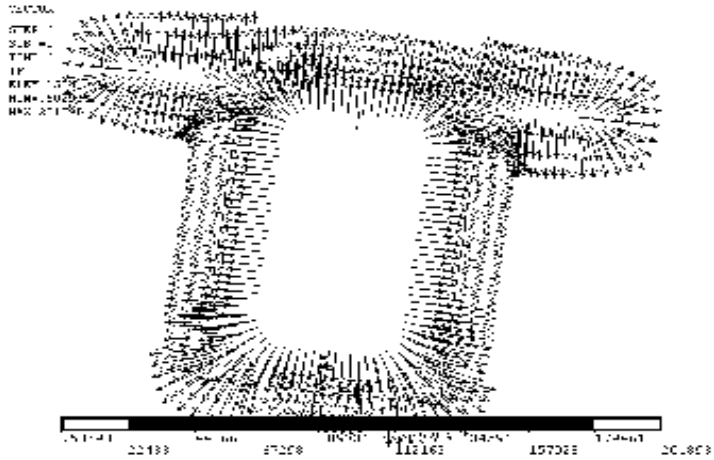

Figure 4. Thermal flux

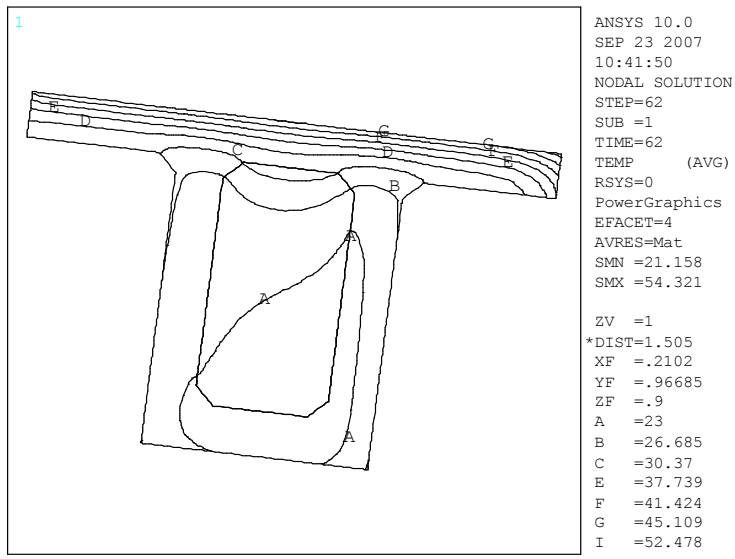

Figure 5. Temperature distribution.

Conclusion

This paper introduces the research of a general secondary development method for ANSYS. Combining Fortran and APDL, the initial and boundary conditions for thermal parameters in transient thermal simulations for bridges due to solar radiation has been developed. The calculation results matches the experimental results. It is shown that by this mean, the powerful functions of the FEA software ANSYS can extend the developing period, effectively reduce the programming works, lower the maintenance of the program needed, and guarantee the stability and the reliability of the program. The technology can be widely used in the pos-processing function of engineering calculation software.

ACKNOWLEDGMENT

This work was supported by 2008 Scientific Research Plan Projects for Higher Education of Liaoning Education Department (Project Number: 2008091).

This research was also supported by China Postdoctoral Science Foundation (Project Number:20080441119) .

REFERENCES

Fernando A. Branco, Pedro A. Mendes (1993) "Thermal actions for concrete bridge design." Journal of Structural Engineering, 119(8), 2313-2331.

Francis T.K. Au , Leslie G. Tham, ManTong, Peter K.K. Lee (2001) "Temperature monitoring of steel bridges." Health Monitoring and Management of Civil Infrastructure Systems, Proceedings of SPIE, 43(2), 282-291.

Josef Schoenauer, Erwin Schlemmer, Franz Mueller (2003). "Finite element modeling of the temperature distribution in the stator of a synchronous generator." The International Journal for Computation and Mathematics in Electrical and Electronic Engineering, 22(4), 909-921.

K.T. Lau, F. Liu (2000) "APDL-based low-power adiabatic programmable logic array." Microelectronics Journal, 31(1),235–238.

M. Tong, L.G. Tham, F.T.K. Au, P.K.K. Lee (2001). "Numerical modeling for temperature distribution in steel bridges." Computers and Structures, 79(1), 583-593.

Peng Yousong, Qiang Shizhong (2007). "Analytical solution to temperature variations in highway concrete bridges due to solar radiation." International Conference on Transportation Engineering ,1,1536-1541.

P. J. Barr, M.ASCE, J. F. Stanton, M.ASCE; M. O. Eberhard (2005) "Effects of Temperature Variations on Precast, Prestressed Concrete Bridge Girders." Journal of Bridge Engineering, 20(2),186-194.

Song Hui, Xie Zi-shan, Zheng Hong-yang, Zhang Wen (2007) "Numerical simulation for temperature field of subgrade on seasonal frozen area." International Conference on Transportation Engineering, 23(1),1753-1758.

Song qing Zhu, Jin-fei Shi, Tong-sheng Sun (2008) "Heat Transfer Model and Numerical Simulation for Microwave Hot In-Place Recycling of Asphalt Pavements." Transportation and Development Innovative Best Practices, 23(2), 462-467.

Troy T. Tindal, Chai H. Yoo (2003) "Thermal Effects on Skewed Steel Highway Bridges and Bearing Orientation." Journal of Bridge Engineering, 10(3), 57-65.

Study on asphalt treated permeable base in permafrost regions

Dong xi-bin and Wang hai-biao and Li li-hui
School of Engineering Technique, Northeast Forestry University. Harbin,China email: xibindong@sina.com Harbin ,China；

ABSTRACT

Setting drainage system in the pavement could improve the pavement performance and extend service life of the road. According to the weather condition in north China, three kinds of open-graded ATPB were designed and their performances were evaluated using the analytic hierarchy process, and then we established the hierarchy model. The permeability, water stability, mechanical properties, and stability under low temperature of the mixtures were tested. It is concluded that ATPB-25 is a better material for permeable base of the pavement in permafrost regions.

Keywords: roads in permafrost region, asphalt treated permeable base, asphalt content; performance

Setting drainage system in the pavement could improve the pavement performance and extend service life of the road. Asphalt treated permeable base (ATPB) is a common case for asphalt pavement with internal water drainage system.

1. Design of Mixture Proportion

1.1 Materials

Dry clean basalt with no weathering and impurities was used in the experiment. Tests show that the basalt meets the quality requirements for the surface layer of asphalt pavement. Fine aggregate and fillers include basalt crumb and mineral powder. It is tested that the materials meet the quality requirements of fine aggregates and fillers for asphalt surface layer specified in “Road asphalt pavement construction technical specifications” (CTS). To meet the modified asphalt specified in the CTS, 4.5% SBS of modifier was added to Pacific Asphalt.

1.2 Design of Mineral Mixture Proportion

ATPB is composed of open graded gravel aggregates which are free or with small amount of fine materials less than 4.75mm in size. According to the mixture ranges specified in the CTS, three graded asphalt mixtures, ATPB-40, ATPB-30, and ATPB-25 were examined in this study.

1.3 Determination of the Asphalt Content

Determination of the asphalt content is the key point for designing of ATPB mixture. Since the asphalt treated permeable base is used below the surface layer, the horizontal shear force caused by loaded vehicle has relatively small impact on it. Therefore, Scattering Loss Test is not necessary. Schellenberg Binder Drainage Test combined with Marshall Test was adopted in this study to determine the optimal asphalt content.

Fund financing projects: the major breakthrough issue in Hei Longjiang Province：（GA06B302-4）；
Author of Correspondence: Wang hai-biao，email:wbcumt@163.com

1.3.1 Schellenberg Binder Drainage Test

Five asphalt contents with 0.4% interval were tested for each mixture (ATPB-40, ATPB-30, and ATPB-25). Among them, it was 1.8% ～ 3.4% for ATPB-40 and ATPB-30, respectively. It was 2.2%～3.8% for ATPB-40. The relationship between leakage loss and asphalt content under different scenarios was shown in Fig. 1.

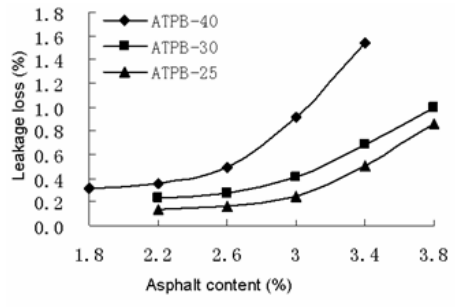

Fig1. Asphalt leakage tes

To determine the maximum asphalt content, dichotomy was used in this study. A function was fitted to the curve first, and then the second derivative of the function was calculated. The largest point of the second derivative could be obtained by dichotomy. Since the accuracy of asphalt content was 0.1, the error allowed could be ε=0.1.

The steps for determining the maximum asphalt content were as following：

Fitted function： $y = -0.472x^4 + 5.0781x^3 - 19.483x^2 + 32.172x - 19.135$

Where, x —asphalt content，%； Y —asphalt leakage loss，%。The second derivative of the function： $y'' = -5.664x^2 + 30.4686x - 38.966$。The biggest value of the y " determined by dichotomy is shown in Tab. 1。The approximate maximum point of the second derivative was calculated as 2.7%. Therefore, the maximum asphalt content for ATPB-40 was 2.7%。Similarly, the maximum asphalt content for ATPB-30 and ATPB-25 was 2.9% and 3.1%, respectively.

Tab 1. The maximum asphalt content of ATPB-40 determined by dichotomy.

Iterations	ak	bk	xk	f"(ak)	f"(bk)	f"(xk)	Reservation interval
1	2.2	3.0	2.6	0.6512	1.4638	1.9637	（2.6，3.0）
2	2.6	3.0	2.8	1.9637	1.4638	1.9403	（2.6，2.8）
3	2.6	2.8	2.7	1.9637	1.9403	2.0087	

1.3.2 Marshall Test

Five asphalt contents were prepared as the specimen for the large-scale Marshall Test. The results were shown in Tab 2-4.

Tab 2. Marshall Test for ATPB-40.

Asphalt content %	1.8	2.2	2.6	3.0	3.4
Gross bulk density ρ g/cm^3	1.972	1.986	1.999	2.027	2.065
Porosity vv %	26.22	25.23	24.25	22.22	20.27

Tab 3. Marshall Test for **ATPB-30.**

Asphalt content %	2.2	2.6	3.0	3.4	3.8
Gross bulk density ρ g/cm^3	1.964	1.978	2.001	2.029	2.047
Porosity vv %	25.18	24.19	22.83	21.27	20.07
Stability MS kN	8.27	10.25	10.43	9.67	9.24

Tab 4. Marshall Test for **ATPB-25.**

Asphalt content %	2.2	2.6	3.0	3.4	3.8
Gross bulk density ρ g/cm3	1.961	1.982	1.996	2.026	2.040
Porosity vv %	25.15	23.89	22.87	21.23	20.22
Stability MS kN	8.32	9.11	11.05	10.43	9.87

According to the Schellenberg Binder Drainage Test, the maximum asphalt content for ATPB-40, ATPB-30 and ATPB-25 was 2.7%, 2.9% and 3.1%, respectively, which were a little bit higher than the ones obtained by Marshall Test. To increase the water stability of the ATPB, higher asphalt content was encouraged. Therefore, the maximum asphalt content for ATPB-40, ATPB-30 and ATPB-25 was determined as 2.7%, 2.9% and 3.1%, respectively.

2 Permeability Test

Permeability coefficient is the index for evaluating the permeability of a material. A simplified test method was used in order to better meet the pavement actualcondition [4]. The time interval for 400 ml water completely seapage in a large Marshall specimen which was already immersed in water for one hour was recorded. The permeability coefficient (K) was calculated (Tab 5)

The permeability coefficient decreased from ATPB-40 to TPB-30, and to ATPB-25. But the difference is not significant. The permeability coefficients for all three mixtures meet the requirements of less than 0.35cm/s specified in "Design specifications for Highway Drainage".

Tab 5. Testing results for permeability coefficient.

Type of mixture	Asphalt content (%)	Porosity (%)	Time interval (t) (s)	Permeability coefficient (K)	
				cm/s	cm/s
		23.95	11.3	0.777	
ATPB-40	2.7	24.96	10.5	0.836	0.790
		23.54	11.6	0.757	
		23.03	12.1	0.725	
ATPB-30	2.9	24.27	11.1	0.791	0.751
		23.50	11.9	0.737	
		21.66	14.6	0.601	
ATPB-25	3.1	22.43	13.1	0.670	0.661
		22.92	12.3	0.713	

3 Analysis of Water Stability

ATPB drainage layer itself may be immersed in water for a long time period. Water damage may occur under water immersion and loaded vehicle passing. Therefore, water stability is required to the drainage ATPB. Immersed Marshall Test and Freeze-Thaw Splitting Test were used to evaluate the water stability of the mixture.

3.1 Immersed Marshall Test

The immersed residual stability MS_0 was calculated as $MS_0=MS_1/MS\times100\%$

Where MS is the Marshall stability of large-scale Marshall test specimen after compaction and molding, MS_1 is the Marshall stability of the specimen after immersion in the water for 48 h under constant temperature of 60℃. Testing results

were shown in Tab 6.

Tab 6. Marshall Testing results for three kinds of mixtures.

Mixture	Porosity （%）	Stability MS (kN)	Stability MS1 (kN)	Residual stability after immersion in water （%） MS0 （%）	
				Observed value	Required value
ATPB-40	24.29	10.02	9.03	90.1	＞75
ATPB-30	23.05	10.56	9.81	92.9	＞75
ATPB-25	22.92	11.17	10.57	94.6	＞75

3.2 Freeze-Thaw Splitting Test

Freeze-Thaw Splitting Test is used to test the water damage resistance of the ATPB. The requirement for the experiment is stricter than Immersed Marshall Test. Three curing processes of vacuum for water preserving, low temperature for freezing, and high temperature with water immersion are required. The procedure could better represent the real working condition of the ATPB under cold weather condition of north China. Testing results were shown in Tab 7.

After Immersed Marshall Test and Freeze-Thaw Splitting Test, all three mixtures could meet the requirements for water stability in the region with Class I rainfall. From Tab 6 and Tab 7, we noticed that the water stability of the three mixtures follows the sequence of ATPB-25＞ATPB-30＞ATPB-40.

Tab 7. Freeze-Thaw Splitting Test results for three kinds of mixture.

Mixture	Porosity （%）	Splitting tensile strength of the specimen in group B after freeze-thaw cycle R1(MPa)	Splitting tensile strength of the specimen in group B without freeze-thaw cycle R2(MPa)	Tensile strength ratio TSR= R1//R2 （%）	
				Observed value	Required value
ATPB-40	24.35	0.813	0.982	82.8	＞70
ATPB-30	23.09	0.845	0.994	85.0	＞70
ATPB-25	22.88	0.901	1.032	87.3	＞70

4 Analyses of Mechanical Properties

In China, semi-rigid base was adopted for most of asphalt pavements. Drainage ATPB is above the semi-rigid base and has lower rigidity. The ATPB is commonly under compression from the loaded vehicle passing. Therefore, compressive resilient modulus is a good indicator for the mechanical properties of the mixtures. The compressive resilient modulus of the mixture could be determined by uniaxial compression test of the specimen after static compressing (Tab 8).

Tab 8. Testing results of the compressive resilient modulus.

Mixture	Asphalt content （%）	Porosity （%）	Resilient modulus Er(Mpa)
ATPB-40	2.7	21.96	985.9
ATPB-30	2.9	21.35	1058.6
ATPB-25	3.1	21.76	1114.3

Fig. 8 shows that the compressive resilient modulus of all three mixtures of

ATPB fall between 800MPa～1200MPa, which meet the requirement to the material. The more coarse aggregates contained in the mixture, the higher is the porosity. Therefore, increasing the amount of coarse aggregate or asphalt in the mixture will cause the decrease of the material strength. The more asphalt in the mixture, the smaller of the compressive resilient modulus. The compressive resilient modulus of the three mixtures follow the sequence of ATPB-25＞ATPB-30＞ATPB-40.

5 Analyses of Material Stability under Low Temperature

Bending Creep Test was used to evaluate the deformation of the material under low temperature. Creep rate is a good indicator for the ATPB performance under low temperature. According to the weather condition in north China, Bending Creep Test was carried out at -10℃. Due to the large particle size of the mixture, cuboids specimen of 250mm×50 mm×50mm prepared by wheel rolling method were used for the test. Testing results were listed in Table 9.

Creep rate shows the rheological parameters of the material under varied temperature and loading conditions, which reflects the deformation resistance of the material. The higher is the creep rate, the greater is its ability to resist deformation, and the better is the resistance to cracking of the material under low temperature. Results showed that the resistance to deformation of ATPB-25 is higher than that of ATPB-30 and the resistance to deformation of ATPB-30 is higher than that of ATPB-40 under low temperature. The coarser is the ATPB mixture, the larger is the porosity and the lower is the resistance to deformation under low temperature.

Tab 9. Results for Bending Creep Test.

Mixture		Asphalt content (%)	Porosity (%)	Loading (N)	Stress level (MPa)	Creep rate 10^{-8}(1/s/MPa)	
ATPB-40	Specimen 1	2.7	24.73	250	0.59	2.07	2.47
	Specimen 2		23.65	250	0.61	2.46	
	Specimen 3		23.02	250	0.62	3.88	
ATPB-30	Specimen 4	2.9	22.96	250	0.60	2.78	3.04
	Specimen 5		23.44	250	0.58	3.80	
	Specimen 6		24.05	250	0.63	2.56	
ATPB-25	Specimen 7	3.1	22.98	250	0.62	2.73	3.37
	Specimen 8		22.31	250	0.57	3.41	
	Specimen 9		21.54	250	0.63	3.97	

6 General Performance Evaluations

Analytic hierarchy process was used for the general evaluation of the material properties. A hierarchy model with objective layer(Optimum ATPB), index layer （Water Permeability A_1、 Water Stability A_2 、Mechanical Property A_3、Stability under low Temperature A_4）, and scheme later （ATPB-40、ATPB-30、 ATPB-25）。

Among the four factors of A_1 to A_4, water permeability is the most important one while resistance to deformation is also required to the material. Additionally, to the road in permafrost region, water stability and material stability under low temperature have to be met. The factors were ranked by their importance with permeability was the most important, followed by water stability and material stability under low temperature. And permeability and mechanical properties are at

the same important level. Therefore, the judgment matrix is as follows:

$$A=\begin{bmatrix} 1 & 3 & 2 & 3 \\ 1/3 & 1 & 1/3 & 3 \\ 1/2 & 3 & 1 & 3 \\ 1/3 & 1/3 & 1/3 & 1 \end{bmatrix}$$

Root-squaring method was used for an approximation of the eigenvector for each judgment matrix. The single ordering weight value was then obtained. Results showed that the judgment met the requirement of consistency.

w_A=(0.437 0.161 0.309 0.093)。it means that the weight for permeability, water stability, mechanical property, and material stability under low temperature was 0.437, 0.161, 0.309, and 0.093, respectively.

Tab 10 shows that ATPB-25 has the highest score, followed by ATPB-30, and ATPB-40 has the lowest score. Therefore, ATPB-25 has the priority to be selected as the material for the permeable base of asphalt pavement in permafrost regions.

Tab 10 Results of Grading for Performance.

Index	permeability A1	water stability A2	mechanical property A3	stability under low temperature A4	Weighted score
Weight	0.437	0.161	0.309	0.093	
ATPB-40	1.5	0.5	0.5	0.5	0.937
ATPB-30	1.0	1.0	1.0	1.0	1.0
ATPB-25	0.5	1.5	1.5	1.5	1.063

7 Conclusions

The optimal asphalt content of the mixture was determined based on Schellenberg Binder Drainage Test and Marshall Test. Permeability, water stability, mechanical property, and material stability under low temperature of the three mixtures of ATPB were tested and analyzed. Results showed that ATPB-25 was more suitable as permeable base of asphalt pavement in permafrost regions.

References:

Hao P.W., Liu H. Y., Huang W. (1994). Research on Evaluation Low Temperature Anti-cracking Characteristic of Asphalt Mixture by Creep Speed. Petroleum Asphalt, Vol. 3, 1994, pp. 6-10.

Hong B., Yao Z. K. (2000). Permeability of asphalt treated permeable base materials. China Journal of Highway and Transport, Vol. 13, No. 2, 2000, pp. 20-23.

Huang L.K., Zhang Y.C. etc. (2003). Component Design of Asphalt Stabilized Crushed Stone Permeable Mix for Pavement Base. Central South Highway Engineering, Vol. 28, No. 4, 2003, pp. 8-10.

Li L.H., Dong X.B. (2007). Study on the Water Stability of Asphalt Treated Permeable Base. Forest Engineering, Vol. 23, No. 2, 2007, pp. 49-53.

Shen J.A. (2001). Road Performance of Asphalt and Asphalt Mixtures. Beijing, People Transportation Press, 2001, pp. 67-75.

Wang G.Z., Zhao C., Zhang Y. (2005). Analysis of Structure of Asphalt Pavement with Asphalt Stabilized Base Course. Journal of Inner Mongolia Institute of Agriculture and Animal Husbandry, Vol. 26, No. 3, 2005, pp. 61-64.

Continuous Test for Construction Quality of Mixed Filling Roadbed

Caixia Wang [1], Guanghui Xu, Haibin Cai, Dapeng Song
[1]School of Transportation Science and Engineering, Harbin Institute of Technology, Harbin, PH (086)451-86283090 FAX (086)451-86283090, email:wang_ccxx@126.com

ABSTRACT

The components of mixed filling roadbed are complex, and the variability is big. This paper focuses on the monitoring technology of construction quality after compacting mixed filling roadbed. Based on the vibratory roller and roadbed interactive dynamic characters, the dynamic model has been built. By analyzing the model, the relationship between the dynamic response acceleration of the vibratory roller and the roadbed structure resistance has been obtained. The continuous informative response of the vibratory roller can be monitored by using the monitoring system established on the basis of the vibratory roller. The correlation between the dynamic response acceleration and the corresponding deflection is good. After calibrating the acceleration by deflection, the controlled acceleration standard can be developed The feasibility and advanced characteristics have been validated by monitoring the construction quality of mixed filling roadbed.

KEYWORDS

roadbed engineering, mixed filling, dynamic compaction, continuous test

INTRODUCTION

Based on statistic data, the amount of construction trash takes up thirty to forty percent of the whole trash in large or medium size cities, which is the biggest waste source. At present, most of the construction trashes are delivered to the suburb or places near villages without any treatment. They are piled up in the open air, or dumped into big or small pits as fillings, or even into the lake or sea. The places used to dispose the construction trash are getting farther and farther from the city, because the land for keeping trash becomes less. Such waste disposal influences extension of the city construction, especially the exploitation between the city and the country. Trash digging and disposing needs new land and brings pressure to the environment. This means new ways of trash disposal is needed. In this sense, mixed filling is a better choice for environment protection, saving resources and reducing construction cost.

Dynamic compaction is the most common method to deal with the mixed filling in the initial place. It can not only improve the capacity of mixed filling but also improve the uniformity in some extent. Dynamic compaction technique should be designed on the basis of the soil condition, concretion density, construction

efficiency and so on. The quality of dynamic compaction roadbed is unsteady because of so many influential factors. Sand replacement method is the main method to control the construction quality of mixed filling roadbed. The design compaction is the control index. This method is not suitable for grand grains, and the water level is used to measure the compaction difference between the dynamic compactions. Heavy dynamic penetrometer, plate static load test and bearing plate method are also used to measure the capacity. Because the uniformity of mixed filling is bad, these methods all have some limitation sometimes. The continuous monitoring technique has been established based on the dynamic response during rolling by vibratory roller. The relationship between dynamic response and normal index-deflection has been established. The dynamic response is calibrated by deflection. Based on all of these, the continuous monitoring and real-time control of the quality of mixed filling roadbed is realized.

PRINCIPLE OF CONTINUOUS TECHNOLOGY

Recognition principle of roadbed

The continuous monitoring equipment is essential for continuously monitoring the construction quality. The vibratory roller can be treated as dynamic excitation equipment, and the dynamic test can be achieved through its rolling process. The roller wheel is the key of the research. It can be expressed as a reaction from the resistance without considering the condition of the roadbed, which is shown in figure 1.

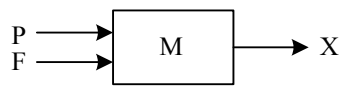

Figure 1. Recognition of roadbed resistance.

This is a problem with single input and multiple outputs. The recognizing work is not so complex because the system is linear. For the linear system, if one input is known, the other input can be obtained by analyzing the response. There are two inputs for the vibratory wheel. One is the exciting force from the roller itself; the other is the resistance from the roadbed. The first is named as P and it is already known, the second is named as F, and it is unknown. The response is named as X, and it can be obtained by monitoring. So F could be obtained with the aid of P and X (Xu and Gao 2007; 2005).

According to figure 1 and Newton second law, the dynamic equation was established as shown in equation 1 and 2.

$$M\ddot{x} + F(x) = P\sin\omega t \qquad (1)$$

$$P = me\omega^2 = 4\pi^2 mef^2 \qquad (2)$$

Where M—quality of roller wheel;

P—amplitude of exciting force;
e—eccentric distance;
m—eccentric quality;
ω—angle frequency, $\omega=2\pi f$;
F(x)—roadbed resistance.

The above equations seem to be simple. In fact, they are very complex. They are nonlinear elastic plastic dynamic equation, and it is difficult to solve. One difficulty is that the nonlinear relationship between F(x) and x is not clear, and the displacement contains elastic part and plastic part. The second difficulty is that the phase angle between exciting force and displacement is unknown. But we can analyze them qualitatively. This is the most common method to deal with nonlinear problems (Zhou 1998)

Theoretical calculation and measured data show that there is linear relationship between acceleration response and system resistance if the vibratory system is steady and the exciting force is fixed. So the acceleration of vibratory wheel is chosen as resistance index. It can reflect the changing information very well.

Continuous testing mode

While testing, the compaction process monitor system (CPMS) is fixed on the vibratory roller, and the dynamic response of the roller can be continuously monitored. The data can be calculated immediately and shown on the system screen. The changing information of roadbed compaction state is reflected by stiffness, intensity and stability, and can be comprehensively reflected by resistance. With the plastic deformation decreasing, the compaction state changes from a low steady system to a high steady system. The roadbed resistance increases continuously, and the dynamic response of roller increases too. All the variation can be reflected by CPMS. The testing mode is shown in figure 2.

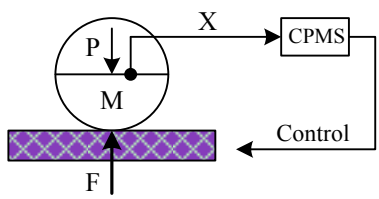

Figure 2. Continuous testing mode for roadbed compaction quality .

MONITORING AND ANALYZING

Test section

A newly constructed road in the suburb of Harbin is studied in this project. This area was lowland in the past, and later became a trash place for construction and

daily life waste. The drill data shows that the components of mixed filling are complex, and the thickness of the mixed fillings is different. There are organic clays containing much water under the layer of the mixed filling. The ground capacity is bad. So it is difficult to deal with it. Dynamic compaction at the initial place was adopted. The hammer weight is 2 tons. The falling distance is 10 meters. After two times of point compaction and one time of row compaction, the surface layer is shoved. Then an 18-ton vibratory roller is used to compact. The resilient modulus is more than 30MPa according to the pavement design.

The relationship between dynamic response X and reflection

YZ16JC vibratory roller is used in compaction of the mixed filling roadbed and the dynamic response testing. The quality of the mixed filling roadbed is measured and evaluated with this roller. The first step is to establish the relationship between the dynamic responses (acceleration) and the normal index (deflection).

When measuring, a section is selected at first, and no less then 30 points' deflections are tested by deflection vehicle. The position of the deflection should also be noted. Then the same section is tested by the vibratory roller with CPMS. After testing, the relationship between the deflection and the dynamic response acceleration are established as shown in Figure 3. The correlation coefficient is 0.87.

According this relationship, the whole section can be tested continuously by adopting the same roller and setting the same parameters.

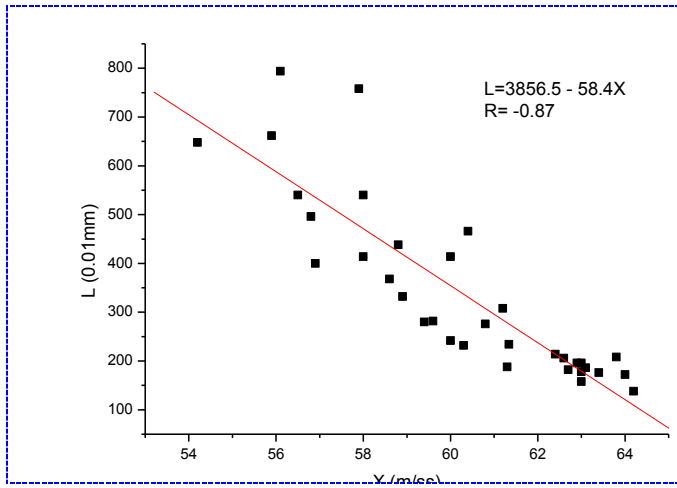

Figure 3. Relationship between deflection and dynamic testing results.

Analyzing the continuous testing results for roadbed quality

According to the pavement design, the resilient modulus should be more than 30MPa, and the corresponding resilient modulus of roadbed should be less than 258.7 (0.01mm) after it is modified by season parameters and roadbed humidity. According to the relationship between deflection and dynamic testing results, the

dynamic response acceleration is calibrated as less than 61.61m/ss. This value is the criterion for roadbed quality. If the acceleration of the testing point is more than this value, it means that this point is eligible. After inputting this value into CMPS, the information for eligible points and ineligible points are shown on the screen of the equipment. Figure 4 is the dynamic response information for the points on the wheel trail. X-axis is the testing distance, and y-axis is the ratio of the testing point acceleration to the criterion. After testing the whole section, the compaction conditions for the whole section are shown in figure 5 and 6. In thes two figures, x-axis is the strip number, and y-axis is the testing distance. Red means eligible and green means ineligible.

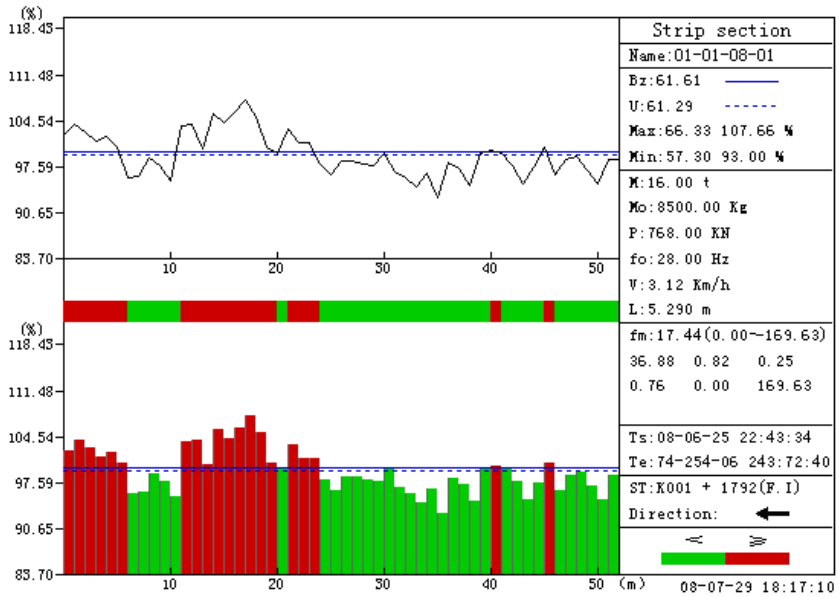

Figure 4. Dynamic response curve of one strip.

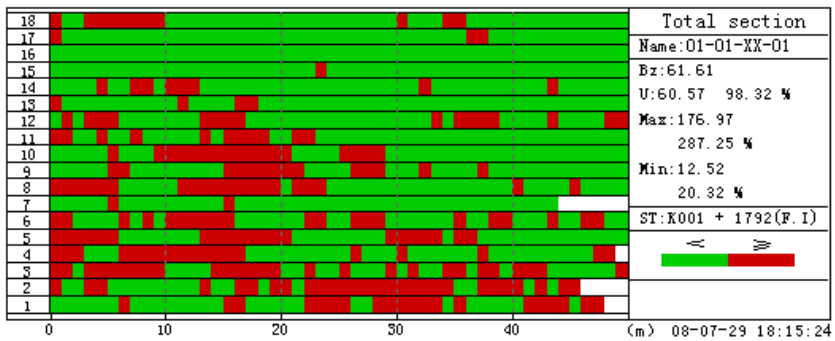

Figure 5. 18 strips results for mixed filling roadbed A.

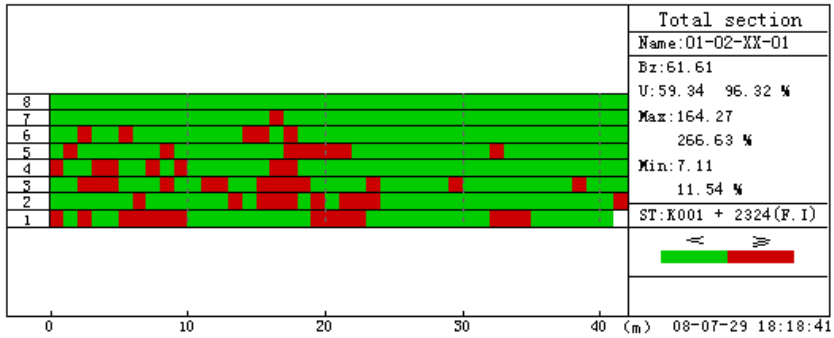

Figure 6. 8 strips results for mixed filling roadbed B .

Using this method, the construction quality after compaction is obtained. As shown in the figures, the ineligible areas are more than 50 percent, and the figure also shows that the compactions are uneven. These are the same with the deflection results. After testing, some representative points including those eligible and ineligible are chosen for further study. Meanwhile, several reasons are identified. One is that the mixed filling does not distribute well. The second is that there are some problems with the dynamic compaction technique. The surface layer is influenced by dynamic compaction greatly. After compaction, the surface layer is shoved and compacted. The compaction layer is so thick, and the deep hole after dynamic compacting can also affect the surface layer. The third reason is that the fine grains in the mixed filling contain a lot of water, sothat the dynamic compaction results are not good.

If the above results can be provided for the construction company and the quality control department, further improvement in construction technology can be made.

CONSLUSION

Continuous dynamic technology can control the overall compation quality during construction, and the output is easy to understand. There are difficulties in normal testing. The relationship between dynamic testing information and normal testing results has been established. Based on this relationship, the dynamic continuous technology can be used in construction quality testing. It is meaningful for monitoring the quality of roadbed, especially for the complex roadbed construction over the long term. It is also important for improving the construction technology, increasing working efficiency and ensuring the construction quality.

REFERENCE

Wu Man-zhen,(1993). “The Utilization of Mix Soil.” Chinese Journal of Geotechnical Engineering, 15(6):103-109

Xu guanghui, Gao Hui.(2007). “Continuous dynamic monitor technology on

subgrade compaction quality."China Journal of Highway and Transpor t.
Xu Guanghui, Gao Hui.(2005). "Analysis of continuous dynamic monitoring on vibrating compaction process of graded broken stone." Chinese Journal of Geotechnical Engineering
Zhou Jiqing (1998). "Nonlinear vibration" Xi'an Jiaotong University Press . 97-137

An Evaluation of the Effectiveness of Geo-textile-Binder-Aggregate System for Surface Treatment of Distressed Asphalt Pavement

Yanping Sheng[1], Shuanfa Chen[2] and Linbing Wang[3]

[1] Virginia Tech Transportation Institute, The Via Department of Civil and Environmental Engineering, Virginia Polytechnic Institute and State University, 301S Patton Hall,Blacksburg,VA24061,PH(001)5405770449; email:shengy08@vt.edu

[2] Key Laboratory for Special Area Highway Engineering of Ministry of Education, Chang'an University, P.O. Box 651, Xi'an, Middle Section of Nan Erhuan Road, PH (86)13609159803, email:chensf@chd.edu.cn

[3]Virginia Tech Transportation Institute, The Via Department of Civil and Environmental Engineering, Virginia Polytechnic Institute and State University, 301N Patton Hall, Blacksburg,VA24061,PH(001)5402315262;Fax(001)5402317532; email:wangl@vt.edu

Abstract

The surface treatment method presented in the paper, a mineral aggregate layer paved on geo-textile coated with asphalt layers on both sides, can improve the performance of existing asphalt pavement surface such as slip resistance, waterproof, and wear resistance. The sample fabrication method is determined by structural characteristic of the treatment method. Eight structures with different asphalt and geo-textile combinations are selected for testing, and the optimal dosage of asphalt and mineral aggregate are determined. The optimal structural combination is obtained on the basis of testing the shear capability of the eight structures. The shear capability of the optimal structural combination is tested under different vertical pressures and temperatures by the shear capability test machine for asphalt road surface structure layers, which is developed by the research team. Test results show that the combination of KLMY90$^{\#}$ base asphalt and short fiber geo-textile with density of 300g/ m^2 is the optimal structure. The friction coefficient of the optimal structure is 0.5989.The results also show that shear capability under high temperature is better than which under low temperature. Finally, the construction procedureis also described . The test road shows that this surface treatment method is economical and effective .

Key Words: Existing asphalt surface, Surface treatment method, Structural combination, Friction coefficient, Shear capability, Construction.

1. Introduction

Surface treatment can be a highly economical highway maintenance option when properly constructed (Khaled, 2007). Surface treatment, usually thinner than 3cm, is constructed by the layer spread method or the mixing method. As the surface treatment layer is very thin, it can't improve the strength of road surface but can seal the cracks, improve the smoothness of road surface, increase the slip resistance and extend the life of pavement (R.Gary, 1997; Chen, 2005). Since the middle 1970s,

surface treatment techniques have been widely used all over the world, in such as France, New Zealand and Australia. Existing research shows that the average life of existing asphalt pavement will be prolonged by using surface treatment techniques (Zane, 2004; Tom, 2004). This paper presents the structure optimization, performance evaluation and construction methods for a surface treatment technique, a mineral aggregate layer paved on geo-textile coated with asphalt layers on both sides. This method has been used in New Zealand and Australia, but has not been used in China (Sheng, 2008).

2. Raw Materials and Sample Fabrication

2.1Raw Materials

Two kinds of asphalt are used in the research. One is KLMY90# base asphalt, the other is KLMY90# base asphalt with 4% SBS. Table 1 shows the test results of asphalt (JTJ052-2000, 2000). For mineral aggregate, macadam granite with single grain size (5~10mm) is used. The test results of the mineral aggregate are showed in the Table 2 (JTJ058-2000,2000).

Table 1. Test Results of Asphalt

Items		Base Asphalt	SBS Modified Asphalt
Penetration(25℃)/0.1mm	25℃	96	76
	5℃	12	16
Penetration Index PI		-0.45	1.77
Ductility/cm	25℃	>150	70
	15℃	>150	37
	5℃	42	28
Softening Point/℃		46	49
Elasticity Comeback(25℃)/%		26	42
Mass Loss/%		0.01	0.06
Penetration Ratio(25℃)/%		63	78
Ductility(5℃)/cm		35	13

Table2. Test Results of Mineral Aggregate

Items			Unit	Test Result
Los Angeles Abrasion			%	21.7
Aggregate Crusing Valve			%	18.1
Ratio of Water Absorption			%	0.64
Content of Slenderness Flat Particle			%	5.36
Viscidity with Asphalt	Base Asphalt		Grade	2
	Anti-stripping Agent(after aging)	3%		4
		4%		5

Apparent Density	g/cm^3	2.68

Geo-textile with long fiber and short fiber, whose density are 300g/ m^2 and 200g/ m^2 respectively , are used in this experiment

AC-16Ⅰconcrete mixture is adopted.

2.2 Sample Fabrication

The surface treatment method proposed in the paper is different from the traditional method for adding geo-textile. A layer spread method is used in the construction. The sequence of construction is asphalt—geo-textile—asphalt—mineral aggregate. The two layers of asphalt should cohere together through the geo-textile layer in order to form the integrity of the structure. A single layer of aggregates of the same size is paved. Meanwhile, the mineral aggregate should be embedded 2/3 into the top asphalt layer to combine with the asphalt adequately and the other 1/3 of the uncovered mineral aggregate provides wear-resistance and slip-resistance. The function of asphalt is to bond the different layers, and the function of geo-textile is to provide waterproof and improvement of the flexibility of pavement. Use of geo-textile can also reduce the temperature stress through controlling the temperature cracking. Geo-textile soaked by asphalt forms a waterproof coating that can prevent rain from infiltrating into the pavement (Jiang, 2000). Figure 1 shows the layer structure of the surface treatment technique. Figure 2 shows the actual effect of determining dosage of each layer's material.

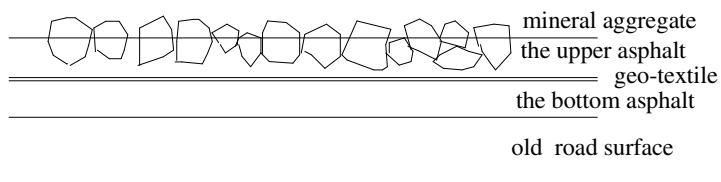

Figure 1. Layer structure of surface treatment

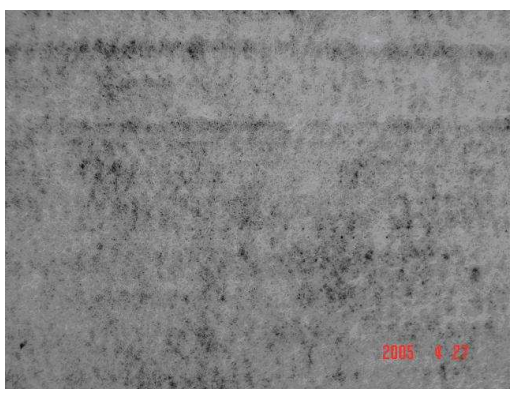

(a)

(b)

Figure 2. Actual effect of determining dosage of each layer's material, (a) Dosage of bottom asphalt and (b) Dosage of top asphalt and mineral aggregate

According to Figure 1 and Figure 2, sample fabrication is obtained after repeated tests. First, a rutting board, which is molded with AC-16 asphalt mixture, is formed as a basic sample. It should be heat conditioned in oven for about 2 hours at 60℃. Then, asphalt (Base asphalt is heated up to 160-170℃, SBS modified asphalt is heated up to 170-180℃) is brushed to the sample surface evenly. Meanwhile, the asphalt quantity of the bottom layer is weighed. Then the geo-textile is spread, after that, the sample is placed on the rutting machine to press twice under the pressure of 0.7MPa. Then, asphalt is evenly brushed to the sample again after heated to the required temperature. The asphalt quantity of the top layer is weighed. Then, an amount mineral aggregate determined beforehand is spread onto the sample surface evenly. The sample is then pressed 6 times under the pressure of 0.7MPa . Since mineral aggregate can't be uniformly arranged in a single layer, whether spalling will appear should be checked. During the test process, if the quantity of spalling of mineral aggregate is too big, the amount of aggregate shall be decreased in the next test, until the optimal quantity is obtained. Finally, the sample fabrication is finished after being pressed 6 times again under the pressure of 0.7MPa.

2.3 Material Dosage Determination

Since the layer of mineral aggregate is one stone diameter thick, dosage of mineral aggregate can be calculated first. The apparent density of the mineral aggregate is 2.65 g/cm^3 by testing. The grain diameter is 4.75mm～9.5mm (intermediate value 7mm is used in calculation). The plane size of the sample is 30cm×30cm. Under the assumption that mineral aggregate is of uniformly sized spheres (the volume of each sphere is (4/3) x π x0.35^3=0.18cm^3), and mineral aggregate is evenly distributed on the sample surface, the total volume can be calculated as 0.18(cm^3)×(30/0.7)×(30/0.7)=330.6 cm ^{3}, so the dosage of mineral aggregate is 330.6(cm^3)×2.65(g/cm ^{3})=876g. Optimal dosages of different structures are obtained on the basis of repeated tests. The results are shown in Tables 3 and 4.

Table 3 Test Results of Mineral Aggregate Dosage

Asphalt	Base Asphalt				SBS Modified Asphalt			
Geo-textile	Long Fiber 300g/m^2	Short Fiber 300g/m^2	Long Fiber 200g/m^2	Short Fiber 200g/m^2	Long Fiber 300g/m^2	Short Fiber 300g/m^2	Long Fiber 200g/m^2	Short Fiber 200g/m^2
Calculated Dosage/g	876	876	876	876	876	876	876	876
Spalling Dosage/g	176	106	156	146	86	106	76	106
Actual Dosage /g	700	770	720	730	790	770	800	770

Unitage/(g/m^2)	7778	8556	8000	8111	8778	8556	8889	8556

Table4. Test Results of Asphalt Dosage

Asphalt	Base Asphalt				SBS Modified Asphalt			
Geo-textile	Long Fiber 300g/m^2	Short Fiber 300g/m^2	Long Fiber 200g/m^2	Short Fiber 200g/m^2	Long Fiber 300g/m^2	Short Fiber 300g/m^2	Long Fiber 200g/m^2	Short Fiber 200g/m^2
Dosage of the Bottom Layer/(g/m^2)	1111	1222	889	1000	1333	1333	1222	1222
Dosage of the Upper Layer/(g/m^2)	1333	1333	1111	1111	1444	1556	1333	1444
Total Dosage/(g/m^2)	2444	2555	2000	2111	2777	2889	2555	2666

Table 4 shows that the dosages of asphalt are different for different kinds of geo-textile. From the test data, the dosage of modified asphalt is more than base asphalt; the dosage of geo-textile with density of 300g/m^2 is more than the geo-textile with density of 200g/m^2 and the dosage of long fiber geo-textile is more than that for short fiber geo-textile.

3. Test of Shear Capability

The road surface should be wear and skid resistant, so shear capability is a key parameter to evaluate the performance. The shear capability test machine for asphalt road surface structure layers, developed by the research team, is used to test the shear capability.

3.1 Testing Machine

The mechanism of the testing machine is to test the friction coefficient *f* between surface treatment layer and a rubber plate. In other words, it is to get the ratio of pull force *F* and vertical load *N*. The pressure *N* is acted on the test piece by a jack. The pressure value can be measured by transducers. Mineral aggregate will be peeled off when both vertical and horizontal forces are applied. At last, the test piece will be removed. The friction coefficient will be measured finally. The diagram of the machine is shown in Figure 4.

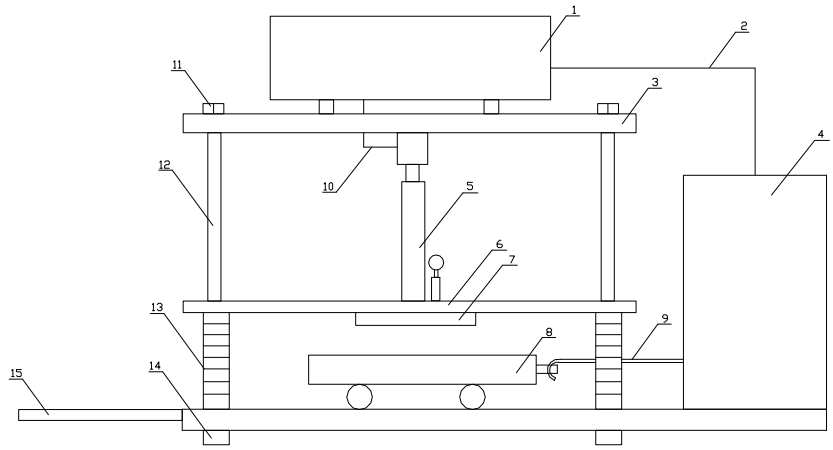

Notes: 1-Intelligent controller;2-Data line;3- Reaction bracket;4-Electromotor;5-Jack;6-Bedplate;7-Rubber board;8-Roll mold;9-Linker;10-Data line;11-Bolt;12-Bracket;13-Spring bracket;14-Bottom bearing;15-Iron rail

Figure 4. Diagram of shear capability test machine for asphalt road surface structure layers

3.2 Test Results and Analysis

3.2.1 Influence of structure

The vertical pressure *N* is basically set as 0.7MPa（25KN）, but it varies with the horizontal pull. A vertical pressure *N* will appear while the horizontal pull reaches the max. The temperature is set as 20C in the experiment. The result is shown in Table 5.

Table 5, Max Horizontal Pull under Fixed Vertical Pressure.

Asphalt	Base Asphalt				SBS Modified Asphalt			
Geo-textile	Long Fiber 300g/m^2	Short Fiber 300g/m^2	Long Fiber 200g/m^2	Short Fiber 200g/m^2	Long Fiber 300g/m^2	Short Fiber 300g/m^2	Long Fiber 200g/m^2	Short Fiber 200g/m^2
Vertical Pressure *N*/KN	26.85	26.04	27.70	27.40	25.33	25.79	25.01	25.12
The Max Horizontal Pull *F*/KN	25.67	25.23	24.94	24.69	23.22	23.84	22.56	22.87
F/N	0.956	0.969	0.900	0.901	0.917	0.924	0.902	0.910

The data in Table 5 indicates that base asphalt is better than SBS modified asphalt. Test results also show that geo-textile with density of 300g/m^2 is better than the geo-textile with density of 200g/m^2. There is no obvious influence by using geo-textile with long-fiber and short-fiber, but geo-textile with short-fiber takes less asphalt dosage than geo-textile with long-fiber. So combination of base asphalt with geo-textile with density of 300g/m^2 and long-fiber is the best structure according to

the test results.

3.2.2 Influence of vertical pressure

Three different vertical pressures are adopted and the temperature is set as 20C in the experiment. The test results are shown in Table 6.

Table 6. Test Results of the Max Horizontal Pull with Different Vertical Pressure

Pressure/MPa	The Max Horizontal Pull *F*/KN	Vertical Pressure *N*/KN	*F/N*
0.5	8.57	14.54	0.589
0.7	12.53	21.07	0.595
0.9	15.91	26.80	0.594

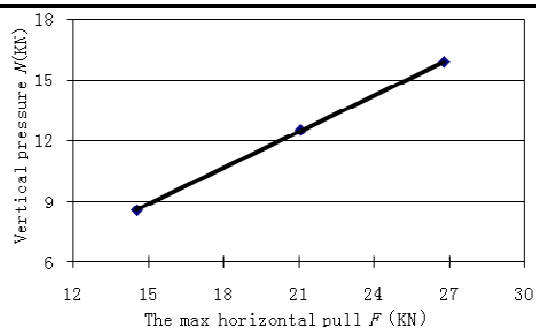

Figure 6. Relation of Max Horizontal Pull *F* and Vertical Pressure *N*

Figure 6 indicates that there is a good linear relationship between the max horizontal pull *F* and vertical pressure *N*. The correlative equation is: $F=0.5989N-0.1219$（$R=0.9999$）.The friction coefficient is 0.5989.

3.2.3 Influence of temperature

Four different temperatures are adopted for testing at the vertical pressure *N* set as 0.7MPa（25KN）. The test results are shown in Table 7.

Table 7. Test Results of the Max Horizontal Pull with Different Temperatures

Temperature/℃	The Max Horizontal Pull *F*/KN	Vertical Pressure *N*/KN	*F/N*
0	15.58	24.64	0.63
20	11.30	19.82	0.57
40	10.60	19.63	0.54
60	8.96	17.23	0.52

Table 7 indicates that the max horizontal pull *F* decreases with the temperature. So the shear capability of the surface treatment is better in low temperature area than in high temperature area.

4. Construction and Testing

4.1 Construction procedure

The construction flow is: Disposal of existing pavement → Sprinkle the bottom layer asphalt → Spread geo-textile → Compact → Sprinkle the top layer asphalt → Spread crushed stones → Compact . The construction flow is shown in Figure 7.

Figure7. Construction flow in fieldwork

4.2 Testing

Table 7 shows the test results of smoothness, structural depth, friction coefficient and seepage conditions. From Table 7, it is evident that pavement performance such as smoothness, slip resistance, friction and waterproof are improved after the surface treatment.

Table 7. Test Results of Test Road

Items	Smoothness/mm	Structural Depth/mm	Friction Coefficient/mm	Seepage Situations/(ml/min)
Technical Requirements Results	≤10	≥0.60	≥54	≤10
Old Surface Pavement	14.5	0.45	30	Seepage*
Pavement After Surface Treatment	8.5	1.1	75	No seepage*

*Under the field acceptance test, since the systematic error of test, if test result of seepage is less than 5mL/min, the pavement is considered impermeable .

5. Conclusion

The method presented in this paper, a mineral aggregate layer paved on geo-textile coated with asphalt layers on both sides，can improve the efficiency of slip resistance, waterproof and wear resistance of existing asphalt pavement surface. Test results of shear capability show that combination of KLMY90# base asphalt, geo-textile with 300g/m^2 density and with short-fiber is the optimal structure. The friction coefficient of the optimal structure is 0.5989 according to the test results of shear capability under different vertical pressures. We have also discovered that the structure is better adapted in low temperature area on the basis of test results of shear capability under different temperatures. Finally, the construction procedure of the surface treatment is described in the paper. The test results show that pavement performance such as

smoothness, slip resistance, wear resistance and waterproof are improved after the surface treatment.

REFERENCES

Khaled, K., Michael,C., and Michal, F.,(2007). Evaluation of Surface Treatment Practices in United States, Transportation Research Record, Washington D.C. ,N0.1545, pp. 26–34.

R.Gary,H., Kimberly, D., and James S.M., (1997). Framework for Selecting Effective Preventive Maintenance Treatments for Flexible Pavements, Transportation Research Record, Washington D.C. ,N0.1597, pp. 1–10.

Zane, L.W.,(2004). Seal Coat and Surface Treatment Manual. Texas Department of Transportation, Austin

Tom, K.,(2004). Surface Treatments: When Your Seals Make Sense, Better Roads, Tuscaloosa

Chen, X.W., (2005).Study on the Modified Asphalt Treatment,Journal of Highway and Transportation Research and Development，Beijing，22(11): 61－64.

Sheng,Y.P., Chen,S.F., Zhang,D.L.,(2008). Study on Surface Treatment Shear Capability of Old Asphalt Pavement, Journal of Chang'an University: Natural Science Edition,Xi'an,28(5):19－22

JTJ052-2000,(2000). Standard test methods of bitumen and bituminous mixtures for highway engineering, Beijing

JTJ058-2000,(2000).Test methods of aggregate for highway engineering, Beijing

Jiang, H.F.,(2000) .Geotextile Applied to Old Asphalt Pavement Strengthening, China Municipal Engineering，Beijing,(4): 29－30

Laboratory Investigation of Reclaimed Asphalt Pavement Mixed with Pure Binder Using X-ray CT Scanner

Cristian Druta[1], Linbing Wang[2], and Tulong Zhu[3]

[1]Virginia Tech Transportation Institute, Virginia Polytechnic Institute and State University, VTTI 2001A, Blacksburg, VA; Ph (540) 231-1056; Fax (540) 231-1555; email: cdruta1@vt.edu
[2]The Via Department of Civil and Environmental Engineering, Virginia Polytechnic Institute and State University, 301N Patton Hall, Blacksburg, VA; Ph (540) 231-5262; Fax (540) 231-7532; email: wangl@vt.edu
[3]Department of Mechanical Engineering, School of Engineering, Widener University, One University Place, Chester, PA; Ph (610) 499-4041; Fax (610) 499-4059; email: tzhu@mail.widener.edu

ABSTRACT

The use of reclaimed asphalt pavement (RAP) has proven to be economical and environmentally safe as being used extensively to produce new asphalt pavements. To examine the "black rock" problem of RAP material, a laboratory investigation was conducted in this study in which the blending process of simulated and actual RAP material with virgin binder was analyzed using an x-ray scanner. For this purpose, new aggregate was mixed with virgin binder containing 25% metal powder (by weight) at 4.5% asphalt content, and then the mixture was oven aged to simulate the RAP binder. Subsequently, the simulated RAP material was again mixed with new binder, without metal powder, to observe if the metal powder from the aggregate surface will combine with the added binder. Also, virgin binder with 25% metal powder was mixed with actual RAP to detect any dispersion of the powder into the asphalt film. Cross sectional images from the x-ray CT scanner indicated that the metal powder has diffused from and into the asphalt film of the aggregate particles during the blending process. Thin layers (microlayers) of metal powder, with varying thicknesses, were observed in the vicinity of the aggregates' surfaces due to x-ray diffraction. The results provide clear evidence that simulated and actual RAP binders partially blend with the virgin binder to a certain extent.

INTRODUCTION

More than 90 percent of the United States roadway system is surfaced with asphalt concrete. Due to this fact, around 500 million tons of hot mix asphalt (HMA) have to be produced every year to cover new placement and rehabilitation works. One-fourth of these tons contain recycled asphalt pavement (RAP) making the HMA industry one of the biggest recyclers in America. The Federal Highway Administration (FHWA) estimates that approximately 90 million tons of asphalt concrete are removed yearly, with more than 80 percent being reused in highway

applications. About one-third of the removed material is recycled into asphalt pavements. Today, RAP is routinely accepted in asphalt paving mixtures as an aggregate replacement and as a portion of the binder for both base and surface courses in most states (McDaniel and Anderson 2001a, b).

Various research studies have been reported in the literature regarding the use different percentages of RAP in HMAs and their performance after placement (Kennedy et al. 1998, Shah et al. 2007). During the blending process, though, there are two major concerns for the engineers and researchers. The first concern relates to the amount of old asphalt binder that actually blends with the new (virgin) asphalt during the mixing process, while the second concern addresses the influence of the aged RAP binder on the composite binder properties. Based on experience and previous test results, the present common belief is that RAP does not act in the new mixture as a "black rock" but the aged asphalt does blend with the new asphalt during the mixing of the materials. These aspects of HMA mix design were addressed in the NCHRP Project 9-12 through fabrication of asphalt concrete specimens that simulated the actual practice, black rock, and total blending. As different cases of blending were evaluated using various Superpave tests at low and high temperatures, it was found out that there were no significant differences among them at low RAP contents. However, at higher RAP contents, usually over 25%, the differences became significant, with the black rock case showing lower stiffnesses and higher deformations than total blending and actual practice cases (Roberts et al. 1996, Soleymani et al. 2000). The partial blending between RAP and virgin binder, especially at high RAP contents, indicates that the hardened RAP binder has to be accounted for in the virgin binder selection (Zhai et al. 2000).

Huang et al. (2005) conducted a laboratory study on asphalt surface mixtures containing screened RAP to evaluate the degree of blending between the two binders. They stated that if the aged asphalt binder cannot fully blend with the virgin asphalt it will form a stiff layer on the aggregate's surface, underneath the virgin binder. Thus, a double-binder layer forms on the RAP's surface which may reduce the internal stresses of the compacted mixtures and eventually enhance their performance (Figure 1).

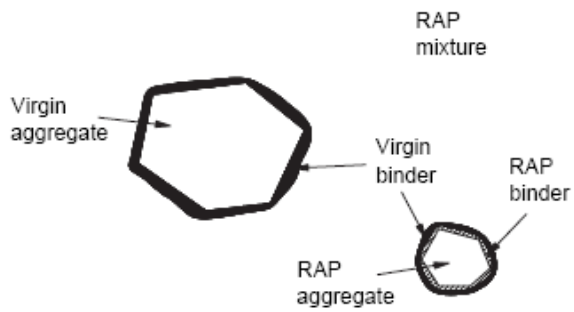

Figure 1. RAP-binder dual-layer system (Huang 2005)

In reality, the actual amount of blending that occurs in a mixture depends on many factors, among which the stiffness of the RAP binder, the compatibility of the RAP

and virgin binders, the characteristics of the hot-mix plant, the mixing temperature, and mix handling are the most important. Also, in the last decade imaging and image analysis techniques have been widely adopted for aggregate and asphalt pavement evaluation. Among these techniques, Computed Tomography (CT) represents a specialized X-ray imaging technique that creates a 3-D image of an object from a large series of 2D X-ray images taken around a single axis of rotation. By spinning the sample around its own axis data is collected from multiple angles, then a computer processes this information to create multiple images. These images are called "cross-sections" or "slices" and can be easily generated for 2D display to analyze the internal structure of the scanned object.

OBJECTIVE

The objective of the present study is to determine to what extent the RAP binder (simulated and actual) will merge with the virgin binder under normal mechanical mixing conditions. For this purpose, metallic powder in the amount of 25% by weight of total binder content was used in order to find out how close to the aggregate surface it “may reach”.

EXPERIMENTAL PLAN

A laboratory experimental plan was developed to investigate the blending effect of the aged asphalt in simulated and actual RAP during a normal mixing operation. This experiment evaluated new aggregate particles coated with asphalt containing 25% metal powder and subsequently mixed with virgin asphalt binder without metal powder. Also, RAP material was mixed with virgin binder containing 25% metal powder. The asphalt binder contents were 4.5% for new aggregate and 2.5% for RAP material, respectively. The amount of binder added to the RAP material was calculated using formulas provided in the NCHRP 452 report. The RAP material originally had 4.4% asphalt content.

Materials and Mixture Production

The virgin aggregate for this study was selected from No. 67 limestone. Only aggregate particles passing the 1/2 in. (12.5mm) sieve and retained in the No. 8 (2.36mm) sieve were used for the mixing with the virgin binder. Properties of the virgin aggregate and binder are presented in Tables 1 and 2. They were provided by Virginia Transportation Research Council (VTRC). The actual RAP material used for blending with the new asphalt binder contained PG64-22 binder. No binder extraction was performed on the RAP material. Also, only particles passing the 1/2 in. sieve and retained in the No. 8 sieve were selected for mixing. The virgin asphalt binder used in this study was a standard PG64-22. The metal powder combined with the virgin asphalt was from industrial grinding processes, with particle sizes ranging from 5 to 50 microns. 25% by weight of metal powder was added to the virgin binder before further mixing it with the new aggregate and RAP. To simulate the aged binder on the virgin aggregate, the mixture was kept for 36 hours in the oven at 120℃.

Subsequently, the simulated RAP containing 25% metal powder was mixed with virgin binder without any powder in it. Similarly, the actual RAP material was combined with virgin asphalt binder containing 25% metal powder. The blending was performed at 175℃ for 5 min. for all material comb inations using a laboratory mechanical mixer after the materials were heated up in a forced draft oven. The blending temperature was selected in order for the RAP particles to completely break down and blend with the virgin materials. As already known, the RAP particles have a coarser gradation than the RAP aggregate, so if the RAP material is not heated sufficiently, the RAP binder does not blend adequately with the virgin binder and the RAP will more likely act as a black rock material.

Table 1. Properties of virgin aggregate

Sieve Size	% Pass
12.5 mm	100
9.5 mm	87
4.75 mm	37.4
G_{sb}	2.651

Table 2. Properties of PG64-22 asphalt binder

Binder test	Test results	Specifications
Rotational viscosity @ 135℃(Pa.s) DSR (G*/sinδ) (kPa) @ 64℃ (Original binder)	0.56 1.64	3 Pa.s max 1 kPa min
RTFO aged binder @ 64℃ DSR (kPa)	3.46	2.20 kPa min
PAV aged binder @ 25℃ DSR (MPa)	3812.2	5000 kPa mi n

X-ray Scanning Equipment

The scanner used in this study was a low energy (50kV) CT scanner using an x-ray cone-beam to collect 2D radiographic (or angular) projections of an object while is rotated 180°or 360°(Figure 2). Its x-ray source has adjustable voltage and can use a range of filters for versatile adaptation to different object densities. Variable magnification (6-30 μm pixel size) is combined with object positioning for easy selection of the object part to be scanned. The x-ray flux is measured by a detector plane located behind the object. This scanning technique, also known as volume CT or 3D scanning uses a special reconstruction algorithm that processes the 2D projections into a volume that is the equivalent of many simultaneous and contiguous CT slices. The reconstruction process includes post alignment optimization and can be focused on a restricted volume of interest. Reconstructed slices can be saved in BMP or JPG data format for subsequent creation of 3D models.

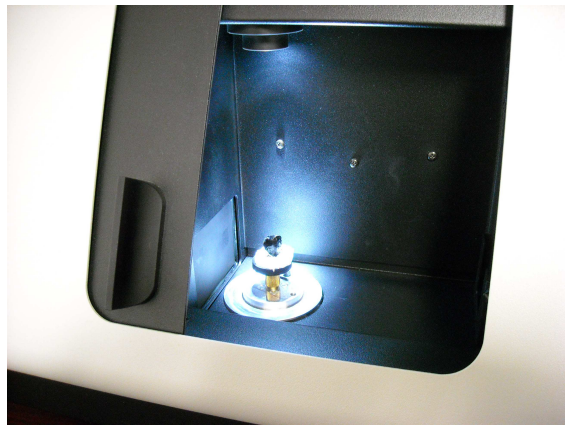

Figure 2. Aggregate particle inside x-ray CT scanner

Aggregate Image Analysis

Ten new coarse aggregate particles and ten RAP particles were randomly selected for X-ray scanning before being mixed with virgin binder. All selected particles were taken from material retained in the 3/8" (9.5 mm) sieve. Same particles were scanned after being mixed with asphalt with and without metal powder in the same orientations and under the same conditions. Three-dimensional radiographic images of the aggregate particles were analyzed with the help of the Computerized Tomography (CT) imaging technique (Wang et al. 2004, 2008). This technique provides non-destructive three-dimensional visualization and characterization of the scanned objects and creates a series of two-dimensional cross-sectional images (slices) of the objects. Figures 3 and 4 show binary radiographic (angular) images of scanned aggregates in the same orientations. Using software capabilities asphalt binder film thicknesses were detected in the range of 15 to 760 microns.

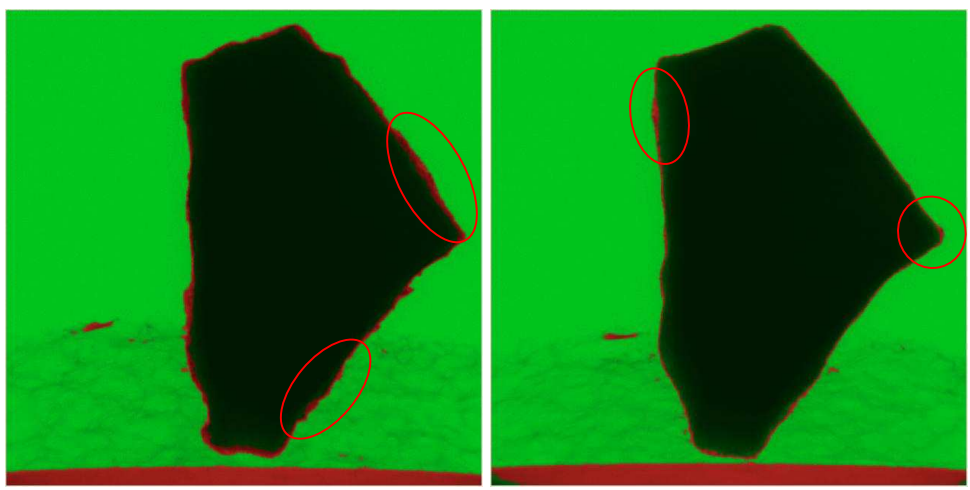

(a) (b)

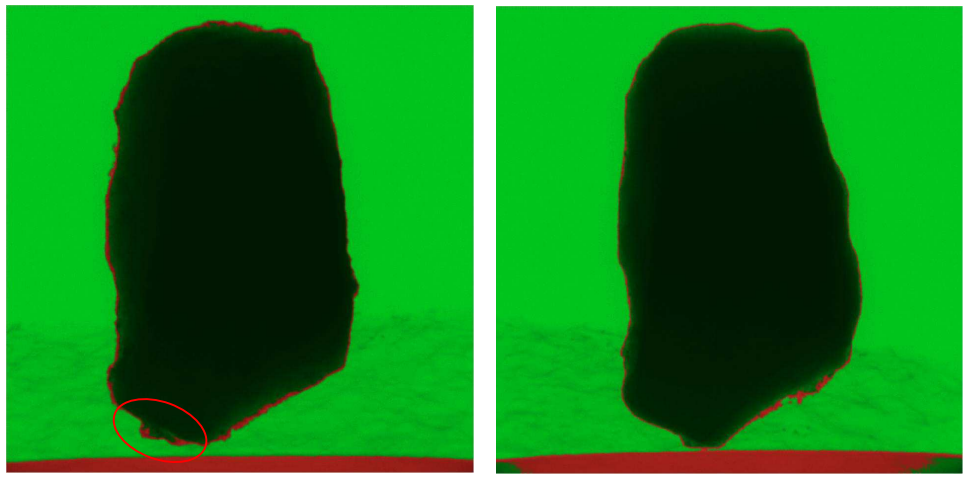

Figure 3. Binary angular images of (a) simulated RAP containing metal powder only and (b) simulated RAP remixed with virgin asphalt

It can be observed from the figures that the asphalt binder is distributed differently on the surface of the aggregates before and after blending with virgin binder. Also, the metal powder (small black spots circled in red), has combined with the newly added or aged binder to different extents. Figures 3(a) and 3(b) picture the same aggregate particle, likewise Figure 4(a) and 4(b).

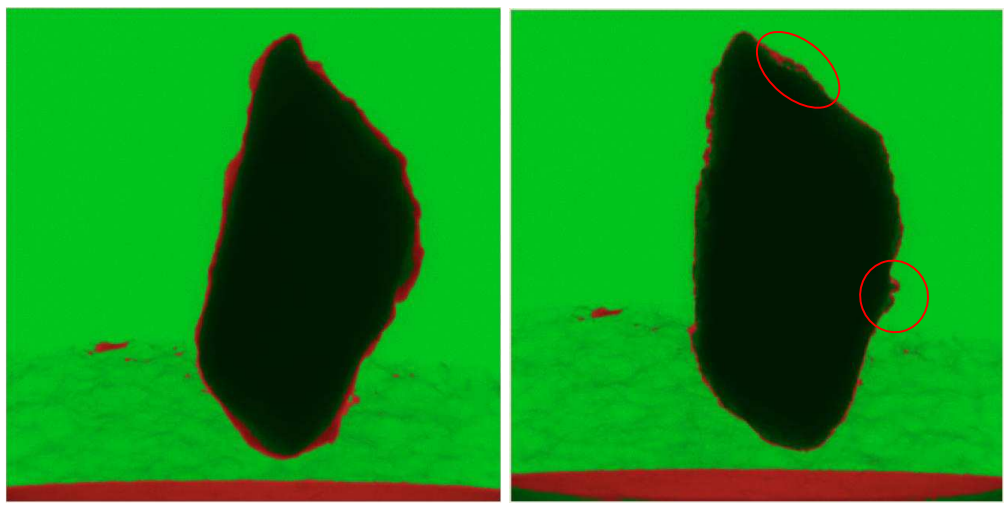

(a) (b)

Figure 4. Binary angular images of (a) actual RAP without metal powder and (b) actual RAP mixed with binder containing metal powder

Figures 5 through 8 present cross-sectional images (slices) of scanned aggregates having thicknesses ranging from 17 to 24 microns. They were acquired at three different locations, closer to the ends and from the middle of the aggregate. Their resolution is 1K x 1K. The contrast in these X-ray CT images is generated from differences in X-ray absorption which relates closely to density differences within the object. During scanning an X-rays cone beam is emitted continuously at different angles and after it has passed through the object the strength of the rays are measured

with a detector. Different contrasts are obtained depending on how dense the material they have passed through is. A computer software subsequently calculates the relative density of the material in the scanned cross section and draws a two-dimensional image of it.

The small white spots (circled in red) in the figures below, representing the x-rays diffraction as they interact with the metal powder, illustrate that the asphalt binder from actual and simulated RAP did blend with the added binder with or without metal powder. It can be observed from Figures 5 and 6 that the new aggregate originally mixed with binder containing metal powder was coated with thicker layers of powder (50 to 340 microns) than the remixed aggregate. Smaller amounts of powder or thinner layers (12 to 72 microns) were detected close to the aggregate's surface for the remixed case. This is illustrated by the red circles in Figure 6. Thus, metal powder layers were detected in the range of 12 to 340 microns for the simulated RAP. The three slices for the two cases were selected at the same z-axis positions for each aggregate at 1K x 1K resolution.

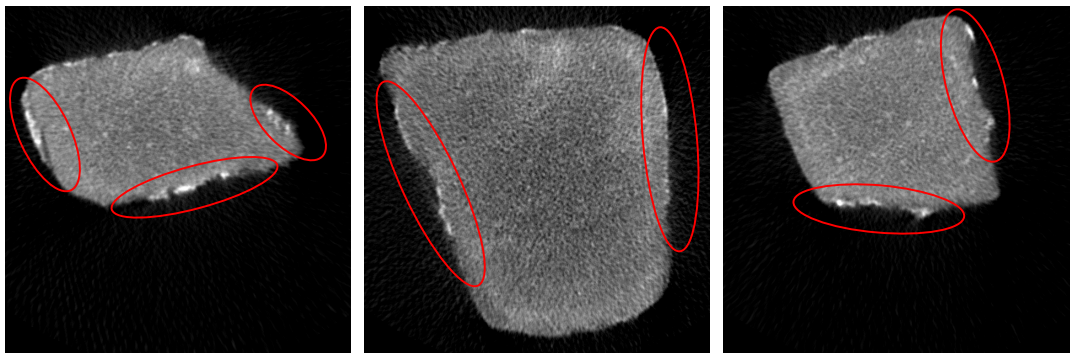

Figure 5. Simulated RAP aggregate coated with asphalt containing metal powder (white spots)

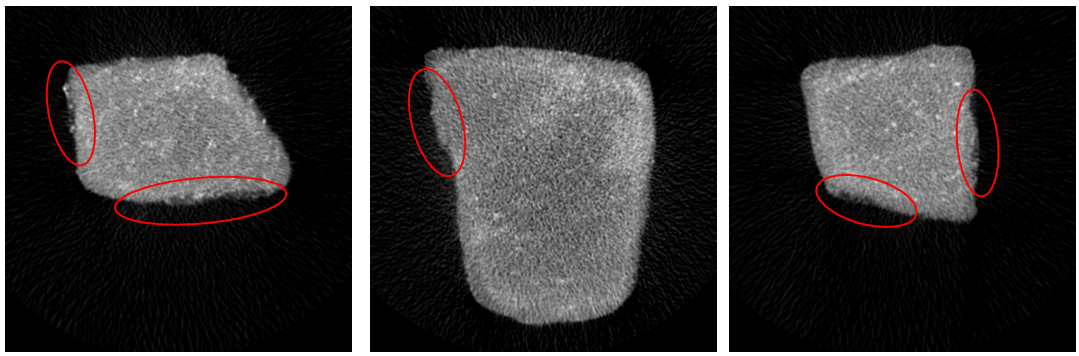

Figure 6. Simulated RAP aggregate remixed with virgin binder without metal powder

Figures 7 and 8 show actual RAP aggregate before and after being mixed with binder containing metal powder. Here also, thin metal powder layers (red circles in Fig. 8), ranging from 15 to 320 microns, have been spotted on the aggregates' surface or in its vicinity, meaning that the aged and virgin binder have combined to a certain extent. In this case, the bright (white) layers only can be observed on the actual RAP

aggregate combined with binder containing metal powder. Figures 5 and 6 present cross-sectional images of the same simulated RAP aggregate particle coated with asphalt binder with and without metal powder, while figures 7 and 8 show images of the same actual RAP aggregate particle before and after it was combined with virgin binder containing metal powder. Cross-sectional images were acquired at same height (z) position.

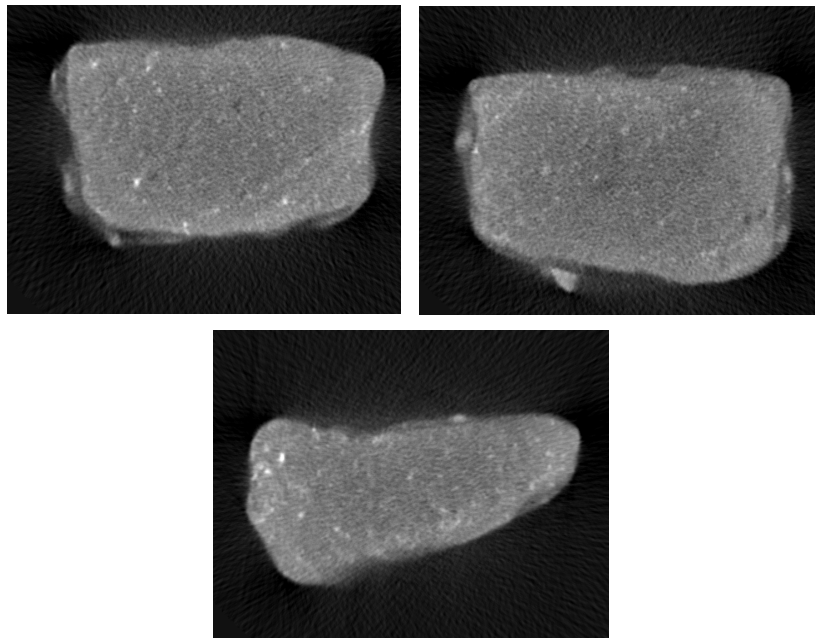

Figure 7. Actual RAP aggregate without metal powder

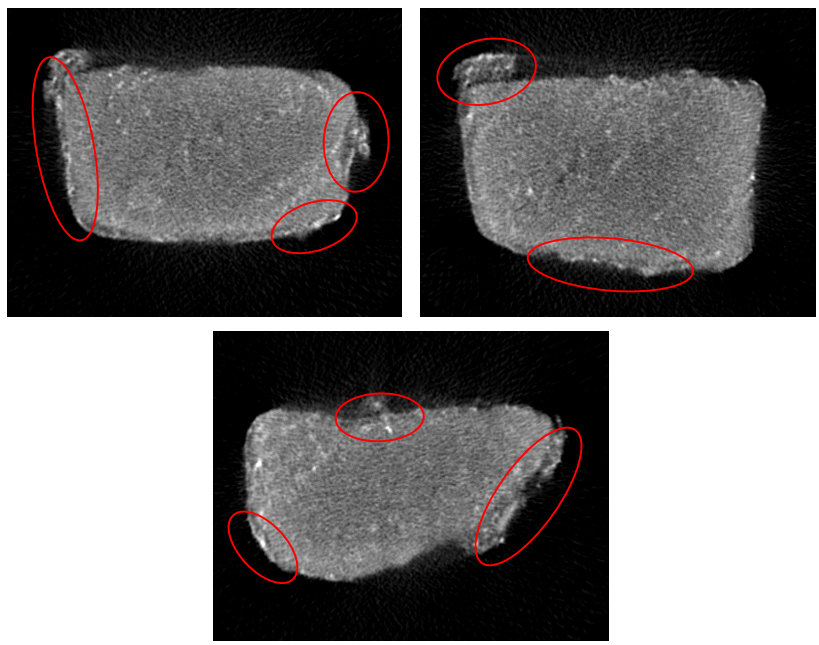

Figure 8. Actual RAP aggregate mixed with binder containing metal powder

SUMMARY AND CONCLUSIONS

This small study was conducted to investigate the blending of actual and simulated RAP binder with virgin asphalt binder with and without metal powder. One type of screened RAP and one type of new aggregate - limestone - were blended under pure mechanical blending along with the binders. It was discovered that partial blending apparently occurred to a certain extent, but it could not be determined if more blending took place in the case of simulated RAP compared to the actual RAP material. Computed tomography images presented in this paper represent only the materials under the test conditions in this study. It should also be mentioned that the mixtures in this study may not reflect the majority of mixtures used by the HMA industry. Additional research investigations are needed to cover a wide variety of materials under various conditions and combinations.

REFERENCES

Daniel, J. S., and Lachance, A. (2005). "Mechanistic and volumetric properties of asphalt mixtures with recycled asphalt pavement." In *Transportation Research Record: Journal of the Transportation Research Board,* Transportation Research Board of the National Academies, Washington, D.C., 1929, 28-36.

Huang, B., Li, G., Vukosavljevic, D., Shu, X., and Egan, B.K. (2005). **"**Laboratory investigation of mixing hot-mix asphalt with reclaimed asphalt pavement." In *Transportation Research Record 1929,* TRB, National Research Council, Washington, D.C., 1929, 37-45.

Kennedy, T.W., Tam, W.O., and Solaimanian, M. (1998). "Optimizing use of reclaimed asphalt pavement with the Superpave system." *Journal of Asphalt Paving Technologists,* 67, 311-328.

McDaniel, R., and Anderson, R.M. (2001a). *NCHRP Report 452: Recommended Use of Reclaimed Asphalt Pavement in the Superpave Mixture Design Method: Technician Manual.* TRB, National Research Council, Washington, D.C.

McDaniel, R. and Anderson, R.M. (2001b). "Recommended use of reclaimed asphalt pavement in the Superpave mix design method: Guidelines." NCHRP, Research Results Digest, 253.

Roberts, F. L., Kandhal, P.S., Brown, E.R., Lee, D.Y., and Kennedy, T.W. (1996). *Hot mix asphalt materials, mixture design, and construction,* 2nd Ed. NAPA Education Foundation, Lanham, MD.

Shah, A., McDaniel, R.S., Huber, G.A., and Gallivan, V.L. (2007). "Investigation of properties of plant-produced reclaimed asphalt pavement mixtures." In *Transportation Research Record,* TRB, National Research Council, Washington, D.C., 1998, 103-111.

Soleymani, H.R., Anderson, R.M., McDaniel, R., and Abdelrahman, M. (2000). "Investigation of the black rock issue for recycled asphalt mixtures." *Journal of Asphalt Paving Technologists,* 69, 366-390.

Wang, L.B., Wang, X., Mohammad, L., and Abadie, C. (2004). "A unified method to quantify aggregate shape angularity and texture using Fourier analysis." In *ASCE Journal of Construction Materials*, 17(5), 498-504.

Wang, L, Druta, C., Zhou, Y., and Harris, C. (2008). "Three-dimensional aggregate evaluation using laser and x-ray acanning." TRB, 87th Annual Meeting, CD-ROM.

Zhai, H., Bahia, H.U., and Erickson, S. (2000). "Effect of film thickness on rheological behavior of asphalt binders. In *Transportation Research Record,* TRB, National Research Council, Washington, D.C., 1728, 7-14.

Influence of Curing Regime on the Ductility of Ultra-High Performance Fiber Reinforced Concrete (UHPFRC)

Yang Songlin[1], Diao Bo[2]

[1] PhD student, Department of Civil Engineering, School of Transportation Science and Engineering, Beihang University, 100191, Beijing, PH(86)10-138 1042 6405, FAX (86)10- 82316111, email: yangsl@ce.buaa.edu.cn
[2] Dr. Prof. Department of Civil Engineering, School of Transportation Science and Engineering, Beihang University, 100191, Beijing,, PH (86)10-136 1110 2221, FAX (86) 10-82316330, email: diaobo@buaa.edu.cn

ABSTRACT

Ultra-High Performance Fiber Reinforced Concrete (UHPFRC), characterized by its outstanding mechanical and ductile performance, have received significant attention recently in the construction. In this paper, curing of UHPFRC cubes and prisms at 20^{o}C and 90^{o}C has been investigated to quantify the differences in both mechanical and ductile performance within the age of 91 days. The results shows that specimens cured at 20^{o}C gives approximately 20%, 10% and 15% lower performance in compressive strength, flexural strength and fracture energy than specimens cured at 90^{o}C, respectively. However, the 20^{o}C-cured specimens not only achieve above 120MPa, 20MPa and 18kJ/mm^2 in compressive strength, flexural strength and fracture energy, but also show advantage in maintaining flexural resistance in the ductile deformation. The results of the research demonstrate the feasibility of in-situ concrete placement and construction of UHPFRC.

INTRODUCTIONUltra-High Performance Fiber Reinforced Concrete (UHPFRC), demonstrates comprehensive high performance in workability, mechanical and durable behavior in the construction. The UHPFRC mix improves the homogeneity by using sand with particle size between 0.15 and 0.6 mm, increases the density by using silica fume as partial cement replacement and improves the ductility by integrating high-quality steel fibers (Richard 1994-96, Soutsos 2005). The current definition of UHPFRC is that the slump, the compressive strength, the flexural strength and the fracture energy are greater than 240mm, 100MPa and 15000 J/mm^2, respectively (Pu 2004, Zhao G. 2004, Chanvillard 2003). In recent years the UHPFRC has been successfully applied to dam repair, bridges, laying pavement, as well as high-level structures (M. E. Schmidt 2005, V.C. Li 2004).

The heat-curing procedure of UHPFRC is used in order to improve the microstructure, reduce curing time and increase early strength (P. Richard 1994, M. Cheyrezy 1994, Z. Helene 1996, T.T. Le 2007, S. Liu 2003, M. Urs 2008). However, it is not only energy-consuming and costly but also restricts the fabrication of UHPFRC products to pre-casting factories. Normal temperature curing would be expected to reduce the early aging material properties, but the increase in usability and the actual long-term material properties may still be sufficiently high. The

comparison of mechanical performance of UHPFRC with and without elevated temperature curing, which could lead to this material being used for in-situ construction instead of factory fabrication, is not yet to be available in the relevant literature. In this paper, the UHPFRC with 0.15 water/binder ratio was produced with steel fiber, polycabonxylate-based superplasticizer and two types of building sands with different maximum particle sizes. Cubes and bending specimens of UHPFRC were tested within the time interval of 91 days (7, 28, 56, 91days) to determine the influence of curing regime on the mechanical performance including compressive strength, flexural strength and fracture energy, and the experimental results shows the possibility of extending UHPFRC from pre-casting factory to the in-situ pouring construction.

MATERIALSPortland cement (52.5N CEM I) and two types of supplementary cementitious materials were used in this study, i.e. ground granulated blast-furnace slag (GGBS) and silica fume (SF). The chemical and mechanical properties of cement, GGBS and SF used in this study are shown in Table 1.

Table1. Chemical and Mechanical Properties of Cement, Silica Fume (SF) and Ground Granulated Blast-furnace Slag (GGBS)

		Cement I 52.5N	SF	GGBS
Chemical composition（%）	SiO_2	18.7	93.1	35
	Al_2O_3	6.3	0.9	12
	Fe_2O_3	3.2	2.0	0.2
	CaO	64.7	0.4	40
	MgO	0.7	1.2	10
	Na_2O_{eq}	0.13	0.3	-
	SO_3	3.1	0.3	-
	Cl^-	0.025	0.09	-
Physical property	Bulk density (kg/m^3)	1200	321.3	1050
	Specific surface (m^2/kg)	460	20000	470

Two types of building sands, Fine Ordinary sand–type I (FOS-I) and Fine Ordinary Sand-type II (FOS-II) were used and Figure 1 shows the particle shape and distribution of FOS-I and FOS-II. The superplasitizer used in this study was polycarboxylate-based, and the steel fibers (BS EN 10016 Part 1) are made using high carbon steel with a tensile strength of 2000MPa and each fiber is coated with brass and is 0.2mm in diameter and 13mm in length.

SPECIMEN PREPARATION The mix design is shown in Table 2. The steel fiber content in UHPFRC is 2% by volume of the total mixture (A. Oner 2007). Use of the polycarboxylate-based superplasitizer enabled a water-binder ratio of 0.15 to achieved, which met the low water requirement of UHPFRC (P. Richard 1995, G. Chanvillard 2003).

Table 2. Mix Proportion of UHPFRC

Cementitious component(level of cement replacement) (kg/m^3)			Aggregate sand (kg/m^3)	Water-binder ratio	Superplasticizer(% solid by weight of binder)
Cement	GGBS	SF			
657	429.8 (35%)	119.4 (10%)	1050	0.15	1.05%

Two groups of UHPFRC specimens were investigated using FOS-I and FOS-II. In each group specimens were cast comprising 50mm cubes for compressive strength (BS EN 1881 Part 116) and 50x50x200mm prisms for flexural strength (BS EN 12390 Part5). The 90°C-cured specimens were stored in a hot water bath from an age of 1 day until 7 days, and then stored in air at room temperature until testing. The 20°C-cured specimens were kept in a standard curing tank until testing.

EXPERIMENTAL TESTS All cube specimens were tested using a loading rate of 0.8kN/s (BS EN 1881 Part 116). The prism specimens were tested under four-point loading using displacement control and using a testing machine controlled by an external displacement transducer, such that the mid-span deflection rate of the prism specimen was held constant throughout the test. The fracture energy (P. Richard 1994) of specimens tested was calculated by integrating the area under the flexural stress versus deflection up to 1.25mm. The mechanical test schedule of UHPFRC specimens is shown in Table 3.

Table3. Test schedule of mechanical properties of UHPFRC

Test age (day)	7	14	28	56	91
20℃ curing	Comp./Flex.	Comp./Flex.	Comp./Flex	Comp. /Flex.	Comp.
90℃ curing	Comp./Flex.	Comp.	Comp./Flex.	Comp. /Flex.	Comp.

NOTE: Comp.: compressive strength test Flex. : flexural strength test

RESULTS AND DISCUSSION

1. Compressive and flexural strength

Figure 2 shows the compressive strength development of UHPFRC using FOS-I and FOS-II under 20°C and 90°C curing. The use of FOS-I and FOS-II had little influence on the compressive strength development. The compressive strength of UHPFRC cubes fell within the range of 160-180MPa from 7 to 182 days, while the 20°C–cured specimens achieved the compressive strength of 120MPa at 20 days and continued to increase. By the age of 180 days, the compressive strength of 20°C–cured specimens stayed at approximately 140MPa which is about 80% of 90°C-cured specimens.

Figure 3 shows the flexural strength development versus the age of UHPFRC. Under 90°C curing, the flexural strength did not change significantly with age and the mean flexural strength was approximately 24MPa. Under 20°C curing, the flexural strength increased from 20MPa at 7 days to 22MPa at 91 days, which is about 90% of 90°C cured specimens.

2. Flexural ductility

Under various curing conditions, failures of the tested UHPFRC specimens show ductile performance under flexural strength tests. Figure 4 shows typical flexural stress versus deflection curve. After crack appeared and started to propagation, fiber bridging effort across the crack section would be dominant in bearing the further loading (K. Y. Leung 1992). The transformation from linear to nonlinear increasing of flexural stress represents the tensile stress transferring from concrete matrix to fibers across the crack section. With the increasing concrete strength by the elevated curing temperature, the higher maximum linear flexural stress was achieved accordingly. After the crack section opening, the stress across the crack section continually distributed which resulted to the unsteady shape of the curve. Stress-deflection curve of 90°C-cured specimens rose faster than 20°C-cured specimens because of stronger adhesion between fiber and concrete matrix.

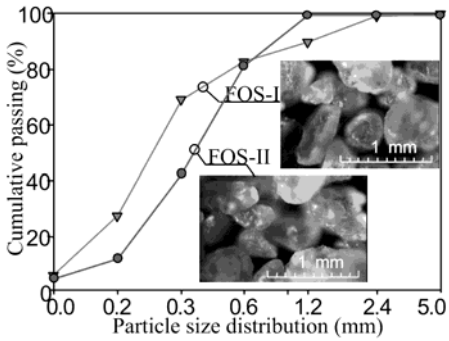

Figure 1. Particle size distribution and micrograph (50x) of the sand particles

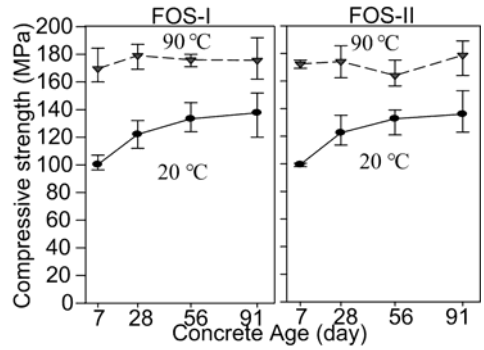

Figure 2. Compressive strength development of UHPFRC

Concrete fracture energy (P. Richard 1994), as the shaded area in Figure 4, can be regarded as the measurement of the efficiency of the fiber bridging effort (M. Cheyrezy 1994). The development of fracture energy of UHPFRC prisms versus age up to 91 days is shown in Figure 5. Although the 90°C-cured UHPFRC specimens exhibited higher compressive strength and fracture energy, the 20°C-cured specimens showed larger mid-span displacement at the peak flexural stress and better ductility at the yielding stage. As shown in Figure 4, $\delta_{20°C}$ and $\delta_{90°C}$ are the mid-span displacement at the peak flexural stress of the UHPFRC prisms cured under 20°C and 90°C, respectively. $\theta_{20°C}$ and $\theta_{90°C}$ are the flexural stress decreasing angle from the mid-span displacement δ_J to $2\delta_J$, respectively. On the whole, a general principle, i.e. $\delta_{20°C}>\delta_{90°C}$ and $\theta_{20°C}<\theta_{90°C}$, was found in all tested specimens. Figure 6a shows the development of deflection at peak flexural stress versus age of UHPFRC. The deflection at peak stress of the tested 90°C-cured specimens stayed approximately at 0.55mm while that the 20°C-cured specimens increased with age and stayed between 0.7mm to 0.75mm. Figure 6b shows the flexural stress decreasing rate from δ_J to $2\delta_J$, i.e. the tangent of $\theta_{20°C}$ and $\theta_{90°C}$ in the unit of MPa/mm, versus age from 7 to 56 days. The decreasing rate of the tested 90°C-cured specimens stayed approximately at -6MPa/mm while that of the 20°C-cured specimens decrease from -3.5MPa to

-4.5MPa from age of 7 to 28 days，it stayed approximately at -4.5MPa/mm from age of 28 to 56 days.

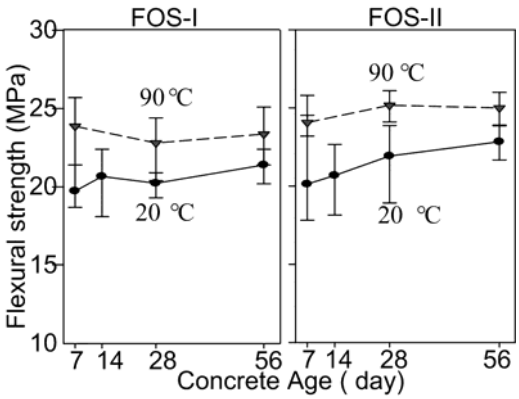

Figure 3. Flexural strength development of UHPFRC

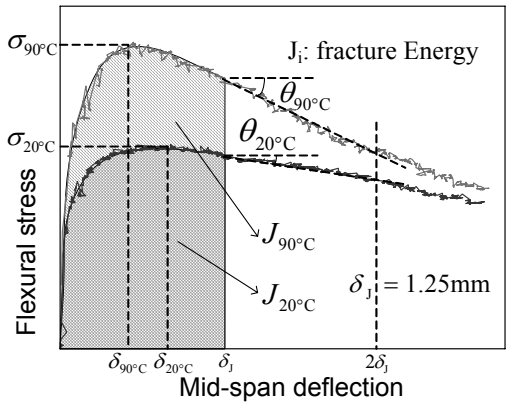

Figure 4. Flexural stress versus mid-span deflection of UHPFRC

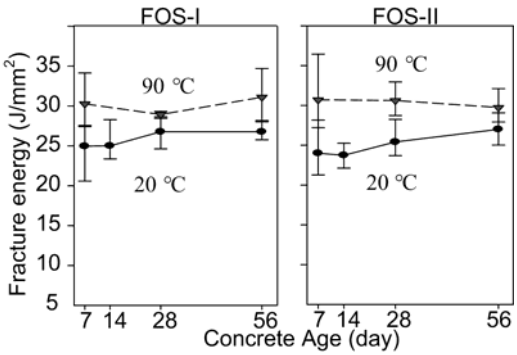

Figure 5. Fracture energy development of UHPFRC

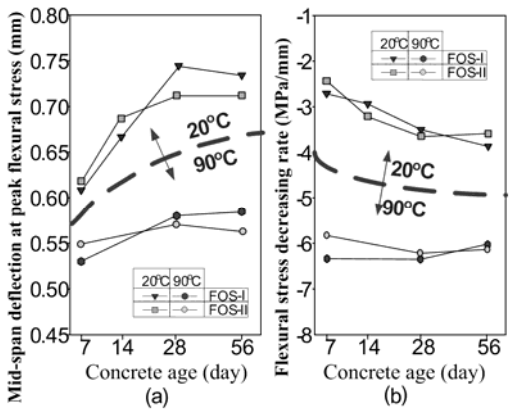

Figure 6. Development of deflection at peak flexural stress and flexural stress decreasing rate from δ_J toδ_{2J}

CONCLUSION

In this paper, experimental investigations have been conduct on the mechanical and ductile performance of UHPFRC under 20°C and 90°C curing within the age of 91 days, and the results shows:

(1) The mechanical performance of 20°C and 90°C cured UHPFRC stabilized after the age of 28 days and 7 days, respectively. Comparison of the mechanical properties from UHPFRC cured at 90°C and 20°C shows that 20°C-cured UHPFRC is approximately 20% lower in compressive strength, 10% lower in flexural strength

and 15% lower in fracture energy than that of 90°C-cured UHPFRC.

(2) The 20°C-cured UHPFRC excelled the 90°C-cured in ductility including displacement at the peak flexural stress and the post flexural stress decreasing rate.

(3) Within parameters investigations, the grading and maximum particle size of aggregate sand do not influence the mechanical strength development of UHPFRC.

Although the 90°C-cured condition leads to higher mechanical strength, the 20°C-cured UHPFRC, similar to the in-situ construction curing, could lead to a more attractive product when considering other aspects related both to economy and to the environment. A small reduction in mechanical properties from the 20°C-cured must be balanced against cost savings from high-temperature curing and pre-casting procedures.

ACKNOWLEDGEMENTThis research work has been partially supported by National Scientific Foundation of China under granted number 50778010. The authors also wish to thank the editors and reviewers of ICCTP 2009 for their assistance during this project.

REFERENCES

Cheyrezy, M.. "Reactive powder concretes with high ductility and Richard, Present and 200-800 MPa compressive strength". *Concrete Technology Past, 1994 Future*, Detroit, Michigan, American Concrete Institute, 507-518.

Chanvillard, G., Rigaud, S.. "Complete characterization of tensile properties of DUCTAL@ UHPFRC according to the French recommendations", *High Performance Fiber Reinforced Cement Composites (HPFRCC4)*, RILEM, USA, 2003.

Helene Z., Marcel C., Vincent M., et al. (1996). "Investigation and pozzolanic reaction in reactive powder concrete(RPC) using Si29 NMR". *Cement and Concrete Research*, 26(1), 93-100.

Leung K. Y., Li V .C. (1992). "Effort of fiber inclination on crack bridging stress in brittle fiber reinforced brittle matrix composites". *Journal Mechanics and Physics of Solids,* 40(6), 1333-1362.

Li, V.C. "Strategies for High Performance Fiber Reinforced Cementitious Composites Development". *North American/European Workshop on Advances in Fiber Reinforced Concrete*, 2004, Italy, 93-98.

Liu, S. (2003). "Preparation and Durability of High Performance Concrete with Natural ultra-fine-doped hybrid materials". *Portland Journal*, 31(11), 1080-1085.

Oner A. , Akyuz S. (2007). "An experimental study on optimum usage of GGBS for the compressive strength of concrete". *Cement and Concrete Composites*. 29(6), 505-514.

Pu, X.. *Ultra-High Performance Concrete*. Chongqing Universiy Press, 2004

Richard, P., Cheyrezy M. "Reactive Powder Concretes With High Ductility and 200 - 800 Mpa Compressive Strength". *Concrete Technology: Past, Present and Future*. 1994,144, 507-525.

Richard, P., Cheyrezy M. (1995). "Composition of reactive powder concretes". *Cement and concrete research*, 25(7), 1501-1521.

Richard, P. "Reactive powder concrete: a new ultra-high-strength cementitious

material". *Fourth International Symposium on Utilization of High-strength/High-performance Concrete*, 1996, Paris, 1343-1352.

Schmidt Fehling E. "Ultra-High-Performance Concrete: Research, Development and Application in Europe". *Seventh International Symposium on the Utilization of High-Strength/High-Performance Concrete*, 2005 Washington, D.C., 51-78.

Soutsos M. N., Millard S. G., Karaiskos K. "Mix design, mechanical properties and impact resistance of reactive powder concrete(RPC)". *International workshop on High Performance Fiber Reinforced Cementitious Composites in Structural Applications*, 2005, Hawaii, 549-560.

Urs M., Birgit M., Hans-Carstan K., et al. "Micro texture and mechanical properties of heat treated and autoclaved Ultra High performance Concrete (UHPC)". *Second International Symposium on Ultra High Performance Concrete*, 2008, Kassel, 213-220.

Zhao G.. (2004). "Introduction to the high performance concrete". *Construction Technology*, 31(4), 1-3.

NURBS Strands Modeling of Prestressed Concrete Bridges

Dawei Yang[1] and Qiao Huang[1]

[1]School of Science and Engineering of Communications, Harbin Institute of Technology, Heilongjiang Harbin 150090; email: yangdawei.hit@gmail.com

[1]School of Science and Engineering of Communications, Harbin Institute of Technology, Heilongjiang Harbin 150090

ABSTRACT

To establish the unified description for strands in prestressed concrete girder bridges, a NURBS strands model is proposed in which Non-Uniform Rational Basic Spline (NURBS) is adopted. Prestressed strands in design and construction are analyzed, which presents the reasons for selection of NURBS as the strands model. Compared with the Fold Line Approximation Model (FLAM), the NURBS model needs fewer parameters for pre-processor and gives higher accuracy in the calculation of prestress equivalent loads and loss of tendon forces. The example using the NURBS model is fit to be a unified description method for strands in all kinds of prestressed structures.

ITRODUCTION

Prestressing effects analysis plays a significant role in design and calculation of prestressed concrete bridges. The quality of structural design, especially for statically indeterminate continuous post-tensioned concrete bridges, significantly depends on the accuracy of prestressing effects analysis. Among the three basic viewpoints or analytical ways of prestressing members, the load balancing as first introduced by Lin (1963), is the predominant method nowadays, in which prestressing is viewed as an attempt to balance a portion of the load on the members. Together with the concentrated force acting on the end of the beam, the vertical forces compose a system of external loads which can be looked upon as a separation body free from the original structure. Respectively, concentrated force is the action arising from the points of anchorage and abrupt turning of tendon, and distributed force is the action arising from curvature part. The distributed force is constant only when the profile is strictly arc because of the invariant curvature. In the actual engineering circumstances, the profiles of tendon are so complex that there are no general functions that can be used to describe them. Accordingly, mathematical modeling of tendon and its relative calculation become important for solving problems of prestressing effects analysis.

Xiao (2002) presented a model of prestressing tendon in which the geometry profile was idealized as a series of straight segments and thus called the fold-line approximate (FLA) method. Theoretically, the fold-lines approximate the original curve at the precision level of engineering and the equivalent loads are accordingly transformed from distributed forces to a series of concentrated forces. Although the

FLA is simple and directly perceived to some extent, there are several associated shortcomings including: (1) as a spatial curve, the profile of tendon is of first and secondary continuity which are lost after transforming into fold-lines and leads to some error; (2) the tedious fold-lines dividing not only increases the preprocess of calculation but also makes it hard to control the error induced from human operation; and (3) the FLA is inconvenient for alignment adjustment, especially during the repetition check in the process of structure design. The above latent defects of the FLA are not negligible according to the theory of prestressing effects analysis.

This paper introduces a spline curve instead of the PLA and offers a new model based on the Non-Uniform Rational Basic Spline (NURBS). This NURBS model, expressing geometry profile with simplicity and accuracy, is easy for evaluating equivalent loads. Through examination of numerical examples, the NURBS model is demonstrated to be a unified way for expressing prestressing tendon and one that can be applied to the actual design of structures.

NURBS MODELING OF TENDON

Engineers are initially familiar with spline functions or curves from their application in the finite strip method. In fact, spline curves can be widely used in more complex circumstances of engineering. Applying spline as model of tendon is indicated by its nature that in the actual construction the tendon is fixed on scattered locations of the duct. So the final result of construction is indeed scattered points fitting the curve of the original one no matter it is a arc curve or a parabolic curve in the working drawing. Spline, however, has been a perfect solution in the field of computer graphics (Qin 1985, Li 1998). The main reason for selecting NURBS as model of tendon is the advantage over other splines—the local modification scheme that means that changing the position of control points only affects the curve on nearby intervals. The local modification scheme provides NURBS curve with necessary flexibility that when some control points are adjusted the other part of the curve does not vary notable. This benefit offers engineers with great efficiency and accuracy for design. There are more advantages that are not stated here (Philippe 1996).

A NURBS of k degree is defined as such：

$$\overline{P}(u)=\frac{\sum_{i=0}^{n}\omega_i\vec{d}_iB_{i,k}(u)}{\sum_{i=0}^{n}\omega_iB_{i,k}(u)} \tag{1}$$

where $\omega_i, i=0,1,...,n$ are the weights，$d_i, i=0,1,...,n$ are control points，$B_{i,k}(u)$ are B-spline basis function of k-degree of point *i,* which is deduced from the recurrence formula of the point vector of B-spline basis function U= [u_0, $u1$, u_{n+k+1}] as Eq. (2).

$$B_{i,m}(x) = \frac{x - x_i}{x_{i+m-1} - x_i} \cdot B_{i,m-1}(x) + \frac{x_{i+m} - x}{x_{i+m-1} - x_{i+1}} \cdot B_{i+1,m-1}(x) \tag{2a}$$

$$B_{i,1}(x) = \begin{cases} 1, & x \in [x_i, x_{i+1}] \\ 0, & x \notin [x_i, x_{i+1}] \end{cases} \tag{2b}$$

The B-spline applied in the finite spline method is actually a special form of Eq. (1) with k = 3 and the knots distributed in uniform or equal-spacing intervals, in which there is a denominator term called uniform non-rational B-spline(UNRBS). Otherwise, it is called the Non-Uniform Rational Basic Spline (NURBS).

When modeling the tendon, it is difficult to ensure a uniform knots vector so that the fixed points in construction become even in the meaning of parameter *x*. Also, the Non-Rational B-spline cannot describe exactly the second order curves except for the parabolic ones. NURBS, however, is not limited to this constraint, and can be used to precisely express all the curves including the straight lines, second order parametric curves and any free curves. For this reason, the NURBS was defined as the unique mathematic method for geometric shape in the 1991 STEP standards for data exchange of industry products.

APPLICATION AND EXTENDING OF NURBS++

The first problem of the NURBS tendon model comes with programming since its algorithm is much more complex than regular curves. Piegl and Tiller (1996) and Shi (1994) discussed or expounded about the NURBS; while much software on CAD exhibit the ability of forming NURBS. Philippe (1996) developed a graphic library for program—the NURBS++ to facilitate the application of NURBS, which is used in this paper to model tendon. The application and extending of NURBS++ are discussed as followed.

NURBS++ is based on two basic data types, the Vector class and Matrix class, both having the powerful mathematic operation and memory to allocate functions and thus can be easily used. Based on the Vector and Matrix curves and surface classes are developed as the child class of NurbsCurve class.

Although the NurbsCurve provides functions to calculate the length of curve and the derivatives of k-1 degree, there are some variables such as curvature at any points that is needed for equivalent load of prestressing tendon and for the accumulation of angles between tendon and horizontal line used for formulating friction loss. These, however cannot be directly obtained from the functions of NurbsCurve. Therefore, it is necessary to extend the original library of NURBS++ for such purposes.

Distribution load induced by the prestressing tendon is defined as:

$$q(x) = N_y(x) \cdot \kappa(x) \tag{3}$$

where $q(x)$, $N_y(x)$, $\kappa(x)$ are the distribution load, prestressing force and curvature at coordination x, respectively. Accordingly, curvature computing actually is a procedure of getting curvature based on the first and second order derivatives of the profile line of tendon：

$$\kappa = \frac{y''x' - x''y'}{[(x')^2 + (y')^2]^{3/2}} \tag{4}$$

It should be noted that the variables x and y in the Eq. (4) are functions of parameter t while the variable x in Eq. (3) is the coordinate. To void abrupt turning of distribution load, that is to keep the second order continuity, the degree is defined as 3. When the function that executes Eq. (3) and (4) is extended in NURBS++, the calculation of distribution load of the prestressing tendon can be used to call this function.

As calculating frictional losses, the angular change of tendon from jacking end to point x is required while generally it is difficult to get as well as curvature. The curvature, however, has been solved with the above function in NURBS++. So, the angular can be gotten with Eq. (5):

$$\theta = \int \kappa(x)dx \tag{5}$$

After extending the NURBS++, the Strand class is programmed with one NurbsCurve object as its member variable and the modeling of tendon and its relative operation is built in this class.

EXAMPLES

Two examples are given here to examine the accuracy and convenience of the NURBS tendon model.

Example 1: A part of tendon is an arc with its radius R = 170 m, x∈ [-30 m, 30 m] and the prestressing force is 1000 kN, as shown in Fig. (1a). The arc is fitted with 5 dispersed points, with coordinates at (-30, -2.668)、(-15, -0.6631)、(0, 0)、(15, 0.6631)、(30, -2.668).

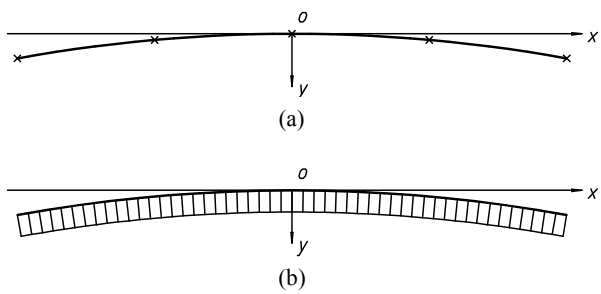

Fig. 1 Arch Tendon Profile

Figure 1(b) shows the curve fitted with NURBS++. The $\kappa(x)$ equals to 5.888×10^{-3} m^{-1}, the length of arc s is 60.316 m，and the angular θ equals 0.355 rad. Theoretically, the geometric parameters of arc are $\kappa \equiv 1/170 = 5.882\times10^{-3}$ m^{-1}，s = 60.315 m，θ = 0.355 rad.. Substituting the value of curvature into Eq. (3), the equivalent load of prestressing can be obtained as $q(x)$ =1 000$\times5.888\times10^{-3}$ = 5.888 kNm^{-1}. Compared with the result of FLA，the total concentrated force $F_y = 5.888\times60$ = 353.28 kN, the NURBS model is obviously better. The results produced from FLA and NURBS are compared in Table.1.

Table 1. Fold Line approximation and the NURBS model

Number of Knots	FLA 5	FLA 17	FLA 33	NURBS 5
Length of arc (m)	60.296	60.315	60.315	60.316
Angular (rad.)	0.2657	0.3324	0.3436	0.355
Force on nodes (kN)	883.00	22.10	11.00	—
Total force (kN)	264.90	336.00	352.00	353.28

Table 1 shows that, with the knots number increasing，the error of PLA become smaller. However, the knots number needs to be higher for the further precision. Conclusively, the NURBS model provides better precision and efficiency while needs fewer parameters than the PLA model.

Example 2: A post-tension prestressed girder bridge is of 2-span with one prestressing tendon as shown in Figure 2. The dispersed knots are expressed with "×". Considering the symmetry about axis Y of the tendon profile, only half coordinate of knots are listed in the Table 2 and the curve of tendon are fitted by the spline function using the engineering graphic software, AutoCAD. The equivalent load (only including distribution loads) is shown in the Figures 2 (a~d).

Table 2 Points coordination of the tendon

Points	1	2	3	4	5	6	7
x(m)	0.00	2.00	5.00	7.00	13	15	20
y(m)	-0.15	-0.30	-1.00	-1.35	-1.70	-1.70	1.00

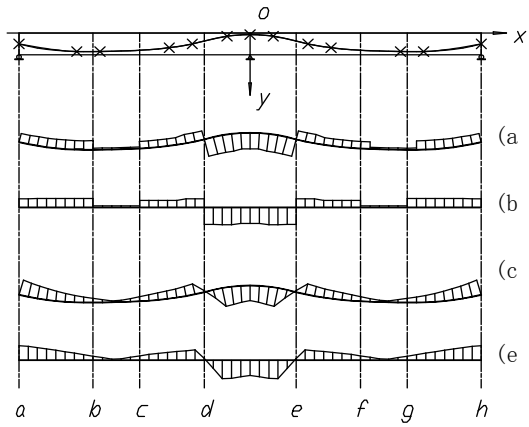

Fig. 2 Tendon with Free Profile

In Figure 2, (a) gives the second order (k=2) NURBS fitting the prestressing tendon and equivalent loads; (b) is the vertical component of (a); (c) gives the third order (k=3) NURBS fitting the prestressing tendon and equivalent loads; and (d) shows the vertical component of (c). This example adopts the second and the third order NURBS curve respectively to fit the tendon profile. Both schemes are good at the precision of lines as shown in Figures 2 (a) and (c). While on the equivalent loads, the result of the second order NURBS curve is not continuous at the points of c、d、e、f、 g, the third order curve apparently gets the continually varying distribution loads. Accordingly, it is necessary to adopt the third order NURBS to obtain reasonable result.

CONCLUSION

In this paper, numerical model of prestressing tendon is discussed and a new one—NURBS model is presented, which provides better precision and much efficiency than the PLA method. It is believed that the NURBS model is especially suitable for the analysis of the post-tensioned prestressing girder bridges. Through extending the library NURBS++, this model is conveniently available in the program. Further, for the flexibility in any plane and spatial curves, the NURBS model can be applied for analyzing more complex structures such as the curve girder prestressed bridges and circle shape prestressing tendons and thus can be used as an unified description method.

REFERENCES

Foley, J. D., van Dam, A., and Feiner, S. K. (1998). "Introduction to Computer Graphics." *Addison-Wesley Publishing Company, Inc.*

Piegl, L. A., Tiller, W. (1996). "*The NURBS Book (2 edition)*."Springer, Berlin.

Li, J. (1998). "Principle of computer graphics."*Electric scientific university press*.

Lin, T. Y. (1963). "Load-Balancing Method for Design and Analysis of Prestressed Concrete Structures." *J. ACI*, 60(6), 719~742.

Lin, T. Y. and Burns, N. H... (1981). "Design of Prestressed Concrete Structures." *John Wiley*.

Philippe, L. (1996). http://yukon.genie.uottawa.ca/lavoie/software/nurbs

Qin, R. (1985). "Spline function method of structure mechanics."*Guangxi People Press*.

Shi, F. (1994). "*Computer aided geometry design and NURBS.*"Beijing Aeronautic and Space University Press.

Xiao, R. (2002). "Analysis system of bridge structures." *People Communications Press*.

Zhang, C. (2004). "Analysis of mathematic on engineering." Scientific press.

Zhang, S. (2004). "*Design principle of reinforced concrete and prestressed concrete bridge.*" People communications press.

Performance Model for Pavement Maintenance of Expressway in Northwest of China

Zhang Yan[1],Zhao Chen[2], Li Wei-sheng[3]

Zhang Yan[1] ,Energy and Traffic Engineering college, Inner Mongolia Agricultural University Huhhot,P.C.010018;PH86-471-4309211;FAX86-471-4309204; email: zhangyanli@imau.edu.cn
Zhao Chen[2],Civil Engineering college, Nanjing Forestry University, Nanjing, P.C.210037; PH 86-25-85427021; FAX 86-25-85427168; email: czh@njfu.edu.cn
Li Wei-sheng[3],Material Science and Art Design college, Inner Mongolia Agricultural University; PH 86-471-4309211; FAX 86-471-4309204; email: liweishengyan@126.com

Abstract

This paper focused on developing pavement formance model for the pavement maintenance of expressway in Northwest of China. It included traffic analysis, identification of typical pavement distresses, and pavement performance evaluation. There were three primary distresses in these expressways, transverse cracking, potholes, and rutting. The performance index and pavement performance evaluation model were developed suitable for expressway maintenance in Northwest. The model was evaluated using fuzzy mathematics. In conclusion, the modeling results agreed with expert evaluation.

Keywords: expressway, asphalt pavement, distress, maintenance, method

Foreword

China began to construct expressway since the 1970´s when it has been common in America and Europe. On Dec.31, 1988, the first expressway from Shanghai to Jiading was opened to traffic. This section of expressway was 18.5 km in length. From then on, the expressway mileage has increased rapidly. There were about 5.4×10^4 km expressway in China by the end of 2007, after 20 years' rapid development. The total length was about 6.03×10^4 km by the end of 2008(China Highway Magazine Agency.2005), which put China in the second position in the world. The freeway network will reach 8.5×10^4 km by 2020, which will be close to that of USA in terms of total mileage, according to "The Plan of National Expressway Network". China plans to construct significant amount of motorways for next decades .

Under the repeated vehicle loads and the environmental impact, the performance of expressway pavement deteriorates in terms of pavement strength, stiffness, stability, roughness and anti-skid ability. The serviceability and life of pavements will be severely affected if the distresses cannot be repaired as needed. This study focused on the maintenance of expressways in the Northwest of China.

1 Performance Evaluation of In-service Expressway

1.1 Traffic

Based on investigation, the traffic consisted of about 32.3%, 28.2 and 18.0% trucks, trailers and cars, respectively. More than 70.7% of trucks were overloaded by 100-200%. Overloading is common in the Northwest of China, due to its abundant natural resources, especially coal. Heavy traffic, especially overloaded trucks, was the major reason of the pavement distresses.

1.2 The typical pavement distress

The expressway asphalt pavement were investigated in terms of distress types and causes, factors affecting performance, maintenance conditions, traffic, geotechnical conditions, and

climate in the field. It was concluded that there were three primary distresses in expressways, transverse cracking, potholes, and rutting.

1.3 Field investigation

The basic cross section of a typical Northwest expressway consists of 2 lanes, one lane for one direction. The lane width is 3.75m, with 3.0m shoulder. For every 1000m within the stationing between k83 and k56, 22 sections were selected for field investigation. The results are shown in Figures 1～4.

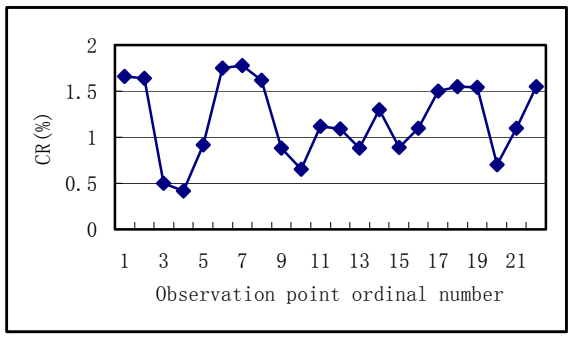

Figure 1. Survey data of transverse cracking.

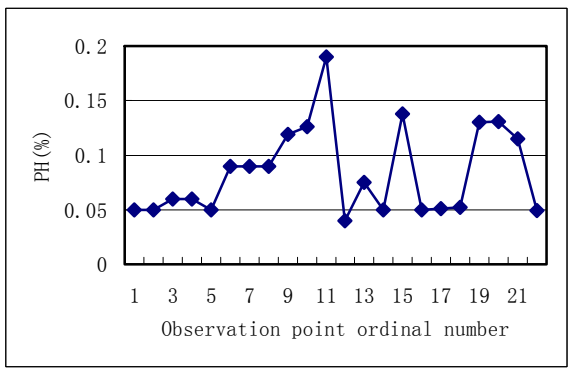

Figure 2. Survey data of potholes.

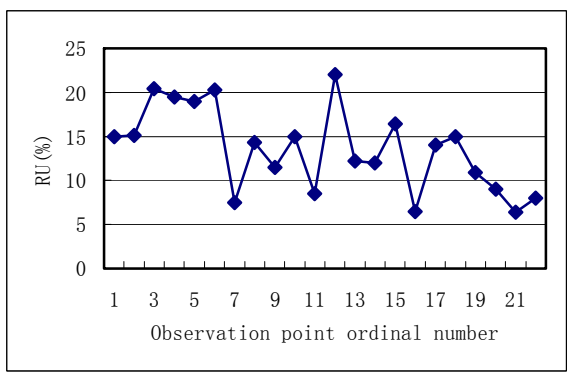

Figure 3. Survey data of rutting.

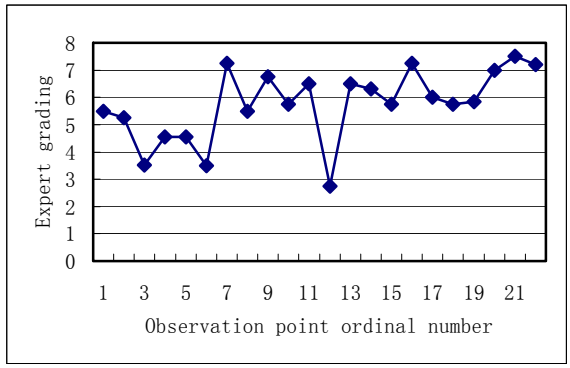

Figure 4. Result of expert grading.

2 Pavement performance evaluation model

The first pavement performance evaluation model was based onpresent serviceability index (PSI) and was developed by the American Association of State Highway Transportation Officials (AASHTO). PSI is essential to the development of pavement maintenance techniques and pavement management systems. Many countries have developed their own models, based on PSI. A pavement performance evaluation model was developed for the expressways in the Northwest of China in this paper.

2.1 Factor selection

The progression rates of transverse cracking, potholes and rutting were selected as primary factors in the model.

2.2 Grading method

The expert system was also used in this study, based on ten-point system. The results were showed in Table 1.

Table 1. Description of Expert System.

Score	Grade	Road condition
10~8	excellent	very smooth
8~6	fine	no or little distresses and smooth
6~4	medium	little distress and rough
4~2	second	some distress, discomfort and very rough
2~0	poor	severely distressed

2.3 Modeling

Equation 1 was selected as the model, based on the three typical distresses.

$$PCI=f(CR, PH, RU) \qquad \text{(Equation 1)}$$

Using multi-variable regression analysis, Equation 1 can be rewritten as Equation 2.

$$PCI=\alpha_1+\alpha_2 f(CR)+ \alpha_3 f(PH)+ \alpha_4 f(RU) \qquad \text{(Equation 2)}$$

Where PCI is pavement performance index, CR is transverse cracking damage rate, PH is potholes damage rate, and RU is rutting damage rate.

Single-variable regression analysis was conducted using different functions like $y = a + bx$,

$y = ae^{bx}$, $y = ae^{\frac{b}{x}}$, $y = ax^b$, $y = a + b\ln x$, $y = a + b\ln(x+1)$, $\frac{1}{y} = a + \frac{b}{x}$,

$y = b(x-c)^2 + a$, $y = \dfrac{1}{a + be^{-x}}$, $y = a + b\sin x$, $y = a + b\cos x$, $y = a + b\tan x$ and so on.

Correlation function between expert grading and survey data are showed in Table 2.

Table 2. Correlation function between expert grading(M) and survey data.

Variable(%)	function	correlation coefficient
CR	$M = 5.6723 + 0.0317\tan CR$	0.2534
PH	$M = 6.9206e^{\frac{-0.0151}{PH}}$	0.3479
RU	$M = 7.6803 - 0.0091RU^2$	0.9640

Using $0.0317\tan CR$, $e^{\frac{-0.0151}{PH}}$ and $0.0091RU^2$ as index of multi-variable regression analysis (Wang Binhui.2003), the results are shown in Table 3.

Table 3. Result of non linearity multi-variable regression analysis.

variable (%)	regression equation	correlation coefficient
CR/RU	$M_1 = 7.6535 + 0.0049\tan CR - 0.0091RU^2$	0.9647
PH/RU	$M_2 = 7.6243 + 0.3373e^{\frac{-0.0151}{PH}} - 0.0092RU^2$	0.9642
CR/PH	$M_3 = 6.8316 + 0.0382\tan CR - 5.3820e^{\frac{-0.0151}{PH}}$	0.4491
CR/PH/RU	$M_4 = 7.6216 + 0.0045\tan CR + 0.2058e^{\frac{-0.0151}{PH}} - 0.0091RU^2$	0.9648

Relationship between M and M_1, M_2, M_3 and M_4 are shown as Figure 1~5

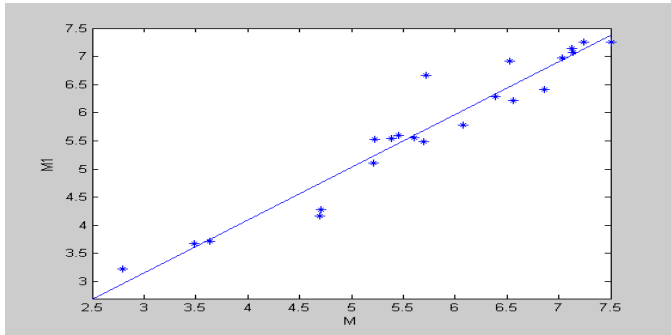

Figure 5. Relationship between M1 and M.

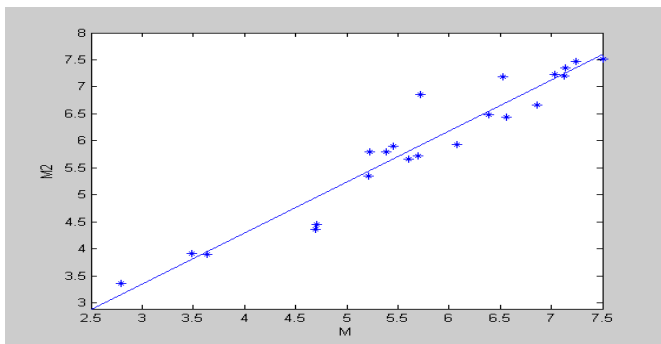

Figure 6. Relationship between M2 and M.

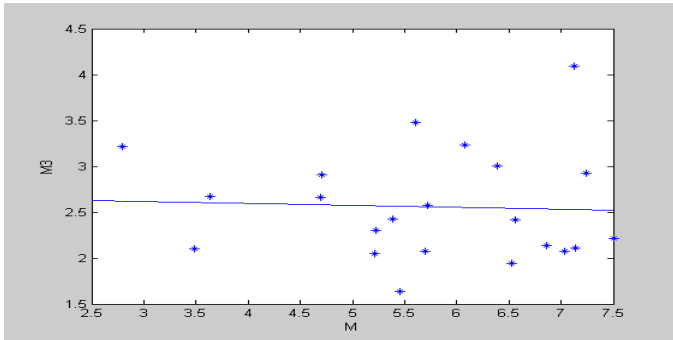

Figure 7. Relationship between M3 and M.

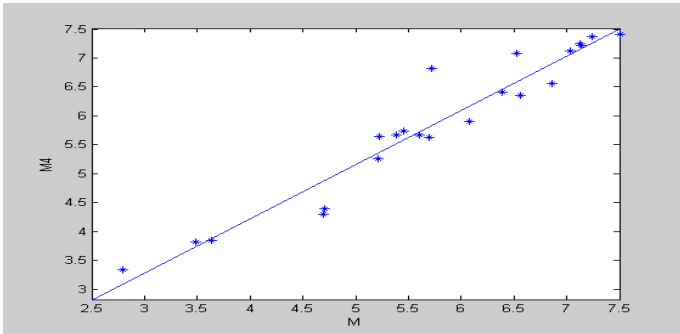

Figure 8. Relationship between M4 and M.

The highest correlation coefficient was 0.9648 between M and M_4. Therefore, M_4 was selected,

$M_4 = 7.6216 + 0.0045 \tan CR + 0.2058 e^{\frac{-0.0151}{PH}} - 0.0091 RU^2$.

2.4 Model Evaluation

Model was evaluated using fuzzy mathematics as below.

Disjoint set is, V={excellent，fine，medium，second，poor}

Result, B=0/ excellent +0.46/ fine +0.36/ medium +0.18/ second +0/ poor

Representation by fuzzy vector, B=（0，0.46，0.36，0.18，0）

The results was found to be either fine ore medium, according to μ_B=0.46 and μ_B=0.36. In conclusion, the modeling results agreed with expert evaluation.

3 Conclusion

The pavement maintenance becomes more and more important with the significant amount of construction of expressway in China. A pavement performance evaluation model was developed for the Northwest of China. The model selected was,

$PCI = 7.6216 + 0.0045 \tan CR + 0.2058 e^{\frac{-0.0151}{PH}} - 0.0091 RU^2$, which can also be used in the maintenance of non-freeway with similiar conditions.

References

China Highway Magazine Agency (2005). “7918 painted expressway network of China”. *China Highway*, 2: 2-4. (Chinese)

Fan Daoshang (1981). “MCI Evaluation Model of Pavement Performance”. *Civil technique*

material. (Chinese)

He Yunmin (2003). "Comprehensive Assessment of Expressway Asphalt Pavement Maintenance". *Engineering Masteral Dissertation* . (Chinese)

K.Majidzadeh (1979). " Evaluation of Pavement Deformation in Asphalt Concrete Pavements" . *Transportation Road Research Lab 719*.

Li Shiyong (2004). "Engineering Fuzzy Mathematics and Appling".*Harbin Institute Technology Press*:96-98. (Chinese)

Wang Binhui (2003). "Excel Applying in multi-variable regression analysis". *Statistics and forecast*. (Chinese)

Xie Zhaohong, Fan Zhengsen and Wang Yinyuan (2003). "Math Modeling Technique". *China Water Conservancy and Hydroelectric Power Press*:4-5. (Chinese)

Zhang Yan,Shi Hongjiang,Wang Guozhong and Li Weisheng (2005). "Study on the pavement distress of the Expressway". *Journal of Inner Mongolia Institute of Agriculture and Animal Husbandry*, 4:80-82. (Chinese)

Zhu Jianmin (2004). "Research and Discussion on Evaluation Method of Pitch Road Surface in Expressway". *Communications Standardization*, 7:33-36. (Chinese)

Pavement Crack Automatic Recognition Based On Wiener Filtering

J. Zhang[1], A. Sha[2], Z. Y. Sun[2] and H. G. Gao[3]

[1]The First Highway Survey & Design Institute of China, Xi'an China, 710068; PH(86)029-87906405; FAX(86)029-87906405;email:zhangjuan0810@163.com
[2]Chang'an University, Xi'an China, 710064; PH(86)029-85217496; FAX(86)029-85217496 email:aiminsha@263.net
[3]Xi'an Electronic Engineering Research Institute, Xi'an China, 710100 PH(86)029-87906405; FAX(86)029-87906405; email:gaohuaigang@163.com

ABSTRACT

System principle and composition including image acquisition, image processing and image interpretation for pavement crack automatic recognition based on digital image processing are presented. In order to improve crack identification rate, pavement image retrogression reasons are introduced and stochastic and complex characteristics for pavement images are analyzed. Wiener filtering theory is investigated to overcome the problem that some classical methods will weaken useful image details when restrain noise. Results show that Wiener filtering can preserve image edge information and remove some noise from non-uniform illumination, imaging systems, pavement material and grain's texture through the analysis for representative examples.

KEYWORDS: pavement non-destructive detection, Wiener filtering, digital image processing, crack recognition

INTRODUCTION

Visual rating systems are used in most pavement cracks surveys. It has disadvantages such as poor repeatability and reproducibility and it is not safe for inspectors. More recently, advances in electronic sensors and computer systems have provided the opportunity of using advanced technologies in pavement distress data collection. Existing automatic real-time detection systems focus on the low identification rate and classification difficulty (Wang et al. 2002). First, a lot of noise in pavement images caused by the road environment itself brings in recognition and classification difficulties. Second, it is lack of easy and effective identification and classification algorithm (Zhang 2004).

Pavement images contain information from road surface, the rough texture, aggregate and uneven illumination. A variety of enhanced technologies including histogram equalization, median filtering, low-pass filtering and high-pass filtering

and fuzzy technology have been applied (Chou et al. 1995, Siriphan et al. 1997, Koutsopoulos et al.1993). A different approach is proposed and discussed in this paper.

PAVEMENT CRACKS IMAGE RECOGNITION SYSTEM PRINCIPLE

The basic function of this system is shown in Figure 1. This system can be divided into three parts: image acquisition, image processing and image interpretation. Image acquisition includes the recording of the pavement distress data by a moving vehicle. Image processing includes following steps: (a) image preprocessing, i.e. reduce noise, (b) image identification (the extraction of pavement distresses in an image from the background and obtaining a binary image), and (c) image interpretation (the identification of distresses, i.e. whether a surface cracking is longitudinal or transverse, as well as their quantification, i.e. the measurement of their extent and severity).

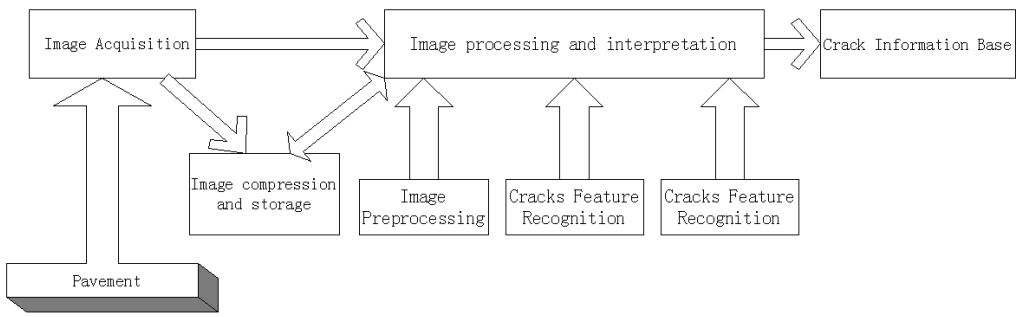

Figure 1. Pavement Cracks Image Recognition System Principle

WIENER FILTERING FOR THE IMAGE

Wiener filtering is a basic and commonly used modern filtering method. It treats minimum mean square error as the optimal standard. and the optimal estimation can be obtained by Fourier transform of the input random signal and noise auto-correlation (Ruan 2001, Yi et al. 2000).

Image filtering using Wiener filtering is to remove image noise and restore degraded images. In order to achieve this goal, mathematical expression about $\hat{f}$ must firstly be formulated to make the indicator reach a limit value. Before the accurate solutions can be solved, the estimation $\hat{f}$ of the original image f is viewed as a random variable so the image can be seen as a random process. Under normal circumstances, it can be treated as a stable random process. Assuming

covariance matrix $R_{ff} = E\{ff^T\}$ and noise covariance matrix $R_{nn} = E\{nn^\tau\}$ of image are known, a linear filtering approach is selected to estimate $\hat{f}$ to make $E\{\|f - \hat{f}\|^2\}$ the smallest. It can be achieved to

$$\hat{f} = R_{ff} H^T (HR_{ff} H^T + R_{nn})^{-1} y \tag{1}$$

If it is assumed that various matrices in Equation (1) are block circulate matrix, it can be solved in discrete frequency domain. Assuming R_{ff} and R_{nn} are block circulant matrix, implicit image and noise signals are stationary random signal, then two-dimensional frequency domain solution is:

$$F(l) = \frac{S_{ff}(l) H^*(l) Y(l)}{S_{ff}(l) \left|H^*(l)\right|^2 + S_{nn}(l)} \tag{2}$$

Since the spectral density of original image and noise is not known in advance in reality, noise spectral density is generally estimated in smoothing region of lower quality image observed and the original image spectral density is replaced by the spectra density of degraded image.

Wiener filtering adjusts the filter's output in accordance to local variance of the image. The larger the local variance is, the stronger the effect of smoothing filter is. It has better selectivity than the corresponding linear filter and has better preservation effect for image edge and high-frequency detail information.

This paper uses an achievable two-dimensional adaptive Wiener filter. The adaptive Wiener filter for pixels is implemented. It estimates the method according to the statistical properties of the pixel local neighborhood. It is calculated as follows.

First, the local mean of the pixels and variance are estimated:

$$\mu = \frac{1}{MN} \sum_{n_1, n_2 \in \eta} a(n_1, n_2) \tag{3}$$

$$\sigma^2 = \frac{1}{MN} \sum_{n_1, n_2 \in \eta} a^2(n_1, n_2) - \mu^2 \tag{4}$$

Where η is M ×N neighborhood of each pixel in the image. T hen gray value for each pixel is estimated using Wiener filtering:

$$b(n_1, n_2) = \mu + \frac{\sigma^2 - v^2}{\sigma^2} (a(n_1, n_2) - \mu) \tag{5}$$

where v^2 is the noise variance of the image.

PAVEMENT CRACKS RECOGNITION BY WIENER FILTERING

Characteristics Analysis of Pavement Crack Image

Identification system of pavement cracks based on CCD works in complex environment and is affected by many factors, such as uneven pavement materials and a variety of dark spots. Meanwhile, the greatest impact on the image feature is whether or not to use auxiliary lighting. Even though a uniform illumination condition is provided, uneven background still exists in the images. Generally speaking, the brightness at the center of the image is higher and is gradually darkening from center to edge. In natural light, there are more influencing factors so that there is a shadow on the pavement and the contrast of each image varies with the intensity of sunlight. In addition, image contrast also varies with the auxiliary lighting intensity for the same equipment. Another effect on image quality is from the camera installation angle relative to the pavement. Due to the impact of field of view, the video image will produce geometric distortion. In addition, installation height of the camera will also affect the image quality. In general, the images include two types of objects: pavement, i.e. the background and the detecting goals such as cracks. Therefore, the digital image pixels can be classified into two sets: the pixels representative of the background and pixels representative of cracks. In ideal circumstances, the cracks should be darker than the background. However, the specific situation is more complex due to following influencing factors:

(1) The uneven road surface materials and uniform road surface texture result into larger changing image background.

(2) Different cracks are different in size, type and severity. If there are as many large particles as the cracks and even brighter than the background color, the cracks image color will be diversified. However, cracks in the image are darker than the normal pavement in general.

(3) The pixels quantity of the cracks is far less than that of the background pixels.

(4) There is the same part of gray value between normal pavement and cracks.

(5) Cracks are composed by a lot of short intertwined and even disconnected lines which are randomly distributed.

(6) Due to the inherent characteristics of CCD cameras, uneven image brightness exists.

Based on the above road surface cracks image characteristics and the basic principle of Wiener filtering, it is reasonable in theory that cracks signal and noise signal in the road image is treated as a random signal. Therefore, crack identification in the complex pavement image is feasible based on Wiener filtering. The following two typical examples are analyzed.

Examples

According to the above theoretical analysis, Wiener filtering is used to deal with the pavement images to extract cracks. The results are as follows.

Figure 2. One of Original Image

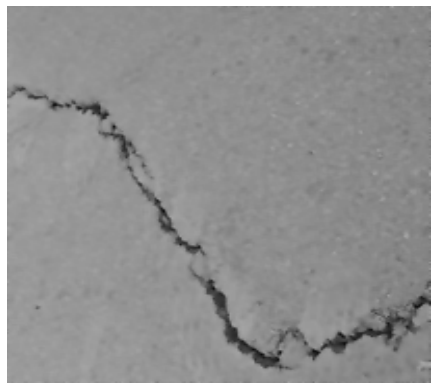

Figure 3 Wiener filtering Result of Fig.2

It can be seen from Figure 3 that Wiener filtering improves the image quality by not only the stress on cracks but also removing parts of noise signal.

In order to analyze more directly the effect of Wiener filter, Wiener filtering and median filtering is separately used in the same image and then Sobel operator is used to detect the crack edge. Figure 4 is a repaired crack with serious tire print on it, which is very difficult to recognize. Figure 5 is the result by Wiener filtering for Figure 4, Figure 6 is the result by Wiener filtering and edge detection by Sobel Operator for Figure 4 and Figure 7 is that by the median filter and edge detection of Figure 4.

Figure 4. One of Original Image

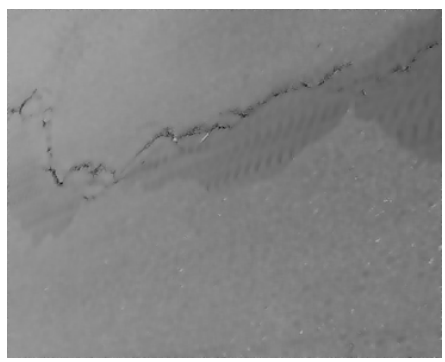

Figure 5. The Result by Wiener filtering

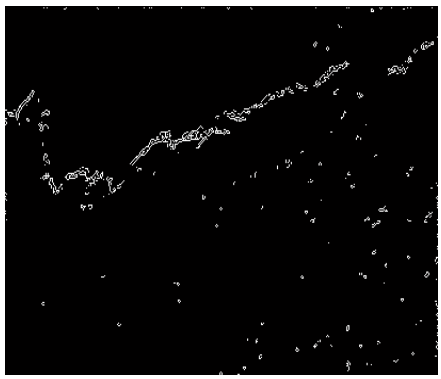

Figure 6. The Result by Sobel

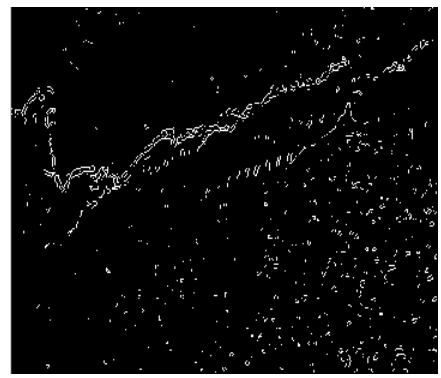

Figure 7. The Result by median filtering

From the comparison, it can be seen that the repaired crack can be clearly detected by Wiener filtering. This also shows that the Wiener filtering has better adaptability to the road conditions. Therefore, it is feasible to improve the road surface image quality by Wiener filtering.

CONCLUSION

How to make use of Wiener filtering to improve the image quality was studied based on the analysis of the characteristics of the road image. Through the experiments, the Wiener filtering can be used to improve road image and can provide a reliable basis for crack extraction, crack evaluation and pavement evaluation. The result has practical significance in the development of automatic identification system.

REFERENCES

Wang, R.B., Wang, C., and Chu X. M. (2002). Developments of Research on Road Pavement Surface Distress Image Recognition[J]. *Journal of Jilin University(Engineering and Technology Edition)*, 32(4):91-97

Zhang, J. (2004). Study on Pavement Crack Identification and Evaluation Technology Based on digital Image Processing[D]. Ph.D. Dissertation of Chang'an University.

Chou, J. C. and O'Neil, W. A. Pavement distress evaluation using fuzzying logic and moment invariants. *Transp. Res. Record.*,1505, Transportation Research Board, Washington D.C.:144-148.

Siriphan, J. (1997). Develioment of a new digital pavement processing algorithm for unified crack index computation[D]. A Dissertation Submitted to the Faculty of the University of Utah.

Koutsopoulos, H. N. and Downey A. B. (1993). Primitive-based classification of pavement cracking images[J]. *J.Transp. Engsr.*, 19(3):136-143.

Ruan Qiuqi. Digital Image Processing. Bei Jing: Publishing House of Electronics Industry, 2001.7

Yi, X. F., Chen, F. J. and Yang, X. J.(2000). Template Matching By Wiener Filtering[J]. *Journal of Computer Research and Development*. 19－21.

Determine Old Asphalt Pavement Milling ThicknessBased on Pavement Surface Deflection Control

WANG Chao-hui[1] and WANG Xiao-zhao[2]

[1]School of Highway, Chang'an University, Postcard 710064, City Xi'an China; PH (86)029-82334836; FAX (86)029-82334836; Email:wchh0205@163.com
[2] Department of Traffic Engineering, Henan University of Urban Construction, Postcard 467044, City Pingdingshan China; PH (86) 0375-3672589; FAX (86) 0375-3672589; Email: wangxz@hncj.edu.cn

ABSTRACT

In order to determine optimum pavement milling thickness when old asphalt pavement structure strength deteriorates to some degree，the back calculation method is usually considered. Based on the multi-layer elastic system theory, the change law of the deflection before and after old pavement milling is calculated using the theory of orthogonal design. The change law of the deflection before old pavement milling and old road equivalent rebound modulus after milling is also calculated using the uniform design method. Meanwhile, this paper developed correlations between the deflections before and after old pavement milling for different milling thickness, and the relationship between the deflection before old pavement milling and the old road modulus after milling using regression analysis. The results indicate that the exponential equation usually gives better correlation. When the deflection value before old pavement milling and milling thickness value are small, the difference between the deflection before and after old pavement milling is relatively small. Finally, according to the calculation results, the design criterion of asphalt pavement milling based on the old pavement surface deflection control is proposed. The example indicates that this criterion is simple and reasonable, and has a good practical value, which can provide the basis for the determination of asphalt pavement milling thickness and the design of asphalt overlay.

Keyword: road engineering, asphalt pavement, pavement surface deflection, milling, design

Nowadays, it's a common practice to control the milling thickness of asphalt pavement according to the level of pavement distress and pavement structure strength, using empirical methods or based on specifications (Wang 2008). If pavement structure strength could not meet certain requirements, two methods are often used to determine the milling thickness of old asphalt pavement. The first method is FWD back calculation (Zha 2002； Wang and Lytton ,1993, which means back calculating each layer's module according to FWD test data and thickness of these layers, and then determining
milling thickness by reference to each layer's module. The second method is to

design the milling thickness based on experiences, representative deflection value of old pavement, design deflection value of overlay and Chinese standard Technical Specifications for Maintenance of Highway Asphalt Pavement (JTJ073.2-2001). This method obtains pavement structure strength index（SSI）according to representative deflection value of old pavement and design deflection value of overlay. Depending on different SSI values, different milling strategies are used. If SSI is very high, only functional recovery is applied after distress treatment. If SSI is high, the asphalt pavement surface is usually milled according to the type of distress. When SSI value is medium, the entire asphalt pavement should be milled. If base strength is deficient, the pavement needs to be milled to the bottom of the base. If the SSI value is poor, engineers mill the whole old pavement structure layers.

In the first method, non-destructive testing is often used to determine each layer's thickness. The FWD back calculated modulus is dynamic modulus which needs to be transferred to static one, so this method is inexact and only used by a few Chinese design unit. When it comes to the second method, if SSI is good and the pavement distress is mild, there is no need to mill the entire asphalt surface, as it will increase the construction cost. . However, how to make further deflection separation to determine whether to mill upper surface, middle surface, or the entire surface, , as well as determine optimum pavement milling thickness according to different pavement surface deflection are still a difficult problem in highway engineering. . Some Chinese and international experts suggest first mill part of the pavement (or a layer of pavement) and then do deflection test, which is not only time-consuming and tedious ,but also could not be accepted by design as well as construction unit.

Consequently, considering the difficulty in controlling milling thickness of old asphalt pavement, it's necessary to propose old asphalt pavement milling criterion based on the old pavement surface deflection control by theoretical analysis, which will provide scientific basis to old pavement milling thickness determination as well as overlay design.

1. Old Asphalt Pavement Milling Thickness Determination

According to the calculation formula of SSI（SSI = l_T/l_s）given in the Chinese Standard Technical Specifications for Maintenance of Highway Asphalt Pavement (JTJ073.2-2001), , the level of representative deflection value l_s can be determined by design deflection value l_T. If l_s is superior, medium or poor, the pavement will be treated accordingly using functional recovery, whole surface milling or whole structure layers milling. In the next paragraph, back calculation method is used to analyze how to determine reasonable surface milling thickness on the basis of design deflection value as well as representative deflection value.

Assume that old pavement milling thickness as well as the maximum overlay asphalt thickness is known, which means the thickness of asphalt overlay is determined. Then, based on overlay design modulus and design deflection value,

back calculate the old road modulus after old pavement milling that meets design requirements and to determine old surface representative deflection value after old pavement milling. However, if the old road modulus after old pavement milling or old surface representative deflection value is known, old asphalt pavement milling thickness meeting corresponding design requirements could be obtained. Because old surface representative deflection value is often tested, deflection value after old pavement milling could not be used as control criterion. If there is relationship between deflection before and after old pavement milling, or there is relationship between deflection before milling and old road modulus after milling, old road representative deflection before milling can be determined by old road deflection or modulus after milling. , This old surface representative deflection value can then be used as control criterion. Therefore, the key of milling design criterion determination is to establish relationship between the deflection before and after old pavement milling, or between the deflection before old pavement milling and the old road modulus after old pavement milling.

2 Analysis of the Change Law of Deflection Before and After Old Pavement Milling

2.1 Orthogonal test calculation

Orthogonal design has advantages such as homogeneous dispersion and unified comparability. If appropriate experimental quantity is designed, the results will be more homogeneous and of a broad range. Consequently, in order to determine the relationship between deflection before and after old pavement milling more properly, orthogonal test analysis method is used. The old asphalt pavement structure is divided into two layers: asphalt surface course as well as base course (those beneath the surface course are equivalent to base), and their Poisson's ratios are 0.25 and 0.3, respectively. Meanwhile, assume that it's half-continuous and half-smooth between surface course and base, and the old pavement has no crack. Then, in the range of variation, four typical levels of modulus of surface course, equivalent rebound modulus of basis, and the thickness of asphalt surface course are selected. When pavement milling thickness is during 4～8cm, the thickness of old asphalt surface course is generally around 4～8cm; while milling more than 8cm, the thickness of old asphalt surface course is generally around 15～18cm. Therefore, the thickness of old asphalt surface course should changes with milling thickness.

According to the table 1, there are 3 varying factors and every factor has 4 numerical levels. Then, to establish orthogonal test table L16 (4^5), , the old road deflection before and after old pavement milling when milling 4cm、6cm、8cm、10cm、12cm are calculated based on multi-layer elastic system theory (the total of thickness of upper and middle surface course is generally no more than 12cm）

Table 1. Calculation Parameter of Pavement Structure

Influence factors	Levels			
	Level 2	Level 3	Level 4	Level 5
（milling between 4～8cm） old asphalt surface course thickness (cm)	10	12	15	18
（milling more than 8cm） old asphalt surface course thickness (cm)	15	16	17	18
modulus of asphalt surface course (MPa)	800	1000	1200	1400
equivalent rebound modulus of base course (MPa)	100	200	300	400

2.2 Results analysis and deflection correlation

In order to establish the relationship between deflection before and after old pavement milling more accurately, SPSS statistical software is applied to analyze the correlation between different data sets, including deflections and their differences before and after milling, and the percentage of deflection increase after milling. The results showed that the deflection before and after milling correlates very well , with R^2 values 0.96 or higher, as given in Figure 1 and Table 2.

According to Figure 1, deflections before and after milling are further treated separately through linear regression fitting and exponentiation regression fitting.

As shown in Figure 1, when the deflection values before and after milling are small, their differences are also relatively small indicating the little effect of milling. . Table 2 indicates that exponential correlation gives a better fit for the deflection relationship before and after milling, and such correlation is recommended for future calculation. . If milling thickness is different from those given in table 2, the deflection before milling can be determined by linear interpolation.

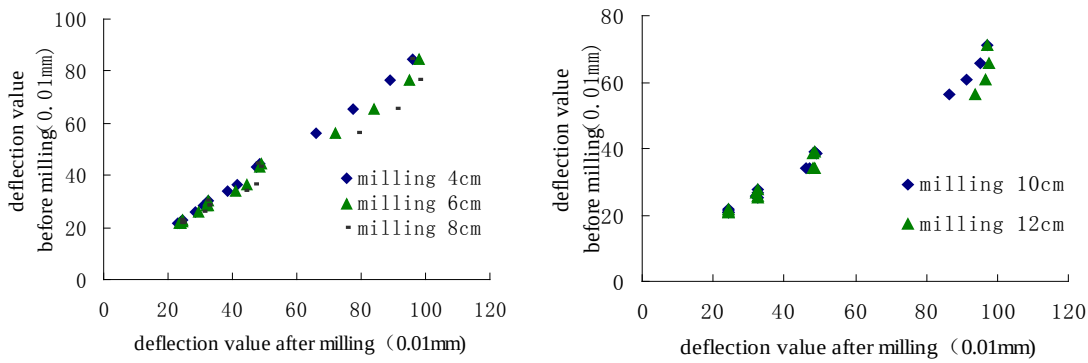

Figure1. Change of the Deflection Before and After Old Pavement Milling

Table 2. Regression Fitting of the Deflection Before and After Old Pavement Milling

milling thickness（cm）	linear regression fitting		exponential fitting	
	regression equations	correlation coefficient	regression equations	correlation coefficient
4	$l' = 0.8373l + 2.4272$	R^2=0.9974	$l' = 1.146l^{0.9357}$	R^2=0.9980
6	$l' = 0.7784l + 3.504$	R^2=0.9879	$l' = 1.2433l^{0.9046}$	R^2=0.9914
8	$l' = 0.7367l + 4.5553$	R^2=0.9610	$l' = 1.3619l^{0.8753}$	R^2=0.9743
10	$l' = 0.6235l + 6.0918$	R^2=0.9880	$l' = 1.4638l^{0.8319}$	R^2=0.9913
12	$l' = 0.586l + 7.2863$	R^2=0.9726	$l' = 1.6219l^{0.8018}$	R^2=0.9836

Annotation: l' means deflection before milling, l means deflection after milling.

3. Correlation Between Deflection Before Milling and Old Road Equivalent Rebound Modulus After Milling

In order to establish correlation between deflection before milling and old road equivalent rebound modulus after milling, the correlation equations between deflection before and after milling in Table 2 could be utilized. , Then these correlation equations of deflections and the prediction equation of modulus as given in the highway asphalt pavement design criterion (JTG D50-2006): $E_t = 1000\dfrac{2p\delta}{l_0}m_1m_2$ should be combined. However, other research shows that this equation has some uncertainty and it changes with environment and structure. Therefore, to make correlation equation between deflection before milling and old road equivalent rebound modulus after milling more representative, and to make milling design process more simple and cost effective, it is necessary to analyze deflection before milling and old road equivalent rebound modulus after milling from theoretical aspect, and explore correlations between them.

In order to conduct the structural analysis, old asphalt pavement structure is divided into two layers: asphalt surface course and base (those beneath the surface course are equivalent to base), and their Poisson's ratios are 0.25 and 0.3 respectively. Furthermore, it is assumed that the interface between the surface and the base course is half-continuous and half-smooth, and the old pavement has no crack. For the determination of parameters, , uniform test analysis method is used to ensure a reasonable development of the equations because this method makes

parameters more homogeneous and dispersed, and it is suitable for establishing regression equations between calculation results and parameters. Then, in the range of variation, seventeen typical levels of modulus of surface course and equivalent rebound modulus of base course are selected to calculate deflections before milling when milling thickness varies from 2 to 14 cm. Finally, the relationship between surface deflection and the equivalent rebound modulus of base course is established.

Using SPSS statistical software to analyze data in Table3, it can be found that exponential equation gives the best fit between surface deflection and equivalent rebound modulus of base course. Therefore, the exponential fitting is used to correlate deflection under different asphalt course thickness to old road equivalent rebound modulus after milling (see Table3). If milling thickness is different from those mentioned above, linear interpolation can be used to determine deflection before milling

Table3. Regression Fitting of the Deflection Before Milling and the Rebound Modulus After Milling

milling thickness（cm）	regression equations	correlation coefficient
2	$l' = 9583.5E_t^{-1.0009}$	R^2=1
4	$l' = 9818.7E_t^{-1.0025}$	R^2=0.9999
6	$l' = 8675.1E_t^{-09803}$	R^2=0.9998
8	$l' = 6847.3E_t^{-0.9423}$	R^2=0.9993
10	$l' = 5320.8E_t^{-0.9039}$	R^2=0.9983
12	$l' = 4175.8E_t^{-0.8683}$	R^2=0.9967
14	$l' = 3331.3E_t^{-0.836}$	R^2=0.9944

Annotation : l' means deflection before milling, l means deflection after milling.

4 DETERMINE MILLING THICKNESS CONTROLLED BY DEFLECTION

4.1 Milling design criterion controlled by deflection

(1) Determine the maximum old pavement surface representative deflection l_1 suitable for direct overlay

According to pavement elevation, determine the maximum thickness h_1 and design modulus E_1 which are suitable for direct overlay. Combined with the design deflection l_0, the old pavement surface minimum rebound modulus E_{t1} suitable for direct overlay can be back calculated using the overlay design method, (from

regression equation The old pavement surface maximum representative deflection l_1 suitable for direct overlay can then be determined based on the regression equation $E_t = 1000\frac{2p\delta}{l}m_1m_2$. Figure 1 shows that, when both the design deflection of old pavement and overlay thickness are small, the old pavement surface maximum and representative deflection l_1 of direct overlay is similar to the design deflection l_0, and they can be considered as equal.

(2) Determine the old pavement surface maximum representative deflection l_2 before milling top layer

First, determine the maximum thickness of overlay $h_2 = h_1 + h_t$ and design modulus E_2 (when the pavement is multi-layer, the design modulus is more than one), where h_t is the thinkness of milling top layer. Combined with design deflection l_0, the old pavement surface minimum rebound modulus E_{t2} before milling top layer can be back calculated. The old pavement representative deflection l_2 before milling top layer can then be determined according to Table 3.

(3) Determine the old pavement surface maximum representative deflection l_3 before milling both top and middle layer

First determine the maximum thickness of overlay $h_3 = h_1 + h_t + h_m$ and design modulus E_3 (when the pavement is multi-layer, the design modulus is more than one), where $(h_t + h_m)$ is the thickness of milling both top and middle layer Combined with design deflection l_0, the old pavement surface minimum rebound modulus E_{t3} before milling both top and middle layer can be back calculated. The old pavement representative deflection l_3 before milling both top and middle layer can then be determined according to Table 3.

(4)Determine the old pavement surface maximum representative deflection l_i before milling some layer

The maximum overlay thickness $h = h_1 + h_i$ and the design modulus E (when the pavement is multi-layer, the design modulus is more than one) are first determined when the milling thickness is unknown (h_i =2cm、3cm、4cm…). Combined with design deflection l_0, the old pavement surface minimum rebound modulus E_{ti} can be back calculated. Finally according to Table 3, the old pavement representative deflection l_i before milling some thickness can be determined.

(5) Determine milling thickness based on deflection control

If the pavement condition with respect to surface deflection is excellent, perform functional recovery.

If the old pavement surface representative deflection $l \le l_1$, the pavement distress is not treated and an overlay asphalt layer can be placed directly.

If the old pavement surface representative deflection $l_1 < l \le l_i$, mill the pavement to the bottom of h_i, and overlay asphalt layer.

If the old pavement surface representative deflection $l_1 < l \le l_2$, mill the pavement to the top layer, and overlay asphalt layer.

If the old pavement surface representative deflection $l_2<l\leq l_3$, mill the pavement to the top and middle layer, and overlay asphalt layer.

If the old pavement surface representative deflection $l>l_3$, and the deflection assessment ranking is good, overlay asphalt layer after all asphalt layers are excavated.

If the assessment ranking of the old pavement surface representative deflection is medium, mill all asphalt layers, excavate part or all base, meanwhile, add flexible or semi-rigid reinforcement layer,, and then overlay the asphalt layer.

If the assessment ranking of the old pavement surface representative deflection is poor, the whole pavement structure should be replaced.

Above are the milling thickness design criterion based on deflection control. In practical engineering application, it is suggested including pavement distress consideration into the milling thickness design.

4.2 Analysis Example

The deflection control milling thickness design is further explained using a Northwestern Expressway project as design example.

The old pavement structure includes a 4cm medium-grained asphalt concrete, a 5cm coarse-grained asphalt concrete, a 7cm hot mix asphalt macadam, a 20cm cement stabilized macadam base, and a 35cm lime-stabilized soil subbase. The design deflection of this old pavement rehabilitation project is 29.3 (0.01mm）. The direct overlay thickness is 4cm, and the design modulus is 1200MPa. It is assumed that the overlay material and the thickness after milling surface layer are the same as the old pavement. The design modulus of adding top layer after milling top layer is 1200 MPa, the design modulus of adding middle layer after milling middle layer is 1000 MPa, and the design modulus of adding lower layer after milling lower layer is 800 MPa.

According to step (1), the old pavement surface maximum representative deflection, which is directly overlaid, is determinated. As to this expressway, both the design deflection of old pavement and overlay thickness are small, so take l_1 as 29.3 (0.01mm); According to step(2), the old pavement surface maximum representative deflection before milling top layer can be determined, l_2 = 30.0(0.01mm). According to step(3), the old pavement surface maximum representative deflection before milling top and middle layer can be determined, l_3= 32.6 (0.01mm）. Then, based on the calculation formula of pavement strength evaluation and structure strength index, SSI=pavement surface design deflection / pavement surface representative deflection, the pavement surface representative deflection for different pavement condition and different highway classification can be calculated, as shown in table 4.

Table4. Assessment Ranking Range of the Surface Deflection

standard	excellent	good	medium	poor	bad

highway grade	expressway, first-class highway	expressway, first-class highway	expressway, first-class highway	expressway, first-class highway	expressway, first-class highway
deflection（0.01mm）	<29.3	29.3～35.3	35.3～44.4	44.4～58.6	>58.6

Therefore, the milling design standard can be determined according to the deflection:

If the old pavement surface representative deflection $l \leq 29.3$(0.01mm），no surface treatment is needed, and only direct asphalt overlay or functional recovery is considered.

If the old pavement surface representative deflection 29.3 (0.01mm）$< l \leq 30.0$ (0.01mm）, mill the top layer, and overlay asphalt layer.

If the old pavement surface representative deflection 30.0 (0.01mm）$< l \leq 32.6$ (0.01mm）, mill the top and middle layer, and overlay asphalt layer.

If the old pavement surface representative deflection 32.6 (0.01mm）$< l < 35.3$ (0.01mm）, and the deflection assessment ranking is good, overlay asphalt layer after all asphalt layers are excavated.

If the old pavement surface representative deflection 35.3 (0.01mm）$\leq l < 44.4$ (0.01mm）, mill all asphalt layer, excavate partial or the entire base, meanwhile, add flexible or semi-rigid reinforcement layer, and then overlay asphalt layer.

If the old pavement surface representative deflection $l \geq 44.4$ (0.01mm）, replace the whole pavement structure. It is suggested that make the milling criterion further determined, considering pavement disease.

5. CONCLUSION

This paper aims to determine the milling thickness of old asphalt pavement based on old pavement surface deflection. According to the calculation results, the design criterion of old asphalt pavement milling thickness based on pavement surface deflection control is proposed. The example indicates that this criterion is simple and reasonable, which has good practical value. It can provide the basis for the determination of asphalt pavement milling thickness and the design of asphalt overlay. In practical engineering application, it is suggested including pavement distress consideration into the milling thickness design.

REFERENCES

Wang, Chaohui(2008). *"Study on asphalt pavement overlay technology."* Xi'an, Chang'an University.

Zha, Xudong (2002）. *"Summary of back calculation methods of pavement layer moduli."* Journal of Traffic and Transportation Engineering, 2(4),1-3.

Wang, F, Lytton, R L (1993). "*System identification method for back calculating pavement layer properties."*Transportation Research Record1384, TRB, National Research Council, Washington,D.C.,1-7.

Stability and Reinforcement Analysis of a High and Steep Cataclastic Rock Slope

ZOU Zuyin[1], ZHU Zhanyuan[2], TAO Lianjin[3] and MO You[1]

[1]Dujiangyan Campus of Sichuan Agricultural University, P.O. Box 611830, City, Dujiangyan, P.R. China; PH (86) 28-89737099; School of Civil Engineering, Southwest Jiaotong University Chengdu; email: zzuyin@126.com

[2]Information and Engineering Technology College, Sichuan Agricultural University, P.O. Box 625014, City, Ya'an, P.R. China; PH (86) 835-8268909; FAX (86) 835-8268909; email: zhuzyuan910@163.com

[3]College of Architecture and Civil Engineering, Beijing University of Technology, P.O. Box 100022, City, Beijing, P.R. China; email: ljtao@bjut.edu.cn

ABSTRACT

This analysis is based on a highway project in Guangdong province, involving a tall, steep, and rock-excavating slope with cataclastic structures. Quantitative analysis of the stress-strain trend, possible failure models and safety factors during the slope excavation were investigated by the discrete element program UDEC. The following results were obtained: (1) The slope with joint fissure developed was in anticlinal core and the stability was greatly influenced by the extroversion of rock level. (2) The primitive balance of the slope was broken during the excavation, which induced large range shear failure zone in the internal part of the slope, and the whole circle-broken similar to soil slope appeared. (3) The excavation slope was in a critically stable state, but wide area landslide could be induced by certain triggering factors. Based on these results, a comprehensive treatment scheme was adopted and implemented through the methods, such as reinforcing the broken rock with concrete lattice beam-anchor (cable); minimizing erosion and preserving the slope strength with an efficient drainage system; and protecting the slope with grouted rubble. The integrity of the high standard highway was maintained and the slope was reinforced during time the plan was carried out.

INTRODUCTION

During the construction process of high-level highways in mountainic areas, cutting slope with a cataclastic structure is always a challenge. At present, the inadequate understanding of the deformation and damage laws of this kind of slope, together with lack of quantitative analyses on the validity during designed anchors, result in the increase of invalidity cases (Song et al 2003, Luo et al 2004, Quan et al 2004, Yu et al 2005). The tall and steep slope excavated, from K93+946 to K94+082 of S223 highway in Guangdong, is located at the middle and lower reaches of the Mei Jiang River. This section belongs to friable and brittle rock excavating slope, over 100 meters high, steeply gradient. There is a power station downstream of the slope, and the distance between power station and the slope is 100 meters approximately. It is possible that a large-scale global landslide would occur under certain triggering factors, which is a great threat to the highway, power station and reservoir downstream. Therfore, it is urgent to find a reliable reinforcement scheme.

Based on the results of engineering geological investigations, a possible destruction pattern during excavation was analyzed by UDEC, and the relative safety factor was calculated. Finally, a specific reinforcing scheme was proposed.

ENGINEERING GEOLOGICAL CONDITION

According to geological conditions of this region, the slope is under the impact of the northeastern regional normal fault and the northwestern regional reverse fault, with original vertical fissures developed, easily weathered superficial zone. Rock strata are intensively cracked under the pressure. The rock masses are mainly made up of flagstone, and partly grooved of thick-bedded easily weathered mulberry sandstone, which are generally inclined to the inside of the slope. Under the impact of long-termed weathering, part of the shallow rock is inclined to the outside of the slope with a low-pitched inclination of NE315°~345°∠9°~30°. The main attitudes of the rock masses are composed of ① NE5°~24°∠7°~21°, ② NE105°~145°∠59°~80°, ③ NE150°~170°∠5°~24°. The rock masses were cut into fragments with the length of 10~20 centimeters by the bedding surface and joint plane, and is approximate to the loose cataclastic structure. The main types of the groundwater are loose rock pore water and base rock fissure water. The groundwater varies with seasons, and often springs out especially in rainy seasons.

STABILITY ANALYSIS

Numerical simulation analysis. The original design scheme of the slope is shown as Fig.1. The excavation height is 66.19 meters with 9 steps. The gradient of the two lower steps is 1:0.5 and the others are 1:0.75. Each step is 8 meters high with a one-meter-width bench. In order to simulate the effects of fractional excavation and the impact of rainfall (annual rainfall is 1400~1700mm), the program of UDEC3.1 (Cundall 1987) was used to investigate changes of the stress and strain state of the slope during excavation under conditions of gravity, and gravity plus rainstorms. Moreover, safety factors of the above two conditions were calculated using the Geo-slope program.

Numerical model and parameters. According to the observed data, the typical section K94+005 was chosen as the calculated cross section and the slope numerical model using discrete element method is established in Figure 2. The thickness of the rock strata is 0.1~0.3m with an inclination of 15°. The distance of each joint is 1.5m with an inclination of 59°~80°. The boundary of the left- and right-hand sides is fixed from movement in horizontal direction and the bottom boundary is fixed from movement in both vertical and horizontal directions. A large deformation mode has been adopted and the constitutive relations of rock masses are assumed to be a Molar-Coulomb model. The physical mechanical parameters are determined based on the results of the geological survey, degree of crushing and weathering of the rock masses, and engineering experiences. The parameters are shown in Table.1.

Table 1. Rock Mechanical Parameters.

Rock mass	Gravity	Cohesive Strength	Internal friction angle	Young's modulus	Poisson's ratio	Tangent stiffness	Normal stiffness
	ρ /g.cm^{-3}	C /kPa	φ / ^{0}	E /MPa	μ	K_s/kPa.m$^-$	K_n/kPa.

						^{1}	m^{-1}
Sandstone	2.5~2.6	20~80	23~40	35000	0.23	-	-
Jointing	-	0~50	20~25	-	-	1×10^{6}	10×10^{6}

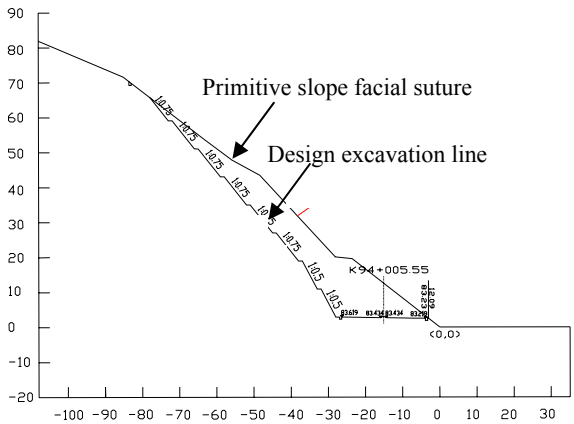

Figure 1. The typical profile of slope excavation scheme.

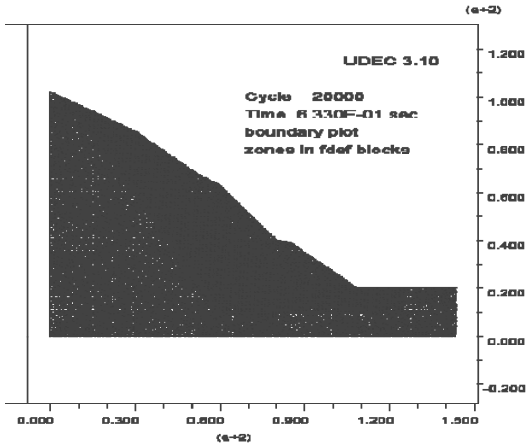

Figure 2. Discrete element model of the slope section.

Results analysis. According to the simulation of UDEC, the stress and displacement results for before and after slope excavation are shown in Figure 3. The geo-stress of the natural slope is uniformly distributed and tensile stress only partly shows on the slope surface. With the process of the excavation, the slope stress field changes visibly. The excavation volume is considerable because of the great excavation height. Under the influence of pressure, the stress near the surface is greatly reduced and the principal stress trajectory is deflected. Moreover, tensile stress is shown not only at free face but also at the slope crest. Stress concentration emerges at the slope free face and the slope toe where the maximum principal stress is increased significantly while the minimum principal stress decreased. The minimum principal stress is translated into tensile stress which results in the compressive tension face parallel to the slope.

According to Figure 4 (a), the slope deformation is concentrated at the middle of the slope after excavation and a series of fissures, as well as continual slip (failure) planes are found at the slope. The slip plane is similar to an arc and the maximum displacement is 30mm. This situation is mainly related to the abundance in joint fissures and serious weathering; the entire slope can be assumed to be a cataclastic texture which is appropriate to soil. According to Figure 4 (b), the horizontal displacement has increased with the maximum displacement of 38mm under the conditions of gravity plus rainstorms, which means an increase of 26.67%, compared to that based on conditions of gravity only. The comparison result indicates rainstorms directly influence the stability of the slope; thus drainage should be seriously considered in the slope design.

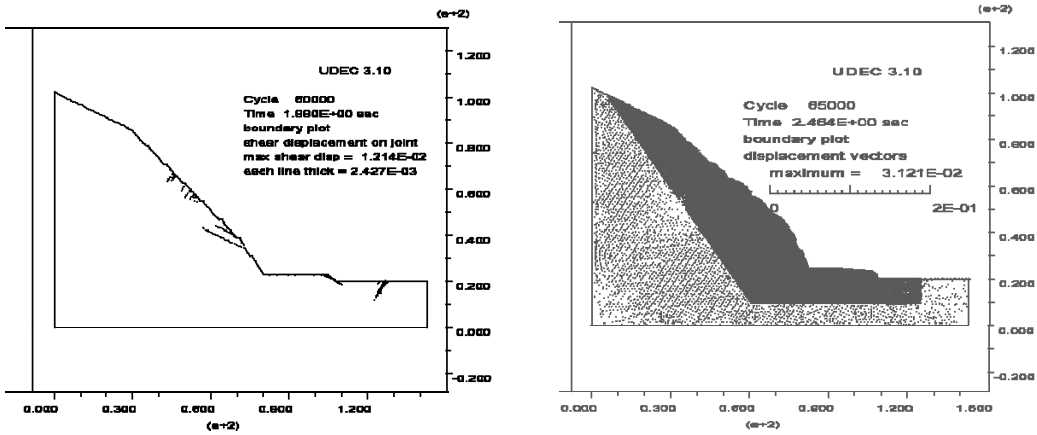

(a) Shear deformation **(b) Displacement vector**

Figure 3. Slope stress and displacement after excavation.

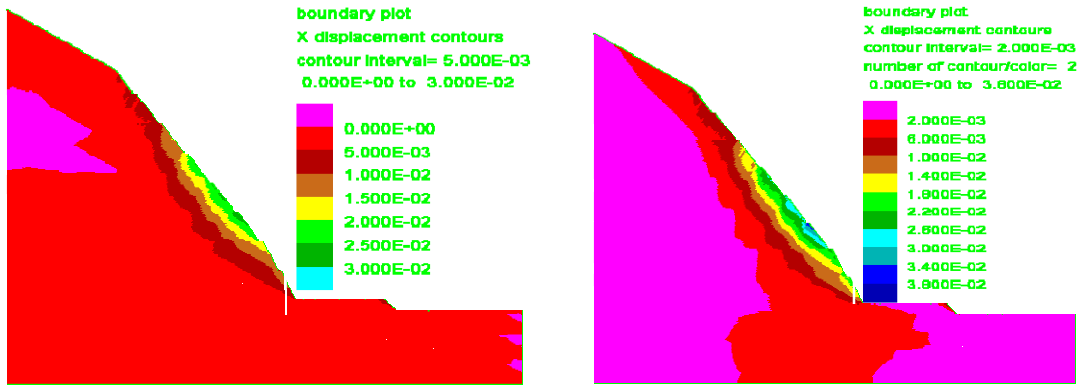

(a) Natural state **(b) Condition of gravity plus rainstorm**

Figure 4. Horizontal displacement comparison.

Stability Evaluation. According to the results of the UDEC program, the sliding slope appeared to be in a curved shape, similar to **that for a** soil slope. The Geo-slope program was used and the Morgenstern-Price method was adopted in the analysis. The physical mechanical parameters are shown in Table 1, and the calculated results are presented in Table 2. The safety factor calculated by Geo-slope program was appropriated to the value calculated by the UDEC.

Table 2. Safety Factor under Different Condition.

Operating mode	Before excavating	After excavating completes	
	Condition	Condition	Condition of gravity plus Rainstorm
Safety coefficient	1.205	1.049	0.964

Before excavation, the safety factor of the slope is 1.205 and the slope is stable. After excavation, the safety factor is only 1.049 under the condition of gravity, which puts the slope basically in critical state. Adding the effects of heavy rains, the factor of safety further decreases to only 0.964, which indicates that the slope is

unstable. The underground water has a great influence on the stability of the high and steep slopes of cataclastic structures along with weathering and rainfalls. The stability level would be quite low if excavated according to the original design and large scale landslides could occur under certain negative conditions. Thus, reinforcement work must be done.

SLOPE REINFORCEMENT SCHEME

At present, even though engineers have obtained much experience in reinforcing slopes, there are still many uncertainties surrounding various conditions such as tall and massive excavation, steep slope, seriously rock mass weathering, potential slip plane, land restrictions, and engineering cost, etc. All of these require that the slope surface excavated according to the original design be well maintained. Moreover, the abundant rainfalls make it even more difficult to maintain the stability of the slope. In order to maintain the slope's long-term effectiveness and cost efficiency, scientific analyses of reinforcement effects are required for the actual situation. Based on full research and analysis on the formation of structures, trends of distortion and damage, and other factors affecting the stability, the following comprehensive reinforcement schemes were proposed through numerical experiments and simulations, as shown in Figure 6.

Water control before slope improvement. Intercepting ditches should be set at about 5 meters away from the top of the cutting and at each of the slope benches. Drains should be set on both sides of the slope, and roadside ditches should be set at the toe of the slope, all of which form a storm sewer system that can drain storm water quickly, thereby preventing the erosion or build up of the hydrostatic pressure on the slope.

Reinforcing toe of the slope. Stress is typically concentrated the most at the toe of the slope, which could cause instability. Accordingly, a reinforced concrete lattic frame beam-anchor bar (cable) is proposed to strengthen the first step of the slope. The anchor is made of full-bond cement mortar and the designed withdrawal resistance is 60kN. The anchored force can be enhanced through second-time high pressure grout. Part of the rock mass that has inferior stability is grouted with cement mortar in order to improve its shear strength and to enhance the sliding resistance of the toe of the slope.

Strengthening slope waist. Because of the high and steep excavation, the slope is highly likely to be unstable under the adverse factors. Thus, the reinforced concrete lattic frame beam-anchor bar (cable) should be applied to the 2nd, 3rd, 5th, and 6th steps in order to enhance the global stability. The total length of anchor cable is 24.0~31.0m in which the length of the anchorage is 10.0m; the designed tension and the lock tension can be reach to 550kN, 600kN respectively through the second-time high pressure grouting.

Slope protection. In order to prevent instability of the slope and reinforce the cataclastic rock mass, the reinforced concrete lattic frame beams-anchor bars

(cable) are also applied to the 4th, 7th, and 8th steps. The anchor is a kind of full-bond cement mortar and second-time high pressure grouting. The anchor's designed tensions for the 4th, 7th and 8th steps are 90kN, 90kN, and 60kN respectively. The M10 mortar rubble masonry pavement of 0.4m thick is applied to the 9th step and both sides of each step. The slope benches adopt M7.5 mortar rubble masonry pavement of 0.3m thick. Moreover, the slope surfaces are protected by grass with six rows of brick, which can prevent slope erosion, rainfall seepage and maintain stability of the slope.

The safety factor for the K94+ 005 section is improved to 1.297 and 1.264 under the conditions of gravity, gravity plus rainstorms respectively through the above measures, which satisfies the design code.

CONCLUSION

The UDEC program can be well utilized to analyze the change of stress and strain during excavation of the cataclastic structure slope. According to the simulation results, mechanism of the damage, stability evaluation, and prediction can be used to optimize design and information-based construction.

If the original design approach is implemented, numerical results indicate that large-scale shear plastic area will occur and the failure plane appropriates to be an arc; the factor of safety is only 1.049 under the condition of gravity, which indicates that the slope is in critical state. Considering the additional adverse effects from heavy rains, the slope will be unstable. Thus reinforcing work needs be done.

The comprehensive reinforcing scheme includes the lattice beam-anchor (anchor cable) system, slope waist strengthening, slope protection, and a proper storm sewer system. It helps satisfy the integrity of a highway through reinforcing the stability of the slope. This reinforcing scheme can be used as a reference to similar rock slope engineering work.

ACKNOWLEDGMENT

This study is supported by Scientific Research Fund of SiChuan Provincial Education Department of China.

REFERENCES

Cundall, P A. (1987). "Distinct Element methods of rock and soil Structure." *In*:*E T Browned.Analytical & Computational methods in engineering rock mechanics*, 129-163.

LUO，Y. H., HE, J. H., HU, B. (2004). "Loose slope landslide governance structure and the importance of strength." *Rock mechanics and engineering journal*, 23(7), 1233–1236. (in Chinese)

QUAN, F. W. (2004). "Fragmentation of rock slope slide mechanism and control." *Highways*, (6), 8-12. (in Chinese)

SONG, C. J., ZHOU, D. P., et al. (2003) "Cutting soft rock reinforcement high slope protection technology research." *Highway*, (12), 76－80.(in Chinese)

YU, Z. H., YAN, E. C., DAI, G. Z., et al.(2005). "Structural fragmentation cutting

rock slope stability evaluation and treatment design." *Highway traffic technology*, 9(22), 137-140.(in Chinese)

Research on the Mechanism for Preventing Reflective Cracks in Old Cement Concrete Pavement Reconstruction

Liang Wang[1],Jinhua Song[1],Sheng Feng[2],Zhiping Jia[2],and Yuchao Lian[3]

[1]School of Civil Engineering, Hebei University of Technology, P.O. Box 383, Tianjin, 300401,China; PH (0) 13820597924; email: wangliang031438@163.com .
[2]Xuanda Express Way Management Office, Zhangjiakou, 075000, China; PH (0) 13903239705; email: wojzpwo@163.com.
[3]Hebei Road &Bridge Group Co. Ltd., Shijiazhuang, 050011, China; PH (0) 15097837188; email: chengchaogaosu23@126.com.

ABSTRACT

Although cracking-seating technology has been applied to engineering practices successfully, the mechanism of this technology in preventing reflective cracks is not very clear yet. This article starts with the expansion mode of reflective cracks, then goes on to study the redistribution of load stress in the fragments by using fracture mechanics theory and finite element methods. By framing analysis model with the method of ANSYS, the article analyzes the change of shear stress and tensile stress in the construction process and reveals how cracking-seating technology can reduce reflective cracks, vehicle load stresses and alleviate the stress concentration in the overlay effectively.

INTRODUCTION

The cement concrete pavements in our country have shown damage to various degrees, among which reflective cracks have been an ever-harassing problem for the highway department. Now the highways in some provinces and cities have entered the stage of conservation and maintenance. So how to conserve and repair damaged roads effectively is the key point in improving the service property and prolonging the lifespan of the roads.

There are many ways for transforming cement concrete pavements, but how to reduce reflective cracks after the transformation effectively is a technical problem. Engineering practices at home and abroad have proved that cracking-seating methods can restrain the emergence and development of reflective cracks.

In the cracking-seating technology, Impact Rollers are used to impact the pavement with low-frequency and high-amplitude vibrations and thus crack the original cement concrete pavement into small-scale fragments of various sizes. In this way the spacing at the bottom of the original cement panel can be eliminated and excessive displacement of the plate which occurs when it is under vehicle loads can

be avoided. On the one hand, this technology enables the usage of the strength of the original concrete; on the other hand, it can reduce waste and thus save the construction investment, which meets the requirements of environmental protection.

THE DEVELOPMENT OF REFLECTION CRACKS

The fact that reflection cracks appear in the asphalt surface when the cement concrete pavement has been modified is mainly caused by the existence of cracks or joints in the original cement slab. According to fracture mechanics, the joints exist in the old cement concrete pavement as original defects, and the tensile stress and shear stress cause stress concentration at the joints, which results in the emergence and expansion of cracks. The vehicle loads will cause shear-type reflective cracks in the added layers. Under partial vehicle loads the deflection and margin of the cracks at the joints will be so increased that it causes the shear destruction of the added layer. The cracks in the joints are shown in Figure 1 and reflective cracks in overlap are shown in Figure 2.

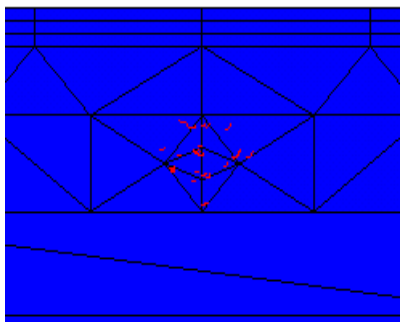

Figure 1. Fracture distribution in the joints

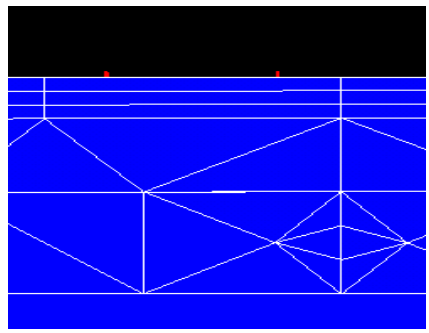

Figure 2. Reflection cracks in the overlay

From all the results above, we can conclude that the main reason for the emergence of reflection cracks is that the stress will be concentrated and accumulated when the joints are under the pressure of vehicle loads, and the repeating vehicle loads will have the cracks reflected to the surface. In Figure 1, the cracks concentrate at the seams of the concrete, and in Figure 2, the cracks are reflected to the surface.

THE MECHANISM OF CRACKING-SEATING TECHNOLOGY

ANSYS finite element methods are adopted to analyze the change of the stress and strain in the joints of cement concrete when cracking-seating technology is applied to old cement pavements.

Model

For the cement concrete pavement, the unit of solid concrete 65 will be chosen and for the grass-roots and soil the unit of solid 45 will be chosen. And the assumptions will be made as follows:

(1) Each structural layer is made of homogeneous, continuous, isotropic, and

linear elastic materials;

(2) The layers are completely and continuously connected with each other;

(3) Interactions between layers are to be taken into consideration.

(4) The overall model: cement board 5m×4m×0.25m, grass-roots 35m × 28m × 0.30m , soil 35m×28m×20 m;

(5) The grass-roots and soil are constrained from all directions while the cement concrete pavement is free from constraint.

The schemes of the units are shown in Figure3, and the schemes of the impact roller position are shown in Figure 4.

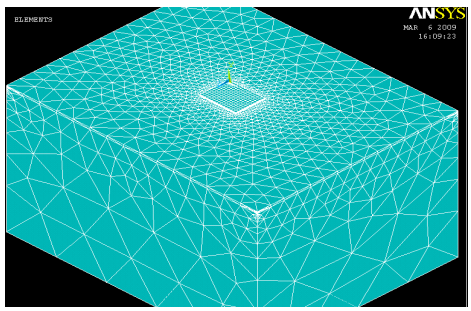

Figure3. Schemes of the units.

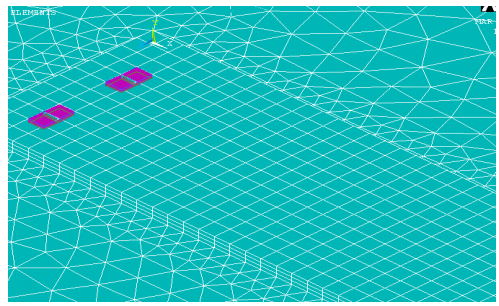

Figure 4. Schemes of the impact roller position.

STRUCTURE ANALYSIS

The development of cracks

In the process of construction, it can be found that when the impact wheel is walking along the central line of the panel, the transverse cracks appear more while the longitudinal cracks develop faster. With the times of impact compaction increasing, the longitudinal cracks begin to appear throughout the panel when it is impacted for the 2nd time. When the loads are on the edge of the plate, the cracks develop from the top to the bottom, forming the longitudinal cracks. When the loads are on the central part of the plate, the cracks will be reflected from the bottom to the top, forming the transverse cracks. The distribution of cracks in the plate and the relationship between tensile stress and compaction times are shown in Figure 5 and Figure 6, respectively.

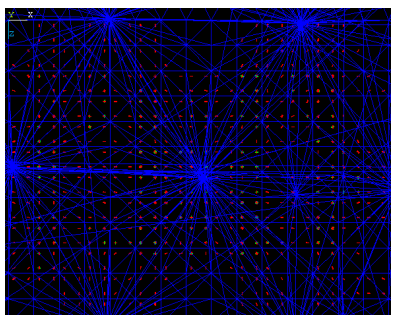

Figure 5. The crack distribution after impact.

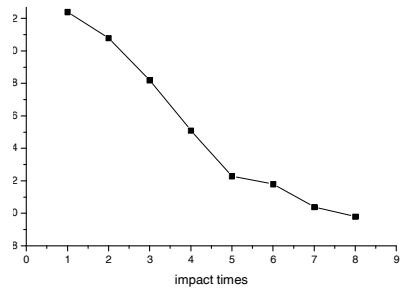

Figure 6. The tensile stress change with compaction times.

Processed by the cracking-seating technology, the cement concrete panels are cracked into small pieces. In this way, all the pieces of the cement fragments can bear the vehicle loads together, which will alleviate the stress concentration at the seams of the cement concrete panels. The stress in the plate under vehicle loads will be reduced as shown in Figure 6, which can be explained as stress release.

MECHANISM OF PREVENTING REFLECTIVE CRACKS

The stress in cement plate before impact

By analyzing the whole process of cracking construction, we can find that before impact stress in the juncture of the plate is concentrated with a maximum shear stress of 0.4MPa and a minimum of 0.025MPa, as shown in Figure 7. The tensile stress in the asphalt concrete layer concentrates at the top of the cement concrete board (which is also the bottom of the asphalt layer) with a maximum of 0.94MPa, as shown in Figure 8. Thus the asphalt surface is easily cracked by the action of repeating vehicle loads and reflective cracks develop. Figure 9 shows the curve of shear stress changing with load position, and Figure 10 shows the curve of tensile stress changing with load position.

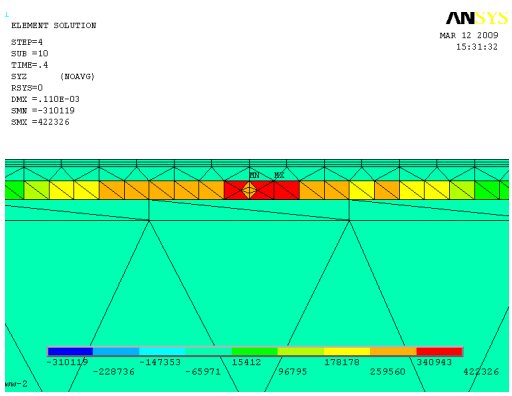

Figure 7. Diagram of shear stress under vehicle loads before cracking.

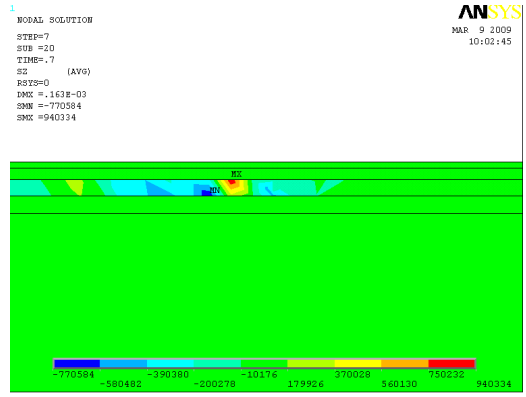

Figure 8. Diagram of tensile stress under vehicle loads before cracking.

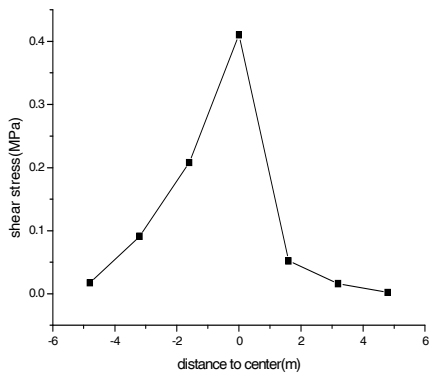

Figure 9. The curve of shear stress changing with load position.

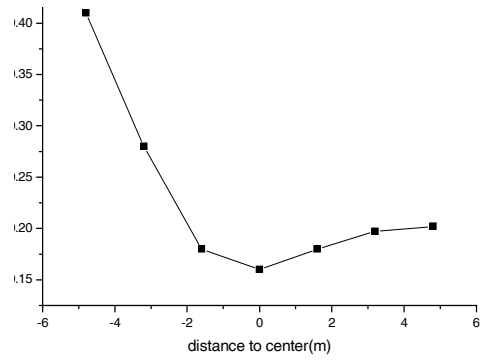

Figure 10. The curve of tensile stress changing with load position.

It is shown in Figure 9 that the shear stress in the seams changes with load position. When the load is at the joint, the value of shear stress is at its largest of 0.4MPa. Figure 10 shows how tensile stress at the bottom of the overlay varies with the change of load position. The tensile stress concentrates mainly upon the bottom of the overlay. Analyzing the stress distribution in the depth direction, we can find that the tensile stress exists in a zone of about one third the thickness of the cement concrete plate. The distribution of the tensile stress is consistent with the bending deformation of the plate.

The stress in the plate after impact

The tensile stress at the bottom after impact is given out in Figure 11, and the shear stress at the juncture after impact is given out in Figure 12.

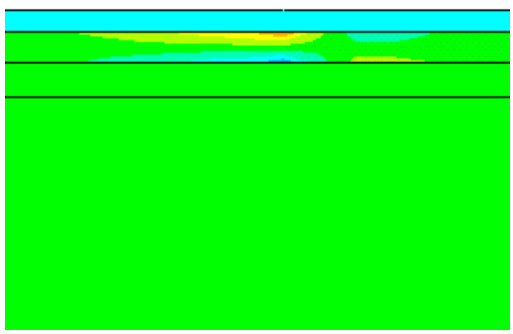

Figure 11. Tensile stress at the bottom after impact.

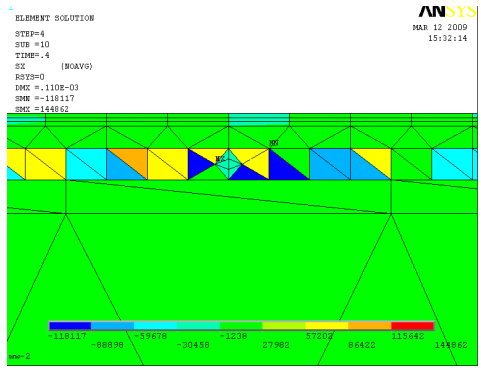

Figure 12. Shear stress at the juncture after impact.

After cracking, the maximum shear stress at the joints under vehicle loads is 0.15MPa, the tensile stress in the asphalt layer is 0.7MPa, and the stress distribution is comparatively even without just concentrating on the deflection joints. It shows that after cracking and seating the stress in the cement panel which is caused by vehicle loads will be reduced significantly. Moreover, comparing Figure 7 and Figure 12, we can see that before cracking the shear stress at the joints is more intensive while after cracking and seating more dispersive.

CONCLUSION

Cracking-seating technology can effectively reduce the emergence and development of reflection cracks. This article is based on using ANSYS to analyze the shear stress and tensile stress before and after the pavement is cracked, then comes to a conclusion that the cracking-seating can reduce reflective cracks effectively :

(1) Owing to the redistribution of the stress in the cement concrete panel, the tensile stress at the bottom and shear stress at the juncture which are caused by vehicle loads are obviously reduced;

(2) As the original cement board is cracked into small pieces, the stress

distribution is more even and the stress concentration is alleviated so that the development of reflective cracks is restrained effectively.

BIBLIOGRPHY

Kamyar C M, Yinhui Liu, David L A. Asphalt overlay and subsurface drainage of broken and seated concrete pavement[J]. *Journal of Transportation Engineering,* 2005,131(8):617-622.

Svinkin，M.R. Prediction and calculation of construction vibrations[J].*DFI 24th Annual Members Conference, Decades of Technology-Advancing into the Future*, 1999, pp.53-69

Hu Changbin, Application of Impact Roller in Rehabilitation of PCCP. *China Communications Press*.2007.5

Dowding C H. Construction Vibration[M] *Prentice Hall Upper Saddle River*.1996`

Study on Prolonging Asphalt Pavement Fatigue Life Based on Vision Transverse Intervention

PAN Xiaodong[1], HU Peng[2], YANG Zhen[3], and CHI Cheng[4]

[1]Professor, Transportation Engineering School, Tongji University, P.O. Box 444, Shanghai; PH (0086) 021-69585721; FAX (0086) 021-69585721; email: panxd6@163.com
[2]Doctor Student, Transportation Engineering School, Tongji University, P.O. Box 444, Shanghai; PH (0086) 021-69583813; email: eimhp@163.com
[3]Senior Engineer, Transportation Engineering School, Tongji University, P.O. Box 444, Shanghai; PH (0086) 021-69585721; email: yangzhen2276@263.net
[4]Graduate Student, Transportation Engineering School, Tongji University, P.O. Box 444, Shanghai; PH (0086) 021-69583813; email: cc851006@sohu.com

Abstract: Rutting and fatigue cracks have been common hazards for pavement with the development of traffic. The correlation of wheel tracking transverse distribution and pavement fatigue failure is studied in this paper to propose a new pavement maintenance method which changes wheel tracks transverse distribution after drivers' vision is intervened. This new method not only prolongs pavement fatigue life but also improves driving safety. Finite element models are established to analyze fatigue life of asphalt pavement in theory. Results show that this new method can prolong pavement service life by 10%-30% when wheel tracks are shifted 25-50cm.

Key words: pavement, vision transverse intervention, wheel tracks transverse distribution, fatigue life

1 Introduction

With the development of transportation in China and higher traffic volume, rutting and fatigue cracks become common hazards (Shen 2004; Zhang and Sun 2004). Currently, fatigue failures in high class highway have a lot to do with vehicle load and traffic channeling. Aiming at solving these problems, typical highways are surveyed and vehicle wheel tracks transverse distribution is studied, and then a method for highway maintenance based on drivers' vision intervention is proposed which will make vehicles stay away from its customary route to achieve a well-distributed vehicle load. As a result, anti-fatigue performance of pavement is exploited, service life of pavement is prolonged and driving safety is improved. It has offered a new method for pavement maintenance and management.

2 Traffic Survey and Analysis on Vehicle Wheel Tracks Transverse Distribution

2.1 Selection of Survey Highways

Vehicle transverse distribution is influenced by many factors such as highway cross section, types of pavement, lane width, traffic volume, traffic composition and driving habits, etc. However, it is stated in many documents (Fwa and Li 2007; Liu and Sun 2005) that vehicle transverse distribution still has a certain discipline under the influence of the factors above. Jiasong north highway located in Shanghai Jiading district and Jingfu freeway in Shandong province are selected as survey roads, seen in the table 1.

Table 1. Basic Information of Highways Surveyed.

Name	Number of lanes	Lane width	Class	Median strip
Jiasong north	4	3.75	first class	Yes
Jingfu	6	3.75	freeway	Yes

2.2 Survey Methods and Data Analysis

The pavement is divided into a number of strips before transverse distribution of vehicle tracks is surveyed. The narrower the strips are divided, the more accurate the result of tracks distribution is. But if strips are too narrow, it will be difficult to survey, so the width of the strip is assumed as 25cm considering 25cm grounding width for single tire and 50cm for double tires. Video camera is employed to shoot at appropriate cross sections for a relatively long time. Video datum is analyzed to get vehicle wheel tracks transverse distribution in laboratory.

2.2.1 Discipline of Wheel Tracks Transverse Distribution of Mixed Traffic.

For mixed traffic, video datum is analyzed to obtain the discipline of transverse distribution. Take Jiasong North road for example with the result shown in figue1.

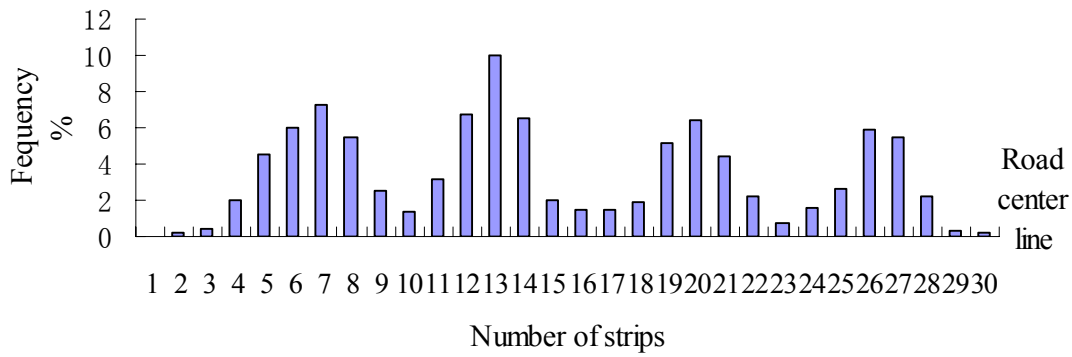

Figure 1. Vehicle wheel tracks transverse distribution for mixed traffic on Jiasong north highway.

From figure 1 it can be known that vehicle tracks are concentrated on just a few strips; more vehicles are distributed in slow lane than in traffic lane.

2.2.2 Vehicle wheel Tracks Transverse Distribution for Standard Axle Load

Damage to the pavement caused by small cars can be neglected when pavement

is designed (Ministry of Communications of the People's Republic of China 2004). When vehicles are converted into standard axle load, wheel tracks transverse distribution of Jiasong North highway is shown as figure 2 and distribution of various kinds of vehicles in different lanes in Jingfu freeway is shown in table 2.

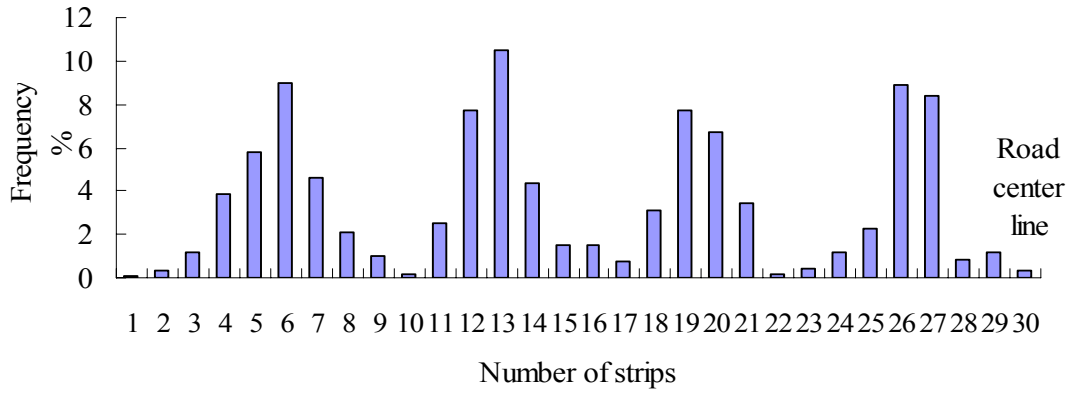

Figure 2. Vehicle wheel tracks transverse distribution for standard load on Jiasong north highway.

From figure 2, it is found that vehicle tracks transverse distribution is more concentrated.

Table 2. Proportion of various vehicles in different lanes of Jingfu freeway.

type of vehicle	slow lane	traffic lane	overtaking lane
special large trucks	0.41	0.48	0.11
large trucks	0.29	0.56	0.14
medium truck	0.38	0.52	0.10
large bus	0.38	0.30	0.33
small car	0.17	0.27	0.55

From the table above, it is known that trucks travel mainly in slow lane and traffic lane with small amount traffic in speed lane; large buses travel in good distribution; cars mainly travel in speed lane with a small amount in slow lane and traffic lane.

3 Principle of Transverse Intervention and Feasibility Analysis

3.1 Principle of Drivers' Vision Transverse Intervention

Basic conception about drivers' vision intervention is that when drivers' vision is intervened by traffic marking or mobile traffic signs, drivers will adjust traffic routes on condition that driving safety is guaranteed.

Documents reveal that with more than 80% of information coming from drivers' vision when driving (Yin et al. 2007)，drivers will adjust their driving behaviors according to what they have seen. If certain kinds of traffic markings or mobile

traffic signs are set up to intervene in drivers' behaviors to make vehicles stay away from its original routes, vehicle load distribution will be changed. The gap between peak point and low point of wheel tracks distribution is 50~100cm, see figure 3. A period after the highway is open, transverse intervention is applied, the peak point of vehicle load distribution is shifted to a position where vehicle load was once less concentrated which makes vehicle load distribution more even in the end. That is the basic principle of drivers' vision transverse intervention.

3.2 Feasibility Analysis for Transverse Intervention

Width of lane is related to highway class and design speed. According to Technical Standard of Highway Engineering (Ministry of Communications of the People's Republic of China 2004), width of lane is 3.75 m if design speed exceeds 80km/h.

According to the related traffic survey (see figure 1), there are more than 95% vehicles traveled within the width of 3.0-3.5m, so there is room for vehicle wheel tracks to be adjusted.

In Japan where traffic accident rate is among the lowest in the world, width of travel lane is 3.5m for high class highways, 3.0m for ordinary roads. Compared with that, 25cm can be adjusted for high class highways in China.

In addition, when traffic markings or signs are used to intervene in drivers' vision in this method without changing width of original lanes, the compressed space becomes fault-tolerance space. Through exploratory experience on freeways in some provinces in China, this method not only adjusts wheel tracks distribution but also warns drivers against fatigue driving to improve driving safety.

4 Finite Element Analysis of Asphalt Pavement Fatigue Life with Vehicle Load Shifting

4.1 Finite Element Model

Two-dimensional finite element model seen in figure 4 is established according to actual pavement structure shown as figure 3. The model length is 1000cm with a total height of 662cm including 600cm subgrade, 50cm base and 12cm pavement. Boundary conditions are: displacement of model bottom is zero, right boundary in direction X is zero and free in direction Y, left boundary is free in X and Y direction.

Considering both model size and loading method, 25*25cm square elements are employed in subgrade and base, 12*25cm rectangular elements are used in pavement.

Calculation reveals that the most vulnerable positions are the places where vehicle wheel tracks are most concentrated, i.e. the peak position of load distribution. The four points A B C and D are selected as fatigue failure calculating points on which vehicle wheel tracks are most concentrated, see figure 4.

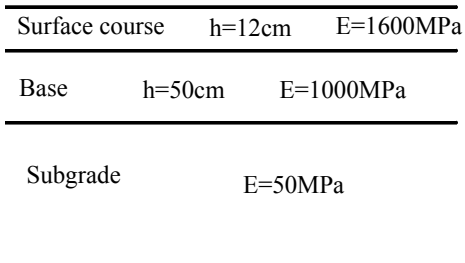

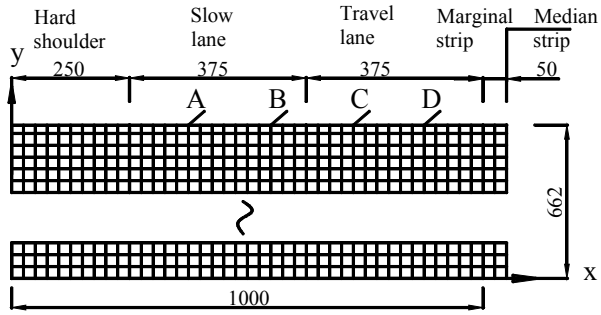

Figure 3. Pavement structure. **Figure 4. Pavement finite element model.**

4.2 Loading Combination and Loading Times Design

4.2.1 Loading Combination Design

After the highway has served for a period, vision transverse intervention is applied, as a result, vehicle wheel tracks are shifted reducing fatigue loss in the positions of A B C and D but increasing fatigue loss in the new positions where wheel tracks distribution concentrates. Based on the consideration above, when the loading times are applied for one half, loading positions are shifted, then the other half loading times are applied which will prolong the pavement service life without causing other points losing fatigue life more than the calculating points.

Loading positions are divided into: original position, shifting 25cm, shifting 50cm and shifting 100cm. Standard load which is 0.7Mpa is applied for 12million times in all. Loading combination cases are: 12million times on original position; 6million times on original positions+6million times shifting 25 cm; 6million times on original positions+6million times shifting 50cm; 6million times on original positions+6million times shifting 100 cm.

4.2.2 Loading Positions and Loading Times

For the convenience of load application, 50cm strips are employed to calculate loading distribution frequency which is used to calculate loading times in 15 positions according to total times, seen in Table 3. The repeated standard load is applied to their own positions according to the calculated times. After repeated load is applied for one position, fatigue analysis is carried out. The loading positions for the four cases are shown as figure 5.

Table 3. Loading Times in 15 Positions (ten thousand).

Total	Positions														
times	1	2	3	4	5	6	7	8	9	10	11	12	13	14	15
1200	3.6	61.2	180	80.4	14.4	120	180	36	46.8	168	43.2	19.2	138	98.4	10.8
600	1.8	30.6	90	40.2	7.2	60	90	18	23.4	84	21.6	9.6	69	49.2	5.4

Note：This table is used to calculate loading times in 15 different positions on condition that total loading times are 12 or 6 million. Loading for the four cases

should refer to this table.

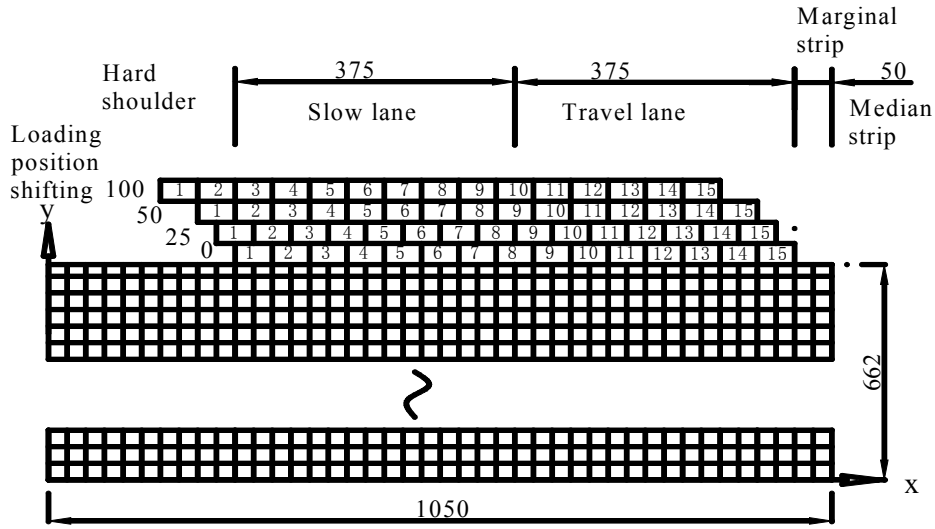

Figure 5. Loading positions (cm).

4.3 Performance of Asphalt Pavement Fatigue Failure

Properties of asphalt mixture fatigue failure vary greatly which are influenced by many factors, such as types of asphalt, porosity of concrete, asphalt content, variation of temperature, test methods, etc. Many scholars (Hugoet al. 2007; Insoo et al. 2008; Zheng et al.2005; Wang 2002.) have studied performance of asphalt mixture with diversified conclusions. Equation (1) is employed as basis in this paper to analyze fatigue life of asphalt pavement (Wang 2002).

$$N_e=N_f\times7\times40\times365/60/0.5=13.7\times10^6\times A_a\times A_g/A_c\times\sigma^{-4.17} \quad (1)$$

Where: N_f fatigue life in laboratory, $N_f = 4025\times A_a\times A_g/A_c\times\sigma^{-4.17}$

A_a coefficient of asphalt type

A_g coefficient of asphalt mixture

A_c coefficient of highway class

The influence from weather is neglected in this paper and vehicle wheel tracks transverse distribution discipline has been in consideration, so weather factor and coefficient of lanes should be ignored, other parameters can be assumed as $A_a=1$, $A_g=1$, $A_c=1$. Then equation (1) will be:

$$N_e=N_f\times7\times40=4025\times280\times A_a\times A_g/A_c\times\sigma^{-4.17}=1127000\times\sigma^{-4.17} \quad (2)$$

Equation (2) is taken as standard for calculating asphalt pavement fatigue life.

4.4 Result Analysis

According to the loading combination cases, loading positions and loading

times, fatigue analysis is carried out. Fatigue life usage coefficient-FLUC (loading times/allowable loading times with the same stress) in position A B C and D can be obtained. The results are shown as figure 6, figure 7, figure 8 and figure 9.

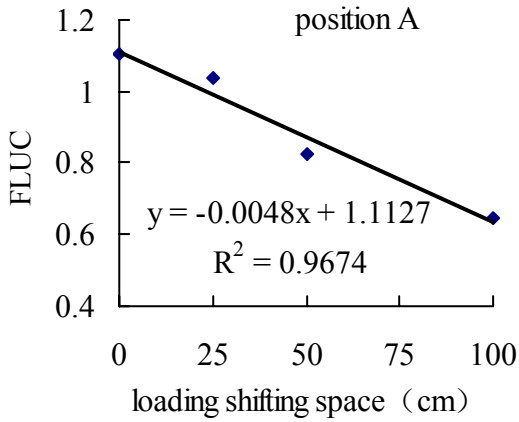

Figure 6. Relationship between fatigue loss in position A and loading shifting space.

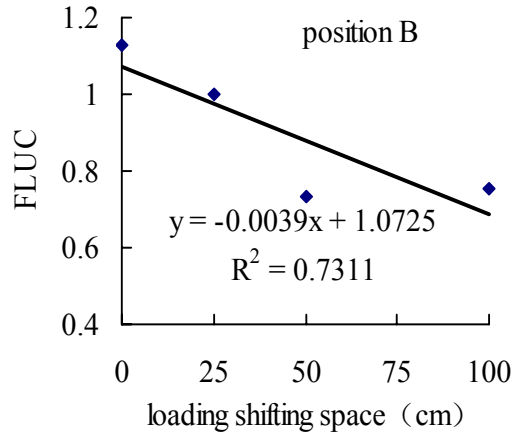

Figure 7. Relationship between fatigue loss in position B and loading shifting Space.

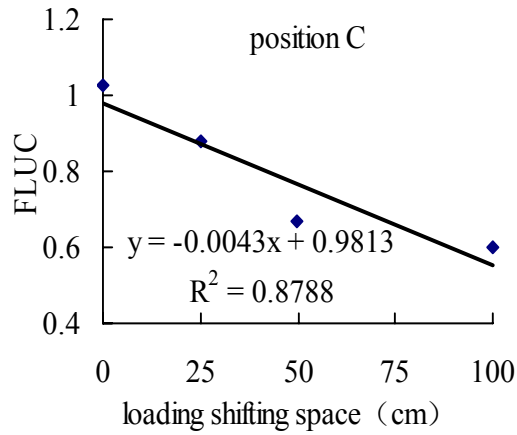

Figure 8. Relationship between fatigue loss in position C and loading shifting space.

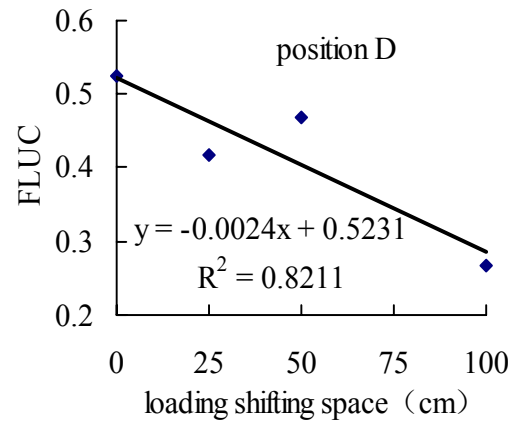

Figure 9. Relationship between fatigue loss in position D and loading shifting space.

From the four figures above, it is known that after loading positions are shifted, the fatigue life usage coefficients in position A B C and D which used to be mostly vulnerable are reduced remarkably although the total loading times is not changed. Calculation reveals that when shifting space is 25cm, fatigue life in position A B C and D are prolonged 7%, 13%, 15% and 11% respectively; when 50cm, they are prolonged 27%, 39%, 35% and 6% respectively; when 100cm, they are prolonged 45%, 37%, 42% and 26% respectively. From the analysis it is known that the larger

the space is shifted, the longer the fatigue life is prolonged within a certain range. Considering limited shifting range and practicability of construction, the best shifting space recommended in this paper is 25~50cm.

5 Vehicle Wheel Tracks Shifting and Improvement of Anti-skid Performance

High friction coefficient and good anti-skid performance of pavement will contribute to driving safety. With the increase of vehicle loading times, surface of pavement is worn that decreases friction coefficient as well as driving safety. With high degree of traffic channeling in high class highways, vehicles usually travel along relatively fixed routes where friction coefficient decreases remarkably threatening driving safety. Related documents (Jing 1990) have manifested it, seen in figure 10.

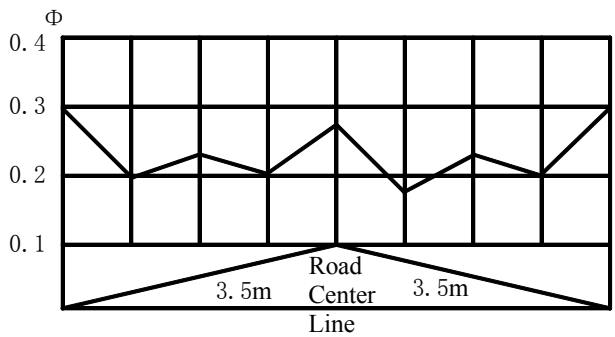

Figure 10.Variation of Friction Coefficient in Different Positions.

When transverse intervention is applied, vehicle load distribution will be shifted, the area with good anti-skid performance can be fully utilized to improve driving safety.

6 Conclusions

The study of vehicle wheel tracks transverse distribution reveals that wheel tracks are concentrated on minor range in lanes which is one of the main reasons causing pavement premature damage. In order to prolong highway service life effectively, a method for highway pavement maintenance and management based on drivers' vision intervention is proposed. Feasibility of this method is analyzed and the finite element models are established according to actual pavement structure. Fatigue analysis on the most vulnerable points is carried out according to vehicle load transverse distribution and certain fatigue properties of asphalt pavement. The results show that when loading positions are shifted 25cm, fatigue life is prolonged about 10%, when shifted 50cm, it is about 30%, when shifted 100cm, it is about 40%. 25~50cm shifting space is recommended based on analysis of the results and construction practicability. Also some related documents are employed to discuss the variation of friction coefficient in travel lanes and concluded that when vehicle wheel tracks are shifted, anti-skid performance of the pavement can be fully utilized for the

improvement of driving safety.

References:

Fwa, T. F., and Li, S. (2007). "Estimation of Lane Distribution of Truck Traffic for Pavement Design." Journal of Infrastructure Systems, 13（2）：24-134.

Hugo, F., Eben.R., and Hilário, T. (2007). "Aspects of cement stabilized Mozambique sand base material performance under MMLS3 and MLS10 APT trafficking." SATC 2007-26th Annual Southern African Transport Conference: The Challenges of Implementing Policy. SATC, Pretoria, South Africa, 821-844.

Insoo, Y., Suh, Y. C., and Mun, S. (2008). "Development of a remaining fatigue life model for asphalt black base through accelerated pavement testing." Construction and Building Materials, 22(8), 1881-1886.

Jing, T. R. (1990). "Traffic Safety From Road Maintenance." Roadway Conditions and Traffic Safety, Tongji university press, Shang Hai, 222.

Liu, L. P., and Sun, L. J. (2005). "Research on Wheel path Lateral Distribution for Freeway Asphalt Pavements." Journal of Tongji University(science edition), 33(11), 1449-1452.

Ministry of Communications of the People's Republic of China. (2004). JTGB01 (2003) Technical Standard of Highway Engineering, China Communication Press, Peiking, 3.1-3.3.

Ministry of Communications of the People's Republic of China. (2007). JTGD50 (2006)Specifications for Design of Highway Asphalt Pavement, China Communication Press, Peiking, 5-6.

Shen. J. A. (2004). "Chapter 2: Premature damage on freeway pavement." Analysis and preventive techniques of premature damage of asphalt Pavement in Expressway, China Communications Press, Peking, 10-35.

Wang, X. D., Sha, A. M., and Xu, Z. H. (2002). "Chapter 5: Asphalt mixtures fatigue performance." Asphalt Pavement Materials Dynamic properties and dynamic state parameters, China Communication Press, Peiking, 94-104.

Yin, Y. H., Pan, X. D., and Yang, Z. (2007). "Relationship between Roadway Visual Environment and Driving Safety." Highways & Automotive Applications, 3, 48-50.

Zhang, Z. X., and Sun, W. Z. (2004). "Investigation and Analysis of Rutting Distress on Asphalt Pavements." Highway, 6, 138-145.

Zheng, J. l., LV, S. T., and Tian, X. G.. (2005). "Prediction of asphalt mixture fatigue life based on damage mechanics." Journal of China & Foreign Highway, 25(3), 94-98.

Reliability Analysis on Pavement Skid-resistant Performance in Expressway Tunnel

Jian-guo YANG[1, 3], Yong-li XIE[1], Xiao ZHANG[2] and Wei MA[3]

[1]Shaanxi Provincial Key Laboratory for Highway Bridge and Tunnel, Chang'an University, Xi'an, Shaanxi 710064, P.R.C; 86-15809202586; asiayjg@163.com
[2]Gansu Province Road and Bridge Construction Group, 568 Gannan Road, Lanzhou, Gansu 730000, P.R.C; zhangxiao6128@163.com
[3]Cold and Arid Regions Environmental Engineering Research Institute, Chinese Academy of Sciences, Lanzhou, Gansu 730000, P.R.C.

ABSTRACT

Driving conditions and durability of pavement skid-resistant are important factors that influence traffic safety of expressway tunnel. To understant the present conditions of pavement skid-resistant performance, mean texture depth (MTD) and British pendulum number (BPN) were measured in different places on an expressway tunnel pavement. Residual life of pavement skid-resistant was predicted based on surveyed traffic volume. Fuzzy cluster was used to analyze pavement skid-resistant performance. The analysis results showed that skid-resistant performance of asphalt concrete pavement is better than that of cement concrete pavement and skid-resistant performance of different places in tunnel has certain regularity, which matched the actual situation well. This paper provided scientific basis to select pavement maintenance strategies and to set speed limits in tunnel, which will lead to a decrease in traffic accidents..

KEY WORDS: expressway tunnel; pavement skid-resistant performance; pavement reliability; fuzzy cluster analysis

1 INTRODUCTION

Expressway tunnel is the bottleneck of highway transportation with poor driving environment and a high occurrence of traffic accidents. Pavement skid-resistance is one of the primary factors that influence the safety of tunnel. Statistical data have indicated that traffic accident rate

of expressway tunnel was 1.34 to 8 times higher than that of other expressway parts. About 81% of the traffic accidents were related to the poor pavement skid-resistance, which led to vehicle side-slip and 19% were related to other factors. These accidents resulted in enormous economic loss. For example, the direct economic loss is up to 2.1 hundred million Euro annually in Europe due to traffic accidents of tunnel and the indirect one is more than 3 to 4.5 hundred million Euro (Shen 2002; Yao, 1985; Ma, et al., 2008).

Pavement skid-resistance is influenced by many factors and these factors are changing all the time, which cannot be described and analyzed quantitatively through traditional mathematical methods. Many variables can be considered in fuzzy cluster analysis; therefore fuzzy cluster analysis has obviously advantages than regression analysis and other traditional methods. In order to learn about the present pavement skid-resistance of tunnels, field tests were conducted and test data were analyzed using fuzzy cluster analysis method. Furthermore, residual life of pavement skid-resistant performance was predicted based on present traffic volume and traffic growth rate. This research provided scientific basis to establish pavement maintenance plan and to take effective measures to improve pavement skid-resistance, which, will lead to a decrease or avoidance in traffic accidents.

The projects discussed in this paper included two separated tunnels of one expressway with four lanes in two ways. One tunnel is 3011m long and the other is 3056m. The tunnels lie in the transition zone between loess plateau and Qinghai-Tibet plateau with semi-arid climate of continental plateau. Asphalt concrete pavement was used outside the tunnels and cement concrete pavement inside.

2 FUZZY CLUSTER ANALYSIS OF PAVEMENT SKID-RESISTANT PERFORMANCE

2.1 EXPRESSION OF FUZZY EQUIVALENT RELATIONSHIP

In order to learn about the whole pavement behavior of the two tunnels, 14 points in different places (See figure 1) were tested by using pavement test equipment.

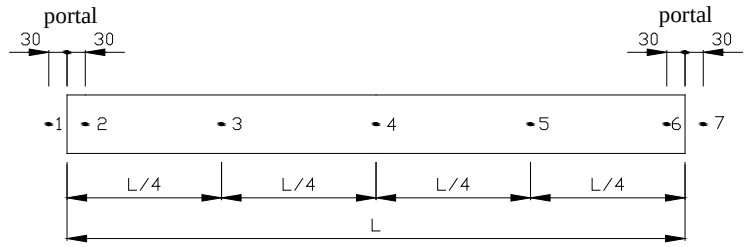

Unit: m

Figure 1. Layout of test points.

Three variables, pavement type, British pendulum number (BPN) and mean texture depth (MTD), were used to express each point. Besides, each variable was determined by the mean test value of three different points at the same cross section of each tunnel. Test data were showed in table 1.

Table 1. Test Value of Tunnel Pavement Skid-resistant Performance.

Points	Pavement type	BPN	MTD(mm)
Z1	0	63	0.39
Z2	1	62	0.26
Z3	1	64	0.35
Z4	1	65.5	0.32
Z5	1	65	0.30
Z6	1	64	0.30
Z7	0	72.5	0.37
Y1	0	60	0.36
Y2	1	59	0.27
Y3	1	62	0.32
Y4	1	63.5	0.34
Y5	1	63	0.33
Y6	1	64	0.36
Y7	0	69	0.36

In table 1, 0 represents asphalt concrete pavement, 1 cement concrete pavement, Z the left tunnel and Y the right tunnel. In order to preclude random effect, test data have to be treated by means of standardization of data range.

Canonical matrix can be obtained based on standardization of data range. Similarity coefficient which used to weigh sample level of similarity can be calculated with cape cosine equation, expressed as:

$$\gamma_{ij} = \frac{\sum_{k=1}^{m} X_{ik} \cdot X_{jk}}{(\sum_{k=1}^{m} X_{ik}^{\ 2} \cdot \sum_{k=1}^{m} X_{jk}^{\ 2})^{\frac{1}{2}}} \qquad (1)$$

where γ_{ij} is the similarity coefficient; X_{ik} is the i-th standard data of the k-th variable; X_{jk} is the j-th standard data of the k-th variable; and m is the number of variables.

According to Eq. (1), fuzzy similarity matrix R was calculated and equation $R^8=R^4$ was derived by means of transitive closure method. Therefore, R^4 is the fuzzy equivalent matrix, which is listed below.

1.00	0.64	0.64	0.64	0.64	0.64	0.89	0.98	0.64	0.64	0.64	0.64	0.64	0.89
0.64	1.00	0.95	0.95	0.95	0.95	0.64	0.64	0.97	0.95	0.95	0.95	0.95	0.64
0.64	0.95	1.00	0.99	0.99	0.99	0.64	0.64	0.95	1.00	1.00	1.00	1.00	0.64
0.64	0.95	0.99	1.00	0.99	0.99	0.64	0.64	0.95	0.99	0.99	0.99	0.99	0.64
0.64	0.95	0.99	0.99	1.00	1.00	0.64	0.64	0.95	0.99	0.99	0.99	0.99	0.64
0.64	0.95	0.99	0.99	1.00	1.00	0.64	0.64	0.95	0.99	0.99	0.99	0.99	0.64
0.89	0.64	0.64	0.64	0.64	0.64	1.00	0.89	0.64	0.64	0.64	0.64	0.64	1.00
0.98	0.64	0.64	0.64	0.64	0.64	0.89	1.00	0.64	0.64	0.64	0.64	0.64	0.89
0.64	0.97	0.95	0.95	0.95	0.95	0.64	0.64	1.00	0.95	0.95	0.95	0.95	0.64
0.64	0.95	1.00	0.99	0.99	0.99	0.64	0.64	0.95	1.00	1.00	1.00	1.00	0.64
0.64	0.95	1.00	0.99	0.99	0.99	0.64	0.64	0.95	1.00	1.00	1.00	1.00	0.64
0.64	0.95	1.00	0.99	0.99	0.99	0.64	0.64	0.95	1.00	1.00	1.00	1.00	0.64
0.64	0.95	1.00	0.99	0.99	0.99	0.64	0.64	0.95	1.00	1.00	1.00	1.00	0.64
0.89	0.64	0.64	0.64	0.64	0.64	1.00	0.89	0.64	0.64	0.64	0.64	0.64	1.00

2.2 CLUSTER RESULTS

Different level cut sets λ were selected for fuzzy cluster analysis. If the corresponding elements are completely identical, they can be put into the same class and new fuzzy equivalent matrixes can be obtained. For example, If λ =0.89, two classes can be obtained such as (Z1, Z7, Y1, Y7) and (Z2, Z3, Z4, Z5, Z6, Y2, Y3, Y4, Y5, Y6). If λ =0.98, six classes can be obtained such as (Z1), (Z2), (Z3, Z4, Z5, Z6, Y3, Y4, Y5, Y6), (Y1), (Y2) and (Z7, Y7). Based on the results, the following observations are made:

1) Skid-resistant performance of asphalt concrete pavement is better than that of cement concrete and skid-resistant performance durability of asphalt concrete pavement is better than that of cement concrete. Besides, pavement skid-resistant performance outside the tunnel is better than that inside the tunnel.

2) In order to adapt to the tunnel environment, continuous deceleration was done by all the drivers when they travel through the tunnel. Therefore, vehicle density increased and pavement skid-resistance performance reduced accordingly. As the frequent brake and deceleration, Z2 and Y2 became the worst points in terms of pavement skid- resistance performance. Point Z7 and Y7 is in the same class, so their pavement skid-resistance performances are the same.

3) Unctuous and thin film often comes into being on top of the pavement as tunnel environment is closed and as the pavement is hygroscopic. Attachment coefficient of point Z3, Z4, Z5, Z6, Y3, Y4, Y5 and Y6 lie in the tunnel decreased in value greatly. So pavement skid-resistance performance in tunnel is worse than that of other parts of expressway.

According to actual survey, the fuzzy cluster results discussed above matched the actual condition well.

3 RESIDUAL LIFE PREDICTION OF PAVEMENT SKID-RESISTANT PERFORMANCE

Pavement skid-resistant performance reduced quickly under traffic loads and then gradually turned to be stable. (Yang 2001; Yang et al. 2002) Residual life of tunnel pavement skid-resistant performance can be predicted based on present traffic volume and traffic growth rate. The tunnels under study have open to traffic for 4 years. The current annual average daily traffic of the left tunnel is 6500veh/d and traffic growth rate is about 10% in initial operation period. Therefore, accumulated applications of standard axle (Ne) can be calculated. According to British pendulum number and texture depth, attenuation rate (K) of tunnel pavement skid-resistant performance can be expressed as

$$K = -\frac{dTD^*(BPN^*)}{dN} = \frac{TD_0(BPN_0) - TD(BPN)}{N\mathrm{e}} \qquad (2)$$

where TD(BPN) is the value of pavement skid-resistant performance in the application period; $TD_0(BPN_0)$ is the value of pavement skid-resistant

performance in the stage of opening to traffic; N is the accumulated applications of standard axle; and $TD^*(BPN^*)$ is the relative value of pavement skid-resistant performance. $TD^*(BPN^*)$ can be calculated as

$$TD^*(BPN^*) = TD(BPN) - TD_S(BPN_S) \quad (3)$$

where $TD_S(BPN_S)$ is the finial stable value.

According to the field test data and laboratory experiments, attenuation equation can be expressed as

$$TD^*(BPN^*) = A_{TD(BPN)} e^{-B_{TD(BPN)}N} \quad (4)$$

where $A_{TD(BPN)}$ is the maximum attenuation fall of skid-resistant performance and $B_{TD(BPN)}$ is the ratio of attenuation rate to the relative value of pavement skid-resistant performance.

$TD_0(BPN_0)$ can be obtained from technical specifications (Ministry of Transport of the People's Republic of China 2001). According to calculation, the residual life of pavement skid-resistant performance of the left tunnel entrance is no more than 0.85 years, which means that the pavement skid-resistant performance will fall to unacceptable level in 0.85 years.

4 CONCLUSIONS

1) The pavement skid-resistance performance of expressway tunnel is different in different places because of vehicle actions, pavement materials, highway traffic environment, etc.

(2) Pavement skid-resistance performance reduced gradually with the increase in traffic volume and the residual life of pavement skid-resistant performance can be predicted based on traffic volume and its growth rate. The results showed that attenuation rate decreased quickly in tunnel entrance. Therefore, some effective measures should be taken to improve pavement skid-resistant performance.

(3) Highway traffic safety is influenced by pavement skid-resistant performance. This paper provided an evaluation method of pavement performance. Besides, this research can also be regarded as references for reliability analysis of the whole tunnel structure.

REFERENCES

Ma, C.X., Guang, X.P. and Qian, Y.S. (2008). "Study on long tunnel traffic safety." *J. Science of disaster*, 23(1), 82-87.

Ministry of Transport of the People's Republic of China, (2001). *Technical specifications of cement concrete pavement maintenance for highway* (*JTJ* 073.1-2001), China Communications Press, Beijing.

Ministry of Transport of the People's Republic of China, (2001). *Technical specifications for maintenance of highway asphalt pavement* (*JTJ 073.2-2001*), China Communications Press, Beijing.

Shen, A.Z..(2002). "Causes and protective measures to traffic accident in tunnel." *Road Traffic Management*, 105(9), 40-41.

Yao, S.G. (1985). *Study on long term performance of pavement skid-resistance*, Position paper of the China's 6th five-year plan, Research institute of highway ministry.

Yang, Z. (2001). *Study on evaluation method of asphalt mixture surface properties*, Tongji University, Shanghai.

Yang, Z. and Guo, Z.Y. et al. (2002). "The acceleration test's method study of the slide-preventing function of slide-preventing wearing course of bituminous concrete." *J. East China highway*, 135(2), 50-54

Influence of Crack Size of Old Concrete Pavement Slab on Structure Stress of Asphalt Overlay

M. Zheng[1] and S. Chen[2]

[1]Associate Professor, Key Laboratory for Highway Engineering in Special Areas, China's Ministry of Education, Chang'an University, Xi'an 710064, Shaanxi, P. R. China; also College of Highway Engineering, Chang'an University, Nan-er-huan Road, Xi'an 710064, P. R. China; PH 86-13630280989; FAX: 86-29-82334846; email: zhengmulian@163.com

[2]Professor and Deputy Head, Key Laboratory for Highway Engineering in Special Areas, China's Ministry of Education, Chang'an University, Xi'an 710064, Shaanxi, P. R. China; chenshuanfa@sohu.com

ABSTRACT

Old concrete pavement with major damage can be reconstructed by paving the asphalt surface after cracked and stabilized with punching technique. But the cracked size is different in every country and there is no corresponding theory basis. Using 3-D finite element method, the relationships between cracked size for concrete slab and load stress, thermal stress, and coupling stress in asphalt overlay together with pressure stress on base surface were analyzed. The results show that the influence of cracked size on thermal stress and coupling stress is much greater than that of load stress. When cracked size decreases, thermal stress and coupling stress in asphalt overlay decrease rapidly. Also, the stress centralization at joints and cracks lessens evidently, while the pressure stress on base surface increases. Considering the factors synthetically, it is reasonable for the cracked size to range from 80 cm to 100 cm.

INTRODUCTION

When old cement concrete pavement slab is largely damaged, it can be reconstructed by paving asphalt surface after it is cracked and stabilized with punching technique. It has been widely used in America and South Africa, and now in some regions of China. There is no consensus about the cracked size of old concrete slab, and no corresponding design and construction specifications in China. Li (1997) suggests that the cracked results of old cement concrete pavement should be blocks with length of sides of 45~60cm, some blocks about 75cm, and blocks exceeding 60cm should be less than 70%. Yao (1999) suggests supplying concrete crack machines to break concrete slab into blocks of 60~100cm, and then using a heavy tyre roller on the blocks. In the United States, the cracked size of concrete pavement, listed in Table 1, differs greatly among the states. The cracked size varies greatly from the minimum size of 45cm to a maximum size of 180cm.

Research shows that the cracked size of old cement concrete pavement slab has great influence on the performance of asphalt overlay. Using an experimental road and adopting a finite element method, this paper studies the relationships of cracked concrete slab size and load stress, thermal stress, coupling stress in asphalt

overlay and pressure stress on base surface in order to determine a reasonable cracked size for old cement concrete slab.

Table 1. Empirical cracked size of cement concrete pavement in American

State	*Cracked size of cement concrete pavement*
Iowa	1.8m
California	1.2～1.8m
Minnesota	0.9～1.2m
New York	0.9m
North Dakota	0.9m
Illinois	0.45～0.6m
Kentucky	0.45～0.6m
Michigan	0.45～0.6m
West Virginia	0.45～0.6m

1 CALCULATION MODEL AND PARAMETERS

We begin with a pavement structure as an elastic layered system. The object of study is composed of asphalt overlay, cracked and stabilized slab of different size and subgrade. The paper utilizes a model of three-dimensional space and takes the length direction as the x axle, width direction as y axle, and depth direction as z axle. To reflect the characters of semi-infinite space subgrade, the subgrade is simulated with expansion size and the model and grid system are shown in Figure 1. In the model, the joint width of old cement concrete pavement is assumed to be 1 cm, and there is no load transmission capability at joints.

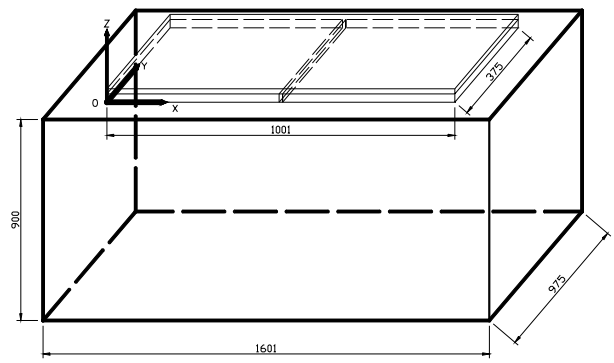

Figure 1. Structure calculation model (unit: cm).

The plane size of cement concrete pavement slab before cracked adopts 500cm×375cm, and the expansion dimension of subgrade is decided as 16.01m×9.75m×9m. The average size of slabs after cracked separately adopts 250cm×188cm, 100cm×94cm, 50cm×54cm.

The traffic load adopts standard axle load BZZ-100 and the tyre inner pressure is 0.7MPa. The loading pattern is shown in Figures 2 and 3.

The reference temperature is approximately adopted as the temperature of -5℃ when calculating thermal stress. The temperature ranging between -10℃ and +10℃. Since the influence of negative difference in temperature is more

unfavourable for pavement structure, the temperature decline of -10□ on an overlay surface is set to calculate thermal temperature. The other main calculation parameters are listed in Table 2.

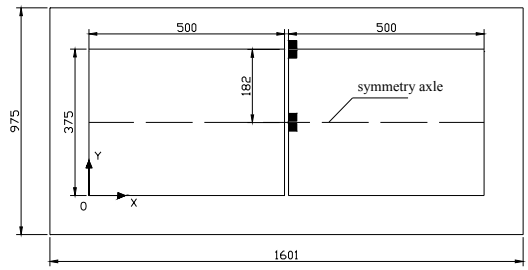

Figure 2. Wheel loading plane (unit: cm).

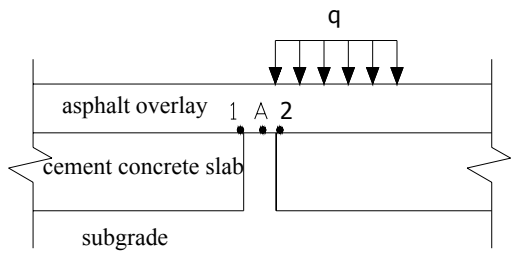

Figure 3. Diagrammatic sketch of wheel loading

Table 2. Main parameters

Structure layer	Thickness/cm	Elastic modulus/ MPa	Passion ratio	Coefficient of heat conductivity /w·(m·□)$^{-1}$	Coefficient of linear expansion /(□$^{-1}$)
Asphalt overlay	12	1200	0.25	1.2	2.1×10^{-5}
Cracking and Stabilized slab	22	30000	0.15	1.5	1.0×10^{-5}
Subgrade	—	100	0.35	1.0	0.5×10^{-5}

Besides, since the crack can transmit shearing, but cannot transmit bending moment and tensile force, the influence of crack contact condition should be considered when calculating the vehicle load stress of overlay. Calculation results show that the equivalent stress σ_e and maximum shearing stress τ_{max} of asphalt overlay decrease with the friction coefficient between crack increasing under the action of vehicle load. Therefore, the calculations are all carried out under the most unfavourable bearing conditions of asphalt overlay, namely the friction coefficient between a crack is 0.

2 Influence of cracked slab size on asphalt overlay stress

When traffic load is 100KN, the reference temperature of pavement structure is -5° and the temperature decline range of asphalt overlay surface is -10°. The influence of pavement slab cracked size on load stress, thermal stress and coupling stress of overlay is calculated and the results are shown in Table 3.

Table 3. Load stress, thermal stress and coupling stress of asphalt overlay.

Cracked slab size /cm×cm	Load type	Stress /MPa										
		σ_x	σ_y	σ_z	τ_{xy}	τ_{yz}	τ_{xz}	σ_1	σ_2	σ_3	σ_e	τ_{max}
500×375	Load	-1.165	-0.353	-0.276	-0.014	0.034	-0.354	-0.146	-0.359	-1.289	1.053	0.572
	Thermal	3.616	1.033	0.181	-0.002	0.000	0.011	3.616	1.033	0.181	3.098	1.718
	Couple	2.446	0.679	-0.094	-0.017	0.034	-0.343	2.491	0.680	-0.141	2.333	1.316
250×188	Load	-1.115	-0.355	-0.273	-0.013	0.038	-0.339	-0.150	-0.362	-1.271	1.031	0.560
	Thermal	2.961	0.859	0.147	-0.001	-0.001	0.021	2.962	0.859	0.147	2.535	1.408
	Couple	1.815	0.507	-0.126	-0.014	0.037	-0.318	1.866	0.508	-0.178	1.802	1.022
100×94	Load	-1.037	-0.326	-0.263	-0.010	0.039	-0.391	-0.093	-0.333	-1.200	1.009	0.554
	Thermal	2.138	0.639	0.104	0.000	0.000	-0.001	2.138	0.639	0.104	1.826	1.017
	Couple	1.119	0.317	-0.157	-0.010	0.039	-0.392	1.230	0.319	-0.270	1.309	0.750
50×54	Load	-0.872	-0.285	-0.259	-0.012	0.034	-0.443	-0.022	-0.289	-1.105	0.977	0.541
	Thermal	1.392	0.437	0.064	-0.001	-0.001	0.000	1.392	0.437	0.064	1.187	0.665
	Couple	0.536	0.157	-0.195	-0.013	0.033	-0.443	0.747	0.156	-0.405	0.997	0.576

2.1 Influence of cracked size on overlay load stress

It can be seen from Table 3 and Figure 4 that the maximum principal stress σ_1 at the bottom of asphalt overlay at joints increases a little with the cracked size of cement concrete slab and decreases under the traffic load action. But the value of σ_1 is always negative. This shows the overlay is under the favourable compressive condition all along, while the equivalent stress σ_e and the maximum shearing stress τ_{max} decline slowly with cracked slab size decreasing, which shows that reducing slab size can decrease the load stress concentration at joints of old cement concrete at a certain extent.

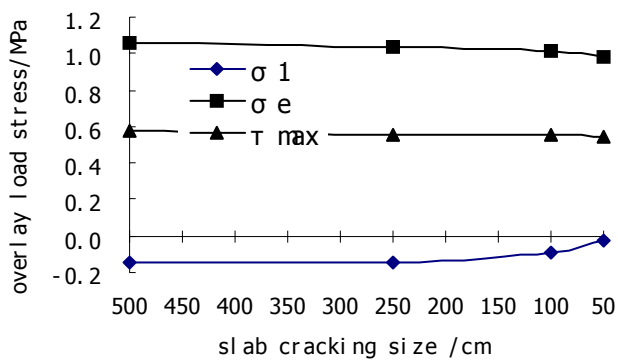

Figure 4. Load stress of asphalt overlay along with cracked slab size variety.

Figure 5 shows that the compressive stress on base surface increases with cracked slab size decreasing. When the cracked size is less than 100cm×94cm, the compressive stress increases quickly.

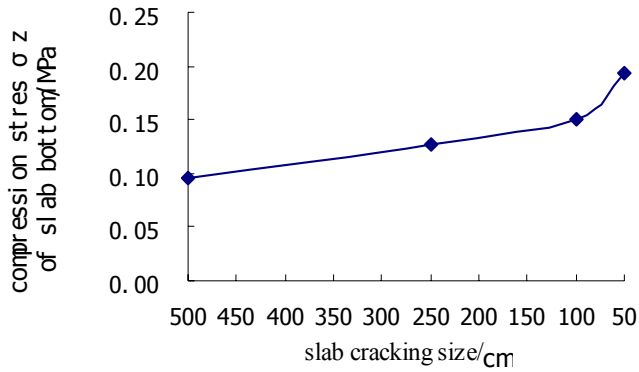

Figure 5. Compressive stress at slab bottom along with cracked slab size variety.

2.2 Influence of cracked slab size on overlay thermal stress

The calculation results of overlay thermal stress are shown as Figure 6, which indicates that the thermal stresses σ_1, σ_e and τ_{max} of asphalt overlay fall quickly with the decreasing size of cracked slab. When the slab size reduces from 500cm×375cm to 50cm×54cm, the values of σ_1, σ_e and τ_{max} decline by 61.5%, 61.7% and 61.3%, which shows that the slab size has great influence on overlay thermal stress.

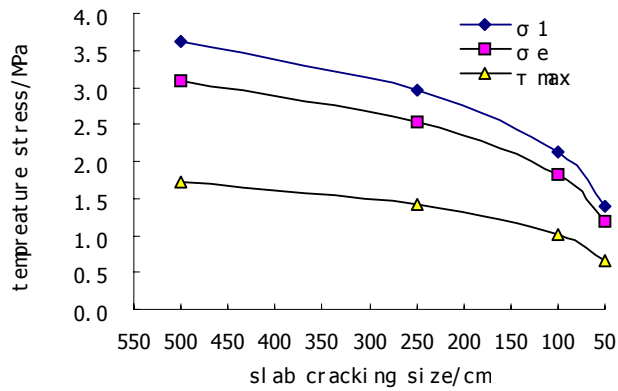

Figure 6. Thermal stress of asphalt overlay with cracked slab size variety.

2.3 Influence of cracked slab size on overlay coupling stress

Table 3 and Figure 7 show that the coupling stressed σ_1, σ_e and τ_{max} of asphalt overlay formed by the joint action of load and temperature decline along with the decreasing size of cracked slab. When the slab size reduces from 500cm×375cm to 100cm×94cm, the values decline by 70.0%, 57.3% and 56.2%, which indicates that the coupling stress of asphalt overlay falls greatly when cement concrete slab is cracked and divided into small slabs.

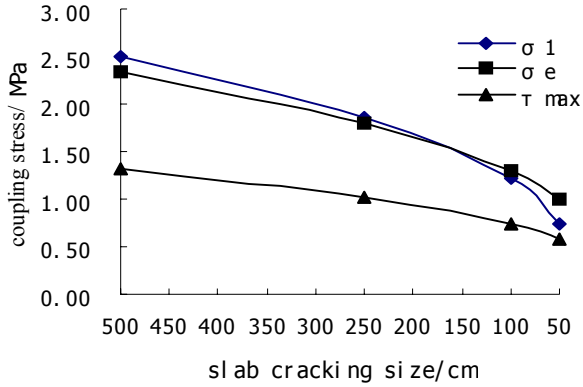

Figure 7. Coupling stress of asphalt overlay along with cracked slab size variety.

3 CONCLUSIONS

(1) The cracked size of pavement slab has some influence on the load stress of asphalt overlay, and the equivalent stress σ_e and maximum shearing stress τ_{max} of overlay have a small decrease along with smaller cracked slab size. The cracked size has great influence on the compressive stress on the base surface, which increases with cracked slab size decrease.

(2) The influence of cracked slab size on thermal stress and coupling stress of asphalt is greater than that on load stress. The thermal stress and coupling stress decline quickly and the stress concentration at joints weakens obviously along with the decrease of cracked slab size.

(3) Based on comprehensive consideration of the influence of cracked slab size on load stress, thermal stress and coupling stress of asphalt overlay, compressive stress on the base surface, research findings are that it is reasonable for the cracked size to be 80~100cm when using punching technique to crack and stabilize cement concrete pavement slab.

REFERENCES

Bozkurt, D. (2002). "Three dimensional finite element analysis to evaluate reflective cracking potential in asphalt concrete overlays," University of Illinois, 54-72.

Cho, Y., Liu, C., Dossey, T. and Mccullough, B. F. (October 1998). "Asphalt overlay design methods for rigging pavements considering rutting, reflection cracking, and fatigue cracking." Research Report 987-9, The University of Texas at Austin, 11-98.

Li, H., Liao, C., and Jin, Z. (1997). *Mending technique of cement concrete pavement*. China Communications Press.

Yao, Z. (1999). *Pavement*. China Communications Press.

Stability Analysis of Excavating Rock Slope Based on the Catastrophe Theory

WANG Xiao-zhao[1] and WANG Si-chang[2]

[1]Traffic Engineering Department, Henan College of Urban Construction, South Road 26th of Zhan-he, Pingdingshan, 467001, Henan, China; PH (0375)3672589; email: wangxz@hncj.edu.cn

[2]School of Highway, Chang'an University, Middle Section of the South 2nd Ring, Xi'an,710064, Shaanxi, China; PH (029) 82334839; email: wsc1257@163.com

Abstract: As a complex system, there are lots of complex non-linear characteristics in excavating slopes. Stability of rock slope was analyzed with the catastrophe theory. A mechanistic model for assessment of the slope stability was derived in this paper. Based on it, the criterion for the mechanistic conditions that can cause the failure and instability of slope were inferred. Compared with the deficiency of the limit equilibrium stability analysis method applied in rigid bodies, it was proved that using catastrophe theory to analyze the stability of rock slope was feasible in practical engineering.

Key words: *rock slope; stability; catastrophe theory; mechanistic model*

0 Introductions

Parameters of the slope system, which is an open system with complex structure and behavior, are uncertain and random. In evolution process of the slope system, mass, energy and information exchange with the out world continually. In fact, the mechanical behavior of rock slope instability is a dynamic, nonreversible and non-linear evolution process and the non-linearity is the basic attribute (Huang Runqiu, Xu Qiang 1996, Huang Zhiquan 2005). Using the catastrophe theory, researchers in China and other countries proposed a number of mechanistic models of slope instability to study the stability of rock slope. However, to the rock slope of the reservoir bank and riverbank, these models don't include the erosion effect of water and the influence of water pressure of posterior margin in slope fissures on the stability of excavating rock slope (Liang Guilan, Xu Weiya, He Yuzhi 2008, Lou Yiqing, Gu Shijun, Li Jun 2008, Qin Siqing 2000, Jiang Yongdong, Xian Xuefu, Yang Gang 2008). Voluminous facts indicate that 90% of landslides are caused by water, which fully demonstrate that, water is an important factor affecting the stability of slope (Xiong Junming 2008, He Keqiang, Wang Ronglu, Li Xinzhi 2008, Liu Bingshan, Li Shihai, Zhao Qing 2008). Considering the influence of water on the stability of excavating slope and compared with the deficiency of the limit equilibrium stability analysis method in evaluating the stability of rock slope, this paper established a the catastrophe theory of rock slope, and furthermore verified the feasibility of using it to analyze the stability of excavating rock slope in engineering.

1. Mechanistic model

Assuming the gliding plane is homogenous and the sheering stress of various point in gliding plane reached the limit damage state at the same time, the limit equilibrium stability analysis method, which determines whether a slope is stable by getting the slide safety coefficient of the sliding block at the moment of destroying the equilibrium of the rock slider, is a common method to analyze slope stability (Chen Zuyu, Wang Xiaogang, Yang Jian 2005). Qin Siqing (2000) and Liu Yaoru (2007) believe that, slope slip surface was not homogenous and it is impossible for the sliding force to reach the limit at the same time. The limit equilibrium stability method could not reflect the real state of gliding plane. Considering the slope was non-homogenous, the mechanistic model, built by Qin Siqing, assumed that the gliding plane was a non-homogenous soft interlayer and the upper rock was a rigid body. Based on the above conditions, the unit width of landslide is studied in this paper. *H, L,* , *h* and *Mg* represent the average height of the upper rock of landslide, the length of landslide, the slope angle, the thick of the soft interlayer and the weight of landslide respectively. Where, $Mg = HL(\rho g + \gamma_w)$ and γ_w is the unit weight of water and g is the acceleration of gravity. Maybe $_w$ is a variable because of the rainfall. Along soft interlayer, rock mass has a displacement represented by u (Fig. 1). In certain section of soft interlayer, where the intensity of medium is great such as locked patch, or suffered shearing stress is little, the medium has flexibility and strain-hardening effect, and the ability of deformation resistant was increased by the increasing of deformation，however, in other sections such as toe of slope, for the medium is crushing, the argillization of water or the medium has the capability of strain-weakening properties because the suffered stress is so great that the stress beyond the peak stress, the ability of deformation resistant is decreased by the increasing of deformation.

In order to simplify the analysis and focus on the physical nature of instability, it is assumed that, the soft interlayer is composed of two different medium, having different mechanical properties with one of strain weakening and the other one of flexibility. Fig.2 shows the relationship between the shearing stress and the deformation of two-section medium.

The constitutive relationship of the medium of flexible section in soft interlayer is,

$$\tau_1 = G_1 \frac{u}{h} \quad (u \le u_1) \qquad \tau_1 = \tau_m \quad (u \succ u_1) \tag{1}$$

where τ_1 is the shearing stress of the medium of flexible section, G_1 is the shearing modules of the medium of flexible section, u_1 is the displacement

corresponded to the peak value of shearing stress and τ_m is the residual shearing intensity of the medium of flexible section.

The constitutive relationship of the medium of strain weakening section in soft interlayer is,

$$\tau_2 = G_2 \frac{u}{h} \exp\left[-\frac{u}{u_2}\right] \qquad (2)$$

where τ_2 is the shearing stress of the medium of strain weakening section, G_2 is the shearing modules of the medium of strain weakening section and u_2 is the displacement corresponded to the peak value of shearing stress.

In equation (2), when $\frac{d^2\tau_2}{du^2} = 0$, it could identify the inflection point of the curve of shearing stress and deformation. The displacement of the medium of soft section is $2u_2$ and the inclination is $-\frac{G_2 e^{-2}}{h}$.

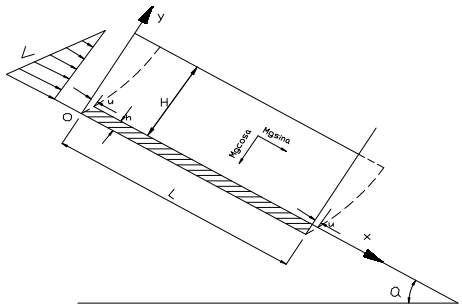

Fig.1 Analysis model of slope gliding

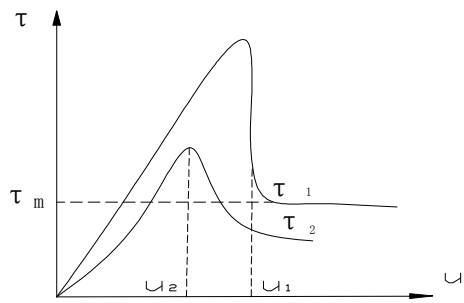

Fig. 2 Relationship between deformation and shearing stress of the medium of two-section soft interlayer

In order to reflect the effect of ground water, Jiang Yongdong (2008) introduced a function reflecting the water-caused weakening effect on the gliding plane.

$$f_{(w)} = (1-\eta)(1-w)^2 + \eta \qquad (3)$$

where w is the saturation and η is softening coefficient of rock body.

Equation (3) is descending monotonously. When slope is dry, $w=0$, $f_{(0)}=1$ and when water is saturated, $w=1$, $f_{(1)}=\eta<1$, the constitutive relationship of the medium of two sections under water-caused weakening effect is,

$$\tau_1 = f_1(w_1)G_1\frac{u}{h} \quad (4)$$

where w_1 is the saturation of the medium of flexible section.

$$\tau_2 = f_2(w_2)G_2\frac{u}{h}\exp\left[-\frac{u}{u_2}\right] \quad (5)$$

where w_2 is the saturation of the medium of strain softening section.

To rock landslide, the fissure water pressure in posterior margin of fracture should be considered. The fissure water pressure is calculated by equation (6).

$$V = \frac{1}{2}r_w h_w^2 \quad (6)$$

where V is the fissure water pressure, kN/m, r_w is the water unit weight and h_w is the height of water in fissure, *m*.

2. Cusp catastrophe model

The total potential energy function of a slope system could be induced by mechanistic model.

$$V_{(u)} = \int_0^u \left| f_1(w_1)l_1\frac{G_1 u}{h} + f_2(w_2)l_2\frac{G_2 u}{h}\exp[-\frac{u}{u_2}] \right| d_u - \left[HL(\rho g + \gamma_w)\sin\alpha + \frac{1}{2}\gamma_w h_w^2 \right] u \quad (7)$$

where l_1, l_2 is the length of flexible section of gliding surface and the length of weakening section of gliding surface respectively and $L = l_1 + l_2$.

Chosen u as a state mutation variable and calculated the derivative of equation (7), the equilibrium surface of slope stability analysis could be achieved.

$$V'_{(u)} = f_1(w_1)l_1\frac{G_1 u}{h} + f_2(w_2)l_2\frac{G_2 u}{h}\exp[-\frac{u}{u_2}] - \left[HL(\rho g + \gamma_w)\sin\alpha + \frac{1}{2}\gamma_w h_w^2 \right] = 0 \quad (8)$$

Equation (8) is the equilibrium condition of force. According to the smooth property of equilibrium, the shear displacement of the equilibrium conditions cusp is $u = u_1 = 2u_2$ by solving $V''_{(U)} = 0$, namely the displacement in cusp is just the inflection point of the constitutive relationship curve of the medium of weakening section.

The equilibrium surface is transformed to equation (9) by using the cubic polynomial of Taylor expansions of equation (8) at state variable u_1 in the cusp point.

$$\frac{2}{3}\frac{f_2(w_2)l_2G_2u_1e^{-2}}{h}\left|\left|\frac{u-u_1}{u_1}\right|^3+\frac{3}{2}\left|\frac{f_1(w_1)l_1G_1e^2}{f_2(w_2)l_2G_2}-1\right|\left|\frac{u-u_1}{u_1}\right|+\frac{3}{2}\left|1+\frac{f_1(w_1)l_1G_1e^2}{f_2(w_2)l_2G_2}-\frac{\left|HL(\rho g+\gamma_w)\sin\alpha+\frac{1}{2}\gamma_w h_w^2\right|he^2}{f_2(w_2)l_2G_2u_1}\right|\right|=0 \quad (9)$$

The equilibrium surface, which is the standard form of the cusp catastrophe theory, could be achieved by carrying out variable substitution of equation (9).

$$V'(x)=x^3+bx^2+c=0 \quad (10)$$

Where, $x=(u-u_1)/u_1$ (11)

$$b=3(fk-1)/2 \quad (12)$$

$$c=\frac{3}{2}\left|1+fk-\frac{\xi}{f_2w_2}\right| \quad (13)$$

$$k=\frac{l_1G_1e^2}{l_2G_2} \quad (14)$$

$$\xi=\frac{\left[HL(\rho g+\gamma_w)+\frac{1}{2}\gamma_w h_w^2\right]he^2\sin\alpha}{l_2G_2u_1} \quad (15)$$

$$f=\frac{f_1(w_1)}{f_2(w_2)} \quad (16)$$

where x is a state variable of the system, b and c are the control variables of the system, k is the stiffness ratio of the medium of flexible section in the softening interlayer to the rigidity of the inflection point of the constitutive section of the medium in strain weakening section, f is the ratio of water-caused weakening coefficient of the medium of flexible section in softening interlayer to water-caused weakening coefficient of strain weakening section, namely the ratio of water-induced weakening coefficient and ξ, related to the weight of the medium, the physical dimension of the system, parameters of the medium and etc, are called geometry-mechanical parameters.

The bifurcation set is: $\Delta=4b^3+27c^3=0$ (17)

By substituting equation (12) and equation (13) into equation (17), it could achieve,

$$2(fk-1)^3+9\left|1+fk-\frac{\xi}{f_2w_2}\right|^2=0 \quad (18)$$

Equation (18) is a necessary and sufficient mechanical condition to determine whether the slope is suddenly instable gliding along softening surface. Only when $b\le 0$, crossing the bifurcations set, the system could mutate. The necessary condition is:

$$k \le \frac{1}{f} \tag{19}$$

Equation (19) shows that, when the stiffness ratio k is smaller than a certain impact factor of the ground water, the system will be instable; in other words, the saturation of the gliding band determines the mutation of the system. Equation (20) could be derived by equation (14) and equation (19).

$$k = \frac{l_1 G_1 e^2}{l_2 G_2} \le \frac{1}{f} \tag{20}$$

Equation (20) shows that, the stiffness ratio is determined by the physical dimension and material properties of the system and mutation of rock are determined by internal property of material and saturation of softening interlayer. The smaller the rigidity in flexible section is and the bigger the rigidity in the weakening section is, the easier the mutation of the system is. The longer the flexible section is or the lower the saturation in the weakening section is, the harder the mutation of system is.

When crossing the left branch of bifurcation set, namely $c \prec 0$, the corresponding point is in the instable state and x will leap suddenly. The displacement at the critical instable point could be calculated using equation (10) and equation (17).

$$u^* = u_1 \left| 1 - \frac{\sqrt{2}}{2}(1- fk)^{\frac{1}{2}} \right| \tag{21}$$

When the control variable satisfies

$$2(fk-1)^3 + 9\left| 1 + fk - \frac{\xi}{f_2(w_2)} \right|^2 \prec 0 \qquad (fk \prec 1) \tag{22}$$

It means that, although the slope body is in the limited equilibrium state, the equilibrium state will have a minor change when control variable has a minor change, which corresponds to the creep phenomena of the slope.

3. Comparison with the limit equilibrium method

Equation (18) could be simplified to

$$\frac{f_2(w_2) G_2 l_2}{\left[HL(\rho g + \gamma_w) + \frac{1}{2}\gamma_w h_w^2 \right] h \sin\alpha} = \frac{e^2}{2u_2 \left| 1 + fk \pm \frac{\sqrt{2}}{3}(1- fk)^{\frac{3}{2}} \right|} \qquad (fk \prec 1) \tag{23}$$

When $b \prec 0$, system cross the left branch of the bifurcation set resulting in the instability and positive sign is taken in equation (23).

$$\frac{f_2(w_2) G_2 l_2}{\left[HL(\rho g + \gamma_w) + \frac{1}{2}\gamma_w h_w^2 \right] h \sin\alpha} = \frac{e^2}{2u_2 \left| 1 + fk + \frac{\sqrt{2}}{3}(1- fk)^{\frac{3}{2}} \right|} \qquad (fk \prec 1) \tag{24}$$

According to the limit equilibrium stability analysis method, the stable coefficient of slope is a ratio of skid resistance to downslide force.

$$K = \frac{f_2(w_2)G_2 l_2 u \exp\left[-\frac{u}{u_2}\right] + f_1(w_1)G_1 l_1 u}{HL(\rho g + \gamma_w) + \frac{1}{2}\gamma_w h_w^2} = \frac{f_2(w_2)G_2 l_2}{HL(\rho g + \gamma_w) + \frac{1}{2}\gamma_w h_w^2}\left[u\exp\left[-\frac{u}{u_2}\right] + fke^{-2}u\right] \quad (25)$$

By substituting equation (24) into equation (25), it could get equation (26)

$$K = \frac{e^2\left|u\exp\left[-\frac{u}{u_2}\right] + fke^{-2}u\right|}{2u_2\left|1 + fk + \frac{\sqrt{2}}{3}(1-fk)^{\frac{3}{2}}\right|} \quad (26)$$

Equation (26) shows that, coefficient of slope stability K is correlated to the stiffness ratio k, u/u_2 and the water-weakening coefficient. K is increased with the increase of u. When the slope is in the critical instability state, namely $u = u^*$, the critical instability coefficient K_c could be obtained by substituting equation (21) into equation (26).

$$K_c = \frac{\left|1 - \frac{\sqrt{2}}{2}(1-fk)^{\frac{1}{2}}\right|\left|\exp\left[2(1-fk)\right]^{\frac{1}{2}} - fk\right|}{1 + fk + \frac{\sqrt{2}}{3}(1-fk)^{\frac{3}{2}}} \quad (27)$$

Equation (27) demonstrates that K_c is related to f and k.

4. Case study

Rock slope topography of the subgrade of the Shan-Man expressway from K110+809 to K110+872 is a steep slope in middle-low mountain and the slope angle is around 45°. Geologic lithology of the rock slope is metamorphic schist which is fulvous and strongly weathered and the structure of rock body is broken. 15 meters below the top of slope, there is a mudstone interbed which is about 10cm thick and the slope with a tendency of landslide.

According to field observation and indoor and outdoor experiments, when the slope was excavated, the saturation of flexible section of soft mudstone interbed is 0.2, the softening coefficient is 0.7, the length is 0.85 meters，shear modulus of medium is 1.47×10^{10}Pa, the saturation of strain weakening section is 0.3, the softening coefficient is 0.5, the length is 18.5 meters and the shearing modules of medium is 0.43×10^{10}Pa.

By equation (3), it could obtained $f_1 = 0.892, f_2 = 0.745$ and $f = \frac{f_1}{f_2} = 1.197$，

$\frac{1}{f} = 0.835$.

By equation (14), it could obtained $k = 1.16 \succ 0.835$. According to equation (19), the slope is stable and the sudden instability will not be happened.

By equation (27), it could obtained $K_c = 0.857$. The limit equilibrium stability analysis method suppose that, if only skid resistant is less than downslide strength, namely the stable coefficient of critical gliding K_c <1, the landslide will be happened. According to this theory, the slope is instable and the landslide will be happened conflicting with the result of the cusp catastrophe theory. However, the fact is, this slope is stable when excavated and not destroyed for instability which better proved that using the cusp catastrophe theory to analyze the stability of excavating rock slope is feasible. The calculated result of limit equilibrium stability analysis method is conservative，resulting waste in engineering.

5. Conclusion

By building the geo-mechanistic model of slope and using the catastrophe theory, the internal and external factors were taken into account, especially the effects of the water-caused weakening factor and the fissure water pressure in posterior margin of fracture and a more perfect cusp catastrophe model was built. Through analyzing influences of certain factors on stability of the slope, the mechanical conditions criterion of the unstable failure of slope was derived. After engineering calculation, analysis and comparing with the deficiency of the limit equilibrium analysis method, it was proved that, using catastrophe theory to analyze the stability of excavating slope was more feasible in practical engineering.

References:

Chen Zuyu, Wang Xiaogang, Yang Jian, and etc (2005). “Rock Slope Stability Analysis: Theory, Methods and Programs.” Bei Jing: China Waterpower Press.

He Keqiang, Wang Ronglu, Li Xinzhi, and etc (2008).“Load-unload Dynamic Law of Ground Water Level and Dynamic Displacement Prediction of Debris Landslide—A Case Study of Bazimen Landslide in Three Gorges Reservoir .” Chinese Journal of Rock Mechanics and Engineering, 19(2),36-43.

Huang Runqiu, Xu Qiang (1996).“Application of Non-linear Theories in Geological Engineering.” Bulletin of National Natural Science Foundation of China, (2),79-84.

Huang Zhiquan (2005).“The Nonlinear Theories of Slope Analysis and Application.” Zheng Zhou, Yellow River Water Conservation Press.

Jiang Yongdong, Xian Xuefu, Yi Jun (2008).“Study on Cusp Catastrophe Mutation of Slope Destability.” Journal of Chongqing Jianzhu University, (2),40-43

Jiang Yongdong, Xian Xuefu,Yang Gang and etc (2008). “A cusp catastrophe model study of destabilization of soft sandwich-rock slope”. Journal of Chong Qing University (Nature Science Edition). 31(6),677-682.

Liang Guilan, Xu Weiya, He Yuzhi, etc (2008). "Application of Catastrophe Progression Method to Comprehensive Evaluation of Slope Stability." Rock and Soil Mechanism, (7),1895-1899.

Liu Bingshan, Li Shihai, Zhao Qing (2008)."Research on The Main Factors Causing Maoping Lanslide Based Upon the Insitu Investigation." Chinese Journal of Geology Hazard and Control, 19(2),36-43.

Liu Yaoru, Yang Qiang, Xue Lijun and etc (2007)." Slope Stability analysis Based on 3-D Nonlinear Finite Element Method." Rock and Soil Mechanisms, 28(9),1894-1898.

Lou Yiqing, Gu Shijun, Li Jun (2008)." Study on the slope failure criterion in strength reduction finite element method based on catastrophe theory. " Journal of Xi'an University of Architecture and Technology (Nature Science Edition), (3),361-367.

Qin Siqing (1994). "New Theory of Planar Sliding Slope Instability—Rigidity Effect Instability Theory ." Hydrogeology and engineering Geology, (5),1-4.

Qin Siqing (2000). "Nonlinear Catastrophe Model of Slope Instability and Chaotic Dynamics Mechanisms of Slope Evaluation Process."Chinese Journal of Rock Mechanics and Engineering, 19(4),486-492.

Xiong Junming (2008). "Cause analysis and Renovating Measures of Landslide of Li Jiashan".West-China Exploration Engineering, (11),9-11.

Reinforcement Learning Control for On-Ramp Metering Based on Traffic Simulation

Xingju Wang[1,2], Bohang Liu[1,2] , Xueqin Niu[1,2] and Toshihiko Miyagi[3]

[1] School of Traffic and Transportation, Shijiazhuang Railway Institute, P.O. Box 050043, Shijiazhuang, Hebei, China. PH +86 311 87936027; FAX +86 (311) 87935516; email: xingjuwang@gmail.com

[2] Traffic Safety and Control Laboratory of Hebei Province, P.O. Box 050043, Shijiazhuang, Hebei, China. PH +86 (311) 87936027; FAX +86 (311) 87935516; email: xingjuwang@gmail.com

[3] Graduate School of Information Sciences, Tohoku University, P.O. Box 9808578, Sendai, Japan; PH +81 (22) 795-7495; FAX +81 (22) 795-7495; email: toshi_miyagi@plan.civil.tohoku.co.jp

ABSTRACT

Traffic congestion on highways causes decreased efficiency in road operation and increased energy consumption and environmental pollution. Various measures for traffic control have been considered for easing traffic congestion. In this paper, we propose the use of ramp metering control by introducing the reinforcement learning model in artificial intelligence, which is then combined with a dynamic micro traffic style simulation. Numerical simulation showed that when effective Reinforcement Learning ramp metering control is completed in the on-ramp section, traffic confusion can be prevented in advance.

INTRODUCTION

A model to simulate the dynamic changes in traffic congestion and to create a control model is needed. Wang and Miyagi created the simulation model which added the lane change model, i.e., the IDM (Intelligent Driver Model), originally developed by Treiber et al. (2000). The phase transition phenomenon that localized clusters and homogeneous congested traffic was pointed out by Kerner (2004). Moreover, the amount of vehicles inflow of the main line and an on ramp is a basic factor of traffic congestion based on the sensitivity-analysis result of the parameters in a simulation by Wang (2007). When effective control of traffic inflow is completed in the on-ramp section, traffic confusion can be prevented in advance and a smooth traffic style can be achieved.

The purpose of this research is to propose the ramp metering of an effective on-ramp section by introducing the reinforcement learning model using artificial intelligence that is then combined with a dynamic micro traffic simulation.

In the following section, the reinforcement learning ramp metering is elucidated. Moreover, reinforcement learning ramp is verified by traffic simulation by metering, and conclusions of our findings are given subsequently.

THE REINFORCEMENT LEARNING RAMP METERING

In order to solve the problem of the ramp metering, reinforcement learning ramp metering is proposed, of which the formula used is rewritten as follows.

$$Q(qin_t, r_t) \leftarrow Q(qin_t, r_t) + a\left[qout + \gamma \max Q(qin_{t+1}, r) - Q(qin_t, r_t)\right] \quad (1)$$

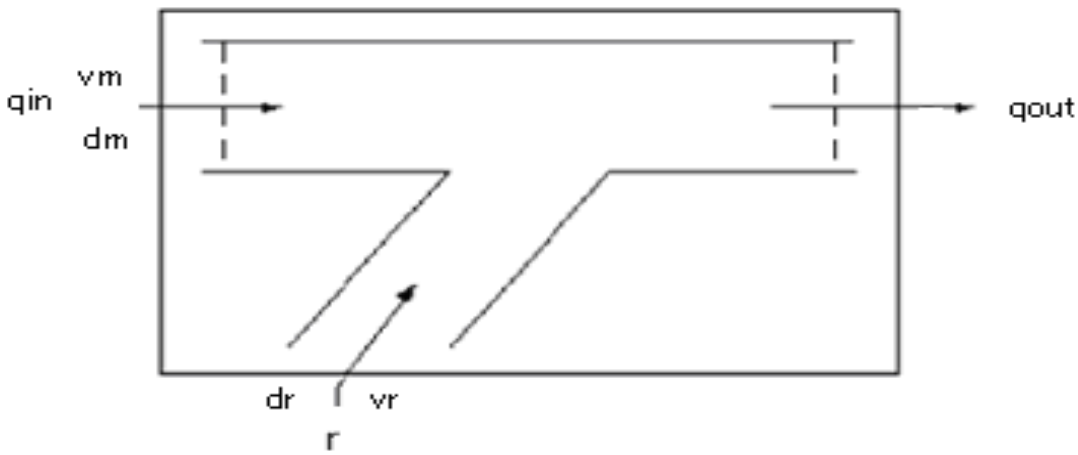

Figure 1. The reinforcement ramp metering.

In Figure 1, the *qin* is the main line upper stream traffic, *r* is the ramp inflow traffic, *qout* is the main line downstream traffic, *dm* is the main line upper stream density, *dr* is the ramp density, *vm* is the main line upper stream average speed, and *vr* is the ramp average speed.

$$q = qin + r - qout \quad (2)$$

In consideration of the stay traffic volume *q,* upper traffic is updated by the following formula.

$$qin_{t+1} \leftarrow qin_{t+1} + q \quad (3)$$

The upper traffic *qin* shall be obtained by observation and treated as a known variable. The ramp inflow traffic volume *r* is set with a selection-action variable as an amount of control. Moreover, *qout* is the reward accompanying action selection. Optimal *Q* is decided using a simulation. Optimization conditions are shown below:

(a) Traffic congestion does not occur in the main line.
(b) Traffic congestion does not occur with a ramp.
(c) Down-stream traffic becomes the maximum.

It is possible that the main line speed is larger than the simulation result by Wang and Miyagi, which could lead to large traffic congestion occurrences, the following conditions (a) and (b) are therefore established.

$$dm < 15 \qquad dr < 15 \tag{4}$$

$$vm < 15 \qquad vr < 10 \tag{5}$$

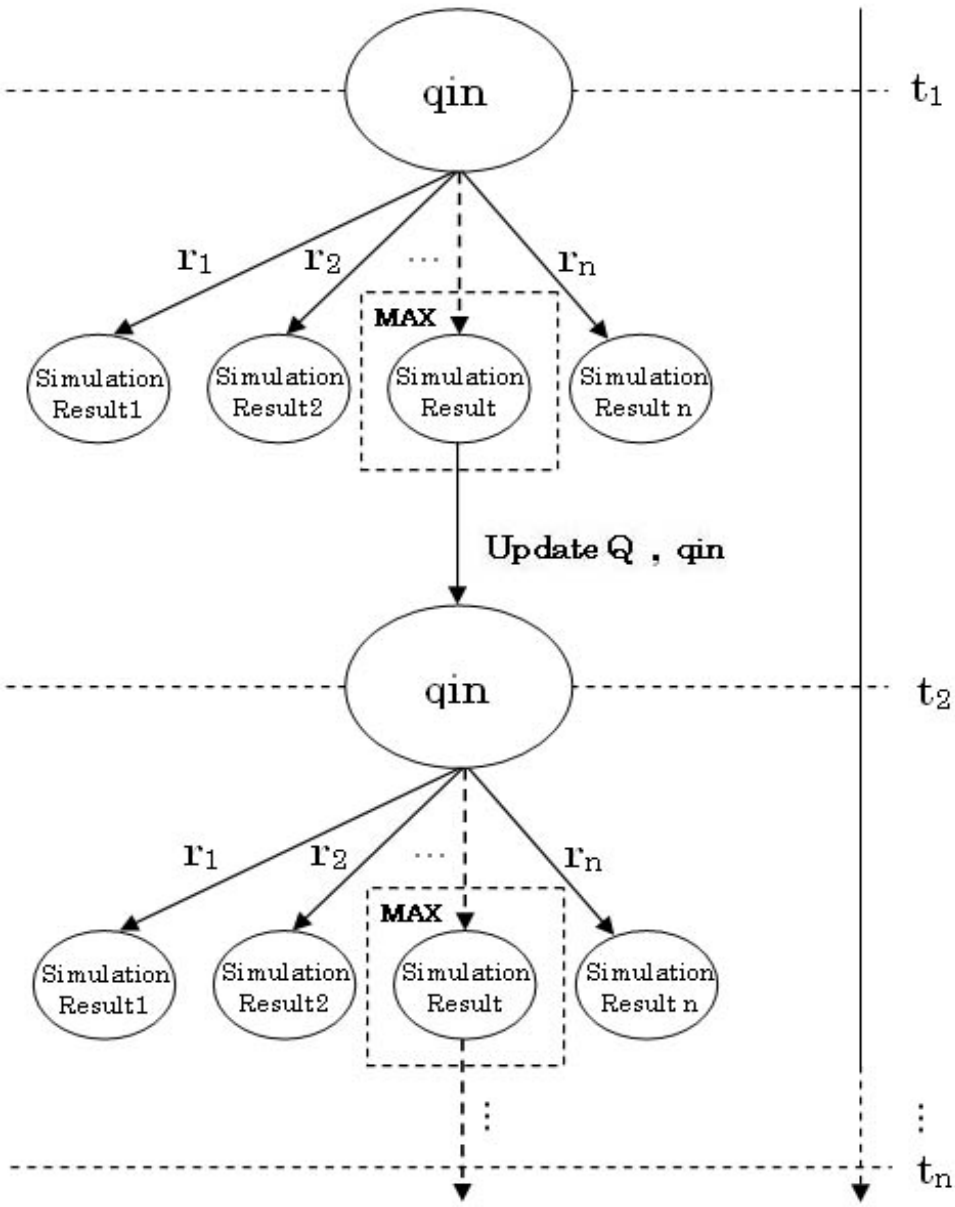

Figure 2. The procedure of td ramp metering.

The procedure of reinforcement learning ramp metering is shown in Figure 2 and follows the steps below:

(1) Input of main line upper stream traffic volume.
(2) Choose action (the amount of ramp traffic inflow), and perform a simulation.
(3) By using the results of the simulation, an optimal control action is selected.
(4) Update total outflow traffic Q and main line upper stream inflow traffic volume.
(5) Perform a repetition at a time unit.
(6) Stop repetition if it is the end of time.

VERIFICATION OF THE REINFORCEMENT LEARNING RAMP METERING

As shown in Figure 3, the merging section consists of a main lane and a side lane 100 m long. Vehicles on the ramp enter the main lane through the side lane. Various combinations of traffic flows of the main lane and the ramp were tested.

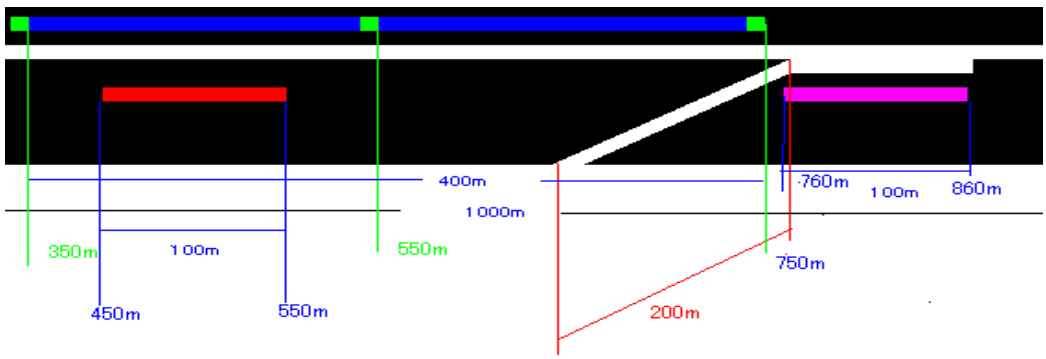

Figure 3. Structure of the road unification part used in the simulation.

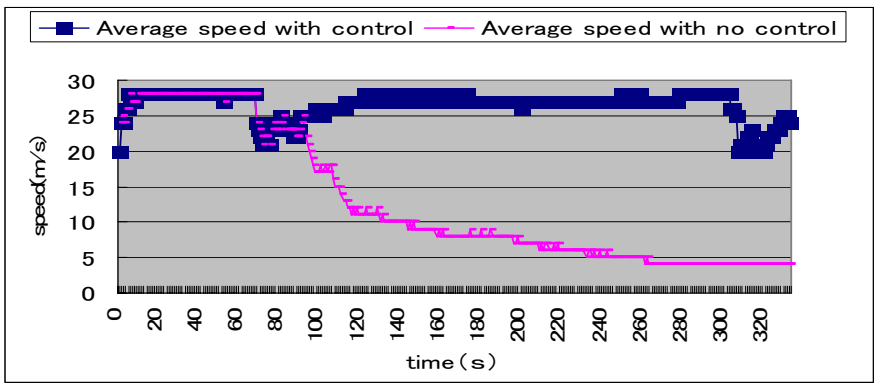

Figure 4. Time change of average speed in case B.

Table 1. Setup of a parameter, and selection of the optimal control action.

Case	time-axis (minute)	Main line traffic volume pcu (passenger car unit)	Ramp traffic volume pcu (passenger car unit)	
			with no control	with control
A	1.5	600	800	800
	3	1200		600
	4.5	1800		0
	6	2200		600
B	1.5	1200	800	800
	3	1800		600
	4.5	2200		0
	6	1600		600
C	1.5	600	800	800
	3	800		600
	4.5	1000		0
	6	1200		600

Table 2. The control effect by traffic and average travel time.

	Case	with no control	with control	The amount of change	Traffic congestion relief rate
A	Traffic volume (passenger car unit)	1850	1860	10	0.54%
	Average travel time (s/ car unit)	73	40	-33	-45.38%
B	Traffic volume (passenger car unit)	1840	2120	280	15.22%
	Average travel time (s/ car unit)	78	38	-40	-51.28%
C	Traffic volume (passenger car unit)	1560	1680	120	7.69%
	Average travel time (s/ car unit)	38	43	5	10.97%

As shown in Table 1, Cases A, B, and C were set up. In "having no control", ramp average traffic volume was set up in 800 pcu (passenger car unit). In the case of "with control", the optimal action brought a result shown in Table 1. If main line traffic volume increases to be 1600~1,800 pcu during traffic congestion, inflow control will be needed for Case B, and the result of choosing action (600 pcu) will be obtained. Moreover, time change of the average speed at this time is shown in Figure 4. If it continues permitting inflow by "he has no control", it will fall to 4 m/s after traffic congestion generating; however, in the case of "with control", average speed can be reduced to approximately 25 m/s. If the traffic volume exceeds 2,000 pcu, it will be necessary to close a ramp temporarily.

The effect of ramp metering by passage traffic and average travel time are shown in Table 2. As for traffic volume, it would increase 280 pcu to Case B, and a traffic congestion relaxation effect would become 15.22%. Moreover, when looking at the average travel time, it decreased for 40 (s/car unit), and the traffic congestion relief rate became 51.28%. The traffic congestion relief rate became 45% or more in the cases of A and B. On the other hand, main lane traffic volume, although traffic volume increased 120 pcu, leads to a few cases of C at average travel time, which takes five more seconds. When there was much main lane traffic, it turned out that the effect of the proposed control measure is large.

CONCLUSION

In order to reduce the traffic congestion in the on-ramp sections, the reinforcement learning ramp metering is investigated and proven to be effective. In this research, the simulation of the main lane upper stream traffic which changes momentarily was conducted. The reinforcement learning ramp metering was proposed to be used as an optimal action selection tool. It was used as a means to verify if a traffic style is carried out smoothly. As for future development, actual field data will be studied and the reinforcement learning ramp metering will be validated.

REFERENCES

Kerner, B. S. (2004). *The Physics of Traffic,* Springer, Germany.

Treiber, M., Hennecke, A. and Helbing, D. (2000). "Congest traffic state in empirical observations and microscopic simulation" *Physical Review E, Vol. 62,* 1805-1824.

Wang, X. J., Miyagi, T. and Ying, J. Q. (2007). "A Simulation Model for Traffic Behavior at Merging Sections in Highways" CD-ROM Proceedings of Second International Conference on Innovative Computing, Information and Control*, No. A04-03*.

Wang, X. J., Miyagi, T., Takagi, A. and Ying, J. Q. (2007). "Analysis of the Effects of Acceleration Lane Length at Merging Sections By Using Micro-Simulations" CD-ROM Proceedings of The 7th International

Conference of Eastern Asia Society for Transportation Conference*, No. 100604*.

A Fatigue Test on Fiber Reinforced Asphalt Mixtures

Yang Guo[1], Yinghua Zhao[2], Naisheng Guo[3]

[1]Ph D, Institute of Road and Bridge Engineering, Dalian Maritime University, 116026, Dalian, China; email:yangyang600eiv@163.com
[2]Professor, Institute of Road and Bridge Engineering, Dalian Maritime University, 116026,Dalian,China;Tel:86-411-84725602;email:yhzhao@newmail.dlmu.edu.cn
[3]Lector, Institute of Road and Bridge Engineering, Dalian Maritime University, 116026, Dalian, China, email:gnsdy@163.com

Abstract

This research focuses on the use of Bonifibers as the reinforcement for improving the fatigue endurance of asphalt mixture, which is an important property of the pavement structure. Fiber reinforcement as an available attempt has been proved to be effective in improving the toughness of asphalt concrete, and is becoming a new method for highway maintenance. For the purpose of examining the influence of the addition of Bonifibers on the durability of asphalt concrete pavement, a fatigue test was developed on MTS-810. 96 beam specimens of two kinds of asphalt mixture including AC-20 densely-graded bituminous concrete and SMA-13 stone mastic asphalt were fabricated and tested. The test results showed that the addition of the fibers decelerates the deflection development and crack evolution significantly. It was concluded that, polyester fiber reinforced asphalt mixtures behaves much better in the resistance to fatigue than that of plain concrete. They are the excellent pavement materials for heavy loading road applications.

Introduction

Fatigue is one of the main deterioration modes of flexible pavements for it induces the major distresses that contribute to the degradation and ultimate failure of asphalt concrete. The study on fatigue performance of asphalt pavements is important not only for the new roads but also for the maintenance of existing pavement. Flexible fiber as a kind of reinforced material is well used in the pavement construction and maintenance because of its wonderful effect on improving the pavement performance, as well as its convenience for construction process. Numerous field trials and laboratory investigation have illustrated that fiber inclusions are effective for reinforcing the asphalt concrete (Dean and Gerald 1989), improving the capacity of deformation (P Peltonen 1991), and retarding the development of reflective crack (Molenaar and M.Nods 1996). Numerous experiments with several types of reinforced fibers, different aggregates and asphalts (Hossam et al. 2005; Vikas Sharma and Shweta Goyal 2006) have demonstrated the significant improvement of fibers on the general performance of asphalt concrete. However, the research on fatigue behavior remains to be improved and some critical

questions need to be answered. The primary purpose of this study is to investigate the reinforcement effect of polyester fibers on the durability of asphalt concrete by fatigue tests.

Materials

The binder is a styrene butadiene styrene modified asphalt. Two gradations including densely-graded asphalt mixture AC-20 and stone matrix asphalt SMA-13 were used in this research. Crushed limestone with the maximal normal size of 20 mm was employed as the coarse grade aggregate of AC-20, while in SMA-13 mixture crushed basalt with maximal normal size of 13 mm was used. Limestone was chosen as fine grade aggregate for both materials. And limestone powder as filler was added into the materials. The gradation of the test materials is described in Table 1.

Table 1. AC-20 and SMA-13 Gradations

Sieve size (mm)	Percent passing (AC-20)	Sieve size (mm)	Percent passing (SMA-13)
26.5	100	16	100
19	95.9	11.4	93
16	87.8	9.5	75.7
13.2	72.5	8	56.2
9.5	57.7	5.6	26.9
4.75	38.4	4.75	23.9
2.36	26.3	2.36	22.5
1.18	19.0	1.18	18.2
0.6	13.5	0.6	14.9
0.3	8.9	0.3	12.7
0.15	6.9	0.15	11.7
0.075	5.6	0.075	10.5

Two kinds of fiber adopted in current experiment included xylogen and Bonifibers. Xylogen is a kind of flocculent fiber that could increase the viscidity of asphalt. Bonifibers as a kind of polyester fiber extracted from petroleum have good workability with bituminous. The properties of Bonifiber are shown in Table 2.

Experiments

Table 2. Properties of Bonifibers

Characteristic	Value
Length (mm)	6±1.5
Diameter (μm)	20±5
Density (g/cm^3)	1.36±0.04
Melting point (℃)	>250
Tensile strength (MPa)	>517 MPa
Strain at failure(%)	50
Water absorption (%)	9%

Binder and Fiber Contents (by weight). The Marshall test was used to define the optimum asphalt and fiber contents. With few experiments, the results showed the optimum asphalt contents of four experiment materials. For AC-20, Bonifibers of 0.20% in weight were added comparing with that without fibers. For SMA-13, the weight fraction of fiber inclusions was 0.10% with Bonifibers and 0.20% with xylogen. The results of Marshall tests are shown in Table 3.

It can be seen that the addition of Bonifibers allowed AC-20 mixture with richer bitumen. The content of asphalt was reduced by 3.0% for Bonifiber reinforced SMA-13, because the viscosity between xylogen and asphalt was prior to that of Bonifibers. As it is shown in Table 4, the stability value and Marshall flow for Bonifiber modified mixture had increased for AC-20. For SMA-13 with Bonifibers, both Marshall parameters decreased. Voids filled with binder were decreased while air voids were increased for both reinforced mixtures. From these aspects, adding Bonifibers may disturb the initial gradation structures.

Table 3. Marshall Test Results

Characteristic	Materials			
	AC-20		SMA-13	
Bonifiber content (%)	0	0.20	0	0.10
Optimum asphalt content (%)	4.17	4.46	6.50	6.30
Marshall density (g/cm^3)	2.472	2.458	2.463	2.468
Air voids (%)	3.2	3.5	3.6	3.8
VMA (%)	12.1	12.8	18.5	18.2
Voids filled with asphalt (%)	73.4	72.7	80.4	79.2
VCA (%)	—	—	39.0	38.8
Marshall stability (kN)	14.53	15.22	9.72	9.32
Flow (mm)	3.22	3.99	4.39	4.29

Fatigue Test. Fatigue tests were conducted on asphalt concrete beams under stress-controlled loading in the laboratory. The beams were cut from the rutting specimens with the size of approximately 300*300*50 mm. The size of the beam samples was 250*30*35 mm. The bending fatigue test was performed by MTS (Material Test System), which is a computer controlled hydraulic loading system. Four point bending test was used. The loading frequency was 10 Hz, without intermittent time. The loading level was adjusted for different conditions in the experiments, and was designed as 0.1 to 0.5 initially. The room temperature was effectively constant, 15℃ and was maintained within ±1℃. During the test period, the displacement of the sample surface was continuously measured and recorded. Loading level of fatigue test was based on the static bending failure test. The test was stopped when the crack propagated to the upper surface of the beam and the failure criterion was set up. A total of 96 specimens were tested.

Table 4. Static Bending Test Results

Characteristic	Materials			
	AC-20		SMA-13	
Bonifiber content (%)	0	0.20	0	0.10
Ultimate loading (kN)	0.979	1.109	1.049	1.448
Deformation (mm)	2.879	3.178	3.894	2.220
Tensile strength (MPa)	3.996	4.527	4.282	5.910
Maximum strain ($\times 10^{-2}$)	2.103	2.321	2.844	1.622
Bending Stiffness (MPa)	190.01	195.05	150.56	364.36

Test Results and Analysis

Bending Failure Test Results. The results of the static bending failure test

are shown in Table 4.

It is seen from table 4 that the reinforcement effects of Bonifibers are significant in ultimate loading, strength and stiffness. Especially for SMA-13 with Bonifibers, the bending stiffness increased 142% compared to plain concrete.

Fatigue Test Results. The stress levels used in the fatigue test and corresponding test results for each mixture are summarized in table 5.

Based on the theory of fatigue life, a fatigue equation was obtained through the regression of the fatigue test results. A linear regression model was developed between Log of the number of load repetitions to failure and Log of the tensile stress as:

$$\log N_f = k - n\log\sigma$$

where N_f is fatigue life (loading times for crack propagating to the top of the specimen); σ is applied tensile stress; k and n are coefficients determined by experiments. The fatigue equations for 4 mixtures obtained from the regression of the fatigue test results were listed in table 6. The high R values in Table 6 indicate the excellent model accuracy for the results of the fatigue tests.

Table 5. Fatigue Test Results

Stress ratio	Fatigue life			
	AC-20 (0%)	AC-20 (0.20%)	SMA-13 (0%)	SMA-13 (0.10%)
0.1		128019	78660	262854
		102762	102894	369102
		49520	135916	
		59410	118765	
		152098		
0.2	26244	34507	6580	26651
	36385	21618	13010	15241
	44756	43752	14236	26284
	38539	14825	13137	18717
		26521		32972
		72104		
		129055		
0.3	14690	21609	5115	8190
	25314	12724	5416	12803
	8277	15836	5808	8610
	14227	8074	4564	9124
	17258	19567		9201
0.4	10960	11884	645	1157
	8355	7607		1750
	6146	8439		2104
	7528	5315		1962
		6980		
0.5		4564		
		3733		
		4226		
		3578		

The fatigue property of AC-20 is shown in figure 1. By looking at the trend, it is clearly shown that Bonifibers reinforced asphalt mixture has better fatigue performance than that of plain concrete for AC-20. The addition of Bonifibers increases the slop of the $\log N - \log\sigma$ fatigue curve. When tensile stress changes the same degree, the diversification of the fatigue life for Bonifibers reinforced asphalt concrete is slighter than that of plain concrete, which means

Table 6. Fatigue Equation

Material	Fatigue equation	Correlation coefficient R
AC20-0%	$\log N_f = 4.380172 - 2.48348\log\sigma$	0.93621
AC20-0.20%	$\log N_f = 4.47672 - 2.25943\log\sigma$	0.97322
SMA13-0%	$\log N_f = 3.99435 - 2.79501\log\sigma$	0.99345
SMA13-0.10%	$\log N_f = 4.87079 - 4.05696\log\sigma$	0.98496

that adding Bonifibers in AC-20 mixture reduces the sensibility of fatigue life to stress level. With the help of fatigue equations, we realize clearly that, comparing to the plain AC-2,0 fatigue life of Bonifibers reinforced mixture is increased by 18.8% at applied stress of 0.8 MPa. And when stress is increased to 1.61 MPa, the growth of the fatigue life of Bonifiber reinforced mixture is 38.9%. It can be seen that with the increasing stress level, the growth of the fatigue life due to Bonifiber reinforcement is more significant compared to that of plain concrete. The closeness of the two curves suggests that the application of Bonifibers did not influence much on the fatigue life of AC-20 mixture.

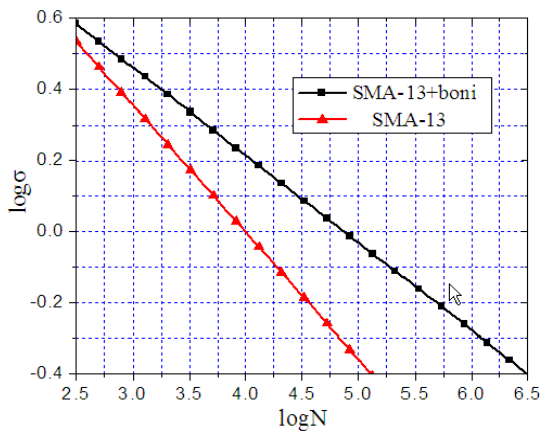

Figure 1. Fatigue curve of AC-20

Figure 2 shows the fatigue curves of SMA-13. From regression curves, we recognize that Bonifibers reinforced asphalt mixture performs much better in fatigue resistance ability compared to that of plain concrete for SMA-13. The exchanging of some xylogen with Bonifibers reduced the slop of the $\log N - \log \sigma$ fatigue curve. It is shown that fatigue life of Bonifibers reinforced asphalt concrete changes more remarkably compared to plain concrete when tensile stress changes the same degree, which means that adding Bonifibers in SMA-13 mixture increased the sensibility of fatigue life to stress level. From the figure we can see that, compared to plain SMA-13 the fatigue life of Boni-fibers reinforced mixture is increased by 1334% at stress of 0.6 MPa. And when the stress applied to specimen is increased to 1.25 MPa, the growth of the fatigue life of Bonifibers reinforced mixture is 475%. The fatigue performance of SMA-13 is different from that of AC-20.

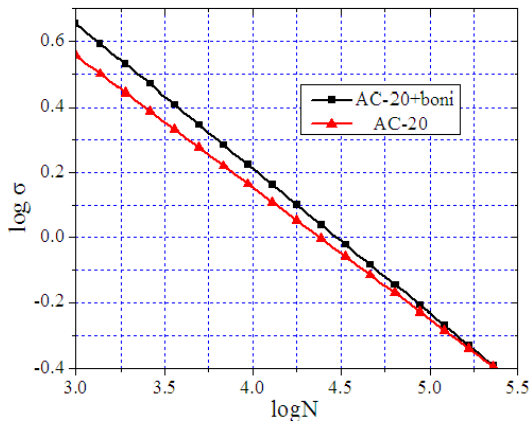

Figure 2. Fatigue curve of SMA-13

The process of fatigue failure for stone matrix asphalt was quite different from that of densely graded asphalt mixture. During the damage process of AC-20 specimens, the cracks started, propagated until penetrating the whole sample. The fatigue failure of SMA-13 specimens did not depend on the crack size, but the extrusion of discontinuously graded aggregate and the cohesive force of asphalt matrix. The coarse aggregates of SMA-13 headed together to bearing the fatigue

loading when the deformation of specimen gradually increased, the asphalt layer blended with aggregates was stretched and became thinner, and the phenomenon was clearly seen during the test period of SMA-13(figure 3). For SMA-13, the cracks appeared in the interface between asphalt and aggregates where asphalt was stretched to thin. For AC-20, the cracks appeared in the location where micro-cracks existed. During the test process of AC-20, there was no phenomenon that asphalt was stretched to thin as that of SMA-13. Cracks appeared later in SMA-13 than in AC-20, and the size of most cracks was smaller in SMA-13. The observations from the fatigue test were conducted to prove that the fatigue test process of AC-20 and SMA-13 was not completely the same.

Conclusions

1) Bending fatigue test perfectly reflected the fatigue performance of asphalt mixture. The fatigue prediction model used for regression was obtained from beam blending fatigue test results; the obtained parameters may reflect the relationship between fatigue life and the loading times. The observations of high R values are also indicative of excellent model accuracy for the results of the fatigue tests.

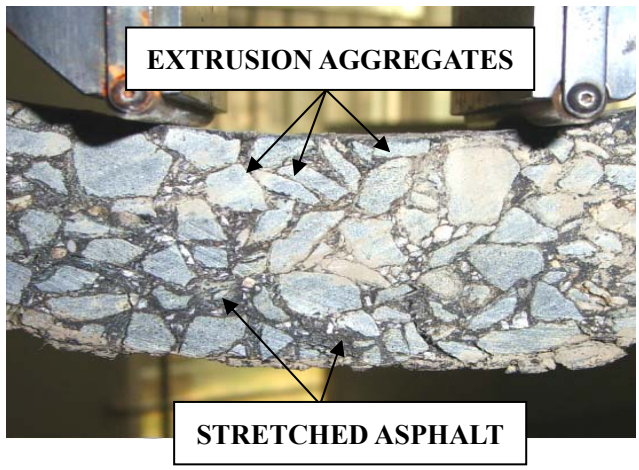

Figure 3. Fatigue phenomenon of SMA-13

2) The addition of Bonifibers to AC-20 mixture improves the fatigue performance of asphalt concrete. Bonifibers modified AC-20 mixture is the perfect material for heavy loading roads. For SMA-13, Bonifibers reinforced asphalt mixture performed much better in fatigue resistance compared to that of plain concrete.

References

Dean A. Maurer, Gerald J. Malasheskie (1989). "Field performance of fabrics and fibers to retard reflective cracking." *Geotextiles and Geomembranes*, 8 (3), 239-267.

P Peltonen (1991). "Wear and deformation characteristics of fibre reinforced asphalt pavements." *Construction and Building Materials*, 5(1), 18-22.

A.A.A.Molenaar, M. Nods (1996). "Design method for plain and geogrid reinforced overlays on cracked pavements." *Reflective Cracking in Pavements, London.*

Hossam F.Hassan, Salim Al-Oraimi, Ramzi Taha (2005). "Evaluation of Open-Graded Friction Course Mixtures Containing Cellulose Fibers and Styrene Butadiene Rubber Polymer." *JOURNAL OF MATERIALS IN CIVIL*

ENGINEERING, 17(4), 416-422.

Vikas Sharma, Shweta Gpyal (2006). "Comparative study of performance of natural fibers and crumb rubber modified stone matrix asphalt mixtures." *Canadian Journal of Civil Engineering*, 33(2), 134-139.

ANALYSIS METHOD FOR THE PRESTRESSED CONCRETE BRIDGES BASED ON TIME-DEPENDENT THEORY

Wu Hong-Lin

School of Transportation Science and Engineering, Harbin Institute of Technology, Harbin, P.O. Box 2524, Harbin, 204 Haihe Rd; PH 8615804505529; email: whlhitb@163.com

ABSTRACT

Based on the equilibrium equation of the section and structure, an analytical method for predicting properties of the bridge structure is proposed in this paper. In the method, time-dependent factors such as shrinkage and creep in concrete, relaxation in the tendon, as well as temperature are synthetically considered. It is shown that the method is more comprehensive, easier, and more accurate than traditional methods. With this method, a long-term evaluation for stresses and deformation on any section of pre-stressed concrete beams at any time from the beginning of construction to opening, even to many years later, can be completed. The results based on the theoretical analysis is proven by practical engineering.

BASIC PRINCIPLE OF TIME-DEPENDENT ANALYSIS

Basic principle on time-dependent analysis. The precise calculation of deformation or secondary internal force of the structure is difficult because of the complexity, even if a partial differential equation can be established (Tang, 1982) Time-dependent analysis is based on numerical calculation, so the following assumptions are given:

(a) Concrete and steel are the ideal elastic material. The modulus of elasticity of concrete is constant.

(b) Section deformation is in accordance with the plane section assumption.

(c) Adopt liner creep theory.

(d) The constitutive relations such as shrinkage and creep in concrete and relaxation in the tendon are known.

(e) When considering the temperature effect, the distribution mode of temperature on the section is known.

1. Stresses and strains relations on the section

Take any beam block section along the span (Figure 1.a). Assume that the longitudinal strain at the bottom surface of the section (x=0) is ε_o and the actual curvature on the central section of the beam block is χ (Figure 1.b, χ is minus) under the whole external load, and shrinkage and creep in concrete, and relaxation in the

tendon. The actual strain of any point (Height is x.) along section ε can be determined as (Figure 1.b)

$$\varepsilon_{act} = \varepsilon_o - \chi\, x \tag{1}$$

Assume the strain on any slice (Height is x) caused by shrinkage and creep in concrete is ε_f (Figure 1.c) and the strain caused by relaxation in the tendon is ε_{sf} under no restriction. All of the above strains are called free strains. The free strains can also include the temperature strains increment when temperature distribution exists on the section. The strains corresponding with elastic stresses in every slice ε_σ can be determined as (Figure 1.d)

$$\varepsilon_\sigma = \varepsilon_f - \varepsilon_{act} \tag{2}$$

The stresses and strains in concrete and the tendon along the section (Height is x) can be determined as:

(a) Stresses and strains relations of concrete:

Actual strains in concrete:

$$\varepsilon_{act} = \varepsilon_o - \chi\, x$$

Stresses in concrete:

$$\sigma = Eh\varepsilon\ \sigma = Eh(\varepsilon_f - \varepsilon_o + \chi\, x) \tag{3-1}$$

(b) Stresses and strains relations of tendon:

Actual strains in tendon:

$$\varepsilon_{sact} = \varepsilon_o - \chi\, x$$

Stresses in tendon:

$$\sigma_s = E_s\varepsilon_{\sigma s} = E_s(\varepsilon_{sf} - \varepsilon_o + \chi\, x_s) \tag{3-2}$$

2. Establishing the equilibrium equation of the section

For pre-stressed concrete bridges, there is often bending moment M and axle

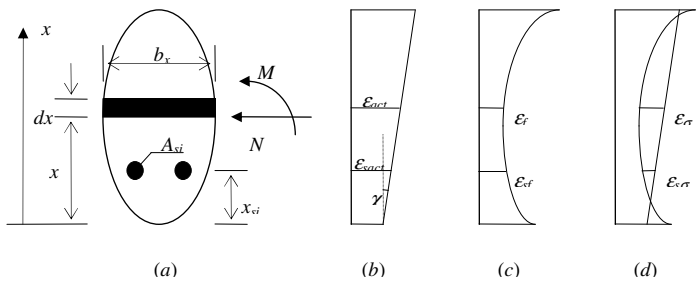

Figure 1. Stresses and strains relations on section

force N on the sections. Shear Q is not considered here. According to the equilibrium between the internal force on the section and the total forces of stresses in concrete and the tendon, the equations can be determined as:

(a) The equation of horizontal force

$$\int_h \sigma dA + \sum_{i=1}^{ns} \sigma_{si} A_{si} - \sum_{i=1}^{ns} E_h \varepsilon_{si} A_{si} = N \qquad (A)$$

in which, n_s is the number of tendon.

(b) The equation of bending moment

$$\int_h x\sigma dA + \sum_{i=1}^{n_s} x_{si}\sigma_{si} A_{si} - \sum_{i=1}^{n_s} E_h x_{si}\varepsilon_{si} A_{si} = M + N \cdot y_x \qquad (B)$$

Considering: $m = E_s / E_h$, then taking equation (1)and (2) to (A) and (B).

Noting that:

$$A_0 = \int_h dA + (m-1)\sum_{ns} A_{si}$$

is the area of transformed section, and

$$A_1 = \int_h x dA + (m-1)\sum_{ns} x_{si} A_{si}$$

is the moment to bottom of transformed section, and

$$A_2 = \int_h x^2 dA + (m-1)\sum_{ns} x_{si}^2 A_{si}$$

is the second moment to bottom of transformed section.

N is the axle force caused by loads on the section; IF there is no axle force, N=0; M is the bending moment caused by loads on section. Therefore, a set of the equilibrium equations (4) on section could be deduced, that is,

$$\begin{cases} \varepsilon_o \left[\int_h dA + (m-1)\sum_{i=1}^{n_s} A_{si} \right] - \chi \left[\int_h x dA + (m-1)\sum x_{si} A_{si} \right] \\ \qquad = \int_h \varepsilon_f dA + (m-1)\sum_{i=1}^{n_s} \varepsilon_{sfi} A_{si} - \frac{N}{E_h} \\ \varepsilon_o \left[\int_h x dA + (m-1)\sum_{i=1}^{ns} x_{si} A_{si} \right] - \chi \left[\int_h x^2 dA + (m-1)\sum x_{si}^2 A_{si} \right] \\ \qquad = \int_h x\varepsilon_f dA + (m-1)\sum_{i=1}^{n_s} x_s \varepsilon_{sfi} A_{si} - \left(\frac{M + N \cdot x_c}{E_h} \right) \end{cases} \qquad (4)$$

Solving the above equations (4), then the solutions on he longitudinal strain ε_o and the actual curvature on central section of beam block χ could be found in formula (5).

$$\begin{cases} \chi = \dfrac{1}{A_0 A_2 - A_1^2} \left[A_0 \xi - A_1 \eta + \dfrac{A_0 M}{E} \right] \\ \varepsilon_o = \dfrac{1}{A_0 A_2 - A_1^2} \left[A_2 \xi - A_1 \eta + \dfrac{A_1 M - A_2 N}{E} \right] \end{cases} \qquad (5)$$

In the equation (5) the parameters ξ and η are related to free strains and

geometric performance of a section, and determined by the following equations:

$$\xi = \int_h \varepsilon_f \, dA + (m-1) \sum_{ns} \varepsilon_{sfi} A_{si}$$

$$\eta = \int_h x \varepsilon_f \, dA + (m-1) \sum_{ns} x_{fi} \varepsilon_{sfi} A_{si}$$

The stresses and strains at any point on a section can be determined by taking curvature χ and strain εo to equation (3-1) and (3-2).

CONCLUSIONS

Based on the equilibrium equation of the section and structure, an analytical method for predicting long-term properties of pre-stressed concrete bridge structures is proposed in this paper, in which time-dependent factors such as shrinkage, creep in concrete, and relaxation in the tendon, as well as temperature are synthetically considered. The following actions, such as interactive action between concrete and tendon, the characteristic of relaxation in tendon, and the interactive effect on sections, could be determined truly by the proposed method in this paper.

The time-dependant analysis theory has been taken into the traditional force method and displacement method, so that the solving of the structure problem becomes easier and more comprehensive. The time-dependant analysis theory can be easily used in pre-stressed concrete bridge structures such as continuous beams, continuous rigid frames, and cable-stayed bridges with the numeric analysis method. By this method, the stresses, strains, internal forces, and deformation at any time from the beginning of construction to the operating stage could be determined easily in the above bridges.

It is unnecessary to save the history of strain and stress changes of elements by the FEM method proposed in the paper. The increment of strains and the total deformation during a period of time are the only factors needed to be saved. Therefore, the method is more suitable to be used in FEM in PC structures. The program based on the above time-dependent theory has been proven successfully in practical engineering.

BIBLIOGRAPHY

Huang Qiao. Long-term properties analysis of long span PC structure. In: Symposium of national bridge structure academical meeting in 1992. Shanghai: Tongji University press, 1992, 808-814.

Jin Wenlu. Uniform theory of Elasticity-creep state for prestressed concrete structure. Beijing: China railway press. 1990, 3-21.

Fan Lichu. Prestressed concrete continuous bridge. Beijing: China communications press, 1988, 18-25.

Tang ChongLi. Mechanics of Creep and technology of research for concrete. Beijing: Water conservancy and electric press, 1982, 18-25.

Huang Qiao. Report on Program Development for the Analysis of Continuous Prestressed Concrete Bridge. London, 1990; 2~9

Wang ZhongLin. Time effect analysis on the whole-life and construction control of Prestressed concrete continuous bridges with long span. [Dissertation]. Harbin: Harbin Institute of Techonology, 1997, 9-11.

An Analytical Method for Predicting the Service Life of Bridge Structures

Xiaoguang Wu[1], Jun Liu[2] and Yanwei Li[3]

[1]Professor, Highway Institute, Chang'an University, Xi'an, China, ST 710064; PH (029) 82334878; FAX (029) 82334878; email: wxgwst.cn@126.com

[2]Senior Engineer, Highway Bureau of Shanxi Province, Taiyuan, China, ST 030006, PH (0351) 7582124; FAX (0351) 7582124; email:liujun.cn@163.com

[3]Professorate senior engineer, Shijiazhuang Transportation Bureau, Shijiazhuang, China, ST 050061; PH (0311) 87819155; FAX (0311) 87819156; email:liyanwei69@vip.sina.com

ABSTRACT

This paper presents an analytical method to predict the confidence level of service life for bridge structures. The analysis uses the Monte-Carlo Analysis to build the resistance model and load model of bridge structures. With the reliability module of ANSYS program, the material properties and load character were set as time-dependant variables. The distribute shape of each variable was also considered. Based on the stress and deformation output of the bridges, the different confidence levels at different time were obtained using two reliability determination criterions. The bridge's time-dependant confidence level curve can be drawn, based on which the confidence level at different time can be directly read.

INTRODUCTION

Research in structural reliability has recently made significant progress in China. Due to the lack of a reasonable assessment mechanism of their service life, a number of collapse accidents occurred to the bridges built in the 1980's or earlier. Within this context, it is urgent to propose a reliability-theory-based method to assess the service life of the old bridges, based on which their rehabilitation and reconstruction can be conducted.

CALCULATION METHOD

Commonly used methods for the reliability analysis of bridge structures include the first-order second-moment central point method, the first-order second-moment check-point method and methods based on their improvements. In recent years, methods for reliability calculation such as Monte Carlo method and response surface method have come into use, b having both advantages and disadvantages. Because of the clarity and simplicity of its structural utility function, hence the ease of its use, the first-order second-moment method is commonly used for structural calculation. When the utility function of a structure takes no specific expressions; however, such use is usually difficult. In such cases, the Monte Carlo method can be used instead.

Monte Carlo method is a numerical simulation to solve practical engineering problems related to random variables. In the current reliability calculation of bridges, it is taken as a relatively precise method. The numerical simulation of random variables is equivalent to a "trial";

the Monte Carlo method is therefore also known as the common method for statistical test. The commonly used methods of sampling include direct Monte Carlo sampling, Latin super cube sample method, and self define method. In the following section, the reliability analysis of life expectancy of bridges will be demonstrated using reinforced concrete bridges for their universal use.

PROPOSED BRIDGE STRUCTURE MODEL

Model of time-varying strength of concrete. The mean and standard deviation functions t (Zou 1998) as an arbitrary point of time can be taken as

$$\mu_f(t) = 1.3998\mu_{fo}e^{\left[-0.0195\left(\ln\left(t+0.0892\right)-1.7322\right)^2\right]} \tag{1}$$

$$\sigma_f(t) = \sigma_{fo}\left[0.318(t+0.03742)+0.9881\right] \tag{2}$$

in which μ_{fo} - average of compressive strength of concrete in 28d; and

σ_{fo} - Standard deviation of compressive strength of concrete in 28d.

Model of time-varying strength of reinforcement. The time-varying strength of reinforcement (Zou 1998) can be expressed as

$$f_{sk} = f_{yk}(0.986 - 1.1992\eta_s) \tag{3}$$

in which f_{sk} - characteristic value of the nominal yield strength of corroded reinforcement;

f_{yk} - characteristic value of the yield strength specified in the current code, and is taken as 320MPa in this paper; and

η_s - corrosion ratio of the cross sectional area of reinforcement (the ratio of corroded cross sectional area to the original one).

Model for the change in cross sectional area of reinforcement. After t years of use, the mean and standard deviation of the cross sectional area of a rebar (Jin and Zhao 2002) can be expressed as Equations 4 and 5, in which μ_0 and σ_0 are the mean and standard deviation of the initial cross sectional area of a reinforcement respectively.

$$\mu_{As}(t) = \lambda(t)\mu_0 \tag{4}$$

$$\sigma_{As}(t) = \eta(t)\sigma_0 \tag{5}$$

$$\lambda(t) = c_1 + c_2\cdot(t-52.5) + c_3\cdot(t-52.5)^2 + c_4\cdot(t-52.5)^3 \tag{6}$$

$$\eta(t) = d_1 + d_2 \cdot (t - 52.5) + d_3 \cdot (t - 52.5)^2 + d_4 \cdot (t - 52.5)^3 \quad (7)$$

In addition, the resistance of a bridge is related to the density of materials, which follows the standard normal distribution in the analysis hereafter.

ANSYS MODULE FOR PREDICTING LIFE EXPECTANCY OF R/C BRIDGES

Introduction has been given to the distribution functions of parameters taken as random variables with respect to time for RC bridges. In the following, from the viewpoint of ANSYS calculation, study will be focused on how to determine the uncertainty level of outcome variables to be found through the uncertainty of parameters in a model. The failure probability of a bridge resulting from the uncertainty of input parameters will then be determined on the basis of certain criteria. The remaining service life can be determined also.

For a R/C bridge, its strength, cross sectional area, and density of reinforcement, tensile and compressive strength of concrete, and its density all follow certain distribution functions. Because of structural failure takes a certain period of time, in the analysis with ANSYS program, it is unnecessary to simulate the reliability of a bridge under load at every minute in a dynamic analysis. This article will, therefore, first divide the service life of a bridge (typically 100 years) into a number of time intervals. At the ends of the time interval the value of each parameter will be taken. For example, when t=10 is substituted into the corresponding time-varying functions for strength, cross sectional area and density, the material properties at the time point will be calculated. The calculated parameters are then assumed to follow normal distributions, with which the reliability of the bridge can be determined using the ANSYS analysis procedures

Reliability calculation of Life expectancy of RC bridge. Below a R/C simply supported girder bridge will be taken as an example for calculating the reliability and analyzing the service life.

A five-girder fabricated simply supported RC bridge was built in 1970, with its flanges rigidly jointed. Its concrete is of C25, calculation span is 20.0 meters, with a net deck width of 7.0 meters. The average thickness of asphalt concrete bridge deck is 9cm (a 4cm-asphalt layer overlying a 5cm concrete one). The full-bridge layout, cross-section and one piece of girder are shown in Figures 1,2 and 3 respectively.

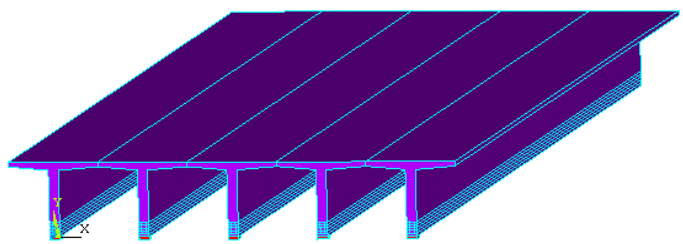

Figure 1. Overall layout of full-bridge.

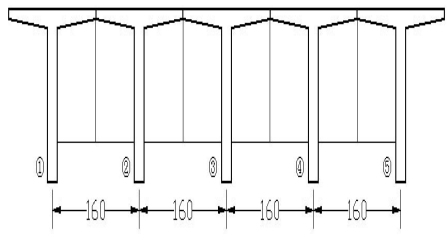

Figure 2. Full-bridge section size (cm).

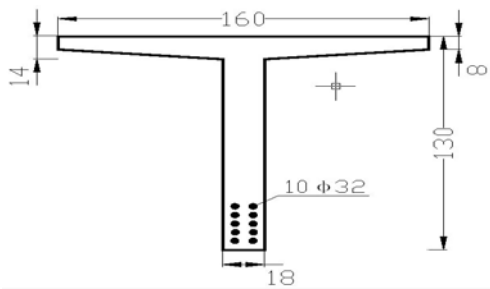

Figure 3.Girder cross-section (cm).

According to rigid cross beam method, Bridge Doctor has been used to find its coefficients of transverse distribution as given in the Table 1.

Table 1. Coefficients of transverse distribution.

Girder No. / Load	1	2	3	4	5
Automotive	0.522	0.461	0.400	0.461	0.523

Criteria for the assessment of RC bridge reliability.

(1) Stress, deformation criteria

a. Stress criteria

Characteristic value of concrete strength of reinforced concrete girders are listed in Table 2 below.

Table 2. Characteristic values of concrete strength (MPa).

Types of strength		Symbol	Concrete grade						
			15	20	25	30	40	50	60
Characteristic value	Axial compressive	R_a	10.5	14.0	17.5	21.0	28.0	35.0	42.0
	Tensile	R_l	1.3	1.60	1.90	2.10	2.60	3.00	3.40

b. Deformation criteria

As far as reinforced concrete bridges are concerned, the calculated maximum vertical deflection of the supper structure under the automobile load shall not exceed the following allowable value: the midspan deflection of girder bridges ≤ L/600 (Li Yang Hai 1997).

(2) Failure probability criteria

For the existing structures, the reliability of assessment criteria is usually based on the reliable indexes, and Dalian University of Technology has conducted a lot of research in this aspect. Taking βt <0.85βo as a criterion of structural failure, that is, at this moment, a structure has come to the end of its service life. The target reliability indexes with design reference period T = 100 years are as listed in Table 3.

Table 3. Target reliability indexes of Road and Bridge structural members.

Structure class / Combination action effect	First class		Second class		Third class	
	Ductile failure	Brittle failure	Ductile failure	Brittle failure	Ductile failure	Brittle failure
Primary combination	4.7	5.2	4.2	4.7	3.7	4.2
Additional combination	4.2	4.7	3.7	4.2	3.2	3.7

In this paper, the reliability of a structure is judged on the basis of its failure probability. At the same time because all the material variables involved obey normal distributions, live loads generally obey type-I extreme distribution, hence the stresses and deformations obtained all follow normal distributions, so that it is reasonable to calculate its failure probability theoretically in terms of 0.85 β_o by using normal distributions. In addition, the calculated results also follow normal distribution. The detailed results obtained are as listed in table 4.In this paper, examples of secondary roads are of ductile failure, so that β_o = 4.2, and 0.85 β_o = 3.57, which is in the interval [3.5, 4.0]. From Table 4 is can be found that P_f = 0.0002, so that when the failure probability of the bridge is less than 0.0002, the structure is considered to be safe.

Table 4. Corresponding relationship between β and P_f.

β	P_f	β	P_f	β	P_f
1.0	0.159	2.5	0.00621	4.0	0.0000317
1.5	0.0668	3.0	0.00135	4.5	0.0000034
2.0	0.0228	3.5	0.000233	5.0	0.00000029

Calculation of the life expectancy of RC bridges. It is known from the coefficients of transverse distribution that maximum values occurs at side girders; therefore, as long as the calculated stresses and deformations of these girders meet requirements of failure criteria, the whole bridge will be safe (Zhao Shang-chuan 2001). In this analysis, t the structural responses of only the first piece of girder are calculated.

(1) The distribution curve of the material properties at time t

With the elapse of time, the material properties of a RC bridge change, hence its carrying capacity. The key point of this paper is to determine when the bridge can no longer carry the imposed loads. In the structural analysis, it is assumed that the material properties follow normal distributions. Figure 4 shows the distribution curves of the material properties at the t = 30 years.

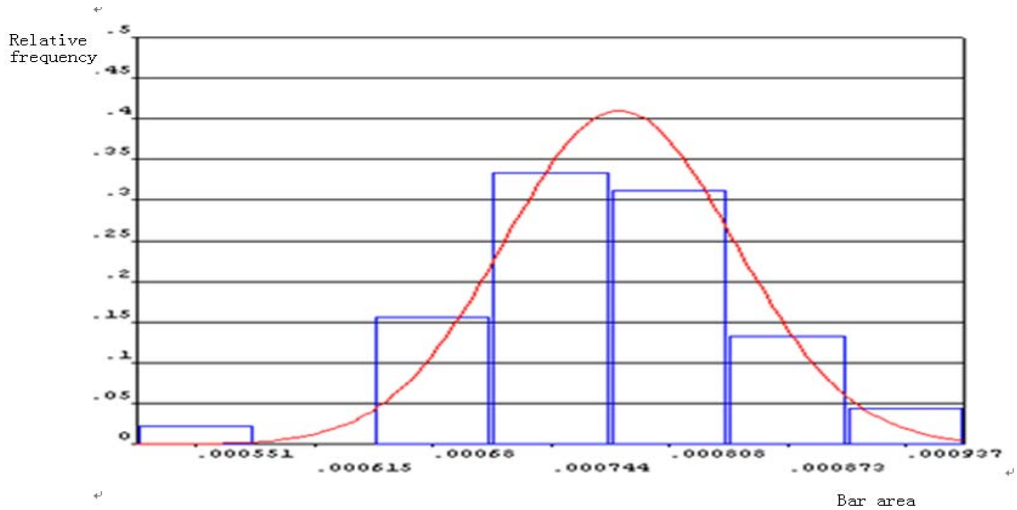

Figure 4. Distribution curves of the material properties (t = 30).

(2) Types of bridge failure under loads

The largest cross-sectional area of concrete: A = 0.11×1.6 +0.18×1.19 = 0.390 m^2, when t = 0, Ag (0) = 10×π×0.0162 = 0.00804 m^2. At this point, reinforcement ratio μ= (0.00804/0.390)% = 2.1%> 1.5%, when t = 100, Ag (100) =$\lambda(t)$, μ_o= 0.858 × Ag (0) = 0.00690 m^2 . At this point, reinforcement ratio μ= (0.00690/0.390)% = 1.8%> 1.5%

Therefore, through out its service life, the girder always acts as an under reinforced concrete one, which is characterized by the occurrence horizontal longitudinal cracks in its compression zone, followed by the crushing of concrete when concrete at the extreme fibers of compression zone reaches the ultimate compression strain of concrete. Therefore, in the simulation of its deformations, only when the compressive stress of concrete in the compression zone reaches the ultimate strength of concrete, or structural deformation exceeds L/600 (the reliable probability is beyond the corresponding allowable limits), can its failure be considered to have occurred.

(3) Deformations, stress distribution curves and probability distribution curve

For the convenience of curve plotting during the stress and deformation analyses, the negative sign of compressive stress was plotted in the curves. However, since what is concerned with is the failure mode when the concrete compressive stress reaches its ultimate value at the time of failure, negative sign is always implicitly inferred. In addition, the girder deflects downward under loads, which is opposite to the positive direction of longitudinal axis of the coordinate system, the deflection is also negative. The two boundary curves for the distribution functions of stresses and deformation indicate the ranges of reliability when the confidence level is 98%.The structure is always safe in these ranges.

At t = 20 years the results of reliability analysis of the bridge are shown in the following figures.

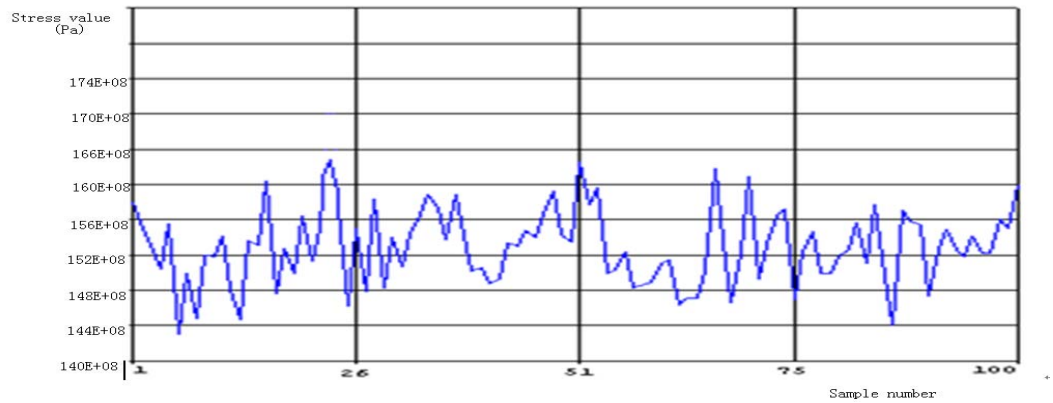

Figure 5. Curve of the sampled stresses.

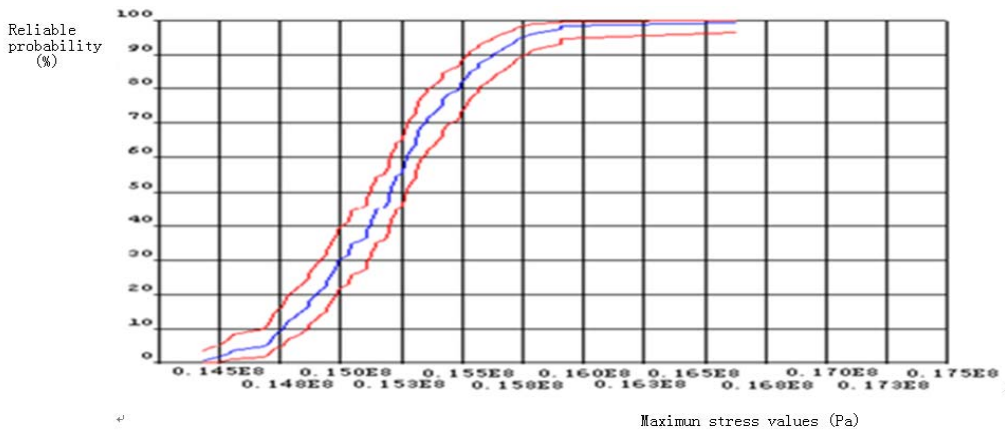

Figure 6. Curve of stress distribution function.

From the curve of sampled stresses in Figure 5, we can clearly see the range of the maximum stress in the sampling process, and the sampled values are all under the characteristic strength of 17.5MPa, thus at t = 20 years the bridge is safe.

In Figure 6, if a vertical line is drawn at characteristic strength of x = 17.5 MPa, it will intersect the curve of stress distribution function at the ordinate of 1.0, at the reliability of 1. It shows the structure is fully reliable at this time. In the following section, the o direct output

module of probability is used to analyze the reliable probability. In the probability output module of program, we select executable documents and the smax for option of reliability design variable, and then fill in the limit with the characteristic strength of 17.5 MPa while keeping the confidence level as 0.98. Running the module at such a condition gives the reliability of 1.0 if the stress is less than 17.5 MPa (see Figure 7) (GE Jun-yin, WANG Li-you 2007).

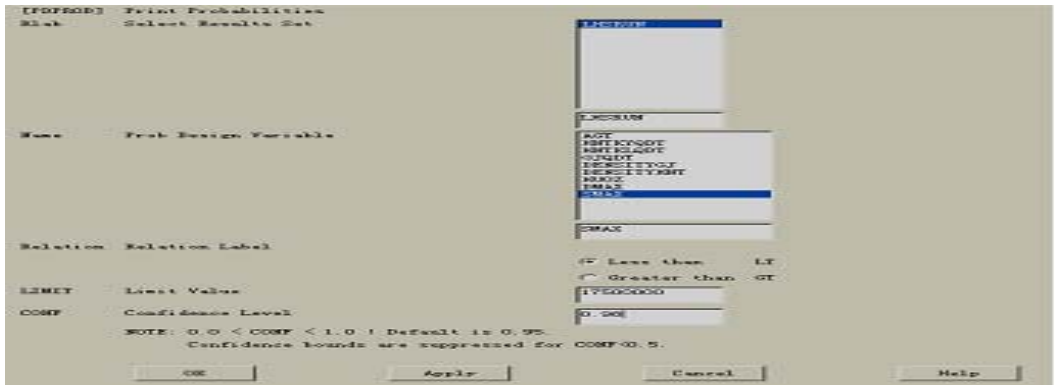

Figure 7. Direct numerical method for reliability.

From the curve of sampled deformations in Figure 8, it can be seen that the sampled maximum deformations are all smaller than the required value of L/600 = 0.033m, hence, from the distribution of deformations the bridge is completely safe at the t = 20 years.

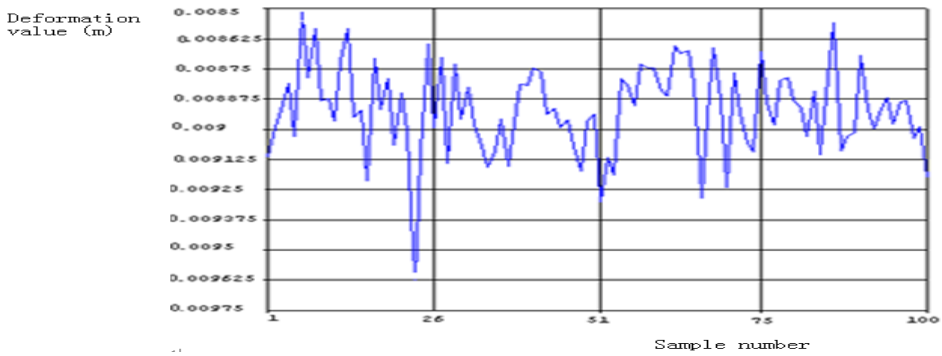

Figure 8. Curve of sampled deformations.

In the curve of deformation distribution function in Figure 9, if a vertical line is drawn at deflection x = 0.033m, it will intersect the curve of the distribution function at the ordinate 1.0. Again, we can use the direct output probability value method to carry out the reliable probability analysis. In Figure 7, we firstly select the executable documents and the dmax in the option of variable selections, and then fill in 0.033m as the value of deflection limit while taking confidence level as 0.98, the reliable probability can be obtained as 1.0 if the deformation is less than 0.033m.

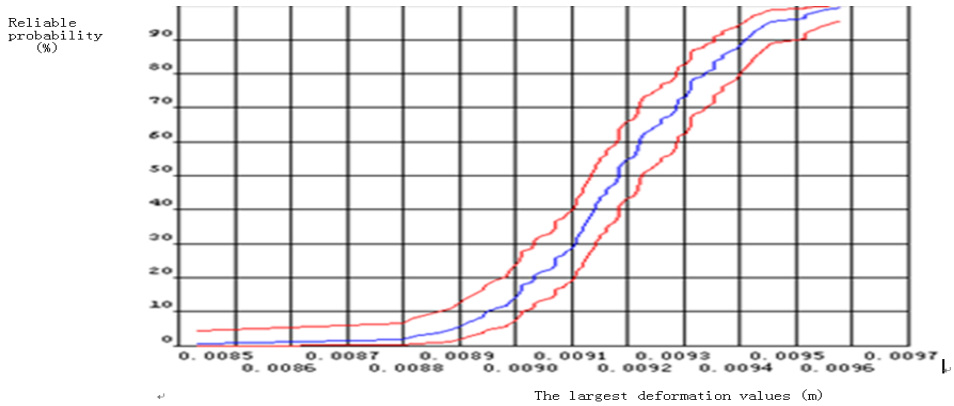

Figure 9. Curve of deformation distribution function.

From the argument above, the stress and deformation of the bridge after 20 years operation are all within ranges of limits. With the reliability of 1, the structure is reliably safe.

Table 5. Time-probability relationship.

Time (years)	20	40	60	75	76	77	78	79	80	81	85
Reliable probability	1.0	1.0	1.0	0.99999	0.99996	0.99993	0.9999	0.99987	0.99984	0.9998	0.998

Using the same method, reliable probability at other time can be obtained as shown by the function between time and reliable probability in Table 5 and Figure 10.

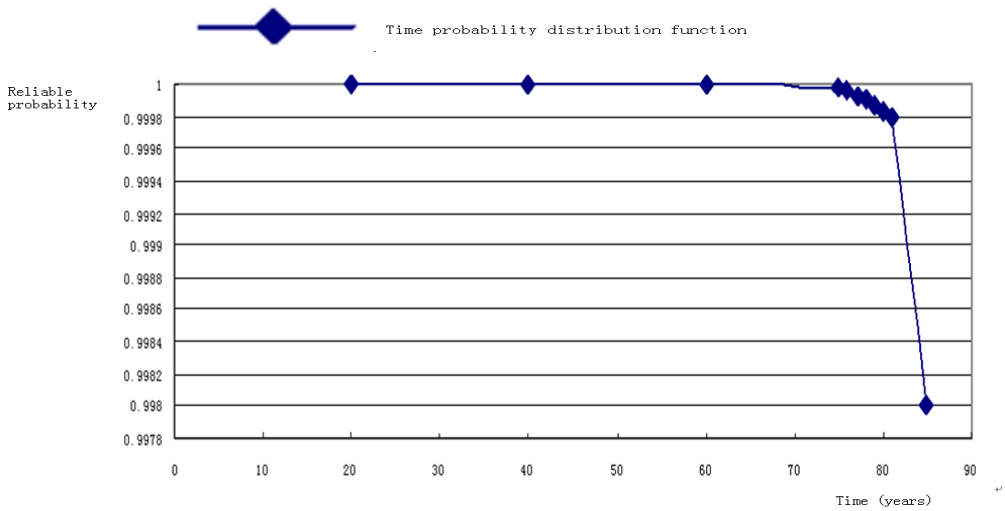

Figure 10. Curve of probability distribution function with time.

Solution of the remaining service life of bridges. As mentioned above, there are various methods for calculating the remaining service life of bridges. As long as the service life of a

bridge can be accurately calculated, its remaining service life can be precisely obtained by directly subtracting the year of operation from its service life. The life of RC bridge algorithm are described in detail above; also it has been obtained that the service life of a certain RC simply supported girder bridge is 81 years; therefore, after operation over 35 years, the bridge is reliably safe. Moreover, the bridge can operate 46 years without overhauls.

CONCLUSION

This paper describes a method which uses the analytical module of ANSYS to determine the stress and deformation of a simply supported R/C girder bridge. The remaining service life of the bridge was subsequently determined in terms of two criteria. The methodology developed provides a theoretical basis for assessing the bridge reliability, calculating their service life, and rehabilitating or rebuilding the bridges.

REFERENCES

GE Jun-yin, WANG Li-you. Bridge Structural Analysis Based on ANSYS [M].China Railway Publishing House, 2007.

Hao Wen-hua. Ansys Civil Engineering Applications [M]. China Water Conservancy Press, 2005.

Hua Xu-gang, CHEN Zheng-qing. Full-mode Flutter Frequency Domain Analysis Method of Bridge Based on ANSYS [J].China Journal of Highway and Transport, 2007, 20 (5):41-47.

Jin, W., and Zhao, Y. (2002). Durability of concrete structures. Science Press.

Li Yang Hai, BAO Wei-Gang, Guo Xiu-wu, Xiang-Yun Cheng. Highway bridges structural reliability and the probability of limit state design [M]. The people traffic Press, 1997.

Zhao Shang-chuan. Reinforced concrete structure durability based on reliability assessment and Experimental Research [M]. Dalian University of Technology doctoral dissertation, 2001. `

Zou, T. (1998). Structural reliability. The people traffic Press.

A Study of Cold In-Place Recycling Mixture Used as Binder Course in China

Jonathan Jia[1], Jinhai Yan[2], Zhuohui Tao[3]

[1]Emulsion Field Support Manager, Shell (China) Limited, 100016, No.43 Liangmaqiao Road, Chao Yang District, Beijing, P.R. China; PH (8610) 65326565 Ext 1809; FAX (8610) 65327195; email: jonathan.jia@shell.com

[2]PHD Candidate.School of Transportation, Southeast of University, 210096, No.2 Sipailou Road, Nanjing, P.R. China; email: jason.yan1@gmail.com

[3]Technical Engineer, MeadWestvaco Corporation, 200231, 5FL, Nami Building, No.18 Lane1305, Huang Jing Road, P.R. China; email: zt7@meadwestvaco.com

ABSTRACT

Partial depth Cold In-place Recycling (CIR) is a cost-effective method for the preventive and corrective maintenance of existing pavements. In recent years, the asphalt emulsion CIR has been used in asphalt pavement preservation and maintenance in China. This study focused on asphalt emulsion CIR mixtures that are used as binder course on roads of various traffic volumes. Performance related testing and evaluation of specification properties of six different recycling mixtures were conducted. In addition the field post-project monitoring has also been evaluated. Based on lab and field performance, it was discovered that emulsion CIR was an effective method for the preventive and corrective maintenance of existing pavement as binder course. Then, performance related specifications of asphalt emulsion CIR mixtures used as binder course was recommended to a local highway agency.

INTRODUCTION

Background

Jiangsu provincial trunk highway network usually has a relative good structural bearing capacity, but it still has some severe distresses, such as rutting, cracking, shoveling, patching, etc in asphalt pavements. Based on the distressed types of old asphalt pavement in Jiangsu, the technology of asphalt emulsion partial depth CIR is a very ideal rehabilitation candidate. This paper presented a study to evaluate the suitability of emulsion recycling mixture used as pavement binder course from lab and field performance aspects.

CIR process

The partial depth CIR process is a single-unit CIR process conducting milling and mixing on existing asphalt pavement with potential addition of new aggregates (if necessary) and asphalt emulsion and cement in proportion. Then it places the mixed material on the ground. A pick-up machine, a paver and a set of compactors will continuously finish the processes of elevating, paving and

compacting the recycled materials under natural environment temperature. Typically, the layer/lift thickness is from 50 to 120 mm.

Project description

Six-project roads having different traffic volumes that belong to Jiangsu provincial trunk highway network were evaluated by Falling Weight Deflectometer (FWD) testing and visual inspection. Pavement conditions including PCI (Pavement Condition Index) and SSI (Structure Strength Index) are listed in Table 1. The typical distresses of the these roads included rutting, moisture damage, cracking, flushing, corrugation and patching. Even the PCIs of G328, S239-I, S239-II, S336 and G104 show good conditions, their rutting is very unstable in summer,. It was shown that all project roads had good structural bearing capacity. Hence, these roads were ideal candidates for using asphalt emulsion partial depth CIR technology based on the distress types.

Table 1. The conditions of old asphalt pavements

Road	Performance Evaluation				Length (km)	AADT
	PCI	PCI Grade	SSI	SSI Grade		
S229	68.8	Fair	0.65	Fair	0.5	16,000
S239-I	68.5	Fair	0.74	Good	2.0	10,000
S239-II	65.3	Fair	0.74	Good	8.0	10,000
S336	56.9	Fair	1.88	Excellent	3.68	8,000
G104	56.0	Weakness	0.88	Good	1.0	5,000
G328	84.4	Good	0.94	Good	0.8	25,000

SAMPLE PREPARATION

Original material

All testing RAP was taken from the original old asphalt pavement of the each project road. RAP is regarded as “black rock” (Forsberg et al., 2002). This research will not study the effect of recovered old asphalt in RAP.

Virgin coarse aggregate was added to enhance the aggregate skeleton and provide higher internal frictional resistance (JTRI 2005). Meanwhile, the fine aggregate can form emulsion-cement / fine mortar to improve the cohesion between asphalt and RAP.

Portland cement was limitedly selected for improving early strength, moisture stability and high temperature stability of recycled mix despite of a little sacrificing its fatigue performance.

An engineered asphalt emulsion that was classified as cationic slow setting was applied on each project. This engineered emulsion had been assessed as compatible with the RAP / virgin aggregate blend to ensure quick mixing, complete coating, quick early strength development, resistance to moisture damage through many projects. Typically, the engineered emulsion has high residue content (not less

than 63%) in order to guarantee a thick asphalt coating film.

Pre-mix water has multiple functions. Chief among these functions is to improve coating of the RAP and virgin aggregate, to lubricate mixture during compaction, and to facilitate / accelerate the cement hydration reaction.

A vary emulsion dosage and pre-mix water content were selected in mix design of each project. The contents of original material used in recycled mixes of CIR projects are listed in Table 2.

Table 2. The contents of original materials used in recycled mixes

Project	RAP	New Aggregate			Portland Cement	
	(%)	Type	Size (mm)	Ratio (%)	Type	Ratio (%)
S229	85	Coarse	10-25	15	32.5	2.0
S239-I	85	Fine	0-3	10	32.5	2.0
		Coarse	15-25	5		
S239-II	84	Fine	0-3	8	42.5	2.0
		Coarse	15-25	8		
S336	85	Coarse	10-20	15	42.5	2.0
G104	85	Coarse	10-25	15	42.5	2.0
G328	85	Coarse	10-20	15	42.5	1.5

Gradation design

The gradation of the combined RAP and virgin aggregate was designed to meet guidelines and specifications from worldwide research road authorities and associations, such as DOTs of U.S., the Federal Highway Administration and the Asphalt Reclamation and Recycling Association (FHWA 1997; Iwoa DOT 2005; Montana DOT 2005; ARRA 2006). To meet the recommended total aggregate gradation, different amounts of coarse aggregate (by mass of recycling mixture) was blended with RAP aggregate. The sieve analysis results of this blended gradation are shown in Figure 1.

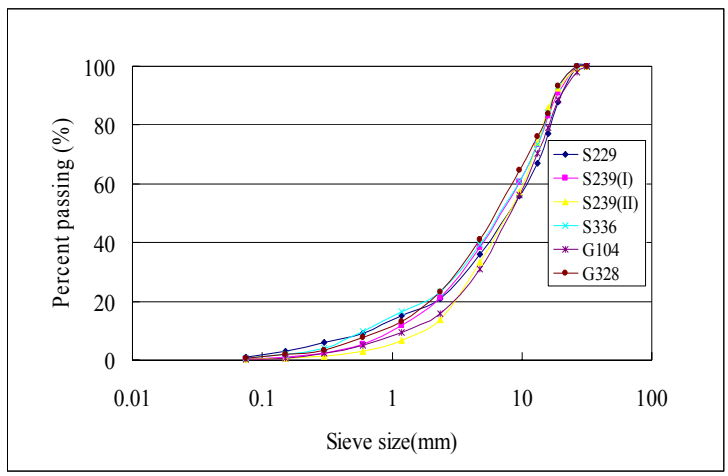

Figure 1. Recycling blended gradation curves

Experimental procedures

Specimen preparation and curing

A laboratory mechanical mixer was used for cold mixing. Superpave™ gyratory compactor was applied for preparing the specimens with 100mm in diameter and 63.5 ± 2.0 mm in height with 30 gyrations (Lee et al., 2003; Tan et al., 2005). The compacted specimens were initially cured at room temperature for 12 hours, and then were cured at 60℃ for 48 hours.

Test methods

The Marshall stability testing was carried out on two sets of specimen at 40 ± 1℃ testing temperature. One set of three replicates was tested directly without conditioning. Another set of replicates was conditioned in water bath at 25℃ for 23 hours. The percentage of retained stability can be expressed as follows:

$$RS = IMS / MS * 100\ \% \quad [1]$$

Where RS, IMS and MS represent retained stability, immersion Marshall stability, and Marshall stability, respectively.

The indirect tensile test (IDT) was conducted with two sets of specimen at 15℃ testing temperature. One set of three replicates was tested directly without condition, and another set of replicates was conditioned in water bath at 25℃ for 23 hours. The percentage of indirect tensile strength ratio is calculated as follows:

$$DWTSR = WIDT / DIDT * 100\% \quad [2]$$

In equation [2], the DWTSR, WIDT and DIDT represent dry-wet tensile strength ratio, immersion IDT strength, and dry IDT strength, respectively.

The freeze-thaw indirect tensile tests were performed at 25°C testing temperature. One set of three replicates was tested directly without conditioning, and the other set of three replicate specimens were vacuum saturated to 55-75% and conditioned at -18°C for 16 hours, and then placed in a water bath at 60°C for 24 hours.

Rut testing was performed with a 0.7 MPa rubber wheel load at a test temperature of 60 ± 1°C for three replicate specimens. The rutting specimen dimensions are 300 mm × 300 mm × 60 mm.

RESULTS AND DISCUSSION

Marshall test

Figure 2 shows that the Marshall stability (MS) has different trend patterns for different recycling mixes. MS no less than 6kN is the criterion for cold recycling mixture used as binder course, and retained stability should be greater than 75％.

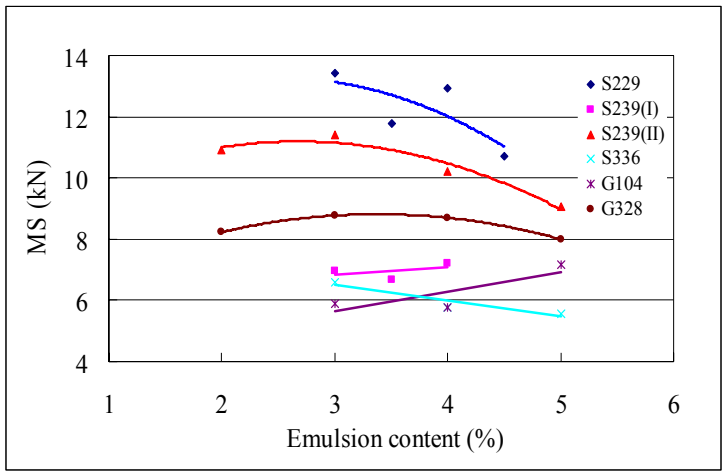

Figure 2. Marshall Stability trend curves

Indirect tensile test

Indirect tensile strength is the most important factor in optimum emulsion content evaluation. Figure 3 shows IDT strength trend patterns of each mix.

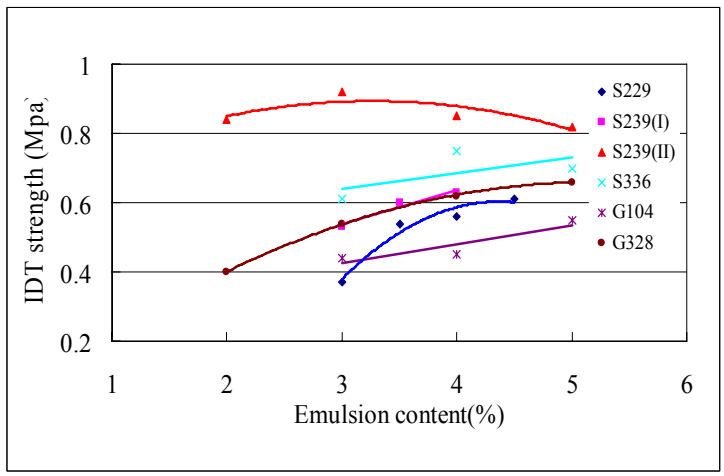

Figure 3. IDT strengths trend curves

Optimum emulsion content and validation test

The optimum emulsion content selection is an integrated judgment that includes all mechanical performance and mixture volumetric properties. The pre-mix water content is determinate by compromise of total liquid content between maximum density and minimum coating requirement.

Table 3 shows that all validation tests were conducted on the optimum formulated with cement, emulsion and water contents for each project. A note is made here: all tensile strength ratios (TSR) are greater than 70% and the Chinese Dynamic Stability (DS) test is more than 2500 times/mm, which indicates that the recycling mixture has good water resistance and high temperature stability and respectively.

Table 3. Optimum contents and performance results of validation test

Project	S229	S239-I	S239-II	S336	G104	G328
Emulsion, %	4.0	3.8	3.6	3.8	4.3	3.5
Pre-mix water, %	2.8	2.4	2.3	2.6	2.0	2.4
Voids, %	12.1	13.6	9.6	10.2	12.9	10.5
Marshall stability, 40℃	12.94	7.05	10.71	6.25	8.79	7.12
Retained stability, %	76.7	85.3	102.3	106.7	89.8	99.0
IDT, 15℃, MPa	0.56	0.61	0.87	0.71	0.56	0.56
Retained IDT, %	139.3	103.2	100.0	86.3	91.1	101.7
TSR, %	75.4	71.2	74.3	73.2	80.2	72.0
Rutting test, 60℃	2951	3080	3080	2548	2762	N/A

Post-project monitoring

For each project, a usual 3-5cm HMA surface course was applied on the CIR binder course. FWD inspection of four roads showed good structural bearing capacity after one year traffic and snow disaster in the winter of 2007. No crack and and no more than 3 mm rutting had been found in all projects. The FWD values of the four pavements were listed in Table 4. It was shown that all trial projects have typical asphalt pavement deflection level with Chinese Semi-Rigid Base.

Table 4. Deflections of old pavements and recycled roads（0.01 mm）

Road	Old pavement	Recycled roads
S229	17	6
S239-I	20	5
S239-II	26	6
S336	23	7

The recommended Performance Related CIR Specifications

Based on the results of performance evaluation and post-project monitoring, for Jiangsu province trunk highway network in China, a summary of the performance specifications recommended for CIR mixture used as binder course is presented in Table 5. However, for the suggested performance specifications, raveling test, fatigue test and low-temperature cracking test will be considered in the next research plan. Highway Bureau of Jiangsu Provincial Communication Department will adopt the specifications after more CIR projects are implemented.

Table 5. The performance related specifications for CIR

Property	Criteria	Purpose
Gyratory Compactor	1.25°, 600 kPa, 30 gyrations	Density Indicator
Voids	8-14%	Compacted Density
Gradation for RAP	Report	Mix design
Marshall stability, 40℃	6kN min	Stability Indicator
Retained stability	75% min	Moisture susceptibility
IDT, 15℃	0.5 MPa min	Strength Indicator

Retained IDT	75% min	Moisture susceptibility
Freeze-thaw IDT, 25℃	70% min	Moisture stability
Rutting test, 60℃	2500 times/mm min	High temperature stability

Discussion

For some project test results, RS and DWTSR ratios were higher than 100%. The possible explanation is that the rest cement continued to undergo strength-building hydration reactions during the immersion process.

The study process used herein involved laboratory performance evaluations and established emulsion percentages that would yield recycled mixes for six projects that met the recommended performance specifications with Superpave™ gyratory compactor. Additional performance tests, such as the raveling test and low-temperature cracking test (Thomas et al., 2003) will be considered in the next research plan, as well as quality evaluation of RAP from the six projects.

CONCLUSIONS

This research work aimed at studying the characteristics of asphalt emulsion recycled mixtures as binder course on six roads with different traffic volumes in Jiangsu province, China. Based on the studies here, the following conclusions were drawn:

According to asphalt emulsion CIR mixture mix design procedures, the performance characteristics of cement asphalt emulsion recycling mixtures that were used as binder course can be evaluated with varying emulsion contents. For the six projects with different traffic volumes, the optimum emulsion contents that are from 3.5% to 4.3% exhibit the most satisfactory performance properties.

Post-project monitoring showed that recycled pavement had good structural bearing capacity after one-year traffic using FWD inspection. Even rut was the major distress on old pavements, only minor rutting about 3mm was observed on recycled pavements. It may be affected by the HMA surface course due to high temperature stability of recycled mixes as shown in results of rut testing.

CIR is the most cost-effective, environmental friendly and socially conscious pavement preservation and maintenance options. Based on performance evaluation and post-project monitoring, the performance specification for asphalt emulsion CIR mixture used as binder course is recommended in Jiangsu province trunk highway network in China.

ACKNOWLEDGEMENTS

This study was a co-operation with South East University and all data was supported by Jiangsu Provincial Transportation Science and Technology Project. We would like to thank Li Xiaoming, Dr. Everett Crews, Dr. Ma Xiang, Li Jian, Xu Biao who assisted in the lab testing and field construction.

REFERENCES

Leonard Dunn, Stephen Cross (2006). "Basic Asphalt Recycling Manual." Asphalt Recycling and Reclaiming Association (ARRA)

Brayton T. E., Lee K. W., Harington J., Kearney E. J. (2001). "Characterization of cold in-place recycling asphalt mixtures." *Construction and Materials Issues,* 193-205.

Brayton T. E., Harrington J. (2003). "New mix-design procedure of cold in-place recycling for pavement rehabilitation." *Transportation Research Board*, Washington, D.C.

Cross, S. A., Ramaya B. M.(1995). "Evaluation of cold in-place recycling." *Report No. K-TRAN: KU-93-1*, Kansas DOT.

Epps J. A. (1990). "Cold-recycled bituminous concrete using bituminous materials, NCHRP synthesis of highway practice 160", *Transportation Research Board*, Washington, D.C..

Federal Highway Administration (1997), "Pavement recycling guidelines for state and local governments." *FHWA-SA-98-042*, 1997.

Iwoa DOT (2005). "Development specifications for cold in-place recycled asphalt pavement (engineered emulsion)." *DS 01040*.

Jiangsu Transportation Research Institute (JTRI), (2005). "The report of Huning freeway's asphalt pavement recycling technique's research." Nanjing, 22-30.

Lee K. W., Brayton T. E., Harrington J. (2003). "New mix-design of cold in-place for pavement rehabilitation." *Transportation Research Board*, Washington, D.C..

Murphy D. T., Emery J. J. (1996). "Modified cold in-place asphalt recycling." *Transportation Research Record*, Washington, D.C..

Thomas T., Kadrmas A. (2003). "Performance-related tests and specifications for cold in-place recycling: lab and field experience." *Transportation Research Board*, Washington, D.C

Optimization of Vehicle Routing for Plowing and Snow Disposal

Zhang Dali[1]

[1]Highway Administration of Heilongjiang Province, No.169, Yiman Street, Nangang District, Harbin, Heilongjiang Province, PRC, 150090, PH:(86) 13766862168; email: hitliugang@live.cn

ABSTRACT

Plowing, snow loading, and hauling operations involve a number of vehicle routing problems where roads have to be traversed by plows, snow blowers, and trucks. This paper analyzes the problem of designing efficient routes for plowing and hauling trucks in snow emergencies. The plow routing and haul routing problems are determining a set of routes, each performed by a vehicle that starts and ends at its own depot, so that all the road segments are serviced, all the operational constraints are satisfied, and the total deadhead distance is minimized. Firstly, the typical characteristics of vehicle routing problems related to plowing and snow disposal operations are analyzed by considering their main components. Then, by using network transformation, a Capacitated Arc Routing Problem (CARP) is formulated to find the routes for vehicles. Heuristic procedures are applied because the problem has been shown to be NP-hard..

INTRODUCTION

Cleaning or reducing snow and ice in time on roads can improve the safety. Snow on pavement may be removed by chemical, thermal, or mechanical techniques. Plowing and snow disposal operations are usually performed on a regular basis in urban regions with frozen precipitation or significant snowfall (Blackburn et al, 2004). The snow removal and disposal problem includes many sub-problems including: what kind and how much deicer to use; where to locate the depots; how to assign snow emergency routes for the vehicles; and how to schedule the personnel. These problems are very difficult because of the diversity of operation conditions. Many solutions based on local search techniques are proposed. However, many planning and routing decisions are not so efficient. Recent developments in modeling and algorithmic tools, the increased performance of computers, and the increased pressure of maintaining or enhancing service levels and minimizing environmental impacts, all motivate the more widespread use of optimization models (Perrier et al, 2006a).

Plowing and snow disposal involve a number of vehicle routing problems where streets have to be traversed by plows, snow blowers, and trucks. The routes must satisfy several operational constraints imposed by the level of service policies and the characteristics of the transportation network, road segments, sectors, vehicles, and crews. This problem has many features. First, the snow route design problem can be classified into the category of Arc Routing Problems (ARP) in which the vehicles should service some or all arcs in a network. Second, in snow emergency operations we are dealing with a network in which every link has a direction. Since a truck can service two lanes at the same time, some two-lane streets can be serviced in one pass

from either direction. Therefore, these streets in the network do not have direction. That means some links are directed and some are not. Third, the underlying network is a hierarchical network. This means that there is a precedence structure for servicing the roads. Since most primary highways that are in the snow emergency route network belong to the 1st class, we have only focused on this class and do not deal with the different classes of roads (Perrier et al, 2006b).

In general, the route design in snow emergency operations is classified as Capacitated Arc Routing Problem (CARP). Based on the operational extensions，it can be viewed as a multiple Hierarchical Chinese Postman Problem (m-HCPP) with class upgrading possibilities and vehicle-road segment dependencies. The m-HCPP generalizes the hierarchical Chinese Postman Problem (HCPP), calling for the determination of a single route starting and ending at a depot and servicing all road segments of a network in such a way that the service hierarchy is satisfied and a time objective is minimized. The HCPP is NP-hard, but can be solved in polynomial time if the precedence relation is linear and all subgraphs induced by the classes are connected. Since the HCPP with no assumption on class connectivity is a special case of the m-HCPP, it follows that the m-HCPP is NP-hard. Ghiani and Improta (2000) have described exact algorithms for this case. Cabral et al. (2004) showed that it is possible to solve the HCPP with linear precedence relations and no assumption on class connectivity by transforming it into a rural postman problem. The heuristic could sequentially solve the HCPP for each class, starting with the highest class, considering all traversed edges in any of the classes of lower priority as already serviced. As highlighted by Korteweg and Volgenant (2006), declaring a deadheading edge as already serviced could not increase total completion time, but may generate routes with a shorter time.

Dealing with snow emergencies involves a number of different operations. Because each area has its own unique environmental conditions, most papers published for this problem have different operational area backgrounds. For example, Campbell and Langevin (1994) were dealing with snow removal and disposal problem for Montreal Urban Community. Because different areas have different operations, the formulation and solution approaches can be very different. The previous literature focuses more on heuristic algorithms instead of finding exact solution algorithms and mathematical formulations. The main reason for this is that the field operations have many constraints that are very hard to be described mathematically. And even if we can find a mathematical formulation for the problem, it is very hard to solve.

Campbell and Langevin (1994) provide a detailed description of the snow removal and disposal operation in Montreal. They also list major problems related to snow operations. These problems include site location, section design, section assignment, fleet mix and routing. An Integer programming formulation for snow disposal site location and assignment problem (SLAP) is given and a decision support system is discussed in that paper, but no routing algorithm or formulation is suggested or discussed. Eglese (1994) presents a heuristic to minimize the distance traveled by gritting vehicles. The solution procedure includes partitioning the network, creating the cycle node network and constructing the route. The heuristic allows multiple depots and different road priorities. Simulated Annealing is used to

solve the constrained problem. Perrier et al. (2006c) give a formulation models for general precedence relation constraints with no assumption on class connectivity, different service and deadhead speed possibilities, separate pass requirements for multi-lane road segments, class upgrading possibilities, and vehicle-road segment dependencies. Two objectives are considered: a hierarchical objective and a make span objective. The resulting model is based on a multi-commodity network flow structure to impose the connectivity of the route performed by each vehicle.

An integrated overview of the most relevant operations research literature on arc routing was presented by Eiselt et al (1995a, 1995b). The paper gives a directed transportation network G (V, A) with arc demands q_{ij} for each $\text{arc}(i, j) \in A$. It must be satisfied by a fleet of vehicles k, each of which has a capacity W_k, The number of cycles (routes) which pass always through the arcs and satisfy the demands at minimal total cost are found. The geographical region (or network) is usually partitioned into non-overlapping subareas (sub networks), called districts, each including one depot at which a number of vehicles are based. The traditional approach for the design of districts in the context of winter road maintenance consists in partitioning the road network into districts by assigning road segments to their closest depot. Kandula and Wright (1995, 1997) and Muyldermans et al (2002, 2003) used this approach for designing districts for plowing and spreading operations. A similar approach for designing small clusters of streets in the context of snow disposal operations was developed by Labelle et al. (2002) and Perrier et al (2008). For a recent survey of optimization models and algorithms for the design of districts for winter road maintenance, the reader is referred to the work of Perrier et al. (2007a, 2007b).

In this research, we focus on how to design the service routes for snow emergency operations. Efficient route design and planning for snow vehicles can not only save agencies operational cost, but also improve level of service and social benefits. The objective of this research is to reduce the total cost of snow emergency operations. As discussed earlier, the total cost includes operational costs and social costs. There is a tradeoff between the two components. We can reduce one by increasing the other. For example, we can reduce the service time (social cost) by increasing the number of trucks. In an extreme case, every truck can service only one link in the network. In this research, our objective is to minimize the operating costs given operational conditions while improving or maintaining the level of service to reduce the social costs. The operation cost is mainly composed of the truck costs, the personnel costs and the fuel costs. The objective is to reduce the total deadhead distance, so the fuel and other costs are reduced and the level of service is improved since the overall execution time is reduced.

MATHEMATICAL FORMULATIONS

In this chapter, we will try to formulate the Snow Emergency Routing Problem as Capacitated Arc Routing Problem with several extensions that are required for field operations. Service continuity constraint is very important for practicality of the operation. The service continuity can be defined as follows: the links that are serviced by one truck should be connected. Also we need to expand the

single depot formulation to multi-depot formulation. After expanding to multi-depot formulation, the original illegal sub-tour elimination methods in CARP formulation cannot be applied directly. The details of this problem will be discussed later. A network transformation that duplicates the depots is needed to make sure that illegal sub-tours can be eliminated. As discussed before, the objective is to find the minimum deadhead distance for a given number of trucks.

We can deal with a mixed network as directed network and add constraints for the undirected links that ensures that the sum of the service of both directions should be one. The load balancing extension is also easy to implement. We can simply add a lower bound for total demands of the links in an assignment. The multi-depot extension is a little difficult, because the illegal sub-tour breaking constraints will not work in this case directly. Some network transformations are needed to eliminate the illegal sub-tours. In this section, we will present the formulation.

The following notation is defined:

G	A directed network
V	The vertex set $\{1,\cdots,q,\cdots q+n\}$
V_d	Set of depots $\{V_1,\cdots,V_q\}$
A	$\{\tau_i \mid i=1,2,\cdots,m\}$ is the arc set
$\omega(\tau_i)$	The cost of arc τ_i
R	The set of the arcs that is need service, $R \subset A$
λ	1 Only if $\tau_i \in R$
	0 Otherwise
X	The number of the vehicle fleet
W_l	The capacity of the vehicle $1 \le l \le X$
q_{ij}	The demand of arc $\{(i,j)\}$
M	$\{T_i,T_i,\cdots,T_K\}$ is the set of routes
$\mathrm{X}_{ij\|T_i\|}$	1 Only if edge $\{(i,j)\}$ is traversed from vertex i to vertex j on route T_i
	0 Otherwise
$\mathrm{Y}_{ij\|T_i\|}$	1 Only if edge $\{(i,j)\}$ is serviced from vertex i to vertex j on route T_i
	0 Otherwise
R_k	The set of serviced arcs on route k
A_{kt}	The number of the serviced arcs on route k
A_{kr}	The number of the traversed arcs on route k
v_w	The average servicing speed
v_f	The average traversing speed
L	The maximum working time

The problem formulation is as follows:

Minimize

$$\sum_{T_i \in M} \sum_{(i,j) \in A} \omega(\tau_i) X_{ij|T_i|} \tag{1}$$

Subject to:

$$\sum_{(i,j) \in A} X_{ji|T_i|} - \sum_{(i,j) \in A} X_{ij|T_i|} = 0 \qquad i \in V \text{ for all } T_i \tag{2}$$

$$\sum_{i=1}^{k} |T_i| = \xi \tag{3}$$

$$R_k = \left\{ T_{ki} \mid T_{ki} \in \left\{ T_k, \cdots, T_{k|T_k|} \right\} \right\} \tag{4}$$

$$R_i \cap R_j = \varnothing \ (i \neq j; 1 \leq i, j \leq K) \tag{5}$$

$$Y_{ij|T_i|} - Y_{ji|T_i|} = 0 \qquad \text{For all k, and } (i,j) \in A \tag{6}$$

$$\sum_{(i,j) \in A} q_{ij} Y_{ij|T_i|} \leq W_l \qquad \text{For all } T_i \tag{7}$$

$$\sum_{i \in V_d} X_{ji|T_i|} = 1 \qquad \text{For all } T_i \tag{8}$$

$$0 \leq |T_i| \leq \xi \ \ (1 \leq i \leq K) \tag{9}$$

$$\sum_{k=1}^{N_l} \left(\sum_{i=1}^{A_{kt}} \frac{\tau_i}{v_W} + \sum_{j=1}^{A_{kr}} \frac{\tau_j}{v_f} \right) \leq L \quad (l = 1, 2, \cdots, X) \tag{10}$$

$$\begin{cases} \sum_{i,j \in S} X_{ij|T_i|} \leq |S| - 1 + n^2 u_k^s \\ \sum_{i \in S} \sum_{j \notin S} X_{ij|T_i|} + w_k^s \geq 1 \\ u_k^s + w_k^s \leq 1 \\ u_k^s, w_k^s \in \{0,1\} \end{cases} \qquad \text{For all k}, S \in V / V_d \tag{11}$$

$$X_{ij|T_i|}, Y_{ij|T_i|} \in \{0,1\} \qquad \text{For all k, and } (i,j) \in A \tag{12}$$

The objective function (1) seeks to minimize the total travel distance for all trucks. Constraints (2) ensure the route continuity. Constraints (3), (4) and (5) ensure that each arc should be serviced as required. Constraints (6) require that both directions of a link be serviced by the same trucks. Constraints (7) are the capacity constraints. Constraints (8) require that the in-degree of a depot should be one for each route. Constraints (9) require that the serviced arcs of one route are less than the serviced arcs of all routes. Constraints (10) require that the working time of every truck is less than the maximum working time. Constraints (11) are the sub-tour breaking constraints.

HEURISTIC SOLUTION

Based on the basic operations in the arc routing problems, we proposed an algorithms to generate an initial solution. In the proposed algorithm, the network is initialized as follows. The network is composed of a vector of nodes and a vector of links. The vector of nodes contains the information about the index of the nodes, for example, node No. 0 means that the node is the depot. The vector of links contains

the links pertinent information that include start node, end node, start service time, end service time, cost (distance), travel time, number of times of service, etc. In network initialization, we also maintain the information regarding the shortest paths and distances between any pair of nodes. Since we use the shortest paths and distances frequently, when we initialize the network we use Floyd's shortest path algorithm to generate all pair-wise shortest paths and distances and save the information for later use.

The steps of the procedure are as follows:

Step 1. For existing links that are not serviced, find the furthest link to the depot.
Step 2. Find the shortest path from the depot to the start node of this link and from the end node of this link to the depot. Establish an initial route using the links in the shortest path and the link found in step 1.
Step 3. Find the nearest link to the current route.
Step 4. Insert the link found in step 3 in the route.
Step 5. Loop until the capacity constraint for vehicle is violated.
Step 6. Loop until no link that requires service remains.

CONCLUSION

The mathematical formulation of the Snow Emergency Routing Problem is presented and discussed for the traditional CARP. The difficulties come from the mufti-depot extension. By duplicating the depots and their related links, we expanded the single depot CARP formulation into a mufti-depot formulation. One formulation is based on the dynamic binding of subset of links that a vehicle services. Since CARP is a NP-complete problem, we try to find the good lower bounds to assess the solutions generated by heuristic algorithms.

From the CARP formulation, most decision variables result was observed. Actually, not all of these constraints are necessary. If the solution consists of an illegal sub-tour, then we just add the respective illegal sub-tour elimination constraints to the problem and solve it again. This method uses the same basic idea of cutting plane methods. A branch and cut method can be used if the relaxed problem is still difficult to solve. Finding good lower bound for NP-complete problem is always a challenging work for researchers. For a field application, it is more important to find a good or acceptable solution efficiently. From this aspect, it is more important to design a good algorithm.

REFERENCES

Blackburn RR, Bauer KM, Amsler DE, Boselly SE, McElroy AD. (2004). "Snow and ice control: guidelines for materials and methods". *NCHRP report 526,Washington, DC.*

Cabral E.A., Gendreau M., Ghiani G., Laporte G. (2004). "Solving the hierarchical Chinese postman problem as a rural postman problem". *European Journal of Operational Research* 155, 44-50.

Campbell, J.F., and Andre Langevin. (1994). "Operations Management for Urban SnowRemoval and Disposal". *Transportation Research A*, p. 359-369.

Eglese, R.W.. (1994). "Routing Winter Gritting Vehicles". *Mathematics*, p. 231-244.

Eiselt HA, Gendreau M, Laporte G. (1995a). "Arc routing problems, Part I: the

Chinese postman problem". *Operations Research* 43, 231-242.

Eiselt HA, Gendreau M, Laporte G. (1995b). "Arc routing problems, Part II: the rural postman problem". *Operations Research* 43, 399-414.

Ghiani G., Improta G. (2000). "An algorithm for the hierarchical Chinese postman problem". *Operations Research Letters* 26, 27-32.

Kandula P., Wright J.R. (1995). "Optimal design of maintenance districts". *Transportation Research Record* 1509, 6-14.

Kandula P., Wright J.R. (1997). "Designing network partitions to improve maintenance routing". *Journal of Infrastructure Systems* 3, 160-168.

Korteweg P., Volgenant T. (2006). "On the hierarchical Chinese postman problem with linear ordered classes". *European Journal of Operational Research* 169, 41-52.

Labelle, A. Langevin, J.F. Campbell. (2002). "Sector design for snow removal and disposal in urban areas". *Socio-Economic Planning Sciences* 36, 183-202

Muyldermans L., Cattrysse D., Van Oudheusden D., Lotan T. (2002). "Districting for salt spreading operations". *European Journal of Operational Research* 139, 521-532.

Muyldermans L., Cattrysse D., Van Oudheusden D. (2003). "District design for arc-routing applications". *Journal of the Operational Research Society* 54, 1209-1221.

Perrier N., Langevin A., Campbell J.F. (2006a). "A survey of models and algorithms for winter road maintenance Part I: system design for spreading and plowing". *Computers & Operations Research* 33, 209-238.

Perrier N., Langevin A., Campbell J.F. (2006b). "A survey of models and algorithms for winter road maintenance Part II: system design for snow disposal". *Computers & Operations Research* 33, 239-262.

Perrier N., Langevin A., Amaya V., (2006c). "Routing for Urban Snow Plowing Operations". *Les Cahiers du GERAD* G-2006-33.

Perrier, N., Langevin, A., Campbell, J.F., (2007a). "A survey of models and algorithms for winter road maintenance Part III: vehicle routing and depot location for spreading". *Computers & Operations Research* 34, 211-257.

Perrier N., Langevin A., Campbell J.F. (2007b). "A survey of models and algorithms for winter road maintenance Part IV: vehicle routing and fleet sizing for plowing and snow disposal". *Computers & Operations Research* 34, 258-294.

Perrier A., Langevin A., Campbell J.F. (2008). "The sector design and assignment problem for snow disposal operations". *European Journal of Operational Research* 189, 508-525.

Expressway Pavement-Performance Indexes Prediction Based on Gray Model GM(1,1,λ)

Zhang Li-juan[1,2] and Xu Fu-you[3]

[1]Key Laboratory of Road and Traffic Engineering of the Ministry of Education, Tongji University, 200092,Shanghai;PH(86)13671683893; FAX (86) 21-54153622; email:20070214xy@163.com

[2]College of Civil Engineering, Shanghai Normal University, Shanghai 201418, China

[3]School of Civil & Hydraulic Engineering, Dalian University of Technology, 116024, Dalian, China; PH(86)21-54153622; email: fuyouxu@hotmail.com

ABSTRACT

The gray model GM(1,1,λ) method was applied to fit the pavement performance indexes (international roughness index, pavement deflection value , BPN)of asphalt expressway. To obtain the optimal value of parameter λ, the random search method and the cyclic search method were established by minimizing the mean absolute error, the average relative error or the average square of Absolute Error. The results show that forecast precision of gray model GM(1,1,λ) method is higher than that of GM(1,1) method. The optimal value of parameter λ can be obtained easily and accurately by random search method and the cyclic search method. The parameter λ is very close to 0.5 by minimizing the average square of Absolute Error. To improve the forecast precision，it is more appropriate to minimize the mean absolute error or the average relative error.

INTRODUCTION

Pavement-performance indexes prediction model is the core of the highway facilities-management system. Viewing of the different type of road facilities, there are many kinds of models. Up to date, the models have been divided into deterministic model and probabilistic model(Yao,1993). The deterministic model has been further divided into mechanical-model, mechanical-empirical-model and regressive-model(Hass,1994). The regressive-model and the Markov-chain- model are the most popular. For the regressive-model, the multiple regression is used to predict the pavement-performance indexes influenced by the influencing variables, such as service time，traffic flow and pavement structure. The three following models all belong to regressive-model: The PSI prediction model drawn from the American AASHO test road, the PCI prediction model of the American air-force PAVER management system and the general deterioration equation for pavement performance established by Sun li-jun. In the regressive-model，the statistical fitting method is used. Its authenticity not only depends on the information adequacy and accuracy, but also on how the researchers interpret the relationship between the pavement-performance indexes and the influencing variables. The Markov-chain-model can reveal uncertainty of the pavement-performance indexes. But considering the current management level, the administrators are unwilling to accept this model. And because the model is established on the regressive method, the error can not be ignored.

Some researchers adopted other methods to investigate the subject(Bi,1999), such as the Bayesian-method of the Canadian-strategic-expressway-research-project, the dynamic- model and the adaptive- algorithm method adopted by Zou pei-guo. In

recent years, the artificial neural network began to apply in this field (Wang,2001;Zhou,2006). But for the above models, large sample size is needed and can not be obtained in the engineering practice. Because of its nonlinear character, the artificial neural network can take the vehicle load factor and the environmental factor into account simultaneously. But it can not avoid the influence of the local least value, and requires trial calculation.

Some researchers adopted gray theory to study the pavement performance (Hu,2006;Wang,2002). Gray theory focuses on uncertainty system. The theory is quite easy, its forecast precision is rather high, and it is convenient for programming. For example, based on discrete data sequence of the independent variables and dependant-variables, the traditional gray model GM(1,1,λ) can be applied to establish explicit functions for data fitting and prediction(Liu,2004). But for ordinary data sequence, the fitting and forecast precision is rather low.

In view of this background and condition, the purpose of this paper is to modify the traditional gray model GM(1,1) by introducing the parameter-λ and improving the adjacent-data weight. So the new gray model GM(1,1,λ) method is established, and the forecast precision is improved. To obtain the optimal value of parameter λ, the random search method and the cyclic search method are used .By minimizing the mean absolute error, the average relative error or the average square of absolute error, the feasibility and characteristic of GM(1,1,λ) method is discussed .

1 GRAY MODEL GM(1,1,λ) METHOD(Xu,2003;Xie,2000)

N-gram vector is supposed to be $\left\{X_i^{(0)}\right\}$, $i=1,2,\ldots,N$

By one-accumulating，the generating sequence is $\left\{X_i^{(1)}\right\}$, $i=1,2,\ldots,N$

$$B=\begin{pmatrix} -(\lambda X_1^{(1)}+(1-\lambda)X_2^{(1)}) & 1 \\ -(\lambda X_2^{(1)}+(1-\lambda)X_3^{(1)} & 1 \\ \cdot & \cdot \\ \cdot & \cdot \\ -(\lambda X_{N-1}^{(1)}+(1-\lambda)X_N^{(1)} & 1 \end{pmatrix} \tag{1}$$

$$Y_N=(X_2^{(0)},X_3^{(0)},\ldots,X_N^{(0)})^T \tag{2}$$

According to Least Square Principle：

$$\begin{pmatrix} a \\ b \end{pmatrix}=\left(B^TB\right)^{-1}B^TY_N \tag{3}$$

The formula(3)can be converted to：

$$a=\frac{\sum_{i=2}^{N}[\lambda X_{i-1}^{(1)}+(1-\lambda)X_i^{(1)}]\sum_{i=2}^{N}X_i^{(0)}-(N-1)\sum_{i=2}^{N}[\lambda X_{i-1}^{(1)}+(1-\lambda)X_i^{(1)}]X_i^{(0)}}{(N-1)\sum_{i=2}^{N}[\lambda X_{i-1}^{(1)}+(1-\lambda)X_i^{(1)}]^2-\{\sum_{i=2}^{N}[\lambda X_{i-1}^{(1)}+(1-\lambda)X_i^{(1)}]\}^2} \tag{4}$$

$$b=\frac{\sum_{i=2}^{N}X_i^{(0)}\sum_{i=2}^{N}[\lambda X_{i-1}^{(1)}+(1-\lambda)X_i^{(1)}]^2-\sum_{i=2}^{N}[\lambda X_{i-1}^{(1)}+(1-\lambda)X_i^{(1)}]\sum_{i=2}^{N}[\lambda X_{i-1}^{(1)}+(1-\lambda)X_i^{(1)}]X_i^{(0)}}{(N-1)\sum_{i=2}^{N}[\lambda X_{i-1}^{(1)}+(1-\lambda)X_i^{(1)}]^2-\{\sum_{i=2}^{N}[\lambda X_{i-1}^{(1)}+(1-\lambda)X_i^{(1)}]\}^2} \tag{5}$$

So the model data is generated：

$$\hat{X}_{i+1}^{(1)} = e^{-ai}(x_1^{(0)} - \frac{b}{a}) + \frac{b}{a} \quad (6)$$

where i is Generally regarded as integral number($1,2,\ldots,N$). It can also be regarded as decimal. By inverse accumulated generating operation of model data, data restoration is realized.

2 PARAMETER DETERMINATION FOR GM(1,1,λ) METHOD

For the original sequence, the parameter λ is the decisive factor for the forecast precision of gray model GM(1,1,λ) method. To obtain the optimal value of parameter λ, the error-fitting minimization principles are established by minimizing the mean absolute error, the average relative error or the average square of Absolute Error. The concrete method is discussed in the below.

2.1 Random search method

(1) The error-fitting minimization principle should be established by choosing one form the above there principles. The initial value of parameter λ is λ_1 and can be supposed to 0.5.

(2) If the value of parameter λ equals to λ_i, the fitting error ε_i is obtained based on gray theory.

(3) The random search method is used within certain interval according to the following method: $\lambda_{i+1} = \lambda_i + [0.5 - rand(0,1)] \cdot T$, where $rand(0,1)$ is random number satisfying uniform distribution on [0, 1] interval; T has an effect on the chasing step, and the value can be defined within [0.01, 0.001] interval.

(4) The value of ε_{i+1} is obtained. If ε_{i+1} is less than ε_i, λ equals to λ_{i+1}, the feedback information is obtained as follows: with the value of parameter λ changing form λ_i to λ_{i+1}, the corresponding fitting error decreases. So the value of λ can be successively changed into $2\lambda_{i+1} - \lambda_i$, $3\lambda_{i+1} - 2\lambda_i$, $4\lambda_{i+1} - 3\lambda_i$ ……, and the procedure should continue until the last error is greater than the last but one error; If not, the procedure should return to (3);

(5)The procedure from (3) to (4) should be repeated until the minimization of the fitting error tends to be stable. Then the optimal value of parameter λ is obtained and the corresponding fitting error ε is got.

2.2 Cyclic search method

(1) The error-fitting minimization principle is established by minimizing the mean absolute error, the average relative error or the average square of Absolute Error. The initial interval $[\lambda_b, \lambda_t]$ of parameter λ is generally determined as interval $[0,1]$.

(2)The interval $[\lambda_b, \lambda_t]$ is divided equally into m parts, and the coordinate of segmentation point λ_k ($k = 0,1,\ldots,m$)is obtained.

(3) If the value of parameter λ equals to λ_i, the fitting error ε_k is obtained based on loop calculation.

(4)The minimum fitting error $\varepsilon_{\min}$ is determined and the corresponding value

of parameter λ is obtained.

(5)The latest value of parameter λ is used as the loop interval center of the next time, and the chasing step of the last time is used as the loop interval of the next time. Then the obtained loop interval is divided equally into m' parts (m' can be equal to m), and the coordinate value of segmentation point $x_{k'}$ ($k' = 0,1,\ldots,m'$)is obtained.

(6) The procedure from (3) to (5) should be repeated until the step is small enough or the fitting error ε of the last time is very close to the fitting error of the last but one time.

3 INSTANCE STUDY

In this paper, the measured pavement-performance indexes of asphalt expressway (Shenda Expressway, some expressway in Jiangsu, Hujia Expressway) in recent years are provided(Hu,2006;Wang,2002;Highway,2007). The indexes consists of international roughness index(IRI), pavement deflection value(l) , British pendulum number(BPN). Based on the gray model GM(1,1,λ) method , the random search method and the cyclic search method are applied to imitate and forecast these indexes. The relative percentage error between the fitted values and the measured values is given in the table 1 and table 2. In the row"0", the fitting errors based on GM(1,1) method are shown(C=0.5). In the row"1" 、"2"、"3", the fitting error based on GM(1,1,λ) method is shown. For the row"1"，the corresponding error fitting minimization principle is established by minimizing the mean absolute error；for the row "2"，the average relative error and for the row "3"，the average square of Absolute Error.

Table 1 Fitting errors of pavement performance index for Shen-Da highway

year / index			1989	1990	1991	1992	1993	1994	1995	1996	1997	mean absolute error
IRI (mm)	site data		1.2	1.22	1.39	1.57	1.81	1.97	2.01	2.11	2.40	/
	fitting error (%)	0	0	3.01	-0.5	-6.0	-5.8	0.56	4.42	0.07	7.66	3.5238
		1	0	2.96	-0.6	-6.0	-5.9	0.50	4.36	0.00	7.61	3.5063
		2	0	2.59	-1.0	-6.4	-6.3	0.04	3.86	-0.5	7.26	3.5038
		3	0	3.00	-0.5	-6.0	-5.8	0.56	4.42	0.07	7.66	3.5225
l (0.01mm)	site data		27.9	28.5	29.8	31.1	33.7	35.3	36.9	39	40.3	/
	fitting error (%)	0	0	0.01	0.66	1.51	-1.4	-0.9	-0.2	-0.7	1.14	0.8313
		1	0	0.22	0.88	1.75	-1.1	-0.6	-0.0	-0.4	1.43	0.8213
		2	0	0.23	0.89	1.75	-1.1	-0.6	0.00	-0.4	1.43	0.8225
		3	0	0.02	0.67	1.52	-1.4	-0.9	-0.2	-0.6	1.16	0.8300
BPN	site data		49	48.4	46.7	45.3	43.2	41.8	39.9	38.7	37.2	/
	fitting error (%)	0	0	0.26	0.04	-0.7	0.23	-0.2	0.58	-0.1	-0.0	0.2850
		1	0	0.22	0.00	-0.7	0.20	-0.3	0.55	-0.2	-0.0	0.2838
		2	0	0.22	0.00	-0.7	0.20	-0.3	0.55	-0.2	-0.0	0.2838
		3	0	0.27	0.05	-0.7	0.24	-0.2	0.59	-0.1	0.00	0.2838

Table 2 Fitting errors of pavement performance index of certain highway

year / index			Express highway in Jiangsu						Hujia express highway					
			1996	1997	1998	1999	2000	mean absolute error	2002	2003	2004	2005	2006	mean absolut error
	site data		1.56	1.799	1.905	1.999	2.127		2.15	2.37	2.51	2.62	2.72	
IRI (mm)	fitting error (%)	0	0	-0.05	-0.26	0.44	-0.25	0.2500	0	0.59	-0.63	-0.39	0.38	0.4975
		1	0	0.16	-0.04	0.68	0.00	0.2200	0	0.25	-0.98	-0.76	0.00	0.4975
		2	0	0.17	-0.03	0.68	0.00	0.2200	0	0.25	-0.98	-0.76	0.00	0.4975
		3	0	-0.02	-0.23	0.47	-0.22	0.2350	0	0.60	-0.61	-0.38	0.40	0.4975
	site		12.994	16.097	19.521	20.111	24.133	/	17.6	24.6	27.0	29.3	31.6	/
l 0.01mm	fitting error (%)	0	0	1.80	-4.96	4.45	-1.45	3.1650	0	0.50	-0.54	-0.45	0.26	0.4375
		1	0	2.92	-3.80	5.85	-0.01	3.1450	0	0.29	-0.76	-0.69	0.00	0.4350
		2	0	2.93	-3.79	5.86	-0.01	3.1475	0	0.29	-0.77	-0.69	0.00	0.4375
		3	0	1.95	-4.81	4.63	-1.26	3.1625	0	0.56	-0.48	-0.39	0.33	0.4400
	site		57.1	47.98	50.94	46.4	39	/	44.5	43.0	42.1	41.4	40.8	/
BPN	fitting error (%)	0	0	5.63	-6.80	-4.14	6.84	5.8525	0	-0.17	0.20	0.13	-0.16	0.1650
		1	0	0.00	-11.62	-8.96	1.63	5.5525	0	0.00	0.37	0.29	0.00	0.1650
		2	0	0.00	-11.62	-8.96	1.63	5.5525	0	-0.30	0.07	0.00	-0.29	0.1650
		3	0	5.65	-6.78	-4.12	6.86	5.8525	0	-0.16	0.21	0.13	-0.15	0.1625

Based on the result of table 1 and table 2，the conclusion is drawn as follows：

(1)For the three pavement-performance indexes (IRI, pavement deflection value , BPN)，based on different model and different error-fitting minimization principle，the results of the same year are different and the fitting errors are either negative or positive.

(2)Because of the gray model's own characteristics, no matter what kind of model and error-fitting minimization principle are used, the fitting error of the first data is zero.

(3)For IRI of road A, the maximum value of the relative fitting error is close to 8%，the minimum value is close to 0,and the mean of absolute value is 3.5%; for the pavement deflection value of road A, the maximum value of the relative fitting error is close to 2%，the minimum value is close to 0,and the mean of absolute value is 0.8%; for BPN of road A, the maximum value of the relative fitting error is close to 1%，the minimum value is close to 0,and the mean of absolute value is 0.3%.Generally speaking, the fitting error of pavement deflection value is smaller than that of IRI, and the fitting error of BPN is smallest.

(4) For the IRI of road B, the maximum value of the relative fitting error is close to 0.7%，the minimum value is close to 0,and the mean of absolute value is 0.25%; for the pavement deflection value of road B, the maximum value of the relative fitting error is close to 6%，the minimum value is close to 0,and the mean of absolute value is 3.2%; for BPN of road B, the maximum value of the relative fitting error is close to 12%，the minimum value is close to 0,and the mean of absolute value is 6%.Generally speaking, the fitting error of pavement deflection value is smaller than that of BPN, and the fitting error of IRI is smallest.

(5) For the IRI of road C, the maximum value of the relative fitting error is close to 1%，the minimum value is close to 0,and the mean of absolute value is 0.5%; for the pavement deflection value of road C, the maximum value of the relative fitting error is close to 0.8%，the minimum value is close to 0,and the mean of absolute value is 0.44%; for BPN of road C, the maximum value of the relative fitting error is close to 0.4%，the minimum value is close to 0,and the mean of absolute value is 0.17%. Generally speaking, the fitting error of pavement deflection value is smaller than that of IRI, and the fitting error of BPN is smallest.

(6)The results show that for the three indexes，it is difficult to choose which one is most suitable for the gray model to fit.

(7)For the three pavement-performance indexes，the fitting-error values of the different year is independent on the error-fitting minimization principle.

(8)For the three pavement-performance indexes，the absolute-values mean of the fitting-error based on different principles is very close. So it is very difficult to determine which principle is most reasonable. In general, based on the minimizing the mean absolute error principle or minimizing the average relative error principle, the relative fitting error is rather small. It also reflects the advantage of the GM(1,1,λ) model. But , for the problem discussed in this paper, the fitting precision of the GM(1,1,λ) model and the traditional GM(1,1) model is rather close.

For the three pavement-performance indexes, the mean absolute error, the average relative error, the average square of absolute error and the corresponding parameter λ are all listed in Tab.3.

Table 3 Average fitting errors of pavement performance index

index		λ		mean absolute error		λ		average relative error		λ		average square of absolute error	
Highway A	IRI	0.5	0.4949	0.0528	0.0525	0.5	0.4556	3.1337	3.1163	0.5	0.4998	0.0050	0.0050
	l	0.5	0.5405	0.2565	0.2502	0.5	0.5416	0.7380	0.7303	0.5	0.5035	0.0990	0.0990
	BPN	0.5	0.5104	0.1092	0.1079	0.5	0.5104	0.2531	0.2514	0.5	0.4969	0.0224	0.0224
Highway B	IRI	0.5	0.5378	0.0040	0.0034	0.5	0.5378	0.1997	0.1757	0.5	0.5046	0.0000	0.0000
	l	0.5	0.5819	0.5006	0.4780	0.5	0.5819	2.5321	2.5162	0.5	0.5105	0.3888	0.3879
	BPN	0.5	1.4117	2.1504	2.1428	0.5	1.4117	4.6813	4.4427	0.5	0.4962	6.0175	6.0174
Highway C	IRI	0.5	0.4268	0.0101	0.0101	0.5	0.4268	0.3986	0.3972	0.5	0.5036	0.0001	0.0001
	l	0.	0.47	0.09	0.09	0.	0.47	0.35	0.34	0.	0.50	0.01	0.01

		5	55	66	61	5	55	02	94	5	67	21	18
	BPN	0.5	0.4016	0.0549	0.0549	0.5	0.5753	0.1311	0.1309	0.5	0.4955	0.0039	0.0039

Form Tab.3, we can conclude that:

(1)The fitting error of the GM(1,1,λ)method is lower than that of GM(1,1) method.

(2)For the three indexes of the highway discussed in the paper, the relationship between 0.5 and the value of λadopted by model GM(1,1,λ) is uncertain.

(3)Under most conditions, the value of λis within the interval(0.4,0.6).While for the BPN of highway B, the value is 1.4117. It shows the optimal value of λwill be far from 0.5 when the a set of data is not suitable for gray method fitting. So the optimal value of λ can be used to decide whether the data is suitable for gray method fitting.

(4) For highway A and C the average-relative fitting-error of IRI, pavement deflection value , BPN decreased successively; For highway B, the average-relative fitting-error value of IRI, pavement deflection value , BPN increased successively. So it is difficult to choose which index is fit for gray method fitting.

(5)For IRI, the fitting error of highway B、 C、 A is increasing successively;for pavement deflection value and BPN, the fitting error of highway C、A、B are increasing successively. So it is difficult to choose which highway is fit for gray method fitting.

The relationship between the fitting error of different error principle and the parameter λ is listed in Fig. 1. For the feasibility of comparison, the different coefficient is multiplied to unify the range.

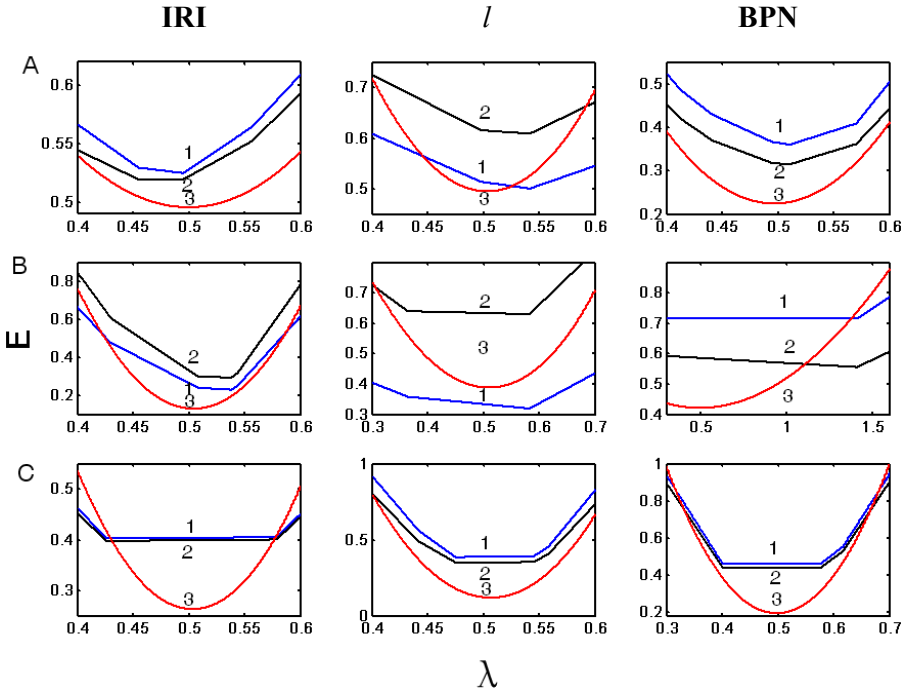

Fig.1 Graphs of pavement performance index fitting error versus parameter λ

(1)When the third principle (minimizing the average square of absolute error) is used, the fitting error and the parameter λ is Symmetric with 0.5. In other words, 0.5 is approximately regarded as the optimal value of λ based on least-square theory. There is second order relationship between the average square of Absolute Error and λ.

(2) When the first or second principle (minimizing the mean absolute error or the average relative error) is used, there is piecewise-linear relationship between the mean absolute error (or the average relative error) and λ. Especially for express C, when λ is approximate to 0.5, the error doesn't change. While λ falls into the bilateral of the interval, the error is increasing and is basically symmetric with the vertical axis(whenλ=0.5).

(3)When the first or second error principle (minimizing the mean absolute error or the average relative error) is used, the relationship curve between the mean absolute error (or the average relative error) and λ is similar, and the turning point of the curve is also similar.

4 CONCLUSIONS

(1)In this paper, the feasibility of GM(1,1,λ) method applied to fit the pavement performance indexes(IRI, pavement deflection value , BPN) is discussed. The method is proved to be feasible by practice. But it is difficult to choose which index is most suitable for GM(1,1,λ) method to fit.

(2) To obtain the optimal value of parameter λ, the random search method and the cyclic search method were established. It shows the methods are shortcut and accurate.

(3) The forecast precision of gray model GM(1,1,λ) method is higher than that of GM(1,1) method, but the difference is not large. By minimizing the average square of Absolute Error, the GM(1,1,λ) will degenerate into GM(1,1) based on least square principle. To improve the forecast precision，it is more appropriate to minimize the mean absolute error or the average relative error.

REFERENCES

Bi,Y.X.(1999). *Study on prediction model of pavement performance,* Shanghai: Department of Road and Traffic Engineering, Tongji University.

Hass, R, Hudson, W. R. and Zanicwski (1994). *Modern Pavement anagement* .USA. Krieger Publishing Company.

Highway Administration Department of Shanghai (2007).*Pavement and Bridge Condition Analysis Report of Arterial Highway(express highway) in Shangha*i.

Hu, G.X., Liu, Y.(2006). "Application of Gray Theory in Forecast of Pavement Performance ." *Journal of Yangtze University*. 3(4).

Liu, S.F., Dang, Y.G. (2004).*Gray System Theory and Its Application* Beijing: Science Press.

Wang, G.X., An, J.F., Chen, R.S. (2002). "Application of Gray Theory in Forecast of Pavement Performance." *Journal of Highway and Transportation Research and Development*. 19(3)

WANG, Y.L., WANG B.G. (2001). "Prediction of pavement performance using

artificial neural network.". *Journal of Xian High way University*, 21(1):42.

Xie, K.G. (2000). "Gray Model GM(1,1, λ) Based on genetic algorithm". *Journal of Systems Engineering*. 15(2)

Xu, F.Y., Zhang ,J.R., Hao, H.X. (2003). "Gray Model GM(1,1, λ)Method for Fitting Relation Curve of Engineering Structure." *Journal of CHANGSHA COMMUNICATIONS UNIVERSITITIY*. 19(3)

Yao, Z.K.(1993). *Pavement management system*. Beijing: China Communications Press.

Zhou, W.X.,LI, M.L.,SUN, L.J.(2006). "Portland Cement Concrete Pavement Performance Prediction Model Based on Improved Neural Network." *Journal of Tongji University(Natural Science)*,34(9)

Experimental Tests and Finite Element Modeling of Shrinkage Behavior in Cement Stabilized Aggregate Base

Qiang LI[1], Fujian NI[2] and Zaixin LI[3]

[1]Department of Civil and Environmental Engineering, Sejong University, 98 Gunja-Dong, Gwangjin-Gu, Seoul, 143-747, Republic of Korea; PH (082) 010-5825-0926; FAX (086)025-83794931; email:lq2526@163.com **(Corresponding Author)**
[2]School of Transportation, Southeast University, Si Pai Lou 2#, Nanjing, 210096, China; PH (086)025-83794931; FAX (086)025-83794931; email: Nifuji an@gmail.com
[3]Baicheng Construction and Investment Ltd, Xiamen, 361009, China; PH (086)0592-8267511; FAX (086)0592-8269500; email: lizaixin.2001@163.com

ABSTRACT:

The objective of this paper is to develop regression functions of material properties based on experimental results and finite element method (FEM) model to simulate shrinkage behavior in cement stabilized aggregate base. Firstly, material properties were obtained from physical property tests. The correlations were established among cement content, strength, modulus and shrinkage coefficients by statistics regression. Secondly, a FEM model was developed to simulate dry and thermal shrinkage in base. Thirdly, a simplified method to predict shrinkage cracking spacing was obtained. Finally, FEM model was validated by comparison analysis with analytical solutions and field observations in roller compacted concrete (RCC) pavement due to similar shrinkage behavior. It is discovered that the strength and shrinkage properties of cement stabilized aggregate have good correlations with the 7-day unconfined compressive strength. It is also observed that from relationships of pavement length and shrinkage stresses, shrinkage cracking spacing can be predicted by FEM calculation. It is proved that proposed FEM model is an accurate tool to simulate shrinkage behavior and prediction results are consistent with actual pavement performance.

KEY WORDS: *Cement Stabilized Aggregate, Property Tests, FEM, Shrinkage*

INTRODUCTION

One of major distresses for cement stabilized aggregate base is shrinkage cracking at the early stages after construction. It appears in the base when accumulated tensile stresses caused by dry and thermal shrinkage reach material

strength. Eventually, cracks would reflect up to asphalt surface under combined effects of traffic, temperature and moisture, and thus accelerate pavement deterioration rate.

There are many factors contributing to shrinkage cracking in cement stabilized aggregate base, such as moisture loss, cooling, interface friction, and material properties, etc.(George,1968). Historically, cement content is accepted as an important factor for shrinkage. Some researchers concluded that shrinkage decreased with increasing cement content, while others indicated that there was optimal cement content existing to minimize shrinkage; however, still others found no relationship between cement content and shrinkage (Sebesta,2005). With regard to theoretical research, the performance and space distribution of shrinkage cracking were analyzed during base construction period (Sun et al. 2003). Based on the elastic theory and concrete strength theory, a theoretical model for predicting thermal cracking spacing in cement stabilized base was developed (Shi et al. 2004).

The goal of this study is to develop regression functions of material properties based on experimental results and FEM model to simulate shrinkage behavior in cement stabilized aggregate base.

MATERIAL PROPERTIES

The 32.5 composite silicate cement and typical gradation of cement stabilized aggregate used in China were selected for tests, as shown in Table 1.

Table 1. Aggregate Gradation.

Sieve Size(mm)	*31.5*	*26.5*	*19*	*9.5*	*4.75*	*2.36*	*0.6*	**0.075**
Percent Passing	100.0	94.7	82.6	54.3	42.0	27.2	13.9	2.5

The following laboratory and filed tests were performed:

- Unconfined compressive strength test: The 150 mm diameter×150 mm height cylindrical specimens sealed in plastic bags at optimum moisture content are kept in standard curing room (temperature=25℃, moisture≥95％), and then immerged in the water for 24 hours before testing.
- Indirect tensile strength (IDT) test: The same specimens as compressive strength test are tested by MTS with a loading rate of 1mm/min.
- Dry shrinkage test: Test system consists of static resistance strain surveying instruments, transform boxes, resistance strain gauges and connection lines. Initial temperature and moisture conditions in the lab were 25℃ and 50％,

respectively. Specimen size is 100 mm length×100 mm (width) × 400 mm (height).

- Temperature shrinkage test: It is operated in high-low temperature cycling box where the temperature decreases from 55℃ to -25℃ with a rate of 1℃/min. When accumulated decrease reaches 10℃, test is paused and temperature is kept constant for 2 hours before restarting.
- Field tests: FWD test is carried out in test pavement sections and cored samples from field are obtained for laboratory strength test.

Empirical correlations among cement content, laboratory strength, in-situ strength, resilient modulus and shrinkage coefficients of cement stabilized aggregate were developed from test results. Using σ_w as an intermediate variable, functions for material properties are shown in Equation (1)-(5). If σ_w or σ_7, which can be obtained more easily from labtests, are known, other parameters such as resilient modulus, shrinkage coefficients and IDT strength can be calculated from these functions.

$$\alpha_d = 1.1688\sigma_w^2 - 21.9181\sigma_w + 151.56 \quad (1)$$

$$\alpha_T = 0.1243\sigma_w + 0.601 \quad (2)$$

$$\sigma_{IDT} = 0.05164\sigma_w^{1.0407} \quad (3)$$

$$\sigma_w = \frac{-161.63 + \sqrt{26124.26 - 140.72(400.5 - E)}}{70.36} \quad (4)$$

$$\sigma_w = 2.4353\sigma_7 = 2.7361X \quad (5)$$

where, σ_w=unconfined compressive strength of cored specimens from field, MPa; σ_{IDT} =IDT strength, MPa; α_d =average dry shrinkage coefficient, 10^{-6}/%; α_T =average thermal shrinkage coefficient, 10^{-6}/℃; E=resilient modulus, MPa; σ_7=7-day unconfined compressive strength, MPa; X =cement content, %.

DEVELOPMENT OF FEM MODEL

The FEM model is based on following assumptions: (1) Mixture for each layer is homogeneous, isotropic and linear elastic, using analysis method of concrete pavement for reference. (2) Dry shrinkage strain distributes evenly in whole base, and (3) thermal shrinkage strain also distributes evenly in whole base. Thus, the model can be simplified to a plane strain problem.

Exponential functions (Wu et al, 1996) were used to simulate temperature distribution, while dry shrinkage stress was achieved by converting moisture loss to temperature decrease with equivalent shrinkage strain. The interface contact friction between base and lower layer has a significant effect on shrinkage stresses in base.

The Coulomb friction model was introduced to simulate interface contact between two layers (Dowson, 2003). The 8-node plane parametric finite element was used for calculation in this research. A contact pair was applied between the base and subbase to simulate interface constraint. A total depth of one meter was modeled since significant effect of temperature variation on pavement structure usually occurred within the thickness. Due to the symmetry, only half of the system needed to be modeled. In order to save calculation cost, mesh was designed to be coarser and coarser from middle to edges, seen in Figure 1. Minimum mess size was 5mm.

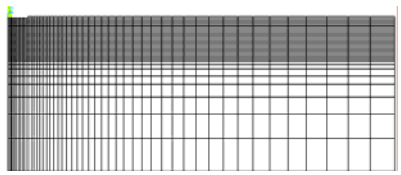

Figure 1. FEM model mess.

DETERMINATION OF SHRINKAGE CRACKING SPACING

In order to determine shrinkage cracking space in cement stabilized aggregate base, relationships of pavement length and shrinkage stresses need to be determined first. Pavement structure used in this analysis consisted of 30 cm base, 30 cm subbase (E-1000MPa, α_T-10^{-5}/℃), and Subgrade (E-60MPa, α_T-2×10^{-5}/℃). The material properties of cement stabilized aggregate base, as shown in Table 2, were calculated from Equation (1)-(5).

Table 2. Material Properties of Cement Stabilized Aggregate.

Structure	Resilient Modulus E (MPa)	IDT Strength R_{sp} (MPa)	Dry shrinkage coefficient α_d (10^{-6}/%)	Thermal shrinkage coefficient α_T (10^{-6}/℃)
1	2000	0.27	70.4	6.7
2	4000	0.45	51.2	7.0
3	6000	0.60	50.4	7.3
4	8000	0.72	60.8	7.6
5	12000	0.93	115.9	8.2

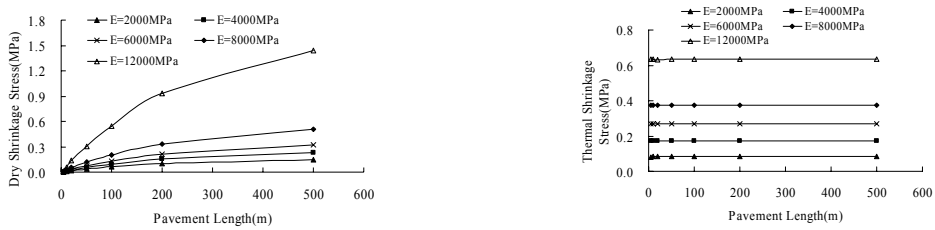

(a) Dry shrinkage stress (Δw=1%) (b) Thermal shrinkage stress (ΔT=10℃)

Figure 2. Effect of pavement length on shrinkage stresses.

Figure 2 shows that higher dry shrinkage stress tends to occur in longer base, while there is negligible effect of thermal shrinkage stress on pavement length. Thus, if no-cracking section is shorter than a certain value, shrinkage stresses can be controlled below tensile strength, which can be utilized to predict shrinkage cracking spacing in cement stabilized base. In other words, shrinkage cracking spacing is the same as critical pavement length in which shrinkage stresses are equal to material tensile strength under certain shrinkage condition. The fracture criterion is expressed by failure stress, as seen in Equation (6).

$$\gamma_r \sigma_m \le \sigma_{IDT} \tag{6}$$

where, σ_m=shrinkage stress, MPa; σ_{IDT} =IDT strength, MPa; γ_r= reliability coefficient 1.20-1.33 for the 95% target reliability.

Using this FEM model, a sensitivity analysis was performed and the results indicated that the base course with lower modulus has less shrinkage cracking and there are no radical changes in shrinkage stresses with different intervals of construction time between asphalt surface and base (Ni et al, 2008).

VALIDATION OF FEM MODEL

The accuracy of theoretic methods for shrinkage prediction in RCC has been well documented in previous studies (Yu et al, 1997). Because of lack of field data on cement stabilized aggregate base and in order to validate the proposed FEM model, a RCC pavement, due to similar shrinkage behavior, was employed as a trial object. The comparison of predicted results by FEM model with existing theoretic solutions and field observations could be used to judge the accuracy of the model. Only dry shrinkage was considered in this simulation since it is the key factor to determine the slab size for RCC. Analytical solutions of shrinkage stress were obtained from thermal stress equations for pavement slab induced by interface friction (Zhu et al, 1985), substituting dry strain for thermal strain. The selected pavement structure for simulation consisted of 24 cm RCC (E-33000MPa,

α_d-2-4×10^{-4}/℃), 15cm lime-fly-ash stabilized base (E-1500MPa, α_d-8×10^{-5}/℃) and subgrade (E-60 MPa). It was assumed that moisture of RCC pavement changed from the optimum moisture content 5.5% to final state 2%.

Table 3. Comparison of FEM and Analytical Solutions.

Shrinkage coefficients (10^{-6}/%)	Slab length (m)	FEM Solutions (MPa)	Analytical Solutions (MPa)	Error
200	5	0.544	0.564	3.7%
	10	1.315	1.352	2.8%
	15	2.214	2.150	-2.9%
	20	3.332	3.492	4.8%
300	5	0.815	0.844	3.5%
	10	1.969	1.993	1.2%
	15	3.316	3.217	-3.0%
	20	4.989	4.949	-0.8%
400	5	1.089	1.141	4.8%
	10	2.63	2.564	-2.5%
	15	4.429	4.495	1.5%
	20	6.666	6.713	0.7%

For engineering practice, Table 3 shows that FEM model is accurate enough to simulate shrinkage stresses in pavement, since maximum relative error is less than 5%. As general tensile strength of RCC is 2.9MPa, predicted control slab lengths is 18.2m, 13.4m and 10.7m for shrinkage coefficients 200×10^{-6}/%, 300×10^{-6}/% and 400×10^{-6}/%, respectively. Transverse shrinkage spacing in field is often between 10m and 20m for RCC (Yu et al, 1997). Thus, it is proved that the simulation results are consistent with actual pavement performance.

CONCLUSIONS

From many lab and field experiments of cement stabilized aggregate, 7-day unconfined compressive strength, which can be obtained easily in the lab, is found to have good correlations with other parameters and can be used to predict strength and shrinkage properties as an intermediate variable. From the FEM analysis, it is found that higher shrinkage stresses occur in longer base. Thus, in combination with failure stress, relationships of pavement length and shrinkage stresses are introduced to predict shrinkage spacing cracking in cement stabilized aggregate base. Verified by research results in RCC pavement, the proposed model is proved to be an accurate tool to simulate shrinkage behavior in pavement.

REFERENCES

Dowson, D., (2003). *History of Tribology*, Longman Ltd, London.

George,K.P.(1968). "Final Report on the Study of Criteria for Strength and Shrinkage Control of Cement-Treated Bases", *University of Mississippi*, Oxford.

Ni, F.J., LI, Q., GU, X.Y., and LI, Z.X.(2008). "Prediction Model for Shrinkage Cracking Spacing of Cement Stabilized Base" in *Transportation Research Board 2008 Annual Meeting*, Washington, D.C., Paper 08-0716.

Sebesta.S.(2005). "Use of Microcracking to Reduce Shrinkage Cracking in Cement Treated Bases", in *Transportation Research Board 2005 Annual Meeting*, Washington, D.C., Paper 05-0805.

Shi, W.M. and Jiang, Z.S. (2004). "Research on the Calculation Method of Temperature Stress of Cement Treated Crushed Stone Base and the Method of Controlling Temperature Shrinkage Crack". *Journal of Highway and Transportation Research and Development* 21(4) 23-27.

Sun, T.B. and Cong, L. (2003). "A Study on Drying Shrinkage Procedure of Semi-rigid Base Coarse during Construction", *Highway* 712(3) 111-115.

Wu, G.C., and Zhang, G.S. (1996). "Thermal Stress Intensity Factor Analysis for Asphalt Concrete Pavement", *China Journal of Highway and Transport*. 9(1) 37-44.

Yu, J.R and Chen, R.S. (1997). "Plane Size of Roller-compacted Concrete Pavement Plate with Asphalt Overlay", *China Civil Engineering Journal.* 30(2) 56-62.

Zhu, Z.H., Wang, B.G. and Guo, D.Z. (1985). *Pavement mechanics calculation*, China Communications Press, Beijing.

Research on Automatic Identification Method of Pavement Sag Deformation

Wang Jiaqiu[1]; Ma Songlin[2] ; Jiang Li[2]

[1]Department of Mathematic and Mechanism， Heilongjiang Science and Technology Institute，Harbin 150027, P.R. China; PH:86-13945050837；Email: wjqqiu@163.com

[2]School of Transportation Science and Engineering, Harbin Institute of Technology, Haihe Road 202, Nangang District, Harbin 150090,P.R.China;Tel.：86-451-86282120; Fax ： 86-451-86283779; E-mail: masonglin@hit.edu.cn

ABSTRACT

In order to identify pavement sag deformation automatically，this article proposed an automatic identification method of pavement sag deformation: fitting base level method based on assumption pavement flatness. This method is based on the 3-D data collected by automatic pavement distress detection system, and the theory in mathematics morphology: how to identify the character of vertex in concave/convex polygon. The automatic identification of pavement sag deformation can be realized by using this method. In this method, the influence like rutting, cracking etc. on the identification progress was excluded. A computer programme was compiled for automatic identification, location, classification, area calculation and graduation of pavement sag deformation. The method and compiled programme were examined by comparing data of programme and data of actual measurement in pavement sag deformation. The result shows that this method can reflect the actual configuration of pavement sag deformation and perceive the parameters of the sag deformation accurately.

INTRODUCTION

There will be a variety of road damage when asphalt pavement is in use, and sag deformation is one of pavement damages. Sag deformation will have negative impact to the road and traffic. For example, excessive deformation would affect pavement roughness; rain water depressed region could lead to vehicle drift slide and impact on traffic safety; at the same time, water easily penetrate into the pavement, and induce other damage. To ensure good pavement performance, traffic safety & riding comfort, and carry out maintenance of pavement in a timely manner, it is necessary to collect information on pavement damage timely and accurately (David.H.K et al. 1997).

Compare with other pavement damage like pavement cracking, rutting, it is more difficult to detect and identify pavement sag deformation. The realization of automatic identification sag deformation is conducive to accurate and automated data processing of the pavement, as well as to develop countermeasure of pavement maintenance for scientific basis. Apart from the manually identification, the pavement photo information is used as the main method to identify sag deformation (Jiebo Luo et al. 2002). And the researchers used digital image processing technology, pattern recognition, neural networks, mathematical morphology and other methods to conduct in-depth study. Because of complicated reasons for road surface deformation and diversity of sag deformation, the existing methods are complex to use. In addition, poor real-time data, difficult to classify and accuracy for recognition do not meet use requirements (Rucckert D. et al. 1996, Serve Belongie 2002). Thus, this paper proposed an identification

method of pavement sag deformation: fitting base level method based on assumption pavement flatness.

SPECIATION ANALYSIS OF SAG DEFORMATION

Pot hole and depression are the basic types of sag deformation. For pot hole the elevation change in is relatively small in damaged area, but the elevation change is relatively large in damaged edge and non-damaged areas. For depression the elevation changes slowly in depression area; elevation change is small between adjacent points; and the difference of elevation between edge area and non-depression area is not significant. Because pavement depression is mainly caused by sub-grade depression or pavement structural damage, deformation of the scope usually is larger.

AUTOMATIC IDENTIFICATION METHOD OF PAVEMENT SAG DEFORMATION: FITTING BASE LEVEL METHOD BASED ON ASSUMPTION PAVEMENT FLATNESS BASIC DATA

The pavement surface elevation data comes from three-dimensional data acquired by the integrated road surface detection system. Data form is that horizontal & vertical spacing of 20cm; and detection width in the road cross-section is 3m. Rows and columns of the matrix elements correspond to measuring point elevation values of the road cross-section and the longitudinal section respectively. The impact of longitudinal gradient of the road can be ignored because the data collected is the relative difference of the uneven pavement and longitudinal gradient impact of the road offsets each other in the difference. The impact of road cross slope can be ignored also (Tsai Du Ming, 1997).

BASIC IDEA OF AUTOMATIC IDENTIFICATION METHOD OF PAVEMENT SAG DEFORMATION

The algorithm is by simulating the original pavement design lines, the original calculation of the road line and the actual measured surface elevation points online counterparts to determine the points of the embossing; thus the number of lines constitutes a cross-section mesh-like surface. Given a minimum depth of depression and minimum area threshold, depression can be identified. The level of depression is classified by the maximum depth value and the area value. Algorithm process is shown in **Figure 1**.

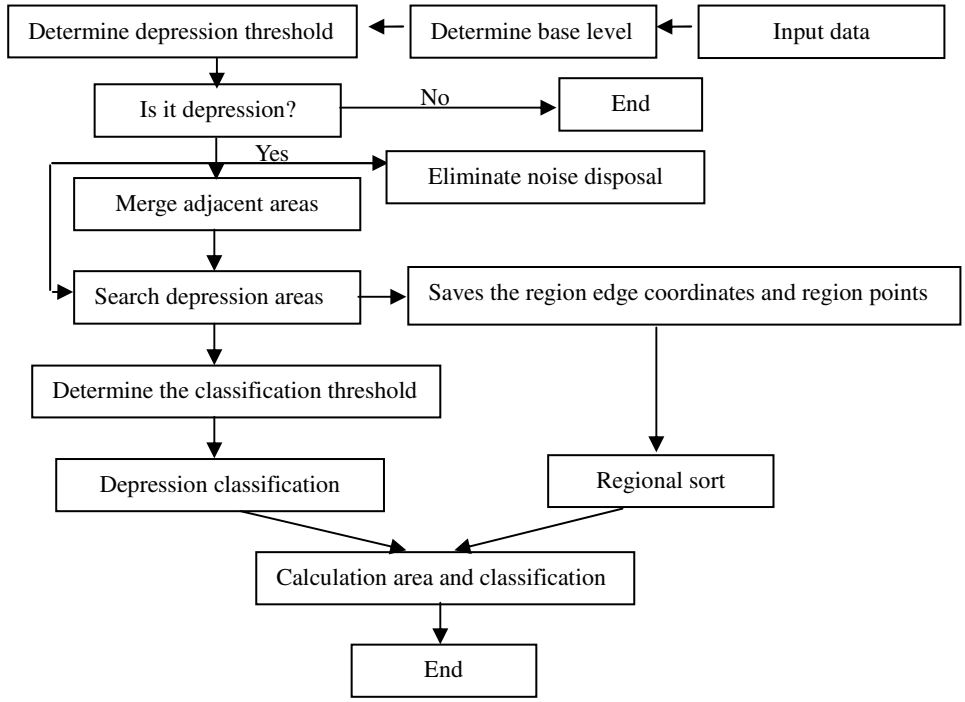

Figure 1. Algorithm flow chart of automatic identification

BASE LEVEL DETERMINATION

It is assumed that the average value measured in the longitudinal direction (longitudinal section) is as the original surface elevation line. Because of existence of a lot of small depression and rut, local data would have large deviation impact for fitting results. Hence it is needed for an amendment to the value. First calculate the average value and standard deviation of every longitudinal elevation, and then amend three-dimensional data on the road by using the method of 2 times square deviation.

$$\overline{h^j} = \frac{\sum_{i=1}^{n} h_i^j}{n} \qquad (1)$$

$$\sigma^j = \sqrt{\frac{\sum_{i=1}^{n} \left(h_i^j\right)^2 - \frac{\left(\sum_{i=1}^{n} h_i^j\right)^2}{n}}{n-1}} \qquad (2)$$

Note: h_i^j — elevation data of measure point i (i =1,2,……,n) in jth longitudinal section(j=1,2,……,m)

$\overline{h^j}$ 、 σ^j — average value and standard deviation of h_i^j

n — the number of measure point in every longitudinal section

m — the number of measure point in every cross-section(the number of longitudinal section)

Method of amendment:

When $h_i^j > \overline{h^j} + \sigma^j$, $h_i^j = \overline{h^j}$

When $h_i^j < \overline{h^j} - \sigma^j$, $h_i^j = \overline{h^j}$

When $\overline{h^j} - \sigma^j \le h_i^j \le \overline{h^j} + \sigma^j$, $h_i^j = \overline{h^j}$

The amended data would be used of cubic polynomial fitting and the data after fitting would be used as base level data. As seen from Figure 2, the curve on behalf of the original road changes is in the larger bump. If the datum directly fitting, then the larger part of the value of the convex-concave fitting results have a greater impact. Thus it is necessary to amend the data, remove the impact of embossing in larger parts, and make longitudinal section curve to be shown as a smooth curve which close to the design line of the road. Finally a number of longitudinal and cross section fitting base level line of the road constitute a fitting base level.

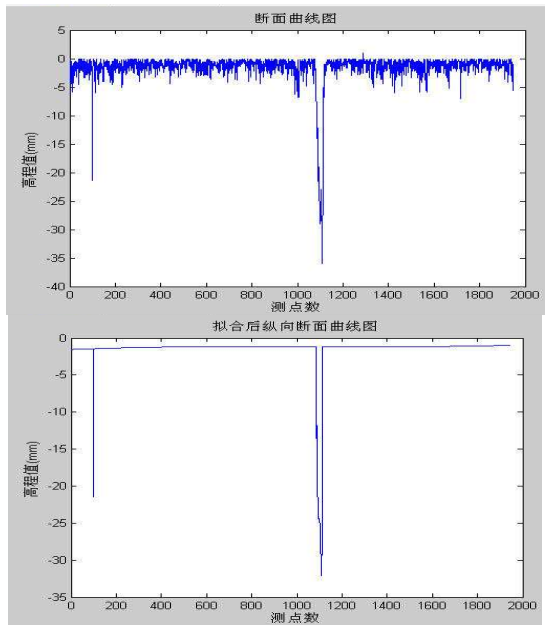

(a) Longitudinal section before fitting (b) Longitudinal section after fitting

Figure 2. Comparison of longitudinal section before & after fitting

IDENTIFICATION OF SAG DEFORMATION

After determining the base level of assumption, the high-margin data of corresponding points between base level and actual measurement data would be calculated. If the difference is greater than the minimum depth of depression, it is deemed to be one of the points in the depression region and it would be recorded. This article assumes that the minimum depth of depression in line with the normal distribution and mathematical Statistics 3σ theory would be used as original data for testing. When 3σ and 5σ are used respectively as a minimum depth of surface depression to identify the value of the results in comparative analysis, the result shows that when the value of the minimum depth is 5 times the standard deviation, the identification accuracy is higher, and it is in line with the true extent of the traffic. Therefore when difference of which corresponding points between base level and actual measurement data of road curves greater than 5 times the standard deviation, the point would be considered as feature point in depression area.

DETERMINATION OF THE EDGE OF DEPRESSION

Because of the depression minimum depth value has some limitations; it can be used to identify significant regional of sag depression only and sometimes it cannot reflect the actual border of sag depression completely. The elevation

changes of original position in depression edge are often in the framework of pavement roughness, but it belongs to a point in depression area. Therefore secondary search is used in algorithm for such areas in marginal depression. The performance for such a depression is shown in Figure 3.

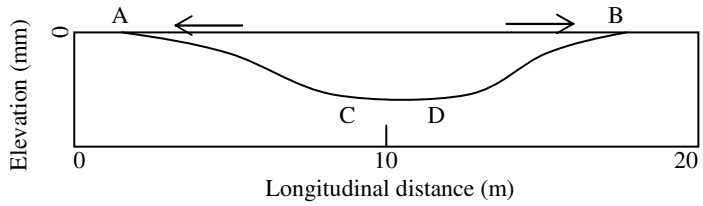

Figure 3. Depression form

As it can be seen from Figure 3, the trend of elevation changes in the edge of the depression regional is the same as its adjacent area, but the elevation changes is smaller of prior one. Based on this result, this method is used in edge searching in depression area of this algorithm (e.g. searching edge changing point A and B). Coordinates C and D are starting points in recorded depression area and the searching direction is along the arrow. From points C, D out, the elevation difference between previous coordinate point and next coordinate point is calculated point by point. If the difference is more than 0, then it means that the trend of elevation changes of these two points is the same as previous two points. Keep calculating till the difference closed to the given threshold. Then recording the last point of the two points; this point is the final point of the edge of the depression.

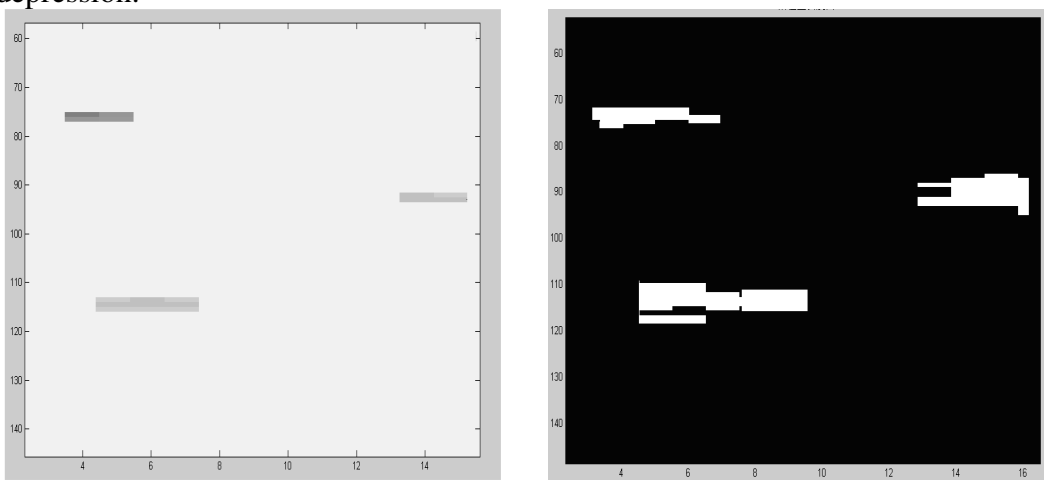

(a) Before searching edge changing point (b) After searching edge changing point

Figure 4. Depression area (abscissa: cross-sectional measurement points; ordinate: longitudinal section measurement points)

From figure 4, it can be seen that there is less data in depression area before searching edge changing point. The reasons are: the minimum depression determining value provided by algorithm is relatively big; only the significant deformation of depression area would be identified; the slight deformation of depression area may be ignored. After searching edge changing point, there is more slight depression can be identified. Thus recognition effect and calculation accuracy of depression are increased.

DEPRESSION CLASSIFICATION

By comparing the elevation changes between edge of depression region

and edge of non-depression region, pot hole and depression can be identified. The main difference between pot hole depression and depression is reflected in the depth of its marginal changes. In this paper, the edge density factor λ (formula 3) is used to determine the type of depression. When the density factor λ larger than 5, the point (i, j) would be recorded. By comparison of a large number of the actual pot holes and depression in edge area, it is defined that the depression area is pot hole when these points are more than 80% of the total number of border points; otherwise it is defined to be depression. After a large number of calculations and artificial identification test comparison, it is proofed that this method is good for identification.

$$\lambda = \frac{\Delta h_i^j}{\Delta h_i'^j} \quad \text{(i= 1,2,3,……,n)} \qquad (3)$$

Note: λ —depression edge density factor

Δh_i^j —elevation changes of row i, column j in depression area

$\Delta h_i'^j$ —elevation changes of row i, column j in the edge of non-depression area

CALCULATION OF DEPRESSION AREA

The data spacing is 0.2m, and every measure point represents a square with side length of 0.2m. So every measure point represents 0.04 m2 and the depression area S is equal to the cell area times the number of measure points.

$$S=0.2 \times 0.2 \times n \qquad (4)$$

CONCLUSION

Based on the research of characteristics of pavement sag deformation, this paper proposed minimum depth of depression and edge density factor as the characteristic parameters for identifying and classifying depression and fitting base level method based on amendment of 2 times square deviation. By using this method, it can realize automatic identification, location, classification, area calculation and graduation of pavement sag deformation. It is simple and fast to get the result. After a large number of calculations and artificial identification test comparison, it is proofed that this method is good for identification.

REFERENCES

David.H.Kil, Frances B.(1997). “Shin.Automatic Road-Distress Classification and Identification Using a Combination of Hierarchical Classifiers and Expert Systems-Subimage & Object ”;Processing.IEEE,414~417, 1997.

Jiebo.Luo, Stephen. (2002). “A Photographic Images Physical Model-Based Approach to Detecting Sky Transaction on Image.” ,Processing. IEEE,ll(3),201~212, 2002.

Rucckert D, Urger P. (1996). “Shape-based Tracking and Analysis of the Aortic Cardiac MR Images Using Geometrically Deformable Templates. ”, Computer Assisted Radiology, (6), 274~279, 1996.

Serve Belongie, Jitendra Malik. (2002). “Shape matching and object recognition using shape contexts.” IEEE Transactions on Pattern Analysis and Machine Intellinence,24(24), 509~521, 2002.

Tsai Du Ming. (1997). “Boundary2 based corner detecting using neuralnet works.” Pattern Recognition,30(1), 85~97, 1997.

The Experimental Study of Effects of Herbaceous Plant Protecting Slope in Cold Area

WANG Hai-biao[1] and JIANG Bi-feng[1] and Dong Xi-bin[1] and Yang Hai-xu[2]
[1]School of Engineering Technique, Northeast Forestry University. email: whbcumt@163.com.Harbin,China
[2]School of Civil Engineering , Northeast Forestry University; Harbin ,China;

ABSTRACT

Five kinds of herbaceous plants commonly distributed in cold regions were selected as experiment plants for protecting slopes. According to the study of coverage, proportion of the root system, and shear strength of root-soil composite in the growth period of plants, the affectivity of slope protection of herbaceous plants in cold regions was verified. By experimentation of the root system, the Lucerne and June grass have a large extent of root system sand robust main roots. In the experiment of the shear strength of root-soil composite, the Lucerne had the largest shear strength and was followed by the White clover. The results of experiments verified that the herbaceous plants selected with good adaptability could protect slopes and enhanced slope stability, which produces better landscape effects under representative soil conditions in cold regions.

Key words: cold region, herbaceous plant, slope protection

Since slope protection using plants can effectively decrease noise and light pollution, it has a significant impact on reducing drivers' fatigue and ensuring traffic safety, promoting the degradation of organic pollutants, purifying the atmosphere and regulating micro-climate, and so on. In September 1994, the first international conference specifically for the slope protection plants was held at Oxford University, which marked that slope protection using plants had been paid extensive attention in the world by the academic community. The conference also effectively enhanced the awareness of using vegetation in slope protection, restoring the damaged eco-environment, and set up an idea to study systematically the plants in slope protection. This paper selected five kinds of herbs that are commonly used for slope protection in the north to carry out the experimental study systemically on plants for slope stability. The study results of this paper can provide scientific and effective methods and technique bases for road slope protection in cold regions.

1 Experiment site

The experiment site is located in the experimental forest farm of Northeast Forestry University in Harbin, Heilongjiang Province. Harbin City is located in south of Heilongjiang Province, Northeast China (125°42' - 130°10' E, 44°04' -46°40' N). It is dominated by the temperate continental monsoon climate with long winters and the short summers. It has four distinct seasons in the year. The annual mean temperature

was 3.1 ℃, the extreme minimum and maximum temperatures reached -41.1 ℃ and 36.2 ℃ respectively, the annual average rainfall was 400-600mm, and the annual frost-free and ice period was 150d and 190d respectively.

The slope gradient of the experiment site was 1:1.5 and the soil was clay soil, which is a common type in the Northeast. The soil was measured by the potentiometry method to be alkaline with a PH value of 8.69. The organic matter content was measured by the ferrous sulfate titration method (GB7848-7858-87) to be 1.198%. These measurements showed that the slope soil has low nutrients and a strong alkaline, which is the common after-construction soil of the highway slopes in Heilongjiang.

2 Coverage of herbaceous plants

The highway vegetation has the functions of cutting off rainfall and reducing the landslides in shallow slopes[5]. The herbaceous plants and litters may decrease the sediment loss of the slope surface. If there was no vegetation cover on the slope, the runoff capacity carrying sediment is enhanced. The greater the coverage the less the carrying sediment content with runoff. The herbaceous plants and litter on the slope increased the surface roughness, thereby reduced sediment loss. A good herbaceous vegetation cover on slope can effectively control runoff and reduce soil erosion, which plays an important role to protect the slope. The function can be described as equation 1.

$$E = \begin{cases} veg \cdot p & (P \le P') \\ E' & (P > P') \end{cases} \qquad (1)$$

Where, E is rainfall cut off by vegetation, veg is vegetation coverage, E' is maximum cut-off rainfall, P' is critical rainfall, and P is rainfall.

For each species, the acupuncture method was employed every month to measure the plant coverage after grass seed germinating.

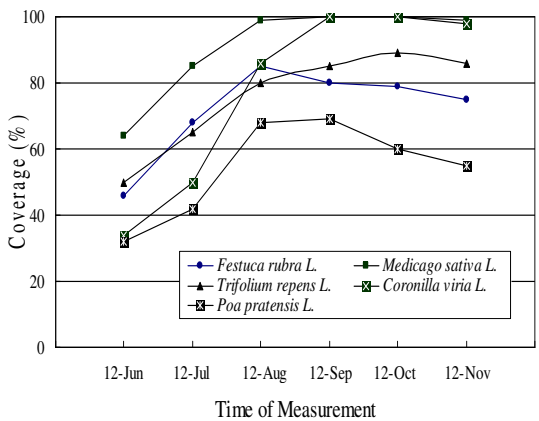

Experiments showed the overall trend that the coverage of all grass species increased first and decreased afterwards. The first measure was carried out in June 12, 2006 while plants were still in the seedling stage, so the coverage values for all species were relatively low. During July and August, with good rainfall condition, all plants grew fast and the coverage increased rapidly, approaching or reaching the maximum. **Figure1 Grass coverage in different periods.** At Harbin, the temperature started to drop in September and the average temperature was less than 10℃ from then on. During this period, the metabolism ability of plants was lower and coverage no longer increased. With further temperature drops, the coverage

lowered slightly while plant leaves started to become yellow, wilt, and the plants even died. The measurement results of each grass species showed that, the coverage of *Medicago sativa L.* is in a leading position followed by that of *Coronilla varia L.*, *Trrifolium repens L* and *Festuca rubra L.*, and the last one is that of *Poa pratensis L.*

3 Proportion of herbaceous root system

The shape of the plant root system affects the touching area between roots and soil, consequently the shear strength of soil-with-roots. L. DUPUY and T. FOURCAUD conducted the detailed studies with regard to this. They analyzed the deformation angle of roots, the number of fibers, touching area of root-soil, root volume, root diameter, and other factors on the ability of resisting pullout power and accordingly evaluated the root capability to stabilize soil. Our experiment started from September 12, 2007, and the root systems of all alternative plants were extracted and shown in Figure2 to Figure 6.

Figure2 ***Festuca rubra L .root.***

Figure3 ***Rrrifolium repens L root.***

Figure4*Coronilla varia L. root.*

Figure5 ***Poa pratensis L root.***

Figure6 ***Medicago sativa L .root.***

Table1. Status of the root system of different herbs.

Herbs	Root density (Five-month growing period)	Fibre (or root)diameter/ mm	Root status
Festuca rubra L.	97-98% of roots distributed within 0-50cm depth of soil, and only about 2-3% of roots distributed in greater than 50cm depth of soil.	<0.2	Developed fibres
Poa pratensis L.	95-97% of roots distributed within 0-50mm depth of soil, and only about 3-5% of roots distributed in greater than 50cm depth of soil.	3.0-5.0	Robust main roots, and more lateral roots
Trrifolium repens L.	Roots distributed in the soil within 0-10cm depth, and the root density steadily declined as soil depth increasing.	1.5-2.0	Obvious main roots, and developed lateral roots
Medicago sativa L.	85-90% of roots distributed within 0-30cm depth of soil, and the root density declined rapidly within 30-50cm depth of soil.	3.0-5.0	Robust main roots, and less lateral roots
Coronilla varia L.	88-92% of roots distributed within 0-30cm depth of soil, and the root density declined rapidly within 30-50cm depth of soil.	<0.2	More fibres

4 Principles of slope protection using herbs

Losing stability, which leads to soil slide, is mainly due to weakened soil shear strength. Many scholars found that by mixing a small amount of reinforcement materials the shear strength of soil can be significantly improved[7]. Herbaceous roots distribution can reinforce soil just as the same as fibers do, and their acting model is shown in Figure 7.

From the observation of the plant root system, we could find that herbs root system can fully access soil particles and had apparent effects on reinforcing soil. Study on root-soil composite shear strength may explain the mechanics action of stabilizing soil and slope by the root system and further reveal the soil mechanics performance of stabilizing soil and slope by trees and herbaceous vegetation.

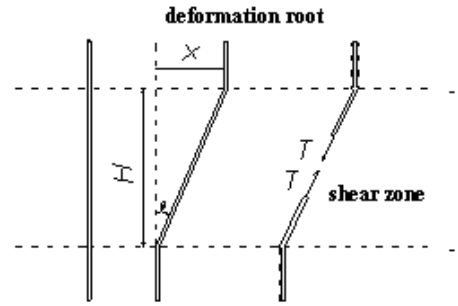

Figure7 Interaction model between single root and soil.

The root-soil composite shear strength is in line with Coulomb's law and it is described as equation (2):

$$\tau = c + (\sigma - \mu)\tan\varphi = (c_0 + \Delta c) + \sigma(\mu \quad)\tan(\varphi_0 + \Delta \quad) \qquad (2)$$

The paper analyzed the stress state of slope soil according to the principle of reinforced soil, which considers the soil distribution as the three dimensional fiber-reinforced distribution. This reinforcement provided additional cohesion Δc for soil. On one hand, it moved the original shear strength of soil up over in distance Δc; on the other hand, the maximum shear stress decreased due to limiting the lateral expansion of soil. Both actions improved the loading capacity of slope soil.

5 Experiment of soil moisture content

Soil moisture content very closely relates to both slope stability and strength. Before the experiment, the soil moisture content of each experiment point was calculated by averaging three measures at the same point. Meanwhile, using the same method, the soil moisture content of the upper, central, and lower part of the slope were measured. It can be seen that the soil moisture contents of experiment slopes were sorted as follows: slope soil without vegetation >*Coronilla varia L.* >*Festuca rubra L.* > *Trrifolium repens L.* > *Poa pratensis L.* > *Medicago sativa L.*

The water consumptions of different plants were varied since their rates of photosynthesis were different. Moreover, the rainfall cutoff and surface runoff were varied among different plants due to the different vegetation coverage. Furthermore, the slope soil moisture content was affected. The moisture contents of tested soil with *Festuca rubra L.*, *Trrifolium repens L.*, *Poa pratensis L.* and *Medicago sativa L.* were similar, *Coronilla varia L.* was higher.

4 Shear experiment

Starting from September 12, 2007, we extracted the soil samples with roots of the site-planted herbs from depths of 0-50cm underground. Soil samples with roots were

used for the shear experiment and comparing the shear strength of soil-with-roots of herbs. In this experiment, the non-consolidated and un-drained fast-shear mode was employed and the speed of the electric hand wheel of the direct-shear instrument was 4r/min. For each of the four soil samples, this test was carried out at 5kPa, 10kPa, 15kPa and 20kPa, respectively, under the vertical pressure.

(1)Experiment data

In the experiment, the shear stress was equal to the dynamometer readings multiplied by the dynamometer coefficient. The stress-strain relationship diagram was established using shear stress as the horizontal axis and shear displacement as the vertical axis. We considered the shear stress peak in curves as the shear strength of soil samples under the corresponding vertical pressure. Under the vertical pressure, the root-soil composite shear strength of 4 duplicate experiments for each herb is shown in Figure 8.

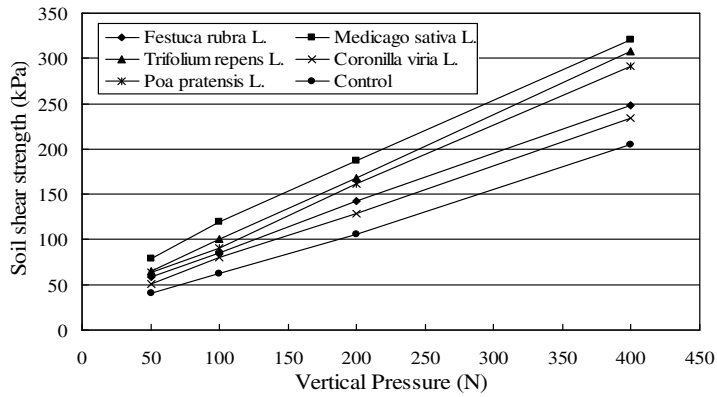

Fig8 Shear strength curves of soil-with-roots and soil-without-roots of herbs.

Table2 Equations of shear strength curves of different soil-with-roots.

	Linear expressions of shear strength	Correlation coefficient	Effective cohesion *c* /kPa	Internal friction angle /(°)
Festuca rubra L.	y_1=0.5446*x*+31.297	0.9995	31.297	28
Medicago sativa L.	y_2=0.6808*x*+48.852	0.9995	48.852	34
Trrifolium repens L.	y_3=0.6932+30.741	0.9999	30.741	34
Coronilla varia L.	y_4=0.519*x*+26.084	0.9994	26.084	27
Poa pratensis L.	y_5=0.6545*x*+29.194	0.9993	29.194	33
Soil-without-roots	y_6=0.4726*x*+14.657	0.9991	14.657	25

(*x* represents the vertical pressure, and y_i (*i*=1、2、3、4、5、6) represents the shear strength of different herbs)

(2) Data analysis

There were shear strength differences between samples of soil-with-roots and soil-without-roots. With increasing vertical pressure, the shear strength of each soil increased; the shear strength differences among soils increased also. From individuals, the shear strength of *Medicago sativa L.* was higher under each of the

vertical pressures, so its shear strength line is always at the top. It is followed by *Trrifolium repens L.*, *Poa pratensis L.*, *Coronilla varia L.* and soil-without-roots respectively. The effective cohesion *c* of soil-with-roots was significantly higher than that of soil-without-roots, which agreed with many other scholars' conclusion that plant roots can enhance the soil shear strength.

5 Conclusions

Slope protection plants on roads can effectively reduce the slope surface erosion and reduce the sliding of shallow slopes. Within the range of roots entangled, the soil with roots can be seen as composite material of soil and roots. The roots of the herbaceous plants played the same role as the fiber did. The number of roots contained in the soil of per unit volume is varied from the herb species. The greater number of roots, the greater the soil shear strength. Roots can not only improve soil cohesion but also improve the friction angle of soil, thereby increasing the shear strength of soil and enhancing the stability of the slope. All these indicators showed that, among all alternative herbaceous plants, the *Medicago sativa L.* is the most suitable species to protect the highway slopes in cold regions.

In the work of slope protection, in order to meet the requirements of road slope stability and landscape, we can determine the protection of plant varieties, planting plants, and reasonable configuration of the shrubs and herbaceous plants from the basis of scientific data.

Reference

Cheng Hong, Xie Tao etc. Overview of mechanism of plant poots improving soil reinforcement and Slope stabilization[J]. Bullentin of Soilland Water Conservation, 2006,26(1) :97~102

Fu Haifeng, Jiang Zhiqiang, Zhang Shufeng. Numerical simulation of root reinforcement to stability of slope[J]. Bullentin of Soilland Water Conservation, 2007,27(1)：92~98

He Hongliang，Wang Qiong，Yang Zhijian，Yan Jingcai. Slope vegetation：present situation and its Prospcet[J]. Central South Highway Engineering, 2007,32(2): 150~153

Liu Xiangdong, Wu Qinxiao ect. Vertical interception of forest plants acts on conservation of water and soil[J]. Research of Soil and Water Conservation, 1994, 1(3): 8~13

Song Yun. The research on the mechanism of vegetation for slope stailization and the design and management of the vegetation[D]. South Central Forestry College, 2005 :3

Tian Jia, Liu Yaohui. Mechanics characteristic of root system of some plants commonly used for slope afforestation in North China Region[J]. Soil and Water Conservation in China, 2007(10)：34~36

Effect of Inorganic Salts on Frost Resistance of Concrete

Yong Ge[1], Wencui Yang[2], Jie Yuan[3], Baosheng Zhang[4]

[1]School of Transportation Science and Engineering, Harbin Institute of Technology, 202 Haihe Road, Nangang District, Harbin 150090, P.R. China; PH (86)45186282191; email: [1]hitbm@163.com, [2]keriy@126.com, [3]hityuanj@163.com, hitzbs@163.com

ABSTRACT

Effects of water-binder ratio and inorganic salt additive，including NaCl, $NaNO_2$ and Na_2SO_4, on frost resistance of concrete were investigated using the orthogonal experimental test. There were two criteria, i.e., the relative dynamic elastic modulus (RDEM) and weight loss that can be used to evaluate the resistance of concrete subjected to fast freeze-thaw tests. The results show that the effect of water-binder ratio on frost resistance of concrete is obvious and that the salts have different effects: adding NaCl and Na_2SO_4 into concrete decreases frost resistance and that the worst effect occurs when the dosage of NaCl and Na_2SO_4 is about 0.5% and 1.25% of cement, respectively. Adding $NaNO_2$ into concrete improves frost resistance but the effect is not obvious. The influential effects of these salts are ranked to be NaCl>Na_2SO_4>$NaNO_2$.

INTRODUCTION

In cold regions of China, chemical admixtures are widely used in concrete as antifreeze agents or high-early strength agents including many inorganic salts such as chloride, sulfate, nitrite, nitrate, carbonate, and some organic admixtures such as triethanolamine, formate, acetate, propionate (Wang 2005, Chen 2004). In fact, some inorganic salts used as high-early strength agents can improve hydration of cement and increase the early strength of concrete; some inorganic salts used as antifreeze agents can lower freezing point of solution in pores and make concrete ice-free before hardening. However, inorganic salts also cause some problems. For example, steel corrosion of reinforced concrete structures is usually enhanced by chlorides used as traditional antifreeze agents. Studies on alkali-silica reaction, corrosion of steel induced by chlorides and effect of corrosion inhibitors have been reported (Sideris 2005, Tritthart 2001, Muralidharan 2004, and Rivard 2003).

Orthogonal test is a mathematical method to carry out multifactor experiments. It is based on the principle of statistics and orthogonal theory. Orthogonal tests select sufficient typical and representative sample tests to analyze the relationship among the factors and the test results. Orthogonal test is widely used since it could handle a complex issue with much lower cost and less time. There is a series of orthogonal tables in correspondence with different amounts of factors and values. Different orthogonal tables are applied when the numbers of factors or values are different.

Frost resistance of concrete is very important in cold weather and is affected by inorganic salts when antifreeze agents or high-early strength agents are used. Research of concrete deterioration due to freeze-thaw action in Heilongjiang province and east of Inner-Mongolia showed that deterioration of concrete with high-early strength agents or antifreeze agents was more severe. Within this context, frost resistance of concrete containing inorganic salts was investigated by orthogonal experimental test in this study.

EXPERIMENTAL PROCEDURE

Scheme of the experiment. Orthogonal tests were applied to analyze the influence of four factors on the frost resistance of concrete. Experimental factors to be considered were water-binder ratio, NaCl dosage, $NaNO_2$ dosage, and Na_2SO_4 dosage. Four levels of each factor should be mentioned. According to the orthogonal tables, $L_{16}(4^5)$ orthogonal table was applied in this paper. Experiment schemes used are shown in Table 1.

Table 1. Orthogonal table, $L_{16}(4^5)$, for frost resistance of concrete

Factors / Levels	*W*/*B*	NaCl dosage (%)	$NaNO_2$ dosage (%)	Na_2SO_4 dosage (%)	Blank
1	0.55	0.0	0.0	0.0	—
2	0.42	0.50	1.0	0.50	—
3	0.34	1.25	2.0	1.25	—
4	0.26	2.00	3.0	2.00	—

Materials and mix proportions. The raw materials used in test and their properties are shown in Table 2. A series of non-air-entrained concrete were prepared with water-binder ratio values of 0.55, 0.42, 0.34 and 0.26, respectively. The water-reducing agent dosage was adjusted to keep the slump of fresh mixed ordinary concrete in the range of 70mm~90mm. The proportions of concrete mixes are given in Table 3.

Table 2. Raw materials and properties.

cement	Chinese standard 42.5 ordinary Portland cement
river sand	fineness modulus of 2.49 and apparent density of 2590kg/m^3
crushed basalt stone	maximum size of 20mm and apparent density of 2740kg/m^3
Grade I fly ash	15% weight replacement for cement
water-reducing agent	Naphthalene-type water-reducing agent, UNF-5

Samples and testing programs. The specimens with size of 100mm×100mm×200mm were cast for each mixture. All specimens were demolded 24 hours later and cured for 24 days in standard condition (20±2℃ and 95% RH), and then immersed in water for 4 days before being subjected to freezing and thawing cycles. Three specimens were tested for each mixture. The sound velocity and weight

of the specimens were measured at different freeze-thaw cycles. The relative dynamic modulus of elasticity (RDEM) is the ratio of the dynamic modulus of elasticity for a certain cycles to the initial value before subjected to freeze-thaw cycles. The RDEM is calculated by the following expression: RDEM $=E_n/E_0=(V_n/V_0)^2$, where E_n is the dynamic modulus of elasticity of n cycles and E_0 is the initial value. V_n and V_0 are the sound velocity of n cycles and initial value, respectively.

Table 3. Proportions of concrete mixes.

W/*B*	Cement (kg/m^3)	Water (kg/m^3)	Sand (kg/m^3)	Coarse aggregate (kg/m^3)	Fly ash (kg/m^3)
0.55	222	150	720	1305	51
0.42	290	150	667	1273	67
0.34	359	150	616	1240	82
0.26	469	150	547	1171	108

The weight of specimens was measured using electronic balance with a precision of 0.1 g. According to the test procedures, the specimen failed if its RDEM dropped to below 60% or its weight loss exceeded 5.0%.

RESULTS AND ANALYSIS

Table 4. Number of freeze-thaw cycles of concrete.

No.	*W*/*B*	NaCl dosage (%)	$NaNO_2$ dosage (%)	Na_2SO_4 dosage (%)	Blank	Number of freeze-thaw cycles
F1	0.55	0	0	0	—	55
F2	0.55	0.5	1.0	0.5	—	25
F3	0.55	1.25	2.0	1.25	—	23
F4	0.55	2.0	3.0	2.0	—	24
F5	0.42	0	1.0	1.25	—	53
F6	0.42	0.5	0	2.0	—	81
F7	0.42	1.25	3.0	0	—	82
F8	0.42	2.0	2.0	0.5	—	85
F9	0.34	0	2.0	2.0	—	213
F10	0.34	0.5	3.0	1.25	—	115
F11	0.34	1.25	0	0.5	—	61
F12	0.34	2.0	1.0	0	—	138
F13	0.26	0	3.0	0.5	—	403
F14	0.26	0.5	2.0	0	—	296
F15	0.26	1.25	1.0	2.0	—	384
F16	0.26	2.0	0	1.25	—	347

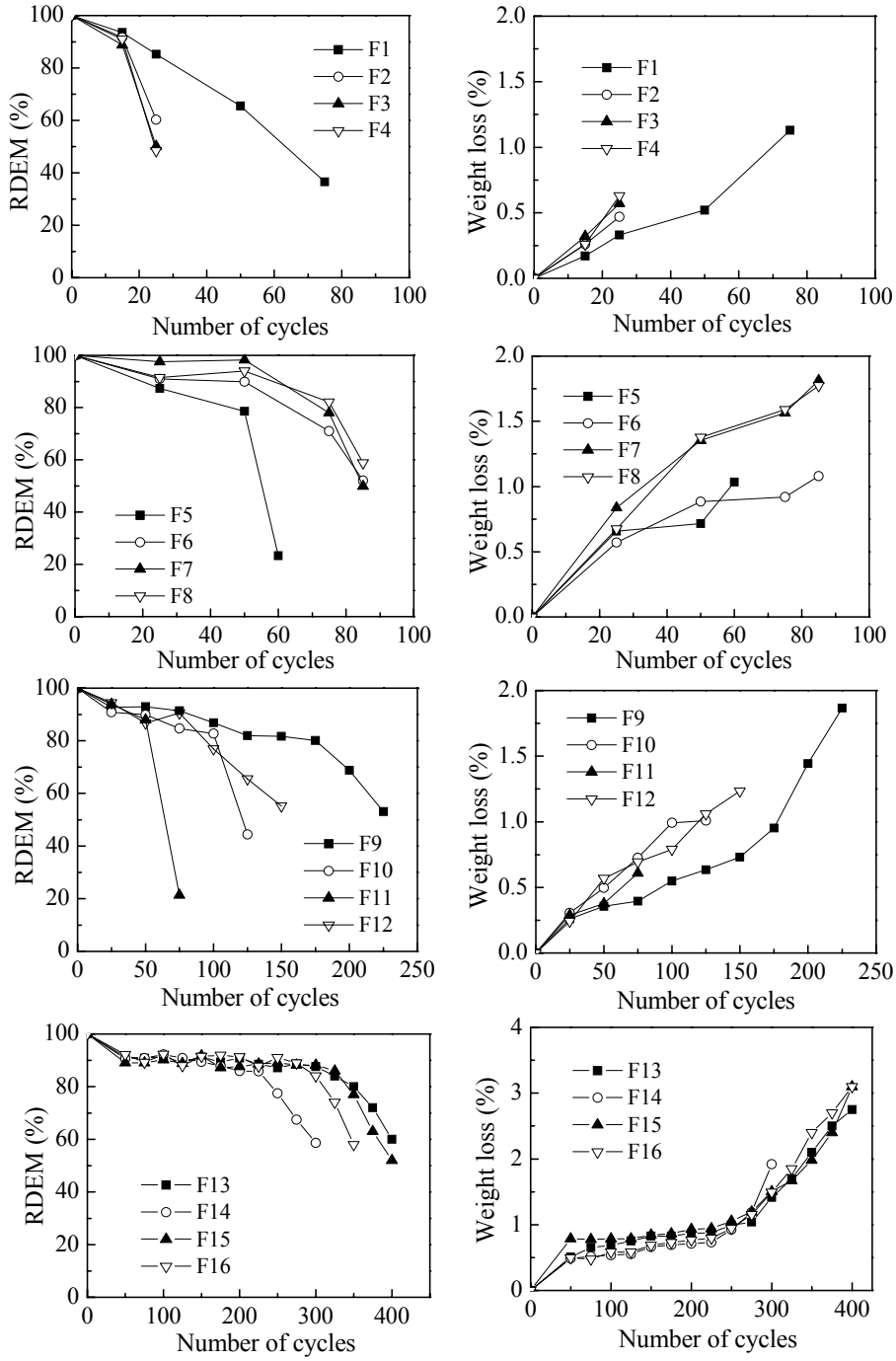

Figure 1. RDEM and weight loss of concrete subjected to freeze-thaw cycles.

Experiment results. Frost test results of the specimens prepared in the experiments are shown in Table 4 and Figure 1. It could be seen from Figure 1 that the drop of dynamic modulus of elasticity was faster than that of the weight loss. So all specimens failed due to the RDEM below 60%. The effect of *W*/*B* on frost resistance of concrete was obvious. For the concrete with the same *W*/*B*, RDEM and weight loss

after some freeze-thaw cycles were very different, which indicated that inorganic salts added into concrete had influence on frost resistance. Moreover, the effects of salts were remarkable on frost resistance of concrete with higher *W*/*B*.

Mean values of every four numbers of cycles corresponding to the same factor were calculated as shown in Table 5. Considering the differences between the maximum mean value and the minimum mean value of each factor, it is obvious that the most effective factor affecting frost resistance of concrete is *W*/*B*, followed by the material in the order of NaCl, Na_2SO_4 and $NaNO_2$.

Table 5. Mean value of each factor in correspondence with levels.

No.	*W*/*B*	NaCl dosage (%)	$NaNO_2$ dosage (%)	Na_2SO_4 dosage (%)	Blank
1.	31.750	181.000	136.000	142.750	159.750
2.	75.250	129.250	150.000	143.500	166.750
3.	131.750	137.500	154.250	134.500	161.250
4.	357.500	148.500	156.000	175.500	108.250
Difference of the mean value	325.750	51.750	20.000	41.000	58.250

Taking the levels of the experimental factors as X-coordinate and the corresponding mean values of damping ratio results as Y-coordinate, the trend curves showing the relationship between the considered factor levels and damping ratio results could be drawn as shown in the Figure 2.

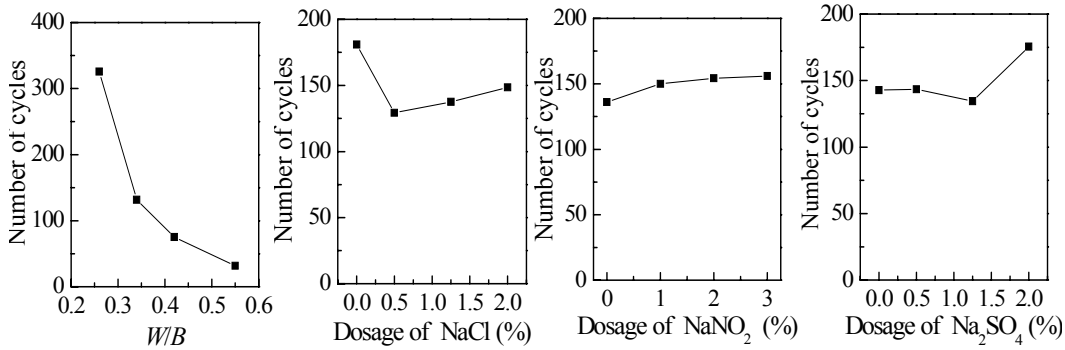

Figure 2. Effects of four factors on number of cycles.

It could be seen from Figure 2 that as *W*/*B* decreased, cycles of concrete subjected to action of freeze-thaw increased. The average number of cycles of four concrete with *W*/*B* of 0.55 were 32, which rose to 75 when the *W*/*B* of concrete was 0.42. Cycles of the four concrete samples with *W*/*B* of 0.26 can exceed 300. As dosage of NaCl increased, the number of cycles first decreased and then increased. The minimum cycles was obtained when NaCl dosage was 0.5%. Moreover, the number of cycles of concrete with NaCl was lower than the concrete without salt. $NaNO_2$ had no side effects as a frost resistance agent for concrete. Frost resistance of concrete was improved appreciably when $NaNO_2$ was used. Effect of Na_2SO_4 dosage

on number of cycles was similar to that of NaCl. As the dosage of Na_2SO_4 increased from 0% to 1.25%, the number of cycles decreased and the minimum cycles was obtained at the dosage of 1.25%.

CONCLUSIONS

(1) Orthogonal test was carried out and results show that water-binder ratio is the most important factor affecting frost resistance of concrete. Inorganic salts also have influence on frost resistance of concrete, and effect of NaCl is obvious, followed by the Na_2SO_4 and $NaNO_2$.

(2) NaCl and Na_2SO_4 could reduce frost resistance of concrete. Number of freeze-thaw cycles for concrete with salt is minimum when NaCl dosage is 0.5% or Na_2SO_4 dosage is 1.25%. $NaNO_2$ can improve frost resistance of concrete appreciably at the dosage between 1.0% and3%.

(3) When inorganic salts are used as antifreeze agents or high-early strength agents in concrete, the water-cement ratio or water-binder ratio should be reduced properly to avoid harmful effects of salts on frost resistance of concrete.

ACKNOWLEDGMENTS

This work was supported by the Foundation of the Natural Science Funds of China (Project No. 50778055).

REFERENCES

Wang, Y., Ye, Y., and Zhong, X. (2005). "Research and application of a new high-early strength agent of concrete." *Journal of Sichuan Architectural* (in Chinese), (4), 105-106.

Chen, J. (2004). *Theory and application of concrete additives (Second edition)*. Planning Press, Beijing, China, 101-112, 498-525.

Sideris, K. K, and Savva, A. E. (2005). "Durability of mixtures containing calcium nitrite based corrosion inhibitor." *Cement and Concrete Composite*. (27) 277-287.

Tritthart, J, and Banfill, P. F. G. (2001). "Nitrite binding in cement." *Cement and Concrete Composite*. (31) 1093-1100.

Muralidharan, S., Saraswathy, V, and Merlin Nima, S. P. (2004). "Evaluation of a composite corrosion inhibiting admixtures and its performance in Portland pozzolana cement." *Journal of Materials Chemistry and Physics*, (86) 298-306

Rivard, P., Berube, M., and Ballivy, G. (2003,). "Effect of drying–rewetting on the alkali concentration of the concrete pore solution." *Cement and Concrete Research*, (33) 927-929.

EFFECT OF LIGHTWEIGHT AGGREGATE WITH DIFFERENT MOISTURE ON AUTOGENOUS SHRINKAGE AND STRESS UNDER PARTIALLY RESTRAINED CONDITION

DONG Shuhui[1], ZHANG Baosheng[2], GE Yong[3], YUAN Jie[4]

School of Transportation Science and Engineering, Harbin Institute of Technology, 202 Haihe Road, Nangang District, Harbin 150090, P.R. China; PH 86-451-86282191; E-mail: [1]ailsa_hit@yahoo.com.cn, [2]hitzbs@163.com, [3]hitbm@163.com, [4]hityuanj@163.com

ABSTRACT

A study of the efficiency of lightweight aggregate (LWA) in controlling restrained shrinkage cracking of low water-to-cement ratio concrete is presented. Free autogenous shrinkage test of concrete specimens and restrained test with ASTM C 1581-04 were performed. Autogenous shrinkage and restrained stress of concrete with different moisture content (0%, 20%, 40%, 60%, and 100%) LWA at the same water-to-cement ratio of 0.30 were investigated by experiments that provided date on free autogenous shrinkage and restrained shrinkage. The results showed that the pre-wetting LWA effectively reduced autogenous shrinkage, restrained shrinkage and tensile stress in the restrained conditions. Also, it was found that the shrinkage stress was relaxed more and more with degree of saturation of LWA increasing, and can be mitigated by 45.7% in the concrete with the saturated LWA.

KEY WORDS

Concrete; lightweight aggregate; autogenous shrinkage; restrained shrinkage; tensile stress

1. INTRODUCTION

Development of high-performance concrete (HPC) with high-performance and improved durability has brought new opportunities to the construction industry. However, some attention was given to characteristics of such concrete, in particular with respect to their cracking sensitivity. HPC is generally made of a low water-cement ratio, which makes it susceptible to self-desiccation (Jensen, 1996). This self-desiccation process is directly related to autogenous shrinkage. Autogenous shrinkage results in tensile stresses in the cement paste, due to the external restraint. It has been argued and demonstrated experimentally that a low water-to-cement ratio concrete may undergoes shrinkage due to self-desiccation. If this shrinkage is restrained, the concrete may crack. This autogenous shrinkage cracking is a major concern for the durability and aesthetic of concrete structures (Takafumi Noguchi, 2005). One possible method to reduce the adverse effects of cracking due to autogenous shrinkage is the addition of LWA for internal curing (Hammer, 1992).The pre-wetted porous LWA can be used as an internal source of water and release gradually in the internal concrete under the capillary tension function.

The research on the effect of water absorption and desorption of LWA on adjusting the internal relative humidity of concrete and improving the properties of fracture and deformation is very necessary. This article addresses the issues outlined above both with experiments and with calculations. Autogenous deformation of LWAC realized with pre-wetted LWA (ceramsite) was measured. The aims at evaluating mechanical properties of concrete such as various types of strain and shrinkage stress with pre-wetted LWA, which were measured on the corresponding normal weight concrete (NWC) mix.

2. EXPERIMENTAL PROGRAM

2.1 MATERIALS AND MIX PROPORTIONS

Mixtures were prepared using P·O 42.5 cement. The fine aggregate is river sand with a specific gravity of 2.61 and fineness modulus of 2.82. In the corresponding normal weight concrete (NWC) case, with a continuous grading of 5mm~20mm. Specific gravity of the crushed limestone coarse aggregate is 2.81. The non-air entrained and high-effective naphthalene-based superplasticiser (SP) used was a type of UNF-5, with a water reducing ratio of 20%. The LWA used was one type of shale ceramisite(BY) with a maximum size of 16mm and cylinder compressive strength of 5.9MPa, with an water-absorbing ratio 6.6% for 1hrs, a saturated water content of 24%, The variations curves of shale ceramsite water absorption and desorption versus time were shown in Figure 1.

The shale ceramsite were pre-wetted before mixing. The drying ceramsite was soaked in water (saturation refers to maintain 20 min in water under 5 MPa hydraulic pressure. The saturation level of the LWA obtained by impregnating under pressure was higher compared to vacuum impregnation, other pre-wetting treatment refers to atmospheric pressure) for a specified time to make them have five different saturated water contents (100%, 60%, 40%, 20% and 0%), so the ceramsite would have different initial water content. The LWA concrete and normal weight concrete were prepared with a water-cement ratio of 0.3, a cement dosage of 500kg/m^3, a fine aggregate dosage of 678kg/m^3. The LWA concrete were prepared with a ceramsite dosage of 495kg/m^3, normal weight concrete was prepared with crushed aggregate dosage of 1067kg/m^3. In order to study the autogenous shrinkage, the restrained shrinkage and the restrained tensile stresses by contrast, the used proportions are shown in Table 1.

2.2 TEST PROCEDURE

The primary tests that will be described in this paper consist of ring test that was performed using a ring with a steel wall thickness of 12.5 mm, an inner diameter of 305 mm, an outer diameter of 330 mm, a specimen outer diameter of 406 mm, and a height of 75 mm. Four strain gages were fixed to each steel ring at mid-height and their strain was measured at 10 minute intervals from the time water came into contact with the cement (MA Xinwei, 2006). After removing the mould at an age of 24 hours, the rings were sealed with duct tape around their outer circumference, in

this research the specimens were allowed to dry from the top to the bottom surface.

Table 1 Mix proportions of concrete and properties of concrete specimens

Sign of concrete	Degree of Pre-wet /%	Net Time-to-Cracking /Days	Steel Ring Strain at cracking /μ-strain	Maximum restrained Stress (σ_{max}) /MPa	Tensile Strength at cracking /MPa	Compression strength at 28d /MPa
NWC	0	3.71	54.40	3.57	4.38	62.80
IC00	0	5.08	35.60	3.01	3.62	41.80
IC20	20	6.96	41.34	2.71	3.54	40.60
IC40	40	10.40	40.34	2.65	3.42	40.50
IC60	60	13.46	37.70	2.48	2.98	40.30
IC100	100	26.08	29.43	1.94	2.54	39.50

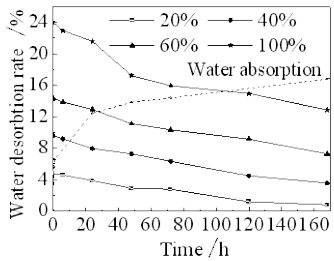

Fig.1 Water desorption rate of ceramsite at RH=91%

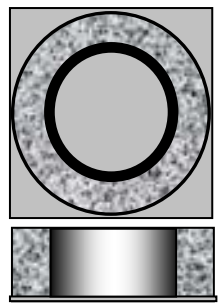

Fig.2 Top view and cross sectional view of the ring specimens

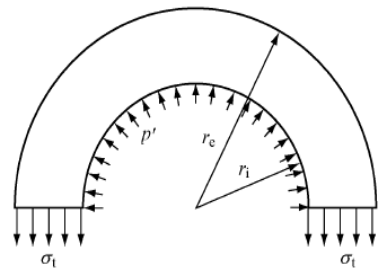

Fig.3 Stress of concrete under ring restrained condition

The restrained tensile stresses of concrete ring can be calculated by Equation 1:

$$\sigma_t = \frac{p \cdot r_{ic}}{h_c} \tag{1}$$

where: σ_t is the restrained tensile stresses of concrete ring; p is the internal pressure of the concrete ring; r_{ic} is the inner radius of the concrete ring; h_c is the thickness of the concrete ring.

The fictitious pressure acting on the steel (at the interface with concrete) can be calculated by Equation 2, which incorporates the strain value that is equivalent to the strain measured in the steel ring.

$$\sigma_{st} = E_{st} \cdot \varepsilon_{st} = \frac{p \cdot r_{es}}{h_{st}} \tag{2}$$

where: σ_{st} is the pressure stresses of the steel ring; E_{st} is the elastic modulus of the steel ring, where is 200GPa; r_{es} is the inner radius of steel ring; ε_{st} is the strain pressure of steel ring; h_{st} is the thickness of the steel ring.

The strain that develops at the inner surface of the steel ring can be used to determine the force that is exerted by the shrinking concrete. After recording the

strain in the steel at ten minute intervals, the ring system is analyzed by separating the problem into one that considers a steel ring with a fictitious external pressure and a concrete ring with a fictitious internal pressure. Equilibrium requires that the fictitious external pressure equals the fictitious internal pressure. So, combining Equation 1 and Equation 2 and allowing the stress to be computed when $r_{ic} = r_{es}$ enables the maximum tensile stress σ_t that develops in the ring to be calculated using the measured strain $\varepsilon_{st}(t)$ as shown in Equation 3:

$$\sigma_t = \frac{E_{st} \cdot h_{st}}{h_c} \cdot \varepsilon_{st}(t) \tag{3}$$

In order to avoid deviation due to the move of the specimen (Dong Shuhui, 2008), one micrometer gauge was fixed on each specimen to measure the length change of it. Autogenous shrinkage was tested with the equipment. Three specimens were cast in cylindrical mould (100mm×400mm) for each mix ratio and a temperature probe embedded in the specimens. After casting, specimens were sealed immediately and set up in the test equipment. The measurement of autogenous shrinkage began 3hrs after casting and measurement of temperature began.. All autogenous shrinkage data used in analysis were averages of the data of three specimens. As change of internal temperature in concrete due to hydration has great impact on autogenous shrinkage of concrete, so a method from literature (Ahmed Loukili, 2000, Erika E Holt, 2001) was adopted to amend the experimental data for autogenous shrinkage to eliminate this impact. Amendment was also made to erase effect of settlement during plastic stage.

3. RESULTS AND DISCUSSIONS

3.1 EFFECT OF LWA WATER CONTENT ON CONCRETE AUTOGENOUS SHRINKAGE

The effect of water content of ceramsite on concrete autogenous shrinkage was studied, the test result were shown in Figure 4.

The test results indicate that, autogenous shrinkage of concrete develops very quickly at the early age, the majority completes within 48hrs. For later period shringkage grows slowly. Autogenous shrinkage value of the LWA concrete at the age of 12h is about 50%~70% of that at the age of 120h, but the normal weight concrete reaches 80%. With the increase of ceramsite initial water content, the autogenouse shrinkage of LWA concrete reduces obviously, and also lower than that of normal weight concrete.

In the hardening process, a great amount of free waters is consumed for the cement hydration, so the concrete internal humidity decreases steadily, and the water stored in pre-wetted ceramsite would migrate to the cement paste around under the capillary tension, and provide water for the no hydrated cement particles, this could reduce the capillary water consumption, thereby reduce the self-desiccation shrinkage. The higher the ceramsite water content and the more the migration water,

the compensation effect for the concrete self-desiccation shrinkage becomes more significantly. It can be seen that, the addition of pre-wetted LWAs has obviously effect on eliminating the autogenous shrinkage.

3.2 EFFECT OF SATURATION DEGREES OF LWA ON RESTRAINED SHRINKAGE OF CONCRETE

Three replicates were prepared for each specimen and average of two closer values was considered. In Figure 5, the restrained shrinkage of concrete with different degrees saturation of the ceramsite and 30NWC were presented.

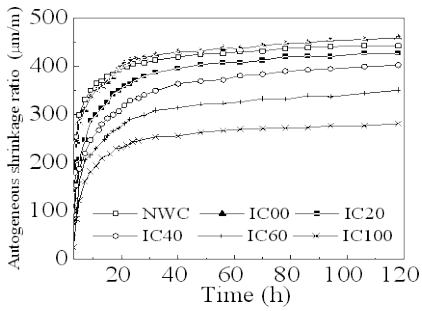

Fig.4 Effect of ceramsite water content on autogerous shrinkage

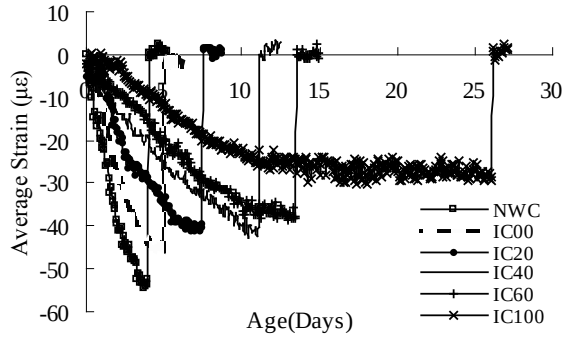

Fig.5 Effect of saturation degrees of ceramsite on restrained shrinkage

It was observed that the rate of restrained shrinkage development in each of the specimens was dissimilar before the specimen cracked. The restrained shrinkage was initialized at zero at the setting time of concrete. The restrained shrinkages of NWC specimens occurred at a rapid rate in the first few days and the shrinkage reached a maximum of 54.4 μstrain at 3.71days. The restrained shrinkages of IC00 specimens occurred at a rapid rate in the first few days but the shrinkage reached a maximum of 35.6 μstrain at 5.08 days, lower and later than NWC. The restrained shrinkage of IC100 specimens reached a maximum of 29.43 μstrain at 26.08 days and the shrinkage rate was the lowest than other mix specimens. That was, with the increase of ceramsite initial degree of saturation, the restrained shrinkage of concrete reduces obviously, and the time of reaching maximum restrained shrinkage had a much delay, also lower than that of normal weight concrete.

However, as was shown in Figure 5, an abrupt change of shrinkage was observed in several instances for all specimens at different age, which corresponds to cracking in the specimen. It was observed that this abrupt change in shrinkage for all specimens corresponds to the age of visible cracking in the specimen. The residual shrinkage in ring specimens was found to be reduced to almost zero after the visible crack developed.

3.3 EFFECT OF SATURATION DEGREES OF LWA ON RESTRAINED TENSILE STRESSES OF CONCRETE

Figure 6 shown the development of tensile stresses of all specimens that were computed using the measured strain values obtained (using Equation 3) for the

mixtures tested in this study. The trend of tensile stress development in each specimen was found to be fairly similar as the restrained shrinkage development, before the specimen cracked. The concrete specimens NWC restrained stress occurred from the start of setting. The stress reached a maximum of 3.57MPa at 3.71 days, an abrupt change of stress was observed after the peak. The mixture with 100% saturated ceramsite showed slowly development rate of restrained stress in the all stage of measuring. After 26.08 days the stress peak occurred, reaching a maximum of 1.94MPa. Figure 6 illustrated the stress that had developed before and after visible cracking occurred in all specimens. The restrained stress in the ring specimen was found to be reduced to almost zero after the first crack developed in the specimens.

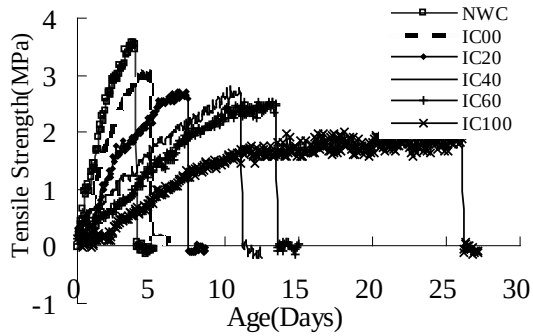

Fig. 6 Effect of saturation degrees of ceramsite on tensile stresses

The effect of the degree of saturation of the aggregate on the stress development is significant. For the mixtures with an actual degree of saturation of 0% and 20%, stresses are higher than those of the mixtures with an actual degree of saturation of 60% and 100%. These maximum stresses were 3.01 MPa and 2.71 MPa, respectively. With the increase of ceramsite initial degree of saturation, the restrained stress of concrete reduces obviously, and the time of reaching maximum restrained stress had a much put off, also lower than that of normal weight concrete. The maximum restrained stress value (1.94MPa) of the mixture with 100% saturated ceramsite can reduce to 54.3% than the value of the corresponding normal weight concrete. Test results of compressive strength at 28 days and splitting tensile strength at crack occurring were shown in Table 1. The results represent the average value of three 100×100×100mm concrete specimens. The measured splitting tensile strength values higher than the computed restrained stress values in every mixture.

The theory of pre-wetting LWA can reduce the restrained shrinkage and the restrained stress of low water-cement ratio concrete was conform to the reason of autogenous shrinkage reduction.

4. CONCLUSIONS

(1) The addition of pre-wetting LWA can obviously reduce the autogenous shrinkage of high-performance concrete with low water-cement ratio, at early age. When the initial degree of saturation of ceramsite increases from 20% to 100%, the 120h-shrinkage values of LWA concrete reduces from 3.6% to 36.4% respectively as compared to that of normal weight concrete.

(2) With the increase of ceramsite initial degree of saturation, the restrained shrinkage of concrete reduces obviously, and there is a big delay on the time to reach maximum restrained shrinkage. When the initial degree of saturation of ceramsite are 60% and 100%, the restrained shrinkage values of LWA concrete reduces 30.7% and 45.9% respectively as compared to that of normal weight concrete.

(3) With the increase of ceramsite initial degree of saturation, the restrained stress of concrete reduces obviously, and the time to reach maximum restrained stress had a much put off, also lower than that of normal weight concrete. The pre-wetting LWA effectively reduced tensile stress in the restrained conditions. It was found that the restrained stress was relaxed more and more with degree of saturation of LWA increasing, and can be mitigated by 45.9% in the concrete with the saturated LWA.

REFERENCES

Ahmed Loukili. (2000). A new aproach to determine autogenous shrinkage of mortar at an early age considering temperature history. Cement and Concrete Research. 2000, (30):915-922.

Dong Shuhui, Ge Yong, Yuan Jie, Zhang Baosheng. (2008). Study on Shrinkage Property of Lightweight Aggregate Concrete. Concrete. 2008, (2): 47-49.

Erika E Holt. (2001). Early age autogenous shrinkage of concrete. Ph.D. Thesis, Washington: Philosophy University of Washington Press, 2001, 34-98.

Hammer T.A. (1992) High strength LWA concrete with silica fume - Effect of water content in the LWA on mechanical properties, Supplementary Papers in the 4th CANMET/ACI Int. Conf. On Fly Ash, Silica Fume, Slag and natural Pozzolans in Concrete, Istanbul, Turkey, 1992, pp. 314-330.

Jensen, O.M., Hansen, P.F. (1996). Autogenous deformation and change of the relative humidity in silica fume-modified cement paste, ACI Mater J, 1996, 93(6): 539-543.

MA Xinwei, LI Xueying, ZHU Weizhong, NIU Changren. (2006). Cracking Prediction of Medium and Low Water-Cement Ratio Concrete under Partially Restrained Condition. Journal of Building Materials. 2006, (5) : 598-602.

Takafumi Noguchi, Park Sun-Gyu, Ippei Maruyama. (2005). Mechanical properties of high-performance concrete with expansive additive and shrinkage reducing admixture under simulated completely-restrained condition at early age. Self-desiccation and its importance in concrete technology B Persson, D Bentz and L O Nilsson, Proceedings of the Fourth International Research Seminar, Gaithersburg, Maryland, USA, June, 2005: 67~77.

Dynamic Response of Saturated Asphalt Pavement Based on Three Dimensional Finite Element Simulation

Dong Zejiao[1], Cao Liping[2] and Cheng Xiaoliang[3]

[1]Ph.D, Associate Professor, School of Transportation Science & Engineering, Harbin Institute of Technology, Harbin, P.R.China; PH (86) 451-86282120; FAX (86) 451-86282118; email: hitdzj@hit.edu.cn

[2]Ph.D, Assistant Professor, School of Transportation Science & Engineering, Harbin Institute of Technology, Harbin, P.R.China; PH (86) 451-86282120; FAX (86) 451-86282118; email: hitclp@hit.edu.cn

[3]Master, Candidate of Ph.D., School of Transportation Science & Engineering, Harbin Institute of Technology, Harbin, P.R.China; PH (86) 451-86282120; FAX (86) 451-86282118; email: xiaoliang1985412@163.com

ABSTRACT

It has been recognized that asphalt pavement performance will be weakened with the presence of water within pavement structure. However, current mechanistic analysis does not take into account the moisture influence on the dynamic response of pavement appropriately. In this paper, finite element meshing, boundary conditions, material properties and dynamic loading were introduced, followed with the analysis of typical time history pore pressure. Then, the mechanism of premature failure related to water damage was discussed based on on-site damage phenomenon combined with the finite element simulation according to the spatial distribution of pore pressure and the comparison between the saturated and dry cases. Finally, the influence of surface drainage conditions on the dynamic response of saturated pavement is presented here. The result indicates that the presence of water changes stress distribution in pavement structure. What's more, it is interesting to find that the worst positions are the middle and bottom HMA layer according to the distribution of pore pressure, which was consistent with the initial failure phenomenon of asphalt pavement due to water.

INTRODUCTION

It is generally accepted that newly placed HMA pavements are placed at a higher air void (6-7%) than designed value with the assumption that traffic loadings will decrease the air void content over time. The air void can allow water to move through the pavement. Infiltration of water into the pavement can develop pore pressure leading to excessive deflection, cracking and reduction in load carrying capacity of pavement.

It is general that all pavements have some degree of saturation, which indicates that water should not be ignored in asphalt pavement mechanics analysis.

Therefore, some related researches have been done. Masad et al. (2003) used two dimensional SEEP/W finite element modeling to study the relationship between the water flow patterns and the gradients in percent air voids in HMA. Novak et al. (2002) used theory of mixture to describe the saturated asphalt pavement and studied the effects of vehicle speed and permeability on pore pressure by a two dimensional finite element code-PlasFEM. Kringos et al.(2005) developed a finite element tool RoAM (Raveling of Asphalt Mixes) to describe the raveling of asphalt Mixes due to moisture damage from the micro-mechanics point of view. Dong (2006) carried out theoretical derivation and FEM simulation for the saturated pavement subject to transient vehicle loading.

FINITE ELEMENT MODELING

Three dimensional finite element meshes are shown in Figure 1. Eight-node brick element is used. The nodes, when analyzed in a transient dynamic saturated state, have seven degrees of freedom corresponding to fluid and solid displacements in X, Y and Z direction as well as pore pressure. The size of the finite element model is 3.0m by 3.0m by 3.0m. Elements are finer near the top and middle (where the wheel load will be applied) and gradually grow coarser towards the sides and bottom of the pavement.

For solid phase, it was assumed that there is no vertical, transverse or horizontal movement at the bottom of the model, thus the bottom of the model was completely restrained. The top was free to move in all directions. Horizontal movement perpendicular to the perimeters was also restrained whereas the remaining two directions were considered free. For fluid phase, the surround boundaries and upper boundary, except for the loading area, were pervious while the bottom boundary and loading area were impervious.

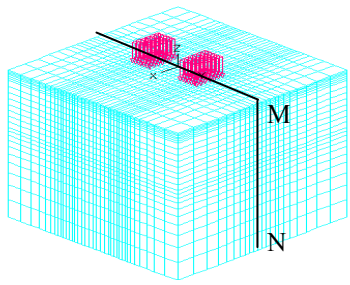

Figure 1. Three dimensional finite element meshes.

TRANSIENT DYNAMIC LOADING

The standard wheel load was assumed to be 0.24m long and 0.16m wide with a contact pressure of 651kPa for a single rectangle loading area, and the distance between the two loading areas is assumed to be 0.24m. A transient haversine loading function with a recovery time is used to simulate the actual vehicle loading action on asphalt pavement. The peak of uniform loading is defined

as $P_{\max}$, loading duration as T and the whole analysis time as T_a. At any time t in the analysis period, the applying uniform loading is:

$$p = \begin{cases} P_{\max} \sin(\frac{\pi t}{T}) & 0 \le t \le T \\ 0 & T < t \le T_a \end{cases} \quad (1)$$

The duration of the load is based upon the vehicle speed v and the assumption that the tire, with length l, has no effect at a distance of $6l$. This paper looked at a wheel load traveling at 60 km/h, or haversine load duration of 0.0864s.

MATERIAL PARAMETERS

Typical material parameters of asphalt pavement are used, shown in Table 1.

Table 1. Material parameters of saturated asphalt pavement.

Layer	Thickness cm	Young's modulus/MPa	Poisson Ratio	Density kg/m^3	Permeability cm/s
Upper HMA	5	1400	0.3	2400	1.0E-04
Middle HMA	6	1400	0.35	2400	1.0E-05
Bottom HMA	8	1400	0.35	2400	1.0E-05
Upper Base	20	1600	0.2	2100	1.0E-04
Bottom Base	20	600	0.3	1900	1.0E-05
Subgrade	250	50	0.4	1900	1.0E-06

ANALYSIS OF TIME HISTORY OF PORE PRESSURE

Figure 2 shows the time history of pore pressures at different depths on the longitudinal center section (M-N section) of the applied load. As shown in Figure 2, the pore pressures increase very rapidly as load increases at the initial stage, as the applied load is transferred to the fluid in the voids. Subsequently, as the fluid starts to escape the voids, the pore pressures decrease. Then the positive pore pressures change to negative suction pressures and the surrounding material skeleton recovers from the load and sucks the water back into the voids between the aggregates gradually. The maximum negative suction pressure reaches when the wheel load is almost gone. Finally, as the loading is gone the negative pressure starts to dissipate. It is noted that the peak time of pore pressure is earlier than that of applied loading, after the initial stage of loading there has certain time for the fluid to escape through the around interconnected void. Although the applied loading reaches its peak value, the transferred pressure to fluid can't continue to increase.

The similar reversals from positive pore pressures to sizable suction, as the wheel load is applied, are found at all the depth, while the different point is their peak value.

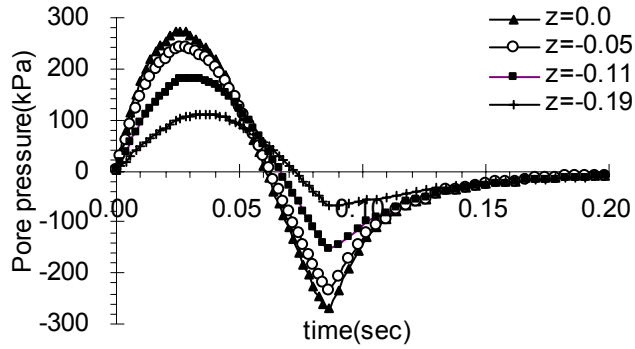

Figure 2. Pore pressure histories at different depths.

PRELIMINARY ANALYSIS OF PREMATURE DAMAGE DUE TO WATER

Figure 3 shows the pore pressure distribution at different times for M-N section. Pore pressures mainly focus on asphalt layers within the depth of 0.2m, both in the arising and dissipating phases. What's more, the transverse influence scope is the biggest at the depth from 0.05 to 0.2m, which is just the middle and bottom asphalt layer. This means that the worst position is the middle and bottom asphalt layer once water enters the pavement structure, consistent with the initial failure phenomenon of asphalt pavement due to water. This can be thought as one of the reasons for the premature failure caused by water similar to Figure 4, from the theoretical point of view.

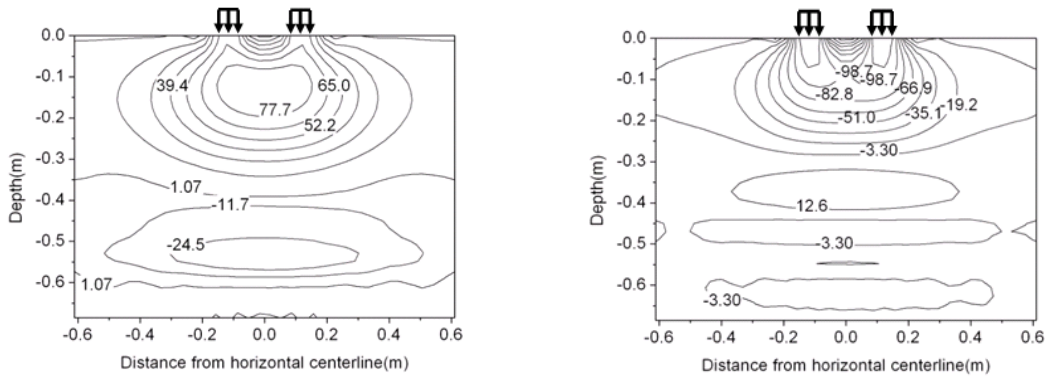

(a) t=0.026(sec) **(b) t=0.082(sec)**

Figure 3. Pore pressure distribution for different time.

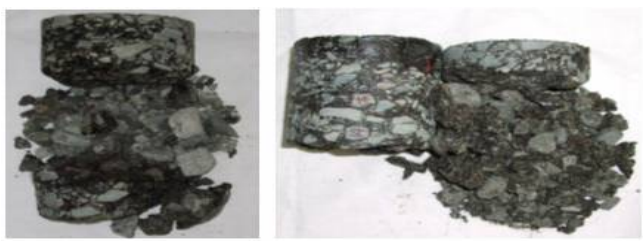

Figure 4. Coring results from the initial failure site of asphalt pavement.

INFLUENCE OF SURFACE DRAINAGE CONDITION

When carrying out theoretical calculation and analysis about the dynamic response of saturated asphalt pavement, surface drainage condition needs to be considered, i.e. surface draining condition and surface non-draining condition. Surface draining condition is defined that water near the surface can flow freely to get into or get out of pavement structure. Generally, asphalt pavement with no sealing or water-proofing should use this boundary condition. Surface non-draining is defined that water cannot be drained out of the pavement structure. When surface course is used for sealing or water resisting such as slurry seal and Micro-surfacing, it should be regarded as non-drainage condition. Figure 5 gives the results of pore pressure distribution along the depth at *t=0.036s* and *t=0.075s* for surface draining condition and surface non-draining condition.

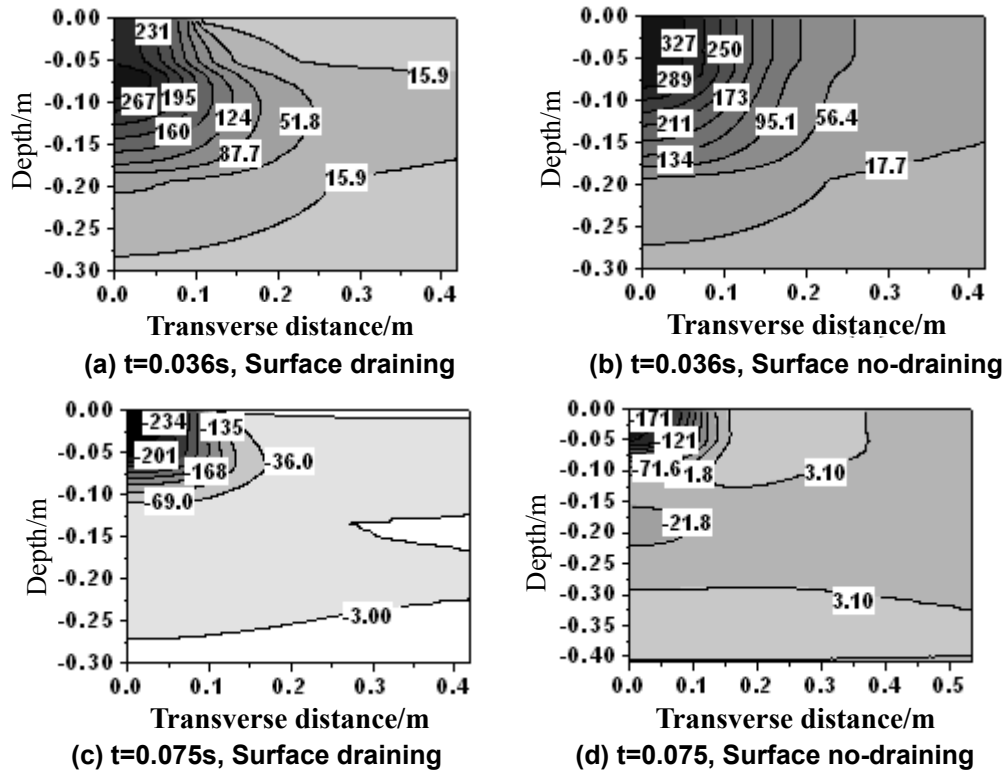

Figure 5. Pore pressure distribution along depth

It can be seen that the distributions are different for the two cases. For the draining condition, the absolute value of positive and negative pore pressure is roughly equal, while for the non-draining condition, the absolute value of negative pore pressure is obviously lower than the former. What's more, the pore pressure distributions are different. Influence of pore pressure is mainly concentrated on wheel load region, and along the depth. This region gradually expands to maximum

width at the middle asphalt layer in surface draining condition. The largest influence of pore pressure is at surface asphalt layer because water can't be discharged. With the depth increasing, the influence reduces gradually in surface non-draining condition. According to the comparison, it shows it is more detrimental for pavement structure in surface draining case.

CONCLUSIONS

This paper presents three dimensional finite element simulation of dynamic response for a saturated pavement system subject to the dynamic vehicle loads. It shows that a reversal of pore pressures occurs in saturated asphalt pavement due to dynamic vehicle loading, which may induce stripping and raveling damage. The worst position is the middle and bottom layer of pavements because the arising and dissipating of pore pressure concentrates at here, which is consistent with the initial failure phenomenon of asphalt pavement due to water. Furthermore, it is more detrimental for pavement structure in surface draining case, as the influence of pore pressure is the largest at the surface of asphalt layer because water can't be discharged

It is recommended that analysis between permeability and pore pressure should be performed, as the former highly influences the latter. Further laboratory test considering the action of pore pressure induced by vehicle loading should be carried out.

ACKNOWLEDGEMENTS

The authors are grateful to the fund from "Development Program for Outstanding Young Teachers in Harbin Institute of Technology (HITQNJS.2007. 032)", "Specialized Research Fund for the Doctoral Program of Higher Education (SRFDP) for young teachers (20070213014)" and "National Natural Science Foundation of China (50808056) ".

REFERENCES

Kringos, N. and Scarpas, A. (2005). "Raveling of asphaltic mixes due to water damage: computational identification of controlling parameters." *the 84th Annual Meeting of the Transportation Research Board*, Washington, D.C., 1-19.

Masad, E., Birgisson, B., Al-Omari, A. and Cooley, A. (2003). "Analysis of permeability and fluid flow in asphalt mixes." *the 82th Annual Meeting of the Transportation Research Board*, Washington, D.C., 1-33.

Novak, M., Birgisson, B. and McVay, M. (2002). "Effects of permeability and vehicle speed on pore pressure in Hot Mix Asphalt pavements." *the 81th Annual Meeting of the Transportation Research Board*, Washington, D.C., 1-19.

Dong, Zejian (2006). *Dynamic response analysis of saturated asphalt pavement based on porous medium theory*, Ph.D. Dissertation, Harbin Institute of Technology, Harbin.

Permanent Deformation Characteristic of Asphalt Mixture Considering Pavement Temperature Distribution

Cao Liping[1], Dong Zejiao[2], Sun Lijun[3]

[1]Dr., Assistant Professor, School of Transportation Science and Engineering, Harbin Institute of Technology, Harbin, P.R.China; PH (86) 451-86282120; FAX (86) 451-86282118; email: hitclp@hit.edu.cn

[2]Dr., Associate Professor, School of Transportation Science and Engineering, Harbin Institute of Technology, Harbin, P.R.China; PH (86) 451-86282120; FAX (86) 451-86282118; email: hitdzj@hit.edu.cn

[3]Professor, School of Transportation Engineering, Tongji University, No.4800, Caoan Road, Shanghai 201804, China; e-mail: ljsun@mail.tongji.edu.cn

ABSTRACT

Permanent deformation(PD) of asphalt mixture caused by high temperature (above 50°C), instead of the accumulative deformation caused by moderate temperature (20°C to 50°C), attracts more attention. First, distributions of pavement temperature based on continued hourly average pavement temperature data in Shanghai and Wilson County were introduced. The result indicated that percentage frequency of pavement temperature below 50°C is more than 90%, and that above 50°C is less than 5. Second, PD of two asphalt mixtures measured by APA (asphalt pavement analyzer), dynamic stability (DS) of four mixtures tested by wheel tracking device and shear strength of five mixtures tested by uniaxial penetration test were introduced. The results show that PD at 40℃ is almost 50 percent of that at 60°C, and that the ranking of high temperature performance for the same mixture changes with temperatures. At last, result of rutting depths calculated by the Mechanistic-Empirical Pavement Design Guide (MEPDG) suggests that rutting depth for high temperature months is almost two to three times of that for moderate temperature months. Therefore, PD of asphalt mixtures should be evaluated considering pavement temperature distribution.

INTRODUCTION

Rutting of asphalt pavements is a serious concern for a long time due to the increased traffic and wheel loads in China. Thus, it is necessary to predict the PD of a mixture before construction. Several test methods are in practice to assess the PD. The commonly used test methods include diametral tests, uniaxial tests, triaxial tests, shear tests, empirical tests, simple shear tests and simulative tests which are basically accelerated laboratory PD prediction tests (Sousa et al., 1991). However, almost all the tests evaluate the PD at constant high temperature such as 60°C or PG (performance grade) high temperature, while PD at moderate temperature was

nearly neglected. In fact, rutting occurs at both high temperature and moderate temperatures. In addition, pavement temperature changes frequently. For a certain mixture, it is difficult to conclude whether it is enough to evaluate high temperature performance at one temperature. Consequently, the PD characteristic should be investigated considering the distribution of pavement temperature at different depths of asphalt layers and taking pavement temperature variation into account.

DISTRIBUTION OF PAVEMENT TEMPERATURE

The temperature profile in asphalt pavement structure plays an important role on performance of asphalt pavement owing to the susceptibility of asphalt mixture. Many researches have been carried out to measure and predict the temperature distribution in asphalt pavement.

Distribution of Pavement Temperature in Shanghai

Qin (2005) measured pavement temperature data of asphalt pavement sections in Shanghai. In the test section, there were 12 thermal-probes were instilled at different depths in the asphalt layers. The frequency histograms of hourly average pavement temperature for different averaging intervals are given in Figure 1 based on collected data at four depths in asphalt layers from August 20th to September 14th, 2002. The time region represented typical high temperature season in Shanghai, and the depths were 5mm, 17mm, 39mm and 61mm below the surface.

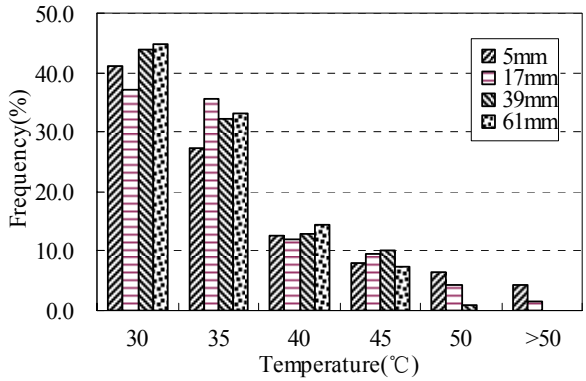

Figure 1. Hourly average pavement temperature distribution for different averaging intervals in Shanghai.

As shown in Figure 1, percentage frequency of pavement temperature interval from 30 to 40°C is about 70, while that from 40 to 50°C is about 20 and that above 50°C is less than 5 at four depths. As a result, moderate temperature contributes large proportion even in high temperature season.

Distribution of Pavement Temperature in Texas

There are three pavement temperature measurement methods in the LTPP program: infrared surface pavement temperature, manual in-depth pavement temperatures and Seasonal Monitoring Program (SMP) pavement temperatures (Drumm et al., 2003). All SMP sites are monitored with temperature, moisture, and

weather instrumentation. The temperature instrumentation in the pavement consisted of 300-mm stainless steel tubes or rods fitted with three thermistors, one at each end and one in the middle. A data logger monitored the thermistors and the weather instruments, with a recording frequency of one minute. A data logger recorded the average hourly reading at the end of each hour(LTPP, 1994).

Since all the SMP data was available online, SMP section 48-1122-1 in Wilson County, Texas was selected. This site is located southern of the United States. Hourly average pavement temperature distribution for different averaging intervals at three depths (1.3cm, 4.0cm and 12.3cm) in 1994 was analyzed. Frequency histograms are shown in Figure 2. Cumulative frequency of moderate temperature exceeds 90, while frequency of pavement temperature above 50°C is less than 5 for three depths.

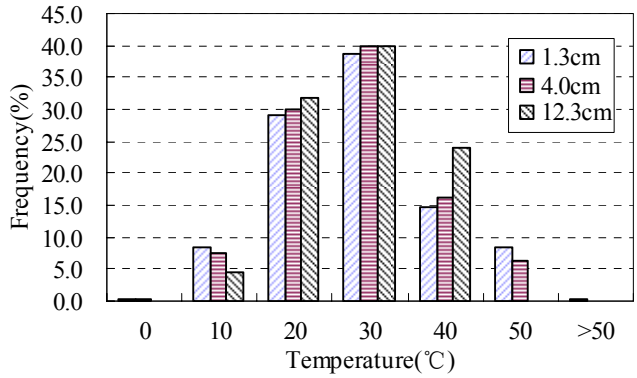

Figure 2. Hourly average pavement temperature distributions for different averaging intervals.

In conclusion, whether in Shanghai (China) or Wilson County(Texas), the proportion of high temperature in a year is far lower than that of moderate temperature. Then, is it proper to state that PD of asphalt mixtures should be evaluated at moderate temperature as well?

PD OF ASPHALT MIXTURES TESTED BY DIFFERENT METHODS

The performance tests are basically accelerated laboratory PD prediction tests and relatively easy to use and ready for immediate adoption. There are several performance tests in practice. Of the different laboratory rut testers, APA is a widely used load wheel tester. In addition, Hamburg Wheel Tracking Device and wheel tracking tester are also wildly used in their respectively country.

PD of Asphalt Mixtures Tested by APA

PD can be evaluated by using APA test which simulates the traffic loading and temperature effects on compacted asphalt mixtures. The APA allows for an accelerated evaluation of rutting potential after volumetric design of mixes. Cylindrical specimens compacted using the Superpave gyratory compactor (SGC) of two gradations with the same aggregates and asphalt were chosen. The testing time

used in this study was 135 minutes (8000 cycles). A load of 100 pounds and a hose pressure of 100 psi were used for all tests (Pavement Technology INC, 2003). Temperatures used in APA test were 20, 30, 40, 50 and 60°C .

In order to simplify the explanation, two surface course mixtures (13.2 mm mixtures) with the same aggregate sources (diabase for coarse aggregates and limestone for fine aggregates) and asphalt binder were used to prepare mixtures. The penetration of base asphalt was 68(0.1mm) at 25℃. The two gradations meet the requirement of *technical specifications for construction of highway asphalt pavements* in China. Two design aggregate structures are given in Table 1.

TABLE 1 Aggregate Gradation for Two Mixtures

Sieve Size(mm)	Percent Passing (%)										Actual air void content (%)
	16	13.2	9.5	4.75	2.36	1.18	0.6	0.3	0.15	0.075	
Upper limit of gradation	100	100	85	68	50	38	28	20	15	8	
Lower limit of gradation	100	90	68	38	24	15	10	7	5	4	
Design gradation 1	100	95	70	41.5	30	22.5	16.5	12.5	8.5	6	4.03
Design gradation 2	100	96	84	60	45	30	19.5	13.5	8	5	4.11

PD of two mixtures at five temperatures is shown in Figure 3. PD increased with temperature for both mixtures. In addition, the PD of design gradation 1 was higher than that of design gradation 2 at all the temperatures except for 40°C. PD at 40°C was almost 50% of that at 60°C for these two mixtures, which indicates that the PD at moderate temperature can be compared to that at high temperature even if without distribution of pavement temperature considered.

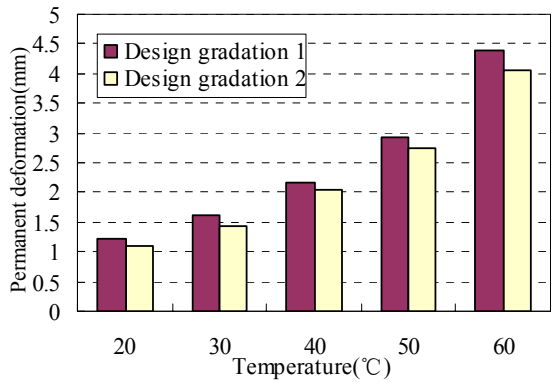

Figure 3. PD at five temperatures for two mixtures tested by APA.

DS of Four Asphalt Mixtures Tested by Wheel Tracking Device

The wheel tracking test measures rut depth and the number of passes of tire loads at high temperatures to evaluate the PD characteristics of mixtures. Test results are presented by a curve relating deformation with loading time (or loading cycles). The rate of rut depth (i.e., rut depth per minute) was monitored during 15 minutes of testing (from 45 to 60 minutes during the test) and was considred as an indicator to estimate DS. At present, wheel tracking device is widely used in China to assess

high temperature performance of asphalt mixtures with DS as evaluation index. Test results of four mixtures (HXL, LHE, SLI and CHA) typically used in China were analyzed. Results of these four mixtures are shown in Figure 4.

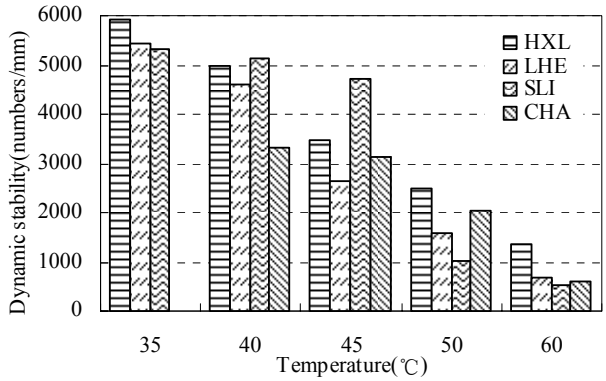

Figure 4. DS of four mixtures at five temperatures tested by Wheel tracking device in China.

As shown in Figure 4, DS of four mixtures decreased with the increase of temperature. The general trend of was that HXL presented higher DS, followed by LHE, CHA, and SLI at 60°C. The trend changes as HXL presented higher DS followed by CHA, LHE and SLI at 50°C. At 45°C, DS of SLI had highest DS, followed by HXL, CHA and LHE. For 40°C, SLI still ranks first, however followed by HXL, LHE and CHA. HXL again had highest DS at 35°C, followed by LHE and SLI. The change of ranking at different temperatures indicates that these four mixtures had different temperature sensibility. In other words, the trends of DS variation with temperature are different. Therefore, it is misleading to assess PD characteristic only at constant high temperature?

Shear strength of Asphalt Mixtures Tested by Shear test

As it was previously mentioned, shear test is another test used to assess high temperature performance of asphalt mixtures. Considering the deficiencies in the existing shear tests, a surrogate test method, the uniaxial penetration test (UPT), was developed by Sun (2006), as illustrated in Figure 5. Compared with triaxial shear test, the UPT can directly determine the shear strength of asphalt mixture in pavement structure.

Figure 5. The Uniaxial Penetration Test (Lijun Sun, 2006).

The cylindrical specimens were with both diameter (R) and the height (H) 100mm. The diameter and height of the plunger for the uniaxial penetration test were respectively 28.5mm and 50mm. In addition, the test temperature was from 20°C to 60°C, and the loading rate was set to 1mm/s. The mixtures are the same as that tested by APA. Mixture 1 and mixture 2 correspond to design gradation 1 and design gradation 2. Shear strength of both mixtures are given in Figure 6.

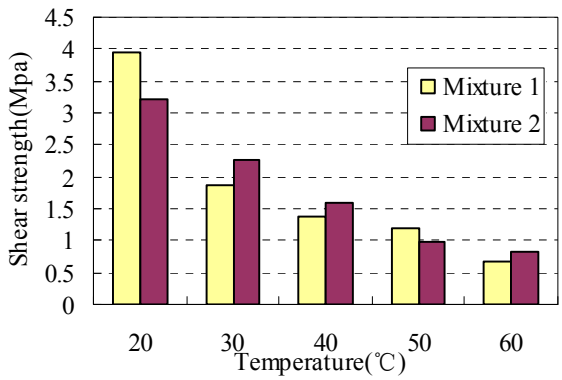

Figure 6. The uniaxial penetration test result of two mixtures.

Figure 6 shows that shear strength decreased with the increase of temperature. In addition, the shear strength of mixture 1 is higher than mixture 2 at 20℃ and 50℃. However, the trend is opposite at the other temperatures. In other word, the fact that the high temperature performance was good at a constant high temperature does not mean its high temperature performance would be good at other temperatures.

RUTTING PREDICTION OF ASPHALT PAVEMENT USING MEPDG

The MEPDG released by the National Cooperative Highway Research Program (NCHRP), is a significant improvement in pavement performance prediction methodology. Therefore, result of rutting prediction was imported to analyze the difference of PD at months with high temperature and the other months. The difference of parameters would not influence the result of this research so much. For this reason, level 3 was chosen and hypothetical data was input to the software in this study. The site is located in Texas, and the design life was 15 years. The

climate data was also from Texas. Rutting prediction for asphalt layers is given in Figure 7.

As shown in Figure 7, rutting of asphalt layers increased with pavement age. At the end of design life (180 months), rutting depth was up to 10mm, while rutting depth reached to 2mm at the end of the first year. Afterwards, increment of rutting for each year decreased gradually. Average pavement temperatures for June, July and August all exceeded 35℃, and were defined as high temperature months. The other months were defined as moderate temperature months. Then rutting depth of high temperature months and moderate temperature months were compared for the first nine years. Histogram of rutting depth with pavement age is given in Figure 8.

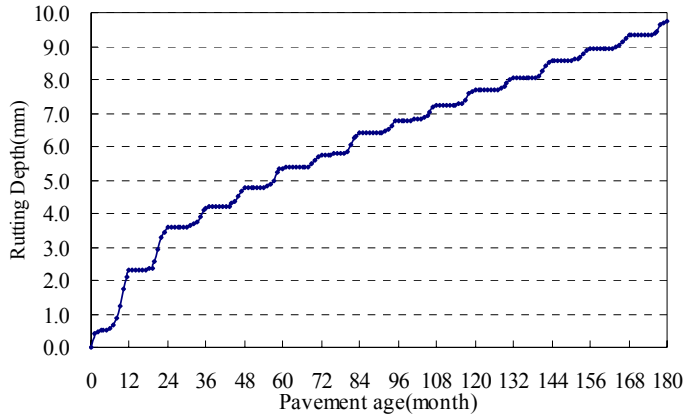

Figure 7. Rutting predictions for asphalt layers using MEPDG.

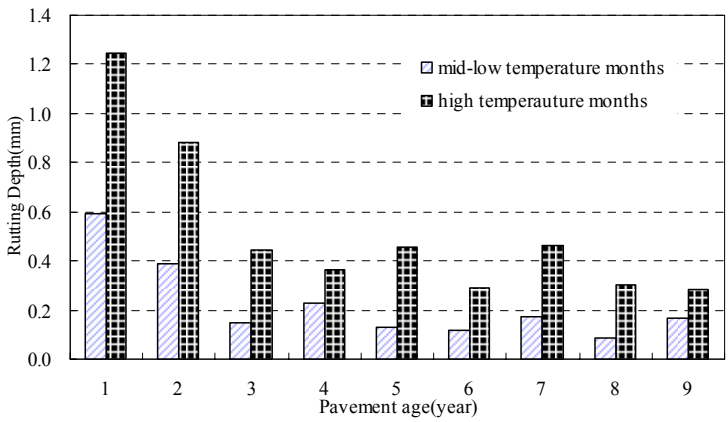

Figure 8. Comparison of rutting depth for high temperature months and moderate temperature months.

As shown in Figure 8, rutting depth at high temperature months was only two to three times of that at moderate temperature months. It indicates that rutting depth for moderate temperature months should not be ignored.

In conclusion, results of PD characteristic of asphalt mixtures measured by several test methods showed that the PD property at moderate temperature was of the equivalent importance as that at high temperature. Furthermore, research on the

PD property with varying temperature is of benefit to better understand the PD property of asphalt mixture and to more rationally estimate the rutting in asphalt pavement.

CONCLUSIONS

Based on the testing and analysis presented, the following conclusions may be made:

1. The frequency of high pavement temperature is less than 5%, while that of moderate temperature is more than 90% according to pavement temperature data in Shanghai and Wilson County.
2. PD or other evaluation indexes at moderate temperature is close to or compared with that at high temperature.
3. The high temperature performance is good at a constant high temperature does not mean its high temperature performance would be good at other temperatures.
4. PD of asphalt mixtures should be evaluated considering pavement temperature distribution.

ACKNOWLEDGEMENTS

The authors are grateful to "Key Laboratory of Road and Traffic Engineering of the Ministry of Education" of Tongji University. And, the authors are grateful to the fund from "Development Program for Outstanding Young Teachers in Harbin Institute of Technology (HITQNJS.2008.047)" and "Specialized Research Fund for the Doctoral Program of Higher Education (SRFDP) for young teachers (200802131011)".

REFERENCES

Eric C. Drumm. and Roger Meier et al.(2003). LTPP Data Analysis: Daily and Seasonal Variations in Insitu Material Properties. *National Cooperative Highway Research Program*. Transportation Research Board.

Jorge B. Sousa, Joseph Craus, and Carl Monismith(1991). Summary Report on Permanent Deformation in Asphalt Concrete. SHRP-A-318. *Strategic Highway Research Program,* National Research Council, Washington, D.C.

Lijun Sun, Xiaodi Hu, Yufeng Bi, Xiao Hu, Feng Li(2006). Top-down Cracking Analysis and Control for Asphalt Pavements. *Proceedings 10th Conference of the International Society for Asphalt Pavement(ISAP)*.

LTPP Seasonal Monitoring Program(1994): Instrumentation Installation and Data Collection Guidelines, *FHWA-RD-94-110*, McLean, VA: Federal Highway Administration.

Pavement Technology INC. Asphalt pavement analyzer user's guide [2003-03-28]. http://www.pavementtechnology.com/ manuals/APAManual.pdf.

QIN Jian(2005). Research on prediction of temperature field in asphalt pavements. Master dissertation. *Tongji University*.

Basic Study on Fractal Characteristic of Pore Structure in Cement Mortar

JIN Shanshan, ZHANG Jinxi, LI Shuang, FAN Meng

Key Laboratory of Traffic Engineering, Beijing University of Technology, Beijing 100124, P.R. China; Tel: +86-10-67391583 (O); Fax: +86-10-67391509; email: zhangjinxi@bjut.edu.cn

ABSTRACT

Mercury intrusion porosimetry (called MIP) was used to test the pore structure of cement mortar with different water-cement ratios at different ages. The fractal characteristic of the pore structure of cement mortar was studied, and the pore surface fractal dimension was computed based on the Menger sponge model. The relations between the fractal dimension and water-cement ratio, age, strength were investigated. The results indicated that, the fractal dimension was not unique in the whole range of pore size tested by MIP, and it could be divided into three regions by pore diameter: larger than 100nm, between 10nm and 100nm and smaller than 10nm. The pore fractal characteristic in the regions of larger than 100nm and between 10nm and 100nm were remarkable. The regular relations between pore surface fractal dimension and water-cement ratio, age and strength were obtained.

KEY WORDS: Fractal; Pore size; Mortar; Strength

1 INTRODUCTION

The pore structure is a very important part of the microstructure of concrete. It strongly influences the macroscopical physical and mechanical performance of concrete. The result of the SEM indicates that the pore structure of concrete is so disordered that its complexity cannot be described effectively by traditional methods (Tang and Huang, 2007). Therefore, the fractal theory as a new method describing the material complexity is used in the study of pore structure of concrete. Fractal theory can express the complexity of pore structure as fractal dimension quantitatively. It brings a new way on study of the complexity of concrete pore structure and the relation between pore structure and macroscopical performance of concrete. In recent years, fractal theory has been advanced greatly (Hu, 1997; Tang, 2000; Tang and Huang, 2007; Zhang and Li, 1995), and becomes a very important research direction gradually on the study of concrete pore structure. However, at the present time, the study of concrete pore fractal characteristic is still at the initial stage. The physical meaning of the pore fractal dimension is not very clear; and the pore test technology and pore fractal modeling method are different. All of these have caused the experimental results of pore fractal dimension to be terribly various. Therefore, the study on fractal characteristic of concrete pore structure is urgently needed.

Mercury intrusion porosimetry (called MIP) was used to test the pore structure of cement mortar with different water-cement ratios at different ages in the research. The pore surface fractal dimension of cement mortar was computed based on the Menger sponge model, and the relations between the pore surface fractal dimension and water-cement ratio, age and strength were analyzed.

2 RAW MATERIAL AND TEST METHOD

2.1 Raw materials and mix proportion

The raw materials included: Chinese standard P·O 42.5 Portland Cement, nature sand and artificial sand, water and water reducing agent. The fine aggregate was mixed with nature sand and artificial sand with the ratio of 4:6. The fineness module of the fine aggregate is 2.85. The mix proportion of the mortar is shown in Table 1.

Table 1. Mix proportion of cement mortar/ (kg /m^3)

Water-cement ratio	Cement	Natural sand	Artificial sand	Water	Water reducing agent
0.4	510	612	918	204	13.3
0.5	510	612	918	255	—
0.6	510	612	918	306	—

2.2 Strength test

The experimental methods were referred to "Test Methods of Cement and Concrete for Highway Engineering (JTG E30-2005)". The specimen size for strength experiment is 4cm×4cm×16cm. The specimens should be placed in the standard curing room with 20±2℃ and more than 90% relative humidity after demoulding. The flexural strength and compressive strength were tested at prescriptive age.

2.3 Pore structure test

The AutoPore IV 9510 MIP, which is manufactured by Micromeritics Instrument Corporation of USA, was used in this study. The MIP test parameters are as follows: the initial pressure of the low pressure is 1.03Psi, the terminal pressure is 30Psi; the initial pressure of the high pressure is 30Psi; the terminal pressure is 60000Psi. The tested range of diameter is between 3.3nm and 360000nm.

3 FRACTAL MODEL OF PORE STRUCTURE

Concrete contains pores of a large diameter interval, so it can be associated to the Menger sponge fractal model. The construction process of the Menger sponge fractal model is as following. A cube with edge R is assumed, and then the cube is divided into m^3 small cubes. In a designated rule, there are N_1 small cubes left after removing parts of the small cubes. Repeating the above process step by step. Consequently the size of the remained cubes continuously decreases but the number of the cubes unceasingly increases. Finally, after k times, edge length of the remnant cubes is $r_k=R/m^k$, and the remnant cubes quantity is $N_k = (r_k/R)^{-D_f}$. D_f represents the fractal dimension (Zhu, 2004). Linking it to MIP test, the remnant cubes constitute

the substrate of the material, and their volumes are $V_k = N_k \cdot r_k^3$; and the removed small cubes in different steps constitute the different steps' pore of material, and their volumes are $V_\phi = R^3 - V_k$. V_ϕ can be calculated with cumulative intrusion volume of mercury V at a given pressure P, r_k is the pore diameter D at the same pressure. It is deduced that the intrusion volume curve should obey the relation (Tang, 2000):

$$\lg\left(-\frac{dV}{dD}\right) \propto \left(2 - D_f\right)\lg D \tag{1}$$

Using the relations in Eq.1, the surface fractal dimension can be calculated. The logarithm of derivative cumulative intrusion volume is plotted vs. diameter logarithm, and if pore surface is fractal between a range of pore diameters, a linear tendency should be observed, and from the slope of that line D_f is calculated.

4 DATA PROCESSING METHOD

The experimental data of MIP were imported into Microsoft Office Excel. Lg(−dV/dD) and LgD at different pressures were calculated and scatter plots were made in Excel. The linear equation and Correlation coefficient were obtained by adding the trend line for Lg(−dV/dD) ~ LgD. If the Correlation coefficient is high, the fractal characteristic is remarkable. According to Eq.1, the pore surface fractal dimension can be calculated by the slope of the trend line of Lg(−dV/dD) ~ LgD.

The scatter plot of Lg(−dV/dD) ~ LgD for cement mortar with 0.6 water-cement ratio at 3d age is shown in Figure 1(a). It can be seen that the trend line of Lg(−dV/dD) ~ LgD is not linear in the whole range of pore size tested by MIP, and there are inflexion points. The plot can be divided into three regions according to the inflexion points as shown in Figure 1(a). Taking inflexion points and pore classification method in account, the three regions divided by pore diameter were: D>100nm, 10nm<D<100nm and D<10nm. The scatter plot of Lg(−dV/dD) ~ LgD, linear regression equation and the correlation coefficient in three regions are shown in Figure 1 (b), (c) and (d) respectively. It can be seen that the correlation coefficient is higher in the region of D>100nm and 10nm<D<100nm, so the fractal characteristic is remarkable for these two regions. The correlation coefficient is equal to 0.4812 in the region of D <10nm, so the fractal characteristic is not remarkable. The reason may be that the error exists in the data of MIP at the small pore size near to the test limit. The absorption method can be used to study the pore fractal characteristic in the region of D <10nm. For analysis convenience, D_{f1} and D_{f2} were proposed to represent the pore surface fractal dimension for the region of D >100nm and 10nm<D<100nm respectively.

The pore surface fractal dimension (D_{f1} and D_{f2}), correlation coefficient (R^2), compressive strength (R_c) and flexural strength (R_f) with different water-cement ratios (w/c) and ages are shown in Table 2. The fractal dimensions calculated in two pore size regions are different. D_{f1} is large, and general between 3.1 and 3.5; D_{f2} is small, and general between 2.6 and 3.2. The correlation coefficients show that, the

correlation coefficients of D_{f1} are high, which are general greater than 0.97. Relatively, the correlation coefficients of D_{f2} are lower, most of which are greater than 0.80 with some between 0.7 and 0.8. It indicates that the pore fractal characteristic of mortar is more obvious with the pore diameter D>100nm. According to fractal dimension definition (Zhu, 2004), the surface fractal dimension should be between 2 and 3, but some pore surface fractal dimensions calculated in the study are large than 3. The reasons why this happened need to be further studied. .

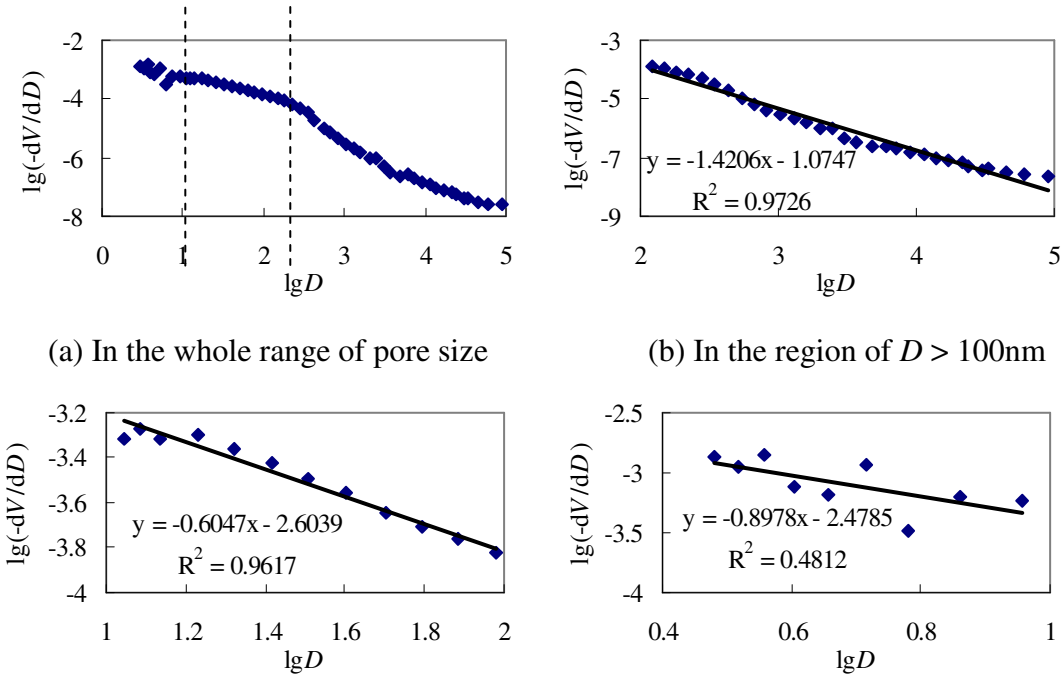

(a) In the whole range of pore size

(b) In the region of D > 100nm

(c) In the region of 10nm< D <100nm

(d) In the region of D <10nm

Figure 1. Scatterplot of Lg(−dV/dD) ~ LgD of different pore diameter ranger for cement mortar with 0.6 water-cement ratio at 3d age

Table 2. Data of pore surface fractal dimension and strength of cement mortar

w/c	Age	D_{f1}	R^2	D_{f2}	R^2	R_c/Mpa	R_f /Mpa
	3d	3.2775	0.9844	2.6936	0.7052	36.5	7.5
0.4	7d	3.1893	0.9880	3.0294	0.7895	46.5	7.9
	28d	3.2187	0.9749	3.4292	0.8406	95.9	10.2
	3d	3.3455	0.9779	2.6523	0.9867	29.3	6.9
0.5	7d	3.2934	0.9804	2.6974	0.9702	41.9	8.0
	28d	3.2271	0.9766	3.1346	0.8699	89.7	10.0
	3d	3.4206	0.9726	2.6047	0.9617	23.1	4.9
0.6	7d	3.4057	0.9720	2.7127	0.9865	35.3	7.0
	28d	3.3238	0.9707	2.9129	0.9656	79.5	9.9

5 EXPERIMENT RESULTS AND DISCUSSION

5.1 Influence of water-cement ratio and age on pore surface fractal dimension

The pore surface fractal dimension with different water-cement ratios and

ages are plotted in Figure 2. From Figure 2, it can be seen that the pore surface fractal dimension varies with water-cement ratio and age regularly, but the relations between the fractal dimensions D_{f1}, D_{f2} and age, water-cement ratio are different. For D_{f1}, the pore surface fractal dimension becomes lower as the age of mortar grows and water-cement ratio decreases . For D_{f2}, the relations are just opposite from D_{f1}.

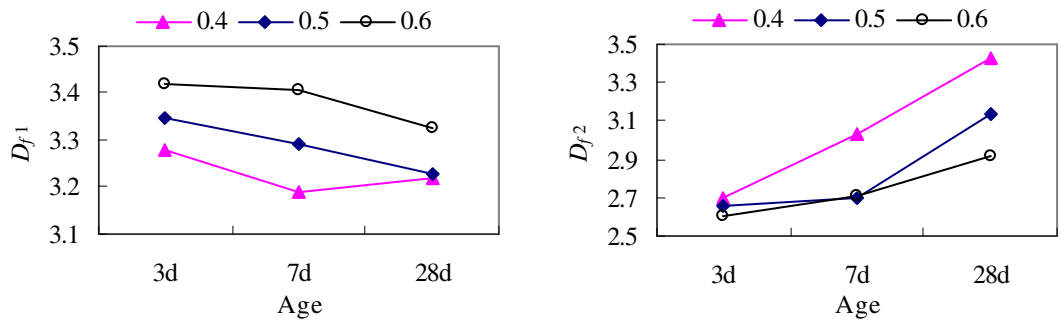

(a) D_{f1} ~ Age (b) D_{f2} ~ Age

Figure 2. Pore surface fractal dimension varies with water-cement ratio and age

The larger the fractal dimension is, the more complex is the surface, so the results show that as the hydration progresses and the water-cement ratio decreases, the pore distribution (D >100nm) becomes simpler, and the pore distribution (10nm<D<100nm) becomes more complex. It means that the number of larger pores decreases and the number of small pores increases when age grows and water-cement ratio decreases , which fits the development rule of pore structure in mortar. Therefore it is suitable for using pore surface fractal dimension to describe the pores characteristic.

5.2 The relationship between strength and pore surface fractal dimension

Strength is the most important macroscopical performance parameter of cement-based materials, and it is influenced by pore structure strongly. The scatter plots of compressive strength and flexural strength with pore surface fractal dimension are shown in Figure 3 and Figure 4.

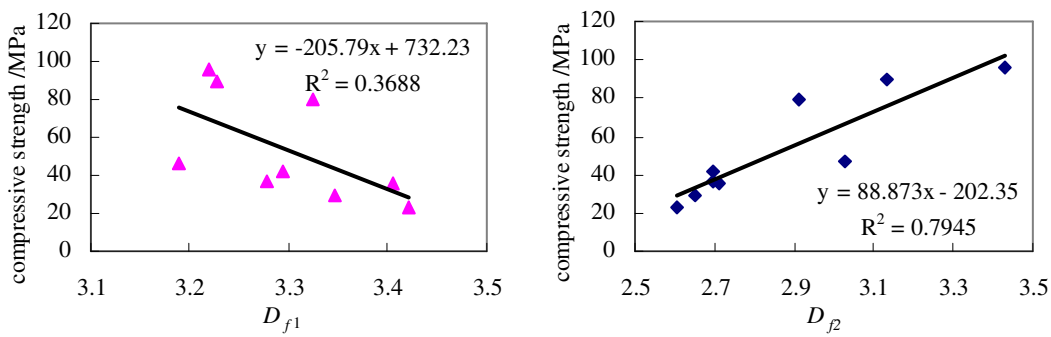

(a) Compressive strength~ D_{f1} (b) Compressive strength~ D_{f2}

Figure 3. Relations between compressive strength and surface fractal dimension

It can be concluded that the compressive strength and flexural strength vary

with pore surface fractal dimension regularly, and the regular patterns are the same. That is, the compressive strength and flexural strength grow to higher as D_{f1} decreases and D_{f2} increases. Considering the influence of water-cement ratio and age on pore surface fractal dimension, as pore surface fractal dimension D_{f1} decreases and D_{f2} increases, the number of large pores gets smaller and the number of small pores gets bigger. Therefore the specific surface area of the pores gets larger. It means that the pore structure becomes optimized, and so the compressive strength and the flexural strength increase.

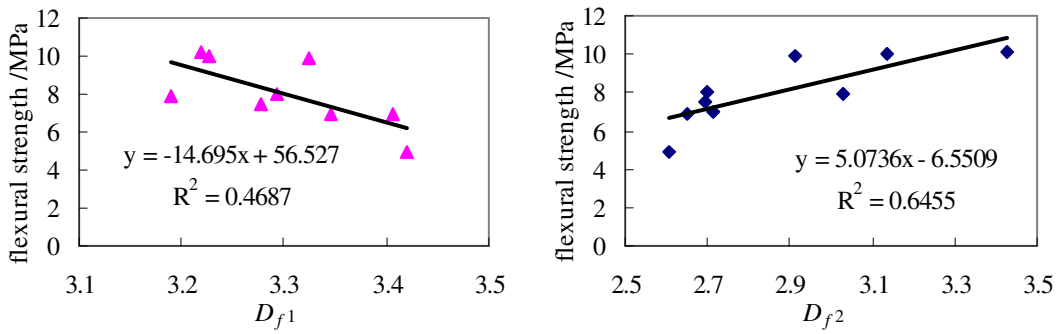

(a) Flexural strength ~ D_{f1} (b) Flexural strength ~ D_{f2}

Figure 4. Relations between flexural strength and surface fractal dimension

6 CONCLUSIONS

(1) The fractal dimension is not unique in the whole range of pore size tested by MIP. Three regions divided by pore diameter were: D>100nm, 10nm<D< 100nm and D<10nm. The pore fractal characteristic in the regions of D>100nm and 10nm<D<100nm are more remarkable, and the pore surface fractal dimensions calculated in the two regions are general in range of 3.1~3.5 and 2.6~3.2 respectively.

(2) The pore surface fractal dimension varies with water-cement ratio and age of the cement mortar regularly. As the age grows and water-cement ratio decreases , the pore surface fractal dimension D_{f1} becomes smaller and D_{f2} becomes larger .

(3) The compressive strength and flexural strength of mortar vary with pore surface fractal dimensions regularly. Their regular patterns are the same. The compressive strength and the flexural strength increases as D_{f1} decreases and D_{f2} increases.

REFERENCES

W. Hu (1997), Modeling the Influence of Composition and Pore structure on Mechanical Properties of Autoclaved cellular concrete. PhD. thesis, Univ. of Pitt.

M. Tang (2000), Research on fractal characteristics of concrete materials pore with MIP, J. Shenyang Arch. and Civ. Eng. Univ., 8, 272-275 (In Chinese)

M. Tang, Z. Huang (2007). Evaluation on the Fractal Characteristics of Pore in SEM Photo of Cement Matrix Materials with the Measure Relation. J. Shenyang

Arch. and Civ. Eng. Univ., 23(6), 952-956 (In Chinese)
B. Zhang, S. Li (1995). Determination of the Surface Fractal Dimension for Porous Media by Mercury Porosimetry, Ind. and Eng. Chem. Res., 4, 1383-1386
W. Zhu (2004).the fractal in material science. Chemical Industry Press, Beijing

Node-Importance-Degree-Based Logistics Node Analysis

Li Li[1] and Guoquan Yao[2]

[1]Hebei University of Technology, No. 1 Road Dingzigu, Hongqiao district, Tianjin, China; Tel:13672006506; email: danmama95@sina.com
[2]Hebei University of Technology, Beichen district, Tianjin, China; Tel: 15822502567; email: yaoguoquan_001@163.com

ABSTRACT

Port is an important hub of the integrated transport network. It is necessary to build the logistics centre in the port industrial zone, which will provide comfortable logistics services and enhance the competitiveness. Based on the theory of the node important degree, the traffic location and the indexes of the nodes, the paper calculates the importance of the logistics node index, which uses Analytic Hierarchy Process (AHP) to determine the weights. Combined with related data and documents, the paper analyzes the logistics node of the iron and steel industry of Caofeidian.

INTRODUCTION

The analysis of the logistics node important degree is an important aspect for the logistics center building and investment decisions. Determining the logistics node is one of the main subjects for Industrial Park Planning. A reasonable set of logistics nodes can ease the operation pressure of a logistics center and increase the investment profit of the logistics node.

NODE IMPORTANCE DEGREE

The concept of node is widely used in graph theory, economic geography, regional science and other fields. Traffic location theory believes that a small number of the region (1/3) node traffic generated by the corresponding region accounts for all the traffic generated most of the (2/3).As a result, the logistics node analysis of the characteristics of the traffic is particularly important. Node important degree is a quantitative indicator that studies the transport network represented by the proposed distribution node transport capacity and has become the main basis that is used to measure the importance of the transportation hub in road planning.

NODE IMPORTANCE DEGREE CALCULATION

Modeling

Node important degree is an important index of relative degree that describes a node in the region and compares different functions of the strength of the relativity between nodes. It is a comprehensive measure of importance for every node in the area. In industrial areas of logistics planning, the choice of logistics distribution, warehousing centers for the consideration of the link nodes, and its importance

degree by the following formula:

$$D_i = \sum_{j=1}^{m} \omega_i \frac{P_{ij}}{\sum_{k=1}^{n} P_{kj}} \qquad (1)$$

Where: n = the number of nodes; m = the evaluation of the number of indicators; and P_{ij} = the i-node department j (j = 1,2, ..., m) index value.

Model

Although the Equation 1 is given all nodes importance degree of quantitative terms, it cannot reflect the limits of the division of nodes, which means that it cannot be given an important degree of range. In this system, analysis of the cluster ideas was used. According to the major index, summing all nodes into the required categories must be done in order to better determine the extent of the important nodes.

Suppose there are n samples: X_1, X_2... X_n, and each of the samples were found to have m characteristics or indicators. These indicators will be quantified (that is to use the digital representation of their targets), for each sample corresponding to a set of indicators for its characterization of a number of Y_1, Y_2... Y_m. This group represents the number of samples for m-value targets. It is clear that a different sample of the corresponding indicator is not the same as that used in this X_{ij}. The first i samples of the first j-value targets are not the same, so the targets of the n samples are shown in Table 1.

Table 1. Method of samples.

Sample	Index			
	index 1	index 2	…	index m
X_1	X_{11}	X_{12}	…	X_{1m}
X_2	X_{21}	X_{22}	…	X_{2m}
…	…	…	…	…
X_n	X_{n1}	X_{n2}	…	X_{nm}

We can see from Table 1, samples X_i can be lined up (X_{i1}, X_{i2}... X_{im},) and recorded for X_i = (X_{i1}, X_{i2}... X_{im}) from the broad use of standardized square Euclidean distance to reflect the close of the two samples between X_i and X_j, the formula becomes:

$$D_k = | X_i - X_j | = \sum \frac{(X_{ik} - X_{jk})^2}{S_k^2} \qquad (2)$$

Where: K = 1, 2... m; D_k for between two points the generalized distance; and S_k for the X variable variance.

This comprehensive reflection of the distance between the two samples of the different indicators of size, the smaller of $| X_i - X_j |$ the smaller differences and closer in the two samples and can be grouped into the same otherwise the greater of $| X_i - X_j |$, that is the larger different samples, and not in the same category. The specific approach is as follows.

Step 1: calculate the distance between the sample $|X_i–X_j|$ and seek min ($|X_i–X_j|$)

Step 2: make the samples with min ($|X_i–X_j|$) characteristics in the same category and form a new sample and make the assignment. Samples of the new indicators represent the value of the average of all the corresponding samples.

Step 3: repeat steps 1 and 2 above and place all the samples into a category.

Following the above classification process,Figure 1 shows:

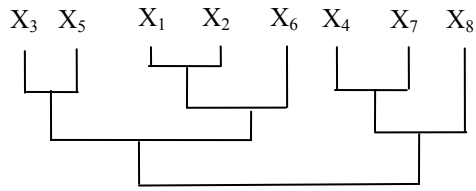

Figure 1. Clustering logistics node hierarchy.

The cluster analysis is to better partition node types, determine the different levels of the main line, and carry out the layout of the road network well. On the basis of cluster analysis principles and methods calculating all nodes importance degree of group cities node, the node can generally be divided into three categories: the firstly important node, the secondly nodes and the generally nodes.

NODE IMPORTANCE DEGREE ANALYSIS

The logistics node function is closely related to the material flow and personnel flow. As a result, material and human traffic flow are the important indexes of decision logistics nodes importance degree. At the same time, relevant economic indicators directly impact important nodes, such as the evaluation of the economic efficiency of enterprises in selected logistics park business profits tax. Usually calculated the node important degrees use the Analytic Hierarchy Process (AHP). AHP has been widely applied in many fields. This paper mainly relates using the methods to analyze the importance node process. Specific theories can be found in the reference section.

Indicators Weight

Determining the index weight is a clear indicator influencing the degree of the target level. The extent of the impact of the target layer is often based on experience and the weight of certain subjectivity. The Analytic Hierarchy Process makes the rules of the quantitative process to reduce the weight determined by the subject and to improve accuracy.

To establish the hierarchy model. The hierarchy model is the result of the analysis of the study and makes all factors at division different levels, such as the target layer, indicators layer, and programs layer and so on. Using the diagram shows the form of note-level hierarchical structure and factors of affiliation.

The chart below is the location of logistics nodes analysis hierarchy model. .

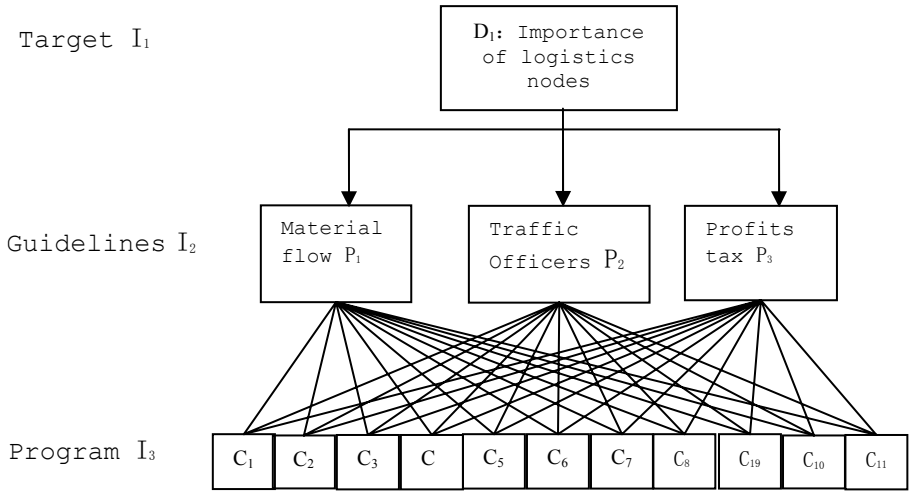

Figure 2. Logistics node location hierarchy.

Node important degree evaluation indicators

According to the AHP, create the target level (logistics nodes important degrees) and indicators layer (materials flow, personnel flow, profits tax) that impact on the important node concrete structure shown in Table 2.

Table 2. Nodes important undicator of its analysis of weight.

Target layer I_1	Indicators layer I_2	I_2 to I_1 weight ω_i
Importance of logistics nodes D_i	Material flow P_1	0.65
	Traffic officers P_2	0.13
	Profits tax P_3	0.22

Node important degree calculations

Access to the index weight, and calculate the logistics node i (i = 1, 2,…, n) index major D_i. According to the State has approved Caofeidian harbor planning documents and related materials summarized Caofeidian the logistics center of the relevant data show in Table 3.

Based on the above data, calculate the importance of the logistics nodes. Importance of coal distribution centers, D_1 , is：

$$D_1 = 0.65\times\frac{6280}{4279.245}+0.13\times\frac{0.07}{1.25}+0.22\times\frac{0.314}{4.495}=0.97$$

By the same token, power plant $D_2 = 0.215$, cement plant $D_3 = 1.754$, iron and steel industrial base $D_4 = 4.37$, cement logistics center $D_5 = 0.121$, railway station $D_6 = 2.061$, building materials plant $D_7 = 0.104$, ore logistics center $D_8 = 1.907$, steel logistics center $D_9 = 0.635$, steel wharf $D_{10} = 0.256$, and plastic logistics center $D_{11} = 0.031$.

Table 3. Caofeidian data summary.

Serial number	**Logistics node name**	**In total material handling / 10,000**	**The number of district /**	**Tax**

		tons	thousand	profits / billion
1	Coal logistics center	6280	0.7	0.314
2	Power plant	1210.7	0.22	0.156
3	Cement plant	775	188	0.045
4	Iron and steel industrial base	8452	10.9	40.092
5	Cement logistics center	750	0.05	0.042
6	Railway station	13450	0.1	0.204
7	Building materials plant	409	0.31	0.151
8	Ore logistics center	11120	0.08	4.260
9	Steel logistics center	3220	0.05	2.852
10	Steel wharf	1270	0.05	1.198
11	Plastic logistics center	135	0.04	0.128

Table 4. Node importance.

Serial number	Logistics node name	Important node index	Importance ranking
1	Coal logistics center	0.088	4
2	Power plant	0.019	8
3	Cement plant	0.028	6
4	Iron and steel industrial base	0.398	1
5	Cement logistics center	0.011	9
6	Railway station	0.188	2
7	Building materials Plant	0.007	10
8	Ore logistics center	0.174	3
9	Steel logistics center	0.058	5
10	Steel wharf	0.024	7
11	Plastic logistics center	0.003	11

Table 5. Node importance.

Important node	Logistics node name	Iron and steel industrial base	Railway station	Ore logistics center	
	Importance	0.398	0.188	0.174	
Major node	Logistics node name	Coal logistics center	Steel logistics center	Cement plant	Steel wharf
	Importance	0.088	0.058	0.028	0.024
General node	Logistics node name	Power plant	Cement logistics center	Building Materials Plant	Plastic logistics center
	Importance	0.019	0.011	0.007	0.003

Table 4 and Table 5 show all nodes important degree, but the Caofeidian iron and steel Industrial Zone logistics center construction sequence program is not in accordance with the node important degree or the planning of a logistics center size to building. It's based on node important degree, considered Caofeidian Industrial Zone of development direction in the future and the cycle of economic models and other factors to sort. It can reflect the Caofeidian Industrial Zone Logistics Center construction and Industrial Zone circular economy is consistent patterns.

CONCLUSION

The evaluation index system of logistics node is complex and effective solutions are not yet presented because of the lack of the standards of a logistics market in China. In this paper, the AHP is applied to calculate the relative weightings of the major factors and the important index of the nodes is calculated in terms of theory of transportation, where an authentic and operable solution is given to determine the index system and evaluate the logistics nodes.

BIBLIOGRPHY

Qu, D. Y., Wang, W., and Deng, W. (2000). "Order of item in the process of highway network planning based on AHP." *China Journal of Highway and Transport*, 13 (3):64–68.

Hu, G.. (2003). "Order of item in the process of distribution [ark [lanning based on AHP and multi-object decision." *J. of Highway and Transportation Research and Development*, 20 (2):157–161.

Guan, C. D. (2001). "Transportation location." Beijing: People's Communications Press.

Hu, L. G., Xu, G. L., and Xie, H. (2006). "Layout of roads link provinces based on the layou method combining node important degree with area location." *J. of Railway Science and Engineering*, 3(1):50–55.

Saaty, T. L. (1980). *The Analytic Hierarchy Process*. New York: McGraw Hill.

Study on Evaluation Method of Expressway Roughness

WANG Shuyun1, ZHANG Jinxi 1, CUI Yaping2

[1]Key Laboratory of Traffic Engineering, Beijing University of Technology, Beijing 100124，P.R. China. Tel: +86-10-67391583 (O), Fax: +86-10-67391509, email: zhangjinxi@bjut.edu.cn

2 Beijing AOK-REAL Communications Technology Development Co.,Ltd., Beijing 100176，P.R. China. Tel: +86-10-67805858-2208 (O), email: cuiyaping1977@yahoo.com.cn

ABSTRACT

International roughness index has become a well-recognized standard for measurement of pavement roughness in the world. In China, the current evaluation rules are such that the average value of IRI measured from road test sections is used to evaluate road quality. However this evaluation method is not proper in judging road quality in practical application. In this study, moment method is utilized to statistically analyze the IRI data distribution of expressway pavement. In Beijing city, 8 expressways of different road ages are selected as test samples, and then a time series of IRI data are employed .By statistical analysis, a comprehensive evaluation system, which is composed of 3 indictors such as the average of IRI, skewness coefficient and kurtosis coefficient is established. Practical application testified that the evaluation system can truly reflect expressway riding quality.

KEY WORDS

Expressway, Roughness evaluation, Riding quality, Moment method

1 INTRODUCTION

Pavement roughness as an important indicator to evaluate pavement serviceability directly reflects traffic comfortability and safety level (Zhang, 2005). International roughness index (IRI) is a standardized roughness indicator, which uses mathematical model to simulate quarter-car driving on test road section (M.W., 1986). The relative displacement between the sprung masses and un-sprung masses at 80Km/h caused by the dynamic suspension system is called IRI. IRI has two advantages: time stability and easy conversion between different test equipments, and then it has a wide use all around the world. According to the current specification: "highway performance assessment standards" (JTG H20 - 2007), expressway pavement riding quality is also assessed by average of IRI (AOI) in China. At present, an IRI value per 100m is defined as an evaluation unit, ultimately the arithmetic mean value of all units is calculated to judge road riding quality.

Table 1 shows two expressways' IRI test value in Beijing city (Cui, 2006). The evaluated section of A expressway is 45.6Km long and B expressway's assessed

section has a distance of 9.5 Km. A expressway had 456 IRI values and B expressway had 95 IRI values. The arithmetic means of the IRI of two expressways are calculated separately and the results are 0.78m/Km for A expressway and 2.24 m / Km for B expressway. According to specification JTG H20 - 2007, when expressway's IRI is less than 2.3 m/Km in Ride Quality Index (called RQI) of roads is defined as excellent. Therefore, it can be seen that two expressways' RQI are both excellent. Careful analysis of Table 1 finds out that all the IRI sample values of A road are less than 2.3 m/Km, that is, all samples can meet the criteria. The number of units of B highway with AOI greater than 2.3 m/Km is 30, which account for 31.6 percent of all assessed units. It means that only 68.4 percent of the units should be excellent. Clearly, there is a significant careless omission in the present evaluation indictor AOI, which can't accurately reflect the actual riding quality of expressway.

Table 1. Test result and evaluation of IRI of expressway.

IRI (m/Km)		0.7	0.9	1.1	1.3	1.5	1.7	1.9	2.1	2.3	2.5	2.7	2.9	3.1	3.3	3.5	3.7	3.9	4.1
Nu.	A	282	166	6	2	0	0	0	0	0	0	0	0	0	0	0	0	0	0
	B	1	1	8	14	16	6	5	10	4	2	9	4	4	2	5	3	0	1
Tot.	A	456		Mean	A	0.78													
	B	67			B	2.24													

Note: 1. Nu. represents the number of samples per IRI zone.
2. Tot. represents the total number of samples.
3. Mean represents the IRI average of tested expressway.

2 METHODLOGIES

Moment method(*Wang,2008*) is one statistical methods ,and it is based on two important statistical indicators which are used to describe the numerical distribution of variable values, namely, skewness coefficient (SC) and kurtosis coefficient (KC). So the moment method is also named skewness and kurtosis test method.

SC and KC of random variable x respectively represent standardized variables x's third-order center moment and fourth-order center moment. When random variable x are subordinated to normal distribution， g_1(represent SC) and g_2 (represent KC) from the overall samples are:

$$g_1 = B_3 / B_2^{3/2} \quad , \quad g_2 = B_4 / B_2^2 \tag{1}$$

Among them, B_K (k = 2, 3, 4) represents k-order center moment of samples.

If random variable x obeys normal distribution, it can be certified when n is sufficiently large. The approximations are:

$$g_1 \sim N(0, \frac{6(n-2)}{(n+1)(n+3)}), \qquad g_2 \sim N(3-\frac{6}{n+1}, \frac{24n(n-2)(n-3)}{(n+1)^2(n+3)(n+5)})$$

Generally, SC reflects the degree and direction of single-peak distribution, and the distribution corresponding to $g_1 > 0$, $g_1 = 0$, $g_1 < 0$ is separately known as the normal-skewness, positive skewness and negative skewness.

KC reflects the kurtosis case of single-peak distribution, with $g_2 > 3$, $g_2 = 3$, $g_2 < 3$, the corresponding peak is called leptokurtosis, normal peak kurtosis and flat kurtosis respectively.

3 TEST CONDITIONS OF EXPRESSWAY

Eight expressways located in Beijing are selected as test samples for evaluating the riding quality. Table.2 shows the construction structure, design life, completion time and road age of 8 expressways. All 8 expressways have similar structure composed of semi-rigid base plus asphalt surface, belong to the same climate zone, and the traffic volume of them has an insignificant difference, so the samples data can approximately be used to analyze the IRI-age relationship. Data used in this study were collected in 2004, and then road age is calculated accordingly.

Table 2. Structure Conditions of Expressway.

Expressway Name	Pavement structure of expressway	Design Life (year)	Completion time (year)	Road ages (year)
1	asphalt chip surface 2cm Medium-grained asphalt concrete 4cm Bituminous macadam mixture 5cm Inorganic binder base36cm Lime stabilized soil 18cm	15	1990	14
2	Medium-grained asphalt concrete 3.5cm Coarse-grained asphalt concrete 4.5cm Bituminous macadam 7cm Lime and fly-ash stabilized gravel 40cm Lime stabilized gravel 20cm	15	1993	11
3	Dense-Graded medium-grained asphalt concrete 5cm Coarse-grained asphalt concrete 7cm Bituminous macadam 8cm Lime and fly-ash stabilized gravel 40cm Natural gravel 20cm	15	1996	8
4	SMA-16 4cm Coarse-grained asphalt concrete (AC-25)6cm Coarse-grained asphalt concrete (AC-30)8cm Lime and fly-ash stabilized gravel 40cm Lime stabilized soil 30cm	15	2001	3
5	SMA-16 5cm Dense-Graded medium-grained asphalt concrete 6cm Coarse-grained asphalt concrete 7cm Lime and fly-ash stabilized gravel 54cm	15	2001	3

6	SMA-16 4cm Coarse-grained asphalt concrete 5cm Coarse-grained asphalt concrete 7cm Lime and fly-ash stabilized gravel 54cm	15	2002	2
7	SMA 4cm Dense-Graded coarse -grained asphalt concrete 5cm Coarse-grained asphalt concrete 6cm Lime and fly-ash stabilized gravel 40cm Natural gravel35cm	15	2002	2
8	SMA-16 5cm Dense-Graded medium-grained asphalt concrete 6cm Coarse-grained asphalt concrete 7cm Lime and fly-ash stabilized gravel 54cm	15	2003	1

4 DATA ANALYSIS

4.1 IRI analysis of expressway with different ages.

Expressway test sections are selected randomly, and then IRI values are measured by laser road condition test equipment. Sampling frequency is one IRI value per 100 m. IRI distribution curves of test expressways are mapped as shown in Fig.1, in which abscissa value represents IRI, longitudinal coordinates represent frequency number. As can be seen from Fig.1, with the road ages increasing, the peak of the distribution curve gradually decreases, the AOI increases and the slope grow flatter.

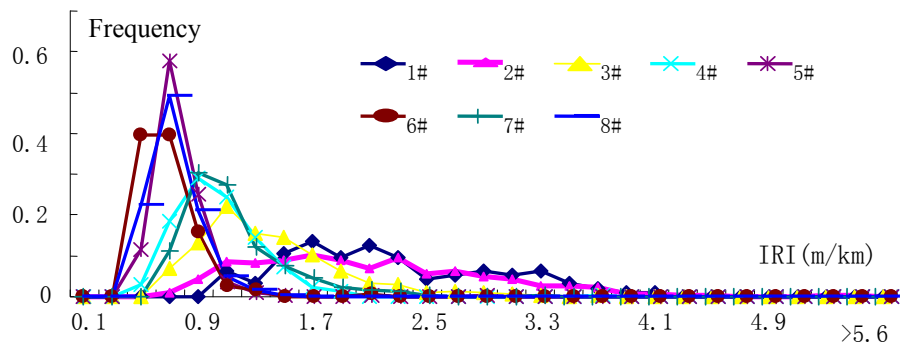

Figure 1. IRI distribution curve of different expressway

4.2 SC and KC analysis of expressway with different ages

Based on the theory of moment method , normality test of all the curves in Fig.1 is conducted, in which it is found that only IRI distribution of 1 # expressway was subordinated to normal distribution. SC and KC of each curve are calculated separately, and then the rules that SC and KC gradually decrease with the increase of road ages is found (see Figure 2 and Figure 3).

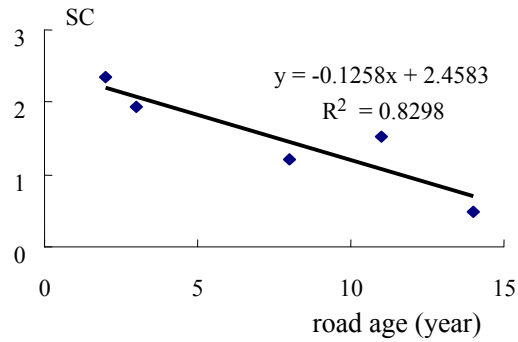

Figure 2 SC-age-related regression curve

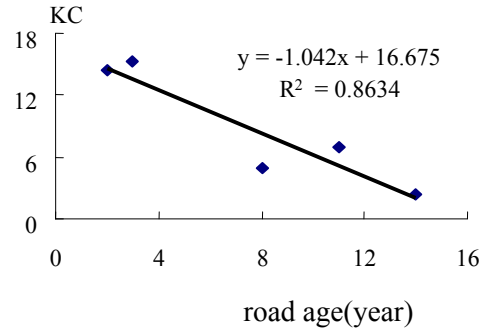

Figure 3 KC-age-related regression curve

Because expressway with road age of 2 years includes two roads and expressway with road age of 3 years does so, then the average of SC and KC is defined as SC and KC value corresponding to these two kinds of road age. When road age is one year old, SC and KC value are all larger than those of other road ages, which makes it impossible to establish a better correlation between different road ages. Taking into account the excellent practicality of one year road age expressway, SC and KC of one year road age are discarded. Data of SC and KC from five kinds of road age was mapped into scatter chart and made a straight-line fitting separately (see Figure.2 and Figure.3). The square of correlation coefficient between SC and road age is 0.8298, and it is 0.8634 between KC and road age.

4.3 Evaluation system establishment

According to these expressway s' IRI data, IRI decay curves varying with road age were given (Cui, 2006). Fig.4 shows the IRI-age-related regression curve of expressway with road age below 5 years. The IRI-age-related regression curve of expressway with road age above 5 years is shown in Fig.5.

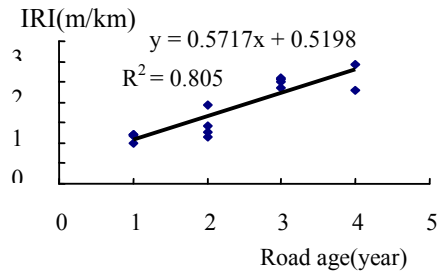

Figure4. IRI-younger road age regression curve

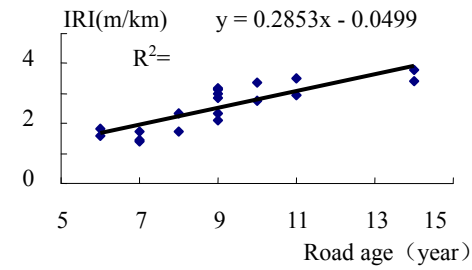

Figure5. IRI-older road age regression curve

In accordance with the RQI-IRI relationships ruled by " Highway Performance Assessment Standards" (JTG H20-2007), comparing IRI value of each grade to Fig. 4 and Fig.5 respectively, then the corresponding road age is obtained according with every RQI level (or IRI level)(see table 3).

Then according to the conclusions of Figure 2 and Figure 3, SC and KC value corresponding to road age obtained above can be found. Filling all the data in Table 3, and then a comprehensive evaluation system is established based on the AOI, SC and KC. i.e., when 3 indictors simultaneously meet the demand in Tab.3, the quality grade of RQI could be judged. When 3 indictors locate in three

different RQI Levels, the treatment should accord with the most adverse situation.

Table3. RQI – IRI – g_1 –g_2 corresponding relationship.

RQI(score)	90（excellent）	80（good）	70（medium）	60（bad）
IRI	2.3	3.5	4.3	5.0
Road age(year)	3.1	12.4	15.3	17.7
g_1 (SC)	2.07	0.90	0.53	0.23
g_2 (KC)	13.44	3.75	0.73	-1.77

5 PRACTICAL APPLICATIONS

Computing SC and KC of B expressway (shown as Table1.) based on moment method, the results are 0.49，2.40 respectively. From the above analysis, when AOI is less than 2.3m/km, RQI has a score larger than 90 points. But the road SC value falls into the scope between 70 ~ 60 scores, by interpolation method, RQI score is 68.7; then by KC's interpolation value, RQI score is 75.5. In accordance with the most disadvantaged rules, the riding quality score is 68.7 points, and this score can truly reflect riding quality of B expressway.

The calculation formula of g_1 and g_2 is attached as below:

$$A_1=\frac{1}{n}\sum_{i=1}^{n}x_i\ ;\qquad A_2=\frac{1}{n}\sum_{i=1}^{n}x_i^2\ ;\qquad A_3=\frac{1}{n}\sum_{i=1}^{n}x_i^3\ ;\qquad A_4=\frac{1}{n}\sum_{i=1}^{n}x_i^4\ ;$$

$$B_2=A_2-A_1^2\ ;\qquad B_3=A_3-3A_2A_1+2A_1^3;\qquad B_4=A_4-4A_3A_1+6A_2A_1^2-3A_1^4;$$

$$g_1=\frac{B_3}{B_2^{3/2}},\qquad g_2=\frac{B_4}{B_2^2}$$

6 CONCLUSIONS

6.1 Findings

In this study, moment method theory is utilized to analyze IRI data. SC-age-related and KC-age-related regression curve were set up. Based the rule of current "Highway Performance Assessment Standard" (JTG H20-2007) and Cui Yaping's study conclusions, an evaluation system was established, which is composed of 3 indictors including mean IRI, SC and KC. When 3 indictors located in three different score region, the lowest value is suggested as RQI score by the most disadvantaged principle. Testified by practical application, the evaluation system has a better effect on evaluating RQI and can diminished the bad effect caused by the single indictor-AOI. The evaluation system is practical in use and is very useful in the maintenance and management of expressway.

6.2 Future

This study is based on statistic principle, so the sample data should further

increase in order to obtain more accurate result. In data acquisition, the tested IRI's error caused by irregular maintenance should be avoided. RQI evaluation system should be separately set up corresponding to road grade and climate region, because asphalt pavement performance is greatly affected by materials, construction techniques, climatic factors and traffic volume etc.

ACKNOWLEDGEMENT

This study was sponsored by National Natural Science Foundation of China (GM: 50522201).

REFERENCE

J.X., Zhang, Y.P., Cui, et al. "Analysis of Present Condition of Beijing's Expressway". Sino-Netherlands Seminar Proceedings, pp.9-16, 2005.

Sayers, M.W., T.D., Gillespie, et al. "Guidelines for the Conduct and Calibration of Road Roughness Measurements". World Bank Technical Paper 46.World Bank, Washington, D.C., 1986.

Y.P., Cui, J.X., Zhang, et al. "Analysis on the Evenness Changeable Characteristics of the Expressway in Beijing". International Slurry Sealing Proceedings, 2006.

X.M., Wang . "Misunderstanding of Skewness and kurtosis". Statistics and Decision-making, No.12, pp.145-146, 2008.

JTG H20-2007: Highway Performance Assessment Standards[S].Beijing, the People's Traffic Press, 2008.

Research on Cost Control in Logistics Enterprises

Lingxiang Jian[1,2] and Dongbing Li[3]

[1]Transportation Management College, Dalian Maritime University, P.O. Box 116026, Dalian, China
[2]School of Management, Dalian University of Technology, Dalian, China, PH (0411) 8472- 8808; email: jian8808@126.com
[3] City Institute, Dalian University of Technology, P.O. Box 116023, Dalian, China; PH (0411) 8472- 8808; email: li8808@126.com

ABSTRACT

At present, competition among domestic logistic enterprises is fierce. If they want to endure and become more advanced, they must calculate cost accurately and control cost effectively. Based on the management characteristics of logistic enterprises, this paper brings the Activity-Based Cost (ABC) into cost control practice in order to probe a new method to reinforce cost control and raise economic benefit in the logistic enterprises.

INTRODUCTION

Since the 1980s, enterprises' direct artificial cost has dropped and indirect expense has increases greatly. The information cost obtained by indirect expense assignment, based on sole quantity traditionally, has been serious distorted. Staubus (1971) and Cooper (1988, 1992) explained that ABC can not only provide more accurate cost information, but also has vital significance in cost control, budget management, new product design and development and more. The application domain of ABC has also expanded from the initial advanced manufacturing industry to commercial, financial, transportation enterprises, as well as the logistics industry. Since the 1990s, Yu (1995), and Wang (1999) have conducted extensive research on utilization theory and its practical application and significance and on prospects for the application of ABC. Jian's (2004) has done research on logistics enterprises activity cost calculation, but there is little research on cost control in logistics enterprises with the ABC method.

ASCERTAINING THE BEST DESIGNED ABILITY OF ACTIVITY OF LOGISTICS ENTERPRISE

Logistics enterprise designed ability of activity refers to the activity ability that enterprises design or the contract stipulates. The designed ability of activity cost is cost caused by the enterprise signing an agreement to buy resources in advance. We can summarize Its characteristics: Before satisfying the activity demand, the enterprise has obtained the activity ability, by the way of cost, either by payment or by pledging future payment by contract or agreement. The result is that, whether these activity abilities are used or not, the activity ability cost will surely occur. The designed ability of activity

cost is the sum of the surplus activity ability cost and already used activity ability cost. If the logistics enterprise is able to ascertain the designed ability of activity according to the future demand change of logistics activity, it may clearly understand and measure the surplus activity ability or the bottleneck activity ability. The enterprise's manager can make decisions scientifically at the right moment, change the designed ability of activity level in future periods, and thus control the ability of activity cost effectively.

Assuming we know the standard cost of each increment of value activity, this paper ascertains the best designed ability of activity for a logistics enterprise. The basic approach is: First, scientifically forecast the enterprise future logistics demand; next, ascertain the future activity demand according to logistics demand; then, ascertain the expectation cost of activity function according to the mutual existing relationship of activity and the cost; and, finally, in the situation of satisfying the logistics demand, extract the designed ability of activity with the smallest expectation cost of activity, namely the best designed ability of activity. The concrete method follows:

Supposing that the logistics enterprise has many kinds of activities $j = 1,2,\cdots,J$, provides many kinds of logistics service products $i = 1,2,\cdots,I$, faces uncertain demand market, and later observes an incomplete demand signal vector $\Psi = (\Psi_1, \Psi_2, \cdots, \Psi_i)$ (Ψ_1 is the demand signal of logistics service product of 1, Ψ_i is the demand signal of logistics service product of i) of each logistics service product. Suppose as well that the logistics enterprise has a designed ability of activity level of j is $\overline{Y}_j$, $\bar{x}_i(\Psi_i)$ is the anticipated demand for logistics service product i observed by the enterprise of demand signal Ψ_i, η_i is the random variable or the random error of uncertain market elements related to the anticipated demand, with the expectation value $E(\eta_i) = 0$, the variance of Ψ_i is $V_{ar}(\Psi_i) < \infty$. Then the enterprise actual service level $x_i(\Psi_i)$ is:

$$x_i(\Psi_i) = \bar{x}_i(\Psi_i) + \eta_i \qquad (1)$$

According to incomplete demand signal $\bar{x}_i(\Psi_i)$ that determines the best logistics service level $x_i^*(\Psi_i)$, as a result of the uncertainty of market and the influence of internal factors, the actual demand $x_i(\phi_i)$ may not be equal to the best logistics service level.

The consumption of activity demand is a linear model, supposing y'_{ij} represents activity demand j of providing i service product, then provides x_i unit service product actually consuming j activity demand $Y_{ij} = y'_{ij}x_i$, the actual activity demand $Y_j(\phi)$ of activity j that all services products consume is:

$$Y_j(\phi) = \sum_{i=1}^{1} y'_{ij}x_i(\phi_i) + \varepsilon_j \qquad (2)$$

In the formula, ε_j represents the correlative measuring error of activity

consumption linear function, supposing the random error ε_j and x_i with Ψ_i is independent and not related, then $\mathrm{E}(\varepsilon_j)=0$.

According to the principle of the ABC method, the cost of product consuming each activity is equal to product of the quantity of consumed resources and the price, that is the product of resources agent quantity and the resources agent rate. Each activity cost can be divided into the fixed part and the variable part. Thus, the activity cost function $ZC_j(\overline{\mathrm{Y}}_j, \mathrm{Y}_j)$ of activity j may be described as follows:

$$ZC_j = b_j \mathrm{Y}_j + \overline{d}_j \overline{\mathrm{Y}}_j + \theta_j \overline{d}_j \Delta \mathrm{Y}_j + \delta_j \quad (3)$$

In the formula: b_j expresses unit activity variable cost of activity j; $\overline{d}_j$ expresses designed ability of activity cost of activity j; $b_j\mathrm{Y}_j$ is the variable cost of activity j; $\overline{d}_j$ is the fixed cost of activity j; δ_j is the disturbance factor independent with Ψ_i ,and $\mathrm{E}(\delta_j)=0$; supposing θ_j is the exceeded activity cost coefficient of activity j, it is equal to the ratio of the resources price of the part that actual need activity ability surpasses the designed ability of activity ($\theta_j > 1$), $\theta_j \overline{d}_j$ indicates exceeded activity cost of the activity unit j; $\Delta \mathrm{Y}_j$ is the quantity that the demand surpasses the designed ability of activity, $\Delta \mathrm{Y}_j = \mathrm{Y}_j - \overline{\mathrm{Y}}_j$, （ $\mathrm{Y}_j > \overline{\mathrm{Y}}_j$ ）.

Make $\overline{\mathrm{Y}}$ and Y separately represent the designed activity ($\overline{\mathrm{Y}}_1 \sim \overline{\mathrm{Y}}_j$) and the vector of actual consumed activity ($\mathrm{Y}_1 \sim \mathrm{Y}_j$), after it observes the demand signal Ψ_i and before it realizes the actual demand, the enterprise needs to choose the level of designed activity resources $\overline{\mathrm{Y}}$. Considering the formula of (1), (2), (3), the relations of expectation activity cost the signal Ψ is like the formula (4) showing.

$$\mathrm{E}[ZC(\overline{\mathrm{Y}}, \mathrm{Y}(\Psi) \mid \Psi)] = \mathrm{E}[\sum_{j=1}^{J} ZC_j(\overline{\mathrm{Y}}_j, \mathrm{Y}_j(\Psi) \mid \Psi)] = \mathrm{E}[\sum_{j=1}^{J} (b_j \mathrm{Y}_j(\Psi) + \overline{d}_j \overline{\mathrm{Y}}_j + \theta_j \overline{d}_j \cdot \Delta \mathrm{Y}_j(\Psi) + \delta_j) \mid \Psi]$$
$$= \mathrm{E}[\sum_{j=1}^{J} (b_j \mathrm{Y}_j(\Psi) + \theta_j \overline{d}_j \Delta \mathrm{Y}_j(\Psi) \mid \Psi] + \sum_{j=1}^{J} \overline{d}_j \overline{\mathrm{Y}}_j \quad (4)$$

Insert formula (1) into formula (2):

$\mathrm{Y}_j(\Psi) = \sum_{i=1}^{\mathrm{I}} y'_{ij} \overline{x}_i(\Psi) + \sum_{i=1}^{\mathrm{I}} y'_{ij} \eta_i + \varepsilon_j$, supposing $\mathrm{Z}_j(\Psi) = \sum_{i=1}^{\mathrm{I}} y'_{ij} \overline{x}_i(\Psi)$ and $h_j = \sum_{i=1}^{\mathrm{I}} y'_{ij} \eta_i + \varepsilon_j$, then $\mathrm{Y}_j(\Psi) = \mathrm{Z}_j(\Psi) + h_j$, in the formula, $\mathrm{Z}_j(\Psi)$expresses anticipated demand $\overline{x}_i(\Psi)$ of service product i that corresponds to anticipated activity j, h_j expresses the probability density function set of the probability density function of η_i and ε_j , and $\mathrm{E}(h_j) = \mathrm{E}(h_j \mid \Psi) = 0$. Supposing $f(h_j)$ represents the boundary probability density function of h_j, $F(h_j)$ is the corresponding accumulation density function, because the distribution of h_j has nothing to do with Ψ (because η_i and ε_j is

independent with Ψ), therefore the formula (4) can be transfigured as follows:

$$\mathrm{E}[ZC(\overline{\mathrm{Y}}, \mathrm{Y}(\Psi) \mid \Psi)] = \sum_{j=1}^{J} [b_j \mathrm{Z}_j(\Psi) + \overline{d}_j \overline{\mathrm{Y}}_j + \theta_j \overline{d}_j \int_{\overline{\mathrm{Y}}_j - \mathrm{Z}_j}^{\infty} (\mathrm{Z}_j(\Psi) + h_j - \overline{\mathrm{Y}}_j) f(h_j) dh_j] \quad (5)$$

$$= \sum_{j=1}^{J} [b_j \mathrm{Z}_j(\Psi) + \overline{d}_j \overline{\mathrm{Y}}_j + \theta_j \overline{d}_j (\mathrm{Z}_j(\Psi) - \overline{\mathrm{Y}}_j) \int_{\overline{\mathrm{Y}}_j - \mathrm{Z}_j}^{\infty} f(h_j) dh_j + \theta_j \overline{d}_j \int_{\overline{\mathrm{Y}}_j - \mathrm{Z}_j}^{\infty} h_j f(h_j) dh_j$$

In order to get the best designed ability of activity level, suppose the first derivative of $\overline{\mathrm{Y}}_j$ is equal to 0, namely

$$\frac{\partial \mathrm{E}(ZC)}{\partial \overline{\mathrm{Y}}_j} = \overline{d}_j - \theta_j \overline{d}_j \int_{\overline{\mathrm{Y}}_j - \mathrm{Z}_j}^{\infty} f(h_j) dh_j = \overline{d}_j - \theta_j \overline{d}_j [1 - F(\overline{\mathrm{Y}}_j - \mathrm{Z}_j)] = 0 \quad (6)$$

We can get the best designed ability of activity level $\overline{\mathrm{Y}}_j^*(\Psi)$

$$\overline{\mathrm{Y}}_j^*(\Psi) = \mathrm{Z}_j(\Psi) + G_j = \sum_{i=1}^{1} y'_{ij} \overline{x}_i(\Psi) + G_j \quad (7)$$

In the formula, $G_j = F^{-1}(1 - 1/\theta_j)$ is the inverse function of the accumulation density function of h_j which has nothing to do with Ψ .

From the formula (7), the best designed ability of activity level is mainly determined by the demand of anticipated logistics service and the activity amount of each activity.

CASE ANALYSIS

A logistics enterprise provides three kinds of logistics service of 1, 2 and 3, their anticipated demand is 30000 pieces, 100000 pieces and 30000 pieces respectively. Each freight vehicle may install 1,000 pieces of $\overline{x}_1$, each freight vehicle may install 2,000 pieces of $\overline{x}_2$, and each freight vehicle may install 500 pieces of $\overline{x}_3$. In order to simplify the question, suppose an enterprise's actual demand and the anticipated demand are same, and it only determines four kinds of best designed ability of activity. The amount of activity and the existing ability of activities for three different activity levels are shown in Table1 as follows.

Table 1. The amount of activity and the existing ability of activities for different activities.

Level of Activity	Logistics service demand	$\overline{x}_1$	$\overline{x}_2$	$\overline{x}_3$
Unit level	Unit load and unload time (hour/vehicle)	1	1	2
	The most load and unload ability (hour)			260
	Product quantity of each value-added service (piece/ time)	1000	1000	500
Batch level	Preparing time of each value-added service d （hour/ time）	2	2	4
	Preparing ability of value-added service （hour）			500

	Product quantity of each distribution e （piece /set）	4000	4000	1000
	Distribution time of each batch c (time/batch)	5	8	12
	Distribution ability （time）			950
Product level	Information disposal time of each logistics service k （hour）	100	100	300
	Logistics information disposal ability （hour）			600

Calculating four kinds of activities according to the formula (7) and the above data, the best designed ability of activity is:

The best designed ability of activity in unit level activity loading and unloading

$$\overline{Y}_{\text{loading and unloading}}^{*} = \overline{x}_1 / 100 \times y'_{11} + \overline{x}_2 / 200 \times y'_{21} + \overline{x}_3 / 50 \times y'_{31} = 200 \ hours$$

The best designed ability of activity of preparing ability of value-added service and distribution in batch level

$$\overline{Y}_{\text{value-added}}^{*} = \overline{x}_1 \times y'_{12} + \overline{x}_2 \times y'_{22} + \overline{x}_3 \times y'_{32} = \overline{x}_1 \times d_1 / b_1 + \overline{x}_2 \times d_2 / b_2 + \overline{x}_3 \times d_3 / b_3$$

$$= 500 \ hours$$

$$\overline{Y}_{distribution}^{*} = \overline{x}_1 \times y'_{13} + \overline{x}_2 \times y'_{23} + \overline{x}_3 \times y'_{33} = \overline{x}_1 \times c_1 / e_1 + \overline{x}_2 \times c_2 / e_2 + \overline{x}_3 \times c_3 / e_3$$

$$= 1000 \ times$$

The best designed ability of activity of logistics information processing ability of activity in product level

$$\overline{Y}_{\text{logistics information processing}}^{*} = k_1 + k_2 + k_3 = 500 \ hours$$

According to the existing activity ability of the four kinds of activities in Table1, through further calculation one may get: This enterprise has 60-hour surplus abilities of loading and unloading activity. The logistics information processing activity also has a 100-hour surplus processing ability left. Value-added service preparation has no surplus ability. Distribution activity is insufficient, and still lacks fifty times distribution.

CONCLUSION

The best designed ability of activity level $\overline{Y}_j^*$, obtained above of four kinds of activities, will be the theoretical basis of management making future correct decisions for the logistics enterprise.

(1) When the existing activity ability $\overline{Y}_j > \overline{Y}_j^*$, the difference of $\overline{Y}_j$ and $\overline{Y}_j^*$ is the surplus activity ability, just like the handling operation and the logistics information processing activity in the example above. In the situation that business income is invariable, the enterprise may through a series of measures, like the reduction of unnecessary temporary workers, reducing the wage disbursement of temporary workers, selling or the hiring unnecessary equipment and property and so on, reduce extra

resources consumption or reduce surplus activity ability, increasing profit, or develop the new logistics service through resources shifting to fully use surplus activity ability to increase business income, thus enabling the enterprise to squeeze out profit from the use of activity ability.

(2) When $\overline{Y}_j < \overline{Y}_j^*$, the difference of $\overline{Y}_j$ and $\overline{Y}_j^*$ is the insufficient activity ability, like the distribution activity in the example above. In this situation, the enterprise needs to decide whether to expand its own designed ability of activity or to outsource to supplement the insufficient productivity. In the situation that it expands, the enterprise may consider the method of introducing new technology and so on, enhancing the activity efficiency, expanding the bottleneck activity productivity, to satisfy the enterprise's demand of this activity productivity. Because the bottleneck activity is an important economic influence in the enterprise, it has vital significance in determining what enterprise's bottleneck activity is for the continuous improving and increasing profit.

(3) When $\overline{Y}_j = \overline{Y}_j^*$ is the latent restrained activity ability, like the value-added service preparation activity in the example above, this kind of activity will transform into insufficient activity ability when the enterprise will fully use the surplus activity ability to develop new logistics service or the future logistics demand will expand further.

Therefore, it is the important to ascertain the activity with the greatest potential, as well as the latent restrained work in the process of continuous improving of the logistics enterprise, to enhance the activity efficiency and the ability to implement the activity cost management.

REFERENCES

Cooper, R., and Kaplan, R. S.(September-October, 1988). "Measure cost right make the right decisions." *Harvard Business Review*, 43(2), 96-106,

Cooper, R., Kaplan, R. S., Maisel, L. S., Morrissry, E., and Oehm, R. (1992). "Implementing activity-based cost management moving from analysis to action," Institute of Management Accountants, Preface, 27.

Staubus, G.. J. (1971). *Activity costing and input-output accounting*, Richard D. Irwin, Homewood, IL..

Jian, L., and Li, D. (Dec. 2004). Analysis of using activity-based costing management in logistics enterprises, The 9th Conference of Hong Kong Society for Transportation Studies, Hong Kong, 475-481,

Wang, P., Han, X., and Jin, Q. (1999), Activity cost calculation, activity management and its application feasibility in our country. *Accounting Research*, (8), 37-40.

Yu, X. (1995). Briefly discusses new development of modern management accounting, *Accounting Research*, (7), 1-4.

Simulation Study on a Freeway Climbing Lane

Xiaomeng. Cai[1], Q. Li [2], and Z. Wang[3]

[1]Civil Engineering, Hunan University,Changsha 410082, P. R. China; PH (86) 13755030617. Email: caixiaomeng2003@163.com

[2]Gudong ChangDa Highway Engineering Co, Ltd, Guangzhou 510260, P. R. China; PH (86) 13609636664; email: liqidasa@163.com

[3]Civil Engineering, Hunan University, Changsha 410082, P. R. China; PH (86) 13739074779. email: wangzibang@hotmail.com

ABSTRACT

Since the influence of a moving bottleneck varies with time and space, a climbing lane is proposed to alleviate it based on the effect law of trucks. The north section of Beijing-Zhuhai Freeway in Guangdong Province of China is selected as the experiment site. A Corsim model in TSIS which has been calibrated is used, and a cost-effectiveness graph is chosen to analyze the investment effect under conditions of different volumes and percentages of trucks.

INTRODUCTION

With an increase in volume, freeway level of service (LOS) decreases rapidly. As far as the causes are concerned, only a few freeways achieve capacity. On most of China's freeways, there are many overloaded and overrun vehicles with poor performances mixed with other high-speed vehicles in freeways. This leads to a great number of "moving bottlenecks" (Gazis and Herman, 1992) on the freeways. Different from a fixed physical bottleneck, a moving bottleneck causes widespread problems. How to choose a reasonable method to relieve the effect of a "moving bottleneck" on freeways has become a top priority in China's traffic system. Based on an investigation and analysis of the law of "moving bottleneck" in trucks, a climbing lane is proposed by selecting the north section of Beijing-Zhuhai Freeway as test section. A simulation confirms the calibrated and validated model.

DEVELOPMENT OF MOVING BOTTLENECKS

Gazis and Herman (1992) noticed that some heavy trucks cause several or even a large number of cars to decelerate and follow. This creates a clustered fleet in low speed contradicting normal freeway traffic flow. They developed the concept "Moving Bottleneck" to describe this phenomenon. When a truck moves on a multi-lane freeway, it often causes the cars behind to queue. This is not an actual obstacle on the lane, but rather it happens when the flow behind the trucks accumulates a certain amount because of speed differences.

Later, moving obstructions were introduced into the kinematic wave theory of Lighthill and Whitham (1955) and Richards (1956). This lead to a complete theory of moving bottlenecks (Newell, 1998). Additional work was done on moving bottleneck parameter investigation (Munoz, 2002) and the discretization method (Daganzo, 2002,

among others. However, relevant research is just beginning in China.

THE INFLUENCE OF TRUCKS

Investigation was done on the Xiaotang-Gantang section. A rader gun was used to collect speed data, and the data from the freeway monitoring system was applied. Table 1 and Table 2 indicate the data.

Table 1. Volume and Percentage of Trucks on Xiaotang -Gantang Section.

Detector number	Stake number	2006.12.25				2006.12.26			
		Volume(veh/h)		% of trucks		volume (veh/h)		% of trucks	
		N	S	N	S	N	S	N	S
1	K11+183	237	230	55	52	238	228	49	45
2	K22+703	221	100	54	44	219	107	49	38
27	K36+800	232	175	57	56	236	186	57	51
28	K37+305	223	155	51	51	228	165	48	46
30	K38+315	225	98	50	49	239	96	46	44
31	K38+800	237	115	59	47	243	118	55	42
55	K51+505	226	125	58	48	237	150	57	46
79	K104+705	226	195	46	39	231	227	43	45
113	K76+312	349	94	58	53	364	98	56	53

Notes: N-Northbound, S-Southbound

Table 2. S peed on Xiaotang -Gantang Section.

Stake number	Direction	Grade (%)	Speed of each vehicle type（km/h）			
			car	Medium truck	Large truck	coach
K29+700	N	-1	107	67	63	97
K43+250	N	2	76	38	29	65
K31+300	S	2	77	37	34	64
K37+000	S	5	72	31	24	57
K38+900	S	4	75	30	24	54
K44+700	S	-3	99	62	56	91

Notes: 1. The survey time is 2007.4.23-28. The percentage of trucks and the flow are obtained by detectors, the speed is measured by Rader gun.

2. The upgrade sections are all sustained upgrades.

As can be seen from Table 1, the two-way average daily traffic is not so large, ranging from 200veh/h to 400veh/h, and belongs to LOS 1. But the percentage of trucks is relative high, mostly exceeding 40%. Table 2 also shows that the speed of cars slows down under the condition of low volumes, and the phenomenon becomes more obvious on the upgrade section. It occurs mainly because of the speed reduction of trucks on the upgrade section and the intensified influence the moving bottleneck has enforced. Meanwhile, the data reflect the present situation of Chinese freeways: the flow is not large, but the percentage of trucks is high, and the delay of other vehicles is relatively large as well (Lin Hangfei, 2007).

The entry of heavy vehicles such as trucks into the traffic stream affects the number of vehicles that can be served. Heavy vehicles have poorer operating capabilities than passenger cars, particularly with respect to acceleration, deceleration, and the ability to maintain speed on upgrades. The inability of heavy vehicles to keep pace with passenger cars in many situations creates large gaps in the traffic stream, which are difficult to fill by passing maneuvers. The resulting inefficiencies in the use of roadway space cannot be completely overcome (HCM2000) and leads to the increasing delay of passenger cars, thus forming a moving bottleneck.

CLIMBING LANE

The paper proposes to establish a climbing lane for heavy trucks in order to reduce the influence of moving bottlenecks. When the flow increases in the future, other parts can be extended into three lanes in each direction. According to the "Design Specification for Highway Alignment", when the running speed of a loaded truck which moves along the sustained upgrades is slowed down to the minimal allowable speed as shown in Table 3, it is better to establish climbing lanes on the right side of the driving lane. It is obvious that all the speeds in Tabel 2 are lower than the minimal allowable one, and that meets the requirement.

Table 3. The Minimum Allowable Speed on the Upgr ade Section.

Design speed（km/h）	120	100	80	60	40
The minimum allowable speed（km/h）	60	55	50	40	25

APPLICATION OF MICROSCOPIC SIMULATION

The Xiaotang-Gantang segment (K28+000~K48+000) of Beijing-Zhuhai Freeway in the north of Guangdong Province with sustained upgrades and complicated terrain is selected as the section for research. Microscopic Simulation Software TSIS was used to verify the effectiveness of climbing lanes.

Calibration of CORSIM model. In the CORSIM model, parameter calibration is divided into known parameter calibration and unknown parameter calibration.

First, we analyze the model parameters and calibrate known parameters according to the data from the survey, and then find the sensitive parameters by adjusting unknown parameters. Based on Tables 1 and 2, the evaluating indexes of volume and mean speed will be tested until the model is calibrated successfully.

1. Known parameters: From the road design materials and traffic investigation, we can obtain road geometric parameters and traffic composition. In China, there are many types of vehicles, quite different from their counterparts abroad in terms of classification criteria. Therefore, it is significant to calibrate vehicle types. The paper divides vehicles into four types, i.e. passenger car, coach, medium truck, and large truck. For the purpose of matching the actual vehicle situation (trucks are featured by low capability and overloading in China) with the vehicle types in TSIS, the parameters of simulated vehicles (such as geometrical features, dynamic performance, etc.) must be adjusted,

especially the performance index of acceleration which directly reflects different climbing performances.

2. Unknown parameters should be adjusted constantly according to the actual traffic situations. Upon sensitive analysis, cars following the sensitivity multiplier in the car-following model, advantage threshold for discretionary lane change in lane changing model, and free-flow speed multiplier are highly sensitive parameters.

Roadway Conditions. 1. Scheme 1: The basic section of two-lane freeway in each direction K28+000 ~K48+000, with a total length of 20 km. This scheme is to simulate existing roads. 2. Scheme 2: Three-lane freeway in each direction K28+000~K48+000 extended from two lanes, with a total length of 20 km. 3. Scheme 3: Setting climbing lanes. Based on the vehicle operating situation, several climbing lanes were set at the northbound and southbound directions.

Traffic Conditions. To verify the effectiveness of climbing lanes, volume is divided into four grades: 500, 1000, 1500, 2000 veh/h (those over 2000veh/h will not be discussed here, for they have exceeded the capacity of this section), and the percentage of trucks selected is 30%, 40%, 50%, and 60%. With a 95% confidence level and a 5% allowable error range, after running ten times, the effectiveness of setting the climbing lanes is verified in terms of different flows and percentages of trucks.

Selection of Index. The influence of trucks is multi-dimensional, such as speed reduction, increased delay, density changes and so on. Speed is not significantly affected by volume over a wide range of demand (HCM2000). If speed does not vary with flow rate over a broad range of flows, it becomes difficult to use speed as the sole measure. This important characteristic is the major reason why such measures as density have been introduced as primary measures of effectiveness, with travel time playing a secondary role.

ANALYSIS OF RESULTS

According to the simulation model calibration and the condition settings above, travel time (min/veh), density(pcu/km/ln) and LOS with different road conditions and percentage of trucks are gained after the simulation experiments (see Tables 4, 5, 6)

Table 4. MOEs of Scheme 1.

% of trucks	Volume（veh/h）											
	500			1000			1500			2000		
	TT	D	LOS	TT	D	LOS	TT	D	LOS	TT	D	LOS
30	19.3	6	1	21.6	12	2	23.1	18	2	25.1	25	3
40	19.7	6	1	22.4	12	2	23.6	19	3	26.5	25	3
50	20.3	6	1	22.8	13	2	24.0	19	3	27.6	26	4
60	21.2	6	1	23.0	13	2	24.1	19	3	27.9	26	4

Table 5. MO Es of Scheme 2.

% of trucks	Volume（veh/h）											
	500			1000			1500			2000		
	TT	D	LOS	TT	D	LOS	TT	D	LOS	TT	D	LOS
30	15.7	4	1	18.6	7	1	20.0	11	2	21.7	15	2
40	16.8	4	1	19.5	8	2	21.3	11	2	22.4	16	2
50	17.7	4	1	20.6	8	2	21.9	12	2	23.0	16	2
60	18.6	4	1	21.1	8	2	22.5	12	2	23.4	16	2

Table 6. MOEs of Scheme 3.

% of trucks	Volume（veh/h）											
	500			1000			1500			2000		
	TT	D	LOS	TT	D	LOS	TT	D	LOS	TT	D	LOS
30	16.3	5	1	19.5	10	2	22.4	16	2	27.0	21	3
40	17.6	5	1	20.7	10	2	23.6	16	2	28.6	21	3
50	18.5	5	1	21.5	10	2	24.5	16	2	29.7	21	3
60	19.1	5	1	22.1	10	2	25.4	16	2	30.9	20	3

It can be observed that the road conditions in Scheme 2 and Scheme 3 are obviously improved, compared with Scheme 1. For instance, the density gets smaller and the travel time becomes shorter at varied levels. Scheme 3 still keeps its LOS even after the flow has increased to 1500 veh/h and reduces the influence of moving bottlenecks effectively on the freeway.

However, the investment varies from different schemes. Whether to choose Scheme 2 or Scheme 3 is up to decision-makers after the two schemes are compared in terms of investment benefits. A cost-effective graph is used in this paper (HCM2000). According to the associated cost, the travel time of different schemes is shown as Figure 1. I represents scheme 1, II and III are extension schemes, respectively representing schemes 2 and 3. The solid lines indicate the relative cost effectiveness of moving from I to II or I to III. The slope of the line between the schemes represents the travel time saved per dollar of cost. The steeper the slope, the better the effectiveness.

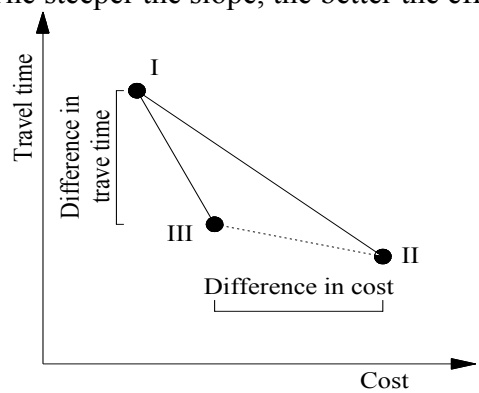

Figure 1. Example of a Cost -Effectiveness Graph.

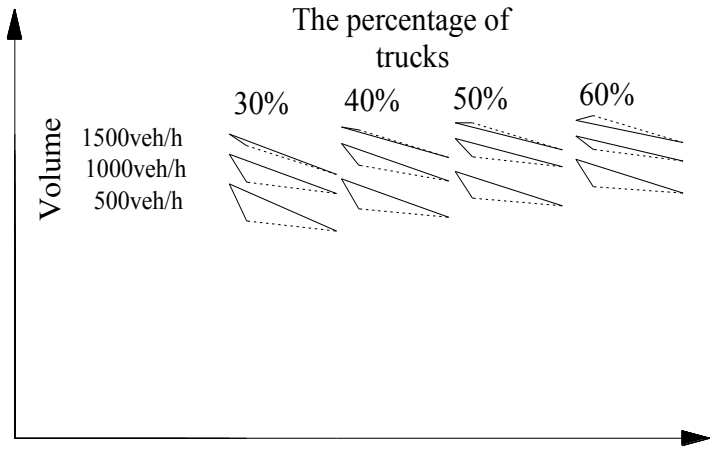

Figure 2. Cost -Effectiveness Graph with Schemes.

From Figure 2, conclusions are drawn as follows:

1. The cost-effectiveness ratios of Scheme 2 and Scheme 3 are various with different flows and percentage of trucks, so reasonable schemes according to different traffic conditions should be selected in the formulation of the extension scheme.

2. When the percentage of trucks is 30% or 40%, the slope of Scheme 3 is bigger, and the cost-effectiveness of setting climbing lanes is obviously better.

3. When the percentage of trucks reaches 50% or 60% and the volume is below 1500 veh/h, the slope of Scheme 3 remains comparatively bigger, so the effect of setting climbing lanes is still notable. However, when the flow is above 1500 veh/h, Scheme 2 has a bigger slope, and then it will be time to consider the extension of the road into six lanes.

Analyzing the cost-effectiveness graph, it is proposed that the setting of climbing lanes can effectively shorten travel time within a certain range of flows and percentage of trucks. It is feasible for the small volume and high percentage of trucks on freeways in China. This method costs less and produces more investment benefits and, thus, it can be carried out during the initial period of freeway reconstruction and extension.

CONCLUSION

The current traffic of most two-lane freeways in each direction in China has not reached the capacity yet, but the percentage of trucks is relatively high. After setting climbing lanes on the sustained upgrades, the travel time and delay can evidently be reduced. In addition, its investment cost is lower than that of extending it into a six-lane, and its adaptability is good as well. Nevertheless, the climbing lane can not be applied for all situations. For example, when the volume and the percentage of trucks are high, the fixed bottleneck and insecurity factors might appear at the merge segment. Then an extension to six-lane freeways should be considered.

REFERENCES

Daganzo, C. F., and Jorge, A. (2002). "Laval: on the numerical treatment of moving bottlenecks." Transportation Research Part B , 31-32.

Daganzo, C F. (2002). "A behavioral theory of multi-lane volume. Part I: long homogeneous freeway sections." Transportation Research , Part B, 36, 131.

Gazis, D. C., and Herman, R. (1992). "The moving and phantom bottleneck." Transportation Science , 26, 223.

Lin, H., Fu, Q., and Zhang, H. M. (2007). "Moving bottleneck theory-based new countermeasure for influence of heavy vehicles." Journal of Tongji University, 35(9), 1209-1213.

Ministry of Communications P.R.C. (2006). JTG D20-2006 decide specification for highway alignment. Beijing, 39.

Newell, G. F,.(1998). "A moving bottleneck." Transportation Research Part B , 32 , 531.

Transportation Research Board (TRB). (2001). Highway capacity manual 2000. Transportation Research Board, Washington D. C., 4-6, 8-23.

Hybrid Genetic and Taboo Search Algorithm for Solving the Bus Timetable Problem

C. Ren[1], W. Lu[1], L. Zhao[1], C. Yin[1], and H. Wang[1]

[1] College of Information and Electrical Engineering, Shandong University of Science and Technology, Qingdao 266510, China; email: ren_chx@sina.com

ABSTRACT

The non–uniform bus timetable is presented, and then the optimization model is formulated. The Genetic Algorithm (GA) and Taboo Search (TS) algorithm are analyzed and combined to become hybrid Genetic Algorithms, namely GATS. The GATS is used to solve the bus timetable model and the non–uniform bus timetable is obtained. The final results of the simulation indicate GATS has higher efficiency than simple GA and is one effective way to solve the bus timetable. Simultaneously, it is proved that the non–uniform bus timetable can reduce the passengers' waiting time and meet the passengers' need and also could improve agency efficiency.

INTRODUCTION

The bus operation and dispatching plan is the core basic content of the public transportation system. The bus timetable is one of the most important steps in the bus planning process (Wang, 2001). A better bus operation plan can improve a city's traffic environment, resident travel status and agency services and products.

The bus timetable problem is a typical multi-objective optimization problem. It also is a None-determinist Polynomial time hard problem, because it must take into account the passengers' waiting time and the bus agency's benefit. Many researchers have formulated the bus timetable by analyzing the bus dispatching process and computed it by traditional methods and Genetic Algorithm (Hurdle, 1973; Chakroborty, 1995; Zhang, 2003). Traditional methods have difficulty with the problem, because of increscent dimensions and computing complexity. The Genetic algorithm also has difficulty reaching the optimal solution, because of slow evolving and early convergence. Much research on the bus timetable utilizes a uniform time interval in the time period. This ignores the difference of passenger numbers and so it can not better meet the needs of passengers and the agency. In addition, with the application of the intelligent transportation system's advanced technologies, it is now feasible and convenient for the bus to be dispatched on a none-uniform timetable. Based on above analysis, the GA and Taboo Search are combined to become Hybrid Genetic Algorithms, namely GATS, which can overcome the shortcomings of GA. Simultaneously the none-uniform bus timetable in the time period is computed.

BUS TIMETABLE OPTIMIZATION MODEL

The bus timetable is related to the passengers' waiting time and the bus agency's

benefit. So the passenger waiting time and the cost for the bus agency are computed, and then the bus timetable model is formulated. Its objective is to minimize the passengers' waiting time and the bus agency's operating cost.

Cost for the passenger . The cost for passenger relates to the passenger waiting time at station, and this is the sum of all passengers' waiting time at every station. If the arrival rate of passenger at station k is $P_{ak}(t)$, then the formula of the passengers' waiting time at all stations in the day as follows:

$$T_{pw} = \sum_{k}\sum_{m}\int_{t_{ak,m-1}}^{t_{ak,m}} P_{ak}(t)\times(t_{ak,m}-t)dt \qquad (1)$$

Where k is the index of station, m is the index of bus, $P_{ak}(t)$ is arrival rate of passenger at station k, and $t_{ak,m}$ is the time of bus m arrival at station k.

Based on the Eq.1, we obtain the passenger cost as the formula:

$$E_{pw} = r_{pw} * T_{pw} = r_{pw}\sum_{k}\sum_{m}\int_{t_{ak,m-1}}^{t_{ak,m}} P_{ak}(t)\times(t_{ak,m}-t)dt \qquad (2)$$

Where r_{pw} is the value of passenger waiting time (yuan per minute).

Cost for the a gency. The cost for the agency consists of the fixed and variable fare. The fixed fare comes from the depot and bus line building, and so on. The variable fare mainly includes the fare of vehicle parts, oil fee and depreciation charge (Wang, 2001). The bus timetable problem relates to the variable fare, so if we can compute the variable cost for the bus running the whole route once, the cost for the agency can be computed as the formula:

$$E_a = r_a \times N \qquad (3)$$

Where r_a is the variable cost for the bus running the route once (yuan per bus), N is the bus number of the whole operation time.

The optimization model . Based on the Eq.1, Eq.2 and Eq.3, we can compute the total cost of the day for the agency and passenger, so the objective function is expressed as follows:

$$\text{Min} \quad r_{pw}\sum_{k}\sum_{m}\int_{t_{ak,m-1}}^{t_{ak,m}} P_{ak}(t)\times(t_{ak,m}-t)dt + r_a N \qquad (4)$$

Subject to: $t_{ak,m} - t_{ak,m-1} \leq h^{max}$

$t_{ak,m} - t_{ak,m-1} \geq h^{min}$

Where h^{max} is the maximal headway, h^{min} is the minimal headway.

THE HYBRID GENETIC TABOO SEARCH ALGORITHM

Genetic Algorithm . GA was first put forward by Holland in 1975 (Holland.,1992). It is a biologically inspired method for function optimization that is loosely based on the theory of evolution. GA starts from a population of pairs, with

their coded attributes and their fitness, and then selection, crossover and mutation will result in the next generation population. Lastly, the population converges to the global optimum or proximately optimum.

GA can simultaneously explore many points in the search space and does not require problem specific auxiliary knowledge. Also, it has proved to be robust in the selection of optimization parameters and noise. It is not necessary to give specific rules for parameter settings and the number of mutation and crossover operators can be selected freely. However, GA's shortcomings are that it evolves slowly and converges early.

Taboo Search Algorithm . Taboo Search was developed by Glover (1986). Taboo Search is an expanding local neighborhood search, an iterative optimization procedure, and a simulation for human intelligent activity It is also a newer heuristic optimization algorithm.

TS searches the solution space by flexible memory system and aspiration criteria, and the best solution in the neighborhood is always selected, even if it is worse than the current solution. So TS has the stronger ability of "hill climbing", and can escape from the local optima, then finds the global optima solution. However, it relies on the initial solution excessively and its search process is from one solution to another, so it reduces the probabilities of finding global solution.

Genetic Algorithm Taboo Search . To overcome GA's evolving slowly and convergence earliness, one solving method is to combine GA with another artificial intelligent search method to become hybrid genetic algorithms (Wang, 2001). A TS algorithm has the characteristic of short memory and can escape the local optima. In this paper we bring TS into GA and combine them to become Hybrid Genetic Algorithm, namely GATS (Genetic algorithm taboo search). In GATS, GA is the whole frame, while TS is adopted to explore the local space to generate new and better population. The major steps of the GATS algorithms are as follows:

(1) Determine the parameters, such as population size, crossover probability, mutation probability, and so on.

(2) Initialize population by randomly generating a set of feasible solutions.

(3) Compute the fitness value and employ selection operation to the population.

(4) Apply crossover and mutation operator to produce new population.

(5) Apply TS algorithm to the new population, improve the individuals' quality and generate newer population.

(6) If the stopping rule is met, then out put the optimal solution and terminate, others return to step (3).

SIMULATION AND DISCUSSION

This paper examines one route of some city and optimizes the route direction bus timetable. The route has thirteen stations, and the bus start and end time is known. The passenger arrival rate of every station during operating time is given, i.e.

Figure 1. We assume the bus departs the station on time. The optimization objective is to find the none-uniform timetable which minimizes the cost of the passenger and the bus agency.

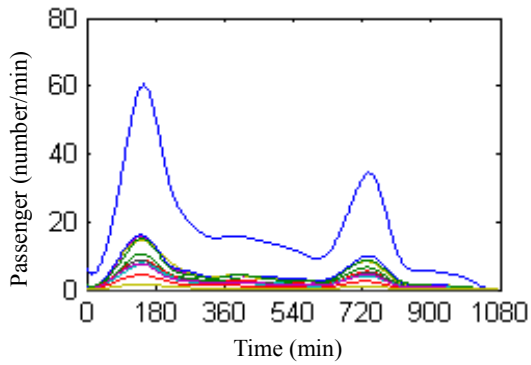

Figure 1. Passenger arrival rate at station.

Design GATS parameters . (1) Chromosome coding. The binary coding method is chosen and genes consist of zero and one. The size of the chromosome is the length of the bus dispatching time T, and it is sixty in this paper. The gene of the chromosome is corresponding to the minute in the time T, and also it represents the state of the bus, namely "1" presents bus depart at this time and "0" is others.

(2) Chromosome decoding. Find and record the position of "1" in the chromosome and compute the number of one state, so the bus timetable and the bus frequency can be determined.

(3) Fitness function. Fitness function can compute the good degree of every chromosome approaching optimal solution. Fitness value must be not negative generally, and the bus timetable optimization belongs to minimizing the objective problem, so the fitness function can be derived as follows:

$$F(X) = C_{max} - f(X)$$

Where $F(X)$ is fitness function, $f(x)$ is the objective value based on Eq.4 and C_{max} is the maximal objective value of the same population.

(4) Selection operation. A fitness proportional model is used in GA. The selection probability can be computed as follows:

$$G_i = f(X_i) / \sum_{i=1}^{n} f(X_i)$$

Where G_i is the probability of chromosome X_i, X_i is the i chromosome in the population, $f(X_i)$ is the fitness value of chromosome X_i, n is the population size.

At the same time a penalty operation is applied. When the bus operation term is not met, the individual fitness will be given a maximum. This will forbid the individual passing down.

(5) Crossover and mutation operation. Single point crossover and uniform mutation are selected in GA.

(6) Neighborhood structure. The TS algorithm is based on the neighborhood search and the neighborhood structure is very important in TS. The solution of bus scheduling is headway serial, which can be expressed in one point of multi-dimension space or solution space, and the space is made up of all points which meet the bus operation constraints. In the solution space the neighbor points of

every point combine the neighbor set.

Simulation and t he result analysis . The optimization model is set up based on the Eq. 4 in the one hour and the timetable is computed by applying the standard GA algorithm and hybrid GATS algorithm to the model respectively. In the GA and GATS algorithm the population size is 200, the crossover probability P_c is 0.85, mutation probability P_m is 0.005 and generation number is 200 after many test simulations. Moreover, the uniform timetable is computed by GA in order to compare with the non-uniform timetable.

Figure 2 compares the convergence process between GA and GATS. Table 1 is the results of a computed non-uniform timetable and uniform timetable by GA and GATS algorithms.

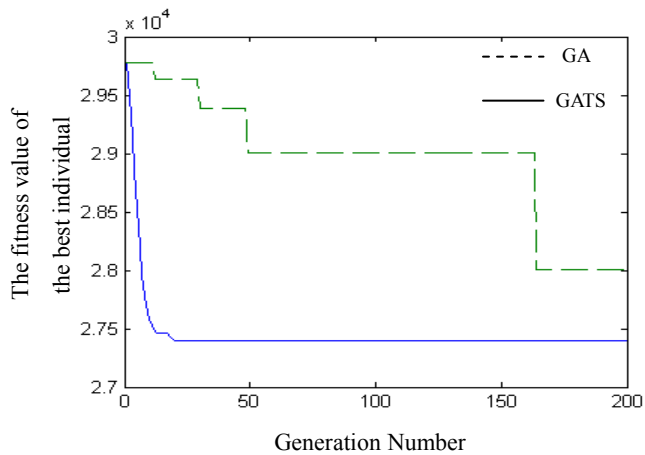

Figure 2. The convergence of G ATS and SA .

Table 1 . Results of different cases .

	Method	Bus number	Cost for Passenger (yuan)	Cost for agency (yuan)	The total cost (yuan)
Non-uniform Timetable	GATS	7	13393	14000	27393
	GA	8	12001	16000	28001
Uniform timetable	GA	7	13767	14000	27767

Figure 2 shows that the GATS algorithm converges earlier and gets the better solution than standard GA. This also shows that GATS overcomes the evolving slow and convergence earliness of GA. From Table 1 we see that GATS achieves the better timetable, the low cost of passenger and the agency. Standard GA gets the local solution of the timetable problem, so this is also confirmed with results in Figure 2. Furthermore, we see that the non-uniform timetable of GATS can make the passengers' waiting time short and can meet the passengers' need better than the uniform timetable from Table 1. Finally, the bus number is equal in the uniform and non-uniform timetable, but reducing the passengers' waiting time needs to reduce the bus depart time interval in the uniform timetable. This must result in an increasing number of buses and so wastes resources.

CONCLUSIONS

In this paper a model is formulated based on the benefits for the passenger and agency to research and solve the bus timetable problem. A Taboo search algorithm is merged into GA to develop a hybrid GATS which overcomes the bad local search capability of GA. Finally, GATS and GA are designed and applied to the bus timetable problem respectively. Results have proved GATS algorithms to be efficient tools for the development of an optimal bus timetable. Findings also indicate that the non-uniform timetable can better meet the needs of passengers and reduce the resource waste than can the uniform timetable.

ACKNOWLEDGMENT

The research is supported by the Research Project of "SUST Spring Bud" (2008AZZ069), the "Taishan Scholarship" Construction Engineering and the National Nature Science Foundation of China (60804034).

REFERENCE S

Chakroborty, P., Deb, K., and Subrahmanyam, P. S. (1995). "Optimal scheduling of urban transit systems using genetic algorithms." Journal of Transportation Engineering, 121(6), 544-553.

Glover, F. (1986). "Future paths for integer programming and links to artificial intelligence." Comput. & Ops. Res., 13(5), 533-549.

Holland., J. H. (1992). Adaptation in nature and artificial systems. MIT Press, Cambridge.

Hurdle, V. F. (1973). "Minimum cost schedules for a public transportation route-II. Examples." Transportation Science, 7, 138-157.

Wang, L. (2001). Intelligent optimization algorithms with applications. Tsinghua University Press, Beijing.

Wang, X. (2001). Operation dispatching management of urban transit. China railway publishing house, Beijing.

Zhang, F., and Yan, L. et al. (2003). "Research on dispatching methods of public traffic vehicles in intelligent transport system." China Journal of Highway and Transport, 16(12).

Analysis of the Competitive Strategy of the Core Enterprises in Virtual Intermodal Freight -Transportation Enterprise

Dapeng Liu[1], Xiamiao Li[1], Minghua Zeng[1], and Xiaodong Cao[1]

[1]School of Traffic & Transportation Engineering, Central South University, Changsha 410075, China. PH: ++86-15874160884; email: liudabird@163.com

ABSTRACT

The formation of a virtual intermodal freight-transportation enterprise and the determination of the core enterprise strategy is the primary solution for the cooperation and competition between freight-transportation enterprises. This paper seeks maximization of business income in the core freight business through analysis of the economic benefits of the core freight-transportation business with virtual intermodal freight-transportation enterprise, individually and cooperatively. The paper seeks to establish a gain matrix based on Game Theory. In sum, when the business income of cooperatively-constructed enterprise is higher than the individual one, two enterprises will choose to construct cooperatively. When two enterprises with the same characteristics are in different cities, the optimal strategy is cooperative construction. When other enterprises are unwilling to develop an intermodal transportation business, the core enterprise should seize the opportunity to establish the virtual intermodal freight-transportation enterprise individually. The results of a computational example show that every enterprise can use the conclusion to make useful decisions.

INTRODUCTION

With the establishment and improvement of a market economy and the rapid development of transportation in China, the development of an integrated transportation system has become a basic national policy. Zhang (2008) observes that the focus in the establishment of an integrated transportation system is to set up the chain of integrated multimodal transportation. Luo (2002) suggests that how to cope with relationships of cooperation and competition in different modes of transportation enterprise is becoming an important issue in transportation development. Zhang (2001) and Liu (2001) studied core enterprise partner choice in different enterprises. Others, using a fuzzy evaluation model, optimal technology and GIS space technology, examined the capacity and dispatch of combined transport in different enterprises. Xie (2004) and Chen (2005) identified two types of organization in cooperative-transport. Based on the work of Ye and Sun (2005) on the concepts and features of virtual enterprise, this paper solves the problem of cooperation and competition in different modes of transport enterprises through the construction of virtual intermodal freight-transportation enterprise. In the process of

the virtual enterprise, the core freight-transportation enterprise will have a wide range of choices. This paper sets up a gain matrix of core-transportation freight-transportation enterprises based on the game theory and discusses the decision of core freight-transportation enterprises with the purpose of maximization of benefits.

THE CONCEPT OF THE CORE FREIGHT -TRANSPORTATION ENTERPRISE

The core freight-transportation enterprise is the transport enterprises in the virtual intermodal freight-transportation enterprise with several functions, such as collecting information to identify market opportunities, confirming the core competitiveness and identifying risks, identifying and choosing partners, perfecting the comprehensive information infrastructure, establishing a leadership structure and supervising partner's operation. This enterprise has the capacity to collect information, recognize market opportunities, confirm their own core competitiveness and avoid risk, distinguish and select their partners, have an information infrastructure, and can establish the lead agency. In terms of technical features and business models of transportation, the core freight-transportation enterprise must have the ability to take the major transport trip, such as railway, waterway and air transport enterprises.

ANALYSIS OF THE EFFECTIVENESS IN CORE FREIGHT - TRANSPORTATION ENTERPRISE

In the intermodal transportation network, transport enterprises are separated in geo-spatial location. Each enterprise has a spatial superiority which is one of the basic conditions for them to cooperate with each other. Meanwhile, every enterprise has its own customer resources, include long-term and retail customers. There is no competition for customers between enterprises. So the core freight-transportation enterprise in the intermodal transportation network can make use of the other enterprise's resources to achieve mutual benefits and reduce the overall cost of the intermodal transportation system.

Set up the virtual intermodal freight -transportation enterprise individually

For enterprise A in city A, which sets up the virtual intermodal freight-transportation enterprise individually to deliver goods between city A and city B, enterprise A should associate with motor transport enterprises and ship cargoes to the warehouse of enterprise A. Then enterprise A must transport goods to city B and distribute them to customers in city B. When enterprise A transports goods from city A to city B, it should also do the same work. Through such an organization, enterprise A sets up a Virtual Intermodal Freight-Transportation Enterprise V_A, if the

transportation costs are C_A per unit, and the total Traffic is x_A. Then, enterprise B can do the same work, and the transportation costs are C_B per unit, and the total traffic is x_B. We assume that the coefficient of income distribution of enterprise A includes the business income from V_A is k_A, $0.5<k_A<1$. In the same way, the coefficient of enterprise B includes the business income from V_B is k_B, $0.5< k_B <1$. Then V_A and V_B provide the same transportation services between the two cities. Based on the demand function which is commonly used in the transport industry (Chen 2002), the inverse demand function of transportation services is $P = a - x_A - x_B$. Then the decision of V_A about this market is

$$\max\{\pi_A = (a - x_A - x_B)x_A - x_A C_A\} \quad . \qquad (1)$$

Derivative expression (1) we can obtain $x_A = (a - x_B - C_A)/2$. On the same principle, the decision of V_B about this market is

$$\max\{\pi_B = (a - x_A - x_B)x_B - x_B C_B\} . \qquad (2)$$

Derivative expression (2) we yield $x_B = (a - x_A - C_B)/2$. Then we can get the solutions $x_{A*} = (a - 2C_A + C_B)/3$ and $x_{B*} = (a - 2C_B + C_A)/3$. Then the business income of V_A and V_B are $\pi_A = (a - 2C_A + C_B)^2/9$ and $\pi_B = (a - 2C_B + C_A)^2/9$. So the business income of enterprise A and B are $m_A = k_A(a - 2C_A + C_B)^2/9$ and $m_B = k_B(a - 2C_B + C_A)^2/9$.

Cooperatively set up the virtual intermodal freight -transportation enterprise

If enterprise A and B cooperate and they set up a new virtual intermodal freight- transportation enterprise V_C, then the transportation costs are C_c per unit, and the total traffic is x_c. The inverse demand function of transportation services is $P = a' - x_C$ ($a' > a$). And the two core freight-transportation enterprises have the same status in V_C, Assuming the coefficients of enterprise A and B got in business income from V_C are equal, $k_C = k_{A*} = k_{B*} < 0.5$; and the decision of V_C about this market is

$$\max\{\pi_C = (a' - x_C)x_C - x_C C_C\} . \qquad (3)$$

Derivative expression (3) we have $x_C = (a' - C_C)/2$. Then the business income of V_C

is $\pi_C = (a' - C_C)^2/4$. So the business income enterprise A and B receive from V_C are $m_{A*} = m_{B*} = k_C(a' - C_C)^2/4$.

The game analysis of the cor e freight -transportation enterprises

In conclusion, there are two choices when a core freight-transportation enterprise wants to set up a virtual intermodal freight-transportation enterprise. That is to say, every enterprise will have two choices for this decision, 'cooperatively' or 'individually'. The core freight-transportation enterprise must decide which strategy is the better one and how to select the better one. Game theory can help enterprise management do this. The analysis above leads to the following table:

Tab le 1.The strategy about business income matrix of each enterprise A and B .

enterprise		core enterprise B	
	strategy	individually	cooperatively
core enterprise A	individually	(m_A, m_B)	(m_A, m_{B*})
	united	(m_{A*}, m_B)	(m_{A*}, m_{B*})

From the work of Nash (1997, 2007) and Gardner (2003), we know that there are two Nash equilibria, which are (individually, individually) and (cooperatively, cooperatively). When $m_{A*} > m_A$ and $m_{B*} > m_B$, the Nash equilibrium is (cooperatively, cooperatively). If $m_A > m_{A*}$ and $m_B > m_{B*}$, the Nash equilibrium is (individually, individually). Generally, if two enterprises in different cities cooperate, they will save the cost at opposite city where they want to establish an institution. They will reduce the no-load rate, so the costs are lower than they are individually. Namely: $C_C < C_A$, $C_C < C_B$. Then we will discuss the conditions of those two Nash equilibria.

1) When $m_{A*} > m_A$ and $m_{B*} > m_B$, namely

$$m_{A*} - m_A = \frac{k_C(a' - C_C)^2}{4} - \frac{k_A(a - 2C_A + C_B)^2}{9} > 0; \quad (4)$$

$$m_{B*} - m_B = \frac{k_C(a' - C_C)^2}{4} - \frac{k_B(a - 2C_B + C_A)^2}{9} > 0. \quad (5)$$

Only when expression (4) and (5) are satisfied simultaneously do enterprises A and B in different cities unite and set up a virtual intermodal freight-transportation enterprise V_C, deformation expression (4) and (5), namely

$$3(a' - C_C)\sqrt{k_C} > 2(a - 2C_A + C_B)\sqrt{k_A}, 3(a' - C_C)\sqrt{k_C} > 2(a - 2C_B + C_A)\sqrt{k_B}. \quad (6)$$

It can reach the following conclusions, if the costs of the transportation services are low enough, namely $C_A \to 0$, $C_B \to 0$ and $C_C \to 0$, and the limits of expression (6) are $k_C > 4k_A/9$ and $k_C > 4k_B/9$. In practice, the transportation costs cannot be zero, if the conditions $k_C < 4k_A/9$ and $k_C < 4k_B/9$ exist, organizing the enterprise together is

impossible.

2) If the transportation costs and profit distribution rate of two transport enterprises are equal, namely C_A=C_B and k_A=k_B. Then considering geospatial characteristics of the two cities, distribution partner enterprise of the two core transport enterprises are of the same quantity, assuming the profit distribution rate is unchanged. In this case, we can think that $k_C \approx \frac{1}{2} k_A$, $k_C \approx \frac{1}{2} k_B$. Let $C = C_A = C_B$, $k = k_A = k_B$, and we have $3(a' - C_C) > 2\sqrt{2}(a - C)$. In this expression, from C_C< C, we have a'- C_C >a -C, the expression is obviously hold. Then the only difference between the two transport enterprises is they are in different cities. Their optimal strategy is setting up a virtual intermodal freight-transportation enterprise cooperatively.

3) When only one core transport enterprise identifies the market opportunity, the other core transport enterprise does not know it and does not want to join in the alliance. Assumping it is enterprise A, the decision-making model of enterprise A is

$$\max\{\pi_{A*} = (a - x_A)x_A - x_A C_A\}. \quad (7)$$

Then the business income of V_A is $\pi_A = (a - C_A)^2/4$. So the business income of enterprise A can get from V_A is $m_A = k_A(a - C_A)^2/4$.

In this case, only one enterprise develops combined transport service, and the core enterprise can earn more profits than the preceding two modes. Moreover, this enterprise will have the dominant market position for the future.

CASE STUDY

For enterprise A in city A, enterprise A sets up V_A, and the transportation costs are C_A=20 YUAN/kg, and the total traffic is x_A. And for V_B , the transportation costs are C_B=20 YUAN/kg, and the total traffic is x_B, and k_A= k_B =0.7. The demand function is $P = 200 - x_A - x_B$. For V_C , the transportation costs are C_B=10 YUAN/kg, and k_C= 0.4, the demand function is $P = 400 - x_C$. The analysis above leads to the following table:

Tab le 2. The business income matrix of each enterprise A and B (YUAN) .

enterprise		core enterprise B	
	strategy	individually	cooperatively
core enterprise A	individually	（2,662，2,662）	（2,662，3,083）
	united	（3,083，2,662）	（3,083，3,083）

We can see from Table 2 that when the two core transportation enterprises construct the virtual intermodal freight-transportation enterprise cooperatively, they will earn 3,083 YUAN. This is more than they earn individually (2,662 YUAN). The results indicate that each enterprise can use the above conclusion to adopt a strategy

that will produce more business income.

CONCLUSIONS

We conclude from the market opportunities analysis in two cities the appropriate strategies for transport enterprises: When the two core transportation enterprises are iso-enterprises, the optimal solution is to cooperatively construct the virtual intermodal freight-transportation enterprise. When they both want to provide combined transport services, they will get more profit when they cooperate. When the other core transportation enterprise is unwilling to develop the intermodal transportation business, the core transportation enterprise should grab the chance to construct the virtual intermodal freight-transportation enterprise.

REFERENCE S

Chen, N., Liu, H., and Fu, W. (2005).“Research on collaborative transportation dispatch among enterprises,” Journal of Wuhan University of Technology, 29(3), 440-443.

Chen, Y., and Shao, Z. (2002). Transport economics, The People’s Traffic Press, Beijing.

Gardner, R. (2003). Games for business and economics, Wiley, New York.

Liu, K., Wang, R., and Jin, B. (2004). “A fuzzy evaluation model and its implement for supplier,” Journal of Wuhan University of Technology, 28(3), 420-423.

Liu, Z. (2001). The design of the logistics & distribution system. China Material Press, Beijing.

Luo, X., and Zhang, X., and Zhang, G. (2002).“Research on transportation Enterprise virtual organization based on MAS,” Computer Engineering, 28(12), 66-68.

Nash, J. F. (1997). Essays on game theory . Edward Elgar Publishing, London.

Nash, J. F. (2007). The essential John Nash. Princeton University Press, Princeton .

Xie, H., and Du, J. (2004). “A method on bus station planning based on Optimization theory and technique of GIS spatial analysis,” Journal of Wuhan University of Technology, 28(6), 907-910.

Ye, F. and, Sun, D. (2005). Formation and operation of virtual enterprise in life cycle. Machinery Industry Press, Beijing.

Zhang, G. (2008). “The theoretical foundation and the construction of the platform in comprehensive transportation,” Communication and Transportation Systems Engineering and Information, 8(5),1-9.

Zhang, X., and Zhang, G.. (2001). “Application of MAS coorperation approach in transport enterprise management,” Communication and Transportation Systems Engineering and Information, 8(3), 226-231.

Optimization of Transportation Enterprises Pricing Strategies

Bailing. Wang[1] and Hui. Li[1]

[1]Transportation Management College, Dalian Maritime University, DaLian, 11602 China; PH/FAX (0411) 8472-6998; email: wanda_519@yahoo.com.cn

ABSTRACT

The market adaptability of the price mechanism of China's transportation is still relatively weak. Many of the effective regulatory mechanisms have not yet been established, so prices can not adapt to transport demand changes in the market. As a result, building a scientific and reasonable optimization model of the transportation pricing system is very important for the development of the industry. According to economic theory, transportation enterprises can get the highest profits from a pricing model consistent with the theory of price elasticity. A price discrimination strategy can help transportation enterprises establish the best price to keep high profit levels and competitive advantages in the transportation market.

INTRODUCTION

As is well known, price is a permanent problem faced by any enterprise. Both parties in a transaction are very sensitive to it. Transportation enterprises are not an exception. The profitability and competitiveness of an enterprise are relative to transportation price to a great extent. In addition, the products of transportation enterprises have their own special properties. That is to say, production and sale are realized simultaneously. This makes the pricing in the transportation market more complicated than that of other product markets.

The government has strictly conrolled prices in China's transportation market for many years. The flexible change mechanism of price is affected and restricted by various factors. China railway transportation is basically owned and operated solely by the government. The transportation price of the stated-owned railway is generally controlled by the central government (Wang, 2009).

However, civil aviation transportation in China has many airlines, including some foreign airlines, in the market. Competition in the civil aviation system has been very fierce, and the flexibility of price change is obviously higher here than for rail transportation.

The competitive mechanism in highway and water transportation has been formed. There is no need to mention maritime enterprises, where price is completely decided by the supply and demand in the international shipping market. There is keen competition among various transportation modes, and this requires a relatively uniform transportation price policy.

MAIN FACTORS AF FECTING TRANSPORTATION ENTERPRISES

Transportation enterprises find that setting prices is complicated and that many factors affect the process. These factors usually include the following:

Transportation cost is an important basis for pricing, because it is the basic measure of the labour expended in producing transportation services. Production in successful transportation enterprises require prices that generate sufficient revenue to compensate for their costs. Therefore, transportation enterprises widely adopt a pricing method on the basis of cost.

Profit level is also a basis of pricing. Profit level is a very important factor affecting price. Transportation price is generally charged on the basis of cost plus fixed proportional profit.

The state of market supply and demand affects pricing as well. Generally, when the demand for transportation increases, the transportation price should rise accordingly. When the demand for transportation decreases, the transportation price should drop. Under the circumstances of constant development of the market economy and the gradual improvement of transportation market, transportation pricing according to market supply and demand is a significant feature of transportation price formation.

Transportation pr ice policies, usually instructed and supervised by state macroeconomic policies, are important because transportation is a basic industry of national economy. State regulation of transportation prices may shift over time, from quite stringent to rather relaxed. In either case, transportation price policies are very important factors that affect the pricing.

OPTIMAL MODEL OF TRANSPORTATION ENTERPRISE PRICING

Here the optimal pricing model analyzes the best price for enterprises' greatest profit, according to the demand elasticity index of transportation service under the economics elasticity theory. No consideration is given to other influential factors except price, and we then correct the price with other influential factors changing. The theoretical model is applicable for China's shipping companies, airlines and road transport businesses with a relatively high degree of marketization.

Demand function and elasticity index of demand. The transportation demand function reflects the relationship between demand and supply of transportation. Setting up the demand function of transportation enterprise is the essential prerequisite. Suppose transportation demand and price satisfy Q=f (p). Actual equations can be calculated and regressed according to the historical data. This then sets up the possible mode of demand function and decides the parameters in that demand function. Demand price elasticity index can be calculated by deriving the demand function as: $|Ed| = \frac{dQ}{dP} \cdot \frac{P}{Q}$

Defining the theoretical price adjusting rang e. Suppose the present price of a transportation enterprise is P_0, the amount is Q_0, fixed transportation cost is F, variable cost is V, price adjusting range is ΔP, the change in amount of transportation caused by price adjusting is ΔQ. We can get:

The profit before adjusting price = $P_0Q_0 - F - VQ_0$ （1）

The profit after adjusting price （2）

The change in the profit: $\Delta\pi = \pi_1 - \pi_2 = P_1Q_1 - P_0Q_0 - \Delta QV$ （3）

And $P_1 = P_0 + \Delta P$, $Q_1 = Q_0 + \Delta Q$, put them in （3）, and we get:

$$\Delta\pi = \Delta QP_0 + \Delta PQ_0 + \Delta P\Delta Q - \Delta QV \quad (4)$$

From （4） we know ΔQP_0 is the change in income caused by transport amount changes; ΔPQ_0 is the change in income caused by transport price changes; $\Delta P\Delta Q$ is the change in income caused by both changes in price and amount at the same time; ΔQV is the change in cost caused by transport amount. According to the principle of economics, the demand elasticity index is:

$$|Ed| = \frac{dQ}{dP} \cdot \frac{P}{Q}$$

Bringing it into（4）, we get:

$$\Delta\pi = \Delta PQ_0\left[1 - |Ed|(1 - \tfrac{V-\Delta P}{P_0})\right] \quad (5)$$

The first and the second derivative of （5）are:

$$\frac{d\Delta\pi}{d\Delta p} = Q_0 - (1 - |Ed|) + \frac{|Ed|VQ_0}{P_0} - \frac{2|Ed|\Delta PQ_0}{P_0}$$

$\frac{d^2\Delta\pi}{d(\Delta p)^2} = \frac{2|Ed|Q_0}{P_0} \prec 0$, so $\Delta\pi$ must have the optimal result. Suppose $\frac{d^2\Delta\pi}{d(\Delta p)^2} = 0$, we can get the most optimal price adjusting range theoretically:

$$\Delta P = \tfrac{1}{2}(\tfrac{P_0}{|Ed|} - P_0 + V) \quad (6)$$

From （6）we can see the most optimal price adjusting range varies inversely with the demand elasticity index when the original price and variable cost are relatively stable. So if the demand elasticity index of an transportation enterprise is greater, the price adjusting range is more narrow for the maximization of its profit,

and vice versa.

APPLICATION OF PRICE DISCRIMINATION STRATEGY IN PRICING OF TRANSPORTATION

According to the above model, we know that different enterprises' optimal pricing is decided by demand elasticity in the transportation market. Different transport enterprises under any transport mode have different price elasticity. Generally speaking, a transport enterprise with better service quality, more security, higher waiting cost of customers, and more additional services to satisfy customers, will have a lower degree of demand elasticity in the transport service market and have more room for pricing. So the theoretical price adjusting model of transportation enterprise determines the feasibility of applying a price discrimination strategy in the transportation market.

Definition of price discrimination. According to economic theory, any enterprise with some degree of market power can decide its output and market price, which leads to the greatest possible monopoly profits through a price discrimination strategy. Charging different buyers different prices (third-level price discrimination) or charging the same buyer with different buying amounts different prices (second-level price discrimination) for the same goods or service is a practice known as price discrimination (Schiller, 1996). This pricing can not appear in the fully competitive market, because in the fully competitive market individual firms cannot affect prices. Rather they are passive acceptors of market prices, but enterprises with some degree of market power can definitely influence price.

Enterprises with some degree of market power use price discrimination in order to obtain monopoly profits. Successful implementation of a price discrimination strategy requires that the market should have the following characteristics:

The market is incomplete. When market competition is insufficient, with poor market information and lots of segmentations for various reasons, the enterprises with market power can take advantage of these features and utilize a price discrimination strategy. At present, many modes of China's transport markets are in this situation.

Different customers have different price elasticity for even the same product or service, and enterprises have the ability to grasp and to distinguish this difference. Thus, enterprises charge different consumers different prices. In fact, different transportation modes and enterprises are able to do so.

Differences in transport services and the expectations of the owners determine the application of price discrimination. As the price mechanism of China's transportation is perfected and effective regulatory mechanisms are established, the price system can adapt to market demand changes more fully. Further, differences in transport enterprises' service quality, transit time, security, and

customers' other special requirements should be necessarily reflected through the pricing system. Given its service products, transport enterprise pricing also should follow the law of supply and demand in the market (Wohl and Hendrickson 2004.

With the increasing opening of a transport market, competition has strengthened. Differences among different transport modes and differences among different enterprises in the same mode of transport are also growing significantly. So, many enterprises pay more attention to upgrading their service quality, which is reflected in saving transport time, improving transportation quality, strengthening security, meeting the special requirements of goods, and so on.

The above differences must bring different utilities to clients (the owner). The price elasticity of demand for different clients is not the same, so transport enterprises can set different prices, that is, to implement a price discrimination strategy as an important tool to realize the highest profits (Dewan and Mendelson, 1990).Therefore, transport enterprises should flexibly adjust prices, taking full account of demand elasticity reflected by the enterprise (industry) and external market conditions.

INFLUEN TIAL F ACTORS FOR TRANSPORTATION PRICING STRATEGY

The situation of supply and demand between transport capacity and transport demand. In the case that the transport capacity is greater than the demand, the elasticity of demand is bigger, price level should be appropriately reduced; if the transport capacity is less than the demand, the demand in that market becomes inelastic, and therefore the price has more room to rise.

Alternative modes of transport or numbers of enterprises which can provide the same service. If there are more alternative transport modes and substitutive enterprises, then this transport has the greater elasticity of demand and there is a need for lower prices.

Seasonal factors, such as low season and busy season. For example, the railway should adjust prices throughout the year according to traffic volume changes. Prices can be raised in the transport peak period and reduced appropriately in the low season.

Customer (the owner) market division factors. Offer differential pricing for different transport customers (shippers) with different elasticities of demand. For example, the tourist train, football fans train, the students train, high speed carriage and general speed carriage, and so on, may have targeted and specific tariffs.

Transport time, speed and comfort factors. Compared with competitors, a transport business with more timely, faster, and more comfortable services has lower elasticity and can enjoy higher prices and more revenue than competitors.

Regional factors. Affordability for clients from different economic regions is not the same. That is, differences in income level in different regions determine different levels of tariffs. Transport enterprise should activate market through

flexible, different forms of pricing. In addition, the situation of socio-economic conditions, inflation, the proportion of freight in cost and other factors should also be taken into account.

In fact, in recent years, various means of transportation have utilized a flexible pricing strategy to stimulate demand and expand market share. For example, since 1998, a number of railways have stimulated market demand greatly through flexible pricing (Dequan, 2007). Civil aviation companies and shipping enterprises also often employ a discount fare strategy to attract more customers.

CONCLUSIONS

The application of a price discrimination strategy in the transport market can help transport companies make optimal prices to maximize profits based on projections of demand elasticity. At the same time, it will help them appreciate the importance of market research and improvement in their transport service quality, develop characteristic transport services, enhance security and convenience, and pay attention to energy-saving and emission reduction.

Price system reform must also be synchronized with the reform of management mechanisms. Based on different investment relations, different tariff forms and implementation scope, the implementation of layered decision-making in railway freight is needed. This may result in the formation of new management mechanisms organized at different levels of the central and local governments, the railway authorities, and railway transportation enterprises.

REFERENCES

Schiller, B. R. (1996). Essentials of economics. 2nd ed., McGraw-Hill, New York.

Dequan H. (2007). The system, modal and practice of pricing in transportation market. Shang Hai finance and economics publishing house, 60~73.

Dewan, S., and Mendelson, H. (1990). "User delay costs and internal pricing for a service facility." Management science, 36(12), 1516~1520.

Wang, P. L. (2009). Transportation price reform and its tendency in China. Research speech of academy of macroeconomic research, Beijing.

Wohl, M., and Hendrickson, C. (2004). Transportation investment and pricing principles: introduction for engineers, planners and economists, John Wiley, Chapter 6.

Coordinated Development between Trans portation System and Socio-economic System Research based on SEM

Lu Shengrong[1], Jiang Huiyuan[2] and Liu Yao[3]

[1]School of Transportation, Wuhan University of Technology, P.O. Box Y17, Wuhan, ST 430063; PH 13807174044; email: allanlsr1986@163.com
2School of Transportation, Wuhan University of Technology, P.O. Box Y17, Wuhan, ST 430063; PH 13971110418; email: jianghuiyuanpanh@163.com
3School of Transportation, Wuhan University of Technology, P.O. Box Y17, Wuhan, ST 430063; PH 13437260440; email: mantha.pipi@163.com

ABSTRACT

Transportation System and Socio-economic System have mutual connections and influences. Their coordinated development has become an important guarantee to achieve the overall optimization of national economy. But in reality the situation is that one is often relatively ahead of or legged behind the other. So it becomes necessary for us to research on their coordinated development. Structural Equation Model (SEM) is a combination of Factor analysis and Path analysis, and it is suitable for dealing with such problems of finding out the relationship between large-scaled systems that contain lots of attributes and targets. For this reason, this paper has established a SEM-based model to study the situation of coordinated development between Transportation System and Socio-economic System. In the model, we build an evaluation index system, and take Wuhan City Circle for empirical study on its status of coordinated development between Highway-Waterway Transportation System and Socio-economic System. The paper gives out the path figure by LISREL and calculates out the coordination degree according to the coordination degree model; at last it puts forward some strategies for improving the coordination between the two systems.

INTRODUCTION

The coordination between Transportation System and Socio-economic System refers to the ability of coherency and sustainable development of all aspects of the two systems; it also can be understood as the problem of how to develop the Transportation System at a certain stage or level of Socio-economic System. When Transportation System is able to adjust to Socio-economic development, it can stimulate the Socio-economic growth; when it lags behind the development of Socio-economic, it plays the role of "dragging down"; and high speed of Socio-economic development also tends to generate new transportation need, thereby promoting the development of transportation industry. So it is of great guiding significance to know clearly the mutual coordination between them in the process of making investment decisions. As an integrated statistical technique of Factor and Path analysis, Structural Equation Modeling (SEM) is suitable for dealing with problems of researching the relationship between

large-scaled systems that contain many goals and properties. By SEM, this paper makes a structural validity evaluation on the given evaluation index system and gets the correlation between the two systems and their indicators. Then we apply the coordination degree model to calculate the coordination degree of the Highway-Waterway Transportation and Socio-economic System of Wuhan City Circle. In the end, this paper puts forward some strategies for improving the coordination between the two systems.

THEORIES OF SEM

Structural Equation Model supposes that there exists a causal relationship between latent variables; these variables can be calculated by a group of significant variables, and they are linear combinations of a number of significant variables. By verifying the covariance between significant variables, we can get the estimated coefficients in linear regression models. Then we may decide whether the assumed model is suitable for research in statistical. If confirmed appropriate, it can be said that the relationships between latent variables are reasonable. Structural Equation Model is composed of measurement model and structural model, and it can be represented by three matrix equations. When using SEM, we should assume a necessary pre-model (such as a given evaluation index system). Once set, we can do parameter estimation based on variance and covariance variables. The estimation process of SEM is different from traditional statistical methods. It derivates a variance and covariance matrix or correlation matrix from the variable covariance matrix or correlation matrix and makes the matrix elements as close as possible to observed variance and covariance matrix. If the model performs well, it will be very close to the original matrix, so the process is estimated to use a special fitting function so that the difference between the two matrixes becomes minimal.

Traditional multivariate statistical methods, such as Factor analysis and Path analysis, provide a powerful theoretical support and analytical tool to a certain extent for researchers to explain the relationship between variables, but each of them can only test single relation between the independent variables and dependent variables. Despite that the multi-variance analysis can deal with the relationship between multiple dependent variables and independent variables, this relationship is also single. SEM combines Regression analysis, Factor analysis, Path analysis and other methods. When dealing with the relationship between multiple variables, it simultaneously changes the test capacity from exploratory analysis to verifying analysis. It supplies strong theoretical support on statistical hypothesis testing, and also permits measurement errors of independent variables and dependent variables. These make it possible to analyze the structural relationship between potential variables.

Therefore, this article builds an evaluation index system of Highway-Waterway Transportation System and Socio-economic System of Wuhan City Circle. Each of the two systems has six indicators. Through questionnaire survey, this paper uses LISREL to make an evaluation of constructed validity of the index system. The result shows that it performs well.

Through the path figure, this paper gets the correlation between system and its indicators. These lay foundation for calculating coordination degree between the two systems.

EMPIRICAL STUDIES

In this paper, we select Socio-economic System and the Highway-Waterway Transport System of Wuhan City Circle as the research object, and establish an evaluation index system as shown in Table 1 .

Table 1.E valuation Index System .

Socio-economic System	Added value of Primary industry(X1)
	Added value of Secondary industry(X2)
	Added value of Third industry(X3)
	Total retail sales of society(X4)
	The level of urbanization(X5)
	Engel Coefficient(X6)
Highway-Waterway Transportation System	Transportation net connectivity(Y1)
	Transportation scale of matching(Y2)
	Road network density(Y3)
	Port throughput capacity fitness(Y4)
	Passenger volume(Y5)
	Cargo turnover(Y6)

In order to define the correlation between the indicators, this paper carries out a questionnaire on the index system. We use Likert-scale (5 scales) for the evaluation. Each title has 5 options: not important (1), not so important (2), general (3), important (4), very important (5). In the survey, we release 150 pieces, and recover 150 one week later; the recovery rate was 100%. According to survey results, we apply LISREL, and the programming is as follows:

```
Transportation System and Socio-economic System
DA NI=12 NO=150 MA=KM
KM SY
1
0.561 1
0.335 0.417 1
0.476 0.621 0.494 1
0.687 0.743 0.593 0.462 1
0.788 0.712 0.480 0.698 0.491 1
0.880 0.437 0.646 0.667 0.725 0.431 1
0.620 0.624 0.468 0.664 0.672 0.620 0.678 1
```

0.508 0.674 0.703 0.702 0.661 0.614 0.879 0.663 1
0.664 0.877 0.813 0.877 0.371 0.672 0.648 0.766 0.721 1
0.592 0.860 0.429 0.352 0.362 0.800 0.756 0.785 0.623 0.499 1
0.646 0.464 0.845 0.697 0.618 0.725 0.615 0.604 0.750 0.627 0.855 1
MO NX=12 NK=2 LX=FU, FI PH=ST TD=DI, FR
PA LX
6(1 0)
6(0 1)
PD
OU MI SS SC

After running the programming, we get the path figure as shown in Figure 1:

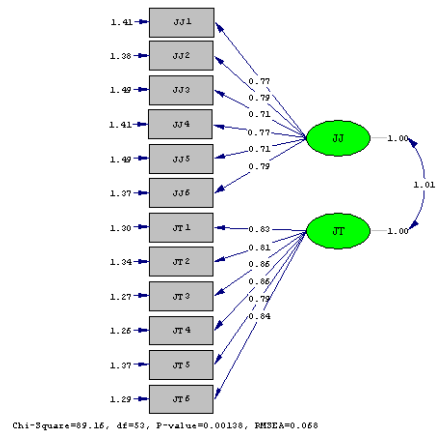

Figure 1. Path Figure in LISREL.

In addition, the main fitting parameters of the model are given in Table 2:

Table 2. Main fitting parameters and their s tandard values .

fitting parameters	X^2	RMSEA	NFI	NNFI	CFI	GFI
standard values	Near 0	≤0.08	Near 1	Near 1	Near 1	Near 1
fitting parameters	89.16	0.068	0.89	0.93	0.94	0.91

From the table, we can see that the main fitting parameters such as X^2, RMSEA, CFI and NNFI are close to their standard values. It means that the fitting situation is good, the constructed validity of the index system is permit and it can be used for evaluating the two systems in this article. According to the calculation method of coordination degree, the article is required to calculate the respective system-ordering of the two systems in advance. From the path figure, we can get the correlations between the two systems and their indicators. Combining the original data (as shown in Table 3) of the two systems in Year 2000-2007, we can calculate the system-orderings out. In addition, the formula of coordination degree is as follows: $D(t) = \sqrt{\frac{2 f_1 f_2}{f_1 + f_2}}$, where f_1 expresses Socio-economic System, f_2 expresses Waterway-Highway Transport System. The coefficients can be calculated by normalizing the coefficient in the Figure 1.

Table 3. Original data and Calculated C oefficients.

	2000	2001	2002	2003	2004	2005	2006	2007	Coefficients
X1	364.68	366.18	378.95	404.64	467.57	488.91	490.02	493	0.170
X2	1116.44	1228.72	1348.67	1508.53	1767.95	2034.01	2213.04	2452	0.174
X3	1018.01	1127.1	1249.92	1382.59	1570.37	1753.83	1925.26	2234	0.156
X4	1091.16	1209.48	1357.8	1475.04	1656.58	1890.54	2204.15	2405	0.170
X5	36.1%	36.7%	37.3%	39.6%	41.2%	43.1%	45.2%	46.9%	0.156
X6	45.8%	44.6%	43.2%	42.6%	41.4%	40.2%	39.6%	38%	0.174
Y1	1.1435	1.1602	1.1603	1.1914	1.2424	1.2692	1.2856	1.3202	0.166
Y2	2.4748	2.4998	2.4923	2.5665	2.6593	2.7139	2.7881	2.8376	0.162
Y3	0.5655	0.5738	0.5738	0.5939	0.6145	0.6278	0.6351	0.6541	0.172
Y4	0.1531	0.1624	0.1711	0.1885	0.209	0.2231	0.2288	0.2444	0.172
Y5	1643104	1672545	1765998	1680901	1724582	2377600	2586829	2814470	0.158
Y6	2151866	2077667	2260381	2451248	3837621	5152600	5970318	6917807	0.168

After normalizing and further calculating, we can get the coordination degree.

Table 4. C oordination Degree of all the years.

	2000	2001	2002	2003	2004	2005	2006	2007
f_1	1.000	1.061	1.136	1.224	1.363	1.493	1.608	1.741
f_2	1.004	1.018	1.051	1.093	1.252	1.449	1.551	1.681
D(t)	0.99	0.98	0.95	0.93	0.87	0.82	0.79	0.76

The respective system-ordering degrees are as follows:

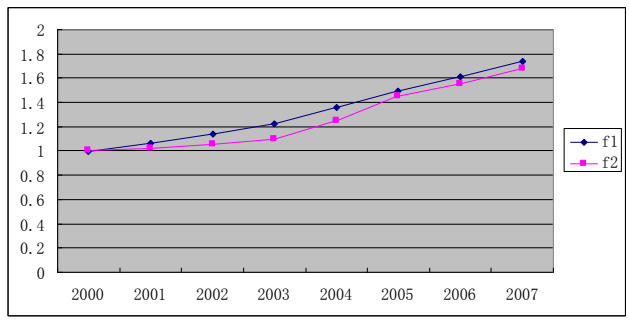

Figure 2 . Respective system -order ings of Year 2000 -2007.

From Table 5 and 6 , we can finally see the coordination degree grading.

Table 5. C oordination Degree grading standard.

D(t)	0.9-1.0	0.80-0.90	0.70-0.80	0-0.70
Grading	Overall adapting	Basically adapting	Lagging behind	Seriously constraint

Table 6. C oordination Degree grading in Year 2000 -2007.

	2000	2001	2002	2003	2004	2005	2006	2007
Grading	Overall adapting	Overall adapting	Overall adapting	Overall adapting	Basically adapting	Basically adapting	Lagging behind	Lagging behind

From the situation of system-ordering in Figure 2, we can see that the system- orderings of Socio-economic System are basically lower than those of the Highway- Waterway Transport System. We can also see that the coordination degrees change from overall adaptation to basically adaptation, and then to

lagging behind. The reason lies in fast development of socio-economic in recent years, while insufficient investment in the Highway-Waterway Transport System. These make the coordination between the two systems worse gradually. These are problems that relevant departments should pay attention to. The local government should make full use of the market. Through competition, it should enhance the vitality of market, improve its efficiency to speed up the development of Transportation system and implement reasonable division and efficient operation of various transportation modes in order to adapt to the development of Socio-economic System.

CONCLUSIONS

The innovation of this paper is that we apply Structural Equation Model to evaluate the constructed validity of the given index system, and get the correlation between the system and its indicators. After these, by combining the original data of Wuhan City Circle in recent years and the coordination degree model, we calculate out the values of coordination degree and divide the coordination grades. This article can provide some references for relevant departments in the process of making investment decisions.

BIBLIOGRAPHY

Anderson J C, Gerbing D W (1988). Structural Equation Modeling in Practice: A Review and Recommended Two-Step Approach [J]. Psychological Bulletin, 1988, 103 (3):411-423.

Chen Kaiming (2006). The characteristics and applications of Structural Equation Modeling [J]. Statistics and Decision, May., 2006, pp. 22-25.

Cheung G. W, Rensvold R B (2002). Evaluating goodness of fit indices for testing measurement invariance [J]. Structural Equation Modeling Journal, 2002, 9(2), 233–255.

Lei Huaiying (2007). Coordination Evaluation of Transportation and Economic development based on DEA. Statistics and Information Forum, Vol.22, No.1, Jan., 2007, pp. 50-53.

Shook, Ketchen, Hult, Michele Kacmar (2004). An assessment of the use of structural equation modeling in strategic management research [J]. Strategic Management Journal, 2004(25): 397-404.

Xu Wenxue, Jia Yuanhua (2007). Traffic development strategies and measures of Wuhan City Circle [M]. Beijing: People's Traffic Press, May., 2007, pp. 224-250.

Study on the Structure of Digitized Transport Network s and Evaluation of some Logistics Policies

YANG ZhongZhen, JIANG Yonglei, JIN Lianjie

College of Transport Management, Dalian Maritime University, Dalian, 116026, China; TEL/FAX (0411) 8472-6756; E-mail: yangzhongzhen@263.net

Abstract : This paper presents a method to construct an integrated transport network model based on the attributes and structures of the modes and path choice behavior of users. First, a conception of integrated transport networks is given and the meanings of dummy links and their construction methods are discussed. Three kinds of dummy links are created. Then three kinds of network models are constructed for the Chinese Northeast region, and their performance is evaluated. Finally, we evaluate some logistics techniques and policies with the integrated transport network.

INTRODUCTION

An integrated transport network is a network consisting of links and nodes of several kinds of transport modes (Jin et al, 2006). When organizing multi-mode transport, the cost, time and reliability of the combination of different modes must be considered; therefore, the shortest path between the origin and destination, the mode combination of the shortest path and the transfer cost/time from one mode to another should be considered. Thus integrated networks are necessary to analyze multi-mode transport schemes. Recently, many studies have focused on integrated transport, among them a quantitative analysis mainly focused on terminal location (Guo et al, 2001), and an analysis of multi-mode transport and path choice (Beuthe et al, 2001, Sun and Yang, 2005, Zhang and Guo, 2002). In the field of integrated transport networks, many researchers have built simple network models and have developed the shortest path algorithms (Lozano and Storchi, 2001, Wei et al, 2006, Kozan, 2001). There is scant literature discussing the transfer process in the integrated network. Based on the analysis of the attributes and structures of each mode, and path choice behaviors of users, this paper presents a method for constructing integrated transport networks. Three kinds of construction methods are presented based on different kinds of links, and a set of logistics techniques and policies are listed and evaluated based on the network.

INTEGRATED TRANSPORT NETWORK MODEL

The integrated transport network model means a mathematical configuration recorded in the computer, which can represent the topological structure of the combination of multi-mode transport networks in the real world (Southworth and

Peterson, 2000, Wang and Wang, 2005). In the network, ordinary links represent railways, highways, waterways and airways, and dummy links represent the transfer routes. The ordinary links have the attributes of time, cost and capacity, while dummy links have time and cost attributes. Figure 1 is a simple example, which contains highway, railway, and dummy links and transfer terminals. The main task in constructing a integrated network model is to represent the dummy links suitably.

DUMMY LINKS IN AN INTEGRATED TRANSPORT NETWORK MODEL

Transfer Attributes based Dummy Links

Figure 2 shows the method of creating dummy links based on transfer attributes, where the attributes of dummy links record the needed time, cost and reliability of the transfer. On a macro level, the node to connect highway and railway may not be in the same location but at two terminals in a city; thus urban roads will be used for transfer. Consequently, the static shortest path is one attribute of a dummy link, and the cost and time of loading, unloading and storage are the others.

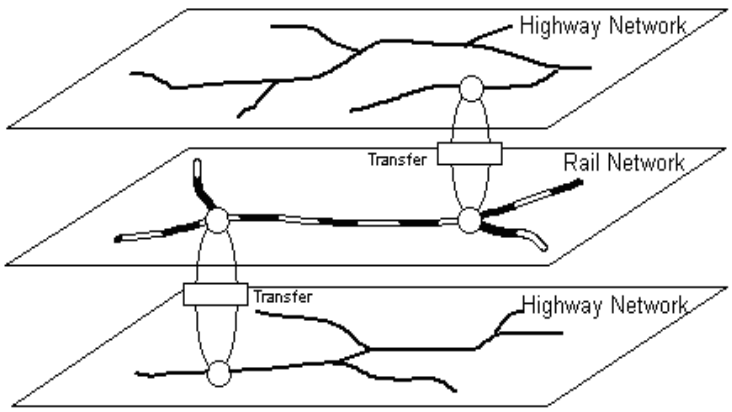

Figure 1. Integrated Transport Network

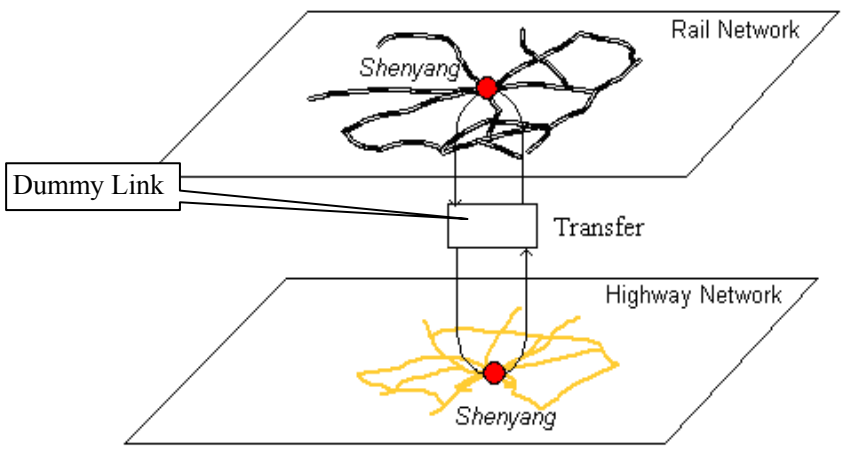

Figure 2. Transfer Attributes based Dummy Links

There may be more than one dummy link for a node because freight with different destinations may require different paths, resulting in different needed time and costs in urban road network. Moreover, due to the different schedules of trains, waiting time and costs in stations may differ; different dummy links should be created correspondingly. An integrated network model based on this method has a simple structure and is easy for computing. However, the disadvantage is that the method for representing dummy links is too simple to precisely account for the dynamic attributes of road traffic.

Urban Road Ne twork based D ummy Links

In this method, dummy links are the connectors linking urban road networks and highway networks; thus the integrated transport network model with these dummy links contains railway links, highway links, urban road links, transfer terminals and dummy links, where railway and highway are at the same macro level and an urban road is represented in micro degree. The solid line in Figure 3 represents the dummy link, and the dash line represents the direct connected roads without any impedance. This is because that urban road commonly links directly with inter-city highways.

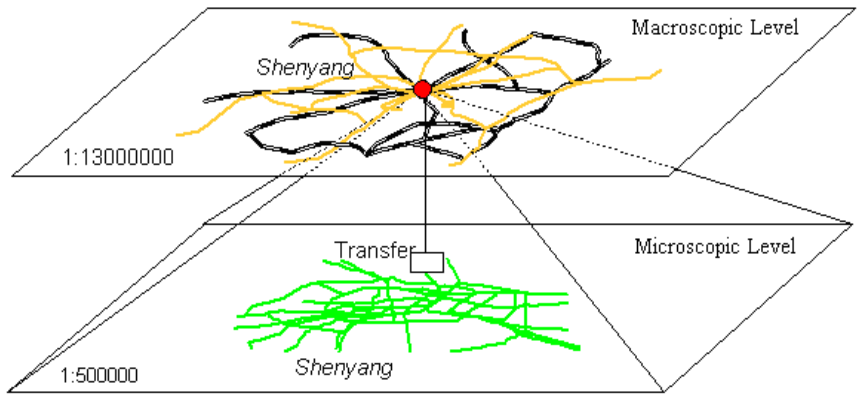

Figure 3. Urban Road Network based Dummy Links

Compared with the first kind of dummy link, dummy links here only represent the transfer process, and movement of freight in a city can be shown clearly with urban road networks. The integrated network model here can reflect the transfer process, the moving status of trucks in a city and the impact of trucks specifically on urban traffic. However, when the corresponding region is too large, the network model also becomes large, since many urban roads should be included. Therefore, in this kind of network, urban road networks should be simplified.

Multi -scale based Dummy Links

Different scales represent different information densities (Hu & Yan, 2006). Spatial data can be represented as different geometrical forms under different scales. Here we use two scales to represent an integrated transport network model. As

shown in Figure 4, under macroscopic level (small scale), attributes of dummy links are used to represent the information of urban roads and terminals, while under microscopic level (large scale), both attributes of dummy links and urban roads are used.

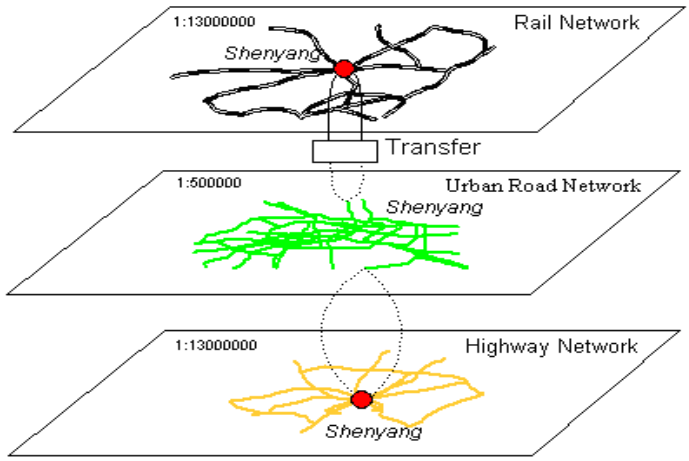

Figure 4. Multi -scale based Dummy Links

This means that at the macroscopic level, the transfer process is abstracted as dummy links; while at the microscopic level, the dummy links are changed back to urban road network and transfer links. The multi-scale based dummy links are stored in two levels: the first includes railway, highway and dummy links, and the second includes urban roads and dummy links to represent the transfers. The two layers are connected with indexes. This integrated transport network uses two kinds of dummy links and connects urban road networks, highway networks and railway networks closely.

PERFORMANCE OF THE THREE KINDS OF MODELS

The first kind of integrated network model presents transfer in urban road and terminals with dummy links. The network is simple, but highly generalized dummy links make it difficult to analyze truck behaviors in urban roads. The second kind connects urban road networks with inter-city highway networks; it reflects the interaction between truck flow and urban traffic flow. However, with the addition of urban road networks, it becomes larger and more complicated. The third one divides the whole model into two scales. Therefore, for finding the shortest path, we can search the nodes at the macroscopic level. Then, the information of urban road networks is obtained by indexing the dummy links at the macroscopic level, and thus Dijsktra's algorithm can be used in urban road networks by taking the entrance node into the urban road network as the origin and terminal as the destination. Finally, the two level shortest paths obtained are integrated by their scales and indexes. Therefore, this method can not only depict the detailed moving

characteristics of trucks in urban road networks, but also avoids the undue increase of search space through the macroscopic-level dummy links.

To evaluate the performance of the three methods, we constructed three kinds of integrated transport network models for the Chinese Northeast region, where roads, railways, dummy links and terminals etc. are included and urban road networks in Dalian, Shenyang, Changchun, Harbin, Yanji, Manzhouli are constructed. Table 1 shows their attributes. We found that the attribute of the first model is similar to that of the second one, and their physical structures are also same. The only difference is the number of nodes and links.

Table 1. Links in the Integrated Transport Network Models

Model Type	Link Number	Link Length (km)
Attributes based dummy link		
Road sub-network	224	29,823
Rail sub-network	232	20,844
Dummy links	67	332
Urban road network based dummy link		
Road sub-network	224	29,823
Rail sub-network	232	20,844
City sub-network	523	1,263
Dummy links	67	0
Multi-scale based dummy link		
Road sub-network	224	29,823
Rail sub-network	232	20,844
City sub-network	523	1,263
Dummy links	134	332

We used Dijsktra's algorithm to test the three models; the calculation times for them are 0.30s, 0.62s and 0.47s, respectively (CPU=Pentium 2.2G).We can see that the first model needs the least time due to having the fewest links, dummy links and nodes. The third model balances the calculation efficiency and the details of the network well. Because the third model uses two scales to express the information and has two levels of physical structure, thus the process of Dijsktra's algorithm is divided into steps as follows.

- Step 1: Find the shortest path by Dijsktra's algorithm at the macroscopic level. If there are transfers in the path, go to Step 2; otherwise, stop;
- Step 2: Find all the dummy links in the shortest path; get urban road information among them by the index of dummy links, use Dijsktra's algorithm to find the shortest path in the urban road network with taking the entrance node into the urban road network as the origin and the terminal as the destination;

- Step 3: Integrate the two shortest paths with their scales and indexes to meet the output demand for different scales.

EFFECTS OF SOME TRANSPORT POLICIES AND TECHNIQUES

We summarized 11 policies or techniques used to improve the container integrated transport. They are: 1) operation of railway liner; 2) use of double-deck container trains; 3) increment of liner frequency; 4) raising railway speed; 5) setting freight dedicated railway; 6) price discounts; 7) construction of expressways to connect ports and railway terminals; 8) construction of container yards; 9) use of new handing equipment; 10) construction of information systems for integrated transportation; and 11) digitally managed container yards. Through combination of these policies and techniques we developed the following improvement schemes.

Schemes 1=without any change; Schemes 2=7)+ 8)+ 9)+ 10)+ 11)；Schemes 3=4)+ 5)+ 6); Schemes 4=1)+ 2)+ 3); Schemes 5=1)+ 4)+ 7); Schemes 6=1)+ 2)+ 4)+ 5)+ 7)+ 8)+ 9); Schemes 7=1)+ 2)+ 3)+ 4)+ 5)+ 6)+ 7)+ 8)+ 9)+ 10)+ 11).

Then by taking Dalian, Shenyang, Changchun, Harbin and Manzhouli as centers, we built an integrated network and five transport zones (Figure 5) and obtained the container OD metric per two weeks as Table 2 shows. Assigning the OD onto the networks corresponding to the 7 schemes with the least cost rule, we obtained transport costs as shown in Table 3.

Table 2. Regional Containers O -D (TEU)

O/D	1	2	3	4	5
1	0	506	168	96	24
2	4900	0	402	154	14
3	1634	186	0	152	12
4	922	106	98	0	32
5	230	26	16	12	0

Figure 5. Network and the Zon e

We found that compared with Scheme 1, Scheme 2 saves 1.2 million RMB, Scheme 3 and Scheme 4 save 2 million RMB respectively. The effects of Scheme 3 and Scheme 4 are more obvious because of the increment of railway capacity, although the increment is limited subject to transfer capacity. In Scheme 2 only transfer methods were taken, and thus transfer cost is reduced but transfer quantity did not change. Schemes 5, 6 and 7 implemented a series of policies and techniques and resulted in more obvious outputs. Through the comparison it can be understood that effects of a single method are much less than the effects of a set of methods, meaning that multi-model transport is a whole system; improved efficiency and cost savings are realized only through cooperating and compromising policies and methods. Then the advantages of the integrated transport can be realized.

Table 3. Transport Costs obtained through Traffic Assignment (million RMB)

Scheme	Cost on Road	Cost on Rail	Transfer Cost	Total
1	18.91	1.08	0.35	20.33
2	17.96	1.01	0.14	19.10
3	15.27	2.19	0.88	18.34
4	13.93	3.06	1.08	18.08
5	14.07	2.63	0.83	17.53
6	13.93	2.55	0.76	17.24
7	12.83	2.72	0.60	16.15

CONCLUSION

This paper studied the method of building integrated transport networks. In the integrated network model, transfer terminals are abstracted as dummy links. Three methods of constructing dummy links were proposed. The performances of the three kinds of models were evaluated. Through testing the Shortest Path Searching, it was found that the integrated network model, made up of multi-scale-based dummy links, is more efficient and can reflect the transfer behaviors in the networks precisely.

We also used the integrated network model of multi-scale-based dummy links to test policies or techniques that are designed to improve the efficiency or reduce the cost of the transport. We found that the increment of railway capacity can reduce transport cost, and that a combined set of policies and techniques are better than a single policy or technique.

REFERENCES

Beuthe M. et al (2001). “Freight transportation demand elasticity’s: a geographic multimodal transpiration network analysis.” Transportation Research Part E , 37, 253-266.

Guo Z.J., Wang N., Huo H. (2001). “Study of model of port planning for multimodal container transportation.” J. of Dalian University of Technology, 41(5), 598-601.

Hu Z., Yan H.W. (2006). “Research on multi-scales expression of spatial data.” J. of Lanzhou Jiaotong University (Natural Sciences), 25(4), 35-38.

Jin Z.H., Piao H.S., Yang H.L. (2005). "Optimization of co-ordinate container loading and transportation in the multimodal transportation system." Systems Engineering, 23(11), 1-6.

Kozan E. (2001). "Optimising container transfers at multimodal terminals." Mathematical and Computer Modeling, 31(10), 235-243.

Lozano A., and Storchi G. (2001). "Shortest viable path algorithm in multimodal networks." Transportation Research Part A , 35, 225-241.

Southworth F., and Peterson B E. (2000). "Intermodal and international freight network modeling." Transportation Research Part C , 8, 147-166.

Sun Z., and Yang Z. Z. (2005). "A GIS-based path searching system on the combined network of roads and transit." J. of Eastern Asia Society for Transportation Studies, 6, 2223-2233.

Wang T., and Wang G.(2005). "A combined optimization model for transportation modes of multimodal transport." Engineering Science, 7(10), 46-50.

Wei H., Li J., and Liu N. Z. (2006). "An algorithm for shortest path with multi-modal in time-varying network." Chinese J. of Management Science, 14(4), 56-63.

Zhang J. Y., and Guo Y. H.(2002). "A multimode transportation network assignment model." J. of the China Railway Society, 24(4), 114-116.

Research on Optimization of Crew Scheduling of the Passenger Dedicated Line Based on a Genetic Ant Colony Algorithm

Z. Tian[1], S. Ni[1], T. Chen[1], Q. Song[1]

[1]College of Traffic and Transportation, Southwest Jiaotong University, Chengdu, Sichuan, 610031, China; PH(+86)28-87634680;email: tianzhiqiang_1128@126.com

ABSTRACT

Crew scheduling is an important part of the passenger dedicated line plan system, and also the main factor influencing operating expenses of passenger dedicated lines. After analyzing a crew scheduling problem, the following two steps are chosen to solve this problem. First, the train running paths are divided into crew paths, which are then combined into crew routes according to related constraint conditions of the crew scheduling plan, the relationship between train numbers and the motor train set routes. Then, a mathematical model is given with the aim of minimizing the operating expenses of the crew scheduling problem, and a Genetic Ant Colony Algorithm is designed for solving this model.

1. INTRODUCTION

Crew scheduling is an important problem faced by every transportation method. In airline transport and urban transport, the cost of a crew is second only to the total production cost; in railway transport and maritime transport, the cost of a crew is also an important part of the total cost.

In response to market demands, the adjustment of train diagrams becomes more frequent, and so too does the corresponding adjustment of the crew scheduling become more frequent too. If we still use the manual weaving method, long time will be needed, thus not fitting the need of the transport organization. According to these factors, we apply an effective optimization method and utilize computers to weave crew scheduling as the only choice to satisfy the transport organization.

2. PROBLEM FORMULATION

In ZhaoPeng et al. (1998), the crew scheduling problem was divided into two sub problems: the crew scheduling problem and the crew rostering problem. Crew scheduling consists of all crew routes, which indicates the total crew members needed by the crew works of the train diagram and the detail of the crew routing. A crew rostering plan is such a plan that stipulates the work and the rest dispatched to every crew member. This paper only focuses on the research of the crew scheduling problem.

The existing research results have usually treated the crew scheduling problem as a Set Covering Problem (SCP) or a Set Partition Problem (SPP), and

various algorithms have been developed to solve it. J.E. Beasley et al. (1996) adopted a tree search algorithm to solving the crew scheduling problem, and the lower bound of the problem was found by Lagrangian relaxation. Shangyao Yan et al. (2002) have pointed out that the pure network model can be used to represent crew scheduling problems when the scale of the problem is relatively small. However, using a Genetic Ant Colony Algorithm to solve the crew scheduling problem has not been explored in previous research. The related knowledge of Genetic Algorithm and Ant Colony Algorithm could refer to J.E. Beasley (1996) and Marco Dorigo (2006).

3. MODELING

The crew scheduling of passenger dedicated lines is a very difficult problem; to reduce the complexity of the problem, we adopted a method which divides the weaving problem into the following two steps: (1) divide the travel line into crew paths based on the distribution of the relief station; (2) combine the crew paths into crew routes that qualify all restrictions.

3.1 The division of crew paths

The travel line can be divided into crew paths based on two factors: first, the distribution of the relief stations, and second, the stops on the stations stipulated by the train diagram (excluding the direct trains). The divided crew paths could be expressed as follows:

$$p_i = (TN, n_i, JN, S_i^s, T_i^s, S_i^e, T_i^e) \qquad i = 1, 2, ..., m$$

where *TN* is the train number of the crew path; n_i is the *No.* of the crew path; *JN* is the motor train set route number of the crew path; S_i^s is the start station of crew path *i*; T_i^s is the start time of crew path *i*; S_i^e is the end station of crew path *i*; T_i^e is the end time of crew path *i*; *m* is the total number of all crew paths.

3.2 The combination conditions of the crew paths

Constrained by the distribution of the relief station, the length of the crew paths is usually not very long , so when forming the crew route, we could combine the divided crew paths into crew routes with ideal length by satisfying all restrictions such as total working time criterion, relief time criterion etc.

In this process, the following restrictions should be satisfied:

(1) Every crew path should belong to one and only one crew route. (2) For the connected two crew paths, the end station of the first crew path and the start station of the second crew path should be the same station. (3) The time interval between two crew paths must be longer than the relief time criterion. (4) The total time of each crew route should not exceed the maximum working time. (5) The continuous working time in each crew route should be no longer than the criterion.

The constructed crew routes can be expressed as follows:

$R_j = (RN, k_j, S_j^s, T_j^s, S_j^e, T_j^e)$

Where k_j is the relief time happened in crew route j, other variables have the similar definition with crew path.

3.3 Optimization model

The most important goal of the crew scheduling problem is to minimize the cost of the crew operation. In order to reduce the difficulty of the problem, some of the researchers only considered the number of the crew members in the optimization model, but in practicality, the various costs involved by the crew scheduling plan may affect the result of the scheduling. The set-covering model of crew scheduling problem is as follows:

$$\min Z = \sum_{j=1}^{n} c_j \cdot x_j + \sum_{i=1}^{m} \left(T_i \cdot c_{zc} + \left(\sum_{j=1}^{n} a_{ij} \cdot x_j - 1 \right) T_i \cdot \beta \cdot c_{zc} \right) \quad (1)$$

$$c_j = c_{wage} + k_j \cdot c_h + \sum_{l=1}^{k_j} (\omega_l - T_{hc}) \cdot c_{zc} \cdot \alpha$$

Subject to:

$$\sum_{j=1}^{n} a_{ij} x_j \geq 1 \qquad i = 1, 2, ..., m \quad (2)$$

In the objective function, each crew path should be covered at least one time. Once the crew path is decided, the total time of it is fixed, so the objective function can be simplified as follows:

$$\min Z = \sum_{j=1}^{n} c_j \cdot x_j + \sum_{i=1}^{m} \left(\left(\sum_{j=1}^{n} a_{ij} \cdot x_j - 1 \right) T_i \cdot \beta \cdot c_{zc} \right)$$

When constructing a feasible solution, the following constraint should be satisfied:

$$S_{i_1}^e x_{i_1 j} = S_{i_2}^s x_{i_2 j} \qquad 1 \leq i_1 \leq m, \ \ 1 \leq i_2 \leq m, \ \ i_1 \neq i_2, \ \ j = 1, 2, ..., n \quad (3)$$

$$T_{i_2 j}^s - T_{i_1 j}^e \geq x_{i_1 j} x_{i_2 j} T_{hc} \ 1 \leq i_1 \leq m, \ \ 1 \leq i_2 \leq m, \ \ i_1 \neq i_2, \ \ T_{i_2}^s > T_{i_1}^e, \ \ j = 1, 2, ..., n \quad (4)$$

$$T_j^e - T_j^s \leq T_{bz} \qquad j = 1, 2, ..., n \quad (5)$$

$$T_{v+\delta}^s - T_v^e \leq T_{lx} \qquad \prod_{v}^{v+\delta} r_i = 1 \qquad 1 \leq v < v + \delta \leq n_j \qquad j = 1, 2, ..., n \quad (6)$$

In the optimization model, m is the number of all crew paths, n is the number of the crew routes, x_j is a 0-1 binary value that equals 1 if crew route R_j was selected and 0 otherwise. c_j is the total cost of crew route j which consists of fixed costs and variable costs. The fixed cost consists mainly of the basic wage of crews c_{wage}; the variable cost is determined by the duty time T_j, the number of relief times k_j and the

length of invalid relief time $\sum_{l=1}^{k_j}(\omega_l - T_{hc})$, ω_l is the time spent in each relief, T_{hc} is the time criteria of the relief, c_h is the average relief cost, c_{zc} is the cost of the crew duty per time unit, α is the coefficient of invalid relief time versus normal duty, β is the coefficient of invalid relief time versus normal duty, a_{ij} is a 0-1 variable that equals 1 if crew path p_i belong to crew route R_j and zero otherwise, n_j is the total number of crew paths in crew route R_j, T_{bz} is the maximum working time in one route, T_{lx} is the continuous working time, δ is the number that undertaken by one crew continuously, r_i is a 0-1 binary value that equals 1 if the connection time after crew path i longer than the rest time and 0 otherwise.

The restrictions (2)-(6) correspond to the combination rules of crew paths in 3.2, respectively.

4 GENETIC ANT COLONY ALGORITHMS (GACA)

4.1 The basic steps of GACA

The basic steps of GACA used in this paper are as follows:

Step1: Generate some relatively better solutions to the problem by genetic algorithm and initial the pheromones by these solutions,

Step2: $nc \leftarrow 0$，(nc is the number of iterations).

Step3: Place m ants on the starting node of the construction graph, and for each ant k (k=1, 2,…, m), choose the next node j with the probability decided by the pheromones and the heuristic information until the construction of the solutions is finished.

Step4: Choose some pair of solutions to carry out the crossover operation according to the crossover probability. Receive the new solutions generated by crossover if the value of the objective function has been improved, and reject otherwise.

Step5: Decide whether to carry out the mutation or not according the mutation probability. Receive the new solution generated by mutation if the value of the objective function has been improved, and reject otherwise.

Step6: Calculate the length of each route L_k (k=1, 2,…, m) and update the best-so-far solution.

Step7: Select the best s solutions to update the pheromones of the edges by the update equation.

Step8: $nc \leftarrow nc+1$.

Step9: Turn to step 3 if nc is less than the given iteration times and without degradation, otherwise, turn to step 10.

Step10: Output the best-so-far solution.

4.1 Coding of the problem

This paper uses a column-based method to represent the solution of the crew scheduling problem, forming the n columns of the problem by sorting the feasible

crew routes in certain sequence. Then it describes the solution with a binary character string in which 1 means the column *i* is contained in the final solution.

4.2 The operations of Genetic Algorithm

(1) The generation of the initial solution

We selected some crew routes randomly from the set of all crew routes to generate the initial solution of the problem, considered the feasibility of these solutions, and adopted the repair method and post optimization technology. We repeated this procedure several times to get the initial group and then chose the better initial solution of the problem by their fitness value.

(2) Selection

The selection method used in this paper is roulette wheel selection.

(3) Crossover

The crossover adopted is the crossover operator based on the fitness value which both considered the construction and fitness value of the parents.

Let P_1, P_2 be the chromosome of the parents, and f_{p1}, f_{p2} be the fitness value of the parents, C represent the chromosome of the child, so the crossover can be represented as follow:

When $P_1[i] = P_2[i]$, let $C[i] = P_1[i] = P_2[i]$, otherwise, let $C[i] = P_1[i]$ by the probability of $p = f_{P2} / (f_{P1} + f_{P2})$ and let $C[i] = P_2[i]$ by the probability of $1 - p$.

Because the feasibility of the solution can not be ensured after the crossover operation, the repair method and the post optimization technology is adopted to handle the solutions determined by the crossover.

(4) Mutation

The purpose of mutation is to preserve diversity and it avoids local optima entrapment. Each chromosome carries out mutation by the mutation probability. The method adopted is turnover one of the gene in the chromosome by small probability. In order to assure the feasibility of the solution, the repair method and the post optimization technology is used after the mutation.

4.3 The operations of Ant Colony Algorithm

(1) The representation, update and initialization of pheromones

Pheromones τ_j is the expectation that crew route *j* is contained in the final solution, the larger τ_j is, the greater the probability of selecting the crew route *j* into the final solution. The formulation for update the pheromone is as follows:

$$\tau_j(n+1) = \rho \tau_j(n) + \Delta \tau_j \tag{7}$$

Where ρ is the evaporation rate, *n* is the iteration times, $\Delta\tau_j$ is the quantity of pheromones laid on column *j* by the ants.

(2) The construction of the solution

The construction of the solution is an important content in ant colony

algorithm. In this paper, each ant starts from an empty solution and constructs the solution by adding the crew routes step by step. The probability of choosing crew route *j* is as follows:

$$p_j^k(t) = \frac{\tau_j[\eta_j]^\beta}{\sum_{l \in N^k} \tau_j[\eta_j]^\beta}, \qquad if \ \ j \in N^k \tag{8}$$

Where η_j is the heuristic information that equals c_j / e_j, e_j is the row number covered by column *j*, so η_j indicates the average cost of the newly covered rows when adding column *j* into the solution.

After the construction, the post optimization technology is used to ensure there are no redundant columns in the solution.

4.4 The termination condition

The algorithm will be terminated when one of the following conditions is satisfied:

(1) The algorithm has already found the best solution whose value equals f^*, or the solution found located in an expected range with the best solution.

(2) The solution found by the algorithm or the iteration time of the algorithm has reached maximum.

(3) The CPU time of the algorithm has reached maximum.

(4) The algorithm has stagnated.

5 CONCLUSION

This paper analyzed the crew scheduling problem and created a mathematical model to minimize the total cost of crew expense. The model considered almost all costs that will affect the result of the crew scheduling, therefore describing the crew scheduling problem accurately. However, this paper researched only the crew scheduling problem and does not address the problem that must be faced in the second stage when weaving the crew plan—the crew rostering problem. Therefore, a key point for future work will be creating a reasonable mathematic model of the crew rostering problem and designing an effective solution algorithm.

ACKNOWLEDGEMENTS

This research is supported by National Natural Science Foundation of China in 2008 (60870004).

REFERENCES

Beasley, J. E., and Cao, B. (1996). "A tree search algorithm for the crew scheduling problem." *European Journal of Operational Research*, 94, 517-526.

Beasley, J. E., and Chu, P. C. (1996). "A genetic algorithm for the set covering

problem." *European Journal of Operation Research*, 94, 392-404.

Dorigo, M., Birttari, M., and Stützle T. (2006). "Ant colony optimization." *Computational Intelligence Magazine*, 11, 28-39.

Yan, S., and Tu, Y. (2002). "A network model for airline cabin crew scheduling." *European Journal of Operational Research*, 140, 531-540.

Peng, Z., Anzhou, H., and Hao, Y. (1998). "Research on Optimization of Crew Scheduling." *Journal of the China Railway Society*, 20(4), 8-13.

Analysis for Principal-agent Relationship between Owner and Construction Agent of Agent-construction Project

Wenyi ZHAO[1], Xuancang WANG[1] and Ting ZHAN[1]

[1]School of Highway, Chang'an University, Xi'an China, PH (86) 29-82334387; email: chd-zwy@163.com

ABSTRACT

According to the basic logic of principal-agent theory in information economics, and in combination with the connotation of management mode for agent-construction project, a principal-agent model for the relationship between owners and constructions agent was established. The model has been used to analyze the principal-agent problem of owners and construction agents. As is shown in the analysis results, incentive mechanisms and supervision mechanisms can stimulate construction agents to do better; however, the traditional mode that increases in fixed remuneration has no effect on it. In addition, an increase in fixed remuneration is only the precondition for cooperation between owner and construction agent. A supervision mechanism has a negative impact on the construction agent; for the owner, it is necessary to use it with caution.

1 INTRODUCTION

An agent-construction project means a project is constructed by adopting a management mode of principal-agent. It originally came from innovations in the management mode of governmental investment projects; however, it has been widely used in non-governmental investment projects, including private, government-private, foreign investment projects, and so on in this day and age (Zhao 2006). The essential characteristic of the agent construction mode is that the agent-construction owner decides who owns project on its behalf (Yin and Yan 2006). In the agent construction mode, the owner must sign a contract with the construction agent. Normally, what the construction agent can earn is predetermined agent-construction fees and part of the project investment remainder. In the view of information economics, the relationship between the owner and the construction agent belongs to the principal-agent.

The principal-agent theory of information economics attempts to model the following issues: the principal is originally intent to make agent action as the former's advantages, however, principal can not get to know what the agent do, in addition, all that the principal can observe are just other variables. These variables are affected by the agent's action and other random factors, so that the principal only gets incomplete information about the agent. The principal's main problems is how to award or punish the agent according to the information gained from observations

so as to inspire the agent to choose the most beneficial action (Zhang 2007). The owner of the agent-construction project is the principal and the construction agent works for the owner. The construction agent's fees are fixed, but the project investment remainder can serve to inspire the agent. This paper tries to analyze the relationship between the owner and the agent through the principal-agent model, and provides references for the design of an incentive and supervision mechanism.

2 HYPOTHESES AND ILLUSTRATION OF MODEL

Assume a is a one-dimensional endeavor variable, and productive function is linear form, as is shown in (1). k_1 expresses productive coefficient of endeavor variable. θ is a random variable which mean = 0 and variance = σ_θ^2. It represents uncertain exterior factors. The supervisory signal, p, is the benefit to supervise and calculate a. Because a is related to p and affected by it, so p is a function of a. As is shown in (2), in which ε is a random variable which mean = 0 and variance = σ_ε^2 (Yang and Zhang 2008).

Productive function:

$$\pi = k_1 a + \theta \qquad \theta \sim N(0, \sigma_\theta^2) \tag{1}$$

Supervisory signal:

$$p = k_2 a + \varepsilon \qquad \varepsilon \sim N(0, \sigma_\varepsilon^2) \tag{2}$$

Var(θ)= σ_θ^2 reflects ectogenic environmental risk. Var(ε)= σ_ε^2 reflects accuracy of monitoring signal. θ and ε are both independent, so we can get covariance cov(θ, ε)=0.

Under the condition of the monitoring signal, the reward payment function of the owner not only depends on production π but also depends on the monitoring signal p, so we can get (3).

$$s(\pi, p) = \alpha + \beta\pi + \delta p \tag{3}$$

Where α is fixed income of the construction agent; β is the productive share of the construction agent under the condition of $0 \le \beta \le 1$; δ reflects the reward of the construction agent regarded the monitoring signal as a reference. Then, the expectant utility function of the owner is:

$$E(v) = E[\pi - s(\pi, p)] \tag{4}$$

Suppose the expectant utility function of the construction agent has the invariable character of absolute risk elusion, i.e. $U = -e^{-\rho\omega}$. Where ρ is the absolute risk elusion degree; ω is practical currency income. Supposing the effort cost of the

construction agent is $c(a)=\frac{b}{2}a^2$， here, $b(b>0)$is cost coefficient; negative effect of a increases with increase of b. Then, the practical income of construction agent can be expressed as follows:

$$\omega = s(\pi, p) - c(a) \tag{5}$$

Determining equivalent income is:

$$E(\omega)-\frac{\rho}{2}(\beta^2\sigma_\theta^2+\delta^2\sigma_\varepsilon^2)=\alpha+(k_1\beta+k_2\delta)a-\frac{b}{2}a^2-\frac{\rho}{2}(\beta^2\sigma_\theta^2+\delta^2\sigma_\varepsilon^2) \tag{6}$$

Where $E(\omega)$ is expectant income of construction agent; $\frac{\rho}{2}(\beta^2\sigma_\theta^2+\delta^2\sigma_\varepsilon^2)$ is risk cost of construction agent. Supposing $\overline{\omega}$ is reserved income level of construction agent, participation restriction of construction agent can be expressed as follows:

$$\alpha+(k_1\beta+k_2\delta)a-\frac{b}{2}a^2-\frac{\rho}{2}(\beta^2\sigma_\theta^2+\delta^2\sigma_\varepsilon^2)\geq\overline{\omega} \tag{7}$$

Maximizing left side of (7), we can get a by inducement.

$$a=\frac{k_1\beta+k_2\delta}{b} \tag{8}$$

3 ESTABLISHMENT AND ANALYSIS OF MODEL

3.1 Establishment of Model

Through analyzing and supposing of chapter 1 in the paper, selection of （α,β） and optimization problem as follows should be considered by owner (Chen 2006).

$$\max E(v)=k_1a-E(\alpha+\beta\pi+\delta p)$$

$$\text{s.t.}\quad (\text{IR})\quad \alpha+(k_1\beta+k_2\delta)a-\frac{b}{2}a^2-\frac{\rho}{2}(\beta^2\sigma_\theta^2+\delta^2\sigma_\varepsilon^2)\geq\overline{\omega}$$

$$(\text{IC})\quad a=\frac{k_1\beta+k_2\delta}{b}$$

By substituting (IC) into (IR), we can get

$$\alpha=\overline{\omega}-\frac{(k_1\beta+k_2\delta)^2}{2b}+\frac{\rho}{2}(\beta^2\sigma_\theta^2+\delta^2\sigma_\varepsilon^2) \tag{9}$$

$$\max E(v)=k_1\frac{k_1\beta+k_2\delta}{b}-\overline{\omega}+\frac{(k_1\beta+k_2\delta)^2}{2b}-\frac{\rho}{2}(\beta^2\sigma_\theta^2+\delta^2\sigma_\varepsilon^2)$$

$$-\beta k_1 \frac{k_1\beta + k_2\delta}{b} - \delta k_2 \frac{k_1\beta + k_2\delta}{b}$$

The first order condition of β is

$$\beta = \frac{k_1^2 - k_1 k_2 \delta}{k_1^2 + b\rho\sigma_\theta^2} \tag{10}$$

The first order condition of δ is

$$\delta = \frac{k_1 k_2 - k_1 k_2 \beta}{k_2^2 + b\rho\sigma_\varepsilon^2} \tag{11}$$

In order to discuss conveniently and universally, supposing k_1 and k_2 both equal to 1, combined with Eq.(10)and Eq.(11), we can get

$$\beta = \frac{1-\delta}{1+b\rho\sigma_\theta^2} \tag{12}$$

$$\delta = \frac{1-\beta}{1+b\rho\sigma_\varepsilon^2} \tag{13}$$

3.2 Analysis of Model

(1) Influence of incentive mechanism and supervision mechanism on effort of construction agent is analyzed. According to(8), an increase of β>0 or δ>0 makes increase of a. It shows that a productive share and a monitoring signal can induce or encourage the effort of the construction agent. If the owner hopes to increase the construction agent's level of effort, the productive share should be increased to stimulate construction the agent under weak monitoring ability of owner. The effort of the construction agent is realized by β and by monitoring signal under δ=0 and β=0 respectively.

(2) An increase of the fixed reward has no incentive effect on the effort of the construction agent. According to (8), the construction agent's degree of effort does not relate to the fixed reward of the construction agent. It shows that the fixed reward institution can not incent the construction agent. Especially when β and δ are all equal to 0, we can get a=0 by (8). It means that the construction agent's degree of effort is 0 without incentive and supervision mechanisms because of the lack of incentive mechanisms to construction agent, but it does not mean that design of fixed reward is not necessary in agent-construction contract. According to (9), when the fixed reward of construction agent reaches necessity of (9) at least, payment for the project provided for owner will be accepted by construction agent. Otherwise, they will not cooperate with each other and the benefit of owner will not be realized.

(3) The relation between the productive share and the monitoring signal is studied. According to (12) and (13), β decreases with increase of δ and β increases with decrease of δ. It indicates that productive share and monitoring signal are correlative in the establishment of a substitute contract. When δ tends to 0, β is determined by the risk abominating degree of the construction agent and environment risk. When δ tends to 1, the productive share is 0, agent-construction contract is only designed by using monitoring information.

4 CONCLUSIONS

Incentive mechanisms and supervision mechanisms of the agent-construction owner's relationship to the construction agent can be combined with each other by principal-agent theory. It can provide beneficial information for the design of an agent-construction contract. Both incentive mechanisms and supervision mechanisms can encourage efforts of construction agents; productive share will increase with a decrease of supervision; and supervision will increase with a decrease of productive share; increasing of a fixed reward has no incentive effect on the efforts of the construction agent.

REFERENCES

Chen, Z. (2006). "Information and incentive economics." Shanghai: Shanghai People's Publishing House, 30-110.

Yang, X. and Zhang, X. (2008). "Gambling analysis of substitute project based on bi-level commission agent model." *Statistics and Decision*, (10), 62-64.

Yin, Y., and Yan, X. (2006). "Theory and practice of substitute institution of government investment projects." Tianjin: Tianjin University Press, 108-126.

Zhang, W. (2007). "Gambling theory and information economics." Shanghai: Shanghai People's Publishing House, 235-256.

Zhao, W. (2006). "Research on management mode of substitute project." Xi'an: Chang'an University, 121-123.

Research on Calculation of Important Parameters of Freeway Financial Post-evaluation

Y. Wang[1], S. Zhu[2], H. Wang[3], W. Xin[4], and M. Li[5]

[1]Postgraduate, Dept. of Traffic Engineering, Wuhan University of Technology, 430063, 1040 Heping Ave., Wuchang, Wuhan, Hubei, China; Tel: +86-13297974166; email: wangyf1573@163.com

[2]Professor, Dept. of Traffic Engineering, Wuhan University of Technology, 430063, 1040HepingAve., Wuchang, Wuhan, Hubei, China; Tel:+86-13995680983; email: zhusy2001@163.com

[3]Associate Professor, School of Transportation, Wuhan University of Technology, 430063, 1040 Heping Ave., Wuchang, Wuhan, Hubei, China; Tel: +86-027-62597390; email: wanghong2004317@sina.com

[4]Postgraduate, Dept. of Traffic Engineering, Wuhan University of Technology, 430063, 1040 Heping Ave., Wuchang, Wuhan, Hubei, China; Tel: +86-13871178942; email: qqyyxwh@163.com

[5]Postgraduate, School of Transportation, Wuhan University of Technology, 430063, 1040 Heping Ave., Wuchang, Wuhan, Hubei, China; Tel: +86-13297974168; email: lm19842003@163.com

ABSTRACT

The objective of the paper is to solve the new problems in freeway financial post-evaluation stage. Considering normal operating conditions, major freeway maintenance or expansion construction, Build-Operate-Transfer (BOT), Build-Transfer (BT) etc., an investigation was made on calculating the evaluation periods from 4 circumstances. The influencing factors of the residual value rate include design service life of different freeway structures, recycling of discarded building materials due to scientific advancements, appreciation of scarce resources, and sustainable freeway use. Then, based on current laws and regulations on financial evaluation and freeway post-evaluation in China, with a combination of quantitative and qualitative analysis, a methodology was then developed to calculate the residual value rate. Finally, we demonstrated how to determine the two parameters according the actual situation of Huanghuang (HH) freeway in Hubei province.

Key words : freeway; financial post-evaluation; evaluation period; residual value rate

INTRODUCTION

Economic post-evaluation of a freeway is generally carried out after operation and is seen as an important part of investment decision-making and management. However, new financing modes, such as BT and BOT, freeway major maintenance required ahead of schedule as a result of poor quality, and other new problems have emerged in economic post-evaluation. Hence, it is necessary to investigate the evaluation period (EP) and residual value (RV). With occurrence of situations such as

BOT, major freeway maintenance or expansion construction, there will be a number of evaluation periods, making it difficult to determine the EP. In accordance with relevant laws and regulations, RV of a freeway is usually calculated by qualitative methods. However, considering that different parts of a freeway have different values at the end of EP, the decision of whether or not to adopt quantitative methods to calculate residual value rate (RVR) has a significant impact on the accuracy of results. Wang Mei (2006) pointed out that there are problems in the calculation of EP and RV in financial evaluation of BOT projects. She argued that the operation period had best consistent with the concession period and that calculating RV or not has impacts on evaluation results. But she did not investigate the parameters of calculation. The existing research and practices in economic evaluation (Hui,2001; Ruan,2000; Zhu,2007; Robert,1997; Luenberg,1998) which do not solve these new problems, calculated the two parameters only based on current laws and regulations. In this paper, according to laws and regulations, a methodology combining quantitative analysis with qualitative analysis was developed to calculate EP and RVR.

EVALUATION PERIOD

Economic Evaluation Methods and Parameters of Construction Project (3rd Edition) (EEMPCP) says that the EP of a project in economic evaluation refers to the period for dynamic analysis, including the construction period and operation period. The construction period should be determined reasonably based on the construction time limit or construction plan. The operation period is determined according to the reasonable economic service life of projects (NDRC and MC 2006). EP mostly depends on characteristics of projects and therefore can not be calculated uniformly. In general, a project corresponds to an EP.

In general, the EP is the sum of the construction and operation periods, as shown in Table 1. Compared with the construction period, a number of factors need to be considered to define the operation period. So the EP should be developed based on a variety of factors. Considering the conditions of normal operation, freeway major maintenance or expansion construction, BOT, BT etc., the thesis investigated the calculation of the EP from 4 circumstances.

1)BOT Transfer of Freeway. The freeway transferee recovers its investment and profits through tolling in the toll period. Whether or not to consider the toll period in calculating the EP has great effects on evaluation results. Therefore, the EP should be calculated to the end of toll period, in order to reflect the investors' actual financial situation and to ensure the investors' proceeds in a reasonable scope. Thus, the EP includes the construction period, the operated period and the toll period. The formula is offered in Table 1.

2)Freeway major maintenance or expansion construction happened ahead of schedule during the design service life. This extends its service life. The EP, which includes the construction period, the operated period and the service life after major

maintenance or expansion construction, should be calculated to the extended freeway service life, as seen in Table 1. This helps to maintain the continuity of freeway finance and further study the effectiveness of investment decision-making.

3) Both BOT transfer and freeway major maintenance or expansion construction. Combining the two calculation methods, the EP should be calculated in chronological order. If they happened successively, the EP is calculated to the latter, as seen in Table 1. If they happened simultaneously, the EP could be calculated to the greater one. The formula is given in Table 1.

4) Project financing of BT. After completion the project is transferred to the government from the investors at the agreed price. Then the government operates it. Hence, the EP contains the construction period and the operation period. Under normal circumstances, the operation period is the service life. When freeway major maintenance or expansion construction happens ahead of schedule due to freeway quality, the EP should be calculated to the freeway service life, as seen in Table 1.

Table 1. Calculation Methods of Evaluation Period .

Type	Calculation Method
Normal Situation	$T = T_C + T_O$, T =EP, T_C =construction period, T_O =operation period
BOT Projects	$T = T_C + T_{HO} + T_B$, T_{HO} =the operated period, T_B = the toll period of BOT
Major Maintenance or Expansion Construction of A Freeway	$T = T_C + T_{HO} + T_{MM}$, T_{MM} = the extended service life of freeway after major maintenance or expansion construction
Both BOT and Major Maintenance or Expansion Construction	If the two happened successively, $T = T_C + T_{HO} + T_1 + T_2$, T_1=the interval between the two(namely, the actual period happened), T_2 =the period of the latter(namely, $T_2 = T_B$ or $T_2 = T_{MM}$); If the two happened simultaneously, $T = T_C + T_{HO} + \max\{T_B, T_{MM}\}$
Project financing of BT	$T = T_C + T_O$
Both BT and Major Maintenance or Expansion Construction	$T = T_C + T_{HO} + T_{MM}$

Transfer Rules of Rights and Interests of Toll Roads (TRRITR) says that the cumulative sum of toll periods of toll-repayment road is not more than 20 years (toll-repayment roads from the country's central and western provinces, autonomous regions and municipalities directly under the Central Government, 25 years) and that the cumulative sum of toll periods of operating roads should not be longer than 25 years (operational roads from the country's central and western provinces, autonomous regions and municipalities directly under the central Government, 30 years). According to freeway classification and location region, the longest toll period is selected, that is, the longest operation period, T_O^{max}. In conclusion, the EP is

calculated by the following formula: $T_O \le T_O^{max}$, $T = T_C + T_O$; $T_O > T_O^{max}$, $T = T_C + T_O^{max}$.

In addition, the results of each evaluation require vertical comparison to verify the effectiveness of investment decision-making. Therefore, the current EP should be consistent with the former one. In brief, according to specific circumstances and needs of projects, more than one period can be determined to meet different purposes.

RESIDUAL VALUE RATE

Economic Evaluation Practices of Highway Construction Project (EEPHCP) shows that RV of a freeway generally accounts for 50 percent of the project expenditure, in the form of negative value reckoning in costs(MCs, 1996). But at the end of the EP, different freeways correspond to different RV. The RV of components of a freeway must be estimated in order to improve the accuracy of evaluation.

Different parts of a freeway have different values. In light of particularities of individual freeways, the RVR of a freeway should be calculated by integrating its components' values. The factors variables set of RV, $A = \{a_1, a_2, \cdots\cdots, a_m\}$, was set up where a_i is the initial value of factors variables, m is the number of factors variables. After operation in EP, the freeway value reduces in the overall trend. Then variables set $B = \{b_1, b_2, \cdots\cdots, b_m\}$ was set up, where b_i is the final value of factors variables. This paper selects five variables to calculate RV, such as design service life of different freeway structures, recycling of discarded building materials due to scientific advancement, appreciation of scarce resources, sustainable use of a freeway, and rest value.

1) Design Service Life of Different Freeway Structures. The factor mainly includes the design service life of freeway structures and service area buildings. Individual parts of a freeway vary in their design life, the lowest being 20 years, and the longest, of grand bridges, 100 years. Freeway structures and buildings will depreciate. Then the remaining freeway value which has not depreciated at the end of EP is calculated, i.e. RV of freeway structures and buildings. The formula is presented in Table 2. Financial Management Practices Of the Freeway Company: Adopting the Workload Method, the freeway structures are depreciated without expected RV. The paper adopts a depreciation period of 30 years. The depreciation method used for service area buildings is the Average Period Method, taking a 40-year depreciation period.

2) Recycle Use. With the development of science and technology, the discarded materials of a freeway with recycling values should be classified and recycled, including road pavement and so on. The abandoned pavement can be smashed and processed on-site and used as base course and subgrade or other products. Value of recycle use is calculated in term of market price for various uses and discounted to the base year. The formula is presented in Table 2.

3) Value Appreciation. With economic development land is a scarce resource, and land occupied by freeways is appreciating with time. This appreciation is another

important production factor. Therefore it is necessary to estimate the land value reasonably by the method referring to the estimation model of land prices. Regional population, economy, land area and other factors are considered to amend the growth factors of land prices. Then the land value is discounted to the base year. A specific calculation is offered in Table 2.

4) Continuous Utilization. This type includes the freeway subgrade and so on. Due to continuous development of transportation, traffic demands are on the rise, requiring corresponding traffic supplies. At the end of the EP, the freeway will not be abandoned, but rather will be used continuously, and the life expectancy of the subgrade is greater than 20 years. So the freeway subgrade has both function value and use value and could be used in reconstruction and expended construction. Freeway subgrade does not need depreciation. Value of continuous utilization is calculated according to the construction cost of subgrade in reconstruction or expansion construction of a freeway, discounting to the base year. The formula is provided in Table 2.

Table 2. Calculation of Influence Variable s of Residual Value Rate .

Type	Component	Calculation Method
Design Service life of different structures	Bridge, culvert, tunnel, intersection projects and service area buildings etc.	$b_1 = V_K - \sum_{i=1}^{T-T_C} D_i + D[40-(T-T_C)]$, annual depreciation values of structures $D_i = \frac{V_K}{W} \times \omega_i$, annual depreciation values of buildings $D = \frac{V_K - V_L}{N}$, where, V_K=original value of fixed assets, V_L=expected net residual value of fixed assets, W=predicted traffic volume in depreciation period, ω_i=actual or predicted annual traffic volume, N=depreciation period, other parameters as noted before
Recycle Use	Freeway Pavement etc.	$b_2 = C_{recycle} \times (1+i_d)^{-T}$, $C_{recycle}$=recycle value of pavement, i_d=discount rate
Value Appreciation	Land occupied by the freeway etc.	$b_3 = S \times V_{bm} \times \lambda_{amend} \times (1+i_d)^{-T}$, S=land area, V_{bm}=benchmark land price, λ_{amend}=amended growth factor of land price
Continuous Utilization	Freeway subgrade etc.	$b_4 = C_{subgrade} \times (1+i_d)^{-T}$, $C_{subgrade}$=cost of subgrade in reconstruction and expended construction
Rest Value	Rest projects and facilities etc.	$b_5 = \beta a_5$, β=RV of the rest projects and facilities

RVR is calculated by the following formula.

$$R = \frac{V_K - \sum_{i=1}^{T-T_c} D_i + D[40-(T-T_c)] + (C_{recycle} \times S_{bm} \lambda_{amend} C_{subgrade}(1-i)^{-T_i}) + \beta_d}{\sum a_i}$$

where R is RVR, a_i is the initial value of factors variables, b_i is the final value of factors variables.

CASE STUDY

Project Description

HH freeway has two parts: the mainline from Huangshi to Huangmei and the lateral from Huangmei to Jiujiang Yangtze River Bridge. The freeway was started in November 1996 and put into operation in January 2000. In April 2003, Hubei Provincial Communications Department officially signed the assignment contract with Hong Kong Fude Company. The transfer period of tolling equity is 20 years, beginning January 1, 2003. The expansion construction was started in April 2005 and completed in May 2006. In this study, the mainline will be evaluated as an example.

Financial Evaluation Period

As to the particularity of HH freeway, the transfer of tolling equity and the major maintenance happened successively. In accordance with the foregoing methods, the calculation of the EP should consider the following two aspects.

1) Occurrence of BOT and major maintenance. The major maintenance was carried out in 2005 because of the decline in pavement quality and the service life is 20 years. Based on the above methods, EP is calculated as follows: $T = 3 + 4 + 4 + 20 = 31$ years.

2) In the project feasibility research report, the EP takes on the values of 23 years, of which the operation period is 20 years. Therefore, EP is offered as follows: $T = 23$ years.

HH freeway is located in the central and western regions of China and is considered an operational road. The calculation operation period (28 years) is less than the longest accumulated tolling period of freeway (30 years). Therefore, this paper identified two EPs to carry on financial evaluation respectively, namely: 1) EP I is 23 years, from 1996 to 2018; 2) EP II is 31 years, from 1996 to 2026.

Residual Value Rate

After calculation of the EP, a combination of quantitative and qualitative analysis was used to calculate RVR. Based on the circumstances of HH freeway, five influence variables were taken into account and provided in Table 3. According to the project assets statistics of HH freeway, RVR was calculated, as shown in Table 3.

Table 3. Calculation of Residual Value Rate (Unit: 10 Thousand Yuan).

Type	Initial Value of Variables(a)	Final Value of Variables(b)
Design life of different structures	87472.90	10915.75

Recycle use	45402.90	27468.75
Value appreciation	14215.65	50490.30
Continuous utilization	45170.10	45170.10
Rest value	33589.35	1007.68
Summation	225850.90	135052.59

In accordance with the factual situation of Hubei Province and areas along HH freeway, the aforementioned methods were used to calculate the RV of every factor, and finally RVR is obtained: $R = \frac{135052.59}{225850.90} = 0.589 = 58.9\%$.

Evaluation Parameters and Indicators

Evaluation parameters and indicators are selected in accordance with EEMPCP, EEPHCP, and other relevant laws and regulations. The main indicators adopted by the project are Financial Internal Rate of Return (FIRR), Financial Net Present Value (FNPV), Payback Period (Pt), Loan Repayment Period (Pd) and Financial Benefit-cost Ratio (FBCR)(NDRC and MC,2006;MCs,1996).

Financial Evaluation and Evaluation Conclusion

Financial costs and benefits were calculated. Then annual financial costs and benefits are discounted to the present value of the base year using dynamic discount methods. The discount rate is selected according to the relevant regulations, 6.5%. Finally, financial evaluation indicators were calculated, as given in Table 4. In conclusion, calculating the appropriate EP and RVR, it is proved that the project is feasible from a financial point of view.

Table 4. Values of Main Financial Evaluation Indicators .

Evaluation items	Mainline(1996-2018)		Mainline(1996-2026)	
Evaluation indicators	After income tax	Before income tax	After income tax	Before income tax
Pt (Year)	20.1	17.5	20.1	18.7
FNPV (10,000 Yuan)	38898.0	134347.8	143184.2	432668.9
FIRR (%)	8.47	9.63	11.03	12.22
FBCR	1.11	1.22	1.30	1.50

SUMMARY

Major maintenance or expansion construction of a freeway carried out during the operation period requires substantial funds. As a result, value of the freeway increases and service life is extended. The freeway company could have the right to toll continually, in theory. But as it is a policy-oriented concern, the freeway toll period needs taking into account the national legislation and policies.

If BOT took place before the promulgation of TRRITR and the transfer toll

period of a freeway exceeds the cumulative sum of toll periods by law, there is a conflict between the transfer contract protected by relevant national laws and regulations and TRRITR. Therefore, a post-evaluation period of this type should be further studied.

REFERENCE S

Hui, X. (2001). "Financial Evaluation Model Research of Highway Companies." Journal of Industrial Engineering and Engineering Management, (3), 24-26.

Luenberg, D. G.. (1998). "Investment Science." Oxford University Press, New York, Oxford.

Ministry of Communications (1996). "Economic Evaluation Practices of Highway Construction Project ." China Communications Press, Beijing.

National Development and Reform Commission, Ministry of Construction (2006). "Economic Evaluation Methods and Parameters of Construction Project (3rd Edition)." China Jihua Press, Beijing.

Ruan, L. (2000)."Economic Evaluation Method for Upgrading & Revising Road[D]."Chengdu: Southwest Jiaotong University, 5-15.

Tiong, R. (1997). "Evaluation of Proposals for BOT Projects." International Journal of Project Management, (15), 67-72.

Wang, M. (2006)."Discussion on Several Issues of Financial Evaluation of BOT Projects." Technical Economy, (3), 78-79.

Zhu, W. and Wen, Y. (2007)."Research on Selecting Indicators of Financial Evaluation of Freeway Companies." Highway, (5), 119-120.

Empirical Research on Applicable Principle for Toll Mode of Highway

Ying ZHANG[1], Guang YANG[2]

[1] Assistant Research Fellow,Research Institute of Highway Ministry of Transport, Add: No.8 Xitucheng Road, Haidian District, Beijing, China; Post Code: 100088; Tel: 13241777792; Fax: 62370155; Email: ying.zhang@rioh.cn
[2] Research Fellow, Research Institute of Highway Ministry of Transport, Add: No.8 Xitucheng Road, Haidian Districtt, Beijing, China; Post Code: 100088; Tel: 13701362837; Fax: 62370155; Email: g.yang@rioh.cn

ABSTRACT

The objective of this paper is to take two typical highways as examples to discuss the applicable principles for the Barrier System and the Closed System which are currently applied to the most toll collection systems of Chinese highways. For the first step, this paper picks out two typical highways from Xinjiang Uygur Autonomous Region highway network. The first highway is the Tulufan to Urumqi (TU) highway whose toll collection system applies the Barrier System. The second highway is the Heshuo to Korla (HK) highway whose toll collection system implements the Closed System. For the second step, this paper analyzes the historical data on the toll systems of these two highways respectively, including the cost of construction and management which was spent on the toll collection system before the year of 2005, the historical data of traffic volume and every year's total charges of these two highways. Based on these data, this paper forecasts the traffic volume, total charges and management cost about these two highways by applying several kinds of forecasting model comprehensively. Fully considering the influence of time value of funds, this paper analyzes the difference of economic benefit between these two types of toll mode. At the end, several applicable principles for the Barrier System and the Closed System are concluded respectively by taking synthetically economic analysis, considering the traffic flow characteristics of these two highways. The initial data of this paper comes from the research report--Toll Collection Technique Research on Xinjiang Uygur Autonomous Region Roads, which is the key research for the Department of Transport of Xinjiang Uygur Autonomous Region.

MAIN IDEA AND ANALYTICAL METHODS

Since the 1980s, traffic mileage of Chinese highway has been grown rapidly. By the end of 2008, the total mileage of Chinese highway has surpassed 60,300 km, ranking second in the world. More than 90% of these highways are toll highways. The discussing objectives of this paper are toll highways, and the following are referred to the highways. At present, the Barrier System and the Closed System are implemented on most of Chinese toll highways. It is showed that the choice of toll

mode has a significant impact on the selection of highway toll collection facilities, and it will affect the whole highway's investment benefit (YANG, 2008).

The initial data of this paper comes from the research report--Toll Collection Technique Research on Xinjiang Uygur Autonomous Region Roads. For the first, two typical highways are selected as analytic objects from Xinjiang Uygur Autonomous Region highway network. The first highway is the Tulufan to Urumqi (TU) highway whose toll collection system applies the Barrier System. The second highway is the Heshuo to Korla (HK) highway whose toll collection system implements the Closed System. For the second step, this paper analyzes the historical data about toll systems of these two highways respectively, including the cost of construction and management which were spent on the toll collection system before the year of 2005. Based on the historical data of traffic volume and total charges of every year, this paper forecasts the traffic volume and total sum of toll about these two highways respectively, applying several kinds of forecasting model comprehensively. Considering the influence of time value of funds and the increase of management cost, this paper obtains the income and expenses of these two highway's toll systems. At last, based on the traffic flow characteristics of these two highways, this paper discusses application principles of the Barrier System and the Closed System.

In short, this article obtains the economic benefits difference between these two kinds of toll mode, and sums up some application principles for these two types of toll mode. It is hoped this article can provide a reference for the highway toll mode selection.

COLLECTED DATA

The highway toll collection facilities mentioned in this paper belongs to subsidiary facilities of highway, including the toll station building, toll plaza and other electro-mechanical Systems.

Kinds of data collected for those two sample highways toll collection facilities by this paper include:

(1) the traffic volume and vehicle composition data for the sample highways;
(2) the sum of toll for the sample highways;
(3) the construction costs and facilities update costs for the samples highways;
(4) the annual management costs for the samples highways;
(5) toll period limited and loan interest for the samples highways.

THE EVALUATION INDICATORS

Because the toll collection facilities are parts of toll highway, toll fees collected by

toll collection facilities are generated by the whole toll highway. According to "the principle of consistency between cost and benefit"(The World Band Research Report (1998)), the toll collection facilities can not be evaluated separately for its investment and economic benefits. So this paper uses such two indicators as net income and ratio of income to expenditure.

(1) Net income

Net income = charges-expenditure, divided into annual net income and total net income of toll period limited separately.

Expenditures include all kinds of cost (including building construction and electro-mechanical Systems investment) and all kinds of the business expenses (including management expenses and interest expense). The level of net income depends on the toll highway's characteristics and the rationality of toll collection facilities. When there are multiple toll modes available, this indicator should play an important role (The World Band Research Report (1998)). The dynamic analysis method of the net present value concept (FNPV) is used in the calculation of net income.

$$FNPV = \sum_{t=1}^{n} (CI - CO)_t (1 + i_c)^{-t}$$

Where: Cl: cash inflow; CO: cash outflow; $(Cl\text{-}CO)_t$: the t years of net cash flows; n: the calculation period the number of years; i_c: discount rate. (The World Band Research Report (1998))

(2) Ratio of income to expenditure

the ratio = Toll station revenue expenditure / Toll station charges, divided into annual ratio and total ratio. The indicator reflects the efficiency of toll station.

The World Bank provided a set of experience data in the assessment report for Jingjintang highway: In the effective operations, the Barrier System ratio of income to expenditure is 5% ~ 10%for the Barrier System and 10% ~ 15% for the Closed System. In poor management the ratio of income to expenditure for the Closed System may be as high as 30%. (The World Band Research Report (1998))

PREDICTION METHOD

In order to predict the total charge of every year for these two highways, multiple linear regression method and Elasticity coefficient prediction are used to predict the increase of area traffic productions and attractions related these two highways. Second, Fratar method is applied in the prediction of the trip distribution. The third, this paper obtains the traffic volume of these two highways by using stochastic user equilibrium model in the traffic distribution. Considering the charge rate of these two highways, this paper works out the total charges of every year about these two highways. Besides, this paper predicts the management cost on the basis of related provisions. At last, this paper obtains the Ratio of income to expenditure of these two

highways' toll system.

CASE STUDY

ANALYSIS OF THE TU HIGHWAY TOLL CLLECTION FACILITIES

The TU highway was opened to traffic in 1998, passing through the city of Turpan and Urumqi. This highway had a dramatic impact on connection between Urumqi and its surrounding cities (YANG, 2006).

After investigation, TU highway traffic flow characteristics are as follows((YANG, 2006):

(1) the traffic flow of Urumqi to Turpan vary from large to small and is composed mainly by long-distance and cross-border vehicles. The AADT of Urumqi to Chaiwopu interchange reaches to the 6000 ~ 8000 pcu/d. However the AADT of Turpan toll station falls to 4000 pcu/d.

(2) Few vehicles pass through the interchanges along this highway. The interchange of Jidong owns the most heavy traffic flow among those interchanges, which can reach 1600 pcu/d. Other interchange's traffic flow are less than 1000 pcu/d y and even some interchange's traffic are less than 100 pcu/d.

After comprehensive analysis, the main economic indicators of the TU highway toll station are showed as follows in table 1 below:

Monetary unit: Million RMB

Toll Station	Traffic Flow(pcu/d)	Total Income FNPV	Total Expenditure FNPV	Ratio of Income to Expenditure
Wulabai Main line Toll Station	7,594	477	64	13.5%
Nanquanzi Main line Toll Station	1,988	610	51	8.2%
Toutunhe Main line Toll Station	5,968	1479	74	5.0%

Table 1: the main economic indicators for the TU highway toll stations

ANALYSIS OF THE HK HIGHWAY TOLL COLLECTION FACILITIES

The HK Highway is an important component of Chinese State Highway 314, whose total length is 92.4km. Its starting point connects with Tuokexun to Heshuo Highway. After comprehensive adjustment, a length of 41.17km highway from Wushitala to

Heshuo is merged into the HK highway. The toll mode of this highway is the Closed System, with a total of seven toll stations and a management center (YANG, 2006).

This highway is the unique highway connecting the northern and the southern of Xinjiang Uygur Autonomous Region across the Tianshan Mountains. Because cities and towns distribute relatively sparsely, the main line traffic flow takes the most portion of total highway volume. The traffic volumes of most interchanges are low, except the interchanges entering the city of Heshuo and Korla (YANG, 2006).

Applying such analytical methods mentioned above, the total net income and total expenditure is 1.35 billion Yuan and 316 million Yuan respectively for the toll period limited of the HK highway, and the ratio of income to expenditure is 18.9%, which is less than optimal operational efficiency. The main economic indicators of the HK highway toll station are illustrated as follows in table 2 below:

Monetary unit: Million Yuan

Toll Station	Traffic Flow(pcu/d)	Total Income FNPV	Total Expenditure FNPV	Ratio of Income to Expenditure
Korla Main line Toll Station	5,343	629.3	62.2	9.9%
Tashidian Ramp Toll Station	715	23	38.5	167.6%
Ziniquan Ramp Toll Station	967	29.5	35.9	121.8%
Yanqi Ramp Toll Station	2,558	166.2	48.8	29.4%
Gaoqiao Ramp Toll Station	607	71.9	36.9	51.3%
Heshuo Ramp Toll Station	722	75.4	39	51.7 %
Heshuo Main line Toll Station	1,649	355.7	54.8	15.4%

Table 2: the main economic indicators for the HK highway toll stations

Supplementary Analysis for Table 2

(1) because the 41.17km of Wushitala to Heshuo highway is merged into this highway toll range, the charge length of the HK highway increases by near 1/3. Therefore, the main economic indicators have been greatly improved. But the management efficiency of this highway is still less than ideal. The conclusion is that

the Closed System does not fit in this highway's traffic flow characteristics and has a negative effect on the HK highway's investment benefit.

(2) The traffic flow of the HK highway is very concentrated, and the traffic volume of interchange along this highway is very small. Among the seven toll stations, Korla Main line Toll Station, Heshuo Main line Toll Station and Yanqi Ramp Toll Station own larger traffic flow and better operational efficiency. The total charge of this three toll stations accounts for 85.2 percent of whole highway income. The charge of other four toll stations is low and operating efficiency is poor. For example, the income of Tashidian Ramp Toll Station is lower than its expenditure and the same situation happens to the Ziniquan Ramp Toll Station. The income proportions of these seven toll station are showed as detailed in Figure 1.

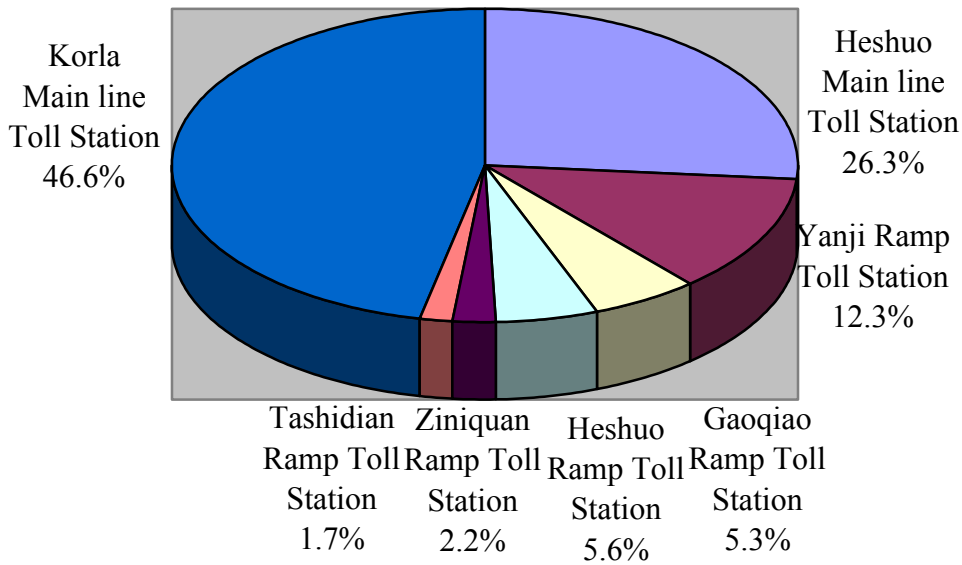

Figure1: The income proportion of the HK highway toll stations

CONCLUSION

Based on the analysis above, this paper obtains two conclusions for the Barrier System and the Closed System:

(1) In the area where cities and towns distribute relatively sparse, the Barrier System is more appropriate than the Closed System. Because the Barrier System's economical efficiency is good than the Closed System. As long as there is no major turning traffic flow, the toll range of the Barrier System toll station should be extended as far as possible to reduce its ratio of income to expenditure. On the other side, in the areas where the cities and road network are relatively intensive, the Closed System is a more reasonable choice. It is suitable for highway whose traffic

flow distributes more evenly and the traffic volume of every interchange along the highway is relatively large.

(2)If the traffic flow has such characteristics as cities and towns along the highway distribute relatively sparsely, main line traffic flow of the highway is low and most of interchanges traffic flow except connection with large and medium-sized cities is very small, the highway toll system should adopt the Barrier System. The Barrier System applied in the TU highway match the characteristics of the highway, so its economic indicator is well. On the other hand, the HK highway toll system's economic indicator is not ideal because the Closed System does not match with the highway traffic flow characteristics. To sum up, different kinds of toll model play an important influence on the highway's investment benefit. All in all, highway toll system should be carefully chosen in order to enhance the highway's investment benefit, based on the characteristics of the highway's traffic flow.

REFERENCES

Guang YANG (2006), Toll Collection Technique Research on Xinjiang Uygur Autonomous Region Roads, the Department of Transport of Xinjiang Uygur Autonomous Region Research project report.

Guang YANG (2008), "Review of Several Problems on Chinese Toll Highway", Chinese ITS Journal, No.8, 2008.

The World Band Research Report (1998), Beijing to Tianjin and Tanggu Highway Construction Project Evaluation Report.

Research on Travel Behavior Changes under Vehicle-Use-Restriction Measures during the Olympic Games

Li Chun Yan[1], Sun Sheng Yang[2], and Guo Ji Fu[3]

[1]College of Architecture and Urban Planning, Tongji University & Beijing Transportation Research Center; PH (8610) 6337-2682; FAX (8610) 6337-2715; Email: lichyan@gmail.com
[2]Parsons Brinckerhoff Beijing Co. Ltd; PH (8610)6719-9389;FAX (8610) 6714-8124; Email: sun.sy@pbworld.com
[3]Beijing Transportation Research Center; PH (8610) 6337-2701; FAX (8610) 6337-2715; Email: guojf@bjtrc.org.cn

ABSTRACT

During the Olympic Games, Beijing implemented a series of transport demand management (TDM) measures that have effectively reduced traffic congestion. It would be useful if we could get a clearer understanding of behavior changes in the influence of TDM measures. Drawing on data from the household interview travel survey, this paper analyzes the travel behavior changes of Beijing residents under the influence of TDM. Data concerning trip rate, trip purpose, ridership of motor vehicles, mode share, and travel time were collected to reflect travel behavior changes. The accumulated travel behavior data will help long-term TDM measures research.

INTRODUCTION

The Beijing 2008 Summer Olympic Games were held from August 8 to August 24 and placed Beijing in the world spotlight. The Beijing 2008 Olympic Games have completed successfully. During the 16 days of competition, hundreds of thousands of visitors flooded to Beijing, presenting a challenge to the urban transport system. There were more than 200 International Olympic Committees, more than 5,000 officials of 28 events, more than 16,000 athletes and 2,500 team officials, more than 22,000 members of the media and 40,000 sponsors, more than one million staff and volunteers, and more than 6 million spectators (Beijing Transportation Research Center 2008, Yan 2008). At the same time, with the urban population and the ownership of motor vehicles increasing rapidly, traffic congestion in Beijing is becoming heavier. Coordinating the huge Olympic transport demand along with the daily travel demand of local residents is one of the most important things. From other countries' experiences, we find examples; the Atlanta Olympic Games implemented reducing commuter travel, and the Sydney Olympic Games implemented a free public transport policy, increased parking fees, etc. Based on the experiences of these countries holding mega events, implementing transport demand

management (TDM) measures is a good solution to transport system (Guo, J. *et. al.* 2008).

During the Olympic Games, Beijing implemented a series of TDM measures from Jul. 20 to Sep. 20, including the following: stopping all registered motor vehicles according to the last number of the license; odd number motor vehicles running only on odd days, and even number vehicles running on even days; motor vehicles owned by the Beijing government and company reduced by 70% of total numbers; and the establishment of a prohibited area within the 5th ring road of Beijing city proper area (Beijing Municipal Committee of Communications 2008).

The TDM measures greatly affected the people's travel behavior. It would be useful to get a clearer understanding of behavior changes resulting from the TDM measures. Drawing on data from the household interview travel survey, this paper analyzes the travel behavior changes of Beijing residents under the influence of TDM. Trip rates, trip purpose, occupancy rate of motor vehicles, mode share, and travel time were collected to reflect travel behavior changes. The accumulated travel behavior data also will help to long-term research of TDM measures.

QUESTIONNAIRE SURVEY

The Beijing household interview travel survey was a cross-sectional travel-diary survey of household travel behavior changes in Beijing before and under Olympic TDM measures. The household interview survey was carried out during two periods. The first survey period ran from May 10 to 28 without TDM measures, and the second survey period was from Aug. 8 to 28, during Olympic Games with TDM measures.

Sample size

The sample size was about 3600 households (net response) for each period. The survey compiled data on travel behavior, providing information on approximately 18,000 trips made by 10,000 individuals during each period.

Survey scope

The samples were distributed at random within the 5th ring road of Beijing city proper area, shown in Figure 1.

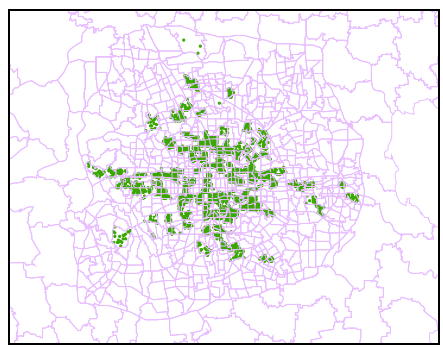

Figure 1. survey samples distribution.

Questionnaire includes three kinds of data:

- Basic household information, including household members, age, occupation, income, car ownership, etc.
- Travel diary of days during which car use is limited for household members, including travel time, trip purpose, travel mode, etc.
- Travel diary of days during which car use is permitted for household members, including travel time, trip purpose, travel mode, etc.

HOUSEHOLD BASIC INFORMATION FROM SURVEY

Car ownership rate

There are 35.6% households owning cars from survey data. Of these, 96% households have only one car; 4% households have more than one car..

Age distribution

Participants ranging from 26 to 55 years old account for 60% of the samples and within this age range, and 45 to 55 years old participants cover the highest proportion, accounting for 25%. Moreover, survey data indicates that middle-aged (35-55 years old) persons are the primary group of car users.

Occupation distribution

Occupation in the questionnaire includes worker, government staff, student, teacher, retiree, professional driver, police, independently employed, and unemployed person. The top three occupations of car owners within the samples are government staff, independently employed, and worker, which accounts for 87.2% of the total. Notably, government staff owned cars account for 60.2%, followed by those independently employed, accounting for 16.8%.

Household income distribution

From the survey data, we found that groups owning cars are high-income groups. In the samples, groups having monthly household income of 3,500-5,500 RMB Yuan reach 40.7%. Groups having monthly household income of more than 5,500-10,000 Yuan account for 30.1%.

TRAVEL BEHAVIOR CHANGES UNDER TDM MEASURES

TDM measures have triggered changes in daily travel patterns. For example, changes in trip rate, trip purpose, trip destinations choice, and travel mode choice were noted (Gärling 2002, Loukopoulos 2005).The survey results show travel behavior changes under car-use-restriction during Olympic Games.

Average trip rate of residents

Survey data indicated that average trip rate of all residents generally reduced from 1.88 times/day to 1.70 times/day under TDM measures, or a 9% decline. In particular, trip rate change of persons with cars was most apparent, from 1.9 times/day to 1.61 times/day, a 15.3% decrease; the trip rate among persons without cars fell by only 5.4%.

Comparison of car limited running and permitted running day

Moreover, there were different results when cars were limited or permitted. When car use was limited, it presented much travel inconvenience to car users. The trip rate was 1.59 times/day when car was limited, while 1.76 times/day when car was permitted, accounting for a 9.6% reduction in use when cars were limited.

Comparison of different occupations

From the survey data, we concluded that different occupations have different trip rates, mainly shown in Figure 2.

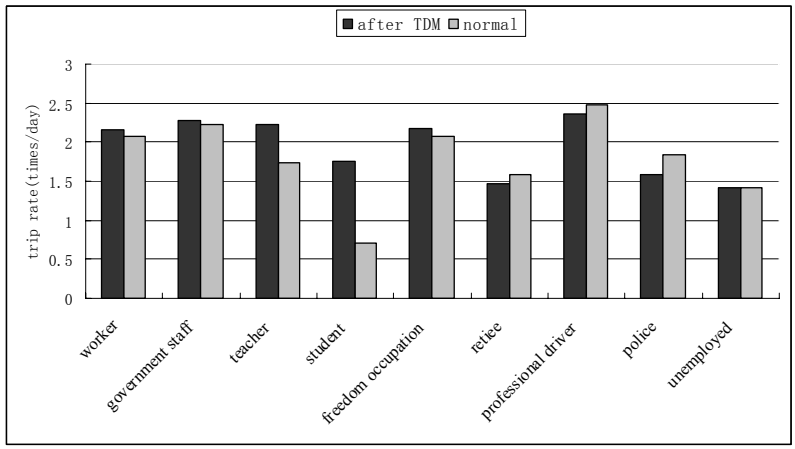

Figure 2. Trip rate changes by occupation under TDM measures.

The trip rates of worker, government staff, teacher, student, freedom occupation and unemployed persons decreased. Most notably, the trip rate of students declined significantly, from 1.75 times/day to 0.70 times/day, because temporary vacation policies were carried out for less school-related travel. School vacation schedules were prolonged according to the Olympic Games, and students enjoyed their Olympic vacation from June 28 to August 31. Trip rates of full-time drivers, police, and retiree increased a little, by about 10%. The reason for this was that use of motor vehicles owned by the Beijing government and company was reduced by 70%, which resulted in an increase in the trip rate of full-time drivers. Moreover, in order to achieve the "peace Olympics" goal, more security measures and volunteer missions resulted in the trip rate of police and retirees increasing.

Car using characteristic changes: Car using rate

Generally speaking, rate of car use declined under the influence of TDM measures. The use rate of private cars reduced from 2.26 times/day to 2.22 times/day, accounting for a 1.8% reduction. While the use rate of official car increased from 2.62 times/day to 3.32 times/day, accounting for a 26.7% increase, fewer cars were given almost the same assignments because motor vehicles owned Beijing Government and company were reduced by 70% of total numbers.

Car using characteristic changes: Ridership rate of car

Because half of the total number of cars were limited every day during the

Olympic Games, car-pooling became more popular. Ridership rates of car increased under TDM measures. Ridership of private cars increased from 1.17 persons/car to 1.27 persons/car; ridership rate of official cars increased even more, from1.19 persons/car to 1.51 persons/car.

Trip purpose

Trips are commonly divided into mandatory trips and elastic trips. From the survey data, we found that the proportion of mandatory trips increased, such as work commuter travel, while elastic travel decreased, such as shopping, leisure, work-related business, etc. Elastic trips accounted for 40% of the total reduced trips, shown in Figure3.

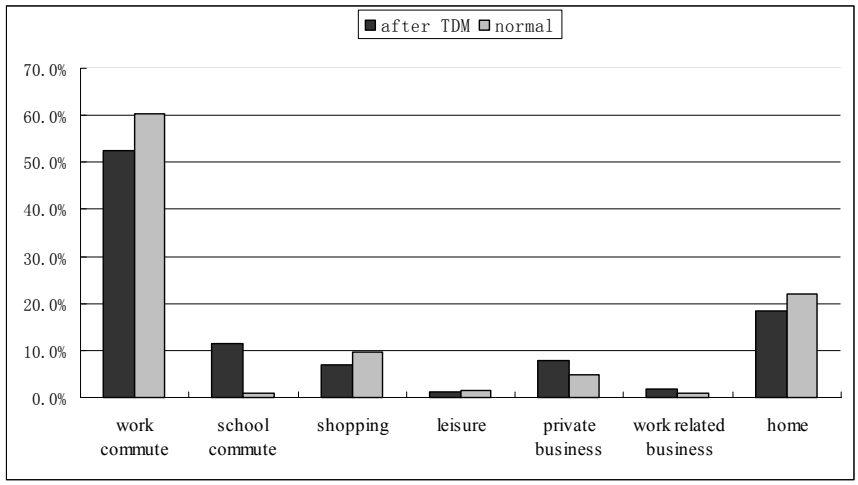

Figure 3. Trip purpose changes under TDM measures.

Mode share

Car-use-restriction policy resulted in obvious changes to mode share, namely a sharp decline in car share and promotion of the use of mass transit, such as bus and metro. In conclusion, bus, metro and bicycle became the major alternative travel modes. When the car was permitted, car share of car-owners reached 94.2%. When the car was limited, bus share increased 32.8%, bicycle share increased 22.5%, walk share increased 11.3%, metro share increased 9.4%, and taxi share increased 7.3%. Figure 4 shows the mode share shift under TDM measures influence.

Moreover, the shift of transport mode differs slightly for different travel purposes. For example, mass transit was the major alternative to commuting trips, taxi was the main alternative to work-related business trips, while bus and bicycle were the main alternative modes to private business trip.

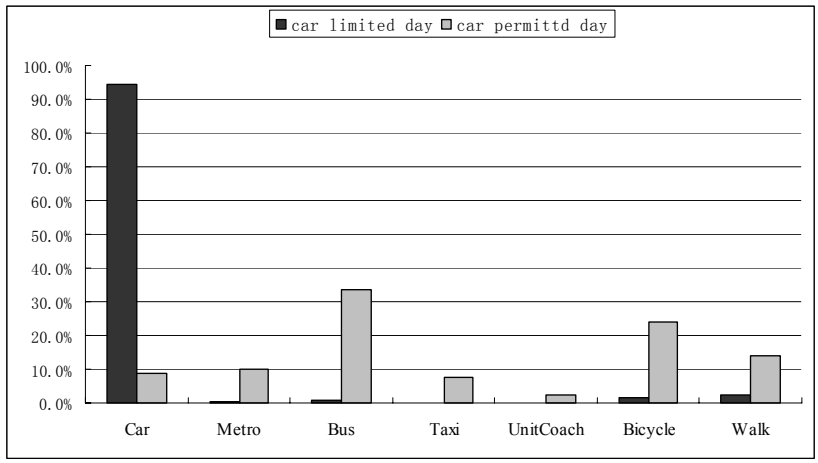

Figure 4. Trip purpose changes under TDM measures.

Travel time

Car and bus travel time shortened by 8 minutes under the TDM measures, and metro travel time decreased by 12 minutes. Table 1 lists the travel time changes during the AM peak period under TDM measures.

Table 1. Travel time changes in AM peak period under TDM measures

Travel time (min)	car	metro	bus	bicycle	walk
Normal	44.6	72.6	63.5	21.4	12.1
After TDM	36.2	60.5	55.1	21.7	11.1

CONCLUSION

The implementation of TDM measures during the Olympic Games has effectively reduced urban traffic congestion and ensured Olympic transport success. The traffic volumes of road networks decreased by 23% and the average travel speed of road networks increased by 26.9%, reaching 30.2 km/h in AM peak period. The passenger volumes reached 15 million per day for bus systems and 3.8 million per day for metro systems, accounting for 15.3% increases.

Also, drawing on data from the household interview travel survey before and after TDM measures, we determined the travel behavior changes of Beijing residents under TDM influence. We found that the residents' average trip rate fell from 1.88 times/day to 1.70 times/day. Moreover TDM measures have considerable effects on car-owners, whose average trip rate fell from 1.90 times/day to 1.59 times/day. The use rate of private cars declined 0.07 times/day and the ridership rate increased 0.10 person/car, while the official cars' use rate increased 0.70 times/ day and ridership rate increased 0.32 person/car. The implementation of TDM measures changed travel patterns and modified travel demand. Trips for schooling, shopping and leisure purposes decreased. The mode share of public transport increased sharply.

The travel time of subway, bus and car decreased by 12 min., 8 min., and 8 min., respectively.

In conclusion, Beijing hosted a special and successful Olympic Games and left a unique transport legacy to China and to the world.

REFERENCES

Beijing Municipal Committee of Communications. (2008). *A General Compilation of Traffic Assurance Plan during 2008 Beijing Olympic and Paralympics Games and Support Measures*.

Beijing Transportation Research Center. (2008). *Research on urban traffic operation simulation system during the Olympic Games*.

Gärling T., Eek, D., Loukopoulos, P., Fujii, S., Johansson-Stenman, O., Kitamura, R., Pendyala, R., Vilhelmson, B.(2002). A conceptual analysis of the impact of travel demand management on private car use [J]. *Transport Policy*, 9(1), 59-70

Guo, J., Chen, J., Sun, J., Wang, S., Quan, Y. (2008). "An Analysis of Impact of TDM Measures on Traffic Operations in Beijing." *Proceedings of the Sixth International Conference on Traffic and Transportation Studies*, ASCE, USA, 7-25.

Loukopoulos, P., Gärling, T., Vilhelmson, B. (2005). "Mapping the potential consequences of car-use reduction in urban areas." *Journal of Transport Geography*, 13, 135-150.

Yan, L. C.. (2008). "An Exploration of Demand Model for Beijing 2008 Olympic Games." 2008 TRB Conference, Washington.

Study on Congestion Pricing Model of Bus Lane Mixed Use by Carpool Vehicles

Pan Dawei[1], Deng Wei, Qian Renjie

[1]School of Transportation, Southeast University, Nanjing 210096, China;
PH: 15850539537; email: pandaweijt@yahoo.com.cn

ABSTRACT

Making use of bus lanes' excess capacity by opening them to carpool vehicles is a method that can effectively mitigate traffic jams and improve the operating efficiency of roads. In order not to influence buses' operation in bus lanes, congestion pricing is needed to regulate the volume of carpool vehicles in bus lanes. This paper analyzed the travel choice between carpool vehicles and single-occupancy vehicles when congestion pricing is used in bus lanes, and then proposes the congestion pricing model, in which the lowest average people cost and maximum road operating efficiency are the upper-layer objective model and the user equilibrium is the lower-layer objective model. The objective function of the model was solved by an advanced heuristic solution algorithm based on sensitivity analysis. Finally, a simple numerical example is given to illustrate the proposed model and algorithm.

INTRODUCTION

With the rapid increase in the number of the urban vehicles, the limited road traffic resources are becoming more and more strained. The problems of traffic congestion, traffic pollution, and traffic safety, which are caused by the large number of travelers' trips, have also become important restrictive factors in cities' development. Devoting major efforts to develop urban public transport is one of the most effective measures to solve the problem, and the operating efficiency of buses is further improved by opening bus lanes to give the exclusive right-of-way to the buses. However, during peak periods it is not uncommon to see fewer buses in bus lanes and excessive private vehicles in other lanes, reducing the total efficiency of the road system. Allowing carpool vehicles to take advantage of the excess capacity of the bus lanes can effectively alleviate the problem of congestion and improve the efficiency of the road operation. This paper proposed a travel choice model of travelers following research of traffic impedance and utility function, and then put forward the two-layer congestion pricing model, in which the lowest average people cost and maximum road operating efficiency are the upper objective function and the user equilibrium model is the lower objective function. The influence of traffic congestion pricing on travelers' model choice and road operation efficiency is analyzed by the advanced heuristic solution algorithm based on sensitivity analysis.

UTILITY ANALYSIS OF THE METHOD

The method of carpool vehicles using excess capacity of the bus lanes combines bus lanes and pricing strategies by allowing carpool vehicles carrying more than two passengers to gain access to bus lanes by paying a toll.

Figure 1 illustrates how the concept of excess capacity for bus lanes can be used to manage overall roadway congestion. The excess capacity is the white gap from the curve line to the top. The key to effective use of this strategy is to actively manage, using dynamic toll collection, how many vehicles can use the excess capacity. The traveler has the option of paying for a congestion-free restricted freeway lane or traveling freely on a congested general purpose freeway lane.

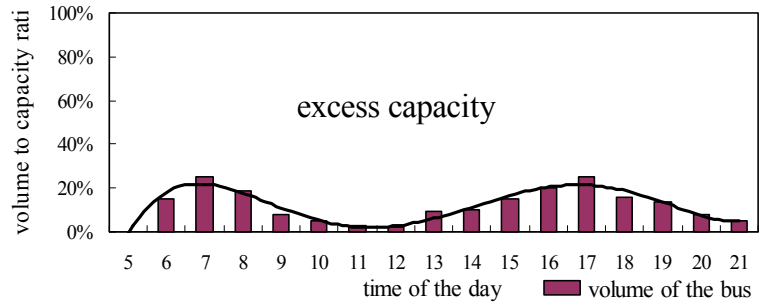

Fig 1. The excess capacity of bus lane.

When the method is applied, the toll-paying carpool vehicles move into bus lanes and the demand on the mixed flow lanes is reduced, as shown in Figure 2. The initial maximum delay is the upper dashed horizontal line. After the carpool vehicles move to the bus lanes, the maximum delay is reduced to a portion of that line. The total delay is reduced by the area between the initial and final demand, and the traffic congestion disappeared earlier than ever.

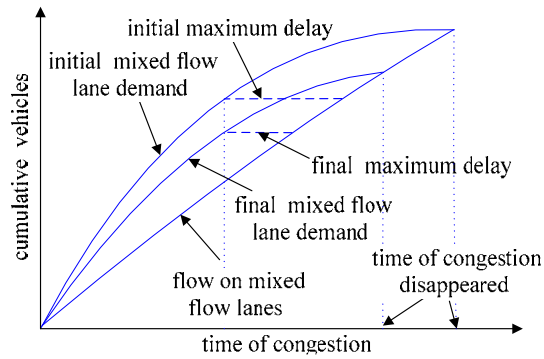

Fig 2. The utility of the method for reducing the traffic congestion.

The intent of the method is not to force individuals to make changes against their will. Rather, the objective is to provide a cost-effective travel alternative that a significant volume of commuters will find attractive enough to change from driving alone to use a carpool vehicle mode. So, with both travel time savings and more predictable travel times, the person-movement capacity of the roadway is increased by carrying more people in fewer vehicles.

THE ANALYSIS OF IMPEDANCE AND TRAVEL CHOICE

Impedance Function

By empirical formula (Wu 2008) and considering the influences among the different types of vehicles in different lanes, we get the impedance function as:

$$t_{k1g1} = t^0_{k1g1}[1+\alpha_{11}(f_{k1g1}/c_{k1})^{\beta_{11}}]\times[1+\alpha_{12}(f_{k1g2}/c_{k2})^{\beta_{12}}]+u_{k1g1} \quad (1)$$

$$t_{k1g2} = t^0_{k1g2}[1+\alpha_{21}(f_{k1g1}/c_{k1})^{\beta_{21}}]\times[1+\alpha_{22}(f_{k1g2}/c_{k1})^{\beta_{22}}]+u_{k1g2} \quad (2)$$

$$t_{k2g2} = t^0_{k2g2}[1+\alpha_{31}(f_{k2g2}/c_{k2})^{\beta_{31}}]\times[1+\alpha_{32}(f_{k2g3}/c_{k2})^{\beta_{32}}]+u_{k2g2} \quad (3)$$

$$t_{k2g3} = t^0_{k2g3}[1+\alpha_{41}(f_{k2g2}/c_{k2)}^{\beta_{41}}]\times[1+\alpha_{42}(f_{k2g3}/c_{k2})^{\beta_{42}}]+u_{k2g3} \quad (4)$$

Where k is the type of the lanes, *k1* represents mixed flow lanes, *k2* represents bus lanes; g is traffic modes, *g1* represents the mode of single-occupancy vehicle, $g2$ represents the mode of the carpool vehicle, *g3* represents the mode of the bus; t_{kg}, t^0_{kg} are the traffic impedance and the free flow time of the traffic mode type g in lane type k; f_{kg}, u_{kg} are the traffic volume and the congestion toll rate of the traffic mode type g in lane type k; α、β are the regression parameters, often taken value of 0.15 and 4, respectively.

Travel Choice Model

A disaggregate modal-split model can be used to analyze the relationship between the traffic mode split rate and the congestion toll rate (Xu 2008). The probability of the traveler choosing traffic mode i is as:

$$p(i) = e^{U_i}/\sum_{i=1}^{4} e^{U_i} = e^{\xi_i+mF_i^*+nB_i^*+kT_i^*}/\sum_{i=1}^{4} e^{\xi_i+mF_i^*+nB_i^*+kT_i^*} = e^{-\theta t_{kg}}/\sum_{k\in K}\sum_{g\in G} e^{-\theta t_{kg}} \quad (5)$$

where F is the cost that can be saved under the condition of traffic congestion tolls; B is the ratio between economic profit and personal income; T is the cost that can be saved when choosing one type of traffic mode; ξ_i is the constant for model adjustment; m, n, k denote respectively the constant of toll rate, economic benefit, and travel time; θ is an nonnegative constant, represent the travelers' comprehensive degree of travel cost.

BI-LEVEL MODEL OF TRAFFIC CONGESTION

Upper Model (P1): $$\min F(u) = \sum_{k\in K}\sum_{g\in G}\lambda_g f_{kg}(u) t_{kg}(f_{kg},u) \quad (6)$$

$$s.t. \quad u_{kg} \ge 0;\ \sum_{k\in K} d_g f_{kg} \le C_k;\ f^{\min}_{bus} \le f_{k2g3} \le f^{\max}_{bus} \quad (7), (8), (9)$$

where λ is the weight coefficient, it is proportional to the average number of passengers of the vehicle type g; d_g is the equivalent conversion factor to a standard vehicle; $f^{\min}_{bus}$ and $f^{\max}_{bus}$ are the lower limit and upper limit of the volume of the buses.

Lower Model (P2): $$\min Z = \frac{1}{\theta}\left\{\sum_{k\in K}\sum_{g\in G}[\Gamma_g f_{kg}(\ln f_{kg} - 1)] - \sum_{g\in G}[\Gamma_g q_g(\ln q_g - 1)]\right\}$$

$$+\sum_{g\in G}\Gamma_g \Phi_g(u_g + y_g)q_g - \sum_{g\in G}\Gamma_g\int_0^{q_g}[D_g(f)]^{-1}df + \int_0^{q} t(f)df \quad (10)$$

$$s.t. \quad \sum_{g\in G} q_g = \sum_{k\in K}\sum_{g\in G} f_{kg};\ \ q_g \ge 0;\ f_{kg} \ge 0 \quad (11), (12), (13)$$

where Γ_g is the influence coefficient of the vehicle of the traffic mode type g

compared with standard car to traffic flow; q_g is the volume of the traffic mode type g; Φ_g is the conversion factor between toll and time value; y_g is the sum of travel costs and individual preference costs of the vehicle of the traffic mode type g; D_g is travel demand function of traffic mode type g.

HEURISTIC ALGORITHM BASED ON SENSITIVITY ANALYSIS

Sensitivity Analysis

In the problem of bi-level programs, it is necessary to gain a feasible descending searching direction when solving upper-level problems, which requires the gradient to decision variable from the objective function (Zhou 2001).

Make the decision variable u of upper-level as the lower-level's disturbing variable of users' equilibrium distribution, then derive the gradient ${}^{u}_{\Delta}f$ of f to u by sensitivity analysis. Using Kuhn-Tucker's first condition, for a given solution u^0 of upper-level problem, $(\mathbf{f}^{*T}, \mathbf{m}^{*T}, \mathbf{I}^{*T})$ is made as the optimal path volume and Lagrange multiplier vectors of lower-level problem .Because the Lagrange multiplier vector has no effect, assume it as 0. So Kuhn-Tucker's condition can be simplified as:

$$\ln f_{kg}{}^{*} + \theta \sum_{g \in G} \Phi_g (u_g + y_g) q_g + \int_0^q t(f)df - m_k{}^{*} - l^{*} = 0, k \in K, g \in G; \tag{14}$$

$$\sum_{k \in K} \sum_{g \in G} f_{kg}{}^{*} - C_k = 0; \quad \sum_{k \in K} \sum_{g \in G} f_{kg} = \sum_{g \in G} q_g = q \tag{15), (16}$$

where q_g is related to cost vector $\mathbf{u}$, multiplier l, and $m = (m_1, m_2, \cdots)$, so to simplify, the above equations can be represented by vectors as:

$$\mathbf{\Phi}(\mathbf{f}^{*}, \mathbf{u}^{0}) - A^{T}\mathbf{m}^{*} - B^{T}\mathbf{I}^{*} = 0, \quad A\mathbf{f}^{*} - \mathbf{C}^{*} = 0, \quad B\mathbf{f}^{*} - \mathbf{q}(\mathbf{u}^{0}, \mathbf{m}^{*}, \mathbf{I}^{*}) = 0 \tag{17}$$

$\mathbf{\Phi}(\mathbf{f}^{*}, \mathbf{u}^{*})$ is the vector composed by element of $\ln f_{kg}{}^{*} + \theta \sum_{g \in G} \Phi_g (u_g + y_g)$,

let: $\mu = \begin{vmatrix} \mathbf{m} \\ \mathbf{I} \end{vmatrix}$, $\Lambda = \begin{vmatrix} A \\ B \end{vmatrix}$, $z(\mathbf{u}^0, \mu^0) = \begin{vmatrix} \mathbf{k} \\ \mathbf{g}(\mathbf{u}^0, \mu^*) \end{vmatrix}$,

then: $\mathbf{\Phi}(\mathbf{f}^{*}, \mathbf{u}^{0}) - \Lambda^{T}\mu^{*} = \mathbf{0}$, $\Lambda\mathbf{f}^{*} - \mathbf{z}(\mathbf{u}^{0}, \mu^{*}) = \mathbf{0}$ (18)

The Jacobian matrix of $(\mathbf{f}^{T}, \mu^{T})$ at $\mathbf{u}^0$ of the equation mentioned above is:

$$J_{f,\mu}{}^{*} = \begin{vmatrix} {}^{f}_{\Delta}\mathbf{\Phi}(\mathbf{f}^{*}, \mathbf{u}^{0}) & -\Lambda^{T} \\ \Lambda & -{}^{\mu}_{\Delta}z \end{vmatrix} \tag{19}$$

let: $[J_{f,\mu}{}^{*}]^{-1} = \begin{vmatrix} J_{11} & J_{12} \\ J_{21} & J_{22} \end{vmatrix}$, according to the formula of inverse matrix:

$$J_{11} = {}^{f}_{\Delta}\mathbf{\Phi}(\mathbf{f}^{*}, \mathbf{u}^{0})[I + \Lambda^{T}J_{21}], \quad J_{12} = {}^{f}_{\Delta}\mathbf{\Phi}(\mathbf{f}^{*}, \mathbf{u}^{0})\Lambda^{T}J_{22}, \tag{20), (21}$$

$$J_{21} = -J_{22}\Lambda {}^{f}_{\Delta}\mathbf{\Phi}(\mathbf{f}^{*}, \mathbf{u}^{0}), \quad J_{22} = [-{}^{\mu}_{\Delta}z + \Lambda {}^{f}_{\Delta}\mathbf{\Phi}(\mathbf{f}^{*}, \mathbf{u}^{0})\Lambda^{T}]^{-1}, \tag{22), (23}$$

I represents the proper dimension unit matrix in the above formula. For ${}^{f}_{\Delta}\mathbf{\Phi}(\mathbf{f}^{*}, \mathbf{u}^{0})$ is a diagonal matrix containing diagonal element $1/f_r^{w^*}$, it must be positive definite. According to the quantitative method of nonlinear programming in sensitivity analysis,

Then: $\begin{vmatrix} {}^{u}_{\Delta}\mathbf{f} \\ {}^{u}_{\Delta}\mu \end{vmatrix} = -J^{*}_{f,\mu}{}^{-1} J^{*}_{u}$;

$$ {}^{u}_{\Delta}\mathbf{f} = -J_{11}\ {}^{u}_{\Delta}\mathbf{\Phi}(\mathbf{f}^{*},\mathbf{u}^{0}) + J_{12}\ {}^{u}_{\Delta}z(\mathbf{f}^{0},\mu^{*}) \quad (24) $$

$$ {}^{u}_{\Delta}\mu = -J_{21}\ {}^{u}_{\Delta}\mathbf{\Phi}(\mathbf{f}^{*},\mathbf{u}^{0}) + J_{22}\ {}^{u}_{\Delta}z(\mathbf{u}^{0},\mu^{*}) \quad (25) $$

Because of positive definiteness of the matrix, the derivative above exists (Tobin, 1988). Thus the heuristic algorithm based on sensitivity analysis can be used to solve the problem of a bi-level program.

Heuristic Algorithm Based on Sensitivity Analysis

For the obtained solution $\mathbf{u}^{0}$, solve the lower-level problem and get the corresponding solution $v(\mathbf{u}^{0})$,then linearize the upper-level problem at $\mathbf{u}^{0}$and get the linear programming problem as (LP1),

$$ \min\left|\partial\mathbf{F}(\mathbf{u}^{0})/\partial\mathbf{u} + (\partial\mathbf{F}/\partial f)\,{}^{u}_{\Delta}f(\mathbf{u}^{0})\right|^{T}(\mathbf{u}-\mathbf{u}^{0}) \quad \text{s.t.}\ \ \mathbf{u}^{\min} \le \mathbf{u} \qquad (26),(27) $$

Solving the linear programming problem above yields the optimal solution $\mathbf{u}'$, $\mathbf{u}'$–$\mathbf{u}^{0}$ is the feasible descending direction. Finally, we get the heuristic algorithm of bi-level programming problem, the algorithm steps are as:

Step 1 Give an initial structure of congestion pricing u which is feasible;

Step 2 Solve problem (P2) with **u**, then we can get f;

Step 3 Calculate the information of sensitivity analysis ${}^{u}_{\Delta}f$;

Step 4 Linearize the problem (P1) at **u**, we can get the problem (LP1);

Step 5 Calculate $\mathbf{u}: = \mathbf{u} + \alpha(\mathbf{u}'–\mathbf{u})$, which α is the step size in search;

Step 6 If the **u** is closed enough at two adjacent times, iterative is end; if not, return to step2.

NUMERICAL EXAMPLE

Supposing the road is composed of mixed flow lanes and bus lanes, the types of vehicles driving in the lanes are composed of: single-occupancy vehicles, carpool vehicles and buses. t^{0}_{k1g1}, t^{0}_{k1g2} are equal to 8unit time value t^{0}_{k2g2}, t^{0}_{k2g3} are equal to 6 unit time value; λ_{g1}=1, λ_{g2}=3, λ_{g3}=50; c_{k1}=400, c_{k2}=500. In a peak hour, supposing the initial volume of the single-occupancy vehicles, carpool vehicles and buses are 300, 200, and 10, respectively, the simulation results of the model are as follows:

Table 1. Traffic flow distribution and the optimal toll with different θ

θ	Optimal toll	f_{k1g1}	f_{k1g2}	f_{k2g2}	f_{k2g3}
0.1	3	300	158	42	10
0.5	2.1	280	155	65	10
2	1.9	230	187	83	10

Table 2. The volume ratio of different vehicle types with different θ

θ	the volume ratio of different vehicle types		
	single-occupancy vehicle	carpool vehicle	bus
0.1	60%	38%	2%
0.5	56%	42%	2%
2	46%	52%	2%

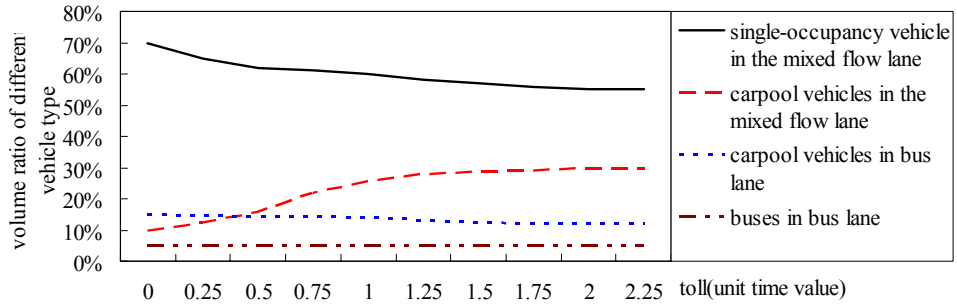

Fig 3. The volume ratio of different vehicle types with different toll rate.

From the tables and the figures above, it is clear that: (1) With the increase of θ, more travelers convert from single-occupancy vehicles to carpool vehicles, because the more the travelers learn about the traffic situation the better they can choose the most suitable trip modes to avoid traffic jams. Therefore it is important to provide real-time information to travelers. (2) With the increase of toll, the number of carpool vehicles converting to the bus lanes reduced, and when the toll decreased the situation reverses, so the toll is an effective way to regulate the number of carpool vehicles in bus lanes .

CONCLUSION

In this paper, we proposed that carpool vehicles utilize excess capacity of bus lanes as well as the implementation of congestion pricing in order to to regulate the number of carpool vehicles in bus lanes. We then put forward a bi-level programming model, using an advanced heuristic solution algorithm based on sensitivity analysis to solve a numerical example. The paper found that traffic volume changes with the changing of θ and toll, and the optimal toll in the condition of different volumes is also supposed. The method and the model proposed by the paper are therefore practical.

ACKNOWLEDGMENTS

This work is supported in part by National 863 High Technology Research and Development Program of China (2007AA11Z202).

REFERENCES

Wu, J., Huang, J., Liu, M., and An, N. (2008). "Double-mode modeling for the traffic congestion toll." *Journal of ChangSha Communications University*, 24(2), 54-59.

Xu, W., He, S., Song, S., and Li, J. (2008). "Disaggregate Modal-split Model Considering Congestion Pricing." *Journal of Transportation Systems Engineering and Information Technology*, 8(3), 96-102.

Zhou, J., Sheng, Z., and He, J. (2001). "Optimal fare design for public transport networks with elastic demand." *Acta Automatica Sinica*, 27(5), 637-643.

Tobin, R. L., and Friesz, T. L. (1988). "Sensitivity analysis for equilibrium network flow." *Transportation Science*, 22(3), 243-250.

Principle analysis and state evaluation on coordinated development among transportation modes

Hai-bo Zou[1]

[1]Department of Transportation, School of Economics and Management, Chang'an University, Middle of South 2nd Ring Road, Xi'an; PH (86)29-82335577; FAX (86)29-82334507; email: zhb207766@163.com

ABSTRACT

Based on the viewpoint of system theory and synergetics, this paper advocates the coordinated development among transportation modes and cooperation among modes. According to the component of every transportation mode, an index system was built up from quantity and quality aspects, and principal component analysis was used to evaluate the development level of every mode from 1995-2005. Then the model of degree of membership was established to evaluate the coordinated state among modes. The results indicate that the average static coordinated degree is 0.298, and that all modes develop quickly, but their developments are not coordinated. The ways to change the situation are to develop a united development plan, combine policies, and exploit and use all modes fully, building a true comprehensive transportation hub and so on.

0 INTRODUCTION

In recent years, five transportation modes have made substantial progress and have exerted the best history role. But a misbalanced comprehensive transportation system is still prominent, and does not correspond with the development of a national economy, for each transportation mode emphasizes its own benefits. These affect the system's exerting function, so promoting more coordinated development needs to be a priority. The coordinated development of a comprehensive transportation system includes three aspects, which are the coordinated development between the system and economy, among transportation modes, and among sub-systems of every mode. This paper only studies the coordinated development among transportation modes.

Numerous scholars have contributed research on the coordinated development of comprehensive transportation systems, but the results are not abundant. Zhang et al. (2002) theoretically discussed the coordinated development of transportation systems, but a suitable method does not now exist to realize quantitative evaluation according to his viewpoint. Xiong et al. (2006) used DEA to quantitatively evaluate the coordinated development state among transportation modes, but the indexes chosen were too simple. Xu et al. (2003) quantitatively analyzed the principle and character of the coordinated development among transportation modes. This paper builds upon previous research by systematically setting up an index system that can reflect the developing level of every transportation mode from the angle of its composition, and according to system theory and synergetics, attempts to analyze the principle and evaluate the state of the coordinated development among modes.

1 COMPONENT OF TRANSPORTATION MODE

To analyze the principle and evaluate the state of coordinated development among transportation modes, every mode is separated into five sub-systems from the angle of its component in the paper: (1) Route infrastructure sub-system (RIS), for example, aviation routes, shipping routes, highways, railways, and pipelines;(2) transportation infrastructure sub-system (TIFS), which provides conditions for the transportation instrument's working normally on the route, mainly including stations, hubs, monitoring facilities, communication facilities, and other auxiliary facilities; (3) transportation instrument sub-system (TISS), which is set up around the transportation instrument's operation; (4) transportation human resources sub-system (THRS), which includes all kinds of personnel relating to transportation supply; and (5) transportation software sub-system (TSS), which includes transportation organization and management, traffic science, technology and others.

2 PRINCIPLES ON COORDINATED DEVELOPMENT AMONG TRANSPORTATION MODES

In accordance with system theory, character, function, and move law of a system shows only as a whole. If all elements of one system cooperate with each other, the function of the whole system is greater than the sum of every element's function. Therefore, in order to have the transportation system's function optimized, the coordinated development among transportation modes is necessary.

Synergetics puts forward that the function which one system displays is the result that its sub-systems reach the synergetic state by self-organizing under some condition. In the self-organizing process, the coordinated development among sub-systems plays a decisive role in realizing the system's order, and there are several key factors, called order parameters, which indicate the ordered structure and type of a system and display the sum of all sub-systems' contributions to the synergetic movement. So if order parameters are found, the developing state of a system can be described. According to synergetics, under the conditions of a market economy, the self-organization among five transportation modes is the process that each of them develops in its own proper field and they cooperate with each other in some fields, and that any of them cannot finish tasks individually at the same time, ultimately making the transportation system more and more ordered as a whole.

Summarizing the above analysis, the coordinated development among transportation modes is not that they develop complying with the stable static proportion, but the developing trends that they adapt to, promoting and cooperating with each other to realize the overall objective of the system. Based on this, the paper attempts to make successive research.

3 DEVELOPING LEVEL INDEX SYSTEM OF TRANSPORTATION MODE

According to the layer, system, reality, representation, and other principles, the indexes which can describe the state of every mode's sub-systems and every whole mode are chosen from the quantity and the quality aspects—because pipeline transportation has little relationship with the other four modes and in order to simplify the calculation, it is not addressed in this paper. Moreover, the indexes of TSS are very difficultly divided into the quantity indexes and the quality indexes, so

they are not chosen separately. The index system is shown in Table 1.

Table 1. Developing level Index system of transportation modes.

		Quantity index	Quality index
Railway	RIS	Length of national railways in operation	(Double tracking,automatic blocking) length proportion of national railways in operation, railway density
	TIFS		
	TISS	(Locomotives, passenger coaches, freight cars) number of national railway	(Diesel locomotives, electric locomotives, berth coaches, non-general freight cars) proportion of national railway, technical speed of passenger (freight) trains of national railway
	THRS	Number of staff and workers	Average wage of staff and workers
	TSS	(Punctuality rate at departure, punctuality rate in running, traveling speed)of passenger (freight) trains of national railway, daily distance per passenger (freight) locomotive of national railway, average transport distance of passengers(freight)	
	Whole mode	Passenger (freight) (traffic, ton kilometers), fixed assets investment	{ Passenger (freight) (traffic, ton kilometers)} proportion
Highway	RIS	Length of highways, highway and bridge construction investment	Expressway proportion, highway density
	TIFS		
	TISS	Possession of (civil vehicles, trucks, civil passenger vehicles), possession of (vehicles, trucks, passenger vehicles) for highway transportation	Proportion of (large passenger vehicles, non-ordinary trucks)for highway transportation
	THRS	Number of staff and workers	Average wage of staff and workers
	TSS	Average transport distance of passengers(freight)	
	Whole mode	Passenger (freight) (traffic, ton kilometers), highway construction investment	{ Passenger (freight) (traffic, ton kilometers)} proportion
Water	RIS	Length of navigable inland waterways, waterways and navigation mark construction investment	
	TIFS	Number of berths in major coastal ports for productive use, port construction investment	Ratio of berths in major coastal ports 10000 ton class for productive use, cargo handled at seaports per berth
	TISS	Possession of civil transport vessels	Proportion of civil transport (motor vessels, barges)
	THRS	Number of staff and workers	Average wage of staff and workers
	TSS	Average transport distance of passengers(freight)	
	Whole mode	Passenger (freight) (traffic, ton kilometers), water transport construction investment	{ Passenger (freight) (traffic, ton kilometers)} proportion
Air	RIS	Number(length) of civil aviation routes	Number (length) proportion of civil aviation international routes
	TIFS	Number of civil airports	
	TISS	Number of (civil aircraft, civil aero transport)	Large and medium civil aircraft proportion
	THRS	Number of staff and workers	Average wage of staff and workers
	TSS	Utilization rate of aero transport, average loading rate, average passenger seated rate, average transport distance of passengers(freight)	
	Whole mode	Passenger (freight) (traffic, ton kilometers), fixed assets investment	{ Passenger (freight) (traffic, ton kilometers)} proportion

4 STATE EVALUATION OF COORDINATED DEVELOPMENT AMONG TRANSPORTATION MODES

4.1 DEVELOPING LEVEL EVALUATION OF EVERY MODE

There are many quantitative methods on evaluating a system's development level, but none has been generally accepted at this point. Principal component analysis is chosen to evaluate every transportation mode's developing level in this paper because according to this method weight for indicators are distributed objectively, and a set of correlated variables are transformed into a set of uncorrelated ones, which are ordered by reducing variability, and the uncorrelated ones are linear combinations of the original variables with minimum loss of real data. Order parameters controlling every mode's development situation can be obtained by this method. Its main steps are: (1) make the index data x_{ij} $(i = 1,2,\cdots, p, j = 1,2,\cdots n)$ standardized:

$$y_{ij} = (x_{ij} - \overline{x_j})/\sigma_j, \quad \overline{x_j} = \frac{1}{p}\sum_{i=1}^{p} x_{ij}, \sigma_j = \sqrt{\frac{1}{p}\sum_{i=1}^{p}(x_{ij} - \overline{x_j})^2};$$

(2)construct matrix $R = (r_{kj})_{n\times n}$, $r_{kj} = \frac{1}{p}\sum_{s=1}^{p} y_{ik} y_{ij}$, $k = 1,2,\cdots, n$;

(3) calculate R's eigenvalue λ_k and assume $\lambda_{k+1} \geq \lambda_k$, and its feature vector is $\beta_k = (\beta_{k1}, \beta_{k2}, \cdots, \beta_{kn})^T$;

(4)calculate every component's contribution ratio: $p_j = \lambda_j / \sum_{i=1}^{n} \lambda_k$;

(5)calculate the score of type-i sample in the direction of every principal component: $\begin{bmatrix} Z_1^i \\ Z_2^i \\ M \\ Z_m^i \end{bmatrix} = \begin{bmatrix} \beta_{11} & \beta_{12} & \cdots & \beta_{1n} \\ \beta_{21} & \beta_{22} & \cdots & \beta_{2n} \\ \cdots & \cdots & \cdots & \cdots \\ \beta_{m1} & \beta_{m2} & \cdots & \beta_{mn} \end{bmatrix} \begin{bmatrix} y_{i1} \\ y_{i2} \\ \cdots \\ y_{in} \end{bmatrix}$, $m(m < n)$ is the minimum positive number which satisfies with $\sum_{j=1}^{m} \lambda_j / \sum_{j=1}^{n} \lambda_j \geq e$, generally e=0.85;

(6)calculate the score of type-i sample: $q_i = p_1 \left|Z_1^i\right| + p_2 \left|Z_2^i\right| + \ldots + p_m \left|Z_m^i\right|$.

The data of the indexes was collected from 1995-2005 in China; SPSS12.0 is used to go on principal component analysis, and the developing level value of every transportation mode is obtained (listed in Table 2). According to Table 2, the developing level value of every mode increased year by year, which illustrated that all of them had realized continuous and rapid development during those years.

Table 2. Developing level of every transportation mode.

Year	Railway	Highway	Water	Air
1995	-4.850	-4.698	-4.150	-4.488
1996	-4.360	-4.124	-3.424	-3.530
1997	-3.009	-3.396	-2.560	-2.782
1998	-2.148	-2.705	-1.821	-1.817
1999	-1.350	-1.317	-0.893	-1.210
2000	-0.368	-0.360	-0.271	-0.257
2001	1.018	0.868	0.562	0.003

2002	1.871	2.130	0.680	1.422
2003	2.823	3.072	2.077	2.053
2004	4.435	4.737	4.174	4.790
2005	5.937	5.794	5.625	5.816

4.2 EVALUATION OF COORDINATED DEGREE AMONG MODES

Coordinated development is an indistinct concept, in which content is definite and its extension is indefinite, so its link with fuzzy mathematics is quoted to describe it. The coordinated degree function is set up to reflect the change law of system's coordinated extent, and its formula is:

$$U = \exp\left\{-(w - w')^2 / s^2\right\} \quad (1)$$

In (1): U stands for static coordinated degree, w stands for actual value, w' stands for coordinated value, s^2 stands for variance.

To illustrate conveniently, X_i , X_j , X_k and X_l respectively stands for railway, highway ,water and air transportation.

$U_{i/j}$ is the coordinated degree of X_i to X_j and describe the degree that X_i's actual value is approach to the coordinated value of X_j demanding X_i, the others also comply with this rule. So $U_{i/j}$ and $U_{j/i}$ describe the coordinated degree of one system to another, the coordinated degree between X_i and X_j is $U_{i,j}$, its formula is:

$$U_{i,j} = \min\left(U_{i/j}, U_{j/i}\right) / \max\left(U_{i/j}, U_{j/i}\right) \quad (2)$$

According to the same law, the coordinated degree among 3 systems and among 4 systems can be determined, and the formulas are:

$$U_{i,j,k} = (U_{i/j,k}U_{j,k} + U_{j/i,k}U_{i,k} + U_{k/i,j}U_{i,j}) / (U_{j,k} + U_{i,k} + U_{i,k}) \quad (3)$$

$$U_{i,j,k,l} = (U_{i/j,k,l}U_{j,k,l} + U_{j/i,k,l}U_{i,k,l} + U_{k/i,j,l}U_{i,j,l} + U_{l/i,j,k}U_{i,j,k}) / (U_{j,k,l} + U_{i,k,l} + U_{i,j,l} + U_{i,j,k}) \quad (4)$$

In the above formulas, the coordinated value is the value that one system adapts to another, and linear regression analysis is used to get it. The evaluation of the coordinated degree among systems need be gone on from the static and the dynamic ways, and relative definitions are given:

Definition 1: $U(t)$ stands for the static coordinated degree among systems at time t, and it can be determined with the formula (2) ~ (4), $0 \le U(t) \le 1$.In general, define $U(t) < 0.5$ as uncoordinated, $0.5 \le U(t) < 0.8$ as approximately uncoordinated, $0.8 \le U(t) < 0.9$ as approximately coordinated, $0.9 \le U(t) \le 1$ as coordinated.

Definition 2: $U(t-T+1)$, $U(t-T+2)$,…, $U(t-1)$, $U(t)$ are the static coordinated degree among systems at the different times during time $(t-T+1)$ to t. And $\overline{U}(t) = \frac{1}{T}\sum_{i=0}^{T-1} U(t-i)$ is the dynamic degree, T is the starting time. Assume $t_2 > t_1$ (two randomly different times); if $\overline{U}(t)$ does not keep decreasing, the system is approaching the coordinated state (Wang, 1998).

Using the above formulas and definitions, the static and the dynamic coordinated degree among 4 transportation modes (listed in the table 3) is obtained. According to Table 3, from 1995-2005 the average static coordinated degree among 4 modes was 0.298<0.800, which indicates that 4 modes were in the uncoordinated development situation in China; and the dynamic coordinated degree displays that

the uncoordinated situation among them had been improving since the year 2000, but the trend was not obvious. As a result, the conclusion is that the transportation modes developed uncoordinatedly in China those years, and the uncoordinated state did not markedly improve.

5 CAUSES AFFECTING COORDINATED DEVELOPMENT

(1) The prevalent management system in China leads to the absence of a united plan for whole transportation system development, and there has not been one real comprehensive perfectly functioning hub to this point. (2) The goal of transportation policies is not clear and the systematization is not strong. For example, the united price implemented hinders the railway freight transport development to some extent. (3) The theories guiding the coordinated development of transportation systems are not complete. (4) Every mode does not hold its proper position in the market and somewhat blindly competes with other modes (Wu et al., 2006).

Table 3. Static coordinated degree and dynamic coordinated degree.

year	1995	1996	1997	1998	1999	2000
$U_{i,j,k,l}$	0.209	0.091	0.187	0.058	0.259	0.637
$\overline{U}_{i,j,k,l}$	0.209	0.150	0.162	0.136	0.161	0.240
year	2001	2002	2003	2004	2005	average
$U_{i,j,k,l}$	0.381	0.193	0.441	0.193	0.628	0.298
$\overline{U}_{i,j,k,l}$	0.260	0.252	0.273	0.265	0.298	

6 COUNTERMEASURES FOR COORDINATED DEVELOPMENT

(1) A united transportation management system should be established quickly, and a real comprehensive hub should be built. (2) To provide a better development environment for transportation modes, the policies should be drafted and reform efforts should be particularly focused on investment and financing policy and price policy. (3) The special research on development of transportation system should be consolidated, and the operative theories and methods should be put forward. (4) Every transportation mode should set the proper position to develop in the market, at the same time, strengthens cooperation with other modes (Antoni et al., 2005).

7 CONCLUSIONS

According to the paper's research results, all transportation modes in China are developing quickly but uncoordinatedly. Therefore, all divisions of departments in charge of traffic should take measures to promote the coordinated development among transportation modes, so that every mode can develop in its proper field and cooperate effectively with other modes.

REFERENCES

Antoni, C., and Albert, S. (2005). "The regional allocation of infrastructure investment." *European Economic Review*, 49(5), 1165-1205.

Wang, W.G. (1998). "Study on theory and method of coordinated development." *Dongbei University of Finance and Economics,* Da Lian.

Wu, Q. Q., and Sun, Q. P. (2006). "Basic point of integrated transport planning

theory.". *Journal of Traffic and Transportation Engineering,* 6(3), 119-122.

Xiong, C. J., and Ning, X. X., and Pan, Y. L. (2006). "Evaluation of coordinated development between chinese comprehensive transportation modes". *Systems Engineering*, 24(6), 1-7.

Xu, L. M., and Hu S. J. (2003). "Discussion on the transportation system coordination." *Technology Economy*, 21(5), 18-20.

Zhang, S. R., and Yan, B, J. (2002). "Analysis of the transportation system coordination." *Journal of Changàn University: Natural Science Edition,* 22(3), 51-53.

Evaluating the Equity Impacts of Rural Road Investment Projects on Household Welfare Based on a Quantile Regression Approach: Evidence from Fujian Province

Y. Tian[1], Y. Li[2], and X. Chen[3]

[1]Key Laboratory of Road and Traffic Engineering of Ministry of Education, School of Transportation Engineering, Tongji University, 201804 BOX13#604, Shanghai, Caoan Road 4800; PH 13764488423; E-mail: tianyuandy@126.com

ABSTRACT

The basic purpose of public investment in rural roads is to increase the social benefits in rural areas. However, it has been difficult to precisely quantify the size and especially the distribution of benefits of rural road investments, due to methodological constraints and data limitations. This paper develops and implements a method for nonparametrically estimating whether the impact of Rural Roads Improvement Projects (RRIP) is equitable. Furthermore, a panel data surveying project and control villages before and after program implementation from Fujian Province is applied to estimate the welfare gain as an empirical approach. It is shown that the proposed quantile nonparametric regression approach can examine whether the rural road projects efficiently reduce inequity in the targeted population.

1. INTRODUCTION

Improved roads can create opportunities for economic growth and poverty reduction through a range of mechanisms. Roads reduce transportation costs and the costs of consumption and production of goods and services. With easier access to markets and technology, improved roads expand farm and nonfarm production through increased availability of relevant inputs and lower input costs (Binswanger, Khandker, and Rosenzweig 1993; Levy 1996). At the household level, road development contributes to higher productivity and demand for labor (World Bank 2000), and improved education and health, including those for women and girls (Bryceson and Howe 1993; Levy 1996). Road-related studies have also suggested that household consumption is likely to get a boost from increased household income, consequently reducing poverty (Fan, Hazell, and Thorat 2000). This problem is compounded by the fact that the effects of rural roads are also long-term, and thus cannot be captured through the use of cross-sectional data, particularly since unobserved fixed area characteristics influence the placement of road investment in a village or community (Binswanger, Khandker and Rosenzweig 1993).

It has been difficult to precisely quantify the benefits of roads, due to methodological constraints and data limitations. The traditional estimates of the

returns on rural roads investments using the internal rate of return approach have also been criticized for not being able to capture the true distributional benefits to the targeted population, particularly to the poor (van de Walle 2002). This paper, applying the data from the Rural Roads Improvement Program (RRIP) in Fujian Province, offers an empirical assessment of the impact and role of roads on economic behavior across different income groups by using a fixed-effects quantile estimation approach.

2. DATA AND ITS CHARACTERISTICS

The data used for the analysis, collected by the Fujian Provincial Communications Department (FPCD), is based on household and community surveys prior to, and following, implementation of RRIP, funded by the World Bank in Fujian province, that allowed identification of control and treated villages. The datasets have a true before/after and with/without structure and are reasonably large, allowing a study of community-level and household-level impacts. The data covers all villages covered by the household surveys; there is complete overlap between these data. This permits the use of both community and households information for analysis.

In the surveys, a multistage PPS random sampling method was used to choose sample villages, and 12 households were selected from each sample village using a stratified random sampling procedure. The distribution of the sample in the survey is showed in Table 1, and Table 2 presents means for outcomes and explanatory variables across project and control households, for both rounds of each survey.

Table 1 Distributional of the Sample (for households and villages).

Type	*Villages*	*Households*
Treated Group	**34**	**426**
Control Group	**34**	**414**
Total	**68**	**840**

Table 2 Summary statistics for outcomes and explanatory variables.

Type	*Treated Villages*		*Control Villages*	
	Mean	*S.E.*	*Mean*	*S.E.*
Outcome				
HH per increase income (*RMB*)	**9340.8**	**751.8**	**6773.1**	**764.9**
Explanatory variables				
Number of HH labors	**3.00**	**0.08**	**2.60**	**0.07**
Number of HH employment	**1.07**	**0.07**	**0.89**	**0.05**
HH landownings (*Mu*)	**3.53**	**0.13**	**4.07**	**0.16**

Type	*Treated Villages*		*Control Villages*	
	Mean	*S.E.*	*Mean*	*S.E.*
Village has RRIP (*Y*=1, *N*=0)	**1**		**0**	
***Observations* (*n*)**	**426**		**414**	

3. METHODOLOGY

In this section, we examine the distributional issue of gains from RRIP investment using quantile regression analysis (Khandker, Bakht, and Koolwal 2006). It is potentially important to investigate changes in outcomes observed at different points in the income distribution. Simply investigating changes in the mean may not be sufficient when the entire shape of the distribution changes significantly (Buchinsky 1998). Studying the distributional impact also sheds light on political constraints on the allocation of infrastructural investment (Jacoby 2002).

Following the model proposed by Koenker and Bassett (1978), assume y_i, i=1,…, n is a sample of observations on the log income, and that x_i is a K x 1 vector (comprising the RRIP (R), household (H), and village (V) level characteristics controlled on the right-hand side of equation (1)).

$$\ln Y_{ij} = \alpha H_{ij} + \beta V_j + \gamma R_j + \varepsilon_{ij} \tag{1}$$

Where Y_{ij} is the per capita income of i-th household living in j-th village, H is set of observed household characteristics, R is an indicator of the road development project at the village level, V represents observed non-road village-level characteristics, and ε is a vector of errors term.

The quantile regression model can be expressed as:

$$y_i = x_i'\beta_\tau + \varepsilon_{\tau i},\ Q_\tau(y_i \mid x_i) = x_i'\beta_\tau, \qquad \tau \in (0,1) \tag{2}$$

Where $Q_\tau(y_i|x_i)$ denotes the quantile τ of log per capita income conditional on the vector of covariates (x) and $Q_\tau(\varepsilon_{\tau i} \mid x_i) = 0$. In general, the τ-th sample quantile of y solves:

$$\min_\beta \frac{1}{n}\left[\sum_{i:y_i \geq x_i'\beta} \tau\left|y_i - x_i'\beta_\tau\right| + \sum_{i:y_i < x_i'\beta}(1-\tau)\left|y_i - x_i'\beta_\tau\right|\right] \tag{3}$$

Parameters using the quantile regression approach are estimated semi-parametrically by minimizing the sum of weighted absolute deviations, which fits medians to a linear function of covariates, and can be performed using linear programming methods (Buchinsky, 1998). Specifically, the quantile's coefficients can be interpreted as the partial derivative of the conditional quantile of Y with respect to one of the regressors such as a road development status variable.

One potential obstacle to applying quantile estimation in this paper is the

difficulty in extending fixed-effects methods to quantile estimation. Unlike Gaussian models, quantiles are not linear operators and thus differencing the dependent and independent variables will not in general be equal to the difference in the conditional quantiles:

$$Q_\tau(y_{i2} - y_{i1} \mid x_i) \neq Q_\tau(y_{i2} \mid x_i) - Q_\tau(y_{i1} \mid x_i) \tag{4}$$

To overcome this, Koenker (2004) proposes a model for fixed-effects quantile regression where the unobserved fixed effect is a location shift on the distribution of the dependent variable; i.e. it is the same for each value of τ. Abrevaya and Dahl (2005) take this approach further and characterize the fixed effect using Chamberlain's unobserved effects model. In this paper, we implement Abrevaya and Dahl's procedure; following Chamberlain's model, we specify η_i as follows:

$$\eta_i = \phi + x_{i1}'\lambda_1 + x_{i2}'\lambda_2 + \omega_i \tag{5}$$

where Ø is a scalar and ω_i is an error term uncorrelated with x_{it}, t=1, 2. Given $y_{it} = x_{it}'\beta + \eta_i + \varepsilon_{it}$, substituting equation (5) yields the following equations for periods 1 and 2:

$$y_{i1} = \phi + x_{i1}'(\beta + \lambda_1) + x_{i2}'\lambda_2 + \omega_i + \varepsilon_{i1} \tag{6a}$$

$$y_{i2} = \varphi + x_{i1}'\lambda_1 + x_{i2}'(\beta + \lambda_2) + \omega_i + \varepsilon_{i2} \tag{6b}$$

If we assume all of the error disturbances (ω_i, ε_{i1}, ε_{i2}) are independent of x_{it}, the conditional quantiles also take the analogous forms:

$$Q_\tau(y_{i1} \mid x_i) = \phi_\tau^1 + x_{i1}'(\beta + \lambda_\tau^1) + x_{i2}'\lambda_\tau^2 \tag{7a}$$

$$Q_\tau(y_{i2} \mid x_i) = \phi_\tau^2 + x_{i1}'\lambda_\tau^1 + x_{i2}'(\beta + \lambda_\tau^2) \tag{7b}$$

Where φ_τ^1 and ϕ_τ^2 are location shifts in the conditional quantiles for each year, λ_τ^1 is the unobserved effect λ_1 for the τ^{th} quantile and λ_τ^2 is the unobserved effect λ_2 for the τ^{th} quantile. Without the independence assumption, the conditional quantile functions would in most cases not assume a linear form; this is also true for most cross-sectional quantile estimations, even if the data-generating process is linear in the covariates. Based on equations (6a) and (6b), we run a pooled linear quantile regression where the observations corresponding to the same household are stacked as a pair. Specifically, a quantile regression (using the estimator for the τ^{th} quantile) would be run using:

$$\begin{bmatrix} y_{11} \\ y_{12} \\ \cdots \\ y_{21} \\ y_{22} \\ \cdots \\ \vdots \\ \cdots \\ y_{N1} \\ y_{N2} \end{bmatrix} = \begin{bmatrix} 1 & 0 & x'_{11} & x'_{11} & x'_{12} \\ 1 & 1 & x'_{12} & x'_{11} & x'_{12} \\ \cdots & \cdots & \cdots & \cdots & \cdots \\ 1 & 0 & x'_{21} & x'_{21} & x'_{22} \\ 1 & 1 & x'_{22} & x'_{21} & x'_{22} \\ \cdots & \cdots & \cdots & \cdots & \cdots \\ & & \vdots & & \\ \cdots & \cdots & \cdots & \cdots & \cdots \\ 1 & 0 & x'_{N1} & x'_{N1} & x'_{N2} \\ 1 & 1 & x'_{N2} & x'_{N1} & x'_{N2} \end{bmatrix} \begin{bmatrix} \phi \\ \pi \\ \beta \\ \lambda_1 \\ \lambda_2 \end{bmatrix} + \begin{bmatrix} \upsilon_{11} \\ \upsilon_{12} \\ \cdots \\ \upsilon_{21} \\ \upsilon_{22} \\ \cdots \\ \vdots \\ \cdots \\ \upsilon_{N1} \\ \upsilon_{N2} \end{bmatrix} \tag{8}$$

Along with the parameters ($\varnothing$ β, λ_1, λ_2), the parameter π is also estimated (representing the "year effect"). Next, since observations are clustered and hence not independent, standard errors for the estimators are obtained via a bootstrap method that repeatedly draws (with replacement) a household from the sample of households, including both observations on that household (Abrevaya and Dahl 2005).

4. RESULTS

The equity impacts assessment of rural roads include horizontal and vertical appraisal; the former refers to the equity of different income level households, and the latter represents the equity in different periods.

Table 3 presents the panel quantile estimates for β (using the software of Stata 10) to assess the distributional effects of the road project on log per capita annual income. There are five quantiles, 0.05, 0.25, 0.50, 0.75, and 0.95. For the observed effect β, the road impact is significant and positive for all quantiles in the RRIP sample, with effects varying between 11 and 21 percent. The results indicate that gains from road investment do not necessarily accrue only to relatively wealthier households. Furthermore, the benefits of road investments are focused primarily among the poor.

The Lorenz curve and Gini coefficient are shown in Figure 1 before and after RRIP. The Lorenz curve is presented by statistician Lorenz and the Gini coefficient by economist Gini. The two indexes are the equity indicators in common use, which can quantify the equity of policy or projects. The diagonal represents the absolute average (AP) which implies that the proximity of the curve to *AP* connotes greater equity. The Gini coefficient after RRIP is 0.339 and 0.437 before the projects, reflecting an equity effect over time, because the small coefficient value expresses the high equity.

Table 3 Quantile regression estimates RRIP impact on log per HH income.

Quantile regression estimates, by quantile of per HH income	*RRIP*	
	β	*S.E.*
0.05	0.173***	0.040**
0.25	0.194***	0.042**
0.50	0.210***	0.036**
0.75	0.168***	0.045**
0.95	0.113***	0.058*

***Notes*: * *significant at* 10%; ** *significant at* 5%; *** *significant at* 1%.**

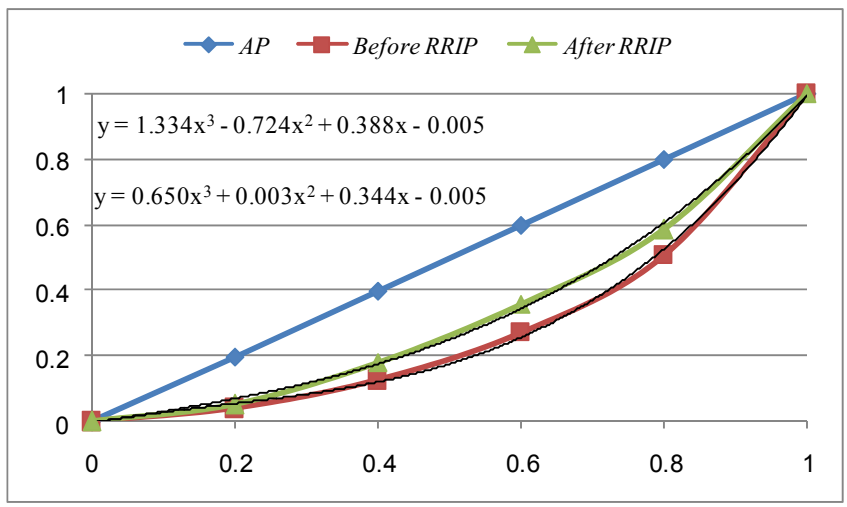

Gini coefficient $_{before}$ = 0.437, Gini coefficient $_{after}$ = 0. 339

Figure 1 Lorenz curve before and after RRIP.

5. CONCLUSION

Rural investment constitutes a major portfolio of public investment in rural areas, reinforcing the notion that rural income depends critically on roads and other public investments. This paper investigates the effects of rural road investments in Fujian Province. It evaluates the equity impact of rehabilitation of rural roads on household wellbeing. The empirical approach for project impact evaluation utilizes the panel structure of the data to control for time-invariant unobservable at the community-level by quantile regression approach – a method of semi-parametric.

The results indicate RRIP returns for HH per income average about 11-21 percent across different per HH income quantiles (with the highest return for households in the 50^{th} quantile), and the households in the 15^{th} to 50^{th} quantiles of the main distribution, with the highest impact for the poorest households. Thus, rural road projects do benefit poorer households.

REFERENCES

Abrevaya, J. and Dahl, C. M. (2005). "The Effects of Smoking and Prenatal Care on Birth Outcomes: Evidence from Quantile Estimation on Panel Data." Working Paper, Purdue University.

Binswanger, H. P., Khandker, S. R. and Rosenzweig, M. (1993). "How Infrastructure and Financial Institutions Affect Agricultural Output and Investment in India." *Journal of Development Economics*, 41, 331-336.

Bunchinsky, M. (1998). "Recent advances in quantile regression models: a practical guide for empirical research." *Journal of Human Resources*, 33(1), 88-126.

Fan, S., Hazell, P. and Thorat, S. (2000). "Government Spending, Growth, and Poverty in Rural India." *American Journal of Agricultural Economics*, 82(4), 1038-1051.

Jacoby. (2002). "Access to Markets and the Benefits of Rural Roads." *Economic Journal* 110(465), 713-737.

Khandker, S. R., Bakht, Z., Koolwal, G. B. (2006). "The Poverty Impact of Rural Roads: Evidence from Bangladesh." World Bank Policy Research Working Paper 3875, 1-34.

Koenker, R. and Bassett, G. (1978). "Regression Quantiles." *Econometrica* 50, 43-61.

Levy, H. (1996). *Kingdom of Morocco: Impact Evaluation Report, Socioeconomic Influence of Rural Roads*. Operation Valuation Department, World Bank: Washington, DC.

Lokshin, M. and Yemtsov, R. (2005). "Has Rural Infrastructure Rehabilitation in Georgia Helped the Poor?" *World Bank Economic Review* 19(2), 311-333.

Van de Walle, D. (2002). "Choosing Rural Road Investment to Help Reduce Poverty." *World Development* 30(4), 575-589.

Study on using OD Traffic Flow to Identify the Special Boundary of the Expressway Influence Zone

Li-Ying Situ[1], Shun-Ying Zhu[2], and Hong Wang[3]

[1]Master Student, Dept.of Traffic Engineering, Wuhan University of Technology, 1040 Heping Ave., Wuchang, Wuhan, Hubei, China, ST 430063; PH +86-13871130824; email: situliying@163.com
[2]Professor, Dept.of Traffic Engineering, Wuhan University of Technology, 1040 Heping Ave., Wuchang, Wuhan, Hubei, China, ST 430063; PH +86-13995680983; email: zhusy2001 @163.com
[3]Associate Professor, School of Transportation, Wuhan University of Technology, 1040 Heping Ave., Wuchang, Wuhan, Hubei, China, ST 430063; PH +86-27-62597390; email: wanghong2004317 @sina.com

ABSTRACT

The definition of the special boundary of the expressway is crucial in analyzing the expressway's social and economic benefits. This paper constructed a boundary method based on a gravitational force model, which describes the traffic intensity between traffic zonings and expressways. Then the spatial influence radius of a crossing was obtained based on the weighting travel distance of the traffic intensity, which can describe the crossing influence zone. Based on the spatial influence radius of all crossings of the expressway, this paper roughly outlines the expressway influence zone, and then adjusts it for topography, and accordingly the special boundary of the expressway influence zone can be identified. Finally, the practicality of this method was explained through an example.

KEY WORDS: expressway; crossing; influence zone; OD traffic flow

INTRODUCTION

Expressways can improve conditions of a regional economy, attract economic development and new various resources, and then change the extent of land use of the main urban area along the route of the expressway. The expressway utilizes each interchange to influence land use along the line mainly, and all crossings form the basic expanding point of the expressway, continuing land influence from key city to peripheral area (David and Wei 2007; Robert and William 2000). How to scientifically determine the border and intensity where expressway crossings influence land development is of great significance in order to accurately analyze economic contribution of areas along the expressway. However, there is still no practical method to solve this problem. This paper

constructed a boundary method based on a gravitational force model, which describes the traffic intensity between traffic zoning and expressways, and then finally makes an empirical study on it.

THE WAYS EXP RESSWAY CROSSINGS AF FECT LAND USE

Expressways have expanded the hinterland of regional traffic area along the line while improving key cities, expanding communication systems of areas from city centers to peripheral regions, and have helped to spread economic areas as well (Zhang et al. 2002; Thomas 2004). Because cars can not leave expressways freely, we consider that the expressway utilizes its crossings to produce connections and exchange between goods, materials, funds and information with the surrounding area. While defining the range of expressway land utilization and economic coverage of urban areas along the line, we usually regard expressway crossings as the target.

THE NEW METHOD TO ID ENTIFY THE SPECIAL B OUNDARY OF THE EXPRESSWAY INFLUENCE ZONE B ASED ON OD TRAFFIC F LOW

C**rossing's** Traffic Intensity of Single Traffic Zoning

At present, freight charges and time are often used as the decisive index to define boundary models (Lu and Huang 2007). But actually, average freight charges and determination of transportation time are limited by numerous conditions such as choosing a route, how to get regional road freight off the route and so on. In addition, the radius of the expressway influence zone is determined by different complex factors. The expressway already put into operation has already formed steady OD traffic flow; the larger the flow is, and the closer to interflow connection to the outside, the greater economic traction will be gained by the area along the line. But in a sense, under the situation of lacking freight charges and time-consuming technical or data, we can use OD traffic flow and its space distribution to indirectly analyze a crossing's traffic intensity of traffic zoning along the line.

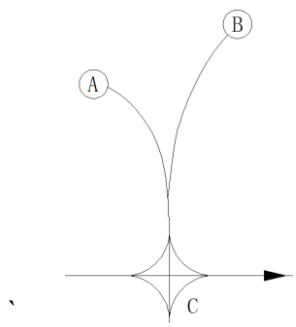

Figure 1. The sketch map for **connecting route between expressway's** crossing and traffic zonings .

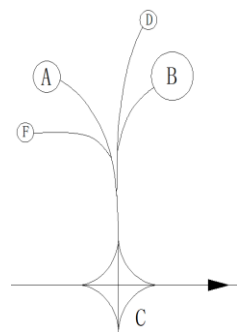

Figure 2. Sketch map for traffic flow between **expressway's** crossing and traffic zonings .

In the Figure1, traffic zonings A and B are separately connected to crossing C by branch lines, which is a result of an expressway having been put into the operation. Because of freight and distance, time consumption and traffic flow among A , B and C had different requirements, and these requirements can be interpreted as interacting forces formed by the traffic flow among A , B and C, just as gravitational forces interacting intimately on each other. In this paper, the above interacting forces are defined as the crossing's traffic intensity, F .

For describing a crossing's traffic intensity numerically, sequence $d=(d_1,d_2,\cdots,d_i,\cdots,d_n)$ denotes the distance of the connecting route (m); sequence $n=(1,2,\cdots,i,\cdots,n)$ denotes the number of traffic zonings connected to crossing by branch lines, so d_i is the distance from traffic zoning i to the crossing; sequence $O=(O_1,O_2,\cdots,O_i,\cdots,O_n)$ denotes origin flow formed from the crossing (pcu), so O_i is the origin flow from the crossing to i ; sequence $D=(D_1,D_2,\cdots,D_i,\cdots,D_n)$ denotes destination flow formed from the crossing (pcu), so D_i is the destination flow from i to the crossing. Then the crossing's traffic intensity of traffic zoning i , F_i (pcu), is as follows:

$$F_i=(F_{Oi},F_{Di})$$

$$\begin{cases} F_{Oi}=G\dfrac{O\cdot O_i}{d_i^2} & (1) \\ F_{Di}=G\dfrac{D\cdot D_i}{d_i^2} & (2) \end{cases}$$

Where Eq. (1) = the crossing's traffic intensity from the origin flow point of view, and in it , $G=\dfrac{O}{\sum_{i=1}^{n}OO_id_i^{-2}}$; Eq. (2) = the crossing's traffic intensity from the destination flow point of view, and in it, $G=\dfrac{D}{\sum_{i=1}^{n}DD_id_i^{-2}}$. More importantly, it is necessary to satisfy $O=\sum_{i=1}^{n}F_{Oi}$ and $D=\sum_{i=1}^{n}F_{Di}$ when G were calculated.

Comprehensive Land Influence Radius of Single Crossing

The above analysis has described the traffic intensity among single traffic zonings and crossings. Under realistic conditions, it should be huge origin-destination traffic flow creating from traffic zonings to all crossings of the expressway, and the traffic zonings do not scatter in the same region space with

different traffic intensity, as shown in Figure 2, the round size expresses the traffic intensity size of traffic zoning contacting to crossing.

In order to scientifically delimit a crossing's traffic intensity of sequence n=(1,2,…,i,…,n),which denotes the number of the traffic zonings connected to the crossing by branch lines, sequence $F_O = (F_{O1}, F_{O2}, \ldots F_{On})$ denotes the crossing' s origin traffic intensity formed from crossing to all traffic zonings connected to it, while sequence $F_D = (F_{D1}, F_{D2}, \ldots F_{Dn})$ denotes the crossing's destination traffic intensity formed from crossing to all traffic zonings connected to it; R_{F_O} denotes the corresponding comprehensive land influence radius of crossing of sequence F_O,while R_{F_D} denotes the corresponding comprehensive land influence radius of crossing of sequence F_d. Based on above-mentioned, the comprehensive land influence radius of a crossing R (km), was obtained found on the weighting travel distance of the traffic intensity, that is:

$$R = \frac{\sum_{i=1}^{n} \alpha_i d_i}{(\alpha_1 + \alpha_2 + \cdots \alpha_n)} \tag{3}$$

where α_i denotes the weight factor of corresponding traffic zoning i , and its value can be applied by the crossing's traffic intensity. R_{F_O} and R_{F_D} can be calculated separately by Eq. (3), and the ultimately reasonable comprehensive land influence radius takes the form as follows:

$$R = \max\left\{R_{F_O}, R_{F_D}\right\} \tag{4}$$

Determination of Expressway Influence Zone of Crossings

According to the calculation method of comprehensive land influence radius in the above chapters, sequence (R_{11},R_{21},…R_{n1}) and sequence (R_{12},R_{22},…R_{n2}) can be calculated appropriately, which denote the influence zone on both sides of crossings on expressway's tending axis. Finally, the zonal shape of the comprehensive land influence radius of all crossings can be outlined, as shown in Figure 3.

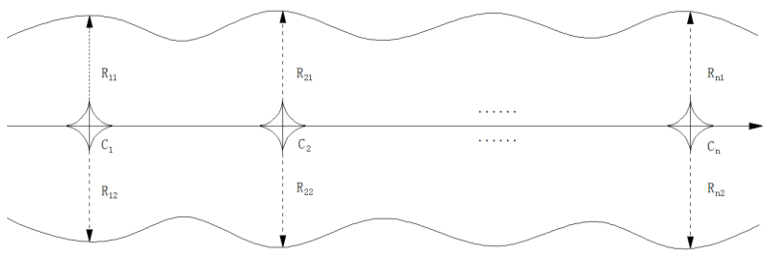

Figure 3. The zonal shape of comprehensive land influence radius of all crossings

Thanks to the different factors of traffic zoning on both sides of crossings, such as natural environment, topography and development of traffic networks, the comprehensive land influence radius of different sides of a single crossing are not the same, so we can calculate the irregular land influence radius of all crossings, and the average land influence radius on both sides of the expressway are different. With social economic development and completion of traffic network construction, the economic belt of an expressway will expand, and the land influence radius of crossings will continue to expand; therefore the influence radius of the whole expressway will increase, too.

CASE STUDY

In this paper, we choose Huang-huang expressway as an analytical object for case study. After an origin-destination study of four important crossings (Sanhua, Qichun, Wuxue, Huangmei), we determined average annual daily traffic of the crossings in 2007. According to the new method of identifying the special boundary of the expressway influence zone based on OD traffic flow, the result of calculations of the comprehensive land influence radius of all crossings is shown in Table 1.

Table1. The comprehensive land influence radius of all crossings

Project \ Crossing		Sanhua	Qichun	Wuxue	Huang mei
On north side of crossing	R_{F_O} (km)	27.43	39.15	33.03	57.54
	R_{F_D} (km)	26.81	41.97	35.84	66.39
	R (km)	27.43	41.97	35.84	66.39
The taking value		27.4	42.0	35.8	66.4
On south side of crossing	R_{F_O} (km)	8.87	21.25	16.86	24.37
	R_{F_D} (km)	8.67	23.32	16.85	23.32
	R (km)	8.87	23.32	16.86	24.37
The taking value		8.9	23.3	16.9	24.4

TransCAD can help outline the zonal shape of the comprehensive land influence radius of the whole expressway, as shown in Figure 4.

As shown in Figure 4, pie charts denote the traffic flow from different crossings to different traffic zonings; real arcs denote the comprehensive land influence radius of all crossings identified by the new boundary method. On the basis of calculations, according to the space position of Huang-huang expressway, it delineates the zonal shape of the comprehensive land influence radius of the expressway with a dashed line. A dotted line shows the comprehensive land influence radius on the north side of the crossing in Wuxue, included in the areas of the crossings in Qichun and Huang Mei; the Changjiang River is south of the crossings in Qichun, Wuxue and Huang Mei, so the comprehensive land influence

radius of the three crossings are limited, for they can not be delineated beyond the Changjiang River.

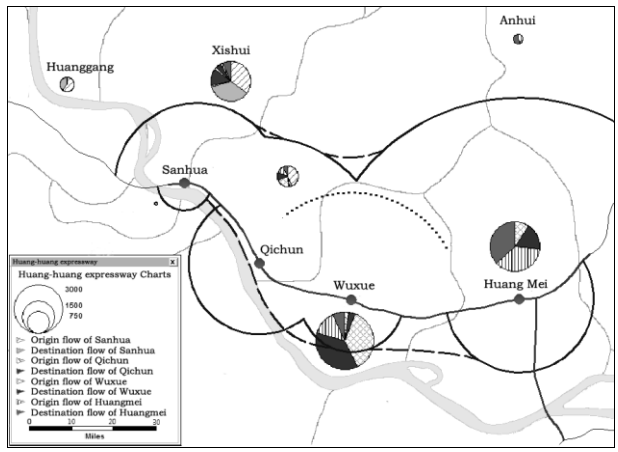

Figure 4. Sketch map for the comprehensive land influence radius of Huang -huang expressway

The radiating range of advantage of industries in counties and cities along the line of the expressway has been widened, and the most important economic zones, such as the Provincial Economic Development Zones of important economic counties and cities, Biochemical Science and Technology Park and Hi-Tech Park, are all in the influence boundary estimated by new method. To sum up, the practicality and rationality of the new method was further explained by this case.

DISCUSSION AND CONCL USION

In this paper, the new method of OD traffic flow used to identify the special boundary of the expressway influence zone does not take into consideration intermodal operation of the comprehensive transportation ways, so it narrows expressway influence zones. To solve this insufficient point, we can analyze indirect influence zones produced by intermodal operation: First, we divide important transport junctions into traffic zonings, then investigate their passenger-cargo through transport OD traffic flow and analyze their space distribution.

How best to identify the expressway influence zone correctly is determined by complex factors such as the characteristics of expressways and traffic characteristics of interrelated traffic networks, peripheral land utilization, topography, etc. At present, finding out one particular influence radius to portray the expressway influence zone still needs to be studied in greater depth.

REFERENCES

Levinson, D., and, Wei Chen. (2007). “Area-Based Models of Expressway Growth.”

Journal of Urban Planning and Development . ASCE, 133(4), 250-254.

Lu, H., and Huang, H. (2007). "Theoretical research Frontiers in Transportation Planning." Tsinghua University Press, Beijing.

Noland, R. B., and Cowart, W. A. (2000). "Analysis of Metropolitan Expressway Capacity and the growth in vehicle miles of travel." Transportation . ISTP, 27(4), 363-390.

Sanchez, T. W. (2004). "Land Use and Growth Impacts from Expressway Capacity Increases." Journal of Urban Planning and Development , ASCE, 130(2), 75-82.

Zhang, W., Jin, F., and Fan, J. (2002). "Traffic Economic Belt." Science Press, Beijing.

Transport Strategy for Sustainable Development of Jiao Dong Economic Region

S. Wang[1], S. Zhang[2], and L. Ren[3]

[1]School of Economics & Management, Yantai University, P.O. BOX 264005, Yantai; PH(86) -535 -6705951, FAX (86) -535 -6902617; email:wsyyt@163.com
[2]School of Economics & Management, Yantai University, P.O. BOX 264005, Yantai; PH(86) -535 -6705951, FAX (86) -535 -6902617; email:shuai_sdjn@163.com
[3]School of Economics & Management,Yantai University, P.O. BOX 264005, Yantai; PH(86) -535 -6705951, FAX (86) -535 -6902617; email: renliting@126.com

ABSTRACT

It is stated that an advanced transport system will help enhance economic performance and promote economic growth. This paper discusses the transport strategy for sustainable development of the Jiao Dong economic region in Shandong province, based on the analysis of the correlation between Yantai's GDP and its total transport volume as a logistics hub, because Yantai is centrally located in the region. Both marginal analysis and elasticity analysis of the correlation of Yantai's economy, along with its transport volume, demonstrates that the contribution of transport to economic growth and development has not yet realized its maximum potential. We conclude that Yantai's transport system could be expanded and improved to promote its economic growth, and thereby to promote regionally sustainable development. To accomplish this, several major steps are in order. First, it should quickly build comprehensive traffic networks to encompass a one-hour economic circle within the region. Second, it should fully engage in traffic infrastructure construction to draw internal demand, and lastly, it should establish an intelligent public traffic system to improve passenger transport services.

1. INTRODUCTION

A transport system that can support and drive national and regional development processes must consist of two basic components, namely, traffic infrastructure and transport services, developed in tandem. It is universally recognized that transport service is crucial for sustained economic growth and modernization of a nation. Transport demand, both freight and passenger, is linked to the level of economic activity and development needs (Kulshreshtha et al. 2001). On the other hand, adequacy of traffic infrastructure is an important determinant of the success of a nation's efforts to diversify its production base, expand trade and link together resources and markets into an integrated economy. It is also necessary

for connecting villages with towns and market centers, and in bringing remote and developing regions closer to one another.

In addition to and because of its primary task of efficient and cost-effective movement of people and goods, transport also has a significant impact on the lives of many people through increased employment opportunities and improved accessibility to social infrastructure and services (Morash and Clinton 1997).

Jiao Dong peninsula cities are mainly composed of Qingdao, Yantai and Weihai (exclusive of Wei fang here) with No.1, No.2 and No.9 GDP rankings respectively in the entire Shandong province. The GDP of this region represents one third of the province.

Geographically, Yantai is located between Qingdao and Weihai, which is a link connecting these three cities. Although Yantai's GDP ranks second in Shandong province, its third industry ratio (about 30%) is lower than that of the average of the province (about 33%). Analyzing the relationship of Yantai's transport system with its economic contribution and providing some strategies as an example are appropriate means of promoting the sustainable development of Jiao Dong peninsula economy and thereby Shandong province's economy.

Following the interpretation of economic impacts of transport and analysis of Yantai's transport to economic contribution, this paper provides some strategies for Jiao dong peninsula's sustainable economic development using Yantai as an example.

2. THE RELATIONSHIP OF TRANSPORT AND SUSTAINABLE ECONOMIC DEVELOPMEMT

2.1 Micro impacts of transport

From the microeconomic view point, traffic and transport infrastructure improvements not only reduce distances between origins and destinations but also reduce congestion and thereby travel time by adding links to a network or enhancing the capacity of existing links. They also provide many new services, such as logistics, by improving networks. In these ways, they make it possible to increase traffic and transportation capacity and to offer freight transportation services less expensively and more reliably. The overall effect is a reduction in the movement cost and yielding direct efficiency. Further gains, however, can arise through a number of mechanisms. Freight transport firms not only provide traditional material flow faster, cheaper and more reliably than before, they also offer new types of transport and logistical services. These new services are characterized by reliability, timeliness, strategic outsourcing of a corporation's distribution functions, and flexibility in destination choices for customer firms. Such new service attributes thereby offer manufacturers and customers additional production value and strategic comparative advantages. Further transportation and distribution concerns are increasingly integrated into strategic decisions of firms. These include where to

locate their production and warehouse facilities, where to source their intermediate goods, and how to manage their value chains. Through these processes, the new transport services firms help gain system-wide cost reduction and value addition. The illustration of microeconomic impacts of transport infrastructure improvements is as depicted in Figure 1 (Lakshmanan and Anderson 2002).

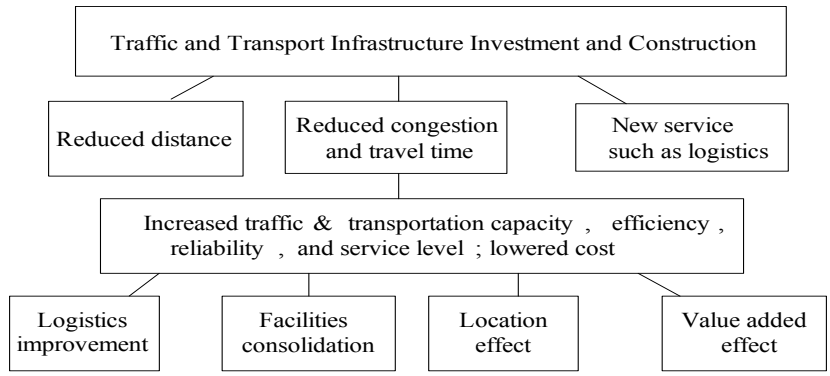

Figure 1. Microeconomic Impacts of Traffic and Transportation .

2.2 Transport infrastructure and full economic effects

When infrastructure networks are improved, as noted above, transport firms will gain lowered costs, efficiency, reliability and more logistics services. All these attributes will help increase the accessibility of inputting suppliers and labor, and customers and realize market expansion and integration. Opportunities for exporting and importing goods are enhanced, in turn opening up several channels of economic effects, both in product markets and in factor markets. The macroeconomic effects of traffic and transport infrastructure are as shown in Figure 2(2002).

First, export expansion will lead to higher levels of output, which allows higher sales to cover fixed costs of operation, yielding efficiencies. Second, increasing imports puts competitive pressures on local prices, which leads not only to the removal of monopoly rents but also to improved efficiency. This is achieved both via the restructuring of the economy (as firms enter and exit) and by promoting leaner production processes, which lower costs of production and raise productivity.

Third, lower transport costs and increased accessibility enlarge the markets for labor and other factor inputs. Firms will likely draw labor from a broader area and with a greater range of attributes, improving labor supply and lowering costs.

Finally, Figure 2 suggests two mechanisms in the oval boxes: one dealing with innovation, and the other with spatial arrangements in the economy. These two mechanisms create, in the context of transport infrastructure improvements, conditions which enhance economic performance, and promote total factor productivity, competitiveness, and internal growth.

Transport improvements can have an internal growth effect to the degree they impact the rate of innovation and transfer of technology, thereby promoting

total factor productivity (TFP) growth and competitiveness. Such impacts of transport improvements can derive from the following sources: industrial restructuring resulting from the entry and exit of firms and the opening of larger markets; the benefits accruing to various economic actors from the likely parallel increase in information flows, especially in locations where industries are spatially agglomerated. Impacts from both of these sources can impact the pace of technology transfer and innovation, thereby increasing economic growth.

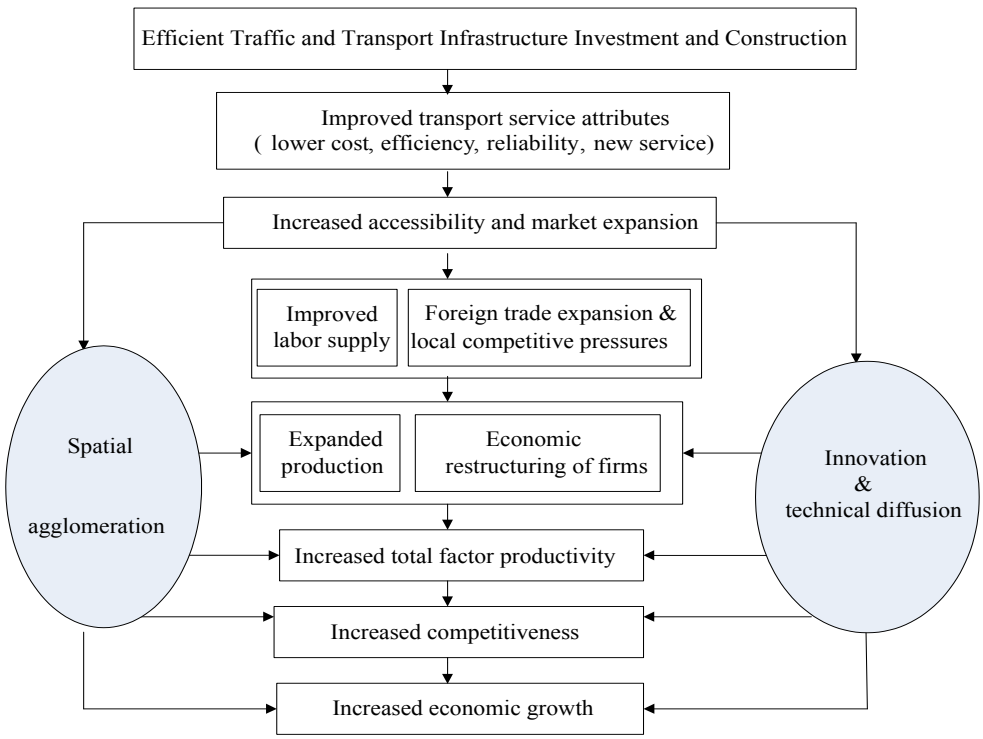

Figure 2 . Transport Infrastructure and its Full Economic Effects.

3. CORRELATION OF YANTAI 'S GDP AND ITS TRANSPORT VOLUME

3.1 Regression analysis of Yantai 's GDP and its transport volu me

From scatter diagram analysis, GDP possesses a positive correlation to transport volume, but the growth is non-linear, showing an S curve feature (2006). This research utilizes the logistic equation to fit the relations of regional GDP growth to total transport volume.

The logistic function is as follows:

$$Y = \frac{1}{C + Ae^{-BX}} \qquad (1)$$

Here, $A > 0, 0 < B \neq 1, \ 0 < C \to 1/Y$

X : The total transport volume in 10 thousand tons

Y : Yantai's GDP in 100 million RMB

Total transport volume shown in Table 1 is the sum of freight and the equivalent of passengers to freight, calculated based on the correlation function of freight volume (G) and passenger volume (L) per G = 241431n(L) – 205514..

Table 1 . Data of Yantai 's Total Transport Volume and its GDP .

Year	t	X	Y
2001	0	15862.43515	980
2002	1	21131.63276	1115
2003	2	21651.76766	1316
2004	3	26244.22941	1639
2005	4	31337.38232	2012.46
2006	5	33002.68034	2402.1
2007	6	38746.82319	2878.97
2008	7	45794.42	3434.19
2015	14	7320.73	8000

Through the transformation and C value estimated, utilizing the least squares method, the logistic function is as follows:

$$Y = \frac{1}{\frac{1}{8000} + 0.00188 * e^{-0.0000424X}} \qquad (2)$$

Here, $A = 0.00188$, $B = 0.0000424$, $C = 1/8000$

3.2 Marginal analysis

Through the marginal analysis according to the function of $Mf = \frac{dY}{dX} = \frac{ABe^{-BX}}{\left(C + Ae^{-BX}\right)^2}$, it is found that the increase of transport volume per ten thousand tons results in 0.0733 of 100 million Yuan GDP increase .

On the other hand, according to the second derivative of $\frac{d^2Y}{dX^2} = AB^2 \frac{Ae^{-BX} - C}{\left(C + Ae^{-BX}\right)^3} e^{-BX}$, the critical value of total transport volume equals 63985.68 units.

Since in 2008 Yantai's transport volume was about 45794.42 units, lower than the above derived critical value, we conclude that the increase of transport per unit would result in a further increase of Yantai's GDP. That is, Yantai should greatly develop a transport system in order to promote the regional GDP growth.

3.3 Elasticity analysis

Through the elasticity analysis based on the equation of $\xi = \frac{dY}{dX} \cdot \frac{X}{Y} = \frac{ABXe^{-BX}}{C + Ae^{-BX}}$ (ξ: the elasticity coefficient of transport to GDP) and $\frac{d\xi}{dX} = AB\frac{Ae^{-BX} - BCX + C}{\left(C + Ae^{-BX}\right)^2}e^{-BX}$ as well as the Newton's method of numerical analysis, the inflection point of the elasticity coefficient is of 1.39 with X nearing 56300 units.

However, in year 2008, Yantai's total transport volume of 45794.42 units was less than the inflection point value of 56300 units, giving an elasticity coefficient of 1.27, lower than the inflection point value of 1.39. We thus conclude that in Yantai the contribution of each 1% transport increment to the economy hadn't realized its optimal level, and therefore, transport should be expanded to promote the increase in GDP increments in the future.

4. STRATEGY OF YANTAI 'S TRANSPORT FOR JIAO DONG ECONOMIC REGION 'S SUSTAINABLE DEVELOPMENT

4.1 Building comprehensive traffic networks to realize one -hour economic circle of Jiao Dong peninsula

To quickly star t the construction of Qingdao -Yantai -Weihai light railway . In order to cope with the financial crisis, the State plans to appropriate 4 trillion RMB to support the construction of infrastructure, and Shandong province should receive about 667.8 billion RMB in the next three years. Qingdao-Yantai-Weihai light railway construction has been planned as part of the program. It is advisable to accelerate the construction pace and put it into operation as soon as possible.

To construct Yantai -Qingdao freeway . To intensify the links with the core city of Qingdao, it is necessary to build a direct freeway between Yantai and Qingdao. The freeway will serve as a major bridge for connecting with air, ports and other transport modes and will therefore accelerate economic and cultural exchanges.

To strength en the links of Yantai -Weihai -Qingdao -Weifang traffic networks. Since the construction of inter-city railways has been included in the agenda, the relevant road network planning and construction must be kept up to ensure the smoothness of intra / inter-city traffic networks.

4.2 Fully embarking on other traffic infrastructure construction

To quickly begin civil airport construction . In order to fully meet domestic and international demands, Yantai should accelerate its construction pace of the civil airport to expand additional domestic passenger routes and international routes, especially the Northeast and Southeast Asia routes. Meanwhile, cargo air transport and its feeder transport should be developed as well.

To impr ove railway coverage and standards . Firstly, it should accelerate the construction of De-Long-Yan Railway to act as the port access of Yantai, Longkou, Weifang, Dongying, Binzhou and the east-west provincial passageway. Secondly, it should accelerate the electrification and informational connectivity, of Lan-Yan railway to facilitate communication between Yantai and the Northeast region, the Yangtze River Delta region and the central and western regions, and expand radiation to the landlocked hinterland (Wang, 2006). Thirdly, it should further enhance the role of the Yantai-Dalian railway ferry to consolidate the economic link of North-east and Shan dong province.

To speed u p port construction . Accelerating the port construction should concentrate on a deep container berth of the new Yantai port and Longkou for coal and liquid chemicals as well as Laizhou for grains and a salt terminal.

4.3 Setting up an intelligent public traffic system

First, it's necessary to issue compatible transport fare cards within the whole urban area for bus transport, taxi transport, short-hall passenger transport and public parking lots. Second, it must expand the card-purchasing channels. In addition to Evergreen Bank, some machines should be installed at Wal-Mart, RT-Mart, business malls, and so forth. Third, the unified-card should be expanded to other businesses, such as tourism, shopping, etc. Lastly, favorable polices should be drafted to encourage use of the cards, for example, giving discounts for more spending.

Besides, Yantai should pay attention to developing contemporary logistics, especially, cold chain logistics, green logistics and bonded logistics.

CONCLUSION

Theoretically, transport systems can contribute to competitiveness and economic growth and promote the sustainable development of regional economy. Both the marginal analysis and elasticity analysis of the correlation of Yantai's GDP and transport as an example of the Jiao Dong peninsula cities demonstrates that the contribution of transport to economic growth and increase has not realized their maximum potential. In the future, the city should greatly develop transport systems to promote economy growth and increase and that of Jiao Dong economic region. The transport strategy may include the construction of comprehensive traffic networks to realize a one-hour economic circle of the region and other traffic infrastructures, including the establishment of an intelligent public traffic system.

REFERENCES

Kulshreshtha, et. al. (2001). "A Multivariate co-integrating Vector Auto Regressive Model of Freight Transport Demand: Evidence from Indian Railways." Transport Research , (1), 1-72.

Morash, E. A., and Clinton S. R. (1997). "The Role of Transportation Capabilities in International Supply Chain Management." Transportation Journal, Spring,

1997, 5-17.

Lakshmanan, T. R., and Anderson P. W. (2002). "Transportation Infrastructure, Freight Services Sector and Economic Growth". www.google.com, 2002.

Wang, S.(2006). "The countermeasures of the development of Shandong's TPL industry." Report of Shandong province's social science planning, 2006.8.

Zhou, J. (2006). "The Influence of regional logistics industry on regional economy. " Statistics and decision-making, (2), 109-111.

Research of Road Transportation Sustainable Development Based on Ecological Footprint Model

WANG Xiao-xia[1], FANG Lei[2], WANG Xiao-xia[3], LU Jian-feng[4]

[1,4] School of Civil Engineering and Traffic Engineering, Guangdong University of Technology, P.O. Box B59, Guangzhou, P.R. China, 510006; PH 86-20-39322528; FAX 86-20-39322528; Email: xiaoxiawang2006@163.com or lujianfeng1983@126.com
[2]School of Civil Engineering and Transportation, South China University of Technology, Wushan RD., Tianhe District, Guangzhou, P.R. China, 510641; PH 86-20-83630583; FAX 86-20-83630583; Email: fangfanglei@tom.com
[3]School of Economics and Management, Chang'an University, Xi'an, P.R. China, 710064; PH 86-29-82334524; FAX 86-29-82334524; Email: joy113@tom.com

ABSTRACT

Many studies have shown that air pollution is typically affected by road transportation. In order to further discuss the relationship between road transportation and regional environment carrying capacity, this article has built a road transportation ecological footprint model. In order to explain how to use this model, quantitative calculation with data derived from China Yearbook has been applied. Calculation results can show that the road transportation ecological footprint mainly consists of a fossil energy ecological footprint, and both of them show a tendency of increasing in recent years. Therefore, it can be concluded that fossil energy consumption and greenhouse gas emission are main factors for restricting road transportation's sustainable development. As a result, to make sure road transportation is developed in a sustainable way, many effective measures should be taken.

INTRODUCTION

With the rapid development of the national economy, road transportation has shown significant growth since 2000, as shown in Fig.1. As we all know, the automobile has made travel convenient for the public, but it is also a major source of energy consumption and air pollution. When totaling the forms of energy consumption in China's transportation system, road transportation accounts for approximately 51.6% (Xi J P. 2008), as shown in Fig.2. Moreover, more than 50% of air pollutants arise from automobile in China. What is worse, more than 80% of CO and more than 40% of NO_X are produced by automobiles in big cities such as Beijing and Guangzhou (National Development and Reform Commission. 2007). Therefore, attention must be paid to the relationship between road transportation, energy consumption, environment protection and sustainable development. Up until now,

many scholars have widely used an ecological footprint model in regional environment evaluations, but no one has used this model in a transportation sustainable development study. This article attempts to do research in this area.

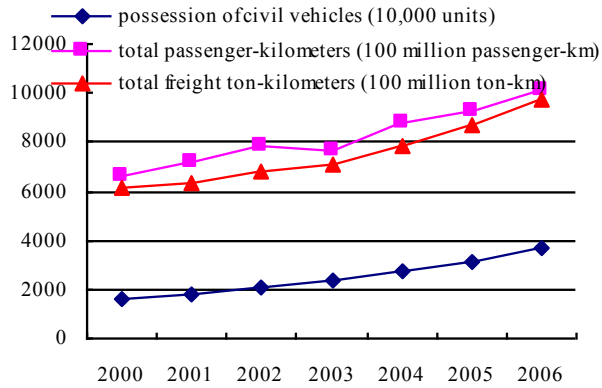

Figure 1. Changes in China's Road Transportation from 2000 to 2006.

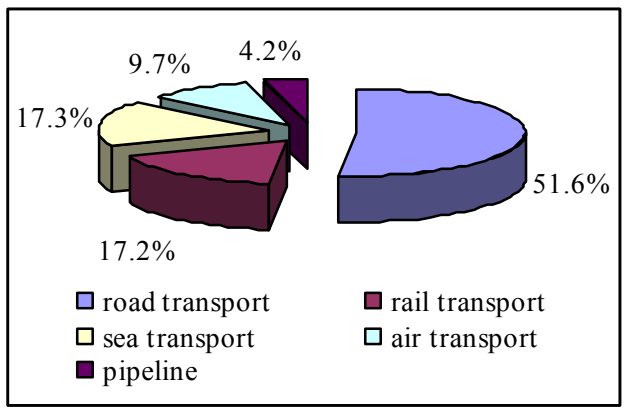

Figure 2. Composition of Energy Consumption of Transportation Systems.

ROAD TRANSPORTATION ECOLOGICAL FOOTPRIN MODEL

Summariz ation of Ecological Footprint Model. The ecological footprint model can clearly demonstrate environmental pressure by comparing ecological footprint demand and ecological carrying capacity. This becomes a quantitative method for the measurement of sustainable development degree.

$$EFD = N \times ef = N \times (\sum r_j \times A_j) = N \times [(\sum r_j \times (O_i + I_i - E_i)/(P_i \cdot N)] \quad (1)$$

Where, EFD is regional ecological footprint demand; N is total population; ef is per capita ecological footprint demand; r_j is balance factors for various biological productivity land (Wackernagel classified biological productivity land as arable land, grassland, forest land, construction land, fossil energy land and waters (Wackernagel

et al. 1999; 2007).), which is determined by unified value (Luan Y, et al. 2008), as shown in Table 1; A_j is per capita No. j kind of biological productivity land; O_i is annual output of No. i kind of consumer items; I_i is annual import volume of No. i kind of consumer items; E_i is annual export volume of No. i kind of consumer items; P_i is annual average production capacity of No. i kind of consumer items.

$$EC = N \times ec = N \times \sum (r_j \times y_j \times a_j) \quad (2)$$

Where, EC is regional ecological carrying capacity; N is total population; ec is per capita ecological carrying capacity; y_j is yield factors, according to value chosen by UN Food and Agriculture Organization , Wackernagel and others who have calculated China's ecological footprint. Yield factors are as follows: arable land and construction land both equal 1.66, grassland is 0.19, fossil energy land and forest land both are 0.91; a_j is per capita No. j kind of biologically productive land.

Table 1: Balance Factors for Six Types of Biologically Productive Land.

land type	arable land	grassland	forest land	construction land	fossil energy land	waters
r_j	2.8	0.5	1.1	2.8	1.1	0.2

Meanwhile, ecological deficit (usually abbreviated as ED) is defined when the ecological footprint demand exceeds ecological carrying capacity. That also indicates regional sustainable development is threatened. Conversely, ecological surplus (usually abbreviated as ES) is defined. That is,

$$ED = EC - EFD \quad (\text{while } EC < EFD) \quad (3)$$

$$ES = EC - EFD \quad (\text{while } EC \geq EFD) \quad (4)$$

Road Transportation Ecological Footprint Model. As the smooth operation of road transportation relies on highways, parking lots, toll station and other facilities, as well as on a large amount of gasoline, diesel oil, natural gas and other energy, biologically productive land mainly refers to construction land and fossil energy land.

(1) Ecological footprint demand for construction land

$$EFD_1 = N' \times \sum (S_i / N') \quad (5)$$

Where, EFD_1 is demand for construction land ecological footprint; N' is total possession of civil vehicles; S_i is an area occupied by No. i kind of transport facility.

(2) Ecological footprint demand for fossil energy land

When an automobile travels, it needs to burn energy to generate driving force. However, at the same time, it will generate numerous pollutants. Because the absorptive capacity of forest for greenhouse gas and pollutants is characterized by heat, it needs to convert energy consumption into heat according to its combustion efficiency. Conversion standards use world united value, as shown in Table 2.

$$EFD_2 = \sum \frac{N_i C_i \lambda_i}{K_i} = \sum \frac{C_i' \lambda_i}{K_i} \quad (6)$$

Where, EFD_2 is demand for fossil energy land ecological footprint; N_i is possession of civil motor vehicles, which burn NO. i kind of energy; C_i is per vehicle consumption of NO. i kind of fossil fuel; C_i' is total consumption of NO. i kind of energy; λ_i is conversion coefficient for NO. i kind of energy; K_i is average calorie absorptive capacity of forest for per energy.

Table 2: Average Calorie Absorptive Capacity of Per Energy and its Conversion Coefficient.

	coal	crude oil	fuel oil	gasoline	diesel oil	natural gas	electricity
absorptive capacity (joule per hectare)	55	93	71	93	93	93	1000
conversion coefficient	20.93①	41.87①	50.20①	43.12①	42.71①	0.034②	0.0036③

Note: ①Joule per ton; ②Joule per cum; ③Joule per KWH

(3) Road transportation ecological footprint demand

$$EFD' = r_1 \times EFD_1 + r_2 \times EFD_2 = r_1 \times N' \times \sum (S_i / N') + r_2 \times \sum \frac{C_i' \lambda_i}{K_i} \quad (7)$$

Where, EFD' is road transportation ecological footprint demand; r_1 is balance factors for construction land, and r_1 equals to 2.8, as shown in table 1; r_2 is balance factors for fossil energy land, and r_2 equals to 1.1, as shown in table 1.

(4) Road transportation ecological carrying capacity

$$EC' = N' \times \sum (r_j \times y_j \times a_j') \quad (8)$$

Where, EC' is road transportation ecological carrying capacity; N' is total possession of civil motor vehicles; r_j is balance factors; y_j is yield factors; a_j' is No. j kind of biological productivity land occupied by per vehicle.

In addition, according to reports from the World Commission on Environment and Development (WCED), 12% of biologically productive land should be set apart to protect biology. Therefore, road transportation effective ecological carrying capacity is gained after 12% of biologically productive land is deducted. That is,

$$REC = (1-12\%)EC = (1-12\%)N \times \sum (r_j \times y_j \times a_j') \quad (9)$$

Where, REC is effective ecological carrying capacity.

As REC is more reasonable than EC when calculating ED or ES, the following formulation is used in this article.

$$ED = REC - EFD' \quad (REC < EFD') \tag{10}$$

$$ES = REC - EFD' \quad (REC \geq EFD') \tag{11}$$

CALCULATION EXAMPLE OF ROAD TRANSPORTATION ECOLOGICAL FOOTPRINT

Example . Because energy consumption of transportation systems is usually calculated together with that of storage as well as with that of post in China, and special statistical data for road transportation energy consumption is lacking, so energy consumption of road transportation is calculated based on the China Yearbook and estimated proportion (In China, gasoline consumption of transportation system occupies about 40% of national gasoline consumption now. Meanwhile its consumption of diesel oil accounts for about 38% of total diesel oil consumed. Beyond that, its consumption of fuel oil accounts for about 10% of total fuel oil consumption.). Road transportation energy consumption is shown in Table 3.

Table 3: Basic Condition of Road Transportation System from 2000 to 2006 .

year	length of highways (10,000 km)	possession of civil vehicles (10,000 units)	possession of private vehicles (10,000 units)	road transport land (10,000 hectare)	gasoline (10,000 ton)	diesel oil (10,000 ton)	fuel oil (10,000 ton)	electricity (100 million KWH)	natural gas (100 million cum)
2000	140.27	1608.91	625.33	192.50	723.42	1328.30	199.84	23.80	0.85
2001	169.80	1802.04	770.78	198.60	742.58	1393.82	207.21	44.50	1.30
2002	176.52	2053.17	968.98	205.70	773.94	1503.52	199.89	58.10	1.95
2003	180.98	2382.93	1219.23	214.52	840.46	1648.99	217.78	59.70	3.20
2004	187.07	2693.71	1481.66	223.32	969.20	1940.24	246.83	68.20	3.60
2005	334.52	3159.66	1848.07	230.90	1001.72	2151.48	218.89	73.80	3.92
2006	345.70	3697.35	2333.32	239.50	1081.89	2320.79	225.41	81.90	4.35

Based on formulation (5) to formulation (11), road transportation ecological footprint demand and ecological carrying capacity are gained, as shown in table 4.

Table 4 Results of road transportation ecological fo otprint (10,000 hectares).

Year	EFD1	EFD2	EFD'	EC'	REC	ES or ED
2000	192.50	1090.70	1738.77	1986.53	1748.14	9.38
2001	198.60	1137.27	1807.08	2061.50	1814.12	7.04
2002	205.70	1199.88	1895.83	2157.17	1898.31	2.48
2003	214.52	1314.81	2046.94	2313.21	2035.62	-11.32
2004	223.32	1530.56	2308.91	2570.08	2261.67	-47.24
2005	230.90	1624.27	2433.21	2699.11	2375.22	-57.99
2006	239.50	1745.67	2590.83	2860.61	2517.34	-73.50

Analysis of Calculation Results. Looking at Fig.3, the following conclusions can be made: Changes in EFD' are similar to that of EFD_2 and both of them show similar rising characteristics year after year, indicating EFD' mainly consists of EFD_2. In addition, EFD_2 is bigger than EFD_1 and their difference is larger and larger as time goes by, indicating EFD_2 contributes more to EFD' than EFD_1 as well as indicating EFD_2 is a main factor for restricting road transportation's sustainable development. Especially in 2003, there is an obvious increase for EFD_2, mainly because there is also an obvious increase in possession of private vehicles (see table 3). Further, energy saving consciousness was weak that year, resulting in larger consumption of fossil energy.

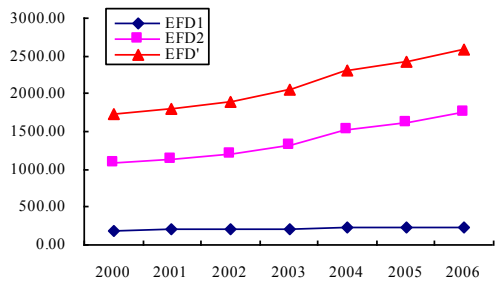

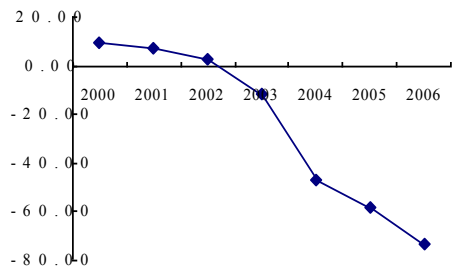

Figure 3. Changes of EFD_1, EFD_2 and EFD. Figure 4. Changes of ES or ED.

In Fig.4, positive values which are above the lateral axis denote ES, while negative values which are below the lateral axis denote ED. From 2000 to 2002, the road transportation ecological footprint is in ES state, indicating road transportation development in a sustainable way. Since 2003, negative values have appeared and continue to increase, indicating that road transportation sustainable development is threatened and will possibly continue to deteriorate. Therefore, in order to adjust ED state to ES state, energy consumption must be saved, greenhouse gas emission must be decreased and road transport construction land must be restricted.

Suggestions. In order to realize the sustainable development of road transportation, it is urgent to strengthen transportation management with the following measures.

First, the energy saving consciousness of road staff must be raised. Good driving habits should be encouraged such as stepping gently on the accelerator pedal, reducing unnecessary braking, cutting down on engine idle time, decreasing air-conditioning use, etc.

Second, energy consumption of vehicles must be decreased. Today, the increase in use of private vehicles can be restricted, and vehicles that are old and high-energy consumption may have to be eliminated.

Third, in order to control the increase of the construction land ecological footprint, maintenance and management of highways must be strengthened. The additional use of road transport land should be reasonably restricted.

CONCLUSIONS

(1) Raising energy saving awareness of road staff, decreasing energy consumption of automobiles, as well as strengthening maintenance of highways is important to realizing road transportation's sustainable development.

(2) This article has only calculated the ecological footprint of gasoline, diesel oil, fuel oil, electricity and natural gas due to availability of data, so the fossil energy land ecological footprint is smaller than its actual value. This discrepancy will be the focus of future study.

REFERENCES

Hu, B. Q., and Yan, Z. Q., etc. (2005). "Theories, methods and practice of regional ecological economy." China Environment Scientific Press, 11.

National Development and Reform Commission. (2007). "Production rules of new energy automobile are promulgated to deal with issues of energy consumption and pollution." http://hzs.ndrc.gov.cn/qhbh/qjfzjz/t20071126_174458.htm> (Nov. 5, 2007).

Luan, Y., and Lü, B. Z. (2008). "The research on urban drainage system management mode innovation." Environment Science and Management, 33(1), 51.

Li, Y. M., Zhang, L., and Yang, T. (2007). "Research of transportation sustainable development based on ecological footprint model." Productivity Research, (1), 55-57.

Wackernagel, M., Lewan, L., and Hansson, C. B. (1999). "Evaluating the use of natural capital with the ecological footprint." Applications in Sweden and Subregions, (28), 604-612.

Wu, Q. L., and Wang, Y. J. (2007). "Calculation and analysis of ecological footprint of Jiaozuo City in 2005." Journal of Pi ngdingshan Institute of Technology, 16(6), 21-23.

Xi, J P. (2008). "Study of energy saving and emission reduction in road transportation." Master's Dissertation of Chang'an University, 43-47.

A Study on Signal Timing Optimization of Individual Intersections Based on an Ant Colony Algorithm

Ling-jie Li[1], Xiao-kuan Yang[2] and Zhi Xu[3]

[1]Transportation Research Center, Beijing University of Technology, Beijing 100124, China; Tel: (0086) 13522110235; Fax: (0086-10) 6739-2991; E-mail: lilingjie185@emails.bjut.edu.cn

[2]Transportation Research Center, Beijing University of Technology, Beijing 100124, China; Tel: (0086-10) 6739-1678; Fax; (0086-10) 6739-2991; E-mail: xiaokuan@bjut.edu.cn

[3]Transportation Research Center, Beijing University of Technology, Beijing 100124, China; Tel: (0086) 13911677094; Fax: (0086-10) 6739-2991; E-mail: xuzhi1984@emails.bjut.edu.cn

ABSTRACT

Because traffic delays and queues have a serious impact on intersections and even entire roadway networks, this paper attempts to study the optimization algorithm of signal timing for individual intersections. The non-linear optimization model which is applicable for an individual intersection can be built up by using an ant colony algorithm based on mesh strategy. The programs are made by MATLAB in which some relevant parameters and algorithm rules are ameliorated. Taking some typical intersections in Beijing as an example, the non-linear model is established through programming in MATLAB. The optimization model is verified by estimating some targets after conducting a contrast study between the ones made by the Webster Method and the current timing condition derived from an ant colony algorithm. The results suggest that the ant colony algorithm based on mesh strategy is suitable for solving the problem of signal timing during peak periods. This new optimization algorithm can improve the condition at signalized intersections and provide a new effective method for solving the problem of signal timing at intersections.

1. INTRODUCTION

The key to solving the signal timing problem at intersections is seeking an optimal signal cycle length and green time. Solving the traffic control problem plays a crucial role in decreasing the delay time and the number of stops at intersections, as well as the road network. At present, foreign scholars' studies for the method of signal timing includes: F. Webster and B. Cobber who put forth an F-B algorithm for fixed signal timing problems in a single-point intersection which had been used for decades. Later some scholars made a few additional and amending suggests for the

F-B algorithm, such as R. Kimber who advanced the algorithm called TRRL. R. Aksay introduced the parameter of "stop compensation factor", that is, ARRB algorithm. The most widely-used and effective systems for signal control include: the TRANSYT system using climbing method, the SCOOT system for optimization with smaller step, the SCATS system with the strategy of comparison-selection, the Cabal system using genetic algorithm and so on.

In China, professor Yang Xiaoguang introduced the stopping-line delay model which improved the traditional algorithm of "F-B" (Yang Xiaoguang et al. 1993). Pu Qi modified the formula for calculating the delay and described the delay time as a discrete variable (Pu Qi et al. 1999). Yang Dongyuan considered the fuzzy-correlation among the parameters of cycle length with flow rate, the number of stops, queue length and volume for critical lane group and came to the conclusion that the factor most associated with cycle length is saturation, followed by flow rate, delay and number of stops (Yang Jindong et al. 2001).

With regard to controlling algorithm, Zhang Shengrui solved the optimization model and obtained some better values with a genetic algorithm and a genetic simulated annealing algorithm (Wang Qiuping et al. 2006). Wang Huiqiu put forth a study method of self-organization in real-time traffic signal control which combined fuzzy control and artificial neural network (Wang Huiqiu et al. 2005). Xu Xunqian used an elite ant colony algorithm to solve a multi-phase real-time model and validated the rationale and effectiveness of this optimal algorithm (Xu Xunqian et al. 2005).

2. SIGNAL TIMING OPTIMIZATION MODEL

In accordance with the actual traffic demands at the intersection, the optimization model is set up with the bound of saturation, which is a single-goal function by two real-time weighted coefficients in order to minimize the delay time and the number of stops. The optimization model is as follows:

$$\begin{aligned} &\min\ f(g_{e1}, g_{e2}, g_{e3}) = \sum_{i=1}^{n} K_i^1 D_i + \sum_{i=1}^{n} K_i^2 H_i \\ &g_{ei,\min} \le g_{ei} \le g_{ei,\max}, 1 \le i \le n; \\ \text{s.t.}\quad &\sum_{i=1}^{n} (g_{ei} + l_i) \le C_{\max}, 1 \le i \le n; \\ &x_{\min} \le \frac{q_i}{\lambda_i s_i} \le x_{\max}, 1 \le i \le n; \\ &x_i \ge 0, 1 \le i \le n. \end{aligned} \tag{1}$$

Where: $g_{ei,\min}$、$g_{ei,\max}$ = the minimum and maximum of effective green time for phase i; l_i = lost time for phase i; $C_{\max}$ = the maximum of cycle length; $x_{\min}$、$x_{\max}$ = the minimum and maximum of ratio; Delay time for phase i

is $D_i = \frac{(C-g_i)^2}{2C(1-q_i/s_i)} + \frac{C-g_i}{2Cq_i} + \frac{q_i C^2}{2s_i g_i (s_i g_i - q_i C)}$; The number of stops for vehicles is $H_i = 0.9 \times \frac{1-\lambda_i}{1-y_i}$; K_i^1， K_i^2 are the weighted coefficients of delay time and the number of stops respectively, $K_i^1 = 2s_i y_i (1-Y)$， $K_i^2 = s_i y_i \frac{1-Y}{0.9}$.

3. ANT COLONY ALGORITHM FOR CONTINUOUS DOMAI N BASED ON MESH STRATEGY

3.1 Basic Idea and Solving Steps for this Algorithm

In the study of signal timing optimization, the application of fuzzy theory, neural networks, traffic flow simulation and genetic algorithms are involved. However, some studies show that the practical application of self-adaptive systems for signal control has poor effectiveness. Most of them use complicated algorithms produce large amounts of calculation and can't satisfy the requirements of real-time control in the actual application. Yan Yanxia and others have used the basic ant colony algorithm to work on the signal timing optimization model (Yan Yanxia et al. 2006). But the basic ant colony algorithm based on discrete theory is aimed at the shortest closed path and the process for searching for solutions. It is a way of hopping based on the analysis of discrete points. An ant colony algorithm for continuous domain based on mesh strategy can overcome these shortcomings, which aims at searching for the most optimal value by making it a gradual iterative search to points and their affected areas. This optimized algorithm has shown very good performance in a series of nonlinear optimization problems.

The idea of the ant colony algorithm based on mesh for a continuous domain has the following features: First, according to the nature of the continuous optimization problem, the range of variables can be estimated. Then, a grid in the variable region is built up. One of the grid points in this space corresponds to a state. Ants moved between these grid points and left different amounts of messaging in terms of the value of goal function at that point, as an impact on the moving direction for the next ant group. After cycling for a period of time, the point with a smaller value of goal function has a larger amount of messages between two adjacent nodes. It would be selected and the range of variables would be narrowed. There the next ant group continues moving. Repeat this process until the conditions of this algorithm have been met (Duan 2005).

The assumption that a variable should be divided into n equal parameters makes the problem have n determined levels. In each level there are n+1 nodes so that the total number of nodes is (n+1)×n which make a connection from the first level to the level n, as a solution space as follows:

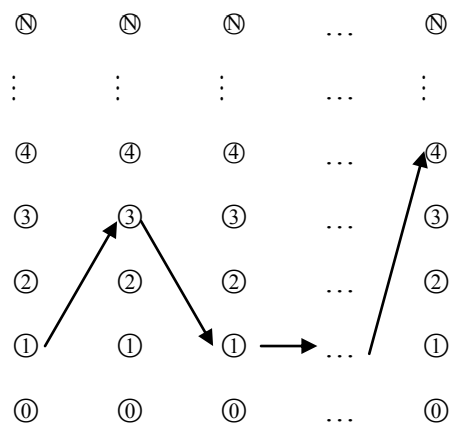

Figure 1 . Diagram of State Space .

As shown in the chart above, the state in this space is (1, 3, 1,…, 4). Its corresponding solution is

$$\begin{aligned}(x_1, x_2, x_3, \ldots, x_n) = (\ & x_{1lower} + \frac{x_{1upper} - x_{1lower}}{N} \times 1, \\ & x_{2lower} + \frac{x_{2upper} - x_{2lower}}{N} \times 3, \\ & x_{3lower} + \frac{x_{3upper} - x_{3lower}}{N} \times 1, \ldots, \\ & x_{nlower} + \frac{x_{nupper} - x_{nlower}}{N} \times 4) \end{aligned} \tag{2}$$

The state-transition probability from the first level to level N can be calculated by the formula as followings:

$$P_{ij} = \frac{\tau_{ij}}{\sum_{i=1}^{N} \tau_{ij}} \tag{3}$$

Assume τ_{ij} to be the node i in the level j, the update equation is

$$\tau_{ij}^{new} = (1-\rho)\tau_{ij}^{old} + \frac{Q}{f} \tag{4}$$

Where, f is the value of goal function.

The solution steps of this algorithm are:

(1) To estimate the range of variables: $x_{jlower} \le x_j \le x_{jupper}\ (j=1,2,...,n)$;

(2) To divide each variable into N equal parameters: $h_j = \frac{x_{jupper} - x_{jlower}}{N}\ (j=1,2,...,n)$;

(3) If $\max(h_1, h_2, ..., h_n) < \varepsilon$, the algorithm stops. The most optimal solution is $x_j^* = \frac{x_{jlower} + x_{jupper}}{2}\ (j=1,2,...,n)$; Otherwise jump to step (4);

(4) When the number of cycle $N_c \leftarrow 0$, give the matrix τ_{ij} the same value and set initial value to Q, ρ and $N_{c\max}$;

(5) Assume the number of ants is num_ant , each ant can select next node by formula (4);

(6) Modify the value of message by the update equation, $N_c \leftarrow N_c + 1$;

(7) If $N_c < N_{c\max}$, jump to step (5); Otherwise select the row what the maximum in each column corresponds in matrix τ_{ij} and narrow the range of variables: $x_{jlower} \leftarrow x_{jlower} + (m_j - \Delta)h_j$, $x_{jupper} \leftarrow x_{jlower} + (m_j + \Delta)h_j$, where $j = 1,2,...,n$, then jump to step (2).

In the process of making programs, some improvements have been made for an ant colony algorithm for continuous domain based on mesh strategy: The proliferation and stagnation problem appeared easily and cannot be ignored. The amount of messaging left on the optimizing path should be restricted within $[\tau_{\min}, \tau_{\max}]$. After every cycle, the most optimized path was saved. Only the ant with the shortest path can modify the value of $\tau_{ij}(t)$. We can select and determine threshold in accordance with the following formula:

$$\tau_{ij}(t+n) = \begin{cases} \tau_{\min}, & \tau_{ij}(t) \le \tau_{\min} \\ \tau_{ij}(t), & \tau_{\min} < \tau_{ij}(t) \le \tau_{\max} \\ \tau_{\max}, & \tau_{ij}(t) > \tau_{\max} \end{cases} \quad (5)$$

3.2 Algorithm Validation

3.2.1 The Case

Using “Xueyuan Southern Road and Zaojunmiao Road” intersection as an example, the survey was conducted at morning, afternoon and evening peak hours in

light of all the necessary parameters that are base dates for signal timing. Volumes in each direction have been recorded in Table 1:

Table 1. Timing Parameters of Each Phase During Morning Peak Period .

Parameters in Webster method	The first phase		The second phase		The third phase			
	Through lane in southern	Through lane in northern	Left lane in southern	Left lane in northern	Through -left lane in eastern	Through-left lane in western	Through lane in eastern	Through -right lane in western
Volume q_i	930	1554	280	190	550	426	550	708
Flow rate S_i	2000×3	2000×3	1800	1800	1500	1500	1698	1674
Flow ratio	0.155	0.259	0.156	0.106	0.367	0.284	0.324	0.423
Flow ratio of critical lane y_i	0.259		0.156		0.423			

3.2.2 Parameter Calibration

Calculating programs of ant colony algorithms for continuous domain based on mesh strategy are made in Matlab 6.5, which is used to calculate the results of signal timing. In this algorithm, initial parameters are calibrated as follows: pheromone evaporation coefficient ρ =0.6; pheromone intensity Q=10000; the number of ants ant=20; the number of cycles NCmax=10; iteration steps step=10; the number of equal parts n=10.

(1) Value of ρ

Ants in this algorithm have human memory function. With time flying, messages left earlier will gradually disappear. Parameter ρ is directly related to global search ability and convergence speed. 1-ρ reflects the interaction between individual ants. When ρ becomes bigger, the path searched preciously would be more likely to be chosen. That affects the randomness and the global search capability of this algorithm; On the other hand, the randomness and search capability can be improved by reducing ρ. But the convergence speed of the algorithm will be reduced. In this case, parameter ρ was set at 0.6 by a large number of experiences with experimental verification.

(2) Value of Q

Q is the total number of messages whose function is to search the global optimal solution under reasonable speed by using the global feedback number of messages in directed graph in the positive-feedback system.。When Q gets bigger, the convergence speed becomes larger and can enhance the ability of positive-feedback. In this case, Q values 10000 in accordance to the goal value under the Webster method whose magnitude is 10^4. From equation (4), we can see the messages have obviously been updated.

(3) Values of ant、NCmax and step

An ant colony algorithm searches the optimal solution from several candidate solutions. If the number of ants is larger; the capacity of global search and stability would be stronger. But when the number of ants increases substantially, the change in solutions tends to average out. At the same time, the capability of positive feedback is reduced and the convergence speed gets lower. In contrast, if there are only a few ants, randomness capability would get weak. Although the algorithm has a high convergence speed, with the stability reduced, the phenomenon of premature stagnation appears.

The scale of this case is small and there are only three variables in the controlling model. In the process of program debugging, ant, NCmax and step should not be too large. In order to avoid searching for a long time, their product should be controlled within 10^3-10^4. After repeated debugging, set ant=20，NCmax=10，step=10。

(4) Value of n

Using the data obtained during morning peak hours as an example, an analysis about the value of n has been implemented. When n is 10, 20, 30, respectively; the results are calculated as follows:

Table 2. Results with Different n .

	g_{e1}	g_{e2}	g_{e3}	C	Z
n=10	36	21	58	130	36215
n=20	38	24	62	137	38292
n=30	40	26	66	146	40827
⋮	⋮	⋮	⋮	⋮	⋮

Figure 2 . Trends of Goal Function Value .

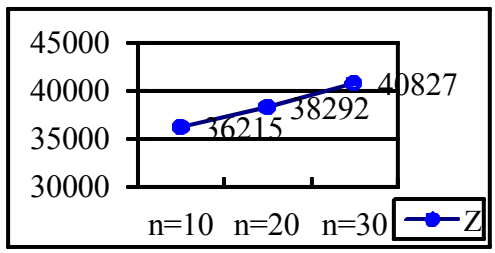

From Table 2 it can been seen that, with n increasing, the effective green time of each phase and cycle length have all increased. As shown in Figure 2, the value of optimal target becomes larger as the value of n increases. The goal of an optimal controlling model is to search the solution which makes the target value the most optimal, or the smallest. In Table 2, when n is 10, the value of the target is the smallest one.

3.2.3 The Calibration of Initial Value of Effective Green Time for Phase i

In this algorithm, it is necessary to set the initial search scope for solutions. According to the results of the Webster method, we calibrate a different search scope for each phase at three periods:

A. Morning peak hours：ylow=[20，20，20]，ymax=[80，80，80]；

B. Afternoon hours：ylow=[5，5，5]，ymax=[35，35，35]；

C. Evening peak hours：ylow=[10，10，10]，ymax=[50，50，50]。

Where ：“y” represents effective green time for phase i.

3.2.4 Algorithm Rule

In this case, Applying the program-making procedure to this case, the original

rule for this algorithm can be described as follows: First, a solution matrix is generated, and then it is determined whether these solutions meet the constraint. If they do, save them and select the best solution. With this kind of rule, satisfying solutions occupies only a very small proportion of the solution matrix at the stage where the original solutions are generated. Consequently, the final solution doesn't achieve the desired optimal result. After modifying the program many times, the algorithm rules would be replaced as follows:

Make the restrictive conditions a determining factor when generating the solution matrix. In other words, whenever a group of solutions is generated, a judgement must be made on whether these solutions meet the demands. If they don't, the program must re-generate a new group of solutions until all of the initial solutions meet the conditions. Finally, a feasible solution matrix is obtained, from which we are able to search the most optimal solution. Thus there is a significant improvement on the optimizing effect.

4. EVALUATION OF ANT CO LONY ALGORITHM

4.1 Comparative Analysis of Calculation Results

The simulation calculation of the ant colony algorithm for continuous domain based on mesh strategy could be done in MATLAB. The results obtained from the ant colony algorithm compared with the ones of the Webster method are shown on the following table:

Table 3 . Comparison of Results .

Period	The name of algorithm	g_1	g_2	g_3	C	$\overline{d_i}$	$\overline{h_i}$
Morning	Ant colony algorithm	37	19	56	130	44.428	0.875
	Webster method	46	25	71	159	53.540	0.877
	Present condition	47	15	72	150	54.441	0.882
Afternoon	Ant colony algorithm	9	2	12	41	15.374	0.873
	Webster method	14	6	24	62	21.315	0.824
	Present condition	31	13	57	117	48.776	0.768
Evening	Ant colony algorithm	18	7	32	75	26.060	0.856
	Webster method	21	8	41	88	29.992	0.870
	Ant colony algorithm	45	27	75	163	51.293	0.886

From Table 1 it can be seen that the average delay time calculated in an ant colony algorithm for continuous domain based on mesh strategy is less than the ones obtained from Webster during any period of the day. It also shows that this algorithm also affects the average delay time at intersections. In addition, the average number

of stops derived from the ant colony algorithm is less than the ones in the Webster method for both morning and evening peak hours. But for the noon peak period, the number of stops with the ant colony algorithm is more than that in the Webster method. Therefore, this algorithm has an apparent effect on decreasing the number of stops during peak periods.

5. CONCOUSION

The simulation results show that the ant colony algorithm is applicable to solving the signal timing problem during peak hours at intersections. Average delay time has been significantly optimized, followed by the number of stops. In this case, the results reveal some bias because saturation flow rates were all taken during morning peak hours. As a result, the signal timing results of the noon period are too small. We should pay more attention to modifying saturation flow rates. From this case, a conclusion can be made that solving the nonlinear optimal model of signal timing with the ant colony algorithm has fully taken the actual situation of the "Xueyuan Southern Road and Zaojunmiao Road" intersection into account. General applicability of this algorithm should be studied for further use.

In conclusion, we can get some satisfactory optimal results by using this new optimization algorithm which can obviously improve the conditions at signalized intersections and provide a new, effective method for solving the problem of signal timing at individual intersections.

REFERENCES

Duan H.. (2005). Principle and application of ant colony algorithm . Sciences Press, Beijing.

Pu Q, and Tan Y. (1999). "Signal- planning optimal model for intersection." Journal of Shanghai Tiedao University (Natural Science Edition). 20(4), 31-34.

Wang H., and Le Y. (2005). "Transport signal control based on fussy neural network." Intelligent Transportation System. 7(1), 23-24.

Wang Q., and Tan X. (2006). "Signal timing optimization of urban single-point intersections." Journal of Traffic and Transportation Engineering . 6(2), 60-64.

Xu X., Huang W. "Multiphase traffic signal real-time controlling model of isolated intersection and its algorithm." Control Theory and Applications. 22(3), 413-417.

Yang J., and Yang D. (2001). "Optimized signal time model in signaled intersection." Journal of Tongji University. 29(7), 789-794.

Yang X., Yang P.. (1993). "Simulative models on signalized intersection stop-line delay." Journal of Tongji University (Natural Science). 21(1), 67-73.

Yan Y., and Li W. (2006). "Ant colony optimization for signalized intersection." Journal of Highway and Transportation Research and Development . 23(11), 116-119.

Study on the Optimization of Vessel Scheduling Design Based on Soft Time Windows Under Voyage Charters

Ming Sun[1], Feifei Fei[2] and Xuefeng Wang[3]

[1]International Shipping Department, School of Transportation, Shanghai Maritime University, Shanghai 200135, P.R. China; email: sunm@shmtu.edu.cn
[2]International Shipping Department, School of Transportation, Shanghai Maritime University, Shanghai 200135, P.R. China; email: feifeifei1357@yahoo.com.cn
[3]International Shipping Department, School of Transportation, Shanghai Maritime University, Shanghai 200135, P.R. China; email: xfwang@cct.shmtu.edu.cn

ABSTRACT

Informed by Vehicle Routing Problems with time windows (mainly soft time windows), this paper incorporates time windows into vessel scheduling problems. After a relevant literature review, this paper proposes an optimization of vessel scheduling design that could control the time deviation from designed discharging time. This optimization is especially important in view of the rough times the shipping market is experiencing as a result of the worldwide economic crisis . . This design of vessel scheduling could effectively yield a comparatively high daily net profit.

1. INTRODUCTION

In traditional Vehicle Routing Problem (VRP) studies, due to a time limitation set by clients, Soft Time Windows (STWs) are often introduced. This means that the service is potentially performed off schedule, but clients should be compensated for this inconvenience. In voyage charters, expenses incurred while waiting for berth are typically charged to the owners' account if the vessel enters the port ahead of time. Wharf storage charges will typically be paid if the vessel voyage is moved up for the next voyage charter party on time. If vessel owners fail to deliver the cargo on time, possible revenue and reputation losses will occur. So every voyage charter party has its corresponding soft time window and the vessel owner will incur punitive charges if this cargo fails to be delivered within its time window.

In practice, vessel owners usually canvass for cargoes first and then after negotiation, sign with charterer's fixture notes or voyage charter parties in which lay days and a cancellation date (LAYCAN) and sometimes estimated time of arrival (ETA) are clearly stipulated. According to these fixture notes or charter parties, vessel owners develop a design for the vessel's schedule.

2. DESCRIPTION OF VESSEL SCHEDULING PROBLEMS

Suppose a certain vessel owner has a fleet of K short-sea sailing vessels with the same dead weight tonnage Q and all these vessels are launched into voyage charter services in the East China/Japan/Korea area. Before vessels sail from the port

of departure, M cargoes are fixed. Each cargo m has a quantity of G_m and is to be carried with a freight rate of R_m. According to the charter parties, the total number of ports to be called is N and every cargo is requested by the charterer to arrive at its discharging port within a time period of $[a_m, b_m]$. If the cargo m is discharged at its port of destination before a_m because of earlier completion of the former voyage or quicker sailing speed, the vessel owner is required to pay an extra wharf storage charge for this cargo; and if cargo m is discharged at its port of destination after b_m because of severe weather, breakdown of machinery and so on, the vessel owner should make reparation for losses suffered by the charterers (Fan et al. 2005). To maximize the vessel owner's daily net profit in respect to the fleet as a whole, how should the vessel scheduling be designed?

3. ASSUMPTIONS AND EXPLANATIONS

In voyage charters, both loading and discharge work exists at every port of call. In other words, a certain cargo is discharged at a port where another cargo is waiting to be loaded onto the same vessel, so the vessel fulfills two voyages consecutively. Cargo m is loaded and discharged at port N_{lm} and N_{dm} respectively, and N_{lm} could be any port among the above defined N ports.

For every vessel among K launched into voyage charter services, it is not supposed to call at the same port more than once. During the voyage, any one vessel should sail in ballast or carry at most one cargo.

Generally, the cargo quantity G_m is mildly less than αQ, α meaning that the vessel's loading capacity will be adjusted according to the utilization of capacity, quantity of gross stores and constant, $\alpha \in (0, 1)$.

For every vessel k in service, the fixed cost per operating day is f. In general situations, the business tax rate is 3% and the rate of commission is 2.5%.

4. MATHEMATICAL MODEL

Define M_n as the number of cargoes that canvassed for port n. Because every vessel could call at every port just once, at most, the number of vessels launched must satisfy the requirement that all the cargoes fixed for each port will be carried. So,

$K = \max\ M_n,\ n \in \{1,\ 2,\ ...,\ N\}$.

Define x_{ijk} and y_{ijk} as binary variables, the port of departure is marked 0 and other ports of call are marked 1, 2, ..., N, then

$$x_{ijk} = \begin{cases} 1, \text{ vessel } k \text{ carries one cargo from port } i \text{ directly to port } j \\ 0, \text{ otherwise} \end{cases}, \text{ and}$$

$$y_{ijk} = \begin{cases} 1, \text{ vessel } k \text{ sails in ballast from port } i \text{ to port } j \\ 0, \text{ otherwise} \end{cases}.$$

So, after vessel k has been loaded at one port of loading, sailed at sea, arrived at the designated port of discharge and the discharge work of cargo has been completed, the time then is defined as t_{jk}.

$$t_{jk} = \sum_{i=0}^{N} x_{ijk}(t_{ik} + t_{li} + t_{ij} + t_{dj}) + y_{ijk}(t_{ik} + t_{ij}^{'}), \qquad j \in \{1,\ 2,\ ...,\ \mathrm{N}\},$$

where t_{ik} refers to the time that vessel k has arrived at port i and completed discharge of previous cargo, and $t_{0k} = 0$; t_{li} refers to the time spent loading at port i; t_{ij} refers to the sailing time of the laden vessel from port i directly to port j, and $i, j \in \{0,\ 1,\ ...,\ N\}$; $t_{ij}^{'}$ refers to the sailing time of the vessel in ballast from port i directly to port j, and $i, j \in \{0,\ 1,\ ...,\ N\}$; and t_{dj} refers to the time spent on discharging at port j.

The total fixed costs and the total variable costs for the fleet could be expressed as $f \times \sum_{k=1}^{K} MAX(t_{jk})$ and $\sum_{i=0}^{N}\sum_{j=0}^{N}\sum_{k=1}^{K}(V_{ij} \cdot x_{ijk} + V_{ij}^{'} \cdot y_{ijk})$ respectively, where V_{ij} refers to the variable costs for a laden vessel and $V_{ij}^{'}$ a vessel sailing in ballast.

In this model, d represents the wharf storage charge per time unit due to an earlier discharge, and e represents punitive charges per time unit because of a delay in delivery of cargo. If the cargo m is discharged at port N_{dm} before a_m, the inconvenience cost is $d_m(a_m - t_{N_{dm}k})$; and if the cargo m is discharged at port N_{dm}

after b_m, the inconvenience cost is $e_m(t_{N_{dm}k} - b_m)$.

The mathematical model for optimization of vessel scheduling with soft time windows under voyage charter is stated below. Its objective function is for the highest daily net profit (Han 2008).

$$\max Z = \left\{ \sum_{m=1}^{M} G_m \times R_m \times 94.5\% - \sum_{i=0}^{N}\sum_{j=0}^{N}\sum_{k=1}^{K}\left(V_{ij}\cdot x_{ijk} + V_{ij}^{'}\cdot y_{ijk}\right) - f \times \sum_{k=1}^{K} MAX(t_{jk}) \right.$$

$$\left. - \sum_{m=1}^{M}\sum_{k=1}^{K} x_{N_{lm}N_{dm}k} \times \left[d_m \times \max(a_m - t_{N_{dm}k},\ 0) + e_m \times \max(t_{N_{dm}k} - b_m,\ 0) \right] \right\} \div \sum_{k=1}^{K} MAX(t_{jk})$$

s. t.
$$\sum_{j=0}^{N} x_{ijk} = 1, \quad \forall i \in N,\ \forall k \in K \tag{1}$$

$$\sum_{i=0}^{N} x_{ijk} = 1, \quad \forall j \in N,\ \forall k \in K \tag{2}$$

$$\sum_{k=1}^{K} x_{N_{lm}N_{dm}k} = 1,\ \forall m \in M \tag{3}$$

Among the above examples, constraint (1) and (2) restrict that any vessel in service could not call at the same port twice or more, and constraint (3) makes sure that every cargo will be carried to its discharging port as designated.

5. EXAMPLE AND ALGORITHMS

5.1 Example

Suppose the owner has two vessels named A and B with both $Q = 10000$ metric tons and a sailing speed 12 knots. There are five cargoes fixed before the vessels start sailing from Shanghai. Distances between ports of loading and ports of discharge are listed in Table 1, and the data of the cargoes and vessels are listed in Table 2. Suppose rates of loading and discharging are 2000 metric tons per day at the five ports. Inconvenience costs are d = USD 40/h and e = USD 60/h.

Table 1. Distances Between Related Ports (Nautical Miles).

	Shanghai (SHG)	Busan (BSN)	Kobe (KOB)	Guangzhou (GGZ)	Qingdao (QDO)
Shanghai		492	783	928	399
Busan			365	1223	502
Kobe				1455	808
Guangzhou					1183
Qingdao					

Table 2. Data of the Cargoes and Vessels.

m	G_m	R_m (USD)	a_m (h)	b_m (h)	f (USD/h)	V (USD/h)	V' (USD/h)	POL	POD
1	8000	12	200	250	125	146	120	Shanghai	Busan
2	7600	25	400	500	125	146	120	Busan	Guangzhou
3	7800	13	300	350	125	146	120	Busan	Qingdao
4	8000	23	700	800	125	146	120	Guangzhou	Qingdao
5	7200	18	550	650	125	146	120	Qingdao	Kobe

An optimum solution could be achieved by spreadsheet linear programming. (see Table 3.) The optimum scheduling of vessel A is Shanghai – Busan – Guangzhou – Qingdao, and the optimum scheduling of vessel B is Shanghai – Busan (in ballast) – Qingdao – Kobe. The value of the objective fuction is $\max Z = \text{USD } 12953.80$.

Table 3. Result of Spreadsheet Linear Programming.

Vessel A (laden)

	SHG	BSN	KOB	GGZ	QDO
SHG	0	1	0	0	0
BSN	0	0	0	1	0
KOB	0	0	0	0	0
GGZ	0	0	0	0	1
QDO	0	0	0	0	0

Vessel A (ballast)

	SHG	BSN	KOB	GGZ	QDO
SHG	0	0	0	0	0
BSN	0	0	0	0	0
KOB	0	0	0	0	0
GGZ	0	0	0	0	0
QDO	0	0	0	0	0

Vessel B (laden)

	SHG	BSN	KOB	GGZ	QDO
SHG	0	0	0	0	0
BSN	0	0	0	0	1
KOB	0	0	0	0	0
GGZ	0	0	1	0	0
QDO	0	0	1	0	0

Vessel B (ballast)

	SHG	BSN	KOB	GGZ	QDO
SHG	0	1	0	0	0
BSN	0	0	0	0	0
KOB	0	0	0	0	0
GGZ	0	0	0	0	0
QDO	0	0	0	0	0

Using this model, we can develop an optimum vessel scheduling design and obtain the theoretically highest daily net profit. Besides this advantage, in a situation where vessel owners are extremely expert at canvassing cargoes or where a shipping market is prospering with a great number of cargo supplies, this model could be used to assess whether a new fixture note or charter party is worth signing or not. Whenever M or G_m is altered, a new daily net profit is obtained. After comparing the new daily net profit with the original one, an optimum choice of cargoes could be determined.

If the vessel owner is insightful enough to pursue a long harmonious relationship with certain cargo owners, this model d_m and e_m could be magnified

to ensure that the cargoes of these owners will be carried and delivered punctually.

5.2 Algorithms

The Vehicle Routing Problem was first proposed by Dantizig and Ramser in 1956. Since then, studies on VRP have yielded additional results including VRPTW. If a large number of nodes exists, then routing becomes an NP-hard problem (Liu et al. 2005). In the above model, if the numbers of cargoes and ports are more, a "combinatorial explosion" problem exists in respect to accurate algorithms, and time problem solving increases exponentially. The improved heuristic algorithms for near optimum solutions include Taboo Search, Genetic Algorithm (Bin et al. 2003), Immune Algorithm, Ant Algorithm (Li 2008) and so on, all of which could apply to the above vessel scheduling problem model. However, each of these solutions has its own deficiencies. Even though studies on VRPTW models have brought about many achievements and the algorithms have been much improved, further improvements still need to be made in these algorithms, especially when VRPTW models are combined with concrete decision-making problems and optimization problems.

6. CONCLUSION

Based on traditional Vehicle Routing Problems, this paper proposed a solution to tvessel scheduling problems with soft time windows under voyage charter parties. Considering the current situation in shipping markets, this paper discussed the problem under the assumption that cargoes are fixed ahead. This model could reduce costs while establishing a reputation for punctual delivery, winning the fleet a strong place in the stagnant shipping market. But the algorithm for this model still needs to be further studied, taking into consideration the practices of voyage charter and the shipping market.

ACKNOWLEDGEMENT

This research is supported by Shanghai Leading Academic Discipline Project, Project Number: 30601.

REFERENCES

Bin, S. and Fu Z.,. (2003). "An improved genetic algorithm for vehicle routing problem with soft time windows." *Systems Engineering*. 21(6), 12-15.

Fan, T., Ma, Z. and Li, Y.. (2005). "Optimization of vessel scheduling with soft time window." *Journal of Dalian Maritime University*. 31(4), 5-14.

Han, S. (2008). "Object planning model for selecting multi-objective distribution route with time window constraints." *Logistics Technology*. 27 (1), 44-46.

Li, Q. (2008). "Application on vehicle routing problem with time windows based on the hybrid strategy of genetic algorithm and ant algorithm." *Mathematics in Practice and Theory*. 38(15), 40-48.

Liu, C., Chen, Z. and Feng, Qi. (2005). "Parallel genetic algorithm for vehicle routing problems with soft time windows of logistic distribution." *Systems Engineering*. 23(10), 7-11.

CONGESTION PRICING REVENUE REDISTRIBUTION STRATEGY BASED ON TRAFFIC BEHAVIOR

Z. B. Zhao[1], Y. Tian[1] and Y. Chen[1]

[1] Harbin Institute of Technology, Harbin, China, 150001; Tel (86) 0451-86412866; FAX (86) 0451-86412866; email: zhaozebin@hit.edu.cn

ABSTRACT

A congestion pricing revenue redistribution strategy is the key to the effective implementation of congestion pricing, whose design is based on mastering travelers' traffic decision behaviors. This paper analyzes the change of travel costs and impact on choice of travel mode and route for different redistribution modes, and then constructs the bi-level planning model of congestion pricing revenue redistribution in a transportation system, which is composed of a transportation plan designer and road user. The upper level model aims to maximize the benefit of the road network and the lower level model is described as a Stochastic User Equilibrium problem. The transportation plan designer acts first, framing the charge strategies and revenue redistribution. The users determine their own travel modes according to the strategies and the network traffic conditions. The transportation plan designer responds to the the users' decisions before they frame the strategies. The results of the calculation examples analysis demonstrates that this bi-level model can effectively mix the the decisions of travelers and traffic managers with proper consideration of the benefits to be gained by both sides.

INTRODUCTION

A strategy for congestion pricing revenue redistribution is the key to the effective implementation of congestion pricing, whose design is based on mastering travelers' traffic decision behaviors, such as traveling modes and route choices. However, present studies on revenue redistribution of congestion pricing are not in-depth. Overall, the greatest difference can be shown as the two views below. Most of the work in this area has concentrated on qualitative analysis or case study of revenue redistribution of congestion pricing. Representative researchers include Hau (1998), Goodwin (1989), Small (1992), Litman (1996), Armelius (2006). Only a limited number of quantitative models of revenue redistribution were established under simple network conditions for direct presentation of distribution policy, or the benefit of traffic management agencies. Representative researchers include Bernstein (1993), Jeffrey (2001), Kockelman and Kalmanje (2005) , Ferrari (2005).

Current road congestion pricing revenue redistribution research focuses on qualitative mode analysis or case studies, and fails to focus on traffic behavioral analysis under congestion pricing revenue redistribution. It should be noted that

traveler utility must be changed after redistribution of revenue from road congestion pricing, a factor that will result in a change in traveler behavior, especially the choice of travel mode. Relative research papers establish models that only benefit traffic management agencies while ignoring travelers' response to traffic policy. Therefore, analysis of traffic behavior is the basic premise of establishing practical policy of redistribution. Research results contain important theoretical and practical approaches to improve road congestion and enhance transportation efficiency.

ANALYSIS OF TRAFFIC BEHAVIORS UNDER DIFFERENT SITUATIONS

Modes of redistribution of revenue from road congestion pricing can be considered under the following three types of situations: The first mode is to compensate motor vehicle travelers by returning cash or through tax offsetting. The second mode is to use the revenue to extend road capacity. The third mode is to improve the running speed, departing frequency, convenience, and reduce fare of public transport. According to efficiency and equity criteria, the first mode goes against efficiency criteria and is not the best way. The second mode improves road capacity and supply ability. In short terms, this mode can improve transport efficiency, but it is not the best long-term plan because the capacity cannot increase infinitely due to the limited earth. The third mode can improve the service of public traffic, decrease operating costs and increase the demand of public traffic. Extending road capacity and improving public transport service are accepted methods and the best way to distribute congestion pricing revenue when we can't extend road capacity.

When the revenue of road congestion pricing is used to extend road capacity, we assume B_a as capacity of vehicle on road a. The new capacity is g_a, c_a, $\overline{c}_a$ is general travel costs of road a for private and public transports after pricing, which can be expressed as:

$$c_a = t(x_a, g_a) + u(x_a) = t_0[1 + \alpha(\frac{x_a}{B_a + g_a})^{\beta}] + u(x_a) \quad (1)$$

$$\overline{c}_a = t(\overline{x}_a, g_a) + \overline{u}(\overline{x}_a) = \overline{t}_0[1 + \alpha(\frac{\overline{x}_a}{B_a + g_a})^{\beta}] + \overline{u}(\overline{x}_a) \quad (2)$$

Where, t_0, $\overline{t}_0$ is the driving time of private and public transport under free flow through road a; u_a, $\overline{u}_a$ is the pricing fee of private transport and bus fare for road a; x_a, $\overline{x}_a$ is private and public traffic flow on road a, α, β are the parameters of road fee function BPR which shows the relationship between travel time and flow of vehicles. Road congestion pricing revenue is used to increase road capacity which will decrease fees and improve welfare when travelers use the road a.

When the revenue of congestion pricing is used to improving public transport service, including decreasing bus fare and increasing send-out frequency, waiting

time is reduced at the bus station. We assume c_m, $\overline{c}_m$ as the generalized cost of private traffic and public traffic each trip between r-s, which can be expressed as:

$$c_m = b_0 + b_1 t_1 + b_2 t_2 + b_3 (c_d + u) \tag{3}$$

$$\overline{c}_m = \overline{b}_0 + \overline{b}_1 \overline{t}_1 + \overline{b}_2 \overline{t}_2 + \overline{b}_3 \overline{u} = \overline{b}_0 + \overline{b}_1 \frac{1}{y} + \overline{b}_2 \overline{t}_2 + \overline{b}_3 \overline{u} \tag{4}$$

Where, b_i, $\overline{b}_i$ are the corresponding factors of private traffic and public traffic, $i = 0,1,2,3$; t_j, $\overline{t}_j$ denotes wait time, in-vehicle time of private traffic and public traffic, $j = 1,2$; c_d denotes vehicle depreciation and fuel costs. y denotes the bus departure frequency. We can find $\overline{c}_m$ will decrease when u is used to the decreasing of $\overline{u}$ and increasing of y in the formula.

According to MNL model, the probability can be derived as follows if private transport and public transport travelers choose path k:

$$p_k^{rs} = \frac{\exp(-\alpha c_k^{rs})}{\sum_k \exp(-\alpha c_k^{rs})}, \quad \overline{p}_k^{rs} = \frac{\exp(-\alpha \overline{c}_k^{rs})}{\sum_k \exp(-\alpha \overline{c}_k^{rs})} \tag{5}$$

Where, c_k^{rs}, $\tilde{c}_k^{rs}$ are the generalized costs of private traffic and public traffic on path k, which can be expressed as:

$$c_k^{rs} = \sum_a c_a(x_a, u_a)\delta_{a,k}^{rs}, \quad \overline{c}_k^{rs} = \sum_a \overline{c}_a(\overline{x}_a, \overline{u}_a)\overline{\delta}_{a,k}^{rs} \tag{6}$$

Where, $\hat{\delta}_{a,k}^{rs}$ $\tilde{\delta}_{a,k}^{rs}$ are the 0-1 variables, they are equal to 1 if private transport or public transport trips' road a is on route k.

The probability can be derived as follows if travelers choose private transport or public transport:：

$$p_{rs} = \frac{1}{1 + e^{\theta(\overline{c}_m - c_m)}}, \quad \overline{p}_{rs} = \frac{1}{1 + e^{\theta(c_m - \overline{c}_m)}} \tag{7}$$

A MODEL FOR CONGESTION PRICING REVENUE REDISTRIBUTION BASED ON TRAFFIC BEHAVIOR

This paper regards the transport system as a mix of transportation planning managers and users of complex systems, where transportation planning managers become the upper decision makers, and network users become the lower decision makers. The establishment of upper planning objectives is based on meeting the city's traffic management objectives. In this paper, road congestion pricing revenue is used for road expansion or public transport. We set the amount of investment for the road expansion at $\sum \varphi(g_a) = d_a g_a$, d_a is the parameter for the investment function, the amount of subsidies for the public transport is $S = C_p y - \overline{uq}$, C_p is the operating costs of each bus travel between the O-D pairs, including vehicle depreciation, maintenance, drivers and conductors' wages, plus related costs such as fuel consumption for each travel. Then the Upper Level Planning Model of road congestion pricing revenue redistribution can be expressed as:

$$\max_{u,\tilde{u},y,g} H = \sum_{rs}\int_0^{q_{rs}} D_{rs}^{-1}(x)dx - \sum_a t_a\left(x_a(u,g),g_a\right)x_a + \sum_{rs}\int_0^{\bar{q}_{rs}} \bar{D}_{rs}^{-1}(x)dx - \sum_a \bar{t}_a\left(\bar{x}_a(\bar{u},\bar{g}),\bar{g}_a\right)\bar{x}_a - S - \sum_{a\in A}\varphi_a(g_a) \quad (8)$$

$$s.t. \quad x_a(u) + \tau\bar{x}_a(\bar{u}) \le B_a + g_a \quad (9)$$

$$\sum_a \varphi(g_a) + S \le \sum_a u x_a \quad (10)$$

$$u_a, \bar{u}_a, g_a \ge 0 \quad (11)$$

Where, τ denote the vehicles' conversion coefficient; q_{rs}, $\bar{q}_{rs}$ denote the demand of private and public transport between r-s.

The lower planning model can be expressed as:

$$\min_{x,v,\hat{q},\tilde{q}} G = \sum_{rs}\sum_k \hat{f}_k^{rs}(\ln \hat{f}_k^{rs} - 1) - \sum_a \hat{q}_{rs}(\ln \hat{q}_{rs} - 1) + \alpha\left[\sum_a\int_0^{x_a} \hat{c}_a(w,\hat{u}_a,g_a)dw - \sum_{rs}\int_0^{q_{rs}} \hat{D}_{rs}^{-1}(w)dw\right] + \sum_{rs}\sum_k \tilde{f}_k^{rs}(\ln \tilde{f}_k^{rs} - 1) - \sum_a \tilde{q}_{rs}(\ln \tilde{q}_{rs} - 1) + \alpha\left[\sum_a\int_0^{v_a} \tilde{c}_a(w,\tilde{u}_a,g_a)dw - \sum_\omega\int_0^{\tilde{q}_{rs}} \tilde{D}_{rs}^{-1}(w)dw\right] \quad (12)$$

$$st. \quad \sum_k f_k^{rs} = q_{rs}, \quad \sum_k \bar{f}_k^{rs} = \bar{q}_{rs} \quad (13)$$

$$x_a = \sum_r\sum_s\sum_k f_k^{rs}\delta_{a,k}^{rs}, \quad \bar{x}_a = \sum_r\sum_s\sum_k \bar{f}_k^{rs}\bar{\delta}_{a,k}^{rs} \quad (14)$$

$$q_{rs} + \bar{q}_{rs} = \hat{q}_{rs} \quad (15)$$

$$q_{rs}, \bar{q}_{rs}, \hat{q}_{rs}, f_k^{rs}, \bar{f}_k^{rs}, x_a, \bar{x}_a \ge 0 \quad (16)$$

Where, α is a parameter of plus values. $\hat{q}_{rs}$ denotes the total demand between r-s, f_k^{rs}, $\bar{f}_k^{rs}$ denote the private and public transport flow on path k.

Because the above-mentioned bi-level optimization model is notsmooth, such traditional methods as interactive and bundle methods are not appropriate for using the bi-level optimization model. The Genetic Algorithms based on natural selection and biogenetics have few limitations on optimization, and are likely to be optimal solutions to the models. Practice proves GA is an efficient tool for the solving of optimization problems, so GA is used here. For more detail see literature (S. An, 2004).

CASE STUDY

When considering the existence of private cars and buses traveling on the road network, most scholars usually choose a four-square city region composed of public transportation grid lines as a numerical example. This example arranged by Holroyd, is the best road network in that all OD are uniformly distributed rectangular lines (Newell, 1979). This paper selects this example of the road network as the basic framework (Ying J. Q & Yang H, 2005), shown in Figure 1.

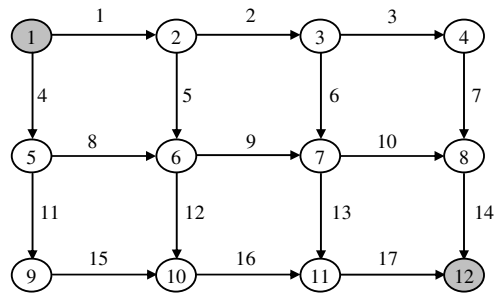

Figure 1: The Network Used for the Numerical Example.

The road network, as shown in Figure 1, consists of 1 O-D pair, 12 nodes and 17 links. We assume that buses share the same streets with private vehicles. Corresponding parameters of road sections are shown in Table 1.

The demand between (1,12) equals 3750, that is $\hat{q}_{rs} = q_{rs} + \overline{q}_{rs} = 3750$. According to congestion pricing revenue redistribution models and the GA algorithm, bus departure frequency y is 8veh/h. The optimal bus fare $\overline{u}$ is 0.51 yuan/veh between (1,12) when revenue from congestion pricing is used to extend road capacity, decreasing bus fare and increasing bus departure frequency. Road congestion pricing and road capacity extension is shown in Table 2.

Table 1: Corresponding Parameters of Road Sections.

Link	t_a^o	B_a	Link	t_a^o	B_a	Link	t_a^o	B_a
1(1,2)	20	1000	7(4,8)	22	500	13(7,11)	26	500
2(2,3)	23	500	8(5,6)	14	1000	14(8,12)	19	1000
3(3,4)	17	500	9(6,7)	17	1000	15(9,10)	7	800
4(1,5)	18	1500	10(7,8)	13	1000	16(10,11)	18	800
5(2,6)	19	500	11(5,9)	24	800	17(11,12)	17	800
6(3,7)	16	500	12(6,10)	20	500			

Table 2: Road Congestion Pricing and Road Capacity Extension.

Link	u	g_a	Link	u	g_a	Link	u	g_a
1(1,2)	4.8	9.78	7(4,8)	0.3	11.26	13(7,11)	0.3	14.21
2(2,3)	2.3	12.00	8(5,6)	4.1	5.35	14(8,12)	6.3	9.04
3(3,4)	0.3	7.56	9(6,7)	4.3	7.56	15(9,10)	3.3	0.17
4(1,5)	7.4	8.30	10(7,8)	6	4.61	16(10,11)	5.6	8.30
5(2,6)	2.4	9.04	11(5,9)	3.3	12.74	17(11,12)	5.9	7.56
6(3,7)	2.1	6.82	12(6,10)	2.2	9.78			

CONCLUSION

This paper proposes that the revenue of congestion pricing can be used to extend road capacity and support public transport. Under two redistribution modes，it is concluded from all of the results of analyses obtained that the costs of private

and public transport will increase, which will cause more use of public transport. On this basis, this paper establishes the bi-level model of congestion pricing revenue redistribution. The results of the calculation examples analysis demonstrate that this bi-level model can represent the variability of transportation demand and the randomness of road user's behavior better than that of traffic managers.

ACKNOWLEDGMENTS

This research is supported by supported by Post-doctoral project in Heilongjian (Project No.AUGA41100032). This work was performed at the National Center of Technology, Policy and Management, Harbin China.

REFERENCES

An S, Wang J, and Li, J. (2004). "Study on pricing for two management modes of on-street parking: Guangzhou case". *Proceedings of the 9th Conference of HKSTS*.Dec. 391-395.Armelius, H., and Hultkrantz L. (2006). "The politico-economic link between public transport and road pricing: An ex-ante study of the Stockholm road-pricing trial", *Transport Policy*. 162-172.

Bernstein, D. (1993). "Congestion pricing with tolls subsidies." *In Proceedings of the Pacific Rim Transportation Technology Conference*, Nov. 145-151.

Ferrari, P. (2005). "Road pricing and users' surplus", *Transport Policy*, 12(6):477-487.

Goodwin, P.B., and Jones, P.M. (1989). "Road Pricing: The Political and Strategic possibilities." *In System of Road Infrastructure Cost Coverage, Round Table 80, European Conference of Ministers of Transport*, Paris. 5-59.

Hau T. D. (1998). "Congestion pricing and road investment", *Road Pricing, Traffic Congestion and the Environment: Issues of Efficiency and Social Feasibility*, Edward Elgar Publishing Limited. 39-78.

Jeffrey L., and Adler, M. C. (2001). "A direct redistribution model of congestion pricing", *Transportation Research Part B*. 447-460.

Kockelman, K.M., and Kalmanje, S. (2005). "Credit-based congestion pricing: a policy proposal and the public's response." *Transportation Research A*, 39: 671-690.

Litman, T. (1996). .."Using road pricing revenue: Economic efficiency an equity considerations", *Transportation Research Record*, 1558: 24-28.

Newell, G.E. (1979). "Some issues relating to the optimal design of bus routes," *Transportation Science* 13, 20–35.

Small, K. A. (1992). "Using the revenues from congestion pricing." *Transportation,* 19:359-381.

Ying, J. Q, and Yang, H. (2005). "Sensitivity analysis of stochastic user equilibrium flows in a bi-modal network with application to optimal pricing". *Transportation Research Part B*, 39: 769–795.

Investment and Financing Influence Analysis and Countermeasures for **Highway Construction in the period of China's 11th** Five-year Plan

Zhang Ruoqi[1], Chen Minglan[2], Cai Xiurong[3] and Liu Fang[4]

[1]Zhang Ruoqi, [3]Cai Xiurong and [4]Liu Fang, Transportation Information Center, China Academy of Transportation Sciences, Ministry of Transport of P.R.China, No. 240, Huixinli Chaoyang District, Beijing 100029, P.R.China; PH (86-10) 65293170, 65293113, 65293153; FAX (86-10) 80115555-ext.301934, 65293125; email: zhangruoqi@catsic.com, cai_xiurong@catsic.com, liufang@catsic.com

[2]Chen Minglan, Department of Development and Strategy, Beijing Automobile Investment Company Limited, No.25, Automobile Tower, South of Third Ring Road, Beijing 100021, P.R.China; PH (86-10) 67699888-ext.8768; FAX (86-10) 87667186; email: chenminglan@ cnbaic.com

ABSTRACT

Highways characteristically provide a basic service, public and social welfare, and economic benefits. The government and the market should both play a role in highway construction. Different types of highways require significantly different types of financing capability. A positive fiscal policy could bring a typical "financial driving-effect" to highway construction. Based on the analysis of influence aroused by the macroeconomic environment change in the period of the "11th five-year plan" (abbreviated as "11FYP") - two aspects of the fiscal policy change and the tax reform, or four suggestions on highway construction investment and financing strategy are put forth regarding legislation, orientation, approach and layout.

INTRODUCTION

Changes in Economic and Social Development During the 11FYP. China's macroeconomic situation continues to develop as a basic "V" during the 11FYP period. There are two reasons for the formation of this trough. On one hand, China's foreign trade dependency is up to 70%. Because of the weakened foreign requirement, the world financial crisis has had negative effects on China's economic development. On the other hand, the domestic economy is in an economic structure transformation and cyclical adjustment, and the economic operation status is the inevitable reflection of "double factors superposition." In view of this, during this period, China's macro-control measures should transform rapidly and policies quickly adjust. Up until now, there have been two big shifts from "two prevents," (prevent the economy from overheating and prevent inflation) to "one keep and one prevent" (keep the economy growing steadily, but prevent the price level from becoming too high). Now there is a focus on "one keep" (keep economic growth at a rate of no less than 8%). Prudent fiscal policy has transformed from a tight to a positive one from the beginning to the mid-term of 11FYP. Financial monetary policy has emerged with a corresponding change. Furthermore, the China State Council has issued an economic stimulus plan for this investment with a scale of

RMB 4 trillion projected by the end of 11FYP, Nearly 38% of this amount is slated for the areas of transportation and water conservancy infrastructure construction. The orientation of the positive Mac policy and coordinated structure adjustments provide an opportunity for rapid highway construction development.

Implementation of Highway Construction Investment Planning in t he Mid-term of 1 1FYP. During the period of 2006-2008, national highway construction has raised funds of 1.68 trillion RMB. Of these funds, the central government fund is 13.5%. Highway construction finished the investment of 1.96 trillion RMB. The total highway length increases 338 thousand kilometers, which means 91% of the task will be completed as part of the "China Highway and Waterway Transportation Development for 11FYP" (hereinafter briefly as "the plan"). The expressway increases by 19 thousand kilometers, which completes 79% of the task in "the plan". Highway that is above II-grade technical condition increases by 67 thousand kilometers and is 54% complete. Rural roads increase 294 thousand kilometers and will be 91% complete. Ninety-three percent of townships and 91.9% of villages have road connections. Twelve national trunk highways run through and national expressway network construction is involved in large-scale construction.

Despite overall highway construction progress and improvements in the highway infrastructure that have happened up until the mid-term of 11FYP, the plan is inevitably affected in the face of great changes in China's macroeconomic policy.

INFLUENCE ANALYSIS

Highway Infrastructure's Attributes and Financing Capability Analysis

1.）Attributes and Characteristics

The highway is a kind of public infrastructure and a means of transporting quasi-public goods. It plays a fundamental role in the national economy and almost all social and economic activities as personnel and goods are moved., Thus, highways have the attribute of providing a basic service function.

Highways will spread and transfer many benefits for social welfare and life, but it is hard to ask for a return and prevent a spillover effect for all users. So the highway has the characteristic of serving public and social welfare.

The cycle of highway construction is long and the investment is huge. But once the highway network is formed, it brings far more social and economic effectiveness than the composition of single roads. Therefore, the highway has net scale economic benefits.

2.）Financing Capability Analysis

Highway financing capability is closely related to the characteristics of its attributes. Since highways are a kind of quasi-public goods, its investment potential is often determined by the government and the market. Under certain conditions, it can be determined by the government, or by the market, or both.

The economic factors and traffic level are important factors that can impact the financing ability of highway projects. For general highways in low-grade technical condition, the investment should come entirely from state and local governments for they have an interest public welfare and low financing capability.

Actually, this should be the government responsibility.

Highways with the higher level of technical condition can provide better services for users, and are used for transporting merchandise. Because toll rights are involved in the deal, they have certain financing capability. However, even the expressway, which has the strong financing capability in the highway construction market, faces problems in the face of rising financing costs and risks. According to the calculations, most of the expressway projects' financial internal rate of return is much lower than the average social discount rate. If there is no guide and support of the related policy and no proportion of direct investment, it is almost impossible for highway investment and construction to completely depending on the market.

HIGHWAY CONSTRUCTION INVESTMENT AND FINANCING INFLUENCE ANALYSIS

The Change of the Central Finance Policy . Central finance capital is not only used in the direct investment in highway construction, but is also used to increase the capital fund, so it can significantly increase project financing capability and then promote input of bank loans and local funds. In fact, the banks regard fiscal funding as the "invisible" support of the government and involvement of this kind helps prevent risks.

From the beginning of 11FYP, the national fiscal and monetary policy has been "tightening" until the fourth quarter of 2008. This affects the total capital in the national budget applied to highway infrastructure, and applications for construction land and bank loans have become harder and harder to obtain. The ratio between highway construction investment and social investment in fixed assets and the ratio between capital of the national budget and financing funds decrease gradually. The growth rate of newly increased highway fixed assets also slows sharply (see Table 1).

Table 1. Highway Construction Investment and Financing Funded Scale from 2004 to 2008.

	Highway construction investment ① (billion RMB)	Rate[1] (%)	Rate[2] (%)	Capital of the National Budget in Highway ② (billion RMB)	Rate[3] (%)
2004	464.50	6.6	26.9	13.75	3.3
2005	541.31	6.1	16.5	11.82	2.6
2006	613.88	5.6	13.4	8.13	1.6
2007	640.01	4.7	4.3	7.74	1.4
2008	675.52	3.9	5.5	15.92	2.7

Note: Rate[1]=①/Social investment in fixed Assets, Rate[2]=annual rate of growth of ①, Rate[3]=②/ Highway construction financing funded.

At the end of 2008, highway construction projects included in the "program with the central budget of 10 billion RMB" have obtained national funding. Highway projects have gained more financing opportunities in the environment of "loose" monetary and fiscal policy. Those projects are promised 15.6 billion RMB in

supporting funds from local government, national banks and even some foreign banks. In the new cycle of stimulating domestic demand and accelerating fixed asset construction, it is expected that highway construction will drive nearly another 2 trillion of total investment scale at the end of the11FYP period.

To meet the requirement of sustainable and balanced development, full use should be made of the existing financing channels and challenged by expanding investment scale to meet the needs of the present economic development, as well as greatly raising investment efficiency in order to strengthen construction structure and quality. That is the real challenge for transportation management departments in "the super-ministries" transformation.

The Influence Analysis of Tax Reform on Highway Construction . Since 2009, fuel tax reform has been carried out in China. After enterprise income tax and value-added tax system reform, it is another very important tax reform. Fuel tax has replaced maintenance fees, additional expenses for the passenger and goods transport, and administration fees for highway and waterway facilities and transport. In addition, the toll fees of the highways above II-grade technical condition whose debts are paid by the local governments will be canceled step by step. On one hand, fuel tax reform rationalizes China's taxation system and establishes the internal mechanism of energy consumption mediation. On the other hand, it changes the pattern from "giving priority fees to tax" to "giving priority tax to fees.". That is, the new tax system primarily takes fuel and vehicles purchase taxes, and takes the toll fees from highways in higher-grade technical condition as auxiliary fees. At the same time, vehicles purchase tax for vehicles whose displacement is less than 1.6 liters is reduced to 5% from January 20th to December 31st 2009.

According to estimates, vehicle purchase tax collected by the State Taxation Administration will decrease about 8 billion RMB, and less than 10% of the total vehicles purchased taxation in 2009. In view of the recent annual vehicles purchase tax contribution to highway construction, which is less than 90% of the amount collected, the effect of vehicle purchase tax expenditure is almost negligible. However, the implementation of fuel tax reform will bring about great influence.

First, the local transport management departments collected and expended the fees mentioned above before the establishment of the new tax system. The central government just macro controlled the criteria and scope of collected fees. Local transport management departments play an active and generative role. They maintain the highways from collected fees, simplify the procedure and administrative of levels of spending and appropriation so as to adapt to seasonal highway construction. After the establishment of the new tax system, tax agencies will impose the fuel tax and hand it over to state finance. State financial departments will arrange the tax according to the strict budget plan that will subordinate financial departments . Financial departments will then transfer it to transport management departments. The capital turnover takes a long time. This pattern may have some problems in the cases of capital used for any purpose other than highway construction and capital not meeting the construction demand of general highways in the lower grade technical condition.

Second, local transport management departments lost the possibility to use fees (such as maintenance and administration fees) as the financial guarantee or backing the need to apply to banks for loans because national financial capital cannot be used as the debt guarantee. To a certain extent, that impacts the construction and the financing channels of highways in higher-grade technical condition. Highway projects that have used transportation fees as the financial guarantee must be handled accordingly. In addition, under the new tax system, highway construction fund management is changed from the non-budgetary pattern to the national financial management pattern, run strictly according to "separate income and expense management." Appropriation is directly paid to construction units. This will cause cash flow reduction and a unitary financing structure for local highway construction. The ability to finance a single project is relatively weak. While investment entities that can replace local transport management departments with finance capital have not been established, the financing capability of highway construction units is weakened. This requires reforming and adjusting the current capital management and financing systems.

COUNTERMEASURE

Highway construction needs to complete the targets and tasks it will be facing as a consequence of the changes that will occur in the later period of 11FYP. So the following strategies and suggestion from the perspective of the government are suggested based on the influence analysis of highway construction investment and financing environment:

The government sho uld lay a solid foundation for highway construction by establishing and improving laws and regulations. There is only the "Highway Law of the People's Republic of China" which rarely includes specific provisions for highway construction investment and financing. The law is hard to comply with and implement. Relevant government orders and administrative regulations about capital financing also exist, but they could not meet the requirements for highway construction because of artificial factors and the vulnerable policy environment. It is urgent to establish laws that will provide the excellent macro environment for investment and financing activity. New laws and regulations should provide stable and legal financing channels or approaches under a fair, reasonable and legal framework, and guarantee the rationalization, supervision of the capital scale, as well as recourses and uses for highway construction.

The government should restrict , guide and coordinate highway construction. On one hand, this would ensure annual financial input by arranging key highway project investments in the public finance system framework, while increasing financial budget appropriations in the field of general highways building and rebuilding. On the other hand, it would make the vehicles purchase tax and fuel tax truly a main and reliable source of policy funds. The government would restrict, guide and coordinate, all aspects of not only scale, but also layout and structure.

The government should ma ke full use of existing financing approaches and social capital, actively expanding financing channels. At present, the existing

financing approaches are effective financing channels for highway construction. These channels include issuing bonds and stocks, utilizing foreign investment, BOT (Build-Operation-Transfer) mode etc. and should continue to be used to help set up the standard operation and management systems for highway construction. In addition, Asset-Backed-Securitization (ABS) is also a suitable financing channel for highway construction when domestic capital markets are allowed. The government can enliven the investment and financing market by encouraging and supporting enterprise capital, social capital and overseas capital access while reducing permission restrictions so as to gradually form a relatively reasonable investment structure and possibly meet the needs of highway construction.

The government should arrange to rationally investment in rural road construction and rea lize the healthy development of highway construction. Solving the problems of "peasant-village-agriculture" is one of the government's and transport management's priority tasks. Rural road construction should be adopted in the framework of public finance where local governments give priority to township and social input. Central financing capital can be the oriented funds which drive and mobilize local financing capital at various levels so as to promote local economic development as well as guarantee national highway construction.

CONCLUSION

Highway infrastructure should take advantage of the opportunities that the government is providing as part of the positive fiscal and monetary policy that will occur during the latter part of 11FYP and adapt to the changes and requirements of the new tax reform. Transportation management departments should set up and improve laws and regulations concerning highway construction investment and financing, broaden the financing channels, optimize capital layout, explore the mechanism established to promote coordinated and sustainable development of highway construction, and lay the solid foundation for the 12FYP of China's highway transportation development.

REFERENCES

Ministry of Transport of the People's Republic of China (2006). "China highway and waterway transportation development for 11th five-year plan".

Ministry of Transportation, the People's Republic of China, "China highway and waterway transportation statistics Yearbook 2008".

Xu, Q. (2008). "The investment and financing problems and countermeasures for China's expressway", Modern Management Science, (3)109-110.

A Study on the Financing Mode of Assets Securitiz ation in Port Project

Yu Su[1]

[1]MBA education center of Shanghai Maritime University, Cell phone: 13918184850; email: yusu@sem.shmtu.edu.cn

ABSTRACT

Through analyzing the asset property of ports, this paper maintains that the high efficiency of port asset provision needs wide multi-channel financing on the basis of clear responsibility. As to the financing channels and mode, this paper combines the theory and operating characteristics of assets securitization, by mainly investigating the function and implementing pattern of port assets securitization. It further proposes an assets securitization financing mode and blueprint for Chinese port projects, and finally proposes an "immune" plan against the possible assets value risk of this financing mode.

INTRODUCTION

Background . China, as an emerging economic power, has 18,000 islands, a coastline of more than 18,000 kilometers and an inland waterway of more than 100,000 kilometers. However, the insufficient investment of port facilities means that the port construction pace cannot catch up with the economic growth rate, a bottleneck which is a difficult situation in port construction financing. While asset securitization is a developing trend in international financing, the investment channel of Chinese civilian capital is very limited. With few investment choices, and a single form of capital market, the stock market is facing high risks. At the same time, port assets have a large capacity for absorbing capital and a steady return, but very few such companies are listed in the security market. Thus, the possibility of expanding port construction through stock market financing is an import subject that we must currently deal with.

The Purpose of the Research . According to international experience, asset securitization is a supplementary financing method that can be used in China. In this essay, I first analyze the property of port project assets, then by combining the theory and operating characteristics of assets securitization, I introduce a feasible mode for port asset securitization financing, and propose a corresponding plan.

PROPERTIES OF PORT ASSETS

Public goods are non-rival in consumption and non-excludable. Based on the efficiency of public goods provision, different types of port assets are provided by different parties, as can be seen in the following table:

Table 1 . Different Types of Port Assets Provision in Chin a.

Types of products	Types of port project	Types of port assets	Investment mainbody
Public goods	Public investment project	The water and land way. Buildings and sites for customs, inspection and quarantine officials, etc.	Government, by levying a tax on the users according to the relevant rules and regulations
Quasi-public goods	fundamental investment project	Wharfs, berths, cable fastening facilities and other floating vessel parking facilities, etc.	Examined and approved by the government ， invest and run by the enterprises
Private goods	Competing investment project	Loading and unloading equipment, transportation conveyance, warehousing facilities	Enterprises, individuals, non-governmental organizations or commercially loaned capital.

The classification in Table 1 is not absolute. There are enterprises in other countries that invest in sea routes and charge for them. There are also governments who invest in the public wharf and make it free to the public.

ENVISION OF THE MODES OF ASSET **SECURITIZATION IN CHINA'S** PORT PROJECT

Single mode of securitization financing for a new port . The precondition of applying this mode is: the newly built port must be developed on virgin soil; there is no existing infrastructure or corresponding facilities that can be borrowed from, such as the Shanghai Luchao port construction project.

To finance a new port project, the government should shoulder the responsibility of infrastructure construction at the early stage of port financing. In the case of a tight budget imposed by the financial department, assets securitization can help fill the gap. The securitization mode conceived in this paper can be illustrated in the following simplified model:

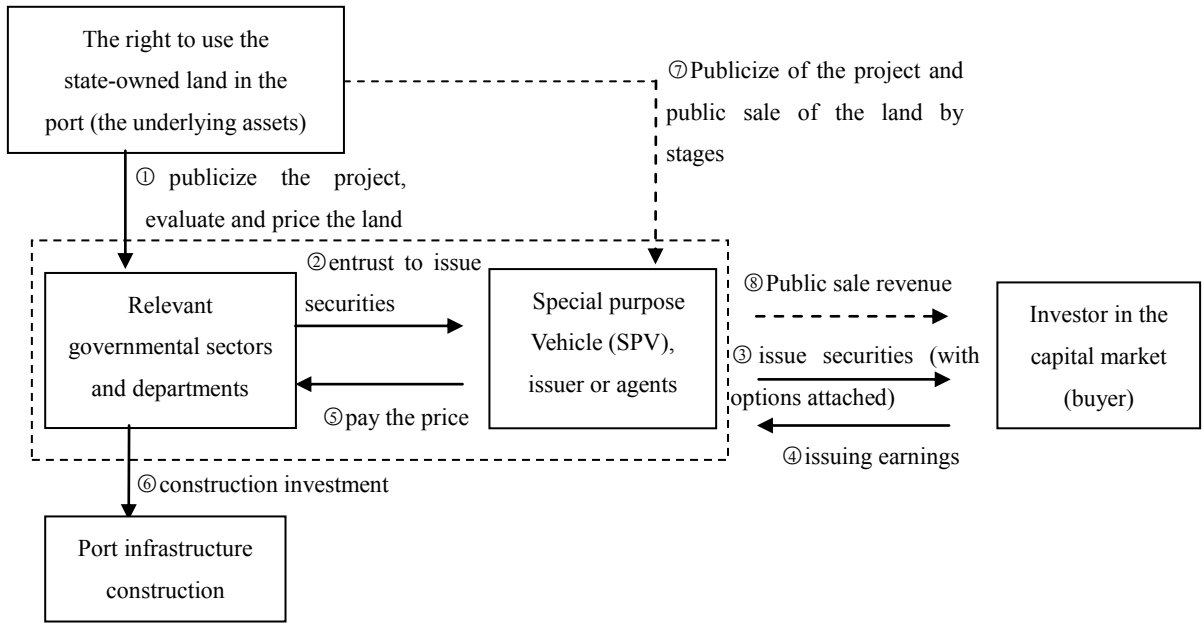

Figure 1 . Single Mode of Securitization Financing for a New Port.

The above mode can be a win-win solution. The government gets the future land-sale proceeds at one time and invests in infrastructure construction of the port. The investor hedges its risks by attached options and get the extra profits of the land.

Mode of Securitization Financing Based on First Phase Project Assets for the Second Phase Construction . The previous financing mode can be extended, when the first phase of the project has been completed. The income gained from the project assets leasing can be used as the underlying assets for the securitized financing of the second phase project. The following chart will give the details:

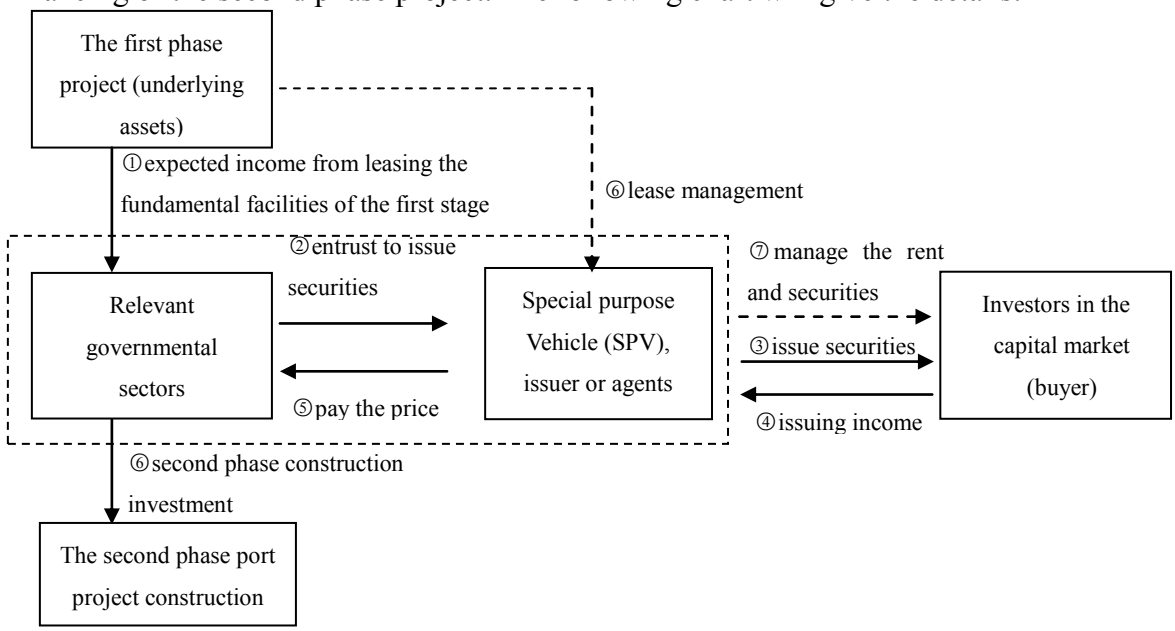

Figure 2 . An Extended Financing Mode.

PROBLEMS OF CAPITAL MANAGEMENT AFTER ASSET S SECURITIZATION IN PORT PROJECT

Duration of Securitized Assets . Capital management after securitized financing is the key factor to the success of the whole project. As the income capital flow of port assets does not match the expenditure cash flow at each term, exposure risk exists all the time. Therefore, we need to introduce "duration" to match these positions, which will be illustrated later.

Macaulay Dration(D): $D = \dfrac{\sum_{i=1}^{n}\left[\dfrac{CF_i}{(1+r)^i}\cdot i\right]}{\sum_{t=1}^{n} PV(CF_i)}$, Modified Duration(MD): $MD = \dfrac{D}{1+r}$

Then we have: $\dfrac{dP}{P} = -MD\cdot dr$

Suppose some securitizable port assets can bring 10 billion Yuan RMB revenue per year (which can be seen as an expected cash flow of 10 billion Yuan/year in the next 5 years). The market yield for a 5-year financial product is 5%. When discounting the yield over the next five years, we can get the present value of the expected yield in the following table:

Table 3 .The Present Value of the Expected Yields (in 100million Yuan) .

Term (year)	1	2	3	4	5
Expected annual yield	10	10	10	10	10
PV of the expected annual yield	9.5238	9.0703	8.6384	8.2270	7.8353

The total present value of five years' expected proceeds is:

$$P = \sum_{i=1}^{5} PV(CF)_i = \sum_{i=1}^{5} \frac{CF_i}{(1+r)^i} = 9.5238+9.0703+8.6384+8.2270+7.8353 = 43.2948$$

Suppose we decide the size of securities issuing according to the present value of the assets, or 4.32984 billion Yuan. We issue the debt securities at face value with coupons attached, and then the real yield rate is 5%, equal to the market rate. We can calculate the cash flow of the debt securities in the next five years:

Table 4. The Present Value of the Expected Payment (in 100million Yuan) .

Term (year)	1	2	3	4	5
Expected annual payment	2.1647	2.1647	2.1647	2.1647	4.5.4595
PV of the expected annual payment	2.0616	1.9634	1.8699	1.7809	3.5.6187

From the above two tables we can see that securitized financing for port assets by issuing the debt securities with coupons attached will mean that the yield and payment cash flow won't match. More specifically, during the first four terms, the cash flow of yield far exceeds that of payment, while in the fifth term, the cash flow of payment far exceeds that of yield.

The Macaulay Duration of expected value of yield:

$$D_1 = \frac{\sum_{i=1}^{n}\left[\frac{PV(CF)_i}{(1+r)^i}\cdot i\right]}{\sum_{t=1}^{n} PV(CF_i)} = \frac{9.5238\times 1 + 9.0703\times 2 + 8.6384\times 3 + 8.2270\times 4 + 7.8353\times 5}{43.2948} = 2.9025$$

Modified duration: $MD_1 = \frac{D_1}{1+r} = \frac{2.9025}{1.05} = 2.7642$

The Macaulay Duration of expected value of payment:

$$D_2 = \frac{\sum_{i=1}^{n}\left[\frac{PV(CF)_i}{(1+r)^i}\cdot i\right]}{\sum_{t=1}^{n} PV(CF_i)} = \frac{2.0616\times 1 + 1.9634\times 2 + 1.8699\times 3 + 1.7809\times 4 + 35.6187\times 5}{43.2948} = 4.5459$$

Modified duration: $MD_2 = \frac{D_2}{1+r} = \frac{4.5459}{1.05} = 4.3294$

The market value of assets is calculated according to the net present value. In the above case, the five-year assets yield 4.32948 billion Yuan, with the Modified Duration being 2.7642; while the total present value of securitized assets is also 4.32948 billion Yuan, but the Modified Duration is 4.3294. This means that when the market rate changes, there will be big differences in these two values. In the end, the market risk will be out of control.

Risk Immunity o f Cash Flow Management . From the duration value calculated above, we can see that there is a big difference between the duration of expected payment of debt securities and the duration of expected yields of the assets. Further, the cash flow of future yields cannot offset that of the payment, which suggests that the position exposure may cause large market risk. The change rate of the value of expected payment will be 56.62% larger than that of the market yield, in which case the market value formed after the securitized assets are listed on the market will fluctuate asymmetrically. This brings great risks to the management of these assets.

As the expected income of port assets is uncontrollable and unchangeable, the

only way to solve the above problem is to change the structure and proportion of expected income that is to change the compound duration of expected income. To reach this goal, we can change the structure of securities issued to combine the issuance of short-term securities, median-term securities, and long-term securities to get a compound duration of payment that is in correspondence with that of the expected income at any time.

To be specific, we can issue a one-year short-term debt security, three at the rate of 3% in addition to the previous five-year debt securities. As there is only one expected future payment cash flow for the one-year debt securities, the Macaulay Duration is $D_3 = 1$

the modified duration is: $MD_3 = 0.9709$

Then, use the risk-immune way to balance the duration, we get:

$$\begin{cases} MD_1 = W_2 \times MD_2 + W_3 \times MD_3 \\ W_2 + W_3 = 100\% \end{cases} \quad \begin{cases} 2.7642 = W_2 \times 4.3294 + W_3 \times 0.9709 \\ W_2 + W_3 = 100\% \end{cases},$$

$W_2 = 53.40\%$; $W3 = 46.60\%$

Therefore, as long as we issue the long-term and short-term securities according to a certain proportion, the interest rate fluctuating risk of future cash flow will be in control.

CONCLUSION

Port asset securitization in China has just come into being, and many problems are still waiting to be explored. There is rarely any past experience to follow in China, and it is also impractical to copy successful examples from foreign counterparts due to systematic differences. In the article, the author first designs two models to analyze port asset securitization in China. The models are based on the basic theories of asset securitization and are adjusted for Chinese port asset classifications. The author then studies the cash flow patterns after port asset securitization, and based on the results, uses duration theory to probe into risk management issues during the securitization, and raises a simple but effective method to control the risk.

As China's security market continues to improve, the theory of duration in risk management will certainly be utilized on a greater scale. This article has only taken the first step in discussing issues in financing process and financing risk in China's port asset management, and the conclusions and suggestions in the article carry the author's intent to invite more contributions to this field of research.

BIBLIOGRAPHY

Huang, Y., and Ning, M. (2006). “Research on multi-financing model of port construction,” Journal of Beijing, Jiaotong University.

Junling, L. and Yanbao, L. (2004). Explore on China port financng mode with capital

structure theory, China Ports.

Kaiguo, W. (1999). On assets securitization, Shanghai University of Finance and Economics Press, Shanghai, China.

Ruiqing, S. (2002). Reference on European, American and Japanese water transportation project financing, China Investment.

Samuelson, P.A. (1954). The pure theory of public expenditure. review of Economics and Statistics, 36.

Song, J., Haifeng, F. and Meiqing, Z. (2006). "Actuality and developing trend of investment and financing direction of the waterage in China," World Shipping.

Study on the Capacity of Right -**Turn Movement Under Pedestrians' Influence at** Signalized Intersections

Wanchao Zhang[1], Xiaokuan Yang[2], Zhi Xu[3]

[1]Transportation Research Center, Beijing University of Technology, Beijing, China.Tel: (8610) 6739-1678; Email: zhangwanchao2008@emails.bjut.edu.cn

[2]Professor, Transportation Research Center, Beijing University of Technology, Beijing, China.Tel: (8610) 6739-1678; Fax: (8610) 6739-2991; Email: xiaokuan@bjut.edu.cn

[3]Transportation Research Center, Beijing University of Technology, Beijing, China. Tel: (8610) 6739-1678; Email: xuzhi@emails.bjut.edu.cn

ABSTRACT

In the big cities of China, pedestrians and bicycles have a great impact on the capacity of right-turn lane vehicle movement at signalized intersections. In most cases, pedestrians become the main factor in the capacity of movement in the right-turn lane, This paper attempts to explore the potential capacity of right turn movement when there are conflicts between right-turn vehicles and pedestrians at signalized intersections. In order to take this impact into account in the capacity calculation, it is assumed that all pedestrians obey the traffic regulations, which means pedestrians cross the intersection only when the pedestrians' signal indication is on. The objective of this study is to quantitatively analyze the impact of pedestrians on the capacity of right-turn vehicles at signalized intersections with regard to different signal phases. In order to reach this objective, a new concept of "Pedestrian Group" is introduced in this paper, where the capacity model of the right-turn lane at signalized intersection is based on gap acceptance theory. The results of this study has great importance for the development of capacity analysis and our own Manual.

INTRODUCTION

The traffic conditions at intersections in China are relatively complicated as compared to other countries. At intersections, there are heavy conflicts between pedestrian traffic and vehicular traffic. Based on traffic regulations, those making a right turn can make that turn during any signal indications for the majority of signalized intersections in China. However there is a conflict between right turn vehicles and pedestrians crossing at intersections during green indication. On these occasions, pedestrians have a great impact on the right turn capacity at signalized intersections. The Highway Capacity Manual (HCM) estimates an adjustment of saturation flow rate of right turn movement during different phases and lane use, but

it does not provide the approaches to estimate the effect of pedestrians. In China, many approaches also do not estimate the effect of pedestrian movement. Therefore, the motivation behind conducting this study is to model the potential capacity of right turn movement under the presence of through pedestrian flow at signalized intersections. This model can, to some extent, represent the real state of signalized intersections in China. This model can also help traffic engineers conduct capacity analysis under mixed traffic conditions. In addition, the results of this study provide useful information for traffic management at signalized intersections.

METHODOLOGY

Analysis of characteristics of right -turn movement

At signalized intersections, right turn vehicles conflict with through pedestrians from two directions. As shown in Figure 1, during the green indication right-turn vehicles have to yield to through pedestrian traffic based on traffic regulations. As a result, the capacity of right- turn movement will definitely decline.

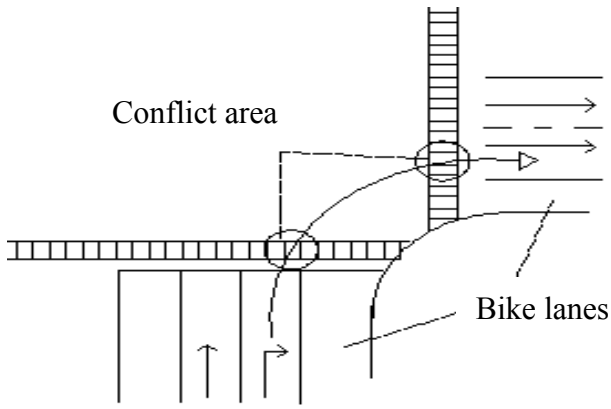

Figure 1. Illustration of Conflicts Between Pedestrians and Rig ht-turn Vehicles.

Characteristics of conflicts

Right turn vehicles and pedestrians have three types of conflict:

(1) No conflict

Because of traffic signal control, pedestrians should wait for crossing at the sidewalk during the red indication for pedestrians. At this time. right turn vehicles have no conflict with through pedestrians.

In this case, the maximum number of right-turn vehicles through the intersection can be estimated by equation 1.

$$n_l = \frac{3600}{T}\left(\frac{t_g}{h_l}\right) \quad (1)$$

Where, n_1 = the number of right turn vehicles through the intersection (veh);
T = cycle length (s);
t_g = green time for right turn movement (s);
h_t = headway of right turn vehicles (s).

(2) At early stage of green indication the number of right-turn vehicles through intersection is n_2.Pedestrians are in constant arrival during the red indication and concentrate at the intersection. When the pedestrian signal turns yellow, pedestrians will be the first to enter the crosswalk. The right turn vehicles must wait for pedestrians to cross at this time. In this case n_2=0.

(3) Pedestrians arrive in a random manner. The number of right turn vehicles through the intersection is n_3.

Pedestrians randomly arrive at the intersection during this period. The right turn vehicles pass through the intersection according to the distance between the pedestrian's flow. The gap acceptance theory is then used to simulate the process of right turn movement traversing through pedestrian flow. Note that pedestrian movement has its own characteristics in passing through the intersection. They often pass through the intersection one-by-one or in groups. However, the traditional gap acceptance model is applied to passing through in a single-stream only. In this paper, pedestrians are divided into groups in accordance with their characteristics of movement. In this way, gap acceptance model can be applied to compute the potential capacity of the right-turn vehicles. The capacity of the right turn lane can be estimated by applying the following equation 2.

$$n = n_1 + n_2 + n_3 \quad (2)$$

Where, n_1 = the number of right turn vehicles through the intersection when there is no pedestrian crossing,
n_2 = its value is 0
n_3 = the number of right turn vehicles through the intersection when pedestrians randomly arrive at intersection.

Estimation of n_3 based on gap acceptance model

Pedestrians have unique characteristics when they pass through the intersection., We can put pedestrians into groups based on these characteristics. Taking pedestrian groups as a study object, we can use the gap acceptance model to estimate the potential quantity of the right turn vehicles.

Analysis of pedestrian group

Movement of pedestrians on crosswalks shows some obvious common features. These features are elaborated in the Highway Capacity Manual (HCM). The common features are as follows:

1) Pedestrian often travel together. They often arrive at the intersection in groups.
2) To avoid collision, when two pedestrians pass each other each should have about 2.5ft of walkway width.
3) Most of pedestrians believe that right-turn vehicles should yield to pedestrian traffic

Based on these features, the "pedestrian group" concept is proposed in this study to explore the potential capacity of right turn movement influenced by pedestrians taking 10 typical signalized intersections in Beijing as study subjects. Pedestrian group is defined as a group of pedestrian who possess the same location and the move at the same speed.\

Approach of dividing pedestrian groups

Pedestrians can be divided into groups based on the distance between two adjacent persons. When the distance between two adjacent persons is greater than L (L is pre-set value that can be calculated according to time and speed).A separated point can be set up. The relationship between pedestrian groups and separated points is as follows:

$$G_P = k + 1 \tag{3}$$

Where

G_P = the number of pedestrian groups;

k = the number of separated point.

According to the distribution of time-headway between pedestrians, the probability P(H>t)can be calculated. H is the time-headway between two adjacent pedestrians. When the traffic volume is Q, the separated points K can be calculated with equation 4.

$$k = QP(H \geq t) \tag{4}$$

The number of pedestrian group can be calculated by equation 5

$$G_P = QP(H \geq t) + 1 \tag{5}$$

We can compute the number of pedestrian groups once we know the distribution of pedestrian arrival with this method.

3 Determine the distribution of pedestrians

After investigating 10 intersections in Beijing, it is found that the arrival of pedestrians complies with the Poisson distribution when the flow of pedestrians is not excessive. Taking Xi Dawang-Bai Ziwan intersection as an example to analyze the distribution of the pedestrian arrival, survey data is

shown in Table 1 with a counting interval of 1 min.

Table 1. Volume Data Obtained from Intersections .

Arrive number	0	1	2	3	4	5	6	7	8	9	〉=10	aggregate
frequency	1	3	8	6	5	5	4	10	1	0	2	41

K-S testing for the above data is conducted by using SPSS software. The outputs are shown in Table 2.

Table 2. k -s Test for the Distribution of Pedestrian Arrival .

		frequence
N		11
Poisson Parameter (a,b)	Mean	4.09
Most Extreme Differences	Absolute	.188
	Positive	.188
	Negative	-.125
Kolmogorov-Smirnov Z		.622
Asymp. Sig. (2-tailed)		.834

From the output it is known that the value of P=0.834>0.05 for this 2-tailed test, which demonstrates that the pedestrian arrival of north-south bound movement complies with the Poisson distribution at this intersection. Likewise, based on the data of east-west bound movement, it can be proved that the pedestrian arrival of east-west movement also complies with the Poisson distribution.

After grouping pedestrians and realizing the pedestrian impact on right turn vehicles pedestrian groups became the object of our study. Gap acceptance theory can be used to simulate the process of right turn movement traversing through pedestrian groups flow as is shown below:

$$n_3 = \frac{G_p \cdot e^{-\lambda t_c}}{1 - e^{-\lambda t_f}} \tag{6}$$

Where

n_3 = potential capacity of right turn vehicle during green indication (veh);

t_f = follow-up time of right-turn vehicle in second (s);

t_c = critical gap for right-turn vehicle in second (s);

G_p = number of the pedestrian groups (s).

MODEL BUILD -UP

Based on the above analysis, the capacity of right turn lane can be calculated by equation 7

$$c = \frac{3600}{T}\left(\frac{t_g}{h_t}\right) + \frac{G_p e^{-\lambda t_c}}{1 - e^{-\lambda t_f}} \quad (7)$$

Where

T = cycle length (s);

t_g = no impact time of right turn vehicles (s);

h_t = headway of through stop-line of right turn vehicles (s);

t_f = follow-up time of right turn vehicle in second (s);

t_c = critical gap for right turn vehicle in second (s);

G_p = number of the pedestrian groups (s);

MODEL VALIDATION

For the validation of the model we cite Xi Dawang-Bai Ziwan intersection as an example. The correlative data is shown in Table 3.

Table 3. Data from Intersection .

	North-south	East-west
Pedestrian volume	293	176
Green time	90s	27s

For this intersection the cycle length is 120 seconds, yellow time is three seconds. The critical gaps and follow-up times for right turn vehicles traversing bicycle flow were observed from video tapes. Critical gap is 5 seconds in this study. The follow-up time is 3 seconds. The pedestrian arrival of this intersection obeys Poisson distribution. When the travel time between two adjacent persons is more than 2 seconds, a separated point can be set up. The separated points K can be calculated with equation 4.

Number of pedestrian groups:

$$m = 187 + 1 = 188$$

Number of right turn vehicles through the intersection during green time (north-south direction):

$$n_3 = \frac{188 \times e^{-0.0814 \times 5}}{1 - e^{-0.0814 \times 3}} = 568$$

Number of right turn vehicles through the intersection during green time (east-west direction) is 195. The capacity of the right turn lane is 568+195=763

(PCE/H)

For two-phase intersections, the right-turn vehicles are always impacted by pedestrians. Therefore, there is no need to calculate n_1. But, for three or four-phase intersections, pedestrians will not interfere with right-turn vehicles. In this case we need to calculate n_1.

CONCLUSION AND FURTH ER STUDY

It is concluded from this study that pedestrian traffic at signalized intersections has a big impact on the capacity of right turn movement. To model the relationship between pedestrian movement and the potential capacity of right turn movement will help traffic engineers and management better understand performances under the mixed traffic conditions at intersections. The concept of pedestrian groups was proposed in this paper to facilitate building up this model. This concept plays a key role in the model building because the movement of pedestrian traffic is different from the movement of automobiles.

This is a preliminary study for the capacity analysis of vehicular traffic under the presence of pedestrians. The follow-up study will be carried out to develop all details of the impact of mixed traffic on the performances of intersections. The mutual impact of both pedestrians and bicycles at signalized intersections will be the focus of further studies in order to fully and completely reflect China's characteristics of traffic movement at intersections.

BIBLIOGRAPHY

Allen, D.P., et al. "Effect of Bicycles on Capacity of Signalized Intersections" Transportation Research Board 77 th Annual Meeting, January 1998, Washington, D.C., CD-ROM.

Landis, B.W, Guttenplan, M. Crider, L.B. (2003) "Intersection Level of Service: Bicycle Through Movement," Transportation Research Board 82 nd Annual Meeting, January 2003, Washington, D.C., CD-ROM.

Xiao-ming, C., and Shao chun-fu (2008). "Computation models of capacity influenced by non-power driven vehicle at signalized intersection." ASCE, 8(2):101-105.

Ramp Metering Strategies in a Corridor Network

Qiong TIAN [1], Haijun HUANG[1], Hai YANG [2]

[1]School of Economics and Management, Beijing University of Aeronautics and Astronautics, PH (86) 10-8231-6608; FAX (86) 10-8232-8037, China;
E-mail: tianqiong@buaa.edu.cn; hjhuang@nsfc.gov.cn
[2]Department of Civil Engineering, The Hong Kong University of Science and Technology; E-mail: cehyang@ust.hk

ABSTRACT

In this paper, which regards highway capacity as scarce resource, we study the ramp metering strategies that have a great effect on commuters' travel behavior. A spatial residence location problem has been incorporated in the travel choice model. Two representative strategies, namely space equality and commuter equality, are investigated. It has been proven that both strategies attract the same total trip demand,. However, while space equality will have less social cost than commuter equality, this is not consistent with our general belief. For long-term planning purposes, local authorities should insist on adopting the space equality ramp metering strategy, which can alleviate traffic congestion and cause no harm to total demand.

INTRODUCTION

Urban traffic congestion is recognized as a significant type of externality arising from vehicle usage in both developed and developing countries (Small et al., 1989). Recently, Lago and Daganzo (2007) focused on an idealized two-origin, single-destination network with limited storage space to analytically study queue spillovers and merging competition phenomena. They found that not considering merging competition will cause the total cost to be over estimated, as the point-queue model did, and with proper ramp metering, may cause some drivers too be better-off without hurting the others. Because the spillover queue will spread backward and may even gridlock the highway by several blocks during peak periods, urban authorities generally want to prevent artery highways from hyper-congesting and maintain traffic flow into the Central Business District (CBD hereafter) at the highway's maximum flow rate.

Shen and Zhang (2009) studied the morning commute problem in a freeway with multiple on-ramp accesses. They analyzed the properties of the system optimum and designed a dynamic road pricing policy to achieve the optimum. The ramp metering strategies, however, are not taken into consideration in their work.

Their ramp metering is obviously an effective tool in helping urban authorities regulate traffic flow. Their paper is focused on investigating the effect of the various ramp metering strategies on social welfare.

In this paper, we study the morning commute problem in a corridor network with multiple bottlenecks along the highway by characterizing the ramp metering strategy. Our analysis considers both departure time and residence location choice. The congestion costs arising from the departure time choice is captured by the bottleneck model formula, , while the residence location choice is based on a general spatial equilibrium model. In the next section, we formulate the basic model and illustrate the two representative ramp metering strategies. Then, we derive the equilibrium trip demand and trip cost based a general spatial equilibrium. Some comparisons between the two strategies are made in the last section to show the core result of our paper. We conclude the paper with remarks and introduce some our on-going work in this areai.

2. BASIC MODEL

As shown in Fig. 1, imagine a linear city where CBD is located at the center (origin of coordinate) and residential areas are developed around the CBD. The land area of the CBD is negligible and the characteristic of each residential location is represented solely by the distance from the CBD. It is assumed that all residents in the city are homogeneous and they have the same desirable arrival time at the CBD, (the same value of time and the same arrival early/late penalty). A highway, B kms long, connects the CBD with the outlying areas of the city. The width of the highway is uniform and the highway capacity is μ vehicles per unit time.

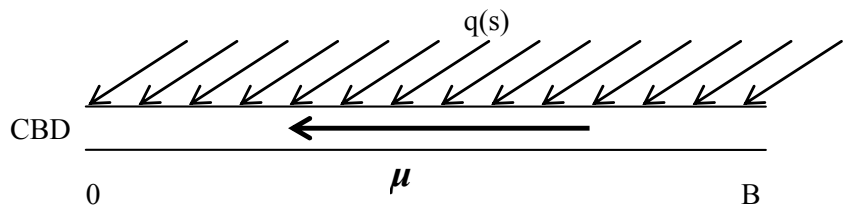

Figure 1. The Study Network.

On each work day morning, an individual makes trips from his/her residence to the CBD by private car. Other types of trips are neglected. Let s be the distance from the CBD, and q(s) denotes the trip demand of a resident located at s. In this section, we assume the trip demand exogenous. Then the (inverse) trip demand function is given as

$$p\big(q(s)\big) = a - bq(s), \quad \forall s \in [0, B] \tag{1}$$

where a, b are positive constants and p(q(s)) represents the private benefit of a trip.

Because the highway is uniform and has limited capacity, some ramp metering strategies must be adopted to assure the total traffic volume will not overstep the limit. Otherwise, there will be a gridlock or even a spill-back phenomenon on the highway, which is a disaster to all commuters and regarded as huge waste (Lago and Daganzo, 2007). Let r(s) denotes the on-ramp capacity of location s, and then we have the conservation condition for highway capacity.

$$\int_0^B r(s)ds = \mu \tag{2}$$

If the trip demand of location s, q(s), exceeds the on-ramp capacity, r(s), the commuters cannot all arrive at the CBD on time and a queue will form in the front of the on-ramp access. Only a small fraction of people who endure the longest waiting time can arrive at the CBD on time. According to the classic bottleneck model (Vickrey, 1969), at user equilibrium the congestion cost of commuters from location s can be expressed as $\theta q(s)/r(s)$, where θ, a positive constant, usually be regarded as the schedule delay parameter (Arnott, et al., 1993).

The total cost of a trip from s to the CBD, C(s), is given by

$$C(s) = f_l + \alpha \cdot s + \theta \cdot \frac{q(s)}{r(s)} \tag{3}$$

where f_l is the fixed cost of travel, such as the maintenance cost of a private car; α is the cost of unit travel distance; The second term of Eqn. (3) is the travel cost of individual from residence s with free flow speed on the highway. The third term of Eqn. (3) reflects the congestion effect of location s.

Because highway capacity is a scarce resource, the ramp metering strategy $\{r(s), s \in [0,B]\}$ plays an important role. In the rest of this section, we will investigate two of the most popular on-ramp strategies.

2.1. Space Equality Strategy

In this subsection, we investigate the space equality ramp metering strategy, which distributes the main road capacity to each access location equally to ensure that commuters from different residences have the same access opportunity to the highway. Then we have

$$r_I(s) = \mu / B, \quad \forall s \in [0, B] \tag{4}$$

where the subscript I represents the space equality strategy hereafter. Substituting Eqn. (4) into Eqn. (3), we have the trip cost

$$C_I(s) = f_l + \alpha \cdot s + \theta \cdot \frac{q(s)}{\mu / B} \tag{5}$$

2.2 Commuter Equality Strategy

One public opinion on the ramp metering strategy is that longer access time should be given to the locations with a larger population. In other words, all the commuters along the corridor should have the same access opportunity. We refer to it as the commuter equality strategy. Then we have

$$r_{II}(s) = \frac{q(s)}{\int_0^B q(y)dy}\mu, \quad \forall s \in [0, B] \tag{6}$$

where the subscript II represents the commuter equality strategy hereafter. Substituting Eqn. (6) into Eqn. (3), we have the trip cost

$$C_{II}(s) = f_l + \alpha \cdot s + \theta \cdot \frac{q(s)}{r_{II}(s)} \tag{7}$$

SPATIAL EQUILIBRIUM

In this section, we assume the trip demand distribution q(s) to be endogenous and follow a general spatial equilibrium. Then, under the space equality ramp metering strategy, we have

$$p(q_I(s)) = C_I(s), \quad \forall s \in [0, B] \tag{8}$$

Substituting equation (1) and (5) into equation. (8) yields

$$q_I(s) = \frac{\mu}{\theta B + \mu b}(a - f_l - \alpha s) \tag{9}$$

Substituting equation. (9) into equation. (1) yields

$$C_I(s) = \frac{\alpha\mu b \cdot s + \theta B a + \mu b f_l}{\theta B + \mu b} \tag{10}$$

From equation. (9) and (10), we can see that the trip demand decreases and the trip cost increases linearly with the distance far away from the CBD.

Under the commuter equality ramp metering strategy, we have

$$p(q_{II}(s)) = C_{II}(s), \quad \forall s \in [0, B] \tag{11}$$

Substituting equation (1) and (7) into equation (11) yields

$$q_{II}(s) = \frac{\mu}{\theta B + \mu b}\left[(a - f_l) + \frac{\alpha\theta B^2}{\mu b} - \frac{\alpha(\theta B + \mu b)}{\mu b}s\right] \quad (12)$$

Substituting equation (12 into) equation (1) yields

$$C_{II}(s) = \frac{\alpha(\theta B + \mu b)\cdot s + \theta Ba + \mu b f_l - \alpha\theta B^2}{\theta B + \mu b} \quad (13)$$

We can also find, for equation(12) and (13), that the trip demand decreases and the trip cost increases linearly with the distance far away from the CBD.

Under the different ramp metering strategies, both the trip demands and the trip costs vary. In the next section, we will compare the characters of these two strategies in detail.

4. COMPARISON OF THE TWO STRATEGIES

It is very easy to verify that $q_{II}(0) > q_I(0)$ and $q'_{II}(0) > q'_I(0)$. As shown in Figure 2, the trip demand is steeper under the commuter equality strategy. The areas between different q(s) and the vertical and horizontal axis, however, are equal to each other.

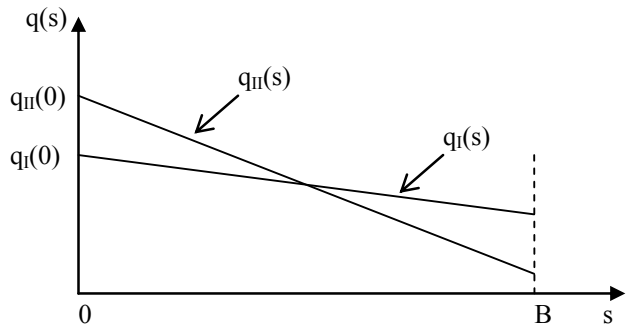

Figure 2. Travel demand under different ramp metering strategies.

We can derive the following proposition with equation. (9) and (12).

Proposition 1. Although the trip demand distribution is different under the two ramp metering strategies, the total trip demand along the corridor is the same. Additionally, under the commuter equality strategy, the trip demand will be more centralized to the CBD.

From Proposition 1, we find that the larger θ is less total demand along the corridor. This can be explained by a tough "on-time" work policy; less people will select work in the CBD. We also find that larger f_l and α also leads to lower population. This is because higher trip costs will force more people to work at home. Furthermore, we investigate the total trip cost along the corridor, namely

$\int_0^B C(s) \cdot q(s) ds$, which is the social cost in this paper, and derive the Proposition 2 as below.

Proposition 2. The total trip cost along the corridor is larger under the commuter equality strategy than under the space equality strategy.

Thus, the space equality strategy is actually more efficient with less total social cost. In reality, the commuter equality strategy is usually more popular with local authorities who believe that that more highway capacity should be given to the residential areas with a higher population. However, for long-term planning purposes authorities should allocate the access priority equally along the corridor to alleviate the traffic congestion and lower the total social cost.

CONCLUSION

In this paper, we study ramp metering strategies' effects in a corridor network. Both space equality and commuter equality strategies are taken into account. We have proven that as both of these ramp metering strategies attract the same total trip demand, space equality will result in less social cost than commuter equality does, which is different from our general belief. These results will be very useful for local authority's urban transportation management purposes.

Our on-going work is to extend the model to a discrete multi-origin framework similar to that of Tian et al. (2007) which is similar to the so-called "corridor problem" in transportation economics. Considering more general demand function will be also an interesting endeavor.

ACKNOWLEDGEMENTS

The work described in this paper was supported by grants from the National Natural Science Foundation of China (70801002, 70521001), the Beijing Natural Science Foundation (9073018), a project (2006CB705503) from the National Basic Research Program of China and the Research Grant Council of the Hong Kong Special Administrative Region (HKUST6215/06E).

REFERENCES

Arnott, R., De Palma, A. and Lindsey, R. (1993). "A structural model of peak-period congestion: A traffic bottleneck with elastic demand." American Economic Review, 83(1), 161-79.

Daganzo, C.F. and Garcia, R.C. (2000). "A areto improving strategy for the time-dependent morning commute problem." Transportation Science, 34(3), 303-311.

Lago, A. and Daganzo, C.F. (2007). "Spillovers, merging traffic and the morning commute." Transportation Research Part B , 41(6), 670-683.

Shen, W. and Zhang, H.M. (2008). "On the morning commute problem in a corridor network with multiple bottlenecks: Its system-optimal traffic flow patterns and the realizing tolling scheme." Transportation Research Part B , 2008, 43(3), 267-284.

Small, K.A., Winston, C.M. and Evans, C.A. (1989). Road Work: A New Highway Pricing and Investment Policy. The Brookings Institution, Washington DC.

Tian, Q., Huang, H.J. and Yang, H. (2007). "Equilibrium properties of the morning peak-period commuting in a many-to-one mass transit system." Transportation Research Part B , 41(6), 616-631.

Vickrey, W.S. (1969). "Congestion theory and transport investment." American Economic Review, 59(2), 251-260.

Efficiency Loss of the Multiclass, Multicriteria Stochastic User Equilibrium Traffic Assignment Against Stochastic System Optimization

Xiaojun Yu[1, 2] Haijun Huang[1] Tianliang Liu[3]

[1]School of Economics and Management, Beijing University of Aeronautics and Astronautics, Beijing 100191; TEL (86) 10 82339327; FAX: (86) 10 82328037. Email: haijunhuang@buaa.edu.cn(H.-J. Huang), xjyu0508@sina.com (X.-J. Yu).
[2]School of Mathematics and Statistics, Guizhou College of Finance and Economics, Guiyang 550004
[3]School of Economics and Management, Tsinghua University, Beijing 100084; TEL (86)10 62795147; Email: liutl@sem.tsinghua.edu.cn

ABSTRACT

In stochastic traffic assignments, if the total perceived travel cost of all users is used as the system performance index, the stochastic system optimum (SSO) assignment will then be to minimize the total perceived travel cost. In this study, we investigate the efficiency loss caused by the stochastic user equilibrium (SUE) traffic assignment against the SSO assignment. The efficiency loss is defined as the difference between these two assignments. Two variational inequality (VI) models are presented to formulate the time-based and monetary-based SUE route choice behaviors respectively, in traffic networks with multiple user classes and fixed demand. The upper bounds of the efficiency losses caused by these two kinds of behaviors are analytically derived and their relations to some network parameters are discussed.

INTRODUCTION

Wardrop (1952) presented two famous principles regarding users' route choice behavior in traffic networks, namely the user equilibrium (UE) traffic assignment and system optimum (SO). The UE principle states that every traveler tries to minimize her/his own cost, so that no traveler can reduce it by unilaterally changing her/his choice at equilibrium. In the case of SO, it is assumed that a central organization exists to minimize the total cost of the system. In stochastic circumstances where travelers cannot accurately compute their costs, a stochastic user equilibrium (SUE) may be achieved, i.e., travelers choose routes for minimizing their perceived travel costs. At the SUE, the perceived travel costs of all actually used paths between each O-D pair are identical and minimal. It is natural to define the stochastic system optimum (SSO) as that which makes the system's total perceived travel cost to be minimal. Yang (1999) proposed a SSO model with a single user class and fixed demand. Maher et al. (2005) further formulated a logit-based SSO model.

It is well known that the UE is generally not identical with but has more or less efficiency loss than the SO, i.e., the UE renders the total travel cost of the whole network as more (Yang and Huang, 2005). Roughgarden and Tardos (2002) introduced the notion of coordination ratio or the price of anarchy, which was first defined by Koutsoupias and Papadimitriou (1999) to quantify the inefficiency of UE

decision making in networks. Since then, many researchers (Roughgarden and Tardos, 2003; Chau and Sim, 2003; Correa et al, 2004; Huang et al, 2006) have extended the investigation on the efficiency loss of the deterministic UE traffic assignment.

However, up to now, few studies have been done to investigate efficiency loss of the equilibrium assignment with multiple user classes. Obviously, different classes of users have different route choice preferences due to their differences in income, age, gender, education, travel destination and so on. Some users may like time-based criterion and others monetary-based ones for route choice. Recently, Liu et al, (2007) investigated the inefficiency of mixed travel behavior in networks with advanced travel information systems. Han and Yang (2008) derived the upper bounds of efficiency loss caused by the multiclass and multicriteria traffic equilibrium. However, the aforementioned researches are just subject to the deterministic traffic assignment.

In this study, we focus our attention on the efficiency loss caused by logit-based SUE and extend the work of Guo et al. (2009) to the case of multiple user classes. All users are classified into several groups according to their values of time. We first formulate the time-based and monetary-based VI models for this multiclass problem, and then derive the upper bounds of the inefficiency caused by the SUE against the SSO. Finally, we examine the relationships between bounds and the network parameters. The value of our study lies in more understanding of complex route choice behavior and their consequences on system performance.

THE MULTICLASS, MULTICRITERIA STOCHASTIC TRAFFIC EQUILIBRIUN MODEL WITH FIXED DEMAND

Notation and assumptions . Let $G=(N, A)$ be a directed transportation network, where N and A denote the sets of nodes and links, respectively. Let W be set of O-D pairs; R_w be set of paths between O-D pair w. There are travel demands that can be subdivided into M classes corresponding to groups of users with difference values of time; $\beta_m > 0$ be the average value of time of user class m. Let d_w^m be the demand of user class m between w, which is assumed to be constant in this paper; v_a^m be the flow of user class m and v_a be the total flow on link $a \in A$; f_{rw}^m be the flow of user class m on path $r \in R_w$, $w \in W$. The travel time function $t_a(v_a)$ is assumed to be continuously differentiable and monotonically increasing.

Let $c_a^m(v_a)$ be the experienced travel cost function of class m on link $a \in A$, C_{rw}^m and c_{rw}^m be the perceived travel cost and experienced one of user class m on path $r \in R_w$, respectively. Therefore, the following relationship must be satisfied, i.e.

$$c_{rw}^m = \sum_{a \in A} c_a^m \delta_{ar}^w, \forall r \in R_w, w \in W, \ m=1,\cdots, M. \tag{1}$$

The flow conservation conditions and nonnegative constraint conditions are

$$v_a^m = \sum_{w \in W} \sum_{r \in R_w} f_{rw}^m \delta_{ar}^w, \forall a \in A, \ m=1,\cdots, M, \tag{2}$$

$$v_a = \sum_{m=1}^{M} v_a^m, \forall a \in A, \tag{3}$$

$$\sum_{r \in R_w} f_{rw}^m = d_w^m, \forall w \in W, \ m = 1, \cdots, M, \tag{4}$$

$$f_{rw}^m \geq 0, \forall r \in R_w, w \in W, \ m = 1, \cdots, M. \tag{5}$$

Where δ_{ar}^w is equal to 1 if the path r between OD pair $w \in W$ otherwise traverses link $a \in A$, and 0. We denote $\Omega_v = \{v \mid v \text{ satisfying (2)-(5) }\}$ and $\Omega_f = \{f \mid f \text{ satisfying (2)-(5)}\}$. Clearly, Ω_v and Ω_f are both closed and convex sets.

The SUE model . Under SUE condition, the multiclass multicriteria stochastic user equilibrium traffic assignment can be formulated as VI (Xu and Zhu, 2007). Therefore, we have the following Lemma 1.

Lemma 1. Under the logit-based path choice assumption, the multiclass SUE with fixed demand is equivalent to the following VI, i.e., find $\bar{f} \in \Omega_f$, such that

$$\sum_{w \in W} \sum_{r \in R_w} \sum_{m=1}^{M} \left\langle c_{rw}^m(\bar{f}) + \frac{1}{\theta} \ln \bar{f}_{rw}^m, \ f_{rw}^m - \bar{f}_{rw}^m \right\rangle \geq 0, \forall f \in \Omega_f . \tag{6}$$

Under the time-based criterion, $c_a^m(v_a) = t_a(v_a), a \in A, m = 1, \cdots, M$. Comparably, under the monetary-based criterion, $c_a^m(v_a) = \beta_m t_a(v_a), a \in A, m = 1, \cdots, M$. Therefore, the time-based VI model can be formulated as

$$\sum_{a \in A} t_a(\bar{v})(v_a - \bar{v}_a) + \frac{1}{\theta} \sum_{w \in W} \sum_{r \in R_w} \sum_{m=1}^{M} \ln \bar{f}_{rw}^m \left(f_{rw}^m - \bar{f}_{rw}^m \right) \geq 0, \forall f \in \Omega_f , \tag{7}$$

Similarly, the monetary-based VI model can be formulated as

$$\sum_{a \in A} \sum_{m=1}^{M} \beta_m t_a(\bar{v})(v_a^m - \bar{v}_a^m) + \frac{1}{\theta} \sum_{w \in W} \sum_{r \in R_w} \sum_{m=1}^{M} \ln \bar{f}_{rw}^m \left(f_{rw}^m - \bar{f}_{rw}^m \right) \geq 0, \forall f \in \Omega_f . \tag{8}$$

Defining the SSO . Following the work of Maher et al. (2005), the total perceived travel cost under the multiclass SUE with fixed demand can be given as

$$F(f) = \sum_{w \in W} \sum_{r \in R_w} \sum_{m=1}^{M} c_{rw}^m(f) f_{rw}^m + \frac{1}{\theta} \sum_{w \in W} \sum_{r \in R_w} \sum_{m=1}^{M} f_{rw}^m \ln f_{rw}^m - \frac{1}{\theta} \sum_{w \in W} \sum_{m=1}^{M} d_w^m \ln d_w^m . \tag{9}$$

The SSO problem is to minimize the total perceived travel cost, namely

$$\min_{f \in \Omega_f} F(f). \tag{10}$$

As a result, we can easily obtain the SSO path flow vectors, $\hat{f}$ and $\tilde{f}$, and the SSO link flow vectors, $\hat{v}$ and $\tilde{v}$, through solving the following minimization problems under time-based and monetary-based criterions, respectively. That is

$$F_{sso}^t = \min_{f \in \Omega_f} F^t(f) = \sum_{a \in A} t_a(v_a) v_a + \frac{1}{\theta} \sum_{w \in W} \sum_{r \in R_w} \sum_{m=1}^{M} f_{rw}^m \ln f_{rw}^m - \frac{1}{\theta} \sum_{w \in W} \sum_{m=1}^{M} d_w^m \ln d_w^m , \tag{11}$$

$$F_{sso}^{c} = \min_{f \in \Omega_f} F^{c}(f) = \sum_{a \in A} \sum_{m=1}^{M} \beta_m t_a(v_a) v_a^m + \frac{1}{\theta} \sum_{w \in W} \sum_{r \in R_w} \sum_{m=1}^{M} f_{rw}^m \ln f_{rw}^m - \frac{1}{\theta} \sum_{w \in W} \sum_{m=1}^{M} d_w^m \ln d_w^m \quad . \tag{12}$$

BOUNDING THE EFFICIENCY LOSS OF THE TIME -BASED SUE AGAINST THE SSO

Let $\bar{v} \in \Omega_v$ and $\bar{f} \in \Omega_f$ be the link and path flow vectors under the time-based SUE, respectively. Correspondingly, the total experienced travel time and the total perceived one is, respectively, $T_{sue}^{t} = \sum_{a \in A} t_a(\bar{v}_a)\bar{v}_a$ and $F_{sue}^{t} = \sum_{a \in A} t_a(\bar{v}_a)\bar{v}_a + \frac{1}{\theta} \sum_{w \in W} \sum_{r \in R_w} \sum_{m=1}^{M} \bar{f}_{rw}^m \ln \bar{f}_{rw}^m - \frac{1}{\theta} \sum_{w \in W} \sum_{m=1}^{M} d_w^m \ln d_w^m$. The efficiency loss of the time-based SUE against the SSO is formulated as $F_{sue}^{t} - F_{sso}^{t}$. Clearly, $F_{sue}^{t} - F_{sso}^{t}$ is generally positive.

Let $f = \hat{f}$ in the VI (7), and then lead to

$$F_{sue}^{t} - F_{sso}^{t} \le \sum_{a \in A} \left(t_a(\bar{v}_a) - t_a(\hat{v}_a) \right) \hat{v}_a + \frac{1}{\theta} \sum_{w \in W} \sum_{r \in R_w} \sum_{m=1}^{M} \hat{f}_{rw}^m \left(\ln \bar{f}_{rw}^m - \ln \hat{f}_{rw}^m \right). \tag{13}$$

Next, we introduce how to get upper bounds on the two terms of the right-hand side of (13). For the first term, its upper bound can be obtained following the method adopted in Yang and Huang (2005). For each link travel time function $t_a = t_a(z_a)$ and nonnegative link flow z_a, we define the following parameter

$$\gamma_a(t_a, z_a) = \max_{v_a \ge 0} \frac{\left(t_a(z_a) - t_a(v_a) \right) v_a}{t_a(z_a) z_a}. \tag{14}$$

Here 0/0=0 by convention. For a given class L of link travel time functions, we let

$$\gamma(L) = \max_{t_a \in \mathcal{L}, z_a \ge 0} \gamma_a(t_a, z_a). \tag{15}$$

Then we have

$$\sum_{a \in A} \left(t_a(\bar{v}_a) - t_a(\hat{v}_a) \right) \hat{v}_a \le \sum_{a \in A} \gamma(L)\, t_a(\bar{v}_a)\bar{v}_a = \gamma(L)\, T_{sue}^{t}. \tag{16}$$

From Gibbs' inequality, we readily have a zero upper bound of the second term of the right-hand side of (13). Namely, the following inequality holds

$$\sum_{r \in R_w} \hat{f}_{rw}^m \left(\ln \bar{f}_{rw}^m - \ln \hat{f}_{rw}^m \right) \le 0, \quad w \in W, \ m = 1, \cdots, M. \tag{17}$$

Substituting (16) and (17) into (13), we have the following theorem.

Theorem 1. For a given separable link travel time function class L, Let T_{sue}^{t} and F_{sue}^{t} be, respectively, the total experienced travel time cost and the total perceived one at the time-based SUE, and F_{sso}^{t} be the minimum total perceived travel time cost, then

$$F_{sue}^{t} - F_{sso}^{t} \le \gamma(L) T_{sue}^{t}. \quad (18)$$

BOUNDING THE EFFICIENCY LOSS OF THE MONETARY -BASED SUE AGAINST THE SSO

In this section, we let $\bar{v} \in \Omega_v$ and $\bar{f} \in \Omega_f$ are the link and path flow vectors under the monetary-based SUE.. Correspondingly, the total perceived travel monetary cost and experienced one are, respectively, $F_{sue}^{c} = \sum_{a \in A} \sum_{m=1}^{M} \beta_m t_a(\bar{v}_a) \bar{v}_a^m +$

$\frac{1}{\theta} \sum_{w \in W} \sum_{r \in R_w} \sum_{m=1}^{M} \bar{f}_{rw}^m \ln \bar{f}_{rw}^m - \frac{1}{\theta} \sum_{w \in W} \sum_{m=1}^{M} d_w^m \ln d_w^m$ and $T_{sue}^{c} = \sum_{a \in A} \sum_{m=1}^{M} \beta_m t_a(\bar{v}_a) \bar{v}_a^m$ .The efficiency loss of the monetary -based SUE against the SSO is formulated as $F_{sue}^{c} - F_{sso}^{c}$. Clearly, $F_{sue}^{c} - F_{sso}^{c}$ is generally positive.

Let $f = \tilde{f}$ in the VI (8), then leads to

$$F_{sue}^{c} - F_{sso}^{c} \le \sum_{a \in A} \sum_{m=1}^{M} \beta_m \left(t_a(\bar{v}_a) - t_a(\tilde{v}_a) \right) \tilde{v}_a^m + \frac{1}{\theta} \sum_{w \in W} \sum_{r \in R_w} \sum_{m=1}^{M} \tilde{f}_{rw}^m \left(\ln \bar{f}_{rw}^m - \ln \tilde{f}_{rw}^m \right). \quad (19)$$

For the first term on the right-hand side of (19), its upper bound can be obtained using the method in Han and Yang (2008). For each link travel time function $t_a = t_a(z_a)$ and nonnegative link flow $z_a \ge 0$ and value of time $\beta_m, m = 1, \cdots, M$, define the following parameters:

$$\gamma_a(z_a, t_a, \beta) = \frac{1}{\left(\sum_{m=1}^{M} \beta_m z_a^m \right) t_a(z_a)} \max_{v_a^m \ge 0} \left\{ \left(\sum_{m=1}^{M} \beta_m v_a^m \right) \left(t_a(z_a) - t_a(y_a) \right) \right\}. \quad (20)$$

$$\gamma_a(t_a, \beta) = \sup_{z_a \ge 0} \gamma_a(z_a, t_a, \beta), \gamma(L, \beta) = \sup_{t_a \in \mathscr{L}} \gamma_a(t_a, \beta). \quad (21)$$

Where L is a given class of link travel time functions on link $a \in A$.

From definition (20) and (21), we have

$$\sum_{m=1}^{M} \beta_m \tilde{v}_a^m \left(t_a(\bar{v}_a) - t_a(\tilde{v}_a) \right) \le \gamma_a(\bar{y}_a, t_a, \beta) \sum_{m=1}^{M} \beta_m \bar{v}_a^m t_a(\bar{v}_a) \le \gamma(L, \beta) T_{sue}^{c}. \quad (22)$$

From Gibbs' inequality, we can obtain

$$\sum_{r \in R_w} \tilde{f}_{rw}^m \left(\ln \bar{f}_{rw}^m - \ln \tilde{f}_{rw}^m \right) \le 0, \; w \in W, \; m = 1, \cdots, M. \quad (23)$$

Substituting (22) and (23) into (19), we have the following theorem.

Theorem 2 . For a given separable link trav el time function class L, let T_{sue}^{c} and F_{sue}^{c} be, respectively, the total experienced travel monetary cost and the total perceived one at the monetary-based SUE, and let F_{sso}^{c} be the minimum total perceived travel monetary cost, then

$$F_{sue}^{c} - F_{sso}^{c} \le \gamma(L, \beta) T_{sue}^{c}. \quad (24)$$

CONCLUSION

In this paper, we have investigated the efficiency loss of multiclass, multicriteria stochastic user equilibrium traffic assignment against stochastic system optimization. Specifically, when considering two kinds of the decision criteria, i.e., time-based or monetary-based, the upper bounds of the efficiency loss under time-based and monetary-based criteria are both independent of network topology and depend on the class of link travel functions and the experienced total travel cost. Furthermore, at the monetary-based SUE, the upper bound is also dependent on the users' socio-economic characteristics. Our ongoing work will focus on examples that validate and study the inefficiency loss of multiclass, multicriteria stochastic traffic equilibrium with elastic demand.

ACKNOWLEDGEMENTS

This research was partly funded by the National Natural Science Foundation of China (70521001), the National Basic Research Program of China (2006CB705503) and China Postdoctoral Science Foundation Funded Project (20080440357).

REFERENCES

Chau, C. K., and Sim, K. M. (2003). "The price of anarchy for non-atomic congestion games with symmetric cost maps and elastic demands," Operations Research Letter, 31(5), 327–334.

Correa, J. R., Schulz, A. S., and Stier-Moses, N. S. (2004). "Selfish routing in capacitated networks," Mathematics of Operations Research. 29(4), 961–976.

Guo, X. L., Yang, H, and Liu, T. L. (2009). "Bounding the inefficiency of logit-based stochastic user equilibrium," European Journal of Operational Research. in press.

Han, D. R., and Yang, H. (2008). "The multi-class, multi-criterion traffic equilibrium and the efficiency of congestion pricing," Transportation Research Part E. 44(5), 753–773.

Huang, H. J., Ouyang, L. Q., and Liu, T. L. (2006). "Upper bounds of efficiency loss for equilibrium behavior in traffic networks," Journal of Beijing University of Aeronautics and Astronautics. 32(10), 1215–1219.

Koutsoupias, E., and Papadimitriou, C. (1999). "Worst-case equilibria," Proceeding of the 16th Symposium on Theoretical Aspects of Computer Science. NCS 1563.

Liu, T. L., Ouyang L. Q., and Huang, H. J. (2007). "Mixed travel behavior in networks with ATIS and upper bound of efficiency loss." Systems Engineering – Theory & Practice. 27(4), 154–159.

Maher, M., Stewart, K., and Rosa, A. (2005). "Stochastic social optimum traffic assignment," Transportation Research Part B. 39(8), 753–767.

Roughgarden, T., and Tardos, E. (2002). "How bad is selfish routing?" Journal of the ACM 49(2), 236–259.

Roughgarden, T., and Tardos, E. (2003). "The price of anarchy is independent of the network topology," Journal of Computer and System Science. 67(2), 341–364.

Wardrop, J. G. (1952). "Some theoretical aspects on road traffic research," In:

Proceedings of Institution of Civil Engineers, Part II, vol. 1: 325–378.
Xu, B., and Zhu, D. L. (2007). "A multiclass and multicriteria stochastic traffic network equilibrium variational inequality model with fixed demand," Journal of Highway and Transportation Research and Development . 24(4), 129–133.
Yang, H. (1999). "System optimum, stochastic user equilibrium and optimal link tolls", Transportation Science , 33 (4), 354–360.
Yang, H, and Huang, H. J. (2005) Mahematical and economic theory of road pricing . Elsevier Ltd, Oxford, UK.

The Application of TUXEDO Middleware in a Network -based Train Working Diagram Compilation System

Hongxia LU [1], Shaoquan NI [1], Jinshan PAN [1], Bin LIU [2]

[1]Traffic and Transportation College of SouthWest Jiaotong University, Chengdu Sichuan, PH (86)- 28-87600706; email: hongxialu@163.com
[2]School of Traffic and Transportation of Lanzhou Jiaotong University, Lanzhou Gansu, PH (86)-931-4938025; email:liubin0909@163.com

ABSTRACT

Establishing a train working diagram system and realizing the modernization of a train working diagram's compilation, management and service is important to railway information construction in China. In this paper, the deficiency of the existing system architecture is apparent after analyzing the features of the existing network-based train working diagram computerized compilation system. Furthermore, the three-layer architectural model is a setup that uses TUXEDO middleware to implement the network-based train working diagram computerized compilation system. Considering the train working diagram system's characteristics, the implementation methods of this system are expounded upon including an analysis of business process division service design and TUXEDO application and development. By verifying the architecture, it is proven that this architecture can well solve the inadequacy of the original one and can meet the needs.

1. INTRODUCTION

A train working diagram is the most important fundamental plan by which different departments organize their railway transportation activities. It reflects the quality level of the railway's service for the other fields of the national economy. The College of Traffic and Transportation of Southwest Jiaotong University has been doing considerable research on train working diagram computerized compilation and has established and put into practicle application a network-based railway passenger train working diagram computerized compilation system based on LAN (Shao Quanni 2001).

When compiling a network-based train working diagram, all users can check any data. Each user's authority is set according to the railway bureau's jurisdiction to which the user belongs. Once one user changes the data, the other user's data must be immediately synchronized. The train working diagram includes lots of data, such as railway line, station, section, train trip route, train running time, train interval and display section, etc. In order to accomplish the train working diagram computerized compilation based on network environment, the network needs to transmit large amounts of data in high frequency. Therefore, the request of the system's network

communication is comparatively high. At present, the architecture of this system adopts C/S 2-layer architecture and realizes the network communication between server and client by using SOCKET (Shaoquan Ni 2003). Practical application indicates that the current architecture still has the following problems: ① the amount of concurrency is limited; ② the stability and safety of network transmission can not be guaranteed; ③ the data logic, business logic and presentation logic's division is not clear. The disposition is very difficult after update. The reusability of the business logic and interface logic is very poor; ④ the data integrity and consistency is difficult to guarantee; ⑤ the system's expansibility and flexibility is comparatively poor.

2. SYSTEM ARCHITECTU RE DESIGN

TUXEDO middleware is the platform software on which a three-layer C/S critical business system can be developed and managed in the distributed computing environment such as enterprise and the Internet. It has unprecedented on-line transaction performance, high reliability and unlimited flexibility, and can provide a powerful supporting platform which can establish, operate and manage a large-scale, high performance and distributed critical business system for enterprise. This middleware provides seven communication mechanisms: synchronous and asynchronous invoking, pipeline, session, broadcast notification, queue and a communication pipeline which releases subscription of a three-layer structure application. It has the advantages of load balancing, failover, etc (Wei Jiang 2008).

Therefore, the three-layer architecture based on TUXEDO middleware can be used for dividing applied user logic, business logic and data logic into three different processing layers. The application system which adopts this architecture not only possesses mainframe performance, such as stability, safety and high processing capacity, but also has numerous advantages such as open systems, e.g. low cost, strong extensibility and short development cycle.

In order to realize the three-layer architecture ground on TUXEDO middleware and reduce modifications to a minimum, the enhancement can be done on the basis of the original architecture. The main modification is as follows: move the client business logic and data logic to the TUXEDO application server and keep the interface logic with the client; replace the original environment with the TUXEDO application service platform; replace the SOCKET communication with TUXEDO communication; bring about service of the server's module according to standards of service interface and service realization.

The logic architecture shown in Figure 1 is composed of a presentation layer, business logic layer and data layer. The main contents of the presentation layer are data input interface, train working diagram graphic display, and interactive adjustment function for client front interface. For the purpose of realizing front interface flexibility and diversification, the presentation layer keeps the configuration

files locally and defines the interface elements and interactive action to bring about a customizable front interface.

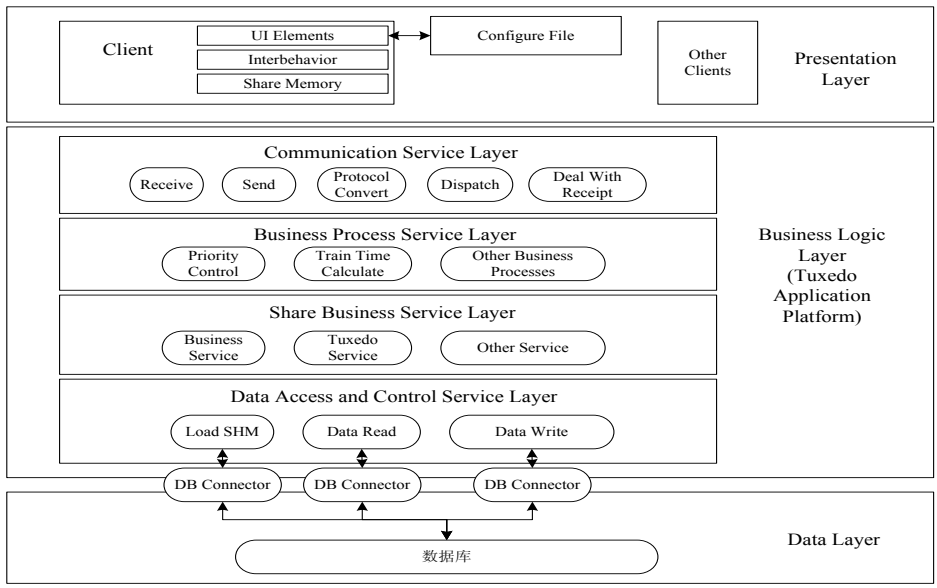

Fig. 1. Logic Architecture .

The business logic layer is on the TUXEDO application server and mainly contains business logic processing, such as pushing line (calculating the train running line), user register, user privileges control, train running time calculation, data synchronization, data storage, etc. According to the necessary functions, this layer can be divided into a communication service layer, a business processing service layer, a sharing business service layer and a data access control layer. The communication service layer mainly contains the TUXEDO communication function, such as receiving/sending data, protocol conversion and distribution service. The business processing service layer primarily includes business logic function of the original architecture, such as privileges control, train running time calculation, pushing line calculation, etc. The sharing business service layer mainly contains some common services. The data access control layer interacts with the data layer and contains services, such as reading/writing data control and loading shared memory data.

3. SYSTEM REALIZATION

In network-based train working diagram computerized compilation systems, the most basic and frequently used operation is train line operation, such as forward direction pushing line, backward direction pushing line, dragging train line, etc. In the following example, the pushing line operation is used in order to elaborate on how to utilize TUXEDO middleware to realize the logic architecture presented in Figure 1.

3.1 Service Designs

The object-oriented application is based on classes and objects. Through modeling technology, the relative objects are classified to a single component according to business function. For function call of cross-components, exposes that in the form of interface and decouples the definition and specific realization of the interface. The above mentioned then forms the corresponding service.

The way to discover service is top-down, bottom-up and align middle mode. The top-down mode is derived from business and carries on domain decomposition, flow decomposition and change analysis of business. Bottom-up is used for the realization of service using existing assets. The existing assets include existing systems, suite and custom applications, occupational standards or service model. Align middle mode is used to help find the align-business services and ensure no omission of critical services during flow decomposition and existing assets analysis.

In this paper, the top-down mode is adopted. Considering the pushing line flow, the service can be determined as follows:

① Data Transmission Service (SHMSVC): Retrieves data from service shared memory and transmits it to the client. ② Service Registry (REG): Client runtime connects with the server and registers through this service. ③ Un-register Service (UNREG): Cancellation through this service when the client logs off. ④ Pushing Line Service (PUSHLINESVC): Receives pushing line operation order from client, calculates pushing line results and sends them to notification service. ⑤ Notification Service (NOTIFY): Sends calculation results to all registered clients. ⑥ Data loading Service (DBLOAD): Acquires data from database and loads it to server shared memory. ⑦Writing Shared Memory Service (SAVESHM): Saves pushing line operation results in shared memory. ⑧Database Update Service (UPDATEDB): Saves pushing line operation results in database.

3.2 Data Packet Size Design

After launching, the client needs to request data from the server and then downloads the train working diagram data whose data size is larger than 100M. The size of the network data packet will directly influence the network performance. In view of determining a reasonable size for the data packet, it is necessary to test the network's occupation and the time-consuming factors of the different data packet sizes. Currently, the railway network-based train working diagram computerized compilation's network environment is 1Gbps, network card 1000M, total amount of test data 100M. The test results are shown in Figure 2.

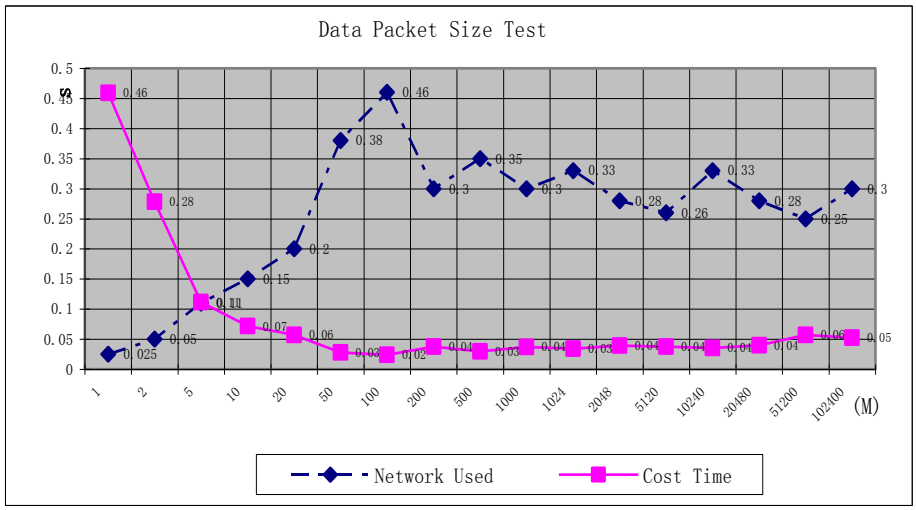

Fig. 2. Result of data packet size test .

An analysis of the test results leads to a number of conclusions as follows: If the data packet is comparatively small, the occupation of network bandwidth is comparatively small, but time-consuming is comparatively larger. With the gradual increase of data packet size, the occupation of network bandwidth gradually increases initially and then reduces and fluctuates around 30M. However, the time-consuming gradually reduces at first, and then increases with the lapse of time, comparatively stable on the whole. It can be clearly seen that “bigger is not better” in the case of the data packet’s size. Through the analysis of Figure 3 and the balance of network bandwidth and time-consuming factors, the selected data packet size under this network environment is 1M. At this time, the time-consuming of 100M data’s transmission is 3.42s, and the occupation network bandwidth is 33M

3.3 TUXEDO Application Development

The application development processes are often divided into compiling and loading configuration files, editing and compiling server programs, editing and compiling client programs and startup application programs.

TUXEDO configuration files contain the various parameters of system operation, including the connection information with databases, service information provided by the server, authentication information necessary for calling service by client, and so on. Through the tmloadcf command, the binary file TUXONFIG is generated for the TUXEDO system runtime to acquire relative information. During startup of the TUXEDO service, TUXEDO will read relatively useful information from TUXCONFIG and then support the realization of the service.

Server and client programs are all written in C language, then the server program and client program are compiled using the buildserver command and buildclient commands respectively. After that, the TUXEDO server service is

launched using the tmboot command and waits for the client's call.

Pushing line service (PUSHLINESVC) is the key part of the pushing line operation. The flow of the client's call of this service is shown in Figure 3. PUSHLINESVC service receives the client's pushing line operation command, calculates the pushing line results, and sends them to NOTIFY service. Afterwards, the NOTIFY service informs all registered clients to update client data and client display.

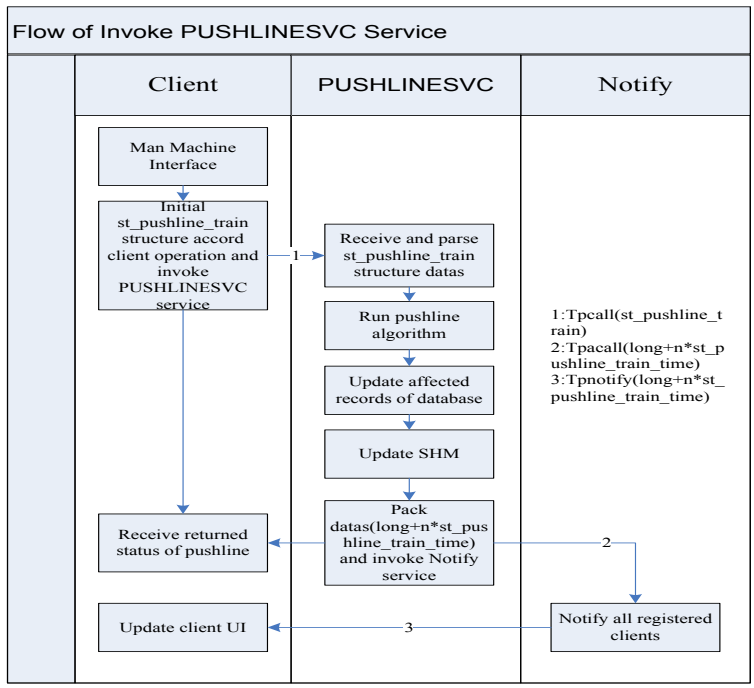

Fig. 3. Flow of Invoke PUSHLINESVC Service .

The pushing line operation command structure (st_pushline_train) includes train number, original station name, destination station name, departure time, parameter setting, etc. The train number is used to select the train to be operated. The original and destination station are used for ascertaining the pushing line's influence scope. The departure time is applied to determine the offset compared to the original time. The pushing line parameter setup is applied in order to decide the input parameters of the pushing line algorithm. Calculation result structure (st_pushline_train_time) includes train number, station index, station name, train arrival time, train departure time and the order number of occupied receiving-departure tracks. The train number is used to select a train. Station index, train arrival time, train departure time and the order number of occupied receiving-departure tracks are used for ascertaining the train's receiving time, departure time and occupied receiving-departure track in the station after pushing line operation.

4. CONCLUSION

This paper accomplishes the verification of network-based railway train working diagram computerized compilation system's transformation from a two-layer architecture to a three-layer architecture. Thus, the stability, safety, and the amount of concurrency of this system have received some improvement and are in accordance with the request of network-based railway train working diagram computerized compilation. Nevertheless, the reality of the fact that the client directly connects with the server creates a little disorder in management of the TUXEDO application at present. We can add Enterprise Service Bus (ESB) between the client and the server to solve this problem. The management of service and the client's call of backend service through ESB will be achieved in the course of future research.

ACKNOWLEDGEMENTS

This paper was prepared based on research project sponsored by Natural Science Foundation of China (No.60870004).

REFERENCES

Jiang, W. F. (2008).”Application and implementation of tuxedo middleware in telecom business system,” Journal of Mianyang Normal University..5(27)

Ni Shaoquan, L., and Hongxia, L. H. (2001).”Research on train working diagram computerized compilation system ” Railway transport and economy, 7, 31-35.

Ni Shaoquan, L., and Hongxia, Y. M. (2003). ”Research on design of train diagram computerized compilation system of railway in China,” Journal of Southwest Jiaotong University. 3, 332-335

Analyzing the Effects of the Growth of M aritime Industries on the Regional Economy with D ynamic Inverse Matrix

Yajun LI[1], Zhongzhen YANG[2]

[1 2]College of Transport Management, Dalian Maritime University, Dalian, China P.O.116026； PH:13804246281; email:liyajun507@163.com

ABSTRACT

The study on the interaction between the growth of the maritime industries and the output of other industries is important to the shipping center in Dalian. Based on an input-output table, this paper first selects five maritime industries according to the construction plan of the Shipping Center and the attributes of the maritime industries. Second, DIM (Dynamic Inverse Matrix) is calculated with the regional input-output table for six years. Then, the contributions of other industries to maritime ones and contributions of the maritime industries to increments of residential and governmental demands are analyzed. The results show that Petroleum and Chemistry, Energy Mining and Supply, Metal Mining and Products industries closely relate to the maritime industries in terms of input and output.

DATA

The I-O model is quite useful for analyzing the sector issues in the national economic context because it recognizes the interdependence of all sectors of the economy. Therefore, the interaction between the maritime industries and others in Liaoning can be explained by the I-O model.

The study uses two sets of 1997, 2002 I-O tables in Liaoning. For the sake of maritime sector-based analysis, original tables (42-sectors) are aggregated into 15-sector tables according to the plan of the Shipping Center and the attributes of the maritime industries (Diao.2006). The main maritime sectors are embodied by ind.7, ind. 8, ind.10, ind.11, and ind.12, as described in Table 1. The paper sets 2000 as the object year and 1997-2001 as the planning years.

The coefficients of and labour means the input of capital and labour in one unit output for every sector. The coefficients of 1997-2002 are from the I-O Table in Liaoning, and the coefficients of 1998 to 2001 are acquired by interpolation.

Table 1. The 15 sectors a fter aggregat ion.

Ind.1	Agriculture	Ind.2	Energy Mining and Supply
Ind.3	Metal Mining and Products	Ind.4	Nonmetal Ores Mining and Products
Ind.5	Processing from Agricultural Products and Light Industry	Ind.6	Petroleum and Chemistry
Ind.7	Transportation	Ind.8	Manufacture of Transport Equipment
Ind.9	Manufacture of Other Manufacturing	Ind.10	The Service for Maritime Operation
Ind.11	The Service for Employed Persons in Maritime	Ind.12	The Harbor Construction
Ind.13	Business	Ind.14	Education and Science
Ind.15	Public Service		

METHOD AND ASSUMPTIONS

Dynamic input-output analysis is derived from the static through consideration of lags of change over time of sectoral interdependences. A dynamic model has the following form:

$$(I - A - B)X_t - B(X_{t+1} - X_t) = \tilde{Y}_t \quad (1)$$

Where I is identity matrix; X is the total gross output in sector; A is a matrix of technical coefficients, which mean the inter-industry purchases; and Y is the final demand for products. In this paper, the technical coefficients matrix A is calculated from the data of the 2002 I-O table in Liaoning and is assumed as fixed in all planning years and the object year; B is the matrix of fixed capital coefficients, $\tilde{Y}_t$ is the vector of final demand, excluding fixed capital investment; t refers to the time period.

We deduce capital coefficients matrix B under the assumption that the demand to intermediate production is the same as the demand to investment for sector j from sector i. It is shown as:

$$\Delta Z_{ij} / \sum_{j=1}^{n} \Delta Z_{ij} = k_{ij} / \sum_{j=1}^{n} k_{ij} = k_{ij} / I_i, i, j = 1,.....n \quad (2)$$

Where, ΔZ_{ij} is the intermediate goods increment, then $\Delta Z_{ij} = a_{ij} \times \Delta X_j$, ΔX_j is the total outputs increment from (t+1) year to t year; k_{ij} is the investment demand of sector j from sector i in t year; I_i is the investment of sector i in t year. The capital coefficients can be calculated as follow:

$$b_{ij} = k_{ij} / \Delta X_j \tag{3}$$

Where, b_{ij}, capital coefficients, defines the stock of products of industry j required per unit of capacity output of industry i and is thus a stock-flow ratio. The date from the 2002 I-O table and 2003、2004 statistical Yearbook in Liaoning is used to calculate the capital coefficients matrix B, which is assumed as fixed in all planning years as well as the object year.

In Eq.1, we set $(I - A + B) = G$ and t=1,2,…,m, hence have a system of n difference equations in difference years:

$$\begin{bmatrix} X(-m) \\ \cdots \\ X(-1) \\ X(0) \end{bmatrix} = \begin{bmatrix} G^{-1} & \cdots & R^{m-1}G^{-1} & R^{m}G^{-1} \\ & \cdots & \cdots & \cdots \\ & & G^{-1} & RG^{-1} \\ & & & G^{-1} \end{bmatrix} \begin{bmatrix} \tilde{Y}(m) \\ \cdots \\ \tilde{Y}(-1) \\ \tilde{Y}(0) \end{bmatrix} \tag{4}$$

Where, $R = G^{-1}B$, it can be described in abbreviated form as $X = U^{-1}\tilde{Y}$. U^{-1} is Leontief's DIM (D. Kendrick.1972). That means the direct and indirect input in all planning years from sector i to sector j which has a one unit increase of final demand in the object year.

RESULTS AND ANALYSIS

In the following analysis in Liaoning, the contributions of the output of other industries to the maritime ones which have one unit increase in demand will be evident. When we also increase the government and citizen demand with one unit in the object year, the input of output labor and capital of maritime industries is received. (0:object year,-1~--5:planning years)

Input from the Output of Other Industries to Maritime Industr ies

The Analysis to I nd. 7. Table 2 shows that the input from most industries to Transportation (ind.7) ascends gradually and steadily except for Education and Science (ind.14). That means most industries directly sustain the development of transportation with the top industry Petroleum and Chemistry (ind.6). The result is consistent with the real condition of Liaoning. Ind.6 is the most important maritime industry in Dalian and most cargo passing through the Dalian Port comes from it. So the growth of input from Ind.6 can meet the increasing demand of Transportation (ind.7).

Table 2.Input from Other Industries with One Unit Increase in Demand of Ind.7 (Unit : 100 million/100 million) .

	-5	-4	-3	-2	-1	0
ind.1	0.00008	0.00033	0.00135	0.00521	0.01823	0.04197
ind.2	0.00017	0.00073	0.00316	0.01417	0.05864	0.12095
ind.3	0.00009	0.00040	0.00171	0.00703	0.02381	0.04403
ind.4	0.00002	0.00008	0.00034	0.00144	0.00484	0.00796
ind.5	0.00010	0.00044	0.00180	0.00702	0.02250	0.03600
ind.6	0.00015	0.00064	0.00275	0.01229	0.06297	0.23038
ind.8	0.00013	0.00058	0.00248	0.01059	0.04269	0.10591
ind.9	0.00001	0.00003	0.00011	0.00047	0.00197	0.00413
ind.10	0.00012	0.00050	0.00217	0.00955	0.04575	0.03453
ind.11	0.00004	0.00017	0.00070	0.00295	0.01217	0.03736
ind.12	0.00001	0.00003	0.00013	0.00055	0.00333	-0.00158
ind.13	0.00010	0.00043	0.00183	0.00777	0.03034	0.06670
ind.14	0.00004	0.00019	0.00074	0.00262	0.00599	-0.00655
ind.15	0.00000	0.00032	0.00136	0.00561	0.01716	0.01528

Additionally, based on a consideration of relationships among maritime industries, we see that, Transportation (ind.7), and Harbor Construction (ind.12) falls below the 0 line which means that Ind.12 is the key devotion to the early development of Transportation (ind.7). So during the construction of the Shipping Center in Dalian, the investment in harbor should be completed before the development of transportation.

Analysis to Ind. 8, Ind. 10, Ind. 11 and Ind. 12. Table 3 shows that most input into Manufacture of Transport Equipment (ind.8), which has one unit increase in demand, come from Metal Mining and Products (ind.3). The development of Ind. 8 depends greatly on the contribution of Ind.3. In addition, the input of Transportation (ind.7) is mostly in favor of the realization of increase in demand of Ind.8.

Table 3. Input from Other Industries with One Unit Increase in Demand of Ind. 8 (Unit : 100 million/100 million) .

	-5	-4	-3	-2	-1	0
ind.1	0.00012	0.00048	0.00191	0.00676	0.01794	0.02362
ind.2	0.00025	0.00108	0.00455	0.01856	0.06237	0.10629
ind.3	0.00014	0.00061	0.00275	0.01415	0.08980	0.34249
ind.4	0.00003	0.00012	0.00052	0.00229	0.00963	0.02360
ind.5	0.00015	0.00064	0.00256	0.00921	0.02584	0.03675
ind.6	0.00022	0.00095	0.00400	0.01642	0.06016	0.13757
ind.7	0.00021	0.00089	0.00383	0.01634	0.06014	0.03303
ind.9	0.00001	0.00004	0.00017	0.00071	0.00312	0.01605
ind.10	0.00018	0.00075	0.00316	0.01282	0.04339	0.03040
ind.11	0.00006	0.00025	0.00105	0.00434	0.01559	0.03454
ind.12	0.00001	0.00004	0.00018	0.00064	0.00083	-0.00051
ind.13	0.00015	0.00064	0.00272	0.01169	0.05273	0.14029
ind.14	0.00007	0.00029	0.00125	0.00526	0.01854	-0.01801
ind.15	0.00000	0.00048	0.00201	0.00808	0.02376	0.02081

We also calculate the input from other industries to the Service Maritime Operation (ind.10), Service for Employed Persons in Maritime (ind.11), and Harbor Construction (ind.12). The results indicate that the biggest contribution to Ind.10 is Transport Equipment (ind.8). For Ind.11 it is agriculture (ind.1) and Processing from Agricultural Products and Light Industry (ind.5). For Ind. 12 it is Nonmetal Ores Mining and Products (ind.4) and Metal Mining and Products (ind.3). These results are consistent with the development character of maritime industries in Liaoning.

Input Analysis of Maritime Industries with Increase in Gov. and Cit. Demand .

Input from the Output of Maritime Industries

The demand of government and citizens is the important component of general demand. In order to meet one unit of increase in demand of government and citizens in the object year, the direct and indirect contributions from maritime industries in planning years are achieved with DIM. (cd: citizen demand; gd: government demand)

From the Fig.1, we can see that to meet one unit of growth in demand from government and citizens, the contribution of Transportation (ind.7) is the greatest. On the other hand, for each maritime industry, the level of input induced by the growth of demand from government is more than from citizens, which means the effect of the increase in government demand on the development of maritime industry is more important in Liaoning.

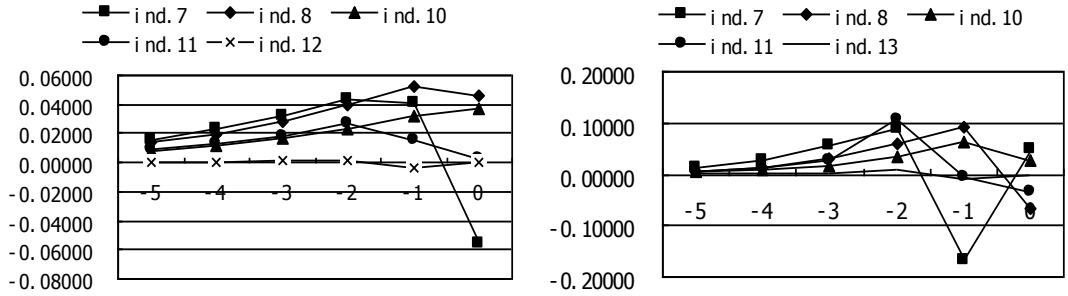

Figure 1: the Input of Maritime Ind. by cd (left) and the Input of Maritime Ind. by gd (right) (unit : 100 million/100 million).

In Fig.1 (left), it can be seen that the time series values of the DIM of most industries are over the 0 line besides Transportation (ind.7), which indicates that the input of most maritime industries to meet the growth in citizen demand is continuously growing. From Fig.1 (right), apart from the Service for Maritime Operation (ind.10), the contributions of other industries are below the 0 line in the object year or before, which indicates that more input during the planning years of the maritime industries in Liaoning is necessary to meeting the increase in the demand of government in the object year.

Labor and Capital Input of Maritime Industries . Fig.2 (left) shows labor input of maritime industries with one unit increase in the demand of government and citizens. The gd-curve is smooth, and in the object year falls below the 0 line, which means the increase in demand of government will inspire more labor input from maritime industries in the early planning years. Fig.2 (right) reflects the required amount of capital input. The input induced by the increase in demand of government and citizens reached the maximum in the last year before the object year, and the gd-curve is higher than the cd-curve. This means the effect of pulling force from the demand increase of government on the development of maritime industries is greater than from citizens.

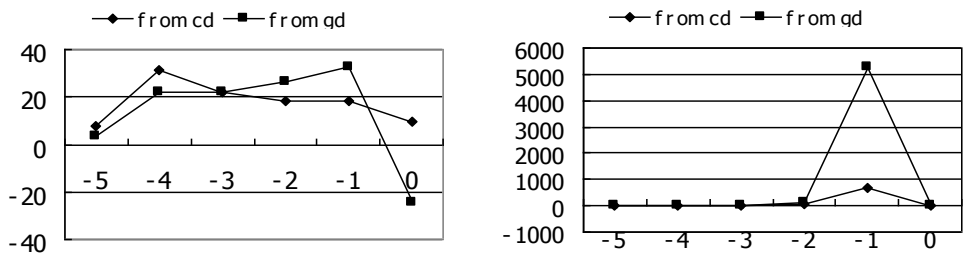

Figure 2: the Lab. Input of Maritime Industries (left) and the Cap. Input of Maritime Industries (right) (unit: 100 people/100 million, million /100 million).

CONCLUSION

Based on the I-O table of Liaoning, this study employs DIM of I-O analysis to examine the character of inter-industry linkage effects on the construction of the international shipping center in Dalian. It can be summarized

that first, the increase of maritime industries in Liaoning needs a different level of input from others, which can provide some guidelines to optimize and allocate investments for the different maritime industries. Second, it can be concluded that the input of maritime industries has a closer relationship to the demand from government than from citizens. The early input during the planning years from the maritime industries is important to accomplishing the increase in government demand. This is helpful in constituting the policy measures for construction of the shipping center in Dalian.

Although the economic level of and the maritime industry of the Dalian Shipping Center accounts for a large proportion in Liaoning, the disadvantage that becomes apparent in this paper is that it will be more typical if we can separate the maritime industries of Dalian from the I-O table of Liaoning. In addition, the industry of raw and processed materials would not be fully reflected in the calculated results because the sectors in the I-O table are combined and a number of irregular factors are off-sett. Those problems provide a focus for further research.

REFERENCES

Chengbao, D., (2006). Dalian Main International Sh ipping Center in Northeast Asia, Dalian Maritime University Press, ISBN 7-5632-1951-X

Enrico, M. ,(2006). "Port Investment: profitability, economic impact and financing," Port Economics Research in Transportation Economics , 16, 17-218.

Leontief, W, (1970). "The dynamic inverse," Contributions to Inputoutput Analysis, A.Caner and A. Brody, Eds. Amsterdam, The Netherlands: North-Holland.

Optimization Theory of Regulation on Rural Transit Market Based on Rule of Transport Equality

Changan Zheng [1], Maosheng Li [2], and Qisen Zhang [3]

[1] Changsha University of Science & technology.
[2] School of Transportation Planning and Traffic Engineering, Central South University.
[3] Hunan Communications Research Institution. PH: +86-0731-5222573; Email: zcajhdd@163.com

ABSTRACT

Transport equality is necessary to a harmonious society. Transport equality is illustrated by means of an assignment of transport resources and reallocation of transportation benefits, and it is carried out by the balanced relationship among all social members' payment for and gain from our society's transportation system, including two aspects of its practical burden and its duty. In order to build a harmonious society and realize transport equality, we need to improve rural economy, health and social service by enhancing rural massive transit services,. Based on historical and realistic rules of transport equality, in this paper optimization theory is adopted to analyze the equilibrium relationship under market conditions of admittance, among power preferences of administrative organization and operational effectiveness of rural transit service and benefit protection of consumers using data of rural residents' income, cluster level of inhabitancy and transport demand of people in the relative areas. Economic data in three rural areas of Hunan province are also used to correct parameters of the game theory model. Results of the model show that proper restriction of administrative power and a reasonable government subsidy policy are useful to motivate the effectiveness and profitability of rural massive transit service. In addition, some practical stratagem can gain consulates from these results.

INTRODUCTION

Passenger transport demand is the required ability to pay which is requested by the social and economic life about the spatial displacement of passengers, and it must possess two conditions: one is the ability to realize this displacement and the other is the ability to pay. Rural passenger transport happens in a range of cities or counties which generally have no other transportation modes except the highway, as in Wang Wei, XU Ji-qian and Yang Tao, et al (1998), and Liu Can-qi (2001). No matter how high the transportation price, when peasants have a need to travel, the highway provides the only transportation mode, (Yu Hong-jun, Li Xu-hong, XuYuan. A, (2002); Yin Hongbin, Wen Huiying, Jin Wenzhou, (2001); Wen Huiying, Zou Xianmin, Xu Jianmin, (2003). The approving system of the passenger transport market leads to the fact that the market is not open and the transportation price is determined by the government while it is not influenced by the market, so that the demand and the supply of the rural transportation is frequently inconsistent. Nowadays, the contradiction between the demand and the supply of rural

transportation has become a bottleneck which constrains development of economic and social aspects in rural areas. In order to accelerate construction of rural public passenger transport systems, promote traffic justice and build a harmonious society, this paper refers to the game theory and basic household income level data, the aggregation degree of residential and travel demand. Research was then applied which is under the regulation of historicity and concreteness of justice in traffic, on a game model of market access regulation about the equilibrium between the management organizations' rights preferences, the efficiency and benefit of management body and interest protection. The optimization model in this paper, which is calibrated by the technical and economic index of a typical area, elaborates the invigorative function and the functional range of which the constraint for the management organization and reasonable policy guidance influences the management body, and will play a guiding role in promoting passenger transport management in rural areas.

1. AN ANALYSIS OF BASIC CHARACTERISTICS OF RURAL PASSENGER TRANSPORT DEMAND DURING THE TRANSITIONAL PERIOD

With the acceleration of the urbanization process in our country, the dualistic social structure of urban and rural areas, which can be described as "urban/industry, countryside/ agriculture", will definitely evolve into urban-rural integration and urban-rural coordinated development. The main characteristics of rural passenger transport during the transitional period are shown as follows:

1) The rural passenger demand is a derived demand. It is derived from the demand of social and economic activities and is designed to serve production or living objectives, while completing spatial displacement which is just as necessary to achieve real aims. The main objectives of social and economic activity include business (the circulation of agricultural products and agricultural means of production), public affairs, visiting relatives, seeking treatment, tourism, and so on.

2) Rural passenger demand is weakly influenced by ticket price. Generally, in a range of city or county, there is no other transportation mode except the highway, so the highway is an irreplaceable service. No matter how much it costs, when peasants have a need to travel, the highway is the only transportation mode available.,. The approving system of the passenger transport market means that the market is not open and the transportation price is determined by the government and is not influenced by the market, so the ticket price is wekly influenced by passenger demand.

3) The heterogeneity and partial substitution of rural passenger transport demand. Because of scattered living conditions, the rural passenger transport demand is heterogeneous in its management of transport quality, technological requirements, transportation distance, direction, time and speed. With the development of modern communication technology, there is a reduction of passengers in rural areas due to smooth information transmission.

4) Certain regularity conditions exist in rural passenger demand during the transitional period. The demand of rural passenger transport is derived from social

and economic activities. Generally, the prosperity of the rural economy can bring growth to passenger transport demand, while the depression of it can cause decline. This imbalance in rural passenger demand can be reflected in the time, space and direction. The imbalance of the time arises mainly from the seasonality of agricultural production, slack and peak seasons of trade activities, holidays, the tourist season and so on. The imbalance of space and direction are mainly caused by productivity, industrial distribution, economic development level, layout of the transportation network, and so on. During the transitional period of urban-rural integration, extremely strong regularity exists in the shift of the rural/surplus labor force, which can be divided into three types: **1)** Living at home but abstaining from the land, which means that labor transfers from agriculture to non-agriculture in the local areas. **2)** Leaving home, but not going to the city, which means that labor shifts betweem different rural areas. **3)** Leaving home and abstaining from the land, which means that rural surplus labor shifts to t urbanareas. As is shown in the Figure 1, M1 and M2 belong to "living at home but abstaining from the land," M5 and M6 belong to "leaving home and abstaining from the land," M3 and M4 belong to "leaving home but not going to city." The different levels of the social and economic development in different areas determines the structure and proportion of the rural surplus labor force flow, which will influence the size and volatility of the rural passenger transport demand. We should notice the differences between the rural passenger transport demand between different areas where the surplus labor force flows in or out. The economics of the former are developed and a large number of the labor force flows in, and the flowing population is one of the main sources of the passenger transport in the daily and holiday period. This can cause the rural passenger transport to change enormously and the scale of it fluctuates according to the proportion of the flowing rural surplus labor force. With the population base M fixed, and letting N_1, N_2, N_3 and $\alpha_1, \alpha_2, \alpha_3$ represent the different average travel times per year and the different proportion in the flowing population of the three different types of flowing population, which is "living home but abstaining from the land," "leaving home but not going to the city" and "leaving home and abstaining from the land." So, due to the flow of the rural surplus labor force, the demand of the rural passenger transport in the areas where surplus labor force flows can be calculated as follows:

$$D = M(N_1\alpha_1 + N_2\alpha_2 + N_3\alpha_3) \quad (1)$$

Even if M and N_1, N_2, N_3 keep invariant, the demand of the rural passenger transport will change greatly when $\alpha_1, \alpha_2, \alpha_3$ keeps different proportion. The figure 2 has shown the change chart when $M = 5000$, N_1, N_2, N_3 equal to 4.5，0.6，0.75 and the different proportion of $\alpha_1, \alpha_2, \alpha_3$ is 3:5:2, 2:7:1and 5:4:1respectively. The different proportion of $\alpha_1, \alpha_2, \alpha_3$ just reflects the configuration effect of how the market and the opportunity cost influences human resources. We can also assume that the change value of the rural passenger transport demand is determined by the portion of the surplus labor force which is absorbed by the local area.

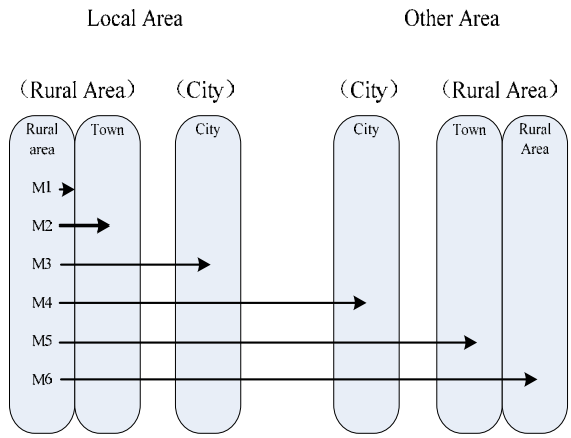

Figure 1 The flowing mode of the rural surplus labor force

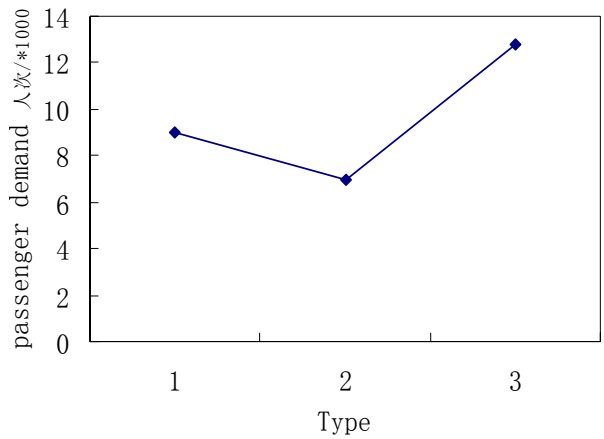

Figure 2. different passenger transport demand under different structure of surplus labor.

These basic characteristics determine that the amount of the occurrence and attraction of the rural passenger transport can be separated into two parts: one caused by the flow of the rural surplus labor force and the other derivative, due to the social and economic activities of other rural areas. Based on basic factors such as gross domestic product, industrial and agricultural output value and population scale, the regression analysis method is most popular in predicting traffic volume which is derived from rural social and economic activities. There are other methods, such as the growth speed method, the growth curve prediction method, the gray system prediction method and so on, as in Jun Zhicai (1998), Zhang Weiying (1999) and Wang Jianjun, Yan Baojie (2004). The traffic volume due to the flow of the rural surplus labor force is determined by the structure and proportion of the flowing labor force. The volume of the rural passenger transport due to the first transferring mode of the labor force which is “living home but abstaining from the land,” is larger and more equal to the other two modes which are “leaving home but not going to city” and “leaving home and abstaining from the land.” However, the volume of

rural passenger transport will change enormously during holidays, when the amount of the labor force due to the two latter modes becomes very large.

2. THE GAME OF RURAL PASSENGER TRANSPORT MANAGEMENT UNDER THE REGULATION OF JUSTICE

Maintaining balance between supply and demand is one of the main objectives of management in rural passenger transportation. Under the regulation of justice in traffic, in order to guarantee that justice is implemented in the balance of the supply and demand in rural passenger transportation, the traffic governing department, which represents the government, must ensure the supply service level of the rural passenger transport on one hand, and the economic benefit which corresponds to the management body of the rural passenger transport on the other hand. Otherwise, harmonious development in rural areas will be hindered and social contradiction will be intensified, or the supply of rural passenger transport will suffer a serious shortage due to the lack of guarantee of economic benefit to the management body in rural passenger transportation. We also need to do our best to help the market invigorate the demand of rural passenger transportation,which is under the regulation of justice and arouses the participation of social resources in the supply of rural passenger transportation.

According to the above analysis, rural passenger transportation has a basic demand fluctuation. For convenience purposes, this paper uses the whole range passenger volume per day Q, which converts the passengers who get on or off at midway to the whole range of passengers and reflects the average traffic flow of the whole range, to describe the demand of the rural passenger transport. $g(Q)$ and $F(Q)$ represents the probability density function and the probability distribution function of the whole range passenger volume Q respectively. The balance between the supply and the demand of the rural passenger transport is reflected by that of the demand of the passenger transport route in the rural areas and is satisfied in some service levels because of the bus service on the route. According to the regulation of justice in traffic, the probability that the passenger transport demand is satisfied by the transport capacity of the daily employee, is no less than β_1 in the normal period or β_2 in the peak period. IC represents the fixed cost of the operation per month which includes management and parking fees, insurance, maintenance costs, bank loans, booking clerk wages and so on. OC represents the oil costs of every employee bus. The normal times of each employee bus on each route per day is t_1, and the average maximum of overtime work times for each employee bus per day is t_2. SN. φ represents the fixed seating number and the maximum of overloading rate for each employee bus respectively. C and MR represent the whole range price of each employee bus on the route and the average income per month in the local area. The number of employee buses on route x should satisfy the normal and peak period service level:

$$\beta_1 < \int_0^{SN \cdot t_1 \cdot x} g(Q)dQ \tag{2}$$

$$\beta_2 < \int_0^{SN\cdot\varphi\cdot t_2\cdot x} g(Q)dQ \tag{3}$$

Second, the number of the buses arranged on route x should satisfy the demand for reasonable profit of the operational bodies:

$$\begin{aligned}&[\int_0^{SN\cdot\phi\cdot t_1\cdot x} Q\cdot c\cdot g(Q)dQ+\int_{SN\cdot\phi\cdot t_1\cdot x}^{SN\cdot\phi\cdot t_2\cdot x}\left\lfloor\frac{Q}{SN\cdot\phi}\right\rfloor\cdot SN\cdot\phi\cdot c\cdot g(Q)dQ\\&+\int_{SN\cdot\phi\cdot t_2\cdot x}^{\infty} t_2\cdot SN\cdot\phi\cdot x\cdot c\cdot g(Q)dQ]\times 30-IC\cdot x-OC\cdot[\int_0^{SN\cdot\phi\cdot t_1\cdot x} t_1\cdot x\cdot g(Q)dQ\\&+\int_{SN\cdot\phi\cdot t_1\cdot x}^{SN\cdot\phi\cdot t_2\cdot x}\left\lfloor\frac{Q}{SN\cdot\phi}\right\rfloor\cdot g(Q)dQ+\int_{SN\cdot\phi\cdot t_2\cdot x}^{\infty} t_2\cdot x\cdot g(Q)dQ]\times 30>2\cdot MR\cdot x\end{aligned} \tag{4}$$

$\lfloor * \rfloor$ represents the integral function here, for example, $\lfloor 3.5 \rfloor = 3$.

According to regulation of justice in traffic, the governing department should make the daily operating cost of route Z smallest when they design the route and number of employee buses. Considering the limited number of buses on the route, we can postulate the maximum number of buses is $V_{\max}$. So the number of the employee buses, which are on the route that are a balance between the supply and the demand of the rural passenger transport under regulation of justice in traffic, should satisfy as:

$$\begin{aligned}&MIN \quad Z = IC\cdot x + OC\cdot x\cdot t_1\\&s.t. \quad (2),(3),(4)\\&\qquad x\in 0,1,2,\cdots,V_{\max}\end{aligned} \tag{5}$$

As shown in the Figure 3, the formulas (2) and (3) of the linear programming above represent the service levels of the daily and peak periods respectively, and formula (4) represents the reasonable profit that the operating body should receive.

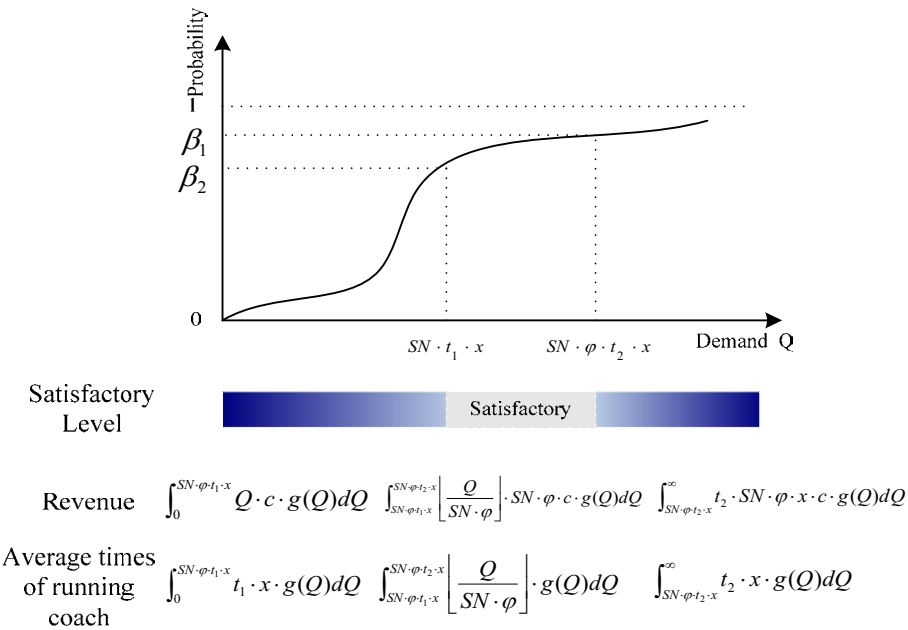

Figure 3. Schematic Diagram of Rural Passenger Management Optimization.

The linear programming (5) can be solved easily by the branch-and-boundor enumeration methods, and the solution can be simplified if the integration can be determined in advance. If the constraint conditions (2), (3) and (4) do not have a feasible region, it shows that the demand of passenger transport is too small to ensure the probability that the transport capacity of the daily employee bus can satisfy the demand because it is higher than the service level β_1, while it is higher than β_2 in the peak period. At this point, relevant policies should be implemented or the service level should be decreased by government in order to keep the balance between passenger transport supply and demand in relevant rural areas.

3. EXAMPLE ANALYSIS

This paper assumes that the daily passenger volume of the whole range Q obeys normal distribution, namely $Q \sim N(585,12^2)$; the fixed cost of and the fuel fees for each employee bus are 7700 yuan per month and 50 yuan per day respectively, and the other parameters are shown as follows:

Table 1. Table of Parameters and Value.

Parameters	β_1	β_2	t_1	t_2	SN (person)	φ	C (yuan)	MR (yuan/month)
Value	0.75	0.9	5	5.4	17	1.2	7	650

Because the number of the employee buses x is an integral, we can solve the linear programming problem with the enumeration method. For $x = 1,2,3,...,n$, we can verify each of the restrictive conditions (2), (3) and (4) as satisfied or not. We also can obtain all of the objective functional values Z for every x, and then the optimum number of the employee buses x can be selected. The solution procedure of the linear programming (5) is simple, so we will not elaborate on that here.

After solving linear programming (5), we can get $x = 7$, which means optimum transport supply is seven employee buses. The value of the objective function is a minimum value, $Z = 55650$. At this time the service level of the normal and peak period is 0.9983 and 0.9999, which satisfies restrictive conditions (2) and (3). The average profit per month of the operational body is 16490 yuan, which is bigger than the average income of 9100 yuan of the local area. So the restrictive condition (4) can be satisfied

If a feasible solution for linear programming (5) cannot be found, it is assumed that the passenger demand in the normal and peak periods will not be satisfied simultaneously with the operating body running sustainably without a subsidy from the government. That means the passenger transportation operational body will never operate well without a subsidy from the government.

We considered that the employee buses are not allowed to overload during the normal or peak period. In this situation, the maximum of overloading rate φ equals 1. We can get $x = 7$, but the service level will drop to 0.7977 in the normal period.

4 CONCLUSIONS

a. Variation is a basic characteristic of rural passenger transport demand curing the transformation period, which determines that the amount of occurrences and attraction of rural passenger transport can be separated into two parts: one is caused by the immigration of the rural surplus labor force and the other one is derived from social and economic activity in rural areas.

b. Under the justice in traffic rule, and in order to guarantee that justice si implemented in the balance of supply and demand in rural passenger transportation, the traffic governing department, which represents the government, must ensure a supply service level of rural passenger transport on one hand, and protection of the economic benefit that corresponds to the running body of rural passenger transport. Otherwise, harmonious development in the rural areas will be hindered and social contradiction will be intensified, or the supply of rural passenger transport will be seriously diminished because the economic benefit of the running body in rural passenger transportation will not be guaranteed. The optimal allocation for daily employee bus transport capacity in rural areas must refer to normal and peak period service levels.

ACKNOWLEDGEMENTS

This paper is partially granted by the novel research project of the Transportation Bureau of Hunan Province (No. 200831).

REFERRENCES

Jun, Zi. (1998). “Economy of road transportation.” *China Communications Press*. Beijing,

Liu, C. (2001). “Advanced traffic planning.” : *China Communications Press*. Beijing.

Wang, W., Xu, J., and Yang, T. 1998). *Urban transportation planning*, Southeast University Press. Nanjing.

Wen, H., Z, X., and Xu, J. (2003). “Development and application of transportation database system for the bus station of guangdong province.” *Journal of South China University of Technology*, *(Natural Science Edition)*. . 31(11), 61-64.

Wang, J., and Yan, B. (2004). “Transportation survey and analysis.” *China Communications Press*. Beijing,

Yu, H., Li, X., and Xu, Y. A. (2002). “Three-Phase approach to passenger transport capacity forecast of passenger transport line on the road. *Journal of Hubei Automotive Industries Institute*,.16(4), 52-55.

Yin H., Wen H., and Jin, W. (2001). “A prediction of passenger volumes of the highway transit lines in guangzhou,” *Journal of South China University of Technology (Natural Science Edition)* ,.27(7), 86-87.

Zhang W. (1999). *Enterprise theory and company reform of China*, Beijing University Press, Beijing,

Analyzing the Motivation of Queue-jumping Driving-action on Transportation Systems by Prospect Theory

Maosheng Li [1], Qinglong Zhong[1], and Dafei Chen [1]

[1] College of Transportation Planning and Traffic Engineering, Central South University, Changsha city, Hunan Province, 410075, China; Phone numbers: +86-0731-2655640; Email: maosheng.li@163.com

ABSTRACT

This paper researches the motivation of queue-jumping driving-action on transportation systemsas compared to the expected utility theory . The drawback of the expected utility theory, which fails to explain the motivation of the queue-jumping driving-action, is illustrated. In addition, when considering three underlying factors, traffic management policy, the delayed time after taking queue-jumping action and audit probability, a critical function about expected disutility, which can reveal whether the driver has the motivation to jump the queue or not relative to these underlying factors, is established. The model established in this paper, which is rooted in the prospect theory for describing the complicated relationships among the three aspects of underlying factors, is calibrated by actual data collected from intersections. Based on the quantitative analysis results, three approaches are offered to decrease the possibility of taking queue-jumping driving-action when a driver encounters a queue. Finally, conclusions and some future research problems are summarized.

1. INTRODUCTION

Although differences exist in eastern and western countries queue-jumping driving-actions in the transportation system can be spotted in our daily lives; , especially in congested urban settings. The minor peccadilloes that occur as a consequence of these actions will subsequently cause different kinds of confusion, from a very short delay of traffic flow to heavy congestion of the transportation system in some areas. Managers all over the world take great efforts to eliminate the affect of queue-jumping driving-actions by different means and transportation policies. The motivation of queue-jumping driving-actions varies under different factors, such as traffic management policy, the exogenous delay time due to the queue, the audit probability and lack of stigmatization from moral a moral standpoint. These actions occur only when there is a queue ahead and the extra-free space is adequate enough for a driver to take a queue-jumping driving-action. For example, some drivers may occupy a left turn lane cheating by going straight instead of turning left, which is followed by a go-ahead phase on the in-leg of the intersection. There is a high probability that this may cause confusion near the outter edge of the intersection. In this paper, we aim to explore the relationship between the motivation of queue-jumping driving-actions and underlying factors in order that most of the queue-jumping driving-actions, except for the motivation of saving somebody's life, will be help up by well planned mechanisms.

The cause of a vehicle's movement can be classified into two types: one is

simple or standard situations that can be well predicted, in which the motion of the mixed agents can be described as if they would be subject to social forces(Helbing and Molnar., 1995). The other is the complex or new situations that may occur with probabilistic models such as expected utility theory (EUT) which is a useful tool for analyzing route choice decisions (Sheffi, 1985). But there is a failure to explain the motivation of queue-jumping driving-action as described in Section 3. The cell transit model (Wolfram, 1983; Daganzo, 1994; Lo, 2002a) which is rooted in Wolfram's rule 184 succeeds in simulating the effect of queue-jumping driving-actions in links or areas of the transportation system and adapts its probability to capture this effect. Although underlying stimuli relationships exist among traffic management policies (i.e. penalty on the action), and the delay time after taking queue-jumping action, audit probability remains to be a mystery.

In this paper, we adopt prospect theory to describe the complicated relationships between traffic management policy, the exogenous delay time due to queue and audit probability. We also offer a critical function that can reveal whether a driver is motivated to jump the queue or not relative to these underlying factors. The new results from an economic standpoint would be useful for designing width of lane and evaluating transportation management policies.

2. A BRIEF INTRODUCTION TO PROSPECT THEORY

Prospect theory is based on the following five main ideas: reference dependence, declining sensitivity, loss aversion, non-linear weighting of probabilities, and susceptibility to frame effects. Unlike EUT, where the utility carriers are equivalent to final levels of wealth (or incomes or commodities), the utility carriers for prospect theory are equivalent to both gains and losses relative to the reference point. Declining sensitivity means that the utility function is concave in the domain of gains and convex in the domain of losses. Loss aversion is based on the idea that losses are more salient than gains. Given an amount of money, $x > 0$, and a utility function, $v(x)$, loss aversion implies that $v(x) < -v(-x)$. Agents facing uncertain situations over evaluate small probabilities but under evaluate large ones. Finally, agents' preferences are influenced by the way a problem is presented. There is a substantial body of evidence to support these building blocks of prospect theory (Tvershy and Kahneman, 2000).

Prospect theory has been successfully used to explain a range of puzzles in economics, such as the disposition effect, asymmetric price elasticity, the elasticity of labor supplies that are inconsistent with standard models of labor supply, the excess sensitivity of consumption to income, and the tax evasion puzzle (Dhami and al-Nowaihi 2006, 2007). But to the best ov my knowledge, there is little literature on the application of prospect theory to solve transportation problems.

3. QUEUE-JUMPING DRIVING-ACTION UNDER PROSPECT THEORY

Facing a queue situation in a transportation system, a driver will encounter exogenous delay time $D > 0$, more than normal transverse time $W > 0$ in a non-queue situation. If the exogenous delay time D could be cut down to some level of proportion $\phi(0 \le \phi < 1)$ of delay time by taking a queue-jumping action, the driver

would possibly be motivated to implement it. Despite the fact that the delay time ϕD that the driver will encounter after taking queue-jumping action is shorter than the exogenous delay time D under taking no action, the queue-jumping driving-action is not always encouraged because it is punished at constant rate s if the action is caught by a policeman. If the queue-jumping driving-action caught by a policeman is recorded as a traffic citation, the driver would suffer additional stigma rate λ. In this paper, we assume that both the penalty rate s and stigma rate λ are relative to exogenous delay time D, and their values are converted to time units rather than money. We also assume that the driver is caught with a probability $P(D) \in [D]$, in which $P(D)$ is continuously differentiable and $P^{'}(D) \geq 0$ (i.e. the driver who takes queue-jumping driving-action is more likely to be caught if the length of queue is too long). Denoted by Y_C and Y_{NC}, respectively, the transverse time of taking queue-jumping action under a queue situation in the transportation system when he is "caught" and when he is "not caught", respectively:

$$Y_C = W + \phi D \tag{1}$$

$$Y_C = W + tD + sD + \lambda D = W + (t + s + \lambda)D \tag{2}$$

When he is caught while taking a queue-jumping action, the transverse time through the queue area is usual longer than the exogenous delay time D. In this paper we assume that the extra delay time is $tD(t \geq 1)$, and the driver has a strictly decreasing, strictly concave and twice continuously differentiable disutility function, $u(Y)$. Under expected utility theory (EUT), his expected disutility is:

$$U(D, s, \lambda, W) = p(D)u(Y_C) + [1 - p(D)]u(Y_{NC}) \tag{3}$$

When combined with equations (1)-(3), we find that the driver's expected disutility is relative to normal transverse time W, which is illogical in our experience. Results indicate that the motivation behind queue-jumping driving-action iss not relative to normal transverse time W. You can image that a driver's willingness to engage in queue-jumping driving-action is very low if the exogenous delay time D approaches zero, although normal transverse time W may probably be long enough in this situation. So we turn to prospect theory to find a reasonable explanation for the motivation behind queue-jumping driving-action.

Let R be the reference transverse time of the driver under a queue situation, and let the time relative to this reference point be:

$$X_i = Y_i - R \tag{4}$$

Where i = C or NC denotes the two states "caught" and "not caught," As in Tversky and Kahneman (1992), and Dhami and al-Nowaihi (2007), the utility associated with a gain (i.e. time-saving) or loss (i.e. time-consuming, penalty and stigma rate) X_i is $v(X_i)$ with minor modifications, and

$$v(X_i) = \begin{cases} (-X_i)^{\beta} & if\ X_i \leq 0 \\ -\theta\, X_i^{\beta} & if\ X_i > 0 \end{cases} \tag{5}$$

Here, $\beta \in [0,1]$ and $\theta > 1$ are preference parameters and v is called the value function. The parameter θ is the parameter of loss aversion. It encapsulates the basic

idea that a loss of x hours (or dollars) is more painful than the pleasure derived from a gain of x hours (or dollars). Based on experimental evidence, Tversky and Kahneman (1992) suggested that $\beta = 0.88$ while $\theta = 2.25$.

Although prospect theory does not provide sufficient guidance to determine the reference point in each possible situation, specifying a suitable reference point is often essential for a successful application of prospect theory.

We take the legal transverse time as the reference point in this paper, so

$$R = W + D \tag{6}$$

The assumption below shows that this will be the case if, and only if, the reference point is the legal transverse time of queuing link or area.

Assumption: For a driver who jumps the queue, if both the penalty rate s and stigma rate λ are larger than zero, he/she is in the domain of gains if not caught, $X_{NC} \le 0$, but in the domain of losses if caught, $X_C > 0$. If both the penalty rate s and stigma rate λ equal zero, he/she is in the domain of gains no matter whether he/she is caught or not. Then the reference point must be $R = W + D$.

Using equations (4) and (6), we get:

$$X_{NC} = -(1-\phi)D \le 0 \tag{7}$$

$$X_C = (t + s + \lambda)D > 0 \tag{8}$$

Let w^+ and w^- be the driver's probability weighting function for the domains of gains and losses, respectively. Then, according to cumulative prospect theory, the driver maximizes:

$$V(D, \phi, s, \lambda) = w^-[p(D)]v(X_C) + w^+[1 - p(D)]v(X_{NC}) \tag{9}$$

Comparing equation (9) with the analogous expression for expected utility theory, equation (3), we see the following differences. First, the carriers of utility in prospect theory are gains and losses relative to some reference point rather than levels. Second, one uses decision weights in prospect theory to aggregate outcomes while one uses objective probabilities under expected utility theory. From equations (5), (7), (8) and (9), we get:

$$V(D,\ \phi, s, \lambda) = -\theta w^-[p(D)][(t + s + \lambda)D]^\beta + w^+[1 - p(D)][(1-\phi)D]^\beta \tag{10}$$

Let:

$$h(\phi,\ s, \lambda) = -\theta w^-[p(D)](t + s + \lambda)^\beta + w^+[1 - p(D)](1-\phi)^\beta \tag{11}$$

Equation.(10) can be rewritten in the following form:

$$V(D, \phi,\ s, \lambda) = D^\beta h(\phi, s, \lambda) \tag{12}$$

The value of function (12) reveals whether a driver has motivation to jump the queue or not. He will take queue-jumping driving-action if $V(D, \phi, s, \lambda) > 0$, and takes no action to jump queue if $V(D, \phi, s, \lambda) < 0$. If $V(D, \phi, s, \lambda) = 0$. The driver who

is risk-preferring is more likely to jump the queue because he/she does not care about the losses if he/she is caught. The driver who is risk-averse is more likely to not jump the queue. Comparing function (12) with equation (3), we see the difference that the value of equation (3) is related to both the exogenous delay time D and normal transverse time W, but the value of function (12) is only relative to the exogenous delay time D. The above is summarized by the following assumption:

4. MODEL CALIBRATION

4.1 The Probability Weighting Function

For our calibration exercise, we adopt the weighting function of Prelec (1998) because it is parsimonious, which is consistent with much of the available empirical evidence and has an axiomatic foundation. Let P be the case of audit probability $P(D)$. The Prelec weighting function has the following form:

$$w^+(p) = w^-(p) = w(p) = e^{-(-\ln p)^\alpha} \text{ for } p \in (0,1],\ w(0) = 0 \text{ and } 0 < \alpha < 1 \tag{13}$$

Note that $w(p)$ is a strictly increasing function onto $[0,1]$, $w(0) = 0$, $w(1) = 1$, $w(e^{-1}) = e^{-1} \cong 0.37$, $w(p)$ is strictly concave on $(0, e^{-1})$ with $w(p) > p$, $w(p)$ is strictly convex on $(0, e^{-1})$ with $w(p) < p$. Using Eq.(12) and the Prelec weighting function (13), the $(t + s + \lambda, p)$ locus at the value $V(D, \phi, s, \lambda) = 0$ under prospect theory while other parameters be assumed to be fixed is given by:

$$(t + s + \lambda) = (1 - \phi)\Gamma(p)^{(1/\beta)}\theta^{-(1/\beta)}\left(\frac{1-p}{p}\right)^{(1/\beta)} \tag{14}$$

Where $\Gamma(p) = \exp(-\ln p)^{0.35} - (-\ln(1-p))^{0.35}]$, we have substituted the value of $\alpha = 0.35$ in $\Gamma(p)$ in this paper.

4.2 Queue-jumping Driving-action in Front of the Intersection

The queue caused by the red light at the intersection is ubiquitous in the transportation system. If a driver decides to jump the queue while he faces it and the extra-free space is wide enough, the expected delay time $E(\phi D) = E(\phi)D$ which the driver will encounter after taking queue-jumping action is $0.5D$. Equuation.(14) takes expected value in both sides, then we get:

$$(t + s + \lambda) = 0.5\Gamma(p)^{(1/\beta)}\theta^{-(1/\beta)}\left(\frac{1-p}{p}\right)^{(1/\beta)} \tag{15}$$

According to equation (15), the relationship between the penalty adding stigma rate $t + s + \lambda$ and the audit probability p is given in Table 1, and is also depicted in Figure 1, while $t = 1$. A policeman who works eight hours per day is in charge of four legs of the intersection, so the audit probability p for queue-jumping driving-actions

by the policeman is no more than (1/4)*(8/24) in front of the intersection, which is 0.075, because he can only monitor one of four legs of the intersection at any moment. Table 1 gives 18 groups of value for $(t+s+\lambda, p)$. When audit probability p increases in range of intervals 0.001-0.01, value of $t+s+\lambda$ drops very fast. That means very small improvements in audit probability, and more saved in the value of p. We can see that this measure, where auto-surveillance cameras are installed in front of an intersection to increase audit probability p in some countries, is very effective. This is why the possibility of taking queue-jumping driving-actions in front of an intersection drops quickly after auto-surveillance cameras are installed though the value of penalty and stigma rate $t+s+\lambda$ is actually very low.

Table. 1 Value of $(t+s+\lambda, p)$ at Critical Point of Equation(12) While $\phi=0.5$.

Items	Audit probability p	Penalty & stigma rate $t+s+\lambda$ (dollar)	Items	Audit probability p	Penalty & stigma rate $t+s+\lambda$ (dollar)
1	0.001	566.5251	9	0.009	31.0524
2	0.002	230.8286	10	0.01	26.8731
3	0.003	135.6122	11	0.02	10.1901
4	0.004	92.6554	12	0.03	5.6710
5	0.005	68.7959	13	0.04	3.7007
6	0.006	53.8521	14	0.05	2.6371
7	0.007	43.7258	15	0.06	1.9876
8	0.008	36.4708	16	0.07	1.5576

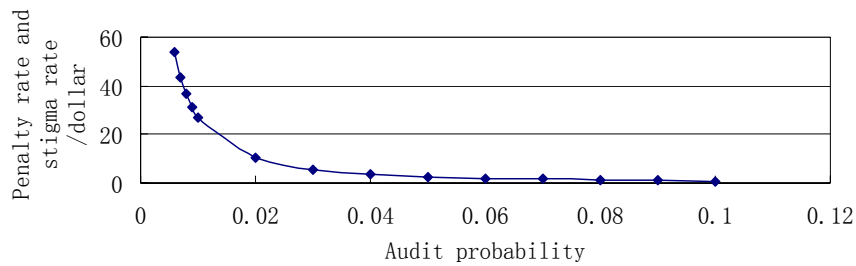

Figure 1. Relationship Between Penalty and Stigma Rate and Audit Probability Described by Equation (14) While $\phi=$ 0.5.

In Figure.1, the horizontal axis represents the audit probability p, and the vertical axis represents the penalty rate adding stigma rate $t+s+\lambda$. Considering that the actual penalty rate is about \$25-\$50 and the stigma rate is very small in most Chinese cities today, we can deduce that the actual audit probability of queue-jumping driving-action is in the range 0.006-0.01, so the horizontal axis is shown as a maximum value of 0.011. We can also see from Figure 1 that the higher the actual probability p is, the less the penalty rate adding stigma rate $t+s+\lambda$ needs to be for

keeping the value function of equation (12) equal to zero, namely, let the critical point of the value function appear.

Equation(10) can be rewritten as:

$$V(D,\phi,\ s,\lambda) = D^{\beta}[-\theta \cdot e^{-(-\ln p)^{\alpha}} \cdot (t+s+\lambda)^{\beta} + e^{-[-\ln(1-p)]} \cdot (1-p) \cdot (1- \quad (16)$$

From equation. (16), we observe that there are three basic ways to change the value of $V(D,\phi,s,\lambda)$. By changing the value of one of the variances, the penalty rate adding stigma rate $t+s+\lambda$, the audit probability p and the proportion ϕ of delay time we arrive at:

Approach 1. The first approach is to set a proper level of penalty and stigma rate on queue-jumping driving-action. For example, the penalty rate remains in the range of \$25-\$50 and we increase stigma rate up to \$25 or more. Other parameters remain unchanged, because the audit record of the transportation system is not employed to cite personal credit, and the current stigma rate equals close to zero in most Chinese cities. On the contrary, the stigma rate in European countries and America is very high. This is a very important reason why drivers in western countries are willing to follow queues in intersections without taking queue-jumping driving-action. A high penalty rate is not currently favored by Chinese drivers or governors.

Approach 2. The second option is to increase the audit probability on queue-jumping driving-action, such as installing auto-surveillance cameras in front of the intersection. This way requires more policemen or cameras to supervise drivers so the cost of transportation management is increased. Although a small improvement in audit probability will cause a large decrease in queue-jumping driving-action as seen in Figure1 or Table 1, achieving a small improvement in audit probability is very hard.

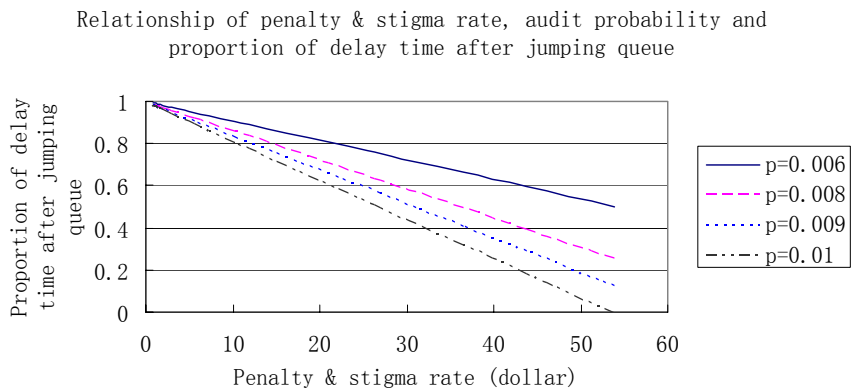

Figure 2. Relationship of Penalty and Stigma Rate, Audit Probability and Proportion of Delay Time After Jumping Queue at Critical Point.

Approach 3. The last option is that the delay time which the driver will encounter after taking queue-jumping action is connected to the exogenous delay time of taking no action by some methods (i.e. changing audit place, setting a limited width of the lane entering the intersection or other means so that the delay time is hard to cut after a driver makes a queue-jumping driving-action.).

An integrated policy may be more effective in decreasing queue-jumping driving action.. The larger the value of proportion ϕ, shorter the saving time will be when a driver makes a queue-jumping action. To provide deterrents to jumping queue, Figure 2 clearly depicts the relationship of the penalty and stigma rate, the audit probability and the proportion of delay time y.

5. CONCLUSION

The motivation behind queue-jumping driving-action is researched under prospect theory while considering three aspects of underlying factors: traffic management policy (i.e. penalty, stigma rate on the action), the delay time after taking queue-jumping action, and the audit probability. Some new characteristics of prospect theory allow us to get some new results. , These include where the carriers of utility in prospect theory are gains and losses relative to some reference points rather than levels in expected utility theory (EUT), as well as where decision weight in prospect theory is used to aggregate outcome while objective probability is employed under EUT.. These quantitative analysis results show that there are three approaches to decrease the possibility of a driver's taking queue-jumping driving-action when he encounters a queue.

The first approach is to set a proper level of the penalty rate on queue-jumping driving-action and increase the stigma up to $25 or more. The second approach is to increase the audit probability on queue-jumping driving-action.

The last approach is to delay the time the driver will encounter after taking queue-jumping action, tending to the exogenous delay time of taking no action by some methods.

The data of queue-jumping driving-action collected near four legs of the intersection is used to calibrate the model. Queue can be classified into two classes: recurrence and non-recurrence., While the proposed analysis method is suitable for non-recurrence cases, A method for the elimination of cases of non-recurrence queues is worthy of further research.

REFERENCES

al-Nowaihi, A., Dhami, S. (2006). "A simple derivation of Prelec's probability weighting function." *Journal of Mathematical Psychology* 50(6), 521–524.

Daganzo, C. F. (1994). "The cell transmission model: A simple dynamic representation of highway traffic." *Transportation Research Part B*, 28, 269-287.

Dhami, S., al-Nowaihi, A. (2007). "Why do people pay taxes? Prospect theory versus expected uility theory." *Journal of economic behavior & organization*. Forthcoming.

Helbing, D., Molnar, P. (1995). "Social force model for pedestrian dynamics." *Physical Review E,* 51(5), 4282-4286.

Lo, H. K. and Szeto, W. Y. (2002a). "A cell-based variational inequality formulation of the dynamic user optimal assignment problem." *Transportation Research Part B*, 36, 421-443.

Prelec, D. (1998). "The probability weighting function." *Econometrica* 60, 497–528.

Sheffi, Y. (1985). *Urban Transportation Network: Equilibrium Analysis with Mathematical Programming Methods*. Prentice Hall, New York.

Tversky, A., Kahneman, D.(1992). "Advances in prospect theory: cumulative representation of uncertainty." *Journal of Risk and Uncertainty* 5, 297–323.

Wolfram, S. (1983). "Statistical mechanics of cellular automata." *Rev. Mod. Phys*. 55, 601-644.

Modeling Passenger Choice Behavior in Chinese Multi-Airport Regions

LIU Jiangtao[1]

[1]School of Economics, Wuhan University of Technology, Hubei, 430070, P. R. China; email: liujiangtaoljt@sohu.com

ABSTRACT

Passenger choice is a crucial factor in determining airports' success or failure. As a developing country, Chinese travelers have their own choice indicators. Application of existing models of passenger choice behavior developed by countries outside of China has not had any effect on passenger choice behavior in China. In this paper, a nested logit model is constructed to predict airport choice in a multiple-airport region and estimated using passenger data from Chinese metropolitan areas. A two level nested logit model with the airport choice at the top level and the access mode choice at the lower level is preferred. The estimation results show that business travelers have higher access time elasticity than leisure travelers, while leisure travelers have higher fare elasticity. In addition, airport access time and passenger experience are of great importance in Chinese airport choice behavior for both business and leisure travelers.

INTRODUCTION

Intercity travel has grown steadily over the past decade, and recent studies suggest that such travel is only likely to grow over the next two decades (Basar and Bhat 2004). Within the development of Chinese economy and its standard of living, air travel is the fastest growing intercity mode of travel in China. Many of the world's largest cities are served by more than one commercial airport and this is not dissimilar for Chinese metropolitan areas. Airports in a multiple airport region have to compete with other airports for passengers. Therefore, airport choice is an important air travel-related decision in multiple airport regions.

The study of such multiple-airport systems has long been considered an important research area. To date, a number of papers have modeled airport choice in multi-airport regions. Most studies use the discrete choice models, such as the binomial or multinomial logit approach to investigate the primary determinants of passengers' airport-choice decisions, e.g. airfare, airport access time, airport access cost, and flight frequencies. Some of these studies have focused on airport choice in isolation (e.g. Skinner 1976; Harvey 1987; Thompson and Caves 1993), while others have examined airport choice along with other dimensions of air travel (Furuichi and Koppelman,1994; Pels et al. 2001, 2003; Warnock-Smith and Potter, 2005; and Hess et al. 2007). These studies have important implications for airport managers and planners. However, the choice of airport access mode has been studied only sporadically in the literature. Harvey (1986) studies the airport access mode in the San Francisco Bay Area, and, finds that travel time and travel costs are strong determinants of the airport access mode. Bondzio (1996) estimated nested logit models to explain the joint access mode-departure airport choice for German airports, using access time to the airport, access costs, and frequency of service as explanatory

variables. Pels et al. (2001, 2003) finds that a nested logit model with the airport choice at the upper level and the airline choice at the lower level best explains the joint airport–airline choice for both business and leisure travelers in the San Francisco Bay Area. However, airfare was not included in the analysis. In this paper, airfare is included, but since it is not available for all airlines (only average fares on a route level are available), the airline choice deleted from the model and the access mode choice is included.

In addition, previous researchers generally studied airport choice in developed countries and seldom concern themselves with the multi-airport regions in developing countries. This paper aims to provide insight into passenger sensitivity to fare, frequency, airport access time, airport access cost, and passenger experience, and furthermore, we extend the research on airport choice to developing countries. A nested logit (NL) model is constructed to predict airport choice in a multiple-airport region and estimated use of passenger data from Chinese metropolitan areas. The modeling results indicate that business travelers have higher access time elasticity than leisure travelers, while leisure travelers have higher fare elasticity. In general, airport access time and passenger experience is of greater importance in airport choice behavior for both business travelers and leisure travelers.

PROPOSED MODEL

Suppose a traveler has decided to fly to a particular airport. The traveler then has to choose a departure airport (d) and an airport access mode (a). The log of the average fare on a route will be used as an explanatory variable for the airport choice. There are two options for modeling these choices. In the simple option, airport and access mode are made independently; first one chooses an airport and later one chooses the access mode. Although travel time to the airport may depend on the access mode, while the airport is chosen, the passenger does not decide on the access mode. At a later stage, the passenger decides on the access mode based on access time, access cost, and experience. For example, a passenger buys a ticket at the airport and thus has to choose in advance what airport is preferred and how to get there, or, a ticket is bought in advance, but this choice, which also includes the airport choice, also depends on access mode; the passenger chooses the alternative, which maximizes the total utility of the airport access mode combination.

Let there be a set (d) of airports and set (a) of access modes. The probability model for choosing alternative (airport) (d) in the first option is:

$$P(d) = \frac{\exp[\alpha_d + \alpha_{fare} \ln fare_d + \alpha_{freq} \ln freq_d + \alpha_{expe} \cdot expe_d]}{\sum_{d \in D} \exp[\alpha_d + \alpha_{fare} fare_d + \alpha_{freq} \ln freq_d + \alpha_{expe} \cdot expe_d]} \quad (1)$$

for the airport choice and:

$$P(a) = \frac{\exp[\beta_a + \beta_{cost} \cos t_a + \beta_{time} time_a]}{\sum_{a \in A} \exp[\beta_a + \beta_{cost} \cos t_a + \beta_{time} time_a]} \quad (2)$$

for the access mode choice. In Equation (1), $freq_d$ is the daily frequency of service, included in logarithmic form, as it is an indication of the "size" of an airline in a market to a certain destination; $\alpha_{freq}>0$. The average fare and distance to the airport are also included; $\alpha_{fare}<0$ and $\alpha_{expe}>0$. α_d is an airport-specific constant. In Equation (2), β_a is a mode-specific constant, cost is the access cost and time is the

access time.

In the second option, the passenger chooses the airport and access mode simultaneously. The chosen alternative is therefore a combination of an airport and an access mode. According to the independence from irrelevant alternatives (IIA) assumption, a passenger's choice probability ratio of two alternatives is not affected by the utilities of other alternatives. To overcome this problem, we specify a nested logit model, which recognizes that there are clusters of alternatives of which the utilities are correlated through random disturbances. In this case, clusters of alternatives can have a common airport or a common access mode. If we specify the model with nests determined by a common airport, we have:

$$P(a/d)=\frac{\exp[\frac{\beta_a+\beta_{cost}\cos t_{a,d}+\beta_{time}time_{a,d}}{\mu_d}]}{\sum_{a\in A(d)}\exp[\frac{\beta_a+\beta_{cost}\cos t_{a,d}+\beta_{time}time_{a,d}}{\mu_d}]} \quad (3)$$

$$P(d)=\frac{\exp[\alpha_d+\alpha_{fare}\ln fare_d+\alpha_{freq}\ln freq_d+\alpha_{expe}\cdot expe_d+U_1]}{\sum_{a\in A(d)}\exp[\alpha_d+\alpha_{fare}\ln fare_d+\alpha_{freq}\ln freq_d+\alpha_{expe}\cdot expe_d+U_1]} \quad (4)$$

$$U_1=\mu_d\ln\left\{\sum_{a\in A(d)}\exp[\frac{\beta_a+\beta_{cost}\cos t_a+\beta_{time}time_a}{\mu_d}]\right\} \quad (5)$$

U_1 is the maximum expected utility. The passenger chooses an access mode based on the access cost and access time, and an airport based on the fare, frequency and the expected value of the subset of access modes available to the airport. Simply put, if an airport has better accessibility in terms of access time, access cost and the number of available modes, it has a higher probability of being chosen. μ_d is an inclusive value parameter, which can also be interpreted as a heterogeneity parameter; alternatives within a nest become closer substitutes if μ_d gets closer to 0. In theory, a heterogeneity parameter could also be included in similar fashion in Equation (4), but this parameter is standardized to 1. The model in Equations (3) through (5) is consistent with the theory of utility maximization if $0<\mu_d<1$. When $\mu_d=1$, the model reduces to the multinomial logit (MNL) model.

We can also formulate a model with nests determined by access modes. Since the access time and access cost are dependent on the departure airport, these variables now appear in the airport's utility function. The conditional probability of choosing airport (d), conditional on the choice of access mode (a) is:

$$P(d/a)=\frac{\exp[\frac{\beta'_a+\beta'_{cost}\cos t_{a,d}+\beta'_{time}time_{a,d}+\alpha_{fare}\ln fare_d+\alpha_{freq}\ln freq_d+\alpha_{expe}\cdot expe_d}{\mu_a}]}{\sum_{d\in D(a)}\exp[\frac{\beta'_a+\beta'_{cost}\cos t_{a,d}+\beta'_{time}time_{a,d}+\alpha_{fare}\ln fare_d+\alpha_{freq}\ln freq_d+\alpha_{expe}\cdot expe_d}{\mu_a}]} \quad (6)$$

The marginal probability of choosing access mode (a) depends on mode-specific factors and the log of the denominator of (6) multiplied by μ_a. In this model, the access mode choice is dependent on the fares, frequencies, and experiences.

SURVEY DATA

Data for calibrating the models were collected in the Shanghai region from the passenger survey conducted by four university students in the study area during the summer of 2007. In the survey, the passengers were asked to provide information on their recent trip (e.g., trip destination and purpose of trip), ground access trip to the airport (e.g., origin of trip, ground access mode, access time, and access cost), airport choice (e.g., primary reasons for choosing airport over other airports and other airports considered), experience (that is, whether or not a passenger has ever used a candidate airport in the past, and the times every year, and his/her impression in the airport), and their personal characteristics (e.g., age, sex and income). The survey was distributed to the passengers in the study area by the intercept survey. The four students worked on 4-hour shifts for two weeks, one week at each airport. Their shifts were carefully scheduled on every day of the week. Only those passengers who lived in the study area were surveyed. The number of surveys collected included 112 business travelers and 98 leisure travelers in airport I; and 126 and 109 in airport II, respectively.

In the airport-choice studies, we use the following airport-choice variables: (a) airfare at each airport, (b) flight frequency to the passenger's destination from each airport, (c) access time to each airport, (d) access time to each airport, (e) passenger's experience with airports. The airfare variable measures a passenger's perceived level of airfare at each airport. Flight frequency was obtained by counting the number of scheduled flights from each airport to the passenger's destination using the official airline guide. The access time to each airport and experience variables were collected directly from the survey data. The value of passenger experience is -4, 2, 0, 2, and 4. "-4" denotes that the traveler has a very bad experience in this airport; "0" denotes no experience or common experience; "4" represents a very pleasant experience.

ESTIMATION RESULTS

Estimation results of the nested logit model for choice of airport and access mode are presented in Table 1. Estimation results suggest that, if everything else is equal, a passenger tends to choose the airports that have lower average airfares, more flight frequency, prior good experience, and less access time and access cost. These five variables explaining the conditional access mode choice are proved to be insignificant.

From the estimations in Table 1 we can calculate the value of time based on access cost and access time parameters. For business travelers the value of time is 0.125/0.44=2.84 yuan/min, while that for leisure travelers is 0.092/0.048=1.92 yuan/min.

Table 1. Estimation results of the nested logit model.

Variables	Business travelers		Leisure travelers	
	Coefficients	Error level	Coefficients	Error level
Ln(fares)	-0.168	0.005	-0.249	0.004
Ln(frequency)	0.857	0.093	0.638	0.086
Experience	1.592	0.030	1.251	0.036
Access time	-0.125	0.085	-0.092	0.092
Access cost	-0.044	0.032	-0.048	0.036

Table 2. Elasticity of choice probabilities of airport and access model.

	Conditional				*Marginal*		
	Time	**Cost**	**Fares**	**Frequency**	**Experience**	**Time**	**Cost**
Business travelers	**-1.43**	**-0.10**	**-0.69**	**0.85**	**1.23**	**-1.91**	**-0.12**
Leisure travelers	**-1.16**	**-0.16**	**-0.85**	**0.56**	**1.06**	**-1.32**	**-0.15**

As shown in Table 2, access time and experience are two dominant explanatory factors of airport choice. Airport access time, as well as experience, is clearly higher elasticity than fare, flight frequency or access cost. This implies that access time and experience are of greater importance in the competition between airports in a multiple airport region.

CONCLUSION

This paper has extended the studies of multi-airport choice into Chinese metropolitan areas using a nested logit model. The most significant findings are the following:

(a) The important airport-choice variables in Chinese multi-airport choice are airfares, experience, access time, access cost, and flight frequency.

(b) Business travelers and leisure travelers have different elasticities. Business travelers have higher access time elasticity than leisure travelers, while leisure travelers have higher fare elasticity.

(c) Airport access time and passenger experience are of greater importance in the airport choice behavior for both business travelers and leisure travelers. A passenger tends to choose airports that have less access time. In addition, passengers who have used an airport will tend to continue to use the same airport, all other factors being equal. Airport managers may benefit by attempting to attract nonusers and providing high-quality service.

REFERENCES

Ashford, N., and Benchemam, M. (1987). "Passengers' choice of airport: An application of the multinomial logit model." *Transportation Research Record.* Transportation Research Board, Washington, D.C., Issue no.1147, 1-5.

Basar, G., and Bhat, C. (2004). "A parameterized consideration set model for airport choice: an application to the San Francisco Bay Area." *Transportation Research Record*, Part B: Methodological, 38(10), 889–904.

Bondzio, L. (1996). Models for the passengers' access to airports. Ph.D. Thesis, Ruhr-University, Bochum.

Furuichi, M., and Koppelman, F. S. (1994). "An analysis of air travelers' departure airport and destination choice behavior." *Transportation Research Record,* Part A: Policy and Practice*,* 28(3), 187–195.

Harvey, G. (1987). "Airport choice in a multiple airport region." *Transportation Research Record.* Part A: Policy and Practice*,* 21(6), 439–449.

Hess, S., Adler, T., and Polak, J. W. (2007). "Modelling airport and airline choice behaviour with the use of stated preference survey data." *Transportation Research Record,* Part E: Logistics and Transportation*,* 43(3), 221–233.

Pels, E., Nijkamp, P., and Rietveld, P. (2001). "Airport and airline choice in a multiple airport region: an empirical analysis for the San Francisco Bay Area." *Regional Studies,* 35(1), 1–9.

Pels, E., Nijkamp, P., and Rietveld, P. (2003) "Access to and competition between airports: a case study for the San Francisco Bay Area." *Transportation Research Record,* Part A, 37(1), 71–83.

Skinner, R. E. J. (1976) "Airport choice: an empirical study." *J. Transportation Engineering,* ASCE, 102(4), 871–882.

Thompson, A., and Caves, R. (1993) "The projected market share for a new small airport in the north of England." *Regional Studies,* 27 (2), 137–147.

Warnock-Smith, D., and Potter, A. (2005) "An exploratory study into airport choice factors for European low-cost airlines." *J. Air Transport Management,* 11(6), 388–392.

Design and Realization of Decision-making and Analysis Assistant System on National Integrated Transportation Information

J. Zhang[1], C. Shao[2], C. Zhang[3], Z. Ma[4]

[1]MOE Key Laboratory for Transportation Complex Systems Theory and Technology, School of Traffic & Transportation, Beijing Jiaotong University, Beijing 100044; China; PH(86)10-51687415, email: y4zhangjuan@126.com
[2]MOE Key Laboratory for Transportation Complex Systems Theory and Technology, School of Traffic & Transportation, Beijing Jiaotong University, Beijing 100044; China; PH(86)10-51688344, email: cfshao@center.bjtu.edu.cn
[3]Microsoft Research Asia, Beijing 100080; China; email: zhangchiqing@gmail.com
[4]MOE Key Laboratory for Transportation Complex Systems Theory and Technology, School of Traffic & Transportation, Beijing Jiaotong University, Beijing 100044; China; email: 06114185@bjtu.edu.cn

ABSTRACT

With the development of modern transportation methods, there is huge body of transportation data related to road, railway, waterway, and air transportation networks. A decision-making and analysis system is requisite in intelligent management and transportation planning. Using the Visual C++ platform and MapInfo, GIS software, the national integrated transportation decision-making and analysis assistant system is designed and realized in this paper. The system has many characteristics, such as friendly interface, handy operation, intuitive query and analysis result, convenient management, etc. The system not only can be used in the analysis of transportation actuality and the data extraction of traffic information, but also is a basic condition of the scientific and data management in the integrated transportation fields.

INTRODUCTION

With the continuing development of roads, railways, water ways, and air transportation, there is an accumulation of valuable traffic data and information such as road traffic, passenger-cargo traffic volume of railways, water ways, and air transportation, etc. It is crucial, therefore, to mine this data with particular emphasis placed on researching the developing law and trends.

The electronic map of various national transportation systems can be viewed on MapInfo software and can assist in the understanding of national integrated transportation information decision-making and analysis assistance system that functions with the electronic map, data query statistic analysis, and data mining, etc. combined with traffic volume for the past several years. Only then can the

information management level be improved and a better system given for a modern, reasonable and intelligent control of transportation information.

SYSTEM REQUIREMENT ANALYSIS

Feasibility analysis. In recent years, the Ministry of Communications, Civil Aviation Administration, and the Ministry of Railway have done and continue to do more about traffic information statistics related to various transportation modes, such as the handbook of national highways traffic, national railways passenger-cargo traffic schematics, the passenger-cargo throughput schematics about some main seaports and airports, etc. so that traffic information collection is practicable. From a technical viewpoint, the continual development of the hardware and software is feasible (Wang, Yuan, and Li 2004). The windows platform Visual C++, which can form 32-bit application as a powerful and complicated development tool, is simple and quick to be utilized. The MapInfo software system has a powerful image function with which the bidirectional conversion of many types of data platforms can be accomplished. Suitable program language, Map Basic, makes the data maintenance, management, and application convenient and clear.

Necessity analysis. The traffic networks of four traffic modes differ from each other in spatial distribution. The traditional data management in report form does not meet the current requirement of traffic data statistics and analysis, convenient deep data mining, and difficulty with actual problems solving (Feng, Tong and Wang 2004). In order to relieve traffic conflicts and other traffic problems, it is imperative to improve the traffic management level and construct a more integrated transportation information management system that takes full advantage of GIS (geographical information systems) and computer technology.

SYSTEM DESIGN

System functional design. In this paper, the main objective of the system discussed is to collect shared data from data rooted in multi-channels, then organize real time data and the prevenient data, and at last realizing the intuitionistic query, statistic analysis, and types of thematic maps and statistic report forms about the transportation data of various transportation means. Thereby, the development law of national integrated transportation is researched and a basic platform is supplied for the deep analysis.

According to the system functions, the system includes four modules: electronic map operation model, information query model, statistic analysis model, and thematic map analysis model (Zhang and Shao 2007).

The electronic map model is shown in Figure 3.1. Transportation information about roads, railways, water ways, and air transportation can be shown in different layers. The user can do some basic work, such as move, zoom, choose shown layer and label the information of the map element, e.g., traffic point or traffic line.

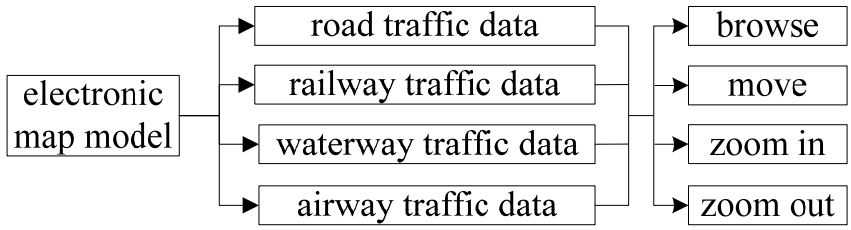

Figure 3.1. Electronic map model.

The information query model is shown in Figure 3.2. There are two parts to this model: attribute query and condition query. The attribute query means choosing one specific traffic point or line and finding its attribute information, such as the orientation and the throughput of a port. The condition query refers to screening out the attribute information of one or more map elements and fixing a position according to one specific restriction condition (e.g. screening out airlines from one particular airport from the national air transportation network).

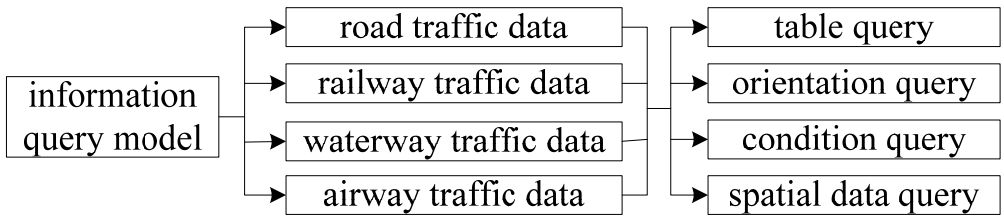

Figure 3.2. Information query model.

The statistic and analysis model is shown in Figure 3.3. The function means, according to different province, traffic line or traffic point, comparing and analyzing the structure and distribution of corresponding passenger-cargo volume, and viewing the statistic reform forms. For example, the amplitude of the passenger-cargo volume in the past five years at one certain port.

The thematic map analysis model is shown in Figure 3.4, mainly contains thematic map about different provinces' traffic distribution of a given transportation mean and thematic map about different traffic load. In the thematic map, different colors and different linewidths express different traffic loads, and then the traffic volume distribution and the traffic load of national transportation networks can be viewed intuitively.

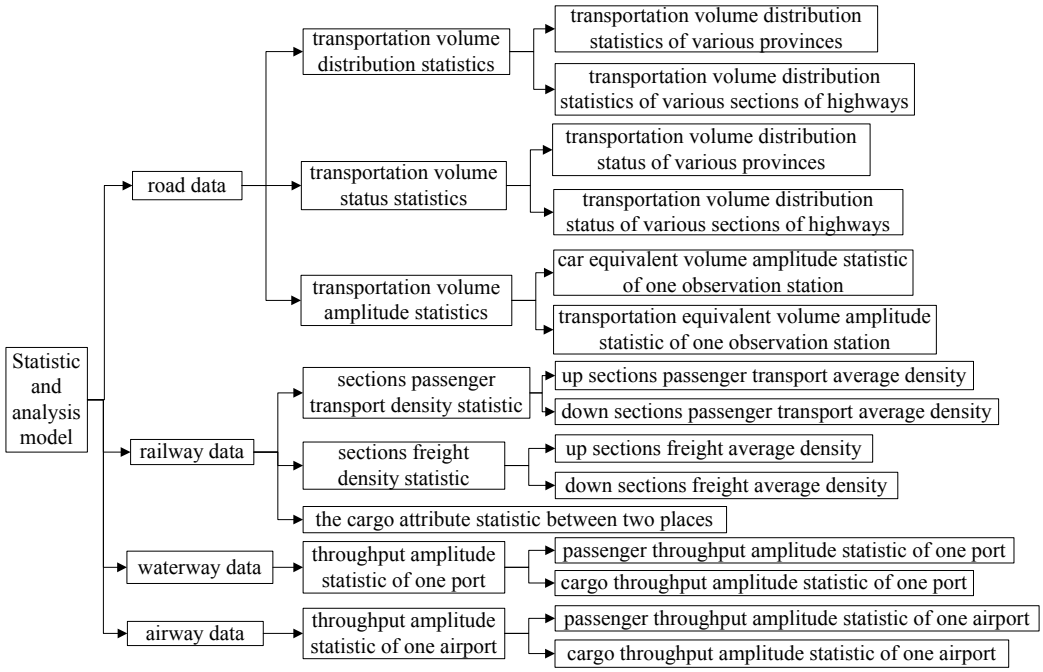

Figure 3.3. Statistic and analysis model.

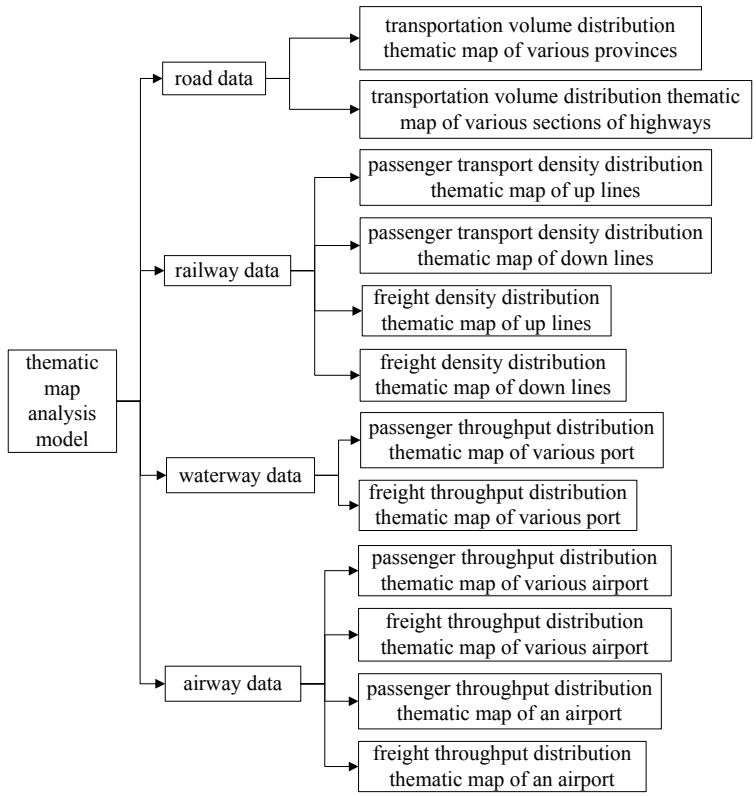

Figure 3.4. Thematic map analysis model.

Database design. Database design includes the creation of attribute database, the creation of spatial database, and a design about the attribute table and the attribute relationship (Wang, Zhu, and Zhou 2005). The hard core is the creation of the relationship pattern with complete content even the one-to-one relation between attribute database and spatial database according to the 3NF law.

The creation of attribute database refers to designing field type and field length of the data record, and appending the key words. The creation of spatial database means gathering and compiling the traffic information with different spatial geography character, and then the different data types can be converted to one identified and used by the computer. Then the spatial data could be managed conformably. At the same time, the independency and the data integrality should be ensured and the data redundancy should be avoided in order to conveniently realize the maintenance and update of the spatial data, and the user's requirement of the timely and quick visit.

METHOD AND KEY TECHNIQUE

Result. Spatial data processing is realized in MapInfo software system with the data processing algorithm compiled by the matched program language Map Basic, and then the attribute data and the spatial data would be matched.

On the basis of the national integrated transportation information database, the functions of the system realized are illustrated as follows:

Figure 4.1 shows the distribution of national main airports. In the map, after choosing Lanzhou airport, the take-off and landing number, and the passenger-cargo throughput about the airport could be viewed. Figure 4.2 shows the amplitude statistic analysis of the passenger-cargo throughput from the year 2000 to 2005 about Xi'an airport. Figure 4.3 shows the thematic map about passenger-cargo throughput of national main ports. Figure 4.4 shows the thematic map about the traffic volume of the airlines passed Urumqi airport, and in the figure, the traffic load was expressed by various shades of gray.

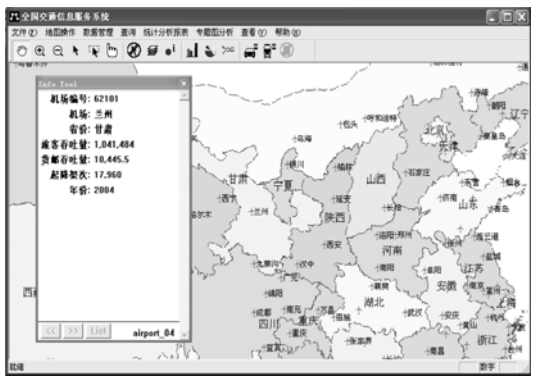

Figure 4.1. Distribution of national amplitude, main airports.

Figure 4.2. Passenger-cargo throughput statistical analysis about Xi'an airport.

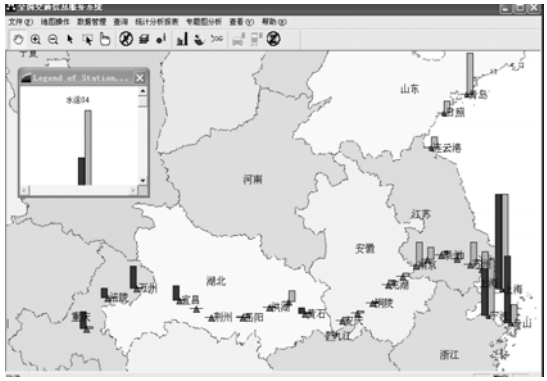

Figure 4.3. Passenger-cargo throughput thematic map about national airport main ports.

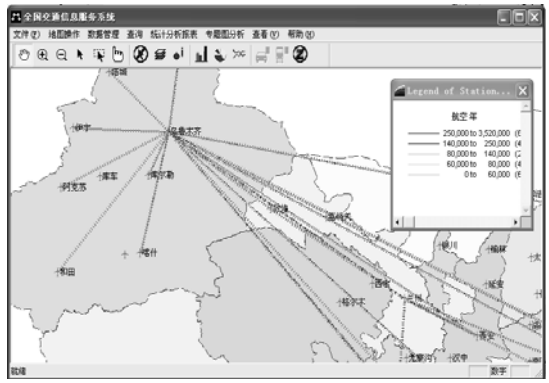

Figure 4.4. Traffic volume thematic map about the airlines passed Urumqi airport

Key technology. *Integrated secondary development*. Integrated secondary development refers to an integrated development integrated professional MapInfo software that can be used to realize the basic GIS functions on an universal visual software, such as Visual C++ (Shang, Wang, and Li 2005). In the whole process, the OLE (Object Linking and Embedding) automation technology is the core (Li, Lu, and Che 2004). The foreground application is developed by Visual C++ and the GIS software is executed in the background through OLE automation technology, and at last all the spatial data processing would be realized.

Integrated secondary development can not only take full advantage of the management and analysis about the spatial data of MapInfo software, but also the advantages of visual programming language, such as high efficiency, convenience etc. Therefore, the development efficiency of the system would be greatly advanced with these advantages and the application developed by visual programming language would have more elegant appearance, a more powerful database, better reliability, and easier to manage system maintenance and updating.

Call-back technology. The information query is realized mainly through the call-back technology of MapInfo software. After a map element is chosen, the corresponding coordinate would be queried from the database via a match made between the map information and the coordinate saved in the database. The attribute data corresponding to the selected map element would then be returned through call back technology by the map element number, the unique identifier (Zhang and Shao 2007).

Thematic map. One of the most powerful functions of MapInfo software is intuitively visual analysis to the data, mainly for statistic map and thematic map in the system, such as, statistic report forms, amplitude passenger-cargo traffic volume statistic analysis, the distribution thematic map of the traffic volume and the traffic load, etc. On the thematic map, the attributing data would be intuitively viewed in the form of figure, so that the changing law and trend of the traffic data can be showed through the intuitive graphical show of traffic distribution.

Data mining. Data mining (also called KDD – Knowledge Discovery in Database) refers to a process of extracting the connotative but useful information from a great deal incomplete and random data. The large amount of transportation data reflects a certain law after a long data accumulation. For the traffic management and development research departments, it is favorable to find the underlying and valuable information, the contributing factors, even the intuitive graphical representation about traffic data to do assistant analysis. The main data mining technology used in the realization of the system functions are as follows: first, data mining of the basic attribute information about spatial map elements the intuitive graphic representations. It is relatively simple and less strict in the complexity of spatial data, e.g., the traffic volume structure statistic of all national highways. Second, the data mining of the time series and the spatial series for spatial map elements data, the changing law varied along with time would be researched after the analysis of the spatial data influenced by time series and spatial series. Therefore, the intending traffic would be forecasted by the changing law. For example, the changing trends of one particular port's passenger-cargo throughput from the year 2000 to 2005. Third, the data mining of the spatial distribution law about the traffic volume according to different data sorts. For example, the distribution law of the traffic volume by air about different airlines.

CONCLUSIONS

Based on MapInfo software system, the integrated transportation database is built using national transportation data about roads, railways, water ways and air transportation, and then national integrated transportation information decision-making and analysis assistant system is developed on the platform Visual C++ by integrated secondary development technology. In the system, the MapInfo server is called backstage by OLE automatic technology. It can realize the query and representation of the basic attribution of traffic lines and traffic points regarding various transportation means. From this, traffic data mining based on time series and spatial series is understood. The system provides a data mining platform, a new assistant method for the analysis, and statistical information of traffic data and an advanced technology for the planning and management of national traffic network. Thereby, the management level of various transportation modes is advanced and a solid foundation is laid for the reasonable, intelligent, and integrated transportation information decision-making and management system.

ACKNOWLEDGEMENTS

This paper was supported by the research projects sponsored by the National Basic Research Program of China (973 Program, 2006CB705500).

REFERENCES

Feng, Y., Tong, X., and Wang, C. (2004). "Analysis and design of the highway management information based on GIS." *Computer and Communications,* 22(5), 61-64.

Li, S., Lu, Y., and Che, S. (2004). "MapInfo GIS redevelopment instance." *Publishing House of Electronic Industry*.

Shang, L., Wang, D., and Li, H. (2005). "Building of an intelligent integrated information service system." *Computer and Communications*, 23(6), 32-34.

Wang, J., Zhu, Y., Zhou, H. (2005). "Design on the integrated information platform frame of traffic management based on GIS-T." *Transportation Systems Engineering and Information*, 5(2), 116-120.

Zhang, C. and Shao, C. (2007). "Design and realization of rational highway traffic information management system." *Modern Transportation Technology*, 4(3),65-68.

Wang, Y. Yuan, K., and Li, T. (2004). "GIS-T and the application in the ITS." *China Railway Publishing House*.

Pricing Model for Expressway with Elastic Demand

Lu Huapu [1] Yu Xinxin [1] Wang Haiwei[1,2] Bian Changzhi[1]

[1]Institute of Transportation Engineering, Tsinghua University, Beijing, 100084; PH (010) 627-72615; email: weixx03@mails.tsinghua.edu.cn
[2]Military Transportation College, Tianjin, 300171

ABSTRACT

Many researchers have studied the pricing model for expressways with the economic principle of marginal cost pricing. However, there is also much interesting and important work to still do. The objective of this paper is to enhance the insights into the expressway pricing mechanism with elastic demand. We proposed two specific models by considering the scenario under different market conditions, including the monopoly model and the monopolistic competition model. This paper analyzed the differences between the two scenarios. A numerical example is presented in order to illustrate how the pricing policies affect the demand and the social-welfare of the whole transportation system.

KEY WORDS

Road pricing; network equilibrium; elastic demand; monopoly; monopolistic competition

1. INTRODUCTION

Road-use pricing as an effective means of both managing road traffic demand and raising additional revenue for road construction has been studied extensively by both transportation researchers and economists.

Roth stated that private firm can provide public roads which is an efficient answer to deal with rapid growing traffic demand (Roth 1996). Gomez-Ibanez considers that the public sector may simply be unable to finance facilities that the private sector would be willing and able to undertake for a profit (Gomez-Ibanez 1991). Huang analyze a bi-modal system will be significantly different from that of a single mode system (Huang and Yang 1996). Yang presents a rigorous quantitative modeling of a highway B-O-T project under different market condition (Yang and Meng 2000).

This paper presents two models of an expressway pricing problem by considering the scenario under different market conditions, including the monopoly model and the monopolistic competition model. Private firm profit and total social welfare gain generated from an expressway system are investigated under each condition. Mathematical models are developed to characterize price under either monopolistic or monopolistic competitive markets. The characteristics of the problem are illustrated with a numerical example.

2. MARKET STRUCTURE AND THE OBJECTIVES OF COMPANY

2.1 Notations

C_a capacity of link a
x_a flow on link a
rs OD pair index, rs $\in$ RS
d_{rs} OD demand between pair rs, it depends on p
f_{rs} commuter path flow on rs
k_{rs} path between OD pair rs
$\delta_{a,k}^{rs}$ link-path incidence parameter; 1 if link a is on path k, zero otherwise
t_a travel time on link a
α a parameter that represents value per hour
β a parameter in the SUE
d a vector of all O-D demands
x a vector of all link flows
r required rate of return by the company
r_{tax} tax rate
Dep annual depreciation
Inv initial investment which is given
N the number of years of the project existing
l_a the length of the link a
c_a the variable cost of the link a per kilometer per vehicle
p_a price of the link a which charges the users
NPV net present value of the project

2.2 The objectives of firm

The firms use several important criteria to evaluate capital investment (Richard Brealey, Stewart Myers 2007). The most comprehensive measures of whether a project is profitable or unprofitable is the net present value (NPV), which is the present value of the future after-tax cash flow minus the investment outlay, or

$$NPV = \sum_{t=1}^{n} \frac{CF_t}{(1+r)^t} - Inv \tag{1}$$

Because the NPV is the amount by which the investor's wealth increases as a result of the investment, the objective of the firm is to obtain the largest NPV.

Annual after-tax operating cash flow CF_t:

$$\begin{aligned} CF_t &= (\text{Sales} - \text{Variable Cost})(1\text{-tax rate}) + \text{tax rate} \times \text{Depreciation} \\ &= (\sum_a (l_a x_a p_a - l_a x_a c_a) - Dep)(1 - r_{tax}) + Dep \times r_{tax} \end{aligned} \tag{2}$$

The required rate of return form the project can be computed from CAPM and is equal to the risk-free interest rate plus the risk premium:

$$r = r_f + \beta_1 (r_m - r_f) \tag{3}$$

2.3 Monopoly model

When only one supplier exists in the market, we call the firm a monopolist. Because there is no competition, a monopolistic firm does not respond to price changes. The firm that monopolizes its industry finds the price and output rate that maximizes profit. The monopolist is a "price maker," not a "price taker." The model is formulated as:

$$\max_{p} \ \mathrm{NPV} = \sum_{i}^{N} \left[\frac{(\sum_{a} (l_a x_a p_a - l_a x_a c_a) - \mathrm{Dep})(1 - r_{tax}) + \mathrm{Dep} \times r_{tax}}{(1+r)^i} \right] - \mathrm{Inv} \qquad (4)$$

That means the firm finds an optimal price which maximizes the NPV of the project.

2.4 Monopolistic competition model

Monopolistic competition is a common market form. Monopolistically competitive markets have the following characteristics:

1. There are many producers and many consumers in a given market.
2. Consumers perceive that there are non-price differences among the competitors' products.
3. There are few barriers to entry and exit.
4. Producers have a degree of control over price.

The characteristics of a monopolistically competitive market are almost the same as in perfect competition, with the exception of heterogeneous products and the fact that that monopolistic competition involves a great deal of non-price competition. A firm making profits in the short run will break even in the long run because demand will decrease and average total cost will increase. This means that in the long run a monopolistically competitive firm will make zero economic profit.

$$\mathrm{NPV} = \sum_{i}^{N} \left[\frac{(\sum_{a} (l_a x_a p_a - l_a x_a c_a) - \mathrm{Dep})(1 - r_{tax}) + \mathrm{Dep} \times r_{tax}}{(1+r)^i} \right] - \mathrm{Inv} = 0 \qquad (5)$$

That means that in the long-run the NPV of the project is zero.

3. MODEL FORMULATION

3.1 A bi-level framework for the pricing problem

The pricing problem is to determine the optimal price to maximize some measures, while taking into account the effects of the implementation of the price toward the travel demand and link flow. The problem can be generally formulated as follows:

$$\max_{p} F(d, x) \qquad (6)$$

Subject to: $G(d, x) \le 0$ (7)

$$\min \sum_a \int_0^{x_a} [t_a(\omega) + \alpha p_a l_a] d(\omega) + \frac{1}{\beta} \sum_k f_k^{rs} (\ln f_k^{rs} - 1) \quad (8)$$

$$\text{st:} \quad \sum_k f_k^{rs} = d_{rs}(p) \quad \forall r, s \quad (9)$$

$$f_k^{rs} \geq 0 \qquad \forall r, s \quad (10)$$

Where link flow is defined by:

$$x_a = \sum_r \sum_s \sum_k f_k^{rs} \delta_{a,k}^{rs} \quad \forall a \quad (11)$$

The low-level sub problem (9)-(12) is a SUE network equilibrium problem with variable demand. The up-level sub problem has been descried in Section 2.

3.2 Evaluat ing the social-welfare

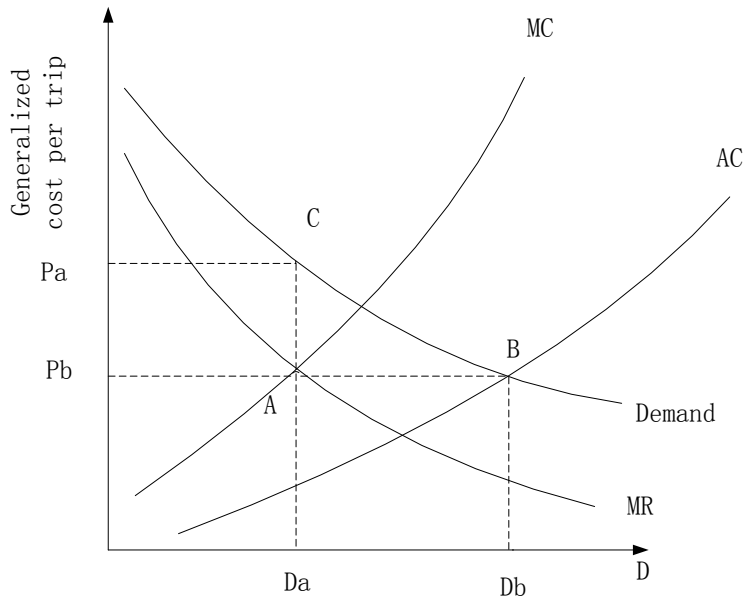

Figure 1. Equilibrium under Monopoly and Monopolistic competition

As shown in Figure 1, the AC curve represents the average cost of the firm, and the MC curve represents the marginal cost of the firm, which is the additional cost of adding one extra vehicle to the expressways.

Under the monopoly model, monopolist will maximize its profit by supply Da where MR=MC (Point A in Figure 1). Under the monopolistic competition model, the firm earns zero profit where P=AC (Point B in Figure 1).

The total network user benefit (UB) from travel is evaluated as:

$$UB = \sum_{rs \in RS} \int_0^{d_{rs}} d_{rs}^{-1}(x) dx \quad (12)$$

The firm cost (FC) incurred by all network links is given by:

$$FC = \sum_a l_a x_a c_a + \frac{1}{N} \times Inv \quad (13)$$

Therefore, the social-welfare of the whole transportation system can be formulated as:

$$SW = UB - FC = \sum_{rs \in RS} \int_0^{d_{rs}} d_{rs}^{-1}(x)\,dx - \left(\sum_a l_a x_a c_a + \frac{1}{N} \times Inv\right) \quad (14)$$

4. NUMERCIAL SAMPLE

4.1 Problem setting

Here we use a simple numerical example to demonstrate some interesting characteristics of the pricing problem. The network is depicted in Figure 2 with 1 O-D pair. The following form of the O-D demand function is adopted:

$$d_{rs} = d_0 - p \times \gamma \quad (15)$$

Where d_0 is the demand under zero price, here d_0=1000. γ is a scaling parameter which reflects the sensitivity of demand to price, here γ=10.

The following link volume-delay function is used:

$$t_a = t_0\left(1 + 0.15\left(\frac{x_a}{C_a}\right)^4\right) \quad (16)$$

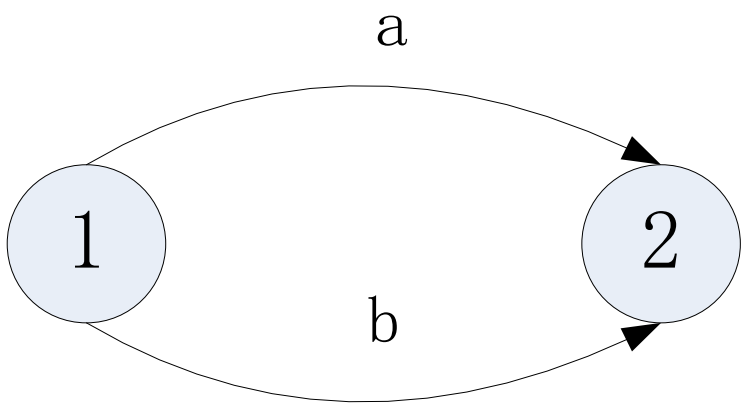

Figure 2. The network used for the numerical example

Table 1 . Input data for the link volume -delay function

Link No.	Free-flow travel time(h)	$c_a l_a$(RMB/(veh)	Link capacity (veh/h)	Length(km)
a	4	50	500	100
b	5	50	300	120

4.2 Numerical results

The changes in the OD demand, link flow, price, profit and welfare gain generated by the expressway under the two models are depicted in Table 2.

Table 2. Numerical results

	Monopoly	Monopolistic competition
d_{12}	250	490
p	75	51
x_a	215	421.4
x_b	35	68.6
t_a	4.14	4.26
t_b	5	5
NPV	5750	0
social-welfare	8875	11995

In this sample, the monopolist supplies a lower quantity of goods at a higher price than firms would in a monopolistic competitive market, which leads to a lower social-welfare. The monopoly will secure monopoly profits by appropriating some or all security of the stop consumer surplus. Since the loss in consumer surplus is higher than the monopolist's gain, it creates deadweight loss, which is inefficient and a form of market failure.

5. CONCLUSION

This paper proposed the model of an expressway in equilibrium networks. Our study differs from the conventional analytical economic analyses mainly in three aspects. Firstly, the traffic demand is not constant but depends on the price which is charged by the firm. Secondly, profit, price, demand, and social welfare are considered under two different scenarios, including the monopoly model and the monopolistic competition model. Thirdly, the firm operates the expressway system over many periods which makes it consider maximizing the NPV of the project instead of the profit. The result of the numerical sample demonstrates that the monopoly leads to deadweight loss and inefficiency. Therefore, our modeling approach is significant to help government regulate the firms that invest in the expressway system.

ACKNOWLEDGEMENTS

This research is supported by National High-Tech Research and Development Program of China (863 Program) (Grant No.2007AA11Z202 & No.2007AA11Z233).

REFERENCES

Arnott, R., and Yan, A. (2000). “The two-mode problem: Second-best pricing and capacity. ” Review of Urban and Regional Development Studies 12,170–199.

Brealey, Richard, and Myers, Stewart. (2007). Principles of Corporate Finance , Mc Graw Hill.

Huang, H.-J. (2002) . “ Pricing and logit-based mode choice models of a transit and highway system with elastic demand. ”European Journal of Operational Research 140,562-570.

Mohring, H. (1985). “Profit maximization, cost minimization, and pricing for congestion-prone facilities.” Logistics and Transporta tion Review 21,27–36.

Verhoef, Erik T. (2007). “Second-best road pricing through highway franchising.” Journa l of Urban Economics 62, 337-361.

Yang, H., and Lam, W.H.K. (1996). “Optimal road tolls under conditions of queuing and congestion. ”Transportation Research A30, 319-332.

Yang, H., Huang, H. J. (1996). “Principle of marginal-cost pricing : how does it work in a general road net work . ” Transportation Research A32, 45-54.

Yang, H. , and Huang, H. J. (1997). “Analysis of the time-varying pricing of a bottleneck with elastic demand using optimal control theory.” Transportation Research B31, 425-440.

Yang, H., and Meng, Q.. (2002). “Highway pricing and capacity choice in a road network under a build–operate–transfer scheme.” Transportation Research A 36, 659-663.

Research on Conversion Coefficients between Bicycle, Electric Bicycle and Pedestrian on Urban Road Intersection

Ai-Zeng Li[1], Xin-Sheng Song[2], Wei Wang[3] and Wen-Quan Li[4]

[1]Department of Traffic Engineering, Henan University of Urban Construction, Postcode: 467044, Pingdingshan, Henan, China; Cellphone +86-15837551819; email: liaizeng@163.com
[2]Department of Traffic Engineering, Henan University of Urban Construction, Postcode: 467044, Pingdingshan, Henan, China; email: sxs@hncj.edu.cn
[3]School of Transportation, Southeast University, Postcode: 210096, Nanjing, Jiangsu, China; email: wangwei@seu.edu.cn
[4]School of Transportation, Southeast University, Postcode: 210096, Nanjing, Jiangsu, China; email: wenqli@seu.edu.cn

ABSTRACT

In order to analyze traffic flow running characteristics and provide basis for capacity research on urban road intersection, velocity characteristics and occupied space resources of bicycle, electric bicycle and pedestrian were studied. Based on method of time-space resource occupancy, models calculating conversion coefficients between bicycle, electric bicycle and pedestrian were established. Then, taking pedestrian as a conversion standard, conversion coefficient values, 1.67 and 1.58, of bicycle and electric bicycle were obtained. Taking the bicycle as a conversion standard, conversion coefficient values 0.60 and 0.95 of pedestrian and electric bicycle respectively were obtained as well. This research indicates that time-space resources occupied by bicycle, electric bicycle and pedestrian are different and the conversion coefficient values and effects of them on motor vehicles are different as well.

INTRODUCTION

There are many bicycles, electric bicycles and pedestrians on urban road intersections in China. This activity forms remarkable characteristics of the intersection and has considerable impact on powered vehicles. Because time-space resources occupied by bicycle, electric bicycle and pedestrian are different when they pass through intersections, their effects on vehicles are different as well. Thus, in order to analyze the combined effect of them on powered vehicles, it is necessary to study conversion coefficients between bicycle, electric bicycle, and pedestrian.

Until now, most research results about conversion coefficients have concerned vehicles (Yuan 2001, Li 2001, Cesar 1987, Benekohal et al. 2000, Elefteriadou et al. 1996). There is only limited research on the bicycle, electric bicycle, and pedestrian, especially on urban road intersections. Zhao (2004) studied conversion coefficients among bicycle, pedestrian, and pedestrians pushing bicycles on urban road intersection. Li (2004) and Li et al. (2006) researched conversion coefficients between bicycle, electric bicycle, and pedestrian on a street crosswalk. Until now, there has been no research studying conversion coefficients between bicycle, electric bicycle, and pedestrian on urban road intersection. Taking time-space resources occupied by bicycle, electric bicycle, and pedestrian into consideration, based on method of time-space resource occupancy, the conversion

coefficients between them on urban road intersections are studied. This research lays the foundation for further study on traffic flow running characteristics and capacity on urban road intersections.

VELOCITIES

In order to get velocity characteristics of bicycle, electric bicycle, and pedestrian on urban road intersections, an investigation was made on Shuguang-Guangming intersections in Pingdingshan, Henan Province. Statistical analyses of velocity samples of 206 for each of them were made. The results are shown in Figure 1, 2, and 3 and Table 1. It can be seen that the velocities of bicycle, electric bicycle, and pedestrian all followed normal distribution. Taking velocity mean as its velocity value, let v_b, v_e and v_p be velocity of bicycle, electric bicycle, and pedestrian respectively, then v_b=3.08 m/s, v_e=3.75 m/s and v_p=1.22 m/s.

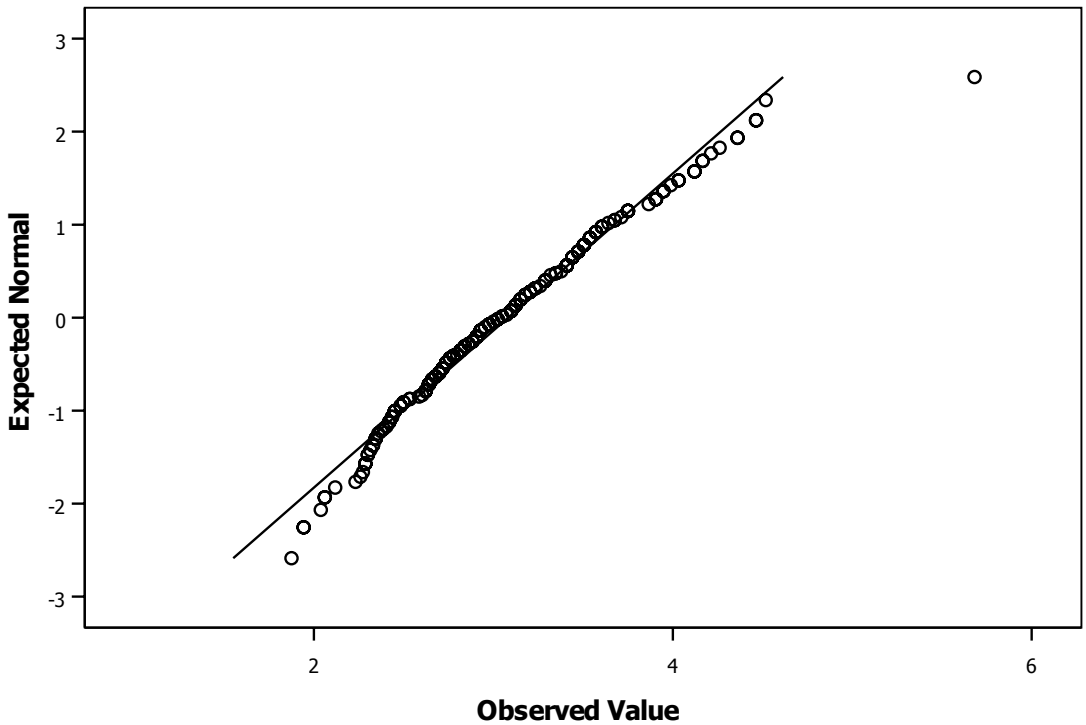

Figure 1. Q-Q normal probability graph of bicycle velocity.

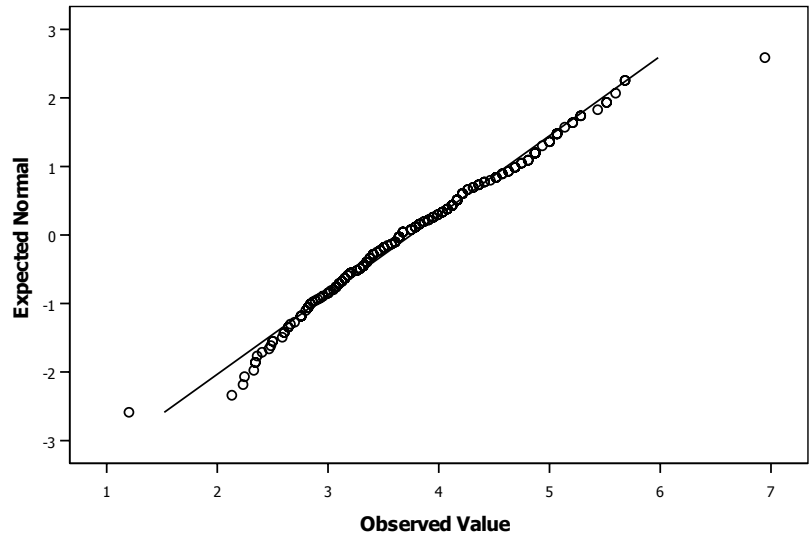

Figure 2. Q-Q normal probability graph of electric bicycle velocity.

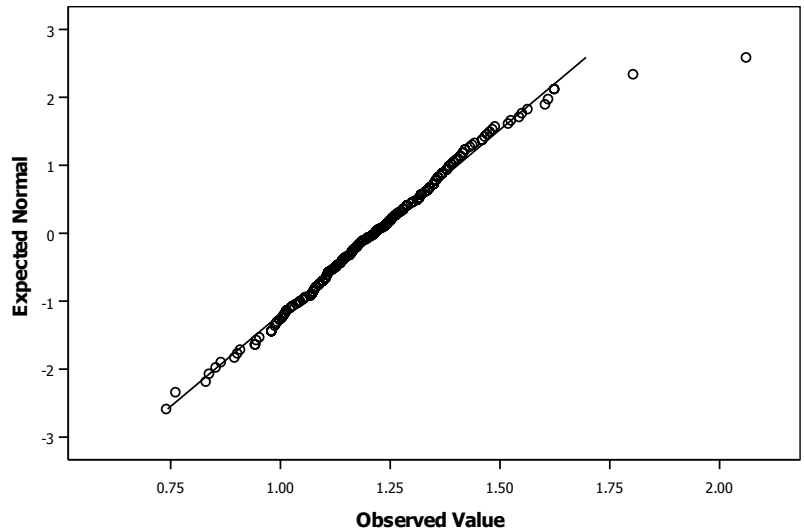

Figure 3. Q-Q normal probability graph of pedestrian velocity.

Table 1. Velocities of bicycle, electric bicycle and pedestrian.

Traffic Flow	Sample Number	Average Velocity (m/s)	Sample Standard Deviation (m/s)	95% Confidence Interval
Bicycle	206	3.08	0.59	3.00~3.16
Electric Bicycle	206	3.75	0.86	3.63~3.87
Pedestrian	206	1.22	0.18	1.19~1.24

ROAD SPACE RESOURCES

When bicycle, electric bicycle, and pedestrian pass though a street, road space resources occupied by them can be expressed by following equation:

$$S_i = l_i \cdot w_i \quad (1)$$

where S_i = road area occupied by a bicycle, electric bicycle, and pedestrian when they pass through a street (m^2), $i = b$, e and p, respectively; and l_i , w_i = dynamic length and width of a bicycle, electric bicycle, and pedestrian when they pass through a street (m), $i = b$, e and p, respectively.

Road Area Occupied by a Bicycle. From Equation (1), road area occupied by a bicycle when it passes through a street is $S_b = l_b \times w_b$. Dynamic length of a bicycle can be expressed as $l_b = v_b t / 3.6 + v_b^2 / 254(\varphi \pm i) + l_0 + l_v$, where t = reaction time (s), φ = adhesion coefficient; i = road longitudinal gradient; l_0 = safety stopping distance (m); and l_v = vehicle length (m) (Li et al. 2006).

Through analysis in section 2, let v_b = 3.08 m/s. Let t = 0.7 s, φ = 0.5, i =0, l_0 = 0.8 m, and l_v = 1.9 m. Then:

$$l_b = v_b t / 3.6 + v_b^2 / 254(\varphi \pm i) + l_0 + l_v = 3.08 \times 0.7 / 3.6 + 3.08^2 / (254 \times 0.5) + 0.8 + 1.9 = 3.37(\text{m}) .$$

Let w_b =1 m, thus $S_b = l_b \times w_b$ = 3.37 m^2.

Road Area Occupied by an Electric Bicycle. From Equation (1), road area occupied by an electric bicycle when it passes through a street is $S_e = l_e \times w_e$. Dynamic length of an electric bicycle can be expressed as $l_e = v_e t / 3.6 + v_e^2 / 254(\varphi \pm i) + l_0 + l_v$ (Li et al. 2006). Through analysis in section 2, let v_e =3.75 m/s. Let t = 0.7s, φ = 0.5, i =0, l_0 = 0.8 m, and l_v = 1.9 m. Then:

$$l_e = v_e t / 3.6 + v_e^2 / 254(\varphi \pm i) + l_0 + l_v = 3.75 \times 0.7 / 3.6 + 3.75^2 / (254 \times 0.5) + 0.8 + 1.9 = 3.54(\text{m}) .$$

Let w_e =1.1 m, thus $S_e = l_e \times w_e$ = 3.89 m^2.

Road Area Occupied by a Pedestrian. From Equation (1), road area occupied by a pedestrian when he passes through a street is $S_p = l_p \times w_p$.

A pedestrian's walking stride is about 0.66 m. When a pedestrian is walking, the distance before and after their position is one and a half steps approximately, so let l_p = 1 m. Dynamic width of a walking pedestrian is about 0.8 m, so let w_p = 0.8 m. Thus $S_p = l_p \times w_p$ = 0.8 m^2.

CONVERSION COEFFICIENT VALUES

Taking Pedestrian as a Conversion Standard. Taking a pedestrian as a conversion standard, let its conversion coefficient value be one, namely let pce_p = 1. Based on method of time-space resource occupancy, the conversion coefficient calculation formulas of bicycle and electric bicycle can be expressed as follows:

$$pce_b = S_b t_b / S_p t_p = S_b v_p / S_p v_b = l_b \cdot w_b \cdot v_p / l_p \cdot w_p \cdot v_b \quad (2)$$

$$pce_e = S_e t_e / S_p t_p = S_e v_p / S_p v_e = l_e \cdot w_e \cdot v_p / l_p \cdot w_p \cdot v_e \quad (3)$$

where pce_b, pce_e = conversion coefficient of bicycle and electric bicycle respectively; t_i = walking time of bicycle, electric bicycle, and a pedestrian passing though the same length road section, $i = b$, e and p, respectively.

Substitute parameters into Equations (2) and (3), conversion coefficient values of bicycle and electric bicycle are as follows: $pce_b = S_b v_p / S_p v_b = 3.37 \times 1.22/(0.8 \times 3.08) = 1.67$, and $pce_e = S_e v_p / S_p v_e = 3.89 \times 1.22/(0.8 \times 3.75) = 1.58$.

Taking a Bicycle as a Conversion Standard. By traffic investigation, on some urban road intersections, the number of bicycles and electric bicycles are greater than pedestrians at peak period. So it is necessary to calculate conversion coefficient values of pedestrian and electric bicycle taking a bicycle as a conversion standard.

Taking bicycle as a conversion standard, let $pce_b = 1$. Based on method of time-space resource occupancy, the conversion coefficient calculation formulas of pedestrian and electric bicycle are as follows:

$$pce_p = S_p t_p / S_b t_b = S_p v_b / S_b v_p = l_p \cdot w_p \cdot v_b / l_b \cdot w_b \cdot v_p \quad (4)$$

$$pce_e = S_e t_e / S_b t_b = S_e v_b / S_b v_e = l_e \cdot w_e \cdot v_b / l_b \cdot w_b \cdot v_e \quad (5)$$

Substitute parameters into Equations (4) and (5), conversion coefficient values of pedestrian and electric bicycle are as follows: $pce_p = S_p v_b / S_b v_p = 0.8 \times 3.08/(3.37 \times 1.22) = 0.60$, and $pce_e = S_e v_b / S_b v_e = 3.89 \times 3.08/(3.37 \times 3.75) = 0.95$.

CONCLUSIONS

Here we may draw the following three conclusions. First, velocity characteristics of bicycle, electric bicycle, and pedestrian on urban road intersections were analyzed. Velocities of the three all followed normal distribution. Their velocity values are 3.08, 3.75, and 1.22 m/s respectively.

Second, space resources occupied by a bicycle, electric bicycle, and a pedestrian on urban road intersections were studied. Road areas occupied by them are 3.37, 3.89, and 0.8 m^2 respectively.

Third, based on the method of time-space resource occupancy, taking the pedestrian as a conversion standard, conversion coefficient values, 1.67 and 1.58, of bicycle and electric bicycles were obtained. Taking bicycle as a conversion standard, conversion coefficient values, 0.60 and 0.95 of bicycle and electric bicycle were obtained as well.

REFERENCES

Benekohal, R. F., and Zhao, W. X. (2000). "Delay-based passenger car equivalents for trucks at signalized intersections." *Transportation Research Record,* Part A: Policy and Practice, 34(6), 437-457.

Cesar, J. J. (1987). "Development of passenger car equivalencies for large trucks at signaled intersections." *ITE J.of Institute of Transportation Engineers)*, 57(11), 33-37.

Elefteriadou, L., Torbic, D., and Webster, N. (1996). "Development of passenger car equivalents for freeways, two-lane highways, and arterials." *Transportation Research Record*, 1572, 51-58.

Li, L. L. (2001). Research on capacity of unsignalized intersection. M.S. Dissertation, Harbin Institute of Technology, China.

Li, N. (2004). Research of Signal Coordination of Mid-Block Street Crossing and Intersection. M.S. Dissertation, Southeast University, China.

Li, W. Y., Chen, X. W., and Wang Q. (2006). "Algorithm of mid-block street crossing

capacity and cross-street green time." *J. of Wuhan University of Technology (Transportation Science and Engineering)*, 30(5), 751-754.

Yuan, T. (2001). Research on system simulation and traffic conversion coefficients on signalized intersection. M.S. Dissertation, Chang'an University, China.

Zhao, J. L. (2004). Study on pedestrian traffic at signalized intersections with mixed traffic flow. M.S. Dissertation, Beijing Jiaotong University, China.

Simulation Analysis of Merging Area on Urban Expressway in Alternate Rules Based on Cellular Automata Model

FANG Shun[1], ZHANG Xiaoning[2] and H.M. ZHANG[3]

[1.]Key Lab of Road and Traffic Engineering in the Ministry of Education, Tongji University, Shanghai 200092, China; PH(8621)-69585245; Email: fangshun03@126.com

[2.]Key Lab of Road and Traffic Engineering in the Ministry of Education, Tongji University, Shanghai 200092,China; Email: cexzhang@mail.tongji.edu.cn

[3.] Department of Civil and Environment Engineering, University of California Davis, CA 95616, USA

ABSTRACT

Merging area is a typical type of carrying out merging on urban expressway; It is usually a traffic congested bottleneck. Under the heavy traffic demand, it easily occurs when vehicles on the mainline and on ramp contesting the right way without any regulation, and making the 'forced entry' manoeuvre at the junction of merging area. This disturbance results in a severe decrease of traffic capacity. The alternate traffic rules, however, could make an orderly merging. Starting from analysis of merging mechanism, the comparative traffic flow models are established based on the Cellular Automata Model, using alternate rules or no alternate rules. The effects of a new alternate strategy are obtained by numerical simulation. Finally, this paper presents a conclusion that traffic state with these rules is much better than not using these rules, and the capacity is improved to some extent as well.

KEY WORDS: alternate rules, merging area, expressway, Cellular Automata Model

1. INTRODUCTION

Traffic congestion has been one of the major challenges facing contemporary cities around the world, which adversely affects mobility, safety, and air quality. The majority traffic jams frequently occur at bottleneck sections. As a significant amount of daily commuting time is spent on urban expressway, it plays a greater role in alleviating traffic pressure. However, more and more sections and bottlenecks fall into serious jam. Not-unblocked passing at merging area has been innegligible in treating expressway management. Uncontrolled free entering flow from on-ramp is the main reason, especially, when the traffic demand is heavy (Jiang, R. *et al.* 2002). Therefore, it occurs easily that drivers from the mainline and ramp contest the right way at this bottleneck. In addition, various traffic streams competed merging freely, inevitably causing potential conflicts which may induce frequent accidents

Microscopic simulation of road traffic has received increasing attention in the last decades. Cellular Automata Models comprise a type of particle hopping models and are hence of microscopic nature while being quite efficient in

computational time. The first cellular automata model for traffic simulation was proposed by Nagel and Schreckenberg (1992) (often referred to as the NaSch model). And since then the several modifications have been used for traffic applications more frequently.

2. LITERATURE

Helbing, D. *et al.* (1998) observed the hysteretic transitions to "synchronized traffic" with high values of both density and traffic flow on German freeways. And the results suggest a general mechanism for the formation of probably the most common form of congested traffic.

Lee, H. Y. *et al.* (1998) found that the presence of the external vehicle flux through ramps generates a new state of “recurring humps” with the hydrodynamic traffic flow model. This novel dynamic state is characterized by temporal oscillations of the vehicle density and velocity which are localized near ramps, and found to be the origin of the synchronized traffic flow reported recently.

The phase diagram of different kinds of congested traffic which are triggered by disturbances were presented by Helbing, D. *et al*.(1999), when passing ramps or other spatial inhomogeneities of a freeway. They allowed one to understand the observed transitions between free and various congested traffic conditions, among them were localized clusters, stop-and-go waves, and different types of "synchronized" traffic.

Pedersen, M. M. *et al*. (2002) described a way of including entry ramps in the NaSch traffic model by placing what is so-called shadow cars on a highway next to cars on entry ramps, which enables the drivers to take ramp cars into account. The model is shown to capture important real-life traffic phenomena that have not been included in previous models.

How to manage the merging at the merging area? In article 44 of Law of the People's Republic of China on Road Traffic Safety，it has been clearly stipulated that “The motor vehicles shall, when driving on a road section or at a road junction where the driveways are decreasing, or when parked for waiting in a queue or running slowly at an intersection without any traffic signal lamp, traffic sign, or command of traffic policeman, pass alternately in turn.” What influence do the alternate rules have on traffic, when the mainline has multi-lanes instead of single lane (Lei, L *et al*.2007, Li, F. 2007)? The paper aims at conducting research on the traffic characteristics pre-and post alternate rules enforcement, based on modeling the traffic flow under various traffic flows with improved Cellular Automata model.

3. THE MODEL

Both on-ramp systems are divided into three sections: the upstream, consisting of *A1, A2* lanes (*A*); the downstream with two lanes, *C1* and *C2*(*C*) (see Figure 1 and 2). The length of each section is indicated as shown. Differently, in the current on-ramp, the two-lanes of on-ramp merge into a single lane in front of the junction firstly, just like status quo (Current Free Merging Model) (see Figure 1). Meanwhile, in order to simulate the phenomenon of contesting the right of way, an additional short section is set up in current free merging model, which is a

virtual lane just as shown in the shaded parts. Comparatively, the system with alternate rules is shown in the Figure 2 (Alternate Rules Model), which means vehicles from the ramp and mainline will pass alternately in turn (the familiar signal control is used to state the rules more convenient instead of the alternate rules).

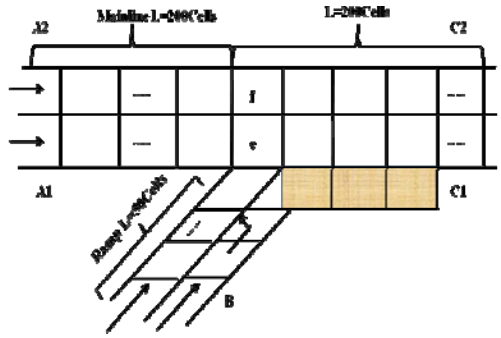

Figure 1. The illustration of the current free merging on-ramp system

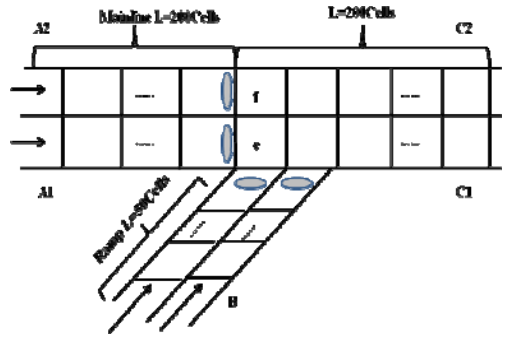

Figure 2. The illustration of the system with alternate rules

In this paper, the simulated system is within open boundaries and the model will be based on NaSch model with additional rules of lane changing. In the discrete NaSch model, each lane is represented by one dimensional chain of cells of length 5*m*, each cell could be empty or occupied by just one vehicle. The velocity of each vehicle can take one of the value varying from 0; 1;…; v_{max} (v_{max}=4 *cells/s*). At each step of discrete time, from t to t+1, the state of the road can be obtained by applying the following rules to all vehicles at the same time (parallel dynamics):

Step 1: Acceleration: $v_n \rightarrow \min(v_n+1, v_{max})$;

Step 2: Braking: $v_n \rightarrow \min(v_n, d_n-1)$;

Step 3: Randomization with probability P: $v_n \rightarrow \max(v_n-1, 0)$;

Step 4: Driving: $x_n \rightarrow x_n + v_n$. (1)

Where: x_n and v_n denote the position and velocity of the car *n* respectively. d_n(d_n=x_{i-1}-x_i-1)is the gap of the vehicle *n* (it is assumed vehicle *n-1* precedes *n*). The maximum velocity and slowdown parameter are denoted by v_{max}, *P* respectively.

In the condition of two-lane traffic, it's necessary to introduce an additional set of rules that determine the changing cars between lanes. And the merging means the process of vehicles from on-ramp entering into the mainline, which can also be viewed as a special form of mandatory lane-changing (Kou C.C, 1997). Usually, the updated step is divided into two sub-steps: in the first sub-step, cars may change lanes in parallel according to lane-changing rules and in the second sub-step the two lanes are considered as independent single-lane NaSch models. For all the cars in the sections with two-lanes, we use a symmetric rule set where vehicles change lanes if the following criteria are fulfilled (Chowdhury, D. *et al*.1997):

$$d_n < \min(v_n+1, v_{max}) \text{ and } d_{n,other} > d_n \text{ and } d_{n,back} > d_{safe}$$

(2)

Here denotes the number of empty cells between the n_{th} vehicle and its two neighbor vehicles on the destination lane at time step of t, respectively; d_{safe} is a safety distance to avoid crash.

In the current free merging model, the section of shadow needs a set of different rules for changing lane, so as to model the messy merging in the case of heavy traffic. We assume that only a certain percentage of drivers from the ramp are allowed to entry into this lane to fulfill merging while it is hard for merging on ramp. The maximum velocity of the vehicles on the additional lane is 1*cell/s*; it keeps steady speed when it has accelerated to the maximum. It would finish merging while it meets the condition of $d_{n,other}>d_n$ and $d_{n,back}>d_{safe}$; or else it will wait at the end until the above condition fits after it has come to the end of this lane. If there is one vehicle on this lane, the velocity of the lag-behind vehicle on the adjacent outside lane of the mainline shouldn't be more than 1*cell/s* and the leading car on ramp couldn't entry into the mainline or the additional lane.

Contrastively, in the alternate rules model, we use the traffic signal control instead of this set of rules for convenient statement. To make the problem simple, the color of traffic signal is divided into only two types: green and red. We denote the leading car on road H*A*H and *B* as HA_{lead}H and HB_{lead}H, the last car on road H*C*H as HC_{last}H. When the car HA_{lead}H or HB_{lead}H arrive at the lattice of the junction, H*e*H or *f*, it must stop before the lattice if the signal is red in front, or else it may enter the road H*C*H allodially just as the free merging model. The update of traffic signals on the road H*A*H and H*B*H is alternate, namely when the traffic signal on the main road is green, and red for the on-ramp, vice versa. And in the simulation, the signal will become red from green on the following condition is fulfilled:

$$T_{green}=(t-t_{red})\ mod\ T \qquad (3)$$

Here T_{green} denotes passage time of vehicle in the condition of green signal on the mainline; t and t_{red} means the time step, the end point of last red phase; T is the traffic signal cycle; Green ratio= T_{green}/T.

When vehicles are approaching the lattice of *e* or *f*, they are inevitably influenced by the traffic red signal in front. So an additional set of special update rules are taken for the vehicles in front of the junction. If the vehicle *n* is the leading car on the road *A* or *B* and approaching the junction of *e* or *f*, then it should be pointed out that $d_n=x_{signal}-x_n-1$, where x_{signal} is the position of traffic signal, or else $d_n=x_{n-1}-x_n-1$. In one time step, after all the vehicles of the system are updated, we check the signal time to decide whether to update the color of traffic signal or not.

4. NUMERICAL RESULTS

In this section, the presented simulation results are analyzed and discussed. The simulation system, completed with C# programming language, uses the open boundary condition. A new vehicle with velocity of v_{max} would be injected with probability of $\alpha_1(\alpha_2)$, if x_{Alast} (x_{Blast})> v_{max}, at the left end of mainline and ramp. The first 10,000 time steps are discarded to let the transient time die

out. The results are obtained by the virtual detectors in the simulation system, as shown in figure 3-6.

The flow of free merging against α_1 and α_2 in the downstream of merging area(C), shows the capacity under various traffic flows without any regulation (see Figure 3). From this figure, the traffic flow occurs a transition from free flow to congested flow at a certain value of α_1 according to different given value ofα_2. Generally, they appears a similar characteristic, such as the flow increases with the growth ofα_1 when it is not very large , following that it would become saturated and get into congestion. However, by a comparison, whenα_2 takes a various given value, it can affect the downstream flow state to a large extent. With the continuous increment ofα_2, the downstream would get into congestion at a smaller value ofα_1, and the maximum flow, which we can consider it as its capacity in the given case of constant probability, has a decreasing trend generally. The reason is that, when cars are in the progress of entering into the mainline, an increase in time of waiting would result in drivers' willingness to accept smaller gaps, consequently, in their performing a "forced entry" maneuver to merge into the mainline. As a result, due to this messy merging order which caused by the respectable forced entry, the capacity of the system has a notable reduction, while the traffic demand is heavy.

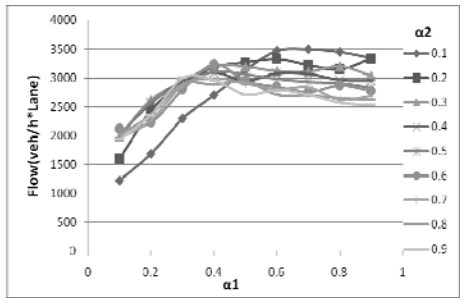

Figure 3. The variations of flow against α_1 about the current system

Expressway merging area performance is dependent upon the ability of the stream to absorb vehicles entering via the on-ramp. Thus we ought to investigate the effect of alternate rules comparing to the current free merging model. The parameters of alternate rules model are obtained by numerical simulation in the below.

The downstream flow changes against various green ratios (which equals to HT_{green}H/T), whenα_1 (α_2) is given by a different value (see Figure 4). To make the problem simple, we just studied the cases of various green ratio in the case ofα_1=α_2. When the probability is not more than 0.3, the flow curve presented a symmetric reversed "bowl-shape". When the probability is larger, the bottom of the "bowl" is narrower until it becomes a reversed "n-shape". Simultaneously, the maximum as well as the minimum flow increases with the growth of the probability. Subsequently, with the increment ofα_1(α_2), the flow nearly presents an approximately linear shape, and appreciably upwarping with the raise of green ratio. The downstream flow has little difference, without consideration of the driver's response delay (see Figure 4). While the traffic demand is very light,

namely$\alpha_1(\alpha_2)$ <0.3, the flow ascends with the growth of$\alpha_1(\alpha_2)$ rapidly. After a rapid increment, meanwhile, the flow reaches its capacity, and keeps stable on a large range of the probability (see Figure 4).

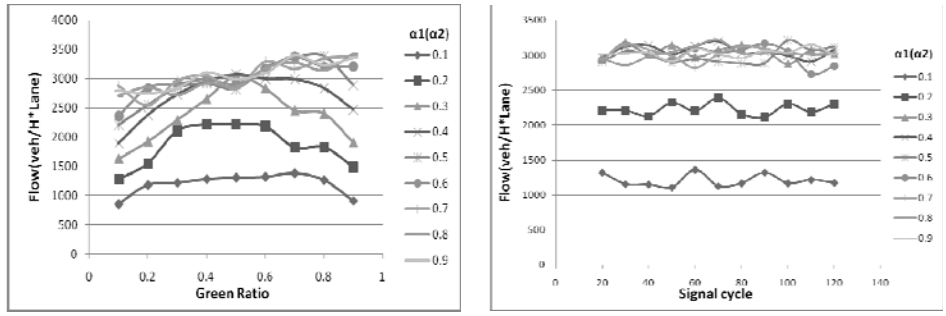

Figure 4. The figures of flow against green ratio and signal cycle

Generally, on the urban expressway, while carrying out the alternate rules, there isn't sufficient parking space for the ramp vehicles queuing on ramp. And from the analysis above, signal cycle has little influence upon capacity. While green ratio equals to 0.5, the optimization of the system could always be investigated under various traffic flow in the condition of$\alpha_1 = \alpha_2$. Therefore, it's feasible to choose the cycle equals to 60s and green ratio is 0.5 for the alternate rules model.

When$\alpha_1(\alpha_2)$ <0.3, the maximum flow of the two models has little difference, that means the alternate rules cannot raise the capacity. With the increase of$\alpha_1(\alpha_2)$, between 0.3 and 0.6, the alternate rules model still do not have any advantage, even the flow of free merging is larger. And when the probability is more than 0.6, the flow would decrease due to the messy merging in free merging model; while in the alternate rules model it has almost no influence on the flow, owing to the regularly orderly merging under the rules (see Figure 5). Against the probability ofα, the ideal flow of single lane increases firstly, which indicates the maximum flow in different conditions. After the growth it occurs that the transition from free flow to congested flow (see Figure 6). Combined with figure 5, it's known that when the averagely original flow of each lane in the upper stream is more than 1400*veh/h*lane*, alternate rules would get the advantage over free merging. The reason for the raise of capacity by these rules is that a stable and ordered merging could always be in progress, which make possible to pass through the system at a steady and large flow.

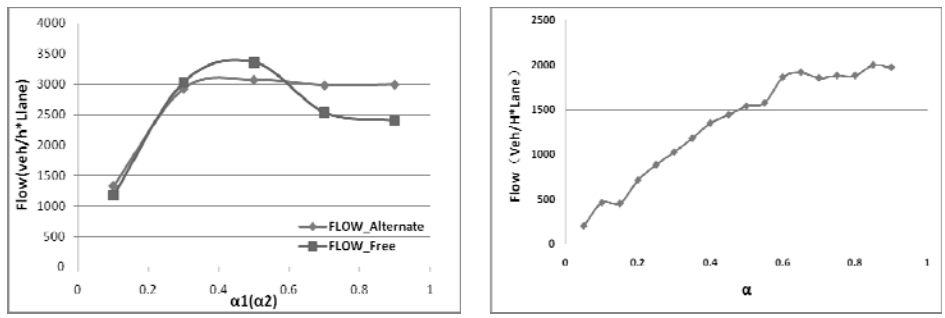

Figure 5. Comparison of flow variation pre & post enforcing alternate method

Figure 6. The diagram of ideal flow against the probability ofαon a single lane

Based on the above research, the alternate rules' enforcement needs the following precondition: Two or multi-lanes merge into one lane; the flow is heavy enough to have apparent synchronization or congestion due to the messy merging.

5. CONCLUSION

By the comparative numerical simulation study, the results indicate that the traffic improvement is significant, especially while the mainline and ramp are under heavy traffic demand(α_1(α_2)>0.6). Whereas, hardly does the model have any improvement when the flow is on the condition ofα_1(α_2)<0.6. Meanwhile, with the help of this set of rules, traffic order could have been improved, and the reduction of mandatory lane-changing could avoid accident possibly.

ACKNOWLEDGMENTS

This study has been supported by two grants from the National Natural Science Foundation Council of China (Project No. 70871092 and 70631002).

REFERENCES

Chowdhury, D., Wolf, D. E., and Schreckenberg, M. (1997). "Particle hopping models for two-lane traffic with two kinds of vehicles: Effects of lane-changing rules." *Physica A*, 235(3-4), 417-439.

Helbing, D., and Treiber, M. (1998). "Gas-kinetic-based traffic model explaining observed hysteretic phase transition." *Physical Review Letters*, 81(14), 3042-3045.

Jiang, R., Wu, Q. S., and Wang, B. H. (2002). "Cellular automata model simulating traffic interactions between on-ramp and main road." *Physical Review E*, 66(3).

Kerner, B. S. (2002a). "Empirical macroscopic features of spatial-temporal traffic patterns at highway bottlenecks." *Physical Review E*, 65(4).

Kou, C. C., and Machemehl, R. B. (1997). "Modeling vehicle acceleration-deceleration behavior during merge maneuvers." *Canadian Journal of Civil Engineering*, 24(3), 350-358.

Lee, H. Y., Lee, H. W., and Kim, D. (1998). "Origin of synchronized traffic flow on highways and its dynamic phase transitions." *Physical Review Letters*, 81(5), 1130-1133.

Lei, L., Dong, L. Y., and Ge, H. X. (2007). "Study of gear-alternating control regulation in the interfluent location of on-ramps with cellular automaton model." *Acta Physica Sinica*, 56(12), 6874-6880.

Li, F., Gao, Z. Y., and Jia, B. (2007). "Traffic behavior in the on-ramp system with signal controlling." *Physica a-Statistical Mechanics and Its Applications*, 385(1), 333-342.

Nagel, K., and Schreckenberg, M. (1992). "A cellular automaton model for freeway traffic." *Journal de Physique I (General Physics, Statistical Physics, Condensed Matter, Cross-Disciplinary Physics)*, 2(12), 2221-9.

Pedersen, M. M., and Ruhoff, P. T. (2002). "Entry ramps in the Nagel-Schreckenberg model." *Physical Review E*, 65(5).

A Study on the Bus Delay Model at Bus Stops

XU Zhi[1], AKPAKLIVincent Kwami[2], YANG Xiaokuan[3]

[1]Transportation Research Center, Beijing University of Technology, Beijing 100124, China; Tel: (0086) 13911677094; Fax: (0086-10) 6739-2991; E-mail: xuzhi1984@emails.bjut.edu.cn
[2] Transportation Research Center, Beijing University of Technology, Beijing 100124, China; Tel: (0086) 13683391376; Fax: (0086-10) 6739-2991; E-mail: vkakpakli@yahoo.com
[3]Transportation Research Center, Beijing University of Technology, Beijing 100124, China; Tel: (0086-10) 6739-1678; Fax; (0086-10) 6739-2991; E-mail: xiaokuan@bjut.edu.cn

ABSTRACT

In this study, the delay of buses at bus stops is defined and classified. According to this classification, parameters that result in bus delay are then proposed. A concept of "bus arrival occupancy rate" is also introduced in this study to quantitatively explain the situation at a bus stop with reference to a typical bus stop in Beijing. A relationship is then established between bus delay and bus arrival occupancy rate. The study also proposes a delay estimation model for buses at two types of bus stops: a bus bay and a curbside bus stop.

Key words: bus stop, delay, bus arrival occupancy rate, bus bay, curbside bus stop

INTRODUCTION

A bus stop is an area on urban roadways where one or more buses load and unload passengers (TCRP 1996). When additional bus lines are added to a bus stop, the frequency of buses using the bus stop increases and a larger portion of the bus stop platform is used. As a result, the bus stop becomes more congested and the bus delay increases. The delay of buses at the bus stop impacts the running and operating efficiency of the public transportation buses. These delays are an inconvenience and a discomfort to commuters who use the public transportation buses.

There are many qualitative researches being conducted by researchers and scholars from home and abroad about delay at or near the bus stops but the quantitative estimation of delay at the bus stops are very few. For example that Ma Hong Wei analyzed the factors which have impact on the bus movement and made a conclusion that the style of platform affect delay (Ma et al. 2006). Zhu Wei and Chen Xue Wu introduced some examples of buses delayed at the urban hub terminals, and based on investigations of some typical terminals, made analysis of the main factors causing such delay with relevant solutions thereto (Zhu et al. 2002). Han Bao Rui also made a qualitative analysis on the factor which impact the delay and got a conclusion that decreasing the bus arrival rate and the time of bus staying at bus stop can make a good help in reducing the delay time (Han et al. 2004). Reebu Zachariah Koshy analyzed the influence of bus stops on traffic flow under heterogeneous traffic conditions using a simulation

technique (Reebu et al. 2005). They examined the effects of variation of the basic parameters, such as bus dwell time, road width and traffic flow for both bus bays and curbside bus stops. However, they did not come up with a formula for calculating delay.

In conclusion, most studies that have been conducted on bus delay at bus stops focus mainly on the qualitative analysis of factors that affect the delays. However, there are very few references discussing delays from a quantitative point of view. For this reason, it is necessary to estimate delay in a quantitative manner, in order to evaluate the level of service of a bus stop and provide a very useful tool to plan, redesign, and manage a bus stop.

DEFINITION AND CATEGORIES OF DELAY AT A BUS STOP

Definition of Delay at a Bus Stop. The process of a bus stopping at a bus stop consists of three parts: the deceleration of the bus into the bus stop, the loading and unloading of passengers, and the acceleration of the bus as it pulls out of the bus stop to rejoin the traffic stream. The delay of a bus at a bus stop is defined as the sum of all delays that happen during this process. Delay is equal to the time the bus is actually dwelling at a bus stop minus the time the bus is expected to be at the bus stop. The expectation time is equal to the time it takes a bus to drive in and pull out of a bus stop without experiencing any difficulties, including the time to load and unload passengers when following a schedule made by its bus company. The difficulties a bus may encounter include a more-than-average number of passengers wanting to enter or leave the bus at a bus stop, engine shutdown, or any man-made incident.

Categories of Delay at a Bus Stop. Based on the movement of buses and the causes of bus delay times, the two categories of bus delay can be described as follows: service delay and non-service delay. Service delay is the extra time a bus may need to load and unload passengers beyond what is expected. Non-service delay is related to the overall time a bus requires from when it pulls into a bus stop to when it exits and is the extra time required beyond the time that a bus typically takes to pull in and pull out of a bus stop without any interruption. The delay of a bus at and near a bus stop is the sum of the service delay and non-service delay, which can be expressed mathematically as follows:

$$d_T = d_1 + d_2$$

Where: d_T -- Delay of the bus at a bus stop, s;

d_1 -- Service delay, s;

d_2 --Non-service delay, s.

FACTORS RESULTING IN DELAY AT A BUS STOP

A bus stop system is composed of three parts: passengers, buses, and the bus stop itself. In this system, passengers and buses form the main dynamic factors and these main factors cause the delay at bus stops.

Passenger Factors . A passenger is an important element of service delay because of two factors including: (a) passenger density and (b) follow-up type of

passengers entering and exiting a bus.

- Passenger Density

If there are many passengers on a bus or there are many passengers waiting at a bus stop, the process of loading and unloading passengers will not be continuous because of the high density of passengers at the bus stop and inside the bus. As a result of these circumstances, a bus will experience a service delay. When passenger density increases, the service delay will significantly increase.

- Follow-up Type of Passengers Entering and Exiting a Bus

If passengers do not enter and exit a bus in a one-by-one fashion, then the bus will again experience a service delay.

Bus Factors . There are two types of bus factors, including bus arrival rate and spacing of buses at bus stops.

- Bus Arrival Rate

When the bus arrival rate exceeds the capacity of a bus stop, buses will eventually form a queue beyond the limits of the bus stop and into the curb lanes. In this situation, the buses movement can be best described as stop-and-go movement and this is how a bus experiences non-service delay.

- Spacing of Buses at Bus Stops

The spacing of buses at bus stops should be done properly when buses stop at bus stops to allow enough space for themselves and buses around them to exit the bus stop when they finish loading and unloading passengers. When the space between stopped buses becomes too small, a bus will not be able to move out of the bus stop when they finish loading and unloading. Consequently, buses have to wait for available space to move out. As a result, the bus that has to wait for available space incurs a non-service delay.

Other Factors . Apart from the factors enumerated above, there are two other factors including (a) traffic organization at bus stops and (b) volume of vehicles near the bus stop. The explanation of these factors is given below:

- Traffic Organization at Bus Stops

Traffic organization has a great impact on the process of buses pulling into and out of a bus stop. As a result of an unreasonable organization of traffic, buses pulling into and out of a bus stop will be out of order, resulting in non-service delays. This is also the reason that buses experience a stop-and-go type movement at a bus stop.

- Volume of Vehicles Near a Bus Stop

If there is a high volume of traffic flow near a bus stop, the process of buses pulling into and out of a bus stop will be heavily influenced. Both deceleration and acceleration time will increase as well. A bus experiences a non-service delay in this situation.

APPROACH TO DELAY ESTIMATION

Bus Arrival Occupancy Rate. A new concept of bus arrival occupancy rate is introduced in this study. It is defined as the ratio of the bus arrival rate to the number of berths at a bus stop. This can be expressed mathematically as follows:

$$\Lambda = \frac{\lambda}{N}$$

Where: Λ--bus arrival occupancy rate, veh$\cdot h^{-1}$;
λ --bus arrival rate, veh$\cdot h^{-1}$;
N--the number of berths at bus stop.

Bus arrival rate only reflects the demand intensity at a bus stop. However, bus arrival occupancy rate considers both the demand intensity at a bus stop and the service capacity at a bus stop. By taking into account both of these two bus stop factors, bus arrival occupancy rate is considered the better indicator for describing the operation of bus stops. Bus arrival occupancy rate is a more objective indicator because it can reflect the actual supply and demand of a bus stop.

Principle of Delay Estimation . When one of the following two conditions is met, it can be assumed that there is no delay and data can be collected for a non-interference situation:

(a) The passengers both inside a bus and on the platform of a bus stop are not crowded. The processes of bus deceleration and bus acceleration are not internally or externally obstructed. There is only one bus that arrives at a particular time at the bus stop. When all of these conditions are met, it can be assumed that this bus experiences no delay at this bus stop.

(b) The passengers both inside a bus and on the platform of a bus stop are not crowded. The processes of bus deceleration and bus acceleration are not internally and externally obstructed. If there are two or more buses arriving at the bus stop at the same time, then it can be assumed that the first bus experiences no delay at this bus stop.

Based on the two basic types of bus stops, namely curbside bus stops and bus bay bus stops, a detailed survey has been conducted to collect field data of bus deceleration time, bus acceleration time, bus dwell time, driver perception-reaction time, the number of berths at the bus stop, bus arrival rate, and the number of passengers that get on and get off the bus. The actual time of the overall bus stop process minus the normal bus deceleration time, bus acceleration time, driver perception-reaction time and the normal time it takes for passengers to get on and get off the bus gives the delay time of a bus. The total delay time is the sum of all delays experienced by buses in the period of an hour and it can be expressed mathematically as follows:

$$d_T = \sum_{1}^{n} (t_i - t_1 - t_2 - t_3 \cdot \max\{m_1, m_2\})$$

Where: d_T -- Total delay time, s;

t_i --Actual total time of a bus from starting to decelerate to a stop, bus dwell time, and time of bus acceleration to join the traffic stream to attain steady speed, s;

t_1 --Average bus deceleration time without any interference from other vehicles, s;

t_2 --Average bus acceleration time without any interference from other vehicles, s;

t_3 --Average time of a passenger boarding or alighting from the bus without any interference from other passengers, s;

n --Bus arrival volume

m_1 --Number of passengers boarding a bus;

m_2 --Number of passengers alighting from a bus.

Data Collection. A total of fifteen bus bays and six curbside bus stops have been selected in Beijing for data collection. The selected bus stops should satisfy the following conditions. First, there should be an area where a digital video camera can be mounted so that it can tape the entire zone affected by the bus stop, or the whole traffic area affected, to ensure that video graphing and on-site observations give valuable, representative, and practical data covering all categories of buses on the road-site. Normally, locations close to the bus stop, such as an overpass for pedestrians, a high-rise building, or flyovers, are good places to mount a video camera. Secondly, the traffic on sections of road near the bus stop should be relatively high, but not to a point of congestion at the bus stop. Thirdly, bus stops selected should be along sections of road where the road is typical, void of interference of basic at-grade intersections, has a larger roadway gradient, and has entrances or exits from the main roads on which the bus stops are located. Fourthly, bus stops located at or near bus terminals of bus lines or bus routes are to be excluded. These could affect bus traffic flow and data collection. Lastly, the selections of the bus stop locations are to be carried out uniformly and equal in all directions as shown in Figure 1. The collection of data from these locations serves as the data for building a model of objectivity and practical value.

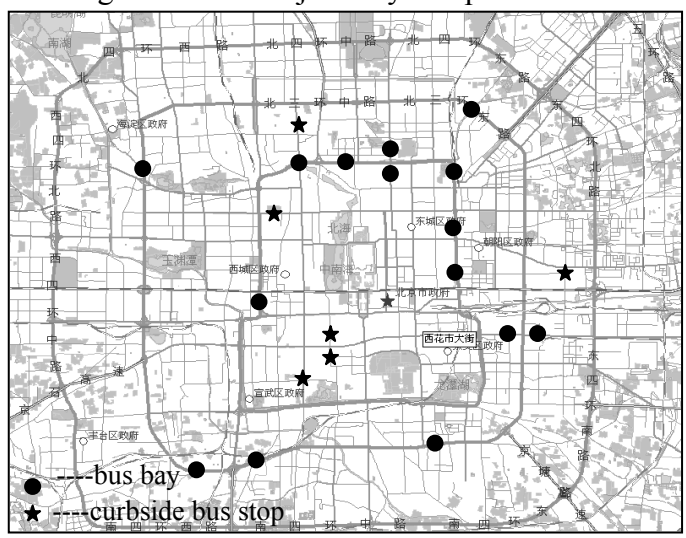

FIGURE 1: Geographical Locations of Selected Bus Stops Surveyed in Beijing

Delay **E**stimation.

- Bus Average Deceleration and Acceleration Time Without Interference

Based on the two scenarios above, average bus deceleration time and average bus acceleration time without interference have been obtained from both curbside bus stops and bus bays. The data distribution is illustrated in Figure 2 and Figure 3.

Table1. Average bus deceleration/ acceleration times under non-interference situation

Types of Bus stops	Average bus deceleration time	Average bus accelera tion time
Bus bay	9.0s	10.7s
Curbside bus stop	8.5s	10.9s

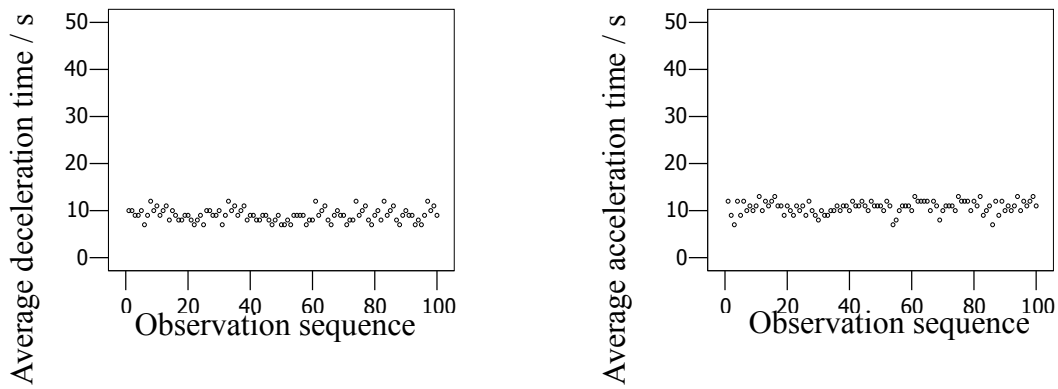

FIGURE2. Distribution of deceleration and acceleration time at bus bay without any interference

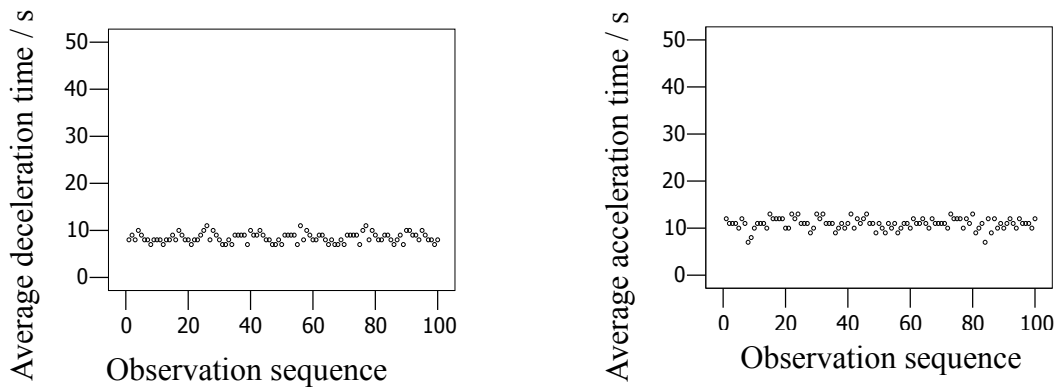

FIGURE 3. Distribution of deceleration and acceleration time at curbside bus sto p without any interference

- Average Time that Passengers take to get On and Off the Bus

In Beijing, the vast majority of bus fares are paid through the IC card. According to the survey, the doors of buses can be divided into the narrow ones and wide ones. The average time for a passenger to get on and get off a bus is quite different between these two types of doors. The results of the average time for passengers to get on and get off a bus, both with the narrow and with the wide doors, are shown in Table 2. Figure 4 and Figure 5 show the distributions of the time for passengers getting on and off the bus.

Table2. Average times of passengers boarding and alighting from the buses

Type of Door	Average time of get on and out of the bus
Narrow door	2.1s
Wide door	1.7s

- Driver Perception-Reaction Time

In this study, the driver door operation time consists of two parts: (a) time taken by the driver to open the door for the first passenger to get on board or alight and (b) time taken by the driver to close the bus door for the bus to start moving again. From the survey of these two types of driver door operations, the times are both less than one second. Therefore, the driver door operation time is not considered or taken into account during the calculation.

- Delay Estimation of Bus Bay Bus Stops

The final processed data has been analyzed with the aid of a Statistical Program for Social Sciences (SPSS 13) for Windows. The scatter plot and the curve of best fit are shown below for the regression analysis of the bus bay:

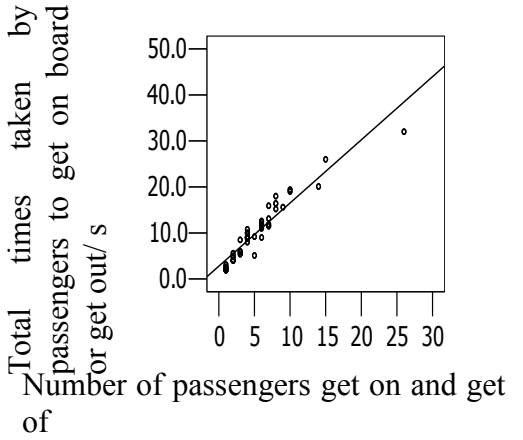

Figure 4. Graph of total times taken by passengers to board or to alight versus number of passengers getting on or off the bus. (Narrow door)

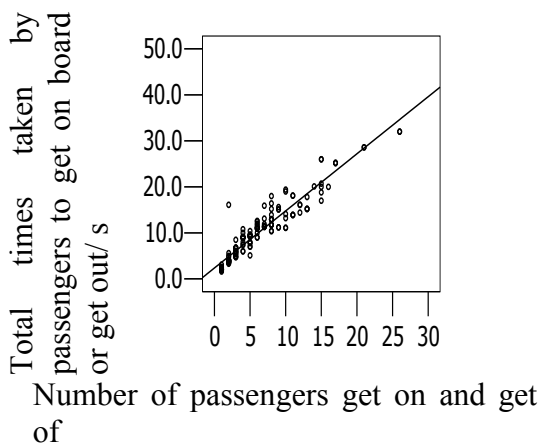

Figure 5. Graph of total times taken by passengers to board or to alight versus number of passengers getting on or off the bus. (Wide doors)

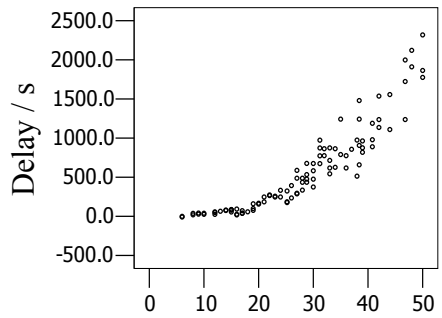

FIGURE 6. Scatter plots of the delay and bus arrival occupancy rate of bus bay

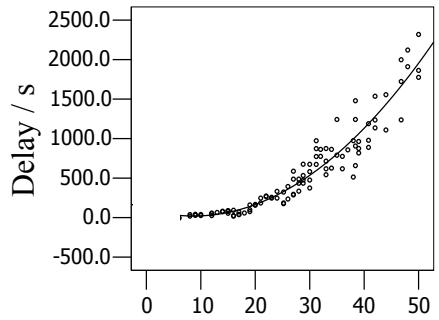

FIGURE 7. A curve of best fit of regression analysis for bus bay surveyed data

From Figure 7 above, when the bus arrival occupancy rate is less than 20veh/h, it is observed that delay at a bus bay bus stop is quite small. As the bus arrival occupancy rate increases to more than 30veh/h, the delay at a bus bay bus stop increases significantly. Using a logarithmic model, quadratic model and linear model, and comparing their test parameters (R^2 – square of correlation coefficient and F-statistic test), the model which has the highest value is selected. Table 3 illustrates the summary of the three models and the estimate of parameters or the results of regression analysis for various regression models.

Table3 . Model Summary and Parameter Estimates (bus bay)

Model		R^2	F
Logarithmic model	$T = b_0+b_1 ln\lambda$	0.652	183.9
Quadratic model	$T = b_0+b_1\lambda+b_2\lambda^2$	0.912	505.7
Linear model	$T = b_0+b_1\lambda$	0.830	476.9

The results of the statistical correlation (Model Summary and Parameter Estimates), as shown in Table 3, show that the best fit curve comes from the Quadratic Model because the R-square and F-test parameters proved to be of the highest values for the Quadratic Model when compared to the test parameters of the Logarithmic and Linear models. Therefore, for bus bay bus stops, the correlation between bus arrival occupancy rate (Λ) and delay time (d_T) can best be expressed as:

$$d_T = 105.5-19.666\Lambda+1.133\Lambda^2 \quad (\Lambda>20\text{veh/h})$$

➢ Delay Estimation of Curbside Bus Stops

The scatter plot and the curve of best fit for the regression analysis of curbside bus stops are shown below:

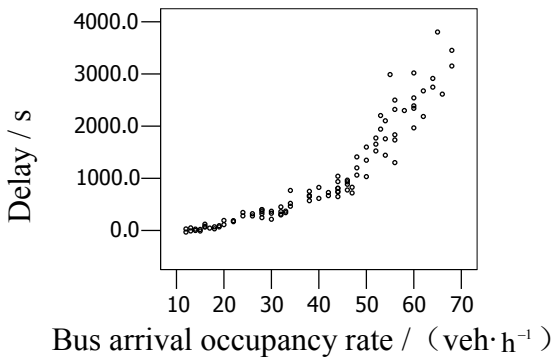

FIGURE 8. Scatter plots of the delay and bus arrival occupancy rate of curbside bus stop

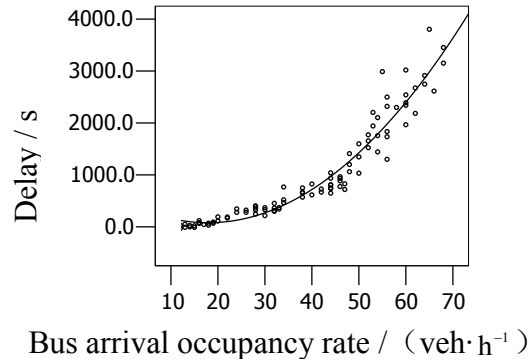

FIGURE 9. A curve of best fit of regression analysis for curbside bus stops surveyed data

From Figure 9, we can clearly see that the situation for curbside bus stops is quite the same as for bus bay bus stops. When the bus arrival occupancy rate is less than 20veh/h, it is obvious that delay at a curbside bus stop is quite small. As the bus arrival occupancy rate increases to more than 30veh/h, the delay at a curbside bus stop increases significantly. We again use the logarithmic model, quadratic model and linear model with regression analysis and choose R^2 and F as our test parameters. Table 4 illustrates the summary of the three models and the estimation of the parameters or the results of regression analysis for various regression models.

Table4. Model Summary and Parameter Estimates (curbside bus stop)

Model		R^2	F
Logarithmic model	$T = b_0+b_1 ln\lambda$	0.680	199.7
Quadratic model	$T = b_0+b_1\lambda+b_2\lambda^2$	0.929	612.5
Linear model	$T = b_0+b_1\lambda$	0.826	445.6

The results of the statistical correlation (Model Summary and Parameter Estimates), as shown in Table 4, indicate that the best fit curve for curbside bus stops is the Quadratic Model because the R-square and F-statistics test values proved to be the highest for the Quadratic Model when compared to the values of the Logarithmic and Linear models. Therefore, for curbside bus stops, the correlation between bus arrival occupancy rate (Λ) and delay time (d_T) can best be expressed with a quadratic relationship as follows:

$$d_T = 498.8-46.944\Lambda+1.31\Lambda^2 \quad (\Lambda>20\text{veh/h})$$

CONCLUSIONS

From the analysis of the bus bay bus stop and curbside bus stop surveyed data, it is concluded that bus arrival occupancy rate has a statistical correlation

with delay at and near the bus stops. A concept of "bus arrival occupancy rate" is introduced in this study to explain the situation near and at the bus stop. From this study, it has been shown that when the bus arrival occupancy rate of a bus stop is less than 20veh/h, the delay at the bus bay bus stop is quite small. When the bus arrival occupancy rate increases to more than 30veh/h, the delay a bus experiences at a bus bay bus stop increases significantly. From the analysis, a bus arrival occupancy rate of 30veh/h can be used as the reference for bus stop design standards. If the bus arrival occupancy rate is more than 30veh/h, steps can be taken to zone the platform of a bus stop into two or more zones in order to maximize the operating efficiency of the bus stop.

Empirical models have been set up for bus arrival occupancy rate and delay for both bus bay and curbside bus stops, which are used to estimate the delay at the bus stops, and also to provide a basis for determining the level of service of a bus stop.

REFERENCES

Han Bao rui, Lin Li, Fan Xiao. (2004). "survey and analysis of bus delay in bus stop." Traffic Analysis and Design.2 (4), 68-71.

Ma Hong Wei, Li gang Yan, Hu Jian.(2006). "delay analysis and countermeasure of urban bus stop." Highways & Automotive applicants. (06), 25-27.

Reebu Zachariah Koshy, and V., Thamizh Arasan.(2005). "Influence of Bus Stops on flow Characteristics of Mixed Traffic." Journal of Transportatio n Engineering, 131(8), ASCE, 640-643.

Transit Cooperative Research Program (TCRP).(1996). "Guidelines for location and design of bus stops." Report No.19, Transportation Research Board, National Research Council , Washington, D.C.

Wang Qian, Yang Xiaoguang. (2003). "Impact of Bus Stops on Delay and Capacity of Shared Approaches at Signalized Intersections." China Civil Engineering Journal , 36, No.1, 58 -64.

Zhu Wei, Chen Xue wu.(2002). "Analysis of Traffic Delay at Bus Stop Hubs and Solutions."china municipal engineering. 97(2),7-9.

A Google-map Integrated Web -based Stated Preference Survey for Modeling Personal Mobility

Kai LIU[1], and Yasuo ASAKURA[2]

[1]Center of Transportation Research, Dalian University of Technology, No.2 Linggong Street, Ganjingzi, Dalian, 116024, CHINA; PH/FAX: +86-411-84707761; email: lk_liukai@hotmail.com

[2] Graduate School of Civil Engineering, Kobe University, Hyogo 657-8501, JAPAN; PH/FAX: +81-78-803-6208; email: asakura@kobe-u.ac.jp

ABSTRACT

An internet stated preference (SP) survey was developed in order to investigate an operational strategy in practice for a new kind of personal travel assistance mode - Low Speed Private Transportation Mode (LSPTM) system. This article outlines the idea and methodology of developing an SP survey which applies the recent innovations of Google-map API and Ajax models. Details regarding the dynamic location based information provision through various overlapping elements on Google-map and the experimental design with respect to different respondents/situations are explained. Results proved that the combination of environmental information provision through Google-map and efficient generation of attribute settings allows for an attractive SP survey design.

INTRODUCTION

Recently, a new kind of personal travel assistance mode (e.g. iSwing, iUnit, Segway, and so on) that was designed for improving the mobility and flexibility of personal transportation is receiving increasing attention. This kind of generally Low Speed PrivateTransportation Mode (LSPTM) is recognized as a possible link or complement to existing travel modes within city areas. A deeper behavioral understanding of traveler response to LSPTM is necessary, which will increase insight into policy issues for projecting a strategy of new travel mode service as a mobility management tool.

Stated Preference (SP) survey was proved to be an efficient method for modeling stated choices under various conditions and believed to offer a reliable treatment of influence factors (Hensor, D.A. 1994). Since almost all possible responders had no user experiences of LSPTM up to now, it is really not so easy for them to imagine the established settings and make a decision on use or not. It is certainly better to interview test riders, whereas a more flexible alternative that will

be introduced in this article is to develop a web application system which supports the visualization of LSPTM vehicles and maps of real urban networks.

Seymour and his colleagues (2007) developed a traveler assistance system in which a large amount of traffic related information were overlapped onto Google maps and can be easily accessed through the internet. It is our opinion that the advanced web technologies may extend/enrich the flexibility and efficiency of SP survey by providing respondents more location-based environmental information, as well as by offering more flexibility in the environmental attributes setting. This article aims at developing a Google-map integrated web-based SP discrete choice survey system. The main objective focus is on the implementation of embedding Google-map into the internet SP survey and the experimental design implemented through internet technology, rather than the discussion of a discrete choice model. To our knowledge this study is the first SP experiment survey by which the web functions are resorted to fully performed in order to realize the merits of web-based SP survey.

The remainder of the contents are organized as follows. The next section reviews some existing Internet-based SP surveys and Google-map incorporated web applications in transportation fields. Section 3 focuses on the architecture and technologies for survey design and SP experimental design. Subsequently, a test survey of intentions of LSPTM usage in Kobe Sannomiya area, as well as the preliminary analysis, is depicted. This article ends with our conclusions and future research proposal.

LITERATURE REVIEW

During the last decade, transport surveys through e-mails or web sites were promoted significantly and have been employed for wide applications (e.g. Iragüen and Ortúzar, 2004; Arentze et. al, 2005; Polydoropoulou and Papola, 2006; Fleming and Bowden, 2007). These studies provided valuable references on fully performed web survey design and various discrete choice analyses. Arentze and his colleges (2005) alleged that well designed internet-based surveys are even capable of providing reliable data for quite complex stated adaptation experiments.

Among all recent innovations in web technologies, Google-map API and Ajax model allow for implementation of more advanced SP surveys, more flexibility (with more possible cases for various changing conditions), and better amusement (dynamic provided contents with interesting expression, such as location-based information).

Since the Google map Application Programming Interface (API) was released in 2005, Google's mapping capabilities have been incorporated freely into various web applications. Seymour and his colleagues (2007) developed an Internet–based

traffic information system. Similarly, Welch and his colleagues (2007) reported a traffic data management and archive system. Wu and Wang (2008) established a Google-map-based online platform, GATI, for arterial traveler information broadcast and analysis, which has operated online using the City of Bellevue's data since January 1, 2007. These significant works generate an efficient framework for Google-map API applications in transportation fields. The methodology of embedding Google-map into a web site is omitted in this article due to space limitation. Please refer to above literatures and the web site of Google API (http://code.google.com/apis/maps/) for detailed instructions. Google-map API also provides many other functions, such as dynamic map behaviors (zoom, pan, and so on), open/close information window, and overlapping elements (points, polylines and polygons) with expected color, shape, and transparency, which do extend the way of presentation of location-based information and enrich the flexibility of SP experimental design.

Ajax (shorthand for Asynchronous JavaScript + XML) is another recent web innovation which incorporates several technologies for improving the interactive communication between web servers and user interfaces. Google-map is actually a successful example of the Ajax application.

SURVEY FRAMEWORK AND EMPERIMENT DESIGN

The core of survey design is to embed Google-map into the survey contents and to provide various-situations-specified information, considering that the location-based information may enrich interviewees' knowledge and therefore make choices easier. Besides realizing the affluent information through Google-map, another innovation of this web-based SP survey is the way of experimental design. Here the Ajax model is employed to efficiently exploit the way in which various attribute combination settings are generated. The popular combination of Apache-PHP-MySQL was chosen as the web server because it is free of charge and is an abundant open-source. Moreover, numerous features are built-into the PHP language which allows web applications to be quickly developed.

Giving an imaging leisure trip from their homes to the city center at weekends, all participants are informed that they have to initially go to one of the car parks near the destination by private vehicle or one of the nearest stations by train. Upon arrival they are asked to make a choice of terminal mode among electric bicycle, LSPTM, and walk, for arriving at the destination. The web survey (in Japanese) was framed into three main categories: Category 1 made an introduction on the survey objective and LSPTM characteristics with an image photo of iReal vehicle; Category 2 concerned participants' personal characteristics and their usually choice of travel mode (by train or by private car), as well as comparative ride frequency in case of

both mode users, for a weekend leisure trip to their resident city center; Category 3 focused on the stated choice survey designed for three groups: car user, train user, and both mode users. The survey architecture is depicted in Figure 1.

A hypothetic private-car forbidden area around the destination, as a common traffic regulation practice during events, is established (as shown in Fig. 2). At least one nearest park outside is no more than 300m away (about 4mins by walk) from the destination. For all three groups, two types of situations differentiated by providing unique or two available transfer place(s) as included. Subsequently participants are asked to select an egress mode. Considering that it is better to keep a moderate level of complexity , three egress modes are set to be available for the case of unique transfer place (randomly selected from four pre-set parks with differing distances to the destination shop) while only walk and LSPTM are set to be available for the case of two transfer places. The first type of situation provides three alternatives and the second one has four alternatives. Each situation consists of five settings and participants are asked to make a total of 10 to 15 choices.

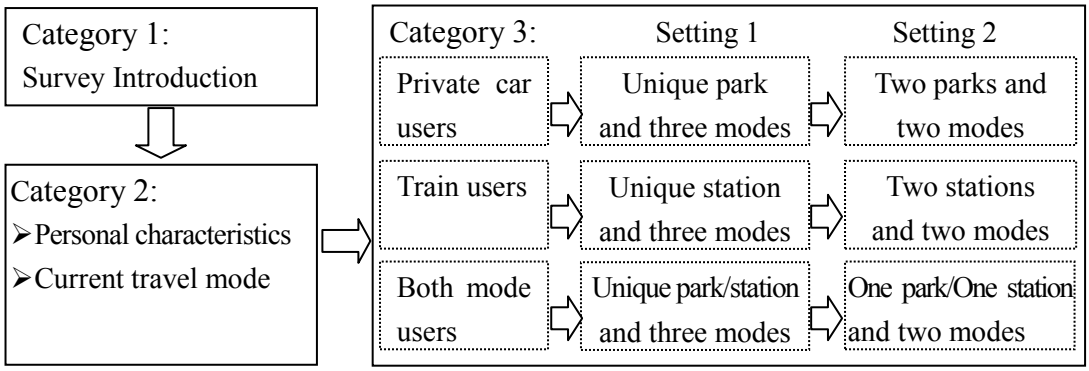

Figure 1: The architecture of survey

Location-based information, such as the stated destination, private-car forbidden area (polylines or polygons), as well as available locations for car parks and LSPTM parking garages (points), are provided overlapping Google-map (see Figure 2). Respondents can also explore information through the zoom in and drag functions of Google map.

Figure 2: Location -based information overlapping on Google -map

The fractional factorial experiment design (Henser, D.A. 1994) was employed to optimize these independent variables in order to generate a more efficient attribute combination. Each attribute was set to have several levels; parking charges have 7 levels from 200 JPY /2h to 500 JPY/2h, travel times depend on the real route distances (with 4 levels for each mode), waiting times have 3 levels (with 1min, 5mins and 10mins for each mode), and 3 levels for rental charges (with 50JPY, 100JPY and 200JPY for bicycle and LSPTM, and zero for walk). In order to reduce the number of choices for respondents, the yielded attribute combinations were separated into four groups and each group included 5 sets. One group of sets was randomly chosen and sent from the server database to the user interface if respondents press the "Start choices" button when they have already understood the environment settings and have determined their choices. Weather and temperature information are also provided randomly as two-level dummy variables, that is, raining or sunny for weather, and sizzling hot or comfortable for temperature.

In order to take advantage of not only Google-map's enormous database, but also the appealing map behaviors that comes with it, some dynamic map functions were designed. For example, the blinking marks highlighted available car parks, and information windows dynamically appear as "mouse-on" events happen, and so on.

DATA COLLECTION AND PRELIMINARY MODELING RESULTS

The beta-test version of this internet-based SP survey was has been available since December 20, 2008. The test area is Kobe city, Japan, and the destination is set as Kobe municipal museum. Data collected from a pre-test (on Dec.21, 2008 and Jan.5, 2009) by 25 students/researchers members is used to check the effectiveness of this web survey and investigate the implication of LSPTM characteristics and environmental attributes. All interviewees proved the efficiency of the web survey and enjoyed both the ease and interactive method of filling form fields in comparison

to conventional paper-based survey methods.

Multinomial logit (MNL) model and nested logit (NL) model are used separately to model the choice behaviors associated with two types of situations. A total of 100 samples was used for the first situation and 105 samples for the second situation. Personal attributes are not considered this time because of sample limitation. The results of estimated parameters for both models are omitted here due to space limitation. The preliminary results show that the waiting/running time and the usage/parking charge are significant influence factors. It is disclosed that respondents when confronted with rain or sizzling heat are more likely to choose LSPTM. An interesting result is that for the case of second situation (two available car parks and two transfer modes), students have a tendency to walk and females tend to use LSPTM, while no trend can be found for the first situation (unique station and three transfer modes).

CONCLUSIONS

This article focuses on an introduction of an Internet-based stated choice survey which was developed to collect the data and model personal mobility needs. The electric-derived LSPTM vehicles are designed for improving personal mobility within the city, while the operational strategy that satisfies both environment sustainability and personal mobility needs is still an open issue.

Some advanced web technologies were employed to take our web survey to new levels of power and usability, especially Google Maps and the Ajax model. It is proved that the embedded location-based environmental information through dynamic Google maps improve the understanding of interviewees, and the Ajax model when incorporated with experimental design methods provides a more efficient choice attribute design. In short, these web technologies provide more likely conversation survey possibility than paper-based methodologies.

The large-scale data collection is still in progress and only a portion of preliminary results are reported in this article. More analysis and models will be carried out in the near future. Also, more consideration on the sampling frame and sampling bias, the typical pitfalls of Internet-based surveys showed by Arentze and his colleges (2005), are necessary in future studies.

REFERENCES

Arentze, T., Bos, I., Molin, E. and Timmermans, H. (2005). “Internet-based travel surveys: selected evidence on response rates, sampling bias and reliability.” Transportmetrica , 1 (3), 193-207.

Chorus, C.G., T. A. Arentze, H. J. P. Timmermans, E. J.E. Molin, and B.V. Wee. (2007). “Travelers' Need for Information in Traffic and Transit: Results from a Web Survey.” Journal of Intelligent Transportation Systems , 11 (2), 57-67.

Fleming, C.M. and Bowden M. (2009). "Web-based surveys as an alternative to traditional mail methods." Journal of Environmental Management , 90 (1), 284-292.

Hensher, David A. (1994). "Stated preference analysis of travel choices: the state of practice." Transportation 21 (2), 107-133.

Iragüen, P. and Ortúzar, J. (2004). "Willingness-to-pay for reducing fatal accident risk in urban areas: an Internet-based Web page stated preference survey." Accident Analysis & Prevention, 36 (4), 513-524.

Polydoropoulou, A. and Papola, A. (2006). "Shopping-Related Travel in Rich ICT Era: Case Study on Impact of E-shopping on Travel Demand." 85th Transportation Research Board Anural Meeting, Washington, D.C.

Seymour P.E., Edward James, and Bryan Miller. (2007). "Use of A Google-Based Mapping System for Traffic Management Center Web Navigation." 86th Transportation Research Board Annual Meeting , Washington, D.C.

Welch, T.J., K.A. Tufte, R.S. McCourt, R.L. Bertini, and Alan Snook. (2007). "Implementing a User-Oriented Web-Based Traffic Data Management and Archive System." 86th Transportation Research Board Annual Meeting.

Wu, Yao-Jan, and Yinhai Wang. (2008). "Google-Map-Based Online Platform for Arterial Traffic Information and Analysis." 87th Transportation Research Board Annual Meeting, Washington, D.C.

Evaluation of Supervision Engineer 's Control over Investment Based on AHP

T. Lu [1] and Q. Li [2]

[1]Management College of Hebei Agriculture University, Engineering Management Department of Shijiazhuang Railway Institute, Shijiazhuang 050043, China; email: tiejunlu2003@163.com
[2]Engineering Management Department of Shijiazhuang Railway Institute, Shijiazhuang 050043, China; email: lqj_wuqiao@sina.com.

ABSTRACT

The Supervision Engineer's performance plays an important role in the investment control of a construction project. The effect of the Supervision Engineer's control over investment can be evaluated from two aspects. One aspect is the Employer's target. The other is the interest of the Contractor. Control over investment requires the Supervision Engineer to provide good professional consultation and management service by imposing strict audits and effective control over the contractor's expenses involving management work in technique, contract, organization, coordination and measurement, etc. The factors that influence the Supervision Engineer's performance in these two aspects are complicated: some factors are common to both aspects while others are particular to only one. In order to use the AHP method to appraise the performance of the Supervision Engineer's performance in investment control, these factors are divided into certain indicators and an analytical hierarchy model is formed. The relative significance of the factors in each hierarchy are judged based on expert experience and quantitatively expressed with the weights of superiority of the factors of each hierarchy determined mathematically.

INTRODUCTION

As a useful tool in multi-target analysis, AHP (Analytical Hierarchy Process) was first introduced to China in the 1980s. AHP has been widely adopted for systemic analysis and decision-making process due to its advantage in combining qualitative analysis with quantitative analysis of concerned elements. AHP decomposes the decision problem into a hierarchy of more easily comprehended sub-problems, each of which can be analyzed independently. Decision makers then systematically evaluate its various elements, comparing one to another in pairs. AHP converts these evaluations to numerical values that can be processed and compared over the entire range of the problem. A numerical weight or priority is derived for each element of the hierarchy. In the final step of the process, numerical priorities are derived for each of the decision alternatives (Yang et al. 2006).

The effect of the Supervision Engineer's control over investment can be

evaluated from two aspects. One aspect is the Employer's target. The other is the interest of the Contractor. Control over investment requires the Supervision Engineer to provide good professional consultation and management service by imposing strict audits and effective control over the contractor's expenses involving management work in technique, contract, organization, coordination and measurement, etc (Huang et al. 2002). In order to use the AHP method to appraise the performance of the Supervision Engineer's performance in investment control, the elements that influence the Supervision Engineer's performance are divided into certain sub-elements, as explained below.

STRUCTURING OF THE P ROBLEM INTO A HIERARCHY

According to the above discussion and based on practical experience in construction management, the appraisal model of the Supervision Engineer's investment control effect can be structured as shown in Figure 1, involving five levels and seven influencing factors (C_1~C_7). These are further divided into fourteen elements (D_1~D_{14}) (Liang 2004).

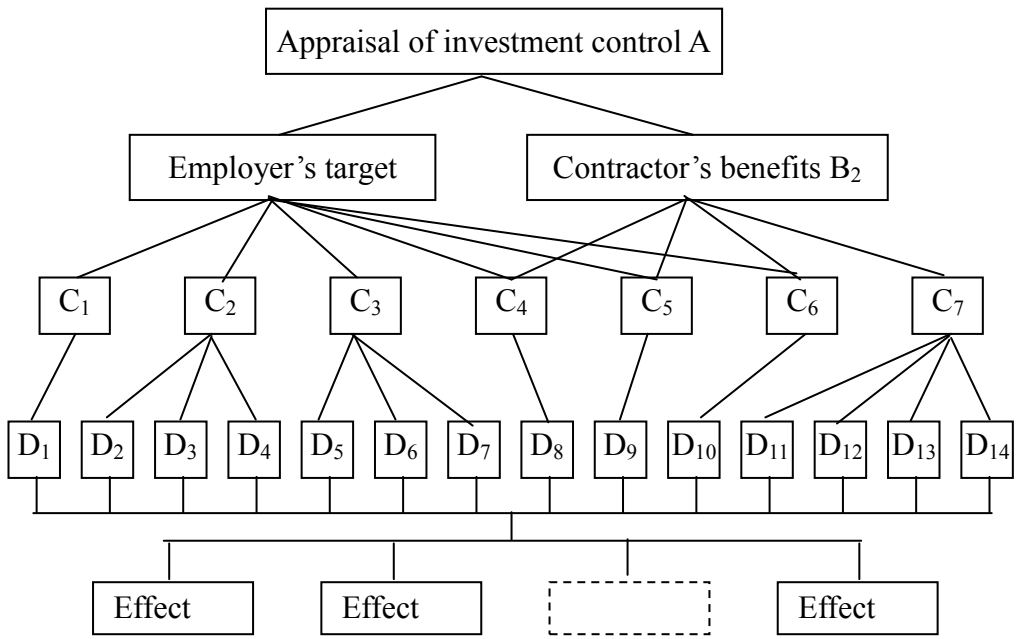

Figure 1. Appraisal model of investment control effect.

The seven influencing factors and fourteen elements as shown in Figure 1 are defined as follows:

C_1 (Supervision defficiency) . Supervision Engineer's defficiency rate D1 = (loss due to supervision engineer's defficiency)/(project total cost estimate).

C_2 (Reduction through Control) . Budget reduction rate D_2 = (budget reduction)/(budget total). Certified reduction rate D_3 = (certified reduction)/(certified total). Final payment reduction rate D_4 = (final payment reduction)/(final payment total).

C_3 (Economic measures) . Claim reduction rate D_5 = (relative claim reduction)/(relative claim original). Total cost reduction rate D_6 = (relative cost reduction)/(estimated cost total). Advice-based reduction rate D_7 = (relative reduction)/(estimated cost total).

C_4 (Coordination) . Coordinate disputes between parties D_8.

C_5 (Contract management) . Urge each party to perform in accordance with the Contract D_9.

C_6 (Technological Man agement) . Checking and approving technological plans D_{10}.

C_7 (Contractor 's Measurement) . Budget compensation rate D_{11} = (budget compensation)/(estimated cost total). Certified compensation rate D_{12} = (certified compensation)/(certified total). Final payment compensation rate D_{13} = (final payment compensation)/(final payment total). Employer's claim reduction rate D14 = (Employer's claim reduction)/(relative claim original).

COMPARISON MATRIX

The comparison matrix reflects the relative significance of each element at one level to the related elements at the preceding level, which is accomplished through pair comparisons and quantified with 1-9 scales as shown in Table 1.

Table 1 . Meanings of Different Scale Values .

Scale	Meaning
1	elements u_i and u_j have equal significance
3	u_i is slightly more significant than u_j
5	u_i is remarkably more significant than u_j
7	u_i is intensely more significant than u_j
9	u_i is extremely more significant than u_j
2, 4, 6,8	Medium values of 1-3, 3-5, 5-7, 7-9

ELEMENT PRIORITY

Individual element priority reflects the influence of each individual element at one level on a specific element at the upper level. Individual element priority can be established by calculating the feature vector of the comparison matrix. The root method can be conveniently used to calculate the feature vector with required accuracy.

(1) Calculate the product M_i of the elements at each row of Matrix A:

$$M_i = \prod_{j=1}^{n} a_{ij}, \quad i = 1, \quad 2, \quad \cdots, \quad n$$

(2) Calculate the nth root of M_i, $\overline{W_i}$, $\overline{W_i} = \sqrt[n]{M_i}$

(3) Normalizing vector $\overline{W} = \left| \overline{W_1} \quad \overline{W_2} \quad \cdots \quad \overline{W_n} \right|^T$, $W_i = \dfrac{\overline{W_i}}{\sum_{j=1}^{n} \overline{W_i}}$

Hence the feature vector: $W = [W_1, \quad W_2, \quad \cdots, \quad W_n]^T$

CONSISTENCY CHECKING

For consistency checking, use the following method:

(1) Calculate the maximum feature root of the comparison matrix:

$$\lambda \max = \frac{1}{n} \sum_{i=1}^{n} \frac{|AW_i|}{W_i}$$

Where: AW_i is the ith element of AW, the vector obtained by multiplying comparison matrix A and its feature vector W.

(2) Calculate the consistency index CI: $CI = \dfrac{\lambda \max - n}{n-1}$

If CI = 0, the comparison matrix is completely consistent and the checking is over. If CI ≠ 0, then continue to the next step.

(3) Calculate random consistency CR: $CR = \dfrac{CI}{RI}$

Where: the value of RI can be obtained by referring to Table 2.

If CR < 0.1, the consistency of the comparison matrix and individual element priority is acceptable, otherwise, the elements of the comparison matrix need to be

revalued.

Table 2 . Average Random Consistency Index (RI) .

Order	1	2	3	4	5	6	7	8	9	10
RI	0.00	0.00	0.58	0.96	1.12	1.24	1.32	1.41	1.45	1.49

GENERAL PRIORITY

General Priority reflects the relative significance of all elements of each level to the upmost level. The priority value of a certain level is calculated based on the General Priority value of the previous level and the individual element priority values of this level, thus the General Priority must be calculated from the upmost level downwards. Consistency should also be checked from up to down.

SUPERVISION EFFECT EVALUATION

The indexes include qualitative indexes (D_8, D_9 and D_{10}) and quantitative indexes (D_1~D_7, D_{11}~D_{14}). Among the quantitative indexes, some prefer lower values, such as D_1. In this case, the ratio of two effects on index D_i may be calculated:

$$Q_{12}^{(i)}, Q_{12}^{(i)} = \frac{M_1^{(i)}}{M_2^{(i)}} \times 100\%$$

Where: $M_1^{(i)}$ —the actual value of effect M_1 on index D_i;

$M_2^{(i)}$ —the actual value of effect M_2 on index D_i.

Consult Table 3 for the corresponding comparison scale value $D_{12}^{(i)}$, establish the comparison matrix, and calculate the individual priority of the effect.

Some other quantitative indexes prefer higher values (D_2~D_7, D_{11}~D_{14}). If this is the case, then consult Table 3 with $\frac{1}{Q_{12}^{(i)}}$ to obtain $D_{12}^{(i)}$. For index D_6, if one effect is negative, adopt 9 for $D_{12}^{(i)}$. If both are negative, then consult Table 3 with $Q_{12}^{(i)} = \frac{\left|M_1^{(i)}\right|}{\left|M_2^{(i)}\right|} \times 100\%$ to get $D_{12}^{(i)}$.

Table 3 . Scale Valuation .

$Q_{12}^{(i)}$ %	<50	50~ 60	65~ 75	85~ 95	98~ 102	105~ 115	125~ 135	140~ 150	>150
$D_{12}^{(i)}$	9	7	5	3	1	1/3	1/5	1/7	1/9

APPLICATION IN ENGINEERING CASES

In order to minimize the unfairness of the supervision effect evaluation,

projects should be properly classified into several categories by location, function or structure, etc., and by the qualifications of the contractor. Supervision effects should be compared only between projects in the same category. It should also be noted that the cost only refers to the cost of the project in construction stage, and does not include the expenditures incurred in the stages prior to construction, such as land, removal, and resettlement, etc.

M_1 and M_2 are two highway construction projects of the same category that are supervised by Supervision Company S_1 and S_2 respectively. According to the statistical data at completion, the related indexes are given in Table 4.

Table 4 . Indexes for Evaluation of Investment Control for M_1 and M_2 (%).

	D_1	D_2	D_3	D_4	D_5	D_6	D_7	D_{11}	D_{12}	D_{13}	D_{14}
M_1	0	18.94	30.70	5.69	52.17	11.35	2.42	1.16	1.61	0.55	17.62
M_2	0.13	12.39	43.24	6.61	45.71	8.66	5.28	1.78	2.32	0.83	12.79

According to the structure model as shown in Figure 1 and the quantification procedure described above, the comparison matrix can be established, individual element priority can be obtained, and consistency can be checked. Calculations are then made for General Priority. Finally, the priority values of investment control effects of the two supervision companies are obtained as shown in Table 5.

Table 5 . Calculation Result of GP for Investment Control Effect of M_1 and M_2.

Index	Weight	$M_1^{(i)}$%	$M_2^{(i)}$%	$1/Q_{12}^{(i)}$%	$Q_{12}^{(i)}$%	$D_{12}^{(i)}$	$W_1^{(i)}$	$W_2^{(i)}$
D_1	0.060	0	0.13	-	0	9	0.90	0.10
D_2	0.049	18.94	12.39	65.4	152.9	5	0.83	0.17
D_3	0.096	30.70	43.24	140.8	71	1/7	0.125	0.875
D_4	0.024	5.69	6.61	116.2	86.1	1/4	0.20	0.80
D_5	0.042	52.17	45.71	87.6	114.1	3	0.75	0.25
D_6	0.140	11.35	8.66	76.3	131.1	4	0.80	0.20
D_7	0.078	2.42	5.28	218.2	45.8	1/9	0.10	0.80
D_8	0.130	-	-	-	-	2	0.667	0.333
D_9	0.130	-	-	-	-	1/2	0.333	0.667
D_{10}	0.130	-	-	-	-	3	0.75	0.25
D_{11}	0.032	1.16	1.78	153.4	65.2	1/9	0.10	0.90
D_{12}	0.052	1.61	2.34	145.3	68.8	1/7	0.125	0.875
D_{13}	0.020	0.55	0.83	150.9	66.3	1/9	0.10	0.90
D_{14}	0.017	17.62	12.79	72.6	137.8	5	0.83	0.17
GP							0.516	0.484

As shown in Table 5, the General Priority value for M_1 and M_2 are 0.516 and 0.484 respectively. Thus it is concluded that supervision company S_1 has achieved a better investment control effect than supervision company S_2.

CONCLUSION

The elements that influence the Supervision Engineer's performance are complicated. These elements, however, can be divided into certain sub-elements and an analytical hierarchy model formed. The relative significance of the elements in the hierarchy can be judged based on expert experience and quantitatively expressed with the weights of priority of each element determined mathematically. AHP provides a useful method to appraise the performance of the Supervision Engineer in investment control, which may be used as reference for employers in their choice of good supervision companies in the consulting market.

REFERENCES

Huang, X. and Wei, C. (2002). "AHP Model for Bid Evaluation of Civil Engineering Projects." Journal of Qingdao Architecture Engineering Institute , 2002(2).

Liang, L. (2004). Study on Supervision Target Control System for Construction Projects (Masters Thesis). Hebei Engineering Institute, May 2004.

Yang, B. and Li, H.M. (2006). "Study on Investment Decision-making Model for Construction Engineering." Journal of Xi'an University of Science and Technology, 2006(2).

Technical Efficiency of Container Terminals in China Using a Multi-Activity Data Envelopment Analysis Model

LI Ying[1], MIAO Lixin[1]

[1]Research Centre for Modern Logistics, Graduate School at Shenzhen, Tsinghua University, Shenzhen 518055; PH (86) 755-26036772; FAX (86) 755-26036005; email: lying99@mails.tsinghua.edu.cn

ABSTRACT

The aim of this paper is to provide a multi-activity data envelopment analysis (DEA) model which can represent both quayside and landside operations in a unified framework. The model is applied to simultaneously estimate the overall container terminal efficiency: quayside operation efficiency and landside operation efficiency. To do this, 20 selected container terminals in China for the year 2006 are selected for empirical applications. The results show that the average quayside operation efficiency is higher than the average landside operation efficiency (0.630 vs. 0.588), but these measures differ significantly for individual terminals. The main advantage of the multi-activity DEA model is that it can be utilized to detect the source of poor performance of container terminals rather than just evaluating the overall efficiency as in the traditional DEA model.

INTRODUCTION

To remain competitive, a container port must satisfy the specific demands of its customers and facilitate cost reductions. In short, the port must improve its operational efficiency. As a consequence, many researchers have focused attention on the measurement of efficiency in the container port or terminals. For example, Valentine (2001), Tongzon (2001) and Cullinane (2006) all apply various single-measure DEA models to study the port performance of different countries.

However, the current literature still treats these sub-technologies as a "black box" with no information about what happens inside container terminals. If the performance measurement model enables a description of the sub-activities: quayside and landside operations, it will provide extra management information that the traditional DEA models cannot address. Therefore, measuring quayside operations efficiency (QTE), landside operations efficiency (LTE), and the overall efficiency (TE) in a unified multi-activity DEA analysis model provides for a more realistic and reasonable view of container terminal systems.

With these objectives, the rest of this paper is structured as follows. The following section describes the framework for the estimate of a container terminal system and is followed by the proposed methodology for assessing QTE, LTE and TE for container terminals in a unified framework. The sample data is then described, the

three measures are estimated, and the results are discussed.

FRAMEWORK OF CONTAINER TERMINALS PERFORMANCE ESTIMATE

Container terminals can be described as open systems of material flow with two main activities. These activities are the quayside operations dealing with loading and unloading of ships, and the landside operations where containers are stored in stacks in the yard area and then loaded and unloaded onto and off of trucks and trains.

Specific cranes are used in terminal operations. The quay crane (QC) is used for loading and unloading ships in quayside operations. The stack crane (SC) is applied to stacks in landside operations. Container trailer (TRL) is a shared resource employed for the horizontal transport between both quayside and landside. Container throughput (THRT) is the most important output for container terminals system to reflect its handling capacity. Both quayside and landside operations contribute to the value-added services on container throughput.

The analytical framework portrayed in Figure 1 describes two vital parts of container terminals' operations, the specific inputs (QL, QC and SC), the shared input (TRL) and shared product produced (THRT) among these activities.

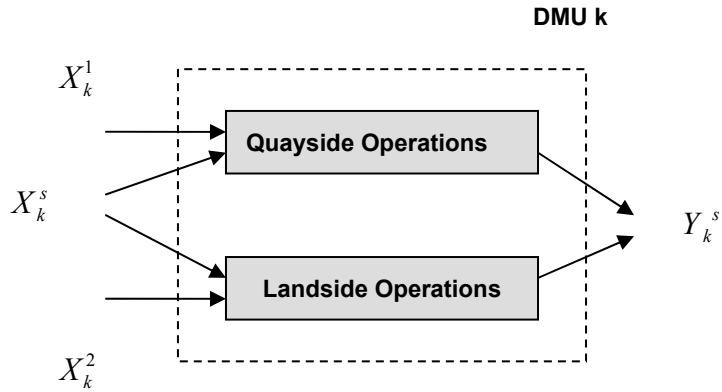

Figure 1. Analytical framework in multi-activity DEA model for port.

METHODOLOGY

First developed by Charnes et al. (1978), DEA is a non-parametric programming technique used to evaluate the relative efficiency with which a DMU transforms inputs into outputs. In most real applications, a single measure of production efficiency provided by DEA is an adequate and useful means for comparing performances and identifying best practices.

Assume that there is a set of container terminals $k = \{1, 2...n\}$. Each uses the input quantities $X_k^{\ 1}, X_k^{\ 2}, X_k^{\ s}$ to generate final output $Y_k^{\ s}$ shown in Figure 1. The input, output, and other variables used in the model are shown in Tables 1 and 2.

Table 1. Input and output used in the model.

Input		Output	
QL	**Quay length (m)**	**THRT**	Total throughput (1000 TEU)
QC	**No. of quay cranes**		
SC	**No. of stack cranes**		
TRL	No. of container trailers		

Table 2. Variables used in the model.

Variables (DMU k)	
$X_k^{\ 1}$	Dedicated input for quayside operations, including QL and QC
$X_k^{\ 2}$	Dedicated input for landside operations, including SC
$X_k^{\ s}$	Shard input for both activities, including TRL
$Y_k^{\ s}$	The sole shared output for both activities, including THRT
α_1	portion of working time per X_k^s distributed between two activities with a range [0,1]
α_2	portion of processing time per $Y_k^{\ s}$ distributed between two activities with a range [0,1]
μ^{s1}, μ^{s2}	multiplier vectors of two activities respectively for Y_k^s, the created value ratio by per Y_k^s to two activities
v^{s1}, v^{s2}	multiplier vectors of two activities respectively for $X_k^{\ s}$, the created cost ratio by per $X_k^{\ s}$ to two activities
v^1, v^2	multiplier vectors for $X_k^{\ 1}$ and $X_k^{\ 2}$ respectively the created cost ratio by per $X_k^{\ 1}$ and $X_k^{\ 2}$ respectively

To maximize the overall efficiency, consider the following multi-activity DEA model of container terminals portrayed in Figure1 for some DMU *o*:

$$\max \quad e_o^a$$

$$\text{s.t.} \quad TE = e_k^a = \frac{\mu^{s1}(\alpha_2 Y_k^s) + \mu^{s2}[(1-\alpha_2)Y_k^s]}{v^1 X_k^1 + v^{s1}(\alpha_1 X_k^s) + v^2 X_k^2 + v^{s2}[(1-\alpha_1)X_k^s]} \le 1, \qquad \forall k$$

$$QTE = e_k^1 = \frac{\mu^{s1}(\alpha_2 Y_k^s)}{v^1 X_k^1 + v^{s1}(\alpha_1 X_k^s)} \le 1, \qquad \forall k$$

$$LTE = e_k^2 = \frac{\mu^{s2}[(1-\alpha_2)Y_k^s]}{v^2 X_k^2 + v^{s2}[(1-\alpha_1)X_k^s]} \le 1, \qquad \forall k \qquad (1)$$

$$0 \le \alpha_i \le 1, \qquad \forall i$$

$$(\mu^{s1}, \mu^{s2}) \in S_1, \ (v^1, v^{s1}, v^{s2}, v^2) \in S_2$$

$$\mu_j^{\ s1}, \mu_j^{\ s2}, v_j^{\ 1}, v_j^{\ 2}, v_j^{\ s1}, v_j^{\ s2} \ge \delta, \qquad \forall j$$

The sets S_1 and S_2 are assurance regions defined by any restrictions imposed on the multipliers according to their respective measurement meanings. The multi-activity DEA model (1) can be transformed to the alternative form (Cook et al 2000):

$$
\begin{aligned}
&\max\ e_o^a = \mu^{s1}(\alpha_2 Y_o^s) + \mu^{s2}[(1-\alpha_2)Y_o^s] \\
&\text{s.t.}\ \ v^1 X_o^1 + v^{s1}(\alpha_1 X_o^s) + v^{s2}[(1-\alpha_1)X_o^s] + v^2 X_o^2 = 1 \\
&\quad \mu^{s1}(\alpha_2 Y_k^s) + \mu^{s2}[(1-\alpha_2)Y_k^s] - v^1 X_k^1 - v^{s1}(\alpha_1 X_k^s) - v^{s2}[(1-\alpha_1)X_k^s] - v^2 X_k^2 \le 0, \forall k \\
&\quad \mu^{s1}(\alpha_2 Y_k^s) - v^1 X_k^1 - v^{s1}(\alpha_1 X_k^s) \le 0, \qquad \forall k \\
&\quad \mu^{s2}[(1-\alpha_2)Y_k^s] - v^{s2}[(1-\alpha_1)X_k^s] - v^2 X_k^2 \le 0, \qquad \forall k \\
&\quad 0 \le \alpha_i \le 1, \qquad \forall i \\
&\quad (\mu^{s1}, \mu^{s2}) \in S_1, \quad (v^1, v^{s1}, v^{s2}, v^2) \in S_2 \\
&\quad \mu_j^{s1}, \mu_j^{s2}, v_j^1, v_j^2, v_j^{s1}, v_j^{s2} \ge \delta \qquad \forall j
\end{aligned}
\tag{2}
$$

EMPIRICAL STUDY

Data. The required data are mainly taken from *Yearbook of Ports in China* (2006) with a size of 20. Important statistics related to the sample are summarized in Table 3.

For solution purposes, we have restricted α_1 and α_2 to lie in the range 1/3–2/3. For shared input and output we take $2 \le \mu^{s1} : \mu^{s2} \le 3$ and $0.5 \le v^{s1} : v^{s2} \le 2$ by the realistic conditions of container terminals.

Table 3. Descriptive statistics for the input and output.

	Input			**Output**	
	QL	**QC**	**SC**	**TRL**	THRT
Max	**3,418**	**38**	**154**	**670**	8,295.657
Min	**231**	**1**	**2**	**4**	19.147
Mean	**1,137.37**	**10.78**	**29.86**	**60.67**	1,464.322
S.D.	**894.16**	**10.28**	**33.71**	**100.62**	1,809.968
Count	49	49	49	49	49

Results. The results for TE, QTE, LTE, and the distribution of the shared input and output are shown in Table 4. The average QTE is higher than the average LTE (0.630 vs. 0.588).

Table 4. Performance comparison and the distribution of shared inputs and output.

Container terminal	TE	QTE	LTE	α_1	α_2
1. Dalian Dagang	**0.618**	**0.637**	**0.525**	**0.373**	0.667
2. Dalian Port	**0.069**	**0.067**	**0.071**	**0.333**	0.333
3. Dalian Container Terminals	**0.852**	**0.865**	**0.776**	**0.333**	0.667
4. Fuzhou Qingzhou	**0.846**	**0.848**	**0.837**	**0.366**	0.667
5. Guangzhou Nansha	**0.741**	**0.766**	**0.618**	**0.667**	0.667
6. Guangzhou	**0.665**	**0.700**	**0.511**	**0.333**	0.667
7. Haikou	**0.945**	**1.000**	**0.712**	**0.667**	0.667
8. Jinzhou New Age	**0.299**	**0.281**	**0.320**	**0.333**	0.333
9. Lianyungang New-Oriental	**1.000**	**1.000**	**1.000**	**0.472**	0.333
10. Longkou Haishen	**0.243**	**0.188**	**0.344**	**0.333**	0.333
11. Port of Nanjing Longtan	**0.563**	**0.521**	**0.613**	**0.333**	0.333
12. Nantong Port	**0.437**	**0.374**	**0.525**	**0.333**	0.333
13. Ningbo Port Beilun	**0.964**	**1.000**	**0.795**	**0.667**	0.667
14. Port of Ningbo Daxie	**0.056**	**0.046**	**0.073**	**0.667**	0.333
15. Daxie Ningbo China Merchants	**0.259**	**0.264**	**0.230**	**0.667**	0.667
16. Ningbo Port Beilun 2nd	**0.964**	**1.000**	**0.791**	**0.333**	0.667
17. Ningbo Port-Gangji	**0.488**	**0.514**	**0.374**	**0.667**	0.667
18. Ningbo Port- Gangwu	**0.589**	**0.536**	**0.652**	**0.667**	0.333
19. Qingdao Port-Qianwan	**1.000**	**1.000**	**1.000**	**0.333**	0.667
20. Qingdao Port-Yuangang	**0.995**	**0.990**	**1.000**	**0.333**	0.333
Average	*0.630*	*0.630*	*0.588*	*0.461*	*0.517*

Table 4 reveals that some container terminals, such as Lianyungang New-Oriental (no. 9) and Qingdao Port-Qianwan (no. 19) are technically efficient both in quayside and landside production terms. Some others appear to have relatively greater difference between QTE and LTE. In such cases, the higher QTE or LTE does not imply a higher corresponding TE.

The average share of container trailers assigned to quayside is lower than that assigned to landside (0. 461 vs. 0.539). As for throughput, the average share of TEUs assigned to quayside is higher than that of landside (0.517 vs. 0.463). However, their distributions among different container terminals differ greatly.

Management implications. Based on the results, we construct the TE matrix in which the horizontal axis represents QTE and the vertical axis LTE, and where each container terminal is located. We can divide the matrix into four sub-matrixes based on the average scores as shown in Figure 2.

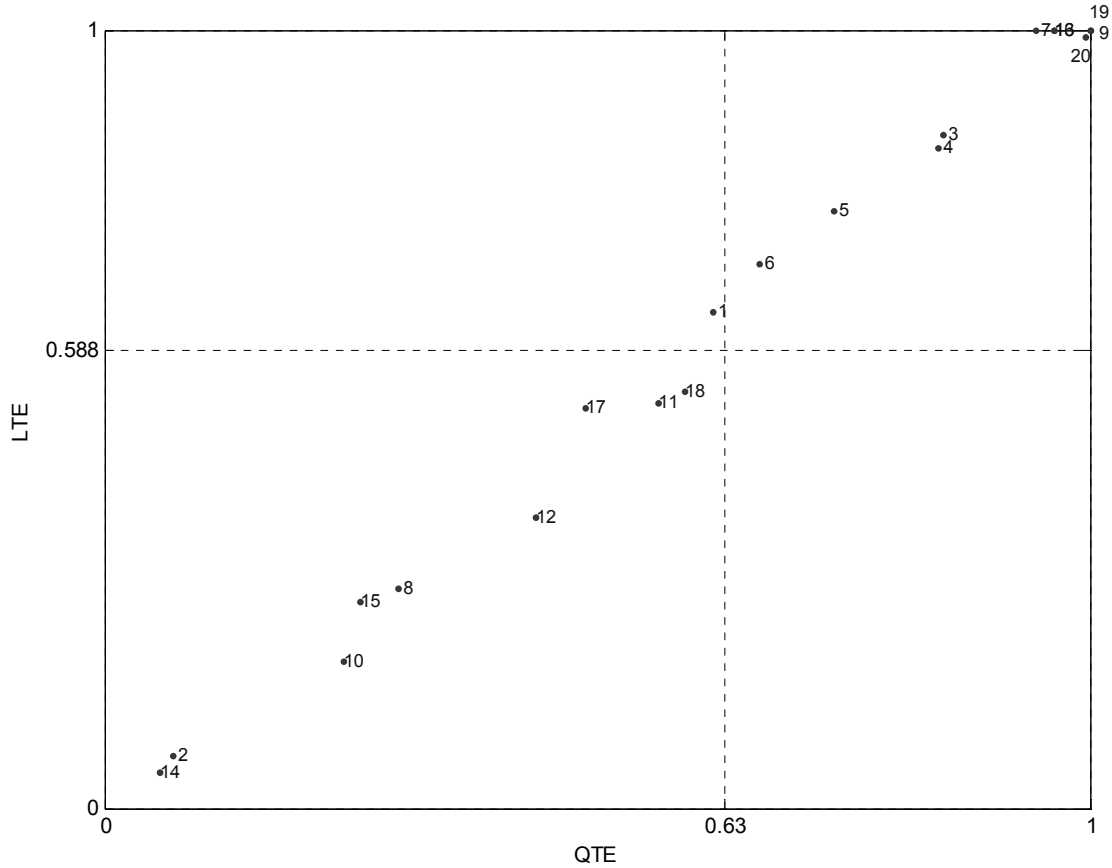

Figure 2. The efficiency distribution of quayside and landside operations.

Those container terminals located in the second quadrant (for instance, Dalian Dagang (no.1) represents lower QTE but higher LTE. A management implication for these container terminals is that they need to first improve quayside operations before their landside operations. Those terminals located in the third quadrant should consider improving both operations. There are no terminals located in the fourth quadrant that exhibit higher QTE but lower LTE.

CONCLUSION

This paper has proposed a multi-activity DEA model different from traditional DEA models in evaluating multiple activities in the container terminals simultaneously. Using the multi-activity model proposed in this paper, one can further identify the sources of poor performance and gain a proper understanding for improving a ports performance in quayside or landside operations.

In this study, we made some strong assumption on the constraints of multipliers imposed on the input and output due to the lack of available data from the annual yearbook. If the data difficulties are to be overcome in future research, a more

rational approach will necessitate construction of improved models of container terminals.

REFERENCES

Chinese Ministry of Communications, *Yearbook of Ports in China* (2006).

Charnes, A., Cooper, W.W., Rhodes, E. (1978). "Measuring the efficiency of decision making units." *European Journal of Operational Research* 2, 429–444.

Cook, W.D., Hababou, M. and Tuenter H. (2000). "Multicomponent efficiency measurement and shared inputs in data envelopment analysis: An application to sales and service performance in bank branches." *Journal of Productivity Analysis* 14, 209-24.

Cullinane. K. P. B. (2006). "The technical efficiency of container ports: Comparing data envelopment analysis and stochastic frontier analysis." *Transportation Research A: Policy and Practice* 40(2006) 354–374.

Tongzon, J.L. (2001). "Efficiency measurement of selected Australian and other international ports using data envelopment analysis." *Transportation Research A: Policy and Practice* 35(2), 113–128.

Valentine, V.F., Gray, R. (2001). "The measurement of port efficiency using data envelopment analysis." *Proceedings of the 9th World Conference on Transport Research, 22–27 July, Seoul, South Korea*.

Expressway Operation Financial Benefit Evaluation under Uncertainty

Liye Zhang[1] and Chang Li[2]

[1]School of Traffic and Transportation Engineering, Changsha University of Science & Technology, No.45, Chiling Road, Changsha, China; PH (86) 13874957585; email: chinazhangly@126.com
[2]Changsha Planning Administrative Bureau, Changsha, China; email: lichang_cs@126.com

ABSTRACT

Expressway operation financial benefit evaluation is the basis of expressway operation decision-making. There are many uncertain factors in the expressway operation process. In this paper, the main factors influencing the operation financial benefit are analyzed. An expressway operation financial benefit evaluation model based on Monte-Carlo simulation method is proposed. The evaluation model is applied to an expressway operation financial benefit evaluation and the simulation is carried out with SciPy, a Python science library. The results show that the proposed evaluation model is practical and effective.

INTRODUCTION

The expressway is a type of capital intensive project, the demand for which increases with economic development. In many countries where investment in expressways exceeds the capability of the government, private investors are permitted to participate in expressway building. In developing countries, private funds become the main sources of expressway construction investment (Walker 1995). The duration for expressway operation is very long and the operation benefit can be influenced by many factors, such as transportation policy, land use, currency exchange rate, etc. At present, the main methods for financial benefit evaluation assume a deterministic environment and most uncertain factors are not considered (Froud 2003; Al-Bahar 1990). Most researchers undergo these kinds of studies before the expressway construction phase, so few studies are undertaken during the expressway operation period (Chuan-de 2006; Subprasom 2001). Expressway operation financial benefit evaluation is the basis for scientific operation decision-making. Therefore, it is of great importance to research expressway operation financial benefit evaluation method under uncertainty.

OPERATION FINANCIAL BENEFIT AND UNCERTAINTY ANALYSIS

Calculation **method** of **financial benefit** under **uncertainty.** When private

capital has been involved in expressway construction, the expressway has obvious commodity characteristics. Because maximizing profit is one of the most important goals for an expressway operation company, managers pay more and more attention on financial benefit. Expressway operation financial benefit evaluation is to evaluate the financial benefit during the operating period and it is of great help for the companies to promote the decision-making level and to reduce the operation risk.

There are many uncertain factors in expressway operation, but the classic financial evaluation methods do not reflect this feature. The evaluation result under uncertainty must at least contain two kinds of information, one is the value which indicates the level and the other is the possibility of this level.

Uncertainty **analysis.** The factors that influence the expressway operation financial benefit include internal and external factors. Internal factors are factors that can be controlled directly by the company, such as operation cost, management level, and operation efficiency. External factors are harder to control, such as traffic policy, currency exchange rate, and regional road network planning.

Traffic demand is one of the main uncertain factors in expressway operation. At present, traffic volume forecast methods are made without consideration of uncertainty. In fact, most of the factors related with traffic volume are uncertain, such as social and economic development, population growth, and so on (Chen et al 2003; Feng and Chen 2003). According to research by Skamris and Flyvbjerg, travel demand forecasts often deviate at least 20% to 60% when compared with real world data (Skamris and Flyvbjerg 1996). According to the mechanism of traffic volume, there are uncertainties in the process of traffic demand production, distribution, assignment, and the modal split.

There are many factors that impact traffic demand. Firstly, traffic demand is impacted by the toll rate. Expressway toll is the main income of an expressway operation company and for some Chinese expressway operation companies, toll is their only income. The uncertainty of travel demand is mainly due to social and economical progress influenced by the international environment, the country's policy, and so on. There are also many other factors that can influence travel demand, such as road network structure, land use patterns, traveler's driving behavior, etc. Many studies show that traffic demand is determined by the potential demand and the travel time (Subprason 2004).

Expressway toll rate is a prime uncertain factor. The toll rate will influence the financial income and the profit of the project directly. At present, there is no uniform standard of the toll rate and every road has its own standard.

Another uncertain factor in expressway operation is interest rate. Interest rate is one of the most important parameters of the project financial benefit evaluation

and it is also the basis of the basic discount rate calculation. One main factor that influences the interest rate is social average profitability.

The fourth uncertain factor in expressway operation is exchange rate. Usually, the financial evaluation indexes are calculated without considering inflation and assuming the internal value of the currency remains stable. The profit index of the project using foreign funds may change if the exchange rate varies during the operation period (Chandra and Chang 2000). There are many factors that determine exchange rate. During a given period, the main factor is international payments, but over a long period, the exchange rate is determined by the economy's development and the growth rate of the currency.

EVALUATION METHOD BASED ON MONTE-CARLO SIMULATION METHOD

Evaluation index calculation under uncertainty. Financial benefit evaluation indexes that do not take into account uncertainty include FIRR, FBCR, FIRR and FRP. These kinds of indexes can not reflect uncertainties of the real world. From these indexes, we can know their value, but we can not learn their probability. Monte-Carlo is an efficient simulation method whereby we can discern the real situation of expressway operation.

Principle of Monte-Carlo **simulation method.** Monte-Carlo simulation is a method for resolving mathematical and physics problems. Its mechanism is as follows. Once the probability model is confirmed to have common features with the target problem, a relationship between the two of them is established on the basis of these common features (such as the mean of the random parameter, variance, and so on). A random simulation analysis or sampling method is applied to the model and the statistic and estimation values of the results are considered as the approximate solution of the mathematical computing problem.

Random numbers are generated according to a certain distribution that is the same as the distribution of the random parameter related to the problem. Experiments are carried out using this data and then statistical analysis is applied on the forecast random parameters. The statistic and estimation values are consider as the statistic eigenvalues of the random parameter.

EVALUATION METHOD

Selection of main factors and determination of distribution functions. First, select the main factors from all of the uncertain factors. Then, determine the distribution functions that may be normal, triangular, uniform, lognormal or others. The possibility distribution function can be determined empirically or fitted by the survey data.

Long-term forecasted data such as traffic volume is considered as a random variable with a normal distribution function. The forecasted result is considered as the most probable event; the shorter the forecasting period, the more precise the forecasted result, and the smaller the standard deviation (see Figure 1). For example, the distribution function of traffic volume is considered as $N(\mu,\sigma^2)$, where μ is the traffic volume forecasted, $\sigma=\mu\times(at+b)\%, t=1,2,\cdots$ a , b are coefficients.

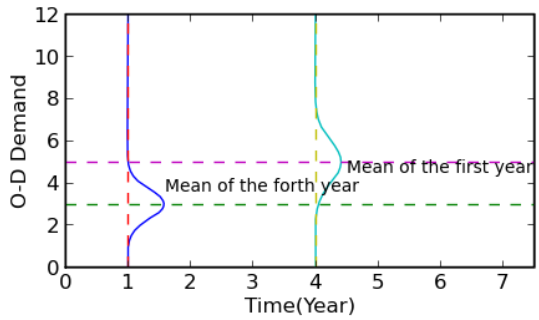

Figure 1. Stochastic O-D demand.

Financial benefit evaluation index calculation. Generate the numbers according to the possibility distribution function of the variable parameter as the input data. Calculate the evaluation index to get n samples.

Result analysis. Provide the distribution an assumption according to the sample and test the distribution. Then, estimate the parameters of the distribution functions that are to be tested. After this, the expressway operation financial benefit can be analyzed using these distribution functions. The index risk and index reliability are calculated as follow:

$$FD=\frac{VAX-(EX-X_0)}{EX} \tag{1}$$

Where VAX is standard deviation. EX is the mean. X_0 is the value of a certain parameter. The reliability is:

$$p=\{x\le x_0\}=\int_{-\infty}^{x_0} f(x)d_x \tag{2}$$

, Where x_0 is a preset value and p is the reliability.

CASE STUDY

Project **introduction.** Tan-Shao expressway is located in Hunan province south of China. Ten-Shao is a segment of the national ShangHai-RuiLi expressway and is a part of the national highway network. The 218 kilometer long expressway

goes through XiangTan, LouDi, and ShaoYang, including 10 counties. The financial indexes calculated during the feasibility study stage were as follows: FIRR=9.96%, FNPV=95321million Yuan, FBCR=1.37 and FRP=16 year.

Financial benefit evaluation under uncertainty. The distribution functions of the random variables of the uncertain factors were determined by the data from the experts and the expressway operation data between 2003 and 2006 offered by Tang-Shao Expressway Operation Company. The simulation model is carried out with Python, an open-source programming language. With the help of the statistic model from the SciPy library of scientific tools, the Monte-Carlo simulation can be implemented easily. The output is plot with the Python library matplotlib. Indexes such as FNPV, FIRR, FBCR and FRP are calculated in the experiment. The simulation is made 1000 times and the statical result is shown as Figure 2.

According to the statistical results (Figure 2), the probability that the FNPV can reach 95321 is 55% and the probability that the FNPV is between 24000 and 10000 is 92.5%. The operating state of the expressway is therefore good. The project is profitable and quite capable of resisting risks (Table 1). Depending on the results from the Monte-Carlo simulation model, a decision-maker can make a more effective decision according to their risk-bearing capability than with an evaluation that does not consider uncertainty.

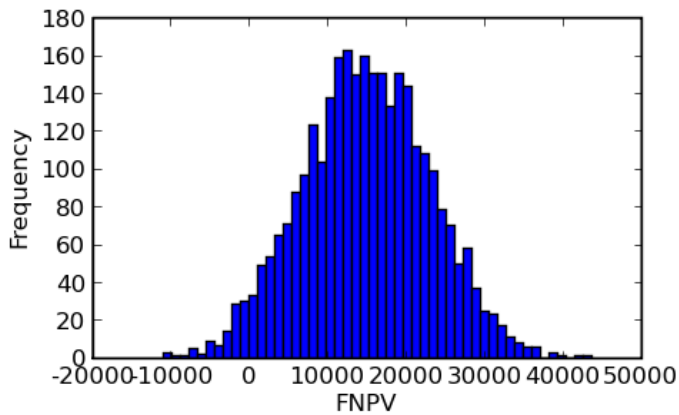

Figure2. Stochastic NPVR.

Table 1. Financial benefit evaluation indexes.

	value	stability	risk	mean
FNPV	95321	0.551	0.73	5061
FBCR	1.37	0.45	0.82	1.16
FIRR	9.96%	0.553	0.73	7.4%
FRP	16	0.68	0.63	19

CONCLUSION AND RECOMMENDATIONS FOR FUTURE RESEARCH

The main factors that influence the operation financial benefit are analyzed and the distribution functions of the uncertain factors are confirmed. An evaluation model based on the Monte-Carlo simulation method is proposed and the reliability index and risk index are also proposed in the evaluation process. According to the result of the application of the evaluation model on Tan-Shao expressway operation financial benefit evaluation, the proposed model is deemed practical. Using this evaluation model, both values and probabilities can be obtained from the expressway operation evaluation indexes. With this evaluation model, the state of the expressway operation can be estimated with precision, thus supporting the operation decision-making process.

REFERENCES

Al-Bahar, J. (1990). "Systematic Risk Management Approach for Construction Projects." Journal *of Construction Engineering and Management,* 116(3), 533–546.

Chen, A., Subprasom, K., and Ji, Z. (2003). "Mean-variance Model for the Build-operate-transfer Scheme under Demand Uncertainty." *Transportation Research Record*, 1857, 93–101.

Chandra, F. and Chang, L.M. (2000)."The Impact of Foreign Currency on BOT Projects." *Proceedings of the 6th Construction Progress*, Florida, 878–888.

Chuan-de, C. and Ming-yuan, Z. (2006). "Investment Decision for Highway Project Based on Risk Analysis." *China Journal of Highway and Transport*, 19(1), 99–103.

Feng, W. and Chen, X.H. (2003). "Risk Assessment in Freeway Volume Forecast." Journal *of Changàn University:Natural Science Edition* , 23(6), 90–93.

Froud, J. (2003). "The Private Finance initiative: Risk, Uncertainty and the state, Accounting." *Organizations and Society*, 28(6),567–589.

Skamris, M. K. and Flyvbjerg, B. (1996). "Accuracy of Traffic Forecasts and Cost Estimates on Large Transportation Projects." *Transportation Research Record*, 1518, 65–69.

Subprason, K. (2004). *Muti-party and Multi-objective Network Design Analysis for the Build-operate-transfer Scheme*, Ph.D. dissertation, Utah State University, Utah.

Subprasom, K. and Chootinan, P. (2001). "Assessing Financial Feasibility of Build-operate-transfer Project under Uncertain Demand." *Transportation Research Record,* 1771, 124-131.

Walker, C. and Smith, A. (1995). *Privatized Infrastructure: the Build Operate Transfer Approach,* Thomas Telford, London.

Research on the Differences in Regional Economy and Transportation among the Three Regions in China

Sun Kechao,[1] Zhang Qingnian[2] and Zhang Xinjie[3]

[1]School of Transportation, Wuhan University of Technology, P.O. Box Y17, Wuhan, 430063; PH (86) 13607166236; email:sunkechao2004@163.com
[2]School of Transportation, Wuhan University of Technology, P.O. Box Y17, Wuhan, 430063; PH (86) 13308633268; FAX (86) 02786561629; email: zqnwhut@163.com
[3]School of Transportation, Wuhan University of Technology, P.O. Box Y17, Wuhan, 430063; PH (86) 13476137801; email: jessice864@163.com

ABSTRACT

There are distinct differences among the regional economic and transportation aspects of the three regions of China (eastern, middle and western). This paper investigates differences between the indexes of GDP, GDP per capita, freight turnover, and the Average Density of Transport Line (ADTL) from 1996 to 2007. Indexes in eastern China were found to be significantly higher than those in the middle and west. Moreover, the coefficients of differences in ADTL were estimated among the three regions, and their developing trends were explored by employing the R/S analysis method within fractal theory. The result indicates that the differences in transportation development would decrease from 2008 to 2019 among the three economical regions, but would increase gradually from 2015 to 2019.

INTRODUCTION

As China reforms and opens up, the differences in regional economic and transportation develop rapidly, especially among the three regions in China (eastern, middle and western). In recent years, the differences between the three regions in China have attracted wide attention both at home and abroad.

In this paper, the eastern region includes 11 provinces (municipalities and districts): Beijing, Tianjin, Liaoning, Hebei, Shandong, Shanghai, Jiangsu, Zhejiang, Fujian, Guangdong and Hainan. The middle region comprises 8 provinces including Heilongjiang, Jilin, Shanxi, Anhui, Jiangxi, Henan, Hubei, and Hunan. The western region comprises 12 provinces including Inner Mongolia, Guangxi, Chongqing, Sichuan, Guizhou, Yunnan, Tibet, Shaanxi, Gansu, Qinghai, Ningxia, and Xinjiang.

Utilizing data from 1996 to 2007, this paper investigates the differences in the indexes of GDP, GDP per person, freight turnover, and the Average Density of Transport Line (ADTL) by. The coefficients of differences in ADTL are estimated among the three regions, and their developing trends further explored by employing the R/S analysis method within Fractal Theory.

DISCUSSION ON DIFFERENCES IN CHINA'S REGIONAL ECONOM Y AND TRANSPORTATION AMONG THE THREE REGIONS

This section investigates the differences in the indexes of GDP, GDP per capita, freight turnover and ADTL from 1996 to 2007. The trends of indexes can be seen in the figures below:

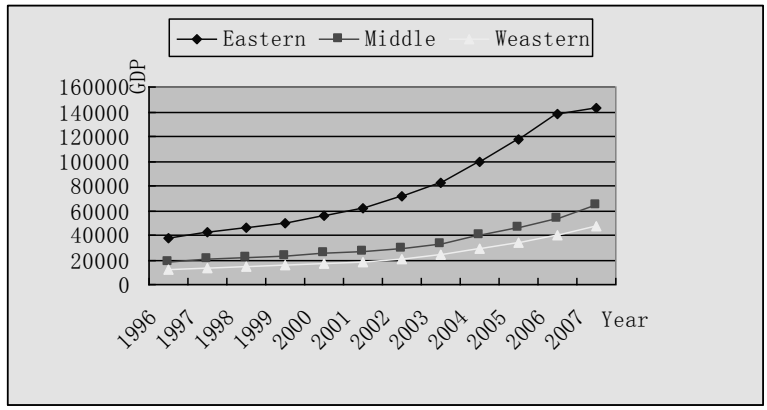

Figure 1. GDP among the three regions from 1996 to 2007 .

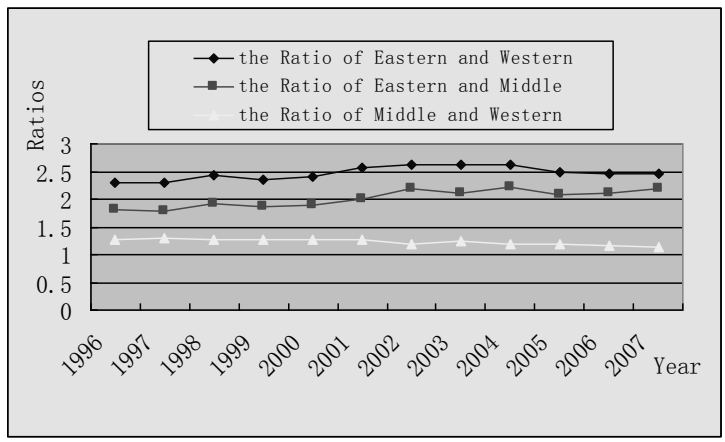

Figure 2. Ratio of GDP per capita among the three regions from 1996 to 2007 .

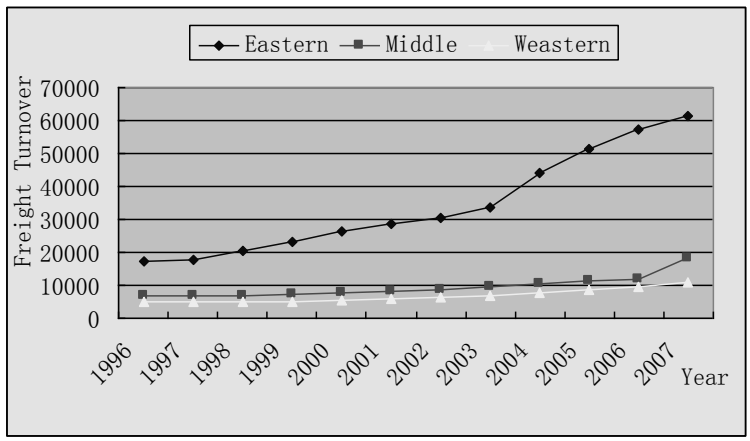

Figure 3 . Freight turnover among the three regions from 1996 to 2007.

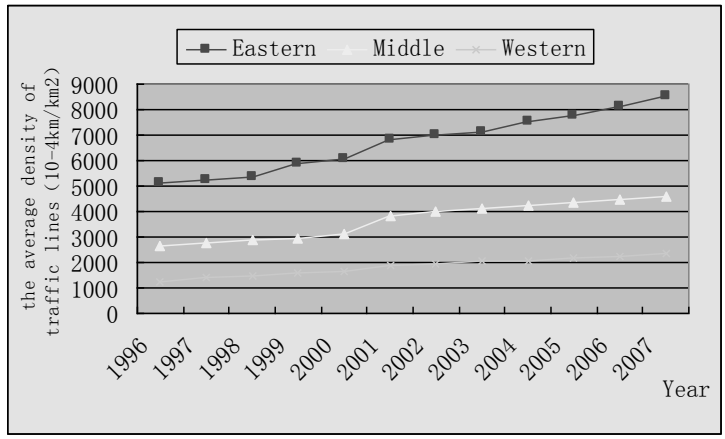

Figure 4. ADTL among the three regi ons from 1996 to 2007.

As shown in Figures 1, 3 and 4, the indexes of GDP, GDP per capita, and ADTL in the eastern region are significantly higher than those in the middle and western regions. The trend is similar between the middle and the western regions. As shown in Figure 2, there are significant changes between the ratios of eastern and western as well as eastern and middle, while it changes little between the ratio of middle and western.

THE ORIES

A fractal is a mathematical abstraction of an irregular shape, the basic characteristic of it being neither smooth nor continuous and the constituent parts of which, when broken down, are self-similar. The birth of fractal theory came in 1975 when Benoît Mandelbrot, a French-American mathematician, published Fractal: Form, Chance and Dimension. Using R/S analysis (Rescaled Range Analysis) in fractal theory, we can study a fractal's characteristics, identify the change laws, and predict its trend. The Hurst Exponent (H) is a statistic named after Harold Hurst, a British hydrologist who did long term research on the water level of Nile River. While inspecting a pre-existing time-series $B(t)$ (Cv in this paper, Table 1), Hurst found that R/S can be described in the following empirical formula:

$$R/S = (a\tau)^H$$

Where: R is the range of the cumulative deviation, S is standard deviation, τ is the observed frequency, and a is a constant (we make $a = 0.5$ in this paper). According to statistics, when $H \neq 0.5$, the observation is not independent and each

observation has its initial case's memory. This memory will continue to exist ad infinitum. The impact of recent events is greater than long-term, and the impact's residue will persist indefinitely. Theoretically it is proven by the correlation function as follows:

$$C(t) = \frac{[-\Delta B(-t)\Delta B(t)]}{[\Delta B(t)^2]} = 2^{2H-1} - 1$$

Then, we can obtain H using the Least Square Method in the double logarithmic coordinates $(\ln(a\tau), \ln R/S)$. H has three types.

1. When $H = 0.5$, $C(t) = 0$, the last increment $\Delta B(-t)$ has nothing to do with the future increments $\Delta B(t)$, and this means the sequence is random.
2. When $H < 0.5$, $C(t) < 0$, there is a negative correlation of time series, that is, the last increment $\Delta B(-t)$ has a negative correlation with the future increments $B(t)$. This feature relies on the closeness of H to 0.
3. When $H > 0.5$, $C(t) > 0$, it shows that $B(t)$ and $\Delta B(-t)$ have a positive correlation. If the last increment is up (below), then the future increment will continue to be up (below). This feature relies on the closeness of H to 1.

Compared with the traditional forecasting methods (i.e., linear regression, gray theory, and neural networks, etc.), R/S analysis starts from the historical data and predicts the trends in the same environment. The environment of the Global Financial Crises which burst in 2008 is similar to that of the Southeast Asian's Financial Storm in 1997. In addition, China takes the increasing input of the transport infrastructure as the economic stimulus program. So in similar situation, using R/S analysis is more appropriate. In general, while the accuracy of forecasts falls rapidly when using traditional forecasting methods, R/S analysis is less influenced by time.

EMPIRICAL STUDIES

Inputs of the model. This section analyzes the differences of regional economic and transportation among the three regions from 1996 to 2007. Using R/S analysis, this section calculates the coefficient of variation (Cv) of ADTL to perform further research on the differences of regional transportation. The difference coefficient of ADTL is calculated as follows:

$$Cv = \frac{S}{\bar{x}} = \bar{x}\sqrt{\sum_{i=1}^{n}\left(x_i - \bar{x}\right)/\left(n-1\right)} = \sqrt{\frac{\sum_{i=1}^{n}\left(k_i - 1\right)^2}{n-1}} \quad , \quad \text{where} \left(k_i = \frac{x_i}{\bar{x}}\right) \quad (i=1,2,\cdots,n)$$

Notes: S expresses the sample standard deviation; x_i, $\bar{x}$ express ADTL in the area i and sample mean respectively; the formula indicates that the greater the Cv values, the more extent of the disparities is, and vice versa. The results are shown in Table 1.

Table 1. Coefficient of variation of ADTL among the three regions .

Year	1996	1997	1998	1999	2000	2001	2002	2003	2004	2005	2006	2007
Cv	0.654	0.612	0.606	0.628	0.623	0.597	0.585	0.578	0.596	0.590	0.595	0.605

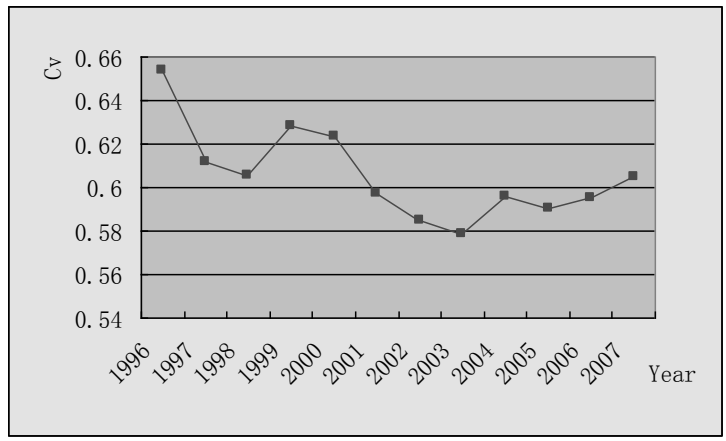

Figure 5. Coefficient of variat ion of ADTL among the three regions .

Results. Based on the R/S analysis, input the time-series $B(t)$ (Cv in this paper, Table 1), the results showing the Hurst exponent are as follows: (see Table 2)

Table 2.R/S analysis results: Hurst exponent .

	1996	1997	1998	1999	2000	2001	2002	2003	2004
1999	0.5883								
2000	0.5852	0.8537							
2001	0.8032	0.5971	0.5995						
2002	0.7630	0.6307	0.6583	0.7018					
2003	0.6903	0.6217	0.6404	0.7106	0.7499				
2004	0.4104	0.7669	0.861	0.6457	0.6471	0.8132			
2005	0.4207	0.7094	0.7713	0.6379	0.6338	0.7546	0.8531		
2006	0.4358	0.7397	0.7979	0.7245	0.7519	0.5942	0.6049	0.5441	
2007	0.5388	0.7672	0.8234	0.7979	0.8061	0.6683	0.4167	0.7188	0.7554

From Table 2, we can see, H (1996-2007) = 0.5388 > 0.5, C (t) > 0. Therefore, in the years 2008-2019, the differences in regional development will have the same development trend as in the years 1996-2007. Since H is closer to 0.5, regional differences will be reduced overall, but relatively have strong randomness. H (1996-1999) = 0.5883 > 0.5, C (t) > 0, and thus the difference between 2008 and 2011 will have the same trend with the year 1996-1999. H (1999-2003) =0.7106 > 0.5, C (t) > 0, and thus the regional differences will continue to decrease in 2011-2015. H (2003-2007) = 0.7188 > 0.5, C (t) > 0: because the regional differences between the three regions significantly expanded from 2003-2007, so regional differences will continue to expand from 2015-2019.

CONCLUSION S

From a theoretical perspective, the following conclusions are reached. Firstly, according to the indicators about the indexes of GDP, GDP per capita, the freight turnover and ADTL from 1996 to 2007, the indexes in the eastern region are significantly higher than those in the western and middle regions (especially GDP and freight turnover). Due to the open-door policy in coastal cities, the economy of the eastern region has developed faster, and so the differences of the three regions are more obvious. Secondly, the R/S analysis indicates that the differences in transportation development will decrease from 2008 to 2019. From 2008 to 2011, they will decrease, but still have the potential to expand. Between 2015 and 2019, the regional differences will continue to expand. The results of this paper can provide a theoretical basis to the traffic department on planning and decision-making.

BIBLIOGRAPHY

Cheng, Q.C. (2007). “Analysis on Spatial Differentiation of Land Transport Density and Influential Human Factors in China.” Journal of Subtropical Resources and Environment. 2(4), 60-68.

Chinese Bureau of Statistics. http://www.stats.gov.cn.

Li, C.F. (2003). “Rescaled-range and power spectrum analyses on well-logging data,” Geophysical Journal International . 153(1), 201-212.

Jacquin, A.E. (1992). “Image coding based on a fractal theory of iterated contractive image transformations.” IEEE Trans Image Process. 1(1), 18-30.

Li, Q. (2006), “Research on the differences in regional economy and R/S analysis.” Southeast Academic Research.

Zhang, X.S., Chen, H.N., and Yang, G.Q. (2008). “The Evolution and Genesis of Income Gap Among China's Three Major Economic Zones.” Shandong Social Sciences.

Evaluation and optimization of public transport subsidies for alternative energy

Yuan Fang[1], Xiqun Chen[2], and Xinmiao Yang[3]

[1]Institute of Transportation Engineering, Department of Civil Engineering, Tsinghua University, 100084, Beijing, PH (8610) 62792260; PH (8610) 62792252; email:fangy03@mails.tsinghua.edu.cn
[2]Institute of Transportation Engineering, Department of Civil Engineering, Tsinghua University, 100084, Beijing, PH (8610) 62792260; PH (8610) 62792252; email:chenxq04@mails.tsinghua.edu.cn
[3]Institute of Transportation Engineering, Department of Civil Engineering, Tsinghua University, 100084, Beijing, PH (8610) 2792260; PH (8610) 62792252; email:xmyang@tsinghua.edu.cn

ABSTRACT

This paper proposes a nonlinear integer optimization model which takes into account both economic and environmental effects in order to evaluate the benefits of government subsidies for alternative energy public transit vehicles. When an interim assessment of a five-year transit fleet conversion plan requires evaluation due to budget limitations, this model can inform an optimal choice between economy and environmental protection to achieve a win-win situation for both government and transit agencies. The government achieves pollution reduction and maximizes social benefits while the budget stimulates the innovation of transit agencies. This paper uses data from the Beijing Public Transportation Group to employ the proposed model to analyze the operational and environmental costs of replacing an existing bus fleet with new hybrid electric buses over several years. The results show that altering the preference variable of economic/environmental benefits influences the results. Governments should consider a range of preference variables when making optimum proposals.

INTRODUCTION

After World War II, only five major American cities—Cleveland, Detroit, New York, San Francisco, and Seattle—owned and operated their transit systems; by the 1970s most transit systems in large American cities were operated by the public sector (Saltzman, 1992). Since the 1990s, when the public transit systems of cities in China became market based and opened to the private sector, the negative effects of marketization practices in several cities have caused them to return to public sector operation. Government subsidies play an increasingly important role in public

transit systems, as urban public transport companies usually operate under deficit conditions (Ubbels, 2002). These subsidies represent an income transfer from taxpayers to transit users (Iseki, 2001).

The aim of subsidies is to create more efficient, less costly, and less energy-dependent urban transport, as well as a better urban environment (Bly, 1980). Subsidised public transport also provides environmental benefits, as private urban transportation contributes to climate change and is associated with other negative environmental effects such as traffic congestion and air pollution. For example, Beijing suffers from high local external costs due to motor vehicle use that, together with global climate change externalities, cost the equivalent of between 7.5% and 15.0% of Beijing's GDP (Creutzig, 2009). Since burning gasoline and diesel fuel is unfriendly to the environment, and the costs of these fuels is rapidly increasing, the purchase and operation of buses that use alternative energy sources has become a target of public transit subsidies. Although electric vehicles contribute least to local air pollution, hybrid electric vehicles, which use both conventional internal combustion engines and electric motors as their major sources of power (Tzeng, 2005), can provide an interim solution until the development of viable electric vehicles.

The economic and environmental impacts of subsidies for low emission vehicles (LEVs) are difficult to quantify. A bootstrap data envelopment analysis (DEA) method was applied to estimate technical efficiency scores for Canadian urban transit systems (Attah, 2004). However, it was difficult to attain accurate figures for cost savings and emissions reductions, since much of the shortfall can be attributed to the elimination or significant delay of anticipated grant programs for installing fast fuel stations and other fueling infrastructure (Haller, 2007).

This paper proposes an original Subsidy Optimization Model (SOM) which considers both economic revenue of the public transit company and environmental benefits for the whole society. It then uses this SOM to analyze options for subsidy distribution for Beijing's public transit system over a five year period. Optimized results and limitations of the proposed model are considered, and conclusions are summarized.

SUBSIDY OPTIMIZATION MODEL

Government subsidies for LEVs for public transit offer two separate benefits, the economic benefit to public transit companies and the environmental benefit to the whole society. In order to optimize these benefits we have formulated a Subsidy Optimization Model (SOM) structured as a nonlinear integer optimizing problem.

The parameters are defined as follows:

F: Total revenue over T years under investment program $x_1, x_2, \ldots x_T$;

T: Time duration in years;

A: Total budget over T years;

β: Weighting coefficient of economic benefits;

m: Number of projects included in cost calculation system;

x_i: Subsidies during year i;

$c_j(x_i)$: Cost variance of project j in year i with subsidy x_i;

d_i: Environment cost of year i without subsidy x_i;

$f(x_1, x_2, \ldots, x_T)$: Environment cost over T years with subsidy x_i;

$n_i(x_i)$: Number of LEVs purchased in year i with subsidy x_i;

L: Limitation on the number of LEVs purchased each year.

The general objective function for total revenue is as follows:

$F = \Delta P_{BC} + \Delta E$

The two terms on the right side are the changes in economic (P) and environmental (E) costs after subsidies contribute to transit companies. Changes in economic costs may include the following:

- purchase costs of LEVs;
- cost of energy use of LEVs;
- operation and maintenance costs of LEVs;
- Construction and maintenance of gas stations/service stations etc.

Changes in environmental costs may include the following:

- reduction in CO_2 emissions caused by reduction in fuel consumption;
- reduction in major pollutants including HC (hydrocarbons), CO (carbon monoxide), NO_x (nitrogen oxide), and $PM_{10}/PM_{2.5}$ (respirable suspended particulates).

In the equation below, β represents the weighting of economic benefits while 1-β represents the weighting of environmental benefits.

$$F = \beta \sum_{i=1}^{T} [x_i - \sum_{j=1}^{m} c_j(x_i)] + (1-\beta) \sum_{i=1}^{T} d_i - f(x_1, \ldots, x_T)$$

The SOM can then be expressed in the following form:

$$\max \quad F = \beta \sum_{i=1}^{T} [x_i - \sum_{j=1}^{m} c_j(x_i)] + (1-\beta) \sum_{i=1}^{T} d_i - f(x_1, \ldots, x_T)$$

$$s.t. \begin{cases} \sum_{i=1}^{T} x_i \le A \\ n_i(x_i) \le L, (i = 1, 2, \ldots, T) \\ x_i = 0, \quad \sum_{j=1}^{m} c_j(x_i) \le 0, (i = 1, 2, \ldots, T) \end{cases}$$

1) The total amount of subsidy does not exceed a total budget of A over T years;

2) The number of LEVs purchased each year does not exceed a specific number (or a certain proportion when the total number of vehicles changes);

3) The amount of subsidy is less than the loss of revenue resulting from purchase and operation of LEVs in each year.

CASE STUDY

The adaptability and accuracy of this model was tested with data from the Beijing Public Transportation Group. For this experiment the following conditions were assumed:

- Bus companies receive ￥5 billion in government subsidies to support the purchase and operation of LEVs over five years;
- Bus companies plan to buy parallel hybrid electric vehicles (PHEVs) to replace diesel hauled buses (DHBs);
- Bus companies will spend all the subsidy money available to purchase PHEVs.

Table 1. Cost Calculation System (10,000￥).

Power	Cost calculation system	2009	2010	2011	2012	2013
DHB	Acquisition cost	73.40	72.67	71.94	71.22	70.51
	Fuel cost	126.10	129.89	133.78	137.80	141.93
	Maintenance cost	10.80	10.80	10.80	10.80	10.80
	Total economic cost	**210.30**	**213.36**	**216.52**	**219.82**	**223.24**
	Upper environmental cost	11.22	12.34	13.58	14.93	16.43
	Lower environmental cost	18.62	20.48	22.53	24.78	27.26
	Total environmental cost	**29.84**	**32.82**	**36.11**	**39.71**	**43.69**
PHEV	Acquisition cost	123.60	102.42	91.06	81.95	75.47
	Fuel cost	113.49	115.73	118.01	120.33	122.70
	Maintenance cost	11.88	11.77	11.67	11.59	11.51
	Total economic cost	**225.67**	**221.92**	**220.74**	**220.87**	**221.68**
	Upper environmental cost	10.10	11.00	11.98	13.04	14.20
	Lower environmental cost	16.76	18.25	19.87	21.64	23.57
	Total environmental cost	**26.86**	**29.25**	**31.85**	**34.68**	**37.77**

Source: Beijing Public Transit Group

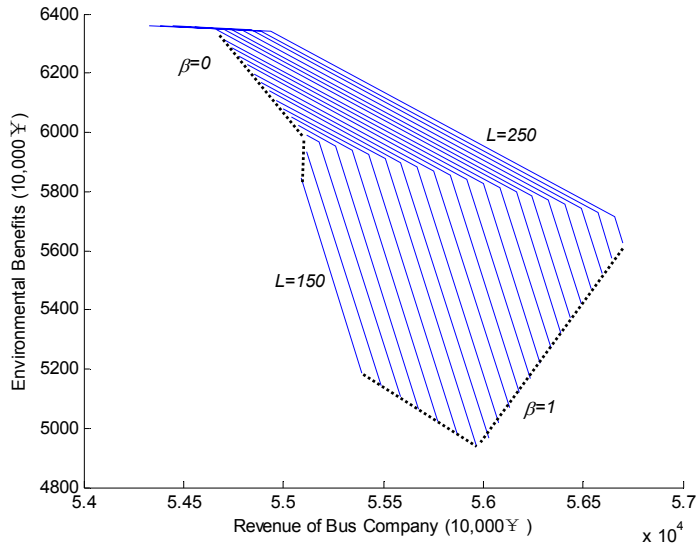

Figure 1. Optimizing Results under Different Scenarios.

Values were calculated using the following assumptions:

- The cost of PHEV acquisition includes the cost of engines/motors/batteries, research and development, and non-power systems;
- Price trends over the period of analysis were corrected for linearity;
- Vehicles travel 50,000 kilometers each year;
- Fuel consumption of a DHB (diesel-hauled bus) is 40 liters per 100 kilometers, while PHEVs are assumed to consume 90% of this rate and to reduce every year;
- Diesel fuel prices increase 3% annually;
- The environmental cost of CO_2 increases 10% annually.

Using these assumptions, the model was optimized for values of β between 0.00 and 1.00 in increments of 0.01; and for values of L between 150 and 250 in increments of 5. The resulting graph is shown in Figure 1, and selected results are shown in Table 2.

Table 2. Optimized Results (x_1~ x_5, **10,000￥**).

β	L	x_1	x_2	x_3	x_4	x_5
0.00	150	18510	15405	13785	2300	0
0.50	150	18510	15405	13785	2300	0
1.00	150	8630	15405	13785	12180	0
0.00	250	30850	19150	0	0	0
0.50	250	1350	25675	22975	0	0
1.00	250	0	25675	22975	1350	0

The results showed that the optimal strategy changes for different weightings of benefits preference. When β is relatively small and more concern is given to environmental benefits, environmental benefits are higher in earlier years and thus subsidies should be focused on earlier years. As β increases and concern for environmental benefits decreases, benefits are higher in later years and thus subsidies should be focused on later years. The value of limitation on the number of PHEVs bus companies purchase (L) also influences the optimization results, in that the total revenue boundary extends as the limitation constraint increases.

The results show that increasing weighting of environmental benefits may greatly decrease economic benefits; this is indicated by the dotted lines in Figure 1, whose slope are relatively small. It is therefore important to fix an appropriate value for β to balance between the economic interests of bus companies and the environmental interests of society.

CONCLUSIONS

This paper proposes a metrological model to evaluate and optimize the subsidy strategies of encouraging transit companies to purchase and operate LEVs, using different weightings of environmental benefits. The results of the case study using this model show that varying the weighting coefficient has the potential to influence the optimal result.

ACKNOWLEDGEMENTS

This work is supported by National High-Tech Research and Development Program of China (863 Program) (Grant No. 2007AA11Z233) and National Key Technology R&D Program (Grant No. 2007BAK35B06).

REFERENCES

Attah, K. B. (2004). "The technical efficiency of Canadian urban transit systems." *Transportation Research Part E* 40 (5), 401-416.

Bly, P. H., Webster, F. V. and Pounds, S. (1980). "Subsidization of urban transport. Department of Transport", *Transport and Road Research Laboratory Supplementary Report* 541.

Creutzig, F. and He, D. (2009). "Climate change mitigation and co-benefits of feasible transport demand policies in Beijing." *Transportation Research Part D* 14 (2), 120-131.

Haller, M., Welch, E., Lin, J., Fulla, S. (2007). "Economic costs and environmental impacts of alternative fuel vehicle fleets in local government: An interim assessment of a voluntary ten-year fleet conversion plan." *Transportation Research Part D,* Dec, 219-230.

Iseki, H. and Taylor, B. D. (2001). "The demographics of public transit subsidies: a case study of Los Angeles." *The 81th Annual Meeting of the Transportation Research Board*.

Saltzman, A. (1992). "Public transportation in the 20th century." In G. E. Gray and L. A. Hoel, *Public transportation,* 24-45.

Tzeng, G. H., Lin, C. W., and Opricovic, S. (2005). "Multi-criteria analysis of alternative-fuel buses for public transportation." *Energy Policy* 33(11), 1373-1383.

Ubbels, B. and Nijkamp, P. (2002). "Unconventional funding of urban public transport." *Transportation Research Part D*7 (5), 317-329.

Study on the Control Strategy of Gas Injection of Gas Engines

Gao Song[1], Li Yu-ming [2] and Zhang Ling-yong[3]

[1]School of Transportation and Vehicle Engineering, Shandong University of Technology, 12 Zhangzhou Rd. Zibo, China, P.O. Box 255049, PH (86)533-2786028; FAX (86) 533-2786837; email: gs6510@163.com
[2]School of Transportation and Vehicle Engineering, Shandong University of Technology, 12 Zhangzhou Rd. Zibo, China, P.O.Box 255049, PH (86)533-2786028; FAX (86) 533-2786837; email: lym820825@126.com
[3]School of Transportation and Vehicle Engineering, Shandong University of Technology, 12 Zhangzhou Rd. Zibo, China, P.O.Box 255049, PH (86)533-2786028; FAX (86) 533-2786837; email: zhanglingyong3@163.com

ABSTRACT

It is very important for the gas engine to improve its fuel economy, low emission and power performance. To solve this problem, the air fuel ratio should be controlled accurately. In order to keep the air fuel ratio around 16.7, an air-fuel ratio parallel control method, which is based on CMAC neural network and PID, is adopted and its arithmetic is elaborated in this paper. The parallel control method is also compared with the one using PID only. The simulation result shows that air fuel ratio could be controlled at the range of 16.7 by the parallel control method.

PURPOSE OF CONTROL SYSTEM

The A/F ratio control system could adjust the gas injection automatically when its concentration changes, so that the A/F ratio keeps at the range of the ideal value. Therefore, the engine could operate steadily, and the power and rotate instability, the inlet backfire, the blow of the outlet could be avoided.

DESIGN PROPOSAL OF THE CONTROL SYSTEM

The control system as shown by Fig. 1 consists of four parts: sensor signals\sensor processing circuit, A/F ratio controller, gas injecting valve.

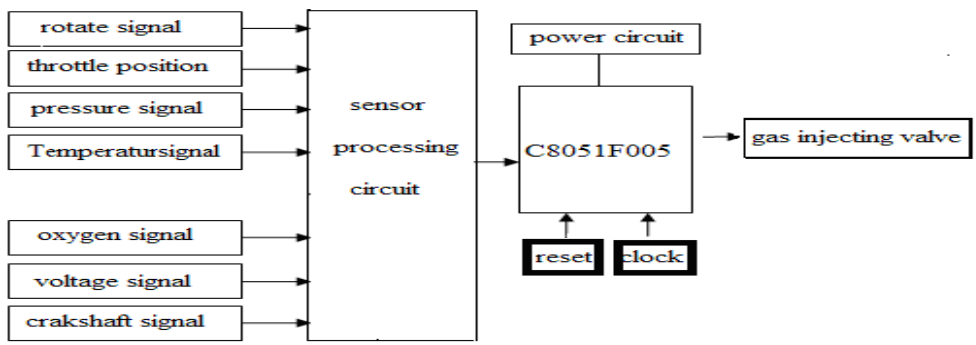

Fig. 1. Gas engine A/F ration control schematic.

After processing, sensor signals are put into the electronic control unit (ECU). With analysis, the needed optimal A/F ratio is determined and according to the A/F ratio, the injecting pulse is calculated. The single chip microcontroller (SCM) then adopts the PWM to adjust the suitable pulse width.

REACH ON CONTROL STRATEGY OF SYSTEM

The core of the control system is to determine and realize the control arithmetic (*Martin Brown, 1994*). The suitable control arithmetic should have the tiny steady state error, quick dynamic response, and good robustness. In terms of A/F control system, the purpose is to make the A/F ratio mean value of the steady working condition close to the ideal value. Besides, the A/F ratio deviates from the target value as the engine working condition changes suddenly, at that moment, the control system should respond quickly and control the A/F close to the target value, wile avoiding the situation occurrence of poor engine emission. In view of the engine high nonlinearity and its time delay, the A/F ratio control method based on CMAC and PID parallel control is put forward.

PID Control Theory and Its Problem. PID control has strong robustness, little dependence on model, and is prone to realize in engineering, so it is widely used in industry. The control method only using PID could not realize the control of large pure-lag and big inertia segments. Additionaly, the controlled plant has some variability, the conventional PID parameters possess no self-adapting ability, and it is difficult to meet the actual control needs. At the present time, the setting and optimizing of PID parameters depends mainly on the technicist regulating manually and the control effect is limited by their experience and level largely, besides, plenty of manpower, physical resources and time are wasted.

Summarize of the CMAC. Cerebellar Model Articulation Controller (CMAC) is a query by form self-adapting neural network; it is used to express complicated nonlinear functions (*C. C. Lin, 2001*). The network could change the content of the form by learning and has the ability to store information classically.

CMAC is acknowledged as the important part of the associate memory neural network. It could learn any dimensions nonlinear mapping (*Hecht-Nielsen R, 1989*). CMAC arithmetic could be effectively used in nonlinear approximation of function, dynamic modeling, control system designing, and so on. CMAC has better nonlinear approaching ability, is suitable to control nonlinearly, and is timely in the complex dynamic situation.

CMAC consists of an input layer, a middle layer, and an output layer. Between the input layer and middle layer, the function relation is the input layer nonlinear mapping, and between the middle layer and the output layer is the output weight self-adapting linear mapping.

CMAC designing way consists of three steps:

(1) Quantizing (concept mapping)

In the input layer, the N-dimension space is divided, and every input is in the hypercube unit of N-dimension grid. To any input, the output is a nonzero value only in several space intervals. The number of the nonzero value space

intervals is norm parameter C, and the size influencing the network output area in the inner network is determined by the norm parameter.

(2) Address mapping (actual mapping)

By dividing the remainder, the input sample is mapped to the concept storage address, and divide a number, the remainder is the actual storage address. That is, C numbers of units in the concept storage are mapped to the C numbers of addresses in the actual storage.

(3) CMAC function calculating (CMAC output)

After the input is mapped to C numbers of units of the actual storage, every unit store the corresponding weight value, and the CMAC output is the weighting sum of C numbers of actual storage units.

Gas Injection Control Strategy of Gas Engine Based on CMAC and PID Parallel Control. CMAC and PID parallel control method is adopted in the control system, CMAC is the feed forward control, and PID realizes the feedback control of the inverse dynamics model of the controlled plant. The stability of the system is guaranteed and the perturbation is inhibited. That makes the system have better stability and robustness in the high-responding speed and nonlinear conditions (*Lino Guzzella, 1995*). A control diagram is shown in Fig.2. Firstly, the A/F value is compared with the setting value, adjusted by the PID controller, and the output controls the system; the sampled rotate signal, throttle position signal, cylinder temperature signal, gas pressure signal, and the oxygen signal is processed. Those and the output of the PID controller are then both used to train the CMAC control arithmetic.

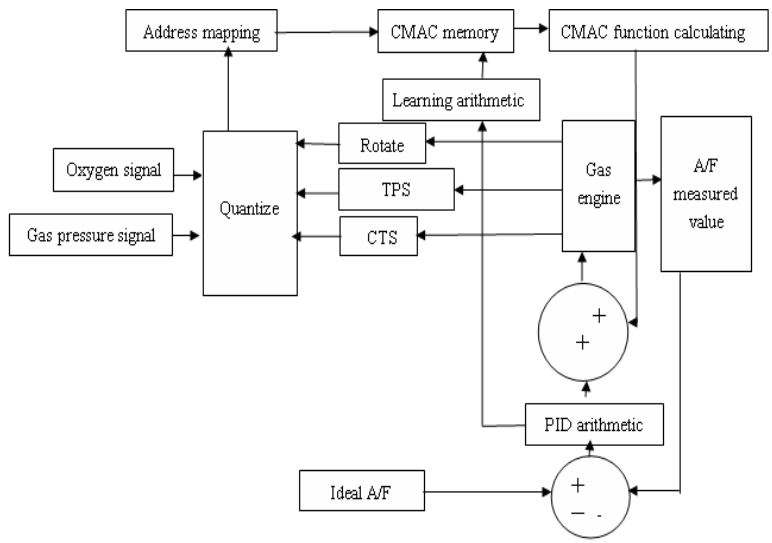

Fig. 2. CMAC and PID parallel control diagram.

SIMULATING AND ANALYZING OF THE CONTROL STRATEGY

The A/F control method of coal bed gas engine is simulated by Simulink. Fig.3 shows the simulation diagram based on the PID and the control diagram based on the CMAC and PID parallel control is shown in Fig.4.

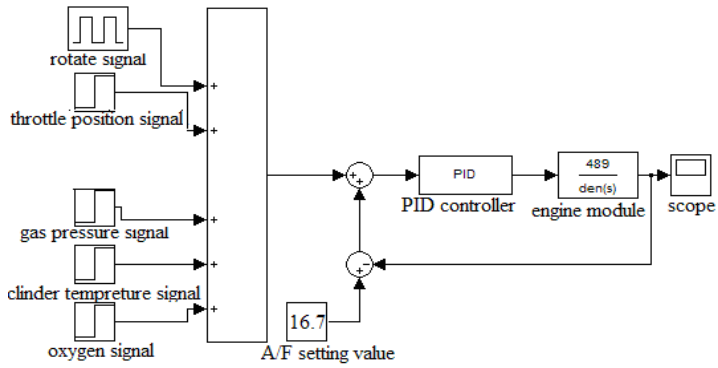

Fig. 3. Simulating diagram of A/F control based on PID.

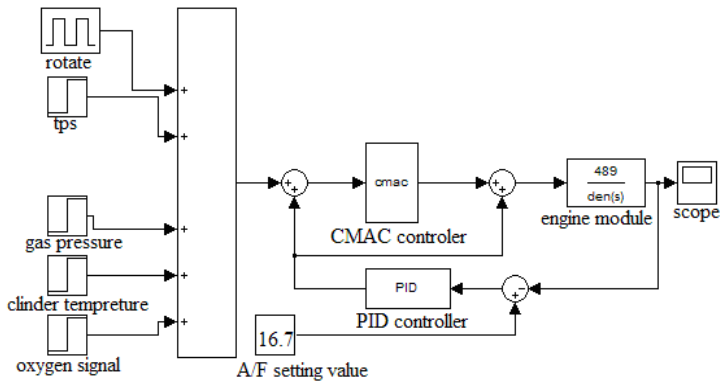

Fig. 4. Simulation diagram of A/F parallel control based on CMAC and PID.

The input signals include a rotate signal, throttle position signal, cylinder temperature signal, gas pressure signal, and A/F setting value and measuring value. When simulating, the step signal or pulse signal are the input signals. The A/F setting value is 16.7, and PID controller calls for the PID function of the simulation toolbox and CMAC is compiled using M-function.

Fig.5 and Fig.6 shows the simulation results.

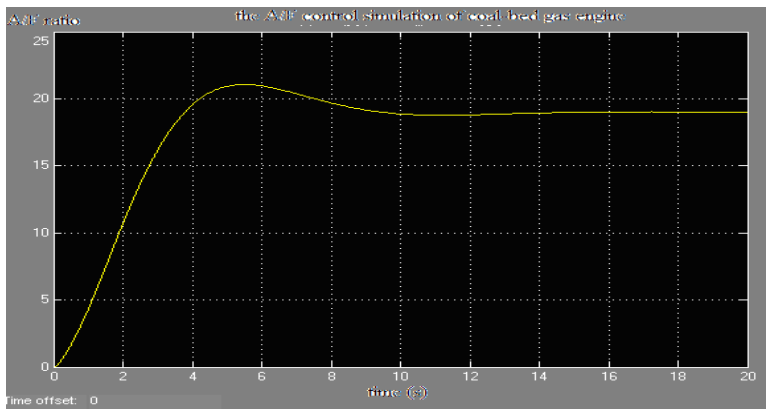

Fig. 5. Simulation result of A/F control based on PID.

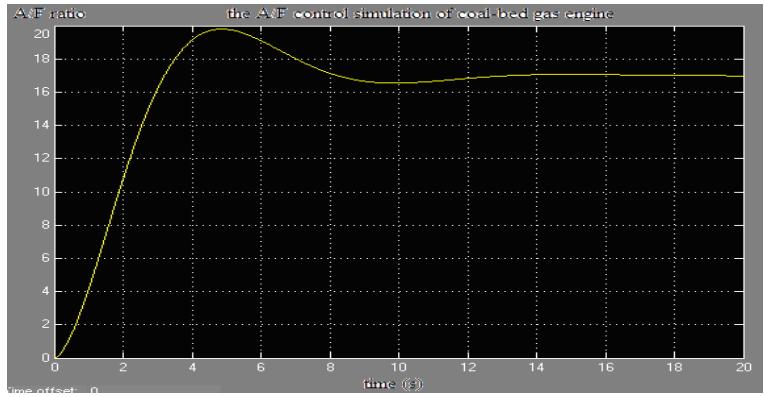

Fig. 6. Simulation result of A/F parallel control based on CMAC and PID.

The simulation result shows that:

(1) Steady state response

After adjusted by PID, the A/F is only controlled about 19, and the steady error is bigger; however, by the parallel control based on CMAC and PID, the A/F could be steadily kept among the range of 16.7.

(2) Dynamic response

After adjusted by PID, the overshoot, adjusting time, raising time and peak-time is shown in Table 1.

But by the parallel control based on CMAC and PID, the overshoot, adjusting time, raising time and peak-time is shown in Table 2.

Table 1. Dynamic PID response.

overshoot (δ_p)	adjusting time (t_s)	raising time (t_r)	peak-time (t_p)
$\delta_p \approx 30\%$	$t_s \approx 11s$	$t_r \approx 3.5s$	$t_p \approx 5.5s$

Table 2. Dynamic CMAC and PID response.

overshoot (δ_p)	adjusting time (t_s)	raising time (t_r)	peak-time (t_p)
$\delta_p \approx 17\%$	$t_s \approx 13s$	$t_r \approx 3s$	$t_p \approx 5s$

From the results, we can come to the conclusion that by adding CMAC, the steadily state error becomes smaller and the control accuracy is improved, while the overshoot becomes smaller.

CONCLUSIONS

The simulation results show that at the beginning, only the conventional PID controller takes effect in the parallel controller based on CMAC and PID. After learning from the output of conventional controller, the CMAC plays the role of controlling instead of PID gradually. In this method, some drawbacks that the conventional controller could not avoid, are overcome to some extent, and the

control effect is improved accordingly. The controller in the paper has better self-adapting ability and strong robustness and could follow the desired value of engine A/F well. The power performance and fuel economy are both improved in addition to avoiding a less effective emission

REFERENCES

Lino Guzzella (1995). "Models and Modelbased Control of IC - Engines- a Nonlinear Approach." *SAE paper,* 950844.

C. C. Lin and F. C. Chen (2001). "On&New CMAC Control Scheme and Its Comparisons with the PID Controllers." *Proceedings of the American Control Conference*, 11-32.

Martin Brown, Chris Harris (1994). "Neurofuzzy adaptive Moeling and Control." *Prentice Hall*, 114-284.

Hecht-Nielsen R (1989). "Theory of the back propagation neural networks." *Proceedings of the International Joint Conference on Neural Networks*, Vol.1.593-611.

Design of Intelligent Decision Module for Storage Location Assignment in AS/RS

ZHU Yanru [1], ZHOU Guiliang[1] and MAO Lina[1]

[1]Transport Engineering Department, Huaiyin Institute of Technology, Huaian 223003, China; e-mail: zgl_transport@126.com

Abstract: The paper points out the importance of storage location optimization in Automated Storage and Retrieval Systems to the logistics enterprises, analyzes the general situation of current storage location assignment methods and reveals their shortcomings. It then designs the intelligent decision module for storage location assignment, including the background and flow of the design, the mathematical model construction on optimizing the storage location assignment, the model solution based on the genetic algorithm, the operation tested by simulation, etc. Finally, it concludes that the module provides technical support for the logistics enterprises to develop the automated warehouses, and has positive significance for leading the development of automated warehouse to intellectualized direction.
Key words: AS/RS, storage location assignment, optimization, simulation

1 Introduction

The Automated Storage and Retrieval Systems (AS/RS) is a modern logistics facility which integrates storing, handling, conveying, and distribution into one system. It is an important part of plant logistics system. In order to manage the AS/RS effectively, improve the whole operation efficiency, reduce the cost of goods handling and storing, decrease the overstocking of the funds, reduce the time loss during the process of storing and handling, and then reduce the logistics cost, and increase the income accordingly, it is necessary to optimize the storage location. It is based on this thought that the paper constructs the intelligent decision module on storage location assignment by making use of the intelligent, information technologies. It plays an important role in promoting the utilization ratio of the storage location, cutting down unnecessary workload, and saves large amounts of manpower and material resources and helps the managers to make rapid, proper decisions in the increasingly fierce competition.

2 Analysis on the Methods of Storage Location Assignment in AS/RS

For the storage location assignment in AS/RS, there are primarily three types of principles: random storage, designated storage and classified storage. Aiming at that there are some shortcomings in practical application of the principles mentioned above, for example, the storage location assignment policy lacks pertinence in the

real-time operation of stacker, the paper constructs the intelligent decision module for storage location assignment by taking the minimum stacker travel time as principle and using the simulation optimization technology to avoid these problems.

3 The Intelligent Decision Module Design on Storage Location Assignment in AS/RS

3.1 Environment and flow of the intelligent decision module design

The paper takes the AS/RS of Jiangsu Feiliks International Logistics Inc. as an example to study. The warehouses of Feiliks contain general warehouse, constant temperature warehouse and high-value warehouse. The functional areas of warehouses are divided into receiving area, pending disposal area and dispatch area, etc. The area of general warehouse is 26,000 square meters; the shelves are standardized 20 floors entirely, with 29,500 storage locations. The handling operation equipments consist of 7 sets of forklifts and stackers respectively. It is the background and basis to design the intelligent decision module. The module has taken Microsoft Access 2000 as the back-end database, the advanced language Microsoft Visual Basic6.0 as the front-end development tool (Chen, Ning et al 2007). It has integrated the optimization simulation model with GA optimization algorithm and Flexsim simulation platform. The design has adopted the object oriented idea and made full use of the flexibility and reliability of the Intelligent Decision Support System (IDSS). The design flow chart of the module is shown in figure 1.

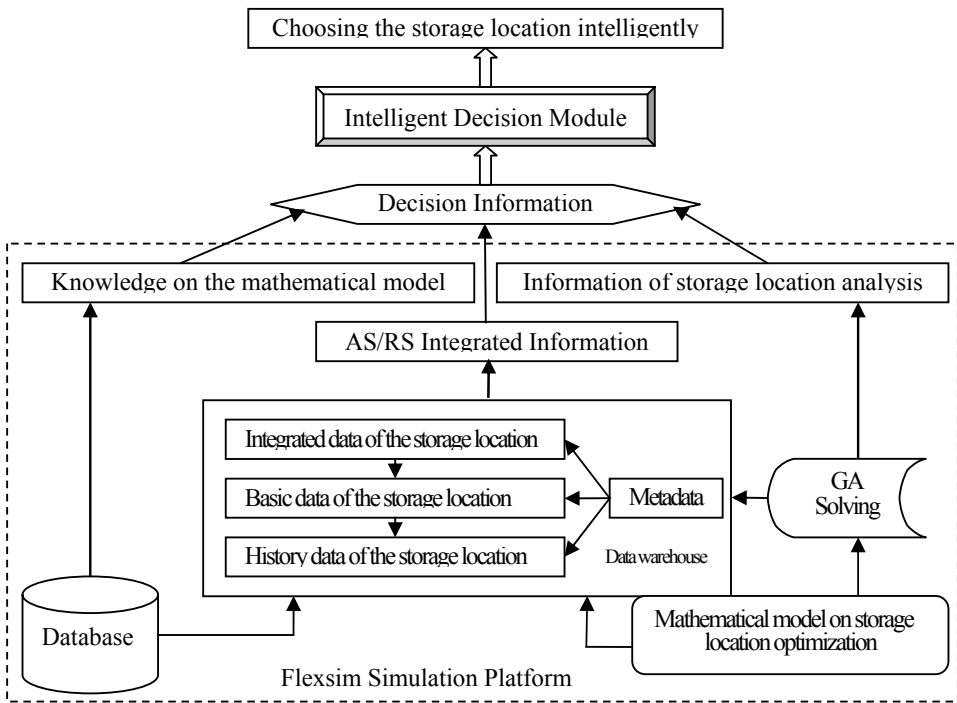

Figure 1. Design flow chart of the module

3.2 Constructing of the mathematical model on storage location optimization

Due to the complexity and diversity of the goods stored in AS/RS, we construct the mathematical model on storage location optimization with main considerations of several principles as below: (1) Heavy cargoes should be placed on the lower shelves in warehouse and light cargoes should be placed on the upper shelves, as to stabilize the force on shelves. The materials should be stored dispersedly lest the excessively concentrated storage lead to uneven loading on the shelves (Cou, Yang et al 2003). (2) When assigning the storage location, it is necessary to take improving the warehousein/warehouseout efficiency into account as much as possible. (3) The goods should be dispersedly placed beside several laneways lest the obstruction of certain laneway affect the passing of some materials. (4) Adopt the "First In First Out" principle (FIFO), that is, for the same kind of goods, the earlier it enters the warehouse, the earlier it leaves, as to accelerate the turnover of the materials and avoid loss caused by overstocked materials (Liu, S. C. et al 2003). In order to optimize the storage location in AS/RS, the paper makes pre-division of the storage location with consideration of the stacker running speed; and then establishes a mathematical model on the assignment problem considering many comprehensive affecting factors such as the storage characteristic code of the goods and so on.

Given the actual situation of the AS/RS in the example, the warehouse area is divided into 7 parts: A, B, C, D, E, F, and G. There are 7 laneways, 14 rows of shelves in total. Each shelf has 20 floors in a row and 20 columns in a floor with 500×500 cell-grids. In the process of calculating the operating cycle, the given constants are: the horizontal velocity of the stacker v_x =80m/min, the vertical velocity of the stacker v_z =63 m/min, the height of the shelf H=10,000mm. The mathematical model on storage location optimization is constructed as below:

$$\min \sum_{i=1}^{n}\sum_{j=1}^{n}\sum_{k=1}^{n} a_k \frac{2\times abs\{\max[\frac{(Z-1)h_0}{v_z}\ ;\frac{(X-1)l_0}{v_x}]\}}{t_c} x_{ijk}$$

In:

$$\sum_{i=1}^{n_1} x_{ijk}=1 \qquad j,k=1,2,3,...,n; \qquad \sum_{j=1}^{n_2} x_{ijk}=1 \qquad i,k=1,2,3,...,n;$$

$$\sum_{k=1}^{n_3} x_{ijk}=1 \qquad i,j=1,2,3,...,n; \qquad x_{ijk}=0 or 1 \qquad i,j,k=1,2,3,...,n$$

$x_{ijk}=1$ Denotes that the goods j be placed in area i by using NO. k stacker;

a_k ——the gravity effect coefficient on the shelf when using the NO. k stacker;

t_c——storage time of the goods ; Z——layer numbers ; X——number of columns ; v_z——the vertical velocity of the stacker; v_x——the horizontal velocity of the stacker; h_0——height of single storage location; l_0——width of single storage location.

3.3 Solving of the mathematical model

There are many methods to solve the mathematical model, mainly including Hungary algorithm and GA. Considering the actual situation of the model and example and the convenient operation, strong robustness and optimizing ability of the GA on solving the combinatorial optimization problem, the paper mainly uses GA to optimize the storage location assignment problem. The paper has constructed GA to solve the decision problem on goods warehousein by using the ergodicity of optimization and the searching mechanism of GA. The basic idea is: coding the alternative storage location with the natural number through the natural number coding method. The genic value of each individual in chromosome is the storage location of corresponding goods. In the genetic operation, in order to avoid the partial optimum and accelerate the searching speed, the adaptive adjusting crossover and mutation probability is adopted. The parameters of the model are chosen as bellows: the population number of the GA P=20, the crossover probability pc=0.7, the mutation probability pm=0.02. The fitness value graph of solving the model by GA is shown in Figure 2. By solving the basic steps such as obtaining the algorithm data, calculating the fitness value of the current chromosome, choosing the fitness value for the function, judging the ending criterion, carrying out crossover and mutation on chromosomes and outputting the final solution, etc. The final solving results of the model are shown in Table 1.

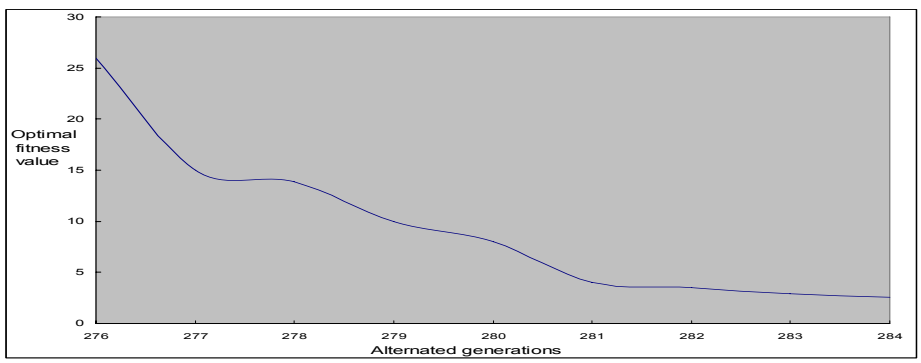

Figure 2. The fitness value graph of solving the model by GA

Table 1. Solving results of the intelligent decision model on storage location assignment

Number of the warehousing goods	Sub area number	Length (mm)	Width (mm)	Height (mm)	Weight (kg)	Results of manual decision	Results of algorithm decision
						Storage location number	Storage location number
20090211822	A	450	300	380	18	A020413	A020413
20090211823	A	450	300	250	12	A020515	A020512
20090211824	G	480	450	450	25	G140205	G140205
20090211825	C	300	300	300	10	C091618	C091717
20090211826	D	300	350	380	14	D100713	D100714
20090211827	B	480	300	300	16	B070609	B070609

From figure 2 and table 1, we can see that the model algorithm can choose the suitable storage location for each goods to be put into the warehouse quickly. With the increase of the cyclic alternated generations, the optimization effects become more obvious.

3.4 Simulation of the intelligent decision module

In order to evaluate the mathematical model above, we need to carry out simulation for it. We choose Flexsim as the simulation tool. The Flexsim has adopted the object-oriented technology and possessed the three-dimensional display (3D) function. Moreover, the important characteristics of the software lie in quick and convenient modeling and the powerful displaying ability. The functions provided by this software contain original data fitting, input modeling, graphic model constructing, virtual reality (VR) displaying, operating the model to do simulation tests, optimizing the results and generating the 3D animation image files, etc. The running interface of the intelligent decision module through Flexsim is shown in figure 3. The dynamic variation graph of the storage location during certain time segment is shown in figure 4.

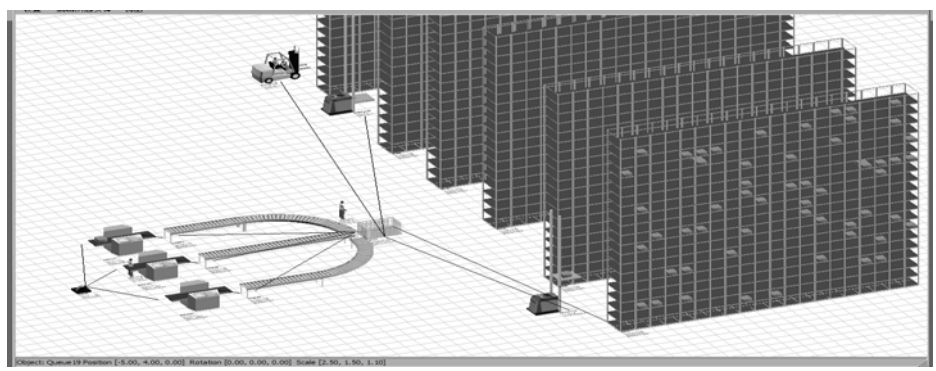

Figure 3. The simulation running interface of the module

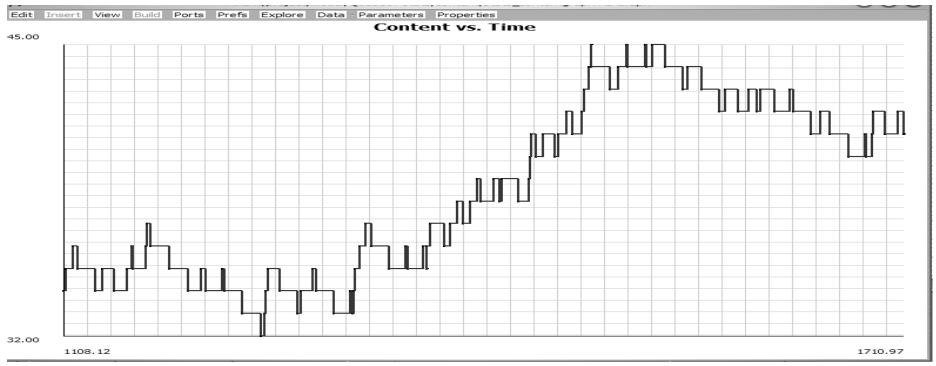

Figure 4. The dynamic variation graph of the storage location during certain time segment

According to the simulation running situation, the intelligent decision module for storage location assignment has promoted the warehousein/warehouseout efficiency of the goods, shortened the operating path of the stacker and achieved comparatively satisfactory results.

4 Conclusions

Based on the simulation result and practical application, the intelligent decision module for storage location assignment is able to choose the appropriate storage location relatively correctly according to the nature and characteristics of the goods. Meanwhile, it has reduced the waiting time of the warehousein/warehouseout operation evidently and has the ability to respond to much higher frequency operations. Thus, it has provided technology support for establishing rapid and efficient material warehousing system with high flexibility as to adapt to the increasingly fierce market competition and the diversity and convenience requirements of the customers. It has positive significance for leading the development of automated warehouse to intellectualized direction.

References

Chen, Ning and Zhou, Guiliang (2007). "Design and Realization of IMIS for Container Freight Station." *Port and Waterway Engineering*, 10, 26-28

Cou, Yang and Cheng, M. C. (2003). "Developing a PDM/MRP integration framework to evaluate the influence of engineering change on inventory scrap cost." *International Advanced Manufacture technology*, 22, 161-174.

Liu, S. C. and Lee, S. B. (2003). "A two-phase heuristic method for the mutt-depot Location routing problem taking inventory control decisions into consideration." *International manufacturing technology*, 22, 941-950.

Optimization of Open Vehicle Route to Reduce Fuel Consumption Based on Genetic Algorithm

PENG Yong[1], ZHU Haiying

[1]Key Laboratary of Traffic & Transportation, Chongqing Jiaotong Univ., Chongqing 400074, China; Phone: (86)13637948336; Email: pengyong818@sohu.com

Abstract: In the classical version of Vehicle Routing Problems, the vehicles are required to return to the depot after completing service. In open Vehicle Routing Problems, however, the vehicles need not do so. Just like Vehicle Routing Problems, almost all the research papers of open Vehicle Routing Problems focus on minimizing the sum of travel distance. However, vehicle managers are also interested in vehicle routing schedules that minimize fuel consumption. This paper presents a new open vehicle routing problem based on reducing fuel consumption. That is, the optimization objective of the open vehicle routing problem is to minimize the fuel consumption. Then the paper formulates a mathematical model for this problem and develops a genetic algorithm to solve this NP-hard problem. A numerical example is used to demonstrate the operation validation of our genetic algorithm, and to compare the different routing schedules of the open and closed versions of the same problem.

Keywords: open VRP, fuel consumption, routing schedule, genetic algorithm

1 Introduction

In the classical version of Vehicle Routing Problems (VRPs), the vehicles are required to return to the depot after completing service. In open VRPs (Tarantilis, C. D. et al 2005; Li, L. and Fu, Z., 2002; Tarantilis, C. D. et al 2002; Fu, Z. et al 2005), however, the vehicles need not do so. As a result, the vehicle routes are not closed paths but open ones, starting at the depot and ending at one of the customers. Just like VRPs, almost all the research papers of open VRPs focus on minimizing the sum of travel distance (travel time). However, vehicle managers are also interested in vehicle routing schedules which minimize fuel consumption due to two factors. First, reducing fuel consumption means reducing the service cost. Second, reducing fuel consumption means reducing its impact on our environment (green-house effect), our health (air pollutants), and our economy (increased fuel prices).

This paper will present a new open vehicle routing problem based on reducing fuel consumption. That is, the optimization objective of the open vehicle routing problem is to minimize the fuel consumption. Then the paper will provide this problem's mathematical model and develop a genetic algorithm (GA) to solve this NP-hard problem. A numerical example will be used to demonstrate the

operation validation of our genetic algorithm, and to compare the different routing schedules of the open and closed versions of the same problem.

2 Problem Formulation

Our problem can be formally described in the following way: there is one central depot, which uses some independent delivery vehicles with identical delivery capacity to serve demands of some customers. We know the amount of fuel consumption for each kilometer without load, and the addition amount of fuel consumption for each kilometer with unit load. The vehicles must accomplish the delivery with minimum total fuel consumption.

Let N denote the set of indices of customers with node 0 denoting the depot, and V denote the set of indices of vehicles. All feasible vehicle routes correspond to paths start from one depot and end at the same depot. Let $d_{ij}, i, j \in N$ be the distance from i to j. Let $d_{i0} = 0, i \in N$, then we can treat the open vehicle routing problem as VRP.

Let $q_i, i \in N$ be the demand of node i, and C be the capacity of vehicle. Since node 0 denotes the depot, let $q_0 = 0$. Let $Q_{ik}, i \in N, k \in V$ be the load on the vehicle k when arriving at node i. Let c_0 be the amount of fuel consumption for unit distance without load. Let c_1 be the addition amount of fuel consumption for unit distance with unit load.

We define the decision variables $x_{ijk} = 1(i, j \in N, i \neq j, k \in V)$ if arc ij is part of the route for vehicle k, otherwise, $x_{ijk} = 0(i, j \in N, k \in V)$. Since the vehicle k loads goods of all the customers at the depot (node 0), let $Q_{0k} = \sum_{j \in N} q_j x_{ijk}$.

Then the problem can be formulated as follows:

$$\min \quad z = \sum_{k \in V} \sum_{i \in N \setminus \{0\}} \sum_{j \in N, j \neq i} (c_0 + c_1 Q_{jk}) d_{ij} x_{ijk} \tag{1}$$

s.t.

$$\sum_{j \in N} \sum_{i \in N, i \neq j} q_j x_{ijk} \leq C, \forall k \in V \tag{2}$$

$$\sum_{i \in N} x_{ijk} = \sum_{i \in N} x_{jik}, \forall j \in N, \forall k \in V \tag{3}$$

$$\sum_{k\in V}\sum_{i\in N} x_{ijk} = 1, \forall j \in N \setminus \{0\} \tag{4}$$

$$\sum_{i\in N} x_{0ik} \le 1, \forall k \in V \tag{5}$$

$$\sum_{k\in V}\sum_{i,j\in U} x_{ijk} \le |U| - 1, \forall U \subseteq N \setminus \{0\} \tag{6}$$

$$(Q_{ik} - q_i - Q_{jk}) x_{ijk} = 0, \forall i \in N, \forall j \in N \setminus \{0\} \tag{7}$$

The objective function (1) is to find the vehicle routing schedule with minimal fuel consumption. Constraint (2) ensures that the load of each vehicle cannot exceed its capacity. Equation (3) tells us that if vehicle k visits a node then it will also leave from the same node. Equation (4) guarantees that every customer is served by one and only one vehicle. Constraint (5) ensures that a vehicle departs only once from depot 0. Constraint (6) forbids routes that are not connected with depot 0. Constraint (7) ensures that, when $x_{ijk} = 1$, the load Q_{jk} of vehicle k between node i and node j equals the load Q_{ik} of vehicle k arriving at node i minus the demand q_i of node i unloading at node i.

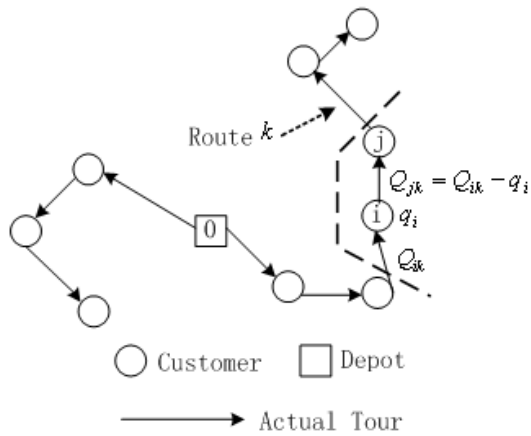

Fig.1 The relationship between Q_{ik} and Q_{jk}

3 GA algorithm for our problem

3.1 Encoding

To solve our problem with GAs, we can represent each individual by just one chromosome, which is a chain of integers, each of them representing a customer or a vehicle. So that each vehicle identifier represents in the chromosome a separator between two different routes, and a string of customer identifiers represents the sequence of deliveries that must cover a vehicle during its route. In the figure below

we can see a representation of a possible solution for our problem with 9 customers and 4 vehicles. Each route begins at the depot (it will be assigned the number 0) and ends at the last customer of the route. If we find in a solution two vehicle identifiers not separated by any customer identifier, we will understand that the route is empty and, therefore, it will not be necessary to use all the vehicles available.

$$\underbrace{1 \to 3 \to 2}_{\text{route1}} \to 10 \to \underbrace{7 \to 4 \to 9 \to 6}_{\text{route2}} \to 12 \to 11 \to \underbrace{5 \to 8}_{\text{route3}}$$

Fig.2 A representation of One Individual

3.2 Fitness function

The fitness function is given by the following equation:

$$fitness \qquad z = \sum (\sum \sum (c_0 + c_1 Q_{jk}) d_{ij} + \psi)$$

Where, ψ is a large number if constraint (2) is violated. Otherwise, $\psi = 0$.

3.3 GA algorithm

Now, we can provide the GA algorithm based on Inver-over operator (Michalewicz Z. et al., 2000) as follows.

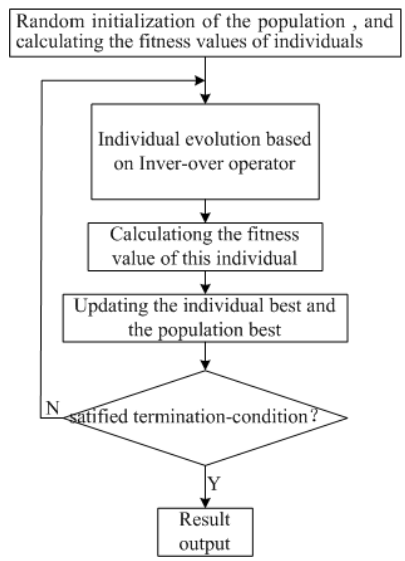

Fig.3 The calculating process of our GA

4 Numerical Example

Provided that there are 20 customers, all the information is shown as follow.

Table 1 Customer Data

Index	Location	Demand	Index	Location	Demand
0(depot)	(94,99)	-	-	-	-
1	(98,43)	6	11	(49,19)	4
2	(58,90)	6	12	(19,73)	1
3	(97,93)	2	13	(38,23)	3
4	(11,65)	5	14	(67,17)	2
5	(75,85)	5	15	(38,5)	3
6	(69,36)	2	16	(74,36)	1
7	(30,85)	2	17	(63,68)	1
8	(22,14)	3	18	(12,68)	3
9	(57,16)	4	19	(103,8)	1
10	(55,13)	1	20	(71,15)	2

Table 2 Model Parameter Settings

Parameter	Value
Vehicle Capacity	20
c_0	0.1
c_1	0.0005

Let the population size be 50, maximum generation be 2000, and $p = 0.2$ (the selection probability our GA based on Inver-operator needs). With our GA, the result suggests that the vehicle number is 4. The total optimal fuel consumption is 43.006. Figure 4 gives one of the solutions by our GA.

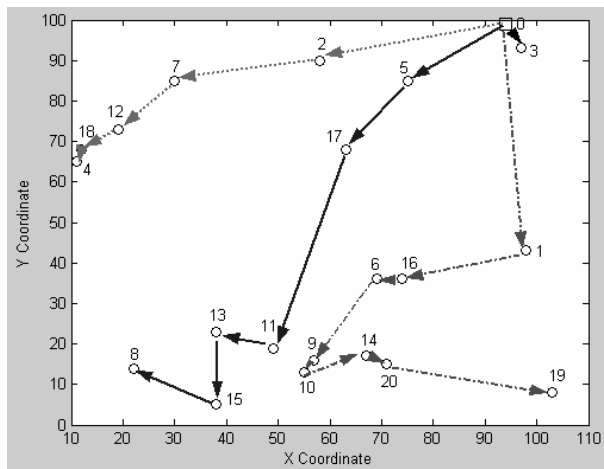

Fig.4 One solution by our GA

The routes are:

$0 \to 1 \to 16 \to 6 \to 9 \to 10 \to 14 \to 20 \to 19$;

$0 \to 5 \to 17 \to 11 \to 13 \to 15 \to 8$;

$0 \to 2 \to 7 \to 12 \to 18 \to 4$;

$0 \to 3$.

Compared to the closed version of the same problem shown in figure 5, the open version of this problem really has a different routing schedule. If we restrict the

vehicle number to 3, we get the solution shown in figure 6, the fuel consumption of which increases to 48.166.

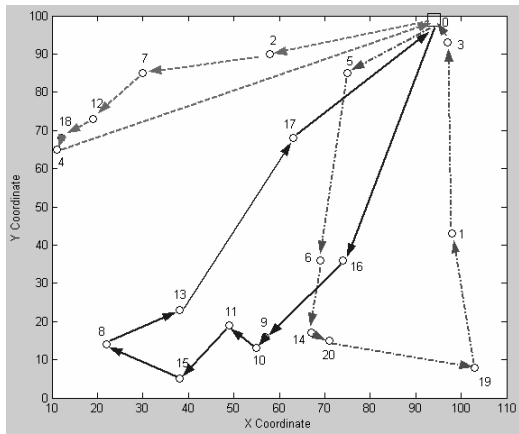

Fig.5 Solution of the closed version of the same problem

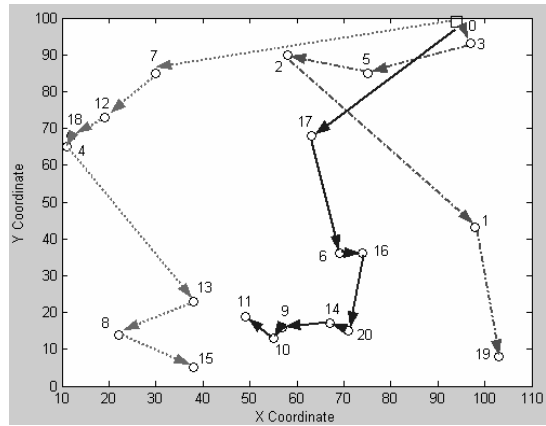

Fig.6 Solution of our problem with 3 vehicles

5 Conclusion

Due to various reasons, vehicle managers are interested in the open vehicle routing schedules which minimize fuel consumption. This paper presents a new open vehicle routing problem based on reducing fuel consumption. That is, the optimization objective of the open vehicle routing problem is to minimize the fuel consumption. Then the paper provides this problem's mathematical formulation and develops a genetic algorithm to solve this NP-hard problem. A numerical example is used to demonstrate the operation validation of our genetic algorithm, and to compare the different routing schedule of open and closed versions of the same problem.

Acknowledgement

This work is supported by Chongqing key laboratory of traffic and transportation.

References

Fu, Z., Eglese, R., and Li, L. Y. O. (2005). "A new tabu search heuristic for the open vehicle routing problem." J. of the Opl Res. Soc., 56: 267–274

Li, L. and Fu, Z. (2002). "The school bus routing problem: a case study." J Oper Res Soc, 53: 552–558

Michalewicz, Z. et al. (2000). "How to Solve It: Modern Heuristics. Springer-Verlag," Berlin, 2000

Tarantilis, C. D., Ioannou, G., Kiranoudis, C. T., and Prastacos, G. P. (2005). "Solving the open vehicle routeing problem via a single parameter metaheuristic algorithm." J. of the Opl Res. Soc., 56: 588–596

Tarantilis, C. D., Kiranoudis, C. T. (2002). “Distribution of fresh meat.” J Food Eng, 51: 85–91

Research on Location of Railway Logistics Center

Xionghuan Jin, Haihong Xie, Bo Jiang, Lan Xu

MOE Key Laboratory for Transportation Complex Systems Theory and Technology, School of Traffic and Transportation, Beijing Jiaotong University, Beijing 100044, China. Email: 07121344@bjtu.edu.cn. Tel: (0086)13811921647

Abstract: Transportation has been greatly influenced by the development of logistics with its characteristics of new management concept and organizational form. Logistics center has been a new trend for railway freight stations. This paper brings forward a location method for logistics center based on existing railway freight stations. It first analyzes location influencing factors of railway logistics centers and proposes to select alternative logistics centers by cluster analysis. It then constructs a mathematical location model to re-select within alternative logistics centers. At the same time, genetic algorithm is applied to seek the optimal solution, and the result is that one or more freight stations are selected to be developed into logistics centers. Finally, a numerical example is given to validate this method.
Key word: Railway logistics, genetic algorithms, cluster analysis, location

INTRODUCTION

Railway transportation has played a crucial role in general freight transportation in China with its outstanding advantages of large volume, round-the-clock operation, less pollution and safety. But the development of modern logistics in railway industry lags behind the requirements of society and China's economy, which hinders the complete utilization of abundant resources and capability of railway transportation, making it difficult to improve the efficiency and benefit of railway transportation. The small-scale, scattered and disorderly freight stations are the main reason that limits the development of modern railway logistics. Thanks to the massive railway construction and layout optimization of railway transportation capability as a whole, it's possible today to transform some existing freight stations into logistics centers. Taking into consideration of regional economic characteristics, technology, equipment conditions and railway facilities, this article preliminary explores the location method of railway logistics center based on the existing freight stations, so as to provide technical reference for railway system planning. This article first adopts cluster analysis to obtain alternative logistics centers after analyzing the location influencing factors of railway logistics center, then constructs mathematical location model and solves this model. The optimal site is determined at the end. It gradually narrows the scope of options in accordance with macro to micro principle.

INFLUENCING FACTORS OF RAILWAY LOGISTICS CENTER LOCATION

To determine the location of railway logistics center, we should first

understand the influencing factors of railway logistics center location. Since this location is based on existing freight stations and environment of economic logistics associated, we can consider it from the areas of the economic environment, policy environment, transport facilities, natural environment and geographical environment.

Table 1 Influencing factors of railway logistics center location

Influencing factors	Detailed influencing factors	Variables and description	
Economic and traffic	Railway turnover	A_{11}	
	Road network density	A_{12}	
	GDP per capita	A_{13}	
	Number of logistics enterprises in the area	A_{14}, take average distance between stations as radius	
	Number of transport hub node	A_{15}, take average distance between stations as radius	
	Land price	A_{16}, take local average level as criteria	
Policy environment	Degree of district administration	$A_{11,}$ according to relative degree, records as 1 to3 individually from low to high	
	Regional supporting policy	A_{22}, 1 expresses enjoyed ,otherwise 0	
Conditions of transport infrastructure	Area of freight station	A_{31}	
	Line capacity	A_{32}	
	Available area of logistics operation	A_{33}	
	External traffic conditions	A_{34}, according to convenience and timeliness, records as 1to3 from low to high	
	Outspread of station	A_{35}, according to degree, of expansion, records as 1 to3	
	Technical condition of railway lines: degree of railway, number of lines, limiting slope, minimum curve radius, traction type, locomotive type, effective length of railway, method of blocking	A_{36}, according to the degree of appropriate, records as 1 to3 from low to high	
	Railway station circumstances: drainage system, box area, road, subgrade and land, yard	A_{37}, same as above	
Natural geographical conditions	Weather conditions	A_{41}	according to the degree of appropriate, records as 1 to3 from low to high
	Hydrological conditions	A_{42}	
	Terrain conditions	A_{43}	

Economic environment is the inherent condition for logistics. The more developed the economy is, the faster the freight flows. Thus it will be more appropriate to set up logistics center. Policy environment is the external condition for the promotion of logistics and is associated with national planning, regional planning and special support; Environmental advantages and disadvantages of transport facilities for the railway system are especially important since the cost of infrastructure transformation of railway lines and stations is relatively high; Natural environment is a main factor to be taken into account. Some factors above are qualitative factors which need to be quantified. Description and treatment of influencing factors are shown in Table 1.

LOCATION MODEL OF RAILWAY LOGISTICS CENTER

Alternative logistics center meets requirements in the railway and economic environment. The following discusses re-location optimization by applying genetic algorithm from the economic view. Railway logistics centers are divided into different types based on their functions. The type of logistics center discussed in this article is mainly based on transportation and has taken other business into account.

Model assumptions

(1) The category and quantity of demand and supply can be predicted in future years. Here it is replaced by existing data;

(2) Railway logistics center collects and distributes bulk cargo, and there are several categories. Here the cost rate is simplified to a unified rate based on the proportion of every cargo;

(3) Transportation costs are linear function;

(4) Railway logistics center is not only the transport entity, but also a third-party service center. Its operating costs is a concave function of flow inside, $W^{\theta} \in (0,1)$, and θ equals 0.5 in this model.

Description of model and parameter

Objective function:

$$\min f(x,z) = \sum_{i=1}^{m}\sum_{k=1}^{l} a_{ik}x_{ik} + \sum_{k=1}^{l}\sum_{j=1}^{n} b_{kj}y_{kj} + \sum_{k=1}^{l} z_k \frac{C}{1+q_k} + \sum_{k=1}^{l} z_k V_k W_k^{\theta}$$

Subject to:

$$\sum_{k=1}^{l} x_{ik} \le S_i \qquad i = 1,2,3.....m$$

$$\sum_{k=1}^{l} y_{kj} \ge D_j \qquad j = 1,2,3.....n$$

$$\sum_{i=1}^{m} x_{ik} = \sum_{j=1}^{n} y_{kj} \qquad k = 1,2,3.....l$$

$$\sum_{i=1}^{m} x_{ik} \le z_k M_k \qquad k = 1,2,3.....l$$

$$\sum_{k=1}^{l} z_k \le P \qquad P = 1,2,3.....N$$

$x_{ik} \ge 0$, $y_{kj} \ge 0$ $(i = 1,2,3.....m\ ;\ j = 1,2,3.....n\ ;\ k = 1,2,3.....l)$

Where:

α_{ik}, x_{ik} ——Unit rates, flow from supply place i to alternative logistics center k;

b_{kj}, y_{kj} ——Unit rates, flow from alternative logistics center k to demand place j;

z_k ——0, 1 variable, 1 expresses selected, otherwise 0;

V_k ——Changeable cost coefficient of alternative logistics center k;

W_k ——Flow of alternative logistics center k (flow of arrival equals flow of departure);

M_k ——Maximum limit flow of alternative logistics center k;

D_j ——User's demand of No j;

S_i ——Supplier's supply of No i;

P ——Max number of railway logistics center in the area;

$\frac{C}{1+q_k}$ ——Fixed operating cost of alternative logistics center k;

Denote $\frac{C}{1+q_k}$ as F_k can be divided into two parts. One is the fixed operating cost for the station, and the other is construction cost of the logistics center. Construction cost varies greatly because of different investment conditions, but here we do not consider it much. The fixed operating cost is mainly incurred by occupying tracks and tasks in tracks. In order to represent the advantages of stations with private lines or potentials of direct transport, denote fixed cost as $\frac{C}{1+q_k}$, in which constant C is the total construction cost, q_k is the number of private lines of station k.

Model solution

The calculation process of genetic algorithm is a typical continuous iterative process. Key steps and parameters are described as follows:

(1) Initialize groups. Choose binary code to give some 5-bit binary string in initialization. The string represents five alternative logistics centers. 1 indicates the alternative logistics center is selected. 0 indicates it is not selected.

(2) If the stop rules are satisfied, the algorithm stops and outputs the result. Otherwise, calculate $f(x,z)$ for every gene code according to the objective function, compare the values of $f(x,z)$, and select the largest $f(x,z)$ and save it in $C_{\max}$ in each generation.

(3) Take $g(x,z) = C_{\max} - f(x,z)$ as fitness function; $C_{\max}$ varies with different

generations. If C_{max} in the next round of iteration appears better than the previous one, upgrade C_{max} as the optimal solution.

(4) In this paper, the standard roulette method is applied to select outstanding code in groups. Adopt decreasing function to obtain crossover probability, from 75% of the first generation to 25% of the last generation, while mutation probability increases with the evolutionary process. The above two tasks ensure fast convergence. Adjust genetic code according to the probability of crossover and mutation of each evolutionary, and prepares for the next round of iteration.

EXAMPLE AND SOLUTION

To verify the correctness of the above algorithm, simulation is done with sample data. Suppose that there are 4 supply places (the largest supply volume are 40, 60, 50, 50), 10 large customers (customer demands are 20, 25, 25, 20, 20, 25, 20, 15, 20, 10 respectively), 5 alternative logistics centers, and no more than 2 logistics centers should be selected. C equals 100 in this model, other relevant data are shown in Table 2 and 3.

Table 2 Rates table

Alternative logistics center	Supply point to the alternative logistics center a_{ik}				From Alternative logistics center to demand points b_{kj}									
	1	2	3	4	1	2	3	4	5	6	7	8	9	10
1	8	7	9	12	7	8	8	7	17	6	9	10	8	7
2	7	9	10	10	9	12	13	6	20	5	7	9	12	11
3	12	17	15	7	12	13	7	9	8	6	5	8	7	8
4	13	14	17	8	6	5	7	9	10	4	3	3	6	5
5	19	13	10	5	6	8	8	7	13	8	9	5	7	9

Table 3 Cost parameters of alternative logistics center

Alternative logistics center (C_j)	1	2	3	4	5
The maximum limit traffic (M_k)	120	100	110	130	105
Fixed costs ($F_k/(1+q_k)$)	100	100	100/3	100	50
Variable cost coefficient (V_k)	75	80	75	80	75

After applying genetic algorithm, the result shows that one logistics center couldn't meet the demand (because the maximum volume for any alternative logistics center is less than 200). The optimal code is 00101, which means the best solution is to choose the third and the fifth alternative logistics center. If iterations are more than 700 times, the fitness value is stabilized at around 900, and the volume through the 2 railway logistics center shows little difference.

Takes 790 times of iteration as example, its fitness value and flow is shown in Table 4.

Table 4 Results of allocation

Optimal genetic code	0	0	1	0	1
Fitness value	0	0	914.0	0	902.0
Flow volume	0	0	57.0	0	47.9

If the amount of supply and demand is stable, we can also perform linear programming to further determine the amount from supply place to railway logistics center and from railway logistics center to the place of demand.

CONCLUSIONS

In this paper, an optimization method of railway logistics center location is proposed. Due to the complexity of the railway system, the factors that need to be considered are complex. We choose cluster analysis method to do hierarchical analysis in macro-level for the purpose of finding alternative logistics centers. As for re-selection, combine railway characteristics to set up the model and introduce genetic algorithm to solve it. The result is some freight stations are selected from the view of economy. Finally it verifies with a numerical example that this method is feasible and reasonable. This paper seeks to make the model match railway operations to the maximum extent. However, the uncertainty of railway flow pathway and diversity of technical standards of railway lines increases the difficulty. Future work is needed to address these issues.

BIBLIOGRAPHY

Gen, M., Cheng, R. W. (2007). Genetic algorithms and engineering optimization. *John Wiley & Sons*, New York.

Li, X. M., She, Y. (2005). Applications of fuzzy cluster analysis at railway express network planning. *Railway science of china,* June

Wu, J., Shi, Z. K. (2004). Study of site selection of distribution center based on genetic algorithm. *Journal of south china technology university*, June

Xiao, H., Yang, D. Y., Chen, Y. L. (2007). Research on Container Freight Station position to extend inside with clustering analysis. *Computer Engineering and Applications,* China, 184-187.

Yu, J. Y., He, X. H. (2005). "Chapter 8: Cluster analysis and discriminant analysis" *Statistical data analysis and application of SPSS,* 8.1-8.2

Zhang, X. D. (2006) "Chapter 6: Analysis of level classification factors in macro layout of logistics parks" *Logistics park planning theory research,* China, 6.1-6.3

Study on Logistics Center Location Bi-Level Programming Model and Algorithm Based on Competition

Xiaojun Guan,[1] Xifu Wang,[2] Cuihua Wang,[3] Yana Yan[4]

[1]Doctor of System Engineering, School of Traffic & Transportation, Beijing Jiaotong University, Beijing 100044, China
[2]Professor, School of Traffic & Transportation,Beijing Jiaotong University, Beijing 100044,China; PH (10) 5168- 8663; email: wangxifu@jtys.bjtu.edu.cn
[3]Master of System Engineering, School of Traffic & Transportation, Beijing Jiaotong University, Beijing 100044, China; PH (10) 5146-5282; email: 07121239@bjtu.edu.cn
[4]Master of System Engineering, School of Traffic & Transportation, Beijing Jiaotong University, Beijing 100044, China

ABSTRACT

At present, the development of the logistics industry is very rapid. Logistics centers play a very important role in a logistics system, and so their location is very important for the effective operation of a logistics system. Introducing the relevant research, this paper presents a logistics center location bi-level programming model based on competition. The bi-level programming model takes into consideration two decision-makers, the distribution center (DC) location planner and the consumer, and also addresses the problem of consumer selection after the distribution center is built. This model has great significance for weighing the total costs of the decision-makers and customers and for studying the optimal location of logistic centers over a long period based on the upper- and lower-level decision-makers in logistic centers. The paper solves the bi-level programming model with a genetic algorithm and proves the model to be more practical.

Key words: Logistics; distribution center; bi-level programming model; genetic algorithm

INTRODUCTION

At present, the development of the logistics industry is very vigorous. Logistics centers play an important role in a logistics system, and their location is very important to the effective functioning of a logistics system. Logistics center location refers to the planning process of selecting a place to establish a logistics center at supply sites and needs sites. A good logistics center location program should take into account adaptability, coordination, economic efficiency, and strategic principles. A logistic center can store, transport, and distribute goods, thus increasing efficiency.

In recent years, many methods related to logistics center location and

network layout have been researched and developed as part of location theory. Regardless of which method is used, the necessary preconditions for success are obtaining accurate data and applying various models. The traditional models of logistics center location have advantages and disadvantages. Table 1 shows an analysis and comparison of variety of methods (Hong, 2004; Xiaodong et al., 2004; Huijun et al., 2003).

Table 1. Analysis and Comparison of Variety of Methods.

	Advantage	Disadvantage	Scope of Application
Gravity Model Approach	Simple principle, convenient computation, easy to solve.	Only for a single center location; sometimes has large difference with the actual situation when the actual road conditions are replaced for straight lines.	For a single location, and in the region, the actual distance and straight-line distance have less difference.
Wolfe's Method	Provides a simple heuristics.	Cannot guarantee that ultimate solution is optimal solution; solution does not involve new distribution center fixed investment costs.	Factory to distribution center costs and distribution center to user's less-than-truckload transportation costs have a linear relationship to carryings into the user's location; the demand is known.
CFLP	Intuitive modeling, can improve model according to the actual situation.	Difficult to get pre-determined options set; lack of theoretical proof.	Alternative set determined according to actual situation and influencing factors; a stepwise refinement process.
BLP	Can concurrently analyze two different, conflicting objectives in decision-making process, can clearly show interaction of higher level policy-making departments and public	Bi-level programming problem is NP-hard problem, so difficult to solve.	Many people involved in making decisions at different levels; decentralized decision-making system optimization.

In this paper, a bi-level programming model based on competition for logistics center location is established and solved according to the analysis listed in Table 1 for a variety of models and approaches. Validity is shown through an example.

MODEL

The bi-level programming model is a system optimization model of a two-layer hierarchical structure. Decision-making variables in the model will affect the two participants in decision-making. The upper-level decision makers and the lower-level decision-makers have their own objective functions and constraints; the upper-level decision-makers give decision-making variables, and the subsystems of lower-level decision-makers use the variables as parameters to achieve optimal value and provide feedback to the upper-level decision makers. The upper-level decision-makers then find the overall optimal solution according to the reflections of the lower-level decision-makers (Amouzegar, 1999).

Upper Model

Upper programming (U) can be described as determining the best location of the new logistics center to minimize the total costs within the fixed range that is allowed, while the lower programming (L) describes the distribution patterns of customer demands between different logistics centers in conditions where there are a number of logistics centers; the goal is for every customer to have the lowest costs. Specific models are shown below.

$$U: \quad \min F = \sum_i \sum_j c_{ij} x_{ij} + \sum_j f_j z_j + \sum_j \sum_q p_{jq} w_{jq} \tag{2-1}$$

$$s.t. \quad \sum_{j=1}^{n} f_j z_j \le B \tag{2-2}$$

$$\sum_{j=1}^{n} z_j \ge 1 \tag{2-3}$$

$$\sum_{j=1}^{n} w_{jq} \le M_q \qquad \forall q = 1, \ldots, p \tag{2-4}$$

$$\sum_{i=1}^{m} w_{ik} \le V_i \tag{2-5}$$

$$\sum_{i=1}^{m} x_{ij} = \sum_{q=1}^{p} w_{jq} \qquad \forall j = 1, \ldots, n \tag{2-6}$$

$$z_j \in \{0,1\} \tag{2-7}$$

Where

c_{ij} - unit cost for distribution center j services the customer i

x_{ij} - demand satisfied at distribution center j of customer i

f_j - fixed investment costs of building the distribution center j

z_j - if build distribution center j, this value is 1, otherwise 0

B - total investment budget to construct the distribution center

w_{jq} - traffic from factory q to distribution center j

P_{jq} - transportation unit price from factory q to distribution center j

M_q - supply capacity of factory q

V_i - supply capacity of distribution center i

Lower Model

In a real distribution system, a distribution center cannot satisfy the demand of a single customer, and there is much competition from other distribution centers. Therefore, in the lower target planning, if there is a distribution center, then the K customers distribute their demands between n+1 distribution centers. This problem can be described as follows:

$$L: \quad \min T = \sum_i \sum_k x_{ik} y_{ik} \tag{2-8}$$

$$s.t. \quad \sum_{k=1}^{n+l} x_{ik} = A_i \qquad \forall i = 1, \ldots, m \tag{2-9}$$

$$\sum_{i=1}^{m} x_{ik} \le v_k \qquad \forall k = 1, \ldots, n+1 \tag{2-10}$$

$$x_{ik} \le M \cdot z_k \qquad \forall i = 1, \ldots, m; \forall k = 1, \ldots, n+1 \tag{2-11}$$

$$x_{ik} \ge 0 \tag{2-12}$$

Where

x_{ik} - demand satisfied at distribution center k of customer i

Y_{ik} - unit cost needed when customer i selects distribution center k to be serviced

A_i - total demand of customer i

V_k - total supply capacity of distribution center k

M - arbitrary large positive number

MODEL SOLUTION

Genetic Algorithm

A genetic algorithm is a search algorithm that combines survival of the fittest rules in the biological evolution process and the same group of chromosomes random information exchange mechanism. A genetic algorithm solves optimization problems by the initial population variation, crossover and recombination, and natural selection, etc. It can receive the most suitable new individual through limited iteration, which is the overall (or similar) optimization solution of the problem (Xiaoping et al., 2002). Figure 1 shows the basic flow diagram of a simple genetic algorithm.

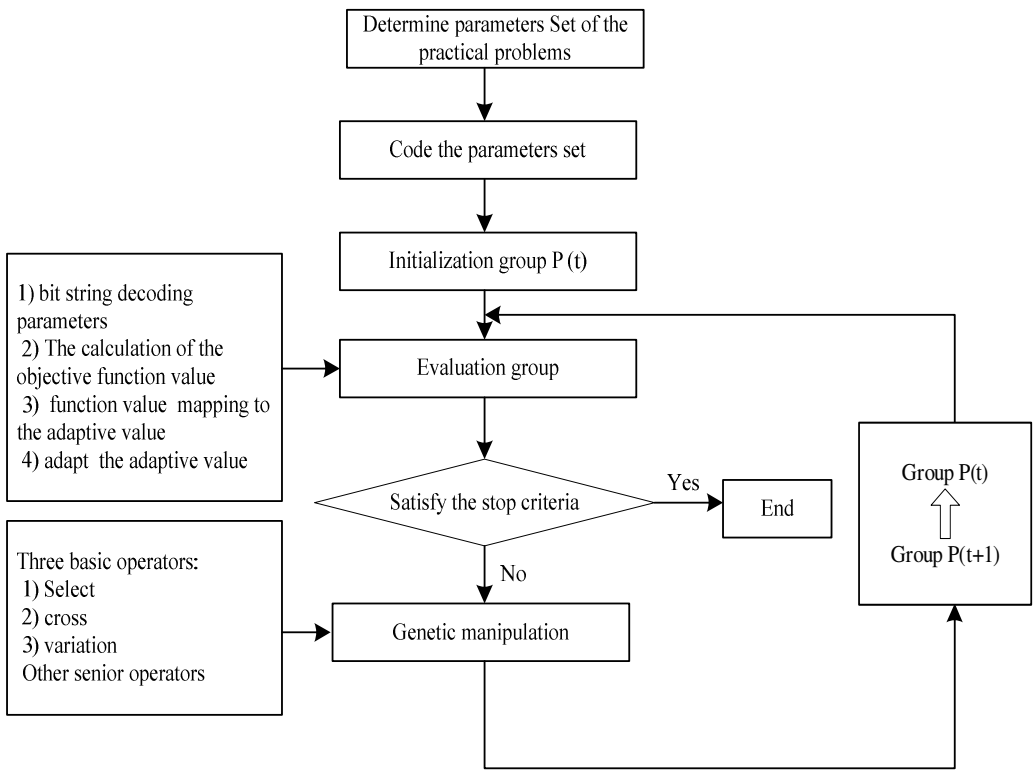

Figure 1. Basic flow diagram of simple genetic algorithm.

Process of Solving the Model

Thinking that some variables are discrete variables in these issues, we can see from the analysis of L, restrictive condition (2-11) shows the relationship between the demand distributed by every customer at distribution centers and the distribution center site selection program under an equilibrium state. That is, for the lower problem, z_k is known; if z_k=0, then x_{ik}=0, this restrictive condition can be deleted. If z_k=1, then $x_{ik} \le M$. M is an arbitrarily large number. This constraint naturally is okay and can be deleted. However, to get the concrete form of response function, restrictive condition (2-11) can be changed into the following form (but not to join the model).

$$x_{ik} = M \cdot z_k - s_{ik} \quad i = 1, \ldots, m; \qquad k = 1, \ldots, n \tag{3-1}$$

Here, s_{ik} is the slack variable. When z_k=0, we can get the values of x_{ik} and s_{ik} .When z_k=1, solve L using the existing methods, then we get customer demand x_{ik}^* in every distribution center under a balanced state. Then, the value of the slack variable s_{ik} is calculated using (3-1). Thus, all the functions can be written as follows:

$$x_{ik} = M \cdot z_k - s_{ik}^* \tag{3-2}$$

The above relationship is put into the upper objective function, and then the function is solved. For the optimal solution from the upper problem, we solve the lower problem once again to get the customer demand distribution between the distribution centers. Repeating the processes, we can get a new location program. Such double counting, the final is expected to converge to the optimal solution of the top programming model. Specific calculation steps are as follows:

Step 1: Set an initial solution z_k^0, the number of iterations r=0

Step 2: For given z_k^r, solving the lower problem, we get x_{ik}^r

Step 3: According to (3-2), calculate s_{ik}^r, put $x_{ik} = Mz_k - s_{ik}^r$ into the upper objective function; solving the upper problem combined with C_{ik}^r, we can get a new value z_k^{r+1}

Step 4: If $\left|F^{r+1} - F^r\right| \le \varepsilon$, stop. Otherwise, set r=r+1, turn to the second step; ε is the iterative precision.

EMPIRICAL STUDY OF LOGISTICS CENTER LOCATION

Case Description

A Dairy (Group) Company Limited is China's largest milk collection agricultural industrialization enterprise. The company has a factory in a region where there is a distribution center. Products are shipped to the distribution center first, then shipped by special vehicles from the distribution center to a retail shop where customers buy the products. The company now needs to establish at least one new distribution center at three candidate sites because of the expanding needs. In addition, the region has a number of other distribution centers that have a unified name, "social distribution center." These centers also serve customers in this region, so there is competition for this company. The demands of the five distribution centers are 7,000, 15,000, 13,000, 10,000, and 9,000. The network is shown in Figure 2. Related costs and a list of known parameters are shown in Table 2 - Table 6.

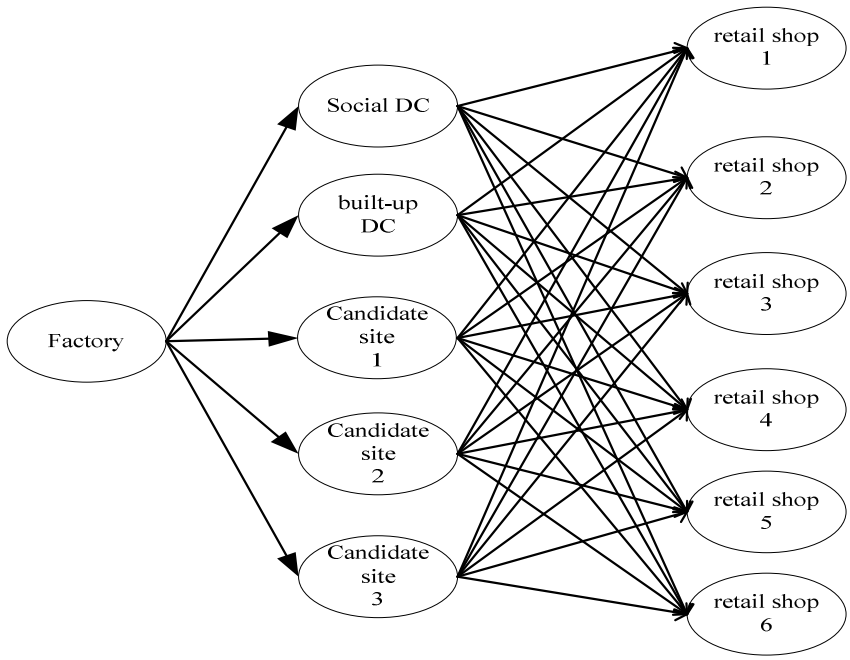

Figure 2. Network diagram.

Table 2. Transport Rates of Distribution Center to Retail Shop.

	Social DC	*Built-Up DC*	*Candidate Site 1*	*Candidate Site 2*	**Candidate Site 3**
1	30	25	19	20	24
2	26	21.5	33	18	23
3	25.5	27	20	23	21
4	19.5	20.5	23	21.5	28
5	31	27	25.5	21	17
6	22.4	23.6	26.4	26	21

Table 3. Distribution Center's Largest Annual Handling Capacity and Unit Volume Cost.

	Social DC	Built-Up DC	Candidate Site 1	Candidate Site 2	Candidate Site 3
Largest annual handling capacity	88,000	13,000	20,000	21,000	19,000
Unit volume cost	0.32	0.41	0.38	0.35	0.33

Table 4. Construction Costs and Operating Expenses of Candidate DC.

	Candidate Site 1	Candidate Site 2	Candidate Site 3
Construction costs	89	98	67
Operating expenses	2,500	2,600	2,800

Table 5. Transport Distance.

	Built-up DC	Candidate Site 1	Candidate Site 2	Candidate Site 3
1	215	120	200	135
2	198	145	350	150
3	145	200	200	120
4	202	194	195	175
5	173	185	135	195
6	184	215	215	205

Table 6. Transportation Price and Distance from Factory to Distribution Center.

	Built-up DC	Candidate Site 1	Candidate Site 2	Candidate Site 3
Transportation price (Yuan/box)	11	10	12	15
Distance	165	120	190	155

CASE ANALYSIS

We solve the problem with the bi-level goal programming location model. In the upper planning, the upper objective function makes the total costs of the construction of distribution centers and the costs that are used to meet the consumers' demand the smallest from the decision-makers' point of view. The

lower objective function aims at distributing the demands among all distribution centers to achieve the lowest customer spending costs from the customers' (distributors') point of view. In this case, the corresponding parameter settings are as follows:

Population size (popsize) = 80
Cross-rate (pcross) = 0.6
Mutation rate (pmutation) = 0.05

The main program of solving the example using MATLAB is:

[x endPop bpop trace] = ga([0 1] 'fitness'[][][1e-6 1 1],'maxGenTerm'20 'normGeomSelect', [0.08] ['arithXover'] [2 0] 'nonUnifMutation', [2 1 3])

The genetic algorithm used to obtain a general approximate optimal solution, rather than the optimal solution and the convergence of genetic algorithm, is related to its initial value. So we repeat the commands many times to get the approximate optimal solution, using different initial groups randomly. Table 7 shows the final results of the five running programs.

Table 7. Location Probability of Candidate Sites 1, 2, 3.

	1	2	3	4	5
Candidate Site 1	0.8964	0.9871	0.8878	0.9827	0.9053
Candidate Site 2	0.1381	0.631	0.5818	0.0841	0.6976
Candidate Site 3	0.2239	0.3461	0.3938	0.1287	0.591

According to the varying methods of the encoding scheme, we conclude the location is not here when the location probability is between [0, 0.8]; when the location probability is larger than 0.8, then the site is here. From the results above, we conclude it is better to build a new distribution center at Candidate Site 1. Figure 3 shows the tracking chart for optimizing performance of the genetic algorithm. As can be seen from the chart, when the genetic algebra reaches 20 generations, the changes in solution and the average population begins to stablize.

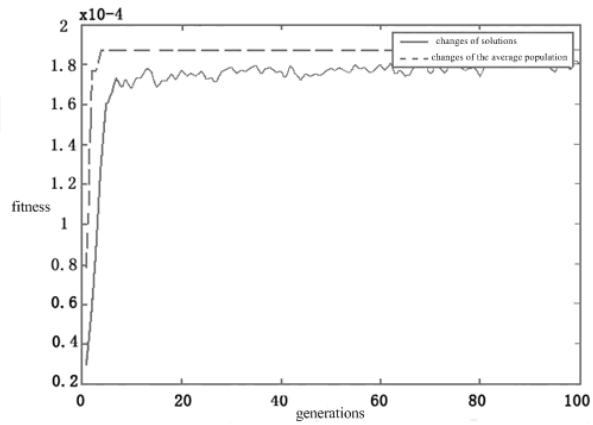

Figure 3. Changes of solutions and populations.

From the examples above, we can see the model is effective. This model has better adaptability and cost savings than the common location models and is more convenient and faster.

CONCLUDING REMARKS

This paper presents a logistics center location bi-level programming model based on competition. Upper programming (U) can be described as determining the best location for the new logistics center to minimize total costs within an allowed fixed range, while lower programming (L) describes the distribution patterns of customer demands between different logistics centers under the condition that there are several logistics centers. The goal is to make every customer have the lowest costs. The upper objective function makes the total costs of the construction of distribution centers and the costs that are used to meet the consumers' demand the smallest from the decision-makers' point of view. The lower objective function aims at distributing the demands among all distribution centers to achieve the least customer spending costs from the customers' (distributors') point of view. This paper analyzes the model and algorithm by means of a case study of a milk company and shows that the model and algorithm are both effective and practical.

REFERENCES

Amouzegar. (1999). "A global optimization method for nonlinear bi-level programming problems." *IEEE Trans on Systems, Man, and Cybernetics*, 29(6), 771-777.

Hong, Huo. (2004). "Research of distribution center." *Logistics Technology,* 27(2), 50-52.

Huijun, Sun, and Ziyou, Gao. (2003). "Bi-level programming model and algorithm of the logistics distribution center location considering the routing." *China Road Journal,* 16(2), 115-119.

Xiaoping, Wang, and Liming, Cao. (2002). *Genetic algorithm - theory, application and software implementation*. Xi'an Jiaotong University Press.

Xingdong Miao and Yinghong Li. 2004. "The exploration of gravity method location." *Traffic Standardization,* (10), 50-52.

A Model and Heuristic Algorithm for Inventory Routing Problem in Emergency Logistics

Xie Binglei and Hu Xiaoming

Shenzhen Graduate School, Harbin Institute of Technology, Shenzhen, Guangdong, 518055，China;Email: xbl7586@tom.com, frank0127@126.com

ABSTRACT

Model and heuristic algorithm are designed to solve inventory routing problem in emergency logistics with fuzzy demands and split delivery. Fuzzy demands are converted to deterministic demands by Yager's fuzzy number ranking method. A model which considers effects of stock-out is designed to optimize distribution period of the affected areas. Meanwhile, a modified vehicle routing model with split delivery is provided by tightening some constraints in order to decrease search space. A heuristic algorithm is used to coordinate inventory control and route optimization for minimizing total cost. The result shows that the benefits can be obtained from the integration of inventory and transportation.

Key words: emergency logistics; inventory routing problem; fuzzy demand; split delivery

INTRODUCTION

In recent years, as disasters which may occur abruptly and come with enormous consequences have brought great loss to human beings, such as Wenchuan Sichuan earthquake (2008), SARS (2003) in China, the 911 terrorist attack in US (2000), efficient and effective emergency logistics has became a worldwide noticeable problem.

One of the main missions in emergency logistics is to carry out relief delivery from distribution centers to affected areas. Both inventory controlling and vehicle routing are two fundamental and crucial items in logistics management. The inter-relationship between inventory and vehicle routing has recently motivated some authors to model these two activities simultaneously, which is known as the integrated Inventory Routing Problem (IRP). IRP can be seen as an extension of Vehicle Routing Problem (VRP). However, IRP does not include delivery routes only but also quantity to deliver to each customer as well as time for delivery.

Most researchers employ some strategies that allow IRP to be decomposed into two underlying problems, namely inventory problem and travelling salesman problem. The inventory problem is solved to determine replenishment quantities as well as replenishment times. The solution methods either find the routes first and then solve IRP formulation, or solve the inventory control problem first and then construct the routes for each demander. However, emergency system is unique in many aspects that may amplify complexity and difficulty in solving IRP. For example, in most of disaster cases demand information is provided by affected people under emergency conditions. Such information is rather fuzzy and hardly predicted due to lack of relative historical data, especially in the immediate

aftermath.

In the paper, a model and heuristic algorithm is designed to solve inventory routing problem in emergency logistics with fuzzy demands and split delivery.

DESCRIPTION OF THE IRP WITH FUZZY DEMAND AND SPLIT DELIVERY

The problem can be described as follow: a emergency distribution center serves affected areas which are geographically dispersed in a given area. Let 0 represent the distribution center, {1, 2, …, N} represents a set of affected areas. In a planning horizon T, every affected area faces a fuzzy, independent demand per day in which the membership function is known. Distribution is fulfilled without any delay by a fleet of homogenous vehicles with limited capacity V. No backorder is allowed at each area but each area may hold a local inventory used to meet future demands with a holding cost. The delivery to each area in each period can be performed by multiple vehicles. The objective is to minimize total cost, which includes fixed cost, cost of stock-out, cost of storage, and routing cost. Hereafter, notations are defined as follows

(1) *Parameters*

$c = \{c_{ij}\}$ Transportation cost of a vehicle send out product per unit from i to j where satisfy $c_{ij} = c_{ji}$ and $c_{ik} \le c_{ij} + c_{jk}$, for any i, j, k

$c^e = \{c^e_{ij}\}$ Transportation cost of an empty vehicle from i to j

$\tilde{\xi} = \{\tilde{\xi}_i\}$ Fuzzy demand of affected area i per day, $\tilde{\xi}_i$ and $\tilde{\xi}_j$ are independent for any $i \neq j$

s Price of product per unit

$p = \{p_i\}$ Stock-out penalty cost of product per unit per day in area i

$h = \{h_i\}$ Holding cost of product per unit per day in area i

(2) *Decision variables*

$q = \{q_{ij}\}$ Quantity of products transported through a directed arc (i, j)

$x = \{x_{ij}\}$ Number of vehicles visited a directed arc (i, j)

$d = \{d_i\}$ The optimal replenishment period of affected area i

SOLVING IRP WITH FUZZY DEMAND AND SPLIT DELIVERY

Inventory problem with fuzzy demand

In emergency logistics, the demand is believed subjectively to be a fuzzy number $\tilde{\xi}$. It's described as a general membership function $\mu_{\tilde{\xi}}(x)$

$$\mu_{\tilde{\xi}}(x) = \begin{cases} L(x), & r_1 \le x \le r_2, \\ R(x), & r_2 \le x \le r_3, \\ 0, else \end{cases} \tag{1}$$

where $L(x)$ and $R(x)$ are left and right shape functions。

In order to solve IRP with fuzzy demand in emergency logistics, a fuzzy demand is converted to a deterministic demand. Assuming the deterministic demand

is Q, increment cost $\tilde{T}(Q)$ between fuzzy demand and deterministic demand is

$$\tilde{T}(Q) = sQ + p\max\{0, \tilde{\xi} - Q\} + (h - s)\max\{0, Q - \tilde{\xi}\} \quad (2)$$

For a specified order quantity Q, the cost is only dependent on real demand x. Because $T(x|Q)$ is a linear function about x, the demand x and the cost $T(x|Q)$ have the same membership grade. In other words, the memberships functions of $\tilde{\xi}$ and $\tilde{T}(Q)$ have the same shape.

Since $\tilde{T}(Q)$ is a fuzzy variable, whose membership function is unknown, it can be ranked by the existing ranking methods. Chiang Kao and Wen-Kai Hsu (2000) had given a process of dealing with fuzzy variable with unknown membership function by Yager fuzzy number ranking method (1981). Therefore the calculation process is omitted here. The computing formula of Q is

$$Q = \begin{cases} L^{-1}(2(p-s)/(p+h-s)), & p < s+h, \\ R^{-1}(2h/(p+h-s)), & p \geq s+h, \end{cases} \quad (3)$$

On one side, decision makers can adjust subjectively the deterministic demand by controlling penalty cost p. On the other side, the transformation that $\tilde{\xi}$ is substituted by Q avoids solving complex fuzzy demand.

In IRP, if total cost is the sum of fixed cost (FC), cost of stock-out (OC), cost of storage (SC), and routing cost (RC) in a distribution period, average cost in per day is

$$AC = (FC + RC + OC)/d + hdQ/2 \quad (4)$$

Claudia、Savelsbergh and Speranza (2006) showed that the ratio of the optimal cost of the SDVRP over that of the corresponding VRP approaches 1/2 when the number of demand points goes to infinite. Here, $(cdQ + c^e)/2$ is used to estimate routing cost.

At the beginning of day 1, there are enough products. Assuming that if a stock-out happens on ith ($i \neq d$) day, then a replenishment is made immediately on that day and next replenishment is updated to $d+i$ and so on. Defining $OC(T,d)$ to be total cost of stock-out.

Let $p_i (1 \leq i \leq d)$ be the credibility that a stock-out first happens on day i, so the credibility that a stock-out happens in the next d days is $\sum_{i=1}^{d} p_i$, the credibility of no stock-out happens during period is $p_{d+1} = 1 - \sum_{i=1}^{d} p_i$. Here, the credibility p_i is give as: $p_i = Cr((i-1)\tilde{\xi} \leq dQ < i\tilde{\xi})$. The following relationships are hold

For $d \geq T \geq 2$, $OC(T,d) = \sum_{j=1}^{T} p_j (OC(T-j,d) + P)$; (5)

For $T \geq d+1$, $OC(T,d) = \sum_{j=1}^{d} p_j (OC(T-j,d) + P) + p_{d+1} OC(T-d,d)$; (6)

where P is the loss of a stock-out which is a constant。

For a fixed period d, $OC(T,d)$ is dependent on T. Defining $y_T = OC(T,d)$, the following equations are obtained.

$$y_T = \begin{cases} \sum_{j=1}^{T} p_j y_{T-j} + P\sum_{j=1}^{T} p_j, 2 \le T \le d \\ \sum_{j=1}^{d} p_j y_{T-j} + P\sum_{j=1}^{d} p_j + p_{d+1} y_{T-d}, T \ge d+1 \end{cases}, y_1 = 0 \quad (7)$$

However, only the condition that $T \ge d+1$ is considered. From the associated homogeneous equation $y_T - \sum_{j=1}^{d} p_j y_{T-j} - p_{d+1} y_{T-d} = 0$, $y_T = f(T,d) + \alpha(d)$ is hold, where $f(T,d) = \sum_{i=1}^{d-1} \omega_i r_i^T$ ($r_i (|r_i| \le 1)$ is the solution of the equation, ω_i is a constant, $\alpha(d)$ is independent on T). Subsequently, a particular solution needs to be found. Assuming the form of a particular solution is $y_T = \beta(d)T$ where $\beta(d)$ is independent on T. Replacing y_T by $\beta(d)T$, the formulation of $\beta(d)$ is obtained.

$$\beta(d) = P\sum_{j=1}^{d} p_j / (\sum_{j=1}^{d} j p_j + d p_{d+1}) \quad (8)$$

Therefore, the total cost of stock-out for $T \ge d+1$ is described as follow.

$$OC(T,d) = f(T,d) + \alpha(d) + \beta(d)T \quad (9)$$

Noticing that $\lim_{T \cdots d} OC_T(d)/T = \beta(d)$, let $\beta(d)$ be the average cost of stock out during period. Therefore, the optimal replenishment period d^* needs to satisfy the condition that $d^* = \min_d (\beta(d) + dhQ/2 + (FC + 0.5c^e)/d)$.

Modified SDVRP model

Split delivery vehicle routing problems (SDVRPs) were introduced by Dror and Trudeau in 1989. Unlike VRPs, SDVRPs allow delivery to a demand point to be split by two or more vehicle. Since SDVRPs are NP-hard, instances of realistic size is difficult to solve directly. Heuristics algorithms are often used to find good solutions to various routing problems in reasonable time. In this section, a modified SDVRP model is provided by tightening some constraints in order to decrease search space.

Theorem 1 (Dror and Trudeau, 1990). If $c_{ij}, i, j = 1, \cdots, N, i \ne j$ satisfy the triangle inequality, then no two routes in optimal solution have more than one common customer.

From theorem 1, it's easy to deduce that $x_{ij} \in \{0,1\}$, and $x_{0i}, x_{0j} \ge 0$ are integers.

Property 1. If the same conditions of Theorem 1 hold, then the optimal solution (x^*, q^*) satisfies $x_{0i}^* = [q_{0i}^*/V], i = 1, \cdots, N$. Here, $[q_{0i}^*/V]$ is the nearest integer less than or equal to q_{0i}^*/V.

Proof: Because $x_{0i}^*, i = 1, \cdots, N$ are integers, $x_{0i}^* \ge [q_{0i}^*/V], i = 1, \cdots, N$ holds. If in optimal solution (x^*, q^*), there exists $i \in \{1, \cdots, N\}$ not satisfying $x_{0i}^* = [q_{0i}^*/V]$, namely $x_{0i}^* \ge [q_{0i}^*/V] + 1$. Consequently, there exits another demand area j satisfying $x_{ij}^* = 1$ and $q_{0i}^* \ge q_{ij}^*$. Variables $x_{ij} = x_{ij}^* - 1 = 0$, $x_{0i} = x_{0i}^* - 1$, $x_{0j} = x_{0j}^* + 1$, $q_{0i} = q_{0i}^* - q_{ij}^*$, $q_{ij} = 0$, $q_{0j} = q_{0j}^* + q_{ij}^*$ are substituted in the solution, and other variables remain unchanged. The modified solution is also a feasible solution of the problem. However, the transportation cost of the new solution is reduced by

$(c_{0i}+c_{ij}-c_{0j})q_{ij}^*$. The above operation can be repeated until $x_{0i}^*=[q_{0i}^*/V]$. Therefore, $q_{0i}^*/V \le x_{0i}^* < q_{0i}^*/V+1$ holds. Furthermore, $x_{ij}^*=0$ holds when $q_{ij}^*=0$. So $q_{ij}/V \le x_{ij} < q_{ij}/V+1, i=0,1,\cdots,M, j=1,\cdots,M$ and $q_{ij}(1-x_{ij})=0$ is hold. With the above theorem and property, a modified model of SDVRP with tighter constraints can be proposed.

A Heuristic algorithm

After distribution periods are determined, the problem is similar to a periodic IRP. A heuristic algorithm to integration inventory and vehicle routing problem is designed as follows.

Step 1: Determining the initial optimal replenishment period and quantity of every affected area.

Step 2: Computing the expect cost include inventory cost and routing cost. Let iterative time $NC=0$ and $t'=1$.

Step 3: Improving the value of objective by modulating distribution dates in the planning period. Calculating increment inventory cost and routing cost of each affected area by moving the next replenish time t up to $t'(t'<t)$.

Step 4: Using greed algorithm to choose the substitute plan. The total cost and relevant information are updated.

Step 5: $t'=t'+1$. If $t'=T$, outputting the total cost, else go to step 3.

Step 6: $NC=NC+1, t'=1$. If NC is more than the maximal iterative time, the algorithm is terminated; otherwise, go to step 3.

NUMERICAL STUDY

The main purpose of numerical study is to demonstrate efficiency of the proposed method that can save cost by integrating inventory and vehicle routing in emergency logistics. Given a planning period 10 days, 20 affected area dispersed stochastically and consistently in region of [-5,5]×[-5,5], in which the coordinate of the distribution center is assumed to be (0,0). The capacity of vehicle V is equal to 100, and demands are supposed to be triangle fuzzy numbers simply. Other parameters are generated stochastically by computer.

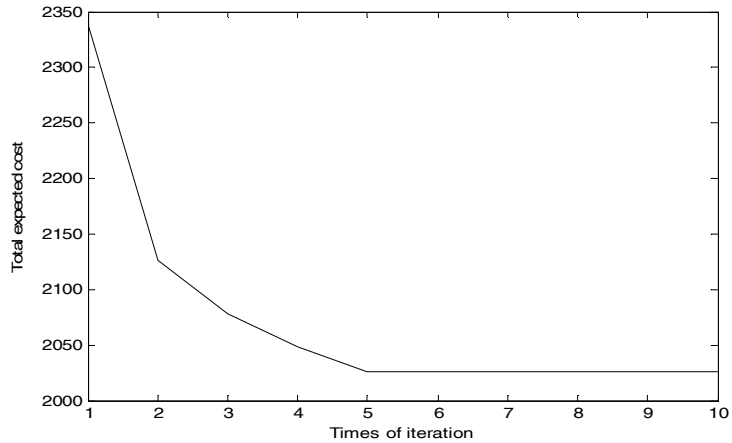

Figure 1. Iterations of the heuristic algorithm

Here, total cost is the sum of fixed cost, cost of stock-out, cost of storage and

routing cost in planning horizon T. From **Figure. 1**, in the early iteration, the value of total cost is improved obviously, but with development of iteration, the improvement is decelerated gradually until the cost is stable. The total cost goes down by 12.9% which is caused by integrating inventory and vehicle routing.

CONCLUSIONS

In the paper, minimizing total cost of IRP, a model and heuristic algorithm to solve the IRP in emergency logistics have been presented. The proposed approach involves four major steps: (1) describing demands in emergency logistics by fuzzy numbers, and converting fuzzy demands to deterministic demands with Yager fuzzy number ranking method; (2) optimizing distribution period by minimizing average expect cost; (3) modifying split delivery vehicle routing problem with tightened some constrains; (4) integrating inventory and vehicle routing by heuristic algorithm.

A numerical study was provided to illustrate efficiency of the method in solving IRP in emergency logistic. By comparing the total cost at initial step with that at convergence step, the numerical results reveal that cost could go down by 12.9%, resulting from the integration inventory and vehicle routing.

Nevertheless, there is still a great potential for improving performance of IRP in emergency logistics. One orientation is integrating time window and resource constrains. Furthermore, it will be conducted to improve the proposed algorithm. Alternative heuristic rules and meta-heuristic features will be examined to enhance efficiency and reducing computational time.

ACKNOWLEDGEMENT

The authors wish to acknowledge the financial support from National Soft Project Research Plan of The Ministry of Science and Technology of P. R. C. (Project No. 2009GXS5D130).

REFERENCES

Campbell A.M., Clarke L., and Savelsbergh M.W.P.(2002). Inventory routing in practice: the vehicle routing problem, SIAM Monographs on Discrete Mathematics and Applications, 309-220

Chiang K., and Wen-kai H. (2000). A single-period inventory model with fuzzy demand, Computers and Mathematics with Applications, 43(6/7):841-848

Claudia A., Savelsbergh M.W.P., and Grazin S. (2006). Worst-case analysis for split delivery vehicle routing problem, Transportation Science, 40(2):2226-2234

Claudia A., and Grazin S. (2008). The split delivery vehicle routing problem: a survey, Springer Science+Business Media, LLC 2008:103-122

Dror M., Laporte G.. and Trudeau P. (1989). Vehicle routing with stochastic demands: properties and frameworks, Transportation Science, 23:166-176

Dror M., and Trudeau P. (1990). Split delivery routing, Naval Research Logistics, 37:383-402

Jaillet P., Bard J., Huang L., Dror M. (2002). Delivery cost approximations for inventory routing problem in a rolling horizon framework, Transportation Science, 36(3):292-300

Martin S., and Song J-H. (2007). Inventory routing with continuous moves,

Computers & Operations Research,34: 1744-1763

Moin N.H., and Salhi S. (2007). Inventory routing problems: a logistical overview, Journal of Operational Research Society, 58:1185-1194

Xie B.l., An sh., and Wang j. (2005). Stochastic inventory routing problem under B2C E-commerce, Proceedings of the 2005 IEEE international conference on e-business engineering

Yager R.R. (1981). A procedure for ordering fuzzy subsets of the unit interval, Information Science, 24: 143-161

Yu Y.G, Chen H.X, and Chu F. (2008). A new model and hybrid approach for large scale inventory routing problems. European Journal of Operational Research, 189:1022-1040

Study on Multi-dimensional Structure Model for Agricultural Products Logistics Organization in China

Yao Xinsheng, Xu Guangyin, Qu Jianhua, Wei Jianguang and Fan Shasha

College of Mechanical and Electrical Engineering, Henan Agricultural University, P.O. Box 450002, Zhengzhou, Wenhua ST 95; PH (086) 0371-63978179; FAX (086) 0371-63558368; email: yaoxsh@163.com

ABSTRACT

Affected by the traditional consciousness of small-scale peasant economy and the related national basic policy, the small and medium-sized self-employed individuals have been the main parts in the agricultural products logistics in China for a long time. Such agricultural products logistics have many shortcomings, such as its chaotic and dissipative nature and the low efficiency. In this paper, a multi-dimensional structure model of agricultural products logistics organization is developed, based on operating order, space order, time order, evaluation order and its evolution mechanism. The logistics elements evolved from the two-dimensional discrete operation point, to the three-dimensional independent logistics line, and then to the four-dimensional value added curve. Through the evolution of logistics elements, the efficiency of the agricultural products logistics organization can be improved continuously. At last, the implementations of the model are discussed.

1 INTRODUCTION

In recent years, the development of the agricultural products logistics in China has been behind the development of the socioeconomics, not only in operation but also in efficiency and benefit. It is very necessary to study the structural characteristics and the internal evolution rule of agricultural products logistics organization, in order to improve its efficiency and ensure its healthy development. Previous studies on agricultural products logistics are generally based on qualitative macro analysis rather than the basic law of organization. According to the problems in logistics organization of agricultural products in China, this paper investigates the inherent law of logistics organization of agricultural products and discusses the effective ways to promote its development.

2 THE CURRENT SITUATION

Agricultural products are the main sources of farmers' income and the basic insurance of their public life. With the continuous increase of living standard, the demand for the diversity, safety and timeliness of the agricultural products also increases. Agricultural products logistics is an economic activity to meet the user's needs by realizing the value of agricultural products and providing relevant information between producers and consumers. It includes a series of activities, such as gathering, transportation, storage, loading and unloading, packaging, processing, distribution and logistics information. Through this process the value of agricultural

products and the organizational objectives are realized. (Huang, 2005). The typical structure of the process of agricultural products logistics is shown in Figure 1.

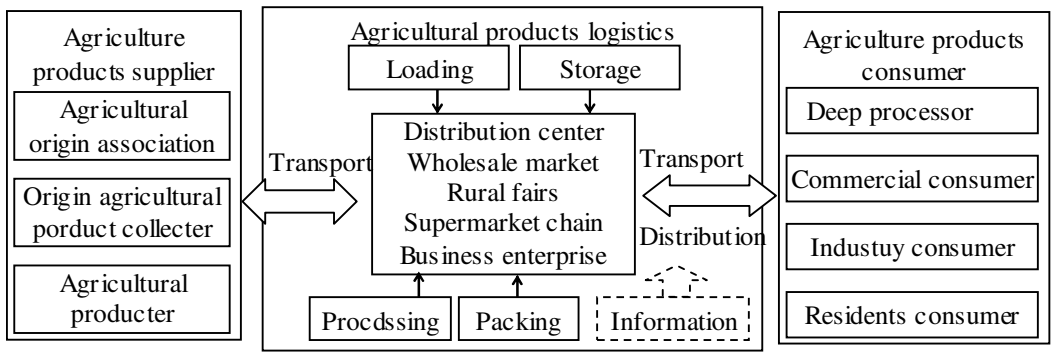

Figure 1. Typical processes of agricultural products logistics in China

In recent years, the National "Three Agriculture" policies have been promoting the development of agriculture in a new phase. Except that only small parts of agriculture products are for farmers' self-use, most of the products are put into agricultural commodity circulation, which generates the real or potential great logistics. In Henan province in 2007, for example, there are 9.46 million hectares of crops, 12.2 thousand hectares more than the previous year; 52.45 million tons of grain yield, increased by 2.6 million tons; 483.98 tons of oil production, increased by 5.2%; 74.74 tons of aquatic products, increased by 21.7% (NBS, 2007). The year-round logistics added 863.1 billion RMB, increased by 12.9%. The average annual growth rates of vegetable planting in China are nearly 10% in the 1980s and 14.5% in the 1990s. In 2007, 260 million Mu (a unit of area in China, 1 Mu is approximately equal to 666.67 square meter) of vegetable planting yields the total output of 565 million tons. However, compared with the developed countries, China's current agricultural products logistics has many problems, which seriously restrict its development. The agricultural logistics in China appears with low efficiency, high cost, high loss and laggard technology (see Table 1).

Table 1. The comparison of the agricultural products logistics

County	Logistics cost	Loss Rate	Processing proportion	Processing added	Supermarket chain operation proportion
Developed county	10%	5%	80%	1:(3-4)	80%-95%
China	40%(corps)	15%	10%	1:0.8	Less 30%
	60%(Fruits and vegetables)	25%	10%	1:0.8	Less 30%

According to the statistics of FAO, China's fruit planting area and the aggregate yields accounted for 18% and 13% of the entire world, while the vegetable planting area and the aggregated yields accounted for 43% and 49% of the entire world. All of these percentages rank first among other countries in the world. However, the logistics costs of vegetable and fruit are high. Every year there are

nearly 1200 tons and 1.3 million tons of corrosion damages for fruit and vegetable respectively, with the total economic losses more than hundred billions RMB (Zhang, 2007). In logistics organization, the market system has some faultiness, leading to the results that some agricultural products cannot be put into circulation or realize their value. (1) Because of the numerous small-scale, unregulated business owners, the overall intensive degree is too low. These small farmers, who lack market power, can hardly respond to the impact of the market and modern large-scale logistics enterprises. (2) The level of information technology for agricultural products logistics is too low. The required information of supply chain is distorted seriously, which greatly destroys the coordination in supply chain. (3) Harvesting, drying, sorting, portage and other logistics operation are mostly conducted manually. The major transportation is by ragtops. Only 30% of the transportation vehicles are vans and less than 1/10 vehicles are equipped with refrigeration machinery. In some rural regions, transportation system is inadequate without inter-modal transportation network. (4) There is no specialized training system or intelligent mechanism for agricultural products logistics in China. The agricultural products logistics personnel are in short supply. (5) Government has issued many policies to promote the legislation and investment for the agricultural cooperation, but its implementation is inadequate.

3 DATUM ORDER FOR AGRICULTURAL PRODUCTS LOGISTICS ORGANIZATION

Agricultural products logistics can be a network, a chain, or a combination of some chains (Bouckova, 2002). Before logistics, there exists “former logistics business”, including agricultural production, agricultural planning, material supply and other supporting activities. After logistics, there exists “latter logistics business," including fashioning, marketing and many other activities related to food market.

Affected by the small-scale peasant economy, agricultural products logistics reveals obvious scattered characteristic. The logistics of agricultural products need to be fully considered with the time and regional characteristics. This paper investigates the agricultural products logistics organization in four datum orders: the operation order, the time order, the space order and the evaluation order. The operation order, which includes type and volume, is the basis of the agricultural products logistics. The type includes five general logistic operations and other additional content. The volume is the number of indicators. For a real logistics business it is the actual business volume. The time order refers to the relationship of the agricultural products logistics in the time dimension, including the specific logistic business relations before and after order, as well as the connections among other logistic operations. The space order refers to the location-based geographic relationships involved in agricultural products logistics. The evaluation order is the overall evaluation of the completed agricultural products logistics, including quality indicator, efficiency indicator and benefic indicator.

4 EVOLUTIONAL ORGANIZATION STRUCTURE MODEL

Based on the datum orders of organization degree of the agricultural products logistics, this paper analyzes the different levels of agricultural organizations. Figure

2 represents three modes of agricultural products logistics organizations in the evolution of three typical logistics patterns in China.

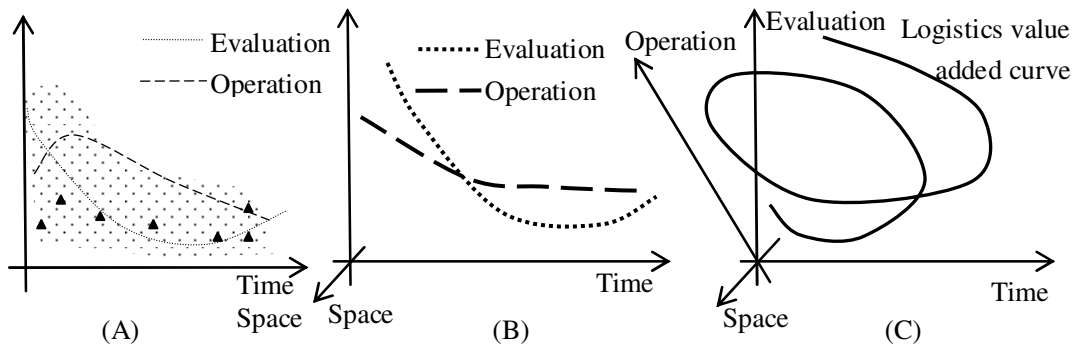

Figure 2. Organization degree of agricultural products logistics and its evolution

Figure 2A represents the primary stage of the agricultural products logistics. At this stage, the logistics is at a very low level. Many so-called logistic companies can only complete a few types of operations and low logistic volume. There is no collaboration or sustainability among the logistics operations. In the time dimension, it is mainly short-term, showing that the longer the time interval the less the period logistic demand there is. In space dimension, it is mainly regional, indicating that the bigger the space the smaller the operation volume will be. Moreover, logistics mainly focuses on small areas. The greater the space interval, the greater the time interval is. The supply chain for agricultural products is almost nonexistent. There is no contact between the various logistic segments. Thus the overall evaluation is bad. Only few rapid or long-distance logistics have a better evaluation. As shown in the figure, all the logistic business are presented as some sporadic scattered points; the volume and type of operation are not increased with the space and time. Most logistics of the agricultural products wholesales, distributions and markets in rural areas and towns in China were still in this stage.

By integrating some operations, the logistic operation mode of agricultural products has made great progress. The logistics of agricultural products has a certain development and has gradually evolved into three-dimensional logistic curve, which is shown in Figure 2B. At this stage, some entities reveal the archetypal features of logistics enterprises. They are able to complete two or more kinds of logistic operation and engage in a relatively stable and professional agricultural logistics system. Moreover, they have a certain amount of logistics volume, and a certain extension in time order and space order. However, it is still at a relatively low-level stage and it is not a completely continuous logistic curve. The overall evaluation is also ordinary. Currently, China's major logistic enterprises related to agricultural products, including some 3PL and 4PL, as well as some supermarkets and wholesale markets for agricultural products, are in this stage.

Based on the analysis of the previous two stages, this paper proposes a higher-level organizational model for agricultural products logistics, which is shown in Figure 2C. In this stage, the participated logistic enterprises can be involved in at least 2-4 types of logistic operations and professionally engage in logistics operation activities. In the time demission, most operation can be realized as an effective link

of all logistics operation to a certain extent. Some business can achieve JIT. In the space demission, the logistics can cross geographical boundary and cover a relatively large area. It has a certain degree of industrial concentration and forms a relatively stable industrial chain. Therefore, the logistic organization in this stage can achieve higher evaluation in quality, efficiency, effectiveness, social service and other aspects. It develops continuously and forms a logistic value curve. At present, there are hardly any logistic enterprises in China in this stage. Some model enterprises, such as Shuanghui Group and Sunxin Agriculture have shown the preliminary features. In this stage, "company + production + farmers" business model would be more prevalent. The awareness of quality, safety and efficiency is improved obviously. In addition, the integrated entity or enterprise, which combines production, processing, logistics, management and service, is being brought up gradually.

5 MEASURES TO IMPROVE THE ORGANIZATION LEVEL

In view of the industrial organization, we hope the logistics of agricultural products have a high level of organization, so that it can be improved in scale, efficiency, effectiveness, quality, etc. There are already a lot of approaches to improve the logistics organization level, such as the methods of information, networks, decision-making and administration proposed by many scholars and entrepreneurs. With this understanding, this paper proposes several ways to improve the organization degree of agricultural products logistics, based on the theories of swarm intelligence.

Considering logistics individuals of agricultural products have the similar characteristics with the intelligent agents, and the dynamic alliance or enterprises can be formed with scale economies. In order to save logistic resources and to achieve the maximum social benefits, the swarm intelligence theory is adopted as the solution algorithm. For a given logistic business, there is a four-dimensional order in time, space, operation and evaluation, where the intelligent agents can move. Through the collaboration of the autonomous action of multiple agents, the logistics value is enhanced. The algorithm is described as follows. Assume the data set of logistic business members is $B=\{Bi=(b_{i1}, b_{i2}, \ldots,b_{im}), i=1,2,\ldots,N\}$, representing the set of N members in agricultural products logistic enterprise. For one logistic enterprise Oi, $o_{i1},o_{i2},\ldots,o_{im}$ are the performance index, and m equals 4.

$$\text{Consider } d_{ij} = \left\| P(B_i - B_j) \right\| = \sqrt{\sum_{k=1}^{m} w_k (b_{ik} - b_{jk})^2}$$

where $dij(B_i, B_j)$ is the Euclidean distances between B_i and B_j, representing the cooperation likelihood between B_i and B_j in the real world. P represents the weighted integration and w is the weight. For the virtual enterprise, the weight w of the operation may be bigger, while for the dynamic alliance, the performance indices for the time and space may be bigger. The candidate *area* (B_i, r) represents the cooperation field of data object B_i, which expresses a group of logistics individuals who cooperate closely. r is a four-dimensional radius. In operation, individual selects its cooperation set $A = \{Ai=(a_{i1},a_{i2},\ldots,a_{ik}), a_{ik}\in O\}$ in $area(O_i,r)$, by optimizing the objectives using the multiple-agent algorithm. In application, the cooperation must be optimized in some aspects. The detailed algorithm can be found in other studies (e.g. Yao, 2008).

In addition, other measures should be made to improve the organization level of agricultural products logistics, such as reinforcing information construction, improving market mechanism and vitality, talented personnel training, system standardization construction, improving industrial concentration, and so on.

6 CONCLUSION

Efficient logistics can reduce the costs of production and circulation of agriculture and promote the process of modernization of agriculture. Moreover, it can also increase the flow speed and protect the fundamental profit of both urban and rural residents, in order to improve the overall benefit of agriculture. At present, the small and medium-sized self-employed individuals are the main parts in the agricultural products logistics in China. The agricultural products logistics is in a mess, low efficient and dissipative. Therefore, the theoretical study which focuses on the organization structure of the agricultural products logistics is very essential.

In this paper we present the problems in agriculture products logistics in China, such as the high costs and loss rate, less value-added capability, the lack of specialied logistic personnel etc. We then propose a multi-dimensional organization evolution model of agricultural products logistics in theory. At last, based on the swarm intelligence theory, we discuss the information standardization technology and other recommendations to improve the efficiency of the logistics organization of agricultural products in China. This study intends to explore the suitable development path and to provide some theoretical reference for the healthy and rapid development of agriculture products logistics industry, and thus to promote the agricultural production and rural economy in China.

REFERENCES

Bouckova, B. (2002). “Agricultural Co-operatives: Perspectives for the 21st Century.” *Journal of Agricultural Economics*, 48(4), 166-170.

Huang, Z. (2005). “China's Logistics System for Agricultural Products: Their Development and Institutional Aspects.” *Issues in Agricultural Economy*, (4): 94-99.

National Bureau of Statistics. (2007). *China agricultural statistics* (2001-2007).

Ngai, E., and Gunasekaran, A. (2004). “Information Systems in Supply Chain Integration And Management.” *European Journal of Operational Research*, 159, 269-295.

Yao, X., Li, S., and Cui, Y. (2008). “Study on Virtual Logistics Enterprise Organization of Agricultural Products Based On Swarm Intelligence.” *Guangdong Agricultural Sciences*, (8), 174-178.

Zhang, R. (2007). “Integrative Innovation of Cold Storage Chain Technologies in Modern Logistics of Fruit and Vegetable.” *World Agriculture*, (9), 47-49.

Mean-CVaR Model of Wholesale Price Contracts and Dual Purchase Contracts in the Supply Chain

Y. G. Mu, Q. Mai, Z. B. Zhao, Y. J. Feng

Harbin Institute of Technology, No.92, West Da-Zhi Street, Harbin 150001, P.R. China; PH (86) 0451-86412866; FAX (86) 451-86412866; email: muyg_hit@163.com

ABSTRACT

Wholesale price contracts and dual purchase contracts are the most common contract styles in the supply chain because they are price-only contracts. The CVaR model of loss in revenue of retailers in the two styles of contracts under a two-level supply chain is proposed in this paper according to the definition of Conditional Value at Risk (CVaR), which previously has been used in financial engineering. Consequently, the mean-CVaR model, which aims at revenue maximization with CVaR risk explosion constraints, is proposed. The numerical results indicate that dual purchase contracts achieve strict Pareto improvement over wholesale price contracts, with more revenue and less risk explosion.

INTRODUCTION

Supply chain contracts can ensure the cooperation between both parties of a contract and realize the "win-win" condition based on information-sharing. As Arrow (1985) and Lariviere and Porteus (2001) point out, most of the research on these contracts ignores the administrative costs that occur in reality. The difficulties associated with administering complex contracts are also criticized by many practitioners. This paper focuses on price-only contracts, wholesale price contracts (WPC), and dual purchase contracts (DPC).

Research on wholesale price contracts falls into three areas. In the first, some papers examine the effect of wholesale price contracts on profit improvements in a supply chain. Cachon (2004) researched the order of retail after and before demand realization and addressed inventory risk-sharing based on a news vendor model. Taylor (2006) addressed the impact of forecast updating on order timing. Ye Fei (2006) investigated the mechanism of supply chain coordination under flexible demand. The second area studies forecast information asymmetry, such as Ozer and Wei (2006). The third area focuses on the effect of advance ordering on the supply chain.

None of these papers consider the risk aversion of the decision maker. This paper introduces the Conditional Value at Risk (CVaR), which is broadly used in finance engineering, into wholesale price contracts and dual purchase

contracts to consider the risk aversion of the decision maker. Mean-CVaR models are proposed in a two-level supply chain constituted by some suppliers and some retailers under random market demand. Based on the simulation analysis, this paper shows the effect on supply chain profit by risk aversion and the Pareto improvement caused by dual purchase contracts.

MEAN CVaR MODEL

In the research of Jiang Min et al. (2007) and Yu Chun-yun et al. (2007), the objective was to minimize α-CVaR. But, according to the research of Krokhmal (2002), by considering different expected returns, an efficient frontier can be generated. Theorem 3 in that research proves that the following three optimization problems are equivalent in the sense that they produce the same efficient frontier.

Theorem 1 Considering the function $\Phi(\mathrm{x})$ and $\Pi(\mathrm{x})$ dependent on the decision vector x, and the following three problems:

$$\text{(P1)} \qquad \min_{\mathrm{x}} \quad \Phi(\mathrm{x}) - \beta\Pi(\mathrm{x}), \quad \mathrm{x} \in X \quad \beta \geq 0$$

$$\text{(P2)} \qquad \min_{\mathrm{x}} \quad \Phi(\mathrm{x}), \quad \Pi(\mathrm{x}) \geq \rho \quad \mathrm{x} \in X$$

$$\text{(P3)} \qquad \min_{\mathrm{x}} \quad -\Pi(\mathrm{x}), \quad \Phi(\mathrm{x}) \leq \varpi \quad \mathrm{x} \in X$$

If $\Phi(\mathrm{x})$is convex, $\Pi(\mathrm{x})$ is concave and the set x is convex, then the three problems, (P1)-(P3), generate the same efficient frontier.

Based on the above theorem, the following part will adopt the structure of model (P3). The objective of optimization programming is to minimize the negative expectation of revenue, and the CVaR will be considered as a constraint. In this way, when maximizing the expectation of revenue, the risk will be controlled within a given bound. This method can give many effective frontiers based on different risk level.

Mean-CVaR Model under Dual Purchase Contracts

Revenue and Loss Function. In dual purchase contracts, there are two prices, an advance purchase price w_b and the regular wholesale price w. The retailer pays w_b for each unit ordered before observing the forecast update and w after the forecast. The sequence of events for the retailer is as follows: (1) he parties agree on a w_b and w; (2) the retailer decides how much to order in advance of obtaining the forecast update and pays w_b per unit of advance order; (3) the retailer obtains the forecast update and decides how much more to order and pays w per unit; (4) market uncertainty is realized, and the retailer satisfies the demand from on-hand inventory as much as possible at a per-unit price.

Based on the above assumptions, the revenue function of the retailer in a

dual purchase contract is

$$\Pi^r(\mathrm{x}_1,\mathrm{x}_2,\mu_1,\mu_2) = \mathrm{r}E_{\mu_1}E_{\mu_2}\min\{\mathrm{x}_1+\mathrm{x}_2,\mu_1+\mu_2\}-\mathrm{w}_b\mathrm{x}_1-\mathrm{w}\mathrm{x}_2 \quad (1)$$

Similarly, substituting $\min\{\mathrm{x},\mu\}=\mathrm{x}-(\mathrm{x}-\mu)^+$ into equation (1), we get

$$\Pi^r(\mathrm{x}_1,\mathrm{x}_2,\mu_1,\mu_2) = \mathrm{x}_1(\mathrm{r}-\mathrm{w}_b)+\mathrm{x}_2(\mathrm{r}-\mathrm{w})-\mathrm{r}E_{\mu_1}E_{\mu_2}(\mathrm{x}_1+\mathrm{x}_2-\mu_1-\mu_2)^+ \quad (2)$$

Then, in a dual purchase contract, the loss in revenue of retailer is given by

$$f^r(\mathrm{x}_1,\mathrm{x}_2,\mu_1,\mu_2) = \mathrm{r}E_{\mu_1}E_{\mu_2}(\mathrm{x}_1+\mathrm{x}_2-\mu_1-\mu_2)^+-\mathrm{x}_1(\mathrm{r}-\mathrm{w}_b)-\mathrm{x}_2(\mathrm{r}-\mathrm{w}) \quad (3)$$

CVaR Constraint. If $\varpi \in R$ is the threshold of loss risk explosion, risk function $\Phi_\alpha(\mathrm{x}_1,\mathrm{x}_2)$ α-CVaR of loss function, then the linear constraints of α-CVaR can be given by

$$\varsigma+(J(1-\alpha))^{-1}\sum_{j=1}^{J}z_j \le \varpi$$

$$z_j \ge \sum_{i=1}^{n}\left(r_i\left(x_{1i}+x_{2i}-\mu_{1ij}-\mu_{2ij}\right)-x_{1i}\left(r_i-w_{bi}\right)-x_{2i}\left(r_i-w_i\right)\right)-\varsigma$$

$$z_j \ge 0, \qquad j=1,\ldots,J \quad (4)$$

Bounds on Ordering Quantity. Similar to a wholesale price contract, the size of the ordering quantity can affect the price. This also considers the bounds on ordering quantity. Therefore, the ordering quantity about x_1 and x_2 can be bounded as

$$0 \le \underline{x}_{1i} \le x_{1i} \le \bar{x}_{1i},$$

$$0 \le \underline{x}_{2i} \le x_{2i} \le \bar{x}_{2i} \qquad i=1,\ldots,n \quad (5)$$

The Optimization Problem. Based on the above assumptions and models, the optimization problem, whose objective is to maximize the revenue of retailer with α-CVaR constraints about loss in revenue, is given by

$$\min_{\mathrm{x}_1,\mathrm{x}_2,\varsigma} \quad \sum_{i=1}^{n}\mathrm{w}_{bi}\mathrm{x}_{1i}+\mathrm{w}_i\mathrm{x}_{2i}-\mathrm{r}E\min\left(\mathrm{x}_{1i}+\mathrm{x}_{2i},\mu_{1ij}+\mu_{2ij}\right) \quad (6)$$

subject to

$$\varsigma+(J(1-\alpha))^{-1}\sum_{j=1}^{J}z_j \le \varpi$$

$$z_j \ge \sum_{i=1}^{n}\left(r_i v_{ij}-x_{1i}\left(r_i-w_{bi}\right)-x_{2i}\left(r_i-w_i\right)\right)-\varsigma$$

$$z_j \ge 0 \qquad j=1,\ldots,J$$

$$v_{ij} \ge x_{1i}+x_{2i}-\mu_{1ij}-\mu_{2ij}, \quad v_{ij} \ge 0$$

$$0 \le \underline{x}_{1i} \le x_{1i} \le \bar{x}_{1i}$$

$$0 \le \underline{x}_{2i} \le x_{2i} \le \bar{x}_{2i}, \qquad i=1,\ldots,n$$

Mean-CVaR Model under Wholesale Price Contracts

In a wholesale price contract, the sequence of events for the retailer is as follows: (1) the parties agree on a wholesale price $\mathrm{w} \in R^N$ and sign the contract; (2) the retailer orders N products $\mathrm{x} \in R^N$ according to the forecast of market demand; (3) the retailer satisfies the demand from on-hand inventory at a fixed price.

Based on the above assumptions and models, the optimization problem, whose objective is to maximize the revenue of retailer with α-CVaR constraints about loss in revenue, is given by

$$\min_{\mathrm{x},\varsigma} \sum_{i=1}^{n} \left(w_i x_i - r_i E \min\left(x_i, \mu_{ij}\right)\right) \tag{7}$$

subject to

$$\varsigma + \left(J\left(1-\alpha\right)\right)^{-1} \sum_{j=1}^{J} z_j \le \varpi$$

$$z_j \ge \sum_{i=1}^{n} \left(r_i v_{ij} - \left(r_i - w_i\right)x_i\right) - \varsigma, \quad z_j \ge 0 \quad j = 1,\ldots,J$$

$$v_{ij} \ge x_i - \mu_{ij}, \quad v_{ij} \ge 0$$

$$0 \le \underline{x}_i \le x_i \le \overline{x}_i, \qquad i = 1,\ldots,n$$

By solving this problem, we get the optimal vector x^*, which is the optimal ordering quantity, and the corresponding VaR, which equals ς^*. The efficient return-CVaR frontier is obtained by taking different risk tolerance level ϖ.

NUMERICAL EXAMPLE

This section proposes a numerical example to compare revenue considering the CVaR constraints under wholesale price contracts and dual purchase contracts. For simplicity, the retailer orders only two products from the manufacturer. Assume the market demand for the first product follows truncated normal distribution on $[8,24]$ with mean 16 and standard deviation 4; the market demand of the second product follows truncated normal distribution on $[-8,8]$ with mean 24 and standard deviation 2. The forecasts for the two products all follow truncated normal distribution on $[-8,8]$ with mean 0 and standard deviation 5. The per-unit market prices of the two products are 10 and 6, respectively. Based on these assumptions, Table 1 illustrates the revenue and VaR of the retailer under different α and different contract prices, giving the fixed risk explosion threshold 10.

Table 1. Revenue and VaR of Retailer with Fixed Risk Explosion Threshold of 10.

α	Wholesale Price Contract (7,4)		Dual Purchase Contract (5,7;3,4)	
	Revenue	VaR	Revenue	VaR
0.6	143	6.9	294.4	4.8
0.75	142.5	8.8	291.6	3.3
0.95	142	10	284.9	10

Table 2 illustrates the revenue and VaR of the retailer under different risk explosion thresholds and different contract prices, giving the fixed α, which is 0.75.

Based on the above solutions, we get following results:

(1) By comparing the revenue and VaR in Table 1 and Table 2, we see that the revenue under a dual purchase contract is larger than that under a wholesale price contract, and the VaR under a dual purchase contract is less than that under a wholesale price contract. Therefore, although the forecast of market demand by the retailer requires more uncertainty, the dual purchase contract not only improves the revenue but also decreases the risk explosion of revenue. In another word, this kind of contract provides the strict Pareto improvement.

Table 2. Revenue and VaR of Retailer with Fixed α 0.75.

Risk Explosion Threshold	Wholesale Price Contract (7,4)		Dual Purchase Contract (5,7;3,4)	
	Revenue	VaR	Revenue	VaR
10	142.5	8.8	291.6	3.3
15	145	13.8	296.6	8.3
20	147.5	18.8	301.6	13.3

(2) Table 1 illustrates that the revenue of the retailer decreases and the VaR increases under not only a wholesale price contract but also a dual purchase contract, with the gradually increasing of confidence level α. This means that the revenue decreases when the retailer is more risk averse. But the effect is not outstanding, because when confidence level α changes to 0.95 from 0.6, which means the probability of loss in revenue not exceeding 10 increases to 0.95 from 0.6, the revenue under a wholesale price contract decreases 1, and the revenue under a dual purchase contract decreases 10, not reaching the 3.5% of initial revenue. Accordingly, it is absolute to fix a little small confidence level α, which can guarantee a higher revenue while satisfying the risk preference.

(3) Table 2 illustrates that the revenue of the retailer increases under not only a wholesale price contract but also a dual purchase contract, with the

gradually increasing threshold of risk explosion. This means that the revenue increases when the retailer is risk preference. But the table also illustrates that when the threshold of risk explosion increases times two, from 10 to 20, revenue under a wholesale price contract decreases 5, and revenue under a dual purchase contract decreases 10, which does not reach the 3.5% of initial revenue. Accordingly, it is good to be risk preference for the retailer. Under a fixed confidence level, revenue will be higher if given a lower threshold of risk explosion.

CONCLUSION

This paper researched the risk caused by the uncertainty of market demand and the forecast of market demand in a two-level supply chain constructed by manufacturers and retailers. Based on the risk model, this paper proposes Mean-CVaR models under wholesale price contracts and dual purchase contracts, which have been transformed into linear programming to get the optimal order quantity under the two contracts. The numerical example illustrates that dual purchase contracts increase retailer revenue and decrease the VaR, hence creating strict Pareto improvement. If the retailer is a risk preference and the confidence level is lower, the revenue of the retailer will reach a higher level while satisfying the risk threshold of risk explosion.

REFERENCES

Arrow, K. J. (1985). "The economics of agency." In Pratt, J. P., and Zeckhauser, R. J. (Eds.), *Principals and Agents*. Harvard Business SchoolPress, Cambridge, MA.

Cachon, G. (2004). "The allocation of inventory risk in a supply chain: Push, pull, and advance-purchase discount contracts," *Management Science,* 50, 222–238.

Erhun, F., Keskinocak, P., and Tayur, S. (2003). "Sequential procurement in a capacitated supply chain facing uncertain demand." Working paper, Stanford University.

Jiang min, Meng zhi-qing, and Zhou Gen-gui. (2007). "Conditional risk decision model of ordering portfolio multiproduct and inventory problem in supply chain," *Systems Engineering-Theory & Practice,* 12, 29-35 (in Chinese).

Krokhmal, P., Palmquisl, J., and Lrvasev, S. (2002). "Portfolio optimization with conditional value-at-risk objectives and constraints," *Journal of Risk,* 42(2), 124-129.

Lariviere, M, and Porteus, E. (2001). "Selling to the news vendor: An analysis of price-only contract,"*Manufacturing & Service Operations Management,* 3, 293–305.

Ozer, O., and Wei, W. (2006). "Strategic commitment for an optimal capacity

decision under asymmetric forecast information," *Management Science,* 52, 1238-1257.

Rockafellar, T., and Uryasev, S. (2002). "Conditional value-at-risk for general loss distributions," *Journal of Banking Finance,* 26, 1443-1471.

Tang, C. S., Kumar, R., Alptekinoglu, A., and Ou, J. (2003). "The benefits of advance booking discount programs: Model and analysis," *Management Science,* 50, 465–478.

Taylor, T. (2006). "Sale timing in a supply chain: When to sell to the retailer?" *Manufacturing & Service Operations Management,* 8, 23–42.

Ye, Fei, Li, Yi-na, and Fu, Shao-lin. (2006). "Research on supply chain wholesale price coordination mechanism with demand elasticity," *Industrial Engineering,* 9(5), 18-22 (in Chinese).

Yu, Chun-yun, Zhao, Xi-nan, Peng, Yan-dong, and Pan, De-hui. (2007). "Study of supply chains optimization and coordination model based on conditional value-at-risk," *Chinese Journal of Management Science,* 15(3), 31-39 (in Chinese).

Structure System Model of Modern Logistics

Chen Lijun[1], Chen Xuewu

[1]Key Laboratory of Transportation Planning and Management of Jiangsu Province, Transportation College, Southeast University, Nanjing, 210096, P.R. China
PH 15850550543; email: 2006clj@sina.com

ABSTRACT

It is a very important task to build a structured system for modern logistics development from the experiences of logistics developmental stages. However, at present the construction idea of modern logistics lack a complete and scientific structured system. First, several concerned points of developmental stages of modern logistics are elucidated. Secondly, a structured system model of modern logistics is proposed to be build, with characteristics of: one subject, two systems, three platforms, four logistics developmental modes, and five logistics service styles, in order to provide scientific guidance. According to the structure system model, the characteristics of specific components are analyzed from five aspects: subject, policy, platform, developmental mode and service style.

KEYWORDS

modern logistics; structure system model; guiding analysis

1 INTRODUCTION

The key to develop modern logistics mainly focuses on promotion and reformation of traditional logistics from the aspect of management ideas and operation. In the management ideas aspect, the goal is to realize optimal deployment of resources. In the operational aspect, the goal is to reflect advantages from service, management, technology and efficiency. Fen, H proposed a modern regional logistic system (Fen, H. 2006). He suggested that the full system of regional logistics include a logistics subject, two support systems and two basic platforms. His points mainly focus on management ideas of logistic without the operation aspect. We propose a structure system model of modern logistics with its characteristics for both management idea and operation aspects.

2 GUIDING ANALYSIS ON DEVELOPMENT STAGES OF MODERN LOGISTICS

2.1 Stage I: Resource Integration for Intensive Construction

Resource integration for intensive construction is the short-term goal of modern logistics development. In this step, new logistics projects are launched and logistics platforms of infrastructures are established by creating new logistics resources and integrating existing ones. A series of goals should be determined at this stage, ranging from production value of modern logistics, economic contribution, to the number of cultivated logistics enterprises with demonstration or leading effect.

2.2 Stage II: Platform Creation for Rapid Development

The second stage focuses on the improvement of the logistics network systems,

the construction of logistics information and organization platforms, and the maturation of policy systems. The construction of logistics network architecture is finished with logistics parks, logistics centers, distributing centers and logistics service stations as basic elements. Logistics industries are also encouraged to seek for their own characteristics and gradually increase the scales and the benefits of intensive management. Lastly, large-scale and professional modern logistics enterprise groups should be cultivated with band strength and core competitiveness.

2.3 Stage III: Function Enhancement for System Perfection

The third stage focuses on the overall enhancement and sustainable development of logistics system's functions. It is suggested that we should explore new developing spaces for industrial logistics, improve the service quality of various industrial logistics, and finally arrive at a real system with its own industrial characteristics. This system will rely on local area, radiating surrounding regions facing China, and aimed at the international world.

3 STRUCTURE SYSTEM MODEL OF MODERN LOGISTICS

The system model of modern logistics industry structure could be summarized in a numbered style as: one subject, two systems, three platforms, four logistics developmental modes, and five logistics service styles. This relationship is illustrated in Figure 1.

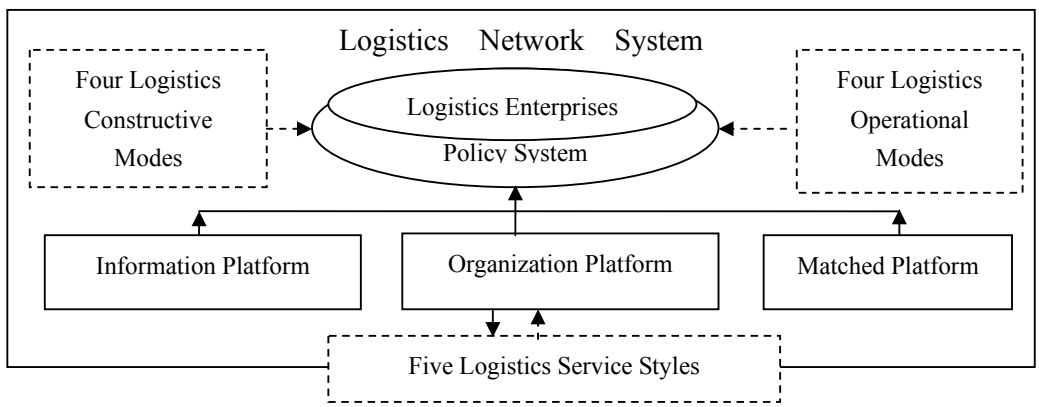

Figure 1. Structure System Model of Modern Logistics

3.1 One Subject

Traditional logistics enterprises, such as transportation enterprise, storage enterprise, agent enterprise and internal logistics department, are guided to transform to be third-party logistics enterprises. They are to improve competitiveness of logistics enterprises during modern logistics development.

3.2 Two systems

3.2.1 Policy system

In the process of policy system establishment, we should abide by the characteristics of market rules and benefits in accordance with city economics

features (Wen, K. 2007). Table 1 outlines the logistic policy system classes in detail.

Table 1 Logistics Policy System

Class	Detailed Content
Supportive Policy	Transportation management policy, tax policy, land-use policy, financing policy, government investment policy
Guiding Policy	Structure leading policy of logistics industry, network spatial layout leading policy, business firm leading policy
Developmental Policy	Cultivation policy for key logistics enterprises, introduction policies for foreign logistics enterprises and talents

3.2.2 Logistics Network System

The key elements of modern logistics network system, outlined in Figure 2, include logistics nodes hierarchical layout and logistics channel system (J. Bloomberg, D. 2004). The major task in this process is to make explicit the logistics nodes' location and the function orientation.

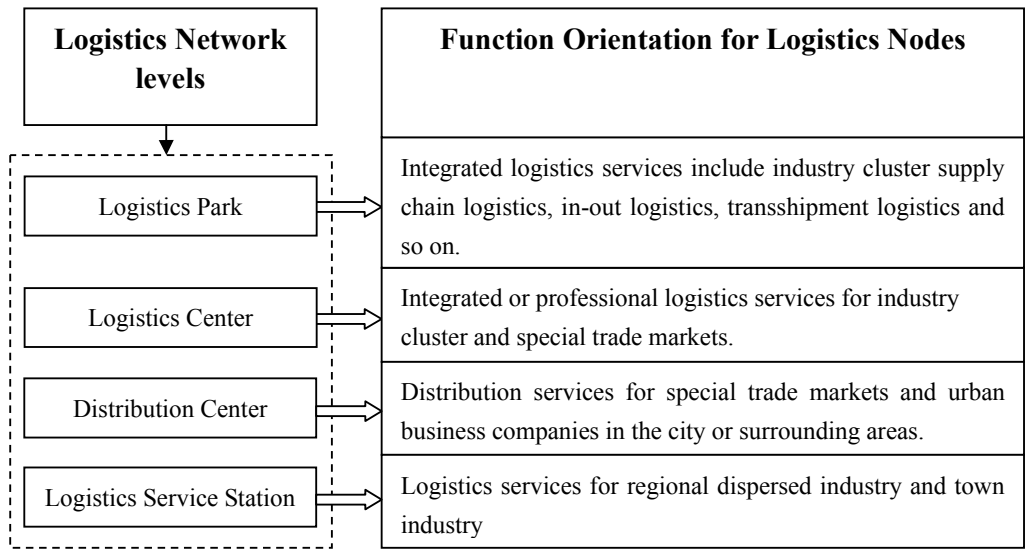

Figure 2. Logistics Network and Function Orientation

3.3 Three Platforms to Be Created

3.3.1 Infrastructure and Supporting Facility Platform

The planning for logistics infrastructure and supporting facility platforms focuses mainly on three aspects.

1. specifying the building object at all levels of the logistics network system;
2. according to local land using status, designing the spatial distribution of logistics nodes in detail, and establishing a structured system of logistics spatial distribution consisting of major logistics nodes and related transport routes as logistics channels,

3. planning the logistics nodes in detail.

3.3.2 Logistics Information Platform

It is expected that enterprises, markets, logistics nodes and some specific external interfaces be considered. Consequently, this provides a series of approaches for information exchange with provincial and municipal information platforms in the upper level, information resources sharing with platforms of other cities in the same level. In the lower level, a variety of accesses to information system of logistics nodes is provided as well as industrial management departments.

3.3.3 Logistics Organization Platform

Mainly by creating logistics industry association, logistics organization platforms are expected to play an important role in broadcasting industrial management standards, safeguarding legitimate rights and interests, promoting technical standards, exchanging industrial development information, and contacting with industrial enterprises (Liu Yinbing, L. X., Xiong Li 2008).

3.4 Four Logistics Developmental Modes

3.4.1 Four Logistics Constructive Modes

3.4.1.1 Trade logistics mode based on specialized market

In the background of existed regional commodity circulation, this mode converges on several links such as market trade service, storage, packaging and processing, and commodity distribution depicted in Figure 3. In the course of logistics activities, the characteristics are embodied as small batch and multi-batch, with diversification of logistics entities circulation varieties. The main businesses are focused on storage and commodity distribution. The key to run it effectively is the consistency of commercial flow and logistics and agility degree of information service.

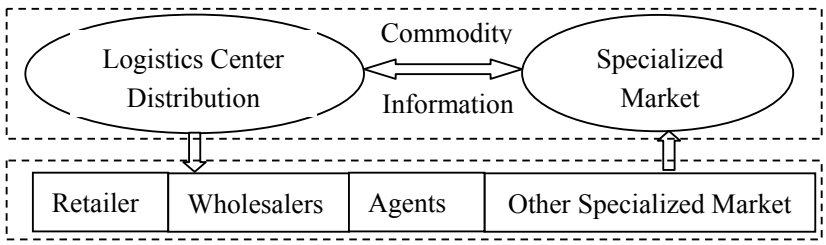

Figure 3. Trade Logistics Mode Based on Specialized Market

3.4.1.2 Integrated Logistics Mode Based on Freight Transit Hub

This mode undertakes regional logistics activities or logistics activities inner city with freight transit hub's function. It is base on special geographical position, such as ports and airport terminals. In the course of logistics activities, the characteristics are: embodied as huge batch of handling, loading and storage, scale and special logistics facilities and equipments, logistics value-added services such as health quarantine, insurance, declaring dutiable goods, international freight

forwarding, vessel-agency and so on. The key how to run it effectively is construction and operation capacity of logistics infrastructure. Logistics value added services based on freight transit hubs are outlined in Figure 4.

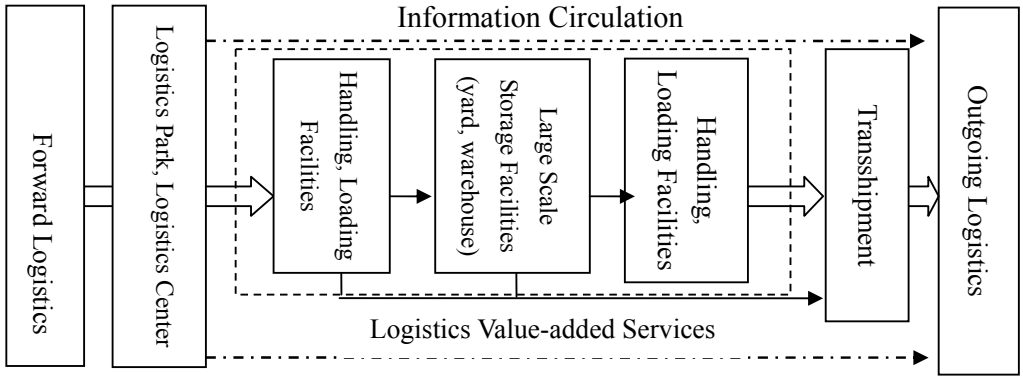

Figure 4. Integrated Logistics Mode Based on Freight Transit Hub

3.4.1.3 Multifunctional service logistics mode based on industry cluster district

The logistics layout relies on the geographical position and regional transportation condition. The different industries, depicted in Figure 5, in the cluster district are the main service objects. The mode demands establish a perfect logistics network which covers a certain range. Logistics demands service presents the characteristics of diversification. Logistics enterprises begin to supply customization and specialized logistics services.

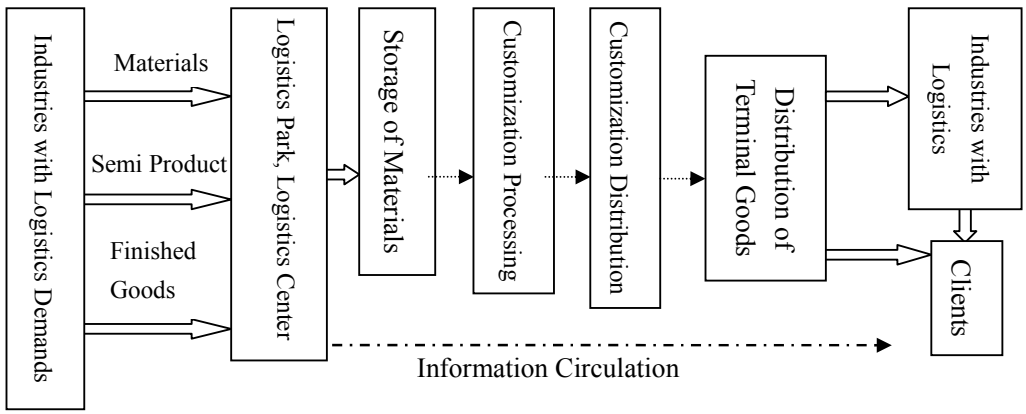

Figure 5. Multifunctional Service Logistics Mode Based on Industry Cluster District

3.4.1.4 Integrated purvey chain service logistics

The mode main supply stable purvey chain logistics service is the lead in the industry. In the logistics course, flow volume, flow direction, process and variety of freight in the purvey chain are grossly fixed. Logistics activities mainly emphasize distribution speed and quality assurance. According to order information and feedback information, logistics business request “just in time” logistics offer high

quality protection. Besides, it is necessary to set an exact regulation. Figure 6 provides order information and feedback for integrated purvey chain service logistics.

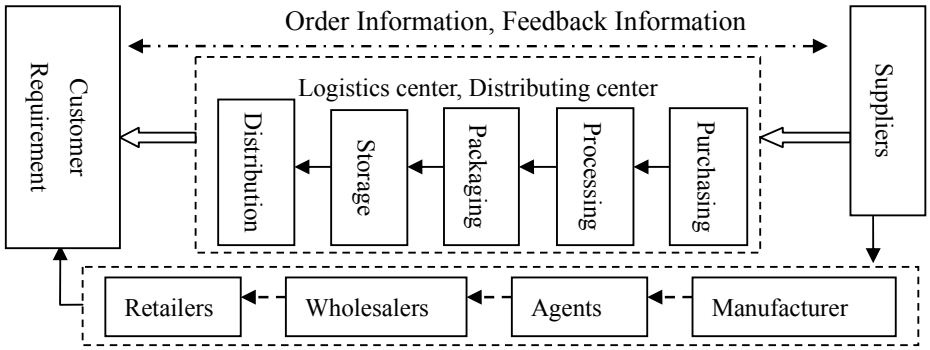

Figure 6. Integrated Purvey Chain Service Logistics

3.4.2 Four Logistics Operational Modes

The economic development zone mode treats logistics parks as a project similar to an economic, industrial, or high-tech development zone. One for well-organized development and construction is often under the organization of particular planning, policies, and development departments. The principle enterprises leading mode, which is the most commonly used operation mode today, allocates logistics and industrial resources effectively from the view of the market economy development. It performs business operation using logistics technology, offers preferential supports to enterprises advanced in enterprise supply chain management, and finally step by step realizes the aggregation of industries under the guidance of reasonable macroeconomic polices and the introduction of industrial and commercial enterprises based on logistics environments.

Industrial real-estate dealer mode considers the construction of logistics nodes as industrial real estate projects. Industrial park developers conduct the investing and building of logistics warehouse, other infrastructures and basic equipments, while managing these infrastructures in terms of lease, transfer, joint venture and cooperative operation under appropriate policies. Comprehensive operation mode is the comprehensive application of the above three modes.

3.5 Logistics Service Styles

Comprehensive logistics service style expands its services to city-wide, regional and international scope. The comprehensive logistics service style could offer services including some value-added logistics services. Industrial logistics service center style provides complete logistics services to a cluster of enterprises from a single industry or enterprises from various industries with the aid of manufacturing, processing industries and others in the industrial agglomeration zone, with related industrial bases as logistics regions. It is in this approach that, port

logistics service style provides logistics bulk freight services using harbors as transportation junction. The radiation of this style could cover the regional or even the entire international scope.

Professional trade market service style mainly delivers logistics services to local markets based on the professional trade market. The main logistics service function of the commerce distribution logistics service style lies in warehousing and distribution. Its service area focuses on the commercial industries in the city.

4 CONCLUSIONS

The modern logistics structure system is comprehensively concerned with enterprises, market, network system, infrastructure and information and policy & organization management. Combined with different main points of development, the characteristics of modern logistics structure system model could be illustrated as "one subject, two systems, three platforms, four logistics developmental modes, and five logistics service styles".

5 REFERENCES

Fen, H. (2006). "Regional Logistics Theory: Theories, Demonstrations and Cases." *Economy & Management Publishing House*, Beijing.

J. Bloomberg, D. (2004). "Logistics. "*Tsinghua University Press*, Beijing.

Liu Yinbing, L. X., Xiong Li (2008). "Logistic Strategies Planning and Implementation". *Publishing House of Electronics Industry*, Beijing.

Wen, K. (2007). "Logistics Industry and Policy Study Based on Modern Logistics." *Dongbei University of Finance & Economics.*

Multi-objective Interval Number Model of Intermodal Transport under Uncertain Environment

YANG Longhai[1], HU Xiaowei[2] and WANG Jian[3]

[1]School of Transportation Science and Engineering, Harbin Institute of Technology, No. 202, Haihe River Road, Nangang District, Harbin, Heilongjiang Province, PRC, 150090, PH:(86) 13936131585; email: yanglonghai@hit.edu.cn
[2]School of Transportation Science and Engineering, Harbin Institute of Technology, No. 202, Haihe River Road, Nangang District, Harbin, Heilongjiang Province, PRC, 150090, PH:(86) 13936646128; email: hxwhit@163.com
[3]School of Transportation Science and Engineering, Harbin Institute of Technology, No. 202, Haihe River Road, Nangang District, Harbin, Heilongjiang Province, PRC, 150090, PH:(86) 13030092006; email: wang_jian@hit.edu.cn

ABSTRACT

Intermodal transport can improve the efficiency, safety, and adaptability in the transportation process, and to a certain extent, it can reduce transport costs. Due to the time-varying characteristics of transport network, market demand and natural conditions, the goods' transport price and travel time are uncertain. Since it is often difficult for the carriers to correctly forecast the transport costs and travel time, intermodal transport is by natural an optimization problem of transportation choices under uncertain environment. This paper describes the uncertain environments by interval numbers, and establishes a multi-objective interval number intermodal transport model. We first create the intermodal virtual transport network by expanding every transfer node into multiple inflow and outflow nodes. The problem boils down to a multi-objective shortest path problem, which can be solved by Dijkstra's algorithm. An example is provided to demonstrate the effectiveness of the model.

Keywords: *uncertain environment, intermodal transport, interval number, multi-objective model*

1 INTRODUCTION

Intermodal transport uses two or more transport modes to deliverer the goods from the origin to the destination, and is the best way in modern logistics system (Bontekoning et al. 2004). The research on transport mode choice problem in intermodal transport system has vital practical significance (Copperman et al. 2004), because it can achieve cost or time savings, improve the transport level of service, competitiveness, and social benefits or efficiency,. Researchers often chose the total transport time (Ziliaskopoulos et al. 2000), the total transport cost (Reddy et al. 1995), or the level of service (Boardman et al. 1997) as the objective in the intermodal transport mode choice problem, and eventually transformed the problem

into a shortest path model (Ziliaskopoulos et al. 2000; Reddy et al. 1995), or a multi-objective combinatorial optimization model (Chang, 2008).

None of the studies mentioned above considers the integration of transport time and transport costs, and the studies only focus on the cases with deterministic freight transport costs and time. However, due to the uncertain characteristics of transport network, market demand and natural conditions, it is often difficult for the carriers to grasp and identify the information of a variety of costs and transport time, and thus impossible to accurately forecast them. Therefore, intermodal transport is an optimization problem of transportation choices under uncertain environment. For uncertainty problem, interval analysis is an essential mathematical tool. The use of interval numbers may describe the complex real-world uncertain problem more realistically, and is more consistent with people's fuzzy thinking habits.

This paper describes the uncertain environments by interval numbers, and establishes a multi-objective interval number intermodal transport model. We first create the intermodal virtual transport network by expanding every transfer node into multiple inflow and outflow nodes. The problem then becomes a multi-objective shortest path problem. Taking the decision-makers' preferences information into account, we introduce decision-makers' preference operator and then use Dijkstra's algorithm to solve for the shortest path.

2 MULTI-OBJECTIVE INTERVAL NUMBER MODEL OF INTERMODAL TRANSPORT UNDER UNCERTAIN ENVIRONMENT

2.1 Problem Description

Suppose intermodal transport carriers attempt to establish an intermodal transport path from city O to city D. There are n cities as internal nodes, where adjacent cities have a number of transport modes in between. The problem is to determine the best transport routes and modes combination, which has the minimum total transport cost and total transport time. The basic assumptions of this paper are as follows:

1) The transport network can be divided into phases. There is no path within the same phase and between non-adjacent phases;

2) The freight can not be divided at a node, that is, between a particular nodes pair only one transport mode can be chosen, and transfer only happens at the interim node;

3) The transport times and costs of different transport modes are different between any two adjacent cities, and the capacity of each mode is large enough;

4) There is transfer time and cost associated with mode transfer.

2.2 Model Foundation

Similar to Ziliaskopoulos et al. (2000) and Reddy et al. (1995), we establish the multi-objective interval number model for intermodal transport problem under uncertain environment as follows:

$$z = \min\left(\sum_i \sum_k x_{i,i+1}^k \tilde{c}_{i,i+1}^k + \sum_i \sum_k \sum_l y_i^{kl} \tilde{f}_i^{kl} + \sum_i \sum_k x_{i,i+1}^k \tilde{t}_{i,i+1}^k + \sum_i \sum_k \sum_l y_i^{kl} \tilde{g}_i^{kl} \right) \quad (1)$$

Subject to:

$$\sum_k x_{i,i+1}^k = 1, \forall i \in N \quad (1\text{-}1)$$

$$\sum_k \sum_l y_i^{kl} \le 1, \forall i \in N, k \in K, l \in K \tag{1-2}$$

$$x_{i-1,i}^k + x_{i,i+1}^l \ge 2 y_i^{kl}, \forall i \in I, k \in K, l \in K \tag{1-3}$$

$$y_i^{kl}, x_{i,i+1}^k \in \{0,1\}, \forall i \in I, k \in K, l \in K \tag{1-4}$$

$$x_{i,i+1}^k = \begin{cases} 1 & \text{if mode } k \text{ is chosen from node } i \text{ to node } i+1 \\ 0 & \text{otherwise} \end{cases}$$

$$y_i^{kl} = \begin{cases} 1 & \text{if transfer from mode } k \text{ to mode } l \text{ at node } i \\ 0 & \text{otherwise} \end{cases}$$

Here $\tilde{c}_{i,i+1}^k = \left[c_{i,i+1}^{k-}, c_{i,i+1}^{k+}\right]$ is the interval number associated with the transport cost of mode k from node i to node $i+1$; $\tilde{f}_i^{kl} = \left[f_i^{kl-}, f_i^{kl+}\right]$ is the interval number for transfer cost from mode k to mode l at node i; $\tilde{t}_{i,i+1}^k = \left[t_{i,i+1}^{k-}, t_{i,i+1}^{k+}\right]$ is the interval number for transport time of mode k from node i to node $i+1$; $\tilde{g}_i^{kl} = \left[g_i^{kl-}, g_i^{kl+}\right]$ is the interval number for transfer time from mode k to mode l at node i; K is the set of available transport modes; and N is the set of all nodes.

For the constraints, (1-1) guarantees only one mode of transport is chosen between two adjacent nodes; (1-2) means at each node only one transport mode change is allowed; (1-3) ensures the transport continuity and internal consistency, if mode transfer occurs at node i from mode k to mode l, then mode k must be used from node $i-1$ to i, and similarly mode l must be chosen from node i to $i+1$; and (1-4) shows the decision variables are 0-1 variables.

2.3 Model Conversion

The objective function of model (1) is a function of various costs and time. Since the units of these costs and time might be different, they are not directly additive. Here we use the occupancy cost rate of capital per unit time and the total value of goods for the time-cost conversion. For transport time, if the occupancy cost rate of capital per unit time is $\rho_{i,i+1}$, the total value of goods is $p_{i,i+1}$, then the transport time can be converted to $p_{i,i+1}\left[\left(1+\rho_{i,i+1}\right)^{x_{i,i+1}^k \tilde{t}_{i,i+1}^k} - 1\right]$. For transfer time, if the occupancy cost rate of capital per unit time is ρ_i, the total value of goods is p_i, then the transfer time can be converted to $p_i\left[\left(1+\rho_i\right)^{y_i^{kl} \tilde{g}_i^{kl}} - 1\right]$.

The generalized transport cost of using mode k from node i to node $i+1$ includes transport cost and transport time cost, which can be expressed as $\vec{C}_{i,i+1}^k = x_{i,i+1}^k \tilde{c}_{i,i+1}^k + p_{i,i+1}\left[\left(1+\rho_{i,i+1}\right)^{x_{i,i+1}^k \tilde{t}_{i,i+1}^k} - 1\right]$. The generalized transfer cost from mode k to mode l at node i includes transfer cost and transfer time cost, which can be expressed as $\vec{C}_i^{k,l} = y_i^{kl} \tilde{f}_i^{kl} + p_i\left[\left(1+\rho_i\right)^{y_i^{kl} \tilde{g}_i^{kl}} - 1\right]$. The objective function of model (1) can then be converted to the generalized total cost, which can be expressed as:

$$\tilde{z} = \min\left(\sum_i \sum_k \left(x_{i,i+1}^k \tilde{c}_{i,i+1}^k + p_{i,i+1} \left[\left(1+\rho_{i,i+1}\right)^{x_{i,i+1}^k \tilde{t}_{i,i+1}^k} - 1 \right] \right) + \sum_i \sum_k \sum_l \left(y_i^{kl} \tilde{f}_i^{kl} + p_i \left[\left(1+\rho_i\right)^{y_i^{kl} \tilde{g}_i^{kl}} - 1 \right] \right) \right)$$

$$= \min\left(\sum_i \sum_k \vec{C}_{i,i+1}^k + \sum_i \sum_k \sum_l \vec{C}_i^{k,l} \right)$$

In order to reduce the cost-time multi-objective model into a single objective one, we adopt the interval number conversion method. By defining a decision-maker's preference operator, it is possible to map the sequence relationship of the interval numbers to the ordering relationship of real number. The order of the interval numbers can be sorted as:

$$O: I \to R, w_\lambda(\tilde{a}) = m(\tilde{a}) + \lambda w(\tilde{a})$$

where I is the interval number scale, R is the real number scale, and λ is the preference operator, $m(\tilde{a}) = 1/2 \cdot \left(a^- + a^+\right)$ is the center of interval $\tilde{a}$, and $w(\tilde{a}) = a^+ - a^-$ is the width of interval $\tilde{a}$. We let $-1/2 \le \lambda < 0$ for risk-taking, $\lambda = 0$ for risk-neutral, and $0 < \lambda \le 1/2$ for risk-averse decision-makers. This way we are able to map the interval numbers to real numbers, and incorporate decision-makers' preference as a parameter into the shortest path selection. We then use Dijkstra's algorithm to find the shortest paths under different preferences.

3 THE CONSTRUCTION OF INTERMODAL TRANSPORT NETWORK

The basic intermodal transport network is composed by nodes and arcs between adjacent nodes, where each arc is associated with one mode. Denote N as the set of nodes, K the set of transport modes, and A the arc set. Any arc $a \in A$ can be expressed by $(i, i+1, k)$, where $i, i+1 \in N$ and $k \in K$.

1) If mode transfer is not allowed, we will leave the basic network as it is, with parallel links connecting two adjacent nodes, where each link is associated with one possible mode and its generalized transport costs.

2) If mode transfer is allowed, each transfer node will be expanded into two groups: inflow and outflow nodes. Virtual transfer lines are introduced into the network as shown in Figure 1.

3) According to the above expansion idea, we construct the intermodal virtual transport network. In a complex intermodal transport network, mode transfer may occur at every node. Therefore, every node except the origin node O is expanded to k virtual nodes. For the purpose of computation convenience, we introduce a virtual destination D', where the transfer time and cost between every destination node D_i and D' is equal to 0.

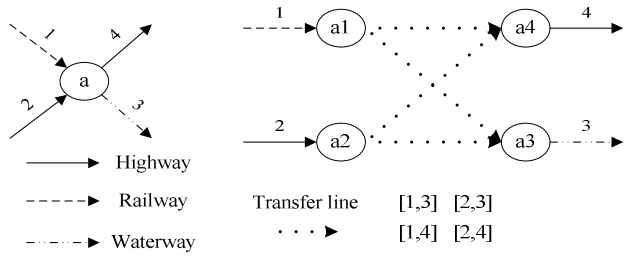

Figure 1. The expansion of transfer node

4 EXAMPLE ANALYSIS

Assume there are six internal nodes, n_1 to n_6, from the original node O to destination D. According to the node expansion idea, we construct the intermodal virtual transport network, as shown in Figure 2. Outgoing arcs of virtual nodes P_{i1} are associated with the railway, those of P_{i2} take highway as the transport mode, and those of P_{i3} refer to waterway.

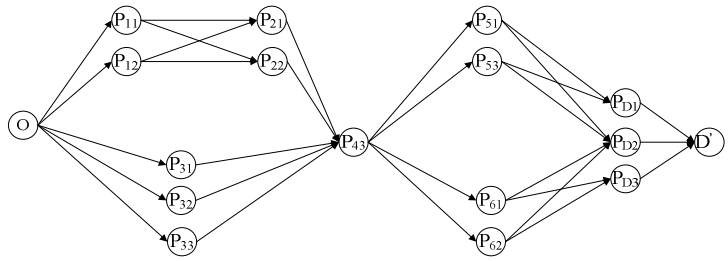

Figure 2. The intermodal virtual transport network of the example

The transport costs / transport time costs of alternative transport modes between the nodes are shown in Table 1, and blank cell means the corresponding mode is not available between the two cities. Table 2 shows the transfer costs / transfer time costs between different modes. According to different values of the decision-maker's preference parameter λ, three cases are solved. For each case, the shortest paths with respect to cost, time, and the multi-objective function value are obtained respectively. The results, as shown in Table 3, provide optimal integrated route and mode choices for the intermodal transport routing problem.

Table 1. The transport costs / transport time costs of alternative transport modes between the nodes

	O-n1	O-n3	n1-n2	n2-n4	n3-n4	n4-n5	n4-n6	n5-D	n6-D
Railway	[2,4]/[4,8]	[3,5]/[5,9]	[2,4]/[4,6]			[6,10]/[9,15]	[6,10]/[10,16]	[7,11]/[12,18]	
Highway	[3,5]/[4,6]	[2,4]/[4,8]	[1,3]/[4,8]				[5,9]/[8,14]	[8,12]/[10.16]	[6,10]/[11,17]
Waterway		[1,3]/[8,12]		[2,4]/[9,15]	[4,6]/[11,17]	[4,6]/[12,20]			[4,8]/[12,20]

Table 2. The transfer costs/transfer time costs between different modes

Transport modes	Railway	Highway	Waterway
Railway	0/0	[1,3]/[1,3]	[2,4]/[2,4]
Highway	[1,3]/[1,3]	0/0	[3,5]/[1,3]
Waterway	[2,4]/[2,4]	[3,5]/[1,3]	0/0

Table 3. The solving results of intermodal transport routing model

	Path and transport modes		Transport cost	Transfer cost	Transport time cost	Transfer time cost	Total cost
	the shortest cost	O -P_{33}-P_{43}-P_{53}-P_{D1}- D'	16	2	--	--	18
$\lambda = -1/2$	the shortest time	O -P_{32}-P_{43}-P_{62}-P_{D2}- D'	--	--	34	2	36
	multi-objective	O -P_{33}-P_{43}-P_{62}-P_{D2}- D'	16	3	38	1	58
	the shortest cost	O -P_{33}-P_{43}-P_{53}-P_{D1}- D'	21	3	--	--	24
$\lambda = 0$	the shortest time	O -P_{32}-P_{43}-P_{62}-P_{D2}- D'	--	--	45	4	49
	multi-objective	O -P_{33}-P_{43}-P_{62}-P_{D2}- D'	22	4	49	2	77
	the shortest cost	O -P_{33}-P_{43}-P_{53}-P_{D1}- D'	26	4	--	--	30
$\lambda = 1/2$	the shortest time	O -P_{32}-P_{43}-P_{62}-P_{D2}- D'	--	--	56	6	62
	multi-objective	O -P_{33}-P_{43}-P_{62}-P_{D2}- D'	28	5	60	3	96

5 CONCLUSIONS

From the numerical example, we educe the following conclusions:

1) Single-objective model has different optimal paths for different objective functions, i.e., the shortest cost path and the shortest time path are not the same. And by taking into account both the transport costs and time, the optimal solution to the multi-objective model may vary with different weighting factors.

2) The optimal path remains the same but has different total cost for different values of the decision-maker's preference parameter λ. According to the numerical results, the cost of the minimal cost / time path is [18, 30] and [36, 62] respectively, and the total cost of the minimal multi-objective path is [58, 96].

REFERENCES

Boardman, B. S., Malstrom, E. M., Butler, D. P., and Cole, M. H. (1997). "Computer assisted routing of intermodal shipments." *Computers & Industrial Engineering,* 33(1/2), 311-314.

Bontekoning, Y. M., Macharis, C., and Trip, J. J. (2004). "Is a new applied transportation research field emerging?-A review of intermodal rail-truck freight transport literature." *Transportation Research Part A,* 38, 1-9.

Chang, T-S. (2008). "Best routes selection in international intermodal networks." *Computers and Operations Research*, 35(9), 2877-2891.

Copperman, R. B, Devlin, M. P., Ewalt, R. M., et al. (2004). "Coordinating and prioritizing multimodal transportation projects." *Proceedings of the 2004 Systems and Information Engineering Design Symposium,* 113-119.

Reddy, V. R., and Kasilingam, R. G. (1995). "Intermodal transportation considering transfer costs." *Proceedings of the 1995 Global Trends Conference of the Academy of Business Administration.* Aruba.

Ziliaskopoulos, A., and Wardell, W. (2000). "An intermodal optimum path algorithm for multimodal networks with dynamic arc travel times and switching delays." *European Journal of Operational Research,* 125(3), 486-502.

A Model on Risk Evaluation for Emergency Guarantee Mechanism of Food Logistics

Huang Xiangrong[1, 2] and Xie Ruhe[2]

[1]School of Traffic and Transportation Engineering, Central South University, Changsha, Hunan, China, 410083; PH: (0086) 13342885911;email: chamwin@163.com
[2]Business School, Guangzhou University, Guangzhou, Guangdong, China, 510006, FAX: (0086) 020 39366822; email: huangxr@gzhu.edu.cn, rhxie@gzhu.edu.cn

ABSTRACT

This paper proposes a new approach to evaluate the total risk degree for emergency guarantee mechanism of food logistics. Firstly, it reveals the composition of emergency guarantee mechanism of food logistics. Secondly, it puts forward a two-level risk evaluation index system on the basis of path analysis with AHP method. Thirdly, it develops a model which combines fuzzy comprehensive evaluation with hierarchy variable weight method, in order to improve the accuracy and reliability of risk evaluation by solving the deferred problem of risk. Finally, the paper verifies the efficiency and applicability of the model with a simulation example.

KEY WORDS: fuzzy comprehensive evaluation; hierarchy variable weight; emergency guarantee mechanism; food logistics; risk evaluation

INTRODUCTION

Emergency guarantee refers to the process of controlling, handling and managing various activities in sudden events by effectively integrating relevant resources (Ji et al., 2006). Therefore emergency guarantee mechanism is provided to react to various emergencies during all phases of emergency management (Yao and Gao, 2006). It may include but is not limited to the following five components: early warning mechanism, monitoring mechanism, rapid reaction mechanism, urgent disposal mechanism and rehabilitation mechanism (Zhao et al., 2006). However, the supply of rescue materials, especially food, is often affected by sudden events. Perishable loss often happens in food logistics during transportation, handling and storage (Xu, 2007). Thus, how to recognize and prevent the risks in emergency guarantee process of food logistics is extremely crucial.

Many researches have studied the risk analysis and evaluation methods, such as investigation method, Delphi, net present value method, hierarchy analysis, antd sensitivity analysis, etc. (Yan et al., 2004). But most methods regard the uncertainty of risk as randomness, and measure it by means of probability distribution. However, the uncertainty of risk is not only random but also fuzzy in nature (Steed, 2000). Furthermore, it's very important to deal with the deferred characteristic of risk in its

evaluation, which means that the risk in early stage will be gradually enlarging during its backward transmission. Therefore, the hierarchy variable weight method can be used to improve the accuracy of risk evaluation (Li et al., 2004).

This paper proposes a two-level risk evaluation index system for emergency guarantee mechanism of food logistics on the basis of path analysis with AHP method. A model which combines fuzzy comprehensive evaluation with hierarchy variable weighting method is then built. Finally, a simulation example is conducted to verify the applicability and effectiveness of the model. The model can also be considered as the means of recognizing and preventing risks.

RISK EVALUATION INDEX SYSTEM

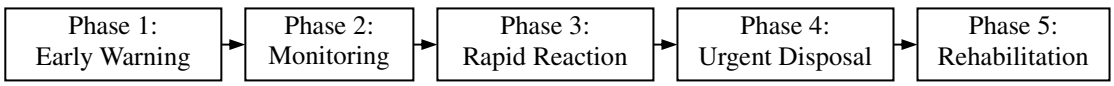

Figure 1. Horizontal path map of emergency guarantee mechanism.

First of all, according to the five corresponding components of the emergency guarantee mechanism, a path which is composed of five phases can be obtained through Path Analysis (PA) as shown in Figure 1. We can outspread the above path longitudinally, and arrange the risk factors within each phase through AHP method. Considering the special characteristics of food logistics, this paper establishes a two-level risk evaluation index system for emergency guarantee mechanism of food logistics as shown in Table 1.

MODEL CONSTRUCTION

Building factor sets and weight sets. As shown in Table 1, the factor set of the top-level indexes is $U = \{U_1, \cdots, U_5\}$, and the relative weight set is $A = \{A_1, \cdots, A_5\}$. The sub-factor set of the sub-level indexes is $U_i = \{u_{i1}, \cdots, u_{ij}\}$, while the relative weight set is $A_i = \{a_{i1}, \cdots, a_{ij}\}$, where $i = 1, \cdots, 5$ and j is the number of the sub-factors (i.e., sub-level indexes) corresponding to U_i.

Constructing the risk degree-marking vector. In order to effectively describe the risk evaluation of all factors, the five-grade marking system can be used. The risk degree of a certain factor is slim as its marking value is 1, and it is large when the value is 5. Then we may construct the risk degree marking vector as $V = (v_1, v_2, v_3, v_4, v_5) = (1, 2, 3, 4, 5)$.

Calculating the fuzzy evaluation values. The fuzzy evaluation value c_{ij} of each sub-factor u_{ij} can be calculated by fuzzy statistics method. Firstly, experts can be invited to evaluate the risk degree of each sub-factor u_{ij} according to the given evaluation criterion. They independently give the evaluation marking values for each sub-factor u_{ij}. Then we can summarize the frequency of $u_{ij} \in v_k (k = 1,2,3,4,5)$, and make further calculations as follows:

$$m_{v_k}(u_{ij}) = w_{ij}^{(v_k)} / N \qquad (0 \le m_{v_k}(u_{ij}) \le 1)$$

where $m_{v_k}(u_{ij})$ is a fuzzy membership function, which denotes the fuzzy membership degree of $u_{ij} \in v_k (k = 1,2,3,4,5)$; $w_{ij}^{(v_k)}$ refers to the frequency of $u_{ij} \in v_k (k = 1,2,3,4,5)$; N is the number of experts. Therefore, the fuzzy membership vector of each u_{ij} is $M_{ij} = \left(m_{v_1}(u_{ij}), m_{v_2}(u_{ij}), m_{v_3}(u_{ij}), m_{v_4}(u_{ij}), m_{v_5}(u_{ij})\right)$, and the fuzzy evaluation value c_{ij} of u_{ij} can be calculated as follows:

$$c_{ij} = V \times M_{ij}^T = \sum_{k=1}^{5} v_k \times m_{v_k}(u_{ij}) \qquad (1 \le c_{ij} \le 5)$$

Table 1. Risk Evaluation Index System.

No.	The top-level indexes	Evaluating variables	The sub-level indexes	Evaluating variables
1	Early Warning	U_1	early warning on large-scale sudden events outbreak	u_{11}
			early warning on food manufacture and supply shortage	u_{12}
			early warning on food safety threat	u_{13}
			early warning on food logistics condition	u_{14}
2	Monitoring	U_2	Monitoring on food resources	u_{21}
			Monitoring on food safety	u_{22}
			Monitoring on food transportation and distribution	u_{23}
			Monitoring on organization	u_{24}
			Monitoring on tech equipments	u_{25}
3	Rapid Reaction	U_3	rapid reaction on emergency food manufacture and supply	u_{31}
			rapid reaction on emergency food safety inspection	u_{32}
			rapid reaction on emergency food transportation and distribution	u_{33}
4	Urgent Disposal	U_4	urgent disposal on food manufacture and supply interruption	u_{41}
			urgent disposal on food safety hazard	u_{42}
			urgent disposal on food transportation and distribution disturbance	u_{43}
			urgent disposal on food redistribution and compensation	u_{44}
5	Rehabilitation	U_5	rehabilitation on food manufacture and supply accident	u_{51}
			rehabilitation on food safety accident	u_{52}
			rehabilitation on food transportation and distribution accident	u_{53}
			rehabilitation on organization disorder	u_{54}
			Rehabilitation on tech equipments failure	u_{55}

Constructing the state vectors. The state vector value x_{ij} of u_{ij} can be calculated as follows:

$$x_{ij} = c_{ij} / \sum_j c_{ij} \qquad (0 \le x_{ij} \le 1)$$

Then we may construct the state vectors $X_i = (x_{i1}, \cdots, x_{ij})$ of factors $U_i (i = 1, \cdots, 5)$.

Constructing the state variable weight vectors. The state variable weight vectors $S_i = (s_{i1}, \cdots, s_{ij})$ of factors U_i can be constructed according to the relative state vectors $X_i = (x_{i1}, \cdots, x_{ij})$ (Li et al., 2004). There are three types of state variable weight vectors, which are punishment-type, stimulation-type and hybrid-type. They denote three kinds of variable weight methods respectively (Hou et al., 2005). The state variable weight value s_{ij} of u_{ij} can be defined as follows:

$$s_{ij} = x_{ij}^{\alpha} \qquad (0 < \alpha \le 1)$$

It is obvious that state variables weight vector $S_i = (s_{i1}, \cdots, s_{ij}) = (x_{i1}^{\alpha}, \cdots, x_{ij}^{\alpha})$ belongs to the stimulation type as $0 < \alpha \le 1$. Furthermore, if α becomes smaller and smaller, the "stimulation" effect of variable weight method becomes more and more strong, indicating that the deferred characteristic of risk become larger.

Calculating the variable weight evaluation value. The variable weight a_{ij}^* of u_{ij} can be calculated as follows:

$$a_{ij}^* = a_{ij} s_{ij} \Big/ \sum_j a_{ij} s_{ij}$$

Therefore, the variable weight evaluation value U_i^* of corresponding top-level factor U_i can be calculated as follows:

$$U_i^* = A_i^* \times X_i^T = \sum_j (a_{ij}^* \times x_{ij}) \qquad (i = 1, \cdots, 5)$$

Then we may construct the top-level variable weight evaluation vector as $U^* = (U_1^*, \cdots, U_5^*)$. Eventually, the weight evaluation value for the top-level variable U^*, which describes the total risk degree for the emergency guarantee mechanism of food logistics, can be obtained by this vector through the same calculation.

SIMULATION EXAMPLE

In order to illustrate the application of this model, a simulation example is given below. It takes source data from a certain simulative emergency guarantee process of food logistics by using simulation software.

Fuzzy evaluation calculation. We may calculate the fuzzy membership degree $m_{v_k}(u_{ij})$ of u_{ij} according to experts' evaluation marking values, then obtain c_{ij} and x_{ij} of u_{ij} as in Table 2.

Calculation for hierarchy weight fuzzy evaluation. Considering the deferred characteristic of risk, the α value in the first four phases of emergency guarantee process should be add one fixed value. The fixed added value of α is 0.15 in the paper, and $\alpha = 1$ for the last phase (i.e., phase 5). Then the calculation is demonstrated in Table 3.

Table 2. Fuzzy Evaluation Calculation.

U_i	u_{ij}	a_{ij}	$m_{v_1}(u_{ij})$	$m_{v_2}(u_{ij})$	$m_{v_3}(u_{ij})$	$m_{v_4}(u_{ij})$	$m_{v_5}(u_{ij})$	c_{ij}	x_{ij}
U_1	u_{11}	0.31	0.25	0.3	0.3	0.1	0.05	2.4	0.2697
	u_{12}	0.29	0.6	0.3	0.1	0	0	1.5	0.1685
	u_{13}	0.21	0.5	0.2	0.2	0.05	0.05	1.95	0.2191
	u_{14}	0.19	0.2	0.15	0.25	0.2	0.2	3.05	0.3427
U_2	u_{21}	0.17	0.5	0.2	0.15	0.1	0.05	2	0.1778
	u_{22}	0.15	0.3	0.3	0.15	0.15	0.1	2.45	0.2178
	u_{23}	0.15	0.15	0.25	0.3	0.25	0.05	2.8	0.2489
	u_{24}	0.25	0.3	0.2	0.2	0.2	0.1	2.6	0.2311
	u_{25}	0.28	0.7	0.2	0.1	0	0	1.4	0.1244
U_3	u_{31}	0.37	0.25	0.15	0.25	0.2	0.15	2.85	0.3775
	u_{32}	0.28	0.2	0.25	0.25	0.15	0.15	2.8	0.3709
	u_{33}	0.35	0.5	0.2	0.2	0.1	0	1.9	0.2517
U_4	u_{41}	0.29	0.2	0.3	0.35	0.1	0.05	2.5	0.2564
	u_{42}	0.23	0.4	0.3	0.1	0.1	0.1	2.2	0.2256
	u_{43}	0.26	0.5	0.25	0.15	0.05	0.05	1.9	0.1949
	u_{44}	0.22	0.15	0.15	0.25	0.3	0.15	3.15	0.3231
U_5	u_{51}	0.21	0.5	0.2	0.15	0.1	0.05	2	0.1843
	u_{52}	0.23	0.3	0.3	0.15	0.1	0.15	2.5	0.2304
	u_{53}	0.18	0.2	0.3	0.3	0.2	0	2.5	0.2304
	u_{54}	0.16	0.3	0.2	0.2	0.2	0.1	2.6	0.2396
	u_{55}	0.22	0.8	0.15	0.05	0	0	1.25	0.1152

As is shown in Table 3, the top-level state variable weight vector can be constructed as $U^* = (0.2491, 0.1990, 0.3385, 0.2548, 0.2083)$. In the same way, we implement the variable weight calculation on vector U^* as shown in Table 4.

Eventually, the top-level hierarchy variable weight fuzzy comprehensive evaluation value of U^* is 0.2232.

Evaluating the total risk degree. Since evaluation value varies from 0 to 1, this paper proposes a five-grade rating system for evaluating the total risk degree according to its value interval, i.e. [0, 0.2] is “slim”, [0.2, 0.4] is “small”, [0.4, 0.6] is “general”, [0.6, 0.8] is “big”, and [0.8, 1] is “large”. Therefore the total risk degree is evaluated as “small”, which shows that the emergency guarantee mechanism basically plays a safe and reliable role in sudden events.

CONCLUSION

This paper thoroughly investigates the risk evaluation for emergency guarantee mechanism of food logistics. The simulation example verifies the applicability and effectiveness of the proposed model. It makes relatively objective evaluation on total risk degree which helps to recognize and prevent the risks effectively. Future research will focus on continuous improvement of evaluation index system and various models under more complicated conditions.

Table 3. Calculation for Sub-level Variable Weight Fuzzy Evaluation.

U_i	α	u_{ij}	a_{ij}	x_{ij}	s_{ij}	a_{ij}^*	U_i^*
(1)	(2)	(3)	(4)	(5)	(6)	(7)=(4)*(6)/Σ((4)*(6))	(8)=Σ ((7)*(5))
U_1	0.35	u_{11}	0.31	0.2697	0.6321	0.323619	0.2491
		u_{12}	0.29	0.1685	0.5362	0.256819	
		u_{13}	0.21	0.2191	0.5878	0.203859	
		u_{14}	0.19	0.3427	0.6874	0.215703	
U_2	0.5	u_{21}	0.17	0.1778	0.4216	0.164599	0.1990
		u_{22}	0.15	0.2178	0.4667	0.160745	
		u_{23}	0.15	0.2489	0.4989	0.171844	
		u_{24}	0.25	0.2311	0.4807	0.275988	
		u_{25}	0.28	0.1244	0.3528	0.226823	
U_3	0.65	u_{31}	0.37	0.3775	0.5309	0.404059	0.3385
		u_{32}	0.28	0.3709	0.5248	0.302277	
		u_{33}	0.35	0.2517	0.4079	0.293665	
U_4	0.8	u_{41}	0.29	0.2564	0.3366	0.298640	0.2548
		u_{42}	0.23	0.2256	0.3039	0.213828	
		u_{43}	0.26	0.1949	0.2703	0.214968	
		u_{44}	0.22	0.3231	0.4050	0.272564	
U_5	1	u_{51}	0.21	0.1843	0.1843	0.196629	0.2083
		u_{52}	0.23	0.2304	0.2304	0.269195	
		u_{53}	0.18	0.2304	0.2304	0.210674	
		u_{54}	0.16	0.2396	0.2396	0.194757	
		u_{55}	0.22	0.1152	0.1152	0.128745	

Table 4. Calculation for Top-level Variable Weight Fuzzy Evaluation.

U_i	α	U_i^*	A_i	X_i	S_i	A_i^*	U^*
(1)	(2)	(3)	(4)	(5)	(6)	(7)=(4)*(6)/Σ((4)*(6))	(8)=Σ((7)*(5))
U_1	0.35	0.2491	0.15	0.1993	0.5687	0.227056	0.2232
U_2	0.5	0.1990	0.1	0.1593	0.3991	0.106229	
U_3	0.65	0.3385	0.35	0.2709	0.4278	0.398604	
U_4	0.8	0.2548	0.3	0.2038	0.2802	0.223744	
U_5	1	0.2083	0.1	0.1667	0.1667	0.044367	

REFERENCES

Hou, H. J., Gu, Y. D., and Wang, J. Y. (2005). "Some problems on nature and construction of state variable weight." *J. of Beijing Normal University (Natural Science Edition)*, 41 (4), 334-338.

Ji, L., Chi, H., and Chen A. (2006) *Emergency management of sudden events*, China higher education press, Beijing.

Li, D. Q., Cui, H. M., and Li, H. X. (2004). "Multi-factors decision based on the hierarchy variable weight." *System Project J.*, 19(3), 258-260.

Li, D. Q., Gu, Y. D., and Li, H. X. (2004). "Several results of state variable weight vector axiomatization definition." *System Project Theory and Practice*, 24 (5), 97-102.

Steed, J. C. (2000). "Engineering project risk management." *Engineering Mgmt. J.*, 10(1), 43-44.

Xu, S. Y. (2007). "Green food logistics and food safety supply chain management." *International Business Technology*, 68(1), 47-49.

Yao, C., and Gao C. (2006). "Study on highway transportation emergency guarantee system." *Highway Traffic and Security*, 6(6), 14-16.

Yan, W. Z., Hou, D. Z., and Yu, Y. M. (2004). "Study on risk evaluation of project investment decision." *J. of Xi'an University of Architecture and Technolo gy (Natural Science Edition)*, 36 (3), 337-344.

Zhao, H., Kang, D. C., and Wang, L. (2006). "Study on emergency management mechanism and system of sudden events." *China Management Science*, 14(10), 784-788.

Logistics Distribution Information System Based on 3rd Generation Mobile Communication Technology

Zhongwei WANG[1], Hongbo WANG[1], Yan PANG[1]

[1]School of Logistics, Central-South University of Forestry and Technology, Changsha 410004, HN, CHINA, TEL/FAX: +86 731 5623939, MOBILE: +86 13755059838, email: wangpmp@163.com

ABSTRACT

On the basis of discussing the characteristics of logistics demand of communication information, communication information is divided into three categories which include dynamic, static and relevance. In order to fully grasp the dynamic communication information, a three layer platform of logistics distribution information system is designed. This is based on the 3rd generation mobile communication technology (3G), and expounding the composition and working principle of regional distribution centers. Then on-board information devices are designed, which is one of the most important logistics information terminals. The benefits of regional distribution information systems, based on 3G mobile communications technology, is illustrated using the example of taking on–board information devices together with real-time communication information to locate the shortest time line. The system can make vehicles receive communication information at anytime and anywhere, so it is more suitable to the characteristics of time-varying and dynamics of regional distribution information.

KEYWORDS

Intelligent regional distribution systems; 3rd generation mobile communication technology; communication information center; on-board information device

1 FORWORD

Logistics is a complicated system touching on several aspects of social economic life. In the course of the logistics process, distribution is an important aspect. The process of logistics distribution is to plan, execute and control the practical process of raw material or final products from the place of origin to the place of usage. Every link in the logistics process involves the problem about how to deal with enormous spatial data and attributive data to shorten logistics time and lower the cost. In general, the transmission of data information adopts wired and wireless styles. The dynamic characteristics of the logistics distribution process decide which of the wireless communication styles should be adopted in the terminal (YANG Li Qiang, 2007). Compared with the wired style, wireless transmission has the features of lower cost, short construction cycle, good adaptability and extension,and easiness of safeguard.

Widely used 2nd mobile communication technology is not suitable for transmitting the multi-media logistics distribution information with enormous data, because of the weakness of a slow transmission rate. Through the combination of the

3rd generation mobile communication technology with other information technology, and the popularization of the 3rd generation mobile communication technology (with the transmission rate of 384kbps to 3Mbps faster) (ZHAO Zhen, 2008), the alternation of logistics distribution information and real-time transmission can be realized effectively. The paper will discuss the application of the 3rd generation mobile communication technology and other relevant information technology in logistics distribution.

2 REQUIREMENTS ANALYSIS OF THE REGIONAL LOGISTICS INFORMATION SYSTEM

The major objective of the regional logistics information platform is oriented to every-grade customer in a given region (HE Jie, 2003). There are related logistics management departments in the government, professional third-party logistics enterprises, manufacturing enterprises demanding logistics services and some units providing services to the links of logistics. Through the perspective of systematical requirements specifications, the principal function should include the following aspects.

(1) Rational distribution scheme: logistics distribution from distribution to custom is a very complex process. In the process, the most difficult issue is how to arrange the distribution plan according to the quantity and time. Formulating the distribution scheme includes the following sub-process: selection of logistics center; selection of vehicle; vehicle loading scheme; and vehicle routing arrangement. In order to reduce cost, if the capacity of the vehicle allows, it is best to put the goods of many customs together. It leads to many problems such as the arrangement of vehicle route, and the decision of dispatching time. The above sub-processes are not independent; they will influence each other (YANG Deng, 2008).

(2) The dynamic acquisition of the distribution information: on-time delivery, determination of the dynamic location.

(3) The storage and disposal of information

(4) Information analysis: the aim of information analysis lies in calculating the process cost and realizing maximization of profit through analyzing the distribution and sales data, vehicle route, and the stock of the distribution center.

(5) Real-time information transmission

(6) Disposal of the distribution sheet

3 STRUCTURE DESIGN OF THE LOGISTICS DISTRIBUTION INFORMATION SYSTEM

3.1 Logistics distribution system structure design

Based on the demand of the logistics distribution system, the system involves seven models: gathering model, distribution pattern model, preprocessing model, distribution model, transportation optimization model, allocating model and tabulating model (WANG Xiaokun, 2008). The seven models are included in the model base. In addition, ten relevant databases should be built for the data

procession of the models. They are: custom applying for delivering database, inventory database, overall application database, overall stock database, commodity distribution database, distance matrix database, good allocation database and distribution center database. In order to combine the model part and data part, a general control program should be built. It is conducive to the process of every model and the effective storage of data. The structure of the process is as follows in Figure 1.

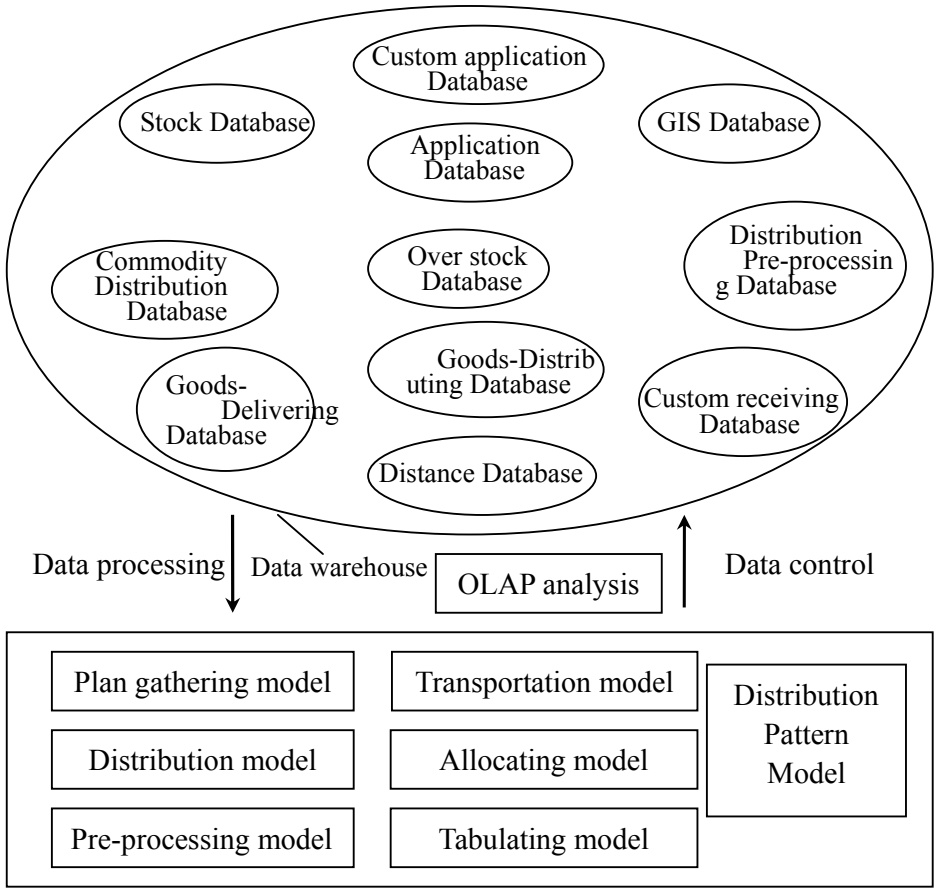

Figure 1. The overall structure of the logistics distribution system.

3.2 The information pack of distribution business

In the general construction design of the logistics distribution system, the design of the data warehouse is very important. During the construction of the data warehouse, the information pack oriented to the data warehouse of logistics distribution is adopted, as Figure 2 demonstrates. When constructing the data warehouse, there are many kinds of parameters to define. In order to make the data warehouse both effective and simple, it is important to choose correct parameters to make detailed descriptions of the distributed goods. The following dimensions are

defined in the figure of information pack: time dimension, goods dimension and vehicle dimension.

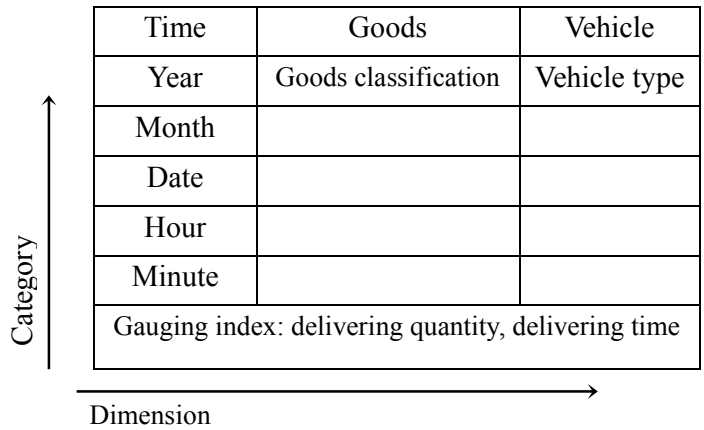

Figure 2. Information pack of distribution business.

Through the comprehensive analysis of the distribution business pack, we can get the details of the distribution business. For example, through the analysis on vehicle dimension and time dimension, we can check the situation of the vehicle. Through the analysis on vehicle dimensions and goods dimensions, we can check the status of distributing goods and analyze the loading capacity of every vehicle. Different dimensions have different polymerization levels. In the logic design of a data warehouse, an important issue is to decide the grading division level of the data warehouse, whether the grading division level is suitable or not will have influence on the data quantity in the data warehouse and suitable query type (YANG Feng, 2008).

3.3 The design of the distribution platform scheme

Every kind of business information in the distribution process can be acquired by automatic collection and artificial collection. Having been standardized, they can be transmitted to the information disposal centers through special medium and provide the function of data query, data classification and data storage for realizing the function of the distribution information system. The function of collecting, classifying and processing all dynamic information, static information and relevant information, as well as searching for the optimal distribution route, will be accomplished automatically in the system. Due to the large quantity of data disposal, we use the 3rd generation mobile communication network to acquire the dynamic data. Depending on the 3rd generation network, the transmission of real-time information can be accomplished conveniently. With the fast development of the logistics industry, constructing the special 3rd generation network based on logistics usage and forming the logistics information platform utilizing the 3rd generation technology as the core provides the best choice. The platform scheme includes a

distribution business operation layer, a distribution business management layer and a distribution business decision layer, as shown in Figure 3. The effective implementation of a higher layer is based on the implementation of the lower ones. At the same time, the higher layers play the role of managing the lower ones (XU Wei, 2008).

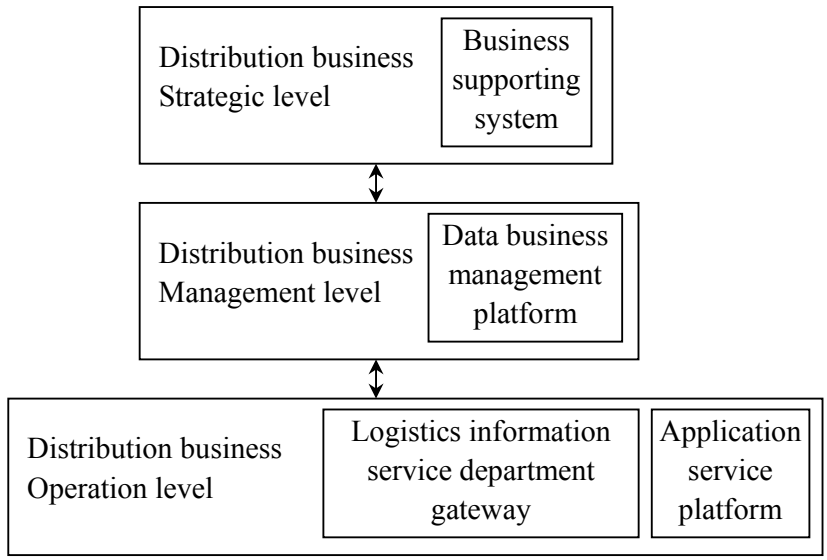

Figure 3. Logistics information platform scheme based on 3G.

4 THE ANALYSIS OF THE SYSTEMATIC FUNCTION

Using the distribution system, we can conduct online analytical processing conveniently. For example, during the distribution process, we can analyze the rate of arriving in the right place, the expenditures, vehicle distribution and vehicle route, etc.

4.1 The analysis of arriving in the right place

In data warehouse design, we consider the vehicle dimension and time dimension but not the route dimension. When the place of distribution is determined, the distance from the distribution to every demand point is fixed. Using the shortest route model (LI Yuming, 2008), the optimal route will be found. To find out if the distribution missions arrive in the right place can be determined by the analysis based on the time window constrained model and the operation on the rate in vehicle dimension table and on the earliest arriving time and latest arriving time in the time dimension table.

4.2 The analysis of the expenditure condition

The best method to make profit is by reducing the fixed cost and variable cost by using the present resources. Variable cost includes manpower cost such as drivers, loaders and vehicle attrition. Fixed cost includes the purchasing cost and depreciation cost of the vehicle. Putting the above mentioned cost together is the

distribution cost. Using the least expenditure model, the expenditure of every distribution mission is calculated. The monthly or the yearly sheet is determined by adding the above expenditure. Through the analysis on the monthly or yearly sheet, more detail about the operation condition itself can be beneficial to lay down the strategic plan in the future.

4.3 The analysis of the vehicle distribution

In many circumstances, a truck loaded with as many items of a single good cannot be fully loaded due to the dimension constraints of the single good. At that time, the goods will be mixed-loaded to improve the processing efficiency of the vehicle. In data warehouse design, we have planned the vehicle dimension and goods dimension to satisfy the demand of mix-loading the goods. Through analyzing the load capacity in vehicle dimension and the unit weight in goods dimension we can get the optimal distribution scheme to make use of the load capacity of the vehicle and give full play to the maximum processing efficiency of the vehicle.

4.4 The analysis of the vehicle route

The analysis of the vehicle route mainly depends on the shortest route model. Because the location of every distribution center is fixed, the selection of route lies in the location of every demand point. The execution of distribution mission is a route. Through the long-term data accumulation and analysis on the data, the enterprise is able to find an optimal route (ZHAO Zhengfen, 2004).

4.5 The structure of the on-board information device

A vehicle running in the city should be provided with the function of position and navigation. The drivers can find the traffic information by interactive equipment. The hardware composition of the on-board information device is as follows in Figure 4.

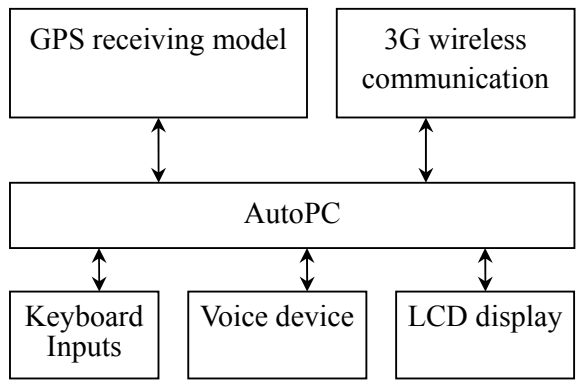

Figure 4. Hardware composition of the on-board information devices.

The vehicle supplies power to the on-board information device. The GPS receiving model calculates the function of position and the function of map-matching and provides navigating by LCD display equipment. Drivers control the query of traffic information by the input device such as keyboard; by 3rd generation mobile communication model, the interconnection between the on-board information device

and TIC is realized. At the same time, voice equipment broadcasts sound information.

4.6 Inquiring traffic information by the on-board device

The drivers can acquire the shortest route from A to B by inquiring the on-board device.

The software calculating the shortest route is installed on the AutoPC. Due to the dynamic traffic information, the shortest route from A to B is continuously changing. So the information interaction is conducted at the crossing. The on-board device makes the suitable regulation based on the dynamic real-time traffic condition to ensure the route shortest (Schumann, 1993).

5 THE MANAGEMENT OF THE DISTRIBUTION SYSTEM

In the distribution information system, to identify the goods, the most convenient method is through Radio Frequency Identification, called RFID. RFID is a non-contact auto-recognition technology. It recognizes the object through radio frequency signals and can track the goods and exchange data quickly. In recognition work, there is no man needed, it can work in adverse circumstances. RFID technology can recognize high speed moving objects and recognize several labels at the same time with easy operation. It benefits for the accomplishment of ERP (enterprise resource planning) and CRM (customer relationship management) business systems and can improve the business and commercial model greatly. Recently, RFID got a great deal of attention because of long-distance readability and high capacity. RFID not only help logistics enterprises improve the efficiency of goods and information management, but connects logistics enterprises with manufacturing enterprises. We can now receive the feedback information, control the demand information, optimize the whole supply chain, and improve the operative efficiency of the logistics information system better.

5.1 The operating principle of RFID

The composition of RFID system: (1) Tag: consists of coupling cells and chips, there is an antenna in the tag for communicating with radio frequency antennas. (2) Reader: to fetch the information in the tag. (3) Antenna: transmit radio frequency information between tag and reader. Some RFID systems can be connected with outer computers through reader's interface of RS232 or RS485 to exchange data.

The operation process of RFID systems is as follows: the reader transmits radio frequency signals through the antenna with a given frequency. When tag comes into the antenna's working area, it will generate induction current. Tag will be activated through the energy, and then it will transmit the code information through the antenna. The system antenna receives the carrier signals and transmits them to the reader through the antenna regulator. The reader modulates and decodes the signals, then sending them to the background system for processing. The principal system will justify the signal by logic operation then take corresponding actions depending on the different situation and send out command signals.

5.2 The features of RFID

The principal features of RFID lie in:

(1) Non-contact information collection, auto-recognition and auto-management.

(2) Supplying the supply chain management and logistics information system with bilateral communication of logistics and information flow.

(3) Satisfying the ever more improved demand for high-capacity information and high processing speed.

(4) Improving the automation degree of collecting data.

(5) Solving the problem of managing information in movement.

(6) Solving the problem of data error and data-filtering by adopting the RFID integrated middle-ware, meanwhile making the seamless integration with present the ERP system come true.

5.3 The advantages of the system

The system is an integration of RFID technology and 3rd mobile communication systems. So, it integrates both the advantages of a RFID system and a 3rd generation mobile communication system. The advantages of the system can be summarized as follows.

(1) The rapid and accurate data-processing. RFID's non-contact technique makes it possible to identify and label parameters of the goods in logistics distribution systems.

(2) Multi-media identification system. The 3rd generation mobile communication technology can provide video images when communicating. This is helpful to identify goods more intuitively.

(3) The system makes it possible to improve the distribution efficiency and lower distribution cost. And, the distribution speed is faster, which means we can improve the efficiency of the whole logistics system.

5.4 The possible disadvantages of the system

As the distribution system is based on the 3rd generation mobile communication system, if something is wrong with the mobile system, the distribution system may be halted. In order to make the system more stable, efforts to keeping the mobile communication system stable is very important. Thanks to the matured technology of 3rd generation mobile communication technology, the system is quite stable with a small margin of error.

In case of any error of the 3rd generation mobile communication sytem, a man-aided module is invented in the system to keep the system operating. When the mobile system is failed, the distribution system can operate well by way of the man-aided module though the speed may not be as fast as normal.

6 CONCLUSIONS

The paper discusses the construction design and platform composition of modern logistics distribution information systems based on 3rd generation mobile communication technology and analyzes the function of the system. In the platform

design, 3rd generation mobile communication technology is adopted to give full play to the function of dealing with a large quantity of data quickly. In database design of the information structure, data warehouse technology is used to integrate several databases. In addition, we conduct data analysis by using OLAP technology, dramatically improving efficiency and accuracy. In identifying the distribution goods, RFID technology is used to make the identification more correct, timely and dynamic with the development of information technology. Constantly reinventing the logistics distribution information platform by using every kind of relevant information technology will be the tendency of the logistics information system, at the same time, the information technology will provide the logistics industry with better technology support.

REFERENCES

HE Jie, LI Xuhong, and MAO Haijun (2003). "Analysis on structure scheme of the provincial information platform of logistics." *Communication Technology,* Science Press, Beijing, Vol. 23, June, pp. 72-74.

LI Yuming, LIU Shanzhong, and LI Xuhong (2008). "Framework analysis of regional logistics information platform." *Journal of Henan University of Science and Technology (Science and technology)*, University of Henan Science and Technology, Zhengzhou, Vol. 25, Jan, pp. 65-68.

Schumann, Fosef (1993). "TIRLS-Leader in radio frequency identification technology."*Texas Instruments Technical Journal*, Texas, Vol. 55, June, pp. 76-80.

WANG Xiaokun, YANG Dongyuan, and ZHANG Jin (2008). "Study on function orientation and structure of logistics public information platform." *Journal of Kunming University of Science and Technology (Science and Technology)*, University of Kunming Science and Technology, Kunming, Vol. 33, April, pp. 137-141.

XU Wei, ZHAO Songzheng, and JIANG Weiyang (2008). "Research on system structure of regional logistics information platform." *Journal of Information,* Science Press, Beijing, Vol. 15, July 2008, pp. 9-12.

YANG Deng (2008). "Analysis and design of a logistics distribution system based on the data warehouse." *Journal of Jilin Institute of Chemical Technology.* Vol. 25, Aug, pp. 146-151.

YANG Feng, ZHOU Guang-tian (2008). "Design and analysis of information system of modern logistics delivery center." *Information Technology*. Nov, pp. 11-14.

YANG Li-qiang, ZHANG Ning, TAO Zhi-xiang (2007). "Application of 3rd generation mobile communication technology in urban transportation information system." *Journal of Highway and Transportation Research and Development*. Vol. 24, Dec, pp. 132-136.

ZHAO Zhen (2008). "Research on the planning of the provincial information platform of logistics." *Computer Engineering & Science*, Science Press, Beijing,

Vol. 30, May, pp. 138-141.

ZHAO Zhengfen, CUI Nanfang, and CHEN Rongqiu (2004). "Study on function orientation and operation mechanism of regional logistics information platform." *Logistics Technology*, Science Press, Vol. 6, April, pp. 63-66.

Theory Study on Correlation Stability and Profit Allocation of Supply Chain

Hui Hu[1] and Chuantao Wang[2]

[1]School of Automobile, Chang'an University, Xi'an, China, PH (0086) 029-82334426; email: huhui@chd.edu.cn
[2]School of Traffic and Transportation, Beijing Jiaotong University, Beijing, China, PH (0086) 010-51687142; email: wangchuantao000@gmail.com

ABSTRACT

In this paper, correlation stability and profit allocation of supply chain are studied. Stability theory of dynamical system is introduced to study the supply chain system. The paper defines correlation stability of supply chain, and analyzes its mechanism. Nonlinear model of the integrated supply chain is then formulated, and its stability is evaluated by Lyapunov stability criterion. Based on the correlation stability analysis, new profit allocation method is proposed. The method considers system stability as a basic condition of reasonable profit allocation. The original profit allocation should be adjusted if system stability condition is not satisfied.

INTRODUCTION

Nowadays fierce competition exists between supply chains. Supply chain members compete and cooperate at the same time. How to coordinate with partners and to make decision jointly is essential for the entire system to operate stably.

In this paper, stability theory in the field of dynamical system is introduced to analyze supply chains. Stability is an important mechanism for system to survive and develop. How to evaluate the stability and to find the measures to guarantee system stability is very important for the system to operate normally. From the end of the 19th century to the beginning of this century, French mathematician Poincaré gave the definition of dynamical system in his studies of classical mechanics and differential equation theories (Ledyaev and Sontag, 1999; Retchkiman, 1998). In 1892, the Russian mathematician Alexander Mikhailovitch Lyapunov introduced his famous stability theory for nonlinear and linear systems (McConley et al., 1998). A complete English translation of Lyapunov's doctoral dissertation "*The general problem of the stability of motion*" was published in the *International Journal of Control* in March 1992 (Buse and Barbu, 1997; Penzl, 1998). He studied the motion stability problem of dynamical system described by differential equations and proposed the architecture and approach of stability theory, which is still widely used now.

Profit allocation is another important problem in supply chain coordination. In these years, cooperative game is applied to solve this problem successfully. The methods include Shapley value method, MRCS method, Nash negotiation method and so on (Nagarajan and Sosic, 2008; Guardiola et al., 2007; Giannoccaro and

Pontrandolfo, 2004). In this paper, new profit allocation method based on stability criteria is presented.

CORRELATION STABILITY ANALYSIS OF SUPPLY CHAIN MEMBERS

Lyapunov Exponent Stability

Supply chain is a network that includes material provider, manufacturer, distributor, retailer, customers and so on. For supply chain, correlation stability means that its members shall keep efficient operation and normal fluctuation when satisfying the customers' demands. They can corporate and coordinate with each other. In the product life cycle, all members adjust their own strategies to optimize the performance of the entire system. Therefore, correlation stability focuses on how supply chain members react to their partners and how their reactions affect system stability.

Lyapunov exponent is an important concept in nonlinear dynamics. It is also a reliable and simple quantitative approach to measure chaos. Lyapunov exponent is useful for distinguishing various types of orbits. It works for discrete as well as continuous systems (Xing, 2000; Benettin et al., 1980; Gukenheimer, 1982).

A stability criterion with the largest Lyapunov exponent is described as blow (Lu, 2004). Consider a dynamical system which satisfies

$$X_{k+1} = F\left(X_k\right) \tag{1}$$

We assume that ΔX_k satisfies

$$\Delta X_{k+1} = \left(\frac{\partial F}{\partial X}\Big|_{X=X_k}\right) \Delta X_k = J_k \Delta X_k$$

Define J_k to be the Jacobian matrix of F at X_k, then

$$\Delta X_{k+1} = J_k \Delta X_k = J_k J_{k-1} \ldots J_1 \Delta X_1$$

where $J^{(k)} = J_k J_{k-1} \ldots J_1$ and $\Delta X_{k+1} = J^{(k)} \Delta X_1$. For dynamical system (1), let $T\left(X\right) = \lim_{k \to \infty} \left[\left(J^{(k)}\right)^T J^{(k)} \right]^{\frac{1}{2k}}$, and denote λ_i its eigenvalue.

The Lyapunov exponent of equation (1) is

$$\sigma_i = \ln\left|\lambda_i\right|, (i = 1, 2, \ldots n)$$

According to the definition of Lyapunov exponent and its relationship with system stability, the stability criterion with the largest Lyapunov exponent is stated in theorems 1 and 2.

Theorem 1. For nonlinear dynamical system (1), we assume the largest Lyapunov exponent of its spectrum is $\sigma_m \left(m \in i, i = 1, 2, \ldots, n\right)$. If $\sigma_m < 0$, this system is stable. If $\sigma_m > 0$, the system is unstable.

Theorem 2. For nonlinear dynamical system (1), if $\left|\lambda_i\right| < 1$ for all *i*, this system is stable. If there exists any $\left|\lambda_i\right| > 1$, the system is unstable.

Theorem 2 is recommended for the nonlinear model of supply chain in this paper, because using theorem 2 we only need to verify whether $\left|\lambda_i\right| > 1$ or not in stead of finding out the exact values of all Lyapunov exponents.

Nonlinear Model of the Supply Chain

Traditionally, some factors are neglected in supply chain modeling, and external environment is often simplified to linearize the nonlinear system. However, this approximation method is not able to describe practical systems accurately. Inspired by the research in the field of dynamical system, similar methods are introduced to evaluate system stability and to analyze the key elements affecting stability.

Without loss of generality, we consider a simplified supply chain system with three phases: product manufacturing, storage and distribution to customers. Our study in this paper can be applied to virtually all supply chains.

The inventory process of the manufacturer is:

$$x_{t+1} = x_t + P_{t+1} - S_{t+1} \ (t = 1, 2, ..., N) \tag{2}$$

where x_t is the inventory level of the manufacturer at the end of period t, P_{t+1} is the manufacturer production quantity in period $t+1$, and S_t is the amount of products sent to storage providers by the manufacturer in period t. In reality, manufacturers often attempt to decrease costs, improve core competence and achieve the goal of zero inventories. Therefore, we assume the manufacturer sends all products to the storage provider once they are produced. Equation (2) can then be written as blow:

$$S_{t+1} = P_{t+1}$$

According to the production model with constant elasticity of substitution (Zhang, 1999), the initial production quantity of the manufacturer can be written as

$$P_1 = A(\omega_1 L^{-\tau} + \omega_2 K^{-\tau})^{-(h/\tau)}$$

where ω_1 and ω_2 are distribution parameters that reflect the weights of labor and capital investments with $\omega_1 + \omega_2 = 1$, h is the order parameter, and $\tau = \frac{1}{\sigma} - 1$ is the substitution parameter. Substitution elasticity σ is the ratio of the capital increasing rate to the labor income increasing rate. To model the production in all other periods, we denote the retailers' actual sales volume in period t as Q_t. We assume Q_t can be observed by all upstream enterprises at the end of period t. The assumption is reasonable because advanced information technology is often utilized nowadays to guarantee high speed information transmission. Moreover, the production of the manufacturer is closely related to the existing inventory and sales volume. The production level is often forecasted based on the demand in the last period, the season factor, the promotion factor and so on. Adopting the promotion response model (Huang, 2000), the production in period $t+1$ can be expressed as:

$$P_{t+1} = N(t)M(\varsigma)\left\{k \tanh\left[k\left(t_f - t\right)\right]\left(y_d - y_t\right) + Q_t\right\} \tag{3}$$

where $k = \sqrt{\frac{h}{C}}$, and h and C are constant weighting factors. y_d is the ideal inventory level, y_t is the inventory level of the storage provider at the end of period t, and $\tanh = \frac{e^x - e^{-x}}{e^x + e^{-x}}$. $N(t)$ is the season exponent, which represents the

changes caused by season or holiday factors. $M(\varsigma)$ is the promotion exponent, which reflects the effects caused by reduced prices, advertisements or other promotions:

$$M(\varsigma) = \prod_{i=1}^{k} \Omega \left[\left(\varsigma_i \Big/ \varsigma_i^* \right) \right]^{V_i}$$

where ς_i is the market variable, and ς_i^* denotes its standard value, and V_i is the elasticity or sensitivity of the market variable. According to equation (3), the manufacturer adjusts its production level based on the sales condition as well as the inventory level. When the actual inventory is more than the ideal level, manufacturing speed decreases; otherwise, it increases.

The inventory process of the storage provider is

$$y_{t+1} = \theta y_t + \delta S_{t+1} - D_{t+1} \quad (t = 1,2,...,N)$$

where $1-\theta$ is the inventory damage rate of the storage provider, $1-\delta$ is the damage rate of the products during delivery from the manufacturer to the storage provider, and D_{t+1} is the amount of products sent from the storage provider to the distributor during period t+1.

In VMI mode, distribution companies manage the inventory levels of the retailers. To reduce retailers' inventory costs, the distributor's lot size must be controlled. On the other hand, storage providers have the incentive to send more products to the distributor to reduce their own costs. Therefore, it is necessary for them to coordinate in determining the distributor's lot size. We assume that when the storage provider's inventory level y_t is higher than the expected value y^*, the distributor agrees to take a portion of the excess to its own lot from the storage providers' warehouse. Therefore, distributor's lot size depends not only on the predicted retailer demands, but also the storage provider's inventory level. The distributor's lot size in period t+1 can then be expressed as:

$$\begin{aligned} D_{t+1} &= \left(D_{l,t+1} + D_{c,t+1} \right) - \rho z_t \\ &= \left[R_{t+1} + \eta \left(y_t - y^* \right) \right] - \rho z_t \end{aligned} \tag{4}$$

where $D_{l,t+1}$ is the delivering lot size for the predicted retailer demands at period t+1, $D_{c,t+1}$ is the amount of excess inventory the distributor takes from the storage provider, z_t is the total inventory level of all retailers during period t, and the damage rate of the retailers' inventory is $1-\rho$. The first term in equation (4) equals to the predicted retailer sales volume R_{t+1}. According to Bass model (Steffens and Murthy, 1992) and the index number smoothing method (Disney and Towill, 2002), R_{t+1} satisfies the following equation:

$$\begin{cases} R_{t+1} = \alpha Q_t + (1-\alpha) R_t, \ t = 1,2,....N \\ R_1 = k \cdot \dfrac{1 - e^{-(a+bk)}}{1 + \dfrac{bk}{a} e^{-(a+bk)}} \end{cases}$$

where k is the potential amount of customers, and a, b, and α are predetermined parameters. Based on the discussion above, the second term in equation (4) equals to $\eta(y_t - y^*)$, where η is the proportion parameter. Variable η is a crucial element to the coordination between the storage provider and the distributor, which directly affects the lot size of the distributor and the inventory level of the storage provider, as well as their profits. In this paper, we treat η as a decision variable of the supply chain system. Obviously, if $y_t < y^*$ then $\eta = 0$; if $y_t > y^*$, η should be greater than zero. The relationship between the parameter η and the stability of the system will be analyzed in the following section to help the players in the supply chain make their decisions.

We assume the distributor delivers products at the end of every period, and retailers receive products at the beginning of the next period. For the distributor, the delivering lot size in period t is the sum of the quantities ordered by all retailers:

$$D_t = \sum_{i=1}^{n} D_{it}, (t = 1, 2, ..., N)$$

And for each retailer i, its inventory at the end of period $t+1$ is

$$z_{i,t+1} = \rho z_{it} + \xi D_{it} - Q_{i,t+1}$$

where the delivering damage rate is $1-\xi$, z_{it} is the inventory level of retailer i at the end of period t, and $Q_{i,t+1}$ is the actual sales volume of retailer i in period $t+1$, which satisfies

$$Q_{t+1} = \sum_{i} Q_{i,t+1}$$

The total retailer inventory level in period $t+1$ is then

$$z_{t+1} = \rho z_t + \xi D_t - Q_{t+1}$$

Finally the dynamical nonlinear model of the supply chain is

$$\begin{cases} y_{t+1} = \theta y_t + \delta P_{t+1} - D_{t+1} \\ z_{t+1} = \rho z_t + \xi D_{t+1} - Q_{t+1} \\ P_{t+1} = N(t)M(\varsigma)\left\{k \tanh\left[k(t_f - t)\right](y_d - y_t) + Q_t\right\} \\ D_{t+1} = \left[\eta(y_t - y^*) + R_{t+1}\right] - \rho z_t \\ R_{t+1} = \alpha Q_t + (1-\alpha) R_t \end{cases} \tag{5}$$

Enterprise Correlation Stability Analysis Based on Lyapunov Exponent Criterion

In this section, enterprise correlation stability will be analyzed by means of Lyapunov exponent criterion. The matrix of model (5) is

$$A = \begin{pmatrix} \theta - \delta u - \eta & \rho & 0 & 0 & -(1-\alpha) \\ \xi\eta & \rho\xi - \rho & 0 & \xi & \alpha(1-\xi) \\ -u & 0 & 0 & 0 & 0 \\ \eta & -\rho & 0 & 0 & 1-\alpha \\ 0 & 0 & 0 & 0 & 1-\alpha \end{pmatrix}$$

where $u = N(t)M(\varsigma)k\tanh\left[k\left(t_f - t\right)\right]$.

We obtain the characteristic equation

$$\lambda^2\left[\lambda - (1-\alpha)\right]\left[\lambda^2 - (\theta - \delta u - \eta + \rho\xi)\lambda + (\rho\xi\theta - \rho\xi\delta u - \rho\xi\eta - \rho\eta)\right] = 0,$$

and

$$\Delta = (\rho + \theta - \eta - \delta u + \rho\xi)^2 - 4\left[\rho\xi\theta - \rho\xi\delta u - \rho\xi\eta - \rho\eta + \rho\eta\right].$$
$$= (\theta - \delta u - \eta - \rho + \rho\xi)^2 + 4\rho\xi\eta$$

Since $0 \le \rho$, $\xi \le 1$ and $\eta \ge 0$, there exists a $\Delta \ge 0$. The solutions to the characteristic equation are

$$\lambda_{1,2} = 0, \quad \lambda_3 = 1-\alpha, \quad \lambda_{4,5} = \frac{\rho + \theta - \delta u - \eta - \rho\xi \pm \sqrt{\Delta}}{2}$$

According to theorem 2, when the absolute values of all characteristic roots are smaller than 1, the supply chain system is stable in the sense of Lyapunov.

PROFIT ALLOCATION BASED ON SYSTEM STABILITY EVALUATION

We discuss the profit allocation problem between supply chain members in this section. In our method, profit allocation must guarantee the stability of supply chain, because considering stability and coordination between supply chain members may lead to reasonable profit allocation and sustainable supply chain operation.

More specifically, the profit allocation method consists of two steps: one fundamental and one modified allocation. Fundamental allocation refers to original allocation between supply chain members, while modified allocation further adjusts the original allocation based on some criteria value obtained from the previous section. It is worth mentioning that it may require multiple modifications before the stability condition is satisfied.

Due to the page limit, the detailed profit allocation model and the case study are omitted. We found that the method is more reasonable and applicable, and taking stability into consideration for profit allocation helps us to analyze cooperation and coordination relationship between enterprises and helps the supply chain to sustain.

CONCLUSIONS

In this paper, we introduce stability theory into the study of supply chains, and construct a dynamical nonlinear model for integrated supply chain. The stability of the proposed model is analyzed by the largest Lyapunov exponent theorem. More specifically, to guarantee the system stability, the value domains of dynamical parameters are discussed and simulated. Based on the investigation of the impact of the dynamical parameter disturbance on the supply chain system, this paper proves that the supply chain system will be unstable if the value of some dynamical parameter exceeds its domain. For example, if the proportion the distributor takes

from the storage provider when the inventory level of the latter is high is too large, the system will lose its stability. This indicates that the entire supply chain system will be unstable if its members make their decisions in terms of local optimization. Finally, a profit allocation method based on correlation stability is proposed.

REFERENCES

Benettin, G., Galgani, L., and Strecyn, J.M. (1980), "Lyapunov Characteristic Exponents for Smooth Dynamical Systems and for Hamiltonian Systems: A method for Computing all of Them." *Meccanica*, vol. 15, 9-20.

Buse, C., and Barbu, D. (1997), "The Lyapunov equations and nonuniform exponential stability." *Studii si Cercetari Matematice*, vol. 49, 25-31.

Disney, S.M., and Towill, D.R. (2002), "A discrete linear control theory model to determine the dynamic stability of vendor managed inventory supply chains." *International Journal of Production Research*, vol. 40, 179-204.

Giannoccaro, I., and Pontrandolfo, P. (2004), "Supply chain coordination by revenue sharing contracts." *International Journal of Production Economics*, 89, 131-139.

Guardiola, L., Meca, A. and Timmer, J. (2007), "Cooperation and profit allocation in distribution chains." *Decision Support Systems.* 44, 17–27.

Guckenheimer, J. (1982), "Noise in Chaotic System," *Nature*, vol. 298, 285-317.

Huang, H. (2000), "Study on the application of control theory in inventory management." Doctoral dissertation, Northeastern University.

Ledyaev, Y. and Sontag, E. (1999), "A Lyapunov characterization of robust stabilization." *Nonlinear Analysis*, vol. 37, 813-840.

Lu, Y. (2004), "Research on the dynamic complexity of integrated supply chains." *Doctoral dissertation*, University of Electronic Science and Technology of China.

McConley M. W., Dahleh M. A., and Feron E. (1998), "Polytopic control Lyapunov functions for robust stabilization of a class of nonlinear systems." *Systems and Control Letters*, vol. 34, 77-83.

Nagarajan, M. And Sosic, G. (2008), "Game-theoretic analysis of cooperation among supply chain agents: Review and extensions." *European Journal of Operational Research*,187, 719-745.

Penzl T. (1998), "Numerical solution of generalized Lyapunov equations." *Advances in Comp. Math,* vol. 8, 33-48.

Retchkiman Z. (1998), "Practical stability of discrete event systems using Lyapunov methods." *Proceedings of the American Control Conference. Phladelphia,* 3627-3628.

Steffens, P.R., and Murthy, D.N.P. (1992), "A Mathematical Model for New Product Diffusion: The Influence of Innovators and Imitators." *Math. Comput. Modeling*, vol. 16, 11-26.

Xing, W. (2000), "Study on system stability and general optimization control." *Doctoral dissertation*, Northeastern University.

Optimal Dynamic Substitution Policy for components in an Assemble-to-order System

LIU Yongqiang[1], CHANG Qing[2], ZHANG Xiaohong[3], and GAO Hui[4]

[1]School of Electronics and Information Engineering, Beijing University of Aeronautics and Astronautics, Beijing 100191, China; PH (010)82317800; email:yongqiangliu@sina.com
[2]School of Electronics and Information Engineering, Beijing University of Aeronautics and Astronautics, Beijing 100191, China; PH (010)82317800; email:changq@263.net
[3]School of Politics and Public Administration, Soochow University, Suzhou 215006, China; email: zhangxh2@sem.tsinghua.edu.cn
[4]China Spacesat Corporation Ltd, Beijing 100191, China; PH (010)82317800

Abstract: In assemble-to-order system, the substitution of higher-class components for lower-class components is often applied when the latter are stock-out. But the decision for substitution should be made in advance in practice. How to manage the substitution in such a system is of managerial interest. We model this scenario as a two-stage mathematical programming where the first step is to determine how many to order for each product at the beginning of the selling season, and the second step is to explore the substitution rule. We exploit the structural properties of the substitution rule and present a dynamic substitution policy. Then we show that our substitution policy is a threshold policy and present the upper bound of the threshold.

Key Words: *assemble-to-order, dynamic substitution policy, threshold, inventory*

1. Introduction

In this paper, we consider a simple assemble-to-order system, where substitution of components is allowed in assembling end-products. We only allow a one-way downward substitution structure in that demand for lower-class components may be satisfied by using the higher-class ones; however the demand for higher-class components can not be satisfied by using the lower-class ones. This downward substitution structure occurs in several practical settings such as semiconductor chips (Hsu and Bassok, 1999), hotel booking, airline seats allocation (Zhao and Zheng, 2001), as well as resource allocation and risk mitigation in news-vendor networks (Van Mieghem, 2007) etc. It has also been adopted as an aid for the mass customization strategies. Besides improving customer service, this substitution policy can mitigate the risk that the types of products may increase rapidly due to customization, especially for products with short life cycle.

Wang et al. (2007) adopts downward substitution and forecast updating to reduce demand uncertainty in a supply chain system, where mass customization and traditional production process exist simultaneously. The authors focus on two stages

of decisions: prior to final demand is known, how many components to purchase; and once demand is realized, how to allocate those components in a profit maximizing manner. However, in today's saturated markets, customers demand greater flexibility and faster reaction from their suppliers. The two-stage process might not serve their needs in practice. Terms like Quick Response and Just-in-Time are becoming increasingly prevalent in business literature and practical management process.

2. The Model

2.1 Symbols and Assumptions

We consider two components denoted by 1 and 2, where component 1 can substitute for component 2 but the opposite is not allowed. We also assume the following events occur in sequence: 1) At the beginning of the selling season, the order is placed based on the initial inventory level and is delivered immediately; 2) Demands for two components are realized; 3) Excess stock of each component is salvaged at the end of each period. Before we proceed our study, we first introduce the following basic notations: c_i –wholesale price per unit of component i; p_i–sales price per unit for component i; $_i$–loss for shortage per unit of component i; s_i–salvage value per unit for component i; h_i–holding cost per unit for component i; Q_i–order quantity for component i, that is, the inventory level of component i at the start time of the selling season. We also define $r_i = _i + p_i$ and the net salvage value of component i to be $v_i = s_i - h_i$.

Further, we make the following assumptions.

Assumption 1. $c_1 \geq c_2$; $p_1 \geq p_2$, $\pi_1 \geq _2$; $v_1 \geq v_2$

Assumption 2. $r_2 \geq v_1$, i.e., $_2 + p_2 \geq v_1$;

Assumption 3. If component 1 is substituted for component 2, then charge p_2 (not p_1)

Assumption 4. $p_i \geq c_i \geq v_i > 0 (i = 1, 2)$.

Assumption 5. Unmet demands of component 1 and 2 after the possible substitution is exercised are lost.

Assumption 6. Customers are allowed to buy only one final product each, and arrive according to a Poisson process with density $_i(t)$ at time t.

2.2 Model Formulation

Let T be the length of the selling season. Let t be the time left until the end of the selling season. The time interval between t_1 and t_2 with $t_1 > t_2$ is denoted by (t_1, t_2) or $[t_1, t_2)$ if t_1 is included. Let the inventory level of component i at the start time of selling season be Q_i $(i = 1, 2)$. Our aim is to find the optimum order quantity Q_i for component i $(i = 1, 2)$, as well as the stopping time for substitution, in order to obtain the highest expected revenue during the whole selling season. In our model we assume that once substitution is ended at a time point, it will not be allowed to restart. We will proceed in two steps: first, to find the optimal stopping time for given Q_1 and Q_2; second, to determine the optimal order quantity Q^*_i for component i $(i = 1, 2)$. We first begin with step 1. Let t_i be the time point when the inventory level of component i $(i = 1,2)$ drops to zero, that is, the hitting/trigger time for stock-out. It is easy to see that substitution is possible only when $t_1 < t_2$, that is, only when there are stocks left for component 1 while demands still arrive for component 2 but its stocks have been used up. Recall that t is the time left until the end of selling season. At any

time $t \in [t_2, 0)$, let $x_1(t)$ be the total number of component 1 that has been sold and $y_1(t) = Q_1 - x_1(t)$ the inventory level at time t. We will make our decisions on whether to exercise substitution, that is, to meet the demand for component 2 by using the stocks of component 1. Clearly, this should be based on $y_1(t)$, the inventory level of component 1, as well as t, the time left until the end of the selling season. Thus, it is an optimal stopping problem. A stopping rule can be characterized by a stopping region S contained in $[t_2, 0) \times \{0, 1. . . \quad Q_1\}$.

Let $N_i(t, s)$, $(t > s)$, denote the total demand for component i (i = 1,2) that occurs between t and s, that is, the number of customers who buy component i. It follows that $N_i(t, s)$ is a Possion random variable with mean $\int_s^t \lambda_i(\tau)\, d\tau$ (which is clearly continuous in t). Let $J_S(y_1, t)$ denote the expected revenue accrued in $[t, 0)$, under a given stopping rule S, starting with y_1 ($y_1 > 0$) left for component 1 while the stocks for component 2 have been used up at time t. Then we have

$$\begin{aligned} J_S(y_1, t) = E[&p_1 N_1(t, s) + p_1 \min\{N_1(s, 0), y_1 - N_1(t, s) - N_2(t, s)\} \\ &+ p_2 N_2(t, s) + v_1 (y_1 - N_1(t, s) - N_2(t, s) - N_1(s, 0))^+ \\ &- \quad _1 (N_1(s, 0) - y_1 + N_1(t, s) + N_2(t, s))^+ - \quad _2 N_2(s, 0)] \end{aligned}$$

where s is the stopping time determined by stopping rule S. We can ensure the non-negativity of $y_1 - N_1(t, s) - N_2(t, s)$ by requiring that $[T, 0) \times \{0\} \quad \subset S$, i.e., substitution is automatically ended as soon as all the stocks for component 1 are used up.

3. Optimal Substitution Policy

3.1 Optimality Conditions and Results

Let $f(y, t)$ be the maximum expected revenue starting with y component 1 in stock at time t, i.e., $f(y,t) = \sup_s J_s(y,t)$. Let $g(y, t)$ be the expected revenue over $[t, 0)$ with y component 1 left and with substitution ended already by time t. Then the optimal stopping region $S^* = \{(s, y) | f(y, s) = g(y, s), s \in [t_2, 0)\}$. On the other hand, if $(t, y) \notin S^*$, $f(y, t) > g(y, t)$ and it is optimal to keep substituting component 1 for 2. Because $g(y, t)$ is the expected revenue accrued in $[t, 0)$ where only the demand for component 1 is met, we have

$$\begin{aligned} g(y_1, t) = E\,[&p_1 \min\{N_1(t, 0), y_1\} \\ &+ v_1 (y_1 - N_1(t, 0))^+ - \quad _1 (N_1(t, 0) - y_1)^+ - \quad _2 N_2(t, 0)] \end{aligned}$$

It is easy to see that, for any fixed y, $g(y, t)$ is continuous in t (because the mean of $N_1(t, 0)$ is continuous in t). For any fixed t, $g(y, t)$ can be determined inductively by the following equations:

$$g(y + 1, t) - g(y, t) = r_1 P_r\{N_1(t, 0) \geq y + 1\} + v_1 P_r\{N_1(t, 0) \leq y\}, \qquad (1)$$

Equation (1) indicates that the expected marginal revenue of component 1 when the substitution is ended equals to the sum of r_1 times the probability that the stocks for component 1 can be used up and v_1 times the probability that there are still stocks left for component 1 at the end of selling season.

We proceed to present the Bellman equation for our dynamic program. At any time t, when the substitution has already been ended, there is no further decision to make. In this case, because both the demand processes of component 1 and component 2 follow Possion distibution, we have

$$g(y, t) = \quad _1(t) \quad t(p_1 + g(y - 1, \quad t - \quad t))$$

$$+(1 - \lambda_1(t)\,\Delta t)(g(y, t - \Delta t) - \lambda_2 c_2(t)\,\Delta t + o(\Delta t) \quad (2)$$

where Δt is the length of a small time interval $[t, t-\Delta t)$. Hence, the first term is the expected total revenue if one unit of component 1 is sold during $(t, t-\Delta t)$, the second is the total expected revenue of component 1 otherwise, and the third is the expected loss for unmet demand of one unit of component 2 during $(t, t-\Delta t)$. Rearranging terms and letting Δt decrease to 0, we obtain the differential form of equation (2).

$$\frac{\partial g(y,t)}{\partial t} = \lambda_1(t)[p_1 + g(y-1,t)] - \lambda_1(t)g(y,t) + \pi\lambda_2 c_2(t)$$

If it is optimal to keep on substitution at (y, t), we have the following dynamic programming equation,

$$f(y, t) = \lambda_1(t)\,\Delta t(p_1 + f(y-1, t-\Delta t)) + \lambda_2(t)\,\Delta t(p_2 + f(y-1, t-\Delta t)) + (1 - \lambda_1(t)\,\Delta t - \lambda_2(t)\,\Delta t)f(y, t-\Delta t) + o(\Delta t)$$

Rearranging terms and letting Δt go to 0, we get the differential form of the dynamic programming equation

$$\frac{\partial f(y,t)}{\partial t} = \lambda_1(t)[p_1 + f(y-1,t)] + \lambda_2(t)(p_2 + f(y-1,t)) - (\lambda_1(t) + \lambda_2(t))f(y,t)$$

The above equation only holds when $(t, y) \notin S^*$. When $(t, y) \in S^*$, we have $f(y, t) = g(y, t)$. Clearly, $f(y, t)$ is continuous in t when $(t, y) \in S^*$. Now we present our dynamic substitution rule: keep on substitution if and only if

$$r_2 > r_1 P_r\{N_1(t, 0) \geq y\} + v_1 P_r\{N_1(t, 0) < y\} \quad (3)$$

where y is the inventory level of component 1 at time t. The rule is optimal for the following static model. Assume that the remaining demand for component 1 is $N_1(t, 0)$ with a known (static) probability distribution. The decision is how many stocks of component 1 should be protected at the time point. The optimality of this rule in this static model is based on the following simple marginal analysis: the left hand side of equation (3) is the revenue accrued from meeting the demands for component 2 with the stocks of component 1; the right hand side is the opportunity cost of the last component 2. The substitution should be kept on if the left hand side is greater. Although intuitive and convenient, the above substitution rule is not optimal but only a heuristic for our dynamic model. It is compelling to know how good it is compared to the optimal dynamic policy. Therefore, in the next subsection, we will pursue the relationship between our substitution rule and the optimal dynamic policy.

For dynamic model, the above substitution rule specifies a stopping region with

$$\{(t, y) | r_2 \leq r_1 Pr\{N_1(t, 0) \geq y\} + v_1 Pr\{N_1(t, 0) \leq y\}\} = \{(t, y) | r_2 - v_1 \leq (r_1 - v_1) Pr\{N_1(t, 0) \geq y\}\}$$

Because $Pr\{N_1(t, 0) \geq y\}$ decreases in y ($Pr\{N_1(t, 0) \geq y_2\} = Pr\{N_1(t, 0) \geq y_1\} + Pr\{y_2 \leq N_1(t, 0) < y_1\} \geq Pr\{N_1(t, 0) \geq y_1\}$ holds when $y_1 \geq y_2$), the above stopping rule is a threshold policy, i.e., there exists $y^*_L(t)$ such that the substitution should be ended if $y(t) \leq y^*_L(t)$.

It is clear that $N_1(t, 0)$, the remaining demand for component 1, is stochastically non-increasing over time, i.e., for any given y, $Pr\{N_1(t_1, 0) \geq y\} \geq Pr\{N_1(t_2, 0) \geq y\}$ for all $t_1 > t_2$. As a result, the threshold is non-increasing over time.

PROPOSITION 1. $y^*_L(t)$ is non-increasing over time, i.e., the closer to the end of the selling season, the lower the threshold.

3.2 Structure of Optimal Policies

In this subsection, we first show that the optimal dynamic policy is a threshold policy. That is, there exists a threshold $y^*(t)$ such that the optimal dynamic policy is to cancel substitution whenever $y(t) \le y^*(t)$.

The optimality of a threshold policy is based on the following observation: the expected marginal revenue is smaller when the substitution has been ended.

LEMMA 1. For any t and y, $f(y+1, t) - f(y, t) \ge g(y+1, t) - g(y, t)$ (4)

Inequality (4) can be rewritten as

$$f(y+1, t) - g(y+1, t) \ge f(y, t) - g(y, t) \quad (5)$$

Inequality (5) indicates that if it is optimal to end substitution at $(y+1, t)$, that is, $f(y+1, t) = g(y+1, t)$, then it must be optimal to end substitution at (y, t), because it follows that $f(y, t) = g(y, t)$ from inequality (5). Therefore, we have shown:

THEOREM 1. The optimal policy is a threshold policy, i.e., there exists a threshold $y^*(t)$ such that it is optimal to end substitution whenever $y(t) \le y^*(t)$, where

$$y^*(t) = \max\{y | f(y, t) = g(y, t)\}.$$

PROPOSITION 2. For any t, $y^*_L(t) \ge y^*(t)$.

PROPOSITION 3. $y^*(t)$ is non-decreasing in t.

4. Determination of Optimal Order Quantities of Q^*_1 and Q^*_2

4.1 Optimal Replenishment Policies

Let $V(Q_1, Q_2, T)$ be the optimal expected revenue accrued from a stock Q_i of component i ($i = 1, 2$) when the time left is T until the end of selling season (see Rahim et al., 2000). Let the stockout of component 2 start at time t with $0 \le t \le T$, and let k denote the quantity of component i sold before the stockout of component 2 was observed. We then have the following:

$$V(Q_1, Q_2, T \mid 0 \le t \le T) = \sum_{k=0}^{Q_1-1} [\max_s J_s(Q_1 - k, t) \quad p_1 k p_{1,k}(T, t)] + \sum_{k=Q_1}^{+\infty} p_1 Q_1 p_{1,k}(T, t) + p_2 Q_2$$

where $p_{i,k}(T, t)$ is the possibility that the sales quantity of component i (i=1,2), which equals the number of customers who purchase this component, is k in a time interval $[T, t]$. Thus,

$$p_{i,k}(T, t) = \frac{1}{k!}\left(\int_t^T \lambda_i(\tau)\, d\tau\right)^k e^{-\int_t^T \lambda_i(\tau)\, d\tau}, (i = 1, 2).$$

On the other hand, if the stockout of component 2 occurs at time t with $t < 0$, that is, there are always stocks left for component 2 throughout the selling season, then

$$V(Q_1, Q_2, T \mid t < 0) = \sum_{k=0}^{Q_1-1} p_1 k p_{1,k}(T, 0) + \sum_{k=Q_1}^{+\infty} p_1 Q_1 p_{1,k}(T, 0) + \sum_{k=0}^{Q_2} p_2 k \; p_{2,k}(T, 0)$$

Thus, we can obtain the optimum order quantity Q^*_i for component i ($i = 1, 2$) by solving the following programming problem:

$$V(Q^*_1, Q^*_2, T) = \max_{Q_1 \geq 0,\, Q2 \geq 0} V(Q_1, Q_2, T)$$

4.2 Numerical Examples

For computational purposes, we discretize $[T, 0]$ into N periods of equal length $\Delta t = \frac{T}{N}$. When N is large, the discrete-time approximation is close to the continuous time model. Let $F[y, n] = f(y, n\Delta t)$, $G[y, n] = g(y, n\Delta t)$, $_i[n] = _i(n\Delta t)\ \Delta t$, $F[y, 0] = 0$, $F[0, t] = 0$, $G[y, 0] = 0$, $G[0, t] = 0$, and $g[y, n] = \max\{ _1[n](p_1 + F[y-1, n-1]) + _2[n](p_2 + F[y-1, n-1]) + (1 - _1[n] - _2[n])F[y, n-1],\ G[y, n]\}$.

Note that y^*_n, the optimal threshold, is the largest y such that $F[y, n] = G[y, n]$.

EXAMPLE 1. We set $T = 100$, $N = 200$, $p_1 = 200$, $p_2 = 100$, $c_1 = 100$, $c_2 = 40$, $_1 = 50$, $_2 = 30$, $s_1 = 60$, $s_2 = 20$, $h_1 = 10$, $h_2 = 8$, $Q_1 = 30$, $Q_2 = 20$, $_1(t) = 0.5$, and $_2(t) = 0.8$. The result indicates that the system obtains its optimal expected revenue, 124.3912 with the order quantity $Q_1 = 10$ and $Q_2 = 2$.

5. Conclusions

In this paper, we have established a two-component inventory model with downward demand substitution and presented a dynamic substitution rule. We have shown that the optimal policy is a threshold policy, which is relatively easy to determine and implement. One of the contributions of this paper is that for the first time, we show that although our substitution rules are not optimal, they are close to optimal. We also have shown that the static threshold determined by our dynamic substitution rule is the upper bound of the optimal dynamic threshold.

Acknowledgements: This work is funded by National Science Foundation of China (60879024, 60872062).

References

Hsu, A., and Bassok, Y. (1999)."Random yoeld and random demand in a production system with downward substitution." Operations Research. 47(2)277-290.

Van Mieghem, J. A. (2007)."Risk mitigation in Newsvendor networks: Resource diversification, flexibility, sharing, and hedging." Management Science. 53(8)1269-1288.

Wang,Y., Gao C., and Li, S. (2007). "Optimal order policies in a custom-made product supply chain with substitution and market signal." 2007 IEEE International Conference on Automation and Logistics, Jinan, China. 1498-1503.

Zhao, W., and Zheng, Y. (2001)."A dynamic model for airline seat allocation with passenger diversion and no-shows." Transportation Science. 35 80-98.

Coordination Policies of Supply Chain where Deterioration Begins at a Random Time Point

LIU Yongqiang[1], CHANG Qing[2], ZHANG Xiaohong[3], and GAO Hui[4]

[1,2]School of Electronics and Information Engineering, Beijing University of Aeronautics and Astronautics, Beijing 100191, China; PH (010) 82317800; email: yongqiangliu@sina.com, changq@263.com
[3]School of Politics and Public Administration, Soochow University, Suzhou 215006 China; email: zhangxh2@sem.tsinghua.edu.cn
[4]China Spacesat Corporation Ltd, Beijing 100191, China; PH (010) 82317800

Abstract: This paper investigates the manufacturer's optimal wholesale price and return policy as well as the retailer's optimum order size and price decisions in a supply chain, where deterioration begins at a random time point. In the current study we assume that the retail price can only be adjusted once at that point according to the lifetime of product in the cycle and current stock level. The numerical example illustrates that the channel coordination of supply chain can be obtained if the manufacturer offers a reasonable wholesale price and return price where they refund retailer full credit for all unsold goods.

Keywords: *Supply Chain, Channel coordination, Return policy, Deterioration*

1. Introduction

In recent years, perishable goods have attracted many supply chain management researchers' attention because of their conspicuous characteristics, such as short sales period, low salvage value, and volatile market environment. They abound in any field in the world, for instance, flight seats, fresh bakery products, personal computer, Christmas trees, etc. Zhao et al. (2004) examines the game of two-stage supply chain for perishable goods in the e-marketplace. However, most related studies are based on the assumption that the deterioration begins at the start point of the operation cycle while the sales price and customer demand rate remain constant during the whole cycle. With the development of inventory management, the advanced storage technology and storage condition have significantly improved the quality of the goods stored. More often, the occurrence of the deterioration depends on some stochastic factors, such as the instrument disruption, natural factor, emergency, etc. It is important to explore the supply chain with perishable products, especially when the deterioration begins at a stochastic time point.

In the current study, we focus on the optimal policies of inventory and price when the start time point of deterioration is stochastic. This paper is organized as follows: section 2 reviews previous literature on return and price policy of a supply chain. Section 3 describes the basic model when deterioration begins at a stochastic time point. Section 4 provides a summary of results and future research directions.

2. Model Formulation

In this paper, we consider a simple supply chain composed of only one manufacturer/supplier and one independent retailer. In such a supply chain, the supplier sells her products at wholesale to the retailer and then the retailer resells the products to the end customers, under the assumption that the item is perishable and the deterioration begins randomly in time. To make the problem traceable, we make the following assumptions: (i) only one selling season or operation cycle is considered; (ii) retailer makes order at the start of the selling season and there is only one opportunity for her to do so during the whole cycle; (iii) once the order is placed, the goods are immediately in stock, i.e. the goods ordered arrive instantly; (iv) retailer sells goods until either all the stock is depleted or the end of selling season; (v) retailer will incur good-will losses when all the stock goods have been sold out, but there is still demand request; (vi) the leftover unsold goods could be returned to manufacturer at the promised return price at the end of selling season. The selling process is divided into two stages. In the first stage, the deterioration does not occur and the items are sold at the original price per unit. In the second stage, the deterioration starts and the sales price is lowered down according to the leftover inventory level and the residual life of leftover stock, in order to promote the sale.

The notations used in the models are as follows:

t – the remaining time until the end of the selling season. Thus, $t=T$ denotes the starting point and $t = 0$ denotes the conclusion of selling season;

w – wholesale price at which the retailer purchases goods from the supplier;

s – retail price before deterioration happens;

c_{sr} – goodwill loss incurred by retailer due to the stock out per unit;

c_r – return price per unit committed to retailer by manufacturer;

c_M – production cost per unit for manufacturer;

$q(t)$ – inventory level when the remaining time is t;

$x(q, t)$ – selling price when the stock level is q and the residual time is t, given that deterioration has started;

$V(q, t)$ – optimal value of expected revenue that can be generated from a stock of size q in t units of time given that deterioration has not yet begun;

$V(q, t; x)$ – expected value of revenue that can be generated from a stock of size q in t units of time when the selling price during the remainder of the period is x and deterioration has started.

To make the study traceable, we further assume $c_M < w < s$ and $c_r \leq w < p$.

2.1 Integrated Supply Chain

We first present and analyze a supply chain under a centralized decision maker (i.e. the manufacturer). We regard this integrated supply chain as a benchmark. The integrated supply chain maximizes the sum of the retailer's profit and the supplier's profit. Let us denote Q^*_T as the optimum order quantity when the residual time is T. Thus, we have

$$V(Q^*_T, T) - c_M Q^*_T = \max_{Q \geq 0} \{V(Q, T) - c_M Q\} \quad (1)$$

2.2 Retailer's Order Policy

The retailer's purpose is to seek his optimum order quantity Q^*_R. Thus we have

$$V(Q^*_R, T) + wQ^*_R = \max_{Q \geq 0}\{V(Q, T) + wQ\} \quad (2)$$

2.3 Retailer's Optimal Order Quantity

We discuss two scenarios as follows.

(i) Let the deterioration start at time t with $t < T$ and let k denote the number of products sold before deterioration is observed. Thus, we have the following:

$$V(Q,T|t<T) = \sum_{k=0}^{Q-1}[\max_x V(Q-k, T-t; x) + ksp_k(t)] + \sum_{k=Q}^{+\infty}[Q(s - c_{sr}(k-Q)]p_k(t) \quad (3)$$

where $p_k(t)$ is the possibility that k items are demanded during t, given that the sales price is s and mean demand rate is . Thus,

$$p_k(t) = (\lambda t)^k(\frac{\exp(-\lambda t)}{k!}). \quad (4)$$

(ii)Let the deterioration start at time t with $t \geq T$, then

$$V(Q,T|t \geq T) = \sum_{k=0}^{Q-1}[ks + c_r(Q-k)]p_k(T) + \sum_{k=Q}^{+\infty}[Q(s - c_{sr}(k-Q)]p_k(T) \quad (5)$$

Therefore,

$$V(Q,T) = \int_0^T V(Q,T|t<T)dF(t) + V(Q,T|t \geq T)[1-F(T)] \quad (6)$$

In order to compute the integral numerically, we propose the following discretization approximation of (5):

$$V(Q,T) = \sum_{t=1}^{T}\{[F(t)-F(t-1)][\sum_{k=0}^{Q-1}(\max_x V(Q-k, T-t; x) + ks)p_k(t)]$$
$$+\sum_{k=Q}^{+\infty}[(Q_s - c_{sr}(k-Q))p_k(t)] + \sum_{k=0}^{Q-1}(ks + c_r(Q-k))p_k(T) \quad (6)$$
$$+\sum_{k=Q}^{+\infty}[(Q_s - c_{sr}(k-Q))p_k(T)][1-F(T)]$$

We could now evaluate $V(q, t; x)$. Suppose that the deterioration is first observed when the residual time is t and the interval of time is δt. If the arrival follows a Poisson process and the decay follows an exponential model, one of the following circumstances would occur when $\delta t \to 0$: (i) no arrival and no decay; (ii) one arrival and no decay; or (iii) no arrival and one decay. Thus, we have the following expression:

$$V(q,t;x) = \{1-[\alpha(x) + q\mu]\delta t\}V(q, t-\delta t; x) + \alpha(x)\delta t(1-\mu\delta t)[V(q-1, t-\delta t; x) + c_r - c_{sr}]$$
$$+\{q\mu\delta t[1-\alpha(x)\delta t]\}[V(q-1, t-\delta t; x) + c_r - c_{sr}] \quad (7)$$

Therefore, taking limits as $\delta t \to 0$, we have

$$\frac{\partial V(q,t;x)}{\partial t} = [\alpha(x) + q\mu][-V(q,t;x) + V(q-1,t;x)] + \alpha(x)(c_r - c_{sr}) + [(x)\mu q] \quad (8)$$

With the boundary conditions

$$V(0, t; x) = 0 \quad (9a)$$
$$V(q, 0; x) = c_r q \quad (9b)$$

In order to determine the optimum value of x for given q and t, we need to maximize $V(q, t; x)$ over x. The following lemma can be used to determine the solution to (8) to obtain $V(q, t; x)$ for $q = 1, 2, \ldots$.

Lemma 1 for $q \geq 1$, the solution to (8) is given by the following:

$$V(q,t;x) = C_{0q} + \sum_{i=1}^{q} C_{iq} \exp\{-[\alpha(x) + \mu_1]t\} \tag{10a}$$

Where,

$$C_{0q} = xa(x)\sum_{i=1}^{q} \frac{1}{a(x) + i\mu_1} - q(c_r - c_{sr}) \tag{10b}$$

$$C_{iq} = C_{i,q-1}\frac{a(x) + q\mu_1}{(q-i)\mu_1}, i = 1, 2, ..., q-1, q > i \tag{10c}$$

$$C_{qq} = c_r q - \sum_{i=0}^{q-1} C_{iq} \tag{10d}$$

The complete proof is omitted here due to the page limit. Interested readers may contact with the authors.

For given values of x, $V(q, t; x)$ can be computed numerically. A Fibonacci search technique can be used to maximize $V(q, t; x)$ with respect to x. This will yield the optimal selling price $x^*(q, t)$ for the given value of stock size q at the residual time t. Equations (1) – (10) will yield an optimum order size of Q^*.

2.4 Numerical Example

For illustrative purposes, we present a very simple example for our model. Consider a single sale season and a situation in which the deterioration of a well-preserved stock is initiated by a sudden shock such as mechanical failure or natural calamities. Let the deterioration occur at a random point in time and follow an exponential distribution. Assume the demand rate (*x*), which depends on the selling price *x*, satisfies (*s*) ≥ . Let the parameters be $F(t) = e^{\theta.1t}$, T=7, s=3.0, (*x*) = 19 2 x^2, w=1.76, = 1, c_{sr}= 0.15, c_r= 1.0, μ_1= 0.1. The computed results for the model are given in Tables 1-3.

Table 1 The Optimal Sales Price

q	$x^*(q, t)$						
	t=1	t=2	t=3	t=4	t=5	T=6	t=7
1	2.84	2.91	2.92	2.93	2.93	2.93	2.93
2	2.78	2.87	2.89	2.90	2.90	2.90	2.90
3	2.73	2.83	2.86	2.87	2.88	2.88	2.88
4	2.68	2.80	2.84	2.85	2.86	2.86	2.86
5	2.64	2.77	2.82	2.83	2.84	2.84	2.84
6	2.60	2.74	2.79	2.81	2.82	2.82	2.82
7	2.57	2.71	2.77	2.80	2.80	2.80	2.80
8	2.54	2.68	2.75	2.78	2.79	2.79	2.79
9	2.52	2.66	2.73	2.77	2.78	2.78	2.78
10	2.50	2.63	2.72	2.75	2.76	2.77	2.77
11	2.49	2.61	2.70	2.74	2.75	2.75	2.75
12	2.48	2.59	2.68	2.72	2.74	2.74	2.74

Table 2 Expected Revenue

q	$V(q, t)$						
	t=1	t=2	t=3	t=4	t=5	t=6	t=7
1	1.85	1.91	1.93	1.93	1.93	1.93	1.93
2	3.52	3.69	3.72	3.73	3.73	3.73	3.73
3	5.04	5.36	5.42	5.43	5.44	5.44	5.44
4	6.43	6.94	7.04	7.06	7.07	7.07	7.07
5	7.72	8.43	8.60	8.63	8.63	8.63	8.63
6	8.90	9.85	10.08	10.13	10.14	10.14	10.14
7	10.00	11.20	11.51	11.58	11.59	11.59	11.59
8	11.03	12.49	12.89	12.99	13.00	13.00	13.00
9	12.00	13.70	14.22	14.34	14.36	14.37	14.37
10	12.92	14.86	15.50	15.66	15.69	15.69	15.69
11	13.80	15.97	16.73	16.94	16.97	16.98	16.98
12	14.67	17.02	17.92	18.17	18.22	18.23	18.23

Table 3 Optimum Order Quantity

Order Quantity	1	2	3	4	5	6	7	8	9	10	11	12
Retailer's Profit	0.53	1.75	2.83	3.75	4.46	4.95	5.20	5.21	5.02	4.67	4.21	3.66

Table 1 shows the optimal selling price x when the stock level is q and the residual time left is t, given that deterioration has started. Table 2 shows the optimal value of the expected revenue generated from a stock of size q in t units of time when the optimal selling price x per unit remains constant over the residual cycle time, given that deterioration has started. From Table 3 we may find that the optimal order quantity is eight units.

2.5 Coordination Policies of Supply Chain

The retailer will decide his optimum order quantity Q^*_R to maximize his own profit. Thus in order to improve the channel revenue (i.e. the performance of supply chain), the manufacturer will properly set the value of parameter w and c_r to encourage the retailer to order $Q^*_R = Q^*_T$ units of products. Let the parameter be $F(t) = e^{\theta.1t}$, T=7, s=3.0, $(x) = 19 - 2x^2$, c_M= 1.75, = 1, c_{sr}= 0.15, c_r= 0.8, μ_1= 0.1, c_s= 0.3. By using the above method, we can find from Table 4 that the optimum order quantity is eight units, which maximize the revenue of the whole supply chain. In order to maximize the profit of the whole supply chain or to coordinate the supply chain, that is to say, let Q^*_R equals Q^*_T, the manufacturer needs to set the value of parameter as w = 1.76 and c_r= 1.0. The computed results are given in Table4.

Table 4 Optimum Order Quantity for Entire Supply Chain

Order Quantity	1	2	3	4	5	6	7	8	9	10	11	12
Total Profit	-0.09	1.31	2.59	3.70	4.61	5.27	5.66	5.80	5.71	5.44	5.04	4.55

The manufacturer will also set the value of parameter as w = 1.77 and c_r=1.0.The computed results are given in Table 5.

Table 5 Optimum Order Quantity for Entire Supply Chain

Order Quantity	1	2	3	4	5	6	7	8	9	10	11	12
Total Profit	0.52	1.73	2.80	3.71	4.41	4.89	5.12	5.13	4.93	4.57	4.10	3.54

3. Conclusions and Future Research

In this paper we investigate the coordination of supply chain in the case that deterioration begins at a stochastic time point. We found that it is possible to obtain the coordination of the supply chain if the manufacturer offers his wholesale price and promised return price properly as well as guarantees to accept the retailer's return of all leftover stock. It is a very interesting conclusion, for it gives us a suggestion on how to improve the performance of the supply chain and how to alleviate the well-studied problem of double marginalization. For future research, we shall investigate the manufacturer's optimal policy, such as wholesale price, return price and the percentage of returned goods, etc., as well as the retailer's optimum order quantity.

Acknowledgements: This work is funded by National Science Foundation of China (60879024, 60872062).

Bibliography

Lin, C. W. R., Hung O. L., and Chen, C. A. (2006). "A strategic quick response approach for dynamic supply chain management of perishable goods." *International Journal of Industrial Engineering*,13 (4) 373-384.

Mukhopadhyay, S. K. and Setaputra, R.. (2007). "A dynamic model for optimal design quality and return policies." *European Journal of Operational Research*, 180 (3) 1144-1154.

Rahim, M. S., Kabadi, S. N. and Barnerjee, P. K. (2001). "A single-period perishable inventory model where deterioration begins at a random point in time." *International Journal of Systems Science*, 31 (1) 131-136.

Taylor, T. A. (2001). "Channel coordination under price protection, midlife returns, and end-of-life returns in dynamic markets." *Management Science*, 47(9) 1220-1234.

Yeu, X. and Raghunathan, S. (2007). "The impacts of the full returns policy on a supply chain with information asymmetry. " *European Journal of Operational Research*, 180(2) 630-647.

Zhao, Q., Xiong, Z., Lin, Y. and Bu, X. (2004). "Game Analysis of Two - Stage Supply Chain for Perishable Goods under E- Marketplace." *Chinese Journal of Management Science*,12(3)91-96.

Grey Correlation Analysis on Logistics Energy Consumption

Lei Zhiyi

College of Traffic and Ocean, Hohai University, 210098, Nanjing, China; PH (86) 025-83787354; email: Lei_zhiyi@hotmail.com

ABSTRACT

Based on related energy statistical data, the general situation of logistics energy consumption in China is explained in this paper. The indicator system of the region's logistics consumption is established and, with grey correlation theory, each indicator and correlation degrees are analyzed quantitatively. At the end, with the data of Jiangsu Province and the nation, the correlation degree is analyzed contrastively, and the order of factors about logistics energy consumption is arranged. The correlation degrees calculated can be the instruction basis for logistics development and energy savings in certain areas.

Key words: Logistics energy consumption; indicator system; grey correlation

INTRODUCTION

Modern logistics is one of the basics of regional economic development, and an efficient logistics system is an important factor in the core competence of regional economics. People have been unfamiliar with logistics systems, especially their energy consumption. Furthermore, there are no subdivisions in the statistics of energy consumption in China, which makes research difficult, but the grey theory can resolve this problem.

GREY CORRELATION ANALYSIS OF LOGISTICS OF ENERGY CONSUMPTION

Model of grey correlation. The basic fundamental of grey correlation is judging correlations among sequence curves according to their comparability. To analyze an abstract system, the data sequence is first chosen, which is the mapping value of the system. Based on the Eigen value and related data, the graphs of every sequence can be obtained and analyzed.

The comparative sequence and the referenced sequence. Essential to grey correlation analysis is the comparability of the geometry of compared sequences. In general, the more approximate their geometries, the closer the correlations are.

Suppose X_0 is a system factor, with the measured values of $X_0(k)$, $k=1,2,,n$, which can be written as $X_0 = \{X_0(k), k = 1,2,\cdots n\}$, namely behavior sequence. If k means time number, $X_0 = \{X_0(k), k = 1,2,\cdots n\}$ is the behavior

time sequence; if k denotes indicator, $X_0 = \{X_0(k), k = 1,2,\cdots n\}$ is the behavior indicator sequence; if k denotes measured object number, $X_0 = \{X_0(k), k = 1,2,\cdots n\}$ indicates behavior transverse sequence. The time sequence, indicator sequence, or transverse sequence can be analyzed by grey correlation.

In this paper, the referenced sequence can be written as $X_0 = \{X_0(k), k = 1,2,\cdots n\}$, and the compared sequence can be written as $X_i = \{X_i(k), k = 1,2,\cdots n\}$.

Initialization. It is necessary to initialize the data because of the different dimensions or units of each factor.

$$x_0^{'}(k) = \frac{x_0(k)}{x_0(l)}, \quad k = 1,2,\cdots l \quad \text{and} \quad x_i^{'}(k) = \frac{x_i(k)}{x_i(l)}, \quad k = 1,2,\cdots l$$

We get the referenced sequence $X_0^{'}(t)$ and compared reference $X_i^{'}(t)$ after initialization.

Absolute difference. The absolute difference of the comparative sequence and the referenced sequence can be obtained by $\Delta_{0i}(k) = \left| X_i^{'}(k) - X_0^{'}(k) \right|$

Extremum. Mark $M = \max_i \max_k \Delta_{0i}(k)$, in which $\max_k \Delta_{0i}(k)$ indicates the maximum distance between each point on curve X_i and the related points on curve X_0. $\max_k \Delta_{0i}(k) = \max\{\max \Delta_{0i}(1), \max \Delta_{0i}(2), \cdots, \max \Delta_{0i}(l)\}$.

Mark $m = \min_i \min_k \Delta_{0i}(k)$, in which $\min_k \Delta_{0i}(k)$ means the minimum distance between each point on curve X_i and the related points on curve X_0. $\min_k \Delta_{0i}(k) = \min\{\min \Delta_{0i}(1), \min \Delta_{0i}(2), \cdots, \min \Delta_{0i}(l)\}$.

Calculate coefficient in grey correlation. We get the coefficients of grey correlation by $\xi_{0i}(k) = \frac{m + \rho M}{\Delta_{0i}(k) + \rho M}, \quad k = 1,2,\cdots l; i = 1,2,\cdots, n$, in which $\rho \in (0,\infty)$ is the distinguishing coefficient, which has an inverse ratio of resolution. We take it generally $\rho = 0.5$.

Calculating grey correlation. The grey correlation can be obtained by the formula $\gamma_{0i} = \frac{1}{l}\sum_{k=1}^{l} \xi_{0i}(k), \quad k = 1,2,\cdots l; i = 1,2,\cdots, n$.

Arranging and analyzing grey correlations. The influence of each comparative sequence on a referenced sequence will be clear, from the arrangement of γ.

INDICATOR SYSTEM FOR GREY CORRELATION ANALYSIS

It is necessary first to establish the indicator system of a logistics system and other systems in the national economy, namely the mapping value of system behavior, and then to research the relationship among logistic energy consumption and other systems by studying the relationships among those systems' mapping values.

For the faultiness of logistics in China, the general indicator system that reflects the logistics status has not been established yet. Some scholars have

researched the indicator system of logistics and the evaluation methods and obtained valuable results. But it is difficult to establish a simple and general evaluation model because of the nonlinear, opening, and dynamic logistics system.

This research has established an indicator system for logistics energy consumption from three aspects: environment, resource, and requirement, as seen in Figure 1. The environment includes the exterior factors influencing logistics requirements and service supply, such as management system and service level. Environment is the exterior factor, while resources and requirements are interior factors.

The indicator of requirements is composed of gross products of primary industries, gross products of secondary industries, total foreign trade value, total retail sales of consumer goods, and total investment in logistics fixed assets. The gross products of primary and secondary industries reflect social economic development; total retail sale of consumer goods is the mapping value of production, consumption, and circulation, reflecting the status and scale of logistics requirements. The more the social consumption is, the more the logistics requirement is, and the more the energy consumption is. In addition, the logistics fixed assets can also influence indirectly logistics energy consumption.

It is noteworthy that there is an absence of statistical data of total social logistics energy consumption in China because of the faultiness of the statistics system and method. The consumption data in the China Statistical Yearbook for transportation (including passenger transport), storage, and the post and telecommunications industries are calculated for logistics energy consumption.

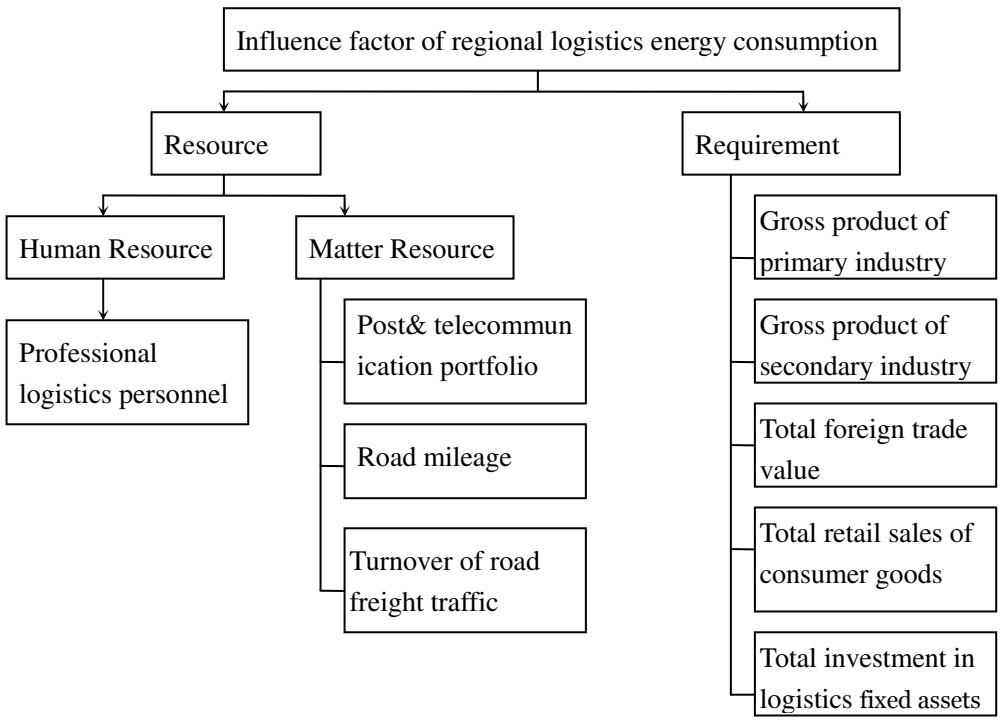

Figure 1. Indicator system of regional logistics.

DEMONSTRATION

To quantify road logistics energy consumption, the referenced sequence is composed of the number of personnel for the transportation, storage, and post and telecommunication industries, X_1; the post and telecommunication portfolio, X_2; road mileage, X_3; turnover of road freight traffic, X_4; gross product of primary industry, X_5; gross product of secondary industry, X_6; total foreign trade value, X_7; retail sales of consumer goods, X_8; and investment in fixed assets of transportation, storage, and post and telecommunication industry, X_9. In this grey system of variable X_i, with the data of Jiangsu Province and the nation from 2003 to 2007, the degree of grey correlations of influence among referenced variables and compared variables X_0 are calculated and arranged, as shown in Table 1 and Table 2.

Table 1. Grey Correlation Degree between Logistics Energy-Consumption and its Influential Factors in Jiangsu Province.

	Degree of Grey Correlation	*Indicators Order*
Personnel in logistics (10,000 people) X_1	0.795	4
Post and telecommunication portfolio (10,000 Yuan) X_2	0.593	9
Road mileage (kilometer) X_3	0.895	2
Turnover of road freight traffic (100 M ton kilometer) X_4	0.919	1
Gross product of primary industry (100 M Yuan) X_5	0.864	3
Gross product of secondary industry (100 M Yuan) X_6	0.747	6
Total foreign trade value (10,000 US dollar) X_7	0.658	7
Retail sales of consumer goods (100 M Yuan) X_8	0.755	5
Investment in fixed assets of logistics (10,000 Yuan) X_9	0.614	8

Table 2. Grey Correlation Degree between Logistics Energy-Consumption and its Influential Factors in China.

Degree of Grey correlation	*Indicators Order*
Personnel in logistics (10,000 people) X_1	0.640	8
The post and telecommunication portfolio (10,000 Yuan) X_2	0.632	9
Road mileage (kilometer) X_3	0.904	2
Turnover of road freight traffic (100 M ton kilometer) X_4	0.949	1
Gross product of primary industry (100 M Yuan) X_5	0.847	6
Gross product of secondary industry (100 M Yuan) X_6	0.860	5
Total foreign trade value (10,000 US dollar) X_7	0.734	7
Retail sales of consumer goods (100 M Yuan) X_8	0.881	4
Investment in fixed assets of logistics (10,000 Yuan) X_9	0.898	3

The grey correlations among logistics energy consumption and its related

factors in Jiangsu Province are calculated, and the order is arranged as follows:

> Turnover of road freight traffic γ_4> road mileage γ_3> gross product of primary industry γ_5> personnel in logistics γ_1> retail sales of consumer goods γ_8> gross product of secondary industry γ_6> total foreign trade value γ_7> investment in fixed assets of logistics γ_9> post and telecommunication portfolio γ_2

The grey correlations among logistics energy consumption and its related factors in China are calculated, and the order is arranged as follows:

> Turnover of road freight traffic γ_4> road mileage γ_3> investment in fixed assets of logistics γ_9> retail sales of consumer goods γ_8> gross product of secondary industry γ_6> gross product of primary industry γ_5> total foreign trade value γ_7> personnel in logistics γ_1> post and telecommunication portfolio γ_2

ANAYSIS

From the arrangement result of the grey correlation coefficients, some conclusions are obtained:

(1) Whether in China or in Jiangsu Province, the correlation degrees between logistics energy consumption and the turnover of road freight traffic, road mileage, and total foreign trade value are in accord and are the same in the qualitative analysis. The correlation between total foreign trade value and logistics energy consumption is not very tight here because only road transport is considered in this paper, while railway transport and water transport are usually included in international logistics. Also, the Yangtze River crosses Jiangsu Province, in which the water transport capacity is very large.

(2) The results also show that the correlations between investments in fixed assets of logistics and logistics energy consumption is very different in China and in Jiangsu Province, namely 3rd and 8th, respectively. This indicates that investment in the fixed assets of logistics are not enough in Jiangsu Province; it must be reinforced by software and hardware.

(3) It is also clear from the results that the correlations between gross product of primary industry and logistics energy consumption are 3rd and 6th, respectively, in Jiangsu Province and China. In Jiangsu Province, agricultural products are the main focus of logistics because Jiangsu is an agricultural province.

(4) The correlation between logistics personnel and energy consumption in Jiangsu is 4th, while it is 8th in China. This indicates that more attention should be paid to training logistics personnel to reduce energy consumption.

The correlations among logistics energy consumption and related economic factors are quantified, which provides some useful recommendations.

CONCLUSION

Through grey correlation analysis, the correlations between logistics consumption and relative economic factors can be analyzed quantitatively, and the influencing degrees calculated can be the instruction basis for logistics development and energy savings in certain areas. But with dynamic logistics development, the main influencing factors will changed, so further analysis should be done to improve the sample's quality for accuracy and reliability.

BIBLIOGRAPHY

David, L., and Steven, E. (2001). "Energy futures for the U.S. transport sectors." *Energy Policy,* (29),1255-1270.

Lai, K. H., Ncai, E. W., and Cheng, T. C. (2000). "Measures for evaluating supply chain performance in transport logistics." *European Management Journal,* 18(4), 398- 410.

Larssjo, S., Gunnar, S., and Eklund, E. (1998). "Transportation and logistics in a joint systems context: A conceptual model and case study of fuel supply to an airport." *Transport Logistics,* 1(3),195-209.

Liu, Ai-qin. (2008). "Grey associated analysis on the relationship between energy consumption and industrial economic growth in Shangdong Province." *China Population, Resources and Environment,* 18(3),103-107.

Liu Sifeng, Dang Yaoguo, and Zhang Qishan. (2004). *Grey System Theory and Application.* Beijing, Science Press.

Markus, H., and Rodrigue, J. P. (2004). "The transport geography of logistics and freight distribution." *Journal of Transport Geography,* (12),171-184.

National Bureau of Statistics of China. (2003-2007). *China Statistical Yearbook*, China Statistics Press, Beijing.

Soner, H., and Halim, C. (2005). "Genetic algorithm approach to estimate transport energy demand in turkey." *Energy Policy,* (33), 89-98.

Statistical Bureau of Jiangsu. (2003-2007). *Jiangsu Statistical Yearbook*, China Statistics Press, Beijing.

Research on Taboo Simulated Annealing Combinatorial Optimization Algorithm of Location Routing Problem with Pickups and Deliveries

Hu Dawei, Xuan Dengdian,Lin Huigangand Guo Xiaofen

Department of Logistics Engineering,Automobile College of Chang'an University,P.O. Box 012,Xi'an, Middle Section, South No. 2 RingRoad,Shaanxi,China;
PH(+86)029-82334745;FAX(+86)029-82334476;email: dwhu@chd.edu.cn.

ABSTRACT:MDLRPPD (Multi-depot Location Routing Problem with Pickups and Deliveries)to be studied in this paper is a kind of problem very close to reality in the optimization of logistics system. In this paper, the complementary restraint relationship between depot selection, transports, pickups and deliveries is analyzed, the mathematical model with the lowest total cost in the logistics system is established, and the verification of correctness of mathematical model established through the application of LINGO software under the condition of small-scale data is conducted. Because of its NP-hard property, the paper designs the taboo-simulated annealing combinatorial optimization algorithm to require a solution, and applies C++ language programming to realize this combinatorial optimization algorithm. Through the comparison with optimum solution obtained from the application of LINGO software, the results show that the taboo-simulated annealing combinatorial optimization algorithm proposed in this paper proves to be a rapid and effective approach in solving MDLRPPD.
KEY WORDS: Logistics System, Location Routing, Pickups and Deliveries, Simulated Annealing, Taboo Search.

1. INTRODUCTION

The exercise of optimal design for logistics system and the provision of logistics optimization solutions for logistics enterprises serve as one of main businesses for the fourth party logistics to carry out the logistics consulting services. MDLRPPD (Multi-depot Location Routing Problem with Pickups and Deliveries), considered as a kind of problem very close to the reality in the optimization of logistics system, is an extension and branch of LRP (Location Routing Problem)model.

Foreign scholars have already begun the research on the issue of logistics system optimization as early as 1980s(Hu Dawei 2008). For example, the comprehensive study (Hu Dawei etal. 2007) on LRP and VRPPD(Vehicle Routing Problem with Pickups and Deliveries)was conducted. However, the current research on LRPPD is basically in a blank. LRPPD optimizes LRP under the premise that the synchronization of pickups and deliveries is taken into consideration. LRPPD, if compared with the traditional logistics system optimization, is closer to the complicated actual characteristics of logistics system.

The paper has analyzed the complementary restraint relationship between depot selection, transports, pickups and deliveries, established the mathematical model with the lowest total cost of logistics system, and conducted the verification of

established mathematical model by utilizing Lingo software under the condition of small-scale data. Because of its NP-hard property, the paper has designed the taboo-simulated annealing combinatorial optimization algorithm to require a solution, applied fairly large scale test data to conduct simulation calculation, and carried out the efficiency analysis on the computed results.

2. MODEL BUILDING

MDLRPPD model to be studied in this paper is based on the following assumptions:

(1) Number, location and demands of customers are known.

(2) Location and capacity of alternative facilities are known.

(3) All the customer demands can be met, and each customer is only served by one specific vehicle.

(4) Each vehicle returns to the starting point after completing all the transport missions.

(5) Overload is not permitted among transport vehicles in all the routes.

(6) Vehicle types are stated in advance.

Definition of variables and parameters:

Decision variable:

x_{ijk} is 1 if the point i is before j on route k, otherwise, it will be 0;y_i is 1 if facility i is to be constructed,otherwise, it will be 0;z_{ij} is 1 if facility i provides service for customer j,otherwise, it will be 0.

Parameters:

R Potential location assembly of facility point;

J Assembly of all the customer points;

V Assembly of all the vehicles;

N Quantity of representative customers;

C_{ij} Distance from point i to point j;

$S = R \cup J$ Assembly of all the customer points and potential facility points;

G_r Fixed costs of construction and operation of facility r;

F_k Fixed costs of vehicle k to be applied;

V_r Maximum capacity of facility r;

p_j Traffic volume of customer j;

q_j Demand of customer j;

Q_k Capacity of vehicle k;

U_{lk} Auxiliary variable.

In the light of problem definition, MDLRPPD can be represented by the following mixed integer linear programming model.

$$Min \qquad \sum_{r \in R} G_r y_r + \sum_{i \in S} \sum_{j \in S} \sum_{k \in V} C_{ij} x_{ijk} + \sum_{k \in V} F_k \sum_{r \in R} \sum_{j \in J} x_{ijk}$$

S.t.

$$\sum_{k \in V} \sum_{i \in S} x_{ijk} = 1, \ j \in J \qquad (1)$$

$$\sum_{i \in S} \sum_{j \in J} p_j x_{ijk} \le Q_k, \ k \in V \qquad (2)$$

$$\sum_{i\in S}\sum_{j\notin J} q_j x_{ijk} \le Q_k,\ k\in V \tag{3}$$

$$\sum_{j\in J} p_j z_{rj} - V_r y_r \le 0, r\in R, \tag{4}$$

$$\sum_{j\in J} q_j z_{rj} - V_r y_r \le 0, r\in R, \tag{5}$$

$$\sum_{i\in S} x_{ipk} - \sum_{j\notin S} x_{pjk} = 0,\ k\in V,\quad p\in S \tag{6}$$

$$\sum_{r\in R}\sum_{j\notin J} x_{rjk} \le 1,\ k\in V \tag{7}$$

$$\sum_{l\in S}(x_{rlk} + x_{ljk}) \le 1 + z_{rj},\quad r\in R,\quad j\in J,\quad k\in V \tag{8}$$

$$U_{lk} - U_{jk} + Nx_{ljk} \le N - 1,\quad l,j\in J, k\in V \tag{9}$$

$$x_{ijk} = 0\ or\ 1,\quad i,j\in S, k\in V, i\ne j \tag{10}$$

$$y_r = 0\ or\ 1,\quad r\in R \tag{11}$$

$$z_{ij} = 0\ or\ 1,\quad i\in R,\ j\in J \tag{12}$$

$$U_{lk} \ge 0,\ l\in J, k\in V \tag{13}$$

In the above-mentioned model, the objective function is the lowest total cost (including the costs of facility construction and operation, transportation cost and running cost of vehicle). Constraint (1) ensures that each customer is only served by one specific vehicle. Constraint (2)-(3) serve as the constraint condition for the capacity of transport vehicles; Constraint (4)-(5) serve as the capacity restrictive conditions for warehouse; Constraint (6) ensure the route continuity; Constraint (7) ensures that the route of every single transport vehicle can only leave from one facility; Constraint (8) ensures that the customers can only be served by the selected facility. Constraint (9) serve as the sub-path restriction; Constraint (10)-(12) stand for 0 & 1 variable restriction; Constraint (13) serve as the auxiliary variables restriction.

3. DESIGN OF TABOO-SIMULATED ANNEALING COMBINATORIAL HEURISTIC ALGORITHM

3.1 Mentality of algorithm design

Taboo search algorithm is the popularization of partial neighborhood searching algorithm, and its features are that taboo technology is applied to avoid getting caught up in local optimum (Xing Wenxun etal. 2005); However, the iterative process of this algorithm is serial. It is only transformation in a single state instead of parallel search, and thus, it leads to longer consumption of search time of this

algorithm. Therefore, with the increase of problem scale to be solved, the computation time experiences rapid growth, and it is likely to bring about the infeasibility of algorithm due to the time relationship in the end. Simulated annealing algorithm, irrelevant to the original value and provided with asymptotic convergence property, has been theoretically proved to be a kind of optimal solution of global optimization algorithm using converge to overall situation with probability (Hu Dawei etal. 2006). Based on the characteristics of these two algorithms, the paper raises the adoption of taboo-simulated annealing combinatorial optimization heuristic algorithm to solve the model. The flow chart is shown in **Figure 1**.

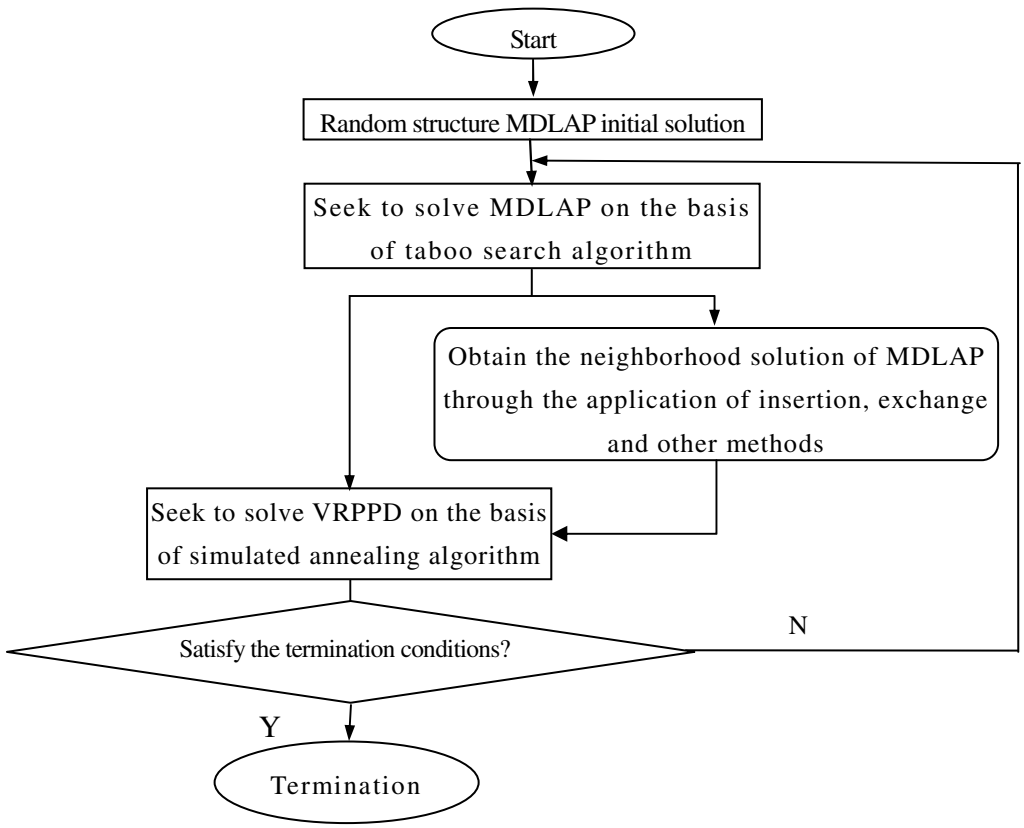

Figure 1. Flow chart for solution of MDLRPPD through application of taboo-simulated annealing combinatorial optimization algorithm.

3.2 Design of initial solution structure and neighborhood search.

In this paper, it is planned to apply the encoding mode directly arranged by customer. Use the natural number from 1 to N to represent the customers, and the random arrangement of these natural numbers is precisely a solution. Sequentially arrange every number (customer) of solution into the delivery route of vehicle according to the constrained condition of questions. Take 12346789 as an example, at first, arrange customer 1 into the first delivery route, and judge whether the constrained condition of questions can be met. If so, the delivery route in terms of 0-1-0 is thus formed. Next, arrange customer 2 into this delivery route, and the rest can be done in the same manner. If the constrained condition of questions can not be met, it shows that customer 2 can not be delivered via this delivery route. At this moment, it is necessary to restart the generation of new delivery route of 0-2-0. Keep

repeating this process until all the customers are arranged into the delivery route.

The taboo search algorithm designed in this paper is mainly to solve MDLAP model. Three kinds of neighborhood search methods, namely, "Depot exchange", "customer exchange" and "customer insertion" operation, are designed in this paper. It is possible to randomly select one kind from these three kinds of neighborhood search methods to generate neighborhood solution, which can strengthen the search performance of taboo search algorithm, expand the search area, and facilitate the avoidance of locally optimal solution.

The schematic diagrams of depot exchange are shown in **Figures 2**.

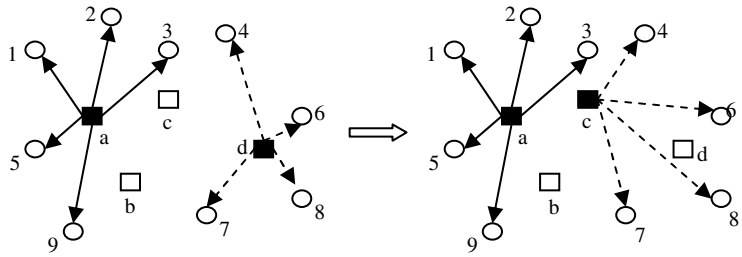

■ Stands for the selected facility □ Stands for the unselected facility
○ Stands for the customers ⟶ And ⇢ Stands for the routes

Figure 2. Schematic diagram of depot exchange method.

The simulated annealing algorithm designed in this paper is mainly to solve VRPPD model. At the stage of route optimization, it is designed to randomly select one kind from three neighborhood search methods in terms of insertion method, 2-swap within the route and 2-swap between the routes to carry out neighborhood transformation, and conduct the route optimization by utilizing 2-opt (Osman, I. H. 1993a) algorithm so as to generate the neighborhood solution. In this way, the optimal performance of simulated annealing algorithm is strengthened, and the optimal solution of search range is expanded so that the better improvement can be obtained in the aspect of vehicle running costs.

The schematic diagrams of insertion method are shown in **Figure 3**.

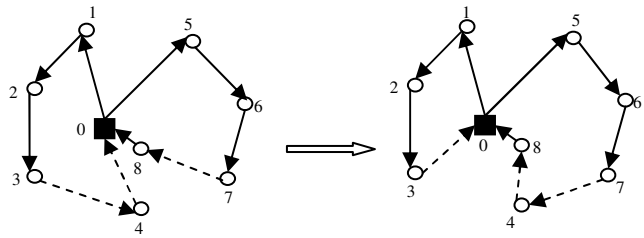

■ Stands for the selected DC
○ Stands for the customers ⟶ And ⇢ Stand for the routes

Figure 3. Schematic diagram of insertion method.

4. ALGORITHM VERIFICATION

The test data proposed by Solomon in 1987 is commonly used in VRP. The data acquisition is divided into six types. The customer locations of R1 and R2 are randomly distributed, customers of C1 and C2 are in the state of aggregation (namely, the node distribution is clustered according to the geographical position), RC1 and RC2 are in the state of semi-aggregation. At the actual problems, the customer

distribution is closer to the states of random and semi-aggregation reflected in R class and RC class data acquisitions in most cases. For this reason, the paper, based on R101 data series of Solomon 25 customers, applies the statement a=rand()%25+1 to generate three random numbers within the range of 1~25, and take the customer coordinates corresponding to these three serial numbers in original data source as the coordinates for alternative facility point in this calculation example. The same method can be applied to once again randomly generate the data corresponding to five customer points from the remaining nodes, and randomly give the supply volume (subject to change according to the actual conditions). A number of parameters for alternative facility points and customer points randomly generated in this way are shown in **Table 1** and **Table 2**. The vehicle capacity is taken as 40 while the fixed cost of vehicle is taken as 30.

Table 1. Coordinates, Capacity and Construction Cost of Potential Facility Points.

	D1	D2	D3
X-coordinate	35	25	10
Y-coordinate	35	30	43
Capacity of facility point	70	70	70
Construction cost	200	200	200

Table 2. Coordinate and Demand of Customer Point.

	C1	C2	C3	C4	C5
X-coordinate	30	50	10	45	45
Y-coordinate	60	35	20	65	10
Customer demand	16	19	19	9	18
Customer supply volume	18	21	14	23	18

Lingo 10.0 is applied to conduct programming calculation for MDLRPPD model so as to obtain the optimal solution, and the results are shown in **Table 3** (calculation time is 39s).The results show that two facilities have been chosen and the corresponding objective function value is 708.47.

Table 3. Computed Result of Lingo.

Selected facility points	Customer route
D1	V1: D1-C1-C2-D1 V3: D1-C4-D1
D2	V2: D2-C5-C3-D2

In order to verify the effectiveness of taboo-simulated annealing combinatorial algorithm designed in this paper, it is to substitute the data in **Table 1** and **Table 2** into the combinatorial algorithm program for the purpose of calculation. The results is fully consistent with the calculation results of Lingo 10.0 (shown in **Table 3**), but the calculation time (203 millisecond) is saved around 200 times. It indicates that the taboo-simulated annealing combinatorial algorithm designed in this paper is rapid and effective in providing solution for this model.

5. CONCLUSION

In this paper, the mathematical model with the lowest total cost of logistics system is established, and the correctness of mathematical model is verified through the application of Lingo software for small-scale data. Because of its NP-hard

property, the paper designs the taboo-simulated annealing combinatorial optimization heuristic algorithm to require a solution, and uses C++ language programming to realize this combinatorial optimization algorithm. It is planned to apply the afore-mentioned same small-scale data to calculate, and the results are completely the same as that of the optimal solution obtained through the application of LINGO. As the heuristic combinatorial algorithm has great advantage in terms of calculation time, it shows that the taboo--simulated annealing combinatorial optimization algorithm is of very practical value in solving the large-scale MDLRPPD model.

REFERENCE

Hu Dawei.(2008). "Research on facility location and vehicle routing problem model and heuristic algorithm."*Doctoral Dissertation of Changȧn University.*

Hu Dawei, Chen Cheng and Guo Xiaofen.(2007). "Research on MDVRP (Multi-depot Vehicle Routing Problem with Pickups & Deliveries) optimization algorithm."*Mathematics in Practice and Theory*, 37(2), 98-104.

Hu Dawei,ZhuZhiqiang,Hu Yong.(2006). "Simulated annealing algorithm for vehicle routing problem." *China Journal of Highway and Transport*, 19 (4),123-126.

Osman, I. H. 1993a."Meta-strategy simulated annealing and tabu search algorithm for the vehicle routing problem." *Annals of operational Research,* 41, 421-451.

Xing Wenxun and Xie Jinxing.(2005). "Modern Optimization Calculation Method." *Tsinghua University Publishing House,* September.

Electrical Appliance Reversion Logistics Network Planning

Zhao Gang, Nan Xi, Lu Kecong

School of Transportation, Shanghai Maritime University; PH (021) 58855200-2310; email: zhaogd@online.sh.cn

ABSTRACT

This article studies obsolete electrical appliance reverse logistics recycling network design. A MILP (Mixed Integer Linear Programming) model is given to optimize the logistics system, and the locations of various facilities are determined. Finally, an example that considers the logistics system of a refrigerator company is taken to demonstrate the model presented in the paper. Linggo8.0 soft is used to resolve the model, and a satisfactory result was gained.

Key words: reverse logistics, network of logistics, Obsolete Electrical Appliances

INTRODUCTION

With the development of the economy and the popularity of electrical appliances, the recycling and reuse of obsolete electrical appliances (OEA) has become a serious problem. Effective recycling and reuse can save resources and energy, lower costs of production. It can also greatly lower the emission of waste, reduce pressure on the environment, and plays an active role in sustainable economic development. From the logistics point of view, this type of cycle (use – recycle – dispose – reuse), used for obsolete products and materials, is leading a new research branch in logistics - reverse logistics.

In the reverse logistics of obsolete electrical appliances, a network should be designed that can reasonably assure that the structure of distribution channels for the obsolete electrical appliances, including various types of reverse logistics facilities, the number and location of facilities, and the transport mode between the facilities of the obsolete products is sensible.

RESEARCH STATUS QUO

Fleischmann et al. (2000) defined the basic characteristics of a reverse logistics network system and determined its design principles. Fleischmann et al. (2002) studied the network structure in which reusable parts could be obtained from the obsolete products and evaluated the financial impact on a company's revenue. Jayarama et al. (1999) analyzed the typical logistics network structure of the American Electronic Equipment Rebuild Company and established a model that can determine storage capacities and locations based on the process in which obsolete products (or core parts) are collected, reused, and redistributed.

Xuhui et al. (2003) described enterprise integration based on the management of the supply chain and the reverse supply chain and introduced the design principles for a product reverse logistics network. Zujun et al. (2004) studied the functions of reverse logistics. Qinli et al. (2004) analyzed the structure of logistics networks, suggesting they could be categorized into open-loop systems and closed-loop systems.

KEY FUNCTIONS OF A REVERSE LOGISTICS NETWORK

Key functions of a Reverse Logistics Network for Obsolete Electrical Appliances (RLNOEA) could be concluded as follows.

Collection This is the starting point of an RLNOEA. Collecting worn-out appliances could be on a paid basis or simply for public interest. Considering the contemporary social situation, the collected items in this study were paid for.

Recycling process This is a primary function of an RLNOEA, which can be divided into three stages: checking, disassembling, and reusing.

Disposal Sometimes disassembled products cannot be recycled due to technical or economic limitations, resulting in burial or burning. However, with the development of recycling technology, this situation has become more and more scarce.

Redistribution Recycled products, parts, or raw materials from this process can be returned to the market.

Although an RLNOEA has distinguishing features, it also shares the same functions of a common system: transporting, stockpiling, moving, and packaging.

RLNOEA PLANNING MODEL

In supply chain management, reverse logistics will impact the production plan, distribution, inventory strategies, and a series of decision-making for forward logistics. This study sets up an integrated logistics network that combines forward logistics and reverse logistics. The network includes factories (remanufacturing plants), distribution centers, recycling centers (testing centers), regional consumption of renewable materials, integrated distribution centers/recycling centers, obsolete product disposal centers, etc.

Parameters and Variables

Let $G=\{1,\cdots,\mathrm{G}\}$,$J=\{1,\cdots,\mathrm{J}\}$,$H=\{1,\cdots,\mathrm{H}\}$,$T=\{1,\cdots,\mathrm{T}\}$denote the set of indices of potential locations for a new plant, a new distribution center, a new recycling center, and a new waste disposal center, respectively. For each g $\in G$, j $\in J$, h $\in H$ and t $\in T$, let c_g^1 , c_j^2, c_h^3 and c_t^4 be the cost for opening a factory, distribution center, recycling center, and waste disposal center, respectively..

Let $F=\{1,\cdots,\mathrm{F}\}$,$I=\{1,\cdots,\mathrm{I}\}$,$L=\{1,\cdots,\mathrm{L}\}$,$S=\{1,\cdots,\mathrm{S}\}$denote the set of indices of locations for the existing plants, existing distribution center, existing recycling center, and existing waste disposal center, respectively. Let $K=\{1,\cdots,\mathrm{K}\}$ denote the set of indices of consumption districts. Let $E=\{1,\cdots,\mathrm{E}\}$ denote the set of indices of the materials market. For $f,i \in F \cup I$, let d_{fi}^1 denote the distance between existing factory f and existing distribution center i, and we define d_{fj}^2, d_{gi}^3, d_{gj}^4, d_{ik}^5, d_{jk}^6, d_{kh}^7, d_{hf}^8, d_{hg}^9, d_{hs}^{10}, d_{ht}^{11}, d_{he}^{12} alike.

For each $k \in K$, let n_k denote the demand for new products in consumption area k each year. Let v_f^1 and v_g^2 denote the production cost of unit products in factory f and g. Let v_i^3 and v_j^4 denote the operation cost of unit products in distribution center i and j. Let v_h^5 , v_s^6 and v_t^7 denote the unit cost of dealing with waste products in recycling center h and waste disposal centers s and t, respectively. Let v_k^8 denote the price of unit new production in

consumption area k. Let w_1 denote the reproducible rate of the product; w_2 the recycle rate of the product material; and w_3 the recycle rate of the waste product. Let a denote the transportation cost for unit mass in unit distance; n the quantity of product delivery to the consumer area; B the proceeds from the recycling material of the unit product; L the proceeds from re-manufactured products of the unit product; R the weight of the unit product. Let A_f^1 and A_g^2 denote the maximum production capacity of the plants each year; A_i^3 and A_j^4 the maximum treatment capacity of distribution centers each year; A_h^5 , A_t^7 and A_s^6 the maximum treatment capacity of recycling centers and waste disposal centers each year. Let α_g, β_j , χ_h and δ_t denote the 0 or 1 that stands for whether to establish a new factory, a new distribution center, a new recycling center, and/or a new waste disposal center or not，1 for positive and 0 for negative.

For $f,i \in F \cup I$, let x_{fi}^1 denote the quantity of product delivery from factory f to distribution center i, and we define x_{fj}^2, x_{gi}^3, x_{gj}^4, y_{ik}^1, y_{jk}^2, z_{kh}, p_{hf}^1, p_{hg}^2, q_{hs}^1, q_{ht}^2, r_{he} alike.

Objective Function

$$\text{MAX } f(c) = \varphi(t) - \varphi(\alpha, \beta, \chi, \delta) - \varphi(x, z, q) - \varphi(x, y, z, p, q) \quad (1)$$

where

$\varphi(t)$ - the proceeds of sale and recycling

$\varphi(\alpha, \beta, \chi, \delta)$- fixed investment of facilities

$\varphi(x, z, q)$ - operation cost

$\varphi(x, y, z, p, q)$- transportation cost

$$\varphi(t) = \sum_{k=1}^{K} v_k^8 \left(\sum_{i=1}^{I} y_{ik}^1 + \sum_{j=1}^{J} y_{jk}^2 \right) + L \left(\sum_{h=1}^{H} \sum_{f=1}^{F} p_{hf}^1 + \sum_{h=1}^{H} \sum_{g=1}^{G} p_{hg}^2 \right) + B \sum_{h=1}^{H} \sum_{e=1}^{E} r_{he}$$

where the first item is the proceeds of the sale; the second item is the proceeds of the re-manufactured products, and the third item is the material's recycle revenue.

$$\varphi(\alpha, \beta, \chi, \delta) = \sum_{g=1}^{G} c_g^1 \alpha_g + \sum_{j=1}^{J} c_j^2 \beta_j + \sum_{h=1}^{H} c_h^3 \chi_h + \sum_{t=1}^{T} c_t^4 \delta_t$$

where the four items denote the fixed cost of building factories, distribution centers, recycling centers, and waste disposal centers, respectively.

$$\varphi(x, z, q) = \sum_{f=1}^{F} \sum_{i=1}^{I} x_{fi}^1 v_f^1 + \sum_{f=1}^{F} \sum_{j=1}^{J} x_{fj}^2 v_f^1 + \sum_{g=1}^{G} \sum_{i=1}^{I} x_{gi}^3 v_g^2 + \sum_{g=1}^{G} \sum_{j=1}^{J} x_{gj}^4 v_g^2 +$$

$$\sum_{f=1}^{F} \sum_{i=1}^{I} x_{fi}^1 v_i^3 + \sum_{f=1}^{F} \sum_{j=1}^{J} x_{fj}^2 v_j^4 + \sum_{g=1}^{G} \sum_{i=1}^{I} x_{gi}^3 v_i^3 + \sum_{g=1}^{G} \sum_{j=1}^{J} x_{gj}^4 v_j^4 + \sum_{k=1}^{K} \sum_{h=1}^{H} z_{kh} v_h^5 + \sum_{h=1}^{H} \sum_{s=1}^{S} q_{hs}^1 v_s^6$$

$$+\sum_{h=1}^{H}\sum_{t=1}^{T} q_{ht}^{2} v_{t}^{7}$$

where the first four items denote the production cost in the factory; the second four items denote the operation cost in the distribution center; the ninth item denotes the operation cost in the recycling center, and the last two items denote the operation cost in the waste disposal center.

$$\varphi(x,\ y,\ z,\ p,\ q)=aR\left(\sum_{f=1}^{F}\sum_{i=1}^{I} x_{fi}^{1} d_{fi}^{1}+\sum_{f=1}^{F}\sum_{j=1}^{J} x_{fj}^{2} d_{fj}^{2}+\sum_{g=1}^{G}\sum_{i=1}^{I} x_{gi}^{3} d_{gi}^{3}+\sum_{g=1}^{G}\sum_{j=1}^{J} x_{gj}^{4} d_{gj}^{4}\right)+$$
$$aR\left(\sum_{i=1}^{I}\sum_{k=1}^{K} y_{ik}^{1} d_{ik}^{5}+\sum_{j=1}^{J}\sum_{k=1}^{K} y_{jk}^{2} d_{jk}^{6}\right)+aR\sum_{k=1}^{K}\sum_{h=1}^{H} z_{kh} d_{kh}^{7}+aR\left(\sum_{h=1}^{H}\sum_{f=1}^{F} p_{hf}^{1} d_{hf}^{8}+\sum_{h=1}^{H}\sum_{g=1}^{G} P_{hg}^{2} d_{hg}^{9}\right)$$
$$+aR\left(\sum_{h=1}^{H}\sum_{s=1}^{S} q_{hs}^{1} d_{hs}^{10}+\sum_{h=1}^{H}\sum_{t=1}^{T} q_{ht}^{2} d_{ht}^{11}\right)+aR\sum_{h=1}^{H}\sum_{e=1}^{E} r_{he} d_{he}^{12}$$

where the first item denotes the product's transportation cost from factory to distribution center, the second item from distribution center to consumption area, and the third item from consumption area to recycling center; the fourth item denotes the waste product's transportation cost from recycling center to factory, the fifth item from recycling center to waste disposal center, and the sixth item from recycling center to renewable materials market.

Constraint Conditions

$$\alpha_g, \beta_j, \chi_h, \delta_t \in \{0,\ 1\} \quad (2)$$

$$\sum_{i=1}^{I} x_{fi}^{1}+\sum_{j=1}^{J} x_{fj}^{2} \le A_f^{1} \ (f=1,2,....F) \quad (3)$$

$$\sum_{i=1}^{I} x_{gi}^{3}+\sum_{j=1}^{J} x_{gj}^{4} \le A_g^{2}\alpha_g \ (g=1,2,....G) \quad (4)$$

$$\sum_{k=1}^{K} y_{ik}^{1} \le A_i^{3} \qquad (i=1,2,....I) \quad (5)$$

$$\sum_{k=1}^{K} y_{jk}^{2} \le A_j^{4}\beta_j \qquad (j=1,2,....J) \quad (6)$$

$$\sum_{k=1}^{K} z_{kh} \le A_h^{5}\chi_h \qquad (h=1,2,....H) \quad (7)$$

$$\sum_{h=1}^{H} q_{hs}^{1} \le A_s^{6} \qquad (s=1,2,.....S) \quad (8)$$

$$\sum_{h=1}^{H} q_{ht}^{2} \le A_t^{7}\delta_t \qquad (t=1,2,.....T) \quad (9)$$

$$\sum_{i=1}^{I} y_{ik}^{1}+\sum_{j=1}^{J} y_{jk}^{2} \le n_k \qquad (k=1,2,.....K) \quad (10)$$

$$\sum_{h=1}^{H} z_{kh} \le w_3 n_k \qquad (k=1,2,.....K) \quad (11)$$

$$\sum_{k=1}^{K} y_{ik}^{1}=\sum_{f=1}^{F} x_{fi}^{1}+\sum_{g=1}^{G} x_{gi}^{3} \qquad (i=1,2,....I) \quad (12)$$

$$\sum_{k=1}^{K} y_{jk}^{2}=\sum_{f=1}^{F} x_{fj}^{2}+\sum_{g=1}^{G} x_{gj}^{4} \qquad (j=1,2,....J) \quad (13)$$

$$w_1\sum_{k=1}^{K} z_{kh}=(\sum_{f=1}^{F} p_{hf}^{1}+\sum_{g=1}^{G} p_{hg}^{2})(h=1,2,....H) \quad (14)$$

$$\sum_{h=1}^{H} q_{hs}^{1}+\sum_{h=1}^{H} q_{ht}^{2}=(1-w_1-w_2)\sum_{k=1}^{K} z_{kh}(h=1,2,....H) \quad (15)$$

All the variables are integer value, which is not less than zero

Constraint (2) sets out the parameters for the 0-1 variables. Constraints (3) - (11) show that the handling volume of facilities such as factory, distribution center, recycling center, and waste disposal center will not to exceed the volume of their capacity. Constraints (12) - (15) express that the commodity volume inbound to and outbound from the distribution centers, consumption districts, and recycling centers is equal.

The above model is a mixed integer linear programming (MILP) model.

CASE STUDY

A refrigerator manufacturer in the area wants to develop a reverse logistics network for its products. According to traffic and transport conditions and the region's products consumption and scrapping situations, the region is divided into 17 districts. After analyzing the various candidates according to the various factors, we can identify the potential locations of various facilities initially. Then we can adopt the above modeling method to confirm the various facilities' quantity and locations. The demand in various districts of the company's refrigerators each year is shown in Table 1.

Table 1. Demand in Various Districts Each Year (unit: piece).

City	D1	D2	D3	D4	D5	D6	D7	D8	D9
Demand	3700	2870	1830	1750	1660	580	5080	1000	1230
City	D10	D11	D12	D13	D14	D15	D16	D17	
Demand	3580	6700	4420	4910	5500	2250	3700	1300	

The company has a factory in D1 already, with a production capacity of A_1^1 = 200,000 (pieces/year). The production cost of each unit is A_1^1 = 200,000 yuan. The distribution centers which have already been built are located in D1, D2, D3, D7. The disposal capacity of the distribution center is $A_1^3 = A_2^3 = A_3^3 = A_7^3 =$ 30,000 (piece/year). The operation cost of each unit is $v_1^3 = v_2^3 = v_3^3 = v_7^3 =$ 10 (yuan/piece). Existing waste disposal centers are located in D1, D9. The maximum disposal capacity is $A_1^6 = A_9^6 =$ 1,500 ton/year (2,500 pieces/year). The cost to deal with each obsolete product is $v_1^6 = v_9^6 =$ 80 yuan/ton (4.8 yuan/piece). The existing renewable materials market region is located in D8.

After analyzing the various candidates according to the various factors, we develop an initial plan: D2, D7 to be an optional factory; D11, D12, D15, D17 to be optional distribution centers; D1, D2, D3, D7, D9, D11, D12, D13, D15, D17 to be optional recycling centers; and D3, D5 to be optional waste disposal centers. According to products and materials market conditions, we can confirm the product price and the prices of recycled materials. The product price is v_k^8 = 2,400 yuan/piece, with $k = 1,2,3,.....16,17$. The unit profit of the remanufactured product is L = 200 yuan. The weight of the refrigerator is R = 60kg. The prices of the materials are shown in Table 2.

Table 2 Materials of Product Composition and Price.

Material	Steel	Copper	Aluminium	Plastic	Other
Percent (%)	49.00	3.5	2.2	43.3	2.0
Price(yuan/ kg)	1.2	20.0	14.5	1.9	6.0

From the above data, we can see a product of reusable material recycling has the profitof B = 40%(60×49%×1.2 + 60×3.5%×20.0 + 60×2.2%×14.5 + 60×43.3%×1.9 +60×2.0%×6.0) = 61 yuan.

The fixed cost of building a new factory is $c_2^1 = c_7^1 =$ 1,000,000 yuan. The production capacity is $A_2^2 = A_7^2 =$200,000 pieces/year; the production cost of each unit is $v_2^2 = v_7^2 =$ 2,000 yuan. The fixed cost of building a new distribution center is $c_{11}^2 = c_{12}^2 = c_{15}^2 = c_{17}^2 =$ 100,000 yuan. The disposal capacity is $A_{11}^4 = A_{12}^4 = A_{15}^4 = A_{17}^4 =$ 330,000 pieces/year. The operation cost of each unit is $v_{11}^4 = v_{12}^4 = v_{15}^4 = v_{17}^4 =$ 10 yuan/piece. The fixed cost of building a new recycling center is $c_1^3 = c_2^3 = c_3^3 = c_7^3 = c_9^3 = c_{11}^3 = c_{12}^3 = c_{13}^3 = c_{15}^3 = c_{17}^3 =$ 100,000 yuan. The disposal capacity is $A_1^5 = A_2^5 = A_3^5 = A_7^5 = A_9^5 = A_{11}^5 = A_{12}^5 = A_{13}^5 = A_{15}^5 = A_{17}^5 =$ 300,00 piece/year. The cost to deal with each obsolete product is $v_1^5 = v_2^5 = v_3^5 = v_7^5 = v_9^5 = v_{11}^5 = v_{12}^5 = v_{13}^5 = v_{15}^5 = v_{17}^5 =$ 20 yuan/piece. The fixed cost of building a new obsolete product disposal center is $c_3^4 = c_5^4 =$ 200,000 yuan. The Maximum is $A_3^7 = A_5^7 =$ 1,500 ton/year (2,500 pieces/year). The cost to deal with each obsolete product is $v_3^7 = v_5^7 =$ 80 yuan/ton (4.8 yuan/piece). Each heavy-duty truck used for transportation has the loading capacity of 15 tons; the transportation cost is 0.3 yuan/ton-kilometer. The maximum manufacture rate is $w_1 =$ 40%. The product material recycle rate is $w_2 =$ 40%. The obsolete product recycle rate is $w_3 =$ 60%.

Using the case data in the model and using *lingo8.0* to get the Maximum of the object function, the max profit is $f(c) =$ 2,024,633 yuan. The optimal of related decision variables are $\beta_{12} = \chi_9 = \chi_{12} = \delta_5 =$1, $x_{17}^1 =$ 22,110, $x_{1,12}^2 =$ 30,000, $y_{72}^1 =$ 2,670, $y_{74}^1 =$ 1,750, $y_{75}^1 =$ 1,660, $y_{7,11}^1 =$6700, $y_{7,12}^1 =$ 4,420, $y_{7,13}^1 =$ 4,910, $y_{12,1}^2 =$3700, $y_{12,2}^2 =$ 200, $y_{12,3}^2 =$ 1,830, $y_{12,6}^2 =$ 580, $y_{12,7}^2 =$ 5,080, $y_{12,8}^2 =$ 1,000, $y_{12,9}^2 =$ 1,230, $y_{12,10}^2 =$ 3,580, $y_{12,14}^2 =$ 5,500, $y_{12,15}^2 =$ 2,250, $y_{12,16}^2 =$ 3,750, $y_{12,17}^2 =$ 1,300, $z_{19} =$1, $z_{29} =$ 1,722, $z_{49} =$ 1,050, $z_{59} =$ 996, $z_{10,9} =$ 2,148, $z_{11,9} =$ 4,020, $z_{12,9} =$ 2,652, $z_{13,9} =$ 2,946, $z_{14,9} =$ 3,300, $z_{1,12} =$ 2,218, $z_{3,12} =$ 1,098, $z_{6,12} =$ 348, $z_{7,12} =$ 3,048, $z_{8,12} =$ 600, $z_{9,12} =$ 738, $z_{15,12} =$ 1,350, $z_{16,12} =$ 2,250, $z_{17,12} =$ 780, $p_{91}^2 =$ 7,534, $p_{12,1}^2 =$ 4,972, $q_{91}^1 =$ 1,267, $q_{95}^2 =$ 2,500, $q_{12,9}^1 =$ 2,486, and the others are zero.

According to the value of the variables, we can make sure that D1 is the location of the factory, with no need to build a new factory; D1, D2, D3, D7, and D12 are distribution centers, and D12 is the new distribution center; D9 and D12 are the new recycling centers; D1, D9, and D5 are the obsolete product disposal centers;

D5 is the new obsolete product disposal center.

CONCLUSION

An optimization model for the design of an integrated logistics network that combines a forward logistics and reverse logistics network is set up and applied to a refrigerator factory's integrated logistics network design. The results were satisfactory.

REFERENCES

Qinli, D., Zuqin, H., and Qin, A (2004). "Reverse logistics system status quo and prospects." *Management Science of China,* 12 (1),131-138.

Fleischmann, M., Krikke, H. R., Dekker, R., Douwe, S., and Flapper, P. (2000). "A characterization of logistics networks for product recovery." *Omega,* 28(6), 653-666.

Fleischmann, M., Van Nunen, J., and Grave, B. (2002). "Integrating closed-loop supply chains and spare parts management at IBM." [R]·ERIM *Report Series Research in Management (*ERS-2002-107-LIS), Erasmus University, Rotterdam, the Netherlands.

Jayaraman, V., Guide, V. D. R., Jr., and Srivastava, R. (1999). "A closed-loop logistics model for remanufacturing." *Journal of the Operational Research Society*, 50(5), 497-508.

Xuhui, X., Fei, L., Chao, Y., and Quanjie, G. (2003). "The supply chain, reverse supply chain management and enterprise integration." *Compute*, 9 (8), 652-656.

Zujun, M., Yin, D., and Zhang, D. (2004). "Reverse logistics network structures and design." *Logistics Technology,* 4, 12-14.

A New Organizational Structure Pattern of Owners Based on Multi-Project

Qiaoting Dong, Yingming Shen, Huijun Li, Zhijun Chen

Shijiazhuang Railway Institute, Shijiazhuang, Hebei, China 050043; PH (86) 311-87935520; FAX (86) 311-87936049; email: shxt7@sohu.com

ABSTRACT

Most projects exist as part of a multi-project environment in the Eleventh Five-Year Program of China and the 2010 Shanghai World Expo, meaning that an era of multi-project management has come. This article suggests that a new organizational model suited for owners' multi-project management should be built and expressed with an organizational structure chart from the owners' perspective, with the owners at the core, and analyzes the relationship of stakeholders with game theory. It also describes the main point of the organizational structure model's implementation to ensure that the organizational structure can be implemented smoothly.

Key words: Multi-project management, organizational structure pattern, owners

INTRODUCTION

In recent years, as key transport infrastructure projects of the National Eleventh Five-Year Plan are carried out and implemented gradually, owners are facing new challenges related to carrying out and coordinating multiple projects simultaneously. With the external environment and conditions changing, the competitive environment of society is increasing. High operating costs of projects are causing owner organizations to examine multi-project management behaviors. They strive to find a new multi-project management pattern to reduce multi-project operating costs, promote the professionalization management, and cultivate the core competitiveness of organizations. This will improve the overall efficiency of organizations and achieve the goal of sustainable development.

CURRENT MULTI-PROJECT MANAGEMENT PATTERN OF OWNERS

In single-project management, project management patterns include self-management projects, namely the traditional triangle pattern of "owners + supervision departments + contractors"; a combination of self-management and commissioned management; and owners' commissioned management. In China, the most common are consultation, total-control, physical, contracting, construction agent patterns, etc. (Yin 2008).

Current multi-project management often adopts the project-centered management pattern (see Figure 1). This project management pattern, which puts the owners, supervision, and contractor together by means of professional project management departments, neglects the central role of owners within the project life cycle.

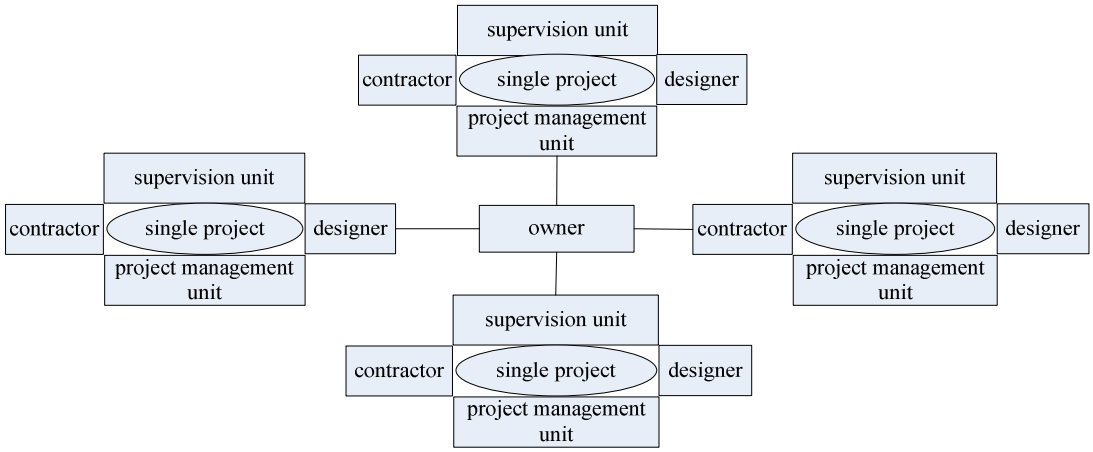

Figure 1. Project-centered multi-project management model.

GAME ANALYSIS OF PROJECT PARTICIPANTS

Single-layer principal-agent game pattern of supervision departments directly commissioned by owners. Assumed conditions are as follows.

In the game, there are owners, contractors, and supervision departments. To increase personal income, contractors use speculative behavior by colluding with (bribing) supervision departments, which decreases project earnings.

Contractors have two choices: to bribe or not bribe; if contractors choose to bribe, supervision departments have two options: to accept or not accept.

If the contractor does not bribe the supervision department, both sides have benefited from zero, and the project has a normal income - the assumption here is zero; If contractors bribe the supervision unit and the supervision unit accepts, the contractor will have an additional income X_1, and bribery amounts X_2. If the supervision unit accepts a bribe, it has the probability of being discovered and can be punished by a fine, an expected loss of X_3. Because of collusion between the two sides, the project is at risk of loss for S. If the contractor offers a bribe and the supervision unit does not accept, then the benefit of both sides is zero and the project has a normal income (see Figure 2). The benefit matrix separately expresses contractor benefit, supervision unit benefit, and project benefit.

We can get a perfect information dynamic game. Sub-game perfect Nash equilibrium is as follows: If X2>X3 and X1>X2, the contractor chooses bribery and the supervision unit chooses accepting bribery. Then the three parties' benefit is (X1-X2, X2-X3,-S). The project suffers from risk losses. If X1<X2, the contractor

chooses not to bribe, the game terminates, and the project proceeds normally.

To prevent project risk caused by the two sides' collusion, it is necessary to prevent the emergence of the balance outcome for the two sides. The keys lie in greater control and punishment of supervision departments.

Double-layer principal-agent game pattern of project management departments and supervision units. Assumed conditions are as follows:

The supervision departments oversee the project implementation of the contractor. For personal enhancement, the contractor may bribe the supervision departments, and the project management department has oversight responsibility for the supervision departments. Once the supervision departments are found to have accepted bribes and are punished, to mitigate punishment, supervision departments have the tendency to bribe the project management department.

Contractors have two choices: to bribe or not bribe. If contractors select bribery, the supervision departments have two options: to accept or not accept. If the supervision departments accept a bribe, they have two choices: to bribe or not bribe. The same project management department has two choices. Both sides benefit, as shown in Figure 3.

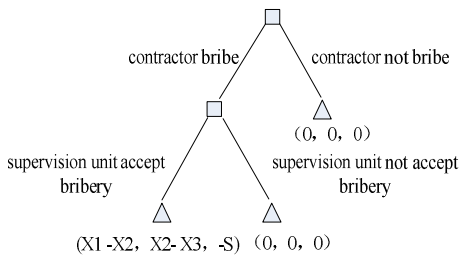

Figure 2. Single-layer principal-agent game model.

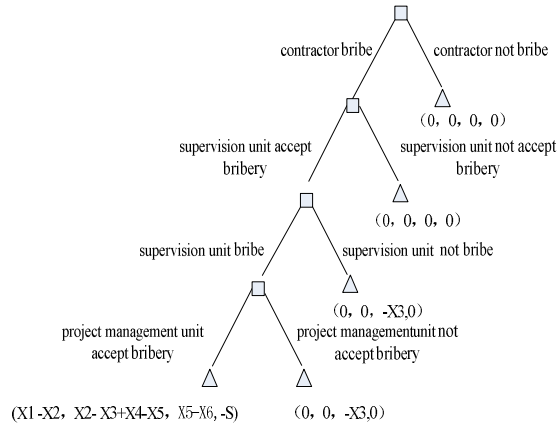

Figure 3. Double-layer principal-agent game model.

Where X1 is the additional revenue of the contractor for the irregularities; X2 is the amount that the contractor bribes supervision departments; X3 is financial penalties of the supervision departments for accepting a bribe; X4 is the reduced punishment amount of the supervision departments for bribing the project management department; X5 is amount of the project management department accepting bribery from the supervision departments; X6 is the punished expectations of the project management department for accepting a bribe; S is the losses of the project.

When X1>X2, X4>X5>X6, X2-X3+X4-X5>0, the sub-game perfect Nash equilibrium for (bribery, accept bribery, bribery, accept bribery), that contractors

bribe supervision departments, supervision departments accept bribery, and, to reduce the punishment amount, they then bribe project management, the project management department accepts bribes, and the owner has the loss of X4+S-X6-X3. X6<X4, so X6+X3-X4-S<X3-S. That is, with the layers of principal-agent increasing, the agent costs of the owner increased X4-X6. When the contractors, supervision departments, and project management departments have collusive behaviors at the same time, the project will have the risk of loss of S. With layers of principal-agent increased, the uncertainty of project income would continue to increase, which is mainly embodied in the risk losses and risk probability (Linchang 2007).

According to the above game analysis, it can be drawn that, with principal-agent layers between owner and supervision units increasing, the probability of the supervision departments' speculative behavior will be great. That is, the damage caused by the contractors' collusion is quite possible. Therefore, this article advocates a project management pattern in which the owner directly commissions the supervision unit as well as increases the punishment, which could be achieved through improved management of the current supervision system.

Game analysis between owners and contractors. To allow the project to be completed ahead of schedule, the owner could award the contractor for early completion. To receive these rewards, the contractor can speed up their own work or adopt jerry-building to shorten project completion time. At the same time, the contractor would like to receive progress payments as soon as possible to reduce advance funds. The owner in capital-limited circumstances, in order to allow multiple projects to proceed smoothly, will try to reduce cost payments. Under conditions of asymmetric information between the two sides in the game, in such a game it is very difficult to achieve a balance of interests.

To resolve the principal-agent disposable game Nash equilibrium problem, vulgar theorem is introduced in the game theory. Based on vulgar theorem, the multi-project organization pattern can choose a two-way principal-agent relationship to form closed circulation, which will achieve infinite repeated game. Repeated game allows both sides to know each other's information to a greater extent, makes more private information become public information for both sides of game, and makes the "eye for an eye" type of retaliation achievable (Zhang 2008).

A two-way principal-agent relationship can be set up between owner and the contractor. After repeated game, both sides will make trade-offs between their short-term benefits and the overall interests of the organization.

Game analysis between owner and project management department. In multi-project management, the owner will entrust projects to project management agencies separately. To achieve the greatest project interest, the project management organization will stand in the perspective of a single item to choose its own behavior. This will cause a difference between the "individual action" of the project organization and the "collective action" of the owner.

Maximizing individual benefit, which is pursued by the project organization, will hamper the strategic goals of the project center to maximize the collective benefits. Contradictions and conflicts between both sides lie in the authority of the owners, the development of incentives, and the reward and punishment mechanisms. Therefore, we can see the relationship between the owner and the project management agency as a commissioned agent relationship. As the client, the owner is responsible for overseeing the agent, supervising the project management organization, and implementing the reward and punishment systems for project management agencies. Every project management organization takes action according to the combination of the project management body of the project and the owners' action. Through analysis on the dual principal-agent pattern, we can see that setting up the double principal-agent relationship between the owner and project management organization can achieve balance after repeated game.

MULTI-PROJECT MANAGEMENT PATTERN WITH THE OWNERS AT THE CORE POSITION BASED ON GAME ANALYSIS

In multi-projects system, the owners are in the core position and coordinate the various participants in overall scheduling. Based on game analysis of the relationship between the project participants, every participant in the projects should be incorporated into the management system to reduce the participants' speculation from the regime. Project management patterns take direct commission as the major style, which can effectively reduce the speculation of the supervision department. For the participants, it will bring the collection into the multi-project management system and set up a double-layer principal-agent project management pattern. In a long-term game, it will eliminate participants who are adverse, introduce new participants, and implement dynamic management.

ADJUST THE ORGANIZATIONAL STRUCTURE OF THE OWNER UNDER NEW MULTI-PROJECT MANAGEMENT PATTERN

In an existing organization, the basic individual projects are at the core, which cannot raise good project management to a multi-project system. With owners of multi-project management, there are a variety of internal and external conflicts of interest.

In the new organizational structure (see Figure 4), increasing the project management center, which is the center of the deployment of resources, will assist the decision-making nerve, achieve coordination of the relationship of the project participation side, organize the internal coordination of various projects, assist in decision-making, increase the group flow of department in the vertical. Pre-planning ministers manage the design departments set, total workers manage the supervision departments set, project engineering ministers manage the contractor set, and materials ministers manage the suppliers set.

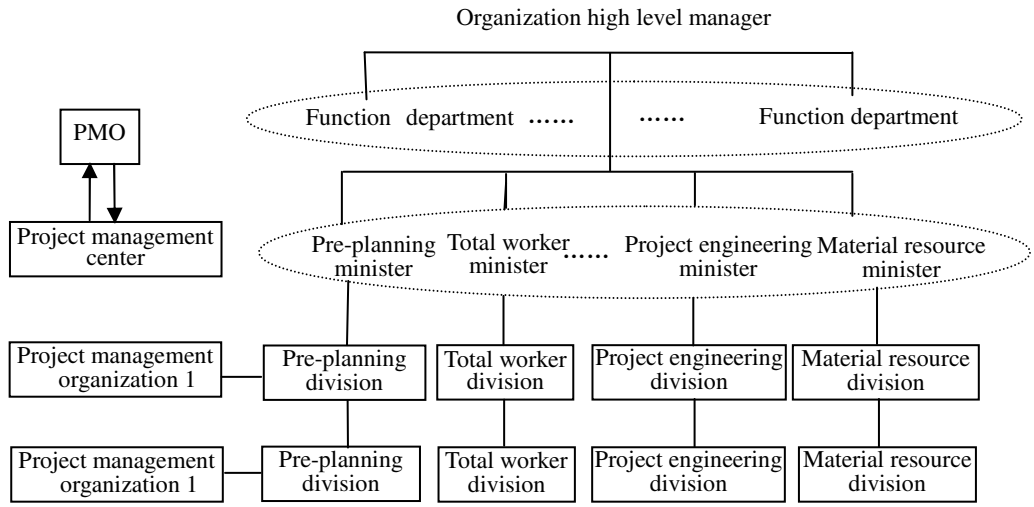

Figure 4. New owner project management organization model.

Increasing this layer changes the previous occlusion information between functional departments and can reduce communication difficulties. These ministers of the flow departments will send professionals to assume the corresponding professional work. The professionals will be commanded and coordinated by the leadership of project management body and can directly report to it. Department managers no longer intervene in the specific aspects of project management and pay more attention to the employment, promotion, career development and learning, and training of department employees and are responsible for the assessment of the staff's professional skills. The project management center coordinates a number of projects, which is a strong decision-making control area, sets a clear separation of powers, authorizes the leadership, and supervises and controls the project management body. According to the information about each project, they determine the input of all project resources and punishments.

The highest decision-making level in the organization setup is the office of project leaders, who are the highest decision-makers on multi-projects and are responsible for the multi-projects, long-term strategic decision-making, and the formation of objectives. The responsible person in the command center manages multi-projects to ensure that the strategic objectives are consistent the highest goals of organization.

CONCLUSION

This article recommends a project-centered multi-project management pattern with the owners and management at the core. The internal organizational structure of the traditional owners should be adjusted to achieve more effective multi-project management. This will improve the overall efficiency of the owner, reduce management costs, and ultimately achieve the strategic objectives of organizations.

REFERENCES

Yin, Yilin, and Zhou, Pei. (2008). "PMO-a new organizational structure pattern of multi-project." *Harbin Commerce College Journal.* (2),11-13.

Yu, Linchang. 2007. "Agent game model of government construction project." *Highway and Transport,* (6),151-153.

Zhang, Qinghua, Wei, Changxing, and Zhao, Yanjuan. (2008). "Organizational structure of project management on owners." *Construction Economy,* (11), 45-48.

Dynamic Alliance of Road Logistics Enterprise Based on Ant Colony Algorithm

Liao Xiaobo[1] and Huo Yamin[2]

[1]College of Traffic and Transportation, Southwest Jiao Tong University; P.O. Box 610031, Chengdu, China; Phone: (86) 28-86466942; Email: jtys001@126.com
[2]College of Traffic and Transportation, Southwest Jiao Tong University; P.O. Box 610031, Chengdu, China; Phone: (86) 28-87634364; Email: huoyamin@163.com

ABSTRACT

Along with the growth of the National Economy and intensive readjustment of industrial structure, the road logistics demands are increasing quickly in quality and quantity. Oppositely, the scattered, weak and disorderly structure adversely affects the healthy development of the road logistics. It is essential to study the logistics service mode suitable for the increasing demands of the road logistics. The paper analyzes the common characteristics between the road logistics individual and the ant colony. Then, by the ant colony intelligence, the dynamic alliance of road logistics is presented, the construction algorithm and the application method are given too. The paper provides a better operable development mode for the road logistics in China, which has a direct impact on improving logistics efficiency for the construction of a harmonious society.

1 INTRODUCTION

Benefited from the quick development of macro economy in recent years, the demands of logistics in China are increasing quickly in quality and quantity. The road logistics is a main mode, which undertakes the majority in volume. However, influenced by the traditional economy thought of 'emphasized production, despised circulation' in China, logistics in China started late and developed slowly, characterized by small-scale, which limits the logistics development seriously (Ding, 2008). Thus, it is very necessary to study the logistics service mode suitable for the increasing demands of the logistics.

At present, there are various problems in the road logistics in China, including low efficiency, poor quality, lack of information and manpower etc. For the logistics individual, there are various modes, including the large-size enterprise, medium-size enterprise, small-size enterprise, self-employed individuals and part-time individuals. Among these individuals, there are great differences in operation, management, specialty, lacking organization and platform. In particular, there are few road logistics enterprises that can operate most types of logistics. In fact, many logistics individuals are competing repeatedly in low efficiency, low-level market.

For the rapid development of the logistics market and to solve the problems

of the logistics individual, it is essential to integrate the road logistics service. The integration targets include enterprises, material suppliers, primary product collectors, and packing, transportation, warehousing, and marketing, product planning, and information service. However, there are a lot of unresolved problems in operation management and benefit distribution, making the integration on entity difficult. And it is impossible for long-term stable organization to exist, since there is many differences between the individuals in domain, manpower, ability and idea etc. Thus, the dynamic logistic organization has more advantages. Researches about logistics integration are mainly on industry logistics (Dai, 2001), and few are on road logistics.

The paper reveals that the road logistics individuals have the characteristic similar to the intelligent individual. By ant colony, the dynamic alliance of road logistics is presented, the forming algorithm and the management of the alliance member are analyzed. Then, the process to create, run, dissolve the road logistics dynamic alliance is discussed.

2 ANT COLONY ALGORITHM AND ROAD LOGISTICS ALLIANCE

Road logistics individuals, with a familiar cognition with itself, can make one or some logistics operation, which is viewed as an individual with some level of intelligence. By ant colony, some road logistics may build up a dynamic alliance according to the coming logistic job.

2.1 Intelligence individual and road logistics individual

The intelligence mainly appears as some form as software or hardware of computer. Yet, they all have some common features, such as highly adaptability and autonomy. Shoham (1993) regards that an entity is intelligence individual if its state includes the psychosis, such as knowledge, idea, promise, ability etc.

An individual who implements some operation of logistics, as an independent entity with knowledge, idea, ability and social duty, can be looked as an intelligence individual. Then, the road logistics individual, as an intelligence individual, has the common features: autonomy, social ability, flexibility, mobility, reaction, consciousness. This is the foundation for making the Ant Colony Algorithm alliance operation.

In general, ant colony shows the characteristic that the entity without intelligence behaves intelligently. Ant colony algorithm provides an approach to solve the distributed problem without centralized control and global model. By applying ant colony, some algorithm has the characteristic of intelligence. Through the interaction between the individual and environment, the algorithm has some self-organization function, robustly and visually. And, the theory of multi individual system is from distributed artificial intelligence, which has been widely adopted in many domains. Multi individual system mainly studies the corresponded intelligence

action of the multi individual separated in logic or physics, and at last solves the problem.

The ant colony algorithm in the paper based on multi individual, not only exerts the initiative and independence of the individual, but also makes the colony to have additional function than the simply combined members have and to present more intelligence function than normal intelligence individual does.

2.2 Road logistics dynamic alliance

Under the well cooperation mechanism and fellowship, road logistics individuals connect and cooperate in related logistics work, and they can build up logistics alliance. In fact, the logistics alliance is an integration platform based on information (Gunasekaran, 2004). The road logistics alliance includes the function like a real logistics enterprise and can implement the same operation, such as warehousing, transportation, packing etc.

In the environment of road logistics integration, the relation between the individuals is the cooperative partnership based on credit and cooperation. Like the traditional integration mode, the fixed logistics alliance has many disadvantages, such as the low adaptability for operation etc. Therefore the alliance needs to form and dissolve frequently to adapt to the logistics demands, which will waste more manpower and resource, increase the cost, reduce the efficiency, and affect the partnership between the individuals.

By the multi individual swarm intelligence, the paper abstracts the fellowship in the forming of the alliance, then build up the road logistics dynamic alliance adapted to the logistics need. Based on the dynamic alliance mechanism, every member understands the participant logistics operation deeply. Then, in cooperation, the members can implement the logistics work that cannot be done by a single member. The dynamic organization is more responsive to the market, can exert more superiority and scale merit compared to a large enterprise.

3 THE MECHANISM OF THE ROAD LOGISTICS DYNAMIC ALLIANCE

The road logistics dynamic alliance is highly active, can be created for the logistics task and disjointed as the task end in a timely manner. Firstly, the system is driven by the upcoming logistics task; the task is then analyzed and decomposed. According to the sub task, the first generation combination of the logistics individual is generated randomly. Each sub task can include one or several logistics individuals. Then, each selected individual can select group cooperation with good fellowship. Repeating the process until the combination is stable. That will be the last generation combination that the task needs.

3.1 Road logistics individuals database management

Based on the understanding of the logistics need, the road logistics individual member database is formed. The database keeps the information of the logistics

member, including operation service area, operation type, enterprise scale, facility, cooperator, operation comprehensive evaluation etc. The system formats the candidate logistics individual and adds it into the database. The system can also maintain and make other operation to the member. Logistics individual member database and its management areshown in figure 1. There, the operation service range includes: the pre-logistics of agriculture products, primary gathering, primary processing, and warehousing, packing, transportation, distributing and information service. There are two types of basic individual, one is the entity logistics enterprise, which is the same as in the real world; the other is the virtual logistics enterprise, which may be a department of a logistics enterprise, or a virtual enterprise combined with certain approach. Some large road logistics enterprise can be added into the database as an enterprise, or be decomposed as several virtual logistics operation and then added into the database. Apparently, these virtual logistics enterprise decomposed from a large enterprise have closer relationship and may select each other for cooperation. However, in other environment, for efficiency and some other reason, some integrated enterprise will select other fellows to complete a logistics work though it may have sub enterprise for that work.

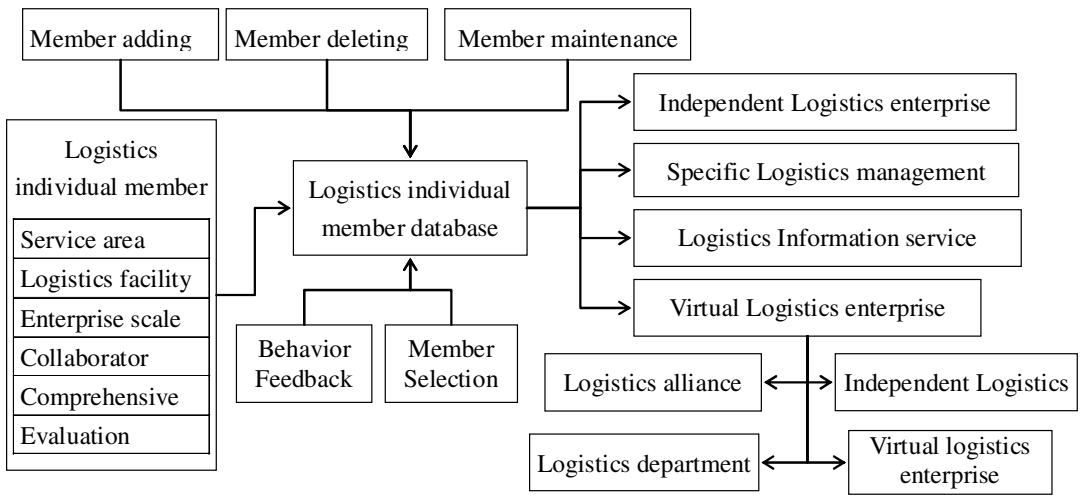

Figure 1. Road logistics individual member management in dynamic alliance

3.2 The Algorithm of road logistics dynamic alliance

For a given logistics task, a multi-dimensional index space with multi order is formed, including the operation, time, place, and service estimate of the logistics task. The same type of intelligence individuals are placed in the multi-dimensional space randomly, where each intelligence individual is assigned to a logistics sub task. The intelligence individuals are moving in the space and evaluated (Himoff, 2004). At last, they are integrated by the multi-dimensional indexes.

Assume that the logistics member data set is $X=\{X_i=(x_{i1}, x_{i2}, \ldots,x_{im}), i=1,2,\ldots,N\}$, is a set including N road logistics enterprise members. For a logistics

intelligence individual xi, x_{i1}, x_{i2}, …, x_{im} are the performance index. The step is as follows:

(1) The logistics task from the management system is analyzed and decomposed. Then, by the task source, select the initial point (member). The selection condition can be the latest distance in space or time.

(2) Initialization. Set the parameters, including the cluster ratio r, cluster error ε and basic probability p_0.

(3) Calculate the Euclidean distances $d_{ij}(X_i, X_j)$

$$d_{ij} = \left\| P(X_i - X_j) \right\| = \sqrt{\sum_{k=1}^{m} p_k (x_{ik} - x_{jk})^2}$$

(4) Calculate the probability, $p_{ij} = t_{ij}^{\alpha} \eta_{ij}^{\beta} / \sum_{s \in S} t_{ij}^{\alpha} \eta_{ij}^{\beta}$

Where, if $d_{ij} > r$, $t_{ij} = 0$, if $d_{ij} \le r$, $t_{ij} = 1$.

(5) If p_{ij} is greater than p_0, X_i and X_j are clustered together.

(6) Return to step 5, until all logistics members are calculated and clustered. Then calculate the total error ε.

(7) If ε is smaller than ε_0, go to the next step; otherwise go to step 1, and select the initial point and Initialization again.

(8) Assign the task to the real enterprise and implement it.

(9) After the task, by the performance of the member in this task, adjust the estimate of the logistics individual member and give feedback in the database.

4 THE IMPLEMENT OF THE ROAD LOGISTICS DYNAMIC ALLIANCE

Road logistics dynamic alliance, centered around the cooperative relation selection algorithm based on the multi individual swarm, driven by logistics task, sustained by logistics individual database management system, implementing the integration of the road logistics (Yao, 2008). The main structure is shown in figure 2.

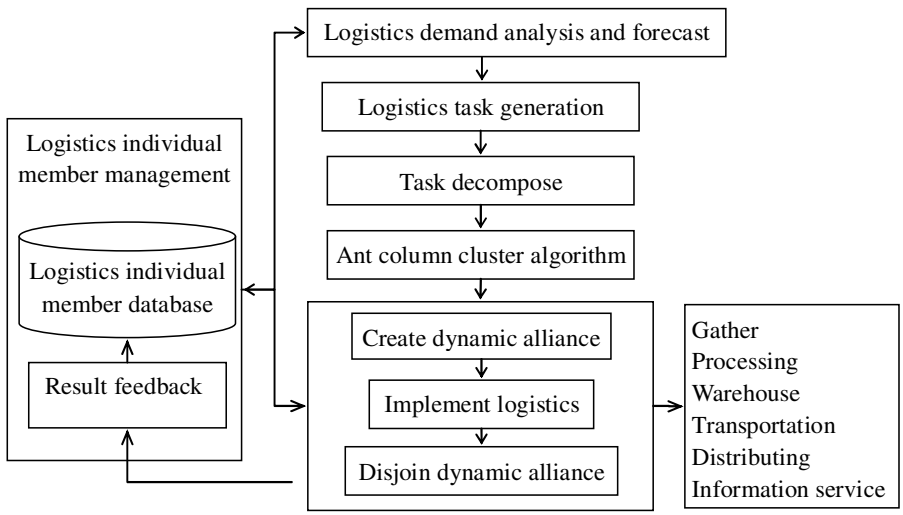

Figure 2. The implement of the road logistics dynamic alliance

The operation of the agriculture products dynamic alliance includes the creating, running and disjointing the alliance. Each member implements one logistics operation, and with the cooperation completes the logistics task in the end. During implementation, the management system and information platform provide the connection for the logistics individuals (Zhao, 2008). There, each member logistics individual can accept task, query the logistics individual database in the information platform, run the algorithm, form the dynamic alliance and execute it.

CONCLUSION

There is serious disharmony between the quickly increasing demands of road logistics and the undeveloped service. Road logistics dynamic alliance provided a suitable mode for road logistics. The paper presents a member cooperative selection algorithm based on ant colony. By using this algorithm, logistics individuals can be dynamically organized together. On one hand, this method can exert the advantage and improve the efficiency of the member; on the other hand, the service ability and quality can be improved. Based on the algorithm, the paper studies the creating, running, disjoining of the road logistics dynamic alliance. The test selects 12 logistics enterprises, including 3 professional road logistics enterprise, 7 traditional road transportation enterprises and 2 part-time logistics individual. For 6 logistics task given, the logistics dynamic alliance generated by the method presented in this paper shows better result than the general selection by the experts.

At last, in application, there are many questions needed further consideration and study, including the operation legislation, member management, credit management, profit assignment and performance evaluation.

REFERENCES

Dai, Y., Lu, J. Q. (2001). “Internet-Based Virtual Logistics Business Alliance IT Platform”. Logistics Sci Tech, (5), 11-13.

Ding, Junfa (2008). “Three Decades of China's Logistics Industry”. Shanghai Logistics, (4), 19-21.

Gunasekaran, A., Ngai, E. (2004). “Information Systems in Supply Chain Integration and Management”, European Journal of Operational Research, 159, 269-295.

Himoff, J., Skobelev, P., Wooldridge, M. (2004). “Magenta Technology: Multi-Agent Systems for Industrial Logistics”. Magenta Technology, August.

Shoham Y. (1993). “Agent-oriented programming”. Artificial Intelligence, 51-92.

Yao, Jianming, Liu, Liwen (2008). “Optimization Model and Algorithm Analysis on Supply Chain Resources Integration Decision in 4PL”. Systems Engineering-Theory & Practice. 28(5), 20-28.

Zhao, Zheng (2008). “Design and Implementation of Logistics Information Platform of Road Transportation”. Computer Engineering, 34(16), 252-255.

Optimization of Emergency Material Dispatch Problem Based on Adaptive Genetic Algorithm

Feng Xuejun[1], Zhang Qinying[2] ,Wang Wei[3]

[1]Transportation & Logistics Engineering Institute of Hohai University; 210098, Nanjing, China; PH: 025-83787270; email: fxj@hhu.edu.cn
[2]College of Traffic and Ocean, Hohai University, 210098, Nanjing, China, PH: 025-83787354; email:zhangqinying@gmail.com
[3]Transportation & Logistics Engineering Institute of Hohai University; PH: 025-83787354; email:jjww888@126.com

ABSTRACT

To pursue the greatest time benefit and the least cost in emergency logistics, an improved emergency logistics system is designed and an operation process in emergency logistics system is proposed by comparing the differences between emergency logistics and common commercial logistics. A multi-material dispatching model is constructed, based on the double objective of the earliest emergency start time and the least cost of emergency logistics. The optimal solution for the model is obtained by an adaptive genetic algorithm (AGA), which has proven to be an effective algorithm. An application example simulated by MATLAB is presented, which shows that AGA has better optimizing resistance than GA; thus, the emergency material dispatching model can be effectively used in the emergency logistics field.

Key words: Emergency logistics; material dispatching; adaptive genetic algorithm (AGA)

PREFACE

China is a country, in which natural disasters occur frequently, and previous earthquakes, floods, etc., have caused tremendous loss, e.g., building damage, personnel casualties, and so on. Massive disaster relief equipment and materials cannot be supplied and distributed in a timely manner due to traffic impediments caused by the disaster. The process of time effects and space effects in logistics is difficult to realize in disaster relief. To minimize losses created by the disaster and to operate the emergency logistics system, there is an urgent need to optimize the dispatching scheme of emergency materials.

In recent years, many domestic and foreign scholars have conducted research on emergency material dispatch problems under different constraints. Hale and Moberg (2005) mainly studied the choice of emergency logistics supply nodes, especially according to the emergency material storage of the nodes, and established a quantitative model. Chunlin et al. (2001) discussed the urgent material dispatch problem under the material demand constraints at several rescue points. This paper, based on the status of China's emergency logistics system construction, presents the design for an improved emergency logistics system and solves the emergency material dispatching problem and selects the appropriate emergency points between them and the transportation line.

ANALYSIS OF EMERGENCY LOGISTICS CHARACTERISTICS

Emergency logistics is a specialized logistics activity for the purpose of providing emergency materials for natural disasters, public health incidents, emergencies, etc., and the pursuit of maximizing time efficiency and minimizing losses in disasters.

Emergency logistics, like common commercial logistics, have space effects, time effects, and form quality effects. However, emergency logistics also has characteristics that are different from common commercial logistics, including paroxysm, uncertainty, emergency of time constraints, and weak economic factors. This study conducted a comparative analysis between emergency logistics and common commercial logistics at the points of purpose, logistics distribution network, and the external environment. The specific content is shown in Table 1.

Table 1. Differences between Emergency Logistics and Common Commercial Logistics.

Sort	Common Commercial Logistics	Emergency Logistics
Purpose	Minimize costs or maximize profits	Primary purpose is to minimize delay time for satisfying demand; secondary purpose is to minimize costs
Logistics Distribution Network	**Characteristics of facility**: permanent **Network structure**: designed distribution nodes and function of network based on demand **Participation role**: various types of economic entities closely linked, such as manufacturers, distributors, transportation companies, etc.	**Characteristics of facility**: temporary **Network structure**: structure and function are simplified **Participation role:** institutions or organizations that are not closely linked such as relevant government departments, various donors, as well as the provisional established
External Environment	Full information, difficult to change	Information missing, easy to change

EMERGENCY LOGISTICS SYSTEM AND OPERATION PROCESS

The rapid and accurate flow of information relies on advanced communications and information transfer mechanisms; the efficient and orderly flow of work relies on sound and rigorous protection mechanisms and related rules and regulations. Quick and timely logistics must rely on the coordinated operation of the procurement of supplies, reserves, transport, and logistics centers. Based on these requirements, emergency logistics systems are made up of an emergency logistics command platform, an emergency logistics information platform, an emergency logistics warehouse platform, emergency logistics transport and distribution platforms, and an emergency logistics policy platform.

When major emergencies occur, the command platform promptly initiates the corresponding level of response in accordance with the type and level of incidents, publishes timely and authoritative information related to the disaster to the public, assesses the type and quantity of materials that disaster-stricken masses

require, organizes rescue materials and issues to the unit the mission, objectives, and requirements and a clear division of responsibilities and specified time node. Adjustments must be flexible according to the actual situation by continuously tracking supervision on the implementation of the operation and timely feedback and information collection. The executive departments organize capable forces and take effective measures to ensure the smooth implementation of emergency logistics of the mission. The information platform conducts real-time tracking of the delivery of materials and timely information collection about changes related to the disaster to make a new materials distribution program. The process is shown in Figure 1.

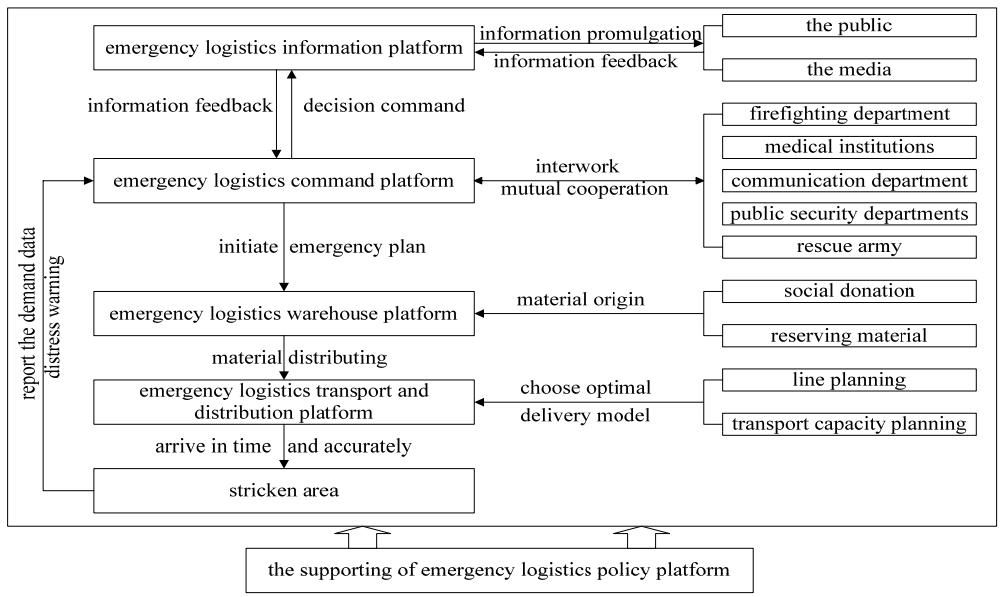

Figure 1. Operation process of emergency logistics.

MULTIPLE EMERGENCY MATERIAL DISPATCHING MODEL

The emergency material arriving at demand points for the first time is important to the successful operation of an emergency logistics system. Emergency logistics seeks the greatest time benefit and realizes the space effects of rescue materials in the shortest delay time, satisfying the rescue materials demand for sudden events disposal. However, China is a developing country, and the capital invested in disaster prevention and rescue is limited. In addition, natural disasters and accidents occur frequently, so it is necessary to spend the limited funds on the most needed aspects of the system. Therefore, this paper considers two goals: how to make the emergency start time the earliest and how to make the emergency cost the least.

Suppose there is an emergency point A at a sudden event, which needs a number of emergency materials $m(m>1)$. The demand of emergency material j is $x_j > 0(j=1,2,\cdots,m)$. There exist $n(n>1)$ emergency rescue points that can provide sufficient emergency materials to A (denoted by $A_1, A_2, \cdots, A_n$), and rescue point i can provide $x_{ij} > 0(i=1,2,\cdots,n; j=1,2,\cdots,m)$ emergency material j ,which x_{ij} satisfies to $\sum_{i=1}^{n} x_{ij} \geq x_j, (j=1,2,\cdots,m)$. The time of the

emergency material from rescue point A_i to emergency point A is $t_i > 0(i = 1,2,\cdots,n)$, and $t_1 < t_2 < \cdots < t_n$. The function $f_j(t)$ is the consumption of material j at the time t.

Because of traffic slowdowns caused by the disaster, transport line planning must adapt to the actual situation after the disaster. This paper considers vehicle travel cost and the cost caused by changing the transport mode; therefore, some parameters display as

CT^r - the transportation cost of the unit section of unit material of transport mode r

$CE_g^{jrr'}$ - the transport mode change cost of unit material j at point g, changing transport mode from r to r'

d_{ef} - the distance from point e to point f

X_{ef}^j - the flow of material j on a radial truck arc (e, f)

$X_g^{jrr'}$ - the flow of material j at point g, changing transport mode from r to r'

$ACAP_{ef}^r$ - the road capacity of transport mode r on a radial truck arc (e, f)

R - the set of transport mode

EF - the set of intermediate transit points

J - the set of materials

For each kind of material j exists various feasible emergency dispatching schemes; that is, for each scheme at any time t arrived material no less than material demand taking t_{sj} as the emergency start time till t. Each scheme corresponds to an earliest emergency time t'_{sj}, and all earliest emergency start times form the set C'_{s_j}. Then the earliest emergency time of emergency material j is $t_{Sj} = \min_{C'sj}(S'_j)$. For one of the emergency material j dispatching schemes $F_j^p = \{(A_1, y_j^1), (A_2, y_j^2), \cdots, (A_p, y_j^p)\}$, $A_i(i = 1,2,\cdots,p)$ is the material supply point, $y_j^i(i = 1,2,\cdots,p)$ is the material quantity of the material supply point i. Then the earliest emergency time of this dispatching scheme is $t_{S_j^p} = \max[t_j^i - t_j^k] \quad i \in \{1,2,\cdots,p\}$, in which t_j^i is the required time of transporting material j from material supply point i to emergency service point. t_j^k is the duration of transport time for material j that has reached emergency point. Its value can be obtained from the type $\sum_{i=1}^{n} x_{ij}^{t_j^k} = \int_0^{t_j^k} [f_j(t)]dt$. ($\sum_{i=1}^{n} x_{ij}^{t_j^k}$ is the emergency material quantity before the time t_j^k arrives at the emergency service point, and $\int_0^{t_j^k} [f_j(t)]dt$ is the material consumption disposing sudden event at the time t_j^k).

In the above analysis, the emergency material dispatching model of the non-uniform speed material continuous consumption with multi-objectives and multi-resources is established and given as follows:

$$\min(\omega_1 \cdot f_1 + \omega_2 \cdot f_2)$$
$$f_1 = \min_{C_{S_j} \neq \phi} S_j \tag{1}$$
$$f_2 = \min \sum_{r \in R} \sum_{e \in EF} \sum_{f \in EF} CT^r \times d_{ef} \times X_{ef}^r + \sum_{j \in J} \sum_{g \in EF} \sum_{r \in R} \sum_{r' \in R} CE_g^{jrr'} \times X_g^{jrr'}$$
$$S.T. \begin{cases} \sum_{i=1}^{n} x_{ij} \geq \int_0^{t_j} f_j(t)dt \\ \sum_{e \in EF} X_{ef}^r = \sum_{r' \in R} X_g^{jrr'} + \sum_{e' \in EF} X_{fe'}^r \\ 0 \leq X_{ef}^r \leq ACAP_{ef}^r \\ X_g^{jrr'} \geq 0 \\ \omega_1 + \omega_2 = 1, \omega_1, \omega_2 \in [0,1] \\ i = 1,2,\cdots,n;\ j = 1,2,\cdots,m \end{cases}$$

OPTIMIZATION SOLUTION TO MODEL BASED ON ADAPTIVE GENETIC ALGORITHM

Since the 1980s, the genetic algorithm, the solution to complex combination optimization problems having general adaptability, has undergone rapid development and is widely used; however, the optimization of the genetic algorithm is easy to fall into local peak, i.e. convergence occurring before mature, but adaptive genetic algorithm's crossover and mutation rates (denoted by p_c and p_m) can adaptively adjust in accordance with the fitness value. When the fitness value of individual in the population tends to be uniform or tends to stick on local optimum, increasing p_c and p_m can help jump out local optimal solution. Nevertheless, when the population fitness value is quite dispersible, decreasing p_c and p_m is benefit for the fine individual survival. Therefore, adaptive crossover and mutation rates can provide the best crossover and mutation rates that relate to some solutions. AGA not only maintains population diversity but also guarantees its convergence. The adaptive parameter formula is as follows:

$$p_c = \begin{cases} p_{c1}, & f < f_{avg} \\ p_{c1} - \dfrac{(p_{c1} - p_{c2})(f' - f_{avg})}{f_{\max} - f_{avg}}, & f \geq f_{avg} \end{cases} \tag{2}$$

$$p_m = \begin{cases} p_{m1}, & f' < f_{avg} \\ p_{m1} - \dfrac{(p_{m1} - p_{m2})(f' - f_{avg})}{f_{\max} - f_{avg}}, & f' \geq f_{avg} \end{cases} \tag{3}$$

Where f_{avg} and $f_{\max}$ are the average fitness value and the maximal fitness value of the population, respectively. f' is the larger of the fitness values of two individuals to be crossed, and f is the fitness value of the individual to be mutated. p_{c1} and p_{c2} are the maximum and minimum crossover rates, respectively, and p_{m1} and p_{m2} are the maximum and minimum mutation rates, respectively.

Based on the above model, the ideal solution L^*_{1j} and L^*_{2j} under the two optimization objectives of the earliest emergency time and the least emergency

cost can be regarded as a special case when weights are $\omega_1 = 1$ and $\omega_2 = 1$. Aiming at any weight ω_1 and ω_2, this paper uses an adaptive genetic algorithm to solve the problem, the concrete steps of AGA is as follows:

Step 1: Initialize the population.
Step 2: Calculate the fitness values
including individual fitness values and average fitness values of the population.
Step 3: Compute the crossover and
mutation rates according to formulas (2) and (3).
Step 4: Execute genetic operations
including selection, crossover and mutation.
Step 5: When the current generation is less than the maximal generation, return to Step 2. otherwise, terminate the program and return to the optimal solutions.

The process is shown in Figure 2.

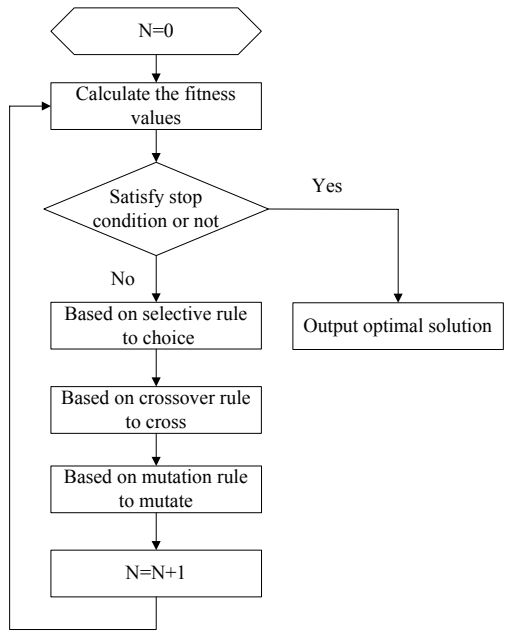

Figure 2. Flow chart of AGA.

ANALYSIS OF EXAMPLE

Suppose at point A a sudden event occurred that required two emergency materials. The numbers of material quantity are X_1 =200 and X_2 =120. Six material supply points exist, $A_1, A_2, \cdots, A_6$. The material quantity of the six material supply points and the arrival time at the emergency service point are shown in Table 2. Suppose the material demand curves are $f_1(t) = -t^2 + 10t$ and $f_2(t) = -t^2 + 4t$, respectively.

Table 2. Supply of Sites and Reach Time from Sites to Facility A.

Supply point	A_1	A_2	A_3	A_4	A_5	A_6
t_i (hour)	2	3	4	11	12	14
x_1	40	30	30	120	60	110
x_2	20	80	20	40	40	160

Assume two transport modes (I and II) can be used after the event. Figure 3 shows the transport line topological graphs. There are two numbers on the arc; the left is the arc's distance (unit: km) and the right is the arc's capacity. Suppose the carry rate of transport mode I is 300, the carry rate of transport mode II is 1,000, and the transformation rate is 260.

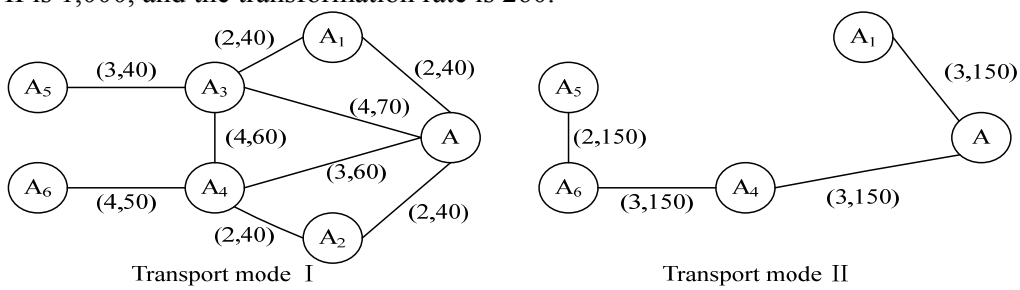

Figure 3. Transport line topological graphs.

Suppose the population size of the algorithm is 50, the maximum evolutional generation is 100. In the genetic algorithm, p_c=0.8, p_m=0.05, and in the adaptive genetic algorithm, p_{c1}=0.8, p_{c2}=0.6, p_{m1}=0.05, p_{m2}=0.005. The scheduling schemes run by MATLAB are:

$$F_1^* = \{(A_1,40),(A_2,30),(A_3,30),(A_4,60),(A_5,40)\}, \text{ and}$$

$$F_2^* = \{(A_1,20),(A_2,40),(A_3,20),(A_4,40)\}$$

The earliest emergency arrival time is 1.5 hours after the sudden event occurred. The relationship of the optimal individual fitness degree and the evolutional generation are shown in Figure 4 and Figure 5.

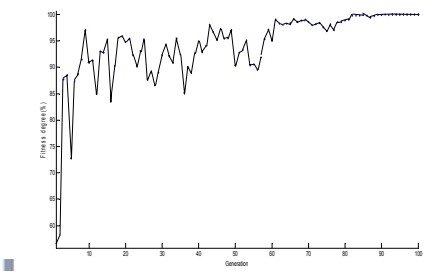

Figure 4. The result of GA.

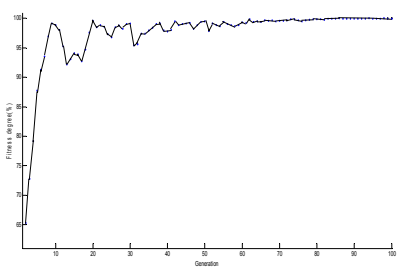

Figure 5. The result of AGA.

Comparing the above figures, the adaptive genetic algorithm has a faster convergence speed and better optimizing resistance than the genetic algorithm; thus, it proves the robustness and effectiveness of AGA, so AGA is effective for the optional solution of the model.

CONCLUSIONS

By the analysis of the adaptive genetic algorithm to the solution of model, we can obtain the optimal transportation route and optimize resource distribution. Applying the model to a practical situation realizes the process of time effects and space effects in emergency logistics and can save manpower, material resources, and financial resources. In this paper, an emergency material dispatch model is constructed under several constraint conditions, but in practicality, many constraint conditions affect emergency material dispatch, so the emergency material dispatch model should be further researched.

REFERENCES

Gong, Ying. (2005). "Study our county disaster relief logistics from Southeast Asia tsunami." *Comprehensive Transportation*, 44-47.

Huang, Jinhu. (2007). "The research and implementation of some emergency logistics key technology." *Shanghai Jiao Tong University,* Shanghai, May 11.

Lin, Chunlin, He, Jianmin and Shi, Jianjun. (2001) "The research on dispatching optimization model of the first class emergency logistics." *Management Science in China*, 11(3), 29-36.

Miao, Cheng. (2007). "The research of transportation optimization problem of emergency logistics under public emergency." *Tongji University*, Shanghai, August 20.

Hale, T., and Moberg, C. R. (2005). "Improving supply chain preparedness decision process for secure site location." *International Journal of Physical Distribution & Logistics Management*, 5, 195-207.

Zhang, Changquan, and Liu, Hong. (2008). "The implementation of adaptive genetic algorithm to solve the function optimization problem." *Software Guide*, 7(1), 152-153.

An algorithm for Vehicle Routing Problem with Soft Time Windows using Tabu Search

Lixin Zhang[1] and Huimin Niu[2]

[1]School of Traffic and Transportation, Lanzhou Jiaotong University, Lanzhou, 730070, China; email: lxzhanglixin@163.com
[2]School of Traffic and Transportation, Lanzhou Jiaotong University, Lanzhou, 730070, China; email: hmniu@mail.lzjtu.cn

ABSTRACT

The vehicle routing problem with soft time windows is studied in this paper. Multiple types of vehicles with different capacities are considered. A mixed-integer programming model subject to capacity and soft time windows constraints is formulated. An algorithm based on tabu search technique is designed to solve the developed model. Initial solution is generated by improved insertion heuristics. Finally, the developed model and algorithm are successfully tested with the help of a numerical example.

INTRODUCTION

Logistics is the process of freight transport activities that considers the social, environment, economic, financial and energy impacts of freight movement. Logistics can facilitate the implementation of cooperative freight transportation and meet various needs in supply chain management systems. The planning and design of vehicle route and service order is very important to the logistics operation process. The Vehicle Routing Problem (VRP) was proposed by Dantzig and Ramser (1959). The classical VRP involves the design of the best set of routes for a fleet of delivery vehicles based at one depot or several depots to distribute goods to a number of customers geographically dispersed, while minimizing the total travel distance or distribution cost.

In the past years, many mathematical models and algorithms have been proposed to the VRP. Solmon (1987) proposed an algorithm for the vehicle routing and scheduling problem with time windows constraints. Balakrishnan (1993) presented a simple heuristics for the VRP with soft time windows. Gendreau and Laporte (1996) proposed a tabu search (TS) heuristic for the VRP with stochastic demand and customers. Dan and Lang (2005) presented a model of multi-vehicle distribution scheduling problem based on TS algorithm. Kara et al. (2007) studied the energy minimizing VRP.

In the previous studies, the objective of VRP research mainly focuses on the total travel distance or distribution cost. However, the real cost of a vehicle traveling between two nodes also depends on the load of the vehicle. Therefore, it is more reasonable to minimize the product of the travel distance and the vehicle load. In

this paper, we proposed a new model for multi-types VRP with soft time windows to minimize the total cost, where the transportation cost is computed as the product of the travel cost per ton per kilometer, the distance traveled and the vehicle load. If the model only considers the distance as the objective, it cannot ensure which customer is served first by the vehicle in a given route. But with our model, it is ensured that the vehicle serves the nearest customer and customers with lager demand first. A TS algorithm is designed to solve the proposed model. We adopt insertion heuristics to construct the initial solution, and three different strategies to generate the neighborhood solutions.

The remaining sections of the paper are organized as follows. In Section 2, we describe the model of the multi-types VRP with soft time windows. The TS solution algorithm is presented in Section 3. And in Section 4, a numerical example is conducted to test the algorithm. Finally, we conclude the paper and outline the potential for future research in related areas.

FORMULATION

Let $G=(N,A)$ denote a network, where $N=\{0,1,\cdots,n\}$ is a set of nodes with 0 denoting the central depot and the remaining nodes representing customers, and $A=\{(i,j)\mid i,j\in N, i\neq j\}$ is a set of arcs. There is a fleet of vehicles $K=\{1,2,\cdots,m\}$ to deliver goods, and Q_k is the capacity of vehicle k. Each customer i has a demand q_i and a time window $[e_i,l_i]$, and requires a service time s_i. For the central depot, $q_0=0$ and $s_0=0$. Let C_f denote the fixed cost of dispatching a vehicle from the depot, d_{ij} the distance between customers i and j, and C_v the vehicle travel cost per ton per kilometer. We then define $C_{ij}=C_v d_{ij}$, which is the vehicle travel cost per ton along arc (i,j).

Let T_i^k be the time vehicle k arrived at customer i, T_0^k the departure time of vehicle k from the central depot, v_{ij}^k and T_{ij}^k the travel speed and travel time of vehicle k from customer i to customer j respectively. If a vehicle k does not arrive at a customer i within its time window, there will be an associated penalty cost denoted as PT_i^k, with p_e and p_l as the corresponding unit time penalty with respect to early and late arrivals respectively. We assume $0<p_e<p_l$.

Decision variable x_{ij}^k takes the value 1 if vehicle k travels directly from customer i to customer j, and 0 otherwise. Decision variable y_{ij}^k, called flow, represents the actually load of vehicle k if vehicle k travels from customer i to customer j, and 0 otherwise.

We can now state the model as follows.

$$Min \quad Z = \sum_{i=1}^{n}\sum_{k=1}^{m} C_f x_{0i}^k + \sum_{i=0}^{n}\sum_{j=0}^{n}\sum_{k=1}^{m} C_{ij} y_{ij}^k + \sum_{i=0}^{n}\sum_{k=1}^{m} PT_i^k$$

s.t.

$$\sum_{\substack{j=0 \\ j\neq i}}^{n} y_{ij}^k - \sum_{\substack{j=0 \\ j\neq i}}^{n} y_{ji}^k = q_i \qquad i \in N \setminus \{0\}; k \in K \tag{1}$$

$$y_{ij}^k \le (Q_k - q_i) x_{ij}^k \qquad i \neq j, i, j \in N; k \in K \tag{2}$$

$$y_{ij}^k \ge q_j x_{ij}^k \qquad i \neq j, i, j \in N; k \in K \tag{3}$$

$$\sum_{i=1}^{n}\sum_{k=1}^{m} x_{ij}^k = 1 \qquad j \in N \setminus \{0\}; k \in K \tag{4}$$

$$\sum_{j=1}^{n}\sum_{k=1}^{m} x_{ij}^k = 1 \qquad i \in N \setminus \{0\}; k \in K \tag{5}$$

$$\sum_{j=1}^{n} x_{0j}^k = 1 \qquad k \in K \tag{6}$$

$$\sum_{\substack{i=0 \\ i\neq h}}^{n} x_{ih}^k - \sum_{\substack{j=0 \\ j\neq h}}^{n} x_{hj}^k = 0 \qquad h \in N \setminus \{0\}; k \in K \tag{7}$$

$$\sum_{i=1}^{n} x_{i0}^k = 1 \qquad k \in K \tag{8}$$

$$T_{ij}^k = d_{ij} \big/ v_{ij}^k \qquad i, j \in N; k \in K \tag{9}$$

$$T_j^k = T_i^k + T_{ij}^k + s_i \qquad i, j \in N; k \in K \tag{10}$$

$$PT_i^k = \max\{p_e(e_i - T_i^k), 0, p_l(T_i^k - l_i)\} \tag{11}$$

$$x_{ij}^k = 0,1 \qquad i, j \in N; k \in K \tag{12}$$

In the above formulation, the objective function is composed of fixed dispatching cost, total travel cost and penalty cost. Constraint (1) is the flow conservation equation balancing inflow and outflow of each node, which also prohibits any illegal subtours. Constraint (2) ensures the capacity restriction, and that y_{ij}^k takes 0 if the arc (i, j) is not on the route of any vehicle. Constraint (3) is the lower bound for the arc flow. Constraint (4) ensures that each customer is served by one and only one vehicle. Constraint (5) ensures that after serving customer *i*, one and only one vehicle leaves. Constraints (6) – (8) ensure that all vehicles will leave and return to the central depot. Constraints (9) – (11) compute the penalty cost associated with early or late arrivals. Constraint (12) defines that decision variable x_{ij}^k is a binary variable.

SOLUTION ALGORITHM

Considered the characteristics of multi-types vehicles, the solution is a combination of the sequence of customers served by a vehicle and the corresponding loads at each customer node.

Initial solution. The calculation formula of the maximum and minimum

numbers of the vehicles needed is as follows:

$$\min_v = \left\lfloor \frac{\sum_{i=1}^{n} q_i}{\max_{1\le k\le m}\{Q_k\}} \right\rfloor + 1, \quad \max_v = \left\lfloor \frac{\sum_{i=1}^{n} q_i}{\min_{1\le k\le m}\{Q_k\}} \right\rfloor + 1$$

An integer as the initial number of vehicles is randomly selected from the interval $[\min_v, \max_v]$. We employ insertion heuristics to construct the initial solution. The feasibility of inserting customer j between $i-1$ and i can be checked by $q_i \le Q_k - q_r^k$ (q_r^k denote the sum of the delivery quantities currently assigned to the route of vehicle k). We add a vehicle to carry the rest goods if the delivery cannot be accomplished by those selected vehicles.

Neighborhood structure. We generate neighborhood solutions using three operations, namely the interchanging, the exchanging and the inserting operations.

In interchanging operation, we switch the orders of two randomly selected customers in a given route. For example, supposed we have a route 0-1-3-5-2-0, and the two elements of random selection are 1 and 2, the new route after the interchanging operation is then 0-2-3-5-1-0.

In exchanging operation, we randomly select one customer each from two different routes, and switch their positions. For example, suppose we select customer 3 from route 1, 0-1-3-5-2-0, and customer 4 from route 2, 0-6-7-4-0. The new routes after exchanging operation are 0-1-4-5-2-0 and 0-6-7-3-0.

In inserting operation, we remove a segment in one route and insert it into another route. Supposed the elements of random selection are as above, we then move nodes 1, 3 from route 1 to route 2. The new routes are denoted by 0-5-2-0 and 0-6-7-1-3-4-0.

Short memory and related parameters. A number of neighbor solutions of the current solution are generated as candidate solutions. The tabu list is composed of three parts: the type of the strategy, the tabu nodes and the mark (0 or 1) that represents whether the tabu solution is improved or not. The algorithm maintains two types of tabu lists: the local and the global tabu list. Local tabu lists record the tabu nodes generated by the three different strategies respectively, And the global tabu list records the common tabu nodes. The size of the tabu list is fixed. The aspiration level is based on the rule of search directions. The algorithm will stop if the best solution remains the same in a given step. The fitness function is calculated according to the following relationship.

$$f = Z + \alpha \cdot \max\{\sum_{j=1}^{n} (y_{0j}^k - Q_k x_{0j}^k), 0\}$$

where α is a lager positive number.

NUMERICAL EXAMPLE

In our numerical example, we assume that there are 8 customers to be served, and there are two types of vehicles with capacities of 10 and 8 respectively. The travel speed of any vehicle is 50km/h. The fixed cost is 10 and the travel cost per ton per kilometer is 2. The time penalty factors are set to $p_e = 100$ and $p_l = 200$.

Table 1 further shows the demand, service time, time window, and coordinates (X, Y) of each customer.

Table 1. Demand, Service time, Time windows and Coordinates

	0	1	2	3	4	5	6	7	8
q_i	0	2	1.5	4.5	3	1.5	4	2.5	3
s_i	0	1	2	1	3	2	2.5	3	0.8
$[e_i, l_i]$	[0,24]	[1,4]	[4,6]	[1,2]	[4,7]	[3,5.5]	[2,5]	[5,8]	[1.5,4]
X	35	41	55	55	15	25	20	10	55
Y	35	17	45	20	30	30	50	43	60

In order to evaluate the effectiveness of the TS algorithm, a genetic algorithm (GA) is also proposed. The proposed algorithms are coded with MATLAB in the Windows environment. Two cases of the problem are solved, one with total distance as the objective function and the other with total cost. The purpose of the former case is to validate our model.

The computational results of both cases are presented in Table 2. Column "Pop" reports the size of the initial population used in GA. The cross probability and mutation probability are set to 0.8 and 0.05 respectively in GA. Column "N" presents the size of the tabu list in TS. We stop the TS algorithm if the objective value is not improved any more within 20 iterations. We conduct multiple runs to compare the two algorithms, and the total number or runs is reported under column "Tn". Columns "Max" and "Min" are the maximum and minimum objective values observed in the multiple runs. Column "MinD" reports the total distance of the optimal solution obtained with respect to the total cost.

Table 2. Computational Results

	Pop	N	Total Distance				Total Cost				
			Tn	Max	Min	Time(sec)	Tn	Max	Min	MinD	Time(sec)
GA	50		18	486.94	480.70	16.5	18	1591.59	1488.90	548.16	18.4
	100		18	480.70	446.46	29.2	18	1591.59	1484.29	431.87	31.0
	200		18	480.70	429.25	55.4	18	1583.99	1481.23	574.99	60.0
		3	18	457.89	429.25	5.6	18	1497.53	1474.91	429.25	4.3
TS		7	18	446.47	429.25	11.3	18	1497.53	1474.91	429.25	10.8
		9	18	434.45	429.25	15.4	18	1573.93	1474.91	429.25	14.9

The comparison indicates that TS performs better and is more efficient. GA also leads to acceptable solutions, but the search time is much longer compared to TS. TS is a good algorithm for this problem in terms of both the computation time and the quality of the solution. Although TS is more complicated to design than GA is in order to reduce the computation time, TS has a great advantage in dealing with optimization problems with complex constraints. Therefore, TS might be the best solution algorithm for VRP with soft time-window constraints.

CONCLUSION

In this paper, a model for multi-types VRP with soft time windows is proposed, where the vehicle loads are treated as decision variables. A TS algorithm

with insertion heuristics is designed. The major contributions of this paper are the incorporation of vehicle load decision variables in the model and the application of insertion heuristics in the solution algorithm. Our future research will take into account more realistic settings such as multi-costs and dynamic environment. This may lead to more valuable and practical models of VRP.

REFERENCES

Balakrishnan, N. (1993) "Simple heuristics for the vehicle routing problem with soft time windows". *Journal of the Operational Research Society,* 44(3), 279-287

Campbell, A. and Savelsbergh, M. (2004). "Efficient insertion heuristics for vehicle routing and scheduling problems". *Transportation Science*, 38(3), 369-378

Dan, H. B. and Lang, M. X. (2005). "Study on the model and its Tabu search algorithm for the JD multi-vehicle distribution scheduling problem". *Journal of Changsha Communications University*, 21(3), 73-77

Gendreau, M. and Laporte, G. (1996). "A Tabu search heuristic for the vehicle routing problem with stochastic demand and customers". *Operations Research*, 44(3), 469-477

Kara, I., Kara, B. Y., and Kadri, Y. M. (2007). "Energy minimizing vehicle routing problem". *Lecture Notes in Computer Science*, 4616, 62-71

Solomon, M. (1987). "Algorithms for the vehicle routing and scheduling problem with time windows constraints". *Operations Research*, 35(2), 254-265

Research on Dynamic Safety Stock Based on Short-Term Weather Forecasting

Wei Liu[1,2], Shuzhi Zhao[1], Wei Wang[1], Bo Peng[1,3]

[1]Transportation College of Jilin University, 5988 Renmin Street, Changchun, Jilin Province, China 130022; PH (431)13504466433; email: wwei@jlu.edu.cn
[2]Management Service Department of FAW-VW, 5 Anqing Road, Changchun, Jilin Province, China, 130000; PH (431)85750092; email: Wei.liu.ms@faw-vw.com
[3]Jilin Public Security Academy, 1399 Boshuo Street, Changchun, Jilin Province, China 130000; PH (431)13944138928; email: wispy76@163.com

ABSTRACT

Based on requirements and short-term weather forecasting, this paper presents a model to calculate dynamic safety stock in MRP (Materials Requirements Planning). Through the setting of dynamic safety stock and advance orders, the model can lower risks in the decline of dynamic safety stock, which may be caused by delivery delay due to weather factors, making the stock better meet our needs and improving the competitiveness of enterprises.

INTRODUCTION

Factors such as market-requirement trends, season, and circle should normally be taken into account in the requirements plan of an enterprise (Hao, 2005; Ho, 2001). For some special parts, an enterprise may increase the safety stock in MRP (Materials Requirements Planning) calculation to meet the timely production in the MRP system.

In reality, safety stock is generally fixed when the supplier's plans for goods in the MRP system are generated, and the risks of decline of dynamic safety stock are ignored, which may cause delivery delay due to weather factors. Rain and fog in the summer significantly affect highway transportation in the south of China, and ice and snow in winter also cause the highway transportation cycle to be lengthened in the north. If the system uses a fixed lead time, the goods may not arrive on time.

This paper takes the highway transportation into consideration and presents a method based on short-term weather forecasting that can dynamically change safety stock and the leading pre-ordered safety stock so as to maintain parts inventory levels. This method ensures that an enterprise will better meet production needs by using leading safety stock even if weather is a factor. As demand is a rolling demand, the supply plan must also be dynamic, so even if high-safety stock is reduced in the next cycle as a result of weather forecasting in the former cycle, the dynamic safety stock would not lead to a high inventory level for long.

DIVISION OF CYCLES IN PROSPECTIVE WEATHER FORECASTING AND THE CALCULATION OF AVERAGE IMPACT FACTORS

In practice, the supply plan generated from the MRP can often be categorized as short-term, medium-term, and long-term. A specific division of time must be set in accordance with the actual situation of the enterprise (Ho, 2001). Normally, a short-term supply plan is an accurate requirements plan; the supplier must provide the goods according to accurate requirements. The medium- and long-term plans can be taken as a forecasting; the supplier must prepare for production according to the forecast. In a short-term supply plan, goods are generally supplied by the week (Xie, 2006; Yu, 2005). This is taken into account for this paper.

Future weather forecasting cycles also can be categorized into short-term, medium-term, and long-term. In short-term weather forecasting, the cycle is divided by the week. According to the characteristics of highway transportation, weather factors that affect the transport cycle can be summarized as Rainfall (R), Fog (F), Snow (S), and Wind (W). Through EDI, information on future weather forecasting can be obtained from the weather bureau; these data can be brought into the system, or an individual weather forecasting database can be established for analysis.

Each weather factor is ranked according to the degree it affects the transport cycle: Rainfall R (0~1), Fog F (0~1), Snow S (0~1), and Wind W (0~1); 0 is the weakest influence, while 1 is the strongest .

Suppose the weather factors of the day are R_j, F_j, S_j, W_j. Each weather factor is ranked by a weight according to the degree it affects the transport cycle. Supposed the weights are PR_j, PF_j, PS_j, PW_j. With the weighted average method, we obtain the average impact factor.

$$G_i = \sum_{j=1}^{7} (R_j * PR_j + Fj * PF_j + S_j * PS_j + W_j * PW_j) / 7$$

$$\text{Restrict: } \begin{array}{l} 0 \le R_j \le 1 \quad 0 \le PR_j \le 1 \\ 0 \le F_j \le 1 \quad 0 \le PF_j \le 1 \\ 0 \le S_j \le 1 \quad 0 \le PS_j \le 1 \\ 0 \le W_j \le 1 \quad 0 \le PW_j \le 1 \\ PR_j + PF_j + PS_j + PW_j = 1 \end{array} \qquad (1)$$

Weights should be dynamically set up to the actual situation in light of MRP. Because it rains a lot in summer, rainfall has a larger weight; it snows a lot in winter, so the weight of snow is larger. According to the method above, the short-term average impact factor per week can be calculated as G_i; it ranks from 0~1. According to the degree it affects, G_i can be divided into grading intervals [0~0.3], [0.4~0.6], [0.7~1]. The weight that each interval affects the supply can be defined as $T_i (i = 1, 2, 3)$, where $T_1 + T_2 + T_3 = 1$. The weights can make some adjustments to the actual situation before the operation of MRP (Xu, 2004).

DYNAMIC SAFETY STOCK CALCULATION MODEL BASED ON SHORT-TERM WEATHER FORECASTING

Suppose the order cycle time is $W_i(1,2,3\ldots\ldots n)$, where n presents the weeks of the short-term order; we can define the main production plan of each cycle $M_i(1,2,3\ldots\ldots n)$, the average weather impact factor, $G_i(1,2,3\ldots\ldots n)$ and the corresponding weights of each level $T_j(j=1,2,3)$, so the dynamic safety stock calculation model are as follows (Figure 1):

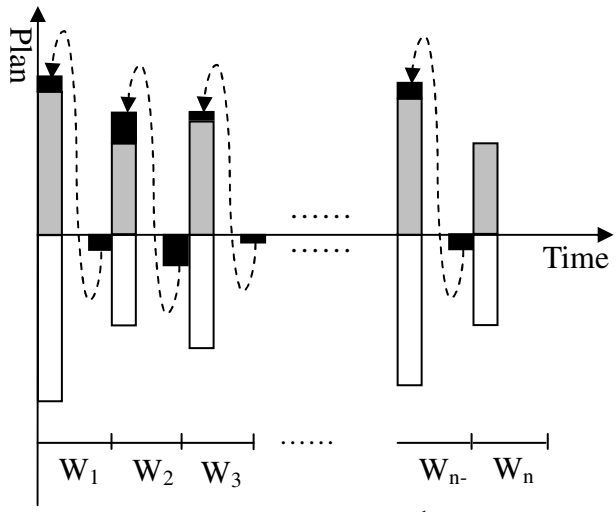

Gross requirements.
Requirements plan except for dynamic safety stock after MRP
Dynamic safety stock in the next cycle
Requirements plan including the dynamic safety stock of the next cycle

Figure 1. Sketch map for the dynamic safety stock model.

1) According to the main production plan MPS and the BOM (Bill of Materials) structure of the products, the gross requirements plan $D_i(i=1,2,3\ldots\ldots n)$ of the parts in each cycle can be obtained (Rabinovich, 2002).

2) Calculating in MRP, we take into consideration the lot-sizing strategy of lot-for-lot and the actual physical inventory. Then an accurate requirements plan $L_i(i=1,2,3\ldots\ldots n)$ in each cycle of the short-term can generated.

3) According to the requirements plan, the average weather impact factor, and the corresponding weights of the coming week, the dynamic safety stock $S_i(i=1,2,3\ldots\ldots n)$ caused by weather can be calculated, where

$$\begin{aligned} S_1 &= L_2 * G_2 * \{T_1 \mid T_2 \mid T_3\} \\ S_2 &= L_3 * G_3 * \{T_1 \mid T_2 \mid T_3\} \\ S_3 &= L_4 * G_4 * \{T_1 \mid T_2 \mid T_3\} \\ &\cdots\cdots \\ S_{n-1} &= L_n * G_n * \{T_1 \mid T_2 \mid T_3\} \end{aligned} \qquad (2)$$

4) Define the requirements plan in each cycle of the short-term $P_i(i=1,2,3\ldots\ldots n)$, Where

$$\begin{aligned} P_1 &= L_1 + S_1 \\ P_2 &= L_2 + S_2 \\ P_3 &= L_3 + S_3 \\ &\cdots\cdots \\ P_{n-1} &= L_{n-1} + S_{n-1} \\ P_n &= L_n \end{aligned} \tag{3}$$

CASE ANALYSIS

Suppose the four-week main production plan of product A is $M_i(1,2,3,4) = (100,200,100,300)$. The BOM structure is as follows (Figure 2):

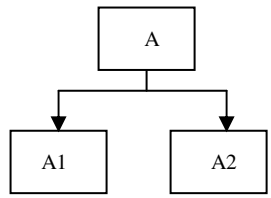

Figure 2. BOM structure of product A.

According to the MPS and BOM of product A, we can draw the four-weeks gross requirements plan of part A_1, $D_i(1,2,3,4) = (100,200,100,300)$.

Suppose the requirements plan except for the dynamic safety stock after MRP is $L_i(1,2,3,4) = (90,195,101,293)$.

Suppose G_i ranks in [0~0.3] in the weight for $T_1 = 0.2$ [0.4~0.6] in the weight for $T_2 = 0.3$ [0.6~1] in the weight for $T_3 = 0.5$.

Calculations for the supply plan for the first week need to consider the dynamic safety stock caused by weather factors in the second week, so the weather forecasting information of the 2-4 weeks obtained from the Bureau of Meteorology through EDI is shown in Table 1.

0.6/0.4 means the grade of rainfall is 0.6, and the corresponding weight is 0.4, so the average impact factor and its corresponding weight of the 2-4 weeks can be calculated according to formula (1): $G_2 = 0.16$

weight of the corresponding grade $T_1 = 0.2, G_3 = 0.13$

weight of the corresponding grade $T_1 = 0.2$ $G_4 = 0.06$

weight of the corresponding grade $T_1 = 0.2$

According to formula (2), the calculated safety stocks of each week are as follows:

$$\begin{aligned} S_1 &= L_2 \times G_2 \times T_1 = 195 \times 0.16 \times 0.2 \approx 6 \\ S_2 &= L_3 \times G_3 \times T_1 = 101 \times 0.13 \times 0.2 \approx 3 \\ S_3 &= L_4 \times G_4 \times T_1 = 293 \times 0.06 \times 0.2 \approx 4 \end{aligned}$$

Table 1. Weather conditions of every day in the fourth week.

Week	Rainfall	Fog	Snow	Wind
2	0.3/0.3	0/0.4	0/0.1	0.1/0.2
	0.4/0.3	0/0.4	0/0.1	0.2/0.2
	0.6/0.3	0/0.4	0/0.1	0.4/0.2
	0/0.3	0/0.4	0/0.1	0.5/0.2
	0/0.3	0.6/0.4	0/0.1	0.1/0.2
	0/0.3	0/0.4	0/0.1	0/0.2
	0.7/0.3	0/0.4	0/0.1	0.2/0.2
3	0.5/0.3	0/0.4	0/0.1	0.3/0.2
	0.4/0.3	0/0.4	0/0.1	0.2/0.2
	0.1/0.3	0/0.4	0/0.1	0/0.2
	0/0.3	0.4/0.4	0/0.1	0/0.2
	0/0.3	0.6/0.4	0/0.1	0/0.2
	0/0.3	0/0.4	0/0.1	0.2/0.2
	0/0.3	0/0.4	0/0.1	0/0.2
4	0/0.3	0/0.4	0/0.1	0.2/0.2
	0/0.3	0/0.4	0/0.1	0/0.2
	0/0.3	0/0.4	0/0.1	0/0.2
	0/0.3	0.6/0.4	0/0.1	0/0.2
	0/0.3	0/0.4	0/0.1	0/0.2
	0.5/0.3	0/0.4	0/0.1	0.2/0.2
	0.2/0.3	0/0.4	0/0.1	0/0.2

According to formula (3), the requirements plan of each week combined with the dynamic safety stock of the former and the coming week could be calculated as follows:

$$P_1 = L_1 + S_1 = 90 + 6 = 96$$
$$P_2 = L_2 + S_2 = 195 + 3 = 198$$
$$P_3 = L_3 + S_3 = 101 + 4 = 105$$
$$P_4 = L_4 = 293$$

We can draw that the total order quality regardless of weather is $L_1 + L_2 + L_3 + L_{34} = 90 + 195 + 101 + 293 = 679$; the four-week total order quality in consideration of the dynamic safety stock is $P_1 + P_2 + P_3 + P_4 = 96 + 198 + 105 + 293 = 692$. With an increase of 2%, the part of the safe stocks can temporarily meet the demands under some special condition.

CONCLUSION

Based on weather forecasting data, this paper presents a model that dynamic safety stock can be calculated through the use of average weather impact factors and their corresponding weights. The additional safety stocks calculated from the model were added to the requirements plan of the former cycle, so that the risks in decline of dynamic safety stock which may be caused by delivery delay due to weather factors would be reduced through advance orders of safety

stock; meanwhile, the increased resilience ensures the continuity and timeliness of the parts supply. As demand is a rolling demand, the supply plan must also be a dynamic one, so that high-safety stock is reduced automatically in the next cycle as the result of the inaccuracy brought on by weather forecasting in the former cycle.

REFERENCES

Hao, Gang, and Wu, Gongyi. (2005). "Research on the MRP based on dynamic lot size and lead time." *Computer Engineering and Applications,* 200515, 230-232.

Ho, C. J., and Chang, Y. (2001). "An integrated MRP and JIT framework." *Computers &Industrial Engineering,* 41,173-18.

Rabinovich, E., and Evers, T.P. (2002). "Enterprise-wide adoption patterns of inventory management practices and information systems." *Transportation Research Part E,* 38, 389-40.

Xie, Qinhua, and Sun, Xianjin. (2006). "Improvements to the design of MRP systems." *Industrial Engineering,* 7(2), 21-24.

Xu, Junzeng, and Peng, Shizhang, (2004). "Neural network model for reference crop evapotranspiration prediction based on weather forecast." *Shuili xuebao,* 37(3), 376-379.

Yu, Liang Liang, Yu, Gang, Wang, Zhiqiang, and Xue, Kean. (2005). "A method of lot-sizing decisions in MRP." *System Engineering Theory Methodology Applications,* 14(1), 74-79.

Study of Operational Characteristics of HAZMAT Vehicles Based on GPS Data

Liu Zhenguo[1], Shi Xiaofa[2] and Hui Ying[3]

[1]School of Transportation Engineering, Tongji University, Shanghai 200092, China; PH(8621)-69585245; email: loe211@163.com
[2]School of Transportation Engineering, Tongji University, Shanghai 200092, China; email: xfshi999@163.com
[3]School of Transportation Engineering, Tongji University, Shanghai 200092, China; email: huiying1975@hotmail.com

ABSTRACT

The transportation of hazardous materials (HAZMAT) is a growing problem worldwide due to increasing transportation volumes. In this paper, the problems of risk assessment methods and the characteristics of hazmat vehicles are discussed. This research is based on a case study in Shenzhen, China. The operation data is acquired with global positioning system (GPS) data acquisition technology. The characteristics of hazmat transportation are obtained through analyzing the vehicle operation characteristics changing by time and space, and the relationship between the hazmat transportation route and urban transportation system. With the conclusions above, the paper gives some advice to support the Government's decision-making about the assessment of the transport risk for hazmat and the planning of the hazmat transportation.

KEYWORDS: hazmat vehicles, GPS data processing, risk assessment, operational characteristics

1. INTRODUCTION

Hazardous materials transportation is a special logistic. Hazardous materials, or dangerous goods, include explosives, gases, flammable liquids and solids, oxidizing substance, poisonous and infectious substance, radioactive materials, corrosive substances, and hazardous wastes. Clearly hazmat transport is an essential component of the nation's freight transportation system.

At the same time, the transportation of hazardous materials (hazmat) is a growing issue worldwide due to the increasing transported volumes. Once a spill occurs during the hazardous materials transportation, it has the potential for great danger which could spread to an enormous area, threaten residents' lives and property, as well as damaging important facilities of communication, electric power and transportation.

In recent years, the Floating Car Data (FCD) is used more and more as an advanced method to get real-time traffic information on the road (Bowen Du, 2008).

For example, in Shenzhen, the city's taxis, buses and hazmat vehicles are all installed with GPS.

With the development of the city intelligent traffic information platform, the authority has a conditional ability to combine GPS information of all logistics firms. Therefore the massive data of the hazmat vehicles may be obtained, which reflect the running characteristics of the vehicles.

This paper is organized as follows: Section 2includes a review of existing related research of hazmat transportation, then describes the problem of calculating the risk. In Section 3, the methods of processing the GPS data are introduced. In Section 4, an analysis of the operation characteristics of the hazmat vehicles in the City of Shenzhen is conducted, with GPS data obtained from the control center. This is followed by some concluding remarks in Section 5.

2. RELATED RESEARCH

2.1 Risk Assessment

The difference between the shipments of hazmat and other materials is the risk associated with an accidental release of these materials during transportation. Almost all the research of hazmat transportation is associated with risk assessment and route selection.

It is common to define the risk of hazmat transport as the consequences of the incident and the probability of the incident. Generally, the consequences of the incident is proportional to the size of the neighborhood population of the incident, where the size of the neighborhood depends on the substance carried; and the probability of an incident occurring depends on the substance carried and the road circumstances.

Using the traditional risk definition (E.Erkut, 1998), the risk of transporting hazmat B over a road link A can be written as:

$$R_{AB} = P_{AB} C_{AB}$$

where

P_{AB} = probability of an incident on the unit road link A for hazmat B, and

C_{AB} = population along the unit road link A within the neighborhood associated with hazmat B.

A path is a collection of several links. Hence, we can express the risk of transporting a pre-specified hazmat along path P as follows:

$$R(P) = \sum_{i \in P} P_i C_i$$

The above formulas show the basic sample model of calculating the risk. In general, we tend to find a path with the lowest level of risk. Risks imposed on the residents living near transport routes can be reduced by explicitly taking the risk of the shipments into account in selecting routes. Thus, the risk minimization problem can be solved by using a shortest path algorithm.

With the development of the research, many factors, such as weather, time, and the distance from the hospital, are taken into account. It is easy to see that risk assessment of hazmat transportation is data intensive and its analysis requires several data sources such as: population density, value of property and environment that could be impacted by a hazmat truck release, and impact radius by hazmat type. However, it was difficult to obtaining all of the data sources. First, it is quite unrealistic to expect the generation of these data sources for all links of a network. Second, the human dose-response for many toxic chemicals is not known; and third, several link attributes, such as the wind direction, the traffic volume and the population in the neighborhood, usually changed by the time (William Carl Frank, 2001).

In China, we don't have the exact information since the GIS platform is not built in many cities. Furthermore, many basic data sources such as the accident rates of the specific road have not been recorded. Meanwhile, a great number of new roads have been built and accident records for these roads are not available. All of the above situations demonstrate that estimating the exact risk of all the links is an impossible task.

2.2 Hazmat Vehicles

In view of the special circumstances of hazmat vehicles, the Department of Transportation regulates hazmat transportation in many countries. The most famous regulation is the European Agreements concerning the international carriage of Dangerous Goods by Road (ADR). ADR has developed many of the technical specifications of the vehicles such as the electrical equipment, the braking equipment and the prevention of fire risks. In China, we also have such regulations. The trucks carrying flammable, explosive or toxic materials over 2 tons are required to install a compression ignition engine and speed limiting device. The maximum speed of a limiting device should be lower than 90 km/h. Many vehicle manufacturers, such as VOLVO, are making features like electronic braking systems (EBS), anti-brake lock system (ABS), air suspension, and GPS equipment that meet ADR regulations. These updates of the vehicle structure will certainly impact the operation characteristics.

Past studies have not sought to address the characteristics of the hazmat vehicles. Ren Changxing & Wu Zongzhi found that traffic accidents were a leading cause of hazmat transport spills, and they happened in a certain random manner through the statistical analysis on 200 typical road transportation accidents of hazmat in China. This paper is confined to considering the risk imposed on hazmat vehicle operation characteristics and the relationship between the hazmat transportation route and urban transportation systems.

3. PROPOSED METHODS AND ILLUSTRATIVE EXAMPLES

Having discussed the methods and the problems of risk assessment, the methods of analyzing the GPS data is discussed. In this section, the data processing

is divided into several steps.

3.1 Data Sources

The GPS data was obtained from the hazmat vehicles equipped with GPS from the Traffic Control Center. Table 1 shows the GPS data format of the hazmat vehicles in Shenzhen.

Table 1. GPS data format of the hazmat vehicles

Field	Examples
Date	20060405
Time	150236
Vehicle ID	13510232563
Firm ID	H
Longitude	114.114117
Latitude	22.550917
Velocity (km/h)	66
Azimuth angle	4
Operation status	1
Usefulness	True/False

3.2 Data Preprocessing

The data preprocessing mainly includes two aspects: excluded invalid data and coordinate transformation.

Invalid data was excluded: (1) when the equipment is under abnormal status or the data when the longitude or the latitude is beyond the scope of the road network; (2) when the velocity is zero since the intent was to analyze the operation characteristics on the road.

Coordinate transformation included transforming the longitude and the latitude of the vehicle data sources, making it consistent with the road network coordinate system.

3.3 Map Matching

Map matching is a method of using digital map data and GPS data to locate the vehicles position relative to the digital map. In general, the vehicle location is not necessarily on the road of the digital map. We try to filter the unreasonable GPS data and remove the biases of GPS signals by using a map-matching system.

After the map matching process, the next work is to match the trajectory of the vehicles data with the corresponding links in the digital map. Since the sampling interval of most GPS data is 30 to 60 seconds, the assumption was made that the vehicle travels along the shortest path between two points in our algorithm. The whole process is carried out by the program through the combination between Visual Basic and Map Object.

3.4 Spatial Distributions of Hazmat Vehicles

By analyzing the GPS data generated by hazmat vehicles from 9:00AM

to11:00AM on Tuesday May 13, 2008 in Shenzhen, 50460 useful data records of 3298 links were obtained.

The distribution of the hazmat vehicles in road networks in Shenzhen are given in Figure 1. It is shown that hazmat vehicles mainly concentrate on the expressway and arterial roads around the city. The roads that connect the harbor to the city are also the main corridor for hazmat transportation.

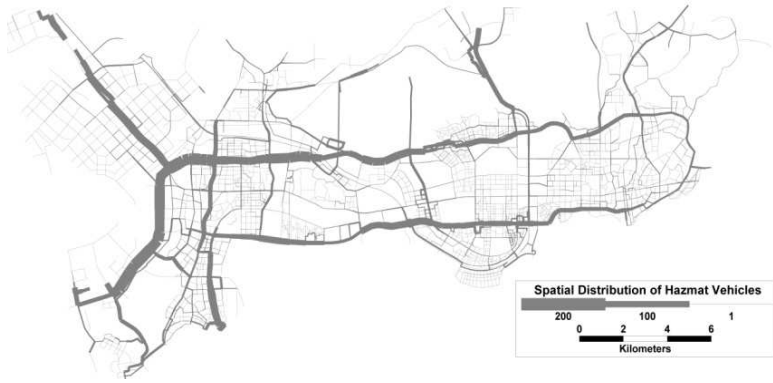

Figure 1. The spatial distribution of hazmat vehicles

Figure 2 shows the distribution of the hazmat vehicles in different road types in Shenzhen. Because of the limitation of the data source amount, 50460 links covered by vehicles trajectories, which account for 67.6% of all road links in the digital map, are collected.

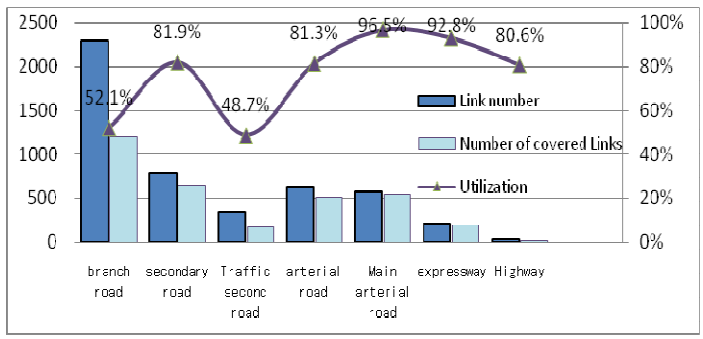

Figure 2. The distribution of hazmat vehicles of different road types

We define utilization as the number of links covered by trajectories according to a certain amount of historical data. It can be seen from Figure 2 that the arterial roads and expressway account for low percentage but high utilization; the circumstances of the secondary roads and the brand roads perform the opposite. In the analysis of the historical data, the trajectories cover the majority of the expressway and the arterial road. The distribution of hazmat vehicles in different road types is consistent with our previous analysis. The distribution of hazmat transportation reflects the authority's management policies at a certain extent.

3.5 Travel Speed of Hazmat Vehicles

After the process of map matching, the trajectory data of the vehicles on the digital map is obtained. The travel speed of each link can be determined since the

time interval of two adjacent points is known.

When studying the running characteristics of certain types of vehicles, the most important indicator is the travel speed. Travel speed impacts the two most important objectives of hazmat vehicles directly – efficiency and safety (see Figure 3).

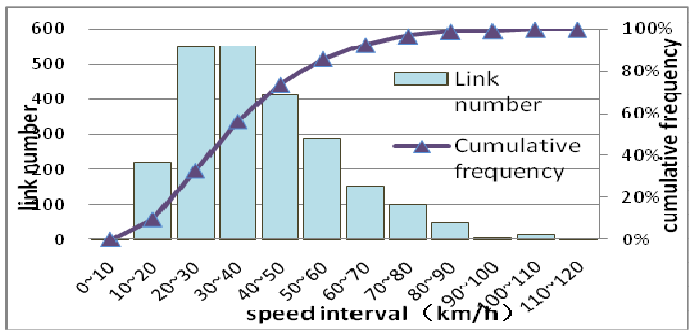

Figure 3. The accumulation histogram of travel speed

We find that most of the link speeds are below 50km/h, the speed between 30km/h and 50km/h account for nearly 60% of all records.

As is shown in Figure 4, the ring line and the roads connecting the conglomerations of the city have a high speed. The roads that connect the harbor to the city and the city roads have a relatively lower speed. Generally, they appear to have a similar characteristic with the spatial distribution.

Figure 4. The distribution of the average speed in the network

The percentage of speed interval on different road types in the road network is quite different. Figure 5 is the distribution.

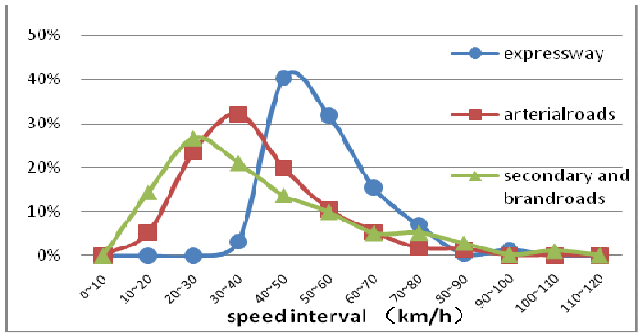

Figure 5. The distribution of vehicle speed of different road types

It can be seen from this figure that the three road types present an arithmetic progression. The speeds of different roads are consistent with the road type. Their average speeds are 50km/h, 40km/h and 30km/h separately. The speed is relatively lower than the cars on the city road.

There are many reasons for the speed difference between hazmat vehicles and cars. Hazmat vehicles are typical large goods trucks and their design speed is much lower than cars, which will lead to the speed difference on the road. Also, the transportation regulations in many countries also specify the requirements of the structure and other ancillary facilities of the hazmat vehicles.

5. CONCLUSIONS

By analyzing the GPS data of hazmat vehicles, the operation characteristics of hazmat vehicles in Shenzhen were obtained. In addition, the identification of spatial distributions and travel speed of hazmat vehicles in the network were acquired. It was determined that the assumption of the risk may also be generalized to incorporate more realistic approaches depending not only on the type of hazmat and the road attributes but also on the operation characteristics of hazmat vehicles.

As the hazmat vehicles mainly concentrate on several road types in the urban network, the authority should pay special attention to these roads; yet it is reasonable for the authority to make some roads of the city inaccessible to truck traffic at different times of the day, which may improve the traffic order of the hazmat transportation, and reduce the accident rate to a large extent. Continued research in the future will analyze other types of vehicles in the road network, which may enable us to find the difference of operation characteristics between hazmat vehicle and other vehicles.

REFERENCES

Bowen Du, Leishi Xu, Dianfu Ma, Weifeng Lv, Tongyu Zhu (2008), “Missing Data Compensation Model in Real-Time Traffic Information Service System", *Fifth International Conference on Fuzzy Systems and Knowledge Discovery*, 371-378.

E. Erkut, and V. Verter (1998) "Modeling of Transport Risk for Hazardous Materials", *Operation Research*, 46(5), 625-642.

Liu Baixiu, Li Gang, Xiao Dianliang ,Liu Saihua(2008), "Analysis on Causes for Truck Accidents on Highway and Special Lane for Trucks", 18(4),157-162.

Ren Changxing, Wu Zongzhi (2007),"Progress of risk assessment and optical routing for hazardous materials transportation by road”, *Journal of Safety and Environment*, 7(3), 127-131.

William Carl Frank (200), *Hazardous Material Vehicle Routing Utilizing a Decision Support System and Temporary Road Attributes*, Ph. D. Dissertation, the State University of New York at Buffalo.

Risk Evaluation Model for Construction of a Logistics Park Based on Principal Component Analysis

Yuzhou Wang[1,2], Qing Huang[1], Bin Chen[3], Dewu Liu[2]

[1]College of Logistics, Southwest Jiaotong University, Chengdu 610031, China; PH (+86) 28-89135700; FAX (+86)28-82680899; email: wangyzcd@163.com
[2]Department of Economy & Management, Sichuan Vocational and Technical College of Communications, Chengdu, Sichuan 611130,China; PH (+86) 28-82680899
[3]Sichuan College Key Laboratory of Road Traffic Safety, Sichuan Vocational and Technical College of Communications, Chengdu, Sichuan 611130, China; PH(+86) 28-82680060

ABSTRACT

Construction of a logistics park has a high risk because of large investment, a long development cycle, etc., and it is influenced by many factors. The failure of logistics park construction can cause large losses, which are difficult to restore. This paper builds an index system on risk evaluation for construction of logistics parks and discusses the problem of how to determine overall risk using individual risk in the risk evaluation. A risk evaluation model is also presented with a concrete example based on principal component analysis by the MATLAB function.

Key words: Logistics park; construction project; risk evaluation; principal component analysis (PCA); model; index system

INTRODUCTION

Logistics parks, which first appeared in Tokyo in 1965, are of great significance for improving logistics at the organization level and intensification degree. In recent years, a logistics park construction wave has emerged rapidly in China. The construction of logistics parks has the following characteristics: large scale land purchase and investment, long development cycle, high specification, long payback period, etc. The failure of logistics park construction can cause large losses over a long period, which are difficult to restore. Risk evaluation and management have become key factors in the success of such construction projects.

Many scholars at home and abroad have presented the concept of risk management for construction projects (Buchan 1994; Miller and Lessard 2000) and have achieved valuable results in theoretical research on risk evaluation methods, such as fuzzy synthetic evaluation (CUI et al. 2002), AHP (Wang et al.2004), ANN (Yang et al. 2004), PERT (Li,2007). Risk grade is determined after the risks occurred in these methods. As a result, there are more disparities between conclusions and the actual state.

This paper presents a risk evaluation index system based on the multi-dimension, multi-layer, and comprehensiveness of logistics park construction connotation referred to in the existing literature on the subject. The paper also presents a risk evaluation model for logistics park construction with a concrete example based on PCA using the MATLAB function, which provides a new idea and approach to risk evaluation of logistics park construction.

ESTABLISHMENT OF INDEX SYSTEM FOR RISK EVALUATION

An index system is the foundation for determining whether the outcome of an evaluation is scientific or not. To establish a scientific risk evaluation index system for logistics park construction, we should consider not only comprehensiveness, systematics, and operability as the index design principles, but also take into account the practical application of methods. Hence, we designed and screened out 15 specific indicators for a risk evaluation index system for logistics park construction from five aspects (Table 1). This was done by analyzing the risk factors for logistics park construction and consulting many experts who having rich practical experience using the Delphi method and by referring to a large number of previous studies.

Table 1. Risk Evaluation System for Logistics Park Construction.

Construction Project Risk of Logistics Park(***A****)*	*Risk of Project Procedure* ***B1***	Macro-control policies related to the construction and the development (X_1)
		Transacting relevant procedures and linking up each necessary content (X_2)
	Environmental Risk ***B2***	Engineering geology and hydrogeology (X_3)
		Planning or design adjustment (X_4)
		Extranet auxiliary projects (water supply and drainage, electricity, transport, etc.) (X_5)
	Economic Risk ***B3***	Materials and equipment prices rise (X_6)
		Working period adjustment (X_7)
		Change of engineering quantity (X_8)
		Adjustment of tax and interest rates (X_9)
		Capital supply (X_{10})
	Construction Technology Risk ***B4***	Construction scheme, craft & technology (X_{11})
		Construction safety (X_{12})
		Construction materials and energy supply (X_{13})
	Management & Quality Risk ***B5***	Quality awareness and quality supervision level (X_{14})
		Bidding and contract management (X_{15})

BASIC PRINCIPLES OF PCA AND MODELING STEPS

Basic Principles

Principal component analysis (PCA), invented in 1901 by Karl Pearson, is a mathematical method of reorganizing information in a data set of samples. PCA

involves a mathematical procedure that transforms a number of possibly correlated variables into a smaller number of new, uncorrelated variables called "principal components" which accounts for the majority of the variability in the data. The first principal component accounts for as much of the variability in the data as possible, and each succeeding component accounts for as much of the remaining variability as possible. Depending on the field of application, it is also named the discrete KarhunenŁoève transform (KLT), the Hotelling transform, or proper orthogonal decomposition (POD). Currently, it is primarily used as a tool in exploratory data analysis and for making predictive models.

Modeling Steps

a) To collect original data x_{ij} (i=1…n, j=1…n), where x_{ij} is evaluation value of expert i to indicator j.

b) To standardize sample value of original matrix $X = (x_{ij})_{n\times m}$ to avoid the influence of difference in dimension and value.

$$y_{ij} = (x_{ij} - \bar{x}_j)/\sigma_j \qquad i=1,2\ldots,n;\ j=1,2\ldots,m \tag{1}$$

Where, $\bar{x}_j = \frac{1}{n}\sum_{i=1}^{n} x_{ij}, \sigma_j = \sqrt{\frac{1}{n}\sum_{i=1}^{n}(x_{ij} - \bar{x}_j)^2}$, σ_j can be achieved by using function *std* in MATLAB. We can get the standardization sample matrix $Y = (y_{ij})_{n\times m}$.

c) To get eigenvalues($\lambda_1 \ge \lambda_2 \ge \cdots \ge \lambda_m \ge 0$) of principal components matrix and covariance matrix by using fuction *princomp* in MATLAB, and to calculate the contribution rate h_j and cumulative contribution rate th_j of eigenvalues.

Where, $h_j = \lambda_j / \sum_{k=1}^{m} \lambda_k, th_j = \sum_{k=1}^{j} \lambda_k / \sum_{k=1}^{m} \lambda_k \ (j = 1,2\cdots m)$

d) To select the principal components and build up the comprehensive evaluation function. According to the size of the contribution rate, to select S principal components F_1, F_2 , …, F_s based on the conditions $\sum_{i=1}^{s} \lambda_i / \sum_{j=1}^{m} \lambda_j \ge 85\%$, thus, the linear combination of pre-s elements as follows:

$$F_i = Z_{i1}x_1 + Z_{i2}x_2 + \cdots + Z_{im}x_m, i = 1,2,\cdots,s \tag{2}$$

To use the compressed S principal components as new decision-making indicators, the principal component decision-making matrix with low-dimensional indicators can be achieved as follows:

$$F = [F_1, F_2 \cdots, F_s] \tag{3}$$

The model for risk evaluation for logistics park construction, which based on S principal components $F_1,F_2,\ldots,F_s$ and their variance contribution rate $h_1,h_2,\ldots,h_s$, is:

$$F = h_1F_1 + h_2F_2 + \cdots + h_sF_s \tag{4}$$

Thus, the total risk value for logistics park construction can be calculated using the comprehensive evaluation function, and the greater F is, the greater the risk of the project.

APPLICATION EXAMPLE

In view of the actual situation of insufficient historical data on the construction of logistics parks, to control the risks from occurring in the construction effectively, relevant departments acquired sample spaces of risk evaluation by inviting senior experts in the related fields to score each type of risk that might exist in the logistics park construction in Chengdu, China. The authors evaluated the risks using PCA.

(1) Experts scored 7 projects of the logistics park/center construction for risk types shown in Table 1. To improve the accuracy of scoring and the objectivity and impartiality of evaluation, the Delphi method was adopted by an group of 15 proficient and experienced experts. Organizers provided the statistical data and evaluation requirements to the group in written form and requested them to give an evaluation value to each risk index of every project independently. The final evaluation value was achieved by integrating all expert evaluation values. If the experts had different opinions, feedback was used so the experts' opinions tend to be in unity. After scoring by the 15 experts and based on the principle of a 1 ~ 10 scoring system, the risk evaluations in Table 2 emerged. The lower the score, the lower the risk.

Table 2. Risk Evaluation Table for Logistics Park Construction.

Risk / Projects	X_1	X_2	X_3	X_4	X_5	X_6	X_7	X_8	X_9	X_{10}	X_{11}	X_{12}	X_{13}	X_{14}	X_{15}
A	4	5	2	4	3	8	5	1	2	5	8	7	4	4	3
B	5	4	3	3	2	4	3	4	3	4	7	8	3	5	4
C	4	6	4	4	3	6	6	2	5	6	6	4	5	8	7
D	3	3	1	3	2	7	5	3	3	4	5	3	2	5	6
E	3	6	4	5	1	5	2	5	3	3	6	5	5	4	5
F	5	4	5	3	3	8	4	6	2	6	4	7	6	6	4
G	4	5	6	4	1	7	6	2	2	6	7	8	7	6	2

(2) The above data were transformed into the matrix P for processing. For small data discrepancies, data standardizing was not needed, and we can directly carry out PCA to the above data using MATLAB.

(3) To carry on PCA to matrix *P* using PCA function *princomp* in MATLAB.

To input the matrix *P* and [pc, score, latent, tsquare] = *princomp* (p), and run it.

Arranged in order of size, the positive eigenvalues of the covariance matrix, the contribution rate and the cumulative contribution rate are shown in Table 3.

Table 3. Eigenvalues, Contribution Rate, and Cumulative Contribution Rate on Covariance Matrix.

Indicators	Eigenvalues	Contribution rate（%）	Cumulative Contribution Rate（%）
1	10.2848	33.91	33.91
2	6.9557	22.93	56.84
3	5.8986	19.44	76.28
4	3.8704	12.76	89.04
5	2.3447	7.73	96.77
6	0.9791	3.23	100

(4) As shown in Table 3, the cumulative contribution rate of the first four principal components has reached 89.04%(more than 85%), which contains almost all the basic information of the indicators, so *S* is 4.

According to the eigenvectors corresponding to the first four eigenvalues, we can get the four following principal components:

$$F_1=-0.1365X_1-0.0247X_2+0.0406X_3+0.1223X_4-0.3916X_5+0.2113X_6-0.1005X_7+0.3373X_8+0.2063X_9+0.0145X_{10}-0.4275X_{11}-0.4277X_{12}+0.1332X_{13}+0.2770X_{14}+0.3733\ X_{15}$$

$$F_2=-0.0794X_1+0.0957X_2+0.0951X_3-0.4502X_4+0.1788X_5+0.4483X_6-0.0930X_7+0.4600X_8-0.0088X_9-0.0659X_{10}-0.1215X_{11}+0.4395X_{12}-0.2851X_{12}+0.1572X_{14}-0.0356X_{15}$$

$$F_3=-0.4190X_1+0.0855X_2+0.3974X_3-0.1749X_4+0.0475X_5-0.2041X_6-0.2910X_7-0.1995X_8+0.2160X_9-0.1071X_{10}+0.2071X_{11}-0.1747X_{12}-0.4361X_{12}-0.1650X_{14}+0.3336X_{15}$$

$$F_4=-0.0261X_1-0.0005X_2+0.0209X_3-0.2907X_4+0.2969X_5+0.1696X_6+0.1089X_7-0.2640X_8-0.3011X_9+0.2291X_{10}-0.4966X_{11}-0.4757X_{12}-0.1733X_{12}-0.1761X_{14}-0.1971X_{15}$$

The model of comprehensive evaluation function for overall risk,which built up by using F_1， F_2 ， ……， F_s and h_1 ， h_2 …h_s , is:

$$F=33.91F_1+22.93F_2+19.44F_3+12.76F_4$$

By comparing the size of the principal component coefficients, it can be seen that the first principal component reflects bidding and contract management and change of engineering quantity; the second reflects materials and equipment prices rise; the third reflects engineering geology and hydrogeology; and the fourth reflects capital supply. According to the calculation, we find that the risk degree from high to low is D, F, C, E, B, G, A.

CONCLUSIONS

Risk evaluation for logistics park construction is a typical multi-indicator problem which involves many factors. We can quantitatively evaluate project risk degree on logistics park construction using the comprehensive evaluation function F, and the greater F is, the greater the risk of the project. Furthermore, we can obtain principal risk factors, which can provide information for circumventing risk by comparing the size of the coefficients of each principal component. The advantages of evaluating construction risk for logistics parks using PCA are as follows:

(1) It reduces the complexity of the risk evaluation and weakens multiple correlations among the indicators through dimensionality reduction. Furthermore, the using of data processing functions in MATLAB reduces the complexity of risk evaluation in the calculation.

(2) The principal components determined by using PCA can better measure the influence extent of specific risks to total risk, which provides a scientific basis for investors or relevant personnel in the logistics park construction to circumvent risk.

ACKNOWLEDGMENT

This research is supported by The Youth Science Foundation of Sichuan Province in China (09ZQ026-001).

REFERENCES

Cui, A. D., and Zhao,Y. L. (2002).“Fuzzy overall evaluation for decision of venture investment projects.” *Scientific Management Research,* (5), 24- 26.

Fan, Jia-Kun. (1993). *Application Multivariate Analysi*s. Nanjing: Hohai University Press.

Guo, Q.,Wub, W., Massarta, D. L., Boucon, C., and de Jong, C. S. (2002). “Feature selection in principal component analysis of analytical data.” *Chemometrics and Intelligent Laboratory Systems,* 61,123-132.

He, Xiao-qun. (2004). *Multivariate Statistical Analysis*. Beijing: People’s University of China Press.

Hotelling, H. (1933). “Analysis complex of statistical variables into principal components.” *Education Psychology,* 24(3), 417-444.

Miller, R., and Lessard, D. (2000). *The Strategic Management of Large Engineering Projects*. Cambridge, MA:The MIT Press.

Wang, Xue-ren, and Wang, Song-gui. (1990). *Static Analysis of Practical*

Multivariate Shanghai: Science and Technology Publishing House of Shanghai.

Wang, S. B., and Wang, S. L. (2004). "Venture capital project evaluation using the analytic hierarchy process." *Science and Technology Management Research,* (1), 106-108.

Yang, J., and Zhang, P. Z. (2004). "Medicine venture capital investment evaluation model based on ANN." *Application of Statistics and Management,* (4), 37-42.

Parameter Sensitivity Analysis of Accident Reconstruction Model Based on Orthogonal Design

Zou Tiefang[1], Yu Zhi[1], Cai Ming[1] and Liu Jike[1]

[1]School of Engineering, Sun Yat-sen University, Guangzhou, 510275, China; email: tiefang@163.com

Abstract: Parameters used in accident reconstruction models are uncertain. How these uncertain parameters influence calculation results can be obtained through parameter sensitivity analysis and then more regard should be paid to these sensitivity parameters in accident measurement. Based on orthogonal design, a parameter sensitivity analysis method in accident reconstruction is proposed. A numerical case is used to illustrate the applications of the presented method, then the influence of uncertain parameters and the interactions between them on calculation results are obtained. Results show that the most sensitive parameter obtained by applying the orthogonal design method is the same as other scholar's; what's more, this method provides availability to inspect the influence of interactions between uncertain parameters on calculation results and the development trend of calculation results versus the variation of parameters.

Key words: *traffic engineering; accident reconstruction; orthogonal design; parameter sensitivity analysis*

1. Introduction

The uncertainty problem is an important issue in accident reconstruction; there are two topics in it: one is uncertainty analysis; the other is parameter sensitivity analysis. Uncertainty analysis has been studied extensively in recent years. Many uncertainty analysis method were presented, such as finite difference method (Wade Bartlett, 2003), Monte Carlo method (Wojciech Wach, 2007; Zbigniew Lozia, 2005), etc. Parameter sensitivity analysis has been studied by some scholars also, like analyzing parameter sensitivity in typical (PEI Jian-ping, 2002) and two-dimension impact (Zou Tie-fang, 2007) model, but the method used in these two papers can not analyze the influence of interactions between uncertain parameters on calculation results. In order to consider the influence, of not only parameters but also interactions between them, on calculation results, some new parameter sensitivity analysis techniques are needed.

In this paper, based on orthogonal design method, a parameter sensitivity analysis method in accident reconstruction is proposed. After that, a numerical case is used to illustrate the applications of the method.

2. Problem description

Models in accident reconstruction vary with the accident modality, the selected methods and many other parameters. But no matter which model is adopted, it can be

described by

$$Y = f(X),\ \mathrm{X} = (x_1, \ldots, x_s)^T \in T \tag{1}$$

where Y is the accident reconstruction results vector, which commonly represents the pre-impact velocity and the collision location; X is independent parameters vector, for example, dimension of vehicle; s is the number of independent parameters; T is the range of the X; f is an equation which characterizes the model.

If the influence of uncertain parameters, not only X but also the interactions between them, on output Y is known, then these sensitivity parameters can be paid more regard in measurement. Therefore, the reconstruction results will be more accurate because of the more accurate inputs. So how these uncertain parameters influence Y is an important issue to be considered. A parameter sensitivity analysis method based on orthogonal design will be proposed in the paper to solve this issue.

3. Parameter sensitivity analysis method based on orthogonal design

Orthogonal design is a kind of multi-factor experiments method. It is a quite efficient method of fraction factorial design (Zhao Xuan-min, 2006).

The basic tool of orthogonal design is the orthogonal table, which can be written as $L_n(t^q)$, where, L represents symbol of orthogonal table, n represents the number of tests, t represents number of levels, and q represents the number of columns in the orthogonal table. For an example, test with 3 parameters and 3 levels, the orthogonal table can be selected as $L_9(3^4)$. When the orthogonal table is chosen, the test table can be got after level translation, and then test results can be obtained through conducting tests according to the test table strictly.

There are two statistical analysis techniques to analyze the test results, which are the extremum difference analysis method and the variance analysis method. The extremum difference analysis method is simple and intuitive, the primary and secondary of parameters sensitivity can be got through a few calculations on the test results, but the test error can not be evaluated by this method. The variance analysis method distinguishes the influence of parameters and error, and then the conclusion, whether the influence of uncertain parameters and/or the difference between different levels of an uncertain factor is significant or not, can be obtained through comparison.

So steps of parameter sensitivity analysis method based on orthogonal design can be given:

1. To select uncertain parameters. There are many uncertain parameters in one issue, and each parameter may influence calculation results. To consider the influence of all parameters will be very hard and not necessary. According to the character of the accident reconstruction model and experience, select the appropriate parameters, and obtain the uncertainty of these parameters.

2. To determine levels of parameters and specify interactions between parameters which need to be estimated. This is the basis for selecting the orthogonal table. Determine these properly according to the actual requirements.

3. To select an appropriate orthogonal table. According to the number and levels of parameters, choose the appropriate orthogonal table, and then arrange the uncertain parameters and their interactions into the chosen orthogonal table. After level translation, the test table can be obtained.

4. To conduct a test, conduct the test according to the experiment table strictly and record the results.

5. To analyze the test results, select the extremum difference analysis method or variance analysis method to analyze the test results.

6. Conclusions, the sensitivity of parameters, interactions between them and the development trend of the calculation results, can be obtained according to step 5.

4. Numerical case

A vehicle impaction pedestrian accident is given in this paper. The model used here can be written as

$$V = \mu\sqrt{2g}\left(\sqrt{h+\frac{l}{\mu}}-\sqrt{h}\right) \tag{2}$$

where V is the velocity of the accident vehicle; l is the throw-out distance of pedestrian, l=18.8±0.5 m; μ is the friction coefficient between the pedestrian and ground, μ=0.6±0.1; h is the throw-out height of the pedestrian, h=0.93±0.1 m; g is acceleration of gravity, g=9.8 m/s^2. The model is validated by Li (Li Yi-bing, 2004) through some tests data once more. All these data of this case are cited from Li.

In this numerical case, the index is V. There are three parameters: μ, h and s. In order to study the nonlinear relationship of index versus parameters, three levels of each factor were selected. Levels of all parameters can be found in Table 1. Therefore, the orthogonal table $L_{27}(3^{13})$ should be selected. The three parameters are arranged in line 1, 2 and 5 respectively, and the interactions items can be arranged according to the interactions tables, test scheme and test results can be found in Table 2. Use the variance analysis method to analyze the test results. The variance analysis results can be found in Table 3. Considering that the experiment error is almost zero here, the significant test on parameters will make no sense because all parameters will have significant effect, so this part will be ignored.

Table 1. Level of all parameters.

Parameters / levels	h [m]	s [m]	μ
1	0.83	18.3	0.5
2	0.93	18.8	0.6
3	1.03	19.3	0.7

Table 2. Test scheme and test results*.

Test No.	1 A	2 B	3 AB	4 AB	5 C	6 AC	7 AC	8 BC	9 Em	10 Em	11 BC	12 Em	13 Em	V [m/s]
1	1	1	1	1	1	1	1	1	1	1	1	1	1	11.5261
2	1	1	1	1	2	2	2	2	2	2	2	2	2	12.44822
3	1	1	1	1	3	3	3	3	3	3	3	3	3	13.27159
4	1	2	2	2	1	1	1	2	2	2	3	3	3	11.70582
5	1	2	2	2	2	2	2	3	3	3	1	1	1	12.64466
6	1	2	2	2	3	3	3	1	1	1	2	2	2	13.48331
7	1	3	3	3	1	1	1	3	3	3	2	2	2	11.88321
8	1	3	3	3	2	2	2	1	1	1	3	3	3	12.83857
9	1	3	3	3	3	3	3	2	2	2	1	1	1	13.69232
10	2	1	2	3	1	2	3	1	2	3	1	2	3	11.42615
11	2	1	2	3	2	3	1	2	3	1	2	3	1	12.33029
12	2	1	2	3	3	1	2	3	1	2	3	1	2	13.13616
13	2	2	3	1	1	2	3	2	3	1	3	1	2	11.60563
14	2	2	3	1	2	3	1	3	1	2	1	2	3	12.52642
15	2	2	3	1	3	1	2	1	2	3	2	3	1	13.34749
16	2	3	1	2	1	2	3	3	1	2	2	3	1	11.78279
17	2	3	1	2	2	3	1	1	2	3	3	1	2	12.72004
18	2	3	1	2	3	1	2	2	3	1	1	2	3	13.55612
19	3	1	3	2	1	3	2	1	3	2	1	3	2	11.33236
20	3	1	3	2	2	1	3	2	1	3	2	1	3	12.21976
21	3	1	3	2	3	2	1	3	2	1	3	2	1	13.00933
22	3	2	1	3	1	3	2	2	1	3	3	2	1	11.51161
23	3	2	1	3	2	1	3	3	2	1	1	3	2	12.41558
24	3	2	1	3	3	2	1	1	3	2	2	1	3	13.22028
25	3	3	2	1	1	3	2	3	2	1	2	1	3	11.68855
26	3	3	2	1	2	1	3	1	3	2	3	2	1	12.6089
27	3	3	2	1	3	2	1	2	1	3	1	3	2	13.42854
I	113.49	110.70	112.45	112.45	104.46	112.40	112.35	112.50	112.45	112.45	112.55	112.45	112.45	
II	112.43	112.46	112.45	112.45	112.75	112.40	112.50	112.50	112.45	112.45	112.40	112.45	112.45	T=337.36
III	111.43	114.20	112.46	112.456	120.146	112.56	112.51	112.36	112.45	112.45	112.41	112.45	112.45	

*A , B and C represent h, l and μ respectively. AB represents the interactions between A and B; AC and BC are similar. I, II and III are the sum of index V corresponding to level 1, 2 and 3 of each factor respectively. Em represents Empty; it means that there is no parameter arranged in this line. T is the total sum of index V.

Table 3. Variance analysis*.

Origin of variance		Sum of squares of deviations	Freedom	Mean square value
h		0.235586	2	0.117793
l		0.680202	2	0.340101
μ		13.67903	2	6.839513
interactions	*hl*	1.1E-06	4	2.8E-07
	hμ	0.0036	4	0.0009
	lμ	0.003	4	0.0008
Error		4E-08	8	5E-09
Sum		14.60138	26	

* *hl*, *hμ* and *lμ* represent the interaction between *h* and *l*, *h* and*μ*, *l* and*μ* respectively.

Through Table 3, the sensitivity of parameters and interactions between them can be ordered as: *μ*>*l* >*h* >*hμ*>*lμ*>*hl*. We can conclude that the friction coefficient between the pedestrian and ground is the most sensitive parameter for the calculation result in model (1); this conclusion is in line with LI's. And the influence on index *V* of the interactions between parameters is little, so we can conclude that only the friction coefficient between pedestrian and ground should pay more regard in accident measurement. In order to make the analysis results intuitive, with the level of parameter as x-coordinate and the sum of velocity, corresponding to the level *i* (*i*=1, 2, 3) of parameters, as y-coordinate, the development trend of velocity versus the variation of parameters can be drawn (Figure 1), the interactions between parameters is consider as factors here.

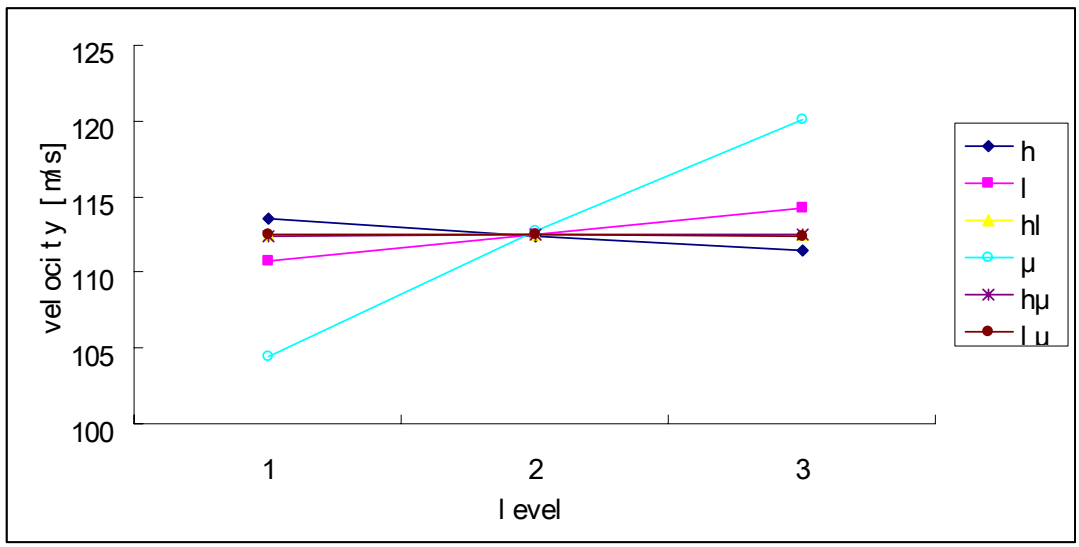

Figure 1. The development trend of velocity versus the variation of level of parameters

From Figure 1, the oblique line with maximum slope is the line represent by μ, the slopes of all of the other lines are small, which means that other parameters and interactions between them influence the calculation results V less. And equation (2) is a nonlinear function, but in Figure 1, the development trend of velocity is approximately linear, which means that equation (2) can be explained by an approximate linear model when the uncertainty of uncertain parameters is small.

5. Conclusions

Based on orthogonal design, a parameter sensitivity analysis method in accident reconstruction is proposed. Using this method to study parameter sensitivity analysis of accident reconstruction, the model can not only study the influence on the index of the parameters, but also the interactions between them, and the development trend of the index versus inputs can also be obtained. It is a useful method in parameter sensitivity analysis, and can be used in the accident reconstruction field.

Acknowledgements

This work is supported by National Natural Science Foundation of China (50808181) and Guangdong Province Science and Technology Program (2007B030102003).

References

Wade Bartlett (2003). Conducting Monte Carlo Analysis with spreadsheet Programs [C]. SAE Paper No.2003-01-0487, sp-1773:29-38.

Wade Bartlett, Albert Fonda (2003). Evaluating Uncertainty in Accident Reconstruction with Finite Differences. SAE Paper No.2003-01-0489, sp-1773:53-63.

Li Yi-bing, Yuan Quan, Chen Li (2004). Study of uncertain parameters in traffic accidents of vehicle impaction pedestrian [J]. China Journal of Highway and Transport. 17(1): 82-85.

Zbigniew Lozia, Marek Guzek (2005). Uncertainty study of Road Accident Reconstruction-Computational Methods [C]. SAE Paper No.2005-01-1195, sp-1930:163-177.

Pei Jian-ping, LI Yi-bing, WU Wei-dong (2002). Parameter Sensitivity of Analysis Typical Impact Models in Traffic Accident Reconstruction [J]. Journal of Highway and Transportation research and Development. 19(4), 130-133.

Wojciech Wach, Jan Unarski (2007). Uncertainty of calculation results in vehicle collision analysis [J]. Forensic Science International. 167(2-3): 181-188.

Zhao Xuan-min (2006). Design of Experiments [M]. Beijing: Science Press.

Zou Tie-fang, Cai Ming, Liu Ji-ke (2007). Parameter Sensitivity Analysis of Two-Dimensional Vehicle Impact Model [J]. ACTA SCIENTIARUM NATURALIUM UNIVERSITATIS SUNYATSENI. 46(3): 17-19.

Study On The Key Technology of Captive Model's Numerical Test

Wang Xiao[1] Xiao Bing[2] Yang Bo[2] and Shi Aiguo[2]

[1] Department of Navigational Engineering, Dalian Naval Academy, P.O.Box ShiKui Road 140#1-2-1, DaLian, ST 116013；PH（86）0411-85855783；FAX（86）0411-85855477；e-mail：WXNV312_6@hotmail.com

[2] Department of Navigational Engineering, Dalian Naval Academy, P.O.Box XiaoLong Road 669#, DaLian, ST 116018；PH（86）0411-85855477；FAX（86）0411-85855477；e-mail：agshi2@tom.com

ABSTRACT

This paper is aimed to realize the numerical simulation, using SCFD, on all functions of PMM (Planar Motion Mechanism) and CMT (circular motion test), in order to get all of the hydrodynamic derivatives, which are vital to ship-maneuverability-design research. So 9 kinds of motions were generalized from captive model tests. And based on the motions' characteristic, the numerical simulations of static drift test, pure sway test , pure yaw test and circular motion test(CMT) were realized, by means of "change inlet-flow's velocity", "Dynamic Meshes" and "region shape design" method. The ship model in this paper is DTMB5415, and in order to advance calculational precision and efficiency, a series of studies on grids, discrimination scheme, scales of computational domain, turbulence model and free surface simulation. The simulation results showed good agreement with that of tank test.

ITRODUCTION

Maneuverability is an important performance of vessels. At present, Captive model test is acknowledged to be the best method which can obtain the hydrodynamic force precisely and be satisfied in engineering. Planar Motion Mechanism (PMM) is one of captive model tests, which can get all of Hydrodynamic derivatives. But the disadvantage of PMM is costly and time consuming; furthermore, modifying the data of ship model is difficult.

Ship Computational Fluid Dynamics（SCFD）method can remedy the disadvantage of PMM fitly, which has the advantage of low consume, time saving and modifying convenient. SCFD has been applied in the ship's investigation more and more widely. But researcher of SCFD has not focused on the numerical simulation of PMM to get all of hydrodynamic derivatives.

The author of this paper attempts to use SCFD method to get hydrodynamic derivatives. This method may offer a new research fundament of numerical tank towing. The thinking that the author studies is: to solve RANS equation in given computational region, based on CFD software "FLUENT", in order to realize the numerical simulation on static drift test, pure sway test , pure yaw test (Figure.1)and circular motion test(CMT).

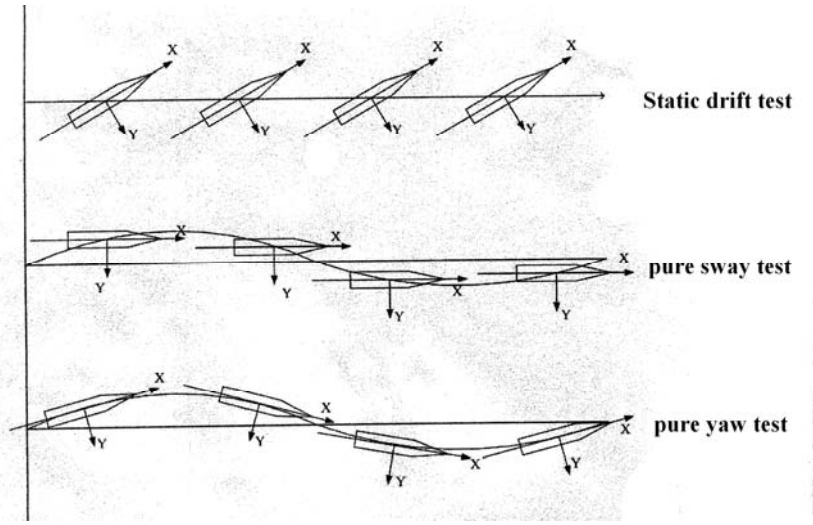

Figure1 all kinds of PMM

2 Implementary scheme of captive model tests' numeric simulation

2.1 Design of implementary scheme

All functions of captive model tests in this paper are summarized to static drift test, static rudder angle test, static drift and rudder angle test, pure sway test, pure yaw test, unstatic drift pure yaw test, zreo drift of CMT, static drift of CMT, and static drift and rudder angle of CMT, amounts to 9 kinds.

In Table 1, all of the schemes are listed.

Table 1 implementary scheme of captive model tests' numeric simulation

Experimental project	Design of simulation	Region and grid	Hydrodynamic derivatives
Static drift test	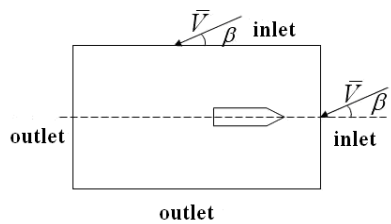	partition hybrid grid	Y_V'、Y_{VVV}'、N_V'、N_{VVV}'

static rudder angle test	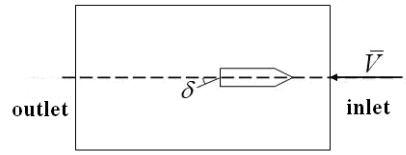	partition hybrid grid	Y_δ'、$Y_{\delta\delta\delta}'$、N_δ'、$N_{\delta\delta\delta}'$
Static drift and rudder angle test	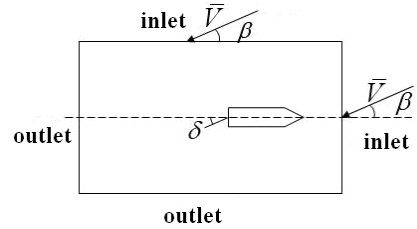	partition hybrid grid	$Y_{V\delta\delta}'$、$Y_{VV\delta}'$ $N_{V\delta\delta}'$、$N_{VV\delta}'$
Pure sway test	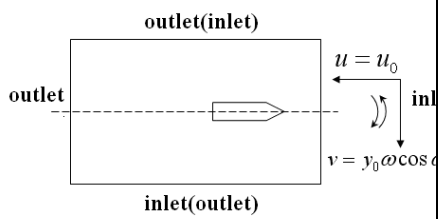	unstructured grid	Y_V'、$Y_{\dot{V}}'$、N_V'、$N_{\dot{V}}'$
Pure yaw test	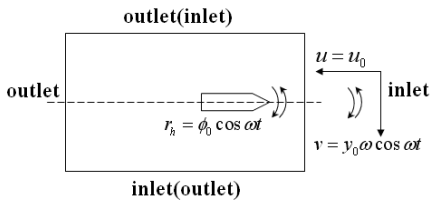	unstructured grid Dynamic Meshes	Y_r'、$Y_{\dot{r}}'$、N_r' $N_{\dot{r}}'$、Y_{rrr}'、N_{rrr}'
unstatic drift pure yaw test	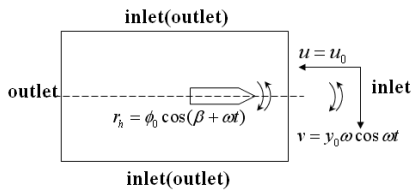	unstructured grid Dynamic Meshes	Y_{rrr}'、Y_{VVr}'、Y_{Vrr}' Y_{VVV}'、N_{rrr}'、N_{VVr}' N_{Vrr}'、N_{VVV}'
zreo drift of CMT	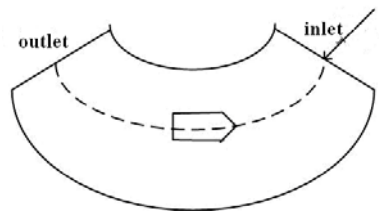	fan-shaped region partition hybrid grid MRF(Multiple Rotating Reference Frames)	Y_r'、N_r'

static drift of CMT	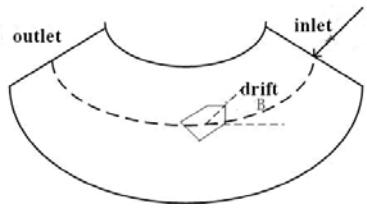	fan-shaped region partition hybrid grid MRF	Y_{Vrr}'、Y_{VVr}'、Y_{rrr}' N_{Vrr}'、N_{VVr}'、N_{rrr}'
static drift and rudder angle of CMT	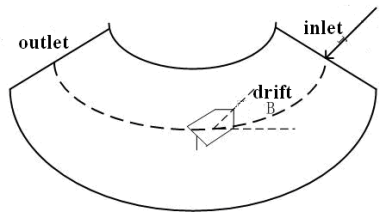	fan-shaped region partition hybrid grid MRF	$Y_{r\delta\delta}'$、$Y_{\delta rr}'$、$Y_{Vr\delta}'$ $N_{r\delta\delta}'$、$N_{\delta rr}'$、$N_{Vr\delta}'$

2.2 Model

In order to validate the feasibility and credibility of this scheme, the author uses DTMB5415 model, which is announced of ITTC. Model's parameters are listed as follows:

Model Length	LPP=4.0023m
Draft	T=0.1736m
Beam	B=0.5382m
Wetted surface area	S=1.571m^2

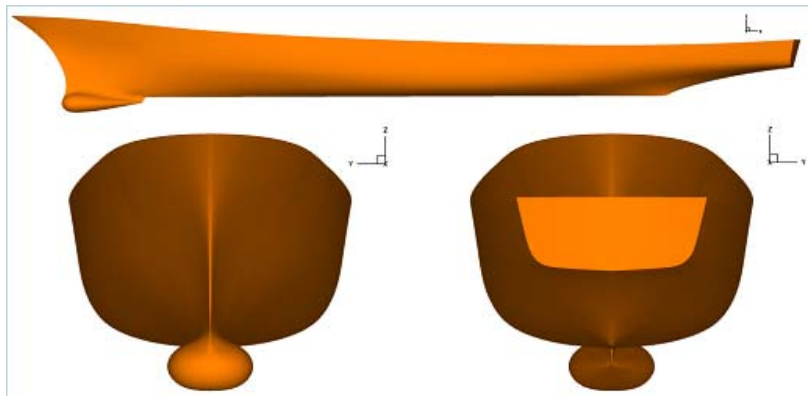

Figure 2 DTMB5415

2.3 Setup of computational region and Generation of grid

2.3.1 Computational region of static drift test, pure sway test and pure yaw test

Computational region of static drift test, pure sway test and pure yaw test is listed as Figure 3. 'L' is Model Length.

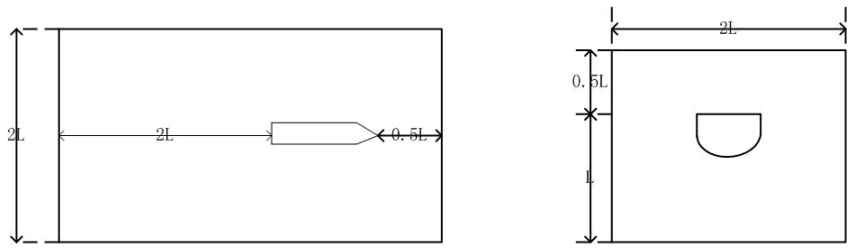

Figure 3 Computational region of PMM

2.3.2 Computation region of CMT

Computation region of CMT is listed as Figure 4. 'L' is Model Length.

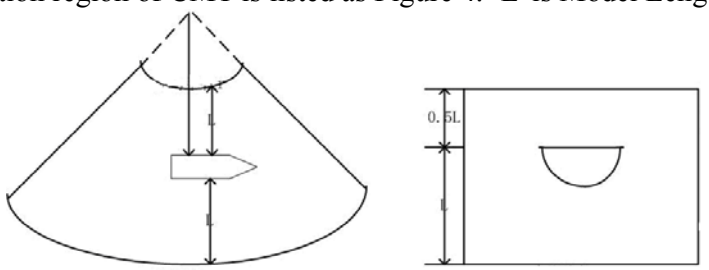

Figure 4 Computational region of CMT

2.3.3 Generation of grid

Different kinds of grid are requested to different PMM numeric simulation test. Such as static drift test is requested to use partition hybrid grid(As Figure. 5 shows), and pure yaw test and pure sway test are requested to use unstructured grid(As Figure. 6 shows).

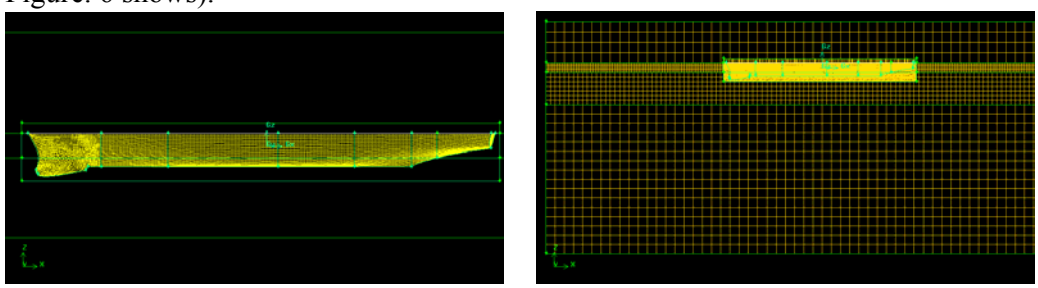

Figure 5 partition hybrid grid

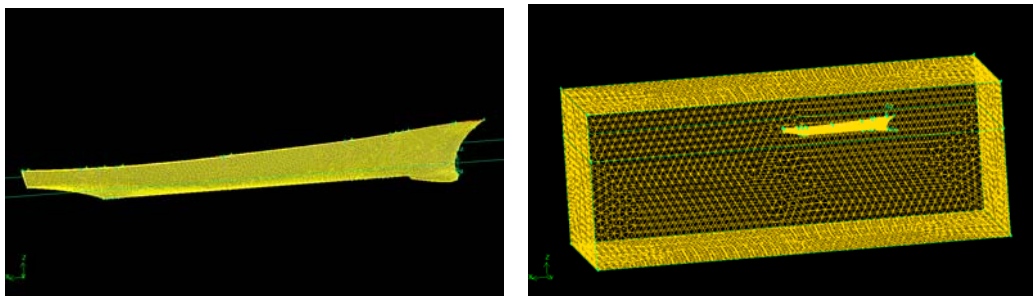

Figure 6 unstructured grid

3 Governing equations

3.1 Continuity equation and momentum equation

Continuity equation

$$\frac{\partial u_i}{\partial x_i}=0 \tag{1}$$

momentum equation

$$\frac{\partial u_i}{\partial t}+\frac{\partial}{\partial x_j}\left(u_i u_j\right)=-\frac{\partial P}{\partial x_i}+\frac{\partial}{\partial x_j}\left(\mu\frac{\partial u_i}{\partial x_j}-\overline{u_i' u_j'}\right) \tag{2}$$

3.2 RNG $k-\varepsilon$ turbulence model

The flow features are very complex in captive model tests' region. So the author chooses RNG $k-\varepsilon$ turbulence model to solve this problem.

$$\frac{\partial \kappa}{\partial t}+\frac{\partial \kappa u_i}{\partial x_i}=\frac{\partial}{\partial x_j}\left(\alpha_\kappa \mu_{eff}\frac{\partial \kappa}{\partial x_j}\right)+G_K+\varepsilon \tag{3}$$

$$\frac{\partial \varepsilon}{\partial t}+\frac{\partial \varepsilon u_i}{\partial x_i}=\frac{\partial}{\partial x_j}\left(\alpha_\varepsilon \mu_{eff}\frac{\partial \varepsilon}{\partial x_j}\right)+\frac{C_{1\varepsilon}^{*}\varepsilon}{\kappa}G_K+C_{2\varepsilon}\frac{\varepsilon^2}{\kappa} \tag{4}$$

3.3 VOF model

To simulate free surface, the author uses the VOF model(volume of fluids model).

The VOF model can model two or more immiscible fluids by solving a single set of momentum equations and tracking the volume fraction of each of the fluids throughout the domain. If the q fluid's volume fraction in the cell is denoted as C_q, then the following three conditions are possible:

$C_q=0$: The cell is empty (of the q fluid).

$C_q=1$: The cell is full (of the fluid).

$0<C_q<1$: The cell contains the interface between the q fluid and one or more other fluids.

Based on the local value of C_q, the appropriate properties and variables will be assigned to each control volume within the domain.

3.4 Solver

The author solves the three-dimensional viscidity incompress RANS equation directly. The discretization scheme of differential eguation is Finite Volume Method (FVM). Second order upwind scheme is used to convective term and diffusive term.

In order to solve the coupled equation of pressure, the author uses SIMPLE method. The dispersed algebraic equation is solved with Gauss-Seidel method.

4 Several typical tests result

4.1 Resistance test

As Fr =0.280 test is the example, the calculational result of resistance force (X force) is showed in Figure. 7, and free-surface wave feature is showed in Figure 8.

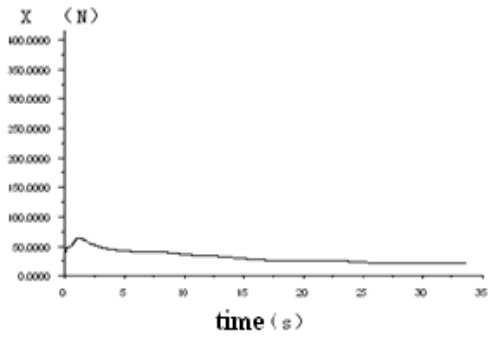

Figure 7 result of X force

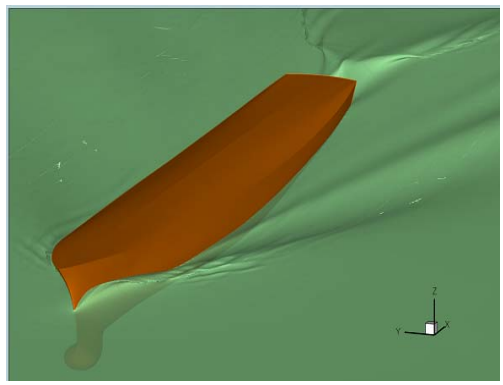

Figure 8 free-surface wave feature

The calculational result and test data from the towing tank are listed as follows:

Table 2 calculational result and test data from the towing tank

Project	Resistance force(N)
Test data from the towing tank	18.797
calculational result	19.45

4.2 Static drift test result

The calculational result and test data from the towing tank are listed as follows:

Table 3 calculational result and test data from the towing tank

Project	Fr=0.138，β=12°		Fr=0.138，β=20°	
	X force(N)	Y force(N)	X force(N)	Y force(N)
Test data from the towing tank	4.3712	21.745	4.6670	48.359
calculational result	4.5722	24.372	4.90	50.839

In order to achieve $Y'(\beta)$ and $N'(\beta)$ curve, the calculational result of β=6°,β=12°, β=15°, β=20° will be non-dimensionalized. Curve slope of zero is hydrodynamic derivative Y'_v or N'_v.

Table 4 hydrodynamic derivative Y'_v and N'_v

Project	Y'_v	N'_v
Test data from the towing tank	0. 2785	0. 002870
calculational result	0. 2964	0. 002681

4.3 Pure sway test result

As Fr =0.280 test is the example, the calculational result of Y force is showed in Figure 9.

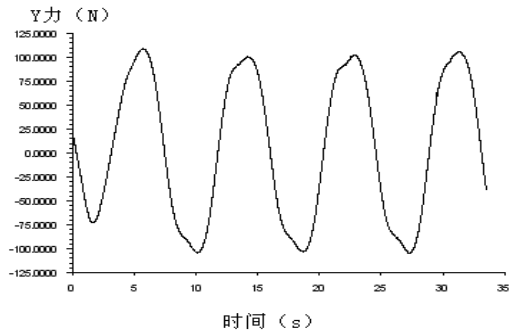

Figure 9 result of Y force

The calculational result of hydrodynamic derivatives are listed as follows:

Table 5 hydrodynamic derivative Y'_V and $Y'_{\dot{V}}$

Project	Y force (N)	transverse displacement (m)	Phasic value (rad)	Y'_V	$Y'_{\dot{V}}$
Test data from the towing tank	108	0. 4292	0. 5872	0. 3120	0. 4500
calculational result	142. 47	0. 4191	0. 5315	0. 4215	0. 5483

4.4 Pure yaw test result

As Fr =0.280 test is the example, the calculational result of Y force is showed in Figure 10.

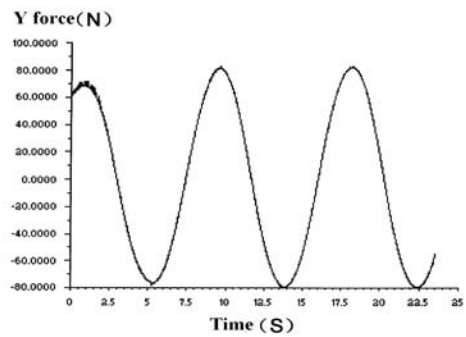

Figure 10 result of Y force

The calculational result of hydrodynamic derivatives are listed as follows:

Table 6 hydrodynamic derivative Y'_{γ} and $Y'_{\dot{\gamma}}$

Project	Y force (N)	transverse displacement (m)	Phasic value (rad)	Y'_{γ}	$Y'_{\dot{\gamma}}$
Test data from the towing tank	79.0	0.4292	1.5414	0.4228	0.06947
calculational result	80.55	0.3270	1.53	0.4159	0.06385

CONCLUSION

(1) CFD simulation of all kinds of captive model tests can achieve all of the hydrodynamic derivatives which are vital in ship maneuverability design research and analysis, especially in nonlinear ship maneuverability application. So it is of great theoretical and practical values to deepen the research of this field.
(2) The effective method of the numerical simulation of all functions of PMM(Planar Motion Mechanism) may be, based on the motion features of model tests, to combine the following three aspects: change of inlet-flow's velocity(include MRF), dynamic change of the ship model (include periodic change) and computational domain (include fan-shaped computational domain). And dynamic meshes is also necessary.
(3) In order to obtain more accurate and more efficient simulation results, the integer simulation design, including the ship features, instead of one special aspect should be taken into account. The simulation design should include discrimination scheme, the quantity and amount of the grids, turbulence model, free surface simulation, computational domain, boundary conditions, and etc.

REFERENCES

Alessandrini, B. (1998). Viscous Free Surface Flow past a Ship in Drift and in Rotating Motion. CD-ROM, Pre-Print of 22"d Symposium on Naval Hydrodynamics Annual Meeting.

Arabshahi A., Beddhu M., and Briley W., et al(1998). A Perspective on Naval Hydrodynamic Flow Simulations. CD-ROM, Pre-Print of 22"d Symposium on Naval Hydrodynamics Annual Meeting.

Cura Hochbaum ,A(1994). A Finite-Volume Method for Turbulent Ship Flows. Ship Technology Research, vol .96 , No.17, pp.135 — 148, October 13, 1994

Cai R.Q., Shen Q.X., and Chen Y.G., et al（2000）. A Numerical Investigation of Free Surface Viscous Flow around the Ship by Combination-of Rankine Source Method with RANSFS. Journal of Ship Mechanics, vol .4 , No.3, pp.1-14.

Claus Daniel Simonsen（2003）. PMM model test with DDG51 including uncertainty assessment. CD-ROM, Pre-Print of 24"d Symposium on Naval Hydrodynamics Annual Meeting.

Tahara Y., Longo J., and Stern F., et al（1998）. Comparison of CFD and EFD for the Series 60 CB=0.6 in Steady Yaw Motion. CD-ROM, Pre-Print of 22"d Symposium on Naval Hydrodynamics Annual Meeting.

Wu Jiankang., and C Shu.,（2001）.Numerical Study of Wave Interaction Generated by Two Ships Moving Parallely in Shallow Water. Comput Methods Appl. Mech. Engrg. vol .190 , No.18, pp. 2099-2110.

Simulation and Analysis for Stick-slip Vibration of Locomotive with Hollow-shaft Drive System

Jianxin Liu[1], Huaiyun Zhao[1], and Wanming Zhai[1]

[1] Traction Power State Key Laboratory, Southwest Jiaotong University; P.O. Box 610031, Chengdu, China; PH (0086) 28-87600290; email: jxliu@home.swjtu.edu.cn

ABSTRACT

For the purpose of investigating the stick-slip vibration of the locomotive with a hollow-shaft drive system, a coupled dynamic model of locomotive and slab track is established based on the theory of the vehicle-track coupled dynamics. The dynamic equations are set up considering the nonlinear relationship between slip velocity and the adhesion coefficient. A simulation program is then compiled using MATLAB/SIMULINK. Simulation results show that the phase trajectories of the torsional vibrations are a set of stable limit cycles when the slip velocity is located at the descending slope of the adhesion coefficient curve, indicating that self-excited torsional vibrations are occurred in the drive system.

1 INTRODUCTION

In railways, the adhesion force between the wheel and the track is the ultimate motivation force to drive the train forward. The adhesion force is directly proportional to the adhesion coefficient, which varies with the slip velocity and the various track conditions (Koan-Sok Baek, 2007). A sudden change of the adhesion force from a high level to a low level leads to the self-excited torsional vibration of the drive system and the excessive slip of the wheels, known as stick-slip vibration (HIROTSU Tetsuji, 1987). The self-excited torsional vibration will cause excessive stress in the drive system, which prevents the train from achieving its best adhesion performance. Moreover, it is well agreed that stick-slip vibration can cause rail corrugations (Clark R.A, 1984) and generate noise which becomes a significant environmental nuisance (W.X. Wu, 1998).

Some research indicated that the main cause of the self-excited torsional vibration of the drive system was the adhesion force became smaller as the slip rate increased (ZHENG Lianzhu, 1996). The adhesion force is also closely related to the locomotive dynamics. This paper will establish a locomotive-track coupled model and study it based on the theory of the vehicle-track coupled dynamics (ZHAI Wanming, 2007).

2 ANALYSIS MODEL AND DIFFERENTIAL EQUATIONS

A complete dynamic model of locomotive is established based on a 2B0 locomotive. This locomotive's bogie is a high-speed power bogie with a wheelset hollow-shaft drive device. Each motor is mounted on the bogie frame by three points, one on the end beam (point A) and the others on the lateral beam (point B and C). The track in the model is slab track.

2.1 Drive system torsional model and dynamic equations

The model of the hollow-shaft drive system torsional dynamics is shown in Figure1, and we can get the torsional dynamic equations below.

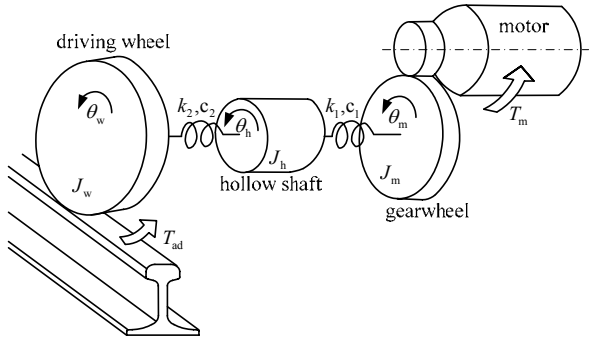

Figure 1. Hollow-shaft drive system torsional model.

$$\begin{cases} J_{\mathrm{m}}\ddot{\theta}_{\mathrm{m}} + c_1(\dot{\theta}_{\mathrm{m}} - \dot{\theta}_{\mathrm{h}}) + k_1(\theta_{\mathrm{m}} - \theta_{\mathrm{h}}) = T_{\mathrm{m}} \\ J_{\mathrm{h}}\ddot{\theta}_{\mathrm{m}} + c_1(\dot{\theta}_{\mathrm{h}} - \dot{\theta}_{\mathrm{m}}) + c_2(\dot{\theta}_{\mathrm{h}} - \dot{\theta}_{\mathrm{w}}) + k_1(\theta_{\mathrm{h}} - \theta_{\mathrm{m}}) + k_2(\theta_{\mathrm{h}} - \theta_{\mathrm{w}}) = 0 \\ J_{\mathrm{w}}\ddot{\theta}_{\mathrm{w}} + c_2(\dot{\theta}_{\mathrm{w}} - \dot{\theta}_{\mathrm{h}}) + k_2(\theta_{\mathrm{w}} - \theta_{\mathrm{h}}) = -T_{\mathrm{ad}} \end{cases} \tag{1}$$

Where T_{m} is the motor traction torque; T_{ad} is the adhesion torque; J_{m} is the motor and gear equivalent moment of inertia; θ_{m} is the torsional angle of the gearwheel; J_{h} is the hollow-shaft moment of inertia; θ_{h} is the torsional angle of the hollow-shaft; J_{w} is the wheelset moment of inertia; θ_{w} is the torsional angle of the wheelset; the c_1, k_1 are the equivalent damping and stiffness between the motor and hollow-shaft, the c_2, k_2 are the equivalent damping and stiffness between the hollow-shaft and wheelset.

The self-excited torsional vibrations are mainly the relative vibrations of the drive parts to the motor. By defining $\Delta\theta_1 = \theta_{\mathrm{h}} - \theta_{\mathrm{m}}$, $\Delta\theta_2 = \theta_{\mathrm{w}} - \theta_{\mathrm{h}}$, equation (1) becomes:

$$\begin{pmatrix} J_{\mathrm{h}} & \\ & J_{\mathrm{w}} \end{pmatrix}\begin{pmatrix} \Delta\ddot{\theta}_1 \\ \Delta\ddot{\theta}_2 \end{pmatrix} + \begin{pmatrix} (1+\dfrac{J_{\mathrm{h}}}{J_{\mathrm{m}}})c_1 & -c_2 \\ -\dfrac{J_{\mathrm{w}}}{J_{\mathrm{h}}}c_1 & (1+\dfrac{J_{\mathrm{w}}}{J_{\mathrm{h}}})c_2 \end{pmatrix}\begin{pmatrix} \Delta\dot{\theta}_1 \\ \Delta\dot{\theta}_2 \end{pmatrix} + \begin{pmatrix} (1+\dfrac{J_{\mathrm{h}}}{J_{\mathrm{m}}})k_1 & -k_2 \\ -\dfrac{J_{\mathrm{w}}}{J_{\mathrm{h}}}k_1 & (1+\dfrac{J_{\mathrm{w}}}{J_{\mathrm{h}}})k_2 \end{pmatrix}\begin{pmatrix} \Delta\theta_1 \\ \Delta\theta_2 \end{pmatrix} = \begin{pmatrix} -\dfrac{J_{\mathrm{h}}}{J_{\mathrm{m}}}T_{\mathrm{m}} \\ -T_{\mathrm{ad}} \end{pmatrix} \tag{2}$$

2.2 Vertical locomotive-track coupled model and dynamic equations

Based on the theory of vehicle-track coupled dynamics, the vertical coupled model of locomotive and slab track and dynamic equations can be as following:

Vertical motion of the carbody:

$$M_{\mathrm{c}}\ddot{Z}_{\mathrm{c}} + C_{\mathrm{s2}}(2\dot{Z}_{\mathrm{c}} - \dot{Z}_{\mathrm{t1}} - \dot{Z}_{\mathrm{t2}}) + K_{\mathrm{s2}}(2Z_{\mathrm{c}} - Z_{\mathrm{t1}} - Z_{\mathrm{t2}}) = M_{\mathrm{c}}g \tag{3}$$

Pitch motion of the carbody:

$$J_{\mathrm{c}}\ddot{\beta}_{\mathrm{c}} + C_{\mathrm{s2}}l_{\mathrm{c}}(2\dot{\beta}_{\mathrm{c}}l_{\mathrm{c}} - \dot{Z}_{\mathrm{t1}} + \dot{Z}_{\mathrm{t2}}) + K_{\mathrm{s2}}l_{\mathrm{c}}(2\beta_{\mathrm{c}}l_{\mathrm{c}} - Z_{\mathrm{t1}} + Z_{\mathrm{t2}}) = 0 \tag{4}$$

Vertical motion of the front bogie:

$$M_t\ddot{Z}_{t1}+C_{s1}(2\dot{Z}_{t1}-\dot{Z}_{w1}-\dot{Z}_{w2})+C_{s2}(\dot{Z}_{t1}-\dot{Z}_c-\dot{\beta}_c l_c)+K_{s1}(2Z_{t1}-Z_{w1}-Z_{w2})+$$
$$K_{s2}(Z_{t1}-Z_c-\beta_c l_c)+K_{tm_A}(2Z_{t1}-Z_{m1}-Z_{m2}-\beta_{m1}l_{m_A}+\beta_{m2}l_{m_A})+ \quad (5)$$
$$K_{tm_BC}(2Z_{t1}-Z_{m1}-Z_{m2}+\beta_{m1}l_{m_BC}-\beta_{m2}l_{m_BC})=M_t g$$

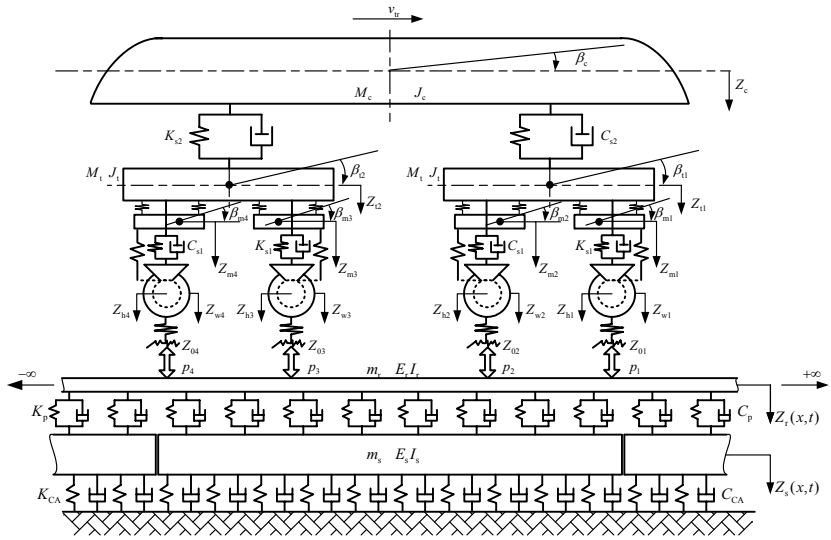

Figure 2. Vertical locomotive-track coupled model

Pitch motion of the front bogie:

$$J_t\ddot{\beta}_{t1}+K_{tm_A}l_{tm_A}(Z_{m2}-Z_{m1}+2\beta_{t1}l_{tm_A}-\beta_{m1}l_{m_A}-\beta_{m2}l_{m_A})+$$
$$K_{tm_BC}l_{tm_BC}(Z_{m2}-Z_{m1}+2\beta_{t1}l_{tm_BC}+\beta_{m1}l_{m_BC}+\beta_{m2}l_{m_BC})+ \quad (6)$$
$$C_{s1}l_t(\dot{Z}_{w2}-\dot{Z}_{w1}+2\dot{\beta}_{t1}l_t)+K_{s1}l_t(Z_{w2}-Z_{w1}+2\beta_{t1}l_t)=0$$

Vertical motion of the rear bogie:

$$M_t\ddot{Z}_{t2}+C_{s1}(2\dot{Z}_{t2}-\dot{Z}_{w3}-\dot{Z}_{w4})+C_{s2}(\dot{Z}_{t2}-\dot{Z}_c+\dot{\beta}_c l_c)+K_{s1}(2Z_{t2}-Z_{w3}-Z_{w4})+$$
$$K_{s2}(Z_{t2}-Z_c+\beta_c l_c)+K_{tm_A}(2Z_{t2}-Z_{m3}-Z_{m4}-\beta_{m3}l_{m_A}+\beta_{m4}l_{m_A})+ \quad (7)$$
$$K_{tm_BC}(2Z_{t2}-Z_{m3}-Z_{m4}+\beta_{m3}l_{m_BC}-\beta_{m4}l_{m_BC})=M_t g$$

Pitch motion of the rear bogie:

$$J_t\ddot{\beta}_{t2}+K_{tm_A}l_{tm_A}(Z_{m4}-Z_{m3}+2\beta_{t2}l_{tm_A}-\beta_{m3}l_{m_A}-\beta_{m4}l_{m_A})+$$
$$K_{tm_BC}l_{tm_BC}(Z_{m4}-Z_{m3}+2\beta_{t2}l_{tm_BC}+\beta_{m3}l_{m_BC}+\beta_{m4}l_{m_BC})+ \quad (8)$$
$$C_{s1}l_t(\dot{Z}_{w4}-\dot{Z}_{w3}+2\dot{\beta}_{t2}l_t)+K_{s1}l_t(Z_{w4}-Z_{w3}+2\beta_{t2}l_t)=0$$

Vertical motion of the motor i ($i=1\sim4$):

$$M_m\ddot{Z}_{mi}+K_{mh}(Z_{mi}-Z_{hi}\pm\beta_{mi}l_{mh})+K_{tm_A}(Z_{mi}-Z_{tj}\pm\beta_{mi}l_{m_A}\mp\beta_{tj}l_{tm_A})+$$
$$K_{tm_BC}(Z_{mi}-Z_{tj}\mp\beta_{mi}l_{m_BC}\mp\beta_{tj}l_{tm_BC})=M_m g \quad (9)$$

Pitch motion of the motor i ($i=1\sim4$):

$$J_m\ddot{\beta}_{mi}+K_{mh}l_{mh}(\beta_{mi}l_{mh}\pm Z_{mi}\mp Z_{hi})+K_{tm_A}l_{m_A}(\beta_{mi}l_{m_A}-\beta_{tj}l_{tm_A}\pm Z_{mi}\mp Z_{tj})+$$
$$K_{tm_BC}l_{m_BC}(\beta_{mi}l_{m_BC}+\beta_{tj}l_{tm_BC}\mp Z_{mi}\pm Z_{tj})=T_{Li} \quad (10)$$

Vertical motion of the hollow-shaft i ($i=1\sim4$):

$$M_h\ddot{Z}_{hi}+K_{mh}(Z_{hi}-Z_{mi}\mp\beta_{mi}l_{mh})+K_{hw}(Z_{hi}-Z_{wi})=M_h g \quad (11)$$

Vertical motion of the wheelset i ($i=1\sim4$):

$$M_{\mathrm{w}}\ddot{Z}_{\mathrm{w}i}+C_{\mathrm{s1}}(\dot{Z}_{\mathrm{w}i}-\dot{Z}_{\mathrm{t}j}\mp\dot{\beta}_{\mathrm{t}j}l_{\mathrm{t}})+K_{\mathrm{s1}}(Z_{\mathrm{w}i}-Z_{\mathrm{t}j}\mp\beta_{\mathrm{t}j}l_{\mathrm{t}})+K_{\mathrm{hw}}(Z_{\mathrm{w}i}-Z_{\mathrm{h}j})+p_i=M_{\mathrm{w}}g+F_{0i}(t) \tag{12}$$

Where M_{c} and J_{c} are the carbody mass and moment of inertia; M_{t} and J_{t} are the bogie mass and moment of inertia; M_{m} is the motor mass; M_{h} is the hollow-shaft mass; M_{w} is the wheelset mass; C_{s1}, K_{s1} are the damping and stiffness of the primary suspension; C_{s2}, K_{s2} are the damping and stiffness of the secondary suspension; $K_{\mathrm{tm_A}}$ and $K_{\mathrm{tm_BC}}$ respectively are the equivalent stiffness of motor suspension at point A or point B/C; K_{mh} is the equivalent stiffness between the gearwheel and the hollow-shaft; K_{hw} is the equivalent stiffness between the hollow-shaft and the wheelset; l_{c} is the half-distance between the two bogies centers; l_{t} is half of the bogie fixed wheel base; $l_{\mathrm{m_A}}$ and $l_{\mathrm{m_BC}}$ respectively are the longitudinal distance from the centre of mass of the motor to the motor suspension point A or point B/C; $l_{\mathrm{tm_A}}$ and $l_{\mathrm{tm_BC}}$ respectively are the longitudinal distance from the motor suspension point A or point B/C to the centre of mass of the corresponding bogie; l_{mh} is the longitudinal distance from the centre of mass of the motor to the centre of mass of the hollow-shaft; p_i are the vertical loads between the wheels and the rails, and it can be calculated using Hertz non-linear contact theory; $F_{0i}(t)$ are the functions of wheel/rail excitation force.

In equations (9),(10) and (12), the subscript j ($j=1,2$) is the number of the bogie, when $i=1,2$, $j=1$ and when $i=3,4$, $j=2$; in equations (9)~(12), when $i=1,3$, the symbol $\pm$ and $\mp$ take the upper value and when $i=2,4$, $\pm$ and $\mp$ take the lower value.

In the equation (10), the T_{L} is the torque on the motor exerted by torsional vibration of the drive system through the gearbox, $T_{\mathrm{L}}=(c_1\Delta\dot{\theta}_1+k_1\Delta\theta_1)/R_{\mathrm{g}}$, where R_{g} is the gear ratio.

The slab track is modeled using the finite element method (ZHAO Huaiyun, 2007).(See the reference for more details of the method.)

2.3 Locomotive traction dynamic model and dynamic equations

The locomotive traction dynamic model shown in Figure3 and the locomotive traction can be represented by the following dynamic equation:

$$M\frac{dv_{\mathrm{tr}}}{dt}=F_{\mathrm{tr}}-R(v_{\mathrm{tr}})=\sum_{i=1}^{4}F_{\mathrm{ad}i}-R(v_{\mathrm{tr}}) \tag{13}$$

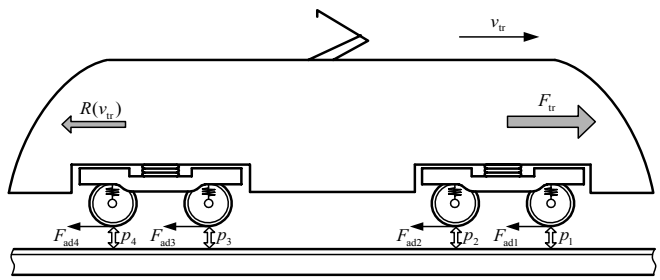

Figure 3. Locomotive traction dynamic model.

Where F_{tr} is the total traction force; F_{adi} are the adhesion forces, $F_{adi} = \mu \cdot p_i$, $T_{adi} = F_{adi} \cdot r_w$, $(i = 1 \sim 4)$; r_w is the wheel radius; μ is the adhesion coefficient; v_{tr} is the train speed (m/s); $R(v_{tr})$ is the running resistance, and the $R(v_{tr})$ can be described by the following expression according to TB/T1407-1998.

$$R(v_{tr}) = [1.02 + 0.0035 \times (3.6 \cdot v_{tr}) + 0.000426 \times (3.6 \cdot v_{tr})^2 \,] \times Mg / 1000$$

2.4 Adhesion coefficient and slip velocity

When the motor traction torque is added to the running wheelset, there is a tangent movement between the wheel and the track on their contact surface. The tangent velocity mentioned above is called slip velocity and can be defined as following:

$$v_{slip} = v_{wh} - v_{tr} = \theta_w \cdot r_w - v_{tr} \tag{14}$$

The adhesion coefficient is assumed to be as bellow (Yoshiki Ishikawa, 1997):

$$\mu(v_{slip}) = a \cdot \exp[-b \times (3.6 \cdot v_{slip})] - c \cdot \exp[-d \times (3.6 \cdot v_{slip})] \tag{15}$$

The values of the parameters *a, b, c* and *d* depend on the rail surface conditions between the wheel and the frictional surface. Table 1 gives the parameters used in this paper. Figure 4 illustrates $\mu(v_{slip})$.

Table 1. Parameters for adhesion coefficient in formula (15).

	a	*b*	*c*	*d*
Dry condition	0.53	0.12	0.53	2.40
Wet condition	0.60	0.20	0.60	0.65

3 SIMULATIONS FOR STICK-SLIP VIBRATION

Based on the models and equations in chapter 2, a simulation program is set up in MATLAB/SIMULINK, the scheme diagram is shown in Figure 5.

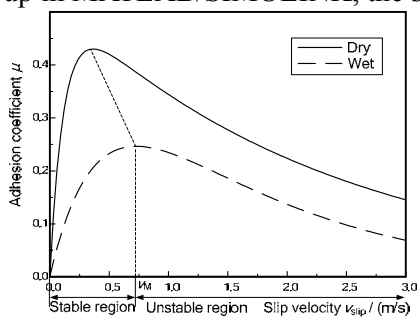

Figure 4. Adhesion coefficient curves in different track conditions.

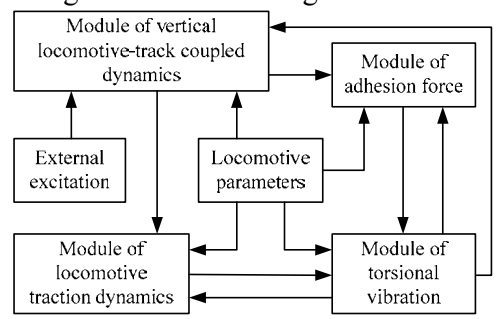

Figure 5. Scheme diagram for simulation.

In this program, there are some modules: the module of locomotive traction dynamics and that of adhesion force can calculate the instantaneous slip velocity; the module of torsional vibration can calculate the drive system torsional dynamics and investigate the self-excited vibration by use of the phase plane method; the module of vertical locomotive-track coupled dynamics can calculate the locomotive vertical dynamics. In this paper, we mainly investigate the self-excited torsional vibration in the drive system; the effects of the self-excited vibration on the locomotive will be discussed in other papers. For the purpose of analyzing the self-excited vibration clearly, the wheel/rail excitation force is temporarily not considered in following calculations.

When the motor traction torque is at a low level, $v_{slip} < v_M$, the v_{slip} is located in the stable region (See Figure 4), where v_M is the slip velocity value corresponding to the maximum adhesion. Each phase trajectory of the hollow-shaft and wheelset (Shown in Figure 6) will be a curve which tends to the initial equalization point (0, 0), indicating that there are no self-excited vibrations occurring in the drive system. This is because the adhesion force between the wheel and the track acts as a positive damping when the slip velocity is located at the ascending slope of the adhesion coefficient curve (ZHENG Lianzhu, 1996), which constantly consumes energy, leaving the drive system in a steady state.

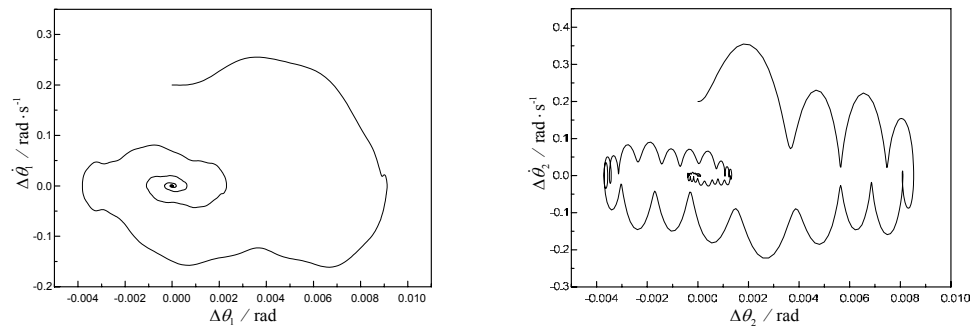

(a) Hollow-shaft (b) Wheelset

Figure 6. Phase diagrams of torsional vibrations when $v_{slip} < v_M$

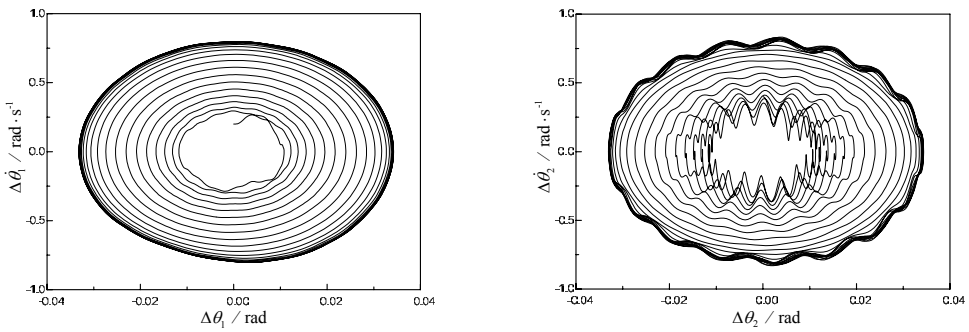

(a) Hollow-shaft (b) Wheelset

Figure 7. Phase diagrams of torsional vibrations when $v_{slip} > v_M$

The slip velocity will increase with the increase of the motor output torque. When $v_{slip_0} > v_M$, the v_{slip_0} is located in the unstable region (See Figure 4), and each phase trajectory (Shown in Figure 7) will tend to a closed curve which is a limit cycle, indicating that a self-excited torsional vibration has occurred. The reason is that the adhesion force between the wheel and the track acts as a negative damping when the slip velocity is located at the descending slope of the adhesion coefficient curve (ZHENG Lianzhu, 1996), which provides energy to the system leading to the self-excited vibration and the phase trajectory will tend to the limit cycle.

4 CONCLUSIONS

In order to investigate the stick-slip vibration of the locomotive with the hollow-shaft drive system, a locomotive-track coupled dynamic model and a simulation program are established based on the theory of the vehicle-track coupled dynamics. Simulation results indicate that the stick-slip vibration will

occur when the slip velocity is located at the descending slope of the adhesion coefficient curve, and the drive system will be in steady state when the slip velocity is located at the ascending slope of the adhesion coefficient curve.

This simulation model could be used to forecast the self-excited torsional vibration of the locomotive drive system and the stability of the self-excited vibration. This model can lay a foundation for further research, such as adhesion control and locomotive dynamics considering the effect of drive system, etc.

ACKNOWLEDGEMENT

The work reported herein was supported by the National Natural Science Foundation of China under grants 50875219, 50821063 and 50823004.

REFERENCES

Clark R.A. (1984). "Stick-slip vibration may hold the key to corrugation puzzle." *Railway Gazette International*. 531-533.

HIROTSU Tetsuji, KASAI Shooji, TAKAI Hideo. (1987). "Self-Excited Vibration During Slippage of Parallel Cardan Drives for Electric Railcars." *JSME International Journal*. 30(266), 1304-1310.

Koan-Sok Baek, Keiji Kyogokua, Tsunamitsu Nakahara. (2007). "An experimental investigation of transient traction characteristics in rolling–sliding wheel/rail contacts under dry-wet conditions." *Wear*. 263(1-6), 169-179.

W.X.Wu, B.V.Brickle, J.H.Smith, R.K.Luo. (1998). "An Investigation into Stick-Slip Vibrations on Vehicle/Track Systems." *Vehicle System Dynamics*. 30(3-4), 229-236.

Yoshiki Ishikawa, Atsuo Kawamura. (1997). "Maximum adhesive force control in super high speed train." *Power Conversion Conference.* Nagaoka, Japan. 951-954.

ZHAI Wanming. (2007). "Vehicle-Track Coupling Dynamics, 3rd edition." *Science Press*. Beijing.

ZHAO Huaiyun, LIU Jianxin, ZHAI Wanming. (2007). "Analysis method of dynamic responses on slab track." *Journal of Traffic and Transportation Engineering*. 7(5), 19-23

ZHENG Lianzhu, JIA Jianzhang, CHENG Yuesun. (1996). "Research on the self-excited vibration in wheeled vehicle powertrain (Part I)." *Transactions of the CSAE*. 12(4), 37-42.

Fatigue Life Prediction of Rubber Nodes

WU Huichao[1], WU Pingbo[1], LAN Qingqun[1]

[1]Traction Power State Key Laboratory, Southwest Jiaotong University, Chengdu 610031, China. Email: wuhuichao1215@yahoo.com.cn

ABSTRACT

Rubber tumbler locating nodes are widely used in railway vehicles as anti-vibration components involving both metal and rubber materials that last many years. It can well control vertical and lateral movements. Damage accumulation due to fatigue, significantly reduces the service life of the rubber tumbler locating nodes. Trains now travelling at higher speeds have led to a poor service environment. Many efforts have been made to optimize the design of rubber tumbler locating nodes. However, experimental methods are limited by costing a great amount of time and money to study the fatigue life of rubber tumbler locating nodes. It is essential to develop a new method to study rubber fatigue life. This paper proposes an effective fatigue life prediction approach for rubber tumbler locating nodes. A non-linear, multi-body model of a rail vehicle is combined with a finite element model of its bogie-frame. Loading histories at tumbler locating nodes were calculated and used as input of fatigue. Fatigue simulation was completed based on stress distribution and stress-time histories. It is shown that a quasi-static simulation for rubber tumbler locating nodes, using nonlinear software, can provide good indication for product design and failure analysis. It is also shown that this approach can be employed at a design stage for both metal and rubber fatigue evaluations.

1 INTRODUCTION

The ability of rubber nodes to control the vertical and horizontal moments has led to them being widely used in the railway vehicle industry. In recent years, the trend toward lighter vehicles and higher speeds has led to the the importance in studying the design and development of competitive vehicles. Because cumulative damage caused by fatigue can seriously reduce the rubber tumbler node service life, we have studied the performance of rubber tumbler node. Rubber tumbler nodes experiencing a sudden fatigue failure is often a threat to the vehicle suspension system. In more serious cases, it may even cause derailment accidentsleading to significant casualties and property losses. It is precisely these reasons that the domestic and foreign scholars have done significant research work in this field. Rubber tumbler nodes consist of metal plates bonded with rubber through a molding process resulting in its fatigue being more complex cthan metal fatigue. Because deformation of rubber materials shows strong similarities in geometry, physics, nonlinear and rubber components with the geometry of the complex, designers in the actual design process have no uniform method of calculation and design (Kim,1998;Oh,1980). In general, engineers have

two tools to assess fatigue toward rubber nodes: tests and simulations. Limited as they are, tests are not possible during the design phase of a new vehicle and require spending a great amount of time and money. With advances in computer technology, simulations based on FEA and multi-body dynamics offer a possibility to predict fatigue.

In this paper, the rigid-flexible coupling dynamic model has been modeled using the software SIMPACK. The fatigue load spectrum can be obtained through simulation with key parameters being studied to analyze the effects of fatigue. Some useful conclusions are drawn from the study. The fatigue design method in this paper can not only greatly shorten the development cycle of new products, but can also provide some guidance for the fatigue test and has a high practical value.

2 THE SIMULATION MODEL

The tumbler axle-box locating node in CRH2 was chosen as a basis for a case fatigue study consisting of rubber and metal.

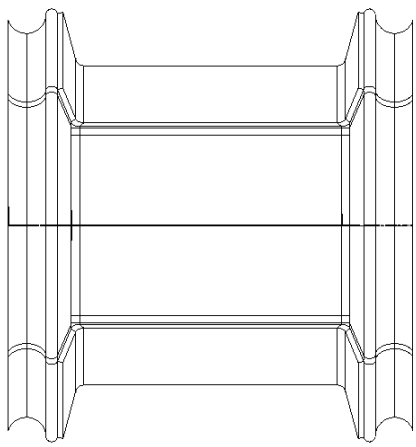

Fig. 1. the whole solid model.

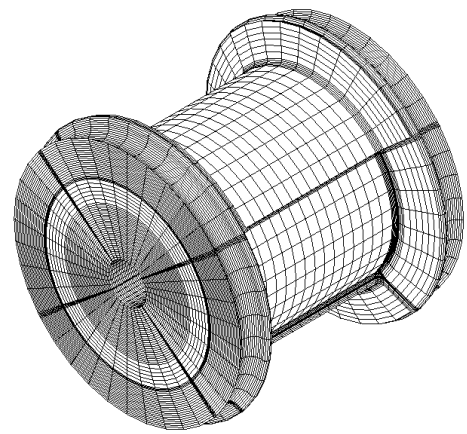

Fig. 2. the finite element model.

It is bonded with rubber and metal through a molding process displaying strong, non-linear mechanical properties. Because of the symmetry of the specimen, in this paper, only a quarter model of the specimen is established. Figure 2 shows the finite element model. The tumbler axle-box locating node is modeled by means of the commercial finite element software ANSYS, giving a model with approximately 23000 degrees of freedom. Solid186 elements represent the corrugated rubber and solid45 elements represent the corrugated metal.

2.1 MATERIALS PROPERTIES

The finite element analysis is used to study the stress distribution of the structure. In order to predict the stress, it is essential to select suitable material models and failure criteria. Rubber is a hyper-elastic material whose mechanical properties are affected not only by the external load but also by time and

temperature. In resent years, there are several hyper-elastic material models that are often used to describe rubber materials based on strain energy potential or strain energy density. The strain energy function can be expressed by the following polynomial series (Ogden,1984):

$$U = \sum_{i+j=1}^{N} C_{ij} \left(\overline{I}_1 - 3\right)^i \left(\overline{I}_2 - 3\right)^j + \sum_{i=1}^{N} \frac{1}{D_i} \left(J_{el} - 1\right)^{2i} \quad (1)$$

Where C_{ij} and D_{ij} are temperature dependent material parameters, J_{el} is the elastic volume strain, $\overline{I}_1$ and $\overline{I}_2$ are the strain are invariant. If $N = 1$, the polynomial formation will become the Mooney-Rivlin hyperelasticity model. The energy potential is as follows:

$$U = C_{10} \left(\overline{I} - 3_1\right) + C_{01} \left(\overline{I}_2 - 3\right) + \frac{1}{D_1} \left(J_{el} - 1\right)^2 \quad (2)$$

The Mooney-Rivlin form was used to model the rubber material. The material constants in Eq.(2) can be determined from experiments (Luo RK,2000; Luo RK,2001). The material constants in Eq.(2) may also be obtained from previously established databases of similar rubber material specimens. Calculating the fatigue life of tumbler axle-box locating nodes require material S-N curves. The curve indicates material failure at a constant dynamic amplitude under a certain number of cycles. S-N curves are generally carried out using the standard fatigue test specimen.

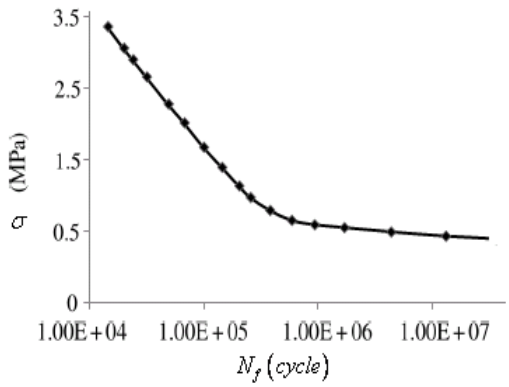

Fig. 3. rubber material S-N curve.

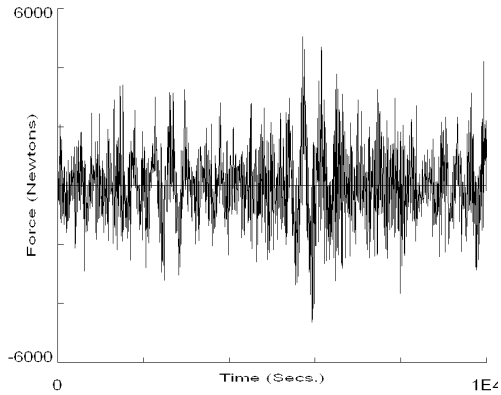

Fig. 4. fatigue load spectrum.

In this paper, material S-N curve is obtained by experiment, shown in Figure.3.

2.2 Fatigue load spectrum

In order to maintain fatigue analysis accuracy, the loading time histories must be able to reflect the actual work condition. In general, loading time histories are measurements of loading for a period of time which must be long enough to

ensure that the measurement reflects a typical duty cycle. However, experiments testing load spectrum require spending a great amount of time and money. In this paper, a rigid-flexible, multibody model of the vehicle including carbody, suspension, bogie and track was set up using the commercial software SIMPACK. The whole vehicle system has 60 degrees of freedom excluding the flexible degrees of freedom. The stress time histories, which indicate the critical locations, are extracted from the simulation results. The stress time histories for the critical locations are translated into input fatigue load spectrum through the rain-flow counting method. The rain-flow counting method, which is considered the non-linear relationship between material stress and material strain, was first introduced by Matsuiski and Endo and has a strong engineering practicability. Through these above processes, random fatigue load spectrum is obtained, shown in Fig.4.

3 NUMERICAL ANALYSIS

3.1 Stiffness Analysis

Rubber nodes are a typical rubber elastic structure working in a pre-stressed state. In this state, the performance of the tumbler axle-box locating node will become extremely complicated. The design of the structure must meet the matching requirements of stiffness making it essential to study the relationship between the performance and radial pre-displacementleading to conclusions that can help the engineering design.

3.1.1 Characteristics radial stiffness

This section studies the influence of pre-displacement on the radial stiffness is studied. According to the symmetry of model structure and load, a quarter model is set up to calculate the stiffness characteristics, which can greatly reduce the simulation time.

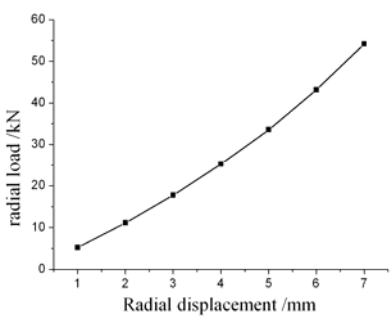

Fig. 5. load and displacement curve.

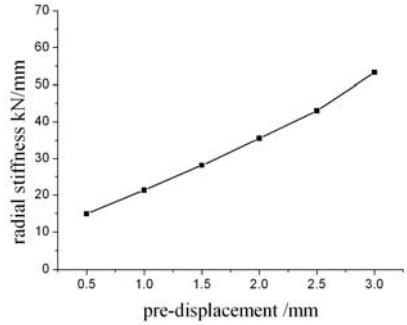

Fig. 6. stiffness and pre-displacement curve.

Fig.5 and Fig.6 show that the radial stiffness increases as the

pre-displacement increases. Radial non-linear properties of tumbler axle-box locating node show more strongly. At the same time, no matter how pre-displacement is applied, its performance often has a certain range of radial linear stiffness; however, when the pre-displacement increases, the scope of the linear stiffness becomes increasingly narrow.

3.1.2 Characteristics of Axial Stiffness

According to the present thesis, pre-displacement will affect axial stiffness. One simple explanation is that the pre-displacement will affect the internal stress distribution; however, the relationship between the axial stiffness and the pre-displacement needs to be studied more carefully. A set of numerical simulations of axial stiffness with different pre-displacements are used.

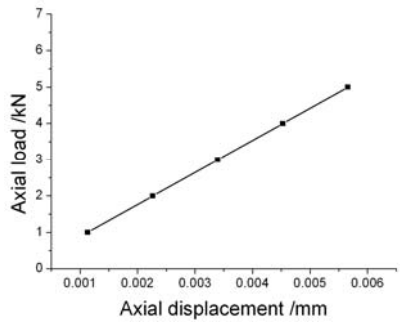

Fig. 7. load and displacement curve.

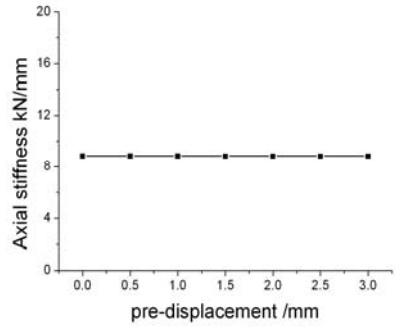

Fig. 8. axial stiffness and pre-displacement curve.

Fig.7 and Fig.8 show that the axial stiffness changes little as the pre-displacement increases. However, the axial stiffness maintains a downward trend, when increasing the pre-displacement and stability of tumbler axle-box locating nodes decreases. In order to improve product stability, it is agreed that the axial performance should stay at a flexible stage.

3.2 Fatigue Life Prediction

In this section, the influence of several factors on the fatigue damage of the tumbler axle-box locating node is studied, using the finite element software ANSYS (ANSYS, 2006).

The pre-displacement of the tumbler axle-box locating node will affect the fatigue damage so it is essential to carefully study the relationship between fatigue life and the stiffness. Some numerical simulations of the tumbler axle-box locating node with different stiffness are calculated.

Fig.9 and Fig.10 show the damage accumulation increase as the pre-displacement increases. In other words, the fatigue life decreases with increasing pre-displacement. The effect of pre-displacement is more significant at the small size pre-displacement stage.

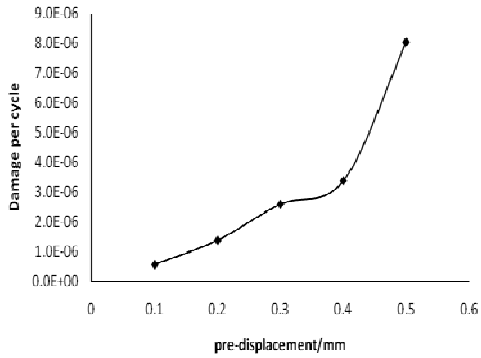

Fig. 9. relation between damage and pre-displacement.

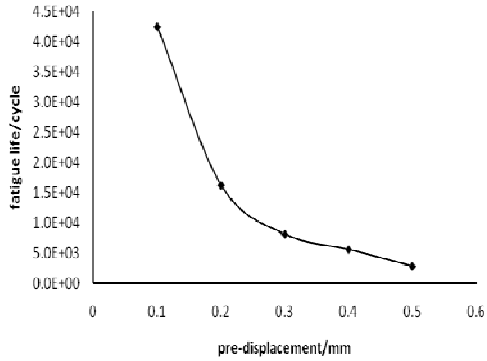

Fig. 10. relation between life and pre-displacement.

4 CONCLUSION

A rigid-flexible multibody model is set up in order to analyze fatigue life of tumbler axle-box locating node, a method used to study the effect of several parameters, namely pre-displacement, on fatigue damage. It is shown that this quasi-static simulation can provide an efficient method of predicting fatigue life of rubber material. Numerical simulation shows that stiffness and fatigue life are significantly affected by pre-displacements. So we should choose suitable pre-displacement in order to prolong life and good dynamic performance for rubber tumbler locating nodes.

ACKNOWLEDGEMENT

This work is supported by the National Natural Science Foundation of China (No. 50675181) and the New Century Excellent Talent Foundation (NCET-07-0717). The 'TIANFU Excellent Youth' Science Innovation Foundation (NO.2)

REFERENCES

Kim WD. "Application of FEA to design of rubber component." Trans Korean Soc Mech Eng 1998;38(12):42–7.

Oh HL. "A fatigue-life model of a rubber bushing." Rubber Chem Technol 1980;53:1226–38.

Ogden RW. "Non-linear elastic deformation." Chichester: Ellis Horwood Limited; 1984.

Luo RK, Wu WX, Mortel WJ. "Effect of loading environment on rubber bolster springs used in railway vehicle bogies." Plast rubber compos 2000;2(29):88-91.

Luo RK, Gahagan PG, Wu WX, Mortel WJ. "Determination of rubber material properties for finite element analysis from actual products." In: Proceedings of the second European conference on constitutive models for rubber. A.A.Balkema;2001. p.257-60.

ANSYS theory reference, release 8.1. ANSYS, Inc. 2006

Application Research of GPS Based on Google Earth Platform

Zhen-Bo Wang[1], Rui-Xiang Chen[2], Niandong Jiang, Hui Zhang, ZhiRen Sha

[1] Graduate, Intelligent Transportation Research Center, Sun Yat-sen University, Guangzhou 510275, China, Phone: 13729340317; FAX (+86) 020-84113689; email: hawk.feather@163.com

[2] Senior Engineer, Intelligent Transportation Research Centre; Sun Yat-sen University; Guangzhou 510275; China.

ABSTRACT

Google Earth has masses of satellite image data, geographic information, and the functional KML interface. By employing these features, this paper realizes GPS serial-port communication, static and dynamic GPS accuracy analysis, GPS error offset, and GPS information publishing are more convenient and effective in offsetting the system error and improving GPS accuracy than traditional methods. Moreover, it brings a vivid and friendly presentation in publishing GPS information with supported satellite image data.

INTRODUCTION

In recent years, automobile and mobile telephones play significant roles in social activities (Colombo OL, Evans AG, 1998). To meet the sharply increasing needs for positioning, GPS (Global Positioning System) technology and applications are widely used in industriesthat improve economics of the society.

The essence of a GPS application is the displaying of the geographic location of a target, including obtaining and publishing information. It is important to check the accuracy of GPS sensors for the distinction among GPS sensors in production. Generally, it is necessary to access the longitude and latitude of a specific location to operate an experiment to verify GPS accuracy. Moreover, to improve the accuracy, differential GPS experiment requests even more specific spots, and GPS sensors have to be set in the exact places. For traditional information publishing, a visual representation of data and graphics is supported by GIS (Geographic Information System).

Though both methods mentioned are effective in obtaining and publishing GPS information, they have flaws. Traditional experiments verifying GPS accuracy request the exact location to place the sensor. Likewise, the existing methods for publishing GPS information demand support by a GIS map, which has to be formed in advance based on a massive data acquisition and is not always accurate enough for location verification. However, the emergence of Google Earth provides a high resolution remote sensing image, which is free and capable of meeting the needs for clearly spotting the target in most of the city. With the support of the Google Earth platform, an accurate location can be achieved, and

the combination of the vivid remote sensing image from Google Earth and graphics from the GIS offers a new option in research (MR Craymer, 1990).

APPLICATION REALITY OF GPS

Raw data parsing.

Almost all the datagram from GPS sensors are in accord with NMEA-0183 protocol, an international standard protocol formed by NMEA (National Marine Electronics Association). In this research, a portable MG/MGL-30 GPS receiver is chosen for its convenience of storing data, which transmits by simulating serial-port communication based on USB Communication Technology (Han S, 1997). Its communication configuration is shown in Table 1.

Table 1. Serial-port communication configuration settings.

Parameter configure	Baud rate	Data bit	parity checkout	Stop bit
value	4800	8	Null	1

NMEA-0183 has its grammar to parse every message. After setting the correct configuration in Table 1, raw data can be received. According to practical demand, it is necessary to parse the message with its beginning "$GPRMC," which is the briefest message to obtain time and geographic information. Thus, the flow chart below (see Figure 1) is designed to parse the "$GPRMC" message in order to store time and geographic data into a database.

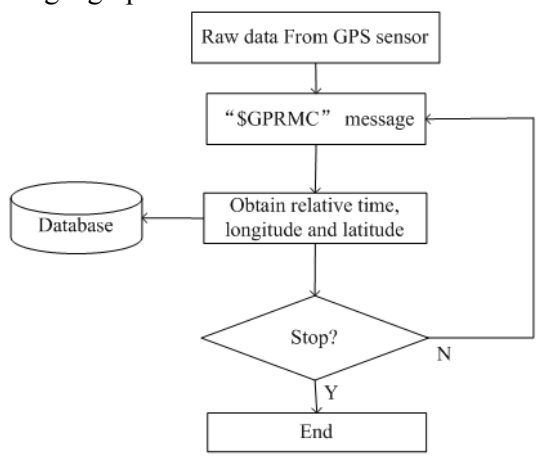

Figure 1. Flow chart of raw data parsing.

Static GPS Accuracy Analysis.

The accuracy of the location position sent by the GPS sensor is influenced by many factors, such as the available number of satellites, the specific satellites, and even the weather and circumstance. Besides the static accuracy, different GPS sensors cause different output delay. As a sequence, dynamic offset could bring considerable error. However, under a similar environment, a GPS sensor presents a stable accuracy.

After Data Extraction from GPS raw data, the relative time, longitude and latitude can be found in database. Then, this information is transferred into KML files so as to be imported into Google Earth software. Compared with the actual spot where the GPS sensor is placed, static offset can be calculated. The static accuracy analysis flow chart (see Figure 2) is below.

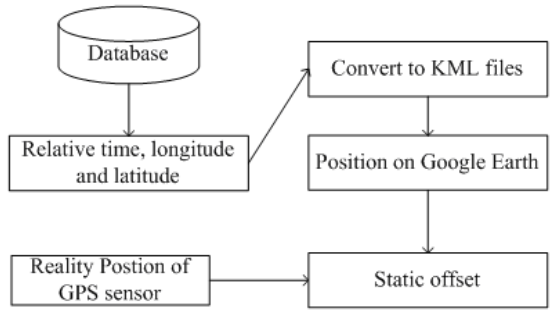

Figure 2. Flow chart of static GPS accuracy analysis.

An experiment has been done at the centre square of the School of Engineering (23°04'00"N 113°22'51"E), Sun Yat-sen University.

Environment: Sunny, Receiving 6-7 effective satellites, 5 minutes of experiment time, 1 time/s of sampling rate; Analysis: The static data of GPS, which distribute in a circle with 5 meter diameter, are shown in Figure 3.

Longitude offset: 00°00'08". Latitude offset: 00°00'24". Distance offset: 7.39m.

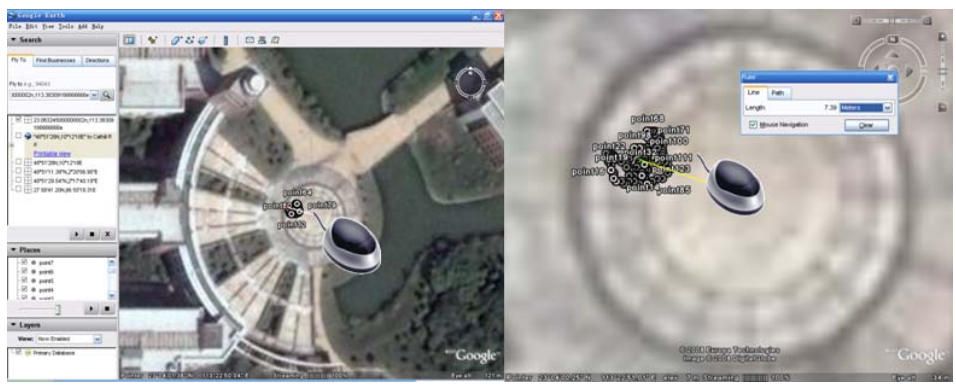

Figure 3. Experiment of static GPS accuracy analysis.

Dynamic GPS Accuracy Analysis.

Besides the static offset, dynamic error exists when it is operated in navigation, for the delay of output data. When a GPS device is mounted on a vehicle, a distance offset caused by a dynamic time delay can not be neglected. It seems difficult to find out the exact time delay directly. However, by taking advantage of a simple formulation “T= S/V”, a technique flow chart (see Figure 4) can be used to obtain time delay indirectly.

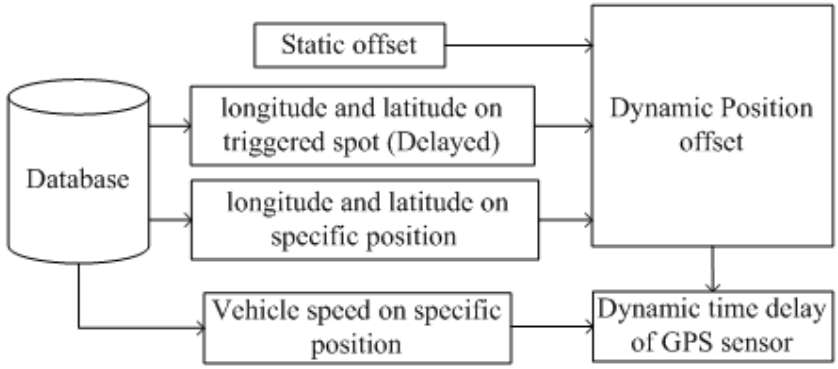

Figure 4. Flow chart of dynamic GPS accuracy analysis.

A dynamic experiment has been done on a laboratorial lane at the School of Engineering at Sun Yat-sen University (see Figure 5). When the vehicle, equipped with mounted a GPS sensor, passed the specific point, events were triggered: the time was marked down, longitude and latitude was stored, and the speed was recorded. Somehow triggered position is not exact the location of the specific point but the delayed one. After comparing it with the correct coordinates, the dynamic position offset could be obtained. Then, the dynamic time delay could be calculated with the vehicle speed.

As a result, an average speed of 38 km/h, caused a 16.5 meter dynamic offset, implying the GPS sensor had a time delay of about 1.5 seconds.

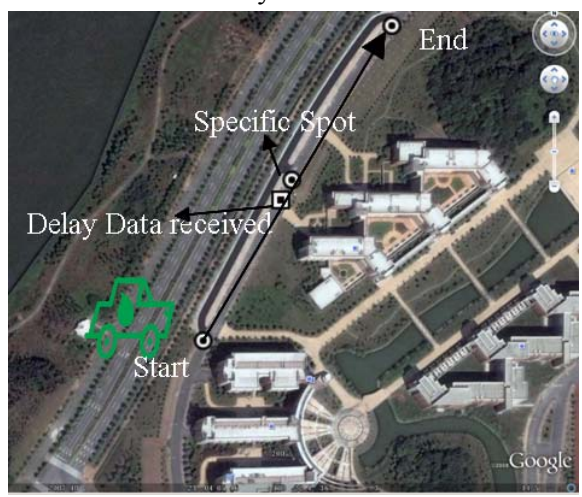

Figure 5. Experiment of dynamic GPS accuracy analysis.

KML Interface in Google Earth.

The layers of map data, landmarks, and other additional information of Google Earth are organized by KML (Keyhole Markup Language) or KMZ files. Google declared that the control of the KML would be open to public after the OOXML (Office Open XML file formats) from Microsoft became an international standard in April, 2008 (Google KML format, 2008). Then, the OGC has taken over the KML, and the KML used in Google Earth and Google Maps

also became an international standard (Google Earth. KML 2.1 Reference, 2007).

KML, which is proposed by Google, is a kind of language and file format based on XML (eXtensible Markup Language). It can be used to store various kinds of information, such as point, polyline and image, and can be used to display the information for the client of Google Earth. KML provides the interfaces for data cross operation, laying stress on the organization of data and the display styles of image and graphic to be loaded into Google Earth for display (Chen Ruixiang et al, 2007).

The GPS data must be transformed before being loaded into Google Earth. The format of the KML file used for the transformation of coordinates is shown by Fig. 6.

```
<?xml version="1.0" encoding="utf-8"?>
    <kml>
    <Placemark> <name>point1</name>
      <Style>   <Icon>
<href>http://maps.google.com/mapfiles/kml/shapes/placemark_circle.png</href>
                </Icon>
      </Style>
      <Point>   <coordinates>  113.3807111,23.06705556,0</coordinates>
      </Point>
    </Placemark>
```

Figure 6. The KML file format of point feature.

The ‘Placemark’ is ab attributes of the landmark; the ‘Icon’ attribute in ‘Style’ points to the icon file used to display point information; and the ‘coordinates’ attribute points to the coordinate of the point information.

Realization Method of GPS Information Release.

The experimental technique proposed in this paper is an error-analysis technique of GPS data based on the Google Earth and is also a kind of method of GPS information release. It can be achieved in the field of vehicle navigation systems and positioning, and safety monitoring based on GPS. For instance, the vehicle navigation information can be sent wirelessly to the server. The server will then transform the GPS data into KML file, showing clients the position of the vehicle on Google Earth platform. As a result, the driver can obtain the real-time navigation information. Extending techniques like these can combine the aerial data from Google Earth, not only reflecting the real-time performance, but also making the information display direct and abundant (see Figure 7).

Figure 7. GPS Information Release.

CONCLUSION

This paper puts forward an experimental technique for dynamic-static error analysis of GPS based on the Google Earth platform. After acquiring and analyzing messages from the receiver, the positioning accuracy of GPS can be improved through reducing system error. It is more direct and rapid compared with the traditional technique. Meanwhile, the technique combined with the Google Earth is superior to the traditional method of information release in the field of GIS.

It is worth noting that the data of Google Earth is soured from aerial images and its error varies in different areas. Therefore, the "correct coordinate" used in this paper tends to adapt the display coordinate of the Google Earth software. And the system error of Google Earth is almost the same in a specific area so that the works can be achieved despite system error.

REFERENCES

Colombo OL, Evans AG (1998). "Testing decimeter-level, kinematic, differential GPS over great distances at sea and on land." *In: Proceedings of ION GPS-1998, Nashville, 15-18 September* , pp 1257–1264

Chen Ruixiang, He Zhaocheng; Huang Min et al. (2007) "The Application of Google Earth in Traffic Information System." *Acta Scientiarum Naturalium Universitatis Sunyatseni* [J],.12

Google Earth. KML 2.1 Reference [Z], 2007.5.2
http://code.google.com/apis/kml/documentation/kml_tags_21.html

Google KML format become international standard [Z], 2008.4.16
http://smb.pconline.com.cn/hydt/0804/1270444.html

Han S (1997). "Carrier phase-based long-range GPS kinematic positioning." *PhD thesis, School of Geomatic Engineering, The University of New South Wales*

MR Craymer. (1990) "Specifications for urban GPS surveys" *Surveying and Land Information Systems.*

A Study of the Fuzzy PID Control over the Hydraulic Semi-active Suspension in Consideration of Automotive Engine and Passenger-seat System

Xiang Chen[1]， Guo-fang Li[2], En-yong wang[3] and Xin-jia Jiang[4]

[1]Associate Professor of Institute of Mechanical Detection and Fault Diagnosis, Lanzhou City University, Lanzhou, 730070, China, PH 13893324116; email: chenxiang-64@126.com
[2]Associate Professor of Lanzhou City University, Lanzhou, 730070, China.
[3]Professor of Lanzhou City University, Lanzhou, 730070, China, PH13609388269.
[4]Associate Professor of Lanzhou City University, Lanzhou, 730070, China.

ABSTRACT

Based on the study of the 1/2 vehicle body of a semi-active suspension with fuzzy control, and taking into consideration such factors as engine and "passenger-seat" system, an automotive dynamic model of 1/4 vehicle body with 4-DOF is created. A parameters-self-tuning fuzzy PID controller is designed for the semi-active hydraulic suspension of the 1/4 vehicle body. The results of simulation by MATLAB/Simulink software show that the high-frequency constant engine excitation has little effect on acceleration of the vehicle seats, and the fuzzy PID controller is more self-adaptable than the fuzzy controller; therefore, ride comfort of the vehicle is better.

1 INTRODUCTION

The design of the automotive suspension system is an essential part concerning the study of automotive dynamics, which is of great importance in improving automotive performances, such as ride, comfort and handling stability. The spring constant and damping coefficient of the passive suspension system are not variable; therefore, it is hard to produce the shock-absorbing effect required by modern automobiles. The semi-active suspension system reduces the vibration of vehicle body and seats, with the spring constant and damping independently adjusted. Compared to active suspension system, it is simple in structure, hardly consumes the power from the system while in operation, and does not produce resonance of the unsprung mass. Its performance is almost equally effective as that of the active control. As a result, it will find a good application(Song et al, 2003).

Currently, many studies done on semi-active suspension systems are based mostly on the 1/4 vehicle body model with 2-DOF. In this type of model, consideration of the affects on ride comfort is only taken of the vehicle body, tire, suspension and road excitation, without considering the engine vibration and "passenger-seat" system. Therefore, it does not reflect the accurate load the vehicle body is subjected to and its dynamic model is confined to a certain degree. Based on our studies of the active and semi-active suspensions , we established

the 1/4 vehicle model of 4-DOF, with comprehensive consideration of many involved factors, such as vehicle body, tire, engine, seat, passenger and suspension, etc.

2 1/4 VEHICLE MODEL WITH 4-DOF

For the convenience of the study, and to be applicable to the real situation of a vehicle, the 1/4 vehicle body is simplified as a vibrating system, as shown in Figure 1, where m_1、m_2、m_3 and m_4 stand respectively for the unsprung mass, mass of the vehicle body, mass of the engine and mass of the passenger, z_1、z_2、z_3、z_4 respectively for their vertical displacement, k_1、k_2、k_3、k_4 respectively for the spring constants of the tire, the suspension, engine support and seat, and c_1、c_3、c_4 respectively for the damping coefficients of the tire, engine support and seat, A_s for the orifice area of the controllable throttle, z_0 for the excitation from the road surface, F for the exciting force of the engine.

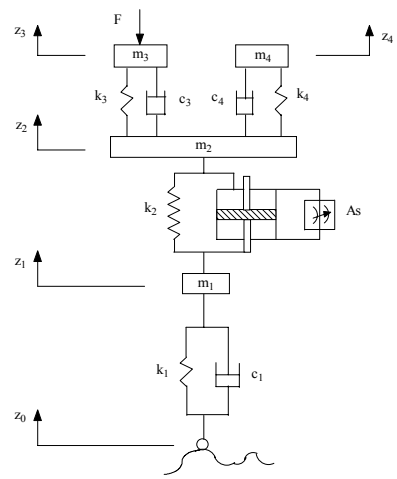

Figure 1. 1/4 vehicle model with 4-DOF.

According to Newton's second law, the dynamic equation of the 1/4 vehicle body with 4-DOF is:

$$\begin{cases} m_1\ddot{z}_1 = k_1(z_0 - z_1) + c_1(\dot{z}_0 - \dot{z}_1) - \left[k_2(z_1 - z_2) + f_d\right] \\ m_2\ddot{z}_2 = k_2(z_1 - z_2) + f_d - \left[k_3(z_2 - z_3) + c_3(\dot{z}_2 - \dot{z}_3) + k_4(z_2 - z_4) + c_4(\dot{z}_2 - \dot{z}_4)\right] \\ m_3\ddot{z}_3 = k_3(z_2 - z_3) + c_3(\dot{z}_2 - \dot{z}_3) - F \\ m_4\ddot{z}_4 = k_4(z_2 - z_4) + c_4(\dot{z}_2 - \dot{z}_4) \end{cases}$$

(1)

$$f_d = A_s(p_1 - p_2) = c(\dot{z}_1 - \dot{z}_2)$$

(2)

Replacing these physical variables in the system dynamic equation with state variables, let

$$x_1 = z_1,\ x_2 = z_2,\ x_3 = z_3,\ x_4 = z_4,\ x_5 = \dot{z}_1,\ x_6 = \dot{z}_2,\ x_7 = \dot{z}_3,\ x_8 = \dot{z}_4$$

$$\boldsymbol{X} = \{x_1, x_2, x_3, x_4, x_5, x_6, x_7, x_8\}^T \tag{3}$$

then the equation of the system state is

$$\dot{\boldsymbol{X}} = \boldsymbol{AX} + \boldsymbol{BU} + \boldsymbol{CF} \tag{4}$$

$$\boldsymbol{A} = \begin{Bmatrix} 0 & 0 & 0 & 0 & 1 & 0 & 0 & 0 \\ 0 & 0 & 0 & 0 & 0 & 1 & 0 & 0 \\ 0 & 0 & 0 & 0 & 0 & 0 & 1 & 0 \\ 0 & 0 & 0 & 0 & 0 & 0 & 0 & 1 \\ -\frac{k_1+k_2}{m_1} & \frac{k_2}{m_1} & 0 & 0 & -\frac{c_1+c}{m_1} & \frac{c}{m_1} & 0 & 0 \\ \frac{k_2}{m_2} & -\frac{k_2+k_3+k_4}{m_2} & \frac{k_3}{m_2} & \frac{k_4}{m_2} & \frac{c}{m_2} & -\frac{c+c_3+c_4}{m_2} & \frac{c_3}{m_2} & \frac{c_4}{m_2} \\ 0 & \frac{k_3}{m_3} & -\frac{k_3}{m_3} & 0 & 0 & \frac{c_3}{m_3} & -\frac{c_3}{m_3} & 0 \\ 0 & \frac{k_4}{m_4} & 0 & -\frac{k_4}{m_4} & 0 & \frac{c_4}{m_4} & 0 & -\frac{c_4}{m_4} \end{Bmatrix}$$

$$\boldsymbol{B} = \begin{Bmatrix} 0 & 0 & 0 & 0 & \frac{k_1}{m_1} & 0 & 0 & 0 \\ 0 & 0 & 0 & 0 & \frac{c_1}{m_1} & 0 & 0 & 0 \end{Bmatrix}^{\mathrm{T}}$$

$$\boldsymbol{C} = \begin{Bmatrix} 0 & 0 & 0 & 0 & 0 & 0 & -\frac{1}{m_3} & 0 \end{Bmatrix}^{\mathrm{T}}$$

where, $\boldsymbol{U} = \{z_0, \dot{z}_0\}^{\mathrm{T}}$, p_1、p_2 stand respectively for the pressure exerted on the up-chamber and down-chamber of the hydraulic cylinder, c for the damping coefficient of the controllable damper

3 DESIGN OF THE SELF-ADAPTABILITY FUZZY PID CONTROL SYSTEM

The ride comfort of a vehicle is directly related to the control strategy of the semi-active suspension. The fuzzy control is of better robustness and can better overcome some uncertainties in the system; however, its control precision is low. The typical PID control is of simple structure, high precision, and has a good control performance for the linear system (Chen et al, 2008). The fuzzy PID control used in this study combines the fuzzy control and typical PID control, making the system faster, with better robustness and higher control precision.

Based on the 1/4 vehicle model with 4-DOF, the speed error of vehicle body e and its rate of change ec are used as the inputs of the fuzzy controller, and 3 gain parameters Δk_p、Δk_i and Δk_d of the PID controller as the outputs. The fuzzy PID controller can adjust online the three parameters according to the fuzzy control principle, and the damping force of the hydraulic damper is changed with the variation of the opening area of the throttle orifice under control so as to produce the damping force in accordance with the running conditions of motor

vehicle, thus achieving the control over the vibration of the vehicle body. The structural theory of the fuzzy PID control system over the 1/4 vehicle body with 4-DOF is shown as in Figure 2.

The basic universes of the input and output variables should respectively be determined according to the maximum value of the road disturbance and the

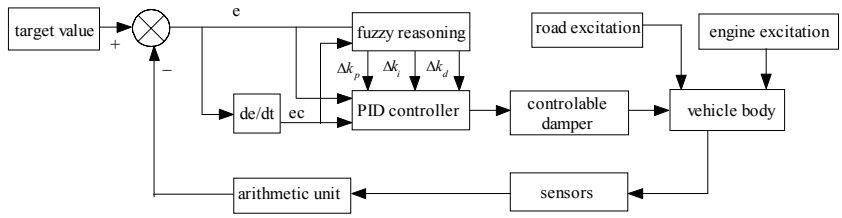

Figure 2. Block diagram of the fuzzy PID control system.

capacity
of maintaining a good performance of the suspensions while running on a rough road. Through the computer simulation of the road condition, the basic universes of the two input variables are taken as $e \in [-3,3]\,\mathrm{m/s}$ and $ec \in [-3,3]\,\mathrm{m/s^2}$, and their fuzzy sets are classified into (NB, NM, ZE, PM, PB). The basic universes of the output variables are $\Delta k_p \in [0,3]$、$\Delta k_i \in [0,3]$、$\Delta k_d \in [0,3]$, and their fuzzy sets are classified into (NB, NM, NS, ZE, PS, PM, PB). The membership functions of input and output variables are assumed to be triangular types.

The role of the proportional coefficient of the PID controller is to increase the response speed and precision of the system and the role of the integral coefficient is to eliminate the static error of the system. The role of the differential coefficient is to improve the dynamic property of the system. The rules of fuzzy control are designed according to the PID control rules and fuzzy control theory. The tuning rules of three parameters are performed as Table 1.

Table 1. Rule table of fuzzy control.

$\Delta k_p / \Delta k_i /$ Δk_d		EC				
		PB	PM	ZE	NM	NB
E	PB	NB/ZE/PB	NB/ZE/PS	NS/ZE/PM	ZE/ZE/PS	PS/ZE/PB
	PM	NB/NB/PB	NB/NM/PM	NS/ZE/PS	PS/PS/PS	PMPS/PM
	ZE	NM/NB/PS	NS/NM/PS	ZE/ZE/ZE	PM/PM/PS	PM/PS/ZE
	NM	ZE/NS/ZE	ZE/NS/NS	PS/ZE/NM	PB/PM/PM	PB/PB/PM
	NB	ZE/ZE/NS	ZE/ZE/NS	PS/ZE/NM	PB/ZE/PS	PB/ZE/PB

The output variables use the centre of gravity method for defuzzification. The

calculating formulas of on-line tuning PID parameters are:

$$\begin{aligned} k_p &= k'_p + \Delta k_p \\ k_i &= k'_i + \Delta k_i \\ k_d &= k'_d + \Delta k_d \end{aligned} \tag{5}$$

where k_p、k_i and k_d are the final control parameters at the PID control, and k'_p、k'_i and k'_d are the initial parameters at the PID control. After testing and adjustment, it is determined that $k'_p = 34$, $k'_i = 0.9$, $k'_d = 0.6$.

4 TIME DOMAIN MODEL OF THE ROAD ROUGHNESS EXCITATION AND ENGINE EXCITATION

4.1 Time domain model of the road roughness excitation

The road power spectral density is used to describe the statistical characteristic of the road roughness, which is taken as the inputs causing vehicle vibration. The road displacement power spectral density recommended by GB7031-86 is in the following form (Yu, 2007)

$$G_q(n) = G_q(n_0)(\frac{n}{n_0})^{-W} \tag{6}$$

where n is the space frequency, n_0 is the referential space frequency. $G_q(n_0)$ is road roughness coefficient. W is the frequency index，taken as W=2. Considering the effect of the vehicle speed, the space spectral density can be converted into the time spectral density, and the result is

$$G_q(f) = G_q(n_0)n_0^2\frac{v}{f^2} \tag{7}$$

where f is the time frequency, v is the vehicle speed. Hence,

$$G_{\dot{q}}(f) = (2\pi f)^2 G_q(f) = 4\pi^2 n_0^2 G_q(n_0)v \tag{8}$$

$$G_{\ddot{q}}(f) = (2\pi f)^4 G_q(f) = 16\pi^4 n_0^4 G_q(n_0) f^2 v \tag{9}$$

It can be seen from the equation (8) that the road input speed power spectrum is a constant at the entire frequency range that is “white noise.” Therefore, the way to produce the random road roughness outline is to allow the white noise to pass a filter, and as a result, the road excitation exerted on wheel can be expressed by the differential equation

$$\dot{z}_0 = -2\pi f_0 z_0 + 2\pi n_0\sqrt{G_q(n_0)v}w(t) \tag{10}$$

where f_0 is the lower end frequency of road input, normally taken as 0.1Hz,

$w(t)$ is the white noise at mean value 0 and power 20dB.

Grade B and Grade C roads of China account for a large proportion; therefore, Grade C road is taken as the excitation input in this simulating test, hence road roughness coefficient is 128×10^{-6} m^2/m^{-1}. Figure 3 shows the excitation single to the vehicle when running at a speed of 25m/s.

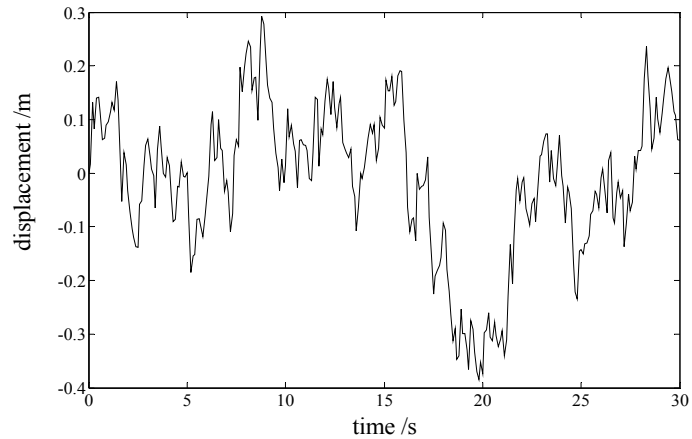

Figure 3. The C-grade road signal.

4.2 TIME DOMAIN MODEL OF ENGINE EXCITATION

The rotating speed of the engine is usually under 6000r/min, and its vibrating source is mainly the second-order mechanical vibration and therefore its frequency is normally under 200Hz. The engine vibration frequency is taken as 25 Hz in the simulating test, using $F = 200\sin 157t$ N sinusoidal to simulate the exciting force of the engine vibration.

5 ANALYSIS OF THE RESULT OF THE SIMULATING TEST

Use MATLAB/Simulink to do computer simulation of the model system. The vehicle model selected is the Red Flag CA 7460 automobile produced by the No 1 Changchun Automobile Works. Its structural parameters are shown as in Table 2.

Table 2. Structural parameters of the Red Flag CA7460.

m_1 / kg	m_3 / kg	k_1 / N· m^{-1}	k_3 / N· m^{-1}	c_1 /(N·s)·m^{-1}	c_3 /(N·s)·m^{-1}
150	120	800	10000	150	3000
m_2 / kg	m_4 / kg	k_2 / N· m^{-1}	k_4 /N· m^{-1}	c_2 /(N·s)·m^{-1}	c_4 /(N·s)·m^{-1}
1800	65	4000	500	2546	150

Table 3 shows the result of simulation of the semi-active suspensions using two different strategies of fuzzy control and fuzzy PID control. Figures 4 and 5 are the graphs of displacement and acceleration of the passenger and vehicle body with engine excitation under fuzzy PID control, while Figure 6 is the graph of acceleration of the passenger with and without engine excitation under fuzzy PID control. Figures 7, 8 and 9 are respectively the graphs of acceleration of passenger,

dynamic load of tire, and dynamic flexibility of suspension under fuzzy PID control and fuzzy control.

Table 3. RMS comparisons of the fuzzy and fuzzy PID control suspension

suspension		fuzzy control	fuzzy PID control
acceleration /m·s^{-2}	passenger	0.0438	0.0357
	vehicle body	0.0624	0.0470
dynamic load /N		69.505	54.575
dynamic flexibility /m		0.019	0.0108

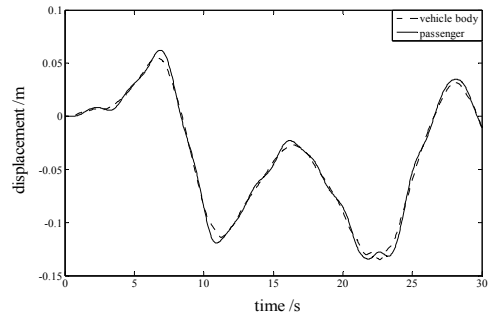

Figure 4. The displacement of passenger and vehicle body.

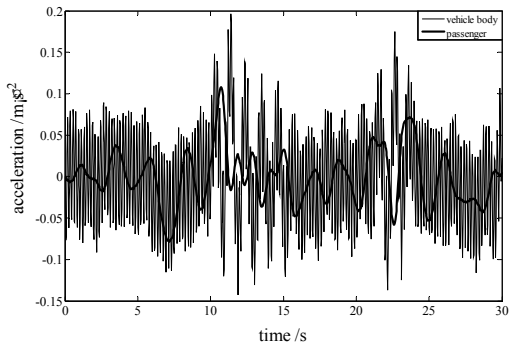

Figure 5. The acceleration of passenger and vehicle body.

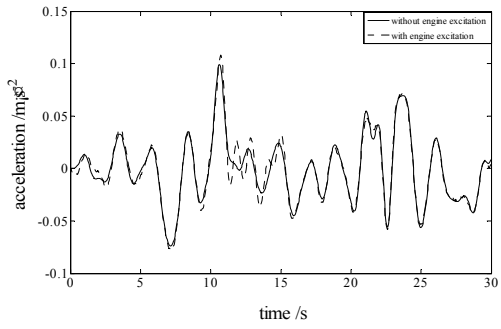

Figure 6. The acceleration of passenger with/without engine excitation.

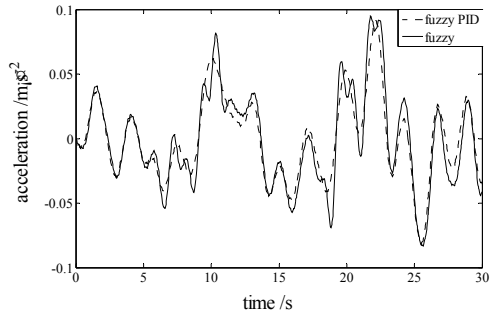

Figure 7. The acceleration of passenger under fuzzy PID/fuzzy control.

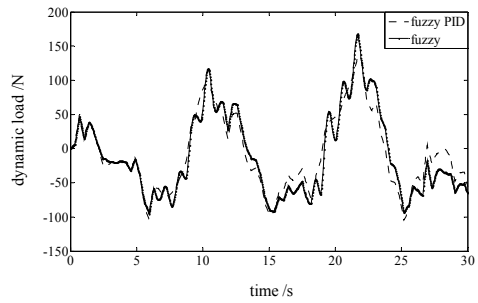

Figure 8. The dynamic load under fuzzy PID/fuzzy control/

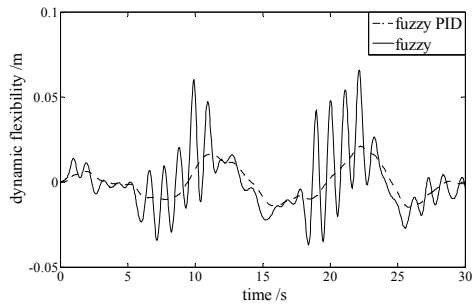

Figure 9. The dynamic flexibility under fuzzy PID/fuzzy control.

6 CONCLUSIONS

(1)The passenger vibration displacement is in perfect harmony with that of suspension, which shows the ride comfort is greatly improved.

(2)The connection between the seat and the suspension is simplified as the connection of the spring and damper. The peak value of its displacement is a bit higher than that of the rigid connection, but the peak value of its acceleration is reduced by 44.931%, which shows the structure of spring and damper is acceptable.

(3)The engine excitation is approximately a high-frequency constant, one compared with the road excitation, and when they both exert on the vehicle body, the RMS of passenger acceleration increases only by 2.61% more than the RMS without engine excitation.

(4)Compared to fuzzy control, fuzzy PID controller reduces the RMS of such

ride comfort values as dynamic load of tire, dynamic flexibility of suspension, etc, to 21.480% and 43.158% respectively, which shows the good self-adaptability of the fuzzy PID control system.

REFERENCES

Chen,X., Wang, E.Y, Qian, Y.S, Zhang, Z.B. (2008). "Simulation of Automobile Hydraulic Semi-active Suspension with Fuzzy PID Controlling System on Simulink." Mechanics in Engineering, 30(5), 57-61.

Song, X.B., Southward S. (2003) "An Adaptive Semi-active Control Algorithm for Vehicle Suspension Systems." Proceedings of ASME MECE 2003, 1-9.

Yu, Z. S. (2007). "Automobile Theory." China Machine Press, 206.

Study On Power Control Of Electric Power Steering System

Chunyan Mu[1], Jingnuo Yu[1], Wansheng Zhao[1], Jianxia Liu[1]

[1] Key Lab of Advanced Manufacturing & Automation Technology, Ludong University, P.O. Box 264025, Yantai Shandong Province, China; PH(+86)13220933388; email: muchunyan1@163.com

ABSTRACT

The method of the proportional control power is analyzed. The oscillations of an Electric Power Steering System are found. On these bases, the improvement measures of the power control carried on a differential calculus compensate is proposed. Proportional plus differential calculus control is designed. Analysis results show that the design of the proportional plus differential calculus control of the power control has a good function. The test shows that the control means is valid, and has a guiding significance to the development of electric power steering.

INTRODUCTION

An electric power steering system relies on electric motors to provide the impetus. EPS, compared with the traditional hydraulic power, to save fuel and improve stability, is beneficial to the environment (Man,H. L,2005). This paper studies the power control methods of an electric power steering system. Using proportional control methods with electrical power steering, the driver will feel a clear vibration in the steering wheel and reduced the stability. The adoption of proportional plus differential calculus control methods can significantly improve performance.

1 ELECTRIC POWER STEERING SYSTEM

When turning, the torque sensor detects steering shaft torque, the speed sensor signal detects the speed signal with the importation of ECU. ECU will process these signals to determine the size and power steering torque to the motor issue directive (Lin Yi,2003). Through deceleration, motor torque from the electromagnetic clutch decelerates to add twisting bodies, plus adjusts the car's steering bodies so that the steering force can adaptto easily provide different help at different speeds to ensure that vehicles in low- speed turns have flexiblity andhigh-speed turns are stable and reliable.

2 ELECTRIC POWER STEERING SYSTEM MATHEMATICAL MODEL

To analyze an electric power steering system power control, the impact of gear-suffered ground as input, the inhabitants applied steering wheel torque on the driver steering wheel as output, and the time-domain response characteristics of

motor steering system represent electric power steering power characteristics of the system. Figure 1 is a power function of the motor control block diagram. We hope that the system can guarantee flexibility in low-speed turning and stability and reliability inhigh-speed turning (Lin Yi ,2001).

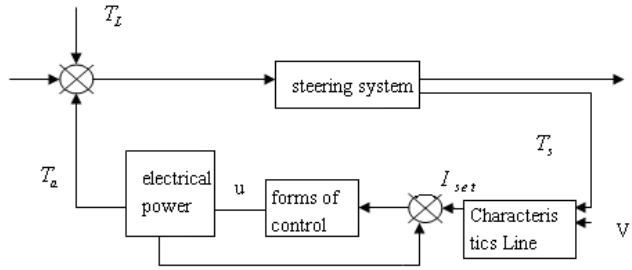

Figure1. Control system diagram.

The steering system dynamics analysis, gets the following equation:

$$T_S = K_s(\theta_h - \theta_c) \tag{1}$$

$$T_h - T_s = J_h \frac{d^2\theta_h}{dt^2} + B_h \frac{d\theta_h}{dt} \tag{2}$$

Where, T_h is imposed for the steering wheel on the steering torque; T_s is the torque sensor detecting the steering torque; K_s is the torque sensor stiffness; θ_h is fthe steering wheel angle; θ_c is equivalent for the front wheel to the steering axis angle; B_h is the steering shaft and bearings for the shift between the friction coefficient; J_h is the moment of inertia for the steering wheel.

For conditions in a tight corner, tire characteristics are linear, and steering resistance torque and the steering angle are in proportion.

That is:

$$T_L = K_c\theta_c \tag{3}$$

$$T_s - T_L = J_c \frac{d^2\theta_c}{dt^2} + B_c \frac{d\theta_c}{dt} \tag{4}$$

Where, T_L is equivalent to the shift shaft for steering resistance torque; K_c is equivalent to turning the front wheel axle cornering stiffness; J_c is the front wheel and steering mechanism to the steering column after the equivalent moment of inertia; B_c is the friction coefficient for the steering mechanism and front wheel equivalent to steering shaft .

The following formula helps determine motor on the steering system: (5)

$$T_m - \frac{T_a}{G} = J_m \frac{d^2\theta_m}{dt^2} + B_m \frac{d\theta_m}{dt} \tag{5}$$

$$T_m = K_T i_m \tag{6}$$

Where, T_m is the electric power generated by electromagnetic torque; G is electric power transmission ratio; T_a is power torque for the electrical power to the steering shaft; θ_m is electric Power Angle; i_m is motor power current; J_m is moment of inertia for power motor; B_m is the friction coefficient between the motor power shaft and the bearing; K_T is the coefficient for power motor electromagnetic torque.

The following formula determines motor current

$$u = Ri_m + L\frac{di_m}{dt} + K_E \frac{d\theta_m}{dt} \tag{7}$$

Where, u is motor armature control input voltage; K_E is the power motor counter electromotive force coefficient; R and L are motor power resistance and inductance respectively.

3 EPS MOTOR POWER CONTROL

3.1 PROPORTIONAL CONTROL MOTOR POWER

It can be assumed that the motor power control system is an ideal system when the relationship between the EPS motor power system dynamic performance and the proportional control is studied (Liu Zhao ,2003). Such an approach studies the transfer of function from the resistance torque input to maintain constant steering wheel angle of the steering wheel required torque. When the proportional control motor power and torque sensors detect volume proportionally, that is: $T_a = K_a T_s$, K_a is the power characteristic curve of the power coefficient. See Figure 2 showing EPS systems transfer function model structure.

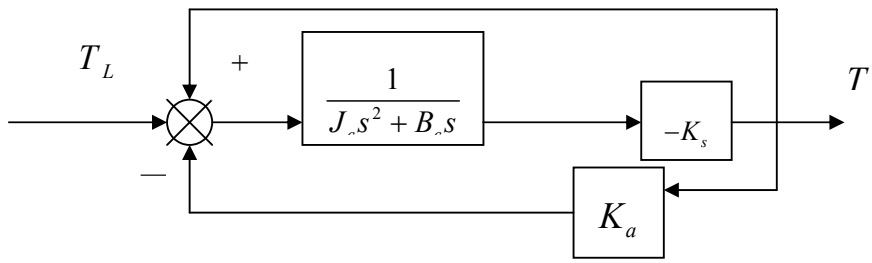

Figure 2. EPS system transfer function model structure diagram.

EPS system transfer function is:

$$G_{eps}(s) = \frac{T_h(s)}{T_L(s)} = \frac{K_s}{J_c s^2 + B_c s + K_s(K_a + 1)} \tag{8}$$

Oscillation frequency and damping coefficient are as follows:

$$\omega_n = [\frac{K_s(K_a+1)}{J_c}] \tag{9}$$

$$\xi = (B_c / J_c)/2\omega_n = \frac{B_c}{2K_s(K_a+1)} \tag{10}$$

This is a second-order system, with applications available at Matlab. Programming system unit impulse response curves are shown in Figure 3.1 where K_a is the smaller value of the response characteristic curves, 2 K_a is the larger value geting the response characteristic curves. From the figure, we can see that the damping ratio is too small, large amounts of overshoot, a strong tendency to respond to the oscillation, and poor stability. Unit pulse also caused a number of steering wheel torque oscillations leaving the system unstable.

When the power factor K_a increases, oscillation frequency will also increase while the damping coefficient will be reduced. This system tends to emphasize the dynamic characteristics and adjust over time, reducing the stability. Selection of a smaller power factor can increase the system damping, which is incentive to suppress high frequency interference from the roadwith the actual shift required in contradiction. Because at low speeds autos shift greater power torque, especially when turning in place, the need for greater torque reduces the proportion coefficient meaning the power torque reduces. Therefore, reducing the proportion coefficients will affect the electric power steering system performance.

Consequently, increasing the proportion of the relationship between power steering and torque should not satisfy the real needs and the need to improve the control algorithm.

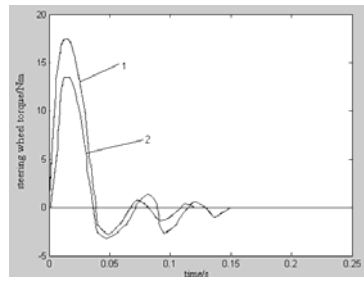

Figure3. Impulse response system.

3.2 PROPORTIONAL PLUS DIFFERENTIAL CALCULUS CONTROL OF MOTOR POWER

By the above analysis, system instability is due to the damping system being too small and the role on the steering gear on the input torque of the high frequency components of the oscillations caused by system. Therefore, if the system remained stable, need will increase system damping and differential control will increase in the original proportional control system.

The motor power using the torque sensor detection is proportional to the amount of torque, coupled with the differential signal, is directly proportional to the compensation items.

That is:

$$T_a = K_a T_s + \frac{K_d dT_s}{dt} \tag{11}$$

K_d is the torque differential coefficient. EPS system transfer function is:

$$G_{eps}(s) = \frac{T_h(s)}{T_L(s)} = \frac{K_s}{J_c s^2 + (B_c + K_s K_d)s + K_s(K_a + 1)} \tag{12}$$

System oscillation frequency is the same type (9), damping coefficient is increased, and the system dynamic performance has improved.

$$\xi = [(B_c + K_s K_d)/J_c]/2\omega_n \tag{13}$$

This system is still a second-order system. By changing the differential coefficient and adjusting the system damping coefficient, system transient stability can be improved and the system also has a strong oscillation suppression.

Application of Matlab programming is available to the system proportional plus differential calculus control, and the role of the steering wheel to shift gears on the flats in the time domain pulse response are shown in Figure 4.1 K_a is the smaller value of the response characteristic curves, 2 K_a is the larger values geting the response characteristic curves. And, Figure 4 comparing, to Figure 5, we can see that oscillation of the system has been significantly inhibited, and the system's response characteristics have markedly improved. The stability of this system has greatly improved and the peak has dropped vibrationrapid convergence. With proportional plus differential control, system transfer functions are always less than the original control system transfer function. That is, the steering wheel shimmy quickly disappears from the impact of the road.

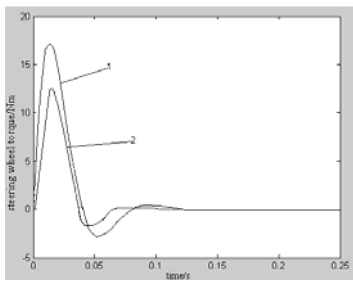

Figure 4. Impulse response system behind add a differential calculus.

4 ANALYSES OF TEST RESULTS

The different signals from the speed sensor and torque sensors in the bench test obtain the power effect. Figure 5 is in the test shows electric power steering system adopting proportional plus differential control of the test results. A

is the relationship of steering wheel torque and time, b is the relationship of the motor current and time. Motor current can better follow the changes in power characteristics which is consistent with previous simulation results. In this paper, the motor power control is effective.

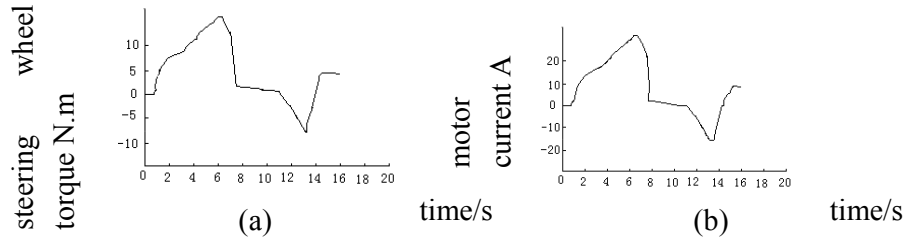

Figure 5. The test result of the comparison add a differential calculus control.

5 CONCLUDING REMARKS

Proportional plus differential control can achieve ideal power characteristics. The system resonance problem in the resonance region effectively eliminates high-frequency problems from the rack, gear, motor, and deceleration agencies inertia. The experimental results show that the control system is relatively stable, manipulative, and improves sensitive performance.

ACKNOWLEDGEMENTS

The author wishes to acknowledge Ludong University which provided financial support for the research projects numbered L20064303. Thank you to the research group of colleagues who made contributions to this project.

REFERENCES

Liu Zhao, Yang Jia-jun, and Liao Dao-xun (2003). “Based on mixed sensitivity method electric power steering system control.” China Mechanical Engineering, 2003(10), 874-876.

]Lin Yi, and Shi Guo-biao (2001). “Automotive electric power steering system technology development status and trends.” Road Traffic Technology, 2001(3), 79-84.

Lin Yi, Shi Guo-biao, and Zhou Chang-feng Etc (2003). “Automotive Power Steering Power Control Strategy.” Automotive Technology, 2003 (3), 8-12.

Man, H. L., Seung, K.H., and Ju, Y.C (2005). “Improvement of the Steering Feel of an Electric Power Steering System by Torque Map Modification.” Journal of Mechanical Science and Technology, Vol. 19, No. 3, 792-801.

Simulation of Wheel/Rail Noise of High Speed Train Running on the Slab Track

Yang Xinwen[1] and Yan Caiyun[2]

[1]School of Mathematics, Physics and Software Engineering, Lanzhou Jiaotong University, Lanzhou, Gansu, ST 730070, CHINA; PH (86) 931-4938667; email: yangxinw_8948@qq.com.
[2]School of Environmental & Municipal Engineering, Lanzhou Jiaotong University, Lanzhou, ST 730070, CHINA; PH (86) 931-7671268; email:ycyyxw@mail.lzjtu.cn.

ABSTRACT

Presented is a model for the prediction of wheel/rail rolling noise generating of a high speed train running on slab track. Using vehicle-track coupled dynamics, the vertical wheel/rail force arises from the roughness excitation on the wheel and railhead running surfaces in time domain. Except for wheels as first rigid, the vertical velocity responses of rail as Timoshenko beam and slab as Euler beam are obtained. The wheel/rail force is transformed into frequency domain as an input of finite element vibration system of the wheels, and then the surface vibration velocities of the wheels are calculated. Based on the sound radiation theory, wheel/rail rolling noise of a train running on slab track is predicted. The results show that wheel/rail noises wayside are higher 5-6dB(A) than on ballasted tracks. Most noise emission energies accumulate in frequency range of 400-4000Hz. Wheel/rail equivalent sound pressure levels increase piecewise linearly as train speed increases.

INTRODUCTION

Compared to ballasted track, slab track has the advantage of structural stability, not easily deformed and requires little maintenance, so slab track has been widely applied to high speed railway all over the world today. In Japan, slab track covers about 90% of Northeast Shinkansen. In China, slab track has been successfully laid in some testing sections of Passenger Dedicated Line and the Beijing-Tianjin Inter-city Railway, and will be extended to newly-built high speed railway in future. But it is well known that slab track has higher environmental noise emissions than ballasted track. So, it is necessary to predict and control noise emission of a train running on slab track. The noise emissions caused by high speed trains are mainly composed of wheel/rail noises, aerodynamic noises, pantograph-catenary noises, etc. This paper investigates wheel/rail noise on slab track.

The first calculation model of wheel/rail rolling noise was presented by P.J. Remington in 1976. In this model, roughness of the wheel and rail running surfaces make the wheel and rail vibrate relative to one another, and these vibrations are transmitted through the structures and thereby radiating noise. This model was developed further and extended by Thompson (1993). Subsequent research funded by the European Rail Research Institute (ERRI) resulted in the implementation of the prediction model in a computer program, TWINS (Track-Wheel Interaction Noise Software) (Thompson 1996).

All the above models are limited to single wheel and single track, and simulated mainly in frequency domain, but the coupling of the wheels of the vehicle

and two rails of the track were neglected. Numerical calculation of high frequency vibration shows that the coupling influences between the two rails through the wheelset cross-admittances and the leading and trailing wheelsets through the rail cross-admittances are great, and cannot be ignored in the high frequency vibration analysis. A vertical model was originally developed by Xu to simulate wheel/rail rolling noise of slab track (Xu 2004). In Xu's model, full vehicles are considered and each rail in the track is modeled as a Timoshenko beam connecting with the discrete fasteners. The vertical vibrations of vehicle and track are simulated. In Xu's works on wheel/rail rolling noise, the vibrations of the wheel axle direction are ignored. It is also important that the axle vibrations of the wheel contribute to the total sound emission of the wheel. This paper attempts to overcome those shortcomings. In order to simulate precisely wheel/rail rolling noises of high speed trains running on slab track, a new model is developed based on the vehicle-track coupled dynamics and the sound radiation theory.

TRAIN-SLAB TRACK COUPLED SYSTEM

Train-track coupled model. A coupled train-slab track dynamic model is depicted in Figure 1. The train-slab track system consists of three subsystems: the vehicles, the track and wheel/rail contact. The interaction of the vehicles subsystem and the track subsystem is implemented by the wheel/rail contact. The passenger cars are considered and modeled as a full dynamic rigid multi-body system. It is equipped with a pair of two-axle bogies with double suspension systems. The wheelset and the bogie are connected by the primary suspension, while the carriage is supported on the bogie through the secondary suspension. It is noted that the car is assumed to move at a constant velocity, v.

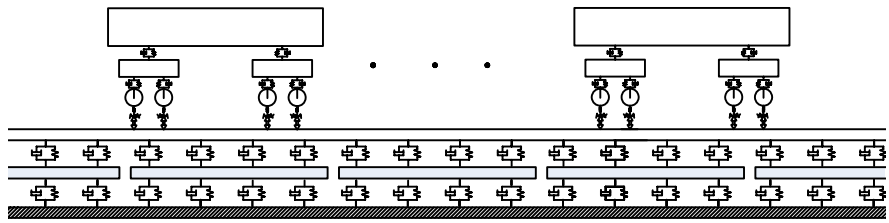

Figure 1. Coupling dynamic model of train-slab track interaction.

A rail in slab track is modeled as a Timoshenko beam connecting at the discrete fasteners. The slab is modeled as an Euler beam with two free ends. The rail pads and slab pads are modeled as spring-damping components. The normal wheel/rail contact force due to roughness excitation of wheel and rail surfaces is calculated using the Hertzian nonlinear contact theory in time domain. In order to simulate the coupled dynamic behavior of wheel/rail system, the passenger cars are assumed to be static with respect to the rail, while running surfaces roughness time historic values move backward. The vibration responses of the rail and the slab are obtained using the modal superposition principle (Zhai 2007). Except for the rail and the slab, the motion equations of the train/track system are second order ordinary differential equations. They are neglected in this paper for simplicity; see in references for details (ibid).

System excitation. In order to investigate high-frequency vibration and rolling noise of wheel/rail system, an expression about roughness (surface irregularity) had been presented by Sato (1977), and is described as follows:

$$S(\Omega) = \frac{A}{\Omega^3}\left(\mathrm{m}^2/\mathrm{rad/m}\right) \qquad (1)$$

Where, Ω is the wave number of roughness; A is the wheel/rail surface roughness coefficient; $S(\Omega)$ is the roughness spectrums. The wavelengths of roughness are between about 5 and 200mm. In the present model, the roughness is taken as an input which is normally assumed to be the same for wheel/rail rolling noise simulation and the roughness filter is considered. Using inverse FFT technique, the values of roughness time history are obtained and input into train-track coupled system to simulate wheel/rail high-frequency vibration (see Figure 2).

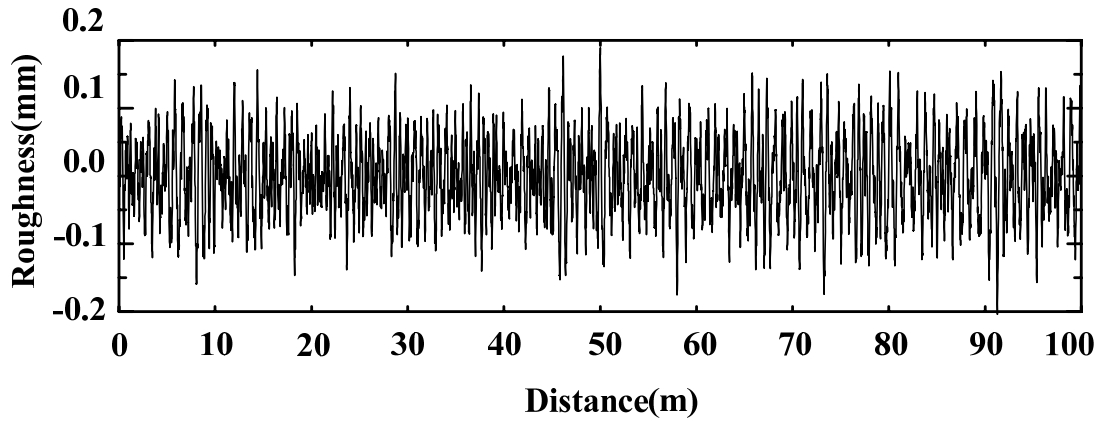

Figure 2. Time history values of roughness.

Solution of dynamic equations. To solve the motion equation of the system, the fast integration methods especially for large-scale dynamic problems in engineering are used to calculate (Zhai 1996). Wheel/rail contact forces are finally transformed into the frequency domain to calculate dynamic responses of the wheels using the finite element method.

MODEL OF WHEEL/RAIL NOISE EMISSION

Because wheel/rail noises are mainly caused by high frequency vibrations of wheel, rail and slab, the main radiating components are wheels, rails and slabs in wheel/rail system. While the vibrations of the carriages, bogies and ballasts take place in low frequency bands and barely contribute to wheel/rail noise, so noise radiations of these components are often ignored. The relationships between acoustic and vibration of wheel and rail have been investigated by Thompson (2002) and Wei (2006), respectively, while acoustic radiation property of railway slab fits to the one of thin plate. A short distance from the rail, wheel sound radiation is described as the summation of a serial of simple point sources, whereas rail and sleep sound radiation are viewed as the finite length line source passing observer point.

RESULTS AND DISCUSSION

Simulation of noise emission is assumed in free-field and takes into account reflections and absorption from the ground plane. Parameters of high-speed train and slab track can be found in the reference (Zhai 2007).

Model validation. In order to verify model validation, an observation point lies at 4.2m side of track center and 1.5m above of railhead. When a high-speed train travels on testing sections of the Passenger Dedicated Line in China at a speed of 200km/h, wheel/rail noise pressure levels are measured. Figure 3 illustrates that a comparison between theory prediction and field measurement for wheel/rail noise generating of a train running on slab track. It can be seen that the predicting values are in agreement with the measure results above those frequency bands of 500Hz, while there is a deviation on them below 500Hz. The causes are analyzed that an increase in train speed will give rise to the contribution of aerodynamic noise below 500Hz. However, wheel/ rail noise energies are predominantly distributed in frequency bands upon 500Hz. It is shown that the present model of predicting wheel/rail noise has satisfactory prediction accuracy.

Wheel/rail noise characters of train running on slab track. When a train runs on slab track at speed of 220km/h, sound pressure level of the observation point lies at 2m at the side of track center and 1.5m above of railhead is calculated. Figure 4 illustrates that some changes of wheel/rail noise frequency spectrums take place. It can be seen from Figure 4 that wheel/ rail noise on slab track is distributed mainly in the frequency range of 400-4000Hz, and the peak frequency of radiation noise is 1000Hz. It is also shown that rail noise occurs mainly in the middle and high frequency range of 500-4000Hz, that wheel noise is chiefly in the high frequency range of 1600-4000Hz, and that slab noise radiates in the frequency range of 125-500Hz. This makes clear that the peak frequency of rail, wheel and slab is 1000Hz, 2500Hz and 500Hz, respectively, which illustrate that the peak frequencies of rail, wheel and slab coincide with main frequencies of their vibrations.

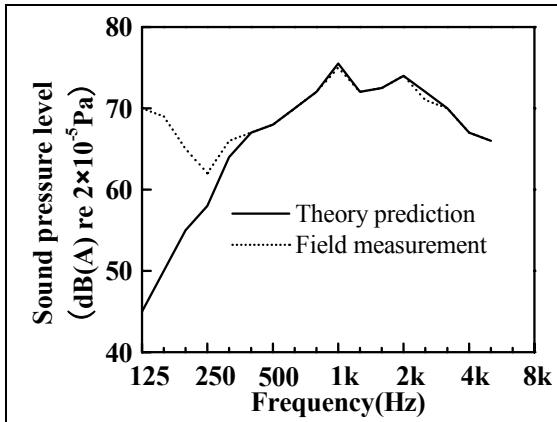

Figure 3. Wheel/rail noise frequency spectrums.

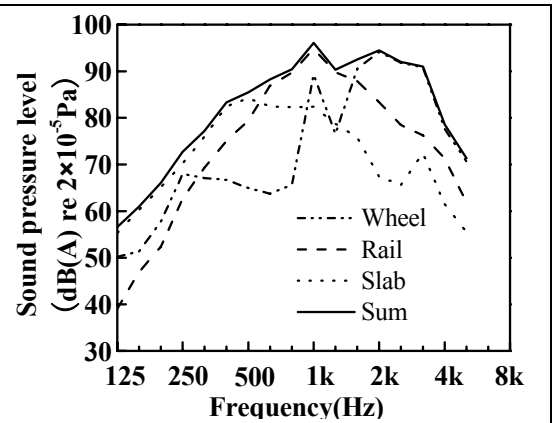

Figure 4. Wheel/rail rolling noise frequency spectrums on slab track.

When a train travels through observation point, the peak values of sound pressure level lie dead ahead of the observation point in full passing time. It can be

seen from Figure 5 that the fluctuation of sound pressure levels occurs the moment when one wheel of the vehicle travels through the observation point.

The influence of train speed on wheel/rail noise. Figure 6 shows the influence of train speed on wheel/rail equivalent sound pressure levels.

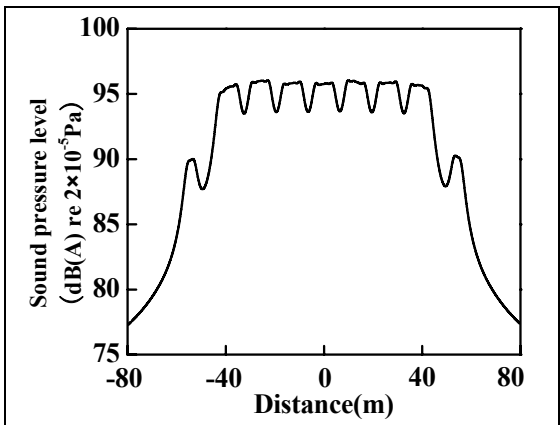

Figure 5. Wheel/rail rolling noise of a train in time domain.

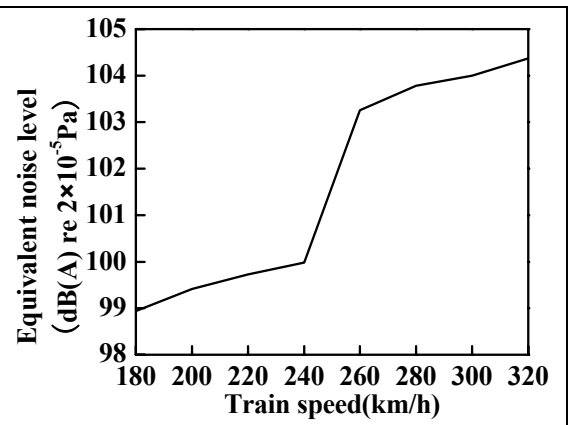

Figure 6. Changes of equivalent sound pressure level with train speed.

Figure 6 shows that wheel/rail equivalent sound pressure levels almost increases piecewise linearly as train speed increases. Sound pressure levels will increase sharply by 3.5dB(A) from 240km/h to 260km/h, while it increases slowly at the other speeds.

CONCLUSIONS

In our simulations, we may reach the following three conclusions for wheel/rail noise caused by high speed train running on slab track.

First, wheel/rail noises wayside are higher 6.2 dB(A) than on ballasted track. Second, most energies of noise emission are predominantly focused in the frequency range of about 400~4000Hz. Third, wheel/rail noise equivalent pressure levels increase picewise linearly as train speed increases.

REFERENCES

Remington, P.J. (1976). "Wheel/rail noise, part IV: rolling noise." *J. of Sound and Vibration,* 46(3), 419-436.

Sato, Y. (1977). "Study on high-frequency vibration in track operation with high-speed trains". *Quarterly Reports*, 18(3), 22-27.

Thompson, D.J. (1993). "Wheel-rail noise generation, Part I: introduction and interaction model." *J. of Sound and Vibration,* 161(3), 387-400.

Thompson, D.J., and Hemsworth, B., and Vincent, N. (1996). "Experimental validation of the TWINS prediction program for rolling noise, part 1: description of the model and method." *J. of Sound and Vibration,* 193(1), 123-135.

Thompson, D. J., and Jones, C. J.C. (2002). "Sound radiation from a vibrating railway wheel". *J. of Sound and Vibration,* 253(2), 401-419.

Wei, W., and Nie, C. (2006). "The prediction of acoustics radiation characteristics of

rails by boundary element method." *J .of the China Railway Society,* 28(5), 78-82.

Xu, Z. (2004). "Study about wheel/rail noise prediction and control in railway traffic." Ph.D. thesis, Southwest Jiaotong University.

Xu, Z., and Zhai, W. (2004). "Prediction of wheel/ rail rolling noise when a high speed train runs on a slab track." *J. of the China Railway Society,* 26(4), 48-52.

Zhai, W.M. (2007). *Vehicle-track coupled dynamics*. 3rd ed. Science Press, Beijing.

Zhai, W.M. (1996). "Two Simple fast integration methods for large-scale dynamic problem in engineering." *International J. for Numerical Methods in Engineering,* 39(4), 199-214.

Study of Influence of Subway Station Excavation on Existing Metro Deformation

LI Yun-Peng[1] and WANG Zhi-Yin[1]

[1]School of Mechanical and Electrical Engineering, China University of Petroleum, Beijing, 102249, China, email: liyp996@163.com

ABSTRACT

Based on the excavation engineering of the subway station across the existing metro tunnel and in situ monitoring displacements, the comprehensive mechanical parameters were obtained by the back analysis. According to the geological engineering conditions and the construction scheme, the numerical model of excavating subway station was established. The structural deformation, settlement and railway incline law of the existing metro caused by new subway station construction were given. The relation of the pipe tent supporting effectiveness to settlement was obtained, and the key excavation step of producing the maximum settlements was given. The evaluation and the prediction of the safety construction and the safety operation on existing subway track were made. The research results had been applied to the subway station across the existing metro tunnel. The obtained results may be referenced in the design and the construction of similar engineering.

INTRODUCTION

With the rapid development of urban rail, underground subway tunnels unavoidably traverse existing buildings, roads, railway tunnel and other existing structures. The research on urban subways, especially the design and construction technology of traversing the shallow tunnel structure, has a long history at home and abroad, and a lot of research results have been collected. For instance, settlement causes, initial supports and the application of grouting auxiliary construction were studied based on the monitoring settlement of Guangzhou metro line 2 (Zhong 2003). Subsidence control problems were researched according to the different requirements of ground settlement and building deformation (Zhong 2005). The basic laws of stratum movement caused by the shallow depth excavation method in weak watery stratum and controlling the large deformation technology were researched (Huang 2004). The control technology of large-span tunnel construction in metro station (Hu 2007); large deformation mechanism and large deformation control principle and technical measures were researched based on the experimental study on soil properties of strata (Lu 2003). And finally, using three-dimensional numerical simulation method, the various construction schemes were compared and simulated by considering the time-space effect and complex external environment factors, including high-rise buildings in flourishing city, ground with heavy traffic, underground pipe (Wu 2004), etc.

However, due to the complexity of the geological conditions in formation, especially the external environment condition of different engineering problems, merely copying existing methods and techniques would not be scientific. According to some subway station engineering across the existing metro line cited in this paper, the comprehensive mechanical parameters of influencing the deformation of soil layers are back analyzed based on the in-situ monitoring

displacements. Using numerical methods, the deformation behaviors of the existing subway structure and the surrounding rock (soil) in the process of traversing excavation are studied, a key step of excavating influence on the existing metro lines is found, and the safety operation of the existing metro lines is evaluated. These results can be supplied to similar engineering as references.

BACK ANALYSIS OF MECHANICAL PARAMETERS

The position and the structural plane layout of two subway stations are shown in Figures 1 and 2. The station structure has twin pillars, three islands, its total length is 208m, total width is 24m, and the width of platform is 14m. Existing tunnel structure is reinforced concrete square frame structure C30. There is a deformation joint every 18m (see Figure 2). The clear distance between the new station and the existing metro ring line is 1.98m. The new line will traverse under the existing line.

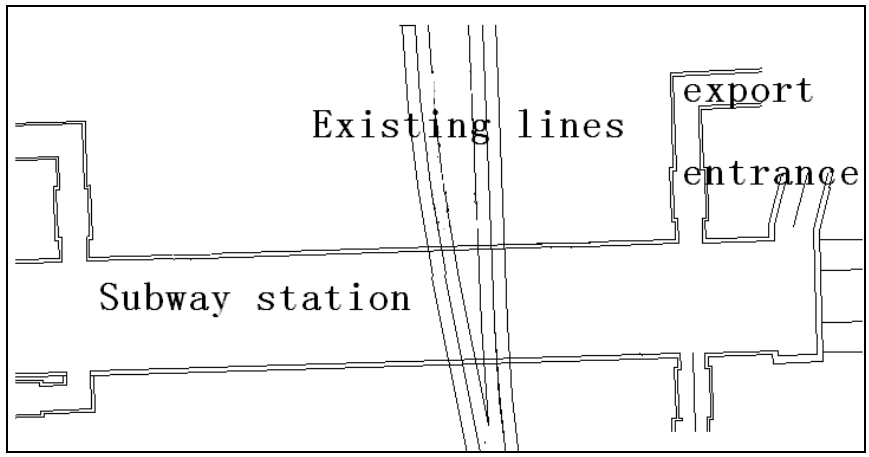

Figure 1. Position of subway station.

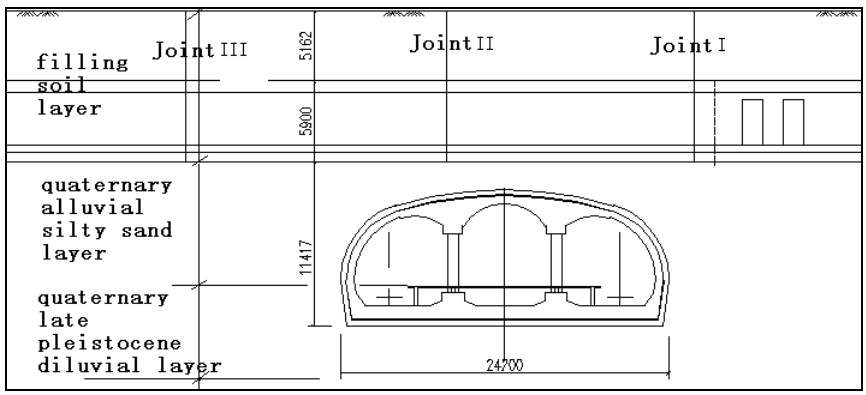

Figure 2. Elevation of metro lines.

It may be seen from the geological sections in the boring log that the formation materials around the new line can be sorted into three layers: earth-filling soil, quaternary alluvial silty sand, and quaternary late Pleistocene diluvial layer. From the in-situ construction data, the soil layers contain construction rubble and waste rock, leaving the mechanical parameters of the soil layers undetermined and fuzzy. In order to solve this problem, the back analysis method of parameters is adopted (Wang 1993, 2008).

According to the structure, construction situation, deformation laws and the corresponding construction characteristics within the intersection region of two subway lines, the back analysis model of the longitudinal section is selected, as shown in Figure 3.

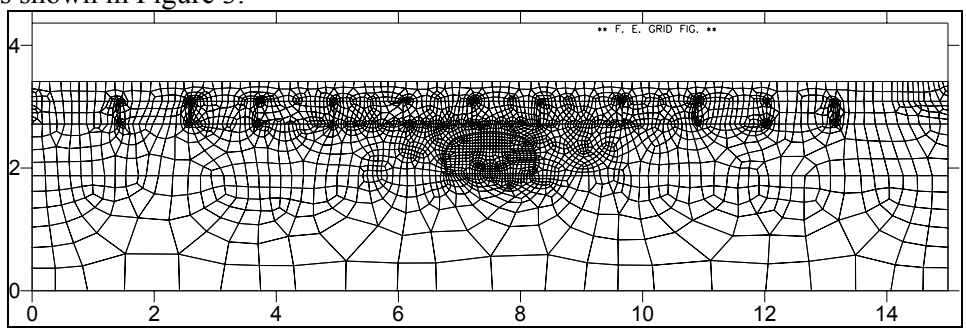

Figure 3. Finite element analysis model.

In order to reflect the rotation and settlement laws of the main structure in the longitudinal axis direction of existing line and the settlement features of expansion joints, taking the central axis of the new subway line as the symmetry axis of analyzing region, the distances from the left and the right boundaries to the symmetry axis are respectively around 120m along horizontal direction, and the upper boundary is the surface, and the lower boundary is 30m below the floor of new line along the vertical direction. The area contains the overburden soil of existing line, main structure, the corresponding soil layers around new station, etc. The fitting deformation points used by inversion are shown in Figure 4.

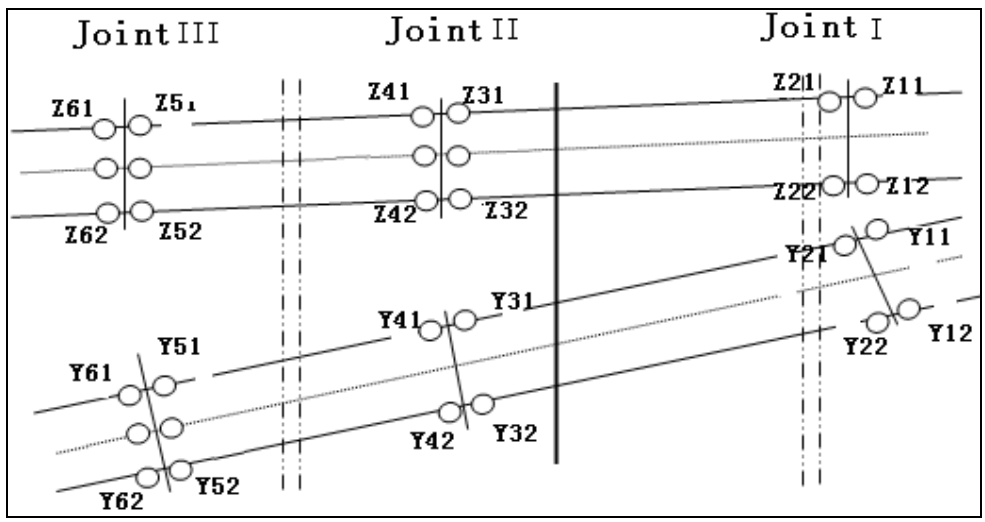

Figure 4. In-situ measuring points.

As mentioned above and seen in Figure 2, the concrete process is as follows: first, the soil formation is divided into three layers, namely, earth-fill, a quaternary alluvial silty sand layer and a quaternary late Pleistocene diluvial layer. The mechanical parameters of each layer take the weighted average values of corresponding soil and other materials as its initial analysis parameters. Then, the fitting inversion is carried out by using in-situ measured deformation at the special points, and the mechanical parameters of three soil layers are gradually

approached.

Through multiple fitting inversion, the comparisons of the longitudinal actual settlement curve of the structure with the inversion result are given in Figure 5 for both left and right lines respectively.

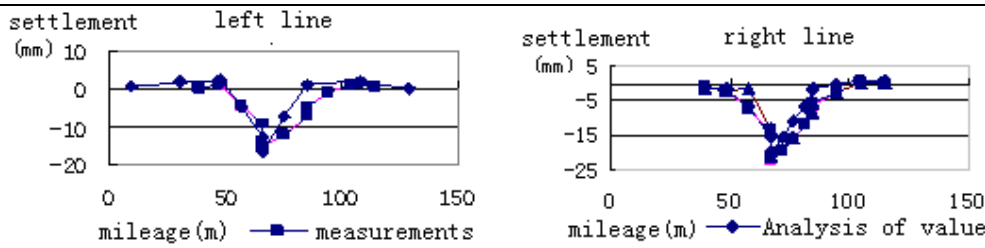

Figure 5. Comparison of settlement of structure with inversion results.

The fitting of three points at the deformation joint II in the left line and its left side is good from Figure 5, and the fitting of the points at two sides of joint II and a measuring point of joint I in the right line is better. Comparing the measured values with the calculated values of the corresponding points, the relative error in the structure at the left line 57m and 66m and the right line 67m is less.

Because the construction process and the subway structure are extremely complex, fitting only above three points is ideal. Through the above inversion and comprehensive analysis, the comprehensive mechanical parameters of soil around the subways are listed in Table 1.

Table 1. Mechanical parameters obtained by back analysis.

Soil layer	E/MPa	μ	C(MPa)	φ	γ(MPa/m^3)	Rt
upper	5.50	0.230	0.019	30	0.0160	0.000
middle	160.00	0.300	0.03	20	0.0195	0.000
lower	20.00-31.00	0.280	0.036	35	0.0200	0.001
C30	30000	0.167	2.000	49	0.0119	2.100

ANALYSIS OF DEFORMATION AND STRESS OF EXISTING LINE

Using the mechanical parameters obtained by inversion, both left and right line structure settlement laws and stress states caused by the new construction are simulated by finite element method.

The settlement results are shown in Figures 6 and 7. In Figure 6, for the left line the longitudinal settlement law of the structure varies with the excavation process of the new line station, and the structure settlement at joint II tends to the stable value after undergoing maximum settlement, and the structure settlement at the joint III undergoes the changing process of subsidence-upper expansion and tends finally to the stable value of upper expansion. The settlement laws of right line structure, as shown in Figure 7, are similar to those of the left line. In the whole construction process, the maximum settlements along existing left and right lines are 6.318cm and 6.473cm respectively, which both locate at the right side of joint II, and the stable settlement values are finally about 4.337cm and 4.997cm. The left and right line structures are expanded up at joint I and joint III to a certain extent, where the up-expanded maximum values on left and right lines are

1.220cm and 0.947cm respectively.

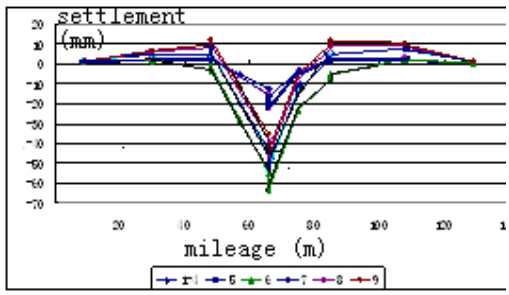

Figure 6. Settlement curves of left line.

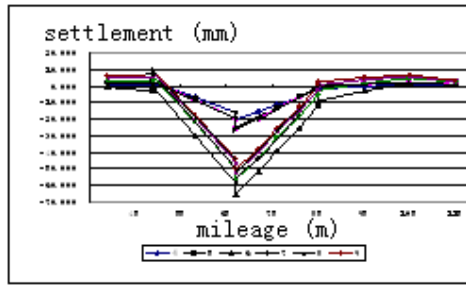

Figure 7. Settlement curves of right line

The displacement contours of longitudinal left and right sections of the existing subway are shown in Figure 8.

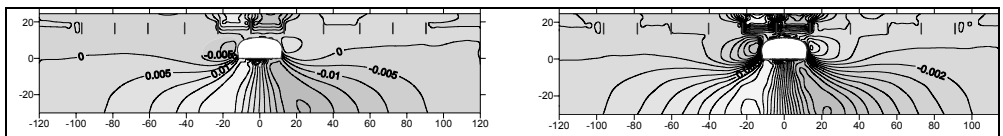

(1) left line (2) right line

Figure 8. Horizontal displacement contours.

It is seen from the horizontal displacement contours of both left and right lines that the displacements of soil mass near the new subway tunnel vary greatly in each construction process and those near the existing line and deformation joints are less, which shows that the possibility of producing the longitudinal extruding deformation in existing line roadbed is less.

The principal stress and the maximum shear stress contours are shown in Figures 9 and 10. It is indicated from both these Figures that the stress concentration occurs mainly near the new subway tunnels and within the existing structure above the new subway tunnels. The tensile stress area appears in either left or right line existing structure and the region between the main structure and the station, and the area locates in the range from 50m to 60m along the transverse axis above new subway station.

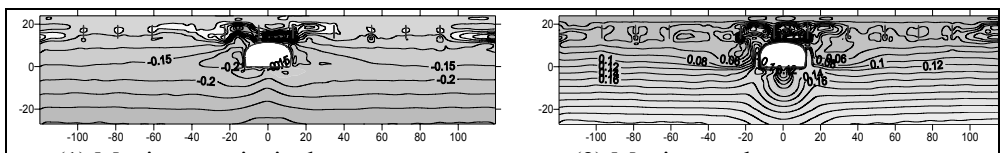

(1) Maximum principal stress contour (2) Maximum shear stress contour

Figure 9. Stress contours of left line structure and soil mass around tunnel.

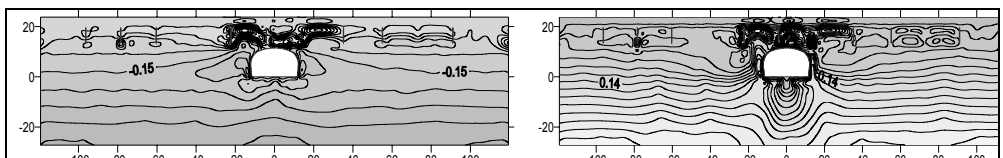

(1) Maximum principal stress contour (2) Maximum shear stress contour

Figure 10. Stress contours of right line structure and soil mass around tunnel.

The above stress and displacement contours are given under the condition that pilot pipes and supporting structure have 50% of the effectiveness. So, to improve the stress concentration, the tensile state and the displacement distribution etc, the supporting stiffness of the tube curtain and the related lining must be strengthened to ensure its effectiveness above 80-90%.

The stress distribution contour after excavating soil mass within the station section is shown in Figure 11.

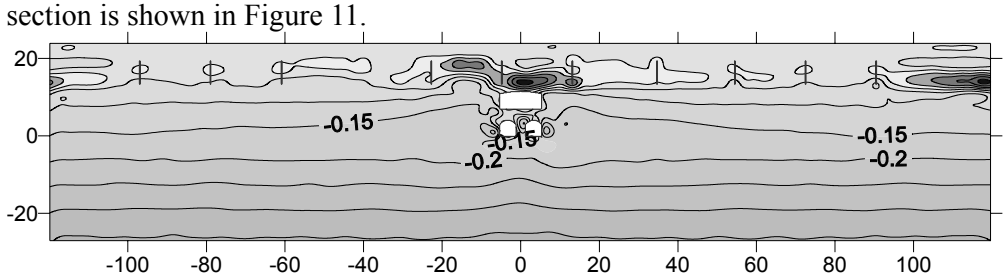

Figure 11. Maximum principal stress contour.

From Figure 11, the tensile stress appears in the connection soil layer of existing and new lines in the new station construction process, especially the serious stress concentration appeared in sandwich. Because the soil layer has no tensile strength, the layer is in tensile damage state and has fully lost its bearing capacity. The imbalance force resulted from tensile damage area is undertaken completely by the new line structure and the pilot pipes. In addition, the existing line structure is partly in tensile state, especially in the area above the new line, and the tensile area is very concentrated at concrete structure joints of existing lines. Although the maximum tensile stress in the area does not exceed the tensile strength of concrete, this will be a potential adverse factor for the existing concrete structure, and the unfavorable factor is in expanding and developing state.

From the plastic area seen in Figure 12, the deep plastic zone appears in soil mass around new line tunnel, the disturbance load within the area is basically undertaken by supporting structure.

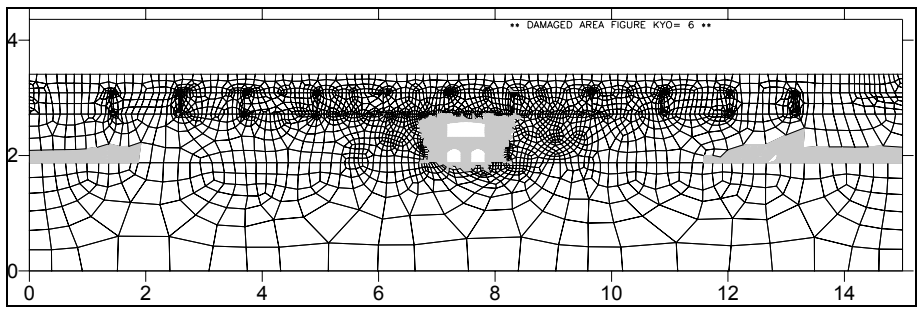

Figure 12. Plastic zone.

It can be seen from the above analysis that the new station construction across the existing lines is very insecure at present. So the strengthening support is suggested based on the current supporting structure, such as strengthening the pilot pipe tent supporting stiffness, whole section pre-grouting and rapidly setting initial support etc. to ensure the engineering safety and stability.

CONCLUSION

Firstly, by establishing the analyzing model of the subway station traversing the existing subway, the comprehensive mechanical parameters of soil around subway tunnels are obtained by the inversion, and the analyzing results are close to in-situ monitoring settlement values.

Secondly, it is shown from the study that there is different subsidence at the expansion joints in the process of construction, and it appears between the joint I and the joint III. The stress concentration area occurs mainly near the subway tunnel and within the existing line structure above the station. The tensile stress area appears in either left or right line existing structure and the region between the main structure and the station, and the area locates in the range from 50m to 60m along the transverse axis above the new subway station.

Lastly, the research indicated that strengthening the pilot pipe tent and supporting stiffness is an effective way of improving the settlement difference, stress concentration and tensile state and ensuring the safety construction of the subway station and the safety operation of the existing subway, and the supporting structures should be set up in time in the late construction process.

REFERENCES

Huang, J. and Zhang, D. (2004), "Analysis of large deformation regularity in stratum above metro tunnel." *Rock and Soil Mechanics*, 25(8), 1288-1301.

Hu, G., Wang B., and Zhang Y., et al. (2007). "Controlling technology of tunnel-group driving in construction of large-span metro station by NATM." *Railway Engineering*, No.8.

Lu, Q., Zhang, D., and Huang, J. (2003), "Mechanism of Stratum Deformation and Its Control Practice in Tunneling Urban Subway at Shallow Depth." *China Safety Science J.*, 13(7), 29-34.

Wang, Z. and Li, Y. (1993). *Methods and programs of back analysis of displacements in underground engineering*. Shaanxi Science and Technology Press, Beijing.

Wang, Z. and Li, Y. (2008). "Rheological Theory and Numerical Simulation of Rock Mass." Science Press, Beijing.

Wu, B., Liu, W., and Gao, B., et al. (2004), "Analysis of space time effect for urban shallow tunneling by excavation." *Chinese J. of Geotechnical Engineering,* 26(3), 340-343.

Zhong, Y. and Luo, C. (2003), "Ground Settlement Monitoring and Control in Metro Construction by Underground Cutting with Shallow Overburden." *West-China Exploration Engineering*, No.4, 91-93.

Zhong, Y. and Li, X. (2005), "Control and Analysis on Tunnel Settlement in Urban Shallow-Buried Mining Subway." *China Resources Comprehensive Utilization* , No.10, 38-40.

Influence of longitudinal connection mode of ballastless slab track on vibration characteristic of train-ballastless slab track-subgrade system

Qing-Yuan Xu[1] and Zhi-Ping Zeng[2]

[1]School of Civil and Architecture Engineering, Central South University, Changsha City 410075, Hunan Province, China; Tel: (86) 731-2655611; email: xuqingyuan1972@163.com
[2]Postdoctoral Work Station of Civil Engineering, Central South University, Changsha City 410075, Hunan Province, China; Tel: (86) 731-2655611; email: hzzp7475@126.com

ABSTRACT

A train-ballastless slab track-subgrade vertical vibration mechanical model was put forward based on finite element method. Vibration equations were formulated by using the principle of total potential energy with stationary value in elastic system dynamics and the "set-in-right-position" rule for formulating matrixes. With the vibration mechanical model, influence of longitudinal connection mode of ballastless slab track on vertical vibration responses of train-ballastless slab track-subgrade system under the load case of track random irregularity was studied. The calculated results show that: longitudinal connection mode of ballastless slab track has little effect on vehicle vertical acceleration, rail vertical acceleration, wheel/rail vertical force and fastener vertical pressure force, but has significant influence on vibration characteristic of ballastless slab track structure. Continuous slab and concrete basement can decrease the vibration of ballastless slab track structure significantly.

INTRODUCTION

Ballastless track is a modern railway technology, and there are many merits for ballastless track compared to ballast track. For example, stability of track is increased, security of train operation is raised, and maintenance work of track is greatly reduced. With the development of ballastless track technology, it has been widely used in high speed railway in many foreign counties, such as Japan, Germany. In China, ballastless track has been successfully used in Beijing-Tianjin intercity high speed railway in 2008, and it will be widely used in many new-built high speed railways, such as Beijing-Shanghai, Wuhan-Guangzhou, Zhengzhou-Xi'an, Haerbin-Dalian railway line for passenger traffic.

There are two kinds of ballastless slab track. One is discontinuous ballastless slab track, and the other is longitudinal connected ballastless slab track. At present, although many researches has been made on vibration characteristic of train-ballastless slab track-subgrade system at home by Zhai W. M., Han W. J., Cai C. B., Wang Q. C.(1999), Cai C. B. (2007), Xiang J., He D., Zeng Q. Y. (2007), and Xuan Y., Wang L. (2005), and abroad by Verbic B. (1997), Esveld C. (2001), and Steenbergen, M.J.M.M., Metrikine, A.V., and Esveld, C. (2007), few studies have been made on the influence of longitudinal connection mode of ballastless slab track on vibration characteristic of ballastless slab track structure, especially on the dynamic stress of ballastless slab track structure.

In this paper, a dynamic model in which different longitudinal connection modes of ballastless slab track can be considered is established, and corresponding calculation program is developed based on MATLAB program language. With the established dynamic model, the influence of longitudinal connection mode of ballastless slab track on vibration characteristic of train-ballastless slab track-subgrade system is studied in detail.

DYNAMIC MODEL OF TRAIN-BALLASTLESS SLAB TRACK—SUBGRADE SYSTEM

Vehicle model**.** Each vehicle is consisted of 7 rigid bodies, and connected with each other by means of elastic and damping linear elements (see Figure 1). For car body and bogie, nodding and vertical motions are considered. For each wheel set, only vertical motion is considered. This results in a total of 10 degree of freedom for each vehicle.

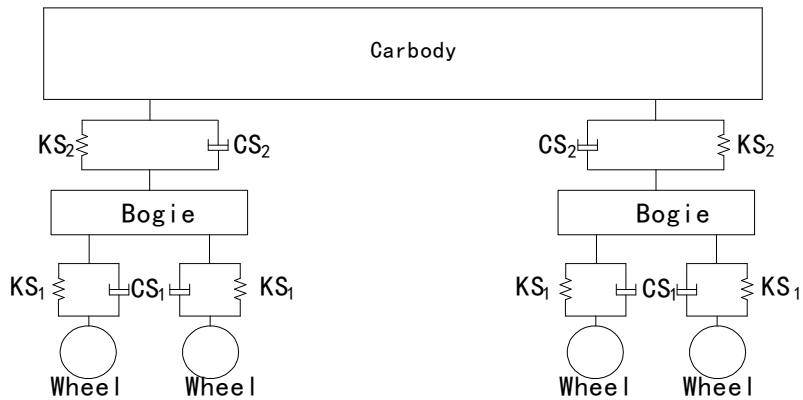

Figure 1. Vertical vibration mechanical model of vehicle.

Ballastless slab track model**.** Dynamic mechanical model of ballastless slab track on subgrade is shown in Figure 2. Rail, slab, concrete basement, longitudinal connections between slabs, longitudinal connections between concrete basements are modeled as beam element respectively. Fastener, CA mortar, and subgrade are modeled as linear spring-damping element respectively.

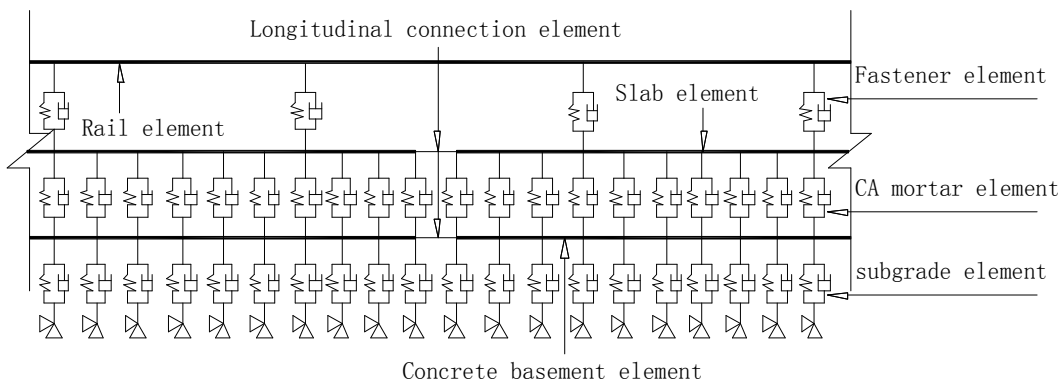

Figure 2. Dynamic mechanical model of ballastless slab track on subgrade.

The longitudinal discontinuity can be simulated by setting the stiffness of longitudinal connection element small enough. The longitudinal continuity can be simulated by setting the stiffness of longitudinal connection element equal to that of slab or concrete basement.

Track irregularity model and its numerical simulation**.** Germany's low disturbance track irregularity power spectrum, which is suitable for high speed railway allowable velocity above 250 km/h, is adopted in this paper. It is expressed as shown in Equation (1) Zhai W. M. (2002):

$$S(\Omega)=\frac{A_v\Omega_c^{\ 2}}{\left(\Omega^2+\Omega_r^{\ 2}\right)\left(\Omega^2+\Omega_c^{\ 2}\right)} \tag{1}$$

where: $S(\ )$ is power spectrum density; is spatial frequency; A_v is roughness constant, and the value is 4.032×10 $^{-7}$ m·rad; $_c$ and $_r$ are cutting off frequency, the values is 0.8246 rad/m and 0.0206 rad/m respectively.

Short wave-length has considerably important influence on ballastless track dynamic characteristic (Zhai W. M. (2002)). But Germany's low disturbance track irregularity power spectrum mainly describes medium and long wave-length track irregularity. Short wave-length track irregularity is added up to medium and long wave-length track irregularity in this paper, and its expression is shown as Equation (2)(Zhai W. M. (2002)):

$$S(f)=0.036f^{-3.15} \tag{2}$$

where: $S(f)$ is power spectrum density; f is spatial frequency.

By using numerical simulation method introduced by W. M. Zhai (2002), the amplitude and random phase can be firstly obtained according to track random irregularity power spectrum, and then track irregularity time domain simulation sample can be gained by inverse Fourier transform.

Wheel/rail interacting model**.** Vertical wheel/rail force can be calculated by Hertz nonlinear contact theory, and its expression is shown as Equation (3).

$$p_j(t)=\begin{cases}\dfrac{1}{G}\left[Z_w(j,t)-Z_r(j,t)-Z_0(t)\right] & wheel/rail \quad contact \\ 0 & wheel/rail \quad seperatoin\end{cases} \tag{3}$$

where: G is wheel/rail contact constant; $Z_w(j,t)$ is j-th wheel displacement at time t; $Z_r(j,t)$ is rail displacement under j-th wheel at time t; $Z_0(t)$ is track irregularity.

Establish and solution of equation set of system**.** Vehicle total potential energy includes inertia potential energy and gravitational potential energy of car body, bogie, and wheelset, and elastic strain energy and damping energy of suspension. Vehicle vibration equation set can be formulated by using the principle of total potential energy with stationary value in elastic system dynamics and the "set-in-right-position" rule for formulating matrixes. Ballastless slab track vibration equation set can be formulated by the same way.

Cross iterative method is used to solve the equation set of system based on wheel/rail interacting model (Lei 2002).

MECHANICAL MODEL VERIFICATION

Because we lack in-site measured data about ballalstless track, vehicle model, ballastless slab track model, and track irregularity models are verified respectively.

Vehicle model verification**.** In 1994, China's Academy of Railway Sciences measured the effect of wave length and wave amplitude on vehicle vibration acceleration on the Guangzhou-Shenzhen railway line. Vehicle vertical acceleration comparison between measured data and calculation data is show in Table 1. (For vehicle and track parameters see Zhai 2002.)

Table 1. Vehicle vertical acceleration comparison between measured data and calculation data.

Test conditions	Track irregularity	λ=10m a=10mm	λ=12m a=9mm	λ=12m a=9mm	λ=24m a=16mm	λ=24m a=20mm
	Vehicle velocity	160km/h	135km/h	150km/h	160km/h	160km/h
Measured data /g		0.12	0.06	0.08	0.12	0.13
Calculation data in this paper /g		0.104	0.078	0.085	0.096	0.120
Calculation data in Ref.8 /g		0.104	0.078	0.085	0.096	0.120

Ballastless slab track model verification**.** It is assumed there is sinusoidal force acting on rail node in the middle of slab. The load function is $F(t)=-100000\times\sin(2\pi vt/10)$, where v=83.33m/h(300 km/h). Slab is discontinuous, and concrete basement is continuous. Other calculation parameters are shown in Table 2. Calculation results by ANSYS and MATLAB program are shown in Figure 3 and 4.

Table 2. Calculation parameter of ballastless slab track.

Item		Unit	Value
Rail		kg/m	60
Vertical stiffness of fastener		kN/mm	35
Slab	Length	m	6.0
	Width	m	2.4
	Thickness	m	0.19
	Young's modulus	GPa	34.5
Concrete basement	Width	m	2.8
	Thickness	m	0.3
	Young's modulus	GPa	32.5
Young's modulus of CA mortar		MPa	400
Vertical stiffness of subgrade		MPa/m	190

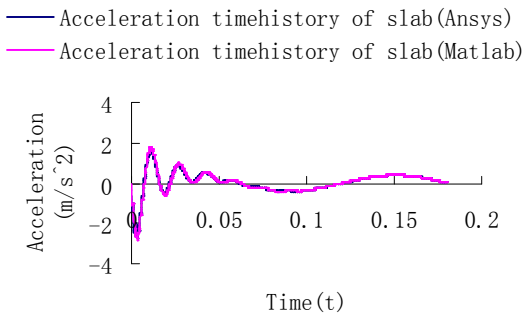

Figure 3. Comparison of time history of slab acceleration at load point position.

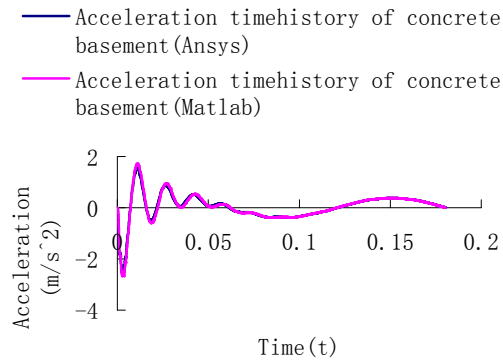

Figure 4. Comparison of time history of concrete basement acceleration at load point position.

Track irregularity model verification**.** Theoretical power spectral density is shown in Figure 5, simulation sample of theoretical power spectral density is shown in Figure 6, sample power spectral density is shown in Figure 7, the error between theoretical and sample power spectral density is shown in Figure 8. From Figure 8, we can see that the error between theoretical and sample power spectral density is very small, which proves the random irregularity simulation is correct.

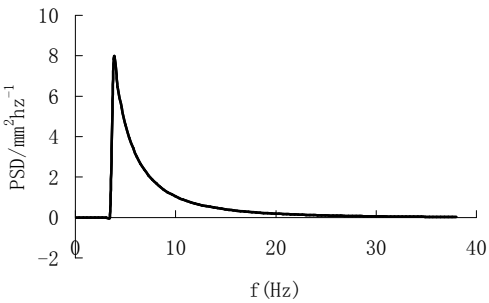

Figure 5. Theoretical power spectral density.

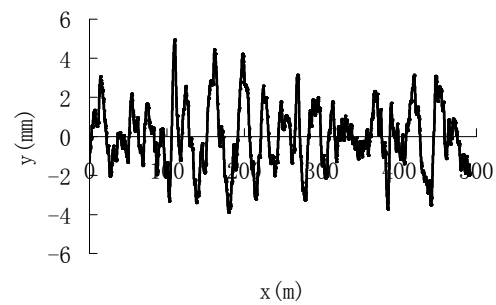

Figure 6. Simulation sample of theoretical power spectral density.

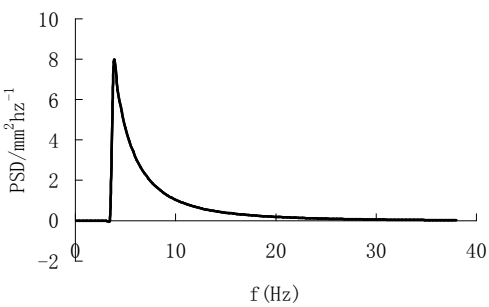

Figure 7. Sample power spectral density.

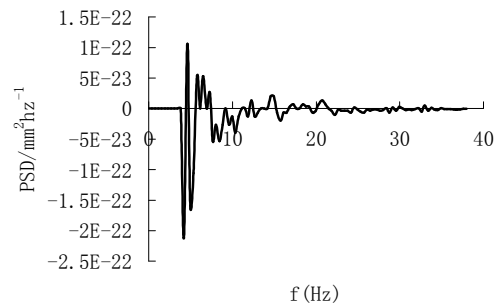

Figure 8. Error between theoretical and sample power spectral density.

INFLUENCE OF LONGITUDINAL CONNECTION MODE ON VIBRATION CHARACTERISTIC OF SYSTEM

Calculation condition. Take a high speed train formed with 4 trailers hauled by a motor car running at 300 km/h on ballastless slab track with different longitudinal connection modes as an example, to study the influence of longitudinal connection mode of ballastless slab track on vibration characteristic of train-ballastless slab track-subgrade system. (For parameters of train see Xuan Y., Wang L. (2005). The main parameters of track are shown in Table 2.) The following 4 load cases are calculated:

Load case 1: both slab and concrete basement are continuous.
Load case 2: slab is discontinuous and concrete basement is continuous.
Load case 3: both slab and concrete basement are discontinuous in the same section.
Load case 4: slab is discontinuous and concrete basement is discontinuous in the middle of slab.

Calculation Results. The effects of different longitudinal connection modes of ballastless slab track on vibration characteristic of train-ballastless slab track-subgrade system are shown in Table 3.

Table 3. Results comparison among different longitudinal connection modes.

Item	Load case 1	Load case 2	Load case 3	Load case 4
Max vertical acceleration of carbody (m/s^2)	0.397	0.397	0.396	0.397
Max vertical acceleration of rail (m/s^2)	1379.020	1376.397	1371.199	1372.617
Max vertical acceleration of slab (m/s^2)	87.969	131.400	127.764	130.100
Max vertical acceleration of concrete basement (m/s^2)	32.226	32.551	49.001	46.011
Max wheel/rail vertical force(kN)	159.694	159.594	159.182	158.877
Max dynamic vertical compressive force of fastener (kN)	38.214	38.198	37.970	38.155
Max dynamic vertical compressive stress of CA mortar (MPa)	0.072	0.102	0.082	0.102
Max dynamic bending stress of slab(MPa)	0.736	0.723	0.699	0.989
Max dynamic bending stress of concrete basement (MPa)	0.524	0.530	0.504	0.525
Max vertical compressive stress on surface of subgrade (MPa)	0.033	0.033	0.048	0.037

Calculation analysis. The effect of longitudinal connection mode of

ballastless slab track on vertical acceleration of car body, vertical acceleration of rail, wheel/rail vertical force, and vertical compressive force of fastener is no more than 1%. When slab is longitudinal continuous, maximum vertical acceleration of slab decreases about 33 percent. When concrete basement is continuous, maximum concrete basement vertical acceleration decreases about 34.2%. When slab and concrete basement are discontinuous in the same section (load case 3), maximum vertical compressive stress on surface of subgrade increases about 31.3%.

CONCLUSIONS

In this paper a general time varying coupling dynamic model is established, in which different longitudinal connection modes can be considered. Taking short, medium and long wave-length track irregularity into account, the influence of longitudinal connection mode of ballastless slab track on vibration characteristic of train-ballastless slab track-subgrade system is studied carefully. The results show that the effect of longitudinal connection mode of ballastless slab track on vertical acceleration of carbody, vertical acceleration of rail, wheel/rail vertical force, and vertical compressive force of fastener is very small, but the effect of longitudinal connection mode of ballastless slab track on ballastless slab track structure is considerable. On the whole, the dynamic characteristic of longitudinal continuous ballastless slab track is better than that of longitudinal discontinuous ballastless slab track.

ACKNOWLEDGEMENTS

This paper is sponsored by Foundation of the Science and Technology of China Ministry of Railway (2008G031-17-1), and China Postdoctoral Science Foundation (20070410769).

REFERENCES

Cai, C. B. (2007). “Dynamics of ballastless track and its application.” *J.of Southwest Jiaotong University,* 42(3).

Esveld, C. (2001). *Modern Railway Track.* TU Delft Press, Delft.

Lei, X. Y. (2002). *Track mechanics and new engineering method.* China Railway Press, Beijing.

Steenbergen, M.J.M.M., Metrikine, A.V., and Esveld, C. (2007). “Assessment of design parameters of a slab track railway system from a dynamic viewpoint.” *J. of Sound and Vibration*, 306(1), 361-371.

Verbic, B. (1997). “Investigating the dynamic behavior of rigid track. *Gazette International*, 153(9), 585-586.

Xiang, J., He, D., and Zeng, Q. Y. (2007). “Analysis method of vertical vibration of train and ballastless track system with the lateral finite strip and slab segment element.” *J. of the China Railway Society*, 29(4), 64-69.

Xuan, Y., and Wang L. (2005). “Simulation Research on dynamic characteristics of vehicle-track coupling system on curved track and the vibration response of

ballastless track structure of passenger traffic railway." China Academy of Railway Sciences, Dec.

Zhai, W. M. (2002). *Vehicle-tack coupling dynamic.* 2nd ed. China Railway Press, Beijing.

Zhai, W. M., Han, W. J., Cai, C. B., and Wang, Q. C. (1999). "Dynamic properties of high speed railway slab tracks." *J. of the China Railway Society*, 21(6), 64-69.

Vehicle Semi-active Suspension System Simulation with Variable Structure Control Method

Li Zhongji[1] and Dai Huanyun[1]

[1]Traction Power State Key Laboratory, Southwest Jiaotong University, Chengdu 610031, China. email: lizhongjiqc@126.com

ABSTRACT

The semi-active suspension system is an effective method to improve riding comfortable. This paper considers variable structure control method with the simplified model for the design of a semi-active suspension system. Firstly, the dynamic model of a vehicle suspension system is built. Secondly, the damp controller with variable structure control method is designed based on that model. Then, the practical dynamic model is built using ADAMS/rail, and the model of the controller is obtained using Matlab/simulink. Finally, the vibration data of car body is obtained by co-simulation using ADAMS and Matlab. The result shows that the VSS (variable structure sliding mode control) controller can reduce the amplitude of car body vertical displacement and acceleration effectively.

INTRODUCTION

The vertical ride quality of railway vehicles could be improved by using the pneumatic active and semi active suspensions. At present, those style systems have been applied in the high-speed trains. The investigation, experiment and application show that the effect of active suspension is ideal. However, the cost of the active suspension system is extremely expensive and the construction is quite complex compared with the semi-active suspension system. Specifically, a power supply is needed in an active suspension system. It may, therefore, be difficult to obtain practical application. On the other hand, semi-active suspension does not need a power supply. More importantly, because there is no power input, the semi-active suspension system is stable and safe. Moreover, the construction of a semi-active suspension system is simple and the cost lower. Taking all this into consideration, semi-active suspension will have broad practicality in actual application.

As the key of semi-active suspension system research, the control policy is given more attention. Some of the commonly control policy include H_∞ control theory, fuzzy logic control, self-adaptation control, variable construction control and so on. But those modern control policies are mostly based on exact model of the practical system. The more exact the system model is, the more ideal the control effect is. Because the vehicle dynamic system has strong nonlinear and time-varying characteristic, the exact vehicle dynamic model would be very complex. Even, it is impossible to build the exact model sometimes. Therefore, according to the complex

model to design the controller, the controller will became more complicated, and the suspension system stability would be decreased. Because of that, it is necessary to simplify the vehicle dynamic model while designing the controller. But it come to the new problem that whether the controller designed base on the simplify model fit the practical system completely. In view of this, the variable structure controller was designed base on 3DOF simplify model in this paper, and the practical vehicle model was built by ADAMS/rail. The performance of VSS controller was verified by co-simulation with ADAMS and Matlab.

CONTROLLER DESIGN

System simplify model. The 3DOF vehicle dynamic model is build for designing the VSS controller. This model consists of two masses, m_b representing the quarter body mass and m_f representing the frame mass. The mass m_b is isolated from m_f by a spring k_b and damper C_b, along with a controllable damp. The controllable damp is represented by the control force u (Stutz, L.T. 2004). The mass m_f is connected to the wheel by a spring k_f and damper C_f. The body vertical displacement is x_b, the frame vertical displacement is x_f. The track disturbance is described by the elevation d and its time derivative. The model is depicted in Figure1.

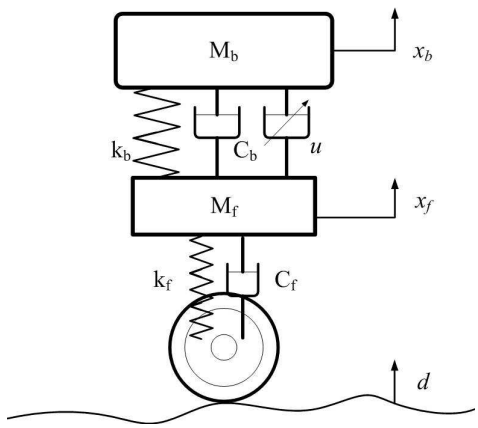

Figure 1. 3DOF vehicle model.

The dynamic behavior of the model is governed by the following equation

$$m_b \ddot{x}_b = -k_s (x_b - x_f) - (\dot{x}_b - \dot{x}_f) C_s + u \tag{1}$$

$$m_f \ddot{x}_f = -k_p (x_f - d) - C_p (\dot{x}_f - \dot{d}) + k_s (x_b - x_f) + C_s (\dot{x}_b - \dot{x}_f) - u \tag{2}$$

Using the following state variables:

$$x_1 = x_f \quad x_2 = x_b \quad x_3 = \dot{x}_f \quad x_4 = \dot{x}_b \tag{3}$$

$$\mathbf{x} = (x_1 \quad x_2 \quad x_3 \quad x_4)^T \tag{4}$$

The equation of motion can be written in state space as

$$\dot{\mathbf{x}} = \mathbf{A}\mathbf{x} + \mathbf{B}u + \mathbf{E}d \tag{5}$$

where:

$$\mathbf{A} = \begin{bmatrix} 0 & 0 & 1 & 0 \\ 0 & 0 & 0 & 1 \\ -\dfrac{k_b + k_f}{m_f} & \dfrac{k_b}{m_f} & -\dfrac{c_b + c_f}{m_f} & \dfrac{c_b}{m_f} \\ \dfrac{k_b}{m_b} & -\dfrac{k_b}{m_b} & \dfrac{c_b}{m_b} & -\dfrac{c_b}{m_b} \end{bmatrix} \quad \mathbf{B} = \begin{bmatrix} 0 \\ 0 \\ \dfrac{1}{m_f} \\ -\dfrac{1}{m_b} \end{bmatrix} \quad \mathbf{E} = \begin{bmatrix} 0 \\ 0 \\ 0 \\ -\dfrac{1}{m_b} \end{bmatrix}$$

Sliding mode motion equation. Consider the following sliding surface

$$s = Cx \tag{6}$$

where C=(c_1,c_2,c_3,c_4), without loss of generality, from now on, one makes $c_4 = 1$, and others are constant.

Because **AB** is controllable, the system can be transformed to into skeleton type through nonsingular transformation (Gao W. 1996). Defining the transformation matrix as follows

$$\mathbf{T} = \begin{bmatrix} 1 & 0 & 0 & 0 \\ 0 & 1 & 0 & 0 \\ 0 & 0 & 1 & \dfrac{m_b}{m_f} \\ 0 & 0 & 0 & 1 \end{bmatrix} \tag{7}$$

$$\bar{x} = \mathrm{T}x\,;\ \overline{\mathbf{B}} = \mathbf{TB}\,;\ \overline{\mathbf{A}} = \mathbf{TAT}^{-1} \tag{8}$$

The skeleton type equation is obtained, as following:

$$\begin{bmatrix} \dot{\bar{x}}_1 \\ \dot{\bar{x}}_2 \end{bmatrix} = \begin{bmatrix} \overline{\mathbf{A}}_{\mathbf{11}} & \overline{\mathbf{A}}_{\mathbf{12}} \\ \overline{\mathbf{A}}_{\mathbf{21}} & \overline{\mathbf{A}}_{\mathbf{22}} \end{bmatrix} \begin{bmatrix} \bar{x}_1 \\ \bar{x}_2 \end{bmatrix} + \begin{bmatrix} \mathbf{0} \\ \overline{\mathbf{B}}_{\mathbf{2}} \end{bmatrix} u \tag{9}$$

$$s = (\overline{C}_1, \overline{C}_2) \begin{bmatrix} \bar{x}_1 \\ \bar{x}_2 \end{bmatrix} \tag{10}$$

where:

$$\overline{\mathbf{A}}_{\mathbf{11}} = \begin{bmatrix} 0 & 0 & 1 \\ 0 & 0 & 0 \\ -\dfrac{k_f}{m_f} & 0 & -\dfrac{c_f}{m_f} \end{bmatrix} \quad \overline{\mathbf{A}}_{\mathbf{12}} = \begin{bmatrix} -\dfrac{m_b}{m_f} \\ 1 \\ \dfrac{c_b m_b}{m_f^2} \end{bmatrix} \quad \overline{\mathbf{A}}_{21} = \begin{bmatrix} \dfrac{k_b}{m_b} & -\dfrac{k_b}{m_b} & \dfrac{c_b}{m_b} \end{bmatrix} \tag{11}$$

To guarantee the existence of $(\overline{\mathbf{C}}_2\overline{\mathbf{B}}_2)^{-1}$, $\overline{\mathbf{C}}_2^{-1}$, the equation $m_f - m_b c_3 \neq 0$ must be satisfied. Therefore, the following equation can be written in sliding mode surface.

$$s = Cx = \overline{C}_1 \bar{x}_1 + \overline{C}_2 \bar{x}_2 = 0 \tag{12}$$

So that, the motion equation on sliding mode surface can be obtained:

$$\dot{\bar{x}}_1 = (\overline{\mathbf{A}}_{11} - \overline{A}_{12}\overline{C}_2^{-1}\overline{C}_1)\bar{x}_1 \tag{13}$$

The characteristic polynomial of this sliding mode motion equation can be written:

$$D(p) = -p^3 + \frac{m_f c_2 - c_f - m_b c_1}{m_f - m_b c_2} p^2 + \frac{c_2 c_f + k_2}{m_f - m_b c_2} p + \frac{k_2 c_2}{m_f - m_b c_2} \tag{14}$$

According the stable theory, require the following:

$$\begin{cases} c_2 > 0 \\ c_1 < \dfrac{m_f c_2 + c_2}{m_b} - \dfrac{k_f c_2}{(c_2 c_f + k_f) m_b} \end{cases} \tag{15}$$

Approach rate and controller. The condition of the sliding mode motion existence and accessibility can be expressed as $s\dot{s} < 0$. Introducing the approach rate limit the approach motion to improve the dynamic qualities in the normal motion stage. This paper selects the exponent approach rate.

$$\dot{s} = -\varepsilon \operatorname{sgn} s - ks \quad (\varepsilon、 k > 0) \tag{16}$$

Consider the following equation:

$$\dot{s} = C\dot{x} = C(\mathbf{A}\mathbf{x} + \mathbf{B}u + \mathbf{E}d) \tag{17}$$

The control force function is expressed as following:

$$u = -(CB)^{-1}(\varepsilon \operatorname{sgn} s + ks + CAx + CEd) \tag{18}$$

Since it is difficult to obtain the track irregularity, the track disturbance must be decoupled from u. So, $CE = c_3 k_f / m_2 = 0$, therefore $c_3 = 0$ (Zhao C, 2007). The control force can be written as follows:

$$u = -(CB)^{-1}(\varepsilon \operatorname{sgn} s + ks + CAx) \tag{19}$$

Constraint condition. Because the semi-active system attenuates vibration through damping force, the controllable damping force does only negative work. Introducing the constraint condition of semi-active suspension, the control force can be express as following:

$$u = \begin{cases} -(CB)^{-1}(\varepsilon \operatorname{sgn} s + ks + CAx + CEd) & \dot{x}_b(\dot{x}_b - \dot{x}_f) \geq 0 \\ 0 & \dot{x}_b(\dot{x}_b - \dot{x}_f) < 0 \end{cases} \tag{20}$$

CO-SIMULATION MODEL

The vehicle dynamic model of a certain style vehicle is created as Figure 2 (Wang, G. 2005). Base on the control force, the model of controller is constructed using Simulink. Finally, the co-simulation model is set up show as Figure 3. The co-simulation of the vehicle dynamic model and controller can be done using Simulink.

Then, the applicability and control performance of the VSS controller base on the 3DOF vehicle model for the practical vehicle are verified (Dong X, 2005).

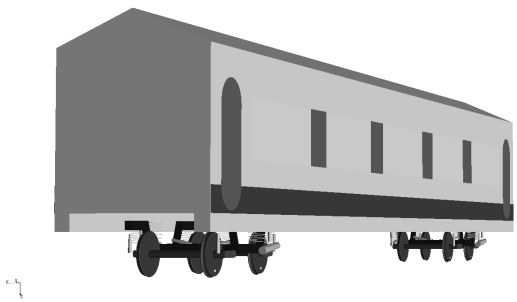

Figure 2. ADAMS vehicle model.

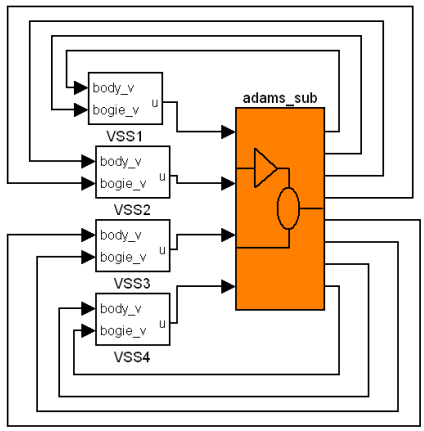

Figure 3. Co-simulation model.

SIMULATION AND RESULTS

According to the vehicle model which is built using ADMAS/rail, the parameter of simulation is presented in Table 1. The track disturbance adopt ORE low interfere spectrum.

Table1. Simulation Parameter

Parameter	Value	Parameter	Value
m_b/kg	32000/4	c_1	-30
m_f/kg	2615/2	c_2	30
k_b/(kN*sm^{-1})	430	c_3	0
k_f/(kN*sm^{-1})	1220*2	k	29
c_b/(kN*m^{-1})	20	ε	0.01
c_f/(kN*m^{-1})	4*2		

The car body displacement and velocity of the passive suspension system and semi-active suspension system are depicted in Figures 4 and 5.

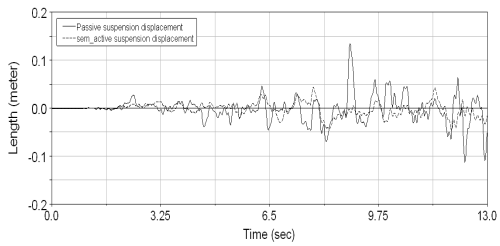

Figure 4. Displacement.

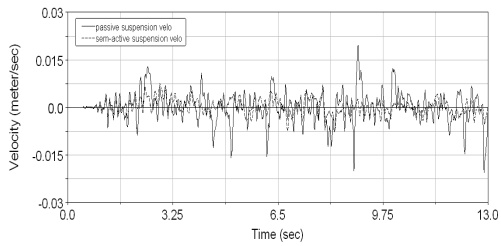

Figure 5. Velocity.

It is clear from Figure 4 that the semi-active suspension attenuates vibration

amplitude effectively. However, the amplitude is enlarged at 7.5 seconds and 11.5 seconds slightly, because the controller designed the base on simplified model does not fit the complex model completely. The car body acceleration of two suspension system is depicted in Figure 6.

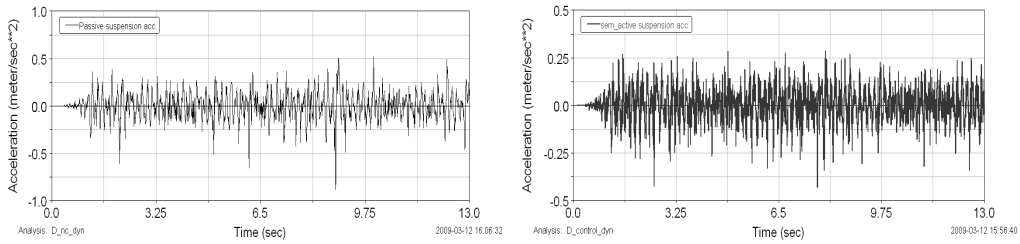

Figure 6. Acceleration of passive suspension and semi-active suspension.

Figure 7 is the acceleration frequency spectrum. The semi-active suspension system is also better than the passive one. From this it is clear that the low frequency vibration is isolated effectively.

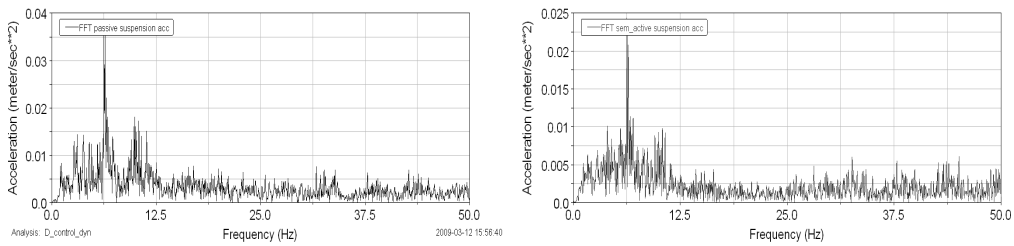

Figure 7. Acceleration frequency spectrum.

CONCLUSION

This paper considers the variable structure control with 3DOF vehicle model for design in a semi-active suspension system. Through the co-simulation, the effect of the VSS controller is studied for the practical complex model. The result shows that the isolating vibration effect of semi-active suspension system with VSS controller is better than the passive one. It is profitable to improve the riding comfort and security.

ACKNOWLEDGEMENTS

This work is supported by National Natural Science Foundation of China (No. 50823004), Special Fund from the Traction Power State Key Laboratory and Southwest Jiaotong University National Basic Research Program of China (973 Program) (No.2007CB714700)

REFERENCES

Zhao, C. (2007). “Semi-active suspension system with VSS control”. *China journal*

of highway and Transport. 20.

Dong, X. (2005). "Simulation of rail vehicle transverse semi-active suspension system," *China railway science.* 26(2).

Gao, W. (1996). "Variable structure control theory and design method." Beijing. 90-133.

Stutz, L.T. (2004). "Variable structure control with model following applied to a quarter car model subjected to random excitation" *ABCM Symposium series in mechatronics,* 1(2),169-176.

Wang, G. (2005). "A basic course of MSC.ADAMS/rail". Science publishing house.

Structural Noise of Longitudinal Stiffened Concrete Cylindrical Shell

XIE Weiping[1] and SUN Liangming[1]

[1]School of Civil Engineering and Architecture, Wuhan University of Technology, Wuhan 430070, China; PH (86) 027-50247564; FAX (86) 027-87664561; email: wpxie@sina.com

ABSTRACT

Structural noise induced by urban viaduct box beam basically comes from the vibration responses with low frequency noises, which may adversely affect humans and the production of high-precision instruments. The mitigation of vibration induced noises becomes a hot, but practical, issue in the field of environmental protection. Aimed at the coupling effect between medium and structure, the characteristics of sound radiation of the longitudinal stiffened concrete cylindrical shell are investigated. Firstly, motion equations of infinite concrete cylindrical shell are established. Secondly, radial velocity of the shell in wave-number domain is obtained based on the wave-number domain approach and transfer matrix method. And then, the forecast model of pressure radiated by the shell is formulated according to the stationary phase method. The results show that longitudinal ribs can effectively reduce the vibration and noise of concrete cylindrical shell. These can provide foundation to the research of reducing vibration and noise of the pipeline structure in practical engineering and the theoretical research on structural noise of railway box beam in urban viaduct rail facilities.

INTRODUCTION

With the rapid development of urban rail industry, the vibration and noise pollution induced by traffic loads have attracted more and more attention in recent years. Structural noises induced by urban viaduct box beam basically comes from the vibration responses with low frequency noises, which may adversely affect humans, the production of high-precision instruments, and the basic operation of hospitals, academic institutions, etc. (Ngai and Ng 2002). The mitigation of vibration induced noises becomes a hot, but practical, issue in the field of environmental protection. The acoustic radiation caused by the vibration of box beam demonstrates the properties of fluid-structure coupling vibration, which is a leading topic in structural acoustics and noise control. The investigation on the acoustic radiation from the box beam based on analytical method or semi-analytical method are quite limited due to the complexity of the equation of motion induced by the curvature varying in the circumferential direction (Junger and Feit 1986).

Ngai (2002) states that the peak level of structure-borne noise is mainly caused by the vibration resonance of the concrete structure, and the frequency range of structure-borne noise generated from concrete box and railway viaduct is within the range from 20Hz to 120Hz. Burroughs (1984) investigated radiation acoustic

pressure in the far field of a fluid-loaded infinite circular cylindrical shell reinforced with doubly periodic ring supporters subjected to a point-driven force with the aiding of the Fourier Transform, modal expansion in circumferential direction and the impedance method. But the model was quite simple because only the radial interacting forces between the stiffeners and the shell were considered. Based on the Burroughs' model, Chen et al (2002) studied the acoustic radiation from the orthogonally stiffened circular cylindrical shells. Wu (2002) examined the double-layer structural-acoustic coupling problem for cylindrical shell through the combination of the wave-number domain approach and the boundary integral equation. Xie et al. (2008) investigated the acoustic properties of the concrete cylindrical shell with/without stiffened ring ribs based on the finite element method.

Present research mainly focuses on the properties of circular cylindrical shells in the fields of military and machine fabrication. Furthermore, the research on the fluid-structure coupling in civil engineering is reported only for experimental and numerical investigation on the circular cylindrical shells. To this end, this paper examines the properties of structural noise of longitudinal stiffened infinite concrete cylindrical shells. The observations made in this study can be provided as beneficial guidelines for the noise mitigation of pipeline structures and railway box beams of urban viaduct rail facilities.

THEORETICAL ANALYSIS OF COUPLING SYSTEM

The configuration of an example longitudinal stiffened infinite concrete cylindrical shell is displayed in Figure 1.

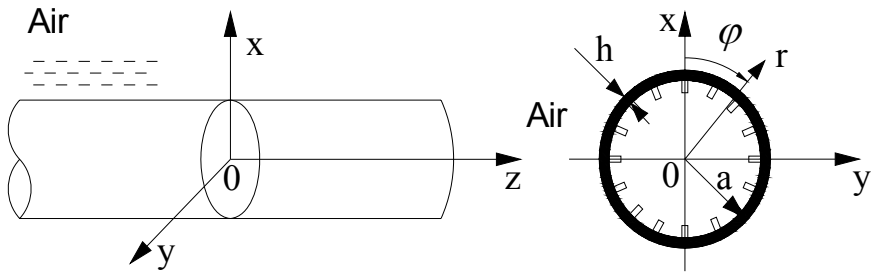

Figure 1. Longitudinal stiffened concrete cylindrical shell.

The exterior of the infinite concrete cylindrical shell is surrounded by air. The air is assumed to be compressible and inviscid. Therefore, only radial reaction on the shell can be observed. The mass density of the air is ρ_0 and the sound speed is c_0. The radius of the middle surface and the thickness are a and h respectively. Donnell's thin shell theory is utilized to describe the motion of the shell. The external excitation force is a point force towards the shell in the normal direction on shell outside surface. All of the loadings have a harmonic time dependence $e^{-i\omega t}$, where ω is the radian frequency, as an algebraic convenience, $e^{-i\omega t}$ is suppressed throughout. The observation point for the acoustic radiation is located in the far-field, such that $k_0 r >> 1$, where $k_0=\omega/c_0$ is the acoustic wave-number and r is the radial distance of the observation point from the z axis.

Following the classical assumption of Donnell, the equation of motion of the

shell can be expressed as:

$$[R]\cdot\begin{bmatrix} u_z(a,\varphi,z) \\ u_\varphi(a,\varphi,z) \\ u_r(a,\varphi,z) \end{bmatrix} = \frac{1-\mu^2}{E^* h}\begin{bmatrix} 0 \\ 0 \\ -p_l(a,\varphi,z) - F(a,\varphi,z) - p(a,\varphi,z) \end{bmatrix} \tag{1}$$

$$[R]=\begin{bmatrix} \frac{\partial^2}{\partial z^2}+\frac{1-\mu}{2a^2}\frac{\partial^2}{\partial\varphi^2}+\frac{\omega^2}{c_l^2} & \frac{1+\mu}{2a}\frac{\partial^2}{\partial z\partial\varphi} & \frac{\mu}{a}\frac{\partial}{\partial z} \\ \frac{1+\mu}{2a}\frac{\partial^2}{\partial z\partial\varphi} & \frac{1}{a^2}\frac{\partial^2}{\partial\varphi^2}+\frac{1-\mu}{2}\frac{\partial^2}{\partial z^2}+\frac{\omega^2}{c_l^2} & \frac{1}{a^2}\frac{\partial}{\partial\varphi} \\ \frac{\mu}{a}\frac{\partial}{\partial z} & \frac{1}{a^2}\frac{\partial}{\partial\varphi} & \frac{1}{a^2}+\beta a^2\nabla^4-\frac{\omega^2}{c_l^2} \end{bmatrix}$$

in which $u_z(a,\varphi,z)$, $u_\varphi(a,\varphi,z)$, and $u_r(a,\varphi,z)$ are the axial, circumferential and radial displacement at the cylinder's mid-surface, respectively. They are positive if they are in the positive direction of the coordinate axis. The mechanical excitation force is expressed as $F(a,\varphi,z)$. The acoustic pressure on the exterior surface of shell is $p(a,\varphi,z)$ and the reaction pressure due to the attachment of the axial ribs on the shell surface is $p_l(a,\varphi,z)$. ρ is the mass density of the shell; $E^*=E(1+i\eta)$ is the complex Young's modulus of the shell; μ is the Poisson's ratio of material; $\beta=h^2/12a^2$, $c_l=(E^*/\rho(1-\mu))^{0.5}$ is the longitudinal wave speed of the shell.

To define the Fourier Transform (FT) as:

$$\tilde{f}_n(r,\zeta)=\int_{-\infty}^{+\infty} f_n(r,z)e^{-iz\zeta}dz=\int_{-\infty}^{+\infty}(1/2\pi)\int_0^{2\pi} f(r,\varphi,z)e^{-in\varphi}d\varphi e^{-iz\zeta}dz \tag{2}$$

By using FT in the z direction and φ direction, the equation of motion of the shell in the wave-number domain can be written as:

$$\begin{bmatrix} \tilde{u}_{z,n}(a,\zeta) \\ \tilde{u}_{\varphi,n}(a,\zeta) \\ \tilde{u}_{r,n}(a,\zeta) \end{bmatrix} = \frac{1-\mu^2}{E^* h}\tilde{\Gamma}_n\begin{bmatrix} 0 \\ 0 \\ -\tilde{p}_{ln}(a,\zeta) - \tilde{F}_n(a,\zeta) - \tilde{p}_n(a,\zeta) \end{bmatrix} \tag{3}$$

where n denotes the order of FT in the φ direction; $\zeta=(k_0^2-\gamma_0^2)^{0.5}$ is the axial wave-number in the air; γ_0 is the radial wave-number in the exterior air. Therefore, the spectral radial velocity of the neutral surface of the shell is:

$$\tilde{\dot{u}}_{r,n}(a,\zeta)=i\omega[(\mu^2-1)/E^* h]\cdot\tilde{\Gamma}_{n3}^3\cdot[-\tilde{p}_{ln}(a,\zeta)-\tilde{F}_n(a,\zeta)-\tilde{p}_n(a,\zeta)] \tag{4}$$

Moreover, the spectral radial velocities among the inner surface, the neutral surface and the outer surface of the shell are identical. Based on the transfer matrix equation of the shell, the spectral radial velocity of the outer surface of the shell is:

$$\tilde{\dot{u}}_{r,n}(a,\zeta)=\tilde{F}(a,\zeta)/[-\tilde{Z}_{l,n}(a,\zeta)-\tilde{Z}_{s,n}(a,\zeta)-\tilde{Z}_{0,n}(a,\zeta)] \tag{5}$$

where the radial mechanical impedance is:

$$\tilde{Z}_{s,n}(a,\zeta)=E^* h/[i\omega(\mu^2-1)\tilde{\Gamma}_{n3}^3] \tag{6}$$

With harmonic time dependence, the acoustic pressure in the air surrounding the shell satisfies the following Helmholtz equation:

$$(\nabla^2+k_0^2)p(r,\varphi,z)=0 \tag{7}$$

The solution to Equation (7) in the wave-number domain is:

$$\tilde{p}_n(r,\zeta) = A_1(n,\zeta)J_{|n|}(\gamma_0 r) + A_2(n,\zeta)H_{|n|}(\gamma_0 r) \tag{8}$$

where $J_n()$ is the nth-order Bessel function and $H_n()$ is the nth-order Hankel function.

At the fluid-structure interface, the radial displacement of the air is equal to the radial displacement of the shell. From the momentum equation, it has:

$$\partial \tilde{p}_n(a,\zeta)/\partial r = i\omega\rho_0 \tilde{\dot{u}}_{r,n}(a,\zeta) \tag{9}$$

It is noted that the spectral radial velocity of the outer surface of the shell can be calculated when the exterior acoustical radiation impedance are determined. Based on the Sommerfield radiation condition, the exterior acoustical radiation impedance can be written as follows:

$$\tilde{Z}_{0,n}(a,\zeta) = i\omega\rho_0 H_{|n|}(\gamma_0 a)/(\gamma_0 H'_{|n|}(\gamma_0 a)) \tag{10}$$

The force on the shell surface exerted by axial ribs is given by:

$$p_l(a,\varphi,z) = \sum_{j=1}^{M} p_l^j(a,z) \sum_{n=-\infty}^{+\infty} \delta\{a[\phi - (\phi_j + 2\pi n)]\} \tag{11}$$

where $p_l^j(a,z)$ is the normal distributed force on the surface per unit length in the x direction, which is produced by the j-th axial rib, and the delta function has dimension [m^{-1}] in order to convert the force per unit length into the force per unit area on the cylinder; $\Phi_j=(2\pi/M)j$, M being the number of the axial ribs.

Here, the axial ribs are modeled as Euler beams, and the shear deformation and rotation inertia are neglected. On the basis of the continuity of the radial displacements between the shell surface and the FT, we have:

$$\tilde{p}_{\ln}(a,\zeta) = \frac{k^4 E_l I_l - \rho_l A_l \omega^2}{-2i\omega\pi a} \sum_{m=-\infty}^{+\infty} \sum_{j=1}^{M} e^{i(m-n)\phi_j} \tilde{\dot{u}}_{r,n}(a,\zeta) = Z_l \sum_{m=-\infty}^{+\infty} A_{nm} \tilde{\dot{u}}_{r,n}(a,\zeta) \tag{12}$$

where the cross-sectional area of the axial rib is A_l, the inertia moment is I_l, the material density is ρ_l, and Young's modulus is E_l. Because the n-order modal force of exterior shell by longitudinal ribs can not only determine by the n-order modal radial velocity, but also by the other order modal radial velocity. If longitudinal ribs are evenly arranged along the circumferential direction, circumferential modal coupling caused by them is a very weak coupling. The Equation (12) can be written as follows:

$$\tilde{p}_{\ln}(a,\zeta) = Z_l \cdot M \cdot \tilde{\dot{u}}_{r,n}(a,\zeta) \tag{13}$$

By applying the external force at the point (z_0,φ_0) from outside the shell, the expression for the external applied pressure is:

$$F(a,\varphi,z) = F_0 \delta(z - z_0)\delta(\varphi - \varphi_0)/a \tag{14}$$

where F_0 is the magnitude of the applied force. Taking the FT Equation (14) yields:

$$\tilde{F}_n(a,\zeta) = (1/2\pi)\int_0^{2\pi} e^{-in\varphi} \int_{-\infty}^{+\infty} F(a,\varphi,z) e^{-i\zeta z} dz d\varphi = (F_0/2\pi a) e^{-in\varphi_0 - i\zeta z_0} \tag{15}$$

Substituting Equations (10), (12), (15) into Equation (5) yields the spectral

radial velocity of the outer surface of the shell in the wave-number domain.

It should be noted that the crucial parts are the prediction of the acoustic radiation at far field. Let *(R, θ, ψ)* be the coordinates of an observation point *N* at the far field (see Figure 2), then according to the boundary integral equation and the stationary phase method, the far field acoustic pressure is expressed as:

$$p(R,\theta,\psi)=\frac{\rho_0 c_0 e^{jk_0 R}}{\pi R\sin\theta}\sum_{n=-\infty}^{\infty}\frac{(-i)^{|n|}}{H'_{|n|}(k_0 a\sin\theta)}\tilde{u}_{r,n}(a,k_0\cos\theta)e^{jn\psi} \tag{16}$$

where $\tilde{u}_{r,n}(a,k_0\cos\theta)$ is given by Equation (5), in which $\zeta=k_0 cos\theta$.

Thus, the far field acoustic pressure level is given by $L_p=20\lg[p(R,\theta,\psi)/p_{ref}]$, where $p_{ref}=2\times10^{-5}Pa$.

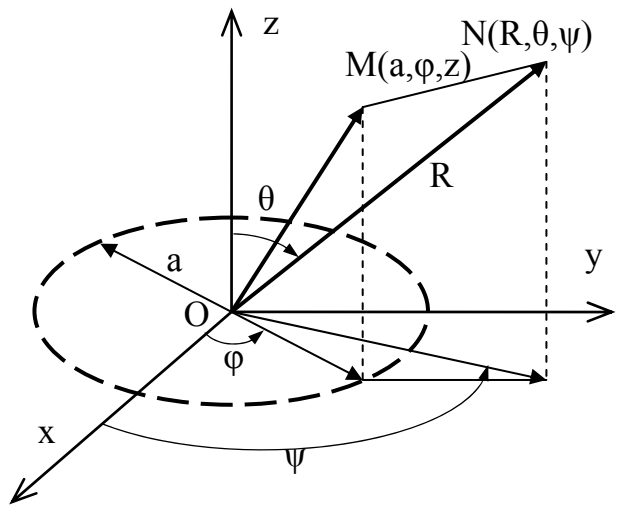

Figure 2. The source point and the observation point of geometry sketch map.

NUMERICAL INVESTIGATIONS

In this section, numerical results based on Equation (16) are presented for the far field acoustic pressure levels of the acoustic radiation from a longitudinal stiffened infinite concrete cylindrical shell immersed in air. It is demonstrated based on numerical observations that the effects of longitudinal ribs on the rule of infinite concrete cylindrical shell are important. The following parameters for the model are used in the calculations. $a=1m$, $h=0.05m$, $\mu=0.2$, $E=3.25\times10^{10}N/m^2$, $\rho=2550kg/m^3$, $\eta=0$, $(z_0,\varphi_0)=(0,0)$, $F_0=100N$, $\rho_0=1.21kg/m^3$, $c_0=343m/s$, $N_1(5m,\pi/2,0)$, $A_l=5.22\times10^{-3}m^2$, $I_l=3.28\times10^{-5}m^4$.

From Figure 3, it can be found that, the axial ribs have an evident effect on the acoustic radiation and vibration of the shell and the sound pressure levels (SPL) decrease.

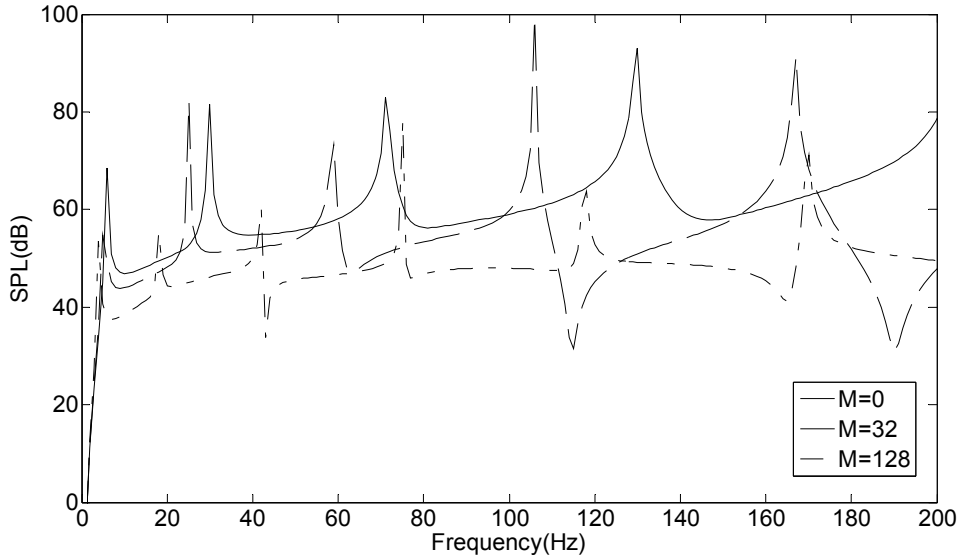

Figure 3. The curves of SPL and frequency with different ribs.

CONCLUSIONS

The analytical approach for rating noise effects of longitudinal stiffened infinite concrete cylindrical shell is actively investigated in this study. The key of computing the acoustic radiation from the infinite concrete cylindrical shell is the solution the equation of motion with fluid-structure coupling effects, the Helmholtz equation, the Sommerfield radiation condition and the coordination condition which is at the interface between air and concrete cylindrical shell. The predicting model of pressure radiated by the shell is deduced based on the wave-number domain approach and transfer matrix method. The results show that longitudinal ribs can effectively reduce the vibration and noise of concrete cylindrical shell. The observations made in this study can be provided as beneficial guidelines for the noise mitigation of pipeline structures and railway box beams of urban viaduct rail facilities.

ACKNOWLEDGEMENT

The authors are grateful for the financial support from the National Natural Science Foundation of China under Grants NNSF-50678141.

REFERENCES

Burroughs, C.B. (1984). Acoustic radiation from fluid-loaded infinite circular cylinders with periodic ring supports. *J. of the Acoustical Society of America*, 75(3), 715-722.

Chen, J.M., Huang, Y.Y. and Zeng, G.W. (2002). Vibration and acoustic radiation from orthogonally stiffened infinite circular cylindrical shells in water. *China Ocean Engineering*, 16(4), 437-452.

Junger, M.C. and Feit, D. (1986). *Sound, structures and their interaction.* 2nd ed. MIT Press, Cambridge.

Ngai, K.W. and Ng, C.F. (2002). Structure-borne noise and vibration of concrete box structure and rail viaduct. *J. of Sound and Vibration*, 255(2), 281-297.

Wu, C.J. (2002). Double-layer structural-acoustic coupling for cylindrical shell by using a combination of WDA and BIE. *Applied Acoustics*, 63(10), 1143-1154.

Xie, W.P., Chen, X.D. and Pan, Z.M. (2008). Analysis of acoustic radiation from reinforced concrete cylindrical shell in air. *Noise and Vibration Control*, 28(3), 109-112. (Chinese)

Research on Greedy Train Rescheduling Algorithm

Z. He [1], H. Li, J. Miao, L. Meng, B. Mao

[1]State Key Laboratory of Rail Traffic Control and Safety, Beijing Jiaotong University, 100044, Beijing, China; PH (86)10-51688564; email: hezhenhuan@jtys.bjtu.edu.cn

ABSTRACT

Train rescheduling is the key work in railway operation. Due to its complexity, it is very difficult to achieve optimal results and the heuristic algorithms become the most popular and effective solving techniques. The paper presents a greedy algorithm for train rescheduling, in which conflicts are resolved respectively with the greedy principle. The algorithm has an excellent efficiency and enables dispatchers to take part in the optimization process more broadly. As a result, it can take more factors into account and make full use of experts' experience to make the solution more practical and efficient.

INTRODUCTION

Railways play a vital role in many countries, which has researchers focusing on train rescheduling a great deal of the time. Branch and bound algorithm is often applied to resolve the problem. The most recent research was done by Dessouky et al. (2006) and D'Ariano et al. (2007). There is, however, an unavoidable disadvantage in that the models are sometimes difficult to resolve, although powerful computers and programming software can resolve the problems. As a result, the application of the models must be limited to small-sized problems and sometimes "unimportant" factors have to be ignored. Furthermore, the experience of dispatchers can hardly be added into the models. All the above prevent the models from being applied in real-time operation. Since 2007, many heuristic algorithms have been developed to achieve satisfactory solutions, though not optimal, but are good enough.

Zhou (1994) used discrete event system (DES) to describe the railway system and presented an algorithm for train rescheduling based on DES firstly. Medanic and Dorfman (2001), (2002), (2004) researched greedy TAS algorithms based on DES with the objective of time or energy efficiency for single-track railway line. Cai et al. (1998) also developed a greedy heuristics algorithm for rapid scheduling of trains on a single line. The algorithm was so efficient that it could be used to tackle large numbers of trains. Cheng (1998) provided a hybrid simulation algorithm that tried to combine the advantage of event-driven and network simulation together to resolve each conflict more easily and effectively. Ismail (1999) provided an algorithm that handled immediate conflict according to dynamic priority of the trains. Adenso-Diaz (1999) presented a heuristic procedure to choose the most appropriate solution from solutions spaces. Jin ([2004) developed a non-delay dispatch algorithm with multiple objectives, which, in fact, is based on DES. In Dessouky's and D'Ariano's research,

some heuristic rules were added that greatly increased the efficiency of the algorithm in order to make it useful in real-time operation. All of the above research proved especially helpful for this paper.

MODELING PROBLEM

The most common objective is to minimize total weighted or unweighted delay time. Other possible objectives include the minimization of the total quantity of delayed trains and energy consumption, and so on.

In this study, we made the following assumptions and definitions:

1) The railway line in the paper has double tracks;

2) There are totally m stations ($s_1, s_2, \cdots, s_m$) in the problem ordered by inbound direction;

3) According to assumption 2, there are totally m-1 sections ($q_1, q_2, \cdots, q_{m-1}$) in the problem where s_i and s_{i+1} are the immediate stations of q_i.

Taking the minimization of overall weighted delay time as the optimizing objective, the model of the problem could be described as follows:

$$\min \sum_{i=1}^{n} \omega_i dt_i$$

Subject to:

$$(-1)^{d_{i,j}} \cdot t_{i,j+1}^{a} - (-1)^{d_{i,j}} \cdot t_{i,j}^{d} \geq (1 - d_{i,j}) \cdot r_{i,j}^{out,\min} + d_{i,j} \cdot r_{i,j}^{in,\min} \quad (1)$$

$$t_{i,j}^{a} \Theta t_{k,j}^{a} \geq I_{i,k}^{a,j} \quad (2)$$

$$t_{i,j}^{d} \Theta t_{k,j}^{d} \geq I_{i,k}^{d,j} \quad (3)$$

$$t_{i,j}^{d} - t_{i,j}^{a} \geq \tau_{i,j}^{s\min} \quad (4)$$

$$t_{i,j}^{d} \geq t_{i,j}^{*d} \quad (5)$$

$$\sum_{i=1}^{n} g_{i,j}^{s,t} \leq n_j^{gs} \quad (6)$$

$$C(t_{i,j}^{f}, {}^{d}_{i,j}, t_{k,j}^{wb}, t_{k,j}^{we}) \cdot O(g_{i,j}^{q}, G_k^{w}) < 1 \quad (7)$$

$$C(t_{i,j}^{f}, t_{i,j+1}^{d}, t_{k,j+1}^{f}, t_{k,j}^{d}) \cdot Q(g_{i,j}^{q}, g_{k,j}^{q}) \cdot D(d_{i,j}, d_{k,j}) < 1 \quad (8)$$

where :

ω_i, dt_i are the weight and overall delay time of train *i*;

$d_{i,j}$ is the direction of train *i* in section *j*, 0 is outbound and 1 is inbound;

$t_{i,j}^{a}, t_{i,j}^{d}$ are the arrival and departure time of train *i* in station *j*;

$t_{i,j}^{*a}, t_{i,j}^{*d}$ are original arrival and departure time of train *i* in station *j* ("original" in the paper refers to the data in last rescheduled plan or initial timetable if the last rescheduled plan doesn't exist) ;

$r_{i,j}^{in}, r_{i,j}^{in,\min}, r_{i,j}^{out}, r_{i,j}^{out,\min}$ are the standard and minimum running time of train i in section j inbound or outbound direction;

$I_{i,k}^{a,j}, I_{i,k}^{d,j}$ are arrival and departure headway interval between train i and k in section j;

Θ is defined as: $t_{i,j}^{d} \Theta t_{k,j}^{d} = \begin{cases} t_{i,j}^{d} - t_{k,j}^{d}, & t_{i,j}^{d} \geq t_{k,j}^{d} \\ \infty & t_{i,j}^{d} < t_{k,j}^{d} \end{cases}$

$\tau_{i,j}^{s\min}$ is the minimum dwell time of train i in station j;

n_j^{gs}, n_j^{gq} are siding quantity of station i and section i;

$g_{i,j}^{s,t}$ is a 0-1 value variable. 1 means train i occupies a siding in station j at t moment, otherwise 0;

$C(t_{i,j}^{a}, {}^{d}_{i,j}, t_{k,j}^{wb}, t_{k,j}^{we})$ is defined as: $C(t_{i,j}^{a}, t_{i,j}^{d}, t_{k,j}^{wb}, t_{k,j}^{we}) = \begin{cases} 1 & t_{i,j}^{d} \leq t_{k,j}^{wb} \quad or \quad t_{i,j}^{a} \geq t_{k,j}^{we} \\ 0 & otherwise \end{cases}$

where $t_{k,j}^{wb}, t_{k,j}^{we}$ are begin and end time of section blockage k in section j;

$O(g_{i,j}^{q,t}, G_k^{w})$ is defined as: $O(g_{i,j}^{q}, G_k^{w}) = \begin{cases} 1 & g_{i,j}^{q} \in G_k^{w} \\ 0 & g_{i,j}^{q} \notin G_k^{w} \end{cases}$, where $g_{i,j}^{q}$ is the track used by train i in section j; G_k^{w} is the set of track involved in window k;

$Q(g_{i,j}^{q}, g_{k,j}^{q})$ is defined as: $Q(g_{i,j}^{q}, g_{k,j}^{q}) = \begin{cases} 1 & g_{i,j}^{q} = g_{k,j}^{q} \\ 0 & g_{i,j}^{q} \neq g_{k,j}^{q} \end{cases}$

$D(d_{i,j}, d_{k,j})$ is defined as: $D(d_{i,j}, d_{k,j}) = \begin{cases} 1 & d_{i,j} = 1 \quad and \quad d_{k,j} = 0 \\ 0 & otherwise \end{cases}$

GREEDY ALGORITHM

Main idea and process of the algorithm. There are usually over 100 pairs of trains in a dispatcher's territory with double tracks. As a result, the solution of the model above has obvious great complexity. It is generally impossible to get optimal solutions in a short time. Therefore, this paper presents a greedy algorithm for the problem. The main idea of the algorithm is to resolve only one conflict in each iteration and obtain the current optimal solution aiming at only the "current" conflict, until all conflicts are resolved. So that the optimization of the problem with large size is divided into a sequence of problems with small size and the solution can be gotten in a short time. Besides the objective and constraints described previously, the experience of experts can be introduced as dispatching strategies to enable the solutions more realistic and optimized. In addition, the algorithm is flexible and can be easily extended to deal with the new type of conflict, since each of the conflicts is resolved independently.

The process of the algorithm is shown as Figure 1.

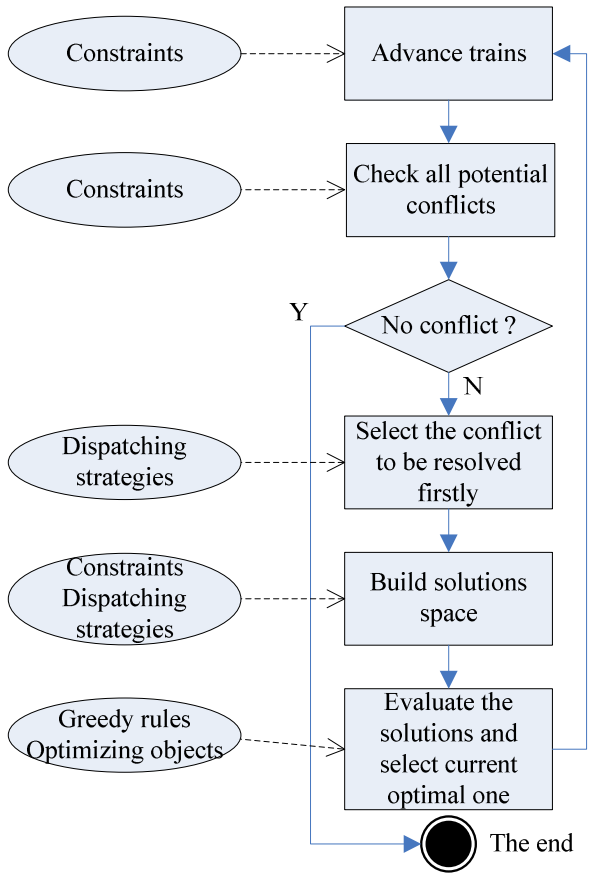

1. Advance relative trains. The arrival and departure time of the delayed trains are recalculated from the changed location regardless the potential conflicts.
2. Detect potential conflicts according to the constraints described in the model. If no conflict exists, the process is accomplished and a new schedule is obtained.
3. Select the conflict that should be addressed firstly. In this step, some strategies such as "time priority" will be applied.
4. Build solutions space according to the constraints and dispatching strategies.
5. Evaluate each solution in solutions space and select the current optimal one. Then, turn to step 2 and a new iteration will begin.

Figure 1. Process of the algorithm.

Types of conflicts. Conflicts here refer to any events that make the current plan infeasible. In the real cases, conflicts usually interweave with each other especially in rush hours and it seems possible that each conflict involves several trains, which greatly increases the complexity of dispatching. Hence in this study, we assume that each conflict involves at most two trains. This means that conflicts occur either between two trains or between the train and other factors, such as section blockage. Therefore, a complicated conflict will be divided into several conflicts and each resolved separately. Six types of conflicts will be mentioned in the study:

- *Headway conflict*: headway interval between two trains is not enough. There are two subtypes: arrival headway conflict and departure headway conflict.
- *Facing in section conflict*: two trains meet in the same track in the section
- *Siding occupancy conflict*: two trains use the same siding at the same time while both/one of them must use it exclusively.
- *Route conflict*: two opposite routes are used at the same time.
- *Section blockage conflict*: the train runs through blocked area within the duration of section blockage.
- *Station blockage conflict*: the train uses the blocked device (siding, switch or

part of rail) of a station.

Train advancing. When abnormal events occur, the arrival and departure time of involved trains will have to be recalculated from the current station (if the delay occurred in station) or the next station (if the delay occurred in the section) mainly according to constraint 1, 4 and 5.

In some cases like Figure 2, some extra constraints could be added in order to improve the efficiency of the algorithm.

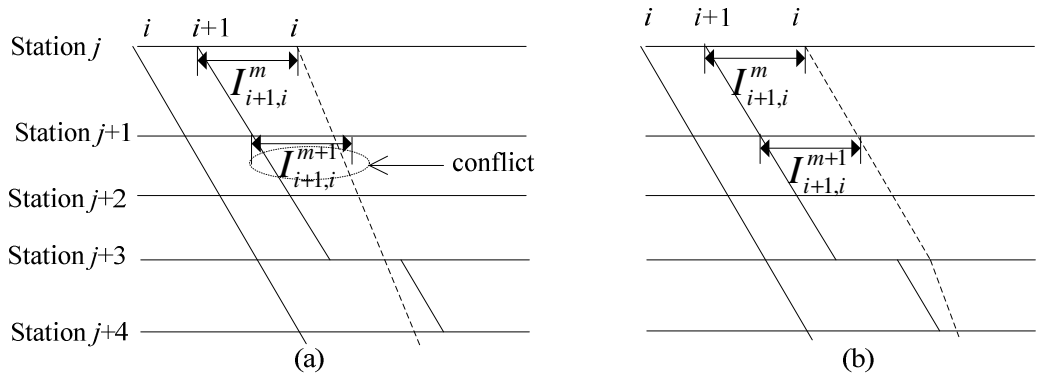

Figure 2. A case about train advancing.

In this case, train i and i+1 have a headway interval conflict in section j and the solution is to move train i behind of train i+1, shown as Figure 2(a). Since the minimum running time is used for train i, but train i+1 runs still by normal running time, the headway time between the two trains will become shorter and shorter. Since then, in a certain section, generally the section j+1, a new conflict occurs. According to previous solution, train i will be moved again. In the following iterations, similar situations will repeat again and again until train i+1 stops at a station. In fact, the following iterations can be avoided since it is always train i that is moved. Therefore, constraints 2 and 3 should be considered in this case and a new arrival time should be calculated as following from station j+1 to j+3 (station j+3 is the first station where train i+1 stops after station j) like Figure 2(b).

$$t^a_{i,j+1} = \max((1-d_{i,j}) \cdot r^{out,\min}_{i,j} + d_{i,j} \cdot r^{in,\min}_{i,j}, t^a_{i+1,j+1} + I^j_{i+1,j}) \quad (9)$$

Now there is no conflict from section j+1 to j+2 and much computation time is saved.

Approach to resolve the conflicts. The former four types of conflicts indicate that two trains want to occupy the same resource at the same time. The key to the solution is to determine which one should first use the resource and how to assign another resource or another time to the second train. Some strategies can help us in this process to determine the priority of the two trains directly. If none of the strategies can determine the final solution directly, a solutions space including two or

more possible solutions will be constructed and evaluated as follows:

Headway interval conflict. There are generally two possible solutions to this conflict: move train *i* while keeping train *k* unchanged or the contrary. The key to the approach is to reassign a new arrival or departure time to moved train.

Generally speaking, the moved train will arrive or depart as soon as the condition of headway interval can be fulfilled. Hence, if the current conflict is a departure headway interval conflict and occurs in station *j*, the solutions seem like Figure 3(a) and (b). In this case the new departure time of moved train (taking train *i* as example) is reassigned as: $t_{i,j}^{d} = t_{k,j}^{d} + I_{k,i}^{d,j}$. If the current conflict is an arrival headway interval conflict, the solutions have two possibilities, shown as Figure 3 (c) and (d). In the case of (c), the front train *i* is moved from station *j* and then the new departure time is: $t_{i,j}^{d} = t_{k,j}^{d} + I_{k,i}^{d,j}$. If train *k* is moved, the new arrival time in station *j*+1 will be reassigned as: $t_{k,j+1}^{a} = t_{i,j+1}^{a} + I_{i,k}^{a,j+1}$.

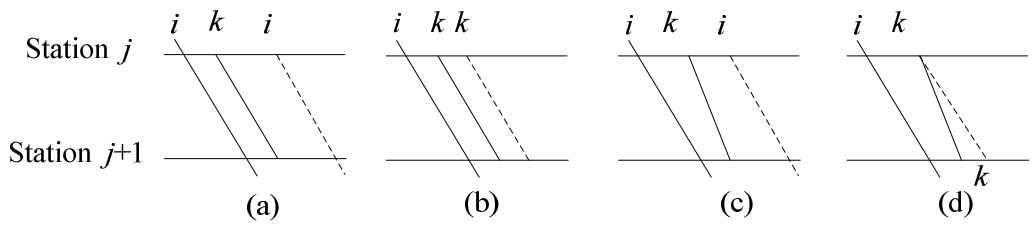

Figure 3. Approaches to resolve headway conflict.

Once a new departure or arrival time is changed, the moved train should be advanced from the station where change takes place to the destination of the train according to the method described in 3.3. Now overall weighted delay time of the two solutions in the solutions space can be calculated respectively according to the objective of the problem and the solution with less delay time will be the final solution for current conflict.

Facing in section conflict. The approach is similar to that described above. The difference lies in the determination of departure time of moved train. If outbound train *k* should be moved in station *j*+1, its departure time is changed to: $t_{k,j+1}^{d} = t_{i,j+1}^{d} + \tau_{j+1}^{ad}$, where τ_{j+1}^{ad} is the minimum interval between two trains needed by station operations.

Siding occupancy conflict. The main approach to resolve the conflict is to try to move each train to each siding of the station separately, and then evaluate the overall delay time of each solution and select the best one as the final solution of the conflict.

1) We assume that train *i* occupies the current siding, and train *k*

will be moved to another siding of the station *j* in turn. When train *k* is moved to siding *x*, the occupancy time slice of train *k* ($ts_{k,j}$) will be compared with the time slice of other trains that occupy siding *x* to calculate overlapped time of each two time slices. If $ts_{l,j}$ has the longest overlapped time with $ts_{k,j}$, train *l* and train *k* are the bottleneck of current operation and they will construct a solution. If none of the time slice have overlapped time with $ts_{k,j}$, train *k* will construct the solution itself.

2) If two trains construct the solution, the subsequent work is to postpone the later train to resolve the conflict between two trains. If train *l* is the later train, its earliest arrival time will be rearranged as $t_{l,j}^{a} = t_{k,j}^{d} + \tau_{j}^{o,\min} + \tau_{j}^{c,\min}$. Then train *l* should be re-advanced from station *j* and a solution is accomplished.

3) Continue the operations above, and finally *n* (*n* is the quantity of siding in the station) solutions will be obtained.

4) Assume that train *k* occupies the current siding and repeat operations above, and other *n* solutions will be obtained.

Now the solutions space has been constructed and the final work is to calculate overall delay time of each solution and select the one with least delay time as a final solution for this conflict.

Route conflict. The possible solutions include changing another route or even another siding and postpone arrival or departure time of one of the two trains. Since the duration of this conflict is usually pretty short and changing to another route will more likely lead to potential conflicts, we can just postpone the arrival or departure time of the train. Then the solutions space has also two solutions: to postpone train *i* or train *j*. Subsequent work is also to evaluate each solution and select one.

Section blockage conflict. The only solution for this conflict is to prevent the train from entering the blocked segment and postponing the departure time is the most common measure. In the algorithm, the departure time will be postponed to the end of blockage firstly. Some headway conflicts maybe occur after this operation. However, that is the work of next iteration and will not be considered here.

Station blockage conflict. If a siding is blocked, the resolving process is almost the same as with that of siding occupation conflict. The only difference is the blocked siding should not be considered. If other devices are blocked, the solution is to select another route for the train. At last, if there is no practicable route currently, the train has to be postponed in the previous station.

Tracing-back in the algorithm. If there are headway interval conflicts between train *i* and *k*, *k* and *m*, but no conflict between train *i* and *k*, shown in Figure 4(a). According to this algorithm, we should resolve the conflict between train *i* and *k* first, and get the new train diagram shown in Figure 4(b). Then, the conflict between *k* and *m* is handled and finally train *k* is moved. Now train *k* and *i* conflict again, and train *i* has to be moved second time. The final solution shown as Figure 4(c) is obtained. In this solution, train *i* is moved two times and becomes the last

train.

When we think over the whole process carefully, something unreasonable will be found. Train *i* moved firstly because the better solution is to keep train *k* unchanged. However, at the next step, train *k* is also moved. It means that the reason for the first movement of train *i* does not exist any longer and the first moving is unnecessary at that time. Thus, this solution is obviously not the result we need and some measures should be introduced into the algorithm to avoid this phenomenon in this situation.

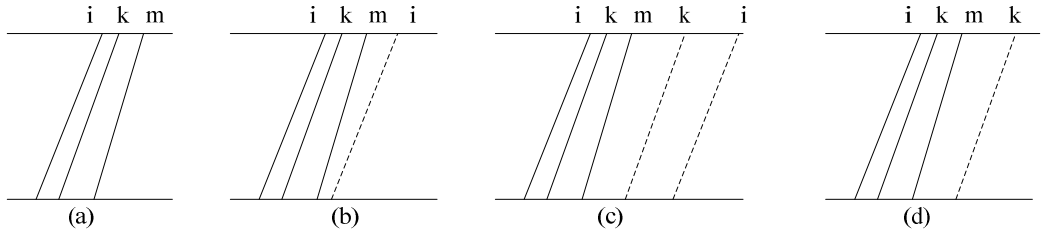

Figure 4. Example of rescheduling process.

Tracing-back in the algorithm is designed aiming at the circumstance described above. Firstly, when a train is moved, original information will be recorded in this train and the index information, generally the train ID, will be recorded in another train in the solution. Taking the instance above as an example, the information about train *i* will be recorded into a set of train *k* as $N_k^{move} = \{i\}$ when train *i* was moved in the first step. Then, in the following step, N_k^{move} will be checked once train *k* was determined to be moved. If the N_k^{move} is not null, the trains recorded in it will return back to their original status. The solution of the instance above is changed as Figure 4(d) when tracing-back is introduced.

Tracing-back should be introduced in handling not only headway interval conflicts, but also all the other types of conflicts. Once anything of the train, no matter arrival and departure time, route or siding, is determined to be changed in the process of rescheduling, the original information should be recorded in the train itself and the index of the train should be recorded in the other object (the other train or blockage). Once the latter is also changed (the train is moved or the blockage is canceled), the former will return back to its original status by the help of the information recorded previously.

In addition, the relative information in any train will be deleted when all the conflicts are resolved and current rescheduling is completed lest the information will influence next rescheduling.

EXAMPLES

We take Wu-guang line, a constructing passenger dedicated line (PDL) in China as the example which has double-track mainlines and 18 stations to test the algorithm. We construct a timetable that includes 115 pairs of high-speed trains (HS)

and 30 pairs of middle-speed trains (MS). The weight of HS and MS is 3 and 1 respectively. We set 4 scenarios in which delay rate and average delay time of HS and MS are: 1) 3%, 5 min, 5%, 5min; 2) 3%, 5 min, 10%, 10min; 3) 5%, 10 min, 10%, 15min; 4) 5%, 10 min, 20%, 15min.

Thirty experiments were made aiming at each scenario. The rescheduling result was shown in Table 1.

Table 1. Result of Rescheduling Test.

Scen-arios	Initially delayed trains				Finally delayed trains						WTDT	ASRT
	HS		MS		HS			MS				
	QDT	ADT	QDT	ADT	QDT	ADT	TDT	QDT	ADT	TDT		
1	3.6	5:20	1.7	4:57	1.9	1:56	3:45	1.8	16:45	29:27	40:42	0.68
					2.1	5:14	11:00	1.2	8:45	10:31	43:31	
2	3.6	5:20	3.4	10:00	3.1	1:56	6:04	3.5	17:04	59:27	1:17:39	0.8
					3.1	4:42	14:32	3.1	13:11	41:26	1:25:02	
3	5.9	09:46	3.2	15:01	7.5	03:31	26:26	5.4	17:02	1:32:36	2:51:54	2.93
					5.9	07:52	46:30	5.3	28:06	2:29:55	4:49:25	
4	5.9	10:02	6.5	14:59	9.1	03:15	29:43	7.7	19:30	2:30:10	3:59:19	3.5
					6.7	06:57	46:35	8.8	25:49	3:46:20	6:06:05	

* QDT: Quantity of Delayed Trains; ADT: Average Delay Time; TDT: Total Delay Time; WTDT: Weighted Total Delay Time; ASRT: Average System Running Time for each experiment (Seconds).

The data with gray background is the result of a typical class-based algorithm. According to this algorithm, when a conflict occurs between HS and MS, the HS will generally run firstly or the trains will run by their current orders. Furthermore, HS can also wait for MS under some special conditions.

As we can see from Table 1, WTDT of greedy algorithm are always better. The differences are remarkable especially in the scenarios with serious delay. On the other hand, the efficiency of the algorithm is quite high. Even in the scenario with serious delay, the rescheduling can also accomplished within several seconds. It is another outstanding advantage of the algorithm.

CONCLUSION

The greedy algorithm offers a quick method for train rescheduling. It can make full use of the experience of the experts and take more factors into account so as to make rescheduled plans more practicable. Furthermore, it is very simple to realize and it also can be extended easily to new networks. All the above make it suitable to real-time railway operation.

In the algorithm, all potential conflicts are ignored when we made the solutions space and evaluate the solutions. It is not doubtful that if the potential conflicts are taken into account, the quality of solutions will be better. The average

meeting and average overtaking delay models proposed by Petersen (1975) has given a good reason for the further study.

REFERENCES

Adenso-Diaz, B., Gonzalez, M.O., and Gonzalez, P. (1999). "On-line timetable rescheduling in regional train services." *Transportation research Part B,* 33(6), 387-398.

Cai, X., Goh, C.J., and Meeset, A.I. (1998). "Greedy heuristics for rapid scheduling of trains on a single track." *IIE Transactions* 30(5), 481-493.

Cheng, Y. (1998). "Hybrid simulation for resolving resource conflicts in train traffic rescheduling." *Computers in Industry*, 35(3), 233-246.

D'Ariano, A., Pacciarelli, D., and Pranzo, M. (2007). "A branch and bound algorithm for scheduling trains in a railway network." *European J. of Operational Research,* 183(2), 643-657.

Dessouky, M.M., Lu Q., Zhao, J., and Leachman, R. (2006). "An exact solution procedure to determine the optimal dispatching times for complex rail networks." *IIE Transactions* 38(2), 141-152.

Jin, F.C. (2004). Study on theory and methods of multi-objective optimization of train operation adjustment. Dissertation. Beijing Jiaotong University.

Sahin, I. (1999). "Railway traffic control and train scheduling based on inter-train conflict management." *Transportation Research Part B*, 33, 511-534.

Medanic, J., and Dorfman, M.J. (2001). "Time efficient strategies for scheduling trains on a line." Presented at the 15th IFAC World Congress, Barcelona, Spain.

Medanic, J., and Dorfman, M.J. (2002). "Energy efficient strategies for scheduling trains on a line." Proceedings of the 15th IFAC World Congress, Barcelona, Spain, 15(1).

Medanic, J., and Dorfman, M.J. (2004). "Scheduling trains on a railway network using a discrete event model of railway traffic." *Transportation Research Part B,* 38(1), 81-98.

Petersen, E.R. (1975). "Interference delays on a partially double-tracked railway with intermediate signaling." Petersen, E.R., Fullerton, H.V., eds. *The Railcar Network Model*. CIGGT Report No. 75-11, Canadian Institute of Guided Ground Transport, Queens University at Kingston, Ontario, Canada, 33-59.

Zhou, L.S. (1994). Study on the theory and approaches of making train operation adjustment plan with computer. Dissertation. Northern Jiaotong University.

Impact on Regularity of Track from Pile Underpinning of Light Railway Bridge

Xiangguo Li[1], Hailong Wang[2], Quan Zhou[3], Jianqing Bu[4] and Musong Li[5]

[1]School of Civil Engineering, Shijiazhuang Railway Institute, No.17 North 2nd-Ring East Road, Shijiazhuang, Hebei Province, China, 050043; PH(0311), 85281531; email: lxg7936636@sina.com

[2]President Office, Hebei Institute of Architecture and Civil Engineering, No.33 Jianguo Road, Zhangjiakou, Hebei Province, China, 075024; PH(0313), 2050871; email: wanghl@hebiace.edu.cn

[3]School of Civil Engineering, Shijiazhuang Railway Institute, No.17 North 2nd-Ring East Road, Shijiazhuang, Hebei Province, China, 050043; PH(0311), 87935555; email: zhouquan1980@126.com

[4]School of Civil Engineering, Shijiazhuang Railway Institute, No.17 North 2nd-Ring East Road, Shijiazhuang, Hebei Province, China, 050043; PH(0311), 87936227; email: bujq@sjzri.edu.cn

[5]School of Civil Engineering, Shijiazhuang Railway Institute, No.17 North 2nd-Ring East Road, Shijiazhuang, Hebei Province, China, 050043; PH(0311), 87935555; email: lims106@126.com

ABSTRACT

The regularity of track is a control factor which influences the safety of vehicles. For many foundation underpinning projects crossing existing rail transit tracks, the displacement of the underpinned foundation must be controlled within a reasonable range, which helps ensure the regularity of the track. Using the pile underpinning project of Tianjin-Binhai light railway as an example, this paper analyzes the impact on the regularity of track imposed by simulation calculation with software of ANSYS and Adams/Rail and test. The research results indicate: during underpinning, the change of static track regularity was lower than the controlled value of the criterion; the running safety indicators including the derailment coefficient (DC) and the reduction rate of wheel load (RRWL) were both under the limited value of norms. The underpinning of Tianjin-Binhai light railway bridge did not impose obvious impact on the regularity of the track, and the allowable displacement of underpinned pier is reasonable.

INTRODUCTION

With the popularizing of underpinning projects, pile underpinning technology has a rapid development in recent years. In 1930s, an engineer of Fondedile Company of Italy, proposed root piles at first (Lizzi, F. 1980). Then, Masuda et al. introduced a new method which can save construction period and cost by using some temporary structures, cast-in-situ diaphragm walls and piles, as elements of the new structures (Masuda et al. 1992). Ke et al. made model test and study of Shenzhen metro pile underpinning project which was considered as the highest load on single pile all over the world (Ke et al. 2003). Xiong et al.

carried out elastic and elasto-plastic analysis of reinforce concrete frame during underpinning construction using software-Ansys (Xiong et al. 2003). Lin, L. R. gave introduction to monitoring, recording, analysis and strain treatment during the positive dynamic replacement of railway bridge pile foundation which employed information technology (Lin, L. R. 2003). Li et al. analyzed the stress acting on rail located at beam gap when underpinning the bridge of railway or urban transit (Li et al. 2008).

The regularity of track is a control factor which influences the safety of vehicles. New track irregularity is produced during underpinning of rail transit tracks, which may bring a potential threat to the safety of the train when running. Based on simulation calculation and testing, this paper analyzes the impact of track regularity on the safety performance of vehicles during pile underpinning of the Tianjin-Binhai light railway. The results may be used as reference for future underpinning construction.

ENGINEERING SITUATION

The No.4 Road Tunnel of Central Avenue, New Coastal Region of Tianjin, crosses the viaduct of Jinbin Light Railway. In order to guarantee the safety of the viaduct, two piers should be underpinned. The cross-sectional diagram of pile underpinning is shown in Figure 1. The underpinned bridges are two linked 3-pan continuous beams; the A339 pier is designed as a braking pier, and the A340 is a linking beam. The underpinning structure is a 2-span rigid frame.

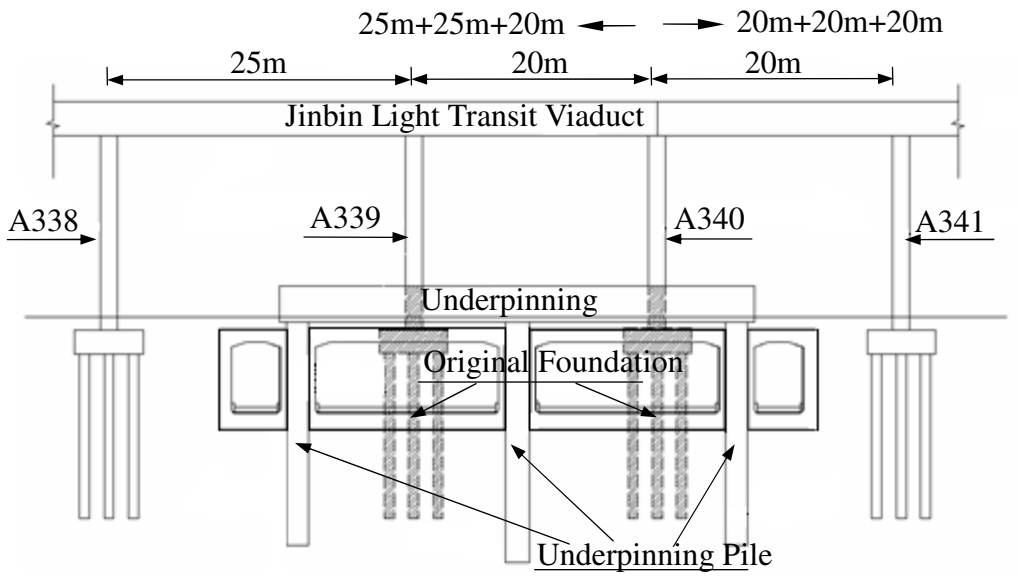

Figure 1. Pile underpinning cross-sectional diagram.

The section is located between Teda and Citizen Plaza Station. The line is in a transition curve whose length is 120 m, the radius of circular curve is 450 m, and the superelevation of the outer rail is 0.125m. Low Vibration Track is adopted with CHN60 rail and WJ-2 fastenings and the spacing of the elastic-bearing-block is 0.6m.

Jacks were installed on the top of the underpinning piles to bear the load of the underpinning beam during construction. During pre-jacking, arch camber occurred on the upper track, and settlement occurred when the state of the original foundation changed. Based on railway-related norms and the experience of Shenzhen Metro pile underpinning, the allowable vertical displacement of the underpinned pier is -3mm and 3mm (Yin et al. 2008). The settlement difference of adjacent piers should not exceed 5mm.

SIMULATION STUDY

Static simulation. Based on a discrete elastic support model，a finite element model for the track structure on the bridge was proposed by using finite element analysis code ANSYS. The model is shown in Figure 2. SOLID45 was used to build the box girder and support the rail bed; BEAM189 was used to build the rail; and COMBIN14 was used to build the series spring which is reduced by rail fastening and elastic shoe.

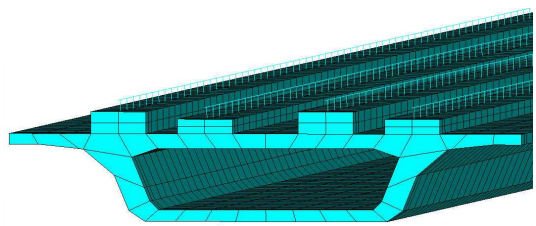

Figure 2. Finite element model of track structure on bridge.

Because A339 and A340 are both braking piers, they were simplified as fixed hinge supports. The others are simplified as movable hinge supports, including two non-braking piers (A338 and A341) and three linked piers (A337, A340 and A343). The constraint condition of the bridge model is shown as Figure 3. The rail was assumed as infinite long beam, and the effect of underpinning becomes small at the ends of the rail, so the ends were simplified as fixed supports.

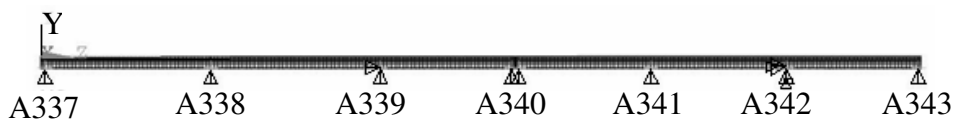

Figure 3. Constraint condition of bridge model.

During the calculation of track deformation, the displacement of the pier was loaded on the bottom of the box girder. There were two types of jacking forms: uniform jacking and differences jacking. The former refers to applying the same load at A339 and A340; the latter refers to imposing different when the underpinned piers are different. The track deformations in different jacking cases are shown in Figure 4.

The results indicate: the maximum displacement occurred at the mid-span

during uniformity jacking, and it was located close to the higher load during differences jacking. The result was consistent with the calculated result using structure mechanics.

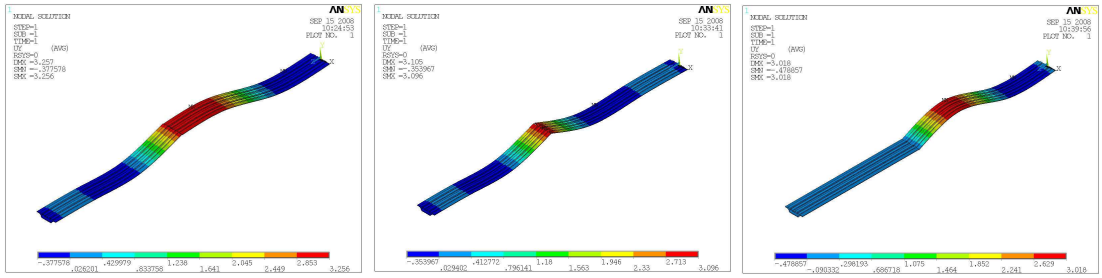

(a) Both A339 and A340 are jacked. (b) Only A340 is jacked. (c) Only A339 is jacked.

Figure 4. Track deformations in different jacking cases.

The maximum displacement loads (5mm) were applied on the models in different cases, and the vertical irregularities (y) of track were carried out. The results are shown in Figure 5. According to the related provisions in TB10082-2005, the criteria for static vertical profile regularity are that 10m-bowstring versine should be less than 4mm.

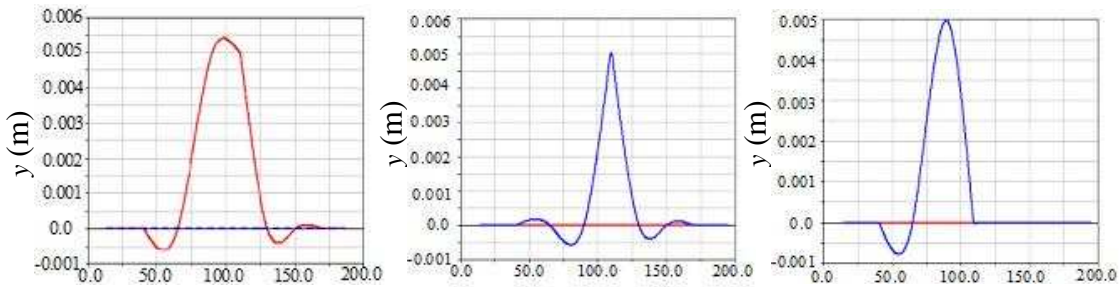

(a) Both A339 and A340 are jacked.(b) Only A340 is jacked. (c) Only A339 is jacked.

Figure 5. Track irregularities in different jacking cases.

The results indicate: during underpinning, the change of static track regularity was within the allowable value of the criterion, so running simulation could be made.

Running simulation. Using Adams/Rail dynamic simulation software of vehicle-track, the vehicle-track model was built which is shown in Figure 6. The assumptions are that the track foundation is rigid, and the railway line adopts a cubic parabolic transition curve to link straight line and circular curve. The track was considered to have no irregularity before jacking, and the deformation of the track caused by jacking was considered as an additional irregularity during the calculation. The Benchmark vehicle-1 model was adopted, which is a general two-bogie coach model in Manchester Benchmarks.

Before introducing the additional irregularity to the track model, the vehicle was simulated running at different speeds. The variation curves of DC

and RRWL along with running distance are shown respectively in Figure 7 and in Figure 8. In the graphics, the negative value presents variations of the wheel running on the inner rail of curve.

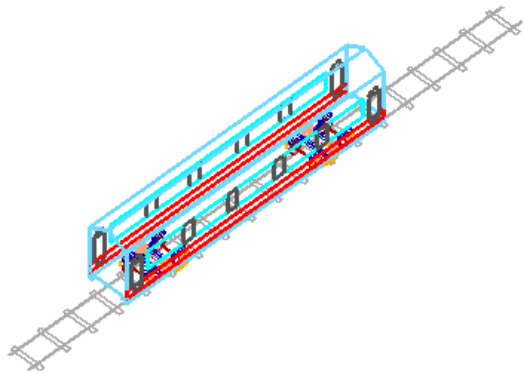

Figure 6. Dynamic simulation model of vehicle-track.

The results indicate: when the running speed was lower than the design speed (80 km/h), the DC and RRWL increased gradually with an increase in velocity. In the case when the vehicle ran at a lower speed, a surplus superelevation occurred, so the DC of the inner wheel was larger than that of the outer one, while it was contrary for the RRWL, viz, the RRWL of the inner wheel was smaller than that of the outer one. Moreover, the nearer the vehicle was to the circle curve from the transition curve, the higher the surplus superelevation, the DC of inner wheel and the RRWL of the outer wheel, until a constant one when the vehicle ran into the circular section entirely.

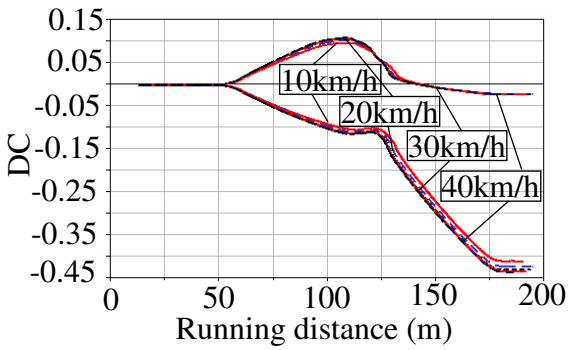

Figure 7. Variation of DC before jacking.

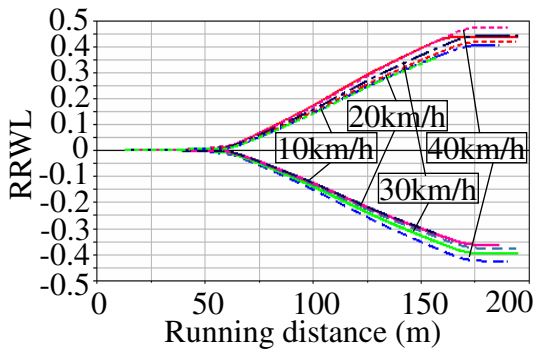

Figure 8. Variation of RRWL before jacking.

After introducing the possible additional-irregularity (as in Figure 5) to the track model, the DC and RRWL were calculated when the vehicle ran at 30 km/h. Simulations were conducted for three possible additional irregularities. Results from all three were similar and only the results from one test are shown in Figure 9 and in Figure 10 – both A339 and A340 were jacked up 5mm simultaneously.

The results indicate: when the vehicle ran at 30 km/h, the variation of DC and RRWL almost coincided with the values before jacking. The additional-irregularity would not impose obvious impact on the safe performance of a running vehicle.

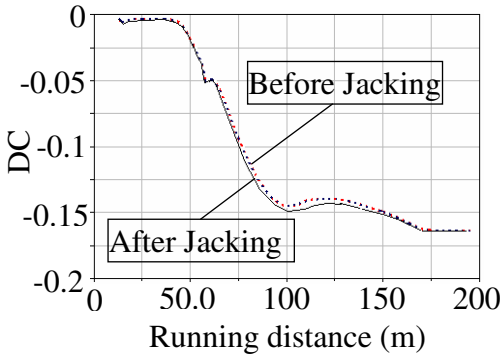

Figure 9. Comparison curve of DC.

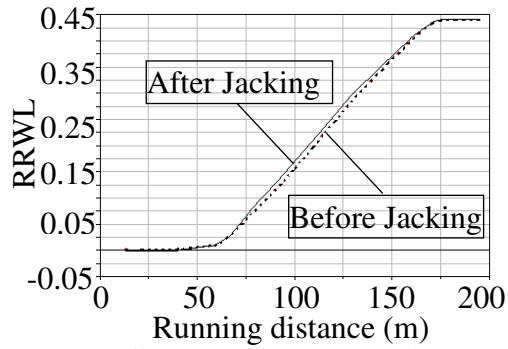

Figure 10. Comparison curve of RRWL.

TEST STUDY

Description of the test. As shown in Figure 11, the strain gauges were installed at the beam gap where the dangerous cross-section A340 is located. Under dynamic load, wheel-rail vertical force P and lateral force Q were tested, and then safety performance indicators, including the DC Q/P and the RRWL $P/\overline{P}$, were derived. The safe running speed of the vehicle was selected before underpinning. The safety performance indicators under different conditions were tested during underpinning. Speed tests were carried out under increasing speed conditions and safety indicators were retested after underpinning.

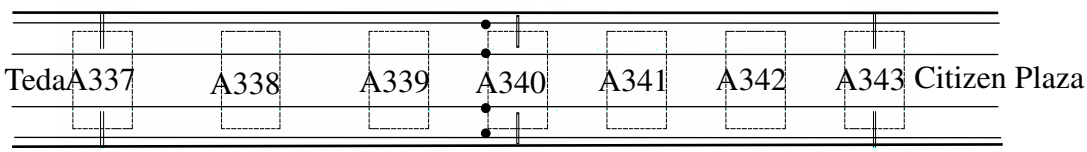

• Strain gauge on rail

Figure 11. Dynamic test point layout.

Test method and criteria for safety evaluation. The "shearing method" was adopted for the test of wheel-rail vertical force P and lateral force Q. DASP2000 data acquisition system with 2048Hz sampling frequency was applied. Railway wheel-rail analysis software was used for the calculation of safety performance indicators. According to the related provisions in GB5599-85 and TB/T2360-93, the criteria for safety evaluation are as following: (1) The DC $Q/P \leq 0.7$; (2) The RRWL $P/\overline{P} \leq 0.6$.

Test results. The test results are listed as following:

(1) Before underpinning, the maximum testing values of DC and RRWL at different speeds are shown in Table 1. The relationship between the safety performance indicators and speed are shown in Figure 12 and in Figure 13. In the table and graphics, "Up" presents the up direction of the train running from Citizen Plaza to Teda, "Down" presents the negative direction; "Inner" presents the wheel on the inner rail of the curve, "Outer" presents the wheel on the outer rail of the curve.

The results indicate: when running speed v ≤ 40 km/h, the safety

performance indicators increased with the increase of speed generally with the exception of 20 km/h, where it decreased slightly.

Table 1. Maximum value of safety performance indicator at different speeds.

Velocity ($km \cdot h^{-1}$)	Q/P				$P/\overline{P}$	
	Up outer	Up inner	Down outer	Down inner	Up outer	Down outer
5	0.022	0.13	0.041	0.17	0.281	0.352
10	0.028	0.15	0.043	0.19	0.286	0.358
15	0.035	0.16	0.042	0.20	0.282	0.360
20	0.040	0.11	0.048	0.15	0.269	0.292
30	0.075	0.16	0.040	0.19	0.291	0.379

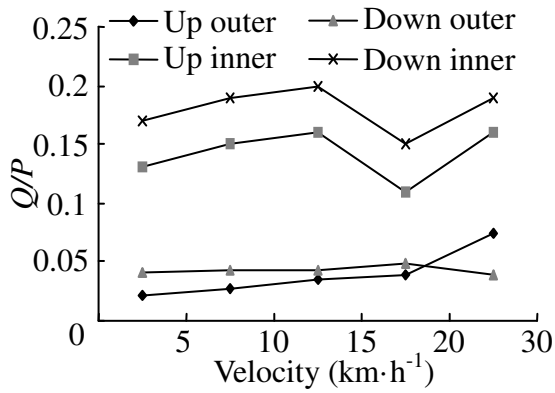

Figure 12. Relationship between Q/P and velocity before.

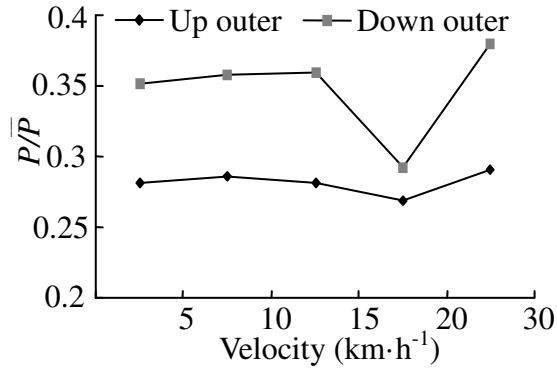

Figure 13. Relationship between $P/\overline{P}$ and velocity before underpinning.

(2) Considering the requirements of construction and operation, the running speed was limited at 10 km/h during construction. The maximum of safety performance indicators are shown in Table 2. The construction conditions are signed as "1" (before jacking), "2" (during underpinning), "3" (after cutting original piers) and "4" (after excavating foundation pit).

Table 2.Maximum of safety performance indicator at limited speed 10km/h.

Construction conditions	Q/P				$P/\overline{P}$	
	Up outer	Up inner	Down outer	Down inner	Up outer	Down outer
1	0.02	0.13	0.04	0.17	0.28	0.35
2	0.04	0.17	0.21	0.46	0.31	0.38
3	0.05	0.18	0.12	0.26	0.31	0.40
4	0.04	0.16	0.05	0.17	0.36	0.39

The results indicate: during the whole construction, the safety performance indicators did not vary obviously except the DC of the Down direction, which increased slightly.

(3) After having finished the underpinning construction, an increasing speed trial was done in order to improve the operation quality. The maximum test

results are shown in Table 3. The relationship between the safety performance indicators and speed are shown in Figure 14 and in Figure 15.

Table3. Maximum of safety performance indicator in speed increasing test.

Velocity ($km \cdot h^{-1}$)	Q/P				$P/\overline{P}$	
	Up outer	Up inner	Down outer	Down inner	Up outer	Down outer
20	0.02	0.16	0.04	0.19	0.31	0.36
50	0.05	0.20	0.06	0.20	0.27	0.29
70	0.05	0.17	0.08	0.12	0.24	0.16
80	0.06	0.15	0.09	0.14	0.23	0.17

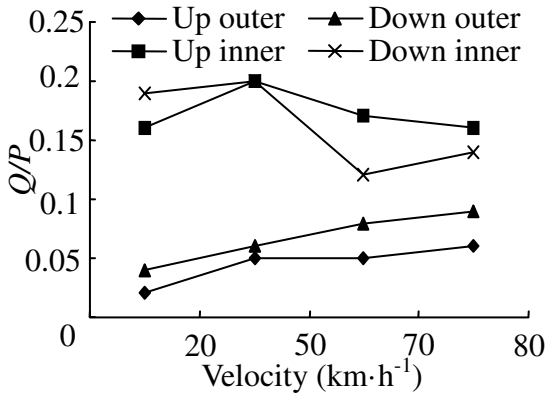

Figure 14. Relationship between Q/P and velocity before.

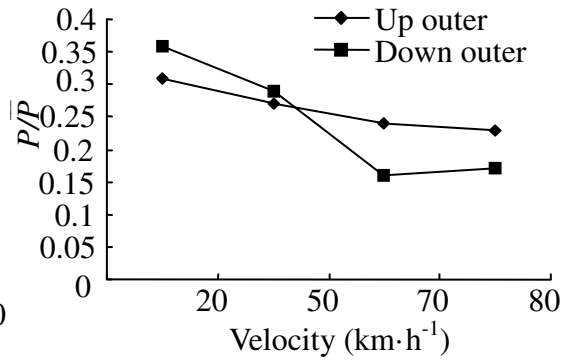

Figure 15. Relationship between $P/\overline{P}$ and velocity before.

The results indicate: as the speed increased to design speed, the DC of the outer wheel increased, while the DC of the inner wheel and the RRWL decreased.

CONCLUSIONS

Using the pile underpinning project of Tianjin-Binhai light railway as a research object, this paper analyzed the impact on the regularity of track from underpinning by simulation calculation and test study. Conclusions are as follows:

(1) During underpinning, the change of the static track regularity was within the allowable value of the criterion.

(2) The running safety indicators including the DC and RRWL are both under the limited value of norms. The simulation calculation and the test study had a similar variation law.

(3) The underpinning of Tianjin-Binhai light railway bridge would not impose an obvious impact on the regularity of the track, and the allowable displacement (Yin, 2008) of underpinned pier was reasonable.

ACKNOWLEDGEMENT

This project was supported by the National Natural Science Foundation of China (No.50878134) and the Natural Science Foundation of Hebei Education Department (No. 2006142).

REFERENCES

Ke, Z. T., Gao, Y. and Zhang, S.Z. (2003). Test and Study of Shenzhen Metro High-Load Pile Foundation Underpinning Model. China Railway Science, Vol.24(5) ,19-22.

Li, Z. X., Lu, Y. R. and Sun, N. (2008). Calculation and Analysis of Stress on Track under Pile Foundation Underpinning. Modern Urban Transit.Vol. (1), 25-26.

Lin, L. R. (2003). Information Technology in Replacement of Railway Bridge Pile Foundation. Journal of Changsha Railway University. Vol.21(3),41-46.

Lizzi, F. (1980). The Use of Root Pattern Piles in the Underpinning of Monuments and Old Buildings and in the Consolidation of Historic Centres. The Italien Technical Magazine“L' Industria Delle Construzion”. Nr. 110, Dec. 1980, Rome.

Masuda, Y., Minoshima, T. and Makino, H. (1992). Large-Scale Underpinning for an Underground Urban Railway Station. Tunneling Underground Space Technology, Vol.7(2),133-140.

Xiong, X. G. and Jiang, J. J. (2003). Elastic and Elasto-plastic Analysis of Reinforced Concrete Frame During the Underpinning Construction. Special Structures. Vol.20(1),8-10.

Yin, J and Ke, Z. T. (2008). Statically Indeterminate Analysis of Active Underpinning System to Control Deformation of Super Structure during Replacing Pile Foundation with Another One. Railway Engineering. Vol.(11),24-26.

Train-Carried Rail Signal Parameters Test System Based on Spectrum Correction Method and Virtual Instrumentation

Y. Guo[1] and G. Cheng[2] and S. Sha[3]

[1]School of Civil Engineering, Changchun Institute of Technology, Changchun 130012, PH: (86) 431-85711590; email: ccgcxygyf@163.com
[2]School of Transportation Science and Engineering, Harbin Institute of Technology, P.O.Box 2531, Harbin, 150090;PH(86)451-86282117; email:guozhucheng@126.com
[3]Jilin Provincial Freeway Engineering Ltd. Changchun 130022, PH: (86) 431-85711590; email: 19774412@sohu.com

ABSTRACT

A new test system is put forward to understand the FSK modulated track signal parameters in real time. The system model and design is based on the spectrum correction method. Carrier frequency is firstly identified by energy distribution in the frequency domain. Then, the signal is filtered and zoomed within a specific range centering on carrier frequency to obtain the spectrum lines. The frequency, amplitude and phase of each spectrum line are corrected using the centrobaric correction method. Lastly, signal parameters were calculated according to spectrum symmetry. Virtual instrumentation techniques were adopted during system implementation and software realization. The programming methodology is described in detail. Trial tests show that the test system is efficient and easy to use; all of the requirements are satisfied.

INTRODUCTION

Track circuit plays an important role in the whole Automatic Train Control (ATC) system. It serves as the path through which an FSK modulated railway signal is transmitted continuously, carrying vital information about potential blocks ahead. Exposed to the harsh environment, such as rain, snow, rust, etc., track-bed conductivity is not stable, which causes track circuit malfunctions. Hence, the track circuit must be tested onboard in real time to ensure transmission reliability.

The major requirements for the onboard test system are described as follows.

Various Types of FSK Modulated Signals Must be Identified. There are two kinds of FSK modulated signals in the railway system -- the YiPin signal and the French UM71 signal. For YiPin signals, carrier frequencies are 550Hz and 750Hz for a down line, and 650Hz and 850Hz for an up line, the frequency deviation is 55Hz, and the modulating frequencies, which contain the vital information of the light mode ahead, are from 7 to 26Hz at the interval of 0.5Hz. For UM71signals, carrier frequencies are 1700Hz and 2300Hz for a down line, and 2000Hz and 2600Hz for an up line, frequency deviation is 11Hz,and the modulating frequencies are from 10.3 to 29Hz at the interval of 1.1Hz (Fei, X. K.,1993).

The test error requirement. Frequency resolution: Central frequency 0.2Hz, Modulating frequency 0.02Hz.

Amplitude error (absolute value) $\leq$ 2mV $\pm$ 2%*value indicated

Parameters must be tested in real time. Test results must be presented at an interval of less than 200ms so as to accord with the train speed at 250Km/h.

SPECTRUM CORRECTION ORIENTED PROGRAMMING METHODOLOGY

Energy Centrobaric Correction Method. During signal processing, only limited numbers of samples of the signal can be acquired. Thus, energy leakage happens. The method of centrobaric correction normally used in vibration analysis is migrated here. The method is based on the theory that most windowing functions such as Henning, Blackman, etc. when sampled, have an energy distribution centered on the zero in the frequency domain. Thus, the actual central frequency can be corrected with several spectrum lines around itself (Ding, K., and Xie, M., 1996).

Supposing the sample rate is fs, sample points for fft is N, the spectrum line number with maximum amplitude is m, the amplitude of the i_{th} line in the power spectrum is Y_i, then the actual central frequency x_0 can be obtained as shown in Equation (1).

$$x_0 = (\sum_{i=-n}^{n} Y_i(m+i)fs/N) / \sum_{i=-n}^{n} Y_i \qquad (1)$$

According to Parseval theory, the actual amplitude is obtained as shown in Equation (2):

$$A = \sqrt{k_t \sum_{i=-n}^{n} Y_i} \qquad (2)$$

where coefficient k_t can be calculated by numerical method.

The actual phase is shown as in equation (3).

$$\Phi_m = tg^{-1}(\frac{\mathrm{Im}}{R_m}) + (x_0 - mf_s/N)(f_s/N)\pi \qquad (3)$$

Programming Methodology. Railway signal is acquired continually by DAQ card at the sample rate of 9600S/s and sample duration of 1.28s. Analysis was done as follows:

Judging Carrier Frequency (F_c). Since the F_c of UM71 and YiPin signals are different, they can be identified by setting a frequency threshold. The frequency threshold must be selected between the maximum F_c of YiPin (850hz) and the maximum F_c of UM71 (1700hz).After judging the signal type, the actual F_c is roughly estimated based on the energy distribution in the frequency domain.

Spectrum preprocessing. Many noises are useless or irrelevant to the actual signal, preventing us from discerning the actual spectrum (Zhou, Q. S., Hou, F. Y. and Zhang, L. P., 2007). To avoid this, the signal required can be preprocessed to find a few lines around F_c which are high-valued relatively. Reduce the noises by discarding the minor-valued spectrum lines when there are several lines too close to each other.

Spectrum Correcting. Correct the spectrum lines obtained according to Equations (1), (2), and (3).

FSK Signal Parameter Calculation. Based on the result of spectrum correction, the parameters can be calculated based on the spectrum characteristics of

the FSK modulated signal. An FSK signal with a continuous phase modulated by a square wave is composed of many ingredients in the frequency domain. Suppose C_n is the n_{th} side frequency amplitude, then (Ding, K., 2008).

$$C_0 = (2A_0 / m\pi)\sin(m\pi / 2) \quad (4)$$

$$C_n = (2m / \pi(m^2 - n^2))\cos(m\pi / 2) \quad \text{n is odd} \quad (5)$$

$$C_n = (2m / (\pi(m^2 - n^2)))\sin(m\pi / 2) \quad \text{n is even} \quad (6)$$

For UM71signal, we adopt the F_c and the several lines nearest to the F_c

Rearrange the spectrum lines corrected by the amplitude. Find the very line around which the other pair of lines are symmetrically located and have similar amplitudes to each other. The corresponding frequency is the actual F_c .

Find the pair of lines within the specified restriction of the relative error in magnitude. Obtain the modulating frequency (F_m) according to this pair's relative position to F_c , as shown in Figure 1.

Based on the C_m and C_n , frequency deviation（ΔF）can be estimated by using the polynomial curve fit method.

Modulation index (m) can be gained as shown in Equation (7):

$$m = \Delta F / F_m \quad (7)$$

According to Equation (4), the amplitude of the signal (Amp) can be obtained as shown in Equation (8)

$$Amp = (C_0 m\pi / 2)\sin(m\pi / 2) \quad (8)$$

For YiPin signal, its spectrum features are: the spectrum line located on F_c is minimum, while most lines are scattered on the side frequencies.

Find enough pairs of lines, each of which are similar in value and located symmetrically. Then F_c can be estimated with the average frequency values of each pair of lines.

Based on the distance within each pair of lines, the modulating frequency (F_m) can obtained as shown in Figure 2.

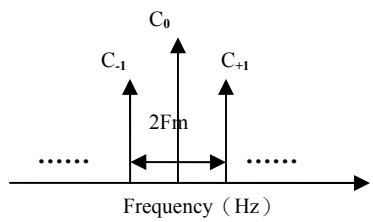

Figure 1. UM71 signal spectrum.

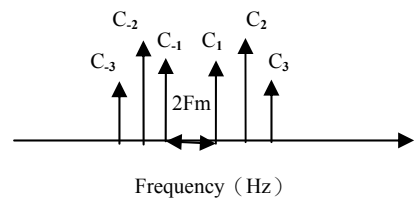

Figure 2. YiPin signal. spectrum

Suppose n1 and n2 are both the index of side frequencies, n1 ≠ n2, if n1 and n2 are both odd or even, then from Equations (5) and (6), m can be estimated in Equation (9):

$$m = \sqrt{(cn_1^2 - n_2^2)/(c-1)} \quad (9)$$

where, $c = C_{n1} / C_{n2}$.

So, m can be obtained by selecting the desired side frequency lines from the above pair of lines, and the amplitude of the signal can be estimated in Equation (5).

ΔF can be calculated as shown in Equation (10):

$$\Delta F = mF_m \quad (10)$$

SYSTEM CONFIGURATION AND SOFTWARE REALIZATION

System Configuration. The general architecture of the test system is shown as Figure 3, where the DAQ card is PXI 6221 multifunction DAQ card, and the software is LabWindows/CVI, a visualized virtual instrument developing environment (Liu, J. H., 2001; Ding, T. X., 2002).

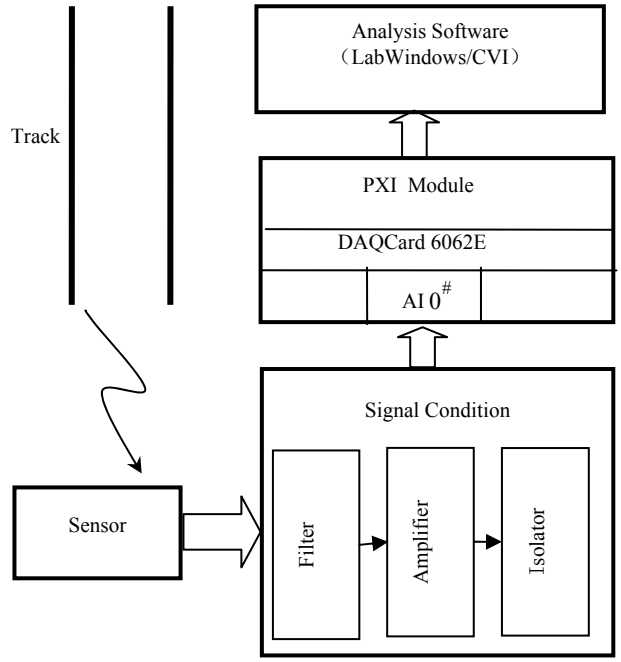

Figure 3.Railway signal parameter automatic onboard test system.

Software Realization. The main panel of the test system software is shown as Figure 4. The left area is for displaying the parameters of the track circuit signal acquired including the original signal in time domain, the original power spectrum and the zoom spectrum. The listboxes “Results in real time” in the upper right area are for displaying the results after spectrum correction, while the area named “FSK parameters” is for displaying the FSK modulated signal’s parameters.

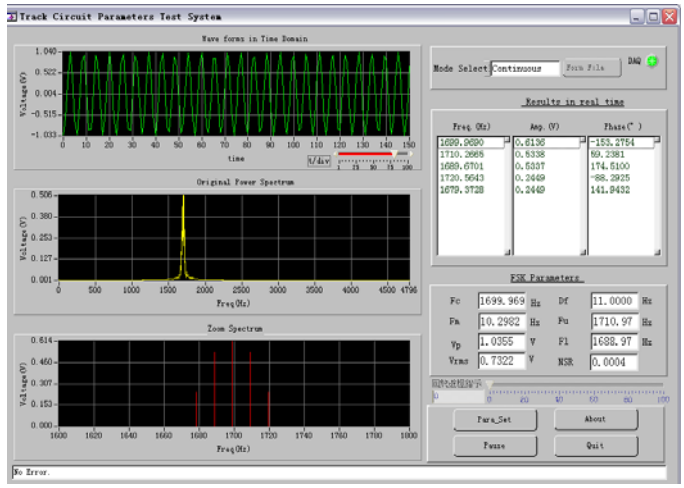

Figure 4. Railway signal parameter onboard test system software.

TESTING CASE EVALUATION

In the testing case, Monte Carlo simulation is used to generate simulated FSK modulated signal and white noise. The above mentioned algorithm is evaluated as follows.

Error Test for YiPin signals. The error test result is shown in Table 1. In this test, a pure YiPin signal was generated with an amplitude of 1V and an initial phase from 0 to 360 degrees at random and then processed. The sample rate is 9600 S/s, the sample duration is 1.28 seconds, samples for analysis is 4096, F_c is 550Hz. The table shows that: the maximum absolute error of F_c and amplitude are both within the error restriction.

Table 1. Error test result for YiPin signal

Modulating frequency（Hz）		7	9	13.5	17.5	20
Maxi-mum error of F_c	Hz	8.2e-2	5.5e-2	2.3e-1	1.3e-3	4.0e-6
	%	1.4e-2	1.0e-2	4.2e-2	2.4e-4	7.2e-7
Maxim-um error of amplitude	V	6.8e-3	1.8e-3	4.4e-3	6.7e-3	2.6e-3
	%	6.8e-1	1.8e-1	4.4e-1	6.7e-1	2.6e-1

Error Test for UM71 Signals. The error test result is shown in Table 2. In this test, a pure UM71 signal was generated with an amplitude of 1V and an initial phase from 0 to 360 degrees at random and then processed. The sample rate is 9600 S/s, the sample duration is 1.28 seconds, the samples for quantitative analysis is 4096, F_c is 1700Hz. The table shows that: the maximum absolute error of both F_c and amplitude are within the test error limit.

Trial tests show that:

As the quantity of samples for analysis decreases, the test error accelerates accordingly, yet at a very lower speed. Even when the number of samples for analysis is 512, the F_c can be judged.

Amplitude error can be reduced by enlarging the dynamic range of the AD converter. It has been verified that when the dynamic range is 200mV, amplitude error can be confined to 1mV.

Table 2. Error test result for UM71 signal

Modulating frequency（Hz）		10.3	13.6	16.9	20.2	29
Maxi-mum error of F_c	Hz	7.8e-3	7.4e-3	7.3e-3	7.7e-3	2.7e-2
	%	4.5e-4	4.3e-4	4.3e-4	4.5e-4	1.5e-3
Maxim-um error of amplitude	V	2.3e-4	5.0e-4	3.4e-4	4.8e-4	2.8e-4
	%	2.3e-2	5.0e-2	3.4e-2	4.8e-2	2.8e-2

CONCLUSION

(1) The spectrum correction oriented methodology is proposed to ensure railway signal parameters can be obtained with high precision in real time.

(2) The software is developed under a powerful visualized environment, i.e. LabWindows/CVI, which facilitates the programming realization, including friendly man-machine interface and visualized presentation of the measurement results.

REFERENCES

Ding, K. (2008). *Discrete spectrum correction technology and theory*, Science Press, 54-57.

Ding, K., and Xie, M. (1996). "A new method of amplitude, phase and frequency correcting in discrete spectrum." *Journal of Dynamic Analysis and Technique of Measurement and Test*, 14(1),10-29.

Ding, T. X. (2002). *Virtual instrumentation technology*, Science Press, 10-15.

Fei, X. K. (1993). "Jointless track circuit theory and analysis." China Railway Publishing House, Beijing, 96-109.

Liu, J. H. (2001). Virtual instrumentation developing environment LabWindows /CVI tutorial, Electronic Industry Press, 60-71.

Zhou, Q. S., Hou, F. Y., and Zhang, L. P. (2007). *Small Signal Detection and Evaluation*, Beijing University of Aeronautics & Astronautics Press, 64-71.

Study on Style Protection and Urban Traffic Planning of Harbin Jingyu Street

X. Yao[1], Y. Zhang[2] and Y. Liu[3]

[1]School of Transportation Science and Engineering, Harbin Institute Of Technology, Harbin, Heilongjiang, ST 150010; PH 86-451-84636911; FAX (0451) 84615434; email: hrbyao@163.com
[2]School of Transportation Science and Engineering, Harbin Institute Of Technology, 202 Haihe Road, Nangang District, Harbin, Heilongjiang, ST 150090; email: zxlt0905@163.com
[3]Harbin Urban Planning and Design Research Institute, Harbin, Heilongjiang, ST 150010; PH 86-451-84636911;FAX (0451)84615434; email: xinliuying163@163.com

ABSTRACT

The local and regional traffic problems of Harbin's Jingyu Street are analyzed. Because of the traffic, business functions are restricted. Two traffic modes are proposed: complete protection and restricted protection. Consideration must be given to the protection and redevelopment of Jingyu Street. Evaluation factors for traffic improvement schemes for a style protection district are discussed. These are based on three indexes: land zone, style protection, and traffic access degree. A fuzzy evaluation method to appraise schemes is presented which discusses experiences for protecting a traditional style protection district.

INTRODUCTION

Since early in the 20th century, there has been an increasing amount of attention devoted to the protection of urban historical and cultural heritage places all over the world. Since the reform and opening of our country, there has been rapid development of the urban economy and much new construction. Historical buildings and blocks have been destroyed to different degrees, and therefore, there is an increasingly urgent need to protect cultural and historical places.

Protection of historical and cultural legacy is done at different levels. It begins with the protection of landmarks, and then develops into protection at the city level and finally at the historical block level. Because of its values in the society, humanities and application, the protection of historical blocks become the most important in a multi-level protection system of historical and cultural heritage. Harbin is a national historical and cultural city and is facing the problem of protecting its historical blocks in the old region of the city. The problem of having modern traffic in historical blocks is becoming an urgent research subject

The traditional business style protection region of Jingyu Street, located in the Daowai district, is an important ingredient in Harbin's history and cultural protection blocks. With the acceleration of the urbanization process, traffic problems in protection blocks are emerging. As the process of land-use

replacement and building renovation in the old region occurs, it is important that planning efforts follow historical and cultural protection planning principles. This includes effectively organizing regional traffic and correctly locating and protecting the style of Jingyu Street.

PRESENT STATE

The style protection district of Jingyu Street covers an area of 53.11 hectares. Its functions include commercial, residential and transportation. The present state of the Jingyu Street protection district is divided into two categories according to different functions. The first category is mainly for commercial functions which has typical business streets, and where there is commercial retail, wholesale markets, as well as financial and business functions. Its traffic flow is a stream of commercial, passengers, and trucks. This category maintains a traditional street style, and Baroque architecture is distributed intensively and continuously on both sides of the street. The decorative style of the external walls is uniform and the aesthetic value is relatively high. Therefore, the historical and cultural conservation value is very important. The other category is mainly for residential functions, which has relatively developed business functions, but the scope of service is small.

PROTECTION LOCATING

The traditional style protection district of Daowai is the old region in Harbin. It has witnessed the effects of development due to the changes in the national economy and it has typical areas that combine Chinese and Western cultures. This region is the third largest traditional business district, following the business centers of Central Avenue and Qiulin. The protection and rejuvenation of this area will help fully exploit the functions of commercial, cultural, tourism, leisure and residential. By improving the infrastructure and the spatial environment, and by balancing the social, cultural, economic, and environmental benefits, it is possible to create a vibrant commercial, cultural, and tourist center that adapts to the requirements of modern life.

PLANNING PRINCIPLES

First, planning must be done according to the requirement of style protection, adaptation to local conditions, determining the planning standard for adjusting arterial roads, and adopting various treatment methods for different regions and protection hierarchies (Li 2006).

A second principle is to adjust the branch system according to bystreet theory and the spatial dimensions of the protection district

A third principle is the determination of the cross-sectional width that will satisfy style protection and preferably consider the relationships among traffic, public facilities, the urban landscape, and the ecological environment.

A fourth principle is to increase the branch system density in the commercial district and in dangerous rebuilding regions.

STUDY OF TRAFFIC MODES

According to the different protection aspects of Jingyu Street, this paper proposes two traffic modes. One is a completely protected traffic mode. This mode strengthens commercial functions, weakens both residential and motor vehicle traffic functions, and becomes a full-time commercial pedestrian street. The model applies to the first category protection area and mainly benefits booming commerce of the whole region. The other is a restricted protection traffic mode.

The commercial function is a key function in the model. The roads in the model are charged with motor vehicle traffic, and develop to time-limit commercial pedestrian streets (Li and Li 2006). The mode applies to the second category. At the same time, this model can also include streets that are restricted to pedestrian traffic at specific times, or at all times. This can be done for the traditional protection area of Jingyu Street by expanding the traffic capacities of the surrounding roads, which will enhance the commercial function

.

THE TRAFFIC IMPROVEMENT SCHEME

The key to accomplishing the above two traffic organizations are having a unified plan and managing the traditional style protection district. At the same time, it also key to excavate the road potentiality of the surrounding region, alleviating traffic pressures on Jingyu Street.

Firstly, the regional road network should be opened up to through traffic. Secondly, auxiliary lanes should be constructed on each side to further shunt traffic (Li 2006). Thirdly, the bystreet mechanism of the traditional style protection district should be applied to strengthen internal traffic connections. The traffic organizing methods of the traditional business street are that when pedestrian traffic volume is small, especially during off-peak hours, surrounding roads should be used to share traffic volume. When pedestrian traffic volume reaches a certain threshold, usually during the commercial peak hours, the street should be closed to vehicle traffic. To determine the specific scheme, it is important to consider the entire area of Jingyu Street and systematically consider the road network structure, the traffic organization, and so on.

Following the upper traffic organization principle and bystreet mechanism, this paper puts forth traffic organization strategies and schemes that are separate from the surrounding road network facilities, the static and dynamic traffic organization, the public transport organization, and the pedestrian traffic organization. The schemes are as follows:

The road network system structure is “three horizons, six verticals.” The three horizons are Beihuan Street., Jingyu Street, and Nanxun Street. The six verticals are Jingyang Street, First Street, Fifth Street, Seventh Street, Ninth Street, and Tenth Street. It is important to implement the following measures: rebuild Taigu Street; broaden the lanes from two lanes to four lanes; open up Binjiang Street; and, plan six lanes. To coordinate the relationship between the regional

protection and the sustainable transportation development, solve the bottleneck problems at the intersection of Seventh Street and Jingyu Street by using some traffic management tools, such as planning two one-way streets which include Seventh Street from south to north and Ninth Street from north to south.

According to "the norms on the protection of historical and cultural city planning" and combining with this specific situation, this paper puts forth the idea to open streets to full-time commercial pedestrian traffic in the part of the region which is surrounded by Jingyang Street, Shengping Street, Fifth Street, and Nanxun Street. At the same time, it is recommended that other areas of the protection district are restricted to commercial pedestrian traffic between 19:00 to 23:00. Also, building a branch system to strengthen the connections between east and west will help create a smooth and convenient shopping environment.

THE SELECTION PRINCIPLE OF EVALUATION FACTORS

Evaluation factors should be chosen that unify the characteristics of style protection, so both the shared characteristics and the differences can be identified

First, apply the dynamic principle. Consider the important characteristics of the study region, which are in accord with the new idea of applying protection knowledge. Choose characteristics that will be relevant under changing circumstances. Second, apply the universality principle. Ensure that the evaluation factors have common characteristics, that they are easy to grasp, and create a comparatively unified dimension in the process of evaluation. Third, apply the importance principle. Choose the factors that have the most effect. Fourth, apply the gathered principle. The evaluation factors should have gathered characteristics. Fifth, apply the comparative principle. The selected factors should rationally respond to various aspects of old city's historical and cultural protection district, and show differences when comparing them. Sixth, apply the irrelevance principle. The correlation of factors can affect objectivity and the accuracy of the evaluation.

EVALUATION FACTORS

Because of the restrictions of cultural relics, ancient trees, and protection bystreet mechanics (Eckholm 1998), the cultural protection district is not able to rebuild at large scales. Therefore, cultural protection factors (Zhang 2008) need to be added. The norm of historical and cultural protection city planning, which was announced in 2005, specifically defines that it should include improving residents' living environments and protecting district activities. An evaluation system for traffic improvement schemes for style protection districts uses three factors in the guidelines layer and ten evaluation factors in sub-layer and is illustrated in Figure 1.

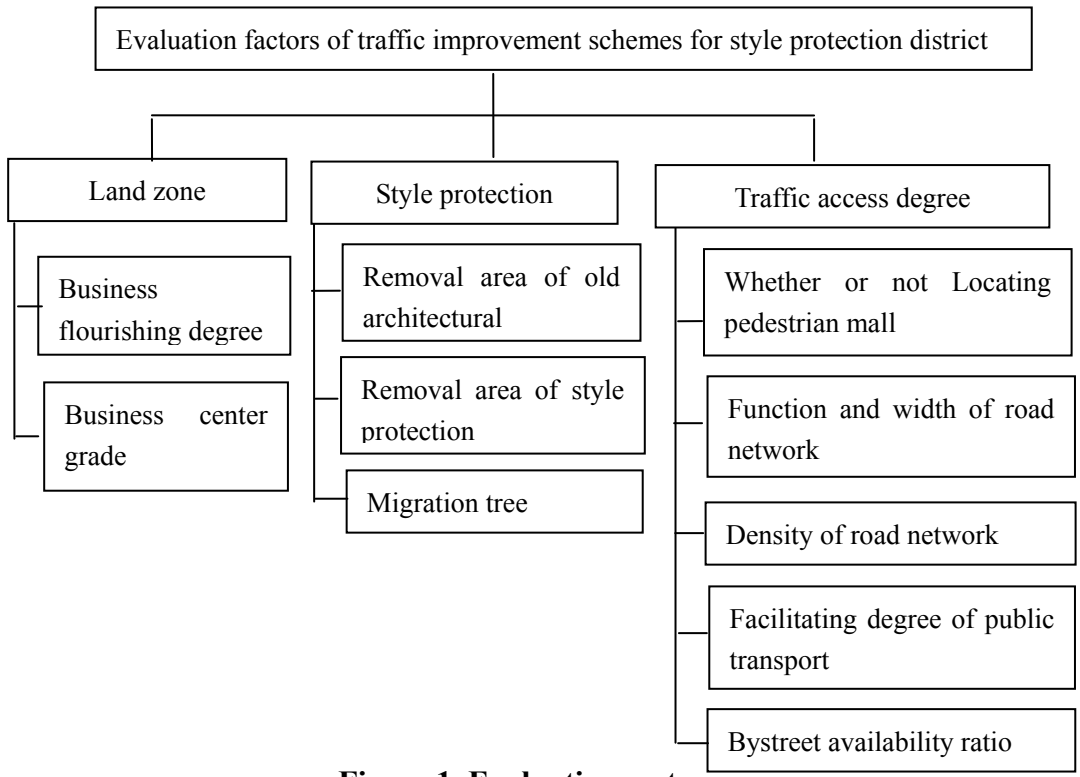

Figure 1. Evaluation system.

EVALUATION METHOD

At present, a commonly used evaluation method uses expert experience to determine a qualitative index and compares the options of the program. This method is simple and clear, and easy to program as a mathematical evaluation method. Moreover, the method is not completely divorced from the people's participation; the experience judgment is still present and by using mathematical evaluation tools, it is possible to break down complex issues and reduce the final evaluation effect of individual partial results. This method of evaluation is more objective and favors of program comparisons.

A fuzzy comprehensive evaluation method, the gray relational grade evaluation method, and AHP have been widely used in many industries (Zhang 2008). A fuzzy comprehensive evaluation is suitable for a multi-factor, multi-level, and multi-program evaluation and is also decision-making system. It is especially useful for system problems that have both qualitative and quantitative factors. This method can more easily carry out a comprehensive evaluation and yield the best solution for decision-making. A fuzzy comprehensive evaluation is based on a fuzzy mathematical approach to evaluation. The evaluation process uses a multi-level evaluation. It is a system that combines a number of factors or objects to give an overall evaluation. Therefore, the traffic organization program of a traditional style protection district such as that of Jingyu Street can be evaluated by a fuzzy comprehensive evaluation method using the three factors of land zone, style protection, and traffic access degree. Through experience

certificate, the evaluation results can scientifically reflect the advantages and disadvantages of various programs.

CONCLUSION

This paper studies the classification of the present state and the localization of a traditional style protection district, and analyzes current problems from the perspective of urban traffic. At the same time, this paper studies the impacts and constraints of regional traffic on the protection district, and puts forth two traffic modes: full protection and restricted protection. Moreover, this paper also proposes using a traffic improvement evaluation system based on land zone, style protection, and traffic access degree, and suggests applying a fuzzy comprehensive evaluation method to compare programs. The study objectives of the paper provide several lessons for protection and traffic improvement of a traditional style protection district.

REFERENCES

Eckholm, E. (1998). "A burst of renewal sweeps old Beijing." *New York Times,* New York.

Li, J. (2006). "Conservation-oriented transportation improvement planning for historical districts: a case study of Guangzhou historical districts in Guangdong province, China." *Urban transport of China*, Sep. 4(5):63-68.

Li J., and Li, Y. (2006). "The style protection and urban traffic of Qilou St. in Guangzhou." *Building saving urban transport system memoir*, (2):52-55.

Li, X. (2006). "Beijing old city traffic and old city protection." Building saving urban transport system memoir, (2):115-118.

Zhang, Q. (2008). "Study on traffic improvement method for protection of historical culture area in Beijing." *Beijing University of Technology.* Beijing.

Study on the System Design and Optimal Models of Urban Rail Transit Traction Calculation System

Hongbo LIU[1] Hongxia LU[2] Miaomiao LU[2] Jie ZHANG[2]

[1] School of Economics and Management, Southwest Jiaotong University, 111,North Second Round Road, Chengdu City, Sichuan Province, P.R.China, zip code: 610031, PH (86) 028-87600706 ; FAX (86)028-87600706; email:lmm_316@163.com
[2] School of Traffic and Transportation, Southwest Jiaotong University.

ABSTRACT

Urban rail transit traction calculation plays an important role in the urban rail transit design. In this paper, the design objectives of this system are determined, which are to simulate the rail transit traction operation dynamically and real-time optimize the train operation through the dynamic combination of basic control strategies. Furthermore, the architecture and function of this system are analyzed and designed, and the system structure can be divided into four parts, including a basic data management subsystem, a traction automatic calculation subsystem, a human-computer interaction subsystem, and a data out subsystem. Moreover, the key technologies of the system are studied, including a multi-objective train operation model and traction calculation algorithm design. Finally, the system is proved to be effective by simulation train operation in Guangzhou Metro Line 3.

INTRODUCTION

With the growth of transportation demand and the rapid development of rail transit technology, urban rail transit has developed in many big or media-sized cities, and urban rail transit traction calculation can provide essential technical data for rail transit operation, important reference value in vehicle type selection, line design, signal equipment arrangement, etc. But present traction calculation software and algorithms are mostly based on railways, for example, traction calculation software developed by HE Hongyun (He 2000), a train operation simulation system developed by GUO Youmin (Guo,2002), a general-purposed simulation system on train movement developed by MAO Baohua (Mao 2000). Traction calculation software based on urban rail transit is quite rare. So, the development of traction calculation system suitable for the characteristics of urban rail transit is urgent.

1 SYSTEM STRUCTURE DESIGN

The functions of the system are determined through the analysis of current traction calculation software and the investigation of urban rail transit traction calculation software users, including designing a simple data management mode with certain compatibilities for using already existing data resources of other departures, realizing train automatic operation and the operation mode conversion between automatic control mode and manual control mode; completing perfect output function so that system data can be demonstrated intuitively by the way of graphs, animation, etc., and all data can be output by all kinds of standard output units. The architecture of urban rail transit traction calculation system is described in

Figure 1. On the whole, the system can be divided into four parts, including a basic data management subsystem, a traction automatic calculation subsystem, a human-computer interaction subsystem, and a data out subsystem.

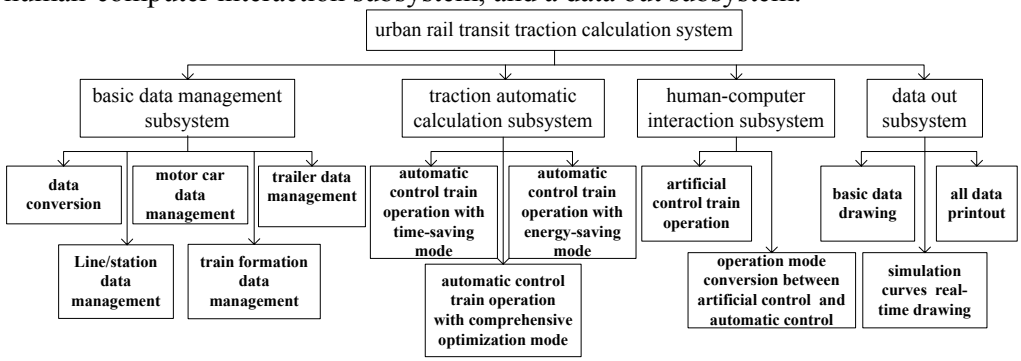

Figure 1: The architecture of urban rail transit traction calculation system.

1.1 Basic data management subsystem

The system includes four kinds of data: motor car data, trailer data, line and train data, and train formation data. The operation on basic data includes the addition, the deletion, the revision and the inquiry; uniformity of the data must be ensured in the operating process. Meanwhile, in order to use already existing data resources of other departures and improve the data input efficiency while decreasing error probability, a special-purpose data import subsystem is designed.

1.2 Traction automatic calculation subsystem

Three traction strategy modes are provided for automatic train control, including a time-saving mode, an energy-saving mode and a comprehensive optimization mode. Trains will realize automatic operation according to calculation parameters and a control mode selected by user, combined with practical operation situations such as vehicle characteristics, line conditions, and so forth.

1.3 Human-computer interaction subsystem

The user can use a mouse to control train operation by selecting the train running condition. The user can not only analog control whole course of train operation, but can also control train operation in the course of automatic operation at any time, moreover, the train can run back at any location and the running condition can be reselected at the location. Better operation effects are realized through the convenient conversion between automatic operation and artificial control, which gives full latitude to the experience of operators.

1.4 Data out subsystem

The basic data of a system such as speed restriction of a ramp, ramp profile, station location, and so forth can be draught, and in the course of train operation, speed-distance curve, time-distance curve, motor voltage-distance curve, motor current-distance curve, source current-distance curve can be real-time displayed by way of animation. All graphics and result reports can be output through all kinds of

standard output units.

2 MULTI-OBJECTIVE TRAIN OPERATION MODEL

According to the characteristics of urban rail transit, time-saving and energy-saving are determined as the control objectives of train operation; safety, accurate stopping, and such are determined as constraints. So, a multi-objective train operation model can be established as follows:

Objective of energy-saving: min $\alpha E = \alpha \sum E_i = \alpha \sum U_i I_i t_i$

Objective of time-saving: min $\beta t = \beta \sum t_i$

Constraints:

$$S(0) = S_b \qquad S(t) = S_e \qquad v(0) = v_b \qquad v(t) = v_e \qquad 0 \le v_i \le v_{max}$$

$$v_{max} = \min\{v_p, v_g, v_y\}$$

Where, α , β = the input parameters which will be explained in section 3.1; S_b= the starting position of train operation; S_e= ending position of train operation; v_b = starting speed, usually it is 0; v_e= ending speed, usually it is 0; v_i = speed of train at time i; v_p = speed restriction of ramp, it is a stage function of train operation position; v_g = design velocity of train (determined by the lower design velocity of motor car and trailer; v_y = operation speed restriction, including temporary speed restriction, etc., which is usually a constant.

Motion equation: $S_{i+1} = S_i + \frac{v_{i+1} + v_i}{2}\Delta t \qquad v_{i+1} = v_i + \Delta t F(v_i, f)$

Where Δt = time step for calculation, $F(v_i, f)$ = train operation acceleration at time i

Traction condition: $F_q(v_i, f) = \frac{f_{qy} - w_i}{(D+T)g}$ Coasting condition: $F_d(v_i, f) = \frac{-w_i}{(D+T)g}$

Braking condition: $F_z(v_i, f) = \frac{-f_{zd} - w_i}{(D+T)g}$

The control mode of nearly stepless traction is adopted in metro motor and light rail motor, so, the maximum tractive effort can be calculated according to speed, actual tractive effort can be obtained by interpolation method, as well as brake force.

$$f_{qy} = af_1(v) \qquad f_{zd} = bf_2(v)$$

where fq_y= train tractive effort, w_i= train running resistance, f_{zd}= train brake force, D= motor car weight , T= trailer weight , $f_1(v)$ = curve of traction characteristic, $f_2(v)$= braking curve, a= usage coefficient of tractive effort , b = usage coefficient of brake force.

Energy consumption for traction: $E_{i+1} = E_i + U_{qy}\left(I_{qy} + I_{zy}\right)\Delta t$

Energy consumption for breaking: $E_{i+1} = E_i + U_{zd}\left(I_{zd} + I_{zy}\right)\Delta t$

Where U_{qy}= traction voltage, I_q= traction current, I_{zy}= traction self-consumption current, U_{zd}= braking voltage, I_{zd}= braking current, I_{zy}= braking self-consumption current.

3 SYSTEM ALGORITHM DESIGN

3.1 The selection of coasting point

In the process of practical train operation, coasting is adopted according to the operation state, line situation and vehicle condition, etc. In many situations, coasting is adopted but the train speed is less than the restricted speed, so there is significant subjectivity in the selection of a coasting point. Several relatively simple cases are presented in Figure 2. If $\alpha = 0$, $\beta = 1$, a time-saving traction strategy is adopted, there is only "idle time" between traction condition and braking condition, shown as curve 1; if $\alpha = 1$, $\beta = 0$, an energy-saving traction strategy is adopted, a coasting condition is adopted until the speed decreases to the calculated speed, the coasting condition is furthest adopted, shown as curve 3; if $0 < \alpha < 1$, $0 < \beta < 1$, a comprehensive optimization traction strategy is adopted. Suppose the distance between a coasting point of a time-saving traction strategy and a coasting point of energy-saving traction strategy in traction curve is l, then, the coasting condition is adopted at the point $\frac{\beta}{\alpha+\beta}l$ apart from the coasting point of an energy-saving traction strategy until the coasting curve crosses with the back-stepping braking curve, following, and the braking condition is adopted, shown as curve 2.

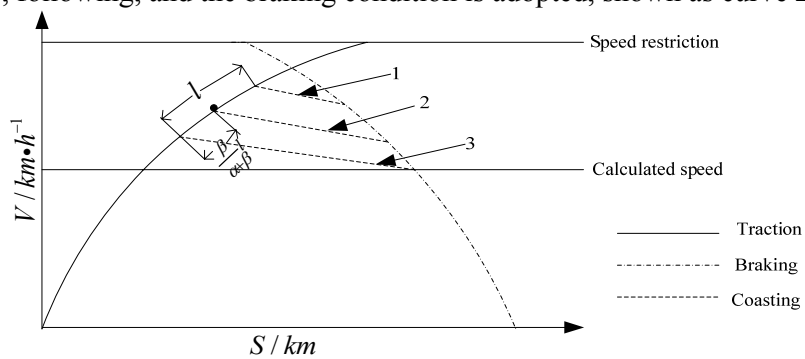

Figure 2: The selection of a coasting point.

3.2 Optimization algorithm of typical transition grade section

In the starting process, maximum tractive force should be adopted in train operation, either from the view of time-saving or from the view of energy-saving (Jin 1997); in the stopping process, based on the method of coasting point selection proposed above, a coasting condition should be adopted; after operation in coasting condition for a while, the braking condition should be adopted. So, the selection of an operation condition in the process of intermediate operation is emphasized in the algorithm. In the practical operation process, the combination of actual ramps is very complicated; control methods of train operation in typical ramps such as straight

ramps, long steep up-gradients, long steep down-gradients, and fragmentary ramps are analyzed as follows:

(1) Straight ramp. When operating on a straight ramp, according to a time-saving traction strategy, a train will run continuously around speed restrictions; according to an energy-saving traction strategy, a train will accelerate to its speed restriction, then a sawtooth operation mode is adopted, that is, the condition of traction—coasting—traction is adopted, and in turn, the operation speed fluctuates between speed restriction and calculated speed; according to a comprehensive optimization traction strategy, the coasting condition will be adopted when the speed of a train is close to speed restriction; coasting point and coasting distance are determined according to the method mentioned above and the parameters α,β input by users.

(2)Long steep up-gradient. When the train location is close to a long steep up-gradient, a traction condition will be adopted for a long time so that the train can run over the gradient by momentum. If the speed of train operation decreases when operating on a long steep up-gradient, traction will be adopted until the train runs over the ramp; if the speed of train operation accelerates continuously, a coasting condition will be adopted when the train operation speed is close to the speed restriction, and the coasting point and coasting distance are determined based on the parameters α,β input by users and the method mentioned above; then the traction condition is adopted, and the train condition of traction—coasting—traction is adopted in turn until the train runs over the ramp.

(3)Long steep down-gradient. When the train location is close to a long down-gradient, the coasting condition will be adopted for a long time in order to take full use of the ramp's potential energy. If operation speed is less than the speed restriction, a coasting condition is adopted until the train runs over the ramp; otherwise, a braking condition is adopted.

(4)Fragmentary ramp. When the train is operating on a fragmentary ramp, uniform motion should be kept; if the time for the conversion of operation condition is less than the specified time, target speed should be determined according to the line condition, and the train can run near the target speed by adopting the condition of coasting— traction — coasting in turn, giving consideration to both time-saving and energy-saving.

4 SYSTEM APPLICATION CASE

In order to prove the effectiveness of the algorithm, practical data of intervals between Eastern Guangzhou and Western Tiyu Road in Guangzhou Metro Line 3 are adopted for simulated train operation, and the main parameters are presented as follows:

(1)Line data: there are three stations between Eastern Guangzhou and Western Tiyu Road intervals, respectively, Eastern Guangzhou, Western Linhe, and Western Tiyu Road. The distance between Eastern Guangzhou and Western Linhe is 1107 meters, and the distance between Western Linhe and Western Tiyu Road is 1179.2 meters.

(2) Motor car data: Length is 60 meters, dead weight is 22 tons, passenger

capacity is 1950 persons, motor number is 1, gross weight is 158.5 tons, braking mode is electrically and pneumatically blended braking, power supply mode is pantograph, traction self-consumption current is 10A, coasting self-consumption current is 5A, braking self-consumption current is 10A, pantograph net voltage of traction condition, pantograph net voltage of coasting condition, pantograph net voltage of braking conditions are all 1500V.

(3)Calculated parameters: time step for calculation is 400ms, the time for the conversion of operation condition is 2s, error of speed restriction is 5km/h.

A simulation curve of train operation is shown in Figure 3, where ——represents the traction condition，---------- represents the coasting condition，---------- and represents the braking condition.

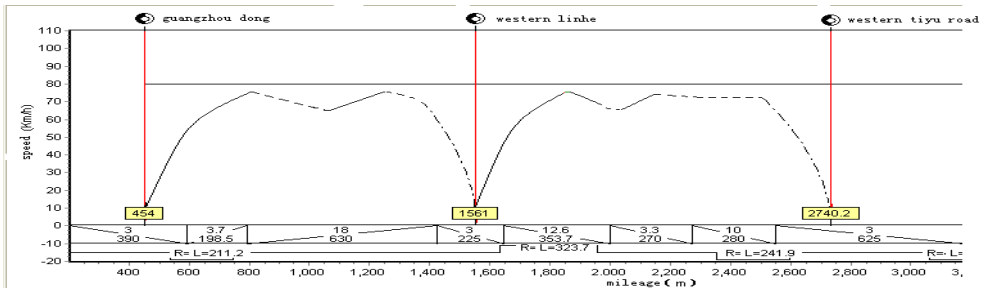

Figure 3 Simulation curve of train operation.

Table 1. Statistical results.

Interval	Distance between interval (m)	Total operation time (s)	Average speed(Km/h)	Traction time (s)	traction rate	energy consumption for traction (Kwh)	total energy consumption (Kwh)
Eastern Guangzhou = western linhe	1100.5	76	52.1	42	0.55	1.9	2.1
Western linhe = Western tiyu road	1179.2	81	52.4	32	0.40	1.5	1.6

5 CONCLUSION

Comprehensive optimization of train operation is very complicated. In this paper, an urban rail transit traction calculation system is established and the key technology comprehensive optimization traction strategy is analyzed. The system is proved to be effective by simulation train operation in the interval of Guangzhou metro line 3, therefore, it can be used in optimization of train operation and in comparison with operation control schemes under different operating conditions, etc.

ACKNOWLEDGEMENTS

This paper was prepared based on a research project sponsored by Natural Science Foundation of China (No.60870004).

REFERENCES

Guo, Y., Wang, Z., Wu, F., et. al. (2002). "Train operation and movement simulation system." *Journal of Lanzhou Railway University*. 21(6), 125-127.

He, H., and Zhu, J. (2000.10). "Design of software for traction calculation and operation schematic diagram of trains." *Journal of Southwest Jiaotong University*. 35(5),514-516.

Jin, W., Wang, Z., Li, C., et. al. (1997). "Study on optimization method of train operation for saving energy." *Journal of the China Railway Society*. 19(6), 58-59.

Mao, B., He, T., Yuan, Z., et. al. (2000). "A general purposed simulation system on train movement." *Journal of the China Railway Society*. 22(1), 1-5.

Characteristic Analysis of Urban Rail Transit Network Considering Demand and Operation: A Case on Shanghai

C. Yang[1] and Y. Wang[2]

[1]School of Transportation Engineering, Tongji University, No. 4800 Cao'an Highway, Shanghai, 201804, China; PH (86) 21-69583704; email: tongjiyc@tongji.edu.cn
[2]School of Transportation Engineering, Tongji University, No. 4800 Cao'an Highway, Shanghai, 201804, China; PH (86) 21-69583248; email: evonne.w@126.com

ABSTRACT

In this paper, we define network characteristic indices from three aspects including topology, demand and operation, to investigate the characteristics of a rail transit network in Shanghai. First, we analyze the degree distribution, and show that the two stations with maximum degree are respectively the social and economic centers of the Pudong and the Puxi areas in Shanghai. Then, considering the demand and operation, we calculate the node closeness and weighted closeness of all the stations. Isoline analysis shows the concentric circle structure, whose centers represent the stations with better accessibility. Furthermore, considering the spatial locations of stations, we calculate weighted straightness for all stations, and use a new presentation to compare it with degree. The results show that the stations with high connectivity are still the hub stations. This research has theoretical significance in promoting the development of complex networks and guiding the planning practice of rail transit networks.

Key words: *rail transit, complex networks, network characteristic index, topology, demand and operation*

INTRODUCTION

In recent years, studies on complex networks have thrived. The development of transport networks represents a complex and dynamic process. However, most research that can be found about transport networks is centered on the topological study of railway, aviation, urban roads and public transport networks, and only a few on rail transit networks. Furthermore, transport networks are located in real space, where nodes and links occupy precise positions in Euclidian space, and links represent physical connections. It is insufficient to study the characteristics of transport networks using topology only. It is more realistic to also consider the spatial location of the nodes, as well as demand and operation when researching transport networks.

Nowadays, many urban rail transit lines are under construction in the metropolises of China. Since the Rail Transit Line 1 (South Section) opened to traffic in 1993, Shanghai, as China's economic and trade center, has formed a rail transit network that consists of Line 1, 2, 3, 4, 5, 6, 8 (Phase 1) and 9 (Phase 1).

By the end of 2007, the network had 148 operation stations and the operation mileage was 234km. The network pattern of '1 ring, 7 radials, 11 interchange stations' is formed and rated as No. 1 in size and dimensions among all the major cities in China. The rapid development of rail transit makes it increasingly important to urban transport.

This paper selects the indices commonly used in studies about complex networks. This paper also selects the indices which consider demand and operation to analyze the characteristics of the Shanghai rail transit network.

THE DEFINITION OF THE RAIL TRANSIT NETWORK

In network analysis, the actual network is usually abstracted as a planar graph: G= {V, E}, where V is a collection of nodes connected by links (edges) E. In this paper, the current rail transit network in Shanghai will be abstracted to planar graphs (see Figure 1). Nodes represent different stations in the network. Links represent actual operational rail transit lines. The length between nodes is the actual travel distance between different stations.

Figure 1 clearly shows the network pattern of '1 ring, 7 radials, and 11 interchange stations.' Particularly, '1 ring' refers to Line 4 -- the only ring line in the rail transit network of Shanghai. '7 radials' refers to the 7 radial lines of 1, 2, 3, 5, 6, 8, and 9. '11 interchange stations' refers to 4 stations intersected with 3 lines including the People's Square Station, the Century Avenue Station, the Zhongshan Park Station and the Shanghai Railway Station, as well as 7 other stations intersected with 2 lines. In addition, there are 9 common stations that belong to both Line 3 and Line 4.

Figure 1. Shanghai rail transit network pattern.

CHARACTERISTIC INDICES OF RAIL TRANSIT NETWORKS

Topological index. Degree represents the number of adjacent nodes connecting to a certain node. Normally, important nodes have more adjacent nodes - just like hub stations.

Indices considering demand and operation. Node closeness. Closeness measures the inverse of the average shortest path distance from node i to all other

nodes in a given network (Sabidussi, 1966). Considering the operation of the rail transit network, closeness is defined as:

$$C_i = (N-1) \Big/ \sum_{j \in N, j \neq i} T_{ij} \tag{1}$$

where T_{ij} represents the travel time using the shortest path.

Weighted closeness. Considering traffic demand, the peak-hour passenger flow of all the stations is selected as demand weight. The weighted closeness is calculated as follows:

$$C_i^w = \sum_{j \in N, j \neq i} \frac{W_j}{T_{ij}} \Big/ \sum_{j \in N, j \neq i} W_j \tag{2}$$

where W_j is the peak-hour passenger flow of station j. Higher C_i and C_i^w values represent better accessibility.

Indices considering spatial location of nodes. Weighted straightness. Latora and Marchiori (2001) proposed to measure the efficiency of spatial networks by comparing the length of the shortest paths between nodes with the crow-fly distance, which captures how much the travel paths deviate from crow-fly paths and considers the impact of spatial location of nodes on the network. Considering operation and demand, $T_{ij}^{crowfly}$ means crow-fly travel time. Thus, weighted straightness can be described as:

$$S_i^w = \sum_{j \in N, i \neq j} W_j \frac{T_{ij}^{crowfly}}{T_{ij}} \Big/ \sum_{j \in N, i \neq j} W_j \tag{3}$$

CALCULATIONS AND ANALYSIS

Degree. In network analysis, nodes with degree 1 usually are the terminal stations. Nodes with degree 2 occupy a higher portion of the whole network as illustrated in Figure 2. In the Shanghai rail transit network, the two stations with maximum degree 6 are People's Square Station and Century Avenue Station, which both are intersected with 3 lines. Actually, they are also social and economic activities of the Puxi and the Pudong areas in Shanghai.

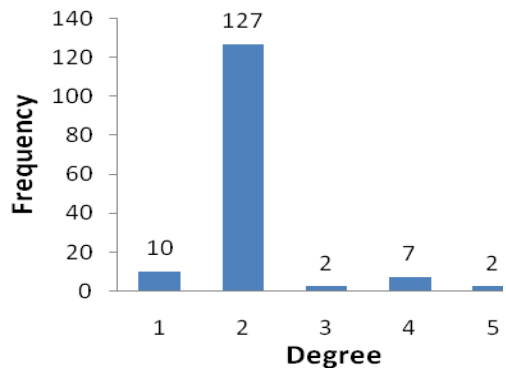

Figure 2. Degree distribution.

Node closeness and weighted closeness. Using Equation (1) and Equation (2), the node closeness and weighted closeness were calculated separately for the rail transit network of Shanghai. (Morning peak-hour passenger flow for all the stations was used as the demand weight for 7:00-9:00am, Thursday, April 21st 2008.) The results represent the accessibility of different stations. ***Isoline analysis*** shows that the spatial pattern is centered by one or several major stations, forming a concentric circle structure. These central stations have higher accessibility, which is defined as the closeness center (CC). As marked with "small ball" in Figure 3, the CCs of the spatial pattern of node closeness are located in People's Square Station, Shanghai Railway Station, Zhongshan Park Station and Century Avenue Station. The CCs of weighted closeness are People's Square Station and Zhongshan Park Station.

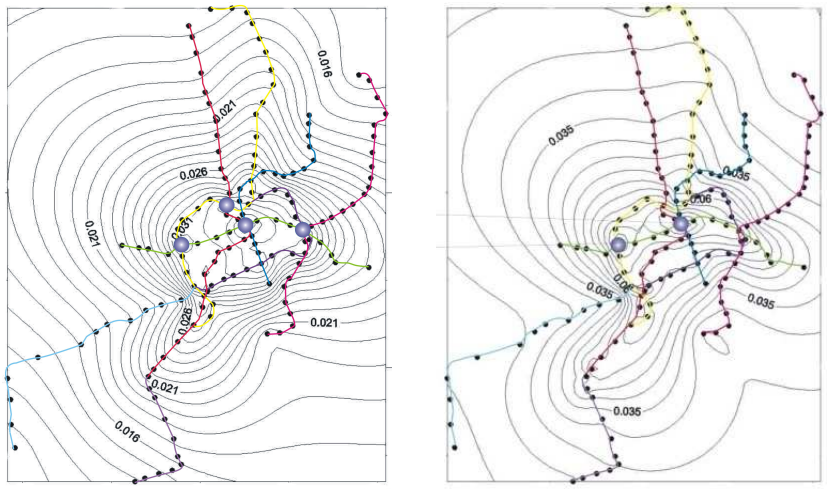

a）node closeness b) weighted closeness

Figure 3. Isoline analysis of spatial pattern of closeness.

The linear correlation analysis between node closeness and weighted closeness in 2008 (see Figure 4) proves that they are correlated. This indicates that stations with higher node closeness also had higher weighted closeness.

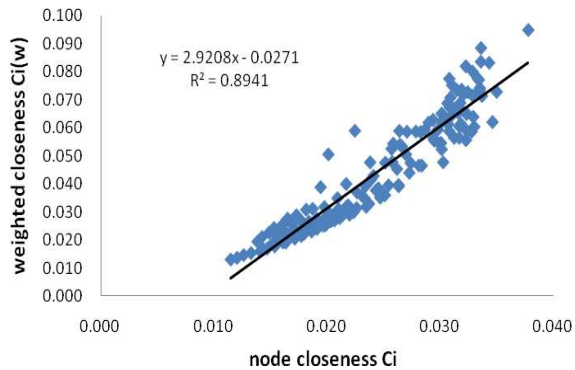

Figure 4. Linear correlation between C_i and C_i^w.

To further investigate the impact of demand on the node and weighted closeness, we ranked the passenger flow of the six stations in decreasing order

(see Table 1). We found that stations with higher closeness also had higher passenger flow. Moreover, these stations are intersected by 3 lines. However, Xinzhuang Station and Zhangjiang Hi-Tech Park Station, which were ranked No. 2 and No. 4 in passenger flow volume, both have lower closeness scores. This indicates that there is a mismatch between their demand and accessibility. Hence, it is necessary to improve the accessibility in future planning and construction efforts.

Table 1. The impact of passenger flow on closeness.

Rank	Station	Passenger flow (W_j)	Ci	Ci(w)	Number of lines
1	Shanghai Railway Station	23,864	0.035	0.073	3
2	XinZhuang	21,469	0.022	0.040	2
3	People's Square	18,087	0.038	0.095	3
4	Zhangjiang Hi-Tech Park	15,297	0.024	0.041	1
5	Century Avenue	13,998	0.033	0.077	3
6	Zhongshan Park	13,825	0.034	0.088	3

Comparison between degree and weighted straightness. In this section, we offer a special representation to investigate the relation between the degree and weighted closeness in the Shanghai rail transit network (Blumenfeld-Lieberthal, 2008). It is based on the assumption that connectivity of stations can be defined by its degree and weighted closeness, rather than by each of them alone. By examining the relations of these two indices, not only the ***connectivity level*** of various stations can be analyzed, but also the ***operational efficiency*** of the whole network can be measured. As illustrated in Figure 5, the graph is divided into 9 regions, of which Region A—D represents four different types of stations, and Region 1—5 represent intermediate situations of development between A—D.

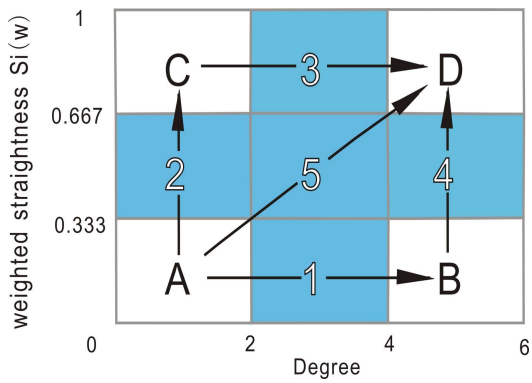

Figure 5. Regions division of degree vs. weighted straightness.

Region A: a low-importance station in a low-efficiency network. Stations in this region are typical of a low-connectivity network with unreasonable line settings.

Region B: a high-importance station in a low-efficiency network. Stations in this region are typical of hub stations in a low-connectivity network.

Region C: a low-importance station in a high-efficiency network. Although stations in this region have fewer adjacent stations, further degree gains would have been possible because of the reasonable line settings of the whole network.

Region D: a high-importance station in a high-efficiency network. Stations in this region are typical of hub stations in a high-connectivity network.

Applying this method to the Shanghai rail transit network, Figure 6 shows that most of the stations appear in Regions 2 and 5; fewer are located in Regions 3 and D; and, no stations appear in Regions 1, A, or B. This means that the rail transit network in Shanghai is still developing towards a better orientation. Besides, the 5 stations in Region D are all hub stations with a high connectivity level. They are the People's Square Station, the Shanghai Railway Station, the Zhongshan Park Station, the Century Avenue Station, and the Shanghai Indoor Stadium Station.

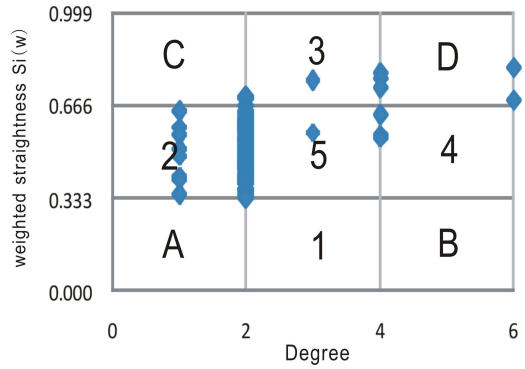

Figure 6. Degree vs. weighed straightness.

CONCLUSIONS

This paper selected the indices of topology, demand, and operation, and used these three aspects to analyze the characteristics of the current rail transit network in Shanghai.

(1) Degree was selected as a topological index. The analysis showed that the two stations with maximum degree 6 are the People's Square Station and the Century Avenue Station, which are also the centers of social and economic activities of the Puxi and the Pudong areas in Shanghai.

(2) Considering demand and operation, the spatial pattern of the node closeness and weighted closeness both showed concentric circle structures. Stations with better closeness (better accessibility) were focused on the 4 stations that intersected with 3 lines. Furthermore, the node closeness and weighted closeness (using passenger flow as the weighting factor) showed linear correlation with each other. For stations with lower closeness and higher passenger flow, future planning and construction should consider improving the accessibility of these stations.

(3) With further consideration of the spatial location of stations, weighted

straightness was defined. By comparing it with degree, we classified different types of stations by their stages of connectivity. The results show that high-connectivity stations are also the hub stations.

Future research will further investigate the correlation among network expansion, land development, and traffic demand, and try to grasp the relationship between transport and land use from the growth perspective of complex networks.

ACKNOWLEDGEMENT

This research is sponsored by Shanghai Rising-Star Program (Grant No: 08QA14066).

REFERENCES

Blumenfeld-Lieberthal, E. (2008). "The topology of transportation networks: a comparison between different economies", *Netw Spat Econ.*

Latora, V., and Marchiori, M. (2001). "Efficient behavior of small-world networks." *Phys Rev Lett* 87:198701.

Sabidussi, G. (1966). "The centrality index of a graph." *Psychometrika,* 31, 581–603.

Adaptability Assessment and Maintenance Technology Research of Existing Railway Line Speed Increases to 200 km/h

Ping WANG[1]，Rong CHEN[2]， Xiaoping CHEN[3]

[1]School of Civil Engineering，Southwest Jiaotong University，Chengdu, 610031，China; PH: (86)028-87601210; Email: wping@home.swjtu.edu.cn
[2]School of Civil Engineering，Southwest Jiaotong University，Chengdu, 610031，China; PH: (86)028-87601210; Email: chenrong@home.swjtu.edu.cn
[3]School of Civil Engineering，Southwest Jiaotong University，Chengdu, 610031，China; PH: (86)028-87601210; Email: cxp193@163.com

ABSTRACT

A section was selected to carry out both dynamic and static tests in order to assess the operation adaptability of existing line speed increases to 200 km/h and to put forward corresponding railway maintenance technology. It assessed the 200km/h EMUs operation safety on existing reform line, and analyzed operation adaptabilities of special sections, such as at the transition between road and bridge, R = 2200m curve and rail welded joints, etc. The results show that for a railway line with a speed increase to 200km/h, a roadbed-bridge transition section should be set up to reduce the additional dynamic impact caused by the changes in track stiffness. It is appropriate to increase the speed of 2200m radius curve to 180km/h, and its speed should be increased accordingly with the speed of freight trains. For a railway line of mixed passenger and freight traffic with speeds up to 200~250km/h, welding joint irregularity should be strictly controlled, and a timely polishing should be arranged when the irregularity is over 0.3mm. Based on the challenges for the China railway and the in-depth analysis of foreign high-speed railway maintenance characteristics, this proposes a maintenance technology system of raising the speed reform railway line by focusing on 4 aspects: the maintenance system, the track management standards, the track detection mode, and maintenance operations.

INTRODUCTION

To realize train speeds of 200km/h or more, two methods are mostly used: 1) construct a dedicated high speed passenger line, which separates passengers and freight transportation; the highest speed can reach 350km/h, such as in France and Japan; and 2) transform the equipment on existing lines, mix passengers and freight transportation; the highest speed can reach 250km/h, such as in Germany and England. On April 18, 2007, the China railway implemented the sixth speed increase: 200 – 250km/h for EMUs, 80 – 120km/hr for 5000t freight trains and double-decker container trucks running on existing reform lines; the railway speed increased to 200km/h along 6003km, of which there are 846km with a speed over 250km/h. This change means China has stepped into world's advanced class (Xi, 2006). In order to assess the operation adaptability of the existing line speed increases to 200 km/h and put forward the corresponding track maintenance

technology, Infrastructure Equipment Test Center of China Railway, Southwest Jiaotong University and Tsinghua University together carried out a study on "Adaptability Assessment and Maintenance Technology Research of Existing Railway Line Speed Increases to 200 km/h."

INTEGRATED ASSESSMENT OF REFORMED RAILWAY OPERATION ADAPTABILITY

A section was selected to carry out dynamic and static tests to assess the 200km/h EMUs running safety on the existing reformed line, and to analyze the operation adaptability of several special sections, such as at the transition between road and bridge, R = 2200m curve and rail welded joints, etc. The track dynamic and static regularities of the reformed track were tested also.

Transition of road and bridge. The track stiffness at the transition between the road and the bridge changes gradually with less additional dynamic impact. Dynamic performance is obviously better than that of the existing bridgehead line (Zhang, 2007). For 200km/h EMUs, the track integral stiffness at the transition between the road and the bridge is 83% of that on the bridge. The additional dynamic coefficient is 5%, and the maximum dynamic irregularity is only 0.1mm. This ensures the safety and comfort of EMUs running at 250km/h. Track stiffness changes abruptly on the existing bridgehead line, and the additional dynamic impact is big. At 195km/h EMUs, the track integral stiffness at the railroad outside bridge is 39% of that on the bridge. The additional dynamic coefficient is 20%, and the maximum dynamic irregularity is 0.7mm. Therefore, a transition between the rail and the bridge should be set up for railway lines with speed increases up to 200km/h so as to decrease the additional dynamic impact caused by stiffness changes. Test results are shown in Table 1.

Table 1. Dynamic test results of transition of road and bridge.

Measuring point	Vehicle	Velocity	Maximal Rail Vertical force (KN)	Maximal rail vertical force variational value(KN)	Additional dynamic coefficient	Maximal Rail Vertical displacement (mm)	Maximal rail vertical displacement variational value(mm)	Vertical displacement variation	Track dynamic stiffness on bridge (KN/mm)	Track dynamic stiffness of transition section (KN/mm)	Track Entire Stiffness ratio
Transition between road and bridge	EMUs	240	86.8	4.3	5%	0.843	0.115	14%	121	101	83%
	passenger train (locomotive)	131.2	162.8	16.36	11%	1.388	0.244	18%	143	111	78%
	Double-decker container truck	119.2	173.46	22.04	15%	1.672	0.473	28%	132	99	75%
	The indicators ratio between EMUs and passenger train		0.53			0.61					
	The indicators ratio between EMUs and double-decker container truck		0.5			0.5					
Existing Bridgehead line	EMUs	195	92.9	15.2	20%	1.203	0.711	59%	175	68	39%
	passenger train (locomotive)	121.6	177.49	16.67	10%	2.041	0.868	43%	147	80	54%
	passenger train (locomotive)		0.52			0.59					

Curve R=2200m. When EMUs pass a curve (R=2200m, superelevation 90mm, maximal deficient superelevation 125mm) at the speed of 200km/h or less, test results show that running stability indexes are all within the allowable safety limits and the dynamic impact is less than that of ordinary trains. See Figure 1. The speed difference between passenger and freight trains and freight train density are comparatively large (MORPRC 2007), so for a curve where R = 2200m, it is

better to increase speed to less than 180km/h which considers passenger comfort and curve maintenance. The speed should be increased with the velocity of freight trains.

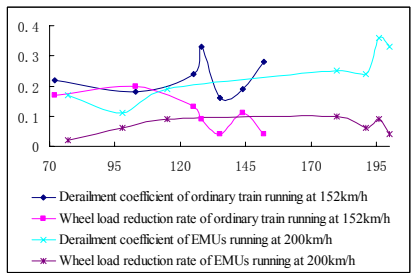

Figure 1. Test results comparison on curve.

Rail Welded Joints. The dynamic impact of EMUs on rail welded joints is comparatively little. For rail welded joints with an irregularity value of 0.25mm, when the EMUs pass at speeds of 240km/h, the wheel-rail vertical force and the acceleration of the rail are both 50% of that of a passenger train running at 120km/h. The impact of the irregularities of rail welded joints on the dynamic performance of the EMUs increases with the increase of speed. For rail welded joints with irregularity values of 0.25mm, when EMUs run respectively at 200km/h and 240km/h, the wheel-rail vertical force of the latter is 2% larger than that of the former, while acceleration is increased 18%. The impact of the irregularity of the rail welded joints on ordinary train dynamic performance increases significantly with the increase of the irregularity of the joints. When EMUs runs at 240km/h and passenger trains and double-decker container trucks run at 120km/h, the wheel-rail vertical force and acceleration of rail welded joints with 0.47mm irregularity are respectively increased by 11% - 18% and 21% - 100% as compared with rail welded joints with 0.25mm irregularity. The impact of the irregularity of rail welded joints on the dynamic performance of 25T axle load double-decker container trucks is comparatively severe. For rail welded joints with a 0.25mm irregularity value, and when a double-decker container truck runs at 120km/h, its acceleration (109.2g) is 1.7 times as large as that of a passenger train(65.30g) running at 120km/h. It is 3.2 times as large as that of EMUs (33.89g) running at 240km/h. The wheel-rail vertical force of rail welded joints with a 0.31mm and 0.25mm irregularity value is slightly different from those of neighboring other rail test points, around 5%. Thus, as for railway lines of mixed passenger and freight transport increase speeds up to 200 – 25km/h, the irregularity values of rail welded joints should be strictly controlled. When it is over 0.3mm, the rail will need grinding.

Safety of EMUs. Three EMUs dynamic performance tests were carried out on Jiao-Ji railway. The test results of frame transversal acceleration show that there is no transversal instability. Maximal lateral wheelset force is less than the operation limits (MORPRC 2005). The derailment coefficient was over 0.8 only once. The maximal wheel load reduction rates are generally less than 0.80; only

a few of which are over 0.80 and they are all single peak unloading. No two peaks appear successively over 0.80. Maximal average values of both transversal and vertical stability of the tested vehicle are less than 2.50, reaching the superior grade. The reformed test section satisfies the safety and comfort requirements of EMUs running between 200～250km/h.

Track Irregularity Spectrum. The track quality of Jiao-Ji railway has greatly improved since its electrification innovation reform in July, 2005. Due to two years of fine maintenance, from between February 2006 to June 2007, the average TQI decreased from 10.16 to 6.93, which is a 32% reduction. The track irregularity spectrum is almost lower than the German Low Interference Spectrum; i.e. the irregularity spectrum of a partial wave band is slightly higher, but none is higher than High Interference Spectrum. See Figure 2. Between July 2006 and June 2007, there were no grade IV over limits, and grade III over limits were within 0 -- 10. Until the sixth raising the speed reform, each dynamic quality index remained stable and the track quality satisfies the criterion of speed increases between 200 -- 250km/h.

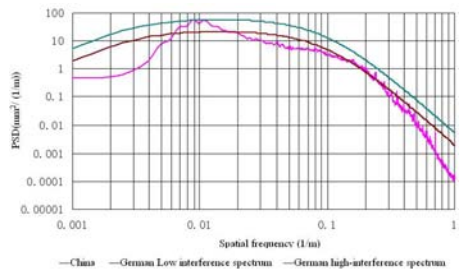

Figure 2. Horizontal irregularity spectrum of Jiao-Ji line.

CHALLENGES FOR RAISING SPEED RAILWAY MAINTENANCE IN CHINA

The integrated assessment of operation adaptability deepens the understanding of the challenges for raising the speed railway line maintenance in China:

(1) To realize high railway regularity based on the operation mode of high speed, high density, big axle weight, and mixed passenger and freight transport.

(2) To improve safety and comfort based on the status of the existing line raising speed reform, but the existing raising speed reform criterion is comparatively low, such as less curve radius, weak roadbed and the stiffness of existing bridgehead line changes dramatically, etc.

(3) To ensure the operation safety under the condition of mixed passenger and freight transport and setting up type V “skylight” for construction operation.

STUDY OF RAISING SPEED RAILWAY MAINTENANCE TECHNOLOGY

Characteristics of Overseas Railway Maintenance and Management.

(1) Advanced concept of design and construction. Make overall plans of

new railway construction and maintenance operation; consider less track maintenance while designing a new line so as to pursue optimized economic benefits. Attach importance to the quality of constructing new lines and strictly control the track starting irregularity. Adopt the principle of equipment first, decrease the influence of artificial factors, i.e., replace personal judgment and operation with equipment. Suit the fixture by mobile equipment to improve the train performance and lighten train axle load and unsprung mass so as to decrease the impact of the train on the track.

(2) Scientific track management. Stipulate integrated criteria for track condition evaluation and management; establish an investigation system with advanced survey techniques, reasonable investigation cycle and dynamic constant velocity testing first with static testing second; predict and control the change of infrastructure equipment scientifically to guide the maintenance. Thoroughly implement guiding ideology of preventive maintenance; rely on an advanced railway information management system, set up "skylight" by adopting a large track maintenance machine according to absolute reference to carry out rail grinding; realize "Equipment Status Repair", efficiently eliminate rail long wave irregularity and rail surface short wave irregularity; improve maintenance precision and track durability so as to extend the track maintenance cycle. See Figure 3 for track irregularity change trends in Germany.

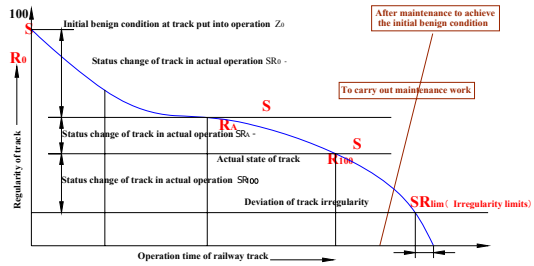

Figure 3.Track irregularity change trends in Germany.

(3) Strict safety management. Establish a disaster prevention and safety monitoring system for high speed railway; carry out complete, accurate and real-time safety controls so as to prevent a sudden disastrous attack (Yu, 2004).

Raising Speed Railway Maintenance for China. Based on integrated assessment results of raising speed railway operation adaptability and in-depth analysis of foreign high speed railway maintenance and management characteristics, this paper put forth a maintenance technology system for raising the railway line speed to 200km/h.

(1) Track maintenance system. Separate systems for management and detection should be put into practice. Establish a detection and monitoring center, which manages the equipment detection, measuring, data analysis, rail flaw inspection, scheduling and computation uniformly.

(2) Track quality management criteria. Complete track quality evaluation criteria are put forward here, including management standards for track dynamic irregularity, track static geometry size allowable errors, and track surface short

wave irregularity. The management standards for track dynamic irregularity contain part irregularity (peak value management), entire irregularity (average value management) and wheel-rail force assessment. See Table 2 for tolerance values for track part dynamic irregularity at different levels. All tolerance levels are divided into four levels: Level I: maintenance standard, level II: comfort standard, level III: temporary repair standard, and level IV: speed limit standard.

Table 2. Dynamic quality tolerance of track.

Items			200km/h≤v≤250km/h			
			I	II	III	IV
Gauge(mm)			+4 -3	+6 -4	+8 -6	+12 -8
Cross-level(mm)			5	8	10	13
Track twist irregularity (gauge length 2.5m)（mm）			4	6	8	10
Comfort indexes	Wave length 1.5～42m	Rail vertical irregularity (mm)	5	8	11	14
		Rail alignment (mm)	5	7	8	10
	Constant velocity detection	Car body vertical acceleration（g）	0.10	0.15	0.20	0.25
		Car body transversal acceleration（g）	0.06	0.10	0.15	0.20
	Wave length 1.5～70m	Rail vertical irregularity (mm)	6	10	15	
		Rail alignment(mm)	6	8	12	
Gauge change rate(gauge length 2.5m)（‰）			1.0	1.2		
Curvature change rate (gauge length 18m)（1/m2×10-6）			1.2	1.5		
Car body transversal acceleration change rate (gauge length 18m)（m/s3）			0.8			

(3) Railway track inspection. It is necessary to adopt a new inspection mode for raising railway speed, which includes dynamic constant velocity detecting first, with static testing second, advanced detection techniques, reasonable inspection cycle, and fast data processing.

(4) Maintenance and repair work. The guiding ideology of preventive maintenance should be implemented, adopt advanced track management technology and equipment status repair regulations to improve maintenance precision, reliability, and achieve the comfort standards.

In detail, six aspects of transformation are needed: (A) Put preventive maintenance into full practice, and track maintenance target switches from safety management to comfort management; (B) Use large railway track maintenance machinery by adopting an absolute reference measurement system; Track maintenance changes from improving track status to completely renewing design, geometry, and shape; (C) Emphasize rail regularity, change from ballast tamping first to reducing ballast tamping by rail grinding; (D) Adopt advanced track management technology, change from traditional experience management to digital, information and customization management; (E) Attach great importance to safety of type V “skylight” operations; as for quality check after construction, it should change gradually from static inspection to dynamic inspection confirmation; (F) Spare no effort to establish a cubic safety barrier for raising speed lines, change from ordinary open railway to raising speed fully-closed railway line.

CONCLUSIONS

(1) Transition between road and bridge should be set up for speeds up to 200km/h so as to reduce the additional dynamic impact caused by track stiffness changes; make overall plan of EMUs comfort and curve maintenance, for

R=2200m curve, it is better to limit speed to not more than 180km/h, moreover, it should be increased with the speed increase of freight train; for raising the speed of mixed passenger and freight transport, the rail welded joints irregularity should be strictly controlled, and the rail needs grinding when it is over 0.3mm.

(2) Raising the railway speed should be based on the principle of preventive maintenance, and it should rely on advanced management technology, and realize comfort target management through equipment status repair.

(3) More research should be carried out soon to determine the mode at which large railway track maintenance machinery works by adopting an absolute reference measurement system in China. Meanwhile, problems such as decreasing additional dynamic impacts caused by track stiffness changes and improving railway dynamic regularity, and tracking integral stiffness proper matching of existing bridgehead railway line, etc., are also urgent research tasks.

REFERENCES

Ministry of Railways of the People's Republic of China (MORPRC) (2005). Design Interim Code for Newly-built 200 km/h Railway Line Shared by Passenger and Freight Trains[S]. Beijing: China Railway Publishing House.

Ministry of Railways of the People's Republic of China (MORPRC) (2007). Maintenance Rules of Track and Bridge in Existing Railway Line Speed Increases to 200～250km/h[S]. Beijing: China Railway Publishing House.

Xi, W. (2006), "China's speed-raising of existing line stride forward into the advanced ranks in the world" [J]. *Chinese Railways*, (12), 1-4.

Yu, J., Miao, L., Li, K. (2004). *New Technology of Design, Construction and Speed Increase Reform in Modernization High-Speed Railway.*[M]. Changchun: Jilin Science and Technology Press.

Zhang, X., Gao, L. (2007). "Research on Track Geometry Status Variation of Road and Bridge Transition in Railway Line Speed Increases to 200km/h."[J]. *Railway Engineering*, (5):81-83.

Analysis on Mechanical Performances of High-speed Railway Transition Curves

Xiangguo Li[1], Musong Li[2], Chao Ma[3], Jianqing Bu[4] and Liangliang Zhu[5]

[1]School of Civil Engineering, Southwest Jiaotong University, No.111 1st-North 2nd-Ring Road, Chengdu, Sichuan Province, China, 610031; PH(0311), 85281531; email: lixiangg12009@126.com
[2]School of Civil Engineering, Shijiazhaung Railway Institute, No.17 North 2nd-Ring East Road, Shijiazhuang, Hebei Province, China, 050043; PH(0311), 87935555; email: lims106@126.com
[3]School of Civil Engineering, Shijiazhaung Railway Institute, No.17 North 2nd-Ring East Road, Shijiazhuang, Hebei Province, China, 050043; PH(0311),87936809; email: mach_74@163.com
[4]School of Civil Engineering, Shijiazhaung Railway Institute, No.17 North 2nd-Ring East Road, Shijiazhuang, Hebei Province, China, 050043; PH(0311), 87936227; email: bujq@sjzri.edu.cn
[5]School of Civil Engineering, Shijiazhaung Railway Institute, No.17 North 2nd-Ring East Road, Shijiazhuang, Hebei Province, China, 050043; PH(0311), 87935535; email: zhuliangliang616@163.com

ABSTRACT

Whether the type of high-speed railway transition curves is suitable or not affects a train's running stability and passengers' comfort directly. The lateral change of acceleration (LCA) plays an important role in determining the transition curve parameters. Based on vehicle movement dynamics, the motions with positive or negative acceleration are taken into account to deduce the equation of lateral change of the vehicle acceleration. The LCA of several common transition curves were compared in five different motion models. The results show that the LCA which considers motion with positive or negative acceleration can be used for the optimization of high-speed railway transition curves as a theoretical basis.

INTRODUCTION

As train speed increases, to ensure that vehicles run safely and are stable, higher requirements on track geometry should be met. Transition curves are normally inserted between straight lines and circular curves in order to make the train pass smoothly from a straight line to a circular curve or from a circular curve to a straight line. Studies on transition curves have been carried out for about 100 years and much information can be found in the literature (Baykal, O. and Tari, E. 1998; Baykal, O. and Tari, E. 2005; Lipicnik, M. 1998; Wang, X. W. 1997; Zhou, X. Z. 1996; Zhu, W. S. 1997). However, there is still much dispute about the selection of transition curve shapes (Wang, X. W. 1997; Zhu, W. S. 1997). Several transition curves are used in the world at present, such as cubic parabola (CP), half-wave-length sinusoidal (HS) and sinusoidal (SI). However, only CP and HS are used in wheel-rail high-speed railway (Liu, X. and Liu, Z. J. 2004). The LCA

plays an important role in determining the transition curve parameters. Based on the vehicle movement dynamics, and assuming that the conditions of the vehicle and the track are sound, simplifying the vehicle as a particle, and taking into account of the motions with positive or negative acceleration, the equation of the lateral change of the vehicle acceleration is deduced in this paper. Additionally, the values of LCA for several familiar transition curves such as CP, HS, and SI are compared.

DEDUCTION OF LCA FUNCTION

Forces acting on a vehicle that is moving on curve are the gravitational force (mg), the centrifugal force ($\boldsymbol{J}=mkv^2$), the reaction force of the track ($\boldsymbol{N}$), and the motor or resistance force (ma_t). See Figure 1(a) and (b). According to Figure 1(a), the gravitational force (mg)/the centrifugal force ($\boldsymbol{J}=mkv^2$) can be divided into two: $mg\cos$ /$mkv^2\sin$ and $mg\sin$ /$mkv^2\cos$ perpendicular and parallel to the track plane, respectively. The component $mg\cos$ and $mkv^2\sin$ are balanced with the reaction of the track plane (N) and becomes effective in only the vertical change of acceleration. The $mg\sin$ and $mkv^2\cos$ are the forces which form the LCA.

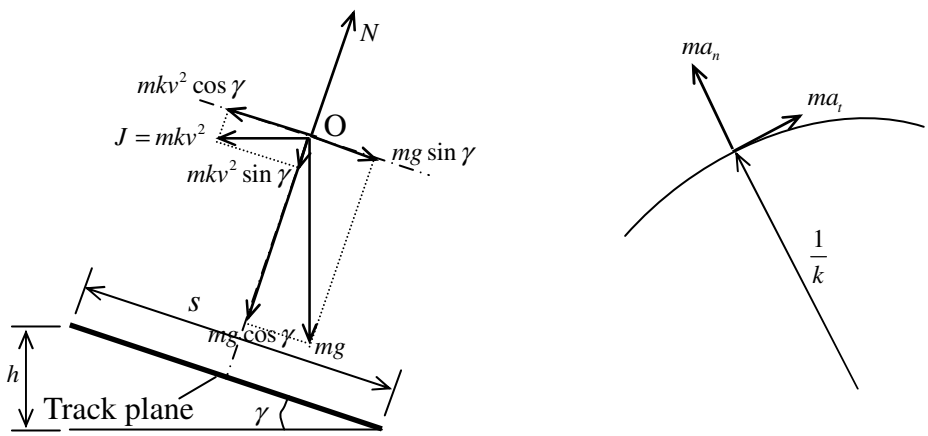

(a) Cross section **(b) Plane view**

Figure 1. Forces acting on a vehicle moving on curve.

From Figure 1(a)

$$\boldsymbol{a}_n = (kv^2\cos\gamma - g\sin\gamma)\ \mathbf{n} \tag{1}$$

can be derived, where $\boldsymbol{a}_n$ is the acceleration along the direction of the curve normal on an inclined track plane (m/s^2); k is the curvature of orbiting curve defined on a horizontal plane (m^{-1}); v is the vehicle velocity; is the bank angle; g is the gravitational acceleration (9.81 m/s^2); and $\mathbf{n}$ is the unit vector along the curve normal.

The tangential acceleration caused by the motor or the resistance force is

$$\boldsymbol{a}_t = \frac{dv}{dT}\ \mathbf{t} \tag{2}$$

where $\mathbf{t}$ is the unit vector along the direction of the tangent of the curve; T is time

(s), and the resultant acceleration of the motion is

$$\boldsymbol{a} = \frac{dv}{dT}\,\mathbf{t} + (kv^2\cos\gamma - g\sin\gamma)\,\mathbf{n} = \frac{dv}{dT}\,\mathbf{t} + \left(kv^2\sqrt{s^2-h^2}\,/\,s - gh/s\right)\mathbf{n} \tag{3}$$

where s is the distance between the centers of the rails (1.5 m); and h is cant (m). In the case where the velocity (v) is constant (a_t=0) along the transition curve and the bank angle (<<1) is small, Equation (3) which is a common function of the lateral acceleration,.can be simplified as

$$a = kv^2 - gh/s \tag{4}$$

where $v = v(l)$ is a function of the velocity related to the track; $k = k(l)$ is a function of the curvature related to the track; and $h = h(l)$ is a function of cant related to the track. The derivative of Equation (3) with respect to the track is

$$\frac{d\boldsymbol{a}}{dl} = \frac{dv}{dT}\frac{d\mathbf{t}}{dl} + \frac{d\left(kv^2\sqrt{s^2-h^2}\,/\,s - gh/s\right)}{dl}\,\mathbf{n} \tag{5}$$

where

$$\frac{d\mathbf{t}}{dl} = k_e\,\mathbf{n} \qquad \text{(O. Baykal 1996)} \tag{6}$$

k_e is the curvature of the orbiting curve defined on the inclined plane of the track; and l is the horizontal distance measured along the transition curve. Since the curvature of the orbital curve is defined on a horizontal plane, as a rule it should be traced on to the inclined plane, such as

$$k_e = k\cos\gamma = \frac{\sqrt{s^2-h^2}}{s}k\,. \tag{7}$$

Introducing (6) and (7) into (5) and multiplying both sides by **n**

$$\frac{d\boldsymbol{a}}{dl}\mathbf{n} = \left(k\frac{dv}{dT} + v^2\frac{dk}{dl} + 2kv\frac{dv}{dl}\right)\frac{\sqrt{s^2-h^2}}{s} - \left(kv^2\frac{h}{s\sqrt{s^2-h^2}} + \frac{g}{s}\right)\frac{dh}{dl} \tag{8}$$

can be obtained. In addition, the following can be written

$$\frac{d\boldsymbol{a}}{dT} = \frac{d\boldsymbol{a}}{dl}\frac{dl}{dT} = v\,\frac{d\boldsymbol{a}}{dl} \tag{9}$$

$$\frac{dv}{dl} = \frac{dv}{dT}\frac{dT}{dl} = \frac{1}{v}\frac{dv}{dT} = \frac{a_t}{v}\,. \tag{10}$$

Introducing (9) and (10) into (8), the equation of the LCA can be derived as follows:

$$f = \frac{d\boldsymbol{a}}{dT}\mathbf{n} = v\left[\left(3ka_t + v^2\frac{dk}{dl}\right)\frac{\sqrt{s^2-h^2}}{s} - \left(kv^2\frac{h}{s\sqrt{s^2-h^2}} + \frac{g}{s}\right)\frac{dh}{dl}\right]\,. \tag{11}$$

Equation (11) can also be written as follows:

$$f = \frac{d\boldsymbol{a}}{dT}\mathbf{n} = v\left[\left(3ka_t + v^2\frac{dk}{dl}\right)\cos\gamma - \frac{kv^2\tan\gamma + g}{s}\frac{dh}{dl}\right]\,. \tag{12}$$

LCA FUNCTIONS OF TRANSITION CURVES

Characteristics of transition curves. The characteristics of CP, HS, and SI are listed in Table 1 where h_0 is maximum cant; R is the radius of a circular curve; and L is the total horizontal length of a transition curve.

Table 1. Characteristics of transition curves.

Characteristics	CP	HS	SI
k	$\frac{l}{RL}$	$\frac{1}{2R}\left[1-\cos\left(\frac{\pi l}{L}\right)\right]$	$\frac{1}{R}\left[\frac{l}{L}-\frac{1}{2\pi}\sin\left(\frac{2\pi l}{L}\right)\right]$
h	$\frac{h_0 l}{L}$	$\frac{h_0}{2}\left[1-\cos\left(\frac{\pi l}{L}\right)\right]$	$h_0\left[\frac{l}{L}-\frac{1}{2\pi}\sin\left(\frac{2\pi l}{L}\right)\right]$

LCA function of CP, HS and SI. Taking vehicle passes from a straight line to circular curve for example, the function of the LCA of the transition curves are derived from Equation (11) by taking into consideration the characteristics in Table 1 as follows:

LCA function of the CP:

$$f=\frac{v}{RLs}\left(3a_{\mathrm{t}}lA+Av^2-Rgh_0-\frac{v^2h_0^2l^2}{LA}\right) \tag{13}$$

where $A=\sqrt{s^2-\left(\frac{h_0 l}{L}\right)^2}$.

LCA function of the HS:

$$f=\frac{v}{4RLs}\left\{3a_{\mathrm{t}}LBC+\left[\frac{2\pi v^2(2s^2-h_0^2B^2)}{C}-2\pi Rgh_0\right]\sin\left(\frac{\pi l}{L}\right)\right\} \tag{14}$$

where $B=1-\cos\left(\frac{\pi l}{L}\right)$, $C=\sqrt{4s^2-(h_0B)^2}$.

LCA function of the SI:

$$f=\frac{v}{RLs}\left\{3a_{\mathrm{t}}LDE+\left[\frac{2v^2(s^2-2h_0^2D^2)}{E}-2Rgh_0\right]\sin^2\left(\frac{\pi l}{L}\right)\right\} \tag{15}$$

where $D=\frac{l}{L}-\frac{1}{2\pi}\sin\left(\frac{2\pi l}{L}\right)$, $E=\sqrt{s^2-(h_0D)^2}$.

CALCULATING

Five different motion models are established by taking into account

motions with positive or negative acceleration.

Calculation parameters. The line is flat; the radius of the circular curve R=5000 m; the length of the transition curve L=300 m; the length of the circular curve L_0=600 m; and the maximum cant h_0=0.055 m.

Model 1-Motion model with constant velocity. In this model, velocity (v=300 km/h) is assumed to be constant (a_t=0) along the total curve. To compare the curves, the graphs of the LCA of the curves for model 1 are illustrated in Figure 3 by introducing the calculation parameters into Equations (13), (14) and (15).

Model 2 and 3-Motion model with constant acceleration. The acceleration is assumed to be constant (a_t=constant) along the total curve. The following equations of velocity and acceleration are valid (where the velocity is v_0 at ZH (l=0) and v_e at HZ (l=2L+L_0) in Figure 2).

$$a_{\mathrm{t}} = \frac{v_{\mathrm{e}}^2 - v_0^2}{2\left(2L + L_0\right)}; \qquad v = \sqrt{v_0^2 + 2a_{\mathrm{t}} l} \tag{16}$$

According to Equation (16), the motion with positive acceleration is valid for v_0 (v_0=150 km/h) < v_e (v_e=300 km/h) (model 2), and the motion with negative acceleration is valid for v_0 (v_0=300 km/h) > v_e (v_e=150 km/h) (model 3). To compare the curves, the diagram of the LCA of the curves for model 2 and model 3 are illustrated in Figure 4 and in Figure 5 by introducing Equation (16) and the calculation parameters into Equations (13), (14) and (15).

Model 4 and 5 Motion model with variable accelerations. The velocities at ZH, M (l=L+L_0/2), and HZ are assumed as v_0, v_c and v_e, respectively. The velocity and the acceleration equations are given for two sections, ZH-M, M-HZ, and are valid as

$$a_{t,1} = \frac{v_c^2 - v_0^2}{2\left(L + L_0/2\right)}; \qquad v_1 = \sqrt{v_0^2 + 2a_{t,1} l}\ ; \qquad (0 \le l \le L + L_0/2) \tag{17a}$$

$$a_{t,2} = \frac{v_e^2 - v_c^2}{2\left(L + L_0/2\right)}; \quad v_2 = \sqrt{v_c^2 + 2a_{t,2}\left(l - L - L_0/2\right)}; \quad (L + L_0/2 \le l \le 2L + L_0) \tag{17b}$$

where a_{t1} (a_{t2}) and v_1 (v_2) is the acceleration and velocity of the former (latter) section, respectively.

According to Equation (17), the motion with negative acceleration - positive acceleration is valid for v_0 (v_0=150 km/h) < v_c (v_c=300 km/h) > v_e (v_e=150 km/h) (model 4), and the motion with positive acceleration - negative acceleration is valid for v_0 (v_0=300 km/h) > v_c (v_c=150 km/h) < v_e (v_e=300 km/h) (model 5). To compare the curves, the diagram of the LCA of the curves for model 4 and model 5 are illustrated in Figure 6 and Figure 7 by introducing Equation (17) and the calculation parameters into Equations (13), (14), and (15).

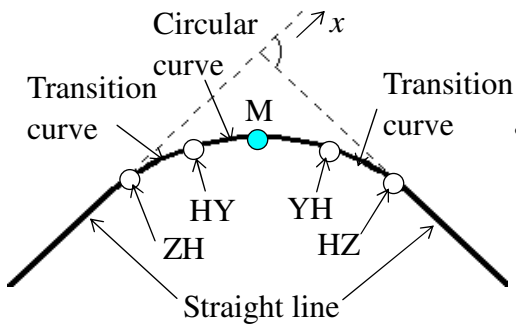

Figure 2. Horizontal geometry of curve.

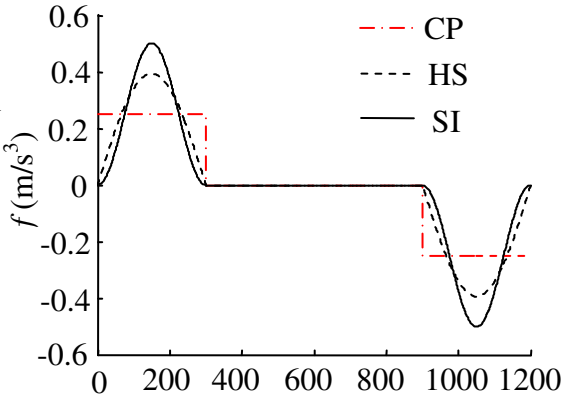

Figure 3. Graphs of LCA in model 1.

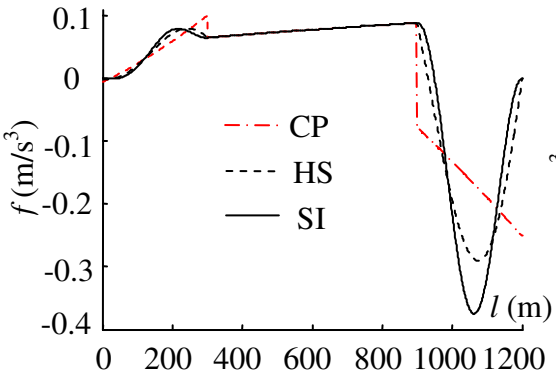

Figure 4. Graphs of LCA in model 2.

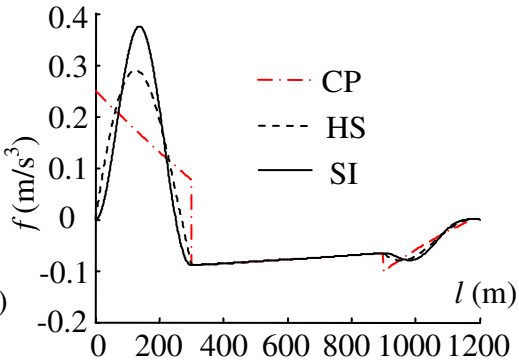

Figure 5. Graphs of LCA in model 3.

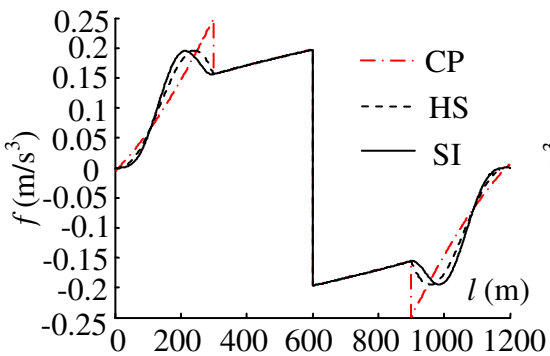

Figure 6. Graphs of LCA in model 4.

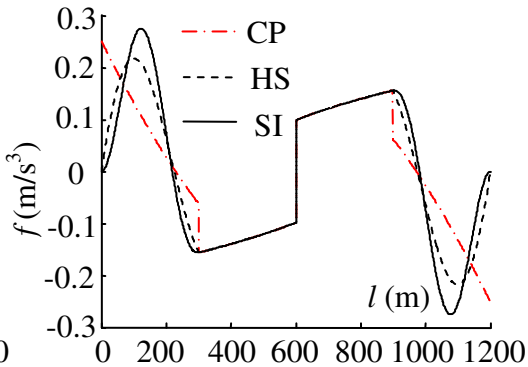

Figure 7. Graphs of LCA in model 5.

COMPARISONS

The continuity of the LCA function is the most important criterion in the comparison of transition curves for several reasons: because discontinuities in the form of jumps affect travel comfort on railways; it changes the geometry of the rails; and more importantly, it causes wear on wheels and rails in railways. The comparisons of the LCA of CP, SI, and HS transition curves with each other using five different motion models as follows:

(1) We can see from Figures 3-7 that the CP has discontinuities at 4, 3, 3, 3 and 5 points, respectively; the HS and SI do not have any discontinuities in the

form of a jump in Figures 3-5, and in Figures 6 and 7 there are discontinuities at one point only. Therefore, according to the criterion the HS and SI are better than the CP.

(2) There are magnitudes of discontinuities in the form of jumps on the diagrams of the LCA. The jumps of the function of the LCA at point ZH, HY, M, YH and HZ and the sums of absolute values of the jumps are given as the criterion listed in Table 2. From Figures 3-7 and Table 2 we can see that the maximum sums of jumps of the transition curves with five different motion models are 1.0032, 0.4584, 0.4584, 0.5883 and 0.8868 m/s^3 for CP. We can also see that the jumps of HS are the same as that for SI. Therefore, according to the criterion, the HS and SI are better than the CP, especially in models 4 and 5.

(3) To better compare the LCA of transition curves, the absolute maximum values of the function of the LCA are given as one of the criteria and are listed in the last column of Table 2. We can see from Figures 3-7 and from Table2 the largest absolute values of the function of the LCA are 0.2508, 0.3937 and 0.5013 m/s^3 for CP, HS and SI, therefore the HS is better than the others.

Table 2. Discontinuities of LCA in the form of jumps (m/s^3).

Point number		Discontinuity Magnitude ZH	HY	M	YH	HZ	Sum of jumps	Maximum
Model 1	CP	0.2508	0.2508	0	-0.250	-0.250	1.003	0.2508
	H	0	0	0	0	0	0	0.3937
	SI	0	0	0	0	0	0	0.5013
Model 2	CP	-0.006	0.0352	0	-0.166	-0.250	0.458	0.2508
	H	0	0	0	0	0	0	0.2902
	SI	0	0	0	0	0	0	0.3752
Model 3	CP	0.2508	0.0166	0	-0.035	0.0061	0.458	0.2508
	H	0	0	0	0	0	0	0.2902
	SI	0	0	0	0	0	0	0.3752
Model 4	CP	-0.006	0.0939	-0.394	-0.093	0.0061	0.588	0.2498
	H	0	0	-0.394	0	0	0.394	0.1972
	SI	0	0	-0.394	0	0	0.394	0.1972
Model 5	CP	0.2508	-0.094	0.1972	0.0940	-0.250	0.886	0.2508
	H	0	0	0.1972	0	0	0.197	0.2172
	SI	0	0	0.1972	0	0	0.197	0.275

CONCLUSION

In this paper, the function of the LCA is obtained by taken into account the motions with positive or negative acceleration based on vehicle movement dynamics. And, Equation (11) is suitable for the optimization of transition curves. However, this article is only a theoretical derivation and useful for comparison purposes. It is necessary to conduct further research and do simulation analyses by using vehicle-track coupling dynamics theory.

By comparing several types of transition curves, we can see that the HS curve is superior to the other two. Due to a lack of construction and maintenance experience about the HS and SI curves, most countries still choose the CP as railway transition curves if a long enough long transition curve can be ensured. In order to improve passengers' comfort, we suggest that the HS curve should be used when the length of the transition curve is constrained by the surroundings, especially at both ends of the station area where there are changes in vehicle acceleration.

ACKNOWLEDGEMENT

The Project Supported by National Natural Science Foundation of China (No.50878134) and Natural Science Foundation of Hebei Education Department (No. 2006142).

REFERENCES

Baykal, O. (1996). "Concept of LCA." *Journal of Surveying Engineering*, 3, 132-141.

Lipicnik, M. (1998). "New Form of Road/Railway Transition Curve." *Journal of Transportation Engineering*, 11/12, 546-556.

Liu, X. and Liu, Z. J. (2004). "Rail/Wheel Dynamics Simulation for the Transition Curve of the High Speed Test Section of the Qinshen Passenger Railway Line." *Journal of the China Railway Society*, 1, 82-87.

Tari, E. and Baykal O. (1998). "An Alternative Curve in the Use of High Speed Transportation Systems." *Canadian Journal of Civil Engineering*, 5, 913-923.

Tari, E. and Baykal, O. (2005). "A New Transition Curve with Enhanced Properties." *Canadian Journal of Civil Engineering*, 5, 913-923.

Wang, X. W. (2001). "Study on Choice of Transition Curve for Quasi-High Speed and High Speed Railway." *Journal of the China Railway Society*, 2, 81-85.

Zhou, X. Z. (1996). "A Discussion on China's Transition Curve on High Speed Railway." *Journal of Southwest Jiaotong University*, 1, 69-74.

Zhu, W. S. (1997). "The Main Features and the Differences between Transition Curves of 4-3-4 Shape and 3 Power Improved Shape." *China Railway Science*, 2, 36-45.

Research on Dynamic Measuring System and Model of Novel High Speed Railway Vehicle Bogie

X. Wang [1], J. Su [1], Y. Liu [1], D. Zhou [2]

[1]Railway Vehicle Bogie Testing Laboratory, College of Transportation, Jilin University, P.O. Code 130025,Changchun, People Street 5988; PH 15948068596; FAX (0431) 85095506; email:maklcewxy@163.com
[2]Changchun Railway Vehicles CO., LTD., P.O. Code 130062, Lvyuan, Qingyin Road 435; PH (0431) 85095506; FAX (0431) 85095506; email:sujianjd@163.com

ABSTRACT

In view of the actual disability and inaccuracy of evaluating railway vehicle bogie stiffness parameters, a more reasonable design scheme about novel bogie dynamic testing system is discussed. The system can satisfy dynamic testing and static testing of stiffness parameters about the whole vehicle bogie and the unattached bogie. Some testing models are given based on the technical features of the system. Testing models such as the H-type bogie of the CRH3 high-speed multiple unit, were investigated. In addition, an optimized neural network PID controller was researched. Results show that the manufacture of a novel bogie dynamic testing system can measure bogie stiffness parameters accurately. The foundation for the application and popularization of a novel bogie parameter testing system has been established.

INTRODUCTION

In order to improve the technical content about high-speed trains and heavy-haul trains, railway manufacturers need to research multifunctional parameter test equipment urgently. The bogie, which is the unique running mechanism of railway vehicles, is the structural parameter and the important factor that affects running security, stabilization, and high effectiveness, etc. Therefore, the need to conduct research for a multifunctional parameter test system of bogie is significant (P.R.China Ministry of Railways, 2003; Broom, M. L., 1990). Although there are massive correlation studies of bogies abroad and in China, as well as the fact that some test equipment has been developed, it is difficult to test the whole vehicle bogie and meet requirements of primary spring and secondary spring for vertical stiffness, transverse stiffness, longitudinal stiffness, and rotary stiffness (Eikhoff, B. M., 1995). Hence, the successful development of a dynamic testing system of bogie is significant for the quality control, product development, and for shortening the development cycle, etc.

THE SYSTEM COMPOSITION

Composition of a bogie dynamic test system such as is shown in Figure 1, the anti-thrust gantry system can be used to test vertical stiffness of a bogie dynamically. It includes two vertical cylinders and two position adjusting motors. The two vertical cylinders can load in both synchronous and asynchronous manners and have the following parameters: the maximum loads are 200KN, the loading waveform uses a sine wave, the maximum amplitude is ±6mm, the maximum dynamic loading frequency is 5Hz, and the two motors can be used to adjust the position of two vertical cylinders in the X-direction for different types of bogies. The anti-thrust

gantry system, which includes the bogie anti-thrust location screw and the vehicle body anti-thrust location screw, can be used in the process of testing.

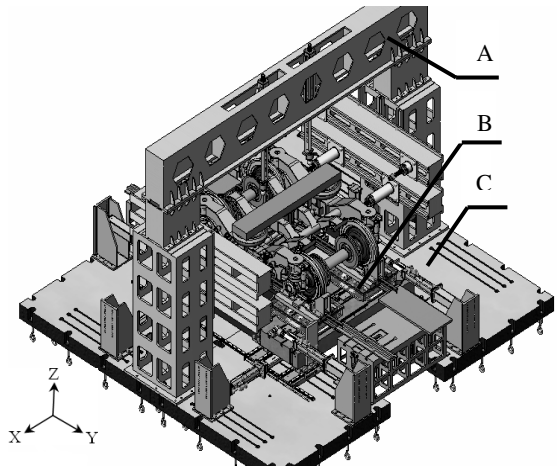

Figure 1. Novel bogie stiffness test system (A. Anti-thrust gantry system B. Cross slipway force system C. Foundation Platform).

It is worthwhile to note that while testing, the whole vehicle needs to remove the anti-thrust gantry system except for the vehicle body anti-thrust location screw. The cross slipway force application system can be used to test vertical stiffness, transverse stiffness, longitudinal stiffness, flexural stiffness, rotary stiffness, shear stiffness, and wrap stiffness, etc. Besides that, it includes a wheel-set clamp device and a guidance orbit device for the positioning function. The hydraulic system uses an optimized neural network PID controller (force-closed feedback control) to control servovalves. The industrial computer can be used to collect, treat and analyze signals of sensors which include force, displacement and angle to complete the testing, recording, and displaying of the parameters and the curve to be measured.

Considering that every single wheel will bear a different force in a different direction, there are four 3-D force sensors under each respective wheel. All hydraulic cylinders use ball-ends and hinges to ensure freedom of cross slipway.

PARAMETERS TEST MODEL

The test of bogie stiffness includes collecting collect force, moment, linear displacement and angular displacement mainly, fix frame in the testing process, meanwhile, load to wheelset slowly and periodically, neglect all inertial mass (Ji, Q. 2005). The system can simulate the forced state of a bogie and draw a curve in the process when the system working. The method and model of testing in this full-text are based on the simplified bogie model that was proposed by Wickens (a British railway expert in the 1960s) (Wickens, A. H. 1965). Using the test models in this paper, we take the H-type bogie of CRH3 multiple unit as an example. Due to the restriction on the length of this paper, the author analyzed some models and methods partially. Other testing models and testing methods are homologous, according to

the parameters of bogie stiffness. It is worth pointing out that the frame must be fixed in the testing process.

DYNAMIC TEST MODEL OF BOGIE VERTICAL STIFFNESS

Locate frame via the four bogie anti-thrust location screws. Next, locate wheel-sets via the four wheel-set location and clamp devices, where the four wheel-set location and clamp devices have been installed on the cross slipway. In addition, a force sensor has been installed at the front-end of every single hydraulic cylinder to constitute a force-closed feedback control. To avoid measurement error caused by the lateral force of a bar in the cylinder, every single force sensor is connected with the supporting body by means of a . The dynamic model can be expressed using the following equations:

$$\begin{cases} m_1\ddot{Z}_{1i} + C_{Z_{1i}}\dot{Z}_{1i} + K_{Z1i}Z_{1i} = F_{Z1i}I(t), (i = 1,2,3,4) \\ m_2\ddot{Z}_{2j} + C_{Z_{2j}}\dot{Z}_{2j} + K_{Z2j}Z_{2j} = F_{Z2j}I(t), (j = 1,2) \end{cases} \quad (1)$$

Equation (1): Z_{1i} -dynamic displacement between frame and axle boxes; Z_{2j} - dynamic displacement between frame and bolster; $C_{Z_{1i}}, C_{Z_{2j}}$ -suspension damping coefficient of primary and secondary; t -time variable (forced); m_1, m_2 -weight on spring; $F_{Z1i}I(t)$ -vertical measured value of 3-D force sensor; $F_{Z2j}I(t)$ -force of two vertical cylinders; $I(t)$ -unit step function.Using $I(t)$ can test vertical stiffness dynamic and instantaneous, let $\delta_{1i} = [Z_{1i}(\infty) - Z_{1i}(0)]$, let $\delta_{2j} = [Z_{2j}(\infty) - Z_{2j}(0)]$; $Z_{1i}(\infty), Z_{2j}(\infty)$ - steady state terminal value of the dynamic displacement in primary and secondary; $Z_{1i}(0), Z_{2j}(0)$ -steady state initial value of the dynamic displacement in primary and secondary.

PRIMARY VERTICAL STIFFNESS OF BOGIE

The force of the vertical hydraulic system needs to transfer downward, which passes through a secondary suspension (air spring), a primary suspension, a vertical hydraulic shock absorber, an axle box, a wheel flange, and a tread, etc. In case the force of the four wheels is unequal, the testing process needs to realize nearby wheels. Measurements are made of the displacement by using the grating displacement transducers of the magnetic base mode, the contact of four grating displacement transducers are rebound, one end is absorbed to the frame, the other end is supported on the axle box. The primary stiffness values are calculated by means of measured values of the four grating displacement transducers and the four 3-D force sensors in the vertical direction, such as is shown in Figure 2. The calculation formula is as follows:

$$K_{Z1i} = F_{Z1i}I(t) / \delta_{1i}, (i = 1,2,3,4) \quad (2)$$

where K_{Z1i} is the primary vertical stiffness of the bogie, and i is one of the four wheels.

SECONDARY VERTICAL STIFFNESS OF BOGIE

The testing process of the secondary vertical stiffness needs to use the nearby bolster and the displacement sensor as in the previous section 2.1.1. However, the

connect type is different. The one end is absorbed to the frame and the other end is supported on the bolster. The secondary stiffness values are calculated by means of a measured value of the four grating displacement transducers and the two force sensors that are installed at the front-end of the vertical hydraulic cylinder, such as is shown in Figure 3. The calculation formula is as follows:

$$K_{Z2j} = F_{Z2j} I(t) / \delta_{2j}, (j = 1, 2) \quad (3)$$

where K_{Z1i} is the secondary vertical stiffness of bogie, and j is one of the two air springs.

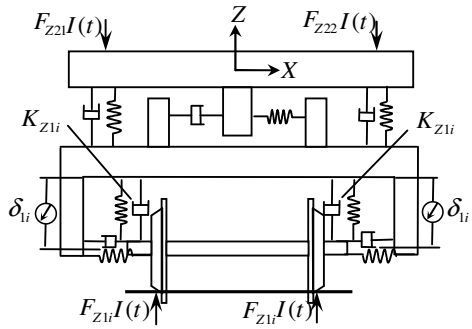

Figure 2. Test of primary vertical stiffness.

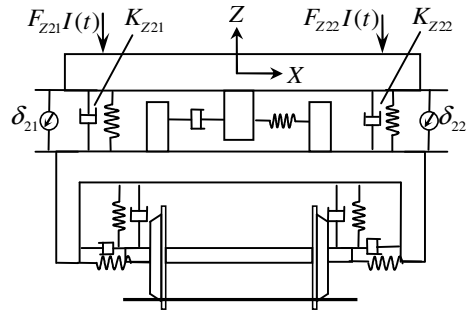

Figure 3. Test of secondary vertical stiffness.

STATIC TEST MODEL OF BOGIE IN XOY PLANE

The stiffness parameters in the XOY plane include primary transverse stiffness, primary longitudinal stiffness, and primary rotary stiffness, etc. These parameters can be measured on a dual cross slipway based on the design features, so it is necessary to conduct movement analyses.

MOVEMENT TENDENCY ANALYSIS OF DUAL CROSS SLIPWAY

The cross slipway force system includes six hydraulic cylinders and the dual cross slipway can move in different directions, as shown in Figure 4. This can test transverse stiffness, longitudinal stiffness, rotary stiffness, shear stiffness, and wrap stiffness, etc. The author has introduced test methods and test models of transverse stiffness and rotary stiffness in this paper.

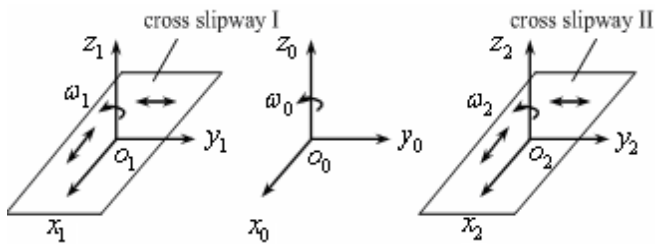

Figure 4. Movement tendency of dual cross slipway.

PRIMARY TRANSVERSE STIFFNESS OF BOGIE

With the two transverse hydraulic cylinders loading synchronously, the 3-D sensors measure the transverse force of the wheel-sets. The four displacement sensors measure the transverse displacement of the wheel-sets that are relative to the

frame. The sensor is the same as that discussed in section 2.1.1, whose one end is absorbed to the frame. The other end is supported on the axle box. The primary transverse stiffness is measured by the four displacement sensors and the 3-D force sensors, such as is shown in Figure 5. The calculation of the formula is as follows:

$$K_{Yi} = F_{Yi} / Y_i , \quad (i = 1,2,3,4) \qquad (4)$$

where K_{Yi} is the primary transverse stiffness of the bogie, F_{Yi} is the transverse measured value of every single 3-D force sensor; and Y_i is the transverse measured value of every single displacement sensor.

ROTARY STIFFNESS OF BOGIE

With the four longitudinal hydraulic cylinders loading respectively, the 3-D sensors measure the transverse force and the longitudinal force of the wheel-set. The angle sensors measure the angle of the wheel-set that is relative to the foundation platform. The rotary stiffness is the measured value of the angle and the 3-D force sensors, such as is shown in Figure 6. The calculation of the formula is as follows:

$$K_\tau = (*F \times L) / \varepsilon \qquad (5)$$

Where $*F$ is the resultant force of the four longitudinal hydraulic cylinders; L is the distance between the two longitudinal hydraulic cylinders; ε is the rotation angle of the cross slipway; M , M' is the torque reaction of the wheel-set; and, ψ is the angle of the frame ($\psi = 0$).

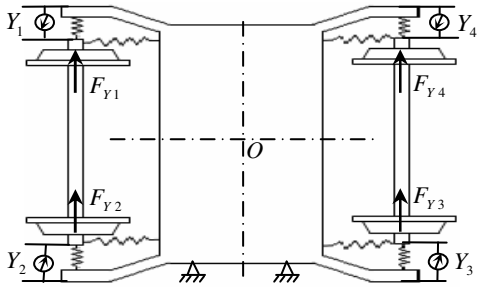

Figure 5. Primary transverse stiffness test.

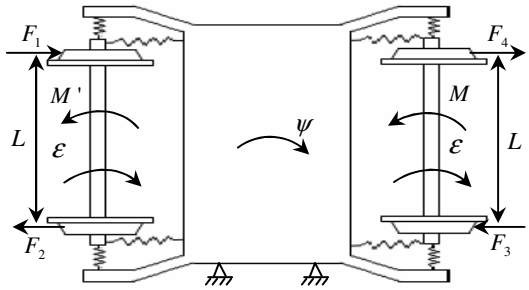

Figure 6. Rotary stiffness test.

OPTIMAL CONTROL MODEL OF NEURAL NETWORK-PID

The accuracy of the testing results about bogie stiffness except the test models and test method mentioned in previous paper, the control accuracy of electro-hydraulic servo system is essential too. In order to reduce the error that is caused by step mutation and external disturbance effectively, an optimized neural network PID controller should be used in the electro-hydraulic servo system; the controller should include a PID controller, a NNI (neural network identification), and a NNC (neural network controller), such as is shown in Figure 7. Firstly, the NNI identifies the 'servo mechanism,' while the accuracy of the identification is up to the requirement, it will transfer the weight to the NNC, and then finds the control parameters which can meet the control requirement via the optimization algorithm and transmit these parameters to the controller. After that, the system by means of the controller which controls the 'servo mechanism', the NNI transmits the optimal estimation of the 'servo mechanism' to the NNC and itself, which is used to regulate

the weight. Via the tonsure algorithm of the neural network, the K_P, K_I, K_D is controlled to reach the optimal performance index.

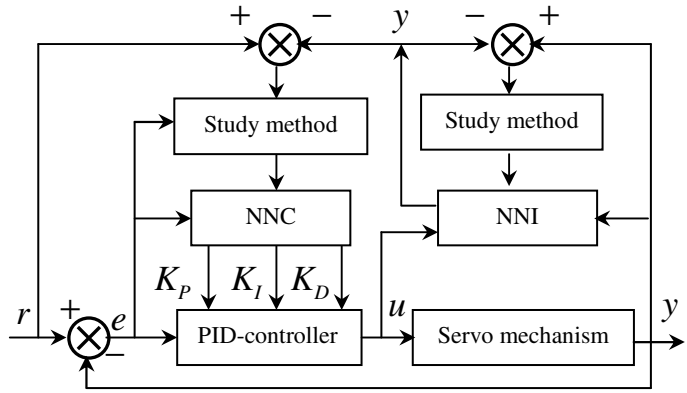

Figure7. NN-PID controller frame.

EXPERIMENTAL VERIFICATION

Because the bogie stiffness is unknown and nonlinear, the author made a pertinent simulation verification based on the models and methods of the previous paper. Due to the restriction on the length of this paper, the author introduced the main control parameters and control results. Figure 8 shows the dynamic simulation results of the system about the sine wave tracking. Among them $K_p = 20.75$, $K_i = 12.68$, $K_d = 0.26$, $\alpha = 0.6$, where α is the inertia coefficient $(0 < \alpha < 1)$), and $\eta = 0.65$ (η is the learning efficiency), $-1 < f(*) < 1$, $-1 < g(*) < 1$. Other training parameter settings are based on control requirements. Figure 9 is the corrected static simulation result. Among them $K_p = 500, K_i = 0, K_d = 0.21$. It is easy to see that the optimized neural network PID controller possesses accurate control precision by comparing Figure 8 and Figure 9. The system can meet the dynamic testing requirement and static testing about bogie stiffness.

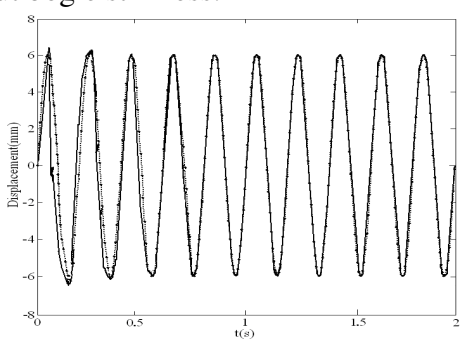

Figure 8. The control result of sine wave tracking.

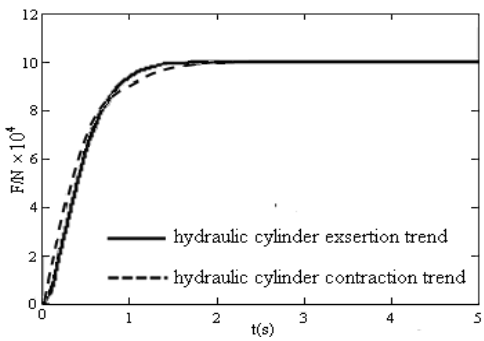

Figure 9. The response curve of time domain characteristics.

CONCLUSION

The novel dynamic testing system of bogies takes the actual situation of railroad cars as the research object, and via reasonable design about structure can test

the main kinetic parameters of bogies objectively and accurately. The system can also actualize testing of stiffness parameters about the whole vehicle bogie and the unattached bogie. We have achieved the goal of multiple test items at one test bench. Detailed research has been introduced about test model, the test method, and the control model in this paper. The successful development of a dynamic testing system about bogies has very wide application prospects, which is significant for accelerating the update of railway vehicles.

REFERENCES

P.R. China. Ministry of railways.TB/T740-2003. (2003). "Technical Condition for Bogie of Diesel Locomotive." *P.R. China Standard Press,* Beijing.

Broom, M. L., and Smart, G. W. (1990). "The Design, Manufacture and Assembly of the Wheel set for the British Rail Class91, 25kV, 225km/h Locomotive." *Journal of Rail & Rapid Transit*, 26(2):13-19.

Eikhoff, B.M., and Evans, J. R. (1995). "A Review of Modeling Methods for Railway Vehicle Suspension Components." *Vehicle System Dynamist*, 24 (3):469-496.

Ji, Q. (2005). "Research on Performance Parameter Test Rig of Freight Car." *Southwest Jiao Tong University*, Chengdu.

Wickens, A. H. (1965). "The Dynamic Stability of Railway Vehicle Wheel-set & Bogies Having Profiled Wheels." *Inst. J. Solids Structure*, 1965(1):318-339.

Empirical Research on Urban Rail Transit Operation Performance Based on FCE~~A~~HP

Xinlong Jiao[1,2]

[1]School of Traffic and Logistics, Ningbo University of Technology, P.R.China, 315211; PH (0) 13705741519;email: jxlfly001@yahoo.com.cn
[2]School of Economics and Management, Chang'an University, P.R.China, 710064; PH (0) 13805898019; email: jxlchina001@163.com

ABSTRACT

Increasingly, urban rail transit has become the focus of Social Economic Development. This is encouraging comprehensive evaluations of urban rail transit which will enhance operation efficiency. This paper sets up an analysis model of an urban rail transit arrangement based on the application of the Delphi and Analytical Hierarchy Process (AHP) and analyzes the shortcomings of AHP. Furthermore, this paper proposes a design of a more comprehensive and more scientific evaluation index system of urban rail transit performance assessment. The proposed system calculates every index weight using the weighting method -- G_1 – which is based on the differential principle. It appraises comprehensive performance using a fuzzy comprehensive evaluation method. Verification of the proposed system was done by conducting an experiment using the Shanghai rail transit systems to measure its performance status. Results provide the theoretical foundation for the development and correction of the Shanghai urban rail transit system

INTRODUCTION

The development of urban modernization has created a need to improve the situation of urban transit congestion, and the fast collection and distribution of passenger flow. Urban rail transit saves parking expenses, reduces traffic accidents, increases car-free mobility, improves people's living standards, and promotes economic development. Urban rail transit plays a very important role (Litman 2004, 2003).

Zadeh, L. A. established a fuzzy mathematical method in the 1960s. Fuzzy synthesis assessment is based on fuzzy mathematics and is a method which fixes the quantities of some factors within a fuzzy margin (Pengfei 2007). At present, research about fuzzy mathematical methods is being done around the world; Xiang, H. of Chongqing Jiaotong University proposed a fuzzy mathematical method and applied it to the assessment of traffic flow forecasting. Li, C., of Nanjing University of Aeronautics and Astronautics proposed a fuzzy mathematical model and applied it to evaluating the synthesis of the competitive capacity of enterprises. Jiang, F., of Hehai University researched the performance evaluation of supply chain management using a fuzzy synthetic evaluation. A proposed method was applied to the risk assessment of

transporting hazardous chemical materials by Guo, P., of Nanjing University of Technology. However, assessing urban rail transit performance based on FCE-AHP has not been studied so far. This reasonable and scientific evaluation method combines quantitative description and qualitative analysis to evaluate the performance of an urban rail transit system. Based on fuzzy evaluation theory, a comprehensive evaluation method for evaluating urban rail transit performance is proposed in this paper, which combines objectivity and subjectivity, static and dynamic analyses, and uses quantitative analysis as the main one.

ESTABLISHMENT OF FCE—AHP MATHEMATICAL MODEL

Shortcomings of Analytic Hierarchy Process. The Analytic Hierarchy Process (AHP) (Wu 2002) is a qualitative and quantitative method of system analysis that was developed by T. L. Saaty, a famous American operations research specialist in the 1970s. By using five steps such as confirm the problem, establish the structural model, build a judgment matrix, create a hierarchy for single ranking and general ranking, AHP calculates the combined weight of interactive influencing factors on the general goal. It draws a comprehensive evaluation value based on different feasible schemes. And, it provides the theoretical foundation for an optimal plan. Establishment of the judgment matrix is the key of the AHP. Whether the judgment matrix is reasonable or not can influence the results of the AHP. Much recent research suggests that there are some shortcomings in AHP (Zhang 2000). It is difficult to check the consistency of the judgment matrix. It is necessary to get the biggest characteristic root $_{max}$ for a consistent test, and observing whether $_{max}$ is equal to n. If $_{max}$=n, it is consistent. When the order is larger, the workload of calculating $_{max}$ is great. When it is not consistent, it is necessary to adjust the elements of the judgment matrix to make it consistent. Only after multiple adjustments and tests is consistency achieved. If is often impossible to achieve this and apply the method in practice. The concept of a fuzzy matrix can solve these problems.

Establishment of FCE—AHP Mathematical Model and Factor Set. It is necessary to introduce the definition and character of the fuzzy matrix for the best analysis. In the analytic hierarchy process, comparing judgments between two factors about which is more relevant offers the following quantitative expression, that is:

Definition: if matrix $A=(a_{ij})n\times n$ can satisfy $0\leqslant a_{ij}\leqslant 1$, ($i$=1,2,…,n; j=1,2,…,n), then call A fuzzy matrix (Xu 1988).

According to the investigation result of urban rail transit, this paper initially constructs the comprehensive evaluation system of urban rail transit operation performance using the Delphi method and the AHP method. Through 2-4 consultations, which are based on optimization theory, an evaluation index set is defined according to the 7±2 psychological extreme limit concept (Cai 2004). Using the function and characteristics of rail transit, this paper eventually constructs an evaluation index system of rail transit performance in accordance with three main factors (rail network structure, operation management level, and

passenger service performance), and corresponding twenty one sub-factors such as the total length of the rail network, the daily total of passengers, operation cost, passenger ticket price etc. (Xi 2008; Ji 2004; Du 2003). (See Figure 1.)

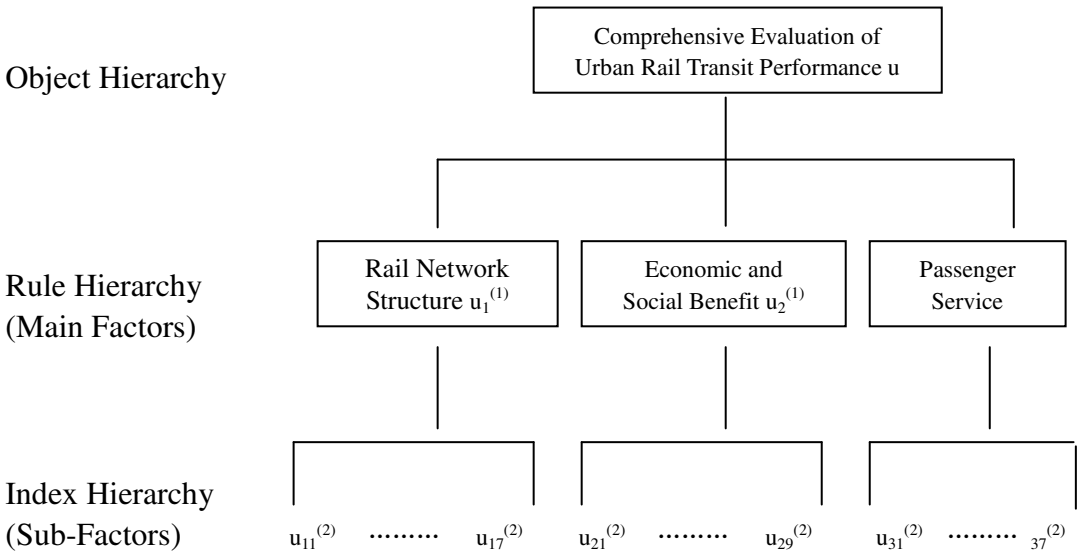

Figure 1. Comprehensive Evaluation Index System of Urban Rail Transit Performance.

The rail network structure $u_1^{(1)}$ (weight, $_1$=0.3125): mainly includes the total length of the rail network $u_{11}^{(2)}$ (ω_{11}=0.1736), the density of the center area rail network $u_{12}^{(2)}$ (ω_{12}=0.1364), a non-linear coefficient $u_{13}^{(2)}$ (ω_{13}=0.0968), transfer joint numbers $u_{14}^{(2)}$ (ω_{14}=0.2211), the rate of covering the center region areas $u_{15}^{(2)}$ (ω_{15}=0.1035), the cohesion number of large passenger flow distributed points $u_{16}^{(2)}$ (ω_{16}=0.0829), and the daily total of passengers $u_{17}^{(2)}$ (ω_{17}=0.1967).

The economic and social benefit $u_2^{(1)}$ (weight, $_2$=0.4613): mainly includes the investment cost $u_{21}^{(2)}$ (ω_{21}=0.0981), operation costs $u_{22}^{(2)}$ (ω_{22}=0.1034), operational revenue $u_{23}^{(2)}$ (ω_{23}=0.0897), the influence on economic development $u_{24}^{(2)}$ (ω_{24}=0.1327), the increase in residents' quality of life $u_{25}^{(2)}$ (ω_{25}=0.1068), resource consumption $u_{26}^{(2)}$ (ω_{26}=0.1201), the environmental capacity $u_{27}^{(2)}$ (ω_{27}=0.1132), the requirement rate of travel-time $u_{28}^{(2)}$ (ω_{28}=0.1097), and the prourban rail transition of transit trip $u_{29}^{(2)}$ (ω_{29}=0.1263).

The passenger service performance $u_3^{(1)}$(weight, $_3$=0.2262): mainly includes the running speed(ω_{31}=0.1727), service frequency $u_{32}^{(2)}$ (ω_{32}=0.1196), the punctuality rate $u_{33}^{(2)}$ (ω_{33}=0.0825), circumstances inside the vehicle and comfort $u_{34}^{(2)}$ (ω_{34}=0.1637), service attitude $u_{35}^{(2)}$ (ω_{35}=0.1290), passenger ticket price $u_{36}^{(2)}$ (ω_{36}=0.1892), and the price of the completed facility $u_{37}^{(2)}$ (ω_{37}=0.1433).

ESTABLISHMENT OF THE WEIGHT SET AND THE EVALUATION SET (THE REMARK SET)

The Determination Method of Weight. The value of the index weight is determined by a statistical analysis method and by an expert evaluation method

(Ahamed, T., 2000). The author determines the weight using a subjective weighting method based on the differential principle—G_1. The specialists on urban rail transit evaluate the rule hierarchy (i.e., the main factors) and index the hierarchy (the sub-factors) for standardization.

Establishment of the Weight Set. The weight of every sub-factor $_{ij}$ (i=1,2,⋯,m; j=1,2,⋯ ,n) is defined by membership degree of the sub-factors to the main factors, then weight sets of sub-factors $_i$={ $_{i1}$, $_{i2}$,⋯; $_{in}$}, among them, $_{ij}\geqslant 0$

and $\sum_{j=1}^{n}$ $_{ij}$ = 1 (Zou, K., 1990).

According to the degree of influence of the main factors to the urban rail transit performance of the object hierarchy $u_i^{(1)}$ (i=1,2,⋯ ,n) , all of the main factors are calculated by adding the proper weights $_i$ (i=1,2,⋯ ,n). We get the weighted set of main factors = ($_1$, $_2$, $_3$).

Define the Remark Set. The remark set V=(v_1 ,v_2 ,⋯,v_m), v_t(t=1,2,⋯,m) shows remarks from high to low at all levels. This paper adopts the 5-grade scoring system. For example, when m=5, that is V=very good; good; general; poor; poorest (Wangqing, W., 2007).

Define Ratings and Scale Score of Factors. According to the actual situation, this paper determines ratings, remarks, and scale scores of factors. In this paper we use 5-point scales, H=excellent; good; middling; general; no. The corresponding scale scores are 0.9; 0.8; 0.6; 0.4; 0 (Yan, B. 2007).

FUZZY COMPREHENSIVE EVALUATION OF URBAN RAIL TRANSIT PERFORMANCE

A fuzzy comprehensive evaluation (FCE) is a multi-layer comprehensive evaluation starting at the bottom and proceeding layer by layer, resulting in an objective hierarchy. An evaluation index of the k-th layer is the membership degree of the k-1 layer. In this paper the second-level comprehensive evaluation is completed from sub-factor to multi-layer and the like may be deduced by analogy.

If $\tilde{R}_1$, $\tilde{R}_2$, and $\tilde{R}_3$ are single factor evaluation matrixes of $u_1^{(1)}$, $u_2^{(1)}$, $u_3^{(1)}$ respectively, single factor assessment results are obtained by the following fuzzy transformation.

$$\tilde{B}=\omega.\tilde{R}=\tilde{A}_1\circ\begin{pmatrix}\omega_1.\tilde{R}_1\\ \omega_2.\tilde{R}_2\\ \omega_3.\tilde{R}_3\end{pmatrix}$$

Mathematic Model of Urban Rail Transit Performance Evaluation. Comprehensive evaluation $\tilde{B}$ is a fuzzy set from the remark set, that is, $\tilde{B}=\omega\circ\tilde{R}$.

"∘" is called the operator, such as the main factor determination model $(\wedge, \vee)$,the main factor outstanding model $(\cdot, \vee)$, the weighted mean model $(\cdot, \oplus)$ etc. (Liu 2000). These are necessary for an assessment of urban rail transit although each factors' effect on the system and its weight values are different. When the operator is adopted in the compound operation of fuzzy matrixes, the operation itself must consider the weight contributions of all of the factors, including influence on the urban rail transit system, and the weighted mean model is adopted. Models of a comprehensive evaluation are as follows:

The first level evaluation model: $\tilde{B}_i = \bar{\omega}_i . \tilde{R}_i$

The second level evaluation model: $\tilde{B} = \bar{\omega} . \tilde{B}_i$

Fuzzy Evaluation Example Analysis. The first level comprehensive evaluation. Currently, there are 5 urban rail transit lines operating in Shanghai, which have 94 stations and covers 144.6km. The average passenger volume is 180,000 person-time/day, and the maximum is 243,000 person-time/day. The Shanghai traffic mileage and average passenger volume is the largest rail system in China. The fuzzy comprehensive evaluation method is used to do a qualitative analysis of the performance evaluation of Shanghai's urban rail transit system.

The result of the first level comprehensive evaluation: $u_{11}=0.318\times 0.9+0.613\times 0.8+0.069\times 0.6+0\times 0.4=0.8180$, is good. Similarly obtain other u_{ij} and evaluations.

The final evaluation space divided $(u_i^{(1)}, V, \tilde{R}_i)$ has been evaluated. $\tilde{R}_i$ is a single evaluation matrix of sub-factor sets $u_i^{(1)}$.

$\tilde{B}_1 = \bar{\omega}_1 . \tilde{R}_1 = (0.1736 \quad 0.1364 \quad 0.0968 \quad 0.2211 \quad 0.1035 \quad 0.0829 \quad 0.1967)$.

$$\begin{pmatrix} 0.318 & 0.613 & 0.069 & 0 \\ 0.354 & 0.459 & 0.178 & 0.077 \\ 0.363 & 0.496 & 0.085 & 0.056 \\ 0.449 & 0.370 & 0.094 & 0.087 \\ 0.264 & 0.493 & 0.168 & 0.075 \\ 0.277 & 0.333 & 0.306 & 0.084 \end{pmatrix}$$

$$\begin{matrix} 1 & 0 & 0 & 0 \end{matrix}$$

$= (0.485 \quad 0.377 \quad 0.108 \quad 0.050)$

$u_1=0.485\times 0.9+0.377\times 0.8+0.108\times 0.6+0.050\times 0.4=0.8229$

We believe that the rail network structure evaluation $u_1=0.8229$ is good. Similarly, other factors influencing urban rail transit $\tilde{B}_i$ and u_i are obtained, $\tilde{B}_2 = (0.436 \quad 0.257 \quad 0.273 \quad 0.040)$, $\tilde{B}_3 = (0.279 \quad 0.357 \quad 0.321 \quad 0.043)$; the economic and social benefit $u_2=0.436\times 0.9+0.257\times 0.8+0.273\times 0.6+0.040\times 0.4=0.7778$ is middling; and passenger service performance evaluation $u_3=0.279\times 0.9+0.357\times 0.8+0.321\times 0.6+0.043\times 0.4=0.7465$ is middling.

The second level fuzzy comprehensive evaluation. The second grade comprehensive evaluation is an analysis of the sub-factors. The single factor evaluation matrix is constructed from the result of the first level comprehensive evaluation $\tilde{B}_i$.

$$\tilde{B} = \bar{\omega} \cdot \tilde{B}_i = (0.3125 \quad 0.4613 \quad 0.2262) \cdot \begin{bmatrix} 0.485 & 0.377 & 0.108 & 0.050 \\ 0.436 & 0.257 & 0.273 & 0.040 \\ 0.279 & 0.357 & 0.321 & 0.043 \end{bmatrix}$$

$$= (0.4158 \quad 0.3171 \quad 0.2323 \quad 0.0438)$$

$u = 0.4158 \times 0.9 + 0.3171 \times 0.8 + 0.2323 \times 0.6 + 0.0438 \times 0.4 = 0.7795$. The result of the evaluation is middling.

The results of the first level comprehensive evaluation shows that transfer joint numbers $u_{14}=0.6891$ and the requirement rate of travel-time $u_{28}=0.6953$ are the lowest, while their combined weight numbers of the index are correspondingly higher. Because of limited regional land resources in Shanghai, traffic capacity has always been a bottleneck problem in the city. This question warrants careful consideration. The total length of the rail network $u_{11}=0.9$, and the increase in residents' quality of life $u_{25}=0.9$ are the highest numbers. The results show that the total length of the rail network of the Shanghai urban rail transit system is at the national forefront, residents' quality of life has risen significantly in recent years. We can see that the evaluation results coincide with the actual situation of Shanghai.

The general comprehensive evaluation results show that the rail network structure is $u_1=0.8229$ and the evaluation is good; the economic and social benefit is $u_2=0.7778$ and the evaluation is middling; passenger service performance is $u_3=0.7465$ and the evaluation is middling. The general evaluation result of Shanghai's urban rail transit performance is $u=0.7795$ and the evaluation is middling. This means that Shanghai's urban rail transit system still needs further development and improvements.

CONCLUSIONS

This paper adopts a fuzzy comprehensive evaluation method to evaluate the performance of urban rail transit and convert a qualitative appraisal into quantitative results. Practical applications truly reflect the present situation of urban rail transit in Shanghai. By careful analysis of the evaluation results, the crux of the problems and the weak points of rail transit management can be identified. Some concrete and effective measures for rectifying the above mentioned evaluation results are put forth to solve problems in the development of rail transit promptly and to improve the level of rail transit management.

Based on the evaluation of urban rail transit performance, the main conclusions are as follows: 1) Urban rail transit performance evaluation is a multi-attribute fuzzy comprehensive evaluation. The key to effective evaluations is to establish an evaluation system. This paper establishes an analytic hierarchical

model of rail transit performance using the Delphi and AHP method, and constructs a comprehensive evaluation index system of performance. 2) The method calculates every index weight using the G_l weighting method, which is based on the differential principle. 3) The verification of the method was done by conducting an experimental evaluation of the actual urban rail transit system in Shanghai. A fuzzy comprehensive evaluation was used. Results provide a theoretical foundation for the development and correction of Shanghai's urban rail transit system.

REFERENCES

Ahamed, T. R. N., Rao, K. G., and Murthy, J. S. R. (2000). "Fuzzy class membership approach to soil erosion modeling"[J]. *Agricultural Systems,* 2000,63(2):97-110.

Cai, C. and Jing, G. (2004). "Study on Way of Predicting Coal and Gas Outburst Scale by Fuzzy Synthesis Evaluation." *Journal of Safety and Environment*, 2004,4(2):54-56(in Chinese).

Du, S., Kong, J., and Xiong, L. (2003). "On Evaluation System of Urban Rail Transit Network Planning." *Journal of Wuhan University of Technology* (transportation science & engineering), 2003,27(6):841-844.

Ji, J. and Li, F., (2004). "A Study on the Synthetic Evaluation Index System of Urban Rail Transit Line Network Planning Scheme." *Systems Engineering Theory & Practice*, 2004(3):129—133.

Litman, T. A., (2004). .Rail Transit In America:ComprehensiveEvaluationofBene?tS[J/OL].(2004-07-01) [2008-03—06].http: // www.vtpi.org / railben.pdf.

Litman, T. A., (2003). Evaluating Rail Transit Criticism[J / OL] (2003—11-09) [2008-03-06].http: // WWW.vtvi.org / railcrit.pdf.

Liu, P., and Wu, M., (2000). *Fuzzy Theory and Application*. National University of Defense and Technology Publishing House, 2000:199 (in Chinese).

Pengfei,Y. (2007). Research on Exponential Effective Function for Comprehensive Evaluation. Statistical Research, 2007,(12):30(in Chinese).

Wangqing, Q. (2007). "Matching Degree Calculation of Talents Post Based on AHP-fuzzy Comprehensive Evaluation." *Chinese Journal of Ergonomics.* 2007,(2):19 (in Chinese).

Wu, X., and Chen, X., (2002). Decision-making System for Programming Urban Mass Transit Network. China Railway Science, 2002(5):6-10.

Xiang, B., and Sun, Y., (2008). "An Evaluation Index System of Passenger Service Performance of URT." *Urban Mass Transit*, 2008(9):15-18.

Xu, S. (1988). Principle of Analytic Hierarchy Process [M],Tianjin University Publishing House, 1988. (in Chinese).

Yan, B., (2007). "AHP and Fuzzy Evaluation of the Competitiveness of China's Auto Industrial Clusters." *Journal of Southwest Jiaotong University(Social Sciences)*, 2007,(4):15-16 (in Chinese).

Zhang, J. (2000). Fuzzy Analytical Hierarchy Process. Fuzzy systems and

mathematics, 2000 (2):80—88. (in Chinese).

Zou, K., and Jin, Z., (1990). *Fuzzy Mathematics Method.* Dalian Maritime University Publishing House, 1990 (in Chinese).

The Application of Functionally Gradient Material to Problems of Wheel-Rail Contact

Jun Zhang[1], Liping Sun[1], Shengwu Wang[1] and Xuesong Jin[2]

[1]School of Transportation Engineering, Modern Railway Transportation Research Institute, Dalian Jiaotong University, Dalian 116028 China, PH (86) 411-84106386; FAX (86) 411-84105786; email: zhangjun@djtu.edu.cn, slp@djtu.edu.cn, wangsw@djtu.edu.cn

[2]State Key Laboratory of Traction Power, Southwest Jiaotong University, Chengdu 610031, China, PH (86)28-87634355; FAX (86)28-87600868; email: xsjin@home.swjtu.edu.cn

ABSTRACT

Based on the parametric variational principle (PVP), the wheel/rail relation problem is analyzed in this paper with the help of the elastic-plastic contact model and the FE parametric quadratic programming method. The precise computational models are constructed according to the contact between the wheel tread and the rail top. The influence of functionally gradient material on wheel-rail contact performance is also investigated. Analysis of the results shows that the maximum stress on rails made of functionally gradient material is smaller than those made of homogeneous material when the wheel-rail contact is loaded.

INTRODUCTION

Currently, there is a world trend for developing high speed trains and heavy haulage. The problems of wheel-rail performance are becoming more serious, and include problems such as rail corrugation resulting from wheel-rail wear, rail fatigue strength caused by rolling contact, derailment, and so on. Large economic losses in international railway transport services are produced due to these problems every year. The damage to China's railways is about 8 billion RMB every year.

Functionally gradient materials are new materials developed in the 21st Century and used in many fields, such as spaceflight, aircraft, chemical engineering, bioengineering, and so on (Williamson, 1993; Tanigawa, 1995; Yang, 2003). They are widely used because of their wear-resistant, thermophilic and corrosion-resistant properties (Koizumi, 1993). Applying functionally gradient materials at the contact surface between wheel and rail could decelerate wheel-rail wear. In this paper, wheel-rail contact is calculated under different load cases when wear-resistant gradient material is used. An FE parametric quadratic programming method and the substructure technique that is developed in this paper is used to calculate results.

COMPUTATIONAL THEORY

In this paper, an FE parametric quadratic programming method is used to solve the elastic-plastic contact problem of wheel-rail. This method is based on the PVP which was put forth in 1985 by Professor Zhong Wanxie, who is a member of the Chinese Academy. This method is very efficient at solving undetermined boundary problems in mathematical physics (Zhong, 1997).

The basic equations of elastic-plastic contact mechanical boundary problem in domain $\Omega = \Omega(1) + \Omega(2)$ are:

1. Equilibrium equation

$$A^{(\nabla)} d\sigma + db = 0 \tag{1}$$

2. Strain-displacement relations

$$d\varepsilon = L^{(\nabla)} du \tag{2}$$

3. Boundary conditions

On the force-prescribed boundary S_p

$$n d\sigma = d\bar{p} \tag{3}$$

On the displacement-prescribed boundary S_u

$$du = d\bar{u} \tag{4}$$

The boundary conditions on the possible contact boundary S_c is determined by state equations of the contact system, i.e.,

$$\begin{cases} f(du_c, \tilde{\lambda}) + \tilde{\nu} = 0 \\ \tilde{\nu}^T \tilde{\lambda} = 0, \tilde{\nu}, \tilde{\lambda} \geq 0 \end{cases} \tag{5}$$

4. Constitutive relations

$$\begin{cases} f(d\varepsilon, \lambda) + \nu = 0 \\ \nu^T \lambda = 0, \quad \nu, \lambda \geq 0 \end{cases} \tag{6}$$

The PVP of elastic-plastic contact problems can be described as follows: among the admissible displacement incremental fields, which satisfy the strain-displacement relations (2) and geometrical boundary conditions (4), the exact solution renders the index of the total potential of the elastic-plastic contact system as follows:

$$\begin{aligned} \Pi\left[\lambda(\cdot), \tilde{\lambda}(\cdot)\right] = & \int_\Omega \left[\frac{1}{2} d\varepsilon^T D d\varepsilon - \lambda^T R d\varepsilon - db^T du \right] d\Omega \\ & + \int_{S_c} \left[\frac{1}{2} d\varepsilon_c^T D_c d\varepsilon_c - \tilde{\lambda}^T \tilde{R} d\varepsilon_c \right] dS - \int_{S_p} d\bar{p}^T du dS \end{aligned} \tag{11}$$

Minimum values under control of state equations (5) and (6), where $d\sigma$, db, $d\varepsilon$ and du are stresses, body forces, strains and displacement increments, respectively; $d\bar{p}$ and $d\bar{u}$ are prescribed surface tractions and prescribed displacement increments; λ and $\tilde{\lambda}$ are variables which do not join variation and according to their physical meaning they are flow and slip parameters; $R = \left(\frac{\partial g}{\partial \sigma} \right) D$, $\tilde{R} = \left(\frac{\partial g}{\partial p_c} \right) D_c$.

It can be proved that the PVP may be changed into a quadratic programming problem through derivation. A normal quadratic programming problem is a convex programming problem; it has a mature solution method (e.g., Lemke algorithm), and can ensure a highly efficient computation.

THE COMPUTATIONAL MODEL OF WHEEL-RAIL

The computational model is constructed according to actual sizes of diesel locomotive wheel sets and 60kg/m standard rail. Only half of a wheel set and one side rail are used owing to symmetrical structure and loads. Besides the wheel set and the rail, the model also includes the sleepers and ballast.

The computational mesh of wheel-rail contact system is shown in Figure 1.

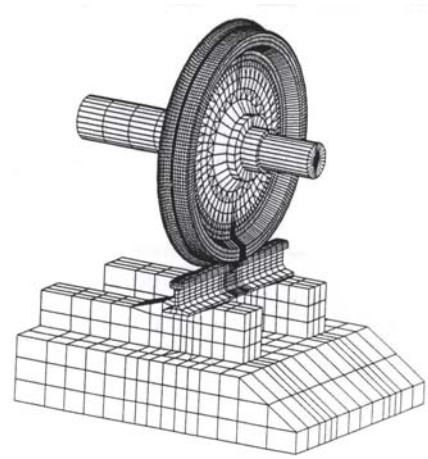

Figure 1. The computational mesh of wheel-rail contact.

In order to investigate the influence that the composition of the material has on the stress distribution of the structure, the mesh must be divided very fine. This reduces the computational efficiency and makes it difficult to analyze the gradient material. To solve this problem, a multi-level and multi-branch substructure method is used for the model and the mesh of the substructures containing the gradient material mesh is very fine.

A hardened layer with a thickness of only a few millimeters on the contact surface is produced, although the heat treatment is performed and wear-resistant material is used on the detail. In order to analyze the influence of the material gradient change on stress distribution in the structure under contact loads, only a thin part including the contact spot is computed. One-point contact between the wheel and the rail is computed and the wheel-rail internal contact force is used as the applied load (Zhang, 2004). The contact forces between the wheel and rail are shown in Figure.2.

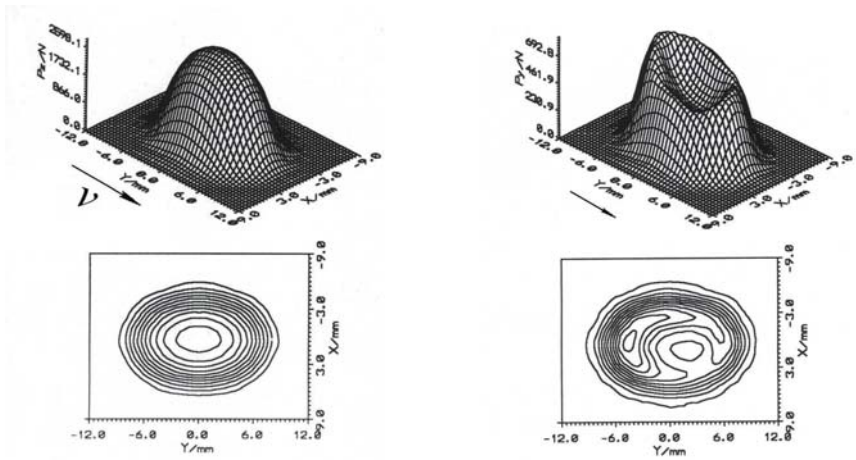

(a) Normal forces (b) Longitudinal friction forces

Figure 2. The computed forces of the wheel-rail contact model.

The functionally gradient material is applied on top of the top of the rail with a layer thickness of 2mm. Furthermore, both the wheel and the rail are made of low carbon steel with an elastic module of 200 -- 400 GPa. The distribution law of elastic module is linear, i.e., 400 GPa on the surface and 200 GPa at a depth of 2mm. In

addition, an isotropic structure is analyzed using the same model and the elastic module is 200 GPa.

THE COMPARISON OF STRESS STATES FOR TWO MATERIALS UNDER SINGLE AXLE LOAD

Computational results state that the stress distribution law under the wheel-rail contact force produced by a single axle load is close to that of Hertz's hypothesis, i.e., the stress distribution is symmetrical along longitudinal and lateral center lines. The maximum von Mises stresses of two materials are all located 2.4 mm from the contact spot center. Their values are 908.48 MPa and 887.24 MPa, respectively. The maximum von Mises stresses for isotropic material at depths of 0.8, 2.4, 4.0, and 5.6 mm from the contact surface are 829.86, 908.48, 884.70, and 792.39 MPa, respectively. Those stresses for gradient material at the same depths are 870.16, 887.24, 834.08, and 668.24 MPa. The stresses of the gradient layer are a little larger than those of the isotropic material and the stresses of the lower gradient layer are smaller than those of the isotropic material.

THE COMPARISON OF STRESS STATES FOR TWO MATERIALS UNDER A COMBINED AXLE LOAD AND DRIVING TORQUE

The maximum von Mises stresses for the isotropic material under the wheel-rail contact force produced by the combined axle load and driving torque at depths of 0.8, 2.4, 4.0, and 5.6mm from the contact surface are 882.47, 943.99, 924.70, and 849.75 MPa respectively. Those stresses for the gradient material at the same depths are 903.40, 921.72, 888.20, and 781.01 MPa, respectively. Results are similar to the case of a single axle load. The stresses of the gradient layer are a little larger than those of the isotropic material and the stresses of the lower gradient layer are smaller than those of the isotropic material.

Since there are larger tangential forces at the contact spot, the wheel-rail stress distribution is complicated. The stress level in the contact layer between the wheel and the rail is increased and the high-stress area is larger than at the single axle load area obviously. The maximum von Mises stresses of the two materials are 943.99 MPa and 921.72 MPa respectively and are located at a depth of 3.2 mm in the rear of the contact spot center. This is the result of a combined effect of the normal force and the longitudinal tangential force at the contact spot.

The stress curves of the above-mentioned four models at different depths under the center of the contact spot are shown in Figure 3. The stress curves of the four models in the longitudinal direction at a 3 mm depth under the contact spot are shown in Figure 4. It can be seen that the distribution level of stress changes at a 3 mm depth when the wheel passes the rail.

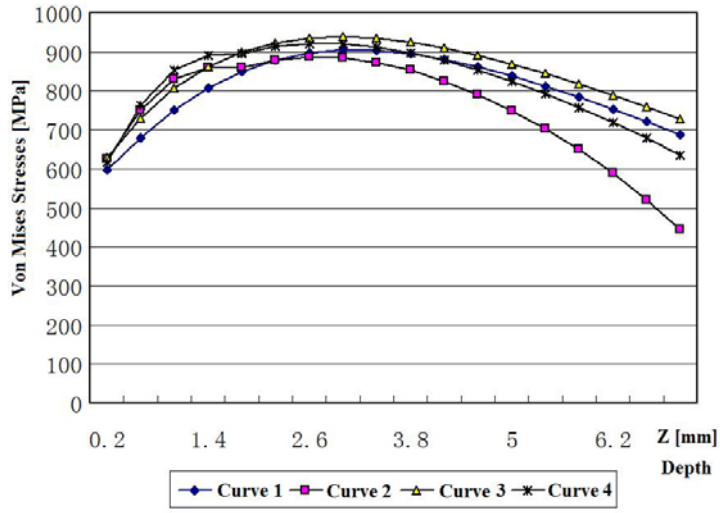

Curve1: for isotropic material under single axle load
Curve2: for gradient material under single axle load
Curve3: for isotropic material under the combined axle load and driving torque
Curve4: for gradient material under the combined axle load and driving torque

Figure 3. The comparison of stress distribution along the depth under the contact spot center.

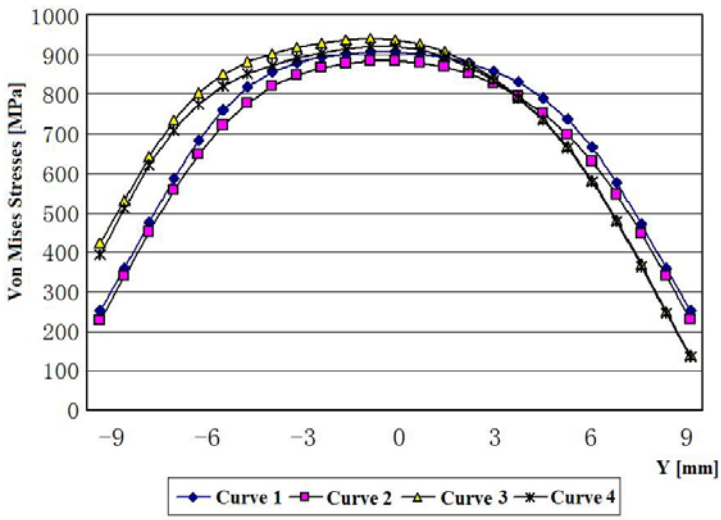

Curve1: for isotropic material under single axle load
Curve2: for gradient material under single axle load
Curve3: for isotropic material under the combined axle load and driving torque
Curve4: for gradient material under the combined axle load and driving torque

Figure 4. The stress curves of different models in longitudinal direction at a 3 mm depth under the contact spot.

Figures 3 and 4 show that the stresses at the center of contact spot under the combined axle load and driving torque are larger than those under the single axle load

at every depth. The stresses of the gradient layer are larger than those of the isotropic material, and the stresses out of the gradient layer in the gradient material are smaller than those at the same location in the isotropic material. But the total stresses in the gradient material are smaller than those in the isotropic material and thus the gradient material can decrease the maximum stresses at the wheel-rail contact surface.

CONCLUSION

The problem of the wheel-rail relation is an elastic-plastic frictional contact problem. The computations performed in this paper show that using an FE parametric quadratic programming method and derived from the parametric variational principle can solve various complicated wheel-rail contact problems successfully.

The shape of the contact spot and the distribution of the adhesion and creep regions can be precisely determined by using the FE parametric quadratic programming method. Under a single axle load, the contact spot is an oval, which entirely coincides with Hertz's hypothesis. Under the combined conditions of axle load and driving torque, the contact spot is also an oval.

The maximum stress on the rail of gradient material will be smaller than that of isotropic material under wheel-rail contact load, i.e., in the case of equal stresses, the carrying capacity of gradient material rail is high and gradient material rail can bear the heavy load.

ACKNOWLEDGEMENTS

This work was supported by the Natural Science Foundation Committee of China that grants the research project (50605003, 50875218). It is also supported by Liaoning BaiQianWan Talents Program and the Department of Education of Liaoning Province.

REFERENCES

Koizumi M. (1993). "The concept of FGM. Ceramic Transactions", *Functionally Gradient Materials*, 34, 3-10.

Tanigawa, Y. (1995). "Some basic thermoelastic problems for nonhomogeneous structural materials." *Appl. Mech. Rev.*, 48, 287-300.

Williamson, R. L., Rabin, B. H., and Drake, J. T. (1993). "Finite element analysis of thermal residual stresses at graded ceramic metal interfaces. Part I. Model description and geometrical effects." *J. Appl. Phy.*, 74, 1310-1326.

Yang, S. Y., Zhang Q. J., and Zhai, P. C. (2003). "Computational Micromechanics Analysis of the Functionally Graded Materials under Thermal Shock Loading." *Materials Science Forum*, 423-425: 687-692.

Zhang, J., Zhong, Z., and Wu, C. (2004). "A study on wheel-rail elastic-plastic frictional contact problem." *Key Engineering Materials*, Trans Tech Publications Ltd, 274-276, 1029-1034.

Zhong, W. X., Zhang, H. W., and Wu C. W. (1997). *The Parametric Variational Principle and its Applications in Engineering*. Science Press, Beijing.

Analysis about Business Investing and Financing Models of Urban Rail Transit

Cui XiaoTian[1,2] and Xie Hui[3]

[1] Tongji University; the School of Transportation Engineering, Room No.423, Shanghai, 201804, P.R.China; email: cxt@sutpc.com
[2]Shenzhen Urban Transport Planning & Design Center Co., Ltd, Hong'li Rd.8009, Shenzhen,518034, P.R.China; email: cxt@sutpc.com
[3] Tongji University; Students' apartment 13#722, Cao'an Rd. 4800, Shanghai, 201804, P.R.China; email: xiehui110@126.com

ABSTRACT

The rapid development of rail transit inevitably needs large capital investments. As a huge investment in urban infrastructure projects, financing is the key to the implementation of the construction. In this paper, the Business Investing and Financing Model (BIFM) of a Rail Transit Project is proposed which includes not only the project construction but also the land development along the rail transit line. Its aim is to attract private capital injection through the interests in the land development. At the same time, the calculation method of the impact area of the rail transit's development interests is amended for reasonable providing land development area to investors. Finally, using the Changsha City Rail Transit Line2 (CCRTL2) as an example, the investing and financing strategy is analyzed. The result shows that the model can reduce the pressures of government from financing and can increase the social benefits at the same time.

INTRODUCTION

According to the "Analysis and Investment Consulting Report on China Urban Rail Transit and Equipment Industry, 2008", in China, more than 10 cities have rail transit projects in operation at present, such as Beijing, Shanghai, Tianjin, Guangzhou, etc. As urban infrastructure projects with huge investments, financing is the key to the implementation of the construction.

There is much research on the investing and financing of rail transit at home and abroad, such as Jie-fen Zheng (2002), Tsinghua University, Wang Hao (2002), Beijing Mass Transit Railway Corporation, and so on. All consider that rail transit projects should be given adequate operating concessions for land development, commerce, advertising and so on, in order to create basic commercialization operating conditions and attract a wide range of investors. On the basis of that, Zhou Jun (2002) analyses the corridor-effect of rail transit on the calculation of development interests of rail transit. Xia-Fei Ye (2002) from Tongji University has studied methods for calculating the rail transit development interest along the track based on the value of the assets in the outskirts of the city and has put forward the

basic ways and means to restore rail transit development interests. However, the gradient effect factors of the corridor-effect are difficult to determine; Ye's calculation is based on the scope of 2km around the railway stations. According to the rail transit planning and design, the distance between two closed mass transit stations is 1 to 2 km. If a 2km distance is used, the benefits calculated can include the effectiveness of another station, so it has some error when calculating the investing and financing benefit of the rail transit. In this paper, a Marketization Investment and Financing Model (MIFM) of urban rail transit based on land revaluation is proposed. The impact area of the rail transit is analyzed reasonably as well as the development interests of the rail transit, and the investing and financing strategies of the rail transit are discussed.

ANALYSIS OF THE DEVELOPMENT INTERESTS IMPACT AREA (DIIA) OF RAIL TRANSIT

For the development interests impact area of the rail transit, there is a low-cost function method (such as Jean-Jacques Filleul 2002; Enrico 2006). According to Ye (2002), the typical model can be changed as:

$$\Delta P_i = a_1 \cdot \ln x_{i1} + a_2 \cdot \ln x_{i2} + a_3 \quad (1)$$

Where: ΔP_i is the land price gap (RMB / m^2); x_{i1} is the distance(m) between the nearest subway station from the block i and the central area (CBD); x_{i2} is the travel distance (m) from the center of the plot to the closest rail station; a_1, a_2 and a_3 are the parameters . It can be seen that ΔP_i is an interval of [0, 1]. For instance, the price gap of land for commerce and office surrounding Hong Kong's MTR is [0, 0.51] and [0, 0.59] respectively.

Because the impact on the land price at the edge of the impact area may be smaller than the impact of other public facilities in the vicinity, the price gap should be in a certain range. Namely,

$$\Delta P_i = a_1 \cdot \ln x_{i1} + a_2 \cdot \ln x_{i2} + a_3 \geq p_i \quad (2)$$

When Equation (2) is met, take the value of x_{i2}, as the radius of the impact areas, while $\Delta P_i = p_i$ (p_i is a given value, depending on the nature of the rail station). As a result, the shape of the region may not be regular round.

DESIGN AND ANALYSIS OF RAIL TRANSIT PROJECT BUSINESS FINANCING MODEL

The Business Investing and Financing Model of Rail Transit project is a Market-oriented Investing and Financing Model (MIFM) for profit. (See Figure 1.)

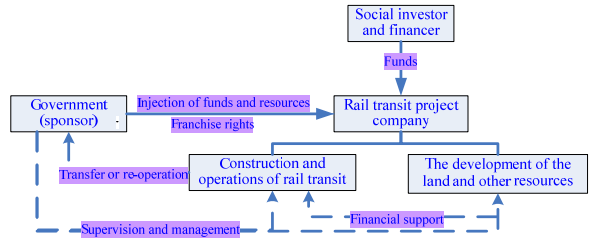

Figure 1. Market-oriented investing and financing process map.

Because the nature of the land varies by section along the rail transit, a reasonable and comprehensive development approach should be undertaken. According to the main industries of each node district, some corresponding markets in the vicinity of the station are set up properly. In the outer suburbs with small populations, the development of logistics types of industries is suitable, as well as the development of various large-capacity and high-tech parts and accessories production industries, machinery industries and farm produce processing industries. The specific models follow.

(1) Ground resource development model (GRDM)

Land resources along the rail transit line on the outskirts are the most important resources for rail transit firms. The local government may consider selling some land to the rail transit company at low-cost or provide it for free according to the specific conditions of some sections.

(2) Underground resources development model (URDM)

With the ground space limited and price question, some bigger entertainment leisure facilities are shifted into the underground spaces. Using the underground space effectively and saving the aboveground space can satisfy different consumer's multi-level expense requirements, and make the service industry stronger in the node district and provide more employment opportunities and tax revenues.

(3) Diversified development model (DDM)

Recently, the rail transit company adopted the DDM where the operating revenue is taken as the principal part, and the real estate industry, the logistics, retail business, travel and tourism and hotel services, etc., were taken as supplements. This and changed the situation so that operation income is not their only income.

The essence of MIFM is that the public welfare and business of the project is clearly defined before the investment is made in the projects, and the loss of rail transit operation is no longer subsidized by the government. The MIFM has a little difference with a PPP (public-private partnership) model with respect to the development of land. The former is that the government hands over the land along the rail transit line to the investors for development. The project company and the government sign a franchise contract, and control the rights of the land in the development interests impact area of the rail transit. The government assesses the enterprises by some indexes provided by the project company which may include the quality of services and their effectiveness status.

The comparison of MIFM and the traditional PPP model are shown in Table 1.

Table 1. Comparison of MIFM and the traditional PPP model.

		MIFM	Traditional PPP model
Investors		Government, Private investors	Government, Bank loans, Private investors
Advantages	Government	Enough Finance, land development well and social benefits increasing	Enough finance
	Private investors	Signed a franchise contract, Control right of the land along, Capital return quickly and Profit space large	Signed a franchise contract
Disadvantages	Government	Land revenue cut a little	Finance pressure and land development slower
	Private investors	Huge finance and With risk in finance return if operation improper	Little Profit space

CASE ANALYSIS

The total investment of CCRTL2 project. CCRTL2 (which includes line 1A and 2A) consists of 36,848 km and needs about 16.676 billion ￥ gross investment. The 1A line needs about 12.873 billion￥ investment. According to the needs of the construction period, the 1A line will be finished by 2013 and the 2A line completion is set for 2017 (TJJT, 2008).

Determine the development interest's impact area of rail transit. In this paper, sections of the CCRTL2 are used to perform a sample analysis of the impact area. These sections include Huangxing road (HXR) station, Furong Road (FRR) station, Jiefang Road (JFR) station and Railway (RW) station. (See Figure 2.) The CBD of Changsha City is located in the region between the Wuyi Road and the Jiefang Road. For the sake of convenience, the CBD is considered as the mid-point of the region.

According to reference [4], the land characteristics surrounding the blocks and the distances to the FRR station are given. According to Equation (2), the development interest's impact area of the four stations can be drawn as shown in Figure 3.

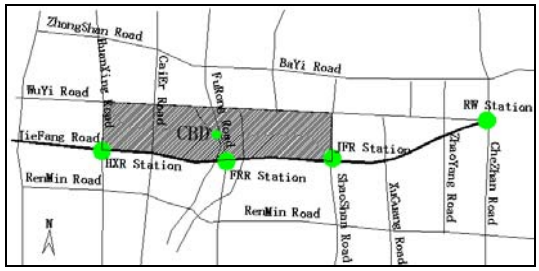

Figure 2. Parts of Changsha metro line 2.

Figure 3. Impact area of four-set.

According to Zhang, et al., 2005, the value of the parameters in Equation (2) are: $a_1 = 919.9$, $a_2 = -379.3$, $a_3 = 1274.9$;

According to the history variance of the three types of land price growth rate (commercial, residential, office), there is $p_{commerce} = 0.03$, $p_{resident} = 0.02$, and $p_{office} = 0.01$.

Table 2 shows the impact area and the land revaluation of the four stations.

Table 2. The land revaluation along Rail Transit (4.488 km)

The Type of Land	Commercial	Residential	Office	Total
Area（m^2）	977,061	1,072,312	191,082	2,240,445
The revaluation of land (100million RMB）	30.87	11.47	1.89	44.23

The proportion of investing and financing. The construction funds for the project are divided into project capital and debt. The government's special funds and the city land revenue constitute the project capital, which is 40% of the total funds; the debt comes from financing, 60% of the total funds (see Table 2).

As shown in Table 2, the total revaluation of CCRTL2 is about 363 billion RMB. If the benefit to the rail transit company is twice their cost, we can attract about 180billion RMB as social investment. So, the private investment (10 billion RMB) of CCRTL2 is guaranteed.

According to the "Study on economic and social development in Changsha City, 2008," from 2008 to 2017, the Changsha City local fiscal revenue is expected to reach 467.200 billion RMB. If 10% will be used for rail transit construction, 4.6 billion of special funds are guaranteed. According to the "Report on National Economic and Social Development of Changsha city, 2006," Changsha City collected 1.796 billion RMB of land deed taxes in 2005. Assuming Changsha City lands maintain a stable situation, and assuming a 2% growth rate, the governors can collect 17.735 billion RMB of the city's land revenue between 2008 and 2017. The 2.0703 billion for the construction of rail transit is feasible.

Table 3. The proportion of the investing and financing.

Types	Special	Land revenue	Private investment	Total
Financing (100million￥)	46	20.703	100.054	166.757
Proportion	27.59%	12.41%	60.00%	100%

Comparison with a traditional investing and financing model. The traditional investing and financing (CRSDG co., LTP 2008) is shown in Table 4.

Table 4. The proportion of the traditional investing and financing.

Types	Special	Land revenue	Bank loans	Equipment leasing	Long-term debt	Total
Financing (100million￥)	46.88	24.83	55.03	23.346	16.68	166.76
Proportion	28.11%	14.89%	33.00%	14.00%	10.00%	100%

According to the traditional model, the government needs to give subsidies to rail transit—about 5.0 billion RMB/year. Therefore, the additional cost to the government reaches 100 billion in the next 20years. So, adding the 5 billion repayment, the total additional cost to the government is more than 105 billion RMB/20years.

However, the MIFM shows that the government lost 19.07 billion RMB for the construction and operation of the rail transit project. By comparing to the traditional investing and financing model, the former will save about 80 billion in costs, if the rail transit ticket sales aren't considered. Besides, the social benefits will be unimaginable, if the land development and the construction of the rail transit are combined perfectly. It is very clear which strategy for investing in rail transit the government should choose.

CONCLUSIONS

The investing and financing strategies of urban rail transit projects can determine the success or failure of a project. The MIFM, which is based on land revaluation, is a cooperative method according to investors "expertise" and reasonably allocates the work. Firstly, the impact area of the development interest of the rail transit is calculated, and then the rail transit companies comprehensively develop the rail transit and the land. It is a deviation from the traditional PPP model. However, this model increases the difficulty of determining the cost of the work at the pre-construction stage. How to form a series of legal documents so as to carefully balance the interests of all parties needs to be solved for similar construction projects in the future.

REFERENCES

China railway si yuan survey and design group co., LTP(CRSDG co., LTP) (2008). "The study report on Feasibility of Changsha metro line 2." Beijing.

Filleul, J., (2002). Renconters parlementaires Le financement des infrastructures. Parliamentary Meetings on Transport Infrastructure Financing Parlamentarisches Treffen über den Verkehr Die Finanzierung der Infrastrukturen, Revue Générale des Chemins de Fer.

Lai, Q., (2006), "Analysis of PPP Financing Conditions and Suggested Framework for Rail Transit Project," *modern urban transit*. Beijing.

Musso, E., Ferrari, C., and Benacchio, M., (2006). "Port Investment: Profitability, Economic Impact and Financing." *Research in Transportation Economics Volume 16*, USA.Pages 171-218.

The school of transportation engineering of Tongji University (2008). "Report on evaluation and chose of location and direction of Changsha metro line 2".Shanghai

Wang, H., (2007), "Study and suggestion on the investing and financing of Beijing rail transit," *economic & financing, metro & light rail1*. Beijing.P4-10.

Ye, X. and Cai, W., (2002). "Fundamental study on return method of development benefits for urban rail transit." *Journal of the china railway society, vol.24*. Beijing.

Zhang, X., Hu, Z., and Ye, X., (2005). "Study of Impact of Urban Rail Transit Development on Surrounding Areas." *Journal of Tongji University (Natural science), vol.33 No.8*.Shanghai.

Zheng, J., Liu, H., (2002). "Comprehensive Development of Rail Transport and Land Resources in Hong Kong." *China railway science*, Beijing.

Zhou, J., Xu, J., (2002). "The Corridor Effects of Rail Transportation on Urban Land Using." *Urban rail transit study*, Beijing.

Characteristics of Fundamental Data for Railway Maintenance and the Construction of Integrated Data Platform

Futian Wang[1], Mei Sun[2] and Jianglin Zhou[3]

[1]State Key Laboratory of Rail Traffic Control and Safety, Beijing Jiaotong University, Beijing, 100044, China; PH (+86-10)51687154; FAX (+86-10) 51687154; Email:wangfutian@jtys.bjtu.edu.cn
[2]Information Tech Center of Ministry of Railway, Beijing, 100844, China; PH (+86-10)5191548; FAX (+86-10) 51891548; Email: sunmei@sinorail.com.cn
[3]School of Mechanical Engineering, Xinjiang University, Wulumuqi, 830008, China; PH (+86-991)4558604; FAX (+86-991)4558604; Email: zhoujl33@126.com

ABSTRACT

This paper summarizes the background information for the establishment of the Integrated Data Platform for Railway Maintenance (IDPFRM). It analyzes the spatial characteristics, the subject characteristics and the time characteristics of Fundamental Data for Railway Maintenance (FDFRM) generally. Then it proposes the thoughts of integrating the FDFRM based on these characteristics. It proposes to construct the IDPFRM through regarding the spatial location as ligament, the single facility as the center, and the maintenance management flow as the master line. Finally, it gives an application example of the IDPFRM in Kunming Railway Bureau.

1. INTRODUCTION

The goal of constructing the Chinese digital railway was envisioned in "Railway Informationization Overall Plan" (MOR, P.R.China, 2005). Its fundamental purpose is to integrate the massive, static or dynamic, multi-resolution, three-dimensional data of railway departments of transportation (locomotive, maintenance, communication and signaling, vehicle, operation management, etc.), according to the unified geographic coordinates, and to construct the fundamental database of the railway.

It is necessary to establish the unified countrywide database of the transportation facilities, the technical state of the facilities, study the technology of synthetically inspection, state estimation, reinforcement and reconstruction about the track, roadbed, bridge and tunnel of the speedup lines, study the regularity of rail wear and defects, and to install the preventive maintenance technical system for the speedup lines (MOR, P.R.China, 2007).

At present, there are many problems about the data management in the

railway maintenance departments, such as decentralized data, non-uniform data standards, and so on. It led to the fact that the current information systems are unable to support the above requirements (Gao, Y. F. etc, 2006).

Therefore, finding ways to collect and integrate the various data resources in track maintenance departments according to the uniform data standard and to install the IDPFRM accordingly have become an extremely urgent research topic.

About the data platform, a 3-tier service architecture of the application service sharing platform for China railway geographic information system has been put forward. The system can provide 5 kinds of data services: access, analysis, visualization, metadata and application integration (Jia, L.M., etc, 2003). A scheme for constituting a synthetic information platform for inspection data, as well as the detailed descriptions of the methods to collect, store, and manage the different track inspection data has been given (Liu J., etc, 2006).

The authors will analyze the characteristics of the FDFRM and propose motions of integrating the FDFRM by constructing the IDPFRM.

2. BASIC CHARACTERISTICS OF THE FDFRM

Although the fundamental data produced in the track departments has decentralized sources and too many categories, its basic characteristics may be induced into the following:

(1) Spatial characteristics. Spatial characteristics refer to the geometry characteristics of the space object, such as position, shape, and size, as well as the topological relations with its neighboring objects.

The fundamental data of the railway track departments is extremely spatially characteristic. According to the preliminary analysis about the data structure of the PWMIS which is widely used in the railway track departments at present, over 95% of the data records have the fields with space position attribute “the central kilometrage”, “the beginning kilometrage”, “the end kilometrage” and so on. For example, in the curve table of PWMIS, “the beginning kilometrage” expresses the beginning of a curve, and “the end kilometrage” expresses the end of a curve (see Table 1). These two fields reflect the curve space position information. But the radius field and the super elevation field reflect the curve’s own geometric characteristics. In the bridge table, “the central kilometrage” expresses the central point of a bridge (see Table 2).

Table 1. Data structure of curve data table in PWMIS (part).

LINE_ CODE	BEGIN_KILO-METRAGE	END_KILO-METRAGE	CURVE_ HAND	RADIUS
0954	302.31449	302.63857	LEFT	1400.0
0954	304.26343	305.01648	RIGHT	600.0
0954	305.06381	305.48275	LEFT	600.0
0954	305.53302	305.91298	RIGHT	800.0

Table 2. Data structure of bridge data table in PWMIS (part).

LINE_ CODE	LINE_NAME	BRIDGE_CODE	CENTTAL_KILOMETRAGE	BRIDGE_ LENGTH
0954	NANJIANG	277	304.085	15.40
0954	NANJIANG	278	304.963	117.30
0954	NANJIANG	279	305.942	6.50
0954	NANJIANG	280	306.010	12.50

Remembering the position of a space object, human beings are not generally prone to memorize its space coordinates, but to determine the space position relations with the neighboring objects with which they are more familiar. The relations are generally called the topological relations. For example, the relations between a curve and two stations (which two stations is the curve between?), the relations between a curve and a tunnel (whether the curve is located in a certain tunnel), the relations between a curve and a bridge (whether the curve is located on a certain bridge). The second curve of Table 1 and the second bridge in Table 2 have the intersecting relations on the space position (see Figure 1). These relations reflect how the curve facilities relate to other facilities.

Figure 1. A bridge on Nanjiang Line.

(2) Subject characteristics. The subject characteristics refer to the other characteristics of the spatial phenomenon beside the time characteristic and the spatial characteristic. For example, a certain region has the characteristics of annual rainfall, land cover type, population density, air pollution degree and so on.

The subject characteristic of the railway facilities data has not only too many data types, but also a huge amount of records. The chief data characteristics of the track facilities are listed below:

A) Fundamental data of the facilities produced in the designing and producing stage, such as specification, model, and material.
B) Inspection data produced by the process of the facilities being used. It includes dynamical and static inspection data. The dynamic inspections include the inspection by track inspection cars, locomotive-mounted dynamic inspection instrument, portable inspection instrument, managers on trains, and rail detector cars. The static inspections include the manual line inspection, track instrument inspection, and line patrolling.
C) The facilities' flaw data produced in the process of the facilities being used.
D) The maintenance data produced in the process of the facilities being used. The track maintenance must take one of the three different repair methods of major repair, medium maintenance, and maintenance, according to different line condition. The maintenance is an operation for eliminating the common line defects or the planned preventive work between two repairs of major or medium maintenance. The Line maintenance may divide into synthetical maintenance, daily maintenance and temporarily repair according to its work pattern (MOR, P.R.China, 2006).
E) The train load data produced in the process of the facilities being used. It includes the information of gross train weight, the speed, the rolling stock type, the axis weight and so on when the train passes the facilities.
F) Management data produced in the process of the facilities being used. It includes the facilities' ownership units, the principals, the data's collecting persons, inputting persons, renewal frequency, and management standards.

(3) Time characteristics. The spatial data or the subject data is always collected or computed at some specific time or in some time span. The time characteristics of basic data of track facilities are the key aspect for tracing the reasons for facilities' failures and forecasting the trend of the facilities' changing states.

3. CONSTRUCTION OF THE IDPFRM

The important foundation of the track maintenance informationization is to manage the FDFRM with multi-sources, different structures massive amounts, to

construct the IDPFRM. These data resources are the enterprise assets that the track maintenance departments hold, with equal importance to the materiality assets. To achieve this goal, we study how to make the data coding standard, dictionary standard, quality specification and so on, and how to establish the data interface program with PWMIS, TMIS and the inspection devices that the Chinese railways commonly use, such as track inspecting cars, track static intelligent inspection instrument, a train-mounted track inspection tester, etc., and to construct the integrated track facilities database in Railway Bureau using the ETL pattern (Inmon W. H., 2005), which will lay the foundation for data mining of a track's state. A description about the data collecting process is given (see Figure 2).

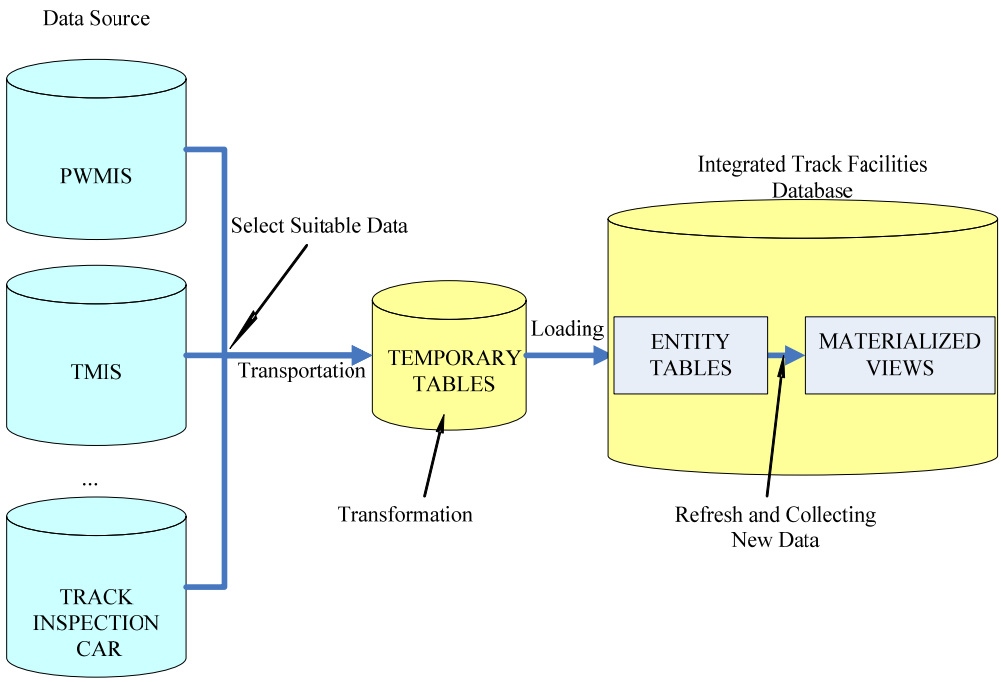

Figure 2. Data Gathering Process in Integrated Track Facilities Database.

Although the data categories of the integrated track facilities' databases that are shown in Figure 2 differ from each other, they have close relationships in time and space, according to characteristics described in the above section. They can be collected and integrated from the following aspects according to these relations.

(1) Information integration by regarding the spatial position as the ligament. All track data is assigned a certain kilometrage in the unified one-dimensional coordinate system (kilometrage), and all related data are gathered with kilometrage as the ligament. It provides the foundation for analyzing the track facilities' state evolution regularity based on time and space.

(2) Track facilities' centered information integration. Except for being

assigned a certain kilometrage, the track data is assigned the code of the facility it belongs to, for the convenience of data integration with the facilities as the ligament. It provides the foundation for analyzing a single facility's state evolution regularity.

(3) Information integration with the track maintenance management process as the master line. All track data is assigned to the step of the track maintenance management process that their source belongs to, for the convenience of data integration with the process as the ligament. It provides the foundation for realizing the track facilities closed-loop management of "inspection → state analysis → prediction → repairing → evaluating→ inspection".

4. AN APPLICATION EXAMPLE OF THE IDPFRM

An application system had been developed for rail track safety and maintenance in Kunming Railway Bureau in 2008, which was based on the IDPFRM, and the rail track facilities' data was fully considered. The system has worked uninterrupted for one year, and the information integration with space, facilities and work flow has been achieved. We can perform the following innovations for track safety and maintenance with the system.

(1) The dynamic and static track quality index (TQIs) computation, single item computation, TQI history changing regularity of the line with arbitrary length.
(2) Track geometric size changing regularity analysis and forecast the data of track inspection cars.
(3) Redrawing waves and contrasting analyses of many kinds of inspection data at one kilometrage (or same facility, especially essential key facilities, such as rail switches, curves, welded joints, joints between line and bridge, and so on).
(4) Maintenance plans made based on track's state changing regularly.
(5) Construction of facilities' trouble database based on the IDPFRM.
(6) Flow designing with "defects" as the master line, and the "defects" tracing management.
(7) Realization of the closed loop management of track maintenance.

These innovations will change the maintenance idea of the traditional "repairing after limits have been exceeded", "repairing after trouble has taken place", and "periodically repairing," to the idea of "selective maintenance", mainly by "preventive maintenance". They will sustain the decision making.

5. CONCLUSION

Analyzing the characteristics of the FDFRM is of great importance to the establishment of the IDPFRM, which will carry out the information integration of

the space position, facilities, and maintenance management processes, and will bring many innovations in the track maintenance management.

REFERENCES

Gao, Y. F., Wang, F. T., and Liu R. K. (2006). "Design and Realization of Analytical Information System for Railway Track State." *China safety Science Journal*. 16(7), 127-132.

Inmon, W. H. (2005) *Building the Data Warehouse*, John Wiley & Sons Inc., Indianapolis, Indiana.

Jia, L.M., Qin Y., and Liu F. (2003). "Research on Application Service Sharing Platform for China Railway Geographic Information System." *China Railway Science*., 24(2), 24-28.

Liu J., Wang F.T., and Liu R.K. (2006). "Design and Implementation of Synthetical Information Platform on Railway Engineering Inspection Data." *Railway Computer Application*, 15(8), 26-28.

MOR, P.R.China (2005). *Railway Informationization Overall Plan*, MOR, Beijing.

MOR, P.R.China (2006). *Regulation of Railway Line Maintenance*, Chinese Railway Press, Beijing.

MOR, P.R.China (2007). *The 11th Five Years' Plan of Railway's Science and Technology Development*, MOR, Beijing.

Track Structure Vibration Characteristic Analysis Based on FEM 3D Model

Linya Liu[1]; LU Zhuqing Lu[1]

[1] School of Civil Engineering and Architecture, East China JiaoTong University, Nanchang, JX; 330013; China; PH: (0086)791-7046080; Email: liulinya@sohu.com

ABSTRACT

A new track structure calculation model is proposed with the characteristics of track noncontinuous supports and rail 3-dimension. Track structure responses at different high frequencies are obtained using Harmonic Response Analysis. The new model can better describe the response of track structure to high-frequency excitations. It excels the traditional beam model in calculation precision and applicable range. Rail foot and rail head vibration response in response to high-frequency excitations and their corresponding vibration distributions are studied, and track structure high-frequency vibration impedance characteristic is determined. Also, vertical vibration propagation decay rates are calculated. It is shown that rail cross-section vibrates mainly as a whole below 1000Hz; but produces deformation when vibratess at high frequencies.

1. INTRODUCTION

Noise pollution produced by high-speed trains has become a prominent problem in the development of high-speed railway system. It has attracted extensive attention from various government agencies and research institutes. Wheel-rail noise is one of the most important parts of railway noise, and high-frequency vibration is the main source of wheel-rail noise. In order to reduce the wheel-rail noise, it is critical to study high-frequency track vibration characteristics [P. J. Remington. (1987)]. The rail is effectively an infinite structure. Timoshenko beam and Eular beam models are often used to simulate the rail in previous studies. These studies are limited to modeling continuously supported beam (D. J. Thompson. 1993) and periodically supported beam (M. A. HEl CKL. 1992). Also, the traditional models did not consider the deformation of track cross-section for high-frequency excitation very well. A more precise model and calculation method are established in this paper to analyse the track structure vibration characteristics.

2. THE ANALYSIS METHOD OF VIBRATION CHARACTERISTICS

Any sustained cyclic load will produce a sustained cyclic response (a harmonic response) in a structural system. Through the harmonic (or sinusoidal) excitation, the amplitude ratio and phase difference between excitation and

response can be employed directly to determine the system impedance:

$$Z_j = F_j / V_j \tag{1}$$

Where: *Z_j represents the vibration impedance of structure. F_j and V_j represent the excitation and response, respectively.*

Sinusoidal force can be expressed as a plural:

$$f(t) = Fe^{i(\omega t+\varphi_1)} \tag{2}$$

Where: *F represents the amplitude of excitation force; ω denotes frequency; t is time; and φ_1 is phase angle of force*

The corresponding displacement, velocity, and acceleration can also be expressed as plural too:

$$x = Xe^{i(\omega t+\varphi_2)}, \dot{x} = i\omega Xe^{i(\omega t+\varphi_2)}, \ddot{x} = -\omega^2 Xe^{i(\omega t+\varphi_2)} \tag{3}$$

Where: *X represents for the amplitude of sinusoidal displacement response amplitude; φ_2 is phase angle of response.*

Equation (1) can be rewritten as:

$$Z_j = \frac{Fe^{i(\omega t+\varphi_1)}}{Ve^{i(\omega t+\varphi_2)}} = \frac{F}{V}e^{i(\varphi_1-\varphi_2)} \tag{4}$$

Where: *V denotes the amplitude of response*

Harmonic response analysis makes it possible to predict the sustained dynamic behavior of structures in Finite Element Method. The idea is to calculate the structure's responses at different frequencies and to obtain a mapping between response quantities (usually displacements) and frequency [ANSYS, Inc. (2005)].

Consider the equation of motion for a structural system:

$$[M]\{\ddot{x}\} + [C]\{\dot{x}\} + [K]\{x\} = \{F^a\} \tag{5}$$

where: *[M] represents structural mass matrix; [C]: structural damping matrix; [K]: structural stiffness matrix; {x} : nodal displacement vector; and {F_a}: applied load vector*

As mentioned above, all points in the structure are moving at the same known frequency, however, not necessarily in phase. Also, it is known that the presence of damping causes phase shifts. Therefore, the displacements may be defined as:

$$\{x\} = \{x_{\max}e^{i\phi}\}e^{i\Omega t} \tag{6}$$

where: *x_{max} : maximum displacement; Ω:imposed circular frequency (radians/time); Φ : displacement phase shift (radians)*

Note that x_{max} and Φ may be different at each degree of freedom (DOF).

The use of complex notation allows a compact and efficient description and solution of the problem. Equation (6) can be rewritten as:

$$\{x\} = \{x_1\} + i\{x_2\}e^{i\Omega t} \tag{7}$$

Where: *{x1}: real displacement vector; {x2}: imaginary displacement vector*

The force vector can be specified analogously to the displacement:

$$\{F\} = \{(F_1)\} + i\{F_2\})e^{i\Omega t} \tag{8}$$

where: *Ω represent force phase shift; {F1} represent real force vector; {F1} represent imaginary force vector.*

Substituting equations (7) and (8) into equation (5), The dependence on time ($e^{i\Omega t}$) is the same on both sides of the equation and may therefore be removed, then the follow equation can be get:

$$([K] - \Omega^2[M] + i\Omega[C])(\{x_1\} + i\{x_2\}) = \{F1\} + i\{F2\} \tag{9}$$

The response can be obtained by the solution to equation (9).

3. The track structure model

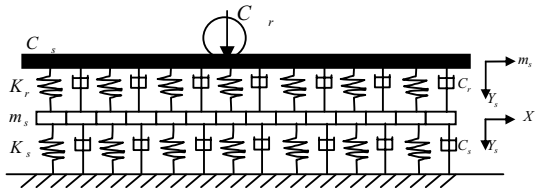

Figure 1. Two degrees of freedom vibration system with sleeper quality model.

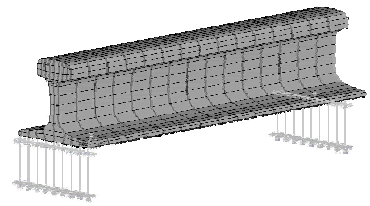

Figure 2. Three-dimensional track structure model.

Two DOF vibration system with sleeper quality model is established in reference [LIU linya. (2004)]. Rail vibration mechanical analysis model is shown in Figure 1. For further optimization of the model, the rail is simulated with three-dimensional solid element shown in Figure 2. In this model, spring-damper combination and mass element are employed to describe the rail support and sleeper, respectively.

4. THE VIBRATION CHARACTERISTICS OF TRACK STRUCTURE

4.1 Track vibration impedance

Based on the model described in Section 3, track responses are calculated. Track parameters are selected from reference [LIU Linya.(2006)]. Figure 3 gives

impedance amplitude and phase angle of rail head and rail foot when excited in the head centerline of rail at mid-span. Figure 4 shows the same value when excited in the head centerline of rail at sleeper supporting point.

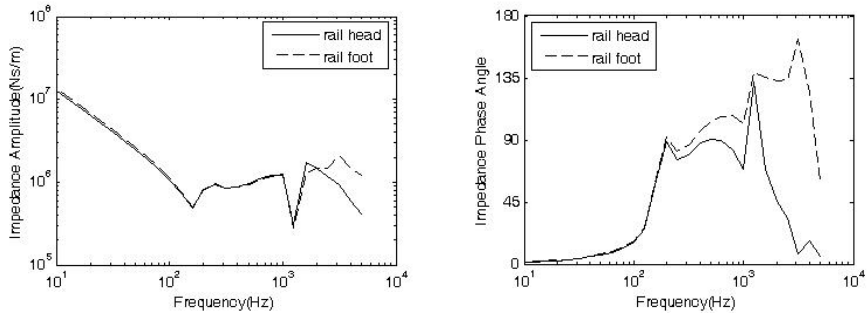

Figure 3. Impedance of track structure when excited in the head centerline of rail at mid-span.

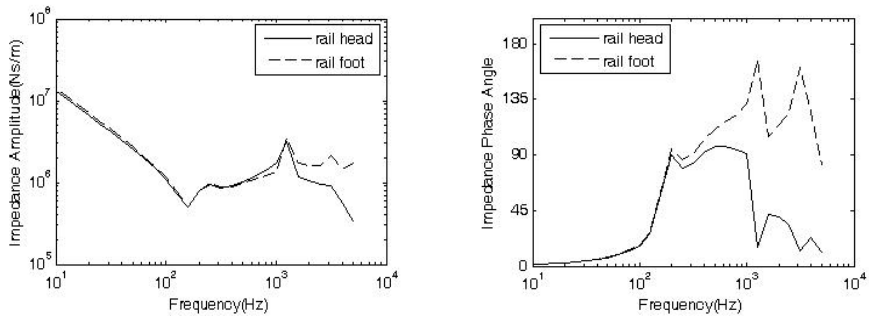

Figure 4. Impedance of track structure when excited in the head centerline of rail at sleeper supporting point.

Both Figures 3 and 4 show that vibration impedance amplitudes of rail head and rail foot are very close when the frequency is lower than 1000Hz. This similarity indicates that rail vibrates mainly as a whole. In the high-frequency part, rail impedance amplitudes of rail head and rail foot are significantly different, which shows that rail cross-section produces deformation vibration at high frequencies.

The traditional models can not effectively reflect the rail cross-section deformation at high frequencies. Thus they cannot precisely simulate the track structure vibration at high frequencies. The model introduced in this paper can describe the deformation very well, thus providing better calculation precision than the beam model.

Comparison between Figures 3 and 4 shows that the track structure vibration characteristics are very similar when excited at mid-span and sleeper supporting point at low frequencies (less than 1000Hz). However, the vibration difference between excitations at mid-span and sleeper supporting point become very large at high frequencies. Particularly, when excited at mid-span there is a resonance point at about 1250Hz. At around the same frequency, there is also an anti-resonance point when excitated at sleeper supporting point.

4.2 Track vibration distribution

Figure 5 gives the typical vibration distributions along the track direction. Some vibration rules can be drawn:

Below 125Hz, vibration distributes with half-wavelength around 4 spans and attenuates in the track length direction rapidly.

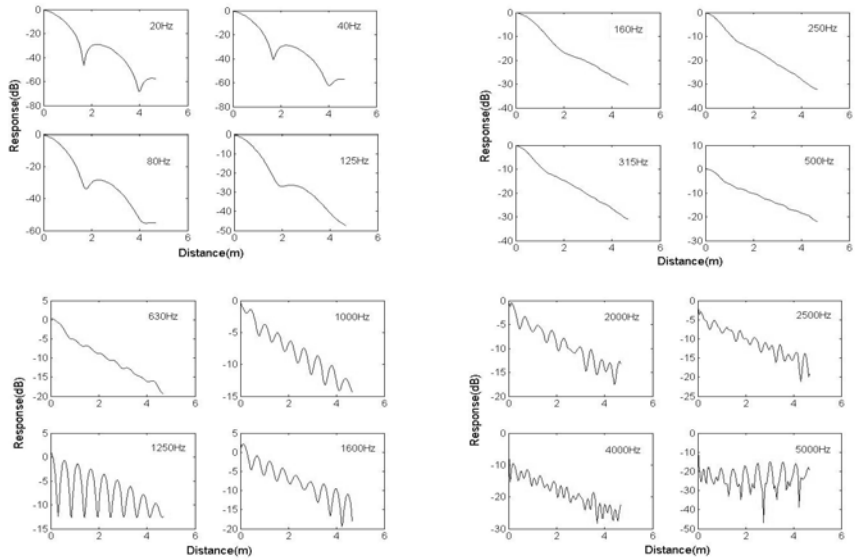

Figure 5. Vibration distribution along the track direction.

Between 160Hz and 500Hz, track vibration attenuates linearly with respect to the track length.

Ranging from 630Hz to 1600Hz, track vibrates in pinned-pinned mode with a span length of half-wavelength especially for 1000Hz.

4.3 Track vibration propagation decay rate

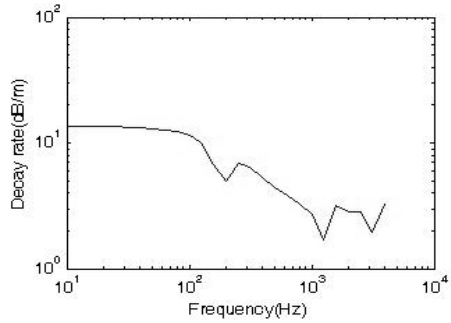

Figure 6. Vibration propagation decay rate.

As illustrated in Figure 5, the track vibration attenuation along the track direction is directly related to frequency. The propagating wave decay rate is obtained [C.J.C. Jones. (2006)] and shown in Figure 8.

It can be seen from Figure 8 that vibration attenuates rapidly at low frequencies; and track structure has comparatively longer transmission distance at

high frequencies.

5. CONCLUSIONS

Based on a three-dimensional track structure vibration model, harmonic response analysis is employed to investigate the vibration characteristics of track structure. This three-dimensional model can better describe the rail cross-section deformation at high frequencies, therefore producing better calculation precision at high frequencies compared to the traditional beam model. Impedances of different exciting and pick-up points are obtained by calculating the track structure. In addition, some interesting rules of track structure vibration at high frequencies are observed:

1. Rail cross-section vibrates mainly as a whole below 1000Hz; At high frequencies, rail cross-section produces deformation when vibrates.
2. Track vibrates in a pinned-pinned mode with a span length of half-wavelength for 1000 Hz.
3. Vibration attenuates rapidly at low frequencies; track structure has comparatively longer transmission distance at high frequencies.

6. ACKNOWLEDGEMENTS

The work reported herein was supported by China Natural Science Foundation (50768004) and Jiangxi Province Natural Science Foundation (2007GQC058).

REFERENCE

ANSYS, Inc. (2005). “Section 17.4. Harmonic Response Analyses”. *Release 10.0 Documentation for ANSYS.”*

C.J.C. Jones, and Thompson D.J., Diehl R.J.. (2006). The use of decay rates to analyse the performance of railway track in rolling noise generation. *J. of Sound and Vibration* 293, 485–495

D. J. Thompson. (1993). Wheel-rail Noise Generation, Part III: Rail Vibration. *J. of Sound and Vibration,* 161(3), 421-446.

LIU Linya, and LEI Xiaoyan.(2004). Study on High Frequency Vibration of Wheel/Rail System. *China Railway Science*, 25(2), 52-55.

LIU Linya. (2006). Theoretical Calculation and Analysis of Wheel-rail Noise for Speed-up Train and High-speed Train. *Ph.D. thesis, Tongji University, Shanghai, China*.

P. J. Remington. (1987). Wheel rail rolling noise, I: theoretical analysis. *J. of the Acoustical Society of America,* 81 (6), 1805-1823.

Measurement and Simulation Study on Ground Subsidence Induced By Shield Tunneling In Sandy Stratum

Haixia Sun[1], Wen Zhao[2], and Lihua Lu[3]

[1,2]Instructor lecturer of Shenyang University of Technology; Ph. D candidate of Northeastern University, Shenyang, China; School of Architecture and Civil Engineering, Shenyang University of Technology, 574#,110178; email:sunhx99@126.com; PH 15998878286

[2] Professor, Ph. D, College of Resources and Civil Engineering, Northeastern University, 110001; email: wenneu@163.com; PH 024-83681391

[3] Associate professor, Ph. D candidate; School of Architecture and Civil Engineering, Shenyang University of Technology, 110178; email: llh_wxy@yahoo.com.cn; PH:024-25496533

ABSTRACT

This paper presents a study of the ground subsidence law caused by tunnel excavation with EPB shield machine, in which a Metro site was selected for data collection. With the data measured in field and tools of general FEM program ABAQUS, three-dimensional finite element model was established and a simulation study was conducted to analyze the construction progress under influences of all possible factors. Major regional and sub-regional factors influencing the ground subsidence were estimated, and the terrain types affecting vertical surface during construction and the amount of ground subsidence in various stages of construction are analyzed. Based on comprehensive understanding of these influencing factors, the prediction model for estimating ground deformation was studied. With the actual values of stratum and construction parameters as well as other relevant data for samples, the established model was applied to forecast the ground deformation and verification the availability and satisfactory results were produced.

1 INTRODUCTION

Construction method for shield tunneling has the virtue of less traffic impact, less excavated earth, short construction period, so it is more and more applied in urban metro construction. But, during construction, this method inevitably caused stratum loss and ground subsidence. When the stratum deformation is out of range, it will

endanger adjacent buildings, urban roads, underground utilities and other a series of geotechnical problems.

Study methods on ground subsidence induced by shield tunneling at home and abroad may come down to: theory and empirical formula method, numerical simulation, model experiment and so on. In this paper, use FEM program ABAQUS to simulate the excavation processes and analyze the ground subsidence law induced by shield tunneling in sandy stratum.

2 INFLUENCING FACTORS ANALYSIS OF GROUND SUBSIDENCE BY SHIELD TUNNELING

Synthesizing home and abroad successful experiences, it can thus be concluded that the stratum loss give major cause for ground subsidence. The subsidence mainly appears on the period of construction. The reason is found expression in over-excavation, unmatched propulsion parameter, insufficient grout or grouting untimely, gesture adjustment and so on. Besides, some factors such as planning, design, local geological conditions can also cause ground subsidence, which happen during construction and long time after construction.

3 MEASURE AND ADVANCING FACTOR

3.1 Project description

Tunnel interval is simple cavity and simple line circle section, whose diameter is 6m, the thickness of lining is 0.3m. The maximal buried depth of the tunnel top is 13.723m, and the minimum is 7.86m, the buried depth of the measured district is 11m, and the stratums are made of expanding granular, such as clay, silt, medium sand, grit, gravelly sand and pebble. The pressure in soil store is 0.18Mpa, the advance rate is 3~4m/min, two grouting hole work at the same time and the pressure is 0.4 Mpa, the amount of grout is $4m^3$.

3.2 Scope of measure and disposition

Measure the horizontal and vertical displacement, there is a measure section per 20m in range of 100m while shield is departure and lifted out, and per 50m in other districts. Concrete factory is as shown in Figure1. The range of 50m before cutter head and 20m after shield tail is considered in this paper.

Ground subsidence observation spot should penetrate road structural layer, and fit in natural soil. The style of the measured spot is shown in Figure 2.

3.3 Analysis of measured results

Taking the section where spot Y4 locates for example, the data is as indicated in Figure2 and Figure3. From Figure2, the conclusion that the subsidence rise and maximize near by spot Y4 can be drawn. After that, the subsidences tend to decrease and uplift begins to emerge. The subsidence shows over-excavated and uplift shows that grouting takes effect, so grouting in time is necessary.

See Figure3, the subsidence of spot Y3 (20m after shield tail) is stable. The uplift and subsidence of spot Y4 and Y5 is also stable before 20m, and make small changes after 20m. But, the uplift and subsidence of spot Y6 and Y7 make big changes; it shows that the thrust of jack and over-excavated play a part. So, measuring range, from 20m after shield tail to 50m before 50m before cutter head, is reasonable.

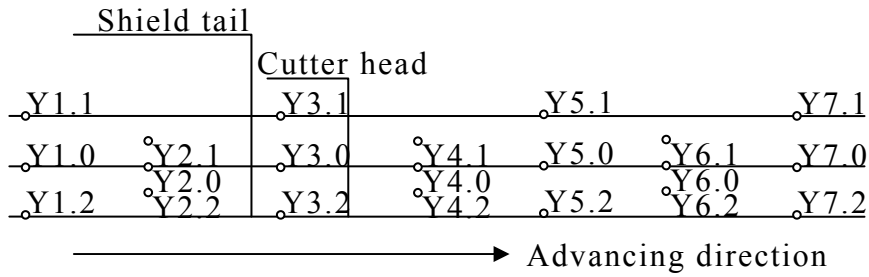

Figure1. Measure site (part).

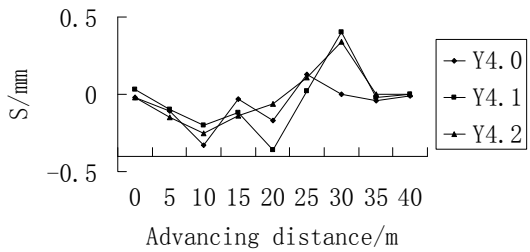

Figure 2 Lateral measured data.

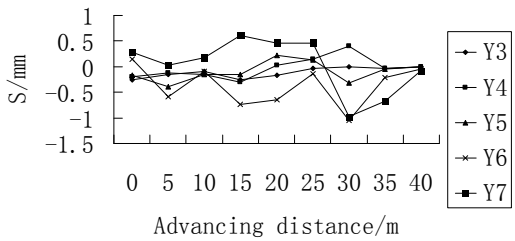

Figure 3 Longitudinal measured data.

4 FINITE ELEMENT MODELS

4.1 Calculation hypothesis

Simplify tunnel lining as homogeneous and linear elasticity material. Time effect is without consideration and only space deformation is considered. The ground surface and solum of soil is homogeneous and flat bedded. Constitutive model of the soil body is Drucker-Prager model, which combine ABAQUS/Explicit destruction model to define stiffness reduction, removing element and so on. Physics mechanics index of earth is shown as Table1.

4.2 Finite element model

On the basis of the width estimation formula from Peck sedimentation tank and solum condition on site, estimate Section size of the model: 60m width, 50m height and 100m length. The top surface is free, the bottom is two-way restraint, the left and right is horizontal restraint and the front and back is also horizontal restraint. The boundaries except the top use infinite element. The solum is simulated by solid elements, which is C3D8R. The tunnel lining is simulated by skin elements, which is applicable to three-dimensional model and can superiorly model the weighted conditions of linings. The excavated step is 1.2m length. As aforesaid, the finite element model is build as below. See Figure 4.

Table 1 Physics mechanics index.

Depth of Stratum (m)	Geotechnical name	Volume weight Γ (kN/m^3)	Cohesion C(kPa)	Internal frictional angle standard φ_k (°)	Coefficient of compressibility α(1/MPa)	Modulus of compression $Es_{0.1}$(MPa)
4.7	Silty clay	18.9	34.0	11.3	0.281	6.65
5.8	Silty fine sand	17.1	9.8	29.8	0.132	12.57
8.4	Medium rough sand	17.7	1.7	33.9	0.132	12.39
5.1	Silty fine sand	19.0	1.5	34.0	0.132	11.99
8.6	Gravelly sand	19.9	1.7	41.8	0.103	14.77

4.3 Computation simulation

Use the ADD technology to activate part lining element, and REMOVE technology to remove excavated soil element. The analysis step is set up as below.

(1) Initial geostatic stress equilibrium: Use step GEOSTATIC to simulate Initial stress field.

(2)The first step is tunnel excavation (release part load). The process of simulating tunnel to be excavated is not absolute stress relaxation. On condition of initial geostatic, diminish modulus of elasticity to soften soil to be excavated. Put it this way to diminish supporting force of country rock, and amount to once stress relaxation. Use command TEMPERATURE to change modulus of elasticity and release 60% geostatic stress.

(3) Assemble lining: Use commands REMOVE to remove lining elements before excavation, and activate a lining (1.2m width) after excavation.

(4) Release remnant stress: Remove the first part soil to release 40% stress.

Repeat step (2)~(4) to excavate to be finished. Only thirty lining(that is 36m width) is simulated in this paper because of the computer' s work. By this time, the ground subsidence is basically stable and can satisfy the analysis required. The part result is shown in Figure 5.

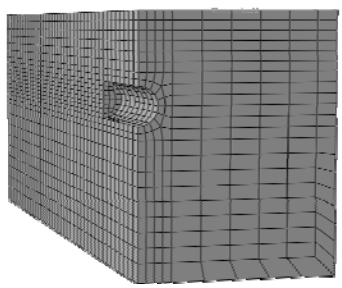

Figure4. Finite element model

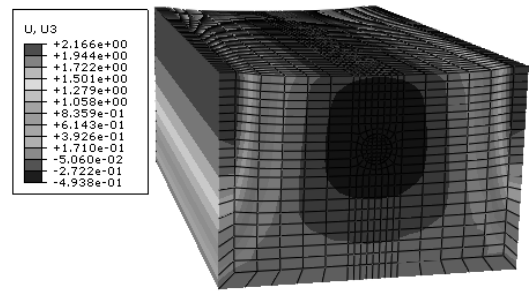

Figure5. Initial geostatic stress equilibrium.

5 CONTRAST OF MEASURED AND SIMULATED RESULT

5.1 Lateral subsidence

The contrast data come from 15m before cutter head to 15m after shield tail. Take points Y4 (Y4.0, Y4.1 and Y4.2) for example and the data comes from 20m before section where Y4 locates. The measured and simulated result of the lateral subsidence is as shown Figure 6. See it from the Figure6 that the measured subsidence increase and then decrease up to uplift, but the simulated can't reflect the increasing part. That is because that the stress relaxation of the model differ from over-excavated solum, and this is a problem to be solved in follow-up work.

5.2 Longitudinal subsidence

Take the three point Y3.0, Y4.0 and Y5.0 right above the tunnel axes for example and inspect changing situation of their ground subsidence during excavation. Because the interval of measured section is longer (20m) and the simulated and calculated model is only 36m length, so the overall changing situation of the longitudinal subsidence cannot be made known.

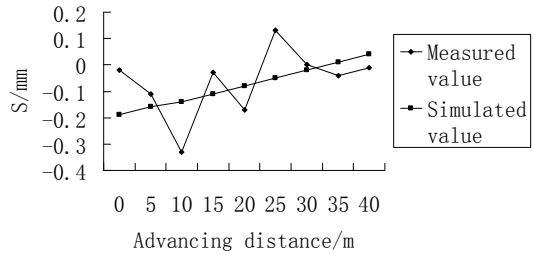

Figure 6. Measured value Compared to simulated value.

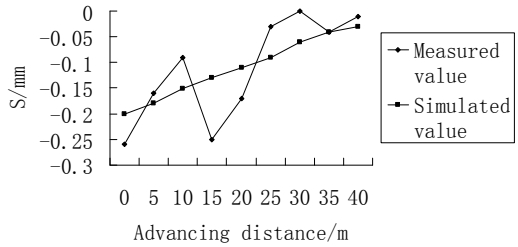

Figure7. 20m far from shield tail (Y3section).

Part match Results are shown in Figure 7 to Figure 8. It can be see that the trend is basically same and the model on the whole can reflect the change law of subsidence.

6 CONCLUSIONS

The measure data make known the ground subsidence law of sandy stratum. Establish three dimensional finite element model by software ABAQUS to simulate the subsidence, and result is as follows.

(1) The simulated value of ground subsidence is approximate to measured value after contrasting and analyzing the value, and the simulation can better give expression to lateral ground subsidence law.

(2)Three-dimensional numerical method can effectively simulate dynamic construction and the change of ground subsidence. Consequently, the simulation results are more accurate and open up a new way to forecast the subsidence cause by excavation.

(3)The three dimensional finite element model established by ABAQUS can superiorly simulate kinds of materials, such as soil, lining, and grout. The stress and deformation, excavation and timbering can all be simulated. The infinite elements of boundaries preferably correspond with Actual projects. The results provide a foundation of next steps, that is, advancing parameter and seepage flow coupling.

REFERENCES

Jiangxinliang, Cuiyi.(2005). *Measurement and simulation of ground settlements of Tianjin subway shield tunnel construction* [J]. Rock and Soil Mechanics, 26(10):1613-1616.

New, B. M., and O'Reilly, M. P. (1991). *Tunnelling induced ground movements*, *predicting their magnitude and effects*[J]. Proc., 4th Conf on Ground Movements and Structures. 671-697.

Shijianyong,Zhangjing.(2002). *Semi analytical method of soil*

deformation induced by tunneling construction, Journal of Hehai Universit, 30 (6):22-25.

Wangjinchang,Chenyekai. (2006). *Application of ABAQUS in civil engineering*[M].Zhejiang: Zhejiang University Press,220-224.

Zhangfengxiang,Zhuhehua,Fudeming.(2004). *Shield tunneling method*[M]. Beijing: China Communications Press,867-874.

Zhouwenbo.(2004). *Shield tunneling technology*[M].Beijing: China Building Industry Press, 248-250.

A | B | C | D | E | F | G | H | I | J | K | L | M | N | O | P | Q | R | S | T | U | V | W | X | Y | Z

Author Index

A

Abraham, John Edward
Modeling Logistics and Supply Chain with an Integrated Land Use Transport Model: PECAS

Ai, Chuan-zhi
Study on Safety Stability of Excavating Shallow Depth Neighborhood Tunnel in Traversing Construction

Ai, Jun
Vehicle Trajectory Model in Two-Dimension Collision Accidents
Uncertainty Analysis of Collision Velocity in Motor Vehicle Crash Using Evidential Reasoning Algorithm

Ai, Qingyi
Integrated Arterial Signal and Access Control Strategy under Non-Notice Emergency Evacuation: Modeling and Simulation-Based Analysis

Akpakli, Vincent Kwami
A Study on the Bus Delay Model at Bus Stops

An, Shi
Gray-Periodic Extensional Combinatorial Model for Road Traffic Accidents in Cold Regions
Study on the Model of Hub Location under Earthquake Conditions
A Framework of the Traffic Organization Simulation System for Freeway Emergency Response
Capacity Reliability of Road Network under Adverse Weather Conditions Based on Fuzzy Theory

Asakura, Yasuo
A Google-Map Integrated Web-Based Stated Preference Survey for Modeling Personal Mobility

B

Bai, Haijian
Conventional Bus Stop Capacity in Peak
Capacity Model of Low Channeling Roundabout Based on Vehicle Arrival Characteristics

Bai, Hua
Empirical Correlation Analysis of Parking Arrival and Departure Rates for Urban Parking Facilities

Bai, Yu
Association of Signal-Controlled Method at Roundabout and Capacity

Bao, S.
Real-Time Optimization Model of Intelligent Public Transport Network and Its Algorithm

Bao, X.
Research on Numerical Simulation of Pollutant Dispersion at Expressway Toll Plazas Based on Multi-Influencing Factors

Bian, Changzhi
Urban Transport Network Capacity Considering Level of Service
Pricing Model for Expressway with Elastic Demand

Bu, Jianqing
Bridge Damage Assessment by Dynamic Response in Time Domain
Impact on Regularity of Track from Pile Underpinning of Light Railway Bridge
Analysis on Mechanical Performances of High-Speed Railway Transition Curves

C

Cai, Haibin
Continuous Test for Construction Quality of Mixed Filling Roadbed

Cai, Ming
Parameter Sensitivity Analysis of Accident Reconstruction Model Based on Orthogonal Design

Cai, W. P.
A Study of Vehicle and Materials Depot Location Problems for Winter Road Maintenance

Cai, Wen-Ping
The Application of the Maximal Coverage and Partial Coverage Model in the Shelter Location Problem
Real-Time Dispatching and Routing for Emergency Vehicles after Earthquake Disasters

Cai, Xiaomeng
Simulation Study on a Freeway Climbing Lane

Cai, Xin-jiang
Seismic Hybrid Simulation of a Multi-Span Bridge

Cai, Xiurong
Investment and Financing Influence Analysis and Countermeasures for Highway Construction in the Period of China's 11th Five-Year Plan

Cai, Yiyi
Investigation of the Relationship between Red-Light-Running Frequencies and Intersection Features

Cao, Gang
A Time-Varying Route Optimization Model for Urban Hazmat Transportation

Cao, Guohui
Study on Long-Term Behavior and Ultimate Strength of CFST Columns

Cao, J.
An Interval-Varying Floating Car Data Clustering Approach Based on Self-Organizing Maps

Cao, Jing
Study on the Carrying Capability of Preplanned Regional Earthquake Evacuation Corridor Based on Macro-Simulation
Analysis on Standards Used in Traffic Impact Study

Cao, Liping
Dynamic Response of Saturated Asphalt Pavement Based on Three Dimensional Finite Element Simulation
Permanent Deformation Characteristic of Asphalt Mixture Considering Pavement Temperature Distribution

Cao, W. S.
A Study of Vehicle and Materials Depot Location Problems for Winter Road Maintenance

Cao, Xiaodong
Analysis of the Competitive Strategy of the Core Enterprises in Virtual Intermodal Freight-Transportation Enterprise

Cao, Xintao
An EEG Predictor of Driving Fatigue

Cao, Yi
Vehicle Dynamics Model in Two-Dimension Collision Accident
Vehicle Trajectory Model in Two-Dimension Collision Accidents

Cen, Guo-ping
Performance of Pavement Plate Reinforced with Modified Unsaturated Polyester Fiberglass Reinforced Plastic

Chai, Gan
A Multi-Objective Decision Model of Traffic Rescue Service Site Location on Road

Chai, X.
Research on Simulation of Train Tracing Operation Based CBTC

Chang, A.
Link Average Speed of Traffic Flow Estimation Method Based on Floating Car

Chang, Chun-qing
Viscoelastic Mechanical Properties of Crumb Rubber Modified Asphalt Mixture

Chang, Liang
The Numerical Analysis of Sound and Vibration from a Tire by FEM and BEM

Chang, M. F.
Study on Permanent Deformation Characteristics of Asphalt Pavement Based on Discrete Element Method
Mechanism of Rutting Formation in Long and Steep Climbing Sections of Asphalt Pavement

Chang, Qing
An Improved Ant Colony Algorithm for the Shortest Path Problem in Time-Dependent Networks
Optimal Dynamic Substitution Policy for Components in an Assemble-to-Order

System
Coordination Policies of Supply Chain Where Deterioration Begins at a Random Time Point

Chang, Yun-tao
Analysis and Evaluation of Expressway Planning Schemes Based on Integrated Macro and Micro Simulation
Evaluation of Traffic Impact on Land Development Projects Based on Matter-Element Analysis

Chang, Zhenwen
The Analysis of Traffic Flow State on Foggy Expressway Based on Fuzzy Clustering

Chao, Huanhuan
Empirical Correlation Analysis of Parking Arrival and Departure Rates for Urban Parking Facilities

Chen, A. R.
Flutter Derivatives Identification of Aeroelastic Model of Hangzhou Bay Bridge

Chen, Bin
Risk Evaluation Model for Construction of a Logistics Park Based on Principal Component Analysis

Chen, Dafei
Analyzing the Motivation of Queue-Jumping Driving-Action on Transportation Systems by Prospect Theory

Chen, Dingjun
An Improved Ant Colony Algorithm for Placing-In and Taking-Out of Wagons in Branch-Shaped Sidings

Chen, Gangliang
Multi-Section Short-Term Traffic Flow Prediction Based on Multi-Dimensional Time Series

Chen, Hanzhen
Research on the Crashworthiness of Two-Layer Thin-Walled Structures

Chen, Hong
The Evaluation of Micro-Benefit on Highway Construction Investments
An Active Parking Guidance Information System Based on Dynamic Agent Negotiation

Chen, Hongyun

Evaluating the Impacts of Ramp Configurations and Influential Factors on Freeway Exit Ramps

Chen, J.
Optimal Setting of the VMS's Future Range Based on the Characteristics of Driving Speed

Chen, Ji-hong
A Nonlinear Model for Decision-Making for Container Slot Chartering and Allocation under Liner Shipping Alliance

Chen, Jian
Design of 3D Virtual Simulation and Evaluation System for Road Traffic Signs

Chen, Juan
The Application of the Maximal Coverage and Partial Coverage Model in the Shelter Location Problem

Chen, Jun
Empirical Correlation Analysis of Parking Arrival and Departure Rates for Urban Parking Facilities
The Attitude and Psychological Demand Related Determinants of Public Transport Use

Chen, Lijun
Structure System Model of Modern Logistics

Chen, Minglan
Investment and Financing Influence Analysis and Countermeasures for Highway Construction in the Period of China's 11th Five-Year Plan

Chen, Nianhe
A Study on Cable-Removing Scheme of the Cable-Stay System of the Zhijing River Bridge

Chen, Ningning
Adaptive Control Method of Multi-Phase Intersection Based on Traffic Status Identification

Chen, Rong
Adaptability Assessment and Maintenance Technology Research of Existing Railway Line Speed Increases to 200 km/h

Chen, Rui-Xiang
Application Research of GPS Based on Google Earth Platform

Chen, S.
Influence of Crack Size of Old Concrete Pavement Slab on Structure Stress of Asphalt Overlay

Chen, Shijun
Vibration Characteristics of Permafrost Embankment Induced by Passing Trains in Qinghai-Tibet Railway in Winter

Chen, Shuanfa
An Evaluation of the Effectiveness of Geo-Textile-Binder-Aggregate System for Surface Treatment of Distressed Asphalt Pavement

Chen, Sili
Study on Experiment of Concrete Mixed with II Degree Flyash under the Corrosion of Freeze Thawing

Chen, Suping
A Comprehensive Bus Line Evaluation Method Based on Fuzzy C-Means Clustering Algorithm

Chen, T.
Research on Optimization of Crew Scheduling of the Passenger Dedicated Line Based on a Genetic Ant Colony Algorithm

Chen, Tao
A Traffic Accident Reconstruction Study on Continuous Collision of Three Cars
Study and Implementation on JPEG Image Enhancement System of Tire Mark

Chen, Tianhong
Stability and Reinforcement Methods of a High Slope at the Hang-Yong Natural Gas Pipeline in China

Chen, Wanji
A Speed Limit Model of Vehicle for Urban Road Hazmat Transportation

Chen, X.
Study on the Rules of Crash Distribution
Evaluating the Equity Impacts of Rural Road Investment Projects on Household Welfare Based on a Quantile Regression Approach: Evidence from Fujian Province

Chen, Xi
Finite Element Analysis on Shear-Lag Effect in Curved Continuous Box Girder with Corrugated Steel Webs

Chen, Xiang

A Study of the Fuzzy PID Control Over the Hydraulic Semi-Active Suspension in Consideration of Automotive Engine and Passenger-Seat System

Chen, Xiao

Damage Model Analysis of SBS Modified Asphalt Mixture

Chen, Xiaohong

The Analysis of Traffic Landscape from Users' Perspective: The Case of the Zhangjiang Tram

Investigation of Relationship between Level of Service and Safety

Investigation of the Relationship between Red-Light-Running Frequencies and Intersection Features

Chen, Xiaoping

Adaptability Assessment and Maintenance Technology Research of Existing Railway Line Speed Increases to 200 km/h

Chen, Xin-dong

A Calculation Method for the Information Utility of Traffic Guide Signs

Chen, Xiqun

Evaluation and Optimization of Public Transport Subsidies for Alternative Energy

Chen, Xuewu

Study on the Relationship of Traffic Flow Complexity and Traffic Conflict on Urban Road

The Key Technology of "One Road One Line with Straight Driving" Public Transportation System

Assessing Performance of Public Transit Network Using Network-Based Accessibility Measures

A Comprehensive Bus Line Evaluation Method Based on Fuzzy C-Means Clustering Algorithm

Transit Network Optimization Method Based on BRT Attracting Region: A Case Study of Changzhou

Structure System Model of Modern Logistics

Chen, Y.

Research on Urban Intersection Vehicle Emission Reduction Based on Microcosmic Simulation

Mechanism of Rutting Formation in Long and Steep Climbing Sections of Asphalt Pavement

Congestion Pricing Revenue Redistribution Strategy Based on Traffic Behavior

Chen, Yanyan
Research on Pedestrian Safety under Rapid Development of Motorization
Pedestrian Simulation Research of Subway Station in Special Events

Chen, Yi
A Time-Varying Route Optimization Model for Urban Hazmat Transportation

Chen, Yuanzhao
Research on Rapid Curing Technology of Lime-Flyash-Cement Stabilized Macadam

Chen, Zheng-jin
Research on Flame-Retardant Technique in Application of Asphalt Pavement in Highway Tunnel

Chen, Zhiguo
Study on the Frost Resistance Test Method of Lime-Fly Ash Stabilized Material Base Course

Chen, Zhijun
A New Organizational Structure Pattern of Owners Based on Multi-Project

Cheng, G.
Train-Carried Rail Signal Parameters Test System Based on Spectrum Correction Method and Virtual Instrumentation

Cheng, Gong
Research on Urban Public Transit Dispatching System Based on Real-Time Prediction and Game Theory

Cheng, Guozhu
Methods of Setting Maximum Speed Limits on Freeways

Cheng, Lin
Multi-Section Short-Term Traffic Flow Prediction Based on Multi-Dimensional Time Series
Study on Road Network Reserved Capacity on Different Levels of Service and Stochastic Conditions

Cheng, Shaowu
A Framework of the Traffic Organization Simulation System for Freeway Emergency Response

Cheng, X.
Effect of Electro-Mechanical Coupling on Dynamic Performance of Crankshaft of ISG HEV

Cheng, Xiaoliang
Dynamic Response of Saturated Asphalt Pavement Based on Three Dimensional Finite Element Simulation

Cheng, Yong-chun
Experimental Research on the Shear Strength Deterioration between the Freezing and Thawing Surface of Melting Soil Slope in Seasonal Frozen Regions

Chi, Cheng
Study on Prolonging Asphalt Pavement Fatigue Life Based on Vision Transverse Intervention

Chong, L.
Research on Simulation of Train Tracing Operation Based CBTC

Ci, Yusheng
A New Cellular Automaton Traffic Flow Model for an Off-Ramp Junction of a Chinese Urban Expressway

Cui, Hongjun
Case Study on the Computing Model of the Driving-Into Rate of Service Area

Cui, J. X.
A Study of Transit Evacuation Route Planning Based on Time-Expanded Network

Cui, K.
Analysis of a New Combined Micropile Structure for Preventing Slope Slippage and Its Application in a Practical Project

Cui, Xiao Tian
Analysis about Business Investing and Financing Models of Urban Rail Transit

Cui, Xiaotian
Algorithm of PFE and Its Application in Shenzhen Urban Transport Simulation System
Study of the Parking Guidance Reliability of Urban Parking Variable Message Signs

Cui, Yaping
Study on Evaluation Method of Expressway Roughness

D

Dai, Huanyun

Vehicle Semi-Active Suspension System Simulation with Variable Structure Control Method

Dai, Jingguo
A Manual Calibration Method for Simulation of a Freeway Weave Section

Dai, Leilei
Road Traffic Safety Micro-Evaluation Based on Bayes Theory

Deng, Ke
Calculation Method on Traffic Noise Pollution of Interchange Based on Geometric Alignment

Deng, Shuanglong
The Method of Determining Traffic Impact Range of Developing Project Based on Threshold Value

Deng, Wei
Study on Congestion Pricing Model of Bus Lane Mixed Use by Carpool Vehicles

Deng, Ziyin
Urban Transport Network Capacity Considering Level of Service

Di, Di
Travel Mode Choice in Large Cities of China Based on Loss Aversion Theory

Diao, Bo
Influence of Curing Regime on the Ductility of Ultra-High Performance Fiber Reinforced Concrete (UHPFRC)

Ding, Heng
Accident Prevention and Inducement Strategy in Highway Tunnel

Ding, Jianmei
An AHP-Based Performance Evaluation Model of Transportation Control System: The Experience from West Liaohe Rd., Dalian
An Optimized Signal Control Method for a Freight Arterial Transport System

Ding, Nan-Hong
A Safety Evaluation Method of Existing Flexible Suspension Bridge with Double Cable

Ding, Tongqiang
Study on Accident Reconstruction Model Based on Reverse-Reasoning Method

Ding, Zhenglin

Grey Relational Analysis Method of Main Reasons of Road Traffic Accidents

Dong, Qiaoting
A New Organizational Structure Pattern of Owners Based on Multi-Project

Dong, Ruijuan
Conventional Bus Stop Capacity in Peak
Capacity Model of Low Channeling Roundabout Based on Vehicle Arrival Characteristics

Dong, S.
Study on Spatial Information Model and Database of Traffic Facilities Management Systems Based on ArcGIS

Dong, Shuhui
Effect of Lightweight Aggregate with Different Moisture of Autogenous Shrinkage and Stress under Partially Restrained Condition

Dong, Wang
Optimum Choice for the Construction Management Plan Based on Entropy Weight

Dong, Xi-bin
Experimental Research on the Combined-Method of Vacuum Well-Point Dewatering and Preloading
Study on Asphalt Treated Permeable Base in Permafrost Regions
The Experimental Study of Effects of Herbaceous Plant Protecting Slope in Cold Area

Dong, Yu-pu
Impact Analysis on Countdown Device on Transit Priority Signal Control

Dong, Zejiao
Dynamic Response of Saturated Asphalt Pavement Based on Three Dimensional Finite Element Simulation
Permanent Deformation Characteristic of Asphalt Mixture Considering Pavement Temperature Distribution

Dong, Zhi
The Analysis of Transportation Demand Generation Mechanisms of the Urban Agglomerations in China

Druta, Cristian
Laboratory Investigation of Reclaimed Asphalt Pavement Mixed with Pure Binder Using X-Ray CT Scanner

Du, Huabing
Expansion and Validation of Beijing Household Interview Survey Data

Du, Rongqiang
Application of High Performance Concrete Mixed with Steel Slag Powder in Concrete Pavements

Du, Xi-kai
Experimental Research and Damage Model of Square Concrete-Filled Steel Tube Subjected to Cyclic Loading

Du, Ye-fan
Study on Traffic Impedance Based on Grey Theory

Du, Ying-chun
A Study on Vehicle Trip Distribution Forecasting Based on BP Neural Network

Du, Yuchuan
ALINEA-Based Urban Expressway On-Ramp Metering Strategy

E

E, Wenjuan
Research on Urban Intersection Vehicle Emission Reduction Based on Microcosmic Simulation

F

Facanha, Cristiano
Repositioning of Empty Containers in the Transpacific Market: A Case Study

Fan, Dongxu
Research on Dynamic Characteristics of Road Network in Snowy Conditions

Fan, Meng
Basic Study on Fractal Characteristic of Pore Structure in Cement Mortar

Fan, Shasha
Study on Multi-Dimensional Structure Model for Agricultural Products Logistics Organization in China

Fang, Chengwei

A Multi-Objective Decision Model of Traffic Rescue Service Site Location on Road

Fang, Jia
Individual and Population Learning in Route Choice Behavior of Drivers: Experiment and Model

Fang, Lei
Research of Road Transportation Sustainable Development Based on Ecological Footprint Model

Fang, R.
Experimental Study on Sound Countermeasures against Driver Fatigue

Fang, S.
Analysis of the Influence of Emergent Incident on Expressways by Simulation
Probabilistic Pedestrian-Vehicle Conflict Micro-Model in Non-Signal Controlled Multi-Lane Segments

Fang, Shun
Simulation Analysis of Merging Area on Urban Expressway in Alternate Rules Based on Cellular Automata Model

Fang, Xuejiao
Influence Analysis of Deep Discount Policy on Public Transit Ridership

Fang, Yuan
Evaluation and Optimization of Public Transport Subsidies for Alternative Energy

Fang, Zhengpeng
Design of 3D Virtual Simulation and Evaluation System for Road Traffic Signs

Fei, Feifei
Study on the Optimization of Vessel Scheduling Design Based on Soft Time Windows under Voyage Charters

Feng, De-cheng
Research on Relationship between Fine Aggregate Angularity and Asphalt Mixture’s Anti-Shear Ability

Feng, Decheng
Impact of Gradation Types on Freeze-Thaw Performance of Asphalt Mixtures in Seasonal Frozen Region
Function Design of Cement Stabilized Crushed Stone Drainage Base
Heat Reflection Coating Design and Performance
Experimental Analysis of Interface Bond Performance of UTW

Feng, Deyou
Experimental Analysis of Interface Bond Performance of UTW

Feng, J.
Analysis of a New Combined Micropile Structure for Preventing Slope Slippage and Its Application in a Practical Project

Feng, Qian
Technology Research on the Vehicle Collision Accident Self-Alarm System

Feng, Sheng
Research on the Mechanism for Preventing Reflective Cracks in Old Cement Concrete Pavement Reconstruction

Feng, Xiating
Study on Experiment of Concrete Mixed with II Degree Flyash under the Corrosion of Freeze Thawing

Feng, Xuejun
Optimization of Emergency Material Dispatch Problem Based on Adaptive Genetic Algorithm

Feng, Y. J.
Mean-CVaR Model of Wholesale Price Contracts and Dual Purchase Contracts in the Supply Chain

Feng, Yuqin
An Estimate Method for Accuracy of Fitting Horizontal Alignment in Old-Highway Based on Fitting Normal Error

Fu, Tao
Research on a Risk Analysis System of Vessel-Bridge Collision

Fu, Zhi
Analysis of Elastic Slab on Non-Uniform Support Foundation Using a Weighted-Residual Method

Fu, Zhipeng
Effect by Different Factors on Ductility of Evaporated Residue of Modified Emulsion Asphalt

G

Gang, Long-Hui
Study on the Method for Calculating Ship Squat in the Restricted Channel

Gao, H. G.
Pavement Crack Automatic Recognition Based on Wiener Filtering

Gao, H. Z.
Public Transport Incident Prediction Method by Road Traffic Delays

Gao, H.
Frequency Optimization Model for a Public Traffic Scheduling System

Gao, Han
Effect of Sunlight Glare on Drivers' Psychophysiological Characteristics

Gao, Hui
An Improved Ant Colony Algorithm for the Shortest Path Problem in Time-Dependent Networks
Optimal Dynamic Substitution Policy for Components in an Assemble-to-Order System
Coordination Policies of Supply Chain Where Deterioration Begins at a Random Time Point

Gao, Qingping
Locating Emergency Response Facilities for Hazardous Materials Transportation with Probabilistic Response Time

Gao, Shuling
Experimental Study on Performance of the Bridge Deck Pavement of SF-PFSC

Gao, Song
Choice of Reasonable Longitudinal Gradient at Alignments of Mountain Highways Based on Driver's Physiological Reactions
Impacts of Road Sight Distance on Safe Driving Conditions
Bus Location Display System Based on GPRS
Study on the Control Strategy of Gas Injection of Gas Engines

Gao, T.
Study on Spatial Information Model and Database of Traffic Facilities Management Systems Based on ArcGIS

Gao, X.
Shake Table Test on Seismic Response of Non-Free Liquefiable Site

Gao, Xia
Case Studies for Shaking Table Tests on Seismic Soil-Pile Group-Bridge Structure Interaction in Liquefiable Ground
Freeze-Thaw Stability of Slopes in Seasonally Frozen Regions of the Northeast China

Gao, Yan
Grey Relational Analysis Method of Main Reasons of Road Traffic Accidents

Gao, Yang
Analysis of Runway Incursion in Civil Airport Based on Bayesian Network
An Improved A* Algorithm for the Intelligent Transportation System
A Novel Real-Time Road Shape Describing and Parameter Obtaining Method

Gao, Yuee
Forecast the Automobile Population Based on Scenario Analysis

Ge, Qi
Experimental Research on the Shear Strength Deterioration between the Freezing and Thawing Surface of Melting Soil Slope in Seasonal Frozen Regions

Ge, Yong
Effect of Inorganic Salts on Frost Resistance of Concrete
Effect of Lightweight Aggregate with Different Moisture of Autogenous Shrinkage and Stress under Partially Restrained Condition

Ge, Zhe-sheng
Effect of Density Variation of Coarse Aggregate on Asphalt Mixture Properties

Gong, Bowen
Dynamic Model of Transit Signal Priority on Colored Time Petri Net

Gong, Lingling
Experimental Research on Shear Connectors' Stress of Composite Beam Bridge under Complex Stress Condition

Gong, Wei-yong
Signal Intersection Optimal Control Model of Small Region Based on Traffic Equilibrium Theory

Gu, Hongbin
Restraint Efficacy Analysis and Structure Optimization for the Design of Airplane Metal Chocks

Gu, Hongjiang
Design and Validation of Wireless Dynamic Testing System for Bridge Based on the 941B Type Vibration Sensor

Gu, Jiuchun
Study on Pedestrian Safety and Countermeasures in Crosswalks around Campus—Case Study at Ludong University in Yantai

Guan, Hong-zhi
Individual and Population Learning in Route Choice Behavior of Drivers: Experiment and Model

Guan, Hongxin
Rut-Resisting Capacity of the Whole Surface Course in Continuous Upgrade under Heavy Loading

Guan, Hongzhi
Influence Analysis of Deep Discount Policy on Public Transit Ridership

Guan, Jizhen
Expressway Data De-Noised Approach Based on Wavelet Analysis

Guan, L.
Detecting the Type of Multi-Fractality in Traffic Time Series

Guan, Q.
The Study on Design Method of Vehicle Intake Silencer Based on Three-Dimension/One-Dimension Models Coupling

Guan, Xiaojun
Study on Logistics Center Location Bi-Level Programming Model and Algorithm Based on Competition

Guan, Z.
Safety Evaluation Methods of Road Traffic Based on Gray Cluster Theory

Gui, Wengang
Research on the 25kW FCPS's Temperature Controlling Simulation

Guo, D.
Research on Urban Intersection Vehicle Emission Reduction Based on Microcosmic Simulation

Guo, Fengxiang
Evaluation Study of the Median Markings in Undivided Highway Tunnels

Driving Simulation Study on Traffic Flow Characteristics on the Climbing Lane on a Two-Lane Rural Road

Guo, Gao

The Application of the Maximal Coverage and Partial Coverage Model in the Shelter Location Problem

Real-Time Dispatching and Routing for Emergency Vehicles after Earthquake Disasters

Guo, Hongwei

Analysis of Crowd Behavior in Route Choice Based on Dynamic Programming

Guo, Hua

Risk Assessment of Road Operation Environment under Atrocious Weather Condition

Guo, Ji Fu

Research on Travel Behavior Changes under Vehicle-Use-Restriction Measures during the Olympic Games

Guo, Jifu

Research on Pedestrian Safety under Rapid Development of Motorization

Guo, Naisheng

A Fatigue Test on Fiber Reinforced Asphalt Mixtures

Guo, Qianqian

An Improved Ant Colony Algorithm for Placing-In and Taking-Out of Wagons in Branch-Shaped Sidings

Guo, Tangyi

Operational Performance Evaluation of Different Exit Ramps on Florida’s Freeways by Considering Number of Lane Change

Guo, Xiaofen

Research on Taboo Simulated Annealing Combinatorial Optimization Algorithm of Location Routing Problem with Pickups and Deliveries

Guo, Y.

Train-Carried Rail Signal Parameters Test System Based on Spectrum Correction Method and Virtual Instrumentation

Guo, Yang

A Fatigue Test on Fiber Reinforced Asphalt Mixtures

Guo, Zhiyong

The Key Technology of "One Road One Line with Straight Driving" Public Transportation System

Guo, Zhong-yin
Risk Assessment of Road Operation Environment under Atrocious Weather Condition

Guo, Zhongyin
Identification of Hazardous Locations Based on Integrated Highway Safety State Analysis

H

Han, Chang-ling
Study on Safety Stability of Excavating Shallow Depth Neighborhood Tunnel in Traversing Construction

Han, Chenglin
Study of Anti-Slide Pile Composed of Arch and Truss Structure Based on FEM

Han, Junhee
Advanced Traveler Information Impact on Truck Route Choice

Han, Ping
A Study on the Headway Distribution of the Xueyuan Roundabout

Han, Y.
Wavy Road Elevation Measurement Based on the Principle of Inertia
Public Transport Incident Prediction Method by Road Traffic Delays
Highway Traffic Parameters Estimation by Using Cell Dwell Time
Real-Time Optimization Model of Intelligent Public Transport Network and Its Algorithm
Frequency Optimization Model for a Public Traffic Scheduling System

Han, Yan
Influence Analysis of Deep Discount Policy on Public Transit Ridership

Hao, Yubo
Analysis of Characters and Causes of Road Traffic Accident Migration

He, Baoxi
Discussion on Methods of Traffic Routes' Alignment Survey and Application of Principle of Least Squares

He, Cao
Research on the Impact of Drivers' Heart Rate on Longitudinal Slope of Freeway Tunnel

He, Hongming
Experimental Research and Damage Model of Square Concrete-Filled Steel Tube Subjected to Cyclic Loading

He, J.
Research on Numerical Simulation of Pollutant Dispersion at Expressway Toll Plazas Based on Multi-Influencing Factors

He, Jun-hui
Study on the Influence of Coarse Aggregate on the Pavement Performance of Road Cement Concrete

He, Lei
Real-Time Dispatching and Routing for Emergency Vehicles after Earthquake Disasters

He, Minai
Real-Time Monitoring System Architecture of Hazardous Goods Logistics Based on RFID

He, Peng
A Novel Real-Time Road Shape Describing and Parameter Obtaining Method

He, Ran
Study on Long-Term Behavior and Ultimate Strength of CFST Columns

He, Ren
Calculation Method for Braking Torque of Self-Excited Retarder
Fuzzy Control of AMT Clutch Engagement during the Vehicle Starting

He, Shuan-hai
Nonlinear Analysis of Time-Dependent Effect for Reinforced Concrete Thin-Wall Box Girders Exposed to Fire
Relation of Stability Coefficient to Design Parameters for Curved Continuous Rigid Frame Bridges with Long-Span and High-Pier

He, Y.
Highway Accidents Analysis with Panel Data Model
Impact of Posted Speed Limits on Operating Speed in Urban Expressways

He, Yan
Experimental Research on the Shear Strength Deterioration between the Freezing and Thawing Surface of Melting Soil Slope in Seasonal Frozen Regions

He, Yulong
The Impacts of Differential Speed Limits on Speed
Road Safety in Sections under Mixed Flow Traffic Environment

He, Z.
Research on Greedy Train Rescheduling Algorithm

He, Zhaocheng
Adaptive Control Method of Multi-Phase Intersection Based on Traffic Status Identification

He, Zhenfeng
From Time Based Speed Series to Behavior Sequence: The Transformations and Applications of VTDR Data

Hou, Shijing
Research on the Crashworthiness Optimization of Curved-Road Concrete Barriers

Hou, Shuzhan
The Impacts of Differential Speed Limits on Speed

Hou, Xiang-shen
Gradually Rolling Prediction of the Use-Level of Road Network Based on BP Neural Network

Hou, Xiangshen
Research on Structural Design of Interlocking Concrete Block Pavement for Rural Road
The Analysis of Dowel and Tie Bars Effects on Curling Up in Concrete Pavement Slabs
The Analysis of the Correlation between International Roughness Index and Body Ride Comfort

Hou, Xianjun
Research on the 25kW FCPS's Temperature Controlling Simulation

Hou, Zhaoguang
Study on the Preventive Maintenance Time for Asphalt Pavement

Hsu, Li-Yen

Enhancing Airport Security and Place Marketing with Spider Web Networking

Hsu, Ping
Effects of Roadway Lighting Level on the Pedestrian Safety

Hu, Chen
A Study on Speeding Driving Based on Expected Speed

Hu, Chunbin
Bus Service Frequency Multi-Objective Optimal under Snowy Day

Hu, Dawei
Research on Taboo Simulated Annealing Combinatorial Optimization Algorithm of Location Routing Problem with Pickups and Deliveries

Hu, Hui
A Particle Swarm Optimization Algorithm for Bilevel Programming Models in Urban Traffic Equilibrium Network Design
Theory Study on Correlation Stability and Profit Allocation of Supply Chain

Hu, Jiangbi
An EEG Predictor of Driving Fatigue

Hu, Jinxin
A Study on the Location Selection of Public Traffic Transfer Hub Based on Improved Particle Swarm Algorithm

Hu, Liwei
Evaluation of Road Traffic Safety Based Improved Fuzzy-AHP Method

Hu, Peng
Study on Prolonging Asphalt Pavement Fatigue Life Based on Vision Transverse Intervention

Hu, Q. F.
The Simulation Analysis of Passenger Evacuation in One Metro Station Based on Exodus

Hu, Qingwu
A "Reality Vision" Navigation Technique Based on Sequence Geo-Referenced Image Databases

Hu, X. L.
Flutter Derivatives Identification of Aeroelastic Model of Hangzhou Bay Bridge

Hu, X.

Effect of Electro-Mechanical Coupling on Dynamic Performance of Crankshaft of ISG HEV

Hu, Xiaoming
A Model and Heuristic Algorithm for Inventory Routing Problem in Emergency Logistics

Hu, Xiaowei
Bus Service Frequency Multi-Objective Optimal under Snowy Day
Analysis of City Transportation Networks' Travel Time Reliability during Adverse Weather
Multi-Objective Interval Number Model of Intermodal Transport under Uncertain Environment

Hu, You-chang
Experimental Study on Behavior of Geotextile-Reinforced Soil

Hu, Yucong
Study on a Passageway Location Model on Underground Expressway

Hu, Zhaofang
A Fuzzy Neural Network Technique for Crack Assessment of RC Bridges

Hu, Zhaotong
Finite Element Analysis on Shear-Lag Effect in Curved Continuous Box Girder with Corrugated Steel Webs

Hu, Zhijian
A Fuzzy Neural Network Technique for Crack Assessment of RC Bridges

Hu, Zuoan
Optimization of Dynamic Dispatching Decisions of Local Wagon-Flows in Terminals with IRTS

Huang, Bao-shan
Fracture Mechanics Analysis of Cracking in Asphalt Pavement Widening

Huang, Caihong
Bending Vibration Suppression of High Speed Railway Passenger Car Body

Huang, H. W.
The Simulation Analysis of Passenger Evacuation in One Metro Station Based on Exodus

Huang, Haijun
Ramp Metering Strategies in a Corridor Network

Efficiency Loss of the Multiclass, Multicriteria Stochastic User Equilibrium Traffic Assignment against Stochastic System Optimization

Huang, Haixin
Influence Factors Analysis of Buffeting Response of Self-Anchored Cable-Stayed Suspension Bridge

Huang, Jing
Evaluation of Fire Risk at Highway Tunnels

Huang, Min-shui
Study on Different Residual and Weight Coefficient in Model Updating of Bridge Structure

Huang, Q.
Lane Change Behavior Character and Its Influence to Traffic Safety on Urban Roads

Huang, Qiao
NURBS Strands Modeling of Prestressed Concrete Bridges

Huang, Qing
Risk Evaluation Model for Construction of a Logistics Park Based on Principal Component Analysis

Huang, Shan
Individual and Population Learning in Route Choice Behavior of Drivers: Experiment and Model

Huang, Shunquan
Study on Energy Consumption by Land Cargo Transportation

Huang, Xiangrong
A Model on Risk Evaluation for Emergency Guarantee Mechanism of Food Logistics

Huang, Yuqiang
Experimental Analysis of Interface Bond Performance of UTW

Huang, Z.
Safe Spacing Research Based on the Theory of Cellular Automation on Freeways in Foggy Weather

Huang, Zhengdong
Information Needs of Urban Transit Travelers—The Case of Wuhan, China

Huang, Zhenzhi

From Time Based Speed Series to Behavior Sequence: The Transformations and Applications of VTDR Data

Hui, Hongqi
Case Study on the Computing Model of the Driving-Into Rate of Service Area

Hui, Ying
Investment and Finance for the Intelligent Transportation System in China
Study of Operational Characteristics of HAZMAT Vehicles Based on GPS Data

Hunt, John Douglas
Modeling Logistics and Supply Chain with an Integrated Land Use Transport Model: PECAS

Huo, Yamin
Dynamic Alliance of Road Logistics Enterprise Based on Ant Colony Algorithm

I

Inaishi, M.
Collision Avoidance among Multiple Ship Agents

J

Ji, H.
Influencing Factors Contributing to Rear-End Collisions on Highways: PCA Based Investigation and Findings

Ji, Heng
The Research of Control Strategy of Permanent Magnet Synchronous Motor for Hybrid Electric Vehicles

Ji, Lun
Research on Flame-Retardant Technique in Application of Asphalt Pavement in Highway Tunnel

Jia, Jonathan
A Study of Cold In-Place Recycling Mixture Used as Binder Course in China

Jia, Yanmin
Nonlinear Analysis of Prestressed Steel Box Beams

Jia, Zhiping
Research on the Mechanism for Preventing Reflective Cracks in Old Cement Concrete Pavement Reconstruction

Jian, Lingxiang
Research on Cost Control in Logistics Enterprises

Jiang , Li
Research on Automatic Identification Method of Pavement Sag Deformation

Jiang, Bi-feng
The Experimental Study of Effects of Herbaceous Plant Protecting Slope in Cold Area

Jiang, Bo
Research on Location of Railway Logistics Center

Jiang, G.
Link Average Speed of Traffic Flow Estimation Method Based on Floating Car

Jiang, Haifeng
Design of 3D Virtual Simulation and Evaluation System for Road Traffic Signs

Jiang, Huiyuan
Coordinated Development between Transportation System and Socio-Economic System Research Based on SEM

Jiang, Niandong
Application Research of GPS Based on Google Earth Platform

Jiang, Xiaobei
Analysis of Crowd Behavior in Route Choice Based on Dynamic Programming

Jiang, Xin-jia
A Study of the Fuzzy PID Control Over the Hydraulic Semi-Active Suspension in Consideration of Automotive Engine and Passenger-Seat System

Jiang, Yonglei
Road Traffic Control Information and Traffic Resource Analysis System
An Optimization Model for Bus Rapid Transit
Study on the Structure of Digitized Transport Networks and Evaluation of Some Logistics Policies

Jiang, Zitian
Design and Validation of Wireless Dynamic Testing System for Bridge Based on

the 941B Type Vibration Sensor

Jiao, Chengwu
Analysis of Characters and Causes of Road Traffic Accident Migration

Jiao, Hai-xian
Signal Intersection Optimal Control Model of Small Region Based on Traffic Equilibrium Theory

Jiao, Xinlong
Empirical Research on Urban Rail Transit Operation Performance Based on FCE–AHP

Jie, Mou
Optimum Choice for the Construction Management Plan Based on Entropy Weight

Jin, Lianjie
Study on the Structure of Digitized Transport Networks and Evaluation of Some Logistics Policies

Jin, Shanshan
Basic Study on Fractal Characteristic of Pore Structure in Cement Mortar

Jin, W.
Analysis of the Influence of Emergent Incident on Expressways by Simulation

Jin, Wenzhou
Study on a Passageway Location Model on Underground Expressway

Jin, Xionghuan
Research on Location of Railway Logistics Center

Jin, Xue
Research on the 25kW FCPS's Temperature Controlling Simulation

Jin, Xuesong
Model of High Speed Railway Wheel Ovalization
The Application of Functionally Gradient Material to Problems of Wheel-Rail Contact

Jing, Hai-min
Gradually Rolling Prediction of the Use-Level of Road Network Based on BP Neural Network

Jing, Lin
Effect by Different Factors on Ductility of Evaporated Residue of Modified Emulsion

Asphalt

Jun, H.
Influencing Factors Contributing to Rear-End Collisions on Highways: PCA Based Investigation and Findings

K

Kang, Haigui
Road Traffic Control Information and Traffic Resource Analysis System

Kang, Hourong
The Bearing Character of Bridge Piles in Karst Areas

Kang, Yongzheng
Research on Model of Public Transportation Network Optimization Based on the Demand of Citizen Trips

Kong, Fanying
Application of High Performance Concrete Mixed with Steel Slag Powder in Concrete Pavements

Kong, Xiangya
Stiffness Reduction Factor of Reinforced Concrete Bridge Pier Considering Characters of Nonlinear

Kui, H.
Study on Spatial Information Model and Database of Traffic Facilities Management Systems Based on ArcGIS

L

Lai, Anxing
Application of Fractal Theory in Pavement Surface Texture Measurement

Lan, Qingqun
Fatigue Life Prediction of Rubber Nodes

Lan, Rong
New Methods for Research in Multi-Agent Traffic Signal Control

Lan, Xiang

Nonparametric Analysis of Timely Distribution of Traffic Crash
Research on the Bicycle Capacity of Signalized Intersection Based on Fluid Diffusion Characteristics

Lei, Lei
Analysis on Standards Used in Traffic Impact Study

Lei, Li
Study on Intersections with Median BRT Stations: Focused on Pedestrian Street-Crossing Characteristics

Lei, Quan
Research on Relationship between Fine Aggregate Angularity and Asphalt Mixture's Anti-Shear Ability

Lei, Shuai
Technology Research on the Vehicle Collision Accident Self-Alarm System

Lei, Zhengbao
Research on the Crashworthiness Optimization of Curved-Road Concrete Barriers

Lei, Zhiyi
Grey Correlation Analysis on Logistics Energy Consumption

Leng, Junqiang
Assessment Methodology for Road Network Travel Time Reliability under Ice and Snowfall Conditions

Leng, Yuquan
Assessment Methodology for Road Network Travel Time Reliability under Ice and Snowfall Conditions

Li, Ai-Zeng
Research on Conversion Coefficients between Bicycle, Electric Bicycle, and Pedestrian on Urban Road Intersection

Li, B.
Impact of Posted Speed Limits on Operating Speed in Urban Expressways

Li, Chang-hong
Study on the Green Traffic Planning System of New Rural Communities

Li, Chang-yu
Experimental Research on the Mechanical Parameter of Fly Ash Soil
Sensitivity Analysis of the Dynamical Parameters on Road Materials

Li, Chang
Expressway Operation Financial Benefit Evaluation under Uncertainty

Li, Chaoyang
Study on Inter-regional Transportation Infrastructure Integration Planning in China

Li, Chengbing
An Improved Ant Colony Algorithm for Placing-In and Taking-Out of Wagons in Branch-Shaped Sidings

Li, Chun Yan
Research on Travel Behavior Changes under Vehicle-Use-Restriction Measures during the Olympic Games

Li, Dongbing
Research on Cost Control in Logistics Enterprises

Li, Dongping
Study of the Parking Guidance Reliability of Urban Parking Variable Message Signs

Li, Feng-chen
Reliability Analysis of Cable-Stayed Bridge under Reaction of Seldom Occurred Earthquake

Li, Fuhai
Restraint Efficacy Analysis and Structure Optimization for the Design of Airplane Metal Chocks

Li, Guang-yuan
Performance of Pavement Plate Reinforced with Modified Unsaturated Polyester Fiberglass Reinforced Plastic

Li, Guangyuan
New Concrete Improving Performance of Airfield Pavement

Li, Gunan
A Speed Limit Model of Vehicle for Urban Road Hazmat Transportation

Li, Guo-fang
A Study of the Fuzzy PID Control Over the Hydraulic Semi-Active Suspension in Consideration of Automotive Engine and Passenger-Seat System

Li, H.
Research on Greedy Train Rescheduling Algorithm

Li, Haifeng
A Study on the Matching of Urban Form and Traffic Pattern

Li, Hiwen
Theoretical Analysis of Design Parameters on Semi-Rigid Asphalt Pavement with Flexible Base

Li, Hong-ping
The Evaluation of Level of Service for Expressway in Operating Stage

Li, Hong-Xi
Study on the Method for Calculating Ship Squat in the Restricted Channel

Li, Hong
The Bearing Character of Bridge Piles in Karst Areas

Li, Hui-Shan
The Application of Anti-Rutting Agent on Improving the High-Temperature Stability of Asphalt Pavement

Li, Hui
Optimization of Transportation Enterprises Pricing Strategies

Li, Huijun
A New Organizational Structure Pattern of Owners Based on Multi-Project

Li, J.
The Study on Design Method of Vehicle Intake Silencer Based on Three-Dimension/One-Dimension Models Coupling

Li, Jiang
Study on Accident Reconstruction Model Based on Reverse-Reasoning Method

Li, Jianglong
Observation and Theoretical Analysis of the Temperature Field on the Cross Section of Concrete Filled Steel Tubes Arch Bridge Rib

Li, Jie
Information Needs of Urban Transit Travelers—The Case of Wuhan, China
Study on Different Residual and Weight Coefficient in Model Updating of Bridge Structure

Li, Ke-ping
Impact Analysis on Countdown Device on Transit Priority Signal Control

Li, Keping
The Comparison of Three Getting Signal Control Delay Video Methods at Signalized Intersection
A Manual Calibration Method for Simulation of a Freeway Weave Section

Li, L.
Traffic Signal Control Optimization of Urban Arterials Based on a Method of Main Intersection Control Strategies
Study on Shear Properties for Adherence of New and Old Concrete and Its Practical Calculation

Li, Li-hui
Study on Asphalt Treated Permeable Base in Permafrost Regions

Li, Li
Node-Importance-Degree-Based Logistics Node Analysis

Li, Lilan
Research on the Bicycle Capacity of Signalized Intersection Based on Fluid Diffusion Characteristics
Gray-Periodic Extensional Combinatorial Model for Road Traffic Accidents in Cold Regions

Li, Lin-bo
Study on the Location Parking Index Based on Function Division of Parking Space

Li, Linbo
The Analysis of Transportation Demand Generation Mechanisms of the Urban Agglomerations in China

Li, Ling-jie
A Study on Signal Timing Optimization of Individual Intersections Based on an Ant Colony Algorithm

Li, M.
Analysis of the Influence of Emergent Incident on Expressways by Simulation
Research on Calculation of Important Parameters of Freeway Financial Post-Evaluation

Li, Maosheng
Optimization Theory of Regulation on Rural Transit Market Based on Rule of Transport Equality
Analyzing the Motivation of Queue-Jumping Driving-Action on Transportation Systems by Prospect Theory

Li, Mingshui
A Study on Spatial Correlation and Power Spectrum of Natural Wind at Xihoumen Bridge

Li, Musong
Test and Analysis of Rail Break Emergency Treatment Device for Railway Switches
Impact on Regularity of Track from Pile Underpinning of Light Railway Bridge
Analysis on Mechanical Performances of High-Speed Railway Transition Curves

Li, Na
The Analysis of Traffic Landscape from Users' Perspective: The Case of the Zhangjiang Tram

Li, Peng-fei
Research on Urban Public Transit Dispatching System Based on Real-Time Prediction and Game Theory

Li, Pengfei
Influencing Factor Analyses of Section Types on Vehicle-Bridge Interaction of Concrete Box Girder with Corrugated Steel Webs

Li, Ping
The Application of Anti-Rutting Agent on Improving the High-Temperature Stability of Asphalt Pavement

Li, Q. Q.
Urban Road Travel Speed Estimation Based on Low Sampling Floating Car Data

Li, Q.
Mixed Traffic Micro-Simulation of Urban Branch Roads
An Interval-Varying Floating Car Data Clustering Approach Based on Self-Organizing Maps
Simulation Study on a Freeway Climbing Lane
Evaluation of Supervision Engineer's Control over Investment Based on AHP

Li, Qiang
Efficient Link Travel Time Estimation for Signalized Link by Small Size Probe Reports
Experimental Tests and Finite Element Modeling of Shrinkage Behavior in Cement Stabilized Aggregate Base

Li, Rongda
Research on Application of Externally Prestressing for Simple-Continuous Bridge

Li, Rui
The Prediction of Urban Bus Travel Time

Li, S.
Research on Urban Intersection Vehicle Emission Reduction Based on Microcosmic Simulation

Li, Shiwu
A Time-Varying Route Optimization Model for Urban Hazmat Transportation
A Speed Limit Model of Vehicle for Urban Road Hazmat Transportation
Application of Locating Technology in the Highway Emergency Response System

Li, Shuang
Basic Study on Fractal Characteristic of Pore Structure in Cement Mortar

Li, W.
Mixed Traffic Micro-Simulation of Urban Branch Roads
Track Access Technology of Traffic Accident Vehicles Based on Video

Li, Wei-sheng
Performance Model for Pavement Maintenance of Expressway in Northwest of China

Li, Wen-quan
A Reserve Capacity Model of Optimal Traffic Lane Allocating
Research on Conversion Coefficients between Bicycle, Electric Bicycle, and Pedestrian on Urban Road Intersection

Li, Wenquan
Conventional Bus Stop Capacity in Peak
Estimation of Original-Destination Matrices for Public Traffic Passenger Flow
The Prediction of Urban Bus Travel Time

Li, X.
Study on Burner Type Diesel Particulate Filter System Using Compressed Air from Turbocharger
Research on Numerical Simulation of Pollutant Dispersion at Expressway Toll Plazas Based on Multi-Influencing Factors

Li, Xi-ying
A Retrograde Vehicle Detection Method Based on the Optical Flow Field

Li, Xiamiao
Analysis of the Competitive Strategy of the Core Enterprises in Virtual Intermodal

Freight-Transportation Enterprise

Li, Xiangguo

Test and Analysis of Rail Break Emergency Treatment Device for Railway Switches

Bridge Damage Assessment by Dynamic Response in Time Domain

Impact on Regularity of Track from Pile Underpinning of Light Railway Bridge

Analysis on Mechanical Performances of High-Speed Railway Transition Curves

Li, Xiaowei

Plastic Behavior for Compaction Pile with Hole Expanded by Blasting or Tamping Techniques

Li, Xin-kai

Gradually Rolling Prediction of the Use-Level of Road Network Based on BP Neural Network

Li, Xinkai

The Analysis of Dowel and Tie Bars Effects on Curling Up in Concrete Pavement Slabs

Experimental Analysis of Interface Bond Performance of UTW

Li, Xuefu

Construction Control of Cable-Stayed Bridges Based on ANN and GA Hybrid Algorithm

Li, Y.

Evaluating the Equity Impacts of Rural Road Investment Projects on Household Welfare Based on a Quantile Regression Approach: Evidence from Fujian Province

Li, Yajun

Analyzing the Effects of the Growth of Maritime Industries on the Regional Economy with Dynamic Inverse Matrix

Li, Yan

An Improved A* Algorithm for the Intelligent Transportation System

Observation and Theoretical Analysis of the Temperature Field on the Cross Section of Concrete Filled Steel Tubes Arch Bridge Rib

Li, Yang

Analysis of Runway Incursion in Civil Airport Based on Bayesian Network

A Safety Protection Technology System on Highway Roadside in China

An Active Parking Guidance Information System Based on Dynamic Agent Negotiation

Li, Yanwei
An Analytical Method for Predicting the Service Life of Bridge Structures

Li, Ying-Hong
Vehicle Tracking from Videos Based on Mean Shift Algorithm
Vehicle Detection from Videos Containing Complex Background Based on Bayesian Statistical Modeling

Li, Ying
Technical Efficiency of Container Terminals in China Using a Multi-Activity Data Envelopment Analysis Model

Li, Yu-ming
Study on the Control Strategy of Gas Injection of Gas Engines

Li, Yun-peng
Study on Safety Stability of Excavating Shallow Depth Neighborhood Tunnel in Traversing Construction
Study of Influence of Subway Station Excavation on Existing Metro Deformation

Li, Yunfeng
Application of High Performance Concrete Mixed with Steel Slag Powder in Concrete Pavements

Li, Z.
Frequency Optimization Model for a Public Traffic Scheduling System

Li, Zaixin
Experimental Tests and Finite Element Modeling of Shrinkage Behavior in Cement Stabilized Aggregate Base

Li, Zheng-Xi
Vehicle Tracking from Videos Based on Mean Shift Algorithm

Li, Zhenxia
Research on Rapid Curing Technology of Lime-Flyash-Cement Stabilized Macadam

Li, Zhijie
Study on the Carrying Capability of Preplanned Regional Earthquake Evacuation Corridor Based on Macro-Simulation

Li, Zhixia
Dilemma Zone Modeling Using Yellow-Onset Vehicular Trajectory Data

Li, Zhongji

Vehicle Semi-Active Suspension System Simulation with Variable Structure Control Method

Li, Zhonglong
Design and Validation of Wireless Dynamic Testing System for Bridge Based on the 941B Type Vibration Sensor

Li, Zimu
Transit Network Optimization Method Based on BRT Attracting Region: A Case Study of Changzhou

Lian, Yuchao
Research on the Mechanism for Preventing Reflective Cracks in Old Cement Concrete Pavement Reconstruction

Liang, Dui-dui
Analysis and Evaluation of Expressway Planning Schemes Based on Integrated Macro and Micro Simulation
Evaluation of Traffic Impact on Land Development Projects Based on Matter-Element Analysis

Liang, Shihua
Dynamic Effects of Moving Vehicular Loads on Continuously Reinforced Concrete Pavements on Winkler Foundation

Liang, Xuerong
The Analysis of the Correlation between International Roughness Index and Body Ride Comfort

Liang, Yanping
Research on Vehicle Information Extraction from High-Resolution Satellite Images

Liang, Ying-hui
Study on Fuzzy Neural Network Model of Vehicle-Bicycle Conflicts at Grade Intersection Based on Failure Tree Analysis
Study and Simulation of Behavioral Decision-Making Model of Through Bicycles Passing Vehicles at Signalized Intersection

Liang, Yubao
Discussion on Methods of Traffic Routes' Alignment Survey and Application of Principle of Least Squares

Liang, Z.
Highway Traffic Parameters Estimation by Using Cell Dwell Time

Liao, Haili
A Study on Spatial Correlation and Power Spectrum of Natural Wind at Xihoumen Bridge

Liao, Xiaobo
Dynamic Alliance of Road Logistics Enterprise Based on Ant Colony Algorithm

Lin, Cheng
Simulation of Turning Stability Control for Two-Motor-Drive Electric Vehicles

Lin, Ciyun
Dynamic Model of Transit Signal Priority on Colored Time Petri Net

Lin, Hangfei
Investigation of Relationship between Level of Service and Safety
Side Road Traffic Considered in Transit Signal Priority Control

Lin, Huigang
Research on Taboo Simulated Annealing Combinatorial Optimization Algorithm of Location Routing Problem with Pickups and Deliveries

Lin, Li-Xia
A Safety Evaluation Method of Existing Flexible Suspension Bridge with Double Cable

Lin, Lifan
A Study on the Location Selection of Public Traffic Transfer Hub Based on Improved Particle Swarm Algorithm

Lin, Tao
Algorithm of PFE and Its Application in Shenzhen Urban Transport Simulation System

Lin, Y.
A Route-Based Model for Determining Interconnection of Isolated Traffic Signals
Research on Dynamic Measuring System and Model of Novel High Speed Railway Vehicle Bogie

Lin, Yu
Locating Emergency Response Facilities for Hazardous Materials Transportation with Probabilistic Response Time

Ling, Ling-yong
Study on the Control Strategy of Gas Injection of Gas Engines

Ling, X. Z.
Shake Table Test on Seismic Response of Non-Free Liquefiable Site

Ling, Xianzhang
Case Studies for Shaking Table Tests on Seismic Soil-Pile Group-Bridge Structure Interaction in Liquefiable Ground
CT Scan on Frozen Roadbed Soil under Dynamic Triaxial Test Condition of Beilu River Section, Qinghai-Tibet Railway of China
Freeze-Thaw Stability of Slopes in Seasonally Frozen Regions of the Northeast China
Stability and Reinforcement Methods of a High Slope at the Hang-Yong Natural Gas Pipeline in China
Stability of Slope with the Weak Structural Plane Based on 2-D Nonlinear Finite Element Method
Vibration Characteristics of Permafrost Embankment Induced by Passing Trains in Qinghai-Tibet Railway in Winter
A New Cellular Automaton Traffic Flow Model for an Off-Ramp Junction of a Chinese Urban Expressway

Liu, B.
Research on the Competitiveness of China’s Ports
Mixed Traffic Micro-Simulation of Urban Branch Roads
Track Access Technology of Traffic Accident Vehicles Based on Video
Traffic Signal Control Optimization of Urban Arterials Based on a Method of Main Intersection Control Strategies

Liu, Baodong
Influencing Factor Analyses of Section Types on Vehicle-Bridge Interaction of Concrete Box Girder with Corrugated Steel Webs

Liu, Bin
The Application of TUXEDO Middleware in a Network-Based Train Working Diagram Compilation System

Liu, Bing
Enhancing Immersion through Adjusting Parameters of Vehicle Driving Simulator
Design Theory for Speed Control by Using Constant Edge Rate
The Reasonable Distance of Unsignalized Crosswalks Based on Traffic Flow, Stability, and Efficiency

Liu, Bo
Influence Factors Analysis of Buffeting Response of Self-Anchored Cable-Stayed

Suspension Bridge

Liu, Bohang
Reinforcement Learning Control for On-Ramp Metering Based on Traffic Simulation

Liu, C.
Research on the Competitiveness of China's Ports

Liu, Cong-hong
Study on the Green Traffic Planning System of New Rural Communities

Liu, D.
Detecting the Type of Multi-Fractality in Traffic Time Series

Liu, Dapeng
Analysis of the Competitive Strategy of the Core Enterprises in Virtual Intermodal Freight-Transportation Enterprise

Liu, Dewu
Risk Evaluation Model for Construction of a Logistics Park Based on Principal Component Analysis

Liu, Dong
Traffic Safety Evaluation of the 30 Provincial Capital in China Based on Principal Component Analysis

Liu, Fang
Investment and Financing Influence Analysis and Countermeasures for Highway Construction in the Period of China's 11th Five-Year Plan

Liu, G.
A Study of Vehicle and Materials Depot Location Problems for Winter Road Maintenance
A Study of Transit Evacuation Route Planning Based on Time-Expanded Network

Liu, Ganbin
Dynamic Effects of Moving Vehicular Loads on Continuously Reinforced Concrete Pavements on Winkler Foundation

Liu, Gui-wei
Mechanical Characteristics of Reinforced Gravity Oblique High U-Shaped Abutment

Liu, Han-bing
Experimental Research on the Mechanical Parameter of Fly Ash Soil
Sensitivity Analysis of the Dynamical Parameters on Road Materials

Liu, Han-Qing
The Application of Anti-Rutting Agent on Improving the High-Temperature Stability of Asphalt Pavement

Liu, Hao-zue
Risk Evaluation for Highway Transportation of "Toxic Gas" Hazardous Materials—Based on a Back Propogation (BP) Neural Network

Liu, Haopeng
Study of Hydrodynamic Pressure on the Cylindrical Pile-Cap Pier in Deep Water Subjected to Seismic Action

Liu, Hongbo
Study on the System Design and Optimal Models of Urban Rail Transit Traction Calculation System

Liu, Hongqi
Evaluation Study of the Median Markings in Undivided Highway Tunnels
Driving Simulation Study on Traffic Flow Characteristics on the Climbing Lane on a Two-Lane Rural Road

Liu, J.
Car-Following Criteria at a Signalized Intersection in Beijing

Liu, Jian-Yi
Choice of Reasonable Longitudinal Gradient at Alignments of Mountain Highways Based on Driver's Physiological Reactions
Impacts of Road Sight Distance on Safe Driving Conditions

Liu, Jiangtao
Modeling Passenger Choice Behavior in Chinese Multi-Airport Regions

Liu, Jianxia
Study on Power Control of Electric Power Steering System

Liu, Jianxin
Simulation and Analysis for Stick-Slip Vibration of Locomotive with Hollow-Shaft Drive System

Liu, Jianyi
Equilibrium Model of Trip Modes in Road Traffic and Orientation of Charge Policy
Optimization of Regional Traffic Structure from the Perspective of Sustainable Development

Liu, Jike
Parameter Sensitivity Analysis of Accident Reconstruction Model Based on Orthogonal Design

Liu, Jin-guang
The Research of Signal Phase Sequences Based on the Conglomeration of Pedestrians and Bicycles

Liu, Jing
Expressway Data De-Noised Approach Based on Wavelet Analysis

Liu, Jun
An Analytical Method for Predicting the Service Life of Bridge Structures

Liu, Kai-zheng
Risk Evaluation for Highway Transportation of "Toxic Gas" Hazardous Materials—Based on a Back Propogation (BP) Neural Network

Liu, Kai
A Google-Map Integrated Web-Based Stated Preference Survey for Modeling Personal Mobility

Liu, Kening
Study on Pedestrian Safety and Countermeasures in Crosswalks around Campus—Case Study at Ludong University in Yantai

Liu, Lan
Research on the Crashworthiness Optimization of Curved-Road Concrete Barriers

Liu, Lihua
Nonparametric Analysis of Timely Distribution of Traffic Crash

Liu, Linya
Track Structure Vibration Characteristic Analysis Based on FEM 3D Model

Liu, Ming
A Study on Spatial Correlation and Power Spectrum of Natural Wind at Xihoumen Bridge

Liu, Peng
Simulation of Turning Stability Control for Two-Motor-Drive Electric Vehicles

Liu, Qin
Study on a Passageway Location Model on Underground Expressway

Liu, Qing

A Study on Vehicle Trip Distribution Forecasting Based on BP Neural Network

Liu, Ruifen

Research on Model of Public Transportation Network Optimization Based on the Demand of Citizen Trips

Liu, Shaotang

Discussion on Methods of Traffic Routes' Alignment Survey and Application of Principle of Least Squares

Liu, Shicui

The Impacts of Differential Speed Limits on Speed

A Study on Speeding Driving Based on Expected Speed

Liu, Shoujun

A "Reality Vision" Navigation Technique Based on Sequence Geo-Referenced Image Databases

Liu, Sisi

Road Safety in Sections under Mixed Flow Traffic Environment

Liu, Su

Several Questions of Highway Influence Assessment on Dongting Lake Ecosystem in China

Computer-Aided Error Detection of Horizontal and Vertical Alignment in Highway Construction

An Estimate Method for Accuracy of Fitting Horizontal Alignment in Old-Highway Based on Fitting Normal Error

Liu, Tai-jun

Study on the Influence of Coarse Aggregate on the Pavement Performance of Road Cement Concrete

Liu, Tianliang

Efficiency Loss of the Multiclass, Multicriteria Stochastic User Equilibrium Traffic Assignment against Stochastic System Optimization

Liu, W.

Safe Spacing Research Based on the Theory of Cellular Automation on Freeways in Foggy Weather

Research on a Generalized Cost Model for Optimization of Ningbo-Zhoushan Port's Collection and Distribution System

Liu, Wei

Stability and Reinforcement Methods of a High Slope at the Hang-Yong Natural

Gas Pipeline in China
Signal Intersection Optimal Control Model of Small Region Based on Traffic Equilibrium Theory
Research on Dynamic Safety Stock Based on Short-Term Weather Forecasting

Liu, Wen-guang
Fuzzy Control of AMT Clutch Engagement during the Vehicle Starting

Liu, X.
Experimental Study on Sound Countermeasures against Driver Fatigue

Liu, Xian
The Balance Lines of International Freight and Incidentals

Liu, Xiangrong
Study on Long-Term Behavior and Ultimate Strength of CFST Columns

Liu, Xiao-ming
The Research of Signal Phase Sequences Based on the Conglomeration of Pedestrians and Bicycles

Liu, Xiaoming
An EEG Predictor of Driving Fatigue

Liu, Xiaoqing
Transit Network Optimization Method Based on BRT Attracting Region: A Case Study of Changzhou

Liu, Xiaoyan
Research on Key Question of Joint of Large Span Pre-Stressed Box-Girder Concrete Continuous Rigid Frame Bridge with High Piers

Liu, Xingwang
The Method of Road Safety Analysis Based on Two-Dimensional Speed Difference

Liu, Xuejun
Information Needs of Urban Transit Travelers—The Case of Wuhan, China

Liu, Y.
Study on Spatial Information Model and Database of Traffic Facilities Management Systems Based on ArcGIS
Noise Source Identification and Noise Reduction of a Double Crank Four Ring-Plate-Type Cycloid Reducer
Study on Style Protection and Urban Traffic Planning of Harbin Jingyu Street

Liu, Ya-Li
Vehicle Tracking from Videos Based on Mean Shift Algorithm
Vehicle Detection from Videos Containing Complex Background Based on Bayesian Statistical Modeling

Liu, Yao
Coordinated Development between Transportation System and Socio-Economic System Research Based on SEM

Liu, Yingshun
Efficiency Evaluation of Urban Transit Terminals Based on the Cloud Model

Liu, Yisheng
Passenger Transport Demand Prediction for Newly-Built Regions

Liu, Yongqiang
An Improved Ant Colony Algorithm for the Shortest Path Problem in Time-Dependent Networks
Optimal Dynamic Substitution Policy for Components in an Assemble-to-Order System
Coordination Policies of Supply Chain Where Deterioration Begins at a Random Time Point

Liu, Ze
Evaluation of Road Traffic Safety Based Improved Fuzzy-AHP Method

Liu, Zhanliang
Effect by Different Factors on Ductility of Evaporated Residue of Modified Emulsion Asphalt

Liu, Zhao-hui
A Study on Multifactorial Prediction Model for the Road Traffic Accidents

Liu, Zhenguo
Study of Operational Characteristics of HAZMAT Vehicles Based on GPS Data

Liu, Zhengwei
Study on Road Network Reserved Capacity on Different Levels of Service and Stochastic Conditions

Liu, Zhili
Expansion and Validation of Beijing Household Interview Survey Data

Liu, Zhongmin

Study on Energy Consumption by Land Cargo Transportation

Long, Kejun
Traffic Management on an At-Grade Signalized Intersection Connecting to Urban Expressway Ramps

Lou, Yanjiang
Forecast the Automobile Population Based on Scenario Analysis

Lou, Yingyan
Robust Optimization Approach for Transportation Network Design under Demand Uncertainty

Lu, Fangqiang
Assessing Performance of Public Transit Network Using Network-Based Accessibility Measures

Lu, Hongxia
The Application of TUXEDO Middleware in a Network-Based Train Working Diagram Compilation System
Study on the System Design and Optimal Models of Urban Rail Transit Traction Calculation System

Lu, Huapa
Pricing Model for Expressway with Elastic Demand

Lu, Huapu
Urban Transport Network Capacity Considering Level of Service

Lu, Jian John
Evaluating the Impacts of Ramp Configurations and Influential Factors on Freeway Exit Ramps
Operational Performance Evaluation of Different Exit Ramps on Florida's Freeways by Considering Number of Lane Change

Lu, Jian-feng
Research of Road Transportation Sustainable Development Based on Ecological Footprint Model

Lu, Jian
A Study on Vehicle Trip Distribution Forecasting Based on BP Neural Network

Lu, Kecong
Electrical Appliance Reversion Logistics Network Planning

Lu, Lihua

Study on Experiment of Concrete Mixed with II Degree Flyash under the Corrosion of Freeze Thawing

Measurement and Simulation Study on Ground Subsidence Induced by Shield Tunneling in Sandy Stratum

Lu, Linjun

Operational Performance Evaluation of Different Exit Ramps on Florida's Freeways by Considering Number of Lane Change

Lu, Miaomiao

Study on the System Design and Optimal Models of Urban Rail Transit Traction Calculation System

Lu, S.

Probabilistic Pedestrian-Vehicle Conflict Micro-Model in Non-Signal Controlled Multi-Lane Segments

Lu, Shengrong

Coordinated Development between Transportation System and Socio-Economic System Research Based on SEM

Lu, T.

Evaluation of Supervision Engineer's Control over Investment Based on AHP

Lu, W.

Hybrid Genetic and Taboo Search Algorithm for Solving the Bus Timetable Problem

Lu, X.

Research on Urban Intersection Vehicle Emission Reduction Based on Microcosmic Simulation

Lu, Zhuqing Lu

Track Structure Vibration Characteristic Analysis Based on FEM 3D Model

Lu, Zi-xu

Individual and Population Learning in Route Choice Behavior of Drivers: Experiment and Model

Lui, Zhili

Research on Pedestrian Safety under Rapid Development of Motorization

Luo, Hui

Analysis of Thermal Stress Response in Asphalt Overlay

Luo, Lianghao

Study on Traffic Noise Characteristics of Large Grade Interchange

Luo, Pengfei
Stiffness Reduction Factor of Reinforced Concrete Bridge Pier Considering Characters of Nonlinear

Luo, Ren
Bending Vibration Suppression of High Speed Railway Passenger Car Body

Luo, Xianglong
Traffic Incident Acoustic Recognition Based on Wavelet Decomposition and SVM
Short-Term Traffic Flow Prediction Based on EMD and Artificial Neural Network

Luo, Yu
Locating Emergency Response Facilities for Hazardous Materials Transportation with Probabilistic Response Time

Luo, Z. W.
RGB Based Crowded Pedestrian Counting in Red Light Time
Short-Term Traffic Flow Prediction with ACD and Particle Filter

Luo, Zhu
Analysis of Elastic Slab on Non-Uniform Support Foundation Using a Weighted-Residual Method

Lv, X.
Mixed Traffic Micro-Simulation of Urban Branch Roads

M

Ma, Chao
Test and Analysis of Rail Break Emergency Treatment Device for Railway Switches
Analysis on Mechanical Performances of High-Speed Railway Transition Curves

Ma, Cunming
A Study on Spatial Correlation and Power Spectrum of Natural Wind at Xihoumen Bridge

Ma, Li-xia
Region Public Transportation Timetable Optimization Based on Node and Line's Wait Analysis

Ma, Qianli

Discussion on Methods of Traffic Routes' Alignment Survey and Application of Principle of Least Squares

Ma, Qing
Plastic Behavior for Compaction Pile with Hole Expanded by Blasting or Tamping Techniques

Ma, Rongguo
A Safety Protection Technology System on Highway Roadside in China

Ma, Sheqiang
Traffic Safety Evaluation of the 30 Provincial Capital in China Based on Principal Component Analysis

Ma, Songlin
Research on Structural Design of Interlocking Concrete Block Pavement for Rural Road
The Analysis of Dowel and Tie Bars Effects on Curling Up in Concrete Pavement Slabs
The Analysis of the Correlation between International Roughness Index and Body Ride Comfort
Research on Automatic Identification Method of Pavement Sag Deformation

Ma, W.
A Route-Based Model for Determining Interconnection of Isolated Traffic Signals

Ma, Wei
Reliability Analysis on Pavement Skid-Resistant Performance in Expressway Tunnel

Ma, Y.
Analysis of the Influences of Fatigue on Driver's Behavior Characteristics

Ma, Yan
Risk Assessment of Road Operation Environment under Atrocious Weather Condition

Ma, Z.
Research on Simulation of Train Tracing Operation Based CBTC
Design and Realization of Decision-Making and Analysis Assistant System on National Integrated Transportation Information

Ma, Zhuanglin
Traffic Safety Evaluation of the 30 Provincial Capital in China Based on Principal Component Analysis

The Method to Identify Black Spots of Long Highway Tunnel

Mai, Q.
Mean-CVaR Model of Wholesale Price Contracts and Dual Purchase Contracts in the Supply Chain

Mao, B.
Research on Greedy Train Rescheduling Algorithm

Mao, Chengyuan
Phase and Timing Optimization at Actuated-Coordinated Signal Control Intersection

Mao, Hongyan
Application of Locating Technology in the Highway Emergency Response System

Mao, K.
Experimental Study on Sound Countermeasures against Driver Fatigue

Mao, Kai
A "Reality Vision" Navigation Technique Based on Sequence Geo-Referenced Image Databases

Mao, Lina
Design of Intelligent Decision Module for Storage Location Assignment in AS/RS

Mao, Xiao-dong
Study on the Rational Size of the Box Girder Used in Cable-Stayed Bridge Based on ANSYS

Mei, Xiao-Ming
Technology Research on the Vehicle Collision Accident Self-Alarm System

Meng, L.
Research on Greedy Train Rescheduling Algorithm

Meng, Xiang-hai
A Study on Vehicle Trip Distribution Forecasting Based on BP Neural Network

Meng, Yan
Travel Mode Choice in Large Cities of China Based on Loss Aversion Theory

Mi, Haijie
Stiffness Reduction Factor of Reinforced Concrete Bridge Pier Considering Characters of Nonlinear

Miao, J.

Research on Greedy Train Rescheduling Algorithm

Miao, Lixin
Technical Efficiency of Container Terminals in China Using a Multi-Activity Data Envelopment Analysis Model

Miwa, Tomio
Efficient Link Travel Time Estimation for Signalized Link by Small Size Probe Reports

Miyagi, Toshihiko
Reinforcement Learning Control for On-Ramp Metering Based on Traffic Simulation

Mo, You
Stability and Reinforcement Analysis of a High and Steep Cataclastic Rock Slope

Mogharabi, Abi
Identifying Alternative Routes with Integration of ITS into Traffic-Diversion Strategies

Morikawa, Taka
Efficient Link Travel Time Estimation for Signalized Link by Small Size Probe Reports

Mu, Chunyan
Study on Pedestrian Safety and Countermeasures in Crosswalks around Campus—Case Study at Ludong University in Yantai
Study on Power Control of Electric Power Steering System

Mu, Liying
Case Study on the Computing Model of the Driving-Into Rate of Service Area

Mu, Y. G.
Mean-CVaR Model of Wholesale Price Contracts and Dual Purchase Contracts in the Supply Chain

N

Nan, Xi
Electrical Appliance Reversion Logistics Network Planning

Ni, Fujian
Experimental Tests and Finite Element Modeling of Shrinkage Behavior in Cement Stabilized Aggregate Base

Ni, S.
Research on Optimization of Crew Scheduling of the Passenger Dedicated Line Based on a Genetic Ant Colony Algorithm

Ni, Shaoquan
An Improved Ant Colony Algorithm for Placing-In and Taking-Out of Wagons in Branch-Shaped Sidings
The Application of TUXEDO Middleware in a Network-Based Train Working Diagram Compilation System

Ni, Tonghe
The Applied Research on Forecasting Cargo Volume of Northeast Economic Zone by Systemic Dynamics

Niu , Huimin
An Algorithm for Vehicle Routing Problem with Soft Time Windows Using Tabu Search

Niu, Guohong
Traffic Incident Acoustic Recognition Based on Wavelet Decomposition and SVM
Short-Term Traffic Flow Prediction Based on EMD and Artificial Neural Network

Niu, Xueqin
Research on Model of Public Transportation Network Optimization Based on the Demand of Citizen Trips
Reinforcement Learning Control for On-Ramp Metering Based on Traffic Simulation

Niu, Yuxin
A Safety Protection Technology System on Highway Roadside in China

P

Pan, Dawei
Study on Congestion Pricing Model of Bus Lane Mixed Use by Carpool Vehicles

Pan, H.
Research on a Generalized Cost Model for Optimization of Ningbo-Zhoushan Port's Collection and Distribution System

Pan, Jinshan
The Application of TUXEDO Middleware in a Network-Based Train Working Diagram Compilation System

Pan, M.
Collision Avoidance among Multiple Ship Agents

Pan, Mu
Research on the 25kW FCPS's Temperature Controlling Simulation

Pan, Xiaodong
Study on Prolonging Asphalt Pavement Fatigue Life Based on Vision Transverse Intervention

Pang, Yan
Logistics Distribution Information System Based on 3rd Generation Mobile Communication Technology

Pang, Yi-Gui
Vehicle Tracking from Videos Based on Mean Shift Algorithm
Vehicle Detection from Videos Containing Complex Background Based on Bayesian Statistical Modeling

Pang, Ying
Analysis and Evaluation of Expressway Planning Schemes Based on Integrated Macro and Micro Simulation
Evaluation of Traffic Impact on Land Development Projects Based on Matter-Element Analysis

Pei, J. Z.
Study on Permanent Deformation Characteristics of Asphalt Pavement Based on Discrete Element Method
Mechanism of Rutting Formation in Long and Steep Climbing Sections of Asphalt Pavement

Pei, Y-L.
Analysis of Deformation Characteristics of Collision Vehicles Using Close-Range Photogrammetry

Pei, Y.
Influencing Factors Contributing to Rear-End Collisions on Highways: PCA Based Investigation and Findings
Analysis of the Influences of Fatigue on Driver's Behavior Characteristics

Pei, Yu-long
Vehicle Dynamics Model in Two-Dimension Collision Accident
Vehicle Trajectory Model in Two-Dimension Collision Accidents

The Evaluation of Level of Service for Expressway in Operating Stage

Pei, Yulong
Methods of Setting Maximum Speed Limits on Freeways
Effect of Sunlight Glare on Drivers' Psychophysiological Characteristics
Evaluation of Road Traffic Safety Based Improved Fuzzy-AHP Method
Road Traffic Safety Micro-Evaluation Based on Bayes Theory
Uncertainty Analysis of Collision Velocity in Motor Vehicle Crash Using Evidential Reasoning Algorithm
Research on the Characteristics of Time Headway Distribution in Expressway Weaving Section of Type A
A New Cellular Automaton Traffic Flow Model for an Off-Ramp Junction of a Chinese Urban Expressway
Phase and Timing Optimization at Actuated-Coordinated Signal Control Intersection

Peng, Bo
Research on Dynamic Safety Stock Based on Short-Term Weather Forecasting

Peng, Junqiang
Study of Driver's EEG and Application in Intelligent Transportation Systems

Peng, Xiaohong
Monitoring Model for Three-Way Catalyst Converter Efficiency Based on Exotherm

Peng, Ying
Study on Signal Timing Methods of Optimizing Urban Transportation Network Efficiency

Peng, Yong
Optimization of Open Vehicle Route to Reduce Fuel Consumption Based on Genetic Algorithm

Peng, Zhong-Ren
Analysis and Evaluation of Expressway Planning Schemes Based on Integrated Macro and Micro Simulation
Evaluation of Traffic Impact on Land Development Projects Based on Matter-Element Analysis

Peng, Zuo
Research on the Crashworthiness Optimization of Curved-Road Concrete Barriers

Perugu, Harikishan
Integrated Arterial Signal and Access Control Strategy under Non-Notice

Emergency Evacuation: Modeling and Simulation-Based Analysis

Pi, X.
Research on a Generalized Cost Model for Optimization of Ningbo-Zhoushan Port's Collection and Distribution System

Ping, Shaohua
Road Traffic Safety Micro-Evaluation Based on Bayes Theory

Pu, Liang
Individual and Population Learning in Route Choice Behavior of Drivers: Experiment and Model

Pu, Yibin
CT Scan on Frozen Roadbed Soil under Dynamic Triaxial Test Condition of Beilu River Section, Qinghai-Tibet Railway of China

Q

Qi, Dongchun
Model Test Study of System Transformation for Jiangdong Bridge

Qi, Guang-yuan
Research on Flame-Retardant Technique in Application of Asphalt Pavement in Highway Tunnel

Qi, Tian
Dynamic Effects of Moving Vehicular Loads on Continuously Reinforced Concrete Pavements on Winkler Foundation

Qi, Z.
Research on Numerical Simulation of Pollutant Dispersion at Expressway Toll Plazas Based on Multi-Influencing Factors

Qian , Hong-bo
Impact Analysis on Countdown Device on Transit Priority Signal Control

Qian, Hongbo
The Comparison of Three Getting Signal Control Delay Video Methods at Signalized Intersection

Qian, Renjie
Study on Congestion Pricing Model of Bus Lane Mixed Use by Carpool Vehicles

Qian, Yu
The Application of Anti-Rutting Agent on Improving the High-Temperature Stability of Asphalt Pavement

Qin, Li-hui
Mechanical Characteristics of Reinforced Gravity Oblique High U-Shaped Abutment

Qin, Wenxiao
Limit Value of Railway Bridge for Traffic Safety

Qin, Xiao
Advanced Traveler Information Impact on Truck Route Choice

Qin, Yaqin
Evaluation Study of the Median Markings in Undivided Highway Tunnels
Driving Simulation Study on Traffic Flow Characteristics on the Climbing Lane on a Two-Lane Rural Road

Qiu, Zhaowen
Monitoring Model for Three-Way Catalyst Converter Efficiency Based on Exotherm

Qiu, Zhuo
Evaluation of Road Traffic Safety Based Improved Fuzzy-AHP Method

Qu, Jianbo
Construction Control of Cable-Stayed Bridges Based on ANN and GA Hybrid Algorithm

Qu, Jianhua
Study on Multi-Dimensional Structure Model for Agricultural Products Logistics Organization in China

Que, Yun
Application of Fractal Theory in Pavement Surface Texture Measurement

R

Ren, C.
Hybrid Genetic and Taboo Search Algorithm for Solving the Bus Timetable Problem

Ren, Gang
Predicting Methods of Trip Modal-Split Based on Structural Model

Ren, Huixing
Application of Thermal Stress Controlling in Construction of Large Bridge Cushion Cap

Ren, L.
Transport Strategy for Sustainable Development of Jiao Dong Economic Region

Ren, Ruibo
Theoretical Analysis of Design Parameters on Semi-Rigid Asphalt Pavement with Flexible Base

Ren, Shao Yun
Evaluation of Fire Risk at Highway Tunnels

Ren, Xian-Qiang
Choice of Reasonable Longitudinal Gradient at Alignments of Mountain Highways Based on Driver's Physiological Reactions
Impacts of Road Sight Distance on Safe Driving Conditions

Ren, Xiao-Qiang
The Application of the Maximal Coverage and Partial Coverage Model in the Shelter Location Problem

Ren, Xiaoqiang
Research on Dynamic Characteristics of Road Network in Snowy Conditions

Ron, J.
Experimental Study on Sound Countermeasures against Driver Fatigue

Rong, J.
Car-Following Criteria at a Signalized Intersection in Beijing

Rong, Jian
The Research of Signal Phase Sequences Based on the Conglomeration of Pedestrians and Bicycles

Ruan, Yong-Fen
Optimum Choice for the Construction Management Plan Based on Entropy Weight

S

Sha, A. M.
Study of an Image-Based Gradation Measurement Techniques of the Asphalt

Mixture

Sha, A.
Pavement Crack Automatic Recognition Based on Wiener Filtering

Sha, S.
Train-Carried Rail Signal Parameters Test System Based on Spectrum Correction Method and Virtual Instrumentation

Sha, ZhiRen
Application Research of GPS Based on Google Earth Platform

Shan, Qiyu
Research on the Crashworthiness of Two-Layer Thin-Walled Structures

Shang, P.
Detecting the Type of Multi-Fractality in Traffic Time Series

Shao, C.
Design and Realization of Decision-Making and Analysis Assistant System on National Integrated Transportation Information

Shao, Chunfu
Traffic Safety Evaluation of the 30 Provincial Capital in China Based on Principal Component Analysis
The Method to Identify Black Spots of Long Highway Tunnel
A Model of Mixed Land Use and Trip Production by BP Neural Network
Short-Term Forecasting of Uncertain Traffic States

Shen, Ai-qin
Study on the Influence of Coarse Aggregate on the Pavement Performance of Road Cement Concrete

Shen, Dongjian
Stiffness Reduction Factor of Reinforced Concrete Bridge Pier Considering Characters of Nonlinear

Shen, Haijun
Calculation Method for Braking Torque of Self-Excited Retarder

Shen, Ruiguang
Uncertainty Analysis of Collision Velocity in Motor Vehicle Crash Using Evidential Reasoning Algorithm

Shen, Ruili

Model Test Study of System Transformation for Jiangdong Bridge

Shen, Yingming
A New Organizational Structure Pattern of Owners Based on Multi-Project

Sheng, Hong-fei
Capacity Reliability of Road Network under Adverse Weather Conditions Based on Fuzzy Theory

Sheng, Hongfei
Observation and Theoretical Analysis of the Temperature Field on the Cross Section of Concrete Filled Steel Tubes Arch Bridge Rib

Sheng, Kejian
Research on Application of Externally Prestressing for Simple-Continuous Bridge

Sheng, Yanping
An Evaluation of the Effectiveness of Geo-Textile-Binder-Aggregate System for Surface Treatment of Distressed Asphalt Pavement

Shi, Aiguo
Study on the Key Technology of Captive Model's Numerical Test

Shi, Jian Fei
The Research of Control Strategy of Permanent Magnet Synchronous Motor for Hybrid Electric Vehicles

Shi, Jian-Jun
A Calculation Method for the Information Utility of Traffic Guide Signs

Shi, Q.
Safe Spacing Research Based on the Theory of Cellular Automation on Freeways in Foggy Weather

Shi, Xiao-Hong
Dynamic Response of a Magnetically Levitated Vehicle in a Crosswind

Shi, Xiaofa
Investment and Finance for the Intelligent Transportation System in China
Study of Operational Characteristics of HAZMAT Vehicles Based on GPS Data

Shi, Xin
Impacts of the Modernization of Global Navigation Satellite Systems on Intelligent Transport Systems

Shi, Yanni

Research on the Impact of Drivers' Heart Rate on Longitudinal Slope of Freeway Tunnel

Situ, Bingqiang
Study on a Passageway Location Model on Underground Expressway

Situ, Li-Ying
Study on Using OD Traffic Flow to Identify the Special Boundary of the Expressway Influence Zone

Song, Bo
Study of Hydrodynamic Pressure on the Cylindrical Pile-Cap Pier in Deep Water Subjected to Seismic Action

Song, Dapeng
Continuous Test for Construction Quality of Mixed Filling Roadbed

Song, Fei
A Study on Driver's Dynamic Visual Characteristics

Song, Hai
Experimental Study on Behavior of Geotextile-Reinforced Soil

Song, Jinhua
Research on the Mechanism for Preventing Reflective Cracks in Old Cement Concrete Pavement Reconstruction

Song, Junjie
Construction Control of Cable-Stayed Bridges Based on ANN and GA Hybrid Algorithm

Song, Q.
Research on Optimization of Crew Scheduling of the Passenger Dedicated Line Based on a Genetic Ant Colony Algorithm

Song, Ti
Region Public Transportation Timetable Optimization Based on Node and Line's Wait Analysis

Song, Xianmin
Study on Signal Timing Methods of Optimizing Urban Transportation Network Efficiency

Song, Xin-Sheng
Research on Conversion Coefficients between Bicycle, Electric Bicycle, and Pedestrian on Urban Road Intersection

Su, Guimin
The Comparison of Three Getting Signal Control Delay Video Methods at Signalized Intersection

Su, J.
Research on Dynamic Measuring System and Model of Novel High Speed Railway Vehicle Bogie

Sun, F.
Effect of Electro-Mechanical Coupling on Dynamic Performance of Crankshaft of ISG HEV

Sun, Feng
The Analysis of Rural Road Safety and Its Strategies

Sun, Guanglin
Analysis of City Transportation Networks' Travel Time Reliability during Adverse Weather

Sun, Haixia
Study on Experiment of Concrete Mixed with II Degree Flyash under the Corrosion of Freeze Thawing
Measurement and Simulation Study on Ground Subsidence Induced by Shield Tunneling in Sandy Stratum

Sun, Hang
Observation and Theoretical Analysis of the Temperature Field on the Cross Section of Concrete Filled Steel Tubes Arch Bridge Rib

Sun, Hao
Research on the Prediction Model of Traffic Accidents Using the Least Square Support Vector Machine

Sun, Jian
Study on Accident Reconstruction Model Based on Reverse-Reasoning Method
A Manual Calibration Method for Simulation of a Freeway Weave Section

Sun, Jing
Study on Pedestrian Safety and Countermeasures in Crosswalks around Campus—Case Study at Ludong University in Yantai

Sun, Kechao
Research on the Differences in Regional Economy and Transportation among the Three Regions in China

Sun, Liangming
Structural Noise of Longitudinal Stiffened Concrete Cylindrical Shell

Sun, Lijun
ALINEA-Based Urban Expressway On-Ramp Metering Strategy
Permanent Deformation Characteristic of Asphalt Mixture Considering Pavement Temperature Distribution

Sun, Liping
The Application of Functionally Gradient Material to Problems of Wheel-Rail Contact

Sun, Lu
Viscoelastic Analysis of Asphalt Pavement Using a Regularized Interconversion Technique between Creep and Relaxation

Sun, Mei
Characteristics of Fundamental Data for Railway Maintenance and the Construction of Integrated Data Platform

Sun, Ming
Study on the Optimization of Vessel Scheduling Design Based on Soft Time Windows under Voyage Charters

Sun, Qi
Research on Vehicle Information Extraction from High-Resolution Satellite Images

Sun, Qian
Research on the Prediction Model of Traffic Accidents Using the Least Square Support Vector Machine
A Study on the Location Selection of Public Traffic Transfer Hub Based on Improved Particle Swarm Algorithm

Sun, Qinmei
Design Theory for Speed Control by Using Constant Edge Rate

Sun, Rui-shan
Research and Application of Graphic-Attributes Integration Based on Web GIS in Aviation Accident Investigation
Research on the Design of Inner Horizontal Surface of the Airport

Sun, Sheng Yang
Research on Travel Behavior Changes under Vehicle-Use-Restriction Measures during the Olympic Games

Sun, Weiyuan
A Time-Varying Route Optimization Model for Urban Hazmat Transportation

Sun, Wen-xia
Region Public Transportation Timetable Optimization Based on Node and Line's Wait Analysis

Sun, Wencai
A Time-Varying Route Optimization Model for Urban Hazmat Transportation
A Speed Limit Model of Vehicle for Urban Road Hazmat Transportation

Sun, X.
Highway Accidents Analysis with Panel Data Model
Impact of Posted Speed Limits on Operating Speed in Urban Expressways

Sun, Xiaoduan
The Impacts of Differential Speed Limits on Speed
Road Safety in Sections under Mixed Flow Traffic Environment
A Study on Speeding Driving Based on Expected Speed

Sun, Xue-xian
Study on the Rational Size of the Box Girder Used in Cable-Stayed Bridge Based on ANSYS

Sun, Z. Y.
Study of an Image-Based Gradation Measurement Techniques of the Asphalt Mixture
Pavement Crack Automatic Recognition Based on Wiener Filtering

Suo, J.
Study on Burner Type Diesel Particulate Filter System Using Compressed Air from Turbocharger

T

Tan, Qulin
Research on Vehicle Information Extraction from High-Resolution Satellite Images

Tan, Yi-qiu
Research on Flame-Retardant Technique in Application of Asphalt Pavement in Highway Tunnel
Effects of Layer Interface Conditions on Fatigue Behavior of Asphalt Pavements

with Semi-Rigid Bases

Tang, L.
Shake Table Test on Seismic Response of Non-Free Liquefiable Site

Tang, Liang
Case Studies for Shaking Table Tests on Seismic Soil-Pile Group-Bridge Structure Interaction in Liquefiable Ground

Tang, Maolin
Model Test Study of System Transformation for Jiangdong Bridge

Tang, Yan-hong
Capacity Reliability of Road Network under Adverse Weather Conditions Based on Fuzzy Theory

Tao, Lianjin
Stability and Reinforcement Analysis of a High and Steep Cataclastic Rock Slope

Tao, Z-M.
Analysis of Deformation Characteristics of Collision Vehicles Using Close-Range Photogrammetry

Tao, Zhouhui
A Study of Cold In-Place Recycling Mixture Used as Binder Course in China

Tian, Da-feng
Ration Effect of Rheological and Combustion Properties of Coal-Oil-Water Slurry

Tian, Jingjing
A Time-Varying Route Optimization Model for Urban Hazmat Transportation
A Speed Limit Model of Vehicle for Urban Road Hazmat Transportation

Tian, Lin
Function Design of Cement Stabilized Crushed Stone Drainage Base

Tian, Qiong
Ramp Metering Strategies in a Corridor Network

Tian, Shi-zhu
Seismic Hybrid Simulation of a Multi-Span Bridge

Tian, Wei
Analysis of Thermal Stress Response in Asphalt Overlay

Tian, Wenling

Experimental Study on Performance of the Bridge Deck Pavement of SF-PFSC
Design and Construction of Overlay with Mechanical Joint Element on Used Concrete Pavement

Tian, Y.
Evaluating the Equity Impacts of Rural Road Investment Projects on Household Welfare Based on a Quantile Regression Approach: Evidence from Fujian Province
Congestion Pricing Revenue Redistribution Strategy Based on Traffic Behavior

Tian, Ying
Ration Effect of Rheological and Combustion Properties of Coal-Oil-Water Slurry

Tian, Yujia
The Evaluation of Micro-Benefit on Highway Construction Investments
Analysis Model for Operating Speed on Two-Lane Secondary Highway

Tian, Z.
Signal Timing and Coordination—An Art of Engineering
Research on Optimization of Crew Scheduling of the Passenger Dedicated Line Based on a Genetic Ant Colony Algorithm

Tian, Zhe-Wen
Technology Research on the Vehicle Collision Accident Self-Alarm System

Tong, Jingjing
Calculation Method on Traffic Noise Pollution of Interchange Based on Geometric Alignment

W

Wan, Huasen
Evaluation Study of the Median Markings in Undivided Highway Tunnels
Driving Simulation Study on Traffic Flow Characteristics on the Climbing Lane on a Two-Lane Rural Road

Wan, Shui
A Multi-Objective Decision Model of Traffic Rescue Service Site Location on Road

Wan, Xia
The Attitude and Psychological Demand Related Determinants of Public Transport Use

Wang, Bailing

Optimization of Transportation Enterprises Pricing Strategies

Wang, Bo
Quick Maintenance for Tunnel Lining Voids with Polymer Grouting Technology

Wang, Bruce X.
Advanced Traveler Information Impact on Truck Route Choice

Wang, C. F.
Study of an Image-Based Gradation Measurement Techniques of the Asphalt Mixture

Wang, Caixia
Continuous Test for Construction Quality of Mixed Filling Roadbed

Wang, Candong
Study on the Model of Hub Location under Earthquake Conditions

Wang, Changhong
An Optimized Signal Control Method for a Freight Arterial Transport System

Wang, Changhoug
An AHP-Based Performance Evaluation Model of Transportation Control System: The Experience from West Liaohe Rd., Dalian

Wang, Chao-hui
Determine Old Asphalt Pavement Milling Thickness Based on Pavement Surface Deflection Control

Wang, Chao
Forecast the Automobile Population Based on Scenario Analysis

Wang, Chuantao
Theory Study on Correlation Stability and Profit Allocation of Supply Chain

Wang, Cuihua
Study on Logistics Center Location Bi-Level Programming Model and Algorithm Based on Competition

Wang, Da-peng
Reliability Analysis of Cable-Stayed Bridge under Reaction of Seldom Occurred Earthquake

Wang, Dejun
Study on Traffic Noise Characteristics of Large Grade Interchange

Wang, Dian-Hai

Inhabitant Trip Behavior Similar to Quantum Transition
A Study on the Headway Distribution of the Xueyuan Roundabout

Wang, Dianhai
Study on Signal Timing Methods of Optimizing Urban Transportation Network Efficiency

Wang, Dongsheng
Impact of Gradation Types on Freeze-Thaw Performance of Asphalt Mixtures in Seasonal Frozen Region

Wang, En-yong
A Study of the Fuzzy PID Control Over the Hydraulic Semi-Active Suspension in Consideration of Automotive Engine and Passenger-Seat System

Wang, Fengxia
The Evaluation of Micro-Benefit on Highway Construction Investments

Wang, Fuming
Quick Maintenance for Tunnel Lining Voids with Polymer Grouting Technology

Wang, Futian
Characteristics of Fundamental Data for Railway Maintenance and the Construction of Integrated Data Platform

Wang, Guanghui
Research on Key Question of Joint of Large Span Pre-Stressed Box-Girder Concrete Continuous Rigid Frame Bridge with High Piers

Wang, H.
Study on Spatial Information Model and Database of Traffic Facilities Management Systems Based on ArcGIS
Impact of Posted Speed Limits on Operating Speed in Urban Expressways
Wavy Road Elevation Measurement Based on the Principle of Inertia
Highway Traffic Parameters Estimation by Using Cell Dwell Time
Hybrid Genetic and Taboo Search Algorithm for Solving the Bus Timetable Problem
Research on Calculation of Important Parameters of Freeway Financial Post-Evaluation

Wang, Hai-biao
Experimental Research on the Combined-Method of Vacuum Well-Point Dewatering and Preloading
Study on Asphalt Treated Permeable Base in Permafrost Regions

The Experimental Study of Effects of Herbaceous Plant Protecting Slope in Cold Area

Wang, Hailong

Impact on Regularity of Track from Pile Underpinning of Light Railway Bridge

Wang, Haiwei

A Time-Varying Route Optimization Model for Urban Hazmat Transportation

Urban Transport Network Capacity Considering Level of Service

Pricing Model for Expressway with Elastic Demand

Wang, Hong

Enhancing Immersion through Adjusting Parameters of Vehicle Driving Simulator

Design Theory for Speed Control by Using Constant Edge Rate

The Reasonable Distance of Unsignalized Crosswalks Based on Traffic Flow, Stability, and Efficiency

Constitutive Relationship of Asphalt Mixture for Finite Element Method

Study on Using OD Traffic Flow to Identify the Special Boundary of the Expressway Influence Zone

Wang, Hongbo

Logistics Distribution Information System Based on 3rd Generation Mobile Communication Technology

Wang, Hua

The Analysis of the Correlation between International Roughness Index and Body Ride Comfort

Wang, Hui

A Time-Varying Route Optimization Model for Urban Hazmat Transportation

A Speed Limit Model of Vehicle for Urban Road Hazmat Transportation

Modeling Study of Coal Allocation and Distribution Plan Based on Graph Theory and Fuzzy Optimization Method

Wang, Jian

Bus Service Frequency Multi-Objective Optimal under Snowy Day

Analysis of City Transportation Networks' Travel Time Reliability during Adverse Weather

Multi-Objective Interval Number Model of Intermodal Transport under Uncertain Environment

Wang, Jianjun

The Analysis of Traffic Flow State on Foggy Expressway Based on Fuzzy Clustering

Wang, Jianxin
Stiffness Reduction Factor of Reinforced Concrete Bridge Pier Considering Characters of Nonlinear

Wang, Jiaqiu
Research on Automatic Identification Method of Pavement Sag Deformation

Wang, Jin-Ping
Optimum Choice for the Construction Management Plan Based on Entropy Weight

Wang, Jin
Study on the Method of "Inverse Four-Step" Regulatory Transportation Planning

Wang, Jun-li
Relation of Stability Coefficient to Design Parameters for Curved Continuous Rigid Frame Bridges with Long-Span and High-Pier

Wang, Junjie
Research on a Risk Analysis System of Vessel-Bridge Collision

Wang, Kaifeng
Establishment of Construction Safety Early-Warning System for Mountainous Freeways

Wang, L.
Real-Time Optimization Model of Intelligent Public Transport Network and Its Algorithm

Wang, Lan
Viscoelastic Mechanical Properties of Crumb Rubber Modified Asphalt Mixture

Wang, Lei
Impact of Gradation Types on Freeze-Thaw Performance of Asphalt Mixtures in Seasonal Frozen Region

Wang, Liang
Research on the Mechanism for Preventing Reflective Cracks in Old Cement Concrete Pavement Reconstruction

Wang, Liangshen
Study on Pedestrian Safety and Countermeasures in Crosswalks around Campus—Case Study at Ludong University in Yantai

Wang, Lijuan
Study on the Preventive Maintenance Time for Asphalt Pavement

Wang, Lina
Freeze-Thaw Stability of Slopes in Seasonally Frozen Regions of the Northeast China
Stability of Slope with the Weak Structural Plane Based on 2-D Nonlinear Finite Element Method
Vibration Characteristics of Permafrost Embankment Induced by Passing Trains in Qinghai-Tibet Railway in Winter

Wang, Linbing
An Evaluation of the Effectiveness of Geo-Textile-Binder-Aggregate System for Surface Treatment of Distressed Asphalt Pavement
Laboratory Investigation of Reclaimed Asphalt Pavement Mixed with Pure Binder Using X-Ray CT Scanner

Wang, Ling-bo
Nonlinear Analysis of Time-Dependent Effect for Reinforced Concrete Thin-Wall Box Girders Exposed to Fire

Wang, Lixia
CT Scan on Frozen Roadbed Soil under Dynamic Triaxial Test Condition of Beilu River Section, Qinghai-Tibet Railway of China

Wang, Long
Runnoff Pollutants Control by Asphalt Permeable Pavement
Resilient Modulus of the Graded Aggregate Material under Long-Term Dynamic Repeat Load

Wang, Longfei
A Safety Protection Technology System on Highway Roadside in China
An Active Parking Guidance Information System Based on Dynamic Agent Negotiation

Wang, Man
Study on the Location Parking Index Based on Function Division of Parking Space

Wang, Ming-Sheng
Topological Properties of Public Transport Networks: A Temporal Perspective

Wang, Mingquan
Investment and Finance for the Intelligent Transportation System in China

Wang, Mingsheng
Test and Analysis of Rail Break Emergency Treatment Device for Railway Switches

Wang, Nan
Experimental Investigation of the First Precast Bi-Pre-Stressing Simple Girder Concrete Bridge

Wang, Ping
Adaptability Assessment and Maintenance Technology Research of Existing Railway Line Speed Increases to 200 km/h

Wang, Qiu-ping
Study on Traffic Impedance Based on Grey Theory

Wang, Ronghui
Experimental Research on Shear Connectors' Stress of Composite Beam Bridge under Complex Stress Condition

Wang, S.
Transport Strategy for Sustainable Development of Jiao Dong Economic Region

Wang, Shen
Study and Simulation of Behavioral Decision-Making Model of Through Bicycles Passing Vehicles at Signalized Intersection

Wang, Shengwu
The Application of Functionally Gradient Material to Problems of Wheel-Rail Contact

Wang, Shuangwei
Grey Relational Analysis Method of Main Reasons of Road Traffic Accidents

Wang, Shuling
Research on Pedestrian Safety under Rapid Development of Motorization

Wang, Shuyun
Study on Evaluation Method of Expressway Roughness

Wang, Si-chang
Stability Analysis of Excavating Rock Slope Based on the Catastrophe Theory

Wang, T.
Optimal Setting of the VMS's Future Range Based on the Characteristics of Driving Speed

Wang, Tao
Association of Signal-Controlled Method at Roundabout and Capacity

Wang, Tie-cheng

Experimental Research and Damage Model of Square Concrete-Filled Steel Tube Subjected to Cyclic Loading

Wang, Wei

The Key Technology of "One Road One Line with Straight Driving" Public Transportation System

Predicting Methods of Trip Modal-Split Based on Structural Model

The Attitude and Psychological Demand Related Determinants of Public Transport Use

Research on Conversion Coefficients between Bicycle, Electric Bicycle, and Pedestrian on Urban Road Intersection

Optimization of Emergency Material Dispatch Problem Based on Adaptive Genetic Algorithm

Research on Dynamic Safety Stock Based on Short-Term Weather Forecasting

Wang, Weili

An EEG Predictor of Driving Fatigue

Wang, X.

Mixed Traffic Micro-Simulation of Urban Branch Roads

Track Access Technology of Traffic Accident Vehicles Based on Video

Traffic Signal Control Optimization of Urban Arterials Based on a Method of Main Intersection Control Strategies

Research on Dynamic Measuring System and Model of Novel High Speed Railway Vehicle Bogie

Wang, Xiao-xia

Research of Road Transportation Sustainable Development Based on Ecological Footprint Model

Wang, Xiao-zhao

Determine Old Asphalt Pavement Milling Thickness Based on Pavement Surface Deflection Control

Stability Analysis of Excavating Rock Slope Based on the Catastrophe Theory

Wang, Xiao

Study on the Key Technology of Captive Model's Numerical Test

Wang, Xiaohuang

Establishment of Construction Safety Early-Warning System for Mountainous Freeways

Wang, Xiaoning

The Method of Determining Traffic Impact Range of Developing Project Based on Threshold Value
Calculation Method on Traffic Noise Pollution of Interchange Based on Geometric Alignment
Study on Traffic Noise Characteristics of Large Grade Interchange

Wang, Xiaowei
Experimental Study on Performance of the Bridge Deck Pavement of SF-PFSC
Design and Construction of Overlay with Mechanical Joint Element on Used Concrete Pavement

Wang, Xifu
Study on Logistics Center Location Bi-Level Programming Model and Algorithm Based on Competition

Wang, Xingju
Reinforcement Learning Control for On-Ramp Metering Based on Traffic Simulation

Wang, Xinzheng
Control and Monitoring of Surface Subsidence for Shallow Tunnel under Existing Railway

Wang, Xiwei
Study on the Frost Resistance Test Method of Lime-Fly Ash Stabilized Material Base Course

Wang, Xuancang
Research on Rapid Curing Technology of Lime-Flyash-Cement Stabilized Macadam
Analysis for Principal-Agent Relationship between Owner and Construction Agent of Agent-Construction Project

Wang, Xuefeng
Study on the Optimization of Vessel Scheduling Design Based on Soft Time Windows under Voyage Charters

Wang, Xuesong
Investigation of Relationship between Level of Service and Safety
Investigation of the Relationship between Red-Light-Running Frequencies and Intersection Features

Wang, Y. L.
Prediction of the Soft Roadbed Deformation Based on a Creep Damage Model

Wang, Y.
Study on Spatial Information Model and Database of Traffic Facilities Management

Systems Based on ArcGIS
Analysis of the Influences of Fatigue on Driver's Behavior Characteristics
Research on Urban Intersection Vehicle Emission Reduction Based on Microcosmic Simulation
Prediction of the Soft Roadbed Deformation Based on a Creep Damage Model
Research on Calculation of Important Parameters of Freeway Financial Post-Evaluation
Characteristic Analysis of Urban Rail Transit Network Considering Demand and Operation: A Case on Shanghai

Wang, Yan
Identification of Hazardous Locations Based on Integrated Highway Safety State Analysis

Wang, Yang
Study on the Carrying Capability of Preplanned Regional Earthquake Evacuation Corridor Based on Macro-Simulation

Wang, Yaowu
Intelligent Emergency Traffic Evacuation Spatial Decision Support System for Urban Disasters

Wang, Yinhai
Identifying Alternative Routes with Integration of ITS into Traffic-Diversion Strategies

Wang, Yunpeng
A Time-Varying Route Optimization Model for Urban Hazmat Transportation
A Speed Limit Model of Vehicle for Urban Road Hazmat Transportation
Application of Locating Technology in the Highway Emergency Response System

Wang, Yuping
Research on the Bicycle Capacity of Signalized Intersection Based on Fluid Diffusion Characteristics

Wang, Yuzhou
Risk Evaluation Model for Construction of a Logistics Park Based on Principal Component Analysis

Wang, Z. L.
Study on Shear Properties for Adherence of New and Old Concrete and Its Practical Calculation

Wang, Z.

Detecting the Type of Multi-Fractality in Traffic Time Series
Simulation Study on a Freeway Climbing Lane

Wang, Zhen-bo
A Retrograde Vehicle Detection Method Based on the Optical Flow Field
Application Research of GPS Based on Google Earth Platform

Wang, Zhenjun
Expressway Data De-Noised Approach Based on Wavelet Analysis

Wang, Zheren
Theoretical Analysis of Design Parameters on Semi-Rigid Asphalt Pavement with Flexible Base
Study on the Frost Resistance Test Method of Lime-Fly Ash Stabilized Material Base Course
A Discontinuous Numerical Method for Asphalt Mixture

Wang, Zhi-Yin
Study of Influence of Subway Station Excavation on Existing Metro Deformation

Wang, Zhijian
Map Matching Algorithm of a Center Terminal Based on the Road Network Topological Structure

Wang, Zhongwei
Logistics Distribution Information System Based on 3rd Generation Mobile Communication Technology

Wang, Zonglin
Research on Application of Externally Prestressing for Simple-Continuous Bridge

Wei, Chenglong
Research on Key Question of Joint of Large Span Pre-Stressed Box-Girder Concrete Continuous Rigid Frame Bridge with High Piers

Wei, H.
RGB Based Crowded Pedestrian Counting in Red Light Time
Short-Term Traffic Flow Prediction with ACD and Particle Filter

Wei, Hai-bin
Experimental Research on the Mechanical Parameter of Fly Ash Soil
Sensitivity Analysis of the Dynamical Parameters on Road Materials

Wei, Heng
Dilemma Zone Modeling Using Yellow-Onset Vehicular Trajectory Data

Integrated Arterial Signal and Access Control Strategy under Non-Notice Emergency Evacuation: Modeling and Simulation-Based Analysis
Identifying Alternative Routes with Integration of ITS into Traffic-Diversion Strategies

Wei, Jianguang
Study on Multi-Dimensional Structure Model for Agricultural Products Logistics Organization in China

Wei, Jianjun
A Study on Cable-Removing Scheme of the Cable-Stay System of the Zhijing River Bridge

Wei, L.
Safety Evaluation Methods of Road Traffic Based on Gray Cluster Theory

Wei, Lang
A Traffic Accident Reconstruction Study on Continuous Collision of Three Cars
Study and Implementation on JPEG Image Enhancement System of Tire Mark

Wei, Xueying
Plastic Behavior for Compaction Pile with Hole Expanded by Blasting or Tamping Techniques

Wei, Z.
Study on the Rules of Crash Distribution

Wen, Hui-ying
Research on Urban Public Transit Dispatching System Based on Real-Time Prediction and Game Theory

Wu, Bing
Study on the Location Parking Index Based on Function Division of Parking Space
The Analysis of Transportation Demand Generation Mechanisms of the Urban Agglomerations in China

Wu, Dayong
Research on Structural Design of Interlocking Concrete Block Pavement for Rural Road

Wu, F.
Frequency Optimization Model for a Public Traffic Scheduling System

Wu, H. N.
Public Transport Incident Prediction Method by Road Traffic Delays

Wu, Haiyan
Strategic Transport Model of Beijing and Application to City Centre Transport Policies Evaluation

Wu, Hong Xing
The Research of Control Strategy of Permanent Magnet Synchronous Motor for Hybrid Electric Vehicles

Wu, Hong-Lin
Analysis Method for the Prestressed Concrete Bridges Based on Time-Dependent Theory

Wu, Huichao
Fatigue Life Prediction of Rubber Nodes

Wu, J.
Traffic Signal Control Optimization of Urban Arterials Based on a Method of Main Intersection Control Strategies

Wu, Jian-Jun
Dynamic Response of a Magnetically Levitated Vehicle in a Crosswind

Wu, Jin-pu
Study on Traffic Impedance Based on Grey Theory

Wu, Jingmei
The Method of Road Safety Analysis Based on Two-Dimensional Speed Difference

Wu, L. Q.
Shake Table Test on Seismic Response of Non-Free Liquefiable Site

Wu, Lina
A New Cellular Automaton Traffic Flow Model for an Off-Ramp Junction of a Chinese Urban Expressway

Wu, Linlin
Equilibrium Model of Trip Modes in Road Traffic and Orientation of Charge Policy
Optimization of Regional Traffic Structure from the Perspective of Sustainable Development

Wu, Liquan
Case Studies for Shaking Table Tests on Seismic Soil-Pile Group-Bridge Structure Interaction in Liquefiable Ground
CT Scan on Frozen Roadbed Soil under Dynamic Triaxial Test Condition of Beilu River Section, Qinghai-Tibet Railway of China

Freeze-Thaw Stability of Slopes in Seasonally Frozen Regions of the Northeast China

Stability and Reinforcement Methods of a High Slope at the Hang-Yong Natural Gas Pipeline in China

Stability of Slope with the Weak Structural Plane Based on 2-D Nonlinear Finite Element Method

Vibration Characteristics of Permafrost Embankment Induced by Passing Trains in Qinghai-Tibet Railway in Winter

Wu, Meng

A Novel Real-Time Road Shape Describing and Parameter Obtaining Method

Wu, Ning

Further Development of the German Highway Capacity Manual (HBS2011)

Wu, Ping

Pedestrian Simulation Research of Subway Station in Special Events

Wu, Pingbo

Fatigue Life Prediction of Rubber Nodes

Wu, Pingdong

Study of Driver's EEG and Application in Intelligent Transportation Systems

Wu, Qian-jiao

New Methods for Research in Multi-Agent Traffic Signal Control

Wu, Qianjiao

Short-Term Traffic Flow Prediction Based on EMD and Artificial Neural Network

Wu, Qisheng

Traffic Incident Acoustic Recognition Based on Wavelet Decomposition and SVM

Wu, Shaopeng

Constitutive Relationship of Asphalt Mixture for Finite Element Method

Wu, Ting

Study on the Preventive Maintenance Time for Asphalt Pavement

Damage Model Analysis of SBS Modified Asphalt Mixture

Wu, Xiaoguang

An Analytical Method for Predicting the Service Life of Bridge Structures

Wu, Ya-ping

Study on the Rational Size of the Box Girder Used in Cable-Stayed Bridge Based

on ANSYS
A Safety Evaluation Method of Existing Flexible Suspension Bridge with Double Cable

Wu, Yaodong
Laboratory Evaluation of the Warm Mix Asphalt Performance in Liaoning

X

Xhao, Jiaqi
Research on the Characteristics of Time Headway Distribution in Expressway Weaving Section of Type A

Xi, Jianfeng
Study on Accident Reconstruction Model Based on Reverse-Reasoning Method
Grey Relational Analysis Method of Main Reasons of Road Traffic Accidents

Xia, Jing
Design Theory for Speed Control by Using Constant Edge Rate
The Reasonable Distance of Unsignalized Crosswalks Based on Traffic Flow, Stability, and Efficiency

Xia, Qingdong
Analysis on Vehicle No-Sideslip Single Side Skid Equivalent Frictional Coefficient

Xian, Kai
Expansion and Validation of Beijing Household Interview Survey Data

Xian, Liang
Modeling Study of Coal Allocation and Distribution Plan Based on Graph Theory and Fuzzy Optimization Method

Xiang, Wen-sen
Vehicle Dynamics Model in Two-Dimension Collision Accident

Xiao, Bing
Study on the Key Technology of Captive Model’s Numerical Test

Xiao, Dianliang
The Evaluation of Micro-Benefit on Highway Construction Investments
Analysis Model for Operating Speed on Two-Lane Secondary Highway

Xiao, Haibing

Plastic Behavior for Compaction Pile with Hole Expanded by Blasting or Tamping Techniques

Xiao, S. G.
Analysis of a New Combined Micropile Structure for Preventing Slope Slippage and Its Application in a Practical Project

Xiao, Shourne
Research on the Crashworthiness of Two-Layer Thin-Walled Structures

Xiao, Wang-Xin
The Numerical Analysis of Sound and Vibration from a Tire by FEM and BEM

Xiao, Xinbiao
Model of High Speed Railway Wheel Ovalization

Xie, Binglei
A Model and Heuristic Algorithm for Inventory Routing Problem in Emergency Logistics

Xie, C.
Highway Accidents Analysis with Panel Data Model

Xie, Chenfeng
The Analysis of Traffic Flow State on Foggy Expressway Based on Fuzzy Clustering

Xie, Haihong
Research on Location of Railway Logistics Center

Xie, Hui
Analysis about Business Investing and Financing Models of Urban Rail Transit

Xie, Ruhe
A Model on Risk Evaluation for Emergency Guarantee Mechanism of Food Logistics

Xie, Shaobo
Simulation of Turning Stability Control for Two-Motor-Drive Electric Vehicles

Xie, Wei-Ping
The Numerical Analysis of Sound and Vibration from a Tire by FEM and BEM

Xie, Weiping
Structural Noise of Longitudinal Stiffened Concrete Cylindrical Shell

Xie, Xiaoguang
Runnoff Pollutants Control by Asphalt Permeable Pavement

Resilient Modulus of the Graded Aggregate Material under Long-Term Dynamic Repeat Load

Function Design of Cement Stabilized Crushed Stone Drainage Base

Xie, Xiaoli

An EEG Predictor of Driving Fatigue

Xie, Yong-li

Reliability Analysis on Pavement Skid-Resistant Performance in Expressway Tunnel

Xie, Zi-nan

Research and Application of Graphic-Attributes Integration Based on Web GIS in Aviation Accident Investigation

Xin, W.

Research on Calculation of Important Parameters of Freeway Financial Post-Evaluation

Xing, Liying

Control and Monitoring of Surface Subsidence for Shallow Tunnel under Existing Railway

Xing, Yong-ming

Viscoelastic Mechanical Properties of Crumb Rubber Modified Asphalt Mixture

Xiong, Chang-Zhen

Vehicle Tracking from Videos Based on Mean Shift Algorithm

Xiong, Huagang

An Improved Ant Colony Algorithm for the Shortest Path Problem in Time-Dependent Networks

Xiong, Hui

Analysis of Crowd Behavior in Route Choice Based on Dynamic Programming

Xiong, Jian-ping

Study on the Influence of Coarse Aggregate on the Pavement Performance of Road Cement Concrete

Xiong, Jian

Evaluation Study of the Median Markings in Undivided Highway Tunnels

Driving Simulation Study on Traffic Flow Characteristics on the Climbing Lane on a Two-Lane Rural Road

Xiong, Wen

The Analysis of Traffic Landscape from Users' Perspective: The Case of the Zhangjiang Tram

Xiong, Zhihua
A Model of Mixed Land Use and Trip Production by BP Neural Network
Short-Term Forecasting of Uncertain Traffic States

Xu, Bin
Resilient Modulus of the Graded Aggregate Material under Long-Term Dynamic Repeat Load

Xu, C.
Public Transport Incident Prediction Method by Road Traffic Delays
Frequency Optimization Model for a Public Traffic Scheduling System

Xu, F. Y.
Flutter Derivatives Identification of Aeroelastic Model of Hangzhou Bay Bridge

Xu, Fu-you
Expressway Pavement-Performance Indexes Prediction Based on Gray Model GM (1,1,λ)

Xu, Fuyou
Influence Factors Analysis of Buffeting Response of Self-Anchored Cable-Stayed Suspension Bridge

Xu, Guanghui
Continuous Test for Construction Quality of Mixed Filling Roadbed

Xu, Guangyin
Study on Multi-Dimensional Structure Model for Agricultural Products Logistics Organization in China

Xu, H.
Influencing Factors Contributing to Rear-End Collisions on Highways: PCA Based Investigation and Findings

Xu, Jia-Qi
Technology Research on the Vehicle Collision Accident Self-Alarm System

Xu, Jia
Voids Classification Standard for Cement Concrete Pavement Slabs Based on Service Life
Side Road Traffic Considered in Transit Signal Priority Control

Xu, Jianguo
Quick Maintenance for Tunnel Lining Voids with Polymer Grouting Technology

Xu, Ke
Effect of Density Variation of Coarse Aggregate on Asphalt Mixture Properties

Xu, Lan
Research on Location of Railway Logistics Center

Xu, P. J.
Shake Table Test on Seismic Response of Non-Free Liquefiable Site

Xu, Pengju
Case Studies for Shaking Table Tests on Seismic Soil-Pile Group-Bridge Structure Interaction in Liquefiable Ground

Xu, Qing-Yuan
Influence of Longitudinal Connection Mode of Ballastless Slab Track on Vibration Characteristic of Train-Ballastless Slab Track-Subgrade System

Xu, T.
Highway Accidents Analysis with Panel Data Model

Xu, Wei
Performance of Pavement Plate Reinforced with Modified Unsaturated Polyester Fiberglass Reinforced Plastic
New Concrete Improving Performance of Airfield Pavement
Application of Thermal Stress Controlling in Construction of Large Bridge Cushion Cap

Xu, Wensheng
Analysis of Thermal Stress Response in Asphalt Overlay

Xu, Xinwei
Design and Construction of Overlay with Mechanical Joint Element on Used Concrete Pavement

Xu, Yang
Rut-Resisting Capacity of the Whole Surface Course in Continuous Upgrade under Heavy Loading

Xu, Yong-gang
Risk Assessment of Road Operation Environment under Atrocious Weather Condition

Xu, Yongneng
Efficiency Evaluation of Urban Transit Terminals Based on the Cloud Model

Xu, Yongpeng
Runnoff Pollutants Control by Asphalt Permeable Pavement

Xu, Zhi
A Study on Signal Timing Optimization of Individual Intersections Based on an Ant Colony Algorithm
Study on the Capacity of Right-Turn Movement under Pedestrians' Influence at Signalized Intersections
A Study on the Bus Delay Model at Bus Stops

Xu, Zhihong
Study on the Relationship of Traffic Flow Complexity and Traffic Conflict on Urban Road

Xu, Zhuokui
Several Questions of Highway Influence Assessment on Dongting Lake Ecosystem in China

Xuan, Dengdian
Research on Taboo Simulated Annealing Combinatorial Optimization Algorithm of Location Routing Problem with Pickups and Deliveries

Xue, Changlong
Research on the Characteristics of Time Headway Distribution in Expressway Weaving Section of Type A

Xue, Kun
Association of Signal-Controlled Method at Roundabout and Capacity

Xue, Lingxiang
Influencing Factor Analyses of Section Types on Vehicle-Bridge Interaction of Concrete Box Girder with Corrugated Steel Webs

Y

Yan, Bo
An Optimization Model for Bus Rapid Transit

Yan, Caiyun
Simulation of Wheel/Rail Noise of High Speed Train Running on the Slab Track

Yan, F.
Collision Avoidance among Multiple Ship Agents
Study on Burner Type Diesel Particulate Filter System Using Compressed Air from Turbocharger

Yan, Jinhai
A Study of Cold In-Place Recycling Mixture Used as Binder Course in China

Yan, Kefei
Study of the Parking Guidance Reliability of Urban Parking Variable Message Signs

Yan, Qipeng
Locating Emergency Response Facilities for Hazardous Materials Transportation with Probabilistic Response Time

Yan, X.
Traffic Signal Control Optimization of Urban Arterials Based on a Method of Main Intersection Control Strategies

Yan, Xiao-Yong
Topological Properties of Public Transport Networks: A Temporal Perspective

Yan, Yana
Study on Logistics Center Location Bi-Level Programming Model and Algorithm Based on Competition

Yan, Yong
Model Test Study of System Transformation for Jiangdong Bridge

Yan, Yusong
Optimization of Dynamic Dispatching Decisions of Local Wagon-Flows in Terminals with IRTS

Yan, Zhanyou
Bridge Damage Assessment by Dynamic Response in Time Domain

Yang, B.
Noise Source Identification and Noise Reduction of a Double Crank Four Ring-Plate-Type Cycloid Reducer

Yang, Bo
Study on the Key Technology of Captive Model’s Numerical Test

Yang, C.
Characteristic Analysis of Urban Rail Transit Network Considering Demand and

Operation: A Case on Shanghai

Yang, Chao
A Multi-Class Multi-Modal Combined Model for TDM Measures Evaluation in Large Scale Urban Transportation Network

Yang, Dawei
NURBS Strands Modeling of Prestressed Concrete Bridges

Yang, Dongyuan
A Multi-Class Multi-Modal Combined Model for TDM Measures Evaluation in Large Scale Urban Transportation Network
Investment and Finance for the Intelligent Transportation System in China
Case Study: Analysis of CO_2 Emissions Caused by Customers Transportation in Shanghai and Shenzhen IKEA

Yang, Guang
Empirical Research on Applicable Principle for Toll Mode of Highway

Yang, Guangwu
Research on the Crashworthiness of Two-Layer Thin-Walled Structures

Yang, Hai-xu
Experimental Research on the Combined-Method of Vacuum Well-Point Dewatering and Preloading
The Experimental Study of Effects of Herbaceous Plant Protecting Slope in Cold Area

Yang, Hai
Ramp Metering Strategies in a Corridor Network

Yang, Jian-guo
Reliability Analysis on Pavement Skid-Resistant Performance in Expressway Tunnel

Yang, Ken
A Collaborative Software Framework Design in Supporting GLITS I-75 Integrated Freeway and Arterial Operation Project

Yang, Longhai
Research on Dynamic Characteristics of Road Network in Snowy Conditions
Multi-Objective Interval Number Model of Intermodal Transport under Uncertain Environment

Yang, Manjuan

Analysis of Characters and Causes of Road Traffic Accident Migration

Yang, Min
A Comprehensive Bus Line Evaluation Method Based on Fuzzy C-Means Clustering Algorithm

Yang, Ou
Reliability Analysis of Cable-Stayed Bridge under Reaction of Seldom Occurred Earthquake

Yang, Qingyan (Ken)
Identifying Alternative Routes with Integration of ITS into Traffic-Diversion Strategies

Yang, Songlin
Influence of Curing Regime on the Ductility of Ultra-High Performance Fiber Reinforced Concrete (UHPFRC)

Yang, Tingting
A Framework of the Traffic Organization Simulation System for Freeway Emergency Response

Yang, Wenchen
Adaptive Control Method of Multi-Phase Intersection Based on Traffic Status Identification

Yang, Wencui
Effect of Inorganic Salts on Frost Resistance of Concrete

Yang, X.
A Route-Based Model for Determining Interconnection of Isolated Traffic Signals

Yang, Xia-lin
Study on the Rational Size of the Box Girder Used in Cable-Stayed Bridge Based on ANSYS

Yang, Xiao-kuan
A Study on Driver’s Dynamic Visual Characteristics

A Study on Signal Timing Optimization of Individual Intersections Based on an Ant Colony Algorithm

A Study on the Bus Delay Model at Bus Stops

Yang, Xiaoguang
Study on the Method of “Inverse Four-Step” Regulatory Transportation Planning

Traffic Management on an At-Grade Signalized Intersection Connecting to Urban

Expressway Ramps
Study on Residential Daily En-Route Travel Choice Behavior with Traffic Information: Application of RP/SP Joint Survey and Disaggregate Model

Yang, Xiaojun
Calculation Method for Braking Torque of Self-Excited Retarder

Yang, Xiaokuan
Study on the Carrying Capability of Preplanned Regional Earthquake Evacuation Corridor Based on Macro-Simulation
Analysis on Standards Used in Traffic Impact Study
Integrated Arterial Signal and Access Control Strategy under Non-Notice Emergency Evacuation: Modeling and Simulation-Based Analysis
Study on the Capacity of Right-Turn Movement under Pedestrians' Influence at Signalized Intersections

Yang, Xinmiao
Evaluation and Optimization of Public Transport Subsidies for Alternative Energy

Yang, Xinwen
Simulation of Wheel/Rail Noise of High Speed Train Running on the Slab Track

Yang, Xueqiang
Dynamic Effects of Moving Vehicular Loads on Continuously Reinforced Concrete Pavements on Winkler Foundation

Yang, Yanhai
Laboratory Evaluation of the Warm Mix Asphalt Performance in Liaoning

Yang, Ze-ping
Reliability Analysis of Cable-Stayed Bridge under Reaction of Seldom Occurred Earthquake

Yang, Zeying
Construction Control of Cable-Stayed Bridges Based on ANN and GA Hybrid Algorithm

Yang, Zhaosheng
Dynamic Model of Transit Signal Priority on Colored Time Petri Net
Map Matching Algorithm of a Center Terminal Based on the Road Network Topological Structure

Yang, Zhen
Study on Prolonging Asphalt Pavement Fatigue Life Based on Vision Transverse Intervention

Yang, Zhongzhen
Road Traffic Control Information and Traffic Resource Analysis System
An Optimization Model for Bus Rapid Transit
Study on the Structure of Digitized Transport Networks and Evaluation of Some Logistics Policies
Analyzing the Effects of the Growth of Maritime Industries on the Regional Economy with Dynamic Inverse Matrix

Yao, G.
Study on Burner Type Diesel Particulate Filter System Using Compressed Air from Turbocharger

Yao, Guoquan
Node-Importance-Degree-Based Logistics Node Analysis

Yao, Hongyu
Restraint Efficacy Analysis and Structure Optimization for the Design of Airplane Metal Chocks

Yao, Rong-Han
Inhabitant Trip Behavior Similar to Quantum Transition

Yao, X.
Study on Style Protection and Urban Traffic Planning of Harbin Jingyu Street

Yao, Xinsheng
Study on Multi-Dimensional Structure Model for Agricultural Products Logistics Organization in China

Yao, Xu
Nonparametric Analysis of Timely Distribution of Traffic Crash

Yao, Yao
Constitutive Relationship of Asphalt Mixture for Finite Element Method

Yao, Zhisheng
Short-Term Forecasting of Uncertain Traffic States

Ye, Lei
Study on the Model of Hub Location under Earthquake Conditions

Ye, Ruimin
Research on the Bicycle Capacity of Signalized Intersection Based on Fluid Diffusion Characteristics

Ye, Xiaofei
A Framework of the Traffic Organization Simulation System for Freeway Emergency Response

Ye, Y. F.
The Simulation Analysis of Passenger Evacuation in One Metro Station Based on Exodus

Yi, Haiming
Construction Control of Cable-Stayed Bridges Based on ANN and GA Hybrid Algorithm

Yi, Junyan
Impact of Gradation Types on Freeze-Thaw Performance of Asphalt Mixtures in Seasonal Frozen Region

Yi, Kai
Experimental Research and Damage Model of Square Concrete-Filled Steel Tube Subjected to Cyclic Loading

Yi, Sheng
Establishment of Construction Safety Early-Warning System for Mountainous Freeways

Yin, C.
Hybrid Genetic and Taboo Search Algorithm for Solving the Bus Timetable Problem

Yin, Jian-ming
Experimental Research on the Combined-Method of Vacuum Well-Point Dewatering and Preloading

Yin, Liang
Study of Anti-Slide Pile Composed of Arch and Truss Structure Based on FEM

Yin, Yafeng
Robust Optimization Approach for Transportation Network Design under Demand Uncertainty

Yin, Yi-xin
Vehicle Detection from Videos Containing Complex Background Based on Bayesian Statistical Modeling

Ying, Ronghua
Damage Model Analysis of SBS Modified Asphalt Mixture

Ying, Ronghue
Study on the Preventive Maintenance Time for Asphalt Pavement

You, Kesi
Viscoelastic Analysis of Asphalt Pavement Using a Regularized Interconversion Technique between Creep and Relaxation

Yu, Bin
An Optimization Model for Bus Rapid Transit

Yu, H.
Study on Spatial Information Model and Database of Traffic Facilities Management Systems Based on ArcGIS

Yu, Huoming
Stability and Reinforcement Methods of a High Slope at the Hang-Yong Natural Gas Pipeline in China

Yu, J.
Detecting the Type of Multi-Fractality in Traffic Time Series

Yu, Jianling
Expressway Data De-Noised Approach Based on Wavelet Analysis

Yu, Jianyi
Establishment of Construction Safety Early-Warning System for Mountainous Freeways

Yu, Jingnuo
Study on Power Control of Electric Power Steering System

Yu, Lu
Computer-Aided Error Detection of Horizontal and Vertical Alignment in Highway Construction

Yu, Q.
Car-Following Criteria at a Signalized Intersection in Beijing

Yu, Qiang
A Traffic Accident Reconstruction Study on Continuous Collision of Three Cars

Yu, Quan
The Research of Signal Phase Sequences Based on the Conglomeration of Pedestrians and Bicycles

Yu, Shijun

Efficiency Evaluation of Urban Transit Terminals Based on the Cloud Model

Yu, Siqin
Study on Energy Consumption by Land Cargo Transportation

Yu, Su
A Study on the Financing Mode of Assets Securitization in Port Project

Yu, X.
Lane Change Behavior Character and Its Influence to Traffic Safety on Urban Roads

Yu, Xiaojun
Efficiency Loss of the Multiclass, Multicriteria Stochastic User Equilibrium Traffic Assignment against Stochastic System Optimization

Yu, Xin
Performance Evaluation of Waterproof Bond Layer Materials Based on Grey Target Theory

Yu, Xinxin
Urban Transport Network Capacity Considering Level of Service
Pricing Model for Expressway with Elastic Demand

Yu, Yanlin
Integration of Fortran with ANSYS in Transient Thermal Simulation

Yu, Zhi
Parameter Sensitivity Analysis of Accident Reconstruction Model Based on Orthogonal Design

Yuan, Ding
Research and Application of Graphic-Attributes Integration Based on Web GIS in Aviation Accident Investigation

Yuan, Jie
Effect of Inorganic Salts on Frost Resistance of Concrete
Effect of Lightweight Aggregate with Different Moisture of Autogenous Shrinkage and Stress under Partially Restrained Condition

Yuan, Yan
Application of Fractal Theory in Pavement Surface Texture Measurement

Yue, Y.
An Interval-Varying Floating Car Data Clustering Approach Based on Self-Organizing Maps

Urban Road Travel Speed Estimation Based on Low Sampling Floating Car Data

Yue, Yongheng
Analysis on Vehicle No-Sideslip Single Side Skid Equivalent Frictional Coefficient

Yun, Meiping
Study on Residential Daily En-Route Travel Choice Behavior with Traffic Information: Application of RP/SP Joint Survey and Disaggregate Model

Z

Zang, L. L.
Public Transport Incident Prediction Method by Road Traffic Delays

Zang, X.
Using VISSIM to Calculate the Capacity of Urban Expressway Interchange

Zeng, Jing
Bending Vibration Suppression of High Speed Railway Passenger Car Body

Zeng, Minghua
Analysis of the Competitive Strategy of the Core Enterprises in Virtual Intermodal Freight-Transportation Enterprise

Zeng, Qingyuan
Limit Value of Railway Bridge for Traffic Safety

Zeng, Sheng
Voids Classification Standard for Cement Concrete Pavement Slabs Based on Service Life

Zeng, Zhi-Ping
Influence of Longitudinal Connection Mode of Ballastless Slab Track on Vibration Characteristic of Train-Ballastless Slab Track-Subgrade System

Zha, Qifen
Equilibrium Model of Trip Modes in Road Traffic and Orientation of Charge Policy
Optimization of Regional Traffic Structure from the Perspective of Sustainable Development

Zhai, Wanming
Simulation and Analysis for Stick-Slip Vibration of Locomotive with Hollow-Shaft Drive System

Zhan, Ting
Analysis for Principal-Agent Relationship between Owner and Construction Agent of Agent-Construction Project

Zhang, Baosheng
Effect of Inorganic Salts on Frost Resistance of Concrete
Effect of Lightweight Aggregate with Different Moisture of Autogenous Shrinkage and Stress under Partially Restrained Condition

Zhang, C.
Design and Realization of Decision-Making and Analysis Assistant System on National Integrated Transportation Information

Zhang, D. L.
A Study of Transit Evacuation Route Planning Based on Time-Expanded Network

Zhang, Dali
Optimization of Vehicle Routing for Plowing and Snow Disposal

Zhang, Dexin
Expansion and Validation of Beijing Household Interview Survey Data

Zhang, Erlong
Experimental Study on Performance of the Bridge Deck Pavement of SF-PFSC

Zhang, Fa
Effects of Lane Changing in Heterogeneous Traffic Flow

Zhang, Fei
ALINEA-Based Urban Expressway On-Ramp Metering Strategy

Zhang, Feng
CT Scan on Frozen Roadbed Soil under Dynamic Triaxial Test Condition of Beilu River Section, Qinghai-Tibet Railway of China
Freeze-Thaw Stability of Slopes in Seasonally Frozen Regions of the Northeast China
Stability and Reinforcement Methods of a High Slope at the Hang-Yong Natural Gas Pipeline in China
Stability of Slope with the Weak Structural Plane Based on 2-D Nonlinear Finite Element Method
Vibration Characteristics of Permafrost Embankment Induced by Passing Trains in Qinghai-Tibet Railway in Winter

Zhang, G. Y.

RGB Based Crowded Pedestrian Counting in Red Light Time
Short-Term Traffic Flow Prediction with ACD and Particle Filter

Zhang, Gang
Nonlinear Analysis of Time-Dependent Effect for Reinforced Concrete Thin-Wall Box Girders Exposed to Fire

Zhang, Guanghou
Pedestrian Simulation Research of Subway Station in Special Events

Zhang, Guoming
Study of Hydrodynamic Pressure on the Cylindrical Pile-Cap Pier in Deep Water Subjected to Seismic Action

Zhang, H. M.
Simulation Analysis of Merging Area on Urban Expressway in Alternate Rules Based on Cellular Automata Model

Zhang, He-feng
Sensitivity Analysis of the Dynamical Parameters on Road Materials

Zhang, Huaizhi
Laboratory Evaluation of the Warm Mix Asphalt Performance in Liaoning

Zhang, Hui
Road Traffic Control Information and Traffic Resource Analysis System
Application Research of GPS Based on Google Earth Platform

Zhang, Huiling
The Comparison of Three Getting Signal Control Delay Video Methods at Signalized Intersection

Zhang, J.
Pavement Crack Automatic Recognition Based on Wiener Filtering
Design and Realization of Decision-Making and Analysis Assistant System on National Integrated Transportation Information

Zhang, Jian
Estimation of Original-Destination Matrices for Public Traffic Passenger Flow

Zhang, Jie
Study on the System Design and Optimal Models of Urban Rail Transit Traction Calculation System

Zhang, Jin

Modeling Study of Coal Allocation and Distribution Plan Based on Graph Theory and Fuzzy Optimization Method

Zhang, Jingjing
The Analysis of Traffic Flow State on Foggy Expressway Based on Fuzzy Clustering

Zhang, Jinxi
Basic Study on Fractal Characteristic of Pore Structure in Cement Mortar
Study on Evaluation Method of Expressway Roughness

Zhang, Juan
The Method to Identify Black Spots of Long Highway Tunnel

Zhang, Jun-hui
Fracture Mechanics Analysis of Cracking in Asphalt Pavement Widening

Zhang, Jun
Limit Value of Railway Bridge for Traffic Safety
The Application of Functionally Gradient Material to Problems of Wheel-Rail Contact

Zhang, Junjian
Research on a Risk Analysis System of Vessel-Bridge Collision

Zhang, Junping
Experimental Research on Shear Connectors' Stress of Composite Beam Bridge under Complex Stress Condition

Zhang, Ke
Nonparametric Analysis of Timely Distribution of Traffic Crash

Zhang, Li-juan
Expressway Pavement-Performance Indexes Prediction Based on Gray Model GM (1,1,λ)

Zhang, Li-na
Reliability Analysis of Cable-Stayed Bridge under Reaction of Seldom Occurred Earthquake

Zhang, Li-xan
Research on the Design of Inner Horizontal Surface of the Airport

Zhang, Lianzhen
Design and Validation of Wireless Dynamic Testing System for Bridge Based on the 941B Type Vibration Sensor

Zhang, Ling-yong
Bus Location Display System Based on GPRS

Zhang, Lixin
An Algorithm for Vehicle Routing Problem with Soft Time Windows Using Tabu Search

Zhang, Liye
Expressway Operation Financial Benefit Evaluation under Uncertainty

Zhang, M.
Lane Change Behavior Character and Its Influence to Traffic Safety on Urban Roads

Zhang, Maomin
Passenger Transport Demand Prediction for Newly-Built Regions

Zhang, Meikin
Study on the Relationship of Traffic Flow Complexity and Traffic Conflict on Urban Road

Zhang, Peng
A Reserve Capacity Model of Optimal Traffic Lane Allocating

Zhang, Qiang
Ration Effect of Rheological and Combustion Properties of Coal-Oil-Water Slurry

Zhang, Qingnian
Research on the Differences in Regional Economy and Transportation among the Three Regions in China

Zhang, Qinying
Optimization of Emergency Material Dispatch Problem Based on Adaptive Genetic Algorithm

Zhang, Qisen
Rut-Resisting Capacity of the Whole Surface Course in Continuous Upgrade under Heavy Loading

Optimization Theory of Regulation on Rural Transit Market Based on Rule of Transport Equality

Zhang, Ruhua
Study on Intersections with Median BRT Stations: Focused on Pedestrian Street-Crossing Characteristics

Zhang, Rui
Strategic Transport Model of Beijing and Application to City Centre Transport Policies Evaluation

Zhang, Ruoqi
Investment and Financing Influence Analysis and Countermeasures for Highway Construction in the Period of China's 11th Five-Year Plan

Zhang, S.
Transport Strategy for Sustainable Development of Jiao Dong Economic Region

Zhang, Shengrui
The Method to Identify Black Spots of Long Highway Tunnel

Zhang, Shibo
Experimental Research on Shear Connectors' Stress of Composite Beam Bridge under Complex Stress Condition

Zhang, Sulan
Research on Vehicle Information Extraction from High-Resolution Satellite Images

Zhang, Tao
Gradually Rolling Prediction of the Use-Level of Road Network Based on BP Neural Network
Integration of Fortran with ANSYS in Transient Thermal Simulation

Zhang, Tianran
A Multi-Class Multi-Modal Combined Model for TDM Measures Evaluation in Large Scale Urban Transportation Network

Zhang, W.
Link Average Speed of Traffic Flow Estimation Method Based on Floating Car

Zhang, Wanchao
Study on the Capacity of Right-Turn Movement under Pedestrians' Influence at Signalized Intersections

Zhang, Wei-hua
Research on the Prediction Model of Traffic Accidents Using the Least Square Support Vector Machine
Accident Prevention and Inducement Strategy in Highway Tunnel

Zhang, Wei
Evaluation of Fire Risk at Highway Tunnels

Zhang, Weihua
Capacity Model of Low Channeling Roundabout Based on Vehicle Arrival Characteristics
A Study on the Location Selection of Public Traffic Transfer Hub Based on Improved Particle Swarm Algorithm

Zhang, X.
Noise Source Identification and Noise Reduction of a Double Crank Four Ring-Plate-Type Cycloid Reducer

Zhang, Xi-qiao
Capacity Reliability of Road Network under Adverse Weather Conditions Based on Fuzzy Theory

Zhang, Xiao
Reliability Analysis on Pavement Skid-Resistant Performance in Expressway Tunnel

Zhang, Xiaohong
Optimal Dynamic Substitution Policy for Components in an Assemble-to-Order System
Coordination Policies of Supply Chain Where Deterioration Begins at a Random Time Point

Zhang, Xiaoning
Simulation Analysis of Merging Area on Urban Expressway in Alternate Rules Based on Cellular Automata Model

Zhang, Xiaowei
Simulation of Turning Stability Control for Two-Motor-Drive Electric Vehicles

Zhang, Xiedong
The Bearing Character of Bridge Piles in Karst Areas
Study of Anti-Slide Pile Composed of Arch and Truss Structure Based on FEM
Establishment of Construction Safety Early-Warning System for Mountainous Freeways

Zhang, Xin
Heat Reflection Coating Design and Performance

Zhang, Xing-qiang
Study on Fuzzy Neural Network Model of Vehicle-Bicycle Conflicts at Grade Intersection Based on Failure Tree Analysis
Study and Simulation of Behavioral Decision-Making Model of Through Bicycles

Passing Vehicles at Signalized Intersection

Zhang, Xinjie
Research on the Differences in Regional Economy and Transportation among the Three Regions in China

Zhang, Xiqiao
Research on Dynamic Characteristics of Road Network in Snowy Conditions

Zhang, Xueshan
Model of High Speed Railway Wheel Ovalization

Zhang, Y.
Lane Change Behavior Character and Its Influence to Traffic Safety on Urban Roads
Frequency Optimization Model for a Public Traffic Scheduling System
Study on Style Protection and Urban Traffic Planning of Harbin Jingyu Street

Zhang, Yan
Performance Model for Pavement Maintenance of Expressway in Northwest of China

Zhang, Yaping
Research of Company Freight Traffic Generation Prediction Models in High-Tech Park
Nonparametric Analysis of Timely Distribution of Traffic Crash
Assessment Methodology for Road Network Travel Time Reliability under Ice and Snowfall Conditions
Research on the Bicycle Capacity of Signalized Intersection Based on Fluid Diffusion Characteristics
Several Questions of Highway Influence Assessment on Dongting Lake Ecosystem in China
Computer-Aided Error Detection of Horizontal and Vertical Alignment in Highway Construction
An Estimate Method for Accuracy of Fitting Horizontal Alignment in Old-Highway Based on Fitting Normal Error

Zhang, Yi
Study on Residential Daily En-Route Travel Choice Behavior with Traffic Information: Application of RP/SP Joint Survey and Disaggregate Model
Study on Inter-regional Transportation Infrastructure Integration Planning in China

Zhang, Ying
Influence Factors Analysis of Buffeting Response of Self-Anchored Cable-Stayed Suspension Bridge
Empirical Research on Applicable Principle for Toll Mode of Highway

Zhang, Yu
Repositioning of Empty Containers in the Transpacific Market: A Case Study

Zhang, Yunqing
Test and Analysis of Rail Break Emergency Treatment Device for Railway Switches

Zhang, Zhiyong
Design of 3D Virtual Simulation and Evaluation System for Road Traffic Signs
Damage Model Analysis of SBS Modified Asphalt Mixture

Zhao, C.
Research on Numerical Simulation of Pollutant Dispersion at Expressway Toll Plazas Based on Multi-Influencing Factors

Zhao, Chen
Performance Model for Pavement Maintenance of Expressway in Northwest of China

Zhao, Gang
Electrical Appliance Reversion Logistics Network Planning

Zhao, Guanghua
Pedestrian Simulation Research of Subway Station in Special Events

Zhao, Guo Ping
The Research of Control Strategy of Permanent Magnet Synchronous Motor for Hybrid Electric Vehicles

Zhao, Hantao
Application of Locating Technology in the Highway Emergency Response System

Zhao, Hong-yuan
Research on the Design of Inner Horizontal Surface of the Airport

Zhao, Huaiyun
Simulation and Analysis for Stick-Slip Vibration of Locomotive with Hollow-Shaft Drive System

Zhao, Jianyou
Research on the Impact of Drivers' Heart Rate on Longitudinal Slope of Freeway

Tunnel

Zhao, Jinhuan
Estimation of Original-Destination Matrices for Public Traffic Passenger Flow

Zhao, Junhai
Plastic Behavior for Compaction Pile with Hole Expanded by Blasting or Tamping Techniques

Zhao, L.
Collision Avoidance among Multiple Ship Agents
Hybrid Genetic and Taboo Search Algorithm for Solving the Bus Timetable Problem

Zhao, Q.
RGB Based Crowded Pedestrian Counting in Red Light Time
Short-Term Traffic Flow Prediction with ACD and Particle Filter

Zhao, Qiang
Analysis on Vehicle No-Sideslip Single Side Skid Equivalent Frictional Coefficient

Zhao, Qiao-xia
Effects of Lane Changing in Heterogeneous Traffic Flow

Zhao, Shuzhi
The Applied Research on Forecasting Cargo Volume of Northeast Economic Zone by Systemic Dynamics
Research on Dynamic Safety Stock Based on Short-Term Weather Forecasting

Zhao, Wansheng
Study on Power Control of Electric Power Steering System

Zhao, Wen
Measurement and Simulation Study on Ground Subsidence Induced by Shield Tunneling in Sandy Stratum

Zhao, Wenyi
Analysis for Principal-Agent Relationship between Owner and Construction Agent of Agent-Construction Project

Zhao, X.
Experimental Study on Sound Countermeasures against Driver Fatigue

Zhao, Xianyao
Study on the Method of “Inverse Four-Step” Regulatory Transportation Planning

Zhao, Xiaoyan
Experimental Study on Performance of the Bridge Deck Pavement of SF-PFSC

Zhao, Xioayan
Design and Construction of Overlay with Mechanical Joint Element on Used Concrete Pavement

Zhao, Yali
A Multi-Class Multi-Modal Combined Model for TDM Measures Evaluation in Large Scale Urban Transportation Network
Investment and Finance for the Intelligent Transportation System in China
Case Study: Analysis of CO_2 Emissions Caused by Customers Transportation in Shanghai and Shenzhen IKEA

Zhao, Yan-qing
Effects of Layer Interface Conditions on Fatigue Behavior of Asphalt Pavements with Semi-Rigid Bases

Zhao, Yanqing
A Discontinuous Numerical Method for Asphalt Mixture

Zhao, Yinghua
A Fatigue Test on Fiber Reinforced Asphalt Mixtures

Zhao, You-ting
A Retrograde Vehicle Detection Method Based on the Optical Flow Field

Zhao, Yue
A Model of Mixed Land Use and Trip Production by BP Neural Network

Zhao, Yufeng
Study on the Frost Resistance Test Method of Lime-Fly Ash Stabilized Material Base Course

Zhao, Z. B.
Congestion Pricing Revenue Redistribution Strategy Based on Traffic Behavior
Mean-CVaR Model of Wholesale Price Contracts and Dual Purchase Contracts in the Supply Chain

Zhao, Zheng-jun
Experimental Study on Behavior of Geotextile-Reinforced Soil

Zhao, Zhong-jie
Accident Prevention and Inducement Strategy in Highway Tunnel

Zhen, Hong
A Nonlinear Model for Decision-Making for Container Slot Chartering and Allocation under Liner Shipping Alliance

Zheng, Bing-qian
Gradually Rolling Prediction of the Use-Level of Road Network Based on BP Neural Network

Zheng, C.
Research on Urban Intersection Vehicle Emission Reduction Based on Microcosmic Simulation

Zheng, Changan
Optimization Theory of Regulation on Rural Transit Market Based on Rule of Transport Equality

Zheng, Jian-long
Fracture Mechanics Analysis of Cracking in Asphalt Pavement Widening

Zheng, Jianlong
Traffic Management on an At-Grade Signalized Intersection Connecting to Urban Expressway Ramps

Zheng, Ke
Research of Company Freight Traffic Generation Prediction Models in High-Tech Park

Zheng, Lili
Study on Accident Reconstruction Model Based on Reverse-Reasoning Method

Zheng, M.
Influence of Crack Size of Old Concrete Pavement Slab on Structure Stress of Asphalt Overlay

Zheng, S.
Probabilistic Pedestrian-Vehicle Conflict Micro-Model in Non-Signal Controlled Multi-Lane Segments

Zheng, Xiao-yan
Accident Prevention and Inducement Strategy in Highway Tunnel

Zheng, Zhong-Yi
Study on the Method for Calculating Ship Squat in the Restricted Channel

Zhong, Lei

Bus Location Display System Based on GPRS

Zhong, Ming
Modeling Logistics and Supply Chain with an Integrated Land Use Transport Model: PECAS

Zhong, Qinglong
Analyzing the Motivation of Queue-Jumping Driving-Action on Transportation Systems by Prospect Theory

Zhong, X.
Study on the Rules of Crash Distribution

Zhou, Chang-hong
Effects of Layer Interface Conditions on Fatigue Behavior of Asphalt Pavements with Semi-Rigid Bases

Zhou, Chang-jun
Research on Relationship between Fine Aggregate Angularity and Asphalt Mixture's Anti-Shear Ability

Zhou, Changhong
A Discontinuous Numerical Method for Asphalt Mixture

Zhou, Chao
The Method of Determining Traffic Impact Range of Developing Project Based on Threshold Value

Zhou, D. P.
Analysis of a New Combined Micropile Structure for Preventing Slope Slippage and Its Application in a Practical Project

Zhou, D.
Research on Dynamic Measuring System and Model of Novel High Speed Railway Vehicle Bogie

Zhou, Guiliang
Design of Intelligent Decision Module for Storage Location Assignment in AS/RS

Zhou, Huaguo
Effects of Roadway Lighting Level on the Pedestrian Safety

Zhou, J.
Effect of Electro-Mechanical Coupling on Dynamic Performance of Crankshaft of ISG HEV

Zhou, Jianglin
Characteristics of Fundamental Data for Railway Maintenance and the Construction of Integrated Data Platform

Zhou, Jiaxiang
A Multi-Objective Decision Model of Traffic Rescue Service Site Location on Road

Zhou, Libo
Rut-Resisting Capacity of the Whole Surface Course in Continuous Upgrade under Heavy Loading

Zhou, Mingjie
Experimental Study on Performance of the Bridge Deck Pavement of SF-PFSC
Design and Construction of Overlay with Mechanical Joint Element on Used Concrete Pavement

Zhou, Minjuan
Experimental Investigation of the First Precast Bi-Pre-Stressing Simple Girder Concrete Bridge

Zhou, Na
Grey Relational Analysis Method of Main Reasons of Road Traffic Accidents

Zhou, Quan
Impact on Regularity of Track from Pile Underpinning of Light Railway Bridge

Zhou, W.
Using VISSIM to Calculate the Capacity of Urban Expressway Interchange

Zhou, Xianyan
Study on Long-Term Behavior and Ultimate Strength of CFST Columns

Zhou, Xiaobo
Enhancing Immersion through Adjusting Parameters of Vehicle Driving Simulator

Zhou, Xuemei
Travel Mode Choice in Large Cities of China Based on Loss Aversion Theory

Zhou, Zhigang
Traffic Management on an At-Grade Signalized Intersection Connecting to Urban Expressway Ramps

Zhou, Zhihui
Limit Value of Railway Bridge for Traffic Safety

Zhou, Zhuping
Predicting Methods of Trip Modal-Split Based on Structural Model

Zhu, Haiying
Optimization of Open Vehicle Route to Reduce Fuel Consumption Based on Genetic Algorithm

Zhu, Hong-ping
Study on Different Residual and Weight Coefficient in Model Updating of Bridge Structure

Zhu, Li-Li
A Calculation Method for the Information Utility of Traffic Guide Signs

Zhu, Liangliang
Analysis on Mechanical Performances of High-Speed Railway Transition Curves

Zhu, S.
Research on Calculation of Important Parameters of Freeway Financial Post-Evaluation

Zhu, Shun-Ying
Study on Using OD Traffic Flow to Identify the Special Boundary of the Expressway Influence Zone

Zhu, Shunying
Enhancing Immersion through Adjusting Parameters of Vehicle Driving Simulator
Design Theory for Speed Control by Using Constant Edge Rate
The Reasonable Distance of Unsignalized Crosswalks Based on Traffic Flow, Stability, and Efficiency

Zhu, Tulong
Laboratory Investigation of Reclaimed Asphalt Pavement Mixed with Pure Binder Using X-Ray CT Scanner

Zhu, W.
Link Average Speed of Traffic Flow Estimation Method Based on Floating Car

Zhu, Xianyuan
Study on Intersections with Median BRT Stations: Focused on Pedestrian Street-Crossing Characteristics

Zhu, Xiaodi
Design and Validation of Wireless Dynamic Testing System for Bridge Based on the 941B Type Vibration Sensor

Zhu, Yanru
Design of Intelligent Decision Module for Storage Location Assignment in AS/RS

Zhu, Yaoting
Viscoelastic Analysis of Asphalt Pavement Using a Regularized Interconversion Technique between Creep and Relaxation

Zhu, Yonggang
The Applied Research on Forecasting Cargo Volume of Northeast Economic Zone by Systemic Dynamics

Zhu, Zhanyuan
Stability of Slope with the Weak Structural Plane Based on 2-D Nonlinear Finite Element Method
Vibration Characteristics of Permafrost Embankment Induced by Passing Trains in Qinghai-Tibet Railway in Winter
Stability and Reinforcement Analysis of a High and Steep Cataclastic Rock Slope

Zi, X.
Study on Burner Type Diesel Particulate Filter System Using Compressed Air from Turbocharger

Zou, H. X.
Urban Road Travel Speed Estimation Based on Low Sampling Floating Car Data

Zou, Hai-bo
Principle Analysis and State Evaluation on Coordinated Development among Transportation Modes

Zou, Jianwen
Application of Thermal Stress Controlling in Construction of Large Bridge Cushion Cap

Zou, Tiefang
Parameter Sensitivity Analysis of Accident Reconstruction Model Based on Orthogonal Design

Zou, Zhichong
Intelligent Emergency Traffic Evacuation Spatial Decision Support System for Urban Disasters

Zou, Zuyin
Stability and Reinforcement Analysis of a High and Steep Cataclastic Rock Slope

Zuo, Wen-xin

Research on Relationship between Fine Aggregate Angularity and Asphalt Mixture's Anti-Shear Ability